Second Edition

Mechanism in Protein Chemistry

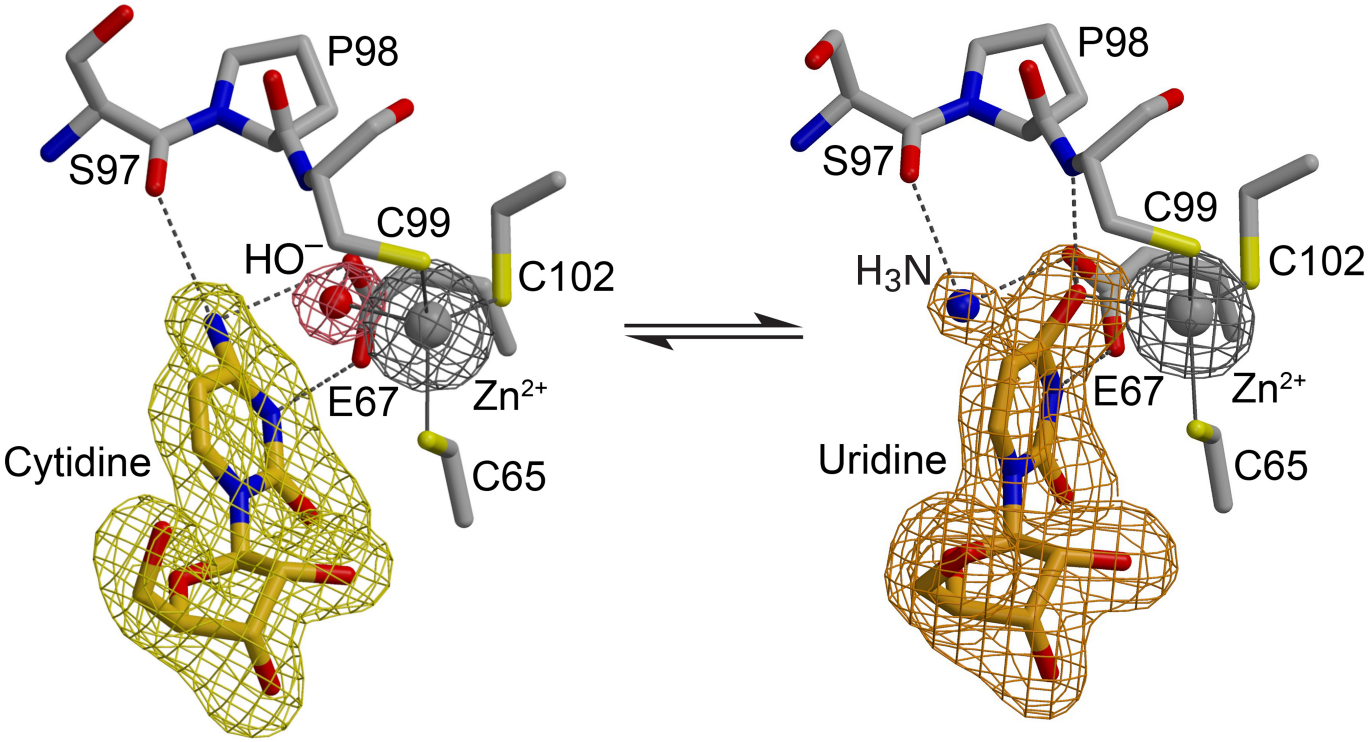

Jack Kyte

with the editorial assistance of
Heather Cammarn

Mechanism in Protein Chemistry

Second Edition

Jack Kyte

Emeritus Professor of Chemistry
University of California at San Diego

With the editorial assistance of

Heather Cammarn

The supplemental material is a list of the Equations, Structures, Figures, and Tables for each chapter in the order in which they appear in the text to make it easier for the reader to find one of them while reading the text.

Erst die Theorie entscheidet darüber, was man beobachten kann.
Attributed to Einstein by Heisenberg

Dedicated to my teachers

Richard Ramette
Charles Carlin
John Edsall
Klaus Weber
Guido Guidotti
Jon Singer
Russell Doolittle
Charles Perrin

Table of Contents

Preface

Over the past 70 years, our understanding of the strategies that are used by enzymes to catalyze their respective reactions has expanded so dramatically that, except for the explanations of every known enzyme, it could well be complete. At the moment, it seems unlikely that some new, as-yet-undescribed strategy will be discovered. It is the purpose of this text to present a comprehensive description of these strategies. It is not, however, intended to be a comprehensive, encyclopedic catalogue of the enzymes for which mechanisms are available, systematically presenting the mechanisms of each in its appropriate category, although this is sometimes done.

It is also the purpose of this book to describe the many techniques that are used to study enzymatic mechanisms. Each method provides information about a particular strategy and can be discussed as the respective strategy is discussed. The most informative observation about the mechanism of an enzyme is a crystallographic molecular model of that enzyme with its active site occupied by substrates in equilibrium with each other in which reactants and products are both observed or by an analogue of a high-energy intermediate in the normal reaction. The majority of our understanding of the mechanisms of enzymatic reactions, however, comes from chemical studies of these mechanisms. In fact, even the design of an analogue of a high-energy intermediate usually requires that a significant amount of chemical information has been gathered. Furthermore, even when a crystallographic molecular model of substrates at equilibrium or an analogue of a high-energy intermediate within an active site is available, its interpretation usually relies heavily on the available chemical information. At the moment, a comprehensive understanding of the methods that are used to study enzymatic mechanisms, as well as the limitations of these methods, is necessary, and for this reason these methods are discussed critically in this text.

Because an understanding of enzymatic mechanisms requires a firm knowledge of mechanistic organic chemistry and molecular association and and because an understanding of the techniques used to study these mechanisms requires a firm knowledge of kinetics, thermodynamics, synthetic organic chemistry, and analytical chemistry, the text places severe demands on the student. The concepts of mechanistic organic chemistry and molecular association are incorporated into structural drawings of individual molecules and chemical reactions. The kinetics and thermodynamics are represented in mathematical equations. The results of the particular techniques used to study enzymes are presented as graphs and tables from the original literature. The crystallographic molecular models are observed in stereo images. The student must have the background necessary to read each of these languages.

Before this book became so comprehensive, it was intended for a course in the mechanism of enzymatic reactions. Consequently, there are suggested readings in which the concepts discussed in each section are applied in an experimental setting. There are citations within the text that support the conclusions drawn but are also intended to direct the student to the research literature, and there are problems at the end of each section, based on actual experimental results, that are to be evaluated by the student. The original purpose of the book was to give the student the wherewithal to take charge of her own education by reading critically the experimental literature. To accomplish such a goal, she must be able to understand the experiments performed and be able to reach the same conclusions as did the authors or to realize that the authors were mistaken. It was my intention to develop in the student the ability to draw her own conclusions from only the experimental results.

The book, however, has expanded somewhat beyond its initial purposes and become a monograph covering the subject of the mechanism of enzymes. The advantage of publishing online is that the student can download the book, and a professor can choose to cover only particular portions of the book. The disadvantage is deciding which portion to choose.

Over the last year I have had the privilege to work with Heather Cammarn, an experienced chemical copyeditor going over the manuscript of this book. Her assistance has been invaluable. Heather was also the copyeditor for the first edition of this book. I have been impressed by the fact that each time she or I have read through a proof, one of us, usually Heather, has found errors I missed as I was

writing the text. I am certain that some still exist and would be grateful to any reader who draws them to my attention.

It is a pleasure to thank everyone who has helped me in the preparation of this book. My wife, Francey, beyond the call of duty, typed the first draft of the manuscript. Jack Kirsch read the entire manuscript of the first edition with remarkable care, understanding of the chemistry, and attention to detail. Individual sections of the manuscript for the first edition were reviewed critically by Charles Perrin, Tom Bruice, Bill Parson, Paul MacPherson, Ted Traylor, David Dolphin, Wallace Cleland, Jonathan Cohen, Howard Schachman, Paul Bartlett, David Matthews, Jeremy Knowles, Judy Klinman, Craig Townsend, Fred Hartman, Paul Saltman, Don Tilley, Bill Trogler, Marion O'Leary, Paul Boyer, and Bruce Kemp. Individual sections of the second edition were reviewed critcally by Tadhg Begley, Faruk Nome, Paul Cook, Harry Gray, Bob Blankenship, Judy Klinman, Neil Marsh, Dave Ballou, Dan Herschlag, Frank Jordan, Hazel Holden, Ivan Rayment, Bill Trogler, Michael Toney, Andrew Bennet, David Silverman, Russ Hille, Roberta Colman, Bob White, Elias Arner, Francesco Tarantelli, Doug Rees, Rick Debus, Johannes Messinger, Chris Murray, Paul Ortiz de Montellano, Janos Lanyi, Donald Hilvert, Ed Solomon, Sean Elliott, Nick Williams, Paul Fitzpatrick, Bob Gennis, Steven Boxer, and Stuart Edelstein. Each of them were kind enough to read the manuscript critically and provide many helpful comments.

Jack Kyte
December 2024
La Jolla, California

Stereodrawings

Almost all the stereodrawings of crystallographic molecular models included in this book were produced by the program Molscript, created by Per J. Kraulis. To understand how the active sites of enzymes achieve their catalysis, anyone interested in understanding enzymatic mechanisms must learn to view these images in stereo. Although a few individuals can view them effortlessly by crossing their eyes, the rest of us need a stereo viewer. Stereo viewers of various qualities can be purchased at:

https://www.walmart.com/ip/American-Educational-Table-Top-Stereo-Glasses/115919914

https://www.forestry-suppliers.com/Search?stext=stereoviewer

https://www.navafresh.com/products/pocket-stereoscope?srsltid=AR5OiO18ZMCEmIJDRadipw54xy402jsC2rXc7pZiJG4fSX6LkabfFbnm_1c

It has been my experience that a student who has never viewed a stereodrawing before will usually complain that although everyone else can learn to use one of these viewers, he cannot. It is also my experience that everyone learns to use one. When I have put a question on an examination where one is asked to write down the sequence of the protein by examining a drawing of a crystallographic molecular model that none of the students has seen before, everyone in the class gets at least 90% of the sequence correct, which would have been impossible unless everyone was able to see the image in stereo. The stereodrawings in the text have been placed on separate pages with their legends so that each of these pages can be printed. Unless they are printed, you cannot view them properly in adequate detail, which is essential. In the text, the drawings are in black-and-white to accommodate a black-and-white printer. In the list of Equations, Structures, Figures, and Tables, the stereodrawings are presented in color. The colors are those of the CPK convention: carbon, black (coal); nitrogen, blue (sky); oxygen, red (fire); phosphorus, orange (an elemental allotrope); sulfur, yellow (elemental); and fluorine and chlorine, pale green (gas). Other colors used are alkali and alkaline earth metals, light gray (metallic); vanadium, pale yellow (VO^{3+}); manganese, purple (permanganate); iron, brown (rust); cobalt, blue (cobalt blue); nickel, dark green (hexaaquo Ni^{2+}); copper, green (cupric oxide); zinc, dark gray (metallic); and molybdenum, dark blue [Mo(V)]. These stereodrawings can be printed on a color printer if one is lucky enough to have access to one, and the printed copies can then be viewed in stereo.

IUBMB and IUPAC

The names of all enzymes are in the nomenclature of the IUBMB (https://www.enzyme-database.org). Unfortunately the committee sometimes changes the names, a practice which is somewhat exasperating. The names of all substrates for enzymes that are used in the reactions given in that database are used for these compounds. The names for all other biochemical compounds that have been assigned by the IUBMB have also been used (https://iubmb.qmul.ac.uk) The terms used in the discussion of enzyme kinetics are those used by the IUBMB (https://iubmb.qmul.ac.uk/kinetics/) All chemical compounds that have not been named by the IUBMB are given the names determined by the IUPAC nomenclature. A searchable copy of those rules can be downloaded (https://iupac.qmul.ac.uk/BlueBook/PDF/), and a list of substituent names is also available (https://www.acdlabs.com/iupac/nomenclature/79/r79_1036.htm). The definitions of many of the chemical and physical terms (albeit in rather awkward rhetoric), units of measure, physical quantities, and physical constants used in this book can be found in the IUPAC Gold Book (https://goldbook.iupac.org/terms). Values for pK_a noted in the text (http://www.fm.ehcc.kyoto-u.ac.jp/pKa_compilation_Williams_RipinEvans.pdf) can be found in the table compiled by William Jencks. The sequences of the amino acids for most, if not all, enzymes discussed can be found in Uniprot (https://www.uniprot.org/) as well as the names of all species from which those enzymes come (select Taxonomy).

Protein Data Bank

The Protein Data Bank (https://www.rcsb.org/ search/advanced) contains the atomic coordinates of almost all crystallographic molecular models that have been constructed. At the moment there are 1,070,000 separate molecular models entered in the data bank. You should look at some of the lists of the full coordinates to get a feeling for what such a file contains. Enter the name of a protein for which there is a stereodrawing in the text of this book, click on the name of one of the molecular models that are then listed, choose “Download Files”, and then choose “PDB File”. The atoms are listed by the name of the amino acid, the position of that amino acid in the sequence of the protein, and their locations within that amino acid. The list tabulates the *x*, *y*, and *z* coordinates of each atom in angstroms (tenths of nanometers). Each file constitutes the raw data on which the Molscript program operates.

Chapter 1
Mechanisms for Reactions

Chemistry is the study of the behavior of electrons. Electrons in molecules behave in a certain, ultimately understandable way and the nuclei follow them passively. A chemical reaction is a sequence of rearrangements of electrons in the molecules involved that turns reactants into products. The rearrangements of the nuclei are automatic and are driven by the rearrangements of the electrons. The exercise of understanding the behavior of the electrons begins with a known chemical reaction for which the reactants, catalysts, and products have been defined by earlier observation. In order to understand that chemical reaction, one first has to account for each pair of electrons and know its location in the molecules that are the reactants and the molecules that are the products. Their locations in reactants and products usually provide insight into what happened to them in the transition states and intermediates in the reaction. A complete understanding, however, comes from learning enough about the behavior of electrons in general to figure out how they behave in a particular reaction as reactants are turned into intermediates and intermediates are turned into products.

Metabolism is the ensemble of the coordinated sequences of chemical reactions and physical processes that occur within all living cells to provide energy (catabolism) and to accomplish biosynthesis (anabolism). Each discrete step in any one of the sequences of reactions in the ensemble is catalyzed by a unique enzyme. An **enzyme** is a molecule of protein that catalyzes a particular chemical reaction. For example, the enzyme fumarate hydratase in the mitochondria from porcine heart is a molecule of protein composed of four identical subunits, each of which is a folded polypeptide 466 amino acids long. The enzyme catalyzes the interconversion of fumarate and (*S*)-malate

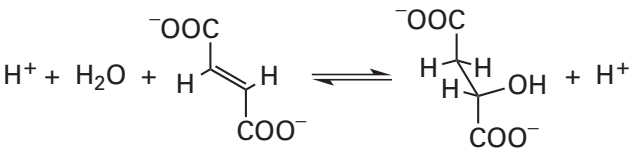

(1–1)

a reaction that is found in the sequence of reactions that comprise the citric acid cycle.* In most instances, the only role that a particular enzyme plays in a particular cell is to catalyze its particular chemical reaction and only its chemical reaction. During the catalysis of its reaction by an enzyme, the electrons in the reactants, the electrons in the catalytic groups on the enzyme that are involved in the reaction, the electrons in the intermediates in the reaction and its transition states, and the electrons in the products behave just as they always do. There is no magic to enzymatic catalysis. An enzymatically catalyzed reaction is a chemical reaction.

The sequences of chemical reactions that constitute the **metabolic pathways**—for example the citric acid cycle—can be written out in an organized scheme and committed to memory systematically. Each reaction in one of these sequences uses as its reactants the products of the reaction or reactions that precede it, and the products of each reaction are the reactants for the enzyme or enzymes that follow it on the chart. The diagrams of metabolic pathways leave the impression that metabolism is a highly organized and neatly ordered system. This organization, however, does not extend to the enzymes themselves, which, as the products of evolution by natural selection, are a motley collection. Within a particular metabolic sequence of reactions, each of the consecutive enzymes is usually a protein with a sequence of amino acids that is unrelated to the sequences of amino acids in the other enzymes; each is usually a protein with a stoichiometry of protomers unrelated to the stoichiometries of the protomers of the other enzymes; and each is usually a protein with a native molecular

*Fumarate and (*S*)-malate are both dianions. In the strictest sense, when referring to them, one should write fumarate ion and (*S*)-malate ion. The International Union of Biochemistry and Molecular Biology, however, in almost all cases omits the word ion, for example, simply using as the name fumarate or (*S*)-malate. In this book, that convention will be followed. When a name ends in –ate, for example phosphate, acetate, and so forth, it will be assumed that the reader understands that this name refers to an anion. When a name ends in –ium, for example ammonium, iminium, and so forth, it will be assumed that the reader understands that this name refers to a cation. Ambiguous names will be followed by the word ion.

structure unrelated to the native molecular structures of the other enzymes.

Consequently, when the enzymes themselves are discussed, they are not arranged in the order in which they occur in metabolic pathways. They can be presented as members of the various **families of proteins** that recapitulate their evolutionary relationships. This approach emphasizes structural homologies. Unfortunately, evolutionally related enzymes often catalyze chemically unrelated reactions. Enzymes can also be presented in categories reflecting the **types of chemical reactions** that they catalyze. Unfortunately, different enzymes sometimes catalyze homologous chemical reactions by different chemical mechanisms. Consequently, it is more effective to discuss the chemical strategies by which enzymes catalyze reactions and to use particular enzymes as examples of those strategies.

The **substrates** of an enzyme are the molecules that are interconverted by that enzyme as it catalyzes its own peculiar reaction. The substrates for the enzyme appear in the equation describing the equilibrium that it catalyzes—for example, water, fumarate, and malate are the substrates for fumarate hydratase. In the cytoplasm of the cell, all of the substrates of an enzymatic reaction are usually present simultaneously. In an experiment, the investigator decides which substrates will be the **reactants** and which will be the **products** of the reaction. This decision is made when a solution is prepared containing only the substrates on one side of the chemical equation—for example, a solution containing only malate—so that those substrates become the reactants, and the substrates produced during the reaction are the products.

An enzyme is a **catalyst**. As with any catalyst, an enzyme controls the reaction that it catalyzes by forming a molecular complex with the reactant or the reactants. The **active site** of an enzyme is the unique location on the surface or in the interior of one of its subunits where the reaction catalyzed by that enzyme takes place. The reactant or reactants must associate with the active site before the catalyzed reaction can occur. As a catalyst, an enzyme displays particular **abilities** and is constrained by particular **rules**.

When an enzyme (for example, fumarate hydratase) is added to a solution containing the reactants designated by the investigator (for example, an aqueous solution of malate), all of the products of the reaction that it catalyzes (for example, fumarate and water) are formed at a **greater rate** than they would have been in the absence of the enzyme. This increase in the rate of the reaction is directly proportional to the molar concentration of the enzyme but is almost never directly proportional to the molar concentration of reactant. At concentrations of reactants less than their dissociation constants from the active site of the enzyme, only a fraction of those active sites are occupied with reactants participating in the reaction at a given instant, but at saturating concentrations of reactants in excess of their respective dissociation constants, all of the active sites are occupied and busy catalyzing the reaction at a given instant. For enzymes that catalyze reactions in which there is only one reactant, the rates of those reactions when they are catalyzed in the respective active sites under these conditions of saturation are usually between 10 s^{-1} and 10^6 s^{-1}. These rates represent accelerations of the respective uncatalyzed rates[1-5] of 10^5 to 10^{21}, which are significant enhancements. On the active site of porcine fumarate hydratase,[6] the rate of the enzymatically catalyzed dehydration of malate at saturation is 700 s^{-1} at pH 6.8 and 37 °C, which represents an enhancement over the uncatalyzed rate[6-8] of between 10^{16} and 10^{17}.

Because of the problem of entropy of mixing, there is no agreement on which units should be used to compare the rate of an enzymatically catalyzed bimolecular or termolecular reaction with the rate of the respective uncatalyzed reaction. The rate of hydrolysis of alkyl sulfates, however, which is technically a bimolecular reaction, is accelerated by sulfatases by a factor of as much as 10^{26} relative to the monomolecular rate of the reaction in aqueous solution.[9] For a bimolecular reaction in which neither reactant is water, regardless of which units are chosen, the difference in rate between the enzymatically catalyzed reaction and the same uncatalyzed reaction is large.

An enzymatically catalyzed reaction is also **more specific** than the respective uncatalyzed reaction. For example, the enzyme fumarate hydratase produces only (*S*)-malate (Equation 1–1), while the uncatalyzed reaction[8] produces both (*S*)-malate and (*R*)-malate, as well as other side products such as maleate. The very **low yield of undesired side products**, which would normally appear in significant yield in an uncatalyzed reaction, is an essential requirement for each enzyme if the sequences of the reactions that comprise metabolism are to operate efficiently.

Under normal circumstances, tens to tens of thousands of molecules of substrate are interconverted during each second by one molecule of

enzyme. Therefore, little enzyme, in terms of its molar concentration relative to the molar concentrations of its substrates, must be added to produce a sufficient increase in the forward and reverse rates of the reaction. For this small amount of enzyme to be able to process these much larger amounts of substrates so efficiently, each molecule of enzyme, ready to process the next molecule of reactant, must be **regenerated in the same state** at the end of each turnover. This rule applies to any catalyst.

Because it is present in the solution in low molar concentration and because it must be regenerated after each transformation, an enzyme cannot be a stoichiometric participant in the chemical reaction. Therefore, an enzyme, under these normal circumstances, **cannot affect the equilibrium constant** and cannot affect the change in standard free energy of the reaction.* There are exceptions to this rule. These exceptions are the frequently encountered situations in which the molar concentration of an enzyme is artificially adjusted by an investigator in a particular experiment to within an order of magnitude of the molar concentrations of the substrates, as well as situations in which the concentration of an enzyme in the cell is actually greater than that of its substrates.[11]

Because an enzyme cannot change the equilibrium constant of a reaction as long as it is not itself a reactant or a product, it necessarily follows that, in spite of the amazement some investigators express at discovering this fact,[12] if the enzyme catalyzes the reaction in one direction, it must also catalyze the reaction in the other direction, even in situations in which the equilibrium constant for the reaction is very large.[13,14] The principle of **microscopic reversibility**, when applied to an enzymatically catalyzed reaction, is that the enzymatically catalyzed reaction must pass through the same transition states but in opposite order in the forward and reverse directions. The enzyme accelerates the reaction by lowering the relative free energy of one or more of the transition states in this sequence. Therefore, it must accelerate the reaction in both directions. For this reason, enzymatically catalyzed reactions are, as are all chemical reactions, **approaches to equilibrium**. It just happens to be the case that most biological reactions have changes in standard free energy between 40 and –40 kJ mol^{-1} and that an enzyme can rapidly bring its substrates to equilibrium, so the equilibria are more obvious. At pH 7 and 25 °C, the ratio between the concentration of fumarate and the concentration of (*S*)-malate is 0.22 at equilibrium.[15]

A **heterolytic reaction** is a reaction in the mechanism of which covalent bonds are always broken in such a way that both electrons in the bond being broken remain with only one of the two fragments between which the bond is broken. In addition, a heterolytic reaction is a reaction in the mechanism of which covalent bonds are formed in such a way that both electrons in a bond being formed arrive on the same reactant. The heterolytic reactions that occur on the active sites of enzymes proceed by mechanisms that often resemble closely the normal chemical mechanisms of similar organic reactions that proceed in solution without enzymatic catalysis. An enzyme usually accelerates a particular heterolytic reaction by controlling the steps that would normally occur even in its absence. It follows that the first step in any examination of the mechanism of a particular enzyme is to write out in exhausting detail one or more realistic chemical mechanisms for the reaction of interest as it would proceed in the absence of enzymatic catalysis and focus upon the specific features of those mechanisms that are vulnerable to manipulation by the enzyme. Therefore, a logical place to begin a discussion of enzymatic catalysis of heterolytic reactions is to examine the established chemical mechanisms of reactions similar to those that are catalyzed by such enzymes.

A **homolytic reaction** is a reaction in the mechanism of which covalent bonds are always broken in such a way that in a bond being broken, each of the molecular fragments between which the bond is broken retains one of the bonding electrons. In addition, a homolytic reaction is a reaction in the mechanism of which covalent bonds are always formed in such a way that in a bond being formed, each of the molecular fragments between which the bond is being formed provides one of the ultimate two bonding electrons. The homolytic breaking of a bond produces two radicals, and the homolytic formation of a bond, **colligation**, combines two radicals. A minority of the extant enzymes catalyze the reactions for which they are responsible homolytically. In the absence of the enzyme, these reactions usually do not occur, or if they do occur, they do not proceed homolytically. In order to catalyze a reaction homolytically, the enzyme must carefully direct the regioselectivity of each step in addition to enhancing its rate. Without an enzyme to direct

*Occasionally, there are publications that seem to indicate that the authors have forgotten the fact that an enzyme cannot alter the equilibrium constant for a reaction.[10]

its regioselectivity, a homolytic reaction usually proceeds along several different paths, one or none of which produces the product that the enzyme produces. Consequently, it is best to refrain from discussing homolytic reactions until the enzymes that catalyze them are discussed.

When a heterolytic reaction is studied as a model for the same reaction or a homologous reaction that is catalyzed by an enzyme, it is usually assumed that the most relevant model reaction is the one that proceeds in aqueous solution. Unless otherwise noted, all of the mechanisms discussed in this chapter will be for **nonenzymatic reactions occurring in water**.

*Transfer of a Hydron**

The molecules to be discussed, be they enzymes, substrates, or prosthetic groups, usually have several or many acidic hydrons and several or many basic lone pairs of electrons. Consequently, it is essential to make a distinction between, on the one hand, the various acidic hydrons and basic lone pairs of electrons in a molecule and, on the other hand, the molecule in which they are located. In other words, in biochemistry the molecules themselves are neither acids nor bases but frameworks on which acids and bases are distributed. For the sake of this discussion, **an acid is an acidic hydron and the atom to which it is attached. A base is a basic lone pair of electrons and the atom with which it is associated.**

Historically, an acid was any molecule that, when added to water, decreased the pH of the water and a base was any molecule that, when added to water, increased the pH. It is also the case that, in the abstract, one can use the term "acidic molecule" to describe a molecule, such as sulfuric acid, in which there are only acidic hydrons. Similarly, one can use the term "basic molecule" to describe a molecule, such as trianionic phosphate, in which there are only basic lone pairs and no acidic hydrons. Such molecules, however, are seldom encountered in biochemistry. It is obvious that the historical definitions and habits are ambiguous when applied to most of the molecules to be discussed here. In fact, water is an excellent example of the ambiguity.

Water is both an acid and a base. When it is performing the role of an acid, water can provide a hydron in two ways: as its conjugate acid, the hydronium, or by itself. Water itself is an acid, albeit a weak one ($pK_a = 15.74$),* but its concentration (55.5 M) can overcome much of this deficit. Every basic lone pair of electrons on any molecule dissolved in an aqueous solution is adjacent to the hydrogen on a neighboring molecule of water and is usually already in a hydrogen bond with one of them, and that lone pair of electrons can immediately accept a hydron from that molecule of water. When it is performing the role of a base, water can remove a hydron in two ways: as its conjugate base, the hydroxide ion, or by itself. Water itself is a base. It is a weak base because its conjugate acid, a hydronium ion, is a strong acid ($pK_a = -1.74$). It is, however, a concentrated weak base (55.5 M). In aqueous solution, every acidic hydron on a dissolved molecule is adjacent to one of the lone pairs of a molecule of water and is usually already in a hydrogen bond with one of them, and that hydron can be immediately transferred to that molecule of water.

The **hydronium ion**, unavoidably present in aqueous solution, is composed of one hydron and some combination of either four molecules of water[16-20]

*According to the rules of the IUPAC, **hydron** is the general name for the cation H^+. Hydron is a general name to be used without regard to the nuclear mass of the hydrogen entity, either for hydrogen in its natural abundance or where it is not desired to distinguish between the isotopes. A **proton** is the nuclear particle of charge number +1 and rest mass of 1.007 276 470(12) unified atomic mass units. When discussing nuclear magnetic resonance spectroscopy, the proper term for the hydrogen nuclei being observed is protons since nuclear magnetic resonance, as it is commonly used, registers absorptions only from nuclei that consist of one proton and no neutrons.

*The only purpose of an acid dissociation constant is to compare acids and bases, one to the other. By the accepted convention, from which no acid is excepted, an acid dissociation constant is defined as the product of the molar concentration of hydronium ion and the molar concentration of the conjugate base of the acid divided by the molar concentration of the acid. Even though, by this convention, the concentration of the conjugate base of the hydronium ion is omitted from every acid dissociation constant, each of them is an equilibrium constant that must apply in any situation at standard temperature (25 °C) in an aqueous solution of any pH. In pure water at pH 7 and 25 °C, the concentration of hydronium ion is $10^{-7.00}$ M; the concentration of the conjugate base, hydroxide ion, is $10^{-7.00}$ M; and the concentration of water, the acid, is 55.5 M. Consequently, the pK_a of water is 15.74. Because, at any given instant, the hydron in a hydronium ion is on a single molecule of water, it is assumed that the conjugate base of a hydronium ion is water. In pure water, at pH 7.00 and 25 °C, the concentration of hydronium ion is $10^{-7.00}$ M; the concentration of water, the conjugate base, is 55.5 M; and the concentration of hydronium ion, the acid, is $10^{-7.00}$ M. Consequently, the pK_a of a hydronium ion is −1.74. At any pH, at standard pressure, and at 25 °C the concentration of hydronium ion times the concentration of hydroxide ion is $10^{-13.995}$ M. This is not an acid dissociation constant, it is the water constant.

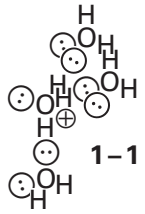

1–1

six molecules of water[17,18,21]

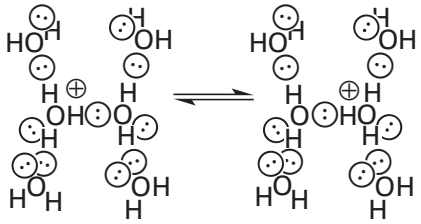

(1–2)

or 21 molecules of water.[22-25] The actual number of waters probably fluctuates, and its mean is unknown. At the periphery of the $H_9O_4^+$ ion (**1–1**), the $H_{13}O_6^+$ ion (Equation 1–2), or the $H_{43}O_{21}^+$ ion are 6, 8, or 10 hydrogen atoms, respectively. Each of these hydrogens is acidic and capable of being transferred within a hydrogen bond to a base in the solution. It is also capable of becoming the hydron of another hydronium simply by being transferred within a hydrogen bond to a neighboring molecule of water. Upon either of these transfers of a hydron, the original hydronium ion disappears. This arrangement makes each isolated hydron in an aqueous solution multivalent. It also enhances the rate of diffusion of the hydron, which appears to be limited not by transfer of hydrons among the waters but by rearrangement of the shells of hydration around the cation as it steps through the solvent.[18] For these reasons, in addition to its low pK_a (–1.74), the hydrated hydron, usually abbreviated H^+, is an efficient acid, a fact that can make up for its low concentration.

The **hydroxide ion**, also unavoidably present in aqueous solution, can be considered as a hydron hole. This hole is shared among the central oxygen and three or more of its nearest neighbors of water[26]

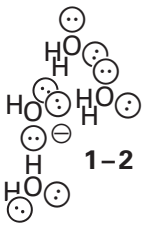

1–2

As with hydronium, this arrangement makes hydroxide a base that can diffuse more rapidly through the solution than any other base by extending its reach simultaneously to at least six lone pairs of electrons. Hydroxide is a strong base because its conjugate acid, a molecule of water, is a weak acid (pK_a = 15.74).

A reaction that occurs at the active site of an enzyme is usually compared to a reaction that occurs in aqueous solution. Because water is both an acid and a base, the mechanism of a reaction occurring in water is rarely hindered for want of hydrons that can be captured or for want of lone pairs of electrons onto which hydrons can be dumped, and these are taken for granted when the mechanism is written. The decision that the appropriate mechanism to use as a model for the one taking place within the active site of an enzyme is the mechanism occurring in aqueous solution implies that an additional assumption has been made about the nature of the active site of an enzyme; namely, that **the active site is at least as efficient a source of hydrons and lone pairs of electrons as an aqueous solution**. A corollary of this conclusion is that all of the removals and additions of hydrons, from and to the reactants, performed by water in the absence of the enzyme must be provided for within the active site of the enzyme by lone pairs of electrons and acidic hydrogens.

There are, however, differences between the transfer of a hydron that occurs in the active site of an enzyme and the transfer of a hydron that occurs in solution. The transfer of a hydron between any two lone pairs of electrons can proceed with the intermediate formation of a direct hydrogen bond[16,27] between acid and base

$$^{(+)}\mathrm{AH} + \odot\mathrm{B}^{(-)} \underset{k_{-1}}{\overset{k_1}{\rightleftharpoons}} {}^{(+)}\mathrm{AH}\odot\mathrm{B}^{(-)} \underset{k_{-2}}{\overset{k_2}{\rightleftharpoons}} {}^{(-)}\mathrm{A}\odot\mathrm{HB}^{(+)} \underset{k_{-3}}{\overset{k_3}{\rightleftharpoons}} {}^{(-)}\mathrm{A}\odot + \mathrm{HB}^{(+)} \qquad (1\text{–}3)$$

This sequence of steps is usually* what happens during the transfer of a hydron in an active site, where the distance and bond angles between a catalytic acid and the base it is to hydronate, or the distance and bond angles between a catalytic base

*There are exceptions in the active site of an enzyme. In those exceptional instances, a hydron is also relayed through a chain of hydrogen bonds, but even in those exceptions the relay is unique rather than promiscuous.

and the acid it is to dehydronate, are those of typical hydrogen bonds.[28] In solution, however, in some if not most instances in which a hydron is transferred from an acid to a base, the hydron is **relayed** from the acid to the base through two or three molecules of water[29]

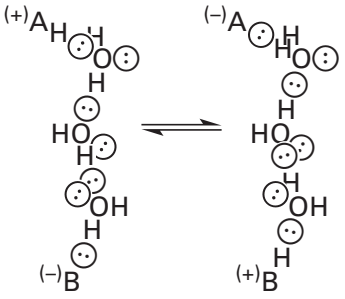

(1–4)

Consequently, the transfer of the hydron in solution can be considered to be the result of the **collision of the layer of hydration around the molecule containing the acid with the layer of hydration around the molecule containing the base.** Each acid in a molecule is incorporated into the surrounding layer of hydration as a donor in a hydrogen bond to a molecule of water in the layer. Each base in a molecule is incorporated into the surrounding layer of hydration as an acceptor in a hydrogen bond to a molecule of water in the layer. It is easy to imagine that whenever the layer of hydration surrounding the molecule containing the acid collides with the layer of hydration surrounding the molecule containing the base, one or more chains of hydrogen-bonded molecules of water connecting the acid to the base form immediately and indiscriminately. The hydron is relayed through one of these chains. In this relay (Equation 1–4), the actual hydron that arrives at the encounter complex on the acid in the one molecule is not the hydron transferred to the base in the other. This relay is the same process that occurs in solution during the transfer of a hydron from hydronium (**1–1** or Equation 1–2) to a base or from an acid to hydroxide (**1–2**). Before the layers of hydration can be penetrated during the collision, the transfer of the hydron from acid to base has occurred within the fused layers of hydration. The hydronated base and the unhydronated acid then dissociate from each other, even though they may never have formed a hydrogen bond with each other.

Consequently, the **relevant equation* in solution** becomes

$$\begin{aligned} {}^{(+)}\mathrm{AH}\cdot(\mathrm{OH_2})_m + (\mathrm{OH_2})_n\cdot\odot\mathrm{B}^{(-)} &\underset{k_{-1}}{\overset{k_1}{\rightleftharpoons}} \\ {}^{(+)}\mathrm{AH}\cdot(\mathrm{OH_2})_m\cdot(\mathrm{OH_2})_n\cdot\odot\mathrm{B}^{(-)} &\underset{k_{-2}}{\overset{k_2}{\rightleftharpoons}} \\ {}^{(-)}\mathrm{A}\odot(\mathrm{H_2O})_o\cdot(\mathrm{H_2O})_p\cdot\mathrm{HB}^{(+)} &\underset{k_{-3}}{\overset{k_3}{\rightleftharpoons}} \\ {}^{(-)}\mathrm{A}\odot(\mathrm{H_2O})_o + (\mathrm{H_2O})_p\cdot\mathrm{HB}^{(+)} & \end{aligned} \tag{1–5}$$

where $m + n = o + p$. This equation is a version of the overall acid–base reaction

$${}^{(+)}\mathrm{AH} + \odot\mathrm{B}^{(-)} \underset{k_\mathrm{R}}{\overset{k_\mathrm{F}}{\rightleftharpoons}} {}^{(-)}\mathrm{A}\odot + \mathrm{HB}^{(+)} \tag{1–6}$$

that has been expanded both in the identity of the participants and in the explicit steps involved. If the mechanism of either Equation 1–3 or Equation 1–5 pertains, k_F and k_R in Equation 1–6 are the composite rate constants[16]

$$k_\mathrm{F} = \frac{k_1 k_2 k_3}{\left(k_{-1} + k_2\right)k_3 + k_{-1}k_{-2}} \tag{1–7}$$

and

$$k_\mathrm{R} = \frac{k_{-1} k_{-2} k_{-3}}{\left(k_{-1} + k_2\right)k_3 + k_{-1}k_{-2}} \tag{1–8}$$

It follows that

$$K_{\mathrm{eq,AB}} = \frac{K_{\mathrm{a,HA}}}{K_{\mathrm{a,HB}}} = \frac{[\mathrm{A}]_{\mathrm{eq}}[\mathrm{HB}]_{\mathrm{eq}}}{[\mathrm{AH}]_{\mathrm{eq}}[\mathrm{B}]_{\mathrm{eq}}} = \frac{k_\mathrm{F}}{k_\mathrm{R}} = \frac{k_1 k_2 k_3}{k_{-1} k_{-2} k_{-3}} \tag{1–9}$$

*In spite of the fact that one woman's acid is another woman's base, the usual convention is to designate an acid with a simple capital A and a base with a simple capital B. Since these designations will be used later in the text for reactants, acids will always be designated as $^{(+)}$AH, $^{(+)}$BH, $^{(+)}$NH, $^{(+)}$OH, $^{(+)}$SH, or $^{(+)}$PH or as $\mathrm{HA}^{(+)}$, $\mathrm{HB}^{(+)}$, $\mathrm{HN}^{(+)}$, $\mathrm{HO}^{(+)}$, $\mathrm{HS}^{(+)}$, or $\mathrm{HP}^{(+)}$. Their conjugate bases will always be designated as $^{(-)}$A⊙, $^{(-)}$B⊙, $^{(-)}$N⊙, $^{(-)}$O⊙, $^{(-)}$S⊙, or $^{(-)}$P⊙ or ⊙$\mathrm{A}^{(-)}$, ⊙$\mathrm{B}^{(-)}$, ⊙$\mathrm{N}^{(-)}$, ⊙$\mathrm{O}^{(-)}$,⊙$\mathrm{S}^{(-)}$, or ⊙$\mathrm{P}^{(-)}$. The charges in parentheses indicate that a monoprotic acid can be neutral or can bear a net formal positive charge on the heteroatom, and the conjugate base of a monoprotic acid can be neutral or can bear a net formal negative charge on the heteroatom.

The observed rate constants, k_F and k_R, for the transfer of a hydron in solution (Figure 1–1)[16] provide insight into the differences in the abilities of various types of acids to provide hydrons and of various types of bases to remove hydrons.

The difference in the values of pK_a between an acid, $HA^{(+)}$, and the conjugate acid, $HB^{(+)}$, of a base, $\odot B^{(-)}$, can be defined by*†

$$\Delta pK_{a,AB} \equiv pK_{a,HB} - pK_{a,HA} = \log \frac{K_{a,HA}}{K_{a,HB}} \equiv \log K_{eq,AB} \quad (1\text{–}10)$$

Usually, when $\Delta pK_{a,AB}$ is positive and greater than 4, and the equilibrium constant for the transfer of the hydron is greater than 10^4, and the transfer of the hydron is significantly **exergonic**, the observed rate constant k_F for transfer of the hydron from the acid to the base falls between 10^9 and 10^{11} M^{-1} s^{-1} (right asymptotes in Figure 1–1). The particular value in a given situation is close to that calculated theoretically for the encounter-controlled bimolecular rate constant, which is the rate constant for simple collisions between the hydrated molecule of the acid, $HA^{(+)}$, and the hydrated molecule of the base, $\odot B^{(-)}$.[16]

The **encounter-controlled bimolecular rate constant** is the rate constant for a reaction in which every encounter between the two reactants results in product. It is referred to as encounter-controlled because the only factor that causes the reaction to be less than instantaneous is the requirement that molecules of the two reactants diffuse through the solution until they encounter and collide with their opposite numbers. If the two respective molecules that must collide in solution are both neutral and of the normal size of hydrated small molecules, the encounter-controlled bimolecular rate constant for the reaction should be between 10^9 and 10^{10} M^{-1} s^{-1} at 25 °C. In pure water, the particular value of the encounter-controlled rate constant is greater by a factor of about 6 if a molecule with at single positive elementary charge reacts with a molecule with a single negative elementary charge than if a neutral molecule reacts with either a neutral or a charged molecule because electrostatic attraction increases the rates of encounter in the former situation.[30]

Because the observed rates for significantly exergonic transfers of hydrons between small molecules are those expected for encounter-controlled reactions, it necessarily follows, in these circumstances, that each time the hydrated acid and the hydrated base collide in solution, a hydrated encounter complex forms and the **exergonic transfer of the hydron** within that complex ($k_2 >> k_{-2}$) occurs faster than the hydrated, hydronated base and the hydrated, unhydronated acid can dissociate.

In a situation where no encounter is required to occur—for example, **when the base is the solvent** and is already adjacent to the acid and forming a hydrogen bond with it—the transfer of the hydron becomes unimolecular. If the transfer of the hydron within the complex is, again, exergonic ($\Delta pK_{a,AB} > 4$), the observed first-order rate constant for the transfer[31] at 25 °C usually falls between 10^{10} and 10^{12} s^{-1}, which is the value calculated theoretically for the encounter-controlled dissociation of two preassociated molecules. This dissociation is governed by the unimolecular rate constant k_3 in Equation 1–3 or Equation 1–5.

All these results demonstrate that, **in an exergonic transfer of a hydron, the rate of the overall reaction is not limited by the rate of the actual transfer of the hydron** either within a direct hydrogen bond (Equation 1–3) or when the transfer of the hydron is relayed through a chain of water molecules (Equation 1–5).

Therefore, when the actual transfer of a hydron between acid and base, which is governed by the unimolecular rate constant k_2 in Equation 1–3 or Equation 1–5, is exergonic, it must be faster than 10^{10} s^{-1}. The value of the unimolecular rate constant for the transfer of a hydron, based on absolute rate theory, if no energy barrier existed, would be $k_B T h^{-1}$, or 6×10^{12} s^{-1} at 25 °C, where k_B is Boltzmann's constant and h is Planck's constant. This calculated value is consistent with an observed value of 10^{-13} s for the lifetime of the H_3O^+ ion at a particular position in ice, where the movement of this ion through the solid phase depends only on the transfer of hydrons in hydrogen bonds.[16]

*In chemical thermodynamics, the difference in a thermodynamic quantity describing a reaction is the value of that quantity for the products minus the value of that quantity for the reactants. For this reason—and for the reason that if this rule is followed, $\Delta pK_{a,AB}$ is equal to the logarithm of the equilibrium constant for the transfer of the hydron (Equation 1–8), which is a useful equality—it was decided that the pK_a of the acid should be subtracted from the pK_a of the conjugate acid of the base.

†The abbreviation for the common logarithm, which is the logarithm to the base 10, will be log, and the abbreviation for the natural logarithm, which is the logarithm to the base e, will be ln. This practice is the one designated by the American Chemical Society.

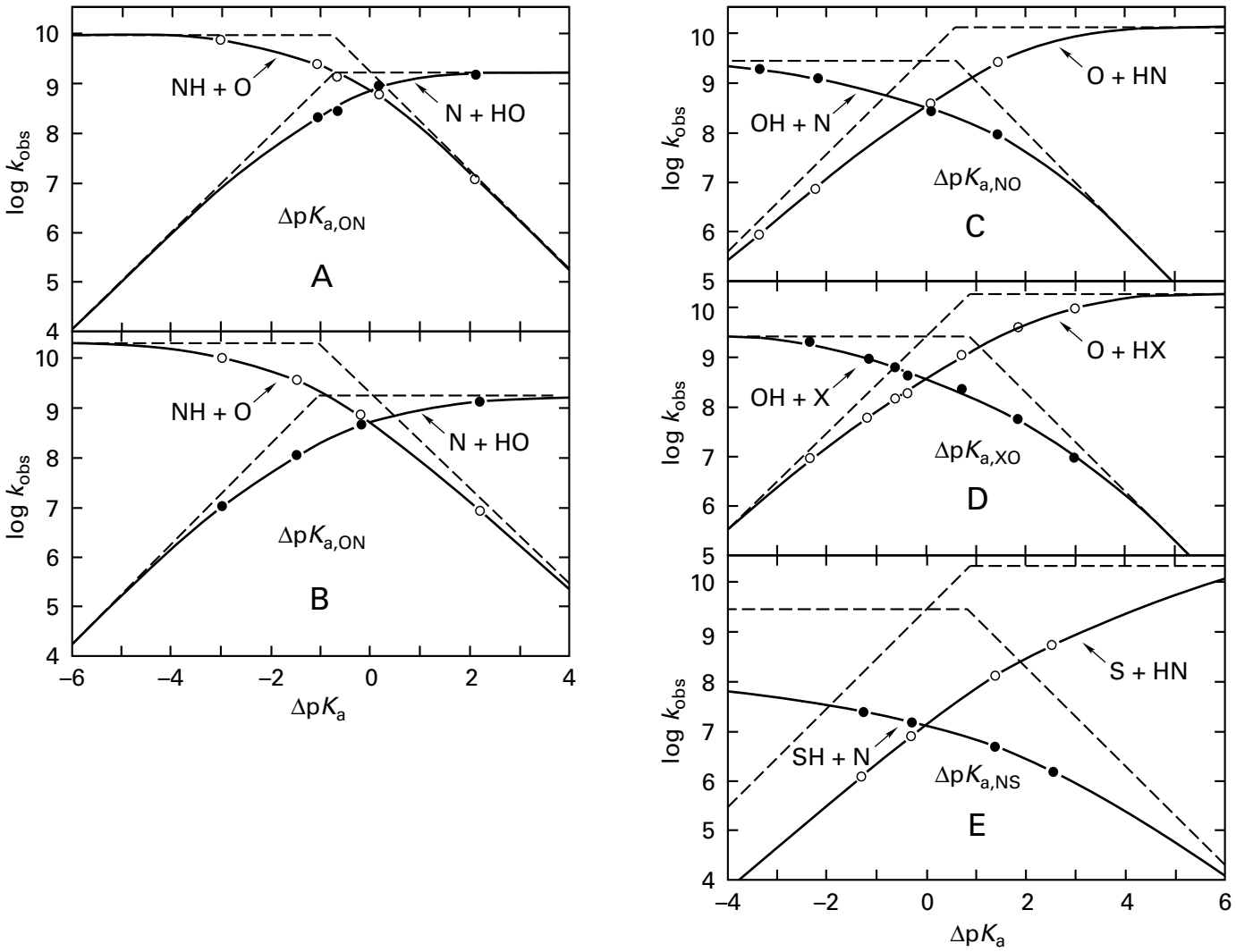

Figure 1–1: Bimolecular rate constants for transfer of a hydron between an acid and a base dissolved in aqueous solution.[16] In each panel, the common logarithms of the observed rate constants, k_{obs}, are presented for (●) the transfer of a hydron from a series of acids to the same common base and for (○) the transfer of a hydron from the conjugate acid of the same common base to the conjugate bases of the same series of acids. With the appropriate choice of reactants, these observed rate constants are the experimentally measured values of the rate constants k_F and k, respectively, of Equation 1–6. Each common logarithm of an observed rate constant is plotted as a function of the difference between the pK_a of the acid and the pK_a of the conjugate acid of the base (Equation 1–10) for that particular transfer of a hydron. **(A)** Common base (N), ammonia; common conjugate acid (NH), ammonium ion; acid series: (OH), D-glucose ($\Delta pK_a = -3$), bicarbonate ($\Delta pK_a = -1.1$), phenol ($\Delta pK_a = -0.7$), boric acid ($\Delta pK_a = +0.1$), and 4-nitrophenol ($\Delta pK_a = +2.1$); (●) transfer from the particular acid (OH) to the common base (N); (○) transfer from the common conjugate acid (NH) to the particular conjugate base (O). **(B)** Common base (N), imidazole; common conjugate acid (NH), imidazolium ion; acid series: (OH), phenol ($\Delta pK_a = -3$), hydrogen diphosphate trianion ($\Delta pK_a = -0.7$), 4-nitrophenol ($\Delta pK_a = -0.1$), and acetic acid ($\Delta pK_a = +2.3$); (●) transfer from the particular acid (OH) to the common base (N); (○) transfer from the common conjugate acid (NH) to the particular conjugate base (O). **(C)** Common base (O), acetate ion; common conjugate acid (OH), acetic acid; acid series: (NH), hydrazinium ion ($\Delta pK_a = -3.3$), imidazolium ion ($\Delta pK_a = -2.3$), anilinium ion ($\Delta pK_a = +0.1$), and 3-chloroanilinium ion ($\Delta pK_a = +1.4$); (●) transfer from the common conjugate acid (OH) to the particular conjugate base (N); (○) transfer from the particular acid (NH) to the common base (O). **(D)** Common base (O), phenolate ion; common conjugate acid (OH), phenol; acid series: (XH), hydrogen phosphate dianion ($\Delta pK_a = -2.4$), piperidinium ion ($\Delta pK_a = -1.3$), propylammonium ion ($\Delta pK_a = -0.6$), bicarbonate ion ($\Delta pK_a = -0.4$), ammonium ion ($\Delta pK_a = +0.7$), hydrazinium ion ($\Delta pK_a = +1.9$), and imidazolium ion ($\Delta pK_a = +2.9$); (●) transfer from the common conjugate acid (OH) to the particular conjugate base (X); (○) transfer from the particular acid (XH) to the common base (O). **(E)** Common base (S), thiolate ion of thioglycol; common conjugate acid (SH), thioglycol; acid series: (NH), dimethylammonium ion ($\Delta pK_a = -1.2$), trimethylammonium ion ($\Delta pK_a = +0.3$), hydrazinium ion ($\Delta pK_a = +1.4$), and imidazolium ion ($\Delta pK_a = +2.4$); (●) transfer from the common conjugate acid (SH) to the particular conjugate base (N); (○) transfer from the particular acid (NH) to the common base (S). The horizontal dashed lines are asymptotes based on the assumption that a sufficiently exergonic transfer of a hydron should have the theoretically calculated encounter-controlled bimolecular rate constant. The dashed lines with slope +1 or slope –1 are the endergonic asymptotes calculated by Equation 1–11.

For hydron transfers in solution that are not significantly exergonic, the behavior of the rate constants is a function of the encounter-controlled rate constant and of the difference in values of pK_a between the acid and the conjugate acid of the base. Within a particular class of hydron transfers—for example, all of the transfers of a hydron from a neutral oxygen to a neutral nitrogen to create an oxygen with a negative elementary charge and a nitrogen with a positive elementary charge—each transfer of a hydron from $^{(+)}$AH to ⊙B$^{(-)}$ in the exergonic direction ($\Delta pK_{a,AB} > 4$) is always encounter-controlled and therefore has the same value for its second-order rate constant k_F. Therefore, the rate of transfer of the same hydron in the reverse direction, or the endergonic direction ($\Delta pK_{a,BA} < -4$) from $^{(+)}$BH to ⊙A$^{(-)}$, must be governed only by $\Delta pK_{a,AB}$ because, from Equation 1–9, it follows that

$$\log k_R = \log k_F - \Delta pK_{a,AB} \qquad (1\text{–}11)$$

Because k_F is always the same in the exergonic direction, the rate constant for transfer of a hydron in the endergonic direction should decrease by a factor of 10 for every increase in $\Delta pK_{a,AB}$ of one common logarithmic unit. This expectation has been demonstrated experimentally. For example, Equation 1–11 defines the diagonal asymptotes in each panel of Figure 1–1. This behavior suggests that the probability the hydron will leave the encounter complex on the weaker base is governed only by the difference in pK_a between the conjugate acids of the two bases and reflects the distribution of the hydron between the lone pair on the conjugate base of the acid and the lone pair on the base in the complex. Consequently, the transfer of the hydron in the complex has reached equilibrium.

The behavior of the transfer of a hydron when the reaction is neither strongly exergonic nor strongly endergonic ($-4 < \Delta pK_{a,AB} < 4$) deviates smoothly from these limits. An example is the transfer of a hydron between a negative oxyanion as one base and a neutral amino nitrogen as the other base (Figure 1–1A)

$$R_1NH_3^+ + {}^-OR_2 \rightleftharpoons R_1NH_2 + HOR_2 \qquad (1\text{–}12)$$

When the transfer is from oxygen to nitrogen (the reverse of Equation 1–12) and exergonic, the encounter-controlled second-order rate constant is less than that for an exergonic transfer from nitrogen to oxygen (the direction of Equation 1–12) because of the asymmetry of charge (horizontal asymptotes in Figure 1–1A). In either direction, when the transfers of the hydrons have become strongly endergonic, the respective rate constants fall off as exponential functions of $\Delta pK_{a,ON}$. The horizontal asymptote, defined by the rate constant for the encounter-controlled exergonic transfer of a hydron from oxygen to nitrogen, intersects the diagonal asymptote, defined by the rate constant for the endergonic transfer from nitrogen to oxygen, when $\Delta pK_{a,ON} = 0$ as required by Equation 1–11. When $\Delta pK_{a,ON} = \Delta pK_{a,NO} = 0$, the actual rate constants for the transfer of the hydron in the two directions are equal, as required by Equation 1–9.

For transfer of a hydron in one direction, the distance at which the smooth curve defining the actual observed second-order rate constant of the transfer lies below the intersection of the two asymptotes, horizontal and diagonal, governing its class of hydron transfers (Figure 1–1) provides information about the **rate of transfer of the hydron within the encounter complex**. If the rate constant k_1 in Equation 1–3 or Equation 1–5 remains constant and encounter-controlled as $\Delta pK_{a,AB}$ is varied, and if k_2 and k_{-2} remain very fast, then k_F, the observed composite rate constant for transfer of the hydron, should have half its asymptotic, encounter-controlled value (horizontal asymptotes in Figure 1–1) at the $\Delta pK_{a,AB}$ at which the horizontal and diagonal asymptotes intersect. If this were the case, the common logarithm of the actual rate constant for the transfer of the hydron should lie a distance of $\log 2 = 0.30$ below the point of intersection. If, however, k_2 is less than k_{-1} because the transfer of the hydron within the encounter complex is not fast compared to diffusion of the reactants apart, then at the $\Delta pK_{a,AB}$ corresponding to the intersection of the two asymptotes, the smooth curve defining the common logarithm of the actual value for the composite rate constant k_F will lie below the intersection of the asymptotes by a distance greater than 0.30, and that distance will be approximately $\log (k_2/k_{-1})$. Consequently, the magnitude of that distance will be dictated by the rate constant k_2 for isoergonic transfer of the hydron within the hydrogen-bonded complex.

The observed rate constant for the transfer of a hydron between a particular acid and a particular base in solution provides a limit for the expected rate constant for the transfer of a hydron between the same acid and the same base during a chemical reaction in the active site of an enzyme. In the active site of the enzyme, there is usually a

direct hydrogen bond between a particular acid and a particular base. In solution, there is often, if not usually, a chain of water molecules connecting the acid and the base that relays the hydron to accomplish the transfer (Equation 1–4). Consequently, the rate constant k_2 for the actual transfer of the hydron in solution is probably a lower limit for the rate constant for transfer of a hydron in a direct hydrogen bond between acid and base. Because, however, most exergonic and even some **isoergonic** hydron transfers occur in solution with rate constants k_2 greater than or of equal magnitude to the rate constants k_3 for dissociations of the respective encounter complexes, the transfer of a hydron through such a relay system, once it is established, must be rapid in all situations in which the hydron transfer is indirect.

The rate constants for the isoergonic transfers of a hydron between various types of acids and bases in solution provide implications about the rate constants for the transfer of a hydron between the same types of acids and bases in the active site of an enzyme. The isoergonic transfer of a hydron to the primary amine or from the primary ammonium in the side chain of a **lysine** should be the most rapid (Figure 1–1A). Even in this case, however, the overall isoergonic reaction in solution is limited by the value of k_2 because the common logarithm of the actual rate constant k_F is more than 0.3 unit below the intersection of the asymptotes. The primary amine or ammonium of a lysine is followed in its efficiency of transfer by the imidazole or imidazolium of a **histidine** (Figure 1–1B), the carboxylate or carboxylic acid in the side chain of an **aspartate** or a **glutamate** (Figure 1–1C), and the phenolate or phenol of a **tyrosine** (Figure 1–1D). Nevertheless, even with carboxylic acids and phenols, which have the slowest transfers within the encounter complex, the distance below the intersection of the asymptotes is only about 1.2 common logarithmic units, and $k_2/k_{-1} \cong 0.06$. If the rate constant for separation of the products, k_{-1}, remains encounter-controlled at $>10^{10}$ s^{-1}, then the rate constant in solution for isoergonic transfer of the hydron, k_2, is still $>10^9$ s^{-1}. In the active site of an enzyme, the rate constant for the transfer of a hydron between any of these side chains and an amine, ammonium, imidazole, imidazolium, carboxylate, carboxylic acid, phenolate, or phenol on a substrate must be at least as rapid as the same type of transfer in solution. **Consequently, all these types of transfer must reach equilibrium in a few nanoseconds.**

If the transfer of a hydron within a hydrogen bond is endergonic, its rate constant, k_2, will be controlled by the equilibrium constant for the transfer of the hydron

$$K_{eq2} = \frac{k_2}{k_{-2}} \qquad (1–13)$$

Consequently, that rate constant should decrease by at most a factor of 10 for each decrease of ΔpK_a by one unit (Figure 1–1A–D). As the reverse reaction, however, becomes more and more exergonic because the forward reaction is becoming more and more endergonic, k_{-2} increases from its isoergonic value, so k_2 decreases by less than a factor of 10 for each change in ΔpK_a of one unit, and equilibrium within the hydrogen bond is nevertheless established rapidly. Consequently, the difference in the values of pK_a between acid and base in the endergonic transfer of a hydron within a hydrogen bond has to be fairly large before the transfer of a hydron between an oxygen and a nitrogen, between two nitrogens, or between two oxygens exerts any significant limitation on the rate of an enzymatic reaction. As long as the differences in the values of pK_a are not large, there is no need for an enzyme to accelerate such a transfer of a hydron.

Two other types of hydron transfer that often take place in enzymatic reactions, however, occur much more slowly in solution. First, the most inefficient heteroatomic acid–base participating in the transfer of a hydron in solution to or from nitrogen and oxygen is a thiol or thiolate (Figure 1–1E). Second, the transfer of a hydron to and from carbon is much slower than that between heteroatoms.

Part of the reason that the **transfer of a hydron from a thiol or to a thiolate** is anomalously slow in solution is that, because sulfur is an element in the third row of the periodic table, a thiol is a poor donor for a hydrogen bond and a thiolate is a poor acceptor for a hydrogen bond to nitrogen or oxygen. As a result, a thiol or thiolate may not be incorporated into the layer of hydration surrounding it by donating or accepting, respectively, a hydrogen bond to or from a molecule of water within the layer. If this is the case, when the hydrated molecule containing the thiol collides with the hydrated molecule containing a nitrogen or an oxygen to which the hydron is going to be transferred, or when the hydrated molecule

containing the thiolate collides with the hydrated molecule containing a hydronated nitrogen or a hydronated oxygen from which the hydron is going to be transferred, a chain of water molecules connecting the hydron of the thiol or a lone pair of the thiolate to that nitrogen or oxygen may not form. If this chain cannot form, it may be necessary for a collision to be energetic enough to penetrate the respective layers of hydration and actually juxtapose the thiol or thiolate with the nitrogen or oxygen that either accepts or donates the hydron before the encounter succeeds in transferring the hydron.

In the active site of an enzyme, however, the situation is different. When the **thiol of a cysteine** is to be used as an acid, it is forcibly juxtaposed immediately adjacent to the base on the molecule of substrate to which it is donating a hydron. Conversely, when the **thiolate of a cysteine** is to be used as a base, it is forcibly juxtaposed immediately adjacent to the acid on the molecule of substrate from which it is accepting a hydron. If, for the transfer of a hydron to or from sulfur in solution, there actually is a unique requirement for the intimate juxtaposition of the reactants, and if this requirement significantly decreases the rate of transfer of the hydron in solution, then the slow rates for these transfers observed in solution do not imply that the transfer of a hydron to or from the sulfur of a cysteine in an active site achieves equilibrium at a significantly slower rate than the transfer of a hydron to or from the heteroatomic bases and acids on the side chains of lysines, histidines, aspartates, glutamates, or tyrosines. In fact, the side chains of cysteines are frequently used as catalytic acids and bases in enzymatic reactions.

The rates for the transfers of hydrons to or from carbon atoms in solution are slow. Almost all of the transfers of hydrons to or from carbon that are relevant to enzymatic catalysis are to an enolate or from a carbon α to a carbonyl or an acyl group, and consequently most of the examples to be considered here are transfers of hydrons of this type. Such rate constants for the transfer of a hydron both to and from carbon exhibit large negative deviations from the asymptotic behavior exemplified by the transfers between heteroatoms displayed in Figure 1–1.

If the transfer of a hydron to or from carbon is severely **exergonic**, such as the transfer of a hydron from hydronium ($pK_a = -1.74$) to the enolate of acetone ($pK_a \cong 20$),[16] it proceeds at encounter-controlled rates,* but the significantly exergonic transfer of a hydron from the acidic carbon on acetylacetone to hydroxide ($\Delta pK_{a,AB} = +7$)

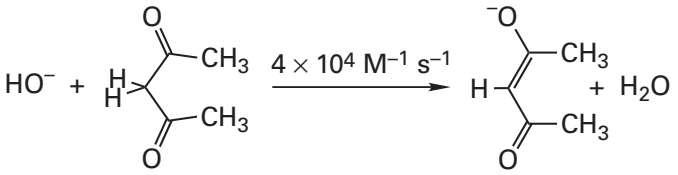

(1–14)

and the significantly exergonic transfer of a hydron from hydronium to the enolate of acetylacetone ($\Delta pK_{a,AB} = +11$)

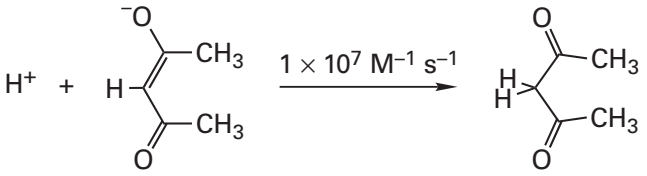

(1–15)

have second-order rate constants of 4×10^4 M^{-1} s^{-1} and 1×10^7 M^{-1} s^{-1}, respectively, which are considerably less than encounter-controlled rates. The rate constant[33] for the exergonic transfer of a hydron from the conjugate acid of 3-quinuclidinone to the enolate of acetone ($\Delta pK_{a,AB} \cong +12$) is 2×10^8 M^{-1} s^{-1} at 25 °C. The rate constants for the exergonic transfers of a hydron to diphenylmethyl anion from a set of acids with different values of pK_a in dimethylformamide at 22 °C[32] vary systematically from 2×10^5 M^{-1} s^{-1} to 2×10^9 M^{-1} s^{-1} within the range of $\Delta pK_{a,AB}$ from 0 to +10 before leveling out near the encounter-controlled limit, and the slope of the line defining log k_F as a function of $\Delta pK_{a,AB}$ is 0.6. If this correlation had been for exergonic transfer to a nitrogen or an oxygen, the rate constants would have reached the encounter-controlled limit at much smaller values of $\Delta pK_{a,AB}$ (Figure 1–1), and below the encounter-controlled limit, they would have been about 1000 times faster at the same respective values of $\Delta pK_{a,AB}$.

*If the transfer of the hydron to carbon becomes exergonic enough, the rate of its transfer from oxygen or nitrogen actually begins to decrease as the acid becomes stronger,[32] but this inverted region is probably well beyond the values of $\Delta pK_{a,AB}$ found in enzymatic reactions.

When the removal of a hydron from carbon is **endergonic**, where it necessarily should be less rapid than a encounter-controlled reaction, it is extraordinarily slow. For example, the rate constant for the removal of a hydron from acetone by hydroxide ($\Delta pK_{a,AB} \cong -5$)

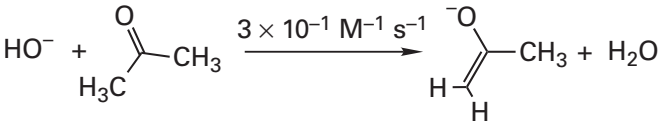

(1–16)

is much less (3×10^{-1} M^{-1} s^{-1})[16] than the rate constant of about 10^5 M^{-1} s^{-1} expected for the rate of transfer of a hydron between two nitrogens or oxygens that differ this much in acid dissociation constants (Figure 1–1). The rate constants[33] for the removal of a hydron by 3-quinuclidinone from acetone ($\Delta pK_{a,AB} \cong -12$) and from ethyl thioacetate ($\Delta pK_{a,AB} \cong -13$) are 5×10^{-4} M^{-1} s^{-1} and 2×10^{-5} M^{-1} s^{-1}, respectively, at 25 °C. The rates of the endergonic transfer of a hydron at 37 °C from carbon 5 of dihydroorotate ($pK_a = 21$)

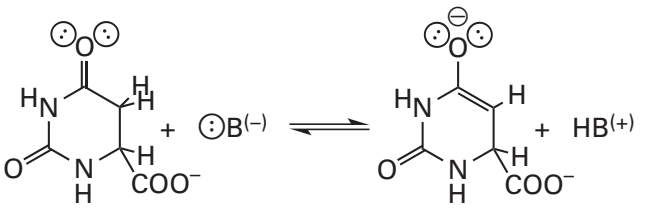

(1–17)

to the lone pairs of a set of bases vary systematically from 10^{-10} M^{-1} s^{-1} to 10 M^{-1} s^{-1} for bases the conjugate acids of which have values of pK_a from –1 to 16, and the slope of the line defining $\log k_F$ as a function of those values of pK_a is 0.8.[34] All these rate constants are more than 100-fold smaller than those expected for transfer of a hydron from oxygen or nitrogen at the same values of $\Delta pK_{a,AB}$ and temperature (Figures 1–1A–D).

The biggest problem in the transfer of a hydron from or to carbon is probably the **inability of a carbon–hydrogen bond or the carbon in an enolate to form a hydrogen bond** with molecules of water or other heteroatomic bases or heteroatomic acids, respectively. A carbon–hydrogen bond cannot act as the donor in a hydrogen bond because the electronegativities of carbon and hydrogen are so similar that a hydrogen–carbon bond has an insignificant electric dipole moment compared to that of a hydrogen–nitrogen bond or a hydrogen–oxygen bond.* The carbon in an enolate cannot act as an acceptor for a hydrogen bond because there is almost no free electron density on the carbon in an enolate. Another way of appreciating this latter problem is to realize that the carbon in an enolate does not have a lone pair of electrons that could act as an acceptor because the pair of electrons is delocalized in the π system and resides mainly on the oxygen. Consequently, as was the case with the thiol or thiolate , the acidic carbon–hydrogen bond or the carbon in an enolate cannot form a hydrogen bond with the molecules of water in the layer of hydration surrounding it. This inability to form a hydrogen bond with the molecules of water in the layer of hydration is even more extreme for carbon than for sulfur, and unlike the situation with a thiol or thiolate, this inability to form a hydrogen bond probably persists even in an encounter complex in which the carbon–hydrogen bond or the carbon in an enolate is immediately juxtaposed to the base that is to remove the hydron or the acid that is to donate the hydron, respectively.

The hydrogen bond that readily forms between a normal heteroatomic base and a normal Brønsted heteroatomic acid when both heteroatoms are from the second row of the periodic table also lowers the free energy of activation for the transfer of a hydron by bringing the reactants significantly closer together than the **van der Waals radii of their atoms** would normally permit. In the transfer of a hydron to or from carbon, advantage cannot be taken of this proximity. This missed opportunity causes the distance between the carbon and the heteroatom of the acid that hydronates the carbon or the base that removes a hydron from the carbon to be longer in the ground state for transfer of the hydron, and it causes the energy barrier for that transfer to be much more significant than the barriers for transfer of a hydron between two heteroatoms.[36]

In solution in both directions, large **changes in solvation** must occur upon transfer of a hydron between any acid and any base.[37] The change in solvation, however, is far more extensive in the removal of a hydron from carbon than in the removal of a hydron from a heteroatom because the resulting increase of one negative elementary charge in the conjugate base of an acidic carbon usually occurs several atoms away from the location within the base

*There are indications that, in the confines of the active site of an enzyme, hydrogen bonds between a carbon–hydrogen bond and a heteroatomic base can be sterically enforced.[35]

that gains the positive elementary charge. For an acidic carbon that has an enolate for its conjugate base, the negative elementary charge in the conjugate base appears primarily on the oxygen of the enolate, which is two atoms away from the atom of the base that gains the positive elementary charge upon hydronation.[38]

In addition, when a hydron is removed from a carbon α to a carbonyl or acyl group (Equations 1–14 and 1–17), **rehybridization** to form the enolate is required as the hydron is removed.

Because carbon does not form normal hydrogen bonds, the transfer of a hydron from and to carbon, a reaction occurring in many **enzymatic reactions**, is slow when it occurs in free solution between two independent solutes. To overcome this difficulty and increase the rate of removal of a hydron from carbon by a heteroatomic base, the lone pair of electrons on the base can be pushed by the enzyme into the hydrogen–carbon bond to enforce an arrangement similar to a hydrogen bond.[39] In the reverse direction, the rate of transfer of a hydron to an enolate can be increased if the excess π electron density on its anionic oxygen can be pushed onto the carbon causing the carbon to be more basic. In addition, in an enzymatic reaction, solvation of the ions is provided by the protein surrounding the location at which the transfer of the hydron occurs, and the surroundings can be tailored by natural selection to provide the necessary changes in solvation as efficiently as possible.

The intramolecular transfer of a hydron can be appreciated in the context of the intermolecular transfers that have been the subject so far. The ideal situation, for both the formation of an effective hydrogen bond and the efficient transfer of the hydron within that hydrogen bond, is that in which the hydrogen of the acid and the σ lone pair of electrons of the base both lie upon the line of centers connecting the nuclei of the two atoms between which the hydron is transferred. This requirement is accomplished in the direct intermolecular transfer of a hydron to and from heteroatoms by the formation of a properly aligned hydrogen bond between two independent, readily oriented molecules. In an ideal hydrogen bond within which the transfer of a hydron is occurring, the *s* atomic orbital of the hydron and the sp^3 or sp^2 orbitals from the two heavy atoms participating in the reaction overlap simultaneously to produce the transition state required for the transfer of the hydron

1–3

Although this transition state is not required to be precisely linear as drawn,[40] overlap of the three atomic orbitals creating it is an inescapable requirement.

In the intramolecular transfer of a hydron, the covalent connection between acid and base can **interfere with the proper alignment** of the orbitals to permit effective overlap. When the oxygen, nitrogen, or sulfur on which the hydron is situated is covalently attached to the same atom as the oxygen, nitrogen, or sulfur on which the lone pair is situated so that only this one atom separates them, the direct transfer of the hydron to the lone pair is impossible.

(1–18)

In such circumstances, a hydrogen bond cannot form because both the hydron and the lone pair lie too far off the line of centers and are held too far apart. In such a situation, if the acid loses a hydron and if the base gains a hydron, it does not result from the direct transfer of the hydron between them. There is always a separate base that removes the hydron from the acid, and the resulting conjugate acid of that base[41] or another acid then transfers a hydron to the lone pair of the base.[42]

When there are two atoms between the atoms on which the hydron and the lone pair are located, the intramolecular transfer of the hydron can occur, but the transfer is slow.[40] The hydrogen bond in which it proceeds, because it is not ideally aligned, is weak and easily disrupted by protic solvents, which consequently interfere with the direct transfer of the hydron.[43] When there are three or four atoms separating acid and base, the hydrogen bond between them is permitted to assume the proper geometry in the resulting five-membered or six-membered ring (not counting the hydron), the hydrogen bond is a strong one,[44] and transfer of the hydron is unimpeded.

Suggested Reading

Eigen, M. (1964) Proton transfer, acid–base catalysis, and enzymatic hydrolysis. Part I: Elementary processes, *Angew. Chem., Int. Ed. Engl. 3*, 1–19. https://doi.org/10.1002/anie.196400011

Nucleophilic Substitution

As is the transfer of a hydron, a nucleophilic substitution is the transfer of an electrophile between two lone pairs of electrons. Nucleophilic substitutions can occur at a saturated electrophilic carbon, at the electrophilic carbon in a carbonyl group, at the electrophilic carbon in an imine, at the electrophilic carbon in an acyl group, and at the electrophilic phosphorus in a phospho group.

The simplest reaction in organic chemistry, other than the transfer of a hydron, is a concerted nucleophilic substitution at a saturated carbon that proceeds without the formation of an intermediate. A **concerted nucleophilic substitution** is a nucleophilic substitution in which the bond between the leaving group and the electrophilic carbon is breaking as the bond between the nucleophile and the carbon is forming. An example of such a concerted nucleophilic substitution is the methylation of glycine by *S*-adenosyl-L-methionine to produce sarcosine

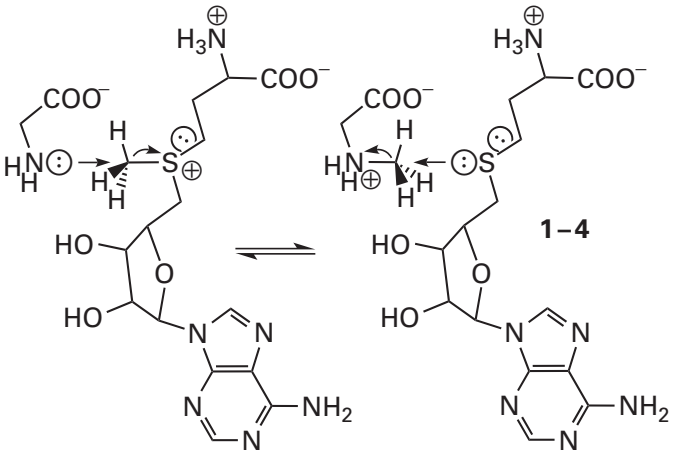

(1–19)

that is catalyzed by glycine *N*-methyltransferase from *Oryctolagus cuniculus*.[45] In this reaction, a bond between the carbon of the methyl group and the sulfur of *S*-adenosyl-L-homocysteine (**1–4**) has been substituted with a bond between the carbon of the methyl group and the amino nitrogen of the glycine. The electrophile, the methyl group, has been transferred from the lone pair of the sulfur of *S*-adenosyl-L-homocysteine to the lone pair of the nitrogen of glycine, as if it were a hydron.

The four electrons participating in a concerted nucleophilic substitution are confined initially in atomic and molecular orbitals of the reactants; they end up confined in atomic and molecular orbitals of the products; and at the apogee of the change in free energy during the reaction, they are confined in a **molecular orbital system of the transition state**. For these electronic transitions to occur, the atomic and molecular orbitals of the reactants that will mix to form the unique molecular orbital system in the transition state must be able to approach each other closely enough and in the proper orientation to **overlap**, and the atomic and molecular orbitals of the product must be such that they can be derived from a permitted unmixing of the molecular orbital system of the transition state.

In the case of the concerted nucleophilic substitution described in Equation 1–19, the sp^3 atomic orbital on the nucleophilic nitrogen occupied by its lone pair of electrons mixes with the molecular orbital system of the σ bond between the carbon and the sulfur to produce the unique molecular orbital system of the transition state (Figure 1–2). This process can be viewed as a smooth transition in which the occupied sp^3 atomic orbital on nitrogen overlaps with the unoccupied σ^* anti-bonding molecular orbital of the σ bond between carbon and

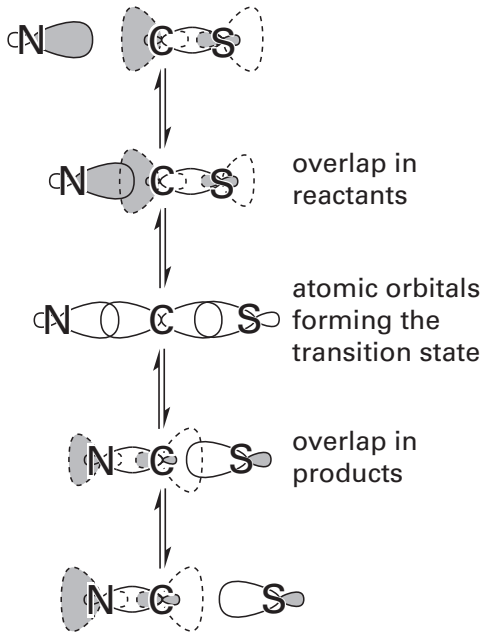

Figure 1–2: Progress of a concerted nucleophilic substitution. An atomic orbital on the nucleophile, occupied by a lone pair of electrons (drawn with solid outline), overlaps the antibonding molecular orbital (drawn with dashed outline) of the carbon–sulfur bond. The overlap proceeds to a transition state formed from a combination of three atomic orbitals, one from each of the three atoms: nitrogen, carbon, and sulfur. The transition state decomposes through an overlap between an atomic orbital on sulfur (drawn with solid outline), which will contain a lone pair of electrons in one product, and the antibonding molecular orbital (drawn with dashed outline) of the carbon–nitrogen bond in the other product. The phases within the molecular and atomic orbitals are indicated with gray shading.

sulfur. This initial overlap leads to a molecular orbital system in the transition state composed of an atomic orbital from the attacking nitrogen, a *p* atomic orbital from the carbon of the methyl group, and an atomic orbital from the sulfur. Therefore, the unique molecular orbital system in the transition state has three molecular orbitals formed from the three atomic orbitals shown in Figure 1–2, and its two molecular orbitals of lowest energy are occupied by the four electrons that are being rearranged. These electrons are the two originally in the lone pair on the nitrogen and the two originally in the σ bond between carbon and sulfur.

When the structure of the methyl group on *S*-adenosyl-L-methionine is examined, one aspect of the **energy barrier** encountered by the lone pair of electrons on the nucleophilic nitrogen can be appreciated. The vacant antibonding orbital on the carbon*

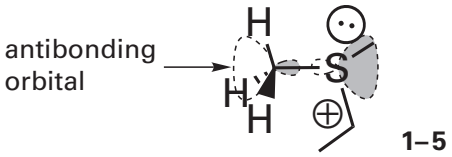

1–5

is in a depression formed from the three σ bonds between the three hydrogens and the electrophilic carbon of the methyl group, and the six electrons in these three σ bonds repel the two electrons in the lone pair on the nitrogen. This **electron repulsion** also results from orbital overlap, but in this case the overlap occurs between filled orbitals rather than between a filled and a vacant orbital. Along the trajectory of the reaction, as the atomic orbital containing the lone pair of electrons on the nitrogen overlaps the occupied bonding molecular orbitals of these three σ bonds between the carbon and the three hydrogens, electron repulsion occurs. This unfavorable overlap is a major contributor to the instability of the transition state relative to the ground state.

The three σ bonds form a repulsive funnel confining the trajectory of the nucleophile and dictating the **stereochemistry** of the reaction. These three σ bonds are pushed forward by the electron repulsion of the lone pair of electrons on the nucleophile as the reaction progresses. As they are pushed forward, they flatten into a plane perpendicular to the σ bond between the carbon and the dissociating sulfur

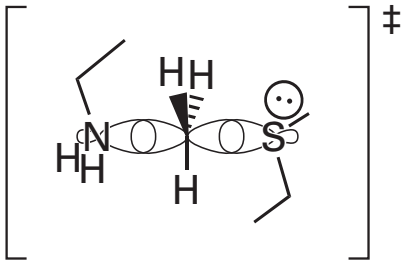

1–6

This reorientation does lead to a decrease in the mutual repulsion of the three σ bonds. Nevertheless, the transition state involves too much electron repulsion to be stable, not to mention a pentavalent carbon, and it breaks down to yield the products. The reaction proceeds with **inversion of configuration** of the methyl group being transferred.

To effect the reaction, the lone pair of electrons on nitrogen must approach a location on the electrophilic carbon opposite the carbon–sulfur bond of *S*-adenosyl-L-methionine with sufficient kinetic energy or, just as effectively, be forced against the carbon with sufficient potential energy to overcome the electron repulsion inherent in the transition state. In solution, the kinetic energy of the reactants, which are freely diffusing prior to the encounter, and the kinetic energy of collisions of molecules of water from the solution with the encounter complex, after the encounter has been effected, provide the kinetic energy to overcome the repulsion in the transition state. Only encounters between two molecules that have kinetic energy greater than the free energy of activation and are correctly aligned can be productive. In the active site of the enzyme, once the reactants are properly aligned, normal thermal fluctuations in the positions of the atoms promote the reaction, but the lone pair of electrons on the nitrogen can also be compressed against the electrophilic face of the methyl group.

There is also an energy barrier to the reaction in solution, resulting from the requirement to **desolvate** the amine. As the nitrogen of the lone pair approaches the carbon, there must be sufficient kinetic energy to peel away the layer of hydration around the lone pair in addition to overcoming the electron repulsion. In the case of the enzymatic reaction catalyzed by glycine *N*-methyltransferase (Equation 1–19), the layer of hydration is stripped

*Because biochemical molecules are often complex and only portions of them are usually shown in chemical drawings, the convention used in this book is to represent a bond to the rest of the molecule as an open line rather than using the convention $-R_n$ as is done in organic chemistry. Instead of using an open line to represent a methyl group, as is commonly done in organic chemistry, a methyl group will always be written explicitly as $-CH_3$.

from the amine as it associates with the active site. This **stripping of layers of hydration** during the association of substrates with an active site is a major contributor to the catalysis performed by enzymes.

A leaving group is the atom or group of atoms that dissociates from the rest of the electrophile during a nucleophilic substitution. The rest of the electrophile contains the electrophilic atom of the reactant, and the leaving group contains the dissociating atom that was originally bound to that electrophilic atom. The leaving group in all of the methylations performed by *S*-adenosyl-L-methionine (Equation 1–19) is the dialkylated sulfur of *S*-adenosyl-L-homocysteine (**1–4**), a sulfide, and the rest of the electrophile is the methyl group. Because the leaving group is an uncharged sulfide, the sulfur in *S*-adenosyl-L-methionine bears the formal single positive charge number of a sulfonium ion, a fact that is responsible for the electrophilicity of its methyl group. This positive elementary charge cannot be delocalized. The other carbons attached to the positively charged sulfur are also electrophilic. For example, the 3-aminopropyl group, rather than the methyl group, in *S*-adenosyl-3-(methylthio)propylamine, the decarboxylated version of *S*-adenosyl-L-methionine, is transferred to butane-1,4-diamine by spermidine synthase from *Escherichia coli* in a concerted nucleophilic substitution that proceeds with inversion of configuration at carbon 1 of the 3-aminopropyl group.[46-48] Likewise, *S*-alkylsulfonium ions are competent alkylating agents[49] in free solution in the absence of enzymatic catalysis.

The leaving group in a nucleophilic substitution can be **improved by making its conjugate acid more acidic**. Because the leaving group dissociates with a lone pair of electrons (Equation 1–19), its dissociation from the electrophilic carbon resembles in its character the dissociation of the same constellation of atoms from a hydron during the acid dissociation of the conjugate acid of the leaving group. For example, the acid dissociation of the conjugate acid of *S*-adenosyl-L-homocysteine, the leaving group in a methylation performed by *S*-adenosyl-L-methionine (Equation 1–19), is

(1–20)

Any alteration in the leaving group that decreases the pK_a of its conjugate acid improves its capacity for dissociation. For example, *S*-adenosyl-L-homocysteine (Equation 1–19) is a better leaving group from *S*-adenosyl-L-methionine than L-homocysteinyl anion, $^{-}SCH_2CH_2CH(NH_3^{+})CO_2^{-}$, is from L-methionine because the cationic conjugate acid of *S*-adenosyl-L-homocysteine (**1–4**; p$K_a \cong -10$) is a stronger acid than is L-homocysteine (p$K_a = 8.9$), the conjugate acid of L-homocysteinyl anion. Consequently, by adenosylating the L-methionine, the leaving group has become the sulfide rather than the thiolate, and *S*-adenosyl-L-methionyl ion is a significantly more effective methylating agent than L-methionine.

Almost all examples of improvements to the ability of the leaving group involve the **addition of electrophiles**. When the oxygen of a hydroxy group in an alcohol has been hydronated, it becomes a better leaving group because it dissociates as water rather than hydroxide ion. The conjugate acid of water, HOH_2^{+} (p$K_a = -1.74$), is a stronger acid than the conjugate acid of hydroxide, HOH (p$K_a = 15.74$). If a phospho group is added to the hydroxy group in an alcohol so that the leaving group is $-OPO_3H^{-}$ rather than –OH, then the bonded oxygen becomes a better leaving group because the conjugate acid of the $^{-}OPO_3H^{-}$ that dissociates, $HOPO_3H^{-}$ (p$K_a = 7.2$), is a stronger acid than the conjugate acid of the ^{-}OH that would have dissociated (p$K_a = 15.74$). If a sulfo group is added to the hydroxy group in an alcohol so that the leaving group is $-OSO_3^{-}$, then the bonded oxygen becomes a better leaving group because the conjugate acid of the $^{-}OSO_3^{-}$ that dissociates, $HOSO_3^{-}$ (p$K_a = 2.0$), is a stronger acid than the conjugate acid, HOH (p$K_a = 15.74$).[50] The hydronation of a monobasic phosphate on another of its oxygens produces an even better leaving group, $^{-}OPO_3H_2$, because the corresponding conjugate acid, $HOPO_3H_2$ (p$K_a = 2.1$), is even more acidic. When the oxygen of a hydroxy group on an alcohol has been acylated with an electrophilic functional group, such as an acetyl group, so that the leaving group becomes $-OC(O)CH_3$, it is a better leaving group because the conjugate acid of the $^{-}OC(O)CH_3$ that dissociates, $HOC(O)CH_3$ (p$K_a = 4.7$), is a stronger acid than the conjugate acid HOH (p$K_a = 15.74$). The hydronation of the sulfur of L-methionine (Equation 1–20), causing it to resemble a sulfonium ion, makes its methyl group more electrophilic.

The hydronation of nitrogen 7 in guanosine

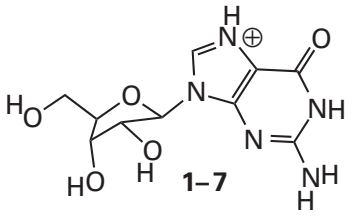

1–7

causes the guanine to become a better leaving group because the cationic conjugate acid of guanine ($pK_a = 3.3$) is a stronger acid than guanine itself ($pK_a = 9.2$). When guanosine is hydronated on the oxygen on carbon 6, when inosine[51] is hydronated on the oxygen on carbon 6, when adenosine[51] is hydronated on nitrogen 1, or when adenosine[52] is hydronated on nitrogen 7, each of the respective nitrogenous bases becomes a better leaving group.

If the leaving group in a nucleophilic substitution at carbon is improved sufficiently that it leaves from the electrophilic carbon before any nucleophile collides with the carbon, it leaves behind a carbenium ion as an intermediate in a dissociative nucleophilic substitution

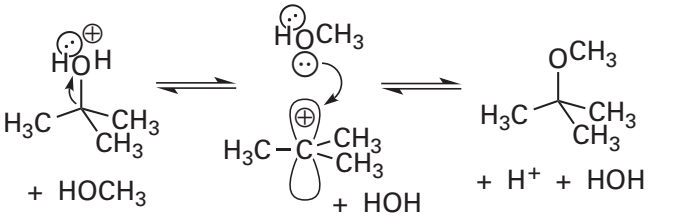

(1–21)

A **dissociative nucleophilic substitution** at carbon is a nucleophilic substitution in which the bond between the leaving group and the electrophilic carbon breaks completely before the bond between the carbon and the nucleophile begins to form. If the resulting carbenium ion then reacts with a nucleophile other than the nucleophile of the leaving group itself, the addition of that nucleophile completes the dissociative nucleophilic substitution. For example (Equation 1–21), the hydronated hydroxy group dissociates and leaves behind a carbenium ion before methanol, the nucleophile, adds. The improvement of the leaving hydroxy group by its hydronation is essential to the formation of the carbenium ion, but the most consequential distinction between the dissociative nucleophilic substitution of Equation 1–21, which is initiated by the formation of the carbenium ion, and the concerted nucleophilic substitution of Equation 1–19, which proceeds through a single transition state with no intermediate, is not so much the enhancement of the leaving group as the fact that the methyl group of the former has a primary carbon as the electrophile while the *tert*-butyl group of the latter has a tertiary carbon as the electrophile. The **hyperconjugation** of the three methyl groups surrounding the carbenium ion is the key to its stability.

During the formation of a carbenium ion by dissociation of the leaving group, the two **molecular orbitals** of the σ bond, bonding (filled) and antibonding (vacant), have been smoothly turned into the filled atomic orbital containing the lone pair of electrons on the leaving group and the vacant *p* orbital of the carbenium ion

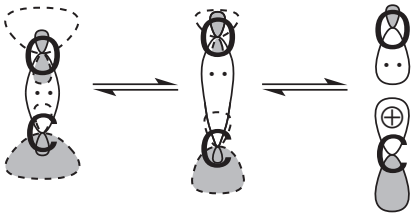

(1–22)

At the same time, the three substituents around the carbon have entered the plane perpendicular to the axis of the *p* orbital (Equation 1–21).

Carbenium ions have the **hybridization** *p*, sp^2, sp^2, sp^2 because of electron repulsion among the three occupied molecular orbitals of the three σ bonds to the substituents, which are no longer repelled by a fourth σ bond and want to be as far apart as possible, and because of the decrease in energy produced by bringing the six electrons in these three σ bonds closer to the nucleus in the more compact sp^2 orbitals. Nevertheless, the reaction is endergonic because a covalent bond—in the example of Equation 1–21, that between carbon and oxygen—is broken with no recompense other than these changes and changes in solvation. The heterolytic cleavage of this bond is the energy barrier to the reaction. In the reverse direction, however, no significant energy barrier exists and the combinations of nucleophiles with carbenium ions are usually encounter-controlled reactions.

Aliphatic carbenium ions are not widely used in **biochemical reactions**. Natural selection presumably has avoided them for the same reasons they are avoided in organic synthesis: the problems of elimination and rearrangement. There is, however, a broad class of enzymatically catalyzed reactions involved in the biosynthesis of carotenoids, steroids, and terpenoids. In each of these reactions, a carbe-

nium ion is generated from the substrate when it is in the active site expressly because it can engage in rearrangement and elimination. The rearrangements and eliminations are carefully controlled sterically by these enzymes and are used to produce dramatic alterations in the structure of their substrates. In each of these reactions, the carbenium ion is generated from a diphosphorylated alcohol ($-OPO_3PO_3^{2-}$) or from a hydronated oxirane, both of which have good leaving groups.

An oxocarbenium ion is a distinct type of carbenium ion. One substituent on the carbon atom in an oxocarbenium ion is an oxygen atom so that the positive charge is delocalized between the carbon and the oxygen. Following the required hydronation of the leaving oxygen, an oxocarbenium ion is formed by the dissociation of that hydronated oxygen from a **hemiacetal**

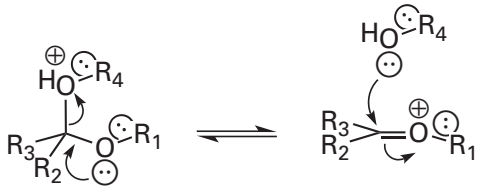

(1–23)

(R_2 = H; R_4 = H; R_1 and R_3 are substituents attached through carbon), a **hemiketal** (R_4 = H; R_1, R_2, and R_3 are substituents attached through carbon), an **acetal** (R_2 = H; R_1, R_3, and R_4 are substituents attached through carbon), or a **ketal** (R_1, R_2, R_3, and R_4 are substituents attached through carbon). When a formally positive nitrogen leaves from a **hemiaminal ether**

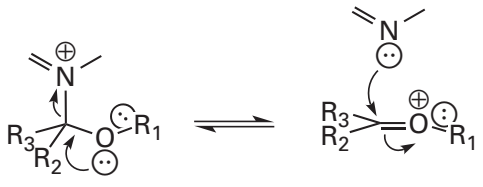

(1–24)

(R_1, R_2, and R_3 are substituents attached through carbon), an oxocarbenium ion is also formed.

When an acetal is formed, almost always from a hemiacetal, the hydroxy group of that hemiacetal, after it has been hydronated, leaves as a molecule of water (forward direction of Equation 1–23, R_4 = H), and the oxygen of an alcohol other than water adds to the resulting oxocarbenium ion (reverse direction of Equation 1–23, $R_4 \neq$ H). When a ketal is formed, almost always from a hemiketal, the hydronated hydroxy group of the hemiketal leaves as a molecule of water and the oxygen of an alcohol adds to the resulting oxocarbenium ion. The replacement of the hydroxy group with an alkoxy group in each of these instances turns a hemiacetal or a hemiketal, which readily reverts to the aldehyde or ketone, into an acetal or a ketal, which, in the absence of enzymatic catalysis, only reverts to the aldehyde or ketone in strong acid.

The **π molecular orbital system of an oxocarbenium ion** contains two electrons, which leaves the system with a net positive formal elementary charge. This formal charge can be represented by **resonance**

1–8

The resonance form drawn to the right in Equations 1–23 and 1–24 and **1–8** for the oxocarbenium ion is the form in which all atoms have octets, but oxygen, the more electronegative element, is required to bear a positive formal elementary charge. In this resonance form, there is a π bond between carbon and oxygen, which is why the oxocarbenium ion is more stable than a simple carbenium ion. An oxocarbenium ion is not so prone to rearrangement and elimination as a carbenium ion because the conjugated oxygen both confines the location of the formal positive elementary charge and moderates its reactivity.

Specific examples of dissociative nucleophilic substitutions involving an oxocarbenium ion as an intermediate would be the nucleophilic substitution of 3-bromoisoquinoline by azide[53]

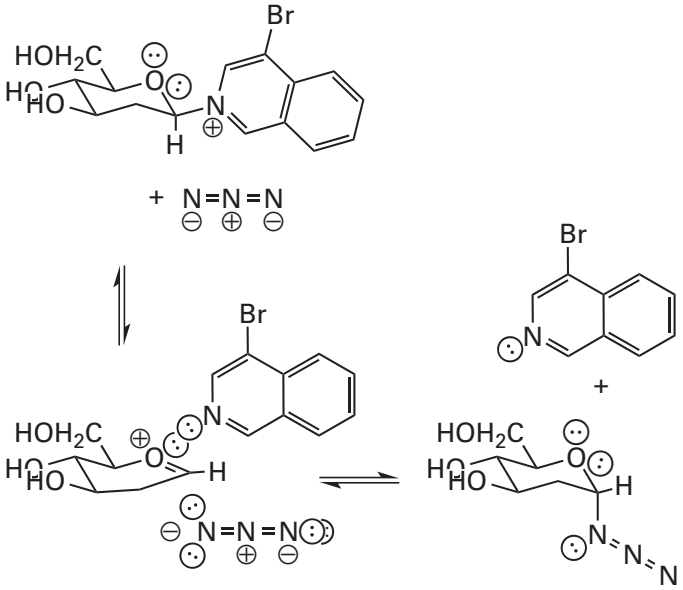

(1–25)

and the acid-catalyzed hydrolysis of adenosine[54] hydronated at nitrogen 7

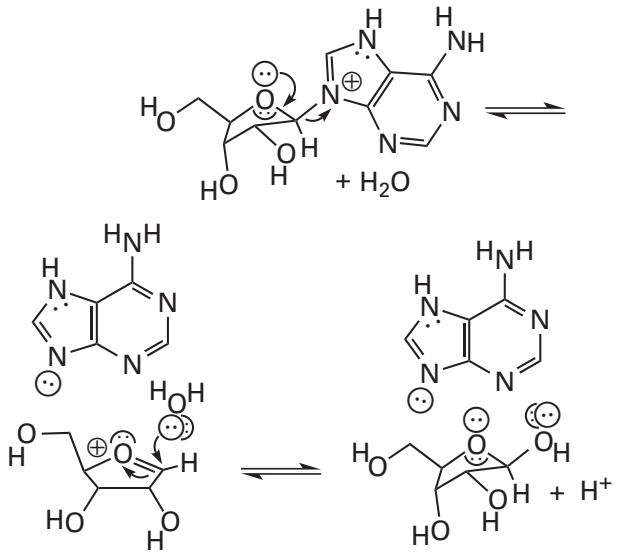

(1–26)

The oxocarbenium ion formed during the acid-catalyzed hydrolysis of acetophenone dimethyl ketal has been identified by trapping it with sulfite[55]

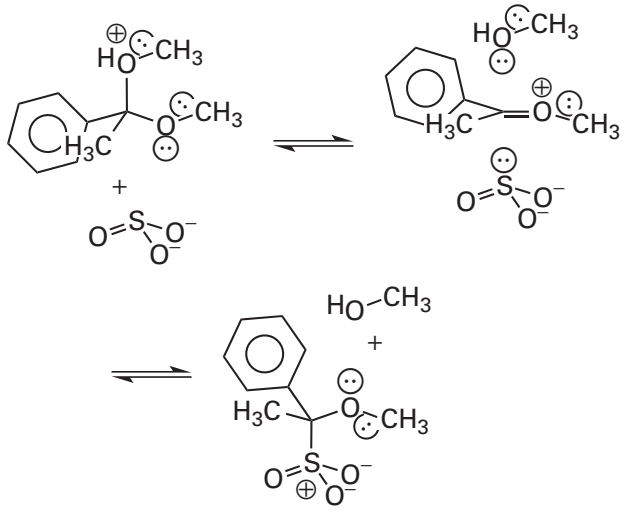

(1–27)

In the latter two reactions, the formation of the oxocarbenium ion requires that the leaving group be hydronated, and in all three reactions, the atom that is leaving bears a formal positive elementary charge in the reactant, as is the case with the leaving oxygen atom in the hydrolysis of any acetal or ketal (see Equation 1–23).[56]

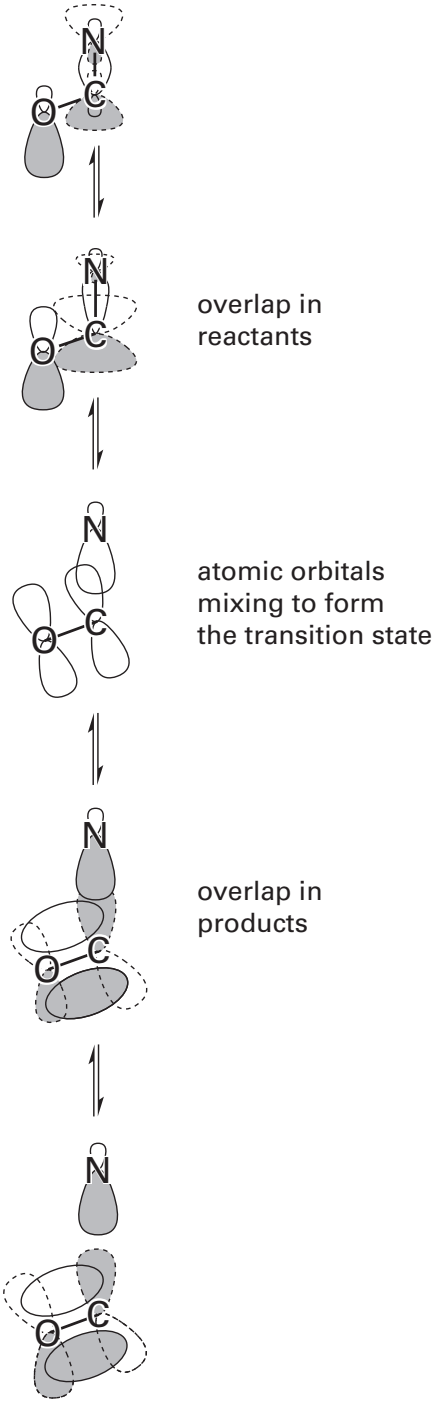

Figure 1–3: Dissociation of a hemiaminal ether to produce an oxocarbenium ion (Equations 1–24 and 1–25). The atomic orbital on oxygen bearing the lone pair of electrons (drawn with solid outline) overlaps the unoccupied antibonding molecular orbital (drawn with dashed outline) of the carbon–nitrogen σ bond to produce the transition state formed from the overlap of three atomic orbitals, one from each of the three atoms, oxygen, carbon, and nitrogen. The transition state decomposes through an arrangement in which the unoccupied antibonding π molecular orbital (drawn with dashed outline) of the oxocarbenium ion in the one product overlaps the atomic orbital on nitrogen (drawn with solid outline) occupied by the lone pair of electrons present in the other product.

The **molecular orbital system of the transition state** in a dissociation that produces an oxocarbenium ion is formed from three atomic orbitals. For example, the orbitals of the reactant that mix to form the molecular orbital system of the transition state lying between the hemiaminal ether and the oxocarbenium ion and the leaving 3-bromoisoquinoline in Equation 1–25 are a *p* atomic orbital on the adjacent oxygen, a *p* atomic orbital on the carbon, and an sp^2 atomic orbital on the nitrogen (Figure 1–3). The unique molecular orbital system of the transition state created from mixing these three atomic orbitals has three molecular orbitals, and the two with lowest energy are occupied by the four electrons participating in the reaction.

Dissociative nucleophilic substitutions that have oxocarbenium ions as intermediates are **accelerated by the push of an adjacent lone pair of electrons on the oxygen**. For example, in the forward direction of the reaction in Equation 1–26, the dissociation to form the oxocarbenium ion can be considered as expulsion of the nitrogen of the leaving group accelerated by the push of a lone pair of electrons on the oxygen.[57] This lone pair of electrons in the reactant is located in an sp^3 atomic orbital on the oxygen. In the approach to the transition state, this occupied sp^3 atomic orbital overlaps with the unoccupied σ^* antibonding molecular orbital of the carbon–nitrogen σ bond (Figure 1–3). This σ^* antibonding orbital is to become the *p* orbital on the carbon (see Equation 1–22). In the absence of the oxygen, it would normally be a simple vacant *p* orbital of a carbenium ion, but in the presence of the oxygen, it will participate in the π molecular orbital system of the oxocarbenium ion. The overlap of the occupied sp^3 orbital of the oxygen with the unoccupied σ^* antibonding orbital of the carbon–nitrogen bond lowers the energy of the transition state relative to the situation in which there is no adjacent heteroatom. There is little doubt that a push is operating in displacements of this type because they are always more rapid than the same reaction in which the oxygen, or a nitrogen (Equation 1–24), is replaced by carbon.

The **direction from which the push is applied** is an issue. The atomic orbital holding the lone pair of electrons on oxygen, which will provide the push during the formation of an oxocarbenium ion, has been shown in Figure 1–3 and Equations 1–23 and 1–24 assuming an antiperiplanar orientation to the dissociating nitrogen

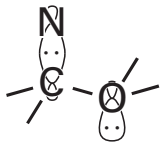

1–9

In **1–9** the nitrogen atom, the σ bond between nitrogen and carbon, the carbon atom itself, the σ bond between carbon and oxygen, the oxygen atom, and the lone pair of electrons on the oxygen atom are all in the same plane so that the lone pair of electrons and the carbon–nitrogen σ bond are periplanar. This **periplanarity** is always necessary for the proper overlaps to occur. In the **antiperiplanar conformation** drawn, when viewed along the carbon–oxygen bond, the lone pair of electrons on the oxygen is oriented at a dihedral angle of 180° from the pair of electrons in the σ bond between carbon and nitrogen. In a **synperiplanar conformation**, which would result from a 180° rotation of the carbon–oxygen bond, the lone pair of electrons is oriented at a dihedral angle of 0° from the σ bond between carbon and nitrogen. There is a proposal, described by the author as **stereoelectronic control**,[58,59] that an antiperiplanar orientation is a necessity of the reaction because the push must be provided through the antibonding orbital (Figure 1–3), from the opposite side of the carbon from which the nitrogen is leaving. In this orientation, the overlap between the atomic orbital containing the lone pair of electrons and the antibonding orbital of the molecular orbital system of the σ bond is at its maximum.

It has been documented in studies of the hydrolysis of cyclic ortho esters[60] that **antiperiplanar push** is stronger than **synperiplanar push**. Even in this situation, however, in which two oxygens rather than one are providing the push, the push from the antiperiplanar side was less than 10 kJ mol^{-1} stronger than the push from the synperiplanar side.[60,61] In other reactions, such as nucleophilic substitution at the anomeric carbon of the pyranose in Equation 1–25, a reaction of the type most common in enzymatic catalysis, there is experimental evidence that the conformation of the pyranose required to effect antiperiplanar push is so sterically disfavored that, in such instances, synperiplanar push dominates.[62-64] For example, in the reaction shown in Equation 1–25, synperiplanar push would be expressed as

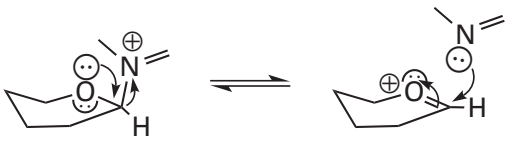

(1–28)

Consequently, the decision as to whether synperiplanar push or antiperiplanar push dominates in a particular reaction is probably more often a steric one than an electronic one because, if there is any electronic advantage to antiperiplanar push, it is a small one. Nevertheless, if there is even a small advantage in a situation in which steric effects do not dominate, that advantage may have been exploited by natural selection.

Periplanar pull may be exerted in the formation of an oxocarbenium ion from an acetal (Equation 1–27) by hydronating a lone pair of electrons on the leaving group that is periplanar rather than orthogonal to the developing π bond of the oxocarbenium ion

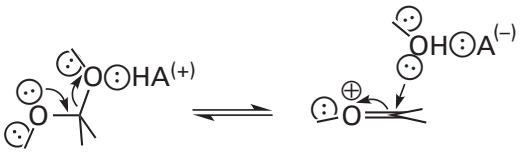

(1–29)

Whether or not periplanar pull can be exerted is of interest for reactions occurring in the active sites of enzymes where the stereochemistry of the acid relative to the acetal can be dictated.[65]

The **addition of a nucleophile to an oxocarbenium ion**, which leads to the product in the second step of a dissociative nucleophilic substitution, is the reverse of the dissociation that produces an oxocarbenium ion (Figure 1–3). Addition of the nucleophile to the oxocarbenium ion can be viewed as being initiated by overlap between the sp^2 atomic orbital on the nucleophile occupied by its σ lone pair of electrons and the vacant π^* antibonding molecular orbital of the molecular orbital system of the double bond between carbon and oxygen in the oxocarbenium ion

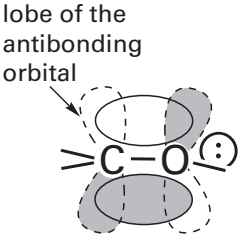

1–10

The resulting transition state separates to produce the two molecular orbitals of the σ bond between carbon and the heteroatom of the nucleophile and the sp^3 atomic orbital on oxygen containing the lone pair of electrons.

During the addition of a nucleophile to the electrophilic carbon in an oxocarbenium ion, a significant portion of the energy barrier is again due to **electron repulsion**. This electron repulsion affects both addition of the leaving group, in the reverse direction, and addition of the original nucleophile, in the forward direction (Equations 1–25 to 1–27) of the dissociative nucleophilic substitution. The lone pair of electrons of the nucleophile on a trajectory toward the **unoccupied antibonding molecular orbital** of the π bond between the carbon and the electropositive oxygen finds itself surrounded by the two pairs of electrons in the two σ bonds between the carbon and its two other substituents and by the pair of electrons in the **occupied bonding molecular orbital** of the π bond between carbon and oxygen. The two electrons in the π bond are delocalized and more concentrated over oxygen because of its electronegativity, so the electron repulsion is not so great as that experienced by a nucleophile in a concerted nucleophilic substitution at a fully saturated carbon. Nevertheless, either the kinetic energy of the nucleophile as it collides or the potential energy of squeezing the nucleophile against the carbon, or a combination of these forces, is required to overcome the energy barrier. As the nucleophile moves in, the two σ bonds are pushed downward and the delocalized electrons in the occupied bonding molecular orbital of the π bond are pushed over onto the oxygen (Equations 1–23 and 1–24).

The lifetime of an oxocarbenium ion measures its electrophilicity. Lifetimes of oxocarbenium ions in water have been estimated by measuring the competition between azide ion and water for trapping them. Because the nucleophilic addition of water extinguishes the oxocarbenium ions, these measurements use water as a reference nucleophile to probe the relative electrophilicities of the oxocarbenium ions. The estimated lifetimes varied from 2×10^{-8} s for methylphenylmethoxocarbenium ion to 5×10^{-11} s for ethylethoxocarbenium ion.[66] As one might expect from the electrophilicities of alkyl carbenium ions, substituents decrease the electrophilicity of an oxocarbenium ion in the order phenyl > alkyl > alkoxymethyl > hydrogen. From these short lifetimes, it follows that an oxocarbenium ion is significantly electrophilic. In fact, it is electrophilic enough to participate in intramolecular electrophilic aromatic substitution.[67]

Various estimates of the lifetime of the D-glucopyranosylium ion

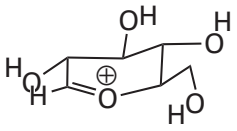

1–11

which is the oxocarbenium ion formed by the dissociation of a leaving group from a D-glucopyranoside, are on the order of 10^{-11} to 10^{-12} s in water at 25 °C.[53,66] These lifetimes are for a situation in which water, a weak nucleophile but nevertheless a nucleophile, surrounds the oxocarbenium ion and solvates it by directing its nucleophilic lone pairs of electrons towards the cation, an orientation in which they are aligned to add to it. The lifetime of the D-glucosyloxocarbenium ion is so short because the two substituents on the electrophilic carbon are a 1-hydroxyalkyl group and a hydrogen. The hydroxy in the the 1-hydroxyalkyl group withdraws electron density, and the hydrogen cannot provide hyperconjugation. Although D-glucopyranosylium ion has never been observed in solution because of its lability, tetramethyl-D-glucopyranosylium ion has been produced in the gas phase and lives long enough for its infrared spectrum to be gathered.[68] In the active site of an enzyme, unlike in solution where nucleophilic molecules of water are immediately adjacent to it, the lifetime of a D-glucopyranosylium ion will depend, as it does in the gas phase, critically on the access of nucleophiles to its two faces. Consequently, the lifetime of the ion in aqueous solution cannot be used as an argument that it is too evanescent to exist as an intermediate in an active site.[69]

"The kinetic equation of a multistep reaction will contain the rate constants of some or all of the successive reaction steps. The last step in this series, the rate constant for which appears in the kinetic equation, is rate-limiting."[70] By this definition, all of the steps that follow the **rate-limiting step**, although they are real, unavoidable steps, must be so fast that they occur immediately relative to the passage through the rate-limiting step, and therefore they have no effect on the observed rate of the reaction. In the hydrolyses of acetals and ketals (Equation 1–27 with H_2O in place of SO_3^{2-}), although hydronation of the oxygen of the leaving group is always required, either the dissociation of the carbon–oxygen bond[71] or the addition of water or hydroxide to the oxocarbenium ion can be the rate-limiting step, depending on the pH of the solution.[72,73]

Although in most cases an oxocarbenium ion is less prone to elimination than a carbenium ion, an oxocarbenium ion is an intermediate in the formation of vinyl ethers by elimination. For example, in an acidic solution, the diethyl acetal of ethanal gives ethyl vinyl ether

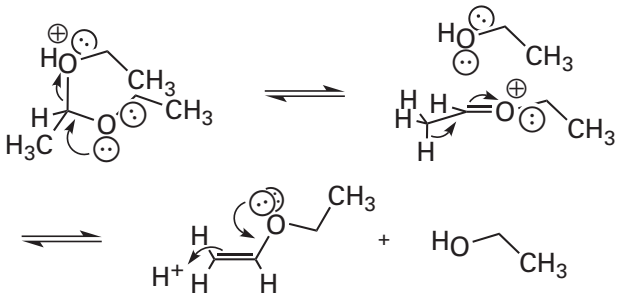

(1–30)

This reaction is analogous to the elimination from a carbenium ion that would be a side product during a simple dissociative nucleophilic substitution. Such an elimination would be an undesired side reaction in a desired nucleophilic substitution at a carbon atom immediately adjacent to an oxygen. Because the loss of the hydron (the second step) is the rate-limiting step in this elimination,[71] such an **undesired elimination** can be prevented from occurring on an enzymatic active site by denying the hydron a base and capturing the oxocarbenium ion by the intended nucleophile before it can eliminate the hydron. In solution, however, for most dissociative nucleophilic substitutions involving oxocarbenium ions as intermediates, the transition state for substitution is of lower energy than the transition state for elimination. The reverse of this type of elimination (Equation 1–30), in which the enol ether is first hydronated at the β carbon to give the oxocarbenium ion, produces the hemiacetal when the nucleophile is water rather than ethanol and leads to the hydrolysis of the vinyl ether.[74] For example, the hydrolysis of ethyl vinyl ether produces ethanal and ethanol.

Tertiary iminiums are the nitrogen equivalents of oxocarbenium ions. During the opening of imidazolines

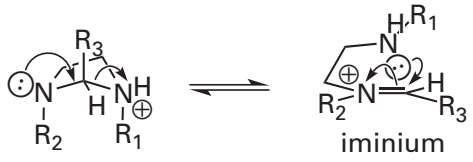

(1–31)

the less basic nitrogen, which is determined by the identity of R_1 and R_2, is the leaving group, but only after it is hydronated.[75] Equation 1–31 serves as an

example of a nitrogen rather than an oxygen providing the lone pair of electrons stabilizing the carbocation by forming an iminium rather than an oxocarbenium ion. Both the fact that the more basic, more electron-releasing nitrogen is better able to stabilize the carbocation while forming an iminium and the fact that the less basic nitrogen, once it is hydronated, is a better leaving group explain the regiochemistry of the reaction. Because a nitrogen is less electronegative than an oxygen, the carbon of an iminium is less electropositive and **significantly less reactive** than the carbon of an oxocarbenium ion. Because it is less electronegative, the nitrogen with a positive elementary charge in a tertiary iminium exerts a weaker electron withdrawal than oxygen with a positive elementary charge in an oxocarbenium ion, and the nitrogen stabilizes the positive elementary charge of the cation more effectively.

A concerted nucleophilic substitution proceeding through a single concerted transition state and a dissociative nucleophilic substitution proceeding through an unassociated, fully intermediate carbenium ion or oxocarbenium ion are two extremes of a continuous spectrum of mechanism.[76] Making a firm distinction between concerted mechanisms and dissociative mechanisms, as well as any other attempts to define boundaries within this continuous spectrum of mechanism, are at best counterproductive.

One way to visualize this continuous spectrum of mechanism is to represent the energetics of a particular nucleophilic substitution on a **three-dimensional surface of potential energy** (Figure 1–4A,B).[77,78] One coordinate for this surface is the distance between the carbon at which the substitution is taking place and the atom (Y) that is leaving the electrophile. Another coordinate is the distance between that same carbon and the nucleophilic atom (X) that is adding to it. These two coordinates define a continuous two-dimensional field.

For every point on this two-dimensional field, there is a potential energy associated with the two distances that are the coordinates of that point. The potential energy is the third coordinate, and these three coordinates together produce the three-dimensional surface of potential energy. This surface of potential energy can be represented topographically with contours of equal potential energy. On this undulating surface of potential energy there will always be a path from reactant to product, the **reaction coordinate** (dashed arrow), through a point of lowest potential energy, a **col**.* The **transition state** of the reaction, which is at the maximum of potential energy experienced between reactant and product, is at this col.

For a **dissociative nucleophilic substitution**, in which the bond to the leaving group is completely broken before the bond to the nucleophile begins to form, there is a carbenium ion or oxocarbenium ion as an intermediate (Figure 1–4A). Before the dissociation begins, there is a minimum of potential energy (lower right corner) at the bond length between the atom of the leaving group and the electrophilic carbon representing the ground state, and the nucleophile is far enough away to have no effect on the potential energy of the electrophile. Following the dissociation, there is a minimum of potential energy (upper right corner) when both the leaving group and the nucleophile are far enough away to have no effect on the potential energy of the carbenium ion or the oxocarbenium ion. After the product has formed, there is a minimum of potential energy (upper left corner) when the leaving group is far enough away to have no effect on the potential energy of the reaction. The reaction proceeds through the first transition state (‡) along a reaction coordinate over a col to produce the carbenium ion or the oxocarbenium ion (vertical dashed arrow) and through the second transition state along a reaction coordinate over a col to give the product (horizontal dashed arrow).

For a **concerted nucleophilic substitution** (Figure 1–4B), in which the bond to the leaving group is being broken while the bond to the nucleophile is being formed, the reaction passes through only one transition state (‡) at a col in the potential energy. In this transition state, the nucleophilic atom and the atom of the leaving group are both closer to the carbon as the bonds are being simultaneously broken and formed than they are when a carbenium ion or oxocarbenium ion is the intermediate. The respective lengths of the bond to the nucleophile and the bond to the leaving group in the transition state of a concerted nucleophilic substitution are determined by the position of the col on the surface of potential energy. For example, it has been estimated from various kinetic isotope effects on the rate of the reaction at pH 6.0 and 50 °C

*A col is a pass in a range of mountains. The term historically applied to this point on a three-dimensional surface of potential energy was a saddle point. Saddle is a term in mountaineering that is more commonly used in certain regions for a col.

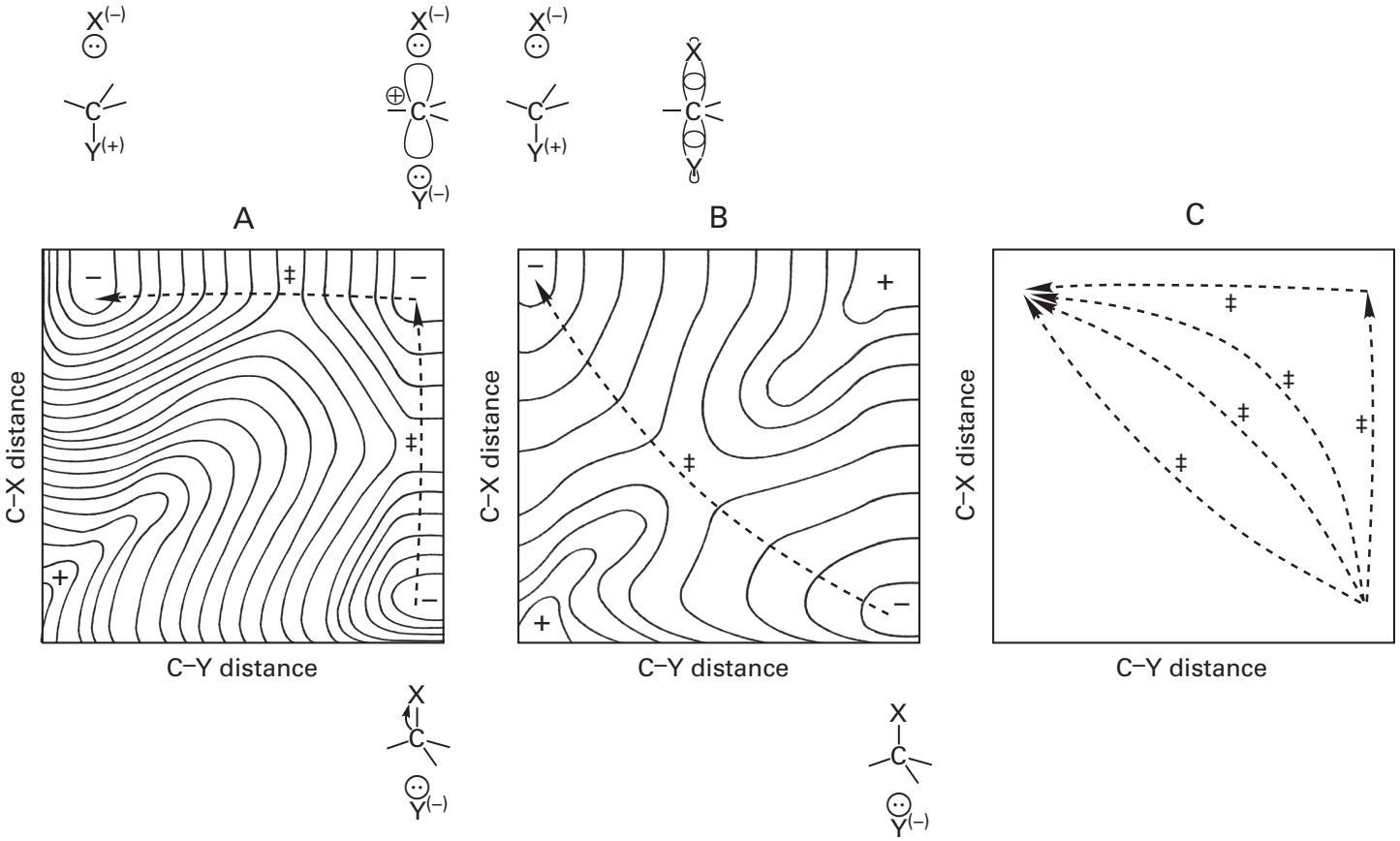

Figure 1–4: Hypothetical three-dimensional representations of surfaces of potential energy[77,78] for a nucleophilic substitution at a saturated carbon. The ordinate of the plot is the distance between the electrophilic carbon and the atom X that is leaving during the substitution. The abscissa of the plot is the distance between the electrophilic carbon and the nucleophilic atom Y that is forming the new bond with the electrophilic carbon. The intersection of these two axes, for the sake of brevity, is not the point at which each has a value of zero, which would be a singularity of potential energy. The point of their intersection has coordinates or distances close to the values for the lengths of the respective covalent bonds, one between the electrophilic carbon and the atom leaving and one between the electrophilic carbon and the nucleophilic atom in the product. The third dimension is the potential energy associated with each value for these two distances. The third dimension is represented topographically by contour lines of equal potential. These contour lines represent a sinuous surface of potential energy. The two topographic maps of potential energy are entirely hypothetical, do not represent the surface of potential energy for any reaction, and are intended only for demonstration. The positive signs identify peaks of potential energy, and the negative signs identify wells of potential energy. The usual sign (‡) for a transition state designates a minimum of potential energy between reactants and products at the col through which the reaction proceeds. The dashed, curved arrows indicate the path of the reaction coordinate along which the reaction proceeds. In all instances of nucleophilic substitution at carbon, the contours nearest the origin of the plot represent a pentavalent carbon, which has such a high potential energy that it has never been observed. The species involved as reactants, intermediates, transition states, or products are represented outside the plots below (reactants) or above (intermediate carbocation, associated intermediate, or products) the location of their respective potential energies. **(A)** Hypothetical surface of potential energy for a dissociative nucleophilic substitution. The atom X, which is the leaving group, dissociates completely (vertical dashed, curved arrow) before the nucleophile Y associates (horizontal dashed, curved arrow) with the resulting carbocation. The carbocation is at a minimum of potential energy as are the reactants and the products. There is a transition state between the reactant and the carbocation and another transition state between the carbocation and the products. **(B)** Hypothetical surface of potential energy for a concerted nucleophilic substitution. The atom X that is leaving dissociates as the bond to the nucleophilic atom Y is forming. Consequently, there is only one col between reactants and products and only one transition state. The position at which a carbocation would be formed is a maximum of potential energy in this instance because the carbocation is unstable. **(C)** Several possible reaction coordinates between reactants and products that represent, in descending order, a more and more unstable carbocation and a more and more associative nucleophilic substitution. Adapted with permission from reference 77. Copyright 1972 American Chemical Society. https://doi.org/10.1021/cr60280a004

that in the transition state for the substitution of a fluoro group on α-D-glucopyranosyl fluoride by an azido group (see Equation 1–25 and **1–14**), the distance from the electrophilic carbon to the fluoride that is leaving is 0.27 nm and the distance from the electrophilic carbon to the nucleophilic nitrogen of the azide is 0.19 nm.[79]

The potential energy is always very large for the situation in which the length of the bond between the nucleophile and the electrophilic carbon is the same as its length in the product at the same time that the bond between the leaving group and the electrophilic carbon is the same length as it is in the reactant (lower left corner) because this would be the situation for a pentavalent carbon, which is so unstable that it has never been observed in solution.* Consequently, there is always a mountain of potential in the lower left corner of the surface of potential energy in both dissociative and concerted nucleophilic substitutions at a saturated carbon.

One way to think about the continuous progression from a dissociative nucleophilic substitution to a concerted nucleophilic substitution is to concentrate on the **stability of the carbenium ion or oxocarbenium ion**, represented by the well of potential energy in the upper right corner of the surface of potential energy for the dissociative substitution (Figure 1–4A). As the carbenium ion or oxocarbenium ion becomes more and more unstable, the well of potential energy becomes a plain and then a hill of potential and then a mountain of potential energy (Figure 1–4B). This increase in the potential energy of the carbenium ion or oxocarbenium ion first creates a col immediately adjacent to the upper right corner and then pushes the col more and more in a lower left direction (Figure 1–4C) until it is a col between two substantial mountains of potential energy (Figure 1–4B). These mountains are the unstable carbenium ion or oxocarbenium ion (upper left corner) and a pentavalent carbon (lower right corner).

This spectrum of mechanism can be considered for the particular case of a reaction involving an electrophilic carbon attached to an alkoxy group for which an oxocarbenium ion is a possible intermediate (Equations 1–25 to 1–30). In a mechanism with a fully developed intermediate oxocarbenium ion, the bond between leaving group and carbon breaks completely before the bond between nucleophile and oxocarbenium ion begins to form (Equation 1–25). Two steps can be distinguished—namely the dissociation of the leaving group followed by the association of the nucleophile—and the reaction has two transition states—one for the first step that produces the oxocarbenium ion and one for the second step that produces the products. This disjunction is the reason for the existence of the oxocarbenium ion as an intermediate. In the single transition state of a concerted nucleophilic substitution proceeding without an intermediate, however, the bond between the leaving group and the electrophilic carbon is breaking in concert with the formation of the new bond to the nucleophile. If the two are fully coordinated, the carbon remains uncharged.

The difference in these two extremes can be also thought of as a matter of **timing**, and the spectrum between these two extremes covers mechanisms in which the formation of the bond to the nucleophile lags behind by a certain degree or precedes by a certain degree the disintegration of the bond to the leaving group. Within this spectrum, an oxocarbenium ion is more or less realized. In the case of nucleophilic substitution at a fully saturated carbon next to an alkoxy oxygen, the formation of the bond between the electrophilic carbon and the nucleophile cannot precede the disintegration of the bond to the leaving group by too much of an interval or the carbon would become pentavalent, but it definitely can lag behind by any interval. The more it lags behind, the more the electrophilic carbon in the transition state resembles an oxocarbenium ion.

One of the traditional distinctions between the two extremes of mechanism for nucleophilic substitution is the molecularity of the observed rate. A concerted nucleophilic substitution proceeding in free solution through a single transition state without the formation of an intermediate (Equation 1–19) is a bimolecular reaction, and its observed rate constant is second-order (S_N2). The rate of the reaction is first-order in electrophile and first-order in nucleophile. The first step of a dissociative nucleophilic substitution, however, which proceeds through an unassociated, intermediate carbenium ion or oxocarbenium ion, is the unimolecular formation of that carbenium ion or oxocarbenium ion (Equations 1–21 and 1–25). Because the second step is almost always more rapid, the first step is the rate-limiting step, and the observed rate for such a dissociative nucleophilic substitution is first-order (S_N1).

*There is a hexacoordinated carbon atom in the center of a metallic cluster in the enzyme nitrogenase.

Consider the following three conditions. First, the nucleophile must be immediately adjacent to the electrophilic carbon within its shell of solvation before the bond to the leaving group can begin to break. Second, after the bond to the leaving group and the electrophilic carbon has completely broken, the new bond to the adjacent nucleophile has not yet begun to form and a full oxocarbenium ion exists. Third, the adjacent nucleophile, while still in the solvent shell, then forms the new bond without having the time to exchange with another nucleophile in the solution because the lifetime of the oxocarbenium ion is so short

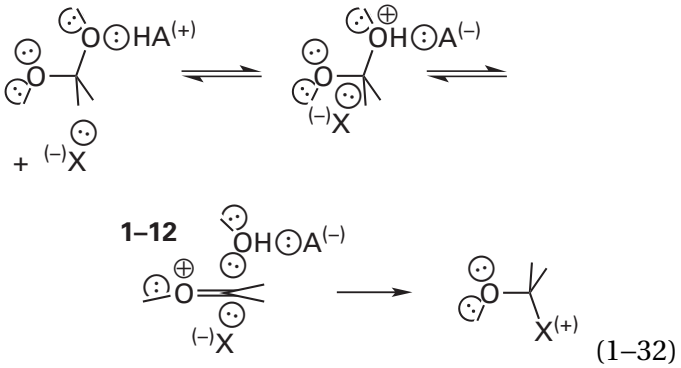

(1–32)

If all three conditions are met, then the reaction is bimolecular, so its rate is first-order in the concentration of the electrophile and first-order in the concentration of the nucleophile, and it proceeds with inversion of configuration at the electrophilic carbon. The reaction, however, also proceeds in two steps with a fully formed, intermediate oxocarbenium ion (**1–12** in Equation 1–32). Such **a mechanism, containing prominent features of the two extremes in the spectrum**, is possible because it has been shown that, in order for an oxocarbenium ion to form, it usually must be solvated above and below the plane of its bonds by lone pairs of electrons from at least the solvent if not the nucleophile.[80] The nucleophile can provide a lone pair of electrons to solvate the oxocarbenium ion on one face, and the leaving group can provide a lone pair of electrons on the other face (**1–12**). Before the solvation by the nucleophile is provided or if the nucleophile dissociates too soon from the shell of sovation, the oxocarbenium ion cannot form.

Nucleophilic substitutions that occur in solution at the electrophilic carbon of a ketal usually have first-order rate constants, and the concentration of nucleophile has no effect on the rate of the reaction. This lack of an effect is presumably because, in a ketal, the oxocarbenium ion that is an intermediate in the nucleophilic substitution is a secondary oxocarbenium ion and the two alkyl substituents on the electrophilic carbon stabilize the carbocation by hyperconjugation, just as a tertiary carbenium ion is stabilized by hyperconjugation.

Most of the **nucleophilic substitutions that occur in solution at the electrophilic carbon of an acetal** (for example Equation 1–27), for which an oxocarbenium ion is a possible intermediate, have second-order rate constants, and the rates of the reactions are first-order in the concentration of the nucleophile. This molecularity is established experimentally by measuring the rate of the nucleophilic substitution as a function of the concentration of the nucleophile and demonstrating that the two are linearly related.[81] From the slope of the line, a second-order rate constant is calculated.

If the reaction takes place in water, one of these nucleophilic substitutions by a particular nucleophile usually proceeds in concert with hydrolysis of the acetal that occurs even in the absence of that nucleophile. For example, as azide ion is added to the solution, the rate of release of 4-bromoisoquinoline from 2-deoxy-β-D-glucopyranosyl-4′-bromoisoquinolinium ion (Equation 1–25) increases. From this increase in rate, an observed second-order rate constant of 1.2×10^{-4} M^{-1} s^{-1} at 65 °C can be calculated for the nucleophilic substitution of 4-bromoisoquinoline by azide ion,[53] which is in addition to the background rate of hydrolysis of the deoxy-D-glucosylisoquinolinium ion that has an observed first-order rate constant of 1.5×10^{-4} s^{-1}. If a particular nucleophilic substitution has a second-order rate constant, the question then becomes how far along is the formation of the bond with the nucleophile and how far along is the breaking of the bond with the leaving group in the transition state responsible for its observed second-order rate constant.

A determination of the degree to which the bond between the carbon and the nucleophile has been formed and the degree to which the bond between the carbon and the leaving group has been broken in the transition state for a nucleophilic substitution can be made from linear free energy relationships.

The **dependence of the observed second-order rate constant for a nucleophilic substitution on the nucleophilicity of the nucleophile** provides an indication of the extent to which the bond is formed between the nucleophile and the electrophilic carbon in the transition state governing the rate constant for the reaction relative to the degree

to which it is formed in the transition state for a purely concerted nucleophilic substitution. The second-order rate constants for several series of nucleophilic substitutions at the same electrophilic carbon by a series of different nucleophiles are measured. The common logarithms of these observed second-order rate constants are plotted in a **Swain–Scott correlation** (Figure 1–5)[81-84] as a function of a set of parameters, known as nucleophilicities, that are related to the common logarithms of the rate constants for the nucleophilic substitutions between the respective nucleophile and methyl iodide. Methyl iodide is used as the reference electrophile because nucleophilic substitutions at methyl iodide are always concerted nucleophilic substitutions that involve a single transition state with no intermediate carbenium ion and there are almost no steric problems associated with this nucleophilic substitution. In the case of the reaction in Equation 1–25, there is little if any dependence (slope of the Swain–Scott correlation is 0.03 ± 0.05) of the observed second-order rate constants on the respective nucleophilicities of the noted set of nucleophiles. This fact indicates that there is little if any bond formed between the nucleophile and the electrophilic carbon in the transition state governing the observed second-order rate constant even though the nucleophile must be present in this transition state to explain the bimolecularity of the reaction.

The greater the dependence of the rate constant for a nucleophilic substitution on the strength of the nucleophile, the more fully developed is the **bond between the nucleophile and the electrophilic carbon** in the transition state governing the observed second-order rate constant. For the nucleophilic substitutions of the azido group in 1-azido-1-ethoxypropane

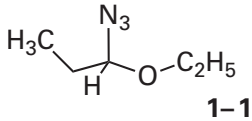

1–13

involving each of a set of nucleophiles, the correlation between the common logarithms of the observed second-order rate constants for the respective nucleophilic substitutions and the respective nucleophilicities of those nucleophiles (Figure 1–5)[81] has a slope of 0.18. This fact indicates that, with this electrophile, the bond between the nucleophile and the electrophilic carbon is only partly developed in the transition state governing this rate constant. When azidomethoxyphenylmethane is used as the electrophile, the slope of the Swain–Scott correlation is 0.4, indicating that with this electrophile the bond between the nucleophile and the electrophilic carbon is further advanced in the transition state than it is with 1-azido-1-ethoxypropane.

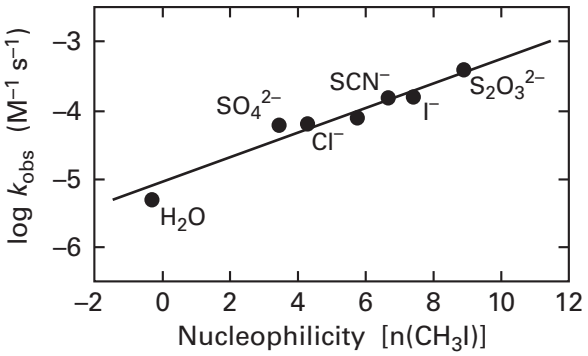

Figure 1–5: Correlation between the rate constants for a common nucleophilic substitution by each of a series of nucleophiles and their respective nucleophilicities.[81] The rate constants for the hydrolysis of 1-azido-1-ethoxypropane (**1–13**) at 25 °C and an ionic strength of 1.0 M were measured by following the production of propanal. Various concentrations of the nucleophilic ions SO_4^{2-}, Cl^-, Br^-, SCN^-, I^-, and $S_2O_3^{2-}$ were added to the solution, and the second-order rate constants for the acceleration of the hydrolysis that they produced were determined from the slopes of plots of observed rate constants against their concentrations. The common logarithms of these observed second-order rate constants, k_{obs} (molar^{-1} second^{-1}), are plotted[82] against parameters [n(CH_3I)] derived from the common logarithms of the respective rate constants of the reaction of these same nucleophiles with methyl iodide in methanol.[83] The line drawn through the points has a slope of 0.18. The observed second-order rate constant of the uncatalyzed hydrolysis is the point[84] labeled H_2O.

The **dependence of the observed rate constant of a nucleophilic substitution on the acidity of the conjugate acid of the leaving group** provides information about the degree to which the bond between the electrophilic carbon and the leaving group is broken in the transition state governing that rate constant. A series of electrophiles, identical except for the leaving group, is synthesized, and the rate of the nucleophilic substitution of each of these electrophiles by the same nucleophile is measured. The common logarithms of the observed rate constants for these nucleophilic substitutions are plotted as a function of the respective values of pK_a for the conjugate acids of the leaving groups (Figure 1–6).[85-88]

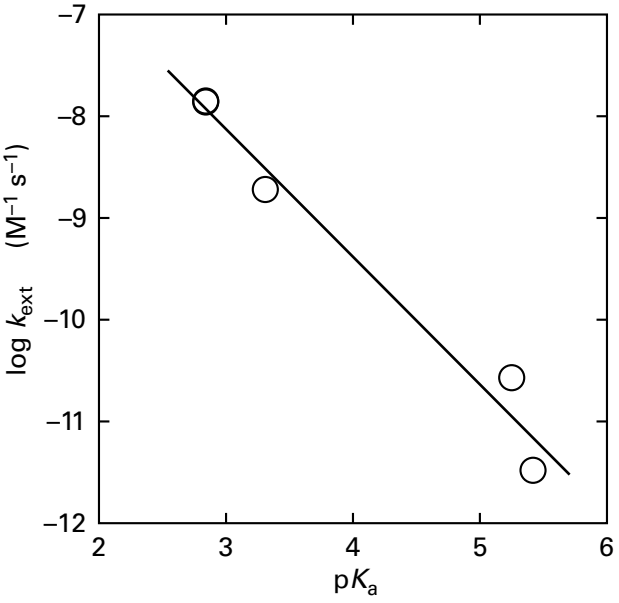

Figure 1–6: Brønsted correlation between the rate constants for the hydrolyses of a series of β-D-galactopyridinium ions and the acid dissociation constants of the conjugate acids of the respective pyridine that is the leaving group.[85] The hydrolyses of 3-chloro-1-(β-D-galactopyranosyl)pyridinium ion, with 3-chloropyridine as the leaving group (pK_a = 2.84); 3-bromo-1-(β-D-galactopyranosyl)pyridinium ion, with 3-bromopyridine as the leaving group (pK_a = 2.84); 4-bromo-1-(β-D-galactopyranosyl)isoquinolinium ion, with 4-bromoisoquinoline as the leaving group (pK_a = 3.31); 1-(β-D-galactopyranosyl)pyridinium ion, with pyridine as the leaving group (pK_a = 5.25); and 1-(β-D-galactopyranosyl)isoquinolinium ion, with isoquinoline as the leaving group (pK_a = 5.42) were measured at pH 6.0 and various temperatures between 48 and 138 °C by following the change in ultraviolet absorption that occurs when the respective pyridine or isoquinoline is released into the solution. Each reaction was monitored at the wavelength at which the change in absorbance is the greatest (276, 290, 350, 260, and 340 nm, respectively). For each D-galactosylpyridinium ion, the rate constant measured for its hydrolysis was extrapolated to a temperature of 25 °C. The common logarithm of each extrapolated first-order rate constant (k_{ext}; seconds^{-1}) is plotted against the respective pK_a for the conjugate acid of the leaving group. The slope of the line, β_{lg}, fit to the data by least-squares numerical analysis is 1.26 ± 0.12. This slope is the Brønsted coefficient for the leaving groups.

A **Brønsted correlation** is any correlation between the common logarithms of a set of rate constants or equilibrium constants for the members of a set of interchangeable participants in a particular reaction—be they reactants, products, or catalysts—and the values of pK_a for the respective participants or for their conjugate acids corrected for the number of acidic hydrons and basic lone pairs of electrons on the participating atom. The distinction between a Swain–Scott correlation and a Brønsted correlation is the use of nucleophilicities in the former and values of pK_a in the latter. The use of a Brønsted correlation is far broader than the use of a Swain–Scott correlation because values of pK_a for a wide variety functional groups are known and variation of the values of pK_a for any of the participants in the reaction produces a Brønsted correlation.

It is usually the case that the common logarithms of equilibrium constants or of rate constants, respectively, are linearly correlated with the common logarithms of the relevant acid dissociation constants. These correlations suggest that what is actually being correlated are changes in the standard free energy or the standard free energy of activation for the reaction, respectively, with changes in the standard free energy of the acid dissociation. Consequently, a Brønsted correlation is an example of the more general class of **free energy correlations**.

A **Brønsted plot** is a graph of the common logarithms of the rate constants or equilibrium constants plotted against the respective values of pK_a for the chosen participant or its conjugate acid. If the data show a linear correlation over a particular range of rate constant and pK_a, the slope of that line is the **Brønsted coefficient**, designated as β. The **Brønsted coefficient for the leaving groups, β_{lg}**, in a series of homologous nucleophilic substitutions, which is the slope of the line on a Brønsted plot (Figure 1–6), is a measure of the degree to which the transition state governing the observed rate constant resembles the fully dissociated conjugate acid. Brønsted plots can also be made for the ability of a leaving group in an enzymatic reaction.[89]

For the hydrolysis of a set of D-galactosylpyridinium ions (similar to Equation 1–25, with D-galactose as the monosaccharide instead of 2-deoxy-D-glucose, water as the nucleophile instead of azide ion, and a set of pyridines as the leaving groups instead of isoquinoline), the value of β_{lg} is –1.26 ± 0.12 (Figure 1–6).[85] This fact indicates that there is a somewhat larger change in the charge of a particular pyridine between the reactant and the transition state controlling the observed rate constant for the hydrolysis of the electrophile than there is upon dissociation of the same pyridine from a hydron.* Consequently, the bond between nitrogen and carbon is fully broken at the transition state.

The value of β_{lg}[53] for the rates of hydrolysis of three different (2-deoxy-β-D-glucopyranosyl)isoquinolinium ions (Equation 1–25) is –1.0 ± 0.1. This fact, and

*That the difference in the case of hydrolysis is greater than 1 is probably because the charge on the nitrogen of the pyridinium ion (the reference for the comparison) is actually less than the charge on the pyridino group in the electrophiles.

the fact that there is only a small effect of the nucleophilicity of nucleophiles other than azide ion (0.03 ± 0.05) on the rate constant for the nucleophilic substitution, together indicate that in this reaction, as shown in Equation 1–25, in the transition state governing the observed rate constant for this reaction, the oxocarbenium ion is fully developed even though the reaction is second-order.

An additional observation indicating that an oxocarbenium ion is formed in the nucleophilic substitutions of D-glucopyranosylpyridiniums[85] as well as phenyl D-glucopyranosides,[90] is that, when the hydrogen on carbon 2 of the D-glucose is replaced by a deuterium, the rates of these reactions decrease by about 10%, a large secondary deuterium kinetic isotope effect. This decrease in rate suggests that this hydrogen participates in hyperconjugation with a double bond between carbon and oxygen in an intermediate oxocarbenium ion.

The **properties of the electrophilic carbon**, by determining the stability of a potential carbocationic intermediate, also affect the timing of formation of the bond to the nucleophile and breaking of the bond to the leaving group. In all of the nucleophilic substitutions at carbon that have been discussed so far, there have been three players: the nucleophile, the leaving group, and the electrophilic carbon. So far, the emphasis of the discussion has been on the properties of the nucleophile and the leaving group that determine the timing of formation of the new bond to the nucleophile and disintegration of the old bond to the leaving group, and hence the type of intermediate that occurs. Substituents on the electrophilic carbon determine its potential to support positive charge and its ability to sustain the vacant *p* orbital that produces this positive elementary charge (Equation 1–21). The substituents of biochemical importance and the order in which they stabilize an adjacent-carbocation with a vacant *p* orbital are $-NH(CH_2-)$ > $-NH_2$ > $-N(CH=)-$ > $-N(CO-$ > $-OCH_2-$ > $-OH$ > $-OPO_3H_2$ > $-OC(O)-$ > =O > $-CH(CH_2-)-$ > $-CH_2-$ > $-CH_3$ > $-CH(NH_2)-$ > $-CH(OH)-$ > $-H$ > $-CONH-$ > $-COOH$. If a hydron is added to any of these substituents, the carbocation is destabilized; if a hydron is removed from any one, the carbocation is stabilized. If the substituents on the electrophilic carbon are ones that increase the stability of a carbocation, then the bond to the leaving group breaks more readily, the bond to the nucleophile forms less readily, and the transition state expands.

Another of the traditional distinctions between the two extremes of mechanism for nucleophilic substitution is the stereochemistry of the reaction. If a concerted nucleophilic substitution proceeds without the formation of a carbenium ion or oxocarbenium ion, complete **inversion of configuration** at the electrophilic carbon (**1–6**) is observed, and the nucleophilic substitution is usually judged to be concerted. If a carbenium ion exists long enough for the leaving group to diffuse away, and if the nucleophile is free to attack either side of the resulting unencumbered carbenium ion with equal facility, the products of **both inversion and retention of configuration** result, in equal concentration, and the nucleophilic substitution is usually judged to be dissociative.

In the **dissociative nucleophilic substitution** of Equation 1–25, however, most of the product (90%) is the α-D-2-deoxyglucosyl azide formed from inversion of configuration. The fact that little retention of configuration (10%) occurs suggests that although the oxocarbenium ion is fully formed in this reaction, it retains contact with the isoquinoline at the one face, blocking entry to that face, long enough that most of the substitution proceeds with inversion of configuration as indicated in Equation 1–25. That some retention of configuration (10%) is observed, however, suggests that the association of the oxocarbenium ion with the isoquinoline is weak enough that the isoquinoline sometimes dissociates from the oxocarbenium ion before the azide ion associates with the oxocarbenium ion at the opposite face, leaving the oxocarbenium ion free in solution to be attacked by the nucleophile from either face.

In the solvolysis of a series of different D-glucopyranosides in mixtures of ethanol and trifluoroethanol,[91] the various nucleophilic substitutions yield products in which retention of configuration varies from 8% to 90% depending on the leaving group.* These results suggest that the oxocarbenium ions produced in some of these reactions have lifetimes long enough for the leaving group to diffuse completely away before the nucleophile ever enters the reaction.

*That the concentration of product resulting from retention of configuration exceeds 50% is due to the fact that the glucopyranosyl oxocarbenium ion in this case is diasteriomeric. Nucleophilic attack at its α face is preferred over nucleophilic attack at its β face. This preference is thought to result from the formation of a hydrogen bond between the oxygen atom of the 2-hydroxy group and the hydroxy group of the approaching alcohol.

When a **concerted nucleophilic substitution** that has only one transition state and in which an oxocarbenium ion is not formed occurs adjacent to an alkoxy group complete inversion of configuration should occur, as in the substitution of azide by bromide in azidomethoxymethylbenzene[81]

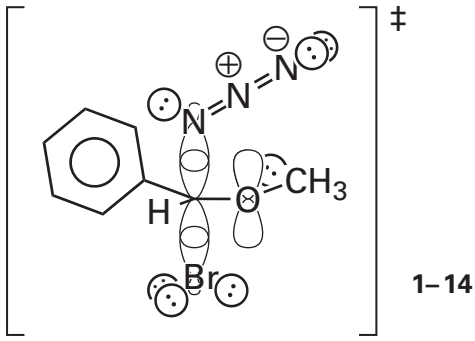

1–14

The dependence of the observed rate constant of the reaction on the nucleophilicity of the nucleophile and the acidity of the conjugate acid of the leaving group should indicate that formation of the bond to the nucleophile occurs in concert with disintegration of the bond to the leaving group. To the extent, however, that the electrophilic carbon in the transition state of a concerted nucleophilic substitution resembles a carbenium ion, the adjacent oxygen should improve its stability by electron donation. In the transition state **1–14**, there are six electrons in the four designated atomic orbitals that mix to form the four molecular orbitals of its unique molecular orbital system. The three of lowest energy are occupied by the three pairs of electrons.

In reactions involving the addition of a nucleophile to an oxocarbenium ion, the oxygen atom has a substituent attached to it in addition to the electrophilic carbon. This substituent fixes a **positive formal elementary charge** on the oxygen and thereby increases its electronegativity and draws the two electrons in the π bond more strongly over it (**1–8**). In a tertiary iminium, such as the one in that is the product of the opening of an imidazoline (Equation 1–31), the nitrogen atom has two substituents attached to it in addition to the electrophilic carbon. These two substituents fix the positive formal elementary charge on the nitrogen, also increasing its electronegativity. If the substituent on the oxygen is replaced by a lone pair of electrons, the oxocarbenium ion becomes a **carbonyl group** (**1–15**),* and if one of the substituents on the nitrogen is replaced by a lone pair of electrons, the tertiary iminium (Equation 1–31) becomes an **imino group** (**1–16**)

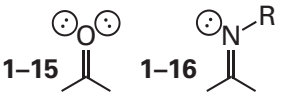

1–15 **1–16**

Although it is far more stable than an oxocarbenium ion because the electronegative oxygen is no longer required to bear a formal positive charge, a carbonyl group is nevertheless susceptible to nucleophilic addition, just as an oxocarbenium ion is. An imino group is also susceptible to nucleophilic addition. The energy barrier experienced by the nucleophile, however, is greater for addition to a carbonyl group or an imino group than to an oxocarbenium ion or a tertiary iminium, respectively, because of the greater electron density over carbon in the bonding molecular orbital of the respective π molecular orbital system. If, however, the carbonyl group or the imino group is hydronated on one

*The hybridization of the two lone pairs of electrons of the oxygen in a carbonyl group or acyl group seems to be conditional on the circumstances. In a liquid of a pure compound containing a carbonyl group or in the gas phase of the pure compound, there are several physical measurements demonstrating that the hybridization of the oxygen is *sp* with one *sp* orbital contributing to the σ bond, one *sp* orbital coaxial with the σ bond and occupied by one of the lone pairs of electrons, one *p* orbital contributing to the π bond, and the other *p* orbital, orthogonal to the π system, occupied by the other lone pair of electrons.[92] In crystallographic molecular models of small molecules, however, in which either one N–H forms a single hydrogen bond with a carbonyl oxygen or acyl oxygen or two N–H form two hydrogen bonds with a carbonyl oxygen or acyl oxygen,[93] the distribution of the angles at which the N–H is oriented is that expected if the carbonyl oxygen or the acyl oxygen is hybridized sp^2, with one sp^2 orbital contributing to the σ bond, the lone *p* orbital contributing to the π system, and the other two sp^2 orbitals in the plane of the carbonyl group. Both when there is one hydrogen bond and when there are two hydrogen bonds, the lines of centers between the oxygen and each nitrogen form angles distributed around a maximum at 120°. In extremely high resolution maps of electron density from X-ray crystallography, valence electron density can be observed. In these maps,[94] the total valence electron density, as opposed to the distribution of electron density in each atomic orbital, is seen to be distributed so that there are maxima of density at the oxygen in the plane of the carbonyl group and quite near the locations occupied by the symbols for lone pairs of electrons in drawing **1–15**. Because all of protein chemistry occurs in surroundings that maximize hydrogen bonding, the hybridization in drawing **1–15** has been chosen for all of the drawings of the oxygen in a carbonyl group or acyl oxygen, but no decision as to the actual hybridization of the particular oxygen is implied.

of its lone pairs, it becomes homologous with an oxocarbenium ion or a tertiary iminium, respectively, and becomes just as electrophilic.

Suggested Reading

Young, P. R., and Jencks, W. P. (1977) Trapping of the oxocarbonium ion intermediate in the hydrolysis of acetophenone dimethyl ketals, *J. Am. Chem. Soc. 99*, 8238–8247. https://doi.org/10.1021/ja00467a019

Huang, X., Surry, C., Hiebert, T., and Bennet, A. J. (1995) Hydrolysis of (2-deoxy-β-D-glucopyranosyl)pyridinium salts, *J. Am. Chem. Soc. 117*, 10614–10621. https://doi.org/10.1021/ja00148a002

Chan, J., Sannikova, N., Tang, A., and Bennet, A. J. (2014) Transition-state structure for the quintessential S_N2 reaction of a carbohydrate: Reaction of α-glucopyranosyl fluoride with azide ion in water, *J. Am. Chem. Soc. 136*, 12225–12228. https://doi.org/10.1021/ja506092h

Nucleophilic Addition and Nucleophilic Substitution at a Carbonyl Carbon

The compounds that can be formed by a nucleophilic addition at a carbonyl carbon or the carbon of an imine are hemiacetals, hemiketals, acetals, ketals, thiohemiacetals, thiohemiketals, and hemiaminals (Table 1–1).

A paradigm of these several reactions is the nucleophilic addition of a thiolate to an aldehyde[96] or a ketone[97] to produce a thiohemiacetal or thiohemiketal, such as the addition of methanethiolate to acetaldehyde

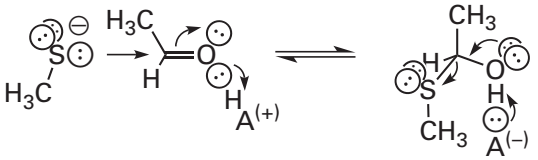

(1–33)

In this reaction, the initial contact between the reactants is the **overlap** between one of the atomic orbitals on sulfur occupied by a lone pair of electrons and the unoccupied antibonding orbital of the π molecular orbital system of the carbonyl group (reverse of the reaction in Figure 1–3 with nitrogen replaced by sulfur). In the process, electron density builds on oxygen at the expense of the nucleophile as the molecular orbital system of the transition state, produced from the three overlapping atomic orbitals, is formed. As the transition state decomposes to the product, the new σ bond is formed by the mixing of an atomic orbital from sulfur and an atomic orbital from carbon as an atomic orbital bearing the lone pair of electrons withdraws onto the oxygen.

As the reaction progresses, **electron repulsion** develops from overlap between the nucleophilic lone pair of electrons on sulfur in the one reactant and the occupied bonding molecular orbital of the π molecular orbital system and two of the three occupied σ bonds to the carbon in the other. Therefore, productive encounters occur only when the trajectory of the lone pair of electrons on sulfur is from above or below the plane of the carbonyl group and from a direction distal to the oxygen

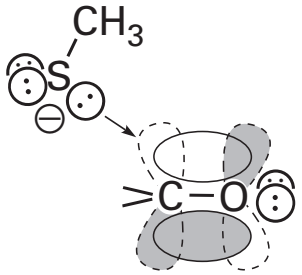

1–17

In the formation of a thiohemiacetal or thiohemiketal, two steps can be formally recognized: formation of the carbon–sulfur bond and **hydronation of the oxygen**. At values of pH greater than 3, the behavior of the reaction as a function of pH is consistent with a mechanism in which the formation of the carbon–sulfur bond precedes the hydronation of the oxygen[98]

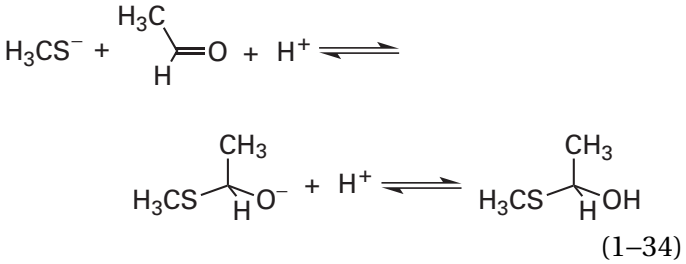

(1–34)

The intermediate anion is unstable and reverts rapidly to reactants unless it is trapped by addition of a hydron from water or other acids in the solution.[99]

Table 1–1: Derivatives of Acetaldehyde or Acetone as Examples of Carbonyl Compounds[a]

derivatives of acetaldehyde[b]		derivatives of acetone[b]	
hemiacetal	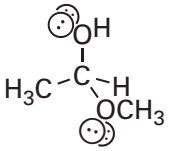	hemiketal	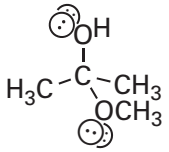
acetal	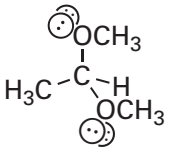	ketal	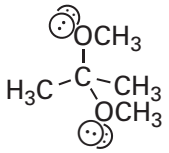
thiohemiacetal	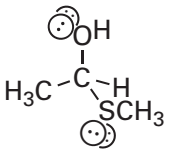	thiohemiketal	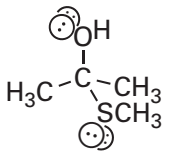
hemiaminal	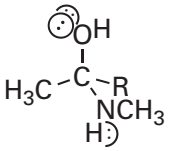	hemiaminal ether	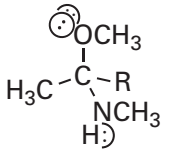
thiohemiaminal	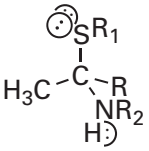	aminal	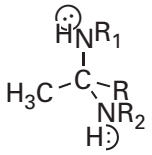

R, R_1, and R_2 can each be either H or CH_3

[a]Derivatives formed from methanol, methanethiol, or methylamine are presented for the sake of simplicity. [b]Only one enantiomer of each derivative is presented.

Consequently, the rate-limiting step in the addition is the hydronation of the oxygen, and the rate of the reaction is determined by the rate at which the anion is hydronated.

A **hemiaminal** (Table 1–1 and **1–18** in Figure 1–7) is formed by the addition of an amine to a carbonyl group.[86-88] This addition initially produces a zwitterion

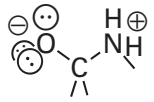

1–19

which is then subject to **tautomerization**. The tautomerization of the initial zwitterion (Figure 1–7) is formally equivalent to the hydronation of the oxyanion that is the second step in addition of the thiolate to a carbonyl group. The tautomerization proceeds by transfer of a hydron from the ammonium to a base in the solution and addition of a different hydron to the oxyanion from the same acid or a different acid in the solution. It cannot occur by intramolecular transfer of the hydron (Equation 1–18) because the acidic ammonium ion is only two atoms away from the basic oxyanion.

Tautomerizations involving the removal of a hydron from an ammonium ion and the addition of a hydron to an alkoxide ion two atoms away or the reverse are encountered frequently in biochemical mechanisms. **Bifunctional acid–bases**, such as phosphate and bicarbonate, catalyze reactions in which

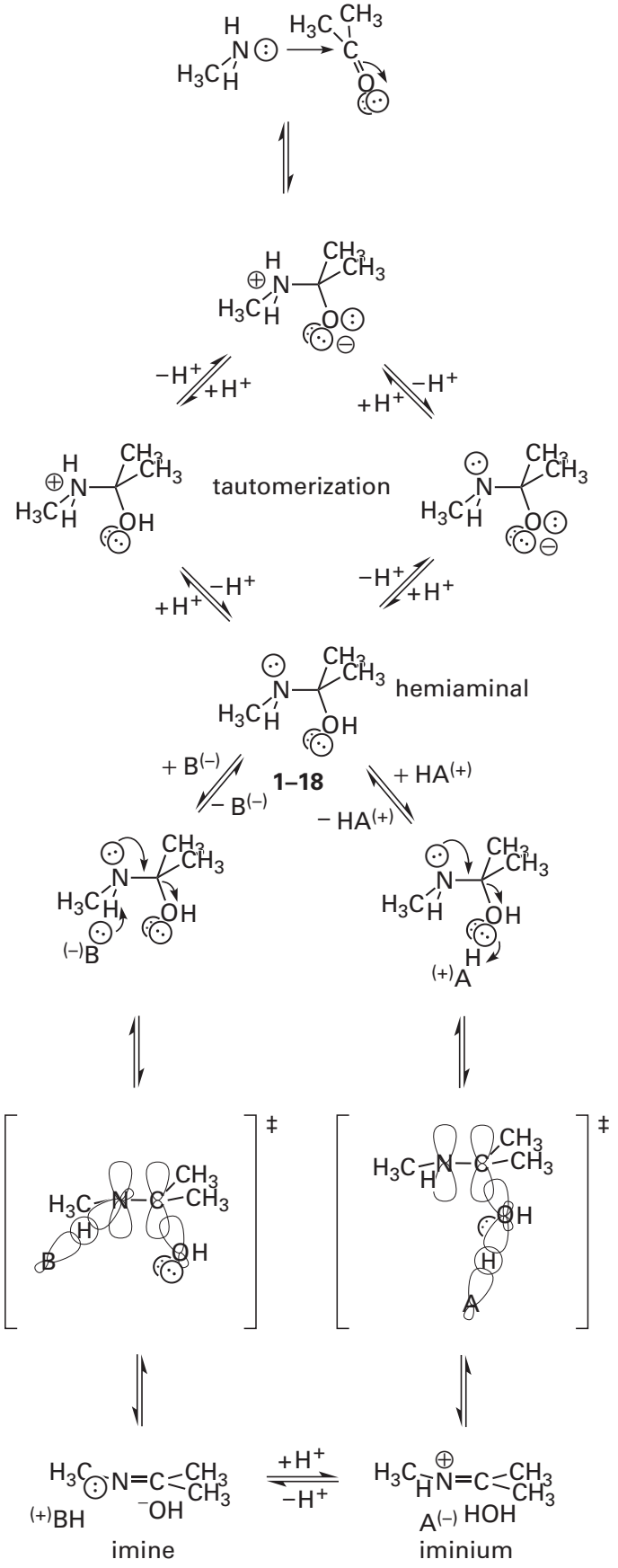

Figure 1–7: Addition of an amine to a carbonyl compound. The conjugate base of the amine adds to the carbonyl group to produce the zwitterion. A base in the solvent removes a hydron from the ammonium ion and an acid in the solvent adds a hydron to the oxyanion to produce the hemiaminal (**1–18**). The hemiaminal is susceptible to elimination in a reaction catalyzed by a general base[87] or a general acid.[86,88] In the reaction catalyzed by a general base, a hydron is removed from the nitrogen at the same time that an orthogonal lone pair of electrons on the same nitrogen pushes out the leaving group, a hydroxide ion. In the reaction catalyzed by a general acid, a hydron is added to a lone pair of electrons on the dissociating oxygen at the same time that the lone pair of electrons on nitrogen is pushing out the orthogonal σ bond to the same oxygen. In both the transition state for the reaction catalyzed by the general base and the transition state for the reaction catalyzed by the general acid, six atomic orbitals mix to form the respective transition states.

the mechanisms require such tautomerizations two to three orders of magnitude more effectively than monofunctional acids or bases with similar values of pK_a. This efficiency has been presented as evidence for the participation of such acid–bases in a cyclic, simultaneous transfer of the two hydrons[100]

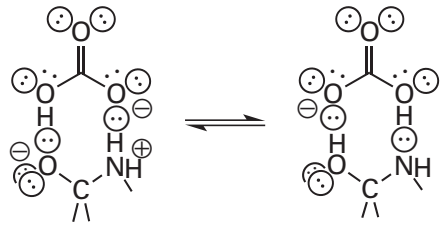

(1–35)

A similar **cyclic intermediate** has been invoked to explain the much less remarkable catalysis of such tautomerizations by primary amines[101,102]

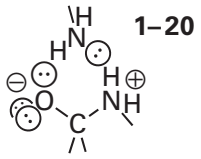

1–20

The hemiaminal (**1–18** in Figure 1–7) that results from the tautomerization is a pseudosymmetric intermediate. There are lone pairs of electrons on oxygen able to **push** away nitrogen to return to the ketone or aldehyde, and there is a lone pair of electrons on nitrogen able to push away oxygen to produce an imine. This abundance of push is another way of looking at the fact that the lone pairs on the heteroatoms in a hemiaminal or any adduct of a carbonyl group produce significant electron repul-

sion. This electron repulsion causes these adducts to be **significantly unstable in solution** relative to the aldehyde or the ketone or the imine. It is possible, however, to form a **stable intramolecular hemiaminal** by using a large synthetic octaphenyl cup to juxtapose sterically an aniline and an anthracene-2-carbaldehyde,[103] just as they can be stabilized on the active site of an enzyme by juxtaposition.

Iminiums are the conjugate acids of imines (Figure 1–7). The carbon of an iminium is electrophilic and **susceptible to addition**, just as a carbonyl group is susceptible to addition. In fact, the electrophilic carbon in an iminium is about 10^{10} times more electrophilic than the electrophilic carbon in the homologous aldehyde or ketone.[104] They are electrophilic enough to participate in the intramolecular electrophilic aromatic substitution of the Pictet–Spengler reaction.[105,106] An enzymatic example of an intramolecular nucleophilic addition to an iminium, which is similar to the Pictet–Spengler reaction, occurs in one of the steps of the reaction catalyzed by (*S*)-norcoclaurine synthase from *Thalictrum flavum*[107]

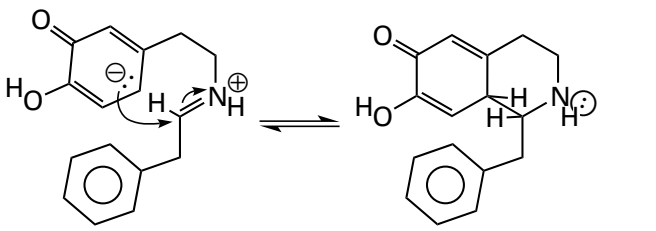

(1–36)

The product of nucleophilic addition of a thiolate to an iminium, the analogue of the addition of a thiolate to a carbonyl group (Equation 1–33 with oxygen replaced by a hydronated, cationic nitrogen), is a **thiohemiaminal** (Table 1–1).

The thiohemiacetals, thiohemiketals, hemiacetals, hemiketals, and hemiaminals formed in all these reactions represent a class of products that can be considered to be the ultimate products of the addition of one nucleophile or two nucleophiles in succession to a carbonyl group. Many biochemical metabolites such as D-glucopyranose (reactant in Equation 1–38) contain such products. In each of these products, the carbon that was the initial **carbonyl carbon** is bonded directly to two heteroatoms and either to two other carbons, to one carbon and one hydrogen, or to two hydrogens (Table 1–1). There is no oxidation or reduction involved in such additions so the carbon is still at the carbonyl oxidation state and can be considered a carbonyl carbon *in maschera*.

Nucleophilic additions to carbonyl groups are susceptible to catalysis by acids and bases. For example, during the nucleophilic addition of an alcohol to a carbonyl group under **catalysis by a base** (Figure 1–8A),[99,108,109] two different reactions occur simultaneously: the formation of the oxygen–carbon bond and the transfer of a hydron from the nucleophilic hydroxy group to the base. A hydroxy group that is already participating at its oxygen in a hydrogen bond with the catalytic base is the nucleophile, and the hydron in this hydrogen bond between the base and the hydroxy group is transferred from the hydroxy group to the base in concert with the formation of the σ bond between its oxygen and the electrophilic carbon of the carbonyl group. The σ lone pair of electrons on the nucleophilic oxygen that is attacking is mixing with the antibonding orbital of the π molecular orbital system of the carbonyl group (reverse of reaction in Figure 1–3, with nitrogen replaced by oxygen). The hydron that is being transferred to the catalytic base from this nucleophilic oxygen during the approach to the transition state is removed from a **different lone pair of electrons** from the pair adding to the electrophilic carbon of the carbonyl group.

During the addition of a nucleophile to a carbonyl group under basic conditions, the carbonyl oxygen becomes an initially unhydronated **oxyanion** (Figure 1–8A). This oxyanion is itself a nucleophile that can participate in a nucleophilic substitution, for example[110]

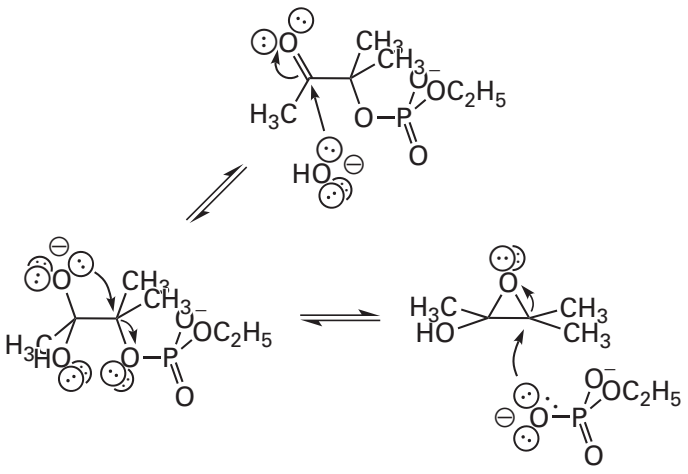

(1–37)

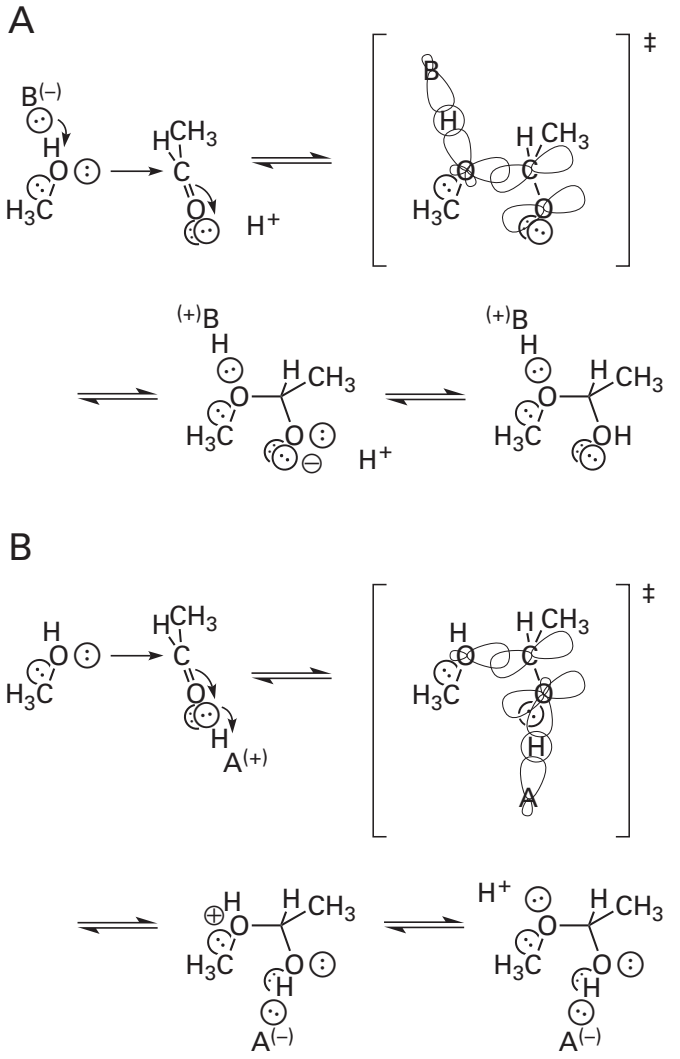

Figure 1–8: Catalysis of the formation of a hemiacetal by a general base or a general acid.[108] **(A)** In catalysis by a general base, the base B⊖, forming a hydrogen bond with the alcohol, removes the hydron from the oxygen at the same time another lone pair of electrons on the same oxygen adds to the carbonyl carbon. The two reactions are orthogonal to each other. The atomic orbitals mixing in the transition state (‡) are an atomic orbital of the base, the 1*s* orbital of hydrogen, two sp^3 orbitals of one oxygen, a *p* orbital of the carbon, and a *p* orbital of the other oxygen. The second step in the reaction is hydronation of the oxyanion to form the hemiacetal. **(B)** In catalysis by a general acid, the acid $HA^{(+)}$, forming a hydrogen bond with the carbonyl oxygen, adds a hydron to this oxygen at the same time that the oxygen of the alcohol adds to the carbonyl carbon. Again, the two reactions are orthogonal to each other. The atomic orbitals mixing to form the transition state (‡) are an atomic orbital of the acid, the 1*s* orbital of the hydron, an sp^2 orbital of one oxygen, a *p* orbital of the same oxygen, a *p* orbital of carbon, and an sp^3 orbital of the other oxygen. The second step in the reaction is dissociation of the hydron from the oxygen of the ether.

During the nucleophilic addition of an alcohol to a carbonyl group under **catalysis by an acid** (Figure 1–8B),[99,108,109] two different reactions again occur simultaneously: formation of the oxygen–carbon bond and transfer of a hydron. A carbonyl group that is already participating at its carbonyl oxygen in a hydrogen bond with the catalytic acid is the electrophile, and the hydron in this hydrogen bond between the acid and the carbonyl group is transferred from the acid to the oxygen of the carbonyl group in concert with formation of the σ bond between the oxygen of the alcohol and the electrophilic carbon. The hydron is transferred from the catalytic acid to a lone pair of electrons already on the carbonyl oxygen that is distinct from and orthogonal to the pair arising from the retraction of the π molecular orbital system of the carbonyl group onto that oxygen.

Catalysis by a base, however, is much more effective than catalysis by an acid because it is easier for a base to remove a hydron from a hydroxy group ($pK_a = 16$) than it is for an acid to add a hydron to a carbonyl group ($pK_a = -10$). This difference is in contradistinction to the absolute requirement for hydronation of the leaving oxygen in the next step in the formation of an acetal or ketal.

A biochemical example in which catalysis either by an acid or by a base or by both of them simultaneously can occur during the dissociation or the formation of a hemiacetal is the reversible **formation of D-glucopyranose**

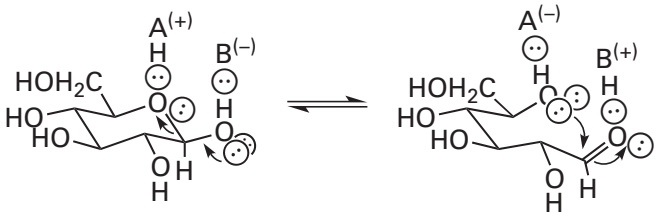

(1–38)

The susceptibility of a particular carbonyl group to addition can be evaluated by referring to its standard free energy of hydration (Table 1–2). The formal reaction defining the hydration of a carbonyl group is

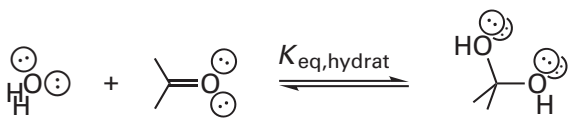

(1–39)

Table 1–2: Standard Free Energies of Hydration of Selected Aldehydes and Ketones at 25 °C[a]

carbonyl compound[b]	ΔG°_{hydrat} (kJ mol^{-1})	carbonyl compound[b]	ΔG°_{hydrat} (kJ mol^{-1})
1–21 	–19	**1–30** 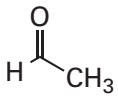	–1
1–22 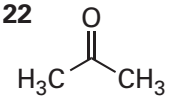	+15	**1–31** 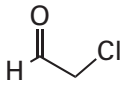	–9
1–23 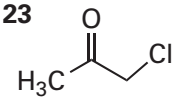	+1	**1–32** 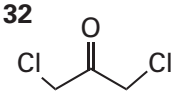	–6
1–24 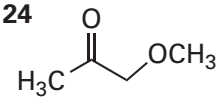	+10	**1–33** 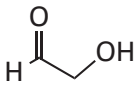	–5
1–25 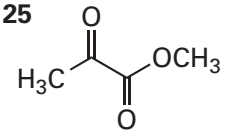	–2	**1–34** 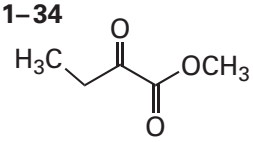	–1
1–26 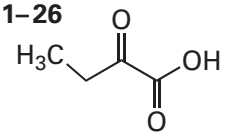	–1	**1–35** 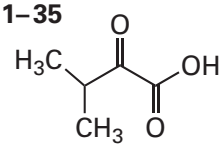	0
1–27 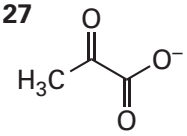	+6	**1–36** 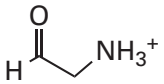	–17
1–28 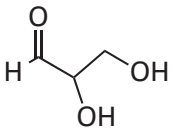	–8	**1–37** 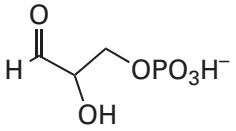	–14
1–29 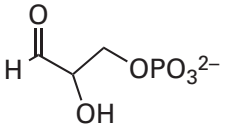	–8	**1–38** 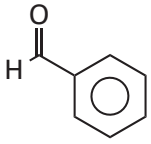	+11

[a]Standard free energy of hydration[96,97,111] based on a standard state of the infinitely dilute solutions and the omission of the concentration of water from the equilibria. [b]The table is arranged intentionally to permit various comparisons in both the horizontal and the vertical directions.

where water is a reference nucleophile. The equilibrium constant for hydration is defined as

$$K_{\text{eq,hydrat}} = \frac{[R_1R_2C(OH)_2]}{X_{H_2O}[R_1R_2C{=}O]} \qquad (1\text{–}40)$$

where the standard state is an infinitely dilute solution of carbonyl compound and its hydrate and X_{H_2O} is the mole fraction of water, which can be less than 1.00 if mixed solvents are used. The standard free energy of hydration

$$\Delta G^\circ_{\text{hydrat}} = -RT \ln K_{\text{eq,hydrat}} \qquad (1\text{–}41)$$

The use of water as a reference for addition to a carbonyl group resembles the use of hydronium as the reference acid and water as the reference base in the definition of the acid dissociation constant.

Values for the standard free energy of hydration* of a large number of aldehydes and ketones are available (Table 1–2).[96,97,111] The more negative the value of $\Delta G^\circ_{\text{hydrat}}$, the more susceptible is the carbonyl carbon to addition.

The **effects of substituents on the value of $\Delta G^\circ_{\text{hydrat}}$** result from their ability to stabilize or destabilize, respectively, the electron-deficient carbonyl carbon in the π system of the unhydrated carbonyl group relative to the saturated *gem*-diol of the hydrated carbonyl group by either donating electron density to the carbonyl carbon or withdrawing electron density from the carbonyl carbon. **Electron-donating substituents**, especially those capable of conjugation or hyperconjugation, decrease the susceptibility of the carbonyl group to addition [compare formaldehyde (**1–21**), acetaldehyde (**1–30**), and acetone (**1–22**)]. **Electron-withdrawing substituents** increase its susceptibility [compare acetaldehyde (**1–30**) to chloroacetaldehyde (**1–31**) or acetone (**1–22**) to chloroacetone (**1–22**) and 1,3-dichloroacetone (**1–32**)]. A hydroxy group or methoxy group is less electron-withdrawing than a carboxy group or esterified carboxy group [compare methoxyacetone (**1–24**) with methyl pyruvate (**1–25**)]. Neighboring negative elementary charge increases electron density at the carbonyl carbon [compare pyruvate anion (**1–27**) with methyl pyruvate (**1–25**)], and neighboring positive elementary charge decreases electron density [compare ammonioacetaldehyde (**1–36**) with acetaldehyde (**1–30**)]. A phosphate in its uncharged acidic form is strongly electron-withdrawing, but it becomes less so as it is titrated [compare glyceraldehyde (**1–28**) with glyceraldehyde 3-phosphate monoanion (**1–37**) and glyceraldehyde 3-phosphate dianion (**1–29**)]. Therefore, lowering the pH will increase the extent of hydration of a carbonyl group near a phosphate in the same molecule because hydration itself neither consumes nor produces hydrons (Equation 1–39) and cannot be affected by pH directly. The second

*The purpose of these standard free energies of hydration is to compare the hydration of the various carbonyl groups, just as the purpose of the acid dissociation constant is to compare the acidity of the various acids. Unlike the situation with the acid dissociation constant, however, where water itself appears in only one of the expressions for the equilibrium constant as an acid and only one of the expressions for the equilibrium constant as a base, by definition in each of these hydrations of a carbonyl group, water appears as a reactant. Consequently, one is free to omit the concentration of water, and all of the comparisons remain valid. In this instance, it was decided that the concentration of water would be omitted. The activities of the particular carbonyl group and its hydrate are expressed as molar concentrations at equilibrium and at infinite dilution. The latter stipulation is to avoid activity coefficients. In practice, the measurements are made at finite concentrations and the activity coefficients are assumed to be negligible. The advantage of omitting the concentration of water is that the tabulated standard free energy of hydration is for the reaction in an aqueous solution. Furthermore, the relative values of the actual free energies of hydration should remain the same for any aqueous solution, such as cytoplasm, in which the concentraation of water remains the same as the comparisons are made. It should be stressed that this is simply a convention, which is a decision agreed to by everyone who measures these values. Both the equilibrium constants and the standard free energies tabulated are not the equilibrium constants and standard free energies that are based on units of molarity, which would require that molarity be used for the concentrations of all reactants and products, as is the case with the acid dissociation constant. The same convention cannot be used for the acid dissociation constant because water appears as a participant only in the acid dissociation constants for hydronium ion and water and none of the others, so the molar concentration of water must be used in these two quotients because in every other quotient the molar concentrations of the conjugate base and the acid are used. It is also the case that by omitting the concentration of water from the equilibrium constant and expressing the concentrations of carbonyl group and hydrate in units of molarity at infinite dilution, the standard free energy of hydration is identical to the standard free energy of hydration if mole fraction had been chosen for the units of concentration. There are convincing arguments that mole fraction is the more defensible choice of units for all standard free energies for participants in any solution. Even if one accepts these arguments and decides that it would be more rigorous to express the concentrations for the acid dissociation constant in mole fractions, this choice would have no effect on the relative values for pK_a. You should convince yourself that if units of mole fraction had been chosen for pK_a rather than molarity, the values of every pK_a, including those for hydronium ion and for water itself, would simply increase by 1.745.

methyl group on an α carbon both donates electrons to the carbonyl carbon and exerts a steric effect, and these two opposite tendencies cancel each other [compare 2-oxobutyrate (**1–26**) to 3-methyl-2-oxobutyrate (**1–35**)].

In aqueous solution aldehydes and ketones are **in equilibrium with their hydrates**. Because the concentration of water is expressed in mole fraction in Equation 1–40, any carbonyl compound with a standard free energy of hydration less than 0 will be present mostly as the hydrate in aqueous solution and any carbonyl compound with a standard free energy of hydration greater than 0 will be present mostly as the unhydrated carbonyl group in aqueous solution. Recall that 5.7 kJ mol^{-1} is equivalent to a factor of 10 in equilibrium constant at 25 °C. In all cases, hydration has the effect of decreasing the concentration of unhydrated carbonyl group, which is the reactive species in any desired addition competing with hydration.

The standard free energies for the addition of thiols to carbonyl groups are linearly correlated to the standard free energies of hydration.[96,97] This correlation is not surprising since the formation of a thiohemiacetal (Equation 1–33) is homologous to the formation of the hydrate (Equation 1–39). Therefore, the relative susceptibility of different carbonyl groups to addition by a thiol can be estimated from the corresponding standard free energies of hydration.

Nucleophilic substitutions at a carbonyl carbon are reactions in which the oxygen of a carbonyl group, the nitrogen of an imine, or the sulfur of a thiocarbonyl group is replaced by the oxygen, nitrogen, or sulfur of a nucleophile. A nucleophilic substitution proceeds through the nucleophilic adduct that is the product of nucleophilic addition of the nucleophile that will replace the oxygen, nitrogen, or sulfur of the leaving group. For example, if the hydroxy group (the leaving group), which began as the oxygen of a carbonyl group, dissociates from the hemiaminal that results from the addition of an amine (the nucleophile) to a carbonyl carbon, then an imine, the product of a nucleophilic substitution, is formed (Figure 1–7). A ketimine is the nitrogen analogue of a ketone, and an aldimine is the nitrogen analogue of an aldehyde. An imine is the product of a nucleophilic substitution of water by an amine at a carbonyl group. A thioketone or thioaldehyde is formally the product of the nucleophilic substitution of water by hydrogen sulfide at a carbonyl group. Nucleophilic substitution at a carbonyl carbon usually involves a discrete, reasonably stable intermediate that is formed by addition of the nucleophile to the carbonyl group (Table 1–1).

The dissociation of oxygen from a hemiaminal (lower half of Figure 1–7) during nucleophilic substitution of the oxygen of a carbonyl group by the nitrogen of an amine can occur under either catalysis by an acid or catalysis by a base. Under **catalysis by an acid** (Figure 1–7), breaking of the bond between carbon and oxygen, assisted by the push of the lone pair of electrons on nitrogen, occurs simultaneously[88] with hydronation[86] of one of the available lone pairs of electrons on the oxygen of the leaving group. This lone pair of electrons that is hydronated by the acid is different from the pair created during the dissociation of the carbon–oxygen bond. Addition of the hydron to the oxygen decreases its electron density and attenuates the σ bond between carbon and oxygen by pulling its electrons toward the oxygen so that the σ bond is weak enough to be broken by the relatively feeble push of a lone pair of electrons on a neutral nitrogen. Under **catalysis by a base**, breaking of the bond between carbon and oxygen, assisted by the push of the lone pair of electrons on nitrogen (Figure 1–7), occurs simultaneously[87] with removal of a hydron by the base from a different lone pair of electrons on nitrogen. Removal of the hydron from the other lone pair of electrons on nitrogen during formation of the transition state increases the electron density on nitrogen and amplifies the push of the initially present lone pair of electrons by electron repulsion so that it is strong enough to push out the poor leaving group, hydroxide ion. Removal of the hydron from nitrogen must occur during formation of the transition state. A hydron cannot be removed from the nitrogen in a pre-equilibrium because of its poor acidity ($pK_a \cong 40$). Usually catalysis by an acid is considerably more effective than catalysis by a base because it is easier to hydronate a hydroxy group ($pK_a = -2$) than it is to remove a hydron from an amino nitrogen.

Suggested Reading

Hine, J., Cholod, M. S., and Chess, W. K. (1973) Kinetics of the formation of imines from acetone and primary amines. Evidence for internal acid-catalyzed dehydration of certain intermediate carbinolamines, *J. Am. Chem. Soc. 95*, 4270–4276. https://doi.org/10.1021/ja00794a025

Sorensen, P. E., and Jencks, W. P. (1987) Acid- and base-catalyzed decomposition of acetaldehyde hydrate and hemiacetals in aqueous solution, *J. Am. Chem. Soc. 109*, 4675–4690. https://doi.org/10.1021/ja00249a034

Appel, R., Chelli, S., Tokuyasu, T., Troshin, K., and Mayr, H. (2013) Electrophilicities of benzaldehyde-derived iminium ions: Quantification of the electrophilic activation of aldehydes by iminium formation, *J. Am. Chem. Soc. 135*, 6579–6587. https://doi.org/10.1021/ja401106x

Nucleophilic Substitution at an Acyl Group

A nucleophilic substitution at an acyl group is a special case of a nucleophilic substitution at a carbonyl group. An example would be the aminolysis of a thioester[112]

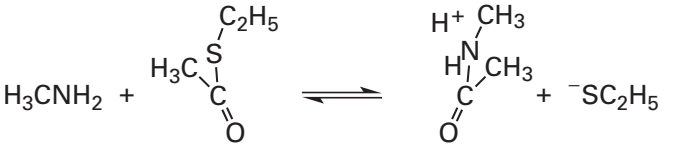

(1–42)

in which a methylamino group is substituted for an ethylsulfanyl group to produce an **amide**.

Most nucleophilic substitutions at acyl groups proceed through a tetrahedral intermediate. The tetrahedral intermediate in a nucleophilic substitution at an acyl group results from nucleophilic addition of the nucleophile to the acyl derivative.[112-114] For example, during the aminolysis of an ester

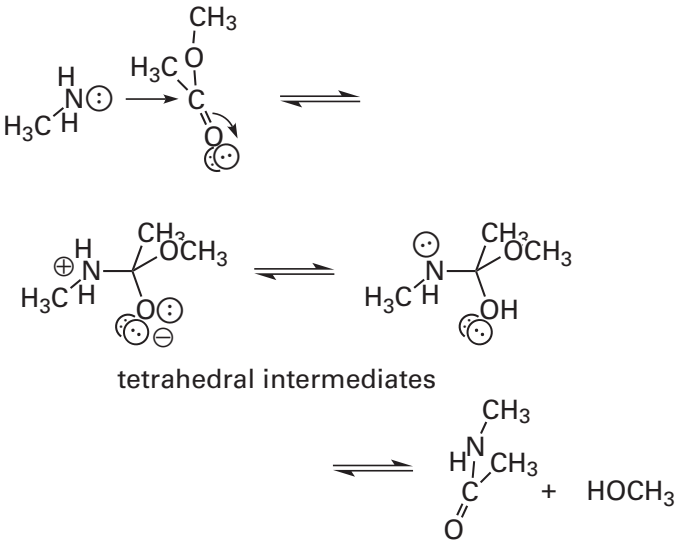

(1–43)

several tautomeric tetrahedral intermediates and their conjugate acids and bases are formed. They resemble the conjugate acids, conjugate bases, and tautomers of the hemiaminal that results from the nucleophilic addition of an amine to an aldehyde or ketone (Figure 1–7).* A nucleophilic substitution at an acyl carbon that proceeds through a tetrahedral intermediate is an example of an associative nucleophilic substitution.

An **associative nucleophilic substitution** is a nucleophilic substitution that proceeds through a tetrahedral intermediate in which a covalent bond is formed between the nucleophile and the electrophilic carbon before the covalent bond between the leaving group and the electrophilic carbon begins to break. The resulting tetrahedral intermediate is a molecule in its own right, albeit an unstable one. It is distinct from the transition state in a concerted nucleophilic substitution at a saturated, electrophilic carbon because that transition state does not have covalent bonds between the carbon and either the nucleophile or the leaving group.

The existence of an intermediate in a nucleophilic substitution at an acyl group is indicated by a **change in the rate-limiting step** from the formation of the intermediate to its breakdown as the pH is lowered.[113] That the intermediate detected in such pH–rate behavior is the proposed tetrahedral intermediate is indicated by the fact that **oxygen exchange** into the initial reactant occurs during the reaction. An example of such isotopic exchange is that observed during the hydrolysis of methyl acetate[115]

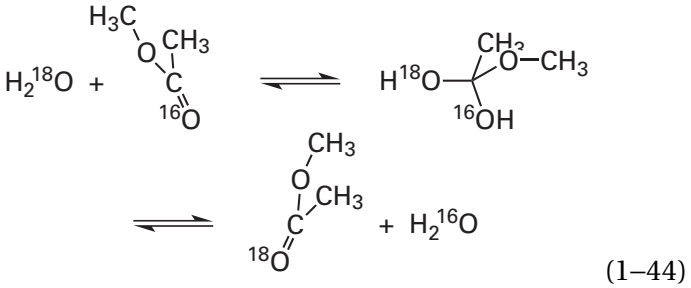

(1–44)

Oxygen exchanges into the initial reactants occur during the hydrolysis of esters, thioesters,[116] anilides,[117] and amides[118] under both strongly acidic[115-117] and strongly basic[115,118] conditions.

*By definition, the various named adducts of a carbonyl group are also tetrahedral intermediates in addition to the tetrahedral intermediates in nucleophilic substitutions at acyl carbons and carbonato carbons.

That a tetrahedral intermediate exists in a nucleophilic substitution at an acyl group is also consistent with observed **secondary kinetic isotope effects**. When the two hydrogens on a carbon immediately adjacent to the carbon in the acyl group are replaced with deuteriums, the rates of the hydrolyses of esters[119-122] increase by about 5%. This significant inverse kinetic isotope effect, an increase in rate rather than a decrease upon substituting hydrogen with deuterium, indicates that the hyperconjugation between these two adjacent hydrogens and the π bond between carbon and oxygen in the acyl group is decreased considerably or lost completely in the transition state of the rate-limiting step or during a pre-equilibrium preceding the rate-limiting step. The hyperconjugation is weaker when the hydrogen is a deuterium, so the deuterated ground state is less stable relative to the transition state than the hydronated ground state. This result is consistent with the formation of a tetrahedral intermediate,* which has no π bond with which hyperconjugation can occur.[123] The effects on the rate constants for aminolysis of methyl formate that result from replacement of the hydrogen on the acyl carbon with deuterium, the acyl oxygen-16 with oxygen-18, the amino nitrogen-14 with nitrogen-15, the ester oxygen-16 with oxygen-18, and the acyl carbon-12 with carbon-13 are all consistent with changes expected for the formation of a tetrahedral intermediate during this reaction.[124]

The molecular details of the formation and dissociation of a tetrahedral intermediate are homologous to those for the formation and dissociation of an adduct to a carbonyl group. All of the considerations—structure of the transition state, electron repulsion on the approach to it, stereochemistry of the attack, energy barriers to the formation of the transition state, push of the adjacent heteroatoms during its dissociation, and the involvement of the atomic and molecular orbitals in the dissociation—that are pertinent to nucleophilic addition to a carbonyl group apply to the formation and dissociation of the tetrahedral intermediate in the associative nucleophilic substitution at an acyl group. Addition of the nucleophile to the acyl group (Equation 1–43) proceeds through overlap of the atomic orbital bearing the lone pair of electrons on the nucleophile with the antibonding π molecular orbital of the carbon–oxygen (**1–17**), carbon–nitrogen, or carbon–sulfur double bond of the acyl group. Expulsion of the leaving group from the tetrahedral intermediate (Equation 1–43) proceeds through overlap of the atomic orbital containing a lone pair of electrons on the oxygen or the nitrogen providing push with the antibonding orbital of the σ bond between carbon and the leaving group (Figure 1–3). For example, in the aminolysis of an ester (Equation 1–43), the lone pairs of electrons providing push in the forward direction and the reverse direction is a lone pair on the hydroxy group that was the oxygen in the carbon–oxygen double bond of the ester, but the lone pair of electrons on the other oxygen also provides push in the reverse direction, and the lone pair of electrons on the nitrogen provides push in the forward direction.

The **difference between an acyl group and a carbonyl group** is that there is a second heteroatom in the former, and the difference between the tetrahedral intermediate in a substitution at an acyl group and the product of addition to a carbonyl group is that there is a third heteroatom attached to carbon in the former. On the one hand, the second heteroatom in the acyl group makes it more stable than a carbonyl group because the lone pairs of electrons on this heteroatom can conjugate with the electropositive acyl carbon. On the other hand, the third heteroatom makes a tetrahedral intermediate much less stable than the product of a nucleophilic addition to a carbonyl group because the lone pair or lone pairs of electrons on the third heteroatom will increase electron repulsion in the tetrahedral intermediate. The net result of these two effects, the one lowering the energy of the reactant and the other raising the energy of the transition state, is that the tetrahedral intermediate in an associative nucleophilic substitution at an acyl group (Equation 1–45) is much less stable than the tetrahedral intermediate in an associative nucleophilic substitution at a simple carbonyl group (Equation 1–46). This instability can be demonstrated by a comparison[96,125] of equilibrium constants*

*These kinetic isotope effects are also consistent with a single transition state for the substitution, in which the bond between the nucleophile and the acyl carbon is forming as the bond to the leaving group is breaking, and the double bond of the carbonyl group is significantly but only partially broken.

*Because the addition of methanol is being compared to the addition of water, these equilibrium constants are for the reactions as written using the molar concentrations of methanol (24.7 M) and water (55.5 M) rather than the mole fractions of methanol and water as was done in Equation 1–40.

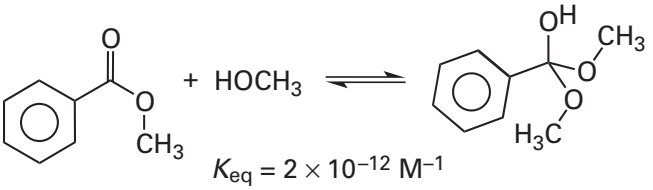

(1–45)

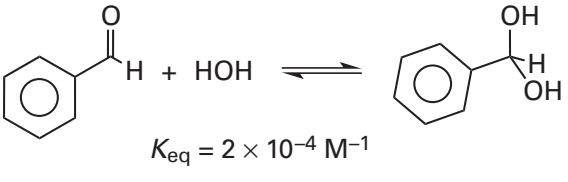

(1–46)

The additional heteroatom also creates a situation in which two lone pairs of electrons can be simultaneously periplanar to the leaving group and provide **greater push**

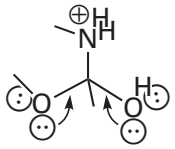

1–39

In every tetrahedral intermediate this double push is possible. It has already been noted that during the hydrolyses of ortho esters (acyl derivatives in which the two lone pairs of electrons providing the push are on two oxygens) antiperiplanar push is stronger than synperiplanar push[60] but by less than 10 kJ mol^{-1}. During the hydrolysis of amidiniums[126] and guanidiniums,[127] acyl derivatives in which the two lone pairs of electrons providing the push in the tetrahedral intermediate are on a nitrogen and an oxygen respectively, antiperiplanar push is also stronger than synperiplanar push but by less than 5 kJ mol^{-1}. To be effective, however, the push must always be **periplanar** for maximum overlap to occur.[60]

Often the tetrahedral intermediate must be formed and **revert to reactants** many times before the expulsion producing a product of associative nucleophilic substitution occurs. If the nucleophile that produces the tetrahedral intermediate in the first place is the most likely leaving group from that tetrahedral intermediate, then the yield of product for every encounter that produces a tetrahedral intermediate will be low because most of the time the initial nucleophile will be expelled from the tetrahedral intermediate to regenerate the reactant. For example, in the esterification of *N*-acetylimidazole by trifluoroethoxide (Figure 1–9)[128] at high pH, the tetrahedral intermediate dissociates to form the reactants about 200 times more rapidly than it dissociates to form the products imidazole and trifluoroethyl acetate.

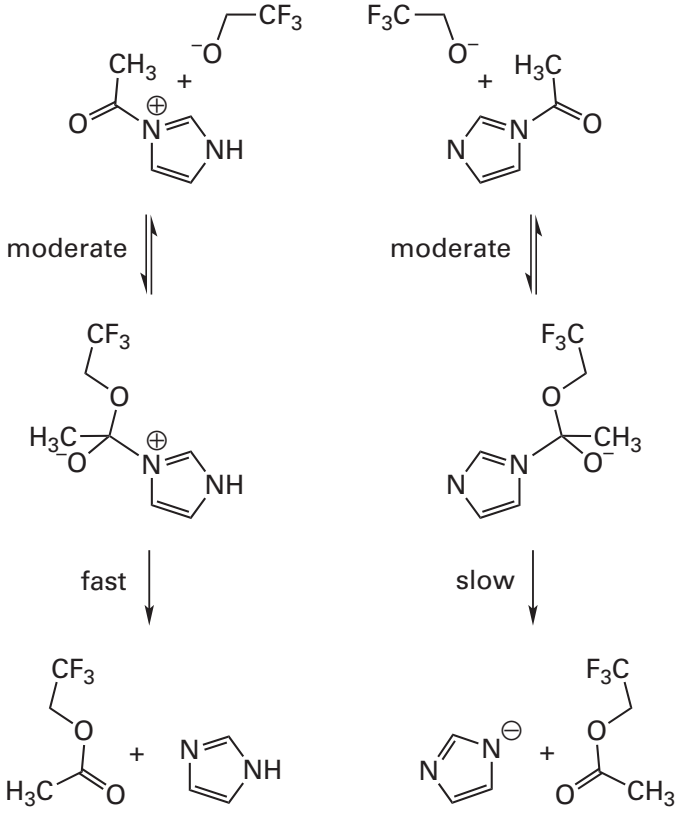

Figure 1–9: Effect of hydronation of the leaving group on the partition in a tetrahedral intermediate.[128] Addition of 2,2,2-trifluoroethoxide ion to *N*-acetylimidazole, in either its hydronated or unhydronated form, produces a tetrahedral intermediate from which either the trifluoroethoxide ion or the imidazole is a potential leaving group. (**Left side**) At low pH, when the imidazole in the tetrahedral intermediate is hydronated, it is the preferred leaving group because its conjugate acid (pK_a = 7.05) is more acidic than the conjugate acid of the trifluoroethoxide ion (pK_a = 12.4). Consequently, imidazole dissociates rapidly from the tetrahedral intermediate relative to the trifluoroethoxide ion (fast against moderate). (**Right side**) At high pH, when the imidazole in the tetrahedral intermediate is unhydronated and must leave as the imidazolate anion, the trifluoroethoxide ion is the preferred leaving group because its conjugate acid (pK_a = 12.4) is more acidic than the conjugate acid of the imidazolate anion (pK_a = 14.5), and the loss of imidazole becomes slower than the loss of trifluoroethoxide from the tetrahedral intermediate (slow against moderate). Because the major change in acidity has been to the imidazole, the major change in rate occurs in its dissociation from the tetrahedral intermediate.

Because there are three heteroatoms in a tetrahedral intermediate and any one of the three can dissociate, there are always **two possible products** that can form in addition to the one formed by the dissociation regenerating the reactants. Consequently, the ratio of the products formed from the tetrahedral intermediate depends on a partition. For example, when ethyl thionobenzoate is hydrolyzed, two products in addition to the reactant form

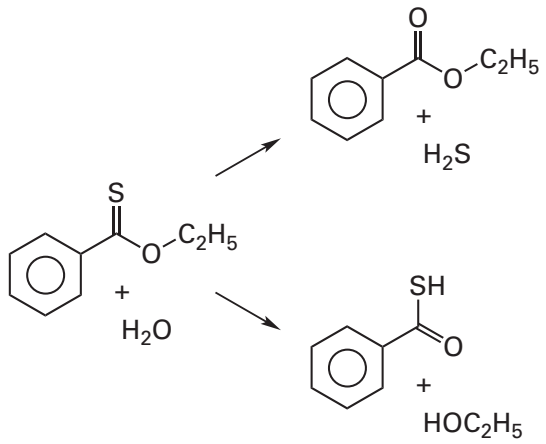

(1–47)

The identity of the leaving group from a tetrahedral intermediate, and hence the acyl derivative that is the product, is usually determined both by hydronation of the leaving group and by the magnitude of the push provided by the different heteroatoms.

The hydrolysis of *O*-ethyl benzenecarbothioate (Equation 1–47) provides an example of the effect of **hydronation** on the identity of the product. During the hydrolysis, ethyl benzoate predominates under weakly acidic conditions, but the fraction of benzenecarbothioic acid increases significantly as the pH is lowered below 1.0.[129] This change in the ratio of the products is due to a shift in the preference for expulsion within the tetrahedral intermediate

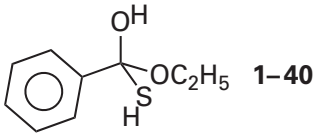

1–40

This conclusion was validated by generating an analogous tetrahedral intermediate through a completely different route involving the decomposition of an ortho ester. The same increase in the yield of thiobenzoate relative to benzoate was observed as the pH was lowered.[130] A reasonable explanation for the shift in the ratio of products is the increased rate for hydronation of the ethoxy oxygen or an increased concentration of the hydronated form of the ethoxy oxygen within tetrahedral intermediate **1–40** at the lower values of pH.* Either of these effects, or both together, will cause the ethoxy oxygen to become a better leaving group than the sulfanyl group, although given the rates at which acid–base reactions reach equilibrium, the latter explanation seems more reasonable.

Another example of the importance of hydronation in determining the identity of the leaving group from a tetrahedral intermediate occurs in the associative nucleophilic substitution of imidazole by trifluoroethoxide in acetylimidazole (Figure 1–9).[128] If the imidazole group is unhydronated (right column), expulsion of trifluoroethoxide from the tetrahedral intermediate predominates; if the imidazole is hydronated (left column), its expulsion predominates. This shift in predominance explains why both the *N*-hydronated and the *N*-methylated acetylimidazolium ions produce the trifluoroethyl ester 200 times more rapidly than unhydronated acetylimidazole.

Hydrolysis of ethyl *N*-methyl-*N*-phenyl-acetimidate ion[131] proceeds by the addition of hydroxide or water to the cationic imidate ester in a slow, rate-limiting step to produce the initial tetrahedral intermediate **1–41**

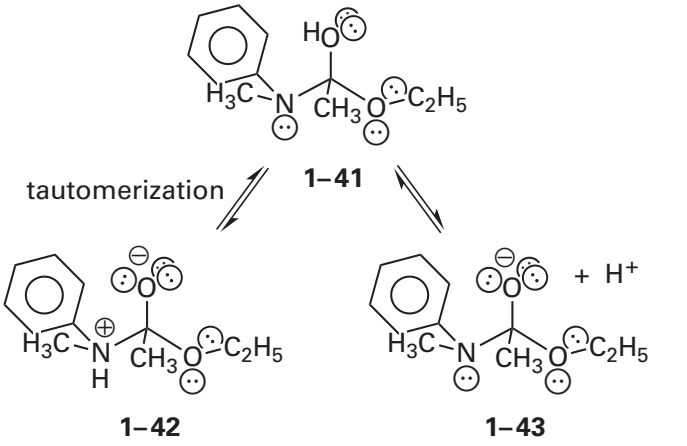

1–41 **1–42** **1–43**

(1–48)

This intermediate can tautomerize to tetrahedral intermediate **1–42** and expel *N*-methylaniline or lose a hydron to produce tetrahedral intermediate **1–43** and expel the ethoxide. The partition between these

*Hydronation of a sulfide ($pK_a \cong -8$) occurs at much lower pH than hydronation of an ether ($pK_a \cong -3.5$).

two outcomes is influenced secondarily by other acids and bases in the solution, but expulsion of the aniline always increases as the pH of the solution is lowered and hydronation of the nitrogen increases.

The magnitude of the **push** available in the tetrahedral intermediate also has a significant influence on the choice of the leaving group. This influence can be appreciated by examining the products formed from the collapse of each of the following hemiaminals and tetrahedral intermediates under catalysis by a general acid[57]

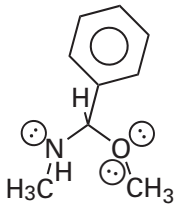

1–44

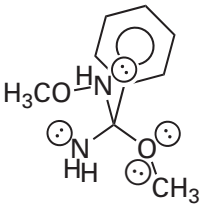

1–45

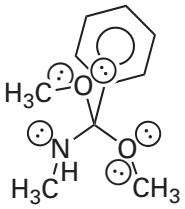

1–46

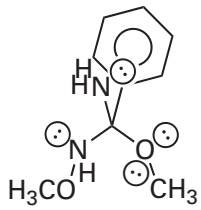

1–47

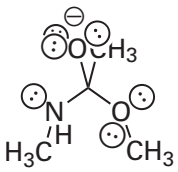

1–48

In the drawings of each of these compounds,* the two potential leaving groups have been placed to the right and left sides of the central carbon, respectively. In each case, the lone pair of electrons on the oxygen to the right is less basic than the lone pair of electrons on the nitrogen to the left, usually by about 14 units of pK_a. Under catalysis by a general acid, the nitrogen will always be hydronated more readily and should be the better leaving group.

The fact that the lone pair of electrons on nitrogen is the more basic, however, also means that it can provide more push. In the hemiaminal **1–44**, nothing other than one of the two potential leaving groups can provide push, so push becomes more important than hydronation, and hemiaminals preferentially expel the alcohol under catalysis by an acid. In either the methoxyamino tetrahedral intermediate **1–45** or the methoxy tetrahedral intermediate **1–46**, the third heteroatom is able to provide only a weak push (pK_a = 5 and pK_a = –3, respectively) but it is enough to enhance the expulsion of nitrogen sufficiently so that its rate of disdissociation becomes equivalent to that of the oxygen under catalysis by an acid. In the amino tetrahedral intermediate **1–47**, the push of the more basic lone pair of electrons on the amino nitrogen (pK_a = 10) predominates over that of the lone pair of electrons on the leaving nitrogen in the methoxyamino group, and the dissociation of the methoxylamine, the more readily hydronated leaving group under catalysis by an acid, is several hundred times more rapid than that of methanol. Finally, in the alkoxy tetrahedral intermediate **1–48**, the push from the lone pair of electrons on nitrogen becomes irrelevant in comparison to the push of the more basic lone pair of electrons of the oxyanion. In the presence of such an abundance, which is able to be directed at either leaving group promiscuously, hydronation of the nitrogen, which is the more basic leaving group, dictates the preference, and alkoxy tetrahedral intermediate **1–48** decomposes almost exclusively through expulsion of amine.

Nucleophilic substitutions at acyl groups can be catalyzed either by acids or by bases. An example relevant to enzymatic catalysis is the **hydrolysis of amides**, which takes place at elevated temperatures in the presence of strong acid or strong base.

In **strong acid** (Figure 1–10A), the acyl oxygen is hydronated[132] in a regular acid–base dissociation

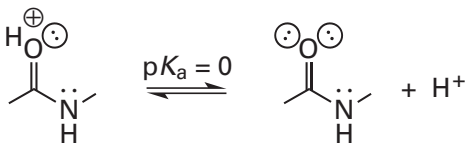

(1–49)

This hydronation causes the acyl carbon to be electrophilic enough to react with water to form a tetrahedral intermediate, but because water is a poor nucleophile, this remains the slowest step in the reaction. Before the tetrahedral intermediate is formed, the lone pair of electrons on nitrogen is unavailable for hydronation (pK_a = –7),[132] but after the tetrahedral intermediate has formed, the nitrogen has become the nitrogen of an amine rather than the nitrogen of an amide. In the case of hydrolysis of primary and secondary amides, the amino nitrogen (p$K_a \cong 9$) in the tetrahedral intermediate initially formed by the addition of water to the hydronated acyl group is immediately and irreversibly hydronated (pH < 0). Because of this immediate hydronation, which makes the amine

*Although **1–45** and **1–47** are enantiomers of each other and both of them would be formed at random in the same nucleophilic substitution, these facts are irrelevant to the present argument. Each is presented as a tetrahedral intermediate that produces a particular product, and each product is different from the other.

the preferred leaving group, insignificant oxygen exchange (see Equation 1–44) is observed during the hydrolysis of amides catalyzed by strong acid. Following its expulsion as the leaving group, the amine is hydronated under acidic conditions, and this hydronation precludes the reverse reaction and provides the free energy necessary to make the hydrolysis favorable.[133]

In **strong base** (Figure 1–10B), hydroxide is the nucleophile during the hydrolysis of an amide. From measurements of the rates of amide hydrolysis in mixtures of ^1H_2O and ^2H_2O, it has been concluded that the hydrated form of hydroxide (**1–2**) is the nucleophile, [134] but whether the actual nucleophile is the lone pair of electrons on the central hydroxide itself or one of the lone pairs of electrons on one of the three surrounding molecules of water[135,136] is unsettled. The hydroxide readily adds to the acyl carbon in a rapid reaction.[133] This addition of the nucleophile creates the oxyanion, ready to push out the leaving group. The amino nitrogen created during this first step is only slowly hydronated because the concentration of hydrons is so low and the transfer of a hydron from water is endergonic. As a result, the transfer of a hydron to the nitrogen is the slow step under basic conditions.[133] Consequently, isotopic exchange (see Equation 1–44) is readily observed during the hydrolysis of amides in strong base, except in the case of tertiary amides.[137] When the nitrogen is hydronated, it leaves in preference to oxygen because the tetrahedral intermediate resembles tetrahedral intermediate **1–48** under acidic conditions. The carboxylic acid produced loses its hydron under the basic conditions, and this ionization precludes the back reaction and provides the free energy necessary to make the reaction favorable.[133]

At **neutral pH**, although transfer of a hydron to the amino nitrogen in the tetrahedral intermediate occurs readily, the acyl oxygen cannot be significantly hydronated so the reaction of water as a nucleophile at the acyl carbon is extremely slow, and the concentration of hydroxide is so low that nucleophilic attack of hydroxide is also slow.[133] Both of these problems luckily cause the hydrolysis of an amide to take years at pH 7 and 25 °C in the absence of catalysis.[1] At neutral pH, both the amine and the carboxylic acid are ionized following the hydrolysis, and both of these ionizations together provide sufficient favorable free energy to cause the

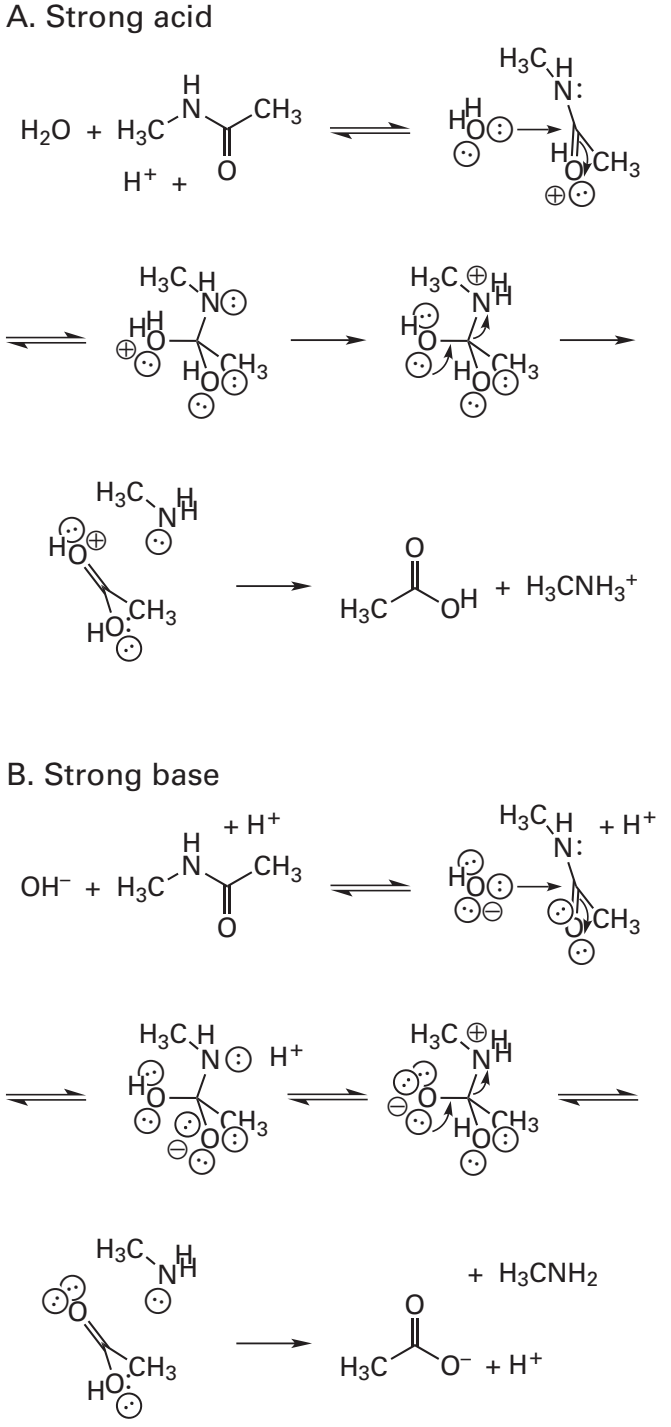

Figure 1–10: Mechanisms of hydrolysis of an amide under specific acid catalysis or specific base catalysis. (**A**) In strong acid, under catalysis by a hydron, a molecule of water adds to the amide, which is hydronated on oxygen, to produce the tetrahedral intermediate. (**B**) In strong base, under specific catalysis, a hydroxide ion adds to the neutral amide to produce the tetrahedral intermediate. In each case, the nitrogen in the tetrahedral intermediate must be hydronated, regardless of whether the pH of the solution in low or high, before it can leave.

hydrolysis, although slow in the absence of catalysis, to be isoergonic rather than endergonic.[133] The equilibrium constant for the hydrolysis of an amide is at a minimum in the midrange of pH and increases at both low pH and high pH.[138]

When the **hydrolysis of an ester** is catalyzed by a base other than hydroxide, and probably by hydroxide as well, a molecule of water, already forming a hydrogen bond with the base, is the nucleophile, just as it is in the addition of an alcohol to a carbonyl group catalyzed by a base (Figure 1–8).[120] During the addition of the molecule of water to the acyl carbon, the hydron in the hydrogen bond is simultaneously transferred to the base.

In addition to catalysis by acids and bases, certain nucleophilic substitutions at acyl groups are susceptible to **catalysis by desolvation**. For example, the rates of nucleophilic substitutions in which the nucleophile is phosphate dianion, which is a common nucleophile in biochemical reactions, are increased by a factor as large as 10^5 when water is replaced by dimethyl sulfoxide, but all anionic nucleophiles exhibit enhancement upon decreases in the concentration of water.[139] This effect is thought to result from the fact that the nucleophilic oxygens of phosphate dianion in particular, but most nucleophilic atoms with a negative elementary charge, usually are masked by a strongly held layer of water molecules solvating the respective ions and the fact that their intrinsic nucleophilicity is revealed upon desolvation. When phosphate or another nucleophilic anion reacts in the **active site of an enzyme**, it has usually been desolvated in the process of associating with the site, and this desolvation should increase its nucleophilicity significantly.

Nucleophilic substitutions at an acyl group are also susceptible to **nucleophilic catalysis**. For example, pyridine is a nucleophilic catalyst for acyl derivatives with good leaving groups. The acceleration of the reaction that occurs in the presence of pyridine results from the fact that pyridine enters and leaves tetrahedral intermediates readily, yet acylpyridinium ions are fairly unstable because the unavoidable positive formal elementary charge on the nitrogen activates the acyl carbon for nucleophilic attack. Therefore, pyridine reacts rapidly with the initial acyl derivative to produce the acylpyridinium ion

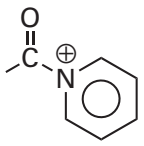

1–49

which then reacts rapidly with the nucleophile to produce the product of the particular reaction and regenerate the catalyst.[140] Many enzymes catalyze substitution at an acyl group nucleophilically, using one or the other of the heteroatoms in the side chains of their amino acids.

In a nucleophilic substitution at an acyl group that passes through a tetrahedral intermediate, there are always at least two steps: combination of the acyl derivative and the nucleophile to create the tetrahedral intermediate and expulsion of the leaving group to create the products. Either of these steps can be the rate-limiting step of the reaction. Usually, as the identity of the nucleophile,[141] the identity of the acyl derivative, the pH, or the identity of the catalyst[142] is changed within a given series of such associative nucleophilic substitutions, the major effect of each of these changes will be on only one step in the mechanism. It often happens that as these parameters are changed systematically, at some point the step that was rate-limiting becomes faster than either a step preceding it or a step following it, and the new slower step then becomes the rate-limiting step. It has already been mentioned that one of the facts consistent with the existence of an intermediate in most nucleophilic substitutions at an acyl group is the observation of such **a change in the rate-limiting step**.

A change in rate-limiting step occurs in a series of nucleophilic substitutions between 4-nitrophenyl acetate and a set of thiolate ions[141]

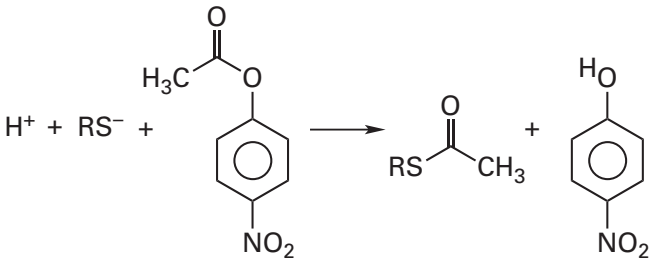

(1–50)

A kinetic mechanism, incorporating a tetrahedral intermediate, can be written for this reaction

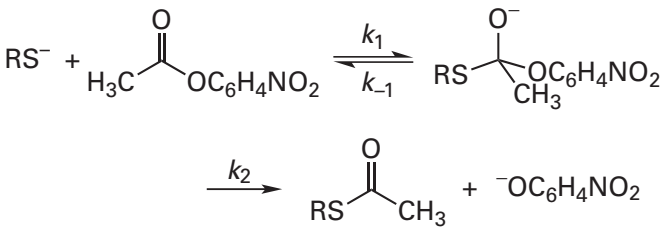

(1–51)

When the rate constant k_{-1} in Equation 1–51 is smaller than the rate constant k_2, the 4-nitrophenolate leaves the tetrahedral intermediate more rapidly than the thiolate, and most of the tetrahedral intermediates formed proceed to molecules of product. If the rate constant k_{-1} is much smaller than the rate constant k_2, almost none of the tetrahedral intermediates can revert to reactants before they proceed on to products. Because a tetrahedral intermediate is always unstable relative to reactants and products and almost none is present in solution at a given instant, the step governed by the rate constant k_1 is rate-limiting because the rate of the reaction depends entirely on the rate at which the tetrahedral intermediate is formed. The observed rate constant for the reaction is simply the rate constant k_1, and the transition state governing the observed rate constant is that of the first step.

When the rate constant k_{-1} is larger than the rate constant k_2, the thiolate leaves in preference to the 4-nitrophenolate, a **pre-equilibrium** establishes an equilibrium concentration of tetrahedral intermediate, and the rate of the reaction is affected by the rate at which this tetrahedral intermediate breaks down to product through the step governed by k_2, now the rate-limiting step. Under these circumstances, however, the rate constants for all three steps—those governed by k_1, k_{-1}, and k_2—determine the rate of the associative nucleophilic substitution because a change of any of these rate constants will affect the observed rate of the reaction, even though only the step governed by k_2 is the rate-limiting step. In this situation, the observed rate constant for the reaction is $K_{eq1}k_2$, where K_{eq1} is the equilibrium constant for the first step, the pre-equilibrium determined by the rate constants k_1 and k_{-1}, and k_2 is the rate constant for the second step.

For the nucleophilic substitution between a series of thiolate ions and 4-nitrophenyl acetate (Equation 1–51), there is a **change in the slope of a Brønsted plot** (Figure 1–11; third curve from the top),[141] in which the common logarithms of the rate constants for the nucleophilic substitutions are plotted as a function of the values of pK_a for the thiols that are the conjugate acids of the respective thiolate ions. The slope of a line on such a plot is the **Brønsted coefficient for the nucleophiles, β_{nuc}.** On moving from right to left on the plot, it can be seen that when the thiolate used in the reaction described in Equation 1–51 becomes sufficiently acidic (pK_a < 6 for the nucleophilic substitutions of

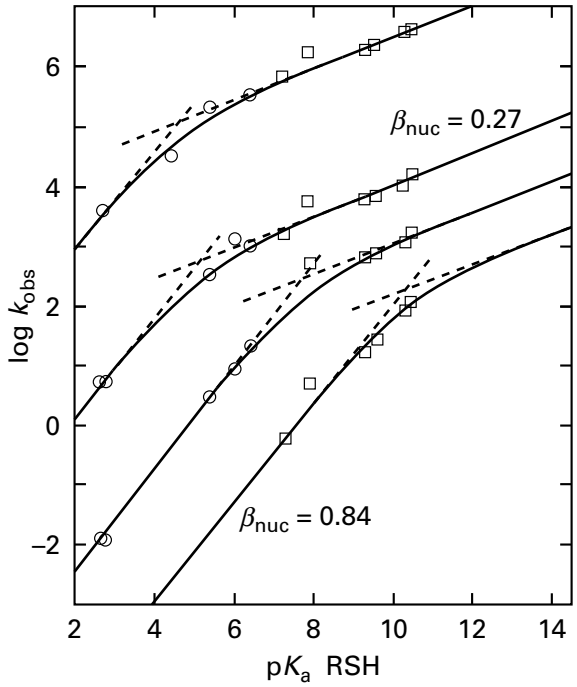

Figure 1–11: Brønsted correlations between the rate constants for nucleophilic substitutions at four different acetate esters by a series of nucleophilic aryl thiolate ions (○) and alkyl thiolate ions (□), the conjugate acids of which have different acid dissociation constants.[141] The rates for each nucleophilic substitution (Equation 1–50) were followed at two or more values of pH at an ionic strength of 1.0 M and at 25 °C. The values of pH chosen in each case were those appropriate to the pK_a of the particular thiol the thiolate ion of which was used as the nucleophile. The pH at which each rate was measured was used to determine the actual concentration of thiolate ion in the solution. For each of the 36 combinations of electrophile and thiolate ion, represented by the 36 points on the graph, the rate constants calculated, based on the actual concentration of thiolate ion, were the same for all values of pH. The common logarithms of the observed rate constants are plotted as a function of the values of the pK_a for the thiol. The thiols chosen, in order of increasing pK_a, were pentafluorobenzenethiol (pK_a = 2.68), 2,3,5,6-tetrafluorobenzenethiol (pK_a = 2.75), 4-nitrobenzenethiol (pK_a = 4.5), 3,4-dichlorobenzenethiol (pK_a = 5.48), 4-acetamidobenzenethiol (pK_a = 6.08), benzenethiol (pK_a = 6.43), 2,2,2-trifluoro-1-sulfanylethane (pK_a = 7.30), methyl 2-sulfanylacetate (pK_a = 7.91), methyl 3-sulfanylpropionate (pK_a = 9.33), 2-sulfanylethanol (pK_a = 9.61), sulfanylethane (pK_a = 10.35), and 1-sulfanylpropane (pK_a = 10.53). Each of the four curves in the figure is for the nucleophilic substitutions of a particular acetate ester. The four acetate esters used as electrophiles, in descending order on the field of the graph, were 1-acetoxy-4-methoxypyridinium ion, 2,4-dinitrophenyl acetate, 4-nitrophenyl acetate, and phenyl acetate. The products produced by the leaving groups were 4-methoxypyridine 1-oxide, 2,4-dinitrophenolate ion, 4-nitrophenolate ion, and phenolate ion, respectively. The curves drawn through the data each have linear asymptotes of the same slope to the left and of the same slope to the right of the respective inflections. The slopes of the linear asymptotes, the values of β_{nuc}, are 0.84 to the left and 0.27 to the right. There is a gradual change in slope in the middle of each curve.

4-nitrophenyl acetate), there is a change in slope (β_{nuc}) from 0.27 to 0.84.

This **change in slope** can be explained as the result of a change in rate-limiting step. The dissociation of 4-nitrophenyl acetate from the sulfur in the tetrahedral intermediate (step governed by k_{-1} in Equation 1–51) is analogous to the dissociation of a hydron from the respective thiol. When the conjugate acid of the thiolate becomes acidic enough, the dissociation of 4-nitrophenyl acetate from the sulfur in the tetrahedral intermediate becomes faster than the expulsion of 4-nitrophenolate from the tetrahedral intermediate. The kinetic mechanism of the reaction changes from one in which the first step, formation of the tetrahedral intermediate, is the rate-limiting step governing the observed rate constant to one in which the second step, expulsion of nitrophenolate, is the rate-limiting step.

For the more basic thiols, before the change in rate-limiting step has occurred, the observed rate constant is governed only by the first step. The **Brønsted coefficient for the nucleophile**, β_{nuc}, is small (0.27) and indicates that, in the transition state for addition of the thiolate to the acyl carbon of the 4-nitrophenyl acetate, the bond between sulfur and carbon is only partially formed.

For the more acidic thiols, after the change in rate-limiting step has occurred, the observed rate constant is governed by both the pre-equilibrium and the second step, expulsion of the leaving group, which is now the rate-limiting step. The Brønsted coefficient for the nucleophile, β_{nuc}, is now large (0.84). If only the rate constant k_{-1}, that for dissociation of 4-nitrophenyl acetate from the sulfur in the tetrahedral intermediate, were affected by the increasing acidity of the thiol, and if dissociation of 4-nitrophenyl acetate from the thiolate when the tetrahedral intermediate dissociates were equivalent to the dissociation of a hydron, then the Brønsted coefficient would have been 1.

Three other acetates were also used in these experiments (Figure 1–11).[141] 1-Acetoxy-4-methoxypyridinium gives the product 4-methoxypyridine 1-oxide (top curve), 2,4-dinitrophenyl acetate gives the product 2,4-dinitrophenolate ion (second curve from the top), and phenyl acetate gives the product phenolate ion (bottom curve). For each of these acetates there also seems to be a similar change in rate-limiting step. These results reinforce the conclusion that a change in rate-limiting step is occurring.

There are nucleophilic substitutions at acyl groups, however, that do not seem to have a tetrahedral intermediate in their mechanism. Evidence for the lack of a tetrahedral intermediate also comes from Brønsted correlations.

In fully associative nucleophilic substitutions in which **both the nucleophile and the leaving group are of the same class of molecules**, at the point that the nucleophile and the leaving group are identical, there should be a change in rate-limiting step as the acidity of the nucleophile is decreased further. In any associative nucleophilic substitution at an acyl group that proceeds through a tetrahedral intermediate, as the acidity of the nucleophile is increased, the rate constant k_{-1} (Equation 1–51) increases. When k_{-1} becomes greater than the rate constant k_2, the rate-limiting step changes from formation of the tetrahedral intermediate to its breakdown. If the leaving group and the nucleophile are both of the same class of compounds—for example, both phenolate ions[143,144] or both pyridines[145]—then the following must be true: As the basicity of the nucleophile is decreased while the leaving group remains unchanged until nucleophile and leaving group are the same molecule, the rate constants k_{-1} and k_2 must become identical because expulsion of the initial nucleophile from the tetrahedral intermediate is chemically identical to expulsion of the initial leaving group. Because the formation of the tetrahedral intermediate and its breakdown are electronically quite different, the rate constant k_1, that for the rate-limiting step when the nucleophile is *more* basic than the leaving group, should have a different dependence on the pK_a of the conjugate acid of the nucleophile than does the rate constant k_2, that for the rate-limiting step when the nucleophile is *less* basic than the leaving group. Consequently, the effect of changing the basicity of the nucleophile on the overall rate of the reaction should be different for nucleophiles of the same class more basic than the leaving group than it is for nucleophiles of the same class less basic than the leaving group.

The rates of nucleophilic substitution of the 4-nitrophenyl group in 4-nitrophenyl acetate by each of a series of phenolate ions were measured. Phenols with values of pK_a both greater than and less than 4-nitrophenol were chosen. The common logarithms of the rate constants for nucleophilic substitutions were plotted as a function of the values of pK_a for phenols that were the conjugate acids of the phenolate ions used as nucleophiles (Figure 1–12).[143]

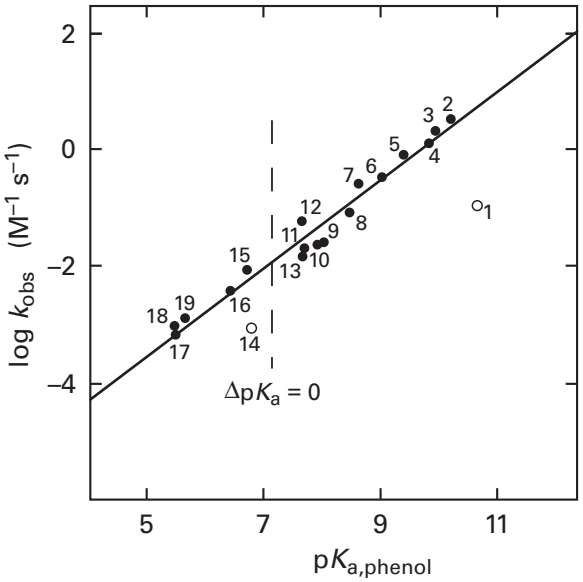

Figure 1–12: Brønsted correlation between rate constants for nucleophilic substitutions of the 4-nitrophenolate ion in 4-nitrophenyl acetate by a series of other phenolate ions.[143] The rate of release of the 4-nitrophenolate ion from 4-nitrophenyl acetate was monitored in water at 25 °C and an ionic strength of 0.1 M by following the increase in absorbance at 400 nm resulting from its production. A buffer strong enough to maintain the pH within 0.02 unit was used in each reaction. The pH chosen was appropriate to the pK_a of the particular phenol being used as the nucleophile. The phenols chosen were (1) 2,6-dimethylphenol; (2) 4-methylphenol; (3) 4-fluorophenol; (4) phenol; (5) 4-chlorophenol; (6) 3-chlorophenol; (7) 3,4-dichlorophenol; (8) 2-chlorophenol; (9) 4-acetylphenol; (10) 4-cyanophenol; (11) 2,3-dichlorophenol; (12) 3,4,5-trichlorophenol; (13) 4-formylphenol; (14) 2,6-dichlorophenol; (15) 2,4,5-trichlorophenol; (16) 2,3,5-trichlorophenol; (17) pentafluorophenol; (18) 2,3,5,6-tetrafluorophenol; and (19) 2,3,4,5-tetrachlorophenol. After the rate of release of 4-nitrophenolate ion resulting from the background hydrolysis of the 4-nitrophenyl acetate was monitored, the nucleophilic phenol was added to the solution to initiate the substitution. The increase in the rate of release of 4-nitrophenolate ion was then measured. It was assumed that the increase in the rate was due to the nucleophilic substitution of 4-nitrophenol by the phenol that had been added to the solution and that the nucleophile responsible for this nucleophilic substitution was the phenolate ion of the phenol that had been added. The phenol was added at a concentration sufficiently in excess of the concentration of 4-nitrophenyl acetate to ensure that its concentration would change insignificantly as the reaction progressed. From the increase in the rate of release of 4-nitrophenolate ion, the concentration of phenol added, and the pH of the solution, a pseudo-first-order rate constant (second^{-1}) could be calculated for the nucleophilic substitution of 4-nitrophenolate ion by the phenolate ion added as the nucleophile. Several different initial concentrations of each phenol were used. From the slope of the line relating the observed pseudo-first-order rate constant to the molar concentration of the nucleophilic phenolate ion, an observed second-order rate constant (k_{obs}; molar^{-1} second^{-1}) for the nucleophilic substitution of 4-nitrophenolate ion by that particular phenolate ion could be calculated. The common logarithm of each second-order rate constant (log k_{obs}) is plotted as a function of the values of the pK_a for the phenol. The slope of the line drawn through the points, β_{nuc}, determined by least-squares numerical analysis, was 0.75. The two points designated with open circles were not included in the analysis. This slope is the Brønsted coefficient for the conjugate acids of the nucleophiles. The vertical dashed line is located at the pK_a of 4-nitrophenol to indicate that the same correlation holds for phenols both more acidic and less acidic than the conjugate acid of the leaving group.

The Brønsted coefficient for the conjugate acids of the nucleophiles, β_{nuc}, which is the slope of the line in Figure 1–12, has a value of 0.75. There is, however, **no change in the slope of the line** as the values of pK_a for the conjugate acids of the phenolate ions used as nucleophiles pass through the point at which they are equal to the pK_a of 4-nitrophenol (pK_a = 7.15). Because there is no evidence for the existence of a tetrahedral intermediate, it was concluded that the nucleophilic substitution of one phenol for another in phenyl acetates proceeds by a concerted nucleophilic substitution with the simultaneous formation of a bond to the nucleophile and disintegration of the bond to the leaving group through a **single transition state**.[143]

Further evidence for this conclusion is that the Brønsted coefficient for the nucleophiles β_{nuc} increases as the pK_a of the leaving group increases and the Brønsted coefficient for the leaving groups, β_{lg}, decreases as the pK_a of the nucleophile increases. These observations imply that the bond to the nucleophile is forming while the bond to the leaving group is breaking in the transition state for the rate-limiting step in the reaction. There is also no change in the Brønsted coefficient for the conjugate acids of the nucleophiles, β_{nuc}, for pyridines reacting with *N*-methoxycarbonylisoquinolium ion[145] as well as for phenols reacting with several phenyl formates,[144] acyl derivatives that should form even more stable tetrahedral intermediates.

Because it was the pronounced break in the plot of the rate constants as a function of the pK_a of the nucleophile for associative nucleophilic substitutions of the 4-nitrophenyl group in 4-nitrophenyl acetate by a series of thiolate ions (Equation 1–50) that indicated the existence of two transition states and a tetrahedral intermediate in each of these reactions (Figure 1–11), the failure to observe the effect of a change in rate-limiting step suggests that, **in these nucleophilic substitutions at an acyl group, no tetrahedral intermediate is formed**.

Kinetic isotope effects also indicate that the bond to the leaving group in this class of nucleophilic substitutions is breaking in the transition

state. In 4-nitrophenyl acetate, the rate of nucleophilic substitution should decrease when the nitrogen-14 atom of the nitro group is replaced by nitrogen-15 if the bond between the 4-nitrophenol and the acyl carbon is breaking in the transition state. That the rate does decrease (by 0.1% ± 0.02%) when phenolate is the nucleophile but does not decrease significantly (0.02% ± 0.01%) when hydroxide is the nucleophile is evidence that a tetrahedral intermediate exists in the latter reaction but not in the former.[146]

The foregoing considerations provide an introduction into **a more comprehensive use of free energy correlations to examine the structures of transition states**. Consider the following coefficients. A Brønsted coefficient for a correlation of any set of rate constants

$$\beta_{rc} = -\frac{d \ln k}{d \ln K_a} \qquad (1\text{–}52)$$

A Brønsted coefficient for a correlation of any set of equilibrium constants

$$\beta_{eq} = -\frac{d \ln K_{eq}}{d \ln K_a} \qquad (1\text{–}53)$$

A Leffler coefficient

$$\alpha \equiv \frac{d \ln k}{d \ln K_{eq}} = \frac{\beta_{rc}}{\beta_{eq}} \qquad (1\text{–}54)$$

A **Leffler coefficient** correlates changes in the standard free energy of activation of a reaction with changes in the standard free energy of the reaction itself.[147] It differs from a Brønsted coefficient in that the reference reaction is not the acid dissociation of a participant but the reaction being monitored itself. As such, a Leffler coefficient is considered to be a more reliable measure of the fraction that the bond to the nucleophile has formed in the transition state when the values of K_a in the two Brønsted correlations (Equations 1–52 and 1–53) are for the conjugate acids of the nucleophiles. A Leffler coefficient is also considered to be a more reliable measure of the fraction that the bond to the leaving group has broken in the transition state when the values of K_a in the two Brønsted correlations are for the conjugate acids of the leaving groups. There is, however, some ambiguity when the Leffler coefficient is equated with the degree to which a bond is broken in the transition state because the Leffler coefficient actually measures the degree to which negative charge has accumulated on the heteroatom of the leaving group in the transition state or the degree to which the negative charge of the nucleophile has diminished on the heteroatom of the nucleophile in the transition state.[148]

For nucleophilic substitution of the 4-nitrophenyl group in 4-nitrophenyl acetate by the series of phenols shown in Figure 1–12, the Brønsted coefficient for the correlation between values of K_a for the conjugate acid of the nucleophile and equilibrium constants[143,149] for the nucleophilic substitutions, $\beta_{eq,nuc}$, is 1.7; and the Brønsted coefficient for the correlation between the values of K_a for the conjugate acids of the nucleophiles and the observed rate constants for the nucleophilic substitutions, β_{nuc}, is 0.75. Consequently the Leffler coefficient for the series of nucleophiles, α_{nuc}, is 0.44. This Leffler coefficient implies that the bond to the nucleophile is only about one-half formed in the transition state, if the reaction actually is a concerted nucleophilic substitution at the acyl group.

For the nucleophilic substitution of one phenol for another at a formyl group, a Brønsted coefficient β_{nuc} of 0.4 to 0.6 and a Brønsted coefficient β_{lg} of –0.3 to –0.5 suggest that formation of the bond to the nucleophile and disintegration of the bond to the leaving group proceed in parallel. These values also suggest that, in the transition state, the oxygen of the entering nucleophile and the oxygen of the leaving group form roughly equivalent partial bonds with the formyl carbon.[144]

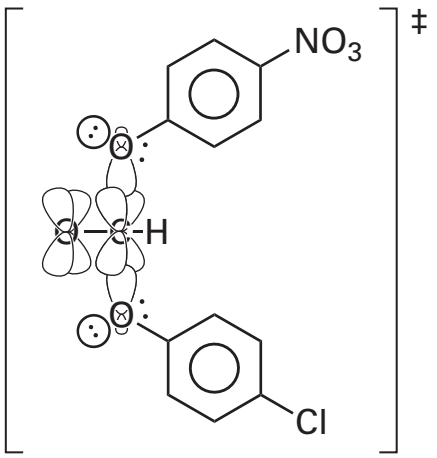

1–50

In the **molecular orbital system of the transition state**, formed from one atomic orbital from each of the two phenolate oxygens, two *p* orbitals from the electrophilic carbon, and two *p* orbitals from the

acyl oxygen, there are six molecular orbitals and eight electrons.

As in any nucleophilic substitution, in the nucleophilic substitution at an acyl group, the σ bond to the leaving group is broken and a σ bond to the nucleophile is formed. Again, it is a matter of timing. If the σ bond to the nucleophile is formed completely before the σ bond to the leaving group begins to break, a tetrahedral intermediate, the homologue of the various products of addition to a carbonyl group (Table 1–1), is produced. This formation of a tetrahedral intermediate is what happens in most nucleophilic substitutions at an acyl group, such as the associative nucleophilic substitution of a 4-nitrophenyl group by a thiolate (Equation 1–50 and Figure 1–11). If the σ bond to the leaving group is breaking in concert with formation of the σ bond to the nucleophile, the nucleophilic substitution is concerted and proceeds through a single transition state with no intermediate just as the concerted nucleophilic substitution at the methyl group of *S*-adenosyl-L-methionine does (Equation 1–19). The concerted formation of the bonds is what happens in the substitution of a phenyl group by another phenyl group in phenyl formates (**1–50**). If the bond to the leaving group breaks before the bond to nucleophile begins to form, an intermediate homologous to a carbenium ion (Equation 1–21) or oxocarbenium ion (**1–8**) forms.

It is when the conjugate acid of the leaving group has a low pK_a that this last possibility is realized. Nucleophilic substitutions at acyl triflates,[150] acyl halides,[151-154] and hindered acyl groups, such as in 2,4,6-trimethylbenzoates,[155] can proceed through **acylium ions as intermediates in dissociative nucleophilic substitutions**

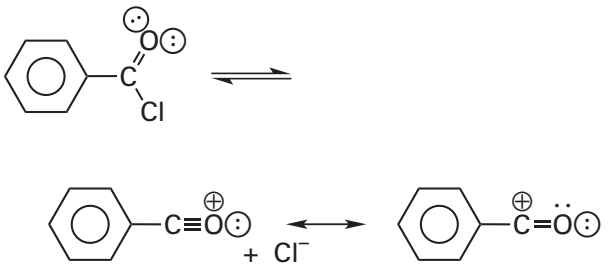

(1–55)

As with any other type of nucleophilic substitution, each nucleophilic substitution at an acyl group falls at a particular point in a continuous spectrum of mechanism. As with a nucleophilic substitution at a tetrahedral, saturated carbon, this spectrum of mechanism can be appreciated by examining a **three-dimensional surface of potential energy** (Figure 1–4). Again, the first coordinate is the distance between the atom of the leaving group and the electrophilic carbon, the second coordinate is the distance between the nucleophilic atom and the electrophilic carbon, and the third coordinate is the potential energy of the system for the point defined by the first and second coordinates.

In the case of a nucleophilic substitution at an acyl group, however, unlike the situation in a simple nucleophilic substitution at a tetrahedral carbon, there is a significant well of potential energy in the **lower left corner**, rather than a mountain of potential energy as in Figure 1–4, because this is the position of the tetrahedral intermediate, in which the carbon is tetravalent, rather than the forbidden pentavalent carbon. The intermediate in a nucleophilic substitution at an acyl group can be tetravalent because the initial electrophile is only trivalent. If the tetrahedral intermediate is the most stable of all the possibilities, there will be two cols of potential energy: one between the reactants and the tetrahedral intermediate and the other between the tetrahedral intermediate and the products.

The **upper right corner** in the three-dimensional surface of potential energy for the nucleophilic substitution at an acyl carbon is the location of the acylium ion, homologous to a carbenium ion or oxocarbenium ion that occupies the upper right corner in a simple nucleophilic substitution. If the acylium ion is the most stable of all the possibilities, as in the organic reactions just discussed that have an acylium ion as an intermediate, there will again be two cols of potential energy: one between the reactants and the acylium ion and the other between the acylium ion and the products, just as is the case when there is a carbenium ion or oxocarbenium ion as an intermediate (Figure 1–4A).

There is, however, always the possibility in a nucleophilic substitution at an acyl group that there is a col of potential energy that occurs when the bond between the nucleophile and the electrophilic carbon is partially formed while the bond between the electrophilic carbon and the leaving group is partially broken and that there is no tetrahedral intermediate nor the creation of a full positive elementary charge on the acyl group in the single transition state.[76] Such nucleophilic substitutions at an acyl group are **concerted nucleophilic substitutions**, just as is the case in a concerted nucleophilic substitution at a saturated carbon (Figure 1–4B).

The properties that determine the position of the transition state or the transition states for a particular nucleophilic substitution at an acyl group on the surface of potential energy are most readily appreciated by considering the **nucleophilic substitutions in which nucleophile and leaving group are identical**:[76] for example, both the same phenol or both the same alcohol. In addition to emphasizing the fact that the leaving group and the nucleophile interchange roles in the reverse reaction, such an identity reaction permits one to focus on only one pK_a, which is the same for the conjugate acid of both the nucleophile and the leaving group.

The effect of the pK_a of nucleophile and leaving group on the rates of such identity reactions with phenyl acetates suggests that when the leaving group and the nucleophile have a pK_a of 7, formation of the bond to nucleophile and disintegration of the bond to leaving group are fully coupled. In this instance, **the poor nucleophile and the poor leaving group** favor a concerted substitution with no intermediate and a single transition state. As the leaving group and nucleophile together become more basic, **the nucleophile becomes stronger and the leaving group becomes poorer**, and formation of the bond to the nucleophile precedes more and more the disintegration of the bond to the leaving group until it precedes it completely and the nucleophilic substitution is associative and proceeds through a tetrahedral intermediate. The combination of a strong nucleophile and a poor leaving group favors a tetrahedral intermediate. As the conjugate acids of the leaving group and the nucleophile in an identity reaction become more acidic, **the nucleophile becomes weaker and the leaving group becomes more able**, and formation of the bond to the nucleophile lags more and more behind the disintegration of the bond to the leaving group until it lags behind it completely and the reaction proceeds through an acylium ion. A weak nucleophile and good leaving group favor an acylium ion as an intermediate.

The same considerations apply to any nucleophilic substitution. The existence of an intermediate carbenium ion, oxocarbenium ion, or acylium ion in a dissociative nucleophilic substitution is more likely when the conjugate acid of the leaving group has a low pK_a and the conjugate acid of the nucleophile also has a low pK_a. The existence of a concerted nucleophilic substitution with a single transition state is more likely when the conjugate acid of the leaving group has an intermediate pK_a and the conjugate acid of the nucleophile also has an intermediate pK_a. When the conjugate acid of the leaving group has a high pK_a and the conjugate acid of the nucleophile also has a high pK_a, a nucleophilic substitution at an acyl group will proceed through a tetrahedral intermediate, but a nucleophilic substitution at a saturated carbon cannot proceed through a pentavalent intermediate and must still proceed through a concerted nucleophilic substitution. There is, however, one other consideration.

In solution, in cases of catalysis resulting from the hydronation of leaving groups, hydronating the acyl oxygen, or dehydronating nucleophiles, the catalytic acid and the catalytic base or the several catalytic acids and catalytic bases have to be supplied simultaneously to the single transition state for a concerted nucleophilic substitution at an acyl group. These participations of catalytic acids and catalytic bases, however, can be divided between the two transition states of an associative nucleophilic substitution with a tetrahedral intermediate. Catalysis increasing the nucleophilicity of the nucleophile and the electrophilicity of the acyl carbon can be supplied during the formation of the tetrahedral intermediate, and catalysis increasing the ability of the leaving group can be supplied during the dissociation of the tetrahedral intermediate. This division of labor is one of the reasons that a nucleophilic substitution at an acyl group under acid–base catalysis usually proceeds through a tetrahedral intermediate in solution. This division of requirements between two transition states, however, is unnecessary **in the active site of an enzyme** because the catalytic acids and bases are assembled and positioned in their proper places before the chemistry begins. In the active site of an enzyme, where catalytic acids and bases are pre-positioned to improve dramatically the ability of the leaving group and the nucleophilicity of the nucleophile, a reaction coordinate for a concerted nucleophilic substitution at an acyl group with a single transition state that passes somewhere on the surface of potential energy between a tetrahedral intermediate and an acylium ion is a reasonable possibility.

In none of the nucleophilic substitutions at acyl groups catalyzed by enzymes, however, is there yet any evidence for such a concerted mechanism, and even in the absence of any evidence, a nucleophilic substitution at an acyl group on an

Table 1–3: Standard Free Energies of Hydrolysis of Selected Acyl Derivatives at 25 °C[a]

acyl derivative[b]	ΔG°_{hydro} (kJ mol^{-1})	pK_a of conjugate acid of the leaving group
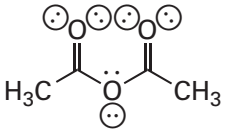	–66	4.7
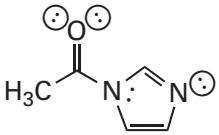	–40	14.5
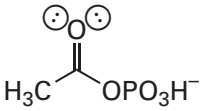	–34[b]	7.2
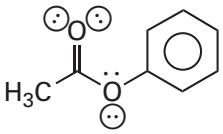	–31	10.0
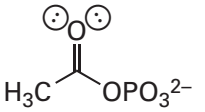	–28[c]	12.4
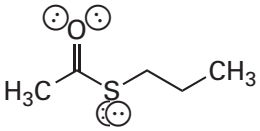	–18	10.5
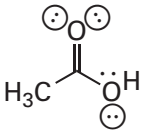	–10	15.7
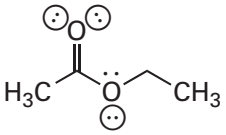	–7	16
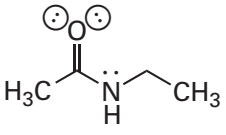	+34	34

[a]Standard free energy of hydrolysis[156,157] (Equation 1–41) based on a standard state of 1 M concentrations of the uncharged reactants and products and an activity of pure water of 1. [b]Based on a pK_a of inorganic phosphate of 7.2 and of an acyl phosphate of 6.2. Value for the monoanions of acetyl phosphate and phosphate. [c]Value for the dianions of acetyl phosphate and phosphate.

enzymatic active site is usually assumed to be associative and to pass through a tetrahedral intermediate. If the pK_a of the conjugate acid of the leaving group is high and that of the conjugate acid of the nucleophile is high, the reaction will certainly proceed through a tetrahedral intermediate. When, however, the biochemical leaving group and the biochemical nucleophile each have a conjugate acid with a low pK_a, the possibility of a concerted mechanism, or even an intermediate acylium ion, should be considered for the enzymatic reaction.

Biochemically relevant acyl derivatives can be arranged in order of their standard free energies of hydrolysis, ΔG°_{hydro} (Table 1–3).[156] These are the changes in standard free energy* for the reaction

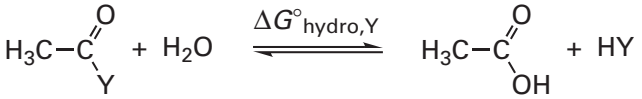

(1–56)

Water acts as a reference nucleophile, permitting the various acyl derivatives to be placed on the same scale of stability.

The **change in standard free energy of any particular nucleophilic substitution** at an acyl group

(1–57)

can be estimated by taking differences between the two values for the two relevant standard free energies of hydrolysis

$$\Delta G^\circ_{YZ} = \Delta G^\circ_{hydro,Y} - \Delta G^\circ_{hydro,Z} \qquad (1–58)$$

For example, the change in standard free energy for the aminolysis of an ester

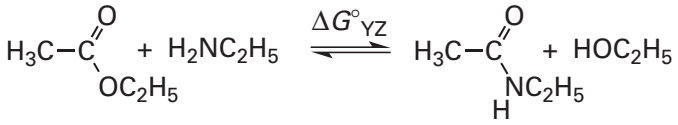

(1–59)

a reaction resembling the formation of a peptide bond during protein synthesis,† should be –41 kJ mol^{-1}.

*See footnote to Table 1–2 on the decision to omit the concentration of water.

†The standard free energy for the dehydronation of ethylamine has to be included when the aminolysis of the ester occurs at a pH less than 11.

When the nucleophilic substitutions of imidates are being considered

(1–60)

the same scale of standard free energies of hydrolysis can be used to estimate roughly the standard change in free energy for the reaction. Consistent with Equation 1–58, the nucleophilic substitutions commonly observed are those that convert an acyl derivative with a more negative standard free energy of hydrolysis into one with a less negative standard free energy of hydrolysis.

The heteroatomic nucleophiles and leaving groups in biochemical nucleophilic substitutions at acyl groups are usually amines, pyridines, phosphates, phenolate ions, alcohols, thiolate ions, enolates, and enamines. For these nucleophiles and leaving groups, **as the leaving groups become stronger bases and their conjugate acids become weaker acids, the standard free energies of hydrolysis increase** (Table 1–3). The acidity of the parent acid of the acyl derivative, however, has much less of an effect, if any.[157]

The dissociation of the leaving group from an acyl carbon resembles its dissociation from a hydron. The equation for the hydrolysis used as the reference (Equation 1–56), however, formally involves the subsequent hydronation of the leaving group. Therefore, the tabulated standard free energies of hydrolysis are actually correlated to the standard free energy for transfer of the leaving group from an acyl carbon to a hydron. If a hydron and an acyl carbon were electrophilically equivalent to each other, there would be no dependence of the standard free energy of hydrolysis on the values of pK_a for the conjugate acids of the leaving groups, and yet there is. For example, within a series of oxygen esters, the equilibrium constant for Equation 1–56, $K_{eq,hydro}$, is correlated to the respective acid dissociation constants of the alcohols that leave (Figure 1–13)[149] by the equation

$$\log K_{eq,hydro} = A + \beta_{eq,lg}\, pK_a \qquad (1–61)$$

where the Brønsted coefficient $\beta_{eq,lg}$ is –0.70.[149] For thioesters, $\beta_{eq,lg}$ is –0.38,[141] and for amides, it is –0.51.[157]

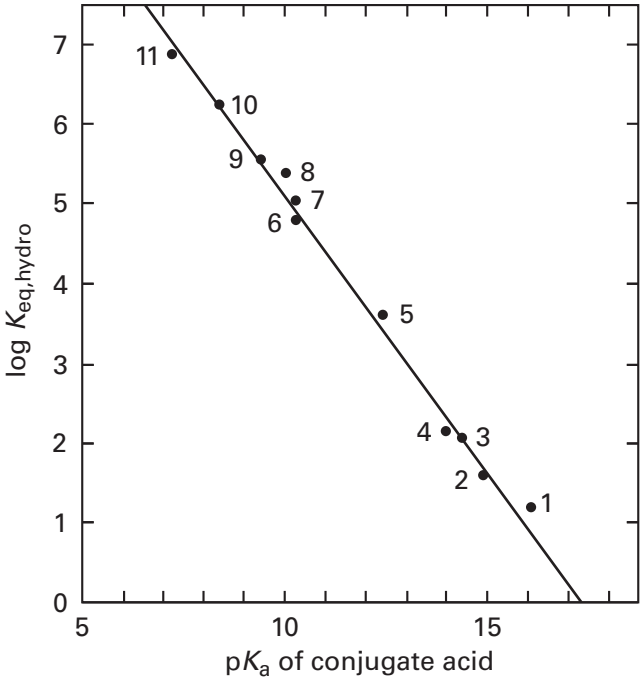

Figure 1–13: Brønsted correlation of the equilibrium constants, $K_{eq,hydro}$, for the hydrolysis of the respective acetate esters of a series of alcohols and phenols with the pK_a of the alcohol or phenol.[149] The esters were (1) ethyl acetate; (2) 2-methoxyethyl acetate; (3) chloroethyl acetate; (4) acetylcholine; (5) trifluoroethyl acetate; (6) 4-methoxyphenyl acetate; (7) 4-methylphenyl acetate; (8) phenyl acetate; (9) 4-chlorophenyl acetate; (10) 3-nitrophenyl acetate; and (11) 4-nitrophenyl acetate. The values for the equilibrium constants were for uncharged reactants, ester and water, and uncharged products, carboxylic acid and alcohol (Equation 1–56). The concentration of water was omitted from the equilibrium constants. The equilibrium constants are plotted as a function of the values for pK_a. The slope of the line drawn through the points (Equation 1–61), which is the Brønsted coefficient for the conjugate acids of the leaving groups, $\beta_{eq,lg}$, is –0.70.

These negative values mean that as the pK_a increases and the conjugate acid of the leaving group becomes less acidic so that the leaving group becomes more basic, the equilibrium constant for hydrolysis of the respective acyl derivative becomes smaller and the standard free energy of hydrolysis becomes more positive. If this is the case, as the leaving group becomes more basic, and more electron-releasing, the acyl derivative of the leaving group becomes more stable, relative to the conjugate acid of the leaving group. This increased stability is almost certainly due to the increasing **ability of the leaving group to conjugate with the carbonyl**

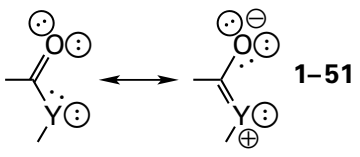

1–51

an ability that increases the stability of the acyl group. This opportunity for conjugation is not available in its conjugate acid, where the leaving group is attached only to a hydron.

Consider an ester, in which the atom bound to the acyl carbon is the oxygen of the leaving group. As the leaving group, RO–, becomes more basic, the electron density in the σ bond between the acyl carbon and the oxygen of the leaving group increases, just as the electron density in the oxygen–hydrogen bond of the alcohol increases, but so does the electron density in the two lone pairs of electrons on the oxygen of the leaving group

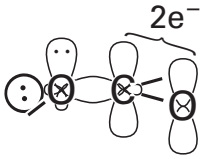

1–52

Either one of these lone pairs of electrons can **overlap with the π molecular orbital system between the acyl carbon and the acyl oxygen**, and this overlap also increases the strength of the bond between the acyl carbon and the acyl oxygen.[158] Such overlap, however, is not possible with a hydron. This presence or absence of overlap explains why the free energies of hydrolysis for oxygen esters increase more rapidly than do the free energies for acid dissociation of their leaving groups, and it also explains why the Brønsted coefficient $\beta_{eq,lg}$ for the hydrolysis of oxygen esters is more negative than that for thioesters. A σ lone pair of electrons on a sulfur overlaps poorly with a *p* orbital on a carbon.

When all four of the bonds to a carbon, single bonds or double bonds, are to heteroatoms, that carbon is in a derivative of carbonic acid (1–53).

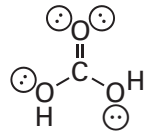

1–53

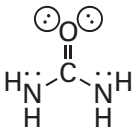

1–54

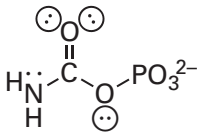

1–55

Examples of such carbons that are of biochemical importance are those in urea (**1–54**), carbamoyl phosphate (**1–55**), and an *N*-alkylguanidinium ion. In the nucleophilic substitutions of derivatives of carbonic acid, the same considerations apply as for nucleophilic substitutions at an acyl group. For example, in nucleophilic substitution at carbamoyl phosphate, either a tetrahedral intermediate or the equivalent of an acylium ion is possible[159]

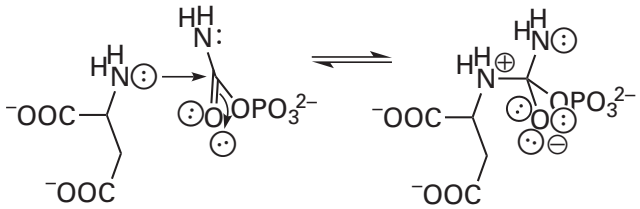

(1–62)

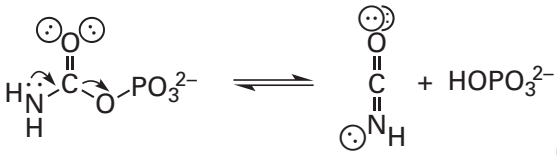

(1–63)

as well as a concerted nucleophilic substitution.

Suggested Reading

Gilbert, H. F., and Jencks, W. P. (1982) Mechanism of the aminolysis of alkyl benzimidates, *J. Am. Chem. Soc. 104*, 6769–6779. https://doi.org/10.1021/ja00388a048

Ba-Saif, S., Luthra, A. K., and Williams, A. (1989) Concerted acetyl-group transfer between substituted phenolate ion nucleophiles: Variation of transition-state structure as a function of substituent, *J. Am. Chem. Soc. 111*, 2647–2652. https://doi.org/10.1021/ja00189a045

Nucleophilic Substitution at Phosphorus

Derivatives of phosphoric acid are susceptible to nucleophilic substitution at phosphorus[160] just as derivatives of carboxylic acids are susceptible to nucleophilic substitution at carbon. An example of such a nucleophilic substitution at phosphorus would be

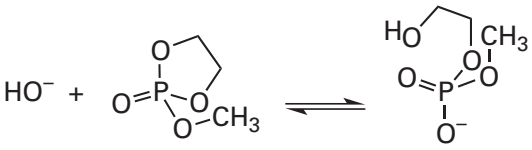

(1–64)

in which the oxygen of hydroxide , the nucleophile, has substituted for one of the two oxygens of the 2-hydroxyethoxy group, the leaving group. The reactant in this reaction is a **phosphotriester**, in which the phosphoric acid has been esterified with

three alcohols. In **phosphodiesters**, such as dinucleotides, the phosphoric acid has been esterified with two alcohols, and in **phosphomonoesters**, such as D-glucose 6-phosphate, the phosphoric acid has been esterified with only one alcohol.

As does nucleophilic substitution at the carbon of an acyl group, nucleophilic substitution at phosphorus includes a continuous **spectrum of mechanism** in which the two dimensions again are the integrity of the bond to the leaving group and the integrity of the bond to the nucleophile. As with nucleophilic substitutions at an acyl group, the two extremes of this spectrum are an **associative nucleophilic substitution,** in which the bond between the nucleophile and the phosphorus has formed completely before the bond to the leaving group begins to break, and a **dissociative nucleophilic substitution,** in which the bond to the leaving group has broken completely before the bond to the nucleophile has begun to form. The former extreme produces a pentavalent intermediate, a pentaoxyphosphorane, while the latter produces a trivalent intermediate, a monomeric metaphosphate. Unlike pentavalent carbon, pentavalent phosphorus can exist both in an intermediate and even in a stable molecule.

The reaction of Equation 1–64 is a nucleophilic substitution at a triester of phosphoric acid. When a series of triesters of phosphoric acid were synthesized with different aryloxy leaving groups and submitted to nucleophilic substitutions with an array of nucleophiles (RO^-)

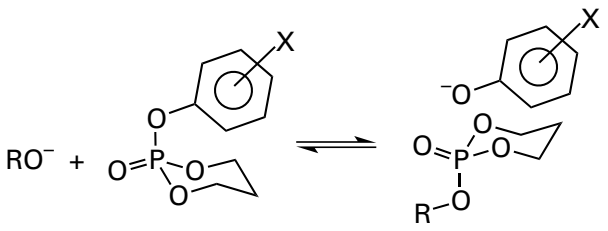

(1–65)

where X indicates the various substitutions at the phenyl group, a plot of the Brønsted coefficient for the leaving groups against the values of pK_a for the nucleophiles shows a pronounced break at a pK_a of 11.[161] The existence of this break in the secondary Brønsted plot, as well as other characteristics of the reaction, suggests that each of the nucleophilic substitutions of these triesters proceeds through at least two steps with at least one intermediate. The fact that oxygen-18 exchanges into the phospho group of the reactant as a nucleophilic substitution in a triester progresses[162] suggests that the intermediate* in such reactions, in analogy to the tetrahedral intermediate in nucleophilic substitution at an acyl group, is a pentaoxyphosphorane and that these reactions are associative nucleophilic substitutions.[163]

Associative nucleophilic substitutions at phosphorus are reactions that proceed through intermediate pentaoxyphosphoranes. Phosphoranes are compounds in which a central phosphorus atom has five substituents. There are pentaoxyphosphoranes that can exist as stable compounds. Simple acyclic examples of stable pentaoxyphosphoranes would be pentaphenoxyphosphorane[164] and pentacyclohexyloxyphosphorane (Figure 1–14A).[165,166] These two molecules are stable, just as an ortho ester of a carboxylic acid is stable, because none of the oxygens can become anionic, increasing the electron repulsion around the phosphorus and, in turn, pushing out one of the phenols or one of the cyclohexanols. The structure of a pentaoxyphosphorane is a **trigonal bipyramid** (Figure 1–14A). Even though all five of the substituents are identical, they are not distributed in such a way that all the angles between the bonds are the same, as they are in a tetrahedral carbon like an ortho ester; this fact indicates that the hybridization of the atomic orbitals on phosphorus controls the structure. In a trigonal bipyramid, three of the substituents lie in a plane containing the central atom at ideally 120° angles to each other (the three horizontal oxygens in Figure 1–14A). These substituents are designated **equatorial**. Two of the substituents are located above and below the plane, respectively, on a line (vertical in Figure 1–14A) passing through the phosphorus and perpendicular to the plane. These substituents are designated **apical**. The angles between each of the equatorial oxygens and each of the apical oxygens are all ideally 90°. The ideal equatorial and apical angles are altered somewhat by steric effects in an actual pentaoxyphosphorane.

The **hybridization of the atomic orbitals** that overlap to form the bonds in a pentaoxyphosphorane can be inferred from its bond angles. The bond angles between the equatorial oxygens are those expected if the central phosphorus in a pentaoxyphosphorane has sp^2 hybridization and each of its sp^2 orbitals participates in a σ bond to one of the three equatorial oxygens.

*Strictly speaking, the intermediate that is responsible for the isotopic exchange could be in a side reaction that is not on the reaction pathway for the hydrolysis.

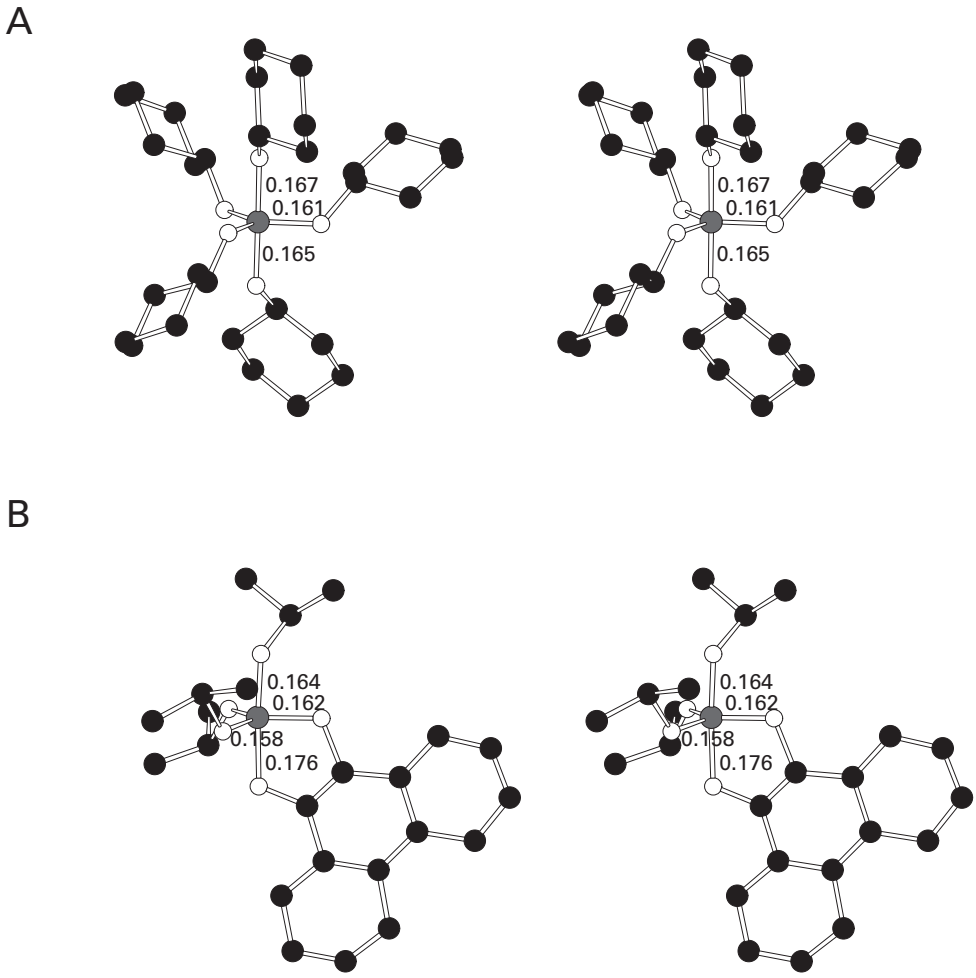

Figure 1–14: Stereodrawings[166] of the arrangement of the five oxygen atoms and the substituents attached to them around the pentavalent phosphorus in crystallographic molecular models of two pentaoxyphosphoranes. Black atoms are carbons, white atoms are oxygens, and the large gray atom is a phosphorus. **(A)** Crystallographic molecular model of pentacyclohexyloxyphosphorane.[165] Pentacyclohexyloxyphosphorane was synthesized by mixing tricyclohexyl phosphite and cyclohexyl benzenesulfenate in pentane at –78 °C. In the crystallographic molecular model, the phosphorus atom lies at the intersection of the five bonds between it and the five oxygen atoms of the cyclohexyloxy groups. Three of the oxygens are in the same plane at the equatorial positions, and the other two oxygens are on a line of centers with the phosphorus at the apical positions. The angles between the equatorial oxygens are almost ideal (120°, 124°, and 116°) and the angles between each equatorial oxygen and the two apical oxygens are also almost ideal (88°, 89°, 92°, 90°, 93°, and 88°). Deviations from the ideal result from the steric effects of the bulky cyclohexyl groups. The bond lengths between the phosphorus and the equatorial oxygens are 0.161, 0.161, and 0.160 nm. The bond lengths between the apical oxygens and the phosphorus are indicated in the drawing (in nanometers). That the apical bonds are longer suggests that they are weaker than the bonds to the equatorial oxygens. The bond angles at the oxygens between carbon 1 of a cyclohexyl group and the phosphorus are 124°,127°, 128°, 128°, and 130°; these angles suggest that the oxygens are all hybridized sp^2. **(B)** Crystallographic molecular model of (9,10-phenanthroquinolyl)triisopropylpentaoxyphosphorane, the adduct that forms between triisopropyl phosphite and 9,10-phenanthroquinone.[174] The phosphorus atom lies at the intersection of the five bonds between it and the five oxygen atoms at the center of a "near [sic] perfect trigonal bipyramid". The angles between the equatorial oxygens are almost ideal (118°, 120°, and 121°) and the angles between each equatorial oxygen and the two apical oxygens are also almost ideal (97°, 85°, 92°, 91°, 87°, and 89°). Within the five-membered ring, the two oxygens from the 9,10-phenanthroquinolyl group occupy one equatorial and one apical position of the trigonal bipyramid, respectively, as expected when there is a five-membered ring, and the other three positions are occupied by the oxygens of the isopropoxy groups. The bond angles at the oxygens between the two carbons of the 9,10-phenanthroquinolyl group and the phosphorus are 113° and 112°, and the angle at the phosphorus between the two oxygens of the 9,10-phenanthroquinolyl group is 89°, so the five-membered ring is distorted to ensure an angle of almost exactly 90° at phosphorus. Four of the bond lengths (in nanometers) are noted in the drawing, and the bond length of the other equatorial phosphorus–oxygen bond is 0.161 nm. The bond angles at the three oxygens of the isopropoxy groups between the carbons and the phosphorus are 126°, 132°, and 127°, these angles again suggest that these oxygens are all hybridized sp^2.

The hybridization of these equatorial oxygens, however, is not so simple. On the one hand, in a calculated structure of pentahydroxyphosphorane,[167] a molecule that for obvious reasons has never been observed, the bond angle at each equatorial oxygen between the phosphorus and the hydrogen is about 110° and the dihedral angle for the hydrogen along a bond between the phosphorus and an equatorial oxygen is around 30°. These angles suggest that, in a normal, unhindered pentaoxyphosphorane,* the three equatorial oxygens have sp^3 hybridization with the usual σ lone pairs and covalent bonds to peripheral substituents

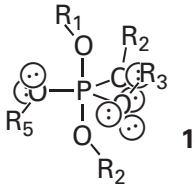

1–56

where the peripheral substituents (R_1–R_5) are either alkyl groups or hydrogens. A dihedral angle of 30°, because it places the two sp^3 lone pairs and the σ bond to the substituent at an equatorial oxygen as far away from the electrons in the two apical bonds as possible, engenders the least electron repulsion. On the other hand, in pentacyclohexyloxyphosphorane the bond angle at each equatorial oxygen between the phosphorus and the cyclohexyl carbon is about 120° (Figure 1–14A).[165] This angle suggests that, in a normal, unhindered pentaoxyphosphorane, the three equatorial oxygens could have sp^2 hybridization with the usual σ lone pairs and covalent bonds to peripheral substituents

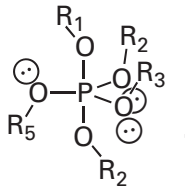

1–57

The bond angles in pentacyclohexyloxyphosphorane, however, could result from steric effects rather than electronic effects. The pK_a of an equatorial hydroxy group in a pentaoxyphosphorane[165] has been estimated to be about 9, which would also be consistent with the equatorial oxygens being hybridized sp^2 because sp^2 hydroxy groups are always more acidic than sp^3 hydroxy groups.

The bonding of the two apical oxygens has not been explained unequivocally, and it probably does not involve simple two-center covalent bonds.[168-172] The *p* orbital on the phosphorus and one sp^3 orbital[167] or one sp^2 orbital[165] from each of the two apical oxygens mix together, by themselves or perhaps with *d* orbitals from the phosphorus and another orbital from each oxygen, to produce the bonding that connects those apical oxygens to phosphorus. The pK_a of an apical hydroxy group[165] has been estimated to be 14, perhaps coincidentally about the same as a normal hydroxy group on carbon.

In an associative nucleophilic substitution at phosphorus that proceeds through a pentaoxyphosphorane, the five oxygens are not equivalent as they are in pentacyclohexyloxyphosphorane or pentaphenoxyphosphorane. The intermediate pentaoxyphosphorane is formed by attack of the nucleophile on the electrophilic phosphorus atom. That attack pushes electron density onto the unsubstituted oxygen or the unsubstituted oxygens of the phospho group

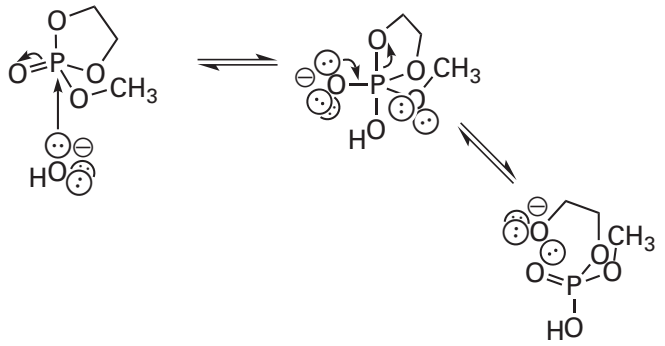

(1–66)

as the addition of a nucleophile to an acyl group pushes electron density onto the former acyl oxygen. Each unalkylated oxygen in the resulting pentaoxyphosphorane is either hydronated and is a hydroxy group or is unhydronated, bears a net negative elementary charge, and is an oxyanion. At neutral pH, each unalkylated equatorial hydroxy group (p$K_a \cong 9$) would be hydronated and only one will be transiently unhydronated and negatively charged at a time. An unhydronated, equatorial oxygen with a negative elementary charge in a pentaoxyphosphorane has a lone pair of electrons, in either an sp^3 orbital or an sp^2 orbital, that can provide **periplanar push to assist in the dissociation of a leaving group** from the phosphorus in the second step of

*If pentacyclohexyloxyphosphorane represents the actual structure of a pentaoxyphosphorane when it is unhindered by the cyclohexyl groups, then the sp^2 lone pair of electrons on each equatorial oxygen would be held by the bonding in the molecule in a periplanar orientation (Figure 1–14A).

the nucleophilic substitution (Equation 1–66). This push, which is essentially inescapable because of the relatively low pK_a of an equatorial oxygen, explains the kinetic instability of a pentaoxyphosphorane that is not completely alkylated.

In associative nucleophilic substitutions at phosphorus involving a pentaoxyphosphorane as an intermediate, the **rule of apical entry and apical exit** provides the best explanation of the observed reactivity.[173] The nucleophile must enter the phospho group at a location that becomes an apical position of the pentaoxyphosphorane, and the leaving group must leave from an apical position of the pentaoxyphosphorane (Equation 1–66). The reason for apical entry is that, to avoid electron repulsion, the lone pair of electrons of the nucleophile must approach the phosphorus atom of the phospho group in one of the four cavities below the faces of the tetrahedron each of which is formed by three of its σ bonds, just as, again to avoid electron repulsion, the nucleophile approaches the electrophilic carbon from the cavity formed by three of the σ bonds in a concerted nucleophilic substitution (Equation 1–19 and **1–5**). Because of the electron repulsion of these three σ bonds between phosphorus and oxygen, the nucleophile has to approach on a trajectory bisecting the three σ bond angles and in line with the fourth σ bond to phosphorus in the tetrahedral phospho group. In the resulting pentaoxyphosphorane, the three substituents pushed forward by the nucleophile end up in the three equatorial positions, the nucleophile ends up at one apical position, and the fourth substituent, the one in line with the nucleophile, ends up at the other apical position (Equation 1–66). That apical entry dictates apical exit follows from microscopic reversibility.

A **second rule**[165,173,174] is that in a five-membered cyclic phosphorane, such as the one in Equation 1–66, **one oxygen in the ring must be equatorial and the other oxygen must be apical** (Figure 1–14B).* This rule follows from the fact that a transition state that would lead to both of the oxygens in the ring being at equatorial positions is more sterically unstable than a transition state that leads to one of the oxygens of the ring being equatorial and the other being apical. The reason this is so is that the interior angles in a regular pentagon are all 72°, which is closer to 90° than 120°. Consequently, in the production of such an intermediate pentaoxyphorane from a five-membered cyclic phosphodiester or phosphotriester, the nucleophile adds to the phosphorus from a direction opposite to one of the oxygens in the ring so that that oxygen ends up in the other apical position, as shown in Equation 1–66.

The crystallographic molecular models of the phosphoranes in Figure 1–14 are for the more biochemically relevant case of phosphorus surrounded by five oxygens, but the most commonly encountered pentavalent compounds of phosphorus are its fluoride and its chloride. Phosphorus pentafluoride has the infrared spectrum of a trigonal bipyramid[177] but the fluorines all have equivalent absorptions in nuclear magnetic resonance spectra. It has been proposed that the five fluorines remain apical and equatorial, respectively, on the time scale of infrared spectroscopy but equilibrate among the apical and equatorial positions of the trigonal bipyramid over the much longer time scale of nuclear magnetic resonance.[178]

The motion in a trigonal bipyramid that accomplishes this equilibration between apical and equatorial positions most efficiently is a **pseudorotation**.[178] One of the pseudorotations available to the trigonal bipyramid of Figure 1–14B would move the equatorial oxygen on the left front backward horizontally into the plane of the page to fall in line with the equatorial oxygen to the right so that these two oxygens become the new apical oxygens while moving the two apical oxygens forward and moving the equatorial oxygen on the back left horizontally back and to the right to form a new plane of three equatorial oxygens.

In instances where **pseudorotation is slower than the entry and exit of nucleophile** and leaving group, the nucleophile in an associative nucleophilic substitution at a phospho group enters the pentaoxyphosphorane at an apical position, and the leaving group is determined only by the direction from which the nucleophile attacked the phosphorus because the leaving group is required to be the substituent that occupies the other apical position, opposite to the point of entry of the nucleophile. There would be three ways to **control the identity of the leaving group**. First, if the nucleophile is forced to enter at only one of the four available points of entry on phosphorus, the leaving group will always be the substituent opposite that point of entry. Such

*The hydrolysis of 2-methoxy-1,3,2-dioxaphospholane 2-oxide (Equation 1–66) is much more rapid (by a factor of 5×10^5) than the hydrolysis of trimethyl phosphate. It was concluded from enthalpies of activation that this increase in rate was due in part to the steric strain destabilizing the cyclic reactant relative to the acyclic reactant but also due to less steric hindrance in the transition state for the formation of the cyclic phosphorane relative to the acyclic phosphorane because the ring ties back the two methylene groups in the cyclic transition state.[175]

stereochemical control is possible in the active site of an enzyme. Second, if only one of the three substituents surrounding the phosphorus in the reactant is a better leaving group than the nucleophile itself, then each intermediate pentaoxyphosphorane in which that substituent is not apical would decompose to regenerate reactants. Third, if all three substituents surrounding the phosphorus in the phosphoester are poorer leaving groups than the nucleophile, the ability of a substituent to leave the intermediate pentaoxyphosphorane can be controlled, as in the situation of nucleophilic substitution at an acyl group (Equation 1–47), by hydronations or dehydronations.

When **pseudorotation in an intermediate pentaoxyphosphorane is fast** enough, however, it can become a third step in the mechanism, between the entry of the nucleophile and the dissociation of the leaving group.[179,180] The products from the reaction of Equation 1–64 are both the one shown, which arises from cleavage of the ring, and the products of exocyclic cleavage

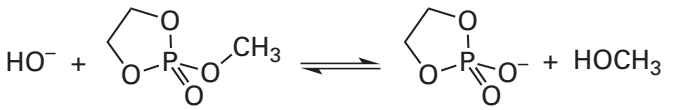

(1–67)

The ratio between these two products varies with pH. If the intermediate is a trigonal bipyramid, and if both the rule of apical entry and apical exit and the rule requiring an apical position of one of the oxygens in a five-membered ring apply, then this variation in the ratio of products can be explained only if pseudorotation occurs in the intermediate pentaoxyphosphorane for this reaction.[181] This additional step and the fact that, as the pH is varied, hydronation of the potential leaving groups varies would permit two or more changes in the rate-limiting steps of the mechanism. Together all these factors can provide an explanation for the rather complex changes with pH in the ratio between the two products (Equations 1–64 and 1–67).

The cyclic phosphotriester that is the reactant in Equation 1–64 is a particularly reactive phosphotriester that has larger than normal rate constants for hydrolysis. In nucleophilic substitutions of less reactive phosphotriesters and phosphodiesters with smaller rate constants for nucleophilic substitution, pseudorotation could easily be so rapid that it would have little or no effect on the overall rate of the reaction. In the particular nucleophilic substitution of Equation 1–64, however, it may be that the saturated five-membered ring in the pentaoxyphosphorane increases the rate of pseudorotation dramatically. If this is so, then in most nucleophilic substitutions at phosphorus pseudorotation is slow relative to entry and exit. These considerations suggest that pseudorotation may or may not be a common feature of nucleophilic substitutions at acyclic phosphoesters.

Just as is the case for nucleophilic substitution at an acyl group (Figure 1–11), observations consistent with the existence of a **change in rate-limiting step** in a nucleophilic substitution at a phospho group is evidence for the existence of an intermediate in the reaction. The intramolecular nucleophilic substitutions of a series of phenolate ions by the 2′-hydroxy group of the uridinyl group in a series of phosphodiesters in solution under catalysis by base[182]

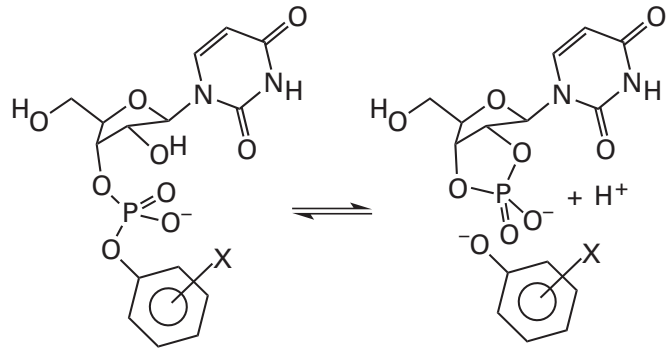

(1–68)

is a model for the cleavage of ribonucleic acid catalyzed by the enzyme ribonuclease

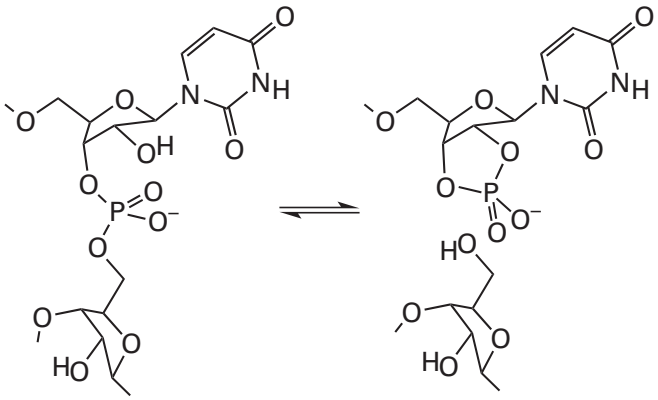

(1–69)

Because there is a pronounced **break in the Brønsted plot** in which the common logarithms of the rate constants for the nucleophilic substitution (Equation 1–68) are plotted against the values of pK_a for the conjugate acids of the phenolates that are the

leaving groups, it was concluded that each of these nucleophilic substitutions at a phosphodiester has an intermediate, presumably the respective pentaoxyphosphorane.[183]

Nucleophilic substitutions at phosphorus in adenosine 3′-phosphate diesters, adenosine 2′-phosphate diesters,[184] and uridine 3′-phosphate diesters under catalysis by acid[185,186] and base,[187] also pass through two transition states[180] with a pentaoxyphosphorane as an intermediate.[179] One piece of evidence for a pentaoxyphosphorane as an intermediate in such nucleophilic substitutions, in which an alcohol is the leaving group rather than phenol, is the effects of the replacement of each of several oxygens-16 with oxygen-18 on the rate of the reaction. Isotopic effects, however, are also consistent with the existence of only a single transition state with significant disintegration of the bond to the leaving group, as in the nucleophilic substitution of 4-nitrophenol by hydroxide in thymidine 5′-(4-nitrophenyl)phosphate.[188]

One side product of an associative nucleophilic substitution at phosphorus, homologous to the reaction in Equation 1–69 in which the leaving group is also an alcohol, is the direct transfer of the phospho group from the 3′-hydroxy group to the 2′-hydroxy group in a nucleoside monophosphate.[184-186,189] Because the two oxygens of a five-membered ring in a pentaoxyphosphorane must be apical and equatorial, respectively (Figure 1–14), and because the 2′-hydroxy group must enter the pentaoxyphosphorane at an apical position and the 3′-hydroxy group must leave from an apical position, pseudorotation must occur in this nucleophilic substitution of the 3′-hydroxy group by the 2′-hydroxy group.[179,187]

Dissociative nucleophilic substitutions at phosphorus proceed through intermediate monomeric metaphosphates. The associative nucleophilic substitutions of phosphotriesters, such as that of Equation 1–64, and of phosphodiesters with poor leaving groups, such as that of Equation 1–69, proceed through intermediate pentaoxyphosphoranes. Nucleophilic substitutions, however, of **phosphomonoesters with good leaving groups by poor nucleophiles**, such as the substitution of the 4-nitrophenoxy group in the *O*-phosphomonoester of 4-nitrophenol by the hydroxy group of 2-methylpropan-2-ol[190] or the substitution of the thiophospho group in the *S*-phosphomonoester of thiophosphate by the hydroxy group of water,[191] proceed under appropriate conditions by the initial release of monomeric metaphosphate from *O*-phospho-4-nitrophenol or μ-thiodiphosphate, respectively

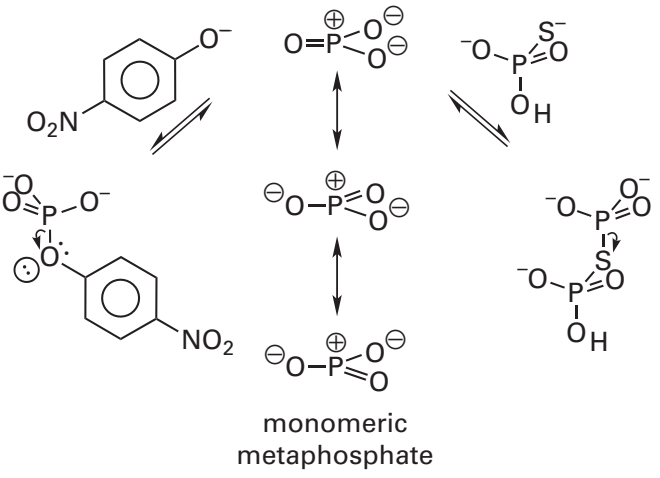

(1–70)

Monomeric metaphosphate is a planar molecule in which phosphorus is trivalent and hybridized sp^2 and forms σ bonds to each of the three oxygens (Equation 1–70). The nitrogen homologue of monomeric metaphosphate is nitrate [192]

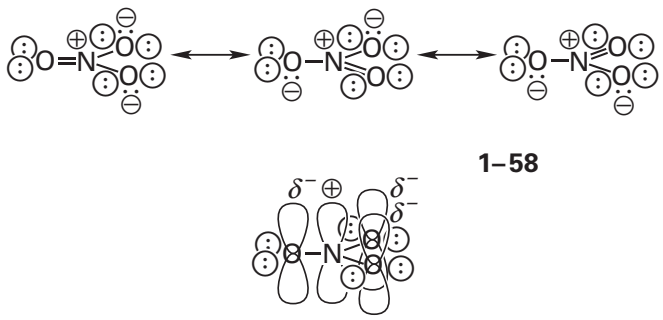

1–58

In nitrate, a *p* orbital from each of the oxygens and a *p* orbital from the central nitrogen comprise its π molecular orbital system. The four *p* orbitals mix to produce four π molecular orbitals in a trimethylenemethane configuration. Three of these four molecular orbitals are occupied by three pairs of electrons, and one is unoccupied. In monomeric metaphosphate there is a similar **π molecular orbital system** containing three pairs of electrons. The only unoccupied π molecular orbital of monomeric metaphosphate, the π^* molecular orbital, is localized almost exclusively on the phosphorus atom.[193] This unoccupied π molecular orbital overlaps with the atomic orbital occupied by the lone pair of electrons on the nucleophile during addition of the nucleophile to monomeric metaphosphate, just as the electrophilic, unoccupied *p* orbital on the carbon in a carbenium ion overlaps with the occupied orbital

on the nucleophile during the second step in a dissociative nucleophilic substitution at a saturated carbon. By microscopic reversibility, when the leaving group dissociates from the phosphoester, the antibonding molecular orbital of the phosphorus–oxygen bond becomes the unoccupied π^* orbital of the monomeric monophosphate, and the bonding molecular orbital and the two electrons in the phosphorus–oxygen bond become the atomic orbital and the two electrons of the lone pair of electrons of the leaving group.

Unlike nitrate , however, which is quite stable, monomeric metaphosphate is so **unstable** that it has never been isolated. Monomeric metaphosphate differs from nitrate because the phosphorus atom in monomeric metaphosphate has *d* orbitals that can overlap with *p* orbitals on the peripheral oxygens. This ***dpπ* overlap** delocalizes pairs of electrons on the oxygens. The pK_a of nitric acid, the conjugate acid of nitrate , is –1.3. The pK_a of the conjugate acid of monomeric metaphosphate should be lower than this because the delocalization of electron density from the oxygens in the monomeric metaphosphate should make them less basic. The pK_a of monomeric metaphosphate in solution has never been measured, but it has been calculated[167] to be around –11.

This calculated pK_a suggests that the neutral, hydronated form of monomeric metaphosphate is even more unstable than the anion. If monomeric metaphosphate had to be anionic to stabilize the electropositive phosphorus, only nucleophilic substitutions at phosphomonoesters could have monomeric metaphosphate as an intermediate. The fact, however, that methyl nitrate is a stable molecule suggests that O-alkylated monomeric metaphosphate might be stable enough to exist. Observations that are consistent with the existence of *O*-methyl monomeric metaphosphate as an intermediate in the solvolysis of a series of α-oxyiminobenzylphosphonate monomethyl esters have been reported.[194] Both of these considerations suggest that ***O*-alkyl monomeric metaphosphate could perhaps be an intermediate in nucleophilic substitutions at phosphodiesters**. An *O,O*-dialkylmetaphosphate, however, is probably so unstable that it is never an intermediate in a nucleophilic substitution at phosphorus. Transition states that resemble an *O,O*-dialkylmetaphosphate are probably also unstable relative to the respective pentaoxyphosphorane. This instability is probably one of the reasons that nucleophilic substitution at the phospho group of a triester usually proceeds through a pentaoxyphosphorane.

That monomeric metaphosphate exists, and that it is of biochemical relevance, follows from the fact that it has been observed in crystallographic molecular models: one from a crystal of porcine fructose-bisphosphatase that had been soaked in a solution of fructose 6-phosphate and phosphate,[195] as well as one of human fructose-bisphosphatase[196] and one of chloride peroxidase from *Curvularia inaequalis* that also catalyzes the hydrolysis of phosphate monoesters.[197] In the case of porcine fructose-bisphosphatase, the monomeric metaphosphate in the complex crystallized at pH 7 has the oxygen of a molecule of water 0.24 nm from the phosphorus, and in the case of chloride peroxidase, the monomeric metaphosphate has the nitrogen of the imidazole of a histidine 0.21 nm from the phosphorus. The van der Waals radii of phosphorus, nitrogen, and oxygen are 0.18, 0.16, and 0.15 nm, so these nucleophilic atoms are well within these radii. The length, however, of a phosphorus–oxygen bond is 0.16 nm, and the length of a phosphorus–nitrogen bond is 0.17 nm. It seems that in each case these nucleophiles are close enough to stabilize the monomeric metaphosphate by orbital overlap, but they are held by the active site too far from the respective phosphorus atoms to form covalent bonds.

Evidence for the production of monomeric metaphosphate during the solvolysis of 4-nitrophenyl phosphate in *tert*-butanol (Equation 1–70) is the **stereochemistry** of the product, *tert*-butylphosphate. To study the stereochemistry of a nucleophilic substitution at a phospho group in a simple monoester, its three oxygens can be labeled respectively with the three isotopes of oxygen: oxygen-16, oxygen-17, and oxygen-18. A single stereoisomer of the reactant can be synthesized, and the absolute stereochemistry of reactant and product can be determined.[198,199] Solvolysis of the dianion of 4-nitrophenyl phosphate in *tert*-butanol proceeds with complete **racemization** as expected for the production of free monomeric metaphosphate as an intermediate.[190]

Other examples of phosphomonoesters with good leaving groups are *N*-phosphopyridine (**1–59**) and *N*-phosphoguanidine (**1–60**)

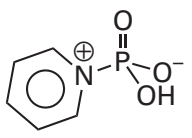

1–59

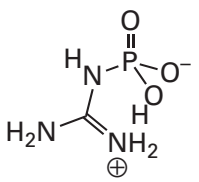

1–60

There are several features[200] of nucleophilic substitutions involving these types of leaving groups that were at one time explained[201] to be the result of the production of monomeric metaphosphate as an intermediate.[202-204] It has been demonstrated, however, that nucleophilic substitutions at phosphorus with these leaving groups nevertheless proceed with **inversion of configuration**.[200] Such nucleophilic substitutions at other monoesters of phosphoric acid with good leaving groups that proceed with inversion of configuration also seem to pass through a single transition state.[205]

Although these results rule out the existence of monomeric metaphosphate completely free of leaving group and nucleophile as an intermediate in these latter nucleophilic substitutions, they do not rule out the existence of monomeric monophosphate that is captured by the nucleophile before the leaving group has the time to diffuse away from the face from which it has dissociated. Such a situation would be analogous to the example of the intermediate complex between the leaving 4-bromoisoquinoline and the oxocarbenium ion of 2-deoxy-D-glucose in the nucleophilic substitution at 2-deoxy-β-D-glucopyranosyl-4′-bromoisoquinolinium (Equation 1–25). In nucleophilic substitutions of pyridylphosphates (**1–59**) either by other pyridines[205,206] or by oxyanions,[207] the transition state governing the observed rate constant seems to be one in which most of the bond (80%) between leaving group and phosphorus has been broken at the same time that only a small fraction (10%–20%) of the bond between nucleophile and phosphorus has been formed. As such, the transition state resembles monomeric metaphosphate sandwiched between the lone pairs of electrons of the two pyridines

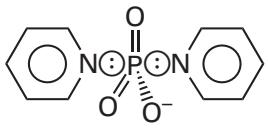

1–61

or of a pyridine and an oxyanion.

Between the two extremes of formation of an intermediate pentaoxyphosphorane and release of free unassociated monomeric metaphosphate are mechanisms in which the formation of the bond to the nucleophile and the disintegration of the bond to the leaving group are concerted, as in the nucleophilic substitutions of pyridylphosphates. The timing within such concerted processes can cause the disintegration of the bond to the leaving group to precede or to follow in some degree the formation of the bond to the nucleophile.

The result of such **differences in timing** is either a steady net decrease or a steady net increase, respectively, in the bond order of the phosphorus atom as the transition state is approached. As a result, the reaction may pass through a single transition state that is partly dissociative or partly associative in character, respectively. For example, for the nucleophilic substitutions of the phenols in a set of phenyl methyl diesters of phosphoric acid with pyridines and amines as nucleophiles,[208] the Brønsted coefficient for the leaving groups, β_{lg}, is –1.0 and the Brønsted coefficient for the nucleophile, β_{nuc}, is 0.35. These Brønsted coefficients suggest that disintegration of the bond to the leaving group is more advanced than formation of the bond to the nucleophile in the transition state, and that the central phospho group in the single, partly dissociative transition state resembles somewhat monomeric metaphosphate. If, however, breaking of the bond to the leaving group is synchronous with formation of the bond to the nucleophile, then the bond order to the phosphorus atom does not change during the process, the bond changes are balanced, and the transition state is neither dissociative nor associative.

Such an analysis can be performed on enzymatic nucleophilic substitutions at phosphorus. The Brønsted coefficient, β_{lg}, for nucleophilic substitution of the diphosphate of the appropriate nucleoside triphosphate by the hydroxy group on the 3′-hydroxy group at the 3′ end of an elongating single strand of DNA catalyzed by human DNA-directed DNA polymerase β could be determined. A series of analogues of the nucleoside triphosphate that adds to the 3′ end of the elongating single strand was synthesized in which the oxygen bridging the β and γ-phospho groups of the nucleotide is replaced with a series of methylenes substituted with fluoro, chloro, bromo, and methyl groups. These various substitutions alter the pK_a of the leaving bisphosphonate which replaces the diphosphate that is the usual leaving group during each step in the elongation. The Brønsted coefficient for the leaving groups, β_{lg}, assessed with these analogues is 0.77 when the nucleoside triphosphate has as its base a thymine, recognizing an adenine on the template.[209] This Brønsted coefficient suggests that the bond to the leaving group is mostly gone in the transition state.

As with nucleophilic substitution at an acyl group, the degree to which the bond to the nucleophile is formed and the degree to which the bond to the leaving group is broken in the transition state governing the observed rate constant for a nucleophilic substitution at phosphorus can be judged by the **Leffler coefficients**, α_{nuc} and α_{lg}, respectively (Equation 1–54). For example, for the transfer of a phospho group from a phosphotyrosine in a peptide, a **monoester**, to $MgADP^-$ catalyzed by non-specific protein-tyrosine kinase Csk, for which peptides with various aryl-substituted phosphotyrosines were synthesized as reactants, the Brønsted coefficient for the leaving groups, β_{lg}, for the rate constants of the enzymatic reaction[210] is –0.33. The Brønsted coefficient for the equilibrium constants for the transfer of a dianionic phospho group between two oxyanions[211] when the values of pK_a for the conjugate acids of the leaving groups are changed, $\beta_{eq,lg}$, is –1.36; that for the transfer of a monoanionic phospho group is –1.74; and that for the transfer of a neutral uncharged phospho group is –1.85. Consequently, the Leffler coefficient, α_{lg}, of around 0.2 was estimated from the Brønsted coefficient for the rates of the enzymatic reactions and the Brønsted coefficients for the equilibrium constants for phosphotransfer.

The Leffler coefficient for this nucleophilic substitution at phosphorus catalyzed by non-specific protein-tyrosine kinase Csk suggests that, in the transition state of the reaction catalyzed by the enzyme, the bond to the leaving group has dissociated by about 20%. The Leffler coefficient for the leaving group, however, is actually a measure of the degree to which a negative charge has accumulated on the leaving group in the transition state as the bond between the leaving group and the phosphorus dissociates. It has been shown that the enzyme is in the process of hydronating the leaving group as the bond is breaking.[212] Consequently, a Leffler coefficient of 0.2 would also be consistent with an almost complete dissociation of the bond between the leaving group and the phosphorus because this concerted hydronation could be neutralizing any accumulation of charge on the oxygen of the leaving group in the transition state.

For the nonenzymatic hydrolysis of **diaryl phosphate ions**,[213] the Brønsted coefficient, β_{lg}, is –1.0, and since the Brønsted coefficient for the equilibrium constant for the transfer of a monoanionic phospho group between two oxyanions, which is analogous to the transfer of an *O*-aryl-phospho group, is –1.74, it can be concluded that the bond to the leaving group in these latter nucleophilic substitutions has dissociated by about 60% in the transition state.

For the nonenzymatic nucleophilic substitutions of a series of aryloxy groups from a series of **aryl diethyl phosphates** by phenoxide anion,[214] the Brønsted coefficient, β_{lg}, is –0.5, and since the Brønsted coefficient for the equilibrium constant for the transfer of a neutral, nonanionic phospho group between two oxyanions, which is analogous to the transfer of an *O,O′*-diethylphospho group, is –1.85, it can be concluded that the bond to the leaving group in these latter nucleophilic substitutions has dissociated by about 30% in the transition state.

The three nucleophilic substitutions just discussed occur at a phosphomonoester, a phosphodiester, and a phosphotriester. In each case, the Leffler coefficients suggested that there was significant, but not complete, disintegration of the bond between phosphorus and oxygen of the leaving group in the transition state. Consequently, it can be concluded that each of these nucleophilic substitutions is concerted and that concerted mechanisms are possible for phosphotriesters as well as phosphodiesters and phosphomonoesters. Presumably this is also the case in nucleophilic substitutions at phosphorus in enzymatically catalyzed reactions. In a concerted reaction, the leaving group is always the oxygen on the opposite side of the phosphorus in line with the nucleophile, and pseudorotation is not an issue. Consequently, the leaving group is determined only by the alignment of nucleophile and phospho group.

The same **considerations that explain the relative timing** for formation of the bond to the nucleophile and for disintegration of the bond to the leaving group in nucleophilic substitutions at an acyl group apply for nucleophilic substitution at phosphorus. The more acidic the conjugate acid of the leaving group and the less nucleophilic the nucleophile, the more likely it is that formation of the bond to the nucleophile will lag behind disintegration of the bond to the leaving group in the transition state and the more likely it is that the phospho group will resemble monomeric metaphosphate in the transition state, until it becomes monomeric metaphosphate. The poor nucleophilicity of *tert*-butanol and the acidity of 4-nitrophenol ensured the production

of monomeric metaphosphate in the nucleophilic substitution of the former by the latter (Equation 1–70). The less acidic the conjugate acid of the leaving group and the more nucleophilic the nucleophile, the more likely it is that formation of the bond to the nucleophile will precede disintegration of the bond to the leaving group in the transition state and the more likely it is that the phospho group will resemble a pentaoxyphosphorane in the transition state, until it becomes a pentaoxyphosphorane. The use of hydroxide as a nucleophile and an alkoxy group as a leaving group in the nucleophilic substitution of 2-methoxy-1,3,2-dioxaphospholane 2-oxide in one case (Equation 1–66), and the use of the 2′-hydroxy group, the nucleophilicity of which is enhanced by approximation, as the nucleophile and an alkoxy group as a leaving group in the nucleophilic substitution of the monophenyl esters of 3′-uridylic acid in another case (Equation 1–68), ensured the production of a pentaoxyphosphorane.

In all the nucleophilic substitutions at phosphorus that have been discussed so far, there are three players: the nucleophile, the leaving group, and the electrophilic phosphorus. So far, the emphasis of the discussion has been on the properties of the nucleophile and the leaving group that determine the timing of formation of the new bond to the nucleophile and disintegration of the old bond to the leaving group. The **substituents on the other oxygens on the phosphorus** that are not the leaving group in a particular situation also affect the nucleophilic substitution. For example, in the nucleophilic substitutions at various triesters of phosphoric acid with several nucleophiles X

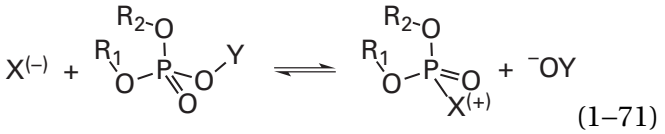

(1–71)

where YO^- is the leaving group, linear Brønsted plots demonstrate that the less basic are the alkoxide ions of the two uninvolved substituents, R_1O^- and R_2O^-, the larger is the rate constant for the nucleophilic substitution.[215] The basicity of an alkoxide ion is a reflection of the ability of the substituent on its oxyanion to stabilize its negative elementary charge; the less basic the alkoxide ion is, the more able the substituent is to stabilize its negative elementary charge. Consequently, the fact that the less basic alkoxy groups have faster rates demonstrates that the ability of the groups that do not leave, R_1O^- and R_2O^-, to stabilize the negative charge developing in the transition state is responsible for these increases in rate. In the active site of an enzyme, anything that makes a substituted oxygen on the phospho group that is not involved in the nucleophilic substitution better able to stabilize adjacent negative charge should increase the rate of the enzymatic reaction.

In situations in which the leaving groups are the same and the nucleophiles are the same, phosphomonoesters are more likely to produce monomeric metaphosphate because they yield its anionic conjugate base and in the ground state they have one or two oxyanions, depending on the pH, to push out the leaving group, and phosphotriesters are more likely to produce an intermediate pentaoxyphosphorane because they cannot give a monomeric metaphosphate as an intermediate and, in the ground state, they have fewer lone pairs of electrons on the uninvolved oxygens to push and they can never have an oxyanion to push.

As with any other type of nucleophilic substitution, the reaction coordinate and the transition state of each nucleophilic substitution at phosphorus fall at a particular point in a continuous spectrum of mechanism. As with a nucleophilic substitution at a tetrahedral, saturated carbon (Figure 1–4) or at an acyl group, this spectrum of mechanism can be appreciated by examining a **three-dimensional surface of potential energy** (Figure 1–15).[77,78] Again, one of the coordinates is the distance between the atom of the leaving group and the electrophilic phosphorus atom, and the other coordinate is the distance between the nucleophilic atom and the electrophilic phosphorus atom. The third coordinate is the potential energy of the system for each pair of coordinates.

In the case of a nucleophilic substitution at phosphorus, as was the case in a nucleophilic substitution at an acyl group, there is a significant well of potential energy in the **lower left corner** of the diagram because this is the position of the respective pentaoxyphosphorane, the pentavalent analogue of the tetrahedral intermediate. If the pentaoxyphosphorane is the most stable of all the possibilities, there will be two cols of potential energy: one between the reactants and the pentaoxyphosphorane, and the other between the pentaoxyphosphorane and the products.

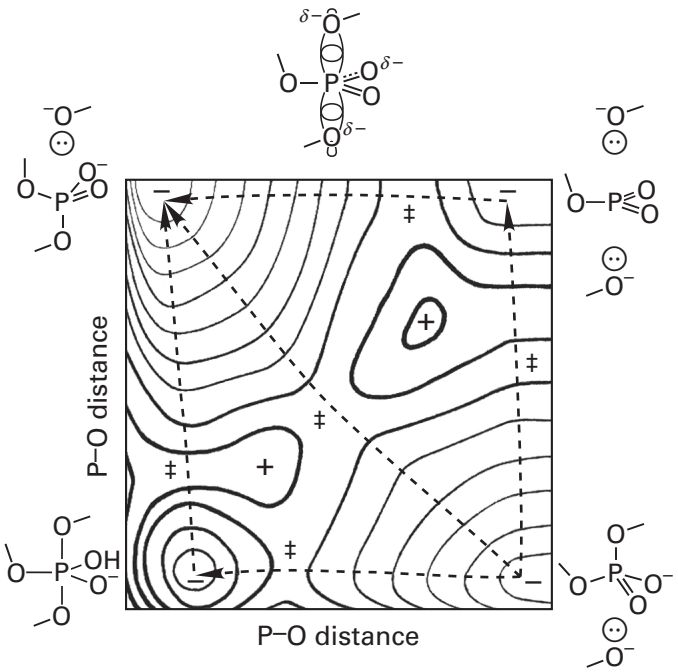

Figure 1–15: Hypothetical three-dimensional representation of a surface of potential energy[77,78] for nucleophilic substitution at phosphorus. The ordinate of the plot is the distance between phosphorus and the oxygen that is leaving during the substitution. The abscissa of the plot is the distance between phosphorus and the nucleophilic oxygen that is forming the new bond. The intersection of these two axes, for the sake of brevity, is not the point at which each has a value of zero, which would be a singularity of potential energy. The point of their intersection has coordinates or distances close to the values of the lengths of the respective covalent bonds: the bond between phosphorus and the oxygen that is leaving in the reactant and the bond between phosphorus and the nucleophilic oxygen that has formed the new bond in the product. The third dimension is the potential energy associated with each value for these two distances. The third dimension is represented topographically by contour lines of equal potential. These contour lines represent a sinuous surface of potential energy. The two topographic maps of potential energy are entirely hypothetical, do not represent the surface of potential energy for any reaction, and are intended only for demonstration. The positive signs identify peaks of potential energy, and the negative signs identify wells of potential energy. The usual sign (‡) for a transition state designates a minimum of potential energy between reactants and products at the col through which the reaction proceeds. The dashed, curved arrows indicate paths on which the reaction coordinate could pass as the reaction proceeds. In this case, three possible paths on which the reaction could proceed were arbitrarily given cols of about the same potential energy to illustrate the three possibilities. In the case of nucleophilic substitution at phosphorus, a pentavalent phosphorane is a possible stable intermediate, as opposed to a pentavalent carbon, so there is a well of potential energy when both distances are short (lower left corner). The species involved as reactants, intermediates, transition states, or products are represented outside the plots to the right (reactants or intermediate monomeric metaphosphate), to the left (intermediate phosphorane or products), or above (associative intermediate) the location of their respective potential energies. The three reaction coordinates are, in descending order of presentation, that for a reaction with monomeric metaphosphate as an intermediate, that for a concerted reaction in which the bond to phosphorus in the product is forming as the bond to phosphorus in the reactant is breaking, and that for a reaction with a phosphorane as an intermediate. Adapted with permission from reference 77. Copyright 1972 American Chemical Society. https://doi.org/10.1021/cr60280a004

The **upper right corner** in the three-dimensional surface of potential energy for the nucleophilic substitution at phosphorus is the location of a monomeric metaphosphate, the trivalent analogue of an acylium ion that occupies the upper right corner in a nucleophilic substitution at an acyl group or a carbenium ion or oxocarbenium ion that occupies the upper right corner in a nucleophilic substitution at a saturated carbon. If a monomeric metaphosphate is the most stable of all the possibilities, there will again be two cols of potential energy: one between the reactants and the monomeric metaphosphate, and the other between the monomeric metaphosphate and the products.

There is, however, always the possibility in a nucleophilic substitution at phosphorus that the lowest col in the surface of potential energy occurs when the bond between the nucleophile and the electrophilic phosphorus is partially formed while the bond between the electrophilic phosphorus and the leaving group is partially broken and that there is neither a pentaoxyphosphorane nor a monomeric metaphosphate as an intermediate. Such nucleophilic substitutions at phosphorus are **concerted nucleophilic substitutions**. The reaction coordinate in all these cases passes through only one col somewhere outside of the corners and has only **one transition state at this one col**.

Metallic cations can accelerate nucleophilic substitutions at phosphorus in solution. In solution, the rate of hydrolysis of thymidine 5′-(4-nitrophenyl)phosphate, an electrophilic phosphodiester, is linearly related to the concentration of the nucleophilic ion $Mg(H_2O)_5(OH)^+$.[216] The second-order rate constant for the reaction of this electrophile with this nucleophile is 5 times the second-order rate constant of the same electrophile with hydroxide even though the pK_a of its conjugate acid, $Mg(H_2O)_6^{2+}$ is only 11.4 rather than 15.74. The substitution of $H_2{}^{16}O$ with $H_2{}^{18}O$ in the solvent decreased the rate of this nucleophilic substitution at phosphorus by 3%, but this was less than the 6% decrease observed for the same nucleophilic substitution when the nucleophile was uncomplexed hydroxide. This latter result suggests that in the

presence of the complexed **Mg^{2+}**, the transition state has become more like a pentaoxyphosphorane.[179]

The rate constant for the hydrolysis of the complex between Mg^{2+} and 4-(4-morpholinyl)-1-phosphonopyridinium by $Mg(H_2O)_5(OH)^+$ is about 100 times greater than that expected from the basicity of the $Mg(H_2O)_5(OH)^+$.[217,218] It was proposed that in the case of this phosphoramide, the nucleophile is either a hydroxide held by one Mg^{2+}, coordinated by both of the anionic oxygens on the phospho group, or a hydroxide held between two Mg^{2+}, each coordinated by one of the two anionic oxygens of the phospho group

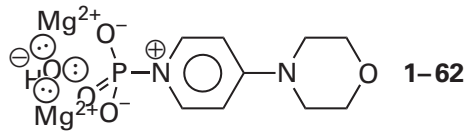

1–62

This proposal assumes that one or two four-membered rings in the transition state (each formed from the phosphorus, two oxygens, and a Mg^{2+}) are effective at positioning the hydroxide. In favor of this possibility, each bond angle at a Mg^{2+} between two coordinated oxygens is required by the octahedral coordination of Mg^{2+} to be 90°, the interior angle of a square.

Magnesium ion, although it is almost always involved in enzymatic nucleophilic substitutions at phosphorus, is not the sole metallic ion that can accelerate such nucleophilic substitutions. Metallic ions of transition metals can also do so.[219] A large organic chelating agent that simultaneously coordinates two **Zn^{2+}** accelerates[220] the hydrolysis of a series of alkyl esters of 3′-uridylic acid by a factor of 10^6, perhaps by a complex resembling that in **1–62**. The association of the phosphodiester, methyl 4-nitrophenyl phosphate, through its two phospho oxygens with a complex of two **Co^{2+}** accelerates[221] the nucleophilic substitution of its 4-nitrophenol by hydroxide by a factor of 10^{11}. The mechanism of the reaction, when it is catalyzed by this complex, is also different from the mechanism of the same reaction in the absence of the complex. The complex causes the reaction to pass through a pentaoxyphosphorane as an intermediate, while the same reaction in solution in the absence of the complex is concerted.[222] This same complex of two Co^{2+} also changes the mechanism of the hydrolysis of the phosphomonoester, 4-nitrophenyl phosphate, from one that passes through an almost dissociative nucleophilic substitution to a concerted nucleophilic substitution with significant bonding to both leaving group and nucleophile in the transition state,[223] which perhaps is stabilized by multidentate coordination of the two Co^{2+}. By associating with the anionic oxygens on a phospho group and decreasing their push, the two Co^{2+} may also shift the mechanisms of these nucleophilic substitutions in the direction of an intermediate pentaoxyphosphorane.

Nucleophilic substitutions at phosphorus catalyzed by the active sites of enzymes have the same spectrum of mechanism: those with intermediate pentaoxyphosphoranes,[179,180,224,225] those with intermediate monomeric metaphosphates,[195,226] and those with concerted mechanisms with no intermediate and a single transition state.[227] For example, the hydrolysis of ribonucleic acid (Equation 1–69) catalyzed by bovine ribonuclease, a reaction in which the nucleophile is enhanced by approximation and the leaving group is poor, passes through a pentaoxyphosphorane intermediate,[224] while the phosphorylation of tyrosines in proteins catalyzed by nonspecific protein-tyrosine kinase Csk, a reaction in which nucleophiles are poor and leaving groups are good, has monomeric metaphosphate as an intermediate.[210]

Regardless of whether the mechanism of a nucleophilic substitution at phosphorus proceeds through a phosphorane or monomeric metaphosphate or is concerted, in the intermediates and the transition state, respectively, the phosphorus and the three oxygens uninvolved in the substitution are all in the same plane and the bond angles between the three phosphorus–oxygen bonds are 120°. It has been pointed out that arginine side chains are often present in the active sites of enzymes catalyzing nucleophilic substitutions at phosphorus, and in many instances these side chains seem to form a cyclic structure with two of these uninvolved oxygens

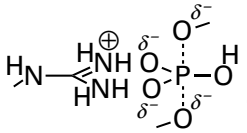

1–63

Presumably this cyclic structure stabilizes the intermediate or the transition state for that reaction.[228]

In at least two instances, it seems that the mechanism of a particular nucleophilic substitution at phosphorus is the same in solution as in the active site of an enzyme.[179,180,224,225,227,229] This result suggests, at least in these instances, that the enzyme does not change the relative timing of formation of the bond to the nucleophile and disintegration of the bond to the leaving group[195] while accelerating[1,2,4] both by factors as large as 10^{20}. There are enzymatic nucleophilic substitutions at phosphorus, however, that appear to employ different mechanisms than those for the same reactions in solution.[230] It seems also to be the case that in enzymatic active sites using metallic caions, usually Mg^{2+}, for the catalysis of nucleophilic substitutions at phosphorus, which is quite a common strategy, the mechanism could also be quite different from the same reaction in solution in the absence of metallic ions.[220] The metallic ion can enter the active site either alone or in complex with one or more of the phospho groups of the substrate.

Suggested Reading

Kluger, R., Covitz, F., Dennis, E., Williams, L. D., and Westheimer, F. H. (1969) pH–Product and pH–rate profiles for the hydrolysis of methyl ethylene phosphate. Rate-limiting pseudorotation, *J. Am. Chem. Soc. 91*, 6066–6072. https://doi.org/10.1021/ja01050a023

Davis, A. M., Hall, A. D., and Williams, A. (1988) Charge description of base-catalyzed alcoholysis of aryl phosphodiesters: A ribonuclease model, *J. Am. Chem. Soc. 110*, 5105–5108. https://doi.org/10.1021/ja00223a031

Lönnberg, H., Strömberg, R., and Williams, A. (2004) Compelling evidence for a stepwise mechanism of the alkaline cyclisation of uridine 3′-phosphate esters, *Org. Biomol. Chem. 2*, 2165–2167. https://doi.org/10.1039/B406926A

Formal Hydride Transfer

Each carbon in a metabolite serves as a representative of one of the five oxidation states of carbon. When a carbon is bonded only to other carbons and hydrogens and not participating in any π bonds, it is **fully reduced** and fully saturated at the **oxidation state of an alkane**. If one of the hydrogens on the carbon is replaced by a hydroxy group, an oxidation of that carbon has occurred. For example, the half-reaction for the oxidation of carbon 1 of butane catalyzed by butane monooxygenase (soluble) is*

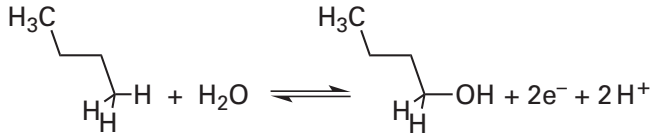

(1–72)

The carbon has undergone a **two-electron oxidation–reduction**. Carbon 1 of the resulting butan-1-ol is at the **oxidation state of an alcohol**. Alcohols can be turned into ethers, amines, thiols, and sulfides by nucleophilic substitution without any net oxidation or reduction. A carbon at the oxidation state of an alcohol can be identified in a molecule by the fact that it has one σ bond to a heteroatom and three other σ bonds to either carbon or hydrogen. If one of the carbons immediately adjacent to a carbon at the oxidation state of an alcohol bears a hydrogen, the two carbons can be converted into an alkene without any net oxidation or reduction

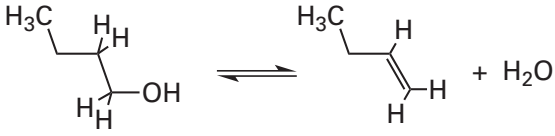

(1–73)

An alcohol can be oxidized to a ketone or an aldehyde, and in reverse, a ketone or an aldehyde can be reduced to an alcohol

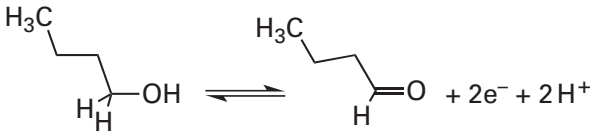

(1–74)

*Formally, Equation 1–72, although it is a balanced chemical equation, is the **half-reaction** of a complete oxidation–reduction. Just as hydrons are never free in solution as cations, electrons are free in solution as solvated electrons only under extraordinary circumstances unrelated to biochemical situations. Just as hydrons, when they are hydronium ions, are always associated with one or more molecules of water, each electron shown in a half-reaction is always associated with another molecule, which appears in the other half-reaction or one of the other half-reactions of the complete oxidation–reduction. In biochemical situations, it is almost always useful to present oxidation–reduction as two or more half-reactions because in this way it is clear where the electrons arose and where they have gone, and it distinguishes the particular molecules that are oxidized or reduced from the general carriers of electrons that receive or provide electrons as the other half of most of the oxidation–reductions in metabolism.

The carbon has undergone a two-electron oxidation–reduction. The carbon in a ketone or an aldehyde is at the carbonyl oxidation state and can be converted by nucleophilic addition or nucleophilic substitution into a hemiacetal, a hemiketal, an acetal, a ketal, a hemiaminal, a *gem*-diamine, an imine, a thiohemiacetal, a thiohemiketal, a thioketone, or a thioaldehyde (Table 1–1). These transformations do not involve any net oxidation or reduction. A carbon at the **carbonyl oxidation state** can be identified in a molecule by the fact that it has two σ bonds to either carbon or hydrogen and either two single σ bonds or a σ bond and a π bond, the two components of a double bond, to the heteroatoms oxygen, nitrogen, or sulfur.

An aldehyde or the derivative of an aldehyde can be oxidized to a carboxylic acid or an acyl derivative of a carboxylic acid, and in reverse, a carboxylic acid or an acyl derivative can be reduced to an aldehyde or the derivative of an aldehyde

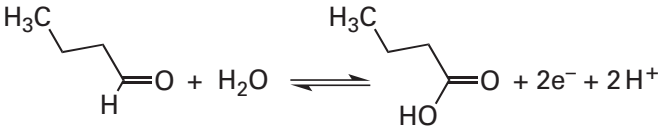

(1–75)

The carbon has again undergone a two-electron oxidation–reduction. Any carbon at the acyl oxidation state can be converted by nucleophilic substitution into an ester, an amide, an imidoester, an amidine, a thioester, a thiocarboxylic acid, or a thionoester, and none of these nucleophilic substitutions involves net oxidation or reduction. A carbon at the **acyl oxidation state** can be identified in a molecule as a carbon that has three bonds, either σ bonds or a mixture of σ bonds and π bonds, to heteroatoms and only one σ bond to carbon or hydrogen. Extreme examples of acyl carbons are the carbon in a nitrile (**1–64**) and the carbon in an ortho ester (**1–65**)

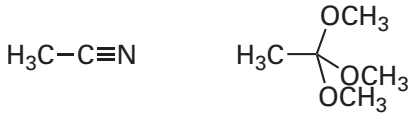

1–64 **1–65**

Formic acid or a derivative of formic acid can be oxidized to carbonic acid or a derivative of carbonic acid, and in reverse, carbonic acid or a derivative of carbonic acid can be reduced to formic acid or a derivative of formic acid

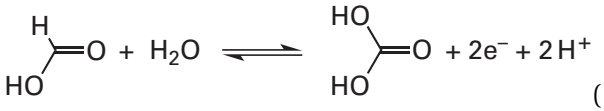

(1–76)

The carbon has again undergone a two-electron oxidation–reduction. For example

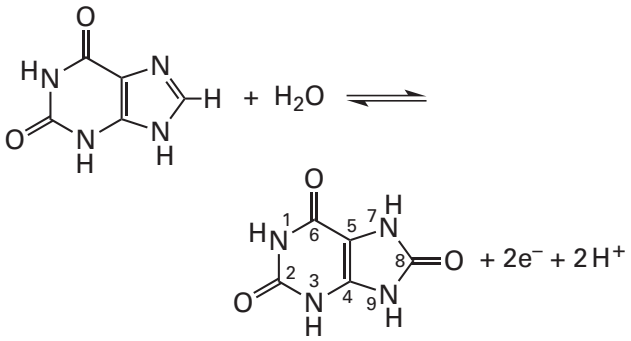

(1–77)

which is the half-reaction catalyzed by xanthine dehydrogenase. Any carbon at the carbonato oxidation state can be converted by nucleophilic substitution, nucleophilic addition, or elimination into carbon dioxide, a carbonato ester, a carbamate, a urea, a guanidine, a thiocarbonate, a thiocarbamate, or a thiourea, and none of these nucleophilic substitutions involves net oxidation or reduction. A carbon at the **carbonato oxidation state** can be identified in a molecule as a carbon that is entirely bonded to heteroatoms, as is carbon 8 of urate (Equation 1–77).

Most of the reactions that occur in metabolism can be placed into this scheme. There are **five oxidation states of carbon**. Within any one of these oxidation states, substrates are transformed by nucleophilic substitution, nucleophilic addition, and elimination. The transitions between any two of these oxidation states are oxidations and reductions that have their own distinct chemistry, which is represented by half-reactions indicating the removal or addition of electrons to the substrates.

In enzymatic reactions that change oxidation states, the oxidation–reductions connecting the oxidation state of an alcohol with the carbonyl oxidation state (Equation 1–74) and the carbonyl oxidation state with the acyl oxidation state (Equation 1–75) often involve the formal transfer of a hydride. A hydride is usually transferred from the nicotinamide ring in reduced **nicotinamide-adenine dinucleotide** (NADH) or reduced nicotinamide-adenine dinucleotide phosphate (NADPH) in one direction and transferred to the nicotinamide ring of oxidized nicotinamide-adenine dinucleotide

(NAD^+) or oxidized nicotinamide-adenine dinucleotide phosphate ($NADP^+$), in the other direction

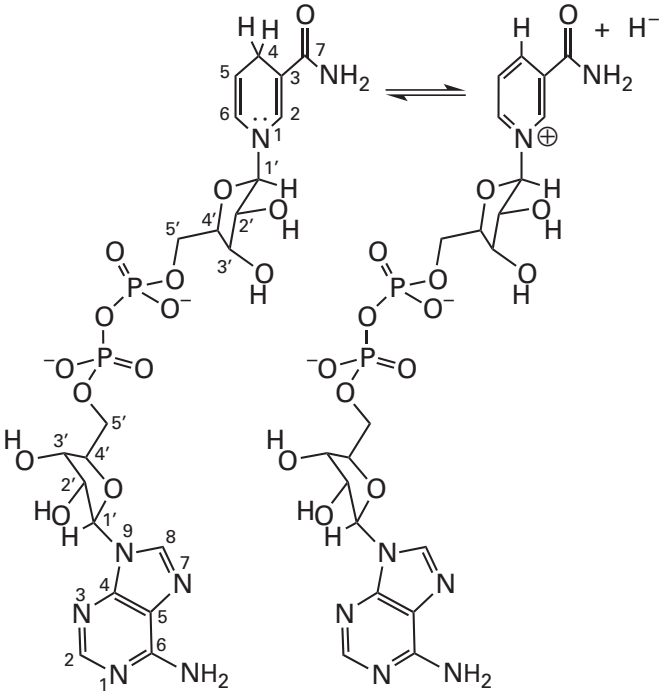

(1–78)

Nicotinamide-adenine dinucleotide phosphate (Figure 1–16),[166,231] which differs by only a 2′-phospho group on the adenosine, which is distant from the nicotinamide ring, performs chemistry that is identical to that performed by NADH, but each enzyme will have its own particular preference for one or the other of these hydride carriers.

A hydride never exists as a free hydride ion, just as a hydron never exists as a free hydron. Equation 1–78 can be written as a half-reaction

(1–79)

which indicates that the hydride that is transferred by NADH is equivalent to a hydron and two electrons, the latter of which also do not exist as free species in solution. Consequently, the half-reaction emphasizes the formality of the hydride transfer.

Just as a hydron, which is formally an electrophile, is transferred from one basic lone pair of electrons to another basic lone pair of electrons, a hydride, which is formally a nucleophile, is transferred from one electrophilic carbon (for example, carbon 4 of NAD^+ in Equation 1–78) to another electrophilic carbon (for example, the carbon on the substrate that is to be reduced). In the direction of reduction, the nucleophilic hydride is usually transferred to an electrophilic carbonyl carbon

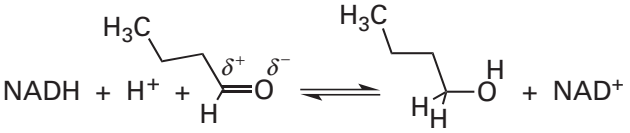

(1–80)

an electrophilic acyl carbon, or an electrophilic carbonato carbon in the substrate, so the reduction is formally a **nucleophilic addition to a carbonyl group, an acyl group, or the derivative of a carbonate.** Formation of the covalent bond between a hydride and the carbon reduces the carbon to the next lower oxidation state. In order for this to occur, the carbon is usually in a double bond to a heteroatom. In the reverse direction, the hydride is transferred from the carbon in the substrate that is to be oxidized to NAD^+, and that carbon is oxidized to the next higher oxidation state. There are also enzymes that use NADH to reduce an imine, such as pyrroline-5-carboxylate reductase

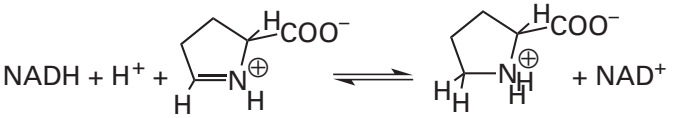

(1–81)

and enzymes that use NADH to reduce alkenes to alkanes.[232]

Usually an enzyme will catalyze the transfer of one hydride from one NADH to a carbonyl carbon, an acyl carbon, or a carbonato carbon to reduce it to a carbon at the oxidation state of an alcohol, a carbonyl carbon, or an acyl carbon, respectively, and vice versa. Hydroxymethyl-glutaryl-CoA reductase (NADPH), however, catalyzes an oxidation–reduction in which two hydrides are transferred consecutively from two molecules of NADPH to the same carbon, converting it from the acyl oxidation state down two levels to the oxidation state of an alcohol

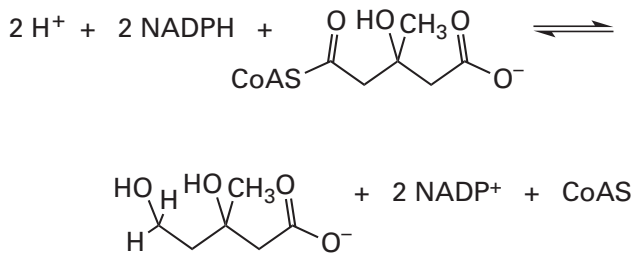

(1–82)

as can be done, much less specifically and only in the direction written, with lithium aluminum hydride.

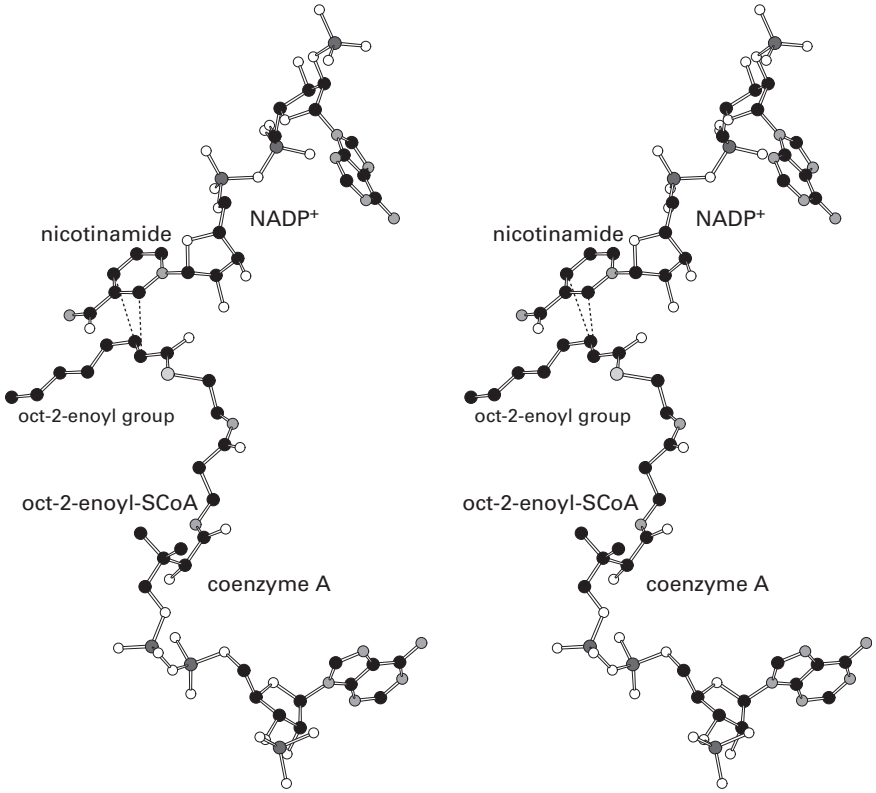

Figure 1-16: Stereodrawing[166] of the stacking of the π molecular orbital system of (*E*)-oct-2-enoyl-SCoA against the π molecular orbital system of $NADP^+$ in the crystallographic molecular model[231] of the active site of octenoyl-CoA reductase/carboxylase from *S. cinnabarigriseus*. Black atoms are carbons, white atoms are oxygens, small gray atoms are nitrogens, the large light gray atom is a sulfur, and the large dark gray atoms are atoms of phosphorus. The gene for octenoyl-CoA reductase/carboxylase from *S. cinnabarigriseus* was expressed in *E. coli* by using a plasmid that adds six histidines to its amino terminus. The protein was purified by the use of an adsorbent to which Ni^{2+} ions are coordinated and with which the histidines associate. After removal of the six histidines, the protein was submitted to molecular exclusion chromatography. A concentrated solution of the protein was crystallized in a buffer containing 10 mM $NADP^+$, 10 mM (*E*)-oct-2-enoyl-SCoA, and 50 mM $NaHCO_3$ at pH 8. A map of electron density was produced from the data set by molecular replacement. In the map of electron density, features were observed into which molecular models of $NADP^+$ and (*E*)-oct-2-enoyl-SCoA, respectively, could be inserted. These features identified the active site. After insertion of the molecular models, the crystallographic molecular model of the resulting complex between enzyme, $NADP^+$, and (*E*)-oct-2-enoyl-SCoA was refined against the data set. Only the molecular models of $NADP^+$ and (*E*)-oct-2-enoyl-SCoA as they are oriented by the active site are drawn. The nicotinamide of the $NADP^+$ and the oct-2-enoyl group and the coenzyme A portion of the (*E*)-oct-2-enoyl-SCoA are labeled. The π molecular orbital system of the oct-2-enoyl group consists of the oxygen, the acyl carbon, and the α and β carbons. The dashed lines connect the α carbon to carbon 2 of the nicotinamide and the β carbon to carbon 4 of the nicotinamide, respectively.

In these oxidation–reductions, **the NADH or the NADPH acts simply as the carrier of a hydride**, much as a catalytic acid acts as a carrier of a hydron. The hydride being carried exists as a lone hydrogen in a large molecule that seems unnecessarily elaborate to an organic chemist (Equation 1–78), but its large size permits it to be bound tightly and to be easily recognized by an enzyme. The extensive interactions between the enzyme and the elaborate substituent attached to the hydrogen atom can also provide free energy that can be used to decrease the free energy of activation of the enzymatic reaction. In its role as the carrier of a hydride, nicotinamide-adenine dinucleotide is a representative of a class of molecules known as coenzymes.

There are several terms that classify molecules, other than substrates, associating with an enzyme. These terms are relevant to oxidation–reductions catalyzed by enzymes, so they should be clarified here.

A **cofactor** is any ion, usually a metallic ion, or any organic molecule that is required by an enzyme for its function. A cofactor can be either a coenzyme, a functional group in a coenzyme, or a prosthetic group.

A **coenzyme** is a small molecule, relative to the enzyme itself, that associates and dissociates from the active site of an enzyme just as a substrate does and that transfers chemical groups, hydrogens, or electrons among active sites. In the case of NADH, the chemical group that is transferred is a hydride in the form of a hydrogen. In the case of *S*-adenosyl-L-methionine (Equation 1–19), another elaborate coenzyme, it is a methyl group, the one on the sulfur. A coenzyme is distinguished from the substrate or the substrates of an enzyme by its promiscuity. The same coenzyme serves the same role in a number of enzymatic reactions, each of which has different unrelated substrates. A coenzyme readily associates with and dissociates from the active site of an enzyme, just as rapidly as the other substrates, and it transfers chemical groups, hydrogens, or electrons within the active site to and from a substrate for that enzyme. A coenzyme enters the active site; donates or accepts the electron, the electrons, a hydrogen, or the chemical group; and then leaves the active site during a single turnover. In most of the enzymatic reactions in which they are involved, NAD^+, $NADP^+$, NADH, and NADPH are coenzymes, acting indistinguishably, except by formal definition, from the other substrates for the enzyme (Equation 1–80). Kinetically, they are the same as a substrate for the enzyme. Because every coenzyme, by definition, is required by at least one enzyme for its function, all coenzymes are cofactors.

Coenzyme A

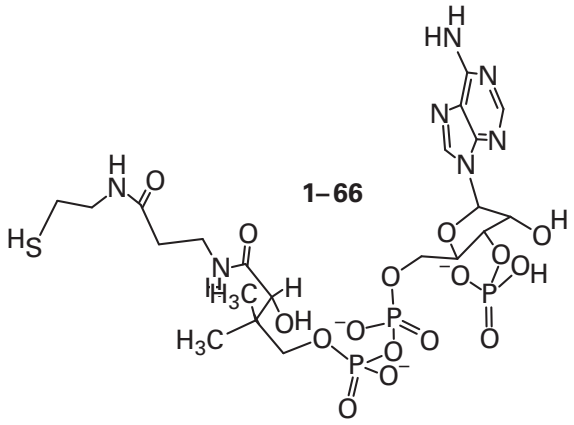

is another elaborate coenzyme. The chemical groups that **coenzyme A** is responsible for carrying between active sites are carboxylic acids. These carboxylic acids are thioesters at the lone sulfanyl group in coenzyme A.* An example of an ester of coenzyme A would be oct-2-enoyl-SCoA (Figure 1–16).[231] In addition to making it easier for an enzyme to recognize the particular thioester of coenzyme A that is its substrate and increasing the free energy of association between the active site and the thioester of coenzyme A, coenzyme A, because it is quite hydrophilic, also increases the solubility of the carboxylic acids that it carries, which are often quite hydrophobic. For example, coenzyme A carries fatty acids of fairly long chain lengths between active sites.

A **prosthetic group** is any group that is neither a protein nor a peptide that is either covalently or tightly attached to a protein and remains tightly bound to the protein for an extended period of time. When it is within the active site of an enzyme, a prosthetic group that is a cofactor for that particular enzyme remains fixed there through many turnovers. The prosthetic group either provides a catalytic group that is chemically unchanged during the enzymatic reaction, or it accepts or donates one or two electrons, a hydrogen, or a chemical group and then donates or accepts, respectively, one or two electrons, a hydrogen, or the chemical group

*Although the rule in IUBMB nomenclature for a thioester of coenzyme A is to append "-CoA" to the name of the acyl group, for example, oct-2-enoyl-CoA, in the current text, the "CoA" is replaced by "SCoA" to remind the reader that the compound discussed is a thioester of coenzyme A, for example, oct-2-enoyl-SCoA.

during a single turnover. At the end of that turnover, a prosthetic group that is a cofactor for the enzyme is chemically identical to its state at the beginning of that turnover. For example, NADH is a prosthetic group in a set of enzymes that catalyze the dismutation of aldehydes[233-236]

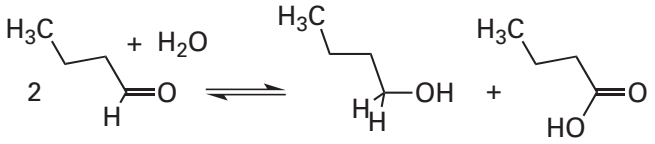

(1–83)

The reduced form of the enzyme, with NADH bound tightly in its active site as a prosthetic group, reduces the first aldehyde to the alcohol. The resulting oxidized form of the enzyme, now with NAD^+ in its active site, then oxidizes the second aldehyde to the carboxylic acid, regenerating the reduced form of the enzyme at the end of the complete turnover. There are prosthetic groups, such as lipids and oligosaccharides, that are attached covalently, or tightly but noncovalently, to a protein but that are not required by any enzymatic activity displayed by that protein. Consequently, unlike coenzymes, some prosthetic groups are not cofactors.

The positive formal elementary charge on the nitrogen of the nicotinamide ring in NAD^+ causes the 2, 4, and 6 positions on the ring to be electrophilic. This effect can be demonstrated by drawing resonance structures

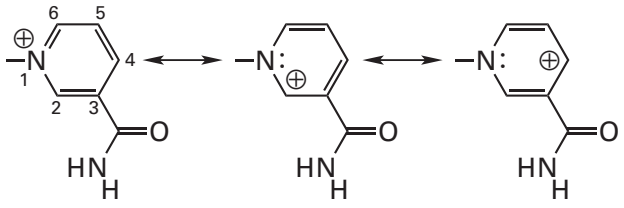

1–67

This enhanced electrophilicity permits carbon 4 in NAD^+ to be an effective acceptor of a formal, nucleophilic hydride.

This electrophilicity is also reflected in the tendency of carbon 4 of NAD^+ to **participate as an electrophile in nucleophilic additions** with carbon nucleophiles. Most of the reactions producing nucleophilic adducts of NAD^+ at carbon 4 are adventitious and counterproductive.[237,238] As part of its mechanism, however, the active site of urocanate hydratase, which catalyzes the hydration of urocanate

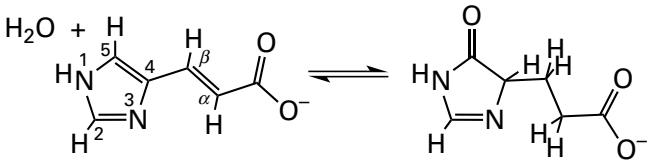

(1–84)

forms adduct **1–68** [239]

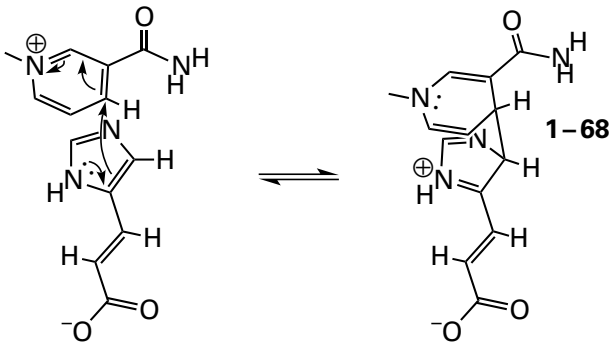

(1–85)

by an electrophilic aromatic addition between carbon 4 of NAD^+, which is the electrophile, and carbon 5 on urocanate, which is within an aromatic ring and hence nucleophilic. Because the NAD^+ in urocanate hydratase is a prosthetic group that never leaves the active site of the enzyme, the adduct must form and unform within the active site during each turnover of the enzyme.

Evidence for the existence of this **covalent intermediate** in the normal enzymatic reaction is the fact that the saturated analogue of urocanate, 3-imidazolylpropionate, forms an analogous electrophilic adduct in the active site of urocanate hydratase from *Pseudomonas putida* that cannot proceed further in the enzymatic reaction because of the lack of a double bond between the α carbon and the β carbon and can be trapped by oxidation with 5-methylphenazinium methyl sulfate

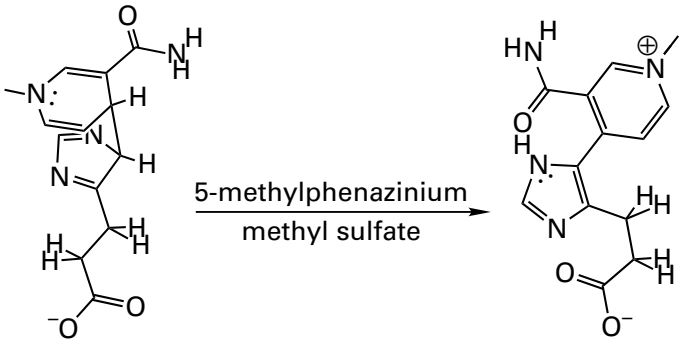

(1–86)

The stable oxidized product could be isolated[240,241] and its identity was verified by nuclear magnetic resonance spectroscopy.[242]

The electrophilicity of carbon 4 of NAD^+ is at its greatest when the **carbamoyl group on the nicotinamide** is in the conformation in which its acyl oxygen is syn to carbon 4 (the conformation shown in Equation 1–78 and **1–67**), and even though the syn conformation is the less stable, the carbamoyl group is usually held within ±30° of the planar syn conformation within the active sites[243,244] of enzymes having NAD^+ as a coenzyme (Figure 1-16). Coenzyme F_{420}

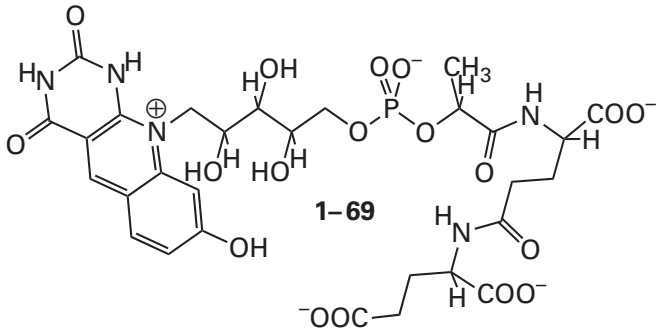

a formal hydride carrier from methanogenic bacteria,[245,246] contains an elaboration of nicotinamide that has a two-electron reduction potential (–0.36 V) similar to that of NAD^+ (–0.33 V) and a structure that locks the acyl oxygen of the analogue of the carbamoyl group of NAD^+ in the conformation in which it is syn to and in the plane of the carbon that is the analogue of carbon 4 of NAD^+.

Upon the reduction of NAD^+ by addition of a hydride to carbon 4, the aromatic π molecular orbital system is broken. Carbon 4 becomes saturated and can no longer support a *p* orbital. A partial compensation for the loss of aromaticity during the reaction is the formation of an extended π molecular orbital system that includes the exocyclic carbamoyl group, the two carbon–carbon double bonds, and the nitrogen within the ring

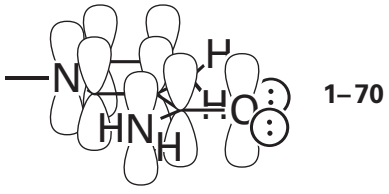

This π molecular orbital system provides an unbroken, acyclic, terminally bifurcated set of 8 *p* orbitals that mix to form a π molecular orbital system containing 10 *p* electrons. This π molecular orbital system explains the fact that the six atoms in the ring, the three atoms in the amide, and the carbon of the functional group attached to the nitrogen in the ring are in the same plane in NADH.[247-249] This extended π molecular orbital system is responsible for the absorbance displayed by NADH or by its phospho derivative, NADPH, at 339 nm.[250]

Oxidized nicotinamide in NAD^+ is aromatic, so all its bonds are of equal length.[251] The **bond lengths** in NADH, however, reflect the uneven distribution of **bond order** over the seven bonds in its molecular orbital system. If the lengths of the bonds in reduced nicotinamide are compared to the lengths of the same bonds in oxidized nicotinamide, the bonds between carbons 2 and 3 and between carbons 5 and 6 each shorten by 0.007 nm to a length equal to the bond length of a normal carbon–carbon double bond,[248] while the bonds between nitrogen 1 and carbon 2 and between nitrogen 1 and carbon 6 each lengthen by 0.007 nm.[248,249] These changes demonstrate that the carbon–carbon bonds gain bond order while the carbon–nitrogen bonds lose bond order upon reduction of nicotinamide (see Equation 1–78). The increase in bond order explains the fact that the double bond between carbons 5 and 6 in NADH is susceptible to hydration[252] as well as an oxidation that converts it to the diol.[253]

The observed bond lengths and bond orders in NADH can be understood by drawing **resonance structures**. Those resonance structures containing double bonds between carbon and nitrogen within the ring are unfavorable relative to the usually drawn resonance structure for NADH (Equation 1–78) because of separation of charge and cross-conjugation

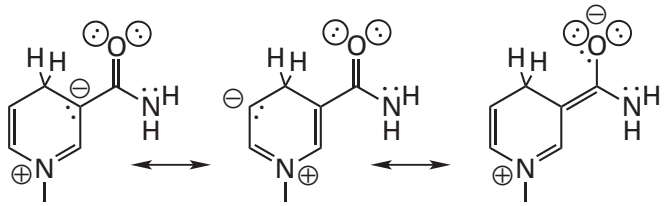

The substrate from which a hydride is to be removed by NAD^+ almost always has at least one lone pair of electrons on an oxygen or a nitrogen that can provide push to the leaving hydride.[254]

This lone pair of electrons can be on an oxygen or a nitrogen that is either attached directly to the carbon to be oxidized or conjugated to that carbon by one or more π bonds

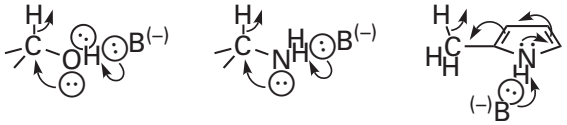

1–72 **1–73** **1–74**

It must be a lone pair of electrons that can be positioned periplanar to the σ bond between the carbon and the hydrogen. This push causes the hydrogen that is to be removed to be more electron-rich and more nucleophilic.

It is also important to have a **hydron on this heteroatom providing the push** before the oxidation takes place rather than an alkyl group so that, as the hydride leaves, that hydron can be simultaneously removed to increase further the nucleophilicity of the lone pair of electrons that is providing the push. The hydron is removed from a lone pair of electrons orthogonal to the pair providing the push. For example, in the active site of ovine phosphogluconate dehydrogenase ($NADP^+$-dependent, decarboxylating), Lysine 183 is responsible for removing the hydron from the 3-hydroxy group of 6-phospho-D-gluconate while the hydrogen on carbon 3 of 6-phospho-D-gluconate is removed by $NADP^+$. The 6-amino group of Lysine 183 is aligned so that it participates in a linear hydrogen bond only when the hydroxy group is in a rotational conformation that places one of its two lone pairs antiperiplanar to the hydride that is being transferred (Figure 1–17).[166,255] When Lysine 183 is mutated to any other amino acid, even to arginine, the rate of the enzymatic reaction decreases by a factor of 1000 or more.[256] In the active site of glucose-6-phosphate dehydrogenase ($NADP^+$) from *Leuconostoc mesenteroides*, Histidine 240 is responsible for removing the hydron from the hydroxy group on carbon 1 of the hemiacetal of D-glucose 6-phosphate while the $NADP^+$ removes the hydrogen from carbon 1. When Histidine 240 is mutated to an asparagine, the rate of the enzymatic reaction decreases by a factor of 50,000.[257] In alcohol dehydrogenase from *Saccharomyces cerevisiae*, however, the hydroxy group of the alcohol is a ligand to a Zn^{2+} ion. This Zn^{2+} lowers the pK_a of the hydroxy group sufficiently so that it has already lost its hydron to form the zinc alkoxide by the time the NAD^+ removes the hydrogen from the adjacent carbon. The Zn^{2+} is placed in the active site in such a way that a lone pair of electrons on the oxyanion, other than the one coordinating the Zn^{2+}, ends up antiperiplanar to the hydrogen that is being removed.[258]

In **aldehydes**, a similar arrangement of hydrogen, carbon, heteroatom, lone pair of electrons, and orthogonal hydron is achieved by forming a hemiacetal, an aminal, a hemiaminal, or a thiohemiacetal

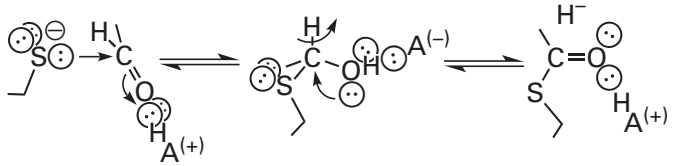

(1–87)

In the **reverse reaction**, the substrate to which a hydride is to be added by NADH or NADPH almost always contains a carbonyl group, an imino group, or an acyl group. This group in the substrate either itself contains the sp^2 carbon to be reduced or is conjugated to that sp^2 carbon by one or more π bonds. Because the sp^2 carbon to be reduced is either in or conjugated to a carbonyl, imino, or acyl group, it is already electrophilic, but its electrophilicity is usually increased by hydronating the oxygen or the nitrogen of the carbonyl, imino, or acyl group as the hydride is being transferred to it (reverse of Equation 1–87). Again, the lone pair of electrons that is being hydronated is in the σ plane of the carbonyl, imino, or acyl group, orthogonal to its π system.

For a reduction accomplished by NADH of an isolated, unconjugated carbonyl group or acyl group in one direction, or for an oxidation accomplished by NAD^+ of an isolated, unconjugated alcohol or hemiacetal in the other direction, the transition state is formed by mixing all nine *p* atomic orbitals of the nicotinamide ring, the *s* atomic orbital of the hydrogen, and the *p* atomic orbitals of the carbonyl or acyl group that is either the reactant in the reduction or the product in the oxidation.

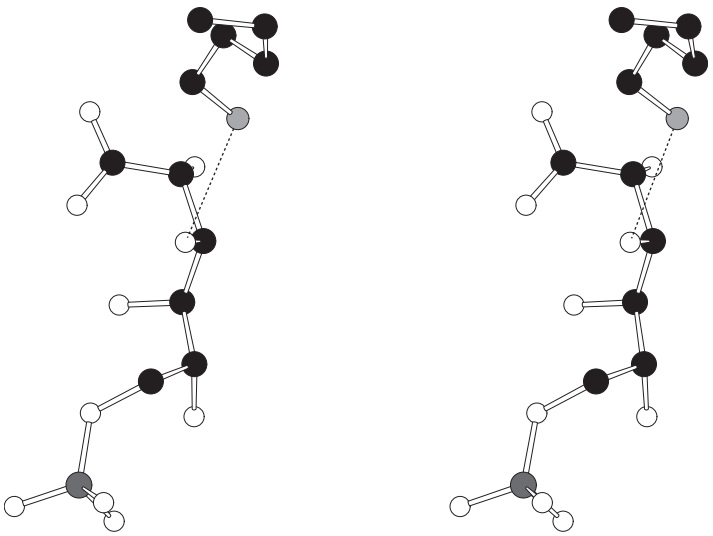

Figure 1–17: Stereodrawing[166] of the orientation of the hydrogen bond between the 3-hydroxy group of the substrate 6-phospho-D-gluconate and Lysine 183 in a crystallographic molecular model of the active site of ovine phosphogluconate dehydrogenase ($NADP^+$-dependent, decarboxylating).[255] Black atoms are carbons, white atoms are oxygens, the small gray atom is a nitrogen, and the large dark gray atom is a phosphorus. The purified enzyme was crystallized from a solution containing 30 mM 6-phospho-D-gluconate. The drawing is of the 6-phospho-D-gluconate bound in the active site of the crystallographic molecular model and the side chain of Lysine 183. In the orientation drawn, the carbon–hydrogen bond on carbon 3 of the 6-phospho-D-gluconate is horizontal and in the plane of the page. Because it is hybridized sp^3, the 3-hydroxy group is held by the hydrogen bond to the 6-amino group of the lysine in a conformation in which one of its lone pairs of electrons is antiperiplanar to the hydrogen on carbon 3 that is to be removed.

In the case of a simple, unconjugated carbonyl group, 12 atomic orbitals are mixing

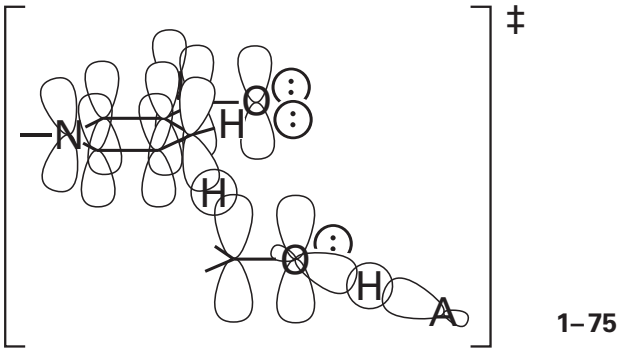

1–75

to produce the 12 molecular orbitals of the transition state, and the 14 electrons fill the seven molecular orbitals of lowest energy. A hydron is usually being removed from or added to, respectively, the oxygen at one of its lone pairs of electrons, which is orthogonal to the molecular orbital system of the rest of the transition state.

At the beginning of the reaction between NAD^+ and a substrate from which a hydride is to be removed, there are two **initial overlaps of molecular orbitals**.[259] One is between the lowest unoccupied molecular orbital of the cation of the nicotinamide and the occupied bonding molecular orbital of the hydrogen–carbon σ bond of the substrate. The other is between the unoccupied antibonding orbital of the carbon–hydrogen bond and the sp^3 atomic orbital on the oxygen occupied by a lone pair of electrons

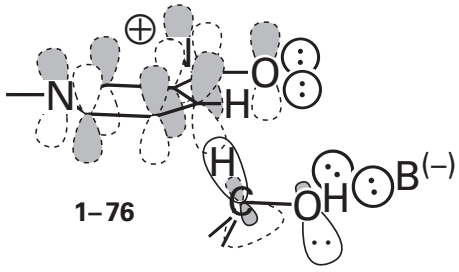

1–76

where gray shading indicates phase within the molecular orbitals and dashed outline indicates antibonding molecular orbitals. The overlap of the unoccupied antibonding molecular orbital of the carbon–hydrogen bond with the occupied atomic orbital of the lone pair of electrons provides the push.

In the reverse direction, at the beginning of the reaction between NADH and a substrate to which a hydride is to be added, there are also two **initial overlaps of molecular orbitals**.[260] One is between the highest occupied molecular orbital of the linear, bifurcated π molecular orbital system of the reduced nicotinamide ring (**1–70**) and the unoccupied antibonding orbital of the σ bond between carbon 4 of the nicotinamide and the hydrogen that will be transferred. This antibonding orbital accepts electron density from the π molecular orbital system of the NADH and will become a p orbital on that carbon in the eventual aromatic system of the NAD^+. The other is between the occupied bonding molecular orbital of the σ bond between carbon 4 of the nicotinamide and its hydrogen and the unoccupied antibonding molecular orbital of the π bond between the carbon and the oxygen of the carbonyl group

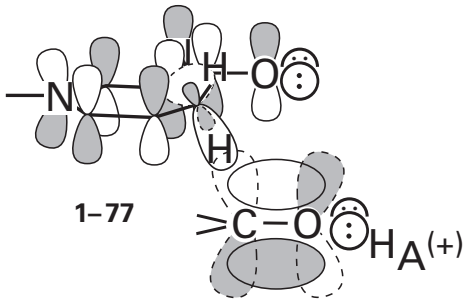

1–77

as is the case with any nucleophile (**1–17**).

Consistent with these assignments, the **favored stereochemistry in the transition state** (**1-75**) for the transfer of a hydride between two electrophilic carbons is one in which the hydrogen being transferred is on a line of centers between the two carbons. This line of centers makes 115° angles with the two σ planes of the respective electrophilic carbons: the plane of the nicotinamide ring and the plane of the carbonyl group. In the transition state, the two carbons are 0.26 nm apart.[261,262]

This favored stereochemistry has been **observed in crystallographic molecular models** of active sites occupied by a substrate and NADH or NAD^+. UDP-Glucose 4-epimerase from *E. coli* catalyzes the epimerization of carbon 4 in the D-glucosyl group in UDP-D-glucose

$$\text{UDP-glucose} \rightleftharpoons \text{UDP-galactose} \qquad (1\text{–}88)$$

In this enzymatic reaction a hydride is removed from carbon 4 of the UDP-D-glucose or UDP-D-galactose by the prosthetic NAD^+ in the active site of the enzyme and then added back to the 4-oxo group of the resulting UDP-4-dehydro-D-glucose with the epimeric stereochemistry, after it has flipped over, to produce the product.[263] In the crystallographic molecular model of the inactive complex between

UDP-glucose 4-epimerase, NADH, and UDP-D-glucose,[264] in which **reduced substrate is paired with reduced coenzyme**, the angle between the carbon–oxygen bond at carbon 4 of D-glucose and the line of centers between carbon 4 of the nicotinamide and carbon 4 of D-glucose is 125° (Figure 1–18).[166,264] In this complex, the distance between the two carbons (0.37 nm) cannot be 0.26 nm because each carbon has a hydrogen on it and they butt up against each other rather than one hydrogen passing between the carbons. The plane of the nicotinamide ring of the NAD^+ makes an angle of 145° with the line of centers rather than the ideal 115°, perhaps because the abutting hydrogens shift the nicotinamide ring from its ideal position. A similar orientation and distance between the carbon from which the hydride is removed and carbon 4 of the nicotinamide is observed in the crystallographic molecular model between shikimate, NADPH, and shikimate dehydrogenase ($NADP^+$) from *Thermus thermophilus*[265] and in the crystallographic molecular model[266] between GDP-D-glycero-α-D-*manno*-heptose, NADH, and GDP-D-glycero-α-D-*manno*-heptose 4-dehydrogenase[267] from *Campylobacter jejuni*. Again, these are complexes between reductant and reductant.

Reduced coenzyme F_{420} (**1–69**) is used by methylenetetrahydromethanopterin dehydrogenase to reduce 5,10-methenyltetrahydromethanopterin at its methenyl carbon. In a crystallographic molecular model of the active site of this dehydrogenase from *Methanopyrus kandleri* occupied by 5,10-methylenetetrahydromethanopterin, the reduced substrate, and reduced coenzyme F_{420}, the hydride on the reduced coenzyme F_{420} points directly at the methylene carbon of 5,10-methylenetetrahydromethanopterin.[268] In this orientation it would be poised for the direct transfer of a hydride to the methenyl carbon if the active site were occupied by 5,10-methenyltetrahydromethanopterin, the oxidized reactant, instead of 5,10-methylenetetrahydromethanopterin.

Dihydroflavonol 4-reductase from *Vitis vinifera* uses NADH to reduce the carbonyl group in (+)-dihydroquercetin. In the crystallographic molecular model of the inactive ternary complex between (+)-dihydroquercetin, NAD^+, and the enzyme, in which **oxidized substrate is paired with oxidized coenzyme**, the line of centers between carbon 4 of the nicotinamide ring of NAD^+ and the carbon of the carbonyl group makes an angle of 105° with the plane of the nicotinamide ring and an angle of 90° with the σ plane of the carbonyl group of (+)-dihydroquercetin. The dihedral angle between the plane of the nicotinamide ring and the plane formed by the carbon of the carbonyl group, nitrogen 4 of the nicotinamide, and carbon 1 of the nicotinamide is 81°, instead of 90° as in **1–75**, and the distance between the two carbons is 0.30 nm.[269] This latter distance is determined by the fact that the π electrons in the carbonyl group of (+)-dihydroquercetin and the π electrons in the aromatic nicotinamide ring of NAD^+ cannot approach any closer because of electron repulsion in the ground state. A similar orientation of the carbon from which a hydride is normally removed and carbon 4 of the nicotinamide can be found in a molecular model for the complex between the active site of L-glutamate γ-semialdehyde dehydrogenase from *T. thermophilus*; NAD^+, the oxidized coenzyme; and the thioester between the substrate L-glutamate and a cysteine, the oxidized intermediate in the enzymatic reaction.[270]

When oxidant is mixed with reductant, however, to form the active complex between NADH and oxidized substrate or between NAD^+ and reduced substrate, the pucker of the reduced nicotinamide at carbon 4 in the former complex or the sp^3 hybridization of the α carbon of the alcohol in the latter complex should shorten the distance between these two carbons.[271] A superposition of NADPH, in the crystallographic molecular model of its complex with dihydrofolate reductase from *E. coli*

$$\text{NADPH} + \text{7,8-dihydrofolate} + H^+ \rightleftharpoons \text{5,6,7,8-tetrahydrofolate} + NADP^+ \quad (1\text{–}89)$$

and folate (an alternative substrate for the enzyme), in the crystallographic molecular model of its complex with dihydrofolate reductase, suggests that in the productive complex between this enzyme, folate and NADPH, carbon 4 of the nicotinamide ends up 0.28 nm away from carbon 6 of the folate,[272] almost the ideal distance for the transfer of a hydride. This juxtaposition, in part, explains why the transfer of the hydride from NADPH to 7,8-dihydrofolate has a rate constant[273] of 940 s^{-1}.

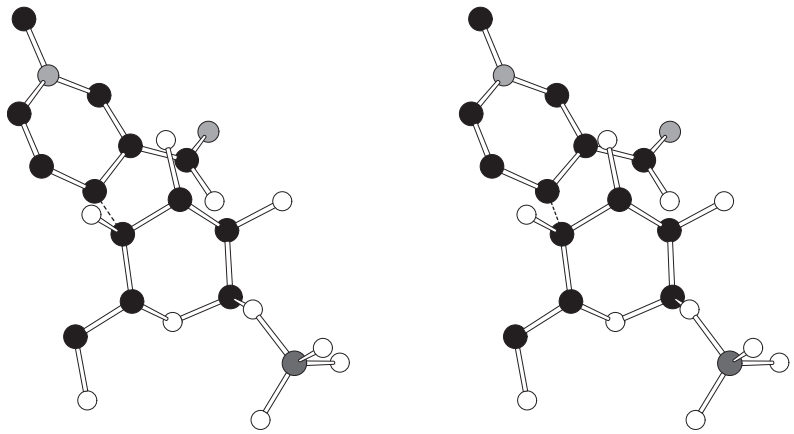

Figure 1–18: Stereodrawing[166] of the in-line transfer of a hydride between carbon 4 of a D-glucosyl group and carbon 4 of the nicotinamide of NADH.[264] Black atoms are carbons, white atoms are oxygens, small gray atoms are nitrogens, and the large dark gray atom is a phosphorus. UDP-Glucose epimerase, purified from *E. coli* with tightly bound NAD^+ at its active site, was mixed with the complex of dimethylamine and borane to reduce the NAD^+ to NADH. UDP-D-Glucose was then added to form a complex at the active site containing both NADH and UDP-D-glucose, reductant and reductant. This complex between the enzyme, NADH, and UDP-D-glucose was crystallized, and a crystallographic map of electron density was calculated. In the active site, a segment of electron density, into which could be inserted a molecular model of UDP-D-glucose, was situated adjacent to the electron density previously assigned to the nicotinamide group of NAD^+. The D-glucose 1-phosphate from UDP-D-glucose and the nicotinamide from NADH (Equation 1–78) in the resulting refined crystallographic molecular model are presented, with NADH to the upper left and the D-glucose 1-phosphate to the lower right. A dotted line is drawn between carbon 4 of the D-glucose 1-phosphate and carbon 4 of the nicotinamide.

Perhaps the most dramatic demonstration of the stereochemistry of hydride transfer is that occurring intramolecularly within (3*S*)-5-(3-carboxy-3-hydroxypropyl)nicotinamide-adenine dinucleotide

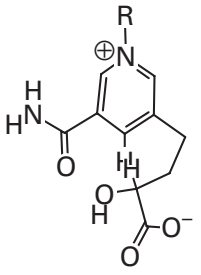

1–78

R ≡ 5′-[(*β*-adenosyl)diphospho]ribosyl

which is a substrate for the enzyme L-lactate dehydrogenase[274]

$$NAD^+ + \text{L-lactate} \rightleftharpoons NADH + H^+ + \text{pyruvate} \qquad (1\text{–}90)$$

When **1–78** is the reactant, the transfer of the hydride occurs intramolecularly. This molecule, in which substrate and coenzyme are fused, fits snugly into the active site of the crystallographic molecular model of the porcine enzyme with the hydrogen that is transferred during the enzymatic reaction immediately adjacent to carbon 4 of the nicotinamide ring in the conformation drawn above for **1–78**.[275] When **1–78** is held by the enzyme in this conformation competent for hydride transfer, the distance between the exocyclic carbon of the alcohol that is to be oxidized and carbon 4 of the oxidized nicotinamide is 0.23 nm. The angle between the line of centers connecting these two atoms and the carbon–oxygen bond of the exocyclic carbonyl group is 105°, but the angle between the line of centers and the plane of the nicotinamide is again about 145°. In the crystal, the hydride is being transferred back and forth between the two carbons continuously.

When the electrophilic carbon in the oxidized form of a substrate is located in a conjugated portion of the substrate for a particular enzyme, the planar *π* molecular orbital system of that substrate often forms a parallel stack with the *π* molecular orbital system of the nicotinamide ring when it is bound in the active site of the enzyme responsible for the oxidation–reduction. A simple example would be that found in the crystallographic molecular model of the active site of octenoyl-CoA reductase/carboxylase from *Streptomyces cinnabarigriseus* when it is occupied by $NADP^+$ and oct-2-enoyl-SCoA (Figure 1–16).[231] In this case, oxidized coenzyme is paired with oxidized substrate. The *π* molecular orbital system, consisting of the first four atoms of the *α*,*β*-unsaturated thioester (the acyl oxygen, the acyl carbon, and the double bond of the oct-2-enoyl group), is found stacked against the aromatic *π* molecular orbital system of the oxidized nicotinamide. The space between the two planes is about 0.34 nm, the usual distance between stacked *π* molecular orbital systems such as those in the stack of nucleotide bases in DNA.

In the crystallographic molecular model of the inactive complex between D-2-hydroxyacid dehydrogenase (NAD^+) from *Lactobacillus casei*, NAD^+, and 2-oxoisocaproate,[276] which is inactive because oxidant is paired with oxidant, the distance between the two electrophilic carbons (0.36 nm) again is not 0.26 nm because, in this instance, the *π* molecular orbital system of the unconjugated oxo group in 2-oxoisocaproate also stacks upon the *π* system of the NAD^+, forcing the carbon–oxygen double bond to sit 0.34 nm above the plane of the ring.

If the substrate has a planar unsaturated ring, its planar *π* molecular orbital system usually tends to form a stack with the nicotinamide of the NADH or the NAD^+ when they are associated with the active site of an enzyme responsible for its oxidation–reduction. A paradigm of this type of arrangement for a cyclic substrate is observed in the crystallographic molecular model of the complex between IMP dehydrogenase from *Tritrichomonas foetus* and its substrates. Inosine monophosphate dehydrogenase catalyzes the reaction

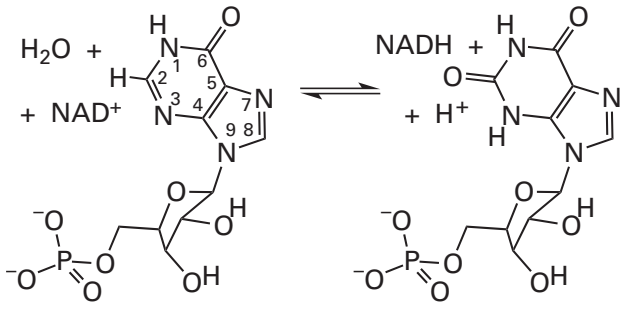

(1–91)

in which a derivative of formic acid is oxidized to a derivative of carbonic acid. In the crystallographic molecular model of the inactive complex between the enzyme, NAD^+, and xanthosine monophosphate, in which again oxidant is paired with oxidant and electrophile with electrophile, xanthine is stacked

flat against the nicotinamide (Figure 1–19).[166,277] The distance between the planes of the two rings is again 0.34 nm. As before, this distance is enforced by the van der Waals widths of the π molecular orbital system of the two rings.

There are **several problems** with all these arrangements in which the π molecular orbital systems stack upon each other. First, the carbons between which the equivalent of a hydride is transferred, carbon 4 of nicotinamide and carbon 2 of xanthine, necessarily end up 0.34 nm apart, and because of **the van der Waals surfaces of the rings**, there seems to be no way they can approach within the necessary 0.26 nm. Second, carbon 2 of the xanthine in xanthosine monophosphate ends up in the complex directly below carbon 4 of nicotinamide in the NAD^+ (Figure 1–19) so that the **angles between the line of centers** and the respective planes of the two rings are both within 10° of 90°. Finally, the most crucial violation is that the hydride is not on the line of centers between the two atoms between which it is to be transferred.

In these stacked complexes—those in which the ring of NAD^+ stacks upon the π molecular orbital system of a extended linear conjugated arrangement, those in which the ring of NAD^+ stacks upon a carbonyl group or an acyl group, and those in which the ring of NAD^+ stacks upon an unsaturated ring—it seems that there should be a **different mechanism operating** for the transfer of the equivalent of a hydride.

It is possible for the reduction of NAD^+ or the oxidation of NADH to occur in **two consecutive one-electron steps**. In organic solvents,[278] mixtures of water and organic solvents,[279,280] and aqueous solution,[281] NADH participates in one-electron oxidations[279-281] and NAD^+ participates in one-electron reductions,[278,282,283] either at the surface of an electrode[278] or with one-electron oxidants or reductants such as ferricyanide,[279] ferrocenium ion,[280] *N,N,N′,N′*-tetramethyl-4-phenylenediamine radical cation,[281] or hydrated electrons.[282,283]

The reduction potential for the one-electron reduction of NAD^+ to form the neutral radical

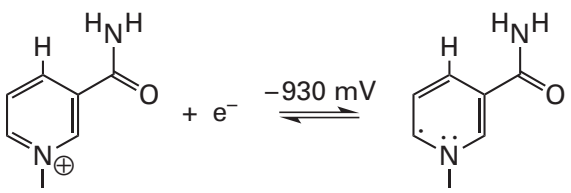

(1–92)

is –930 mV,[280,282,283] and the reduction potential for one-electron reduction of the radical cation of NADH to form NADH is –970 mV.[280,284] This reduction potential means that the potential for the oxidation of NADH by the removal of one electron to form the radical cation

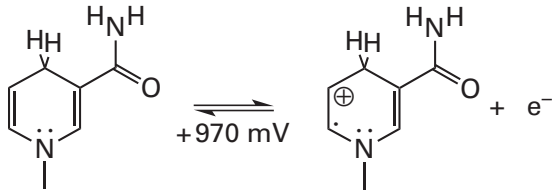

(1–93)

is +970 mV. The neutral radical formed from NAD^+ (Equation 1–92) and the radical cation formed from NADH (Equation 1–93) differ from each other by a hydron and are interconverted by the association or dissociation of a hydron.

The reduction potential for the reduction of NAD^+ is quite negative (Equation 1–92), and the reduction potential for the oxidation of NADH is quite positive (Equation 1–93). These facts state that **both the neutral radical and the radical cation of nicotinamide are unstable species** relative to NAD^+ and NADH, respectively. The radical cation[285] has been observed transiently during the pulsed photooxidation of NADH,[286] but it disproportionates rapidly and completely

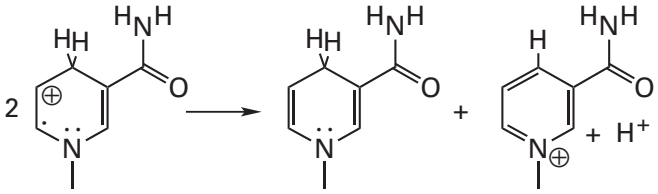

(1–94)

because of its instability relative to NAD^+ and NADH. From the one-electron reduction potentials of NADH and NAD^+ and the two-electron reduction potential of NAD^+, the pK_a of the radical cation (Equation 1–93) can be estimated to be about –5, an estimate indicating that it is a strong acid.[281,287]

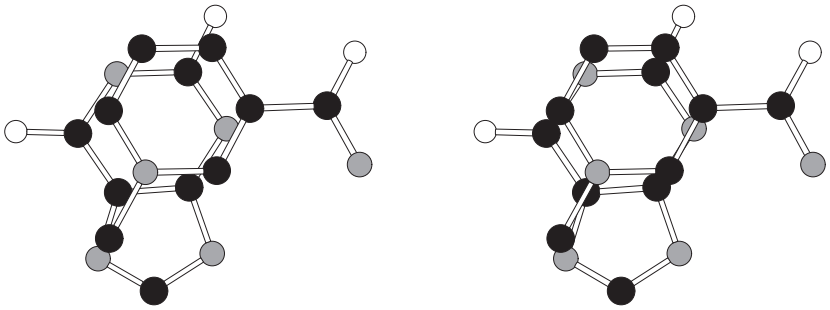

Figure 1–19: Stereodrawing[166] of the π stacking between the nicotinamide of NAD^+ and the xanthine in xanthosine monophosphate in a crystallographic molecular model of IMP dehydrogenase from *T. foetus*.[277] Black atoms are carbons, white atoms are oxygens, and small gray atoms are nitrogens. Inosine monophosphate dehydrogenase from *T. foetus* was mixed with xanthosine monophosphate and then crystallized. The crystals were soaked in a solution of NAD^+ to introduce it into the active site of the enzyme, which was already occupied by xanthosine monophosphate, to form a complex of oxidant and oxidant. In difference maps of electron density, features into which molecular models of xanthosine monophosphate and NAD^+ respectively could be inserted were observed. After insertion of these molecular models, the crystallographic molecular model of the resulting complex between enzyme, xanthosine monophosphate, and NAD^+ was refined against the data set. The xanthine of the xanthosine monophosphate and the nicotinamide of the NAD^+ in the final crystallographic molecular model are drawn: the nicotinamide is shown above and the xanthine is shown below.

The dissociation of the hydron, albeit a significantly exergonic reaction at pH 7, is required before an electron can be removed from the intermediate radical.[279] Consequently, the consecutive steps in the homolytic oxidation of NADH are removal of an electron, dissociation of a hydron, and removal of the second electron. It follows that in the homolytic reduction of NAD^+, which is the reverse reaction of the homolytic oxidation of NADH, a hydron must be added to the neutral radical formed by the addition of a single electron to NAD^+ (Equation 1–92) before the second electron can be added, and the addition of this hydron to this weak base is a significantly unfavorable step.

The significant instabilities of both the radical cation of NADH and the neutral radical of NAD^+ mitigate against the involvement of nicotinamide in one-electron reactions, particularly with two-electron reactants such as alcohols, carbonyl and acyl groups, and derivatives of carbonic acid. Certainly, the stereochemistry of such oxidation–reductions at the active sites of enzymes responsible for their catalysis (Figure 1–18 and **1–78**) suggests that direct two-electron hydride transfer from NADH or NADPH, which proceeds with a reduction potential for the half-reaction (reverse of Equation 1–79) of –330 mV at pH 7, is the favored path if the orientations required by the transition state can be achieved.

A two-electron reduction that may also have a mechanism involving the transfer of an electron, transfers of hydrons, and then the transfer of a second electron is the **reduction by 1,4-dihydropyridines related to NADH** of 1,4-benzoquinone or its derivatives

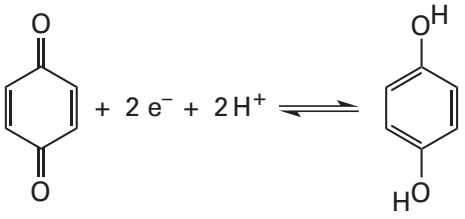

(1–95)

If these reductions do proceed in two one-electron steps, each involves an intermediate charge-transfer complex in which the radical cation of the dihydropyridine is stacked upon the radical anion of the benzoquinone,[288] an arrangement reminiscent of the nicotinamide stacked upon the xanthine in the crystallographic molecular model of IMP dehydrogenase (Figure 1–19). Evidence in favor of a mechanism for this reduction involving the consecutive transfer of one electron after the other[288] and evidence in favor of a mechanism involving only direct hydride transfer[289-291] for these reactions have been presented.

As for enzymatically catalyzed reactions, it has been demonstrated that within the active site of peroxidase from *Armoracia rusticana* (horseradish peroxidase), NADH can be oxidized in a one-electron transfer to the oxoiron(IV) porphyrin$^{\bullet+}$ that is formed at the heme in the enzyme by hydrogen peroxide.[292] This one-electron transfer produces $NADH^{\bullet+}$. A homologous electron transfer also occurs in solution when non-heme oxoiron(IV) complexes oxidize homologues of NADH.[293] Both on the enzymatic active site and in solution, however, the oxidants are strong and also ones that normally engage in one-electron transfers, and for both of these reasons, they are quite different from most of the weak two-electron oxidants that NADH is required to reduce in other enzymatic reactions.

Because of the reduction potentials involved, however, it seems unlikely that an active site, even by stacking the nicotinamide of the coenzyme and the π system of the substrate to facilitate the formation of a charge-transfer complex and by positioning an acid–base for the transfer of the hydron or the hydrons required, could perform a hydride transfer in a process involving the transfer of an electron, the transfer of a hydron, and the transfer of an electron.

There is, however, a more reasonable mechanistic explanation for the common observation of the stacking by an active site of a nicotinamide upon the π molecular orbital system of an extended linear, conjugated system within the substrate or upon a carbonyl group, an acyl group, or an unsaturated ring within the substrate. An intermediate formed during the reduction of (*E*)-but-2-enoyl-SCoA by NADPH in the active site of crotonyl-CoA carboxylase/reductase

$$\text{NADPH} + (E)\text{-but-2-enoyl-SCoA} + CO_2 \rightleftharpoons \text{NADP}^+ + (2S)\text{-ethylmalonyl-SCoA} \quad (1\text{–}96)$$

from *Methylorubrum extorquens* has been isolated, and its structure

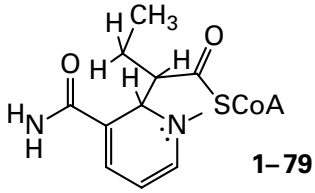

1–79

confirmed by high-resolution mass spectrometry and two-dimensional nuclear magnetic resonance spectroscopy. It is a covalent adduct between NADPH and (*E*)-but-2-enoyl-SCoA. When added to a solution containing crotonyl-CoA carboxylase/reductase, $NaHCO_3$, and carbonic anhydrase, an enzyme that converts $NaHCO_3$ into CO_2, but no (*E*)-but-2-enoyl-SCoA or NADPH, the isolated, purified intermediate is converted rapidly by the crotonyl-CoA carboxylase/reductase into (2*S*)-ethylmalonyl-SCoA and $NADP^+$, the usual products of the reduction.[294] Consequently, the intermediate seems to be on the main path of the enzymatic mechanism. Crotonyl-CoA carboxylase/reductase from *M. extorquens* is a homologue (34% identity; 1.6 gap percent)* of octenoyl-CoA reductase/ carboxylase from *S. cinnabarigriseus*, in the active site of which (Figure 1–16) the substrate (*E*)-but-2-enoyl-SCoA is stacked against $NADP^+$, so it seems to be the case that intermediate **1–79** is the result of an analogous stacking of substrate against coenzyme in the active site of crotonyl-CoA carboxylase/ reductase.

Intermediate **1–79** is **proposed to be the product of an ene reaction**, which is a pericyclic reaction. A **pericyclic reaction** is a concerted reaction that passes through a single transition state formed from a continuous ring of overlapping atomic orbitals creating a π molecular orbital system containing the magic aromatic numbers of electrons, 6 or 10, that make it aromatic. An ene reaction that forms intermediate **1–79** in the reduction of (*E*)-but-2-enoyl-SCoA by NADPH in the active site of crotonyl-CoA carboxylase/reductase

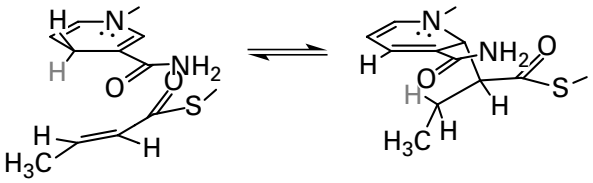

(1–97)

has a transition state arising from remixing of the molecular orbitals of the reactant to form an aromatic transition state and from remixing of the atomic orbitals forming the π molecular orbital system of the transition state to form the molecular orbitals of the product

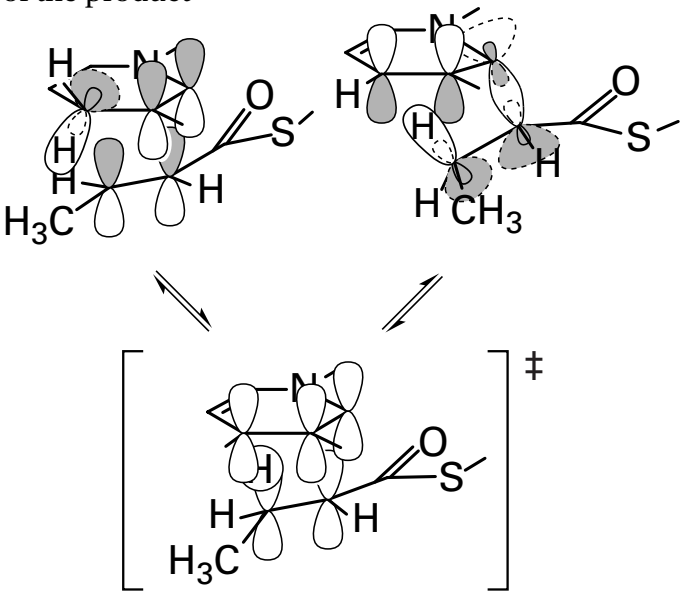

(1–98)

Carbon 4 of the nicotinamide on which the hydrogen transferred is located is only 0.34 nm from carbon 3 of the (*E*)-but-2-enoyl-SCoA to which it is to be transferred, and carbon 2 of the nicotinamide is only 0.36 nm from carbon 2 of the (*E*)-but-2-enoyl-SCoA with which it is to form a σ bond (dashed line in Figure 1–16).

The octanoyl homologue of intermediate **1–79**, in which the methyl group is an *n*-pentyl group, has been isolated from a reaction mixture in which a mutant of enoyl-[acyl-carrier-protein] reductase (NADH) from *Mycobacterium tuberculosis* is reducing (*E*)-oct-2-enoyl-SCoA* to octanoyl-SCoA[295] while oxidizing NADH to NAD^+. In a crystallographic molecular model of the active site of this enzyme,[296] the π molecular orbital system of (*E*)-oct-2-enoyl-SCoA forms a stack with NAD^+. In this instance, however, the enolate of octanoyl-SCoA that dissociates from the intermediate homologous to **1–79** during the normal enzymatic reaction is hydronated at the α carbon instead of being carboxylated because the product of the reaction is to be octanoyl-SCoA. The

*Acyl-carrier protein is a small protein that carries thioesters among the enzymes involved in the biosynthesis of fatty acids. The portion of acyl-carrier protein closest to the thioester is identical to the distal portion of coenzyme A so the two can usually be interchanged in the reaction of an enzyme that normally would have the thioester of acyl-carrier protein as a substrate such as enoyl-[acyl-carrier-protein] reductase (NADH).

*__Percent identity__ is the percent of positions in the two optimally aligned sequences that have identical amino acids. __Gap percent__ is the number of gaps for every 100 amino acids required to obtain the greatest percent identity. A percent identity in excess of 20% is usually a strong indication that the two protein molecules have superposable structures and that the catalytic groups in the active sites, their roles, and the orientation of the substrates when they are associated with the active site are quite similar.

absence of a catalytic acid in the appropriate location in the active site of crotonyl-CoA carboxylase/reductase precludes the hydronation of the enolate in its enzymatic reaction. Enoyl-[acyl-carrier-protein] reductase (NADH) is a much more widely distributed enzyme than crotonyl-CoA carboxylase/reductase because it is essential for the biosynthesis of fatty acids.

There are calculations based on the crystallographic molecular model of the active site of the unrelated[297] enoyl-[acyl-carrier-protein] reductase (NADPH) from *Candida tropicalis*, in the active site[298] of which (*E*)-but-2-enoyl-SCoA also forms a stack with $NADP^+$. These calculations indicate that the direct transfer of the hydride to (*E*)-but-2-enoyl-SCoA in a Michael addition should be more energetically favorable than an ene reaction.[299] The transition state, however, for the transfer of the hydride that is pictured in the report of these calculations does not involve any reorientation of the (*E*)-but-2-enoyl-SCoA to assume the orientation for an in-line transfer, which other calculations indicate is a requirement for the transition state of hydride transfer.[261,262] Following the transfer of the hydride, the carbon–carbon bond holding the two halves of intermediate **1–79** would form through a separate transition state. No explanation, however, is given as to why intermediate **1–79** would be necessary if the hydride has already been transferred.

Intermediate adduct **1–79** between (*E*)-but-2-enoyl-SCoA and NADPH dissociates into $NADP^+$ and the enolate of butanoyl-SCoA (**1–80**)

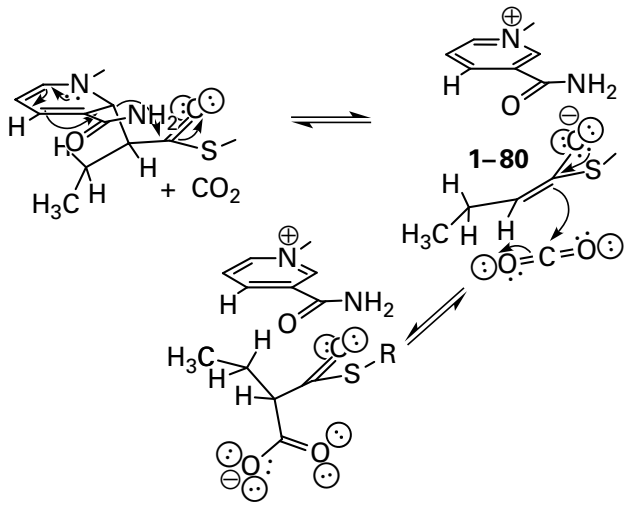

(1–99)

The aromatization of $NADP^+$ drives the dissociation, which would otherwise involve the loss of a σ bond and the formation of a weaker π bond. The enolate of butanoyl-SCoA is nucleophilic at its α carbon. In the active site of crotonyl-CoA carboxylase/reductase, the nucleophilic carbon of the enolate adds to a molecule of carbon dioxide, an electrophile, held by the active site adjacent to the enolate, to give the product (2*S*)-ethylmalonyl-SCoA.

These observations suggest that there may well be a common mechanism for the transfer of the hydrogen from NADH to an electrophilic atom in the enzymes in which the substrate forms a stack with the nicotinamide. This mechanism proceeds with **a pericyclic addition followed by the dissociation of the adduct to form an enolate or the homologue of an enolate, which is then either hydronated or carboxylated**.

Suggested Reading

Powell, M. F., Wu, J. C., and Bruice, T. C. (1984) Ferricyanide oxidation of dihydropyridines and analogues, *J. Am. Chem. Soc. 106*, 3850–3856. https://doi.org/10.1021/ja00325a024

Thoden, J. B., Frey, P. A., and Holden, H. M. (1996) Molecular structure of the NADH/UDP-glucose abortive complex of UDP-galactose 4-epimerase from *Escherichia coli*: Implications for the catalytic mechanism, *Biochemistry 35*, 5137-5144. https://doi.org/10.1021/bi9601114

Rosenthal, R. G., Ebert, M.-O., Kiefer, P., Peter, D. M., Vorholt, J. A., and Erb, T. J. (2014) Direct evidence for a covalent ene adduct intermediate in NAD(P)H-dependent enzymes, *Nat. Chem. Biol. 10*, 50–55. https://doi.org/10.1038/nchembio.1385

One-Carbon Chemistry

Formaldehyde and formic acid are one-carbon compounds widely involved in metabolism. These molecules, however, are rarely found free in the cytoplasm but are, like a hydride, a fatty acyl group, or a methyl group, associated with a coenzyme. **The coenzyme that carries the single carbons equivalent to formaldehyde and formic acid is tetrahydrofolate**

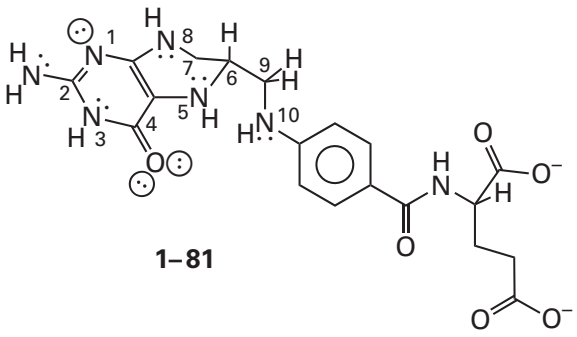

1–81

The formaldehyde or the formic acid is carried on nitrogen 5 or nitrogen 10 of the tetrahydrofolate or on both of them simultaneously. These nitrogens are three atoms apart, so the transfer of the equivalent of formaldehyde or formic acid between them, which involves either a *gem*-diamine or a tetrahedral intermediate, respectively, can occur through an intermediate five-membered ring.

Again, the coenzyme seems far more elaborate than the role of carrying formaldehyde and formic acid should require. In addition, the form of the coenzyme present in the cell is even more elaborate. In a cell, several additional L-glutamates, each linked by its α-amino group to the γ-glutamyl group of the one previously added, are attached to the γ-carboxyl group of the L-glutamate in tetrahydrofolate to form a regular, linear polymer of L-glutamates,[300] and enzymes using tetrahydrofolate associate preferentially with one or the other of the **polyglutamylated forms**.[301]

Other portions of the coenzyme act to adjust the **basicities of nitrogen 5 and nitrogen 10**. The planar pyrimidinyl group of tetrahydrofolate (the ring containing atoms 1–4) is analogous to a heterocyclic pyrimidinyl base in nucleic acid; and, as with the base of a nucleic acid, the three nitrogens exocyclic to the pyrimidinyl group, those attached to carbon 2 and at positions 5 and 8, are planar nitrogens[302] with conjugated π lone pairs of electrons. The exocyclic amino group at carbon 2 of the pyrimidinyl group and nitrogen 8 of the tetrahydrofolate are both directly conjugated to the acyl oxygen at position 4. The lone pairs of electrons on these nitrogens are presumably as weakly basic as the lone pair of electrons on the nitrogen of *N*-methylacetamide, the conjugate acid of which is quite strong ($pK_a = -6$). These two nitrogens will rarely if ever be dihydronated and cationic.

The **values of pK_a for nitrogen 5 and nitrogen 10**, however, are the more relevant to the chemistry of tetrahydrofolate. Nitrogen 5 of tetrahydrofolate (exocyclic to the pyrimidinyl group) is only poorly conjugated to the acyl oxygen at position 4 in the pyrimidinyl group, and the pK_a of its conjugate acid (4.82)[303] is close to that of the conjugate acid of aniline (4.63). If this is also true for the second pK_a of nitrogen 5, that for the neutral secondary amino group, then this second pK_a should be about the same as that for the neutral amino group in aniline ($pK_a \cong 30$). The nitrogen at position 10 is analogous to the nitrogen in 4-carbamoylaniline (estimated $pK_a = 2–3$).* Its conjugate acid, however, has a pK_a of –1.25, which reflects both the electron withdrawal of the carbamoyl group para to the amino group and the fact that at the pH at which the hydron dissociates from the 10-ammonio group, both nitrogen 1 and nitrogen 5 are hydronated and cationic. Consistent with these values of pK_a, the **equilibrium constant between 10-formyltetrahydrofolate and 5-formyltetrahydrofolate** is about 10^7 in favor of the latter.[304-306]

The difference in the values of pK_a between the conjugate acids of nitrogen 5 and nitrogen 10, however, does not seem to be necessary for the role that tetrahydrofolate plays in one-carbon chemistry. Tetrahydromethanopterin is a folate used in one-carbon chemistry in many archaebacteria.[307] The substituent para to nitrogen 10 in 5,6,7,8-tetrahydromethanopterin, unlike that in 5,6,7,8-tetrahydrofolate, is a fully saturated carbon so the pK_a of the conjugate acid of nitrogen 10 should be close to that of aniline and no different from the pK_a of the conjugate acid of carbon 5, and yet tetrahydromethanopterin functions effectively in its role in these bacteria. The two folates, tetrahydrofolate and tetrahydromethanopterin, however, are not interchangeable.[308]

*This estimate is based on the fact that pK_a of 4-ethoxycarbonylaniline is 2.38 and the observation that a carbamoyl group and and ethoxycarbonyl group have about the same ability to withdraw electron density.

An equivalent of formaldehyde is carried as the iminium on nitrogen 5 of tetrahydrofolate

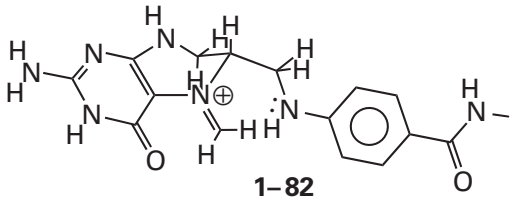

1–82

or, more stably,[309] as the *gem*-diamine in N^5,N^{10}-methylenetetrahydrofolate

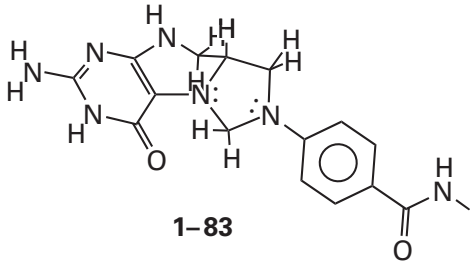

1–83

It is rarely carried on nitrogen 10 alone. In the *gem*-diamine, the two nitrogens remain conjugated to the adjacent π molecular orbital systems of the respective rings. Because of its stability and the fact that it is chemically unreactive, N^5,N^{10}-methylenetetrahydrofolate is the exclusive adduct of formaldehyde found in free solution in the cytoplasm of organisms that use tetrahydrofolate as a carrier of formaldehyde. **N^5-Methylenetetrahydrofolate** (**1–82**), however, is the electrophilic intermediate that usually reacts with a nucleophilic substrate in the nucleophilic substitutions at the methylene carbon in the active sites of enzymes that use N^5,N^{10}-methylenetetrahydrofolate as a donor of the equivalent of formaldehyde.[84]

Because of their toxicity, neither the hydrate of formaldehyde nor the small amount of unhydrated formaldehyde in equilibrium with the hydrate (Table 1–2) usually exists in the cytoplasm. Their toxicity arises from the fact that formaldehyde free in solution reacts with proteins and nucleic acids to modify them and to crosslink them in complex and as yet poorly understood reactions. Its direct, nonenzymatic reaction with tetrahydrofolate to form N^5,N^{10}-methylenetetrahydrofolate may occur under certain circumstances;[310] but most, if not all, of the N^5,N^{10}-methylenetetrahydrofolate in the cell is **made from L-serine** by the enzyme glycine hydroxymethyltransferase

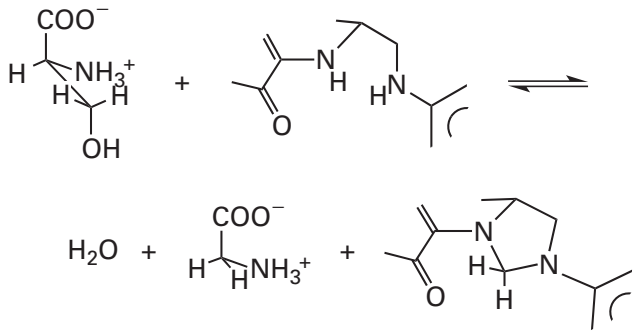

(1–100)

In the reaction between formaldehyde and a model compound for tetrahydrofolate[309]

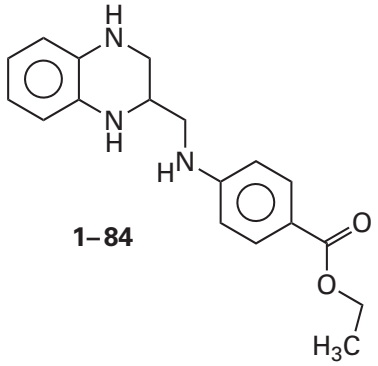

1–84

the iminium of one of the two nitrogens homologous to nitrogen 5 and nitrogen 10 is formed in a rapid equilibrium by a reaction involving a hemiaminal that dehydrates under catalysis by an acid (Figure 1–7). The homologue of this reaction occurs rarely in living organisms, but the iminium that is the product of this nucleophilic addition is homologous to the intermediate in the reaction catalyzed by glycine hydroxymethyltransferase that immediately precedes the formation of the N^5,N^{10}-methylenetetrahydrofolate (**1–83**) that is the final product of the enzymatic reaction. In the model reaction in solution, the ***gem*-diamine is formed from the iminium by nucleophilic addition**

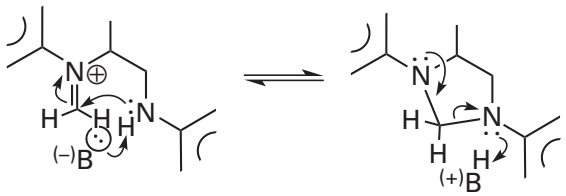

(1–101)

Because the nucleophile in this nucleophilic addition is a weakly basic anilino nitrogen ($pK_a = 2.9$), this step must be catalyzed by a base, which removes the hydron from that nitrogen during its addition

to make it more nucleophilic.[309] The hydron cannot be removed prior to the nucleophilic addition because of its high pK_a.

An equivalent of **formic acid is also carried** at one or both of the two anilino nitrogens, either on nitrogen 5

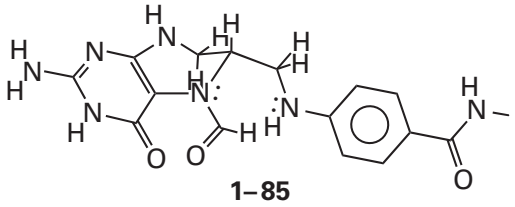

1–85

as the more stable ***N*⁵-formyltetrahydrofolate** (**1–85**), or at nitrogen 10 as the less stable *N*¹⁰-formyltetrahydrofolate, or as the formamidinium between the two nitrogens, as in ***N*⁵,*N*¹⁰-methenyltetrahydrofolate**

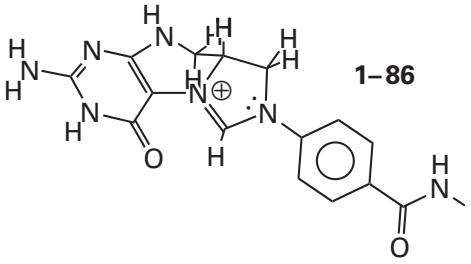

1–86

In its various guises, the formic acid has, as it must, three bonds to heteroatoms. The hydrogen on the methenyl group in *N*⁵,*N*¹⁰-methenyltetrahydrofolate is acidic because the conjugate base is an ylide.[311]

*N*⁵,*N*¹⁰-Methenyltetrahydrofolate (**1–86**) is formed from *N*⁵-formyltetrahydrofolate by a nucleophilic substitution (Figure 1–20). Nitrogen 10 is a poor nucleophile (pK_a = –1.25). Consequently, while nitrogen 10 adds to the formyl group of **1–85** to form this tetrahedral intermediate, a base must simultaneously remove its hydron to make it a better nucleophile, as is the case in the model compound.[312] The reaction proceeds through a tetrahedral intermediate from which the oxygen is the leaving group.

In *N*⁵,*N*¹⁰-methenyltetrahydrofolate (**1–86**) both the 4-*N*-acylaminophenyl ring attached to nitrogen 10 and the pyrimidinyl ring attached to nitrogen 5 are twisted out of the plane of the formamidine by steric effects (Figure 1–21),[302] but the twist is not sufficient to break an extended π system that includes the entire pyrimidinyl group, nitrogen 5, the formyl carbon, nitrogen 10, and the 4-*N*-acylaminophenyl group.

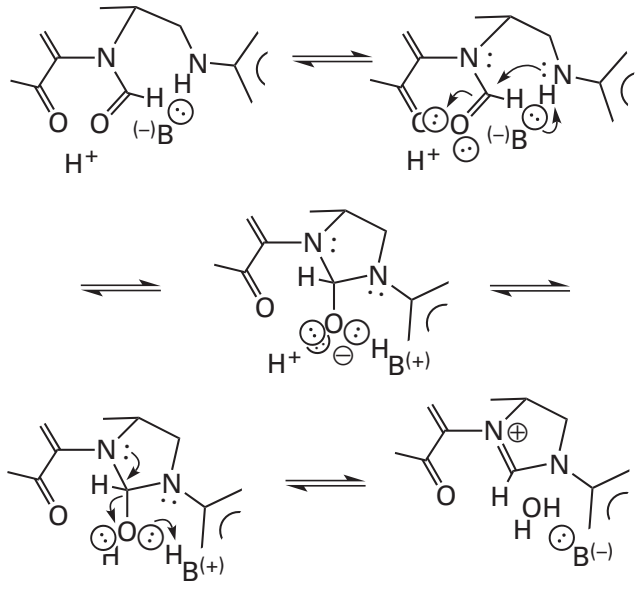

Figure 1–20: Transformation of *N*⁵-formyltetrahydrofolate to *N*⁵,*N*¹⁰-methenyltetrahydrofolate. Formation of the tetrahedral intermediate occurs with catalysis by a general base, and the oxygen of the tetrahedral intermediate must be hydronated before it can leave to yield the amidinium ion.

When they are adducts of tetrahydrofolate, the equivalents of formaldehyde and formic acid are interconverted by an oxidation–reduction involving hydride transfer

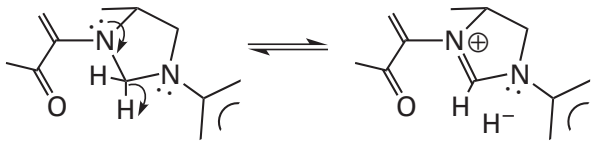

(1–102)

This hydride transfer is catalyzed by the enzyme methylenetetrahydrofolate dehydrogenase, which uses as a source of the hydride either nicotinamide-adenine dinucleotide, nicotinamide-adenine dinucleotide phosphate,[313] or coenzyme F_{420} (**1–69**),[314] depending on the species from which the enzyme is purified.

The reduction of *N*⁵-methylenetetrahydrofolate

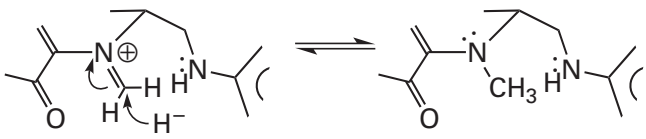

(1–103)

produces ***N*⁵-methyltetrahydrofolate**. This reaction

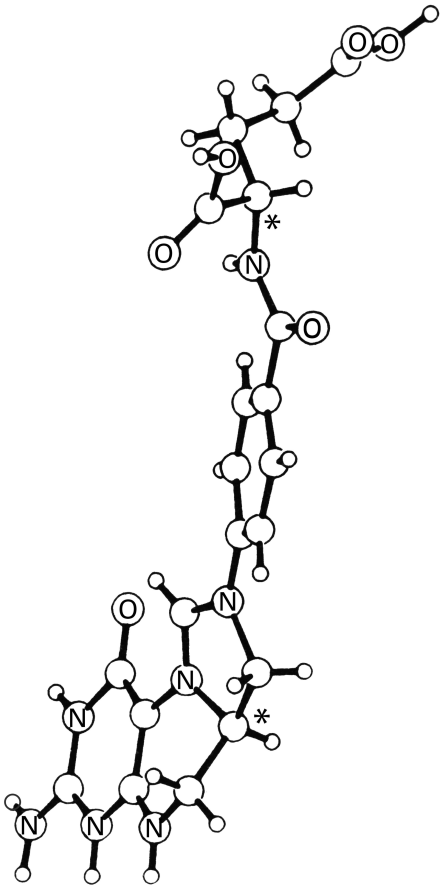

Figure 1–21: Crystallographic molecular model of the conjugate acid of N^5,N^{10}-methenyltetrahydrofolate.[302] White atoms are carbons unless otherwise indicated and the small white atoms are hydrogens. The dication of N^5,N^{10}-methenyltetrahydrofolate was produced from N^5-formyltetrahydrofolate in hydrochloric acid and crystallized as the bromide salt from 50% hydrobromic acid. A map of electron density was derived from X-ray diffraction of these crystals. The asterisks denote the two chiral carbons in this, the naturally occurring diastereomer. The absolute configuration at these carbons was verified with anomalous dispersion. The two formal positive elementary charges of the dication are located in the planar guanidino group in the lower left of the molecule and the amidinium of the methenyl group. Reprinted with permission from reference 302. Copyright 1979 American Chemical Society. https://doi.org/10.1021/ja00514a041

is catalyzed by the enzyme methylenetetrahydrofolate reductase, which also uses either NADH or NADPH. N^5-Methyltetrahydrofolate can act as a simple **methylating agent** (Equation 1–19) in a concerted nucleophilic substitution with strong nucleophiles such as thiolate ion.[315] For example, the archaebacterial analogue of N^5-methyltetrahydrofolate, 5-methyl-5,6,7,8-tetrahydromethanopterin, is the source of the methyl group of *S*-methyl coenzyme M (*S*-methyl-2-sulfanylethanesulfonate). It is this methyl group that is, in turn, the source of the methane produced by these bacteria.[245]

Methionine synthase transfers the methyl group from N^5-methyltetrahydrofolate to L-homocysteine to produce L-methionine. The thiolate of L-homocysteine is the nucleophile, and nitrogen 5 of N^5-methyltetrahydrofolate is the leaving group in a simple concerted nucleophilic substitution. The problem faced by the enzyme is that nitrogen 5 is an anilino nitrogen. Because the pK_a of the conjugate acid of nitrogen 5 in N^5-methyltetrahydrofolate is 5, it is unhydronated at neutral pH, and because the pK_a of the neutral 5-alkylamino group of 5,6,7,8-tetrahydrofolate is around 30, the unhydronated nitrogen is a poor leaving group. The enzyme from *Candida albicans* solves this problem by providing an acid that hydronates the nitrogen before the nucleophilic substitution commences to make it a better leaving group.[316] The hydron on a histidinium side chain is relayed to nitrogen 5 by a molecule of water.[317]

Tetrahydrofolate itself is oxidized and 7,8-dihydrofolate is reduced by hydride transfer in a reaction catalyzed by dihydrofolate reductase

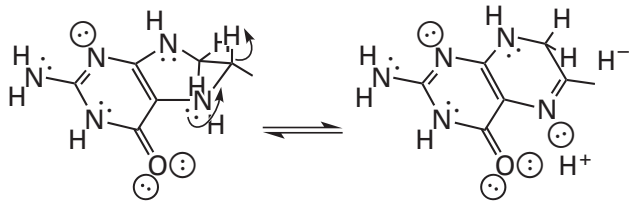

(1–104)

This reaction regenerates tetrahydrofolate by reduction from the 7,8-dihydrofolate produced during the synthesis of thymidine by thymidylate synthase

5,10-methylenetetrahydrofolate + dUMP
$\rightleftharpoons$ 7,8-dihydrofolate + dTMP

(1–105)

and it also participates in the production of tetrahydrofolate from the vitamin folate.

The enzymatically catalyzed reactions involving adducts of tetrahydrofolate with the equivalent of either formic acid or formaldehyde have mechanisms that avoid the formation of free formic acid or free formaldehyde.

The **transfer of a formyl group** from N^5,N^{10}-methenyltetrahydrofolate (**1–86**) is often to a third amine, as in the reaction catalyzed by phosphoribosylglycinamide formyltransferase 1

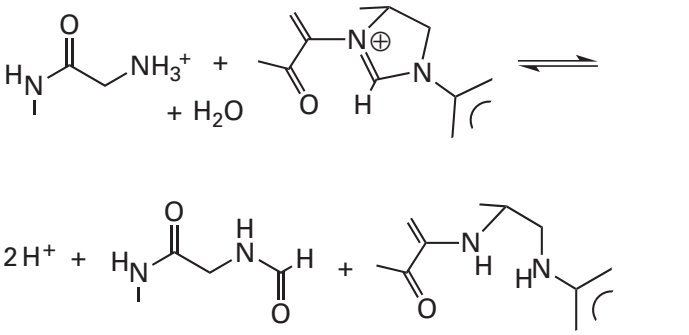

(1–106)

The first step in a reaction of this type is addition of the amine of the acceptor to the formyl carbon in N^5,N^{10}-methenyltetrahydrofolate (Figure 1–22),[318,319] which is an amidine and as a result a strongly electrophilic acyl derivative. After it has been dehydronated, the resulting neutral form of the resulting tetrahedral intermediate has three possible leaving groups, each an amine. The hydronation of one or the other of the two π lone pairs of electrons on the nitrogens of the tetrahydrofolate to make that nitrogen a reasonable leaving group is far more difficult than the hydronation of the aliphatic amine that just associated. If, however, the aliphatic amine is hydronated and leaves, this only regenerates the reactants. In order for the reaction to proceed, one of the anilino nitrogens of the tetrahydrofolate must be hydronated to make it a leaving group. Usually it is nitrogen 5 that is hydronated because it is the more basic nitrogen.[319]

After nitrogen 5 of the tetrahydrofolate leaves, the product of the first nucleophilic substitution is a mixed amidine between nitrogen 10 of tetrahydrofolate and the nitrogen of the amine. To complete the transfer of the formyl group, either hydroxide or water from which a hydron is being removed attacks this mixed amidine to form a second tetrahedral intermediate. At this point a difficulty arises. In free solution the leaving group from this tetrahedral intermediate is always the aliphatic amine rather than the anilino nitrogen,[318] because the aliphatic nitrogen is definitely more basic, and hence more readily hydronated, than the anilino nitrogen. Presumably, in the enzymatic reaction there is a catalytic acid adjacent to nitrogen 10 to hydronate the anilino nitrogen and complete the transfer of the formyl group to the aliphatic amine. If the aliphatic amine were to leave, then the products of the second nucleophilic substitution would be 10-formyltetrahydrofolate and the amine that was the original reactant.

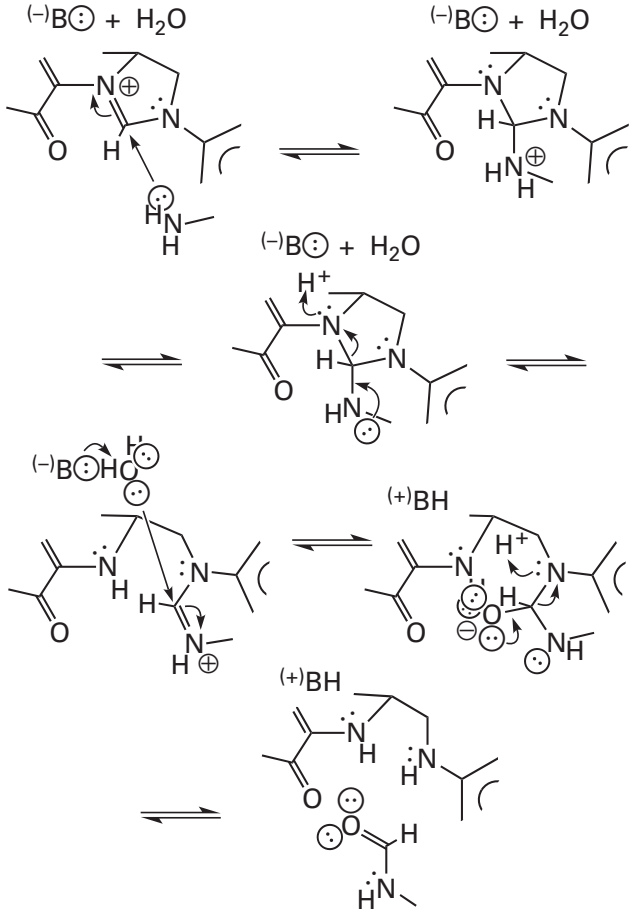

Figure 1–22: Transfer of the formyl group from N^5,N^{10}-methenyltetrahydrofolate to the primary amine on phosphoribosylglycinamide.[318,319] The reaction involves two consecutive nucleophilic substitutions at the formyl carbon: in the first, the amine from the glycinamide enters and an anilino nitrogen of tetrahydrofolate leaves, and in the second, the oxygen of a molecule of water under base catalysis or a hydroxide ion enters and the other anilino nitrogen of tetrahydrofolate leaves.

The **transfer of the equivalent of formaldehyde** from N^5,N^{10}-methylenetetrahydrofolate (**1–83**) to a nucleophile usually proceeds through the electrophilic iminium of N^5-methylenetetrahydrofolate (**1–82**), which can transfer the single carbon to a nucleophile directly. The necessary N^5-methylenetetrahydrofolate is formed in the reverse of the reaction in Equation 1–101. For example, in the reaction catalyzed by 3-methyl-2-oxobutanoate hydroxymethyltransferase

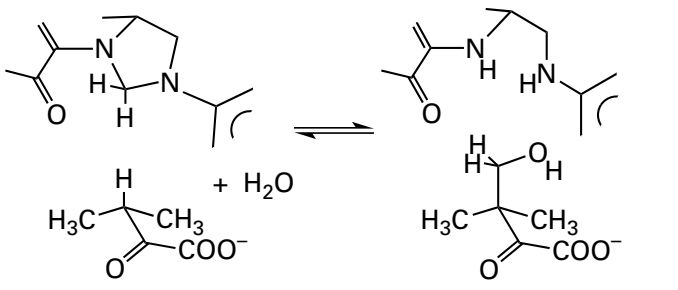

(1–107)

the single electrophilic imino carbon on nitrogen 5 of N^5-methylenetetrahydrofolate is transferred in a nucleophilic substitution (see reverse of the reaction in Figure 1–7) in which the nucleophilic carbon in the enolate of 3-methyl-2-oxobutanoate replaces the anilino nitrogen of tetrahydrofolate. The leaving group in this nucleophilic substitution at the methylene carbon is nitrogen 5 of tetrahydrofolate ($pK_a \cong 30$). Consequently, it is again necessary to provide an acid to hydronate nitrogen 5 during the nucleophilic substitution, or it will not leave.

When **the equivalent of either formaldehyde or formic acid is transferred to nitrogen 5** in tetrahydrofolate from an electrophile, nitrogen 5 is required to act as a nucleophile. It is, however, a poor nucleophile because its conjugate acid is fairly strong ($pK_a = 4.82$). Its **nucleophilicity can be enhanced**, however, by removing the hydron from nitrogen 3 ($pK_a = 10.5$).[303] Although this enhancement cannot be demonstrated by resonance, the negative formal elementary charge resulting from this dehydronation at nitrogen 3, which is shared by nitrogen 3 and oxygen 4, decreases inductively the delocalization of the lone pair of electrons on nitrogen 5 into the pyrimidinyl ring and increases its nucleophilicity. For example, in the active sites of aminomethyltransferase from *Thermotoga maritima*[320] and thymidylate synthase from *E. coli*, [321] both enzymes in which nitrogen 5 of tetrahydrofolate must be nucleophilic in the normal forward direction, the nitrogen–hydrogen bond of nitrogen 3 of the tetrahydrofolate forms a hydrogen bond to a glutamate and an aspartate, respectively, which are significant bases capable of increasing the nucleophilicity of nitrogen 5. There are exceptions to this assistance. In glycine hydroxymethyltransferase from *Geobacillus stearothermophilus*, nitrogen 3 is forming a hydrogen bond with an amido oxygen from the polypeptide backbone,[322] which is not a significant base.

In the reaction catalyzed by 3-methyl-2-oxobutanoate hydroxymethyltransferase (Equation 1–107), the electrophilic methenyl group is transferred from nitrogen 5 of N^5,N^{10}-methylenetetrahydrofolate to carbon 3 of 3-methyl-2-oxobutanoate. The nucleophile in this transfer is the enolate that is the conjugate base of 3-methyl-2-oxobutanoate. This enolate is formed by the dissociation of a hydron from the saturated but acidic carbon 3 of 3-methyl-2-oxobutanoate. This carbon is acidic because it is immediately adjacent to an acyl group.

Suggested Reading

Benkovic, S. J., Barrows, T. H., and Farina, P. R. (1973) Studies on models for tetrahydrofolic acid. IV. Reactions of amines with formamidinium tetrahydroquinozaline analogs, *J. Am. Chem. Soc. 95*, 8414–8420. https://doi.org/10.1021/ja00806a036

Kallen, R. G., and Jencks, W. P. (1966) The dissociation constants of tetrahydrofolic acid, *J. Biol. Chem. 241*, 5845–5850. https://doi.org/10.1016/S0021-9258(18)96349-0

Enolates, Enols, and Enamines

The hydrogen on a carbon immediately adjacent to a carbonyl group or an acyl group is acidic (Figure 1–23)[33,34,38,323-335] because the electronegative oxygen two atoms away from that carbon can support the excess electron density of the conjugate base. The simplest examples of this acidity are that of acetaldehyde, the pK_{aK}* of which is 16.7

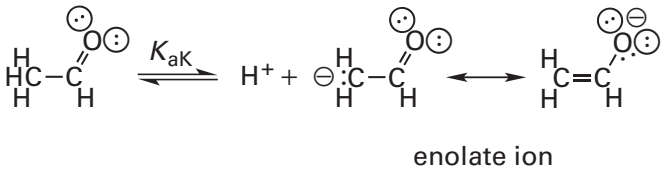

(1–108)

and ethyl acetate ($pK_{aK} = 25.6$)

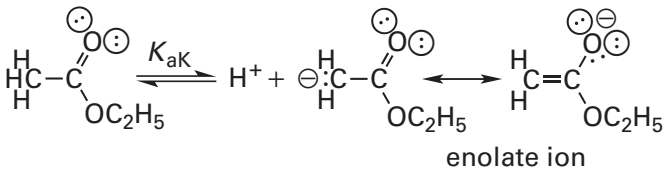

(1–109)

*The subscript K indicates that the pK_a is that for the keto tautomer of the carbonyl compound or the keto form of the acyl derivative. The subscript E indicates that the pK_a is that for the enol tautomer.

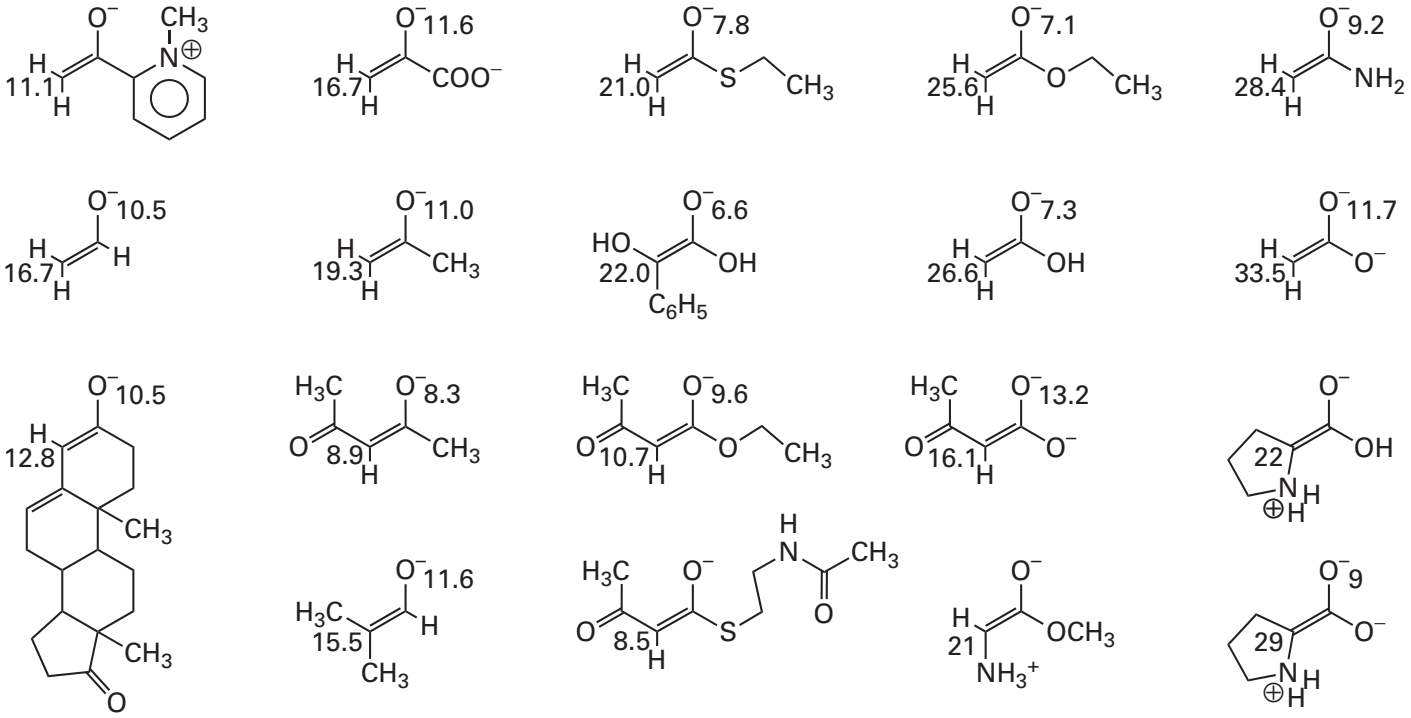

Figure 1–23: Values of pK_a for the acid dissociations of a series of keto tautomers and their enol tautomers.[33,34,38,323-335] The enolate ion of each compound is drawn. The number next to the α carbon of the enolate ion is the pK_a of the keto tautomer of its conjugate acid (pK_{aK}, Equation 1–110); the number next to the oxygen of the enolate ion is the pK_a of the enol tautomer of its conjugate acid (pK_{aE}, Equation 1–110). The value of the respective pK_E (Equation 1–110) is the difference between the two numbers (Equation 1–111). The values of pK_a for the different tautomers of glycine and L-proline containing ammonio groups are estimates from various thermodynamic cycles.[332,334]

The two respective resonance structures demonstrate the conjugation of the neighboring oxygen in the enolate. This conjugation, which shifts negative charge from the carbon onto the more electronegative oxygen to stabilize the enolate, causes the acid dissociation constant of acetaldehyde to be much less than that of propane (p$K_a \cong 50$), in which a methyl group takes the place of the oxygen, and it causes the acid dissociation constant of ethyl acetate to be much less than that of ethyl isopropyl ether (p$K_a \cong 49$).

Because hydroxide can remove a hydron from acetaldehyde many orders of magnitude more rapidly than it can from propane, the neighboring π molecular orbital system must be involved in the **transition state for the dissociation of a hydron on the carbon adjacent to a carbonyl or acyl group** (Figure 1–24). The two electrons in the occupied bonding molecular orbital of the original carbon–hydrogen σ bond remain behind in the π molecular orbital system of the enolate. As the transition state is approached, this occupied σ molecular orbital of the carbon–hydrogen bond overlaps the unoccupied antibonding π^* molecular orbital of the π molecular orbital system between carbon and oxygen. This overlap will create the occupied nonbonding π molecular orbital of the enolate once the hydron has been removed. Also during the approach to the transition state, the occupied atomic orbital of the lone pair of electrons on the base that removes the hydron overlaps the unoccupied antibonding molecular orbital of the carbon–hydrogen bond to gain access to the hydron. In the transition state, the atomic orbital of the base, the 1*s* orbital of the hydrogen, two *p* orbitals, one on each of the two carbons, and a *p* orbital on the oxygen mix, and three of the five resulting molecular orbitals of the transition state are occupied by the six electrons participating in the reaction. The transition state decomposes into the hydronated base and the π molecular orbital system of the enolate through an overlap between the unoccupied antibonding molecular orbital of the σ bond between the base and the hydron and the **nonbonding π molecular orbital of the resulting enolate**

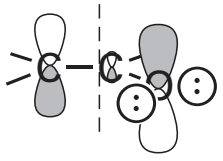

1–87

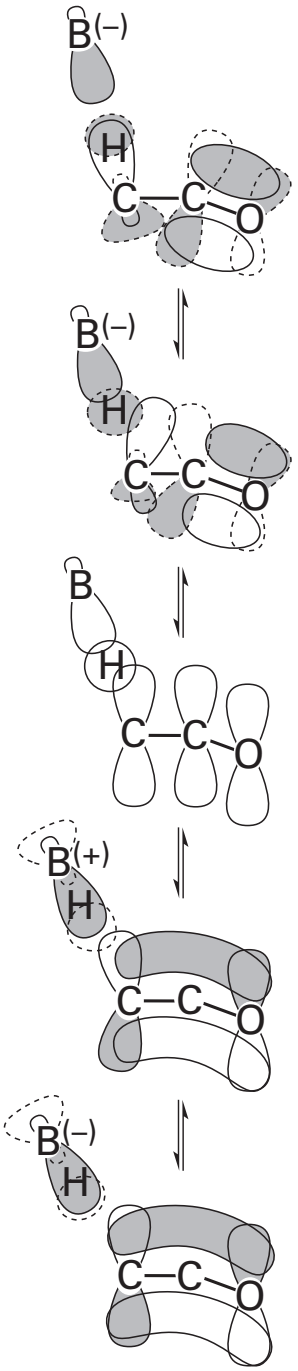

Figure 1–24: Removal of a hydron by a base, B, from a carbon adjacent to a carbonyl group. As the atomic orbital occupied by the lone pair of electrons on the base (solid outline) overlaps the unoccupied antibonding molecular orbital of the carbon–hydrogen bond (dashed outline), the occupied bonding molecular orbital of the carbon–hydrogen bond (solid outline) overlaps the unoccupied antibonding molecular orbital of the π bond between carbon and oxygen (dashed outline). The five atomic orbitals that mix in the transition state are the atomic orbital of the base, the *s* orbital of the hydrogen, and three *p* orbitals on the two carbons and the oxygen. The transition state decomposes through a form in which the unoccupied antibonding molecular orbital of the σ bond between the base and the hydron (dashed outline) overlaps the occupied nonbonding π molecular orbital (composed from the two peripheral *p* orbitals) of the enolate. These overlaps occur in each direction of the reaction.

which is its highest occupied molecular orbital.

For the acid–base reaction to occur in this way, the hydron removed from carbon must be in a **σ bond parallel to the π molecular orbital** system to permit the necessary overlaps and mixing in the transition state

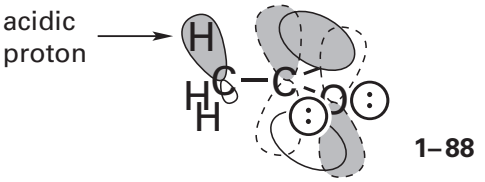

It has already been explained in the section describing the transfer of a hydron why this removal of a hydron from the carbon α to a carbonyl or acyl group by a base, even when the reaction is significantly exergonic, is a slow process.

The highest occupied nonbonding π molecular orbital of the enolate (**1–87**) is **nucleophilic** because it bears the pair of electrons that constitute the excess electron density of the enolate and are responsible for its negative elementary charge. The fact that an enolate can be stabilized by donors for hydrogen bonds directed parallel to this nonbonding π molecular orbital[336] is consistent with the fact that it contains the excess electron density and the nucleophilicity. This nonbonding π molecular orbital accounts for the resonance structures (Equation 1–108) that assign negative charge only to the two end atoms of the three atoms participating in the enolate. The formalism of resonance structures is a reflection of the fact that the highest occupied molecular orbital (**1–87**) has a node close to the central carbon and significant lobes over only the peripheral carbon and the oxygen.

The enolate of a carbonyl compound or acyl compound can be hydronated on oxygen to form the enol tautomer. Examples of enol tautomers would be the enolate of acetaldehyde (Equation 1–108) that has been hydronated on its oxygen

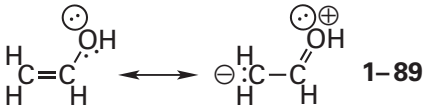

and the enolate of ethyl acetate (Equation 1–109) that has been hydronated on its oxygen

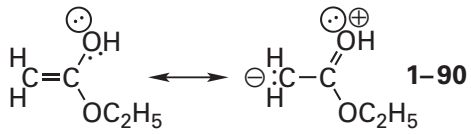

1–90

The enol tautomer of acetaldehyde is acidic at its hydroxy group and is a much stronger acid ($pK_{aE} = 10.5$) than acetaldehyde itself, and the enol tautomer of ethyl acetate is acidic at its hydroxy group and is a much stronger acid ($pK_{aE} = 7.1$) than ethyl acetate itself (Figure 1–23). During the dehydronation of an enol tautomer, the hydron that is removed and that leaves behind a σ lone pair of electrons is in a σ bond to oxygen that is in the σ plane of the enol orthogonal to and uninvolved in the π molecular orbital system of the enol tautomer (see **1–87**). Removal of the hydron from the oxygen of the enol tautomer of acetaldehyde ($\Delta pK_a = 5.2$) or the oxygen of the enol tautomer of ethyl acetate ($\Delta pK_a = 8.6$) by a strong base such as hydroxide is a encounter-controlled reaction.[16] This behavior is consistent with an uncomplicated removal of a hydron from a σ lone pair of electrons on oxygen.

In solution, an enol tautomer is in equilibrium with both its enolate and its **keto tautomer**. An example of these equilibria is shown for acetaldehyde

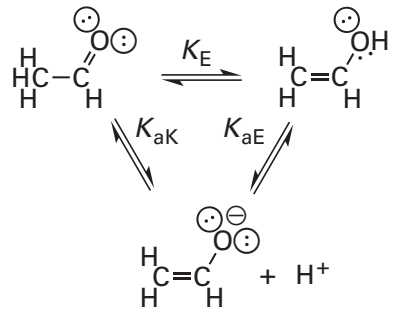

(1–110)

The equilibrium between the keto form and the enol, with the equilibrium constant K_E, is a **keto–enol tautomerization**. Because the three reactions are linked

$$-\log K_E = pK_E = pK_{aK} - pK_{aE} \qquad (1–111)$$

For compounds such as acetaldehyde ($pK_E = 6.2$)[324] and other aldehydes; for acetoacetic acid ($pK_E = 2.2$),[337] other β-oxo acids, and β-oxo esters;[325] and for enol tautomers conjugated to carbon–carbon double bonds,[333] the value for K_E is large enough that measurable amounts of the enol tautomer are present in solution at equilibrium with the dominant keto tautomer. In most other cases, the equilibrium constant for the keto–enol tautomerization, K_E, is so small that the concentration of enol tautomer is undetectable. A **solution of the pure enol tautomer**, however, can be prepared by rapidly mixing a metallic salt of the enolate, dissolved in organic solvent, with water. The enolate is immediately hydronated on the oxygen to produce the enol tautomer[338] before the enol tautomer slowly converts to the keto tautomer because the hydronation of a σ lone pair of electrons on a heteroatom, even though it is less basic, is much faster than the hydronation of a carbon atom in a π molecular orbital system. A solution of the enol tautomer can also be prepared even more rapidly by photolysis of an appropriate precursor.[339] From the kinetics of the subsequent approach to equilibrium between the keto and enol tautomers, the equilibrium constants of Equation 1–110 can be measured.[324] The values of pK_{aK} and pK_{aE} for a series of enol tautomers and their keto tautomers have been measured by these methods and also estimated from the rates[33] at which the hydrons on α carbons adjacent to carbonyl or acyl groups exchange in the presence of base (Equation 1–110).

The acidity of a hydron on the α carbon adjacent to a carbonyl or acyl group in the keto tautomer varies as the substituents attached to the carbonyl or acyl carbon, or to the α carbon itself, are changed (Figure 1–23). These effects are relevant because there are many enzymatic reactions in which a hydron is removed from a carbon α to a carbonyl or acyl group by a catalytic base in the active site. In each of these enzymatic reactions, the pK_a of that particular carbon determines the ease with which it can be transferred to the base in the active site.

When the hydrogen on the carbonyl carbon of acetaldehyde [pK_{aK} (acetaldehyde) = 16.7] is changed to a methyl group, the pK_a of the α hydron increases [pK_{aK}(acetone) = 19.3]. This increase in pK_a reflects the **hyperconjugation** of the carbon–hydrogen σ bonds of the methyl group. In the enolate, the pairs of electrons in these σ bonds push into the π system and destabilize the anion relative to the neutral conjugate acid, and in the neutral conjugate acid, this hyperconjugation releases electron density to the electron-deficient carbon of the carbonyl group to stabilize it.

When the hydrogen on the carbonyl carbon of acetaldehyde is replaced with an ethoxy group or a hydroxy group, the pK_a of the α hydron increases even more [pK_{aK}(ethyl acetate) = 25.6; pK_{aK}(acetic acid) = 26.6] because the **lone pairs of electrons** on the oxygen that has been added push electron density even more strongly into the π molecular orbital system of both the enolate and the keto tautomer than does the methyl group. When the hydrogen on the carbonyl carbon of acetaldehyde is replaced with a carbamoyl group, the pK_a of the α hydron [pK_{aK}(acetamide) = 28.4] increases further because the electrons in the lone pair on the neutral nitrogen are more basic than those on a neutral oxygen. When the hydrogen on acetaldehyde is replaced by an oxyanion, the pK_a of the α hydron [pK_{aK}(acetate ion) = 33.5] increases even further because of the even stronger basicity of lone pairs of electrons on the anionic oxygen. Because the electrons affecting the acidity in these instances are lone pairs of electrons rather than σ bonds as in the case of hyperconjugation, **resonance structures** can be written for each of these electron donations.

When the hydrogen on the carbonyl carbon of acetaldehyde is replaced by an ethylsulfanyl group, however, the pK_a of the α hydron [pK_{aK}(ethyl thioacetate) = 21.0] does not increase so much as when it is replaced by an ethoxy group because the **lone pairs of electrons on a sulfur** do not overlap effectively with the π system of the enolate or the carbonyl group. Consequently, they do not destabilize the enolate and stabilize the carbonyl group as much as do the lone pairs of electrons on an oxygen.[340] This failure of lone pairs of electrons on sulfur, an element in the third row of the periodic table, to overlap effectively with a π system of atoms from the second row[341] results from a mismatch in the size of the respective *p* orbitals. This fact explains why, when a hydron has to be removed by an enzyme from the carbon α to an acyl group, the acyl group will usually be a thioester of coenzyme A, a thioester of a cysteine on the enzyme itself, or a thioester of a pantetheine attached to the enzyme as a posttranslational modification.

When the hydrogen of acetaldehyde is replaced by a carboxy group, the pK_a of the α hydron does not change at all [pK_{aK}(pyruvate ion) = 16.7] because the withdrawal of electron density from the enolate or the carbonyl carbon by the electropositive carbon of the carboxylato group through the σ system is cancelled by the donation of electron density into the π system of the enolate and the carbonyl group from the π system of the carboxylato group. If, however, the hydrogen on acetaldehyde is replaced by an *N*-methylpyridinio group, the pK_a of the α hydron decreases significantly [pK_{aK}(2-acetyl-*N*-methylpyridinium ion) = 11.1] because the withdrawal of electron density through the σ system by the nitrogen bearing a positive elementary charge outweighs the donation of electron density through the π system from the aromatic pyridinyl group.

The acidity of the α carbon in the keto tautomer of a carbonyl or acyl compound is also affected by **substitutions at the acidic α carbon** itself. In particular, when a carbon in an α position is adjacent to **a double bond between the atoms in the β and γ positions**, the π molecular orbital system of that double bond becomes conjugated to the enolate in a π molecular orbital system encompassing five atoms upon removal of the hydron from the α carbon. The pK_a of the α carbon decreases relative to an analogous α carbon that is adjacent to a fully saturated carbon [pK_{aK}(4-andro-stene-3,17-dione) = 12.8; pK_{aK}(acetone) = 19.3] because the loss of the hydron permits extended conjugation to occur. The rate at which the hydron can be removed by a base also increases dramatically in such a situation,[7] a fact suggesting that the π system of the adjacent double bond overlaps the carbon–hydrogen σ bond in the transition state for hydron transfer, lowering its energy. Another example of the effect of a double bond between the atoms in the β and γ positions on the acidity of an α hydron in a keto tautomer is manifest in the iminium

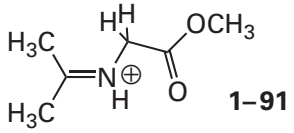

1–91

The removal of the hydron α to the methyl ester creates an sp^2 carbon with a *p* orbital that conjugates the carbon–nitrogen double bond to the resulting enolate. This conjugation again produces a π molecular orbital system spread over five atoms. As a result, the pK_{aK} (14)* of iminium **1–91** is 7 units lower than the pK_{aK} (21) of the cationic conjugate acid of methyl glycinate.[342]

*Again, the pK_a of the iminium cation was estimated indirectly from other acid dissociation constants and rate constants for dehydronation.

When **a second carbonyl or acyl group** is substituted for one of the hydrogens on the carbon α to a carbonyl group or acyl group, the hydron between the two carbonyl groups is much more acidic. For example, acetylacetone ($pK_{aK} = 8.9$) is more acidic than acetone ($pK_{aK} = 19.3$). This increase in acidity reflects the stabilization brought about by delocalization of the negative elementary charge through a π molecular orbital system spread over five atoms in the enolate

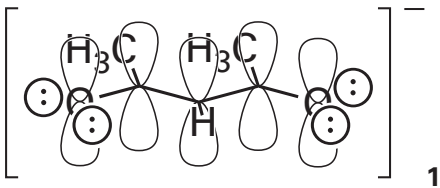

1–92

In this π molecular orbital system, the highest occupied molecular orbital, the orbital containing the excess electron density and the negative elementary charge, has nodes at the two carbons adjacent to the central carbon

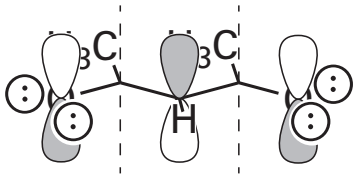

1–93

and lobes over the two oxygens and the central carbon. The highest occupied molecular orbital explains why the negative elementary charge is shared by only the two oxygens and the central carbon in the resonance structures

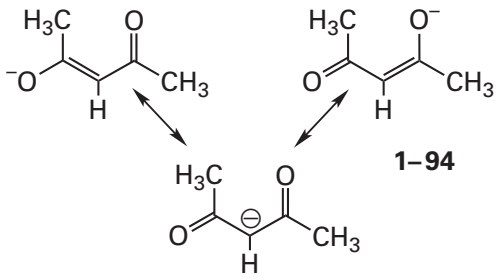

1–94

The fact that the negative elementary charge is shared by two electronegative oxygens instead of one explains the dramatic decrease in the pK_{aK}.

When one of the methyl groups of acetylacetone ($pK_{aK} = 8.9$) is replaced with an ethoxy group, the acidity decreases [pK_{aK}(ethyl acetylacetate) = 10.7], and when the other is replaced by an ethoxy as well, there is a further decrease [pK_{aK}(diethyl malonate) = 13.3]. These decreases in acidity reflect the stronger π electron donation of the lone pairs of electrons on oxygen than the hyperconjugation of the pairs of electrons in the carbon–hydrogen σ bonds of a methyl group. When one of the methyl groups of acetylacetone ($pK_{aK} = 8.9$), however, is replaced by an alkylsulfanyl group, the acidity of the carbon α to the resulting thioester remains essentially unchanged {pK_{aK}[*S*-(2-acetamido)ethylthioacetylacetate] = 8.5}, again because of the ineffective overlap of an atomic orbital on sulfur containing a lone pair of electrons with the π system of the enolate.

It is possible to acidify a hydron on a carbon adjacent to a carbonyl group further by converting the carbonyl group into an iminium[343]

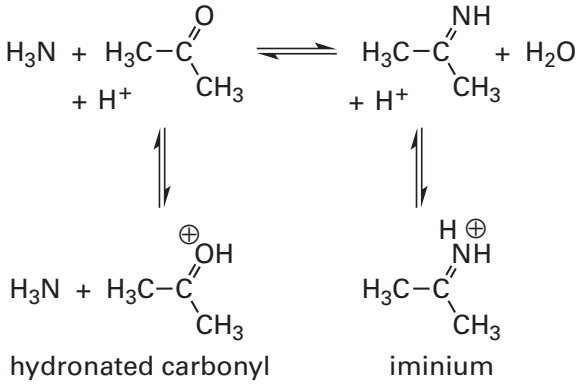

(1–112)

The pK_a of a hydron on acetone is decreased by around 11 units, from $pK_{aK} = 19$ to $pK_{aK} \cong 8$, by this substitution.[343] It has also been observed that, depending on the strength of the base, the rate of hydron removal from the α carbon increases by a factor of 10^5–10^8 in the iminium compared to the parent carbonyl compound.[343,344] Nevertheless, the rates of hydron removal from the α carbon of an iminium are a factor of 10^3 slower than the rates of hydron removal from the respective cationic carbonyl compound hydronated on its oxygen (Equation 1–112), but hydronating an imine, the conjugate acid of which has a $pK_a \cong 8$, is much easier than hydronating a carbonyl oxygen, the conjugate acid of which has a $pK_a \cong -7$.

An **enamine** is the vinylic amine that is the conjugate base resulting from the removal of a hydron from the carbon atom of an iminium

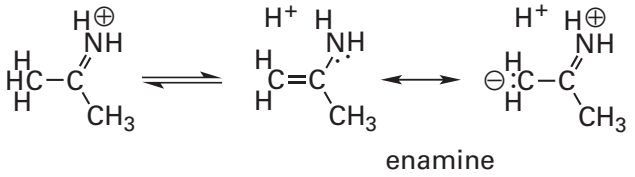

(1–113)

An enamine is more nucleophilic at the carbon than the corresponding enol tautomer (**1–89**) because the electronegativity of nitrogen is less than that of oxygen. All these considerations illustrate the advantages of an enamine relative to an enol at neutral pH in the absence of strong bases and acids.

A hydron α to a **thiocarbonyl** is also acidic.[345] The conjugate base is an **enethiolate,** a vinylic thiolate

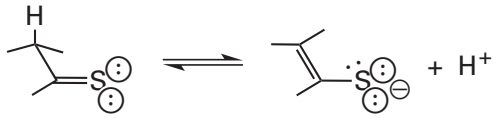

(1–114)

The **acid dissociation constants of the hydroxy groups of enol tautomers** (K_{aE} in Equation 1–110) are affected much less than those of the respective keto tautomers by substitutions at the α carbon or the carbonyl or acyl carbon (Figure 1–23), and often in the opposite direction. The values of pK_{aE} for the hydroxy groups of the enol tautomers usually fall within the range between 7 and 13, a range that makes one of these hydroxy groups a compatible partner with a base on the side chain of an amino acid in an enzyme such as a histidine ($pK_{a1} = 6.6$; $pK_{a2} = 14$), a tyrosine ($pK_a = 9.8$), a lysine ($pK_a = 10.5$), an arginine ($pK_a = 13$), or even an aspartate or a glutamate the pK_a of which has been elevated by its surroundings. Consequently, the transfer of a hydron between the hydroxy group of an enol tautomer and one of these bases will be rapid and uncomplicated. It is simply the removal of a hydron from an otherwise undistinguished heteroatom.

An enol tautomer is less nucleophilic than its conjugate enolate. One way to see this is to examine the effect of hydronation of the enolate oxygen on the distribution of electron density in the nonbonding π molecular orbital of the enolate (**1–87**). When one of the σ lone pairs of electrons on the oxygen of the enolate is hydronated, the oxygen loses the negative charge that was pushing electron density onto the α carbon, and the underlying electronegativity of its oxygen increases the π electron density on that oxygen at the expense of the electron density on carbon. Nevertheless, the carbon in an enol tautomer does retain excess electron density, as illustrated in the right-hand resonance form of **1–89**. On paper, this is an unlikely resonance form because of separation of charge, but it does indicate that the carbon shares the π electron density in the highest occupied molecular orbital and remains nucleophilic. When the enol tautomer is paired with a functional group on a side chain that has similar pK_a in the active site of an enzyme, significant amounts of the more nucleophilic enolate are usually present in rapid equilibrium with the enol. Consequently, once the enolate is formed, it is an effective nucleophile.

The enol tautomer can be produced from the keto tautomer of an aldehyde or a ketone in an acid-catalyzed reaction or base-catalyzed reaction in which either hydronation at oxygen precedes dehydronation at carbon

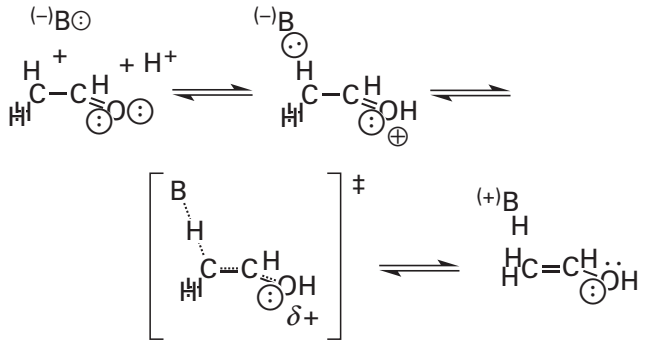

(1–115)

or hydronation at oxygen occurs simultaneously with dehydronation at carbon[346-348]

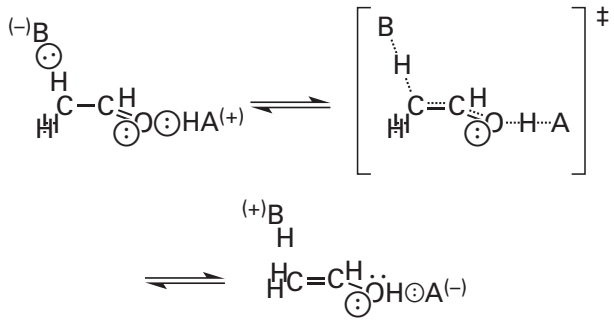

(1–116)

In either case, as indicated in Equations 1–115 and 1–116, the hydron is added to a lone pair of electrons on oxygen orthogonal to the developing π molecular orbital system of the enol tautomer, a hydronation that both increases the electronegativity of oxygen and increases its ability to withdraw electron density from the carbon–hydrogen σ bond.

The **simultaneous hydronation of the oxygen of the carbonyl or acyl group** by a general acid (Equation 1–116) makes it much easier to remove a hydron from the α carbon.[349] In the active site of an enzyme, there will usually be a Brønsted acid acting as the donor in a hydrogen bond to one of the lone pairs of electrons on the oxygen of a carbonyl or acyl group or two Brønsted acids acting as donors to both of the lone pairs. One of these donors will provide the necessary hydron. A dicationic, metallic Lewis acid coordinated to one of the lone pairs will also acidify the α hydron, an acidification making it easier to remove the hydron. Nevertheless, even when it is immediately adjacent to a carbonyl or acyl group, the oxygen of which has been hydronated or is the ligand to a metallic ion, the removal of a hydron from carbon is always slow.

The problem of removing an α hydron is encountered in the extreme in the **removal of the hydron α to a carboxylate** [pK_{aK}(acetate ion) = 33.5; Figure 1–23]. Mandelate racemase from *P. putida* removes a hydron from the α carbon of mandelate (2-phenyl-2-hydroxyacetate ion). In the active site of this enzyme, one of the carboxylate oxygens of mandelate forms a hydrogen bond with the side chain of Glutamate 317, and the other forms a hydrogen bond with the side chain of Lysine 164 and is also a ligand to a Mg^{2+} ion.[350] If the former oxygen in this complex is equivalent to the hydronated oxygen of mandelic acid, then the pK_{aK} of the hydron on the α carbon would be lowered to 22. It has been pointed out that hydronation of the second oxygen would lower the pK_{aK} of the α carbon to 7.4,[351] but the pK_a of the second oxygen should be around –8, which would make it difficult to hydronate. The postulated dihydronated intermediate would be the *gem*-enediol of mandelic acid*

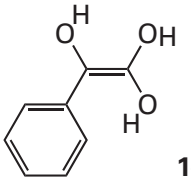

1–95

Although a particularly stable *gem*-enediol has been synthesized,[352] such compounds are usually so unstable that they cannot be observed. In addition, the fact that Mg^{2+} is bound at one of the two carboxylate oxygens when mandelic acid is bound to the active site of the enzyme also would dramatically inhibit its hydronation. The nonenzymatic dehydronation of the α carbon of mandelic acid, however, is accelerated by Mg^{2+} acting as a Lewis acid.[3] It seems to be the case that when mandelate forms a hydrogen bond at one of its carboxylate oxygens with a carboxylic acid and forms a hydrogen bond with an ammonium ion and a complex with Mg^{2+} at the other, the pK_{aK} of the hydron α to that carboxylate is decreased significantly to make its dehydronation relatively rapid.

So far, the nucleophilic substitution of one heteroatom for another at a saturated carbon, a carbonyl carbon, an acyl carbon, or phosphorus; the nucleophilic addition of a heteroatom to a carbonyl group; and the oxidation or reduction of carbon by the transfer of a hydride have been discussed. These several classes of organic reactions account for most of metabolism. They do not, however, involve the making or breaking of carbon–carbon bonds, which is essential to biosynthesis as well as catabolism.

Carbon–carbon bonds are usually made or broken biochemically by the nucleophilic addition of an enolate or an enamine to a carbonyl group or by the nucleophilic substitution of a heteroatom at an acyl group by an enolate or an enamine. An enzymatic example of the nucleophilic addition of an enamine to a carbonyl group is the **aldol condensation** catalyzed by fructose-bisphosphate aldolase

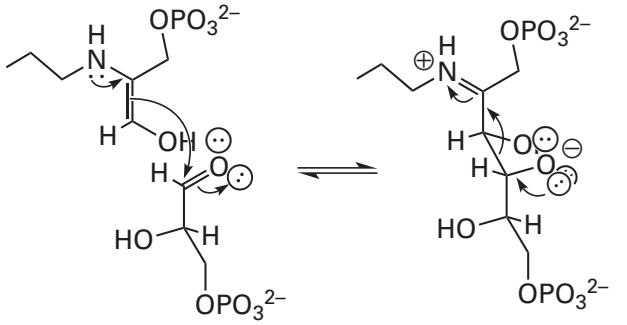

(1–117)

An enzymatic example of the substitution of an enolate for the thiol of a thioester is the **Claisen condensation** catalyzed by the active site for 3-oxoacyl-[acyl-carrier-protein] synthase in fatty acid synthase

*Enetriol **1–95** is a *gem*-enediol that happens to have a hydoxy group at carbon 2. It is the *gem*-enediol, the two hydroxy groups on carbon 1, that would make the intermediate dramatically unstable were it free in solution rather than bound in an active site.

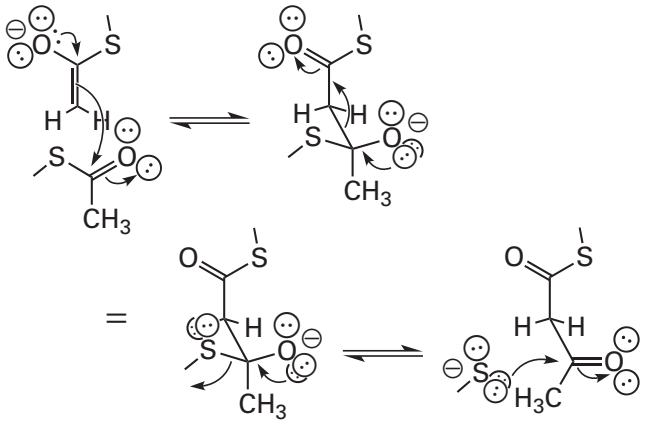

(1–118)

In an aldol condensation in which the enolate is held immediately adjacent to the carbonyl group with which it is to condense, as in the base-catalyzed reaction

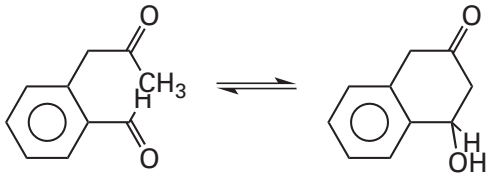

(1–119)

the rate-limiting step of the nucleophilic addition is the removal of the hydron from the α carbon to form the enolate[353] because the rehydronation of the enolate on carbon is much slower[324] than its condensation with the carbonyl or acyl group. Presumably, in the active site of an enzyme, where the enolate or enamine and the carbonyl or acyl group are held even more rigidly, the rate-limiting step of the reaction will usually be the removal of the hydron from carbon.

In enzymatic aldol condensations and Claisen condensations, there is usually a catalytic acid that is the donor for a hydrogen bond to the carbonyl or acyl oxygen on the electrophile: for example, the aldehyde to which the enolate adds in the reaction catalyzed by fructose-bisphosphate aldolase (Equation 1–117) or the thioester to which the enolate adds in the reaction catalyzed by 3-oxoacyl-[acyl-carrier-protein] synthase (Equation 1–118). This hydrogen bond with the acid polarizes the carbon–oxygen double bond and increases its electrophilicity significantly,[349] in addition to providing the hydron required in the formation of the hydroxy group.

In the **reverse reactions** of Equation 1–117 and the first step in Equation 1–118, one of the lone pairs of electrons on the incipient carbonyl or acyl oxygen, respectively, participates in the breaking of the carbon–carbon bond by providing **push**. For example, in the reverse of Equation 1–117

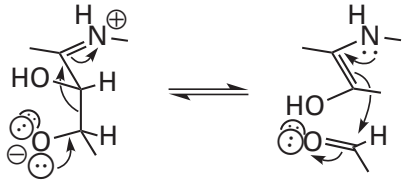

(1–120)

the orbitals that mix to form the transition state, and that also must be able to overlap as the transition state is approached, are the atomic orbital bearing the lone pair of electrons on the oxyanion, the σ molecular orbital system of the carbon–carbon σ bond that is broken, and the π molecular orbital system of the carbon–nitrogen double bond (Figure 1–25). A hydroxy group in a hydrogen bond also provides push, but it is weaker.

In the direction of forming the carbon–carbon bond in Equation 1–117, the orbitals that mix to produce the transition state are the π molecular orbital system of the enamine and the π molecular orbital system of the carbonyl group. For the transition state to be accessible, these atomic orbitals and all the composite atomic orbitals of these molecular orbitals must be parallel to each other, as indicated in Equation 1–120 and Figure 1–25. By microscopic reversibility, if the sp^3 atomic orbital on the oxygen providing the push enters the reaction parallel to the σ bond being broken, it must emerge from the transition state in the reverse reaction parallel to the newly formed σ bond.

Enolates, enols, enamines, and enethiols[345] are intermediates in carboxylations and decarboxylations. The most consequential examples of such reactions are the carboxylation of ribulose 1,5-bisphosphate, which is responsible for the fixation of carbon dioxide during photosynthesis and hence ultimately all the carbon in living organisms, and the decarboxylation of oxalosuccinate, which is responsible for a significant fraction of the expired carbon dioxide in living organisms.

Carbon dioxide

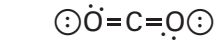

1–96

can be considered to be a dicarbonyl compound*

*Because of the two perpendicular π systems in carbon dioxide that each include all three of the atoms, the oxygens in carbon dioxide are hybridized *sp* and resemble the oxygens in a carbonyl compound in the gas phase or an aprotic solvent.

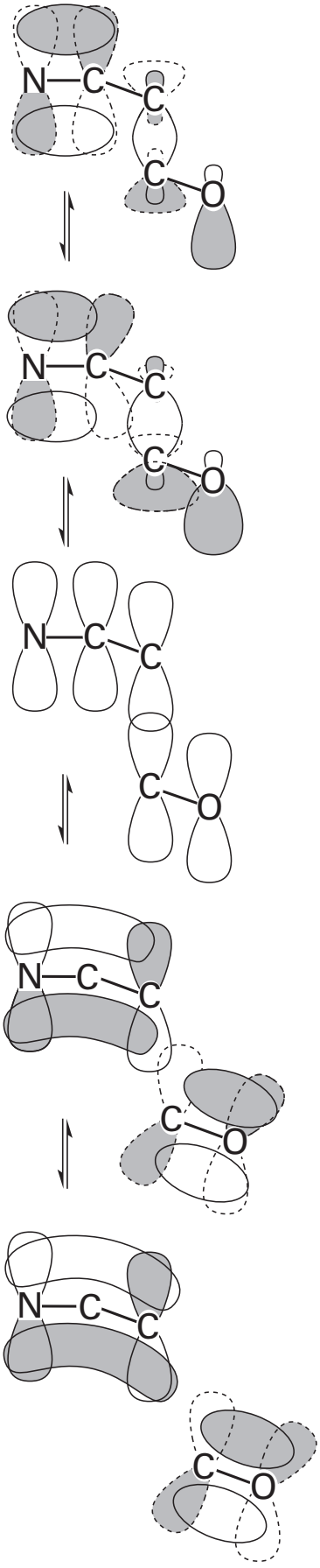

Figure 1–25: Breaking or forming of a carbon–carbon bond adjacent to an imine (Equation 1–117). The reaction breaking the carbon–carbon bond is initiated by overlap of the atomic orbital occupied by the lone pair of electrons on oxygen (solid outline) and the unoccupied antibonding σ molecular orbital of the carbon–carbon bond (dashed outline) and by overlap of the occupied bonding σ molecular orbital of the carbon–carbon bond (solid outline) and the unoccupied antibonding π molecular orbital of the carbon–nitrogen π bond (dashed outline). In the transition state, five p orbitals, one from each of the five atoms, overlap. The transition state decomposes through overlap of the occupied nonbonding π molecular orbital of the enamine (composed from the two peripheral p orbitals of the enamine) and the unoccupied antibonding π molecular orbital (dashed outline) of the carbon–oxygen π bond. The formation of the carbon–carbon bond is the reverse direction.

in which the central carbon is electrophilic and hence a Lewis acid, as is a hydron. In fact, it is educational to consider carbon dioxide and a hydron to be interchangeable, as was the case when the final steps in the respective mechanisms of crotonyl-CoA carboxylase/reductase (Equation 1–99) and enoyl-[acyl-carrier-protein] reductase (NADH) were equated. As a Lewis acid, the central carbon in carbon dioxide associates with a nucleophilic lone pair of electrons during a **carboxylation**. Again, the simplest example of such a nucleophilic addition is **hydration**

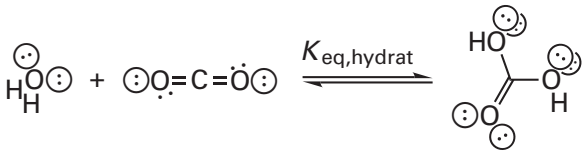

(1–121)

The mechanism of the hydration of carbon dioxide involves removal of a hydron from water and addition of a hydron to one of the carbonyl oxygens during the nucleophilic addition to form the bicarbonate, which is then hydronated as a simple base. As a carbonyl compound, carbon dioxide can also participate in nucleophilic additions to its dicarbonyl group by enolates

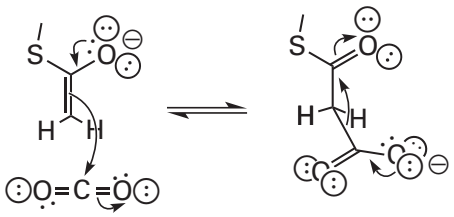

(1–122)

When carbon dioxide dissociates from an acidic carbon during a **decarboxylation**, its dissociation is analogous to that of a hydron from the same acidic carbon. Evidence for this conclusion is that the common logarithms of the rate constants for a series of decarboxylations are linearly related to the values of pK_a for dissociation of a hydron from the respective positions in the respective carbon acids, with a Brønsted slope, β, of –0.7.[354]

Decarboxylations, because they are the reverse of additions of the dicarbonyl group of carbon dioxide to an enolate, are assisted by **push from the lone pairs of electrons on the carboxylate**

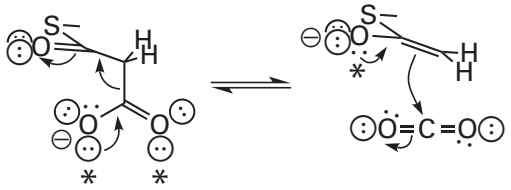

(1–123)

In this equation the negative elementary charge is moved among the three oxygens the lone pairs of electrons of which are indicated by asterisks. The lone pairs of electrons providing the push are parallel to the carbon–carbon bond that is cleaved during the decarboxylation, and that σ bond must also be parallel to the π system of the carbon–oxygen double bond of the adjacent carbonyl or acyl group (reverse of Equation 1–123). This alignment is enforced, for example, by the enzyme isocitrate dehydrogenase ($NADP^+$) from *E. coli* in its complex with the oxalosuccinate that it decarboxylates[355]

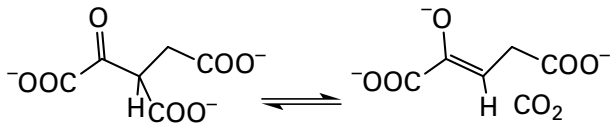

(1–124)

In free solution, **decarboxylations of β-oxo acids** occur more rapidly when the carboxy group is hydronated than when it is unhydronated and anionic, a fact that seems counterintuitive. This increase in rate is usually explained, however, as the result of an **intramolecular transfer of the hydron** between a hydronated lone pair of electrons on the oxygen of the carboxylic acid and the lone pair of electrons on the oxygen of the carbonyl or acyl group

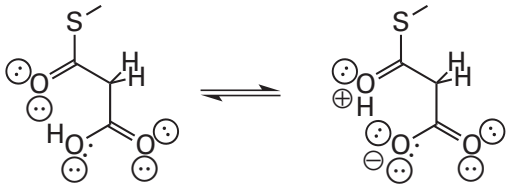

(1–125)

This stereochemically efficient transfer of a hydron from one oxygen to another oxygen that is four atoms away enhances the ability of the acyl or carbonyl group to which the hydron is transferred to withdraw electrons from the carbon–carbon bond to be broken. The transfer of the hydron also increases the push of the lone pairs of electrons on the oxygens of the carboxy group from which the hydron is transferred. Because it is between two lone pairs of electrons, both orthogonal to the orbitals mixing in the transition state for decarboxylation, and because it is sterically impossible while the atomic orbitals of the transition state for decarboxylation are aligned, the transfer of the hydron must precede and must be independent from the decarboxylation itself. The transfer of the hydron and the decarboxylation itself are separated from each other by a rotation around a carbon–carbon bond

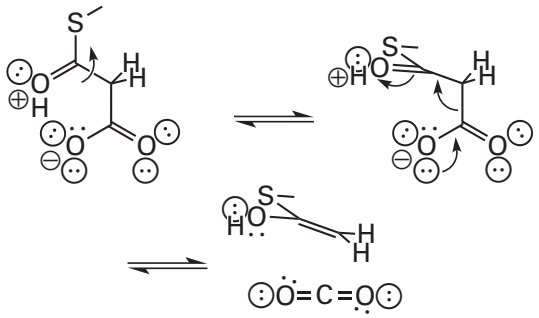

(1–126)

Although it is stereochemically allowed, the transfer of a hydron from a carboxy group to a carbonyl oxygen or acyl oxygen ($\Delta pK_a = +11$) is still thermodynamically unfavorable. In the nonenzymatic decarboxylation of β-oxo acids, this transfer of the hydron from the carboxylic acid to the carbonyl or acyl oxygen permits the enol tautomer to be the immediate product of the decarboxylation (Equation 1–126). Such decarboxylations are also further enhanced by forming the imine at the carbonyl carbon.[356]

Because the transfer of the hydron must precede the dissociation of the carbon–carbon bond and because a rotation is required between transfer of the hydron and dissociation of the carbon–carbon bond, such an intramolecular transfer of the hydron probably cannot occur within the active site of an enzyme, in which substrates are usually held rigidly and seldom permitted to rotate internally, unless required by the reaction. In such a situation, the hydron must be supplied by some other acid, such as the side chain of an amino acid, and the carboxylate must be unhydronated, as it usually is when it enters the active site.

Metallic ions, such as cupric ion, can catalyze the decarboxylation of β-oxodicarboxylic acids, presumably by forming a complex involving the carbonyl oxygen of the β-oxo group and the uninvolved carboxylate in the enolate that will be the leaving group from carbon dioxide

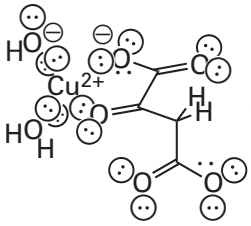

1–97

The metallic ion neutralizes the negative charge forming on the carbonyl oxygen during the reaction.[357] A lone pair of electrons on the uninvolved carboxylate of the dicarboxylic acid provides an additional point of attachment for the copper, the main function of which is to act as a Lewis acid at the oxygen of the incipient enolate and stabilize it as if the metallic ion were a hydron.

The **decarboxylation of 1,3-dimethylorotic acid**, which is an analogue of the reaction catalyzed by orotidine-5′-phosphate decarboxylase, is quite peculiar because it proceeds through a carbanion that, unlike those discussed so far, cannot be stabilized by an adjacent carbonyl or acyl group because it is orthogonal to any that are available. It is believed that the carbanion is stabilized as a **partial ylide** with the electron-deficient nitrogen immediately adjacent to it.[358]

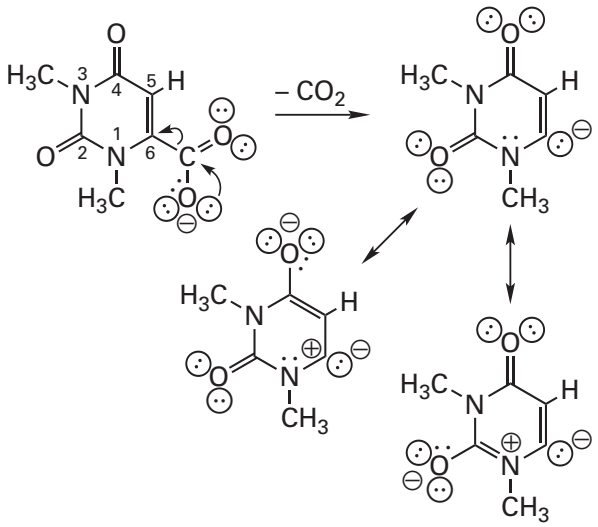

(1–127)

The decarboxylation of 1,3-dimethylorotic acid (Equation 1–127) is enhanced when one of the exocyclic oxygens is hydronated, which would further increase the positive charge on nitrogen 1. In addition, carbon 6 in 1,3-dimethylorotic acid and carbon 6 in uridine are both electropositive because they are each the β carbon in an α,β-unsaturated amide. The exchange of the hydron at carbon 6 of uridine for a deuteron in the solution, which is catalyzed by hydroxide, increases 5000-fold when the hydrogen on carbon 5 of the uridine is replaced by a fluorine.[359] This observation is consistent with a carbanionic partial ylide homologous to the one in Equation 1–127 performing the role of an intermediate in this exchange because electron withdrawal by the adjacent fluorine should stabilize the anion. For reasons that are not obvious because if anything the negative elementary charge is less delocalized in the product and hence in the transition state, the rate constant at 25 °C for the decarboxylation of 1-cyclohexylorotic acid is greater by a factor of 1000 in nonpolar solvents such as dioxane and tetrahydrofuran than it is in water. This observation suggests that the removal of orotidine 5′-phosphate from water as it enters the active site of orotidine-5′-phosphate decarboxylase by itself is responsible for a portion of the catalysis achieved by the enzyme.[360]

Enol tautomers are also intermediates in the isomerizations of α-hydroxy ketones or α-hydroxy aldehydes.[361] An example of such an enzymatic reaction is that catalyzed by triose-phosphate isomerase

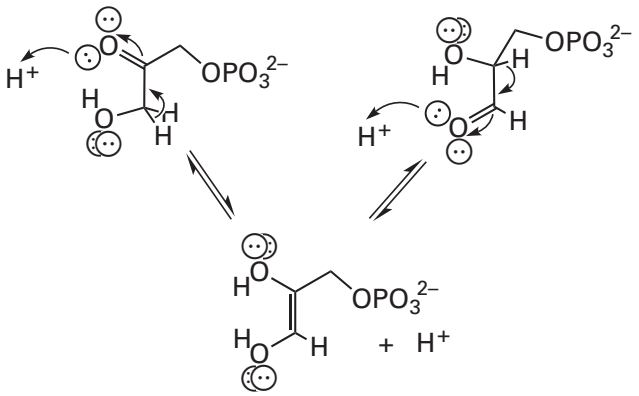

(1–128)

in which the carbonyl group moves between two adjacent carbons. A similar isomerization can interconvert a carbonyl group and an acyl group by the same mechanism[362,363] as in the reaction catalyzed by lactoylglutathione lyase

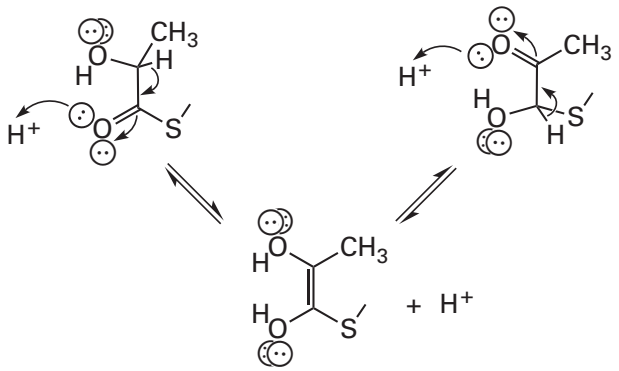

(1–129)

Suggested Reading

Bender, M. L., and Williams, A. (1966) Ketimine intermediates in amine-catalyzed enolization of acetone, *J. Am. Chem. Soc. 88*, 2502–2508. https://doi.org/10.1021/ja00963a026

Chiang, Y., and Kresge, A. J. (1991) Enols and other reactive species, *Science 253*, 395–400. https://doi.org/ 10.1126/science.253.5018.395

Elimination–Addition

In an elimination–addition, an acid or electrophile and a base or nucleophile are removed from two adjacent carbons or two carbons separated by one or more double bonds to produce a double bond or an additional double bond or an acid or electrophile and a base or nucleophile are added to a carbon–carbon double bond or the two ends of a conjugated set of double bonds.* For example, during the elimination[364]

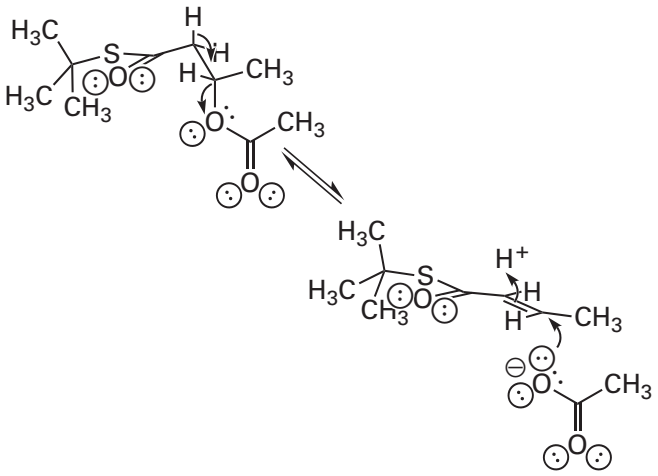

(1–130)

a hydron is removed from one carbon and acetate leaves the adjacent carbon to produce the carbon–carbon double bond. In the addition, which is the reverse reaction, a hydron is added to one carbon and acetate adds to the other carbon in a carbon–carbon double bond. The thioester adjacent to the hydron that is removed facilitates the reaction by acidifying that hydron.

Some elimination–additions proceed through an intermediate carbenium ion and others proceed through an intermediate carbanion but the majority are probably somewhere on a spectrum between these extremes. Two examples of **elimination–additions that proceed through a carbenium ion** are the hydration–dehydration of simple aliphatic olefins such as propene in solutions of strong acids[365] and the more complex elimination of trifluoroacetate and a hydron from 2-(dimethyl-amino)-1-methyl-1-phenyl-2-thioxoethyl 2,2,2-trifluoroacetate[366]

*Most acids are electrophiles and most bases are nucleophiles and vice versa, but each person has a term she prefers for each particular example of an electrophile or an acid and for each particular example of a nucleophile or a base.

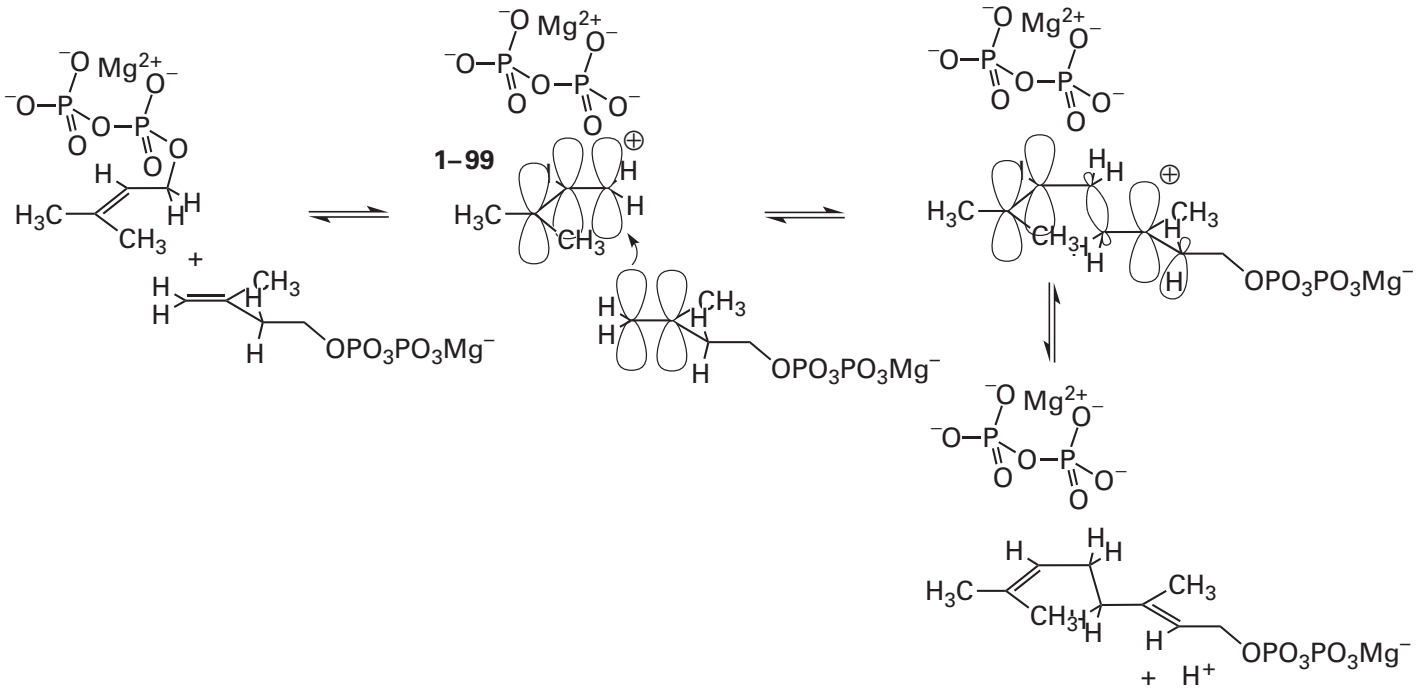

Figure 1–26: Addition of the 3,3-dimethylallyl carbenium ion to isopentenyl diphosphate. The 3,3-dimethylallyl carbenium ion is formed by elimination of diphosphate from 3,3-dimethylallyl diphosphate. The carbon–carbon double bond of isopentenyl diphosphate adds to this allyl carbenium ion to form a new carbon–carbon σ bond in a carbenium ionic adduct. The carbenium ionic adduct loses a hydron in an acid dissociation to produce geranyl diphosphate.

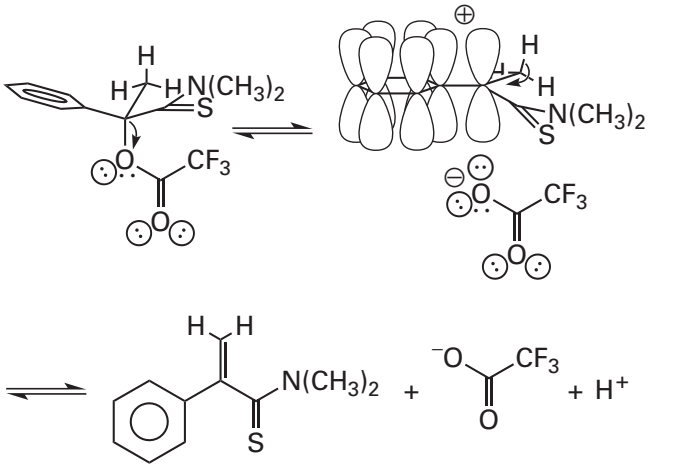

(1–131)

In this latter instance, the intermediate carbenium ion is stabilized by the adjacent phenyl group. In the dehydration–hydration catalyzed by imidazole-glycerol-phosphate dehydratase from *E. coli*,[367] the intermediate carbenium ion is stabilized by an adjacent neutral imidazolyl group

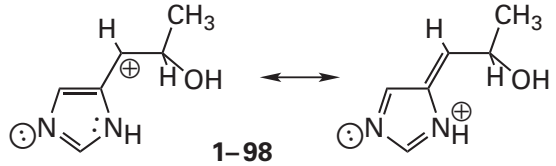

1–98

In this instance, because they are two atoms apart, if either nitrogen is hydronated, the same resonance structures stabilize the carbenium ion: regardless of which nitrogen is hydronated, the formal positive elementary charge ends up on it in the same resonance structure. The resonance structures define the electron donation from the π molecular orbital system of the imidazolyl group to the carbenium ion.

An example of an addition that proceeds through a carbenium ion but involves the initial addition of an **electrophile other than a hydron** occurs in terpene biosynthesis in the reaction catalyzed by dimethylallyl*trans*transferase (Figure 1–26). Carbenium ion **1–99** formed from 3,3-dimethylallyl diphosphate adds to isopentenyl diphosphate, but instead of then reacting with a nucleophile, which is a possibility that the enzyme guards against, the resulting carbenium ion eliminates a hydron to yield the desired product, geranyl diphosphate. The first step in the reaction is the formation of the allylic 3,3-dimethylallyl carbenium ion **1–99**, which consists of three parallel *p* orbitals creating an allyl π molecular orbital system with only two π electrons. It is a Lewis acid, and it adds as would a hydron to the carbon–carbon double bond in isopentenyl diphosphate.

Examples of **elimination–additions that proceed through an enolate** are the elimination of methoxide and a hydron from 4-methoxybutan-2-one under basic conditions to give the respective α,β-unsaturated carbonyl compound[368]

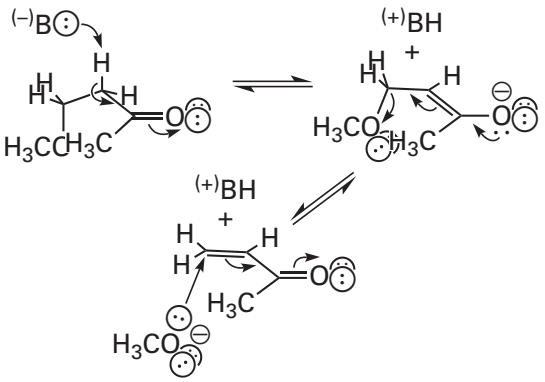

(1–132)

and elimination of the phosphate and a hydron when glyceraldehyde 3-phosphate is exposed to base[361]

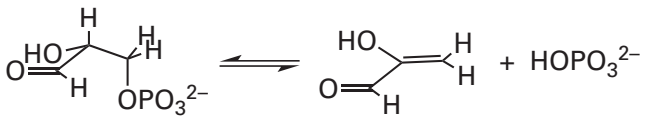

(1–133)

In both of these instances, removal of the hydron on a carbon adjacent to a carbonyl group initiates the elimination rather than dissociation of the leaving group.

The dissociation of the respective leaving group in the second steps of Equations 1–132 and 1–133 is effected by the **push of the enolate**. To experience the push, the σ bond between the oxygen on the leaving group and the carbon from which it is leaving must be aligned parallel to the π system of the enolate before elimination can proceed

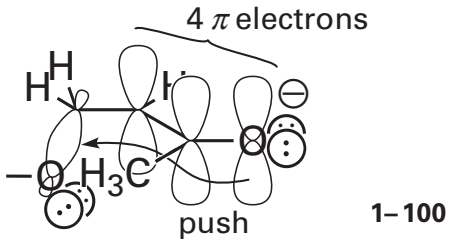

1–100

Electron density in the highest occupied molecular orbital of the enolate (**1–87**) enters the unoccupied antibonding molecular orbital of the carbon–oxygen σ bond on the β carbon and pushes away the two σ electrons of the leaving group that originally were in the bonding σ molecular orbital of the carbon–oxygen bond.

As in Equations 1–132 and 1–133, in most elimination–additions that proceed through a carbanionic intermediate, the intermediate is an enolate. There are, however, other ways to stabilize a carbanion. In the elimination of hydrogen fluoride from 2-(2-fluoroethyl)-1-methylpyridinium in strongly basic aqueous solution, the intermediate carbanion produced by the dissociation of a hydron[369] is stabilized by the adjacent pyridinium group

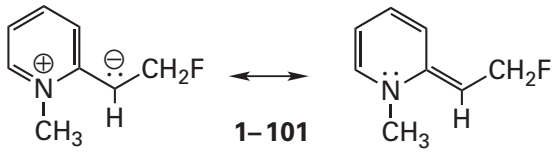

1–101

much as the electron excess in the pentadienyl molecular orbital system of reduced nicotinamide is stabilized by the nitrogen in the ring (Equation 1–78). In effect, however, this stabilization is achieved by the equivalent of an iminium conjugated to the carbanion through two double bonds.

The isomerization of olefins can proceed through either an intermediate carbenium ion or an intermediate carbanion. For example, the isomerization of simple aliphatic olefins under acidic conditions proceeds through a carbenium ion

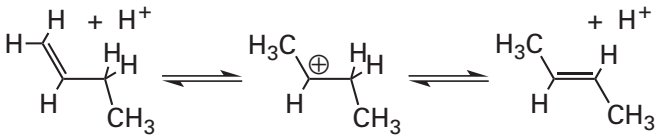

(1–134)

Isomerization of carbon–carbon double bonds α to carbonyl or acyl groups, however, can occur under basic conditions by proceeding through an enolate, which is the conjugate base common to the different isomers. For example, the isomerization of *S*-(1,1-dimethylethyl) but-3-enethioate to *S*-(1,1-dimethylethyl) but-2-enethioate[370] proceeds through the enolate

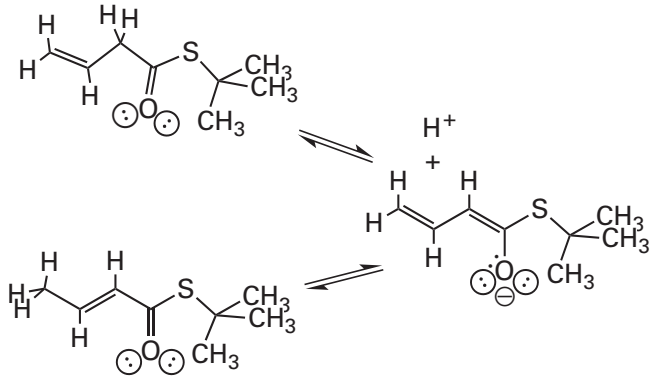

(1–135)

As has already been discussed, the excess negative elementary charge is delocalized over five atoms in the enolate, four carbons and one oxygen. The cis and trans isomers of a carbon–carbon double bond can be equilibrated in the same way.

A **concerted elimination–addition** is one in which there is no carbanionic or carbocationic intermediate because the bond between the one carbon and the base or the nucleophile that is the leaving group is breaking or forming in concert with the breaking or forming of the bond between the other carbon and the electrophile or hydron. The degree to which the bond between the leaving group and its carbon is broken in the transition state of a concerted elimination is assessed by **Brønsted correlations** between the pK_a of the conjugate acid of the leaving group and the rate of the reaction, and the degree to which the bond between the electrophile or the hydron and its carbon is broken is assessed by Brønsted correlations between the pK_a of the conjugate acid of the base that removes the hydron and the rate of the reaction. For example, in the concerted elimination of the respective sulfides from a series of 2-cyanoethyl-sulfonium ions catalyzed by a series of amines

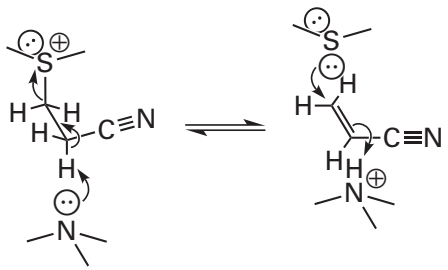

(1–136)

the Brønsted slopes for the catalytic amines ($\beta = 0.62$–0.75) and for the leaving groups ($\beta_{lg} = -0.24$ to -0.38) indicate that, in the transition state for this reaction, the bond between one carbon and the hydron and the bond between the other carbon and the sulfur are both dissociating in concert.[371]

Because the removal of the hydron from the one carbon and dissociation of the leaving group from the other carbon are both proceeding as the transition state is reached, the rate constant of a concerted elimination increases as the strength of the base that removes the hydron increases and as the acidity of the conjugate acid of the leaving group increases.[372] It follows that the rate of a concerted elimination will also increase when **the ability of the leaving group to dissociate** is improved by hydronating it or adding another electrophile to it before it leaves.

In many nucleophilic substitutions, nucleophilic additions, and elimination–additions catalyzed by an acid or a base, the making or breaking of a bond is concerted with the transfer of a hydron (Equations 1–29, 1–33, 1–38, 1–116, and 1–136 and Figures 1–7 and 1–8). In such concerted reactions, a correlation is often observed between the rate of the reaction and changes in both the strength of the acid or the base catalyzing the reaction and the strength of the bond between the two heavy atoms being made or broken brought about by the effect of adjacent substituents. For example, in the acid-catalyzed dissociation of an alcohol from the anionic conjugate base of its hemiacetal with acetaldehyde

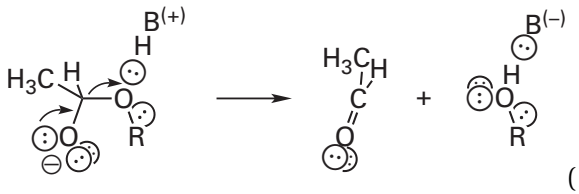

(1–137)

as the alcohol becomes a better leaving group, the effect of acidity of the acid on the rate of the reaction decreases.[373] This interaction suggests that transfer of the hydron and the breaking of the bond to the leaving group occur in the same transition state and are thus concerted. Likewise, in the elimination of sulfides from β-cyanoethylsulfonium salts (Equation 1–136), as the strength of the base that removes the hydron from carbon increases, the effect of acidity of the leaving group on the rate of the reaction, as reflected in the Brønsted coefficient β_{lg}, decreases. This **interaction coefficient** ($\partial\beta_{lg}/\partial pK_{a,BH} = 0.026$) was presented as evidence for the conclusion that the breaking of the bond between the leaving group and one carbon is simultaneous with the transfer of the hydron from the other carbon to the base and that the elimination is concerted.[371]

An elimination–addition passing through an intermediate carbocation and an elimination–addition passing through an intermediate carbanion are two extremes of a spectrum of mechanism, and each concerted elimination–addition occupies a position in this spectrum between these two extremes. The two determinants of this spectrum of mechanism[369] are the degree to which the bond between the acid or the electrophile and the one carbon is broken or formed and the degree to which the bond between the base or the nucleophile and the other carbon is broken or formed in the transition state.[371] As with a nucleophilic substitution at a tetrahedral, saturated carbon (Figure 1–4) or a nucleophilic substitution at phosphorus (Figure 1–15), this spectrum of mechanism can be appreciated by examining a **three-dimensional surface of potential energy** for an elimination–addition (Figure 1–27). In the case of elimination–addition,[78] one coordinate is the distance between the atom of the base or nucleophile that is leaving and the carbon from which it is leaving, and the other coordinate is the distance between the atom of the acid or electrophile and the carbon from which it is being removed. The third coordinate is the potential energy of the system for each pair of coordinates.

For an elimination–addition with an intermediate enolate (Figure 1–27A) or some other carbanionic intermediate, there is a well of potential energy in the **upper left corner** of the diagram because this is the position at which the acid or the electrophile has been removed far enough from its carbon that it no longer affects the potential energy of the system, but the bond between the leaving group and the other carbon has remained intact. If the reaction proceeds through an enolate or another carbanionic intermediate because it is the most stable of all the possibilities, there will be two cols of potential energy: one between the reactants and the carbanionic intermediate and the other between the carbanionic intermediate and the products.

For an elimination–addition with an intermediate carbenium ion (Figure 1–27B), there is a well of potential energy in the **lower right corner** of the diagram because this is the position at which the leaving group has been removed far enough from its carbon that it no longer affects the potential energy of the system, but the bond between electrophile and the other carbon is still intact. If the reaction proceeds through an intermediate carbenium ion because it is the most stable of all the possibilities, there will again be two cols of potential energy: one between the reactants and the intermediate carbenium ion and the other between the carbenium ion and the products.

There is, however, always the possibility in an elimination–addition that there is a col of potential energy, lower than any other col, at a point where the bond between the base or nucleophile and the carbon from which it is dissociating is partially broken while the bond between the acid or electrophile and the carbon from which it is being removed is partially broken. In this case, there would be neither an intermediate carbenium ion nor a carbanionic intermediate (Figure 1–27B). Such elimination–additions are concerted. Each of the reaction coordinates for these concerted elimination–additions passes through only one col **somewhere outside the corners** and has only one transition state at this one col.

The position of the col defining the transition state in an elimination–addition on the surface of potential energy is determined, in part, by the **ability of the leaving group**. In addition to changing the rate of an elimination, changing the leaving group can change the nature of the transition state. The elimination of HF from 1-methyl-2-(2-fluoroethyl)-pyridinium passes through zwitterionic intermediate **1–101**, which is formed by the initial removal of a hydron because fluorine is such a poor leaving group ($pK_{aHF} = 3.2$). When the fluorine is replaced by the better leaving group chlorine ($pK_{aHCl} = -7$) and then by the even better leaving group bromine ($pK_{aHBr} = -9$), rather than passing through the homologous zwitterionic intermediates, the reactions pass through concerted transition states in which dissociation of the bond between the halogen and its carbon becomes greater and greater, and dissociation of the bond between the hydron and the carbon adjacent to the pyridinium becomes lesser and lesser as the halogen becomes a better and better leaving group.[369]

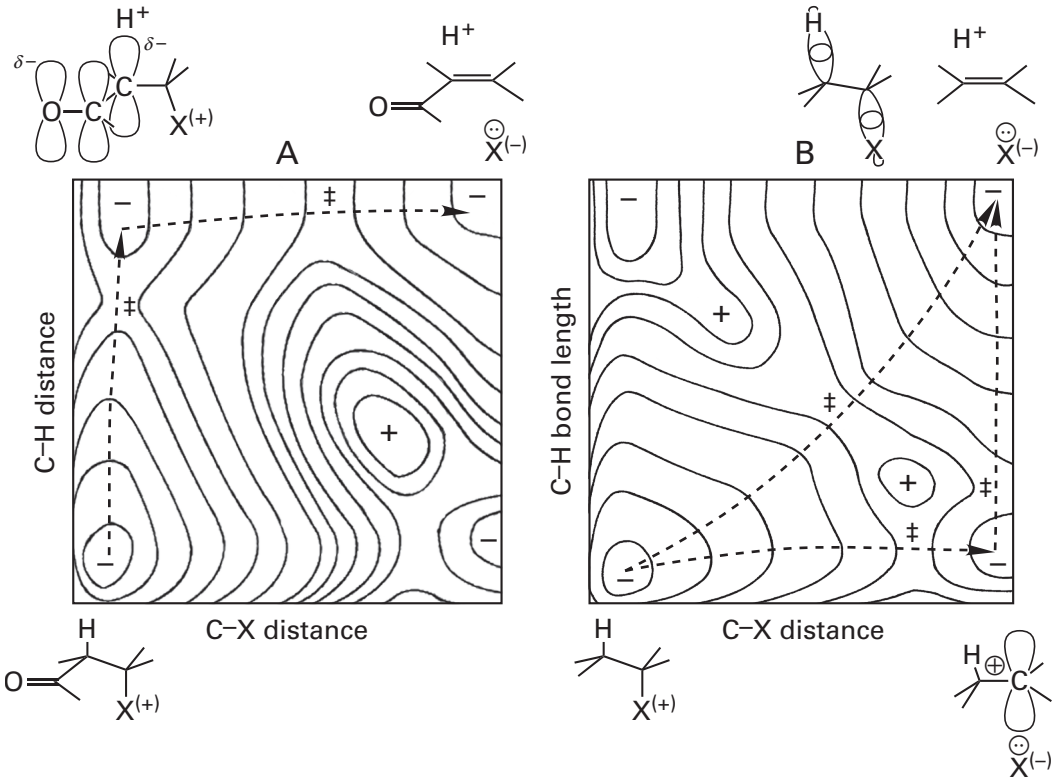

Figure 1–27: Hypothetical three-dimensional representations of surfaces of potential energy[77,78] for elimination–addition. The ordinate of the plot is the distance between the hydron that is being removed during an elimination and its carbon. The abscissa of the plot is the distance between the atom X that is leaving during an elimination and its carbon. The intersection of these two axes, for the sake of brevity, is not the point at which each has a value of zero, which would be a singularity of potential energy. The point of their intersection has coordinates or distances close to the values of the lengths of the respective covalent bonds, that between the hydrogen atom and its carbon and that between the leaving group X and its carbon. The third dimension is the potential energy associated with each value for these two distances. The third dimension is represented topographically by contour lines of equal potential. These contour lines represent a sinuous surface of potential energy. The two topographic maps of potential energy are entirely hypothetical, do not represent the surface of potential energy for any reaction, and are intended only for demonstration. The positive signs identify peaks of potential energy, and the negative signs identify wells of potential energy. The usual sign (‡) for a transition state designates a minimum of potential energy between reactants and products at the col through which the reaction proceeds. Dashed, curved arrows indicate the path of the reaction coordinate along which the reaction proceeds. The species involved as reactants, intermediates, transition states, or products are represented outside the plots, below (reactants or intermediate carbocation) or above (intermediate enolate, associated intermediate, or products) the locations of their respective potential energies. The corresponding addition proceeds along the same reaction coordinate through the same col or cols inthe reverse direction of the elimination. **(A)** Hypothetical surface of potential energy for an elimination with an enolate as an intermediate. The hydron is removed completely (vertical arrow) from its carbon before the leaving group dissociates (horizontal arrow) from the resulting enolate. The enolate is in a well of potential energy, as are the reactants and the products. There is a transition state between the reactant and the enolate and a transition state between the enolate and the products. **(B)** Hypothetical surface of potential energy for an elimination that could proceeds through a carbocationic intermediate or a concerted elimination in which the hydron is removed at the same time that the leaving group is dissociating. In this case, two possible paths on which the reaction could proceed were arbitrarily given cols of the same potential energy to illustrate the two possibilities. In the elimination proceeding through a carbocation as an intermediate, the atom X that is leaving dissociates completely from its carbon before the hydron is removed from its carbon. These two consecutive reactions follow the reaction coordinates represented by the horizontal and vertical arrows, respectively. In the concerted elimination (represented by the diagonal arrow), the atom X that is leaving dissociates from its carbon as the hydron is being removed from its carbon. Consequently, there is only one col between reactants and products and only one transition state. In any particular elimination–addition, the col for the reaction can be located at any point on the surface of potential energy between the coordinates for an intermediate enolate (upper left) or the coordinates for an intermediate carbocation (lower right). Adapted with permission from reference 77. Copyright 1972 American Chemical Society. https://doi.org/10.1021/cr60280a004

The position of the col defining the transition state for a concerted elimination–addition on the surface of potential energy is also determined, in part, by the **substituents on the substrate** from which the acid and base dissociate. In the transition state of a concerted elimination–addition, the bond to the hydron is breaking or forming at the same time that the bond to the leaving group or nucleophile is breaking or forming, and negative charge is accumulating on the former carbon while positive charge is accumulating on the latter. Any alteration in the substrate itself that stabilizes positive charge on the carbon from which the leaving group dissociates, or with which the nucleophile or the base associates, will shift the col in the direction of a carbenium ion as an intermediate. Any alteration in the substrate that stabilizes negative charge on the carbon from which the hydron or the electrophile is removed or added will shift the col in the direction of a carbanion as an intermediate. If one or the other of these accumulations of charge is stabilized sufficiently, the breaking or forming of the bond creating that charge precedes completely the breaking or forming of the other bond, and the reaction passes through an intermediate carbanion or carbocation.

Because negative charge is accumulating on one carbon while positive charge is accumulating on the other, any alteration that stabilizes either of these accumulations of charge will also increase the **rate of a concerted elimination–addition**.[340,372,374] For example, the elimination of HBr from ethyl bromide catalyzed by ethoxide in ethanol is 5 times slower than its elimination from isopropyl bromide, which is 4 times slower than its elimination from 1-phenylethylbromide[372] because these alterations stabilize the partial positive elementary charge that has developed on the carbon from which the bromide is leaving. In the enzymatically catalyzed hydration of *trans*-crotonyl-SCoA

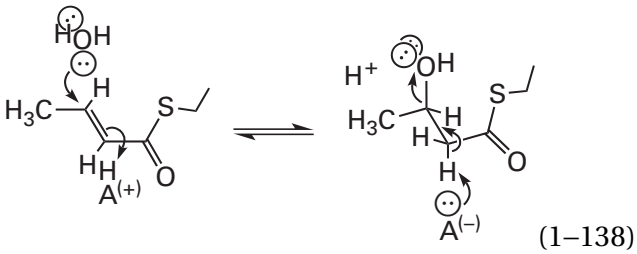

(1–138)

changing the sulfur of the thioester to an oxygen[340] destabilizes the accumulation of negative charge on the α carbon and decreases the acidity of that carbon (Figure 1–23), and the rate of the reaction decreases by a factor of 300.

In a concerted elimination–addition, the pair of electrons in the σ bond between the carbon and either the hydron or the electrophile, which are shifted onto that carbon by dissociation of the hydron or the electrophile and which create the negative charge accumulating on that carbon, provide **push to expel the leaving group**. For example, in Equation 1–136, the atomic orbitals that mix in the transition state of the concerted elimination–addition

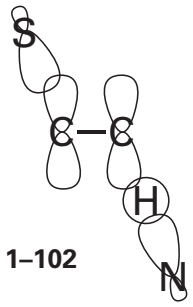

1–102

are the atomic orbital of the amine containing the basic lone pair of electrons that removes the hydron, the *s* atomic orbital of the hydrogen, the two respective *p* atomic orbitals on the two adjacent carbons, and the atomic orbital on the leaving sulfur. All must be parallel to each other. During the approach to the transition state, electrons in the bonding molecular orbital of the σ bond between carbon and the hydrogen that is dissociating are entering the *p* orbitals that are forming on the two carbons, which will become the π molecular orbital system of the carbon–carbon double bond. Through these *p* orbitals they are also entering the antibonding orbital of the σ bond of the carbon–sulfur bond and pushing away the leaving group.

The stereochemistry of a concerted elimination–addition is determined mainly by steric effects. Concerted eliminations are usually anti eliminations as shown in Equation 1–136. An **anti elimination** is an elimination in which the leaving group and the hydron or electrophile dissociate on opposite sides of a plane containing the carbons in a carbon–carbon bond to which they are attached. The orbitals taking part in the elimination, however, are all required to be periplanar. A **syn elimination** is an elimination in which the leaving group and the hydron or electrophile dissociate on the same side of a plane containing the carbons in a carbon–carbon bond to which they are attached. The orbitals are

still periplanar, but the transition state is so crowded as to be sterically disfavored. This crowding, however, is not severe. For example, under basic conditions, the elimination in Equation 1–130, in which the two hydrons, syn and anti, although diastereotopic, have almost the same acidity, proceeds with 15% syn elimination.[364]

When elimination of 4-toluenesulfonic acid from a series of *trans*-2-arylcyclopentyl tosylates

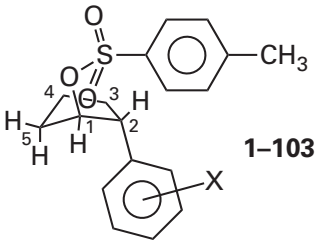

1–103

is catalyzed by *tert*-butoxide in *tert*-butanol, the choice between syn elimination of the hydron at carbon 2 to produce 1-arylcyclopentene and anti elimination of the hydron at carbon 5 to produce 3-arylcyclopentene varies depending on the ability of the phenyl substituent at carbon 2 to stabilize the anionic character that develops at that carbon in the transition state for syn elimination.[375] The yield of the product of syn elimination relative to that for the sum of the products for both syn and anti elimination varies from 10% for *trans*-2-(4-meth-oxyphenyl)cyclopentyl tosylate to 94% for *trans*-2-(3-chlorophenyl)cyclopentyl tosylate.[374] This result is also another example illustrating the increase in the rate of a concerted elimination that occurs when the structure of the substrate is altered to stabilize the negative charge developing on the acidic carbon because it is only the increase in the rate of the syn elimination that leads to the increase in the yield of 1-arylcyclopentene.

The rate of an elimination that occurs adjacent to the carbonyl group of a ketone or aldehyde, and that proceeds through an intermediate enolate under catalysis by a base, can be enhanced by conversion of the ketone or aldehyde to an imine. An example of this enhancement is the dehydration of 4a-hydroxy-*N*-propyl-*cis*-decahydronaphthalen-3-iminium[376]

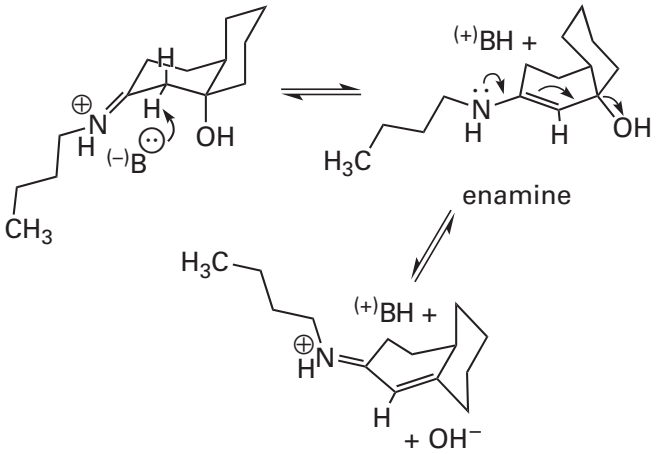

(1–139)

under alkaline conditions. The slow step in the forward direction is the second one: dissociation of the leaving group. The π lone pair of electrons on the intermediate enamine provides the push required to expel the hydroxide, a poor leaving group (arrows in Equation 1–139). The highest occupied π molecular orbital of the enamine must be parallel to the σ bond between the carbon and the oxygen of the leaving group to exert the necessary push (see **1–100**) before the elimination can proceed.

Usually an acyclic enamine, such as the one in Equation 1–139, is unstable relative to the ketone or aldehyde from which it is formed or the unsaturated ketone or aldehyde that is the product of an elimination in which it is an intermediate. The cyclic enamine (7,8-dihydropterin-6-yl)methyl diphosphate (**1–104**), however, is a stable metabolite. The first step in its enzymatic conversion to 7,8-dihydropteroate is the elimination of diphosphate to form the imine[377]

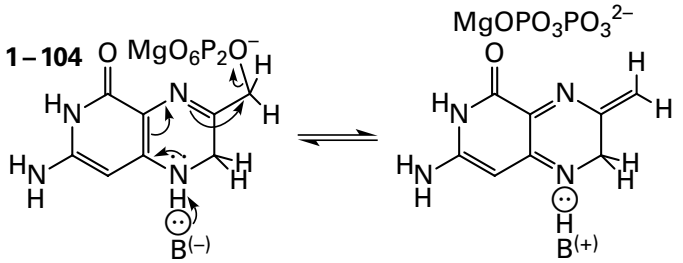

(1–140)

in a reaction that is the vinylogous analogue of the elimination in Equation 1–139 with diphosphate as the leaving group rather than hydroxide.

An addition to a carbon–carbon double bond conjugated to a carbonyl, imino, or acyl group in which a nucleophile adds to the carbon in the double bond peripheral to and a hydron or electrophile adds to the carbon distal to the carbonyl, imino, or acyl group is a commonly encountered reaction. It is common enough to warrant a name, the **Michael addition**. The reverse reactions of Equations 1–132 and 1–133 are Michael additions. If the nucleophile is itself an enolate or another carbanion, the Michael addition is another way, in addition to an aldol condensation or a Claisen condensation, to produce a carbon–carbon bond. An example would be the Michael addition performed by hydroxymethylbilane synthase

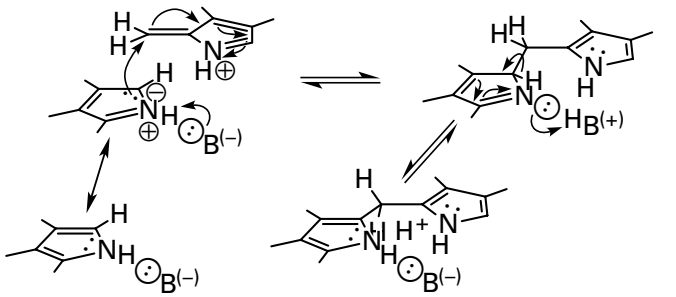

(1–141)

In this instance, the nucleophile is a pyrrolyl group that, under base catalysis, adds to the peripheral, electrophilic carbon in a carbon–carbon bond that is conjugated to an iminium nitrogen rather than being immediately adjacent to it. Instead of a hydron being added to the other carbon originally in the carbon–carbon bond, as in the reverse reactions of Equations 1–132 and 1–133, a hydron dissociates from the intermediate to restore the aromaticity of the pyrrolyl group.

By measuring the rate constants for the Michael additions of a set of eight carbanionic nucleophiles to a set of 15 α,β-unsaturated ketones and acyl derivatives, a scale for the electrophilicity of the respective carbon–carbon double bonds in these electrophiles to addition of a nucleophile can be constructed.[378] The simplest electrophile examined was but-3-en-2-one

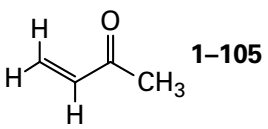

1–105

When the methyl group on the carbonyl in but-3-en-2-one is replaced by an ethoxy group to give the ester, ethyl prop-2-enoate, the electrophilicity of the carbon–carbon bond decreases, and when it is replaced by a dimethylamino group to give the amide, *N,N*-dimethylprop-2-enamide, it decreases further as increasing electron density on the oxygen of the ester and the nitrogen of the carbamoyl group is donated into the π molecular orbital system containing the carbon–carbon double bond. When either the hydrogen on the α carbon or a hydrogen on the β carbon in ethyl prop-2-enoate is replaced by a methyl group to give ethyl 2-methylprop-2-enoate or ethyl but-2-enoate, respectively, the electrophilicity decreases further as a result of sacrificial hyperconjugation donating electron density to the π molecular orbital system of the α,β-unsaturated carbonyl. When the β methyl group on ethyl but-2-enoate is replaced by a phenyl group, the electrophilicity of the carbon–carbon bond decreases even further because the phenyl group donates electron density by resonance rather than hyperconjugation. When the methyl group on the carbonyl of but-3-en-2-one, however, is replaced by a phenyl group, the electrophilicity of the carbon–carbon bond increases, presumably because the phenyl group in this location is not so effective as the methyl group in donating electron density.

Suggested Reading

Hupe, D. J., Kendall, M. C. R., and Spencer, T. A. (1973) Amine catalysis of β-ketol dehydration. II. Catalysis *via* iminium ion formation. General analysis of nucleophilic amine catalysis, *J. Am. Chem. Soc. 95*, 2271–2278. https://doi.org/10.1021/ja00788a028

Banait, N. S., and Jencks, W. P. (1990) Elimination reactions: Experimental confirmation of the predicted elimination of (β-cyanoethyl)-sulfonium ions through a concerted, E2 mechanism. *J. Am. Chem. Soc. 112*, 6950-6958. https://doi.org/10.1021/ ja00175a032

Allgäuer, D. S., Jangra, H., Asahara, H., Li, Z., Chen, Q., Zipse, H., Ofial, A. R., and Mayr, H. (2017) Quantification and theoretical analysis of the electrophilicities of Michael acceptors, *J. Am. Chem. Soc. 139*, 13318-13329. https://doi.org/10.1021/jacs.7b05106

Biotin

Biotin participates in carboxylations. For example, the reaction catalyzed by propionyl-CoA carboxylase

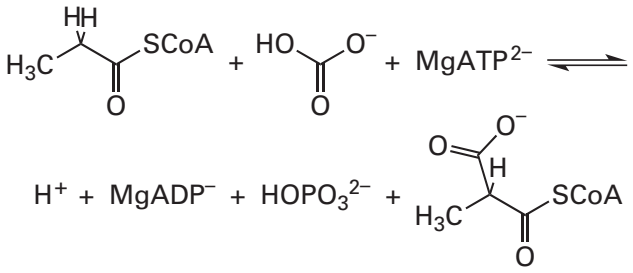

(1–142)

is a carboxylation requiring biotin. In such reactions, an acidic hydrogen on carbon is removed as a hydron and is replaced by the electrophilic acyl carbon of bicarbonate.[379]

Biotin* is a prosthetic group covalently attached to **biotin carboxyl-carrier protein** by an amide between the carboxylate of the biotin and a lysine from the protein[380-382]

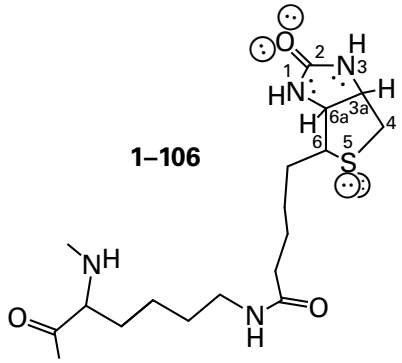

1–106

Biotin carboxyl-carrier protein is either a separate subunit or a domain in a much larger protein.

At one end of the two fused rings in biotin is an ***N,N′*-dialkylurea**. The bond length between the carbonato carbon and the oxygen and those between the carbonato carbon and the two nitrogens are very close to the bond lengths in urea itself .[383] This coincidence suggests that the incorporation of this functional group into the one ring is electronically inconsequential except for the hyperconjugation of the two alkyl groups, which should make the *N,N′*-dialkylurea less acidic. The ring containing the *N,N′*-dialkylurea is absolutely flat (Figure 1–28),[166,383] consistent with a planar structure enforced by the π molecular orbitals of the ureido group. These facts suggest that biotin is simply a complex functional group that is used to hold on to urea.

Because the two bridgehead carbons are tetrahedral, the two rings are tilted with respect to each other at an angle of 122° as if they were the wings of a butterfly. The **cyclic sulfide** is fully saturated, and fully saturated five-membered rings are usually puckered. In biotin, the sulfur occupies the **puckered** position. It is puckered toward the carbonato carbon of the urea rather than away from it. This configuration allows the alkyl group of the side chain of biotin to occupy an equatorial position, and presumably this steric effect explains the direction of the pucker. This configuration also moves the sulfur closer to the urea, perhaps to assist in reactions at this location by a transannular effect,[384] but the sulfur is too far from the carbonate carbon of the urea for significant overlap to occur.[383] The sulfur, however, may be responsible in part for the planarity of the ureido ring because in dethiobiotin the ureido ring is puckered instead of flat.[385]

Decarboxylations are **always significantly exergonic**. An example would be the decarboxylation of oxaloacetate[386]

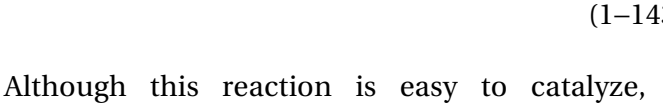

(1–143)

Although this reaction is easy to catalyze, it involves a large waste of free energy, and it is almost never catalyzed in living organisms. In one rare exception, natural selection has discovered the gift, and the oxaloacetate decarboxylase of bacteria such as *Klebsiella aerogenes* stores the free energy of this reaction in the form of an electrochemical gradient of sodium ions.[387]

*The numbering of biotin seems to vary. In this text, the numbering of the IUPAC name will be used.

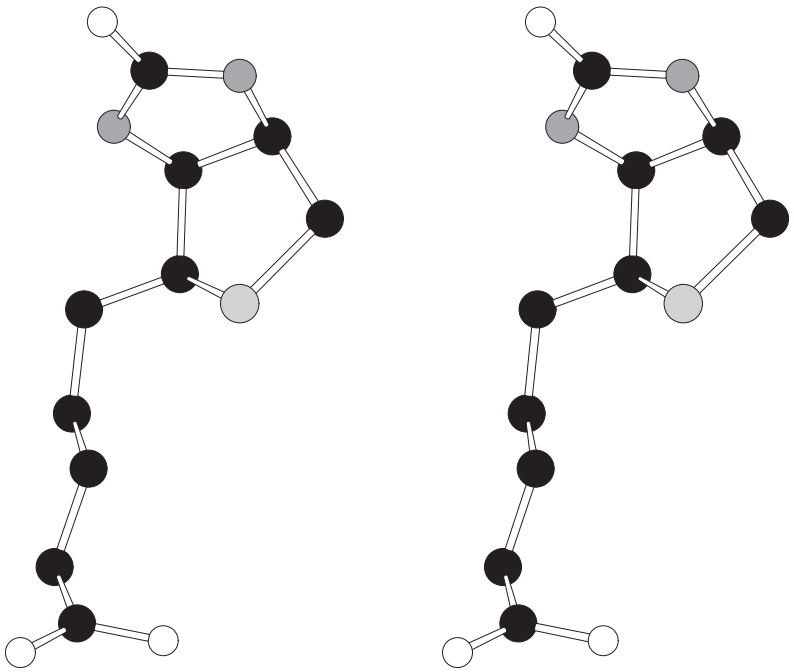

Figure 1–28: Stereodrawing[166] of the crystallographic molecular model of D-(+)-biotin. Black atoms are carbons, white atoms are oxygens, small gray atoms are nitrogens, and the large light gray atom is a sulfur. Crystals were obtained from an aqueous solution of the free acid of D-(+)-biotin by cooling a saturated solution from 95 °C. The two fused rings in the molecule are inclined at 122° with the *N,N′*-dialkylurea at the top.[383]

If it is not to be disadvantageously endergonic, **a carboxylation must be coupled to a reaction that yields energy**. In the case of carboxylations under catalysis by biotin, this energy-yielding reaction is the hydrolysis of $MgATP^{2-}$ to $MgADP^{-}$ and phosphate.* Each time a molecule of carboxylated product is produced, a molecule of $MgATP^{2-}$ is hydrolyzed. An example is the reaction catalyzed by pyruvate carboxylase

$$\text{pyruvate} + HOCO_2^- + MgATP^{2-} \rightleftharpoons HOPO_3^{2-} + MgADP^- + H^+ + \text{oxaloacetate} \qquad (1\text{–}144)$$

with the participation of biotin.

The *N,N′*-dialkylurea is the catalytic center of biotin, and the central intermediate in all reactions involving biotin is *N*³-carboxybiotin[389,390]

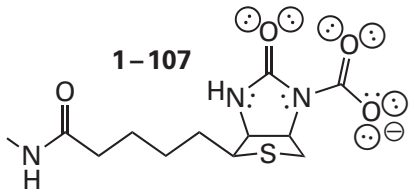

N^3-Carboxybiotin is produced in the active site of biotin carboxylase

$$\text{[biotin carboxyl-carrier protein]-biotin} + HOCO_2^- + MgATP^{2-} \rightleftharpoons HOPO_3^{2-} + MgADP^- + H^+ + \text{[biotin carboxyl-carrier protein]-}N^3\text{-carboxybiotin} \qquad (1\text{–}145)$$

In N^3-carboxybiotin, one of the oxygens on the bicarbonate has been replaced by one of the ureido nitrogens of the biotin in a formal nucleophilic substitution at a carbonato carbon. As a result, N^3-carboxybiotin is the derivative of two carbonic acids: one forms the ureido group and the other forms the carbamate.

The function of biotin carboxyl-carrier protein is to insert the biotin in turn into one or the other of two active sites either in two other subunits or in two other domains of the larger protein. In most instances, these are the active site for biotin carboxylase in which N^3-carboxybiotin is produced from biotin, $MgATP^{2-}$, and bicarbonate and the active site that then transfers the carboxy group on N^3-carboxybiotin to a particular reactant that is to be carboxylated. In methylmalonyl-CoA carboxytransferase, however, biotin is the carrier that transfers a carboxy group between pyruvate and propanoyl-SCoA. Because its role is to transfer a carboxy group between active sites, biotin carboxyl-carrier protein is formally a **coenzyme**, even though the active sites are within the same protein.

The intermediate that precedes the formation of N^3-carboxybiotin in the active site of biotin carboxylase is **carboxyphosphate.**[391] Carboxyphosphate is the product of a nucleophilic substitution at phosphorus

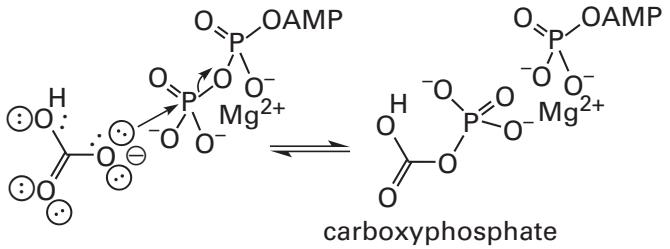

(1–146)

in which bicarbonate is the nucleophile and $MgADP^-$ is the leaving group. It is the carboxyphosphate that accomplishes the coupling of carboxylation to hydrolysis of the $MgATP^{2-}$.

During the overall reaction catalyzed by biotin carboxylase (Equation 1–145), one of the three oxygens-18 of [$^{18}O_3$]bicarbonate is incorporated into the phosphate, and the other two end up in the N^3-carboxylato group (Figure 1–29).[392] This fact, and the fact that the enzymatically catalyzed carboxylation of biotin proceeds with inversion of configuration[393] at the terminal phosphate of $MgATP^{2-}$, are together consistent with nitrogen 3 of the biotin

*At 25 °C, pH 7.0, and a free concentration of Mg^{2+} of 1.0 mM, nominal conditions for cytoplasm but values that vary significantly from organism to organism, $MgATP^{2-}$ (the tridentate complex between ATP^{4-} and Mg^{2+}) accounts for more than 80% of the total ATP in the solution.[388] Under the same conditions, $MgADP^-$ and ADP^{3-} each account for about 45% of the total ADP in the solution. Because the free concentration of Mg^{2+} used in most experiments in which ATP and ADP are substrates usually exceeds 1 mM, and therefore the fraction of nucleotides present as the complexes increases; because $MgADP^-$ is often, if not usually, the actual substrate used by an enzyme; and because the reader should be reminded that Mg^{2+} almost always plays a role in reactions involving ATP and ADP and that the complexes between Mg^{2+} and the respective nucleotide almost always are negatively charged, $MgATP^{2-}$ and $MgADP^-$ will be used from now on to designate ATP and ADP, respectively.

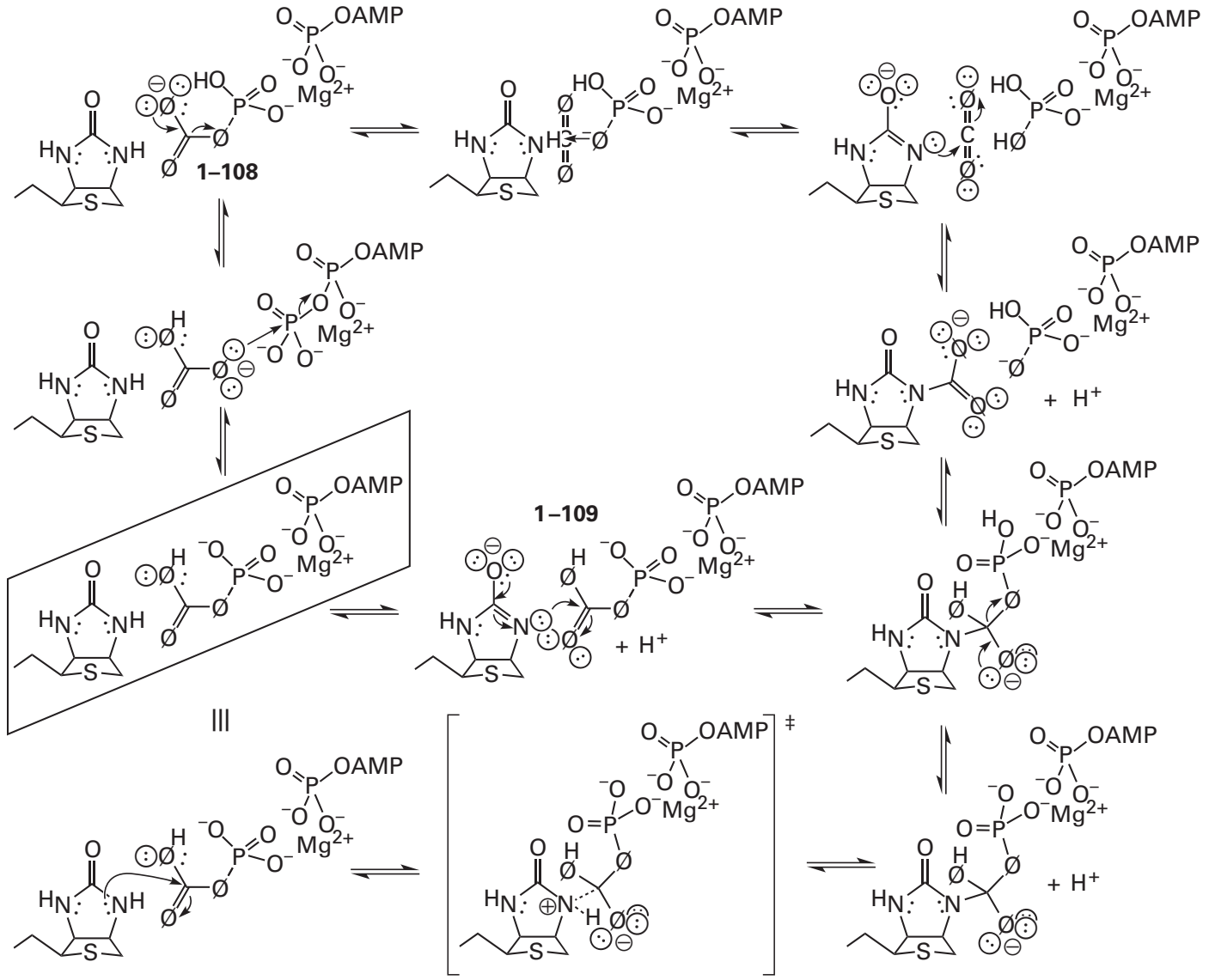

Figure 1–29: Formation of N^3-carboxybiotin coupled to the hydrolysis of $MgATP^{2-}$. There are three presently accepted possibilities for the mechanism. All three begin with biotin, HCO_3^-, and $MgATP^{2-}$ (within the box to the left). (**Upper path**) Carbon dioxide as an intermediate.[391,395] Bicarbonate substitutes nucleophilically at the γ-phospho group of $MgATP^{2-}$ in a direct in-line transfer of the phospho group, with inversion of configuration at phosphorus to produce carboxyphosphate (**1–108**). The leaving group is $MgADP^-$. The intermediate carboxyphosphate then dissociates to carbon dioxide and phosphate. The phosphate, as a catalytic base, removes the hydron from nitrogen 3 of the biotin, and the resulting ureido anion, which is the conjugate base of biotin, adds nucleophilically to the carbon dioxide to produce N^3-carboxybiotin. (**Middle path**) Nucleophilic substitution at carboxyphosphate.[391] Carboxyphosphate (**1–109**) is formed as before by nucleophilic substitution at the γ-phospho group of $MgATP^{2-}$. The ureido anion then adds nucleophilically to the carboxyphosphate to form a tetrahedral intermediate that dissociates to N^3-carboxybiotin and phosphate ion. The carboxy group of the carboxyphosphate is hydronated to improve the electrophilicity of its carbon; and, to improve its capacity as a leaving group, the phospho group of the carboxyphosphate is still coordinated by the Mg^{2+} that coordinated it in the $MgATP^{2-}$. The resulting tetrahedral intermediate decomposes with loss of phosphate to produce N^3-carboxybiotin. (**Lower path**) Neutral biotin as the nucleophile.[397] The π lone pair of electrons on nitrogen 3 of the biotin, which is more nucleophilic than a fully delocalized pair of electrons because of cross-conjugation, is the nucleophile in a nucleophilic substitution that can occur either at the carbonato carbon of the carboxyphosphate (as shown) or at the carbonato carbon of the carbon dioxide that has dissociated from carboxyphosphate (see upper path). In either case, the electrophilic carbon of the carboxyphosphate or carbon dioxide would be adding to the π lone pair of electrons of nitrogen 5, either directly or as the phosphate ion, or another catalytic base was removing the hydron from nitrogen 3. In all three mechanisms, one of the three oxygens of bicarbonate, which are distinguished by the letter Ø, ends up in the phosphate, as required by the observation that the phosphate produced during carboxylation of biotin with $[^{18}O]HOCO_2^-$ bears an equivalent of oxygen-18.

engaging in a nucleophilic substitution at the carbonate carbon of carboxyphosphate with phosphate as the leaving group. The transfer of ^{18}O from [^{18}O]bicarbonate to the phosphate is also observed[394] in the slow, wasteful bicarbonate-dependent ATPase reaction

$$H^{18}OC^{18}O_2^- + MgATP^{2-} + H_2{}^{16}O \rightleftharpoons MgADP^- + H^+ + H^{18}OPO_3^{2-} + H^{16}OC^{18}O_2^- \quad (1\text{–}147)$$

catalyzed by the active site of biotin carboxylase in the absence of biotin in which water slowly hydrolyzes the carboxyphosphate by a nucleophilic substitution at the carbonato carbon with $H^{18}OPO_3^{2-}$ as the leaving group. All these results are consistent with a mechanism involving the intermediate formation of carboxyphosphate.

There are **three current contenders for the mechanism of transfer of the carboxy group** from the carboxyphosphate to nitrogen 3 of the biotin. In the first, the carboxyphosphate dissociates to carbon dioxide and phosphate and the anionic conjugate base resulting from the dehydronation of nitrogen 3 of the ureido group of biotin adds nucleophilically to the electrophilic carbon of the carbon dioxide. In the second, the anionic conjugate base of the ureido group engages in a concerted nucleophilic substitution at the electrophilic carboxy carbon of the carboxyphosphate. In the third, the neutral ureido group is the nucleophile in the nucleophilic substitution, which could be either dissociative or concerted.

In the first proposal, the transfer of the carboxy group is a **dissociative nucleophilic substitution at the carbonato carbon with carbon dioxide as an intermediate** (Figure 1–29, upper path). The equilibrium constant for dissociation of the dianion of carboxyphosphate (**1–108**) to form carbon dioxide and phosphate has been estimated to be 10 M, and the rate of its dissociation has been estimated to be 10 s^{-1}. At the same time, it was demonstrated that carbon dioxide is much more electrophilic than carboxyphosphate.[395] Estimates of the rate of decomposition and the dissociation constant suggest that, once formed on an active site, carboxyphosphate requires little catalysis to dissociate rapidly enough and completely enough for its dissociation to be a step in the overall mechanism for an enzyme that uses biotin as a coenzyme. A molecule of CO_2 would fully dissociate from the carboxyphosphate, and that molecule of CO_2 would be the electrophile to which the anionic conjugate base of biotin would add.[391] If this is the actual mechanism, $MgATP^{2-}$ is not responsible for enhancing the electrophilicity of the bicarbonate by forming carboxyphosphate. Instead, it performs the function of dehydrating the bicarbonate exergonically by converting it into carbon dioxide.

There is **crystallographic evidence** consistent with the participation of CO_2 as an intermediate in the carboxylation of biotin. In a crystallographic molecular model of the active site of biotin carboxylase from *E. coli*, when it is occupied by bicarbonate and $MgADP^-$, one of the oxygens of the bicarbonate is only 0.27 nm from nitrogen 3 of the coenzymatic biotin.[396] The same oxygen of the bicarbonate is also only 0.4 nm from the β phosphorus atom of $MgADP^-$. It is the closest oxygen of the bicarbonate to the β phosphorus atom and should be the oxygen of the bicarbonate that is phosphorylated by $MgATP^{2-}$ during formation of the carboxyphosphate. Consequently, it is destined to be one of the oxygens of the phosphate that is the final product, the one that has gained the oxygen-18 in an isotopic transfer from the bicarbonate (Equation 1–147). If the carboxyphosphate does dissociate to CO_2 and phosphate and that oxygen, which is now on a phosphate ion, remains in the same position, it would be in the perfect location to remove a hydron from nitrogen 3 of the biotin to create the anionic, nucleophilic conjugate base (Figure 1–29, upper path). The carbon dioxide would then move a slight distance to place its carbon immediately adjacent to the now anionic nitrogen 3 for the nucleophilic addition.

In the second proposal, transfer of the carboxy group to biotin is an **associative nucleophilic substitution at the carbonato carbon with a tetrahedral intermediate** (Figure 1–29, middle path). Phosphorylation of the oxygen of the bicarbonate by $MgATP^{2-}$ has turned a poor leaving group (HO^-) into a good leaving group (HO_3PO^{2-}). The electrophile is the carboxyphosphate, with a hydron on the carboxy group to increase its electrophilicity and the Mg^{2+} from $MgATP^{2-}$ still on one of the oxygens of the phospho group to increase its ability to leave. In this proposal, the nucleophile is also the σ lone pair of electrons on the anionic conjugate base of the ureido group.

In both the first and the second proposals, the nucleophile is the anionic conjugate base of the ureido group. A model reaction that is consistent with the anionic conjugate base of the ureido group

being the nucleophile is the rapid (15 s^{-1} at pH 7.4), base-catalyzed exchange of the hydrons on nitrogen 3 of the ureido group in biotin,[384,397] which suggests that these hydrons can be readily removed to form the conjugate base. The problem with this nucleophile is the acid dissociation constants of the ureido group. The difficulty can be understood by examining the acid dissociation constants of urea itself

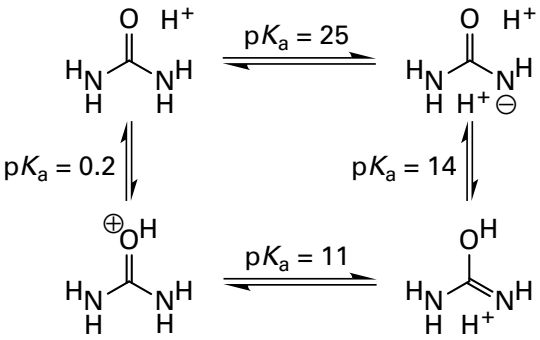

(1–148)

The pK_a for urea[398,399] is 25, so even though the hydron on nitrogen 3 of biotin is susceptible to base-catalyzed exchange and even if the base that removes the hydron from nitrogen 3 were the conjugate base of an arginine (pK_a = 13), only 10^{-12} of the ureido group would be the conjugate base at any instant. If the base that removes the hydron (Figure 1–29, upper path) is the dianion of phosphate (pK_a = 6.8), only 10^{-18} would be the conjugate base. In crystallographic molecular models of the active sites of biotin carboxylase from *E. coli*[396,400] and the almost identical biotin carboxylase (82% identity; 0 gap percent) from *Haemophilus influenzae*[401] when they are occupied by biotin, there are two arginines. One of them forms a hydrogen bond with the carbonato 2-oxo group of the biotin, but neither of them is properly situated to be a catalytic base that removes the hydron from the ureido group of the biotin. There is also a lysine in the active site, the amino group of which might be able to stretch to the hydron,[401] but if it is the catalytic base (pK_a = 10.5), only 10^{-15} of the ureido group would be the conjugate base. The situation would be improved if the carbonato oxygen of the ureido group could be hydronated. This hydronation would lower the pK_a of the hydron on nitrogen 3 to 11, but the pK_a of this oxygen is 0.2. In the active site of biotin carboxylase, the carbonato oxygen is, as noted above, usually in a hydrogen bond with the cationic guanidinio group of an arginine, an unusually weak acid. The fact, however, that the guanidinio group bears a positive elementary charge should at least lower the pK_a of the ureido group.

In the third proposal (Figure 1–29, lower path), the transfer of the carboxy group to biotin would be coincident with the concerted removal of the hydron on that same nitrogen by a base participating in the reaction.[397,401] The observation prompting this proposal is the fact that acid-catalyzed hydron exchange of biotin[397,402] proceeds by hydronation of the π lone pair of one of the ureido nitrogens, which is somewhat more basic than the nitrogen of an amide because of cross-conjugation, to produce the ureido cation (**1–110**)

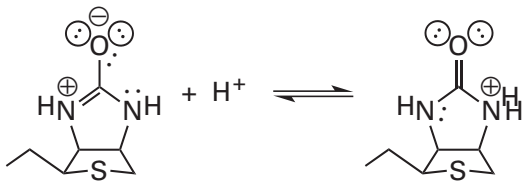

1–110

(1–149)

In this latter acid–base reaction, the π lone pair of the nitrogen has participated as a nucleophile, the reaction of which with an electrophile, the hydron, has preceded removal of the other hydron. In the carboxylation catalyzed by biotin carboxylase, the electrophile would be either carbon dioxide (Figure 1–29, upper path) or carboxyphosphate (Figure 1–29, middle and lower paths) rather than a hydron.

At the moment, in spite of many attempts to do so,[391] there is no unambiguous observation that can establish one or the other of these mechanisms for transferring the carboxy group from bicarbonate to biotin,[400] so all three are possible explanations.

In an active site catalyzing the transfer of the carboxy group from N^3-carboxybiotin to an acceptor, the carboxy group is transferred to an enol or enolate

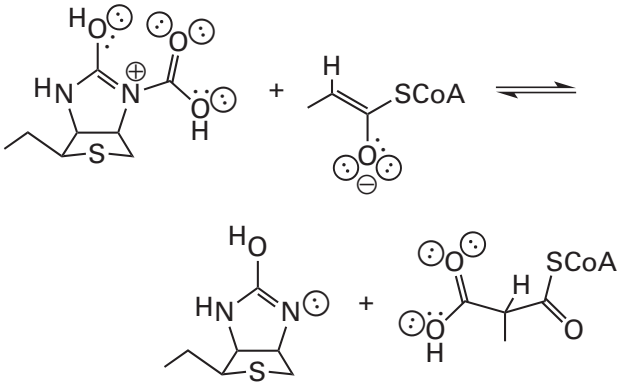

(1–150)

This transfer is usually considered to be a concerted nucleophilic substitution at the carbonato carbon of the N^3-carboxybiotin. If this is the mechanism, because of its acid dissociation constants (Equation 1–148), either hydronation of the biotin on the exocyclic oxygen (as shown in Equation 1–150) or formation of strong hydrogen bonds to it is probably a necessary step in enabling it to be the leaving group. A similar, intramolecular nucleophilic substitution occurs in the intramolecular model reaction[403]

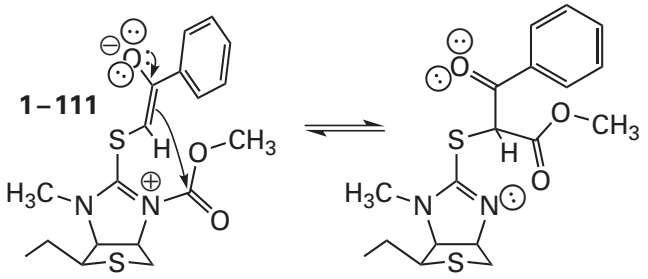

(1–151)

but only if the other nitrogen of the ureido group is methylated to prevent it from losing its hydron. The *N*-methyl-*O*-methyl-*S*-alkenyl model compound **1–111** is the sulfur homologue of the biotinyl cation in Equation 1–150.

Under the proper circumstances, the biotin should be a reasonably good leaving group in a concerted nucleophilic substitution, as illustrated by the fact that the free energy of hydrolysis of N^3-carboxybiotin is –20. kJ mol^{-1} at pH 7 and 0 °C.[386] Because the electrophile has a poor leaving group and the nucleophile, an enolate, is a strong one, an **associative nucleophilic substitution with a tetrahedral intermediate** should be the mechanism.

Another intramolecular reaction that is chemically homologous to Equation 1–150 is catalyzed by 5-(carboxyamino)imidazole ribonucleotide mutase

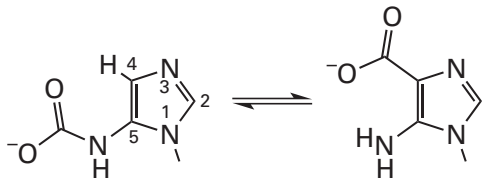

(1–152)

It has been shown that the carboxy group is transferred during this reaction from nitrogen 5 to carbon 4 on the same molecule of substrate.[404] Because a direct, concerted nucleophilic substitution in which carbon 4, as a nucleophile, adds to the carbonato carbon before or while nitrogen 5 leaves is sterically forbidden, it has been proposed that the carboxy group dissociates completely from nitrogen 5 as CO_2, which is then attacked by carbon 4 of the resulting unhydronated enamine. It is possible that the analogous two steps, between which CO_2 would be present as an intermediate, occur in the reaction of Equation 1–150. This disconnection would make it a **dissociative nucleophilic substitution rather than an associative nucleophilic substitution**. The CO_2 would fully dissociate from the N^3-carboxybiotin before the enolate adds to it nucleophilically.[391]

Suggested Reading

Kohn, H. (1976) Model studies on the mechanism of biotin dependent carboxylations, *J. Am. Chem. Soc. 98,* 3690–3694. https://doi.org/10.1021/ja00428a050

Meyer, E., Kappock, T. J., Osuji, C., and Stubbe, J. (1999) Evidence for the direct transfer of the carboxylate of N^5-carboxyaminoimidazole ribonucleotide (N^5-CAIR) to generate 4-carboxy-5-aminoimidazole ribonucleotide catalyzed by *Escherichia coli* PurE, an N^5-CAIR mutase. *Biochemistry 38*, 3012-3018. https://doi.org/10.1021/bi9827159

Electrophilic Aromatic Substitution

There are a number of electrophilic aromatic substitutions catalyzed by enzymes. An example of an **electrophilic aromatic substitution on a phenyl ring** that is encountered in a metabolic pathway is the one catalyzed by trihydroxypterocarpan dimethylallyltransferase

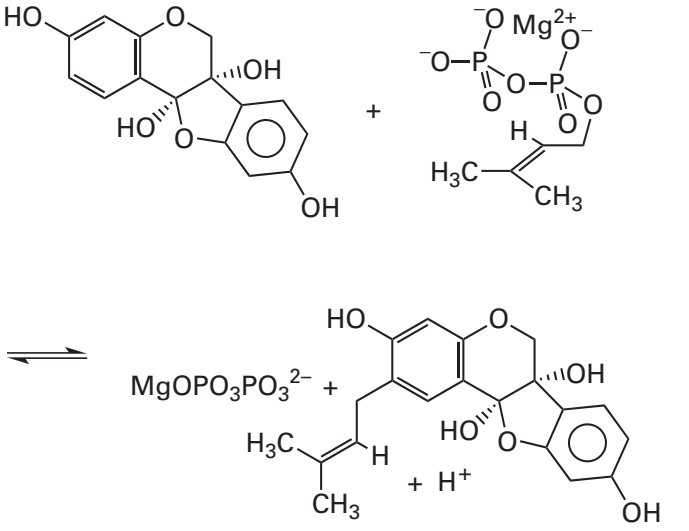

(1–153)

from *Glycine max*.[405] This enzyme participates in the biosynthetic pathway for glyceollin.

The electrophile in the reaction is 3,3-dimethylallyl carbenium ion **1–99** formed by the dissociation of diphosphate from 3,3-dimethylallyl diphosphate (Figure 1–26). The electrophilic allyl carbenium ion adds to the nucleophilic π molecular orbital system of the phenyl ring at a position ortho to the hydroxy group and para to the ether oxygen, both of which increase the nucleophilicity of the ortho position, to produce a pentadienyl carbenium ion as an intermediate. This pentadienyl carbenium ion can be represented by resonance

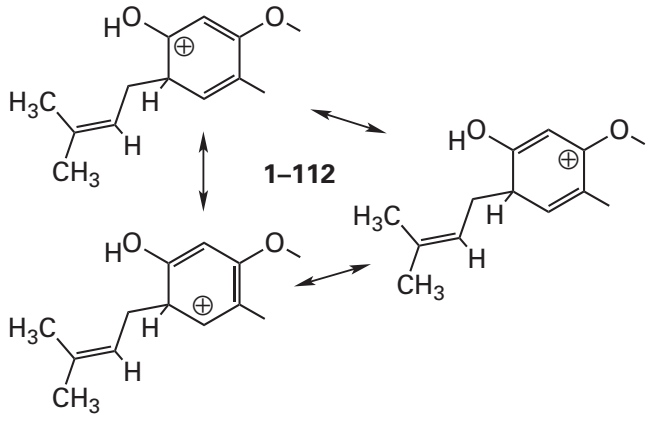

or by its **lowest unoccupied π molecular orbital**

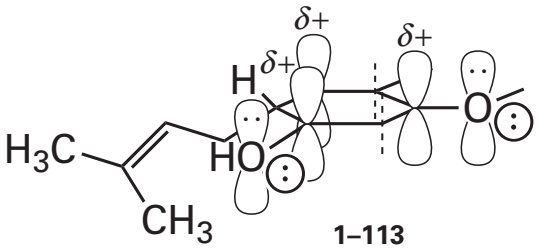

1–113

which contains the electron deficiency of the carbenium ion.

The intermediate in a generic electrophilic aromatic substitution on a phenyl group is a **pentadienyl carbenium ion**. In the particular instance of trihydroxypterocarpan dimethylallyltransferase, the pentadienyl carbenium is defined by the three resonance structures of **1–112** and is formed by mixing the five *p* atomic orbitals in the ring remaining after the electrophilic addition.

In almost all electrophilic aromatic substitutions, with the exception of those on benzene, there are **substituents on the ring** that either withdraw or donate electron density and determine the regioselectivity of the substitution. These substituents withdraw or donate electron density by resonance through the π molecular orbital system of the pentadienyl carbenium ion or by induction through the σ bonds of the system orthogonal to the π molecular orbital system. A withdrawal or donation by resonance, as opposed to one by induction, is represented by aligning the orbital or orbitals on the substituent responsible for it with the π molecular orbital of the pentadienyl carbenium ion as in **1–113**. In the present circumstance, the hydroxy group and the alkoxy group **donate electron density by resonance**, and an orbital on each oxygen containing one of its lone pairs of electrons is aligned with the π molecular orbital system. Each lone pair of electrons is located in a *p* atomic orbital because that permits the greatest overlap and also explains the coplanarity of the alkoxy group. A carbonyl group would be an example of a substituent that **withdraws electrons by resonance**, and in this instance its carbon–oxygen double bond, which is responsible for the withdrawal, would be drawn so that its π molecular orbital system is parallel to the π molecular orbital system of the pentadienyl carbenium ion.

The pentadienyl carbenium ion **1–112** has a π molecular orbital system composed from five consecutive *p* orbitals situated on the five unsaturated carbons around the ring. The two bonding

π molecular orbitals of the pentadienyl carbenium ion, those of lowest energy, are each occupied by a pair of electrons. The lowest unoccupied π molecular **1–113** has lobes at three of the carbons and nodes at the other two. The lobes of this π molecular orbital of the pentadienyl carbenium ion define its electron-deficient positions, and these positions are the same locations at which a carbenium ion is found in each of the three respective resonance structures of **1–112**.

The oxygens attached at two of these three locations stabilize the respective π electron deficiency in these lobes by electron donation from their respective *p* orbitals, each occupied by a pair of electrons. This stabilization is responsible for the regioselectivity of the reaction because it also occurs, but to a lesser extent, in the transition state for the addition. The π electron donation can be represented by two resonance structures in addition to those in **1–112**

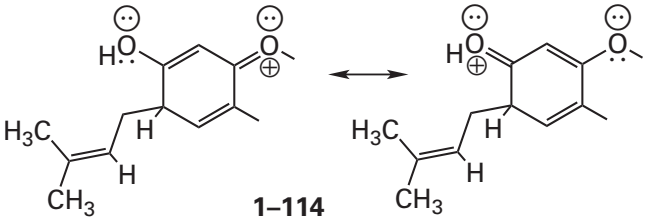

1–114

These resonance structures suggest that the actual π molecular orbital system of this particular pentadienyl carbenium ion includes the two *p* orbitals, one from each of the oxygens. In this case, the π molecular orbital system would be the result of mixing seven *p* orbitals to create seven π molecular orbitals occupied pairwise by eight electrons. The lowest unoccupied molecular orbital of the set would contain the electron deficiency and will have lobes over the atoms identified by the full set of resonance structures.

Addition of the dimethylallyl carbenium ion to the phenyl ring destroys the aromatic π molecular orbital system by introducing a saturated carbon at the one tetravalent position, the position at which both a hydrogen and the dimethylallyl group are attached. The aromatic π molecular orbital system can be regained only by loss of the original electrophile, which yields the reactants, or by loss of the hydron from that saturated carbon. **Loss of the hydron** leaves behind the two electrons formerly in the carbon–hydrogen σ bond and also permits that carbon to rehybridize sp^2, sp^2, sp^2, *p*. The *p* orbital of this carbon, the two electrons, and the pentadienyl carbenium ion together then coalesce to form the aromatic π molecular orbital system of the product

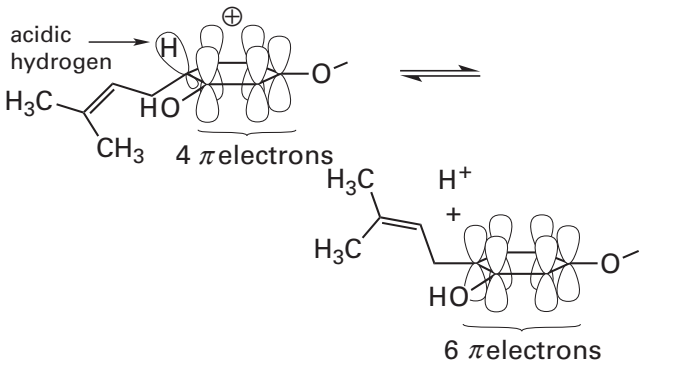

(1–154)

The reason that the carbon from which the hydron dissociates is acidic is that the pair of electrons in the carbon–hydrogen bond are withdrawn into the pentadienyl carbenium ion to complete the aromatic sextet.

Electrophilic aromatic substitutions on indoles are also common. An example of such a substitution, again by dimethylallyl carbenium ion **1–99** formed from dimethylallyl diphosphate (Figure 1–26), is that catalyzed by 4-dimethylallyltryptophan synthase[406]

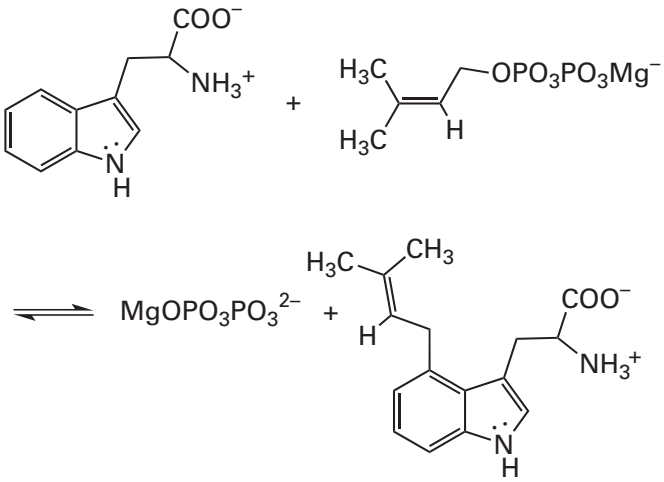

(1–155)

In this reaction, the intermediate carbenium ion is stabilized by the π lone pair of electrons on the nitrogen of the indole ring

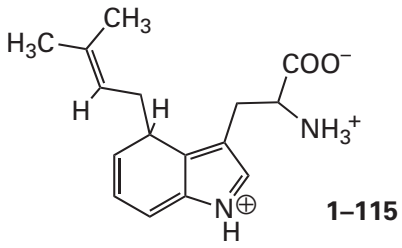

1–115

In this intermediate, an **octatetraenyl π molecular orbital system** encompasses all seven of the unsaturated carbons and the nitrogen in the two rings.

The lone pair of electrons on the nitrogen of indole also stabilizes the intermediate cation in the electrophilic aromatic substitution catalyzed by tryptophan synthase[407,408]

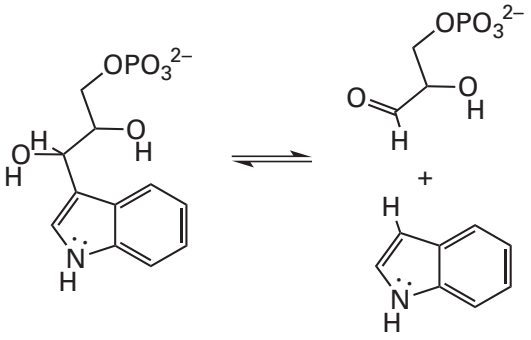

(1–156)

In this electrophilic aromatic substitution on the pyrrolyl ring of the indolyl group, an aldehyde, which is an electrophile, is replaced by a hydron, another electrophile, and the tetravalent carbon in the cationic intermediate is at carbon 3 of the indole rather than at carbon 4 as it is in **1–115**.

Simple pyrroles that are not further conjugated as the one is in indole are also aromatic heterocycles, and as such, they are subject to electrophilic aromatic substitution. In the discussion of the Michael addition catalyzed by hydroxymethylbilane synthase (Equation 1–141), the focus was on nucleophilic addition of the pyrrole to the electrophilic, vinylogous α,β-unsaturated iminium. Here the focus is on the electrophilic aromatic substitution that proceeds at the pyrrole

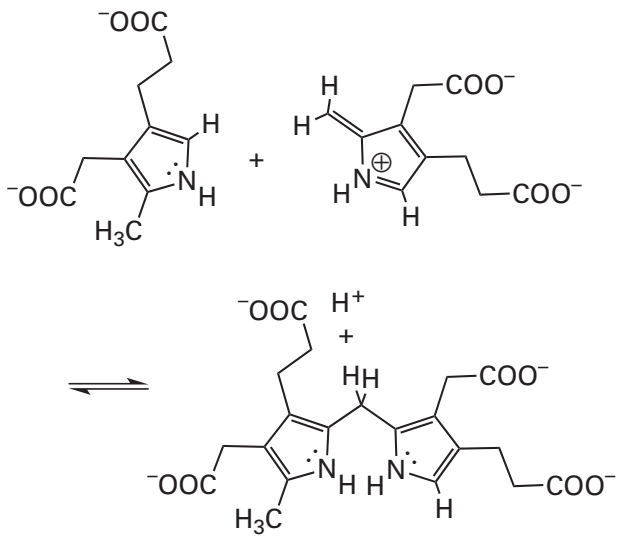

(1–157)

the other substrate in the reaction.[409] In this electrophilic aromatic substitution the cationic intermediate

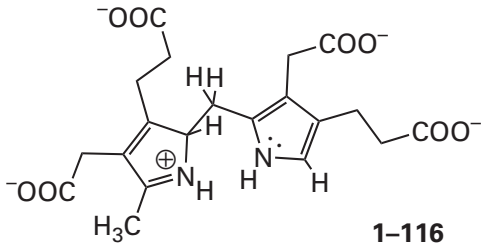

1–116

has a butadienyl π molecular orbital system with four π electrons in which the nitrogen, if hydronated, bears the positive charge. In the next step of the reaction, the hydron on the carbon atom to which the electrophile added dissociates to rearomatize the pyrrole.

There are **electrophilic forms of atomic oxygen** generated enzymatically by flavin that add to phenyl rings in an electrophilic aromatic addition to produce intermediate pentadienyl carbenium ions

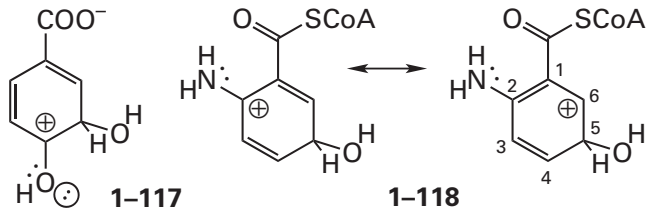

1–117 **1–118**

stabilized by exocyclic oxygens or nitrogens.[410-412]

In the former instance, in which there is a hydroxy group stabilizing the pentadienyl carbenium ion, the usual dissociation of the hydron from **1–117** completes the electrophilic aromatic substitution to give the catechol, the reaction catalyzed by 4-hydroxybenzoate 3-monooxygenase. In the latter instance, in which there is an amino group stabilizing the pentadienyl carbenium ion, the hydrogen at the tetravalent carbon 5 in intermediate **1–118** migrates to cationic carbon 6 as a hydride[412,413]

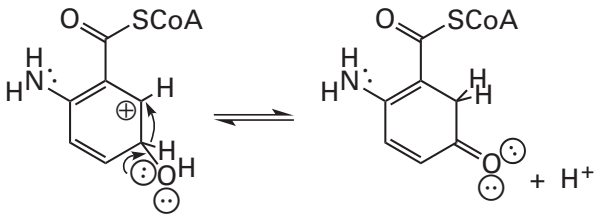

(1–158)

to produce the intermediate ketone in the reaction catalyzed by anthraniloyl-CoA monooxygenase.

One of the more unusual electrophilic aromatic additions is that forming the pentadienyl carbenium ion

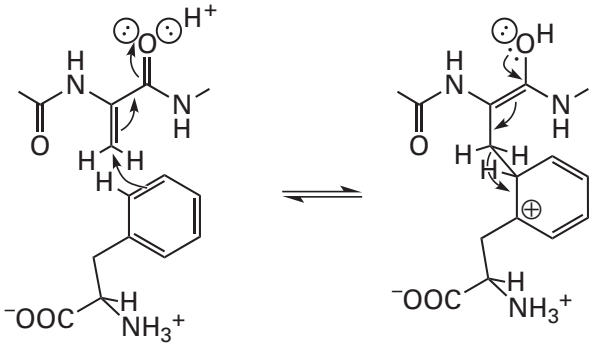

(1–159)

that is an intermediate covalently bonded to the folded polypeptide of phenylalanine ammonia-lyase from *Petroselinum crispum*.[414] This intermediate is formed by Michael addition of the nucleophilic phenyl ring to the **electrophilic dehydroalanine** in the polypeptide of the enzyme, which is an α,β-unsaturated acyl derivative. The purpose of this electrophilic aromatic addition is to acidify one of the β hydrons of L-phenylalanine so that it and ammonia can be eliminated. Once the elimination has occurred, the dehydroalanine rather than a hydron leaves the intermediate to regenerate the phenyl ring. The enzyme must avoid loss of the hydron on the saturated carbon of the pentadienyl intermediate. If the hydron were to dissociate instead of the dehydroalanine, the enzyme would be covalently inactivated.

Nucleophilic aromatic substitutions are rarely encountered in enzymatically catalyzed reactions.[415] One of the few is that catalyzed by 4-chlorobenzoyl-CoA dehalogenase

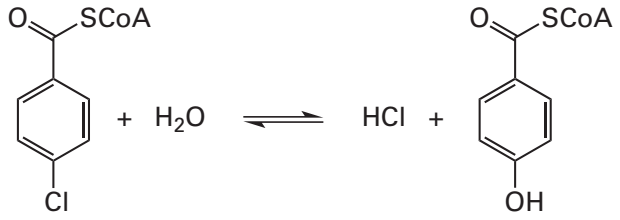

(1–160)

in which the acyl-SCoA substituent stabilizes the intermediate pentadienyl carbanion.

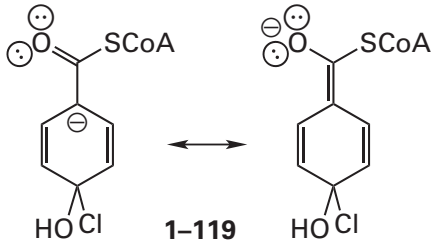

Suggested Reading

Gebler, J. C., Woodside, A. B., and Poulter, C. D. (1992) Dimethylallyltryptophan synthase: An enzyme-catalyzed electrophilic aromatic substitution, *J. Am. Chem. Soc. 114*, 7354–7360. https://doi.org/10.1021/ja00045a004

Pericyclic Reactions

A pericyclic reaction is a rearrangement of covalent bonds that proceeds in a concerted manner through one transition state. The sigmatropic rearrangement catalyzed by chorismate mutase

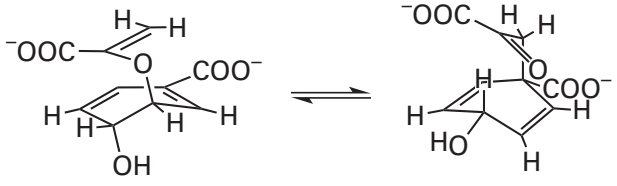

chorismate prephenate

(1–161)

is an example of a pericyclic reaction. It proceeds in one step through a single transition state in which the ether in chorismate is almost fully cleaved heterolytically while only a small fraction of the new carbon–carbon bond has formed.[416-421] As a result, the oxygen of the ether that is leaving bears a partial negative elementary charge; and the pentadienyl group that it leaves, a partial positive elementary charge. These conclusions about the enzymatic mechanism place this rearrangement just within the borderline between a concerted reaction and a stepwise reaction. The same reaction between chorismate and prephenate occurs in free solution in the absence of the enzyme. In this nonenzymatic conversion of chorismate to prephenate, little if any dissociation of the chorismate to *enol*-pyruvate and 4-hydroxy-benzoate occurs,[419] an observation consistent with the reaction proceeding in a concerted mechanism through a single transition state. Were the carbon–oxygen bond to dissociate fully before the carbon–carbon bond had begun to form, the upper and lower fragments of the molecule—the enolate of *enol*-pyruvate and the pentadienyl carbenium ion—would no longer be bonded together and should diffuse apart. This pericyclic reaction is a **sigmatropic rearrangement** because a σ bond allylic to a π bond is broken, a new σ bond allylic to a π bond is formed, and two π bonds migrate to adjacent positions.

Another example of a pericyclic reaction is the ene reaction. The formation of intermediate **1–79** that occurs during the reduction of (*E*)-but-2-enoyl-SCoA by NADPH (Equations 1–97 and 1–98) is presumed to be a concerted pericyclic ene reaction,[294] on the basis of the identity of the reactants and the products, although it has already been mentioned that this conclusion has been challenged.[299] A less controversial example of an ene reaction is the nonenzymatic coupling of 6,6-dimethyl-3-methylidenebicyclo[3.1.1]heptane and maleic anhydride

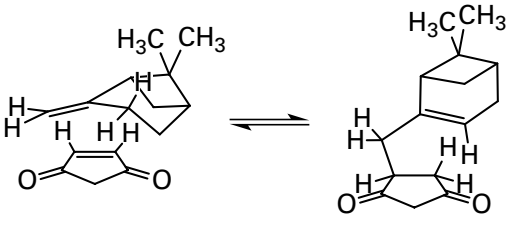

(1–162)

In this reaction, an allylic hydrogen in the 6,6-dimethyl-3-methylidenebicyclo[3.1.1]heptane is transferred to one of the carbons in the double bond of the maleic anhydride while the distal carbon of the methylene group forms a σ bond with the other carbon in the double bond. In an **ene reaction**, the distal atom in the double bond adjacent to an allylic hydrogen adds to an atom in a second double bond unconjugated to the first, either in another molecule or within the same molecule, to form a new σ bond while the allylic hydrogen is transferred to the other atom in the second double bond.

A pericyclic reaction is a concerted reorganization of bonding that takes place through an aromatic transition state that is a cyclic array of overlapping atomic orbitals. The bonding around the ring in the transition state, however, does not need to be a continuous circle of σ bonds. In fact, in most pericyclic reactions one or two of the bonds connecting the atoms in the ring of the transition state are solely π bonds with no σ bond connecting them. To be a true pericyclic reaction, however, the bonds being broken and those being formed must be broken and formed during the passage through a single transition state. Sigmatropic rearrangements, ene reactions, cycloadditions, and electrocyclic reactions are examples of pericyclic reactions.

A pericyclic reaction has an aromatic transition state. The aromatic transition state for the sigmatropic rearrangement catalyzed by chorismate mutase, and the aromatic transition state for the coupling of 6,6-dimethyl-3-methylidenebicyclo-[3.1.1]heptane and maleic anhydride, are both transition states in which there is a continuous ring of six parallel atomic orbitals, each of which overlaps in sequence around the ring with its two nearest neighbors so that they can together form a complete cyclic π molecular orbital system, and the π molecular orbital system in each of these transition states is occupied by six electrons. To satisfy the requirement for an aromatic transition state, there can be atomic orbitals, either *s* orbitals or *p* orbitals, from any number of atoms, as long as they are sterically permitted to overlap and form a continuous, conjugated cyclic transition state, and provided that six or ten electrons (or another aromatic number) participate in the resulting molecular orbital system. Most of the pericyclic reactions catalyzed by enzymes have cyclic transition states of five or six atoms in which only six electrons are rearranged.

In the transition state for the sigmatropic rearrangement catalyzed by chorismate mutase, all six of the atoms involved are hybridized sp^2, and the ring is composed of the six *p* orbitals (Figure 1–30).

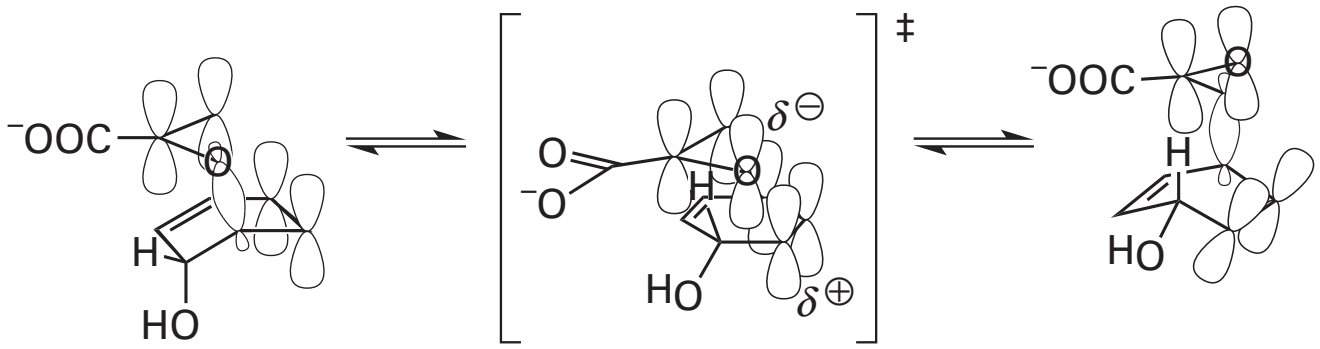

Figure 1–30: Reactant, transition state, and product of the reaction catalyzed by chorismate mutase. The reactant, chorismate, has a σ bond between oxygen and carbon flanked by two carbon–carbon double bonds. In the transition state (‡), the carbon–oxygen σ bond has broken to produce two additional p orbitals, and these new p orbitals and the four p orbitals already in the reactant now form an unbroken ring of six p orbitals. The π molecular orbital system is occupied by six electrons. This aromatic π system holds together the two fragments that are no longer connected by a σ bond. When a σ bond forms between two p orbitals on the opposite side of the ring, the product prephenate (upper right) is produced. It also has a σ bond flanked by two double bonds.

These six p atomic orbitals that mix in the transition state were the two molecular orbitals, bonding and antibonding, that form the σ bond between the carbon and the oxygen and the four π molecular orbitals, bonding and antibonding, that form the two π molecular orbital systems in the two double bonds of the reactant. They will become the four π molecular orbitals that form the π molecular orbital systems in the two double bonds of the product and the two molecular orbitals, bonding and antibonding, that form the molecular orbital system in the new carbon–carbon σ bond in the product. The π molecular orbital system of the transition state (Equation 1–161 and Figure 1–30) is formed from six p orbitals from five carbons and one oxygen. These six π electrons are delocalized and mobile, so it is not surprising that significant negative charge builds up on the more electronegative oxygen in the transition state at the expense of electron density on the five carbons, which become electron-deficient.[421] Because of this imbalance of electron density, the transition state is more polar than the ground state, and the nonenzymatic reaction is more rapid in polar solvents than nonpolar solvents.[419]

The transition state for the ene reaction of 6,6-dimethyl-3-methylidenebicyclo[3.1.1]heptane and maleic anhydride

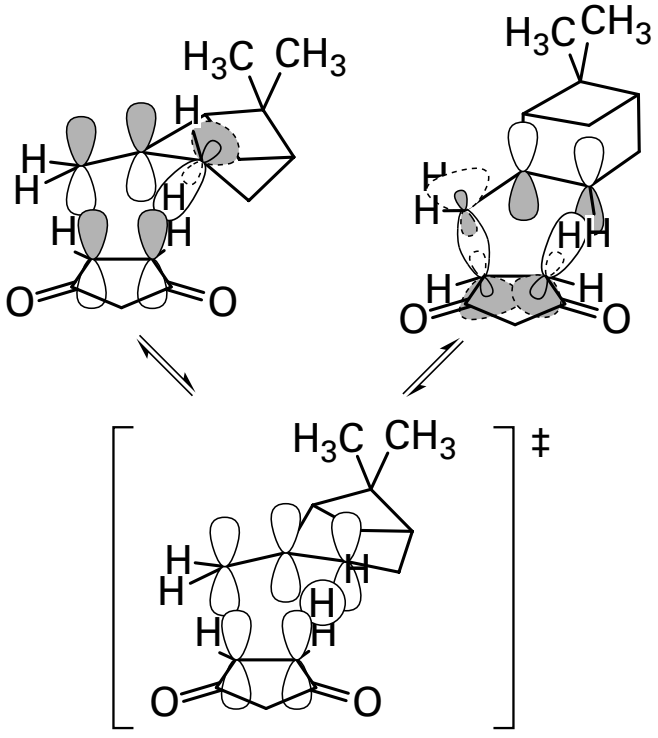

(1–163)

is formed from p orbitals from the five carbons involved and the s orbital of the hydrogen that is transferred from one of the carbons to another. These six atomic orbitals that mix in the transition state were the two molecular orbitals, bonding and

antibonding, that form the σ bond between the carbon and the allylic hydrogen and the four π molecular orbitals, bonding and antibonding, that form the two π molecular orbital systems in the two double bonds of the reactant. They will become the two π molecular orbitals, bonding and antibonding, that form the π molecular orbital system in the double bond of the product and the four molecular orbitals, bonding and antibonding, that form the two molecular orbital systems in the two σ bonds, carbon–carbon and carbon–hydrogen, in the product.

Although aromatic, the transition states in the sigmatropic rearrangement catalyzed by chorismate mutase and in the ene reaction of 6,6-dimethyl-3-methylidenebicyclo[3.1.1]heptane and maleic anhydride are **unstable with respect to reactant and product** because in the reactants and products one or two of the π bonds in the transition state have become σ bonds in the reactant or product. σ Bonds are more stable than π bonds. Each transition state therefore readily decomposes to the reactant or product, either of which is more stable than the transition state. In each case, if the π molecular orbital system of the transition state is examined closely, it can be seen that there are only two ways that it can decompose to form three covalent bonds. In the case of chorismate mutase, the transition state must either form prephenate, in which it has disassembled into two carbon–carbon π bonds and a carbon–carbon σ bond, or form chorismate, in which the transition state has disassembled into two carbon–carbon π bonds and a carbon–oxygen σ bond. In the case of the ene reaction of 6,6-dimethyl-3-methylidenebicyclo[3.1.1]-heptane and maleic anhydride, the transition state must either form 6,6-dimethyl-3-methylidenebicyclo-[3.1.1]heptane and maleic anhydride, in which it has disassembled into two carbon–carbon π bonds and a carbon–hydrogen σ bond, or form the adduct, in which the transition state has disassembled into a carbon–carbon π bond, a carbon–carbon σ bond, and a carbon–hydrogen σ bond.

In pericyclic reactions, the transition state is approached by **overlaps of atomic and molecular orbitals in the reactant or in the product.** The active site of the enzyme catalyzing a pericyclic reaction ensures that a conformation of the two molecules is enforced in which these overlaps are permitted. For example, in the pericyclic, sigmatropic rearrangement catalyzed by chorismate mutase (Equation 1–161)

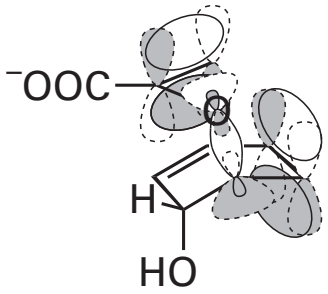

1–120

the following interactions are occurring. First, the lower lobe of the unoccupied antibonding molecular orbital of the carbon–oxygen σ bond overlaps the lower lobe of the occupied bonding π molecular orbital of the lower right double bond. Second, the upper lobe of the unoccupied antibonding π molecular orbital of the lower right double bond overlaps the lower lobe of the occupied bonding π molecular orbital of the upper left double bond. Third, the lower lobe of the unoccupied antibonding π molecular orbital of the upper left double bond overlaps with the occupied bonding molecular orbital of the carbon–oxygen σ bond. Fourth, the occupied bonding molecular orbital of the carbon–oxygen σ bond overlaps with the upper lobe of the unoccupied antibonding π molecular orbital of the lower right double bond. Fifth, the upper lobe of the occupied bonding π molecular orbital of the lower right double bond overlaps with the lower lobe of the unoccupied antibonding π molecular orbital of the upper left double bond. Sixth, the upper lobe of the occupied bonding π molecular orbital of the upper left double bond overlaps with the upper lobe of the unoccupied antibonding molecular orbital of the carbon–oxygen σ bond.

There are other instances of enzymatically catalyzed pericyclic reactions. For example, an enzymatically catalyzed pericyclic ene reaction is that catalyzed by isochorismate lyase from *Pseudomonas aeruginosa*[422]

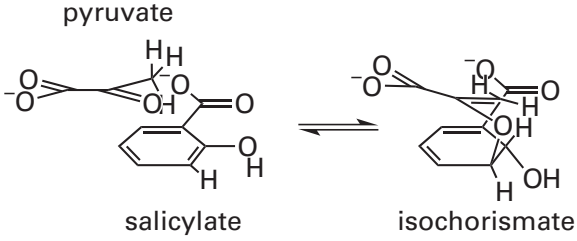

(1–164)

The reaction proceeds through a single aromatic transition state formed from the *s* orbital of the

hydrogen that is migrating and five *p* orbitals from the five heavy atoms, four carbons and an oxygen

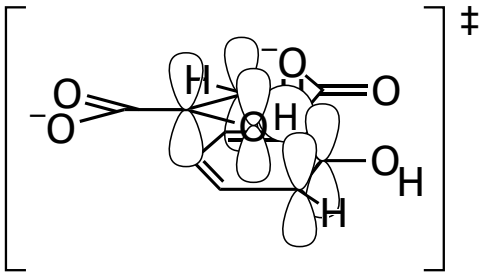

1–121

In the transition state, the σ bond between carbon and hydrogen and the σ bond between carbon and oxygen in the reactant do not exist because their constituent atomic orbitals have been transformed into participants in the π molecular orbital system, but the transition state is held together by that continuous π molecular orbital system. In this ene reaction in the direction of salicylate formation, kinetic isotope effects indicate that dissociation of the carbon–oxygen bond precedes dissociation of the carbon–hydrogen bond but that the reaction is nevertheless concerted and pericyclic.

The proposal that an ene reaction forms intermediate **1–79** during the reduction of (*E*)-but-2-enoyl-SCoA by NADPH was invoked to explain the fact that the π molecular orbital system of the (*E*)-but-2-enoyl-SCoA is stacked against and parallel to the π molecular orbital system of the NADPH. In the case of the ene reaction that is catalyzed by isochorismate lyase the **π molecular orbital systems of the reactants and the products must be parallel** to and stacked against each other. Consequently, the plane of the π molecular orbital system of the pyruvyl moiety must be parallel to the plane of the π molecular orbital system of the salicyl moiety. When the active site of the enzyme is occupied by pyruvate and salicylate, the π molecular orbital system of the pyruvate is parallel to and stacked upon the π molecular orbital system of the salicylate, and the two products are positioned in the orientation they should assume in the transition state (**1–121**).[423]

If the π molecular orbital system of transition state **1–121** is examined closely, it can be seen that there are only two ways that it can decompose to form three covalent bonds. It must either form isochorismate, in which the transition state has decomposed into a carbon–carbon π bond, a carbon–hydrogen σ bond, and a carbon–oxygen σ bond, or form salicylate and pyruvate, in which the transition state has decomposed into a carbon–carbon π bond, a carbon–oxygen π bond, and a carbon–hydrogen σ bond. Although the isochorismate has one more σ bond and one fewer π bond than pyruvate and salicylate, the fact that the salicylate is aromatic while isochorismate is not evens up the reaction.

A **cycloaddition** is a pericyclic reaction in which a total of $(2n + 1)$ double bonds from two unsaturated molecules, or two parts of the same unsaturated molecule, participate and during which a cyclic adduct is produced in which the number of π bonds has decreased by two and the number of σ bonds has increased by two, namely, the two σ bonds creating the cyclic adduct. A **Diels–Alder reaction** is a (4+2) cycloaddition in which four atoms in two adjacent, conjugated double bonds, the diene, form a cyclohexene by combining with a double bond, the dienophile, elsewhere in the same molecule or in another molecule. A Diels–Alder reaction has a single, aromatic transition state formed from a ring of six parallel *p* orbitals through which a cyclohexene is formed or a cyclohexene dissociates. An enzymatically catalyzed example of such a Diels–Alder reaction[424-426] is that catalyzed by prosolanapyrone-III cycloisomerase from *Alternaria solani*, which produces solanapyrone A

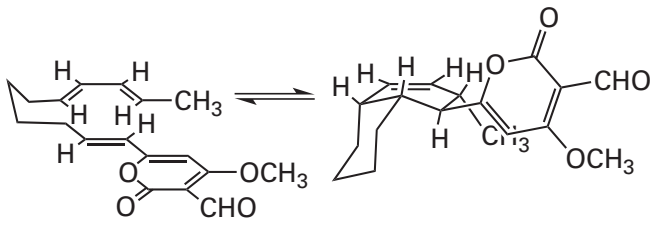

(1–165)

Six parallel *p* orbitals

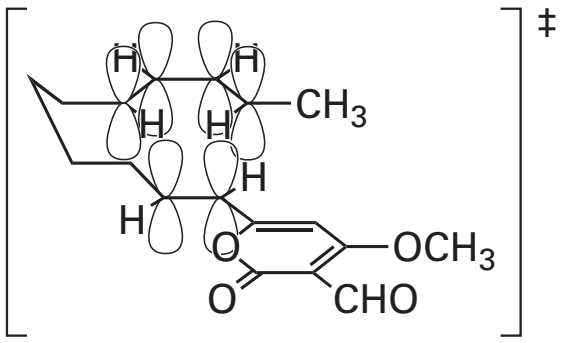

1–122

and six π electrons in the reactant mix to produce the aromatic π molecular orbital system of the transition state. An enzyme catalyzing a similar synthesis of a cyclohexene through a Diels–Alder reaction is involved in the pathway for the biosynthesis of versipelostatin.[427]

A cycloaddition, such as the reaction that produces solanapyrone A, proceeds with an enforced **stereochemistry**, and the product observed in an enzymatically catalyzed reaction, because enzymatic reactions are always stereospecific, is only one of four stereochemical outcomes that can result from this reaction. In the reaction catalyzed by prosolanapyrone-III cycloisomerase, the two possible exo products would be those resulting from the dienophile, with its pyran-2-one pointed away from the diene, approaching the diene either from the bottom as in the drawing or from the top. The two possible endo products would be those resulting from the dienophile, with its pyran-2-one nestled under or above the two double bonds of the diene, approaching the diene either from the bottom or from the top.

In the enzymatically catalyzed reaction, the dienophile approaches from below the diene with its pyran-2-one in the exo orientation as drawn in **1–122**. The dienophile pushes the two central hydrogens of the diene up while the hydrogen and the alkyl group on the dienophile in the center are pushed down by the diene. In response to these steric drives in the center, the carbon–carbon double bond on the periphery of the diene moves downward, and the hydrogen and the pyran-2-one on the periphery of the dienophile twist upward as the two new σ bonds are formed

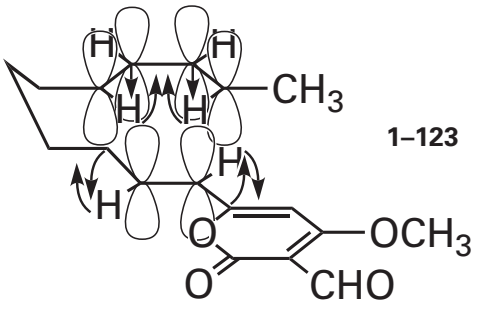

1–123

These drives give the observed stereochemistry of the product (Equation 1–165). The unique feature of this stereochemical enforcement is that the four paired substituents, each of which begins on one of the two sides of the diene or one of the two sides of the dienophile, respectively, remain paired so that each pair ends up only on one side or the other of the cyclohexene. If the stereochemistry of the cyclohexene in the product of an enzymatic reaction that is proposed to proceed by a Diels–Alder reaction satisfies these requirements and furthermore if only one of the four possibilities is observed, then this stereochemistry and the **exclusivity of the product** can be used as an argument for the enzyme catalyzing a concerted, pericyclic cycloaddition passing through a single transition state.

A Diels–Alder reaction is a (4+2) cycloaddition because four *p* orbitals from one fragment combine with two *p* orbitals from the other fragment. In a **(6+4) cycloaddition**, six *p* orbitals from one fragment combine with four *p* orbitals from the other fragment in an aromatic transition state with ten electrons in a decacyclic π molecular orbital system formed from mixing these ten atomic orbitals.

An example of a (6+4) cycloaddition is the reaction catalyzed by the enzyme encoded by the *ngnD* gene in *Nocardia argentinensis* (Figure 1–31).[428] In the first step, a ten-membered ring with three π bonds is formed within a much larger 18-membered ring. During the cycloaddition, five carbon–carbon π bonds are converted into two carbon–carbon σ bonds and three carbon–carbon double bonds through the aromatic transition state*

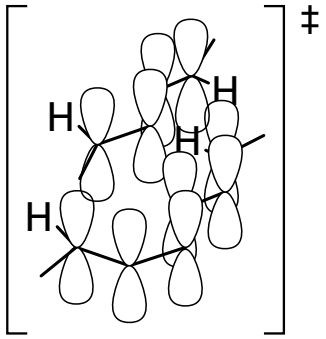

1–124

The product of the cycloaddition is then converted by a sigmatropic ring contraction into a cyclohexene with a ten-membered ring on one side and a six-membered ring on the other side. The stereochemistry† of the hydrogens in the ultimate product is that expected for a (6+4) cycloaddition followed by a sigmatropic rearrangement. An almost identical (6+4) cycloaddition followed by a sigmatropic ring contraction to yield a cyclohexene is catalyzed by an unrelated[428,429] enzyme encoded by the *spnF* gene in *Saccharopolyspora spinosa.*[430-432]

*In order to produce a comprehensible drawing, the structure of the reactant in Figure 1–31 was flipped over so that the fragment with two carbon–carbon bonds approaches the transition state from above rather than from below.

†Professor Hui Ming Ge has written: "The CAS drawing in ChemAbstract's SciFinder is the enantiomer, which we think is not correct based on single crystal X-ray analysis."

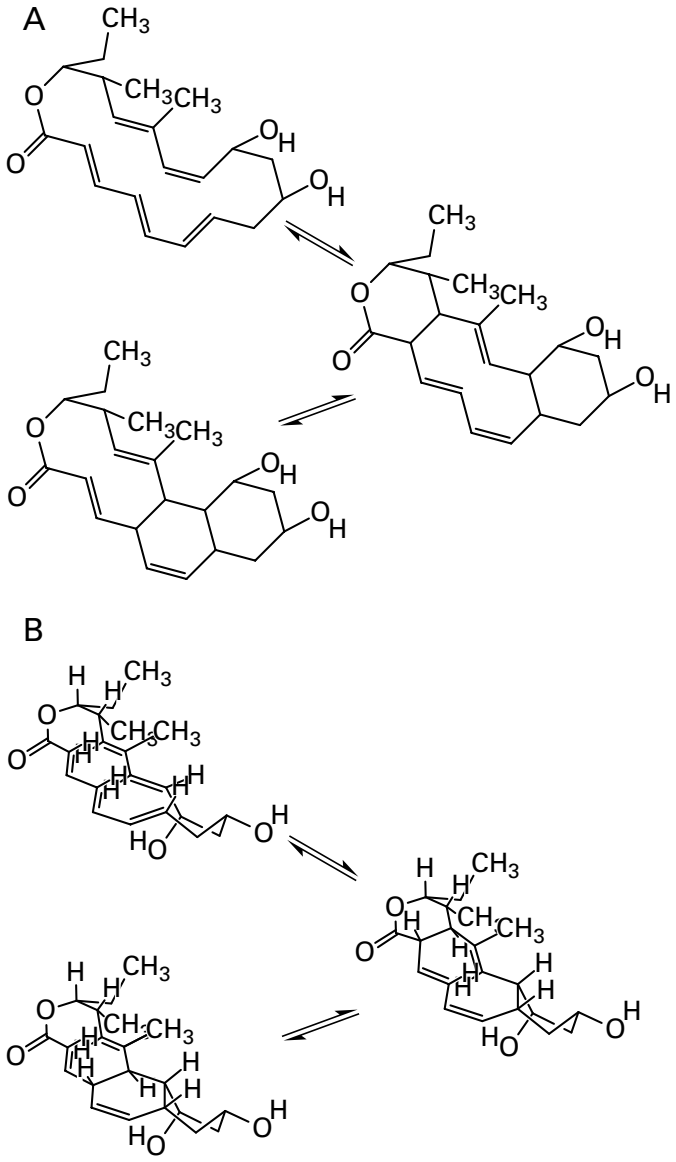

Figure 1–31: The (6+4) cycloaddition and sigmatropic rearrangement catalyzed by the enzyme encoded by the *ngnD* gene in *N. argentinensis*.[428] **(A)** Schematic drawing of the reaction, displaying the (6+4) cycloaddition that converts the octadecacycle into the fused hexacycle, decacycle, and hexacycle and the subsequent sigmatropic rearrangement that produces the fused decacycle, hexacycle, and hexacycle. The initial reactant is the lactone of the linear carboxylic acid (2*E*,4*E*,6*E*,12*E*,14*E*)-9,11,17-trihydroxy-14,16-dimethylnonadeca-2,4,6,8,12,14-pentaenoic acid. **(B)** Stereochemical drawing of the same two reactions. During the (6+4) cycloaddition, the lower left-hand side of the octadecacycle is situated above the upper right-hand side. When the central decacycle forms, the hydrogens and the carbon–carbon bonds attached to the ends of the π bonds rearranging to form the two new σ bonds swing in such a way that those groups in the center on the top and bottom move up and down, respectively, and those pointed away from the center on the top and bottom move down and up, respectively, as in **1–123**. During the sigmatropic rearrangement, the lower left-hand side of the central decacycle is still situated above the upper right-hand side. When the central decacycle contracts, the hydrogens and the carbon–carbon bonds attached to the ends of the π bonds forming the new σ bond swing in such a way that those groups in the center on the top and bottom move up and down, respectively, and those pointed away from the center on the top and bottom move down and up, respectively. As the former σ bond on the upper left dissociates, the two hydrogens swing into the center and the lower left-hand hydrogen ends up above the upper right-hand hydrogen.

An **electrocyclic reaction** is a pericyclic reaction in which a σ bond is formed between the termini of a fully conjugated linear π molecular orbital system containing three (or $2n+3$) π bonds among six (or $4n+6$) atoms that become a ring with two (or $2n+2$) π bonds and the σ bond connecting the former termini. The number of π bonds has decreased by one and the number of σ bonds has increased by one. The transition state is formed from a ring of the six (or $4n+6$) p atomic orbitals of the six (or $4n+6$) atoms participating in the rearrangement. There are many conversions involved in the synthesis of natural products that can be explained as the result of electrocyclic reactions.[433] There is, however, little evidence as yet that they are catalyzed by enzymes. Nevertheless, the fact that such electrocyclic reactions are quite slow at ambient temperatures and should require catalysis, as well as the fact that it is often the case that the biosynthetic products are chiral even though the precursors are achiral, together strongly suggest that enzymatic catalysis is involved.

The assignment of a pericyclic reaction as the mechanism of an enzyme in the absence of direct evidence of such an involvement results from its irresistibility, but in many cases, this may be wishful thinking.[425] For example, prosolanapyrone-III cycloisomerase (Equation 1–165), the enzyme that is involved in the biosynthesis of versipelostatin, and

the enzyme that is encoded by the *ngnD* gene (Figure 1–31) are simply, at the moment, the least controversial of several enzymes that have been proposed to catalyze Diels–Alder reactions.[425,434]

One problem with glibly assigning a pericyclic reaction to the mechanism of an enzyme is that the only mechanism for catalysis of an actual pericyclic reaction seems to be the **alignment of the portions of the reactant** or the two reactants. It should be pointed out, however, that such an alignment of reactants is the most effective way,[435] in which any active site dramatically increases the rate of a reaction. Furthermore, the alignment of the reactant or the reactants by the active site can also explain the **production of chiral products from achiral reactants**. In a reaction such as a cycloaddition, where there are four possible diastereomeric products for the uncatalyzed reaction, the fact that only one enantiomer is observed is strong evidence that the reaction proceeds under the steric control of an active site.

Another problem with the assignment of a pericyclic reaction as the mechanism of an enzyme is that there are usually **alternative mechanisms involving two transition states** and an intermediate rather than the single transition state required of a pericyclic reaction. For example, the formation of intermediate **1–79** in the active site of crotonyl-CoA carboxylase/reductase can be explained[299] by the direct transfer of a hydride from NADPH to (*E*)-but-2-enoyl-SCoA followed by a nucleophilic addition of the resulting enolate to the $NADP^+$ in a nonproductive side reaction. Enzymatic reactions that were at one time considered to be concerted cycloadditions sometimes turn out to proceed through entirely different mechanisms. For example, at one time it was believed[436,437] that the reaction catalyzed by macrophomate synthase from *Macrophoma commelinae* included a Diels–Alder cycloaddition

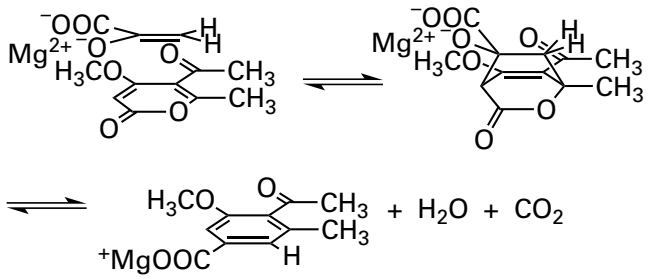

(1–166)

in which the enol of pyruvate was the dienophile. Since then, evidence has been presented[438,439] that is more consistent with a mechanism in which a nucleophilic addition of the enolate of pyruvate to the α,β-unsaturated carbonyl of the exocyclic acetyl group, the carbon–carbon bond of which is also conjugated to the acyl group of the lactone, is followed by a nucleophilic addition of the enolate of the resulting adduct directly to the carbonyl of the pyruvyl group

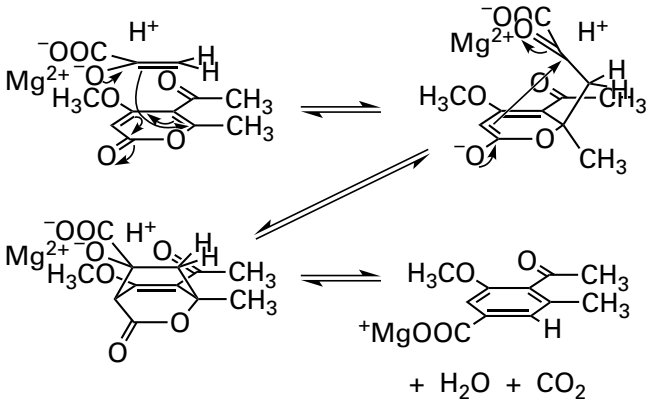

(1–167)

This mechanism involves two transition states and the intermediate adduct.

An enzyme, which is found in both *Yersinia enterocolitica* and *M. tuberculosis*, has an active site[440,441] that catalyzes the same reaction as that catalyzed by isochorismate lyase from *P. aeruginosa* (Equation 1–164), even though this other enzyme is unrelated structurally to isochorismate lyase from *P. aeruginosa* and hence does not share a common ancestor. The active site is completely different, and when the two substrates pyruvate and salicylate are occupying it, unlike what occurs in the active site of the enzyme from *P. aeruginosa*, the π molecular orbital system of the pyruvate is positioned at a 60° angle to the π molecular orbital system of the salicylate, rather than being parallel to it and stacked upon it. This observation is a strong indication that the reaction catalyzed by this other enzyme does not proceed by a pericyclic mechanism, which requires that the pyruvate and the salicylate be parallel to each other (**1–121**).

A mechanism, however, that is consistent with this stereochemical observation is one in which an elimination of the enol of pyruvate precedes the removal of a hydron from carbon 2 of the ring by the resulting enol

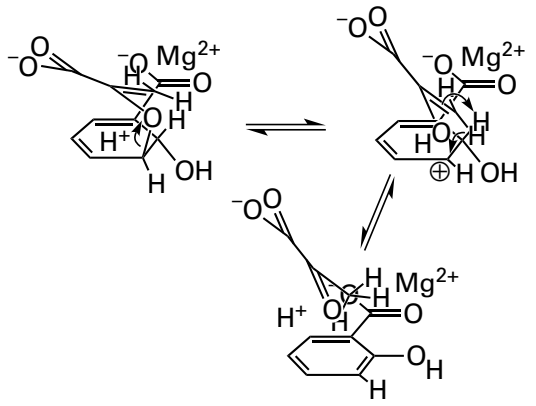

(1–168)

The enol of pyruvic acid should be a good leaving group ($pK_a = 7.3$), the resulting carbenium ion is delocalized over five carbons, and the enolate of pyruvate should be an excellent base (the pK_a of its conjugate acid is 26.6) for removing the hydron from carbon 2 of the ring. In the crystallographic molecular model of the complex between the enzyme from *Y. enterocolitica* and pyruvate and salicylate, the distance between oxygen 2 of the pyruvate and carbon 3 of the salicylate is 0.31 nm, and the distance betweeen carbon 3 of the pyruvate and carbon 2 of the salicylate is 0.38 nm. Both of these distances are within the respective sums of the van der Waals radii of the atoms involved, which is consistent with the proposed steps in the mechanism.

The irresistibility of pericyclic reactions often leads to a proposal that can be rejected by simple consideration of the stereochemistry of the participants. Consider the following mechanism proposed for carboxyl transfer from biotin[442]

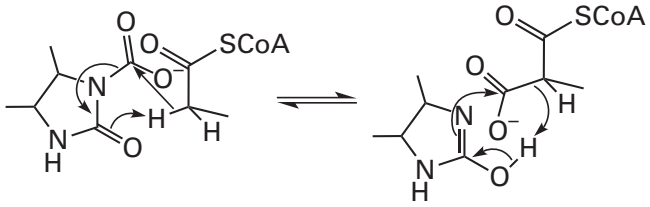

(1–169)

Superficially, it resembles the mechanism of the reaction catalyzed by isochorismate lyase (Equation 1–164). When the details of Equation 1–169 are examined, however, a telling difficulty arises. Although the σ bond between the carbon and the hydrogen of the acyl-SCoA can be parallel to the π molecular orbital system of the urea, the σ bond between the upper right nitrogen of the urea and the carbon of the carboxy group cannot be parallel to the π molecular orbital system of the urea because it is of necessity orthogonal to it. Consequently, the transition state required if this were a pericyclic reaction is impossible. It is not surprising that this reaction has been demonstrated to occur in steps rather than by a concerted mechanism.[443,444]

In summary, a pericyclic reaction is an unequivocal example of a concerted reaction. In a concerted reaction, the making and breaking of two or more bonds occur within the same transition state. Reactions that have been shown to proceed through concerted mechanisms always proceed through simultaneous overlaps between occupied and unoccupied atomic or molecular orbitals that are stereochemically permitted. In addition, overlaps between two occupied molecular or atomic orbitals that would lead to electron repulsion must be avoided. Many more concerted mechanisms have been proposed than have been demonstrated to occur. In many instances, the proposal for a concerted mechanism, when examined closely, has significant problems associated with it.

Suggested Reading

Stubbe, J., Fish, S., and Abeles, R.H. (1980) Are carboxylations involving biotin concerted or nonconcerted? *J. Biol. Chem. 255*, 236–242. https://doi.org/10.1016/S0021-9258(19)86289-0

DeClue, M. S., Baldridge, K. K., Künzler, D. E., Kast, P., and Hilvert, D. (2005) Isochorismate pyruvate lyase: A pericyclic reaction mech-anism? *J. Am. Chem. Soc. 127*, 15002-15003. https://doi.org/10.1021/ja055871t

Problem 1–1: The following reactions are simplified versions of actual reactions that occur in metabolism. In most of them, the complicated functional groups of the actual metabolites have been replaced by methyl or ethyl groups to make it simpler to write the compounds. Therefore, these specific reactions do not necessarily occur anywhere. Nevertheless, as written, the chemistry is identical to the chemistry of the reactions between the more complicated biological molecules that are catalyzed by enzymes. The majority of the chemical reactions that occur in metabolism are represented here. Most of the remaining reactions in metabolism are catalyzed by enzymes that use prosthetic

groups, and these will be discussed in more detail in the next chapter. Assume each reaction occurs in aqueous solution and that donors of hydrons (acids) and acceptors of hydrons (bases) are always available. Write complete chemical mechanisms for these reactions. Where hydrides are shown it is assumed that NAD^+ would be the carrier of them.

(A) $CH_3CH_2OH \rightleftharpoons CH_3CHO + H^- + H^+$

(B) $CH_3COCH_2OH \rightleftharpoons CH_3CH(OH)CHO$

(C) $CH_3CH(OH)CHO + HSCH_2CH_2OH \rightleftharpoons CH_3CH(OH)COSCH_2CH_2OH + H^- + H^+$

(D) $CH_3CH_2NH_3^+ + CH_3COCH_2OH \rightleftharpoons CH_3CH_2\overset{\oplus}{N}HCCH_3CH_2OH + H_2O$

(E) $CH_3CH_2\overset{\oplus}{N}HC(CH_3)CH_2OH + CH_3CHO \rightleftharpoons CH_3CH_2\overset{\oplus}{N}HC(CH_3)CH(OH)CH(OH)CH_3$

(F) $CH_3CH_2NH_3^+ + HCHO + H^- + H^+ \rightleftharpoons CH_3CH_2\overset{\oplus}{N}H_2CH_3 + H_2O$

(G) $CH_3CH_2CONHCH_3 + H_2O \rightleftharpoons CH_3CH_2COO^- + H_3CNH_3^+$

(H) $CH_3COSCH_3 + CH_3CHO \rightleftharpoons CH_3CH(OH)CH_2COSCH_3$

(I) $CH_3COOCH_3 + CH_3NH_3^+ \rightleftharpoons CH_3CONHCH_3 + H^+ + HOCH_3$

(J) $CH_3COCH_2COO^- + H_2O \rightleftharpoons 2CH_3COO^- + H^+$

(K) $2CH_3COSCH_3 \rightleftharpoons CH_3COCH_2COSCH_3 + CH_3SH$

(L) $CH_3CHCHCOCH_3 + CO_2 \rightleftharpoons {}^-OOCCH_2CHCHCOCH_3 + H^+$

(M) $CH_3COSCH_3 + CO_2 \rightleftharpoons {}^-OOCCH_2COSCH_3 + H^+$

(N) $CH_3COSCH_3 + HOPO_3^{2-} \rightleftharpoons CH_3COOPO_3^{2-} + HSCH_3$

(O) $CH_3COSCH_3 + CH_3OH \rightleftharpoons CH_3COOCH_3 + HSCH_3$

(P) $H_2NCOOPO_3^{2-} + CH_3NH_3^+ \rightleftharpoons H_2NCONHCH_3 + HOPO_3^{2-} + H^+$

(Q) $CH_3CONHCH_3 + C_2H_5NH_3^+ \rightleftharpoons CH_3C(NC_2H_5)NHCH_3 + H_2O + H^+$

(R) $H_2NCHNH_2^+ + H_2O \rightleftharpoons H_2NCONH_2 + H^- + 2H^+$

(S) $H^+ + CH_3CONH_2 + CH_3COO^- \rightleftharpoons CH_3CONHCOCH_3 + H_2O$

(T) $CH_3COOPO_3^{2-} + H^- + H^+ \rightleftharpoons CH_3CHO + HOPO_3^{2-}$

(U) $CH_3CHO + H_2O \rightleftharpoons CH_3COO^- + H^- + 2H^+$

(V) $CH_3C(OCH_2CH_3)_2CH_3 + H_2O \rightleftharpoons CH_3COCH_3 + 2C_2H_5OH$

(W) $CH_3C(OCH_2CH_3)_2CH_3 + HOPO_3^{2-} \rightleftharpoons CH_3C(OCH_2CH_3)(OPO_3^{2-})CH_3 + CH_3CH_2OH$

(X) $CH_3CH(OCH_2CH_3)OPO_3^{2-} + CH_3NH_3^+ \rightleftharpoons CH_3CH(OCH_2CH_3)\overset{\oplus}{N}H_2CH_3 + HOPO_3^{2-}$

(Y) $CH_3CH(OH)CH_2COSCH_3 \rightleftharpoons CH_3CHCHCOSCH_3 + H_2O$

(Z) *cis*-$CH_3CHCHCH_3 \rightleftharpoons$ *trans*-$CH_3CHCHCH_3$

(a) $CH_3CHCHCH_2OPO_3^{2-} \rightleftharpoons CH_2CHCHCH_2 + HOPO_3^{2-}$

(b) $CH_2CHCHCH_2 + H_2O \rightleftharpoons CH_3CH_2CH_2CHO$

(c) $CH_3CH(OH)CH_2COO^- + H^+ \rightleftharpoons CH_3CHCH_2 + CO_2 + H_2O$

(d) $CH_3CH(OH)CH_2OPO_3^{2-} + CH_3COCH_3 \rightleftharpoons CH_3COCH_2C(CH_3)_2OH + HOPO_3^{2-}$

(e) 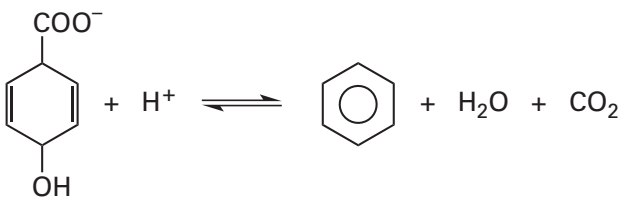

(f) $H_2C(OH)CH(\overset{\oplus}{N}H_2CH_3)OC_2H_5 \rightleftharpoons HCOCH_2\overset{\oplus}{N}H_2CH_3 + C_2H_5OH$

(g) $CH_3CH(OH)CH_2COO^- \rightleftharpoons CH_3CH_2CH(OH)COO^-$

(h) $CH_3COCH_2COO^- + H^+ \rightleftharpoons CH_3COCH_3 + CO_2$

(i) $CH_2CHCH_2OPO_3^{2-} + CH_2CHCH_3 \rightleftharpoons CH_2CHCH_2CH_2CHCH_2 + HOPO_3^{2-}$

(j) $CH_3CH_2OH + HOPO_3^{2-} \rightleftharpoons CH_3CH_2OPO_3^{2-} + H_2O$

(k) $CH_3COOPO_3^{2-} + CH_3OH \rightleftharpoons CH_3COO^- + CH_3OPO_3^{2-} + H^+$

(l) $CH_3COO^- + (CH_3)_2\overset{\oplus}{S}C_2H_5 \rightleftharpoons CH_3COOCH_3 + CH_3SC_2H_5$

Problem 1–2: Write mechanisms for the following reactions:[445,446]

(A)

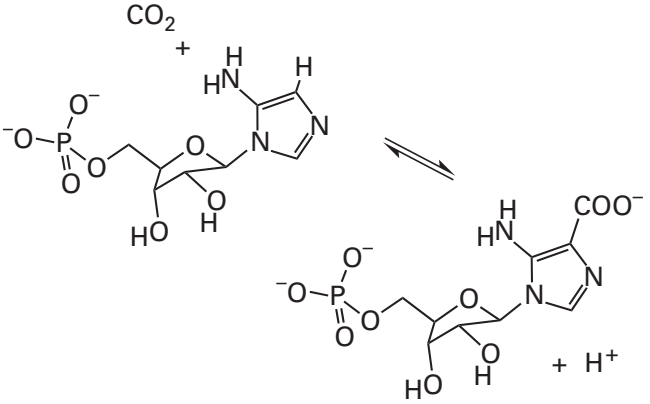

(B)

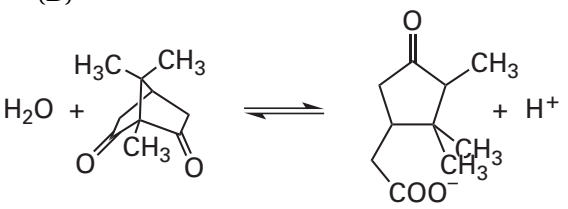

(C)

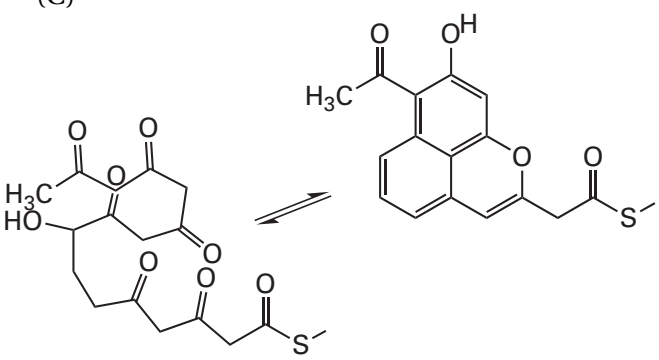

(D) 2-hydroxy-6-oxonona-2,4-diene-1,9-dioic acid $\rightleftharpoons$ succinate + 2-hydroxypenta-2,4-dienoic acid

Problem 1–3: In animal cells, D-glucosamine is made from ammonium ion (NH_4^+) and D-fructose. Write the complete chemical mechanism for this reaction.

Problem 1–4: Write a mechanism[447] for the reaction catalyzed by 1,4-dihydroxy-2-naphthoyl-CoA synthase

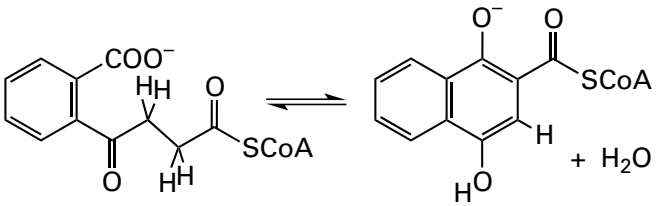

What process drives the reaction to completion?

Problem 1–5: Write a mechanism[448] for the reaction that is catalyzed by coronamic acid synthase

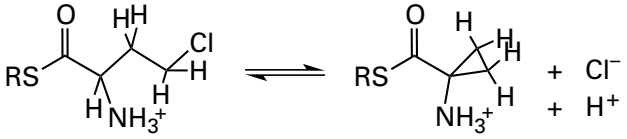

where R is a small protein with a cysteine to which the L-2-amino-4-chlorobutyrate is attached.

Problem 1–6: Write a mechanism for Equations 1–142 and 1–144.

Problem 1–7: Write a mechanism[449] for the reaction that is catalyzed by strictosidine synthase

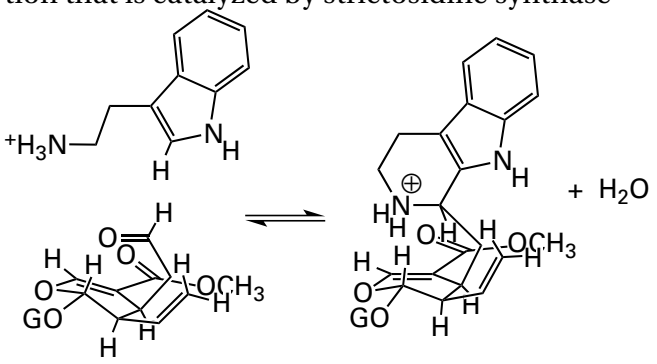

where G is a D-glucopyranosyl group.

Problem 1–8: Write mechanisms for the electrophilic aromatic substitutions of Equations 1–155, 1–156, and 1–157. Write resonance structures for the intermediate carbenium ions that explain their stabilities.

Problem 1–9: The indolyl group in L-tryptophan is susceptible to electrophilic aromatic substitution at nitrogen 1 and carbons 2, 5, 6, and 7, in addition to carbon 4 (Equation 1–155), and to electrophilic addition at carbon 3. Use the dimethylallyl carbenium ion **1–99** (Figure 1–26) as the electrophile and draw the most stable resonance form of the cationic intermediate in each of these six electrophilic aromatic substitutions and the product of the electrophilic aromatic addition at carbon 3.

Problem 1–10: Write a mechanism for this reaction

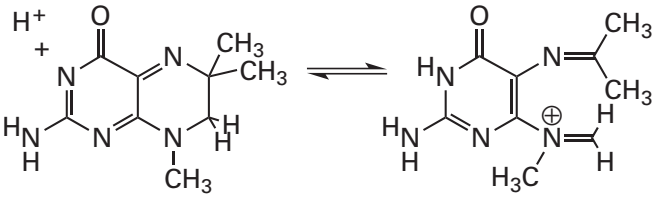

that involves only carbonyl chemistry rather than pericyclic chemistry.

Problem 1–11: Criticize the following proposal for a concerted reaction:

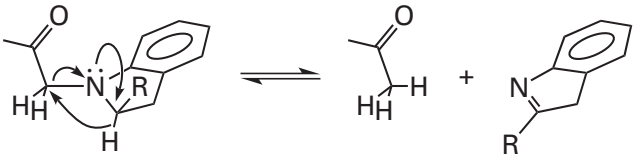

References

1. Radzicka, A., and Wolfenden, R. (1995) A proficient enzyme, *Science 267*, 90–93.
2. Lad, C., Williams, N. H., and Wolfenden, R. (2003) The rate of hydrolysis of phosphomonoester dianions and the exceptional catalytic proficiencies of protein and inositol phosphatases, *Proc. Natl. Acad. Sci. U.S.A. 100*, 5607–5610.
3. Bearne, S. L., and Wolfenden, R. (1997) Mandelate racemase in pieces: Effective concentrations of enzyme functional groups in the transition state, *Biochemistry 36*, 1646–1656.
4. Schroeder, G. K., Lad, C., Wyman, P., Williams, N. H., and Wolfenden, R. (2006) The time required for water attack at the phosphorus atom of simple phosphodiesters and of DNA, *Proc. Natl. Acad. Sci. U.S.A. 103*, 4052–4055.
5. Lewis, C. A., Jr., and Wolfenden, R. (2019) Ether hydrolysis, ether thiolysis, and the catalytic power of etherases in the disassembly of lignin, *Biochemistry 58*, 5381–5385.
6. Brant, D. A., Barnett, L. B., and Alberty, R. A. (1963) The temperature dependence of the steady-state kinetic parameters of the fumarase reaction, *J. Am. Chem. Soc. 85*, 2204–2209.
7. Taylor, E. A., Palmer, D. R. J., and Gerlt, J. A. (2001) The lesser "burden borne" by *o*-succinylbenzoate synthase: An "easy" reaction involving a carboxylate carbon acid, *J. Am. Chem. Soc. 123*, 5824–5825.
8. Bearne, S. L., and Wolfenden, R. (1995) Enzymic hydration of an olefin: The burden borne by fumarase, *J. Am. Chem. Soc. 117*, 9588–9589.
9. Edwards, D. R., Lohman, D. C., and Wolfenden, R. (2012) Catalytic proficiency: The extreme case of S-O cleaving sulfatases, *J. Am. Chem. Soc. 134*, 525–531.
10. Stojanovski, B. M., and Ferreira, G. C. (2015) Asn-150 of murine erythroid 5–aminolevulinate synthase modulates the catalytic balance between the rates of the reversible reaction, *J. Biol. Chem. 290*, 30750–30761.
11. Bloch, W., MacQuarrie, R. A., and Bernhard, S. A. (1971) The nucleotide and acyl group content of native rabbit muscle glyceraldehyde 3-phosphate dehydrogenase, *J. Biol. Chem. 246*, 780–790.
12. Wijma, H. J., Canters, G. W., de Vries, S., and Verbeet, M. P. (2004) Bidirectional catalysis by copper-containing nitrite reductase, *Biochemistry 43*, 10467–10474.
13. Alberty, R. A. (2004) Thermodynamic properties of nucleotide reductase reactions, *Biochemistry 43*, 9840–9845.
14. Yu, X., Niks, D., Mulchandani, A., and Hille, R. (2017) Efficient reduction of CO_2 by the molybdenum-containing formate dehydrogenase from *Cupriavidus necator* (*Ralstonia eutropha*), *J. Biol. Chem. 292*, 16872–16879.
15. Bates, D. J., and Frieden, C. (1973) Treatment of enzyme kinetic data. 3. The use of the full time course of a reaction, as examined by computer simulation, in defining enzyme mechanisms, *J. Biol. Chem. 248*, 7878–7884.
16. Eigen, M. (1964) Proton transfer acid–base catalysis and enzymatic hydrolysis. Part I:

Elementary processes, *Angew. Chem, Int. Ed. Engl. 3*, 1–19.
17. Jiang, J. C., Wang, Y. S., Chang, H. C., Lin, S. H., Lee, Y. T., Niedner-Schatteburg, G., and Chang, H. C. (2000) Infrared spectra of $H^+(H_2O)_{5-8}$ clusters: Evidence for symmetric proton hydration, *J. Am. Chem. Soc. 122*, 1398–1410.
18. Marx, D., Tuckerman, M. E., Hutter, J., and Parrinello, M. (1999) The nature of the hydrated excess proton in water, *Nature 397*, 601–604.
19. Okumura, M., Yeh, L. I., Myers, J. D., and Lee, Y. T. (1990) Infrared-spectra of the solvated hydronium ion: Vibrational predissociation spectroscopy of mass-selected $H_3O^+ \cdot (H_2O)_n$, *J. Phys. Chem. 94*, 3416–3427.
20. Schwarz, H. A. (1977) Gas phase infrared spectra of oxonium hydrate ions from 2 to 5 μm, *J. Chem. Phys. 67*, 5525–5534.
21. Zundel, G., and Metzger, H. (1968) IR spectroscopic study of the hydration of polystyrenesulfonic acid, *Z. Phys. Chem. (München, Ger.) 59*, 225–241.
22. Wei, S., Shi, Z., and Castleman, A. W., Jr. (1991) Mixed cluster ions as a structure probe: Experimental evidence for clathrate structure of water-hydrogen ion clusters ($(H_2O)_{20}H^+$ and $(H_2O)_{21}H^+$), *J. Chem. Phys. 94*, 3268–3270.
23. Yang, X. L., and Castleman, A. W. (1989) Large protonated water clusters $H^+(H_2O)_n$ ($1 \leq n < 60$): The Production and reactivity of clathrate-like structures under thermal conditions, *J. Am. Chem. Soc. 111*, 6845–6846.
24. Shin, J. W., Hammer, N. I., Diken, E. G., Johnson, M. A., Walters, R. S., Jaeger, T. D., Duncan, M. A., Christie, R. A., and Jordan, K. D. (2004) Infrared signature of structures associated with the $H^+(H_2O)_n$ ($n = 6$ to 27) clusters, *Science 304*, 1137–1140.
25. Miyazaki, M., Fujii, A., Ebata, T., and Mikami, N. (2004) Infrared spectroscopic evidence for protonated water clusters forming nanoscale cages, *Science 304*, 1134–1137.
26. Robertson, W. H., Diken, E. G., Price, E. A., Shin, J. W., and Johnson, M. A. (2003) Spectroscopic determination of the OH^- solvation shell in the $OH^- \cdot (H_2O)_n$ clusters, *Science 299*, 1367–1372.
27. Kyte, J. (2007) *Structure in Protein Chemistry*, 2nd ed., pp 204–222, Garland Science, New York.
28. Torrance, J. W., Holliday, G. L., Mitchell, J. B., and Thornton, J. M. (2007) The geometry of interactions between catalytic residues and their substrates, *J. Mol. Biol. 369*, 1140–1152.
29. Siwick, B. J., and Bakker, H. J. (2007) On the role of water in intermolecular proton-transfer reactions, *J. Am. Chem. Soc. 129*, 13412–13420.
30. Debye, P. (1942) Reaction rates in ionic solutions, *Trans. Electrochem. Soc. 82*, 265–272.
31. Perrin, C. L. (1986) Diffusion-controlled unimolecular reactions and the lifetime of a strong acid in water, *J. Am. Chem. Soc. 108*, 6807–6808.
32. Andrieux, C., P., Gamby, J., Hapiot, P., and Saveant, J.-M. (2003) Evidence for inverted region behavior in proton transfer to carbanions, *J. Am. Chem. Soc. 125*, 10119–10124.
33. Amyes, T. L., and Richard, J. P. (1992) Generation and stability of a simple thiol ester enolate in aqueous solution, *J. Am. Chem. Soc. 114*, 10297–10302.
34. Argyrou, A., and Washabaugh, M. W. (1999) Proton transfer from the C_5-*proR*/*proS* positions of L-dihydroorotate: General-base catalysis, isotope effects, and internal return, *J. Am. Chem. Soc. 121*, 12054–12062.
35. Horowitz, S., Dirk, L. M. A., Yesselman, J. D., Nimtz, J. S., Adhikari, U., Mehl, R. A., Scheiner, S., Houtz, R. L., Al-Hashimi, H. M., and Trievel, R. C. (2013) Conservation and functional importance of carbon-oxygen hydrogen bonding in AdoMet-dependent methyltransferases, *J. Am. Chem. Soc. 135*, 15536–15548.
36. Costentin, C., and Saveant, J.-M. (2004) Why are proton transfers at carbon slow? Self-exchange reactions, *J. Am. Chem. Soc. 126*, 14787–14795.
37. Bernasconi, C. F. (1982) The role of solvent reorganization in proton transfer and nucleophilic addition reactions, *Pure Appl. Chem. 54*, 2335–2348.
38. Tobin, J. B., and Frey, P. A. (1996) Electrostatic acceleration of enolization in cationic ketones, *J. Am. Chem. Soc. 118*, 12253–12260.
39. Jogl, G., Rozovsky, S., McDermott Ann, E., and Tong, L. (2003) Optimal alignment for enzymatic proton transfer: Structure of the Michaelis complex of triosephosphate isom-

erase at 1.2 Å resolution, *Proc. Natl. Acad. Sci. U.S.A. 100*, 50–55.
40. Menger, F. M., Chow, J. F., Kaiserman, H., and Vasquez, P. C. (1983) Directionality of proton-transfer in solution: Three systems of known angularity, *J. Am. Chem. Soc. 105*, 4996–5002.
41. Xiang, S., Short, S. A., Wolfenden, R., and Carter, C. W., Jr. (1997) The structure of the cytidine deaminase–product complex provides evidence for efficient proton transfer and ground-state destabilization, *Biochemistry 36*, 4768–4774.
42. Swain, C. G., and Brown, J. F., Jr. (1952) Concerted displacement reactions. VIII. Polyfunctional catalysis, *J. Am. Chem. Soc. 74*, 2538–2543.
43. Sytnik, A., Gormin, D., and Kasha, M. (1994) Interplay between excited-state intramolecular proton transfer and charge transfer in flavonols and their use as protein-binding-site fluorescence probes, *Proc. Natl. Acad. Sci. U.S.A. 91*, 11968–11972.
44. Kyte, J. (2007) *Structure in Protein Chemistry,* 2nd ed., p 227, Garland Science, New York.
45. Heady, J. E., and Kerr, S. J. (1973) Purification and characterization of glycine *N*-methyltransferase, *J. Biol. Chem. 248*, 69–72.
46. Golding, B. T., and Nassereddin, I. K. (1985) The biosynthesis of spermidine. Part 3. The stereochemistry of the formation of the nitrogen-methylene group in the biosynthesis of spermidine, *J. Chem. Soc. Perkin Trans. 1 (1972–1999)*, 2017–2024.
47. Orr, G. R., Danz, D. W., Pontoni, G., Prabhakaran, P. C., Gould, S. J., and Coward, J. K. (1988) Synthesis of chirally deuteriated (*S*-adenosyl-*S*-methylsulfonio)propylamines and spermidines. Elucidation of the stereochemical course of putrescine aminopropyltransferase (spermidine synthase), *J. Am. Chem. Soc. 110*, 5791–5799.
48. Wu, H., Min, J., Ikeguchi, Y., Zeng, H., Dong, A., Loppnau, P., Pegg, A. E., and Plotnikov, A. N. (2007) Structure and mechanism of spermidine synthases, *Biochemistry 46*, 8331–8339.
49. Dietze, P. E., and Jencks, W. P. (1989) General-base catalysis of nucleophilic substitution at carbon, *J. Am. Chem. Soc. 111*, 340–344.
50. Wolfenden, R., and Yuan, Y. (2007) Monoalkyl sulfates as alkylating agents in water, alkylsulfatase rate enhancements, and the "energy-rich" nature of sulfate half-esters, *Proc. Natl. Acad. Sci. U.S.A. 104*, 83–86.
51. Mao, C., Cook, W. J., Zhou, M., Federov, A. A., Almo, S. C., and Ealick, S. E. (1998) Calf spleen purine nucleoside phosphorylase complexed with substrates and substrate analogs, *Biochemistry 37*, 7135–7146.
52. Anand, R., Kaminski, P. A., and Ealick, S. E. (2004) Structures of purine 2′-deoxyribosyltransferase, substrate complexes, and the ribosylated enzyme intermediate at 2.0 Å. resolution, *Biochemistry 43*, 2384–2393.
53. Huang, X., Surry, C., Hiebert, T., and Bennet, A. J. (1995) Hydrolysis of (2–deoxy-β-D-glucopyranosyl)pyridinium salts, *J. Am. Chem. Soc. 117*, 10614–10621.
54. Romero, R., Stein, R., Bull, H. G., and Cordes, E. H. (1978) Secondary deuterium-isotope effects for acid-catalyzed hydrolysis of inosine and adenosine, *J. Am. Chem. Soc. 100*, 7620–7624.
55. Young, P. R., and Jencks, W. P. (1977) Trapping of oxocarbonium ion intermediate in hydrolysis of acetophenone dimethyl ketals, *J. Am. Chem. Soc. 99*, 8238–8248.
56. Kresge, A. J., and Weeks, D. P. (1984) Hydrolysis of acetaldehyde diethyl acetal and ethyl vinyl ether: Secondary kinetic isotope effects in water and aqueous dioxane and the stability of the ethoxyethyl cation, *J. Am. Chem. Soc. 106*, 7140–7143.
57. Gilbert, H. F., and Jencks, W. P. (1982) Mechanism of the aminolysis of alkyl benzimidates, *J. Am. Chem. Soc. 104*, 6769–6779.
58. Deslongchamps, P. (1975) Stereoelectronic control in cleavage of tetrahedral intermediates in hydrolysis of esters and amides, *Tetrahedron 31*, 2463–2490.
59. Perrin, C. L., and Arrhenius, G. M. L. (1982) A critical test of the theory of stereoelectronic control, *J. Am. Chem. Soc. 104*, 2839–2842.
60. Perrin, C. L., and Engler, R. E. (1997) Quantitative assessment by 1D-EXSY NMR of stereoelectronic control in acid-catalyzed exchange between stereoisomeric 2-methoxy-1,3-dioxanes and methanol, *J. Am. Chem. Soc. 119*, 585–591.
61. Perrin, C. L., and Nunez, O. (1986) Absence of stereoelectronic control in hydrolysis of cyclic amidines, *J. Am. Chem. Soc. 108*, 5997–6003.

62. Bennet, A. J., and Sinnott, M. L. (1986) Complete kinetic isotope effect description of transition states for acid-catalyzed hydrolyses of methyl α- and β-glucopyran-osides, *J. Am. Chem. Soc. 108*, 7287–7294.
63. Ratcliffe, A. J., Mootoo, D. R., Andrews, C. W., and Fraser-Reid, B. (1989) Concerning the antiperiplanar lone pair hypothesis: Oxidative hydrolysis of conformationally restrained 4-pentenyl glycosides, *J. Am. Chem. Soc. 111*, 7661–7662.
64. Indurugalla, D., and Bennet, A. J. (2001) A kinetic isotope effect study on the hydrolysis reactions of methyl xylopyranosides and methyl 5-thioxylopyranosides: Oxygen versus sulfur stabilization of carbenium ions, *J. Am. Chem. Soc. 123*, 10889–10898.
65. Sakon, J., Adney, W. S., Himmel, M. E., Thomas, S. R., and Karplus, P. A. (1996) Crystal structure of thermostable family 5 endocellulase E1 from *Acidothermus cellulolyticus* in complex with cellotetraose, *Biochemistry 35*, 10648–10660.
66. Amyes, T. L., and Jencks, W. P. (1989) Lifetimes of oxocarbenium ions in aqueous solution from common ion inhibition of the solvolysis of α-azido ethers by added azide ion, *J. Am. Chem. Soc. 111*, 7888–7900.
67. Zhao, C., Chen, S. B., and Seidel, D. (2016) Direct formation of oxocarbenium ions under weakly acidic conditions: Catalytic enantioselective oxa-Pictet–Spengler reactions, *J. Am. Chem. Soc. 138*, 9053–9056.
68. Elferink, H., Severijnen, M. E., Martens, J., Mensink, R. A., Berden, G., Oomens, J., Rutjes, F., Rijs, A. M., and Boltje, T. J. (2018) Direct experimental characterization of glycosyl cations by infrared ion spectroscopy, *J. Am. Chem. Soc. 140*, 6034–6038.
69. Vocadlo, D. J., Davies, G. J., Laine, R., and Withers, S. G. (2001) Catalysis by hen egg-white lysozyme proceeds via a covalent intermediate, *Nature 412*, 835–838.
70. Rocek, J., Westheimer, F. H., Eschenmoser, A., Moldovanyi, L., and Schreiber, J. (1962) Chromic acid esters as intermediates in the oxidation of alcohols. Rate-limiting esterification of a sterically hindered alcohol, *Helv. Chim. Acta 45*, 2554–2567.
71. Kankaanpera, A., Salomaa, P., Juhala, P., Aaltonen, R., and Mattsen, M. (1973) Isotope-exchange studies with diethyl acetals in ethanol and their mechanistic implications to protolytic reactions of acetals and vinyl ethers, *J. Am. Chem. Soc. 95*, 3618–3624.
72. Fife, T. H., and Natarajan, R. (1986) General acid catalyzed acetal hydrolysis. The hydrolysis of acetals and ketals of *cis*- and *trans*-1,2-cyclohexanediol. Changes in rate-determining step and mechanism as a function of pH, *J. Am. Chem. Soc. 108*, 8050–8056.
73. Fife, T. H., and Natarajan, R. (1986) General acid catalysis in the hydrolysis of 1,3–dioxolanes and 1,3–oxathiolanes. The hydrolysis of acetals and thioacetals of *p*-(dimethylamino)benzaldehyde, *J. Am. Chem. Soc. 108*, 2425–2430.
74. Kresge, A. J., Leibovitch, M., and Sikorski, J. A. (1992) Acid-catalyzed hydrolysis of 5-enolpyruvylshikimate 3-phosphate (EPSP) and some simple models of its vinyl ether functional group, *J. Am. Chem. Soc. 114*, 2618–2622.
75. Fife, T. H., and Pellino, A. M. (1980) General-acid-catalyzed imidazolidine ring-opening: Hydrolysis of symmetrical and unsymmetrical 1,3-imidazolidines of *p*-dimethylaminocinnamaldehyde, *J. Am. Chem. Soc. 102*, 3062–3071.
76. Ba-Saif, S., Luthra, A. K., and Williams, A. (1989) Concerted acetyl-group transfer between substituted phenolate ion nucleophiles: Variation of transition-state structure as a function of substituent, *J. Am. Chem. Soc. 111*, 2647–2652.
77. Jencks, W. P. (1972) General acid–base catalysis of complex reactions in water, *Chem. Rev. 72*, 705–718.
78. O'Ferrall, R. A. M. (1970) Relations between E2 and ElcB mechanisms of β-elimination, *J. Chem. Soc. B*, 274–277.
79. Chan, J., Sannikova, N., Tang, A., and Bennet, A. J. (2014) Transition-state structure for the quintessential S_N2 reaction of a carbohydrate: Reaction of α-glucopyranosyl fluoride with azide ion in water, *J. Am. Chem. Soc. 136*, 12225–12228.
80. Cherian, X. M., Van Arman, S. A., and Czarnik, A. W. (1990) Models for nucleoside glycosylase enzymes. Evidence that the hydrolysis of β-D-ribofuranosides requires a backside preassociation nucleophile, *J. Am. Chem. Soc. 112*, 4490–4498.

81. Amyes, T. L., and Jencks, W. P. (1989) Concerted bimolecular substitution reactions of acetal derivatives of propionaldehyde and benzaldehyde, *J. Am. Chem. Soc. 111*, 7900–7909.
82. Swain, C. G., and Scott, C. B. (1953) Quantitative correlation of relative rates. Comparison of hydroxide ions with other nucleophilic reagents toward alkyl halides, esters, epoxides and acyl halides [Concerted displacement reactions, paper X], *J. Am. Chem. Soc. 75*, 141–147.
83. Pearson, R. G., Sobel, H. R., and Songstad, J. (1968) Nucleophilic reactivity constants toward methyl iodide and *trans*-dichlorodi(pyridine)platinum(II), *J. Am. Chem. Soc. 90*, 319–326.
84. Jordan, P. M., and Akhtar, M. (1970) Mechanism of action of serine transhydroxymethylase, *Biochem. J. 116*, 277–286.
85. Jones, C. C., Sinnott, M. L., and Souchard, I. J. L. (1977) S_N1 Hydrolyses of glycosyl pyridinium salts, and quantification of the main source of catalytic power of *E. coli* (lacZ)-β-galactosidase, *J. Chem. Soc. Perkin Trans. 2 (1972–1999)* 1191–1198.
86. Hine, J., Cholod, M. S., and Chess, W. K. (1973) Kinetics of formation of imines from acetone and primary amines: Evidence for internal acid-catalyzed dehydration of certain intermediate carbinolamines, *J. Am. Chem. Soc. 95*, 4270–4276.
87. Sayer, J. M., and Jencks, W. P. (1977) Imine-forming elimination-reactions: 2. Imbalance of charge-distribution in the transition state for carbinolamine dehydration, *J. Am. Chem. Soc. 99*, 464–474.
88. Funderburk, L. H., and Jencks, W. P. (1978) Structure-reactivity coefficients for general acid catalysis of semi-carbazone formation, *J. Am. Chem. Soc. 100*, 6708–6714.
89. Liu, S. W., Chen, C. S., Chang, S. S., Mong, K. K., Lin, C. H., Chang, C. W., Tang, C. Y., and Li, Y. K. (2009) Identification of essential residues of human α--fucosidase and tests of its mechanism, *Biochemistry 48*, 110–120.
90. Dahlquist, F. W., Rand-Meir, T., and Raftery, M. A. (1969) Application of secondary α-deuterium kinetic isotope effects to studies of enzyme catalysis. Glycoside hydrolysis by lysozyme and β-glucosidase, *Biochemistry 8*, 4214–4221.
91. Sinnott, M. L., and Jencks, W. P. (1980) Solvolysis of D-glucopyranosyl derivatives in mixtures of ethanol and 2,2,2-trifluoro-ethanol, *J. Am. Chem. Soc. 102*, 2026–2032.
92. Mulliken, R. S. (1935) Electronic structures of molecules: X. Aldehydes, ketones and related molecules, *J. Chem. Phys. 3*, 564–573.
93. Taylor, R., Kennard, O., and Versichel, W. (1983) Geometry of the N-H···O=C hydrogen-bond: 1. Lone-pair directionality, *J. Am. Chem. Soc. 105*, 5761–5766.
94. Hirano, Y., Takeda, K., and Miki, K. (2016) Charge-density analysis of an iron-sulfur protein at an ultra-high resolution of 0.48 Å, *Nature 534*, 281–284.
95. Hansen, N. K., and Coppens, P. (1978) Aspherical atom refinements of *p*-nitropyridine-*N*-oxide and ammoniumthiocyanate: Noise filtering in deformation density maps, *Acta Crystallogr A 34*, S24–S25.
96. Kanchuger, M. S., and Byers, L. D. (1979) Acyl substituent effects on thiohemiacetal equilibria, *J. Am. Chem. Soc. 101*, 3005–3010.
97. Burkey, T. J., and Fahey, R. C. (1983) Equilibrium studies of water and thiol addition to ketones: Substituent and solvent effects for methyl ketones, *J. Am. Chem. Soc. 105*, 868–871.
98. Barnett, R. E., and Jencks, W. P. (1969) Diffusion-controlled and concerted base catalysis in decomposition of hemithioacetals, *J. Am. Chem. Soc. 91*, 6758–6765.
99. Gilbert, H. F., and Jencks, W. P. (1977) Mechanisms for enforced general acid catalysis of addition of thiol anions to acetaldehyde, *J. Am. Chem. Soc. 99*, 7931–7947.
100. Cox, M. M., and Jencks, W. P. (1981) Concerted bifunctional proton transfer and general-base catalysis in the methoxyaminolysis of phenyl acetate, *J. Am. Chem. Soc. 103*, 580–587.
101. Bruice, T. C., Hegarty, A. F., Felton, S. M., Donzel, A., and Kundu, N. G. (1970) Aminolysis of esters. IX. Nature of transition states in the aminolysis of phenyl acetates, *J. Am. Chem. Soc. 92*, 1370–1378.
102. Kirsch, J. F., and Kline, A. (1969) Acyl substituent effects in general base catalyzed ammonolysis reactions of esters, *J. Am. Chem. Soc. 91*, 1841–1847.
103. Iwasawa, T., Hooley, R. J., and Rebek, J., Jr. (2007) Stabilization of labile carbonyl addi-

tion intermediates by a synthetic receptor, *Science 317*, 493–496.
104. Appel, R., Chelli, S., Tokuyasu, T., Troshin, K., and Mayr, H. (2013) Electrophilicities of benzaldehyde-derived iminium ions: Quantification of the electrophilic activation of aldehydes by iminium formation, *J. Am. Chem. Soc. 135*, 6579–6587.
105. Klausen, R. S., Kennedy, C. R., Hyde, A. M., and Jacobsen, E. N. (2017) Chiral thioureas promote enantioselective Pictet–Spengler cyclization by stabilizing every intermediate and transition state in the carboxylic acid-catalyzed reaction, *J. Am. Chem. Soc. 139*, 12299–12309.
106. Pictet, A., and Spengler, T. (1911) Über die bildung von isochinolin derivaten durch einwirkung von methylal auf phenyläthylamin, phenylalanin und tyrosin, *Ber. Dtsch. Chem. Ges 44*, 2030–2036.
107. Luk, L. Y., Bunn, S., Liscombe, D. K., Facchini, P. J., and Tanner, M. E. (2007) Mechanistic studies on norcoclaurine synthase of benzylisoquinoline alkaloid biosynthesis: An enzymatic Pictet–Spengler reaction, *Biochemistry 46*, 10153–10161.
108. Funderburk, L. H., Aldwin, L., and Jencks, W. P. (1978) Mechanisms of general acid and base catalysis of reactions of water and alcohols with formaldehyde, *J. Am. Chem. Soc. 100*, 5444–5459.
109. Sorensen, P. E., and Jencks, W. P. (1987) Acid- and base-catalyzed decomposition of acetaldehyde hydrate and hemiacetals in aqueous solution, *J. Am. Chem. Soc. 109*, 4675–4690.
110. Taylor, S. D., and Kluger, R. (1993) Hydrolysis of methylacetoin ethyl phosphate. Competing pathways for carbonyl hydrate participation in a model for biotin carboxylation, *J. Am. Chem. Soc. 115*, 867–871.
111. Bell, R. P. (1966) The reversible hydration of carbonyl compounds, *Adv. Phys. Org. Chem. 4*, 1–29.
112. Fedor, L. R., and Bruice, T. C. (1965) Nucleophilic displacement reactions at the thiol ester bond. IV. General base-catalyzed hydrolysis of ethyl trifluorothiolacetate. Kinetic evidence for the formation of a tetrahedral intermediate, *J. Am. Chem. Soc. 87*, 4138–4147.
113. Satterthwaite, A. C., and Jencks, W. P. (1974) Mechanism of aminolysis of acetate esters, *J. Am. Chem. Soc. 96*, 7018–7031.
114. Satterthwaite, A. C., and Jencks, W. P. (1974) Mechanism of partitioning of intermediates formed in hydrolysis of phenyl imidates, *J. Am. Chem. Soc. 96*, 7031–7044.
115. Bender, M. L. (1951) Oxygen exchange as evidence for the existence of an intermediate in ester hydrolysis, *J. Am. Chem. Soc. 73*, 1626–1629.
116. Bender, M. L., and Heck, H. d'A. (1967) Carbonyl oxygen exchange in general base-catalyzed ester hydrolysis, *J. Am. Chem. Soc. 89*, 1211–1220.
117. Bennet, A. J., Slebocka-Tilk, H., Brown, R. S., Guthrie, J. P., and Jodhan, A. (1990) Concurrent oxygen-18 exchange accompanying the acid-catalyzed hydrolysis of anilides. Implications for the lifetimes of reversibly formed intermediates, *J. Am. Chem. Soc. 112*, 8497–8506.
118. Slebocka-Tilk, H., Bennet, A. J., Keillor, J. W., Brown, R. S., Guthrie, J. P., and Jodhan, A. (1990) Oxygen-18 exchange accompanying the basic hydrolysis of primary, secondary, and tertiary toluamides: 2. The importance of amine leaving abilities from the anionic tetrahedral intermediate, *J. Am. Chem. Soc. 112*, 8507–8514.
119. Adediran, S. A., Deraniyagala, S. A., Xu, Y., and Pratt, R. F. (1996) β-Secondary and solvent deuterium kinetic isotope effects on β-lactamase catalysis, *Biochemistry 35*, 3604–3613.
120. Stefanidis, D., and Jencks, W. P. (1993) General base catalysis of ester hydrolysis, *J. Am. Chem. Soc. 115*, 6045–6050.
121. Hogg, J. L. Secondary hydrogen isotope effects, In *Transition States of Biochemical Processes* (Gandour, R. D. and Schowen, R. L., Eds.), pp 201–224, Springer-Verlag, Boston.
122. Deraniyagala, S. A., Adediran, S. A., and Pratt, R. F. (1995) β-Secondary and solvent deuterium kinetic isotope effects and the mechanisms of base- and acid-catalyzed hydrolysis of penicillanic acid, *J. Org. Chem. 60*, 1619–1625.
123. Melander, L. C. S., and Saunders, W. H. (1980) *Reaction Rates of Isotopic Molecules*, Wiley, New York.
124. Singleton, D. A., and Merrigan, S. R. (2000) Resolution of conflicting mechanistic obser-

vations in ester aminolysis: A warning on the qualitative prediction of isotope effects for reactive intermediates, *J. Am. Chem. Soc. 122*, 11035–11036.
125. McClelland, R. A., and Patel, G. (1981) Rate and equilibrium-constants for the formation and decomposition of the tetrahedral intermediates of the methanolysis of methyl benzoates, *J. Am. Chem. Soc. 103*, 6912–6915.
126. Perrin, C. L., and Thoburn, J. D. (1993) Absence of stereoelectronic control in the hydrolysis of fully and partially *N*-alkylated cyclic amidinium ions, *J. Am. Chem. Soc. 115*, 3140–3145.
127. Perrin, C. L., and Young, D. B. (2001) Is there stereoelectronic control in hydrolysis of cyclic guanidinium ions? *J. Am. Chem. Soc. 123*, 4446–4450.
128. Oakenfull, D. G., and Jencks, W. P. (1971) Reactions of acetylimidazole and acetylimidazolium ion with nucleophilic reagents: Structure–reactivity relationships, *J. Am. Chem. Soc. 93*, 178–188.
129. Edward, J. T., and Wong, S. C. (1977) Effect of sulfuric-acid concentration on rates of hydrolysis of ethyl benzoate, ethyl thiolbenzoate, and ethyl thionbenzoate, *J. Am. Chem. Soc. 99*, 7224–7228.
130. Santry, L. J., and McClelland, R. A. (1983) Kinetics of breakdown of the tetrahedral intermediate of an *O,S*-acyl transfer reaction, *J. Am. Chem. Soc. 105*, 3167–3172.
131. Lee, Y. N., and Schmir, G. L. (1978) Concurrent general acid and general base catalysis in hydrolysis of an imidate ester: 1. Monofunctional catalysis, *J. Am. Chem. Soc. 100*, 6700–6707.
132. Williams, A. (1976) Dilute acid-catalyzed amide hydrolysis: Efficiency of the *N*-protonation mechanism, *J. Am. Chem. Soc. 98*, 5645–5651.
133. Fersht, A. R. (1971) Acyl-transfer reactions of amides and esters with alcohols and thiols: A reference system for serine and cysteine proteinases: Concerning *N*-protonation of amides and amide–imidate equilibria, *J. Am. Chem. Soc. 93*, 3504–3515.
134. Slebocka-Tilk, H., Neverov Alexei, A., and Brown, R. S. (2003) Proton inventory study of the base-catalyzed hydrolysis of formamide. Consideration of the nucleophilic and general base mechanisms, *J. Am. Chem. Soc. 125*, 1851–1858.
135. Marlier, J. F. (1993) Heavy-atom isotope effects on the alkaline hydrolysis of methyl formate: The role of hydroxide ion in ester hydrolysis, *J. Am. Chem. Soc. 115*, 5953–5956.
136. Mata-Segreda, J. F. (2002) Hydroxide as general base in the saponification of ethyl acetate, *J. Am. Chem. Soc. 124*, 2259–2262.
137. Brown, R. S., Bennet, A. J., and Slebocka-Tilk, H. (1992) Recent perspectives concerning the mechanism of H_3O^+ and hydroxide-promoted amide hydrolysis, *Acc. Chem. Res. 25*, 481–488.
138. Ardelt, W., and Laskowski, M., Jr. (1991) Effect of single amino acid replacements on the thermodynamics of the reactive site peptide bond hydrolysis in ovomucoid third domain, *J. Mol. Biol. 220*, 1041–1053.
139. Rucker, V. C., and Byers, L. D. (2000) An assessment of desolvation on rates of acetyl transfer: Insights into enzyme catalysis, *J. Am. Chem. Soc. 122*, 8365–8369.
140. Fersht, A. R., and Jencks, W. P. (1970) Acetylpyridinium ion intermediate in pyridine-catalyzed hydrolysis and acyl transfer reactions of acetic anhydride: Observation, kinetics, structure-reactivity correlations, and effects of concentrated salt solutions, *J. Am. Chem. Soc. 92*, 5432–5442.
141. Hupe, D. J., and Jencks, W. P. (1977) Nonlinear structure–reactivity correlations: Acyl transfer between sulfur and oxygen nucleophiles, *J. Am. Chem. Soc. 99*, 451–464.
142. Cox, M. M., and Jencks, W. P. (1981) Catalysis of the methoxyaminolysis of phenyl acetate by a preassociation mechanism with a solvent isotope effect maximum, *J. Am. Chem. Soc. 103*, 572–580.
143. Ba-Saif, S., Luthra, A. K., and Williams, A. (1987) Concertedness in acyl group transfer in solution: A single transition state in acetyl group transfer between phenolate ion nucleophiles, *J. Am. Chem. Soc. 109*, 6362–6368.
144. Stefanidis, D., Cho, S., Dhe-Paganon, S., and Jencks, W. P. (1993) Structure–reactivity correlations for reactions of substituted phenolate anions with acetate and formate esters, *J. Am. Chem. Soc. 115*, 1650–1656.
145. Chrystiuk, E., and Williams, A. (1987) A single transition-state in the transfer of the methoxycarbonyl group between isoquinoline and substituted pyridines in aqueous solution, *J. Am. Chem. Soc. 109*, 3040–3046.

146. Hengge, A. (1992) Can acyl transfer occur via a concerted mechanism? Direct evidence from heavy-atom isotope effects, *J. Am. Chem. Soc. 114*, 6575–6576.
147. Leffler, J. E. (1953) Parameters for the description of transition states, *Science 117*, 340–341.
148. Deacon, T., Farrar, C. R., Sikkel, B. J., and Williams, A. (1978) Reactions of nucleophiles with strained cyclic sulfonate esters. Brønsted relationships for rate and equilibrium constants for variation of phenolate anion nucleophile and leaving group, *J. Am. Chem. Soc. 100*, 2525–2534.
149. Gerstein, J., and Jencks, W. P. (1964) Equilibria and rates for acetyl transfer among substituted phenyl acetates acetylimidazole *O*-acylhydroxamic acids and thiol esters, *J. Am. Chem. Soc. 86*, 4655–4663.
150. Effenberger, F., Eberhard, J. K., and Maier, A. H. (1996) The first unequivocal evidence of the reacting electrophile in aromatic acylation reactions, *J. Am. Chem. Soc. 118*, 12572–12579.
151. Williams, A., and Douglas, K. T. (1975) Elimination–addition mechanisms of acyl transfer reactions, *Chem. Rev. 75*, 627–649.
152. Jencks, W. P. (1981) How does a reaction choose its mechanism? *Chem. Soc. Rev. 10*, 345–375.
153. Song, B. D., and Jencks, W. P. (1987) Inhibition of the hydrolysis of *p*-(dimethylamino)benzoyl fluoride by potassium fluoride, *J. Am. Chem. Soc. 109*, 3160–3161.
154. Song, B. D., and Jencks, W. P. (1989) Mechanism of solvolysis of substituted benzoyl halides, *J. Am. Chem. Soc. 111*, 8470–8479.
155. Bender, M. L., and Chen, M. C. (1963) Acylium ion formation in the reactions of carboxylic acid derivatives. IV. The acid-catalyzed hydrolysis of methyl 4–substituted-2,6- dimethylbenzoates, *J. Am. Chem. Soc. 85*, 37–40.
156. Jencks, W. P. (1970) *Handbook of Biochemistry* (Sober, H. A., Ed.), pp J181–J186, CRC Press, Cleveland, OH.
157. Fersht, A. R., and Requena, Y. (1971) Free energies of hydrolysis of amides and peptides in aqueous solution at 25 degrees, *J. Am. Chem. Soc. 93*, 3499–3504.
158. Yang, W., and Drueckhammer, D. G. (2001) Understanding the relative acyl-transfer reactivity of oxoesters and thioesters: Computational analysis of transition state delocalization effects, *J. Am. Chem. Soc. 123*, 11004–11009.
159. Estiu, G., and Merz, K. M., Jr. (2004) Enzymatic catalysis of urea decomposition: Elimination or hydrolysis? *J. Am. Chem. Soc. 126*, 11832–11842.
160. Kirby, A. J., and Nome, F. (2015) Fundamentals of phosphate transfer, *Acc. Chem. Res. 48*, 1806–1814.
161. Khan, S. A., and Kirby, A. J. (1970) Reactivity of phosphate esters: Multiple structure–reactivity correlations for the reactions of triesters with nucleophiles, *J. Chem. Soc. B*, 1172–1182.
162. Haake, P. C., and Westheimer, F. H. (1961) Hydrolysis and exchange in esters of phosphoric acid, *J. Am. Chem. Soc. 83*, 1102–1109.
163. Dennis, E. A., and Westheimer, F. H. (1966) The geometry of the transition state in hydrolysis of phosphate esters, *J. Am. Chem. Soc. 88*, 3432–3433.
164. Ramirez, F., Bigler, A. J., and Smith, C. P. (1968) Pentaphenoxyphosphorane, *J. Am. Chem. Soc. 90*, 3507–3511.
165. Davies, J. E., Doltsinis, N. L., Kirby, A. J., Roussev, C. D., and Sprik, M. (2002) Estimating pK_a values for pentaoxyphos-phoranes, *J. Am. Chem. Soc. 124*, 6594–6599.
166. Kraulis, P. J. (1991) Molscript: A program to produce both detailed and schematic plots of protein structures, *J Appl Crystallogr 24*, 946–950.
167. Range, K., McGrath, M. J., Lopez, X., and York, D. M. (2004) The structure and stability of biological metaphosphate, phosphate, and phosphorane compounds in the gas phase and in solution, *J. Am. Chem. Soc. 126*, 1654–1665.
168. Hoffmann, R., Howell, J. M., and Muetterties, E. L. (1972) Molecular orbital theory of pentacoordinate phosphorus, *J. Am. Chem. Soc. 94*, 3047–3058.
169. Gilheany, D. G. (1994) No d orbitals but Walsh diagrams and maybe banana bonds: Chemical bonding in phosphines, phosphine oxides, and phosphonium ylides, *Chem. Rev. 94*, 1339–1374.
170. Dobado, J. A., Martinez-Garcia, H., Molina, J. M., and Sundberg, M. R. (1998) Chemical bonding in hypervalent molecules revised: Application of the atoms in molecules theory to Y_3X and Y_3XZ (Y = H or CH_3; X = N, P or As;

Z = O or S) compounds, *J. Am. Chem. Soc. 120*, 8461–8471.
171. Cundari, T. R. (2013) Chemical bonding involving *d*-orbitals, *Chem. Commun. 49*, 9521–9525.
172. Gaus, M., Lu, X., Elstner, M., and Cui, Q. (2014) Parameterization of DFTB3/3OB for sulfur and phosphorus for chemical and biological applications, *J. Chem. Theory Comput. 10*, 1518–1537.
173. Westheimer, F. H. (1968) Pseudo-rotation in the hydrolysis of phosphate esters, *Acc. Chem. Res. 1*, 70–78.
174. Hamilton, W. C., Laplaca, S. J., and Ramirez, F. (1965) Structure of a pentaoxyphosphorane by X-ray analysis, *J. Am. Chem. Soc. 87*, 127–128.
175. Kluger, R., and Taylor, S. D. (1990) On the origins of enhanced reactivity of 5-membered cyclic phosphate esters: The relative contributions of enthalpic and entropic factors, *J. Am. Chem. Soc. 112*, 6669–6671.
176. Taylor, S. D., and Kluger, R. (1992) Heats of reaction of cyclic and acyclic phosphate and phosphonate esters: Strain discrepancy and steric retardation, *J. Am. Chem. Soc. 114*, 3067–3071.
177. Gutowsky, H. S., and Liehr, A. D. (1952) Infrared spectra of phosphorus trifluoride, phosphorus oxyfluoride, and phosphorus pentafluoride, *J. Chem. Phys. 20*, 1652–1653.
178. Berry, R. S. (1960) Correlation of rates of intramolecular tunneling processes, with application to some group-V compounds, *J. Chem. Phys. 32*, 933–938.
179. Gerratana, B., Sowa, G. A., and Cleland, W. W. (2000) Characterization of the transition-state structures and mechanisms for the isomerization and cleavage reactions of uridine 3′-*m*-nitrobenzyl phosphate, *J. Am. Chem. Soc. 122*, 12615–12621.
180. Breslow, R. (1993) Kinetics and mechanism in RNA cleavage, *Proc. Natl. Acad. Sci. U.S.A. 90*, 1208–1211.
181. Kluger, R., Covitz, F., Dennis, E., Williams, L. D., and Westheimer F. H. (1969) pH–Product and pH–rate profiles for the hydrolysis of methyl ethylene phosphate: Rate-limiting pseudorotation, *J. Am. Chem. Soc. 91*, 6066–6072.
182. Davis, A. M., Hall, A. D., and Williams, A. (1988) Charge description of base-catalyzed alcoholysis of aryl phosphodiesters: A ribonuclease model, *J. Am. Chem. Soc. 110*, 5105–5108.
183. Lonnberg, H., Stromberg, R., and Williams, A. (2004) Compelling evidence for a stepwise mechanism of the alkaline cyclisation of uridine 3'-phosphate esters, *Org. Biomol. Chem. 2*, 2165–2167.
184. Oivanen, M., Schnell, R., Pfleiderer, W., and Lonnberg, H. (1991) Interconversion and hydrolysis of monomethyl and monoisopropyl esters of adenosine 2′-monophosphates and 3′-monophosphates: Kinetics and mechanisms, *J. Org. Chem. 56*, 3623–3628.
185. Kosonen, M., Yousefi-Salakdeh, E., Stromberg, R., and Lonnberg, H. (1998) pH- And buffer-independent cleavage and mutual isomerization of uridine 2′- and 3′-alkyl phosphodiesters: Implications for the buffer catalyzed cleavage of RNA, *J. Chem. Soc. Perkin Trans. 2 (1972–1999)*, 1589–1595.
186. Beckmann, C., Kirby, A. J., Kuusela, S., and Tickle, D. C. (1998) Mechanisms of catalysis by imidazole buffers of the hydrolysis and isomerisation of RNA models, *J. Chem. Soc. Perkin Trans. 2 (1972–1999). 2*, 573–581.
187. Perrin, C. L. (1995) On the mechanism of buffer-catalyzed hydrolysis of RNA Models, *J. Org. Chem. 60*, 1239–1243.
188. Cassano, A. G., Anderson, V. E., and Harris, M. E. (2002) Evidence for direct attack by hydroxide in phosphodiester hydrolysis, *J. Am. Chem. Soc. 124*, 10964–10965.
189. Oivanen, M., Mikhailov, S. N., Padyukova, N. S., and Lonnberg, H. (1993) Kinetics of mutual isomerization of the phosphonate analogs of dinucleoside 2′,5′-monophos-phates and 3′,5′-monophosphates in aqueous solution, *J. Org. Chem. 58*, 1617–1619.
190. Friedman, J. M., Freeman, S., and Knowles, J. R. (1988) The quest for free metaphosphate in solution: Racemization at phosphorus in the transfer of the phospho group from aryl phosphate monoesters to *tert*-butyl alcohol in acetonitrile or in *tert*-butyl alcohol, *J. Am. Chem. Soc. 110*, 1268–1275.
191. Lightcap, E. S., and Frey, P. A. (1992) Discrete monomeric metaphosphate anion as an intermediate in the hydrolysis of micromonothiopyrophosphate, *J. Am. Chem. Soc. 114*, 9750–9755.
192. Guthrie, J. P. (1977) Hydration and dehydration of phosphoric acid derivatives:

Free energies of formation of the pentacoordinate intermediates for phosphate ester hydrolysis and of monomeric metaphosphate, *J. Am. Chem. Soc. 99*, 3991–4001.
193. Loew, L. M., and MacArthur, W. R. (1977) A molecular orbital study of monomeric metaphosphate: Density surfaces of frontier orbitals as a tool in assessing reactivity, *J. Am. Chem. Soc. 99*, 1019–1025.
194. Katzhendler, J., Schneider, H., Ta-Shma, R., and Breuer, E. (2000) Fragmentation of methyl hydrogen β-hydroxyiminobenzylphosphonates: Kinetics, mechanism and the question of metaphosphate formation, *Perkin Trans. 2(2000)*, 1961–1968.
195. Choe, J.-Y., Iancu, C. V., Fromm, H. J., and Honzatko, R. B. (2003) Metaphosphate in the active site of fructose-1,6-bisphosphatase, *J. Biol. Chem. 278*, 16015–16020.
196. Shi, R., Chen, Z. Y., Zhu, D. W., Li, C., Shan, Y., Xu, G., and Lin, S. X. (2013) Crystal structures of human muscle fructose-1,6-bisphosphatase: Novel quaternary states, enhanced AMP affinity, and allosteric signal transmission pathway, *PLoS One 8*, e71242.
197. de Macedo-Ribeiro, S., Renirie, R., Wever, R., and Messerschmidt, A. (2008) Crystal structure of a trapped phosphate intermediate in vanadium apochloroperoxidase catalyzing a dephosphorylation reaction, *Biochemistry 47*, 929–934.
198. Abbott, S. J., Jones, S. R., Weinman, S. A., Bockhoff, F. M., McLafferty, F. W., and Knowles, J. R. (1979) Chiral [^{16}O,^{17}O,^{18}O]-phosphate monoesters: Asymmetric synthesis and stereochemical analysis of [1(*R*)-^{16}O,^{17}O,^{18}O]phospho-(*S*)-propane-1,2-diol, *J. Am. Chem. Soc. 101*, 4323–4332.
199. Buchwald, S. L., and Knowles, J. R. (1980) Determination of the absolute configuration of [^{16}O,^{17}O,^{18}O]phosphate monoesters by using ^{31}P NMR, *J. Am. Chem. Soc. 102*, 6601–6602.
200. Buchwald, S. L., Friedman, J. M., and Knowles, J. R. (1984) Stereochemistry of nucleophilic displacement on two phosphoric monoesters and a phosphoguanidine: The role of metaphosphate, *J. Am. Chem. Soc. 106*, 4911–4916.
201. Kirby, A. J., and Varvogli.Ag. (1967) Reactivity of phosphate esters: Monoester hydrolysis, *J. Am. Chem. Soc. 89*, 415–423.
202. Barnard, P. W. C., Bunton, C. A., Llewellyn, D. R., Oldham, K. G., Silver, B. L., and Vernon, C. A. (1955) The hydrolysis of organic phosphates, *Chem. Ind.*, 760–763.
203. Butcher, W. W., and Westheimer, F. H. (1955) The lanthanum hydroxide gel promoted hydrolysis of phosphate esters, *J. Am. Chem. Soc. 77*, 2420–2424.
204. Clapp, C. H., and Westheimer, F. H. (1974) Monomeric methyl metaphosphate, *J. Am. Chem. Soc. 96*, 6710–6714.
205. Bourne, N., and Williams, A. (1984) Evidence for a single transition state in the transfer of the phosphoryl group ($-PO_3^{2-}$) to nitrogen nucleophiles from pyridino-*N*-phosphonates, *J. Am. Chem. Soc. 106*, 7591–7596.
206. Skoog, M. T., and Jencks, W. P. (1984) Reactions of pyridines and primary amines with *N*-phosphorylated pyridines, *J. Am. Chem. Soc. 106*, 7597–7606.
207. Herschlag, D., and Jencks, W. P. (1989) Evidence that metaphosphate monoanion is not an intermediate in solvolysis reactions in aqueous solution, *J. Am. Chem. Soc. 111*, 7579–7586.
208. Kirby, A. J., and Younas, M. (1970) Reactivity of phosphate esters: Reactions of diesters with nucleophiles, *J. Chem. Soc B*, 1165–1172.
209. Oertell, K., Kashemirov, B. A., Negahbani, A., Minard, C., Haratipour, P., Alnajjar, K. S., Sweasy, J. B., Batra, V. K., Beard, W. A., Wilson, S. H., McKenna, C. E., and Goodman, M. F. (2018) Probing DNA base-dependent leaving group kinetic effects on the DNA polymerase transition state, *Biochemistry 57*, 3925–3933.
210. Kim, K., and Cole, P. A. (1998) Kinetic analysis of a protein tyrosine kinase reaction transition state in the forward and reverse directions, *J. Am. Chem. Soc. 120*, 6851–6858.
211. Bourne, N., and Williams, A. (1984) Effective charge on oxygen in phosphoryl ($-PO_3^{2-}$) group transfer from an oxygen donor, *J. Org. Chem. 49*, 1200–1204.
212. Kim, K., and Cole, P. A. (1997) Measurement of a Brønsted nucleophile coefficient and insights into the transition state for a protein tyrosine kinase, *J. Am. Chem. Soc. 119*, 11096–11097.
213. Kirby, A. J., and Younas, M. (1970) Reactivity of phosphate esters: Diester hydrolysis, *J. Chem. Soc. B*, 510–513.

214. Ba-Saif, S. A., Davis, A. M., and Williams, A. (1989) Effective charge-distribution for attack of phenoxide ion on aryl methyl phosphate monoanion: Studies related to the action of ribonuclease, *J. Org. Chem. 54*, 5483–5486.
215. Kirby, A. J., Medeiros, M., Oliveira, P. S., Orth, E. S., Brandao, T. A., Wanderlind, E. H., Amer, A., Williams, N. H., and Nome, F. (2011) Activating water: Important effects of non-leaving groups on the hydrolysis of phosphate triesters, *Chemistry 17*, 14996–15004.
216. Cassano, A. G., Anderson, V. E., and Harris, M. E. (2004) Analysis of solvent nucleophile isotope effects: Evidence for concerted mechanisms and nucleophilic activation by metal coordination in nonenzymatic and ribozyme-catalyzed phosphodiester hydrolysis, *Biochemistry 43*, 10547–10559.
217. Herschlag, D., and Jencks, W. P. (1990) Catalysis of the hydrolysis of phosphorylated pyridines by $Mg(OH)^+$: A possible model for enzymic phosphoryl transfer, *Biochemistry 29*, 5172–5179.
218. Herschlag, D., and Jencks, W. P. (1989) Phosphoryl transfer to anionic oxygen nucleophiles: Nature of the transition state and electrostatic repulsion, *J. Am. Chem. Soc. 111*, 7587–7596.
219. Linjalahti, H., Feng, G. Q., Mareque-Rivas, J. C., Mikkola, S., and Williams, N. H. (2008) Cleavage and isomerization of UpU promoted by dinuclear metal ion complexes, *J. Am. Chem. Soc. 130*, 4232–4233.
220. Korhonen, H., Mikkola, S., and Williams, N. H. (2012) The mechanism of cleavage and isomerisation of RNA promoted by an efficient dinuclear Zn^{2+} complex, *Chem.–Eur. J.18*, 659–670.
221. Williams, N. H., Cheung, W., and Chin, J. (1998) Reactivity of phosphate diesters doubly coordinated to a dinuclear cobalt(III) complex: Dependence of the reactivity on the basicity of the leaving group, *J. Am. Chem. Soc. 120*, 8079–8087.
222. Humphry, T., Forconi, M., Williams, N. H., and Hengge, A. C. (2002) An altered mechanism of hydrolysis for a metal-complexed phosphate diester, *J. Am. Chem. Soc. 124*, 14860–14861.
223. Humphry, T., Forconi, M., Williams, N. H., and Hengge, A. C. (2004) Altered mechanisms of reactions of phosphate esters bridging a dinuclear metal center, *J. Am. Chem. Soc. 126*, 11864–11869.
224. Wlodawer, A., Miller, M., and Sjolin, L. (1983) Active site of RNase: Neutron diffraction study of a complex with uridine vanadate, a transition-state analog, *Proc. Natl. Acad. Sci. U.S.A. 80*, 3628–3631.
225. Wlodawer, A., Bott, R., and Sjolin, L. (1982) The refined crystal structure of ribonuclease A at 2.0 Å resolution, *J. Biol. Chem. 257*, 1325–1332.
226. Jones, J. P., Weiss, P. M., and Cleland, W. W. (1991) Secondary oxygen-18 isotope effects for hexokinase-catalyzed phosphoryl transfer from ATP, *Biochemistry 30*, 3634–3639.
227. Hollfelder, F., and Herschlag, D. (1995) The nature of the transition state for enzyme-catalyzed phosphoryl transfer: Hydrolysis of O-aryl phosphorothioates by alkaline phosphatase, *Biochemistry 34*, 12255–12264.
228. O'Brien, P. J., Lassila, J. K., Fenn, T. D., Zalatan, J. G., and Herschlag, D. (2008) Arginine coordination in enzymatic phosphoryl transfer: Evaluation of the effect of Arg166 mutations in *Escherichia coli* alkaline phosphatase, *Biochemistry 47*, 7663–7672.
229. Zalatan, J. G., and Herschlag, D. (2006) Alkaline phosphatase mono- and diesterase reactions: Comparative transition state analysis, *J. Am. Chem. Soc. 128*, 1293–1303.
230. McWhirter, C., Lund, E. A., Tanifum, E. A., Feng, G., Sheikh, Q. I., Hengge, A. C., and Williams, N. H. (2008) Mechanistic study of protein phosphatase-1 (PP1), a catalytically promiscuous enzyme, *J. Am. Chem. Soc. 130*, 13673–13682.
231. Quade, N., Huo, L., Rachid, S., Heinz, D. W., and Muller, R. (2011) Unusual carbon fixation gives rise to diverse polyketide extender units, *Nat. Chem. Biol. 8*, 117–124.
232. Ishiyama, N., Creuzenet, C., Miller, W. L., Demendi, M., Anderson, E. M., Harauz, G., Lam, J. S., and Berghuis, A. M. (2006) Structural studies of FlaA1 from *Helicobacter pylori* reveal the mechanism for inverting 4,6-dehydratase activity, *J. Biol. Chem. 281*, 24489–24495.
233. Piersma, S. R., Visser, A. J. W. G., de Vries, S., and Duine, J. A. (1998) Optical spectroscopy of nicotinoprotein alcohol dehydrogenase from *Amycolatopsis methanolica*: A comparison with horse liver alcohol dehydro-

genase and UDP-galactose epimerase, *Biochemistry 37*, 3068–3077.
234. Tanaka, N., Kusakabe, Y., Ito, K., Yoshimoto, T., and Nakamura, K. T. (2002) Crystal structure of formaldehyde dehydrogenase from *Pseudomonas putida*: The structural origin of the tightly bound cofactor in nicotinoprotein dehydrogenases, *J. Mol. Biol. 324*, 519–533.
235. Van Ophem, P. W., Van Beeumen, J., and Duine, J. A. (1993) Nicotinoprotein [NAD(P)-containing] alcohol/aldehyde oxidoreductases: Purification and characterization of a novel type from *Amycolatopsis methanolica*, *Eur. J. Biochem. 212*, 819–826.
236. Henehan, G. T. M., and Oppenheimer, N. J. (1993) Horse liver alcohol dehydrogenase-catalyzed oxidation of aldehydes: Dismutation precedes net production of reduced nicotinamide adenine dinucleotide, *Biochemistry 32*, 735–738.
237. Choe, J., Guerra, D., Michels, P. A. M., and Hol, W. G. J. (2003) *Leishmania mexicana* glycerol-3-phosphate dehydrogenase showed conformational changes upon binding a bisubstrate adduct, *J. Mol. Biol. 329*, 335–349.
238. Benach, J., Atrian, S., Gonzalez-Duarte, R., and Ladenstein, R. (1999) The catalytic reaction and inhibition mechanism of *Drosophila* alcohol dehydrogenase: Observation of an enzyme-bound NAD–ketone adduct at 1.4 Å resolution by X-ray crystallography, *J. Mol. Biol. 289*, 335–355.
239. Kessler, D., Retey, J., and Schulz, G. E. (2004) Structure and action of urocanase, *J. Mol. Biol. 342*, 183–194.
240. Matherly, L. H., DeBrosse, C. W., and Phillips, A. T. (1982) A covalent nicotinamide adenine dinucleotide intermediate in the urocanase reaction, *Biochemistry 21*, 2789–2794.
241. Matherly, L. H., Johnson, K. A., and Phillips, A. T. (1982) Transient-state kinetic analysis of urocanase, *Biochemistry 21*, 2795–2798.
242. Schubert, C., Zhao, Y., Shin, J.-H., and Retey, J. (1994) Mechanism of urocanase reactions: Verification of the structure of NAD^+ inhibitor adducts by direct ^{13}C–^{13}C coupling, *Angew. Chem. 106*, 1331–1332 [see also *Angew. Chem., Int. Ed. Engl.*, (1994) *33*, 1279–1380].
243. Lamzin, V. S., Dauter, Z., Popov, V. O., Harutyunyan, E. H., and Wilson, K. S. (1994) High resolution structures of holo and apo formate dehydrogenase, *J. Mol. Biol. 236*, 759–785.
244. Li, H., and Goldstein, B. M. (1992) Carboxamide group conformation in the nicotinamide and thiazole-4-carboxamide rings: Implications for enzyme binding, *J. Med. Chem. 35*, 3560–3567.
245. DiMarco, A. A., Bobik, T. A., and Wolfe, R. S. (1990) Unusual coenzymes of methanogenesis, *Annu. Rev. Biochem. 59*, 355–394.
246. Eirich, L. D., Vogels, G. D., and Wolfe, R. S. (1978) Proposed structure for coenzyme F_{420} from *Methanobacterium*, *Biochemistry 17*, 4583–4593.
247. Filman, D. J., Bolin, J. T., Matthews, D. A., and Kraut, J. (1982) Crystal structures of *Escherichia coli* and *Lactobacillus casei* dihydrofolate reductase refined at 1.7 Å resolution: 2. Environment of bound NADPH and implications for catalysis, *J. Biol. Chem. 257*, 13663–13672.
248. Karle, I. L. (1961) Crystal structure of *N*-benzyl-1,4–dihydronicoticotinamide, *Acta Crystallogr. 14*, 497–502.
249. Koyama, H. (1963) Structure determination of *N*-propyldihydronicotinamide ($C_9H_{14}ON_2$), *Z. Kristallogr., Kristallgeom., Kristallphys., Kristallchem. 118*, 51–68.
250. McComb, R. B., Bond, L. W., Burnett, R. W., Keech, R. C., and Bowers, G. N., Jr. (1976) Determination of the molar absorptivity of NADH, *Clin. Chem. 22*, 141–150.
251. Wright, W. B., and King, G. S. D. (1954) The crystal structure of nicotinamide, *Acta Crystallogr. 7*, 283–288.
252. Acheson, S. A., Kirkman, H. N., and Wolfenden, R. (1988) Equilibrium of 5,6-hydration of NADH and mechanism of ATP-dependent dehydration, *Biochemistry 27*, 7371–7375.
253. Sulzenbacher, G., Alvarez, K., Van Den Heuvel, R. H., Versluis, C., Spinelli, S., Campanacci, V., Valencia, C., Cambillau, C., Eklund, H., and Tegoni, M. (2004) Crystal structure of *E.coli* alcohol dehydrogenase YqhD: Evidence of a covalently modified NADP coenzyme, *J. Mol. Biol. 342*, 489–502.
254. Kikuchi, A., Park, S.-Y., Miyatake, H., Sun, D., Sato, M., Yoshida, T., and Shiro, Y. (2001) Crystal structure of rat biliverdin reductase, *Nat. Struct. Biol. 8*, 221–225.
255. Adams, M. J., Ellis, G. H., Gover, S., Naylor, C. E., and Phillips, C. (1994) Crystallographic

study of coenzyme, coenzyme analogue and substrate binding in 6-phosphogluconate dehydrogenase: Implications for NADP specificity and the enzyme mechanism, *Structure 2*, 651–668.
256. Zhang, L., Chooback, L., and Cook, P. F. (1999) Lysine 183 is the general base in the 6-phosphogluconate dehydrogenase-catalyzed reaction, *Biochemistry 38*, 11231–11238.
257. Cosgrove, M. S., Naylor, C., Paludan, S., Adams, M. J., and Levy, H. R. (1998) On the mechanism of the reaction catalyzed by glucose 6-phosphate dehydrogenase, *Biochemistry 37*, 2759–2767.
258. Raj, S. B., Ramaswamy, S., and Plapp, B. V. (2014) Yeast alcohol dehydrogenase structure and catalysis, *Biochemistry 53*, 5791–5803.
259. Perpetuo, G. L., Galico, D. A., Guerra, R. B., Moreira, R., Chierice, G. O., and Bannach, G. (2014) Thermal, spectroscopic and DFT studies of solid benzamide, *Braz. J. Therm. Anal. 3*, 5–10.
260. Peng, H. L., Deng, H., Dyer, R. B., and Callender, R. (2014) Energy landscape of the Michaelis complex of lactate dehydrogenase: Relationship to catalytic mechanism, *Biochemistry 53*, 1849–1857.
261. Wu, Y. D., and Houk, K. N. (1987) Transition structures for hydride transfers, *J. Am. Chem. Soc. 109*, 906–908.
262. Wurthwein, E.-U., Lang, G., Schappele. L. H., and Mayr, H. (2002) Rate–equilibrium relationships in hydride transfer reactions: The role of intrinsic barriers, *J. Am. Chem. Soc. 124*, 4084–4092.
263. Nelsestuen, G. L., and Kirkwood, S. (1971) Mechanism of action of the enzyme uridine diphosphoglucose 4-epimerase.: Proof of an oxidation–reduction mechanism with direct transfer of hydrogen between substrate and the B-position of the enzyme-bound pyridine nucleotide, *J. Biol. Chem. 246*, 7533–7543.
264. Thoden, J. B., Frey, P. A., and Holden, H. M. (1996) Molecular structure of the NADH/UDP-glucose abortive complex of UDP-galactose 4-epimerase from *Escherichia coli*: Implications for the catalytic mechanism, *Biochemistry 35*, 5137–5144.
265. Bagautdinov, B., and Kunishima, N. (2007) Crystal structures of shikimate dehydrogenase AroE from *Thermus thermophilus* HB8 and its cofactor and substrate complexes: Insights into the enzymatic mechanism, *J. Mol. Biol. 373*, 424–438.
266. Huddleston, J. P., Anderson, T. K., Spencer, K. D., Thoden, J. B., Raushel, F. M., and Holden, H. M. (2020) Structural analysis of Cj1427, an essential NAD-dependent dehydrogenase for the biosynthesis of the heptose residues in the capsular polysaccharides of *Campylobacter jejuni*, *Biochemistry 59*, 1314–1327.
267. Huddleston, J. P., and Raushel, F. M. (2020) Functional characterization of Cj1427, a unique ping-pong dehydrogenase responsible for the oxidation of GDP-D-glycero-α-D-manno-heptose in *Campylobacter jejuni*, *Biochemistry 59*, 1328–1337.
268. Ceh, K., Demmer, U., Warkentin, E., Moll, J., Thauer, R. K., Shima, S., and Ermler, U. (2009) Structural basis of the hydride transfer mechanism in F_{420}-dependent methylene-tetrahydromethanopterin dehydrogenase, *Biochemistry 48*, 10098–10105.
269. Petit, P., Granier, T., d'Estaintot, B. L., Manigand, C., Bathany, K., Schmitter, J. M., Lauvergeat, V., Hamdi, S., and Gallois, B. (2007) Crystal structure of grape dihydroflavonol 4-reductase, a key enzyme in flavonoid biosynthesis, *J. Mol. Biol. 368*, 1345–1357.
270. Inagaki, E., Ohshima, N., Takahashi, H., Kuroishi, C., Yokoyama, S., and Tahirov, T. H. (2006) Crystal structure of *Thermus thermophilus* Δ^1-pyrroline-5-carboxylate dehydrogenase, *J. Mol. Biol. 362*, 490–501.
271. Bystroff, C., Oatley, S. J., and Kraut, J. (1990) Crystal structures of *Escherichia coli* dihydrofolate reductase: The $NADP^+$ holoenzyme and the folate:$NADP^+$ ternary complex: Substrate binding and a model for the transition state, *Biochemistry 29*, 3263–3277.
272. Reyes, V. M., Sawaya, M. R., Brown, K. A., and Kraut, J. (1995) Isomorphous crystal structures of *Escherichia coli* dihydrofolate reductase complexed with folate, 5-deaza-folate, and 5,10-dideazatetrahydrofolate: Mechanistic implications, *Biochemistry 34*, 2710–2723.
273. Fierke, C. A., Johnson, K. A., and Benkovic, S. J. (1987) Construction and evaluation of the kinetic scheme associated with dihydrofolate reductase from *Escherichia coli*, *Biochemistry 26*, 4085–4092.
274. Grau, U., Kapmeyer, H., and Trommer, W. E. (1978) Combined coenzyme–substrate

analogs of various dehydrogenases: Synthesis of (3*S*)- and (3*R*)-5-(3-carboxy-3-hydroxypropyl)nicotinamide adenine dinucleotide and their interaction with (*S*)-lactate-specific dehydrogenases and (*R*)-lactate-specific dehydrogenases, *Biochemistry 17*, 4621–4626.
275. Grau, U. M., Trommer, W. E., and Rossmann, M. G. (1981) Structure of the active ternary complex of pig-heart lactate-dehydrogenase with *S*-lac-NAD at 2.7 Å resolution, *J. Mol. Biol. 151*, 289–307.
276. Dengler, U., Niefind, K., Kiess, M., and Schomburg, D. (1997) Crystal structure of a ternary complex of D-2-hydroxyisocaproate dehydrogenase from *Lactobacillus casei*, NAD^+ and 2-oxoisocaproate at 1.9 Å resolu-tion, *J. Mol. Biol. 267*, 640–660.
277. Prosise, G., L., and Luecke, H. (2003) Crystal structures of *Tritrichomonasfoetus* inosine monophosphate dehydrogenase in complex with substrate, cofactor and analogs: A structural basis for the random-in ordered-out kinetic mechanism, *J. Mol. Biol. 326*, 517–527.
278. Santhanam, K. S. V., and Elving, P. J. (1973) Electrochemical redox pattern for nicotinamide species in non-aqueous media, *J. Am. Chem. Soc. 95*, 5482–5490.
279. Powell, M. F., Wu, J. C., and Bruice, T. C. (1984) Ferricyanide oxidation of dihydropyridines and analogs, *J. Am. Chem. Soc. 106*, 3850–3856.
280. Carlson, B. W., Miller, L. L., Neta, P., and Grodkowski, J. (1984) Oxidation of NADH involving rate-limiting one-electron transfer, *J. Am. Chem. Soc. 106*, 7233–7239.
281. Zhu, X. Q., Yang, Y., Zhang, M., and Cheng, J. P. (2003) First estimation of C_4–H bond dissociation energies of NADH and its radical cation in aqueous solution, *J. Am. Chem. Soc. 125*, 15298–15299.
282. Farrington, J. A., Land, E. J., and Swallow, A. J. (1980) The one-electron reduction potentials of NAD, *Biochim. Biophys. Acta 590*, 273–276.
283. Anderson, R. F. (1980) Energetics of the one-electron steps in the NAD^+/NADH redox couple, *Biochim. Biophys. Acta, 590*, 277–281.
284. Matsue, T., Suda, M., Uchida, I., Kato, T., Akiba, U., and Osa, T. (1987) Electrocatalytic oxidation of NADH by ferrocene derivatives and the influence of cyclodextrin complexation, *J. Electroanal. Chem. Interfac. Electrochem. 234*, 163–173.
285. Gebicki, J., Marcinek, A., Adamus, J., Paneth, P., and Rogowski, J. (1996) Structural aspects and rearrangement of radical cations generated from NADH analogues, *J. Am. Chem. Soc. 118*, 691–692.
286. Fukuzumi, S., Inada, O., and Suenobu, T. (2003) Mechanisms of electron-transfer oxidation of NADH analogues and chemiluminescence: Detection of the keto and enol radical cations, *J. Am. Chem. Soc. 125*, 4808–4816.
287. Hapiot, P., Moiroux, J., and Saveant, J. M. (1990) Electrochemistry of NADH/NAD^+ analogs: A detailed mechanistic kinetic and thermodynamic analysis of the 10-methylacridan/10-methylacridinium couple in acetonitrile, *J. Am. Chem. Soc. 112*, 1337–1343.
288. Fukuzumi, S., Koumitsu, S., Hironaka, K., and Tanaka, T. (1987) Energetic comparison between photoinduced electron-transfer reactions from NADH model compounds to organic and inorganic oxidants and hydride-transfer reactions from NADH model compounds to *p*-benzoquinone derivatives, *J. Am. Chem. Soc. 109*, 305–316.
289. Miller, L. L., and Valentine, J. R. (1988) On the electron–proton–electron mechanism for 1-benzyl-1,4-dihydronicotinamide oxidations, *J. Am. Chem. Soc. 110*, 3982–3989.
290. Murray, C. J., and Webb, T. (1991) General acid catalysis of the reduction of *p*-benzoquinone by an NADH analogue, *J. Am. Chem. Soc. 113*, 7426–7427.
291. Coleman, C. A., Rose, J. G., and Murray, C. J. (1992) General acid catalysis of the reduction of *p*-benzoquinone by an NADH analog: Evidence for concerted hydride and hydron transfer, *J. Am. Chem. Soc. 114*, 9755–9762.
292. Afanasyeva, M. S., Taraban, M. B., Purtov, P. A., Leshina, T. V., and Grissom, C. B. (2006) Magnetic spin effects in enzymatic reactions: Radical oxidation of NADH by horseradish peroxidase, *J. Am. Chem. Soc. 128*, 8651–8658.
293. Fukuzumi, S., Kotani, H., Lee, Y. M., and Nam, W. (2008) Sequential electron-transfer and proton-transfer pathways in hydride-transfer reactions from dihydronicotinamide adenine dinucleotide analogues to non-heme oxoiron(IV) complexes and *p*-chloranil: Detection of radical cations of NADH

analogues in acid-promoted hydride-transfer reactions, *J. Am. Chem. Soc. 130*, 15134–15142.
294. Rosenthal, R. G., Ebert, M. O., Kiefer, P., Peter, D. M., Vorholt, J. A., and Erb, T. J. (2014) Direct evidence for a covalent ene adduct intermediate in NAD(P)H-dependent enzymes, *Nat. Chem. Biol. 10*, 50–55.
295. Vogeli, B., Rosenthal, R. G., Stoffel, G. M. M., Wagner, T., Kiefer, P., Cortina, N. S., Shima, S., and Erb, T. J. (2018) InhA, the enoyl-thioester reductase from *Mycobacterium tuberculosis* forms a covalent adduct during catalysis, *J. Biol. Chem. 293*, 17200–17207.
296. Rozwarski, D. A., Vilcheze, C., Sugantino, M., Bittman, R., and Sacchettini, J. C. (1999) Crystal structure of the *Mycobacterium tuberculosis* enoyl-ACP reductase, InhA, in complex with NAD^+ and a C16 fatty acyl substrate, *J. Biol. Chem. 274*, 15582–15589.
297. Airenne, T. T., Torkko, J. M., Van den Plas, S., Sormunen, R. T., Kastaniotis, A. J., Wierenga, R. K., and Hiltunen, J. K. (2003) Structure–function analysis of enoyl thioester reductase involved in mitochondrial maintenance, *J. Mol. Biol. 327*, 47–59.
298. Rosenthal, R. G., Vogeli, B., Quade, N., Capitani, G., Kiefer, P., Vorholt, J. A., Ebert, M. O., and Erb, T. J. (2015) The use of ene adducts to study and engineer enoyl-thioester reductases, *Nat. Chem. Biol. 11*, 398–400.
299. Ling, B., Li, H., Yan, L., Liu, R., and Liu, Y. (2019) Conversion mechanism of enoyl thioesters into acyl thioesters catalyzed by 2-enoyl-thioester reductases from *Candida tropicalis*, *Phys. Chem. Chem. Phys. 21*, 10105–10113.
300. Cichowicz, D. J., and Shane, B. (1987) Mammalian folylpoly-γ-glutamate synthetase: 2. Substrate specificity and kinetic properties, *Biochemistry 26*, 513–521.
301. Huang, T., Wang, C., Maras, B., Barra, D., and Schirch, V. (1998) Thermodynamic analysis of the binding of the polyglutamate chain of 5-formyltetrahydropteroylpolyglutamates to serine hydroxymethyltransferase, *Biochemistry 37*, 13536–13542.
302. Fontecilla-Camps, J. C., Bugg, C. E., Temple, C., Rose, J. D., Montgomery, J. A., and Kisliuk, R. L. (1979) Absolute-configuration of biological tetrahydrofolates: Crystallographic determination, *J. Am. Chem. Soc. 101*, 6114–6115.
303. Kallen, R. G., and Jencks, W. P. (1966) Dissociation constants of tetrahydrofolic acid, *J. Biol. Chem. 241*, 5845–5850.
304. Huennekens, F. M., Henderson, G. B., Vitols, K. S., and Grimshaw, C. E. (1984) Enzymic activation of 5–formyltetrahydrofolate via conversion to 5,10-methenyltetrahydrofolate, *Adv.Enzyme Regul. 22*, 3–13.
305. Poe, M., and Benkovic, S. J. (1980) 5-Formyl- and 10-formyl-5,6,7,8-tetrahydrofolate: Conformation of the tetrahydropyrazine ring and formyl group in solution, *Biochemistry 19*, 4576–4582.
306. Guynn, R. W., and Veech, R. L. (1973) Equilibrium constants of the adenosine triphosphate hydrolysis and the adenosine triphosphate–citrate lyase reactions, *J. Biol. Chem. 248*, 6966–6972.
307. Maden, B. E. (2000) Tetrahydrofolate and tetrahydromethanopterin compared: Functionally distinct carriers in C1 metabolism, *Biochem. J. 350 Pt 3*, 609–629.
308. Delle Fratte, S., White, R. H., Maras, B., Bossa, F., and Schirch, V. (1997) Purification and properties of serine hydroxymethyltransferase from *Sulfolobus solfataricus*, *J. Bacteriol. 179*, 7456–7461.
309. Benkovic, S. J., Benkovic, P. A., and Comfort, D. R. (1969) Studies on models for tetrahydrofolic acid: I. The condensation of formaldehyde with tetrahydroquinoxaline analogs, *J. Am. Chem. Soc. 91*, 5270–5279.
310. Vorholt, J. A., Marx, C. J., Lidstrom, M. E., and Thauer, R. K. (2000) Novel formaldehyde-activating enzyme in *Methylobacterium extorquens* AM1 required for growth on methanol, *J. Bacteriol. 182*, 6645–6650.
311. Stover, P., and Schirch, V. (1992) Evidence for the accumulation of a stable intermediate in the nonenzymic hydrolysis of 5,10-methenyltetrahydropteroylglutamate to 5-formyltetrahydropteroylglutamate, *Biochemistry 31*, 2148–2155.
312. Benkovic, S. J., Benkovic, P. A., and Bullard, W. P. (1972) Studies on models for tetrahydrofolic acid: 3. Hydrolytic interconversions of the tetrahydroquinoxaline analogs at formate level of oxidation, *J. Am. Chem. Soc. 94*, 7542–7549.
313. Tan, L. U. L., Drury, E. J., and Mackenzie, R. E. (1977) Methylenetetrahydrofolate dehydrogenasemethenyltetrahydrofolate cyclohydrolaseformyltetrahydrofolate synthetase: Mul-

tifunctional protein from porcine liver, *J. Biol. Chem. 252*, 1117–1122.
314. Ma, K., and Thauer, R. K. (1990) Purification and properties of N^5,N^{10}–methylenetetrahydromethanopterin reductase from *Methanobacterium thermoautotrophicum* (strain Marburg), *Eur. J. Biochem. 191*, 187–193.
315. Whitfield, C. D., Steers, E. J. Jr., and Weissbach.H. (1970) Purification and properties of 5-methyltetrahydropteroyltriglutamate-homocysteine transmethylase, *J. Biol. Chem. 245*, 390–401.
316. Taurog, R. E., and Matthews, R. G. (2006) Activation of methyltetrahydrofolate by cobalamin-independent methionine synthase, *Biochemistry 45*, 5092–5102.
317. Ubhi, D. K., and Robertus, J. D. (2015) The cobalamin-independent methionine synthase enzyme captured in a substrate-induced closed conformation, *J. Mol. Biol. 427*, 901–909.
318. Benkovic, S. J., Barrows, T. H., and Farina, P. R. (1973) Studies on models for tetrahydrofolic acid: 4. Reactions of amines with formamidinium tetrahydroquinoxaline analogs, *J. Am. Chem. Soc. 95*, 8414–8421.
319. Burdick, B. A., Benkovic, P. A., and Benkovic, S. J. (1977) Studies on models for tetrahydrofolic acid: 8. Hydrolysis and methoxyaminolysis of amidines, *J. Am. Chem. Soc. 99*, 5716–5725.
320. Lee, H. H., Kim, D. J., Ahn, H. J., Ha, J. Y., and Suh, S. W. (2004) Crystal structure of T-protein of the glycine cleavage system: Cofactor binding, insights into H-protein recognition, and molecular basis for understanding nonketotic hyperglycinemia, *J. Biol. Chem. 279*, 50514–50523.
321. Montfort, W. R., Perry, K. M., Fauman, E. B., Finer-Moore, J. S., Maley, G. F., Hardy, L., Maley, F., and Stroud, R. M. (1990) Structure, multiple site binding, and segmental accommodation in thymidylate synthase on binding dUMP and an anti-folate, *Biochemistry 29*, 6964–6977.
322. Trivedi, V., Gupta, A., Jala, V. R., Saravanan, P., Rao, G. S., Rao, N. A., Savithri, H. S., and Subramanya, H. S. (2002) Crystal structure of binary and ternary complexes of serine hydroxymethyltransferase from *Bacillus stearothermophilus*: Insights into the catalytic mechanism, *J. Biol. Chem. 277*, 17161–17169.
323. Lynen, F. (1953) Functional group of coenzyme A and its metabolic relations, especially in the fatty acid cycle, *Fed. Proc. 12*, 683–691.
324. Chiang, Y., and Kresge, A. J. (1991) Enols and other reactive species, *Science (Washington, DC, United States) 253*, 395–400.
325. Richard, J., P., Williams, G., O'Donoghue A. C., and Amyes T. L. (2002) Formation and stability of enolates of acetamide and acetate anion: An Eigen plot for proton transfer at α-carbonyl carbon, *J. Am. Chem. Soc. 124*, 2957–2968.
326. Amyes, T. L., and Richard, J. P. (1996) Determination of the pK_a of ethyl acetate: Brønsted correlation for deprotonation of a simple oxygen ester in aqueous solution, *J. Am. Chem. Soc. 118*, 3129–3141.
327. Chiang, Y., Kresge, A. J., and Pruszynski, P. (1992) Keto–enol equilibria in the pyruvic acid system: Determination of the keto–enol equilibrium constants of pyruvic acid and pyruvate anion and the acidity constant of pyruvate enol in aqueous solution, *J. Am. Chem. Soc. 114*, 3103–3107.
328. Le Noble, W. J. (1960) The keto–enol equilibrium of ethyl acetoacetate under high pressure, *J. Am. Chem. Soc. 82*, 5253.
329. Burdett, J. L., and Rogers, M. T. (1966) Keto–enol tautomerism in β-dicarbonyls studied by nuclear magnetic resonance spectroscopy: III. Studies of proton chemical shifts and equilibrium constants at different temperatures, *J. Phys. Chem. 70*, 939–941.
330. Burdett, J. L., and Rogers, M. T. (1964) Keto–enol tautomerism in β-dicarbonyls studied by nuclear magnetic resonance spectroscopy: I. Proton chemical shifts and equilibrium constants of pure compounds, *J. Am. Chem. Soc. 86*, 2105–2109.
331. Mills, S. G., and Beak, P. (1985) Solvent effects on keto–enol equilibria: Tests of quantitative models, *J. Org. Chem. 50*, 1216–1224.
332. Rios, A., Amyes, T. L., and Richard, J. P. (2000) Formation and stability of organic zwitterions in aqueous solution: Enolates of the amino acid glycine and its derivatives, *J. Am. Chem. Soc. 122*, 9373–9385.
333. Houck, W. J., and Pollack, R. M. (2003) Activation enthalpies and entropies for the microscopic rate constants of acetate-catalyzed isomerization of 5-androstene-3,17–dione, *J. Am. Chem. Soc. 125*, 10206–10212.

334. Williams, G., Maziarz, E. P., Amyes, T. L., Wood, T. D., and Richard, J. P. (2003) Formation and stability of the enolates of *N*-protonated proline methyl ester and proline zwitterion in aqueous solution: A nonenzymatic model for the first step in the racemization of proline catalyzed by proline racemase, *Biochemistry 42*, 8354–8361.
335. Guthrie, J. P., and Cullimore, P. A. (1979) The enol content of simple carbonyl-compounds: A thermochemical approach, *Can. J. Chem. 57*, 240–248.
336. Snowden, T. S., Bisson, A. P., and Anslyn, E. V. (1999) A comparison of NH–π versus lone pair hydrogen bonding effects on carbon acid pK_a shifts, *J. Am. Chem. Soc. 121*, 6324–6325.
337. Chiang, Y., Guo, H. X., Kresge, A. J., and Tee, O. S. (1996) Flash photolysis of 2,2,6-trimethyl-4*H*-1,3-dioxin-4-one in aqueous solution: Hydration of acetylketene and ketonization of acetoacetic acid enol, *J. Am. Chem. Soc. 118*, 3386–3391.
338. Chiang, Y., Kresge, A. J., and Walsh, P. A. (1982) Ketonization of enols: Enol content and acid dissociation constants of simple carbonyl compounds, *J. Am. Chem. Soc. 104*, 6122–6123.
339. Haspra, P., Sutter, A., and Wirz, J. (1979) Acidity of acetophenone enol in aqueous solution, *Angew. Chem., Int. Ed. Engl.. 18*, 617–619.
340. Dai, M., Feng, Y., and Tonge, P. J. (2001) Synthesis of crotonyl-oxyCoA: A mechanistic probe of the reaction catalyzed by enoyl-CoA hydratase, *J. Am. Chem. Soc. 123*, 506–507.
341. Zacharias, D. E., Murrayrust, P., Preston, R. M., and Glusker, J. P. (1983) The geometry of the thioester group and its implications for the chemistry of acyl coenzyme-A, *Arch. Biochem. Biophys. 222*, 22–34.
342. Rios, A., Crugeiras, J., Amyes, T. L., and Richard, J. P. (2001) Glycine enolates: The large effect of iminium ion formation on α-amino carbon acidity, *J. Am. Chem. Soc. 123*, 7949–7950.
343. Bender, M. L., and Williams, A. (1966) Ketimine intermediates in amine-catalyzed enolization of acetone, *J. Am. Chem. Soc. 88*, 2502–2508.
344. Roberts, R. D., Ferran, H. E., Gula, M. J., and Spencer, T. A. (1980) Superiority of very weakly basic amines as catalysts for α-proton abstraction via iminium ion formation, *J. Am. Chem. Soc. 102*, 7054–7058.
345. Strauss, E., Zhai, H., Brand, L. A., McLafferty, F. W., and Begley, T. P. (2004) Mechanistic studies on phosphopantothenoylcysteine decarboxylase: Trapping of an enethiolate intermediate with a mechanism-based inactivating agent, *Biochemistry 43*, 15520–15533.
346. Hegarty, A. F., and Jencks, W. P. (1975) Bifunctional catalysis of the enolization of acetone, *J. Am. Chem. Soc. 97*, 7188–7189.
347. Hegarty, A. F., Dowling, J. P., Eustace, S. J., and McGarraghy, M. (1998) Enolization of aldehydes and ketones: Structural effects on concerted acid–base catalysis, *J. Am. Chem. Soc. 120*, 2290–2296.
348. Capon, B., and Zucco, C. (1982) Simple enols: 2. Kinetics and mechanism of the ketonization of vinyl alcohol, *J. Am. Chem. Soc. 104*, 7567–7572.
349. Kurz, L. C., Roble, J. H., Nakra, T., Drysdale, G. R., Buzan, J. M., Schwartz, B., and Drueckhammer, D. G. (1997) Ability of single-site mutants of citrate synthase to catalyze proton transfer from the methyl group of dethia-acetyl-coenzyme A, a nonthioester substrate analog, *Biochemistry 36*, 3981–3990.
350. Landro, J. A., Gerlt, J. A., Kozarich, J. W., Koo, C. W., Shah, V. J., Kenyon, G. L., Neidhart, D. J., Fujita, S., and Petsko, G. A. (1994) The role of Lysine 166 in the mechanism of mandelate racemase from P*seudomonas putida*: Mechanistic and crystallographic evidence for stereospecific alkylation by (*R*)-α-phenylglycidate, *Biochemistry 33*, 635–643.
351. Gerlt, J. A., Kozarich, J. W., Kenyon, G. L., and Gassman, P. G. (1991) Electrophilic catalysis can explain the unexpected acidity of carbon acids in enzyme-catalyzed reactions, *J. Am. Chem. Soc. 113*, 9667–9669.
352. Frey, J., and Rappoport, Z. (1996) Generation and detection of a relatively persistent carboxylic acid enol: 2,2-Bis(2,4,6-triisopropylphenyl)ethene-1,1–diol, *J. Am. Chem. Soc. 118*, 5169–5181.
353. Richard, J. P., and Nagorski, R. W. (1999) Mechanistic imperatives for catalysis of aldol addition reactions: Partitioning of the enolate intermediate between reaction with Brønsted acids and the carbonyl group, *J. Am. Chem. Soc. 121*, 4763–4770.
354. Callahan, B. P., and Wolfenden, R. (2004) Charge development in the transition state

for decarboxylations in water: Spontaneous and acetone-catalyzed decarboxylation of aminomalonate, *J. Am. Chem. Soc. 126*, 4514–4515.
355. Bolduc, J. M., Dyer, D. H., Scott, W. G., Singer, P., Sweet, R. M., Koshland, D. E., Jr., and Stoddard, B. L. (1995) Mutagenesis and Laue structures of enzyme intermediates: Isocitrate dehydrogenase, *Science 268*, 1312–1318.
356. Taguchi, K., and Westheimer, F. H. (1973) Decarboxylation of Schiff-bases, *J. Am. Chem. Soc. 95*, 7413–7418.
357. Raghavan, N. V., and Leussing, D. L. (1976) Kinetic study of copper(II)-catalyzed enolization, ketonization, and decarboxylation of oxaloacetate, *J. Am. Chem. Soc. 98*, 723–730.
358. Beak, P., and Siegel, B. (1976) Mechanism of decarboxylation of 1,3–dimethylorotic acid: Model for orotidine 5′-phosphate decarboxylase, *J. Am. Chem. Soc. 98*, 3601–3606.
359. Tsang, W. Y., Wood, B. M., Wong, F. M., Wu, W., Gerlt, J. A., Amyes, T. L., and Richard, J. P. (2012) Proton transfer from C-6 of uridine 5′-monophosphate catalyzed by orotidine 5′-monophosphate decarboxylase: Formation and stability of a vinyl carbanion intermediate and the effect of a 5–fluoro substituent, *J. Am. Chem. Soc. 134*, 14580–14594.
360. Lewis, C. A., Jr., and Wolfenden, R. (2009) Orotic acid decarboxylation in water and nonpolar solvents: A potential role for desolvation in the action of OMP decarboxylase, *Biochemistry 48*, 8738–8745.
361. Richard, J. P. (1984) Acid–base catalysis of the elimination and isomerization reactions of triose phosphates, *J. Am. Chem. Soc. 106*, 4926–4936.
362. Hall, S. S., Doweyko, A. M., and Jordan, F. (1978) Glyoxalase I enzyme studies: 4. General base catalyzed enediol proton transfer rearrangement of methyl- and phenylglyoxalglutathionylhemithiol acetal to *S*-lactoyl- and *S*-mandeloylglutathione followed by hydrolysis: A model for glyoxalase enzyme system, *J. Am. Chem. Soc. 100*, 5934–5939.
363. Okuyama, T., Komoguchi, S., and Fueno, T. (1982) Reaction of thiols with phenylglyoxal to give thiolesters of mandelic acid: 2. Intramolecular general-base catalysis and change in rate-determining step, *J. Am. Chem. Soc. 104*, 2582–2587.
364. Mohrig, J. R., Schultz, S. C., and Morin, G. (1983) Syn and anti stereochemistry in elimination reactions producing acyclic conjugated thioesters, *J. Am. Chem. Soc. 105*, 5150–5151.
365. Chwang, W. K., Nowlan, V. J., and Tidwell, T. T. (1977) Reactivity of cyclic and acyclic olefinic hydrocarbons in acid-catalyzed hydration, *J. Am. Chem. Soc. 99*, 7233–7238.
366. Creary, X., Casingal, V. P., and Leahy, C. E. (1993) Solvolytic elimination reactions: Stepwise or concerted? *J. Am. Chem. Soc. 115*, 1734–1738.
367. Moore, J. A., Parker, A. R., Davisson, V. J., and Schwab, J. M. (1993) Stereochemical course of the *Escherichia coli* imidazole glycerol phosphate dehydratase reaction, *J. Am. Chem. Soc. 115*, 3338–3339.
368. Fedor, L. R. (1969) Base-catalyzed β-elimination reactions in aqueous solution: 2. Elcb Elimination from β-methoxy ketones, *J. Am. Chem. Soc. 91*, 908–913.
369. Alunni, S., De Angelis, F., Ottavi, L., Papavasileiou, M., and Tarantelli, F. (2005) Evidence of a borderline region between E1cb and E2 elimination reaction mechanisms: A combined experimental and theoretical study of systems activated by the pyridine ring, *J. Am. Chem. Soc. 127*, 15151–15160.
370. Fedor, L., and Gray, P. H. (1976) General acid–specific base catalyzed isomerization of *tert*-butyl thiolbut-3-enoate to *tert*-butyl thiolcrotonate, *J. Am. Chem. Soc. 98*, 783–787.
371. Banait, N. S., and Jencks, W. P. (1990) Elimination reactions: Experimental confirmation of the predicted elimination of (β-cyanoethyl)sulfonium ions through a concerted, E2 mechanism, *J. Am. Chem. Soc. 112*, 6950–6958.
372. Parker, A. J., Biale, G., Cook, D., Lloyd, D. J., Stevens, I. D. R., Takahashi, J., and Winstein, S. (1971) E2C Mechanism in elimination reactions: II. Substituent effects on rates of elimination from acyclic systems, *J. Am. Chem. Soc. 93*, 4735–4749.
373. Coleman, C. A., and Murray, C. J. (1991) Characterization of transition states by isotopic mapping and structure–reactivity coefficients: Solvent and secondary deuterium isotope effects for the base-catalyzed breakdown of acetaldehyde hemiacetals, *J. Am. Chem. Soc. 113*, 1677–1684.

374. Bartsch, R. A., Mintz, E. A., and Parlman, R. M. (1974) Effects of base association and strength upon base-promoted syn eliminations, *J. Am. Chem. Soc. 96*, 4249–4252.
375. Beltrame, P., Ceccon, A., and Winstein, S. (1972) Chloride-induced elimination from 2–phenylcyclopentyl, 2–phenylcyclohexyl, and 2–norbornyl brosylates in acetone, *J. Am. Chem. Soc. 94*, 2315–2320.
376. Hupe, D. J., Kendall, M. C. R., and Spencer, T. A. (1973) Amine catalysis of β-ketol dehydration. 2. Catalysis via iminium ion formation. General analysis of nucleophilic amine catalysis, *J. Am. Chem. Soc. 95*, 2271–2278.
377. Yun, M. K., Wu, Y., Li, Z., Zhao, Y., Waddell, M. B., Ferreira, A. M., Lee, R. E., Bashford, D., and White, S. W. (2012) Catalysis and sulfa drug resistance in dihydropteroate synthase, *Science 335*, 1110–1114.
378. Allgauer, D. S., Jangra, H., Asahara, H., Li, Z., Chen, Q., Zipse, H., Ofial, A. R., and Mayr, H. (2017) Quantification and theoretical analysis of the electrophilicities of Michael acceptors, *J. Am. Chem. Soc. 139*, 13318–13329.
379. Cooper, T. G., and Wood, H. G. (1971) The carboxylation of phosphoenolpyruvate and pyruvate. II. The active species of "CO_2" utilized by phosphoenlpyruvate carboxylase and pyruvate carboxylase, *J. Biol. Chem. 246*, 5488–5490.
380. Moss, J., and Lane, M. D. (1971) Biotin-dependent enzymes, *Adv. Enzymol. Relat. Areas Mol. Biol. 35*, 321–442.
381. Bagautdinov, B., Kuroishi, C., Sugahara, M., and Kunishima, N. (2005) Crystal structures of biotin protein ligase from *Pyrococcus horikoshii* OT3 and its complexes: Structural basis of biotin activation, *J. Mol. Biol. 353*, 322–333.
382. Bai, D. H., Moon, T. W., Lopez-Casillas, F., Andrews, P. C., and Kim, K. H. (1989) Analysis of the biotin-binding site on acetyl-CoA carboxylase from rat, *Eur. J. Biochem. 182*, 239–245.
383. DeTitta, G. T., Edmonds, J. W., Stallings, W., and Donohue, J. (1976) Molecular structure of biotin. Results of two independent crystal structure investigations, *J. Am. Chem.Soc. 98*, 1920–1926.
384. Fry, D. C., Fox, T. L., Lane, M. D., and Mildvan, A. S. (1985) Exchange characteristics of the amide protons of D-biotin and derivatives: Implications for the mechanism of biotin enzymes and the role of sulfur in biotin, *J. Am. Chem.Soc. 107*, 7659–7665.
385. Chen, C. S., Parthasarathy, R., and Detitta, G. T. (1976) Crystal and molecular-structure of D,L-dethiobiotin; Role of sulfur in biotin stereochemistry, *J. Am. Chem.Soc. 98*, 4983–4990.
386. Jencks, W. P. (1976) *Handbook of Biochemistry and Molecular Biology, 3rd Ed., Physical and Chemical Data, Vol I* (Fasman, G. D., Ed.), pp 296–304, CRC Press, Cleve-land, OH.
387. Dimroth, P. (1982) The generation of an electrochemical gradient of sodium ions upon decarboxylation of oxaloacetate by the membrane-bound and Na^+-activated oxaloacetate decarboxylase from *Klebsiella aerogenes*, *Eur. J. Biochem. 121*, 443–449.
388. Alberty, R. A., and Goldberg, R. N. (1992) Standard thermodynamic formation properties for the adenosine 5′-triphosphate series, *Biochemistry 31*, 10610–10615.
389. Guchhait, R. B., Polakis, S. E., Hollis, D., Fenselau, C., and Lane, M. D. (1974) Acetyl coenzyme A carboxylase system of *Escherichia coli*; Site of carboxylation of bio-tin and enzymatic reactivity of 1′-*N*-(ureido)-carboxybiotin derivatives, *J. Biol. Chem. 249*, 6646–6656.
390. Knappe, J., Ringelmann, E., and Lynen, F. (1961) On the biochemical function of biotin: III. The chemical structure of enzymatically formed carboxy-biotins, *Biochem. Z. 335*, 168–176.
391. Knowles, J. R. (1989) The mechanism of biotin-dependent enzymes, *Annu. Rev. Biochem. 58*, 195–221.
392. Kaziro, Y., Hass, L. F., Boyer, P. D., and Ochoa, S. (1962) Mechanism of the propionyl carboxylase reaction: II. Isotopic exchange and tracer experiments, *J. Biol. Chem. 237*, 1460–1468.
393. Hansen, D. E., and Knowles, J. R. (1985) *N*-Carboxybiotin formation by pyruvate carboxylase: The stereochemical consequence at phosphorus, *J. Am. Chem.Soc. 107*, 8304–8305.
394. Ogita, T., and Knowles, J. R. (1988) On the intermediacy of carboxyphosphate in biotin-dependent carboxylations, *Biochemistry 27*, 8028–8033.
395. Sauers, C. K., Jencks, W. P., and Groh, S. (1975) Alcohol–bicarbonate–water system:

Structure–reactivity studies on equilibria for formation of alkyl monocarbonates and on rates of their decomposition in aqueous alkali, *J. Am. Chem. Soc. 97*, 5546–5553.
396. Chou, C. Y., Yu, L. P., and Tong, L. (2009) Crystal structure of biotin carboxylase in complex with substrates and implications for its catalytic mechanism, *J. Biol. Chem. 284*, 11690–11697.
397. Perrin, C. L., and Dwyer, T. J. (1987) Proton exchange in biotin: A reinvestigation, with implications for the mechanism of carbon dioxide transfer, *J. Am. Chem.Soc. 109*, 5163–5167.
398. Rossini, E., Bochevarov, A. D., and Knapp, E. W. (2018) Empirical conversion of pK_a values between different solvents and interpretation of the parameters: Application to water, acetonitrile, dimethyl sulfoxide, and methanol, *ACS Omega 3*, 1653–1662.
399. Bordwell, F. G., Algrim, D. J., and Harrelson, J. A. (1988) The relative ease of removing a proton, a hydrogen atom, or an electron from carboxamides versus thiocarboxamides, *J. Am. Chem.Soc. 110*, 5903–5904.
400. Waldrop, G. L., Holden, H. M., and St Maurice, M. (2012) The enzymes of biotin dependent CO_2 metabolism: What structures reveal about their reaction mechanisms, *Protein Sci. 21*, 1597–1619.
401. Broussard, T. C., Pakhomova, S., Neau, D. B., Bonnot, R., and Waldrop, G. L. (2015) Structural analysis of substrate, reaction intermediate, and product binding in *Haemophilus influenzae* biotin carboxylase, *Biochemistry 54*, 3860–3870.
402. Martin, R. B. (1972) *O*-Protonation of amides in dilute acids, *J. Chem. Soc., Chem. Commun.*, 793–794.
403. Kohn, H. (1976) Model studies on the mechanism of biotin dependent carboxylations, *J. Am. Chem.Soc. 98*, 3690–3694.
404. Meyer, E., Kappock, T. J., Osuji, C., and Stubbe, J. (1999) Evidence for the direct transfer of the carboxylate of N^5-carboxyaminoimidazole ribonucleotide (N^5–CAIR) to generate 4-carboxy-5-aminoimida-zole ribonucleotide catalyzed by *Escherichia coli* PurE, an N^5–CAIR mutase, *Biochemistry 38*, 3012–3018.
405. Hagmann, M. L., Heller, W., and Grisebach, H. (1984) Induction of phytoalexin synthesis in soybean: Stereospecific 3,9-dihydroxypterocarpan 6a-hydroxylase from elicitor-induced soybean cell cultures, *Eur. J. Biochem. 142*, 127–131.
406. Lee, S.-L., Floss, H. G., and Heinstein, P. (1976) Purification and properties of dimethylallylpyrophosphate:tryptophan dimethylallyl transferase, the first enzyme of ergot alkaloid biosynthesis in *Claviceps* sp. SD 58, *Arch. Biochem. Biophys. 177*, 84–94.
407. Crawford, I. P., and Yanofsky, C. (1958) On the separation of the tryptophan synthetase of *Escherichia coli* into two protein components, *Proc. Natl. Acad. Sci. U.S.A. 44*, 1161–1170.
408. Rhee, S., Parris, K. D., Hyde, C. C., Ahmed, S. A., Miles, E. W., and Davies, D. R. (1997) Crystal structures of a mutant (βK87T) tryptophan synthase $\alpha_2\beta_2$ complex with ligands bound to the active sites of the α- and β-subunits reveal ligand-induced conformational changes, *Biochemistry 36*, 7664–7680.
409. Battersby, A. R. (1994) How nature builds the pigments of life: The conquest of vitamin B12, *Science 264*, 1551–1557.
410. Entsch, B., Ballou, D. P., and Massey, V. (1976) Flavine-oxygen derivatives involved in hydroxylation by *p*-hydroxybenzoate hydroxylase, *J. Biol. Chem. 251*, 2550–2563.
411. Ridder, L., Mulholland, A. J., Vervoort, J., and Rietjens, I. M. C. M. (1998) Correlation of calculated activation energies with experimental rate constants for an enzyme catalyzed aromatic hydroxylation, *J. Am. Chem. Soc. 120*, 7641–7642.
412. Hartmann, S., Hultschig, C., Eisenreich, W., Fuchs, G., Bacher, A., and Ghisla, S. (1999) NIH Shift in flavin-dependent monooxygenation: Mechanistic studies with 2-aminobenzoyl-CoA monooxygenase/reductase, *Proc. Natl. Acad. Sci. U.S.A. 96*, 7831–7836.
413. Guroff, G., Daly, J. W., Jerina, D. M., Renson, J., Witkop, B., and Udenfriend, S. (1967) Hydroxylation-induced migration: The NIH shift, *Science 157*, 1524–1530.
414. Schuster, B., and Retey, J. (1995) The mechanism of action of phenylalanine ammonia-lyase: The role of prosthetic dehy-droalanine, *Proc. Natl. Acad. Sci. U.S.A. 92*, 8433–8437.
415. Crooks, G. P., and Copley, S. D. (1993) A surprising effect of leaving group on the nucleophilic aromatic substitution reaction catalyzed by 4-chlorobenzoyl CoA dehalogenase, *J. Am. Chem. Soc. 115*, 6422–6423.

416. Gustin, D. J., Mattei, P., Kast, P., Wiest, O., Lee, L., Cleland, W. W., and Hilvert, D. (1999) Heavy atom isotope effects reveal a highly polarized transition state for chorismate mutase, *J. Am. Chem. Soc. 121*, 1756–1757.
417. Wright, S. K., DeClue, M. S., Mandal, A., Lee, L., Wiest, O., Cleland, W. W., and Hilvert, D. (2005) Isotope effects on the enzymatic and nonenzymatic reactions of chorismate, *J. Am. Chem. Soc. 127*, 12957–12964.
418. Guilford, W. J., Copley, S. D., and Knowles, J. R. (1987) The mechanism of the chorismate mutase reaction, *J. Am. Chem. Soc. 109*, 5013–5019.
419. Gajewski, J. J., Jurayj, J., Kimbrough, D. R., Gande, M. E., Ganem, B., and Carpenter, B. K. (1987) The mechanism of rearrangement of chorismic acid and related compounds, *J. Am. Chem. Soc. 109*, 1170–1186.
420. Chook, Y. M., Gray, J. V., Ke, H., and Lipscomb, W. N. (1994) The monofunctional chorismate mutase from *Bacillus subtilis*. Structure determination of chorismate mutase and its complexes with a transition state analog and prephenate, and implications for the mechanism of the enzymic reaction, *J. Mol. Biol. 240*, 476–500.
421. Zhang, X., Zhang, X., and Bruice, T. C. (2005) A definitive mechanism for chorismate mutase, *Biochemistry 44*, 10443–10448.
422. DeClue, M. S., Baldridge, K. K., Kuenzler, D. E., Kast, P., and Hilvert, D. (2005) Isochorismate pyruvate lyase: A pericyclic reaction mechanism? *J. Am. Chem. Soc. 127*, 15002–15003.
423. Olucha, J., Ouellette, A. N., Luo, Q., and Lamb, A. L. (2011) pH Dependence of catalysis by *Pseudomonas aeruginosa* isochorismate-pyruvate lyase: Implications for transition state stabilization and the role of Lysine 42, *Biochemistry 50*, 7198–7207.
424. Oikawa, H., Suzuki, Y., Naya, A., Katayama, K., and Ichihara, A. (1994) First direct evidence in biological Diels–Alder reaction of incorporation of diene–dienophile precursors in the biosynthesis of solanapyrones, *J. Am. Chem. Soc. 116*, 3605–3606.
425. Klas, K., Tsukamoto, S., Sherman, D. H., and Williams, R. M. (2015) Natural Diels–Alderases: Elusive and irresistable, *J. Org. Chem. 80*, 11672–11685.
426. Kasahara, K., Miyamoto, T., Fujimoto, T., Oguri, H., Tokiwano, T., Oikawa, H., Ebizuka, Y., and Fujii, I. (2010) Solanapyrone synthase: A possible Diels–Alderase and iterative type I polyketide synthase encoded in a biosynthetic gene cluster from *Alternaria solani*, *ChemBioChem 11*, 1245–1252.
427. Hashimoto, T., Hashimoto, J., Teruya, K., Hirano, T., Shin-ya, K., Ikeda, H., Liu, H. W., Nishiyama, M., and Kuzuyama, T. (2015) Biosynthesis of versipelostatin: Identification of an enzyme-catalyzed [4+2]-cycloaddition required for macrocyclization of spirotetronate-containing polyketides, *J. Am. Chem. Soc. 137*, 572–575.
428. Zhang, B., Wang, K. B., Wang, W., Wang, X., Liu, F., Zhu, J., Shi, J., Li, L. Y., Han, H., Xu, K., Qiao, H. Y., Zhang, X., Jiao, R. H., Houk, K. N., Liang, Y., Tan, R. X., and Ge, H. M. (2019) Enzyme-catalysed [6+4] cycloadditions in the biosynthesis of natural products, *Nature 568*, 122–126.
429. Fage, C. D., Isiorho, E. A., Liu, Y., Wagner, D. T., Liu, H. W., and Keatinge-Clay, A. T. (2015) The structure of SpnF, a standalone enzyme that catalyzes [4+2] cycloaddition, *Nat. Chem. Biol. 11*, 256–258.
430. Kim, H. J., Ruszczycky, M. W., Choi, S. H., Liu, Y. N., and Liu, H. W. (2011) Enzyme-catalysed [4+2] cycloaddition is a key step in the biosynthesis of spinosyn A, *Nature 473*, 109–112.
431. Jeon, B. S., Ruszczycky, M. W., Russell, W. K., Lin, G. M., Kim, N., Choi, S. H., Wang, S. A., Liu, Y. N., Patrick, J. W., Russell, D. H., and Liu, H. W. (2017) Investigation of the mechanism of the SpnF-catalyzed [4+2] cycloaddition reaction in the biosyn-thesis of spinosyn A, *Proc. Natl. Acad. Sci. U.S.A. 114*, 10408–10413.
432. Yang, Z., Yang, S., Yu, P., Li, Y., Doubleday, C., Park, J., Patel, A., Jeon, B. S., Russell, W. K., Liu, H. W., Russell, D. H., and Houk, K. N. (2018) Influence of water and enzyme SpnF on the dynamics and energetics of the ambimodal [6+4]/[4+2] cycloaddition, *Proc. Natl. Acad. Sci. U.S.A. 115*, E848–E855.
433. Beaudry, C. M., Malerich, J. P., and Trauner, D. (2005) Biosynthetic and biomimetic electrocyclizations, *Chem. Rev. 105*, 4757–4778.
434. Townsend, C. A. (2011) A "Diels–Alderase" at last, *ChemBioChem 12*, 2267–2269.
435. Page, M. I., and Jencks, W. P. (1971) Entropic contributions to rate accelerations in enzy-

mic and intramolecular reactions and the chelate effect, *Proc. Natl. Acad. Sci. U.S.A. 68*, 1678–1683.
436. Watanabe, K., Mie, T., Ichihara, A., Oikawa, H., and Honma, M. (2000) Detailed reaction mechanism of macrophomate synthase: Extraordinary enzyme catalyzing five-step transformation from 2-pyrones to benzoates, *J. Biol. Chem. 275*, 38393–38401.
437. Ose, T., Watanabe, K., Mie, T., Honma, M., Watanabe, H., Yao, M., Oikawa, H., and Tanaka, I. (2003) Insight into a natural Diels–Alder reaction from the structure of macrophomate synthase, *Nature 422*, 185–189.
438. Guimaraes, C. R. W., Udier-Blagovic, M., and Jorgensen, W. L. (2005) Macrophomate synthase: QM/MM Simulations address the Diels–Alder versus Michael–aldol reaction mechanism, *J. Am. Chem. Soc. 127*, 3577–3588.
439. Serafimov, J. M., Gillingham, D., Kuster, S., and Hilvert, D. (2008) The putative Diels–Alderase macrophomate synthase is an efficient aldolase, *J. Am. Chem. Soc. 130*, 7798–7799.
440. Kerbarh, O., Chirgadze, D. Y., Blundell, T. L., and Abell, C. (2006) Crystal structures of *Yersinia enterocolitica* salicylate synthase and its complex with the reaction products salicylate and pyruvate, *J. Mol. Biol. 357*, 524–534.
441. Zwahlen, J., Kolappan, S., Zhou, R., Kisker, C., and Tonge, P. J. (2007) Structure and mechanism of MbtI, the salicylate synthase from *Mycobacterium tuberculosis*, *Biochemistry 46*, 954–964.
442. Retey, J., and Lynen, F. (1965) Zur biochemischen funktion des biotins: 9. Der sterische verlauf der carboxylierung von propionyl-CoA, *Biochem. Z. 342*, 256–271.
443. Okeefe, S. J., and Knowles, J. R. (1986) Biotin-dependent carboxylation catalyzed by transcarboxylase is a stepwise process, *Biochemistry 25*, 6077–6084.
444. Stubbe, J., Fish, S., and Abeles, R. H. (1980) Are carboxylations involving biotin concerted or nonconcerted? *J. Biol. Chem. 255*, 236–242.
445. Grogan, G., Roberts, G. A., Bougioukou, D., Turner, N. J., and Flitsch, S. L. (2001) The desymmetrization of bicyclic β-diketones by an enzymatic *retro*-Claisen reaction: A new reaction of the crotonase superfamily, *J. Biol. Chem. 276*, 12565–12572.
446. Fu, H., Ebert-Khosla, S., Hopwood, D. A., and Khosla, C. (1994) Engineered biosynthesis of novel polyketides: Dissection of the catalytic specificity of the *act* ketoreductase, *J. Am. Chem. Soc. 116*, 4166–4170.
447. Chen, M., Jiang, M., Sun, Y., Guo, Z. F., and Guo, Z. (2011) Stabilization of the second oxyanion intermediate by 1,4-dihydroxy-2-naphthoyl-coenzyme A synthase of the menaquinone pathway: Spectroscopic evidence of the involvement of a conserved aspartic acid, *Biochemistry 50*, 5893–5904.
448. Kelly, W. L., Boyne, M. T., 2nd, Yeh, E., Vosburg, D. A., Galonic, D. P., Kelleher, N. L., and Walsh, C. T. (2007) Characterization of the aminocarboxycyclopropane-forming enzyme CmaC, *Biochemistry 46*, 359–368.
449. Maresh, J. J., Giddings, L. A., Friedrich, A., Loris, E. A., Panjikar, S., Trout, B. L., Stockigt, J., Peters, B., and O'Connor, S. E. (2008) Strictosidine synthase: Mechanism of a Pictet–Spengler catalyzing enzyme, *J. Am. Chem. Soc. 130*, 710–723.

Chapter 2
Prosthetic Catalysis

In addition to the 20 unmodified side chains of the amino acids and the peptide bonds of the polypeptide backbone, which are provided unavoidably by the protein as catalysts for the chemical transformation performed by an enzyme, prosthetic groups can provide **complicated catalytic functional groups more or less permanently associated with the enzyme.** Prosthetic groups are often attached covalently to the protein as **posttranslational modifications**. In this instance, the prosthetic group is formally equivalent to an amino acid in that it is a covalent participant in the structure of the protein. Often, however, a prosthetic group is merely tightly but noncovalently bound to the protein. Although a tightly bound prosthetic group does not leave the enzyme readily and may remain associated with it for extended periods of time, it is possible for it to dissociate slowly from the protein even when the protein is in its native state. A noncovalently bound prosthetic group always dissociates when the protein is unfolded. As far as the reaction catalyzed by the enzyme is concerned, however, a noncovalently bound prosthetic group is a permanent feature of the molecular structure of the enzyme; and, in this sense, it is also indistinguishable from any of its amino acids. Although most prosthetic groups, other than lipids and polysaccharides, participate directly in the catalytic reactions catalyzed by the enzymes in which they are located, there are examples of otherwise catalytic prosthetic groups that do not seem to be involved in any way in catalysis and seem to perform a purely structural role.[1]

Examples of a **covalently bound prosthetic group** would be the 4′-phosphopantetheines attached covalently to serines as posttranslational modifications of animal fatty acid synthase[2] and fungal L-aminoadipate-semialdehyde dehydrogenase.[3]

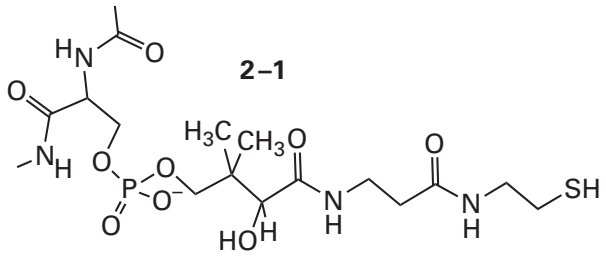

4′-Phosphopantetheine is identical to the portion of coenzyme A (previously **1–66**)*

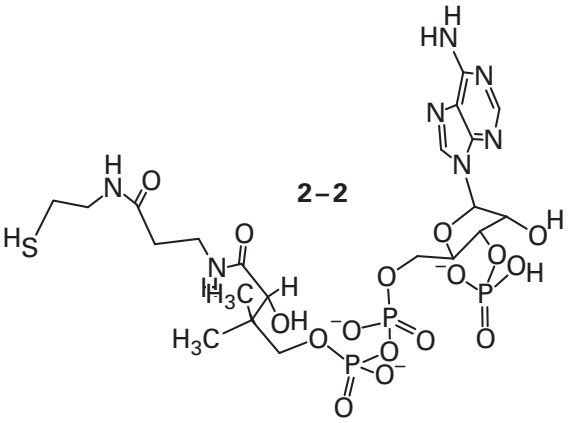

in which the essential sulfanyl group is located, but it is attached to a serine rather than adenosine 3′,5′-diphosphate. The sulfanyl group of the pantetheine, when it is a prosthetic group in the respective active sites, is acylated during enzymatic catalysis, and the resulting thioester participates as an enol in fatty acid synthase or is reduced to the monothiohemiacetal in L-aminoadipate-semialdehyde dehydrogenase. The role of the 4′-phosphopantetheine as a covalently attached prosthetic group in these reactions should be distinguished from its role as a coenzyme when it is incorporated into coenzyme A, even though in both cases the pantetheine is performing the same chemical function. As has already

*From here on, Equations and Structures from previous chapters will be reproduced in the present chapter. The intention is to make it easier for the reader. Instead of having to rummage through an earlier chapter, the reader will find the drawing in the present chapter, usually within pages of any reference to it, and each chapter is self-contained, at least as far as Equations and Stuctures.

been noted, a coenzyme such as coenzyme A, unlike a prosthetic group such as 4′-phosphopantetheine, enters and leaves the active site of the enzyme during every turnover and is functionally indistinguishable from a substrate.

An example of a **tightly but noncovalently bound prosthetic group** would be the NAD^+ that is tightly bound to UDP-glucose 4-epimerase (previously Equation 1–88)

$$\text{UDP-glucose} \rightleftharpoons \text{UDP-galactose} \qquad (2\text{–}1)$$

Because the NAD^+ is regenerated after each catalytic cycle of this enzyme, there is no need for the NAD^+, or the NADH, to enter and leave the active site, and they remain continuously bound as complementary prosthetic groups. The role of the NAD^+ as a prosthetic group in this reaction should be distinguished from its role in almost every other situation where it is a coenzyme, indistinguishable except in name from a substrate, that enters and leaves the active site during each turnover. Many of the prosthetic groups that are noncovalently associated with active sites, such as pyridoxamine 5′-phosphate and thiamine diphosphate, contain one or more phospho groups. These phospho groups can form strong attachments with properly organized cups of donors for hydrogen bonds.

Most prosthetic groups have proven so versatile that they are **used in many different enzymatic reactions** to perform the same, particular function in the respective contexts. A few enzymes, however, carry prosthetic groups unique to themselves, such as the dipyrromethane covalently attached to the active site of hydroxymethylbilane synthase.[4-6]

Most prosthetic groups are **molecules synthesized separately** in their own respective metabolic pathways, each of which encompasses a sequence of successive enzymatic steps, such as the metabolic pathway producing riboflavin. A few, however, are the result of posttranslational modification of the polypeptides forming their enzymes. Such a posttranslational modification can be of a side chain, such as the successive oxidations that produce 2,4,5-trihydroxyphenylalanine[7] or the oxidation that produces dehydroalanine,[8] or it can be a modification of the peptide backbone, such as the one that produces the 4-methyleneimidazol-5-one formed from Serine 143 of histidine ammonia-lyase from *Pseudomonas putida*.[9]

Prosthetic groups exist because they effect chemical transformations beyond those that can be accomplished by the unmodified side chains of the amino acids.

Pyridoxal 5′-Phosphate

Pyridoxal 5′-phosphate

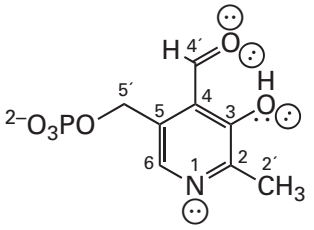

2–3

when acting as a prosthetic group, is usually bound covalently to the resting enzyme as an internal pyridoximine with one of its lysines.[10-12]

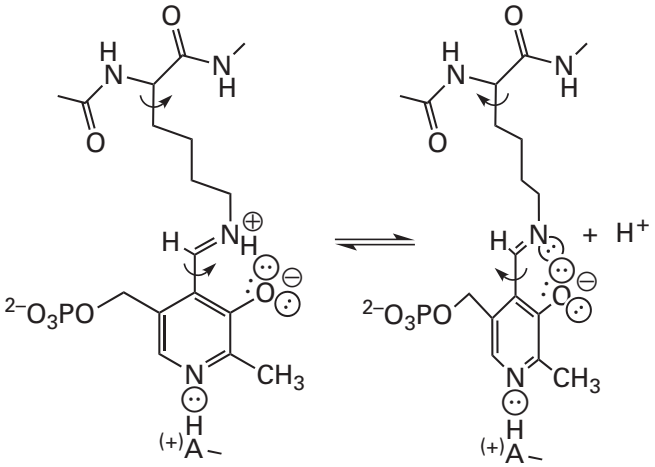

internal pyridoximine

(2–2)

Pyridoxal 5′-phosphate is a 4-azabenzaldehyde. Consequently, it is not prone to the many unfortunate side reactions in which aliphatic aldehydes participate with the amino acids of proteins.[13]

The initial **formation of an internal pyridoximine** between pyridoxal 5′-phosphate and the primary amino group of a lysine in the active site of the enzyme is a simple nucleophilic substitution at a carbonyl and proceeds through the hemiaminal.

The slow step in such a formation of an imine in aqueous solution is usually the loss of water from the hemiaminal, which is also the case in the formation of an internal pyridoximine.[14] The dehydration of a hemiaminal is susceptible to both acid and base catalysis (Figure 1–7). In the case of pyridoxal 5′-phosphate in solution, the phenolic oxygen catalyzes this dehydration intramolecularly.[15] This catalysis is thought to be due to its ability to act as an intramolecular base

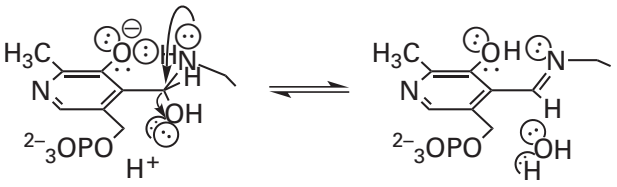

(2–3)

and remove the hydron from imino nitrogen immediately prior to or simultaneously to the breaking of the bond to the hydroxide. Such intramolecular base catalysis augments the push of the lone pair periplanar to the leaving group by increasing its electron density and may be essential within the active site of an enzyme that is shielded from the water, hydroxide, and bases in the surrounding solution, but acids or bases in surrounding side chains of amino acids could also provide catalysis for the formation of the internal pyridoximine.[14]

When it is free in solution, unassociated with an enzyme, the conjugate acid of a pyridoximine (left-hand side of Equation 2–2) is a **zwitterion**: its imino nitrogen is hydronated and its phenolic oxygen is unhydronated.[16] On the active site of an enzyme, such as tryptophan synthase from *Salmonella typhimurium*,[17,18] the internal pyridoximine is usually zwitterionic. In the **absorption spectrum** of the zwitterionic pyridoximine that forms between the amino group of L-valine and pyridoxal in solution, there are maxima of absorbance at 414 and 302 nm. Upon dissociation of the hydron from the iminium nitrogen to form the anionic conjugate base of this zwitterionic pyridoximine (right-hand side of Equation 2–2), the maximum absorbance shifts to 365 nm.[19]

The maximum absorbance at 414 nm manifested by the zwitterion results from the fact that it is an extensive **vinylogous amide**, which can be seen in the resonance structure[16]

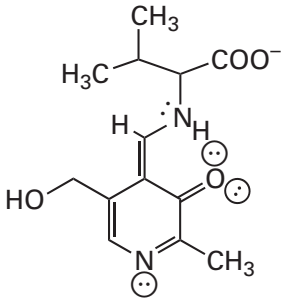

2–4

This resonance structure states that the zwitterion of a pyridoximine, either in solution or in the active site of an enzyme, can be viewed as a ***π* molecular orbital system** encompassing nine atoms

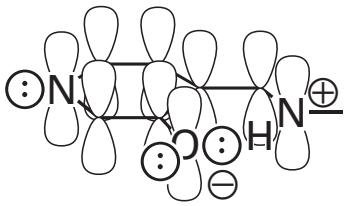

2–5

that has nine molecular orbitals. The five molecular orbitals of lowest energy are occupied by five pairs of electrons. The hydrogen bond between the phenolic oxyanion and the nitrogen–hydrogen bond of the iminium holds the carbon–nitrogen double bond of the iminium ion in the plane of the pyridyl ring to reinforce the conjugation.[20]

When pyridoxal 5′-phosphate is in the active site of porcine aspartate transaminase as the internal pyridoximine (Equation 2–2), the maxima of absorbance for the zwitterion of the internal pyridoximine (left-hand side of Equation 2–2) occur at 430 and 340 nm,[12] and the maxima of absorbance for the zwitterion of the internal pyridoximine in the active site of aspartate transaminase from *Escherichia coli* also occur at 430 and 340 nm (Figure 2–1B).[12,21-26] The zwitterion of the internal pyridoximine between pyridoxal 5′-phosphate and the lysine in the active site of a particular enzyme has the higher maximum absorbance somewhere between 405 and 430 nm depending on the microenvironment that surrounds it. In the active site of aspartate transaminase from *E. coli*, the anionic conjugate base of the internal pyridoximine (right-hand side of Equation 2–2) has a maximum absorbance at 358 nm (Figure 2–1A), and in the active site of porcine aspartate transaminase, the maximum absorbance[12] is at 362 nm.

In the active sites of these aspartate transaminases and the active sites of their close relatives that nevertheless catalyze different reactions, the

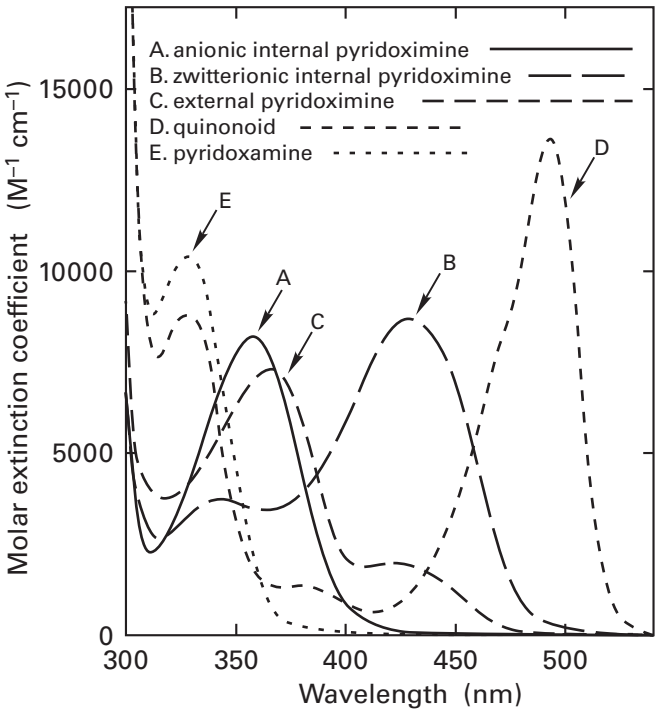

Figure 2–1: Absorption spectra of the pyridoxyl intermediates in the reaction catalyzed by aspartate transaminase from *E. coli*. (**A**) Spectrum[12] for an anionic internal pyridoxime (λ_{max} = 358 nm; ε_{358} = 8300 M^{-1} cm^{-1}),[24] for the enzyme in the absence of substrates, in a solution at pH 9. (**B**) Spectrum[12] for a zwitterionic internal pyridoxime (λ_{max} = 430 nm; ε_{358} = 8200 M^{-1} cm^{-1}),[24] for the enzyme in the absence of substrates, in a solution at pH 5. In (A) and (B), it was assumed that the internal pyridoxime was either completely in the anionic state or completely in the zwitterionic state at the respective pH. These conclusions were based on a spectrophotometric titration. (**C**) Spectrum[22] for an external pyridoxime (λ_{max} = 358 nm; ε_{358} = 7300 M^{-1} cm^{-1}; λ_{max} = 422 nm; ε_{422} = 2000 M^{-1} cm^{-1}),[24] for the enzyme in solutions containing high concentrations of 2-methyl-L-aspartate, at values of pH between 6 and 10.4. The spectrum was invariant with pH. Whether or not this spectrum represents a single species is unknown. It probably represents a fixed internal equilibrium between two species, one the anionic external pyridoxime (λ_{max} = 358 nm) and the other the zwitterionic external pyridoxime (λ_{max} = 422 nm), in a well-closed active site unaffected by the pH of the solution surrounding the enzyme.[22] This proposal is consistent with the fact that the ratio of the two peaks for the complex between aspartate aminotransferase varies with the species from which the enzyme has been purified.[22] (**D**) Spectrum for a quinonoid intermediate (λ_{max} = 494 nm; ε_{494} = 13,600 M^{-1} cm^{-1}),[21,26] for the enzyme in solutions containing high concentrations of L-*erythro*-3-hydroxyaspartate, at values of pH between 6 and 10.4. (**E**) Spectrum for a pyridoxamine in the active site (λ_{max} = 323 nm; ε_{323} = 9100 M^{-1} cm^{-1}),[25] for the enzyme at pH 8, in a solution containing L-cysteinesulfinate, a slow substrate that causes the pyridoxamine to accumulate, presumably stoichiometrically, in the active site. All extinction coefficients are based on the molarity of active sites in the solution. In spectra A, B, and E, only one species of the prosthetic group predominates and the molar extinction coefficient should be close to that for each of these unique species. In the case of spectrum D, it is clear that the majority of the active sites are occupied by the pyridoxamine. The actual molar extinction coefficient for the quinonoid intermediate has been estimated[23] to be 41,000 M^{-1} cm^{-1}.

anionic conjugate base of the internal pyridoxime predominates as the pH of the solution is raised. The **pK_a for the acid dissociation of the zwitterionic internal pyridoxime** (Equation 2–2) in the active site of porcine aspartate transaminase[12,27] is 6.8, and that for aspartate transaminase from *E. coli*[24] is 6.96. Because the value for the pK_a of the pyridoximine[27] formed in solution between *n*-butylamine and pyridoxal 5′-phosphate is 12.4, some feature of the active site must be responsible for the low value for the pK_a of the internal pyridoxime bound to the enzymes in this family.

The decrease in the pK_a of the internal pyridoximine brought about by these two active sites is probably the result of both the **hydronation of the pyridyl nitrogen 1 of the pyridoxal phosphate by the carboxy group of an aspartic acid** that forms a hydrogen bond to it and a twist of the double bond between carbon 4′ and nitrogen 4′ out of the plane of the pyridyl ring brought about by a pull exerted by the active site on the lysine of the internal pyridoximine. When [1-^{15}N]pyridoxal 5′-phosphate is an internal pyridoximine in the active site of aspartate transaminase from *E. coli*, nuclear magnetic resonance absorptions from the pyridinio nitrogen-15 indicate that, in the hydrogen bond, it is hydronated[28] and therefore the donor. The hydronation of the pyridyl nitrogen does not affect the position of the maximum of absorbance for a zwitterionic pyridoximine[19] but would definitely lower the pK_a of the zwitterion. It has been observed that, in a crystallographic molecular model of porcine aspartate transaminase,[29] the carbon–nitrogen double bond of the zwitterionic pyridoximine is rotated 35° out of the plane of the pyridyl ring. This rotation of the double bond out of the plane of the pyridyl ring would cause the iminium to be less conjugated to the pyridyl ring and cause it resemble a normal aliphatic iminium, the pK_a of which should be around 7.[30,31] When the lysine of the internal pyridoximine is mutated to an alanine and methylamine is used to produce a pyridoximine that should resemble an internal pyridoximine,[32] the pK_a of this $N^{4'}$-methylpyridoximine, which cannot be distorted sterically, is 10.2. This result suggests that if the pyridoximine in the active site is not twisted and can remain planar, the pK_a should be normal. In many of the enzymes that have internal pyridoximines in their active sites, however, their respective anionic conjugate bases do not form regardless of how high the pH of the solution is raised, presumably because the pK_a of the pyridoximine has been raised sufficiently by its surroundings that it is out

of the range of pH within which these enzymes remain folded. In these instances, presumably, the pK_a of the respective zwitterionic pyridoximine is increased rather than decreased by the active site. These shifts in the pK_a of the internal pyridoximine may have significance for the particular reactions catalyzed by these enzymes.

As was the case with aspartate transaminase, **the pyridyl nitrogen 1 of an internal pyridoximine is often hydronated by an acidic side chain in the active site**.[33] The pK_a of the pyridinio nitrogen 1 in a pyridoximine[16] is 5.6, so when an internal pyridoximine forms a hydrogen bond with the carboxy group from an aspartic acid (pK_a = 4.0) or a glutamic acid (pK_a = 4.3), the hydron in the hydrogen bond will be on the nitrogen. An internal pyridoximine, however, can also participate in a strong hydrogen bond with a side chain within the active site of the enzyme but remain unhydronated[34] because the partner in this type of hydrogen bond is not noticeably acidic. For example, in tryptophan synthase from *Salmonella enterica*, the pyridyl nitrogen 1 of the internal pyridoximine forms a hydrogen bond with a serine;[35] in cysteine synthase from *S. enterica*, it also forms a hydrogen bond with a serine;[36] and in alanine racemase from *Geobacillus stearothermophilus*, it forms a hydrogen bond with an arginine.[37] In the active site of tryptophan synthase from *S. enterica*, the hydron in the hydrogen bond between the serine and nitrogen 1 of the pyridyl group resides on the serine,[17] and in the active site of alanine racemase from *G. stearothermophilus*, the hydron in the hydrogen bond between the arginine and nitrogen 1 of the pyridyl group resides on the arginine,[28] as expected from the respective values of pK_a for these acids and the pyridyl nitrogen. In these instances, the pyridyl nitrogen is not hydronated.

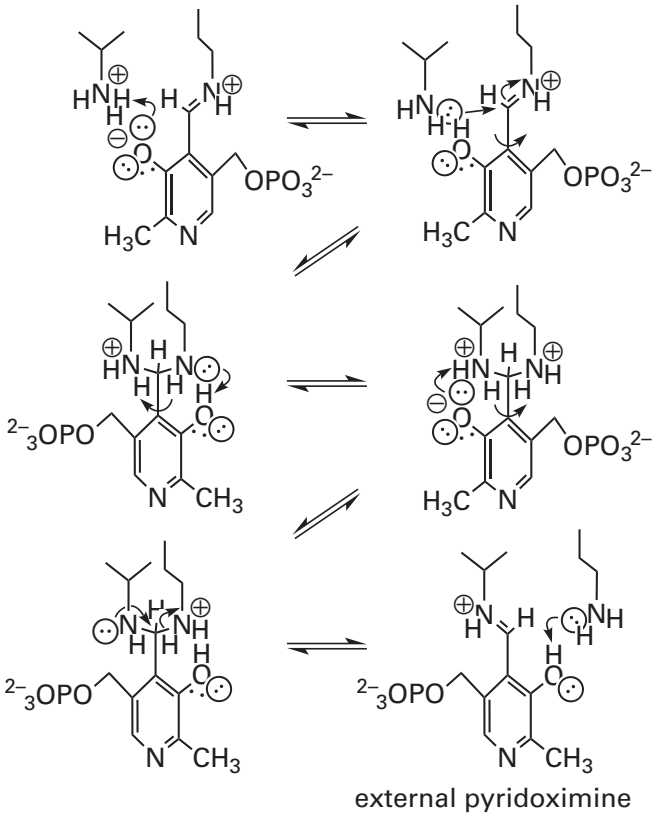

Figure 2–2: Transimination catalyzed by the phenolic oxygen of pyridoxal phosphate. The pyridoxal phosphate is initially the zwitterionic internal pyridoximine with a lysine from the protein (on the right side), and the reactant in the transimination is the conjugate acid of a primary amine (on the left side). As the reaction progresses, hydrons are transferred by the phenolato oxygen from the nitrogen of the reactant to the nitrogen of the lysine. The phenolato oxygen could shuttle both of the hydrons that are transferred from the entering ammonium ion to the dissociating lysinium ion, but other acid–bases may be involved as well. The phenolic oxygen performs each transfer by swinging back and forth between the two nitrogens in this symmetrical reaction.

Almost all the substrates upon which the internal pyridoximines of pyridoxal 5′-phosphate within active sites act prosthetically are primary amines, and the first step in every one of these reactions catalyzed by pyridoxal 5′-phosphate is to form the external pyridoximine between the nitrogen of that primary amine of the substrate and the 4′ imino carbon of the internal pyridoximine. Because the internal pyridoximine is an imine with a lysine in the active site, a **transimination**[38,39] performs the nucleophilic substitution at the carbonyl carbon (Figure 2–2). On an enzyme at neutral pH, the transimination would begin with the cationic conjugate acid of the amino group and the phenolic oxygen of the zwitterionic pyridoximine, the pK_a of which is elevated upon binding of the substrate.[32] This shift in pK_a ensures that the iminium nitrogen of the lysine in the internal pyridoximine is hydronated (Equation 2–2) upon binding of the hydronated primary ammonium of the substrate (Figure 2–2).

There had been some doubt[40] as to whether or not the intermediates in the proposed mechanism for the transimination of imines of pyridoxal 5′-phosphate presented in Figure 2–2 would be stable enough that the reaction could proceed through the

gem-diamine rather than passing through the aldehyde. It was subsequently shown,[39] however, that such a direct transimination in aqueous solution proceeds about twice as fast as the exchange through the indirect route in which the aldehyde, pyridoxal 5′-phosphate itself, is the intermediate. In an active site, shielded from water, the indirect route, which necessarily requires water to provide the oxygen of the aldehyde, would be even slower. Finally, the expected ***gem*-diamine intermediates have been observed in crystallographic molecular models** of mutant enzymes,[41-43] enzymes with which inhibitors have been complexed,[44] or enzymes to which normal substrates have bound nonproductively.[45] Each stratagem prevents the reaction from proceeding further and permits the *gem*-diamine to be observed.

When there is no **phenolic oxygen in an ortho position** to the iminium nitrogen of the imine of a benzaldehyde, a transimination involving that benzaldehyde proceeding in solution displays a requirement for catalysis by both acid and base.[38] This requirement is consistent with the unavoidable requirement to remove hydrons from the amine that is entering and the coincident unavoidable requirement to add hydrons to the amine that is leaving. When the transimination involves imines of pyridoxal 5′-phosphate, however, no requirement for acid or base catalysis is observed.[39] This lack of catalytic requirement can be readily explained by the fact that the phenolic oxygen is four atoms away from both nitrogens and can easily shuttle hydrons between them (Figure 2–2).

In the crystallographic molecular models of enzymes containing a *gem*-diamine of pyridoxal 5′-phosphate, the phenolic oxygen of the 3-hydroxypyridyl group sits on the concave side of the angle formed by the two carbon–nitrogen bonds of the *gem*-diamine, splitting the N–C–N bond angle and sitting within hydrogen-bonding distance of both of the nitrogens.[41] When a crystallographic molecular model of an enzyme containing the internal pyridoximine is superposed on the crystallographic molecular model of the same enzyme that has formed its external pyridoximine with the primary amine of one of its substrates, the two respective carbon–nitrogen bonds of the imines in the two different models form angles of about 100° with each other, as they would in a *gem*-diamine (109°), and again, the phenolic oxygens of the pyridoximines sit on the concave side of this bond angle between the two nitrogens (Figure 2–3).[46-50] This disposition is the one expected for a catalytic base shuttling hydrons between the two nitrogens.

The **freedom of motion required of the pyridoxyl group**, however, to perform this catalysis may not be permitted in the confines of some active sites. In this case, when the phenoxy oxygen is sterically prevented from accomplishing the hydronations and dehydronations, the active site must provide acids and bases to do so because direct transfer of a hydron between two nitrogens on the same carbon cannot occur. For example, in the active site of glycine *C*-acetyltransferase from *E. coli*, there is a histidine side chain positioned properly to perform hydronations and dehydronations of the glycine or the L-2-amino-3-oxobutanoate that are forming the external pyridoximine during the normal reaction in the respective direction, and one of the oxygens of the phospho group of the pyridoxal 5′-phosphate is positioned properly to perform hydronations and dehydronations of the lysine that forms the internal pyridoximine.[51]

Each transimination moves the respective pyridoxal 5′-phosphate from the lysine of the internal pyridoximine to the primary amine of the substrate. There is little electronic difference between an internal pyridoximine and an external pyridoximine. Nevertheless, the external pyridoximine between the active site of aspartate transaminase from *E. coli* and 2-methyl-L-aspartate, an analogue of the normal substrate, L-aspartate, in which the hydron α to the imino nitrogen has been replaced by a methyl group, has an **absorption spectrum** (Figure 2–1C) that resembles a mixture of a zwitterionic pyridoximine and its conjugate base, the anionic pyridoximine, even though the spectrum is invariant with pH.[22-24] Furthermore, the ratio of the peaks for absorbance that seem to originate from the zwitterionic external pyridoximine and its anionic conjugate base differ depending on the species from which the enzyme is purified, but the two molar extinction coefficients add up to around 9000,[22] a fact again suggesting that there is an internal equilibrium between the zwitterion and the anion of the external pyridoximine in a particular active site, and the equilibrium constant varies from species to species.

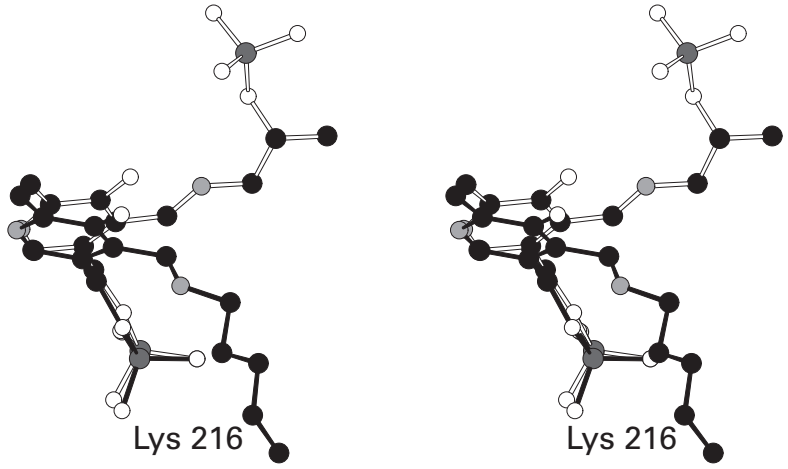

Figure 2–3: Positioning of the iminium nitrogens of the internal pyridoximine and an external pyridoximine adjacent to the phenolic oxygen on carbon 3 of the pyridyl group of pyridoxal 5′-phosphate by the active site of threonine-phosphate decarboxylase from *S. enterica*.[46] The stereodrawing[50] is the superposition of portions of two crystallographic molecular models. Black atoms are carbons, white atoms are oxygens, small gray atoms are nitrogens, and large dark gray atoms are atoms of phosphorus. The internal pyridoximine (black bonds) of threonine-phosphate decarboxylase is found in the crystallographic molecular model of the enzyme purified directly from an overproducing strain of bacteria and crystallized without any alteration. The α carbon through carbon 6 of Lysine 216 and the entire pyridoximine 5′-phosphate are shown in the drawing. The external pyridoximine (white bonds) of the product, (*R*)-1-aminopropan-2-yl phosphate, was formed on the active site by mixing the enzyme with L-threonine phosphate before it was crystallized. At equilibrium, the most stable form of the enzyme under these conditions was found, by direct examination of the map of electron density, to be the external pyridoximine of the product, which is presented in its entirety in the drawing. The two crystallographic molecular models of the entire enzymes were superposed by the crystallographers, and the drawing is of the respective portions of that superposition. The bond between carbon 4′ of the pyridoxylidene and nitrogen 6 of the lysine and the bond between carbon 4′ of the pyridoxylidene and nitrogen 1 of the (*R*)-1-aminopropan-2-yl phosphate in the respective superposed models are at an angle of 106° to each other when viewed down the bonds between carbons 4 and carbons 4′ of the pyridoximines. The respective phenolic oxygens are both on the concave side of this bond angle in position to shuttle hydrons between the nitrogens. The dihedral angle between the plane of the pyridyl ring and the respective imino nitrogen along the bond between carbon 4 and carbon 4′ is 27° in the external pyridoximine and 60° in the internal pyridoximine, probably because the imino nitrogen is mostly hydronated in the former and mostly unhydronated in the latter (Equation 2–2). The hydrogen bond in the hydronated form holds the nitrogen in the plane of the ring so that the imine is conjugated with the pyridinio group, and the repulsion of the lone pairs in the unhydronated form opens up the angle. The 5′ phosphate is held tightly in position by the enzyme and therefore superposes closely, but the superposition illustrates that the pyridinio ring is able to pivot somewhat in the active site, which permits the phenolic oxygen freedom of movement to fulfill its role (Figure 2–2).

When the primary amine of a substrate is coupled as the external pyridoximine of pyridoxal 5′-phosphate and the pyridinio nitrogen 1 of the external pyridoximine is hydronated, the three σ bonds on the carbon of the substrate α to the iminium nitrogen become susceptible to heterolytic dissociation.[16] This susceptibility results from the hydronated pyridinio nitrogen withdrawing electron density from the other end of the π molecular orbital system and increasing the **hyperconjugation** of a σ bond that happens to be aligned parallel to the π molecular orbital system[52]

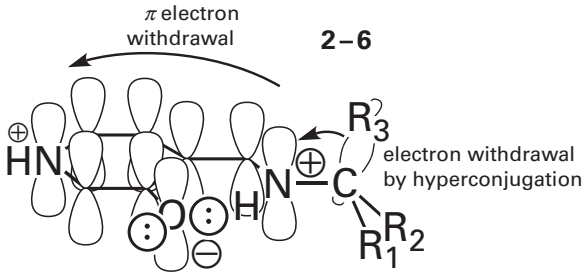

This withdrawal of electron density from the σ bond by hyperconjugation can be realized by writing a resonance structure in which the nitrogen equivalent of a carbenium ion is present on the iminium nitrogen

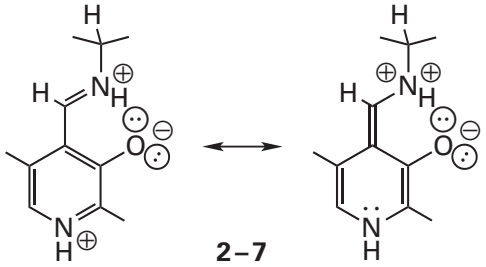

This resonance structure is not so satisfying as the depiction in **2–6** because it involves a dication missing two valence electrons on the iminium nitrogen, albeit somewhat stabilized by the adjacent phenylato oxygen. This resonance structure, however, illustrates that an imine of pyridoxal 5′-phosphate, with its pyridinio nitrogen hydronated, is a vinylogous iminium ion

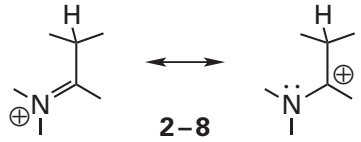

with the exception that nitrogen replaces carbon at the cationic position and has the same effect of weakening a σ bond on the adjacent carbon that is parallel the π molecular orbital system.

For this electron withdrawal by hyperconjugation to operate, the double bond between carbon 4′ and nitrogen 4′ in the external pyridoximine must be **coplanar with the pyridyl ring** (**2–6** and **2–7**). In a crystallographic molecular model of aspartate transaminase from *E. coli*,[53] in which the internal pyridoximine is the anionic conjugate base,[30] the double bond between carbon 4′ and nitrogen 4′ of the pyridoximine is normal (91°) to the plane of the pyridyl ring

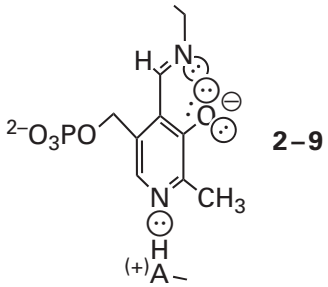

This arrangement is the expected result of electron repulsion between the lone pair of electrons on the phenolic oxygen and the lone pair of electrons on the now unhydronated imino nitrogen, as well as electron repulsion between the carbon–nitrogen double bond at carbon 4′ and the two σ bonds to carbon 4 in the pyridyl ring of pyridoximine 5′-phosphate. For the same reasons, this rotational isomer and its sibling, in which the carbon–nitrogen bond is pointed in the opposite direction, should also dominate in the anionic conjugate base of a pyridoximine when it is free in solution. In solution, the breaking of the conjugation (**2–5**) that results from this rotation of +90° or –90° around the bond between carbon 4 and carbon 4′ (see Equation 2–2) decreases the maximum of absorbance for a pyridoximine from 414 to 365 nm as it is dehydronated. The carbon–nitrogen double bond of the oxime of pyridoxal 5′-phosphate is coplanar with the ring of its pyridyl group because of a strong hydrogen bond (0.256 nm) between its imino nitrogen and its phenolic oxygen.[20] The homologous hydrogen bond between the nitrogen–hydrogen of the iminium and the phenolic oxygen enforces the planarity of an external pyridoximine when the imino nitrogen is hydronated. Because dehydronation of this hydrogen bond forces the double bond between carbon 4′ and nitrogen 4′ to be normal to the plane of the pyridyl ring and breaks the conjugation, **the catalytically active form of an external pyridoximine**

will always be the zwitterion, or its neutral tautomer, never its anionic conjugate base.

Because each of the three σ bonds on the carbon next to imino nitrogen 4′ of an external pyridoximine is weakened by this electron withdrawal by hyperconjugation, if the α carbon* of the external pyridoximine is bonded to an incipient electrophile, **that incipient electrophile can dissociate**.

If the α carbon of an external pyridoximine contains a hydrogen, that hydrogen can **dissociate as a hydron**. An example of this outcome is the first step of the reaction catalyzed by 4-aminobutyrate—2-oxoglutarate transaminase from *Pseudomonas fluorescens*, which proceeds with the dissociation of a hydron from the α carbon[54] of the external pyridoximine formed between 4-amino-butyrate and pyridoxal 5′-phosphate

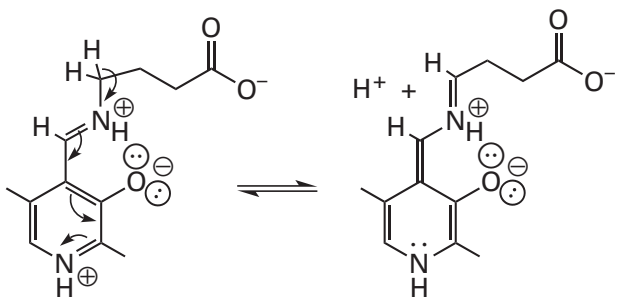

(2–4)

In solution, formation of the pyridoximine between pyridoxal and glycine and hydronation of pyridyl nitrogen 1 decrease the pK_a for dissociation of the hydron from the α carbon of the glycine[55,56] from 29 to 17 and increase the rate of exchange for a hydrogen on the α carbon for a deuterium in ^2H_2O by a factor of 10^7. The hydronated pyridinio nitrogen is essential to this decrease in pK_a and increase in the rate of exchange.[57] Hydronation of both the pyridyl nitrogen and the phenolic oxygen of the pyridoximine lowers the pK_a of the α carbon of the glycine to 11, and hydronation of the pyridyl nitrogen, the phenolic oxygen, and the α carboxylato group of the glycine lowers the pK_a of the α carbon to 6. Each of these hydronations can be accomplished, if necessary, by acidic side chains in an active site.

To explain the ease with which a hydron can dissociate from the α carbon of an external pyridoximine (Equation 2–4) in the active site of an enzyme, it is usually assumed that the α carbon, nitrogen 4′, carbon 4′, and the pyridyl ring are all coplanar (**2–6** and **2–7**) and that the σ bond to the hydron that is to be removed is normal to that plane and parallel to the π molecular orbital system so that its electron density can be withdrawn onto the hydronated pyridinio nitrogen. In the **crystallographic molecular model**, however, of the external pyridoximine of 2-methyl-L-aspartate in the active site of aspartate transaminase from *E. coli*, which also proceeds normally with the removal of a hydron from the α carbon, the σ bond between carbon 4′ and nitrogen 4′ is twisted out of the plane (Figure 2–4).[53] This arrangement seems to result from a steric effect between the 2-methyl group, which is replacing the hydron on the usual substrate, L-aspartate, and the surrounding side chains in the active site, but in a crystallographic molecular model of the external pyridoximine between L-aspartic acid and 1-deazapyridoxal 5′-phosphate in the same active site, in which no such steric effect should occur, the same twist is observed.[58] Neither 2-methyl-L-aspartate, however, nor the external pyridoximine between L-aspartic acid and 1-deazapyridoxal 5′-phosphate is catalytically competent, so this twist may not be relevant to normal catalysis. In a molecular model of the external pyridoximine of L-alanine in the active site of pyridoxamine—pyruvate transaminase from *Mesorhizobium loti*, based on several crystallographic molecular models of the enzyme, rather than just one,[59] all the necessary atoms are coplanar with the pyridyl ring and the σ bond between the α carbon and the hydron that is removed in the normal enzymatic reaction is, as expected (**2–6** and Equation 2–4), normal to the plane of the π molecular orbital system of the pyridoximine and parallel to its constituent *p* orbitals.

*Because at least one (if not more) of the substrates for reactions catalyzed by pyridoxal 5′-phosphate is an α-amino acid and because the carbon attached to the amino group can be considered to be α to that amino group just as it is α to the carboxy group, the designation α carbon will be used for the carbon bonded to the primary amino group of a substrate in an external pyridoximine, β carbon for the carbon that is bonded to the α carbon, other than the carbon of a carboxy group, γ carbon for the carbon bonded to the β carbon, and so forth.

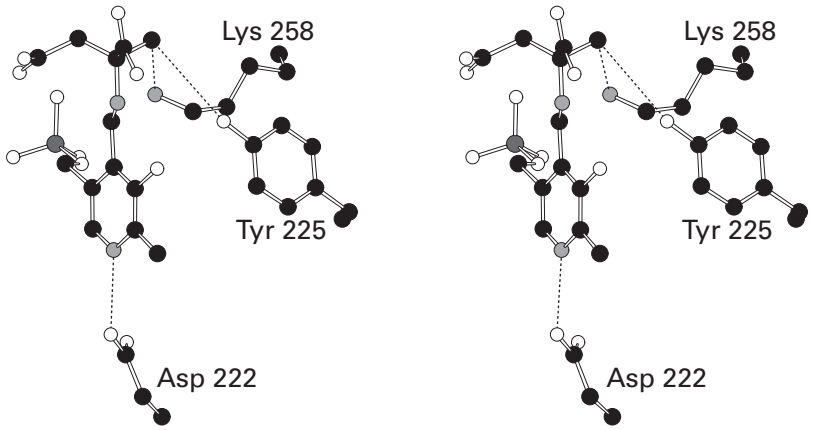

Figure 2–4: Use of the lysine of the internal pyridoximine as an acid–base to add or remove hydrons from the intermediates in a transamination. Black atoms are carbons, white atoms are oxygens, small gray atoms are nitrogens, and the large dark gray atom is a phosphorus. Aspartate transaminase from *E. coli* was mixed with the inhibitor 2-methyl-L-aspartate and then crystallized in its presence. In the map of electron density, it was found that 2-methyl-L-aspartate had formed the external pyridoximine within the active site of the enzyme.[53] Because the hydrogen on the α carbon of the aspartyl group has been replaced by a methyl group, the enzyme cannot proceed with its normal reaction and is locked in the conformation that would normally remove the hydron if it were there. The external pyridoximine and the side chains of Tyrosine 225, Aspartate 222, and Lysine 258, the lysine that forms the internal pyridoximine in the resting enzyme, are included in the stereodrawing[50] from the final crystallographic molecular model. The distances from the 6-amino group of Lysine 258 and the 4-hydroxyphenyl oxygen of Tyrosine 225 to the carbon of the 2-methyl group of the inhibitor, which assumes the position of the hydron that is normally removed during the transamination, are 0.38 and 0.36 nm, respectively (dotted lines). These distances are dictated by the van der Waals radii of the methyl, the amino, and the hydroxy groups and would be shorter if the methyl group were a hydrogen. The 6-amino group of Lysine 258 is also 0.32 nm away from carbon 4′, well within the sum of the length of the nitrogen–hydrogen bond and the van der Waals radii (0.38 nm). Consequently, it is in position to remove the hydron from carbon 2 of the substrate L-aspartate when it has formed an external pyridoximine and then put a hydron onto carbon 4′ of that pyridoximine. The angle between the plane of the pyridyl ring and the bond connecting carbon 2 of the 2-methyl-L-aspartate with the methyl carbon is 87°. Consequently, if the methyl group were a hydrogen, the carbon–hydrogen bond would be positioned by the enzyme almost precisely parallel to the π molecular orbital system of the pyridoximine as drawn in **2–6**. The π molecular orbital system of the α-carboxy group is also parallel to the bond connecting carbon 2 of the 2-methyl-L-aspartate with the methyl carbon and would provide further electron withdrawal. The dihedral angle between the plane of the pyridyl ring and the respective imino nitrogen along the bond between carbon 4 and carbon 4′ is 26° in the external pyridoximine, indicating that the imine is mostly hydronated and that the carbon–nitrogen double bond in the iminium ion is in conjugation with the pyridyl ring. The hydrogen bond between Aspartate 222 and the pyridinio nitrogen of the hydronated pyridoximine (0.289 nm) is indicated with a dotted line.

In many of these reactions in which a hydron is removed from the α carbon of the external pyridoxamine, the 6-amino group of the lysine from the enzyme that formed the original internal pyridoxamine with the pyridoxal 5′-phosphate (Equation 2–2) ends up immediately adjacent to the α carbon of the external pyridoxamine (Figure 2–4)[53,60,61] and is thought to be the base that removes the hydron.[62] In several of these enzymes, however, both the **6-amino group of the lysine and the 4-hydroxy group of a tyrosine** are positioned adjacent to the hydron on the α carbon (Figure 2–4)[53,63] and may cooperate in removing the hydron from it.[64] In the case of glycine hydroxymethyltransferase from *E. coli*, mutation of the lysine that forms the internal pyridoxamine to a glutamine decreases the rate of the conversion of glycine to serine by a factor of only 50.[65] This result suggests that there is a base other than that lysine that is available.

If the α carbon of an external pyridoxamine contains a carboxylato group, that carboxylato group can **dissociate as a molecule of carbon dioxide**. In this instance, as before, carbon dioxide behaves as if it were a hydron. An example of this outcome is the first step in the forward reaction catalyzed by 2,2-dialkylglycine decarboxylase (pyruvate) from *Burkholderia cepacia*,[66] which proceeds with the loss of carbon dioxide from the α carbon of the imine formed between a 2,2-dialkylglycine, such as 2,2-dimethylglycine, and pyridoxal 5′-phosphate

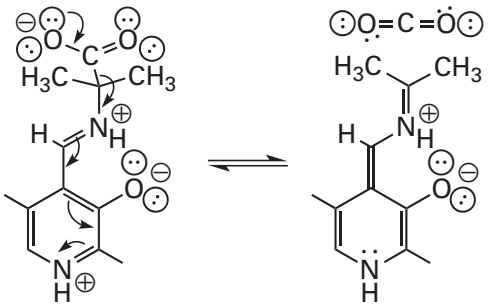

(2–5)

From examination of the crystallographic molecular model of the active site of the enzyme, it was concluded that the σ bond between the carbon α to the iminium nitrogen in the external pyridoxamine and the carboxylato group that dissociates in the usual enzymatic reaction is, again as expected (Equation 2–5 and **2–6**), parallel to the π molecular orbital system of the pyridoxamine. In crystallographic molecular models of the active site of porcine aromatic-L-amino-acid decarboxylase in a complex with an analogue of the substrate[36] and of glutamate decarboxylase from *E. coli* into which the pyridoxamine of L-glutamate has been inserted,[67] similar orientations of the respective carbon–carbon σ bonds leading to decarboxylation are enforced.

If the α carbon of an external pyridoxamine contains an incipient carbonyl carbon, for example, an external pyridoxamine with a β carbon to which a hydroxy group or an amino group is attached, that β carbon can **dissociate as a carbonyl group or imine**, respectively

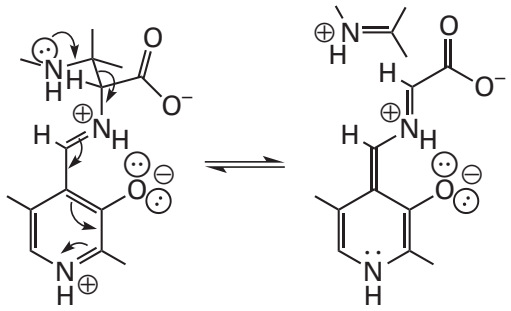

quinonoid intermediate (2–6)

An example of this outcome is the first step of the reaction catalyzed by D-threonine aldolase from *Achromobacter xylosoxidans*,[68] which proceeds with the loss of acetaldehyde from the α carbon of the external pyridoxamine between D-threonine and pyridoxal 5′-phosphate

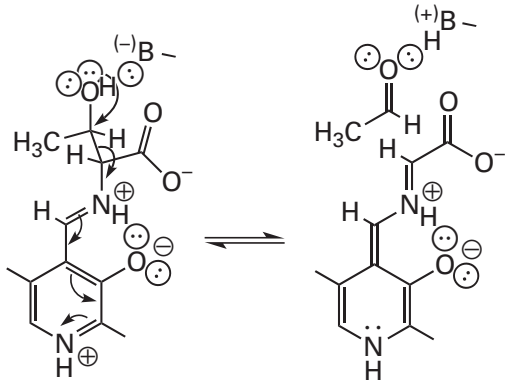

quinonoid intermediate (2–7)

In such a dissociation of a carbonyl group, a base is required to remove a hydron from the hydroxy group.[69,70]

If the α carbon of an external pyridoxamine contains an incipient acyl compound in the form of

a β-oxo group, that β carbon can **dissociate as an acyl derivative** after addition of a nucleophile to the carbon of the β-oxo group. An example of this outcome is the second step in the retro Claisen condensation catalyzed by 5-aminolevulinate synthase,[71-73] which proceeds with the loss of succinyl-SCoA from the α carbon of the external pyridoximine formed between 5-amino-4-oxo-hexanedioic acid and pyridoxal 5′-phosphate

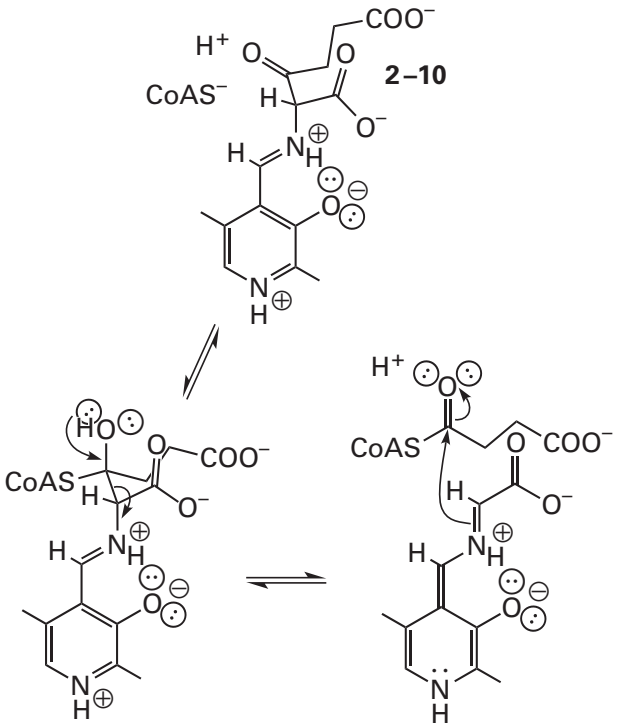

(2–8)

The σ bond that is weakened by the electron withdrawal of the adjacent pyridoximine in an external pyridoximine must be **aligned parallel to the π molecular orbital system** of that pyridoximine for the necessary overlap to occur,[74] as drawn in **2–6** and Equations 2–4 and 2–5. In an enzymatically catalyzed reaction, the necessary alignment is made as the substrate is bound in the active site. This alignment in part **decides which σ bond is broken** during the reaction. At least one of the substrates for an enzyme with an internal pyridoximine 5′-phosphate in its active site is usually one of the twenty canonical L-α-amino acids. For the external pyridoximine formed from an α-amino acid, the most critical discrimination is that between the hydron (Equation 2–4) and the carboxy group (Equation 2–5) on the α carbon. If the σ bond to the carboxylato group is aligned parallel to the π molecular orbital system of the pyridoximine, the enzyme will catalyze the decarboxylation of the amino acid; if the hydron is aligned parallel to the π molecular orbital system, it will catalyze a dehydronation at the α carbon of the amino acid.

2,2-Dialkylglycine decarboxylase (pyruvate)

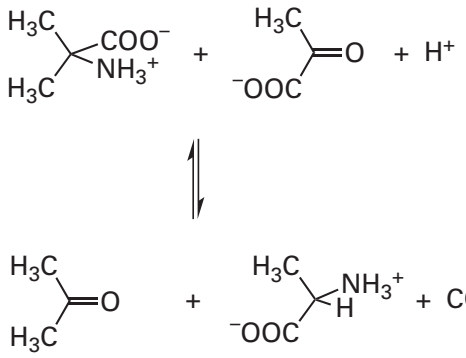

(2–9)

from *B. cepacia* normally catalyzes both a decarboxylation (of dimethylglycine in the forward direction of Equation 2–5) and a dehydronation (of L-alanine in the reverse direction of Equation 2–9). The active site is constructed so that when the σ bond to the carboxylato group of a dialkylglycine is parallel to the π molecular orbital system of its external pyridoximine, the two alkyl groups (R_1 and R_2 in **2–6**) fit comfortably into two open pockets, one that is larger and more polar and the other that is smaller and nonpolar. When the σ bond to the α hydrogen of L-alanine, the amino acid that is a reactant in the reverse direction, is parallel to the π molecular orbital system of its external pyridoximine, its carboxylato group fits into the larger, polar pocket and its methyl group fits into the smaller, nonpolar pocket.[66]

Each of a series of L-amino acids can be used as a reactant instead of the normal L-alanine in the reverse direction (Equation 2–9). As the size of the side chains on these L-amino acids is increased, the rates of their undesired decarboxylations increase as the larger side chain is shunted from the smaller pocket into the larger pocket and the σ bond to the carboxylato group is consequently positioned parallel to the π molecular orbital system rather than the hydrogen. When D-alanine is used as a reactant, because the methyl group can occupy the smaller, nonpolar pocket but its carboxylato group cannot occupy the smaller nonpolar pocket, its carboxylato group is forced to be parallel to the π molecular orbital system of the pyridoximine, and the D-alanine is decarboxylated rather than dehydronated. As the size of the side chains on a series of D-amino acids, however, is increased, the rates of their decarboxylations decrease as the

smaller pocket rejects the increasingly larger alkyl groups and the σ bond to the carboxylato group can no longer be positioned parallel to the π molecular orbital system.[75] All these results are consistent with the necessity of aligning the bond on the α carbon that is weakened by the pyridoximine parallel to the π molecular orbital system of that pyridoximine.

Glycine hydroxymethyltransferase catalyzes the formation of N^5,N^{10}-methylenetetrahydrofolate

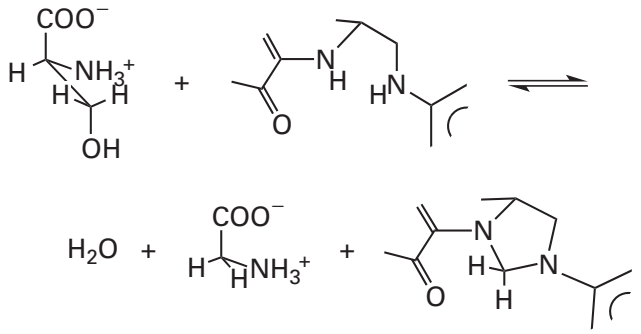

(2–10)

In the **crystallographic molecular model** of glycine hydroxymethyltransferase from *G. stearothermophilus* complexed with L-serine in the absence of tetrahydrofolate, the bond between the α carbon and the β carbon in the external pyridoximine of the L-serine is held parallel to the π molecular orbital system.[76] This orientation causes electron density to be withdrawn from this bond. This electron withdrawal makes the carbon of the hydroxymethyl group of the L-serine electrophilic. Because of this increased electrophilicity, nitrogen 5 of tetrahydrofolate (previously **1-81**)

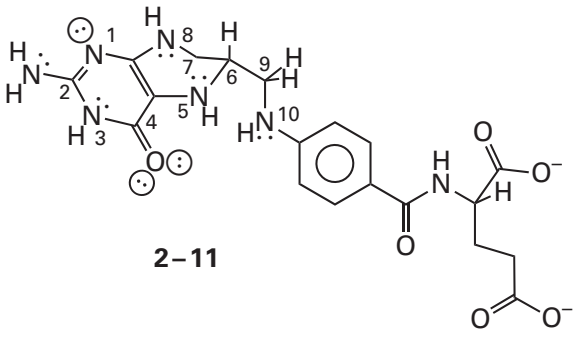

2–11

even though it is a rather nonnucleophilic anilino nitrogen, is able to react with this carbon as a nucleophile in a concerted nucleophilic substitution with *N*-(5′-phosphopyridoxyl)carboxymethanimine as a leaving group.[77]

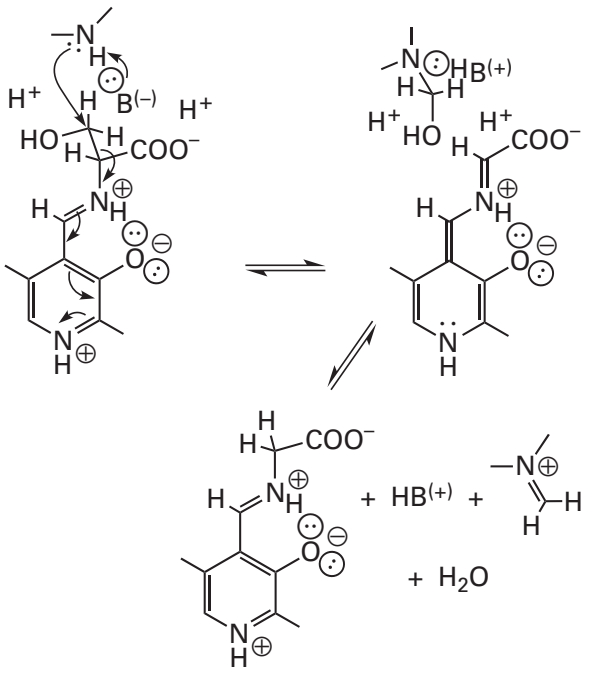

(2–11)

In free solution, pyridoxal 5′-phosphate, supplemented with metallic ions[78] such as **Cu^{2+}, Fe^{3+}, or Al^{3+}, can catalyze dissociations of electrophiles** from the carbon adjacent to an amine with which it has formed an imine. Because free rotation around the bond between the α carbon and the iminium nitrogen is unhindered in solution, all three of the substituents on the α carbon are vulnerable. If the α carbon contains a hydrogen, the usual reaction is loss of a hydron leading to transamination.[79] If, however, there is a carboxylate on the α carbon and no hydrogens, as in 2-aminoisobutyric acid or 2-methyl-L-serine, or there are two carboxylates, as in aminomalonic acid,[80] decarboxylation occurs. The addition of metallic ions to these nonenzymatic reactions suppresses decarboxylation and promotes the loss of alternate electrophiles from the α carbon, presumably because the metal ion forms a complex with the phenolic oxygen of the pyridoximine and the carboxylato group on the α carbon that prevents the σ bond between the carbon adjacent to the iminium nitrogen and the carboxy group in the pyridoximine from becoming parallel to the π molecular orbital system. The required Mn^{2+} in the active site of D-threonine aldolase (Equation 2–7), by associating with the hydroxy group of the D-threonine, orients the carbon–carbon bond between the α carbon and the β carbon that is to be cleaved parallel to the π molecular orbital system of the external pyridoximine.[68] The role of the Zn^{2+} in the active site of D-serine ammonia-lyase from *Saccharomyces cerevisiae*, however, is to associate with the

phospho group of the pyridoximine.[81] These two enzymes are unusual because only a few of the enzymes that use pyridoxal 5′-phosphate as a prosthetic group have a requirement for a divalent metallic ion, even though divalent metal ions can effectively orient the σ bonds of a pyridoximine in solution and catalyze their dissociation.

In all the reactions that have just been described in which a σ bond parallel to the π molecular orbital system of an external pyridoximine is weakened, it has been assumed that the **pyridinio nitrogen 1 of the external pyridoximine is hydronated before the σ bond on the carbon α to the imino nitrogen is broken**. When this nitrogen is hydronated, the electron density in that σ bond can be withdrawn into that electron sink (**2–6**). For this electron withdrawal to occur, however, the nitrogen must be there, and it must be hydronated.

The pyridoxal 5′-phosphate in an active site can be replaced with 1-deazapyridoxal 5′-phosphate in which **pyridyl nitrogen 1 is replaced by carbon**. When this replacement is performed on aspartate transaminase from *E. coli*, the resulting enzyme shows no detectable activity (<10^{-6} percent), and when it is performed on alanine racemase from *G. stearothermophilus*, the resulting enzyme again shows no detectable activity (<0.15%) with L-alanine as a reactant.[82] This altered alanine racemase from *G. stearothermophilus*, however, is able to catalyze the conversion of 3-chloro-L-alanine to pyruvate at a rate about 0.4% of that for the native enzyme, and cysteine synthase from *S. typhimurium* in which the same substitution has been performed is able to catalyze its reaction also at a rate about 0.4% of that for the native enzyme. The most difficult chemical steps in the latter two enzymatic reactions are eliminations, in the first case the elimination of a chloride and a hydron, and in the second case the elimination of an acetate and a hydron. In both eliminations, the hydron that dissociates is on the α carbon of the respective external pyridoximine. Both the chloride and the acetate are excellent leaving groups. It is possible that the absence of the pyridyl nitrogen causes the rate-limiting step of these eliminations to change from dissociation of the leaving group to removal of the hydron from the α carbon. If this is the case, a much larger decrease in the rate of removal of the hydron from the α carbon is masked by the change in the rate-limiting step. It is also possible that, in the absence of the pyridyl nitrogen, the mechanism of the elimination changes from one in which the hydron is removed first because of the weakening of the carbon–hydrogen bond to one in which removal of the hydron and dissociation of the leaving group are concerted.

In enzymes in which an aspartate or a glutamate forms a hydrogen bond with the pyridinio nitrogen, that nitrogen is hydronated in the resting state. In these enzymes, when the aspartate is mutated to alanine, dramatic decreases in enzymatic activity are observed.[33,83,84] In other cases, however, such as tryptophan synthase, cysteine synthase, and alanine racemase, the pyridyl nitrogen of the internal pyridoximine does not participate in a hydrogen bond with an obvious acid. In these enzymes, the possibility arises that the **pyridyl nitrogen in the external pyridoximine is not hydronated** by the active site before the dissociation of the electrophile.[82] The first step in each of these enzymatic mechanisms, however, is the removal of a hydron from the α carbon in the external pyridoximine. After it is removed, even if the pyridyl nitrogen were not initially hydronated, the majority of the net negative elementary charge in the resulting π molecular orbital system in the resulting, unhydronated quinonoid intermediate would necessarily reside on the pyridyl nitrogen because of its electronegativity. Consequently, this nitrogen would probably be basic enough to remove a hydron from the adjacent arginine (pK_a = 13) or serine (pK_a = 14) already forming a hydrogen bond to it. It follows that, in the transition state for the removal of the hydron from the α carbon, a hydron is probably being transferred from the arginine or the serine to the pyridyl nitrogen.

Each of the steps in which an electrophile dissociates from the carbon immediately adjacent to the iminium nitrogen in an external pyridoximine (Equations 2–4 through 2–8) produces a quinonoid intermediate that is electron-rich and capable of push. The normal quinonoid intermediates in such enzymatic reactions are usually unstable and rapidly converted to the next intermediate in the respective reaction.[85] The quinonoid intermediate (λ_{max} = 494 nm; ε_{494} = 13,600 M^{-1} cm^{-1}), however, that is formed after removal of the hydron from the α carbon of the external pyridoximine of the inhibitor L-*erythro*-3-hydroxyaspartate[26] or that is formed after removal of the hydron from the slow substrate L-cysteinesulfinate ($t_{½}$ = 0.3 s; λ_{max} = 520 nm)[86] by the active site of aspartate transaminase from *E. coli* and the quinonoid intermediate formed from L-*erythro*-3-hydroxyaspartate by porcine aspartate transaminase (λ_{max} = 491 nm; ε_{491} = 20,800 M^{-1} cm^{-1})[23] are stable enough that their absorbance spectra

can be recorded (Figure 2–1D). A stable quinonoid intermediate is also formed when tryptophanase from *E. coli* is mixed with its substrate L-tryptophan ($k_{form} = 500\ s^{-1}$; $\lambda_{max} = 505$ nm).[87] When tyrosine phenol-lyase from *Citrobacter freundii* is mixed with 3-fluoro-L-tyrosine, an analogue of its substrate, a stable quinonoid intermediate is formed ($k_{form} = 100\ s^{-1}$; $\lambda_{max} = 502$ nm),[87] and when the enzyme is mixed with L-alanine, a stable quinonoid intermediate forms that can be crystallized.[88] When glycine hydroxymethyltransferase from *G. stearothermophilus* is mixed with glycine and tetrahydrofolate, a stable quinonoid intermediate ($\lambda_{max} = 495$ nm), produced by removal of the hydron from the external pyridoximine of the glycine (reverse of Equation 2–11), can be observed.[89] In the reaction catalyzed by kynureninase, the natural quinonoid intermediate, although of short lifetime ($t_{½} = 0.9$ s; $\lambda_{max} = 494$ nm) has been observed directly.[85]

A quinonoid intermediate is the **leaving group** in its dissociation from the respective electrophile, and as a result, it is an electron-rich species. The net effect of the dissociation of an electrophile from the respective α carbon to form one of these quinonoid intermediates is the **expansion of the π molecular orbital system** of the pyridoximine by one carbon and by the pair of electrons that was in the σ bond. This addition of two electrons to a π molecular orbital system that expands by only one carbon converts it from one that was electron-poor to one that is electron-rich. This excess electron density neutralizes the positive formal elementary charge on the hydronated pyridinio nitrogen (Equations 2–4 through 2–8).

An example of the result of these changes is the quinonoid intermediate that is the product in Equations 2–6 and 2–7. The **π molecular orbital system of this quinonoid intermediate** can be represented as

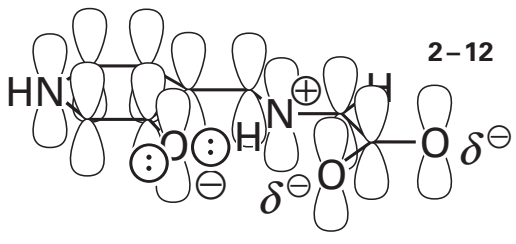

Because it includes the carboxylato group, there are 13 *p* orbitals that combine to produce a π molecular orbital system with 13 π molecular orbitals, and the seven molecular orbitals of lowest energy are each occupied by a pair of electrons. The atoms in the entire π molecular orbital system in quinonoid intermediate **2–12** are coplanar. In the **crystallographic molecular model** of the stable quinonoid intermediate that forms when tyrosine phenol-lyase from *C. freundii* is mixed with L-alanine, which is a quinonoid intermediate that includes a carboxylato group, this complete planarity is unmistakable.[88] In crystallographic molecular models of the external pyridoximine and the quinonoid intermediate in the active site of tryptophan synthase from *S. enterica*, it can be seen that the carboxy group rotates into the plane of the quinonoid intermediate when it is formed from the external pyridoximine.[90] In quinonoid intermediates that lack a carboxylato group (Equations 2–4 and 2–5), only 10 *p* orbitals are combined, and the π molecular orbital system has 10 π molecular orbitals, and the six of lowest energy are each occupied by a pair of electrons. The occupation of the nonbonding molecular orbital with a pair of electrons in the former case (**2–12**) and of an antibonding molecular orbital in the latter case represents the electron excess in a quinonoid intermediate.

The simplest reaction involving a quinonoid intermediate is **racemization**. If a hydron is added back to the opposite side of the α carbon from which a hydron was removed by one base to form the quinonoid intermediate by another acid in the active site,[70] the stereochemistry at that α carbon is inverted. An example of such a racemization would be the reaction catalyzed by alanine racemase from *G. stearothermophilus*,[37] which equilibrates D-alanine and L-alanine.

Because of the excess electron density in the π molecular orbital system, **a quinonoid intermediate is basic and nucleophilic.** Its basicity is manifest in its ability to be hydronated at the carbon α to its iminio nitrogen, as it is in a racemase. Its nucleophilicity is manifest in its ability to add to a carbonyl carbon, as in the addition of the α-carboxyquinonoid intermediate to acetaldehyde in the reverse reaction of Equation 2–7. A dramatic example of the nucleophilicity of the α carbon in a quinonoid intermediate is its ability to displace methyl adenosyl sulfide in the concerted nucleophilic substitution that is the central step of the reaction catalyzed by 1-aminocyclopropane-1-carboxylate synthase[91,92]

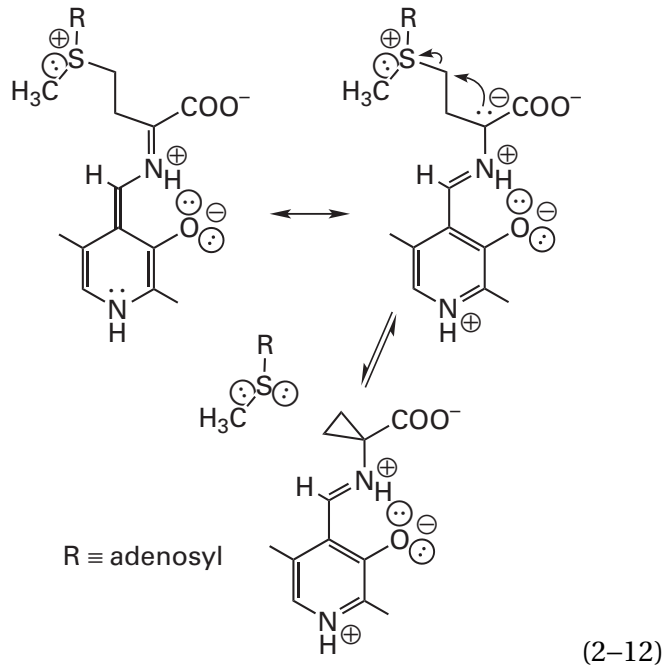

(2–12)

Although the carbon that adds to the carbonyl carbon, the acyl carbon, or the saturated electrophilic carbon in these three reactions appears at first glance to be an imino carbon because of the adjacent imino nitrogen, it is nucleophilic rather than electrophilic because of the electron excess in the complete π molecular orbital system. In all these instances, as illustrated in the resonance structure of Equation 2–12, dehydronation of the pyridinio nitrogen in concert with each nucleophilic addition enhances the nucleophilicity of the quinonoid intermediate and increases the rate of the nucleophilic addition. The active sites in which a weak acid, such as a serine or an arginine, forms the hydrogen bond with pyridyl nitrogen 1 would benefit from the dehydronation that the conjugate bases of these weak acids would necessarily accomplish.

The reverse reaction of Equation 2–8 is the metabolically relevant direction for the Claisen condensation catalyzed by 5-aminolevulinate synthase since the reaction is relied upon to produce 5-aminolevulinate, the precursor in heme biosynthesis. The quinonoid intermediate formed by the removal of a hydron from the α carbon of glycine (reverse of Equation 2–11) adds as a nucleophile to the acyl carbon of succinyl-SCoA in the Claisen condensation to produce the external pyridoximine of 2-amino-3-oxohexanedioic acid (**2–10**). The methyl ester at carbon 6 of 2-amino-3-oxohexanedioic acid has been isolated from a mixture of murine 5-aminolevulinate synthase, the methyl ester of glycine, and succinyl-SCoA. It was identified by gas–liquid chromatography followed by mass spectrometry.[73] These results suggest that the decarboxylation of the α carbon of **2–10** required to produce the final product, 5-aminolevulinic acid, which is 5-amino-4-oxopentanoic acid, occurs after the Claisen condensation (as shown in Equation 2–8) rather than before because the methyl ester cannot and was not decarboxylated during the formation of methyl ester of 2-amino-3-oxohexanedioic acid. This conclusion would make chemical sense because the carboxylato group dissociating as CO_2 would be both on the α carbon of an external pyridoxime and on a carbon that is adjacent to a carbonyl group, both of which would destabilize the σ bond to the carboxylato group.

There is a related (30% identity; 1.3 gap percent) enzyme, 8-amino-7-oxononanoate synthase, that performs a homologous Claisen condensation between L-alanine instead of glycine and 6-carboxyhexanoyl-SCoA instead of succinyl-SCoA to produce 8-amino-7-oxononanoic acid.[93,94] The production of this product also requires both the removal of a hydron and a decarboxylation at the α carbon of successive external pyridoximines. Both murine 5-aminolevulinate synthase[71,95] and 8-amino-7-oxononanoate synthase from *Lysinibacillus sphaericus* [96] exchange one of the hydrogens on glycine and L-alanine, respectively, for a different isotope of hydrogen in the absence of either of the second reactants for the respective enzyme, but these exchanges are significantly slower (250,000 times and 10 times, respectively) than the turnovers for the complete enzymatic reactions when the respective second reactant is present. Nevertheless, these exchanges are consistent with the removal of a hydron from the α carbon in the initial external pyridoximine, rather than the dissociation of carbon dioxide, before the actual Claisen condensation in the mechanisms of each of these enzymes.[97] Also consistent with this conclusion is that when 5-aminolevulinate synthase from *Rhodobacter sphaeroides* is mixed with only glycine, a quinonoid intermediate forms but no CO_2 is produced during the formation of this quinonoid intermediate.[98]

Because it is electron-rich, it cannot absorb the two electrons in another σ bond, but **a quinonoid intermediate can push**. In this role the quinonoid intermediate is acting as a vinylogous enamine

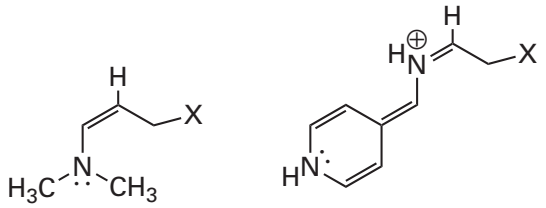

enamine **2–13** vinylogous enamine **2–14**

An enamine is electron-rich and can push out a leaving group (X in **2–13**). When the π molecular orbital system of the quinonoid intermediate is used to provide push, an elimination occurs.[99]

Examples of such an **elimination from a quinonoid intermediate** are encountered in one of the steps in the reaction catalyzed by L-cystine β-lyase from *Synechocystis*[100]

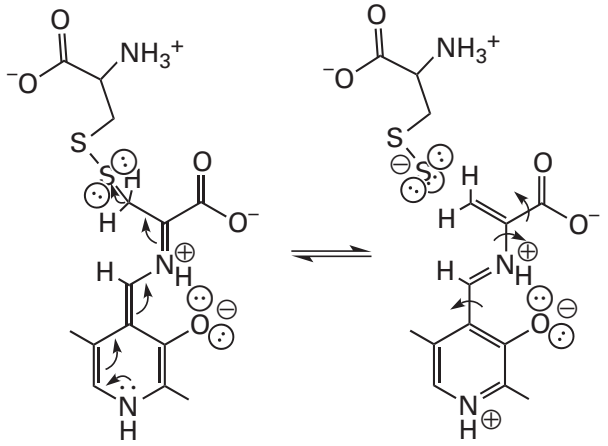

pyridoximine of 2-aminoacrylate

(2–13)

and one of the steps in the reaction catalyzed by tryptophanase[101]

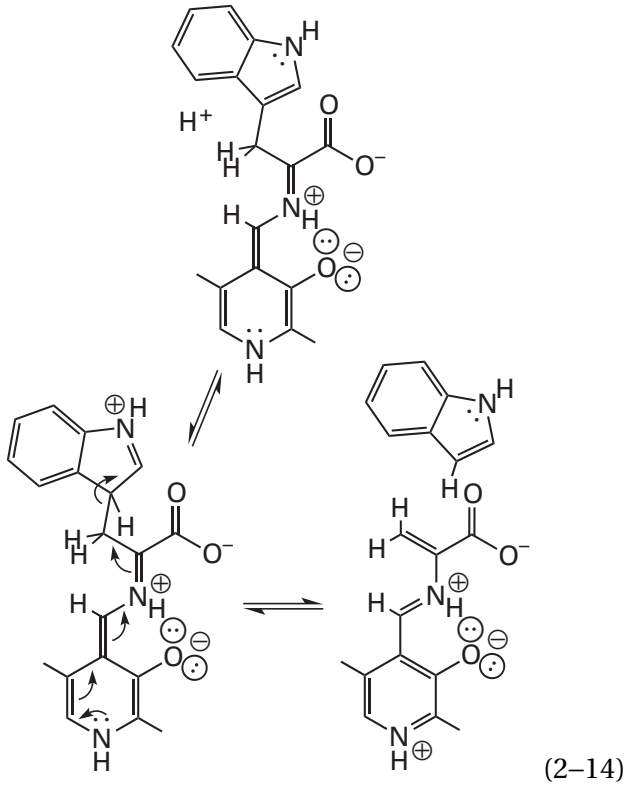

(2–14)

In the latter instance, the indolyl group, when it has been hydronated on carbon 3, is an excellent leaving group because the two electrons in the σ bond connecting it to the quinonoid intermediate can enter its π molecular orbital system and complete an aromatic dectet. The bond is pushed away by the electron excess in the quinonoid intermediate and pulled into the indolyl group[102]

2–15

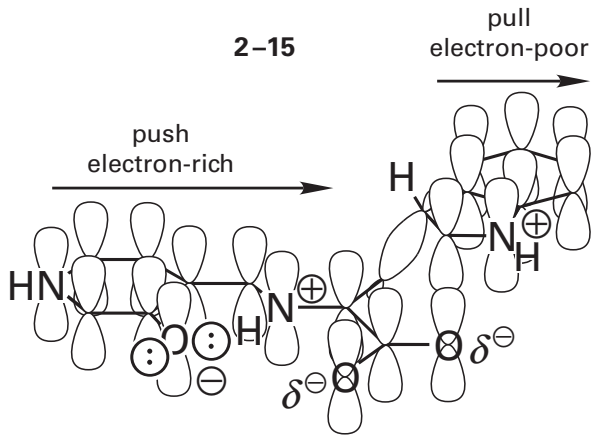

The most difficult step in this electrophilic aromatic substitution is the hydronation of the indolyl group, which might be assisted by the quinonoid intermediate if the hydronation and the dissociation are concerted. The related (41% identity; 0.7 gap percent) enzyme, tyrosine phenol-lyase, catalyzes the homologous reaction in which L-tyrosine is

cleaved into phenol and the enamine of pyruvate rather than indole and the enamine of pyruvate. In the crystallographic molecular model[103] of the active site of a mutant of tyrosine phenol-lyase from *C. freundii*, occupied by 3-fluoro-L-tyrosine, the hydroxy group of Tyrosine 71 in the enzyme is only 0.31 nm from carbon 1 of the analogue, which is the carbon that would be hydronated during the electrophilic aromatic substitution (see first step in Equation 2–14), an observation consistent with it being the catalytic acid.

In the elimination from the quinonoid intermediate catalyzed by L-serine ammonia-lyase, the leaving group is the hydroxy group of the quinonoid intermediate formed from L-serine. In the active site of the enzyme, the phospho group of the pyridoxal 5′-phosphate forms a hydrogen bond with the hydroxy group and is thought to hydronate the hydroxy group as it leaves.[104]

The product resulting from an elimination of a leaving group from the β carbon of a quinonoid intermediate is the external pyridoximine of a 2-aminoacrylate (Equations 2–13 and 2–14). In the active sites of cysteine synthase from *S. typhimurium*[105] and cysteine lyase from *Fusobacterium nucleatum*,[106] the pyridoximine of 2-aminoacrylate (λ_{max} = 330 and 470 nm and λ_{max} = 320 and 460 nm, respectively) forms rapidly when the enzyme is mixed with *O*-acetyl-L-serine.[106] *O*-Acetyl-L-serine is itself not nucleophilic and does not generate a nucleophilic product that can add to the electrophilic carbon–carbon bond in the 2-aminoacrylate. The intermediate external pyridoximine of 2-aminoacrylate has been observed in a crystallographic molecular model[107] of the active site of cystathionine β-synthase (*O*-acetyl-L-serine) from *S. cerevisiae*.

External pyridoximines of 2-aminoacrylate have also been stabilized and observed in active sites in the **crystallographic molecular models** of tryptophan synthase from *S. typhimurium*,[108,109] cysteine synthase from *Mycobacterium tuberculosis*,[110] and alliin lyase from *Allium sativum*.[110] In none of these three molecular models is the pyridoximine of 2-aminoacrylate planar throughout its complete π molecular orbital system. In the active site of tryptophan synthase, the carboxylate of the 2-aminoacrylate is rotated out of the plane defined by the truncated π molecular orbital system; in the active site of cysteine synthase, the completely planar 2-aminoacrylate is tilted out of the plane of the pyridoximine by a rotation about the bond between nitrogen 4′ and the α carbon of the acrylate; and in the active site of alliin synthase, the 2-aminoacrylate is tilted out of the plane of the pyridoximine by a rotation about the bond between carbon 4 and carbon 4′ of the pyridoximine. These three σ bonds are single σ bonds in the only resonance structure of the pyridoximine of 2-amino-acrylate (rotational arrows in Equation 2–13) that do not involve separation of charge and should be the weakest links in the π molecular orbital system. In butadiene, the out-of-plane conformers are at most only about 25 kJ higher in energy than the s-trans conformer.

The 2-aminoacrylate in the pyridoximine can be **released directly** by transimination with the lysine of the internal pyridoximine

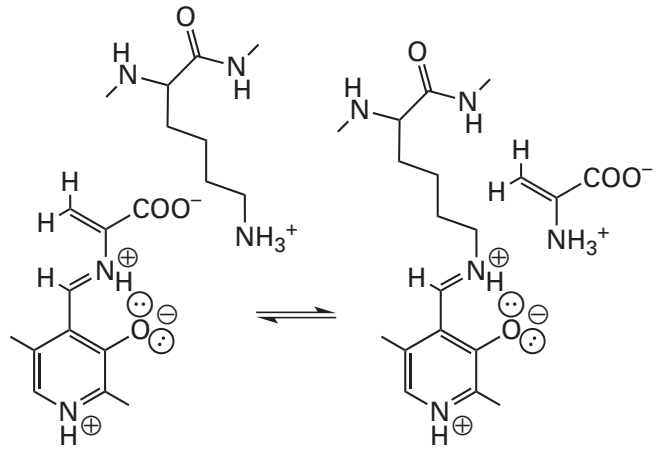

(2–15)

as occurs in the reactions catalyzed by tryptophanase and L-cystine β-lyase. The 2-aminoacrylate released by the transimination tautomerizes to iminopyruvate, perhaps while still within the active site,[111] and the iminopyruvate released into solution rapidly hydrolyzes to pyruvate and ammonia

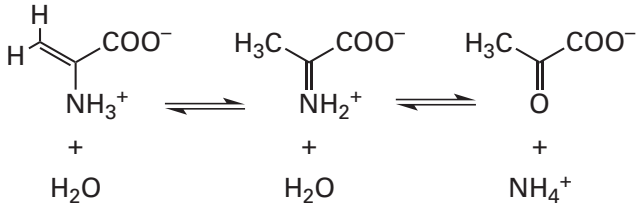

(2–16)

Another nucleophile can add, however, to the external pyridoximine of a 2-aminoacrylate at its β carbon, in the reverse of the reaction that has pushed away the leaving group. If this occurs, then the reaction can proceed in reverse until the amine is liberated from the pyridoxal 5′-phosphate with the

nucleophile that added to the β carbon simply substituting for the leaving group that left it, as in the reactions catalyzed by cysteine synthase, in which a sulfanide has replaced an acetate

O-acetyl-L-serine + HS^- $\rightleftharpoons$ acetate + L-cysteine (2–17)

O-phosphoserine sulfhydrylase,[112] in which a sulfanide has replaced a phosphate

O-phospho-L-serine + hydrogen sulfide $\rightleftharpoons$ $HOPO_3^{2-}$ + L-cysteine (2–18)

or L-seryl-tRNA^{Sec} selenium transferase,[113] in which a selenide has replaced a hydroxide

L-seryl-tRNA^{Sec} + selenophosphate $\rightleftharpoons$ $HOPO_3^{2-}$ + L-selenocysteinyl-tRNA^{Sec} (2–19)

In the case of cysteine synthase (Equation 2–17) from *S. typhimurium*[114] and cysteine lyase from *F. nucleatum*,[106], the external pyridoximine of 2-aminoacrylate in the active site of the enzyme that has been formed from *O*-acetyl-L-serine, when deprived of access the usual nucleophilic cosubstrate, will react with a number of other nucleophiles to produce the respective amino acids in which the respective nucleophile replaces the acetyl group. In the reactions catalyzed by the active site of tryptophan synthase (indole-salvaging) within tryptophan synthase

L-tryptophan + H_2O $\rightleftharpoons$ indole + L-serine (2–20)

the external pyridoximine of 2-aminoacrylate produced from L-tryptophan by the elimination of indole (Equation 2–14 and **2–15**),[102] reacts with water to produce eventually L-serine rather than breaking down to pyruvate and ammonia, as occurs in the reaction catalyzed by tryptophanase (Equation 2–14).

The most remarkable aspect of the reactions catalyzed by cysteine synthase and *O*-phosphoserine sulfhydrylase is that each of these nucleophilic substitutions involves the replacement of a good leaving group, a carboxylate or a phosphate, respectively, by a strong nucleophile, the sulfanide. Rather than proceed through the simplest possible chemical mechanism, a concerted nucleophilic substitution, these enzymes use pyridoxal 5′-phosphate to rearrange hydrons and replace the carboxylate with a distant elimination involving two steps in each direction from the external pyridoximine. This solution seems at a glance not to be an intelligent design.

In many of the enzymatic reactions in which a quinonoid intermediate is formed from a prosthetic pyridoxal 5′-phosphate, rather than exploiting its electron density to push a leaving group from the β carbon, the next step is to exploit its basicity by adding a hydron to carbon 4′ to form the *N*-(5′-phosphopyridoxyl)imine, as occurs in the reaction catalyzed by 4-aminobutyrate—2-oxoglutarate transaminase (Equation 2–4)

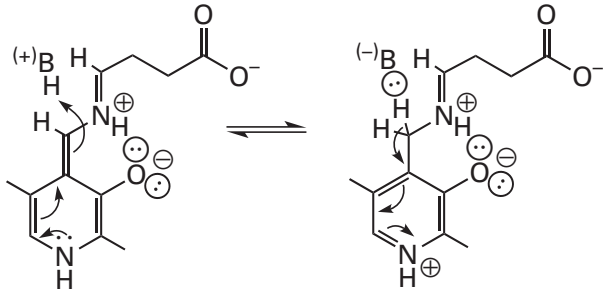

N-(5′-phosphopyridoxyl)imine (2–21)

Carbon 4′ is one of the alternating basic positions in the vinylogous enamine (**2–14**). In the reaction catalyzed by 4-aminobutyrate—2-oxoglutarate transaminase, the removal of a hydron from the α carbon of the external pyridoximine (Equation 2–4) and the addition of a hydron to carbon 4′ of the resulting quinonoid intermediate (Equation 2–21) produce the *N*-(5′-phosphopyridoxyl)-imine, *N*-(5′-phosphopyridoxyl)-3-carboxypropanimine.

The imine in an *N*-(5′-phosphopyridoxyl)imine is disconnected from the remaining **π molecular orbital system** of the pyridyl group by the saturated position at carbon 4′.[85] Two of the 12 π electrons in the π molecular orbital system of the quinonoid intermediate become the two electrons in the new σ bond to the hydron that has associated. The remaining *p* orbitals and π electrons are divided into two unequal sets by the hydronation. Eight of the π electrons remain in the seven π molecular orbitals formed from the seven *p* orbitals of the 3-hydroxy-

pyridyl group. Two π electrons remain in the double bond of the imine (Equation 2–21).

The *N*-(5′-phosphopyridoxyl)imines formed from L-aspartate and L-glutamate, *N*-(5′-phosphopyridoxyl)-1,2-dicarboxyethanimine and *N*-(5′-phosphopyridoxyl)-1,3-dicarboxypropanimine, respectively, have been crystallized in the active site of aspartate transaminase from *Gallus gallus*.[115] In the **two crystallographic molecular models**, the carbon–hydrogen σ bond that would be broken during removal of the hydron from carbon 4′ of the 5′-phosphopyridoxyl group to re-form the quinonoid intermediate (reverse of Equation 2–21) is parallel to the pyridyl ring. This orientation places this σ bond in hyperconjugation with the π molecular orbital system of the hydronated pyridinio ring so that the π molecular orbital system of the pyridinio ring can withdraw electron density from the bond and promote removal of the hydron from carbon.

The two steps that produce any *N*-(5′-phosphopyridoxyl)imine, removal of a hydron from the α carbon and addition of the hydron to carbon 4′, are the two steps in the **tautomerization of an iminium** (the sum of Equations 2–4 and 2–21)

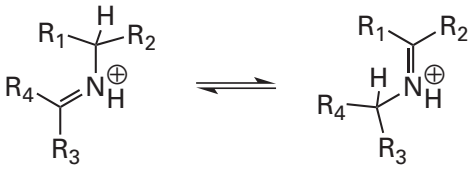

(2–22)

In nonenzymatic situations, simple tautomerizations of this type are catalyzed by bases,[116] which remove the hydron from carbon during the slower of the two steps of the reaction.[117] A weak acid and a weak base together can catalyze the tautomerization of a pyridoxamine, presumably by catalyzing the removal of the hydron from the one carbon and the addition of the hydron to the other carbon.[15] An analogue of pyridoxal 5′-phosphate in which an imidazolyl group has been appropriately incorporated as an intramolecular catalyst can undergo this tautomerization

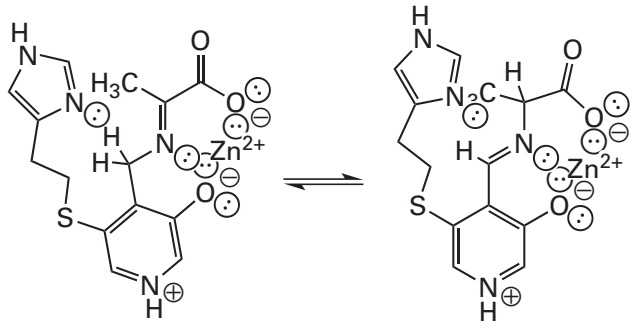

(2–23)

80 times more rapidly than another analogue identical to the first with the exception that the imidazolyl group has been replaced by a methyl group.[118] In this case Zn^{2+} was used as a Lewis acid to maintain the proper orientations within the molecule and promote the reaction. Even with the assistance of the pyridoxal 5′-phosphate in an active site of an enzyme in weakening these σ bonds between carbon and hydrogen, the removal of a hydron from the one carbon and the addition of a hydron to the other carbon are slower reactions than the carbonyl additions necessary to form the pyridoxamine in the first place.

In many cases, the **lysine that formed the internal pyridoxamine** and that is then responsible for removing the hydron from the α carbon (see Equation 2–4) can be positioned by the enzyme so that it is adjacent to both the α carbon and carbon 4′ of the external pyridoxamine (Figure 2–4).[53,60,61,119] In this orientation, the 6-amino group of this lysine can both remove a hydron from the α carbon and then add a hydron to carbon 4′ of the quinonoid intermediate. This arrangement is found in the active site of aspartate transaminase from *E. coli*. The respective *N*-(5′-phosphopyridoxyl)imine that normally participates in the enzymatic reaction, either *N*-(5′-phosphopyridoxyl)-1,2-dicarboxyethanimine or *N*-(5′-phosphopyridoxyl)-1,3-dicarboxypropanimine, can be formed directly from oxaloacetate or 2-oxoglutarate, respectively, and pyridoxamine 5′-phosphate in the active site of the enzyme. When the lysine that forms the internal pyridoxamine in aspartate transaminase from *E. coli* is mutated to alanine, the conversion of the respective *N*-(5′-phosphopyridoxyl)imine into L-aspartate or L-glutamate, which requires the tautomerization to occur, is 10^5 or 10^6 times slower, respectively, in the mutant than in the unmutated enzyme,[120] In the mutant enzyme, presumably, there is no other base present

that is even remotely as effective at removing the hydron from carbon 4′ of the respective *N*-(5′-phosphopyridoxyl)imine and then adding a hydron to the resulting quinonoid intermediate.

An *N*-(5′-phosphopyridoxyl)imine within an active site can be readily hydrolyzed to the corresponding aldehyde or ketone and pyridoxamine 5′-phosphate

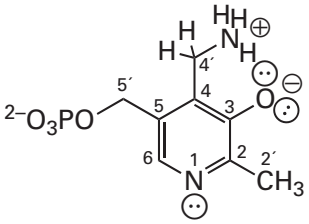

2–16

The upshot of the sequence of events ending in such a hydrolysis is that an **oxo group has replaced the original primary amino group** in the initial reactant. For example, in the reaction catalyzed by 4-aminobutyrate—2-oxoglutarate transaminase (Equations 2–4 and 2–21), when the *N*-(5′-phosphopyridoxyl)-3-carboxypropanimine is hydrolyzed, the products are 4-oxobutanoic acid (succinate semialdehyde), which is one of the products of the overall reaction, and pyridoxamine 5′-phosphate.

In contradistinction to pyridoxal 5′-phosphate, which is covalently attached to an active site as the internal pyridoximine, pyridoxamine 5′-phosphate is a noncovalent prosthetic group that is held in the active site of an enzyme only by strong noncovalent forces. When pyridoxal 5′-phosphate associates with an active site, the dissociation constant for that pyridoxal 5′-phosphate from the enzyme includes the equilibrium constant for the nucleophilic addition that covalently attaches it to the enzyme (Equation 2–3). The dissociation constant for pyridoxal 5′-phosphate from the active site of aspartate transaminase from *E. coli*[83] is 0.4 pM. This dissociation constant is much smaller than the dissociation constant for pyridoxamine 5′-phosphate (1.3 nM) because, even though the rest of the pyridoxamine 5′-phosphate is identical to pyridoxal 5′-phosphate, it does not participate in the covalent attachment. The absorption spectrum of pyridoxamine 5′-phosphate when it is associated with the active site of aspartate transaminase from *E. coli* (Figure 2–1E) has a maximum of absorbance at 323 nm. The short wavelength results from the absence of extended conjugation.

The hydrolysis of an *N*-(5′-phosphopyridoxyl)-imine to form the carbonyl group and the pyridoxamine 5′-phosphate cannot proceed unless there is an acid to provide a hydron that can be added to the iminium nitrogen to make it a competent leaving group, and another hydron is required if the pyridoxamine 5′-phosphate is to end up as zwitterion **2–16**. In the active site of aspartate transaminase from *E. coli*, there is a tyrosine that forms a hydrogen bond (0.28 nm) to the phenolic oxyanion of the *N*-(5′-phosphopyridoxyl)-1,2-di-carboxyethanimine formed from L-aspartate,[115] and the lysine that participated in the internal pyridoximine is near enough (0.39 nm) to reorient and form a hydrogen bond with the tyrosine. The hydron on the lysinium can be shuttled to the imino nitrogen of the *N*-(5′-phosphopyridoxyl)imine during its hydrolysis to provide the mandatory hydron

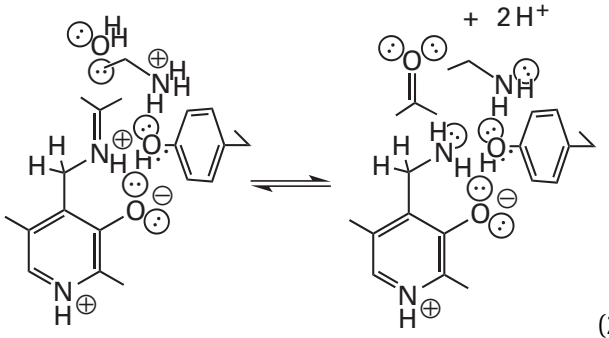

(2–24)

When the tyrosine is mutated to a phenylalanine, the rate of enzymatic activity decreases by a factor of 500 and *N*-(5′-phosphopyridoxyl)-1,2-dicarboxyethanimine accumulates (70%) in the active site, a fact indicating that the hydrolysis of the *N*-(5′-phosphopyridoxyl)imine has been decreased so dramatically by the mutation that it is now the rate-limiting step in the enzymatic reaction.[24,25] The side chain of the lysine is probably flexible enough to pick up another hydron during the hydrolysis to provide the hydron needed to produce the zwitterion of the pyridoxamine 5′-phosphate.

Amino acid decarboxylases are enzymes that catalyze the dissociation of the carboxylato group as CO_2 (Equation 2–5) from an α-amino acid rather than removing the hydron. In the normal reaction of a decarboxylase, the carboxy group dissociates and is replaced by a hydron; for example, in the reaction catalyzed by methionine decarboxylase[121]

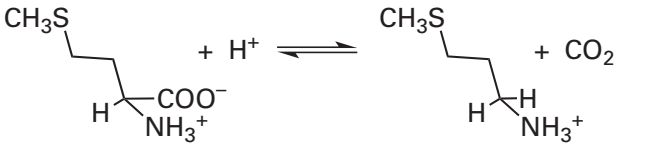

(2–25)

Again, it is usually assumed that the 6-ammonio group of the lysine of the internal pyridoximine, which is liberated upon formation of the external pyridoximine (Figure 2–2), hydronates the quinonoid intermediate (Equation 2–5) at the α carbon following dissociation of the CO_2.[122] The active site in a decarboxylase must be constructed, however, so that the ammonio group of this lysine that is responsible for hydronating the α carbon, or any other acid, cannot hydronate carbon 4′ of the quinonoid intermediate that results from the decarboxylation (Equation 2–21) to produce the *N*-(5′-phosphopyridoxyl)imine, which can then hydrolyze. Methionine decarboxylase from *Dryopteris filixmas* fails to prevent the hydronation of carbon 4′ completely; and during its normal reaction (Equation 2–25), pyridoxamine 5′-phosphate and 3-(methylsulfanyl)propanal are slowly formed as side products in a reaction that inactivates the enzyme.[122]

The formation of an *N*-(5′-phosphopyridoxyl) imine and its hydrolysis are, however, **essential steps in a transamination**. The overall reaction in a transamination is the conversion of an amino group into a oxo group at one carbon and the conversion of an oxo group into an amino group at another carbon resulting in the transfer of ammonia or an amine between the two carbons. In the first sequence of steps in a transamination, the amine of the reactant is converted into a ketone or aldehyde coincident with the conversion of the imino group of the initial internal pyridoximine into the amino group in pyridoxamine 5′-phosphate. In the second sequence of steps in a transamination, which is the reverse of the first sequence of steps, a different ketone or aldehyde that is the other reactant in the enzymatic reaction is converted into the respective amine, coincident with conversion of the pyridoxamine 5′-phosphate into the internal pyridoximine 5′-phosphate, so that the active site can start again.

An **example of a transamination** is that catalyzed by 4-aminobutyrate—2-oxoglutarate transaminase

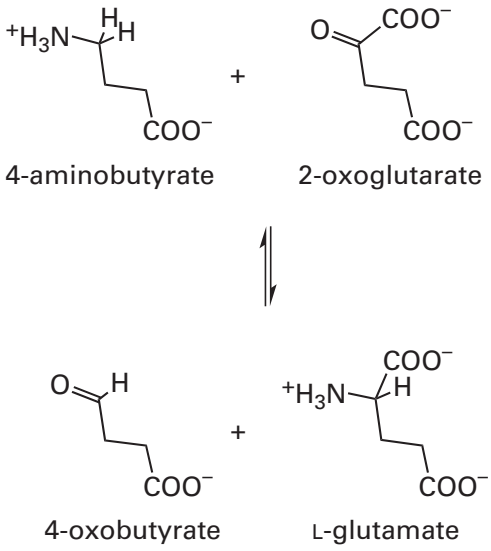

4-aminobutyrate 2-oxoglutarate

4-oxobutyrate L-glutamate

(2–26)

In the forward direction, the external pyridoximine of 4-aminobutyrate is formed from the internal pyridoximine (Figure 2–2), the α hydron is removed (Equation 2–4), carbon 4′ of the quinonoid intermediate is hydronated (Equation 2–21), the resulting *N*-(5′-phosphopyridoxyl)-3-carboxypropanimine is hydrolyzed to produce 4-oxobutyrate and pyridoxamine 5′-phosphate (reverse of Figure 1–7), the 2-oxoglutarate replaces the 4-oxobutyrate, and the reaction proceeds in reverse.

The conversion of 4-aminobutyrate to 4-oxobutyrate in the first half of the overall reaction is an oxidation, the conversion of a carbon from the oxidation state of an alcohol to the carbonyl oxidation state

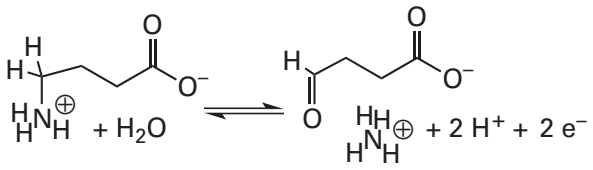

(2–27)

The oxidant in the reaction is the pyridoximine 5′-phosphate

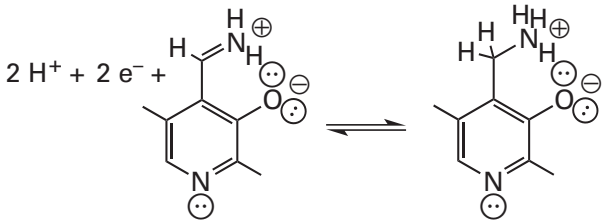

(2–28)

This latter half-reaction demonstrates that a pyridoximine of pyridoxal 5′-phosphate and pyridoxamine 5′-phosphate are at different oxidation states. In the second half of the overall reaction, 2-oxoglutarate oxidizes the pyridoxamine 5′-phosphate back to a pyridoximine of pyridoxal 5′-phosphate while being reduced to a primary amine.

In the complex between the active site of aspartate transaminase

L-aspartate + 2-oxoglutarate
$\rightleftharpoons$ oxaloacetate + L-glutamate

(2–29)

from *G. gallus* and the inhibitor L-*erythro*-3-hydroxyaspartate, the **hemiaminal that is the transient intermediate** (Figure 1–7) in the hydrolysis of the *N*-(5′-phosphopyridoxyl)-1,2-dicarboxy-2-hydroxyethanimine is stabilized by the adjacent, unnatural hydroxy group and can be directly observed.[123]

Transaminations are also catalyzed nonenzymatically by pyridoxal 5′-phosphate in the presence of metallic ions. For example, 2-oxoglutarate and L-alanine are transformed into L-glutamate and pyruvate by pyridoxal 5′-phosphate in solution in the presence of $CuSO_4$.[124]

Just as electron density is withdrawn from any one of the σ bonds on the α carbon of an external pyridoximine (2–6), the iminium in an *N*-(5′-phosphopyridoxyl)iminium withdraws electron density from any one of the σ bonds on the β carbon of the substrate and promotes the dissociation of an electrophile from that β carbon. This electron withdrawal is a property of any iminium (previously Equation 1–113)

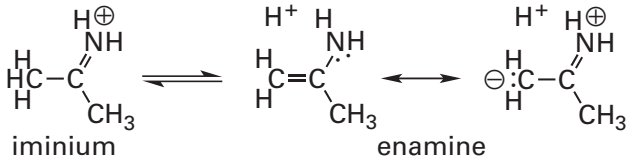

(2–30)

If there is a **hydrogen on the β carbon**, it can be removed as a hydron. For example, cystathionine γ-synthase

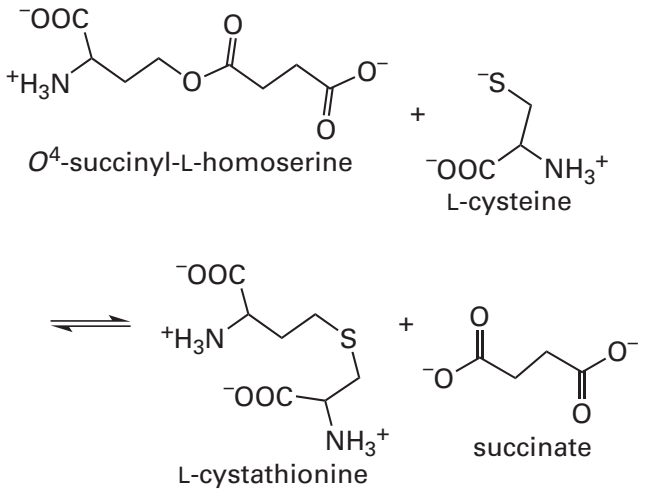

(2–31)

catalyzes a nucleophilic substitution in which the sulfido group of L-cysteine is the nucleophile and succinate is the leaving group. In one of the steps catalyzed by the enzyme, the hydrogen on the β carbon of O^4-succinyl-L-homoserine is removed as a hydron[125] from the *N*-(5′-phosphopyridoxyl)-1-carboxy-3-hydroxy-3-*O*-succinylpropaniminium ion

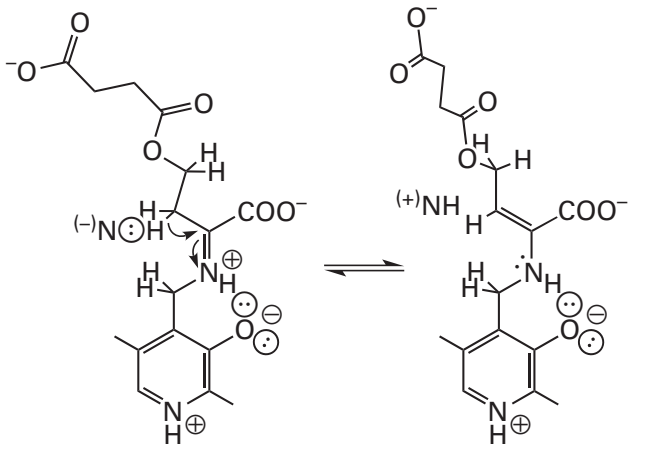

(2–32)

This removal is a simple manifestation of the acidity of a hydron on the carbon adjacent to an iminium (Equation 2–30). The 6-amino group of the lysine that formed the internal pyridoximine, and that is thought to be the base that just removed the hydron from the α carbon of the external pyridoximine and the acid that then hydronated carbon 4′ of the quinonoid intermediate to form the *N*-(5′-phosphopyridoxyl)imine, can also swing up next to the β carbon of that *N*-(5′-phosphopyridoxyl)imine,[60] and its amino group is the prime

candidate for the base that removes the hydron from it in the normal reaction.

If there is a **oxo group on the γ carbon**, the hydrate of that carbonyl group can dissociate from the β carbon as the carboxylic acid in a retro-Claisen condensation, as in the reaction catalyzed by kynureninase[126]

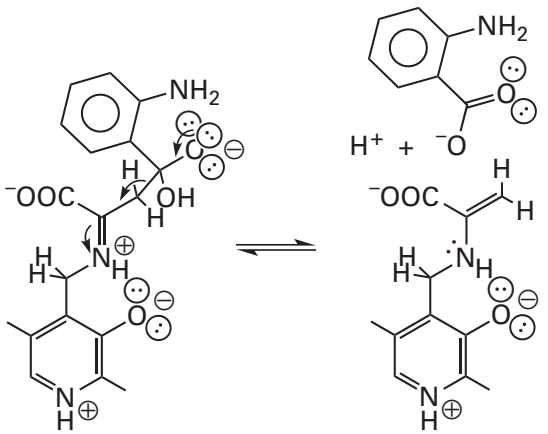

N-(5′-phosphopyridoxyl)enamine
(2–33)

If there is a **hydroxy group on the γ carbon**, it can dissociate from the β carbon in a retroaldol reaction as the respective carbonyl carbon.

When an electrophile dissociates from the β carbon of an *N*-(5′-phosphopyridoxyl)iminium as a result of electron withdrawal by the adjacent iminium (Equation 2–33), an *N*-(5′-phosphopyridoxyl)enamine is formed. As is the case with all enamines (Equation 2–30), an *N*-(5′-phosphopyridoxyl)enamine is electron-rich, basic, and nucleophilic. If the electrophile that dissociated was other than a hydron, the enamine **can be hydronated** on the β carbon, and the reaction can proceed backward until the product, in which the electrophile that dissociated has been replaced by a hydron, is released. This reaction in one direction followed by the reaction in reverse is what happens in the reaction catalyzed by kynureninase (Equation 2–33), in which the products are anthranilate and L-alanine, the amino acid ultimately resulting from hydronation of the β carbon of the *N*-(5′-phosphopyridoxyl)-1-carboxyethenamine. The hydronation of the β carbon converts it to a methyl group.

In the next step of the reaction catalyzed by cystathionine γ-synthase (Equations 2–31 and 2–32), however, the electron excess in the *N*-(5′-phosphopyridoxyl)enamine is used to **push out a leaving group** to extend the reach of the pyridoxal 5′-phosphate to the γ carbon of the amine that was the original reactant

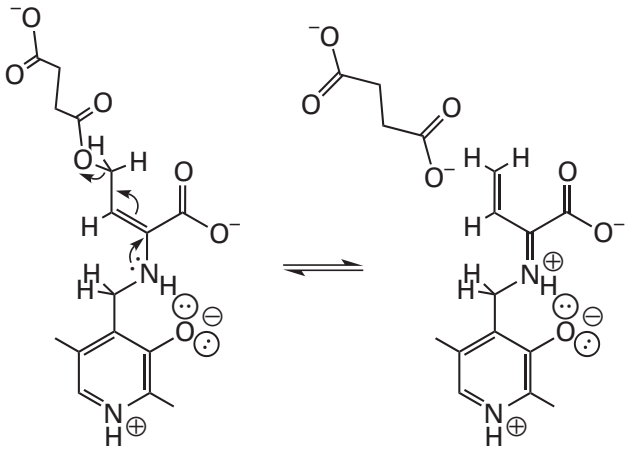

N-(5′-phosphopyridoxyl)-
1-carboxyprop-2-en-1-imine
(2–34)

The intermediate in this elimination is an ***N*-(5′-phosphopyridoxyl)-2-propen-1-imine**, in this particular case, *N*-(5′-phosphopyridoxyl)-1-carboxy-2-propen-1-imine.[127] To complete the reaction, the succinate that is the leaving group is replaced by the sulfido group of L-cysteine, a nucleophile, and the steps producing the 1-carboxy-2-propen-1-imine are reversed to produce L-cystathionine. Again, an excellent leaving group, succinate, is replaced by an excellent nucleophile, the sulfido group of L-cysteine. It would seem that a much simpler enzyme could have been designed in which this reaction was a simple concerted nucleophilic substitution.

An *N*-(5′-phosphopyridoxyl)-2-propen-1-imine is **electrophilic at the γ carbon**. In the reaction catalyzed by cystathionine γ-synthase, the nucleophile that adds to this electrophilic carbon is the sulfido group of L-cysteine. In the reaction catalyzed by the product of the *cndF* gene in *Penicillium citrinum*, *N*-(5′-phosphopyridoxyl)-1-carboxy-2-propen-1-imine is formed in the active site from O^4-acetyl-L-homoserine rather than O^4-succinyl-L-homoserine (Equations 2–31 and 2–34). The enolate of acetoacetate ($pK_a = 16.1$; Figure 1–23) then adds nucleophilically to the *N*-(5′-phosphopyridoxyl)-1-carboxy-2-propen-1-imine[128]

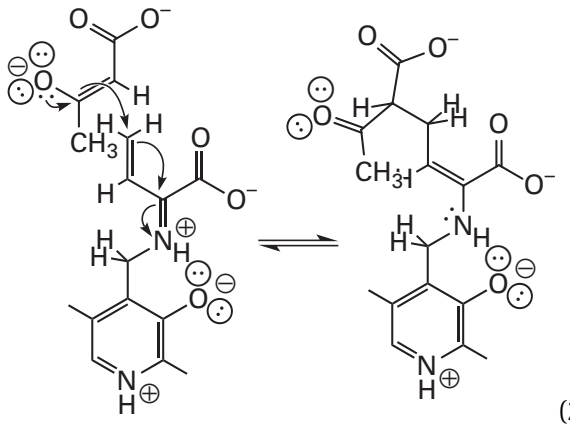

(2–35)

The resulting *N*-(5′-phosphopyridoxyl)enamine is then hydronated on the β carbon, the hydron on carbon 4′ is transferred in the usual tautomerization to the α carbon of the resulting *N*-(5′-phosphopyridoxyl)imine, and the resulting external pyridoximine is transiminated to the L-amino acid. At some point along the way, the carboxylate on the δ carbon of the incipient amino acid, which is on a carbon adjacent to a carbonyl group is decarboxylated. The final product is (*S*)-2-amino-6-oxoheptanoic acid.

In an *N*-(5′-phosphopyridoxyl)prop-2-en-1-imine, the two hydrogens on carbon 4′ of the 5′-phosphopyridoxyl group remain acidic, and one of them can be removed as a hydron. For example, in the reaction catalyzed by threonine synthase from *M. tuberculosis*

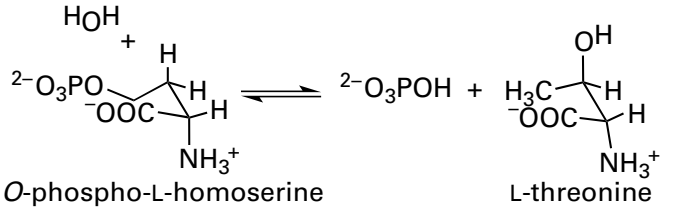

(2–36)

N-(5′-phosphopyridoxyl)-1-carboxyprop-2-en-1-imine is formed as an intermediate after the phospho group of the of the *O*-phospho-L-homoserine leaves as phosphate, an excellent leaving group, just as it is formed as an intermediate after the O^4-succinyl group of O^4-succinyl-L-homoserine leaves as succinate, also an excellent leaving group, in the reaction catalyzed by cystathionine γ-synthase (Equation 2–34). The next step in the reaction of threonine synthase, however, is the removal of one of the acidic hydrons on carbon 4′ of the pyridoxyl group to produce the **quinonoid intermediate of ethenyl glycine (2–18)**

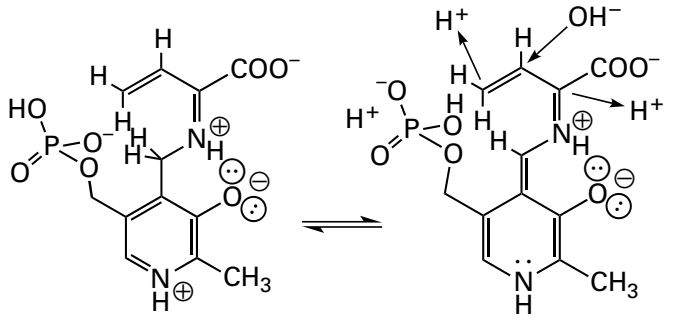

2–17 **2–18**

(2–37)

If the quinonoid intermediate of ethenyl glycine is completely planar within the active site and if it is fully conjugated, 15 *p* orbitals from 15 atoms participate in this **ultimate, fully conjugated π molecular orbital system**. The key to understanding the potential of this quinonoid intermediate of ethenyl glycine is to realize that the imino nitrogen has become a bystander. From here on, the additions are controlled solely by the neutral pyridyl nitrogen 1 or the hydronated cationic pyridinio nitrogen 1 in succession. The product of the enzymatic reaction, L-threonine, results from the addition of a hydron, an electrophile, to the γ carbon that is nucleophilic because of the excess electron density in the π molecular orbital system; the addition of a hydroxide, a nucleophile, to the β carbon that is now electrophilic because of the deficit of electron density in the shorter π molecular orbital system; and the addition of a hydron, an electrophile, to the α carbon that is now nucleophilic and basic because of the excess electron density in the even shorter π molecular orbital system (arrows in **2–18**).

In the crystallographic molecular model of threonine synthase from *Thermus thermophilus*, the active site of which is occupied by *N*-(5′-phosphopyridoxyl)-(*E*)-2-imino-5-phosphonopent-3-enoate, an analogue of the *N*-(5′-phosphopyridoxyl)imine of ethenyl glycine (**2–17**), except for the fact that the 5-phosphono group has not dissociated because it cannot, the π molecular orbital systems on each side of the saturated carbon 4′ are coplanar.[129] Were the analogue the actual quinonoid intermediate of ethenyl glycine, the assumption is that it would be completely planar and fully conjugated over all 15 atoms. A nonbridging phospho oxygen from the phospho group on carbon 5′ of the 5′-phosphopyridoxyl group is only 0.33 nm from carbon 4′ of the 5′-phosphopyridoxyl group,[130] and it has been proposed that this base removes the hydron from carbon 4′ and then hydronates the

γcarbon of the quinonoid intermediate of ethenyl glycine (Equation 2–37).[131] The hydronation of the γ carbon would require that the natural 1-carboxyprop-2-enimine assume the s-cis conformation as in **2–18**, rather than the s-trans conformation seen in the crystallographic molecular model and drawn in Equation 2–34. In another crystallographic molecular model of the same enzyme with its active site occupied by the same external pyridoximine but also occupied by a phosphate, presumably residing where the phosphate that is the product of the overall reaction sits before it leaves, one of the oxygens of this phosphate is located in a position from which it could remove a hydron from a molecule of water as it adds to the β carbon of the quinonoid intermediate of ethenyl glycine (**2–18**).

A quinonoid intermediate of ethenyl glycine is also formed in the elimination catalyzed by methionine γ-lyase

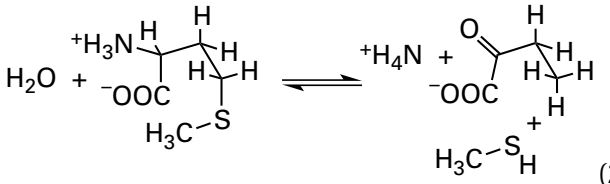

(2–38)

As in the case of cystathionine γ-synthase (Equation 2–34), the leaving group, methanethiol, is pushed out by the *N*-(5′-phosphopyridoxyl)enamine[132-134]

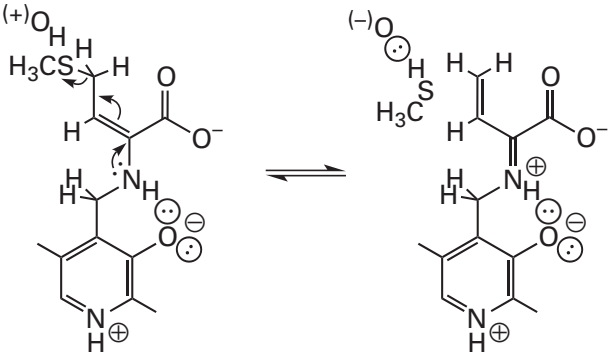

(2–39)

to give the *N*-(5′-phosphopyridoxyl)-1-carboxyprop-2-en-1-imine. A tyrosine in the active site performs the role of catalytic acid that hydronates the leaving group. As in the case of threonine synthase, a hydron is then removed from carbon 4′ of the 5′-phosphopyridoxyl group to produce the quinonoid intermediate of ethenyl glycine (**2–18**), and a hydron is added to carbon 4 of the quinonoid intermediate to accomplish a tautomerization

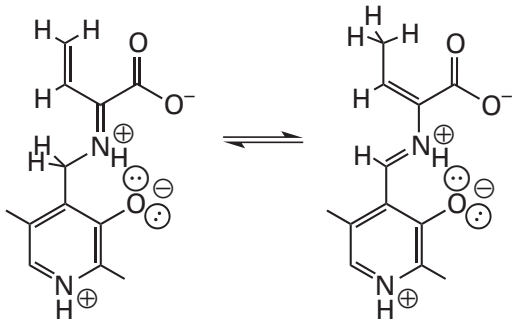

(2–40)

The product of this tautomerization is the pyridoximine of 2-aminobut-3-enoic acid, which is transiminated to give 2-aminobut-3-enoic acid free in solution. This 2-aminobut-3-enoic acid is converted nonenzymatically to the ultimate product of the reaction, 2-oxobutanoic acid (Equation 2–38). In the active sites of the enzymes from *P. putida*[132] and *Entamoeba histolytica*,[134] the catalytic base that removes the hydron from the carbon 4′ of the pyridoxyl group is the lysine forming the internal pyridoximine and the catalytic acid that adds the hydron to carbon 4 of the 1-carboxyprop-2-enimine is a tyrosine, again a cooperation of these two amino acids.

With *N*-(5′-phosphopyridoxyl)-1-carboxyprop-2-en-1-imine and its conjugate base, the quinonoid intermediate of ethenyl glycine, extension of the π molecular orbital system of the pyridoxal 5′-phosphate into an α-amino acid reaches its extreme. The hydronated pyridinio nitrogen at the base of the external pyridoximine functions to withdraw electrons from a σ bond around the α carbon in the external pyridoximine of the α-amino acid that was the original reactant. Upon removal of a hydron from the α carbon, the pyridyl nitrogen becomes a secondary amine and the π molecular orbital system that has been extended by one atom onto the α carbon becomes electron-rich because the two electrons that were in the σ bond to the hydrogen have been added to it. Carbon 4′ of the quinonoid intermediate is hydronated, causing the π molecular orbital system of the 3-hydroxypyridinio group to become dissociated from that of the iminium and the system to become electron-deficient because two of its electrons are now in the σ bond to the hydrogen. The nitrogen of the primary amino group of the α-amino acid that was in the original reactant then functions as a hydronated, cationic iminium to withdraw electron density from a σ bond to the β carbon. Upon dissociation of an electrophile from this carbon and the extension of

the π molecular orbital system by one atom, the electron-deficient iminium has become an electron-rich enamine as a result of the addition of the two electrons from the σ bond. This electron excess is then able to push away a leaving group from the γ carbon of the original α-amino acid. Upon dissociation of an electrophile from this carbon and extension of the π molecular orbital system by one atom, the electron-rich enamine has become an electron-poor, electrophilic 1-carboxyprop-2-enimine as a result of the dissociation of both electrons that were in the σ bond to the leaving group. A hydrogen on carbon 4′ can be readily removed as a hydron from this electron-poor, electrophilic intermediate to connect the two adjacent π molecular orbital systems. The resulting quinonoid intermediate of ethenyl glycine is now electron-rich and basic as a result of the incorporation of two electrons that were in the σ bond to the hydrogen, while the π molecular orbital system has only increased in size by one carbon atom.

Each of these extensions and the subsequent contractions of the successive π molecular orbital systems are usually represented by a series of arrows. "It must be concluded that pyridoxal phosphate was created to provide satisfaction and enlightenment to those enzymologists and chemists who enjoy pushing electrons."[135] The pushing of electrons with arrows, however, is simply a means to indicate the extensions and contractions of the π molecular orbital systems.

The basis for the ability of the two nitrogens, the hydronated pyridinio nitrogen and the hydronated iminio nitrogen, to promote opposite reactions on the same carbon and the same reaction at adjacent carbons is that they are an **odd number of atoms apart** from each other in the external pyridoximine. The influence of these two nitrogens could be propagated even beyond the γ carbon of an amine if incipient electrophiles and leaving groups were properly alternated so that the expanding π molecular orbital systems were not required to become excessively electron-rich or excessively electron-poor.

At each step in the extension of the π molecular orbital systems over the substrate, the electrophile that has just dissociated can be replaced by a different electrophile or the leaving group that has just dissociated can be replaced by a different nucleophile. In the reaction catalyzed by glycine hydroxymethyltransferase (Equation 2–10), the hydroxymethyl group that dissociates as a formal formaldehyde is replaced by a hydron. In the reaction catalyzed by cystathionine γ-synthase, the oxygen of the succinate that dissociates (Equation 2–34) is replaced by the sulfido group of L-cysteine. After these replacements are made, the reaction can proceed in reverse, passing backward through the same steps that led to loss of the electrophile or expulsion of the leaving group to regenerate the amine in which only the one substitution has occurred, as with glycine hydroxymethyltransferase or cystathionine γ-synthase (Equation 2–31), or in which two substitutions have occurred, as with threonine synthase (Equation 2–36).

At each step in the reactions catalyzed by pyridoxal 5′-phosphate, on the way forward or on the way back, the **nitrogen of the original amine** is formally either the nitrogen of an external pyridoximine that can be transiminated to regenerate the internal pyridoximine and a significantly altered derivative of the original amine (Equation 2–15) or the nitrogen of an *N*-(5′-phospho-pyridoxyl)imine that can be hydrolyzed to form pyridoxamine 5′-phosphate and the significantly altered or the unaltered ketone or aldehyde in which an oxo group replaces the original amino group (Equation 2–21). The array of possibilities is breathtaking.

There are peculiar variations on this common theme for the mechanism of the reactions catalyzed by pyridoxal 5′-phosphate.

Pyridoxamine 5′-phosphate is used as a prosthetic group to **deoxygenate carbon 3 of a nucleotide 4-dehydro-6-deoxyhexose**.[136-139] For example, within the active site of CDP-4-dehydro-6-deoxyglucose reductase

$$\begin{aligned}&\text{CDP-4-dehydro-6-deoxy-D-glucose} + \\ &\quad 2\,e^- + 2\,H^+ \rightleftharpoons H_2O + \\ &\qquad \text{CDP-4-dehydro-3,6-dideoxy-D-glucose}\end{aligned} \qquad (2\text{–}41)$$

from *Yersinia pseudotuberculosis*, there is a tightly associated, prosthetic pyridoxamine 5′-phosphate. CDP-4-dehydro-6-deoxyglucose reductase, although it displays no homology in its sequence of amino acids, has a fold that is superposable on the fold of aspartate transaminase, and when four of the amino acids in its sequence are mutated to the respective amino acids that occupy those positions in aspartate transaminase, the mutant displays aspartate transaminase activity,[140] which seems to confirm the evolutionary relationship. Nevertheless, the unmutated enzyme catalyzes a quite different reaction.

The pyridoxamine 5′-phosphate in the active site of CDP-4-dehydro-6-deoxyglucose reductase forms an *N*-(5′-phosphopyridoxyl)imine with the carbonyl group at carbon 4 in CDP-4-dehydro-6-deoxy-D-glucose by the usual nucleophilic substitution of an amino nitrogen for a carbonyl oxygen. Rather than the resulting iminium withdrawing electron density from the β carbon in the imine, however, as it usually would, a hydron is removed from carbon 4′ of the pyridoxamine 5′-phosphate, causing the iminium to become conjugated to the 5′-phospho-pyridoxyl group, and an electron-rich quinonoid intermediate is formed as the two electrons in the carbon–hydrogen bond that was just dissociated join the π molecular orbital system. The quinonoid intermediate then provides push to the elimination of the hydroxy group on carbon 3 of the hexose

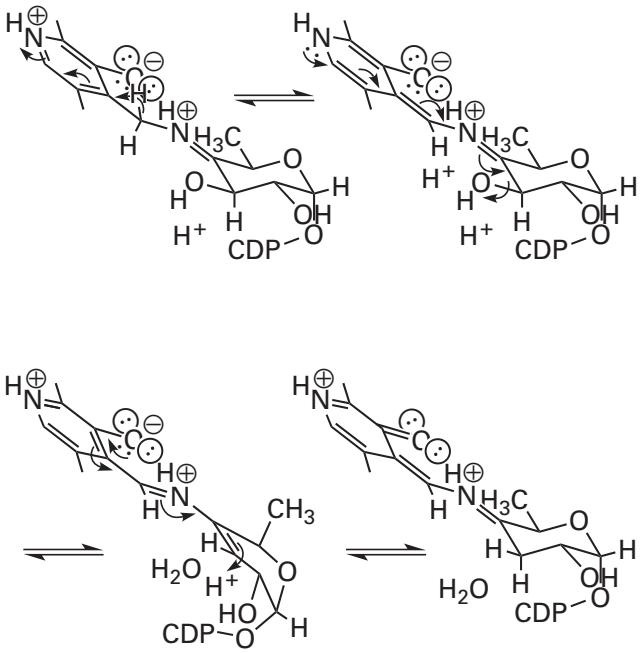

(2–42)

By removing the hydron from carbon 4′, the effect of the pyridoxamine 5′-phosphate on carbon 3 of the hexose has been shifted from its iminio nitrogen to its pyridinio nitrogen, from electron withdrawal, which would lead to the dissociation of a hydron, to electron donation, which leads to the loss of a leaving group. This shift allows the resulting quinonoid intermediate to push out the hydroxy group. A more novel aspect of the reaction, however, is the next step. Instead of withdrawing electron density from the distal carbon–carbon double bond, as usually happens, for example, with the external pyridoxamine of an 2-aminoacrylate, the pyridoxamine recruits the normally overlooked excess electron density of the **anionic, unhydronated 3-hydroxy group** of the pyridoxamine 5′-phosphate, which has gone unmentioned so far in the discussion. This recruitment pushes more electron density into the 2-aminoacrylyl group to permit its hydronation at carbon 3 rather than the usual addition of a nucleophile. This addition of a hydron is coincident with the oxidation of the pyridoxamine 5′-phosphate.[141-143]

There are two ways in which the **oxidized pyridoxamine 5′-phosphate within the adduct** between the now 4-dehydro-3,6-dideoxyhexose and the oxidized pyridoxamine 5′-phosphate is reduced to pyridoxamine 5′-phosphate so that it can begin the next turnover. It can be **reduced by a separate flavoprotein that is in turn reduced by NADH** or NADPH

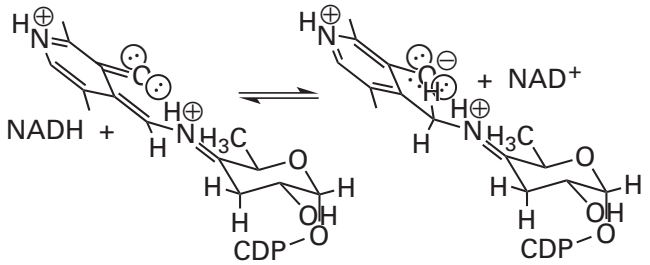

(2–43)

to give the *N*-(5′-phosphopyridoxyl)imine of CDP-4-dehydro-3,6-dideoxy-D-glucose by addition of two electrons and the addition of a hydron to carbon 4′ of the 5′-phosphopyridoxyl group. Hydrolysis of the resulting *N*-(5′-phospho-pyridoxyl)imine produces CDP-4-dehydro-3,6-dideoxy-D-glucose, the product of the reaction, and pyridoxamine 5′-phosphate. There is, however, a related enzyme (31% identity; 1.5 gap percent), GDP-4-dehydro-6-deoxy-α-D-mannose 3-dehydratase, also from *Y. pseudotuberculosis*, that performs the same reaction on GDP-4-dehydro-6-deoxy-α-D-mannose, the reduction of carbon 3 of the 4-dehydro-6-deoxy-α-D-mannose from an alcohol to the saturated carbon. In the active site of this enzyme, however, the final imine homologous to the one in Equation 2–42 is hydrolyzed directly to the oxidized pyridoxamine 5′-phosphate, which is the external pyridoximine of ammonia

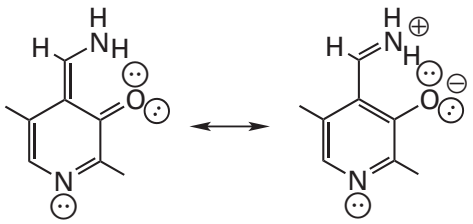

(2–44)

This pyridoximine is hydrolyzed to ammonia and pyridoxal 5′-phosphate, which is then **reduced by L-glutamate** in the usual way to the pyridoxamine 5′-phosphate needed for the next turnover (see Equations 2–26 and 2–29). In this instance, the reduction occurs after the dissociation of the imine, and it is performed by glutamate rather than NADH.

UDP-4-Amino-4,6-dideoxy-*N*-acetyl-β-L-altrosamine transaminase from *Helicobacter pylori*, which is related to CDP-4-dehydro-6-deoxyglucose reductase from *Y. pseudotuberculosis* (25% identity; 1.3 gap percent) and GDP-4-dehydro-6-deoxy-α-D-mannose 3-dehydratase from *Y. pseudotuberculosis*, also contains a prosthetic pyridoxamine 5′-phosphate in its active site, the sole purpose of which is to convert the 4-oxo group of a nucleotide 4-dehydro-6-deoxyhexose into a 4-amino group by a simple transamination rather than performing any reduction of its carbon 3.[144]

A prosthetic group that provides a catalytic capacity similar to that of pyridoxal 5′-phosphate is the covalently attached *N*-pyruvoyl group.[145,146] This group is found in several enzymes that decarboxylate α-amino acids, such as histidine decarboxylase,[145,146] adenosylmethionine decarboxylase,[147] and aspartate 1-decarboxylase.[148] The prosthetic group is a posttranslational modification. In a series of autocatalytic reactions, the peptide bond amino-terminal to a particular serine in the active site is hydrolyzed and the resulting amino-terminal serine is dehydrated to a *N*-pyruvoyl group.

As with pyridoxal 5′-phosphate, during the decarboxylation catalyzed by one of these posttranslationally modified active sites, an imine is formed between the respective amino acid and the *N*-pyruvoyl group. The amido group that is the peptide bond to the amino-terminal *N*-pyruvoyl group is held in the plane of the hydronated iminio group by a π molecular orbital system of five atoms, and it withdraws electron density from the σ bond to the carboxylato group, which is held by the enzyme parallel to the seven atoms and parallel to the π molecular orbital system[148]

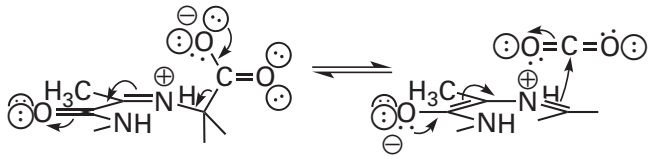

(2–45)

In this instance, the electronegative acyl oxygen of the amido group rather than the pyridinio nitrogen of the external pyridoximine withdraws the electron density. The carbon from which the CO_2 leaves is normally hydronated by an acid on the enzyme to complete the decarboxylation, but in at least one instance, this acid or some other one occasionally hydronates carbon 2 of the *N*-pyruvoyl group (analogous to carbon 4′ of pyridoxal 5′-phosphate) and the enzyme is slowly inactivated by the consequent transimination.[147]

Suggested Reading

Posner, B. I., and Flavin, M. (1972) Cystathionine γ-synthase: Studies of hydrogen exchange reactions, *J. Biol. Chem. 247*, 6402–6411. https://doi.org/10.1016/S0021-9258(19)44707-8

Sun, S., Zabinski, R. F., and Toney, M. D. (1998) Reactions of alternate substrates demonstrate stereoelectronic control of reactivity in dialkylglycine decarboxylase, *Biochemistry 37*, 3865–3875. https://doi.org/10.1021/bi972055s

Stojanovski, B. M., Hunter, G. A., Jahn, M., Jahn, D., and Ferreira, G. C. (2014) Unstable reaction intermediates and hysteresis during the catalytic cycle of 5–aminolevulinate synthase: Implications from using pseudo and alternate substrates and a promiscuous enzyme variant, *J. Biol. Chem. 289*, 22915–22925. https://doi.org/10.1074/jbc.M114.574731

Problem 2–1: Write a complete mechanism for Equation 2–26 under catalysis by pyridoxal 5′-phosphate.

Problem 2–2: Write a complete mechanism for glycine hydroxymethyltransferase (Equation 2–10) incorporating Equation 2–11.

Problem 2–3: Write mechanisms for the following reactions that are mediated by pyridoxal 5′-phosphate:

(A)

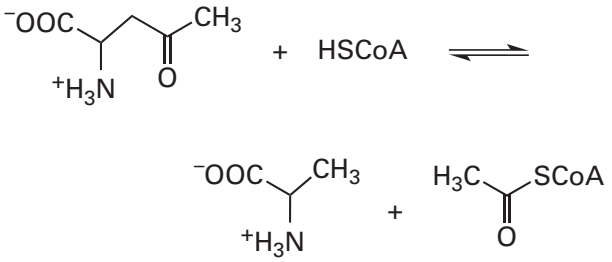

(B)

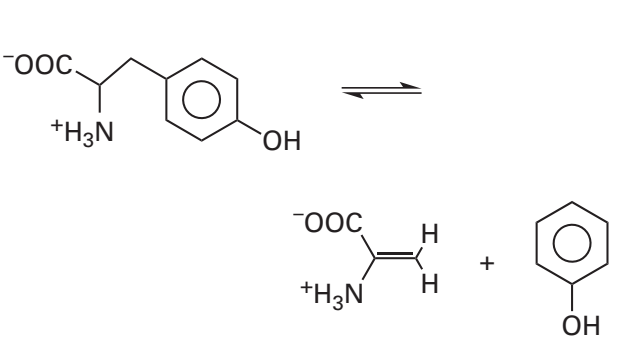

(C)

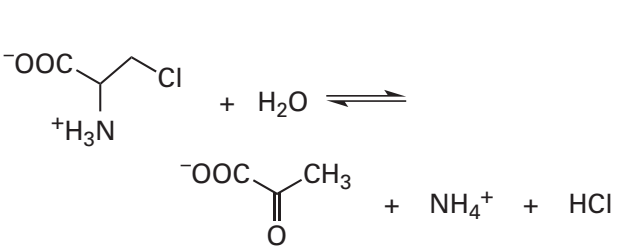

(D)

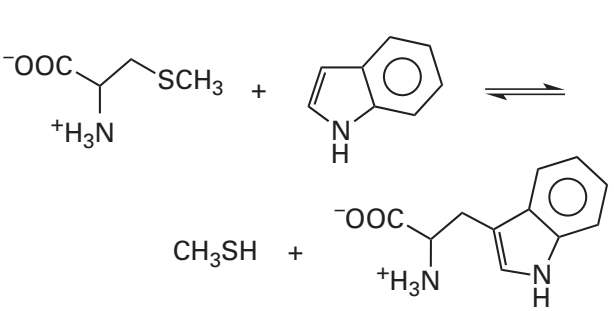

(E)

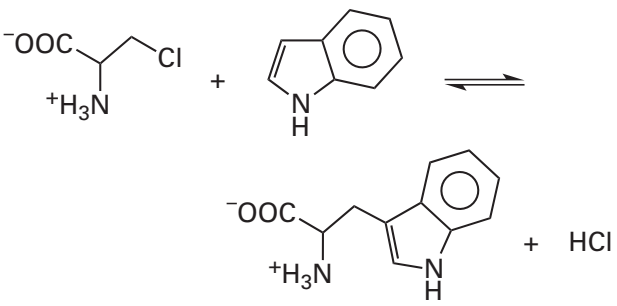

(F)

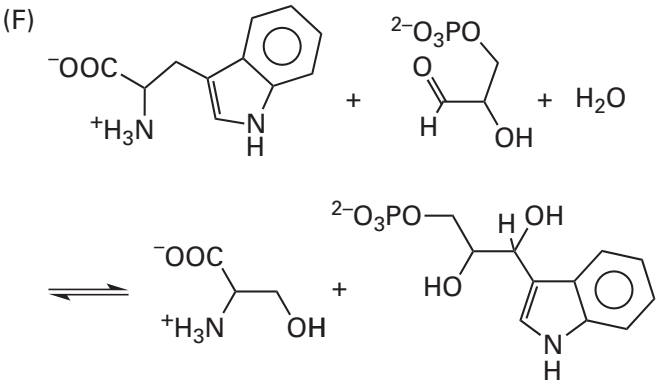

(G)

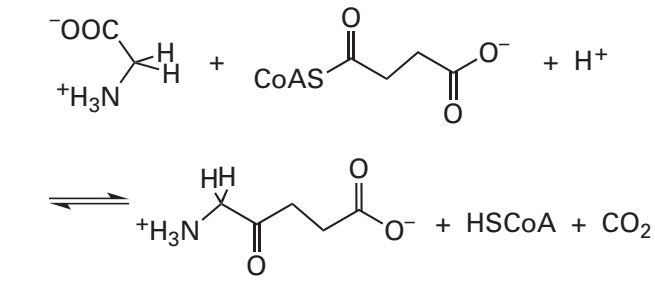

(H)

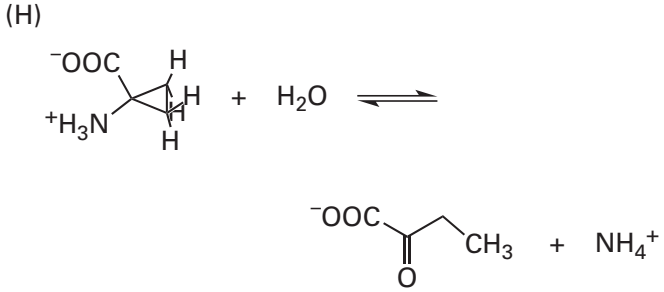

(I)

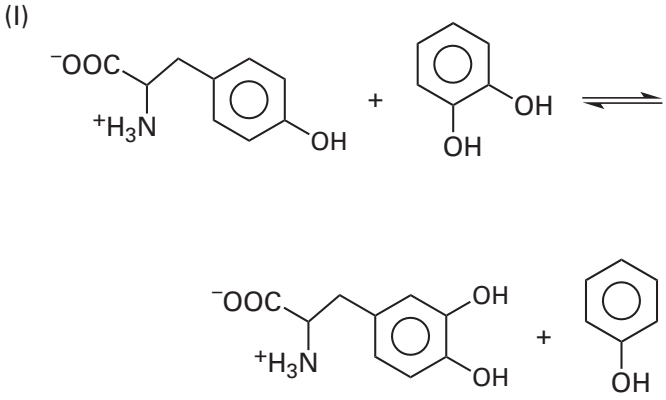

(J)

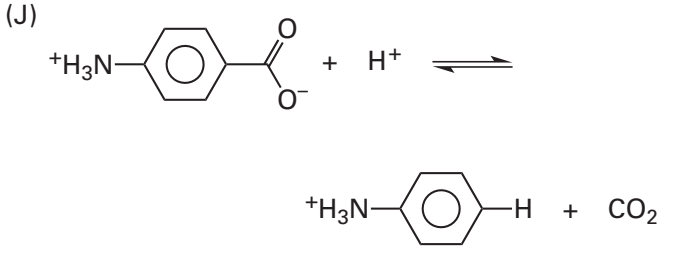

Problem 2–4: Write a mechanism involving pyridoxal 5′-phosphate for the reaction

$$\text{L-serine} + \text{indole} \rightleftharpoons H_2O + \text{L-tryptophan}$$

Show how the same enzyme would also catalyze the reaction[149]

$$\text{pyridoxamine 5′-phosphate} + \text{3-(3-indolyl)pyruvate} \rightleftharpoons \text{pyridoxal 5′-phosphate} + \text{L-tryptophan}$$

Problem 2–5: Write complete mechanisms for the catalysis performed by 5-aminolevulinate synthase[71]

$$\text{glycine} + \text{succinyl-SCoA} + H^+ \rightleftharpoons \text{HSCoA} + CO_2 + \text{5-aminolevulinate}$$

and serine *C*-palmitoyltransferase[150]

$$\text{L-serine} + \text{palmitoyl-SCoA} + H^+ \rightleftharpoons \text{HSCoA} + CO_2 + \text{3-dehydro-D-sphinganine}$$

both of which use pyridoxal 5′-phosphate as a prosthetic group.

Problem 2–6: Write a complete mechanism for the reaction catalyzed by cystathionine γ-synthase (Equation 2–31). In your mechanism, label the intermediates as internal pyridoximine, external pyridoximine, quinonoid intermediate, *N*-(5′-phosphopyridoxyl)imine, and *N*-(5′-phosphopyridoxyl)-enamine.

Problem 2–7: The compound gabaculine

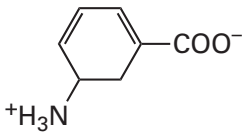

inhibits 4-aminobutyrate—2-oxoglutarate transaminase by forming an aromatic, anilinium adduct with the pyridoxal 5′-phosphate that is the prosthetic group for this enzyme.[151] Write the mechanism for the formation of this adduct.

Problem 2–8: Write the mechanism of the D-serine ammonia-lyase reaction

$$\text{D-serine} \rightleftharpoons NH_4^+ + \text{pyruvate}$$

as it is catalyzed by the pyridoxal 5′-phosphate bound to the enzyme. Show clearly the role of the pyridoxal 5′-phosphate in each step of the reaction. In each step, label every sp^2 carbon conjugated to the aromatic ring. Watch closely the expansion and then contraction of the π system as atoms are turned from sp^3 into sp^2 and back into sp^3. What step in the reaction requires the pyridoxal the most?

Problem 2–9: Write a complete mechanism for the reaction catalyzed by threonine synthase (Equation 2–36) as it is catalyzed by pyridoxal 5′-phosphate.

Problem 2–10: Glutamate-1-semialdehyde 2,1-aminomutase from *Pisum sativum* is an enzyme with either the internal pyridoximine of pyridoxal 5′-phosphate or pyridoxamine 5′-phosphate in its active site, depending on its history. It converts (*S*)-2-amino-4-carboxybutanal (L-glutamate 1-semialdehyde) to 1-amino-4-carboxy-2-oxobutane (5-aminolevulinate).[152]

(a) When 4,5-diaminopentanoic acid is added to a solution of the enzyme, the absorbance at 416 nm, arising from the internal pyridoximine of pyridoxal 5′-phosphate, decreases as the absorbance at 345 nm, arising from pyridoxamine 5′-phosphate, increases stoichiometrically.

(b) When 4,5-dioxopentanoic acid is added to a solution of the enzyme, the absorbance at 345 nm, arising from the pyridoxamine 5′-phosphate, decreases as the absorbance at 416 nm, arising from the internal pyridoximine of pyridoxal 5′-phosphate, increases stoichiometrically.

(c) When a mixture of 4,5-dioxopentanoic acid and 4,5-diaminopentanoic are added to a solution of the enzyme, 1-amino-4-carboxy-2-oxobutane is produced at a rate equal to 40% of the rate of the normal reaction catalyzed by the enzyme.

(d) Increasing the fraction of pyridoxamine 5′-phosphate in the enzyme causes an equivalent increase in the rate of the normal reaction catalyzed by the enzyme.

(A) Write out the structures of the two substrates for the enzyme.
(B) Write a mechanism for the normal reaction catalyzed by the enzyme that involves both the internal pyridoximine of pyridoxal 5′-phosphate and pyridoxamine 5′-phosphate, that involves a *gem*-diamine, and that explains all these results.

Thiamine Diphosphate

Thiamine diphosphate

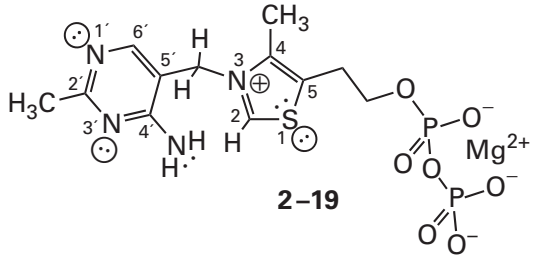

2–19

is a **prosthetic group that is tightly, but noncovalently, bound to the active sites of the enzymes** in which it has a functional role. Thiamine diphosphate is complicated enough that several locations in its structure were sequentially proposed to be the functionally important site[153] before it was identified as carbon 2, sandwiched between the iminium nitrogen and the sulfur in the thiazolium ring.[154] Although enzymes using it as a prosthetic group have a strict requirement for thiamine diphosphate, perhaps because the diphospho group nails it into the active site, the dephospho parent, thiamine, is almost identical chemically to thiamine diphosphate because the diphosphate is so far removed from the thiazole ring. In model studies in solution, thiamine is often used as the catalyst, and it is assumed that the chemistry observed is very similar if not identical to the chemistry that would have been observed with thiamine diphosphate.

Carbon 2 of thiamine is acidic and readily exchanges its hydron with a deuteron in solution[154] by forming the zwitterionic ylide

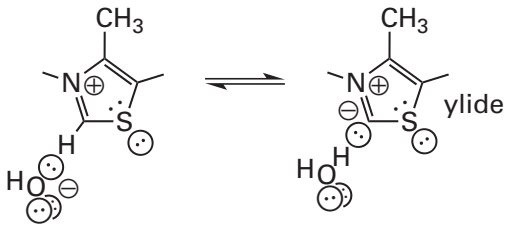

(2–46)

The observed rate constant for exchange of the hydron on carbon 2 of thiamine,[155] at pH 3.5 and 30 °C, is 1.8×10^{-4} s^{-1}, and this observed rate constant is directly proportional to [OH$^-$] with a slight inflection at the pK_a of the aminopyrimidine (5.5) that lowers the rates of exchange by a factor of 2.5 at the higher values of pH.[156,157] The pK_a for the dissociation of the hydron from carbon 2 of thiamine has been measured directly using a rapid kinetic titration to avoid the rapid decomposition of the thiazolium ring that occurs at high concentrations of hydroxide.[158] Nitrogen 1′ is the most basic nitrogen in the 4′-aminopyrimidinyl group in thiamine. When it is hydronated so that the 4′-aminopyrimidinium is cationic, the pK_a for the dissociation of the hydron from carbon 2 is 17.7; when the 4′-aminopyrimidinyl group is neutral, the pK_a is 18.0.[157,159] There are several reasons why thiamine, in which carbon 2 is not α to a carbonyl or acyl group, nevertheless is such a strong carbon acid.

First, because it is within an aromatic heterocycle, **hybridization of the acidic carbon** is sp^2, sp^2, sp^2, p. Because it is formed from one of the sp^2 atomic orbitals of the carbon atom, the σ bond to the hydrogen holds the pair of bonding electrons closer to the nucleus. The sp^2 atomic orbital also holds the lone pair of electrons formed upon dissociation of the hydron closer to the nucleus than if the carbon were hybridized sp^3, sp^3, sp^3, sp^3. These properties cause the carbon–hydrogen bond to be more acidic and the conjugate base to be less basic[153] than those in carbon acids in which carbon is hybridized sp^3, sp^3, sp^3, sp^3.

Second, **the conjugate base of thiamine is an ylide**. An ylide is a compound in which an anionic carbon (or another anionic atom) is attached directly to a heteroatom carrying a fixed formal positive elementary charge. In the case of thiamine, the anionic carbon is produced by dissociation of a hydron from carbon 2 and the heteroatom carrying the fixed positive formal elementary charge is nitrogen 3. Nitrogen 3 has no vacant bonding orbital able to absorb the adjacent negative formal elementary charge by resonance. 1,3-Dimethylimidazoliums, the conjugate bases of which are ylides, display carbon acidity similar to that of 3-methylthiazoliums.[158] In the case of the ylide that is the conjugate base of thiamine (Equation 2–46), the negative formal elementary charge on carbon 2 is stabilized by the electrostatic field of the adjacent formal positive elementary charge on nitrogen 3. The stabilization in the ylide can be seen in semiempirical calculations of the electronic structure of the ylide of thiamine,[160] The adjacent nitrogen with a positive elementary

charge in thiamine from which the hydron on carbon 2 has not dissociated, the conjugate acid of the ylide, weakens the σ bond between the hydrogen and carbon 2. This effect is manifested in the deshielding of carbon 2 observed in the nuclear magnetic resonance spectrum.[161]

Third, the ylides that are the conjugate bases of *N*,*N*′-dialkylimidazoles and *N*-alkylthiazoles, such as thiamine, are further stabilized by **a delocalization that causes them to resemble a carbene**,[162] as illustrated by the resonance form

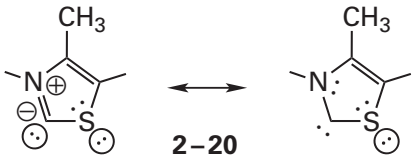

2–20

Fourth, **the neighboring sulfur stabilizes the negative elementary charge** in the σ lone pair on carbon 2 of the ylide of thiamine by $dp\pi$ overlap. This effect can be observed by comparing the rate of hydrogen exchange of 3,4-dimethylthiazolium and 1,3,4-trimethylimidazolium.[156] Although the respective carbon–hydrogen bonds in these two ions are similarly situated with respect to the heteroatoms and the only difference between them is the substitution of a neutral sulfur with a neutral methylated nitrogen, the hydrogen on carbon 2 of 3,4-dimethylthiazolium exchanges 3000 times faster than does the hydrogen on carbon 2 of 1,3,4-trimethylimidazolium. The salient difference is that sulfur has vacant *d* orbitals of suitable size and energy level to accept electron density within the plane of the ring while nitrogen does not.

Finally, the **4′-aminopyrimidinyl group on nitrogen 3 of thiamine enhances its acidity**. 3,4-Dimethylthiazolium ion (with a methyl group at carbon 3) exchanges the hydrogen on carbon 2 about 10-fold less readily than thiamine [with a (4-amino-2-methylpyrimidin-5-yl)-methyl group at carbon 3].[161] This difference results from the fact that the 4′-aminopyrimidine attached through a methylene at nitrogen 3 of the thiazole in thiamine diphosphate (**2–19**) withdraws electrons inductively from that nitrogen.[157] This inductive electron withdrawal is also reflected in the greater susceptibility[163] of thiamine than 3,4-dimethyl-5-(2-hydroxyethyl)thiazolium to addition of hydroxide at carbon 2

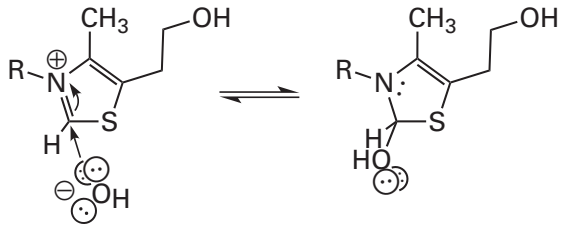

(2–47)

This electron withdrawal is inductive[157] and takes place through the σ bonds between nitrogen 3 and the 4′-aminopyrimidine because there is a saturated benzylic carbon between the two unsaturated rings.

The first step in the enzymatic reactions catalyzed by thiamine diphosphate is removal of the hydron on carbon 2 to form the ylide of thiamine. In the unoccupied active site of human pyruvate dehydrogenase (acetyl-transferring), the pK_a for the hydron on carbon 2 of the prosthetic group has been estimated[164] to be around 9. This value of pK_a is considerably less than that for thiamine diphosphate in solution. In the unoccupied active sites of pyruvate decarboxylase from *S. cerevisiae*, pyruvate decarboxylase from *Zymomonas mobilis*, and transketolase from *S. cerevisiae*, the rate constants[165] at which the hydrogen on carbon 5 of the thiamine diphosphate exchanges for a deuterium in ^2H_2O are 1 s^{-1}, 100 s^{-1}, and 60 s^{-1} at 4 °C. The value of pK_a and these rate constants demonstrate that the ylide of thiamine diphosphate forms readily in the active site of an enzyme, even in the absence of a substrate. One reason for this facile acid dissociation is the assistance of the 4′-anilino nitrogen of thiamine diphosphate (**2–19**) itself.

Although there is no indication that it acts as an intramolecular base to remove the hydron from carbon 2 when it is in free solution,[157] the **4′-amino group of thiamine is intimately involved in the removal of the hydron from carbon 2** when thiamine diphosphate is within the unoccupied active site of an enzyme. In the active sites of enzymes using thiamine diphosphate prosthetically, the thiamine is invariably[166-174] in a conformation in which its own 4′-amino nitrogen, which is five atoms away from carbon 2, ends up within 0.30–0.35 nm of carbon 2 (Figure 2–5A).[172,175,176] If 4′-desaminothiamine diphosphate is incorporated into an active site rather than thiamine diphosphate, the rate at which the hydron on carbon 2 is exchanged for a deuteron decreases by a factor of 30,000 to 700,000.[165]

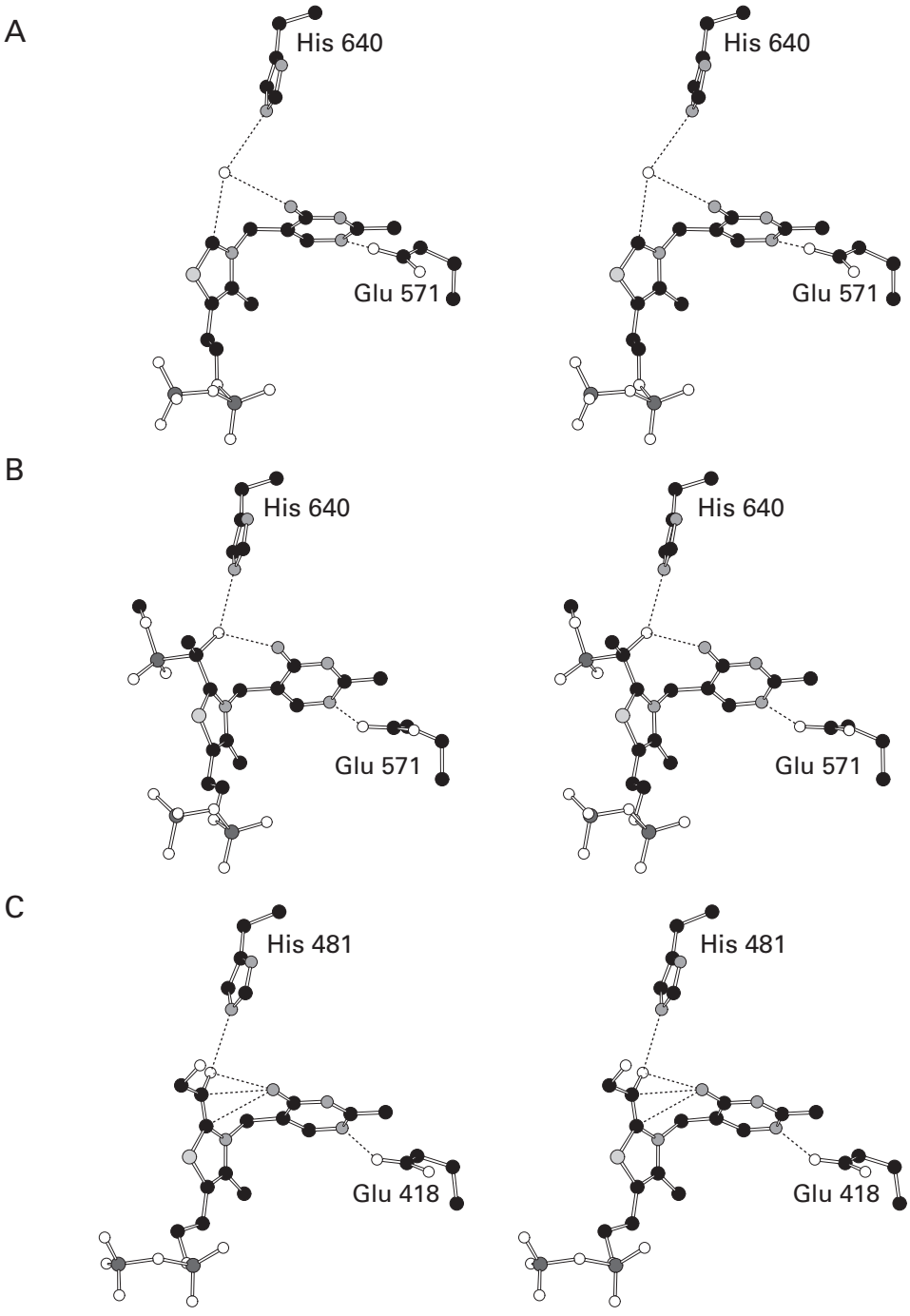
A
His 640
Glu 571
His 640
Glu 571
B
His 640
Glu 571
His 640
Glu 571
C
His 481
Glu 418
His 481
Glu 418

Figure 2–5: Stereodrawings[50] of three crystallographic molecular models of active sites containing prosthetic thiamine diphosphates in three different states: the initial unmodified thiazole, the adduct between the ylide of the thiazole and a carbonyl group, and an α-hydroxy enamine incorporating the thiazole. Black atoms are carbons, white atoms are oxygens, small gray atoms are nitrogens, large light gray atoms are sulfurs, and large dark gray atoms are atoms of phosphorus. In each active site, the carboxylate of a glutamate side chain forms a hydrogen bond with nitrogen 1′ of the thiamine diphosphate; the imidazolyl group of a histidine forms a hydrogen bond with a molecule of water, the hydroxy group of the initial adduct, or the hydroxy group of the α-hydroxy enamine, respectively; and nitrogen 4′ of the 4′-aminopyrimidine of the thiamine diphosphate forms a hydrogen bond to the same molecule of water or the same hydroxy groups. **(A)** The thiamine diphosphate within the active site of pyruvate dehydrogenase (acetyl-transferring) from *E. coli*.[172] The gene encoding the enzyme was transferred to a plasmid, overexpressed in cultures of *E. coli*, purified, and crystallized. The thiamine diphosphate, Glutamate 571, Histidine 640, and a molecule of water (white sphere) from the resulting crystallographic molecular model are presented in the drawing. The molecule of water is in the plane of the thiazole, immediately adjacent to the hydrogen on carbon 2 of the thiazole and only 0.30 nm from carbon 2, a distance much shorter than that dictated by a van der Waals contact, so the interaction is shown as a hydrogen bond. **(B)** The intermediate analogue, 2-(1″-hydroxy-1″-methylphosphonoethyl)thiamine diphosphate, within the active site of pyruvate dehydrogenase (acetyl-transferring) from *E. coli*.[175] The cloned and purified enzyme was cocrystallized with 2-(1″-hydroxy-1″-methylphosphonoethyl)thiamine diphosphate, an analogue of 2-(1″-carboxy-1″-hydroxyethyl)thiamine diphosphate, the adduct formed between pyruvate and thiamine diphosphate in the first step of the enzymatic reaction. In this analogue of the intermediate, the normal carboxy group is replaced by a methylphosphonyl group that cannot be decarboxylated. The σ bond between the methylphosphonyl group and the 1-hydroxyethyl group at carbon 2 of the thiamine diphosphate, which is homologous to the normal σ bond to the carboxy group, is firmly held normal to the plane of the π molecular orbital system of the thiamine by the two hydrogen bonds to the hydroxy group. **(C)** 2-(1″,2″-Dihydroxyethylidene)-2,3-dihydrothiamine diphosphate (Equation 2–57), an α-hydroxy enamine incorporating the thiazole within the active site of transketolase from *S. cerevisiae*.[176] The gene encoding the wild-type enzyme was overexpressed in cultures of *S. cerevisiae*, purified, and cocrystallized with 3-hydroxypyruvate. The 3-hydroxypyruvate, unlike one of the usual ketones that is a substrate for the enzyme, is decarboxylated, and in the absence of an aldehyde to act as an acceptor, the decarboxylated product, 2-(1″,2″-dihydroxyethylidene)-2,3-dihydrothiamine diphosphate, is stable. Nitrogen 4′ of the thiamine diphosphate is 0.30 nm from the hydroxy oxygen, 0.29 nm from the α carbon, and 0.31 nm from the carbon 2 of the thiazole, distances much shorter than those dictated by a van der Waals contact, so the three interactions are shown as hydrogen bonds, even though in the latter two cases there are no hydrogens with which to form a hydrogen bond. The thiamine diphosphate, Glutamate 418, and Histidine 481 from the resulting crystallographic molecular model are presented in the drawing.

The lone pair of electrons on the 4′-amino group in thiamine is not basic ($pK_a = 0$)[157] because it resides on an anilino nitrogen and consequently is conjugated with the pyrimidinyl ring. The σ lone pair of electrons, however, within the plane of the pyrimidinyl ring on the **4′-imino group of the 4′-imino tautomer of the 4′-aminopyrimidinyl group is basic**[157]

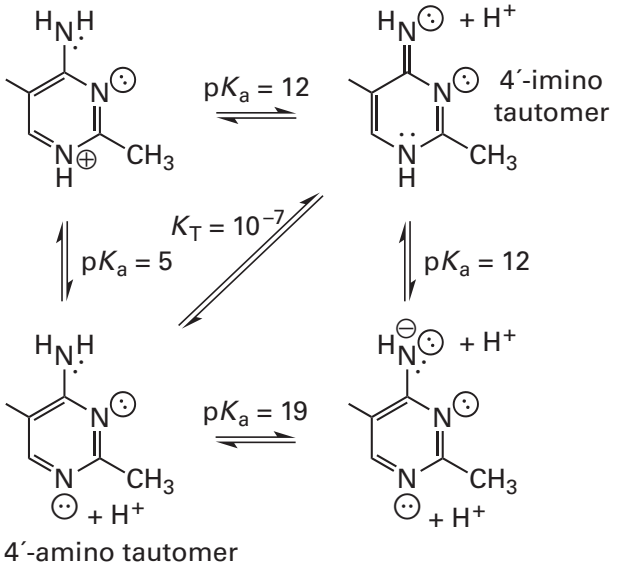

(2–48)

The lone pair of electrons on the 4′-imino tautomer should be basic enough (the pK_a of its conjugate acid is 12) to remove the hydron from carbon 2 of the thiazolium ion to produce the ylide.

In solution, however, the 4′-imino tautomer is unstable relative to the tautomer in which the hydron resides on the nitrogen of the 4′-amino group rather than on nitrogen 1′ ($K_T = 10^{-7}$). In most of the enzymes that use thiamine diphosphate prosthetically, nitrogen 1′ of the 4′-aminopyrimidine forms a **hydrogen bond to the carboxyl oxygen of a glutamic acid** (Figure 2–5).[167-172,174,177] This hydrogen bond, by fixing a hydron on nitrogen 1′ because the carboxy group (p$K_a = 4.3$) is a stronger acid than the hydronated pyrimidinyl group (p$K_a = 5$), should stabilize the desired 4′-imino tautomer by lowering the pK_a of nitrogen 4′ from 19 to 12 (Equation 2–48). When this glutamate in pyruvate decarboxylase from *S. cerevisiae* is mutated to a glutamine, its enzymatic activity decreases by a factor of 2500,[178] and the rate of exchange for a hydron for a deuteron at carbon 2 of the thiamine diphosphate within the active site decreases by a factor of greater than 300.[165]

Because it has a nonpolar side chain, Isoleucine 415 in pyruvate decarboxylase from *S. cerevisiae*, which covers one face of the 4′-amino-

pyrimidine of the thiamine diphosphate, should also stabilize the 4′-imino tautomer by promoting dissociation of the hydron from the 4′-amino group when nitrogen 1′ is hydronated and the 4′-aminopyrimidine is cationic (Equation 2–48). Mutating Isoleucine 415 to valine or alanine decreases the enzymatic activity of pyruvate decarboxylase by factors of 10 or 200, respectively.[179]

That the 4′-imino tautomer does form when thiamine diphosphate is bound by an enzyme for which it is a prosthetic group is indicated by the existence of a maximum absorption around 305 nm in the **circular dichroic spectra** of complexes between those enzymes and thiamine diphosphate.[180-182] The ultraviolet absorption spectrum of the neutral conjugate base of 1-methyl-4-aminopyrimidinium, the stable homologue of the 4′-imino tautomer, has a maximum absorption at 307 nm in dimethyl sulfoxide.[183] The circular dichroic absorption arising from the 4′-amino tautomer (Equation 2–48) when thiamine diphosphate is bound by an enzyme has a maximum at around 330 nm. In the active sites of pyruvate oxidase from *Lactobacillus plantarum* and human pyruvate dehydrogenase (acetyl-transferring), both circular dichroic absorptions, the one with maximum absorbance around 305 nm and the one with maximum absorbance around 330 nm, are observed in approximately equal ratio.[164] This observation indicates that the active site of each of these enzymes, for all the reasons just mentioned, has increased the tautomeric ratio from 10^{-7} to around 1. For each of these enzymes, the two maximum absorptions decrease in magnitude in concert as the solution is acidified as expected for a pair of tautomers turning into their common conjugate acid (Equation 2–48). The apparent pK_a for this conversion of the tautomeric pair to the conjugate acid is 5.6 for pyruvate oxidase and 7.1 for pyruvate dehydrogenase (acetyl-transferring). The apparent values of pK_a for the same conversion for thiamine diphosphate in the active sites of benzoin aldolase from *P. fluorescens* and benzoylformate decarboxylase from *P. putida* are 7.4 and 7.5. These observations and the fact that the tautomeric equilibrium is near 1 in each case suggest that the pK_a for the 4′-imino tautomer in the active site of each of these enzymes is close to that measured for the respective tautomeric mixture, rather than the pK_a of 12 that is observed in solution (Equation 2–48).

All these observations together indicate that, in an active site of an enzyme for which it is a prosthetic group, a significant fraction of the thiamine diphosphate is in the basic 4′-imino tautomer.

The two dihedral angles, however, that are enforced at the methylene carbon connecting nitrogen 3 and carbon 5′ by the active sites of most enzymes when they are unoccupied by substrate usually place nitrogen 4′ in an **unfavorable orientation** (Figure 2–5A) to remove the hydron from carbon 2, which is in the plane of the thiazole.[167-169,172,184] In crystallographic molecular models of the unoccupied active sites of most of the enzymes that use thiamine diphosphate as a prosthetic group, however, there is a molecule of water that forms hydrogen bonds to carbon 2 and the 4′-imino group. This molecule of water participates in a hydrogen bond with the 4′-imino group and the imidazolyl group of a histidine or to the acyl oxygen and carbamoyl nitrogen–hydrogen of a glutamine. Because it is positioned in line with the carbon–hydrogen bond, this molecule of water is in a much more favorable location than the 4′-imino group to remove the hydron from carbon 2. In the crystallographic molecular model of thiamine diphosphate within the active site of pyruvate dehydrogenase (acetyl-transferring) from *E. coli* (Figure 2–5A), the oxygen of the molecule of water is only 0.30 nm from carbon 2 of the thiamine diphosphate. This distance is considerably less than the distance that would be dictated by the sum (0.38 nm) of the van der Waals radii[185] of a hydrogen (0.115 nm) and an oxygen (0.15 nm) and the length of a carbon–hydrogen bond (0.11 nm). The fact that the distance is so short and the fact that this molecule of water is in line with the carbon–hydrogen bond both suggest that this molecule of water, relaying the basicity of the 4′-iminopyrimidine, is the base that catalyzes the exchange of that hydrogen by removing the hydron from carbon 2 of the thiamine diphosphate in the unoccupied active site.

So far the discussion has described the behavior of the unoccupied active site of an enzyme that has a prosthetic thiamine diphosphate. The situation changes significantly when a substrate associates with the active site.

The ylide of thiamine diphosphate reacts with an aldehyde or a ketone to form the product of an addition to a carbonyl

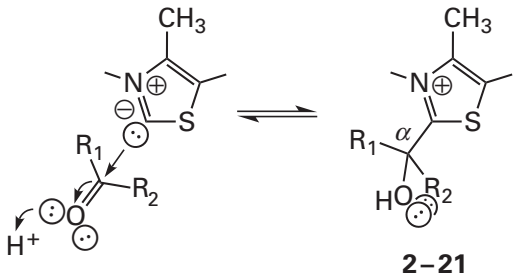

(2–49)

This adduct is analogous to the cyanohydrin that forms between an aldehyde or a ketone and cyanide

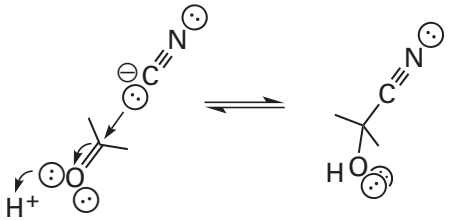

(2–50)

In a cyanohydrin, a weakly basic carbanion that has three bonds to a heteroatom adds to an aldehyde or a ketone.

During formation of the adduct with thiamine diphosphate, the 4′-amino group of the thiamine diphosphate usually ends up in a hydrogen bond with the α-hydroxy group* of the adduct (Figure 2–5B)[175,186] after the addition has occurred. The imidazolyl group of the histidine that had formed a hydrogen bond to the molecule of water adjacent to carbon 2 of the thiamine diphosphate (Figure 2–5A) also forms a hydrogen bond with this hydroxy group,[175,176,186] so the ultimate distribution of hydrons at this location is unclear, but in at least one other enzyme that uses thiamine diphosphate as a prosthetic group, the partner in this hydrogen bond is the carbamoyl nitrogen–hydrogen of a glutamine[167] rather than the imidazolyl group of a histidine. The glutamine would not be able to hydronate the oxygen.

The fact that the carbonyl oxygen of the reactant, now a hydroxy group, replaces the fixed molecule of water that participated in hydrogen bonds with the imidazolyl group of the histidine and the 4′-amino group of the thiamine diphosphate in the adduct between the reactant and thiamine diphosphate is consistent with this molecule of water being the base that removes the hydron from carbon 2 of the thiamine diphosphate in the normal sequence of events. After the it has transferred the hydron from carbon 2 to the 4′-amino group, it would be a molecule of water that can be easily displaced by the oxygen of the carbonyl as the now hydronated 4′-amino group hydronates the oxygen, and it becomes a hydroxy group.

There is no doubt that the thiazolium ring in an adduct between thiamine and a carbonyl group (**2–21**) is aromatic because every bond within the ring displays the shortening expected for a conjugated heterocycle.[187] The $3p$ atomic orbitals of sulfur in the cyclic π molecular orbital system, however, do not overlap efficiently with the $2p$ atomic orbitals of its two neighbors, and the more effective overlap is between a d orbital on sulfur and the p orbitals of the carbons and the nitrogen. Consequently the aromaticity is weak. This weakening of the aromaticity causes the nitrogen within the ring to be less like the nitrogen in an alkylpyridinium and more like the nitrogen of an iminium. The diminution of the aromaticity also explains the facility with which a hydroxide adds nucleophilically to carbon 2 of thiamine itself to form the hemiaminal (Equation 2–47),[158] even though this addition necessarily destroys the aromaticity of the ring.

Because it resembles the cationic nitrogen in an iminium, the cationic nitrogen in the *N,N*-dialkylthioimidoester* in the thiazolio ring of an adduct between thiamine and a carbonyl group (2–21) withdraws electron density from the σ bonds around the former carbonyl carbon and promotes the dissociation of an incipient electrophile.

In the adduct between thiamine diphosphate and an aldehyde, one of the substituents bonded to the α carbon is a hydrogen, and this **hydrogen can dissociate as a hydron**. Adducts between thiamine and aldehydes (R_1 = H in **2–21**) are readily synthesized stable compounds, and the acidity of the hydrogen on the α carbon can be demonstrated by following its exchange with a deuteron in solution[188] or directly by observing the formation of its conjugate base.[189]

*As was the case with adducts of pyridoxal phosphate, the carbon atoms controlled by the thiazolyl group in thiamine diphosphate will be labeled α to indicate that the carbon atom is α to carbon 2 of the thiazole (Equation 2–22), β to indicate the carbon atom is once removed from carbon 2 of the thiazole, and so forth. The carbon designated as α is the carbon that was in the carbonyl group of the original ketone or aldehyde.

*Recall that a thioester resembles a ketone more than it does an ester, so a thioimidoester resembles an imine more than it does an imidoester.

Values of pK_a for these hydrons have been measured in solution for 2-(1″-hydroxyethyl)thiamine (R_1 = H and R_2 = CH_3 in **2–21**; pK_a = 19)[190] and 2-(1″-hydroxybenzyl)-4′-deamino-4′-hydroxythiamine (R_1 = H and R_2 = C_6H_5 in **2–21**; pK_a = 15)[191]

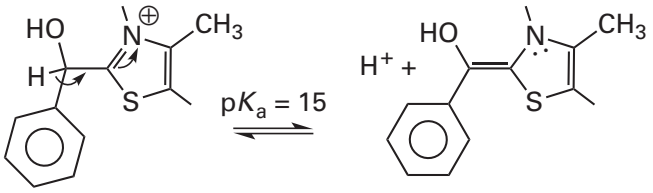

(2–51)

The removal of the hydron from the latter adduct (Equation 2–51) by bases the conjugate acids of which have a $\Delta pK_a \leq -3$ (previously Equation 1–10)

$$\Delta pK_{a,AB} \equiv pK_{a,HB} - pK_{a,HA} = \log \frac{K_{a,HA}}{K_{a,HB}} \equiv \log K_{eq,AB} \qquad (2–52)$$

shows a Brønsted coefficient of 1 as expected (Figure 1–1), but the rates are slower than those expected from the asymptotes in Figure 1–1 by a factor of 10^6 because the hydron is still being removed from carbon.[191]

In the adduct between thiamine diphosphate and a 2-oxo carboxylic acid, one of the substituents bonded to the α carbon is a carboxylate, and the **carboxylate can dissociate as carbon dioxide**. For example, in the reaction catalyzed by the enzyme pyruvate decarboxylase

$$\text{pyruvate} + H^+ \rightleftharpoons CO_2 + \text{acetaldehyde} \qquad (2–53)$$

the immediate adduct between thiamine diphosphate and pyruvate (Equation 2–49; R_1 = COO^- and R_2 = CH_3) accounts for the decarboxylation

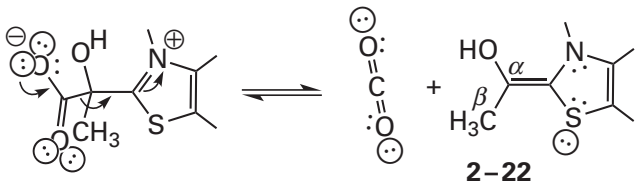

2–22

(2–54)

The analogous adduct of 3,4-dimethylthiazole and pyruvate has been synthesized and shown to decarboxylate readily[192]

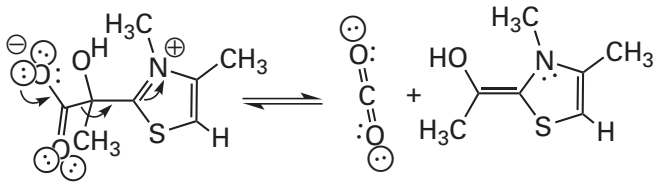

(2–55)

when it is in solution but only when the carboxy group is unhydronated and anionic as written.

The adduct between thiamine itself and pyruvate has also been synthesized, and the rate constants and equilibrium constants for various steps in the **mechanism of its decarboxylation** (Figure 2–6) have been measured.[193] As is required by the fact that both thiamine and pyruvate are achiral, the hydroxyethylthiamine produced by the decarboxylation of the adduct of thiamine and pyruvate and its hydronation is racemic at the α carbon.[194] The decarboxylation of this adduct, once it has formed, is catalyzed by general acids, a fact suggesting that 2-(1″-hydroxyethylidene)-2,3-dihydrothiamine diphosphate (**2–22**), the α-hydroxy enamine* that results from the decarboxylation (Equation 2–55), in a noncovalent complex with the dissociated carbon dioxide, which is the immediate product of the decarboxylation, is hydronated from solution to prevent its recarboxylation (reverse of Equation 2–54) before the carbon dioxide diffuses out of the shell of solvent. The dissociation of carbon dioxide from the solvated encounter complex would be an irreversible, rate-limiting step and therefore must follow the hydronation to explain the general acid catalysis.

An interesting observation made during the study of the decarboxylation of the adduct between 3,4-dimethylthiazole and pyruvate (Equation 2–55) was that, as expected from a reaction in which separated formal elementary charges of opposite sign are neutralized, the decarboxylation is accelerated by performing it in nonpolar solvents rather than polar solvents. In water at 46 °C, the rate of the decarboxylation[192] was 0.48×10^{-3} s^{-1}, but in ethanol

*Just as the sulfur in an *N,N*-dialkylthioiminoester participates only weakly in the π molecular orbital system of an adduct between thiamine and a carbonyl group, the sulfur should also participate only weakly in the π molecular orbital system of 2-(1″-hydoxyethylidene)-2,3-dihydrothiamine diphosphate. Consequently, 2-(1″,2″-dihydoxyethylidene)-2,3-dihydrothiamine diphosphate behaves as an *N,N*-dialkyl-α-hydroxy enamine.

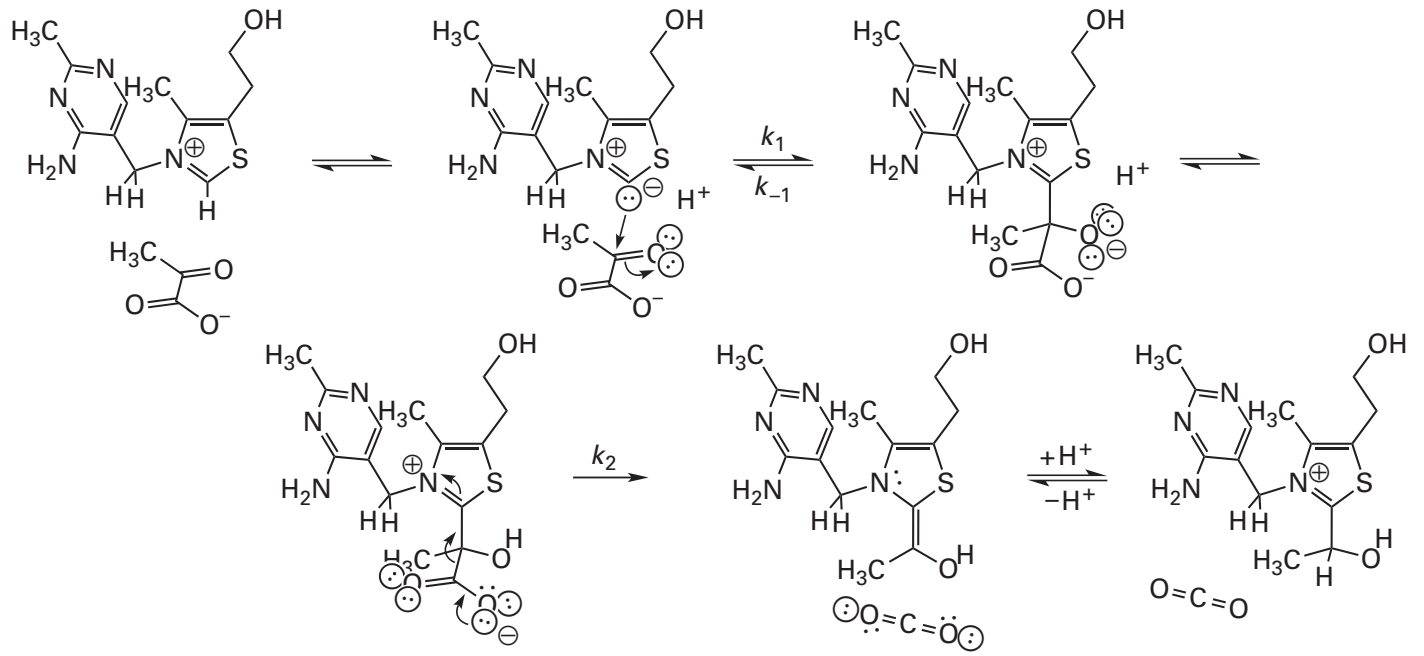

Figure 2–6: Mechanism of the decarboxylation of pyruvate catalyzed by thiamine in solution at 25 °C.[193] The ylide is formed by removing the hydron from carbon 2 ($pK_a = 18$). The adduct between thiamine and pyruvate forms in a bimolecular reaction ($k_1 = 6.5 \times 10^{-2}$ M^{-1} s^{-1}; $k_{-1} = 0.5$ s^{-1}). The oxyanion hydronates to form the conjugate acid ($pK'_a = 13.6$), 2-(1″-carboxy-1″-hydroxy-1″-methyl)thiamine. The 2-(1″-carboxy-1″-hydroxy-1″-methyl)thiamine then decarboxylates ($k_2 = 4 \times 10^{-5}$ s^{-1}) to form the enamine, which hydronates on carbon to give the final product. The final product is in turn the adduct of thiamine and acetaldehyde.

at 26 °C, the rate was 220×10^{-3} s^{-1}. An acceleration of 10^4 in the rate of the decarboxylation of the adduct between pyruvate and thiamine itself also occurs when the solvent is changed from water to ethanol,[195] and an acceleration of 4×10^3 in the rate of the analogous decarboxylation of the zwitterionic tautomer of 4-pyridylacetic acid occurs when the solvent is changed from water to 75% dioxane.[196] The suggestion has been made that enzymes using thiamine diphosphate to catalyze decarboxylations of 2-oxo carboxylic acids may accelerate these reactions in part by providing a **nonpolar environment**.[192]

In the adduct between thiamine diphosphate and an ***α*-hydroxy ketone** or thiamine diphosphate and an ***α*-hydroxy aldehyde**, one of the substituents bonded to the α carbon will be an incipient carbonyl group, and it can dissociate as the respective carbonyl compound. For example, in one of the reactions catalyzed by transketolase

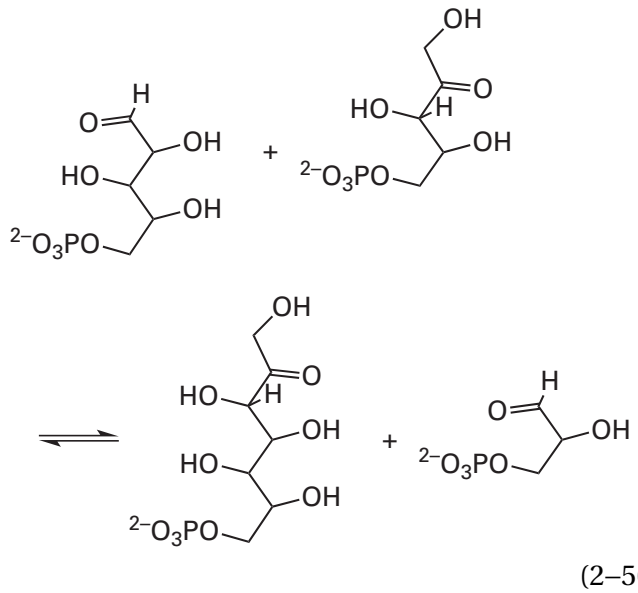

(2–56)

in which a two-carbon fragment is passed between two aldehydes, the product of the addition between thiamine diphosphate and either of the ketones that are substrates in the two respective directions loses the respective aldehyde as a product

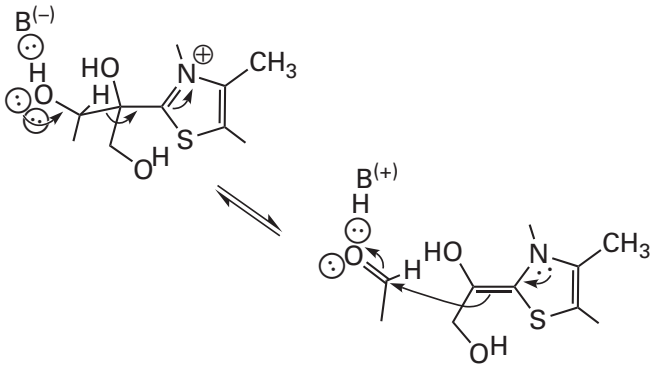

(2–57)

and the two-carbon fragment that will be transferred to the other aldehyde ends up in an α-hydroxy enamine, 2-(1″,2″-dihydroxyethylidene)-2,3-dihydrothiamine diphosphate. In the case of the transketolase from *Streptomyces sahachiroi* involved in the biosynthesis of azinomycin, the same α-hydroxy enamine is formed, but it results from decarboxylation of the adduct of thiamine diphosphate with 3-hydroxypyruvate rather than the dissociation of an aldehyde.[197] In an α-hydroxy enamine formed from dehydronation, decarboxylation, or loss of a carbonyl, the α-hydroxy group is the oxygen that was the carbonyl oxygen of the original aldehyde or the original ketone to which the ylide of thiamine diphosphate added.

In the dehydronation, decarboxylation, or loss of a carbonyl group from the adduct between an aldehyde or a ketone and thiamine diphosphate (Equations 2–51, 2–54, and 2–57), as in the dehydronation, decarboxylation, or loss of a carbonyl or acyl group from the external pyridoximine between an amino acid and pyridoxal 5′-phosphate (**2–6** and Equations 2–4, 2–5, and 2–7), the **σ bond to be broken must be parallel to the π molecular orbital system of the double bond between carbon 2 and nitrogen 3 of the thiamine** and, by extension, the π molecular orbital system of the whole weakly aromatic heterocycle of the thiazole ring. This alignment permits the overlap necessary for the electronegativity of the cationic iminio nitrogen to withdraw electron density from the σ bond between the α carbon and the dissociating electrophile

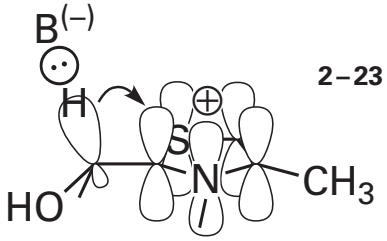

2–23

and this electron withdrawal weakens that σ bond. The electron density in the occupied bonding molecular orbital of the σ bond is withdrawn into the unoccupied antibonding π molecular orbital of the thiazole that has two lobes in phase over carbon 2 and nitrogen 3.

Analogues of 2-oxo carboxylic acids, such as succinylphosphonate

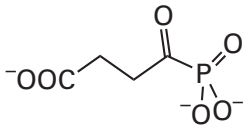

2–24

in which a phosphonate replaces a carboxylate, are excellent inhibitors of enzymes that use thiamine diphosphate prosthetically to decarboxylate the respective 2-oxo carboxylates.[198] They inhibit the enzyme by forming the usual adduct between its thiamine diphosphate and their respective carbonyl groups, but there is then no carboxylate to dissociate as carbon dioxide. In the complex between the adduct of thiamine diphosphate and methyl acetylphosphonate bound in the active site of pyruvate dehydrogenase (acetyl-transferring), the enzyme holds the σ bond between the α carbon and the phosphorus, which is the analogue of the σ bond between the α carbon and the carboxylate carbon in the normal reaction, almost perfectly parallel to the π molecular orbital system of the thiazolium ring and normal to its plane (Figure 2–5B).[175] The same orientation is observed in the complex between methyl benzoylphosphonate and thiamine diphosphate in the active sites of benzoin aldolase from *P. fluorescens*[199] and benzoylformate decarboxylase from *P. putida*.[200] One of the interactions dictating this alignment is the hydrogen bond between the 4′-amino group of the 4′-aminopyrimidinyl group in thiamine diphosphate and the hydroxy group of the adduct.

The α-hydroxy enamine that is the immediate product of dissociation of the electrophile from the adduct between thiamine diphosphate and an aldehyde or ketone (Equations 2–51, 2–54, and 2–57) is now nucleophilic at its α carbon

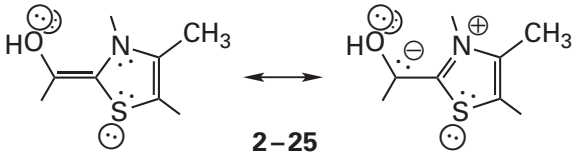

2–25

In the resonance form that places a nucleophilic lone pair of electrons on the exocyclic carbon, the thiazole ring is aromatic. Consequently, even though the aromaticity is weak, this carbon should be somewhat more anionic and nucleophilic than the carbon in an acyclic enamine. Nevertheless, in 2-(1′-methoxyethylidene)-2,3-dihydro-3,4-dimethylthiazole

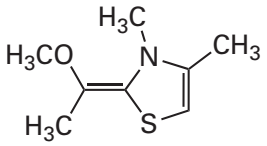

2–26

a methoxy analogue of an α-hydroxy enamine that incorporates a thiazole, synthesized[201]as a mixture of the *E* and *Z* isomers, no rotation around its exocyclic double bond could be detected by nuclear magnetic resonance spectroscopy at 100 °C, a fact indicating that, in spite of the aromaticity of the zwitterionic resonance form, the neutral resonance form of **2–25**, the α-methoxy enamine, is the major contributor to its electronic structure.

An **α-hydroxy enamine formed from thiamine** itself, by decarboxylation of the adduct between thiamine and a 2-oxo carboxylic acid (Equation 2–54), is unstable and **decomposes in solution** in a reaction that rapidly cleaves the bond between nitrogen 3 and the 4′-aminopyrimidine.[202] The properties of this decomposition suggest that it is a pericyclic reaction. It is thought that the enzymes using thiamine diphosphate prosthetically avoid this decomposition, which would be catastrophic, by sterically preventing their thiamines from assuming the conformation necessary for the pericyclic reaction to occur.[203]

While the respective α-hydroxy enamines that incorporate the thiazole of thiamine diphosphate can be observed spectroscopically as intermediates while enzymatic reactions are occurring,[204] they are normally in a low molar ratio to the active sites present. It has been possible, however, to **trap such α-hydroxy enamines** within the active sites of enzymes. In the normal reaction catalyzed by transketolase from *S. cerevisiae*, the α-hydroxy enamine that incorporates the thiazole of thiamine diphosphate is formed reversibly and in low yield from D-xylulose 5-phosphate (Equation 2–56) or a homologous ketone, but one forms irreversibly in the active site in the absence of an aldehyde that can act as an acceptor by the decarboxylation of 3-hydroxypyruvate, which is not a natural substrate for the enzyme. 2-(1″,2″-Dihydroxyethylidene)-2,3-dihydrothiamine diphosphate (Equation 2–57), the α-hydroxy enamine trapped in this way, is stable enough to be observed crystallographically (Figure 2–5C).[176] In this complex between the active site of transketolase and this α-hydroxy enamine that incorporates the thiazole, the hydrogen bonds between the α-hydroxy group of the initial adduct and the imidazolyl group and the 4′-imino group of the 4′-iminopyrimidine (Figure 2–5B) remain intact. 2-(1″-Hydroxyethylidene)-2,3-dihydrothiamine diphosphate (**2–22**), the α-hydroxy enamine formed by the decarboxylation of pyruvate, has been observed crystallographically in the active site of 1-deoxy-D-xylulose-5-phosphate synthase from *Deinococcus radiodurans*, and the same two hydrogen bonds also remain intact.[186] Because it is so basic, however, an α-hydroxy enamine incorporating the thiazole of thiamine diphosphate in the active site of an enzyme usually becomes adventitiously hydronated during the time required to make crystallographic measurements.[205,206] An α-hydroxy enamine that incorporates the thiazole of thiamine diphosphate has also been stabilized so that it can be trapped transiently in the active site of benzoylformate decarboxylase by using 4-nitrobenzoylformate as a substrate[207] rather than benzoylformate. The nitro group withdraws electron density from the basic carbanionic α carbon, discourages its hydronation, and stabilizes the α-hydroxy enamine.

The **π molecular orbital system of an α-hydroxy enamine that incorporates a thiazole** is formed from the *p* orbitals of six atoms

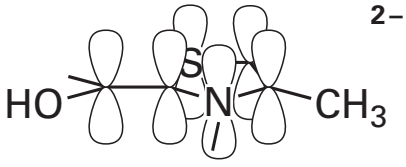

2–27

as is the case in 5-methylene-1,3-cyclopentadiene. The π molecular orbital system of an α-hydroxy enamine that incorporates a thiazole is occupied by eight electrons. In the crystallographic molecular model of 2-(1″,2″-dihydroxyethylidene)-2,3-dihydrothiamine diphosphate (Equation 2–57) in the active site of transketolase (Figure 2–5C)[176] and that of 2-(1″-hydroxyethylidene)-2,3-dihydrothiamine diphosphate (**2–22**) in the active site of 1-deoxy-D-xylulose-5-phosphate synthase,[186] the α carbon is trigonal and its two substituents, the hydroxy group and the hydroxymethyl group or the methyl group, respectively, are coplanar with the thiazole as expected from **2–27**. This coplanarity is not because of the two hydrogen bonds to the α-hydroxy group because it is only in the initial tetrahedral adduct, in which the hydroxy group is out of the plane of the thiazole, that the hydrogen bonds have the optimal geometry (Figure 2–5B); rather, it must be an electronic requirement. The π molecular orbital system contains four pairs of π electrons in its six molecular orbitals. The occupancy of the antibonding orbital of lowest energy by two electrons makes it electron-rich at the exocyclic carbon over which there is a full lobe.

Because of its electron excess, the α-hydroxy enamine that incorporates a thiazole is basic and nucleophilic at its α carbon. The simplest manifestation of this basicity is that the α carbon is readily **hydronated by an acid**. This is what occurs to the α-hydroxy enamine formed in the active site of pyruvate decarboxylase (Equation 2–54) in the next step of the enzymatic mechanism. The hydron that is added then becomes the hydrogen of the aldehyde in the acetaldehyde (Equation 2–53) as the resulting adduct dissociates (reverse of Equation 2–49).

In solution, the hydronation of the α carbon of an α-hydroxy enamine that incorporates a thiazole (see Equation 2–51) is slow. For the α-methoxy enamine 2-(methoxyphenylmethylidene)-3,4-dimethylthiazole the rate of hydronation by a molecule of water,[208] a weak acid ($pK_a = 15.5$), is 0.02 M^{-1} s^{-1}. For the α-hydroxy enamine, 2-(hydroxyphenylmethylidene)-4′-deamino-4′-hydroxythiamine, the rate constants of hydronation by a series of general acids[191] with values of pK_a between 6 and 12 are in the range 1000–100,000 M^{-1} s^{-1}. These latter rate constants are independent of the pK_a of the general acid and are far less than the encounter-controlled limit that would be observed for such an exothermic transfer of a hydron to a heteroatomic base (Figure 1–1), but they are consistent with the slow rate constants for the hydronation of carbon. These slow rates are a further indication that the resonance form with the neutral enamine, in which the thiazole is not aromatic and the carbon is not anionic, is the major contributor to the electronic structure of **2–25**,[189] just as the resonance form of an enamine, in which the pair of electrons is on the nitrogen, is the major contributor to its electronic structure. They also indicate that the density of negative charge on the nucleophilic α carbon in an α-hydroxy enamine that incorporates a thiazole is minuscule.

Another manifestation of the nucleophilicity of the α carbon in an α-hydroxy enamine that incorporates a thiazole is its **addition to a carbonyl group.** In solution, thiamine, like cyanide (Equation 2–50), can catalyze the **formation of α-hydroxy ketones**,[158] for example, the benzoin condensation of benzaldehyde and acetaldehyde[188]

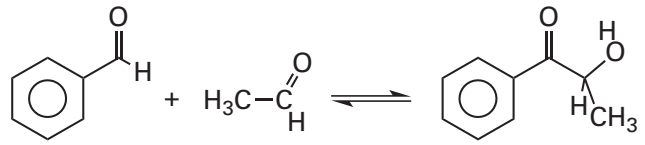

(2–58)

In this reaction the carbonyl carbon of the acetaldehyde, as an electrophile, has replaced the hydrogen that was originally on the α carbon of the benzaldehyde and that dissociated as a hydron, an electrophile, from the adduct between benzaldehyde and thiamine. The hydron that has dissociated is replaced by the acetaldehyde through the nucleophilic addition of the α-hydroxy enamine that incorporates the thiamine to the carbonyl carbon

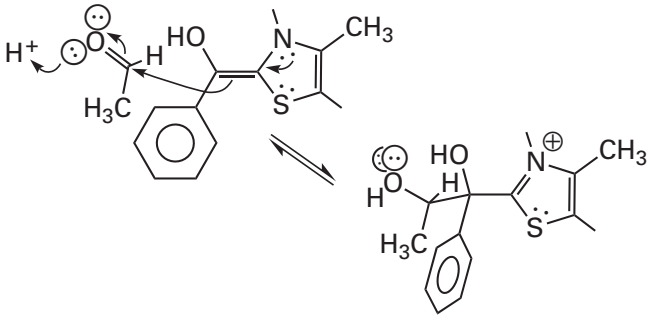

(2–59)

This nucleophilic addition is accompanied by restoration of the aromaticity in the thiazolium ring. The product, 2-hydroxy-1-phenyl-1-propanone, then dissociates in the reverse of the original formation of the adduct between benzaldehyde and thiamine.

In the transketolase reaction (Equations 2–56 and 2–57), the aldehyde that is a reactant, other than the one that has dissociated as a product, adds to the α-hydroxy enamine that incorporates thiamine diphosphate to produce the adduct between the ketone that is the other product and thiamine diphosphate. The ketone that is the product then dissociates from the adduct.

There are also instances in which an α-hydroxy enamine that incorporates a thiazole **adds as a nucleophile to even weaker electrophiles** than an aldehyde, such as an *N*-acylimine in solution,[209] the carbonyl group of a 2-oxo carboxylic acid in the active site of acetolactate synthase,[210] or the β carbon of an α,β-unsaturated carboxylic acid in a Michael addition within the active site of 2-succinyl-6-hydroxy-2,4-cyclohexadiene-1-carboxylate synthase.[211,212] In the active site of 2-succinyl-5-enolpyruvyl-6-hydroxy-3-cyclohexene-1-carboxylic-acid synthase from *E. coli*, 2-(1″-hydroxy-3″-carboxypropylidene)-2,3-dihydrothiamine diphosphate, the α-hydroxy enamine formed by decarboxylation of the adduct between 2-oxoglutarate and thiamine diphosphate, participates in a **Michael addition** to a carbon–carbon double bond in isochorismate. In a crystallographic molecular model of the α-hydroxy enamine in the active site in the absence of isochorismate,[213] the α carbon is not planar but tetrahedral because a lone pair of electrons localized on it is the donor in a hydrogen bond with the 4′-amino group of thiamine diphosphate. It has been proposed that this hydrogen bond concentrates the nucleophilic electron density on the α carbon in preparation for the Michael addition to increase its nucleophilicity.

If the α carbon of the α-hydroxy enamine that incorporates thiamine diphosphate adds to a hydron, the adduct between thiamine diphosphate and an aldehyde is formed;[214] if it adds to carbon dioxide, the adduct between thiamine diphosphate and a 2-oxocarboxylic acid is formed; and if it adds to an aldehyde or ketone, the product of addition between thiamine diphosphate and an α-hydroxy ketone is formed (Equations 2–51, 2–54, and 2–57). Each of these reactions can be considered to be the **addition of an electrophile to the synthon**

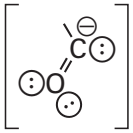

2–28

that was produced by the dissociation of an electrophile from a carbonyl carbon. Considered in this way, the enzymatic reactions in which thiamine diphosphate is used as a prosthetic group are reactions in which one electrophile dissociates from this synthon and a different electrophile adds. In pyruvate decarboxylase (Equation 2–53), a hydron substitutes for carbon dioxide; in transketolase (Equation 2–56), one aldehyde substitutes for another; and in 1-deoxy-D-xylulose-5-phosphate synthase[215,216]

$$\text{pyruvate} + \text{D-glyceraldehyde 3-phosphate} + H^+ \rightleftharpoons CO_2 + \text{1-deoxy-D-xylulose 5-phosphate} \qquad (2\text{–}60)$$

an aldehyde substitutes for carbon dioxide. In these exchanges of the one electrophile for another, the initial electrophile leaves the initial adduct between thiamine diphosphate and the initial aldehyde or ketone, and the electrophile substituting for it reacts with the α-hydroxy enamine to form the final carbonyl adduct of thiamine diphosphate. These carbonyl adducts of thiamine diphosphate can be detected and quantified as the enzymatic reaction is occurring.[217]

As has already been mentioned in passing, the final step in a reaction catalyzed by thiamine diphosphate, following nucleophilic addition of the electrophile to the α-hydroxy enamine that incorporates thiamine diphosphate, is generation of the new aldehyde or ketone by **dissociation of the thiazole from the new carbonyl adduct.** This dissociation is assisted by the fact that the hydroxy group on the incipient carbonyl carbon in the adduct is fairly acidic ($pK_a = 12$),[192] and the removal of its hydron by a base[192,193] either prior to or during the dissociation of the product catalyzes the formation of the product

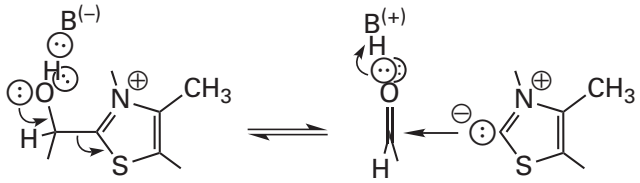

(2–61)

In summary, the **prototypical mechanism** of an enzyme using thiamine diphosphate prosthetically has the following steps. The hydron on carbon 2 of the thiamine diphosphate is removed. The resulting ylide of the thiamine diphosphate adds to the carbonyl

group of an aldehyde or a ketone to form the adduct, the hydroxy group of which ends up in hydrogen bonds to a histidine from the protein and the 4′-amino group of the 4′-aminopyrimidine of thiamine diphosphate (Figure 2–5B), one of which has provided the hydron on the hydroxy group. An electrophile—a hydron, carbon dioxide, or an aldehyde—leaves the α carbon of the adduct to produce the α-hydroxy enamine that incorporates the thiazole (Figure 2–5C). A different electrophile adds to the α-hydroxy enamine to form a different adduct between thiamine diphosphate and a different aldehyde or ketone. The hydron of the hydroxy group of the new carbonyl adduct is removed either before or while the new aldehyde or ketone dissociates, and the ylide of thiamine diphosphate is hydronated on carbon 2.

The puzzle is to define the roles of the 4′-amino group of the 4′-aminopyrimidine in these steps. In the active site of an enzyme, the 4′-amino group of thiamine diphosphate usually forms a hydrogen bond to the α-hydroxy group in both the initial adduct and the α-hydroxy enamine that incorporates the thiazole and abuts the α carbon (Figure 2–5B and 2–5C).[175,176,186] Often there is a histidine in the active site that also forms a hydrogen bond to the same hydroxy group. These dispositions certainly imply that these are the catalytic acids and bases acting on the α-hydroxy group and that the 4′-amino group is a catalytic acid–base that is able to act on the α carbon. One of them hydronates the oxygen of the carbonyl group as the ylide of thiamine diphosphate adds to its carbon, and one of them dehydronates the α-hydroxy group as the ylide of the thiamine dissociates from final adduct to give the ketone or aldehyde that is the final product. In the crystallographic molecular model of 2-(1″,2″-dihydroxyethylidene)-2,3-dihydrothiamine diphosphate (Equation 2–57) occupying the active site, nitrogen 4′ of the 4′-amino-pyrimidinyl group is 0.30 nm from the oxygen of the α-hydroxy group but it is also 0.30 nm from the α carbon of the α-hydroxy enamine (dashed lines in Figure 2–5C). The distance to the α carbon atom is well within van der Waals contact, and this fact indicates that this nitrogen has been forced up against the α carbon by the enzyme. These orientations and distances should permit the 4′-amino group to swing over to the α carbon from the hydroxy group of the α-hydroxy enamine and hydronate it, if indeed the α carbon is supposed to be hydronated,[218] or the 4′-imino group to swing over to the α carbon in the initial adduct and dehydronate it, if indeed it is supposed to be dehydronated. While these movements are occurring, the imidazolyl group of the histidine would maintain the hydron on the hydroxy group.

The next piece of the puzzle is the identity of **the catalytic base that removes the hydron from carbon 2** of thiamine diphosphate to form the ylide and initiate the reaction. Up to this point it has been assumed that it is the molecule of water between the 4′-amino group and carbon 2 (Figure 2–5). It has been observed, however, that, in a single turnover of pyruvate decarboxylase from *S. cerevisiae*, 45% of the tritium in [2-^{3}H]thiamine diphosphate in the active site becomes the hydrogen of the formyl group in the acetaldehyde that is the product.[219] It seems to be the case that the 4′-amino nitrogen of the 4′-aminopyrimidinyl group has to hydronate the α carbon of the α-hydroxy enamine after the initial adduct of pyruvate decarboxylates (Figure 2–5C). If so, nitrogen 4′ of the 4′-imino tautomer of the 4′-aminopyrimidinyl group would seem to be the base that removes the hydrogen from carbon 2 of thiamine diphosphate.[170]

In the crystallographic molecular model of the unoccupied active site (Figure 2–5A), however, nitrogen 4′ is separated from carbon 2 of the thiamine diphosphate by the fixed molecule of water. If the base that removes the triton from carbon 2 in the normal sequence of steps is this molecule of water, relaying the basicity of either the 4′-imino tautomer or the histidine, it should leave the active site with the triton because it is displaced by the carbonyl oxygen of the reactant when it associates. Consequently, the fact that tritium is transferred in high yield seems to argue against this molecule of water as a candidate for the base that removes the hydron from carbon 2 in the usual reaction and seems to leave only the 4′-imino group of thiamine diphosphate.

Nevertheless, the foregoing dispositions and considerations are consistent with the following sequence of events. Before the pyruvate associates with the active site of pyruvate decarboxylase, displacing the molecule of water, the molecule of water freely rotates to equilibrates the triton on carbon 2 of thiamine diphosphate with the hydron on its 4′-imino group. The fact that exchange of the hydrogen on carbon 2 with a hydrogen in the solvent when an active site is unoccupied by a reactant is much slower than the turnover of a reactant would give the molecule of water sufficient time to accomplish this equilibration without dissociating into the solution. At an instant when the ylide of thiamine diphosphate and the tritiated 4′-imino group are

present, the carbonyl group of the pyruvate displaces the molecule of water while Histidinium 640 hydronates its oxygen. The decarboxylation occurs, producing the α-hydroxy enamine. The 4′-[*N*-^{3}H]amino group of the thiamine diphosphate tritonates the α carbon of the α-hydroxy enamine. During dissociation of the tritiated product from its adduct with thiamine diphosphate, the resulting 4′-imino group or the imidazolyl group of the histidine removes the hydron from the α-hydroxy group that the imidazolino group added to it. The only problem with this explanation is that 45%, not less than 33%, of the tritium is transferred.

In the active site of transketolase occupied by 2-(1″,2″-dihydroxyethylidene)-2,3-dihydrothiamine diphosphate (Figure 2–5C), the 4′-imino group is 0.31 nm from carbon 2 of the thiazole of the α-hydroxy enamine, well within van der Waals contact, and the imidazolyl group of the histidine is forming a hydrogen bond with the α-hydroxy group. The only problem with assigning to the 4′-imino group the role of removing the hydron from carbon 2 of the thiamine to initiate the reaction is the **orientation of nitrogen 4′**. Unlike the molecule of water in the unoccupied active site containing the unmodified thiamine diphosphate, which would seem to remove the hydron from carbon 2 in the absence of a substrate, nitrogen 4′ of the prosthetic thiamine diphosphate is not in the plane of the thiazole (Figure 2–5A) where the hydrogen to be removed is located (Equation 2–46) to initiate the reaction, nor is it in the plane of the thiazole (Figure 2–5C) in the location in which the hydron is to be added to the ylide to complete the reaction. One possibility is that, both after the reactant adds at the beginning and following the dissociation of the carbon–carbon bond to the incipient carbonyl carbon at the end, the thiazole pivots to place nitrogen 4′ in its plane.

Both the conversion of the carbonyl in the reactant and the hydronated thiazole in thiamine diphosphate into the adduct between the two and a hydron in the first step of the reaction and the conversion of the adduct between what will be the carbonyl in the product and thiamine diphosphate into the carbonyl of the product and thiamine diphosphate hydronated at carbon 2 at the end of the reaction are formally electrophilic aromatic substitutions. In an actual electrophilic aromatic substitution, the carbonyl group would first add to carbon 2 from the face of the thiazole opposite the 4′-aminopyridine and produce a tetrahedral carbon on which there would be a dramatically acidic hydrogen now pointed at nitrogen 4′ and now in the correct orientation for transfer as a hydron. Even though this gedanken view of the situation is energetically unlikely because the electrophile is so weak and carbon 2 is already so acidic, the removal of the hydron from carbon 2 and the addition of the carbonyl group to carbon 2 could actually be a concerted electrophilic aromatic substitution. By this mechanism in the approach of the system to the roughly tetrahedral transition state, the incoming carbonyl carbon would push the hydrogen on carbon 2 toward the nitrogen of the unhydronated 4′-imino nitrogen, weaken its bond to the carbon, and align it for removal by the 4′-imino nitrogen while the bond to the carbonyl carbon is being formed; or in reverse, the dissociation of the adduct, the incoming hydronated 4′-amino group would push the bond between carbon 2 and the α carbon out of the plane of the thiazole and the hydronated 4′-amino group would enter the almost tetrahedral transition state from a position oblique to the plane of the thiazole.

In a few of the reactions that rely on a prosthetic thiamine diphosphate, the excess electron density of an α-hydroxy enamine that incorporates thiamine diphosphate provides push to expand the π molecular orbital system further out onto and beyond the β carbon of the aldehyde or ketone that was the reactant. One example is the elimination from the β carbon that occurs following decarboxylation of the unnatural adduct formed in the active site of pyruvate decarboxylase from *E. coli* between fluoropyruvate and thiamine diphosphate[220,221]

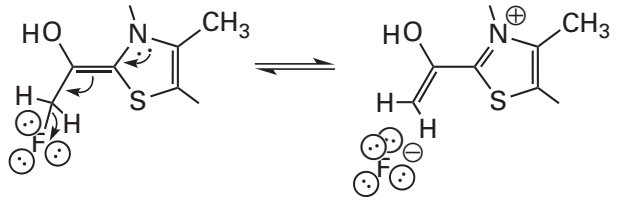

(2–62)

Another example is the elimination from the β carbon that occurs following dissociation of the aldehyde, D-glyceraldehyde 3-phosphate, from the natural adduct formed in the active site of phosphoketolase from *Bifidobacterium breve* between D-xylulose 5-phosphate and thiamine diphosphate[205]

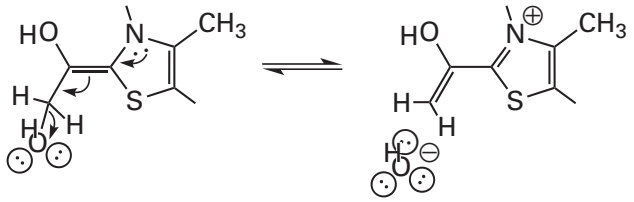

(2–63)

A third example is the elimination from the β carbon that occurs following dissociation of a hydron from the natural adduct formed in the active site of N^2-(2-carboxyethyl)arginine synthase from *Streptomyces clavuligerus* between D-glyceraldehyde 3-phosphate and thiamine diphosphate[222]

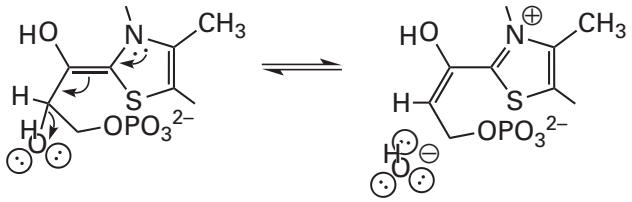

(2–64)

Each of these three eliminations creates an enol incorporating the α carbon and the β carbon that is conjugated to the iminium within the thiamine diphosphate. In the cases of pyruvate decarboxylase and phosphoketolase, the same enol is hydronated at the β carbon, which is a methylene (Equation 2–63), to form 2-acetylthiamine diphosphate.

In the case of N^2-(2-carboxyethyl)arginine synthase, the removal of a hydron from the α-hydroxy group creates an enolate that pushes out the phospho group to **extend the π molecular orbital system onto the γ carbon** while forming 2-(acryloyl)thiamine diphosphate[223]

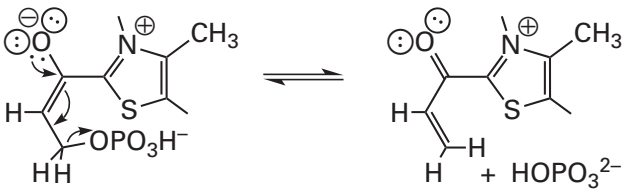

(2–65)

To complete the enzymatic reaction, the phosphate that just left is replaced by the α-amino group of an L-arginine that adds as a nucleophile to the α,β-unsaturated ketone in the reverse of Equation 2–65. The resulting enolate, in which the α-amino group of L-arginine has replaced the phospho group, is then hydronated on the β carbon to give the ketone, and the resulting 2-acylthiamine diphosphate is hydrolyzed with the ylide of thiamine diphosphate as the leaving group to produce thiamine diphosphate and the product N^2-(2-carboxyethyl)-L-arginine.

There are enzymatic reactions in which adducts of thiamine diphosphate are oxidized or reduced. For example, in the reactions catalyzed by both pyruvate synthase[224]

$$\begin{aligned}\text{pyruvate} + 2\ \text{oxidized ferredoxin} \\ + \text{HSCoA} \rightleftharpoons \text{CO}_2 + \\ 2\ \text{reduced ferredoxin} + \text{H}^+ + \text{acetyl-SCoA}\end{aligned} \quad (2\text{–}66)$$

and pyruvate oxidase[225]

$$\begin{aligned}\text{pyruvate} + \text{O}_2 + \text{HOPO}_3^{2-} + \text{H}^+ \rightleftharpoons \\ \text{CO}_2 + \text{H}_2\text{O}_2 + \text{acetyl phosphate}\end{aligned} \quad (2\text{–}67)$$

the pyruvate is oxidized in the forward direction by two electrons in an oxidation that turns it into carbon dioxide and an acetyl group. As such, these two reactions are **oxidative decarboxylations**. In both active sites, the 2-(1″-hydroxyethylidene)-2,3-dihydrothiamine diphosphate (**2–22**) produced by decarboxylation of the adduct of pyruvate and thiamine diphosphate (Equation 2–54) is oxidized and in the process reduces oxidized ferredoxin or reduces an oxidized prosthetic flavin, which in turn reduces molecular oxygen to H_2O_2.

2-(1″-Hydroxyethylidene)-2,3-dihydrothiamine diphosphate (**2–22**) is an electron-rich α-hydroxy enamine, the oxidation of which by the transfer of two electrons restores the aromaticity of the thiazole. Its oxidation in the respective active sites of these two enzymes proceeds in **two successive one-electron steps**. In the active site of pyruvate synthase in the forward direction, each of the two molecules of oxidized ferredoxin, one after the other, can accept only a single electron from the α-hydroxy enamine; and in the reaction catalyzed by pyruvate oxidase from *L. plantarum*, the electrons have been shown to be transferred in the forward direction, one at a time, from the α-hydroxy enamine to the prosthetic flavin in the active site.[226] For both pyruvate synthase from *Moorella thermoacetica*[227,228] and pyruvate oxidase from *L. plantarum* ,[226] the **intermediate radical cation**

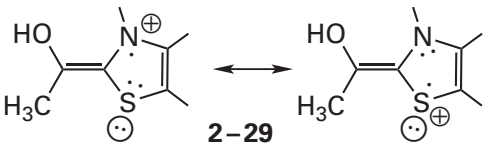

2–29

resulting from transfer of just one electron from 2-(1′′-hydroxyethylidene)-2,3-dihydrothiamine diphosphate during the normal catalytic reaction has been observed; and in the case of pyruvate oxidase, it is stable enough to be observed crystallographically.[229] In cyclic voltammetry, 2-(1′-methoxyethylidene)-2,3-dihydro-3,4-dimethylthiazole (**2–26**) is an electrochemical one-electron reductant with a reduction potential of +70 mV relative to a standard hydrogen electrode.[230] By increasing its π electron density, relative to a hydrogen, the methoxy substituent decreases the reduction potential of the enamine by 250 mV, from +320 to +70 mV, and an unhydronated hydroxy group should decrease it even further. 2-(1′-Hydroxyethylidene)-2,3-dihydro-3,4-dimethylthiazole is able to reduce an analogue of flavin nonenzymatically.[231]

Upon transfer of the second electron, the 2-(1′′-hydroxyethylidene)-2,3-dihydrothiamine diphosphate (**2–22**) in each of the active sites has been converted into **2-acetylthiamine diphosphate**

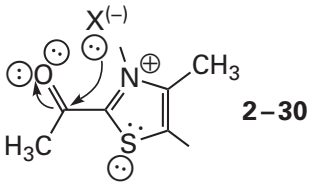

2–30

which then engages in a nucleophilic substitution with either coenzyme A or phosphate, with the ylide of thiamine diphosphate as the leaving group.

Oxalate oxidoreductase

$$\text{oxalate} + 2\ \text{oxidized ferredoxin} \rightleftharpoons 2\ CO_2 + 2\ \text{reduced ferredoxin} \qquad (2\text{–}68)$$

from *M. thermoacetica* is related (24% identity; 3.0 gap percent) to pyruvate synthase (Equation 2–66) and also catalyzes an oxidative decarboxylation in which the two electrons generated in the reaction are transferred to two molecules of oxidized ferredoxin. In this instance, however, the adduct between thiamine diphosphate and oxalic acid (Equation 2–49; $R_1 = COO^-$; $R_2 = OH$) rather than thiamine diphosphate and pyruvate (Equation 2–49; $R_1 = COO^-$; $R_2 = CH_3$) is formed initially

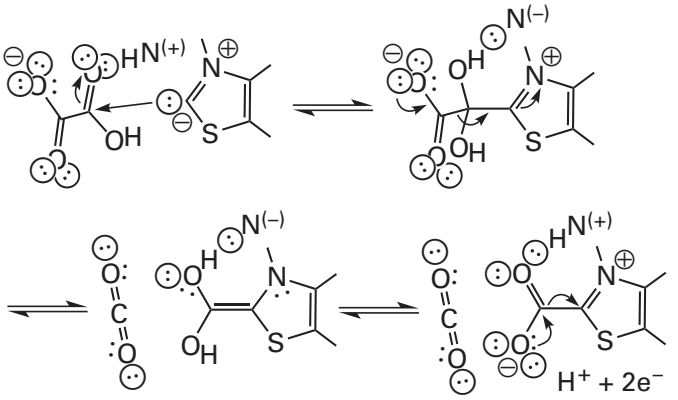

(2–69)

This nucleophilic substitution is an example of the **ylide of thiamine diphosphate that adds to an acyl group** rather than a carbonyl group. The reactions catalyzed by pyruvate synthase (Equation 2–66) and pyruvate oxidase (Equation 2–67) in reverse are also examples of addition of the ylide of thiamine diphosphate to acyl derivatives, acetyl-SCoA and acetyl phosphate, respectively.

The adduct between thiamine diphosphate and oxalic acid in the active site of oxalate oxidoreductase is then decarboxylated, as in the case of pyruvate in the active site of pyruvate synthase. The resulting **dihydroxymethylenethiamine diphosphate**, an even more electron-rich and more reducing α-hydroxy enamine, is then oxidized by transfer of two electrons to two successive oxidized ferredoxins. The resulting intermediate is a derivative of carbonic acid from which the ylide of thiamine diphosphate leaves while the second CO_2 is formed.

Both the initial adduct between the ylide of thiamine diphosphate and the oxalate and dihydroxymethylenethiamine diphosphate have been observed in crystallographic molecular models of oxalate oxidoreductase from *M. thermoacetica*.[232] As expected, the catalytic acid–base that forms a hydrogen bond to the α-hydroxy group in both of these intermediates is nitrogen 4′ of the 4′-aminopyrimidinyl group in thiamine diphosphate, but unlike the situation in the active sites of pyruvate dehydrogenase (acetyl-transferring) (Figure 2–5B) and transketolase (Figure 2–5C), the other participant in a hydrogen bond with the α-hydroxy group is the guanidinio group of an arginine, which would ensure that the hydron on the hydroxy group is within the hydrogen bond to nitrogen 4′.

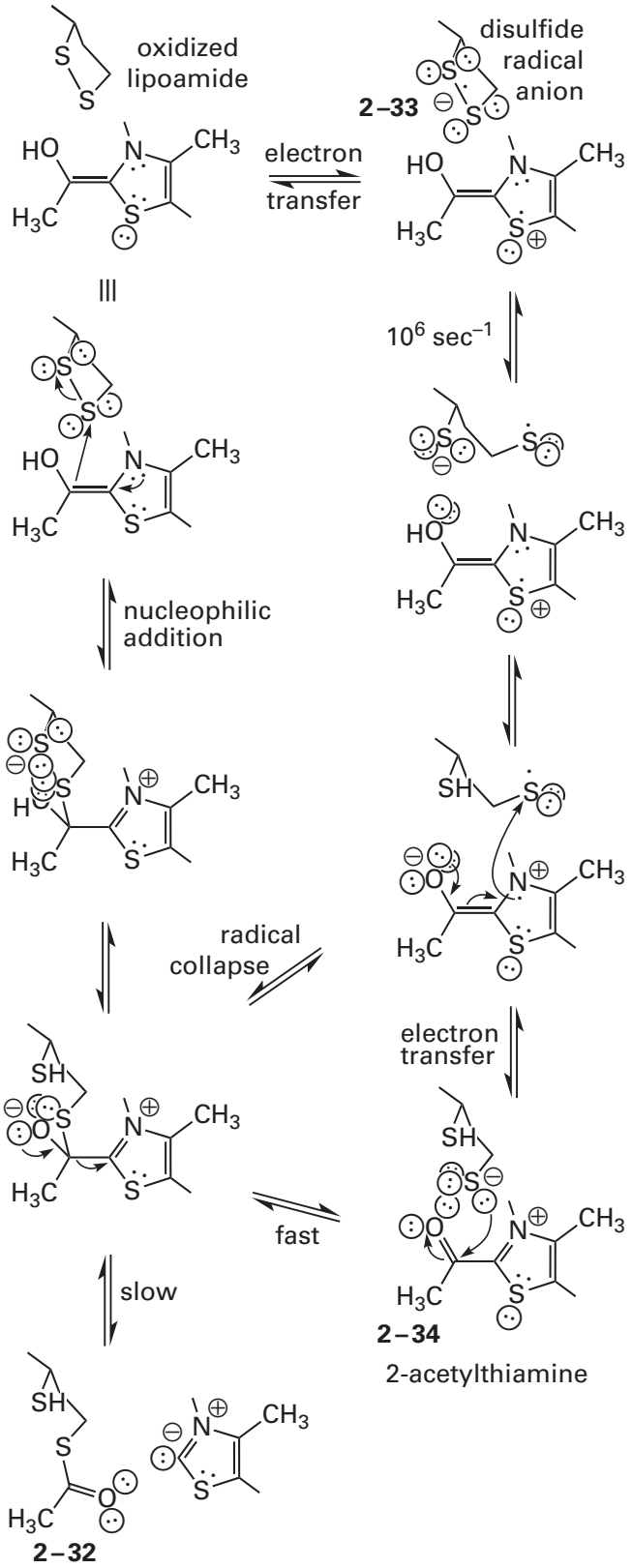

Figure 2-7: Formation of N^6-(*S*-acetyldihydrolipoyl)lysine in the reaction catalyzed by pyruvate dehydrogenase (acetyl-tranferring). There are two possibilities for the mechanism of this reaction, electron transfer[234] or heterolysis.[233] In the first step of the former mechanism (top line and to the right), the electron-rich enamine loses an electron to the disulfide to form the radical anion of the disulfide and radical cation of the thiamine. The radical anion of a disulfide fragments to sulfido group and thiyl radical and the second electron is transferred to the thiyl radical, to give the dithiolate and 2-acetylthiamine. The distal sulfido group adds nucleophilically to the carbonyl carbon of the 2-acetylthiamine to form a tetrahedral intermediate. Another alternative is to have the two radicals collapse directly to the tetrahedral intermediate. In the first step of the heterolytic mechanism (middle left), the enamine as a nucleophile displaces a sulfido group from the disulfide and forms the tetrahedral intermediate. At this point the mechanisms converge and the acetyl group is transferred through the tetrahedral intermediate to one of the sulfido groups of N^6-(dihydrolipoyl)lysine.

The reactions catalyzed by the three related enzymes **pyruvate dehydrogenase (acetyl-transferring), oxoglutarate dehydrogenase (succinyl-transferring), and 3-methyl-2-oxobutanoate dehydrogenase (2-methylpropanoyl-transferring)** are also oxidative decarboxylations. For example, the α-hydroxy enamine incorporating thiamine diphosphate that is formed immediately upon decarboxylation of the adduct of pyruvate and thiamine diphosphate (Equation 2–54) by pyruvate dehydrogenase (acetyl-transferring) reduces the disulfide in N^6-(lipoyl)lysine

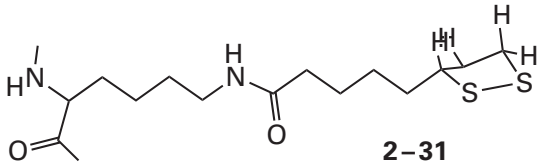

to produce the acetyl thioester of N^6-(dihydrolipoyl)-lysine (**2–32** in Figure 2–7).[233,234] N^6-(Lipoyl)lysine is a prosthetic group that is covalently attached through an amide between lipoic acid and the 6-amino group of a lysine in the polypeptide of a different enzyme, dihydrolipoyllysine-residue acetyltransferase, that forms a noncovalent complex with pyruvate dehydrogenase (acetyltransferring) and presents the lipoyl group to its active site. In the active sites of oxoglutarate dehydrogenase (succinyl-transferring) and 3-methyl-2-oxobutanoate dehydrogenase (2-methylpropanoyl-transferring), the homologous adducts between 2-oxoglutarate or 3-methyl-2-oxobutanoate are formed and decarboxylated, and the resulting succinyl group or 2-methylpropanoyl group is transferred to N^6-(lipoyl)lysine

in the respective acceptor.* There are two possible mechanisms by which the reductive transfer of an acetyl group to N^6-(lipoyl)lysine in the active site of pyruvate dehydrogenase (acetyl-transferring) could take place.

One possibility is a **nucleophilic substitution**. The α-hydroxy enamine that incorporates thiazole, 2-(1′-hydroxyethylidene)-2,3-dihydro-3-benzyl-4-methylthiazole (**2–35**)

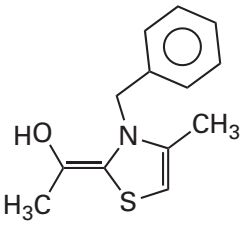

2–35

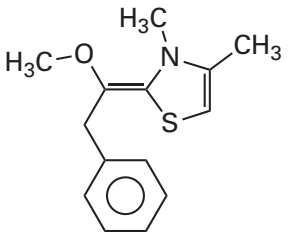

2–36

is nucleophilic enough to participate in a nucleophilic substitution at one of the two sulfurs in an acyclic disulfide,[233] and the α-methoxy enamine 2-(1′-methoxy-2′-phenylethylidene)-2,3-dihydro-3,4-dimethylthiazole (**2–36**) is nucleophilic enough to participate in an intramolecular nucleophilic substitution at one of the sulfurs in the cyclic disulfide of an ester of lipoic acid.[235] If one of these sulfurs is methylated, to mimic the hydronation that would occur in the active site of an enzyme, the α-methoxy enamine 2-(1′-methoxy-2′-phenylethylidene)-2,3-dihydro-3,4,5-trimethylthiazole will participate in a nucleophilic substitution with the other sulfur.[236]

All these results suggest that, within the active site of pyruvate dehydrogenase (acetyl-transferring), 2-(1″-hydroxyethylidene)-2,3-dihydrothiamine diphosphate (**2–22**), the α-hydroxy enamine produced by the decarboxylation of the adduct between thiamine diphosphate and pyruvate (Equation 2–54), should be nucleophilic enough to participate as the nucleophile in a concerted nucleophilic substitution with the disulfide of N^6-(lipoyl)lysine as the electrophile (left side of Figure 2–7). The nucleophilic attack of the electron-rich α-hydroxy enamine resembles the nucleophilic attack of a sulfido group during a thiol–disulfide exchange.[237] If the disulfide is hydronated on the sulfur that is to leave, the nucleophilic substitution liberates one of the sulfurs as a thiol while the other sulfur becomes bonded to the α carbon of the α-hydroxy enamine. This nucleophilic addition of the α-hydroxy enamine creates a **tetrahedral intermediate with the thiazolium as a potential leaving group**. Upon its dissociation, initiated by removal of the hydron from the hydroxy group, the thioester would be the product, and the reaction catalyzed by the enzyme would be accomplished.

The second possibility, however, for the mechanism of pyruvate dehydrogenase (acetyl-transferring) would involve **two transfers, each of one electron**, as in the active sites of pyruvate synthase, pyruvate oxidase, and oxalate oxidoreductase, between the α-hydroxy enamine 2-(1″-hydroxyethylidene)-2,3-dihydrothiamine diphosphate and the disulfide of the oxidized N^6-(lipoyl)lysine (right side of Figure 2–7) to reduce the disulfide to the dithiol and oxidize the α-hydroxy enamine to 2-acetylthiamine diphosphate.[238] The α-hydroxy enamine formed at the active site of pyruvate dehydrogenase (acetyl-transferring) is able to reduce two equivalents of ferricyanide in two successive transfers, each of one electron.[234,238] This observation demonstrates that the radical cation of the α-hydroxy enamine that incorporates thiamine diphosphate, which is shown in the first step of the mechanism for pyruvate dehydrogenase (acetyl-transferring) and which is produced by two successive transfers, each of one electron (right side of Figure 2–7), can be formed in an active site. The radical cation of the α-hydroxy enamine 2-(1″-hydroxy-3″-carboxy-propylidene)-2,3-dihydrothiamine diphosphate, the homologue of **2–29**, has been observed in the active site of oxoglutarate dehydrogenase (succinyl-transferring) when the α-hydroxy enamine is in a complex with the enzyme.[239] The radical cation in this case, however, is believed to result from oxidation of the α-hydroxy enamine by molecular oxygen rather than by the lipoyl disulfide. It was concluded that this radical cation is the result of an adventitious side reaction. Nevertheless, this side reaction demonstrates that the radical cation can be generated in this active site.

The **radical anion of a disulfide** (**2–33**)[240,241] would also be a transient intermediate in the mechanism involving transfer of the electrons one at a time (right side of Figure 2–7). Disulfides can be reduced in two one-electron steps in a reaction

*Dihydrolipoyllysine-residue succinyltransferase and dihydrolipoyllysine-residue (2-methylpropanoyl)transferase form homologous noncovalent complexes with oxoglutarate dehydrogenase (succinyl-transferring) and 3-methyl-2-oxobutanoate dehydrogenase (2-methylpropanoyl-transferring), respectively, also presenting N^6-(dihydrolipoyl)lysine.

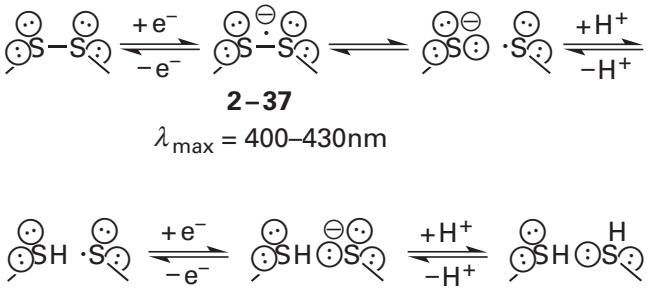

Figure 2–8: One-electron reduction of a disulfide.[240] In the first step, an electron is provided by a reductant to produce the radical anion of the disulfide, **2–37**, with a characteristic electronic absorption at 400–430 nm. This radical anion fragments rapidly (1 μs^{-1}) to form a sulfido group and a thiyl radical. The sulfido group can be hydronated, and the thiyl radical can accept a second electron to produce a second sulfido group.

involving such a radical anion of a disulfide (**2–37**) as an intermediate (Figure 2–8).[240] The one-electron reduction potential of a disulfide, however, is –400 mV.[242,243] The enzyme would have to increase the one-electron reduction potential of the disulfide in N^6-(lipoyl)lysine, for example, by hydronating one of the sulfurs,[236] or decrease the reduction potential of the α-hydroxy enamine,[230] for example, by dehydronating the hydroxy group, for productive transfer of an electron to occur.

Once it has been formed, the rate at which a radical anion of a disulfide spontaneously fragments to a sulfido group and a thiyl radical is 1 μs^{-1}, more than fast enough for this step to participate in the enzymatic reaction. In cyclic radical anions of disulfides, however, such as that of N^6-(lipoyl)-lysine (**2–31**), the equilibrium for ring opening to the sulfido group and thiyl radical is strongly in favor of the closed form, but hydronation of the radical anion of the disulfide shifts the equilibrium constant for ring opening to around 1.[241] Therefore, hydronation of the disulfide in N^6-(lipoyl)lysine by an acid in the active site either before or during transfer of the electron would be necessary both to increase its reduction potential and to promote ring opening. The pK_a of a radical anion of a disulfide is between 4 and 5.[244] The thiyl radical formed in the ring opening would then accept the second electron, either directly or by forming a bond to the radical on the α carbon of the radical cation of the α-hydroxy enamine of thiamine diphosphate by colligation. The unpaired electron in the radical cation is in the antibonding π molecular orbital with a full lobe over the α carbon.

It has been shown that **2-acetylthiamine diphosphate** (**2–30** and **2–34** in Figure 2–7), when it is formed on the active site of pyruvate dehydrogenase (acetyl-transferring), produces N^6-(*S*-acetyllipoyl)-lysine as rapidly as does the α-hydroxy enamine, 2-(1″-hydroxyethylidene)-2,3-dihydrothiamine diphosphate (**2–22**).[245] 2-Acetylthiamine diphosphate has been synthesized[246] and used as a standard to demonstrate that while pyruvate dehydrogenase (acetyl-transferring) is actively catalyzing its reaction, 0.4% of its thiamine diphosphate is present as 2-acetylthiamine diphosphate.[238] These observations have been cited as evidence for the mechanism involving the successive transfer of two electrons because it has been stated that, on the nucleophilic path (left side of Figure 2–7), 2-acetylthiamine diphosphate should not be an intermediate.[238] If the tetrahedral intermediate proposed for the nucleophilic mechanism (left side of Figure 2–7) is examined closely, however, it is clear that sulfur is the better leaving group. It necessarily follows that, in either mechanism, 2-acetylthiamine diphosphate would be formed and unformed many times before the tetrahedral intermediate would decompose to yield N^6-(*S*-acetyllipoyl)lysine.

To complete the reaction catalyzed by the complete pyruvate dehydrogenase system, the acetyl group on N^6-(*S*-acetyllipoyl)lysine is transferred to coenzyme A by dihydrolipoyllysine-residue acetyltransferase, in a simple nucleophilic substitution that liberates N^6-(dihydrolipoyl)lysine

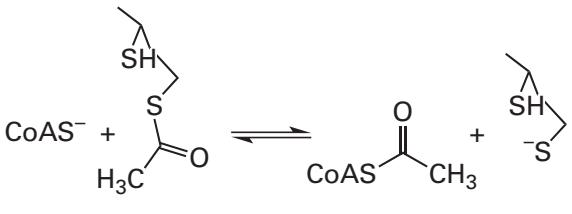

(2–70)

and N^6-(dihydrolipoyl)lysine is converted by dihydrolipoyl dehydrogenase from the reduced to the oxidized form

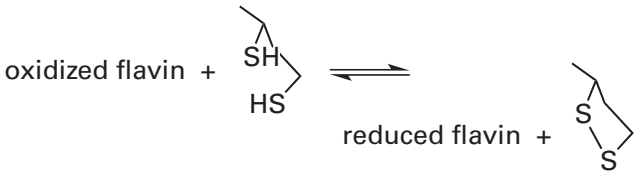

(2–71)

in an oxidation–reduction catalyzed by the prosthetic group flavin.

Suggested Reading

Kluger, R., Chin, J., and Smyth, T. (1981) Thiamin-catalyzed decarboxylation of pyruvate: Synthesis and reactivity analysis of the central, elusive intermediate, α-lactylthiamin, *J. Am. Chem. Soc. 103,* 884–888. https://doi.org/10.1021/ja00394a027

Pan, K., and Jordan, F. (1998) D,L-*S*-Methyllipoic acid methyl ester, a kinetically viable model for *S*-protonated lipoic acid as the oxidizing agent in reductive acyl transfers catalyzed by the 2-oxoacid dehydrogenase multienzyme complexes. *Biochemistry 37,* 1357–1364. https://doi.org/10.1021/bi971835y

Gibson, M. I., Chen, P. Y. T., Johnson, A. C., Pierce, E., Can, M., Ragsdale, S. W., and Drennan, C. L. (2016) One-carbon chemistry of oxalate oxidoreductase captured by X-ray crystallography, *Proc. Natl. Acad. Sci. U.S.A. 113,* 320–325. https://doi.org/10.1073/pnas.1518537113

Problem 2–11: Write a mechanism for the transketolase reaction (Equation 2–56) catalyzed by thiamine diphosphate.

Problem 2–12: There are two enzymes that can catalyze, respectively, the two reactions

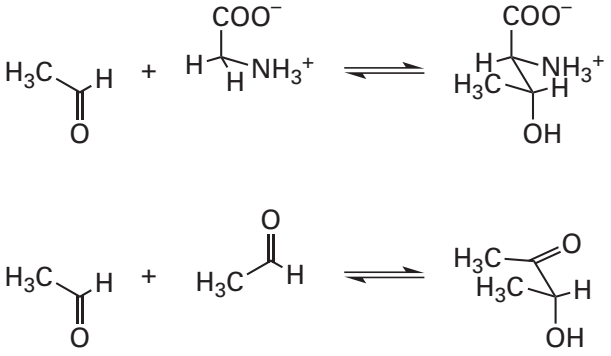

In both of these reactions, a hydron is replaced by acetaldehyde. The two enzymes, however, use different prosthetic groups. Write a mechanism for each reaction, using the proper prosthetic group in each case.

Problem 2–13: 4-(*p*-Chlorophenyl)-2-oxobut-3-enoic acid is an irreversible inhibitor of pyruvate decarboxylase (Equation 2–53).

(A) Write the mechanism of the reaction between this inhibitor and the thiamine diphosphate on the enzyme.

(B) Show by drawing resonance structures why this compound forms an irreversible, covalent adduct with the thiamine diphosphate within the enzyme.

Problem 2–14: Write a mechanism explaining how pyruvate decarboxylase is able to catalyze[247,248]

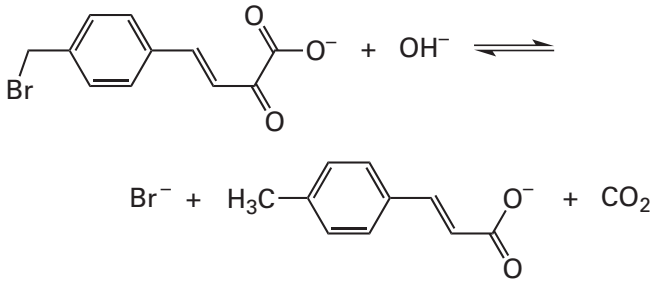

Problem 2–15: Write a mechanism explaining how transketolase is able to catalyze[249]

D-xylulose 5-phosphate $\rightleftharpoons$
hydroxyacetaldehyde +
glyceraldehyde 3-phosphate

Problem 2–16: Write a mechanism for the reaction catalyzed by phosphoketolase[205] and N^2-(2-carboxyethyl)arginine synthase.[223]

3,5-Dihydro-5-methylidene-4H-imidazol-4-one

Histidine **ammonia-lyase** from *P. putida*[9]

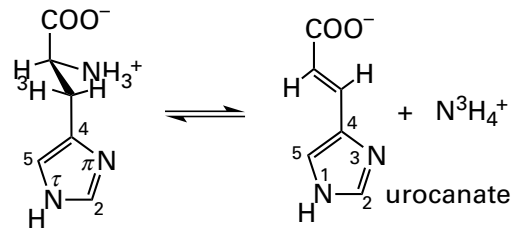

(2–72)

phenylalanine ammonia-lyase from *Rhodosporidium toruloides*[250] and *Petroselinum crispum*[251]

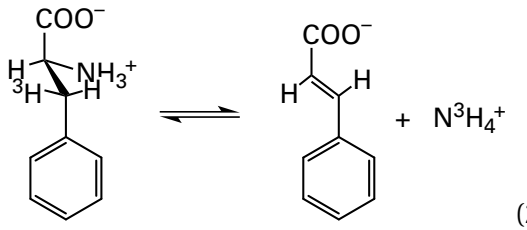

(2–73)

tyrosine ammonia-lyase from *R. sphaeroides*[252]

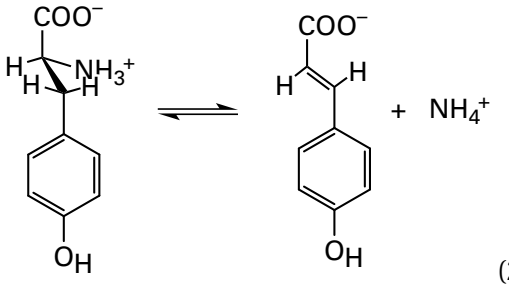

(2–74)

phenylalanine **aminomutase** (L-β-phenylalanine forming) from *Taxus wallichiana*[253]

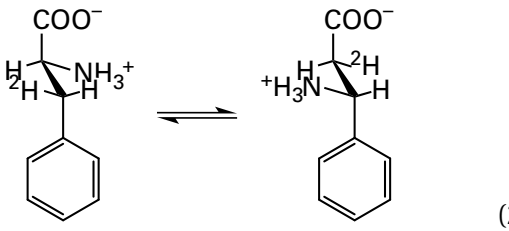

(2–75)

phenylalanine aminomutase (D-β-phenylalanine forming) from *Enterobacter agglomerans*[254]

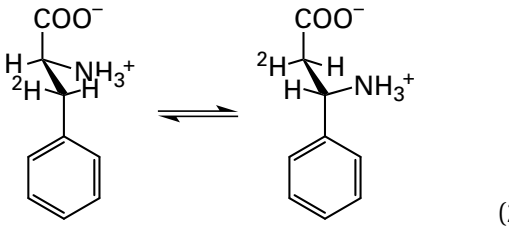

(2–76)

and tyrosine 2,3-aminomutase from *Streptomyces globisporus*[255,256]

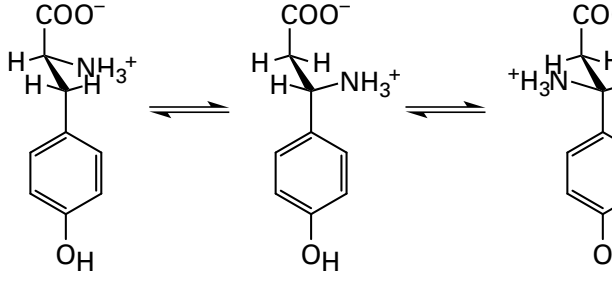

(2–77)

are all homologous enzymes (26–43% identity; ≤2.5 gap percent) catalyzing closely related reactions. The **only difference among the six reactions** is that in the first three reactions, ammonia is eliminated to give the unsaturated product, while in the latter three reactions, ammonia is eliminated and then added back to the resulting carbon–carbon double bond at the carbon adjacent to the one it left. In fact, phenylalanine aminomutase (L-β-phenylalanine forming) from *Taxus cuspidata* produces both L-β-phenylalanine and *trans*-cinnamate, the product of the elimination (Equation 2–73);[257] tyrosine 2,3-aminomutase from *S. globisporus* produces both 3-amino-3-(4-hydroxyphenyl)propanoate and *trans*-4-hydroxycinnamate, the product of the elimination (Equation 2–74);[255] and site-directed mutation can change phenylalanine aminomutase (L-β-phenylalanine forming) from *T. wallichiana* into a phenylalanine ammonia-lyase.[258]

In each of the six eliminations, **the *pro-S* hydron is always removed** from the β carbon of the respective amino acid.[257,259-262] The **stereochemistries of the aminomutases** are more complicated. Phenylalanine aminomutase (L-β-phenylalanine forming) from *T. wallichiana* proceeds predominantly with retention of configuration at both the α and β carbons of the substrates (Equation 2–75)[257,261] so that (*R*)-3-amino-3-phenylpropanoate is the kinetic product. Retention of configuration requires that the carbon–carbon bond of the intermediate *trans*-cinnamate (see Equation 2–73) flip over by rotating around the carbon–carbon bond to the phenyl group before the ammonia and the hydron are added back.[253] Phenylalanine aminomutase (D-β-phenylalanine forming) from *E. agglomerans* proceeds with inversion of configuration at both the α and β carbons of the substrates (Equation 2–76)[262] so that (*S*)-3-amino-3-phenylpropanoate is the other substrate, a fact consistent with the carbon–carbon bond of the intermediate *trans*-cinnamate remaining fixed in its configuration as the ammonia and the hydron are added back. Tyrosine 2,3-aminomutase from *S. globisporus* has both (*R*)-3-amino-3-(4-hydroxyphenyl)propanoate and (*S*)-3-amino-3-(4-hydroxyphenyl)propanoate as the other substrates, but (*S*)-3-amino-3-(4-hydroxyphenyl)propanoate is the kinetic product.

The *pro-S* hydrons on the β carbons of the respective L-amino acids that are the substrates for these enzymes must be acidic enough so each of them can be transferred to the 4-oxidophenyl group of a tyrosine[252,254,263-265] that is located at the homologous position in each active site and that acts as a catalytic base. Mutation of this tyrosine in the active

site of tyrosine 2,3-aminomutase to a phenylalanine[263,266] completely eliminates the enzymatic activity.

Each active site in these enzymes uses a prosthetic group, 3,5-dihydro-5-methylidene-4*H*-imidazol-4-one (**2–38**), that is formed by a **posttranslational modification of the polypeptide** of the enzyme within the internal sequence –ASG–. The modification proceeds by a nucleophilic addition to an acyl carbon followed by two dehydrations

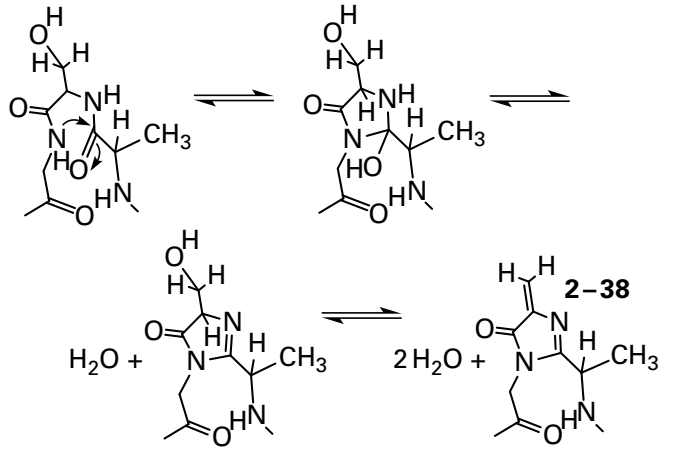

(2–78)

The posttranslational modification is present at the homologous location in each of the proteins.[9,267]

3,5-Dihydro-5-methylidene-4*H*-imidazol-4-one is a strong electrophile at its methylene carbon[268] because addition of a nucleophile, for example a primary amine, to that carbon gives an aromatic product

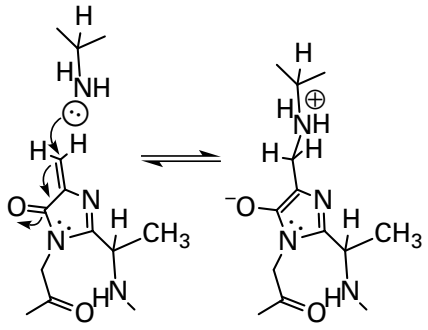

(2–79)

while the reactant, 3,5-dihydro-5-methylidene-4*H*-imidazol-4-one, by itself is not aromatic. The distal carbon of the methylene group is the electrophilic center. Modification of the distal carbon of the prosthetic 3,5-dihydro-5-methylidene-4*H*-imidazol-4-one in the active site of histidine ammonia-lyase from *P. putida* by nucleophilic addition of the conjugate base of nitromethane[260] or cyanide,[269] in the active site of tyrosine 2,3-aminomutase from *S. globisporus* by nucleophilic addition of cyanide[255] to its distal carbon, or in the active site of phenylalanine ammonia-lyase from *P. crispum* by nucleophilic addition of cyanide[270] inactivates the respective enzyme. These facts identify the distal carbon as the crucial location in the prosthetic group. One of the two equivalent, nucleophilic sulfido groups of the conjugate base of (2*S*,3*S*)-1,4-bis(sulfanyl)butane-2,3-diol forms an adduct with the 3,5-dihydro-5-methylidene-4*H*-imidazol-4-one at its distal carbon, which can be observed in a crystallographic molecular model of the active site of phenylalanine ammonia-lyase from *P. crispum*.[251]

There is a crystallographic molecular model of the active site of phenylalanine ammonia-lyase from *R. toruloides* in which the adduct between ammonia and the distal carbon of 3,5-dihydro-5-methylidene-4*H*-imidazol-4-one is present.[250] There is a crystallographic molecular model of the active site of phenylalanine aminomutase (D-*β*-phenylalanine forming) from *E. agglomerans* (Equation 2–76) in which an equilibrium mixture of L-phenylalanine and D-*β*-phenylalanine is present. In this model, the amino group of each substrate in turn forms a nucleophilic adduct with the distal carbon of the 3,5-dihydro-5-methylidene-4*H*-imidazol-4-one (Equation 2–79).[254] There is a crystallographic molecular model of the complex between L-tyrosine and the active site of the inactive mutant of tyrosine 2,3-aminomutase from *S. globisporus* (Equation 2–77), in which the catalytic tyrosine has been changed to a phenylalanine. In this model, the amino group of the reactant L-tyrosine has formed a nucleophilic adduct with the distal carbon of the 3,5-dihydro-5-methylidene-4*H*-imidazol-4-one.[263] There are crystallographic molecular models of the complex between the active site of tyrosine 2,3-aminomutase from *S. globisporus* and (3*S*)-3-amino-2,2-difluoro-3-(4-hydroxyphenyl)propanoate[266] and the complex between the active site and (3*S*)-3-amino-2,2-difluoro-3-(4-methoxyphenyl)-propanoate,[264] both inhibitors of the enzymatic activity. In each of these two complexes, the amino groups of the respective inhibitors have also formed nucleophilic adducts with the distal carbon of the 3,5-dihydro-5-methylidene-4*H*-imidazol-4-one.

On the basis of all these observations, the currently favored mechanism for these enzymes that use 3,5-dihydro-5-methylidene-4*H*-imidazol-4-one as a prosthetic group is that the **adduct between the distal carbon of the prosthetic 3,5-dihydro-**

5-methylidene-4*H*-imidazol-4-one and the amino group of the amino acid that is a reactant for the respective enzyme forms in the first step of the mechanism. Then, in each of the enzymatic eliminations catalyzed by the ammonia-lyases and the aminomutases, the adduct between ammonia and 3,5-dihydro-5-methylidene-4*H*-imidazol-4-one is the leaving group, and in each of the additions catalyzed by the aminomutases, the adduct is the nucleophile that adds. In almost every other elimination that is catalyzed by an enzyme, however, the hydron that is removed during the elimination is α to a carbonyl group or an acyl group and, consequently, acidic ($pK_a = 9–27$; Figure 1-23), but **the β carbons on L-histidine, L-phenylalanine, and L-tyrosine are not acidic**. Consequently, while it would not be surprising that the removal of this hydron is the rate-limiting step in these enzymatic reactions,[261] it is also surprising that it can occur at all if this is the mechanism.

There are two serious **problems with this mechanism**. First, the adduct between the amino group on the substrate and the 3,5-dihydro-5-methylidene-4*H*-imidazol-4-one (Equation 2–79) turns the primary ammonio group into a secondary ammonio group. If anything, the resulting primary amine that would become the leaving group should be a poorer leaving group than ammonia itself because the resulting electron donation by hyperconjugation should increase the pK_a of its conjugate acid relative to that of the conjugate acid of ammonia. Second, this adduct places an additional saturated carbon between the imidazolone and the β carbon of the substrate in the adduct, so there is no way that the adduct with the amino group can solve the fundamental problem of the reaction, which is the extremely poor acidity of the β carbon ($pK_a \cong 43$ in L-phenylalanine and even greater in L-tyrosine).[271] There are no bases in an active site that are capable of removing a hydron from an acid with such a pK_a without some mechanism for lowering its pK_a dramatically.

There is another mechanism, however, that avoids the former problem by avoiding an adduct with the amino group of the substrate and solves the latter problem by directly acidifying the β carbon.[9,272] This acidification is accomplished by withdrawing electron density from the σ bond between it and its hydron, much as pyridoxal 5′-phosphate does with a σ bond between the α carbon and its hydron in the external pyridoximine and as thiamine diphosphate does with a σ bond between a carbonyl carbon and a hydron, an even poorer acid. This other mechanism also explains why the only substrates for the enzymes that use 3,5-dihydro-5-methylidene-4*H*-imidazol-4-one as a prosthetic group are the three aromatic amino acids.

In this mechanism, the 3,5-dihydro-5-methylidene-4*H*-imidazol-4-one, as already noted a strong electrophile, participates in an **electrophilic aromatic addition** to the imidazolyl group, the phenyl group, or the 4-hydroxyphenyl group of the respective substrate to produce an α,β-unsaturated iminium or a pentadienyl cation, respectively. For example, in the active site of histidine ammonia-lyase, adduct **2–39** would result from the electrophilic addition of the 3,5-dihydro-5-methylidene-4*H*-imidazol-4-one to the aromatic imidazolyl group of L-histidine

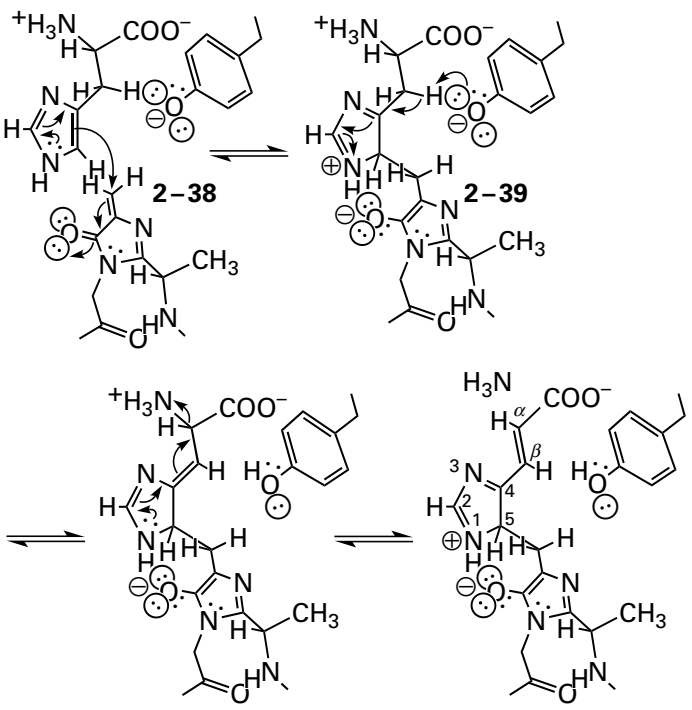

(2–80)

which is analogous to the electrophilic addition of NAD^+ to urocanate (previously Equation 1–85)

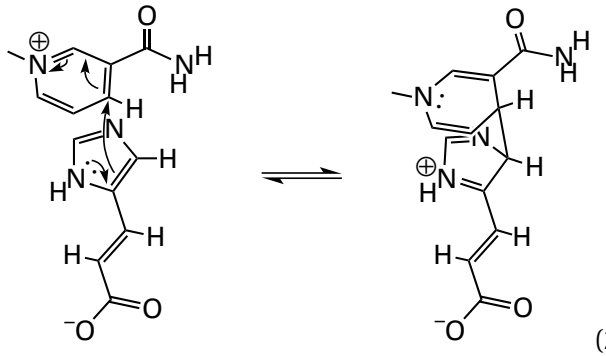

(2–81)

during the reaction catalyzed by urocanate hydratase. During the addition of the 3,5-dihydro-5-methylidene-4*H*-imidazol-4-one to the imidazolyl group (Equation 2–80), the aromatic π system of the imidazolyl group is lost but the 3,5-dihydro-5-methylidene-4*H*-imidazol-4-one has become aromatic in compensation. The homologous adducts of L-phenylalanine (**2–40**) and L-tyrosine (**2–41**)

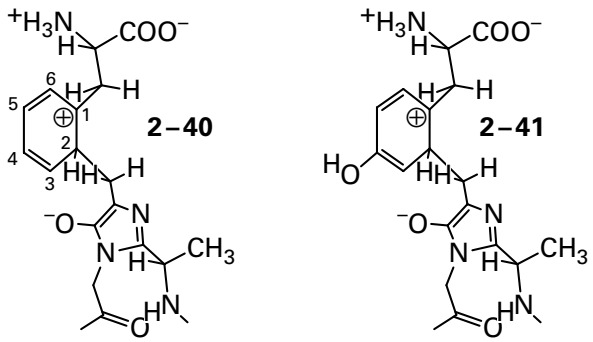

each create a pentadienyl cation in conjugation with the σ bond of the respective β hydron. Electron withdrawal by the α,β-unsaturated iminium (Equation 2–80) or the pentadienyl cation acidifies the β carbon, which permits the oxidophenyl group of the tyrosine in the active site to remove its hydron. Following the removal of the β hydron, the electron excess in the resulting β,γ-unsaturated enamine or the 1,3,5-hexatriene that incorporates the β carbon is able to provide push to assist in the dissociation of the ammonia, just as an enolate provides push during an elimination. There is experimental evidence for such a mechanism.

When L-[β,β,5-$^2H_3$]histidine was used as a reactant with histidine ammonia-lyase (Equation 2–72) from *P. fluorescens* in ^1H_2O for 24 h at pH 9 and 25 °C, 45% of the deuterium at carbon 5 in the product urocanate had been exchanged for protium.[273] This **isotopic exchange** is evidence for the existence of the covalent intermediate **2–39**. In intermediate **2–39** both the hydron on the β carbon of the histidine, the usual target, and the hydron on carbon 5, which are each equivalently placed γ to the iminio group on nitrogen τ (Equation 2–72) and conjugated to it, become acidic. The acidity at the β carbon initiates the elimination; the acidity at carbon 5 is adventitious but unavoidable and an unexpected signature for the intermediate. In the adduct between the α-amino group of L-histidine and 3,5-dihydro-5-methylidene-4*H*-imidazol-4-one, the hydrogen on carbon 5 would not be acidic. One problem with this explanation for the observed isotopic exchange is that the conjugate base of the dissociation of a hydron at carbon 5 in intermediate **2–39** should be the stable bisaromatic product of an electrophilic aromatic substitution, and such a product should inactivate the enzyme. The active site, however, appears to be able to distort sterically the 3,5-dihydro-5-methylidene-4*H*-imidazol-4-one out of planarity at nitrogen 3,[274] an ability that may destabilize the aromatic form of the imidazolone whenever the imidazolyl group or the phenyl group reverts to its aromatic form by loss of the homologous hydron while in the adduct.

When the serine in the sequence –ASG– in the active site of phenylalanine ammonia-lyase from *P. crispum* that becomes 3,5-dihydro-5-methylidene-4*H*-imidazol-4-one during the posttranslational modification (Equation 2–78) is mutated to an alanine, the 3,5-dihydro-5-methylidene-4*H*-imidazol-4-one cannot form. The catalytic constant for the production of *trans*-cinnamate from L-phenylalanine (Equation 2–73) has decreased by a factor of 5000 in the mutant. The wild-type enzyme is able to convert 4-nitro-L-phenylalanine to 4-nitro-*trans*-cinnamate, but with a catalytic constant one-third that for the conversion of L-phenylalanine to *trans*-cinnamate. The mutant, however, has a catalytic constant for the same reaction that is 70 times the catalytic constant for its conversion of L-phenylalanine,[8] so the mutation has decreased the **conversion of 4-nitro-L-phenylalanine to 4-nitro-*trans*-cinnamate** by only a factor of 20. The 4-nitro group, as usual, accomplishes electron withdrawal from carbon 1 of the phenyl group, just as 3,5-dihydro-5-methylidene-4*H*-imidazol-4-one does in electrophilic adduct **2–40**, so the production of 4-nitro-*trans*-cinnamate should be much less affected by the ablation of the 3,5-dihydro-5-methylidene-4*H*-imidazol-4-one than the production of *trans*-cinnamate, as is observed.

There are crystallographic molecular models of a complex between *trans*-cinnamate and phenylalanine ammonia-lyase (Equation 2–73) from *Anabaena variabilis*;[275] complexes between *trans*-

cinnamate and two phenylalanine aminomutases (L-*β*-phenylalanine forming) (Equation 2–76), one from *T. wallichiana*[253] and one from *Taxus canadensis*;[276] and complexes between both *trans*-cinnamate and *trans*-4-hydroxycinnamate and tyrosine ammonia-lyase (Equation 2–74) from *R. sphaeroides*.[252] The ligands are either substrates for the respective enzymes or intermediates in the respective enzymatic reactions. In each of these crystallographic molecular models **the distal methylene carbon of the 3,5-dihydro-5-methylidene-4*H*-imidazol-4-one sits between one of the ortho carbons of the respective phenyl ring and the *β* carbon of the substrate**, from which the amino group would have been removed. In two of the instances, the distal methylene carbon is within van der Waals contact (<0.39 nm) of the ortho carbon, as it should be if intermediate **2–40** is involved in the reaction, and in the others, it is less than 0.5 nm away.

There is also a **model reaction**[277] for the proposed mechanism

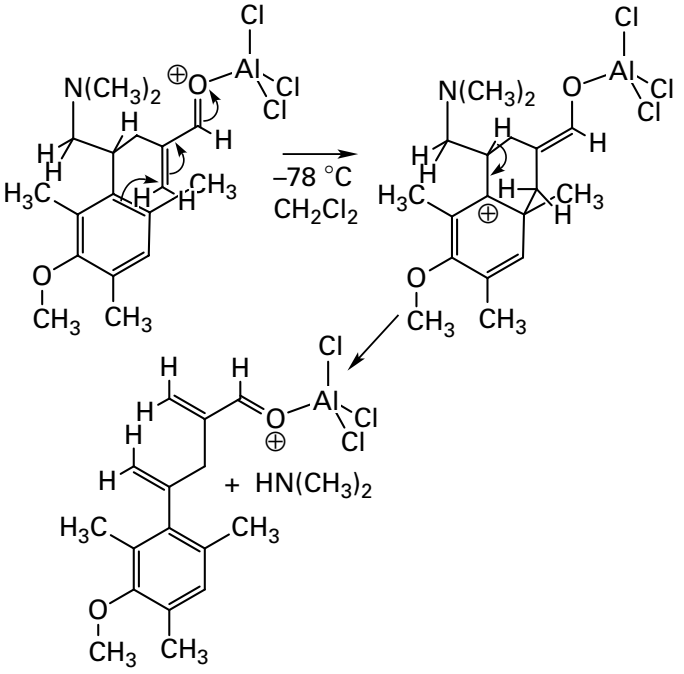

(2–82)

The elimination of the 4-dimethylamino group that is observed in this reaction is believed to proceed by intramolecular nucleophilic addition of the *π* system of the phenyl group to the electrophilic carbon in an aluminum trichloride adduct of a 3-oxoprop-1-en-2-yl group (arrows in Equation 2–82). This addition produces a pentadienyl cation in the phenyl ring, stabilized by a *p*-methoxy group and immediately adjacent to a carbon–hydrogen bond that the cation causes to be acidic. The dissociation of the hydron in this exocyclic carbon–hydrogen bond initiates the observed elimination of dimethylamine. If this is the mechanism of the elimination, then this reaction is a mimic for the proposed mechanism for the enzymes that involves electrophilic additions of the 3,5-dihydro-5-methylidene-4*H*-imidazol-4-ones to the respective aromatic substrates.

Suggested Reading

Schwede, T. F., Retey, J., and Schulz, G. E. (1999) Crystal structure of histidine ammonia-lyase revealing a novel polypeptide modification as the catalytic electrophile, *Biochemistry 38*, 5355–5361. https://doi.org/10.1021/bi982929q

Flavin

The various flavins have, as their catalytically active portion, a 7,8-dimethylisoalloxazine substituted at nitrogen 10

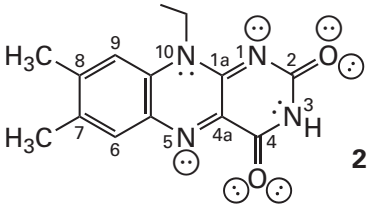

2–42

The substitution at nitrogen 10 is what distinguishes the various flavins: flavin adenine dinucleotide (FAD), flavin mononucleotide (FMN), and riboflavin. Although there are a number of instances, including a family of monooxygenases (EC 1.14.14), in which a flavin participates in an enzymatic reaction as a coenzyme,[278,279] flavins are usually either **covalently or noncovalently incorporated as prosthetic groups** into enzymes and remain bound tightly to the protein during the association of reactants and the dissociation of products.

When it is covalently attached to a protein, the bond to the 7,8-dimethylisoalloxazine is usually between the **carbon of the 8-methyl group** and a nucleophilic amino acid such as histidine,[280] cysteine,[281] or aspartate.[282] This presumably results[283] from a nucleophilic attack on the vinylogous *α,β*-unsaturated imine present in tautomer **2–43** of the conjugate acid of oxidized flavin (**2–42**)

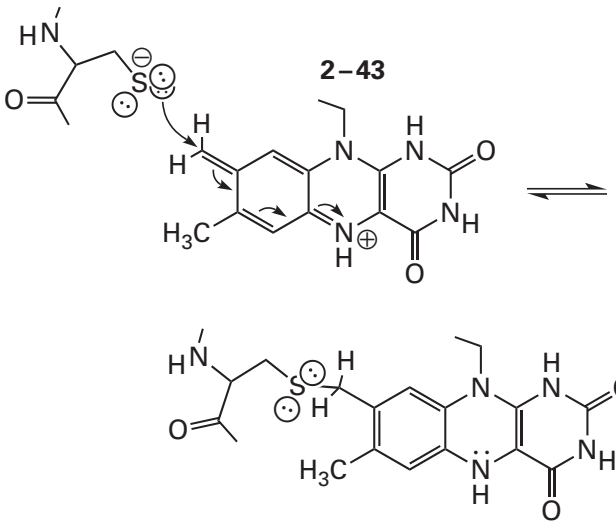

(2–83)

The addition is catalyzed by the active site of the enzyme itself, but there are proteins in the cytoplasm that can accelerate the addition.[284]

If the cysteine in sarcosine oxidase (formaldehyde-forming) from *Bacillus* to which flavin adenine dinucleotide would normally be covalently attached is replaced with alanine, the enzyme binds flavin adenine dinucleotide weakly; and it has to be added to the solution at fairly high concentration for enzymatic activity to be observed.[285] In enzymes in which it is not covalently attached, however, flavin is tightly bound to preclude its loss.

Because flavin is either covalently bound or very tightly bound to a protein and also has a bright yellow color in its oxidized state (**2–42**), which is usually its oxidation state after the specimen is homogenized, a protein with bound flavin can be purified simply by monitoring this color. The absorption spectrum of such a protein can be used to demonstrate that it has the prosthetic group bound to it, and this spectrum designates the protein as a **flavoprotein** or **flavoenzyme**. These terms are sometimes used to designate a protein before its specific function has been determined and a proper descriptive name has been assigned to it. An example would be "old yellow enzyme".

There are three stable oxidation states of flavin that differ sequentially by two one-electron steps (Figure 2–9).[286-289]

Neutral, **oxidized flavin** (**2–42**; HFl_{ox}, Figure 2–9) is the most electron-deficient form occurring naturally. It contains 18 π electrons in a π molecular orbital system with 16 π molecular orbitals constructed from 16 p orbitals. When it is completely unhydronated as the anion (Fl_{ox}^-, Figure 2–9) at high pH, it has seven σ lone pairs of electrons available for hydronation, giving the monohydronated and dihydronated isoalloxazine ample opportunity for tautomerization. In the abbreviations that follow, it will be assumed that the only completely unhydronated form of flavin present under normal circumstances is this anion, and the number of hydrons in each abbreviation, for example, HFl_{ox}, will be based on this designation. Neutral, oxidized flavin mononucleotide (FMN) in solution has a characteristic **absorption spectrum** (Figure 2–10)[290-294] with a maximum absorbance at 446 nm that gives the oxidized flavin its yellow color and a second maximum absorbance at 372 nm. The absorption centered at 446 nm is composed of at least three peaks of absorption that often become even more obvious when flavin is bound in the active site of an enzyme.

The addition of an electron to the neutral, monohydronated form of oxidized flavin (HFl_{ox}, Figure 2–9) forms the radical anion ($HFl^{\bullet -}$). At neutral pH, the radical anion takes up a hydron (pK_a of the conjugate acid is 8.3) to become the neutral radical ($H_2Fl^{\bullet}$, Figure 2–9). A **flavin semiquinone** is a flavin radical. The three normally accessible hydronation states are the radical anion, $HFl^{\bullet -}$, the neutral radical, $H_2Fl^{\bullet}$, and the radical cation, $H_3Fl^{\bullet +}$ (Figure 2–9). In each of these three states of hydronation for the flavin semiquinone, however, because the hydrons are added or removed from σ lone pairs of electrons orthogonal to the π molecular orbital system, if the molecule is fully conjugated, there are formally 19 π electrons in a π molecular orbital system constructed from 16 p orbitals regardless of its state of hydronation. In its neutral form, two of the seven σ lone pairs of electrons on its heteroatoms are occupied by hydrons. The resonance form of the flavin semiquinone, $H_nFl^{\bullet}$, presented in Figure 2–9 is based on its calculated distribution of spin density,[295] which is confined in large part to nitrogen 5 and carbon 4a

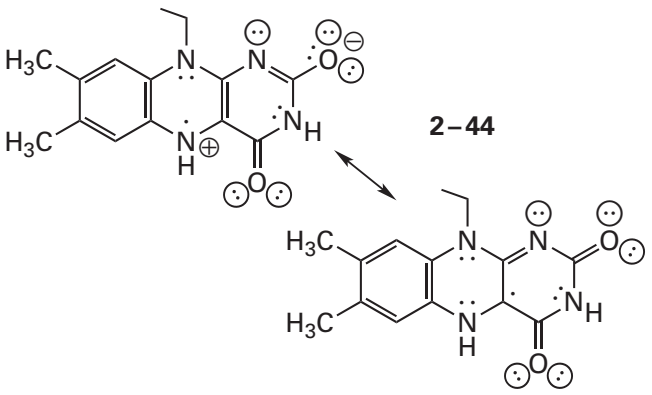

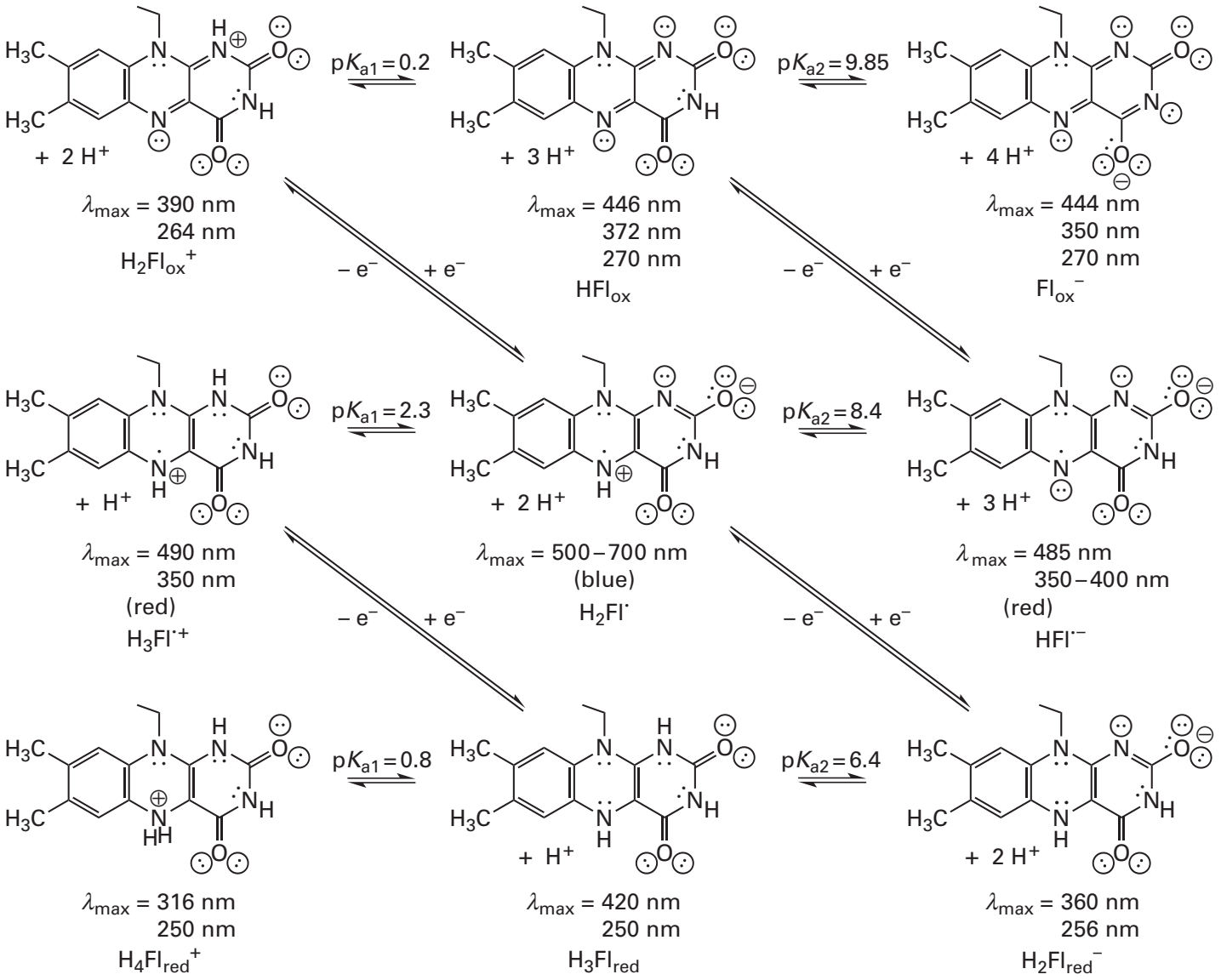

Figure 2–9: The three oxidation states of flavin and the normally accessible conjugate acids and bases at each oxidation state.[286-289] Three conjugate acid–bases of fully oxidized flavin are presented on the top row with their abbreviations and the characteristic maxima in their ultraviolet and visible spectra. Addition of one electron produces the semiquinone, which is a radical (middle row). The most unusual of the three conjugate acid–bases of the semiquinone is the blue neutral radical (λ_{max} = 570 nm). In forming this radical ($H_2Fl^{\bullet}$) directly from the cationic oxidized flavin ($H_2Fl_{ox}^{+}$), the two nitrogens switch basicity and, following a rearrangement of the hydrons, the neutral radical is the opposite tautomer.[289] Addition of a second electron produces fully reduced flavin (bottom row), three conjugate acid–bases of which are presented. The addition of each electron, as expected, increases the basicity of the acid–base to which the electron was added, hence the diagonal arrows for the additions of electrons.

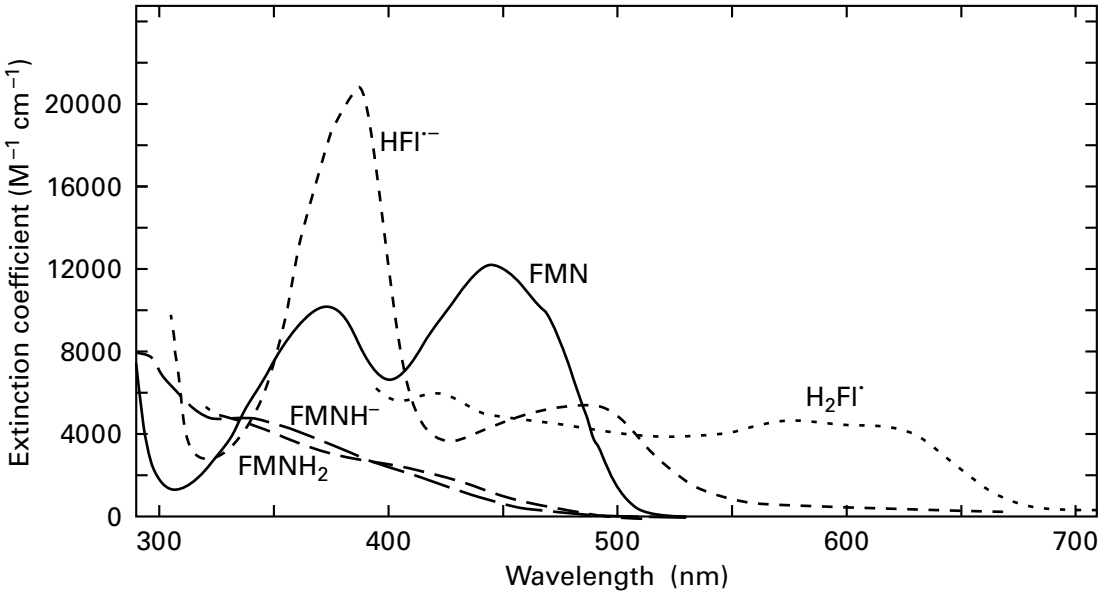

Figure 2–10: Absorption spectra of the five forms of flavin that predominate in the midrange of pH. The extinction coefficient of the spectrum for the neutral, oxidized form of flavin mononucleotide (FMN)[292] (λ_{max} = 446 nm; ε_{446} = 12,200 M^{-1} cm^{-1})[291] was used to scale each of the other spectra because each of these other published spectra had a spectrum of neutral oxidized flavin accompanying it. It was assumed that the extinction coefficient of neutral oxidized flavin in an active site was the same as in solution. The spectra[292] for the neutral reduced form of flavin mononucleotide ($FMNH_2$) and the anionic conjugate base of flavin mononucleotide ($FMNH^-$) have no pronounced maxima of absorbance in the visible range. The spectrum[2608] for the neutral flavin semiquinone ($H_2Fl^{\bullet}$) was obtained by Professor Beinert by reducing completely the oxidized form of the metal-free flavoprotein[294] from *A. vinelandii* with successive additions of $S_2O_4^{2-}$ at pH 7 until the reduction was complete. The initial spectrum of the oxidized flavoprotein provided the reference for the extinction coefficient. The spectrum[293] for the anionic conjugate base of flavin semiquinone ($HFl^{\bullet -}$) was obtained by reducing the oxidized form of L-amino-acid oxidase from *C. adamanteus* by photolysis at pH 7.6 in the presence of 90 mM ethylenediaminetetraacetate until the photoreduction was complete. Again, the initial spectrum of the oxidized flavoprotein provided the reference for the extinction coefficient.

Because of the rapid disproportionation that occurs in solution, the **absorption spectra** of neutral flavin semiquinone, $H_2Fl^{\bullet}$, and the anionic conjugate base of flavin semiquinone, $HFl^{\bullet -}$, are most readily measured in flavoproteins in which these two forms are stabilized. The neutral flavin semiquinone stabilized in the flavoprotein from *Azotobacter vinelandii* (Figure 2–10) absorbs light of long wavelength (λ_{max} = 575 nm and 617 nm) because of its zwitterionic character (Figure 2–9), and this absorption gives it a blue color. The absorption at these long wavelengths is lost when either a hydron is added to one of the σ lone pairs to generate the radical cation, $H_3Fl^{\bullet +}$, or a hydron is removed from one of the σ lone pairs to generate the radical anion, $HFl^{\bullet -}$, neither of which can be zwitterionic. The absorption spectrum of the radical anion of flavin semiquinone in the active site of L-amino-acid oxidase from *Crotalus adamanteus* (Figure 2–10) has maxima of absorbance at 387 and 483 nm. In some flavoenzymes, the peak of absorbance between 350 and 400 nm for the radical anion splits into a broad symmetrical peak around 360 nm and a narrow symmetrical peak of lesser extinction coefficient around 400 nm.[293] These two peaks have coalesced in the case of L-amino-acid oxidase, and that coalescence accounts for the asymmetry in the peak of absorption.

The addition of an electron to the neutral, dihydronated, zwitterionic flavin semiquinone ($H_2Fl^{\bullet}$, Figure 2–9) forms the reduced flavin anion ($H_2Fl_{red}^-$, Figure 2–9). The 7,8-dimethylisoalloxazine that constitutes neutral, trihydronated **reduced flavin**

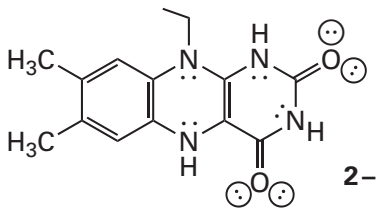

2–45

is conveniently divided in the middle along the axis of nitrogen 5 and nitrogen 10 into *N*-alkyl-1,2-diamino-4,5-dimethylbenzene

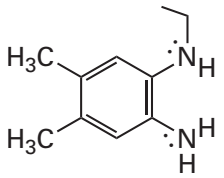

2–46

and N^6-alkyl-5,6-diaminouracil

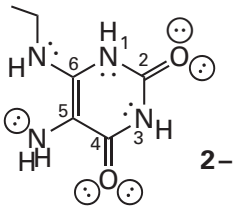

2–47

In this gedanken dissection, reduced flavin is described as a chimera of a dianiline and the substituted base of a nucleic acid. In neutral reduced flavin (**2–45**), the lone pair of electrons on nitrogen 10 is conjugated to both the dimethylphenyl group, **2–46**, and the uracilyl group, **2–47**, and consequently is not basic, while the lone pair of electrons on nitrogen 5 is only conjugated to the dimethylphenyl group and not the uracilyl group, and it is weakly basic (the pK_a of its conjugate acid is 0.8; Figure 2–9).*

The pK_a of neutral reduced flavin for **dissociation of the hydron from nitrogen 1** is 6.4, so when it is in solution at pH 7, reduced flavin is an equilibrium 3:1 mixture of the anion, $H_2Fl_{red}^-$, and the neutral molecule, H_3Fl_{red}. In the active sites of an enzyme, however, the usual form of reduced flavin is $H_2Fl_{red}^-$. Consequently, within the active site of an enzyme, when neutral, oxidized flavin, HFl_{ox}, is reduced by two electrons to reduced flavin anion, $H_2Fl_{red}^-$, only one hydron usually has to be supplied by an acid in that active site, and in the reverse direction, only one hydron must be removed by the conjugate base of that acid. In the anionic form of the reduced flavin, as in any anion of an amide, the greatest density of negative charge is located on the oxygen on carbon 2 ($H_2Fl_{red}^-$, Figure 2–9) because of the disparity of electronegativity between the oxgen and the nitrogen.

Both the **absorbance** of neutral reduced flavin mononucleotide and the absorbance of its anionic conjugate base decrease monotonically between 320 and 500 nm with hints of peaks of absorbance at around 420 and 350 nm, respectively (Figure 2–10). Consequently, for flavins and flavoenzymes, there is an almost complete loss of absorbance at around 450 nm when oxidized flavin becomes reduced flavin.

Whether these three oxidation states of flavin, in the absence of steric effects, are normally **planar or bent** is unclear. Neutral reduced flavin (H_3Fl_{red}, **2–45**), if it is fully conjugated, has 20 π electrons in a π molecular orbital system constructed from 16 *p* orbitals. This **unusually electron-rich π molecular orbital system** is so electron-rich that it may well crack in half along its central axis. One way to relieve the pressure of the electron density would be to **bend the molecule** along an axis between nitrogen 5 and nitrogen 10. This bending would cause the hybridization on these two nitrogens to become [sp^3, sp^3, sp^3, sp^3] and allow them each to confine a pair of those 20 electrons as a σ lone pair and decrease the number of π electrons to 16. This bending would split the π molecular orbital system into two halves—the diaminodimethylbenzene and the diaminouracil. For this splitting to happen, the planes of these two rings must meet at an angle. Ab initio molecular orbital calculations predict that in reduced flavin this angle should be around 150°,[296] but the barrier between this bent conformation and a planar conformation should be a small one.[297]

The available **crystallographic molecular models** of reduced isoalloxazines, when they are not in enzymes, show various departures from planarity, but these departures seem to be due to steric effects, not electronic effects.[298-300] Nuclear magnetic resonance spectra of reduced flavins with no steric complications, in both nonpolar and polar solvents, indicate that these molecules are planar.[301] A planar stereochemistry would also be consistent with the acid–base behavior of the two nitrogens on the 1,2-diaminobenzene (pK_{a1} = 1.3 and pK_{a2} = 4.5), which are considerably less basic than those in 1,2-diaminoethane (pK_{a1} = 7.5 and pK_{a2} = 10.0). This fact indicates that the two nitrogens in a diaminobenzene, and presumably reduced flavin as well, have π lone pairs of electrons rather than σ lone pairs of electrons and are themselves planar. Furthermore, the exocyclic nitrogens of nucleic acid bases, such as 6-aminouracil, are usually planar. The particularly low pK_a (pK_a = 0.8) for nitrogen 5 of reduced flavin (Figure 2–9), which is considerably lower than that for the conjugate acid of aniline (pK_a = 4.6), cannot

*The pK_a of nitrogen 5 is still significantly less than that of 2-amino-4,5-dimethylaniline (pK_a of its monocationic conjugate acid is predicted to be 5). Presumably the low pK_a of nitrogen 5 results from σ electron withdrawal by the 5,6-diaminouracil.

be mistaken for the pK_a of a tetrahedral nitrogen (pK_a = 10) and more closely resembles the values of pK_a for the exocyclic nitrogens in nucleic acid bases. All these considerations indicate that, in solution, in spite of the calculations, reduced flavin seems to have a planar 7,8-dimethylisoalloxazine.

Oxidized flavin (HFl_{ox}) is generally assumed to be completely planar, owing to the conjugation that connects every atom in the three rings. This conclusion is usually based on the crystallographic molecular models of several 10-alkylisoalloxazines, which are perfectly planar.[302] Most of these analogues, however, have been cocrystallized with naphthalene-2,3-diol,[302-304] which sandwiches the isoalloxazines in the crystal and could thereby force them to be planar even if they were not already planar. Therefore, the distinction that is usually made between rigidly planar oxidized flavin and flexible, easily bent reduced flavin may not be so clear-cut as has been assumed, and it is probably not the case that constraining the flavin to one geometry can affect its reduction potential. The nature of the acid–bases around the flavin is probably far more important.[305]

In the **crystallographic molecular models of flavoproteins**, the prosthetic 7,8-dimethylisoalloxazines are planar (Figure 2–11),[306-311] slightly twisted (Figure 2–12),[312-315] or bent (Figure 2–13),[316] sometimes almost as extensively (155°) as predicted in the molecular orbital calculations.[317] The one consistent feature is that the 7,8-dimethylisoalloxazines are tightly surrounded by side chains and the main chain of the protein that hold them in a rigid grip[317,318] and prevent each of them from changing its conformation upon reduction or oxidation.[319] This rigid grip is in marked contrast to how loosely the pyridinium ring of pyridoxal 5′-phosphate, which must reorient during catalysis, is usually held within the active sites of enzymes that use it as a prosthetic group.

A reduced molecule and an oxidized molecule, such as oxidized flavin and reduced flavin, that can be interconverted by subtracting or adding only electrons and hydrons are a redox couple. The **reduction potential**, *E*, of a redox couple under a given set of conditions is the voltage it can provide to move electrons when they are electrochemically transferred from a standard hydrogen electrode to the oxidized molecules of the redox couple to form the reduced molecules. The **standard hydrogen electrode**

$$H_2 \rightleftharpoons 2\,H^+ + 2\,e^- \qquad (2\text{–}84)$$

is an electrode in which diatomic hydrogen gas at 10^5 pascals is poised electrochemically at equilibrium with two hydrons at pH = 0 in aqueous solution.

There are standard electrodes other than a standard hydrogen electrode that are easier to use in electrochemical measurements, but the voltages recorded with these other standard electrodes are usually corrected to voltages that would have been observed with a standard hydrogen electrode. For example, a saturated calomel electrode

$$2\,Hg(l) + 2\,Cl^- \rightleftharpoons Hg_2Cl_2(s) + 2\,e^- \qquad (2\text{–}85)$$

is a paste of Hg_2Cl_2 mixed with liquid mercury, and the concentration of Hg_2Cl_2 at saturation is held constant by using as a solvent a saturated solution of KCl. The voltage of this electrode is +0.241 V relative to a standard hydrogen electrode at 25 °C.

A simple example of a redox couple in an aqueous solution would be ferricyanide and ferrocyanide

$$[Fe^{3+}(CN^-)_6]^{3-} + e^- \rightleftharpoons [Fe^{2+}(CN^-)_6]^{4-} \qquad (2\text{–}86)$$

The voltage that this redox couple can produce to move electrons from molecules of H_2 gas at a standard hydrogen electrode to reduce ferricyanide to ferrocyanide, when the conditions are such that the activities of the ferricyanide and ferrocyanide are equal, is +360 mV. In general chemistry, in such a simple unimolecular oxidation–reduction, the reduction potential provided by the redox couple to move electrons from the standard hydrogen electrode to a mixture of the two members of the redox couple at equal activity at a pH of 0 is the **standard reduction potential**, E°.

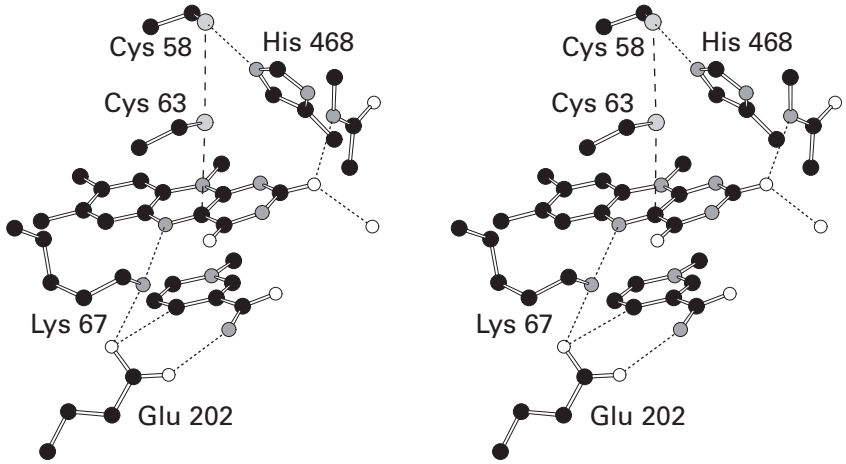

Figure 2–11: Crystallographic molecular model of the active site of reduced glutathione-disulfide reductase from human erythrocytes with bound NADH.[306] Black atoms are carbons, white atoms are oxygens, small gray atoms are nitrogens, and large light gray atoms are sulfurs. Crystals of human glutathione-disulfide reductase were transferred to solutions containing 10 mM NADH in 0.1 M potassium phosphate at pH 7.0. After 3 h, data sets to Bragg spacings of 0.185 nm were collected from these crystals, and the map of electron density was calculated by refinement, beginning with the phases from the refined data set of the enzyme without bound NADH. The stereodrawing[50] is from the resulting crystallographic molecular model. The 7,8-dimethylisoalloxazine of the flavin, which is planar in this active site, is in the center of the drawing, and the nicotinamide ring of the NADH is stacked below the flavin. Lysine 67 forms a hydrogen bond with nitrogen 5 of the flavin, and Glutamate 202 forms a hydrogen bond with Lysine 67 with one of its oxygens and a hydrogen bond with the carbamoyl nitrogen of the NADH with its other oxygen. The latter hydrogen bond can act as a pivot for the carboxy group. The amido nitrogen–hydrogen of the peptide bond between Leucine 339 and Threonine 340 and a molecule of water (white sphere) each donate a hydrogen bond to the oxygen of the 2-oxo group of the flavin. It is at this oxygen that the formal negative elementary charge of the monoanion of reduced flavin ($H_2Fl_{red}^-$) is located (Figure 2–9). Cysteine 58 and Cysteine 63 are the internal thiols that are oxidized to a disulfide by the enzymatic reaction. The two sulfurs of these cysteines are online with carbon 4a of the flavin (vertical thickly dashed line). The Histidine 468 in an identical, neighboring subunit of the enzyme forms a hydrogen bond to the distal sulfur of this pair of cysteines and removes the hydron from this sulfur during the oxidation. When the cystine forms, the dihedral angle, χ_3, along the sulfur–sulfur bond[310] is –138°, which is close to –150°, one of the six dihedral angles, 30°, 90°, 150°, –150°, –90°, and –30°, at which the two lone pairs and the carbon–sulfur σ bonds on each of the two sulfurs are as far from being parallel to each other as possible.[309] The crystallographers note that direct contact between nitrogen 5 of the flavin and the hydride of the nicotinamide is blocked sterically by the side chain of Lysine 67.[311] This steric effect may prevent direct transfer of a hydride to nitrogen 5 of the flavin from carbon 4 of the NADH.

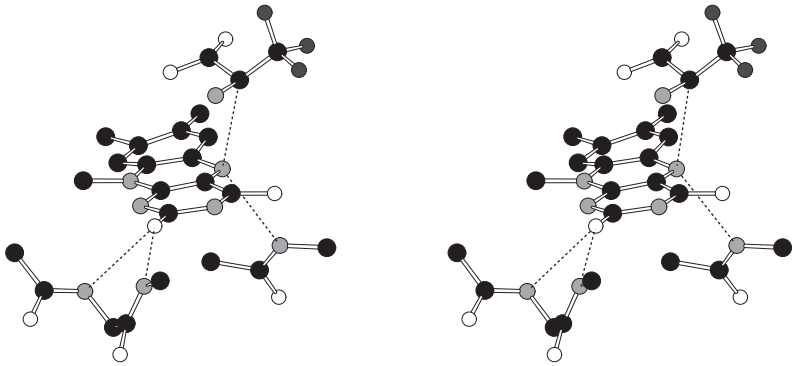

Figure 2–12: Stereodrawing[50] of the crystallographic molecular model of the active site of D-amino-acid oxidase from *R. toruloides* with bound D-trifluoroalanine.[312] Black atoms are carbons, white atoms are oxygens, small gray atoms are nitrogens, and small dark gray atoms are fluorines. Crystals of D-amino-acid oxidase were transferred to solutions containing 10 mM racemic trifluoroalanine. After several hours, data sets to Bragg spacings of 0.172 nm were collected from these crystals, and the map of electron density was calculated by molecular replacement and refinement. The stereodrawing[50] is from the resulting crystallographic molecular model. The 7,8-dimethylisoalloxazine of the flavin, which is slightly twisted in this active site, is in the center of the drawing. The hydrogen on carbon 2 of the D-trifluoroalanine, which is bound selectively by the enzyme and which is above the isoalloxazine in the drawing, is directed toward nitrogen 5 of the isoalloxazine. The amido nitrogen–hydrogen of the peptide bond between Alanine 51 and Glycine 52 (below the isoalloxazine) is the donor for a hydrogen bond to nitrogen 5 of the flavin. The amido nitrogen–hydrogen of the peptide bond between Glycine 337 and Tyrosine 338 and the amido nitrogen–hydrogen of the peptide bond between Tyrosine 338 and Glutamine 339 each donate a hydrogen bond to the oxygen of the 2-oxo group of the flavin. It is at this oxygen that the negative formal elementary charge of the monoanion of reduced flavin ($H_2Fl_{red}^-$) is located (Figure 2–9).

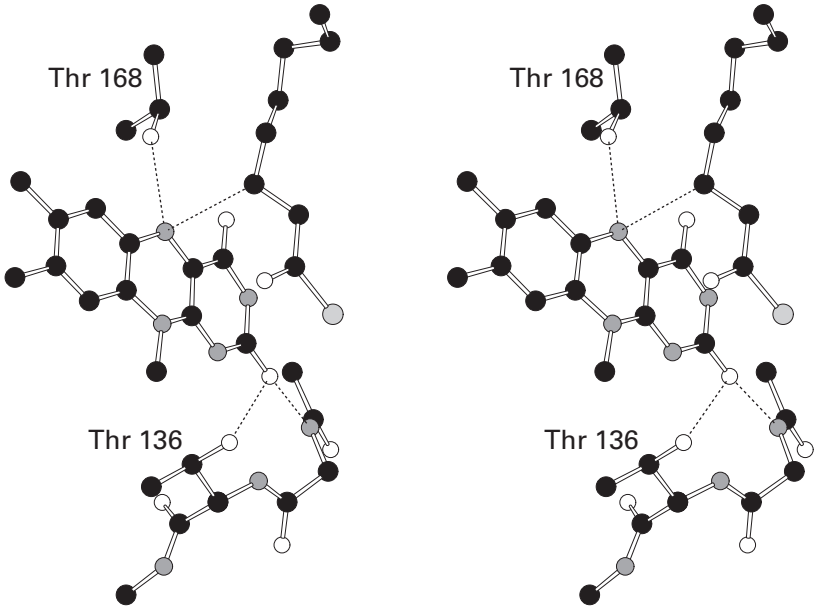

Figure 2–13: Crystallographic molecular model of the active site of porcine mitochondrial acyl-CoA dehydrogenase with bound octanoyl-SCoA.[316] Black atoms are carbons, white atoms are oxygens, small gray atoms are nitrogens, and the large light gray atom is a sulfur. Crystals of acyl-CoA dehydrogenase were grown over a period of a month in an anaerobic solution containing a concentration of octanoyl-SCoA equimolar to the concentration of active sites. Data sets to Bragg spacings of 0.24 nm were collected from these crystals, and the map of electron density was calculated by refinement, beginning with the phases from the refined data set of the enzyme without bound octanoyl-SCoA. The stereodrawing[50] is from the resulting crystallographic molecular model. The 7,8-dimethylisoalloxazine of the flavin, which is bent in this active site, is in the left center of the drawing. The *pro-S* hydrogen on carbon 3 of the octanoyl group of the octanoyl-SCoA, which is to the left of the isoalloxazine in the drawing, is directed toward nitrogen 5. Only the octanoyl group of the octanoyl-SCoA is shown. The oxygen–hydrogen of Threonine 168 is the donor of a hydrogen bond to nitrogen 5 of the flavin. The amido nitrogen–hydrogen of the peptide bond between Cysteine 134 and Valine 135 and the oxygen–hydrogen of Threonine 136 in the segment of polypeptide at the bottom of the drawing each donate a hydrogen bond to the oxygen of the 2-oxo group of the flavin. It is at this oxygen that the negative formal elementary charge of the monoanion of reduced flavin ($H_2Fl_{red}^-$) is located (Figure 2–9).

For biochemical reactions, however, the pH chosen for the standard state of the redox couple is 7.0. By convention, the standard pH for E°, the chemical standard reduction potential, is pH 0, and the standard pH for $E^{\circ\prime}$, the **biochemical standard reduction potential**, is pH 7. The standard hydrogen electrode, however, is always poised at a pH of 0. When standard reduction potentials of either type are stated, the chemical equation for the redox couple to which they refer is the one in which the oxidized species is the reactant and the reduced species is the product.

The more positive the reduction potential, the easier it is to reduce the oxidized molecules of the redox couple and the harder it is to oxidize the reduced molecules. **Electrons move spontaneously from redox couples that have more negative reduction potential to redox couples that have more positive reduction potential** when the redox couples are electrochemically connected. For example, the biochemical standard reduction potential for the redox couple of oxidized flavin and flavin semiquinone anion (Figure 2–9)

$$HFl_{ox} + e^- \rightleftharpoons HFl^{\cdot -} \tag{2–87}$$

is −340 mV,[288] and the biochemical standard reduction potential of ferricyanide is +0.440 V. Therefore, in the following complete stoichiometric chemical reaction

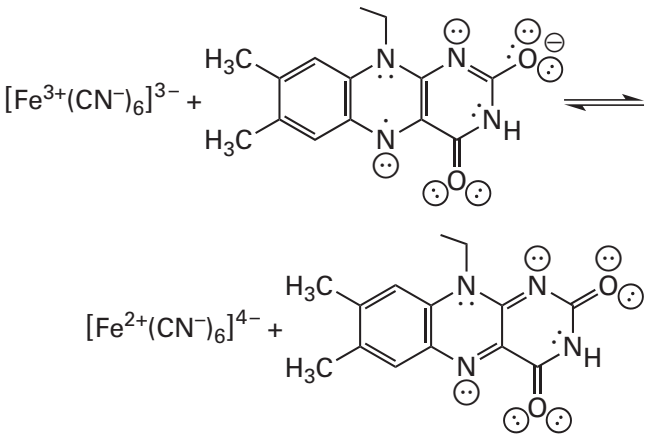

(2–88)

if reactants and products could be present at equal activity, the electron would move spontaneously from the redox couple with a biochemical standard reduction potential of −340 mV to the redox couple with a biochemical standard reduction potential of +440 mV, and this reaction would be favorable when proceeding from left to right. If these redox couples were separated into two compartments, both at pH 7, and connected electrochemically, a voltage of 780 mV moving electrons from flavin semiquinone anion to ferricyanide would be generated between the two compartments if the oxidized flavin and the flavin semiquinone anion could be present at their respective standard states.

The **free energy change of an oxidation–reduction under a particular set of conditions other than standard state**, ΔG, is related to the reduction potentials of the two redox couples under those same conditions by the equation

$$\Delta G = -nF\Delta E \tag{2–89}$$

where n is the number of electrons transferred from reductant to oxidant for the stoichiometric reaction as written, F is the Faraday constant (96,485 J V^{-1} mol^{-1}), and

$$\Delta E = E_{r,ox/p,red} - E_{p,ox/r,red} \tag{2–90}$$

where $E_{r,ox/p,red}$ is the reduction potential for the redox couple of the oxidized reactant that is being reduced and the reduced product that is the result of that reduction and $E_{p,ox/r,red}$ is the reduction potential for the redox couple of the reduced reactant that is being oxidized and the oxidized product that is the result of that oxidation. The designations of reactant and product are defined by the chemical equation as it is written, reactants on the left and products on the right, and the numerical values of E are the reduction potentials of the two redox couples under the particular conditions of the reaction. The more positive the difference between the reduction potentials of the two redox couples, the more negative is the change in free energy for the oxidation–reduction. In this case, net free energy is released during the reaction, and the reaction will proceed in the direction written. Under the same given conditions, however, if the difference in the reduction potentials is negative and the change in free energy is positive, the reaction will necessarily proceed in the direction opposite to that in which it is written.

The reduction potential, E, varies, just as does the free energy, with the **respective concentrations of the two molecules of the redox couple**. As the concentration of oxidized species is increased, the pair becomes easier to reduce, and contrariwise. Quantitatively

$$E = E^\circ - \frac{RT}{nF} \ln\left(\frac{\gamma_{red}[\text{reduced}]}{\gamma_{ox}[\text{oxidized}]}\right) \quad (2\text{–}91)$$

where γ_{red} and γ_{ox} are the activity coefficients of the reduced and oxidized species, respectively, and [reduced] and [oxidized] are their respective molar concentrations. It follows from Equations 2–89 and 2–91 that

$$\Delta G^\circ = -nF\Delta E^\circ \quad (2\text{–}92)$$

where ΔG° is the change in standard free energy when reactants and products are at standard state.

The pH of the solution has a significant effect on the reduction potential of a redox couple that has acidic or basic positions in its structure. When a flavin is free in solution, its reduction potentials change dramatically and predictably as the pH of the solution is changed. When a flavin is tightly bound as a prosthetic group in the active site of an enzyme, its reduction potentials are less affected by the pH of the solution because its acidic and basic positions are usually participating in hydrogen bonds with side chains of the amino acids and are insulated from the solution. Nevertheless, to understand the effects of these donors and acceptors for hydrogen bonds on the reduction potentials of the flavin, it is necessary to understand of the effects of pH on the same flavin when it is free in solution. Initially, the effect of pH on the reduction potential of a simple redox couple is discussed, then the effect of pH on the reduction potential of flavin, and finally the effect of the donors and acceptors for hydrogen bonds on the reduction potential of flavin in an active site.

In most situations, the addition of one or more electrons to the oxidized molecule of a redox couple dramatically changes the pK_a of the lone pairs of electrons in the molecule and causes the reduced molecule to be more basic. For example, the addition of an electron to the neutral form of oxidized flavin (HFl_{ox}) to form the radical anion ($HFl^{\bullet -}$) raises the macroscopic pK_a of its conjugate acid from 0.2 to 8.4 (Figure 2–9) because, with the additional electron, the flavin becomes more electron-rich and more basic and the hydron in the conjugate acid is held more tightly. In fact, **the addition of the electron to a molecule and the dissociation constant of one of its hydrons are linked**. For example, in the case of the reduction of oxidized flavin to the semiquinone and the dissociation of hydrons from reactant and product

$$\begin{array}{ccc} e^- + H_2Fl_{ox}^+ & \overset{K_{a1,ox}}{\rightleftharpoons} & HFl_{ox} + H^+ + e^- \\ E^\circ_{ox/sq,H_2Fl_{ox}^+} \Big\downarrow\Big\uparrow & & E^\circ_{ox/sq,HFl_{ox}} \Big\downarrow\Big\uparrow \\ H_2Fl^\bullet & \overset{K_{a2,sq}}{\rightleftharpoons} & HFl^{\bullet -} + H^+ \end{array} \quad (2\text{–}93)$$

where $K_{a1,ox}$ and $K_{a2,sq}$ are acid dissociation constants (Figure 2–9) and $E^{\circ\prime}_{ox/sq,H_2Fl_{ox}^+}$ and $E^{\circ\prime}_{ox/sq,HFl_{ox}}$ are biochemical standard reduction potentials. The linkage is through the standard free energies

$$E^{\circ\prime}_{ox/sq,H_2Fl_{ox}^+} - E^{\circ\prime}_{ox/sq,HFl_{ox}} = \frac{RT}{F} \ln\left(\frac{K_{a1,ox}}{K_{a2,sq}}\right) \quad (2\text{–}94)$$

It follows from this linkage relationship that just as **the addition of an electron increases the pK_a of the conjugate acid by increasing the total electron density of the molecule, the addition of a hydron increases the standard reduction potential of the redox couple by making the oxidized form more electropositive**. For example, hydronation of neutral oxidized flavin to form the cation ($H_2Fl_{ox}^+$) makes it easier to reduce in a one-electron reaction by +480 mV. For this reason, the nature of the acids that provide donors for hydrogen bonds to the σ lone pairs around the flavin when it is in the active site of an enzyme have a significant effect on the reduction potentials of the redox couple of oxidized flavin and flavin semiquinone and of the redox couple of flavin semiquinone and reduced flavin for an electron.

Frequently when one or more electrons are added to a molecule with σ lone pairs of electrons, the resulting increase in its basicity causes it to take up hydrons immediately. How many hydrons are taken up depends on the pH of the solution and the resulting changes in the values of pK_a for the molecule (Equation 2–94). In turn, the number of hydrons actually taken up, which is determined by the pH of the solution, affects the reduction potential.

Under any particular set of circumstances, a **midpoint reduction potential, E_m, of a redox couple can be defined** as the potential measured when the total molar concentration of reduced participant, $[\text{reduced}]_t$, in all its ionization states and tauto-

mers, is equal to the total molar concentration of oxidized participant, $[\text{oxidized}]_t$, in all its ionization states and tautomers, and the conditions are such that the activity coefficients cancel, usually because the concentrations of the reactants are small. By this definition

$$E = E_m - \frac{RT}{nF} \ln\left(\frac{[\text{reduced}]_t}{[\text{oxidized}]_t}\right) \qquad (2\text{–}95)$$

where E is the reduction potential of the solution. This equation should be compared with Equation 2–91. One difference is that the conditions are those of the solution at hand rather than standard state. Another difference is that the various tautomers and states of hydronation for the two participants in the redox couple are ignored, and only the total concentrations of the two participants are measured.

A simple example of the **effect of pH on the midpoint reduction potential** of a redox couple is encountered in the two-electron reduction of anthraquinone-2-sulfonate

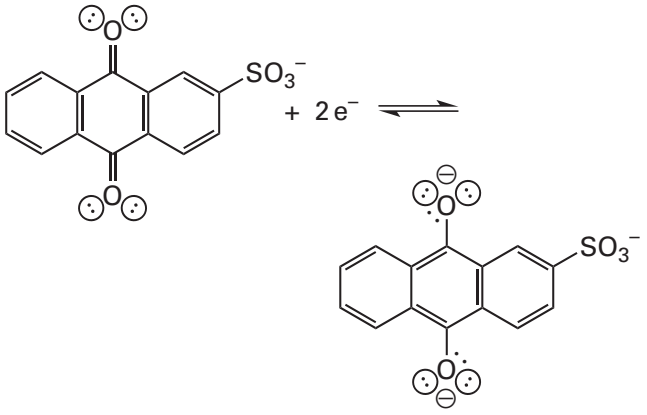

(2–96)

The addition of two electrons to the monoanionic **quinone** to form the quinolate trianion raises the values of pK_a for the conjugate acids of the σ lone pairs of electrons on the two oxygens from below 0 to pK_{a1} = 8.0 and pK_{a2} = 11.3 for the first and second dissociations from the **quinol**, respectively[320]

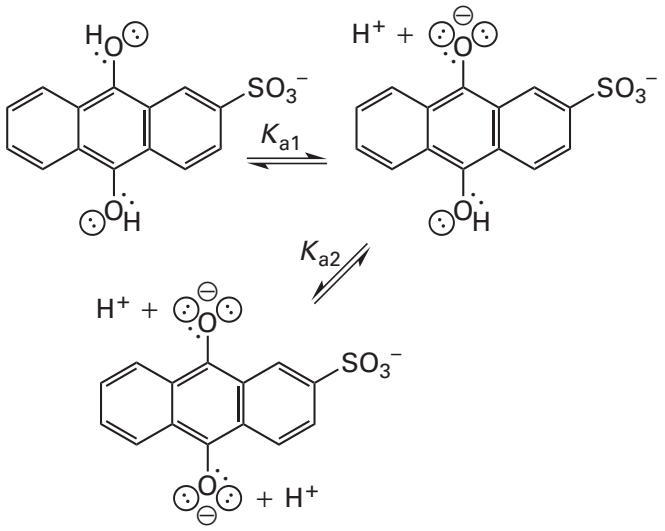

(2–97)

It is easily shown that

$$[Q_{red}^{3-}] = [Q_{red}]_t \left(\frac{K_{a1}K_{a2}}{K_{a1}K_{a2} + K_{a1}[H^+] + [H^+]^2}\right) \qquad (2\text{–}98)$$

where $[Q_{red}^{3-}]$ is the concentration of the quinolate trianion and $[Q_{red}]_t$ is the total concentration of quinol in the trianionic, dianionic, and monoanionic forms. Because the concentration of the neutral conjugate acid of the sulfonato group is negligible at normal values of pH, it is not included in the equation. The redox couple of the monoanion of the quinone and the trianion of the quinol (Equation 2–96) has a chemical standard reduction potential, E°, of –380 mV.[320] This value of reduction potential is invariant with pH because no hydrons are involved when the monoanion of the quinone is reduced by two electrons to the trianion of the quinol. Therefore, at any pH, the observed reduction potential, E, will be equal to

$$E = -380 \text{ mV} - \frac{RT}{2F} \ln\left(\frac{[Q_{red}^{3-}]}{[Q_{ox}^{-}]}\right) \qquad (2\text{–}99)$$

if γ_{red}/γ_{ox} is assumed to be 1. Because the quinone is not a base within the range of pH considered, $[Q_{ox}^{-}] = [Q_{ox}]_t$

$$E = -380\ \text{mV} - \frac{RT}{2F}\ln\left(\frac{[Q_{red}]_t}{[Q_{ox}]_t}\right) - \frac{RT}{2F}\ln\left(\frac{K_{a1}K_{a2}}{K_{a1}K_{a2} + K_{a1}[H^+] + [H^+]^2}\right) \quad (2\text{–}100)$$

By definition (Equation 2–95), when $[Q_{red}]_t/[Q_{ox}]_t = 1$, $E = E_m$. Therefore,

$$E_m = -380\ \text{mV} - \frac{RT}{2F}\ln\left(\frac{K_{a1}K_{a2}}{K_{a1}K_{a2} + K_{a1}[H^+] + [H^+]^2}\right) \quad (2\text{–}101)$$

Equation 2–101 describes the actual behavior, as a function of the pH, of the midpoint reduction potential of anthraquinone-1-sulfonate (Figure 2–14).[320]

When $pH > pK_{a2}$ so that $[H^+] < K_{a2}$

$$E_m = -380\ \text{mV} = E^\circ \quad (2\text{–}102)$$

because only the quinolate trianion is present.

When $pK_{a2} > pH > pK_{a1}$ so that $K_{a2} < [H^+] < K_{a1}$

$$E_m = -380\ \text{mV} - \frac{RT}{2F}(pH - pK_{a2})\ln(10) \quad (2\text{–}103)$$

Because

$$-\frac{RT}{F}\ln(10) = -\frac{(8.314\ \text{J K}^{-1}\text{mol}^{-1})(298.2\ \text{K})(2.303)}{96{,}485\ \text{J V}^{-1}\ \text{mol}^{-1}} = -59.2\ \text{mV} \quad (2\text{–}104)$$

at 25 °C, the slope of the line in this region (dashed line in Figure 2–14) should be –29.6 mV (unit of pH)$^{-1}$ as is observed.

When $pK_{a1} > pH$ so that $K_{a1} < [H^+]$

$$E_m = -380\ \text{mV} - \frac{RT}{2F}(2pH - pK_{a2} - pK_{a1})\ln(10) \quad (2\text{–}105)$$

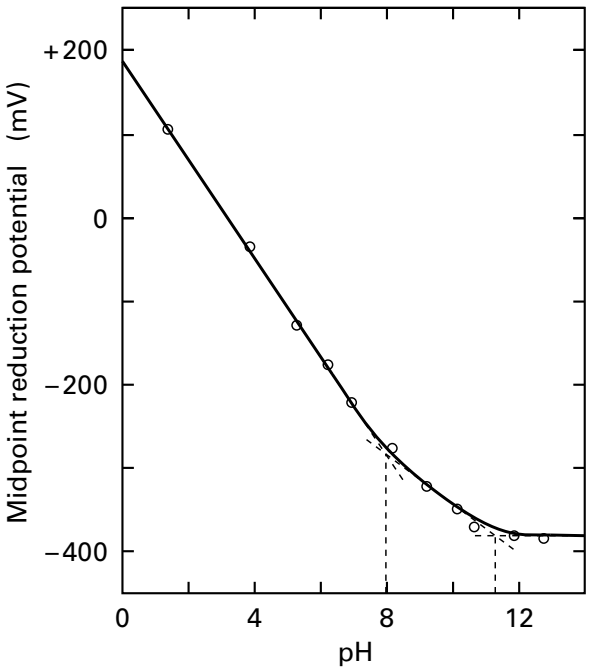

Figure 2–14: Midpoint reduction potential, E_m, of anthroquinone-2-sulfonate as a function of pH.[320] A 3 mM solution of the quinone at the desired pH was titrated with the strong reducing agent sodium hydrosulfite. The reduction potential of the solution was monitored directly with a platinum electrode after each addition. The solution was connected by a salt bridge to a calomel electrode to complete the circuit. The measured potential at the point at which half of the quinone had been reduced, determined by the direct titration, was taken as the midpoint reduction potential at that pH. These potentials are plotted in the figure as a function of pH. The solution also contained a hydrogen electrode that was used to calibrate the readings. The three dashed lines of increasing negative slope from right to left are the lines generated by Equations 2–102, 2–103, and 2–105, respectively, and the two values of pK_a are at the intersections of these lines, as indicated by the two vertical dashed lines.[320]

and the slope of the line in this region (dashed line in Figure 2–14) should be –59.2 mV (unit of pH)$^{-1}$ as is observed.

By solving mathematically for the intersection of the functions described by Equations 2–102 and 2–103 and the intersection of the functions described by Equations 2–103 and 2–105, it can be shown that these two intersections occur when $pH = pK_{a2}$ and $pH = pK_{a1}$, respectively (vertical dashed lines in Figure 2–14).

At values of pH greater than pK_{a2}, the midpoint reduction potential of the reaction is invariant with pH because it involves no hydron uptake (Equation 2–96). At values of pH less than pK_{a1}, the reaction involves the stoichiometric uptake of two hydrons for every two electrons

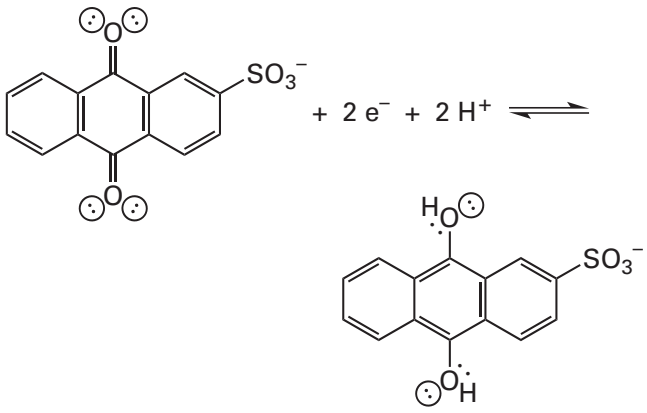

(2–106)

and the slope of the midpoint reduction potential reflects this stoichiometry. At values of pH between the two values of pK_a, the reaction involves the uptake of only one hydron for every two electrons and the slope is half the value that it has at values of pH less than pK_{a1}.

Unfortunately, the **tabulated standard reduction potentials** for most redox couples are for the sum of uptake of both electrons and hydrons as well as any subsequent chemical transformations at standard state. This causes the tabulated standard reduction potentials to be much more complicated, harder to understand, and difficult to correct. For example, the chemical equation for the tabulated reduction of sulfite, which is the reaction catalyzed by sulfite reductase

$$H_2SO_3 + 6\,H^+ + 6\,e^- \rightleftharpoons 3\,H_2O + H_2S \qquad E^\circ = +350\ \text{mV} \qquad (2\text{–}107)$$

is the reaction as written at standard state. In this instance, standard state is equimolar sulfurous acid and hydrogen sulfide at an activity of hydrons of unity (pH = 0). Corrections for both the actual pH of the solution and for the ionization of the reactant and the product as the pH is adjusted to this pH are required to obtain the midpoint reduction potential for this redox couple at a particular pH. This correction is made somewhat easier in the case of standard reduction potentials for biochemical reactions, for which the pH of the standard state is generally taken to be 7.0.

The **midpoint reduction potentials for riboflavin as a function of pH** in solution at 20 °C (middle curve in Figure 2–15)[288,321] reflect its various acid dissociation constants (Figure 2–9). For the redox couple of oxidized riboflavin and reduced riboflavin, involving transfer of two electrons as was the case for the reduction of anthraquinone-2-sulfonate, the midpoint reduction potential ($E_{m,ox/red}$ in Figure 2–15) shows two inflections, one at the pK_a of oxidized flavin (pK_a = 9.85) and one at the pK_a of reduced flavin (pK_a = 6.4). Below pH 6.4 and above pH 9.85, two hydrons are taken up for each two electrons, and the slope of the function is –59.2 mV (unit of pH)$^{-1}$. When the pH is between the pK_a of reduced flavin and the pK_a of oxidized flavin, only one hydron is taken up for every two electrons, and the slope of the function is –29.6 mV (unit of pH)$^{-1}$

For the redox couple of oxidized riboflavin and riboflavin semiquinone, involving transfer of one electron, the midpoint reduction potential ($E_{m,ox/sq}$ in Figure 2–15) should show two inflections, one at the pK_a of the oxidized flavin (9.85) and one at the pK_a of the flavin semiquinone (8.4). Below pH 8 and above pH 10, one hydron is taken up for each electron, and the slope of the function is –59.2 mV (unit of pH)$^{-1}$. The values of $E_{m,ox/sq}$ could be measured below pH 6 and above pH 10 where the concentration of the flavin semiquinone was significant enough to be detected, and the slopes of $E_{app,ox/sq}$ as a function of pH in these regions are –59.2 mV (unit of pH)$^{-1}$ as expected. Between the pK_a of the flavin semiquinone (8.4) and the pK_a of oxidized flavin (9.85), no hydrons are taken up for each electron, and the slope of the function should be zero (horizontal dashed line in Figure 2–15). Because the inflection of the curve for $E_{m,ox/red}$ is at pH 6.4 and the inflection of the curve for $E_{m,ox/sq}$ is at pH 9.85, the concentration of flavin semiquinone becomes immeasurably small relative to the concentrations of reduced and oxidized flavin between pH 6 and pH 10, and the values of $E_{m,ox/sq}$ could not be established in this region. For the redox couple of flavin semiquinone and reduced flavin, also involving the transfer of one electron, the midpoint reduction potential ($E_{m,sq/red}$ in Figure 2–15) should show two inflections, one at the pK_a of flavin semiquinone (8.4) and one at the pK_a of reduced flavin (pK_a = 6.4). Again and for the same reasons, the concentrations of flavin semiquinone could not be measured in the region between pH 6 and pH 10. The two inflections and the invariant region for the behavior of $E_{m,sq/red}$ as a function of pH are indicated by the dashed lines (Figure 2–15).

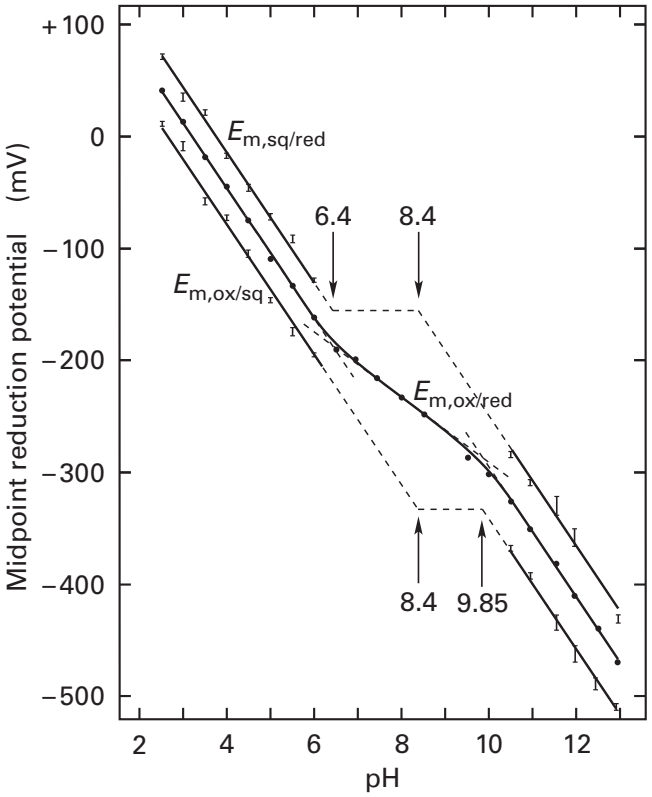

Figure 2–15: Midpoint reduction potentials of riboflavin as a function of pH.[288] A 30 μM solution of oxidized riboflavin, which was shown to be dilute enough that the dimerization of flavin semiquinone was negligible throughout each titration, at a given buffered pH and at 20 °C was flushed with nitrogen in a vessel containing a platinum electrode with which the reduction potential of the solution could be monitored. Measured volumes of the strong reductant sodium hydrosulfite were added to reduce systematically the riboflavin. The potential of the solution was followed as a function of the volume of reductant added to produce a titration curve of the reduction at the given pH. The complete titration curve was that of a two-electron reduction, and the final product was reduced riboflavin. The midpoint reduction potentials, $E_{m,ox/red}$, at the half-reduced point of each two-electron titration curve are plotted as a function of pH (middle curve). In the region below pH 6 and the region above pH 10, the midpoint reduction potentials as a function of pH displayed linear behavior, and the slope of the line in each region was 58 mV (unit of pH)$^{-1}$ (dashed lines), as expected from theory. The shapes of the individual titration curves in the regions from pH 2 to pH 6 and from pH 10 to pH 13 indicated that significant concentrations of flavin semiquinone were present at these values of pH. Each individual titration curve in these ranges of pH was fit to a theoretical function for the behavior of an equilibrium system of oxidized flavin, flavin semiquinone, and reduced flavin to estimate the amount of flavin semiquinone present, from which the midpoint reduction potential, $E_{m,ox/sq}$, for the redox couple of oxidized flavin and flavin semiquinone (lower lines) and the midpoint reduction potential, $E_{m,sq/red}$, for the redox couple of flavin semiquinone and reduced flavin (upper lines) could be calculated. These functions are plotted as well. The midpoint reduction potential $E_{m,ox/red}$ shows two clear inflections between the region of linear behavior below pH 6 and the region of linear behavior above pH 10. Between these two inflections the slope of the function is 29 mV (unit of pH)$^{-1}$ (dashed lines), again as expected. These inflections defined the pK_a of oxidized flavin (p$K_{a,ox}$ = 9.85) and reduced flavin (p$K_{a,red}$ = 6.4). The line of slope 58 mV (unit of pH)$^{-1}$ below pH 6 for the midpoint reduction potential $E_{m,sq/red}$ was extrapolated (dashed line), and a horizontal dashed line was drawn that intersected the line of slope 58 mV (unit of pH)$^{-1}$ above pH 10 for the midpoint reduction potential $E_{m,sq/red}$ at pH = 9.85. The intersection of these two dashed lines is an estimate of the pK_a of flavin semiquinone (p$K_{a,sq}$ = 8.4). The line of slope 58 mV (unit of pH)$^{-1}$ above pH 10 for the midpoint reduction potential $E_{m,ox/sq}$ was extrapolated (dashed line), and a horizontal dashed line was drawn that intersected the extrapolation of the line of slope 58 mV (unit of pH)$^{-1}$ below pH 6 for the midpoint reduction potential $E_{m,ox/sq}$ at pH 6.4. The intersection of these two lines is another estimate of the pK_a of flavin semiquinone (p$K_{a,sq}$ = 8.4).

When flavin is in a protein, the midpoint reduction potential for the two-electron reduction of oxidized flavin to reduced flavin, the one-electron reduction of oxidized flavin to flavin semiquinone, or the one-electron reduction of flavin semiquinone to reduced flavin is controlled, in part, by the acid–bases and the donors and acceptors in hydrogen bonds that surround the flavin. The midpoint reduction potentials of the flavin within a flavoprotein or the active site of a flavoenzyme can also be measured. A mediator such as methyl viologen is added to transfer electrons to and from the flavin within the protein and allow the oxidation–reduction on the active site to come to equilibrium with the potential established in the solution. In the absence of oxygen, successive portions of a strong reductant such as dithionite are added to the solution, and, at equilibrium, the total concentrations of reduced flavin $[Fl_{red}]_t$, flavin radical $[Fl^{\bullet}]_t$, and oxidized flavin $[Fl_{ox}]_t$ are measured spectrophotometrically. The electrochemical potential of the solution at equilibrium, E, is measured either with an electrode[322-324] or by determining spectrophotometrically the concentrations of the reduced and oxidized forms of a dye of known standard reduction potential also present in the solution.[325] The respective concentrations and potentials that have been measured for the successive reductive steps are plotted (Equation 2–95), and from the plot, E_m is obtained for the pH established by the buffer in the solution.

When flavin is bound as a prosthetic group within the active site of a protein, it is, depending on the structure of the site, more or less **shielded from the solution**. This shielding mutes the effects of the pH in the surrounding solution. In addition, acids and bases from side chains of the amino acids in the protein can form hydrogen bonds with the

σ lone pairs and acidic hydrons around the isoalloxazine (Figure 2–9). The **acids and bases from the protein** that form these hydrogen bonds add and remove, respectively, the hydrons transferred to and from the σ lone pairs of the flavin during its reduction or oxidation. In such situations, hydrons from the solution are not the ones transferred. If all the locations around the flavin were occupied by bases and acids from the protein, and both they and the flavin were completely surrounded by protein and isolated from the solution, the midpoint reduction potential of the flavin would be unaffected by the pH of the solution and determined only by the intrinsic values of pK_a for these bases and acids.

Consider the simplest situation in which the flavin is completely surrounded by the protein and the protein provides only one acidic amino acid, $^{(+)}$AH, and that acid is adjacent to the lone pair of electrons on nitrogen 5 of the neutral flavin semiquinone. The addition of an electron to neutral oxidized flavin, HFl_{ox}, to produce flavin semiquinone radical anion, $HFl^{\bullet -}$, and the subsequent transfer of the hydron from $^{(+)}$AH to nitrogen 5, to produce the particular tautomer of neutral flavin semiquinone, $H_2Fl^{\bullet}$, can be described by the following linkage

$$\begin{array}{ccc} e^- + {}^{(+)}AH{:}HFl_{ox} & \rightleftharpoons & {}^{(+)}AH{:}HFl^{\bullet -} \\ \rightleftharpoons & & \rightleftharpoons \\ e^- + {}^{(-)}A{:}H_2Fl_{ox}{}^{+} & \rightleftharpoons & {}^{(-)}A{:}H_2Fl^{\bullet} \end{array} \qquad (2\text{–}108)$$

where the four complexes denote hydrogen bonds between the acid, $^{(+)}$AH, or its conjugate base, $^{(-)}$A:, and the bound flavin. If these are the only forms present, it can be shown[326] that the midpoint reduction potential

$$E^{\circ}_{app,ox/sq} = E^{\circ\prime}_{HFl_{ox}} - \frac{RT}{F}\ln\left[\frac{\left(K_{a,H_2Fl^{\bullet}}\right)\left(K_{a,H_2Fl_{ox}{}^{+}}\right) + \left(K_{a,H_2Fl^{\bullet}}\right)\left(K_{a,AH}\right)}{\left(K_{a,H_2Fl_{ox}{}^{+}}\right)\left(K_{a,H_2Fl^{\bullet}}\right) + \left(K_{a,H_2Fl_{ox}{}^{+}}\right)\left(K_{a,AH}\right)}\right] \qquad (2\text{–}109)$$

where $E^{\circ\prime}_{HFl_{ox}}$ is the biochemical standard reduction potential for the reduction of neutral oxidized flavin in the active site in the absence of transfer of the hydron

$$^{(+)}AH{:}HFl_{ox} + e^- \rightleftharpoons {}^{(+)}AH{:}HFl^{\bullet -} \qquad (2\text{–}110)$$

and $K_{a,H_2Fl_{ox}{}^{+}}$ is the acid dissociation constant of the tautomer of oxidized flavin with hydrons on nitrogen 5 and nitrogen 3, $K_{a,H_2Fl^{\bullet}}$ is the acid dissociation constant for the same tautomer of flavin semiquinone, and $K_{a,AH}$ is the acid dissociation constant for the acid–base in the active site.

Equation 2–109 is the expression that would have resulted for the dependence of $E_{m,ox/sq}$ on pH in free solution if $K_{a,AH}$ were replaced by $[H^+]$. Therefore, if the intrinsic values of pK_a for flavin remain the same when the flavin is within the protein, then the plot of $E_{m,ox/sq}$ against pH for the one-electron reaction in solution ($E_{m,ox/sq}$ in Figure 2–15) would be equivalent to the plot of $E_{m,ox/sq}$ against the pK_a of the acid in the protein that provides the hydron to nitrogen 5 during the one-electron reduction. This relationship is a demonstration of the fact that, by definition, the activity of a hydron on an acid of a given pK_a is equal to the activity of a hydron in a solution with a pH equal to that pK_a. Although none of the values for pK_a in Equation 2–109 or the reduction potential of the oxidized flavin when it is in the active site can ever be known and the equation is of no practical use, nevertheless it shows how the intrinsic acidity of the particular acid that forms a hydrogen bond to nitrogen 5 can control the reduction potential of the flavin when it is within a flavoprotein and, by extension, how **the complete constellation of acid–bases surrounding the flavin controls its reduction potential**.

At the same fixed pH, the two-electron midpoint reduction potentials of flavin differ from one flavoprotein to another (Table 2–1).[322-325,327,328] The tabulated values span a range as large as that for the two-electron midpoint reduction potential of riboflavin between pH 4.5 and pH 8.5 (Figure 2–15). This variation must reflect the identities of the amino acids surrounding the prosthetic flavin in each of these active sites.

It is never the case, however, that the flavin is completely surrounded by the protein, isolated from the solution, and completely surrounded by acids and bases from the protein that in turn are not connected to the solution. If there are particular lone pairs of electrons or acidic hydrogens on the flavin that are exposed to the solution or that are connected to the solution through a network of hydrogen bonds rather than forming hydrogen bonds

Table 2–1: Reduction Potentials of Flavin in the Active Sites of Enzymes

enzyme	pH	temperature (°C)	$E^{\circ\prime}_{app}$ (mV)
salicylate 1-monooxygenase from *B. cepacia*[327]	7.5	10	–88
human medium-chain acyl-CoA dehydrogenase[324]	7.6	25	–114
human short-chain acyl-CoA dehydrogenase[322]	7.6	25	–162
[NAD(P)H] nitroreductase from *Enterobacter cloacae*[323]	7.5	25	–210
methylenetetrahydrofolate reductase [NAD(P)H] from *E. coli*[325]	7.2	25	–237
thioredoxin-disulfide reductase from *E. coli*[328]	7.6	1	–263

with side chains of amino acids in the active site that are not connected to the solution, then the pH of the solution determines whether these positions are hydronated or unhydronated.

Consequently, the midpoint reduction potentials of flavin in an active site are **unpredictably affected by the pH** of the solution. For example, when flavin adenine dinucleotide is the prosthetic flavin in the active site of porcine medium-chain acyl-CoA dehydrogenase,[324] its two-electron midpoint reduction potential ($E_{m,ox/red}$) decreases by –60 mV (unit of pH)$^{-1}$ between pH 6.5 and pH 7.5 at 25 °C. This slope suggests that two hydrons from the solution associate with the flavin upon its reduction by two electrons in this active site. When flavin, however, is in solution, the slope of the midpoint potential as a function of pH is –59.2 mV (unit of pH)$^{-1}$ only below pH 6 and above pH 10 (Figure 2–15). When flavin adenine dinucleotide is the prosthetic flavin in the active site of salicylate 1-monooxygenase from *B. cepacia*,[327] its two-electron midpoint reduction potential decreases by –26 mV (unit of pH)$^{-1}$ at 10 °C between pH 6.5 and pH 7.5. This slope suggests that only one hydron from the solution associates with the flavin upon its reduction by two electrons, as happens when flavin is in solution at 25 °C [–29.6 mV (unit of pH)$^{-1}$] between pH 7 and pH 9. When flavin mononucleotide is the prosthetic flavin in the active site of NAD(P)H nitroreductase from *E. cloacae*,[323] however, its two-electron midpoint reduction potential decreases by –38 mV (unit of pH)$^{-1}$ at 25 °C.

In addition to the effect of donors and acceptors for hydrogen bonds to the σ lone pairs of electrons and acidic hydrons of the isoalloxazine, variations in midpoint reduction potential also result from **other structural features** of the site in which the flavin is bound on the enzyme. A nearby negatively charged side chain within the site decreases the two-electron midpoint reduction potential of the flavin,[324] and a nearby positively charged side chain increases its two-electron midpoint reduction potential.[329,330] The substitution of the methyl group at position 8, as occurs when the flavin is covalently attached to a protein (Equation 2–83), with a group that withdraws electron density increases the two-electron midpoint reduction potential of the flavin, while substitution with a group that donates electron density decreases the two-electron midpoint reduction potential of the flavin.[331,332] The binding of substrates to the active site, because they end up immediately adjacent to the flavin, also affects the midpoint reduction potential of the flavin.[333]

The acid dissociation with a pK_a closest to pH 7 is the **ureido nitrogen 1 in reduced flavin** (Figure 2–9), and upon dissociation of the hydron, the majority of the net negative elementary charge is located on the carbonato oxygen, which is more electronegative than the nitrogen. When reduced

flavin is bound to a protein as a prosthetic group, the protein that surrounds the ureido group at positions 1 and 2 usually insulates nitrogen 1 and the carbonato oxygen on carbon 2. In this way, **the active site stabilizes either the neutral form of reduced flavin, H_3Fl_{red}, or its anionic conjugate base, $H_2Fl_{red}^-$.**[334] As previously noted, the form most often present in an active site is the conjugate base, which, coincidentally, is the more prevalent form at pH 7 in solution. The most commonly encountered form of oxidized flavin in an active site is the neutral form, HFl_{ox}. Consequently, when oxidized flavin in a protein is reduced by two electrons, nitrogen 1 either picks up a hydron or it does not.

Human glutathione-disulfide reductase (Figure 2–11),[306] D-amino-acid oxidase from *R. toruloides* (Figure 2–12),[312] and porcine medium-chain acyl-CoA dehydrogenase, when its substrate is bound (Figure 2–13),[316] are examples of proteins that stabilize the anionic conjugate base of reduced flavin with nitrogen 1 unhydronated.[334] In each of the crystallographic molecular models of these three enzymes, the **carbonato oxygen at position 2** of the flavin accepts two hydrogen bonds from two donors: an amido nitrogen–hydrogen from the polypeptide backbone and a molecule of water; two amido nitrogen–hydrogens from successive amides in the polypeptide backbone; and the hydroxy group of a threonine and an amido nitrogen–hydrogen from the polypeptide backbone, respectively. These donors for hydrogen bonds are typical of the donors that stabilize oxyanions that form in active sites during an enzymatic reaction. **Nitrogen 1 of the flavin** is the acceptor for a hydrogen bond from a threonine in the active site of porcine medium-chain acyl-CoA dehydrogenase, but there are no obvious donors for hydrogen bonds in the other two active sites. The donors for hydrogen bonds that stabilize the oxyanion are not, however, the only reason that the anionic conjugate base of reduced flavin is stabilized in preference to neutral reduced flavin by these proteins. In the crystallographic molecular model of ferredoxin—NADP reductase from *Nostoc*, a protein that stabilizes neutral reduced flavin,[334] the oxygen on carbon 2 of the flavin also engages in two hydrogen bonds, one with an amido nitrogen–hydrogen from the polypeptide backbone and the other with a molecule of water, and there is only a molecule of water, not an obvious acid, forming a hydrogen bond to nitrogen 1, presumably as an acceptor.[335] In choline oxidase, a histidinium ion adjacent to the amide at positions 1 and 2 of the flavin is thought to stabilize the anionic conjugate base of reduced flavin.[336]

In the case of **nitrogen 5 of the flavin**, a lone pair of electrons must be hydronated upon two-electron reduction (Figure 2–9), and donors and acceptors for hydrogen bonds must adjust to this change. In the flavodoxin of *Synechococcus*, the amido group in the polypeptide backbone between Asparagine 58 and Valine 59 flips upon reduction of the flavin so that the amido group that forms an N–H hydrogen bond with the lone pair of electrons on nitrogen 5 of oxidized flavin is replaced by the acyl oxygen of the same amido group that forms a hydrogen bond with the nitrogen–hydrogen of nitrogen 5 in reduced flavin.[337]

When a molecule of flavin is bound to a molecule of protein, its semiquinone radical is often stabilized by the protein. In free solution at all values of pH greater than 2 (Figure 2–15), the midpoint reduction potential for the redox couple of oxidized flavin and **flavin semiquinone** ($E_{m,ox/sq}$) is more negative than that for the redox couple of flavin semiquinone and reduced flavin ($E_{m,sq/red}$). This inversion means that, in solution, two flavin semiquinones participate in a **disproportionation**

$$H_lFl^{\bullet} + H_lFl^{\bullet} \rightleftharpoons H_mFl_{ox} + H_nFl_{red} \qquad (2\text{–}111)$$

with a negative standard free energy change as written ($K_{eq} = 10$ at pH 4.0 and $K_{eq} = 30$ at pH 11.5; Figure 2–15).[288] This disproportionation causes the concentration of flavin semiquinone to become almost immeasurable in the central region of pH.

At an electrode poised at a potential sufficiently negative to reduce oxidized flavin when it is in solution, the anionic flavin semiquinone ($HFl^{\bullet -}$) produced by transfer of an electron at the surface of the electrode immediately picks up a hydron from the solution, and the resulting neutral flavin semiquinone ($H_2Fl^{\bullet}$), because its reduction potential is more positive than that of the electrode, immediately picks up a second electron from the electrode. If no hydrons are available in the solution, however, the second electron is not transferred,[338] and the flavin remains as the radical anion. Denying the anionic flavin semiquinone a hydron is one way to stabilize it.

In an active site, a flavin semiquinone can be stabilized kinetically and thermodynamically. In an active site, a prosthetic flavin is isolated from the solution and sterically hindered from disproportionating at the encounter-controlled rate that it would display in solution. For example, the flavin

semiquinone formed from oxidized flavin adenine dinucleotide on porcine cytochrome-b_5 reductase by a hydrated electron disproportionates much more slowly (1×10^3 M^{-1} s^{-1}) than it would in solution[339] because it is isolated by the surrounding protein. This kinetic protection afforded by the protein is similar to the insulation from disproportionation that an active site affords to a sulfenic acid.[340] When flavin mononucleotide is dispersed at sufficiently low concentration in the absence of oxygen in an agarose matrix, which interrupts diffusion, the semiquinone of the flavin mononucleotide can be produced photolytically in high yield and its lifetime is several days.[341] The matrix precludes disproportionation, just as enclosing the semiquinone in protein does.

In an active site, flavin semiquinone can be stabilized thermodynamically when the environment created by the protein causes the midpoint reduction potential for the redox couple of oxidized flavin and flavin semiquinone ($E_{m,ox/sq}$) to be more positive than that of flavin semiquinone and reduced flavin ($E_{m,sq/red}$), rather than being more negative as it is in solution (Figure 2–15). There are a number of flavoproteins that have dramatically altered these reduction potentials to stabilize the flavin semiquinone (Table 2–2). Unlike flavin when it is free in solution, when flavin is the prosthetic group in a protein that stabilizes the flavin semiquinone thermodynamically, the spectrum of the flavin semiquinone is clearly observed in the midrange of reduction potential (Figure 2–10), and there is no difficulty in measuring changes in its concentration.[342]

By linkage, an active site must stabilize the flavin semiquinone because it binds the flavin semiquinone more tightly than both oxidized flavin and reduced flavin,[348] but the molecular reasons for this preference in association are not well understood, and it is probably due to a combination of factors. When the tyrosine stacked against the flavin in flavodoxin from *Desulfovibrio vulgaris* is mutated to an amino acid other than phenylalanine or tryptophan, the difference in the two one-electron midpoint reduction potentials (Table 2–2) decreases significantly.[330] In model compounds, the presence of an intramolecular donor for a hydrogen bond to nitrogen 5 of flavin

Table 2–2: One-Electron Reduction Potentials in Flavoproteins Stabilizing the Flavin Semiquinone

flavoprotein	$E^{\circ\prime}_{ox/sq}$[a] (mV)	$E^{\circ\prime}_{sq/red}$[a] (mV)
flavin mononucleotide[288]	–240	–170
glycine oxidase from *Bacillus subtilis*[343]	–42	–340
flavodoxin from *Clostridium pasteurianum*[344]	–132	–419
nitric-oxide synthase (NADPH) from *Rattus norvegicus*[345]	–49	–274
flavoprotein of assimilatory sulfite reductase (NADPH) from *E. coli*[342]	–152	–327
NADPH—hemoprotein reductase from *R. norvegicus*[346]		
FMN	–110	–270
FAD	–290	–365
4-hydroxybutanoyl-CoA dehydratase from *Clostridium aminobutyricum*[347]	–140	–240

[a]Standard reduction potentials (pH 7.0) for the redox couples of oxidized flavin and flavin semiquinone ($E^{\circ\prime}_{ox/sq}$) and flavin semiquinone and reduced flavin ($E^{\circ\prime}_{sq/red}$).

stabilizes the flavin semiquinone relative to oxidized and reduced flavin.[349] It is also the case that mutation of the amino acids participating in the hydrogen bonds to nitrogens 5 of flavins in flavodoxin from *Clostridium beijerinckii*[350] and electron-transferring flavoprotein from the methylotrophic bacterium W3A1,[351] respectively, decreases the difference in the two one-electron midpoint reduction potentials responsible for the stabilization of the flavin semiquinone. In flavocytochrome b_2 from *Spinacia oleracea*, the anionic flavin semiquinone is stabilized by an adjacent lysine with a positive elementary charge that encourages its formation from oxidized flavin but discourages the hydronation necessary for its reduction because it is not able to hydronate nitrogen 5.[352]

In some flavoenzymes that stabilize the flavin semiquinone, the form of the enzyme containing this flavin semiquinone is enzymatically active;[353] in others, however, flavin semiquinone, even though it is stabilized by the enzyme, is catalytically inactive.[354,355]

Each of the oxidation–reductions catalyzed by the flavins on flavoenzymes can usually be divided into two half-reactions, each exclusive to a redox couple. The prosthetic oxidized flavin or the prosthetic reduced flavin in the active site of a particular enzyme oxidizes or reduces, respectively, the particular reductant or the particular oxidant of the redox couple of substrates that is usually unique to that flavoenzyme and gives the flavoenzyme its name: for example, dihydrolipoyl dehydrogenase and the redox couple of N^6-(lipoyl)lysine and N^6-(dihydrolipoyl)lysine; (*S*)-mandelate dehydrogenase and the redox couple of 2-oxo-2-phenylacetate and (*S*)-mandelate; medium-chain acyl-CoA dehydrogenase and the redox couple of *trans*-oct-2-enoyl-SCoA and octanoyl-SCoA; D-amino-acid oxidase and the redox couple of pyruvimine and D-alanine; FMN reductase (NADPH) and the redox couple of oxidized flavin mononucleotide and reduced flavin mononucleotide; and glutathione-disulfide reductase and the redox couple of glutathione and glutathione disulfide. To simplify the present discussion, the redox couple unique to a particular flavoenzyme and giving that enzyme its name will be called the **nominal redox couple**.* The resulting reduced flavin or oxidized flavin is then oxidized or reduced, respectively, by a coenzymatic redox couple that is used in many different oxidation–reductions catalyzed by an array of enzymes—for example the redox couple of NAD^+ and NADH, the redox couple of ubiquinone and ubiquinol, the redox couple of oxidized electron-transfer flavoprotein and reduced electron-transfer flavoprotein, or the redox couple of oxidized ferredoxin and reduced ferredoxin—or a redox couple that is not considered coenzymatic but is also used in many different enzymatic reactions, such as the redox couple of oxygen and hydrogen peroxide. To simplify the present discussion, the widely used redox couple in this second half-reaction that returns the flavin to the oxidation state that it had before the first half-reaction occurred will be called the **general redox couple**. The general redox couple connects the particular reaction catalyzed by the enzyme to the overall reduction potential at which the cytoplasm is poised.

Because the nominal redox couple and the general redox couple alternate with each other on the active site, the flavin, as is required of a catalyst, does not participate in the chemical equation for the complete reaction. The facts, however, that the nominal redox couple by itself can either oxidize or reduce the prosthetic flavin and that the general redox couple, also by itself, can either oxidize or reduce the prosthetic flavin permit the overall reaction to be experimentally dissected. Depending on the respective reduction potentials, oxidation of the prosthetic flavin by either the nominal oxidant or the general oxidant can be observed in isolation, and reduction of the prosthetic flavin by either the nominal reductant or the general reductant can also be observed in isolation.

The **complete oxidation–reduction** is the oxidation or reduction of the nominal reactant and the reduction or oxidation, respectively, of the general reactant. Examples of complete oxidation–reductions catalyzed by flavoenzymes would be the reaction catalyzed by dihydrolipoyl dehydrogenase

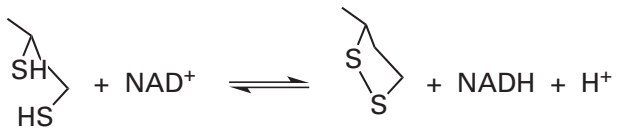

(2–112)

the oxidation–reduction catalyzed by (*S*)-mandelate dehydrogenase from *P. putida*[356]

*A reviewer pointed out that this nomenclature is unprecedented. It is, however, useful.

(*S*)-mandelate + ubiquinone ⇌
2-oxo-2-phenylacetate + ubiquinol (2–113)

the oxidation–reduction catalyzed by medium-chain acyl-CoA dehydrogenase

octanoyl-SCoA +
oxidized electron-transfer flavoprotein
⇌ *trans*-oct-2-enoyl-SCoA +
reduced electron-transfer flavoprotein (2–114)

the oxidation–reduction catalyzed by ferredoxin: thioredoxin reductase from *Clostridium acetobutylicum*[357]

2 thioredoxin + 2 oxidized ferredoxin
⇌ thioredoxin disulfide +
2 H^+ + 2 reduced ferredoxin (2–115)

the oxidation–reduction catalyzed by D-amino-acid oxidase

D-alanine + H_2O + O_2 ⇌
NH_4^+ + pyruvate + H_2O_2 (2–116)

or the oxidation–reduction catalyzed by FMN reductase (NADPH) from *E. coli*

$FMNH^-$ + $NADP^+$ ⇌ FMN + NADPH (2–117)

The direction in which each oxidation–reduction proceeds depends, as always, on its equilibrium constant and the concentrations of reactants and products in the solution.

There are a few enzymatic reactions in which flavin is not used as a redox couple. These reactions should be considered before those in which it does participate as a redox couple because they reveal relevant capabilities of flavin.

In the active site of isopentenyl-diphosphate Δ-isomerase from *Staphylococcus aureus*, nitrogen 5 of the reduced flavin is used as a **catalytic acid–base**[358-360] to add a hydron to one or the other of the substrates, isopentenyl diphosphate or dimethylallyl diphosphate, and then accept a different hydron from the resulting intermediate tertiary carbenium ion to form the other substrate in a reaction involving no oxidation–reduction.

In the enzymatic reaction catalyzed by UDP-galactopyranose mutase

UDP-α-D-galactopyranose
⇌ UDP-α-D-galactofuranose (2–118)

which also does not involve an oxidation or reduction, nitrogen 5 of the central 1,4-dihydropyrazine in reduced flavin is used as a **nucleophilic catalyst**. Nitrogen 5 forms a covalent intermediate with the D-galactopyranosyl group or the D-galactofuranosyl group of the respective reactant in a concerted nucleophilic substitution proceeding with inversion of configuration, with the diphosphate of the UDP as the leaving group, to give the hemiaminal ether between carbon 1 of the now β-D-galactopyranosyl or β-D-galactofuranosyl group and nitrogen 5 of the flavin

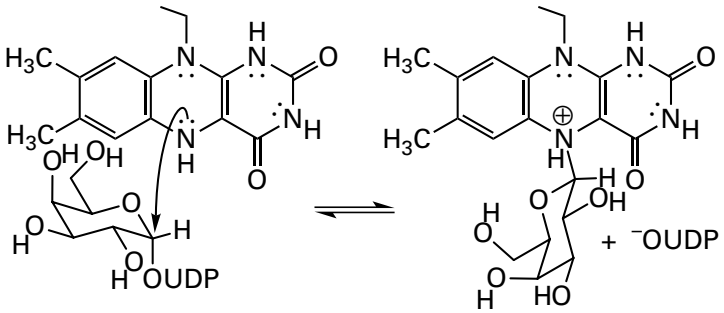

(2–119)

This hemiaminal ether, hydronated on nitrogen 5 as shown, has been observed in a crystallographic molecular model of the active site of a mutant of the enzyme from *Neosartorya fumigata*.[361] The unhydronated hemiaminal ether then opens to produce the iminium of the uncyclized D-galactosyl group at nitrogen 5 of the flavin (**2–48**). This iminium between flavin and the open form of D-galactose in the active site of UDP-galactopyranose mutase[362] from *Klebsiella pneumoniae* has been trapped with $NaCNBH_3$

2–48

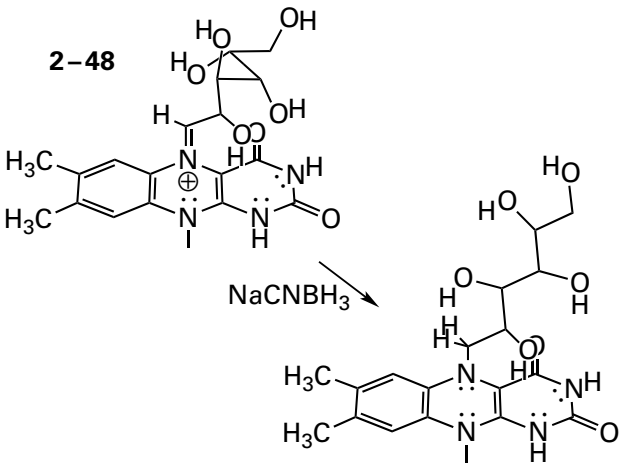

(2–120)

and the trapped product was identified by ultraviolet spectroscopy and mass spectrometry.[363] The reaction then proceeds in reverse to give either UDP-α-D-galactofuranose or UDP-α-D-galactopyranose as the respective product.

There are several other instances in which reduced flavin is a nucleophilic catalyst.[364] In the active site of thymidylate synthase (FAD), nitrogen 5 of reduced flavin nucleophilically adds to the electrophilic methylene carbon in N^5-methylenetetrahydrofolate.[365] In the active site of flavin prenyltransferase, nitrogen 5 of reduced flavin participates as the nucleophile in a nucleophilic substitution at carbon 1 of dimethylallyl phosphate with phosphate as the leaving group during the synthesis of prenylated $FMNH_2$[366]

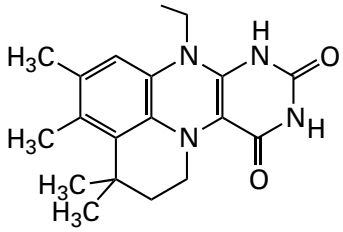

2–49

In the active site of monoamine oxidase, nitrogen 5 of reduced flavin nucleophilically adds to the electrophilic distal carbon of a propargylamine synthesized as a covalent inhibitor of the enzyme.[367]

The strange aspect to these roles of nitrogen 5 of flavin as a catalytic acid or as a nucleophile is that the pK_a of the conjugate acid of nitrogen 5 in neutral reduced flavin is only 0.8 (Figure 2–9), as expected for an anilinium, a fact suggesting that it would be difficult to hydronate nitrogen 5 to form the catalytic acid and that nitrogen 5 should not be nucleophilic. The pK_a for the second dehydronation is well beyond the normal range of pH.

Oxidized flavin is also used as an **electrophilic catalyst**. The reaction catalyzed by alkylglycerone-phosphate synthase

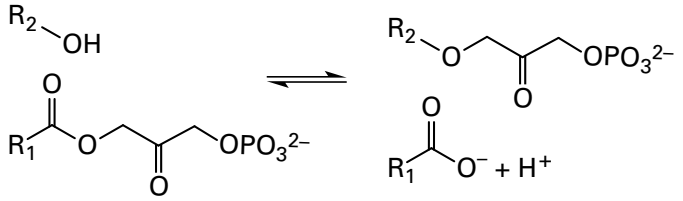

(2–121)

where R_1 is a linear alkyl chain on a fatty acid esterified to glycerone phosphate and R_2 is a linear alkyl chain on a long-chain alcohol, is a formal nucleophilic substitution that involves no oxidation or reduction. The enolate of 1-acylglycerone 3-phosphate adds as a nucleophile to the electrophilic nitrogen 5 of oxidized flavin, and the resulting hemiaminal ester dissociates into the unhydronated fatty acid and the imine of 3-hydroxypyruvaldehyde 1-phosphate at nitrogen 5

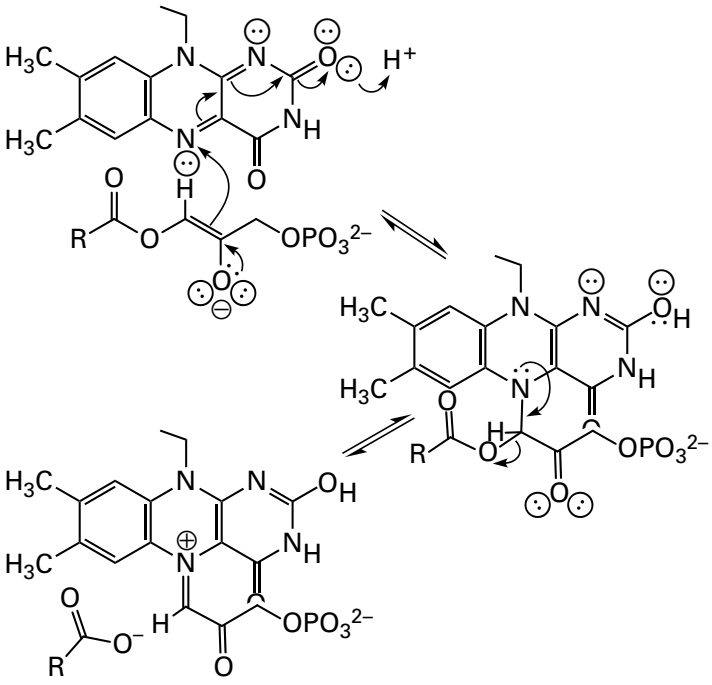

(2–122)

The unhydronated fatty acid is replaced by the long-chain alcohol and the reaction proceeds in reverse to produce the 1-alkylglycerone 3-phosphate.

When alkylglycerone-phosphate synthase from *Cavia porcellus* that has been reconstituted with 5-carba-5-deazaflavin, a synthetic derivative in which nitrogen 5 of the flavin is replaced by a carbon, in place of the flavin, a stable adduct, homologous to the initial adduct in Equation 2–122, between

1-palmitoylglycerone 3-phosphate and the prosthetic flavin forms in the active site.[368] The reaction cannot proceed beyond this initial adduct because nitrogen 5 has been replaced by carbon, which has no lone pair of electrons. In the normal reaction, the enzyme is using nitrogen 5 of the oxidized flavin as an electrophile rather than an oxidant, much as urocanate hydratase (Equation 2–81) uses carbon 4 of a prosthetic NAD^+ as an electrophile rather than as an oxidant.

Prenylated $FMNH_2$ (2–49), a prosthetic group found in active sites of fungal and bacterial enzymes, seems to be used exclusively as a prosthetic catalyst in reactions that again involve no oxidation or reduction.[369] For example, the prenylated $FMNH_2$ in the active site of phenacrylate decarboxylase from *E. coli* forms an adduct with one of its several alternative reactants—(2*E*)-3-phenylprop-2-enoate, (2*E*)-3-(4-hydroxyphenyl)prop-2-enoate, or (2*E*)-4-hydroxy-3-methoxy-3-phenylprop-2-enoate—in a reversible **polar cycloaddition** with the respective (2*E*) double bond[370,371] to facilitate the respective decarboxylation of the carboxylate and replacement of the carbon dioxide with a hydron.

Each of these foregoing examples highlights a chemical property of the flavin that has bearing on the more common oxidation–reductions catalyzed by flavoenzymes. In at least one instance, however, the flavin bound by the enzyme does not seem to participate in the catalytic reaction at all.[372]

Because of the existence of the semiquinone, flavin can be both a one-electron oxidant and reductant and a two-electron oxidant and reductant, an ability that is essential to its dramatic versatility[283] but a fact that obscures the exact mechanism of its participation in a particular oxidation–reduction. Almost all the nominal oxidation–reductions catalyzed by flavoenzymes are formally two-electron oxidation–reductions of the nominal substrate; for example, the reaction catalyzed by (*S*)-mandelate dehydrogenase in which (*S*)-2-hydroxy-2-phenylacetate is oxidized to 2-oxo-2-phenylacetate, a simple oxidation of a secondary alcohol to a ketone. The general redox couples, however, that regenerate the initial oxidation state of the flavin are often one-electron participants such as ferredoxin. The capacity of flavin to act as both a one-electron oxidant and reductant and a two-electron oxidant and reductant leaves in question its specific mechanism of action in many of the nominal two-electron oxidation–reductions. In a formally two-electron oxidation–reduction, are the electrons transferred to and from flavin one at a time or together as a hydride? This question is further complicated by the nucleophilicity and electrophilicity of flavin just described. During the transfer of two electrons, is a covalent adduct formed between a nucleophilic substrate and electrophilic oxidized flavin or between an electrophilic substrate and nucleophilic reduced flavin?

Many of the two-electron reductants oxidized by flavin are nucleophiles, and the products of the oxidations are electrophiles that are reduced in the reverse direction. For example, the flavin in dihydrolipoyl dehydrogenase (Equation 2–71) oxidizes a pair of adjacent cysteines in the polypeptide to produce a cystine, which then oxidizes a lipoyl group. The flavin in monoamine oxidase oxidizes a primary amine to its imine. The flavin in medium-chain acyl-CoA dehydrogenase (Equation 2–114) removes two electrons from the enolate of octanoyl-SCoA. In reactions in which flavin oxidizes a nucleophile, such as a thiolate, amine, or enolate, the question arises of how the two electrons pass from the thiolate, the amine, or the enolate to the flavin during the oxidation.

One possibility is that a thiolate, amine, or enolate is oxidized through **an intermediate produced by its nucleophilic addition to the flavin.** The electrophilic portion of oxidized flavin is the central 1,4-diazabutadiene

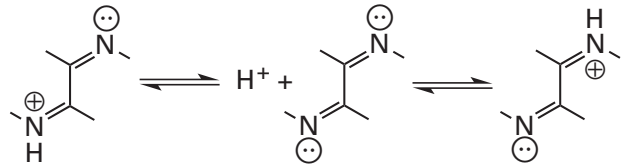

(2–123)

If a thiolate, amine, or enolate participates in a nucleophilic addition with oxidized flavin, the hydronated 1,4-diazabutadiene would be acting as the electrophile.

Because of the existence of this central 1,4-diazabutadiene, **nitrogen 5 of oxidized flavin is electrophilic** when nitrogen 1 is hydronated. Nitrogen 5 is the nitrogen analogue of the electrophilic β carbon in an α,β-unsaturated iminium ion (rightmost tautomer in Equation 2–123). That nitrogen 5 is electrophilic has been demonstrated by using sulfite as a nucleophile. When 7,8-dimethyl-1,10-ethenoisoalloxazinium is modified with sulfite, a crystalline product is obtained[373] that results from addition of the nucleophile to nitrogen 5

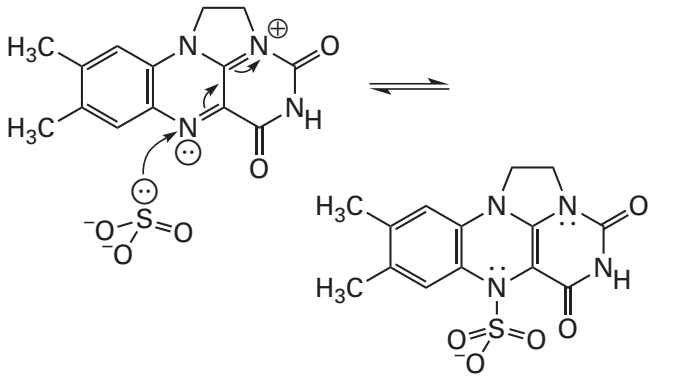

(2–124)

The formation of the adduct interrupts the conjugation of the isoalloxazine, and the strong absorption between 350 and 500 nm disappears. In its place is a peak of absorbance with a maximum at 308 nm (Figure 2–16).[373-375] This reaction demonstrates that when one nitrogen in the central diazobutadiene, in this instance nitrogen 1, is cationic, the other nitrogen is electrophilic.

The analogous adduct at nitrogen 5 (**2–50**)*

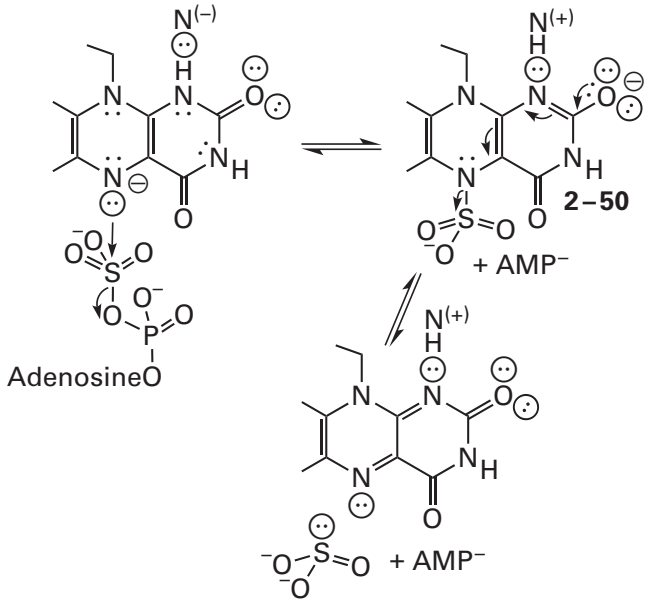

(2–125)

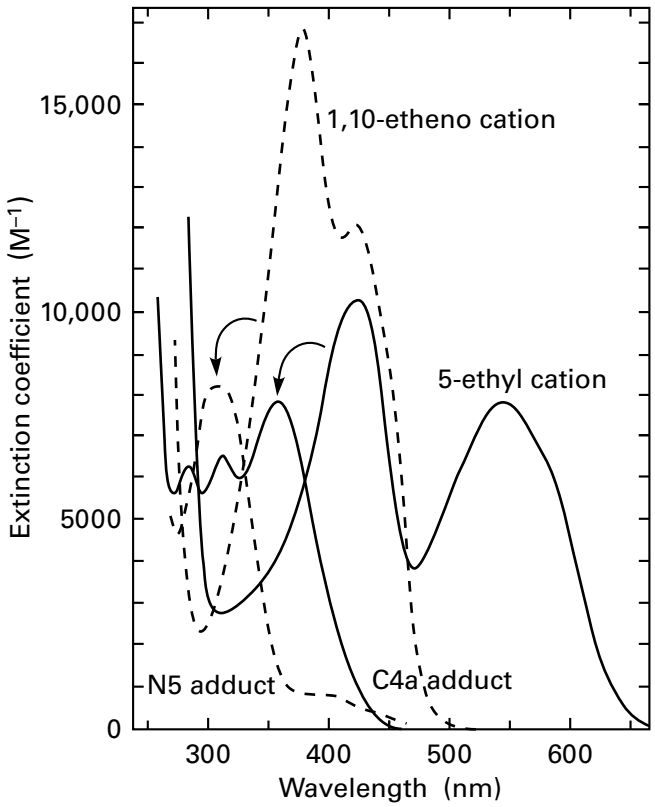

Figure 2–16: Absorption spectra of adducts to oxidized flavin. The spectrum[373] for the adduct of sulfite to nitrogen 5 (N5 adduct) of 7,8-dimethyl-1,10-ethenoisoalloxazinium (Equation 2–124) was obtained by adding sufficient $NaHSO_3$ to a 40 μM aqueous solution of 7,8-dimethyl-1,10-ethenoisoalloxazinium perchlorate at pH 7 to convert all of the isoalloxazinium to the adduct of sulfite at nitrogen 5. The spectrum of 7,8-dimethyl-1,10-ethenoisoalloxazinium (1,10-etheno cation) in the same solution was taken before the sulfite was added. The strong absorbance of the isoalloxazinium between 350 and 500 nm disappeared as the sulfite adduct formed. The spectrum[374] for the adduct of ethoxide to carbon 4a (C4a adduct) of 3,7,8,10-tetramethyl-5-ethylisoalloxazinium ion (Equation 2–128) was obtained by dissolving 3,7,8,10-tetramethyl-5-ethylisoalloxazinium perchlorate in ethanol. The spectrum[375] of the initial 3,7,8,10-tetramethyl-5-ethylisoalloxazinium ion (5-ethyl cation) was obtained by dissolving 3,7,8,10-tetramethyl-5-ethylisoalloxazinium perchlorate in 0.1 M sodium perchlorate at pH 3.

formed by the addition of sulfite to oxidized flavin,[376] is **an established intermediate in the enzymatic reaction** catalyzed by the flavoenzyme adenylylsulfate reductase from *Archaeoglobus fulgidus* and has been observed crystallographically.[377] The σ bond between sulfite and nitrogen 5 of the oxidized flavin in this intermediate is the relay station through which the two electrons pass during reduction of the phosphosulfate in 5′-adenylyl sulfate to sulfite in one direction and during oxidation of the sulfite to the phosphosulfate in the other direction. In one direction, this σ bond between sulfur and nitrogen 5 of the flavin is formed by the nucleophilic substitution of flavin for AMP^- at the electrophilic sulfur in the 5′-adenylyl sulfate, in which the nucleophile is the

*From here on the 7,8-dimethylphenyl ring of isoalloxazine will be truncated to two lines to save space in the equations. This truncation will become more and more appropriate as the equations become larger.

electron-rich nitrogen 5 of reduced flavin. In the other direction, it is formed by the nucleophilic addition of sulfite to electrophilic nitrogen 5 in the 1,4-diazabutadiene of oxidized flavin. The electrons arrive in the nucleophilic lone pair of electrons on nitrogen 5 of the reduced flavin in one direction and arrive in the nucleophilic lone pair of electrons on sulfite in the other direction, and the two electrons in the σ bond that they form leave the flavin on sulfite during the reduction and enter the flavin on sulfite during the oxidation, respectively. In the direction of oxidation of sulfite to form the phosphosulfate, Equation 2–124 suggests that nitrogen 1 will almost certainly be hydronated transiently to make the oxidized flavin more electrophilic.

In the enzymatic reaction catalyzed by nitroalkane oxidase from *Fusarium oxysporum*, the carbanionic conjugate base of a nitroalkane at the carbon α to the nitro group adds nucleophilically to nitrogen 5 of the prosthetic flavin in the active site. After the nitro group leaves and is replaced by a hydroxide, the pair of electrons that was the lone pair of electrons on the carbon α to the nitro group in the anionic conjugate base and that then formed the σ bond to nitrogen 5 is withdrawn into the flavin, reducing it and oxidizing the carbon to the aldehyde. The adduct at nitrogen 5 can be trapped with cyanide ion and observed in a crystallographic molecular model of the enzyme.[378]

On paper, a 1,4-diazabutadiene (Equation 2–123) can also be **electrophilic at either of its two iminium carbons**, which would be carbon 1a and carbon 4a of oxidized flavin, depending on which nitrogen is hydronated. Several products have been isolated[379] that seem to arise from the nucleophilic attack of hydroxide, ammonia, or hydride at **carbon 1a** of 1,3,7,8,10-pentamethylisoalloxazine, but the addition of any one of these heteroatomic nucleophiles leads unavoidably to the decomposition of the pyrimidine ring

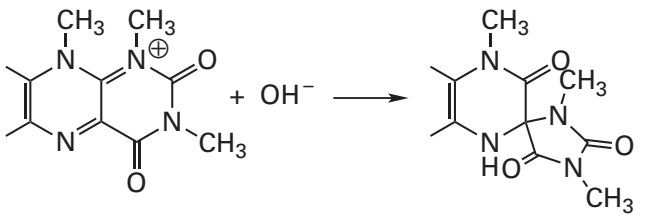

(2–126)

an outcome that would not be salutary for a flavoenzyme. This decomposition requires that nitrogen 1 be hydronated to cause carbon 1a to be electrophilic, and this requirement may explain why most flavoenzymes do not provide a catalytic acid to hydronate nitrogen 1 when flavin is reduced, and the reduced flavin is usually present as the anionic conjugate base. Because of this nucleophilic substitution at carbon 1a and the fact that nitrogen 1 and carbon 1a are always removed from the location at which substrates bind to the active sites of the available crystallographic molecular models for flavoenzymes, nucleophilic adducts at nitrogen 1 and carbon 1a of oxidized flavin have been discounted as intermediates in enzymatic reactions using flavin as a prosthetic group.

Carbon 4a in oxidized flavin is also electrophilic. Sulfite adds to 10-(2,6-dimethylphenyl)-6,8-disulfo-3-methylisoalloxazine[380] to produce a stable derivative at carbon 4a

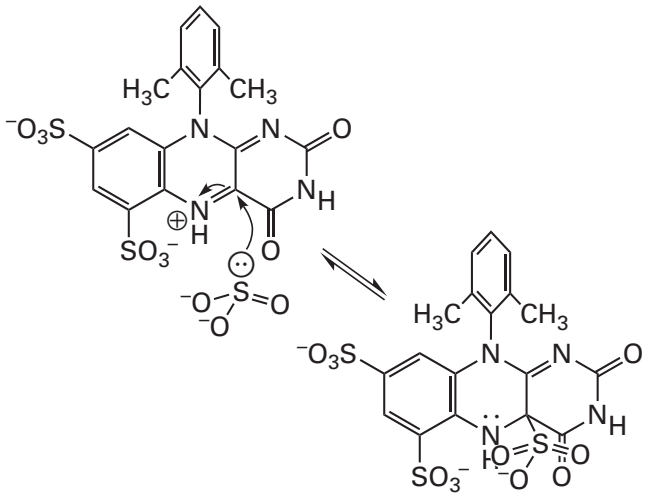

(2–127)

Two equivocal aspects of this observation are that the sulfonates at positions 6 and 8 mildly withdraw electron density ($\sigma_p = 0.1$) from carbon 4a, increasing its electrophilicity, and that the sulfonate on carbon 6 sterically blocks nucleophilic attack at nitrogen 5. Even under these most favorable circumstances, an equilibrium mixture of adducts at both carbon 4a and nitrogen 5 is obtained.[381] When the sulfonates are not present, sulfite adds exclusively[373] to nitrogen 5. The behavior of the rate constant for the decomposition of 4a-(indolylmethyl)-3,7,8,10-tetramethylisoalloxazine, however, as a function of pH can be explained[382] as the result of a rapid equilibrium between the adduct at carbon 4a and the adduct at nitrogen 5. If this is the correct explanation, then in this compound these two locations should have almost equivalent electrophilicities.

Stable, exclusive **nucleophilic adducts to carbon 4a** have been observed with oxidized 5-ethyl-3,7,8,10-tetramethylisoalloxazine. Either hydroxide ion[375]

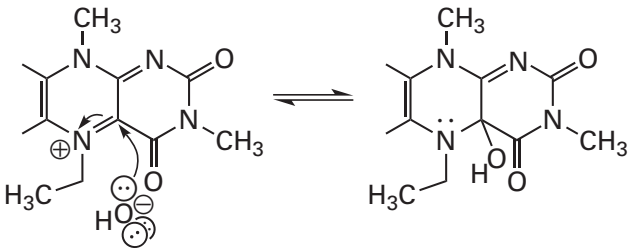

(2–128)

ethoxide,[374] or nitromethane ion ($^{-}$:CH_2NO_2)[383] can add reversibly to carbon 4a of this flavin. In the nucleophilic addition of hydroxide in Equation 2–128, the ethyl group accomplishes the same purpose as hydronation of nitrogen 5, only permanently, but it also sterically hinders addition to nitrogen 5. Nevertheless, this result suggests that, under acid catalysis at nitrogen 5, carbon 4a can be a competent electrophile. As was the case for adducts at nitrogen 5, the addition of a nucleophile at carbon 4a interrupts the conjugation of the oxidized flavin and eliminates its characteristic absorbance between 400 and 500 nm, but the absorption spectrum of an adduct at carbon 4a has a characteristic peak of absorbance between 350 and 400 nm (Figure 2–16).

For normal, oxidized, biochemical flavins, all the foregoing observations, on balance, suggest that **in solution, nitrogen 5 is much more electrophilic than carbon 4a**. This preference may arise from the fact that, because of the ureido oxygen on carbon 2, the addition of a nucleophile to nitrogen 5 can proceed without the need for hydronation of either nitrogen 1 or nitrogen 5

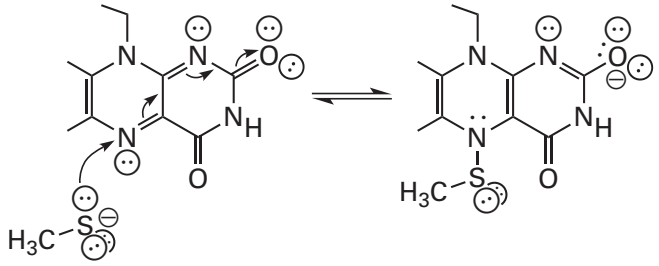

(2–129)

for example, in situations where an active site stabilizes the resulting oxyanion, while addition at carbon 4a requires acid catalysis

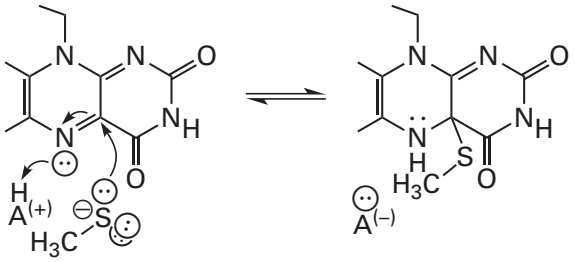

(2–130)

The desire for adducts to carbon 4a in oxidized flavin to be transient intermediates in the reactions catalyzed by flavin arises from the appeal of the following **mechanism for the oxidation of a nucleophile by flavin in which an adduct at carbon 4a is required**

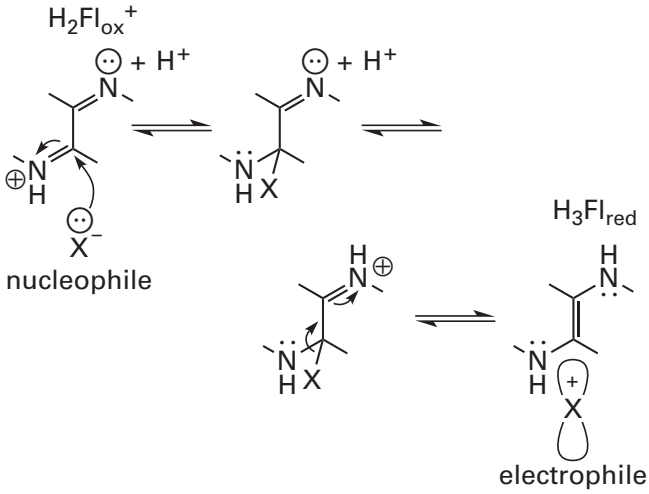

(2–131)

The nucleophilic position of the reactant enters the electrophilic position at carbon 4a with a lone pair of electrons that forms the new σ bond. That new σ bond is now parallel to the π molecular orbital of an adjacent iminium ion that absorbs its electrons. This withdrawal of the electrons releases an electron-deficient, electrophilic, oxidized product and produces reduced flavin. The two electrons entering with the nucleophile remain in the flavin when the electrophile is released. In the reverse direction, the nucleophilic enamine of the reduced flavin would attack the oxidized, electrophilic reactant to form the σ bond to carbon 4a, and the electrons in this σ bond would leave with the dissociating reduced, nucleophilic product. The σ bond to carbon 4a is the transfer point for the two electrons that reduce the oxidized flavin or the electrophile, respectively. In the crystallographic molecular model of 4a-isopropyl-3,7,8,10-tetramethyl-4a,5-dihydroisoalloxazine, which has four σ bonds at carbon 4a, the σ bond

to the isopropyl group at carbon 4a and the π bond of the imine at carbon 1a and nitrogen 1 are parallel,[300] as required in Equation 2–131.

This mechanism for transfer of two electrons through an adduct at carbon 4a has been **validated for several nonenzymatic reactions** catalyzed by flavins. During the reduction of maleimides by reduced 3-(3-sulfopropyl)-7,8,10-trimethylisoalloxazine, an adduct forms between a maleimide and the flavin that is an intermediate in the reaction.[384] The absorption spectrum of this intermediate identifies it as an adduct at carbon 4a

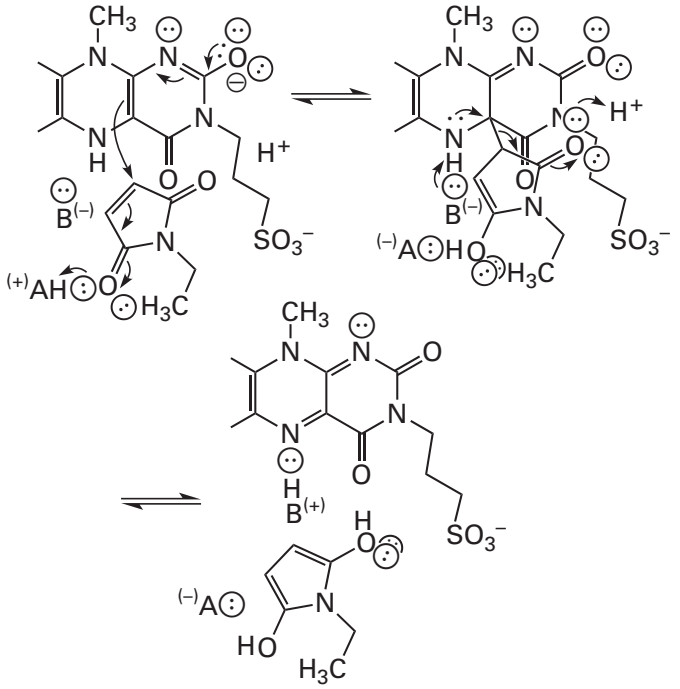

(2–132)

that would result from nucleophilic addition of the nucleophilic anion of reduced flavin to the electrophilic α,β-unsaturated imide. The adduct is formed in a reaction catalyzed by acid, and it decomposes with release of the reduced product in a reaction catalyzed by base.[384]

Benzylamine is oxidatively deaminated to benzylimine by 3,7,8,10-tetramethyl-5-ethylisoalloxazine in a reaction in which the benzylamine adds nucleophilically to carbon 4a. The resulting adduct dissociates in a rate-limiting step in which the electrons in the σ bond are absorbed by the isoalloxazine, reducing it (Equation 2–131), and the hydrogen on the benzylamine at the benzylic position is simultaneously removed by a base as a hydron, producing the benzylimine.[385]

In solution, thiols reduce flavins by forming an adduct at carbon 4a[386]

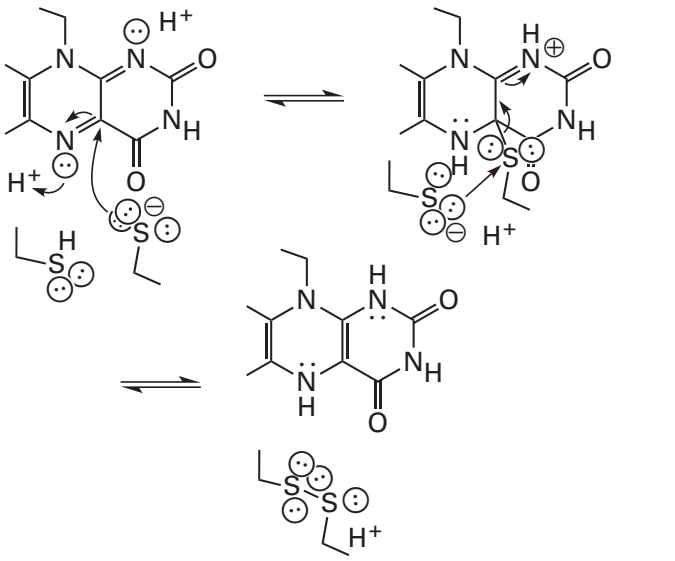

(2–133)

In the reverse direction, the reaction of the reduced flavin is the attack of an enamine on a disulfide and is equivalent to the attack of the enamine of thiamine diphosphate on N^6-(lipoyl)lysine (Figure 2–7). In the forward direction, a lone pair on one of the cysteines becomes a σ bond that is absorbed by the flavin in the second step.

A sulfanyl group is a nucleophile that is often oxidized by a prosthetic flavin. There is a family of related enzymes in which **two nucleophilic cysteines in each of the active sites are oxidized by flavin** and the product of the oxidation is a cystine, which is an electrophile. Glutathione-disulfide reductase is a flavoenzyme that catalyzes the reaction

$$NADP^+ + GSH + HSG \rightleftharpoons NADPH + H^+ + GSSG \quad (2–134)$$

where GSSG is oxidized glutathione, which contains an intermolecular cystine formed from the cysteines in two molecules of reduced glutathione, GSH. The flavoenzyme dihydrolipoyl dehydrogenase catalyzes a reaction

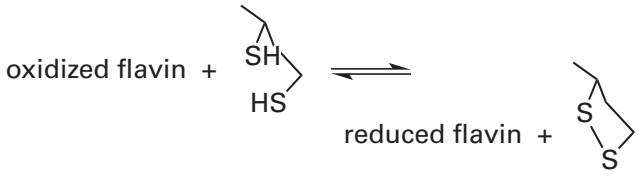

(2–135)

that is equivalent to the one catalyzed by glutathione-disulfide reductase. The flavoenzyme thioredoxin-

disulfide reductase catalyzes the reduction of a cystine in the small protein thioredoxin; the flavoenzyme mercury(II) reductase reduces a cystine in its active site to two cysteines, which then reduce Hg^{2+} to Hg^0; the flavoenzyme 2-oxopropyl-CoM reductase (carboxylating) catalyzes a nucleophilic substitution at the sulfur of a sulfide by a cysteine in its active site; and the flavoenzyme NADH peroxidase catalyzes the reduction of hydrogen peroxide to two molecules of water by reducing a cysteine-sulfenic acid, produced in its active site by the reduction of the hydrogen peroxide, back to a cysteine.

All six of these enzymes use either NADH or NADPH as the reductant, have homologous sequences, have superposable tertiary structures,[387-391] and have very similar if not identical mechanisms for the oxidations and reductions at the flavin. Each of the first five enzymes reduces the respective disulfide or the mercuric ion or catalyzes the nucleophilic substitution by first **reducing a cystine in its active site to two cysteines** and then using the two cysteines to reduce the substrate or one of the cysteines as a nucleophile. NADH peroxidase reduces the cysteine-sulfenic acid in its active site, which is the oxygen homologue of a cystine, to hydroxide and a sulfido group.[392]

In crystallographic molecular models of the five enzymes that each reduce a cystine in its active sites to two cysteines, as well as those of other related homologues, the axis of the sulfur–sulfur bond of the cystine in the active site of the oxidized enzyme and the line of centers between the two sulfurs of the two cysteines in the active site of the reduced enzyme points directly at carbon 4a of the flavin (Figure 2–11).[306,310,387,388,390,393-395] In the most accurate crystallographic molecular model of glutathione-disulfide reductase, the sulfur of the closest cysteine is 0.330 nm from carbon 4a of the flavin, which is within the sum of the van der Waals radii (0.35 nm) of the sulfur and the carbon.[310] The line of centers of the two sulfurs in this molecular model is tilted at an angle of 108° with respect to the bond between nitrogen 5 and carbon 4a, which defines the plane of the flavin, as the σ bond to the closest sulfur would be were it in an adduct at carbon 4a.

Porcine dihydrolipoyl dehydrogenase can be reduced, and one of the two resulting cysteines in the active site can be alkylated with iodoacetamide. When NAD^+ is added to the alkylated enzyme to oxidize the flavin, a spectral change occurs that has been assigned as arising from an adduct between the remaining unalkylated sulfido group and carbon 4a of oxidized flavin.[396] When the flavin adenine dinucleotide in thioredoxin-disulfide reductase from *E. coli* is replaced with 1-carba-1-deazaflavin adenine dinucleotide, in either the active site of the wild type[397] or a variant in which the cysteine farther from the flavin is mutated to serine,[398] and the respective enzyme is reduced, similar spectra, indicative of the formation of the respective 4a adducts, are also observed. When three of the four homologous cysteines in mercury(II) reductase from *E. coli* that are farthest from the flavin are mutated to alanines and the flavin in the enzyme is oxidized with $NADP^+$,[399] the enzyme also has a spectrum consistent with the formation of an adduct at carbon 4a of the flavin. All these spectrally identified intermediates have been presented as evidence for the **formation of an adduct at carbon 4a during the normal reduction of the cystine** or oxidation of the cysteines in the respective active sites of the unalkylated, native enzymes in this family (Equation 2–133).

Glutathione-disulfide reductase from *S. cerevisiae* can also be reduced and alkylated on only one of its two catalytic cysteines.[400] A crystallographic molecular model of this reduced and alkylated enzyme, in a complex with $NADP^+$, is available.[311] Although the unalkylated cysteine is the one closest to the flavin and although the closest atom in the flavin to the sulfur of this cysteine is carbon 4a, there is no bond between the sulfur of the cysteine and carbon 4a of the oxidized flavin. Therefore, the postulated adduct (Equation 2–133) does not form in glutathione-disulfide reductase. In fact, the only adduct that has been observed crystallographically between a sulfido group and carbon 4a in a flavin on an enzyme is one that forms between sulfide ion in solution and the flavin mononucleotide in sarcosine oxidase (5,10-methylenetetrahydrofolate-forming) from *Stenotrophomonas maltophilia*.[401] The lack of such a crystallographic observation cannot disprove the existence of an adduct at carbon 4a, but it is not encouraging.

It is possible that each flavoenzyme in this family of disulfide reductases purposely holds the disulfide of the cystine or the proximal cysteine in its active site at too great a distance to form an adduct with carbon 4a of the reduced or oxidized flavin, respectively, like the one that forms between a thiol and an oxidized flavin in solution (Equation 2–133), because it is faster to **transfer the two electrons between the cystine or the cysteines and the flavin**

one at a time without forming an adduct at carbon 4a than it is to transfer them together through the σ bond of an adduct at carbon 4a. As has been proposed for thiamine diphosphate (Figure 2–7), the electrons would be transferred between reduced flavin and the cystine in the active site in two one-electron steps that have a flavin semiquinone and a cystine radical anion as intermediates. An electron would be transferred from reduced flavin anion to the cystine to produce the disulfide radical anion and the flavin semiquinone. The radical anion of the disulfide would be hydronated on its distal sulfur by an adjacent catalytic acid. The hydronated disulfide radical would cleave to produce the hydronated sulfanyl group and the thiyl radical (Figure 2–8), and the thiyl radical would be reduced by the flavin semiquinone. In the reverse direction, one electron would be transferred from the sulfido group of the proximal cysteine to oxidized flavin to produce the flavin semiquinone and the thiyl radical, which would rapidly form, with the sulfido group of the distal cysteine, a radical anion of a disulfide[241] that would then transfer a second electron to the flavin.

One fact consistent with this possibility is that reduction of the cystine in the active site of thioredoxin-disulfide reductase from *E. coli* decreases the midpoint reduction potential of its flavin by 17 mV,[328] an observation indicating that the cystine and the flavin are electronically coupled. The mutation of the cysteine immediately adjacent to carbon 4a of the flavin adenine dinucleotide in NADH peroxidase from *Enterococcus faecalis*, the cysteine responsible for catalysis, raises the midpoint reduction potential of the flavin by 100 mV.[402] In both instances, the transfer of electron density from a sulfido group could be causing a decrease in the reduction potential. When the cysteine is there, the decrease occurs; when it is not, the decrease does not. Another observation consistent with two successive transfers, each of one electron, between reduced, nucleophilic substrates and oxidized flavin and between reduced flavin and oxidized, electrophilic substrates is the presence of an absorption in the optical spectra of complexes between these flavoenzymes and substrates arising from transfer of charge.

A **charge-transfer complex**[403] forms when a reductant, the donor, transfers an electron in a reversible equilibrium to an oxidant, the acceptor, when they come in contact with each other. Transfer of the electron creates a weak bond between the donor and acceptor that forms a complex between them with a particular dissociation constant. The magnitude of the dissociation constant depends on the equilibrium constant for, and the character of, the electron transfer. A charge-transfer complex will always have an absorption spectrum that contains one or more charge-transfer bands of relatively **long wavelength** (400–800 nm) resulting from the excitation of the transferred electron, which is shared between the donor and the acceptor in an otherwise unoccupied molecular orbital of relatively low energy spread over the complex between the donor and the acceptor rather than being confined exclusively to donor or acceptor.

Although a charge-transfer complex formed by transfer of an electron in the ground state always exhibits such a charge-transfer band in its spectrum, the existence of a charge-transfer band does not require transfer of charge in the ground state; it only requires transfer of charge in the electronically excited state.[404] In solution, the absorption of light by the donor may excite the electron into a charge-transfer orbital formed with an adjacent acceptor even if significant electron density is not transferred to the acceptor in the ground state. In a complex that forms for other reasons, the absorption of light by the donor may also excite the electron into a charge-transfer orbital with an adjacent acceptor even if there is no significant transfer of charge in the ground state.

Charge-transfer bands between the sulfido group of **the proximal cysteine, as a donor, and oxidized flavin, as an acceptor**, have been observed in the absorption spectra of dihydrolipoyl dehydrogenase from *E. coli*,[399,405-409] mercury(II) reductase from *E. coli* (Figure 2–17),[399,405,406,410] and NADH peroxidase from *E. faecalis*.[392,402] With the disclaimer that transfer of the electron may be occurring only in the electronically excited state, these charge-transfer bands demonstrate that a single electron can be transferred from the sulfido group of the proximal cysteine in the active site to the oxidized flavin. If this transfer of an electron does occur in a charge-transfer complex in the ground state even if the equilibrium constant for transfer of the electron is unfavorable, it provides a path for the first, and most difficult, of the two one-electron transfers. The hydronation of nitrogen 5, coincident with the full transfer of one electron, would be followed by formation of the bond between the resulting proximal thiyl radical and the sulfido group of the distal cysteine to form the radical anion of the disulfide, which would then transfer its unpaired

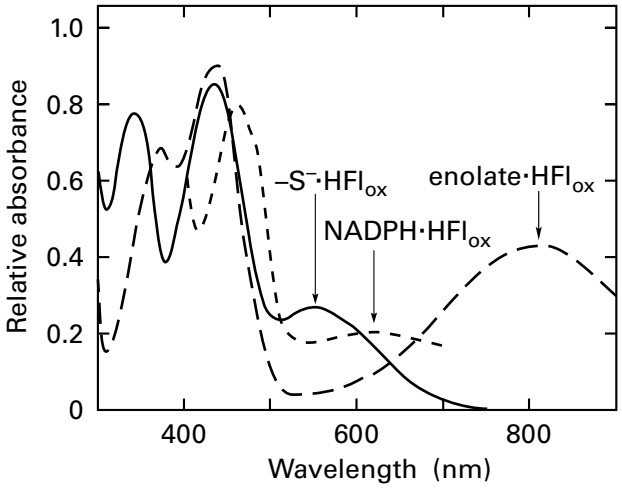

Figure 2–17: Absorption spectra of charge-transfer complexes in which oxidized flavin participates. The maxima of the charge-transfer absorptions are marked by the vertical arrows. The spectrum[399] for the charge-transfer complex (**–S⁻·HFl$_{ox}$**) between oxidized flavin and the sulfido group of the immediately adjacent cysteine in the active site of mercury(II) reductase from *E. coli* was obtained from a sample of a mutant form of the enzyme in which the other three cysteines in the active site had been mutated to alanine. The mutant, oxidized enzyme was dissolved at 2 °C in a solution at pH 9.05 to ensure that the sulfanyl group of the cysteine was the anionic conjugate base. The spectrum[405] for the charge-transfer complex (**enolate·HFl$_{ox}$**) between oxidized flavin and the enolate of 3-thiaoctanoyl-SCoA, octanoyl-SCoA in which carbon 3 is replaced by a sulfur to prevent the removal of the hydrogen on carbon 3 by the oxidized flavin, in the active site of porcine medium-chain acyl-CoA dehydrogenase was obtained from a sample of the oxidized enzyme dissolved in a solution at pH 8.0 to ensure that the enolate of 3-thiaoctanoyl-SCoA was fully formed on the active site. 3-Thiaoctanoyl-SCoA was present in the solution at a high enough concentration (10 μM) to saturate the active site of the enzyme. The spectrum[406] for the charge-transfer complex (**NADPH·HFl$_{ox}$**) between oxidized flavin and NADPH in the active site of the detachable domain of human NADPH—hemoprotein reductase that contains the active site of the intact enzyme in which the prosthetic flavin adenine dinucleotide is normally reduced by NADPH was ob-tained from a sample of the domain dissolved at 25 °C in a solution at pH 7.0 that was rapidly mixed with a solution of NADPH at a concentration high enough to saturate the active sites. The spectrum was gathered within 4 ms of mixing. For each of the three spectra, the absorbance is presented as a fraction of the maximum absorbance of the oxidized flavin in each enzyme that occurs around 450 nm and that was observed before the pH was raised to ionize the sulfanyl group, the 3-thiaoctanoyl-SCoA was added, or the NADPH was mixed with the enzyme, respectively.

electron to the flavin semiquinone. The net result would be the reduction of oxidized flavin to reduced flavin and the oxidation of two cysteines to a cystine.

The ambiguity of mechanism for oxidation of the two cysteines or reduction of the disulfide in the active sites of these related enzyme illustrates the difficulty is assigning a mechanism to flavin because the existence of the semiquinone allows flavin to transfer electrons one at a time and the existence of adducts of flavin allows flavin to transfer electrons two at a time.

In the direction in which the sulfanyl groups in the respective substrates are converted to a disulfide and the flavin is reduced, the **last step** in the reactions catalyzed by glutathione-disulfide reductase, dihydrolipoyl dehydrogenase, and thioredoxin-disulfide reductase is the oxidation of the sulfanyl groups in their respective substrates by thiol–disulfide exchange with the cystine just formed in the active site. For example, the cystine formed in the active site of dihydrolipoyl dehydrogenase by the oxidized flavin (Equation 2–135) in turn oxidizes the pair of adjacent sulfanyl groups in N^6-(dihydrolipoyl)lysine by thiol–disulfide exchange

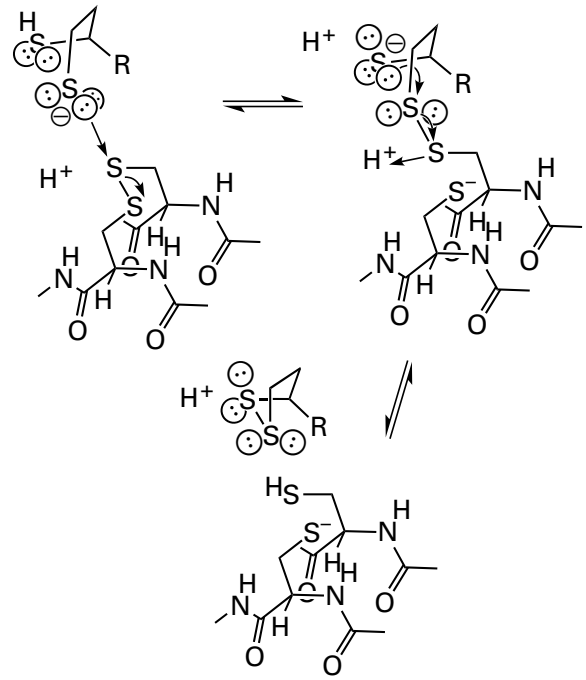

(2–136)

where R is the remainder of the lipoyl group in N^6-(dihydrolipoyl)lysine (Equation 2–70) and N^6-(lipoyl)lysine (**2–31**). In the opposite direction, the first step in the overall reaction catalyzed by dihydrolipoyl dehydrogenase is oxidation of the two cysteines in the active site to the cystine and

reduction of the disulfide in the reactant into two sulfanyl groups.

An amino group is a nucleophile that can also be oxidized by a prosthetic flavin. Flavoenzymes that oxidize amines also display **charge-transfer bands** in their absorption spectra under the appropriate circumstances. Sarcosine oxidase (formaldehyde-forming), which oxidizes *N*-methylglycine to *N*-carboxymethylmethanimine[411]

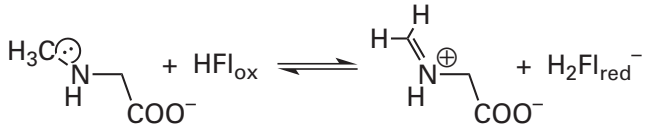

(2–137)

also oxidizes L-proline to the respective imine. L-Proline binds to the enzyme as the usual zwitterionic amino acid, the hydron is removed from the nitrogen, and a charge-transfer band (λ_{max} = 512 nm) between the neutral secondary amine and oxidized flavin is then observed.[412] In dimethylglycine oxidase, however, the charge-transfer band (λ_{max} = 400 nm) observed results from transfer of an electron from reduced flavin to the product of the reaction, *N*-carboxymethylmethanimine.[413] This type of charge-transfer band between an imine and reduced flavin was first observed with D-amino-acid oxidase.[414,415] These observations suggest that an electron can be transferred both between the lone pair of electrons on the amino group in the substrate and oxidized flavin and between the reduced flavin and the imine in the product. The chemistry that would lie between these transfers of electrons would be the removal of a hydron from the radical cation of the reactant[413] and the hydronation of the semiquinone anion of the flavin before an electron is transferred from the neutral radical to the flavin semiquinone

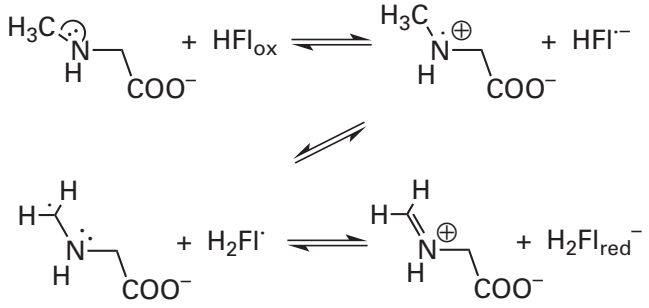

(2–138)

When 4-methylphenol is substituted with 4-bromophenol, a charge-transfer band is observed between the 4-bromophenol and the oxidized flavin in the active site of 4-methylphenol dehydrogenase (hydroxylating) from *P. putida*

$$\text{4-methylphenol} + H_2O \rightleftharpoons \text{4-hydroxybenzaldehyde} + 4\,H^+ + 4\,e^- \qquad (2\text{–}139)$$

There is a close correlation between the wavelength of this charge-transfer band, which registers the energy required to transfer the electron, and the rate of the normal enzymatic reaction for thirty-three variants of the enzyme, either various mutants or enzymes into which various analogues of the flavin had been substituted. The various enzymatic reactions spanned 5 orders of magnitude in rate constant.[416] The lower the energy required to transfer the electron from 4-bromophenol to the oxidized flavin, the faster was the dehydrogenation of the 4-methylphenol catalyzed by the enzyme. This correlation suggests that transfer of one electron is one of the steps in the normal enzymatic reaction.

In many reactions, either enzymatic or non-enzymatic, in which flavin oxidizes a reactant with an acidic carbon adjacent to a carbonyl or an acyl group, the enolate of the reactant is an intermediate. For example, when flavin oxidizes carbons 2 and 3 of an acyl-SCoA or carbon 2 of lactate, the enolate or enol of acyl-SCoA or the enolate or enol of lactate, respectively, is an intermediate in the oxidation.[417]

The evidence for these intermediates in enzymatic reactions is the ability of various flavoenzymes to catalyze the dehydrohalogenation of halogenated analogues of their substrates. For example, porcine D-amino-acid oxidase, a flavoenzyme responsible for oxidizing various D-amino acids to the 2-oxo acids, readily dehydrohalogenates β-chloro-L-alanine,[418] presumably through a β-elimination from its enolate

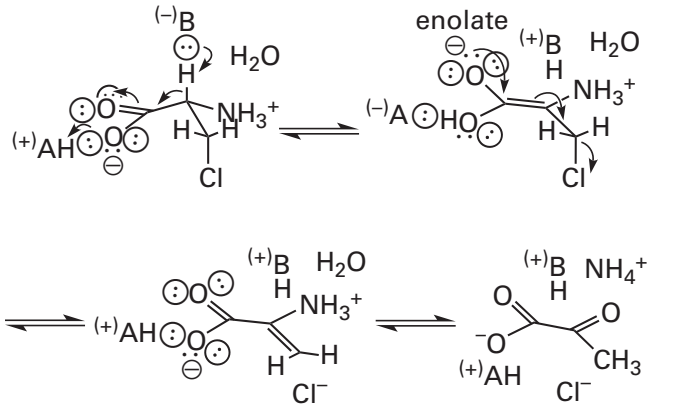

(2–140)

Lactate 2-monooxygenase, a flavoenzyme responsible for oxidizing lactate to acetate and carbon dioxide, has as its first step the oxidation of lactate to pyruvate. This enzyme also catalyzes the dehydrohalogenation of 3-chlorolactate[419]

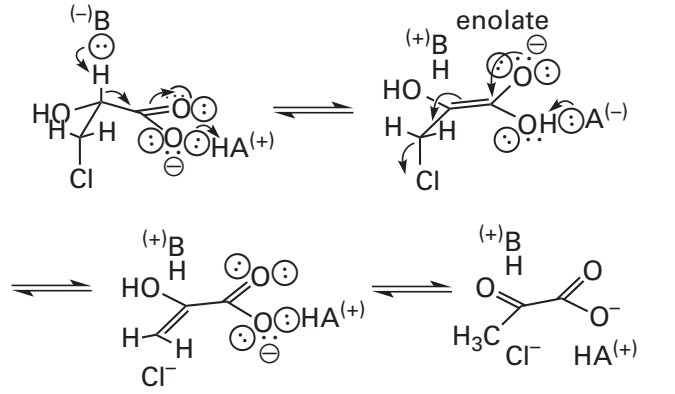

(2–141)

and its ability to catalyze this reaction is consistent with the involvement of the enolate of lactate as an intermediate in the normal enzymatic reaction. Porcine medium-chain acyl-CoA dehydrogenase catalyzes a similar elimination of 1,2-dichlorosulfanylethene from 5,6-dichloro-4-thia-5-hexenoyl-SCoA.[420]

Dehydrohalogenation can also occur in the direction of reduction of the reactant. The reduced form of L-lactate dehydrogenase (cytochrome), an enzyme that also oxidizes lactate to pyruvate and hence the reduction of pyruvate to lactate, can catalyze the dehalogenation of bromopyruvate in a reaction that simultaneously oxidizes reduced flavin. In this reaction, reduced flavin produces the enolate of bromopyruvate, which then eliminates a bromide ion[421]

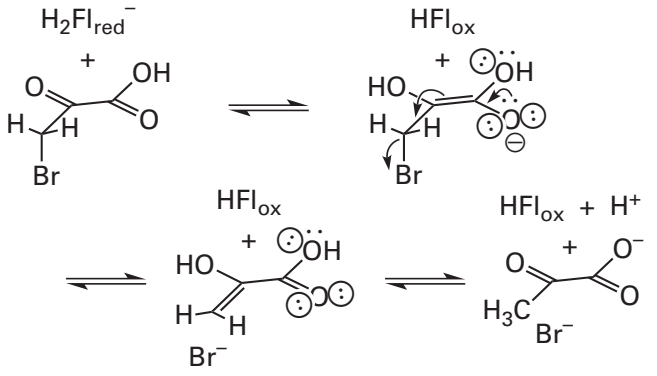

(2–142)

In crystallographic molecular models of the active sites of porcine medium-chain acyl-CoA dehydrogenase, L-lactate dehydrogenase (cytochrome) from *S. cerevisiae*, human isovaleryl-CoA dehydrogenase, and short-chain acyl-CoA dehydrogenase from *R. norvegicus* there is a catalytic base located in the proper position and orientation to remove the respective α hydron on the carbon adjacent to the carbonyl group or the acyl group and form the enol or enolate of the reduced substrate.[316,422-425] When the glutamate that serves as the catalytic base[425] in short-chain acyl-CoA dehydrogenase from *R. norvegicus* was mutated to glutamine, no enzymatic activity could be detected,[426] and when the glutamate in human medium-chain acyl-CoA dehydrogenase was mutated to a glutamine, the rate of the enzymatic reaction decreased[427] by a factor of 10^4.

All these observations have been interpreted to mean that, in the normal oxidation of the respective substrate, its enol or enolate is first formed, and then **two of the electrons in the electron-rich highest occupied molecular orbital of the π molecular orbital system of the enolate are transferred to the oxidized flavin** to oxidize the substrate and reduce the flavin.

Charge-transfer bands have been observed with flavoenzymes that oxidize the enolates of their substrates. (*S*)-Mandelate dehydrogenase, which oxidizes the enol of (*S*)-mandelate

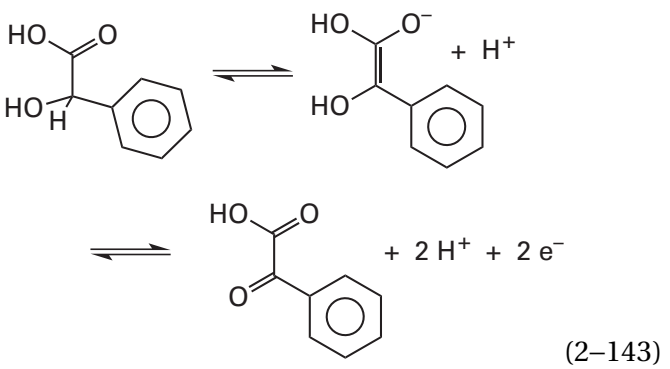

(2–143)

displays a charge-transfer band between 500 and 700 nm. Because the rate of formation of the charge-transfer band is slower when 2-deuteriomandelate is used as the reactant[428] and its formation requires an acyl or carbonyl oxygen α to the hydrogen being removed from the reactant,[429] the charge-transfer band has been assigned as one resulting from electron transfer between the enolate of (*S*)-mandelate and oxidized flavin.

The enolate of octanoyl-SCoA (or of other fatty acyl coenzymes A) is oxidized by medium-chain acyl-CoA dehydrogenase (Equation 2–114) to 2-octenoyl-SCoA (or other α,β-unsaturated fatty acyl coenzymes A). When the enzyme containing oxidized flavin is mixed with octanoyl-SCoA in the absence of electron-transferring flavoprotein, which is its normal general oxidant, the oxidized flavin in the active site oxidizes one octanoyl-SCoA to 2-octenoyl-SCoA, which remains on the active site. This complex between porcine medium-chain acyl-CoA dehydrogenase, reduced flavin, and octenoyl-SCoA displays a broad charge-transfer band between 500 and 700 nm.[430-432] When an analogue of octanoyl-SCoA that can be enolized but cannot be oxidized, such as 3-thiaoctanoyl-SCoA,[433] 2-octynoyl-SCoA,[434] or phenylacetyl-SCoA,[435] is mixed with the oxidized porcine or human medium-chain acyl-CoA dehydrogenase, the α hydron is removed from the analogue by the base in the active site to form the enolate,[434,435] and the absorption spectrum (Figure 2–17) of the complex between the enolate and the oxidized flavin displays a charge-transfer band of long wavelength (λ_{max} = 800 nm).[405]

There are other examples. A transient intermediate with a charge-transfer band (λ_{max} = 565 nm) that has been assigned to electron transfer from the enolate of butyryl-SCoA to oxidized flavin[436,437] has also been observed in rapid kinetic studies of porcine medium-chain acyl-CoA dehydrogenase. Phosphopantothenoylcysteine decarboxylase also displays a charge-transfer band between its enolate and oxidized flavin.[438] If these charge-transfer bands indicate the ability to transfer an electron in the respective ground states, then the chemical steps between transfer of an electron from the enolate of the acyl-SCoA to oxidized flavin, and transfer of an electron from the radical anion of the acyl-SCoA to neutral flavin semiquinone, would be removal of a hydron from the β carbon of the α radical of the acyl-SCoA

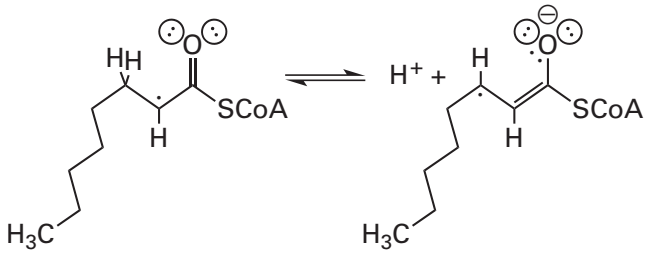

(2–144)

and hydronation of the anionic conjugate base of flavin semiquinone, a hydronation required to occur before the semiquinone can be reduced by one electron (Figure 2–9).

The existence of these charge-transfer bands in the spectra of these flavoenzymes suggests that the **electrons can be passed between the enolate of the substrate and the flavin one at a time.** If so, there must be radical intermediates: flavin semiquinone (Figure 2–9), which would not be surprising since it has been observed routinely in particular active sites, and radicals formed from the substrates (Equations 2–138 and 2–144). The feasibility of one-electron mechanisms involving flavin has been established by calculating standard free energies of formation of radical intermediates.[439] It has even been shown that reduced 3,5,7,8,10-pentamethylisoalloxazine will react with several electron-deficient carbonyl compounds to yield flavin semiquinone, recognized by its blue color, and presumably the carbonyl radical anion,[440] which would be the conjugate base of the radical intermediate in the reduction of an aldehyde or ketone (such as pyruvate) to an alcohol (such as lactate), a reaction always thought to result from direct transfer of a hydride. It has also been observed that scavengers of radicals can lower the yields of enzymatic oxidations catalyzed by flavin that pass through enolates.[441] When flavoenzymes react with analogues of their respective nucleophilic substrates designed to fragment characteristically when they become the respective radical intermediates upon transfer of the first electron, the expected products of those fragmentations are

produced,[442,443] but it has also been shown that such fragmentations can be equivocal.[444] There are also other experimental results obtained with some of the same enzymes suggesting that, in the oxidations of the normal substrates, radical intermediates are not formed.[445]

The mechanisms for the oxidations of the thiolates, enolates, and amines that are suggested by the existence of the various charge-transfer complexes and the fragmentations of analogues of the substrates expected from the formation of their radicals all involve transfer of an electron from the reactant to the flavin to produce the respective radical or radical cation of the reactant and flavin semiquinone radical anion, hydronation of the flavin semiquinone radical anion (Figure 2–9), and transfer of the second electron to the neutral flavin semiquinone, either after or coincident with dehydronation of the appropriate carbon in the radical or radical cation of the reactant. These are, however, the same oxidation–reductions for which mechanisms involving nucleophilic adducts (Equations 2–127 through 2–133) have been proposed as well. These two alternatives are mutually exclusive. Because the two respective members of each of the redox couples in each of these reactions, the reactant and the oxidized product and the oxidized flavin and the reduced flavin, differ from each other by the equivalent of a hydride and a hydron, there is a third, also mutually exclusive alternative.

There is evidence for many enzymes using flavin as an oxidant or a reductant that the mechanisms proceed by direct transfer of a hydride rather than either formation of a nucleophilic adduct or two one-electron transfers. One set of observations in favor of direct transfer of a hydride in two-electron oxidation–reductions of flavin comes from experiments with **5-carba-5-deazaflavins**, in which nitrogen 5 of the isoalloxazine (**2–42**) has been substituted by a carbon. These analogues of flavin retain a hydrogen nucleus at position 5 but in a carbon–hydrogen bond rather than as a hydron that can participate in acid–base exchange in a nitrogen–hydrogen bond as occurs with flavin. A naturally occurring 5-carba-5-deazaflavin is *N*-{*N*-[*O*-(7,8-didemethyl-8-hydroxy-5-deazaphosphoriboflavin)-(*S*)-lactyl]-γ-L-glutamyl}-L-glutamate, coenzyme F_{420} (previously **1–69**)

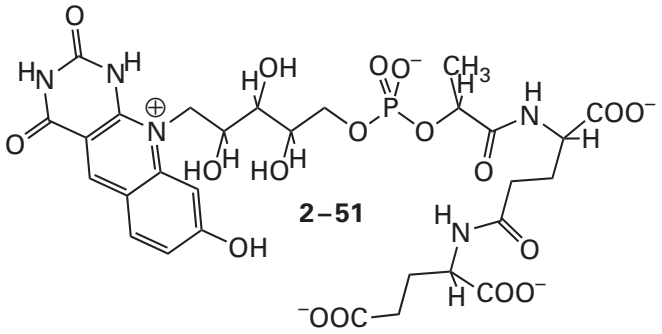

which is used as a coenzyme in methanobacteria.[446] Various enzymes transfer the equivalent of a hydride to and from carbon 5 of this 5-carba-5-deazaflavin.[447,448] The existence of this coenzyme as an acceptable natural analogue of flavin suggests that the unnatural, synthetic substitution of a carbon for nitrogen 5 in a flavin is also acceptable.

In a solution prepared with deuterium oxide, ^2H_2O, NADH is able to reduce 5-carba-5-deaza-3,10-dimethylisoalloxazine

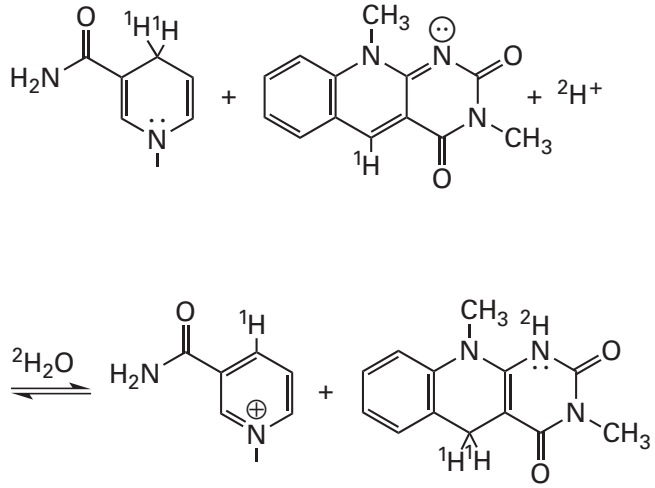

(2–145)

by direct transfer of its hydrogen to carbon 5 of the 5-carba-5-deazaflavin with no interchange with deuterons in the solvent.[449] This observation is consistent with a direct transfer of a hydride and rules out the successive transfer of two electrons, one at a time, punctuated by hydron transfers in this instance because it is unlikely that a hydron lost from carbon 4 of NADH would be transferred directly to carbon 5 of the deazaflavin in free solution. 5-Carba-5-deaza-1,5-dihydro-3,10-dimethylisoalloxazine, the reduced form of 5-carba-5-deaza-3,10-dimethylisoalloxazine, is able to transfer the hydrogen on its carbon 5 directly to the carbonyl carbon of pyridoxal 5′-phosphate,[450] and this ability demonstrates that a reduced flavin, albeit one

missing nitrogen 5, can directly transfer a hydride to a substrate.

The situation is more ambiguous on the active site of an enzyme, however, where the two reactants are held adjacent to each other and formal transfer of a hydride cannot be distinguished from a shielded, directed transfer of a hydron between the reactants. Nevertheless, in each of several enzymatically catalyzed reactions the reduced substrate, the hydrogen of which is labeled as tritium, has been shown to **transfer the tritium, ostensibly as a formal tritide ion, directly to carbon 5 of a 5-carba-5-deazaflavin** that has been substituted for the normal flavin

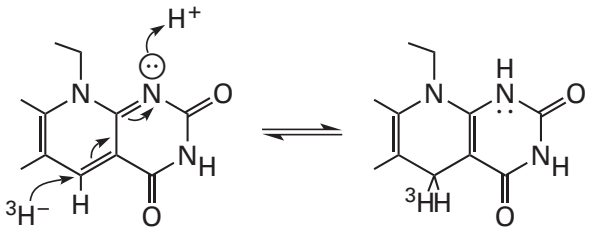

(2–146)

usually in quantitative yield. Examples of donors for hydride in the respective enzymatically catalyzed reductions of a 5-carba-5-deazaflavin have been D-[α-^{3}H]alanine in the active site of porcine D-amino-acid oxidase[451]

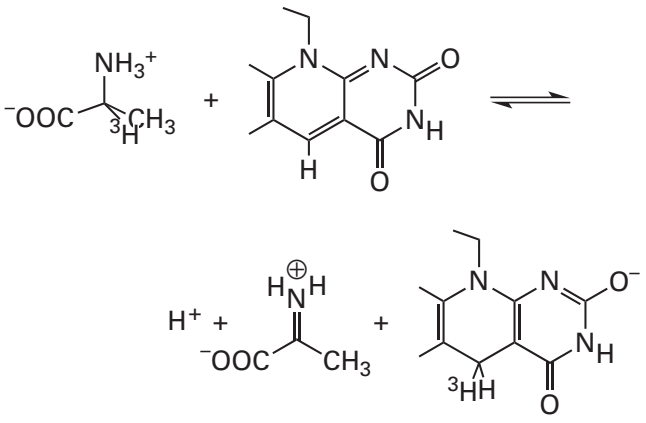

(2–147)

and L-[α-^{3}H]glutamate in the active site of methylamine—glutamate *N*-methyltransferase from *Aminobacter aminovorans*[452]

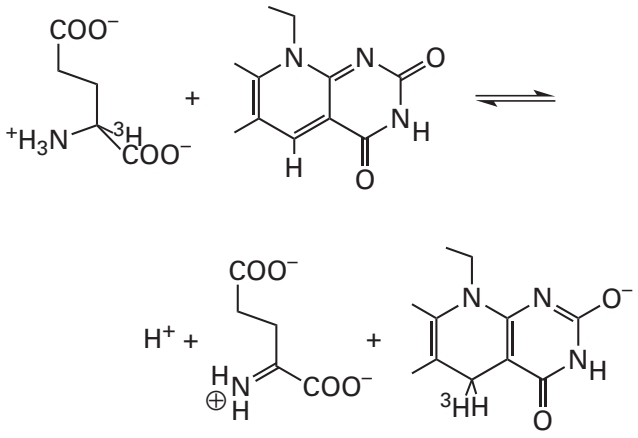

(2–148)

An oxidized substrate can also be reduced by labeled 5-dihydro-5-carba-5-deazaflavin. When crotonyl-SCoA is reduced with [5,5-$^3H_2$]-5-carba-5-deazaflavin in the active site of short-chain acyl-CoA dehydrogenase from *Megasphaera elsdenii*[453]

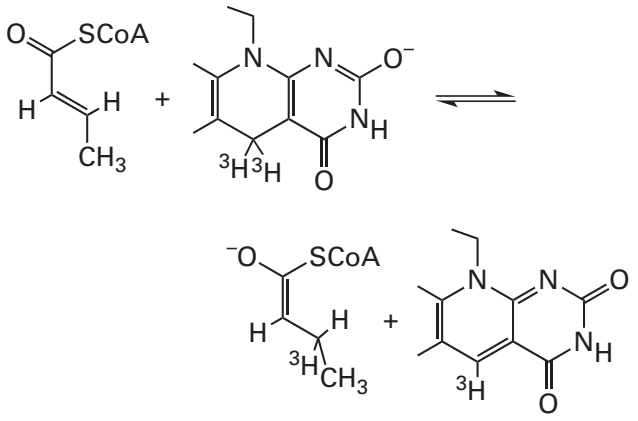

(2–149)

one of the tritiums on the [5,5-$^3H_2$]-5-carba-5-deazaflavin is transferred during a reduction that produces the enol of [3-^{3}H]butyryl-SCoA.

The flavoenzyme porcine methylenetetrahydrofolate reductase (NADPH)

$$N^5,N^{10}\text{-methylenetetrahydrofolate} + \text{NADPH} + \text{H}^+ \rightleftharpoons N^5\text{-methyltetrahydrofolate} + \text{NADP}^+$$

(2–150)

transfers the tritium from (5*S*)-[5-^{3}H]-5-carba-5-deaza-8-demethyl-8-hydroxyflavin quantitatively to form either (4*S*)-[4-^{3}H]NADPH or N^5-([^{3}H]methyl)-tetrahydrofolate.[454] This result shows that the hydride on a 5-carba-5-deazaflavin can be transferred with high stereospecificity to the oxidant in either of the

redox couples, the general and the nominal, of the respective enzymatic half-reactions. The flavoenzyme UDP-*N*-acetylmuramate dehydrogenase catalyzes transfer of the deuterium on carbon 4 of (4*S*)-[^{2}H]NADPH to carbon 11 of UDP-*N*-acetylmuramate with no detectable dilution of the deuterium through exchange with hydrons in solution.[455] This observation suggests that the deuterium is transferred as a hydride from NADPH to the 5-carba-5-deazaflavin and then as a hydride from the flavin to UDP-*N*-acetyl-3-*O*-(1-carboxyethenyl)-D-glucosamine. Before and after each step, the hydrogen is on carbon.

When the formal transfer of a hydride from reduced 5-carba-5-deazaflavin to the β carbon of crotonyl-SCoA (Equation 2–149) was carried out by the enzyme short-chain acyl-CoA dehydrogenase from *M. elsdenii*, the rate was equal to the rate of transfer of a hydride from reduced flavin to the β carbon of crotonyl-SCoA catalyzed by the same enzyme.[453] If the rate-limiting step in these enzymatic half-reactions actually is formal transfer of the hydride, this result suggests that, at least in this case, the reaction of the 5-carba-5-deaza analogue reproduces the normal reaction.

In each of the reactions just described, the hydrogen is required to be on carbon to begin with and on carbon at each step. If it were ever on a heteroatom, it would have been susceptible to exchange. Consequently, these results may not be relevant to reactions involving the oxidation–reduction of thiols discussed above.

In the crystallographic molecular models of the complexes between many flavoenzymes that catalyze formal transfers of hydrides from carbon and their nominal substrates, the carbon on the nominal substrate from which the equivalent of a hydride is removed is often found immediately adjacent to nitrogen 5 of the flavin and points its carbon–hydrogen bond at nitrogen 5.[313,316,456-468] An example would be the complex between D-amino-acid oxidase from *R. toruloides* and D-3,3,3-trifluoroalanine (Figure 2–12).[313] D-3,3,3-Trifluoroalanine is not a substrate for the enzyme[469] because of the electron withdrawal of the three fluorines. In the crystallographic molecular model, the distance between the α carbon of D-trifluoroalanine, from which the hydride would be removed if it were D-alanine, to nitrogen 5 of the flavin is 0.31 nm, well within van der Waals contact. The α carbon–nitrogen 5–nitrogen 10 angle is 104°, close to the angle observed in a covalent, nucleophilic adduct at nitrogen 5 (116°) of flavin,[470] a fact indicating that the hydride would be on a proper trajectory to form a σ bond with nitrogen 5. The carbon–hydrogen bond is not pointed directly at nitrogen 5, but the D-trifluoroalanine is tilted only about 30° out of alignment. The distance and the orientation are almost ideal for direct, in-line transfer of a hydride between the carbon and the nitrogen.

The orientation of the carbon–hydrogen bond is even closer to ideal in the crystallographic molecular model of the complex between cytokinin dehydrogenase from *Zea mays* and the poorly oxidized substrate N^6-benzyladenine. The distance between nitrogen 5 of the flavin and the benzyl carbon, from which the equivalent of a hydride is removed, is 0.27 nm; the benzyl carbon–nitrogen 5–nitrogen 10 angle is 120° (180° – 60°). The carbon–hydrogen bond on the benzyl carbon, which remains reduced in the complex, is tilted only about 10° out of alignment with the line of centers between nitrogen 5 and the benzyl carbon[461]

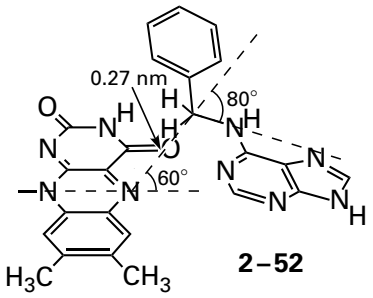

2–52

In the complex between porcine medium-chain acyl-CoA dehydrogenase (Equation 2–114) and octanoyl-SCoA, the octanoyl-SCoA may well be reduced to octenoyl-SCoA and the flavin oxidized, but octanoyl-SCoA was nevertheless inserted into the electron density. In the resulting crystallographic molecular model of the complex between the enzyme and octanoyl-SCoA, the distance between nitrogen 5 of the flavin and the β carbon of octanoyl-SCoA, from which a hydride would be transferred, is 0.30 nm, well within the sum of the van der Waals radii; the β carbon–nitrogen 5–nitrogen 10 angle is 106°; and the β carbon–hydrogen is tilted about 35° out of alignment with the line of centers (Figure 2–13).[316]

All these orientations and distances seem to demand that direct in-line transfer of a hydride from substrate to flavin occur during the normal oxidation–reduction in these cases. Yet complexes between several of these enzymes, in particular D-amino-acid oxidase[471] and porcine medium-chain acyl-CoA

dehydrogenase, and their substrates, both when the substrate is reduced and the flavin is oxidized and when the substrate is oxidized and the flavin is reduced, display charge-transfer bands.

One difference between direct, formal transfer of a hydride to carbon 4 of nicotinamide, for example in the case of alcohol dehydrogenase (previously **1–76**)

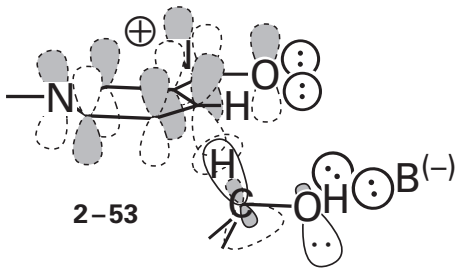

2–53

and direct, formal transfer of a hydride to nitrogen 5 of flavin, for example in the case of cytokinin dehydrogenase (**2–52**), is that carbon 4 of nicotinamide has a hydrogen on it while nitrogen 5 of flavin has a lone pair of electrons. Much more than the hydrogen, this lone pair of electrons on the nitrogen should hinder direct, formal transfer of a hydride by electron repulsion. On the opposite face of the flavin from the position assumed by the nominal substrate that donates the equivalent of a hydride, there is usually a donor for a hydrogen bond.[472] The donor is 0.28–0.34 nm from nitrogen 5 at an angle of 120°–170° to the line of centers between nitrogen 5 and nitrogen 10 of the flavin (Figures 2–12 and 2–13). This is a location ideal (see **2–42**) for **drawing the σ lone pair of electrons on nitrogen 5 into a hydrogen bond** and away from the hydrogen of the nominal substrate that is to be transferred as a hydride.

This donor for a hydrogen bond can be either a nitrogen–hydrogen from the backbone of the polypeptide (Figure 2–12), the donor on a side chain such as the nitrogen–hydrogen of an arginine or the oxygen–hydrogen of a threonine (Figure 2–13), or a molecule of water that forms a hydrogen bond to the 6-amino group of a lysine.[473] It is, however, always a weak acid ($pK_a > 10$), probably because the lone pair, after being pulled away from the hydride being transferred, becomes a delocalized pair of electrons in reduced flavin (Figure 2–9) and should not be localized by hydronation, which would be the drawback of a stronger acid. In the direction of reduction of the nominal substrate, the donor for the hydrogen bond localizes the otherwise delocalized lone pair of electrons (**2–45**) and as a result pushes the hydrogen on nitrogen 5 out of the plane of the ring (see Figure 2–9). These effects would promote the formal transfer of a hydride from nitrogen 5. When the lysine in the active site of tryptophan 2-monooxygenase from *Pseudomonas savastanoi* that performs this role on the opposite face of the flavin is mutated to a methionine,[474] the rate of reduction of the prosthetic flavin by L-tryptophan decreases by a factor of at least 10^5.

In contrast to the frequent examples of orientations of substrates as expected for a direct in-line transfer of a hydride, there are instances in which a π molecular orbital system in a substrate is stacked upon the isoalloxazine. This arrangement is analogous to the stacking of a π molecular orbital system upon nicotinamide adenine dinucleotide (Figures 1–16 and 1–19). In the crystallographic molecular model of the complex between octanoyl-SCoA and porcine acyl-CoA dehydrogenase, the flat π molecular orbital system of the thioester stacks on the π system of the flavin (Figure 2–13).[316,475] The larger π molecular orbital of the enol of the thioester, formed by removing the α hydron, would stack as well. In the crystallographic molecular model between the oxidized form of UDP-*N*-acetylmuramate dehydrogenase from *E. coli* and the oxidized form of its substrate, the carboxyethenyl group of the substrate, which is a carboxyenol ether, is also stacked on the flavin.[476,477] In the crystallographic molecular models of the complexes between the respective substrates and D-amino-acid oxidase (Figure 2–12) and succinate dehydrogenase from *Shewanella putrefaciens*,[456,457] the π molecular orbital system of a carboxylate in the substrate stacks on the π molecular orbital system of the flavin. And in the crystallographic molecular models of complexes between substrate and polyunsaturated fatty acid isomerase from *Cutibacterium acnes*, the π molecular orbital system of a conjugated diene stacks on the π molecular orbital system of the flavin.[462]

In each of these instances, which all involve acyclic, unsaturated nominal substrates, the stacking of a π molecular orbital system in the substrate upon the π molecular orbital system of the flavin does not prevent the hydrogen on the substrate that participates in formal transfer of a hydride to the flavin from assuming the proper orientation and sitting the proper distance from nitrogen 5 of the flavin for direct in-line transfer of a hydride (Figures 2–12 and 2–13). There are, however, several examples of nominal substrates with cyclic π molecular orbital systems in which the almost complete **stacking of a cyclic π molecular orbital system of the substrate**

on the π molecular orbital system of the flavin does seem to place the carbon–hydrogen bond of the substrate in an orientation that should be unfavorable if not forbidden for direct transfer of a hydride.[478-482] The nicotinamide rings of NAD^+ and $NADP^+$ illustrate this problem most dramatically because of their departure from the reasonable positioning performed by other active sites in which the hydride to be removed is in line with the carbon on which it sits and nitrogen 5 of the flavin and at the proper angle for transfer.

Many flavoenzymes use the **general redox couples NAD^+ and NADH and $NADP^+$ and NADPH** as carriers of a hydride in a half-reaction to regenerate the oxidized or reduced flavin, respectively, in preparation for the reduction or the oxidation of the nominal reactant in the next round. Crystallographic molecular models of NADH or NADPH in a complex with the reduced form of the flavin in the active site[306,478,483,484] or crystallographic molecular models of NAD^+ or $NADP^+$ in a complex with the oxidized form of the flavin in the active site[485] or both of these pairings[486] show that, in each case, **the π molecular orbital system of the nicotinamide stacks upon the π molecular orbital system of the flavin** (Figure 2–11).[311] These are not complexes that are normally involved in the enzymatic reaction because they pair reduced flavin with NADH (the reduced form of the nicotinamide) or oxidized flavin with NAD^+ (the oxidized form of the nicotinamide). Consequently, one might argue that they are irrelevant to the actual mechanism of formal transfer of the hydride, but the only atom that is duplicated in or that is missing from the respective complexes is the hydrogen that would normally be transferred between them. Because this is the smallest possible difference and because both flavin nucleotides and nicotinamide nucleotides are large molecules, these complexes probably represent the actual orientation of the ring of the nicotinamide and the rings of the flavin, at least in the Michaelis complex and probably during the actual transfer of the hydride. In the active site of FMN reductase (NADPH) from *E. coli*, the FMN that is the substrate, rather than an NAD^+, also stacks upon the prosthetic $FMNH^-$ in the active site.[487]

The difficulty with all these stacked orientations is that, although carbon 4 of the nicotinamide is always directly adjacent to nitrogen 5 of the flavin in the stack, the distance between them is **fixed at 0.32 nm by the van der Waals radii of the atoms** in the respective rings of π orbitals, and the carbon–hydrogen bond of the hydride on the reduced nicotinamide points well away from nitrogen 5. In a **theoretical calculation of the orientation** that must exist in the transition state for transfer of a hydride between the nicotinamide and the prosthetic flavin in the active site of ferredoxin—$NADP^+$ reductase from *Anabaena*, the plane of the nicotinamide is required to be tilted with respect to the plane of the flavin at a 60° angle before hydride transfer can occur.[488] In a crystallographic molecular model of NADH bound in the active site of a mutant of ferredoxin—$NADP^+$ reductase from *Z. mays* (40% identity; 2.3 gap percent), the nicotinamide, as usual, is stacked upon the flavin.

In order for a nicotinamide that is stacked upon a flavin to tilt through the angle required by this calculation and other similar calculations, either nitrogen 1 of the nicotinamide ring, which is firmly anchored in the active site by the adenosylribose to which it is covalently attached, or nitrogen 10 of the flavin (in the case of ferredoxin—$NADP^+$ reductase, flavin adenine dinucleotide), which is firmly anchored to the active site by its D-ribityl group, would have to move 3 nm. The tilting of one or both of the rings also seems to be sterically precluded in the rather crowded confines of most active sites. For example, in the complex between NADPH and glutathione-disulfide reductase (Figure 2–11), the nicotinamide ring is sandwiched between the flavin and the hydroxyphenyl ring of a tyrosine.[310] All three π molecular orbital systems—tyrosine, nicotinamide, and flavin—are parallel to each other in the stack.

It seems, therefore, that these theoretical calculations of the transition state, if they actually define the required orientation for either direct hydride transfer, rule out the direct transfer of a hydride between carbon 4 of nicotinamide and nitrogen 5 of isoalloxazine if they are stacked one one top of the other in the Michaelis complex, as they are in most if not all crystallographic molecular models of complexes between nicotinamide-adenine dinucleotides and flavoenzymes. Indeed, it would seem that if the calculated orientations are the actual orientations required for hydride transfer, then the active sites that perform transfer of a hydrogen between a nicotinamide and an isoalloxazine would be assembled by natural selection to hold the nicotinamide and the isoalloxazine in those orientations upon their initial association, just as other reactants are held in such favorable orientations in situations in which π molecular orbitals do not stack (**2–52**). It would seem that **in-line transfer of a hydride is precluded** by the actual dispositions. There are

several other possibilities for transfer of the hydrogen between nitrogen 5 of the flavin and carbon 4 of the nicotinamide.

The first possibility is **tunneling**. Theoretical calculations and observed kinetic isotope effects suggest that the formal transfer of a hydride between carbon 4 of nicotinamide and nitrogen 5 of flavin in such a situation could occur by hydrogen tunneling,[489] which is the process generally invoked to explain abnormal, idiopathic kinetic isotope effects in the transfer of a hydron. There are other results, however, suggesting that formal transfer of a hydride from NADH to flavin does not involve hydrogen tunneling.[490] Furthermore, carbon 4 of the nicotinamide and nitrogen 5 of the flavin are farther apart than atoms between which hydrogen tunneling usually occurs, and they are unable to come closer together while stacked upon each other. In the crystallographic molecular model of the complex between 1,4,5,6-tetrahydronicotinamide adenine dinucleotide and the active site of morphinone reductase from *P. putida*, the plane of the tetrahydronicotinamide ring is parallel to the plane of the isoalloxazine ring of the prosthetic flavin and stacked upon it.[491] Theoretical calculations, however, of the transition state for transfer of a hydride from carbon 4 of the nicotinamide to nitrogen 5 of the flavin during the normal reaction in the active site of this enzyme require that, in order to accomplish the transfer of the hydride, when the full effects of tunneling are included, the plane of the nicotinamide ring must tilt away from the plane of the isoalloxazine through an angle of almost 90° so that a normal in-line transfer of the hydride between carbon 4 of the nicotinamide and nitrogen 5 of the flavin, which would bring the two atoms close enough so that tunneling can occur, can be accomplished.[492]

The second possibility is **transfer of an electron, followed by transfer of a hydron from carbon 4 to nitrogen 5, and finally transfer of the second electron**. The standard free energy change for transfer of an electron from reduced nicotinamide ($E^{\circ\prime} = +270$ mV) to oxidized flavin ($E^{\circ\prime}_{ox/sq} = -240$ mV), were each of them in free solution, is +50 kJ mol^{-1}, which is significantly unfavorable ($K_{eq} = 10^9$). Likewise, in the other direction, the standard free energy change for transfer of an electron from reduced flavin ($E^{\circ\prime}_{red/sq} = -130$ mV) to oxidized nicotinamide ($E^{\circ\prime} = -930$ mV), again were each of them in free solution, is +77 kJ mol^{-1} ($K_{eq} = 10^{13}$). These changes in standard free energy seem to indicate that a mechanism of two one-electron transfers in successive steps is unrealistic in either direction because, in each direction, the first step is quite unfavorable. These are, however, changes in standard free energy for transfer of an electron in solution at pH 7. Furthermore, enzymatic active sites often lower free energies of activation for nucleophilic substitutions and additions and elimination–additions by similar amounts.

Unlike the situation in solution, in the active site of an enzyme, the nicotinamide is stacked upon the flavin, and the formation of a charge-transfer complex in this circumstance may permit the rate of the initial transfer of an electron to be rapid enough to participate in the overall reaction. There are many instances in which the first step in the enzymatic reduction by NADH or NADPH of oxidized flavin bound to an active site as a prosthetic group is formation of a complex between the reduced nicotinamide and the oxidized flavin that displays a **charge-transfer band**.[325,406,493,494] These charge-transfer bands are evanescent because reduction of the oxidized flavin follows immediately. For example, when NADPH is mixed with the domain of human NADPH—hemoprotein reductase that contains the active site for reduction of the prosthetic oxidized flavin adenine dinucleotide, within the first 4 ms the NADPH binds to the active site and forms a charge-transfer complex with the oxidized flavin, with a charge-transfer band that has a maximum of absorbance at around 620 nm (Figure 2–17).[406] The formation of this charge-transfer complex precedes removal of the hydrogen nucleus from NADH or NADPH because when the protium on carbon 4 of NADH or NADPH is replaced with a deuterium, the rates of decay of the charge-transfer bands in the next step of several of these enzymatic reactions are decreased[495,496] by a factor of 2–7.

The existence of the charge-transfer band indicates that, in the complex between NADH or NADPH and oxidized flavin in the active site, the nicotinamide and the flavin are **electronically coupled** and that transfer of an electron between the two, under favorable circumstances, will be essentially instantaneous. Consequently, if a hydron must be removed from the NADH or NADPH coincident with transfer of an electron, the removal of that hydron would be the rate-limiting step in the transfer of the electron. This view of the situation is consistent with the fact that when the protium on carbon 4 of NADH or NADPH is replaced with a deuterium, the rate of reduction of oxidized flavin decreases[497-500] by a factor of 3–8. These kinetic isotope effects are consistent with dissociation of a hydron from carbon

but also with dissociation of a hydride from carbon. If the situation is such that the reduced flavin resulting from the formal transfer of a hydride from the nicotinamide to the flavin is not immediately oxidized, the product of the step in which the hydrogen has just been transferred from the nicotinamide to the flavin is now a complex between oxidized nicotinamide and reduced flavin that displays its own characteristic charge-transfer bands.[494,501-504]

With again the disclaimer that these two types of associations may not be charge-transfer complexes in the respective ground states, these results are consistent with **a mechanism in which an electron is transferred from reduced nicotinamide to flavin in a charge-transfer complex** while a hydron is being removed from the developing radical cation of the nicotinamide and a hydron is added to the resulting anionic flavin semiquinone, and then an electron is transferred immediately from neutral nicotinamide radical to neutral flavin semiquinone in a second charge-transfer complex. The fact that the intensity of the charge-transfer bands between nicotinamide and flavin correlated with the rates of normal reduction of the flavin in the reaction catalyzed by 4-hydroxybenzoate 3-monooxygenase [NAD(P)H] from *Pseudomonas aeruginosa*

$$\text{4-hydroxybenzoate} + \text{NADPH} + \text{H}^+ + \text{O}_2 \rightleftharpoons \text{3,4-dihydroxybenzoate} + \text{NADP}^+ + \text{H}_2\text{O} \qquad (2\text{–}151)$$

as the pH of the solution was varied[505] is consistent with participation of the transfer of an electron through a charge-transfer complex in the mechanism of its reaction.

In the crystallographic molecular model of human glutathione-disulfide reductase with NADPH bound at the active site, stacked upon what is probably reduced flavin, the amino group of Lysine 67 is between carbon 4 of the nicotinamide and nitrogen 5 of the flavin. Even though the amino group of Lysine 67 is only 0.37 nm away from carbon 4 of the nicotinamide (Figure 2–11), within the sum of van der Waals radii, nitrogen 5 of the flavin is closer (0.304 nm),[306,310,311] but this contraction is probably the result of a normal hydrogen bond between the two nitrogens. From an examination of the crystallographic molecular model, it was concluded that a hydride could not be transferred from carbon 4 of the nicotinamide to nitrogen 5 of the flavin.[311] Instead, it was proposed that, during the reduction, two electrons would flow from the nicotinamide to the flavin while the hydrogen of NADPH is being removed as a hydron by the oxygen of Glutamate 202, which is within (0.33 nm) van der Waals contact (0.38 nm) of carbon 4.[310] The hydron would be relayed to the 6-amino group of Lysine 67, which is in a hydrogen bond (0.284 nm) with the same oxygen of Glutamate 202, and then transferred from the lysine to the adjacent (0.304 nm) nitrogen 5 of the flavin. Both the charge-transfer complex resulting from the stacking of nicotinamide on flavin and the concerted transfer of the hydron would promote the otherwise difficult movement of the first electron. Following transfer of the hydron, accompanied by transfer of the electron, the second electron would be transferred. When the lysine in dihydrolipoyl dehydrogenase from *E. coli*, the 6-amino group of which is immediately adjacent to nitrogen 5 of its prosthetic flavin and homologous to Lysine 67 in glutathione-disulfide reductase, is mutated to an arginine, the rate of its enzymatic reaction decreases by a factor of 1000.[329]

In the crystallographic molecular models of most if not all complexes between flavoenzymes and nicotinamides, there is a **acid–base adjacent to carbon 4 of the nicotinamide and nitrogen 5 of the flavin** in a position in which it could perform a similar tautomerization. It can be a glutamic acid and a lysine that together participate in a hydrogen bond,[484] the hydroxy group of a serine or a threonine,[483,485] or a molecule of water.[486] In each of these instances the acid–base is at least bidentate. When the serine sitting in this location in NADPH—hemoprotein reductase is mutated to alanine, its proficiency for catalysis of the reduction of its flavin by NADPH decreases by a factor of 100.[506]

The dihydroorotate from which a hydride is transferred to flavin in the active site of dihydroorotate dehydrogenase (fumarate) from *Lactococcus lactis* is stacked upon the flavin,[507] just as the nicotinamide is in the active sites of glutathione-disulfide reductase and other enzymes that catalyze transfer of a hydride from nicotinamide to flavin. The 6-ammonio group of Lysine 43 in dihydroorotate dehydrogenase (fumarate) forms a hydrogen bond to nitrogen 5 of the flavin and is in van der Waals contact with the carbon on the orotate from which the hydride is transferred. When Lysine 43 is mutated to an alanine, the catalytic proficiency of the enzyme decreases by a factor of 7500.[508]

One set of results, however, seems to provide results that contradict the view that NADH or NADPH reduces oxidized flavin by transfer of individual electrons coupled to transfer of a hydron.

This contradiction is the fact that enzymes in which this oxidation–reduction occurs **transfer the hydrogen nucleus from the NADH or NADPH intact to 5-carba-5-deazaflavin** when it replaces the prosthetic flavin. For example, [4-^{3}H]NADH in the active site of FMN reductase (NADPH) from *Vibrio harveyi*[509] is transferred in the active site to 5-carba-5-deazaflavin

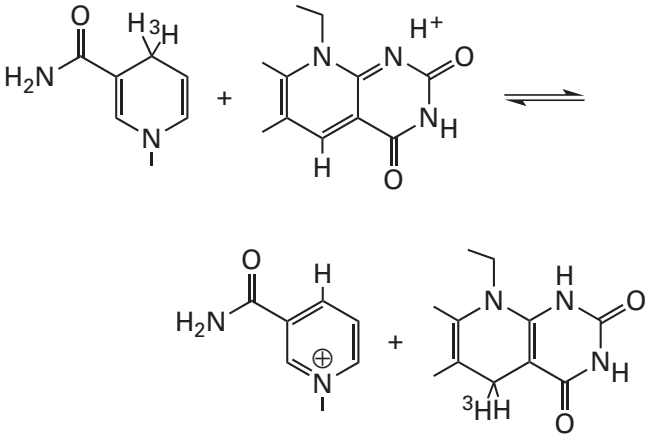

(2–152)

If it were stoichiometric, such a transfer of tritium would be unlikely if the hydrogen nucleus were being transferred as a hydron on a multidentate acid. During the transfer in this instance, however, less than stoichiometric transfer was observed, but the exact percent of transfer could not be determined because the isotope effect for tritium in the reaction was not determined, so it could have resulted from transfer of the hydrogen nucleus as a hydron in the shielded environment of the active site. Nevertheless, if it turns out that, in most cases, when the prosthetic flavin in an active site is replaced by 5-carba-5-deazaflavin and transfer of an isotope of hydrogen is observed to be quantitative, such observations would seem to rule out a mechanism in which a hydron is transferred between flavin and nicotinamide by a multidentate acid.

The third possibility would be transfer of the hydrogen from carbon 4 of reduced nicotinamide to oxidized flavin in an **ene reaction**. Precedent for this mechanism would be the cycloaddition that occurs in the active site of phenacrylate decarboxylase between prenylated $FMNH_2$ and the reactant (2*E*)-3-phenylprop-2-enoate,[370] an enzymatic ene reaction in the biosynthesis of pyridoxatin in *Aspergillus bombycis*,[510] and the apparent, but disputed, ene reaction between NADH and (*E*)-but-2-enoyl-SCoA (previously Equation 1–98)

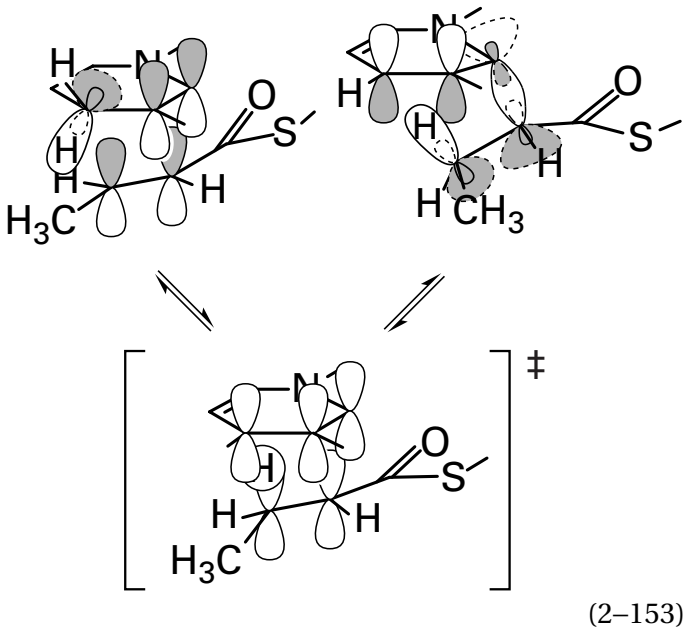

(2–153)

A similar ene reaction should be able to occur between NADH and oxidized flavin

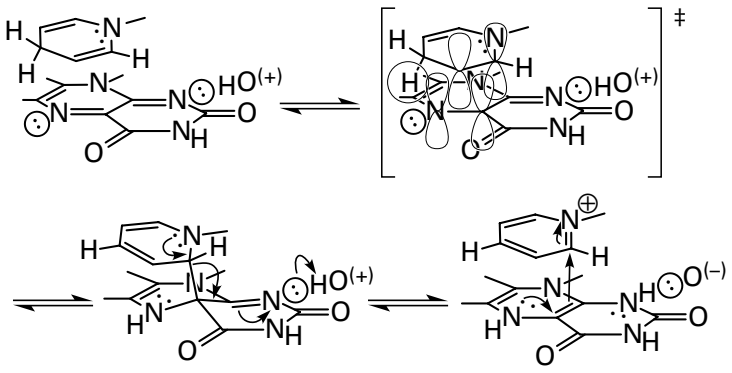

(2–154)

If this is indeed the mechanism for the formal transfer of the hydride, the transfer between carbon 4 of the NADH and nitrogen 5 of the flavin would be quantitative and 5-carba-5-deazaflavin would be as capable a participant in the reaction as flavin, if not a more capable participant. The precedent for the final step in the reaction, reversible nucleophilic addition of reduced flavin to NAD^+, would be the rapidly reversible nucleophilic addition of urocanate to NAD^+ in the hydration catalyzed by the active site of urocanate hydratase (Equation 2–81). Carbon 2 of NAD^+ is as electrophilic as carbon 4, if not more so. In the crystallographic molecular model of the active site of human glutathione-disulfide reductase (Figure 2–11), the nucleophilic double bond between carbon 1a and carbon 4a, which would add

to or dissociate from carbon 2 of the nicotinamide, is immediately adjacent to carbon 2. The distance from carbon 1a or from carbon 4a to carbon 2 is 0.35 or 0.37 nm, respectively. The distance between carbon 4 of the nicotinamide and nitrogen 5 of the flavin is 0.32 nm.

In summary, when oxidized flavin, HFl_{ox}, participates in a two-electron oxidation of a reactant, one or two hydrons and two electrons are removed from that reactant, and two electrons and one or two hydrons are added to the flavin to produce the anionic conjugate base of reduced flavin, $H_2Fl_{red}^-$, or neutral reduced flavin, H_3Fl_{red}. One hydron is usually removed from the reactant as a hydron by a catalytic base properly positioned in the active site. It is removed from a normally acidic position such as a thiol, an amine, or a carbon α to a carbonyl group or an acyl group by a properly positioned base in the active site. It is the other hydron and the two electrons on the resulting conjugate base, all of which end up formally on the oxidized flavin, that are in question. The hydron and the two electrons may be transferred directly as a hydride. The nucleophile left behind by the removal of the first hydron may form an adduct with nitrogen 5 or carbon 4a of the flavin, and the two electrons in the resulting σ bond may be absorbed by the flavin as it dissociates as a nucleophilic leaving group from the electrophilic product. Or the electrons may be transferred one at a time, and during the first transfer of the electron, the remaining hydron may be removed from the substrate radical as a hydron and a hydron added to flavin semiquinone as a hydron. The fact that experimental observations have been reported that are consistent respectively with each of these mechanisms may illustrate the remarkable versatility of flavin. The fact that two or three of these mutually exclusive mechanisms have often been proposed for the same enzymatic reaction, however, may illustrate our ignorance of what flavin actually does. It is possible that evolution by natural selection has been able to choose among these different possibilities and has settled on one or another of them for a particular enzymatic mechanism. Whether it has always made the same choice or made different choices with different flavoenzymes remains to be determined. It is also possible that the actual mechanism for a particular flavoenzyme is some hybrid of two or more of the possibilities, just as a concerted nucleophilic substitution is a mixture of a dissociative nucleophilic substitution and an associative nucleophilic substitution.

Complicating one's judgment of the mechanisms of flavin is the fact that it **participates in one-electron transfers** such as that catalyzed by adrenodoxin-$NADP^+$ reductase

$$2 \text{ reduced adrenodoxin} + NADP^+ + H^+ \rightleftharpoons 2 \text{ oxidized adrenodoxin} + NADPH \quad (2\text{–}155)$$

In this reaction, the redox couple of $NADP^+$ and NADPH oxidizes and reduces the flavin by the equivalent of the transfer of a hydride but the adrenal ferredoxin, the mitochondrial form (33% identity; 5.4 gap percent; human and *E. coli*) of a bacterial ferredoxin, is a one-electron redox couple, and the single electrons are passed one after the other from flavin with flavin semiquinone as an intermediate.[511]

The ability of a flavin to exist as the stable semiquinone (Figure 2–9) permits it to connect a two-electron oxidation–reduction to two successive transfers of single electrons. Flavin sits at the junction between many two-electron oxidoreductants and one-electron oxidoreductants.[283] The two members of almost all nominal redox couples that participate in oxidation–reduction of flavins in flavoenzymes, such as N^5,N^{10}-methylenetetrahydrofolate and N^5-methyltetrahydrofolate, crotonyl-SCoA and butyryl-SCoA, and 2-iminopropanoate and D-alanine, accept or donate the formal equivalent of a hydride and differ from each other by two electrons and one or two hydrons. The two members of several of the general redox couples that act as acceptors or donors to flavin, for example NAD^+ and NADH and O_2 and H_2O_2, also differ from each other by the formal equivalent of a hydride. With all these redox couples, two electrons are transferred to or from flavin and then two electrons are transferred from or to flavin, respectively. In many instances, however, the general redox couple regenerating the oxidized flavin or the reduced flavin, such as a prosthetic metallic ion, a prosthetic iron–sulfur cluster, or a prosthetic heme, is capable of transferring only one electron from or to the flavin. In such instances, the flavin must split a pair of electrons or join a pair of electrons, respectively.

The ability of flavin to split pairs of electrons into two single electrons or join two single electrons into a pair of electrons is one of its key roles in metabolism. When flavin splits a pair of electrons that it has accepted in a two-electron reduction such as a hydride transfer, each electron by

itself can then be **transferred successively** among a subset of the large array of prosthetic groups capable of participating only in one-electron transfer. A single electron transferred to flavin from one member of such a subset of prosthetic groups can also be joined by flavin with a second electron transferred successively on the same path. A prosthetic flavin can also bifurcate two electrons. When flavin **bifurcates two electrons,** they are split between two separate acceptors rather than passed successively to the same acceptor. For example, one of the prosthetic flavins in electron-transfer flavoprotein from *Acidaminococcus fermentans* bifurcates two electrons that it accepts in a hydride transfer from NADH by transferring one to a prosthetic iron–sulfur cluster in a ferredoxin and the other to another prosthetic flavin in the same molecule of electron-transfer flavoprotein situated in an environment that stabilizes the anionic semiquinone.[512] This capacity of flavin to split or join electrons serves as an introduction to biochemical one-electron transfer.

Suggested Reading

Venkataram, U. V., and Bruice, T.C. (1984) On the mechanisms of flavin-catalyzed dehydrogenation α,β to an acyl function: The mechanism of 1,5-dihydroflavin reduction of maleimides, *J. Am. Chem. Soc. 106,* 5703–5709. https://doi.org/10.1021/ja00331a047

Gassner, G., Wang, L., Batie, C., and Ballou, D. P. (1994) Reaction of phthalate dioxygenase reductase with NADH and NAD: Kinetic and spectral characterization of intermediates. *Biochemistry 33*, 12184–12193. https://doi.org/10.1021/bi00206a022

Malito, E., Coda, A., Bilyeu, K. D., Fraaije, M. W., and Mattevi, A. (2004) Structures of Michaelis and product complexes of plant cytokinin dehydrogenase: Implications for flavoenzyme catalysis. *J. Mol. Biol. 341*, 1237–1249. https://doi.org/10.1016/j.jmb.2004.06.083

Problem 2–17: Sarcosine oxidase (formaldehyde-forming) from *Corynebacterium* is a flavoenzyme that catalyzes the reaction[513]

$$H_2O + \text{sarcosine} + HFl_{ox} \rightleftharpoons \text{glycine} + \text{formaldehyde} + H_3Fl_{red}$$

(A) Write a mechanism for the reaction as a direct hydride transfer. What provides the push?
(B) Write a mechanism for the reaction involving an adduct at nitrogen 5 of the flavin.
(C) Write a mechanism for the reaction involving an adduct at carbon 4a of the flavin.
(D) Write a mechanism for the reaction involving successive transfers of single electrons between sarcosine and flavin. Have the hydrogen nucleus removed as a hydron by a base.

Problem 2–18: Write the mechanism by which benzylamine is oxidatively deaminated to benzylimine by 3,7,8,10-tetramethyl-5-ethylisoalloxazine in a reaction in which the amine adds nucleophilically to carbon 4a of the prosthetic flavin.[385]

Problem 2–19: The following reaction is catalyzed by flavin and thiamine diphosphate acting together

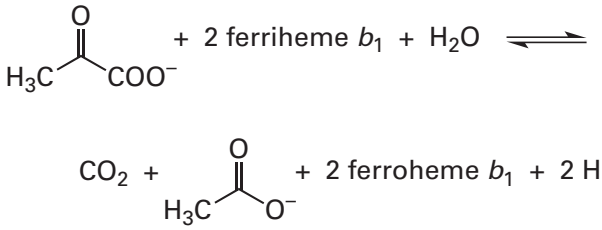

Write a mechanism involving both prosthetic groups.

Problem 2–20: Show how the reaction catalyzed by the flavoenzyme dihydroorotate dehydrogenase (NAD^+)[514]

$$(S)\text{-dihydroorotate} + HFl_{ox} \rightleftharpoons \text{orotate} + H_3Fl_{red}$$

can be written as the formal transfer of a hydride to flavin and how it resembles the reaction catalyzed by D-amino-acid oxidase.

Problem 2–21: 2-Hydroxy-3-butynoate is capable of inactivating the flavoenzyme L-lactate oxidase in the following reaction

2-hydroxybut-3-ynoate + HFl_{ox} ⇌

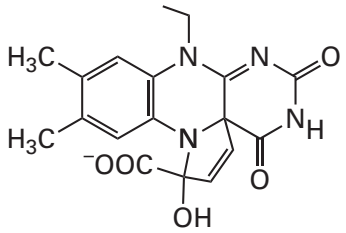

Write a mechanism for this reaction involving hydron removal from 2-hydroxybut-3-ynoate at the carbon analogous to the carbon from which a hydrogen is removed in the regular reaction of lactate with the enzyme.

Problem 2–22: Each of the reactions to the right is catalyzed by either pyridoxal 5′-phosphate, thiamine diphosphate, or flavin.[515] The equations are not necessarily balanced and you may have to add electrons and hydrons to balance them. Balance the equations, decide which prosthetic group is required, and write a mechanism for the reaction involving that prosthetic group. If there are several possible mechanisms, choose only one. There is no exclusively correct mechanism, so the choice is one of personal preference, but the chemistry must be correct.

(A)

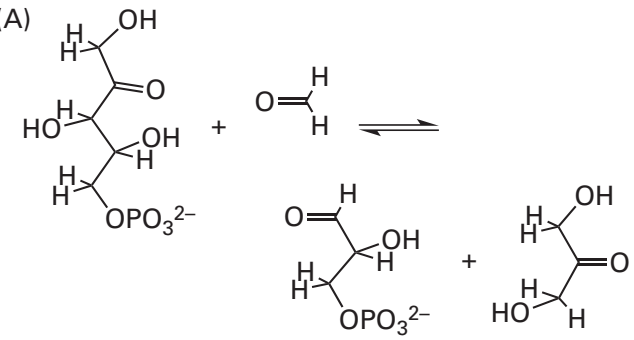

(B)

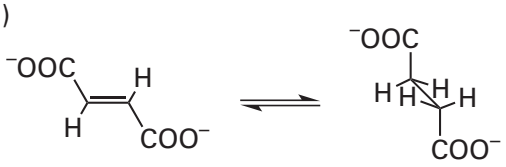

(C)

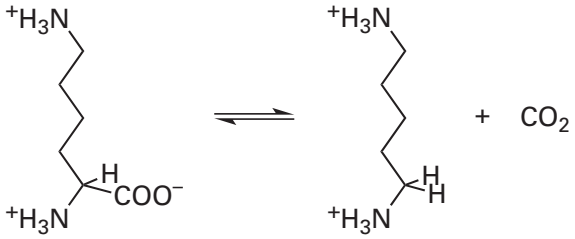

(D)

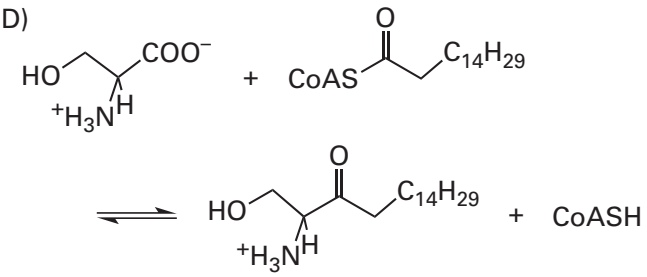

(E)

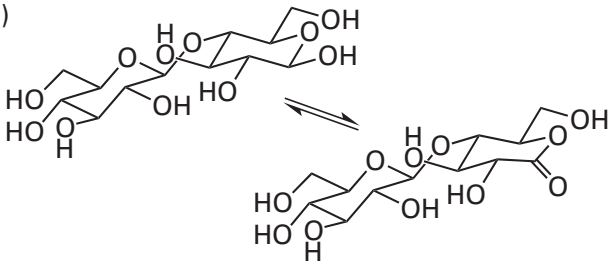

(F)

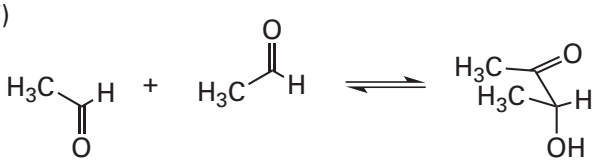

One-Electron Transfer

A prosthetic group capable of participating in transfer of single electrons is a redox couple the two members of which differ from each other by only one electron. If the biochemical standard reduction potential for such a one-electron redox couple is to be in the biochemical range of voltage (approximately −1000 to +1000 mV),[516] both members of the redox couple must have fairly stable electronic structures. For example, flavin semiquinone, because its unpaired electron is delocalized over a large π molecular orbital system, can be a stable organic radical within an active site and can join with either oxidized flavin or reduced flavin to produce in each case a reasonable one-electron redox couple.

There are a set of redox couples that transfer single electrons by forming stable organic radicals. Flavin, because its semiquinone is a stable organic radical, is an example of this class, but many of the members participate only in the transfer of one electron.

Pheophytins

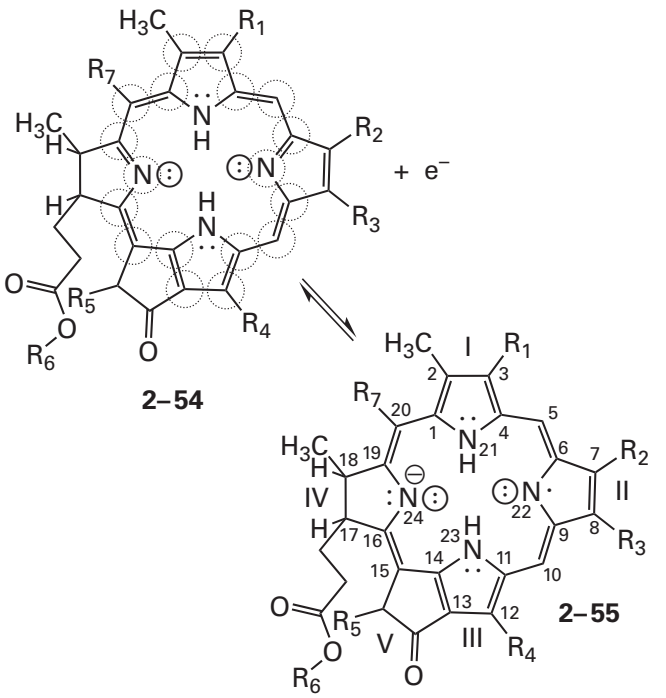

(2–156)

are prosthetic groups capable of participating in one-electron transfer. In the radical anion of pheophytin (**2–55**), as in the radical anion of flavin (Figure 2–9), the unpaired electron is delocalized over a large π molecular orbital system. Within each pheophytin there is an **aromatic ring** of 18 atoms (designated by dotted circles in **2–54**), each of which contributes a *p* orbital to form an unbroken ring with 18 π electrons. In the various pheophytins, some of the carbon–carbon double bonds are reduced to carbon–carbon single bonds, but there is always an unbroken ring of 18 *p* orbitals, although not necessarily in the locations indicated in Equation 2–156. The unpaired electron is added and delocalized into the lowest unoccupied molecular orbital in this aromatic π molecular orbital system.[517] Ring IV has two saturated carbons that lie outside this aromatic π molecular orbital system, and in some of the pheophytins the double bond in ring II, which also lies outside the π molecular orbital system, is either reduced or isomerized into an exocyclic vinylidene group, which is formed from an ethyl group at R_3.

There are more than 15 different pheophytins, which differ from each other by the identity of the substituents around the ring. The substituents R_2, R_3, and R_4 are almost always saturated alkyl groups such as methyl, ethyl, propyl, and isobutyl, but three pheophytins have a formyl group for R_2 and another has an ethenyl group for R_3. The substituent R_1 is an ethenyl, formyl, acetyl, or 1-hydroxyethyl group. The substituent R_5 is either a methoxycarbonyl group or a hydrogen, the substituent R_6 is either a phytyl group or a hydrogen, and the substituent R_7 is either a methyl group or a hydrogen.

The most common pheophytins are pheophytin *a*, pheophytin *b*, bacteriopheophytin *a*, and bacteriopheophytin *b*. In pheophytin *a*, R_1 is an ethenyl group, R_2 is a methyl group, R_3 is an ethyl group, R_4 is a methyl group, R_5 is a methoxycarbonyl group, R_6 is a phytyl group, and R_7 is a hydrogen. Pheophytin *b* is identical to pheophytin *a* except that R_2 is a formyl group. Bacteriopheophytin *a* is identical to pheophytin *a* except that R_1 is an acetyl group and the double bond between R_2 and R_3 has been reduced to a single bond by the addition of a hydrogen to each carbon so that the carbons to which R_2 and R_3 are attached both have *R* stereochemistry. Bacteriopheophytin *b* is the same as bacteriopheophytin *a* except that the R_3 ethyl group has been oxidized to an ethylidene group.

Because the substituents and the ring itself are mostly hydrophobic, pheophytins are essentially insoluble in water and must be dissolved in organic solvents for observation when they are not in a protein or in the hydrocarbon of a phospholipid bilayer.

The **standard reduction potential** in dimethylformamide of the most aliphatic of the pheophytins, bacteriopheophytin *d*, which has alkyl substituents

or hydrogens at positions R_2 through R_7 and a 1-hydroxyethyl group at R_1, is –810 mV.[517] When a formyl group is found in place of the methyl group at R_2, the standard reduction potential of the pheophytin increases to –760 mV; when a methoxycarbonyl group is found in place of the hydrogen at R_5, it increases to –640 mV; and when a methoxycarbonyl group is found in place of the hydrogen at R_5 and an acetyl group in place of the 1-hydroxyethyl group at R_1, it increases to –510 mV. These increases in standard reduction potential result from the electron withdrawal exerted by the various substituents on the electron excess in the reduced state, the radical anion. It is also the case, as with flavin, that when a pheophytin is tightly bound to a protein as a prosthetic group, its standard reduction potential is different from the one it displays when it is dissolved in an organic solvent. It is usually more positive, probably because the protein provides donors that form hydrogen bonds with one or more of its oxygens or direct the positive poles of their dipoles toward the pheophytin.

When the two hydrons on the nitrogens in the center of a pheophytin are replaced by Mg^{2+} and all four of the nitrogens become ligands to the metallic ion, the corresponding **chlorophyll**

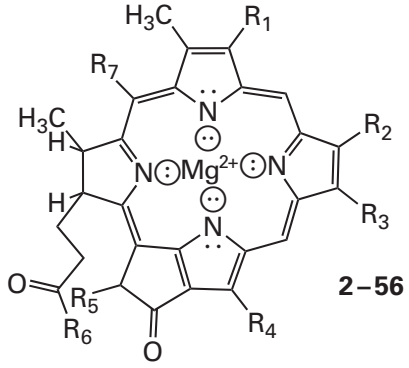

2–56

is formed. Because it replaces two hydrons, insertion of the Mg^{2+} does not alter the charge number of the prosthetic group, nor does the electrochemically inert Mg^{2+} participate in the one-electron oxidation–reduction. As a Lewis acid, it simply substitutes for the two hydrons, which are also Lewis acids. The Mg^{2+}, however, is a weaker Lewis acid than two hydrons, and as a result a chlorophyll has a standard reduction potential that is 200–300 mV more negative than the corresponding pheophytin (see Equation 2–109).[517] Even though chemically they are the same, chlorophylls are more widely recognized than the corresponding pheophytins because they give leaves their green color.

There are a number of **biochemically important quinones such as the ubiquinones** (**2–57**), the **plastoquinones** (**2–58**), the **menaquinones** (**2–59**) and **phylloquinone** (**2–59**)

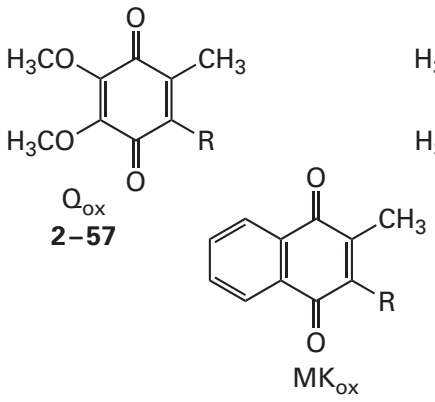

There are also demethylmenaquinones, in each of which the methyl group on the quinone ring of the parent menaquinone is missing. When they are not tightly bound in an active site as prosthetic groups, each of these biochemical quinones transfers electrons between enzymes, and when in this role, they are **electron-transferring coenzymes**. The different versions of these quinones differ in the length of the polyisoprenyl groups attached at position R and the degree of unsaturation of those polyisoprenoids. The polyisoprenyl groups

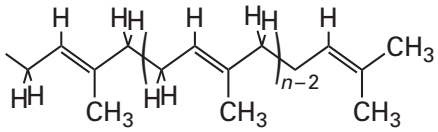

2–60

contain four or more **isoprenoid units** ($n \geq 4$) and can be saturated at any but the most proximal position. For example, in phylloquinone, which is only distinguished from the other menaquinones for historical reasons, the three more distal isoprenoid groups in the phytyl group ($n = 4$) attached at position R are all saturated while in menaquinones, which have the same quinone as phylloquinone but differ in the length of their polyisoprenoids, all the distal isoprenoid units are unsaturated. Because of its polyisoprenoid substituent, each of these quinones is as hydrophobic as the phospholipids forming the bilayer in which they are dissolved. Each of these quinones, like a phospholipid, is an **amphipathic molecule**, with the ring of the quinone providing the hydrophilic end and the polyisoprenoid tail providing the hydrophobic end.

When not tightly bound by membrane-bound proteins as prosthetic groups or weakly bound as coenzymes, these quinones are **solutes dissolved in a phospholipid bilayer**, either the plasma membrane of a bacterium, the inner membrane of a mitochondrion, a chromatophore, or the thylakoid of a chloroplast with which they are associated. When it is an amphipathic solute in one of these membranes, ubiquinone, plastoquinone, menaquinone, or phylloquinone has the diffusional properties of a phospholipid, and most of the time it translates in two dimensions through the bilayer with the quinone at the interface between the alkane and the water. The hydrophilic portion of one of these quinones, however, is much less hydrophilic than the hydrophilic portion of a phospholipid, and unlike phospholipids, they can pass rapidly back and forth across the bilayer between the interfaces.

When they are free solutes in a phospholipid bilayer, these quinones can participate as coenzymes in the two-electron oxidation–reductions that produce the respective quinols. For example, the two-electron oxidation–reduction for ubiquinone is

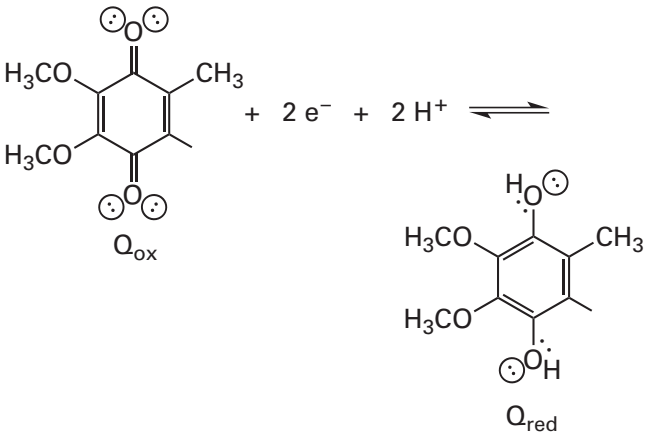

(2–157)

Because the two sequential values of pK_a for the various quinols are greater than 10,[518] the transfer of the two electrons to the π molecular orbital system of the quinone always occurs in a cell with the uptake of two hydrons, one hydron on one of the σ lone pairs on one of the oxygens and the other hydron on one of the σ lone pairs on the other oxygen (as in Equation 2–97). These associations of hydrons cause the **midpoint reduction potentials**, E_m, to vary with pH (as in Figure 2–14) with a slope[519-522] of –59.2 mV (unit of pH)$^{-1}$. When it is a free solute in the membrane of a biological organelle, the biochemical standard reduction potential of a ubiquinone is +70 to +110 mV,[519,520,523] that of a plastoquinone is +80 to +110 mV,[521,522] and that of a menaquinone is around –60 mV.[524] The plasma membranes and the various organelles of the cells in different organisms each have their own particular quinones. For example, anaerobic archaea have only menaquinones in their plasma membranes while bacteria have both menaquinones and ubiquinones.

In addition to the quinone and the quinol (Equation 2–157), each of these quinones can exist as a **semiquinone**. For example, the semiquinone of ubiquinone is ubisemiquinone ($HQ^{\bullet}$), which is the conjugate acid of the ubisemiquinone radical anion ($Q^{\bullet -}$)

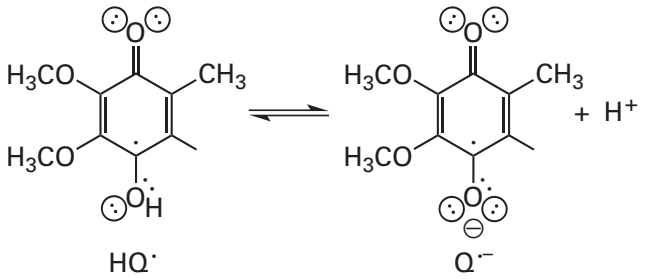

(2–158)

In methanol,[525] the pK_a for **ubisemiquinone** is 6.5, and when it is formed by the transfer of an electron to the quinone (pK_a < 0), the radical anion of the ubisemiquinone will pick up a hydron if the pH is less than its pK_a under the particular circumstances

$$H^+ + e^- + Q_{ox} \rightleftharpoons H^+ + Q^{\bullet -} \rightleftharpoons HQ^{\bullet} \qquad (2\text{–}159)$$

In many instances, however, because its pK_a is often even lower in a particular situation, a radical anion of a quinone remains unhydronated after it is formed, and the two hydrons necessary to form the neutral quinol are picked up only when the second electron arrives.[526,527]

Because they have stable semiquinones, each of these quinones is able to alternate between the oxidized state (the quinone) and the semiquinone or between the semiquinone and the reduced state (the quinol) in one-electron oxidation–reductions and between the quinone and the quinol in two-electron oxidation–reductions. This ability to participate in **both one-electron and two-electron oxidation–reductions** allows these quinones to receive two electrons together and then dispense each electron one at a time or to receive one electron

at a time and then dispense two electrons. Consequently, each of these quinones, like flavin, is able to split or join pairs of electrons. In a particular enzyme, the active site, the substrates, and the surrounding prosthetic groups determine whether one-electron or two-electron oxidation–reductions dominate or if electrons are split in one direction and joined in the other.

In solution, such as the solution of one of these quinones dissolved in a biological membrane, the semiquinone radical is in equilibrium with the quinol and the quinone by a one-electron transfer

$$Q_{ox} + H_2Q_{red} \rightleftharpoons 2\,HQ^{\cdot} \qquad (2\text{–}160)$$

in analogy to the similar disproportionation in which flavin participates (Equation 2–111). The equilibrium constant for the disproportionation of Equation 2–160 is the formation constant for the semiquinone radical

$$K_{f,HQ^{\cdot}} = \frac{[HQ^{\cdot}]^2}{[Q_{ox}][H_2Q_{red}]} \qquad (2\text{–}161)$$

The values of $K_{f,HQ^{\cdot}}$ at pH 7 for plastosemiquinone[528] and menasemiquinone[529] have been estimated to be 10^{-9} and 10^{-8}, respectively. These small values reflect the fact that, outside an active site, the radicals are unstable because the unpaired electron is not delocalized in the highest occupied molecular orbital in a large π molecular orbital system.

Because of these values for this equilibrium constant, when ubiquinone is in free solution in a biological membrane, no ubisemiquinone radical can be detected regardless of the ratio between the concentrations of quinone and quinol.[519] As with flavin, however, when ubiquinone is bound tightly to particular proteins involved in electron transfer, significant quantities of ubisemiquinone radical are observed as the concentrations of quinone and quinol are varied reciprocally.[530,531] In the most common situation, in which only one electron at a time is transferred to one of these quinones bound at an active site on an enzyme or one electron at a time is removed from one of these quinols, the resulting semiquinone radical has to be stable.[526,527] In large part, the **stability of these bound semiquinone radicals** results from the fact that they are isolated and unable to disproportionate as they would if they were free in solution in the surrounding bilayer of phospholipids. They are fixed in dispositions that preclude the conversion of two semiquinone radicals into a quinone and a quinol. Their stability, however, is also controlled by controlling their access to hydrons. Because a hydron is not required for the formation of the radical anion of the quinone upon one-electron reduction, if hydrons are not made available, the radical anion of the quinone cannot be further reduced[532] and is stable. If only weak acids are provided by the protein as donors for hydrogen bonds to the two carbonyl oxygens of the quinone, the semiquinone radical anion will also be stabilized.[533] In any case, the ability of one of these quinones to form a stable semiquinone radical or semiquinone radical anion when it is bound to an enzyme as a substrate or prosthetic group is essential because the quinone is usually required to accept electrons one at a time from other prosthetic groups.

L-Ascorbate is not incorporated into an active site as a prosthetic group, but it can provide a single electron as an electron-transferring coenzyme. For example, it is the electron-transferring coenzyme for peptidylglycine monooxygenase[534]

$$\begin{aligned}&\text{[peptide]-glycine} + 2\ \text{L-ascorbate} + O_2\\ &\quad\rightleftharpoons \text{[peptide]-(2S)-2-hydroxyglycine}\\ &\qquad + 2\ \text{L-monodehydroascorbate} + H_2O\end{aligned} \qquad (2\text{–}162)$$

In this instance, two molecules of L-ascorbate each provide in turn one electron to reduce two prosthetic Cu^{2+} ions on the enzyme to two Cu^{+}, which then in turn provide the two electrons required for catalysis.[535,536]

L-Ascorbate is the monoanionic conjugate base of ascorbic acid ($pK_a = 4.04$)[537] and is the principal form present at pH 7

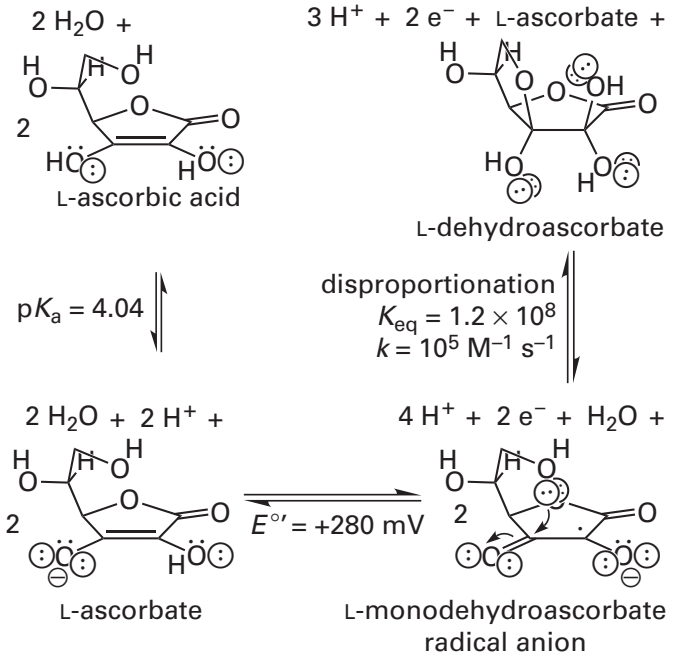

(2–163)

L-Ascorbate is capable of providing single electrons because the radical anion of L-ascorbate,[538] **L-monodehydroascorbate radical anion**, is a relatively stable species as a result of the **captodative effect**.[539] In the radical anion, the unpaired spin is delocalized over the three carbons and the three oxygens, mostly on the carbons but with significant spin density on the three oxygens. The adjacent oxygen donates electron density and the adjacent carbonyls withdraw electron density. L-Monodehydroascorbate radical anion is the analogue of the semiquinone of flavin or the semiquinone of ubiquinol and has almost the same equilibrium constant (8×10^{-9})[540] for disproportionation (see Equation 2–161) as the semiquinone of ubiquinol. In the enzymatic reactions for which it is an electron-transferring coenzyme, L-ascorbate provides a single electron with a biochemical standard reduction potential of +280 mV.[537,540-542]

Following the transfer of the electron and its dissociation from the active site, the resulting L-monodehydroascorbate radical ion rapidly (10^5 M^{-1} s^{-1})[543] disproportionates to give L-ascorbate and **L-dehydroascorbate**. Consequently, the concentration of L-monodehydroascorbate radical ion in the cytoplasm is so small that the enzymatic reactions in which L-ascorbate provides an electron do not proceed significantly in reverse. L-Dehydroascorbate is present in solution at neutral pH as the hydrate at carbon 2 of the internal lactone.[544] L-Dehydroascorbate is reduced by two electrons back to L-ascorbate by either monodehydroascorbate reductase (NADH) in plants and fungi or glutathione transferase, glutaredoxin, and protein disulfide-isomerase in animals.[543]

Because L-ascorbate is not used as a prosthetic group, L-monodehydroascorbate radical anion is not stabilized in an active site and is released as a product after the L-ascorbate has provided the electron. After its dissociation, it is present only evanescently. It follows that, unlike most other electron-transferring coenzymes, L-ascorbate only donates an electron; neither L-monodehydroascorbate radical anion nor L-dehydroascorbate, which are the oxidized forms of L-ascorbate, accepts one electron or two electrons, respectively, from an enzyme other than those that are responsible for the reduction of L-dehydroascorbate back to L-ascorbate. L-Ascorbate is also used, usually in concert with Fe^{2+}, to reduce prosthetic groups in the active sites of enzymes, for example, the iron ion in the active sites of a group of dioxygenases, that have been adventitiously oxidized. In such instances, the L-ascorbate is neither a prosthetic group nor a coenzyme but is used as a reductant that, when called upon, rescues the respective enzyme from occasional oxidative inactivation.

It has already been noted that a **2-(1′′-hydroxyethyl)thiamine radical cation** (Figure 2–7), which distributes its unpaired electron over seven atoms in a π molecular orbital system

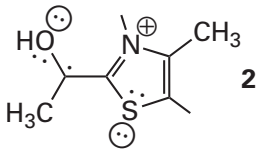

2–61

is an intermediate in the reaction catalyzed by pyruvate synthase.[227] In addition, the *N*-(4,4′-anhydropyridoxyl)imine formed during the biosynthesis of a 3,6-dideoxymonosaccharide (Equation 2–42) is reduced to the *N*-(5′-phosphopyridoxyl)imine in two one-electron steps. In this reduction, an ***N*-(5′-phosphopyridoxyl)imine radical cation**, distributing its unpaired electron over 10 atoms in a π molecular orbital system

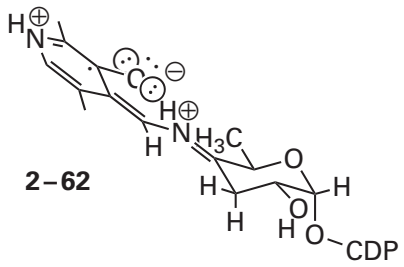

2–62

is an intermediate.[141,142] Each of these two radicals permits the respective prosthetic group to join two electrons that arrive separately to accomplish two-electron reductions. In each of these enzymatic oxidation–reductions, the electrons are transferred to or from these prosthetic groups, one at a time, from or to an iron–sulfur cluster.

There are also prosthetic redox couples that transfer single electrons by the one-electron reduction or oxidation of the ion of a transition metal. Iron–sulfur clusters and hemes are examples of prosthetic groups that, unlike flavin semiquinone radicals, pheophytin radical anions, chlorophyll radicals, quinone radicals, 2-(1″-hydroxyethyl)-thiamine radical cations, and *N*-(5′-phosphopyridoxyl)imine radical cations, accommodate the single electron added or removed in the ion of a transition metal rather than in an organic radical spread over an extended π molecular orbital system.

Iron is a common transition metal participating in prosthetic groups capable of one-electron transfer. When an iron ion is coordinated by six molecules of water, the standard reduction potential for the reaction

$$\left[Fe^{3+}(OH_2)_6\right]^{3+} + e^- \rightleftharpoons \left[Fe^{2+}(OH_2)_6\right]^{2+} \quad (2\text{–}164)$$

is +770 mV. When it is coordinated by six cyanides, the standard reduction potential for the reaction

$$\left[Fe^{3+}(^-CN)_6\right]^{3-} + e^- \rightleftharpoons \left[Fe^{2+}(^-CN)_6\right]^{4-} \quad (2\text{–}165)$$

is +360 mV. When it is coordinated by the four sulfido groups of four cysteines in rubredoxin, the biochemical standard reduction potential is −100 mV. When it is coordinated by six sp^2 nitrogens, four pyrrolinyl nitrogens from a mesoporphyrin and one from each of two imidazolyl groups, the biochemical standard reduction potential is −220 mV.[545] Just in these four simple examples, the biochemical standard reduction potentials of the variously coordinated iron ions span a range of 1000 mV. Most of these differences can be attributed to the identity of the ligands coordinating the iron ions.

The **bonding between iron and its ligands** ranges from mostly ionic with the hard oxygen bases to mostly covalent with the soft sulfur bases. When the ligands are hard bases such as water, cyanide, or nitrogen, six ligands are **arrayed octahedrally** around the iron; when they are soft bases such as sulfido groups or sulfides, four ligands are **arrayed tetrahedrally** around the iron. To sort out the bonding and the overall charge number of such a complex, one can first assume that the iron is the cation appropriate to its oxidation state and that the ligands are the anions or neutral molecules, and then the reader can make her own decision about whether each of the bonds between a ligand and the iron is ionic or covalent. From here on, in order to avoid making any unconditional decision about covalency, the following conventions will be used in figures and equations. Whenever an **oxidation number** can be assigned to a transition metal ion, it will be assumed that the transition metal ion has that charge number—for example, Fe^{III} will be designated as Fe^{3+}—and a charge number will be assigned to each atom of a ligand to a transition metal ion equivalent to the charge number it would bear if that ligand were removed from the ion of the transition metal along with the electron pairs that coordinate the ion. For example, in a tetrahedral complex of a ferrous iron, Fe^{II}, and the sulfido groups of four cysteines, the ferrous iron will be represented by the dication, Fe^{2+}, and the four sulfurs of four cysteines will be represented as the sulfido groups, each with a charge number of −1, giving the ferrous complex with the sulfurs of four cysteines a net charge number of −2. Then the reader can remember that the bonds between the iron ion and any oxygens are mostly ionic, the bonds between the iron ion and any sulfurs are mostly covalent, and the other bonds are intermediate between ionic and covalent. This strategy is applicable to the other prosthetic ions of transition metals in enzymes, such as vanadium, manganese, cobalt, nickel, copper, and molybdenum. In addition, in order again to avoid making any decision about covalency, thick dashed lines will be used to connect each transition metal ion and its ligands. This convention does not mean that these bonds are not covalent or not ionic, simply that they are somewhere in between completely covalent and completely ionic.

The **valence electronic structure** of elemental iron is $3d^6 4s^2$. An Fe^{2+} is dicationic because it is missing the two $4s$ electrons but still has six d electrons, and it is $3d^6$. An Fe^{3+} is tricationic because it is missing its two $4s$ electrons and one of its d electrons so that it is $3d^5$. An Fe^{3+} such as the Fe^{3+} in the hexahydrate, accepts and gives back one electron and passes reversibly between Fe^{3+} and Fe^{2+} because the electron in question at the end of the reduction

ends up in the unfilled 3*d* atomic orbital of lowest energy or one of the five degenerate unfilled 3*d* atomic orbitals of the Fe^{3+} to complete a pair, and in reverse, the electron in question at the end of the oxidation has left that filled 3*d* atomic orbital in the Fe^{2+} or a filled orbital of equal energy. It should be remembered that electrons cannot be followed in a reaction, so only the electron configurations at the beginning and the end of an electron transfer can be assigned.

Iron–sulfur clusters are arrays of iron ions, sulfide ions, and sulfido groups of cysteines. Each of these arrays contains one or more iron ions. Each iron ion is usually surrounded by four sulfurs, either as bridging sulfide ions, S^{2-}, which associate with two or three iron ions simultaneously, or as sulfido groups, $-S^-$, which usually associate with only one atom of iron. For a protein carrying an iron–sulfur cluster as a prosthetic group, the sulfide ions incorporated into the cluster are generated during its assembly by either thiosulfate sulfurtransferase[546,547] or 3-mercaptopyruvate sulfurtransferase,[548] and the sulfido groups are the conjugate bases of the sulfanyl groups of cysteines from the protein. These cysteines incorporate the iron ion, and hence the iron–sulfur cluster, somewhat covalently into the structure of the protein.

In an iron–sulfur cluster, four sulfurs are usually arranged **tetrahedrally around each iron ion**. If the four bonds between the four sulfurs and the iron were completely covalent bonds, then the lone pairs of electrons on the sulfurs would be occupying the four vacant $4sp^3$ atomic orbitals on the iron ion to form the four covalent bonds, which would be arranged tetrahedrally. If the four bonds were completely ionic bonds, then the four sulfurs would be arranged tetrahedrally around the iron ion because electron repulsion between the four sulfurs would be at a minimum in a tetrahedral arrangement. Sulfide is a large ion (0.184 nm) and an iron ion is much smaller (0.06–0.07 nm), so the crowding and the resulting electron repulsion would be significant. The actual bonding is probably somewhere in between these two possibilities.

Mononuclear iron–sulfur clusters, containing one atom of iron, necessarily have all four positions around the iron occupied by the sulfido groups of cysteines in the protein.[549] For example, in the mononuclear iron–sulfur cluster of a rubredoxin,[550,551] the four sulfurs of the four cysteines surround the iron in a tetrahedron modestly distorted by steric effects engendered by the protein (bond angles [S–Fe–S] range from 104° to 114°) with fairly constant iron–sulfur bond distances (0.227–0.233 nm)*

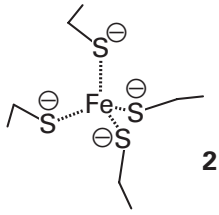

2–63

Rubredoxin from *C. pasteurianum* has a biochemical standard reduction potential of –100 mV[552] for the reaction

$$\left[Fe^{3+}(^{-}S-)_4\right]^- + e^- \rightleftharpoons \left[Fe^{2+}(^{-}S-)_4\right]^{2-} \quad (2\text{–}166)$$

This biochemical standard reduction potential is significantly more negative than that for the redox couple of ferricyanide and ferrocyanide (+360 mV) because the sulfur of a sulfido group is a more effective donor of electron density to iron than is the carbon of cyanide, so the cluster is a better reductant.

Dinuclear [2Fe–2S] iron–sulfur clusters† contain two iron ions, each coordinated tetrahedrally. In proteins containing these clusters, two of the positions around each iron ion are connected by two sulfide bridges, and the other two positions around each iron ion are occupied by the sulfido groups of cysteines (Figure 2–18).[553] This arrangement involves two irons, two bridging sulfides, and four sulfido groups. Such [2Fe–2S] iron–sulfur clusters are found in many of the **ferredoxins**, which are small proteins from animals,[554] plants (Figure 2–18), and bacteria[555] that act as electron-transferring coenzymes. A small **model compound** that contains such an iron–sulfur cluster complexed by two *o*-di(sulfanylmethyl)benzenes

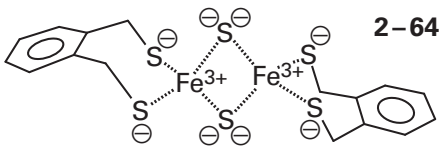

2–64

has been synthesized, and a crystallographic molecular model of high accuracy has been obtained.[556]

*Already it can be seen that insisting that all the iron–sulfur bonds are covalent would require that the formal charge on a ferrous ion in the cluster to be be –2, which seems strange.

†The number of iron ions and sulfide ions in a cluster is traditionally indicated in brackets.

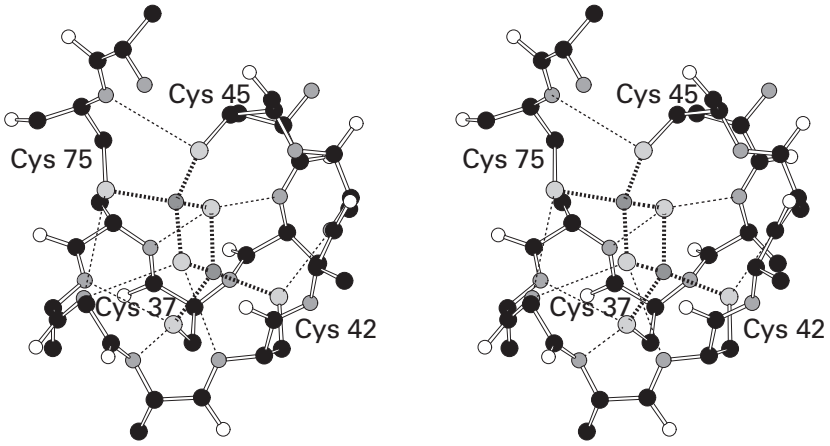

Figure 2–18: Stereodrawing[50] from a portion of the crystallographic molecular model of the [2Fe–2S] ferredoxin (94 aa) from *S. fusca* built from a map of electron density that was calculated from a data set to Bragg spacing of 0.14 nm.[553] Black atoms are carbons, white atoms are oxygens, small gray atoms are nitrogens, and large light gray atoms are sulfurs. In the iron–sulfur cluster, large light gray spheres are sulfides and small dark gray spheres are iron ions. The [2Fe–2S] iron–sulfur cluster in the protein is in the center of the drawing. Cysteine 75 provides a sulfur for a covalent bond to one of the iron ions of the cluster, and the amido nitrogen–hydrogen of the amino-terminal peptide bond of Cysteine 75 provides a dipole directed toward the sulfur of Cysteine 45. The segment of the polypeptide from Serine 36 to Cysteine 45 wraps around the iron–sulfur cluster as the stitches wrap around a baseball. Cysteines 37, 42, and 45 provide the other three sulfurs for the other three covalent bonds to the irons. The amido nitrogen–hydrogens of Serine 36, Arginine 38, Alanine 39, Glycine 40, Alanine 41, Cysteine 42, and Serine 44 in the respective peptide bonds of the polypeptide provide dipoles each directed toward a sulfide or the sulfur of a cysteine in the iron–sulfur cluster. These dipoles are connected to the sulfur to which they are directed by dotted lines. The side chains of only the cysteines are drawn.

In the central rhombus of a [2Fe–2S] iron–sulfur cluster, the angles at the sulfurs are more acute than the angles at the irons. Because the values of these bond angles are the same in the crystallographic molecular model of the model compound (75° and 105°, respectively) and that of the iron–sulfur cluster in the ferredoxin from *Scenedesmus fuscus* (76° and 103°, respectively) (Figure 2–18), the crystallographic molecular model of which was refined without constraints, they appear to represent undistorted energy minima. The iron–sulfide bond distances were also the same in the crystallographic molecular models of the model compound (0.221 ± 0.003 nm) and the ferredoxin (0.220 ± 0.003 nm). The cysteinyl sulfanyl–iron–cysteinyl sulfanyl bond angles are also less than the value for tetrahedral bonding (109.5°) in both the model compound (106°) and the ferredoxin (105°). All these comparisons suggest that steric effects in the protein do not distort the metallacycle and leave the impression that the metallacycle is quite rigid.

The model compound **2–64** crystallizes in its oxidized state, $[(Fe^{3+})_2(^{2-}S)_2(^{-}S-)_4]^{2-}$, and this state has been shown to display electronic, Mössbauer, and nuclear magnetic resonance spectra similar to those of the oxidized form of a dinuclear iron–sulfur cluster in a ferredoxin.[556] Consequently, the biochemical standard reduction potential for a ferredoxin is for the reaction

$$\left[(Fe^{3+})_2(^{2-}S)_2(^{-}S-)_4\right]^{2-} + e^- \rightleftharpoons \left[Fe^{2+}Fe^{3+}(^{2-}S)_2(^{-}S-)_4\right]^{3-} \quad (2\text{–}167)$$

Because the two irons are symmetrically coupled by the bridging sulfides, the odd electron in the reduced state is shared between them equally by occupying a molecular orbital spread symmetrically among the irons and the sulfurs.[557] Because the reduced form of the prosthetic group has an odd number of electrons, it gives an **electron paramagnetic spectrum**. The oxidized form, because it does not display an electron paramagnetic spectrum, must have no unpaired electron spins. The two Fe^{3+}, each formally a species with an odd number of electrons, share the two odd electrons as a pair in the same highest occupied molecular orbital spread over the metallacycle.

The **biochemical standard reduction potentials** of the [2Fe–2S] iron–sulfur clusters in proteins, in which the iron ions are coordinated with only the sulfido groups of cysteines, span a large range (Figure 2–19).[516] The biochemical standard reduction potential of the [2Fe–2S] ferredoxin from *S. oleracea*[558,559] is –420 mV, which is typical of a plant ferredoxin (–450 to –300 mV),[554] while that of bovine [2Fe–2S] ferredoxin is –270 mV, that of the [2Fe–2S] ferredoxin from the bacterium *P. putida*[554] is –230 mV, and that of the [2Fe–2S] ferredoxin from the bacterium *Anabaena*[560] is –180 mV. The biochemical standard reduction potential of one of the [2Fe–2S] iron–sulfur clusters in NADH:ubiquinone reductase (H^+-translocating) is –370 mV, matching it with that of the adjacent flavin ($E^{\circ\prime}_{ox/rad} = -390$ mV),[561,562] but that of the [2Fe–2S] iron–sulfur cluster in succinate dehydrogenase is +10 mV,[563] matching it with that of the redox couple of fumarate and succinate (+30 mV). These differences in standard reduction potential result in part from differences in the number, position, and orientation of several dipoles in the protein surrounding each of these clusters.

In **crystallographic molecular models** of [2Fe–2S] ferredoxins, six or seven amido nitrogen–hydrogen bonds from the polypeptide backbone are pointed at the various sulfurs around the two irons (Figure 2–18).[554,555,560,564,565] The nitrogens in these nitrogen–hydrogen bonds are 0.31–0.37 nm from the sulfurs at which they are pointed. The dipole moment of an *N*-alkylamide is parallel to its nitrogen–hydrogen bond, so this arrangement points the positive poles of the dipoles of these six or seven amido groups at the iron–sulfur cluster and should increase its standard reduction potential. When an alanine in the [2Fe–2S] ferredoxin from *Anabaena* is mutated to serine, putting the even weaker dipole of an alcohol next to the iron–sulfur cluster in addition to all the usual amido groups, its standard reduction potential increased by 24 mV.[566] The standard reduction potential for model compound **2–64**, the [2Fe–2S] iron–sulfur cluster of which is structurally identical to that in a ferredoxin, is –1250 mV in *N,N*-dimethylformamide,[556] a solvent that lacks nitrogen–hydrogen bonds, and it is thought that the **oriented dipoles of the nitrogen–hydrogen bonds** from the polypeptide backbone of the protein are responsible for raising the biochemical standard reduction potential of the iron–sulfur cluster into the range of –450 to –170 mV seen in the ferredoxins.

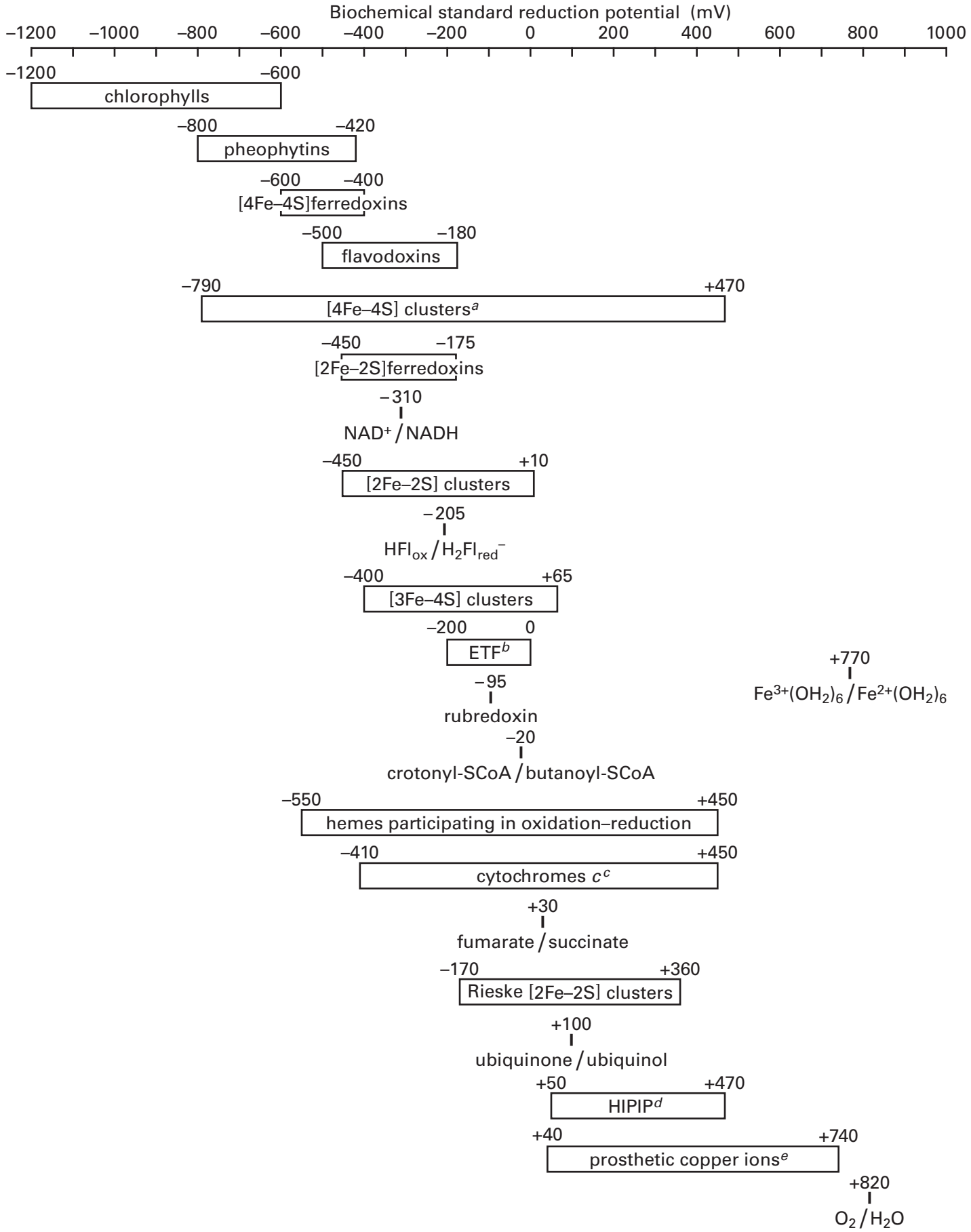
Biochemical standard reduction potential (mV)
–1200 –1000 –800 –600 –400 –200 0 200 400 600 800 1000
–1200 –600
chlorophylls
–800 –420
pheophytins
–600 –400
[4Fe–4S]ferredoxins
–500 –180
flavodoxins
–790 +470
[4Fe–4S] clusters[a]
–450 –175
[2Fe–2S]ferredoxins
–310
NAD+ / NADH
–450 +10
[2Fe–2S] clusters
–205
HFlox / H2Flred–
–400 +65
[3Fe–4S] clusters
–200 0
ETF[b]
–95
rubredoxin
–20
crotonyl-SCoA / butanoyl-SCoA
–550 +450
hemes participating in oxidation–reduction
–410 +450
cytochromes c[c]
+30
fumarate / succinate
–170 +360
Rieske [2Fe–2S] clusters
+100
ubiquinone / ubiquinol
+50 +470
HIPIP[d]
+40 +740
prosthetic copper ions[e]
+820
O2 / H2O
+770
Fe3+(OH2)6 / Fe2+(OH2)6

Figure 2–19: Ranges of the biochemical standard reduction potentials (millivolts) for prosthetic groups and small electron-transferring coenzymes of one-electron transfer. The ranges cited and referenced in the text are presented graphically. The biochemical standard reduction potentials for several redox couples of substrates or coenzymes of central importance in biochemical oxidation–reductions are also presented as individual points on the graph. [a]Biochemical standard reduction potential for reaction of Equation 2–169. [b]Electron-transferring flavoprotein. [c]Span of all small electron-transferring coenzymes containing exclusively one or more hemes *c*. [d]High-potential iron–sulfur protein. [e]Span of biochemical standard reduction potentials for prosthetic copper ions in small electron-transferring coenzymes and enzymes of oxidation–reduction.[516]

There are a number of variations on the ligands attaching a [2Fe–2S] iron–sulfur cluster to the protein surrounding the cluster.[567] One of the sulfido groups of a cysteine can be substituted with the imidazolyl group of a histidine,[568] or the sulfido groups of two of the cysteines can be replaced with the imidazolyl groups of two histidines. An example of the latter type of substitution would be a **Rieske [2Fe–2S] iron–sulfur cluster, in which there are two histidines as ligands to one of the irons instead of two cysteines** (Figure 2–20)[569-571] A substitution of the sulfido group of a cysteine by the imidazolyl group of a histidine increases the biochemical standard reduction potential of a [2Fe–2S] iron–sulfur cluster. The substitution of two cysteines by histidines increases the biochemical standard reduction potential even more than the substitution of only one cysteine.[567] There are also [2Fe–2S] iron–sulfur clusters in which one of the cysteines is substituted by an arginine,[572] which causes a decrease in the biochemical standard reduction potential.[567]

Because an imidazolyl group, when it is a ligand to an iron ion, uses the σ lone pair on only one of its nitrogens to coordinate the iron (Figure 2–20), the other σ lone pair on the other nitrogen is available for hydronation. This availability causes the midpoint reduction potential of these [2Fe–2S] iron–sulfur clusters to become **pH-dependent**. For the Rieske [2Fe–2S] iron–sulfur clusters in their oxidized, $[(Fe^{3+})_2(^{2-}S)_2(^{-}S-)_2(\text{imidazol-4-yl})_2]^0$ state, the conjugate acids of the respective nitrogens that are opposite each of the two nitrogens bound by the iron have acid dissociation constants with values of pK_a between 7 and 12, depending on the protein.[573] Reduction of the iron–sulfur cluster by one electron increases the values of pK_a by 2–5 units as expected from the increase in electron density, and dissociation of the two hydrons from these two available nitrogens decreases the biochemical standard reduction potential by 300–500 mV. For example, for the Rieske iron–sulfur cluster in quinol—cytochrome-*c* reductase from *R. sphaeroides*, the difference in biochemical standard reduction potential between the iron–sulfur cluster hydronated at both available nitrogens and the unhydronated iron–sulfur cluster is –440 mV. The first macroscopic pK_a is 7.6 for the oxidized iron–sulfur cluster and the second is 9.6 while the first macroscopic pK_a for the reduced iron–sulfur cluster is 12.4 and the second is also 12.4. By the use of nuclear magnetic resonance spectroscopy, it was possible to assign each of these values of pK_a to the individual histidines in the Rieske iron–sulfur cluster in quinol—cytochrome-*c* reductase from *T. thermophilus*.[574]

When both of the nitrogens are unhydronated, so the iron is coordinated by two imidazolates, the biochemical standard reduction potentials of Rieske [2Fe–2S] iron–sulfur clusters are between –450 and –100 mV, similar to those of [2Fe–2S] iron–sulfur clusters in which both irons are coordinated by sulfido groups. At neutral pH, however, when both imidazolyl groups are usually hydronated and formally neutral ligands, the biochemical standard reduction potentials are between –170 and +360 mV (Figure 2–19).[575-581] Consequently, the **hydronation of the available nitrogens on the histidines at neutral pH is responsible for the high** biochemical standard reduction potential**s** achieved by Rieske [2Fe–2S] iron–sulfur clusters. When the imidazolyl groups are hydronated and neutral, they donate less electron density than a sulfido group would, so the biochemical standard reduction potentials of hydronated Rieske [2Fe–2S] iron–sulfur clusters are much higher than those of [2Fe–2S] iron–sulfur clusters in which all the ligands are sulfido groups of cysteines. These high biochemical standard reduction potentials permit Rieske [2Fe–2S] iron–sulfur clusters to fulfill their assigned roles in electron transfer. The unusually high biochemical standard reduction potentials of some of these Rieske [2Fe–2S] iron–sulfur clusters permit a second electron to be added to them in a reduction that produces the diferrous $[(Fe^{2+})_2(^{2-}S)_2(^{-}S-)_2(\text{imidazol-4-yl})_2]^0$ state.[579]

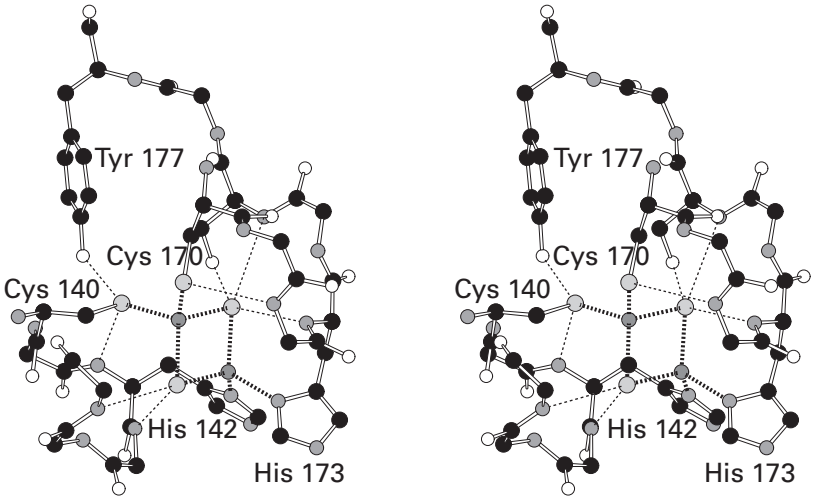

Figure 2–20: Stereodrawing[50] from a portion of the crystallographic molecular model of the domain of the [2Fe–2S] Rieske protein from *S. acidocaldarius* that contains its iron–sulfur cluster.[569] Black atoms are carbons, white atoms are oxygens, small gray atoms are nitrogens, and large light gray atoms are sulfurs. In the iron–sulfur cluster, large light gray spheres are sulfides and small dark gray spheres are iron ions. The complementary DNA for this domain, which comprises the sequence of amino acids for the full protein from Alanine 47 to Glycine 250, was expressed heterologously in *E. coli*. Serendipitously, during its expression the [2Fe–2S] Rieske iron–sulfur cluster was properly inserted. The resulting domain, with the intact iron–sulfur cluster, was purified and crystallized. A crystallographic molecular model was built from a map of electron density that was calculated from a data set to Bragg spacing of 0.111 nm. The [2Fe–2S] Rieske iron–sulfur cluster in the protein is just below the center of the drawing. The numbering of the amino acids in the sequence is that of the intact protein. The segment of the polypeptide in the crystallographic molecular model from Cysteine 140 to Cysteine 145 winds around the cluster below and to its left. Cysteine 140 and Histidine 142 form bonds to the left side of the upper iron ion and the back of the lower iron ion, respectively. The segment of the polypeptide from Cysteine 170 to Tyrosine 177 winds around the cluster above and to its right. Cysteine 170 and Histidine 173 form bonds to the forward side of the upper iron ion and the right side of the lower iron ion, respectively. The amido nitrogen–hydrogens of Histidine 142, Leucine 143, Cysteine 145, Cysteine 172, Histidine 173, Serine 175, and Tyrosine 177 in the respective peptide bonds of the polypeptide provide dipoles each directed toward a sulfide or the sulfido group of a cysteine in the iron–sulfur cluster. The 4-hydroxy group of Tyrosine 177 and the hydroxy group of Serine 175 also provide dipoles directed toward the sulfido group of Cysteine 140 and a sulfide in the iron–sulfur cluster, respectively. Each of these dipoles is connected to the sulfur to which it is directed by a dotted line. Only the side chains of the two cysteines and the two histidines forming bonds with the iron ions and the side chains of the tyrosine and the serine providing dipoles to the sulfurs are drawn.

Unlike in the case of the Rieske [2Fe–2S] iron–sulfur clusters, the biochemical standard reduction potential of a [2Fe–2S] iron–sulfur cluster in which only one of the cysteines has been replaced by a histidine is pH-dependent at lower ranges of pH. In the midrange of pH, the slope of the function defining the variation in biochemical standard reduction potential as a function of pH is –50 mV (unit of pH)$^{-1}$ for an [2Fe–2S] iron–sulfur cluster in which only one of the cysteines has been replaced by a histidine.[582] For Rieske [2Fe–2S] iron–sulfur clusters in which two of the cysteines have been replaced by histidines, the slopes of the biochemical standard reduction potential as a function of pH in the alkaline regions are –110 mV (unit of pH)$^{-1}$.[573] These slopes are those expected if, for the former iron–sulfur cluster with only one imidazolyl group as a ligand, one hydron is taken up by the single available σ lone pair on the imidazolyl group for every electron added; and for the Rieske iron–sulfur clusters, two hydrons are taken up for every electron added by the two available σ lone pairs, one on each imidazolyl group.

A model compound for those [2Fe–2S] iron–sulfur clusters in which only one of the sulfido groups is replaced by an imidazolyl group[583] and model compounds for Rieske [2Fe–2S] iron–sulfur clusters in which two of the sulfanyl groups are replaced by imidazolyl groups[584] have been synthesized. In these synthetic model compounds, each sulfido group is a sulfidophenyl group and each imidazolyl group is a benzimidazolyl group. These model compounds also display values of pK_a that shift upon oxidation or reduction and reduction potentials that shift upon hydronation of the imidazolyl groups. For example, in the model compound for the [2Fe–2S] iron–sulfur cluster in which one of the four sulfidophenyl groups is replaced by a benzimidazolyl group, the reduction potential in acetonitrile increases by 240 mV when the distal nitrogen of the benzimidazolyl group is hydronated.[583]

The **structure of a Rieske [2Fe–2S] iron–sulfur cluster** is almost identical to that of a [2Fe–2S] iron–sulfur cluster in which all four ligands to the iron are sulfido groups of cysteines. The iron–sulfur bond lengths are 0.225 ± 0.002 nm, the S–Fe–S bond angles are 106°, and the Fe–S–Fe bond angles are 74° in crystallographic molecular models in which the iron–sulfur cluster was unconstrained during refinement.[569,585]

From three to seven amido nitrogen–hydrogen bonds from the polypeptide backbone are directed toward sulfurs of a Rieske [2Fe–2S]iron–sulfur cluster (Figure 2–20), with their nitrogens 0.31–0.37 nm from those sulfurs.[569,585-587] The dipoles of the hydroxy groups of a tyrosine and a serine are also directed toward sulfurs in several of these iron–sulfur clusters (Figure 2–20). When the tyrosine is mutated to a phenylalanine, the biochemical standard reduction potential decreases by –50 to –60 mV,[576-578] and mutation of the serine decreases the biochemical standard reduction potential potential by –100 to –130 mV.[576,577] The biochemical standard reduction potentials of these Rieske [2Fe–2S] iron–sulfur clusters are linearly related to the number of amido dipoles directed toward the iron–sulfur cluster, with a slope of around +70 mV dipole^{-1}.[585] Thus the wide range in standard reduction potential seen with Rieske [2Fe–2S] iron–sulfur clusters results, in part, from the wide range in the number of dipoles directed by the protein so that their positive poles are toward the iron–sulfur cluster.

Tetranuclear [4Fe–4S] iron–sulfur clusters have three positions occupied by bridging sulfides around each iron ion (Figure 2–21).[588] Each iron ion also is coordinated to the sulfido group of a cysteine from the protein to complete its tetrahedral coordination. There is a synthetic model compound for a [4Fe–4S] iron–sulfur cluster, in which the four positions that would be occupied by the sulfido groups of cysteines in a protein are occupied by phenylmethanethiolates[589]

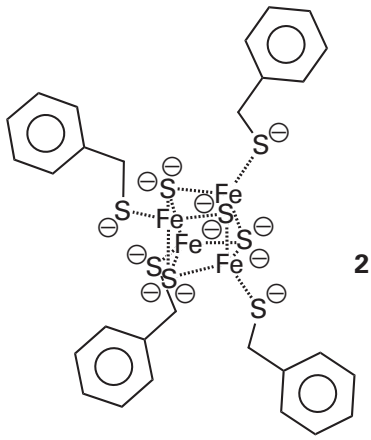

2–65

This synthetic [4Fe–4S] iron–sulfur cluster is indistinguishable within its crystallographic molecular model of high accuracy from the [4Fe–4S] iron–sulfur clusters found in crystallographic molecular models of ferredoxins from data sets with Bragg spacing less than 0.1 nm and in which the atoms of

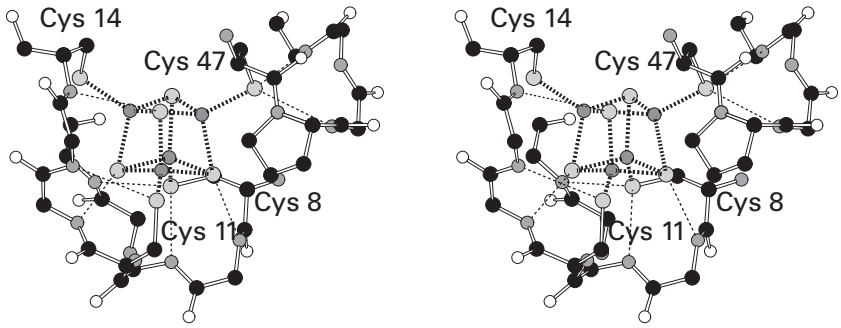

Figure 2–21: Stereodrawing[50] from a portion of the crystallographic molecular model of the ferredoxin (55 aa) from *Clostridium acidurici* that contains two [4Fe–4S] iron–sulfur clusters.[588] Black atoms are carbons, white atoms are oxygens, small gray atoms are nitrogens, and large light gray atoms are sulfurs. In the iron–sulfur cluster, large light gray spheres are sulfides and small dark gray spheres are iron ions. The molecular model was built from a map of electron density that was calculated from a data set to Bragg spacing of 0.094 nm. One of the two [4Fe–4S] iron–sulfur clusters in the protein is in the center of the drawing. The segment of the polypeptide in the crystallographic molecular model from Cysteine 8 to Cysteine 14 winds around the cluster both below and to its left. The sulfido groups of Cysteine 8, Cysteine 11, and Cysteine 14 form bonds to irons in the back, in the front, and to the left side of the iron–sulfur cluster, respectively. The segment of the polypeptide from Cysteine 47 to Alanine 51 is in the upper right corner of the cluster. Cysteine 47 forms a bond to the iron ion on the right side of the cluster. The amido nitrogen–hydrogens of Isoleucine 9, Serine 10, Glycine 12, Alanine 13, Cysteine 14, Valine 49, and Alanine 51 in the respective peptide bonds of the polypeptide provide dipoles each directed toward a sulfide or the sulfur of a cysteine in the iron–sulfur cluster. The amido nitrogen–hydrogen of Tyro-sine 30 in its peptide bond also provides a dipole directed toward the sulfur of Cysteine 8 in the iron–sulfur cluster. Each of these dipoles is connected to the sulfur to which it is directed by a dotted line. Only the side chains of the four cysteines forming bonds with the iron ions are drawn.

the iron–sulfur cluster were unconstrained during refinement (Figure 2-21).[588,590] The iron ions again occupy vertices with wider angles (104 ± 2° in both the model compound and the ferredoxins) than the vertices occupied by the sulfurs of the bridging sulfides (74 ± 2° in both the model compound and the ferredoxins). Again the impression is left that the cluster is a rigid structure.

These bond angles at the irons and the sulfurs are the same as those of a [2Fe–2S] iron–sulfur cluster. In fact, a [4Fe–4S] iron–sulfur cluster seems to be two [2Fe–2S] iron–sulfur clusters that have been stuck together. Two cysteines on the same face of each of the constituent [2Fe–2S] iron–sulfur clusters have been replaced by the two sulfides of the other. This impression is reinforced by the fact that, in [4Fe–4S] iron–sulfur clusters, in both the model compound **2–65**[589] and ferredoxins,[588,590] four of the iron–sulfur bonds that are parallel to each other and that connect two of the rhomboidal faces (the four horizontal bonds most parallel to the plane of the page in Figure 2–21) are shorter (0.224 nm in the model compound and 0.226 nm in the ferredoxins) than the other eight (0.231 nm in the model compound and 0.230 nm in the ferredoxins). This fact sets two of the faces across from each other in the iron–sulfur cluster apart from the other four and breaks the tetrahedral symmetry of the iron–sulfur cluster. Because it is observed in both the model compound and the proteins, this compression appears to be intrinsic to the structure.

As was the case with the [2Fe–2S] iron–sulfur clusters, there are **variations in the ligands attaching a [4Fe–4S] iron–sulfur cluster to the protein** forming an active site.[567] One of the sulfido groups of a cysteine can be substituted by the imidazolyl group of a histidine,[591,592] or the carboxylato group of an aspartate.[593] A substitution of the anionic sulfido group of a cysteine by the neutral imidazolyl group of a histidine again increases the biochemical standard reduction potential of a [4Fe–4S] iron–sulfur cluster. The midpoint reduction potential in tetrahydrofuran for a synthetic [4Fe–4S] iron–sulfur cluster increases by +340 mV when one of the four sulfido groups coordinating the cluster is replaced by 1,2,4,5-tetramethylimidazole.[594] The substitution of an anionic sulfido group by an anionic carboxylato group, however, has no consistent effect on the biochemical standard reduction potential.[567] Although almost all [4Fe–4S] iron–sulfur clusters are attached through their four iron ions to four ligands provided by the protein (Figure 2–21), there are instances in which a [4Fe–4S] iron–sulfur cluster is attached by only three cysteines, leaving one iron open for ligation,[595] or in which one of the irons expands its coordination to form a bond to an additional cysteine.[596,597]

Because there twice as many iron ions in a [4Fe–4S] iron–sulfur cluster, its successive, one-electron biochemical standard reduction potentials are fairly close to each other.[589,598] The **three biochemically accessible oxidation–reductions** are

$$\left[Fe^{2+}(Fe^{3+})_3(^{2-}S)_4(^{-}S-)_4\right]^{-} + e^{-} \rightleftharpoons \left[(Fe^{2+})_2(Fe^{3+})_2(^{2-}S)_4(^{-}S-)_4\right]^{2-} \quad (2\text{–}168)$$

$$\left[(Fe^{2+})_2(Fe^{3+})_2(^{2-}S)_4(^{-}S-)_4\right]^{2-} + e^{-} \rightleftharpoons \left[(Fe^{2+})_3Fe^{3+}(^{2-}S)_4(^{-}S-)_4\right]^{3-} \quad (2\text{–}169)$$

$$\left[(Fe^{2+})_3Fe^{3+}(^{2-}S)_4(^{-}S-)_4\right]^{3-} + e^{-} \rightleftharpoons \left[(Fe^{2+})_4(^{2-}S)_4(^{-}S-)_4\right]^{4-} \quad (2\text{–}170)$$

There has yet, however, to be a documented instance in which more than one of these redox couples is accessible for any particular protein containing a [4Fe–4S] iron–sulfur cluster. Instead, natural selection seems to have designed the environment around a given [4Fe–4S] iron–sulfur cluster to participate in only one specific oxidation–reduction that either requires the higher biochemical standard reduction potential of Equation 2–168 or the lower biochemical standard reduction potential of Equation 2–169. The diamagnetic, completely reduced and significantly anionic iron–sulfur cluster $[(Fe^{2+})_4(^{2-}S)_4(^{-}S-)_4]^{4-}$ of Equation 2–170 has been observed so far in only one protein, in which it is used as a strong two-electron reductant.[599,600] A [4Fe–4S] iron–sulfur cluster that is stable in this fully reduced form has been synthesized, but it was necessary to use four carbenes as the external ligands to the four iron ions rather than four thiolates. This synthetic cluster has a midpoint potential of –1300 mV in tetrahydrofuran.[601]

The diamagnetic species $[(Fe^{2+})_2(Fe^{3+})_2(^{2-}S)_4(^{-}S-)_4]^{2-}$ has an even number of electrons, and all are paired. This species lacks an electron paramagnetic resonance absorption. All the irons are coupled, so several electron pairs are delocalized among them by occupying molecular orbitals spread over the

entire iron–sulfur cluster. If one electron is removed from the highest occupied molecular orbital of these extended, pairwise occupied molecular orbitals (reverse of Equation 2–168) or one electron is added to the lowest unoccupied extended molecular orbital (Equation 2–169), each of the two species formed has an unpaired electron and each is paramagnetic and has a characteristic **electron paramagnetic resonance** absorption.[602] In the reduced species $[(Fe^{2+})_3Fe^{3+}(^{2-}S)_4(^{-}S-)_4]^{3-}$ in a protein, two of the irons are a diferrous pair, and the other two share the unpaired electron that is delocalized over them.[603,604]

The tetranuclear [4Fe–4S] iron–sulfur clusters in proteins that normally participate as the redox couple in Equation 2–168 are referred to as **high-potential [4Fe–4S] iron–sulfur clusters**. The biochemical standard reduction potentials for these iron–sulfur clusters usually lie between +50 and +470 mV (Figure 2–19).[605-607] The iron–sulfur cluster in the high-potential iron–sulfur protein from *Allochromatium vinosum*, for example, has a biochemical standard reduction potential for Equation 2–168 of +350 mV. High-potential [4Fe–4S] iron–sulfur clusters are also found in enzymes such as benzylsuccinate synthase from *Thauera aromatica*.[608] This latter high-potential [4Fe–4S] iron–sulfur cluster has a biochemical standard reduction potential of +80 mV. There is a high-potential [4Fe–4S] iron–sulfur cluster in ferredoxin:thioredoxin reductase from *Synechocystis* in which one of the iron ions has the sulfido groups of two cysteines as ligands in the oxidized $[Fe^{2+}(Fe^{3+})_3(^{2-}S)_4(^{-}S-)_5]^{2-}$ state.[609] Upon reduction of the [4Fe–4S] iron–sulfur cluster with one electron, one of these two sulfido groups is released from the iron and displaces reduced thioredoxin from a mixed disulfide between one of its cysteines and another cysteine in the active site by thiol–disulfide exchange. Consequently, one of the sulfido groups coordinating the [4Fe–4S] iron–sulfur cluster reduces the disulfide between another cysteine in the enzyme and one of the cysteines of the thioredoxin.

The [4Fe–4S] iron–sulfur clusters in proteins that normally participate in Equation 2–169 are **low-potential [4Fe–4S] iron–sulfur clusters.** The biochemical standard reduction potentials for these low-potential iron–sulfur clusters usually lie between –790 and +80 mV (Figure 2–19).[562,605,607,610] For example, both of the [4Fe–4S] iron–sulfur clusters (Figure 2–21) in the ferredoxin from *C. acidurici* have a biochemical standard reduction potential of –430 mV, and each is reduced independently of the other.[611] 2-Deoxy-*scyllo*-inosamine dehydrogenase (AdoMet-dependent) from *Niallia circulans* contains a [4Fe–4S] iron–sulfur cluster,[612] attached to the protein by four cysteines, that has a biochemical standard reduction potential of –765 mV.

The distinction between high-potential and low-potential [4Fe–4S] iron–sulfur clusters is the redox couple, either that of Equation 2–168 or that of Equation 2–169, that is accessible to the members of each group. Although each [4Fe–4S] iron–sulfur cluster in a particular protein is confined to only one of these two common redox couples, the fact that one or the other redox couple is nevertheless available to natural selection is what causes the whole family of [4Fe–4S] iron–sulfur clusters to be able to span the largest range of biochemical standard reduction potentials among the families of one-electron prosthetic groups (Figure 2–19).

The biochemical standard reduction potential for the low-potential oxidation–reduction (Equation 2–169) of a synthetic [4Fe–4S] iron–sulfur cluster similar to **2–65** but with four *N*-(acetyl)-L-cysteine methyl esters rather than benzylthiols as ligands is –740 mV when it is dissolved in dimethyl sulfoxide.[613] In water, the biochemical standard reduction potential is –490 mV. The L-cysteine methyl esters make this model compound as similar as possible to a [4Fe–4S] iron–sulfur cluster in a protein. Because this synthetic [4Fe–4S] iron–sulfur cluster becomes more anionic upon reduction (Equation 2–169), the improved solvation provided by the water for the trianion $[(Fe^{2+})_3Fe^{3+}(^{2-}S)_4(^{-}S-)_4]^{3-}$ relative to the dianion $[(Fe^{2+})_2(Fe^{3+})_2(^{2-}S)_4(^{-}S-)_4]^{2-}$ explains the observed increase in standard reduction potential. Because the reduced synthetic iron–sulfur cluster with the four *N*-acetyl-L-cysteine methyl esters is so anionic, the positive poles of the dipoles of the molecules of water surrounding it will be oriented toward the cluster, just as nitrogen–hydrogen bonds of the polypeptide backbone surrounding a [4Fe–4S] iron–sulfur cluster in a protein direct the dipoles of their amido groups toward the cluster (Figure 2–21). The fact that there are dipoles oriented toward the [4Fe–4S] iron–sulfur cluster in both situations explains in part why the standard reduction potentials for the synthetic iron–sulfur cluster in water and the natural iron–sulfur cluster in a ferredoxin are so similar.

[4Fe–4S] Ferredoxins are low-potential iron–sulfur proteins that function as electron-transferring coenzymes. The range (Figure 2–19) over which the biochemical standard reduction potentials of the various [4Fe–4S] ferredoxins are spread, –400 to –600 mV,[607] is somewhat puzzling because the

number of directed amido dipoles around the iron–sulfur clusters in most [4Fe–4S] ferredoxins is usually eight (Figure 2–21).[588,590,614] The differences in biochemical standard reduction potential may be due to variation in the distances between the oriented dipoles and the [4Fe–4S] iron–sulfur cluster[615] and variation in the **exposure of the [4Fe–4S] iron–sulfur cluster to the aqueous solvent**.[614,616] The oriented amido dipoles in these proteins increase the biochemical standard reduction potential for the redox couple of Equation 2–169 into the accessible range, and they increase the biochemical standard reduction potential for the redox couple of Equation 2–168 out of the accessible range.

The iron protein from nitrogenase contains the only [4Fe–4S] iron–sulfur cluster that participates in the **lowest-potential oxidation–reduction** (Equation 2–170), which requires that the biochemical standard reduction potentials for its [4Fe–4S] iron–sulfur cluster be increased considerably more than they normally are to bring this redox couple into the accessible range. This iron–sulfur cluster not only is surrounded by 10 oriented amido groups from the polypeptide backbone but also is the most exposed to the aqueous phase of any [4Fe–4S] iron–sulfur cluster for which a crystallographic molecular model is available.[617]

High-potential iron–sulfur proteins (HIPIP) are also electron-transferring coenzymes. The [4Fe–4S] iron–sulfur clusters in these proteins are confined by their surroundings to participate in the high-potential oxidation–reduction of Equation 2–168. They have significantly fewer oriented amido groups from the polypeptide surrounding an otherwise identical iron–sulfur cluster than in the case of the ferredoxins, usually only four or five,[607,614,618,619] and the dipoles that are present can account for the observed biochemical standard reduction potential.[616] The environment around the iron–sulfur cluster is also "decidedly hydrophobic."[620] The fact that there are fewer directed dipoles and the fact that the environment is considerably more nonpolar in these high-potential iron–sulfur proteins are the reasons that the biochemical standard reduction potentials for the high-potential oxidation–reduction of Equation 2–168 remain in an accessible range (+100 to +470 mV) and the reasons that the biochemical standard reduction potentials for the low-potential oxidation–reduction of Equation 2–169 remain in an inaccessible range.[605] When one of the oriented amido nitrogen–hydrogens in a high-potential iron–sulfur protein is mutated to an oxygen, the biochemical standard reduction potential decreases by 100 mV,[607] an observation indicating how dramatic an effect these dipoles have, but there are high-potential iron–sulfur proteins that have the same number of oriented dipoles surrounding the iron–sulfur cluster yet differ in biochemical standard reduction potential by as much as 240 mV.[618] Again, these differences may result from differences in the distances between the oriented dipoles and the [4Fe–4S] iron–sulfur cluster and from differences in the exposure of the iron–sulfur cluster to the aqueous phase.

There are **outer-sphere influences other than oriented nitrogen–hydrogen bonds** on the reduction potential of a [4Fe–4S] iron–sulfur cluster. For example, one of the [4Fe–4S] iron–sulfur clusters in hydrogenase (acceptor) from *E. coli* has the imidazolyl group of a histidine instead of the sulfido group of a cysteine as a ligand to one of the iron ions. The π molecular orbital system of the guanidinio group of an arginine is stacked against the imidazolyl group.[592] When this arginine is mutated to a leucine, the reduction potential of the [4Fe–4S] iron–sulfur cluster decreases by 60 mV, as expected for the mutation of a positively charged side chain to a neutral side chain.[621]

Trinuclear **[3Fe–4S] iron–sulfur clusters**, containing three atoms of iron

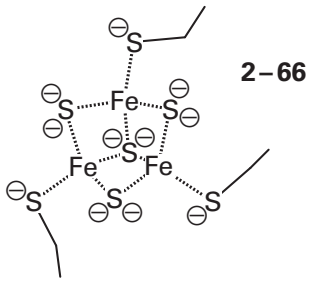

2–66

are [4Fe–4S] iron–sulfur clusters in which one of the four irons has dissociated from the iron–sulfur cluster because a cysteine from the protein that would normally form a strong bond with this iron is either absent or unable to do so.[622-624] In situations in which a naturally occurring [4Fe–4S] iron–sulfur cluster has lost an iron ion during purification or other manipulations of the protein, its trinuclear [3Fe–4S] iron–sulfur cluster can be often be converted back into a [4Fe–4S] iron–sulfur cluster by adding Fe^{2+}.[625,626] These [3Fe–4S] iron–sulfur clusters are adventitious. There are, however, a number of permanently trinuclear [3Fe–4S] clusters that are both natural and essential prosthetic groups.[627-631] Nevertheless, in these instances, the mutation to a cysteine of an amino acid adjacent to the vacant

position in the iron–sulfur cluster can convert the natural [3Fe–4S] iron–sulfur cluster to an unnatural [4Fe–4S] iron–sulfur cluster.[628,632] It is also possible to mutate a cysteine ligating one of the iron ions in a natural [4Fe–4S] iron–sulfur cluster and convert it into an unnatural [3Fe–4S] iron–sulfur cluster.[633]

In **crystallographic molecular models** of a ferredoxin that naturally contains a [3Fe–4S] iron–sulfur cluster[634] and in a model compound of a [3Fe–4S] iron–sulfur cluster,[635] the iron–sulfur bond lengths are 0.227 ± 0.002 and 0.2286 ± 0.0003 nm, respectively, which are indistinguishable from each other and from those in a [4Fe–4S] iron–sulfur cluster. The bond angles within the three intact rhombi are 104° at the three irons and 73° at the four sulfurs in crystallographic molecular models of both the ferredoxin and the model compound, also indistinguishable from those in a [4Fe–4S] iron–sulfur cluster. The three rhombi that are not held together at their vertices by a fourth iron atom open up slightly so that the three S–Fe–S bond angles outside the three intact rhombi (**2–66**) are 112° instead of 104°.

In its most oxidized state, a trinuclear [3Fe–4S] iron–sulfur cluster has an unpaired electron because it contains three Fe^{3+} atoms, each with an odd number of electrons, but pairs of electrons from every other substituent. At pH 7, the **biochemical standard reduction potential**[636,637] for the trinuclear [3Fe–4S] iron–sulfur cluster in the ferredoxin from *A. vinelandii* is –400 mV. The oxidized form displays an absorption in electron paramagnetic resonance but the reduced form does not,[638] so the reduced form must have no unpaired electrons. Therefore, the formal reaction in which this iron–sulfur cluster participates is

$$\left[(Fe^{3+})_3(^{2-}S)_4(^{-}S-)_3\right]^{2-} + e^- \rightleftharpoons \left[Fe^{2+}(Fe^{3+})_2(^{2-}S)_4(^{-}S-)_3\right]^{3-} \quad (2\text{–}171)$$

There is spectral evidence that the pair of electrons formed upon addition of one electron to the [3Fe–4S] iron–sulfur cluster (Equation 2–171) is distributed over only two of the three iron ions,[639] a fact which suggests that one of the irons is actually an unconjugated Fe^{2+} and the other two form a conjugated pair of Fe^{3+} ions. In this reduction, one hydron is taken up by the ferredoxin from *Sulfolobus acidocaldarius* at pH 7,[640] and for the ferredoxin from *A. vinelandii*, one hydron is also taken up but only at values of pH less than 6.[637]

The biochemical standard reduction potentials for [3Fe–4S] iron–sulfur clusters in proteins are between –400 and +65 mV (Figure 2–19).[630,640] Those for just the [3Fe–4S] ferredoxins are between –400 and –140 mV. The [3Fe–4S] iron–sulfur clusters in crystallographic molecular models of two different ferredoxins, the one from *A. vinelandii*[634] and the one from *Desulfovibrio gigas*,[641] have six and eight amido nitrogen–hydrogens directed toward their sulfurs, respectively, which explains in part why the former has a more negative biochemical standard reduction potential than the latter by –290 mV. Trinuclear [3Fe–4S] iron–sulfur clusters in ferredoxins can also engage in a further two-electron reduction[640]

$$\left[Fe^{2+}(Fe^{3+})_2(^{2-}S)_4(^{-}S-)_3\right]^{3-} + 2\,e^- \rightleftharpoons \left[(Fe^{2+})_3(^{2-}S)_4(^{-}S-)_3\right]^{5-} \quad (2\text{–}172)$$

in which two hydrons are taken up by the protein at pH 7 to neutralize the large increase in charge.

In the active site of ferredoxin:CoB-CoM heterodisulfide reductase from *Methanothermococcus thermolithotrophicus*, there are two identical **[3Fe–3S–Fe–S] iron–sulfur clusters** that can be considered the fusion of a [3Fe–4S] iron–sulfur cluster and a [2Fe–2S] iron–sulfur cluster[642]

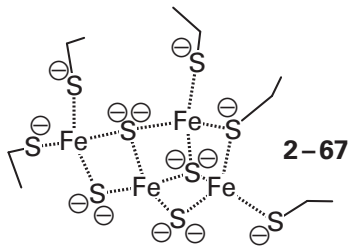

2–67

One of the sulfides in the [3Fe–4S] iron–sulfur cluster (**2–66**) that is the ligand to only two of the iron ions in that cluster and one of the iron ions that the sulfide coordinates are also a sulfide and an iron ion, respectively, in the [2Fe–2S] iron–sulfur cluster. One of the open sulfides in the [3Fe–4S] iron–sulfur cluster has been replaced by the sulfido group of a cysteine, and the open iron ion in the [2Fe–2S] iron–sulfur cluster is coordinated by two sulfido groups from two cysteines, as usual. In the homologous*

*Although the sequences do not align with a significant percentage of identity, every one of the cysteines in the two clusters occupies the same positions in the aligned sequences.

dihydromethanophenazine: CoB-CoM heterodisulfide reductase from *Methanosarcina thermophila*, the reduction potentials[643] of the two clusters are –100 and –400 mV, within the range of both [3Fe–4S] and [2Fe–2S] iron–sulfur clusters (Figure 2–19). The reduced form of each of the iron–sulfur clusters has an unpaired electron and their oxidation states have been assigned as $[(Fe^{2+})_3Fe^{3+}(^{2-}S)_4(^{-}S-)_5]^{4-}$. The two [3Fe–3S–Fe–S] iron–sulfur clusters in dihydromethanophenazine: CoB-CoM heterodisulfide reductase from *M. thermophila* were originally mistaken for two [4Fe–4S] iron–sulfur clusters, in which case that assignment would be reasonable (Equation 2–169). It is also possible, however, that the reduced form of a [3Fe–3S–Fe–S] iron–sulfur cluster with an unpaired electron could be $[Fe^{2+}(Fe^{3+})_3(^{2-}S)_4(^{-}S-)_5]^{2-}$ given the usual one-electron reduced states of a [3Fe–4S] iron–sulfur cluster (Equation 2–171) and a [2Fe–2S] iron–sulfur cluster (Equation 2–167).

A **[4Fe–3S] iron–sulfur cluster** has been observed in crystallographic molecular models of the small iron–sulfur subunits of the membrane-bound hydrogenases (acceptor) from *Cupriavidus necator*[644] and *Hydrogenovibrio marinus*.[645] The common structure of these clusters is again a variation on an [4Fe–4S] iron–sulfur cluster but one in which one of the sulfides is missing rather than one of the iron ions. Two of the three iron ions that would otherwise be coordinated by the missing sulfide are coordinated by the same sulfido group of a cysteine, and the third iron that would have been coordinated by the missing sulfide is coordinated by the sulfido group of an additional cysteine. In effect, two sulfido groups replace one bridging sulfide, and this arrangement distorts the cluster in the region where the single missing sulfide would otherwise be forming bonds with these three iron ions. In both of these [4Fe–3S] iron–sulfur clusters, the oxidized state, $[Fe^{2+}(Fe^{3+})_3(^{2-}S)_3(^{-}S-)_6]^{-}$, is accessible, and in the [4Fe–3S] iron–sulfur cluster from *H. marinus* in this oxidized state, a dehydronated nitrogen from a peptide bond in the polypeptide becomes a ligand to one of the irons, presumably to stabilize the oxidized participant in the redox couple, analogous to that in Equation 2–168.

There are several iron–sulfur clusters that have more than four irons and four sulfurs as well as additional transition metal ions such as molybdenum, copper, or nickel.[646] They appear to be expansions of [4Fe–4S] iron–sulfur clusters, just as a [4Fe–4S] iron–sulfur cluster seems to be the expansion of a [2Fe–2S] iron–sulfur cluster. For example, in the [8Fe–7S] P-cluster of nitrogenase[647]

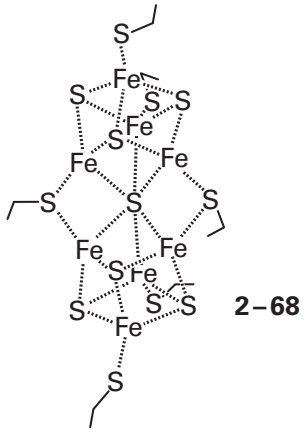

2–68

one of the sulfides of a [4Fe–4S] iron–sulfur cluster coordinates the three iron ions from a [4Fe–3S] iron–sulfur cluster that have open sites for coordination. The FeMo-cofactor of nitrogenase[647] is a [4Fe–3S] iron–sulfur cluster fused by three additional sulfide ions through its three open iron ions to the three open iron ions of a [3Fe–Mo–3S] iron–molybdenum–sulfur cluster, which is a [4Fe–3S] iron–sulfur cluster in which the iron ion in the fully coordinated site has been replaced with a molybdenum ion.

The various types of iron–sulfur clusters can be distinguished spectroscopically to identify the type present in a particular protein. Electron paramagnetic resonance spectra,[581,648] Mössbauer spectra,[649] ultraviolet–visible absorption spectra, and resonance Raman spectra[650] can all distinguish among [4Fe–4S], [3Fe–4S], and [2Fe–2S] iron–sulfur clusters. Electron paramagnetic spectra can also be used to sort out the different iron–sulfur clusters in a protein. For example, five of the individual electron paramagnetic spectra[562] of the seven [4Fe–4S] iron–sulfur clusters and the two [2Fe–2S] iron–sulfur clusters in NADH:ubiquinone reductase (H^+-translocating)[651] can be dissected from electron paramagnetic spectra of the protein taken at different temperatures.

A heme is a visibly colored prosthetic group, always surrounded by protein, that takes on many roles in one-electron transfer. For example, a **cytochrome** is a protein that contains one or more hemes as prosthetic groups and that acts as an electron-transferring coenzyme. Hemes are also prosthetic groups transferring electrons within enzymes responsible for oxidation–reduction.

The parent compound of most of the various hemes is **heme *b***

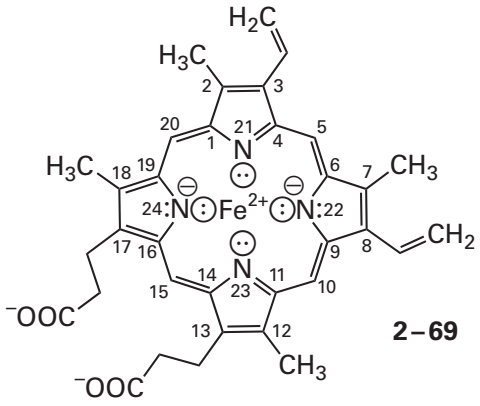

which is the complex between an iron ion and the **porphyrin,** protoporphyrin. Protoporphyrin is derived from uroporphyrinogen III

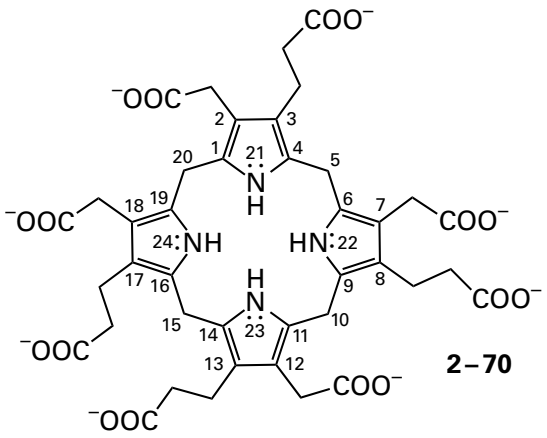

by the decarboxylation of the carboxymethyl groups at positions 2, 7, 12, and 18; the oxidative decarboxylation of the carboxyethyl groups at positions 3 and 8; and oxidation of the central ring coincident with its aromatization. Uroporphyrinogen III is also the precursor to the pheophytins (Equation 2–156) in a series of similar, even more complicated and varied modifications.

As does the magnesium ion in a chlorophyll, the iron ion in the center of a heme replaces two hydrons on the two nitrogens of the porphyrin. Unlike the pheophytins and their respective chlorophylls, however, only the hemes are prosthetic groups, not the respective uncomplexed porphyrins lacking the iron ion. Also, unlike the magnesium ion in a chlorophyll, which is inert to oxidation and reduction in the biochemical range of standard reduction potential, the iron ion in a heme is oxidized or reduced by removing or adding one electron. The iron ion is oxidized to Fe^{3+} or reduced to Fe^{2+}.

There are several **modified versions of heme *b*** that also act as prosthetic groups. Heme *o* is heme *b* in which the ethenyl group at position 3 has been elongated to a 1-hydroxy-5,9,13-trimethyltetradeca-4,8,12-trienyl group (a 1-hydroxyfarnesyl group), which is a long, hydrophobic polyisoprenoid.[652] Heme *a* is heme *o* in which the methyl group at position 18 has been oxidized to a formyl group. Heme *d* is heme *b* in which the double bond at positions 12 and 13 has been oxidized to a trans vicinal diol, a modification that does not affect the aromaticity, and the 2-carboxyethyl group at position 13 has formed a lactone with the hydroxy group now at position 13.[653] Heme d_1

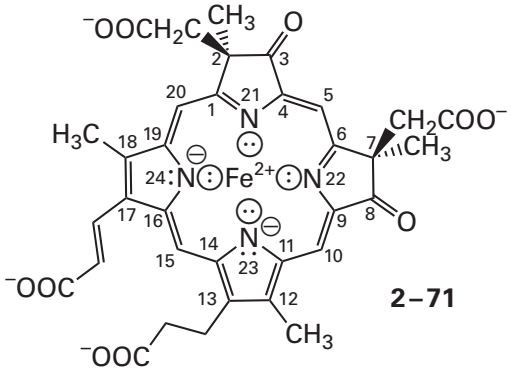

however, is not derived from heme *b* but from uroporphyrinogen III (**2–70**) itself, the common precursor to heme *b* and heme d_1. The carboxyethyl groups at positions 3 and 8 have been oxidized completely to oxo groups while the carbons at the 2 and 7 positions have been methylated with the result that the two respective pyrrolyl groups are no longer unsaturated at positions 2 and 7, and the 2-carboxyethyl group at position 17 has been oxidized to a 2-carboxyethenyl group.[654,655] The unsaturation of the two pyrrolyl groups again does not affect the aromaticity. Siroheme is the complex between an iron ion and a porphyrin which is also a derivative of uroporphyrinogen III (**2–70**), in which the bonds between carbons at positions 2 and 3 and between carbons at positions 7 and 8 are saturated and carbon 2 and carbon 7 are methylated with the same stereochemistry as in heme d_1 (**2–71**).

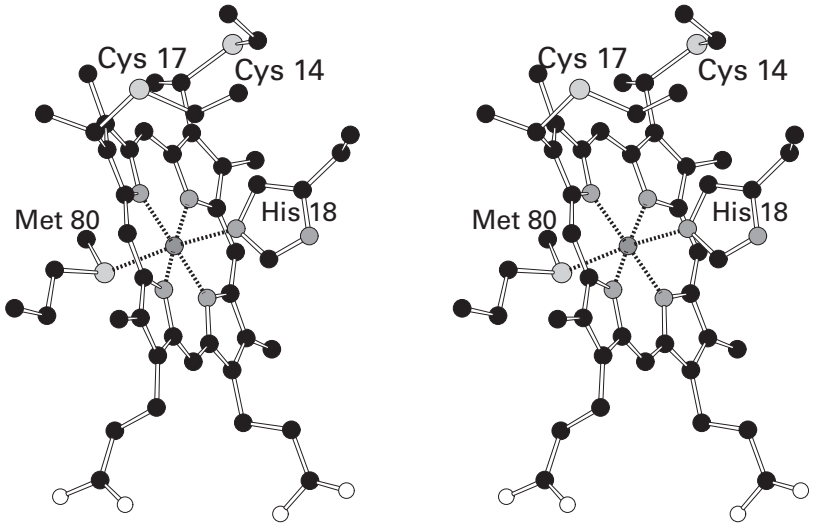

Figure 2–22: Stereodrawing[50] from a portion of the crystallographic molecular model of cytochrome *c* (103 aa) from *T. alalunga* built from a map of electron density that was calculated from a data set to Bragg spacing of 0.15 nm.[656] Black atoms are carbons, white atoms are oxygens, small gray atoms are nitrogens, large light gray atoms are sulfurs, and the small dark gray sphere is an iron ion surrounded by its ligands. The heme *c* in the protein is in the center of the drawing. Cysteine 14 and Cysteine 17 have formed covalent adducts with the two former ethenyl groups at the top of the heme. Histidine 18 and Methionine 80 provide the two axial ligands to the iron ion.

Heme *c* is a heme *b* that is **attached covalently** to the polypeptide of a cytochrome by two sulfides

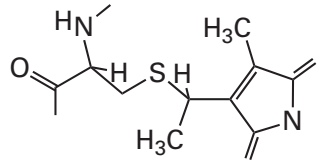

2–72

that are the respective products of nucleophilic addition between two cysteines from the protein and the two ethenyl groups at positions 3 and 8 of heme *b* (Figure 2–22).[656] The heme in hydroxylamine reductase from *Nitrosomonas europaea* is covalently attached to the protein through an adduct between an ortho carbon of Tyrosine 467 that replaces the hydrogen on the methine carbon 5 of heme *b* and the 4-hydroxy group of Tyrosine 467 that has nucleophilically added to carbon 4 of the heme *b* as well as the two sulfides **2–72** from two cysteines.[657] The heme P460 from *N. europaea* is covalently attached to the protein through an adduct between the amino group of Lysine 70 that replaces[658] the hydrogen on methine carbon 5 of heme *b* as well as the two sulfides **2–72** from two cysteines.[659] Both of these latter modifications at the methine carbon require oxidative additions catalyzed by the respective hemes.

An iron ion in a heme, unlike an iron ion in an iron–sulfur cluster, is **octahedrally coordinated**. The four nitrogens of the porphyrin provide four of the ligands, the **equatorial ligands**. The other two, the **axial ligands**, which are opposite each other across the iron, are provided by the protein, the solvent, or solutes in the solution. For example, in eukaryotic cytochromes *c*, the two axial positions are occupied by the lone pair of electrons of the sulfur of a methionine and the lone pair of electrons of the τ nitrogen within the imidazolyl group of a histidine (Figure 2–22). The structure of the heme *c* in the crystallographic molecular model of cytochrome *c* is almost indistinguishable[656] from the crystallographic molecular model of a model compound (Figure 2–23)[660] which was built to incorporate the central features of the heme in cytochrome *c* and which should represent the most stable orientation of the six atoms around the iron unperturbed by steric effects. The protein, however, does move its axial ligands slightly so that they are no longer directly above and directly below the iron ion (Figure 2–22).[656]

One of the axial ligands to the iron ion in a heme is usually[661-663] the τ nitrogen in the imidazolyl

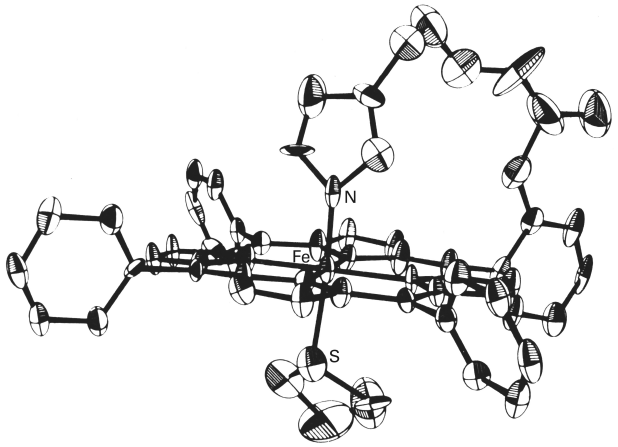

Figure 2–23: Drawing of the crystallographic molecular model of a synthetic heme[660] that incorporates the ligation found in cytochrome *c*. The metallic ion is Fe^{2+}, and the porphyrin is 5,10,15,20-tetraphenylporphyrin. To one of the phenyl groups an *o*-amino group has been added, and this was used to attach *N*-(4-carboxybutyl)imidazolyl group in anilide linkage. This chain of atoms provided an imidazolyl group as the fifth ligand to the Fe^{2+}. The sixth ligand is thiolane, which provides a sulfide to simulate the sulfide in the methionine in cytochrome *c*. The imidazolyl group is above the porphyrin in the drawing, the thiolane is below the porphyrin, and the Fe^{2+} is in the center of the porphyrin. The nitrogen of the imidazolyl group that provides a ligand to the iron, the iron ion, and the sulfur in the thiolane are labeled. Reprinted with permission from reference 660. Copyright 1979 American Chemical Society. https://doi.org/10.1021/ja00507a040

group of a histidine, but the other can be the τ nitrogen in an imidazolyl group of another histidine, the neutral sulfide of a methionine, the amino nitrogen of the amino terminus of the protein, the phenolato oxygen of a tyrosine, a molecule dissolved in the aqueous phase, or a molecule of water. For example, the heme *b* subunit of bovine quinol—cytochrome-*c* reductase contains two hemes *b*. The axial ligands for the iron ion in one heme *b* are the τ nitrogens from the imidazolyl groups of Histidine 83 and Histidine 182, and the axial ligands for the iron ion in the other heme *b* are the τ nitrogens from the imidazolyl groups of Histidine 97 and Histidine 196.[664,665] Cytochrome *c* from *Thunnus alalunga* contains a heme *c*, and the axial ligands to the iron ion in that heme *c* are Histidine 18 and Methionine 80 of the cytochrome (Figure 2–22). The heme *f* subunit of plastoquinol—plastocyanin reductase from *Brassica rapa* contains a heme *c*, and the axial ligands to the iron ion in that heme *c* are the imidazolyl group of Histidine 25 and the amino-terminal primary amine of the protein.[666-669] The most unusual axial ligand to a heme is a cysteine that is found in assimilatory sulfite reductases that contain siroheme. In these

enzymes, the cysteine is simultaneously bound to the iron ion of the siroheme and to one of the iron ions of a [4Fe–4S] iron–sulfur cluster,[661,670,671] which permits this complex to deliver two electrons at a time in three separate steps,[672] as is required for the conversion of sulfate to hydrogen sulfide catalyzed by the enzyme.

In many instances there is only one permanent axial ligand, and the other axial position is open to several different ligands. For example, bovine cytochrome-*c* oxidase contains a heme *a* the iron ion of which has the τ nitrogen in the imidazolyl group of Histidine 376 of subunit I as one of its axial ligands, but the opposite side of the iron ion is uncoordinated by the protein and is occupied by a molecule of water, a molecule of oxygen, or another ligand from the aqueous phase.[673] One of the hemes *c* in cytochrome c_{554} from *N. europaea* has the τ nitrogen in the imidazolyl group of Histidine 64 as one of its axial ligands, and there is no permanent axial ligand

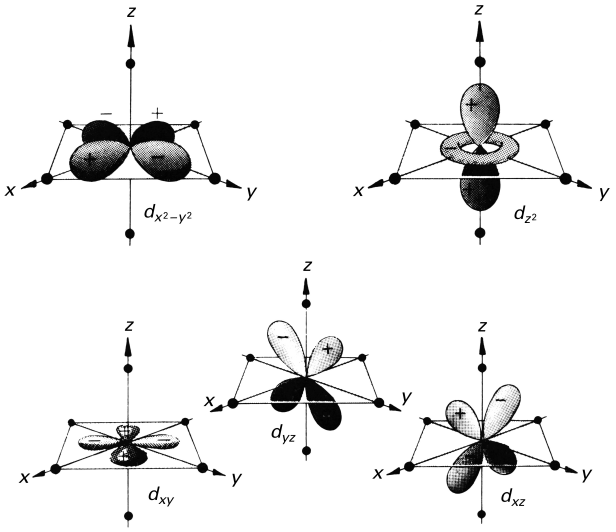

Figure 2–24: The five *d* orbitals of iron in the orientation they assume in the octahedral coordination complex found in hemes.[675] The six ligand positions of the octahedral arrangement are the six small filled circles defining the *x*, *y*, and *z* coordinates. Because three of the orbitals, d_{zy}, d_{yz}, and d_{zx}, lie between the repulsive lone pairs of electrons of the ligands, their energies are lower than the two orbitals, $d_{x^2-y^2}$ and d_{z^2}, that overlap the lone pairs of electrons of the ligands. The basicity of the axial ligands at the fifth and sixth positions controls the energy of the d_{z^2} orbital. The ligands at the four *x* and *y* positions are always the nitrogens of the heme. Reprinted with permission from reference 675. Copyright 1979 Annual Reviews Inc.https://doi.org/10.1146/annurev.bi.48.070179. 001551

on the other side of the iron.[674] When only one of the axial ligands is derived from the protein surrounding the heme, that fixed ligand is designated the **proximal ligand**. Hemes with an open axial coordination site usually catalyze chemical reactions that will be discussed later.

The octahedral coordination of an iron ion in a heme has consequences for the **electronic configuration of the iron ion.** An Fe^{2+} has six 3*d* electrons ($3d^6$), and an Fe^{3+} has five 3*d* electrons ($3d^5$). These are the electrons farthest from the nucleus of the iron ion. Oxygen ligands or nitrogen ligands in octahedral coordination of an iron ion, as are those to the iron in a heme, stabilize either a high-spin state or a low-spin state. The $d_{x^2-y^2}$ and d_{z^2} orbitals are on the axes of octahedral ligation, and the d_{xy}, d_{xz}, and d_{yz} orbitals are between the axes (Figure 2–24).[675] Each ligand directs a lone pair of electrons at the iron ion, and those lone pairs of electrons repel the 3*d* electrons of the iron ion, raise their energy, and split the degeneracy of the *d* orbitals (Figure 2–25A). If the ligands are such that they do not raise the energy of the $d_{x^2-y^2}$ and d_{z^2} orbitals sufficiently by electron repulsion relative to the energy of the d_{xy}, d_{xz}, and d_{yz} orbitals, then, in the case of Fe^{2+}, five of the six *d* electrons will distribute one into each of the five *d* orbitals; the remaining electron will enter either a d_{xy}, d_{xz}, or d_{yz} orbital; and four of the five *d* orbitals will contain an unpaired spin (Figure 2–25B).[676] In the case of Fe^{3+}, the five *d* electrons will distribute one into each of the five *d* orbitals, and each *d* orbital will contain an unpaired spin (Figure 2–25B). In each case, the iron ion will be in a **high-spin state**. If the ligands are such that they do raise the energy of the $d_{x^2-y^2}$ and d_{z^2} orbitals sufficiently by electron repulsion relative to the energy of the d_{xy}, d_{xz}, and d_{yz} orbitals, then, in the case of Fe^{2+}, the six *d* electrons will distribute in pairs into each of the d_{xy}, d_{xz}, and d_{yz} orbitals; and none of the five *d* orbitals will contain an unpaired spin (Figure 2–25C). In the case of Fe^{3+}, four of the five *d* electrons will distribute in two pairs into two of the d_{xy}, d_{xz}, and d_{yz} orbitals; the fifth *d* electron will enter the remaining d_{xy}, d_{xz}, or d_{yz} orbital; and only one of the *d* orbitals will contain an unpaired spin (Figure 2–25C). In each case, the iron ion will be in a **low-spin state**. The identity of the ligands to the Fe^{3+} and Fe^{2+} in a particular redox couple determine both its spin state and its biochemical standard reduction potential. Only the biochemical standard reduction potential, however, determines the ability

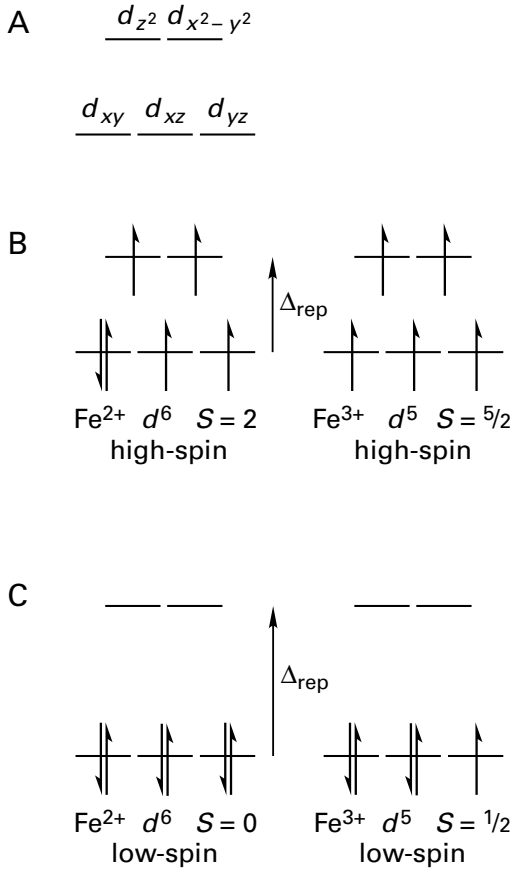

Figure 2–25: Distribution of 3*d* electrons in low-spin and high-spin Fe^{2+} and Fe^{3+} in octahedral coordination.[676] (**A**) The ligands, by electron repulsion, split the energy levels of the five 3*d* atomic orbitals of the iron so that the $d_{x^2-y^2}$ and d_{z^2} orbitals, which are aligned with the six ligands to the iron (Figure 2–24), have a higher energy for occupation by an electron than the d_{xy}, d_{xz}, and d_{yz} orbitals, which lie in between the ligands. (**B**) If the difference in energy (Δ_{rep}) due to the repulsion is small, then the electrons distribute by Hund's rule, which is that every orbital in a sublevel is singly occupied before any orbital is doubly occupied and all of the electrons in singly occupied orbitals have the same spin (to maximize total spin). The six *d* electrons of Fe^{2+} (d^6) distribute one into each of the five *d* orbitals, leaving one to occupy one of the d_{xy}, d_{xz}, and d_{yz} orbitals, which have a lower energy of occupation, giving a spin state of $^4/_2$. The five *d* electrons of Fe^{3+} (d^5) distribute one into each of the five *d* orbitals to give a spin state of $^5/_2$. These two distributions are high-spin. (**C**) If the difference in energy (Δ_{rep}) due to the repulsion is too large, then Hund's rule breaks down. The six *d* electrons of Fe^{2+} distribute in three pairs into each of the d_{xy}, d_{xz}, and d_{yz} orbitals, giving a spin state of 0, and the five *d* electron of Fe^{3+} distribute in two pairs into two of the d_{xy}, d_{xz}, and d_{yz} orbitals, and the remaining electron occupies the other, giving a spin state of $^1/_2$. These two distributions are low-spin.

of a particular redox couple of coordinated Fe^{3+} and Fe^{2+} to participate in an enzymatic one-electron oxidation–reduction.

When passing reversibly between Fe^{3+} and Fe^{2+}, an iron ion in a heme accepts and gives back one electron. During the reduction of the Fe^{3+} in a heme, the electron in question at the end of the reduction ends up in the unfilled 3*d* atomic orbital in the low-spin state of the Fe^{3+} (Figure 2–25C) or in one of the unfilled 3*d* atomic orbitals of lowest energy in the high-spin state of the Fe^{3+} (Figure 2–25B) to complete a pair. In reverse, at the end of the oxidation the electron has left the 3*d* atomic orbital in the Fe^{2+} that was filled or a filled orbital of equal energy. Regardless of whether the iron ion is high-spin or low-spin, the *d* orbital that is filled or that becomes unfilled is **a d_{xy}, d_{xz}, or d_{yz} orbital**. The identity of the ligands determines the energy of that d_{xy}, d_{xz}, or d_{yz} orbital, even though they are not directed toward the ligand, and hence the biochemical standard reduction potential of the iron, regardless of spin state. Whether the iron is high-spin or low-spin, however, does affect the rates at which single electrons can be exchanged; the high-spin states are more reactive in single electron transfer.[676]

The biochemical standard reduction potentials of the iron ions in the hemes involved in one-electron oxidation–reduction span the range from –550 to +450 mV (Figure 2–19).[677-680] For example, in hydroxylamine dehydrogenase from *N. europaea*, the biochemical standard reduction potentials of its eight distinct hemes *c* span the range from –410 to +290 mV.[681] The type of heme seems to be of little consequence because the ranges of biochemical standard reduction potential for cytochromes with different types of hemes overlap extensively. Although the ranges for the cytochromes with hemes *c* (–410 to +400 mV) and with hemes *b* (–200 to +400 mV) are the largest, these are also the most common types of cytochromes and have had the most opportunity for the standard reduction potentials to be manipulated by natural selection.

Variation in the **substituents on the porphyrin** affects the biochemical standard reduction potential of the iron ion in the heme to a degree. When the two ethenyl groups on heme *b* are reduced to ethyl groups, the biochemical standard reduction potential of its biscyano complex decreases by –35 mV; and when one of the ethenyl groups is replaced with a formyl group, it increases by +70 mV.[682] These shifts in standard reduction potential result from increases

(or decreases) in basicity of the nitrogens of the porphyrin resulting from increases in electron donation (or electron withdrawal) at its edges that stabilize (or destabilize) the oxidized Fe^{3+} relative to the reduced Fe^{2+}.

The **identity of the axial ligands** also affects the biochemical standard reduction potential of the iron ion in a heme in solution. When two waters are replaced as the axial ligands of heme *b* by two imidazolyl groups, which are more basic than molecules of water, the biochemical standard reduction potential decreases by –50 mV.[545] When one of those imidazolyl groups is then replaced by a sulfide, which is less basic than water, the biochemical standard reduction potential increases by +110 mV. This latter effect is due both to the decrease in basicity of the ligand and to the ability of the unfilled $3d$ atomic orbitals on sulfur to overlap favorably with the filled $3d$ orbitals on iron.[683]

The effects of the axial ligands are manifested as well in the standard reduction potentials of hemes in proteins. The two hemes *b* in the quinol—cytochrome-*c* reductase from *Rhodobacter capsulatus*, which each have two histidines as axial ligands, have biochemical standard reduction potentials of –90 and +50 mV while the heme *b* of cytochrome b_{558} from *E. coli*, which has a histidine and a methionine as axial ligands,[684] has a biochemical standard reduction potential of +180 mV.[685] Among cytochromes *c*, small proteins that act as electron-transferring coenzymes, those with hemes *c* with one histidine and one methionine as axial ligands have biochemical standard reduction potentials between +100 and +400 mV while those with two histidines have biochemical standard reduction potentials between –400 and –100 mV.[686]

Nevertheless, neither the variation of the substituents around the heme nor the identity of the axial ligands can explain the majority of the **variation in the observed standard reduction potentials** of hemes. For example, among those cytochromes *c* with a single heme *c* with axial ligands from one histidine and one methionine, the biochemical standard reduction potentials vary from +100 to +400 mV.[687] The single heme *b* with two histidines as axial ligands in cytochrome b_5 has a biochemical standard reduction potential of –100 mV[688] while one of the hemes *b* with two histidines as axial ligands in quinol—cytochrome-*c* reductase from *R. capsulatus* has a biochemical standard reduction potential of +50 mV.[575] Aspects of the environment surrounding the heme—such as charged side chains of amino acids in its vicinity, identity of donors or acceptors in hydrogen bonds to the imidazolyl groups of its axial histidines, steric distortions of the heme, extent of its removal from the surrounding solution, surface charge of the protein, and ionic strength of the surrounding solution—all have been shown to affect its standard reduction potential.[680,689,690] For example, when a valine in cytochrome c_{6A} from *Arabidopsis thaliana* is replaced by a glutamine,[691] which is the amino acid at the homologous position in cytochrome c_6 from *Phormidium laminosum*, the biochemical standard reduction potential of the heme increases by +110 mV. This observation explains in part the difference in the biochemical standard reduction potential of cytochrome c_{6A} (+71 mV) and cytochrome c_6 (+325 mV). The heme in the native structure of methyl-accepting chemotaxis protein is distorted significantly out of planarity by the protein. As mutations are made surrounding the heme that decrease this distortion and make the heme more planar,[692] the biochemical standard reduction potential decreases from +166 to –5 mV. In cytochromes with multiple hemes that are close together, each successive electron that is taken up by the cytochrome causes a decrease in the standard reduction potential for the next because of the successive accumulation of negative charge.[674,677,693]

Copper is the second most common transition metal participating in biochemical one-electron transfers. The configuration of valence electrons in elemental, metallic copper, Cu^0, is $3d^{10}4s^1$. The cuprous ion, Cu^+, missing the single $4s$ electron, is the only stable monovalent ion of the transition metals of the fourth period because it has a completely filled $3d$ shell. The cupric ion, Cu^{2+}, is a dication with a partially filled $3d$ shell ($3d^9$), which is the case with all other stable cations of transition metals of the fourth period. In the biochemical oxidation–reductions of prosthetic copper ions, Cu^+ gives up one electron during its oxidation to Cu^{2+}, and Cu^{2+} takes up one electron during its reduction to Cu^+. Unlike the various prosthetic groups containing iron that participate in one-electron transfer, in which the iron has inorganic sulfides or a porphyrin as ligands, prosthetic copper ions usually have lone pairs of electrons only from sulfurs, nitrogens, or oxygens of side chains of amino acids in the protein, acyl oxygens of the polypeptide backbone, or molecules of water as ligands (Figure 2–26).

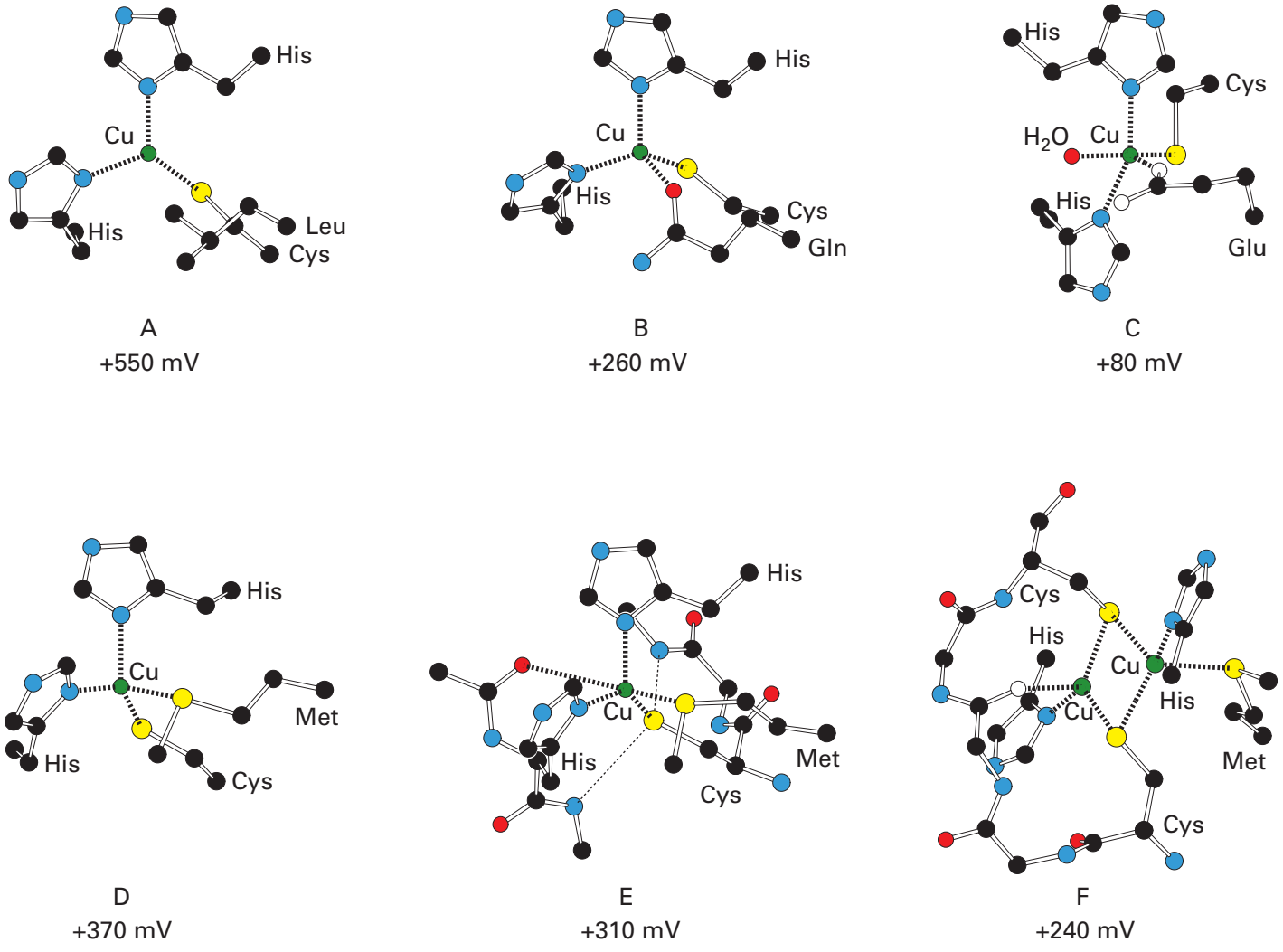

Figure 2–26: Arrangements of the ligands around prosthetic copper ions. Black atoms are carbons, red atoms are oxygens, blue atoms are nitrogens, large yellow atoms are sulfurs, and small green spheres are copper ions surrounded by their ligands. The drawings[50] are of mononuclear copper ions in crystallographic molecular models of (**A**) laccase from *C. cinerea*;[695] (**B**) stellacyanin from *C. sativus*;[740] (**C**) nitrocyanin from *N. europaea*;[742] (**D**) plastocyanin from *P. nigra*;[707] (**E**) azurin from *P. putida*;[722] and (**F**) the dinuclear CuA cluster from cytochrome-*c* oxidase of *T. thermophilus*.[746] The biochemical standard reduction potentials listed are relative to the standard hydrogen electrode and are for a standard state of pH 7.

The simplest arrangement of ligands, which defines the **core ligands present in most of the prosthetic groups containing only one copper ion,**[694] is that found in laccase from *Coprinopsis cinerea* (Figure 2–26A).[695] The copper ion is coordinated by the π nitrogens of two histidines and the sulfur of a cysteine. The bond lengths between the three ligands and the copper are 0.20, 0.21, and 0.22 nm, respectively; the three ligands are arranged trigonally around the copper; and four atoms (the copper, the two nitrogens, and the sulfur) are in the same plane. Again, this arrangement of ligands can be explained as the result of covalent bonding resulting from the occupation of three vacant $4sp^2$ atomic orbitals of the copper ion, the softest of the transition metals, by the lone pairs of electrons on the ligands or as the result of ionic bonding between the lone pairs of electrons and the positive copper ion in which steric and electronic repulsive forces the ligands and their lone pairs to be as far apart as possible, hence trigonal. Laccase is a member of a family of enzymes, each of which contains a prosthetic copper ion that is responsible for removing a single electron from its respective substrate.[696,697] In the case of

laccase, the prosthetic Cu^{2+} removes an electron from a benzenediol. The biochemical standard reduction potential of the copper ion in the active site of laccase from *C. cinerea* is +550 mV,[694] which is more than sufficient to permit the Cu^{2+} to remove an electron from a 1,2-dihydroxybenzene to give its semiquinone. This high biochemical standard reduction potential is in part a result of the fact that there are only three ligands to the copper ion from the protein, so the electron density around the cation is relatively low, which makes the Cu^{2+} more electropositive and more easily reduced. Although trigonally complexed copper is unusual outside a protein, there is a model compound for the prosthetic copper ions in this family of enzymes in which this configuration of ligands is achieved.[698,699]

The **most common arrangement of ligands** for mononuclear, prosthetic copper ions[700-706] is that found in plastocyanin from *Populus nigra* (Figure 2–26D).[707] The core configuration of two nitrogens from two histidines and one sulfur from a cysteine, with respective bond lengths to the copper of 0.19, 0.21, and 0.21 nm,[708-710] is expanded to include the sulfur from a methionine with a long bond to the copper of 0.28 nm. The addition of this ligand, although it is more distant, nevertheless converts the planar, trigonal configuration of ligands into a roughly tetrahedral one.[709] This arrangement of ligands can be explained as the result of covalent bonding resulting from the occupation of four vacant $4sp^3$ atomic orbitals of the copper ion by the lone pairs of electrons on the ligands or ionic bonding between the lone pairs of electrons and the positive copper ion in which steric and electronic repulsion forces the ligands and their lone pairs to be a far apart as possible, hence tetrahedral.

The additional **lone pair of electrons from the sulfide** in the methionine, as expected, decreases the biochemical standard reduction potential of the prosthetic copper ion.[694] If the methionine is mutated to a glycine, the biochemical standard reduction potential of the copper ion increases by about +100 mV,[711] but this observation is equivocal because the space opened by deleting the side chain of the methionine can permit a molecule of water to become the fourth ligand to the copper.[712] When the methionine, however, is mutated to 2-aminohexanoate, which fills the space that the methionine occupied, the biochemical standard reduction potential of the copper ion also increases by +100 mV.[713] When the methionine in amicyanin from *Paracoccus denitrificans* is replaced with a leucine,[714] the biochemical standard reduction potential increases by +130 mV. That the basicity of the lone pair of electrons on methionine is responsible for decreasing the biochemical standard reduction potential of the prosthetic copper ion is supported by the fact that when the methionine is mutated to 6,6,6-trifluoromethionine, a far less basic sulfide, the biochemical standard reduction potential of the copper ion increases by +40 mV. The increase of +100 and +130 mV in biochemical standard reduction potential of the copper ion that is caused by mutating the methionine to a 2-aminohexanoate and a leucine, respectively, however, is much less than the increase of +330 mV that occurs when one of the more intimately associated histidines that are ligands to the copper ion is mutated to a glycine.[715]

The biochemical standard reduction potential of the prosthetic copper ion in plastocyanin from *P. nigra* (Figure 2–26D) is +370 mV,[716,717] but the biochemical standard reduction potentials for prosthetic copper ions with the same four ligands with the same bond lengths[710] vary between +210 and +680 mV.[694,711,712,716-721] These differences are caused, in part, by differences in the distance between the copper ion and the nearby dipole of an acyl oxygen from the polypeptide backbone and by differences in the number of amido nitrogen–hydrogens directed toward the sulfur of the sole cysteine that is a ligand to the copper ion.[694] For example, in the crystallographic molecular model of azurin from *P. putida* (Figure 2–26E),[722,723] the **acyl oxygen from the peptide bond** preceding Histidine 46, which provides one of the π nitrogens that coordinate the copper ion, has been positioned by the protein so close to the prosthetic copper ion that it has become a fifth ligand at a distance of 0.30 nm, and there are two amido nitrogen–hydrogens pointed toward the sulfur of the cysteine that is a ligand to the copper. The distances from the sulfur to the two nitrogens of these nitrogen–hydrogens are 0.35–0.36 nm, well within the sum of the van der Waals radii of sulfur (0.18 nm) and hydrogen (0.11 nm) and the length of a nitrogen–hydrogen bond (0.10 nm). These **oriented nitrogen–hydrogens** are reminiscent of those in the polypeptide backbone surrounding iron–sulfur clusters (Figures 2–18, 2–20, and 2–21).

The biochemical standard reduction potential of the azurin from *P. putida* is +310 mV.[724] In rusticyanin from *Acidithiobacillus ferrooxidans*, there are also two nitrogen–hydrogens in the same relative positions in the sequence of amino acids directed

toward the cysteine, but the acyl oxygen is 0.6 nm away from the copper ion rather than 0.30 nm.[702] The biochemical standard reduction potential of rusticyanin is +680 mV.[694] This increase in standard reduction potential is thought to be due mainly to removal of the lone pair of electrons of the acyl oxygen from the vicinity of the copper.[694] In auracyanin from *Chloroflexus aurantiacus* which also has the same two homologous nitrogen–hydrogens directed toward the sulfur, the biochemical standard reduction potential of the copper ion is less that that of azurin (+210 mV),[721] even though the distance between the copper and the oxygen (0.35 nm)[705] is greater than that in azurin (0.30 nm).

The two nitrogen–hydrogen bonds from the polypeptide backbone directed toward the sulfido group of the cysteine in the crystallographic molecular models of the azurins, rusticyanin, and auracyanin are located in the peptide bond to the carboxy-terminal side of one of the coordinated histidines and the peptide bond two positions carboxy-terminal to the coordinated cysteine (Figure 2–26E). Because they direct the positive pole of the dipoles of their respective amido groups toward the sulfur, they should increase the standard reduction potential of the prosthetic copper ion.[694] In pseudoazurin from *Alcaligenes faecalis*, the amino acid two positions carboxy-terminal to the cysteine is a proline, so there is only one nitrogen–hydrogen directed toward the sulfido group of the cysteine.* When that proline is mutated to an isoleucine, to restore the second hydrogen bond,[725] the biochemical standard reduction potential of the copper ion increases[726] from +280 to +450 mV as expected. The basic blue protein from *Cucumis sativus*, however, does not have a proline at this position and instead has two nitrogen–hydrogens directed toward the sulfur, and the distance from its acyl oxygen to the copper ion (0.38 nm)[727] is the same as that in the pseudoazurin from *A. faecalis* (0.38 nm),[701] yet the biochemical standard reduction potential (+310 mV)[718] is almost the same as that (+280 mV) of pseudoazurin. The copper ions in plastocyanin from *Ulva prolifera*[728] and auracyanin from *C. aurantiacus*[705] are both the same distance from the respective acyl oxygens (0.35 nm). The latter has two nitrogen–hydrogens directed toward the copper while the former has only one, yet the biochemical standard reduction potential of the latter (+210 mV) is significantly more negative than that of the former (+370 mV)[720] instead of the other way around.

All these results suggest that **the biochemical standard reduction potential of a prosthetic copper ion in these proteins is not determined only by the distance between the copper ion and the acyl oxygen and the number of amido nitrogen–hydrogens directed toward the sulfur of the cysteine**.[694] Rather, the biochemical standard reduction potential of the copper ion in a protein seems to be determined by a large array of interactions of the amino acid side chains that surround it. For example four mutants of azurin from *P. aeruginosa* were constructed by mutating just two amino acid side chains in the immediate vicinity of the copper ion, a phenylalanine and an asparagine, neither of which is a ligand to the copper.[729] In the mutants, the biochemical standard reduction potential of the copper ion was decreased by as much as –90 mV or increased by as much as +240 mV.

The prosthetic copper ion in an azurin displays **the full complement of five paradigmatic ligands**. It is surrounded by the sulfurs of a cysteine and a methionine, the nitrogens of two histidines, and an acyl oxygen of the polypeptide backbone (Figure 2–26E). The two sulfurs, the two nitrogens, and the oxygen span, respectively, the complete biochemical spectrum from soft to hard Lewis bases. This list of ligands, however, is not a complete one. For example, one of the copper ions in peptidylglycine monooxygenase from *R. norvegicus*, the one responsible for transfer of single electrons to the active site, is coordinated only by the π nitrogens from the imidazolyl groups of three histidines.[730]

Copper ion is a soft Lewis acid, and in most of its prosthetic groups, it forms a strong, notably short, mostly covalent σ bond with the soft **sulfido sulfur of a cysteine**[731] In addition, in the oxidized cupric state, there is significant **transfer of electron density** from a *p* orbital on this sulfur, occupied by one of its lone pairs of electrons, to the $d_{x^2-y^2}$ orbital of the Cu^{2+}, occupied by its single unpaired electron.[732,733] Consequently, the sulfur must be hybridized *p*, sp^2, sp^2, sp^2. This transfer of electron density is responsible for the strong blue color of all these mononuclear, prosthetic copper ions, and it is thought that the electron entering, or leaving, the copper ion during its reduction, or oxidation, can pass through the *p* orbital on the sulfur that participates in this transfer of electron density.[731] The

*In this pseudoazurin, as well as most of the other proteins with this arrangement of ligands around the copper ion, the nitrogen of the peptide bond immediately adjacent to the respective cysteine is only 0.35 nm from its sulfur,[694] but the dipole of its amide is normal to the vector between the nitrogen and the sulfur (Figure 2–26E) and should have little effect on the standard reduction potential.

sulfur of a methionine is also a soft Lewis base, but as a sulfide it is only weakly basic ($pK_a \cong -9$) relative to the sulfido group of the cyteine ($pK_a = 8.7$), so it is only a weak ligand, a fact reflected in its bond length of 0.28 nm.

The **two nitrogens of the histidines**, although as basic as the sulfido group of the cysteine, are harder bases and do not form such a strong association with the soft copper. The distances between these nitrogens and the copper ion are the same as that between the sulfur of the cysteine and the copper ion even though their van der Waals radii (0.16 nm) are smaller than that of the sulfur (0.18 nm).[185] From crystallographic molecular models of the complex between laccase from *Melanocarpus albomyces* and 2,6-dimethoxyphenol, an analogue of a 1,2-dihydroxybenzene that would be a natural substrate, it was concluded that the electron that is removed by the enzyme and that ultimately ends up on the prosthetic copper ion passes through one of the imidazolyl groups that are ligands to the copper, rather than the cysteine. This imidazolyl group sits between the respective substrate and the copper ion.[734]

The **acyl oxygen of a peptide bond** is an even harder base. The main effect of its lone pair of electrons is to push the cysteine and the two histidines back into a trigonal plane (see Figure 2–26A). The acyl oxygen cannot participate in covalent bonding because it is a hard base and also because it is a weak base ($pK_a = -1$). Consequently, the return to trigonal coordination must be the result of electron repulsion, in which case this reorientation suggests that the tetrahedral orientation distorted by this electron repulsion was not the result of covalent bonding in the first place. The acyl oxygen also lowers the biochemical standard reduction potential of the copper by donating electron density, even though its distance from the copper ion is 0.28–0.32 nm in the azurins.[722,723,735,736]

In the set of prosthetic copper ions[737-739] represented by that of stellacyanin from *C. sativus* (Figure 2–26B),[740] the sulfur of the methionine found in the plastocyanins (Figure 2–26D) has been replaced with the **acyl oxygen in the side chain of glutamine**. The prosthetic copper ion of the stellacyanin from *C. sativus* has a biochemical standard reduction potential of +260 mV,[741] which is about −100 mV less positive than prosthetic copper ions that have methionine as a ligand, such as that in the plastocyanin from *P. nigra* ($E^{\circ\prime} = +370$ mV). In stellacyanin from *C. sativus*, two nitrogen–hydrogens are directed at the sulfur of the cysteine, and the acyl oxygen of the peptide bond to the amino-terminal side of the histidine is at the same distance as it is in the plastocyanin from *P. nigra* (Figure 2–26D). The difference in biochemical standard reduction potential between the stellacyanins and the plastocyanins is due, in part, to the greater basicity of the lone pair of electrons on the acyl oxygen of a glutamine ($pK_a = -1$) relative to that of the lone pair of electrons on the sulfur of a methionine ($pK_a \cong -9$). Consistent with this conclusion is that when the methionine that is the ligand to the prosthetic copper ion in azurin from *P. putida* (Figure 2–26E) is mutated to isosteric 4-methoxy-2-aminobutyrate, which replaces a sulfide with an ether, the oxygen of which has a basicity ($pK_a \cong -4$) closer to that of the acyl oxygen of the side chain of a glutamine, the biochemical standard reduction potential of the prosthetic copper ion decreases by −120 mV.[713] In the stellacyanin from *C. sativus*, the distance between the acyl oxygen of the glutamine and the copper ion (0.21–0.23 nm)[738-740] is significantly shorter than that between the sulfur of a methionine and the copper ion (0.27–0.31 nm),[709,710] which probably is the result of a steric effect because the oxygen is a hard base and less likely to engage in a covalent bond. The acyl oxygen of the glutamine (Figure 2–26B) is also much closer to the copper ion than is the more weakly associated acyl oxygen of the peptide bond (0.28–0.32 nm) in the azurins (Figure 2–26E).

The prosthetic copper ion in nitrocyanin from *N. europaea* (Figure 2–26C)[742] illustrates **the effect of two oxygens** on the biochemical standard reduction potential. In addition to the three core ligands of two nitrogens from two histidines and the sulfur from a cysteine, with bond lengths to the copper of 0.20, 0.20, and 0.23 nm, additional ligands are the oxygen of a molecule of water ($pK_a = 0$) and the oxygen of the carboxylato group of a glutamate ($pK_a = 4.3$) at distances of 0.22 and 0.21 nm, respectively, from the copper. These two oxygens, especially the more basic oxygen from the glutamate, cause the biochemical standard reduction potential of the prosthetic copper ion to be quite low (+80 mV),[743] at the lower end of the range of biochemical standard reduction potentials for prosthetic copper ions (Figure 2–19). In nitrocyanin, the copper has five ligands surrounding it that are all intimate and almost equidistant from the metallic ion and oriented so that they are almost as far apart from each other as possible. It seems likely that the orientation of the four harder ligands other than the sulfido group is determined almost entirely by electron repulsion and steric effects.

When an electron is added to a mononuclear, prosthetic Cu^{2+} during its reduction, the sulfur or sulfurs, the nitrogens, and the oxygen or oxygens of the **ligands move away from the copper** as a result of repulsion between the new electron and their lone pairs of electrons. Because of their strong interactions with the copper ion, the core ligands (the two nitrogens of the histidines and the sulfur of the cysteine) are least affected and usually move out by only about 0.01 nm.[735,738,739] Occasionally, however, one of the two histidines moves away more dramatically;[708,744] in at least one instance by more than 0.1 nm.[745] Upon reduction, the sulfur of the methionine or the acyl oxygen of the glutamine moves away from the copper ion more extensively, by 0.02–0.05 nm.[702] The acyl oxygen of the peptide backbone that is the fifth ligand in the azurins (Figure 2–26E), however, moves very little upon reduction, probably because it is farther away from the copper ion and far more rigidly positioned than the ligands on the side chains.

As with iron ions, prosthetic copper ions participating in the transfer of single electrons can be found in **clusters**. Unlike with iron, the clusters formed by copper ions do not contain sulfide, and they are considerably fewer in number. Two examples of such a cluster are the dinuclear CuA cluster from cytochrome-*c* oxidase of *T. thermophilus* (Figure 2–26F),[746] which is representative of the CuA clusters in other cytochrome-*c* oxidases,[673] and the dinuclear CuA cluster in nitrous-oxide reductase.[747] The central core of two copper ions and two sulfido groups in the dinuclear cluster of prosthetic copper ions in cytochrome-*c* oxidase resembles the central core of a [2Fe–2S] iron–sulfur cluster (Figures 2–18 and 2–20) in its planarity, the bond angles at the two sulfurs of the cysteines (65°), and the bond angles at the two coppers (110° and 118°), but the two sulfurs are not bridging sulfides but sulfido groups from two cysteines.

This central core of the two copper ions and two sulfido sulfurs is covalently bonded with a **molecular z**uted over all four of its atoms.[748] In the oxidized state, Cu^{2+}:Cu^{+}, the single unpaired electron is distributed equally between the two copper ions by the highest occupied molecular orbital of the conjugated system that it occupies. In the reduced state, Cu^{+}:Cu^{+}, the highest occupied molecular orbital of the core is filled by the added electron, and the cluster loses its intense purple color and its characteristic electron paramagnetic resonance spectrum.[748] The biochemical standard reduction potential for reduction of the dinuclear cluster of prosthetic copper ions in cytochrome-*c* oxidase of *T. thermophilus* is +240 mV.[749]

The **ligands to the two copper ions** of a CuA cluster, aside from the two cysteines, are those of the mononuclear copper ion in azurin (Figure 2–26E): two histidines, a methionine, and an acyl oxygen from the polypeptide backbone. The distances between the histidines and the respective coppers (0.19 and 0.21 nm) are typical, but the methionine (0.25 nm) and the acyl oxygen of the polypeptide backbone (0.26 nm) are closer to their respective copper ions than they are to the lone copper ion in the azurins.[746]

A model compound containing a central core almost identical to that in this cluster has been synthesized, but it is stable only in the mixed-valent, paramagnetic oxidation state,[750] unlike the prosthetic CuA cluster in a protein, the reduced, diamagnetic state of which is quite stable. The fact that the **synthetic cluster** is unstable illustrates the fact that when a prosthetic group containing metallic ions is synthesized outside the protein it often fails to display the same range of abilities that it does when it is within the protein, perhaps because the protein that surrounds it prevents its dissociation.

As with flavin, **the effect of pH on the reduction potential** for prosthetic groups participating in the transfer of single electrons is determined by the features of the protein that surrounds them and, in the case of prosthetic groups containing ions of transition metals, by the nature of the ligands provided by the active site for the metallic ions. For example, as has been already noted, the reduction potentials for the Rieske [2Fe–2S] iron–sulfur clusters and the [2Fe–2S] iron–sulfur clusters in which only one ligand is an imidazolyl group are predictably dependent on pH. The reduction potentials of high-potential [4Fe–4S] iron–sulfur clusters, however, are usually invariant with pH. The reduction potentials of some low-potential [4Fe–4S] iron–sulfur clusters are dependent on pH while those for other low-potential [4Fe–4S] iron–sulfur clusters are not. The biochemical standard reduction potential for the heme in bovine cytochrome *c* is +250 mV.[751] Upon addition of the electron, the central core of the heme in cytochrome *c* from *T. alalunga* (Figure 2–22) loses its net positive elementary charge and several amino acids near the sulfur of the methionine rearrange their orientations. These rearrangements are responses of the structure of the protein to the change in elementary charge at the iron.[752] Between pH 8 and pH 3, however, which includes the range

in which the protein normally functions, the reduction of bovine cytochrome *c* proceeds without the uptake of a hydron from the solution, so its biochemical standard reduction potential is not a function of pH.[751] Above pH 8, one hydron is taken up with the electron and no change in net charge on the protein occurs during the reduction. The opposite behavior is observed with plastocyanin, a protein that performs a role similar to that performed by cytochrome *c*. Below pH 6, one hydron is taken up with the electron by the plastocyanin from *P. crispum*, and above pH 6, none is taken up.[753]

The biochemical standard reduction potentials that have been noted above for the various prosthetic groups participating in the transfer of single electrons are usually ascertained by potentiometric titration or cyclic voltammetry.

In a **potentiometric titration**, the reduction potential of the solution is monitored with an electrode. Various small molecules that can be oxidized or reduced by one electron or two electrons are added to the solution as **mediators**. The mediators are ubiquitous redox couples with standard reduction potentials that span the range of reduction potential to be sampled. They are added to bring the potential of the electrode to the reduction potential of the solution by engaging in efficient and rapid oxidation and reduction at its surface; to bring the concentrations of the oxidized and reduced forms of the prosthetic group in the protein into equilibrium with the reduction potential of the solution by oxidizing and reducing it until equilibrium is reached; and to buffer the reduction potential of the solution by maintaining its reduction potential through the equilibrium concentrations of the oxidized and reduced forms of the several mediators (Equation 2–91).

The **reduction potential of the solution is adjusted systematically** in one of two ways. In the first strategy, small portions of a strong reductant, or a strong oxidant, are added in succession to decrease, or increase, the reduction potential of the solution. In the second strategy, the electrode is used to impose a succession of voltages. In the latter instance, the electrode must have a surface area of sufficient capacity to bring the potential of the solution to equilibrium all by itself in a reasonable interval.

After each adjustment, one waits for **equilibrium** to be established. For the titration to be accurate, the measurements must be taken at equilibrium. If the equilibrium is only slowly established and sufficient time is not taken, the ultimate value obtained for the biochemical standard reduction potential will be in error.

After each adjustment, the **reduction potential of the solution that is registered by the electrode** is recorded, and the concentrations of the oxidized form or the reduced form or both forms of the prosthetic group are ascertained spectroscopically. Usually, the reduction potential of the solution is systematically decreased and then systematically increased, or vice versa, to be sure that the same spectra are obtained at the same reduction potential in each direction,[754] a coincidence that demonstrates the reversibility of the oxidation–reduction and the fact that equilibrium was reached in each measurement.

The potentiometric titration of a prosthetic group participating in the transfer of single electrons can be **monitored by gathering visible absorption spectra**. For example, the visible absorption spectrum of equine cytochrome *c* between 500 and 580 nm was monitored as a function of the measured reduction potential of a solution containing cytochrome *c* and the mediators *N*,*N*,*N*′,*N*′-tetramethyl-*p*-phenylenediamine ($E^{\circ\prime}_{2e^-}$ = +260 mV), 2,3,5,6-tetramethyl-1,4-benzenediamine ($E^{\circ\prime}_{2e^-}$ = +240 mV), 5-methylphenazinium methyl sulfate ($E^{\circ\prime}_{2e^-}$ = +80 mV), and 5-ethylphenazinium ethyl sulfate ($E^{\circ\prime}_{2e^-}$ = +55 mV). Ferric ethylenediaminetetraacetate was also present to shuttle single electrons to the mediators from the iron of the heme. The reduction potential of the solution was systematically increased by adding portions of a solution of potassium ferricyanide and was recorded with a gold electrode. The concentration of the reduced form of heme *c* in cytochrome *c* was assessed by its absorbance at 550 nm (Figure 2–27).[755] The data were fit to Equation 2–91 to obtain a value for the biochemical standard reduction potential of the heme *c* in the cytochrome. The value obtained, 257 ± 0.4 mV, agrees closely with the value (256 ± 3 mV) for the same protein that was determined earlier with less accuracy.[751]

The different hemes can be most readily distinguished by their **absorption spectra** in the visible region, between 500 and 580 nm. For example, the ferrous forms of the two different hemes *b* and the heme *c* in quinol—cytochrome-*c* reductase have sharp, characteristic absorption bands at 552.4, 560, and 565.6 nm, respectively, and the three can be followed separately in a potentiometric titration to determine each of their biochemical standard reduction potentials.[756] The strongest visible absorption of a heme is usually at around 400 nm, the Soret band,

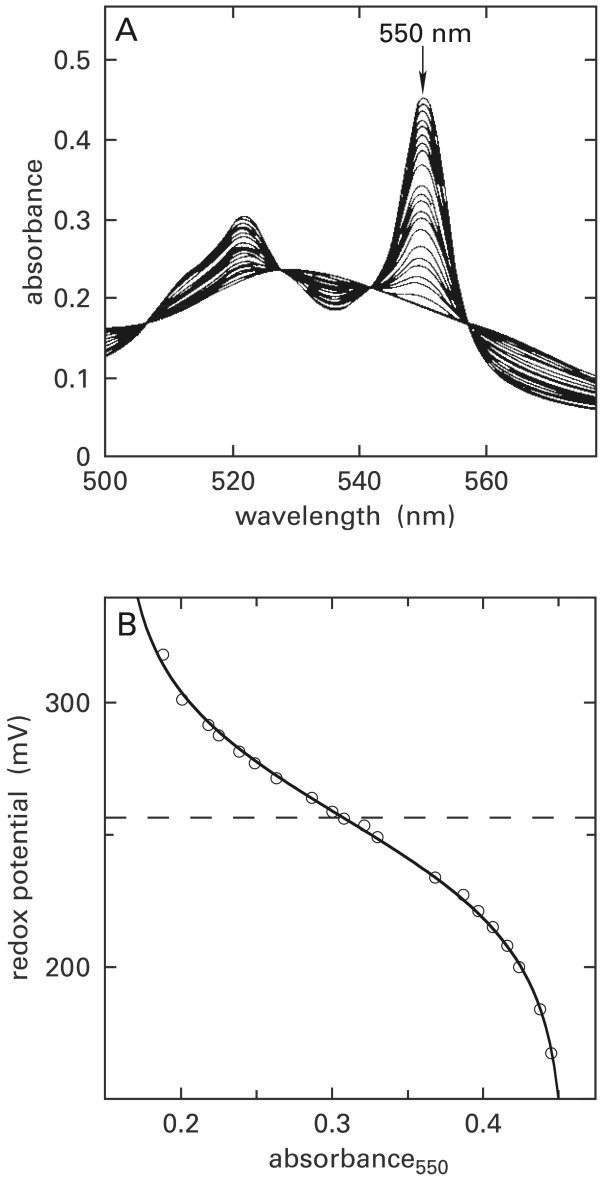

Figure 2–27: Potentiometric titration of equine cytochrome *c*.[755] A solution of the protein (16 μM) in 4.5 M urea, 0.3 mM ferric chloride, 10 mM ethylenediaminetetraacetate, 10 μM *N,N,N′,N′*-tetramethyl-*p*-phenylenediamine, 35 μM 2,3,5,6-tetramethyl-1,4-benzenediamine, 35 μM 5-methylphenazinium methyl sulfate, 35 μM 5-ethylphenazinium ethyl sulfate, and 0.05 M sodium phosphate at pH 7.0 at 25 °C was added to the chamber of an apparatus that permitted the solution to be in contact with a gold-plated platinum electrode and at the same time have its absorbance monitored. The heme *c* in the protein was in the reduced state and was held at an initial reduction potential of 100 mV. Successive additions of a 13 mM solution of potassium ferricyanide were added and, after the solution reached equilibrium, the reduction potential of the solution was recorded as well as an absorption spectrum from 500 to 580 nm. **(A)** Superposed spectra, one for each potentiometric step in the oxidation. The absorbance at 550 nm decreases with each addition of ferricyanide. **(B)** Potentiometric titration. The reduction potentials (millivolts) of the solution at equilibrium are plotted against the absorbance at 550 nm. Equation 2–91 was fit to the data (solid curve). The parameters obtained from the fit were the absorbance of fully reduced cytochrome *c* in the solution, 0.453 ± 0.0003; the absorbance of the fully oxidized cytochrome *c* in the solution, 0.159 ± 0.0007; and the biochemical standard reduction potential of equine cytochrome *c*, +257 ± 0.4 mV (horizontal dashed line).

and potentiometric titrations can also be monitored in this region of the spectrum because the absorption shifts to longer wavelengths upon reduction of the heme,[757,758] but the different hemes all have similar shifts in absorption in this range during a potentiometric titration and cannot be distinguished so readily.

It is also possible to monitor a potentiometric titration with **electron paramagnetic resonance spectra**. For example, the reduction potential of a solution containing lysine 2,3-aminomutase from *Clostridium subterminale*, *S*-adenosyl-L-methionine, and the mediators 1,1′-trimethylene-2,2′-dipyridyl bromide and 4,4′-dimethyl-1,1′-trimethylene-2,2′-dipyridyl bromide was adjusted systematically to voltages in the range between –375 and –525 mV by adjusting the potential of a gold electrode to the desired voltage and waiting for equilibrium to be reached. At each voltage, following equilibration, a sample was removed from the solution and frozen, and the electron paramagnetic resonance spectrum of the [4Fe–4S] iron–sulfur cluster in the enzyme was measured (Figure 2–28A).[595] The differences in the derivatives of the absorption between the maxima of the derivative at 0.345 T and the minima of the derivative at 0.356 T were plotted as a function of the measured reduction potential (Figure 2–28B). These differences are directly proportional to the magnitude of the actual absorption and hence the concentration of the reduced, paramagnetic form of the iron–sulfur cluster (Equation 2–169). The data were fit to Equation 2–91 to obtain a value for the biochemical standard reduction potential (–437 ± 5 mV) of the iron–sulfur cluster in the active site of lysine 2,3-aminomutase.

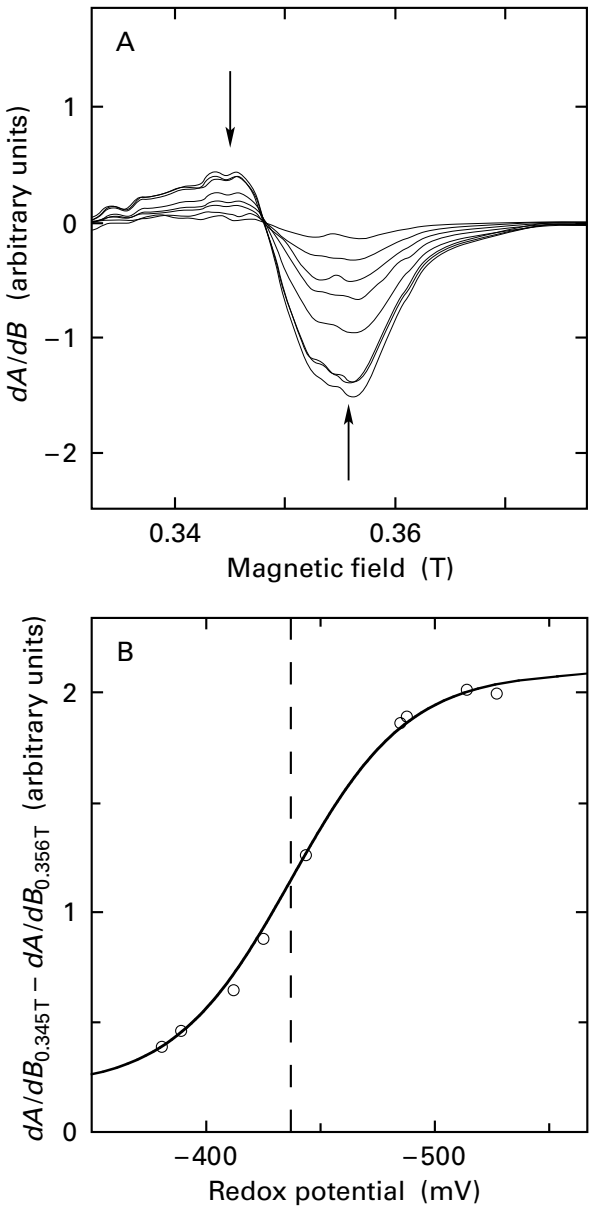

Figure 2–28: Potentiometric titration of the [4Fe–4S] iron–sulfur cluster in lysine 2,3-aminomutase from *C. subterminale*.[595] A solution (1 mL) of the enzyme (40 μM in active sites) in 42 μM *S*-adenosyl-L-methionine, 200 mM KCl, 100 μM of the mediator 4,4′-dimethyl-1,1′-trimethylene-2,2′-dipyridyl bromide, 100 μM of the mediator 1,1′-trimethylene-2,2′-dipyridyl bromide, and 150 mM *N*-(2-hydroxyethyl)piperazine-*N*′-3-propanesulfonate at pH 8.0 was added to the chamber of an of an apparatus at room temperature that permitted the solution to be in contact with a gold electrode poised at a particular potential. After equilibrium was reached between the electrode and the [4Fe–4S] iron–sulfur clusters in the solution, a portion of the solution was immediately frozen, and its electron paramagnetic resonance spectrum was recorded. **(A)** The spectra produced by the apparatus are plots of the first derivative (dA/dB) of the absorption (A; in arbitrary units) of microwave electromagnetic energy, at the fixed carrier frequency of 9.256 GHz, as a function of the flux density of the applied magnetic field (B; in Tesla). The magnetic field was varied from 0.29 T to 0.39 T. **(B)** The differences between the first derivatives (dA/dB) at 0.345 T and the first derivatives (dA/dB) at 0.356 T, which are measures of the concentration of unpaired electrons in the solution, are plotted as a function of the reduction potentials (millivolts) to which each solution was brought to equilibrium before it was frozen. Equation 2–91 was fit to the data (solid curve). The parameters obtained from the fit were the magnitude of the difference at full oxidation, 0.39 ± 0.14; the magnitude of the difference at full reduction, 4.18 ± 0.05; and the biochemical standard reduction potential of the [4Fe–4S] iron–sulfur cluster, -437 ± 5 mV (vertical dashed line). Adapted with permission from reference 595 Copyright 2006 American Chemical Society.https://doi.org/10.1021/bi0519497

Hemes also display electron paramagnetic spectra arising from the unpaired electron in the oxidized ferric form, and potentiometric titrations can be performed by monitoring the intensity of this signal. Most ferric hemes have the central unsplit absorption of their unpaired electron at around $g = 2.29$ and cannot be distinguished in this range, but the different hemes in a protein that contains more than one heme can often be distinguished because each will have characteristic absorptions arising from differences in hyperfine coupling, and each can be potentiometrically titrated independently by monitoring its characteristic hyperfine absorption.[759] Likewise, differences in hyperfine couplig permit the different iron–sulfur clusters in a protein to be distinguished[562] and potentiometrically titrated individually.[760,761] A drawback of using electron paramagnetic resonance to follow a titration is the requirement for much larger quantities of prosthetic group to gather the required data. It is also possible to use both visible spectra and electron paramagnetic spectra in concert to monitor the individual potentiometric titrations of the different prosthetic groups in the same protein.[643]

Cyclic voltammetry is also used to determine the biochemical standard reduction potential of a prosthetic group that participates in a redox couple. In a cyclic voltammogram (Figure 2–29),[762] the current entering or leaving an electrode suspended in a solution is monitored as a function of the potential of that electrode. The initial solution contains a certain concentration of the fully oxidized or the fully reduced prosthetic group within its protein. If the prosthetic group is fully oxidized, the initial potential of the electrode is made sufficiently positive that negligible

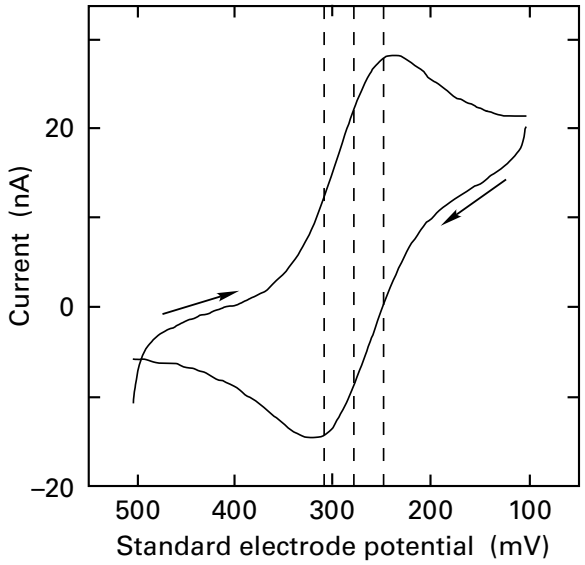

Figure 2–29: Cyclic voltammogram of the prosthetic copper ion in isoform 2 of azurin from *Methylomonas*.[762] A solution of the protein in 0.1 M potassium phosphate at pH 7.0 was added to the chamber of a voltammometer in which there were a Ag/AgCl reference electrode, a platinum wire counter electrode, and a working electrode with a smooth surface of gold that had been modified with bis(4-pyridyl)disulfide. The chamber was flushed with argon. The voltage was then scanned between +300 and −100 mV at 2 mV s^{-1} and then back again, as indicated by the arrows, and the current at the working electrode (nanoamperes) was monitored as a function of its standard potential (millivolts). The two outer vertical dashed lines indicate, respectively, the positions of the maxima of positive and negative current when background has been subtracted from the data for the two sweeps. The distance between these two vertical lines is 60 mV, a number indicating that the apparatus is monitoring a one-electron oxidation–reduction. The central dashed line is halfway between the outer two and is at the biochemical standard reduction potential (+280 mV) of the copper ion in the azurin. Adapted with permission from reference 762, Journal of Biological Inorganic Chemistry, Copyright 1999 Springer Nature. https://doi.org/10.1007/pl00010653

reduction of the prosthetic group occurs. The potential of the electrode is then decreased from the initial value at a certain linear rate (volts $second^{-1}$) until it is significantly more negative than the reduction potential of the prosthetic group. It is then immediately increased at the same rate back to the initial potential, and the full cycle is then repeated until the measurements are reproducible. If the prosthetic group is fully reduced, the initial potential of the electrode is made more negative than its standard reduction potential and is increased at a certain linear rate and then decreased.

Assume that the prosthetic group is initially oxidized and the potential of the electrode is being lowered. At the immediate surface of the electrode, if the rate of the voltage change is slow enough, the concentrations of the oxidized and reduced forms of the prosthetic group will be at the equilibrium appropriate to the voltage at the surface, as determined by Equation 2–91. Initially, if the potential of the electrode is high enough, the concentration of the oxidized form at equilibrium will be its concentration in the solution. As the potential of the electrode decreases, the concentration of the oxidized form of the prosthetic group at the immediate surface of the electrode will decrease below its concentration in the solution. The current due to this decrease will be negligible, but the decrease in the concentration of the oxidized form at the immediate surface of the electrode will create a **concentration gradient** of the oxidized form between the surface of the electrode and the rest of the solution containing the oxidized form at a constant concentration.[763,764] A diffusive flux of the oxidized form will move down this concentration gradient, delivering the oxidized form to the electrode by simple diffusion. Its reduction transfers electrons to the electrode. This **diffusive flux** of the oxidized form down the concentration gradient to the surface of the electrode and its subsequent reduction produces the observed current.

The concentration gradient increases as the voltage decreases, and the concentration of oxidized form at the immediate surface of the electrode becomes smaller and smaller. When the potential of the electrode, however, passes through the reduction potential of the prosthetic group and becomes significantly less than its reduction potential, the concentration of the oxidized form at the immediate surface of the electrode becomes essentially zero and, consequently, invariant. The concentration gradient then decreases as more and more of the oxidized form in the solution surrounding the electrode is consumed, and the current then decreases even though the potential of the electrode is still decreasing.

During a negative sweep such as the one just described, if the oxidation–reduction at the surface of the electrode is always at equilibrium as the voltage is changing[762] and if the diffusion coefficients of the oxidized and reduced forms of the redox couple are the same, **the peak of the current due to reduction of the prosthetic group** (Figure 2–29) under the conditions of the experiment occurs at a potential at a distance $(1.109 \pm 0.002)\ RT(nF)^{-1}$ below the reduction potential of the redox couple,[765]

which at 25 °C is 28.5/n mV. The diffusive current at this peak, i_p (amperes), that arises from only the reduction of the oxidized prosthetic group diffusing to the electrode is defined by the equation

$$i_p = 0.4463\, nFAC\left(\frac{nFvD}{RT}\right)^{1/2} \qquad (2\text{–}173)$$

where A is the surface area (centimeters^2) of a planar electrode, C is the initial concentration (moles centimeter^{-3}) of oxidized prosthetic group in the solution, D is its diffusion coefficient (centimeters^2 second^{-1}), and v is the rate (volts second^{-1}) at which the potential of the electrode is decreasing.[763-766] Both the dimensionless constant 1.109 (given earlier in the text) and the dimensionless constant 0.4463 (Equation 2–173) are the products of terms arising from the diffusion equations.

Upon the positive, return sweep of voltage (Figure 2–29), all the same things happen in reverse, and a peak of current of the opposite sign but of the same magnitude is observed with its maximum at a distance (1.109 ± 0.002) $RT(nF)^{-1}$ above the reduction potential of the redox couple, again only if the oxidation–reduction at the surface of the electrode is always at equilibrium as the voltage is changing. If the oxidation–reduction is fully reversible, successive sweeps should give superposable traces of current.

A cyclic voltammogram provides **several pieces of information** (Figure 2–29). First, if the current in the reverse direction is centrosymmetric to that in the forward direction, as it is in Figure 2–29, and currents in successive sweeps are superposable, the **oxidation–reduction is reversible**. Second, if the oxidation–reduction is reversible and the currents are centrosymmetric, the **reduction potential** of the redox couple is halfway between the potentials at which the two peaks of current occur, at the same potential as that of the point of centrosymmetry. Third, if the oxidation–reduction is reversible, if the oxidized and reduced forms of the prosthetic group are at equilibrium with the potential of the electrode at all voltages, and if the current observed is corrected for background currents that are not due to the redox couple by performing voltammetry on an identical solution not containing the redox couple, then the distance between the maxima of the two peaks (outer vertical dashed lines in Figure 2–29) should be 57/n mV, so this distance provides a determination of n, **the number of electrons involved in the oxidation–reduction**.[767] If the system does not remain at equilibrium as the voltage is decreased or increased, this distance will be greater than 57/n mV, so if it is not too much greater, the value of n can still be determined because n must be an integer. Fourth, if the current observed is corrected for background currents, the corrected current at its peak, which should arise only from the diffusion of oxidant or reductant to the electrode, can be used to estimate the **diffusion coefficient of the protein** containing the prosthetic group.[762,766] From the cyclic voltammogram of isoform 2 of azurin from *Methylomonas* (Figure 2–29), it could be concluded that the oxidation–reduction of the prosthetic copper ion was reversible, that its biochemical standard reduction potential was +280 mV, that only one electron was involved in the oxidation–reduction (ΔE = 61 mV), and that the diffusion coefficient of the azurin was 6×10^7 cm^2 s^{-1}. By varying the rate of the potential sweep and demonstrating that the peak current is directly proportional to its square root (Equation 2–173), it is also possible to show that the current due to the oxidation–reduction is encounter-controlled,[766] a property that is necessary if an accurate diffusion coefficient is to be measured.

Cyclic voltammetry can also be used to determine the same information for hemes in cytochromes[768] and iron–sulfur clusters in ferredoxins and other proteins.[769] If there are several prosthetic groups in a protein,[770] each produces its own individual peak of current on the same cyclic voltammogram. If the several peaks of current overlap too closely, the contributions of the individual prosthetic groups to the cyclic voltammogram can be resolved by eliminating successively each of the prosthetic groups but one by site-directed mutation, performing cyclic voltammetry on each mutant to determine the reduction potential of each prosthetic group in isolation from the others, and then showing that the individual peaks of current sum to give the cyclic voltammogram of the unmutated protein.[771]

Cyclic voltammetry of isoform 2 of azurin from *Methylomonas* was so successful because it is a small protein (124 aa)* with a large diffusion coefficient. One of the drawbacks of cyclic voltammetry arises from the slower rates of diffusion for larger molecules of protein. These slow rates produce smaller currents at the same molar concentration, so they require that higher molar concentrations (0.1 μM–1 mM) of a large protein be used, which is a practical limitation.

*The abbreviation aa is for "amino acids".

In one widely used variation of cyclic voltammetry, which overcomes the requirement for high concentrations of protein, **a thin film of the protein can be adsorbed to the electrode**.[772-774]

There are several ways to produce this thin film on the surface of the electrode. The electrode can be modified so that it has covalently attached amino groups or carboxy groups to which the protein can be attached covalently by amide linkages to carboxy groups or amino groups, respectively, on its surface. The surface of the electrode can be modified so that it is hydrophobic and can absorb hydrophobic patches on the surface of the protein. Fixed molecular elementary charges can also be attached to the surface of the electrode to form a layer of fixed charge. This fixed charge retains the molecules of the protein adjacent to the surface by ion exchange.[775] In each instance, the layer containing the protein is so thin that very little protein is necessary for accurate measurements [on the order of 1 pmol (cm^2 of electrode surface)$^{-1}$].

When cyclic voltammetry is performed on these films, the peaks of current in the forward and reverse directions are still centrosymmetric about the reduction potential of the prosthetic group, but their separation depends on the rate of the sweep in voltage,[776,777] a fact that precludes using the separation to define n, the number of electrons involved in the oxidation–reduction being observed. The number of electrons involved in the oxidation–reduction, however, is proportional to the square of the current at the electrode, i_e^2, and inversely proportional to the peak width at half-height, two independent relationships that can be used to determine the value of n. Because the film contains so little of the protein and its stoichiometric prosthetic group and because the currents measured are from the direct reduction or oxidation of only the prosthetic groups in the protein at the surface rather than arising from the continuous diffusion of prosthetic groups from the bulk solution, the peaks of current due to the oxidation or reduction of the prosthetic group at the surface are quite small and the ratio between the signal and the background is much less, a fact requiring accurate measurement and careful subtraction of background from the signal.[778-780]

The advantage of using a film of protein is that the diffusive currents are almost eliminated, and as a result, the peaks of current are narrower and almost symmetrical. This property permits the peaks from several different prosthetic groups to be examined simultaneously[715,779,781] or permits the investigator to step through several different oxidation states of the same prosthetic group[640] in the same voltammogram. The disadvantage of this procedure is that the protein is not in free solution, so there is always the possibility of denaturation at the surface or steric effects.

The prosthetic groups that are one-electron redox couples are incorporated into electron-transferring coenzymes and enzymes that catalyze oxidation–reductions, and they transfer electrons between or within these enzymes. With few exceptions—the quinones such as ubiquinone, which are often prosthetic groups but are usually free solutes dissolved in a membrane; flavins, which are usually prosthetic groups but in occasional situations are coenzymes in free solution; and L-ascorbate, which is always a free solute—the various prosthetic groups involved in one-electron transfer in living organisms are always tightly bound to particular proteins. Pheophytins and chlorophylls are bound noncovalently in the active sites of proteins but are surrounded so extensively by the polypeptide that they remain attached to the protein over its lifetime. Iron–sulfur clusters do not exist outside proteins and are covalently bound through the cysteines. The hemes of hemoproteins can also be covalently bound through peripheral locations on the heme, as in the case of cytochrome *c* (Figure 2–22 and **2–72**), but in most hemoproteins they are noncovalently bound by the polypeptide that embraces them, and they never leave the protein in which they are enclosed during its lifetime.* Prosthetic copper ions are coordinated to the ligands provided by the polypeptide of the protein and are usually bound covalently to the sulfur of a cysteine (Figure 2–26). Even quinones such as ubiquinone, which are usually free solutes in the membrane, are tightly bound when they are functioning as prosthetic groups at particular locations in a protein, and they may or may not exchange occasionally over the lifetime of the protein. The proteins to which these prosthetic groups participating in the transfer of single electrons are permanently or almost permanently bound vary considerably in their sizes, locations within the cell, complexities, and roles in metabolism.

The largest of these proteins are **enzymes that participate in electron transport chains** and catalyze the transfer of electrons between two widely separated locations. These enzymes are embedded

*In fact, heme that escapes from protein is toxic.[782]

in biological membranes and are large enough to dwarf the phospholipid bilayers that they span. They vary in size from the reaction centers of photosynthetic bacteria, which have asymmetric units of three different subunits and a total of 850 amino acids,[783] to mammalian NADH:ubiquinone reductases (H^+-translocating) with asymmetric units of 45 different subunits and a total of more than 8000 amino acids.[784] The membranes in which these enzymes are dissolved are plasma membranes of bacteria, the inner membranes of mitochondria, the chromatophores of bacteria, and the thylakoids of chloroplasts.

There are also **enzymes that are dissolved in the cytoplasm** or other aqueous phases within the cell and that are responsible for oxidation–reductions. These enzymes are fairly large because they often contain several of the prosthetic groups for one-electron transfers involved in the oxidation–reductions for which they are responsible. Typical asymmetric units for these enzymes vary in size from a single subunit with 300 amino acids to three different subunits with a total of 1200 amino acids.

Operating as lighters among these argosies are small proteins that act as coenzymes responsible for transferring electrons between these large proteins by diffusing rapidly through the cytoplasm or another cellular space or by diffusing over a biological membrane. These small **electron-transferring coenzymes** rapidly associate with and dissociate from the large enzymes and, depending on the circumstances, can either enter or leave with the electron that they are responsible for carrying.

The small electron-transferring coenzymes use prosthetic flavins, prosthetic iron–sulfur clusters, prosthetic hemes, and prosthetic copper ions as carriers of single electrons.

Flavodoxin and **electron-transferring flavoprotein** are small and not-so-small electron-transferring coenzymes, respectively, that each have a single flavin within themselves.[785,786] Flavodoxins are usually monomeric proteins with 140–170 amino acids,[787] and electron-transferring flavoproteins are usually heterodimers with about 600 amino acids in the asymmetric unit.[788] Flavodoxins stabilize the neutral flavin semiquinone significantly, so the biochemical standard reduction potential for the redox couple of neutral oxidized flavin and neutral flavin semiquinone is –240 to –180 mV and that for neutral flavin semiquinone and reduced flavin anion is –500 to –370 mV (Figure 2–19).[789,790] The fact that the former standard reduction potential is so much more positive than the latter, unlike the situation with free flavin (Figure 2–15), favors one-electron transfer, usually that between the redox couple of neutral oxidized flavin and neutral flavin semiquinone (Figure 2–9).[791] If, however, the reductant is strong enough the redox couple of neutral flavin semiquinone, which is created by the first electron, and neutral reduced flavin is available to accept a second electron.[789] If the second electron is accepted, the reduction becomes a two-electron reduction rather than a one-electron reduction. Unlike flavodoxin, electron-transferring flavoprotein stabilizes the anionic semiquinone of its flavin, which cannot be reduced further (Figure 2–9), and usually cycles as an electron-transferring coenzyme between neutral oxidized flavin and anionic flavin semiquinone, a one-electron redox couple with biochemical standard reduction potentials of –200 to 0 mV in these proteins (Figure 2–19).[790]

Rubredoxins and ferredoxins are small, water-soluble proteins with iron–sulfur centers. Rubredoxins are usually monomeric but can be oligomeric,[549] and their monomer or subunit contains 45–60 amino acids and a single iron ion.[551,792] Ferredoxins are monomeric proteins that usually have 60–120 amino acids, but there are a few large ferredoxins resulting from multiple gene duplications with as many as 10 iron–sulfur clusters and 250 amino acids.[793,794] The small unmultiplicated ferredoxins have either a single [2Fe–2S] iron–sulfur cluster,[795] a single [4Fe–4S] iron–sulfur cluster,[598] two [4Fe–4S] iron–sulfur clusters,[796,797] or a [4Fe–4S] iron–sulfur cluster and a [3Fe–4S] iron–sulfur cluster[634] covalently attached to the protein through cysteines. The biochemical standard reduction potentials of the [2Fe–2S] ferredoxins are in the range –450 to –175 mV, and those of the [4Fe–4S] ferredoxins are in the range –600 to –400 mV (Figure 2–19). In the ferredoxins with two [4Fe–4S] iron–sulfur clusters, each iron–sulfur cluster usually accepts an electron independently of the oxidation state of the other iron–sulfur cluster at essentially the same biochemical standard reduction potential, and the protein is able to carry two electrons, one on each iron–sulfur cluster.[798]

There are **small, water-soluble cytochromes**, such as cytochrome *c*, and there are also small anchored, membrane-bound cytochromes, such as cytochrome b_5, that act as small electron-transferring coenzymes between larger enzymes. Cytochrome b_5

can diffuse rapidly over the membrane of the endoplasmic reticulum while carrying an electron between enzymes also located in this membrane. Although there are water-soluble cytochromes containing hemes *b* that are small electron-transferring coenzymes,[799] most of the cytochromes that perform this function contain hemes *c*. These cytochromes *c* are usually, but not always,[800] monomeric proteins. They usually contain 80–140 amino acids, but there are examples of larger cytochromes *c* that are the products of gene duplication.[690] Most cytochromes *c* contain a single heme *c* (Figure 2–22),[801] but some contain more than one heme *c*.[802] The cytochromes *c* that are the products of gene duplication contain two hemes in two separate superposable domains.[803] There are also small unduplicated cytochromes *c* with three closely opposed hemes (70 aa)[804,805] and four hemes (120 aa)[806,807] and a larger membrane-bound cytochrome *c* with four hemes.[808] The hemes *c* in the cytochromes *c* have biochemical standard reduction potentials between –410 and +450 mV (Figure 2–19), which is the broadest range for the small electron-transferring coenzymes. One of the most negative biochemical standard reduction potentials is for one of the hemes *c* in cytochrome c_3, where its four hemes are in such close proximity that the reduction of each heme in turn decreases the biochemical standard reduction potential of the next to be reduced.[809]

The **small electron-transferring coenzymes containing prosthetic copper ions** are usually monomeric proteins but can be homooligomers.[810] Their monomers or subunits contain 90–200 amino acids. Although most are in free solution in one of the aqueous phases in a cell, a few are membrane-bound,[811] presumably diffusing between their donors and acceptors within the same membane. Their range of biochemical standard reduction potential is the same as that for prosthetic copper ions in general (Figure 2–19). Although, for historical reasons, they have many different names—such as amicyanins, auracyanins, azurins, halocyanins, mavicyanins, nitrosocyanins, phytocyanins, plastocyanins, pseudoazurins, rusticyanins, stellacyanins, sulfocyanins, and umecyanins—these small electron-transferring coenzymes with single prosthetic copper ions are all related to each other.[705,742] Within the sequence of amino acids for each member of this group of proteins, one of the histidines that coordinates the copper ion is 35–66 amino acids amino-terminal to the cysteine to which that copper ion is covalently bound; the other histidine is 3–8 amino acids and the methionine is 5–12 amino acids carboxy-terminal to the cysteine. Although they all seem to be the same protein found in the same or different species of organisms, they are nevertheless distinguished from each other because they are specific to the particular enzymes between which they carry electrons. For example, amicyanin accepts single electrons from methylamine dehydrogenase (amicyanin),[812] plastocyanin accepts single electrons from plastoquinol—plastocyanin reductase, azurin accepts single electrons from nitrite reductase (NO-forming),[813,814] amicyanin accepts single electrons from cytochrome *c*-551*i*,[745] and plastocyanin accepts single electrons from photosystem I. The names often reflect the function or location of one of their partners in the transfer of an electron.

Even though each type has its more limited range, as a group the various small electron-transferring coenzymes containing flavins, iron–sulfur clusters, hemes, or prosthetic copper ions provide biochemical standard reduction potentials that span continuously the range from –600 to +740 mV (Figure 2–19), which is almost coincident with the range from the ferredoxin that accepts[815,816] the excited electron from an iron–sulfur center (–550 mV) in photosystem I to molecular oxygen, the strongest biological oxidant (+820 mV) unbound to protein. Within this biological range are all the standard reduction potentials of the prosthetic groups in the enzymes of biological oxidation–reduction that donate electrons to or accept electrons from these small electron-transferring coenzymes.

There are a number of enzymes, both soluble in the aqueous phases within a cell and embedded in cellular membranes, that catalyze the oxidation or reduction of a particular substrate and the subsequent reduction or oxidation, respectively, of one of the small electron-transferring coenzymes by passing single electrons among prosthetic groups within themselves. For example, the flavin in L-lactate dehydrogenase (cytochrome) from *S. cerevisiae*[817,818] or *Wickerhamomyces anomalus*[819]

$$\text{L-lactate} + 2\ \text{ferricytochrome } c \rightleftharpoons 2\ \text{H}^+ + \text{pyruvate} + 2\ \text{ferrocytochrome } c \qquad (2\text{–}174)$$

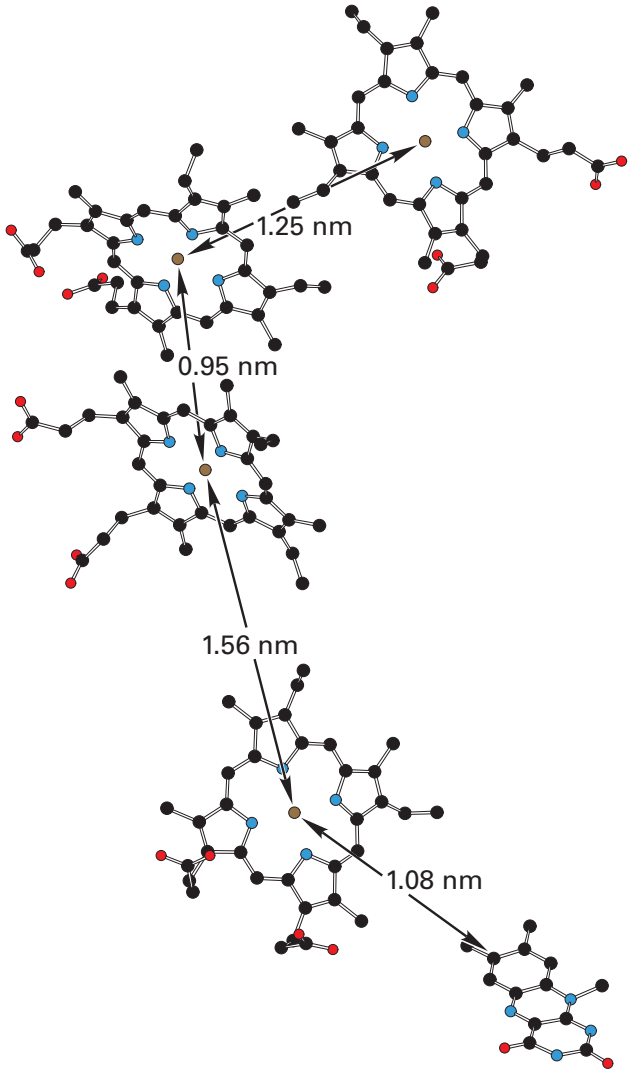

Figure 2–30: Disposition of flavin and four hemes *c* in the crystallographic molecular model of fumarate reductase from *S. frigidimarina*.[456] Black atoms are carbons, red atoms are oxygens, blue atoms are nitrogens, and rusty brown spheres are iron ions. When *S. frigidimarina* is grown under anaerobic conditions, the biosynthesis of this particular fumarate reductase is induced because the purpose of the enzyme is to dispose of the excess electrons from anaerobic glycolysis by reducing fumarate to succinate. The gene for the enzyme was transferred to a plasmid and expressed at a high level in cells of *Shewanella*. The enzyme was purified from the expression system and crystallized. The drawing[50] is of the flavin and the four hemes *c* in the resulting crystallographic molecular model. The distances between the iron ions in the adjacent hemes are noted, as well as the distance from the iron ion in the closest heme to the π molecular orbital system of the flavin.

when it is playing its normal role in metabolism, oxidizes lactate to pyruvate by hydride transfer, and then the resulting two electrons in the reduced flavin are transferred one at a time to a heme *b*, also in the enzyme. From the heme *b*, each electron is transferred to a small, electron-transferring coenzyme, the cytochrome *c* (109 aa in both) in the cytoplasm of each of these two fungi, when it is transiently bound to the L-lactate dehydrogenase (cytochrome).[818,819] Each molecule of ferrocytochrome *c* dissociates from L-lactate dehydrogenase (cytochrome) following its reduction and is eventually replaced on its binding site by a molecule of ferricytochrome *c*, which can then be reduced in turn. One of the intermediate steps in this reaction is

$$H_2Fl^-_{red} + \text{heme } b_{ox} \rightleftharpoons H_2Fl^{\cdot} + \text{heme } b_{red} \qquad (2\text{–}175)$$

in which the stability of the flavin semiquinone is used to accomplish the transfer of only one electron from the flavin to the heme *b*, which can only accept one electron at a time. After the first electron has been passed on to a molecule of cytochrome *c*, the flavin semiquinone then passes the second electron to the heme *b*.

In fumarate reductase from *Shewanella oneidensis* [820] or *Shewanella frigidimarina*,[456,821] when it is playing its normal role in metabolism, the heme *c* on cytochrome CymA, a small electron-transferring coenzyme in the cytoplasm of the bacterium, provides one electron at a time, and each electron is passed consecutively through four hemes *c*,[821] which are covalently bound to the enzyme as prosthetic groups (Figure 2–30),[456] to a flavin also in the enzyme. The flavin joins the electrons in pairs and uses them to reduce fumarate to succinate in a hydride transfer.[822]

In the normal directions of catalysis in the cytoplasm, L-lactate dehydrogenase (cytochrome) uses the flavin in its active site to sunder two electrons, and fumarate reductase uses the flavin in its active site to join two electrons. When these enzymes are catalyzing their reactions in the reverse direction, the flavin in L-lactate dehydrogenase (cytochrome) joins two electrons, and the flavin in fumarate reductase splits two electrons.

Unlike the examples of L-lactate dehydrogenase (cytochrome) and fumarate reductase, it is often the case that, even though one of these enzymes with

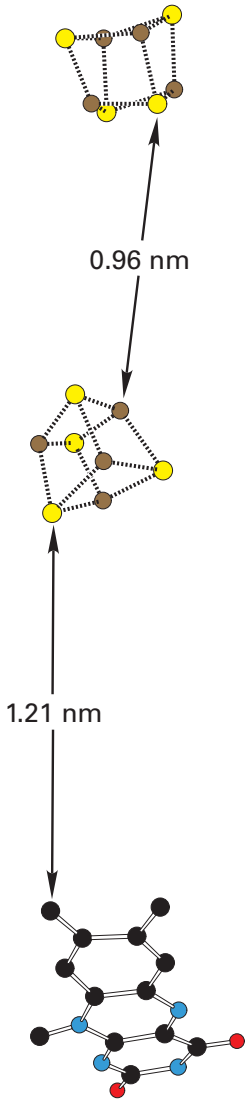

Figure 2–31: Disposition of flavin and two [4Fe–4S] iron–sulfur clusters in the crystallographic molecular model of adenylyl-sulfate reductase from *A. fulgidus*.[377] Black atoms are carbons, red atoms are oxygens, and blue atoms are nitrogens. In the iron sulfur clusters, yellow spheres are sulfides, and rusty brown spheres are iron ions. The enzyme was purified and crystallized in a glove box under strictly anaerobic conditions from cells of *A. fulgidus* that had been cultivated under anaerobic conditions. The distance between the iron–sulfur clusters is noted, as well as the distance from the closest iron–sulfur cluster to the flavin.

multiple prosthetic groups has been purified and extensively characterized, the small electron-transferring coenzyme that provides or removes the electrons during its reaction within the cell is as yet unknown. For example, it was only after many years that the previously[823] **unknown electron acceptor** that removes electrons one at a time from the heme *b* in cellobiose dehydrogenase (acceptor) was identified as another enzyme, lytic cellulose monooxygenase (C4-dehydrogenating), for which cellobiose dehydrogenase (acceptor) provides electrons.[824-826] The heme *b* in cellobiose dehydrogenase (acceptor) in turn removes electrons one at a time from the flavin after it has been reduced by transfer of a hydride during the dehydrogenation of cellobiose to cellobiono-1,5-lac-tone.[823] The identity of the immediate electron donor that provides electrons one at a time to the two [4Fe–4S] iron–sulfur clusters in adenylyl-sulfate reductase from *A. fulgidus* (Figure 2–31) is still unclear.[377] These electrons are passed along one at a time to regenerate the reduced flavin from the oxidized flavin produced upon dissociation of the sulfite from adduct **2–50** during the reduction of adenylyl sulfate (Equation 2–125). Recent studies of mutants suggest that the ultimate source of the electrons is the multiheme cytochrome *c* subunit of menaquinone reductase Qrc in the plasma membrane of the bacterium,[827] but whether that enzyme provides the electrons directly or by reducing an electron-transferring coenzyme which then reduces the peripheral [4Fe–4S] iron–sulfur cluster in adenylyl-sulfate reductase is unknown at the moment. As the experience with cellobiose dehydrogenase illustrates, the natural donor or acceptor of electrons from a particular enzyme, if it is unknown at first, is usually ascertained later on.

When the natural electron donor or acceptor for a particular enzyme that catalyzes an oxidation–reduction in which electrons are transferred one at a time is not known, an **adventitious donor or acceptor** can usually be discovered. In the case of cellobiose dehydrogenase (acceptor) from *Phanerochaete chrysosporium*, either 2,6-dichloroindophenol or equine cytochrome *c* can act as an acceptor of the electron in an assay of the enzyme,[823] while in the case of adenylyl-sulfate reductase from *A. fulgidus*, ferricyanide is used routinely as the one-electron donor in the assay for the enzyme.

There is a family of related enzymes to which dimethyl sulfide:cytochrome c_2 reductase belongs. Each member of this family transfers electrons removed from their respective substrate, dimethyl sulfide in the case of dimethyl sulfide:cytochrome c_2

reductase, through a chain of four [4Fe–4S] iron–sulfur clusters to a prosthetic heme *b* on the enzyme. One might expect that the midpoint potentials of the [4Fe–4S] iron–sulfur clusters would increase as the electron moved from one cluster to the next to encourage efficient transfer of the electron. The midpoint potentials in sequence, however, for dimethyl sulfide:cyto-chrome c_2 reductase from *Rhodovulum sulfidophilum* are +180, −340, +70, and +300 mV. Several of the other enzymes of the family show the same unexplained pattern.[828]

In several enzymes, **one or more one-electron carriers sit between two flavins**. In one direction, one of the flavins splits two electrons and the other ultimately joins them; in the opposite direction, the roles are reversed. For example, in dihydroorotate dehydrogenase (NAD^+) from *L. lactis*, one of the prosthetic flavins removes two electrons from dihydroorotate, oxidizing it to orotate. The reduced flavin passes the electrons one at a time to a [2Fe–2S] iron–sulfur cluster, from which they are transferred to another flavin in the protein that joins them in pairs and then reduces NAD^+ to NADH.[829,830] One of the flavins in porcine dihydropyrimidine dehydrogenase ($NADP^+$) is reduced by transfer of a hydride from either 5,6-dihydrouracil or 5,6-dihydrothymine during its oxidation to uracil or thymine, respectively, and the reduced flavin then passes the electrons one at a time to a [4Fe–4S] iron–sulfur cluster in the protein. From this iron–sulfur cluster, each electron is passed consecutively through three more [4Fe–4S] iron–sulfur clusters to another flavin in the enzyme that joins them in pairs and uses them to reduce $NADP^+$ to NADPH.[478,831] The single flavin in trimethylamine dehydrogenase from *Methylophilus methylotrophus* oxidizes trimethylamine to dimethylamine and formaldehyde. The reduced flavin passes the resulting two electrons one at a time to a [4Fe–4S] iron–sulfur cluster in the enzyme, from which they are transferred one at a time to a flavin not in the protein but in the electron-transferring coenzyme, electron-transferring flavoprotein.[832]

There are many enzymes that **perform two-electron oxidation–reductions of their substrates by transferring single electrons one after the other among one-electron prosthetic groups** without the necessity for flavin to join or split a pair of electrons or transfer a hydride. For example, there are two homologous enzymes, dihydromethanophenazine:CoB-CoM heterodisulfide reductase from *M. thermophila*[643] and H_2:CoB-CoM heterodisulfide,ferredoxin reductase from *M. thermolithotrophicus*,[642] which must use the same mechanism to reduce the heterodisulfide between 2-sulfanylethanesulfonate (coenzyme M; HSCoM) and *N*-[(7-sulfanyl)heptanoyl]-L-threonine *O*-phosphate (coenzyme B, HSCoB). The former enzyme contains two [3Fe–3S–Fe–S] iron–sulfur clusters (**2–67**) and is a subunit in a stable, membrane-embedded heterodimer the other subunit of which contains two hemes *b*. The latter enzyme also contains two [3Fe–3S–Fe–S] iron–sulfur clusters but is in a multienzymatic complex containing several other subunits in which there are twelve iron–sulfur clusters and a prosthetic flavin. The active site of each of the CoB-CoM heterodisulfide reductases is the two [3Fe–3S–Fe–S] iron–sulfur clusters, which are the only prosthetic groups common to both enzymes. An intermediate in the reduction of the heterodisulfide has been observed crystallographically in H_2:CoB-CoM heterodisulfide,ferredoxin reductase from *M. thermolithotrophicus* in which the sulfido group of 2-sulfanylethanesulfonate has become a fifth ligand to one of the iron ions coordinated by only two sulfides in the [3Fe–3S] portion of the [3Fe–3S–Fe–S] iron–sulfur cluster, and the sulfido group of *N*-[(7-sulfanyl)heptanoyl]-L-threonine *O*-phosphate is adjacent to an iron ion in the second [3Fe–3S–Fe–S] iron–sulfur cluster.[642] It has been proposed that the two reduced [3Fe–3S–Fe–S] iron–sulfur clusters, acting in concert, each transfer an electron to the disulfide and that, during the reduction, 2-sulfanylethanesulfonate ends up as a ligand to the iron ion.

Following the reduction of the heterodisulfide, the two resulting oxidized [3Fe–3S–Fe–S] iron–sulfur clusters in dihydromethanophenazine: CoB-CoM heterodisulfide reductase from *M. thermophila* receive electrons from the two hemes *b* in the other subunit. These hemes *b* receive the electrons in turn one at a time from the electron-transferring coenzyme, dihydromethanophenazine

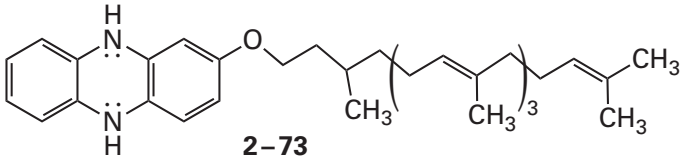

2–73

dissolved in the plasma membrane,[643] which presumably passes through a semiquinone intermediate. The two resulting oxidized [3Fe–3S–Fe–S] iron–sulfur clusters in H_2:CoB-CoM heterodisulfide, ferredoxin reductase from *M. thermolithotrophicus* receive electrons passed through six iron–sulfur clusters, the prosthetic flavin, and then three iron–sulfur clusters. These electron-transferring prosthetic

groups are located in three other subunits in the multienzymatic complex. The electrons are ultimately derived from the reduction of molecular hydrogen to two hydrons and two electrons.

In pyruvate synthase from *Desulfocurvibacter africanus*, the electron-poor adduct 2-acetylthiamine diphosphate

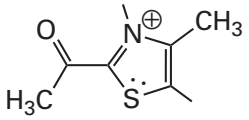

2–74

formed by a nucleophilic substitution at the acyl carbon of acetyl-SCoA by the ylide of thiamine diphosphate, accepts electrons one at a time, with a thiamine radical (Figure 2–7) as an intermediate, from a [4Fe–4S] iron–sulfur cluster in the protein. This [4Fe–4S] iron–sulfur cluster receives electrons one at a time from two other [4Fe–4S] iron–sulfur clusters, the two [4Fe–4S] iron–sulfur clusters in a reduced ferredoxin, associated reversibly with the enzyme, that brings the electrons in.[833]

The large membrane-spanning enzymes that catalyze transfers of electrons in the electron transport chains in bacterial cells, mitochondria, chromatophores, and chloroplasts differ from these water-soluble enzymes of oxidation–reduction because each membrane-spanning enzyme is able to conserve a portion of the free energy of its respective exergonic transfer of an electron. The donor of the electron or pair of electrons to each of these membrane-bound enzymes has a significantly more negative biochemical standard reduction potential than the oxidant that accepts those electrons. For example, the biochemical standard reduction potential of NADH is –310 mV, that of ubiquinone or plastoquinone dissolved as a solute in a phospholipid bilayer is +100 mV, that of mammalian cytochrome *c* is +260 mV, that of the blue copper protein plastocyanin[834,835] is +380 mV, and that of molecular oxygen is +820 mV (Figure 2–19). In these electron transfers, ubiquinone, plastoquinone, cytochrome *c*, and plastocyanin are electron-transferring coenzymes. NADH:ubiquinone reductase (H^+-translocating) transfers two electrons from NADH to ubiquinone; quinol—cytochrome-*c* reductase and its cousin, plastoquinol—plastocyanin reductase, transfer two electrons from ubiquinol or plastoquinol to two cytochromes *c* or two plastocyanins (Figure 2–26D), respectively; and cytochrome-*c* oxidase transfers four electrons from four cytochromes *c* to molecular oxygen. The differences in biochemical standard reduction potential among these steps (150–570 mV) translate into differences of free energy of –14 to –54 kJ for every mole of electrons passing through each of these enzymes. The energy is conserved and used for a number of purposes such as the synthesis of $MgATP^{2-}$ or the transport of metabolites against their concentration gradient across the membrane of a bacterial cell, the inner membrane of a mitochondrion, the chromatophore of a photosynthetic bacterium, or the thylakoid of a chloroplast. This energy realized by these enzymes from their respective oxidation–reductions is stored in the electrochemical gradient of hydrons across the respective membrane.

Mitochondria are the descendants of aerobic, **nonphotosynthetic bacterial cells**, and the inner membrane of a mitochondrion is the descendant of the plasma membrane of the ancestral bacterial cell. The interior of a mitochondrion, inside the boundary of its inner membrane, is the descendant of the cytoplasm of the ancestral bacterial cell. With the exception of alkaliphilic bacteria, both the interior of a mitochondrion and the cytoplasm of a bacterial cell are basic relative to the exterior of the mitochondrion and the exterior of the bacterial cell, respectively. With the exception of acidophilic bacteria, between the interior and exterior of a mitochondrion, or between the cytoplasm and the exterior of a bacterial cell, there is an electric potential, positive on the exterior and negative on the interior.

In photosynthetic bacteria other than cyanobacteria, photosynthesis occurs in chromatophores. **Chromatophores** are either invaginations of the plasma membrane or separate vesicles in the cytoplasm that arise from the pinching off of invaginations of the plasma membrane of a photosynthetic bacterium. The interior of a chromatophore in a photosynthetic bacterium is the descendant of the exterior, extracytoplasmic solution now surrounding the photosynthetic bacterium. **Chloroplasts** are the descendants of a photosynthetic bacterium. Each chloroplast has an outer membrane that is the descendant of the plasma membrane of that photosynthetic bacterium. Inside this outer membrane of a chloroplast or the plasma membrane of a cyanobacterium, there are **thylakoids**, which are flattened vesicles of membrane that are descendants of the

chromatophores that were in the ancestral photosynthetic bacteria. The interior solution inside a thylakoid is the descendant of the exterior, extracytoplasmic solution that surrounded the ancestral photosynthetic bacteria. The stromal solution or the cytoplasm surrounding the thylakoids, between them and the outer membrane of the chloroplast or the plasma membrane of a cyanobacterium, respectively, is the descendant of the cytoplasm of the ancestral photosynthetic bacterium. Because of all these ancestries, the interior of a chromatophore (or thylakoid) is acidic relative to the cytoplasmic (or stromal) solution that surrounds it, and the electric potential in the cytoplasm of a photosynthetic bacterium (or the stromal solution of a chloroplast) is negative relative to the electric potential in the interior of a chromatophore (or thylakoid).

As a consequence of this evolutionary history, the exterior surface of the plasma membrane of a bacterial cell, the exterior surface of the inner membrane of a mitochondrion, the interior surface of the membrane of a chromatophore, and the interior surface of the membrane of a thylakoid face a positive, acidic solution. The opposite surfaces of these four membranes face a negative, basic solution.*

In the process of transferring electrons from NADH or the electron-transferring coenzyme that provides the electrons to the electron-tranferring coenzyme or molecular oxygen that receives the electrons, NADH:ubiquinone reductase (H^+-translocating), ubiquinone, quinol—cytochrome-*c* reductase, plastoquinol—plastocyanin reductase, and cytochrome-*c* oxidase each transport hydrons from the negative, basic side of the respective membrane to the positive, acidic side of the membrane. The resulting current of hydrons, in the absence of the transport of any counterions, is what causes the positive, acidic side on the exterior of a mitochondrion or bacterium or the interior of a chromatophore or thylakoid to have a positive electric potential relative to the negative, basic side and to be more acidic than the negative, basic side on the interior or exterior, respectively. The sum of the free energy stored in the electric potential and the free energy stored in the gradient of hydrons together is the free energy stored in the **electrochemical gradient of hydrons**.

The electrochemical gradient of hydrons between the two sides of a cellular membrane of phospholipid produces a hydron motive force. A **hydron motive force** is a difference in the free energy of a hydron between the two sides. The hydron motive force between the exterior and interior of a mitochondrion or a bacterial cell is such that the free energy of a hydron on the exterior is more positive than the free energy of a hydron in the interior. The hydron motive force between the interior and exterior of a chromatophore or a thylakoid is such that the free energy of a hydron in the interior is more positive than the free energy of a hydron on the exterior. Consequently, when a hydron moves from the positive, acidic compartment to the negative, basic compartment in any of the cells or organelles, the free energy change is negative and favorable. This favorable free energy change is used to perform work.

The most central enzymes catalyzing these electron transfers and the associated transport of hydrons are **quinol—cytochrome-*c* reductase**[836,837] and its sibling **plastoquinol—plastocyanin reductase**.[838] The former enzyme is located in the plasma membranes of bacteria and the inner membranes of mitochondria, and it oxidizes ubiquinol to ubiquinone (**2–57**; +100 mV)[519,520,523] and reduces cytochrome *c* (Figure 2–22; +260 mV).[686] The latter enzyme is located in the membranes of chromatophores and the membranes of the thylakoids in chloroplasts, and it oxidizes plastoquinol to plastoquinone (**2–58**; +100 mV)[521,522] and reduces plastocyanin (Figure 2–26D; +380 mV).[834,835]

The **biological significance of the redox couple of ubiquinone and ubiquinol** and the redox couple of plastoquinone and plastoquinol is their ability to transfer hydrons across the membranes of mitochondria, bacterial cells, chromatophores, and chloroplasts. When one of these quinones is reduced to the quinol, two hydrons are taken up to make the neutral quinol (Equation 2–157). Those two hydrons must come from some aqueous solution. When one of these quinols is oxidized to the quinone, two hydrons are released. Those hydrons must be released into some aqueous solution. When ubiquinone is reduced to ubiquinol, the active site on the enzyme in which this reduction occurs, for example, the active site of NADH:ubiquinone reductase (H^+-translocating) in mitochondria and bacterial cells,[839-841] faces the interior of the bacterium or mitochondrion or the exterior of a chromatophore or thylakoid on the negative, basic side of the membrane that encloses each organelle or organism. This orientation causes the hydrons that add to the quinone when it is reduced to the quinol to be taken up from the more basic, more negative solution, and this uptake increases its basicity and decreases

*Exceptions to this rule are the hydron gradient in alkaliphilic bacteria and the electric gradient in acidophilic bacteria.

its electric potential. When ubiquinol is oxidized to ubiquinone or plastoquinol is oxidized to plastoquinone, the active site in the enzyme at which it is oxidized, for example, the active site in plastoquinol—plastocyanin reductase in chromatophores or thylakoids, faces the exterior of the bacterium or mitochondrion or the interior of a chromatophore or a thylakoid, which is on the positive, acidic side of the membrane enclosing each of them. This orientation causes the hydrons dissociating from the quinol as it is oxidized to the quinone to be released into the more acidic solution.

During the various reactions catalyzed by the enzymes that use them as coenzymes, two hydrons are taken up from the negative, basic solution during the reduction of ubiquinone or plastoquinone by two electrons; the ubiquinol or the plastoquinol diffuses across the membrane; two hydrons are released to the positive, acidic solution during its reoxidation; and the ubiquinone or plastoquinone diffuses back across the membrane. Because the quinone is reduced by a prosthetic group in the active site of the reductase with a more negative biochemical standard reduction potential than the prosthetic group in the active site of the oxidase by which it is later oxidized, the movement of hydrons up their electrochemical gradient from the basic interior to the acidic exterior is driven by the movement of electrons down a **gradient of standard reduction potential**. This strategy accounts for a portion of the electrochemical gradient across these membranes. This strategy works because the quinone is a weak base, the quinolate dianion is a strong base, and neither the cationic conjugate acid of the quinone nor the anionic conjugate base of the quinol is present in significant concentration—nor can they pass readily across the membrane—but it also helps that the semiquinone radical is prone to rapid disproportionation while in solution in a bilayer of phospholipids.

Although the number of different subunits in the asymmetric units in homodimeric quinol—cytochrome-*c* reductase and its homodimeric sibling plastoquinol—plastocyanin reductase differs,[665,842-845] they are clearly related to each other[844,846] and catalyze the same transfers of electrons between their respective reactants and products by passing them in the same sequence among a **Rieske [2Fe–2S] iron–sulfur cluster, two hemes *b*, and a heme *c***,[846-848] which are each bound within their own subunits within the respective enzymes.[849-856]

Plastoquinol—plastocyanin reductase, in addition to these four prosthetic groups in common with those of quinol—cytochrome-*c* reductase, has an additional heme *c*, which is covalently attached by only one sulfide linkage,[857] as well as a chlorophyll *a* and a β-carotene as prosthetic groups.[844,845,858]

The electron transfers catalyzed by these two enzymes among these prosthetic groups constitute the **Q-cycle**.[859,860] The Q-cycle adds a layer of complexity to the oxidation–reduction catalyzed by these enzymes but allows them to transport hydrons across the membranes by using only the respective quinol to carry them across. The simplest place to start in a description of the Q-cycle is the association of a molecule of the appropriate quinol with the enzyme at the quinol binding site (Q_p) facing the aqueous phase on the positive, acidic side of the membrane in which it is located (Figure 2–32).[861,862] An electron is removed from that quinol (+100 mV) by the Rieske [2Fe–2S] iron–sulfur cluster (+300 mV)[575,847] adjacent to the binding site, at the same time that two hydrons dissociate from the quinol into the aqueous phase on the positive, acidic side of the membrane. The resulting radical anion of the semiquinone, which is a much stronger reductant than the quinol, remains in the site. The radical anion of the semiquinone reorients within the binding site[863] so that it now sits next to heme b_p (–100 mV),[575] one of the two hemes *b* in the enzyme (Figure 2–32), and an electron is transferred from the radical anion of the quinone to this heme b_p.*

This sequence of events accomplishes a **bifurcation of the two electrons** by causing each of them to move on a different path. The bifurcation can be achieved because each of these prosthetic groups, the Rieske [2Fe–2S] iron–sulfur cluster and heme b_p, is only a one-electron redox couple; because the Rieske [2Fe–2S] iron–sulfur cluster has nothing in its vicinity to oxidize so that it could take up a second electron; and because only the radical anion of the semiquinone, not the quinol, is a strong enough reductant to reduce heme b_p while the quinol, although

*In many discussions of quinol—cytochrome-*c* reductase, the subscripts o and i are used for the two quinone binding sites, but these designations cannot be applied to the same sites in plastoquinol—plastocyanin reductase because these sites are on the inside and outside of this enzyme, respectively, rather than the outside and inside. Consequently, in this discussion, which emphasizes the similarities of these two enzymes, the subscripts p and n, for positive and negative, will be used for the binding sites for both quinones and the two hemes *b*.

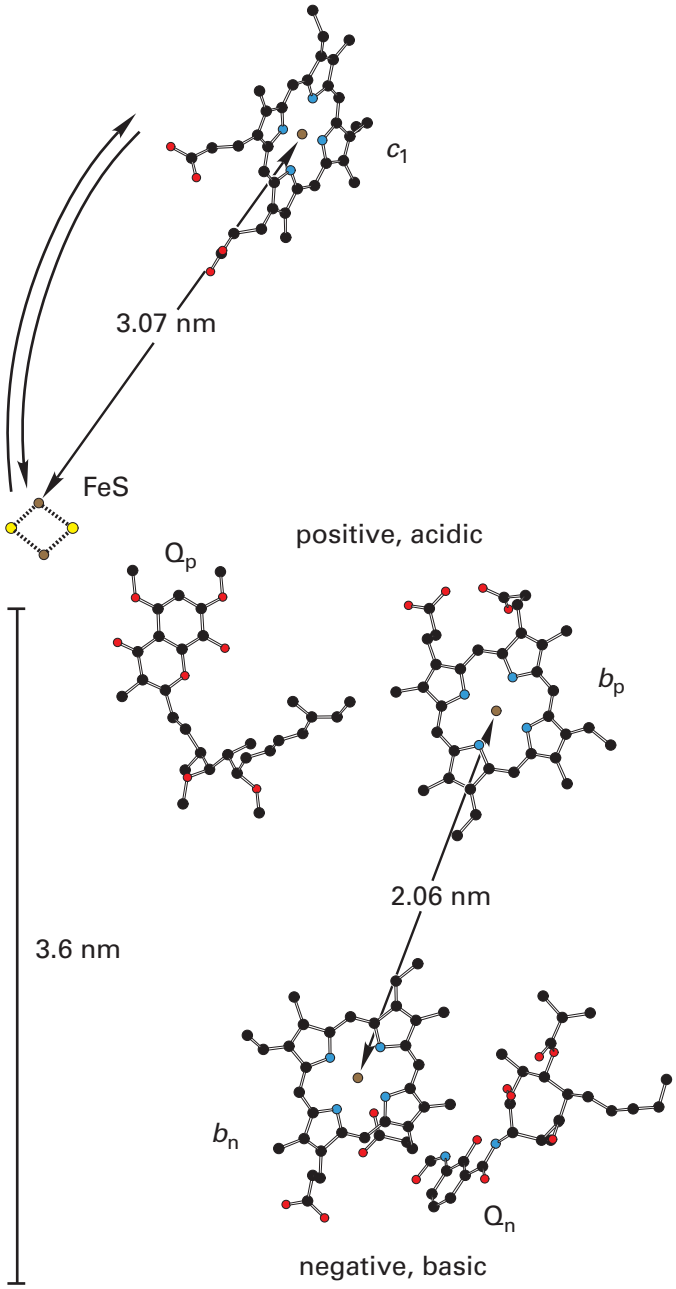

Figure 2–32: Disposition of heme *c*, the Rieske [2Fe–2S] iron sulfur cluster, two hemes *b*, and two quinones in the crystallographic molecular model of bovine quinol—cytochrome-*c* reductase.[861] Black atoms are carbons, red atoms are oxygens, and blue atoms are nitrogens. In the iron–sulfur cluster, yellow spheres are sulfides and rusty brown spheres are iron ions. Intact bovine mitochondria were dissolved in a solution of the detergent dodecyl β-D-maltopyrano-side, and quinol—cytochrome-*c* reductase was purified from the resulting solution by chromatography. Stigmatellin and antimycin A are two inhibitors of the enzyme: stigmatellin binds tightly to the quinone site Q_p on the positive, acidic side of the inner mitochondrial membrane, and antimycin A binds tightly to the quinone site Q_n on the negative, basic side of the inner mitochondrial membrane. These two inhibitors were added to a solution of the enzyme, which was then crystallized with them occupying their respective sites. In this drawing[50] of the prosthetic groups in the resulting crystallographic molecular model, the heme *c* is labeled c_1, the Rieske [2Fe–2S] iron–sulfur cluster is labeled FeS, the heme *b* on the positive, acidic side of the membrane is labeled b_p, the heme *b* on the negative, basic side of the membrane is labeled b_n, stigmatellin is labeled Q_p for the site it occupies, and antimycin A is labeled Q_n for the site it occupies. The approximate position of the planar hydrophobic core of the membrane, which is about 3.6 nm in width, is indicated with the bar. The ability of the Rieske [2Fe–2S] iron sulfur cluster to swing back and forth between heme *c* and quinone site Q_p is indicated by the double arrows. In the crystallographic molecular model, however, the Rieske [2Fe–2S] iron sulfur cluster occupies a stationary position next to quinone site Q_p. The distances between iron ions in the prosthetic groups are noted.

a weaker reductant, is nevertheless a strong enough reductant to reduce the Rieske [2Fe–2S] iron–sulfur cluster. In bovine quinol—cytochrome-*c* reductase, the rate-limiting step in this bifurcation is the removal of the first electron from the quinol by the Rieske [2Fe–2S] iron–sulfur cluster. Following this step, the reduction of heme b_p occurs immediately, so the reduction of the Rieske [2Fe–2S] iron–sulfur cluster and heme b_p occur at the same rate,[864] presumably because the radical anion of the semiquinone is such a strong, reactive reductant. Under certain circumstances, a low amount (0.01–0.1 mole fraction) of the radical anion of the semiquinone, however, can be detected after mixing quinol—cytochrome-*c* reductase from *R. capsulatus* and ubiquinol,[865] a fact that demonstrates its existence. The quinone (Equation 2–157) that is the product of the bifurcation dissociates from the binding site on the positive, acidic side of the membrane but remains as usual in solution in the bilayer.

The **Rieske [2Fe–2S] iron–sulfur cluster is on a loosely tethered domain that can swing back and forth** between the Q_p binding site for quinones on a subunit on the positive, acidic side of the membrane and the prosthetic heme c_1 (Figure 2–32) bound to another subunit of quinol—cytochrome-*c* reductase, or the respective subunit of plastoquinol—plastocyanin reductase containing heme *f*. Both of these hemes are hemes *c*, and both of them are also on the portion of the protein in the aqueous phase on the positive, acidic side of the membrane but quite distant (3 nm) from the site for reducing the quinol.[843,862,866-870] The reduced Rieske [2Fe–2S] iron–sulfur cluster swings through the solution within

its domain from the binding site for quinones to the heme c_1 or heme *f* of the respective enzyme,[667,849,850] its electron is transferred to the heme *c* (+230 mV)[871] in this subunit, and the oxidized Rieske [2Fe–2S] iron–sulfur cluster swings back to the binding site for quinones. The reduced heme c_1 on the subunit of quinol—cytochrome-*c* reductase reduces the heme *c* in a molecule of the small electron-transferring coenzyme cytochrome *c*, or the reduced heme *f* on the subunit of plastoquinol—plastocyanin reductase reduces the copper ion (Figure 2-26D) in the small electron-transferring coenzyme plastocyanin. In either case, the heme *c* in the respective enzyme becomes oxidized as a result. The small electron-transferring coenzymes dissociate and carry the electron away. While all these steps are occurring, the other electron, which had been transferred to the heme b_p (–100 mV), transfers to the heme b_n (+50 mV),[575,872] which is across the enzyme, and hence across the membrane, on its negative, basic side.

A second quinol binds to the binding site for quinones on the positive, acidic side of the membrane, and its two electrons are also bifurcated. The now adjacent, reoxidized Rieske [2Fe–2S] iron–sulfur cluster again removes the first electron; two hydrons are released from the quinol into the aqueous phase on the positive, acidic side of the membrane; the radical anion of the quinone reorients in the binding site; heme b_p, reoxidized after transferring the first electron to heme b_n with the significantly more positive biochemical standard reduction potential and adjacent to the portion of the site now occupied, removes the second electron from the second quinol; and the quinone dissociates from the binding site. At this point, both heme b_p and heme b_n are reduced.

Heme b_n in quinol—cytochrome-*c* reductase is adjacent to the other binding site for quinones (Q_n) on the enzyme (Figure 2–32), which is across the membrane exposed to the solution on its negative, basic side.[862] In the case of plastoquinol—plastocyanin reductase, however, the extra heme *c* in the enzyme, which is electronically coupled to its heme b_n,[873] sits between heme b_n and the binding site Q_n for plastoquinone, and one of the oxygens on the plastoquinone may actually occupy the sixth position on the iron ion in this additional heme *c* when it is bound to this site, permitting it to be reduced directly by that iron ion.[874] The electron on the reduced heme b_n (+50 mV)[575] is transferred to a quinone in the binding site Q_n (Figure 2–32),[862,875] either directly or through the heme *c*, respectively, and this transfer of an electron reduces the quinone to the radical anion. Under appropriate circumstances, a small concentration (0.05–0.25 mole fraction) of the semiquinone can be observed in the Q_n binding site of quinol—cytochrome-*c* reductase from *S. cerevisiae* during its turnover.[876-878] The electron on the reduced heme b_p is transferred to heme b_n, and this second electron on heme b_n is transferred to the radical anion of the quinone as the radical anion of the quinone picks up two hydrons from the aqueous phase on the negative, basic side of the membrane to produce the quinol.[872] The quinol is then released from its binding site on the negative, basic side of the membrane.

Under normal circumstances, the concentration of semiquinone in the Q_n binding site is negligible. This observation suggests that the electrons reducing the quinone arrive one right after the other from two reduced hemes *b*. As noted above, quinol—cytochrome-*c* reductase is a homodimer, which contains two hemes b_p and two hemes b_n, each pair symmetrically arrayed around the twofold axis of symmetry. The two hemes b_p are as close to each other as a heme b_p and a heme b_n on the same subunit, and electrons can be transferred between the symmetrically arrayed hemes b_p as readily[879] as between a heme b_p and a heme b_n. This arrangement may provide additional insurance that the ubiquinone at the Q_n site is reduced by two almost simultaneously arriving electrons.

While all these reactions are occurring, the reduced Rieske [2Fe–2S] iron–sulfur cluster is swinging in its domain from the quinone binding site on the positive, acidic side of the membrane to heme *c* in the heme c_1 subunit or the heme *f* subunit, which it then reduces. That heme *c* in turn reduces another molecule of cytochrome *c* or plastocyanin, respectively, which carries away the electron.

Consequently, the **overall reaction** catalyzed by the respective enzyme is

$$\begin{aligned} 2\,H^+_{neg} + 2\,\text{quinol} + 2\,\text{acceptor}_{ox,pos} \\ + \text{quinone}_{neg} \rightleftharpoons \text{quinol}_{neg} + \\ 2\,\text{acceptor}_{red,pos} + 2\,\text{quinone} + 4\,H^+_{pos} \end{aligned} \quad (2\text{–}176)$$

where pos designates the positive, acidic side of the enzyme, neg designates the negative, basic side of the enzyme, the quinol is either ubiquinol or plastoquinol, the quinone is either ubiquinone or plastoquinone, and the acceptor is either cytochrome *c* or

plastocyanin. The stoichiometry stated in this equation for the hydrons released and taken up on the two sides of the membrane agrees with the numbers measured directly, and this reaction seems to account for all the hydron movements catalyzed by this enzyme.[880] The only purpose for the transfer of electrons from the quinol to cytochrome *c* or plastocyanin down the gradient of standard reduction potential, which is formally transferring hydrons from the negative, basic side of the membrane to the positive, acidic side, is accomplished. The free energy available from oxidation of the quinol and reduction of cytochrome *c* or plastocyanin has been transformed into a chemical gradient of hydrons and an even more dominant electric potential, together comprising an electrochemical potential. The quinols and quinones, which are free solutes miscible in the hydrocarbon of the phospholipid bilayer, rapidly equilibrate across the membrane, with the caveat that neither the monoanionic nor the dianionic conjugate bases of the respective quinols are able to equilibrate across the membrane at a rate that is of any consequence to the overall flux of reducing equivalents through the system.

The hydrons that appear on the positive, acidic side of the membrane are hydrons that were on the two oxygens of ubiquinols or plastoquinols that associated with the enzyme at a site on its positive, acidic side and were then oxidized; the enzyme did not transport these two hydrons across itself from the negative, basic side to the positive, acidic side of the membrane. The hydrons that disappear from the negative, basic side of the membrane are hydrons that were taken up by the two oxygens of ubiquinone or plastoquinone that associated with the enzyme at a site on its negative, basic side as it was reduced to the respective quinol; the enzyme did not transport these two hydrons across itself from the negative, basic side to the positive, acidic side of the membrane. Consequently, this strategy, which is the **formal transport of hydrons**, should be distinguished from the actual **active transport of hydrons** through the portion of the protein embedded in the membrane and spanning it. This distinction is a real one because two other enzymes in the electron transport chain in a mitochodrion perform the active transport of hydrons through the portion of the enzyme that spans the membrane. This active transport requires that there be a continuous path for these hydrons to follow from one side of the enzyme to the other and a physical mechanism to couple the favorable transfer of the electrons to the unfavorable transport of the hydrons, which is not the case for the formal transport of hydrons catalyzed by quinol—cytochrome-*c* reductase and plastoquinol—plastocyanin reductase.

The key to the mechanism of the Q-cycle is the bifurcation of the electrons from the quinol at the binding site for quinones on the positive, acidic side of the membrane; one is transferred to the Rieske [2Fe–2S] iron–sulfur cluster and the other to heme b_p. If both electrons were to pass to the two hemes *b*, heme b_p and heme b_n, quinol would become quinone on the positive, acidic side of the membrane, releasing two hydrons to the aqueous phase on that side, and quinone would become quinol on the negative, basic side of the membrane, absorbing two hydrons from the aqueous phase on that side of the membrane. The stoichiometric reaction would only be the formal transfer of two hydrons from the negative, basic solution to the positive, acidic solution without any net oxidation–reduction. Because the release of hydrons on the positive, acidic side and the absorption of hydrons from the negative, basic side that would occur in this formal transport of hydrons would be significantly endergonic, given the established electrochemical gradient, the reaction would not occur in the direction written; rather, it would occur in the opposite direction, formally transporting hydrons from the more positive, acidic side of the membrane to the more negative, basic side of the membrane and dissipating the electrochemical gradient of hydrons.

Another real concern is the short circuit that would occur if the Rieske [2Fe–2S] iron–sulfur cluster were electronically coupled to heme *c* in the heme c_1 subunit or heme *f* subunit while it was removing an electron from the quinol at the binding site on the positive, acidic side of the membrane. If it were, two electrons would be removed from the quinol instead of one, one ending up on heme *c* (+250 mV) and the other on the Rieske [2Fe–2S] iron–sulfur cluster (+300 mV), and they would be passed from there to cytochrome *c* or plastocyanin. This transfer of these two electrons would be dramatically exergonic ($\Delta E^{\circ\prime}$ = 170–300 mV)[881,882] and certain to occur, and it would defeat completely the strategy used by the enzyme to transfer hydrons formally from the negative, basic side of the membrane to the positive, acidic side because there would be no electrons passing through the membrane to reduce the quinone on the negative, basic side of the enzyme. This **damaging short circuit is prevented** by the fact that the domain in which the Rieske [2Fe–2S] iron–sulfur cluster is located swings a

significant distance through the solution between the binding site for quinones on the positive, acidic side of the membrane and heme *c* in the heme c_1 subunit or heme *f* subunit. For example, in bovine quinol—cytochrome-*c* reductase, when the Rieske [2Fe–2S] iron–sulfur cluster is in position to receive the electron from the ubiquinol, it is 2.70 nm from the closest atom in the π molecular orbital system of the heme *c* (Figure 2–32), too great a distance for effective transfer of an electron. Furthermore, because the domain in which the Rieske [2Fe–2S] iron–sulfur cluster is located is only loosely tethered to the rest of the protein, there is no path through the protein that an electron can follow between the iron–sulfur cluster and heme *c*. Consequently, at any instant, the Rieske [2Fe–2S] iron–sulfur cluster can only be electronically coupled to the quinol or the heme *c*, never to both at the same time. This mutual exclusion precludes the transfer of an electron rapidly and directly from the quinol through the Rieske [2Fe–2S] iron–sulfur cluster to the heme c_1 subunit or heme *f* subunit.

The fact that the quinone binding site on the positive, acidic side of the membrane is constructed in such a way that the quinol can be electronically coupled at a given instant only to the Rieske [2Fe–2S] iron–sulfur cluster or heme b_p, and must reorient to pass between the two,[863] prevents an electron from a reduced heme b_p from being transferred to an oxidized Rieske [2Fe–2S] iron–sulfur cluster that has swung back after it has been oxidized by heme *c*, an unlikely event but one that would also short-circuit the overall reaction.

Nitrate reductase (quinone) spans the plasma membrane of *E. coli* and performs a reaction that also oxidizes a quinol to a quinone and formally transports two hydrons from the negative, basic cytoplasm to the positive, acidic extracytoplasmic solution. This reaction, however, is simpler than that catalyzed by quinol—cytochrome-*c* reductase because it does not require the bifurcation of two electrons. The enzyme oxidizes either menaquinol or ubiquinol to the respective quinone, transfers the electrons across the enzyme and hence the membrane, and uses them to reduce nitrate to nitrite on the other side. The oxidation of the quinol occurs at a site on the extracytoplasmic side of the bacterial membrane and releases the two hydrons into the positive, acidic extracytoplasmic solution, just as does the oxidation catalyzed by quinol—cytochrome-*c* reductase. The reduction of the nitrate (NO_3^-) and two hydrons to nitrite (NO_2^-) and a molecule of water occurs at a site on the cytoplasmic side of the membrane, and the two hydrons that end up on the molecule of water are removed from the negative, basic, cytoplasmic, solution. The quinol is oxidized in two one-electron steps by a heme *b* on the enzyme near its extracytoplasmic surface, and each electron is first passed to a heme *b* in the membrane-spanning portion of the enzyme near its cytoplasmic surface, just as they are in quinol—cytochrome-*c* reductase (Figure 2–32), but the two hemes *b* are only 1.7 nm apart. Each electron is then passed through a [3Fe–4S] iron–sulfur cluster and a chain of four [4Fe–4S] iron–sulfur clusters to its ultimate destination, a molybdopterin at which the nitrate is reduced to nitrite and a molecule of water.[883] In this instance, the overall reaction, the formal reduction of nitrate to nitrite and the molecule of water by the quinol, provides the driving force for the formal transport of the hydrons against their electrochemical gradient. In the absence of an electrochemical gradient of hydrons, this reduction would be significantly exergonic.

The reduction catalyzed by nitrate reductase (quinone) illustrates why quinol—cytochrome-*c* reductase cannot oxidize ubiquinol on the positive, acidic side of the enzyme, pass both electrons through a series of prosthetic groups across the membrane, and reduce a ubiquinone (rather than nitrate) on the negative, basic side of the enzyme because the reaction would be isoergonic in the absence of the electrochemical gradient of hydrons. Consequently, there would be no free energy available to transport the hydrons against their concentration gradient, and the reaction could only operate in reverse.

The ubiquinol that is the substrate for quinol—cytochrome-*c* reductase in mitochondria and heterotrophic bacteria is produced from ubiquinone by a number of different enzymes embedded in the same membrane in which quinol—cytochrome-*c* reductase, ubiquinol, and ubiquinone are dissolved. This coembedment assures that the active sites for reduction of quinones and oxidation of quinols are dissolved in the same solution as their substrates.

Succinate dehydrogenase[884,885] is a flavoenzyme that spans the mitochondrial inner membrane or bacterial plasma membrane.[563] Succinate is oxidized to fumarate (+30 mV) at the prosthetic flavin (-80 mV)[563,886] in the cytoplasmic portion of the enzyme. The two electrons are passed one at a time through three iron–sulfur clusters:[887-889] a [2Fe–2S] iron–sulfur cluster (+10 mV), then a [4Fe–4S] iron–sulfur cluster (–180 mV), and then a [3Fe–4S] iron–sulfur cluster (+70 mV). The electrons are then

passed to a ubiquinone associated with an active site also on the cytoplasmic side of the membrane. This ubiquinone is reduced one electron at a time to ubiquinol (+100 mV), with ubisemiquinone as an intermediate. The only purpose of succinate dehydrogenase is to oxidize succinate to fumarate and transfer the electrons to ubiquinone to produce ubiquinol; no hydrons pass across the membrane, either formally or by active transport. The reason for this lack of hydron transport is that the difference in biochemical standard reduction potential between succinate and ubiquinol (–70 mV) is too small. If the ubiquinone were reduced in an active site on the extracytoplasmic side of the enzyme, the free energy in the electrochemical gradient would reverse the normal direction of the reaction. It seems that the main reason that the enzyme spans the membrane is to ensure access to the ubiquinone and the ubiquinol dissolved in the hydrocarbon.

Succinate dehydrogenase contains a heme *b*, which is not necessary for the enzymatic reaction.[890] Electrons cannot be transferred efficiently between the iron–sulfur clusters and this heme *b* when the binding site for ubiquinone is unoccupied, but they are rapidly transferred back and forth between the heme *b* and ubisemiquinone when the ubisemiquinone is in the site.[891] It seems to be the case that the function of the heme *b* is to stabilize the ubisemiquinone by sharing its unpaired electron while it waits for the second electron. One of the two hemes *b* in nitrate reductase (quinone) from *E. coli* stabilizes the adjacent menasemiquinone that is an intermediate in the transfer of an electron performed by this enzyme.[892]

Under anaerobic conditions, **fumarate reductase (quinol)** is produced in bacteria.[893-896] Fumarate reductase (quinol) is related to succinate dehydrogenase (37% identity; 1.4 gap percent for *E. coli*). It catalyzes the same reaction as succinate dehydrogenase through the same prosthetic groups, but anaerobiosis requires that it mostly reduce fumarate to succinate. Consequently, instead of the ubiquinone (+100 mV) used by succinate dehydrogenase, fumarate reductase (quinol) uses menaquinone (–60 mV) as its substrate. Because the biochemical standard reduction potential of the redox couple of fumarate and succinate is +30 mV, the reaction runs efficiently in one direction with succinate dehydrogenase (ubiquinone) because succinate is enough of a reductant to reduce ubiquinone effectively, and it runs efficiently in the other direction with fumarate reductase (quinol) because fumarate is enough of an oxidant to oxidize menaquinone effectively. Fumarate reductase (quinol) also does not transport hydrons across its membrane.[897,898]

As many as eight different flavoenzymes in the interior of a mitochondrion oxidize their respective nominal substrates and reduce the same general substrate, the flavin in electron-transferring flavoprotein dissolved in the interior solution.[899] The reduced flavin (–20 mV) in the electron-transferring flavoprotein is then reoxidized at the interior surface of the mitochondrial inner membrane by the membrane-anchored enzyme **electron-transferring-flavoprotein dehydrogenase**.[899-901] During the oxidation of the reduced flavin in electron-transferring flavoprotein, the two electrons are distributed singly,[900] one to the prosthetic flavin (+20 mV) in the enzyme, which becomes the semiquinone, and the other to the prosthetic [4Fe–4S] iron–sulfur cluster (+50 mV) in the enzyme.[899,902] They are then passed one at a time to the ubiquinone bound in the active site for its reduction to produce ubiquinol. In this instance, both the active site at which the electron-transferring flavoprotein is oxidized and the site for the reduction of ubiquinone to ubiquinol are in the interior of the mitochondrion, so no hydron transport is involved in the transfer of the electrons. In fact, the enzyme does not even span the inner membrane of the mitochondrion but is only embedded in it by a hydrophobic portion of its surface.

The largest of the enzymes that reduce ubiquinone to ubiquinol in mitochondria and bacterial plasma membranes is **NADH:ubiquinone reductase (H^+-translocating)**,[903-906] which dwarfs the membrane that it spans. Reduced nicotinamide-adenine dinucleotide is oxidized by the flavin within the enzyme[907] by hydride transfer, and the two electrons on the reduced flavin are then transferred one at a time through at least seven of the nine iron–sulfur clusters in the enzyme from *T. thermophilus* (Figure 2–33),[651,908-910] two of which are [2Fe–2S] clusters and seven of which are [4Fe–4S] clusters.[911,912] The [4Fe–4S] iron–sulfur cluster 2.05 nm off the main chain does not participate in electron transfer[913] and exists in only a few bacteria. Aside from the fact that this latter [4Fe–4S] iron–sulfur cluster is missing, the arrangements and orientations of the iron–sulfur complexes in the NADH:ubiquinone reductases (H^+-translocating) in the inner membranes of the mitochondria from animals are the same[839] as their arrangements and orientations in the enzyme from *T. thermophilus*.

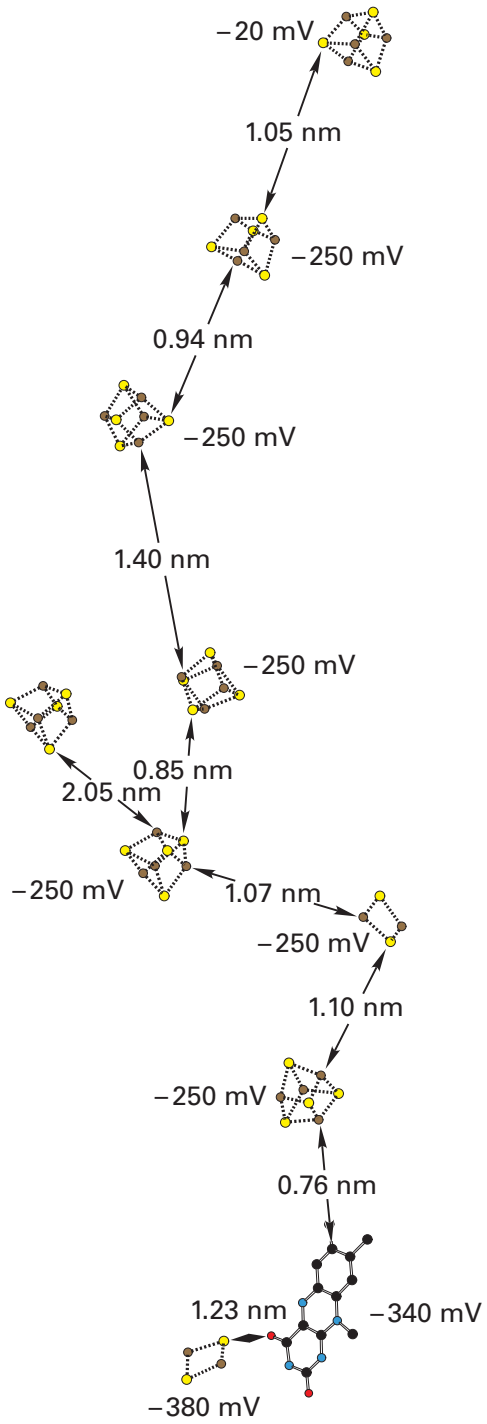

Figure 2–33: Disposition of flavin and nine iron–sulfur clusters, seven [4Fe–4S] and two [2Fe–2S], in the crystallographic molecular model of a portion of NADH:ubiquinone reductase (H^+-translocating) from *T. thermophilus*.[651] Black atoms are carbons, red atoms are oxygens, and blue atoms are nitrogens. In the iron–sulfur clusters, yellow spheres are sulfides and rusty brown spheres are iron ions. Membranes from fragmented bacteria were dissolved in a solution of the detergent dodecyl β-D-maltopyranoside, and the hydrophilic portion of NADH:ubiquinone reductase (H^+-trans-locating) was purified chromatographically.[909] The protein was then crystallized. The drawing[50] is of the flavin and the nine iron–sulfur clusters in the resulting crystallographic molecular model. The distances between the closest atoms in adjacent iron sulfur clusters are noted, as well as the distance from the closest atoms in the two closest iron sulfur clusters to the π molecular orbital system of the flavin. The midpoint potentials listed are those for NADH:ubiquinone reductase (H^+-translocating) from *C. livia* within intact mitochondria.[908,910]

Six of the seven iron–sulfur clusters in the main chain for electron transfer[890,908,910] have the same biochemical standard reduction potential (–250 mV)* and are used to span the distance (>10 nm) in steps of 0.8–1.4 nm between the site for oxidation of NADH and the site at which ubiquinone is reduced.[561] The last iron–sulfur cluster (–20 mV) in the chain is a sink for the electron to pull it along this chain of iron–sulfur clusters. The flavin has a biochemical standard reduction potential of –340 mV, so the initial rise in potential between the flavin and the initial iron–sulfur cluster pushes the electrons forward through the chain.

Ubiquinone is reduced by two electrons on the negative, basic side of the membrane and picks up two hydrons from that solution. The NADH is oxidized to NAD^+ and two electrons, also on the negative, basic side of the membrane, and releases one hydron into that solution. In addition to the resulting net of one hydron removed from the negative, basic solution, known as the scalar hydron, four additional hydrons from the negative, basic side of the membrane are transported to the positive, acidic side for every two electrons passed from NADH to ubiquinone.[915] A strategy for formal transfer of

*There are electrostatic interactions between the clusters in this region of the protein. The reduction of one cluster can lower the midpoint potentials of its neighbors.[914]

hydrons similar to the Q-cycle does not seem to be involved since all the prosthetic groups among which the electrons are transferred are located on the negative, basic side of the membrane outside the membrane-spanning portions of the protein, which contains no prosthetic groups of oxidation–reduction.[651,916-921] Consequently, these four hydrons are actively transported through the enzyme.

In mitochondria, the three reactions catalyzed by NADH:ubiquinone reductase (H^+-translocating), succinate dehydrogenase, and electron-transferring-flavoprotein dehydrogenase, as well as several other oxidation–reductions, receive electrons from diverse sources, but each transfers the electrons to one of the quinones, in particular ubiquinone, to form ubiquinol. This common product passes the electrons derived from each of these enzymes to the central clearinghouse of quinol—cytochrome-*c* reductase. As the concentration of ubiquinone and ubiquinol in the mitochrondrial inner membrane is varied experimentally, the kinetics of electron transfer between either NADH:ubiquinone reductase (H^+-translocating) or succinate dehydrogenase, acting as the donor, and quinol—cytochrome-*c* reductase, acting as the acceptor, are consistent with the following sequence of events. The ubiquinone bound to the donor receives the electrons. The resulting ubiquinol dissociates from the donor, diffuses at random within the mitochondrial membrane, collides with the acceptor, associates with the acceptor, and transfers the electrons to it.[922-924] When ubiquinone is added back to mitochondria that have been depleted of endogenous ubiquinone, the behavior of the increase in electron transfer among these enzymes is also consistent with the postulate that each of them has access to the same mobile pool of ubiquinone and ubiquinol dissolved in the phospholipid bilayer of the membrane.[925]

The reduced cytochrome *c* produced by quinol—cytochrome-*c* reductase in mitochondria and the plasma membranes of bacteria is reoxidized by **cytochrome-*c* oxidase**,[926,927] an enzyme that spans the membrane and catalyzes the reaction[928,929]

$$8\ H^+_{neg} + 4\ \text{ferrocytochrome}\ c_{pos} + O_2 \rightleftharpoons 2\ H_2O + 4\ \text{ferricytochrome}\ c_{pos} + 4\ H^+_{pos} \quad (2\text{–}177)$$

The electron from the ferrocytochrome *c* is first transferred[746] to the dinuclear CuA cluster of copper ions (+240 mV) (Figure 2–26F), and from there to a heme *a* (+250 to +380 mV)[930,931] with the imidazolyl groups of two histidines as axial ligands (heme *a*), and finally to a heme *a* (heme a_3) with only one imidazolyl group from a histidine as a ligand. Heme a_3 is immediately adjacent to an additional prosthetic copper ion coordinated by three imidazolyl groups from three histidines with their nitrogens in a planar trigonal array.[673,746,932] The ultimate receptacle of the electrons is a molecule of oxygen bound between the iron of heme a_3 and the copper ion and occupying simultaneously the vacant sites for ligands on each of them. The site to which the oxygen binds is on the negative, basic side of the membrane. Four of the eight hydrons taken up on this side, the scalar hydrons, end up on the two molecules of water. The other four hydrons are actively transported along a path through the portion of the enzyme that spans the membrane.

One of the two quinol oxidases[933-935]

$$2\ \text{ubiquinol} + O_2 \rightleftharpoons 2\ H_2O + 2\ \text{ubiquinone} \quad (2\text{–}178)$$

located in bacterial plasma membranes is closely related to cytochrome-*c* oxidase.[936] In this quinol oxidase, however, a heme *o*[937,938] replaces heme a_3 and a heme *b*[939] replaces heme *a* of cytochrome-*c* oxidase. The prosthetic copper ion adjacent to heme *o*, in the active site where the oxygen is reduced, is still present, but the CuA copper cluster, which is the entry in cytochrome-*c* oxidase for the electron from cytochrome *c*, is missing. The enzyme has a site with high affinity for ubiquinol and ubiquinone[940,941] where electrons are removed one at a time from ubiquinol and transferred to heme *b*, with a radical anion of ubisemiquinone as an intermediate,[942] and then to heme *o*. Again, reduction of oxygen consumes four hydrons from the negative, basic side of the membrane, but oxidation of two molecules of ubiquinol produces four hydrons on the positive, acidic side of the membrane, and consequently the enzyme accomplishes the formal transport of four hydrons. An additional four hydrons are transferred by active transport through the protein from the negative, basic side to the positive, acidic side of the membrane during the complete reaction catalyzed by the enzyme.[943]

The transfer of electrons between quinol—cytochrome-*c* reductase and cytochrome-*c* oxidase is mediated by cytochrome *c*, each molecule of which accepts an electron from the reductase and donates that electron to the oxidase. Cytochrome *c*

performs this transfer by accepting an electron from quinol—cytochrome-*c* reductase, dissociating from it, diffusing at random through the solution between the outer and inner mitochondrial membranes until it collides with the site for its oxidation on cytochrome-*c* oxidase, associating with that site, and donating the electron.

At physiological ionic strength, cytochrome *c* binds tightly to the cytoplasmic surface of the inner mitochondrial membrane, presumably to quinol—cytochrome-*c* reductase or cytochrome-*c* oxidase at a given instant. When cytochrome *c* is bound tightly to the mitochondrial membrane and then crosslinked to it, the protein to which it becomes covalently attached is cytochrome-*c* oxidase, not quinol—cytochrome-*c* reductase.[944] A similar result is obtained when mixtures of cytochrome *c* and purified cytochrome-*c* oxidase are crosslinked.[945] This observation is puzzling because a complex between cytochrome-*c* oxidase and cytochrome *c* has never been crystallized.

At low ionic strength, cytochrome *c* binds specifically and with high affinity to the heme c_1 subunit purified from quinol—cytochrome-*c* reductase, and there is a crystallographic molecular model of a specific complex between cytochrome *c* and the heme c_1 subunit in an intact molecule of quinol—cytochrome-*c* reductase from *S. cerevisiae*. In this complex, which forms at high concentrations of cytochrome *c* and quinol—cytochrome-*c* reductase at physiological ionic strength, the two hemes *c* from the respective proteins are only about 0.5 nm apart.[946] In more dilute solution, however, the transfer of electrons between purified heme c_1 subunit from bovine quinol—cytochrome-*c* reductase and cytochrome *c* is a purely bimolecular reaction at normal ionic strengths,[947] and at physiological ionic strength, the dissociation constant of cytochrome *c* from the heme c_1 in quinol—cytochrome-*c* reductase from *R. capsulatus*[948] was greater than 0.5 mM. These facts are inconsistent with the existence of a strong, long-lived complex between these two proteins in mitochondria[949] and suggest that, in a mitochondrion, cytochrome *c* may have to associate many times with quinol—cytochrome-*c* reductase before the electron is transferred.

The possibility that cytochrome *c* is bound to both proteins simultaneously has been roundly discounted. The crystallographic molecular model of the complex between cytochrome *c* and the heme c_1 subunit in quinol—cytochrome-*c* reductase[946] places the cytochrome *c* in a location that makes it sterically impossible to bind simultaneously to any location on cytochrome-*c* oxidase, let alone the site thought to be its binding site on cytochrome-*c* oxidase.[950] Furthermore, there is a crystallographic molecular model of a large complex containing both cytochrome-*c* oxidase and quinol—cytochrome-*c* reductase that is thought to represent the state in which these enzymes exist in the mitochondrial membrane. In this complex, the exterior surface of cytochrome-*c* oxidase is so distant from the exterior surface of quinol—cytochrome-*c* reductase that cytochrome *c* could not come close to bridging the gap,[924] and cytochrome *c* must be added to the solution in which this complex is dissolved in order to observe electron transfer between the two enzymes.[951]

In the chromatophores of most photosynthetic bacteria, the ubiquinol oxidized to ubiquinone by quinol—cytochrome-*c* reductase is the product of reduction of ubiquinone by a photosynthetic reaction center, and the reduced cytochrome *c* or high-potential [4Fe–4S] iron protein[952-954] produced by quinol—cytochrome-*c* reductase is oxidized by a photosynthetic reaction center. A **photosynthetic reaction center** is a membrane-spanning enzyme that forces an electron to move from a donor of more positive standard reduction potential to an acceptor of more negative standard reduction potential by coupling that movement to the consumption of the energy in a photon of visible light. A photon of visible light or an exciton resulting from the absorption of a photon of light by prosthetic groups in antenna proteins and passed to the reaction center by electronic energy migration is absorbed to form the electronically excited state of a prosthetic group. The excited electron in this electronically excited state has a much more negative standard reduction potential than it did in the ground state. As a result, the excited electron can pass spontaneously to other prosthetic groups that have more positive standard reduction potentials than the electronically excited state. A photosynthetic reaction center can be viewed as a cage that encloses and positions an array of prosthetic groups that perform one-electron transfers. This array of prosthetic groups in the reaction center from the photosynthetic purple bacterium *R. sphaeroides* (Figure 2–34)[955-957] describes the path taken by the excited electron.

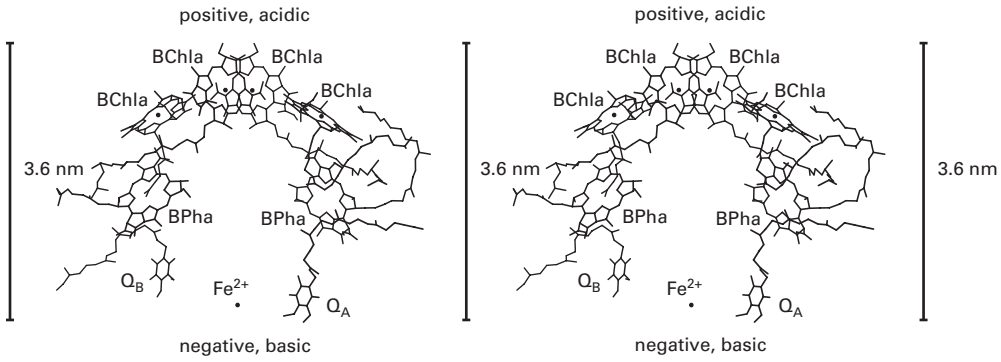

Figure 2–34: Stereodrawing[50] of the disposition of four bacteriochlorophylls *a* (BChla), two bacteriopheophytins *a* (BPha), two ubiquinones (Q_A and Q_B), and a prosthetic Fe^{2+} in the crystallographic molecular model of photosynthetic reaction center from the bacterium *R. sphaeroides*.[955] The bacteriochlorophylls have magnesium ions in their centers, and the bacteriopheophytins are empty. The path of the electron is from the top of the figure downward. It begins in the electronically excited state of the special pair, which is the rotationally pseudosymmetric dimer of bacteriochlorophylls *a* at the top of the array. The local twofold rotational axis of pseudosymmetry within the reaction center itself runs vertically through the Fe^{2+} and the center of the special pair. On each side of the array, right and left, a bacteriochlorophyll *a* bridges the space between the special pair and each of the symmetrically positioned bacteriopheophytins *a*, but the electron, under normal circumstances, transfers from the special pair through the bacteriochlorophyll *a* on the right side of the array in the drawing to the bacteriopheophytin *a* also on the right side. Below each of the bacteriopheophytins is an ubiquinone. The two ubiquinones are on opposite sides of the Fe^{2+}. The electron is transferred from the bacteriopheophytin *a* on the right side of the array to the ubiquinone on the right side (Q_A) and from the ubiquinone on the right side to the ubiquinone on the left side (Q_B). The approximate position of the planar hydrophobic core of the membrane, which is about 3.6 nm in width, is indicated with the bar. The phytyl chains on most of the bacteriochlorophylls *a* and bacteriopheophytins *a* are not complete in the crystallographic molecular model, and the polyisoprenoid on one of the ubiquinones is incomplete also. The polyisoprenoid on the other ubiquinone was truncated in the drawing to save space.

The central prosthetic group in a photosynthetic reaction center in the chromatophore of a photosynthetic purple bacterium is the **special pair** formed from two[958] bacteriochlorophylls (Figure 2–35).[959,960] Two of the pyrrolyl groups, one from each bacteriochlorophyll, are stacked against each other. The two bacteriochlorophylls* of the special pair are arrayed about a twofold rotational axis of pseudosymmetry that runs between the two stacked pyrrolyl groups and is horizontal in the drawing of Figure 2–35. The stacking of the pyrrolyl groups, the resulting overlap of their two aromatic π molecular orbital systems, and the relative orientation of the transition dipoles of the two bacteriochlorophylls that is produced by the juxtaposition shifts the absorption of light by the pair of bacteriochlorophylls to longer wavelengths (800–1000 nm) than that of a lone bacteriochlorophyll (765–785 nm). This shift in the absorption to lower energy permits the special pair to be a much more efficient sink for the exciton that is transferred to it from the prosthetic groups in the light-harvesting antennae, which absorb light of shorter wavelengths and higher energy.

The twofold rotational axis of pseudosymmetry that produces the overlap in the special pair in a photosynthetic purple bacterium exists because two of the three subunits[961] of the reaction center, subunits L and M, are homologous in sequence (30% identity; 2 gap percent),[962] superposable on each other's native structure,[963] span the membrane, and necessarily are arrayed around a twofold rotational axis of pseudosymmetry normal to the plane of the membrane.[964] This rotational axis of pseudosymmetry within the protein relates the two bacteriochlorophylls of the special pair. Because these two subunits in the protein arose from the same common ancestor, the first oligomer containing a reaction center must have been an α_2 dimer of identical membrane-spanning subunits that coincidentally brought the two bacteriochlorophylls together in the proper orientation to display the unique properties of a special pair. In fact, in the crystallographic molecular model of one bacterial reaction center, that from *Heliobacterium modesticaldum*, the structures of the two subunits that surround the prosthetic groups are superposable respectively on the L and M subunits of the other bacterial reaction centers, but both of these two subunits in this reaction center are identical in their sequence of amino acids and are arrayed around a perfect, crystallographic twofold rotational axis of symmetry.[965]

At the same time that the primordial dimerization occurred, each of the identical subunits also brought along one copy of each of the remaining prosthetic groups necessary for the reaction catalyzed by the enzyme: a second bacteriochlorophyll and a bacteriopheophytin. Each subunit also contributed a binding site for ubiquinone or menaquinone. Consequently, in a reaction center, each of these features is duplicated around the twofold rotational axis of pseudosymmetry (Figure 2–34).

Crystallographic molecular models from data sets with short Bragg spacing are available for the photosynthetic reaction centers from the purple bacteria *Blastochloris viridis*,[959,960] *R. sphaeroides* (Figure 2–34), [956,957] and *Thermochromatium tepidum*,[966] which closely resemble each other.[967] The special pair in the photosynthetic reaction center from *R. sphaeroides* absorbs light of wavelength 865 nm, where photons have energies of 138 kJ mol^{-1} (equivalent to a difference in reduction potential of −1430 mV), while the special pair in the reaction center from *B. viridis* absorbs light of wavelength 960 nm,[968] where photons have energies of 124 kJ mol^{-1} (equivalent to a difference in reduction potential of −1290 mV). The reaction centers from *B. viridis* and *R. sphaeroides* accept electrons from a cytochrome *c* and the reaction center from *T. tepidum* accepts electrons from a high-potential iron–sulfur protein, but most photosynthetic bacteria use a high-potential iron–sulfur protein as the electron donor.[969]

Either the absorption of an exciton transferred from an antenna protein by electronic energy migration or the absorption of light within the reaction center itself in a photosynthetic purple bacterium produces an **electronically excited state**. There are several ways for a photon of light to be absorbed within a reaction center that has been purified and lacks its antenna.[970] Although it can be absorbed directly by the special pair, light can also be absorbed by either of the two bacteriochlorophylls that are adjacent to the special pair and symmetrically positioned around the axis of pseudosymmetry (Figure 2–34). Regardless, however, of where the light is absorbed by the purified reaction center, the immediate ($t_{½}$ < 200 fs) result is the same electronically excited state of the special pair in which one electron has been transferred from the highest occupied π molecular orbital of the special pair in its

**Blastochloris viridis* contains bacteriochlorophylls *b* and bacteriopheophytins *b*, while *R. sphaeroides* and *T. tepidum* contain bacteriochlorophylls *a* and bacteriopheophytins *a*.

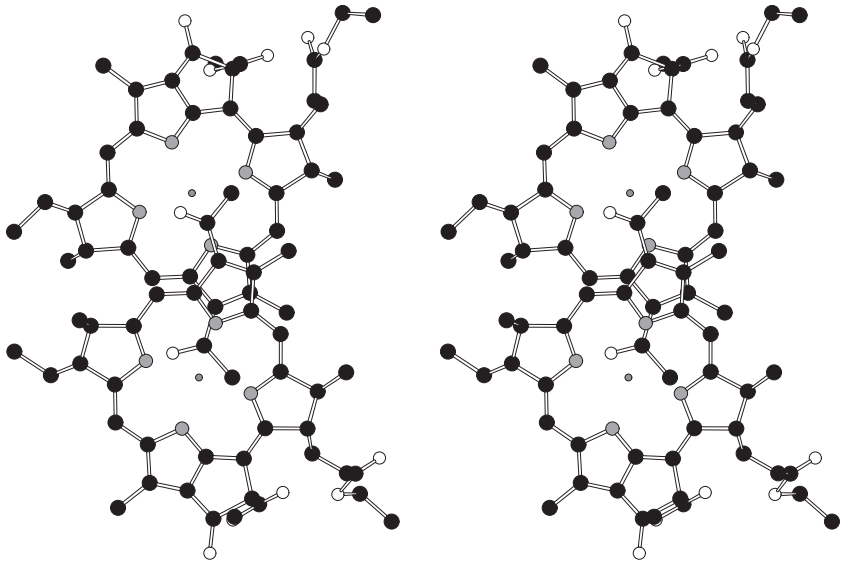

Figure 2–35: Stereodrawing[50] of the special pair of bacteriochlorophylls *b* in the crystallographic molecular model of the photosynthetic reaction center from *B. viridis*.[960] Black atoms are carbons, white atoms are oxygens, small gray atoms are nitrogens, and small dark gray spheres are magnesium ions. The two bacteriochlorophylls *b* of the special pair are held in orientations displayed symmetrically about the twofold rotational axis of pseudo-symmetry of the protein itself. The rotational axis runs horizontally in the plane of the page between the two bacteriochlorophylls *b* and causes them to overlap at the same pyrrole from each. The tetraisoprenoid phytyl groups attached in ester linkage to the 3-(2-carboxyethyl) groups at the carbons 17 of each of the bacteriochlorophylls *a* (R_6 in **2–54**) were not drawn beyond their first two carbons.

ground state to its lowest unoccupied π molecular orbital. Crystallographic molecular models of the special pair in the active site of the reaction center from *B. viridis* in the first 5 ps indicate that, in the initial excited state, the two bacteriochlorophylls move even closer together as they share the excited electron.[971] From here on, unless otherwise noted, the fate of this one electron, now alone in the highest occupied π molecular orbital in the electronically excited state of the reaction center of *R. sphaeroides*, will be followed.

Normally, after the immediate electronic relaxation of the excited state ($t_{½}$ = 0.12 ps),[972] the electron in the electronically excited state of the special pair would return within several nanoseconds to the π molecular orbital of lower energy from which it came and that now contains only one electron, and this process would emit a quantum of light of longer wavelength (920 nm) as fluorescence. In fact, a short time after the absorption of the photon, such fluorescence emission can be observed from a population of electronically excited reaction centers, but it decays rapidly (200 ns^{-1}; $t_{½}$ = 4 ps).[972,973]

The quenching of this fluorescence is due to the **transfer of the excited electron** from the special pair to the lowest unoccupied π molecular orbital on one of the bacteriopheophytins (Figure 2–34) in the enzyme.[973] This transfer is favorable because **the excited electron in the special pair has become a much stronger reductant** than it was when it was in the ground state. After the immediate, automatic relaxation of the electronically excited state, the biochemical standard reduction potential of the special pair has experienced, relative to the ground state, a decrease equivalent to the energy in a quantum of light of a wavelength equal to that of its fluorescent emission (920 nm; $\Delta E^{\circ\prime}$ = –1350 mV).

The transfer of the electron to the bacteriopheophytin creates a radical anion on the bacteriopheophytin (Equation 2–156) and leaves a radical cation behind on the special pair.[974] As soon as the excited electron is passed to the bacteriopheophytin, the π molecular orbital that it occupied on the special pair is no longer occupied but has become the lowest unoccupied π molecular orbital of the special pair. The special pair is now no longer electronically excited because the excited electron has left, and **the radical cation of the special pair is in its ground state**.

Because a bacteriochlorophyll, not involved in the special pair, lies between the special pair and the bacteriopheophytin (Figure 2–34), it is assumed that **transfer of the electron occurs through the bacteriochlorophyll**.[973] There is spectroscopic evidence for the transfer of the electron through this bacteriochlorophyll,[972] and when the bacteriopheophytin is replaced with pheophytin *a*, which has a more negative biochemical standard reduction potential, the electron can be trapped on the bacteriochlorophyll before it returns to the ground state of the special pair (2 ns^{-1}; $t_{½}$ = 430 ps).[975] Under normal circumstances, however, the electron passes through this bacteriochlorophyll to the bacteriopheophytin so rapidly (k_{in} = 100 ns^{-1}, $t_{½}$ = 7 ps; k_{out} = 200 ns^{-1}, $t_{½}$ = 4 ps)[970,972] that it does not reside detectably on the bacteriochlorophyll.[976,977]

In the ground state as opposed to the electronically excited state, the equation for the transfer of an electron from the special pair to this adjacent bacteriochlorophyll would be

$$\mathrm{BChl{\cdot}BChl + BChl \rightleftharpoons BChl{\cdot}BChl^{\cdot+} + BChl^{\cdot-}} \qquad (2\text{–}179)$$

In the ground state, the half-reaction of this overall oxidation–reduction that occurs at the bacteriochlorophylls in the special pair would be

$$\mathrm{BChl{\cdot}BChl^{\cdot+} + e^{-} \rightleftharpoons BChl{\cdot}BChl} \qquad (2\text{–}180)$$

and the half-reaction that occurs at the adjacent bacteriochlorophyll (BChl) would be

$$\mathrm{BChl + e^{-} \rightleftharpoons BChl^{\cdot-}} \qquad (2\text{–}181)$$

As is normally the case for the formation of a radical cation of one molecule and the formation of a radical anion of the same molecule or another, similar molecule, in the ground state, the biochemical standard reduction potential for Equation 2–180 is much more positive than that for Equation 2–181 ($\Delta E^{\circ\prime}$ = +1290 mV)[972] because it involves separation of charge and unpairing of electrons. It follows that, in the ground state, an electron cannot be transferred from a bacteriochlorophyll in the special pair to the adjacent bacteriochlorophyll, but the biochemical standard reduction potential for Equation 2–180 is decreased by –1350 mV upon the formation of the relaxed electronically excited state. This decrease in the standard reduction potential causes the transfer of the electron to the adjacent bacteriochlorophyll on its way to the bacteriopheophytin to become favorable.

When either Histidine L173 or Histidine M202 in the enzyme is mutated to a leucine, one or the other of the bacteriochlorophylls in the special pair loses its magnesium ion; and, as a result, the rate at which the electron is transferred to the bacteriopheophytin is decreased, the lifetime of the electronically excited state is decreased, and the quantum yield of the transfer of the excited electron to the bacteriopheophytin decreases from nearly 1.0 in the native enzyme to about 0.5 in the mutant.[978,979]

As a result of the primordial dimerization that created the special pair, each dimeric reaction center originally contained two **identical paths for electron transfer**. When the gene duplicated and the two subunits began to evolve independently, one of the two paths was shut down. Under normal circumstances, the transfer of the excited electron occurs between the special pair and only the bacteriochlorophyll and its adjacent bacteriopheophytin in the L subunit of the enzyme (on the right side of Figure 2–34). It has been proposed that, at least in part, this preference is due to the hydroxy group of a tyrosine that is oriented so that the positive pole of its dipole is directed toward the bacteriochlorophyll in the L subunit, which would make it the more effective oxidant. The orientation of this dipole stabilizes the radical anion on this particular bacteriochlorophyll (Equation 2–181).[980] The same position in the sequence of amino acids for the homologous subunit is occupied by a phenylalanine. When the identity of these amino acids is switched by site-directed mutation, a portion of the electron transfer is diverted artifactually into the opposite bacteriopheophytin on the M subunit.[981]

If the excited electron can be delocalized to the bacteriopheophytin in the first place, it must be able to **return to the highest occupied π molecular orbital in the ground state of the radical cation of the special pair** that is now occupied by an unpaired electron. If its transfer beyond the bacteriopheophytin is blocked by reducing the ultimate acceptor of the electron,[974] the trapped electron eventually returns to this highest occupied π molecular orbital in the ground state of the radical cation of the special pair, which is at a much lower energy than the highest occupied π molecular orbital on the radical anion of the bacteriopheophytin that it now occupies. Were it to return to the special pair, the energy of the electronically excited state would be dissipated inconsequentially as heat and fluorescence. The rate of decay of the electronically excited state under these circumstances (70 μs^{-1}; $t_{½}$ = 10 ns in *B. viridis* and 50 μs^{-1}; $t_{½}$ = 14 ns in *R. sphaeroides*)[974,982] is less than it would have been if all the excited electron density had remained in the highest occupied π molecular orbital on the excited special pair rather than spreading between the two locations. This decrease in rate is due to the fact that the biochemical standard reduction potential of the electron on the bacteriopheophytin *b* is about +70 mV more positive than in the relaxed electronically excited state of the special pair,[972] and this difference in biochemical standard reduction potential causes most of the electron density to reside on the bacteriopheophytin at equilibrium.

Under normal circumstances, the electron that is now on the bacteriopheophytin transfers **from the bacteriopheophytin to the quinone (Q_A) bound in the A site** adjacent to the bacteriopheophytin at a rate (5 ns^{-1}; $t_{½}$ = 150 ps)[982] that is significantly more rapid that the rate at which it would return to the ground state of the radical cation of the special pair. The product of this next transfer is the radical anion of the semiquinone. In the reaction center from *B. viridis*, this quinone is menaquinone, while in the reaction center from *R. sphaeroides* (Figure 2–34), it is ubiquinone, and each of these respective quinones is bound tightly to the A site as a **prosthetic group**. A crystallographic molecular model of the reaction center from *B. viridis* 300 ps after the absorption of a photon indicates that, upon the arrival of the electron, the now radical anion in the A site moves much closer to the closest imidazolyl group that is a ligand to the iron ion.[971]

At this point, the excited electron located in the semiquinone radical anion of the semiquinone is a good distance (Figure 2–34) from the hole in the highest occupied π molecular orbital in the radical cation of the special pair where it was located before the excitation. Because the biochemical standard reduction potential of the radical anion of the semiquinone is +750 mV more positive than the relaxed electronically excited state of the special pair (Figure 2–36),[968,982] the electron has also lost a significant amount of its original energy. In exchange for this expenditure of –72 kJ mol^{-1} of free energy associated with this increase in standard reduction potential (Figure 2–36), **the electron has gained time**. The observed rate constant[982-984] for the reaction

$$P^{\cdot+}BPhQ_A^{\cdot-} \rightleftharpoons PBPhQ_A \qquad (2\text{–}182)$$

is 8 s^{-1} ($t_{½}$ = 90 ms). This rate constant is considerably smaller than the rate constant for the return of the

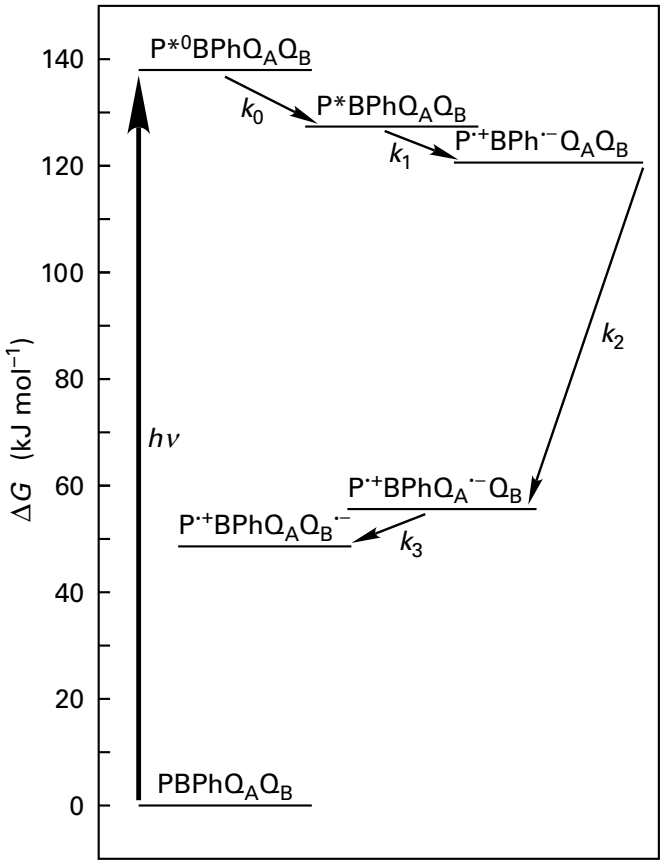

Figure 2–36: Energy diagram for the path of the electron in bacterial photosynthesis.[968,982] The four successive prosthetic groups on the path of the electron (Figure 2–34) are the special pair (P), the bacteriopheophytin (BPh), the tightly bound quinone (Q_A), and the loosely bound quinone (Q_B). The instantaneously populated electronically excited state of the special pair is indicated by P^{*0}; the vibrationally relaxed electronically excited state of the special pair is indicated by P*; its radical cation is indicated by $P^{\bullet +}$; and the successive radical anions are indicated by $BPh^{\bullet -}$, $Q_A^{\bullet -}$, and $Q_B^{\bullet -}$. The energy levels and rate constants are those for the reaction center from *R. sphaeroides*. The energy levels of the various steps relative to the ground state are presented in kilojoules mole^{-1}. The rate constants for transfer of the electron between the various steps are $k_0 = 6000\ ns^{-1}$ ($t_{½} = 0.12$ ps); $k_1 = 200\ ns^{-1}$ ($t_{½} = 4$ ps); $k_2 = 5\ ns^{-1}$ ($t_{½} = 150$ ps); and $k_3 = 5 \times 10^3\ s^{-1}$ ($t_{½} = 140\ \mu s$). Before the electron has time to move from quinone A to quinone B, an electron from the cytochrome c_2 in intact cells of *R. sphaeroides* would normally fill the hole in $P^{\bullet +}$.

electron from the radical anion of the bacteriopheophytin to the radical cation of the special pair ($5 \times 10^7\ s^{-1}$; $t_{½} = 14$ ns). This difference in rate constants is a measure of the time gained by the electron by the expediture of the free energy originally in the electronically excited state. The rate constant for return of the electron to the radical cation of the special pair from the radical anion of the semiquinone (Equation 2–182), however, is still too large to provide sufficient time for the energy to be trapped efficiently. To overcome this dilemma, a second strategy is employed.

Long after the electron has been transferred from the bacteriopheophytin to the quinone (1–30 μs), the hole in the highest occupied π molecular orbital of the radical cation of the special pair, left behind by the departed excited electron and to which it might return, is filled by an **electron from a heme *c* on a cytochrome *c*** or the electron from a [4Fe–4S] iron–sulfur cluster on a reduced high-potential iron–sulfur protein. The enzyme from *B. viridis* binds its cytochrome *c* so tightly that it is purified with the enzyme and is present in the crystallographic molecular model (Figure 2–37).[959] The cytochrome c_2 from *R. sphaeroides* binds to its reaction center less strongly ($K_d = 0.34\ \mu M$)[985] and under normal circumstances transfers its electron to the reaction center in a bimolecular reaction, ($k = 1 \times 10^8\ M^{-1}\ s^{-1}$),[986] and the cytochrome c_2 from *R. capsulatus* at physiological ionic strength does not show any tendency to associate with its reaction center and transfers its electron to the reaction center in a bimolecular reaction with a similar rate constant ($7 \times 10^7\ M^{-1}\ s^{-1}$).[987]

Cells of *R. capsulatus*, in addition to the water-soluble cytochrome c_2, also contain a cytochrome *c* that is anchored in their plasma membranes. This cytochrome *c* diffuses over the surface of the membrane to provide electrons to the reaction centers.[988,989] In other photosynthetic bacteria, only cytochromes *c* that are anchored in the membrane and diffuse over its surface can provide electrons to the reaction center.[990] The cytochrome *c* in *R. sulfidophilum*, which is anchored in the membrane by an extension at its amino terminus and provides an electron to its reaction center, is homologous in sequence with the water-soluble cytochrome c_2 found in its cytoplasm (50% identity; 0.6 gap percent), so both are descended from a common ancestor.[991]

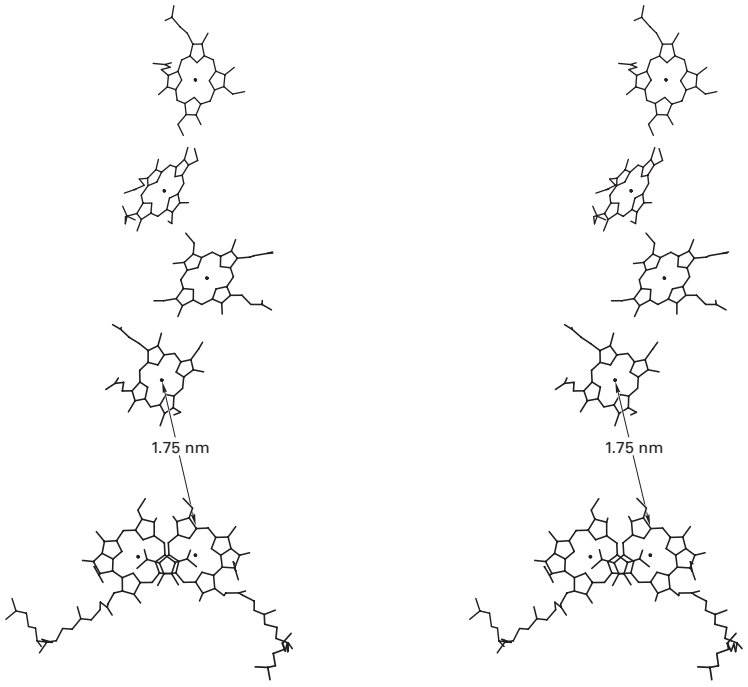

Figure 2–37: Stereodrawing[50] of the special pair of bacteriochlorophylls *b* and four hemes *c* in the tightly bound cytochrome *c* found in the crystallographic molecular model of the reaction center from *B. viridis*.[960] The cytochrome *c* that provides the electron to the radical cation of the special pair copurifies and cocrystallizes with the reaction center from *B. viridis* and is bound to it in the resulting crystallographic molecular model. The four hemes *c* of the cytochrome *c* are to the top of the drawing, and the special pair is at the bottom. The distance from the iron ion of the nearest heme *c* to the nearest carbon atom (carbon 9) within the aromatic π molecular orbital system of one of the chlorophylls *b* in the special pair is 1.75 nm (arrow in the drawing), but the nearest carbon of the double bond of the ethylidene group at position 8 of that chlorophyll *b* (R_3 in **2–54**), which is conjugated to the aromatic π molecular orbital system, is only 1.51 nm away from that iron ion.

In intact cells of photosynthetic bacteria, the **rate constant for the respective transfer of the electron** between the reduced heme *c* on the particular indigenous cytochrome *c* and the hole in the special pair of the reaction center varies from 1.4 μs^{-1} ($t_{½}$ = 0.5 μs) to 0.03 μs^{-1} ($t_{½}$ = 25 μs),[992] which is more than 3000-fold greater than the rate constant for transfer of the electron from the respective radical anion of the semiquinone back to the special pair.

After the excited electron has departed from it, **the radical cation of the special pair** (Equation 2–180), which is now in the ground state, is a **strong oxidant** that readily removes the electron from the reduced cytochrome *c*. Because this is a reaction that proceeds with a negative change of free energy ($\Delta E^{\circ\prime}$ = 200 mV; ΔG° = –19 kJ mol^{-1}), the concentration of the species $P^{\bullet+}BPhQ_A^{\bullet-}$ is decreased by the amount of $PBPhQ_A^{\bullet-}$ that is consequently formed

$$\frac{[PBPhQ_A^{\bullet-}]\,[\text{ferricytochrome } c]}{[P^{\bullet+}BPhQ_A^{\bullet-}]\,[\text{ferrocytochrome } c]} = 4 \times 10^4 \qquad (2\text{–}183)$$

Because so little $P^{\bullet+}BPhQ_A^{\bullet-}$ is present at any instant, the rate constant for the return of the electron from the radical anion of the semiquinone to the special pair (Equation 2–182) is decreased significantly.

The transfer of the electron from the cytochrome *c*, or the high-potential iron–sulfur protein, to the hole in the special pair makes the **overall reaction catalyzed by a photosynthetic reaction center in a purple bacterium upon the absorption of one photon**

$$\text{ferrocytochrome } c_{pos} + Q_{A,neg} + h\nu \rightleftharpoons Q_A^{\bullet-}{}_{neg} + \text{ferricytochrome } c_{pos} \qquad (2\text{–}184)$$

The electron is transferred from a donor of more positive biochemical standard reduction potential, the cytochrome *c*, to an acceptor of more negative biochemical standard reduction potential, the quinone bound at the A site, and the energy of the photon is used to drive the transfer. At this point, the system is still at a higher energy than the ground state, and it is capable of returning, albeit slowly, to the ground state. This return is prevented and the energy is conserved because the electron, at the moment on the radical anion of the semiquinone, subsequently dissociates entirely from the reaction center before the energy can be dissipated.

In a reaction center under normal circumstances, in addition to the quinone Q_A tightly bound as a prosthetic group on the A site (Figure 2–34), which receives the electron directly from the bacteriopheophytin immediately adjacent to it, there is a **second quinone**,[993] usually ubiquinone, even in *B. viridis*.[994] This ubiquinone (Q_B) is a loosely bound electron-transferring coenzyme at the B site, and under normal circumstances, it is freely exchanging with the pool of ubiquinone in the membrane. The B site at which the coenzymatic ubiquinone is located is related by the twofold rotational axis of pseudosymmetry of the LM dimer to the A site at which the prosthetic ubiquinone is found in the crystallographic molecular model of the reaction center from *R. sphaeroides* (Figure 2–34). The two quinones in a given reaction center are pseudosymmetrically displayed around a Fe^{2+} that sits upon the twofold rotational axis of pseudosymmetry. The electron is transferred from the radical anion of the semiquinone at site A to the ubiquinone at site B with a rate constant[995] of 5 ms^{-1} ($t_{½}$ = 140 μs).

The role of the iron ion in this transfer of the electron is unclear. Although reaction centers depleted of iron, either directly or by mutation of one of its ligands, display slower rates of electron transfer between quinone A and quinone B, [979,996] if the iron is replaced by other divalent cations, even ones incapable of participating in electron transfer, the rates of transfer are essentially the same as those of a native reaction center.[997]

Because of a difference in the amino acids that surround the quinones and their orientations in the two sites, quinone B has a more positive biochemical standard reduction potential than the prosthetic quinone in site A so that the equilibrium constant for the reaction

$$Q_A^{\bullet-}Q_B \rightleftharpoons Q_A Q_B^{\bullet-} \qquad (2\text{–}185)$$

is 15.[983,998] Consequently, under usual conditions of illumination the **first electron ends up on quinone B as a radical anion of the semiquinone**, which remains tightly bound to the reaction center until the arrival of a second electron.

The second electron arrives, as did the first, from an electronically excited state of the same special pair, which was regenerated upon the transfer of an electron from the cytochrome *c*. After it is regenerated with the electron from cytochrome *c*, the special pair can absorb the energy of a second photon or exciton to generate a new electronically excited state that passes its electron as before to the quinone in site A, and this transfer forms the radical anion of the semiquinone $Q_A^{\bullet -}$ next to the radical anion of the semiquinone $Q_B^{\bullet -}$ in site B. The radical anion of the semiquinone in site B is **hydronated rapidly** on one of its oxygens as the second electron is transferred from $Q_A^{\bullet -}$ to $Q_B^{\bullet -}$ to form the **ubiquinolate monoanion** Q_BH^-, so the product of the coupled hydron and electron transfers following the arrival of the second electron is $Q_AQ_BH^-$.[999] Site-directed mutation of Serine 223,[984,1000] Aspartate 213,[1001] or Aspartate 210[1002] in the L subunit of the reaction center from *R. sphaeroides* dramatically decreases the rate at which the second electron can be transferred from $Q_A^{\bullet -}$ to $Q_B^{\bullet -}$ by decreasing the rate at which $Q_B^{\bullet -}$ is hydronated. These results are consistent with the conclusion that hydronation of the radical anion of the semiquinone in site B must be concerted with the transfer of the electron to it from the radical anion of the semiquinone in site A.

If a solution of reaction centers is exposed to a saturating flash of light, the absorption spectrum of the radical anion of the semiquinone in site B appears, which remains stable in amplitude over 5 s. When a second saturating flash is administered, the absorption of this radical anion of the semiquinone disappears because the second electron has arrived at site B from the excited special pair and has produced the ubiquinolate monoanion Q_BH^-. If a third saturating flash is administered, however, the absorption of the radical anion of the semiquinone at site B reappears.[1003,1004] This last observation means that the ubiquinolate monoanion formed in the second flash has been replaced by ubiquinone or the third electron could not have been received. Because the radical anion of the semiquinone was bound stably at the instant of the second flash, the replacement must occur only after the ubiquinolate anion is formed.

Site-directed mutation of Glutamate 212[1005] in the L subunit of the reaction center from *R. sphaeroides* does not interfere with the transfer of the first hydron to the radical anion of semiquinone $Q_B^{\bullet -}$ but does interfere with the transfer of the second hydron, the one that hydronates the ubiquinolate monoanion Q_BH^- at site B. Because the side chain of this amino acid is an acid–base in site B in the crystallographic molecular model,[984] this result suggests that the ubiquinolate anion is **hydronated by the enzyme** before it is released from site B. This acid–base and Aspartate 210, Aspartate 213, and Serine 223 from the L subunit are thought to be responsible for ensuring that the two hydrons are efficiently provided and that they are derived from the aqueous solution on the negative, basic side of the membrane. Together they form a chain of acid–bases connected by hydrogen bonds that shuttle hydrons from the aqueous solution on the negative, basic side of the membrane to the two oxygens of the radical anion of the semiquinone or the ubiquinolate monoanion bound loosely as a coenzyme at site B.

The **complete reaction catalyzed by a photosynthetic reaction center in a bacterial chromatophore** upon absorption of the energy of two photons

$$2\,\text{acceptor}_{\text{red,pos}} + \text{quinone} + 2\,h\nu + 2\,\text{H}^+_{\text{neg}} \rightleftharpoons \text{quinol} + 2\,\text{acceptor}_{\text{ox,pos}} \tag{2–186}$$

where the acceptor is either a cytochrome *c* or a high-potential iron–sulfur protein. This equation is the sum of all the steps that have been described.

The energy in each photon of light that has been absorbed by a photosynthetic reaction center has been **divided among three purposes**. Part of it has been used to gain time and prevent the decay of the electronically excited state that would occur if the electron were permitted to return to the hole in the special pair. Part of it has been used to move an electron from a cytochrome *c* (+370 mV for *R. sphaeroides*) to ubiquinone, an acceptor of more negative biochemical standard reduction potential (+100 mV). And part of it has been used to remove two hydrons from the negative, basic side of the membrane.

Bacterial photosynthesis is a cyclic process. A reaction center in the chromatophore of a photosynthetic bacterium uses a photon of light to reduce ubiquinone and two hydrons to ubiquinol. The two hydrons come from the negative, basic solution on the exterior of the chromatophore and are transferred from that solution during the neutralizations

of the radical anion of the semiquinone and the ubiquinolate monoanion Q_BH^-. While it is reducing the ubiquinone with two successive electrons excited from the highest occupied molecular orbital of the special pair, the reaction center is oxidizing two cytochromes *c* or two high-potential iron–sulfur proteins dissolved in the positive, acidic solution on the interior of the chromatophore, which provide two electrons consecutively to the successive holes in the highest occupied molecular orbital in the special pair, which is situated on that side of the membrane (Figure 2–34). The ubiquinol produced at the negative, basic surface of the membrane then dissociates from site B on the reaction center and diffuses across the membrane to the Q_p site on quinol—cytochrome-*c* reductase on the positive, acidic side at which it is oxidized (Figure 2–32). When the ubiquinol is oxidized by quinol—cytochrome-*c* reductase at the Q_p site, it releases two hydrons to the positive, acidic side of the membrane. The two cytochromes *c* or two high-potential iron–sulfur proteins that dissociate in turn from the reaction center into the solution on the positive, acidic side diffuse through that solution[988] to the location on the heme c_1 subunit of quinol—cytochrome-*c* reductase at which they are reduced during the Q-cycle. The ubiquinones dissociate from the quinol—cytochrome-*c* reductase and diffuse across the membrane to be reduced by the reaction center, and the two reduced cytochromes *c* or the two reduced high-potential iron–sulfur proteins diffuse back to the reaction center to be oxidized.

The net result of this cyclic process (the sum of Equation 2–176 and Equation 2–186, realizing that quinones also migrate back and forth across the membrane) is that four hydrons are formally transported from the negative, basic solution on the exterior of the chromatophore to the positive, acidic solution on the interior of the chromatophore, against a significant electrochemical gradient of hydrons. The energy to perform the work of this formal transport of four hydrons is the energy in two photons of light.[1006] These photons may be absorbed consecutively by the reaction center itself, or more often, two photons of light are absorbed in an antenna and transferred to the special pair in the reaction center.

In the absence of the usual electron-transferring coenzyme, either cytochrome *c* or high-potential iron–sulfur protein, the heme c_1 on quinol—cytochrome-*c* reductase can itself provide an electron to the hole in the special pair during collisions within the membrane between the reaction center and heme c_1 on quinol—cytochrome-*c* reductase,[1007] but this process is not so effective as the transfer of the electron by the appropriate electron-transferring coenzyme.

In the chloroplasts of plants and in the membranes of cyanobacteria, photosynthesis is catalyzed by photosystem II and photosystem I. The plastoquinol oxidized by the central enzyme in the process, plastoquinol—plastocyanin reductase, is the product of reduction of plastoquinone at the quinol B site by excited electrons in the reaction center of photosystem II, and the reduced plastocyanin produced by plastoquinol—plastocyanin reductase is oxidized by providing electrons to the radical cation of the special pair in photosystem I. The core of both photosystem II[1008-1013] and photosystem I[1014-1017] is a photosynthetic reaction center. These two respective reactions centers are descendants of the reaction centers of photosynthetic bacteria. Their prosthetic groups are also positioned around a twofold rotational axis of pseudosymmetry, and that rotational axis of pseudosymmetry creates a special pair. Photosystem II has a special pair formed from two chlorophylls *a*; in addition, two chlorophylls *a* replace the two bacteriochlorophylls, two pheophytins *a* replace the two bacteriopheophytins, and two plastoquinones replace the menaquinone and ubiquinones of the bacterial reaction center. In photosystem I (Figure 2–38),[1018,1019] the special pair is also formed from two chlorophylls *a*; in addition, four chlorophylls *a* replace the two bacteriochlorophylls and the two bacteriopheophytins, and two phylloquinones replace the menaquinones and ubiquinones of the bacterial reaction center. All these substitutes play the same roles as their parental prosthetic groups in a bacterial reaction center.

In **photosystem II** in plants and cyanobacteria, the primary excitation of the electron and its transfer to pheophytin *a*[1020] differ somewhat from those in the bacterial reaction center because the special pair is more weakly coupled. The initial separation between the excited electron and the hole can occur in either of two locations. It can occur between one of the chlorophylls *a* of the special pair, which ends up with the hole, and the adjacent chlorophyll *a*, which ends up with the electron, on its way to pheophytin *a* as in the bacterial reaction center. It can also, however,

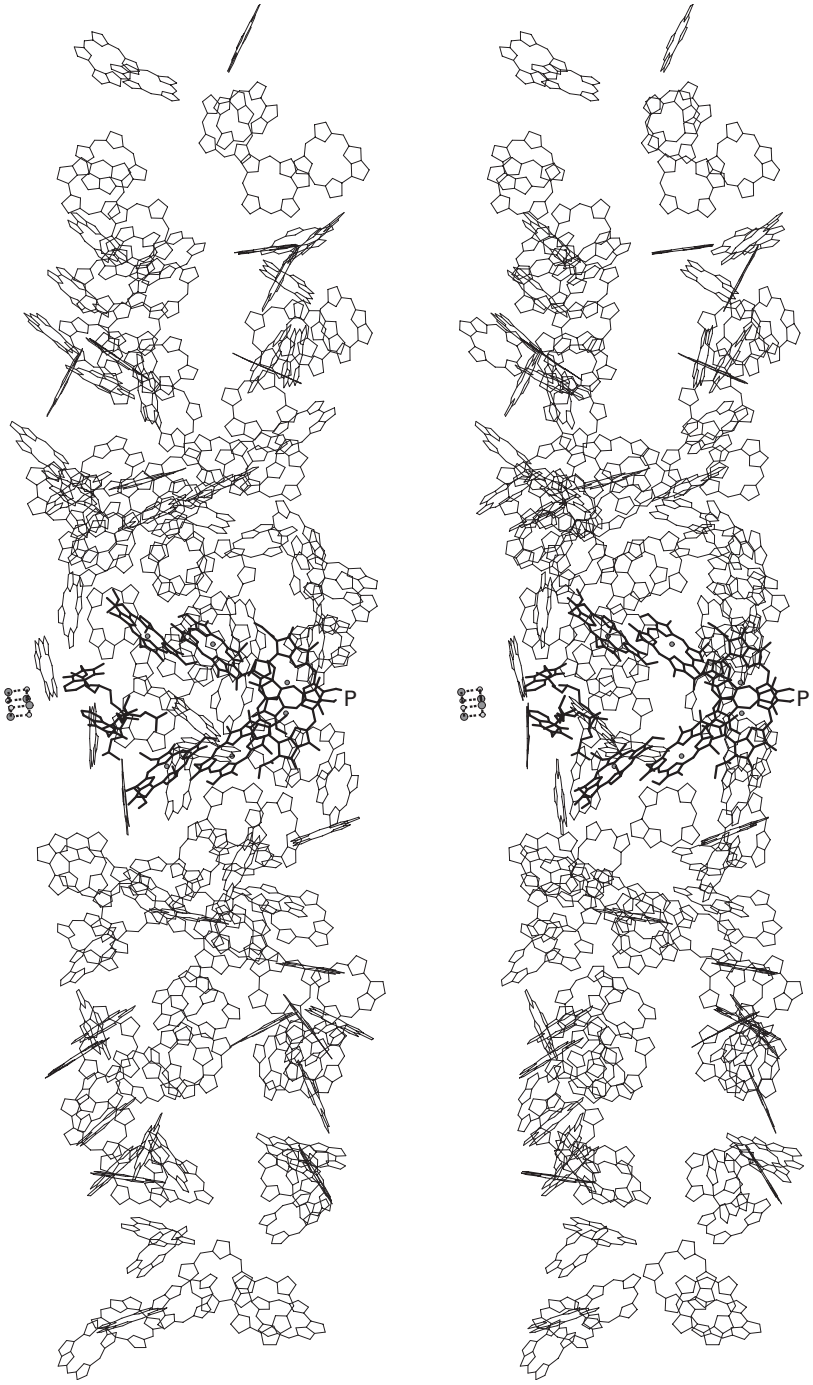

Figure 2–38: Stereodrawing[50] of the distribution of chlorophylls within the crystallographic molecular model of the reaction center of photosystem I from *P. sativum* and the antenna that surrounds it.[1018,1019] Only the central rings of the chlorophylls (thin bonds in the drawing), and not the carotenoids, of the antenna formed by the core protein and light-harvesting complex I are included in the drawing. The reaction center is formed from six chlorophylls *a* and two phylloquinones (thick bonds in the drawing) and a [4Fe–4S] iron–sulfur cluster. The [4Fe–4S] iron–sulfur cluster is embedded in the portion of the core protein that protrudes into the solution on the negative, basic side of the membrane. The special pair (P) is labeled. The plane of the membrane is vertical and perpendicular to the page. The twofold rotational axis of pseudosymmetry that creates the special pair is horizontal and in the plane of the page. The array of chlorophylls embedded in the protein spans the membrane of the thylakoid and defines its boundaries.

occur between this same chlorophyll *a* adjacent to the special pair, which ends up with the hole, and pheophytin *a*, which ends up with the electron. After the initial excitation at either location, the system almost immediately resolves into the normal distribution in which the excited electron is in the radical anion of pheophytin *a* and the hole is in the radical cation of the special pair. This resolution is accomplished by migration of the electron from the adjacent chlorophyll *a* to pheophytin *a* or migration of the hole from the adjacent chlorophyll *a* to the chlorophyll *a* of the special pair.[1021]

The subsequent transfer of the electron from pheophytin *a* to the two plastoquinones[1022] symmetrically bound around the iron ion[1023] in photosystem II is the same as in a bacterial reaction center. After the second electron arrives, the plastoquinol, which has taken up two hydrons from the negative, basic solution, dissociates into the phospholipid bilayer on its way across the membrane to the positive, acidic side of plastoquinol—plasto-cyanin reductase, just as the ubiquinol dissociates from the bacterial photosynthetic reaction center on its way to quinol—cytochrome-*c* reductase. The hole in the special pair, however, is a much stronger oxidant than the hole in the special pair in a bacterial reaction center[1024] because it is mainly located on only one of the two chlorophylls *a* in the special pair,[1021] rather than being delocalized over both. This is the advantage gained from the weaker coupling. This stronger oxidant removes an electron from the 4-oxido group of a particular[1025] tyrosine in the enzyme to form the neutral tyrosyl radical, rather than removing an electron from a cytochrome *c*.[1026,1027] The tyrosyl radical then removes an electron from a cluster of four manganese ions and a calcium ion[1011,1028] responsible for oxidizing water to molecular oxygen, an oxidation that ultimately releases four hydrons into the positive, acidic solution inside the thylakoid.

In **photosystem I** in plants and cyanobacteria, the primary excitation of the electron by a photon and its transfer to the chlorophyll *a* that takes the place of bacteriopheophytin also differ somewhat from those in the bacterial reaction center. The chlorophyll *a* adjacent to the special pair absorbs the photon, and the excited electron is immediately ($3\ ps^{-1}$) passed to the distal chlorophyll *a* that takes the place of the bacteriopheophytin in a bacterial reaction center. The hole then moves from the adjacent chlorophyll *a* to the special pair, and the electron moves from the distal chlorophyll *a* to the phylloquinone,[1029] to produce a distribution homologous to that in the bacterial reaction center, with the hole in the special pair and the electron in the ubisemiquinone.[1030] The hole in the special pair (+480 mV) is filled with an electron from the small electron-transferring coenzyme, reduced plastocyanin (+360 mV),[1031] that freely associates with and then dissociates from the reaction center on its positive, acidic surface on its way to the plastoquinol—plastocyanin reductase,[1032] just as the hole in the bacterial special pair is filled with an electron from a cytochrome *c* that then dissociates on its way to quinol—cytochrome-*c* reductase.

The unique feature of photosystem I (Figure 2–38) is that it produces a radical anion of the prosthetic phyllosemiquinone with a high biochemical standard reduction potential (–700 mV) by using a chlorophyll *a* (–1200 mV) as the acceptor of the excited electron rather than a pheophytin.[815] Because of the excitation process unique to photosytem I, the radical anion of this phyllosemiquinone is formed even more rapidly ($70\ ns^{-1}$; $t_{½} = 10$ ps) than the radical anion of the prosthetic ubisemiquinone in the bacterial system.[1030] This radical anion of phyllosemiquinone transfers its electron rapidly ($0.003\ ns^{-1}$; $t_{½} = 200$ ns) to a prosthetic [4Fe–4S] iron–sulfur cluster[1033,1034] with a biochemical standard reduction potential of around –700 mV[815] that sits on the twofold rotational axis of symmetry of the reaction center of photosystem I (Figure 2–38),[1016,1035] roughly in the location of the single Fe^{2+} in the bacterial reaction center (Figure 2–34). The electron is then transferred rapidly through two prosthetic [4Fe–4S] iron–sulfur clusters to a coenzymatic [2Fe–2S] ferredoxin loosely bound to the enzyme, which then dissociates into the solution on the negative, basic side of the membrane.[1036] The key to this sequence of events is that the radical anion of the phyllosemiquinone is not stabilized by the enzyme, so its full instability and hence its full, low biochemical standard reduction potential can be exerted. The fact that the small electron-transferring coenzyme is a [2Fe–2S] ferredoxin that can accept only one electron means that there is no need for the radical anion of the phylloquinone to wait for a second excited electron. The [2Fe–2S] ferredoxins in higher plants have biochemical standard reduction potentials[559] around –400 mV. The [2Fe–2S] ferredoxins reduced by photosystem I provide reducing equivalents to the plant cell or the cyanobacterial cell; an example would be the reduction catalyzed by ferredoxin—$NADP^+$ reductase, to produce NADPH ($E^{\circ\prime} = -310$ mV), the universal reductant used in biosynthesis, the generation of $MgATP^{2-}$, and in particular, for a plant cell, in carbon fixation.

In chloroplasts, there is a large membrane-spanning enzyme that is structurally homologous to NADH:ubiquinone reductase (H^+-translocating).[1037,1038] A molecular model of this enzyme in chloroplasts, derived from image reconstruction of electron micrographs,[1037] however, has only three of the usual eight iron–sulfur clusters present in most NADH:ubiquinone reductases (H^+-translocating) from mitochondria and bacteria: the upper three in Figure 2–33, which are closest to the membrane. It is possible that several subunits of the intact enzyme are missing in this molecular model,[1038] in particular those containing the other five usual iron–sulfur clusters (the lower five in Figure 2–33) more distal to the membrane and connecting the three that are present in the molecular model to the site at which NADH is oxidized in NADH:ubiquinone reductase (H^+-translocating). The quinone that is reduced by this enzyme while it actively transports hydrons from the negative, basic side of the membrane of the chloroplast to the positive, acidic side, as does NADH:ubiquinone reductase (H^+-translocating), is plastoquinone rather than ubiquinone; and the reduced plastoquinol is then a substrate for plastoquinol—plasto-cyanin reductase. The immediate source of reducing equivalents for this enzyme in the membranes of chloroplasts is unclear. The ultimate source is the reduced ferredoxin produced by photosystem I.[1039,1040] The structural homology with NADH:ubiquinone reductase (H^+-translocating) suggests that the immediate source of reducing equivalents for the enzyme in chloroplasts is the NADPH produced by ferredoxin—$NADP^+$ reductase. In any case, the reducing equivalents in ferredoxin are ultimately used to transport hydrons against their electrochemical gradient by passing through this homologue of NADH:ubiquinone reductase (H^+-translocating). Because the electrochemical gradient is the source of the energy used to synthesize $MgATP^{2-}$, this enzyme serves the purpose of balancing the needs of the cell for reducing equivalents, in the form of NADPH, and energy, in the form of $MgATP^{2-}$.

The achievement that has been accomplished by a photosynthetic reaction center is denying the excited electron access to the hole that it vacated by disconnecting it rapidly enough so that its return to the hole by the normal process of fluorescent decay is precluded. To accomplish this disconnection, the electron is shuttled at an extremely rapid rate to a quinone (ubiquinone, menaquinone, plastoquinone, or phylloquinone) distant enough from the hole and at a positive enough standard reduction potential that the return of the electron to the hole becomes so slow that the electron can be held long enough to be used as a reductant for the respective electron-transferring coenzyme (ubiquinone, plastoquinone, or ferredoxin) and long enough for the hole to be filled by an electron from the appropriate donor (cytochrome *c*, high-potential iron–sulfur protein, a cluster of four manganese ions and a calcium ion, or plastocyanin). This speed and this span can be accomplished because a continuous chain of closely spaced prosthetic groups connects the special pair with the respective quinone in site A (Figure 2–34) and because, along the way, the excited electron is passing through large aromatic π molecular orbital systems of bacteriochlorophylls and bacteriopheophytins that themselves each span a large distance (0.7 nm).[1041] In these enzymes, the **requirement that the electron travel over such a great distance** (about 4 nm) is dictated by two facts. First, the greater the dilution of the electron, the slower its return to the ground state will be. Second, the electron from the respective reduced electron-transferring coenzyme must be received by the hole in the special pair at one side of the membrane, and the excited electron must be added to the respective oxidized electron-transferring coenzyme at the other side of the membrane to create the respective gradient of hydrons. In the reaction center from *R. sphaeroides*, the distances between the closest points in the π molecular orbital systems are 0.63 nm from the special pair to bacteriochlorophyll and 0.65 nm from bacteriochlorophyll to bacteriopheophytin (Figure 2–34). These short distances ensure that the transfer of the excited electron is extremely rapid (200 ns^{-1}; $t_{½}$ = 4 ps). The distance between the closest points in the π molecular orbital systems is 1.09 nm from bacteriopheophytin to the quinone in site A. The greater distance may in part explain the less rapid transfer from bacteriopheophytin to the quinone in site A (5 ns^{-1}; $t_{½}$ = 150 ps), but it does accomplish the final jump to the negative, basic side of the membrane.

In many of the membrane-spanning enzymes catalyzing the transfer of electrons (Figures 2–32 and 2–33) and in many of the water-soluble enzymes catalyzing oxidation–reductions that proceed by the transfer of single electrons (Figures 2–30 and 2–31), there are chains of prosthetic groups that perform one-electron transfers and move electrons over considerable distances. These chains of

prosthetic groups can be formed from iron–sulfur clusters (Figures 2–31 and 2–33)[478] or hemes (Figure 2–30 and 2–32)[1042,1043] or, if the biochemical standard reduction potential of the hole into which the electron is donated is positive enough, the side chains of tryptophans[1044] and tyrosines.

The individual prosthetic groups in one of these chains are usually **spaced at distances that are less than particular limits**.[1045] Because the electron that is transferred to or from each prosthetic group occupies a molecular orbital spread over the entire π molecular orbital system in a flavin, chlorophyll, pheophytin, or quinone, the distance over which the electron is transferred between donor and acceptor in such situations is the distance from the closest edge of the respective π molecular orbital system (Figures 2–30 and 2–31). Because the electron occupies a molecular orbital spread over the entire cluster in a prosthetic group such as an iron–sulfur cluster or a copper–sulfur cluster, the distance over which the electron is transferred between donor and acceptor in such situations is the distance between the closest atoms in the two clusters (Figures 2–31, 2–32, and 2–33). Because the electron occupies an atomic orbital in a single copper ion or an iron ion in a prosthetic group such as a heme, the distance over which the electron is transferred between donor and acceptor in such situations[1046] may be the distance from the metallic ion itself (Figures 2–30 and 2–32).

The distances between the two orbitals in which the electron resides before and after it is transferred through chains of flavins, chlorophylls, pheophytins, quinones, iron–sulfur clusters, clusters of copper ions, and single copper ions are **usually from 0.4 to 1.4 nm** (Figures 2–30, 2–31, and 2–33).[478,651,894,1042-1045,1047,1048] Even in enzymes that have only two such prosthetic groups between which the electron is transferred, the distance between the two orbitals containing the transferred electron before and after the transfer usually fall in this range.[674,817,1049,1050] For example, in nitrite reductase (NO-forming) from *A. xylosoxidans*, the two copper ions between which electrons are transferred are 1.3 nm apart.[1051]

In an apparent exception to the rule, while the distance from the iron in a heme to the nearest electron donor or acceptor frequently falls within the range 0.4–1.4 nm, it is also often greater than 1.4 nm (Figures 2–30 and 2–32).[1047] For example, the distance between the iron in the heme *c* and the iron in the heme d_1 of nitrite reductase (NO-forming) from *Paracoccus pantotrophus* is 2.06 nm.[1691] Partly these larger distances are due to the fact that the heme itself is quite large and hard to approach very closely, especially by another heme, but it is probably the case that the **π molecular orbital system surrounding the iron in a heme** carries a certain fraction of the highest occupied atomic orbital of the iron containing the electron to be donated or of the lowest unfilled atomic orbital of the iron that will be accepting the electron. Consequently, the π molecular orbital system projects a portion of that atomic orbital beyond the iron, bringing it closer to the edge of the heme.

Although in some cases two prosthetic groups are close enough to touch each other,[1052] the space between the molecular orbitals or the iron or copper ions covered by these distances between the prosthetic groups is usually filled with the side chains and polypeptide backbone of the protein enclosing them. Consequently, the question of how the electron is transferred so rapidly from prosthetic group to prosthetic group in these situations is how is an electron transferred through protein.

During a one-electron oxidation–reduction between two redox couples separated from each other in a protein, an unaccompanied electron can transfer through unadulterated protein over a considerable distance (1.5–2.5 nm).[1045,1046,1053,1054] For example, when Histidine 33 in oxidized equine cytochrome *c* is used as one of the ligands to Ru^{3+}, the other five ligands to which are molecules of ammonia, the derivative that results is a cytochrome *c* in which the Fe^{3+} in heme *c* is 1.5 nm from the pentaamminoruthenium at Histidine 33. When Ru^{2+} coordinated with three 2,2′-bipyridines [$Ru(bpy)_3^{2+}$] is dissolved in an aqueous solution of this modified cytochrome *c* and excited by a flash of light with a wavelength of 532 nm, its electronically excited state is a strong enough reductant to transfer an electron rapidly to either Ru^{3+} or Fe^{3+} in the modified cytochrome *c*. This transfer of an electron occurs in a 5:1 molar ratio, respectively, between Ru^{3+} and Fe^{3+}. This kinetic product, in which most of the ruthenium ions are reduced and most of the iron ions remain oxidized, then converts to the thermodynamic product in which most of the iron ions are reduced and most of the ruthenium ions are oxidized.[1053] This conversion results from the intramolecular transfer of an electron from Ru^{2+} to Fe^{3+} through 1.5 nm of unadulterated protein with a rate constant of 20 s^{-1}, which is independent of temperature between

0 and 37 °C. This rate constant is for the approach to thermodynamic equilibrium of a reversible transfer of the electron between the ruthenium ion bound to the protein and the iron ion of the heme.[1055]

It is also possible to observe such an **unnatural transfer of an electron through a protein** without the necessity to modify it. The single disulfide in azurin from *P. aeruginosa* can be reduced to the radical anion of the disulfide by the radical anion $CO_2^{\bullet -}$. The electron in the resulting radical anion of the disulfide is then transferred across 2.0 nm of protein[1056] to the Cu^{2+} at a rate of 50 s^{-1}.

Because cytochrome *c* may not have evolved to transfer an electron from Histidine 33 to its heme and because azurin may not have evolved to transfer an electron from its disulfide to its copper ion, these observations of the transfer of electrons in these two proteins suggest that transfer of electrons may be able to occur through any protein. Azurin and cytochrome *c*, however, have evolved to catalyze electron transfer.

Hemoglobin is a protein that does not normally participate in oxidation–reduction; and it is a protein that definitely has not evolved to be able to support the transfer of electrons through itself. The protein normally contains four hemes *b*, one within each of its subunits. It is an $(\alpha\beta)_2$ heterotetramer, but α and β polypeptides are homologous in sequence, and the native structures of the α and β subunits are superposable. It is possible to separate α and β subunits and reconstitute the protein from these separated subunits. Therefore, a hemoglobin in which the α subunits contained an Fe^{3+} porphyrin and the β subunits contained a Zn^{2+} porphyrin could be constructed.[1057]

When a Zn^{2+} porphyrin is excited by absorbing a photon of light, the excited electron is particularly prone to a spin inversion that produces a triplet electronically excited state, $^3Zn^{2+}$ porphyrin, in good quantum yield. The lifetime of this phosphorescent triplet electronically excited state is much longer (greater than 10 ms) than that of the fluorescent singlet electronically excited state from which it was derived.[1058] The triplet electronically excited state is also a strong enough reductant ($E^{\circ\prime}$ = −1100 mV)

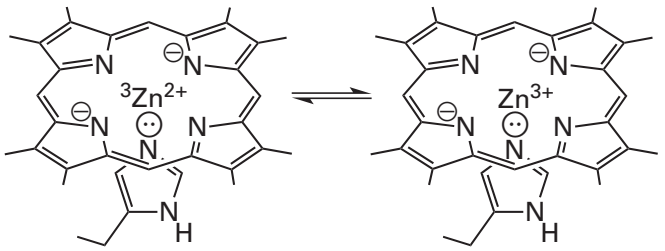

(2–187)

to transfer an electron[1054] to an Fe^{3+} porphyrin ($E^{\circ\prime}$ = +150 mV)

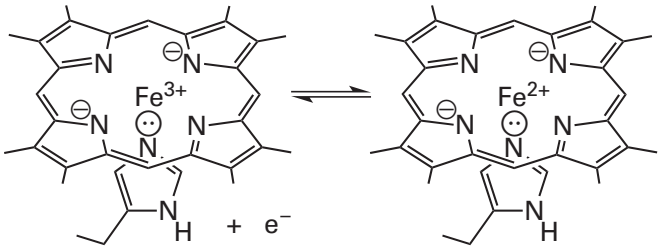

(2–188)

The free energy change of the overall reaction is quite favorable (ΔG° = −120 kJ mol^{-1}).

When hemoglobin containing a Zn^{2+} porphyrin in the β subunits and an Fe^{3+} porphyrin in the α subunits is photolyzed, the decay of the triplet state of the Zn^{2+} porphyrin is more rapid than it is when the Fe^{3+} porphyrin has been reduced to Fe^{2+} porphyrin prior to photolysis.[1054] If it is assumed that this increase in the rate of decay is due to transfer of the electron from the $^3Zn^{2+}$ porphyrin to the Fe^{3+} porphyrin, the first-order rate constant of that transfer is 100 s^{-1} at 25 °C.[1059] In the crystallographic molecular model of a molecule of hemoglobin, the shortest distance between a heme on a β subunit and a heme on an α subunit is 2.5 nm. This experiment demonstrates that the transfer of an electron can occur through any protein and reverses the question from "can an electron transfer through protein" to "how can an electron be prevented from transferring through protein." In this experiment, it is also the case that the electron passes between two subunits of an oligomeric protein.

Traditionally, transfers of electrons have been divided into inner-sphere and outer-sphere transfers. An **inner-sphere electron transfer** is one in which the electronic coupling between the donor (a reductant) and the acceptor (an oxidant) is strong (>20 kJ mol^{-1}) in the transition state. In the original examples of inner-sphere electron transfer, the donor and acceptor, which were transition metallic

ions, were strongly coupled because in the transition state they shared a ligand between themselves. For example, in the oxidation–reduction[1060]

$$\left[(NH_3)_5Co^{3+}Cl^-\right]^{2+} + \left[Cr^{2+}(H_2O)_6\right]^{2+} \rightleftharpoons H_2O + \left[(NH_3)_5Co^{3+}Cl^-Cr^{2+}(H_2O)_5\right]^{4+} \rightleftharpoons \left[(NH_3)_5Co^{2+}(H_2O)\right]^{2+} + \left[Cl^-Cr^{3+}(H_2O)_5\right]^{2+} \quad (2\text{–}189)$$

the transfer of the electron from Co^{2+} to Cr^{3+} occurs within the inner sphere created by the intermediate ion $[(NH_3)_3Co^{3+}Cl^-Cr^{2+}(H_2O)_5]^{4+}$. The electron passes through the chloride that the transition metallic ions share as a ligand and that strongly couples them electronically. An **outer-sphere electron transfer** is one that takes place with weak (<20 kJ mol^{-1}) electronic coupling between the donor and acceptor in the transition state. For example, the transfer of an electron in which two transition metallic ions retain all their ligands during their encounter in the transition state and no ligand is shared between them usually progresses with weak electronic coupling in an outer-sphere transfer.

In enzymatic reactions, inner-sphere transfer of an electron occurs when a bond, anywhere between ionic and covalent, is formed between a substrate and a transition metallic ion, which then oxidizes or reduces that substrate. For example, in nitrite reductase (NO-forming) from *A. faecalis*, the substrate, nitrite, replaces a dissociable ligand in the open coordination site of the prosthetic Cu^+ in the enzyme.[1061] An electron is transferred from the Cu^+ to the nitrite. reducing it to nitric oxide, which then dissociates from the Cu^{2+}. In laccase, an oxygen of the substrate, a benzenediol, replaces a dissociable ligand in the open coordination site of the Cu^{2+} in the enzyme.[695] An electron is instantaneously transferred from the benzenediol to that Cu^{2+}, oxidizing the benzenediol to the hydroxyphenoxy radical, which then dissociates from the resulting Cu^+.

In such **inner-sphere electron transfers**, because the transfer of the electron is to all intents and purposes instantaneous once the complex forms, the rate at which the **ligand initially occupying the open site on the metallic ion exchanges with the substrate** and the rate at which the product on the metallic ion exchanges with a ligand in solution determine the rate of the overall reaction. In aqueous solution, the ligand occupying the open site is usually a molecule of water. The rate constants with which molecules of water exchange at divalent metallic ions[1062,1063] are in excess of 10^4 s^{-1}. For Fe^{2+}, the rate constant is 3×10^6 s^{-1}; and for Cu^{2+}, it is 8×10^9 s^{-1}. The rate constant for exchange of water from $Fe^{3+}(OH_2)_6$, however, is slower, 3×10^3 s^{-1}; and that for chloride,[1064] the main anion in the cytoplasm, from $[Fe^{3+}(OH_2)_5Cl^-]^{3+}$ is slower still, 2.3 s^{-1}. Consequently, the exchange of a substrate into coordination with a prosthetic Fe^{3+} or a product out of coordination with a prosthetic Fe^{3+} will be slow.

Although the transfer of an electron between two prosthetic groups separated by 0.5–2.5 nm of protein is technically between a donor and an acceptor that share the same ligand, namely the protein itself, the distances involved and the number of atoms located in the intervening space cause the electronic coupling between donor and acceptor to be so weak that the transfer of the electron is unmistakably an **outer-sphere electron transfer.**

When the transfer of an electron is inner-sphere, one, two, or three bonds connect the donor and the acceptor, and as soon as the exchange of ligands occurs and these bonds have formed, the transfer of the electron is instantaneous. When transfer of an electron is outer-sphere, the electronic coupling between donor and acceptor is so weak that the **actual transfer of the electron is the slow step** in the reaction. Because the electronic coupling is so weak, the electron has to wait until all the atoms surrounding and between the donor and acceptor reach a configuration that is favorable to the transfer before the electron can transfer from the orbital it occupies on the donor to the orbital it will occupy on the acceptor.[1065]

Because an electron has almost no mass and because, once a favorable configuration has been achieved, the transfer of the electron from the donor to the acceptor is instantaneous, **the Franck–Condon principle requires that the position and momentum of all the nuclei in the system be the same before and after the transfer of the electron.**[1066] The equilibrium positions of the nuclei in the reactants, when the electron is on the donor, however, are different from their equilibrium positions in the products, when the electron is on the acceptor. For example, when the electron is on the donor, the donor is more negative by one elementary charge and the acceptor is more positive by one elementary charge than they are when the electron has transferred to the acceptor. Consequently, the coordination of the charges differs significantly in the reactants and

products of the electron transfer, and the atoms accomplishing that coordination are in significantly different locations. Likewise, the equilibrium bond lengths between a transition metallic ion and its ligands shorten when it loses an electron or lengthen when it gains an electron. The normal spontaneous fluctuations in the positions of the atoms surrounding and between the donor and the acceptor must bring those atoms into a configuration intermediate between their equilibrium configurations in the reactants and in the products, and that intermediate **configuration must be compatible with the transfer of the electron**.

The configuration of the atoms surrounding and between the donor and acceptor is compatible with transfer of the electron when the energy of that configuration is the same in the reactants and the products.[1065] In other words, the configuration of all the atoms surrounding and between the donor and the acceptor must be such that the **energy of the system is the same before and after the instantaneous transfer** of the electron from donor to acceptor.

The atoms surrounding and between the donor and the acceptor are constantly fluctuating in their position and momentum. When they happen to reach a configuration in which the energy before and after the transfer of the electron would be the same, the requirement of the Franck–Condon principle and the requirement that energy be conserved are both met, and the electron can transfer from donor to acceptor. Whether it transfers or not depends on the strength of the electronic coupling. The weaker the electronic coupling, the more often a compatible configuration will be realized before the transfer of the electron actually occurs.[1046]

When an electron is transferred in the outer sphere between a donor and acceptor, such as a reduced prosthetic group and an oxidized prosthetic group in the same protein, the **equation derived from these considerations, the Marcus equation, defines the rate constant of this intramolecular electron transfer**[1067,1068]

$$k_{ET} = \frac{4\pi^2 {H_{AB}}^2}{h\,(4\pi\lambda\, k_B T)^{1/2}} \exp\left[-\frac{(\lambda + \Delta G^\circ)^2}{4\lambda k_B T}\right] \qquad (2\text{–}190)$$

where h is the Planck constant, k_B is the Boltzmann constant, H_{AB} is the **electronic matrix element** quantifying the coupling of the electronic state of the donor with the electronic state of the acceptor when both are in the configuration of the transition state,[1046] ΔG° is the change in the standard free energy of the overall oxidation–reduction (Equation 2–92), and λ is the reorganization energy. The **reorganization energy** is the difference between the free energy of a Franck–Condon state in which the position and momentum of the nuclei and their respective solvation are the same before and after the transfer of an electron and the sum of the free energies of the equilibrium nuclear configuration of the donor, the equilibrium nuclear configuration of the acceptor, and their respective solvations. In the case of self-exchange between an identical donor and acceptor, the reorganization energy is equal to the energy required to alter the nuclear configuration of the donor and acceptor and their solvation from their equilibrium configuration to a configuration that matches the equilibrium nuclear configuration of the products of the electron transfer and their their solvation, and it is often assumed that, in other instances, the reorganization energy is approximately equal to this energy.[1041,1046,1069]

For a given electron transfer, **the values of ΔG°, H_{AB}, and λ can be estimated** by following the temperature dependence of the rate constant for the transfer of the electron (Equation 2–190). The standard free energy of the overall oxidation–reduction at each temperature can be determined by measuring the respective standard reduction potentials (Equation 2–92) by potentiometric titrations. After these measurements are completed, the standard free energy at any given temperature is known, so the only two unknowns in Equation 2–190 are H_{AB} and λ. The measured rates of electron transfer as a function of temperature can be fit with the simplified equation to determine these two parameters.[1070-1072]

Because the reorganization energy is always a positive number, the unexpected prediction made by this equation is that the **rate of transfer for an electron should pass through a maximum as the standard free energy of the oxidation–reduction is decreased** to more negative values, as long as the structure of the reactants and products remain as similar as possible so that the reorganization energy remains about the same, while the reactant is varied to accomplish this decrease in the change of the standard free energy for the reaction. For example, in a series of 17-(4-biphenylyl)androstanes

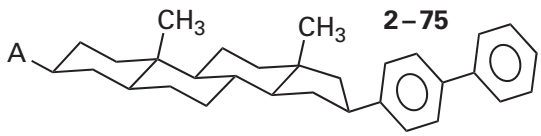

the identity of A, the acceptor, was varied among a set of functional groups with different standard reduction potentials (Figure 2–39).[1069] When the resulting compounds were individually reduced by solvated electrons injected into the solution by an electron beam, the rate at which an electron was transferred from the radical anion of the 4-biphenylyl group, formed by the association of a solvated electron, to the respective acceptor could be measured. The rate constants for these electron transfers do go through a maximum as the standard reduction potential of the acceptor increases and the change in standard free energy for the transfer of the electron decreases. The data could be fit with Equation 2–190 with a reorganization energy of +75 kJ mol^{-1}.

The fact that the rate of an outer-sphere electron transfer passes through a maximum as its change in standard free energy is decreased is a consequence only of the fact that the equilibrium configurations of the atoms surrounding and between the donor and the acceptor lie at the bottom of a potential well for the reactants and the bottom of a different potential well for the products.[1065,1069] The fact that the data seem to fit the behavior predicted by Equation 2–190, and that such behavior was unexpected, validates the equation. This maximum in the rate of electron transfer as the change in standard free energy of the reaction is varied has been observed consistently for simple intramolecular chemical oxidation–reductions,[1073,1074] for intermolecular electron transfer between a donor in which an electron is widely delocalized and a series of small acceptors,[1075] and for intramolecular transfers of electrons through proteins (Figure 2–40).[982,1041,1076-1079] Such a maximum is also observed for the transfer of an electron from a Ru^{2+} ion on Histidine 33 of equine cytochrome *c* to the Fe^{3+} in its heme.[1080] The value for the change in free energy for the oxidation–reduction at the maxima of these observed curves is the negative of the value of the reorganization energy (Equation 2–190). The fits of Equation 2–190 to the data, however, are usually not so convincing as the fits in Figures 2–39 and 2–40, which were chosen for the present discussion to convince.

For transfer of an electron through protein, the reorganization energy is usually around +70 to +110 kJ mol^{-1}. For example, the reorganization energy

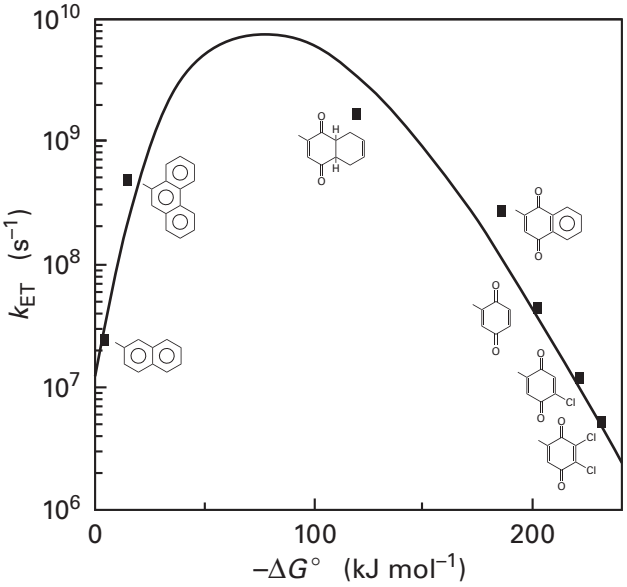

Figure 2–39: Dependence of the rate constant (k_{ET}) for intramolecular transfer of an electron within various versions of the 17-(4-biphenylyl)androstane **2–75** on the difference in standard reduction potential ($-\Delta G^\circ$) between the 4-biphenylyl group and the respective acceptor.[1069] Several versions of 17-(4-biphenylyl)androstane, each with a different acceptor for intramolecular transfer of an electron at carbon 3, were synthesized. The structures of the various functional groups acting as acceptors are drawn next to the points on the graph for their rates of intramolecular electron transfer. Each version was dissolved separately in di(*n*-butyl) ether. The respective solutions were each exposed to a intense, short pulse (30 ps to a few nanoseconds) of an electron beam from a linear accelerator. The resulting hydrated electrons that were formed instantaneously in the solution were trapped by biphenylyl groups to create biphenylyl radical anions, which absorb light of wavelengths between 400 and 650 nm. The decay in the concentration of the biphenylyl radical anion was followed by its absorbance. It was found that when an acceptor was located at carbon 3 of the androstane, the decay of the biphenylyl radical anion was hastened by intramolecular electron transfer. In appropriate cases, the appearance of the radical anion of the acceptor could also be followed. The rate constants for each intramolecular electron transfer (second^{-1}) calculated from these data are plotted as a function of the differences in standard reduction potential (kilojoules mole^{-1}) between a biphenylyl group and the respective acceptor. Note that the difference in rate constant between the most rapid transfer and the slowest transfer is greater than a factor of 100.

for transfer of an electron from bacteriopheophytin to quinone A in the reaction center of *R. sphaeroides* (Figure 2–34)[982] has been estimated to be +60 kJ mol^{-1}, that for the transfer of an electron between a ruthenium ion and the iron ion in the heme in cytochrome b_5 (Figure 2–40)[1076] has been estimated to be +90 kJ mol^{-1}, and that for the transfer

of an electron from the T1 prosthetic Cu^{+} to the NI prosthetic Cu^{2+} of laccase from *Toxicodendron vernicifluum*[1081] has been estimated to be +115 kJ mol^{-1}. The changes in standard free energy for most natural electron transfers in enzymes that catalyze oxidation–reductions are often significantly less than −70 to −80 kJ mol^{-1}. Under these circumstances, the **rate constant for transfer of an electron through protein increases almost exponentially as the change in standard free energy for the reaction decreases** (Equation 2–190).[1078,1082-1084]

Because the rate constant for transfer of an electron, within the normal range of changes in standard free energy, is also increased by decreasing the reorganization energy (Equation 2–190), it is possible that reorganization energy is subject to natural selection.[1065] For example, when the methionine that was placed by natural selection as a ligand to one of the copper ions in nitrite reductase from *A. faecalis* is removed by site-directed mutation,[1085] the reorganization energy for the transfer of an electron from this copper ion to the other copper ion in the enzyme increases by 40 kJ mol^{-1}.

The two parameters that determine the value of the rate constant for an electron transfer, the reorganization energy, λ, and the electronic matrix element describing the coupling of the electronic state of the reactant with the electronic state of the product, H_{AB}, can be separately factored in Equation 2–190 and therefore have independent effects on the rate constant. If the space between donor and acceptor within a protein were not filled by other atoms but were empty vacuum, the magnitude of the electronic coupling would be a function of only the distance between donor and acceptor because it would be determined by the degree of overlap that occurs between the wave functions of the molecular orbitals occupied by the electron on the donor and the electron on the acceptor.[1086]

In the realm of energies in which the reorganization energy is more positive than the change in standard free energy is negative, which is the normal situation in a molecule of protein, **the more negative the change in standard free energy, the greater the rate of electron transfer** (Equation 2–190). In the enzyme laccase, an electron is transferred over a distance of 1.23 nm through the protein between a mononuclear, prosthetic Cu^{+} coordinated by two histidines and a cysteine (Figure 2–26A), at which each of four benzenediols in turn are oxidized by one electron, and a trinuclear cluster of prosthetic copper ions coordinated by the imidazolyl groups of eight histidines,[1087] at which a molecule of oxygen is reduced by the four electrons to two molecules of

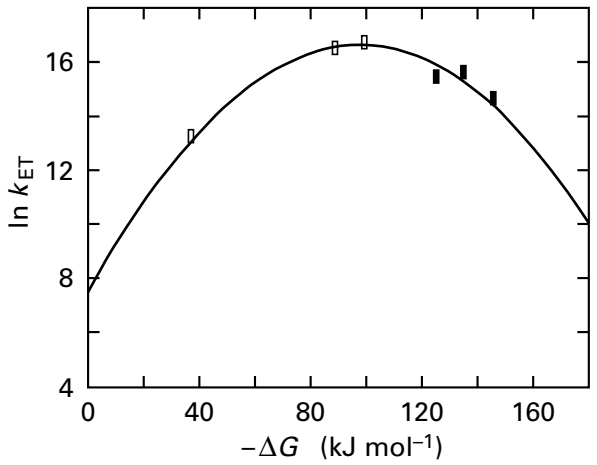

Figure 2–40: Dependence of the rate constant (k_{ET}) for intramolecular transfer of an electron through the folded polypeptide of cytochrome b_5 to and from the Fe^{3+} in its heme on the difference between the standard reduction potential ($-\Delta G^{\circ}$) of the heme and donors attached to the protein, each at the same location.[1076] The gene for cytochrome b_5 from *R. norvegicus* was mutated in the codon for Threonine 69 to to produce a codon for a cysteine. The mutated gene was expressed in *E. coli*, and the mutant protein was purified. The resulting Cysteine 69 is the only cysteine in the mutant, and it was modified in separate reactions with [4-(bromomethyl)-4′-methylbipyridine]bis(bipyridine)ruthenium(II), [4-(bromomethyl)-4′-methylbipyridine]bis(4,4′-dimethylbipyridine)ruthenium(II), and [4-(bromomethyl)-4′-methylbipyridine](bipyridine)(bipyrimidine)ruthenium(II). Each coordinated ruthenium dication that was attached to the protein through Cysteine 69 has a different standard reduction potential in its excited electronic state, and each has a different standard reduction potential in its ground electronic state. The three different modified proteins were dissolved separately and the resulting solutions were excited with short, intense flashes of light that formed the electronically excited states of the respective ruthenium dications. The transfers of an electron to and from the heme in each derivative were monitored at 424 and 556 nm; and the transfers of the electron from and to the ruthenium complexes were monitored at the isosbestic points for the heme at 439 and 547 nm. The natural logarithms of the rate constants (second^{-1}) fortransfer of the electron from the excited electronic state of Ru^{2+} to the Fe^{3+} of the heme (open symbols) and those for subsequent transfer of the electron from the resulting Fe^{2+} in the heme back to the ground electronic state of Ru^{3+} (filled symbols) are plotted as a function of the differences in standard reduction potential (kilojoules mole^{-1}) of the respective donor and acceptor.

water. The transfer between these two prosthetic groups is exergonic because the prosthetic, mononuclear copper ion has a less positive biochemical standard reduction potential than the trinuclear cluster. There are two homologous (25% identity; 1.4 gap percent) laccases, one from *Trametes versicolor* and one from *T. vernicifluum*, in which the biochemical standard reduction potentials for the prosthetic, mononuclear copper ion have significantly different values of +780 and +430 mV, respectively. This difference causes transfer of the electron from the former mononuclear copper ion through the protein to its trinuclear cluster (+1030 mV) to be less exergonic than transfer of the electron through the latter protein to its trinuclear cluster (+970 mV); in other words, the change in standard free energy, ΔG°, in Equation 2–190 is negative in both cases but is less negative in the former laccase (–25 kJ mol^{-1}) than in the latter laccase (–52 kJ mol^{-1}). The reorganization energies, λ, for the electron transfer have been estimated to be +115 and +110 kJ mol^{-1}, respectively, a difference that is most likely within the error of the estimations. The electronic matrix elements, $H_{AB,}$ have also been shown to be the same in the two proteins. The equivalence of these two factors is not surprising since the two proteins are homologues of each other. The observed rate of electron transfer in the laccase from *T. versicolor* is 20 s^{-1}, and the observed rate constant of electron transfer in the laccase from *T. vernicifluum* is greater than 700 s^{-1}. Both values are consistent with the respective values for the change in standard free energy.[1081]

It has been observed in many situations[1041,1088-1093] that, provided ΔG° and λ remain the same, **the function describing the distance dependence of the rate constant for transfer of electrons through molecules other than proteins** is[1067,1069]

$$k_{ET} = k_0 \exp\left[\beta\left(r - r_0\right)\right] \qquad (2\text{–}191)$$

where r is the distance between donor and acceptor, r_0 is the sum of their van der Waals radii or the closest distance they can approach each other, and k_0 is the rate constant for transfer of an electron when donor and acceptor are as close together as possible and the exponential term equals 1. For example, a series of compounds analogous to **2–75** was synthesized in which the donor again was the radical anion of the 4-biphenylyl group and the acceptor R was a naphthyl group (Figure 2–39). The rigid hydrocarbon separating the biphenylyl group and the naphthyl group was varied in length, and the donor and acceptor each occupied equatorial positions of the cyclohexyl rings of the rigid hydrocarbon. The variation in the rate constants for transfer of an electron between the biphenylyl and naphthyl groups satisfied Equation 2–191 with a value of β equal to –12 nm^{-1} (Figure 2–41A).[1069,1088] Although this was not the case in the measurements made with this series of compounds, the most reliable way to ensure that the effects of small changes in ΔG° and λ on the rate constants for transfer of an electron are minimized in such an experiment is to use a donor and an acceptor for which $-\Delta G^\circ \cong \lambda$ (Figures 2–39 and 2–40), a situation in which the derivative of the rate constant for exchange as a function of the change in free energy is 0.

The dependence on the distance *r* between donor and acceptor of the rate constant for transfer of an electron through protein has been extensively measured. In the most extensive set of experiments (Figure 2–42),[1045,1094] ruthenium ions were bound to histidines inserted by site-directed mutation at particular positions in the sequence of amino acids for isoform 1 of cytochrome *c* from *S. cerevisiae* (○; six different positions),[1095-1097] equine cytochrome *c* (○; two different positions),[1098] cytochrome b_{562} from *E. coli* (□; nine different positions),[1099] azurin from *P. aeruginosa* (●; six different positions),[1095,1100,1101] myoglobin from *Physeter macrocephalus* (▼; three different positions),[1046,1102] or high-potential iron–sulfur protein from *A. vinosum* (■; four different positions).[1103] In each case, the ruthenium ion was coordinated by two 2,2′-bipyridines, an imidazole, and the imidazolyl group of the particular histidine that had been placed on the surface of the particular protein.[1098] For each protein, the rate constants for transfer of an electron from Fe^{2+} in its heme, its Cu^+, or its reduced [4Fe–4S] iron–sulfur cluster to Ru^{3+} on the histidine were measured.[1098,1104] These electron transfers are all exergonic enough (ΔG° = –71 kJ mol^{-1} for cytochrome *c*, ΔG° = –76 kJ mol^{-1} for cytochrome b_{562}, and ΔG° = –73 kJ mol^{-1} for azurin) that they are in the range where $\Delta G^\circ \cong -\lambda$.[1080]

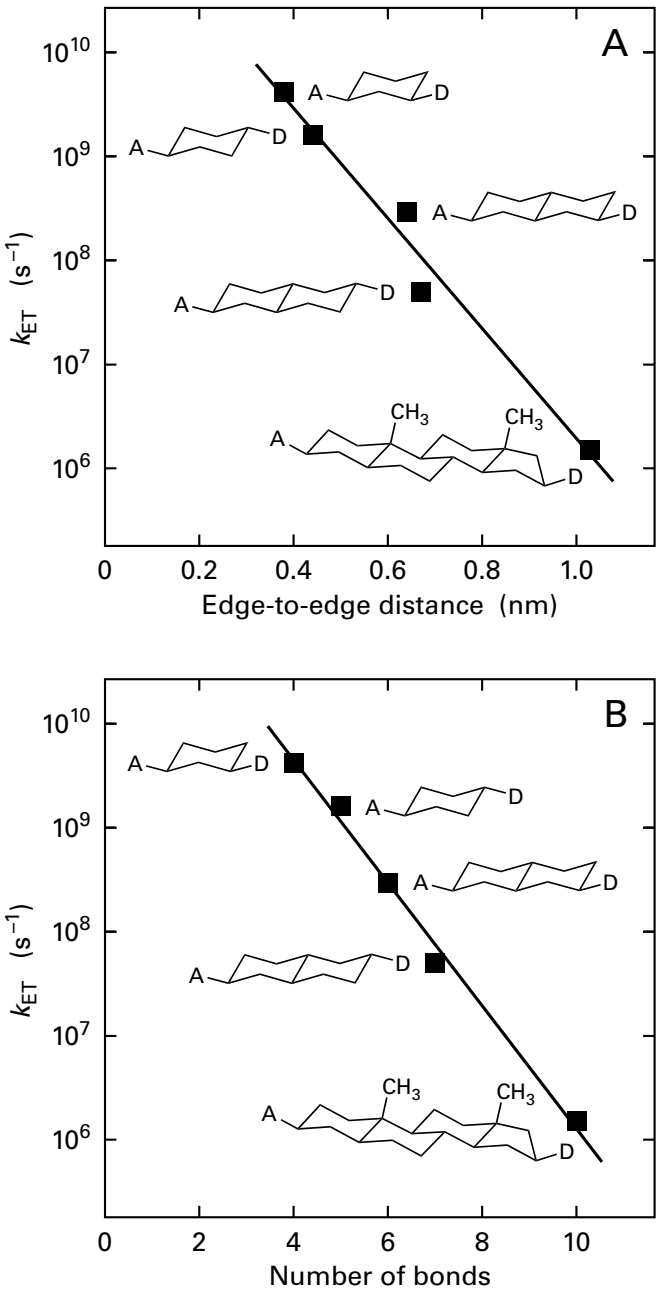

Figure 2–41: Dependence of the rate constant (k_{ET}) for intramolecular transfer of an electron between a 4-biphenylyl group and a 2-naphthyl group, held apart by various rigid hydrocarbons, on the distance between the 4-biphenylyl group and the 2-naphthyl group.[1069] *cis*-1-Naphthyl-3-(4-biphenylyl)-cyclohexane, *trans*-1-naphthyl-4-(4-biphenylyl)cyclohexane, *cis*-2-naphthyl-7-(4-biphenylyl)decalin, *trans*-2-naphthyl-6-(4-biphenylyl)decalin, and *cis*-1-naphthyl-17-(4-biphenylyl)androstane were synthesized. The structure of each of the hydrocarbons positioning the acceptor (A) and the donor (D) at fixed distances from each other is drawn next to the point for the respective rate of electron transfer. Each compound was dissolved separately in tetrahydrofuran. The respective solutions were each exposed to an intense, short pulse (30 ps to a few nanoseconds) of an electron beam from a linear accelerator. The resulting hydrated electrons that were formed instantaneously in the solution were trapped by biphenylyl groups to create biphenylyl radical anions. The decay in the concentration of each of the biphenylyl radical anions was followed by its absorbance. In each instance, it was found that the presence of the acceptor hastened the decay of the biphenylyl radical anion. The amount that the rate was accelerated by the presence of the acceptor was used to calculate the rate constant (second^{-1}) for each intramolecular electron transfer. The natural logarithms of these rate constants are plotted as a function of **(A)** the respective distances (nanometers) between the edges of the aromatic π molecular orbital systems of the biphenylyl group and the naphthyl group and **(B)** the respective number of carbon–carbon bonds between the two edges.

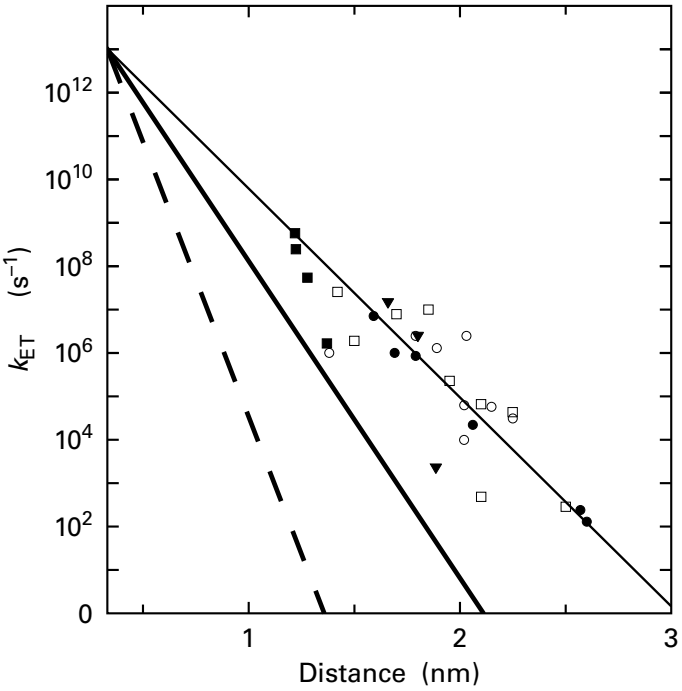

Figure 2–42: Dependence of the rate constant (k_{ET}) for intramolecular transfer of an electron through azurin (●),[1095] cytochrome *c* (○),[1046,1096-1098] cytochrome b_{562} (□),[1099] myoglobin (▲),[1046,1102] and high-potential iron–sulfur protein (■),[1103] as a function of the distance between donor and acceptor.[1094,1099] The amino acids at positions 83, 107, 109, 122, 124, and 126 in azurin from *P. aeruginosa*; at positions 39, 54, 58, 62, and 66 from isoform 1 of cytochrome *c* from *S. cervisiae*; at positions 33 and 72 from equine cytochrome *c*; at positions 12, 15, 19, 63, 70, 73, 86, 89, and 92 in cytochrome b_{562} from *E. coli*; at positions 70, 83, and 95 in myoglobin from *P. macrocephalus*; and at positions 18, 42, 50, and 81 in high-potential iron–sulfur protein from *A. vinosum* were changed one at a time to histidines by site-directed mutation. Each resulting histidine was modified with bis(bipyridine)ruthenium(II) carbonate followed by treatment with imidazole to produce a Ru^{2+} coordinated by two bipyridines, an imidazole, and the imidazolyl group of the respective histidine.[1104] Each modified cytochrome and high-potential iron–sulfur protein was exposed to a short (25 ns) intense pulse of light at 480 nm to form the electronically excited state of Ru^{2+}. An electron then transferred from this electronically excited state to the Fe^{3+} in the ferric heme of cytochrome *c* or the oxidized [4Fe–4S] iron–sulfur cluster of high-potential iron–sulfur protein to produce the ferrous heme or the reduced [4Fe–4S] iron–sulfur cluster and Ru^{3+}. The rate at which the electron transferred from the ferrous heme or the reduced [4Fe–4S] iron–sulfur cluster back to Ru^{3+} was then measured at wavelengths that monitor the transformation of ferrous heme to ferric heme and Ru^{3+} to Ru^{2+}. Each modified azurin or myoglobin was exposed to a short (25 ns) intense pulse of light at 480 nm to form the electronically excited state of the Ru^{2+}. The electron then transferred instantaneously from this electronically excited state to a quencher that had been added to the solution to create Ru^{3+}. The rate at which an electron transferred from the natural Cu^{+} of azurin or the natural Fe^{2+} in the heme of myoglobin to Ru^{3+} was then measured[1101] at wavelengths that monitor the transformation of cuprous azurin to cupric azurin, ferrous myoglobin to ferric myoglobin, and Ru^{3+} to Ru^{2+}. The rates for the transfers of the electrons (second^{-1}) are plotted on a common logarithmic scale as a function of the distances (nanometers) between the respective donors and acceptors as estimated from the crystallographic molecular models of the proteins. The thin solid line is a least-squares fit of the data, the thick solid line is the dependence on distance for transfer of an electron between Ru(2,2′:6,2′′-terpyridine)$_2^{2+}$ and $Fe(OH_2)_6^{3+}$ in a frozen glass of water,[1094] and the dashed line is the dependence on distance for transfer of an electron in the vacuum.[1045,1094]

From the crystallographic molecular models of the unmodified proteins, the distance from the ruthenium ion bound at each histidine to the ion of the transition metal or the nearest ion of the transition metal in the natural prosthetic group was calculated. When the common logarithms of the rate constants for these electron transfers are plotted as a function of these distances, the value of β obtained from a fit of Equation 2–191 to the data is –11 nm^{-1} (Figure 2–42).[1099] The linearity of the rate constants for high-potential iron–sulfur protein suggests that it might be more informative to plot the rate constants for each protein separately, but the scatter of the rate constants for the other proteins suggests that this approach would not reveal any significant differences among the different proteins.

The distances between natural redox couples in proteins can also be used to evaluate this correlation between the rate of electron transfer and distance. When the rate constants for transfer of an electron between the various pairs of prosthetic groups in the reaction center in *R. sphaeroides* (Figure 2–34) are adjusted from their actual values to the values they would have if ΔG° were equal to $-\lambda$, and the natural logarithms of these adjusted rate constants are plotted as a function of the edge to edge distances between the π molecular orbital systems of the prosthetic groups, a linear relationship is observed.[1041] The data in this latter correlation fit Equation 2–191 far more successfully than do the data in Figure 2–42, but these were rate constants that had been significantly adjusted, rather than the actual rate constants. The value of β for the fit of these distances in the reaction center to Equation 2–191 is –14 nm^{-1}.

One problem with the actual rate constants for the artificial electron transfers through protein (Figure 2–42) is that they do not fit Equation 2–191 with much success. This failure as well as theoretical arguments suggest that, rather than through an orbital overlap as would be the case in the vacuum, **the electron is transferred through unoccupied antibonding molecular orbitals** of a continuous sequence of covalent bonds[1105-1107] and hydrogen bonds[1108] that connect the donor of the electron to the acceptor of the electron.* Transfer of an electron also can occur through fixed molecules of water connecting two segments of polypeptide.[1094,1109-1112]

Certainly, transfers of electrons through protein, for which the values of β are –11 to –14 nm^{-1}, are **faster than they would be through the vacuum**, for which the values of β are –28 to –35 nm^{-1} for the same span of distances (dashed line in Figure 2–42),[1045,1094] or even between Ru(2,2′:6,2″-ter-pyridine)$_2^{2+}$ and $Fe(OH_2)_6^{3+}$ through an unbonded glass of molecules of water, for which the value of β is –17 nm^{-1} (thick solid line in Figure 2–42).[1094] The fact that transfer of an electron through a molecule of protein is so fast suggests that it is occurring by some process beyond the overlap of molecular orbitals occupied by the electron in the donor and the acceptor.

In this view, for each intramolecular transfer of an electron through a protein, there are several (or more than several) explicit but often tortuous **paths through the antibonding molecular orbitals** of the chemical bonds, hydrogen bonds, and fixed molecules of water between donor and acceptor, and associated with each path is a particular value of the electronic matrix element H_{AB}.[1113,1114] The actual transfer of the electron occurs along the path or paths with the highest values of H_{AB}.

This view is not inconsistent with the observation that rate constants of intramolecular transfer of an electron through molecules other than protein are usually exponential functions (Equation 2–191) of the distance between donor and acceptor (Figure 2–41A) because they are also exponential functions of the number of covalent bonds between donor and acceptor, and those covalent bonds are usually the same covalent bonds as the length is increased (Figure 2–41B). This equivalence of distance, the number of bonds, and their identity in synthetic molecules is due to the fact that they are usually built from regular repeating structures such as rigid rings of hydrocarbon or rigid regular polymers such as polyproline. Molecules of protein, however, are irregularly folded, irregular polymers interconnected by multiple hydrogen bonds and sometimes fixed molecules of water, so the lengths of the paths through the antibonding molecular orbitals of covalent bonds, hydrogen bonds, and molecules of water connecting donor and acceptor often are uncorrelated with the distance between donor and acceptor.

One indication that an electron might be transferred through a protein along a particular path of covalent and noncovalent bonds is the behavior of the rate constants for transfer of an electron to the prosthetic Cu^{2+} from Ru^{+} coordinated at each of the

*Hydrogen bonds are equivalent to covalent bonds in their ability to catalyze transfer of an electron.[1108]

respective histidines placed by site-directed mutation on the surface of azurin from *P. aeruginosa*. The positions chosen for the histidines in these experiments were along three continuous β strands, each of which contains one of the ligands to the copper ion, Histidine 46, Methionine 121, or Cysteine 112 (see Figure 2–26E). In this case, the distance from each Ru^{+} ion to the Cu^{2+} should be directly proportional to the number of covalent bonds between them, and the correlation between the distances and the common logarithms of the rate constants for transfer of an electron is a good one (filled circles in Figure 2–42). In the case of cytochrome *c*, however, the positions chosen for the histidines were scattered over the structure,[1095] and the correlation between the distances and the common logarithms of the rate constants is poor (open circles in Figure 2–42).

For transfer of an electron that proceeds through a path of the antibonding orbitals in a sequence of bonds connecting donor and acceptor[1113,1115]

$$H_{AB} = H^{\circ}_{AB} \prod_{i=2}^{n_c} \varepsilon_{c,i} \prod_{j=1}^{n_s} \varepsilon_{s,j} \prod_{k=1}^{n_H} \varepsilon_{H,k} \qquad (2\text{–}192)$$

where H°_{AB} is the electronic coupling of the antibonding molecular orbitals immediately adjacent to molecular orbitals in the donor and the acceptor between which the electron is transferred, $\varepsilon_{c,i}$ is the decay parameter for the ith covalent bond of the n_c covalent bonds along the path, $\varepsilon_{s,j}$ is the decay parameter for the jth jump through space of the n_s jumps through space along the path, and $\varepsilon_{H,k}$ is the decay parameter for the kth hydrogen bond of the n_H hydrogen bonds along the path. The decay parameters quantify the decay of the electronic coupling at each step along the path. The value of H_{AB} is calculated for as many paths between donor and acceptor as time will permit, and the one or two giving the largest values are then assigned as the most likely.[242,1048,1114-1116] This exercise provides an explicit chain of covalent bonds, hydrogen bonds, and jumps through space that permits a visualization of the passage of the electron. Unfortunately, the number of parameters required for a calculation by Equation 2–192 is so large and their uncertainty so great that reliable values of rate constants for transfer of an electron cannot be calculated with it for comparison with experimental values.

Although the term electron transfer seems to imply that the same electron leaves the donor and arrives on the acceptor, it is obvious that this is not the case. If transfer occurs through bonds, these bonds contain pairs of electrons, none of which can be distinguished from the electron that is transferred from the donor. If electron transfer occurs through space, there are electrons in the space between donor and acceptor, none of which can be distinguished from the electron that is tranferred from the donor. Strictly speaking, electron transfer through bonds or through space should be referred to as **net electron transfer**.

The argument over outer-sphere intramolecular transfer of an electron is **whether it occurs through bonds (Equation 2–192)**[1113] **or through space (Equation 2–191)**.[1045] In the former view, the failure of the observed rate constants for intramolecular electron transfer through proteins (Figure 2–42) to follow Equation 2–191 is due to the intricacy of the various paths through bonds connecting donor and acceptor. In the latter view, the failure results from variations in the dielectric properties of the intervening medium, in particular the fraction of the space occupied by atoms and the fraction of the space that is vacant. Various molecules have been synthesized to contribute experimental justification for one or the other side in this argument.

There are results suggesting that electron transfer in solution occurs **through space**. For example, two calixarenes have been synthesized that covalently connect a zinc porphyrin with a pyromellitimide group by the same path of covalent bonds, but in one of these calixarenes, the edge of the zinc porphyrin is 0.5 nm from the edge of the pyromellitimide, and in the other, the edges are 1.5 nm apart. In benzene, transfer of an electron is observed between the zinc porphyrin and the pyromellitimide in the former but not in the latter.[1117] Transfer of an electron from the 1,4-dimethoxy-5,8-diphenylnaphthyl group to the 1,1-dicyanoethenyl group in

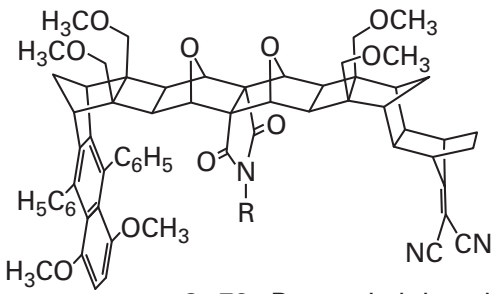

2–76 R = *p*-ethylphenyl
2–77 R = propyl

was measured in acetonitrile. When a phenyl group sits between the donor and acceptor (**2–76**), the rate constant for transfer of an electron ($0.64\ ns^{-1}$) is 2.6 times faster than the rate constant ($0.25\ ns^{-1}$) when a propyl group (**2–77**) sits between them, even though the through-bond paths are identical in each case.[1118,1119]

There are other results, however, suggesting that transfer of an electron in solution occurs **through bonds**. For example, the rate constants for transfer of an electron from a phthalimido group to a *tert*-butyl peroxy group actually increase as the number of α-aminoisobutyryl groups separating them, and the distance between them, increases.[1120] This observation suggests that the increase in the number of hydrogen bonds in the 3_{10} helix formed by these polymers of α-aminoisobutyric acid explains the increase in the rate constants.

It is possible that in some situations transfer of an electron proceeds through space while in other situations it proceeds through the antibonding molecular orbitals of bonds, and in still other situations by some combination of the two.

Side chains of aromatic amino acids such as tryptophan and tyrosine can act as intermediate relay stations through which a hole for an electron is relayed within a protein by hopping from one to the next.[1068,1121-1124] For example, in photoreduction of the oxidized prosthetic flavin in the active site of deoxyribodipyrimidine photo-lyase from *E. coli*, a hole for an electron is transferred from the electronically excited state of the prosthetic oxidized flavin in the active site to Tryptophan 306 on the surface of the enzyme following photolytic excitation of the flavin. Between the flavin and Tryptophan 306 are two others, Tryptophan 382 and Tryptophan 359, that act as relay stations to relay the hole from the electronically excited state of the oxidized flavin to Tryptophan 306.[1125]

While there has never been any doubt that electrons hop from one prosthetic group to another in instances where there is a chain of prosthetic groups, such as pheophytins, chlorophylls, iron–sulfur clusters, or hemes, that normally transfer an electron by successive one-electron reductions, the low standard one-electron reduction potentials for the side chains of tryptophan and tyrosine ($E^{\circ\prime} < -1800$ mV)[1126] to form their respective radical anions preclude transfer of an electron from a donor to one of them and from the resulting radical anion to the acceptor. The biochemical standard reduction potentials, however, for the radical cation of the indolyl group of tryptophan ($E^{\circ\prime} = +1000$ mV)[1127] and for the radical cation of the 4-hydroxyphenyl group of tyrosine ($E^{\circ\prime} = +800$ mV)[1128] are in the reasonable range. Consequently, rather than an electron hopping among the tryptophans and the tyrosines from donor to acceptor, **a hole hops from acceptor to donor.**

The difference is somewhat semantic. For example, in the case of photoactivation of deoxyribodipyrimidine photo-lyase, which reduces the oxidized flavin in its active site to flavin semiquinone, it has been shown[1125] that an electron first transfers from the indolyl group of the closest tryptophan, Tryptophan 382, to the photoexcited oxidized flavin, creating a hole in Tryptophan 382 in the form of an **indolyl radical cation** and the flavin semiquinone. The hole is then transferred to the next tryptophan, Tryptophan 359, when an electron transfers from it to the hole in Tryptophan 382, creating a hole in Tryptophan 359 in the form of an indolyl radical cation. Finally, the hole is transferred to Tryptophan 306 on the surface of the protein when an electron transfers from it to the hole in Tryptophan 359. The net result of this process is that an electron has been transferred from Tryptophan 306 to the photoexcited oxidized flavin.

In ribonucleoside-diphosphate reductase from *E. coli*, which reduces ribonucleoside diphosphates to deoxyribonucleoside diphosphates, a hole is transferred from a stable tyrosyl radical in another protein, which functions as an electron-transferring coenzyme during catalysis, to the sulfido group of Cysteine 439 in the active site of the enzyme to create a thiyl radical. The role of the electron-transferring coenzyme in the reaction is to be a one-electron oxidant and then a one-electron reductant, donating a hole to ribonucleotide reductase and then accepting back a hole each time the ribonucleoside-diphosphate reductase reduces a ribonucleotide to a deoxyribonucleotide. The peculiar aspect of the transfer of this hole is that it is endergonic;[1129] the difference in reduction potential between the tyrosyl radical and the thiyl radical has been estimated to be around +200 mV.* It is the change in overall free energy for enzymatic reduction by ribonucleoside diphosphate that pulls the hole to the sulfido group. There are two tyrosines in ribonucleoside-diphosphate reductase, Tyrosine 731

*Transfer of an electron from a donor of more negative reduction to an acceptor of more positive reduction potential is exergonic, but transfer of a hole from a donor of more negative reduction potential to an acceptor of more positive reduction potential, as is the case here, is endergonic.

and Tyrosine 730, immediately adjacent to the cysteine in the active site that could act as relay stations for the hole from the stable tyrosyl radical in the electron-transferring coenzyme and among which it would hop.[1130] In this instance, an electron in the 4-hydroxyphenyl group of Tyrosine 731 would transfer to a hole arriving from the tyrosyl radical in the electron-transferring coenzyme, then an electron in the 4-hydroxyphenyl group of Tyrosine 730 would transfer to the resulting hole in the radical cation of the 4-hydroxyphenyl group of Tyrosine 731, and then an electron in the sulfido group of Cysteine 439 would transfer to the resulting hole in the radical cation of Tyrosine 730, resulting in the thiyl radical necessary for catalysis.

The biochemical standard reduction potentials for the radical cations of tryptophan or tyrosine can be decreased by positioning a catalytic base adjacent to the nitrogen–hydrogen bond in the indolyl group or the oxygen–hydrogen bond in the 4-hydroxyphenyl group to accept the hydron from the respective radical cation, each of which is a stronger acid than the neutral, unoxidized group. The drawback of stabilizing the hole by removing a hydron from the radical cation, however, is that the rate of transfer of the electron to the hole from the next participant in the chain is decreased. In the case of photoreduction of deoxyribodipyrimidine photo-lyase, the nitrogen–hydrogen bonds on Tryptophan 382, Tryptophan 359, and Tryptophan 306 form hydrogen bonds with the acyl oxygen in the carbamoyl group on the side chain of Asparagine 378, a fixed molecule of water, and a fixed molecule of water, respectively, in the crystallographic molecular model of the protein,[1131] each of which is only a weak base, and in this instance the three successive radical cations remain hydronated and cationic.[1125] In the case of ribonucleotide reductase, however, in the crystallographic molecular model of the enzyme,[1132] the 4-hydroxy group of Tyrosine 731 forms a hydrogen bond with the 4-hydroxy group of Tyrosine 730, which also forms a hydrogen bond with the sulfanyl group of Cysteine 439. It has been proposed that when the hole arrives at Tyrosine 731 to form its radical cation, the 4-oxido group of the conjugate base of Tyrosine 730 removes a hydron from it. This transfer of a hydron turns the radical cation into the **neutral 4-hydroxyphenyl radical**. Then when the hole is transferred to Tyrosine 730, the resulting 4-oxido group of the conjugate base of Tyrosine 731 removes a hydron from it. Finally, when the hole arrives at the sulfanyl group of Cysteine 439, the resulting 4-oxido group of the conjugate base of Tyrosine 730 removes a hydron from it.[1133] The hydron transfers would serve the purpose of stabilizing the hole on each successive relay station.

When Tryptophan 306 in deoxyribodipyrimidine photo-lyase from *E. coli* is mutated to a phenylalanine, the hole ends up in one of the indolyl groups of the tryptophans that act as relay stations rather than on Tryptophan 306.[1134] When either Tyrosine 730 or Tyrosine 731 in ribonucleoside-diphosphate reductase from *E. coli* is mutated to a 3-aminotyrosine, which has a lower biochemical standard reduction potential for the redox couple of the 3-amino-4-phenoxyl group and the 3-amino-4-hydroxyphenyl group (+400 mV)[1135] than for the redox couple of a thiyl radical and a sulfanyl group (+900 mV),[1136] an electron is transferred from that 3-aminotyrosine to the hole in the tyrosyl radical rather than from the sulfanyl group of the cysteine in the active site.[1137] Each of these results has been presented as evidence that, in the normal reaction of each enzyme, the hole hops along the chain of relay stations (tryptophans and tyrosines) from the acceptor (either the electronically excited state of the flavin semiquinone or the tyrosyl radical in the electron-transferring coenzyme) to the donor (the tryptophan or the sulfido group). In the normal reaction of each mutated enzyme, however, a pre-established transfer of an electron must naturally occur from the normal donor to the normal acceptor, so it is not surprising that when the normal donor is eliminated, an even closer donor supplies the electron in its stead, or that when a better donor is placed immediately adjacent to the normal donor, the better donor would simply provide the electron rather than the normal donor.

It has also been observed that when a tyrosine or a tryptophan that could act as a relay station in a protein through which a hole is transferred is **substituted by mutation**, the rate for transfer of the electron decreases. For example, when either Tryptophan 382 or Tryptophan 359 in deoxyribodipyrimidine photo-lyase from *E. coli* is mutated to a phenylalanine, the photoexcited state of the flavin semiquinone decays before the electron can be transferred to it from Tryptophan 306.[1125] When Tyrosine 730 and Tyrosine 731 in ribonucleotide reductase from *E. coli* were mutated in turn to phenylalanine, the enzymatic activity of each mutant was less than 1% of the wild-type enzyme.[1138]

The effects of specific chemical modification of each of 12 lysines on the surface of equine cytochrome *c* on transfer of an electron between it and

bovine cytochrome-*c* oxidase,[1139] as well as computational descriptions of the docking of equine cytochrome *c* and bovine cytochrome-*c* oxidase,[1140] have tentatively defined the structure of the complex between them, in which electron transfer occurs between the heme in cytochrome *c* and the dinuclear CuA cluster of copper ions in cytochrome-*c* oxidase (Figure 2–26F). In that proposed complex, Tryptophan 143 in cytochrome-*c* oxidase from *R. sphaeroides* sits between the heme and the dinuclear CuA cluster. When Tryptophan 143 is mutated to phenylalanine, the rate constant for electron transfer between the reduced heme in equine cytochrome *c* and the oxidized dinuclear CuA cluster in cytochrome-*c* oxidase from *R. sphaeroides* decreases[1141] from 38×10^3 s^{-1} to 85 s^{-1}.

In tyramine β-monooxygenase from *Drosophila melanogaster*, Tyrosine 79 is stacked upon Histidine 172, which is a ligand to one of the two prosthetic copper ions in the enzyme. Tyrosine 79 lies between this copper ion and the other copper ion in the enzyme. When Tyrosine 79 is mutated to alanine, the rate for transfer of an electron from the one copper ion to the other, which in the native enzyme is not rate-limiting, becomes the rate-limiting step in the enzymatic reaction.[1142]

It is also possible to **accelerate an electron transfer by adding a relay station for the hole**. For example, the P450 peroxidase from *S. acidocaldarius* contains a heme with a sulfido group as its axial ligand. Lysine 97, on the surface of the enzyme, was mutated to cysteine, and a ruthenium ion coordinated by two 2,2′-bipyridines and a 1,10-phenanthroline was covalently attached to the sulfanyl group of the cysteine. The ruthenium ion ended up about 2.1 nm from the heme. Histidine 76 is adjacent to the heme and forms a hydrogen bond with one of its carboxyethyl groups.[1143] The homologous enzyme (30% identity; 1.9 gap percent) from *Bacillus megaterium* has a tryptophan in place of the histidine that also forms a hydrogen bond with the same carboxyethyl group of the heme.[1144] No transfer of an electron from an Fe^{3+} in the heme to a photolytically generated Ru^{3+} on the surface of peroxidase from *S. acidocaldarius* is observed in the native enzyme over the lifetime (100 μs) of the Ru^{3+}, but when Histidine 76 in the enzyme is mutated to tryptophan to create a relay station 0.7 nm from the heme and 1.2 nm from the ruthenium ion, an electron is transferred[1145] from the Fe^{3+} to the transient Ru^{3+} during its lifetime.

The rate for transfer of an electron through azurin from *P. aeruginosa* between its prosthetic Cu^{+} (Figure 2–26E) and a Ru^{3+} coordinated by a histidine added to the surface of the protein by site-directed mutation (filled circles in Figure 2–42) is accelerated by the addition of a relay station[1146] for the hole between Cu^{+} and Ru^{3+}. A single histidine was placed by site-directed mutation at position 107 on one strand of β-structure in azurin or at position 124 or 126 on another strand of β-structure in the protein to construct three mutants. A ruthenium ion coordinated by two 2,2′-bipyridines and an imidazole was then coordinated to the imidazolyl group of the inserted histidine in each of these three mutants.[1098] Cysteine 112, which is a ligand to the copper ion (Figure 2–26E), is at the carboxy-terminal end of the first strand of β-structure, and Methionine 121, which is also a ligand to the copper ion (Figure 2–26E), is at the amino-terminal end of the second strand of β-structure. The relay station chosen for the hole, a 3-nitrotyrosyl side chain ($E^{\circ\prime}$ = +1100 mV),[1128] was then placed in turn by mutation on the same strand of β-structure between the inserted histidine to which the ruthenium ion was attached and the respective ligand to the copper ion in each of the three mutants. The relay stations were placed at position 109 on the first strand of β-structure in the mutant with the inserted histidine at position 107, at position 122 on the second strand of β-structure in the mutant with the inserted histidine at position 124, and at position 122 on the second strand of β-structure in the mutant with the inserted histidine at position 126. Both positions to which nitrotyrosyl relay stations were added were amino acids in the wild-type protein, Methionine 109 and Lysine 122, that had side chains incapable of being oxidized and acting as a relay station for a hole, and the positions chosen in each case for the relay stations were between the respective positions chosen for the histidine and the ligand to the copper ion, either cysteine or methionine (Figure 2–26E).

The rate for transfer of an electron from Cu^{+} to Ru^{3+} was determined for each of the three mutants both with and without the inserted relay station. Addition of each nitrotyrosine as a relay station for the hole between Ru^{3+} and Cu^{+} in the three mutants increased the rates of electron transfer by factors of 30, 50, and 15, respectively.[1146] The neutral 3-nitrophenyl radical of nitrotyrosine has about the same biochemical standard reduction potential as a radical cation of the indolyl group of a tryptophan, but the

Ru^{3+} is such a strong oxidant that it is able to abstract an electron readily from the nitrotyrosyl group. This abstraction of an electron creates a hole on the nitrotyrosyl group, which is the hole into which the electron from Cu^{+} is then transferred in the instances in which the relay stations were present.

Hopping of a hole or an electron through one or more relay stations should **significantly increase the rate for overall transfer of an electron over long distance** from a donor to an acceptor. One way to understand this acceleration is to consider an idealized situation in which a relay station sits on the line of centers from donor to acceptor. Assume that the relay station is of an intermediate reduction potential between donor and acceptor, so the standard free energies of each oxidation–reduction are approximately the same. Assume also that the three respective electronic matrix elements and reorganization energies are similar enough that each transfer of the electron—the one from relay station to acceptor, the one from donor to the hole in the relay station, and the one from donor to acceptor in the absence of the relay station—is a function only of the distance between the participants (Equation 2–191). To make the mathematics simpler, it is also better to assume that the relay station is closer to the donor or closer to the acceptor. Suppose that the donor and acceptor are 3 nm apart, the relay station is 1.2 nm from the acceptor and 1.8 nm from the donor, and a β of 11 nm^{-1} (Figure 2–42) applies to this situation. Given the distance between them, the rate constant for transfer of the electron from donor to acceptor in the absence of hopping should be around 2 s^{-1}. Assume that the reverse reactions can be ignored, that the relay station relays a hole, and that the kinetic mechanism for transfer of the electron when the relay station is present is

$$\mathrm{D} \xrightarrow{k_2} \mathrm{RS} \xrightarrow{k_1} \mathrm{A} \qquad (2\text{–}193)$$

where D is the donor, RS is the relay station, and A is the acceptor. If k_1 is 500 μs^{-1} and k_2 is 1 μs^{-1} (Figure 2–42), the rate constant for transfer of the electron from donor to acceptor, after about 100 ns, should be equal to k_2 (1 μs^{-1}). The resulting acceleration of the rate (5×10^5) is significant.

The ideal case just examined, however, represents the maximum acceleration that can be achieved with the stipulated distances. If the reverse reactions are not negligible, if the relay station is not on the line of centers, if the interaction energies are not ideal, or if the differences in free energy of the electron between donor and relay station or between relay station and donor or both are not ideal, then the acceleration in the rate constant for transfer of an electron through a relay station will be less than in the foregoing demonstration, although the acceleration can still be significant. It is possible to take account of all these factors and estimate the rate to be expected for particular values of these parameters.[1122-1124]

In the case of photoreduction of the oxidized flavin in deoxyribodipyrimidine photo-lyase from *E. coli*, the rate constants for each step in which the hole is transferred from the electronically excited state of the flavin to Tryptophan 306 have been determined. Tryptophan 382 or Tryptophan 359 in the enzyme were substituted with phenylalanine, and effects of these mutations on the transient absorptions at 500 and 580 nm following photoexcitation were assessed. These are wavelengths at which the radical cations of the tryptophans absorb. The effects of these mutations on the transient absorption at 800 nm, a wavelength at which the electronically excited state of the flavin absorbs, were also ascertained.[1125] In this way, it was possible to dissect the transients into the contributions of these three chromophores as well as that from Tryptophan 306. The hole is passed from the electronically excited state of the flavin by an electron transfer from the indolyl group of Tryptophan 382 with a rate constant of 1200 ns^{-1}. The hole is then passed from the resulting radical cation of the indolyl group of Tryptophan 382 by an electron transfer from the indolyl group of Tryptophan 359 with a rate constant of 14 ns^{-1}. Finally, the hole is passed from the resulting radical cation of the indolyl group of Tryptophan 359 by an electron transfer from the indolyl group of Tryptophan 306 with a rate constant of 7 ns^{-1}.

There is some electron transfer from the ground state of the flavin semiquinone, which results from relaxation of the electronically excited state of the flavin after it has been reduced by the one electron. This electron transfer fills the hole on the radical cation of the indolyl group of Tryptophan 382 and short-circuits the ultimate oxidation of Tryptophan 306, but once the hole is beyond Tryptophan 382, there is no further short circuit. This situation is reminiscent of the race to move the electron away from the electronically excited state of the special pair to the ubiquinone in site B in the photosynthetic reaction center before it can return back to the ground state of the radical cation

of the special pair, except in this instance it is a hole returning to the source rather than an electron.

The acceleration observed when a 3-nitrotyrosine was installed as a relay station for transfer of an electron in azurin was as much as 50-fold. In this instance, however, the biochemical standard reduction potential of the relay station was not ideally matched to the biochemical standard reduction potentials of the donor and acceptor. In proteins containing chains of prosthetic groups through which an electron hops (Figures 2–30, 2–31, and 2–33) or proteins containing chains of aromatic groups through which a hole hops, it is entirely possible that natural selection has ensured that the differences in free energy and the interaction energies are more successfully matched, and the accelerations achieved by hopping are more significant. In any case, it is hard to see how an electron could be transferred over the large distances that often intervene between donor and acceptor in enzymes that accomplish rapid transfer of an electron without providing relay stations between which the electron or the hole can hop.

Other than a few instances, such as reaction centers and deoxyribodipyrimidine photo-lyase and perhaps cytochrome-*c* oxidase,[1147] the rate constants of normal intramolecular electron transfers between prosthetic groups within enzymes[1045] are usually between 10 s^{-1} and 10^5 s^{-1}. For example, when 5-deazariboflavin semiquinone is produced in solution by flash photolysis, it rapidly reduces the oxidized flavin in trimethylamine dehydrogenase from *M. methylotrophus* to the semiquinone. Transfer of the electron from this semiquinone, monitored by the decrease in its absorption at 470 nm, to the [4Fe–4S] iron–sulfur cluster in the enzyme[1148] has a rate constant of 60 s^{-1}. The rate constant for transfer of an electron from the flavin semiquinone to the heme *b* in L-lactate dehydrogenase (cytochrome) from *S. cerevisiae*[818] is 120 s^{-1}. When the heme *c* in nitrite reductase (NO-forming) from *P. pantotrophus* is rapidly reduced with a hydrated electron, an electron is transferred from it to the heme d_1 in the enzyme, measured by a decrease in absorption at 550 nm and an increase in absorption at 640 nm,[1149] with a rate constant of 1400 s^{-1}. These rates are a **compromise** between the change in standard free energy of the reaction, for which the greater the expenditure of free energy, the greater the rate (Equation 2–190), and the distance between donor and acceptor, for which the greater the distance, the slower the rate (Figure 2–42).[1045]

In the cases of a reaction center and deoxyribodipyrimidine photo-lyase, the unusually rapid rates for transfer of an electron or transfer of a hole, respectively, result from the short distances between the large aromatic π molecular orbitals of the prosthetic groups or between the tryptophans and the flavin, respectively, and the significant increases in standard reduction potential from one to the next in the case of the reaction center. In addition, neither photosynthesis nor photolytic repair of DNA would occur if the rates were not so fast because in each instance there is a race: between transfer of the electron away from the special pair and return of the electron to the ground state of the radical cation of the special pair, or between transfer of the hole away from the flavin and return of the hole to the ground state of the flavin semiquinone. The race is intense because the electronically excited state in each instance is produced photolytically, so the return of the electronically excited state to the ground state is rapid. This last fact explains why natural selection had to guarantee that transfer of the electron was as fast as possible. The fact that a reaction center is immersed in the nonpolar interior of a membrane is also consequential. Because a significant portion of the reorganization energy arises from dielectric reorganization of the solvent, the lower the permittivity of the surroundings, the lower the reorganization energy,[1065] and the larger the rate constant (Equation 2–190). This factor should increase not only the rate constants for transfers of electrons between the prosthetic groups in the reaction center but also those between all the prosthetic groups in those portions of other enzymes that are embedded in the phospholipid bilayers of biological membranes.

Transfer of an electron can occur between subunits of a protein, between domains in a protein, or between prosthetic groups on different molecules of protein. The two extremes of interprotein transfer are transfer of an electron between two subunits permanently associated with each other in the same protein and transfer of an electron during the transient collision of otherwise unassociated proteins. In between these extremes would be the case of an electron-transferring coenzyme that associates with an enzyme as a substrate, accepts or donates an electron while associated, and then dissociates from the enzyme.

Examples of **transfer of an electron between two subunits** associated with each other in the same protein would be transfer of an electron between the flavin on one subunit of the $\alpha\beta$ hetereodimer of

sulfide-cytochrome-*c* reductase (flavocytochrome *c*) from *A. vinosum* and the heme *c* on the other subunit[1150] and transfer of an electron between a heme *c* on a firmly associated subunit of the reaction center from *B. viridis* and the special pair.[959,960]

An example of a similar situation is transfer of an electron between prosthetic groups on two **separate domains** of the same protein that are connected by a single strand of polypeptide distant from the line connecting the two prosthetic groups,[1048,1151] such as between the flavin and the heme each in a separate domain in the NADPH—hemoprotein reductase (flavocytochrome P450 BM-3) of unspecific monooxygenase from *B. megaterium*[1152] or between heme in one domain and two prosthetic copper ions in a second domain naturally tethered to the first by a strand of polypeptide in nitrite reductase (NO-forming) from *Ralstonia pickettii*.[1112]

Domains in an enzyme can swing back and forth between donors and acceptors of electrons, as does the domain in quinol—cytochrome-*c* reductase (Figure 2–32). In NADPH—hemoprotein reductase from *R. norvegicus*, NADPH bound in the active site reduces an adjacent flavin in a prosthetic flavin adenine dinucleotide that then reduces the flavin in a prosthetic flavin mononucleotide. The reduced prosthetic flavin mononucleotide then passes one electron to the oxidized prosthetic heme in a molecule of heme oxygenase (biliverdin-producing) that associates reversibly with NADPH—hemoprotein reductase. Once the prosthetic heme on the first heme oxygenase (biliverdin-producing) is reduced, it dissociates. The next oxidized heme oxygenase (biliverdin-producing) associates with the enzyme, and its prosthetic heme is reduced by the second electron on the semiquinone of the prosthetic flavin mononucleotide, returning the flavin mononucleotide to its oxidized state.

The NADPH and the prosthetic flavin adenine dinucleotide are on a separate hinged domain from the domain in which the prosthetic flavin mononucleotide is located. When the reduced flavin adenine dinucleotide in the enzyme from *R. norvegicus* is reducing the flavin mononucleotide by two electrons, the hinge is closed, the two domains are in intimate contact with each other, and the 7-methyl groups of the two flavins, one on each of the domains, are in van der Waals contact with each other.[1052] When, however, the NADPH—hemoprotein reductase from *R. norvegicus* is associated with heme oxygenase (biliverdin-producing) from *R. norvegicus*, the hinge has opened so that the distance between the flavin adenine dinucleotide and the flavin mononucleotide is now 2.2 nm, but in the complex, the distance between the flavin mononucleotide and the prosthetic heme of the heme oxygenase (biliverdin-producing) is only 0.6 nm, close enough for rapid electron transfer.[1153] These necessary rearrangements of the domains in NADPH—hemoprotein reductase require that the flavin mononucleotide be reduced while the hinge is closed; when the hinge opens, the flavin mononucleotide can then reduce the prosthetic heme on heme oxygenase in the space created by the swinging away of the domain on which the NADPH and the prosthetic flavin adenine dinucleotide are located.

Examples of **transfer of an electron during the collision of two proteins** would be the self-exchange of an electron between two pseudoazurins ($k = 4 \times 10^3$ M^{-1} s^{-1}),[813] the self-exchange of an electron between two azurins from *P. aeruginosa* ($k = 3 \times 10^6$ M^{-1} s^{-1}),[1109] transfer of an electron between ferricytochrome *f* from *B. rapa* and a close homologue of its biological partner cupriplastocyanin from *Phaseolus vulgaris* (5×10^7 M^{-1} s^{-1}),[1154] and transfer of an electron between flavodoxin and its biological partner, photosystem I in *Synechocystis* ($k = 2 \times 10^8$ M^{-1} s^{-1}).[789]

The more common situation is one in which a small electron-transferring coenzyme provides an electron to or removes an electron from an enzyme of oxidation–reduction by forming a complex with the enzyme, and the **electron is transferred intermolecularly within the complex before it dissociates** rather than during a collision with its partner. For example, in *P. putida*, an electron is transferred from putidaredoxin—NAD^+ reductase to putidaredoxin in a complex between these two proteins that has a dissociation constant of 5 μM.[1155] Within the complex, the electron is transferred from the neutral flavin semiquinone of the reductase to the [2Fe–2S] iron–sulfur cluster of putidaredoxin at a rate of 230 s^{-1}. The dissociation constant between amicyanin and methylamine dehydrogenase (amicyanin) from *P. denitrificans*[1156] is also 5 μM, and the rate constant for transfer of the electron is 10 s^{-1}. The dissociation constant between bovine cytochrome *c* and bovine cytochrome-*c* oxidase[1157] is 20 μM, and the rate constant for transfer of the electron is 2600 s^{-1}. Cytochrome c_3 and flavodoxin from *D. vulgaris* form a complex with a dissociation constant of 60 μM in which an electron is transferred between them.[791]

Crystallographic molecular models for the normally transient complexes between an enzyme and a protein serving the role of an electron-transferring coenzyme are available for cytochrome-*c* peroxidase and isoform 1 of cytochrome *c* from *S. cerevisiae*,[1158] methylamine dehydrogenase (amicyanin) and amicyanin from *P. denitrificans*,[812,1159,1160] ferredoxin—$NADP^+$ reductase and ferredoxin from *Z. mays*,[1161] reaction center and cytochrome c_2 from *R. sphaeroides*,[1162] quinol—cytochrome-*c* reductase and isoform 1 of cytochrome *c* from *S. cerevisiae*,[946] human medium-chain acyl-CoA dehydrogenase and human electron-transfer flavoprotein,[1163] aralkylamine dehydrogenase (azurin) and azurin from *A. faecalis*,[1164] carbazole 1,9a-dioxygenase from *Janthinobacterium* and ferredoxin from *Pseudomonas resinovorans*,[1165] rubredoxin—NAD^+ reductase and rubredoxin from *P. aeruginosa*,[1166] ferredoxin—$NADP^+$ reductase and ferredoxin from *Pseudomonas*,[1167] nitrite reductase (NO-forming) and cytochrome c_{551} from *A. xylosoxidans*,[1168] methylamine dehydrogenase (amicyanin) and methylamine utilization protein MauG from *P. denitrificans*,[1169,1170] and L-ascorbate peroxidase and cytochrome *c* from *Leishmania major*.[1171] There is evidence from nuclear magnetic resonance spectra that the complex between methylamine dehydrogenase (amicyanin) and amicyanin is the one that exists in solution,[1160] and the complex between methylamine dehydrogenase (amicyanin) and methylamine utilization protein MauG performs the normal transfer of electrons within the crystal.[1169]

The prosthetic groups on the individual proteins in the crystallographic molecular models of these binary or ternary complexes are **usually within 1.4 nm of each other**,[1159,1161] as is the case for transfer of an electron between prosthetic groups within the same protein, but there is at least one example of a complex in which they are greater than 2.0 nm apart,[1045] which suggests that this complex may not be the natural one. In an electron micrographic reconstruction of the complex between the electron-transferring coenzyme and ribonucleoside-diphosphate reductase, however, the distance between the cysteine in the active site and the tyrosyl radical in the electron-transferring coenzyme, is 3.5 nm.[2610]

Continuous paths of covalent bonds between the prosthetic groups in crystallographic molecular models of these complexes do not exist because the prosthetic groups are on different proteins. Often a continuous path of covalent bonds in one protein can be connected to a continuous path of covalent bonds in the other by a hydrogen bond[1086,1162] or by a molecule of water in the interface fixed in position by hydrogen bonds,[1165,1166] but in other instances, the **connection between the two proteins** along the path is a van der Waals contact between one or more atoms in one protein and one or more atoms in the other rather than a hydrogen bond.[1158,1159,1164,1167,1168,1171] For the complex between quinol—cytochrome-*c* reductase and isoform 1 of cytochrome *c*, it has been proposed that transfer of an electron occurs through space rather than through σ bonds,[1172] even though two of the exocyclic carbon atoms, one from each heme, are in van der Waals contact.[946]

Cytochrome-*c* peroxidase from *S. cerevisiae* catalyzes the reaction

$$2\,H^+ + H_2O_2 + 2\ \text{ferrocytochrome } c \rightleftharpoons 2\,H_2O + 2\ \text{ferricytochrome } c \qquad (2\text{–}194)$$

which serves the purpose of eliminating hydrogen peroxide from the cytoplasm of the fungal cell. The hydrogen peroxide binds to a ferric heme on the enzyme. This complex is converted by the enzyme to a molecule of water; an oxoiron(IV),* $[(Fe^{4+})(^{2-}O)]$, at the heme; and a radical cation of the indolyl group ($\text{indolyl}^{\bullet+}$) of Tryptophan 191 in the enzyme.[1173-1175] Ferrocytochrome *c* from *S. cerevisiae* reduces the radical cation of the indolyl group in a bimolecular reaction[1176] with a rate constant of $2 \times 10^8\ M^{-1}\ s^{-1}$ at an ionic strength of 300 mM. An equilibrium is then established between the oxo-iron(IV) and the indolyl group of Tryptophan 191

$$H^+ + \left[Fe^{4+}O^{2-}\right]^{2+} + \text{indolyl} \rightleftharpoons \left[Fe^{3+}OH^-\right]^{2+} + \text{indolyl}^{\bullet+} \qquad (2\text{–}195)$$

where $[Fe^{3+}OH^-]^{2+}$ is the complex between Fe^{3+} in the heme and hydroxide.[1173] The equilibrium constant (K_{eq}) for this reaction is 0.4 at pH 6 and decreases as the pH is raised because the oxygen of the $[(Fe^{4+})(^{2-}O)]^{2+}$ must be hydronated before the electron can be transferred. A second molecule of ferrocytochrome *c* then reduces the radical cation of the indolyl group with a bimolecular rate constant[1176] of $3 \times 10^7\ M^{-1}\ s^{-1}$ at an ionic strength of 300 mM.

*Oxoiron(IV) is usually abbreviated $[Fe{=}O]^{2+}$ to indicate that there is thought to be both a σ bond and a π bond between the iron and the oxygen. In keeping with the decision to allow the reader to decide on bonding, ionic bonding is used here.

This rate constant is less than the first because the concentration of the radical cation of the indolyl group is decreased by the equilibrium (Equation 2–195).[1177] Addition of two electrons by two successive molecules of ferrocytochrome *c* returns the radical cation of the indolyl group of the tryptophan to the neutral indolyl group and returns the iron to the ferric oxidation state, and the hydroxide is hydronated to become water.

At high ionic strength (>100 mM), the **dissociation constant for the formation of a complex** between cytochrome-*c* peroxidase and cytochrome *c* from *S. cerevisiae* is so great (>10 μM)[1178] that there was no complex present in significant concentration in the foregoing experiments measuring the bimolecular rate constant for transfer of an electron from cytochrome *c* (at less than 1 μM) to cytochrome-*c* peroxidase (at less than 3 μM) and at an ionic strength of 300 mM.[1176] At low, unphysiological ionic strength (20 mM), however, cytochrome *c* from *S. cerevisiae* does form a complex with cytochrome-*c* peroxidase from *S. cerevisiae*[1179,1180] with a dissociation constant of 2 μM.[1178] A crystallographic molecular model of this complex places the iron in the heme of the cytochrome *c* 2.03 nm from the nearest edge of the π molecular orbital system of the radical cation of the indolyl group.[1158] The rate constant for transfer of an electron from heme *c* of ferrocytochrome *c* to the radical cation of the indolyl group[1181] within this complex[1182,1183] is 2 μs^{-1}. It is thought that this complex is the same as that formed transiently during the normal bimolecular transfer of the electron from cytochrome *c* to cytochrome-*c* peroxidase.

At high ionic strength, does transfer of an electron from the iron in ferrocytochrome *c* to the radical cation of the indolyl group of cytochrome-*c* peroxidase nevertheless occur only after this complex, albeit unstable, forms evanescently? Is the electron transferred intramolecularly only within a specific structurally defined complex, formed by the combination of two unique faces on the surfaces of cytochrome *c* and cytochrome-*c* peroxidase to form the unique interface observed in the crystallographic molecular model through which the electron passes,[1184] even though the reaction is kinetically bimolecular as if it resulted simply from the collision of cytochrome *c* and cytochrome-*c* peroxidase? These question can be asked of any transfer of an electron between two proteins that is kinetically bimolecular. Fundamentally, it is a question about the evolution of electron transfer. **Does natural selection have to produce a specific interface and a specific path for the electron to ensure that the required transfer of an electron occurs?**

There are experiments suggesting that any collision between two proteins is capable of accomplishing electron transfer. For example, an electron can be transferred with a rate constant of 2 ms^{-1} over a distance of 2.4 nm between a heme in cytochrome *c* in which a Zn^{2+} has replaced the iron to the Fe^{3+} in a cytochrome *c* adjacent to it in a crystal of cytochrome *c*.[1185] The contacts between molecules of protein in any crystal of protein are adventitious, arbitrary, and certainly not interfaces created by natural selection. The two molecules of cytochrome *c*, however, are held next to each other by the crystal. A specific complex between two faces forming an interface would hold the two proteins together, albeit fleetingly, and it may be that such an immobilization is required for transfer of an electron to occur.

That transfer of an electron from cytochrome *c* to the radical cation of the indolyl group proceeds within the specific complex between cytochrome-*c* peroxidase and cytochrome *c* at low ionic strength does not mean that it does so at high ionic strength. There is one result, however, suggesting that it does. A cysteine was introduced by site-directed mutation at position 193 in cytochrome-*c* peroxidase, which is in the middle of the interface in the specfic complex that forms at low ionic strength. This cysteine was then modified with 3-(*N*-maleimidyl-propionyl)biocytin, which is large enough to prevent the complex from forming. The rate for transfer of an electron from cytochrome *c* to cytochrome-*c* peroxidase at high ionic strength was decreased by a factor of 70 by this modification[1186] but not completely eliminated.

Two other questions are raised by cytochrome-*c* peroxidase. What is an oxoiron(IV) and how does the enzyme produce it?

Suggested Reading

Hunsicker-Wang, L. M., Heine, A., Chen, Y., Luna, E. P., Todaro, T., Zhang, Y. M., Williams, P. A., McRee, D. E., Hirst, J., Stout, C. D., and Fee, J. A. (2003) High-resolution structure of the soluble, respiratory-type Rieske protein from *Thermus thermophilus*: Analysis and comparison. *Biochemistry 42*, 7303–7317. https://doi.org/10.1021/bi0342719

Houser, R. P., Young, V. G., Jr, and Tolman, W. B. (1996) A thiolate-bridged, fully delocalized mixed-valence dicopper(I,II) complex that models the Cu_A biological electron-transfer site. *J. Am. Chem. Soc. 118*, 2101–2102. https://doi.org/10.1021/ja953776m

Deisenhofer, J., Epp, O., Miki, K., Huber, R., and Michel, H. (1984) X-ray structure analysis of a membrane protein complex: Electron density map at 3-Å resolution and a model of the chromophores of the photosynthetic reaction center from *Rhodopseudomonas viridis, J. Mol. Biol. 180*, 385–398. https://doi.org/10.1016/S0022-2836(84)80011-X

Chang, I. J., Gray, H. B., and Winkler, J. R. (1991) High-driving-force electron transfer in metalloproteins: Intramolecular oxidation of ferrocytochrome *c* by Ru(2,2'-bpy)$_2$(im)(His-33)$^{3+}$. *J. Am. Chem. Soc. 113*, 7056–7057. https://doi.org/10.1021/ja00018a064

Problem 2–23: The midpoint reduction potential of cytochrome *c* is invariant with pH between pH 2 and pH 7.8 and decreases with a slope of 60 mV (unit of pH)$^{-1}$ above pH 7.8.[751] Explain these observations in terms of the pK_a of an amino acid in oxidized cytochrome *c* and its pK_a in reduced cytochrome *c*.

Problem 2–24: Draw the structure of heme d_1. Draw circles around the 18 atoms that provide *p* orbitals to the aromatic π molecular orbital system of the heme. How many π electrons are there in this molecular orbital system?

Problem 2–25: The biochemical standard reduction potentials of the flavin adenine dinucleotide, the [2Fe–2S] iron–sulfur cluster, the [4Fe–4S] iron–sulfur cluster, the [3Fe–3S] iron–sulfur cluster, and the heme *b* of succinate dehydrogenase from *E. coli* are −80, +10, −170, +70, and +30 mV, respectively.[563] If the flavin is reduced to $FADH_2$ by two electrons from succinate while the other four centers are initially in the fully oxidized states, what is the distribution of those two electrons among the five centers at equilibrium? It is thought that the two electrons being transferred from reduced flavin to ubiquinone bound to the enzyme do not pass through the heme *b*. Why is it there?

Migration of Electronic Excitation

The photon responsible for excitation of an electron in a photosynthetic reaction center is almost never absorbed directly from the ambient light by the special pair; instead it is absorbed nearby by an array of accessory light-harvesting prosthetic groups. The electronically excited state produced upon absorption of a photon by a prosthetic group in this array then migrates* to the special pair in the reaction center through the array along a **network of the same or similar prosthetic groups**. The individual subunits of protein enclosing one or more of these light-harvesting prosthetic groups associate with each other to form antennae. An **antenna** is a large structure in a photosystem the prosthetic chromophores of which are responsible for absorbing photons of incident light and in which the resulting electronic excitation, an exciton, migrates to the special pair of the reaction center. The light-harvesting prosthetic groups in an antenna are positioned and oriented by the protein of the subunits in which they are found. Individual light-harvesting prosthetic groups or clusters of electronically coupled light-harvesting prosthetic groups capture photons of light, and within the network formed by the array each of the resulting electronically excited states migrates to a reaction center. The advantage of a large antenna is to increase the cross-sectional area associated with each reaction center that contains prosthetic groups capable of absorbing a photon and hence increase its ability to capture photons.

Migration of electronic excitation occurs among the light-harvesting prosthetic groups in the network. Any one of the light-harvesting prosthetic groups, or a cluster of these prosthetic groups, has two abilities. It can either absorb an ambient photon or act as **a conductor of electronic excitation** between its neighbors. Once a photon is absorbed by a light-harvesting prosthetic group or a cluster of light-harvesting prosthetic groups in an antenna, the electronic excitation rapidly migrates among the prosthetic groups it contains. Eventually it reaches the special pair in the reaction center with which

*As it migrates to the special pair of the reaction center, the electronic excitation is often considered to be an "**exciton**", as if it were a quasi-particle moving through the network, to distinguish it from the electronically excited state on a single, isolated chromophore. When, however, an exciton is located on one of the prosthetic groups transferring it, that prosthetic group is in an electronically excited state.

the antenna is associated, and migration of the electronically excited electron in the special pair takes over. The individual prosthetic groups found in these antennae that are responsible for absorption of the photon and migration of the resulting electronic excitation to the special pair are chlorophylls, carotenoids, and bilins.

Carotenoids contain extended, linear π molecular orbital systems. β,β-Carotene

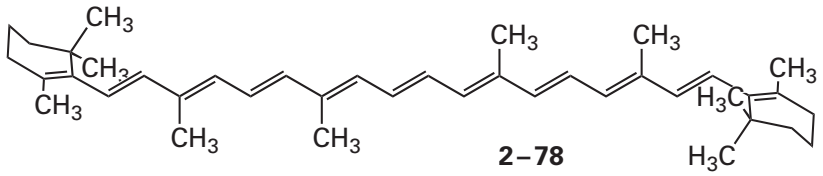

2–78

and its parent ψ,ψ-carotene (lycopene)

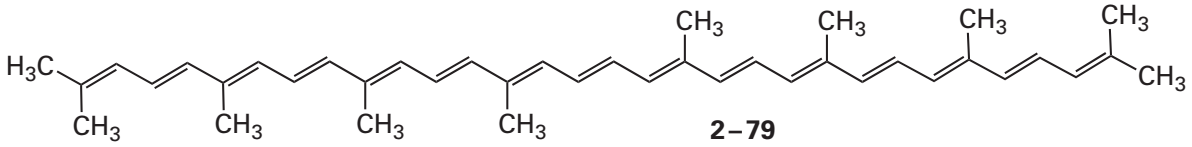

2–79

are examples of carotenoids.* They are octaisoprenoids that each contain 40 carbon atoms and a linear conjugated π molecular orbital system of 22 or 30 carbon atoms that is all trans and fairly rigid throughout its length. Rotation about the carbon–carbon bonds is hindered by the extended π molecular orbital system, as is rotation about the carbon–carbon bond in buta-1,3-diene. Most, if not all, of the carotenoids in a chloroplast or chromatophore are tightly bound to its proteins and each is uniquely oriented by its protein. Most carotenoids are related to ψ,ψ-carotene, and most differ from it only at the two ends, where the isoprenoid units are substituted, saturated, or cyclized as in β,β-carotene. Examples of carotenoids that are light-harvesting prosthetic groups, in addition to β,β-carotene, are neurosporene, chloroxanthin, zeaxanthin, violaxanthin, rhodopin, and peridinin.

Bilins are linear, extensively conjugated tetrapyrroles. All bilins are derived from biliverdin, which is derived from heme *b* (**2–80**) as are all hemes. **Biliverdin** (**2–81**) is produced by oxidative cleavage of heme *b* at carbon 5 by heme oxygenase (biliverdin-producing, ferredoxin) that uses three molecules of molecular oxygen to cleave the porphyrin

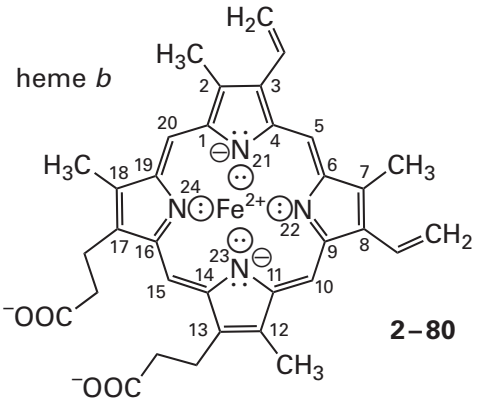

2–80

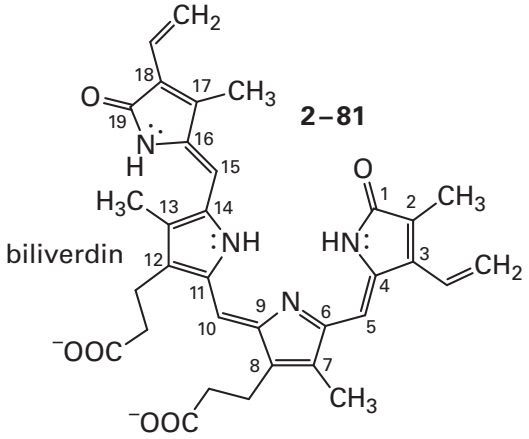

2–81

*Lycopene is the red color in tomatoes. Because of its long conjugated system, it absorbs light of fairly high energy, 380-520 nm, in the green to blue range, causing the tomato to have a red color.

by turning carbon 5 into carbon monoxide. The oxygenation leaves oxo groups at carbons 4 and 6 of heme *b* while breaking the ring and releasing the iron.

Examples of bilins that are used as light-harvesting prosthetic groups are phycocyanobilin, phycoerythrobilin, 15,16-dihydrobiliverdin, and phycourobilin. In both **phycocyanobilin**[1187]

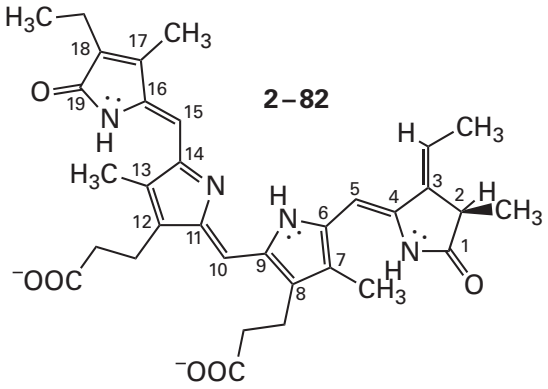

and **phycoerythrobilin**, a hydride has been added to the distal methylene of the ethenyl group at carbon 3 of biliverdin (**2–81**) and the resulting enolate is hydronated at carbon 2. In phycocyanobilin (**2–82**), the ethenyl group that was at carbon 18 of biliverdin (**2–81**) has been reduced to an ethyl group, but it remains a ethenyl group in phycoerythrobilin. In phycoerythrobilin, the double bond that was between carbons 15 and 16 of the biliverdin has been reduced rather than the ethenyl group. In **15,16-dihydrobiliverdin** only the double bond between carbons 15 and 16 of biliverdin has been reduced,[1188] but in phycourobilin the carbon–carbon double bonds between carbons 4 and 5 and carbons 15 and 16 in biliverdin have been reduced and the ethenyl groups at carbon 3 and carbon 18 have been reduced to ethyl groups. Running through a bilin is an extended π molecular orbital system that permits it to absorb visible light.

In most cases, phycocyanobilin is covalently attached to the proteins in which it is found through a sulfide to a cysteine side chain[1189,1190]

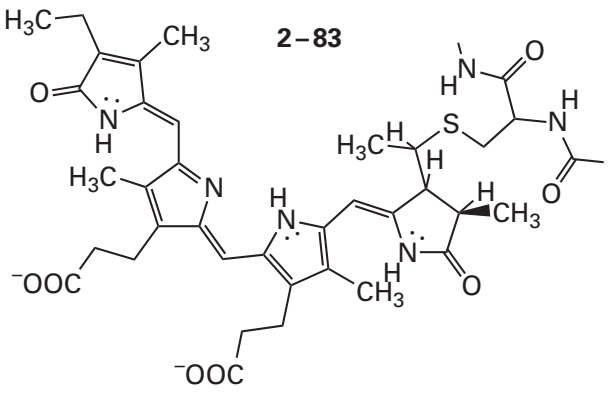

The sulfido group of the cysteine adds to the exocyclic carbon of the double bond of the 3-ethylidene group in phycocyanobilin (**2–82**) with a vinylogous enamine as an intermediate. Phycoerythrobilin[1191] and 15,16-dihydrobiliverdin[1192] are covalently attached to a cysteine with the same linkage at the same carbon, but they can also be covalently attached to a second cysteine at the distal carbon of their respective ethenyl groups at carbon 18 (see **2–81**).[1188,1193] The sulfido group of the cysteine adds to the carbon–carbon double bond in the respective ethenyl group, also with a vinylogous enamine as an intermediate.

Although the reaction centers in different classes of photosynthetic organisms are the same, the antennae associated with these reaction centers are wildly diverse from class to class in the identity of the prosthetic groups, their number, their distribution, and the mechanism for migration and capture of the excited electrons.[1194]

In higher plants and green algae, the antennae on the reaction centers of photosystems I and photosystems II are quite different from each other, but each is formed from a large number of subunits that are embedded in the phospholipid bilayer of the membrane and span it. All these subunits and the reaction center form large intact, discrete proteins. The protein in each extended antenna entraps from 50 to 170 molecules of chlorophyll, both *a* and *b*, and from 10 to 40 carotenoids, almost all within the membrane.

In some cyanobacteria and red algae, antennae are made from subunits that contain bilins rather than chlorophylls. These subunits form cylindrical disks, which stack upon each other to form cylindrical rods that are assembled into phycobilisomes. Rather than being embedded in the membrane of the thylakoid, phycobilisomes are arrays of these rods that radiate out into the negative, basic cytoplasmic solution surrounding the thylakoids, on

the opposite side of the reaction center from the special pair (Figure 2–34). They are attached to the reaction center by a central, multisubunit core.

In cryptophyte algae, the lumen of the thylakoid, on the positive, acidic side of the reaction center closest to the special pair, is packed with large multisubunit biliproteins, each of which binds eight bilins. This solution of biliproteins is the common antenna for reaction centers in the membrane of the thylakoid that encloses them. The antennae in dinoflagellates are also proteins that are not attached to the reaction center but dissolved at high concentration in the lumenal, positive, acidic space of the thylakoid. The protein in each identical subunit in these homotrimers entraps, instead of bilins, eight carotenoids and two chlorophylls.

In purple bacteria, each antenna consists of two concentric rings with a total of 32 subunits, each of which spans the membrane of a chromatophore. The two concentric rings surround the reaction center, and each subunit in the rings contains only one bacteriochlorophyll, either *a* or *b*, depending on the species.

In green sulfur bacteria, the antennae are large vesicles, each formed from a continuous bilayer of phospholipids containing some embedded proteins. Each vesicle contains large **crystalline arrays** that together contain 50,000 to 200,000 bacteriochlorophylls as well as carotenoids. These huge antennae are attached to the cytoplasmic membrane of one of these bacteria, in which reside the reaction centers, by proteins that each contain eight bacteriochlorophylls *a* that act as relays.

The crystallographic molecular models of **photosystem I** from *P. sativum* (Figure 2–38)[1018,1019,1195] contain its antenna. These molecular models constitute a paradigm for the photosynthetic antenna in a higher plant. **The antenna is almost completely embedded within the membrane** and consists of around 140 chlorophylls *a*, around 10 chorophylls *b*, and around 30 carotenoids.* The six chlorophylls *a* of the reaction center (thick bonds) and the [4Fe–4S] iron–sulfur cluster in the reaction are in the center of the photosystem. There is an external subunit on the negative, basic side of the photosystem, adjacent to the [4Fe–4S] iron–sulfur cluster within the reaction center, that contains the two additional prosthetic [4Fe–4S] iron–sulfur clusters (not shown in the drawing) that pass electrons to ferredoxin, the electron-transferring coenzyme that is the ultimate acceptor. In addition to this external subunit, 11 polypeptides, two long ones (758 aa and 734 aa) and nine short ones (40–168 aa), that are folded within the thylakoid membrane in intertwined associations of 32 membrane-spanning α helices comprise the core of the photosystem. On one side of this central core there are four additional subunits of light-harvesting complex I, each of which has three membrane-spanning α helices.

With the exception of the external subunit containing the two prosthetic [4Fe–4S] iron–sulfur clusters, most of the mass of the protein comprising the central core of the photosystem is embedded in the membrane, and segments from 9 of the 11 constituent polypeptides forming the central core span the membrane in one or more α helices. The two folded long polypeptides contain the reaction center. They are homologous (44% identity; 1.5 gap percent) to each other and arrayed around the usual twofold rotational axis of pseudosymmetry that creates the special pair and the pseudosymmetry of the reaction center. Although the two long folded polypeptides are also homologous in the portions of their structures that surround the reaction center to the L and the M subunit in a bacterial reaction center, in particular, five of the α helices from each of them, they are each around 450 amino acids longer than the respective folded polypeptides in an L or M subunit. Within this additional protein, these two large subunits, unlike the L and M subunits, enclose most of the prosthetic groups that form the antenna for the reaction center. The two large subunits each span the membrane with 11 α helices. In addition to surrounding the reaction center, these two long subunits entrap and orient among their membrane-spanning α helices around 10 β-carotenes and around 80 chlorophylls *a* in addition to the 6 chlorophylls *a* in the reaction center itself. These prosthetic groups are the contribution of these two large subunits to the antenna. Around 10 chlorophylls *a* and around 10 β-carotenes are enclosed by the 10 membrane-spanning α helices of the small subunits.

Associated with the core protein of photosystem I is another protein, **light-harvesting complex I**. Four subunits, with homologous sequences 252–275 amino acids in length, and hence superposable structures, comprise light-harvesting complex I that spans the membrane and encloses around 50 chlorophylls *a*, around 10 chlorophylls *b*, and around 10 carotenoids among its 12 membrane-spanning

*There is a slight disagreement between the two crystallographic molecular models of the same protein[1018] as to the number of prosthetic groups and the subunits with which they are associated.

α helices, three in each subunit. The four subunits of light-harvesting complex I are in a row, flush against the surface of the core protein within the membrane.

The rotational axis relating the two large subunits in photosystem I from *P. sativum* is a rotational axis of pseudosymmetry (passing through the special pair in Figure 2–38). Consequently, the surface of the pseudosymmetric heterodimer of the two large subunits within the membrane, which is composed of α helices spanning the membrane, is not duplicated across the rotational axis and is different on the opposite sides of the heterodimer. It turns out that there is only one face on the heterodimer within the membrane with which light-harvesting complex I associates. This face is not duplicated across the rotational axis. As a result, only one light-harvesting complex I of four subunits associates with the heterodimer of large subunits on only one of its sides, which makes the entire photosystem lopsided even though it has a rotational axis of pseudosymmetry.

The chloroplasts of plants contain an additional light-harvesting complex, **light-harvesting complex II**, that is also embedded in the membrane of the thylakoid, that absorbs around half the light used for photosynthesis, and that transfers the resulting electronic excitation to both photosystem I and photosystem II. It diffuses in the membrane as a protein separate from the two photosystems. Each monomer of this homotrimeric protein in the thylakoids of *S. oleracea* contains eight chlorophylls *a*, six chlorophylls *b*, and four carotenoids: two luteins, a neoxanthin, and a violaxanthin.[1196,1197] The transition dipoles of two of the chlorophylls *a* in each subunit of light-harvesting complex II are so strongly coupled that they act as a single chromophore with a dipole strength two times larger than that of an isolated chlorophyll *a*.[1198] This dimer of chlorophylls *a* gathers the electronic excitation from the others and passes it on to one or the other of the photosystems. In a thylakoid, the concentration of light-harvesting complex II is so high that it paves the membrane. Consequently, electronically excited states migrate among adjacent molecules of light-harvesting complex II on their way to a photosystem.[1199]

Photosystems II in higher plants,[1200] algae,[1013] and cyanobacteria,[1011] like photosystems I, are also asymmetric. In the molecular model of photosystem II from *S. oleracea* derived from image reconstruction from electron micrographs,[1200] the two subunits that are homologous to the L and M subunits and homologous to each other (25% identity; 2.2 gap percent) are, unlike those in photosystem I, only about 50 amino acids longer than their bacterial counterparts, and each encloses only one chlorophyll *a* and one β-carotene of the antenna. The remaining 48 chlorophylls *a*, 7 chlorophylls *b*, 8 β-carotenes, 3 luteins, 2 neoxanthins, and a violaxanthin of the antenna are distributed among 15 different membrane-embedded subunits of various sizes. As in photosystem I (Figure 2–38), all these prosthetic groups entrapped within the α helices of these subunits are within the membrane, and the antenna created, although significantly smaller, is similar to that in photosystem I. The partners in several pairs of these subunits are homologous to each other and distributed pseudosymmetrically around the twofold rotational axis creating the reaction center. In the molecular model, one homotrimer of light-harvesting complex II is docked at a site on photosystem II. Again, there is only one face on the membrane-embedded surface of the pseudosymmetric photosystem with which the trimer of light-harvesting complex II associates. Two photosystems II of higher plants, however, also participate in a larger complex in which they are arranged around a twofold rotational axis of true symmetry, and this larger complex contains two copies of an additional membrane-spanning subunit arrayed across the axis of symmetry and two additional symmetrically arrayed light-harvesting complexes II, for a total of four docked light-harvesting complexes II and two photosystems II.[1201]

In the asymmetric unit of the crystallographic molecular model of **photosystem I from the cyanobacterium** *Synechococcus elongatus*, there are 90 chlorophylls *a* responsible for harvesting light that are bound at locations distributed at random through the protein. Most of them are spaced far enough apart that their transition dipoles are not strongly coupled, but there are three pairs of chlorophylls *a* and a group of three chlorophylls *a* in which the π molecular orbital systems are stacked upon each other.[1016] These clusters are thought to be responsible for the absorption of light at longer wavelengths and to act as a sink for electronic excitation, which then migrates from them to the reaction center at the core of the photosystem.[1202] There are also 22 β,β-carotenes in each asymmetric unit of this photosystem I.

Phycobilisomes are additional antennae associated with reaction centers in the thylakoids of some cyanobacteria and red algae that harvest light of shorter wavelengths (450–650 nm). The units from which a phycobilisome is constructed are **cylindrical rods**, formed from two to five individual cylindrical disks stacked one upon the other.[1203] Each disk in one of these cylindrical rods is a **phycobiliprotein** the subunits of which each enclose one or two bilins.

The paradigm of such a phycobiliprotein would be **C-phycocyanin** from *Fremyella diplosiphon* (Figure 2–43)[1204]. The prosthetic group in this protein is phycocyanobilin (**2–82**), and it is an $(\alpha\beta)_6$ hexamer with dihedral symmetry of point group 322(D_3).[1205] The central core of each $(\alpha\beta)_6$ hexamer, along its threefold rotational axis of symmetry, is hollow, and the three twofold axes of symmetry normal to this threefold axis relate $\alpha\beta$ heterodimers in the opposed $(\alpha\beta)_3$ trimers composing the $(\alpha\beta)_6$ hexamer. The α polypeptides are homologous to the β polypeptides in sequence (22% identity; 1.8 gap percent), and the α subunits in the crystallographic molecular model are superposable on the β subunits. Each α subunit, however, has only one covalently attached phycocyanobilin, while each β subunit has two covalently attached phycocyanobilins, one in a location homologous to that occupied in an α subunit. In the $(\alpha\beta)_6$ hexamer, the eighteen prosthetic groups (one from each α subunit and two from each β subunit) are distributed evenly with the dihedral symmetry of the oligomer over the volume of the protein. The arrangement of the prosthetic groups in a rod formed from phycocyanin can be deduced from the spontaneous stacking of the individual $(\alpha\beta)_6$ hexamers of C-phycocyanin one on top of the other that occurs in the crystals of this protein.

Phycoerythrin and **allophycocyanin** are two phycobiliproteins closely related to phycocyanin, and their crystallographic molecular models are superposable on that of C-phycocyanin.[1193,1206] Each $\alpha\beta$ asymmetric unit of phycoerythrin, however, has three phycoerythrobilins as prosthetic groups,[1193] while each $\alpha\beta$ asymmetric unit of allophycocyanin has only two phycocyanobilins instead of three.[1206]

The cylindrical rods of $(\alpha\beta)_6$ hexameric phycobiliproteins are gathered into phycobilisomes, each of which contains 20–70 $(\alpha\beta)_6$ hexameric phycobiliproteins. There are four different ways that have been identified in electron micrographs in which the rods are assembled into phycobilisomes: hemidiscoidal,[1207] hemiellipsoidal,[1208] block-type,[1209] and bundle-type.[1210] The different ways in which the rods are assembled are determined by the particular collection of **linker proteins** that join the rods together. In each instance, however, the rods are arranged around a central core of phycobiliproteins that is attached to the negative, basic surface of the reaction center and that funnels each electronically excited state originating in the bilins in the rods and the core into the reaction center of a photosystem I in a thylakoid.[1190] Because the phycobiliproteins absorb light of shorter wavelengths, migration of the excited states into the membrane-embedded antenna of the associated photosystem II is exergonic. Each photosystem II in the thylakoid, however, is associated with a photosystem I in a megacomplex within the membranes of the thylakoids of cyanobacteria, and the electronic excitations gathered by the phycobilisomes can also migrate within this complex to photosystem II.[1211] Molecular models of the block-shaped phycobilisome from *Griffithsia pacifica*[1212] and the hemiellipsoidal phycobilisome from *Porphyridium purpureum*[1213] have been constructed from image reconstructions of electron micrographs.

The molecular model of the block-shaped phycobilisome from *G. pacifica* contains 62 $(\alpha\beta)_6$ hexameric phycobiliproteins and 72 linker proteins. The linker proteins, in addition to assembling the cylindrical rods, also have bilins within them and bring the total number of bilins in the phycobilisome to 2048. The cylindrical rods of two to five $(\alpha\beta)_6$ hexameric disks of the phycobiliproteins (Figure 2–43) radiate outward from the central core in a structure resembling a fan. The rods are held together in the structure by linker proteins that run down the hollow center of each rod, as well as linker proteins holding the rods to the core and linker proteins holding the phycobiliproteins in the core together. The distal phycobiliproteins in each rod radiating from the core are phycoerythrobilins. The linker proteins in the center of each rod, beyond those linker proteins within the first phycoerythrobilin in each rod, have phycourobilins within their sites for binding bilins. In about half of the rods, the phycobiliprotein most proximal to the core is a phycocyanobilin, and the phycobiliproteins in the core closest to the reaction center are allophycocyanins.. Because the linker proteins running through the center of each rod contain phycourobilins that have a maximum absorbance at 500 nm, because the phycoerythrobilins in

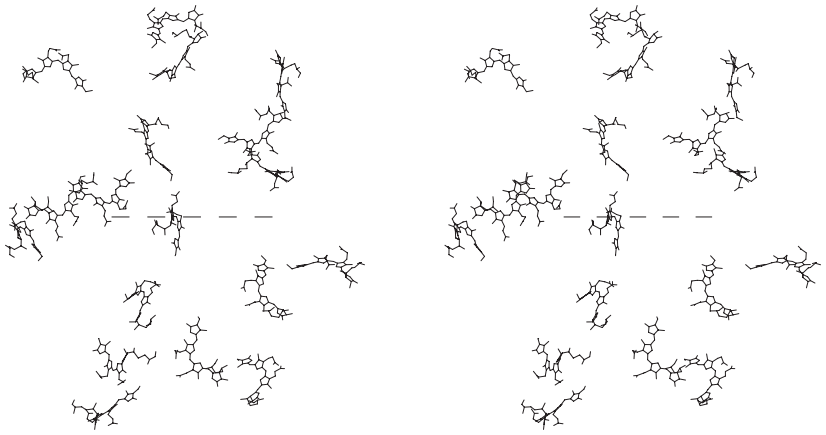

Figure 2–43: Stereodrawing[50] of the distribution of phycocyanobilins within the crystallographic molecular model of C-phycocyanin from *F. diplosiphons*.[1204] In the photosynthetic bacterium, $(\alpha\beta)_6$ hexamers of the protein, each assembled with dihedral symmetry of point group 322(D_3), stack one on top of each other to form the cylindrical rod of a phycobilisome, and this arrangement is preserved in the crystal, which is formed from continuous cylindrical columns of hexamers packed side by side. In the drawing, the distribution of the phycocyanobilins in a single hexamer from one of these columns is presented. A crystallographic threefold rotational axis of symmetry runs through the center of each column and, consequently, through the center of the distribution of phycocyanobilins in each $(\alpha\beta)_6$ hexamer. In the drawing, this exact threefold rotational axis of symmetry (dashed line) is horizontal and inclined at a 40° angle to the plane of the page.

the distal portion of each rod have maximum absorbances at 540 and 565 nm, because the phycocyanins have a maximum absorbance at 620 nm, and because the allophycocyanins have a maximum absorbance at 650 nm,[1206] this distribution of the various bilins, in addition to covering a wide range of absorption wavelengths, creates a gradient of energy for electronic excitation from absorption at shorter wavelengths to absorption at longer wavelengths, down the rod and into the core. The electronic excitation produced by absorption of a photon by one of the prosthetic groups is passed down this gradient in the rods in the direction of the photosystem.

In the hemiellipsoidal phycobilisome from *P. purpureum*, which contains 52 phycobiliproteins, the rods of two to four $(\alpha\beta)_6$ hexameric disks also radiate from the core, but the arrangement of the rods is wider and more splayed than in the block-shaped phycobilisome from *G. pacifica*. The same gradient—formed from distal linker proteins with phycourobilins (500 nm), distal phycoerythrobilins (540–565 nm), proximal phycocyanins (620 nm), and a core of allophycocyanins (650 nm)—is still found in this phycobilisome.

Two concentric elliptical rings—an inner ring of sixteen α subunits (60 aa), each contributing one membrane-spanning α helix, and an outer ring of sixteen β subunits (50 aa), each contributing one membrane-spanning α helix—together comprise **light-harvesting protein LH1**, which surrounds each reaction center in a **purple bacterium**.[1214,1215] The reaction center is in the center of these two concentric rings of sixteen membrane-spanning α helices, which cleave tightly to it and completely enclose it. These two rings of α helices entrap the thirty two bacteriochlorophylls *a* and sixteen spirilloxanthin molecules that comprise the primary antenna intimately associated with each reaction center. Although the structure is elliptical because the reaction center is not circular, it has a twofold rotational axis of symmetry that superposes the eight $\alpha\beta$ sectors in each half ellipse, each sector enclosing their two bacteriochlorophylls *a* and their spirilloxanthin, on the eight in the other half. In addition to this primary antenna, however, there is an additional protein in the chromatophores, light-harvesting protein LH2. **Light-harvesting protein LH2** from the purple bacterium *Rhodoblastus acidophilus* is an $(\alpha\beta)_9$ nonamer that spans the membrane of the chromatophore. The $\alpha\beta$ asymmetric units are arrayed around a ninefold rotational axis of symmetry and create two concentric rings each containing nine α helices. Each α subunit (53 aa) within the inner ring and each β subunit (41 aa) within the outer ring contributes one transmembrane α helix to the entire structure. Eighteen **bacteriochlorophylls *a*** in an eighteenfold rotationally symmetric circular array are enclosed between the two rings of nine α helices (Figure 2–44),[1216] and nine additional bacteriochlorophylls *a* are interspersed between the nine α helices of the β subunits in a more widely spaced ninefold rotationally symmetric circular array deeper in the membrane. There are also nine rhodopin D-glucosides arrayed around the ninefold rotational axis of symmetry.

The light-harvesting protein LH2 in purple photosynthetic bacteria, such as *R. acidophilus*, diffuses over the membrane of a chromatophore,[1217] colliding frequently with the primary antenna, light-harvesting protein LH1, or it is in a weak association with light-harvesting protein LH1. The fact that the electronically excited state resulting from capture of a photon by light-harvesting protein LH2 always ends up in its ring of 18 bacteriochlorophylls *a*, while moving among the bacteriochlorophylls *a* in this ring with a rate constant of around 10,000 ns^{-1}, means that whenever an excited molecule of this protein collides at random with a molecule of light-harvesting protein LH1 or is in a particular evanescent complex with light-harvesting protein LH1, the electronically excited state will arrive at the point of contact between the two proteins almost instantaneously. It then migrates within the complex from light-harvesting protein LH2 (λ_{max} = 860 nm) to light-harvesting protein LH1 (λ_{max} = 875 nm) with a rate constant[1218] of 200 ns^{-1}, and it eventually migrates to the special pair of the reaction center in the complex with a rate constant[1219] of 30 ns^{-1}.

The physical explanation for absorption of the photon by the arrays of light-harvesting prosthetic groups in an antenna and migration of the resulting electronic excitation among them is not entirely clear.[1194,1220-1223]

If two light-harvesting prosthetic groups, the chromophores, are far enough apart and the initial absorption of the photon is confined to only one of these two chromophores, the consequent migration of electronic excitation from the initially excited chromophore, the donor, to the other chromophore, the acceptor, can be described satisfactorily by the process of **radiationless transfer of energy by resonance**.[1224,1225] This formalism describes the migration of electronic excitation, without photon emission or absorption, to be the consequence of a

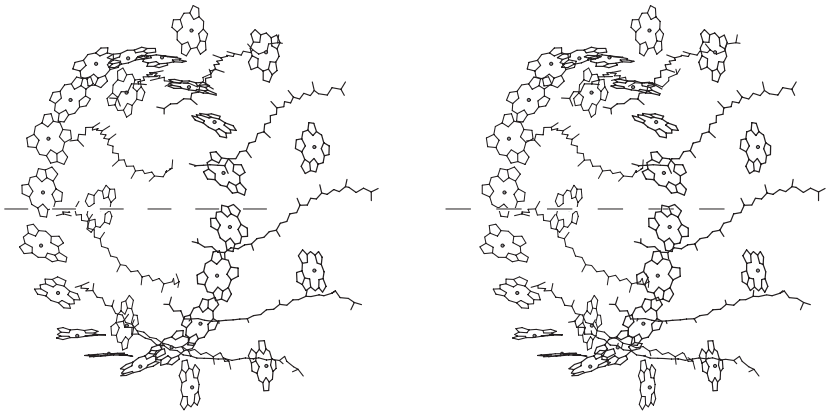

Figure 2–44: Stereodrawing[50] of the distribution of bacteriochlorophylls *a* and rhodopin glucosides within the crystallographic molecular model of light-harvesting protein LH2 from *R. acidophilus*.[1216] In the photosynthetic bacterium, $(\alpha\beta)_9$ nonamers of the protein, each assembled with cyclic symmetry of point group $9(C_9)$, are integral membrane-bound proteins that diffuse translationally in a crowded membrane. In the figure, the distribution of the prosthetic groups in the crystallographic molecular model of one of these $(\alpha\beta)_9$ nonamers is presented. A ninefold rotational axis of symmetry (dashed line) runs through the center each array and, consequently, through the center of each $(\alpha\beta)_9$ nonamer. The 27 bacteriochlorophylls *a* that are bound within the protein are distributed by this rotational axis of symmetry into two circular rings, one containing 18 bacteriochlorophylls *a* and the other 9 bacteriochlorophylls *a*. In the ring of eighteen, the bacteriochlorophylls *a* are tightly packed and touch each other, and each chlorin ring is perpendicular to the plane of the membrane. The ring of eighteen bacteriochlorophylls *a* is on the side of the protein facing the positive, acidic surface of the membrane. In the ring of nine, the bacteriochlorophylls *a* are in a larger circle and more widely spaced and each chlorin ring is parallel to the plane of the membrane. The ring of nine is in the center of the membrane. Only the chlorin rings of bacteriochlorophylls *a* have been drawn; phytol chains, 2-carboxyethyl groups, and alkyl groups on each of them were not drawn in order to simplify the figure. The nine rhodopin glucosides are the long polyisoprenoids located between the bacteriochlorophylls *a* in the ring of nine. They are also distributed by the ninefold rotational axis of symmetry and oriented roughly perpendicular to the plane of the membrane, and they span its hydrophobic core. Only the carotenoid portions of the rhodopin glucosides are drawn. The glucosyl groups are at the end of each rhodopin-glucoside farthest from the ring of eighteen bacteriochorophylls *a* on the negative, basic surface of the membrane. The glucosyl groups are hydrophilic enough to anchor that end of the polyisoprenoid at the surface of the membrane. The ninefold rotational axis of symmetry is exactly normal to the plane of the membrane.

dipole–dipole interaction the magnitude of which depends on the spectral overlap between the donor and acceptor states, the intermolecular distance between them, and the relative orientation of the transition dipole moments of the molecules. The symmetrically arrayed phycocyanobilins responsible for harvesting light in C-phycocyanin from *F. diplosiphon* (Figure 2–43), are spaced far enough apart that an electronically excited state produced by the absorption of a photon is always situated immediately only on one of the prosthetic groups, yet they are close enough together for efficient radiationless transfer of energy by resonance to occur.

The efficiency of radiationless transfer of energy by resonance, the ratio between the quanta transferred before the return of the electronically excited state to the ground state and the quanta absorbed that created that electronically excited state, depends inversely on r^6, where r is the distance between the transition dipoles of the chromophores. It has been estimated that R_0, the distance at which the efficiency for transfer of an electronic excitation between two phycocyanobilins in a C-phycocyanin by radiationless transfer of energy by resonance should be 50%, is 5.0 nm.[1226] In an individual phycobiliprotein and in the rods into which phycobiliproteins are assembled, each of the respective bilins, which in this case are the chromophores, is within 5 nm of at least one other,[1204] and many of the pairs of bilins are less than 3 nm apart.[1227] Since the dependence is to the sixth power, the difference between 5 and 3 nm is a factor of 20, which would increase the efficiency of transfer to 96%.

If prosthetic groups in an array, however, are close enough together and rigidly held in the proper orientation, the electronically excited state that results upon absorption of a photon is **delocalized over the entire array**, as is the case with a special pair. This delocalization results from the strong coupling of their adjacent, stationary transition dipoles. In effect, the electronic excitation is not actually migrating among the closely and rigidly held prosthetic groups but distributed instantaneously among them, as is the case in any delocalization.

The light-harvesting protein LH2 from *R. acidophilus* (Figure 2–44) illustrates the **two extremes in mechanism** for migration of electronic excitation. The eighteen bacteriochlorophylls *a* in the closely spaced continuous ring have strongly coupled transition dipoles, and at low temperature at least, the electronic excitation does not migrate among them but is delocalized among them. The nine bacteriochlorophylls *a* in the more widely spaced ring, however, absorb photons as individual chromophores and the electronic excitation migrates among themselves and to the ring of eighteen bacteriochlorophylls *a* by radiationless transfer of energy by resonance.

For the eighteen bacteriochlorophylls *a* in the closely spaced continuous ring, the electronically excited state that results upon absorption of a photon is delocalized over the entire ring at a temperature of 1.2 K.[1228] Although this complete delocalization requires the rigidity of the low temperature, at a temperature of 7 K, the electronic excitation migrates among the eighteen bacteriochlorophylls *a* in the ring with a rate constant[1229] of 10 ps^{-1} rather than instantaneously, and there is strong coupling of their transition dipoles at room temperature.[1230] The strong coupling of these eighteen bacteriochlorophylls *a* in the ring permits the electronic excitation to migrate among them more rapidly than the radiationless transfer of energy by resonance from one of the nine, more distant bacteriochlorophylls *a* to the ring of eighteen.[1231]

When one of the nine widely spaced bacteriochlorophylls *a* absorbs light, the electronically excited state that results upon absorption of a photon is localized initially in the bacteriochlorophyll *a* that absorbed the photon.[1228,1230] Migration of electronic excitation from one of the bacteriochlorophylls in the ring of nine to the ring of eighteen has a rate constant of 0.5 ps^{-1} at 77 K[1219] and 0.4 ps^{-1} at 300 K.[1232]

The strong coupling of the transition dipoles of bacteriochlorophylls *a* within the ring of eighteen and the relative orientation of those transition dipoles also **shift the absorption** of the bacteriochlorophylls *a* in this ring to longer wavelengths (850 nm), just as the enforced orientation of the transition dipoles in the special pair of a reaction center shifts the absorption of its bacteriochlorophylls *b* to longer wavelengths. The nine more widely spaced bacteriochlorophylls *a* in the ring at the center of the protein, however, absorb photons as individual chromophores with unperturbed absorption maxima at 800 nm. In each of the nine asymmetric units of light-harvesting protein LH2 from *R. acidophilus* (Figure 2–44), there is also a **carotenoid**, in this instance the D-glucoside of rhodopin (1,2-dihydro-1-hydroxy-ψ,ψ-carotene),[1233] that absorbs light with wavelengths from 450 to 550 nm. The resulting electronic excitation migrates from the carotenoid to the bacteriochlorophylls *a* with a rate

constant[1232] of 4 ps^{-1} and an efficiency approaching 100%.* Consequently the whole array is able to absorb light at 450–550 nm and 800–860 nm. Absorption at the shorter wavelengths, and hence higher energies, is funneled from the other prosthetic groups into the bacteriochlorophylls *a* in the ring of eighteen, from which it migrates to the antenna surrounding the reaction center.

The problem with describing migration of electronic excitation within the arrays of prosthetic groups in most photosynthetic antennae is that their spacing, orientation, and the rigidity with which the chromophores are held is **intermediate between the extremes of radiationless transfer of energy by resonance and electronic delocalization**. In many, if not most, situations, the magnitude of the electronic coupling between light-harvesting prosthetic groups is so large that the point dipole assumption of radiationless transfer of energy by resonance breaks down, but the spacing, orientation, and the rigidity with which the prosthetic groups are held is not such that widely distributed delocalization of the electronically excited state can occur. The situation is further complicated by the fact that migration of electronic excitation in an antenna can also display properties indicating that quantum coherence contributes significantly to the migration, even at ambient temperatures.[1220] It seems that natural selection has discovered several different means to transfer electronic excitation rapidly and with high efficiency. The issues in a physical description of migration of electronic excitation in a particular antenna are controversial enough and complicated enough to be beyond the scope of the present discussion. Nevertheless, efficiencies and rates of migration can be measured, and there is little doubt that the excitation is successfully funnelled from the point of initial absorption to the special pair.

The role of harvesting light is not confined completely to chlorophylls, carotenoids, and bilins. Deoxyribodipyrimidine photo-lyase, the photoreduction of which has been described, is a widely distributed enzyme responsible for photolytically repairing cyclobutadipyrimidine dimers that result from unavoidable photolytic damage to double-stranded DNA. In the different varieties of deoxyribodipyrimidine photo-lyase, either 5,10-methenyltetrahydropteroylpolyglutamate,[1234] 7,8-didemethyl-8-hydroxy-5-carba-5-deazariboflavin,[1235] flavin mononucleotide,[1236] or flavin adenine dinucleotide[1237] acts as a light-harvesting prosthetic group, absorbing a photon and transferring the electronic excitation to the anionic conjugate base of flavin adenine dinucleotide, $H_2Fl_{red}^-$, responsible for providing the excited electron to the cyclobutadipyrimidine.[1238] The unpaired electron in the highest occupied molecular orbital of the electronically excited state of the reduced flavin is passed through the indolyl group of an adjacent tryptophan to the cyclobutanyl group of the cyclobutadipyrimidine to form the radical anion of the cyclobutanyl group that then dissociates to produce the two undamaged pyrimidines.[1239]

*The transfer of electronic excitation from carotenoid to bacteriochlorophyll is usually less efficient. Depending on the type of carotenoid and the energy levels for excitation of the bacteriochlorophyll, the efficiency can be as low as 30%.

Suggested Reading

Shirmer, T., Huber, R., Schneider, M., Rode, W., Miller, M., and Hackert, M. L. (1986) Crystal structure analysis and refinement at 2.5 Å of hexameric C-phycocyanin from the cyanobacterium *Agmenellum quadruplicatum*: The molecular model and its implications for light harvesting, *J. Mol. Biol. 188,* 651–676. https://doi.org/10.1016/S0022-2836(86)80013-4

Hess, S., Visscher, K. J., Pullerits, T., Sundstrom, V., Fowler, G. J. S., and Hunter, C. N. (1994) Enhanced rates of subpicosecond energy transfer in blue-shifted light harvesting LH2 mutants of *R. sphaeroides*. *Biochemistry 33*, 8300–8305. https://doi.org/10.1021/bi00193a017

Problem 2–26: Draw the structure of heme *b*, the structure of phycoerythrobilin, the structure of phycocyanobilin, and the structure of 15,16-dihydrobiliverdin.[1240] Phycocyanobilin and phycoerythrobilin both have two isomers at carbon 3.

(A) Draw each of the isomers.
(B) Why should there be a reasonable equilibrium between the two isomers?
(C) Draw phycoerythrobilin and 15,16-dihydrobiliverdin attached at their two ends to cysteines.[1188,1193]

Photoisomerization

There are several prosthetic groups in which a particular double bond is isomerized from the initial *E* or *Z* conformation to the opposite conformation as a result of absorption of a photon of light. Such **photoisomerizations** also occur in nonenzymatic chemical reactions. For example, when a molecule of (*E*)-stilbene dissolved in a 4:1 mixture of ethanol and methanol at 25 °C absorbs a quantum of light at 313 nm, the *Z* isomer and *E* isomer are produced during the decay of the electronically excited state in a 1:1 ratio,[1241] even though (*Z*)-stilbene is significantly less stable in the ground state than (*E*)-stilbene. When a quantum of light is absorbed by a molecule of (*E*)-stilbene, an excited singlet state is produced in which the excited electron occupies an antibonding molecular orbital. The isomerizing bond is at a node in the antibonding orbital. The electron repulsion of the *p* orbitals across the isomerizing bond is relieved by twisting one side of the bond relative to the other. This torsional rotation produces a state in which the dihedral angle across the bond that is isomerizing is significantly less than the 180° of the ground state.[1242,1243] From this twisted transition state, the electronically excited state decays to the *E* isomer or the *Z* isomer in the observed ratio of 1:1.[1244]

One of the simplest biochemical prosthetic groups that undergoes photoisomerization is the (*E*)-4-hydroxycinnamic acid esterified to Cysteine 69

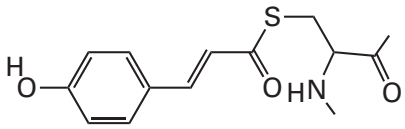

2–84

in **photoactive yellow protein** from *Halorhodospira halophila*.[1245,1246] Upon excitation with blue light of wavelength 445 nm, which is the maximum of its visible absorption within the protein, the quantum yield for the *Z* isomer from the electronically excited state is 0.64.[1247]

There are crystallographic molecular models of the various conformational changes that occur to the chromophore and its surroundings over an interval from 150 fs to 10 ms following the absorption of light.[1248-1252] From one of these crystallographic time courses, it could be determined that the rate constant for isomerization of the carbon–carbon double bond to the *Z* conformation[1248] is 3 ns^{-1}.

In crystallographic molecular models of the ground state, the peripheral 4-hydroxyphenyl group of the 4-hydroxycinnamoyl group is held firmly by two hydrogen bonds between its 4-hydroxy group and the 4-hydroxyphenyl group of Tyrosine 42 and the carboxy group of Glutamate 46. The thioester is in the trans conformation, and its acyl oxygen forms a hydrogen bond with the amido nitrogen–hydrogen bond of the cysteine to which it is esterifed, as in **2–84**. After an interval of 100 ns, two different conformations of the active site are observed in approximately equal concentrations.[1249] In one conformation, the two hydrogen bonds to the 4-hydroxy group remain intact, the thioester has flipped over in response to the photoisomerization but remains in the trans conformation,[1252] and its hydrogen bond to the amido group has broken. In the other conformation, the two hydrogen bonds to the 4-hydroxy group have broken, the thioester has not flipped over and remains in the trans conformation in the same location as it was in the ground state, and the 4-hydroxyphenyl group, freed from the hydrogen bonds, has flipped over.[1250] After an interval of 100 μs following the absorption of light, only one conformation of the *Z* isomer has become predominant. In this conformation, the two hydrogen bonds to the 4-hydroxy group have been broken, the 4-hydroxyphenyl group has flipped over, the thioester, which remains in the trans conformation, is no longer flipped over, the hydrogen bond between the amido group of the cysteine and the acyl oxygen of the thioester has reformed, and the thioester is in the same position as in the ground state.[1251] At this point, a global conformational change in the protein has occurred.[1253] This global conformational change initiates, for example, a repellent response of the bacterium *H. halophila* toward intense blue light.[1254] The prosthetic group slowly (3 s^{-1})[1255] returns thermally to the *E* isomer, and the conformation of the ground state is resumed to complete the **photocycle**.

Phytochrome is a protein that contains a **phytochromobilin**. Phytochromobilin is closely related to phycocyanobilin (**2–82**), the only difference being that the ethenyl group at carbon 18 in biliverdin (**2–81**) is not reduced to an ethyl group during its modification to phytochromobilin. Phytochromobilin is attached as usual through a sulfide linkage at carbon 3 (**2–83**). Upon absorption of light at 670 nm, the double bond at position 15 photoisomerizes from the more stable *Z* isomer (see **2–82**) to the *E* isomer.[1256,1257] The photoisomerization initiates a sequence of events that, in five discrete steps taking about 0.25 s, produces a conformational change of the protein[1258] that registers the fact that light has

been absorbed. This altered conformational change initiates responses to light in a higher plant that control germination of seeds, biosynthesis of chlorophyll, inhibition of stem elongation in the dark, expansion of leaves, and flowering.[1259] The return of the phytochromobilin to the *Z* isomer at at position 15, although exergonic, is achieved photochemically rather than thermally through another photoisomerization requiring light of 730 nm and with a composite rate constant[1260] of 200 s^{-1}. The return of the prosthetic group to the *Z* isomer following the second photoisomerization completes the photocycle.

Retinal, which is the aldehyde of one half of *β*,*β*-carotene (**2–78**)

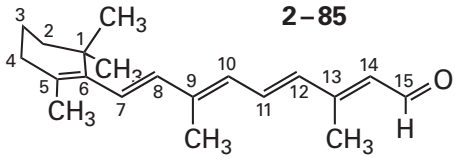

is a carotenoid that is covalently bound as a prosthetic group through an imine with a lysine in an opsin to produce a **rhodopsin**. An opsin is a protein composed of a single polypeptide of 250–450 amino acids, depending on the species, that is embedded in a biological membrane. The polypeptide is folded into seven *α* helices, each of which is about 20 amino acids long and spans the membrane, with loops of variable length connecting the helices.

The visual pigments in a mammalian eye are rhodopsins. They are a set of homologous proteins: visual rhodopsin, long-wave-sensitive visual rhodopsin, medium-wave-sensitive visual rhodopsin, and short-wave-sensitive visual rhodopsin. Their function is to register photons of visible light. The chromophore in each of these proteins is retinal, which is present in the active site as a retinyl group linked to the protein through an imine with the amino group of a lysine. In the dark-adapted retina, the retinyl group within **visual rhodopsin** is in the *Z* isomer at position 11. When retinal is in free solution in an organic solvent or in the phospholipid bilayer of the membrane in which the visual rhodopsin is located, this (7*E*,9*E*,11*Z*,13*E*)-retinal is the less stable isomer relative to (7*E*,9*E*,11*E*,13*E*)-retinal (*all-trans*-retinal). Nevertheless, in the dark and in solution, (7*E*,9*E*,11*Z*,13*E*)-retinal, like any other compound containing a cis double bond, does not isomerize spontaneously in the absence of a catalyst.

In the crystallographic molecular model of bovine visual rhodopsin,[1261-1263] the cis double bond at position 11 is twisted out of planarity by 45°, making the retinyl group even less stable. Upon the absorption of light by the (7*E*,9*E*,11*Z*,13*E*)-retinyl group attached to the lysine of the opsin in visual rhodopsin, the instantaneously formed Franck–Condon electronically excited state decays with a rate constant[1264] of 5 ps^{-1} to an excited intermediate in which the dihedral angle of the double bond at position 11 has increased even further as a result of repulsion from the antibonding molecular orbital occupied by the excited electron.[1265] This form of the electronically excited state, which is distorted even further toward the thermally more stable (7*E*,9*E*,11*E*,13*E*) isomer by the protein itself,[1266] then decays to a static 2:1 mixture of the *E* and *Z* isomers at position 11. In this mixture, the two stereoisomers do not equilibrate with each other. The isomerization of the retinyl group in the bovine visual rhodopsin, in addition to changing the double bond from cis to trans, causes the bond between nitrogen 7 of the lysine and carbon 15 of the retinyl group to rotate almost 180° and the cyclohexyl ring also to rotate 180°[1267]

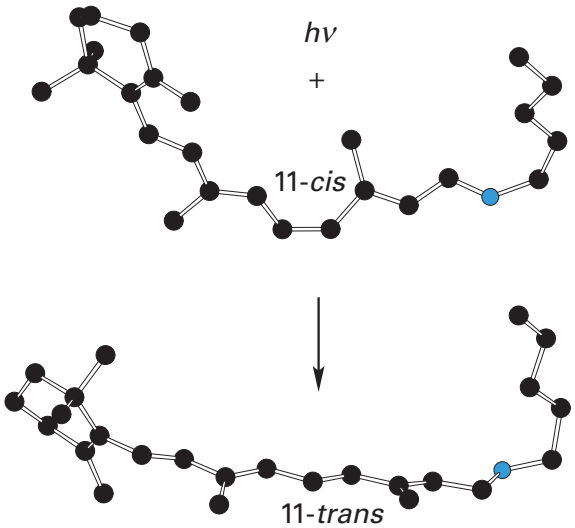

(2–196)

The conformational change of the retinyl group in the visual rhodopsin from *Todarodes pacificus*, however, upon isomerization of the double bond at position 11 produced by the absorption of light, is much less dramatic.[1268]

Coincident with absorption of a photon and isomerization of the retinyl group from *Z* to *E*,[1269,1270] bovine visual rhodopsin undergoes a change in conformation in response to the dramatic change

that has occurred in the structure of the retinyl group (Equation 2–196). This change in conformation of the protein is the event that registers absorption of the photon and leads to visual perception.

Following the change in conformation of the visual rhodopsin, the thermally more stable (7*E*,9*E*,11*E*,13*E*)-retinal is released from the opsin and the less stable (7*E*,9*E*,11*Z*,13*E*)-retinal is regenerated in a sequence of enzymatic steps[1271] that proceed while the retinal and the other intermediates in the sequence are free solutes in the phospholipid bilayer of the membrane of the rod or cone. The enzyme that catalyzes the actual reisomerization, retinoid isomerohydrolase, couples the unfavorable conversion of the double bond at position 11 from trans to cis with the favorable hydrolysis of the ester between (7*E*,9*E*,11*E*,13*E*)-retinol and palmitic acid.[1272-1274] The isomerization involves an allylic carbocationic intermediate[1275] at positions 12, 13, and 14 resulting from the hydronation of carbon 11. The reassociation of (7*E*,9*E*,11*Z*,13*E*)-retinal with a molecule of opsin completes the photocycle.

There are a number of bacteria and archaea that have a **bacteriorhodopsin**, particular to their species, in their membranes. In contrast to the retinyl group in visual rhodopsin, the retinyl group in bacteriorhodopsin from *Halobacterium salinarum*, in the light-adapted, continuously cycling state immediately prior to the absorption of a quantum of light, exists as the thermally more stable (7*E*,9*E*,11*E*,13*E*) isomer. Also in contrast to visual rhodopsin, the *Z* isomer at carbon 13, rather than the *Z* isomer at position 11, is produced by the photoisomerization.[1276-1279] The initial absorption of a photon is followed by a photocycle with a number of different intermediates, distinguished by their absorption spectra.[1280] Crystallographic molecular models[1281,1282] of all the intermediates in this photocycle are available.[1281,1283-1288] The function of bacteriorhodopsin in *H. salinarium* is to use the energy stored in the photoisomerization to **move a hydron across the membrane**. The hydron is transported from the negative, basic solution on the one side of the membrane to the positive, acidic solution on the other. In the flavobacterium *Dokdonia eikasta*, there is a homologous (22% identity; 3.3 gap percent) bacteriorhodopsin that uses a similar mechanism to transport a sodium ion from a solution of low concentration to a solution of high concentration.[1289]

In the initial state, immediately prior to photoisomerization, the nitrogen–hydrogen bond of the hydronated iminium at carbon 15, adjacent to the *E* double bond at position 13 (see **2–85** and Equation 2–196) in the bacteriorhodopsin from *H. salinarum*, is pointed in the direction of the positive, acidic side of the membrane[1281] and is the donor in a hydrogen bond to a molecule of water pinned in place by hydrogen bonds[1290] to Aspartates 85 and 212. After the electronically excited state produced by absorption of a photon has relaxed and the double bond at position 13 has isomerized to the *Z* isomer, a torque is exerted on this imine by the *Z* configuration of the adjacent double bond. Both crystallographic molecular models[1290] taken at 16, 290, and 760 ns and solid-state nuclear magnetic spectra taken in the same interval[1291] indicate that as the isomerization proceeds, the hydronated iminio group swings past the hydroxy group of Threonine 89, which is a donor in a hydrogen bond with the carboxylato group of Aspartate 85 in the ground state, and that as it swings by, the hydron is transferred from the lysyl iminium to the hydroxy group of Threonine 89 and relayed through the hydroxy group to the carboxylato group of Aspartate 85 on the side of the retinyl group closest to the positive, acidic side of bacteriorhodopsin. The hydron is relayed from the carboxy group of Aspartic Acid 85 through two molecules of water to the guanidinio group of Arginine 82 and eventually to the positive, acidic side of the protein. Following the transfer, the two molecules of water dissociate from the protein as a result of slower conformational changes to the carboxy groups holding them in place that are induced by the isomerization of the retinyl group,[1290] so there is no path on which the hydron can return.

The unhydronated imino group has been turned by the torque of the adjacent *Z* double bond, so its lone pair of electrons, from which the hydron was transferred to the hydroxy group of Threonine 89, faces in the opposite direction toward the negative, basic side of the bacteriorhodopsin, just as the imine in visual rhodopsin rotates almost 180° following the photoisomerization of the retinyl group (Equation 2–196). Following this pivot, the lone pair of electrons on the imino nitrogen picks up a hydron relayed from the carboxy group of Aspartic Acid 96 on the negative, basic surface of the bacteriorhodopsin. A conformational change in the protein, induced by the photoisomerization of the retinyl group, opens a channel between the carboxy group of Aspartic Acid 96 and the lone pair of electrons on the imino nitrogen. This channel becomes occupied by three molecules of water that form a continuous

chain of hydrogen bonds, from the carboxy group of Aspartic Acid 96 to the lone pair of electrons on the imino nitrogen,[1292] through which a hydron from the negative, basic solution is transferred to the imino nitrogen. In this instance, the conformational change has assembled rather than disassembled a chain of molecules of water joined by hydrogen bonds.

Following all these more rapid steps, the more stable (7*E*,9*E*,11*E*,13*E*)-retinyl group is regenerated thermally with a rate constant of 200 s^{-1}. During this regeneration, the nitrogen–hydrogen bond of the hydronated iminium rotates back to the initial position, pointed in the direction of the positive, acidic side of the membrane.[1284] During this thermal isomerization, the hydron must remain on the nitrogen so that it is pointed to the positive, acidic side of the membrane. The net result is that one hydron is released into the solution on the positive, acidic side of the membrane and one hydron is taken up from the negative, basic side for every photon absorbed, and the free energy required to formally transport the hydron against the electrochemical gradient from the negative, basic solution to the positive, acidic side of the membrane is supplied by the photon of light absorbed by the retinyl group.

The answers to the most important questions, however, remain unclear. What forces the imine to be hydronated before it begins to flip during its conformational change in response to the photolytic isomerization of the retinyl group from all trans to 13-cis? What forces the imine to be dehydronated by the hydroxy group of Threonine 89 while it passes by so that, when it completes the flip, it is dehydronated? What forces the imine to be hydronated before it can flip back in response to the thermal isomerization of the retinyl group from 13-cis to all trans? What forces the iminium to remain hydronated as it presumably again passes by the hydroxy group of Threonine 89 so that it brings the hydron to the other side of the retinyl group? The answers to these questions probably rely on a careful tabulation of the positions of all the hydrons in the hydrogen bonds in which the hydroxy group of Threonine 89 participates and all the hydrogen bonds among the atoms that relay a hydron to the positive, acidic solution and a hydron from the negative, basic solution. Similar issues will arise later with regard to H^+-transporting two-sector ATPase.

The retinyl group is long and bulky. Because it is hydrophobic along its entire length, there are no donors or acceptors for hydrogen bonds to enforce a particular rotational isomer. In the various rhodopsins, the retinyl group is almost completely surrounded by mostly hydrophobic side chains.[1267] There can be little doubt that the **structure of the active site** formed by this constellation of hydrophobic amino acids surrounding a particular rhodopsin influences the course of the particular photocycle for which it is responsible. For example, the structure of the active site of bacteriorhodopsin must determine that the (7*E*,9*E*,11*E*,13*Z*) isomer is the major product of the photoisomerization rather than the (7*E*,9*E*,11*E*,13*E*) isomer and then must determine that the major product of the thermal equilibrium between the two isomers, when a photon has not just been absorbed, is the (7*E*,9*E*,11*E*,13*E*) isomer of the retinyl group, which happens to be the inherently most stable isomer in solution but not necessarily the more stable on an active site. The active site in visual rhodopsin distorts the double bond at position 11 in the (7*E*,9*E*,11*Z*,13*E*) retinyl group (Equation 2–196), presumably to weaken it, but does not distort it enough to break it and cause it to isomerize because, in the dark, the (7*E*,9*E*,11*Z*,13*E*) isomer remains unisomerized. The active site of visual rhodopsin then exploits the inherent stability of the (7*E*,9*E*,11*E*,13*E*) isomer, which the active site has caused to be the major photoproduct, to leverage the conformational change.

Suggested Reading

Nango, E., Royant, A., Kubo, M., Nakane, T., Wickstrand, C., Kimura, T., Tanaka, T., Tono, K., Song, C., Tanaka, R., Arima, T., Yamashita, A., Kobayashi, J., Hosaka, T., Mizohata, E., Nogly, P., Sugahara, M., Nam, D., Nomura, T., Shimamura, T., Im, D., Fujiwara, T., Yamanaka, Y., Jeon, B., Nishizawa, T., Oda, K., Fukuda, M., Andersson, R., Bath, P., Dods, R., Davidsson, J., Matsuoka, S., Kawatake, S., Murata, M., Nureki, O., Owada, S., Kameshima, T., Hatsui, T., Joti, Y., Schertler, G., Yabashi, M., Bondar, A. N., Standfuss, J., Neutze, R., and Iwata, S. (2016) A three-dimensional movie of structural changes in bacteriorhodopsin, *Science 354*, 1552–1557. https://doi.org/10.1126/science.aah3497

Yan, M., Manor, D., Weng, G., Chao, H., Rothberg, L., Jedju, T. M., Alfano, R. R., and Callender, R. H. (1991) Ultrafast spectroscopy of the visual pigment rhodopsin. *Proc. Natl. Acad. Sci. U. S. A. 88*, 9809–9812. https://doi.org/10.1073/pnas.88.21.9809

Oxides and Hydrides of Hydrogen, Nitrogen, Oxygen, and Sulfur

Molecular nitrogen is diatomic and has 10 valence electrons, and molecular oxygen is diatomic and has 12 valence electrons. The molecular orbital systems (Figure 2–45)[675] occupied by these electrons to form the bonds in molecular nitrogen (N_2) and molecular oxygen (O_2) are the same, and they are the same as the molecular orbital systems of the other diatomic molecules of the elements of the second period, such as molecular fluorine (F_2), carbon monoxide (CO), and nitric oxide ($NO^{\bullet}$) and the diatomic ions of the elements of the second period,[1293] such as the conjugate base of nitroxyl (ON^-), carbide ion (CC^{2-}), and cyanide ion (CN^-) as well as diatomic intermediates of atoms from the second period in enzymatic reactions. The nuclei, however, and, consequently, the energy levels of the respective molecular orbitals in each of these molecules and ions differ because the energy levels of the atomic orbitals that mix to form the molecular orbitals differ. In the diatomic molecules and ions in which the two atoms are different, the shapes of the molecular orbitals are asymmetric because of the differences in electronegativity of the two atoms. There are both σ molecular orbitals and π molecular orbitals between the two respective atoms in these diatomic molecule or diatomic ions.

The two **σ molecular orbital systems**, σ_s and σ_p, are formed by the combination of two $2s$ atomic orbitals, one from each atom, and the combination of two $2p_z$ atomic orbitals, one from each atom, respectively (Figure 2–45). The $2p_z$ orbitals are the $2p$ orbitals that lie along the line of centers between the atoms. These two pairs of atomic orbitals, s and p, combine to create two pairs of σ molecular orbitals. Each pair contains a bonding σ molecular orbital and an antibonding σ molecular orbital. Because all four of the constituent atomic orbitals, the two $2s$ atomic orbitals and the two $2p_z$ atomic orbitals, were cylindrically symmetric with the axis between the two nuclei before they mixed, the four molecular orbitals in the two σ molecular orbital systems that they create are also cylindrically symmetric around the axis between the atoms,[675,1294-1296] but they are asymmetric about axes perpendicular to the central axis when the atoms are different. The resulting four molecular orbitals are considered to be σ molecular orbitals because they form bonds and antibonds along the line of centers between the two atoms.

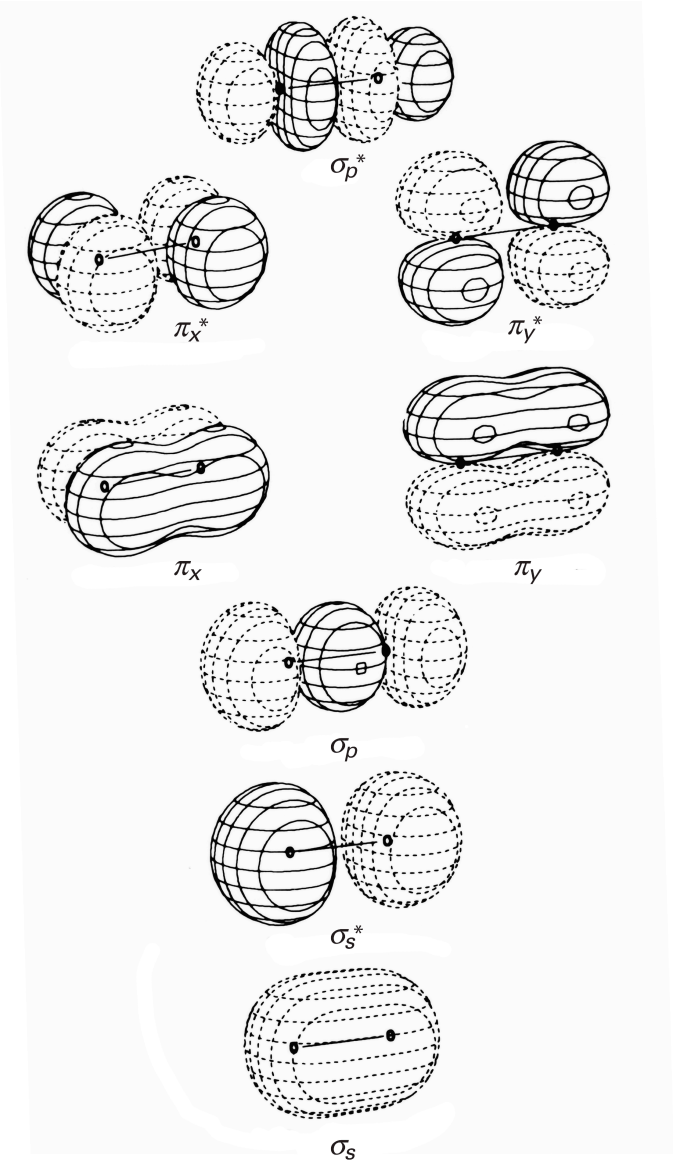

Figure 2–45: One of several ways to depict the molecular orbitals of the O_2 molecule.[675] The drawings of the individual molecular orbitals are distributed and labeled as they are in **2–87**. The two lowest, cylindrically symmetric σ molecular orbitals along the line of centers between the two oxygen atoms (σ_s and σ_s^*) are formed from the overlap of two s atomic orbitals, one from each oxygen atom. The two highest cylindrically symmetric σ molecular orbitals along the line of centers between the two oxygen atoms (σ_p and σ_p^*) are formed from the overlap of two p_z atomic orbitals, one from each oxygen atom. The two pairs of π molecular orbitals, which are orthogonal and degenerate to each other, are formed from the p_x orbitals (π_x and π_x^*) and the p_y orbitals (π_y and π_y^*) of the two oxygen atoms. In the ground state, the distribution of electrons in these orbitals is as in **2–87**. Reprinted with permission from reference 675. Copyright 1979 Annual Reviews, Inc.

The two **π molecular orbital systems**, π_x and π_y, are formed as shown in Figure 2–45. The π_x molecular orbital system is formed by the overlap of the two parallel p_x orbitals, one from each atom, which creates a bonding π molecular orbital (π_x) and an antibonding π molecular orbital (π_x^*). The π_y molecular orbital system is formed by the overlap of the two parallel p_y orbitals, one from each atom, which also creates a bonding π molecular orbital (π_y) and an antibonding π molecular orbital (π_y^*). Because the p_x and p_y orbitals on each atom were orthogonal and degenerate, the two π molecular orbital systems they create are perpendicular to each other, orthogonal, and degenerate; as, for example, are the two π molecular orbital systems in ethyne.

The energy levels of these molecular orbitals are distributed in the order of the atomic orbitals that form them

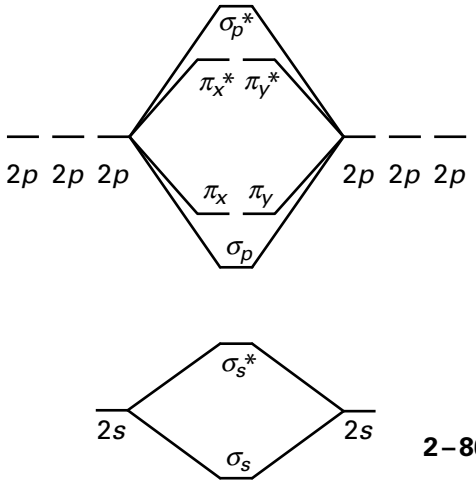

2–86

To the right and to the left, the diagram shows the energy levels of the atomic orbitals of the two atoms that mix among themselves to produce the molecular orbitals of the molecule, which are displayed in the center. The total number of molecular orbitals is always equal to the sum of the atomic orbitals that mixed together.

The first ten **valence electrons** in a diatomic molecule or ion fill the molecular orbitals in order of their energy: the two bonding σ molecular orbitals (σ_s and σ_p,) the antibonding σ molecular orbital of lowest energy (σ_s^*), and the two bonding π molecular orbitals (π_x and π_y). Because two bonding σ molecular orbitals and one antibonding σ molecular orbital are occupied by six electrons, there is a **net number of one σ bond**. Because two bonding π molecular orbitals are occupied by four electrons, there is a **net number of two π bonds**. This distribution of electrons completes the catalogue of occupied molecular orbitals of N_2, as well as CO, CC^{2-}, and CN^-. In each case, the five molecular orbitals of lowest energy are filled with the ten valence electrons, and there is a net number of three bonds between the two atoms, two π bonds and one σ bond. As a result, one way to represent molecular nitrogen is N≡N.

The remaining two valence electrons in **molecular oxygen**, however, are found in the two separate **antibonding π molecular orbitals**,[675,1294-1296] formed from overlap out of phase (Figure 2–45) of the two $2p_x$ and the two $2p_y$ atomic orbitals, respectively

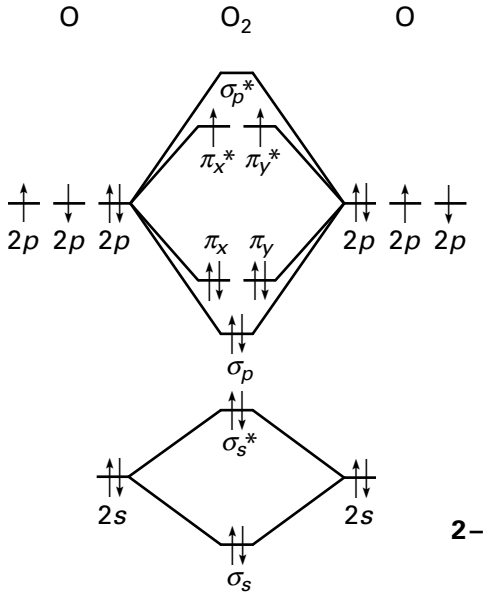

2–87

The two orthogonal, antibonding π molecular orbitals, π_x^* and π_y^*, are degenerate, and by Hund's rule, each is occupied by an unpaired electron. This distribution of electrons causes molecular oxygen in its ground state to be a triplet diradical and paramagnetic. Only one of these two antibonding π molecular orbitals is occupied by the single unpaired electron in $NO^{\bullet}$, which is a stable radical.

The four electrons in the two bonding π molecular orbitals and the two electrons in the two antibonding π molecular orbitals in molecular oxygen produce the **equivalent of one π bond**. Consequently, molecular oxygen can be abbreviated as if it had a double bond, one σ bond and one π bond, O=O, as is the case in a carbon–carbon double bond. Another way of abbreviating it, however, would be :O≒O:, which accounts for all twelve valence electrons and indicates approximately where they are, but this representation is cumbersome and difficult to set in type. Even though the two unpaired electrons

are in separate antibonding orbitals, with a node between the two oxygens, they are delocalized over the two atoms of oxygen, and this delocalization does provide extra stabilization to the bonding in the π molecular orbital system beyond what would be realized by only a single π bond.[1297] The fact, however, that the antibonding molecular orbitals in the σ molecular orbital systems are filled weakens the oxygen–oxygen σ bond and makes it more susceptible to dissociation.

The two unpaired electrons of molecular oxygen in the two degenerate π molecular orbitals have spins of the same sign in the **triplet ground state**. Upon excitation in an appropriate fashion, one of the two electrons can have its spin inverted to create an **excited singlet state** in which the two electrons are of opposite spin. There are two excited singlet states: one in which the two electrons of opposite spin are in the same antibonding π^* molecular orbital and one in which they are split between the two antibonding π^* molecular orbitals. The triplet state of molecular oxygen engages in homolytic radical chemistry and single electron transfer. The heterolytic, singlet electronically excited state of molecular oxygen, in which the two electrons are in the same antibonding π^* molecular orbital, can participate as an electron-deficient dienophile in a cycloaddition reaction with an electron-rich diene and can participate in a [2 + 2] cycloaddition with an olefin to produce a dioxetane, and the pair of electrons in the π bond of an olefin as a nucleophile can add to one of the oxygen atoms in singlet oxygen acting as an electrophile to form a peroxirane.[1298]

In molecular oxygen, the two π molecular orbitals that are each occupied by an unpaired electron are antibonding but only half-filled. The addition of one electron to one of these two antibonding orbitals produces the **superoxide radical anion**

$$O_2 + e^- \rightleftharpoons O_2^{\cdot -} \qquad (2\text{–}197)$$

This reaction, even though it fills an orbital, is not a favorable one [$E^{\circ\prime}$ = –330 mV (standard state of 10^5 pascals of oxygen)][1299,1300] because the electron is added to an antibonding orbital. Unlike the other intermediates in the reduction of molecular oxygen, as well as molecular oxygen itself, the superoxide radical anion is a mild reducing agent.

The addition of a second electron to the remaining unfilled, antibonding π molecular orbital, which is very favorable under standard conditions, makes the dioxygen diamagnetic because all electrons are now paired. It also produces an electron-rich molecule, the peroxide dianion, that is quite basic and picks up two hydrons at pH 7 to form two oxygen–hydrogen σ bonds, one to each oxygen. This one-electron reduction and dihydronation forms **hydrogen peroxide**[1300,1301]

$$O_2^{\cdot -} + 2\,H^+ + e^- \rightleftharpoons H_2O_2 \qquad E^\circ = +940\ \text{mV} \qquad (2\text{–}198)$$

The **acid dissociation constants** of the conjugate acids of superoxide radical anion and of hydrogen peroxide define the character of the respective lone pairs of electrons in these two molecules. Molecular oxygen is not basic because the two pairs of nonbonding σ electrons it contains (Figure 2–45) are, at best, located in two *sp* atomic orbitals or, at worst, delocalized into molecular orbitals cylindrically symmetric to the axis of the molecule, and pairs of electrons in π bonds are always poor bases.

After an electron is added to molecular oxygen to produce the superoxide radical anion, the molecule becomes considerably more basic[1302]

$$HO_2^{\cdot} \rightleftharpoons H^+ + O_2^{\cdot -} \qquad pK_a = 4.7 \qquad (2\text{–}199)$$

This basicity suggests that the σ electrons in superoxide radical anion are not all delocalized as they are in molecular oxygen. This pK_a is low enough relative to that of water (pK_a = 15.7) to suggest that there is considerably less *p* character in the σ lone pair of electrons accepting the hydron in superoxide radical anion than there is in an sp^3 σ lone pair of electrons on hydroxide, which is the conjugate base of water, even when the electron withdrawal of the other oxygen is taken into account.

The pK_a of dihydrogen superoxide radical cation[1301]

$$H_2O_2^{\cdot +} \rightleftharpoons H^+ + HO_2^{\cdot} \qquad pK_a = 1.2 \qquad (2\text{–}200)$$

is 1.2. This value suggests that the **basic lone pairs of electrons** in the conjugate base, hydrosuperoxide radical, are similarly hybridized to those in superoxide radical anion, the conjugate base of hydrosuperoxide radical (Equation 2–199). The two successive acid dissociations resemble the two successive acid dissociations in a diprotic acid. The only difference

between the basic lone pairs of electrons in hydrosuperoxide radical and superoxide radical anion is that in the former case the oxygen on which they reside is immediately adjacent to a hydroxy group and in the latter case they are immediately adjacent to an oxyanion. It is also the case that the pK_a for dihydrogen superoxide radical cation (Equation 2–200) is higher than the pK_a for the oxygen of the conjugate acid of formaldehyde

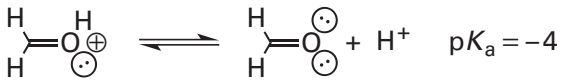

(2–201)

The replacement of a methylene carbon with a hydroxy group should only lower the pK_a of the sp^2 oxygen. This comparison suggests that there is more *p* character in the σ lone pair of electrons accepting the hydron in hydrosuperoxide radical than in the sp^2 σ lone pair of electrons on formaldehyde.

If the hybridizations of the basic lone pairs of electrons in superoxide radical anion and those in hydrosuperoxide radical are similar, if not the same, the conclusion that the basic lone pairs in these two molecules have less *p* character than a lone pair of electrons on the sp^3 oxygen of a hydroxide and more *p* character than the sp^2 oxygen on formaldehyde suggests that their hybridization is somewhere in between.

After a second electron has been added to molecular oxygen, there would be as many antibonding π electrons (four) as bonding π electrons (four) if the molecular orbital structure of molecular oxygen (**2–87**) were retained. For this reason, the π molecular orbitals become even weaker, and in a hydrogen-bonding solvent like water, they decompose completely into **localized σ lone pairs** of electrons on each oxygen. This rehybridization is reflected in the acid dissociation constant of **hydrogen peroxide**

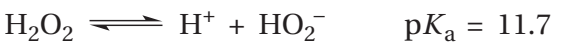

(2–202)

which is that expected of a simple hydroxy group with a strong electron-withdrawing group attached to it [for example, pK_a(CF_3CH_2OH) = 12.5]. That only a single σ bond remains is also reflected in the long bond length (0.148 nm) of hydrogen peroxide. The dihedral angle between the two hydrogens (92°) in hydrogen peroxide can also be explained by the consideration that, were the value of this angle 90°, each of the two sp^3 lone pairs on one oxygen would be as far as possible from being parallel to either of the two sp^3 lone pairs on the other oxygen. This dihedral orientation of 92° minimizes electron repulsion.

In molecular oxygen, the σ molecular orbital system is delocalized and there are no basic lone pairs of electrons. In hydrogen peroxy ion, the basic lone pairs are similar if not the same as the oxygens on a hydroxy group that are hybridized sp^3. The hybridization of the lone pairs of electrons on the superoxide radical anion and the hydrosuperoxide radical is somewhere between sp^2 and sp^3. For the sake of argument and for simplicity, it will be assumed that the two oxygens in the superoxide radical anion, although they are weak bases, are effective **acceptors for hydrogen bonds** and that when superoxide radical anion is dissolved in water, a hydrogen-bonding solvent, it is hybridized so that, in one plane, each oxygen has two sp^2 lone pairs of electrons accepting hydrogen bonds and, in the orthogonal plane, there is a π molecular orbital system occupied by three electrons

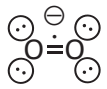

2–88

This electronic structure in aqueous solution resembles, at each oxygen, the electronic structure at the oxygen of formaldehyde (Equation 2–201). It is promoted by the weakening of the π system to the benefit of the σ system, owing to addition of the extra electron to one of the antibonding π molecular orbitals on molecular oxygen. The result of the consequent breakdown of the π molecular orbital system to which the electron has been added is that the now-filled antibonding π molecular orbital becomes a localized σ lone pair of electrons on one oxygen and the associated, filled bonding π molecular orbital becomes a localized σ lone pair of electrons on the other oxygen. Either the occupation of the one antibonding π molecular orbital in the gas phase or this reconfiguration of the electronic structure in water lowers the bonding order from 2 to 1.5, which is reflected in the lengthening of the oxygen–oxygen bond from 0.121 nm in molecular oxygen to 0.133 nm in superoxide radical anion, about half the distance to the single bond in hydrogen peroxide.

There are two more one-electron steps in the reduction of oxygen to two molecules of water. When one electron is added to hydrogen peroxide, the σ bond dissociates and hydroxide and **hydroxyl radical** are produced.[1300,1303] The hydroxide ($pK_a = 15.7$) immediately associates with a hydron to form water as the ultimate product

$$H_2O_2 + H^+ + e^- \rightleftharpoons HO^{\cdot} + H_2O \qquad E^{\circ\prime} = +380\ \text{mV} \tag{2–203}$$

Hydroxyl radical is a strong and dangerous oxidant that can pull an electron[1300]

$$HO^{\cdot} + H^+ + e^- \rightleftharpoons H_2O \qquad E^{\circ} = +2310\ \text{mV} \tag{2–204}$$

or a hydrogen atom

$$HO^{\cdot} + H^{\cdot} \rightleftharpoons H_2O \qquad \Delta H^{\circ} = -500\ \text{kJ mol}^{-1} \tag{2–205}$$

from almost anything during its reduction to hydroxide or water.[1303] In biochemical situations, the two final steps in the reduction of molecular oxygen (Equations 2–203 and 2–204) are usually forced to be concerted[1300,1303]

$$H_2O_2 + 2\,H^+ + 2\,e^- \rightleftharpoons 2\,H_2O \qquad E^{\circ} = +1350\ \text{mV} \tag{2–206}$$

to avoid the production of hydroxyl radical.

There are several **chemical features of molecular oxygen** that must be taken into account by the prosthetic groups that react with it. Its σ lone pairs of electrons are neither basic nor nucleophilic. It is a triplet molecule, a diradical with two unfilled π molecular orbitals. These molecular orbitals are antibonding, so their occupation rearranges the electronic structure of the molecule.

There are flavoenzymes that use molecular oxygen as a general oxidant to reoxidize reduced flavin produced during oxidations of their respective nominal reactants.* For example, in glucose oxidase, oxidized flavin oxidizes D-glucose to D-gluconolactone, and the resulting reduced flavin is then reoxidized by molecular oxygen to then oxidize the next D-glucose. During the reaction catalyzed by glucose oxidase and the other flavoprotein oxidases, molecular oxygen is reduced by the two electrons from the reduced flavin to hydrogen peroxide (Equations 2–197 and 2–198). In most cases, oxidation of the nominal reactant is the purpose of the flavoprotein oxidase, and the hydrogen peroxide is an undesired product that is usually disproportionated to water and molecular oxygen by catalase. In the case of aryl-alcohol oxidase from *Pleurotus eryngii*, however, the production of hydrogen peroxide is the purpose of the enzyme, and the nominal substrate, an aromatic primary alcohol such as veratryl alcohol, is recycled.[1304]

When molecular oxygen is used in a flavoprotein oxidase as the final receptacle for the two electrons passing through the flavin, there is no reason to invoke any type of covalent intermediate between flavin and molecular oxygen;[352] **simple electron transfer** should be sufficient. The reduced form of flavin in glucose oxidase is the anion ($H_2Fl_{red}^-$ in Figure 2–9), and its standard two-electron reduction potential in glucose oxidase from *Aspergillus niger* is –174 mV,[1305] which is close to the two-electron biochemical standard reduction potential (–203 mV) of the anionic form, $H_2Fl_{red}^-$, of riboflavin when it is free in solution (Figure 2–15). If the offset for the one-electron biochemical standard reduction potential (+44 mV) for the redox couple of $H_2Fl^{\cdot}$ and $H_2Fl_{red}^-$ in glucose oxidase is similar to that for riboflavin, then the one-electron biochemical standard reduction potential for the flavin in glucose oxidase should be around -130 mV, but the enzyme may well stabilize the semiquinone, in which case the biochemical standard reduction potential would be more negative. On the basis of these considerations, **transfer of an electron from $H_2Fl_{red}^-$ to molecular oxygen** [$E^{\circ\prime} = -160$ mV (standard state of 1 M O_2 and 1 M $O_2^{\cdot-}$)][1295]

$$H_2Fl_{red}^- + O_2 \rightleftharpoons O_2^{\cdot-} + H_2Fl^{\cdot} \tag{2–207}$$

should be almost isoergonic.

In glucose oxidase, the rate for transfer of the first electron from reduced flavin anion ($H_2Fl_{red}^-$) to molecular oxygen to form **superoxide radical anion as an intermediate**[1306] is accelerated at least 100-fold when a histidine adjacent to the oxygen in the active site is hydronated so that it can form an ionized hydrogen bond to the superoxide radical anion[1307] or even transfer a hydron to the superoxide

*In such situations the flavoenzyme is usually called an "oxidase". The nominal reactant gives the particular name to the oxidase—for example, D-glucose and glucose oxidase—and the general oxidant is a molecule of oxygen.

radical anion ($\Delta pK_a = +2$). Because molecular oxygen is not a base while superoxide radical anion is (Equation 2–199), the hydrogen bond forms or the hydron is transferred as the electron is being transferred, a consequence that stabilizes the superoxide radical anion and makes the transfer more favorable. In glucose oxidase, this transfer of the electron between $H_2Fl_{red}^-$ and oxygen to form superoxide radical anion and the neutral flavin semiquinone ($H_2Fl^\bullet$ in Figure 2–9) is the rate-limiting step in the reoxidation of the flavin.[1307]

The superoxide radical anion formed transiently in certain flavoprotein oxidases[1308] rapidly accepts the second electron from the flavin semiquinone to **form hydrogen peroxide in a strongly exergonic reaction**, provided hydrons are available from immediately adjacent acids in the active site of the enzyme[352,1309] or from the water surrounding the enzyme

$$H_2Fl^\bullet + O_2^{\bullet -} + H^+ \rightleftharpoons HFl_{ox} + HO_2^- + H^+ \rightleftharpoons H_2O_2 + HFl_{ox} \quad (2\text{–}208)$$

The fact that molecular oxygen so readily reoxidizes reduced flavin by unembellished transfer of two electrons suggests that enzymes that are required to reoxidize reduced flavin with other oxidants, such as NAD^+, must purposely prevent molecular oxygen from doing so.[1310]

Reduced flavin anion ($H_2Fl_{red}^-$) in free solution, at early times in the reaction before other side reactions become important, reacts with molecular oxygen to produce superoxide radical anion,[286,291,1308,1311] albeit slowly (rate constant of around 100 $M^{-1}\,s^{-1}$). In these **reactions in solution**, the superoxide radical anion and the flavin semiquinone can dissociate before a second electron is transferred, but on an enzyme, the active site retains the superoxide radical anion long enough for a second electron to be transferred. Therefore, the reduction of molecular oxygen to hydrogen peroxide performed by reduced flavin, as the terminal step in the reactions catalyzed by flavoprotein oxidases, can be thought of as a simple two-electron transfer, within the encounter complex, to the π molecular orbital system of the molecular oxygen concerted with transfers of hydrons to the σ lone pairs of the developing peroxide dianion and hydroperoxide anion.

The involvement of **both superoxide radical anion and hydrogen peroxide** in the reoxidation of reduced flavin by molecular oxygen is illustrated by the reoxidation of reduced xanthine oxidase.[1312] Fully reduced xanthine oxidase has six more electrons than the fully oxidized enzyme: two on a prosthetic molybdenum ion, one in each of its two iron–sulfur clusters, and two in its reduced flavin. The reoxidation of the reduced complex by molecular oxygen occurs at the flavin. The first four electrons are removed by two molecules of oxygen during reoxidation, and they are transferred rapidly enough that two molecules of hydrogen peroxide are produced at the flavin. When only two electrons remain on the enzyme, however, the electrons are distributed over the other prosthetic groups at equilibrium such that the flavin exists as a mixture of oxidized flavin and its semiquinone. In an active site occupied at a particular instant by the semiquinone, only one electron can be transferred to molecular oxygen, and as a result, superoxide radical anion, rather than hydrogen peroxide, is produced. When xanthine oxidase is functioning normally, it produces a variable mixture of hydrogen peroxide and superoxide radical anion, depending on its steady-state level of reduction.

There is a remaining **difficulty with transfer of the electrons during the reoxidation of flavin**

$$H_2Fl_{red}^- + {}^3O_2 + H^+ \rightleftharpoons H_2O_2 + HFl_{ox} \quad (2\text{–}209)$$

Molecular oxygen is a diradical because the two unpaired electrons have parallel spins in the triplet ground state, $^3O_2$. The products of the reaction, oxidized flavin and hydrogen peroxide, and the reactant, reduced flavin, are all singlet molecules in which each of the electrons is paired with one of opposite spin. Therefore during the overall reaction, one electron must invert its spin. Such a **spin inversion** is normally a slow process, but it can be catalyzed.

Spin inversions can be **accelerated by electron transfer**. For example, in the active site of glucose oxidase, after transfer of the electron from reduced flavin to molecular oxygen to form $O_2^{\bullet -}$ and $H_2Fl^\bullet$, the two unpaired electrons of the still triplet state are now located, respectively, on flavin and superoxide radical anion rather than both being on molecular oxygen. Because they are single unpaired electrons on different atoms (nitrogen and oxygen) in different molecules (flavin and superoxide radical anion), spin inversion becomes rapid. There is no indication that the second step in reoxidation of the flavin in glucose oxidase, the step in which the triplet state of the separated electrons formally

becomes a singlet state, is hindered by spin inversion.[1307]

Spin inversions are also **catalyzed by transition metallic ions.** For example, triplet oxygen combines with a ferroheme with an open site for ligation on Fe^{2+} to form a complex between the heme and oxygen, as in hemoglobin. The complex is diamagnetic,[1313] so its formation necessarily involves a spin inversion. As this spin inversion is essentially instantaneous, it can be concluded that it is catalyzed by Fe^{2+}. Transition metallic ions other than iron are also used to catalyze spin inversion. Galactose oxidase catalyzes the reaction

$$\text{D-galactose} + {}^3O_2 \rightleftharpoons H_2O_2 + \text{D-}\textit{galacto}\text{-hexodialdose} \quad (2\text{–}210)$$

During the reaction, spin inversion must take place because both products are singlet molecules. Instead of flavin, the reduced prosthetic group in the active site of galactose oxidase is a complex between a copper ion and a 2-(*S*-cysteinyl)tyrosine.[1314,1315] This complex, in its reduced state, is the immediate electron donor to triplet oxygen. Either transfer of an electron from the Cu^+ to triplet oxygen, to split the triplet between oxygen and Cu^+, or direct complexation of singlet oxygen with copper[1316] accomplishes the necessary spin inversion.

There are many monooxygenases that use flavin as a prosthetic group in the monooxygenation of a substrate by molecular oxygen. Examples are melilotate 3-monooxygenase[1317]

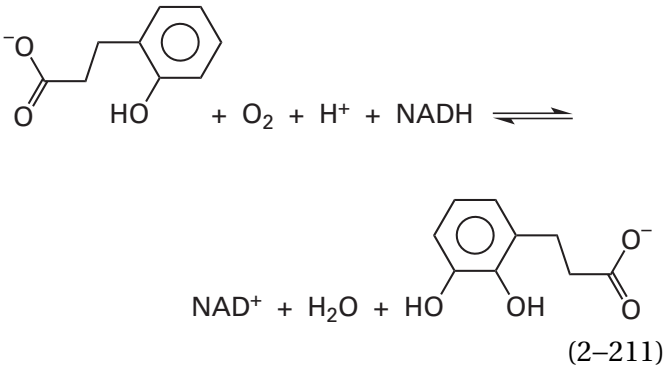

(2–211)

4-hydroxybenzoate 3-monooxygenase[1318]

$$\text{4-hydroxybenzoate} + \text{NADPH} + H^+ + O_2 \rightleftharpoons \text{3,4-dihydroxybenzoate} + NADP^+ + H_2O \quad (2\text{–}212)$$

cyclohexanone monooxygenase[1319]

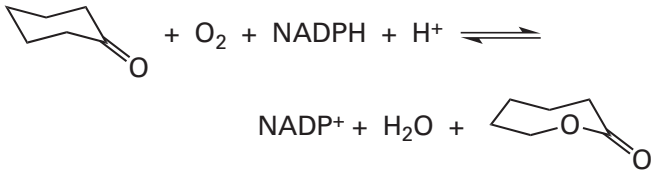

(2–213)

6-hydroxynicotinate 3-monooxygenase[1320]

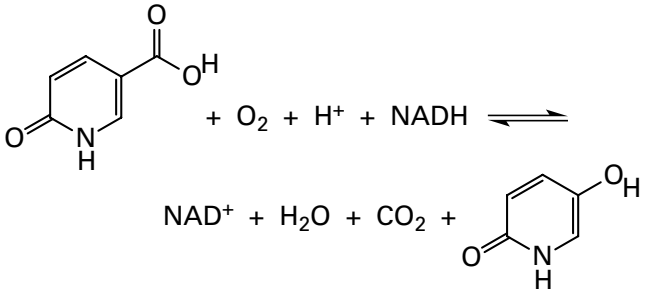

(2–214)

and the epoxidation of the carbon–carbon double bond in the center of fumitremorgin C catalyzed by a flavin monooxygenase from *Aspergillus fumigatus* that is related to 4-hydroxybenzoate 3-monooxygenase. In this last case, the epoxide produced then dissociates at one of the carbon–oxygen bonds, and the resulting carbenium ion undergoes an alkyl migration as in a pinacol rearrangement to form the spiro carbon in spirotryprostatin A.[1321] In the reaction catalyzed by a monooxygenase, by definition, one of the two oxygen atoms of molecular oxygen is incorporated into the product and the other into water.*

Melilotate 3-monooxygenase, 4-hydroxybenzoate 3-monooxygenase, and 6-hydroxynicotinate 3-monooxygenase are enzymes that catalyze **hydroxylations**. 6-Hydroxynicotinate 3-monooxygenase catalyzes an unusual hydroxylation in which a hydroxy group replaces a carboxy group rather than a hydrogen, a fact that reiterates the equivalence between carbon dioxide and a hydron. These three enzymes catalyze the hydroxylation of aromatic rings. Long-chain alkane monooxygenase from *Geobacillus thermodenitrificans*, however, is able to convert a linear alkane of up to 36 carbons into the corresponding primary alcohol.[1322,1323] The bond dissociation energy for a primary carbon–hydrogen bond (+410 kJ mol^{-1}), which seems to be the only logical first step in this reaction at an alkane, is quite large.

*Dioxygenases are enzymes that incorporate both atoms of molecular oxygen into their reactants.

In these hydroxylations and the reaction catalyzed by cyclohexanone monooxygenase, the species that reacts with the molecular oxygen is reduced flavin.[1317-1319] The flavin is usually reduced by either NADH or NADPH. The reduced flavin then reacts with molecular oxygen to produce an intermediate that performs the actual monooxygenation, after which the resulting oxidized flavin is again reduced by either NADH or NADPH.

The spectral characteristics of the **initial intermediate formed in one of these flavin monooxygenases** (Figure 2–46)[1319,1324-1327] from reduced flavin and molecular oxygen are indistinguishable from those of a 4a-peroxyflavin or its conjugate acid, a 4a-hydroperoxyflavin. 4a-Peroxyisoalloxazines or 4a-hydroperoxyisoalloxazines can be formed in solution nonenzymatically from an isoalloxazine and superoxide radical anion or hydrogen peroxide, respectively. For example, superoxide radical anion reacts in dimethylformamide with the neutral semiquinone radical of 5-ethyl-3,7,8,10-tetramethylisoalloxazine[1328] to produce its **4a-peroxyisoalloxazine anion** (**2–89**)

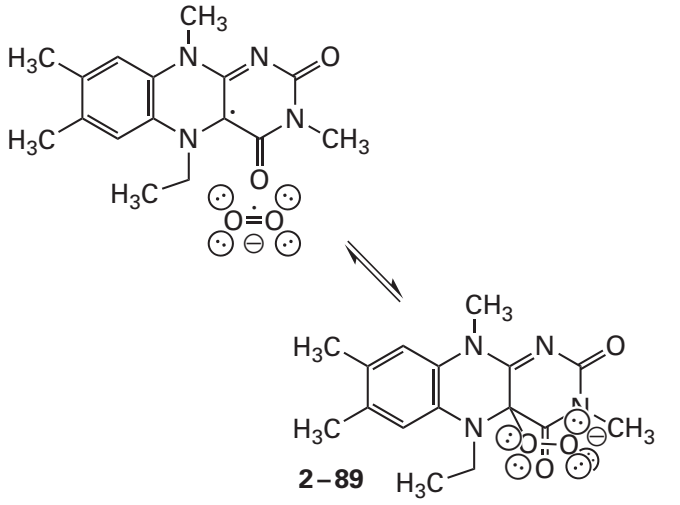

(2–215)

by a simple colligation.* The respective **4a-hydroperoxyisoalloxazine** (**2–90**) has been produced from the reaction between peroxide and an oxidized isoalloxazine in nonpolar solvents[1329]

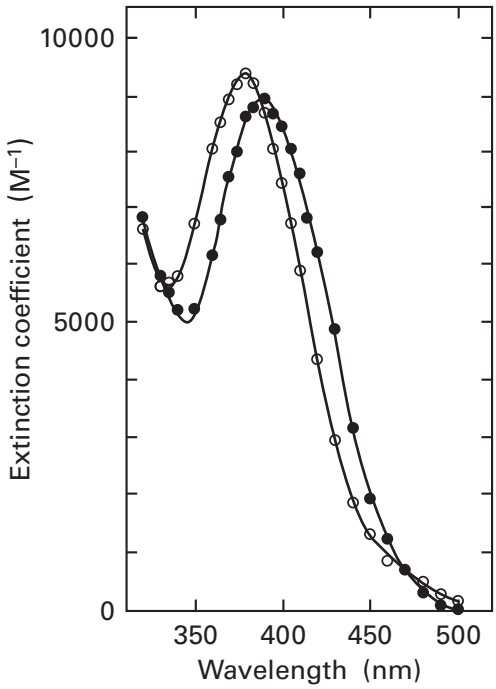

Figure 2–46: Absorption spectra of the two intermediates in the reaction of molecular oxygen with reduced flavin in the active site of 4-hydroxybenzoate 3-monooxygenase from *P. aeruginosa*.[1324] 4-Hydroxybenzoate 3-monooxygenase, the prosthetic flavin adenine dinucleotide of which was in the reduced state and to which the substrate 4-hydroxybenzoate was already bound, was mixed with a solution of O_2 so that the final concentrations of reactants would be 13 μM active sites, 1.1 mM oxygen, and 2.5 mM 4-hydroxybenzoate in a solution of 50 mM potassium phosphate at pH 6.55 at 3.5 °C. The absorbances of the solution at wavelengths separated by 5 or 10 nm were monitored as a function of time. Following the mixing of the reduced enzyme with oxygen, two sequential intermediates were observed. The first was formed in a bimolecular reaction between the enzyme and the O_2 with a rate constant of 2.6×10^5 M^{-1} s^{-1} (a pseudo-first-order rate constant of 280 s^{-1} at 1.1 mM O_2) and the second with a rate constant of 45 s^{-1}. The measurements were repeated at a series of wavelengths and the extinction coefficients of each of the two intermediates is plotted as a function of the wavelength. The intermediates were identified as 4a adducts of the reduced flavin (Figure 2–16) by comparison with spectra of model compounds. The intermediate that formed first (●) was identified as 4a-hydroperoxyflavin adenine dinucleotide. The intermediate that formed afterward (○) was identified as 4a-hydroxyflavin adenine dinucleotide.

*A colligation is the combination of two radicals to form a covalent bond.

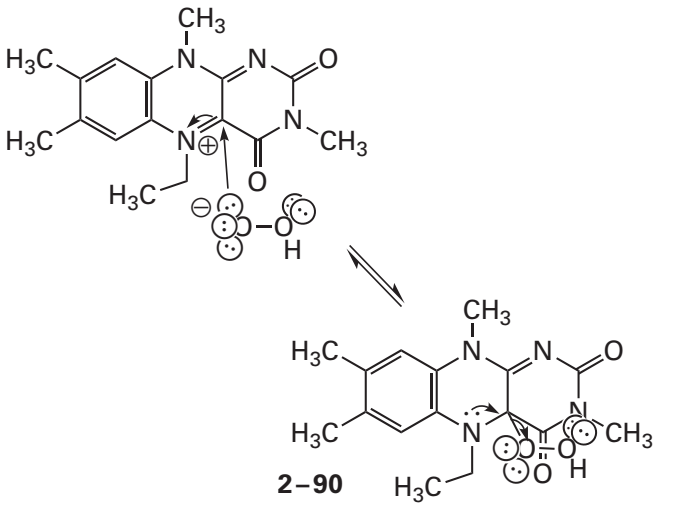

(2–216)

The neutral 4a-hydroperoxyflavin **2–90** reverts readily to reactants because the reaction is a simple addition of the conjugate base of hydrogen peroxide, HO_2^-, as a nucleophile, to the iminium ion in the oxidized 5-ethylflavin to produce the peroxy homologue of a hemiaminal.

A 4a-hydroperoxyflavin (see **2–90**) may be an intermediate in the nonenzymatic formation of hydrogen peroxide from oxygen by reduced flavins in solution.[286] In at least one flavoprotein oxidase, pyranose oxidase from *Trametes ochracea*, molecular oxygen oxidizes the reduced flavin, produced by oxidation of a pyranose, by forming a 4a-peroxyflavin anion (see **2–89**), which is then hydronated and dissociates into oxidized flavin and hydrogen peroxide (Equation 2–216),[1330] rather than transferring electrons one at a time to molecular oxygen. In this instance, the 4a-hydroperoxyflavin was identified spectroscopically (see Figure 2–46).

In the active sites of flavin monooxygenases, formation of the 4a-hydroperoxyflavin proceeds in a similar manner (Equations 2–207 and 2–215)

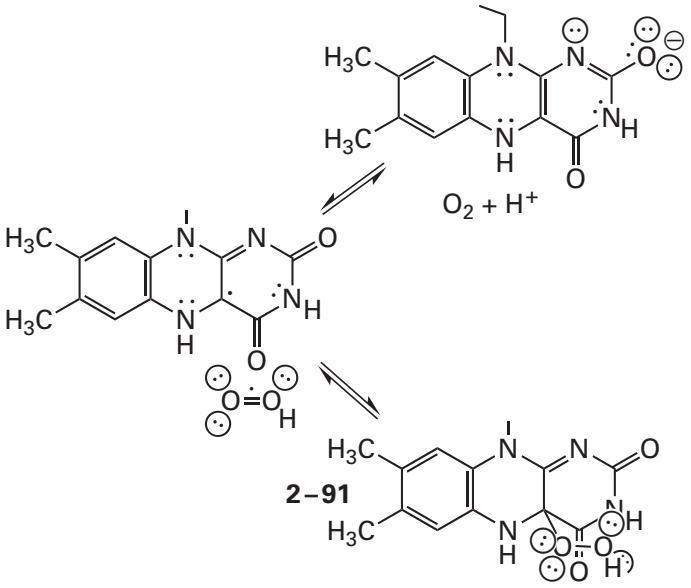

(2–217)

During its formation, **a hydron is provided by the active site**. In the active site of 4-hydroxyphenylacetate 3-monooxygenase from *Acinetobacter baumannii*, the molecule of oxygen is hydronated by the imidazolio group of Histidine 396 as the electron is transferred from the reduced flavin to molecular oxygen. Following transfer of the electron, the system is still in the triplet state, but it rapidly undergoes a nearly barrierless spin inversion to the singlet state before the hydronated superoxide radical anion, which is hydroperoxy radical (Equation 2–199), combines with the semiquinone of the flavin[1331] in a colligation. In the active site of L-ornithine N^5-monooxygenase [NAD(P)H] from *A. fumigatus*, the catalytic acid is the 2′-hydroxy group of the $NADP^+$ that has just provided the hydride to reduce the flavin.[1332] The 2′-hydroxy group relays a hydron from the δ-ammonio group of the substrate L-ornithine.[1333]

A 4a-hydroperoxyflavin or 4a-peroxyflavin that forms in an active site of a flavin monooxygenase either dissociates into hydrogen peroxide and oxidized flavin (a wasted reaction) or oxygenates the substrate.[1318] Two strategies are used to **prevent the production of hydrogen peroxide** under normal circumstances. In the first strategy, which has been adopted by monooxygenases that hydroxylate phenyl groups, the rate of reduction of the oxidized flavin by NADH or NADPH is usually hindered in the absence of the nominal reactant. For example, reduction of the oxidized flavin by NADPH in 4-hydroxybenzoate 3-monooxygenase [NAD(P)H] is 2×10^5 times slower in the absence of 4-hydroxybenzoate than in its presence.[1334] In the second strategy, which

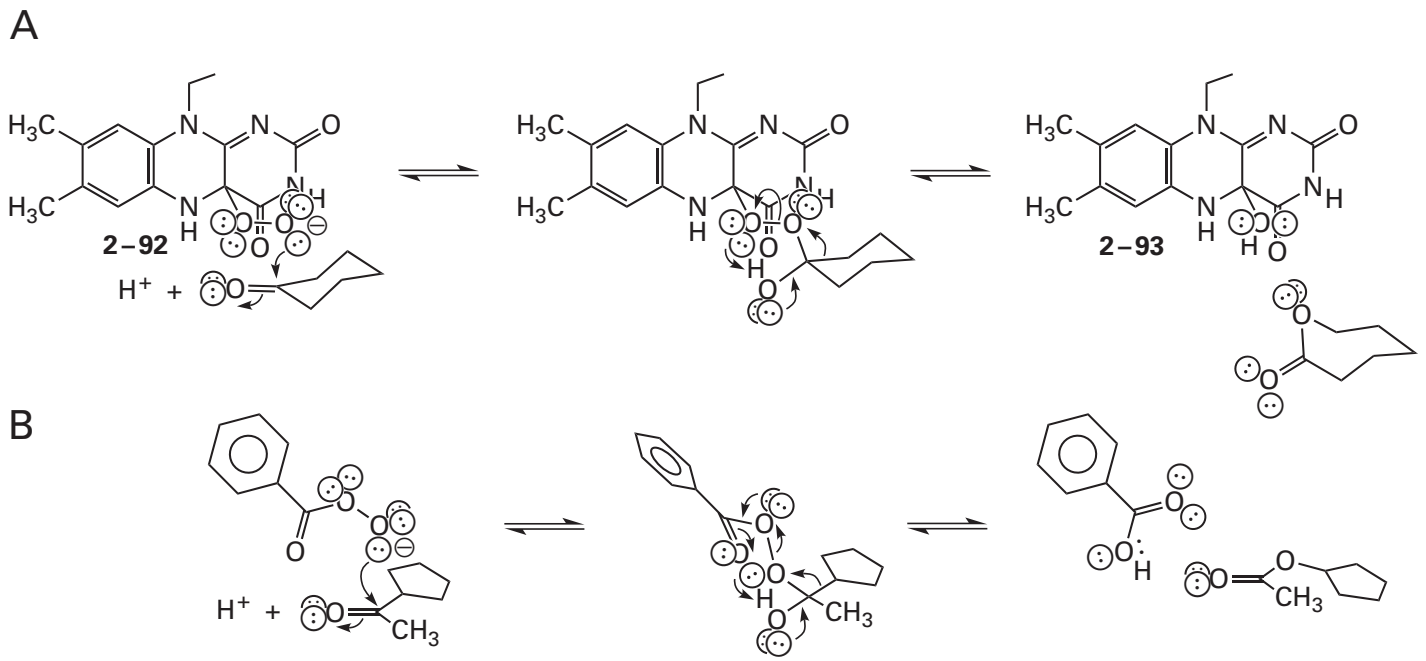

Figure 2–47: Mechanisms for **(A)** the Baeyer–Villiger monooxygenation catalyzed by cyclohexanone monooxygenase and **(B)** a nonenzymatic Baeyer–Villiger oxidation (Equation 2–219). **(A)** In the enzymatic reaction, the anionic distal oxygen of the 4a-peroxyflavin anion adds as a nucleophile to the electrophilic carbonyl carbon of the cyclohexanone. The resulting dialkyl peroxide cleaves heterolytically at the oxygen–oxygen bond, coincident with the migration of one of the alkyl carbons of the cyclohexanone to the adjacent oxygen. The migrating alkyl carbon is pushed by a lone pair of electrons on the alkoxide oxygen. The products of the rearrangement are the lactone and the 4a-hydroxyflavin. **(B)** In the nonenzymatic reaction, the anionic conjugate base of the peroxy acid adds as a nucleophile to the electrophilic carbonyl carbon of the acetylcyclopentane. The resulting dialkyl peroxide cleaves heterolytically at the oxygen–oxygen bond, coincident with the migration of the cyclopentyl group of the acetylcyclopentane to the adjacent oxygen. The migrating carbon of the cyclopentyl group is pushed by a lone pair of electrons on the oxygen of the hydroxy group. The migration of the carbon is coincident with the intramolecular transfer of the hydron on the hydroxy group to the acyl oxygen of the peroxy acid. The transfer of the hydron makes the benzoic acid a better leaving group and increases the push of the lone pair of electrons on the hydroxy group. The products of the rearrangement are cyclopentyl acetate and benzoic acid.

has been adopted by monooxygenases that hydroxylate other substrates and by the enzymes that catalyze Baeyer–Villiger oxidations, the flavin is reduced by NADPH in the absence of the nominal reactant, and after reduction of the flavin, the $NADP^+$ remains bound. The reduced flavin reacts with molecular oxygen to form the 4a-hydroperoxyflavin, which is quite stable as long as the $NADP^+$ remains bound. If the flavin is reduced with NADH or dithionite, no 4a-hydroperoxyflavin is observed. The 4a-hydroperoxyflavin lurks on the enzyme until an unsuspecting nominal reactant is bound and becomes oxygenated. If no reactant is bound, hydrogen peroxide is slowly formed and the reduction is wasted. Thus, inhibition of the production of hydrogen peroxide can occur either at the reduction step or at the step in which the nominal reactant is oxidized.

4a-Hydroperoxides of isoalloxazines in solution are as active as peroxycarboxylic acids [–C(O)OOH],[1335] which are routinely used as oxidants for Baeyer–Villiger oxidations (Figure 2–47B), for the monooxygenations of alkenes to epoxides, and for the oxidation of amines and sulfides to amine *N*-oxides and sulfoxides, respectively.[1336,1337] The oxygenated flavin in the active site of cyclohexanone monooxygenase from *Acinetobacter* has been shown to participate in a series of monooxygenations characteristic of a peroxy acid[1319] as well as the oxidation of sulfides to sulfoxides,[1338] a reaction that is also characteristic of a 4a-hydroperoxyisoalloxazine. It has been shown that the oxygenating species in the active site for all the various reactions catalyzed by cyclohexanone monooxygenase is the 4a-peroxyflavin itself (**2–92** in Figure 2–47A),[1339] or 4a-hydroperoxyflavin, its conjugate acid. These observations suggest that the enzymatic

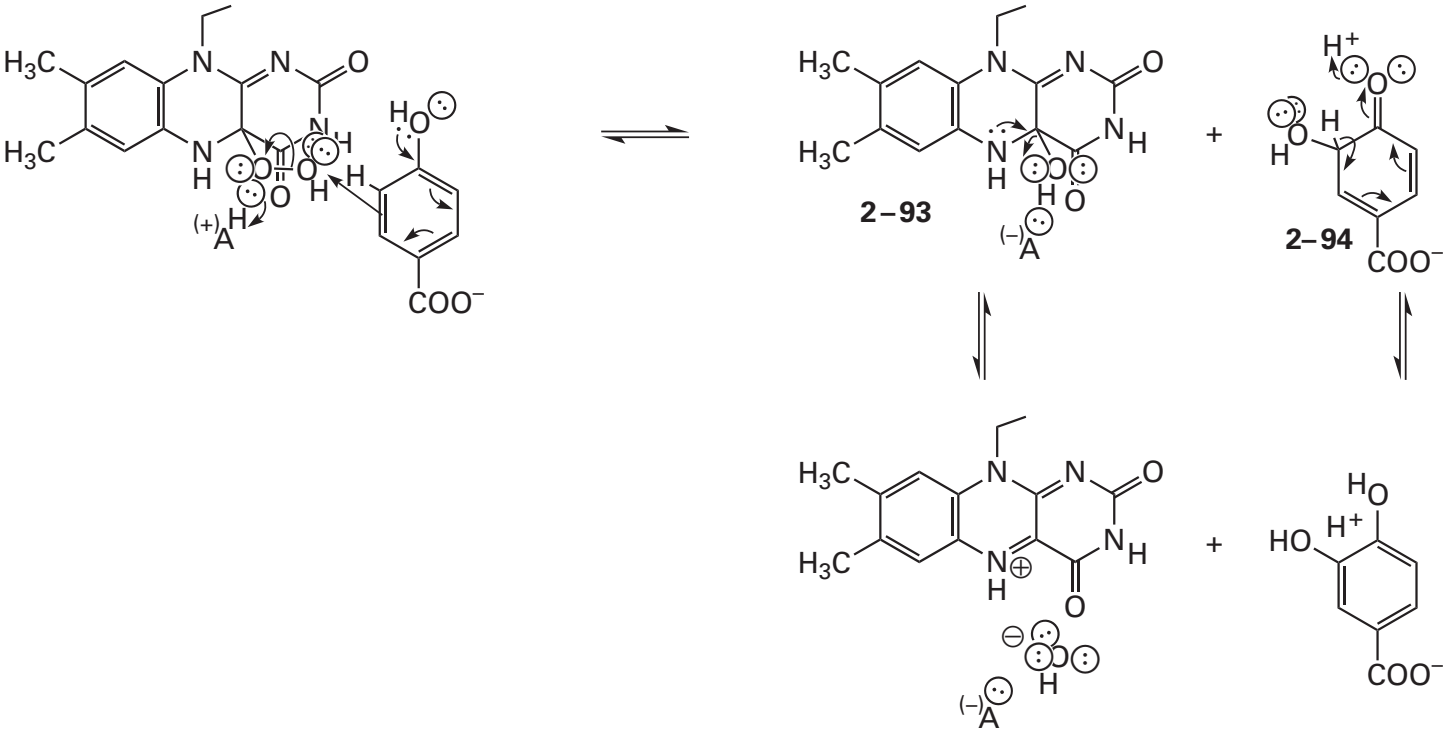

Figure 2–48: Mechanism for the hydroxylation of 4-hydroxybenzoate by 4a-hydroperoxyflavin in the reaction catalyzed by the flavoenzyme 4-hydroxybenzoate 3-monooxygenase (Equation 2–212). The electrophilic hydroperoxy group of the 4a-hydroperoxyflavin, formed by the reaction of molecular oxygen with reduced flavin, is attacked by a pair of the nucleophilic π electrons in the aromatic π molecular orbital system of the 4-hydroxyphenyl group of the 4-hydroxybenzoate at the same time that a catalytic acid hydronates the proximal oxygen of the hydroperoxy group to increase its electrophilicity. The resulting 4a-hydroxyflavin **2–93**, a hemiaminal, dehydrates to oxidized flavin. A hydrogen on the carbon adjacent to the 6-hydroxycyclohexa-2,4-dienone (**2–94**), which is the other product of the first step, dissociates as a hydron to restore the aromaticity of the phenyl group.

monooxygenations in which 4a-hydroperoxy-flavins and 4a-peroxyflavins are the oxidants have mechanisms similar to those for the oxidations performed by peroxycarboxylic acids and peroxycarboxylates.

The 4a-peroxyflavin in the active site of cyclohexanone monooxygenase is likely formed by the **colligation of the neutral flavin semiquinone and superoxide radical anion**, which in turn are formed by direct transfer of an electron from reduced flavin anion $H_2Fl_{red}^-$ (Figure 2–9) to molecular oxygen (Equation 2–217).[1339] In the enzymatic monooxygenations performed by melilotate 3-monooxygenase (Equation 2–211), 4-hydroxybenzoate 3-monooxygenase (Equation 2–212),[1340] or 6-hydroxynicotinate 3-monooxygenase (Equation 2–214), the 4a-hydroperoxyflavin performing the hydroxylation is also probably formed by this colligation of the flavin semiquinone and the superoxide radical anion, followed by a hydronation of the distal oxygen of the resulting 4a-peroxyflavin. This conclusion follows from the fact that hydrogen peroxide in solution cannot produce a 4a-hydroperoxyflavin from the flavin in the active sites of these former enzymes, so it is probably not hydroperoxy ion, HO_2^-, the conjugate base of hydrogen peroxide formed from molecular oxygen by two successive one-electron transfers from reduced flavin (Equations 2–207 and 2–208), that adds nucleophilically to oxidized flavin (Equation 2–216).

Melilotate 3-monooxygenase, 4-hydroxybenzoate 3-monooxygenase, and 6-hydroxynicotinate 3-monooxygenase catalyze the **hydroxylation of an aromatic ring**.[1327,1341,1342] The distal hydroxy group of the 4a-hydroperoxyflavin (**2–91**) is transferred to the aromatic ring, ortho or para to a hydroxy group or an amino group on that ring (Figure 2–48). An intermediate has been observed in transfer of the hydroxy group to various phenols by 4-hydroxybenzoate 3-monooxygenase from *P. fluorescens*[1318,1343,1344] and phenol 2-monooxygenase (NADPH) from *S. cerevisiae*[1345] that has an absorption spectrum similar

to the sum of the spectrum of enzyme-bound 4a-hydroxyflavin (Figure 2–46) and the spectrum of cyclic pentadienyl radical **2–95** of the respective aromatic ring.[1346,1347]

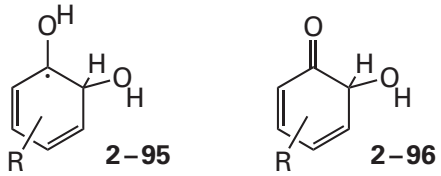

Consequently, it is possible that a cyclic pentadienyl radical is an intermediate in the formation of the usual cyclic pentadienyl cation in an electrophilic aromatic substitution. Because, however, no evidence for unpaired electrons in this spectral intermediate has been obtained,[1344] it seems more likely that the derivative of the aromatic reactant in this intermediate is actually the respective 2-hydroxycyclohexa-3,5-dieneone **2–96**.

The effects of electron-withdrawing groups in the 4-hydroxybenzoate on the rate of 4-hydroxybenzoate 3-monooxygenase,[1348] as well as the effects of electron-donating and electron-withdrawing substituents on the flavin,[1340] are most consistent with an **electrophilic aromatic substitution** in which the π molecular orbital system of the aromatic ring, as a nucleophile, attacks the distal oxygen of the 4a-hydroperoxyflavin, the electrophile, with the anionic conjugate base of the 4a-hemiaminal of the flavin, probably being hydronated in concert, as the leaving group (Figure 2–48).[1349] Certainly the facts that 4-hydroxybenzoate 3-monooxygenase and 6-hydroxynicotinate 3-monooxygenase are related to each other[1350] and that the former replaces a hydrogen with a hydroxy group while the latter replaces a carboxy group with a hydroxy group are consistent with a mechanism in which the hydrogen on carbon 3 of 4-hydroxybenzoate leaves as a hydron, as it would in an electrophilic aromatic substitution. There are also results from kinetic isotopic effects that are consistent with the conclusion that 6-hydroxynicotinate 3-monooxygenase from *Bordetella bronchiseptica* catalyzes the hydroxylation through an electrophilic aromatic substitution.[1320] In the crystallographic molecular model of 4-hydroxyphenylacetate 3-monooxygenase from *A. baumannii*, the imidazolyl group of a histidine is positioned to hydronate the proximal oxygen of the 4a-hydroperoxyflavin to improve its ability as a leaving group,[1342] and there is a molecule of water located in the active site of 4-hydroxybenzoate 3-monooxygenase (Equation 2–212) that can perform the same function.[1351]

That the conjugate base (**2–94**) of the usual cyclic pentadienyl cation in an electrophilic aromatic substitution is an intermediate in the reactions of these monooxygenases is demonstrated by a 1,2 sigmatropic rearrangement that is observed in some of them. When the hydroxy group is being added para to an electron-donating substituent, such as a hydroxy, alkyl, or amino group on the reactant, as in anthraniloyl-CoA monooxygenase

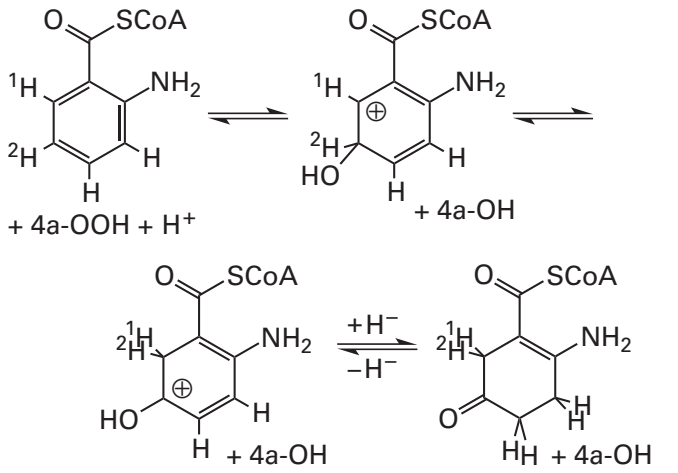

(2–218)

a deuterium located on the reactant at the site of the hydroxylation is found to migrate to the adjacent carbon.[1341] Such a 1,2-hydride migration is evidence for a carbocationic intermediate[1352] in an electrophilic aromatic substitution.

In these hydroxylations, the nucleophilic aromatic ring adds the distal hydroxy group of the **electrophilic 4a-hydroperoxyflavin**. In the active site of premalbrancheamide halogenase from *Malbranchea aurantiaca*, the distal hydroxy group of the prosthetic 4a-hydroperoxyflavin also acts as an electrophile that participates in a concerted nucleophilic substitution with a chloride as the nucleophile and the 4a-hydroxyflavin as the leaving group to produce hypochlorite (OCl^-). The hypochlorite chlorinates the 5-amino group of Lysine 108 to produce a chloramine that performs the actual halogenation of the anilino group in premalbrancheamide.[1353]

The **nucleophilic 4a-peroxyflavin** formed in the initial step in the enzymatic reaction of cyclohexanone monooxygenase (Equation 2–213) performs a **Baeyer–Villiger oxidation**. A nonenzymatic example of a Baeyer–Villiger oxidation[1354] in which the oxidant is a peroxycarboxylic acid would be

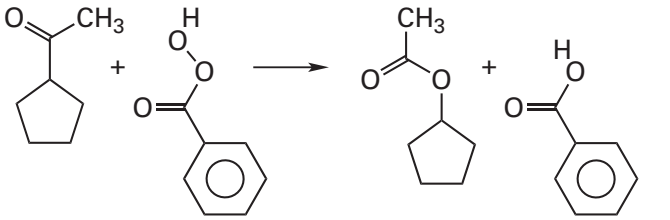

(2–219)

The step following the formation of the 4a-peroxyflavin in the active site of cyclohexanone monooxygenase (Figure 2–47A), by analogy with a Baeyer–Villiger reaction in solution (Figure 2–47B), is proposed to be the nucleophilic addition of the anionic oxygen in the 4a-peroxy group to the carbonyl of the cyclohexanone. In the crystallographic molecular model of the active site of cyclohexane monooxygenase from *Rhodococcus* occupied by $NADP^+$ and cyclohexanone, in which the flavin is in the oxidized state but not the 4a-peroxyflavin, the carbonyl carbon of the cyclohexanone is 0.39 nm from carbon 4a of the flavin, an appropriate distance for the two oxygens of a 4a-peroxy group to span.[1355]

The accepted mechanism for the Baeyer–Villiger oxidation performed in solution by a peroxy acid relies on the ability of the acyl oxygen of the peroxy acid to be **intramolecularly hydronated** and the resulting incipient carboxylic acid to function as the leaving group in a **1,2-alkyl migration**. The 4a-peroxy group of the 4a-peroxyflavin resides on a fully saturated carbon, but the proximal oxygen of the peroxy group could be hydronated by the hydoxy group of the hemiketal in a similar way to improve the ability of the **4a-hydroxyflavin (2–93)** as a leaving group (Figure 2–47A). In at least one Baeyer–Villiger monooxygenase,[1356] the guanidinio group of an arginine is stacked upon the π molecular orbital system of the flavin and its δ nitrogen could also act as the donor for a hydrogen bond to the proximal oxygen of the 4a-peroxyflavin, improving its ability to leave as a 4a-hydroxy group. The ring expansion concerted with the leaving of the 4a-hydroxyflavin results from a 1,2-alkyl migration.

In the Baeyer–Villiger oxidations, prosthetic 4a-peroxyflavin is formed by electron transfer from reduced flavin anion to molecular oxygen (Equation 2–207) followed by the colligation of the two radicals (Equation 2–215). The distal oxyanion of 4a-peroxyflavin then participates as a nucleophile that adds to the carbonyl group in the reactant (Figure 2–47A). Carbon 4 of uracil is an acyl carbon in an *N*-[(alkylamino)carbonyl]amide, and it also participates in nucleophilic substitutions. In the apparent hydrolysis of this amide catalyzed by pyrimidine oxygenase

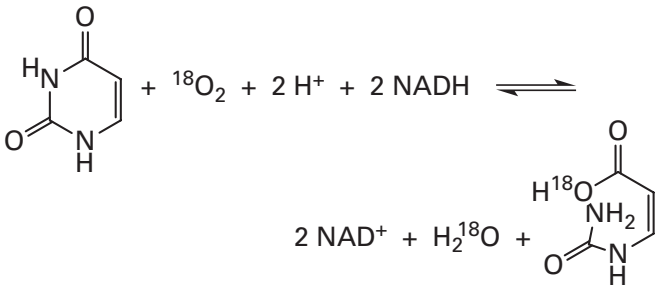

(2–220)

from *E. coli*, in which the *N*-acylurea is substituted by a hydroxy group, it has been concluded that rather than a hydroxide, which would usually be the reactant in a hydrolysis, the distal oxyanion of the 4a-peroxyflavin formed from molecular oxygen and the prosthetic flavin in the active site adds as a nucleophile to acyl carbon 4 in the first step in a nucleophilic substitution because one of the oxygens from oxygen-18 in enriched molecular oxygen ends up as one of the oxygens in the carboxy group of the product.[1357] The peroxy acid that results from this nucleophilic substitution by the hydroperoxy group then oxidizes the flavin to form an *N*-oxide on nitrogen 5 and the carboxylic acid that is the product of the enzymatic reaction (Equation 2–220). This flavin N^5-oxide has been isolated from an enzymatic reaction.[1358] The *N*-oxide is then reduced back to the reduced flavin by two successive hydride transfers from two NADH.

In the hydroxylation of nucleophilic aryl groups, a 4a-hydroperoxyflavin acts as an electrophile at the distal oxygen, but in the Baeyer–Villiger monooxygenations and the monooxygenation performed by pyrimidine oxygenase, a 4a-peroxyflavin acts as a nucleophile, also at the distal oxygen. The **only difference is a hydronation**. The hydronation of the distal oxygen is required to produce the electrophile, just as a hydronation of a carbonyl group significantly increases the electrophilicity of the carbonyl carbon, and the dehydronation of the distal oxygen is required to produce the nucleophile, just as the dehydronation of a molecule of water significantly increases the nucleophilicity of its oxygen. The identity of the other reactant, however, be it a nucleophile or an electrophile, respectively, dictates the course of the reaction, not the hydronation.

At the completion of either the hydroxylation of an aromatic ring (Figure 2–48) or a Baeyer–Villiger monooxygenation (Figure 2–47A), the other

oxygen atom of molecular oxygen remains at the 4a-position of the flavin on a carbonyl carbon, presumably as a hydroxy group. The resulting 4a-hydroxyflavin, a hemiaminal (Figures 2–47 and 2–48), loses hydroxide to the solution in a reaction that is the reverse of the addition of hydroxide to oxidized flavin

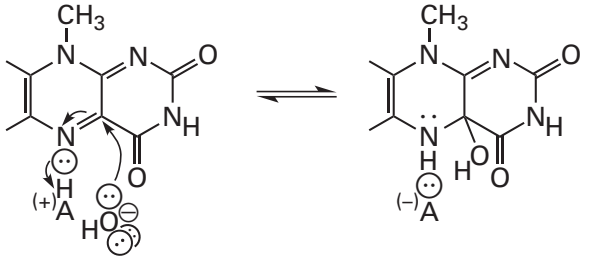

(2–221)

Menaquinones and phylloquinones are both 2-alkyl-3-methyl-1,4-naphthoquinones

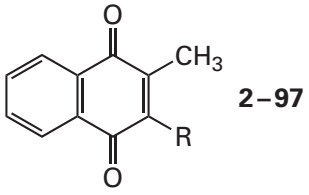

2–97

and 2-alkyl-3-methyl-1,4-naphthoquinones are vitamins K. Vitamins K are a group of coenzymes that differ only in their isoprenoid 2-alkyl groups, which are irrelevant to their function, and they are **used interchangeably and indistinguishably** in their enzymatically catalyzed reactions with molecular oxygen.

An enzyme that catalyzes the reaction of a vitamin K with molecular oxygen is peptidyl-glutamate 4-carboxylase. In the active site, molecular oxygen is combined with the reduced quinol of a vitamin K to produce a base ($:B^{(-)}$) strong enough to **remove a hydron from carbon 4 of a glutamate** in one of several proteins so that the resulting enolate can be carboxylated[1359]

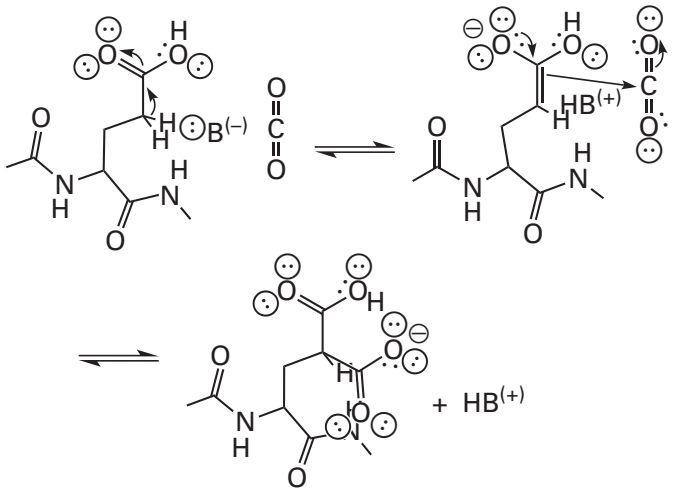

(2–222)

in a posttranslational modification of the respective protein. Coincident with the **carboxylation**, which does not incorporate either oxygen of molecular oxygen into the γ-carboxyglutamate, the quinol of vitamin K is monooxygenated by one of the two atoms of molecular oxygen to form its 2,3-epoxyquinone[1360]

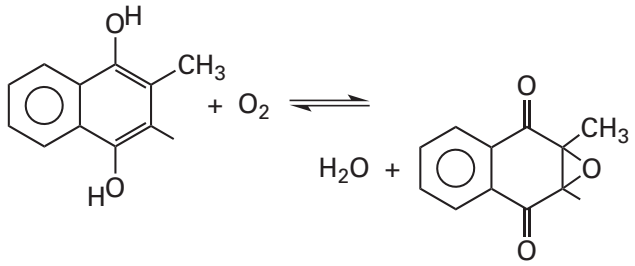

(2–223)

During this epoxidation of vitamin K, the necessary base is formed.[147]

When there is sufficient carbon dioxide present, one mole of the epoxide of vitamin K is produced for every mole of glutamic acid carboxylated.[1361] When there is insufficient carbon dioxide present, the enolate formed by the base eventually picks up a hydron from the solution to regenerate the glutamate,[1359] and the ratio of epoxide to peptidyl-4-carboxyglutamate increases accordingly. Both the carboxylation (Equation 2–222) and the epoxidation (Equation 2–223) are performed by peptidyl-glutamate 4-carboxylase.[1362] The 2,3-epoxide of vitamin K is reduced back to the quinol by a different enzyme or pair of enzymes to be used again.

There is a nonenzymatic, intramolecular Claisen condensation that is a **model for the enzymatic reaction**

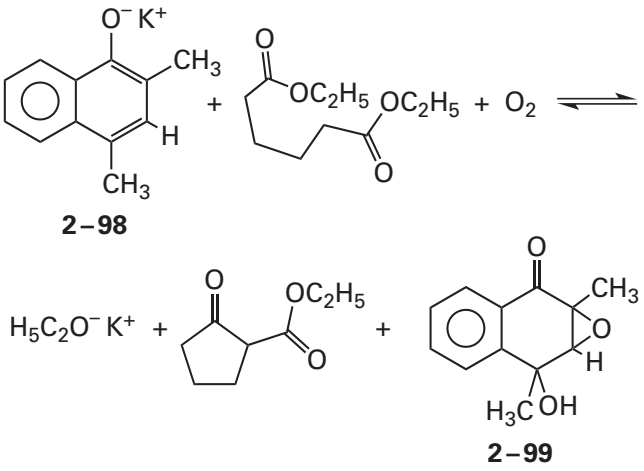

(2–224)

Under the conditions of the reaction, the initial 2,4-dimethyl-1-naphtholate **2–98** is too weak a base ($pK_a \cong 10$) to remove a hydron α to one of the esters in the diethyl 1,6-hexanedioate to form the required enolate, but it combines with molecular oxygen to produce a base that is strong enough to do so.[1363]

There are several other observations that provide an explanation for the mechanism of this reaction. The conjugate acid of naphtholate **2–98**, 2,4-dimethyl-1-naphthol, reacts with molecular oxygen in chloroform to give the stable 4-hydroperoxide (**2–100**)[1364]

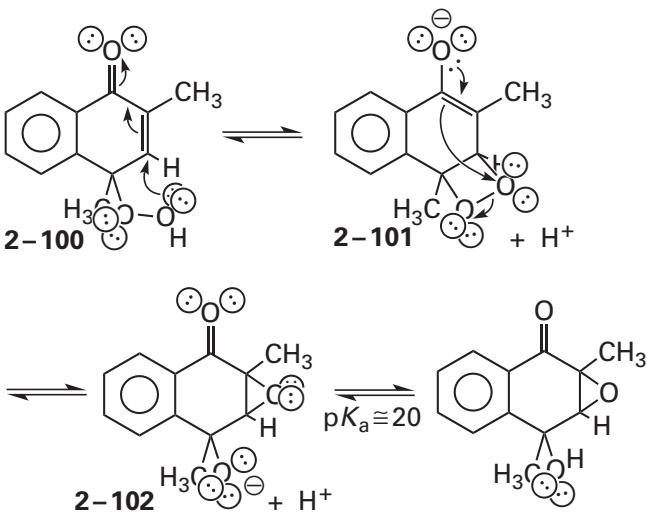

(2–225)

In aqueous solution, the 4-hydroperoxide **2–100** turns into tertiary alcohol **2–99**, the product in the model reaction (Equation 2–224), in an intramolecular rearrangement.[1365] Both this rearrangement and the model reaction itself produce the two diastereoisomers of **2–99**, in each of which the oxygen of the epoxide is cis to the oxygen of the tertiary alcohol. It is proposed that an intermediate **dioxetane** (**2–101**) explains the cis stereochemistry of the product.[1364] When molecular oxygen reacts with the 2,4-dimethyl-1-naphtholate **2–98** to produce the tertiary alkoxide **2–102**, the standard enthalpy change of the reaction[1366] is around –200 kJ mol^{-1}, an observation demonstrating that there is more than enough energy released in the oxidation to convert a weak base, the naphtholate, into a strong base, the tertiary alkoxide ($pK_a \cong 20$),[1366] which is strong enough to produce the enolate responsible for the intramolecular condensation (Equation 2–224).

All these observations suggest a particular **mechanism for the enzymatic formation of a strong base** from the quinol of a vitamin K and molecular oxygen (Figure 2–49).[1367] As with the reaction of flavin with molecular oxygen, transfer of an electron from the quinol of vitamin K to oxygen under catalysis by a general base[1368] separates the electrons of the triplet state of molecular oxygen and permits rapid spin inversion. The two radicals then combine to form the 4-peroxynaphthoquinone, which converts to the anionic conjugate base of a 4-hydroxy group in the 2,3-epoxynaphthoquinone **2–103** through intermediate dioxetane **2–101**. The alkoxide ion **2–103** is not so strong a base as the tertiary alkoxide **2–102** because the electron-withdrawing hydroxy group in place of the electron-donating methyl group should lower the pK_a of its conjugate acid by about three or four units, but hydronation of the alkoxide by the hydron on carbon 4 of the glutamate can be concerted with dehydration of the hydrate of the 2,3-epoxynaphthoquinone, which is a significantly favorable reaction (Table 1–2).

When carboxylation of a glutamate by vitamin K is performed with $^{18}O_2$, about 15% of the 4-oxo group of the 2,3-epoxide of the vitamin K that is the product of the reaction[1369-1372] ends up as oxygen-18. This observation supports the mechanism (Figure 2–49) because it indicates that one of the oxygens of the molecular oxygen was attached at some point to carbon 4 of the vitamin K. It also indicates that dehydration of the hydrate is not completely stereospecific. When [4-^{3}H]-L-glutamate is used as a reactant, the enzyme exchanges the tritium at the *pro-S* position[1373] with a protium from the solution

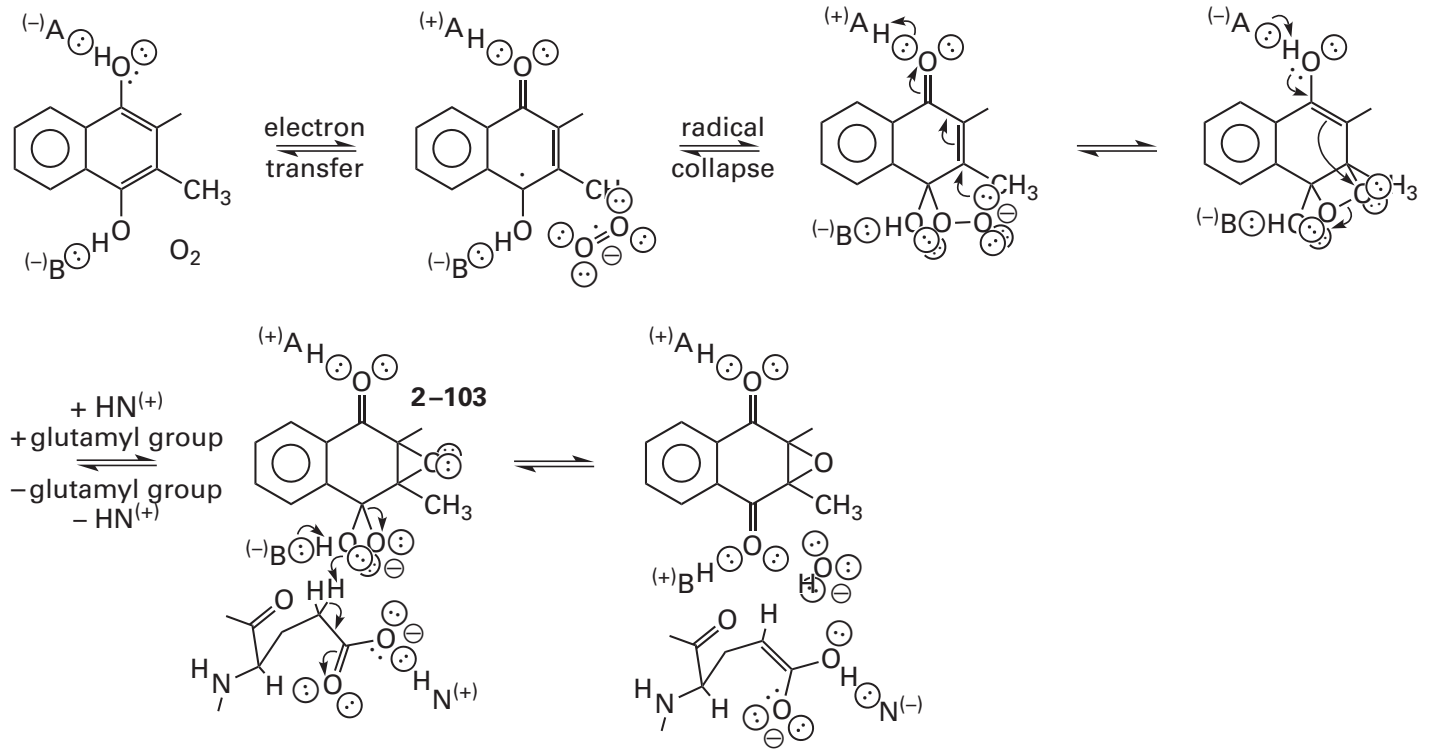

Figure 2–49: Mechanism for the formation of a glutamyl enolate by molecular oxygen and a vitamin K. Transfer of an electron from the vitamin K to molecular oxygen produces superoxide radical anion and the radical cation of the vitamin K, from the now oxo oxygen of which a hydron dissociates to produce the neutral radical. The separation of the unpaired electrons onto two molecules permits spin inversion to occur rapidly. Radical collapse forms a bond between the superoxide radical anion and the vitamin K radical, to form an adduct in which the superoxide has become a peroxy group. The anionic distal oxygen of the peroxy group participates as a nucleophile in an intramolecular conjugate addition to the *α,β*-unsaturated ketone to produce a dioxetane. The resulting enolate of the vitamin K adds nucleophilically and intramolecularly to the adjacent electrophilic oxygen of the dioxetane to produce the epoxide of the vitamin K. During the addition, the other oxygen is the leaving group from the dioxetane and becomes the oxyanion. This newly formed oxyanion removes the hydron from carbon 4 of the glutamatic acid to form its enolate. If, as is drawn, it uses the hydron that was on carbon 4 of the glutamatic acid as the acid required during its ejection as a hydroxide from the hydrate of the ketone, the free energy of the dehydration of the ketone is coupled to the removal of the hydron, a strategy that would increase its basicity even further.

2.5 times more rapidly than it catalyzes the carboxylation of the glutamate.[1374] Consequently, the hydroxide (Figure 2–49) bearing tritium must exchange with hydroxide ions in solution, which each bear a protium, rapidly and reversibly, a process that will also dilute the ^{18}O in the 4-hydrate of the 2,3-epoxide of the vitamin K. This consideration suggests that the dehydration of the hydrate is even less stereospecific than it seems to be. It is difficult to reconcile the high stereospecificity of the hydron abstraction with the low stereospecificity of the dehydration.

Aside from enzymes using flavin and vitamin K as prosthetic groups and coenzymes, almost all[1375-1377] of the enzymes that use molecular oxygen, molecular nitrogen, molecular hydrogen, superoxide radical anion, hydrogen peroxide, oxides of nitrogen, oxides of sulfur, and carbon monoxide as substrates have transition metals such as iron, copper, nickel, manganese, and molybdenum as prosthetic cations.* With the exception of peroxidases, the reactions catalyzed by these enzymes are oxidation–reductions that proceed by inner-sphere electron transfers during which the respective substrates occupy an open, exchangeable coordination site on the transition metallic ion.

*There is an oxidase in *Streptomyces wadayamensis* of unknown mechanism that uses only a prosthetic pyridoxal phosphate to catalyze a four-electron oxidation of L-arginine to 2-oxo-4(*S*)-hydroxy-5-guanidinovalerate and that uses two molecules of molecular oxygen only as general oxidants to accept the four electrons.[1378]

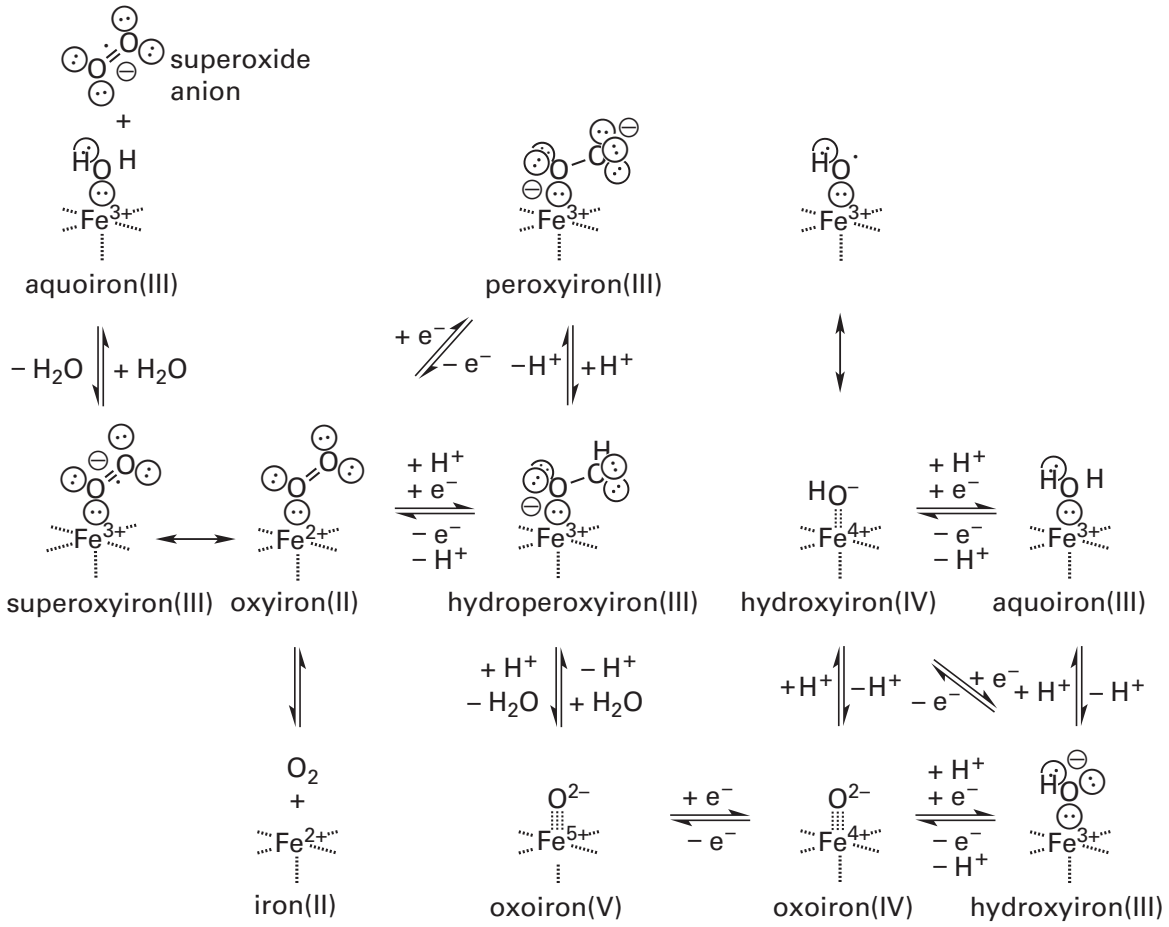

Figure 2–50: Complexes formed between iron ions and the different oxidation states of oxygen. Superoxide radical anion combines with Fe^{3+} (top) or molecular oxygen combines with Fe^{2+} (bottom) to produce the same complex, oxyiron(II), which stereochemically resembles a superoxide radical anion on Fe^{3+} but has the oxygen–oxygen bond length of molecular oxygen. The addition of a hydron and an electron to this complex produces hydroperoxyiron(III), identical to the complex resulting from the addition of hydroperoxide ion, the conjugate base of hydrogen peroxide, to Fe^{3+}. Hydroperoxyiron(III) is the conjugate acid of peroxyiron(III). The addition of a hydron to the distal oxygen in hydroperoxyiron(III) and the heterolytic loss of water produces oxoiron(V), which, if it is in a porphyrin, abstracts an electron from the aromatic π molecular orbital system of the porphyrin coincident with its formation to produce oxoiron(IV) porphyrin radical. The addition of an electron to oxoiron(V) produces oxoiron(IV). The hydronation of oxoiron(IV) produces hydroxyiron(IV), which is a resonance hybrid of hydroxide ion, OH^-, on Fe^{4+} and hydroxyl radical, ·OH, on Fe^{3+}. The addition of an electron to hydroxyiron(IV) produces hydroxyiron(III), the complex between hydroxide and Fe^{3+}, which is the conjugate base of aquoiron(III), the complex between water and Fe^{3+}.

One of the simplest examples of such a prosthetic metallic ion participating in such an **inner-sphere transfer of an electron** is the iron ion in superoxide reductase from *Pyrococcus furiosus*. In its ferric form, the Fe^{3+} is octahedrally coordinated, strongly by the imidazolyl groups of four histidines and the sulfido group of a cysteine and loosely by the carboxylate of a glutamate.[1379] In its ferrous form, the carboxylato group of the glutamate dissociates from the iron in response to the decrease in charge number of the iron ion, and a superoxide radical anion associates in a encounter-controlled second-order reaction at the open site on the Fe^{2+} made available by the dissociation. During the association of the superoxide radical anion, a hydron is transferred (Equation 2–199) to it, coincident with transfer of an electron from the Fe^{2+} to the superoxide in the inner sphere, to produce hydroperoxyiron(III), the equivalent of a complex between hydroperoxide (HO_2^-) and Fe^{3+} (Figure 2–50). After the rate-limiting transfer of a hydron to the hydroperoxide ion (Equation 2–202), the resulting hydrogen peroxide dissociates[1380] from the Fe^{3+}. With its open site again occupied by the carboxylato group of the glutamate, the Fe^{3+} is reduced by rubredoxin in the outer sphere back to Fe^{2+}, and the carboxylate

dissociates. The Fe^{2+} in a synthetic complex with 1,4,8,11-tetramethyl-1,4,8,11-tetraazacyclotetradecane, to which a sulfanyl group has been appended so that it can act as one of the axial ligands to the iron, is able to reduce superoxide radical anion catalytically at the other axial location when it is supplied with a reductant able to supply electrons one at a time to the iron.[1381]

Superoxide dismutase catalyzes a reaction

$$2\,H^+ + O_2^{\cdot -} + O_2^{\cdot -} \rightleftharpoons O_2 + H_2O_2 \qquad (2\text{–}226)$$

in which superoxide radical anion is also a substrate. As in the case of superoxide reductase, an electron is again transferred in the inner sphere from a reduced prosthetic transition metallic ion to a bound superoxide radical anion (Equation 2–198), coincident with the necessary hydron transfers. After dissociation of the resulting hydrogen peroxide and association of a second superoxide radical anion with the now-oxidized transition metallic ion, the metallic ion is reduced by one electron transferred in the inner sphere from that superoxide radical anion, which becomes molecular oxygen (Equation 2–197).

In the different species of superoxide dismutase, different prosthetic metallic ions are used. Although the superoxide dismutases do not run the gamut of transition metallic ions, they come close. Depending on the species of superoxide dismutase, the prosthetic transition metallic ion is either a **copper ion**,[1382] which alternates between Cu^+ and Cu^{2+}; a **nickel ion**,[1383] which alternates between Ni^{2+} and Ni^{3+}; a **manganese ion**,[1384] which alternates between Mn^{2+} and Mn^{3+}; or an **iron ion**,[1385] which alternates between Fe^{2+} and Fe^{3+}. One superoxide dismutase may be closely related to another yet have a different prosthetic ion. For example, superoxide dismutase from *M. tuberculosis* is closely related to superoxide dismutase from *Mycobacterium leprae* (80 percent identity, 0 gap percent), but the former has an iron ion in its active site and the latter has a manganese ion.[1386] The superoxide dismutases containing a prosthetic nickel ion[1387] or a prosthetic copper ion,[1388] however, are unrelated to those that have an iron ion or a manganese ion.

The **coordinations of the metallic ions differ significantly** among the superoxide dismutases. Superoxide dismutases containing a prosthetic nickel ion coordinate the ion with the α-amino group of the protein, the amido nitrogen of a peptide bond, the sulfido groups of two cysteines, and the imidazolyl group of a histidine.[1387] Superoxide dismutases containing an iron ion and those containing a manganese ion coordinate the ion with the same side chains, the imidazolyl groups of three histidines and the carboxylato group of an aspartate, in the homologous positions in the sequences of amino acids.[1389-1394] The ligands around the manganese ion in the superoxide dismutase from *E. coli* are arranged octahedrally. The ligand position opposite one of the imidazolyl groups is occupied by a molecule of water, but the position opposite the single carboxylato group can be either vacant or occupied by a molecule of water. When a hydroperoxide associates with Mn^{3+}, it binds side-on and occupies the two positions occupied by molecules of water.[1395]

In the active site of a superoxide dismutase that contains a single mononuclear copper ion, the copper ion is coordinated in the reduced state by three imidazolyl groups from three histidines in an almost planar, trigonal array.[1396] In the reduced cuprous state of bovine superoxide dismutase, there are only these three ligands to the copper ion,[1397-1400] but there is a fourth imidazolyl group from another histidine nearby. This imidazolyl group is a ligand to a Zn^{2+} at its π nitrogen. In the reduced state, its τ nitrogen is 0.34 nm from the copper ion and therefore not a ligand.[1401] In the oxidized, cupric state of bovine superoxide dismutase, however, this **zinc-imidazolyl group**, in response to the change in charge number, has swung over and become a fourth ligand to the copper ion at its τ nitrogen, while the other three imidazolyl groups remain in the trigonal plane.[1388,1402]

The standard reduction potentials of aquo d^4 Mn^{3+} ($E^{\circ\prime}$ = +1510 mV) and aquo d^5 Fe^{3+} ($E^{\circ\prime}$ = +770 mV) are quite large, making them strong oxidants. Both the superoxide dismutases containing a prosthetic iron ion and the related superoxide dismutases containing a manganese ion have evolved to lower the **biochemical standard reduction potential of the respective metallic ion** into the range of −100 to +300 mV,[1403,1404] which is appropriate for the dismutation, being between the biochemical standard reduction potential of the redox couple of oxygen and the superoxide radical anion (–330 mV), the superoxide of which will reduce the oxidized metallic ion to form molecular oxygen, and the redox couple of superoxide radical anion and hydrogen peroxide (+940 mV), the superoxide radical anion of which will oxidize the reduced metallic ion to form hydrogen peroxide. When the correct metallic

ion, Fe^{2+} or Mn^{2+}, is replaced by the incorrect metallic ion, Mn^{2+} or Fe^{2+}, respectively, the respective environment still performs the same net shift in biochemical standard reduction potential, which brings the biochemical standard reduction potential for the wrong transition metallic ion to the wrong value, either too high or too low, respectively, to perform the dismutation.[1404] In contradistinction to this evolution of the protein to accommodate the properties of the metallic ions, there is a protein that binds either an iron ion or a nickel ion, and the respective metalloenzymes that result perform different oxygenations of the same reactant.[1405] The biochemical standard reduction potential of bovine superoxide dismutase containing a prosthetic copper ion is +120 mV,[1403] again appropriate to the task at hand.

A **detailed mechanism** has been presented for superoxide dismutases, such as those from *Bos taurus* and *S. cerevisiae*, containing a prosthetic copper ion in their active sites. A neutral, hydronated superoxide radical anion associates with Cu^{2+} at the axial coordination site and displaces the zinc-imidazolyl group. During this displacement, the τ nitrogen of the imidazolyl group removes the hydron from the hydrosuperoxide radical.[1406] Upon coordination, an inner-sphere transfer of an electron occurs instantaneously between the resulting superoxide radical anion and the Cu^{2+}, and the resulting molecule of molecular oxygen dissociates.[1407] A neutral hydrosuperoxide radical, which is a hydroperoxy radical (Equation 2–199), associates with the trigonally coordinated Cu^{+} at the open axial site. After the instantaneous inner-sphere transfer of an electron to the peroxy group, a hydroperoxy ion[1408] is sitting on a Cu^{2+}. The hydroperoxy ion is hydronated on its proximal oxygen by the adjacent zinc-imidazolium.[1406] The resulting unhydronated zinc-imidazolyl group recoordinates with the Cu^{2+} replacing the hydrogen peroxide and completing the catalytic cycle.

There is a manganese superoxide dismutase, with a manganese ion coordinated by the same ligands as those used by the enzymes in the family of iron and manganese superoxide dismutases,[1409] that can catalyze the reaction of oxalate oxidase

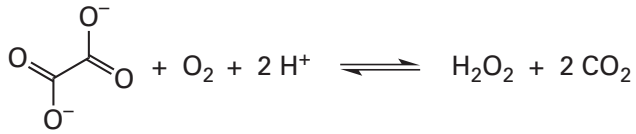

(2–227)

as well as the usual dismutation of superoxide radical anion. The oxidized Mn^{3+} form of the enzyme removes an electron from oxalate dianion, rather than from superoxide radical anion, and the resulting radical anion of oxalate decarboxylates almost immediately, as do most if not all radicals at the oxygens of carboxylic acids, to produce the first molecule of CO_2. The remains of the decarboxylation—a radical anion of carbon dioxide, a strong reductant, that is bound tightly by the now Mn^{2+}—reduces molecular oxygen to superoxide radical anion and becomes the second molecule of CO_2, which can no longer be a ligand to the Mn^{2+} and dissociates to be replaced as a ligand by the superoxide radical anion. The superoxide radical anion is reduced as usual to hydrogen peroxide by the Mn^{2+}, regenerating the Mn^{3+}.[1405]

There are a number of enzymatic reactions in which hydrogen peroxide is a substrate and a heme is the prosthetic group and in which the hydrogen peroxide oxidizes the iron in the heme to a high-valent state. The enzymes with hemes as prosthetic groups that have hydrogen peroxide as a substrate are hemoperoxidases.

There are synthetic examples of high-valent **oxoiron(IV)** (Figure 2–50).[1410-1414] One is the oxoiron(IV)

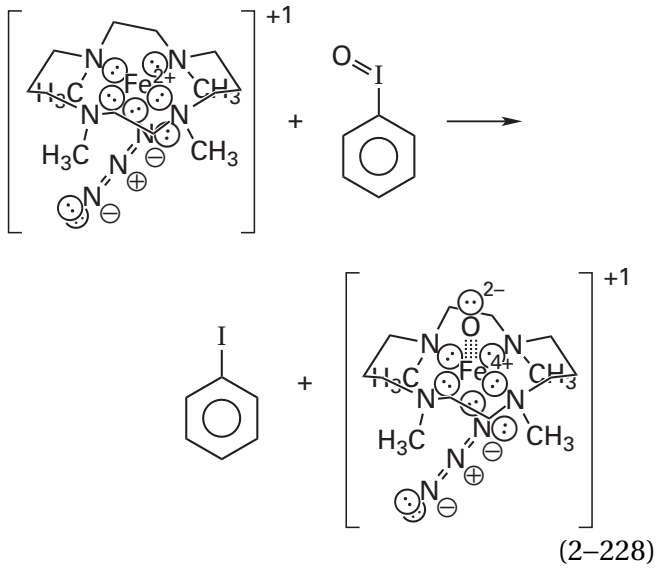

(2–228)

that is the product of two-electron oxidation of a pentacoordinated Fe^{2+} by iodosylbenzene.[1411] The neutral tertiary amino nitrogens in the cyclic tetraamine coordinating the iron ion in Equation 2–228 are basic and contribute sufficient electron density to the iron ion to permit it to achieve the +4 oxidation state. In the product of the oxidation, the formal oxidation state of the iron is +4 and that of the oxygen

from the iodosylbenzene that has become an axial ligand is –2. Similar oxoirons(IV) in cyclic tetraamines can be produced by using hydrogen peroxide[1410] or molecular oxygen itself[1414] as the oxidants.

A more extreme example of high-valent iron is the **oxoiron(V)** (Figure 2–50)[1415,1416]

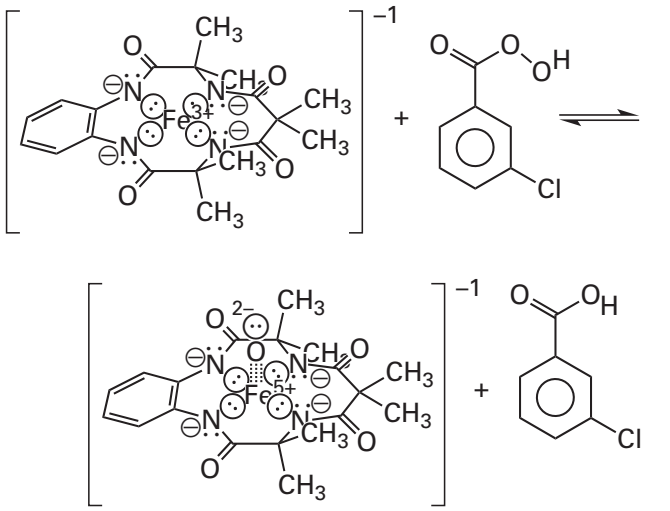

(2–229)

that is the product of oxidation of a coordinated Fe^{3+} by *m*-chloroperoxybenzoic acid. In the product of the oxidation, the formal oxidation state of the iron is +5 and that of the oxygen is –2

$$\underset{(5e^-)}{Fe^{3+}} + \underset{(14e^-)}{ROOH} \longrightarrow \underset{(3e^-)}{Fe^{+5}}=\underset{(8e^-)}{O^{-2}} + \underset{(8e^-)}{ROH} \qquad (2\text{–}230)$$

The strong electron donation of the four strongly basic, anionic amido nitrogens in the tetraamido macrocycle coordinating the Fe^{3+}, which are significantly more basic than four tertiary amino groups, is in part responsible for the capacity of the iron ion to achieve the +5 oxidation state when it is within this ligand.* The tetraamidooxoiron(V) in Equation 2–229 is in square pyramidal pentacoordination with the oxo group at the apex. When an iron(V) is generated in a more flexible ligand, again by the use of a peroxy acid, a complex between the peroxy acid and an iron(III) could be identified[1418] in which the acyl oxygen and the distal oxyanion of the peroxy acid had become the fifth and sixth ligand to a hexacoordinated, octahedral Fe^{3+}, a result that suggests that such an intermediate might be involved in the oxidation of Equation 2–229 and that the oxygen–oxygen bond of this intermediate dissociates to give the oxo group and the *m*-chloroperoxybenzoate, which then dissociates from the oxoiron(V).

The **porphyrin of a heme (2–69) is the biological equivalent** of the 1,4,8,11-tetramethyl-1,4,8,11-tetraazacyclotetradecane in Equation 2–228 or the tetraamido macrocyclic ligand in Equation 2–229. The main difference among these three macrocyclic ligands is the values of pK_a for their respective nitrogens. In the cyclic tetraamide (Equation 2–229), each of the nitrogens is equivalent to the nitrogen in *N*-phenylacetamide (pK_a = 15) or the nitrogen in 2-methylpropionamide (pK_a = 17). In the cyclic tetraamine (Equation 2–228), each of the nitrogens is equivalent to the nitrogen in *N*-methyl-*N,N*-diethylamine (pK_a = 10.5). In the cyclic tetrapyrrole of protoporphyrin (**2–69**), the situation is complicated by the existence of two different types of nitrogen. A net of two of the nitrogens are similar to the nitrogen in pyrrole (pK_a = 17.5), and the net of two of the nitrogens are similar to the nitrogens in pyridine (pK_a = 5.2). These are net values because all four of the unhydronated nitrogens in a heme are essentially equivalent and have some hybrid of these two values of pK_a.

Hemes are one of the classes of prosthetic groups that form complexes directly with molecular oxygen, superoxide radical anion, hydrogen peroxide, and water. In the hemes that form these complexes, unlike in the hemes in proteins involved in electron transfer (Figure 2–22), the **sixth coordination site** on the iron ion, one of the two sites for an axial ligand in a heme transferring electrons, **is not occupied** by a basic amino acid from the protein but is occupied by ligands from the solution, or in a ferroheme, it is sometimes even unoccupied. The chemistry proceeds at the single open site on the iron, as in superoxide reductase.

Synthetic ferrihemes that are properly constructed to prevent destructive side reactions also react with peroxy acids

*When a bis[1-(2,4,6-trimethylphenyl)imidazol-2-ylidene], which is an even more basic, dicarbanionic ligand, coordinates an iron ion, an Fe^{6+} can be stabilized.[1417]

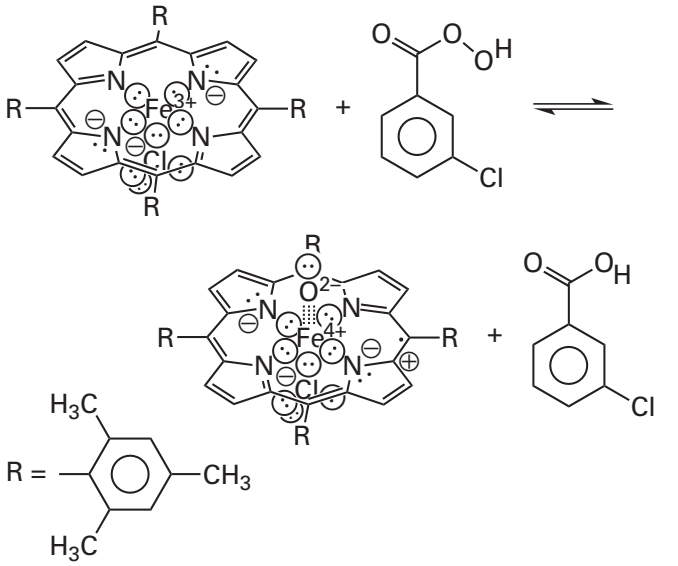

(2–231)

to produce a high-valent iron. The main difference between a porphyrin and the tetraamido macrocyclic ligand of Equation 2–229 is that because of its extensive, continuous, cyclic π molecular orbital system, the redox couple of dihydronated porphyrin radical cation and dihydronated neutral porphyrin has a much more negative reduction potential than the redox couple of dihydronated radical cation of the tetraamido macrocycle and dihydronated tetraamido macrocycle. Consequently, an electron is transferred from the highest occupied π molecular orbital of this π molecular orbital system of the porphyrin to the iron ion as the oxoiron(V) porphyrin is formed during the reaction with the peroxy acid, and the iron ends up in the +4 oxidation state and the porphyrin ends up as a π radical cation (porphyrin$^{\bullet+}$) to give **oxoiron(IV) porphyrin$^{\bullet+}$**. As the designation indicates, the electron deficiency, and hence the positive formal elementary charge of the hole, is in the π molecular orbital system of the radical cation* of the porphyrin.[1419,1420]

When an iron ion is inserted into a heme, the ligand field of the four nitrogens orients its five *d* orbitals (Figure 2–24) while affecting their energies (Figure 2–25). In the oxoiron(IV) porphyrin$^{\bullet+}$ (Equation 2–231), there are **four σ molecular orbitals and four *dp*π molecular orbitals among the iron and the oxygen**. These molecular orbitals resemble the molecular orbitals in a diatomic molecule (Figure 2–45 and **2–86**). The single **σ molecular orbital system** is formed by a combination of the $2s$ atomic orbital on the oxygen, the $4s$ atomic orbital on the iron, the $2p_z$ orbital on the oxygen, and the $3d_{z^2}$ orbital on the iron. These four atomic orbitals together combine to create four molecular orbitals: two bonding σ molecular orbitals and two antibonding σ molecular orbitals. Because all four of these atomic orbitals are cylindrically symmetric with the axis between the oxygen and the iron, the four molecular orbitals in the σ molecular orbital system that they create must also be, as are those in molecular oxygen. Unlike molecular oxygen, however, they are asymmetric about the two perpendicular rotational axes because the atoms are different. There are two perpendicular ***dp*π molecular orbital systems**. One *dp*π molecular orbital system is formed by overlap of the $2p_x$ orbital of the oxygen and the $3d_{xz}$ orbital of the iron ion, which creates a bonding *dp*π molecular orbital and an antibonding *dp*π molecular orbital, and the other is formed by overlap of the p_y orbital of the oxygen and the d_{yz} orbital of the iron, which also creates a bonding *dp*π molecular orbital and an antibonding *dp*π molecular orbital. Because the two *p* orbitals on the oxygen were orthogonal to each other and degenerate and the two *d* orbitals on the iron were also orthogonal to each other and degenerate, the two π molecular orbital systems they respectively create are perpendicular to each other, orthogonal, and degenerate. Except for the fact that these latter two overlaps are *dp*π overlaps rather than *pp*π overlaps, the two *dp*π molecular orbital systems are homologous to the two π molecular orbital systems in molecular oxygen itself.

Upon dissociation of the *m*-chlorobenzoic acid with two electrons that were in the oxygen–oxygen bond, two electrons are required to complete the octet around the remaining oxygen. One is contributed by the iron and the other by the π molecular orbital system of the porphyrin. Formally, this creates an oxide dianion, O^{2-} (8 valence electrons), bonded to Fe^{4+} (4 valence electrons), which together account for **12 valence electrons**, the same number as in molecular oxygen. Six of these electrons occupy three of the σ molecular orbitals for a net of one σ bond; and the six remaining valence electrons occupy the two orthogonal, degenerate *dp*π molecular orbital systems, just as six valence electrons occupy the two orthogonal, degenerate π molecular

*Since the porphyrin in a heme is a dianion, when the radical forms, the charge on the entire porphyrin is –1. There is, however, a positive formal charge and an unpaired electron delocalized over the π molecular orbital system of the porphyrin, which make the π molecular orbital system a radical cation.

orbital systems of molecular oxygen (**2–87**). The same result occurs in the *dpπ* molecular orbital systems. Four of the electrons occupy the two bonding *dpπ* molecular orbitals, and two of the electrons are split between the two antibonding *dpπ* molecular orbitals to create a paramagnetic triplet state and a net of one *dpπ* bond.

Consequently, the oxygen–iron bond in an oxoiron(IV) porphyrin$^{\bullet+}$ is usually abbreviated Fe=O as if it were a double bond, one σ bond and one π bond; but another way of abbreviating it would be :Fe≒O:, which accounts for all 12 of the valence electrons (Equation 2–229). This latter formalism resembles the formalism that can be used for molecular oxygen. Unlike molecular oxygen, however, there is a significant difference in electronegativity between iron and oxygen, a difference of nuclear elementary charge, a difference in the type of atomic orbitals from the iron and the oxygen used to form the molecular orbitals, and the presence of the other axial ligand and the four lone pairs of electrons from the nitrogens of the heme that are ligands to the iron ion. All these factors affect the distribution of electrons between the iron and the oxygen. From here on, however, the bonding will simply be represented by three vertical dashed lines to indicate that there is a sigma bond and two *dpπ* overlaps, and the decision on covalency and distribution of electrons, as usual, will be left to the reader.

A **synthetic oxoiron(IV) porphyrin**$^{\bullet+}$ (Equation 2–231) can be produced with both hydrogen peroxide and alkyl hydroperoxides[1421,1422] as well as with peroxy acids. The former two reactions are most relevant to biochemical oxoiron(IV) porphyrins$^{\bullet+}$. The reactions proceed with general acid catalysis[1421,1423-1428] to promote the heterolysis of the respective oxygen–oxygen bond*

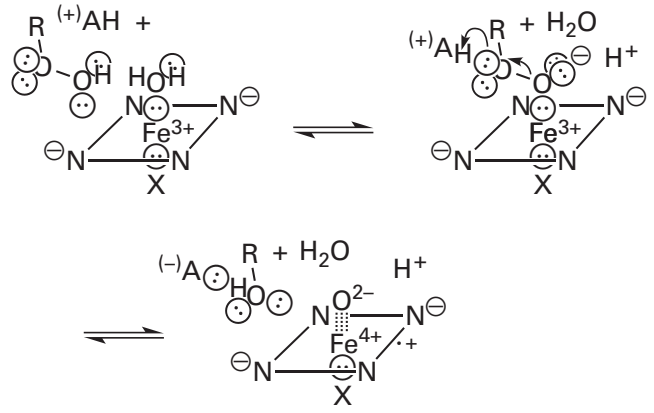

(2–232)

where R is a hydrogen (hydrogen peroxide), an alkyl group (a hydroperoxide), or an acyl group (a peroxy acid) and the leaving group (ROH) is a molecule of water, an alcohol, or a carboxylic acid, respectively.

In the absence of effective general acid catalysis, the oxygen–oxygen bond can also break homolytically[1424,1426,1429-1432]

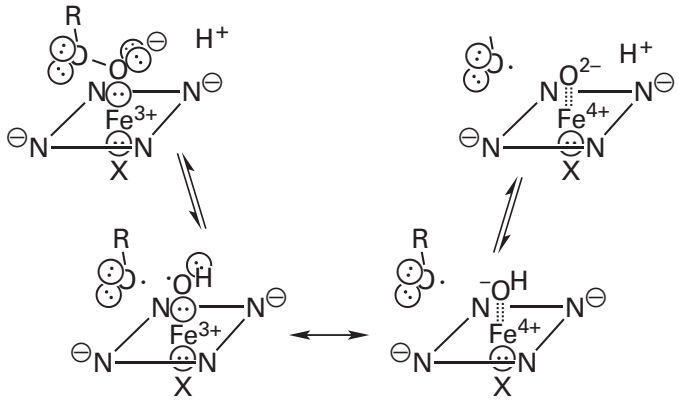

(2–233)

to give a **synthetic hydroxyiron(IV) porphyrin** within an unoxidized heme. A hydroxyiron(IV) is formally equivalent to either a hydroxyl radical bound to Fe^{3+} or a hydroxide bound to Fe^{4+} (Figure 2–50). The conjugate base of a hydroxyiron(IV) is an **oxoiron(IV)** (Figure 2–50).

Alkyl hydroperoxides (R = alkyl) are more prone to homolysis than hydrogen peroxide (R = H), which is more prone to homolysis than peroxy acids (R = acyl).[1422,1429] Peroxy acids are more prone to heterolysis than hydrogen peroxide, which is more prone to heterolysis than alkyl hydroperoxides. The former sequence is that expected from the stability of the corresponding oxy radicals that are the homolytic leaving groups from the hydroxy group of the

*From here on, a heme will be abbreviated by a square with nitrogens at its vertices.

peroxide or peroxy acid, and the latter sequence is that expected from the ability of the corresponding oxyanions to be heterolytic leaving groups from the hydroxy group of the peroxy acid or peroxide. Under appropriate conditions, the reaction with a peroxy acid, which provides the best leaving group for heterolysis, proceeds with no homolysis.[1421,1423]

The **hydroperoxyiron(III)** (Figure 2–50) in 1,4,8,11-tetramethyl-1,4,8,11-tetraazacyclotetradecane (see Equation 2–228) has been produced as a relatively stable compound and examined spectroscopically.[1413,1433] When a hydron and an electron, from triethylammonium and triethylamine, respectively, are then provided, the hydroperoxyiron(III) converts to oxoiron(IV). It is thought that the first step in this conversion is heterolytic dissociation of the oxygen–oxygen bond under acid catalysis by triethylammonium to give oxoiron(V), which, as a strong oxidant, then takes up an electron from triethylamine to become oxoiron(IV). This sequence of events suggests that when the nitrogens in the cyclic ligand are not strong anionic bases, as in Equation 2–229, a source of electrons is required to form oxoiron(IV). In the case of a heme, the **porphyrin is an intramolecular source of the necessary electron**. The same oxoiron(IV) can be formed from the complex between hydrogen peroxide and an Fe^{2+} in the same cyclic ligand by adding catalytic amounts of a base to catalyze the tautomerization in which a hydron dissociates from the proximal oxygen of the hydrogen peroxide and a hydron is added to the distal oxygen to permit heterolysis of the oxygen–oxygen bond. Because the iron begins as iron(II), no electron is needed to produce oxoiron(IV).

An oxoiron(IV) porphyrin$^{\bullet+}$ is so electrophilic that its oxygen is not basic enough to be hydronated at any pH. The oxygen atom in an oxoiron(IV) porphyrin, however, because an oxoiron(IV) porphyrin has one more electron than an oxoiron(IV) porphyrin$^{\bullet+}$, is a base. Its basicity depends on the identity of the proximal ligand on the other side of the heme.[1434] In the active site of an enzyme, the **pK_a of the oxygen atom in a hydroxyiron(IV) porphyrin** in which the proximal ligand is the imidazolyl group of a histidine[1435] is usually less than or equal to 3.5, so it is normally unhydronated.[1436] When the ligand is the sulfido group of a cysteine, which is a much stronger donor of electron density that an imidazolyl group, the pK_a of the oxygen atom[1434,1437] in a hydroxyiron(IV) porphyrin is between 10 and 12, so it is normally hydronated. The fact that the oxygen atom in an oxoiron(IV) porphyrin is basic indicates that, in its reactions, it should be susceptible to acid–base catalysis regardless of the identity of the proximal ligand.

A synthetic **oxoiron(IV) porphyrin$^{\bullet+}$ is able to convert an alkene into its epoxide**[1420,1438-1440]

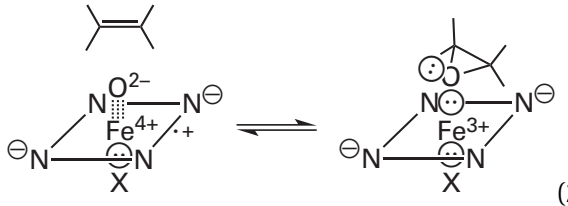

(2–234)

The reaction proceeds with a kinetic intermediate, and the rearrangements of the alkene observed during its epoxidation suggest that this intermediate is a carbocation. The correlation between the rate constant of the epoxidation and the ionization potential of the carbon–carbon double bond suggests that the intermediate is a radical carbocation

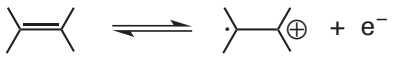

(2–235)

resulting from transfer of one electron from the π bond of the carbon–carbon double bond to the oxoiron(IV) porphyrin$^{\bullet+}$.[1441] If so, the intermediate is both a radical and a carbocation. The oxygen incorporated into the epoxide is that of the oxo group on the iron, but this fact was difficult to determine because the oxygen in a synthetic oxoiron(IV) porphyrin$^{\bullet+}$ is capable of rapid exchange with the oxygen in any water present in the solvent[1420,1426] before it performs the epoxidation. There has, however, been no evidence suggesting that the oxygen in an oxo group at a heme in an enzyme is capable of exchange with the water in the solution. A synthetic hydroxyiron(IV) porphyrin produced by homolysis (Equation 2–233) also performs epoxidation of olefins,[1426,1431,1442] but the distribution of products is quite different from that produced by oxoiron(IV) porphyrin$^{\bullet+}$, an observation suggesting that it proceeds by a different mechanism.

Both synthetic oxoiron(IV) porphyrins$^{\bullet+}$ and synthetic hydroxyiron(IV) porphyrins are **also able to hydroxylate alkanes to alcohols**,[1426,1443,1444] but the heme in the hydroxyiron(IV) porphyrin has to have substituents that withdraw electrons to make the hydroxyiron(IV) a strong enough oxidant. If a hydrocarbon chain is intramolecularly positioned over the iron in a heme model compound and the

heme is converted to oxoiron(IV) porphyrin$^{\bullet+}$, the closest methylene in the chain to the oxygen is converted into a secondary alcohol.[1445] If, however, there are several carbon–hydrogen bonds equally accessible to the oxygen of an oxoiron(IV) porphyrin$^{\bullet+}$, the carbon in the carbon–hydrogen bond with the smallest bond dissociation energy (BDE) is the one that is hydroxylated. This result suggests that the first step in the hydroxylation is abstraction of a hydrogen atom from the alkane. A synthetic oxoiron(IV) porphyrin is able to turn xanthene into xanthone,[1446] presumably by a hydrogen abstraction from the xanthene (BDE = 350 kJ mol^{-1}) followed by an electron transfer and then a hydrogen abstraction from the intermediate xanthydrol (BDE = 340 kJ mol^{-1}) followed by an electron transfer to give xanthone. The oxoiron(IV) in the cyclic ligand 1,4,8,11-tetramethyl-1,4,8,11-tetraazacyclotetradecane (Equation 2–228) is able to abstract hydrogens from the oxygen of a phenol.[1411] The bond dissociation energy (340 kJ mol^{-1}) for the hydroxy group of a phenol, however, is significantly less than that for an alkane (400 kJ mol^{-1}). A synthetic oxoiron(V), however, is a strong enough oxidant to hydroxylate alkanes.[1416] Providing an acidic donor for a hydrogen bond, in particular 2,6-dimethylpyridinium ($pK_a = 6.6$), to the oxygen of a synthetic hydroxyiron(IV) porphyrin increases its reactivity, both in rate and in the bond dissociation energies of its reactants,[1446] by increasing its electrophilicity. The active sites of enzymes often have one or two donors for hydrogen bonds to the oxygen of a prosthetic oxoiron.

A synthetic oxoiron(IV) porphyrin$^{\bullet+}$ is also able to **participate in one-electron transfer**[1432]

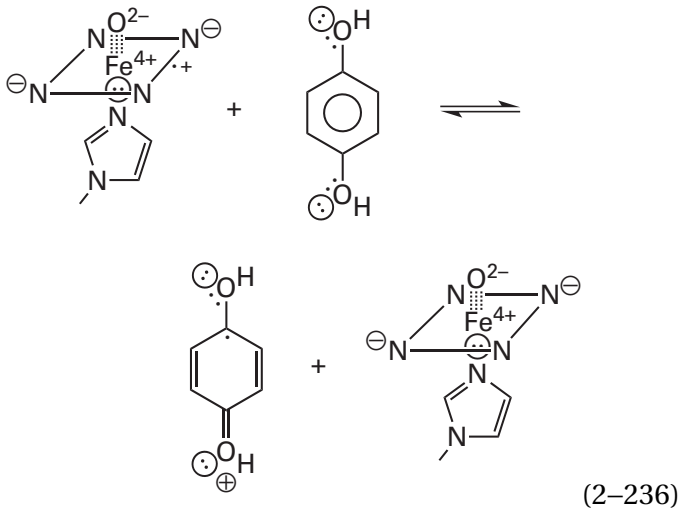

(2–236)

Hemoperoxidases use hydrogen peroxide or an alkyl hydroperoxide as a reactant to produce prosthetic oxoiron(IV) porphyrin$^{\bullet+}$ or oxoiron(IV) porphyrin from their ferric hemes. They use these high-valent intermediates either as a means to remove from the cytoplasm the hydrogen peroxide or the particular alkylperoxide that are the reactants

$$ROOH + 2\,H^+ + 2\,e^- \rightleftharpoons ROH + H_2O \qquad (2\text{–}237)$$

or use these intermediates to oxidize particular substrates. An uncomplicated example of the former purpose is L-ascorbate peroxidase, which reductively removes hydrogen peroxide from the cytoplasm and uses two molecules of the one-electron-transferring coenzyme L-ascorbate (Equation 2–163) to provide the necessary two electrons (Equation 2–237). An uncomplicated example of the latter purpose is myeloperoxidase

$$H^+ + H_2O_2 + Cl^- \rightleftharpoons HOCl + H_2O \qquad (2\text{–}238)$$

which produces oxoiron(IV) porphyrin$^{\bullet+}$ from hydrogen peroxide to oxidize chloride to hypochlorous acid[1447,1448]

$$H_2O + \text{oxoiron(IV) porphyrin}^{\bullet+} + Cl^- \rightleftharpoons HOCl + \text{hydroxyiron(III) porphyrin} \qquad (2\text{–}239)$$

where **hydroxyiron(III) porphyrin** (see Figure 2–50) is the complex between a hydroxide and the ferric heme. The same reaction is catalyzed by another peroxidase in mammalian tissue that oxidizes bromide to hypobromous acid but does not oxidize chloride.[1449]

In the resting state of a hemoperoxidase, the heme is usually an **aquoiron(III) porphyrin** (see Figure 2–50), the complex between a molecule of water and the ferric heme. In a few instances, however, the coordination site on the iron is not occupied by a molecule of water or any other ligand and is open to a strong enough ligand. The first step in the formation of oxoiron(IV) porphyrin$^{\bullet+}$ at the heme in a hemoperoxidase is replacement of the water on the open coordination site of the aquoiron(III) porphyrin by hydrogen peroxide or alkyl hydroperoxide

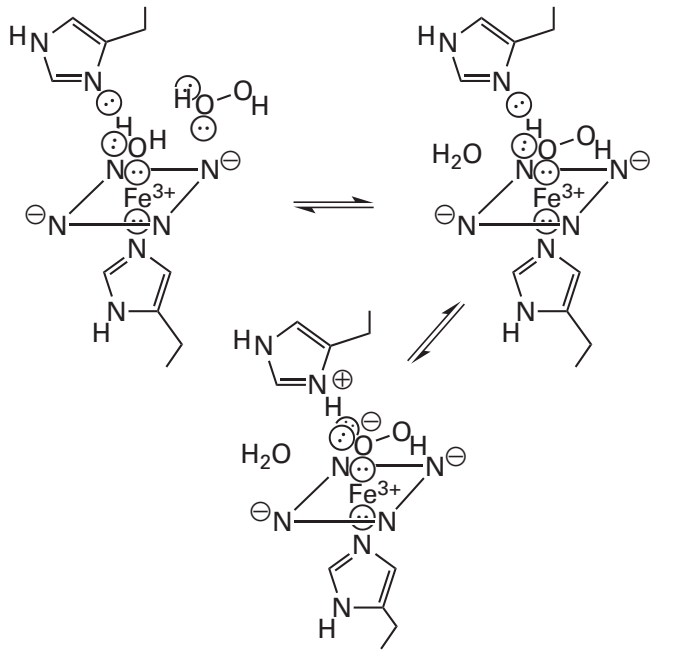

(2–240)

In the active site of most hemoperoxidases, there is the side chain of a histidine forming a hydrogen bond with the water initially on the Fe^{3+}.[1450,1451] This histidine must be both present and unhydronated[1452,1453] so that it can remove the hydron from the proximal oxygen of the hydrogen peroxide, either as the complex is forming or after it has formed.[1454]

The result of the replacement of the molecule of water and transfer of the hydron is a **hydroperoxyiron(III) porphyrin** (see Figure 2–50), the complex between a hydroperoxide ion and the ferric heme. A hydroperoxyiron(III) porphyrin has been observed transiently in the peroxidase from *Armoracia rusticana*[1455] and could be trapped as a stable species at low temperature.[1456] The bond formed between oxygen and iron is between a σ lone pair of electrons from the conjugate base of hydrogen peroxide and the empty, axial d_{z^2} atomic orbital on the iron.[1294]

In the next step of the reaction, heterolytic cleavage of the oxygen–oxygen bond occurs.[1457] The histidine that has just removed the hydron from the proximal oxygen of the hydrogen peroxide (Equation 2–240) hydronates its distal oxygen[1458,1459] to provide the necessary **acid catalysis**

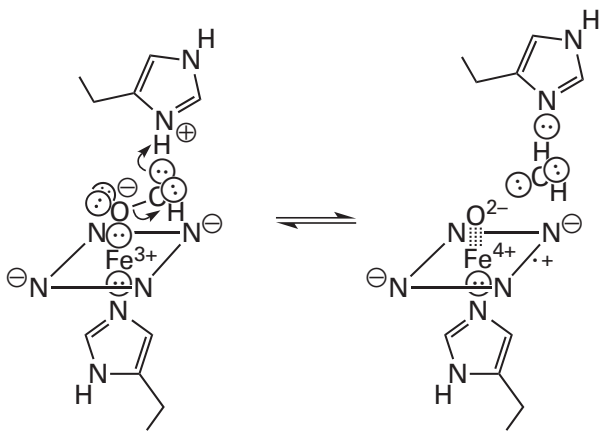

(2–241)

for dissociation of the oxygen–oxygen bond and formation of the oxoiron(IV) porphyrin$^{\bullet+}$. The net of one double bond between iron and oxygen in the oxoiron(IV) porphyrin$^{\bullet+}$ in the active site of a hemoperoxidase that is the product of this sequence of steps has an infrared absorption band at a wavelength in the same range as the one for the net double bond in a synthetic oxoiron(IV) porphyrin$^{\bullet+}$.[1460,1461] The crystallographic molecular model of an oxoiron(IV) porphyrin$^{\bullet+}$ in catalase from *Penicillium janthinellum*, a hemoperoxidase, shows a single oxygen sitting on the iron in the heme (Figure 2–51).[1430,1457]

Chlorite O_2-lyase from *Dechloromonas aromatica* uses chlorite rather than hydrogen peroxide to produce an oxoiron(IV) porphyrin$^{\bullet+}$ in its active site. Chlorite ($OClO^-$) associates through one of its oxygens with the ferric heme in the active site to form an adduct homologous to a hydroperoxyiron(III) porphyrin. Instead of the distal oxygen being hydronated to create a leaving group, in this case the leaving group is hypochlorite (ClO^-) and its dissociation produces the oxoiron(IV) porphyrin$^{\bullet+}$. The hypochlorite reorients in the active site and the oxoiron(IV) porphyrin$^{\bullet+}$ then abstracts the oxygen atom from it. The final products of the reaction are Cl^-, molecular oxygen, which is formed from the two peripheral oxygens of the chlorite, and iron(III) porphyrin.[1462] In this case, an oxygen–oxygen bond is made rather than being broken.

In most of the peroxidases, the electron that reduces oxoiron(V) to oxoiron(IV) is provided by the porphyrin itself to produce oxoiron(IV) porphyrin$^{\bullet+}$. In cytochrome-*c* peroxidase from *S. cerevisiae*[1463,1464] and lignin peroxidase from *P. eryngii*,[1465,1466] however, the radical cation arising from transfer of the electron to oxoiron(V) during heterolysis of the oxygen–oxygen bond ends up located on the nearby indolyl group of a tryptophan in an oxoiron(IV) indolyl$^{\bullet+}$.

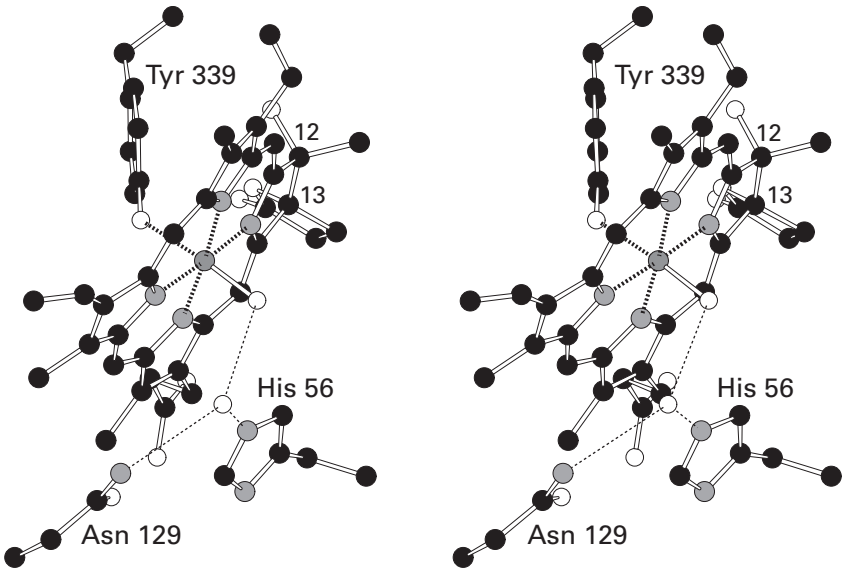

Figure 2–51: Stereodrawing[50] from the crystallographic molecular model of oxoiron(IV) porphyrin$^{\bullet+}$ in the active site of catalase from *P. janthinellum*.[1430] Black atoms are carbons, white atoms are oxygens, gray atoms are nitrogens, and the small dark gray sphere surrounded by ligands is an iron ion. A crystal of catalase from *P. janthinellum* was soaked for 2 min in 125 mM peroxyacetic acid, during which time its color turned from brown to green, suggesting that its heme had become oxoiron(IV) porphyrin$^{\bullet+}$. It was immediately brought to 100 K and stored at this temperature. In the crystallographic model derived from this crystal, there was a single atom of oxygen on the iron ion of the heme at a bond length expected for an iron–oxygen double bond (0.172 nm). The other axial ligand to the iron ion in the heme of this enzyme is the 4-oxido group of Tyrosine 339. The heme *b* (**2–69**) originally present in this catalase has been oxidatively modified during its lifetime of performing catalysis in the cell before it was purified. In addition to the methyl group at position 12, there is a hydroxy group (upper right corner in drawing) and the bond between carbon 12 and carbon 13 is a single bond instead of a double bond. In addition to the 2-carboxylatoethyl group on carbon 13, there is also a hydroxy group, and these two groups have formed a lactone (upper right corner in drawing). The oxygen of the oxo group is participating in a hydrogen bond with a molecule of water, which is held in place by the carbamoyl group of Asparagine 129 and the imidazolyl group of Histidine 56.

The tryptophan in cytochrome-*c* peroxidase is located in a pocket that stabilizes its radical cation,[1467] and when that tryptophan is mutated to a phenylalanine, the usual oxoiron(IV) porphyrin$^{\bullet+}$ forms instead.[1468] It has already been noted that, in cytochrome-*c* peroxidase, the two successive electrons transferred from two successive molecules of cytochrome *c* are both transferred to the **π radical cation of the tryptophan**. In the case of lignin peroxidase, the radical cation of the tryptophan actually oxidizes the lignin by abstracting electrons from it.[1469] In L-ascorbate peroxidase, however, which has a tryptophan in the homologous location, a normal oxoiron(IV) porphyrin$^{\bullet+}$ is formed[1470,1471] rather than an oxoiron(IV) indolyl$^{\bullet+}$.

In methylamine utilization protein, a peroxidase from *P. denitrificans*, there are two hemes: one at which the hydrogen peroxide is converted to an oxoiron(V) porphyrin and the other that provides the extra electron to convert the oxoiron(V) porphyrin to an oxoiron(IV) porphyrin. The iron ion in the other heme has a tyrosine and a histidine as axial ligands, and the Fe^{3+} is converted to the oxidation state of Fe^{+4} after providing the electron. The extra electron is transferred back and forth between the hemes by hopping through a tryptophan that serves as a relay station.[1472]

In many hemoperoxidases, in addition to the imidazolyl group that performs the acid catalysis, there is also the **guanidinio group of an arginine** located appropriately[1473,1474] to provide a hydrogen bond to a molecule of water that in turn forms a hydrogen bond to the distal oxygen of the hydrogen peroxide. This arrangement should polarize the oxygen–oxygen bond and hasten its cleavage.[1475] After the bond cleaves and the water leaves, this guanidinio group then swings over to form a hydrogen bond with the oxygen of oxoiron(IV) in the oxoiron(IV) porphyrin$^{\bullet+}$.[1451,1476] The fact that this hydrogen bond can form is an indication that there must be sufficient electron density on the oxygen to act as an acceptor.

In catalase

$$H_2O_2 + H_2O_2 \rightleftharpoons 2\,H_2O + O_2 \qquad (2\text{–}242)$$

the **proximal axial ligand to the iron in the heme, opposite its open site, is the 4-oxido group of a tyrosine** (Figure 2–51),[1458,1477,1478] rather than the more common imidazolyl group of a histidine (Equation 2–240).[1459] A portion of the spin density of the π radical cation in the oxoiron(IV) porphyrin$^{\bullet+}$ in catalase is delocalized into the tyrosinate ligand on the iron.[1479] An electron from the highest occupied π molecular orbital system of the tyrosinate is transferred into the highest occupied π molecular orbital of the porphyrin radical cation. It fills the hole left by the electron that was transferred to the oxoiron(V) and pairs with the electron in the highest occupied π molecular orbital of the porphyrin, and it leaves behind a hole and an unpaired electron in the highest occupied π molecular orbital of the tyrosinate. The degree to which the unpaired electron and the hole reside on the tyrosine varies among the catalases from different organisms,[1430] but in at least one case, the majority of the **spin density of the radical resides on the tyrosine**.[1480] In the catalase-peroxidase KatG from *M. tuberculosis*, the indolyl group of Tryptophan 107 is stacked against the heme. When the oxoiron(IV) porphyrin$^{\bullet+}$ is formed, as long as the radical cation remains on the heme, the enzyme is a peroxidase performing hydrogen abstraction from various reactants. When, however, the unpaired electron transfers to the indolyl group to form an indolyl radical cation, the resulting oxoiron(IV)porphyrin indolyl$^{\bullet+}$ becomes a catalase (Equation 2–242) and converts a molecule of hydrogen peroxide to a molecule of water. In the process it becomes a superoxyiron(III) porphyrin indolyl$^{\bullet+}$ that dissociates into a molecular oxygen and an iron(III)porphyrin, which again can act as either a catalase or a peroxidase.[1481]

The length of the iron–oxygen bond in the oxoiron(IV) within the cyclic ligand 1,4,8,11-tetramethyl-1,4,8,11-tetraazacyclotetradecane (Equation 2–228),[1410] is short (0.165 nm). When the radical cation remains localized to the porphyrin, the **length of the iron–oxygen bond** in the oxoiron(IV) porphyrin$^{\bullet+}$ in a crystallographic molecular model of a synthetic model compound is longer (0.172 nm),[1482] a fact indicating that there is less π bonding between iron and oxygen because the porphyrin radical cation, a weaker base, provides more electron density to the antibonding $dp\pi$ molecular orbitals of the oxoiron than the cyclic ligand. When the radical cation is localized on the tyrosinate or elsewhere in the protein, the length of the iron–oxygen bond in the oxoiron(IV) porphyrin that results is long (0.182 nm), a fact indicating that there is much less π bonding between iron and oxygen because the porphyrin, no longer the radical cation, provides even more electron density to the antibonding $dp\pi$ molecular orbitals. As a result, the σ lone pair of electrons is more localized on the oxygen so that it can be hydronated (right resonance structure in Equation 2-233).[1430]

Figure 2–52: Stereodrawing[50] of the crystallographic molecular model of a compound that serves as a model for the heme in an oxygen-binding hemoprotein in its oxygenated form.[1514] Black atoms are carbons, white atoms are oxygens, gray atoms are nitrogens, and the small dark gray sphere surrounded by ligands is an iron ion. The porphyrin in this model compound is a tetra(*o*-aminophenyl)porphyrin. Four molecules of pivalic acid [$(CH_3)_3CCOOH$] have been attached as amides, one to the anilino nitrogen in each of the four *o*-aminophenyl groups. These four pivalamides form a dome over one side of the heme. The axial position on the iron opposite the dome is occupied by a 2-methylimidazole to give the heme properties similar to the heme in hemoglobin or myoglobin. The ferrous model compound was recrystallized from refluxing ethanol in the absence of molecular oxygen. The resulting crystals were exposed to 1–2 atm of molecular oxygen saturated with ethanol vapor for several days and then prepared for crystallography. The map of electron density of the crystal that had been treated in this way showed that the iron of the heme in the crystals was occupied by molecular oxygen at its open axial position. In this complex between heme and molecular oxygen, the molecular oxygen assumes four different rotational isomers around the iron–oxygen bond because the heme has a fourfold rotational axis of pseudosymmetry coincident with the iron–oxygen bond. There are four orientations of equal energy, at rotational angles of 90° to each other, that are assumed by the molecule of oxygen. In the drawing only one of these four equally populated orientations is shown. Crystallographic molecular models were made for both the unoccupied heme and the heme occupied by oxygen. In the unoccupied heme, which is not shown, the iron is pulled 40 pm out of the plane of the porphyrin in the direction of the 2-methylimidazole by steric effects arising from the methyl group of 2-methylimidazole. When oxygen binds, as shown in the drawing, the iron returns almost to the plane of the porphyrin (final displacement of only 9 pm). In the heme occupied by molecular oxygen, the bond angle between the iron–oxygen bond and the oxygen–oxygen bond is 129°.

In many of the reactions catalyzed by hemoperoxidases, the oxoiron(IV) porphyrin$^{\bullet+}$, oxoiron(IV) phenoxy$^{\bullet}$, or oxoiron(IV) indolyl$^{\bullet+}$ **accepts a single electron during the oxidation of its natural substrate** or can accept a single electron from an appropriate unnatural substrate. Examples of the former case would be L-ascorbate peroxidase, cytochrome-*c* peroxidase, and manganese peroxidase, each of which accepts two successive single electrons in two separate outer-sphere transfers from two successive molecules of the one-electron donors that are their natural substrates: L-ascorbate (Equation 2–163), cytochrome *c*, and Mn^{2+}·oxalate^{2-}, respectively.[1483,1484] Examples of the latter case would be transfer of one electron from amines[1485] and sulfides[1486] to the oxoiron(IV) porphyrin$^{\bullet+}$ of the peroxidase from *A. rusticana*, which normally removes single electrons from phenols. When a single electron is transferred to oxoiron(IV) porphyrin$^{\bullet+}$, oxoiron(IV) porphyrin (Equation 2–233) is formed,[1487,1488] which in the cases of L-ascorbate peroxidase, cytochrome-*c* peroxidase, and manganese peroxidase then accepts the second electron.

Both oxoiron(IV) porphyrin$^{\bullet+}$ and oxoiron(IV) porphyrin in a hemoperoxidase are strong oxidants. In L-ascorbate peroxidase, the one-electron biochemical standard reduction potential for the redox couple of oxoiron(IV) porphyrin$^{\bullet+}$ and oxoiron(IV) porphyrin is +1160 mV and that for the redox couple of oxoiron(IV) porphyrin and aquoiron(III) porphyrin is +750 mV.[1489] In cytochrome-*c* peroxidase, the two-electron reduction potential at pH 6.1 for the redox couple of oxoiron(IV) indolyl$^{\bullet+}$ and aquoiron(III) indolyl is +740 mV.[1490] In a model compound in which an oxoiron(IV) is coordinated equatorially by the nitrogens of four pyridines and has a proximal axial ligand of a trialkylamine,[1491] a coordination similar to that of heme, the biochemical standard reduction potential for the redox couple of oxoiron(IV) and hydroxyiron(III) at pH 4 is +650 mV. These significantly **positive standard reduction potentials** permit such intermediates to participate as strong one-electron acceptors.

In an oxoiron(IV) porphyrin$^{\bullet+}$, the highest occupied molecular orbital of the porphyrin, which is occupied by the unpaired electron and the hole, has its **greatest spin density at the four meso positions** (carbons 5, 10, 15, and 20 in **2–69**),[1430] and these positions should be locations at which transfer of an electron can occur. In the peroxidase from *A. rusticana*, the channel that leads from the solution to the heme, in which the substrates are oxidized by the enzyme, is centered on one of these meso positions.[1492] During the oxidation of phenylhydrazine by the peroxidase from *C. cinerea*, which leads to inactivation of the enzyme, phenyl radical is produced within the active site by the successive abstraction by the enzyme of the equivalent of three hydrogen radicals from the two nitrogens of the phenylhydrazine, which leads to the production of molecular nitrogen and the phenyl radical. The phenyl radical then phenylates one of the meso positions of the heme.[1493] Because the phenyl radical (bond dissociation energy = 470 kJ mol^{-1}) is so reactive, its insertion at the meso carbon suggests that the meso carbon was immediately adjacent to it when it was formed.

In the reaction catalyzed by L-ascorbate peroxidase and cytochrome-*c* peroxidase, the hydrogen peroxide or alkyl hydroperoxide that produces the oxoiron(IV) porphyrin$^{\bullet+}$ associates with Fe^{3+} of the heme (Equation 2–240) and is turned into a molecule of water or alcohol, respectively, and the oxygen of the oxoiron(IV) porphyrin$^{\bullet+}$ (Equation 2–241). The oxygen of the oxoiron(IV) porphyrin$^{\bullet+}$ becomes a molecule of water following the formal transfer of two electrons and two hydrons. The net result is either that the hydrogen peroxide is turned into two molecules of water or that the alkyl hydroperoxide is turned into a molecule of alcohol and a molecule of water. Either result accomplishes the purpose of **removing peroxides**. In the process, two one-electron reductants, L-ascorbate and ferrocytochrome *c*, respectively, provide the required reducing equivalents.

Catalase (Equation 2–242) uses the oxoiron(IV) porphyrin$^{\bullet+}$, or the oxoiron(IV) porphyrin phenoxy$^{\bullet}$, formed in its active site (Figure 2–51) from hydrogen peroxide to **oxidize a second molecule of hydrogen peroxide to molecular oxygen**, a reaction that is of course only appropriate to aerobic organisms and that serves twice over the role of removing hydrogen peroxide from the cytoplasm. It has been demonstrated that oxoiron(IV) porphyrin$^{\bullet+}$, formed nonenzymatically in a synthetic heme, can readily abstract a hydrogen atom from hydrogen peroxide[1432] to produce hydrogen superoxide radical

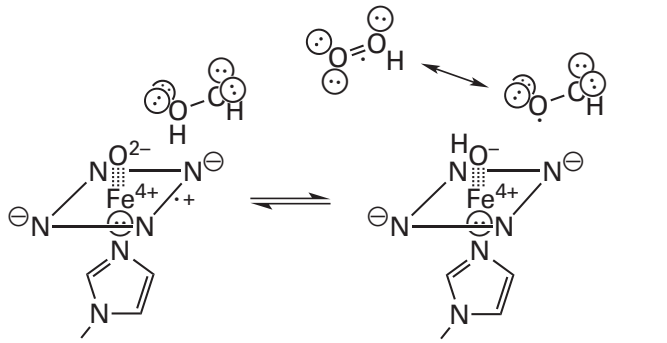

(2–243)

The bimolecular rate constant of this nonenzymatic reaction in solution at 25 °C is 10^7 M^{-1} s^{-1}, and the magnitude of this rate constant suggests that no catalysis is required at this step in the enzymatic reaction. The other product of this reaction is the hydroxyiron(IV) porphyrin,[1494] an intermediate formed stably when the oxoiron(IV) porphyrin$^{\bullet+}$ of catalase is reduced by a one-electron donor rather than a two-electron donor such as hydrogen peroxide.

The last step in the enzymatic reaction of catalase could be transfer of an electron from hydrogen superoxide radical coupled to removal of a hydron

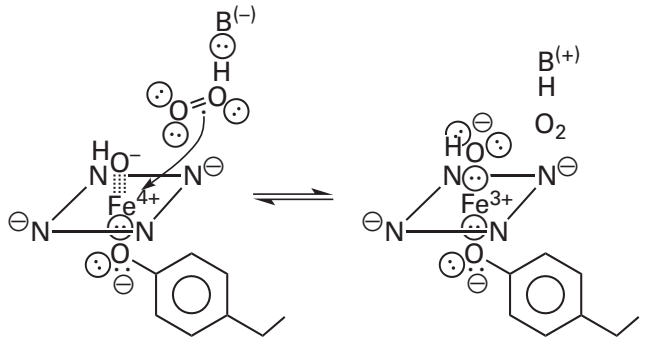

(2–244)

The imidazolyl group of the histidine, which removed the hydron from the proximal oxygen of hydrogen peroxide (Equation 2–240) and added the hydron to the distal oxygen (Equation 2–241), could remove a hydron from hydrogen superoxide radical while an electron is transferred from the superoxide radical anion to Fe^{4+}. In this case, the hydroxyiron(IV) porphyrin is acting as a hydroxide on Fe^{4+}, which is a strong oxidant. The imidazolium ion could then add a hydron to the hydroxide on hydroxyiron(III) porphyrin (Equation 2–244) to return the heme to aquoiron(III) porphyrin.

An alternative possibility for the last step is the abstraction of a second hydrogen atom by the hydroxyiron(IV) porphyrin from the hydrogen superoxide radical that has turned around within the active site of the enzyme[1432]

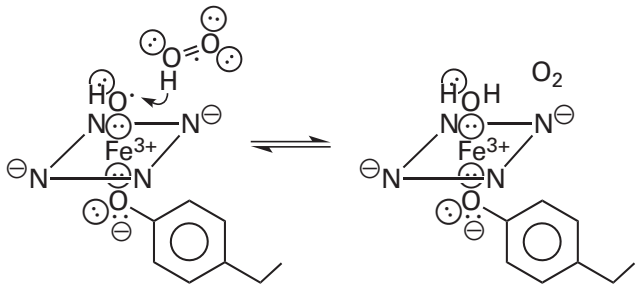

(2–245)

In this reaction the hydroxyiron(IV) porphyrin would be functioning as a hydroxyl radical on Fe^{3+}. A hydroxyl radical (bond dissociation energy = 497 kJ mol^{-1}) is capable of abstracting a hydrogen atom from almost anything. Either scenario is consistent with the fact that when a mixture of $H_2{}^{18}O_2$ and $H_2{}^{16}O_2$ is used as substrate for catalase, the molecular oxygen produced had the same percentage of doubly labeled $^{18}O_2$ as the percentage of doubly labeled $H_2{}^{18}O_2$ in the mixture,[1495] a result requiring that the σ oxygen–oxygen bond of the $H_2{}^{18}O_2$ remains intact during the enzymatic reaction.

There are, however, as already noted, many **peroxidases that use the oxoiron(IV) porphyrin$^{\bullet+}$ to perform useful oxidations of particular substrates**, rather than just removing hydrogen peroxide from the cytoplasm. For example, manganese peroxidase uses its oxoiron(IV) porphyrin$^{\bullet+}$ in two successive removals of an electron from each of two Mn^{2+}·oxalate^{2-} ylides. Each Mn^{3+}·oxalate^{2-} ion it produces is a strong oxidant that is used to degrade lignin, one of the components of wood and one of the most difficult biological polymers to degrade. The inability to degrade lignin was responsible for the Carboniferous period. Lignin peroxidase also uses its oxoiron(IV) porphyrin$^{\bullet+}$ productively to remove two successive electrons from methoxyphenols in lignin by an outer-sphere electron transfer[1451] or an inner-sphere electron transfer[1496] to produce π radical cations in the lignin that lead to its fragmentation.[1497] In mammalian prostaglandin-endoperoxide synthase, there is a hemoperoxidase the only purpose of which is to regenerate the tyrosyl radical in the active site of the enzyme that is required for prostaglandin synthesis[1498] when that tyrosyl radical is occasionally lost by an adventitious reduction. This peroxidase uses its oxoiron(IV) porphyrin$^{\bullet+}$ to abstract either a

hydrogen or an electron from the tyrosine to regenerate the necessary tyrosyl radical.[1499,1500] The oxoiron(IV) porphyrin$^{\bullet+}$ in the active site of a dehaloperoxidase from *Amphitrite ornata* removes two electrons, one at a time, from a single molecule of chlorophenol to produce 4-benzoquinone and chloride.[1501]

During the oxidations of substrates catalyzed by hemoperoxidases, the hydrogen abstractions and electron transfers performed by oxoiron(IV) porphyrin$^{\bullet+}$ and hydroxyiron(IV) porphyrin often generate reactive oxidants in the vicinity of the heme. In many of these enzymes, these reactive oxidants adventitiously modify the heme itself or amino acids nearby. In catalase, the heme *b* in the active sites of the initially synthesized enzyme is often modified by oxidation to heme *d* (Figure 2–51);[653] in lactoperoxidase and iodide peroxidase, the hemes *b* are modified by oxidation to hemes *l*;[1502] and in myeloperoxidase, the heme *b* is modified by oxidation to heme *m*.[1503,1504] Such **adventitious oxidations** account for the existence of many if not most of these unusual hemes. In several of these instances, the oxoiron(IV) porphyrin$^{\bullet+}$ modifies amino acids in the protein as well. In a catalase, an adjacent sulfanyl group of a cysteine[1477] or the nitrogen of an adjacent imidazolyl group from a histidine[1478] is often oxidatively coupled to the β carbon of the tyrosinate that coordinates the iron ion. In catalase-peroxidase from *M. tuberculosis*, a methionine, a tryptophan, and a tyrosine have all been oxidatively coupled together.[1505,1506] Perhaps, originally, this coupling was adventitious, but presently this covalent complex is the location of a radical that forms during turnover of the enzyme and is essential for its enzymatic activity.[1507-1509] In cytochrome-*c* peroxidase from *S. cerevisiae*, an electron is removed adventitiously from each of two tyrosines in the protein during catalysis.[1510]

Hydrogen peroxide-dependent heme synthase from *G. stearothermophilus* is an enzyme that turns coproheme III, the complex between an iron ion and uroporphyrinogen III (**2–70**) and hence a precursor of heme *b*, into heme *b* (**2–69**), which is the precursor of almost all prosthetic hemes. Coproheme III has 2-carboxyethyl groups at positions 3 and 8 instead of vinyl groups, and the enzyme turns those two carboxyethyl groups into the vinyl groups that are in heme *b*. In the active site of the enzyme, the Fe^{3+} in coproheme that is a reactant is turned into an oxoiron(IV) tyrosine$^{\bullet}$ in the usual way with hydrogen peroxide.[1511] The tyrosine radical abstracts a hydrogen from carbon 1 of a 2-carboxyethyl group that then undergoes **oxidative decarboxylation** to become a vinyl group. The oxidative decarboxylation is then repeated at the other 2-carboxyethyl group. During the oxidative decarboxylation, an electron is transferred to the oxoiron(IV) porphyrin to regenerate the hydroxyiron(III) in the heme that was the reactant for the enzyme. This reaction resembles the adventitious reactions in which hemes in the active sites of peroxidases are oxidatively modified, but instead of a prosthetic heme being modified, it is a heme that is the reactant for the enzymatic oxidation.

A hemoperoxidase is usually inhibited by superoxide radical anion, which forms a complex with Fe^{3+} in the resting state of its heme (Figure 2–50). This complex is identical to the one that results when molecular oxygen binds to an Fe^{2+} in its heme[1512]

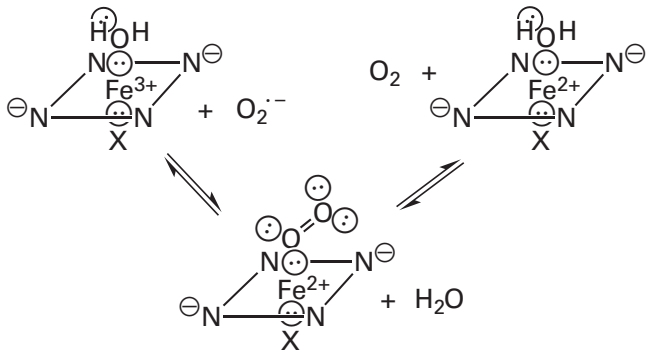

(2–246)

The complex between a ferrous heme and molecular oxygen is an **oxyiron(II) porphyrin** (see Figure 2–50).

Ferrous hemes in hemoproteins such as hemoglobin and myoglobin form reversible complexes with molecular oxygen. In these proteins, the proximal axial ligand to the iron, opposite the open site, is the imidazolyl group of a histidine in the protein and the open ligand position opposite this imidazolyl group is the one occupied by the molecular oxygen. Because an Fe^{2+} is less acidic when it is in a heme than when it is in solution, it forms complexes with bases such as water or hydrogen peroxide poorly. Consequently, when a ferrous heme is in aqueous solution in the absence of molecular oxygen, carbon monoxide, or similar ligands, the open site is vacant or fitfully occupied. The purpose of the complex between molecular oxygen and the Fe^{2+} in the heme in a hemoglobin at the open site is to carry the molecular oxygen from a location of high concentration to a location of low concentration: for example, from

the lungs to the skeletal muscles in a mammal. The heme in at least one hemoglobin, that from *A. ornata*, is able to double as a carrier of molecular oxygen and as a peroxidase. In its ferrous form it carries molecular oxygen, and in its ferric form it is a peroxidase.[1513]

There are several **facts that are known about the complex** between oxygen and a ferrous heme. It is diamagnetic.[1313] This fact states that all electrons in the complex are paired. The Fe–O–O angle in the oxygen complex of a heme model compound, the crystallographic molecular model for which can be constructed with high accuracy (Figure 2–52),[1514] is 129°. The Fe–O–O angles in crystallographic molecular models of oxymyoglobin from *P. macrocephalus* (123°)[1515-1518] and human oxyhemoglobin (125°)[1519] from data sets collected to Bragg spacings of 0.12 nm are almost the same as that in the model compound. Nuclear magnetic resonance spectra of $^{17}O_2$ bound to heme model compounds are in agreement with this bent ligation.[1520] In complexes between molecular oxygen and the hemes in hemoglobin[1519,1521] and myoglobin,[1517,1518,1522] a hydrogen bond forms between the distal oxygen of the molecular oxygen and the imidazolyl group of a histidine (Figure 2–53).[1523,1524] In a complex between molecular oxygen and the heme in the hemoglobin from *Ascaris suum*, there are hydrogen bonds between the distal oxygen and the 4-hydroxyphenyl group of a tyrosine and between the proximal oxygen and the carbamoyl group of a glutamine.[1525]

The Fe–O–O bond angle of 126° and the observed hydrogen bonds suggest that there are **two sp^2 lone pairs of electrons** on each oxygen (Equation 2–246) when it is bound by the iron. The **oxygen–oxygen bond length** in the complex (0.123 ± 0.01 nm),[1514,1516,1517,1519] however, is almost indistinguishable* from that of molecular oxygen itself (0.121 nm) and is much shorter than that of superoxide radical anion (0.133 nm)[1295] or hydrogen peroxide (0.148 nm). This fact only states that the bond order is the same as that in molecular oxygen and that the net of one π bond remains in the oxygen–oxygen bond. In other words, there are two more electrons in bonding π molecular orbitals than there are in antibonding π molecular orbitals. This conclusion does not mean, however, that the bound molecule of oxygen has the same π molecular orbital systems as an unbound molecule of oxygen.

Iron(II) has an even number of electrons (6 valence electrons and 18 core electrons); but it is paramagnetic in the high-spin state, as is molecular oxygen in the triplet state, because there are four unpaired electrons in the five $3d$ atomic orbitals (Figure 2–25). Upon the entry of Fe^{2+} into a heme, the high-spin state becomes less stable, but it is still more stable than the low-spin, diamagnetic state in which all electrons would be paired. Upon formation of the complex, the six formerly unpaired electrons, four from iron and two from oxygen, must become paired because the complex is diamagnetic.[1313] In the process of pairing these electrons, the proximal of the two oxygens becomes bonded to the iron.

Although there is little agreement on the details of the electronic structure, even though there is little ambiguity in the facts, several features of the bonding of molecular oxygen to the ferrous ion in a heme are commonly emphasized. Mixing between one or two d atomic orbitals on iron (d_{xz} and d_{yz} or both) and one or more of the four off-axial p atomic orbitals on the two oxygen atoms (p_x orbitals and p_y orbitals, or some set of both of these off-axial orbitals) creates one or two $dp\pi$ molecular orbital systems, each with a bonding and an antibonding molecular orbital. There is also the possibility of a third nonbonding molecular orbital formed from two p atomic orbitals, one from each oxygen, and a d atomic orbital from the iron ion. The occupied, bonding $dp\pi$ molecular orbitals provide energy to the bond. The **entry of d electrons from iron into antibonding π molecular orbitals** on molecular oxygen in turn enhances the basicity of one of the σ lone pairs of electrons on the proximal oxygen so that it can form a σ bond with the d_{z^2} orbital on iron.[1294] The atomic orbital on the oxygen that participates in the σ bond with iron must have gained sufficient p character to cause the oxygen atom in the bond to have almost sp^2 hybridization because the Fe–O–O bond has an angle of around 125° and the proximal oxygen that is bonded directly to the iron can also accept a hydrogen bond, presumably with the pair of electrons in the other sp^2 orbital. If the σ orbitals of the lone pairs of electrons on molecular oxygen had not gained extra p character, they would have remained

*This equivalence assumes that the oxygen–oxygen bond was unconstrained in the several refinements.

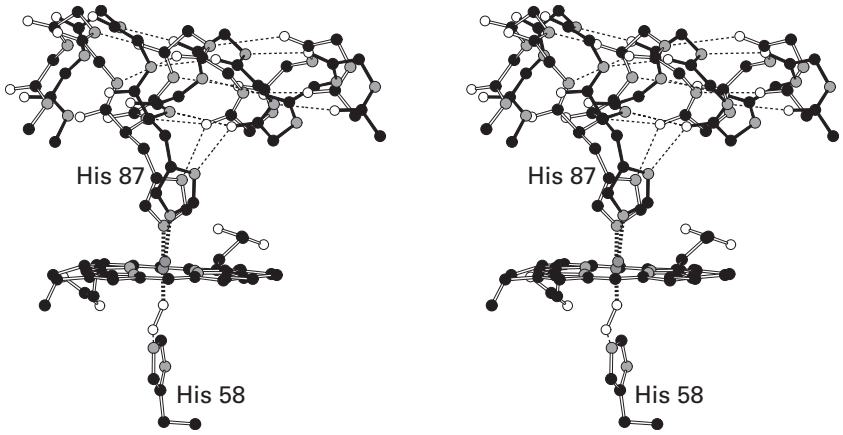

Figure 2–53: Stereodrawing[50] of portions of the superposed crystallographic molecular models of human oxyhemoglobin (white bonds) and human deoxyhemoglobin (black bonds) in the regions surrounding the histidine that is the fifth ligand to the iron in the heme from the α subunit.[1523,1524] Black atoms are carbons, white atoms are oxygens, gray atoms are nitrogens, and dark gray spheres surrounded by ligands are iron ions. The hemes in the two crystallographic molecular models have been superposed so that the changes demonstrated in the drawing between oxyhemoglobin and deoxyhemoglobin are relative to the fixed hemes. The α helices from both oxyhemoglobin and deoxyhemoglobin that contains the respective histidines (Histidines 87) are drawn as well as the iron ions in each heme, the molecule of oxygen bound to the iron in oxyhemoglobin, and the imidazolyl group of Histidine 58 that forms a hydrogen bond to the molecule of oxygen bound to the iron in oxyhemoglobin. For clarity, however, only the heme from oxyhemoglobin, viewed edge-on, is drawn because the two hemes, which have been purposely superposed, overlap each other throughout their structures, and this superposition would complicate the drawing. Aside from the side chains of the respective Histidines 87, only the peptide backbones of the two α helices are presented. The hydrogen bonds within each α helix and the hydrogen bond between the molecule of oxygen and Histidine 58 are drawn as thin dashed lines. The bonds between the respective iron ions and the imidazolyl groups of the coordinated histidines and the molecule of oxygen are drawn with thick dashed lines. In the deoxy conformation of the protein, the position of the imidazolyl group in Histidine 87 is such that it pulls the iron out of the plane of the heme. In the oxy conformation of the protein, the α helix shifts its position to the left, the imidazolyl group comes closer to the center of the heme, and the iron drops into the plane of the porphyrin. The binding of oxygen, because it is much stronger when the iron is in the plane of the porphyrin than when it is pulled away from the center, shifts the equilibrium between the deoxy conformation and the oxy conformation in favor of the oxy conformation.

aligned with the axis of the two oxygen atoms, and the Fe–O–O bond angle would have been 180° because the σ molecular orbital system in molecular oxygen is required to be axially symmetric. Presumably, this extra p character in the σ bond to the iron results from occupation of antibonding π molecular orbitals on oxygen by electrons from the iron ion. This intrusion of electron density causes pairs of electrons in the delocalized π molecular orbitals to become localized, just as they are either during the production of superoxide radical anion or during the production of hydrogen peroxide. In each of these cases, an electron is added to an antibonding π molecular orbital during the respective reduction.

As electron density, entering what were formerly antibonding orbitals, is gained from iron in the π molecular orbitals on oxygen and all the valence electrons become paired, the net π bonding between the two oxygen atoms—the difference between occupation of bonding and antibonding orbitals—must not change because the oxygen–oxygen bond length remains the same. After these readjustments have taken place, there is excess electron density on the molecular oxygen, creating negative formal elementary charge on the distal oxygen.[1526] Therefore, iron, in the electron-rich, ferrous state, has contributed more electron density to the $dp\pi$ molecular orbital system than the oxygens, both more electronegative atoms, has contributed to the σ bond. The unique feature of Fe^{2+} in this reaction is the ability of its d orbitals to overlap with the π molecular orbital system of oxygen and donate sufficient electron density through the resulting π molecular orbital systems. This **back donation of π electron density to the π molecular orbital system of the molecular oxygen** is a common feature of the prosthetic cations of transition metals that interact directly with molecular oxygen.

The reversible association between hemoproteins and oxygen can be duplicated quite closely with the **synthetic heme**

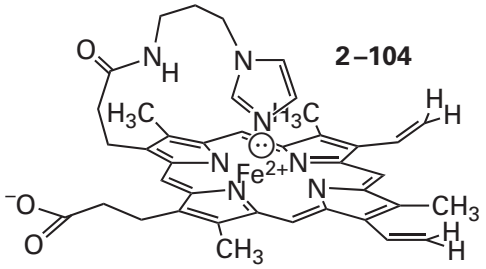

2–104

and its homologues when they are dissolved in aqueous solutions of detergents.[1527,1528] The detergent provides micelles into which these hemes can dissolve. Properties of hemes in globins that are duplicated by the synthetic heme include changes in optical spectra upon ligation, dissociation constants, and on and off rates. These observations suggest that the protein of monomeric globins such as myoglobin simply provides a convenient way of simultaneously dissolving the otherwise insoluble heme in water, sterically preventing the formation of stable heme dimers held together by peroxide dianion, and providing the required axial ligand opposite the open site on the Fe^{2+}.

The **affinity for oxygen of the heme** in oligomeric globins such as hemoglobin, which contains four hemes, is further influenced by the structure of the protein. Depending on the conformation of the protein, the hemes in hemoglobin have either low or high affinity for oxygen. The Fe^{2+} is displaced in the direction of the imidazolyl group in the uncoordinated heme, which usually has no sixth ligand, by the electron repulsion between the four lone pairs of electrons on the pyrrole nitrogens and the lone pair of electrons on the nitrogen of the imidazolyl group. When molecular oxygen binds, the Fe^{2+} moves into the center of the heme[1514] because the σ bond and the $dp\pi$ bonds to the oxygen balance the electron repulsion on the two sides of the heme. Because the iron must move into the plane of the heme during the association of molecular oxygen, any steric constraint that hinders this movement should decrease the affinity of the heme for molecular oxygen. When alterations are made in the structure of heme model compound **2–104** that pull the imidazolyl group away from the plane of the porphyrin and consequently hinder the movement of the iron into the plane, the affinities for oxygen decrease.[1529]

It is also possible to compare crystallographic molecular models of hemoglobin in the conformations of high affinity and low affinity.[1530] In the conformation of low affinity, the α helix in which the histidine providing the axial ligand opposite the open site is located has moved relative to its position in the conformation of high affinity. This movement pulls the imidazolyl group farther away from the plane of the heme. Because the iron should respond to this tug, the movement of this α helix should be at least part of the explanation for the lower affinity

for molecular oxygen in this conformation (Figure 2–53).[1523,1524] In the conformation of high affinity, the imidazolyl group is not pulled away from its unconstrained position.

Occasionally the iron–oxygen bond in the complex between molecular oxygen and a ferroheme splits heterolytically to yield superoxide radical anion and iron(III) porphyrin

$$O_2{\cdot}Fe^{2+}{\cdot}\text{porphyrin} \longleftrightarrow O_2^{\cdot -}{\cdot}Fe^{3+}{\cdot}\text{porphyrin} \rightleftharpoons O_2^{\cdot -} + Fe^{3+}{\cdot}\text{porphyrin} \qquad (2\text{–}247)$$

The molecular oxygen bound reversibly to a heme in hemoglobin or myoglobin, however, is almost inert to this dissociation. It has already been pointed out that oxyiron(II) is not simply a molecule of oxygen associated through its σ molecular orbital system with an Fe^{2+}. Nor is it simply a superoxide radical anion associated by the bonding of one of its σ lone pairs of electrons with an Fe^{3+}. In some contexts, however, it is useful to assume that oxyiron(II) has properties expected of a superoxide radical anion associated with an Fe^{3+}, a superoxyiron(III). Some justification for this assumption is that in the active site of the TxtE protein from *Streptomyces scabiei*, which nitrates the phenyl ring of L-tryptophan, the prosthetic oxyiron(II) porphyrin participates in a colligation with the neutral radical nitric oxide to form peroxynitrite ion as the axial ligand to iron(III) porphyrin.[1531] This colligation acts as a detection of a radical.

The advantage of considering oxyiron(II) porphyrin as superoxyiron(III) porphyrin, which is similar to what is done when the properties of a molecule are considered to be the consequence of only one of its resonance forms, is illustrated by the indole dioxygenases. Tryptophan 2,3-dioxygenase[1532] and indoleamine 2,3-dioxygenase[1533] are two distantly related enzymes[1534] that both use hemes for the dioxygenation of the respective indolyl group

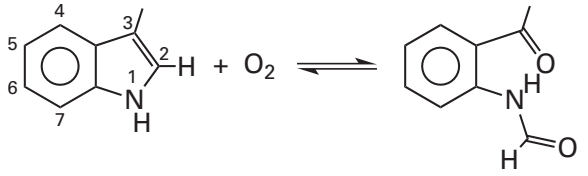

(2–248)

They are often present together in the same species, and they are assumed to have the same mechanism. In the reactions catalyzed by tryptophan 2,3-dioxygenase from *Pseudomonas*[1535] and by human tryptophan 2,3-dioxygenase,[1536] the respective products, each *N*-formyl-L-kynurenine, contain both oxygens from the molecular oxygen, a fact that causes tryptophan 2,3-dioxygenase to be designated a dioxygenase.

The first step in the mechanism of tryptophan 2,3-dioxygenase is the binding of molecular oxygen to the ferroheme adjacent to an already bound L-tryptophan to produce the usual oxyiron(II) porphyrin. The identical complex can be produced by association of superoxide radical anion with the ferric heme.[1537] Synthetic complexes between superoxide radical anion and several similarly coordinated Fe^{3+} are able to convert a number of indoles into the corresponding 2,3-dioxygenated products.[1538] In the crystallographic molecular model of the complex between L-tryptophan and tryptophan 2,3-dioxygenase from *Xanthomonas campestris*,[1534] the closest carbon of the indolyl group to the iron of the heme is carbon 2, and in the crystallographic molecular model of the complex between L-tryptophan, molecular oxygen, and human tryptophan 2,3-dioxygenase,[1539] the closest carbon to the distal oxygen is also carbon 2, which is 0.31 nm away, within the sum of the van der Waals radii (0.33 nm).

After the association of molecular oxygen with ferrous heme, the equivalent of a superoxide radical anion (Equation 2–247) on an iron(III) porphyrin is then thought to participate in a radical addition at carbon 2 of the indolyl group[1540,1541] to produce the equivalent of an alkylperoxyiron(III) porphyrin and a tertiary radical at carbon 3 of the indolyl group

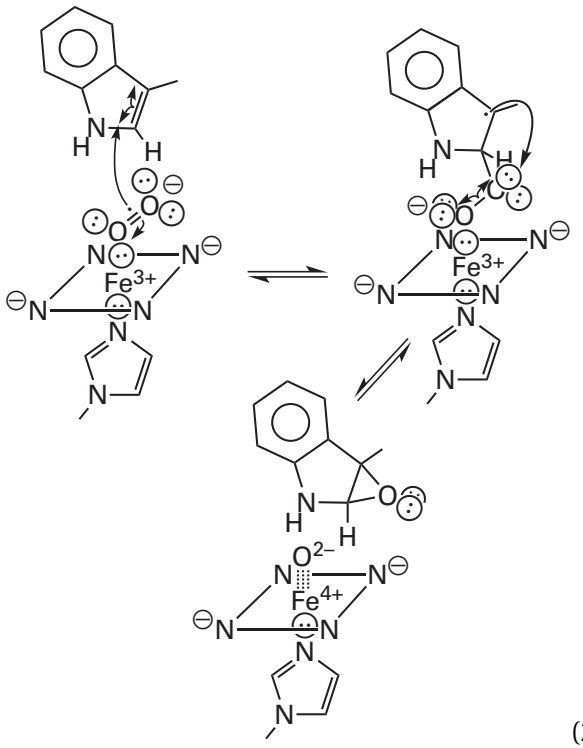

(2–249)

significantly stabilized by delocalization into the phenyl ring. During **addition of the radical in the superoxide radical anion to the double bond,** π electron density is withdrawn onto the proximal oxygen as the bond between the distal oxygen and the carbon forms. When substituents that withdraw more and more of this π electron density into the heme are added to the porphyrin, the rate of disappearance of the oxyiron(II) porphyrin, a measure of formation of the σ bond, increases,[1542] and in the synthetic complexes, the most electron-deficient superoxyiron(III) complexes and the most electron-rich indoles are observed to form the oxygenated products with the greatest rates.[1538]

The alkylperoxyiron(III) then dissociates homolytically, rather than heterolytically, into the **2,3-epoxide of the indolyl group** and oxoiron(IV) porphyrin,[1541] rather than the oxoiron(IV) porphyrin$^{\bullet+}$. There is a side product of the enzymatic reaction catalyzed by both human tryptophan 2,3-dioxygenase and human indoleamine 2,3-dioxygenase that could reasonably arise from intramolecular nucleophilic addition of the α-amino group of L-tryptophan to carbon 2 of the 2,3-epoxide,[1536] and this side product is considered to be an indicator of the existence of the epoxide in the normal mechanism. The MarE protein from *Streptomyces* is a hemoprotein that is a distant relative of tryptophan 2,3-dioxygenase and indoleamine 2,3-dioxygenase. It catalyzes the monooxygenation of indole to 1,3-dihydroindol-2-one, a product that would result from dissociation of the 2,3-epoxide of indole at carbon 3 to form the tertiary carbenium ion, stabilized by delocalization into the phenyl ring, followed by a hydride migration[1543] from carbon 2 to the carbenium ion on carbon 3.

In the active sites of tryptophan 2,3-dioxygenase and indoleamine 2,3-dioxygenase, however, oxoiron(IV) porphyrin and the 2,3-epoxide are converted to the products, *N*-formyl-D-kynurenine and iron(II) porphyrin. All that is known about these latter steps is that the oxygen of oxoiron(IV) porphyrin, as well as the other oxygen from the original molecular oxygen, is incorporated into the products, but the results from the MarE protein suggests that dissociation of the epoxide at carbon 2 to form the iminium of nitrogen 1, rather than the tertiary carbenium ion at carbon 3, could initiate oxidative cleavage of the carbon–carbon bond.

Proteins containing hemes P450 comprise a family of enzymes in which a complex between molecular oxygen and ferroheme can be reduced by one electron to peroxyiron(III) porphyrin or hydroperoxyiron(III) porphyrin. Historically, the members of this family have been referred to as cytochromes P450 even though they are not responsible for electron transfer. Each member of this family of enzymes has a heme in which the proximal axial ligand opposite its open site is the sulfido group of a cysteine.[662,1544,1545] This sulfido group is responsible for the absorption maximum of the heme at 450 nm, which gives this family the name cytochromes P450. Although the criterion for membership in this family of enzymes is only the possession of a heme with a sulfido group as the proximal axial ligand, most members of the family catalyze similar oxidations and have superposable tertiary structures.

The **resting state** of a prosthetic heme P450 is aquoiron(III) porphyrin (see Figure 2–50), the ferric heme with its open site occupied by a molecule of water. In most of these enzymes, reduction of the heme to the ferrous state by transfer of one electron is performed either by a [2Fe–2S] ferredoxin[1546,1547] or by flavoenzyme NADPH—hemoprotein reductase, which can be either a separate protein[1548] or a separate domain of the enzyme containing the heme P450 itself.[1152] Following production of the ferrous heme by transfer of one electron, oxygen binds to form a complex stereochemically indistinguishable from oxyiron(II) porphyrins in model compounds (Figure 2–52)[1514,1549,1550] except that, as in hemoglobin and

myoglobin, the dioxygen is confined to a single orientation by steric effects and by a hydrogen bond between a side chain from the protein and the distal oxygen.

Usually **reduction of the heme to the ferrous state**, which initiates the catalysis; the **association of the oxygen**; the eventual production of an unstable oxoiron(IV) porphyrin$^{\bullet+}$; and then its conversion to an unstable hydroxyiron(IV) porphyrin occur efficiently only after the reactant to be oxidized has bound to the active site of the enzyme so that it is prepared for the oxidation.[1551] Binding of the reactant also changes the spin state of Fe^{3+} in the aquoiron(III) porphyrin from low-spin to high-spin,[1552,1553] increases the biochemical standard reduction potential of the aquoiron(III) porphyrin, and stabilizes the subsequent complex between ferrous heme and molecular oxygen.[1554]

Following the binding of molecular oxygen to the iron(II) porphyrin, there is a second one-electron reduction. The second electron is provided by another molecule of the same ferredoxin or by the second electron from the flavin semiquinone of NADPH—hemoprotein reductase. The complex between molecular oxygen and Fe^{2+} in the heme is reduced by one electron to give **peroxyiron(III) porphyrin**[1555,1556]

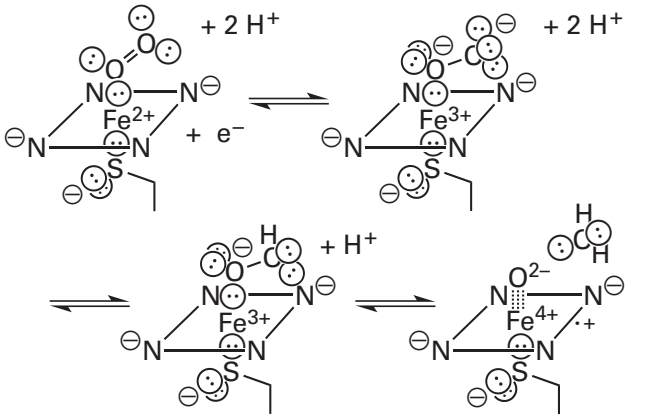

(2–250)

where peroxyiron(III) is the complex (Figure 2–50) between peroxide dianion and Fe^{3+}. This intermediate has been produced in a stable form in solution with a synthetic heme by reducing the complex between its Fe^{2+} and molecular oxygen by one electron, and its spectroscopic properties have been documented.[1557]

The peroxyiron(III) porphyrin is then hydronated on its distal oxygen to form **hydroperoxyiron(III) porphyrin** (see Figure 2–50),[1555,1558,1559] which is the same as the complex between the ferriheme in a hemoperoxidase and hydroperoxide ion (Equation 2–240) except for the identity of the catalytic acid–bases that surround it. Again, this intermediate has been produced in a stable form in the same synthetic heme by hydronating the peroxyiron(III) porphyrin.[1557]

As in a peroxidase, the hydroperoxyiron(III) porphyrin is heterolytically cleaved under acid catalysis[1560] to give oxoiron(IV) porphyrin$^{\bullet+}$.[1549,1561,1562] The peroxyiron(III) porphyrin in the active site of chloride peroxidase from *Leptoxyphium fumago* can be trapped as a stable species at 77 K and converts first to the hydroperoxyiron(III) porphyrin, which is also stable until the temperature is raised further, at which point it then converts to the oxoiron(IV) porphyrin$^{\bullet+}$, but this intermediate can be observed only at temperatures below 220 K.[1456]

Because, in most cases, none of these transformations leading to the production of oxoiron(IV) porphyrin$^{\bullet+}$ in a heme P450 can occur until the reactant is bound and ready to be oxidized, most studies of the oxoiron(IV) porphyrin$^{\bullet+}$ in these enzymes have of necessity been of the evanescent intermediates in the enzymatic reaction, which almost immediately oxidize the substrate. For example, at 4 °C, the complex between iron(II) porphyrin, camphor, and molecular oxygen in the active site of camphor 5-monooxygenase from *P. putida* can be rapidly reduced by hydrated electrons to hydroperoxyiron(III) porphyrin, which then decays with a rate constant 96 ms^{-1} to iron(III) porphyrin, but no intermediates are observed.[1563] This observation demonstrates that the rate-limiting step, at least in this case, is heterolytic dissociation of the hydroperoxyiron(III) porphyrin and that all the steps in the reaction following formation of the resulting oxoiron(IV) porphyrin$^{\bullet+}$ are so fast that they are hidden from observation.

Stable forms of the oxoiron(IV) porphyrin$^{\bullet+}$, however, have been produced in chloride peroxidase from *L. fumago*[1564,1565]and in the peroxidase from *S. acidocaldarius*,[1566,1567] both of which contain hemes P450 by virtue of having sulfido groups as their proximal ligands. In chloride peroxidase, the **length of the iron–oxygen bond** (0.165 nm) is shorter than that in a hemoperoxidase (0.172 nm) that has an imidazolyl group as its proximal ligand rather than a sulfido group[1565] because electron donation from the sulfido group of the cysteine that is the axial ligand to the iron opposite the oxygen of the oxoiron(IV) fills in the π molecular orbitals and gives the

bond between the iron ion and the oxygen greater triple-bond character. When the oxoiron(IV) porphyrin$^{\bullet+}$ of the peroxidase from *S. acidocaldarius* is reduced unnaturally by one electron and spontaneously hydronates to become hydroxyiron(IV) porphyrin, the bond length of the iron–oxygen bond increases to 0.182 nm as more electron density is withdrawn onto the oxygen from the π molecular orbitals and the bond becomes more like a single σ bond.[1568]

Although most enzymes containing hemes P450 use molecular oxygen as the substrate to produce oxoiron(IV) porphyrin$^{\bullet+}$ coincident with two one-electron reductions, there are examples that use only hydrogen peroxide and no reductant to produce oxoiron(IV) porphyrin$^{\bullet+}$, just as a peroxidase would.[1569-1571] Regardless of how the enzyme containing a heme P450 produces the oxoiron(IV) porphyrin$^{\bullet+}$, however, it seems to have the same capabilities, as a result, in part, of the cysteine that is the ligand to the iron ion opposite the oxygen.[1562]

Enzymes containing hemes P450 catalyze several different types of oxidations. The oxoiron(IV) porphyrin$^{\bullet+}$ of a heme P450 can engage two successive **one-electron transfers**,[1572] as it does in a hemoperoxidase. It can **epoxidize olefins** (Equation 2–234),[1573,1574] just as it does in nonenzymatic reactions. It can **abstract a hydrogen atom** from a carbon adjacent to an amino nitrogen[1575]

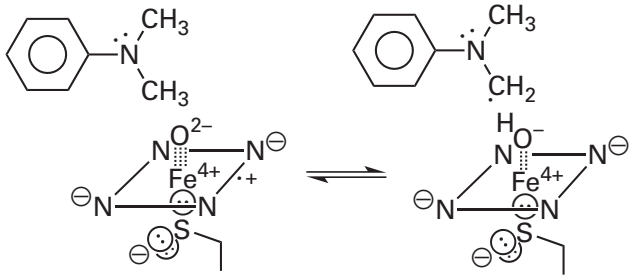

(2–251)

And it can **remove the equivalent of a hydride** from a secondary alkane.[1576]

The most common oxidations catalyzed by hemes P450, however, are **hydroxylations of alkanes**. An example of the hydroxylation of an alkane is the stereospecific exo hydroxylation of camphor catalyzed by camphor 5-monooxygenase

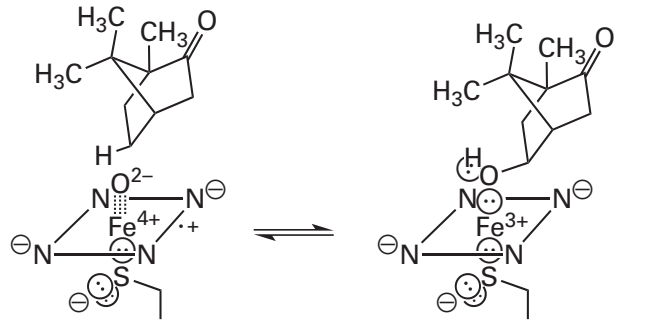

(2–252)

To hydroxylate a saturated carbon requires a strong oxidant. It has been proposed that the advantage of a sulfido group as the proximal ligand is that it decreases the biochemical standard reduction potential of the oxoiron(IV) porphyrin$^{\bullet+}$, which is one of the intermediates in these reactions, into a range in which it is a strong enough oxidant to hydroxylate a saturated carbon but not strong enough to pull an electron irreversibly out of the tyrosines elsewhere in the protein.[1434]

Theoretical calculations[1577] have led to the suggestion that the **mechanism of hydroxylation** takes place in three steps. The oxoiron(IV) porphyrin$^{\bullet+}$ that is formed in the active site first abstracts the hydrogen atom of the carbon–hydrogen bond to be hydroxylated. The resulting hydroxy group on the hydroxyiron(IV) porphyrin (see Figure 2–50) and the alkyl radical reorient so that the orbital containing the unpaired electron on the hydroxyl radical of the hydroxyiron(IV) porphyrin and the orbital containing the unpaired electron of the alkyl radical can overlap. The two unpaired electrons in these two orbitals colligate to form a covalent bond between the carbon of the alkyl group and the oxygen of the hydroxy group.

There are **a number of facts** that are consistent with this suggestion. When the hydrogen to be replaced by the hydroxy group is replaced by a deuterium, the rate of the enzymatic hydroxylation at that location decreases[1578] by a factor of as much as 10.[1579] Because the initial hydrogen abstraction is usually the rate-limiting step in a hydroxylation catalyzed by a heme P450 , the postulated hydroxyiron(IV) porphyrin has rarely been observed, but in the active site of terminal olefin-forming fatty acid decarboxylase from *Jeotgalicoccus*, an enzyme containing a heme P450, even though the rate of the reaction decreases by a factor of 8 when the hydrogen abstracted is replaced by a deuterium, the hydrogen abstraction is not completely rate-limiting, and hydroxyiron(IV) porphyrin has been observed as a

transient intermediate in the enzymatic reaction.[1580] The hydroxylation of an asymmetric carbon with a deuterium and a hydrogen, on which the hydrogen is replaced by a hydroxy group, proceeds with significant but not complete racemization.[1579,1581,2609] Both results suggest that a planar intermediate such as a carbenium ion or carbon radical is formed by removal of a hydride or a hydrogen atom, respectively, from the carbon to be hydroxylated. The rate constants for hydroxylation of a series of alkanes by the oxoiron(IV) porphyrin$^{\bullet+}$ in the active site of unspecific peroxygenase from *Agrocybe aegerita* decrease monotonically as the bond dissociation energies of the hydrogen that is replaced increase.[1582] This correlation is consistent with abstraction of the hydrogen being the rate-limiting step in the hydroxylation catalyzed by this heme P450.

When a complex between [5-$^2H_2$]camphor, oxygen, and iron(II) porphyrin in the active site of camphor 5-monooxygenase from *P. putida* at 74 K is reduced radiolytically and the temperature is raised to 190 K, the oxoiron(IV) porphyrin$^{\bullet+}$ forms and then hydroxylates the camphor at carbon 5. The product, (+)-*exo*-5-hydroxycamphor, remains as a ligand through its oxygen to the resulting iron(III) porphyrin, but the hydrogen of the hydroxy group is a deuteron,[1583] which could only have come from carbon 5 of the camphor. This observation is consistent with abstraction of a deuterium from carbon 5 of the camphor by the oxygen of the oxoiron(IV) porphyrin$^{\bullet+}$ to form deuterohydroxyiron(IV) porphyrin, the deuterohydroxy group of which colligates with the radical at carbon 5 of the camphor. Similar results were observed with the heme P450 in bovine cholesterol monooxygenase (side-chain-cleaving).[1584]

A number of compounds known as **radical clocks** have been submitted to hydroxylation.[1585] These compounds, such as methylcyclopropane or *trans*-2-methyl-1-phenylcyclopropane, rearrange rapidly when the respective radical is produced at the respective methyl group, and the rate constant of each rearrangement is known. The fact that rearranged products in these reactions are observed suggests that abstraction of a hydrogen atom is involved in the mechanism even if it is only occurring in a transition state with radical character. Also consistent with the conclusion that hydrogen abstraction is involved in the mechanism is that when the hydrogens that would be abstracted from the methyl group of *trans*-2-methyl-1-phenylcyclopropane are changed to deuteriums, the yield of oxidation of the phenyl ring increases.[1586] From the observed ratios of the alcohols with unrearranged and rearranged structures for a series of these radical clocks, the lifetime of a radical intermediate in the hydroxylation catalyzed by hemes P450 that are unspecific monooxygenases has been estimated to be around 100 fs[1587-1589] or around 50 ps.[1590,1591] The former seems too fast for a radical to be an intermediate, while the latter is consistent with a radical as an intermediate. One explanation of these discrepancies in the rates is that the active site of the enzyme may hinder sterically the rearrangements of the radicals of some of these molecular clocks, cause the lifetimes of the unrearranged radicals to increase, and lead to longer lifetimes of the radicals.[1589] This explanation, however, seems at odds with the rather large, hydrophobic pockets in crystallographic molecular models of these unspecific monooxygenases[1592] that arise from their need to hydroxylate an array of alkanes nonspecifically.

In contradistinction to these results from isotope effects, stereochemistry, and rearrangements of radical clocks, which are consistent with hydrogen abstraction as the first step, a high yield of products resulting from the rearrangements expected for an **oxocarbenium ion** and none of the products resulting from the rearrangements expected for a radical have been observed during the hydroxylation of (*trans*, *trans*-2-*tert*-butoxy-3-phenylcyclopropyl)methane by unspecific monooxygenase from *R. norvegicus*[1593]

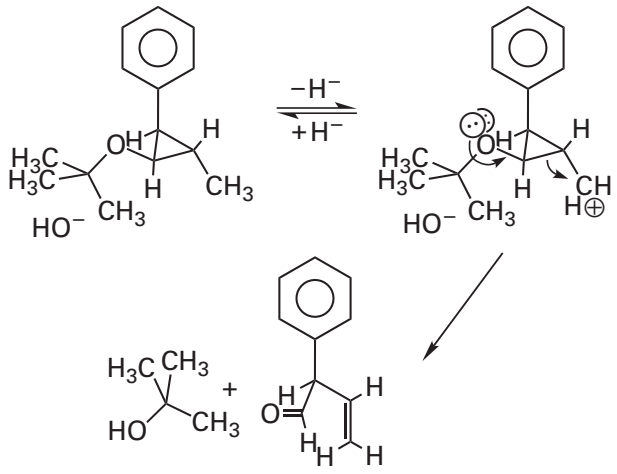

(2–253)

The radical would rearrange to the benzyl position rather than to the carbon with the *tert*-butoxy group.

There is little doubt about the fact that the oxoiron(IV) porphyrin$^{\bullet+}$ formed on an appropriate heme P450 is able to hydroxylate a saturated carbon.

For example, the stable oxoiron(IV) porphyrin$^{\bullet+}$ that can be produced in the active site of the epoxidase from *S. acidocaldarius* is able to hydroxylate dodecanoic acid at the fully saturated carbons at positions 9, 10, 11, and 12.[1567,1594] The oxoiron(IV) porphyrin$^{\bullet+}$ formed transiently in the active site of unspecific peroxygenase from *A. aegerita* is stable enough to be observed and has been shown to be able to hydroxylate alkyl carbons in a series of 10 carboxylic acids and ethers.[1595]

It is also possible, however, that in some situations the peroxyiron(III) porphyrin or hydroperoxyiron(III) porphyrin that is an intermediate preceding formation of the oxoiron(IV) porphyrin$^{\bullet+}$ can also perform hydroxylations. When the step in the mechanism in which hydroperoxyiron(III) porphyrin is converted to oxoiron(IV) porphyrin$^{\bullet+}$ by a nonspecific monooxygenase, cytochrome P450 2B4 from *R. norvegicus*, is inhibited by mutating a threonine serving as the required catalytic acid, the rates of hydroxylation of alkanes decrease but not so much as they should were the oxoiron(IV) porphyrin$^{\bullet+}$ the only species hydroxylating them, and the rates of epoxidations of alkanes actually increase.[1596] The homologous mutation in camphor 5-monooxygenase from *P. putida* eliminated hydroxylation completely while decreasing the rate of epoxidation by only about 80%.[1597] At the least, these results suggest that peroxyiron(III) porphyrin or hydroperoxyiron(III) porphyrin, the immediate precursors of oxoiron(IV) porphyrin$^{\bullet+}$, can perform the epoxidations and perhaps also the hydroxylations catalyzed by these enzymes, but not so effectively as the oxoiron(IV) porphyrin$^{\bullet+}$. In model reactions, a *m*-chlorobenzoylperoxyiron(III) porphyrin (Equation 2–232; R = *m*-chlorobenzoyl) is able to hydroxylate alkanes.[1443] There are results from various measurements of the effects of deuteration on the rates of hydroxylations catalyzed by enzymes containing hemes P450 that are interpreted to mean that oxoiron(IV) porphyrin$^{\bullet+}$ is responsible exclusively for the hydroxylation[1598] or that it is not.[1599,1600] Theoretical calculations, however, lead to the conclusion that peroxyiron(III) porphyrin is too weak an oxidant to perform a hydroxylation.[1577]

Enzymes containing hemes P450 also perform **monooxygenations of arenes**.[1601] For example, an unspecific peroxygenase from *A. aegerita* catalyzes the epoxidation of naphthalene

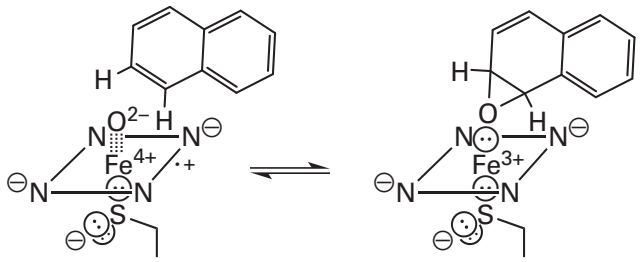

(2–254)

In this case, the oxoiron(IV) porphyrin$^{\bullet+}$ is formed by association of hydrogen peroxide with the prosthetic iron(III) porphyrin in the active site, followed by the usual heterolytic dissociation. The immediate product of this oxidation is the arene epoxide that undergoes an acid-catalyzed ring opening after its dissociation from the active site to give the ultimate product of the reaction, which is 1-hydroxynaphthalene,[1602] in addition to the water that dissociated during formation of the oxoiron(IV) porphyrin$^{\bullet+}$. A hydrogen on a carbon in an aromatic system is quite difficult to abstract (470 kJ mol^{-1}), so the monooxygenation of an arene proceeds by electrophilic aromatic substitution.

An analysis of the rates of aromatic monooxygenation by a synthetic oxoiron(IV) porphyrin$^{\bullet+}$ suggests that the first step in monooxygenation of an arene is electron transfer[1603] from the aromatic π molecular orbital system to the significantly electron-deficient oxoiron(IV) porphyrin$^{\bullet+}$. This electron transfer would be followed by a colligation to form a carbon–oxygen bond between the oxygen of the resulting oxoiron(IV) porphyrin and a carbon of the resulting radical cation of the arene. This colligation would form the usual intermediate in an electrophilic aromatic substitution. In the case of naphthalene, this intermediate would be a nonatetraenyl carbenium ion, with the oxygen of the now oxidoiron(III) and a hydrogen at the tetrahedral carbon at carbon 2 breaking the ring of *p* orbitals.[1604] Either the electrophilic aromatic substitution is completed as usual by dissociation of the hydron to give the hydroxylated arene as a product, or the oxido oxygen on the oxidoiron(III) porphyrin adds as a nucleophile to the carbocationic carbon immediately adjacent to it in the adduct to give the arene epoxide, as is the case in the nonspecific peroxygenase from *A. aegerita* (Equation 2–254).

In part because of the electron donation from the axial sulfido group (Equation 2–250), the **peroxyiron(III) porphyrin of a heme P450 is nucleophilic** at its distal oxygen[1556] and can add to a carbonyl.[1605-1609]

17α-Hydroxyprogesterone deacetylase is responsible for an oxidative cleavage

$$H_2Fl_{red}^- + O_2 + 17\alpha\text{-hydroxyprogesterone} \rightleftharpoons HFl_{ox} + \text{acetate} + \text{androstenedione} + H_2O \quad (2\text{–}255)$$

where $H_2Fl_{red}^-$ and HFl_{ox} are the reduced and oxidized flavin, respectively, in a separate enzyme, NADPH—hemoprotein reductase, that acts as an electron-transferring coenzyme for 17α-hydroxyprogesterone deacetylase. The acetyl group at carbon 17 of the 17α-hydroxyprogesterone becomes the acetate that is a product, and carbon 17 becomes a carbonyl group in the androstenedione that is the other product. The oxidation requires two electrons and breaks the bond between carbon 17 and the carbonyl carbon of the acetyl group. An intermediate in the reaction catalyzed by human 17α-hydroxyprogesterone deacetylase has been trapped at low temperature after adding O_2 to the complex between 17α-hydroxyprogesterone and human 17α-hydroxyprogesterone deacetylase in which the heme had already been reduced by NADPH—hemoprotein reductase. This intermediate had a resonance Raman infrared spectrum consistent with **ferric peroxy hemiketal 2–105**, which is the product of nucleophilic addition of a peroxyiron(III) porphyrin to the carbonyl in the acetyl group at carbon 17 of 17α-hydroxyprogesterone[1610]

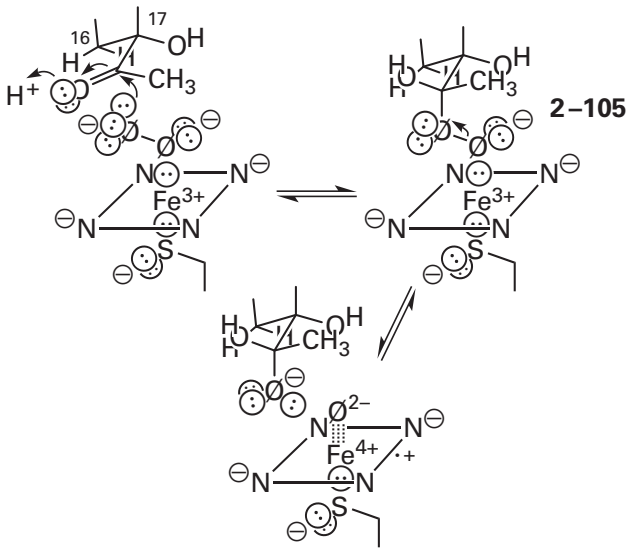

(2–256)

In the crystallographic molecular model of the complex between human 17α-hydroxyprogesterone deacetylase and progesterone, the acetyl group is in the proper location and orientation[1611] for the nucleophilic addition.

In the normal enzymatic reaction, the peroxyiron(III) porphyrin that is the nucleophile is formed in the usual way from iron(III) porphyrin and an electron, molecular oxygen and the resulting iron(II) porphyrin, and a second electron. The normal complete cleavage (Equation 2–255) also occurs, however, when iodosylbenzene is substituted in the reaction catalyzed by human 17α-hydroxyprogesterone deacetylase for the molecular oxygen and the NADH that reduces the flavin.[1612] Iodosylbenzene produces oxoiron(IV) porphyrin$^{\bullet+}$ directly from iron(III) porphyrin in a two-electron oxidation (see Equation 2–228) requiring no other oxidant or reductant. This observation suggests that the only role of the initial addition of peroxyiron(III) porphyrin to the acetyl group to form **2–105** is that the electrophilic acyl carbon of the acetyl group acts in place of a hydron to permit heterolytic dissociation of the oxygen–oxygen bond to produce the *gem*-diol, which could otherwise form by a simple hydration, and oxoiron(IV) porphyrin$^{\bullet+}$ from peroxyiron(III) porphyrin (Equation 2–256). If this is the case, then the iodosylbenzene simply takes the place of the usual stratagem used by the enzyme to form an oxoiron(IV) porphyrin$^{\bullet+}$. One of the oxygens in the acetate produced from the conversion of 17α-hydroxypregnenolone by porcine 17α-hydroxyprogesterone deacetylase is an oxygen-18 that was the oxygen-18 of an [^{18}O]acetyl group on a reactant,[1605] and the other oxygen atom is an oxygen-18 from [$^{18}O_2$]molecular oxygen.[1612,1613] These two facts would require that the intact *gem*-diol proceed to the next steps in the reaction rather than dehydrating.

It is unclear, however, how the oxoiron(IV) porphyrin$^{\bullet+}$ and the *gem*-diol would proceed from this point to accomplish the cleavage. All, or almost all, of the most obvious mechanisms[1612] seem to be ruled out by the preceding and following observations. The other atom of oxygen-18 in [$^{18}O_2$]oxygen ends up as the oxygen in the carbonyl group at carbon 17 of the product, rather than the oxygen in the hydroxy group that was there in the reactant and already forming a covalent bond to carbon 17. The fact that both deuteriums in a 16,16-$^2H_2$-labeled reactant remain on carbon 16 in the product[1613] and the fact that all deuteriums in a $^2H_3$-labeled acetyl group at position 17 in the reactant also remain in the [$^2H_3$]acetate that is the product[1612,1613] together seem to rule out the abstraction of any hydrogen on a carbon by the oxoiron(IV) porphyrin$^{\bullet+}$. The fact that the bond dissociation energy of the oxygen–

hydrogen bond of a hydroxy group is quite large (445 kJ mol^{-1}) argues against the abstraction of a hydrogen from the hydroxy group at carbon 17 in the reactant, even though, in a crystallographic molecular model of a complex between 17α-hydroxyprogesterone and human 17α-hydroxyprogesterone deacetylase, the oxygen in the 17-hydroxy group is one of the closest (0.45 nm) atoms in the steroid to the iron ion in the heme. In this molecular model, the carbonyl carbon and the carbonyl oxygen of the 17-acetyl group and carbon 16 of the steroid are also all between 0.4 and 0.5 nm from the iron ion, so any one of them or all of them could be involved in the rearrangement leading to the cleavage.

All these considerations seem to rule out a heterolytic cleavage of the peroxy group (Equation 2–256) as a step in the oxidative deacetylation of 17α-hydroxyprogesterone deacetylase. Before the observation was made that iodosylbenzene could substitute for oxygen, the accepted mechanism for the oxidative cleavage performed by 17α-hydroxyprogesterone deacetylase was a homolytic one (Figure 2–54).[1556,1606-1609,1614] The homolytic proposal takes advantage of a spontaneous dissociation of the carbon–carbon bond adjacent to the radical of a *gem*-diol and the fact that a radical on carbon 17 of the steroid adjacent to the hydroxy group (BDE = 396 kJ mol^{-1}) is even more stable than a radical on a tertiary carbon (BDE = 400 kJ mol^{-1}). The fact that one of the oxygens in the molecular oxygen ends up in the carbonyl group of the androstenedione requires that the resulting hydroxyiron(IV), which is equivalent to a hydroxyl radical on Fe^{3+}, colligate with the radical on carbon 17 to form another, different *gem*-diol, but in the crystallographic molecular model, carbon 17 is 0.52 nm from the iron ion, albeit because it is a tetrahedral carbon in the 17α-hydroxyprogesterone, and it would have to move closer, presumably as the acetate that is the product of the reaction shifts away. The observation that iodosylbenzene can substitute for the molecular oxygen would require that the oxoiron(IV) porphyrin$^{\bullet+}$ formed by the iodosylbenzene remove the equivalent of a hydrogen atom from a *gem*-diol of the 17α-hydroxyprogesterone that is the reactant to produce the usual radical of the *gem*-diol and the oxoiron(IV)porphyrin. This abstraction would be difficult (BDE = 450 kJ mol^{-1}) unless a catalytic base

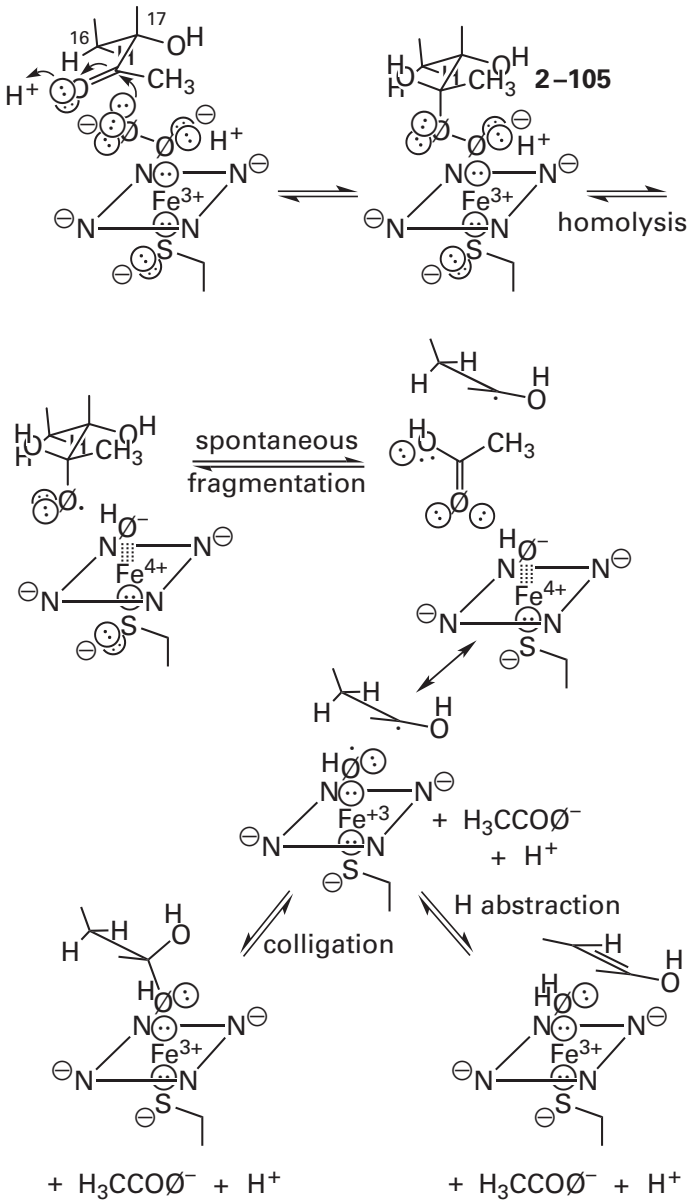

Figure 2–54: Homolytic deacetylation performed by the peroxyiron(III) porphyrin (Equation 2–250) in the active site of human 17α-hydroxyprogesterone deacetylase.[1606-1609] The nucleophilic[1556] peroxy group of the peroxyiron(III) porphyrin adds to the carbonyl of a methyl ketone to form peroxy hemiketal **2–105**. Upon hydronation of the oxygen proximal to the Fe^{3+}, the oxygen–oxygen bond of the peroxy group undergoes homolysis to produce hydroxyiron(IV) and the oxy radical of a geminal diol. The oxy radical of the geminal diol undergoes spontaneous fragmentation to produce acetate and the radical of the deacetylated hydroxyhydrocarbon. The radical of the hydroxyhydrocarbon ends up adjacent to the hydroxyiron(IV), which is the resonance hybrid of a hydroxyl radical on Fe^{3+}. The hydroxyl radical either reacts directly with the unpaired electron of the radical of the hydroxyhydrocarbon to produce the hydrate at carbon 17 of the final product, androstenedione, bound to the Fe^{3+} or abstracts a hydrogen immediately adjacent to the unpaired electron of the radical of the hydroxyhydrocarbon to produce the enol of androstenedione. The product that predominates in this last step depends upon the enzyme in which it occurs.[1606-1609]

removed the hydron from the hydroxy group first or the electron is removed from the oxyanion of the immediate product of the addition of hydroxide to the carbonyl.

A different enzyme containing a heme P450, cholest-4-en-3-one 26-monooxygenase [(25*S*)-3-oxocholest-4-en-26-oate forming] from *M. tuberculosis* turns the terminal *pro-S* methyl group in the linear 1,5-dimethylhexyl side chain of cholest-4-en-3-one into a carboxy group by three successive hydroxylations at that carbon. A significant portion (40%) of the products formed by the enzyme, however, when cholesterol, which has the same 1,5-dimethylhexyl side chain, is the reactant rather than cholest-4-en-3-one result from the deformylation of the (5*S*)-1,5-dimethyl-6-oxohexyl side chain. The (5*S*)-1,5-dimethyl-6-oxohexyl side chain is an intermediate in the overall reaction. It is formed by the first two hydroxylations and dehydration of the resulting *gem*-diol. In addition to the formic acid common to this deformylation of the side chain in cholesterol, the five other products making up this portion of the products of the reaction are those expected from various reactions between a hydroxyiron(IV) porphyrin in the active site and a radical at carbon 5 of the side chain resulting from dissociation of the formic acid. Both a hydroxyiron(IV) porphyrin and a radical at carbon 5 of the side chain should be produced by nucleophilic addition of the distal peroxy oxygen of peroxyiron(III) porphyrin to the 6-oxo group of the side chain that results from the first two hydroxylations followed by homolytic cleavage (see Figure 2–54). These five products are a fingerprint identifying the final oxidation of at least cholesterol as a homolytic process.

The oxoiron(IV) porphyrin$^{\bullet+}$ of a heme P450 can also function as a **strong electrophile.** Cholesterol monooxygenase (side-chain-cleaving), which is an enzyme containing a heme P450, is responsible for cleaving the bond between carbons 1 and 2 in the 1,5-dimethylhexyl side chain of cholesterol (carbons 20 and 22 of the cholesterol). The cleavage proceeds in three successive steps, each involving an oxoiron(IV) porphyrin$^{\bullet+}$ as a intermediate.[1615] The first two steps are simple hydroxylations at carbons 1 and 2 in the side chain, respectively. In the crystallographic molecular model of the complex between the human enzyme and 20,22-dihydroxycholesterol, which is the product of these first two hydroxylations of the side chain and the reactant for the final oxidation leading to cleavage of the carbon–carbon bond, the two hydroxy groups at carbon 1 and carbon 2 of the side chain sit astride the iron of the heme. When an oxygen atom is added to the heme in the molecular model to mimic the oxoiron(IV) porphyrin$^{\bullet+}$ that performs the cleavage of the carbon–carbon bond, the hydroxy group on carbon 2 of the side chain is only 0.23 nm from that oxygen.[1616] The conclusion drawn from this observation is that the 2-hydroxy group adds as a nucleophile to the electrophilic oxygen of the oxoiron(IV) porphyrin$^{\bullet+}$ to produce the peroxyiron(III) porphyrin with carbon 2 of the 1,2-dihydroxy side chain still attached to the distal oxygen of the peroxy group. The bonds in this intermediate then rearrange heterolytically, and the rearrangement produces hydroxyiron(III) porphyrin, pregnenolone, and 4-methylpentanal, the products of the side-chain cleavage.

Cytochrome-*c* oxidase catalyzes the complete reduction of molecular oxygen

$$4\,H^+ + 4\,e^- + O_2 \rightleftharpoons 2\,H_2O \qquad (2\text{–}257)$$

by a mechanism that is similar to the mechanism of an enzyme containing a heme P450. The four electrons required in the reaction are supplied to the enzyme by four molecules of the reduced form of the small electron-transferring coenzyme cytochrome *c*. The enzyme contains just enough prosthetic groups to store all four of these electrons at once. These prosthetic groups are a CuA dinuclear copper cluster (Figure 2–26F); a heme *a* or a heme *b*, depending on the species, in which the iron ion is fully coordinated and diamagnetic in its ferrous state and that acts as a one-electron donor; a heme *a*, heme *b*, or heme *o*, again depending on the species, that has an open site to which the molecular oxygen binds and that is high-spin and paramagnetic in its ferrous state; and a copper ion coordinated by three histidines that also has an open site.[932,1617-1621] One of the histidines that is a ligand to this mononuclear, prosthetic copper ion is the histidinyl group participating in the posttranslational modification that produces the 3-(N^{τ}-histidinyl)tyrosine (Figure 2–55), which is formed by a covalent crosslink between this histidine and a nearby tyrosine in the protein.[1047,1622-1624] The simultaneous presence of **four metallic electron donors** permits the fully reduced enzyme to reduce the molecular oxygen completely in one fell swoop without the

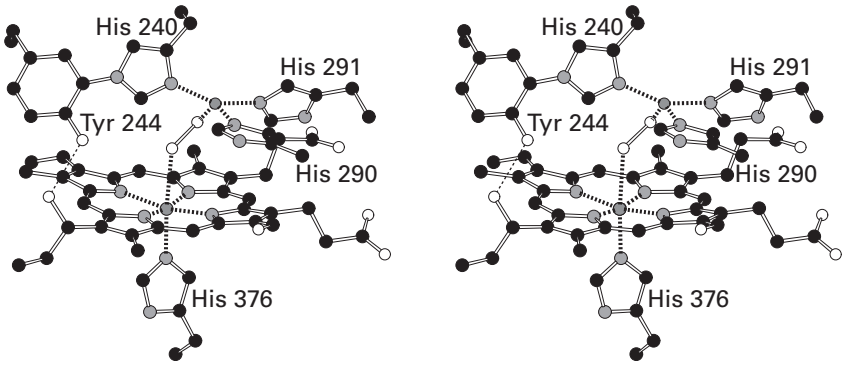

Figure 2–55: Stereodrawing[50] of one of the hemes *a* and one of the prosthetic copper ions complexed with a peroxide dianion in the crystallographic molecular model of bovine cytochrome-*c* oxidase.[1047] Black atoms are carbons, white atoms are oxygens, gray atoms are nitrogens, and the two dark gray spheres surrounded by ligands are an iron ion and a copper ion. Bovine cytochrome-*c* oxidase was purified from mitochondria under ambient aerobic conditions.[1624] The enzyme purified in this way and then recrystallized aerobically was fully oxidized, and six moles of electrons for every mole of enzyme were required to fully reduce its hemes and copper ions.[1623] This titration is consistent with the presence of the equivalent of a peroxide dianion in its active site. In the map of electron density from crystals of this enzyme, a feature of electron density equal in volume and shape to a peroxide dianion was observed spanning the iron ion of heme *a*, to which oxygen is known to bind, and the mononuclear copper ion adjacent to it. This feature of electron density was assumed to be a peroxide dianion and was modeled as such, in spite of the fact that the final oxygen–oxygen bond length following refinement was 0.17 nm,[1622] which is somewhat longer than the 0.14–0.15 nm of the usual peroxide dianion complexed by two metallic ions. The drawing is of the heme *a* and the side chain of Histidine 376 that is its axial ligand; the copper ion and the side chains of the three histidines, Histidines 240, 290, and 291, that are its ligands; and the peroxide dianion of the final crystallographic molecular model.[1047] One of the histidines, Histidine 240, is a 3-(N^{τ}-histidinyl)tyrosine with Tyrosine 244. The peroxide dianion is a ligand to Fe^{3+} in the heme *a* at one of its oxygens and a ligand to the copper ion at the other.

accumulation of intermediates that might release superoxide radical anion or hydrogen peroxide or, even worse, hydroxyl radical into the cytoplasm. During reduction of the fully oxidized bovine enzyme, the rate-limiting step is reduction of the iron in the heme with the open site with which the oxygen associates when it is in its reduced ferrous state (Figure 2–52) and at which the oxygen is reduced.[1625] Consequently, molecular oxygen usually does not bind to the enzyme nor does catalysis commence until the enzyme is fully reduced.

The iron ion in the fully coordinated heme that acts as the donor of a single electron in the bovine enzyme has as one of its axial ligands the imidazolyl group of a histidine that is only two positions in the sequence of amino acids away from the histidine providing the only axial ligand to the heme with the open site at which the reduction of the oxygen occurs.[1618] This connection provides a **continuous path for an electron** on which it can pass rapidly by outer-sphere electron transfer between the iron ions in these two hemes.[1626] The copper ion that is coordinated by the three histidines in bovine cytochrome-*c* oxidase is only 0.45 nm from the iron that has the open catalytic site, and there is nothing between these two metallic ions. This distance would be spanned by the two oxygen atoms in a peroxide dianion coordinated to the iron at one oxygen and the copper ion at the other (Figure 2–55). The dinuclear CuA cluster is coupled electronically to the iron of the fully coordinated heme participating in electron transfer, and a single electron equilibrates rapidly between their respective oxidized states.[1627,1628] The other copper ion, adjacent to the open site on the other heme, is coupled antiferromagnetically to the iron of that heme.[1629] All these arrangements guarantee the rapid arrival of four electrons at the site of reduction.

In the enzymes containing a heme P450 that hydroxylate alkanes, molecular oxygen is initially converted into water and an oxoiron(IV) porphyrin$^{\bullet+}$ (Equation 2–250). Occasionally, the oxoiron(IV) porphyrin$^{\bullet+}$ is converted by mistake in a two-electron reduction into a hydroxyiron(III) porphyrin (see Figure 2–50), and hence a second molecule of water, by absorbing two electrons from the reduced flavin of the NADPH—hemoprotein reductase[1630,1631] or by oxidizing the alkane, which normally is hydroxylated, to an alkene rather than an alcohol.[1632,1633] This abortive side reaction for a heme P450 mimics the actual reaction catalyzed by cytochrome-*c* oxidase.

When the reaction begins with fully reduced cytochrome-*c* oxidase, molecular oxygen is bound at the open site on the iron(II) porphyrin of the catalytic heme,[1634] perhaps by binding initially to the adjacent prosthetic Cu^+ and then moving to the iron[1635] to produce the prosthetic copper(I)oxyiron(II) porphyrin where the molecular oxygen is a ligand to both the Cu^+ and the Fe^{2+}. In several model compounds in which a ferroheme is properly positioned adjacent to a triply coordinated Cu^+, when oxygen binds between the two metallic ions, it is reduced in the inner sphere by an electron from the Fe^{2+} and an electron from the Cu^+ to give[1636-1640] the **complex between the ferriheme, a peroxide dianion, and the Cu^{2+}**, copper(II)peroxyiron(III) porphyrin. In bovine cytochrome-*c* oxidase, cytochrome-*c* oxidase from *P. denitrificans*, and cytochrome-*c* oxidase from *Columba livia*, the same reaction takes place following the binding of oxygen to produce a copper(II)peroxyiron(III) porphyrin[1641-1647] in which the prosthetic Cu^{2+} is coordinated by the distal oxygen of the peroxide dianion.[1629] The initial complex, copper(I)oxyiron(II) porphyrin, and the peroxy complex, copper(II)peroxyiron(III) porphyrin, must be in extremely rapid equilibrium because transfer of the electrons is in the inner sphere, but the question of which of the two complexes predominates at this stage of the reaction seems to be controversial.[1648] Either a copper(II)-peroxyiron(III) porphyrin or a copper(I)-oxyiron(II) porphyrin, which are isosteric and hence indistinguishable as well as being in equilibrium with each other, has been observed crystallographically in the bovine enzyme,[1648-1650] and in this crystallographic molecular model, the peroxide dianion or the molecule of oxygen is coordinated by both the iron ion at the proximal oxygen and the copper ion at the distal oxygen (Figure 2–55).[1047]

In the next step of the mechanism, the distal oxygen of the copper(II)peroxyiron(III) porphyrin is hydronated. The source of the hydron is unclear. It has been proposed that, because it is the closest catalytic acid to the bound oxygen, the source of the hydron is the hydroxy of the 4-hydroxyphenyl group of the adjacent 3-(N^{τ}-histidinyl)tyrosine, the histidinyl group of which is a ligand to the copper ion.[1047,1651-1653] The distance, however, from this hydroxy group to the distal oxygen[1650] in bovine cytochrome-*c* oxidase is 0.54 nm, and the orientations of these two groups are incompatible with such a hydron transfer (Figure 2–55). In one crystallographic molecular model of bovine cytochrome-*c* oxidase, however, there is a fixed molecule of water

forming a hydrogen bond to the hydroxy group of the 3-(N^{τ}-histidinyl)tyrosine, and it would be between the hydroxy group and the distal oxygen of the molecular oxygen. There are also thought to be other disordered molecules of water in the immediate vicinity.[1648] Consequently, one or two molecules of water could relay the hydron from the hydroxy group of the 3-(N^{τ}-histidinyl)tyrosine to the distal oxygen of the copper(II)peroxyiron(III) porphyrin. Nevertheless, the copper(II)hydroperoxyiron(III) porphyrin resulting from the hydronation dissociates heterolytically to produce **an oxoiron(IV) porphyrin and a hydroxide** bound[1643,1644,1654-1658] by the Cu^{2+}. The copper(II)-hydroperoxyiron(III) porphyrin that precedes the dissociation has been observed in a model compound that has a triply coordinated copper ion covalently attached to a heme positioned in the proper orientation.[1659]

Just as the tryptophan in cytochrome-*c* peroxidase provides an electron to the oxoiron(V) porphyrin formed initially by heterolysis of the hydroperoxyiron(III) porphyrin in its active site, in the active site of bovine cytochrome-*c* oxidase, the 3-(N^{τ}-histidinyl)tyrosine provides an electron from its electron-rich π molecular orbital system to the oxoiron(V) porphyrin formed initially by heterolysis of the copper(II)hydroperoxyiron(III) porphyrin so that, after a second hydronation, the intermediate at this step is a hydroxyiron(IV) porphyrin adjacent to a **neutral radical on the 3-(N^{τ}-histidinyl)tyrosine**,[1652,1660-1663] rather than the oxoiron(IV) porphyrin$^{\bullet+}$ that usually forms from an oxoiron(V) porphyrin. This hydroxyiron(IV) porphyrin with the adjacent imidazolyl-4-hydroxyphenyl radical has been reproduced in a model compound,[1664] which is able to catalyze the entire reduction of oxygen to water with electrons supplied by an electrode.[1665] In fact, another model compound in which a peroxyiron(III) porphyrin, the distal oxygen of which is a ligand to a Cu^{2+}, oxidizes 2,4,6-tri-*tert*-butylphenol to the neutral 2,4,6-tri-*tert*-butylphenoxy radical. In this reaction, the tri-*tert*-butylphenol hydronates the distal oxygen of the peroxyiron(III) porphyrin that is a ligand to the copper initiating the dissociation of the oxygen–oxygen bond, and the resulting oxoiron(V) porphyrin then removes an electron from the tri-*tert*-butylphenoxide.[1666] A complex between a different model compound also containing a peroxyiron(III) porphyrin, the distal oxygen of which is a ligand to a Cu^{2+}, forms a complex with 4-nitrophenol in which there is a hydrogen bond between the 1-hydroxy group and the distal oxygen of the peroxyiron(III) porphyrin.[1667]

The final steps in the reaction catalyzed by cytochrome-*c* oxidase are outer-sphere transfer of an electron from the other heme to the imidazoylphenoxy radical,[1647] rapid equilibration of the remaining electron between the CuA copper cluster and the other heme,[1668] and transfer of this second electron from the other heme to the hydroxyiron(IV) porphyrin to produce hydroxyiron(III) porphyrin.[1654]

In bovine cytochrome-*c* oxidase and cytochrome-*c* oxidase from *P. denitrificans*, this last transfer of an electron can be resolved into two steps. The first step is transfer of an electron from a nearby tryptophan to the hydroxyiron(IV) porphyrin to produce a tryptophan radical and the hydroxyiron(III) porphyrin, and the second step is transfer of the remaining electron from the other heme to the **tryptophan radical** to produce fully oxidized enzyme with one hydroxide ion on the Fe^{3+} and one on the Cu^{2+}, and the regenerated tryptophan.[1641,1669] The participation of this tryptophan is another example of an indolyl group acting as a relay station in the transfer of an electron.

The hydroxide that ends up on the ferric heme in bovine cytochrome-*c* oxidase can exchange rapidly with molecules of water in the solution.[1670] Nevertheless, the hydroxyiron(III) porphyrin is hydronated on its hydroxy oxygen, presumably the same hydronation permitting the exchange of the hydroxy group, to release water.[1671]

There is a model compound in which a copper ion is triply coordinated by two imidazolyl groups and a 2-(*N*-imidazolyl)phenol. These ligands are covalently attached to a heme in such a way that the copper and the iron are positioned at the proper orientation and distance to share a peroxide dianion. This model compound reduces molecular oxygen to two molecules of water, using electrons supplied by cytochrome *c*.[1672]

Oxides of nitrogen (Figure 2–56)[1673,1674] **are substrates for enzymes that use the same prosthetic groups that service the various oxides of oxygen.** Sulfite, an oxide of sulfur, also is a reactant for such enzymes. An example of a prosthetic group that is used in oxidation–reductions with either an oxide of nitrogen as a substrate or molecular oxygen as a

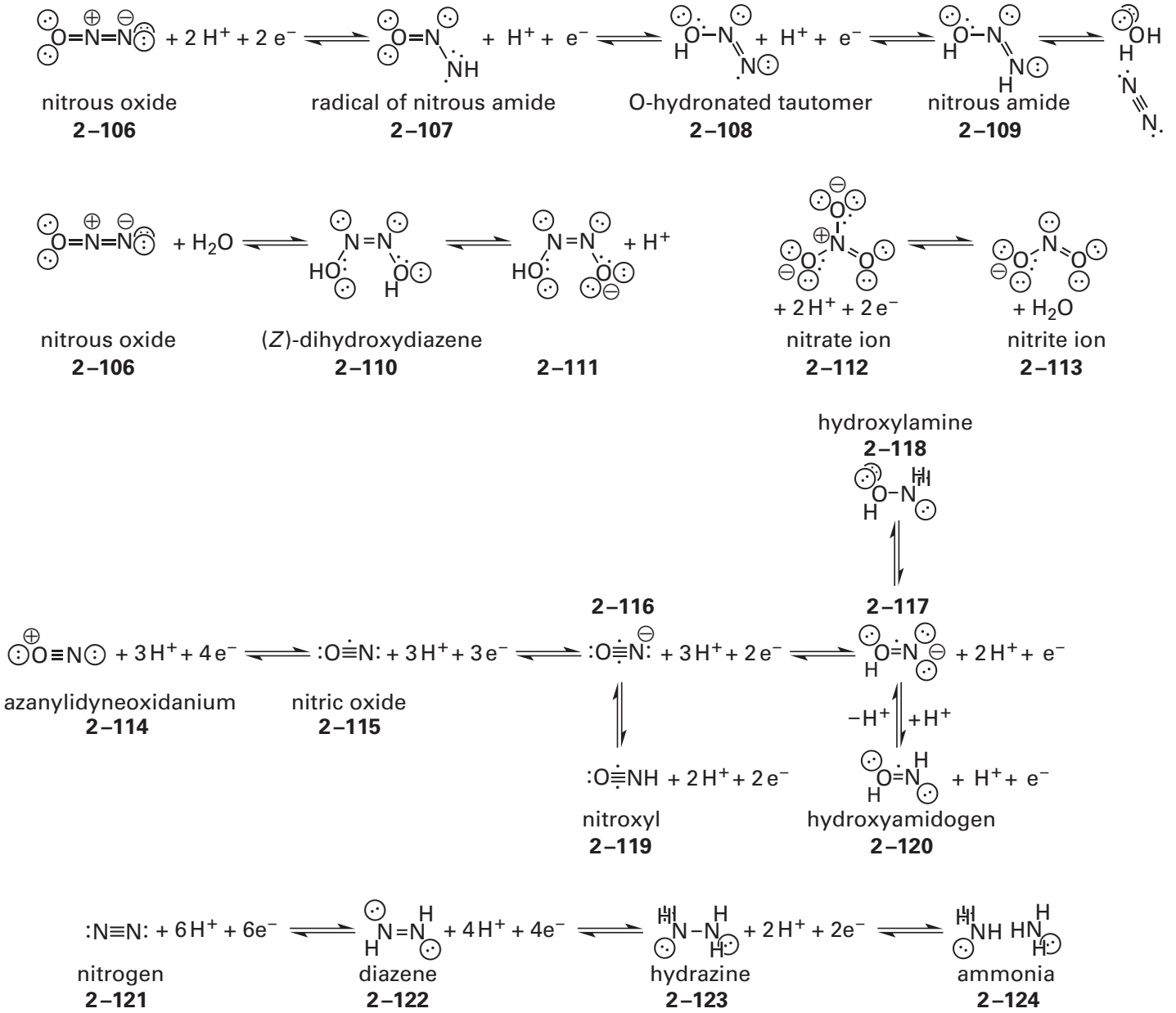

Figure 2–56: Oxides and hydrides of nitrogen and their interconversion by oxidation–reduction. Dihydroxydiazene and nitroxyl exist in the gas phase in equilibrium with each other, and dihydroxydiazene decomposes in water.[1673] Hydroxyamidogen has not been isolated, but its properties have been calculated.[1674] The remaining compounds and ions are relatively stable and can be purchased.

substrate would be a **heme P450.** Nitric oxide reductase [NAD(P)$^+$, nitrous oxide-forming] is an enzyme containing a heme P450 that performs a two-electron oxidation–reduction

$$H^+ + NADH + 2\,NO^{\cdot} \rightleftharpoons NNO + H_2O + NAD^+ \qquad (2\text{–}258)$$

Nitric oxide, NO$^{\cdot}$ (**2–115**), is molecular oxygen in which one of the oxygen atoms and its six valence electrons has been substituted by a nitrogen atom and its five valence electrons, so it has one fewer electron than molecular oxygen. As a result, nitric oxide is a stable radical. One of the two highest occupied π^* molecular orbitals of the diatomic molecular orbital system (Figure 2–45 and **2–86**) occupied by the unpaired electrons in molecular

oxygen (**2–87**) is unoccupied in nitric oxide, and the remaining unpaired electron occupies the other π^* molecular orbital. Unlike oxygen, which associates with only ferroheme, or the superoxide radical anion, which is isoelectronic with nitric oxide but associates with only ferriheme, **nitric oxide binds with almost equal affinity to both ferroheme and ferriheme**.[1675,1676] In these complexes, the nitrogen is on the iron.

The nitrogen of one of the two nitric oxides associates with the ferriheme of nitric oxide reductase [NAD(P)$^+$, nitrous oxide-forming] from *F. oxysporum*. During its association, the nitric oxide is oxidized by transfer of its unpaired electron to the Fe^{3+} to produce an Fe^{2+} coordinated by an **azanylidyneoxidanium ion** (**2–114**)

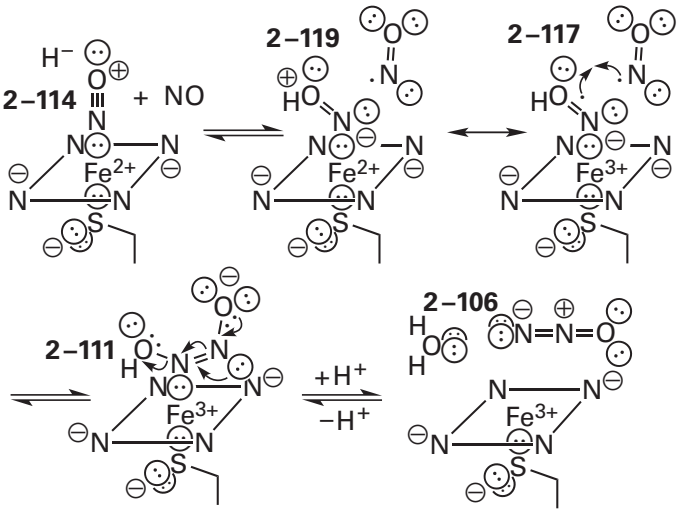

(2–259)

a cation that is diamagnetic because all its molecular orbitals are occupied by pairs of electrons. Because azanylidyneoxidanium is a cylindrical ion, it should associate as a coaxial ligand on the resulting Fe^{2+}, which is the case for a synthetic model complex that can be formed between an iron(III) porphyrin and nitric oxide. This synthetic model complex has been identified as that between azanylidyneoxidanium and iron(II) porphyrin.[1677] In the active site of nitric oxide reductase [NAD(P)$^+$, nitrous oxide-forming], NADH reduces this complex directly by formal transfer of a hydride to the electrophilic, cationic distal oxygen of the azanylidyneoxidanium,[1678-1680] just as a hydride from BH_4^- is able to reduce the synthetic model complex between the iron(II) porphyrin and azanylidyneoxidanium.[1677]

The resulting reduced intermediate[1681] is the complex between **nitroxyl** (**2–119**) and Fe^{2+}. Nitroxyl is isoelectronic with molecular oxygen and should be, as is molecular oxygen, a bent ligand to the Fe^{2+}. As in the case of the complex between a ferroheme and molecular oxygen, there is a resonance form of the complex, in which an electron is transferred from the Fe^{2+} to the nitroxyl to give the complex between Fe^{3+} and the anionic conjugate base (**2–117**) of **hydroxyamidogen** (**2–120**),[1674] which is isoelectronic with hydrosuperoxide radical (Equation 2–199). This resonance form illustrates how the nitroxyl on Fe^{2+} is able to participate in a colligation with a second molecule of nitric oxide to form the conjugate base (**2–111**) of **(*Z*)-dihydroxydiazene** (**2–110**). This colligation is followed by a heterolytic dissociation with water as the leaving group to give nitrous oxide, NNO (**2–106**), and H_2O.

An example of a set of prosthetic groups that is used both in oxidation–reductions with an oxide of nitrogen as a reactant and in oxidation–reductions with molecular oxygen as a reactant would be the set of prosthetic groups in cytochrome-*c* oxidase. In addition to nitric oxide reductase [NAD(P)$^+$, nitrous oxide-forming], which contains a heme P450 (Equations 2–258 and 2–259), there are also nitric oxide reductases

$$2\,H^+ + 2\,e^- + 2\,NO \rightleftharpoons NNO + H_2O \qquad (2\text{–}260)$$

namely nitric oxide reductase (cytochrome *c*) and nitric oxide reductase (menaquinol), from bacteria such as *Bradyrhizobium japonicum*, *P. aeruginosa*, *P. denitrificans*, and *Schinkia azotoformans* that are **evolutionarily related to cytochrome-*c* oxidases** and the homologous bacterial quinol oxidases.[1682,1683] As might be expected from this relationship, the two electrons needed for the reduction are provided by either a cytochrome *c*[1684,1685] or a quinol.[1686] Each of these related nitric oxide reductases contains a fully coordinated heme *b* acting as a one-electron donor and a heme *b* with an open site to which, in its ferrous state, the nitric oxide (**2–115**) binds. These two hemes are in homologous locations to the two in cytochrome-*c* oxidase, and as in cytochrome-*c* oxidase, an electron can be transferred rapidly (>1 ms^{-1}) between them.[1687] In place of the coordinated copper ion with an open site in the active site of cytochrome-*c* oxidase, however, there is a coordinated nonheme iron ion, also with an open site.[1684,1688]

In the active site of one of these nitric oxide reductases, unlike in the active site of nitric oxide

reductase [NAD(P)$^+$, nitrous oxide-forming], the nitric oxide associates when the iron ion in the catalytic heme and the nonheme iron ion are both Fe^{2+} ions. The nitric oxide binds with its nitrogen on the Fe^{2+} in the heme and its oxygen on the nonheme Fe^{2+}, just as the isosteric molecular oxygen binds between the iron and the copper ion in cytochrome-*c* oxidase (Figure 2–55). The nonheme Fe^{2+} provides one electron in the inner sphere to the nitric oxide to produce the intermediate, $[FeNOFe]^{4+}$, the complex between the anionic conjugate base (**2–116**) of nitroxyl and the Fe^{2+} in the heme and the nonheme Fe^{3+}. Because the conjugate base of nitroxyl is isoelectronic with molecular oxygen, the complex with the Fe^{2+} in the heme is isoelectronic with a molecule of oxygen on an Fe^{2+} in a heme. This intermediate is also homologous with the intermediate, $[FeNOH]^{2+}$, the complex between the conjugate acid of nitroxyl (**2–119**) and the Fe^{2+} in the heme after the first step in Equation 2–259 with the nonheme Fe^{3+} replacing the hydron, H^+.

The second nitric oxide then participates in a colligation as it does in Equation 2–259 to produce again the conjugate base (**2–111**) of (*Z*)-dihydroxydiazene. Computations[1689] suggest that, following the colligation, both oxygens of the conjugate base or the dianionic dibase of (*Z*)-dihydroxydiazene are ligands to the nonheme Fe^{3+} to form a pentacyclic metallacycle of the two nitrogens, the two oxygens, and the Fe^{3+}. Consequently, it is probably the case that the oxygen of the second nitric oxide, after it enters the active site, also becomes a ligand to the nonheme Fe^{3+} before the colligation occurs. The heterolytic dissociation then proceeds as before (Equation 2–259). The NNO then dissociates from the active site and leaves behind an oxido oxygen held between the two now Fe^{3+} ions but somewhat closer (0.04 nm) to the nonheme Fe^{3+}, which is the substitute for a hydron.[1688] A synthetic heme with a nonheme Fe^{2+} held in the proper location relative to the Fe^{2+} in the heme is able to convert two molecules of nitric oxide nonenzymatically to NNO.[1690]

The two electrons from the reduced heme *b* within the enzyme and a molecule of reduced cytochrome *c* or a quinol then successively reduce the two Fe^{3+} ions, the one in the heme and the nonheme Fe^{3+}, to Fe^{2+} ions, and the oxido oxygen picks up two hydrons and dissociates as a molecule of water.[1690] As the diferric oxide is unreactive, there is no need for the two electrons to arrive simultaneously as there is in cytochrome-*c* oxidase. These nitric oxide reductases are another, quite different, example of the **ability of the same arrangements of prosthetic groups to process both an oxide of oxygen and an oxide of nitrogen.**

Oxides of nitrogen can also be oxidized or reduced by the **removal or addition of only one electron** instead of two. In the active site of nitrite reductase (NO-forming) from bacteria such as *Pseudomonas stutzeri*, *P. pantotrophus*, and *P. denitrificans*, the Fe^{2+} in a heme d_1[654,1691] with the imidazolyl group of a histidine as the proximal axial ligand is responsible for the reduction of nitrite ion, ONO^- (**2–113**), the central nitrogen of which reversibly associates with the iron as its sixth ligand.[1692] The nitrite ion is reduced by one electron to nitric oxide (NO) and a molecule of water. During the reaction, two hydronated imidazolio groups from two histidines provide the two hydrons to one of the two oxygen atoms of the nitrite ion that leaves as a molecule of water. The Fe^{2+} in the heme provides the single electron. Following dissociation of the molecule of water from the nitrogen, the resulting complex between nitrous oxide (**2–106**) and the Fe^{3+} has the properties of a complex between Fe^{2+} and azanylidyneoxidanium ion (Equation 2-259).[1693] The Fe^{3+} in the heme d_1, either with the nitric oxide still bound or after its dissociation, is reduced by an electron from a heme *c*[1149] covalently attached as a prosthetic group to a separate structural domain in the protein.[1050,1691] The heme *c* in turn is reduced with an electron from the small dissociable electron-transferring coenzyme cytochrome c_{550}.

Ferredoxin—nitrite reductase from plants such as *S. oleracea*[1694] catalyzes the complete reduction of nitrite ion to ammonium ion, a **reduction requiring six electrons**

$$8\,H^+ + 6\,e^- + ONO^- \rightleftharpoons NH_4^+ + 2\,H_2O \qquad (2\text{–}261)$$

The enzyme uses a heme for the reduction, but the heme is a siroheme

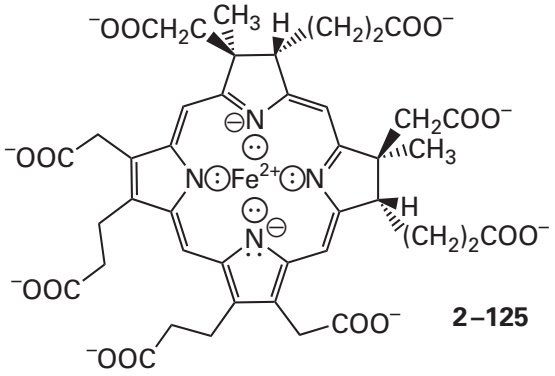

2–125

The ligand to the iron at the axial position is the sulfido sulfur of a cysteine, as in a heme P450, but what disqualifies the enzyme from being an enzyme containing a heme P450 is that the same sulfido sulfur is also the ligand to one of the irons in a **[4Fe–4S] iron–sulfur cluster**.[1695] The two redox couples, the siroheme and the [4Fe–4S] iron–sulfur cluster, act as independent electron-transferring prosthetic groups,[1696] but they are strongly coupled in the inner sphere by the bridging sulfur of the cysteine that they share.[671] The reductants providing the six electrons are six [2Fe–2S] ferredoxins in a sequence of outer-sphere, one-electron steps involving association of the reduced form and dissociation of the oxidized form of each of these small electron-transferring coenzymes. When a reduced ferredoxin is bound to the enzyme and the prosthetic [4Fe–4S] iron–sulfur cluster has already been reduced, two electrons are available to be simultaneously transferred to the siroheme.

The lone pair of electrons on the central nitrogen of the nitrite ion (**2–113**) associates with the open site on the ferric siroheme to become a sixth ligand,[1695,1697] and the two electrons passing through the prosthetic [4Fe–4S] iron–sulfur cluster and a hydron perform a **reductive heterolytic dissociation** of a nitrogen–oxygen bond of the nitrite ion to produce the complex between nitric oxide (**2–115**) and ferrous siroheme[1698] and a hydroxide ion[1699]

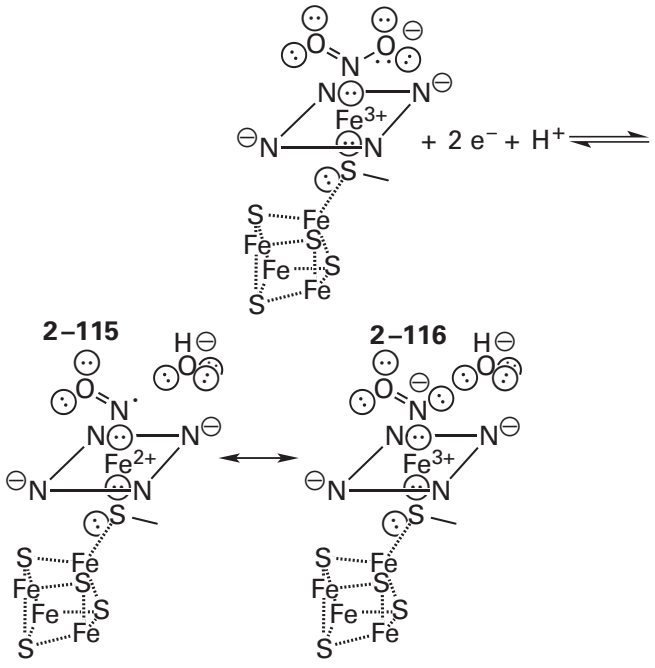

(2–262)

In the active site of the enzyme from *S. oleracea*, the hydron is provided by the ammonio group of Lysine 224.[1695] A complex between nitric oxide and ferrous heme has been stabilized in the unrelated, pentaheme nitrite reductase (cytochrome; ammonia-forming) from *S. oneidensis*, which catalyzes the same reduction (Equation 2–261), by controlling the reduction potential of the solution to prevent the later steps in the overall reaction.[1700]

In the active site of ferredoxin—nitrite reductase, the reductive heterolytic dissociation is accomplished by transfer of one of the arriving electrons from the reduced ferredoxin and the reduced prosthetic [4Fe–4S] iron–sulfur cluster through a d_{xz} or d_{yz} orbital on the iron ion (Figure 2–24) into a vacant antibonding π molecular orbital in the allyl π molecular orbital system on the nitrite ion. The **push of the electron density** arriving on the nitrogen and the fact that it is entering an antibonding π molecular orbital of the nitrite ion weaken the nitrogen–oxygen bond for heterolysis.[1701]

The resulting complex between nitric oxide (**2–115**) and iron(II) porphyrin is equivalent to the complex between nitroxyl ion (**2–116**) and iron(III) porphyrin. Nitroxyl ion is the conjugate base of nitroxyl (**2–119**), a fact that explains how the nitrogen is then hydronated. Following hydronation of the nitrogen, the next two electrons are transferred to the resulting complex between nitroxyl and iron(III) porphyrin, while a hydron is transferred to the oxygen and another hydron is transferred to the nitrogen to produce the complex between hydroxylamine, $HONH_2$ (**2–118**), and ferric siroheme.[1698] This complex is then reduced by two electrons, and two hydrons are added to produce a molecule of water, ammonia, and uncoordinated ferrisiroheme. In this final reduction, the electrons have to arrive two at a time to avoid the formation of hydroxyl radical, hence the prosthetic [4Fe–4S] iron–sulfur cluster in ferredoxin—nitrite reductase.

Assimilatory sulfite reductase (NADPH)

$$8\,H^+ + 6\,e^- + SO_3^{2-} \rightleftharpoons H_2S + 3\,H_2O \qquad (2\text{–}263)$$

from bacteria such as *E. coli* and *D. vulgaris* is an enzyme evolutionarily related (22% identity; 2.3 gap percent) to ferredoxin—nitrite reductase (Equation 2–261). In fact, many sulfite reductases also catalyze the reduction of nitrite ion to ammonia. Sulfite reductases contain a subunit homologous to ferredoxin—nitrite reductase[1695] in which there is the same inner-sphere complex[1697] of an [4Fe–4S] iron–sulfur cluster and a siroheme.[661,1702]

The main difference between assimilatory sulfite reductase (NADPH) and ferredoxin—nitrite reductase is the presence in the former of an additional subunit containing sites at which two flavins are bound as prosthetic groups.[1703] One of the flavins is reduced by successive hydride transfers from molecules of NADPH; and the other, by transfer of two electrons from the first. When the enzyme is fully reduced, there are **six electrons immediately available for each turnover**, two on each of the flavins, one on the[4Fe–4S] iron–sulfur cluster, and one on the siroheme. All six of these electrons are ultimately derived from NADPH. Having them all immediately available ensures that sulfite can be fully reduced in one blast without the need for additional associations and dissociations of molecules of NADPH.

The nucleophilic lone pair of electrons on the central sulfur of the sulfite ion (see Equation 2–124) associates with the Fe^{2+} of the reduced siroheme, and its three oxygens form hydrogen bonds with the guanidinio nitrogens of two arginines, two ammonio nitrogens of lysines, and two molecules of water.[1697] These **catalytic acids** successively provide the eight hydrons needed for hydronation of the oxygens and the sulfur so that the hydrons are all immediately available as well. Overlap between the vacant *d* orbitals on the sulfur of the sulfite and the occupied d_{xz} and d_{yz} orbitals on the Fe^{2+} in the electron-rich siroheme permits efficient transfer of electron density onto sulfur, and the push of this electron density weakens each of the sulfur–oxygen bonds in turn to permit their successive reductive heterolytic dissociation,[1699] as happens to nitrite ion in the active site of ferredoxin—nitrite reductase. The rate-limiting step in the reaction is the reductive heterolytic dissociation of the first molecule of water to give a hydrosulfinate ion associated with the iron ion of the heme, and the further reduction by four electrons and the consumption of six hydrons proceeds so rapidly that no intermediates that could dissociate are allowed to accumulate, nor have any intermediates been observed.

As with assimilatory sulfite reductase (NADPH), nitrite reductase (cytochrome; ammonia-forming) from bacteria such as *Sulfurospirillum deleyianum* and *Wolinella succinogenes*, which catalyzes the same reaction as ferredoxin—nitrite reductase (Equation 2–261), contains enough prosthetic groups, which in this case are five prosthetic hemes *c*, to provide simultaneously, along with its small electron-transferring coenzyme cytochrome *c*, the six electrons needed to accomplish the reduction and **avoid the problem of having intermediates accumulate**. Four of the prosthetic hemes *c* have as their two axial ligands imidazolyl groups from histidines and transfer electrons, and the fifth, at which the reaction proceeds, has nitrogen 7 of a lysine as its proximal axial ligand opposite the open site.[1704,1705] The reaction also requires eight hydrons (Equation 2–261). In the active site of nitrite reductase (cytochrome; ammonia-forming) from *W. succinogenes* with a nitrite ion bound to the iron of the heme, the imidazolyl group of a histidine forms a hydrogen bond with one of the oxygens of the nitrite ion. There is a cluster of eight molecules of water and the 4-hydroxyphenyl group of a tyrosine that are all held together by hydrogen bonds, and two of the molecules of water in this cluster form hydrogen bonds with the other oxygen of the nitrite ion. This cluster is continuous with the surrounding solution and is responsible for shuttling the necessary hydrons into the active site, rather than having all the hydrons immediately at hand.[1701,1706] Other than the immediate availability of at least six electrons in the fully reduced enzyme, the mechanism of the reaction and the intermediates are the same as those of ferredoxin—nitrite reductase (Equation 2–262).[1701] Nitrite reductase (cytochrome; ammonia-forming) from *W. succinogenes* also reduces sulfite to hydrogen sulfide, a reaction also requiring six electrons and eight hydrons (Equation 2–263), at a rate that is actually faster than assimilatory sulfite reductases (NADPH).[1707]

Hydroxylamine dehydrogenase from *N. europaea*, however, contains **more than enough prosthetic groups**, seven hemes *c* in addition to the heme with the open site at which the oxidation occurs, to absorb all four of the electrons produced during the oxidation of hydroxylamine (**2–118**)[1042]

$$H_2O + H_2NOH \rightleftharpoons NO_2^- + 5\,H^+ + 4\,e^- \qquad (2\text{–}264)$$

The hemes *c* are grouped in pairs, a fact suggesting that the electrons are removed two at a time during the oxidation

$$H_2O + H_2NOH \rightleftharpoons H_2O + NO^- + 3\,H^+ + 2\,e^- \rightleftharpoons NO_2^- + 5\,H^+ + 4\,e^- \qquad (2\text{–}265)$$

while the intermediate conjugate base of nitroxyl, NO^- (**2–116**), remains tightly bound to the iron ion of the heme. Nitrite reductase (cytochrome; ammonia-forming) from *Thioalkalivibrio nitratireducens*, which only uses six electrons for its enzymatic reaction (Equation 2–261), contains eight hemes *c*,[1708] again more than enough.

In all the reactions involving a prosthetic heme that have been discussed so far, the axial ligand opposite the open site on the prosthetic heme usually does not involve itself directly in the oxidation–reduction performed by the heme other than to tune the iron ion to a reduction potential appropriate to the oxidation–reduction. The axial ligand to the iron ion in the prosthetic heme in ferredoxin—nitrite reductase (Equation 2–262) is an exception to this general rule because of its coordination of the prosthetic [4Fe–4S] iron–sulfur cluster. Another exception is the sulfido group of Cysteine 123, which is the axial ligand to the prosthetic heme in thiosulfate dehydrogenase from *A. vinosum*, which oxidizes two thiosulfates to tetrathionate, the disulfide between two thiosulfates. In this instance, the sulfido group of Cysteine 123 participates in a mixed disulfide between itself and one of the thiosulfates that is the result of a two-electron oxidation mediated by the heme. The second thiosulfate participates in a thiol–disulfide exchange with the mixed disulfide to regenerate the sulfido group of the axial ligand and tetrathionate.[1709]

Nitric-oxide synthase[1710,1711] contains a heme P450 that catalyzes two successive monooxygenations, one at a guanidinio nitrogen and the next at the carbonate carbon of the hydroxylated guanidinio group[1712-1715]

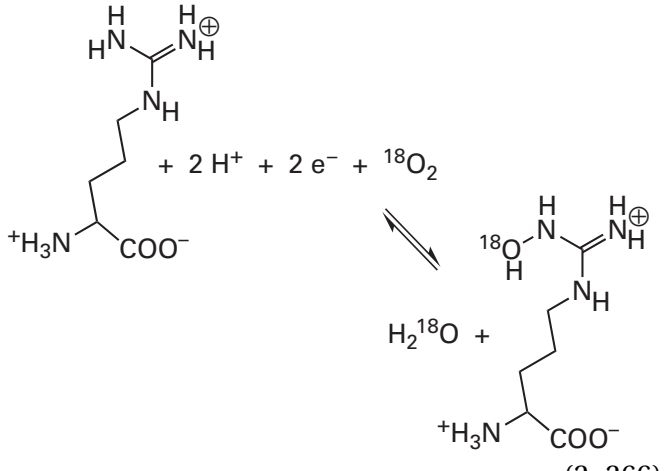

(2–266)

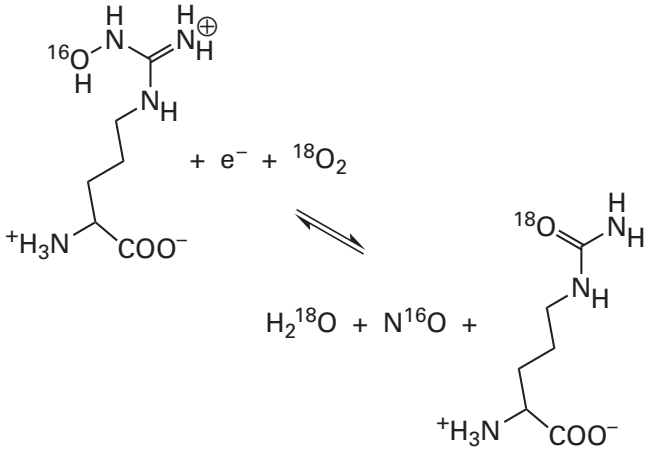

(2–267)

The consequential product of the reaction, as the name implies, is NO, nitric oxide (**2–115**).

The first reaction catalyzed by nitric-oxide synthase, the hydroxylation of a guanidinio nitrogen (Equation 2–266), has the usual stoichiometry of an enzyme containing a heme P450 and a mechanism that proceeds through the usual oxoiron(IV) porphyrin$^{\bullet+}$. Although **the second of the successive reactions catalyzed by nitric-oxide synthase (Equation 2–267) requires only one electron**, the ultimate source of that single electron is nevertheless the flavin of the NADPH—hemoprotein reductase that is a domain of nitric oxide synthase in animals and that is homologous (31% identity; 4 gap percent) with the aforementioned, detached independent NADPH—hemoprotein reductase that provides electrons to hemes P450.[1716,1717] Because NADPH can supply electrons only two at a time, the **overall stoichiometric reaction** catalyzed by the enzyme is

$$3\,\text{NADPH} + \text{H}^+ + 4\,\text{O}_2 + 2\,\text{L-arginine} \rightleftharpoons 2\,\text{L-citrulline} + 2\,\text{NO} + 3\,\text{NADP}^+ + 4\,\text{H}_2\text{O} \quad (2\text{–}268)$$

and a single electron or a hole has to be stored on the enzyme between the production of the first nitric oxide and the production of the second.

In addition to the stoichiometric fact that the conversion of N^{ω}-hydroxy-L-arginine to citrulline and nitric oxide requires only one electron, this reaction is unusual because an oxygen atom from molecular oxygen ends up where the oxygen atom of a molecule of water would end up were there a hydrolysis at the guanidinio carbon of the N^{ω}-hydroxy-L-arginine that ends up as citrulline. The second monooxygenation **does not involve an oxoiron(IV)**

porphyrin$^{\bullet+}$ because when an oxoiron(IV) porphyrin$^{\bullet+}$ is formed at the heme in the enzyme from *R. norvegicus* by using hydrogen peroxide as the oxidant rather than molecular oxygen, N^{ω}-hydroxy-L-arginine is converted by that oxoiron(IV) porphyrin$^{\bullet+}$ to N^{δ}-cyano-L-ornithine and nitroxyl ion, ON^- (**2–116**)[1718-1720]

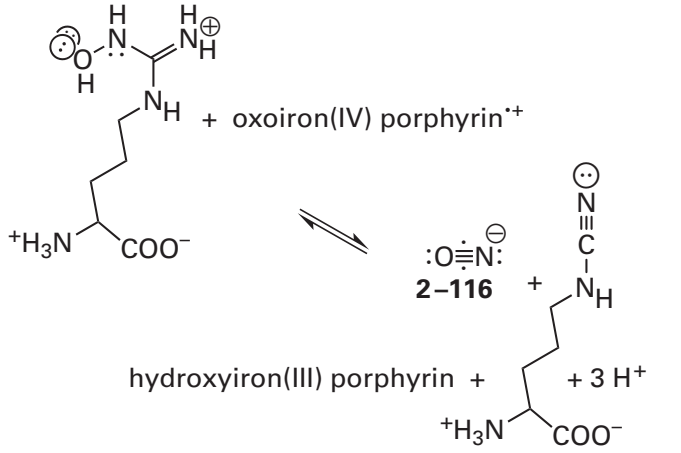

(2–269)

a two-electron oxidation, instead of the normal L-ornithine and nitric oxide (Equation 2–267), a one-electron oxidation.

In addition to the heme, the active site of nitric-oxide synthase contains a prosthetic **(6*R*)-L-*erythro*-5,6,7,8-tetrahydrobiopterin,**[1721-1723] a homologue of flavin. The (6*R*)-L-*erythro*-5,6,7,8-tetrahydrobiopterin (BH_4) participates in the enzymatic reaction by providing a single electron and becoming the **radical cation** ($BH_4^{\bullet+}$)

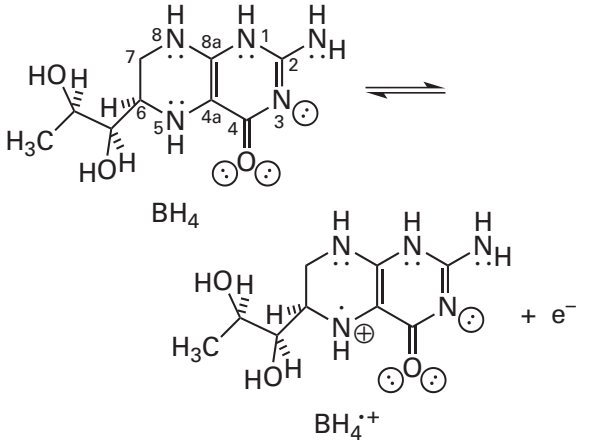

(2–270)

The radical cation participates in the enzymatic reaction by taking up a single electron.[1724-1727] The BH_4 is located in the crystallographic molecular model of the murine and the human enzymes with its 2-imino group forming a hydrogen bond to the carboxy group of the 17-(2-carboxyethyl) group of the heme (see **2–69**)[1728,1729] but directed 180° away from the heme and far from the open site on the iron. Consequently, it can participate only in outer-sphere electron transfer, albeit over a short distance and through a hydrogen bond.

During catalysis, the $BH_4^{\bullet+}$ that is a required intermediate in the enzymatic reaction is slowly and inescapably converted by adventitious oxidation to 6(*R*)-L-*erythro*-6,7-dihydrobiopterin,[1730] which dissociates from the enzyme and must be replaced by free BH_4 either from the cytoplasm or from the solution of the enzymatic assay. Depending on how rapidly the enzyme is turning over, many cycles of oxygenation are completed before this replacement is necessary. Consequently, the BH_4 does not appear in the overall equation (Equation 2–268).

The BH_4 **participates during the hydroxylation of L-arginine**. When a form of murine nitric-oxide synthase lacking the domain for NADPH—hemoprotein reductase and its flavin and having a ferroheme and L-arginine in its active site is mixed with molecular oxygen, oxyiron(II) porphyrin is formed immediately by association of the oxygen with the ferroheme and then decays coincident with both the appearance of $BH_4^{\bullet+}$ and the hydroxylation of the L-arginine to N^{ω}-hydroxy-L-arginine.[1725,1731,1732] This observation indicates that the BH_4 is responsible for the outer-sphere electron transfer necessary to produce the peroxyiron(III) porphyrin[1726,1733-1735] that precedes the formation of oxoiron(IV) porphyrin$^{\bullet+}$, which is required to hydroxylate the guanidinio nitrogen of L-arginine[1727]

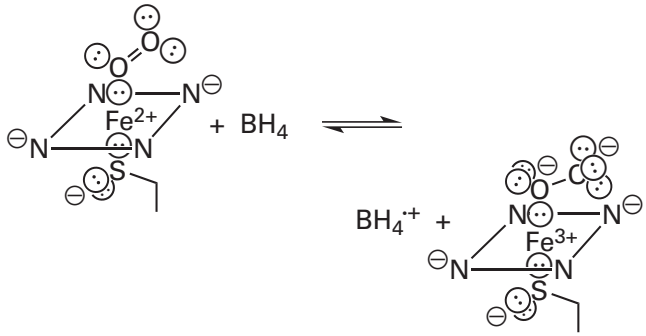

(2–271)

Unlike in the foregoing reaction in which the heme was chemically reduced, in the intact nitric-oxide synthase from *R. norvegicus*, the reduced flavin in the active site of the attached NADPH—hemoprotein reductase is responsible for one-electron reduction of the heme from aquoiron(III) porphyrin

to iron(II) porphyrin, and as a result, the reduced flavin becomes the semiquinone. The production of nitric oxide and L-citrulline from L-arginine and molecular oxygen depends on the ability of the flavin in the NADPH—hemoprotein reductase domain to form a stable semiquinone.[1736]

Consequently, in the **reaction in which L-arginine is hydroxylated**, reduced flavin reduces the heme from iron(III) porphyrin to iron(II) porphyrin and becomes the semiquinone, molecular oxygen binds to the Fe^{2+}, and BH_4 provides the electron necessary to produce peroxyiron(III) porphyrin and becomes $BH_4^{\bullet+}$. The kinetics of these two steps have been followed by using hydrated electrons to reduce the iron(III) porphyrin and rapidly initiate the reaction.[1737] Molecular oxygen associates with the iron(II) porphyrin with a rate constant of $3 \times 10^8\ M^{-1}\ s^{-1}$, and the BH_4 then transfers the necessary electron with a rate constant of $2\ ms^{-1}$. The hydron required to hydronate the peroxyiron(III) porphyrin to form the oxoiron(IV) porphyrin$^{\bullet+}$ (Equation 2–250) is provided by the L-arginine itself.[1738] Following hydronation, the hydroperoxyiron(III) porphyrin becomes oxoiron(IV) porphyrin$^{\bullet+}$, which hydroxylates the ω nitrogen of the L-arginine in the usual manner.

At the end of these steps, the flavin is the semiquinone, the BH_4 is the radical cation,[1725] the heme is the iron(III) porphyrin, and the L-arginine has become N^{ω}-hydroxy-L-arginine. The $BH_4^{\bullet+}$ is then reduced to BH_4 by the flavin semiquinone[1725] with the heme serving as a relay station.[1730,1734] When it is fully reduced, the flavin is able to reduce by one electron the iron(III) porphyrin to iron(II) porphyrin, so it must be the case that the semiquinone can also do so. The reduced heme in turn is able to reduce $BH_4^{\bullet+}$ to BH_4. The oxidized flavin is then reduced by an NADPH.

In the **conversion of N^{ω}-hydroxy-L-arginine to nitric oxide and L-citrulline** (Equation 2–267) by nitric-oxide synthase from *B. subtilis*,* in which N^{ω}-hydroxy-L-arginine occupies the active site instead of L-arginine, the now-reduced flavin reduces iron(III) porphyrin to iron(II) porphyrin, and the BH_4 provides the electron necessary to form peroxyiron(III) porphyrin (Equation 2–271), just as both of these prosthetic groups did before. The peroxyiron(III) porphyrin, however, is only slowly hydronated because there is no catalytic acid, which in the first step was the guanidinio group of the L-arginine, in its vicinity.[1739] As a result, in the bovine enzyme, the peroxyiron(III) porphyrin becomes a detectable intermediate that immediately precedes the formation of nitric oxide and L-citrulline.[1740] Because peroxyiron(III) porphyrin is a nucleophile (see Figure 2–54),[1556] because it is the intermediate that immediately precedes formation of the products, and because one of its oxygen atoms ends up at the acyl oxygen of L-citrulline,[1719,1741] it must be the distal oxyanion of the peroxide in the **peroxyiron(III) porphyrin that is the nucleophile** that adds to the carbonate carbon in the nucleophilic substitution that occurs at that carbon of the N^{ω}-hydroxy-L-arginine and that ultimately produces L-citrulline, just as the distal oxygen of 4a-peroxyflavin adds to the acyl carbon in uracil during the analogous nucleophilic substitution catalyzed by pyrimidine oxygenase (Equation 2–220).

In crystallographic molecular models of the complexes of both N^{ω}-hydroxy-L-arginine and nitric oxide with nitric-oxide synthases from *B. subtilis*[1739] and *R. norvegicus*,[1742] the nitrogen of the nitric oxide occupies the open coordination site on the iron. In this instance, nitric oxide was bound to the active site not as a product of the reaction but as an inert analogue of a peroxide dianion in peroxyiron(III) porphyrin. This complex between the heme and nitric oxide is isosteric with a peroxyiron(III) porphyrin, but the nitric oxide is not a nucleophile. In the crystallographic molecular models, the oxygen of the nitric oxide, taking the place of the nucleophilic distal oxygen of peroxyiron(III) porphyrin (see Figure 2–54), is 0.36 nm from the carbonate carbon of the *N*-hydroxyguanidino group. If, however, the peroxy group in place of the nitric oxide were to rotate around the iron–oxygen bond, a rotation for which there is no hindrance, it would be in the proper location to add nucleophilically to the carbonate carbon of the *N*-hydroxyguanidino group. In these crystallographic molecular models, the hydroxylated nitrogen on the N^{ω}-hydroxy-L-arginine forms a hydrogen bond (0.28 nm) with the nitrogen of the nitric oxide that sits upon the iron ion.

When all these dispositions are considered, the following **nucleophilic substitution**

*Although murine nitric-oxide synthase and nitric-oxide synthase from *B. subtilis* are quite different in size (1144 aa and 363 aa, respectively), the catalytic domain (365 aa) in murine nitric-oxide synthase is essentially the same (44% identity; 0.5 gap percent) as the entire enzyme (363 aa) from *B. subtilis*, and the two enzymes share the same mechanism.

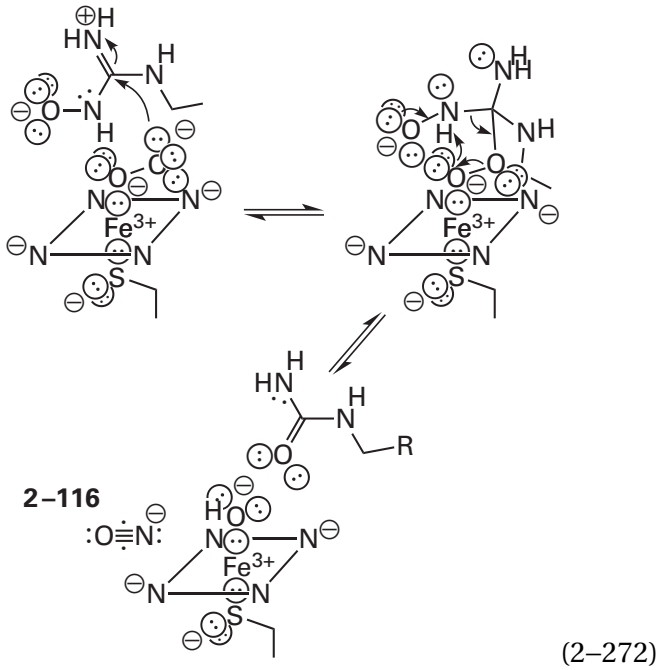

(2–272)

should be a part of the mechanism for the production of nitric oxide. The fact that the hydroxide produced in the reaction ends up on the Fe^{3+} at the end of the reaction catalyzed by murine nitric-oxide synthase[1743] is consistent with this proposal. The nucleophilic substitution as written, however, yields nitroxyl ion, ON^- (**2–116**), instead of nitric oxide, ON (**2–115**). Nitroxyl ion has one more electron than nitric oxide (Figure 2–56), hence the negative charge number, and it is isoelectronic with molecular oxygen, with the additional electron occupying the other π^* molecular orbital (**2–87**). The negative charge number can be explained by the fact that the nucleus of a nitrogen atom has one fewer proton than the nucleus of an oxygen atom.

If the BH_4 in the active site of murine nitric-oxide synthase is present as the radical cation, the heme is in the ferric state, and N^{ω}-hydroxy-L-arginine is added along with hydrogen peroxide to form the hydroperoxyiron(III) porphyrin by direct association with iron(III) porphyrin, the active site, in a single turnover, produces nitric oxide and L-citrulline and ends up containing BH_4 rather than $BH_4^{\bullet+}$.[1744] If, however, the active site contains BH_4 instead of $BH_4^{\bullet+}$, the products are L-citrulline and nitroxyl, ONH (**2–119**), the conjugate acid of nitroxyl ion, ON^- (**2–116**), as in Equation 2–272. When the enzyme from *R. norvegicus* is depleted of BH_4, L-arginine is turned into N^6-cyano-L-ornithine and nitroxyl ion (Equation 2–269), the anionic conjugate base of nitroxyl, rather than L-citrulline and NO.[1733,1745]

In other words, the presence of $BH_4^{\bullet+}$ is essential to the production of nitric oxide (**2–115**) instead of nitroxyl ion (**2–116**), two oxides of nitrogen that differ by only one electron (Figure 2–56). It is essential because **$BH_4^{\bullet+}$ is the acceptor for the electron on nitroxyl ion**. It has been shown that when nitroxyl ion is generated in solution, it associates with the ferric heme of murine nitric-oxide synthase in which the tetrahydrobiopterin is $BH_4^{\bullet+}$, and the nitroxyl ion is oxidized to nitric oxide while the $BH_4^{\bullet+}$ is reduced to BH_4.[1744] It is not surprising that a complex between ferric heme and nitroxyl ion is able to reduce $BH_4^{\bullet+}$ because nitroxyl ion is a strong reductant (–810 mV). The fact that it can, however, provides a role for $BH_4^{\bullet+}$ and explains why nitroxyl is the product when $BH_4^{\bullet+}$ is not present.

In the crystallographic molecular model of nitric-oxide synthase in the complex with nitric oxide, replacing the peroxide ion, and N^{ω}-hydroxy-L-arginine, the π molecular orbital system of the *N*-hydroxyguanidino group is stacked flat against the π molecular orbital system of the porphyrin, and the hydroxyamino group is immediately adjacent to the nitrogen of one of the pyrrolyl groups in the porphyrin, and both the nitrogen and the oxygen are in van der Waals contact (0.36 nm) with that nitrogen. Consequently, the nitroxyl ion released in the nucleophilic substitution (Equation 2–272) would be right up against this nitrogen of the pyrrolyl group, and the nitroxyl ion, as a strong reductant, should be able to reduce $BH_4^{\bullet+}$ easily by injecting an electron into the π molecular orbital system of the heme, through which it would transfer directly to $BH_4^{\bullet+}$ through the hydrogen bond between the heme and the $BH_4^{\bullet+}$. Because the $BH_4^{\bullet+}$ is electronically coupled to the heme, it probably withdraws electron density from the highest occupied molecular orbital of the porphyrin, which has a lobe over the nitrogen of the pyrrolyl group. This **electron transfer from nitroxyl ion to $BH_4^{\bullet+}$** immediately following the nucleophilic substitution (Equation 2–272) completes the reaction.

When all these observations are considered, the overall enzymatic reaction (Equation 2–268), which is a **three-electron reduction**, can be divided into **two cycles**.

Before **the first cycle**, the initial enzyme contains as its prosthetic groups reduced flavin, BH_4, and aquoiron(III) porphyrin, which together have an odd number of valence electrons. The first L-arginine then associates, and at the end of the first cycle, the enzyme from which the first nitric oxide and the first L-citrulline have dissociated and which has

consumed one NADPH contains, as its prosthetic groups, the semiquinone of flavin, BH_4, and aquoiron(III) porphyrin, which together have an even number of valence electrons because the single electron required in the second half of the first cycle has departed with the products (Equation 2–267). After the first cycle, there is probably an equilibrium mixture of reduced flavin, flavin semiquinone, oxidized flavin, iron(III) porphyrin, iron(II) porphyrin, BH_4, and $BH_4^{\bullet+}$, as well as radicals at any relay stations between the flavin and the heme.

In the **second cycle**, this collection of prosthetic groups with an even number of electrons binds L-arginine, and the electrons distribute in such a way that the heme is iron(II) porphyrin, the flavin is oxidized, and the pterin is BH_4, a configuration with an even number of electrons in the proper distribution to hydroxylate L-arginine (Equation 2–271). The hydroxylation is a reaction that requiries two electrons and that leaves the prosthetic groups with again an even number of electrons. At some point, before the intermediate N^{ω}-hydroxy-L-arginine is converted to nitric oxide and L-citrulline during the second half of the second cycle, the oxidized flavin is reduced by a second molecule of NADPH. The flavin then reduces, by the transfer of one electron, the $BH_4^{\bullet+}$ formed during the conversion of L-arginine to N^{ω}-hydroxy-L-arginine, and the resulting flavin semiquinone reduces the aquoiron(III) porphyrin to iron(II) porphyrin. The oxidized flavin is then reduced by a third molecule of NADPH. After the N^{ω}-hydroxy-L-arginine has been oxidized in the second half of this second cycle (Equations 2–271 and 2–272) and the second nitric oxide and the second L-citrulline have dissociated, the flavin is reduced, the heme is aquoiron(III) porphyrin, and the pterin is BH_4. The prosthetic groups with an odd number of valence electrons are ready to repeat the first cycle, and the overall reaction (Equation 2–268) has been accomplished.

In each cycle, at the point at which nitroxyl ion dissociates from the tetrahedral intermediate during the nucleophilic substitution (Equation 2–272), the BH_4 is the radical cation ready to accept the undesired electron. The difference in the active sites at this point in the two cycles is whether or not the flavin is the semiquinone.

During the first cycle, N^{ω}-hydroxy-L-arginine can dissociate from the active site to leave it with $BH_4^{\bullet+}$, aquoiron(III) porphyrin, and flavin semiquinone. The flavin semiquinone then reduces the $BH_4^{\bullet+}$ to BH_4 using the heme as a relay station, the flavin is reduced by a molecule of NADPH, and the active site is returned to the state that precedes the first cycle. During the second cycle, N^{ω}-hydroxy-L-arginine can dissociate from the active site to leave it with BH_4, aquoiron(III) porphyrin, and flavin semiquinone, the state in which the enzyme exists after the full first cycle and before the second. Eventually, any N^{ω}-hydroxy-L-arginine that has dissociated into the solution reassociates with one of these two forms of the enzyme to be converted to nitric oxide and L-citrulline.

There are hemoproteins the purpose of which is to bind nitric oxide.[1746] One property of its binding to a heme is that, unlike oxygen, nitric oxide significantly weakens the affinity of the iron ion for the axial ligand opposite the open site to which it binds—for example, the affinity of the iron for the imidazolyl group of a histidine. This weakening of the bond to the proximal axial ligand may trigger the conformational changes that these hemoproteins undergo upon binding nitric oxide[1675] and that are responsible for their function.

Hemes, because of the rigid, sterically defined arrangement of their ligands, provide the clearest introduction to high-valent iron and to the complexes between iron ions and the oxides of oxygen, sulfur, and nitrogen. A number of enzymes that react with the oxides of oxygen, however, have nonheme iron ions as prosthetic groups (Figure 2–57). The nonheme iron ion in *all-trans*-8′-apo-β-carotenal 15,15′-oxygenase from *Synechocystis* (Figure 2–57A)[1747] is the most similar to the iron ion in a heme, as it is octahedrally coordinated with four sp^2 nitrogens from the imidazolyl groups of four histidines at four of the octahedral positions. In the resting ferrous enzyme, one open position is occupied by a molecule of water and the other is vacant. The two open positions, however, are adjacent to each other rather than opposite each other as in a heme, so the comparison with a heme would be that three of the nitrogens from three of the imidazolyl groups take the place of three of the nitrogens in the heme, the octahedral position occupied by the fourth nitrogen of the heme is vacant, the axial ligand to the iron ion is the fourth imidazolyl group, and the other axial ligand is the molecule of water.

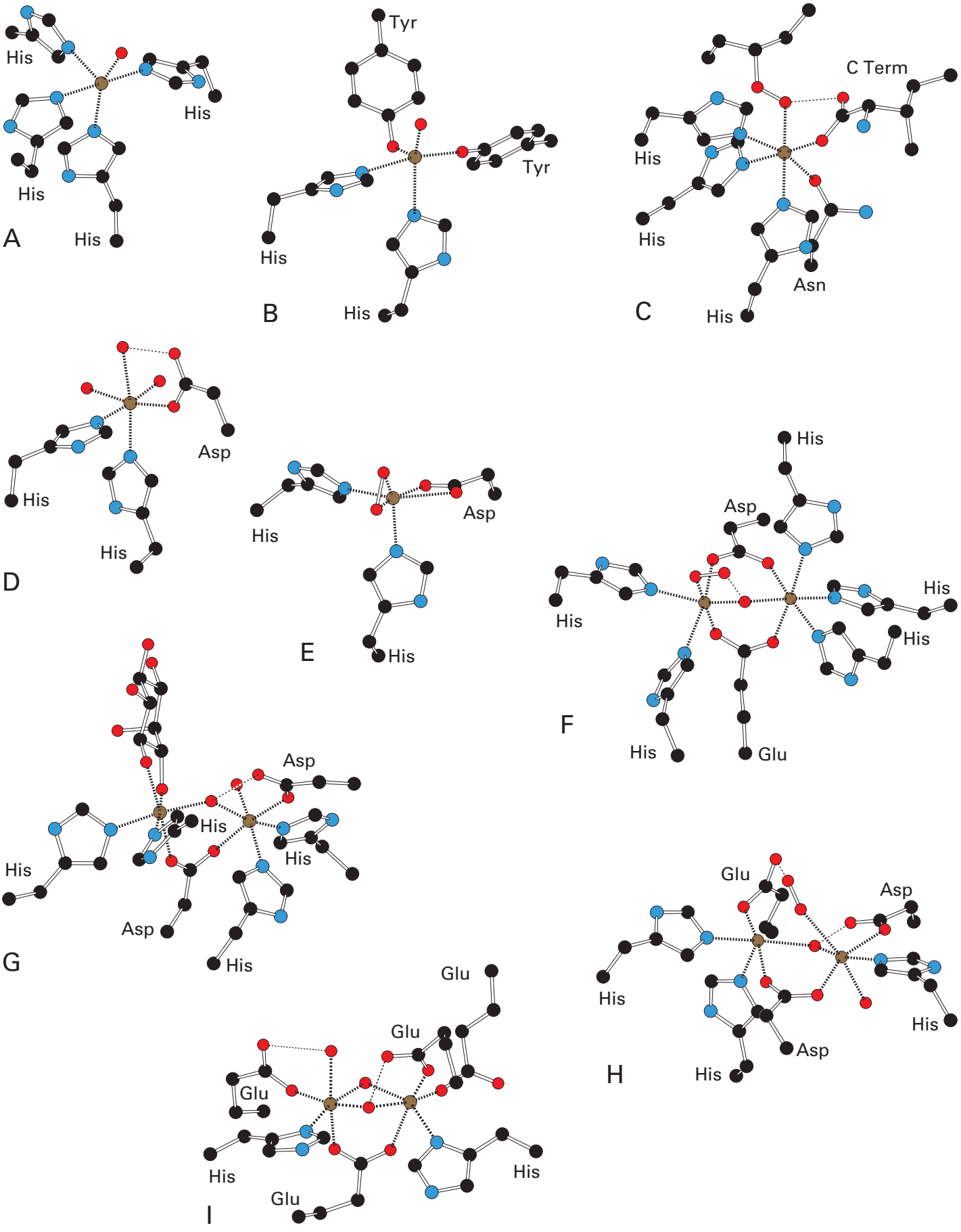
His
His
His
His
A
Tyr
Tyr
His
His
B
C Term
His
His
Asn
His
C
Asp
His
His
D
Asp
His
His
E
His
His
His
Glu
F
Asp
His
His
His
Asp
His
G
Glu
Asp
His
Glu
Glu
His
His
Glu
I
Glu
Asp
His
His
Asp
His
H

Figure 2–57: Drawings[50] of the ligands to prosthetic nonheme iron ions in the crystallographic molecular models of **(A)** *all-trans*-8′-apo-β-carotenal 15,15′-oxygenase from *Synechocystis*,[1747] **(B)** protocatechuate 3,4-dioxygenase from *P. putida*,[1758] **(C)** linoleate 13*S*-lipoxygenase from *G. max*,[1763] **(D)** cephalosporin synthase from *S. clavuligerus*,[1780] **(E)** naphthalene 1,2-dioxygenase from *P. putida*,[1790] **(F)** hemerythrin from *Themiste dyscritum*,[1876] **(G)** murine inositol oxygenase,[1883] **(H)** rubredoxin:oxygen oxidoreductase from *D. gigas*,[1893] and **(I)** methane monooxygenase (soluble) from *M. capsulatus*.[1904] Black atoms are carbons, red atoms are oxygens, and blue atoms are nitrogens. Iron ions are the rusty brown spheres surrounded by their ligands. In most cases, there are six ligands to each iron ion, sometimes in undistorted and sometimes in distorted octahedral array. The side chains acting as ligands are labeled. The lone red spherical ligands in Panels A, B, D, H, and I are molecules of water or hydroxide ions. Often the coordinated molecule of water or the hydroxide forms a hydrogen bond to the carboxy group of an aspartate (D) or a glutamate (I). In Panel C, a portion of the alkyl hydroperoxide that is the product of the lipoxygenase reaction, which was coordinated to the iron ion in the enzyme in the crystal submitted to diffraction, is drawn; and in Panel G, a complete molecule of *myo*-inositol, which was coordinated to the one of the iron ions in the inositol oxygenase in the crystal, is drawn. In Panels E, F, and H, the complex between the respective enzyme and molecular oxygen was present in the crystal and the molecule of oxygen is drawn. In naphthalene 1,2-dioxygenase (E), the molecule of oxygen forms two bonds to the iron ion; in hemerythrin (F), one oxygen forms a bond to an iron ion and the other forms a hydrogen bond with a μ-oxo group; and in rubredoxin:oxygen oxidoreductase (H), one oxygen forms a bond to an iron ion and the other forms a hydrogen bond with the carboxy group of a glutamate. In prosthetic clusters of more than one iron ion, there are often μ-oxo groups between two of the irons. In the drawings (F, G, H, and I), they are the white spheres that connect two iron ions. Often a μ-oxo group will form a hydrogen bond to the side chain of an amino acid (G, H, and I) or an oxygen in a molecule of oxygen (F). A single iron ion can be coordinated by the two oxygens of the same carboxylate (E). In prosthetic clusters of more than one iron ion, two of the iron ions are often coordinated by the same carboxylate of an aspartate (F, G, and H) or a glutamate (F, H) with each of its oxygens coordinating a different iron ion.

There are three related enzymes: *all-trans*-8′-apo-β-carotenal 15,15′-oxygenase (Figure 2–57A), carotenoid oxygenase 1 from *Neurospora crassa* (27% identity; 3.1 gap percent), and β-carotene 15,15′-dioxygenase from *G. gallus* (26% identity; 3.7 gap percent).[1749] The first oxidatively cleaves *all-trans*-8′-apo-β-carotenal at the central carbon–carbon double bond to *all-trans*-retinal (**2–85**) and (2*E*,4*E*,6*E*)-2,6-dimethylocta-2,4,6-trienedial, the second oxidatively cleaves stilbenoids at the central carbon–carbon double bond to two substituted benzaldehydes, and the third oxidatively cleaves β,β-carotene (**2–78**) at the central carbon–carbon double bond to two molecules of retinal (**2–85**). In each case, a carbon–carbon double bond is cleaved and the two carbons end up as the carbonyls of the two aldehydes that are the products. No electrons other than those in the respective reactants and those in the molecular oxygen are required. The two atoms in molecular oxygen end up as the two atoms of oxygen in the carbonyl groups of the two aldehydes, so these enzymes are dioxygenases.[1748]

The first steps in the respective oxidative cleavages are the association of the respective reactant with the active site followed by the association of molecular oxygen with Fe^{2+}.[1749] In a crystallographic molecular model of the active site of carotenoid oxygenase 1 occupied by a reactant for the enzyme, the position on the iron ion occupied by the molecule of water homologous to the one in the active site of *all-trans*-8′-apo-β-carotenal 15,15′-oxygenase (Figure 2–57A) is pointed at the reactant and only 0.31 nm from the double bond that will be oxidatively cleaved, an orientation and proximity stating that the position on the prosthetic Fe^{2+} at which the molecular oxygen binds is the position occupied by the molecule of water. The vacant position is pointed away from the reactant. It is unclear how the oxidative cleavage proceeds, but the fact that the products are aldehydes and the fact that oxygen in the carbonyl group of each aldehyde was one of the oxygens in molecular oxygen suggests that a dioxetane (see **2–101**) is an intermediate in the reaction.[1748]

In cysteine dioxygenase from *R. norvegicus*, the Fe^{2+} in the resting active site is coordinated by three imidazolyl groups from only three histidines.[1750-1752] L-Cysteine, as a reactant, associates with the active site by coordinating the Fe^{2+} with its sulfido group and its α-amino group,[1753] which provides the fourth nitrogen in the coordination of the Fe^{2+}, so that the complex then resembles the coordination in *all-trans*-8′-apo-β-carotenal 15,15′-oxygenase (Figure 2–57A). Molecular oxygen binds to the remaining open site on the octahedral Fe^{2+}, which is only partially occupied by loosely bound water,[1754] and the sulfido sulfur then forms a covalent bond with the proximal oxygen atom, which is adjacent to it in the complex, to form the adduct

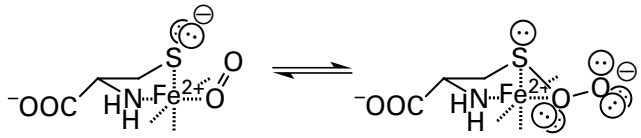

(2–273)

through a colligation between a thiyl radical and a superoxyiron(III).[1755] This adduct has been observed crystallographically.[1756,1757] The colligation does not result in any change in the oxidation state of the Fe^{2+}, which in this instance is approximating the sulfido group and the proximal oxygen, but the ability of Fe^{2+} to form superoxyiron(III), the ability of the Fe^{3+} in superoxyiron(III) to promote a radical on sulfur, and the ability of the iron to catalyze intersystem crossing are all exploited. Whether or not this adduct is an intermediate in the normal enzymatic reaction, however, is controversial, but it does result in the formation of a covalent bond between the sulfur and the oxygen, which would be one of the two covalent bonds between sulfur and oxygen in L-3-sulfinoalanine, which is the final product of the enzymatic reaction.

Unlike the preceding examples, most prosthetic nonheme iron ions are **coordinated both by the nitrogens of the imidazolyl groups of histidines and by the oxygens in the 4-oxido groups of tyrosines, in the carboxylates of aspartates or glutamates, or in the acyl oxygens of the carbamoyl groups of asparagines or glutamines**. For example, in protocatechuate 3,4-dioxygenase from *P. putida*,[1758,1759] two of the four imidazolyl groups found in *all-trans*-8′-apo-β-carotenal 15,15′-oxygenase (Figure 2–57A) have been replaced by two tyrosinates and the coordination is roughly bipyramidal, with one of the tyrosines and one of the histidines at the axial positions of the bipyramid (Figure 2–57B).[1758,1760] In this active site, the **basic oxyanions of the 4-oxido groups of two tyrosines stabilize the Fe^{3+} oxidation state.** In human persulfide dioxygenase, which, although unrelated, has a mechanism analogous to that of cysteine dioxygenase (Equation 2–273),[1761] the prosthetic Fe^{3+} is coordinated by two imidazolyl groups and the carboxylato group of an aspartate[1762] rather than three imidazolyl groups.

In linoleate 13*S*-lipoxygenase from *Glycine max*, the two oxygens in the coordination sphere of the iron ion are provided by the carboxylate of the carboxy terminus of the protein and the carbamoyl group of an asparagine (Figure 2–57C),[1763] but there are three imidazolyl groups instead of two, which together produce an octahedrally coordinated iron ion with only one open site.[1764,1765] Nevertheless, the two oxygens stabilize the ferric state. The 12*Z* double bond in the linoleate [(9*Z*,12*Z*)-9,12-octadecadienoate)] that is a reactant for linoleate 13*S*-lipoxygenase associates with the open site on the Fe^{3+}. Transfer of an electron from that double bond, probably concerted with the dissociation of a hydron from the methylene carbon between what were the 12*Z* double bond and the 9*Z* double bond on the linoleate, produces a stable, neutral **pentadienyl radical** delocalized over carbons 9 through 13. The pentadienyl radical has been defined by electron paramagnetic resonance spectroscopy.[1766] Transfer of the electron to the Fe^{3+} reduces it to Fe^{2+}.[1767,1768] The unpaired electron density at carbon 13 in the highest occupied molecular orbital of the pentadienyl radical then adds to the distal oxygen of a molecule of oxygen that has associated as usual at the now open octahedral site on the now Fe^{2+}. This radical addition to the molecular oxygen forms an acyclic lipid peroxy radical, (9*Z*,11*E*,13*S*)-13-peroxyoctadeca-9,11-dienoate. The ability of molecular oxygen to add rapidly to an alkyl radical and form the more stable alkylperoxy radical is a well-known reaction. A common example of such a radical addition is the use of molecular oxygen to terminate radical polymerizations. The electron needed to turn the resulting peroxy radical into the peroxy ion is provided by the Fe^{2+}, so at the end of the reaction, the anionic conjugate base of (9*Z*,11*E*,13*S*)-13-hydroperoxyoctadeca-9,11-dienoate ends up as a ligand to the octahedrally coordinated Fe^{3+} (Figure 2–57C) The conjugate base of the alkylperoxide is then hydronated on its peroxy oxygen by the carboxy-terminal carboxy group[1763,1769] to form the product of the enzymatic reaction, (9*Z*,11*E*,13*S*)-13-hydroperoxyoctadeca-9,11-dienoate.

Protocatechuate 3,4-dioxygenase is a member of the family of **intradiol dioxygenases**. A member of this family dioxygenates a vicinal dihydroxyphenyl group and turns it into a (2*Z*,4*Z*)-hexa-2,4-dienedioate. For example, protocatechuate 3,4-dioxygenase turns protocatechuate (3,4-dihydroxybenzoate) into (2*Z*,4*Z*)-3-carboxyhexa-2,4-dienedioate

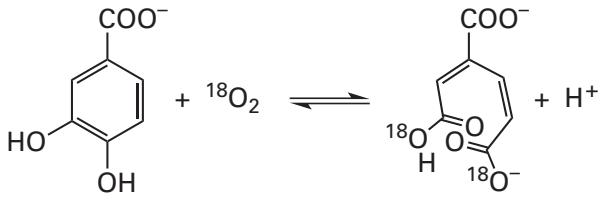

(2–274)

In the active site of protocatechuate 3,4-dioxygenase, one of the hydroxyls of the dihydroxyphenyl group in the reactant displaces the 4-hydroxyphenyl group of the axial tyrosine (Figure 2–57B) from the Fe^{3+}, and the adjacent hydroxy group of the catechol displaces the equatorial molecule of water, so the diol

becomes a bidentate ligand[1770] to the Fe^{3+}. When the axial tyrosine in protocatechuate 3,4-dioxygenase from *P. putida* is replaced by a histidine, the anionic imidazolio group of which is a much stronger ligand to Fe^{3+}, the rate of association of protocatechuate with the Fe^{3+} is decreased by at least 600-fold.[1771]

Following the association of the diol, the Fe^{3+} withdraws electron density from the phenyl ring and creates a partial radical at carbon 3 of the protocatechuate.[1772] The resulting partial radical of Fe^{2+} associates with a molecule of oxygen to approximate it to the radical. The radical of protocatechuate at carbon 3 then reacts as an alkyl radical with the bound molecular oxygen.[1773] In the case of protocatechuate 3,4-dioxygenase, the partial radical at carbon 3 of protocatechuate enters one of the half-occupied, antibonding π molecular orbitals of the molecule of oxygen, and this molecular orbital and an atomic orbital of carbon 3 form a bond between the carbon and the distal oxygen atom. An electron from the now Fe^{2+} enters the other half-occupied, antibonding π molecular orbital of the molecular oxygen, and the two electrons in this latter orbital become a pair of σ electrons sitting between the distal oxygen atom and the now Fe^{3+},[1774,1775] coordinating the Fe^{3+} and forming a **metallacyclic peroxide** (**2–126**)

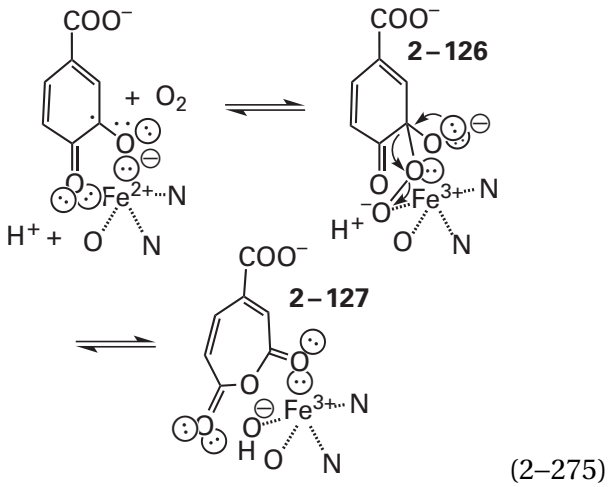

(2–275)

The cyclic peroxide rearranges to the anhydride (**2–127**) of the product[1775-1777] in a ring expansion analogous to a Baeyer–Villiger reaction (Figure 2–47). There are crystallographic molecular models of metallacyclic peroxide **2–126** and ring-expanded anhydride **2–127** formed from 4-fluoro-2-hydroxyphenol in the active site of protocatechuate 3,4-dioxygenase from *P. putida*.[1778] The anhydride is hydrolyzed by the adjacent hydroxide on the Fe^{3+}, which was originally derived from molecular oxygen,[1759,1770] and both atoms from the molecular oxygen are incorporated into the product (Equation 2–274).

The **most prevalent coordination of a mononuclear, prosthetic, nonheme iron ion** is one in which the nitrogens of **two imidazolyl groups** and one or both[1779] of the oxygens from **one carboxy group**, either an aspartate or a glutamate, provide three or four of the octahedral ligands to the iron ion and, in the resting unoccupied enzyme, the oxygens of three or two waters, respectively, provide the remaining octahedral ligands (Figure 2–57D).[1780] When only one of the oxygens of the carboxylate is a ligand, the other can form a hydrogen bond to one of the waters on the iron ion and is available as a catalytic acid–base. Any one of the molecules of water can be replaced by an oxygen, nitrogen, or sulfur in one of the substrates or, when the iron ion is Fe^{2+}, by molecular oxygen. This coordination is capable of several different types of oxygenation.

The **extradiol dioxygenases** are a family of enzymes that, by and large, use this coordination of an iron ion by two imidazolyl groups and the carboxy group of a glutamate. The reactants for these dioxygenases are dihydroxyphenyl or aminohydroxyphenyl groups. The two hydroxy groups or the hydroxy group and the amino group on the phenyl group can be either ortho to each other or para to each other. A member of this family converts a dihydroxyphenyl group or an aminohydroxyphenyl group into the respective 6-oxohexa-2,4-dienoate by oxidatively cleaving the carbon–carbon bond adjacent to one of the hydroxy groups but not the carbon–carbon bond between two vicinal ortho hydroxy groups. For example, 3-carboxyethylcatechol 2,3-dioxygenase

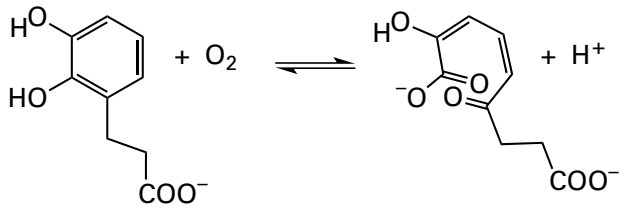

(2–276)

converts 3-(2,3-dihydroxyphenyl)propanoate to (2*E*,4*Z*)-2-hydroxy-6-oxonona-2,4-diene-1,9-dioate. 3,4-Dihydroxyphenylacetate 2,3-dioxygenase

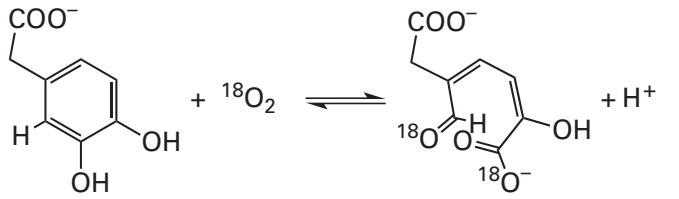

(2–277)

from *Brevibacterium fuscum*[1781] converts 3,4-dihydroxyphenylacetate to (2*E*,4*Z*)-2-hydroxy-5-carboxymethyl-6-oxohexa-2,4-dienoate, and biphenyl-2,3-diol 1,2-dioxygenase from *Pseudomonas*[1782] converts biphenyl-2,3-diol to (2*E*,4*Z*)-2-hydroxy-6-oxo-6-phenylhexa-2,4-dienoate.

Unlike the intradiol dioxygenases, **in the resting state, the iron in the active site of an extradiol dioxygenase is an Fe^{2+}**, in part because there is only one weakly basic anionic oxygen coordinating the iron ion. The Fe^{2+} in the active site of gentisate 1,2-dioxygenase from *Pseudaminobacter salicylatoxidans*, however, which is a member of a separate family of extradiol dioxygenases, is coordinated by three histidines and no carboxylate.[1783] When the Fe^{2+} in 3,4-dihydroxyphenylacetate 2,3-dioxygenase (Equation 2–277) from *B. fuscum* is changed to a Mn^{2+}, there is almost no change in the rate of the enzymatic reaction.[1784] Consequently, because the biochemical standard reduction potentials of Mn^{2+} and Fe^{2+} differ by 700 mV, the oxidation state of the metallic ion probably is not required to change during the enzymatic reaction and its role is to assemble the reactants.

The mechanism of the extradiol dioxygenases begins when the hydroxy group of the substrate that is adjacent to the site of cleavage associates with the Fe^{2+} in the active site. In a crystallographic molecular model of the complex between the Fe^{2+} and the reactant 3,4-dihydroxy-L-phenylalanine in the active site of 3,4-dihydroxyphenylalanine 2,3-dioxygenase (see Equation 2–277) from *Streptomyces sclerotialus*, both the 3-hydroxy group, adjacent to the site of cleavage, and the 4-hydroxy group become ligands to the Fe^{2+}, and the 2-imidazolyl groups and the carboxy oxygen fill three of the other octahedral positions around the Fe^{2+}, an arrangement that leaves an open site.[1785] A molecule of oxygen then binds to the open site—or when the reactant does not have vicinal diols, to one of the two open sites—on the Fe^{2+} to form an oxyiron(II). The oxyiron(II) withdraws an electron from the phenyl ring to form a **radical on the carbon adjacent to the hydroxy group** next to the site of cleavage, just as in the intradiol dioxygenases (see Equation 2–275).

The conclusion that this radical exists is based on results from **radical probes**. The 3-carboxyethylcatechol 2,3-dioxygenases (Equation 2–276) from both *E. coli* and *C. necator* catalyze the isomerization of the radical probe *cis*-2-(2,3-dihydroxyphenyl)-cyclopropane-1-carboxylate to *trans*-2-(2,3-dihydroxyphenyl)cyclopropane-1-carboxylate, an isomerization that requires that the 2,3-dihydroxyphenyl group in these radical probes be converted in the active site to the 2,3-dihydroxyphenyl radical.[1786] Two different complexes between 2-hydroxy-4-nitrophenol and the oxyiron(II) in the active site of 3,4-dihydroxyphenylacetate 2,3-dioxygenase from *B. fuscum* (Equation 2–277) have been examined spectroscopically.[1787] The various spectra of the first complex identify it as 2-hydroxy-4-nitrophenol associated through its 2-hydroxy group to oxyiron(II), and those of the second complex are consistent with it being 2-hydroxy-4-nitrophenol radical bound to superoxyiron(II). In the second complex, an electron from the 2-hydroxy-4-nitrophenol has been withdrawn onto the molecular oxygen to form the superoxide radical anion.

Because the oxidation state of the Fe^{2+} probably does not change during formation of the initial radical, it must be the molecule of oxygen on the Fe^{2+} that forms this initial radical. Either the complex between homogentisate and oxyiron(II) or homogentisate radical and superoxyiron(II), which are indistinguishable, has been observed crystallographically in the active site of homogentisate 1,2-dioxygenase from *P. putida*,[1788] and either the complex between 3,4-dihydroxynitrobenzene and oxyiron(II) or 3,4-dihydroxynitrobenzene radical and superoxyiron(II), which are indistinguishable, has been observed crystallographically in the active site of 3,4-dihydroxyphenylacetate 2,3-dioxygenase from *B. fuscum*.[1789] In these complexes, either the molecule of oxygen or the superoxide radical anion is **bound sideways** to the iron ion (see Figure 2–57E),[1790] and the homogentisate (2,5-dihydroxyphenylacetate), or its radical, is coordinated to the iron ion by the 2-hydroxy group

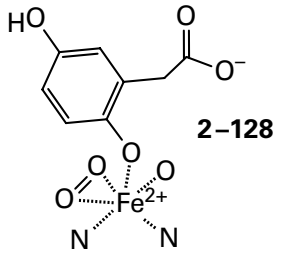

2–128

or the 3,4-dihydroxynitrobenzene, or its radical, is coordinated to the iron ion by both the 3-hydroxy group and the 4-hydroxy group. In the crystallographic molecular model of the occupied active site of homogentisate 1,2-dioxygenase (**2–128**), the closest oxygen atom in the molecular oxygen is 0.26 nm from carbon 2; and in the crystallographic molecular model of the occupied active site of 3,4-dihydroxyphenylacetate 2,3-dioxygenase, the closest oxygen atom in the molecular oxygen is 0.24 nm from carbon 3. In both of these cases, the distances are well within the sum of the van der Waals radii. This disposition suggests that the radical at the respective carbon in each of these two active sites is the result of an inner-sphere electron transfer from the highest occupied π molecular orbital for the aromatic π molecular orbital system of the respective phenyl group to one of the half-occupied π^* molecular orbitals on the oxygen molecule. A model compound that mimics this complex between a hydroxyphenyl radical and an Fe^{2+} has been synthesized.[1791]

The next step in the reaction of an extradiol dioxygenase, for example, 3,4-dihydroxyphenylacetate 2,3-dioxygenase

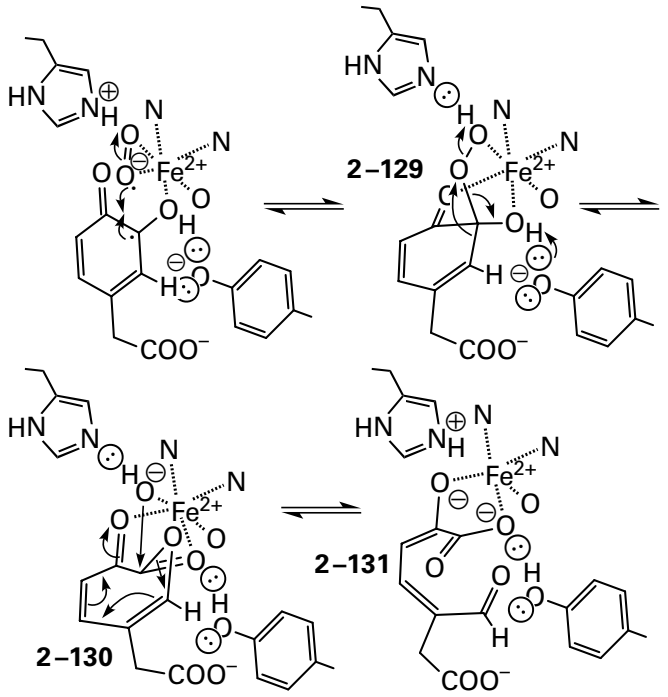

(2–278)

is the addition of the radical at the carbon on which the coordinated hydroxy group is located to the closest oxygen of the superoxide radical anion in a colligation to form **metallacyclic peroxide 2–129**, analogous to the one in protocatechuate 3,4-dioxygenase (**2–126**) but on an Fe^{2+} rather than a Fe^{3+}. This intermediate metallacyclic peroxide has been observed crystallographically in the active sites of 3,4-dihydroxyphenylacetate 2,3-dioxygenase from *B. fuscum*[1789] and homogentisate 1,2-dioxygenase from *P. putida*[1788] and has been identified spectroscopically in the active site of 3,4-dihydroxyphenylacetate 2,3-dioxygenase from *B. fuscum*.[1787]

Given that the distance between the carbon and the oxygen is only 0.24–0.26 nm, it seems odd that formation of the bond producing the peroxide is not coincident with formation of the radical, and that the radical and the superoxide radical anion are identifiable intermediates. Because molecular oxygen is a triplet molecule and the peroxide is a singlet molecule, however, the existence of these intermediates may result from the fact that intersystem crossing must occur before the peroxide can form and that separation of the two electrons into the two reactants and coordination to the Fe^{2+} hastens but does not eliminate this usually slow process. It may also be slow because the spin density on the carbon is meager.

The cyclic peroxide then rearranges to form the lactone of the product (Equation 2–278), which in the case of 3,4-dihydroxyphenylacetate 2,3-dioxygenase would be **2–130**. This ring expansion is again an analogue of a **Baeyer–Villiger rearrangement** (Figure 2–47B) with the leaving group being a hydroxyiron(II) instead of a carboxylate. The 4-oxidophenyl group of a tyrosine in the active site of 3,4-dihydroxyphenylacetate 2,3-dioxygenase from *B. fuscum* (0.25 nm) removes a hydron from the hydroxy group that becomes one of the acyl oxygens during this rearrangement.[1789]

In the crystallographic molecular model of the complex between the active site of 3,4-dihydroxyphenylacetate 2,3-dioxygenase from *B. fuscum* and 2-hydroxy-4-nitrophenol, which is a slow substrate for the enzyme, the respective metallacyclic peroxide (see **2–129**) that precedes the ring expansion is observed.[1789] In this intermediate, the imidazolyl group of a histidine forms a hydrogen bond (0.30 nm) to the oxygen of the peroxy group that is on the iron ion. 2,2-Hydroxy-4-sulfonatocyclohexa-2,4-dienone is isosteric and isoatomic but not isoelectronic with the product of only a heterolysis of the oxygen–oxygen bond in the respective metallacyclic peroxide (see **2–129**) but not a rearrangement. In a complex of the same enzyme with this analogue, the imidazolyl group of the same histidine forms a hydrogen bond (0.28 nm) to a hydroxide on the Fe^{2+}.[1792] It can be concluded that this imidazolyl group **hydronates the proximal oxygen** of the peroxy

group in **2–129** during the actual rearrangement (Equation 2–278) so that the leaving group in the heterolysis of the oxygen–oxygen bond that occurs during the rearrangement is ferrous hydroxide.

2-Hydroxy-2-hydroxymethylcyclohexa-3,5-dien-1-one is an analogue of peroxy intermediate **2–127** that is missing the carboxymethyl group and the other hydroxy group and in which the oxygen atom of the peroxy group on carbon 2 has been replaced with a methylene carbon. When 2-hydroxy-2-hydroxymethylcyclohexa-3,5-dien-1-one is mixed with 3-carboxyethylcatechol 2,3-dioxygenase from *E. coli*, 2-hydroxy-1-oxocyclohepta-2,4,6-triene is produced by the enzyme[1793]

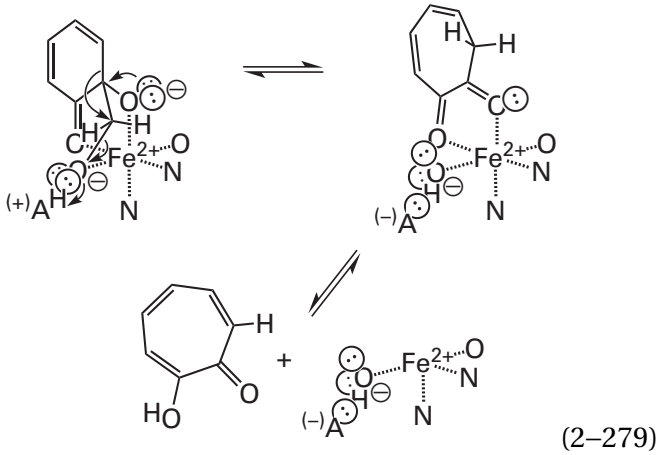

(2–279)

The cycloheptatriene ring in this rearranged intermediate is a carbon analogue of the lactone of the product (**2–130**) in which the oxa group in the ring of the latter is a methylene carbon in the former. This ring expansion is analogous to a pinacol rearrangement with neighboring group participation. This rearrangement catalyzed by this extradiol dioxygenase is the homologue of the usual ring expansion that occurs in the active site of an extradiol dioxygenase (Equation 2–278).

In the crystallographic molecular model of the active site of 3,4-dihydroxyphenylacetate 2,3-dioxygenase from *B. fuscum* occupied by the respective metallacyclic peroxy intermediate (**2–129**) of 2-hydroxy-4-nitrophenol, the hydroxy oxygen of a tyrosine side chain distorts the ring of the intermediate 2-hydroxy-4-nitro-1-oxo-2-peroxycyclohexa-3,5-diene by pushing the bond between carbon 2 and carbon 3 of the phenyl ring toward the oxygen of the peroxy group.[1794] Such a distortion in the normal enzymatic reaction would encourage the migration of the bond between carbon 2 and carbon 3 of the phenyl ring to that oxygen (Equation 2–278).

Following the migration of the σ bond during ring expansion, the resulting **lactone is hydrolyzed** by the hydroxide on the Fe^{2+} that was the leaving group in dissociation of the peroxyiron(II). The imidazolyl group of the histidine dehydronates the oxygen of the hydroxy group on the Fe^{2+}, itself a Lewis acid, during the nucleophilic addition to increase its nucleophilicity. The hydrolyzed lactone has been observed in crystallographic molecular models of the active site of homogentisate 1,2-dioxygenase from *P. putida*[1788] and the active site of 3,4-dihydroxyphenylacetate 2,3-di-oxygenase from *B. fuscum*.[1789]

So far the prosthetic nonheme iron ions that have been discussed have either remained in the same oxidation state throughout the respective reactions or changed back and forth from Fe^{2+} to Fe^{3+}, but no high-valent intermediates have been evoked or have been needed. There are a collection of enzymes in the active sites of which there are prosthetic, nonheme iron ions that do pass through high-valent intermediates.

The same coordination of an iron ion by two imidazolyl groups and a carboxylate oxygen (Figure 2–57D) is used by oxidases and oxygenases that require two electrons from the electron-transferring coenzymes, L-ascorbate or (6*R*)-5,6,7,8-tetrahydrobiopterin (Equation 2–270), or 2-oxoglutarate, a cosubstrate, to accomplish the oxidation or oxygenation of their respective nominal substrates through high-valent intermediates.[1780,1795-1800] An example of an oxidase that uses L-ascorbate (Equation 2–163) as a reductant is aminocyclopropanecarboxylate oxidase[1801]

$$\begin{aligned}&\text{1-aminocyclopropane-1-carboxylate} + O_2 + \\ &2\ \text{L-ascorbate} \rightleftharpoons 2\ \text{L-monodehydroascorbate} \\ &+ 2\,H_2O + H^+ + \text{cyanide} + \text{ethylene} + CO_2\end{aligned} \qquad (2\text{–}280)$$

The two L-monodehydroascorbates then disproportionate to an L-dehydroascorbate (Equation 2–163) and an L-ascorbate. An example of a monooxygenase that uses BH_4 as a reductant is phenylalanine 4-monooxygenase

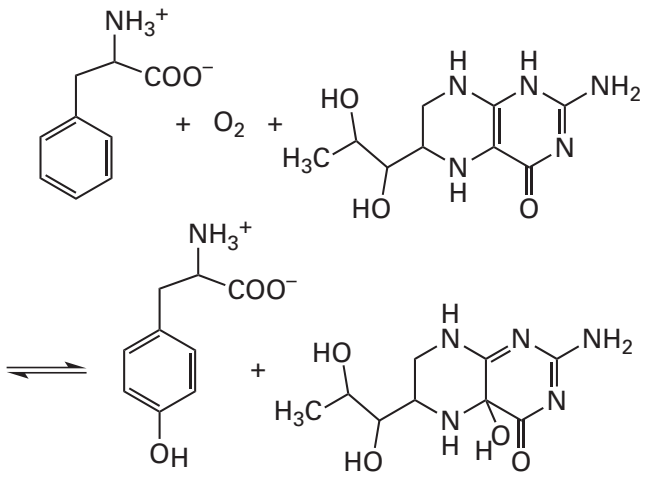

(2–281)

In this latter reaction (Equation 2–281), the 4a-hydroxyhemiaminal of 6,7-dihydrobiopterin,[1802] which, as shown, is the actual product of the enzymatic reaction,[1803,1804] is dehydrated to 6,7-dihydrobiopterin by 4a-hydroxytetrahydrobiopterin dehydratase,[1805] and the resulting 6,7-dihydrobiopterin is enzymatically reduced back to BH_4 by 6,7-dihydropteridine reductase. An example of an oxygenase that uses 2-oxoglutarate as a reductant is procollagen-proline 4-dioxygenase

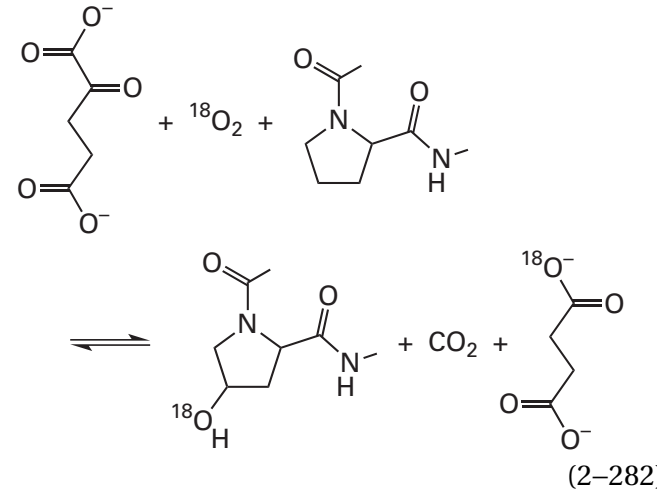

(2–282)

The product of this reaction is succinate, which is a common metabolite in the citric acid cycle, as is 2-oxoglutarate. Bovine procollagen-proline 4-dioxygenase incorporates one oxygen-18 from $^{18}O_2$ into the hydroxy group on the proline in the procollagen and the other oxygen-18 from $^{18}O_2$ into the carboxylate of the succinate.[1806]

The conversion of two L-ascorbates to two L-monodehydroascorbates, the conversion of tetrahydrobiopterin to 4a-hydroxytetrahydrobiopterin, and the conversion of 2-oxoglutarate to carbon dioxide and succinate in each case provides the **two electrons needed to convert an oxyiron(II) to an oxoiron(IV)**

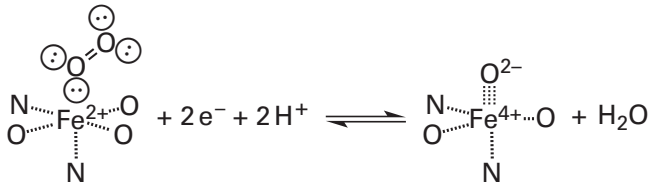

(2–283)

within the respective active sites,[1796,1807-1812] and this prosthetic high-valent iron oxide participates in the observed oxygenations.[1813] Nuclear resonance vibrational spectra of the oxoiron(IV) in such an active site are consistent with pentacoordination with the two imidazolyl groups and the carboxylato group as three of the ligands, the oxo group as the fourth ligand, and an oxygen atom from a molecule of water or a reactant as the fifth ligand.[1814]

L-Ascorbate provides two electrons to the active site, one at a time as required, in outer-sphere transfers. The first electron converts the nonheme oxyiron(II) to peroxyiron(III) (see Equation 2–250). A hydron and the second electron, in place of an electron from a surrounding porphyrin (Equation 2–241), are needed to convert the peroxyiron(III) to an oxoiron(IV).

In contrast to L-ascorbate, BH_4 and 2-oxoglutarate engage in **covalent intermediates** while providing the two electrons needed for the respective oxygenations.

Tetrahydrobiopterin converts oxyiron(II) to the **hemiaminal of a peroxyiron(II)**[1815]

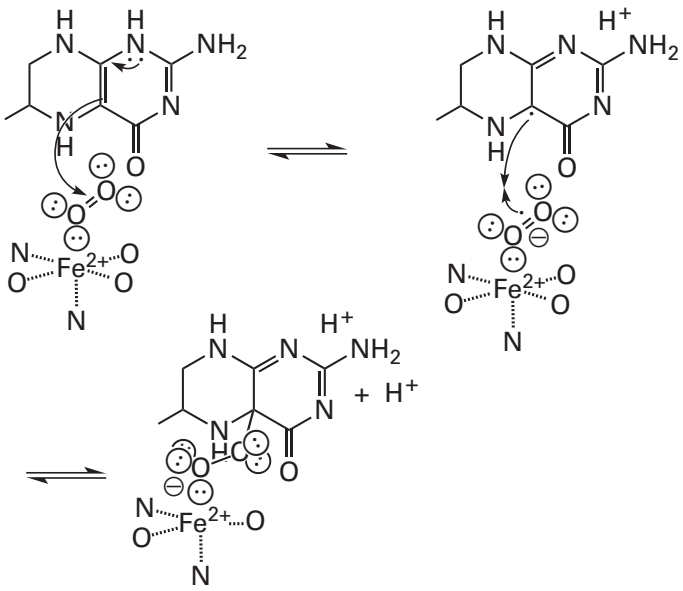

(2–284)

Although formation of this 4a-[peroxyiron(II)]-dihydrobiopterin is formally a nucleophilic addition of a pair of electrons in the electron-rich BH_4 to the molecular oxygen, the actual reaction probably involves two steps. The first is the transfer of an electron from BH_4 to the molecular oxygen of the oxyiron(II) to form superoxyiron(II). The second is the colligation of the two radicals, as in the active site of 3,4-dihydroxyphenylacetate 2,3-dioxygenase (Equation 2–278). These two steps permit rapid intersystem crossing. In this instance, the two radicals that colligate are the semiquinone of tetrahydrobiopterin, $BH_3^{\bullet}$, and superoxyiron(II).[1816]

2-Oxoglutarate converts oxyiron(II) that is formed between molecular oxygen and the Fe^{2+} of the active enzyme,[1817] and which is equivalent (Figure 2–50) to superoxyiron(III), to a **succinylperoxyiron(II)**[1780,1818-1822]

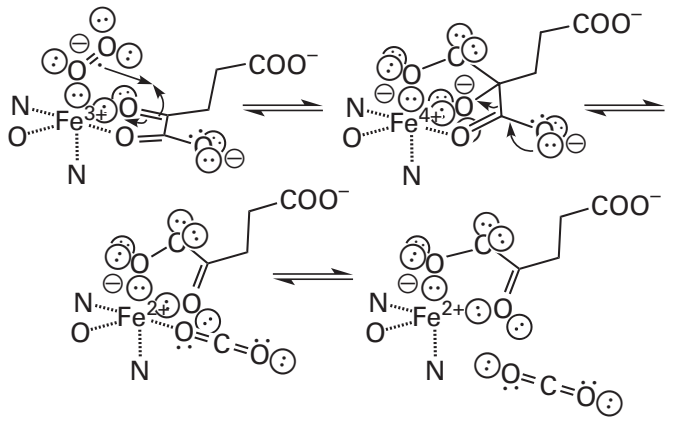

(2–285)

which is the complex between monoperoxysuccinic acid and Fe^{2+}. This complex has been observed in a crystallographic molecular model of L-arginine hydroxylase from *Streptomyces vinaceus*.[1821]

From both the hemiaminal of a peroxyiron(II) (Equation 2–284) and the acylperoxyiron(II) (Equation 2–285), upon the usual heterolytic cleavage, an **oxoiron(IV)** is formed

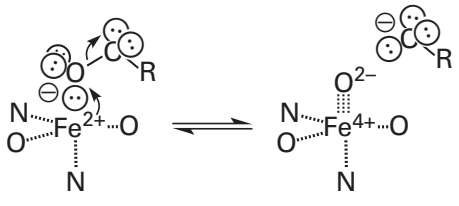

(2–286)

with the respective oxygens, those of 4a-hydroxydihydrobiopterin and succinate, respectively, as leaving groups. This oxoiron(IV) intermediate has been detected spectroscopically in several of these enzymes.[1823-1827] In the case of the oxoiron(IV) formed by 2-oxoglutarate, the succinate that is one of the products remains a ligand to the iron ion until the oxygenation catalyzed by the enzyme has been completed, when both the oxidized product and the succinate dissociate.[1821]

The only purpose of formal nucleophilic addition to BH_4 (Equation 2–284) or decarboxylation of 2-oxoglutarate (Equation 2–285) is to provide the two electrons necessary during the conversion of oxyiron(II) to oxoiron(IV). Phenylalanine 4-monooxygenase from *R. norvegicus*, stripped of BH_4, is able to hydroxylate L-phenylalanine if hydrogen peroxide is used to produce oxoiron(IV) from the iron(II) in its active site, bypassing the normal route in the cytoplasm that relies on BH_4.[1828]

There is a **model compound for a nonheme oxoiron(IV)** in which the iron ion is coordinated by three guanidino nitrogens and an amino nitrogen and the iron–oxygen bond is of the appropriate length (0.165 nm). The arrangement of the five ligands in this model compound is a trigonal bipyramid.[1829] In a similar model compound, the four ligands to the iron are three pyrimidinyl nitrogens and an amino nitrogen and the iron is in the ferric state. The Fe^{3+} in this model compound is able to associate with hydrogen peroxide, and the ferric hydroperoxide dissociates to form oxoiron(V) rather than oxoiron(IV).[1830] This observation demonstrates that with the proper ligands a nonheme oxoiron(V) can be a stable product, but it may not be attainable in the active site of an enzyme.

The two nonheme oxoirons in these synthetic models for high-valent, nonheme iron ions in enzymes illustrate an **important distinction between an iron ion in a heme and an iron ion that is not in a heme**. When a hydroperoxyiron(III) porphyrin in a heme is provided with a hydron by an acid, the oxygen–oxygen bond dissociates heterolytically to form initially an oxoiron(V) porphyrin, which immediately or coincidently removes an electron from the highest occupied π molecular orbital of the porphyrin and becomes an oxoiron(IV) porphyrin$^{\bullet+}$. This latter option is not available to a nonheme iron ion. A nonheme hydroperoxyiron(III) can dissociate in solution under acid catalysis to produce a nonheme oxoiron(V), but because an oxoiron(V) is so unstable in most instances, it is difficult to form, and an oxoiron(V) has not yet been observed in the active site of an enzyme. If an electron is provided along with the hydron, as occurs in a heme, a hydroperoxyiron(III) dissociates to form an oxoiron(IV). A

nonheme oxyiron(II), however, which is formed by the association of molecular oxygen with a nonheme Fe^{2+}, upon two-electron reduction and the addition of a hydron becomes the equivalent of a hydroperoxyiron(II) which dissociates heterolytically to form an oxoiron(IV). In this case, the electron required is provided before the dissociation of the peroxide rather than during its dissociation.

Depending on the specificity of the particular oxidase, monooxygenase, or dioxygenase, the oxoiron(IV) formed on the prosthetic nonheme iron ion (Equation 2–286) in an active site that obtains the necessary two electrons from ascorbate, BH_4, or 2-oxoglutarate can perform **one of several different types of oxidation**. The oxoiron(IV) can **hydroxylate an aliphatic carbon**;[1799,1819,1831,1832] hydroxylate the carbon adjacent to either a sulfonato group[1831,1833] or a carbamoyl nitrogen[1834] to produce ultimately a carbonyl group from that carbon upon hydrolysis of the resulting 1-hydroxy-1-sulfonate or the resulting hemiaminal, respectively, hydroxylate a methyl group to a hydroxymethyl group, hydroxylate the resulting hydroxymethyl group to the formyl group, and hydroxylate the resulting formyl group to the carboxy group in three separate steps.[1835]

The first step in the hydroxylation of an aliphatic carbon–hydrogen bond by oxoiron(IV) is the **abstraction of hydrogen from the carbon**. In the hydroxylation of L-arginine by 2-oxoglutarate dioxygenase (ethene-forming) from *P. savastanoi*, when the hydrogen on the L-arginine that is replaced by the hydroxy group is substituted with a deuterium, the rate at which the oxoiron(IV) formed in the active site decays during the enzymatic reaction decreases[1836] by a factor of greater than 16. In the hydroxylation of the normal substrate 2-amino-ethanesulfonate by taurine dioxygenase from *E. coli*, a hydroxyiron(III) is the intermediate that is formed directly from oxoiron(IV), the result expected (Figure 2–50) for abstraction of a hydrogen atom as the first step in the actual hydroxylation.[1837] In a crystallographic molecular model of the active site of the enzyme in which the oxoiron(IV) has been replaced by an inert oxovanadium(IV) and 2-aminoethanesulfonate is bound, the nearest hydrogen on carbon 1 of the 2-aminoethanesulfonate is only 0.20 nm from the oxo group on the vanadium ion, well within van der Waals contact (0.26 nm), and its carbon–hydrogen bond is pointed at the oxo group.[1838] In the reaction catalyzed by deacetoxycephalosporin-C synthase from *S. clavuligerus*, the role of the oxoiron(IV) formed in its active site is only that of abstracting a hydrogen from a methyl group to initiate a ring expansion.[1839] In verruculogen synthase from *A. fumigatus*, the radical produced on the substrate by abstraction of a hydrogen atom by oxoiron(IV), instead of becoming an alcohol, reacts with a second molecule of molecular oxygen to form the peroxy radical (see Equation 2–275).[1840]

If the first step in hydroxylation of an aliphatic carbon is the abstraction of a hydrogen by oxoiron(IV), then the result at the iron ion would be hydroxyiron(III), and the next step should be the **combination of the carbon radical with the hydroxyiron(III)** to produce the hydroxy group in the product coordinated to iron(II).[1837] In the aliphatic halogenase SyrB2 from *Pseudomonas syringae*, the oxoiron(IV) abstracts a hydrogen from a saturated carbon, and the resulting aliphatic radical reacts with a chloride, which is a ligand to the hydroxyiron(III), rather than its hydroxy group, to give a chloro group on the product rather than a hydroxy group.[1841] There is a synthetic model compound containing a hydroxyiron(III) pentacoordinated by two pyrimidino nitrogens, a tertiary amino group, and a hydroxy group in addition to the hydroxy group of hydroxyiron(III). The hydroxy group on Fe^{3+} in this model compound adds to a carbon radical to give the alcohol as the product.[1842] Consequently, just as hydroxyiron(IV) is equivalent to a hydroxyl radical on an Fe^{3+} (Figure 2–50), hydroxyiron(III), although formally a simple ferric hydroxide, is also equivalent to a hydroxyl radical on an Fe^{2+}, or a chloride as a ligand on a hydroxyiron(III) is equivalent to a chlorine radical on hydroxyiron(II).

There are epoxidases in this family of enzymes that use oxoiron(IV) to **convert a carbon–carbon double bond into an epoxide**[1822] or produce the diol from a carbon–carbon double bond,[1834] presumably by an intermediate epoxidation. For example, the epoxidase AsqJ, which is involved in a step in the biosynthesis of aspoquinolone mycotoxin by *Emericella nidulans*, monooxygenates the electron-rich carbon–carbon bond of an enamine adjacent to a 4-methoxyphenyl group. In the active site of the 2-oxoglutarate-dependent enzyme, the prosthetic oxoiron(IV) acts as an electrophile to which the nucleophilic α position of the enamine adds, and during the addition the iminium is formed

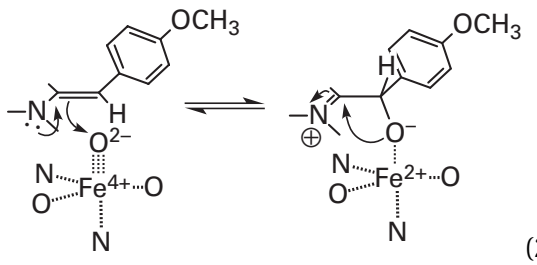

(2–287)

This intermediate has been observed in a crystallographic molecular model of the enzyme.[1822] In the intermediate, the oxygen–carbon bond of the oxido group is normal to the plane of the enamine and parallel to its π molecular orbital system as expected, but the 4-methoxyphenyl ring is rotated so that in the reactant it would have been out of conjugation with the enamine. Following the nucleophilic addition, the oxyanion of the oxido group on the resulting Fe^{2+} then nucleophilically adds intramolecularly to the iminio carbon to form the epoxide that is the product of the reaction. The initial addition of the carbon–carbon double bond to the oxoiron(IV) is only marginally affected by the substitution of the 4-methoxy group, a strong electron-donating group, with strong electron-withdrawing groups. This result is consistent with weak conjugation of the 4-methoxyphenyl ring with the enamine.

In the enzymes that use BH_4 as a coenzyme and that **hydroxylate an aryl carbon–hydrogen bond**, such as in the hydroxylation of L-phenyl-alanine at carbon 4 (Equation 2–281), L-tyrosine at carbon 3, and L-tryptophan at carbon 5, oxoiron(IV) forms an intermediate that is chemically equivalent to pentadienyl carbenium ion **2–132**

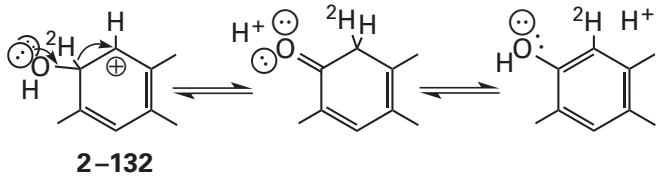

2–132

(2–288)

A fact that is consistent with the existence of this carbenium ion is the observation of a **1,2-hydride migration** (Equation 2–288) or a 1,2-methyl migration from the carbon that is hydroxylated to an adjacent carbon when deuterated or methylated substrates, respectively, are used.[1352,1843-1847] In the crystallographic molecular model of the complex between L-tryptophan and tryptophan 5-monooxygenase from *G. gallus*, carbon 5 of the L-tryptophan is 0.39 nm from the iron ion, but carbon 4 is only 0.43 nm from the iron ion.[1779] These are appropriate distances if the oxygen of oxoiron(IV) is sitting between the iron and the double bond between carbon 4 and carbon 5 during an epoxidation to produce, perhaps,[1848] an intermediate arene epoxide,[1849] which would then dissociate to pentadienyl carbenium ion **2–132**.

In addition to hydroxylation and epoxidation, oxoiron(IV) in one of the enzymes in this family can also **remove a hydride**[1850] or aggressively **withdraw, in the inner sphere, two electrons** from 1-aminocyclopropane-1-carboxylate also bound to iron(IV) to produce ethene, carbon dioxide, and hydrogen cyanide.[1851] Each of these reactions regenerates iron(II) ready to begin again.

With many of the enzymes that activate molecular oxygen by using a nonheme Fe^{2+}, in particular the 2-oxoglutarate dioxygenases, a serious flaw arises in practice. When molecular oxygen is bound to an Fe^{2+}, there is always a significant probability that the complex will **dissociate to produce superoxide radical anion and Fe^{3+}** (Equation 2–246). As superoxide radical anion is rapidly disproportionated in the cytoplasm by superoxide dismutase (Equation 2–226), it does not accumulate sufficiently to reduce the Fe^{3+} back to Fe^{2+}, and the enzyme is inactivated by its own reaction. In most oxygenases, especially those using nonheme iron, the usual mechanism for reducing the iron back to the ferrous form and reactivating the enzyme is to use L-ascorbate (Equation 2–163) as a one-electron reductant. When one of these leaky oxygenases, such as procollagen-proline 4-dioxygenase (Equation 2–282), is operating, **L-ascorbate** must be present continuously. Even at its maximum rate, a molecule of procollagen-proline 4-dioxygenase can oxygenate only about 50–200 molecules of substrate in the absence of L-ascorbate before the iron becomes adventitiously oxidized. Procollagen-proline 4-dioxygenase can be rereduced only at the expense of one electron from L-ascorbate (Equation 2–163).[1852,1853] A failure to hydroxylate collagen causes scurvy, a result of ascorbic acid deficiency. In other oxygenases, however, reductants other than L-ascorbate, and even superoxide radical anion itself, can substitute in this role.[1854]

There are a number of enzymes in the nonheme, iron-dependent dioxygenase family that have Fe^{2+} ions in their active sites also coordinated by two imidazolyl groups from two histidines and one or two of the oxygens of a carboxylate from aspartate or glutamate (Figure 2–57D) but that obtain electrons

for their oxygenations from sources other than L-ascorbate, 2-oxoglutarate, or BH_4. In 4-hydroxymandelate synthase

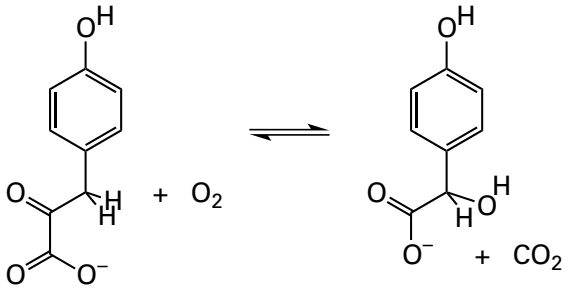

(2–289)

from *Amycolatopsis orientalis*, the substrate 4-hydroxyphenylpyruvate has within itself a 2-oxo carboxylic acid that forms oxoiron(IV) just as 2-oxoglutarate does by decarboxylation. The oxoiron(IV) then hydroxylates the methylene carbon of the intermediate 2-(4-hydroxyphenyl)acetate.[1855]

In (*S*)-2-hydroxypropylphosphonic acid epoxidase from *Streptomyces wedmorensis*,[1855,1856] 2-hydroxyethylphosphonate dioxygenase from *Streptomyces viridochromogenes*,[1857-1860] and isopenicillin-N synthase from *E. nidulans*,[1861,1862] the respective prosthetic iron ion coordinated by two imidazolyl groups and a carboxylato oxygen begins the respective oxygenation in the ferrous state; binds molecular oxygen to form the usual oxyiron(II), which as always is equivalent to superoxy-iron(III). The superoxyiron(III) then converts to hydroperoxyiron(III) upon the transfer of an electron and a hydron or hydrogen atom from the respective reactant. A subsequent, transient intermediate oxoiron(IV) has been identified spectroscopically in the oxidation catalyzed by 2-hydroxyethylphosphonate dioxygenase.[1863] This oxoiron(IV) would result from the homolytic dissociation of a hydroxyl radical from hydroperoxyiron(III). A computationally reasonable proposal for the epoxidation catalyzed by (*S*)-2-hydroxypropylphosphonic acid epoxidase is that the resulting **hydroxyl radical**, which is reactive enough (BDE = 497 kJ mol^{-1}) to abstract a hydrogen from any carbon atom, then abstracts a hydrogen from carbon 1 of 2-hydroxypropylphosphonic acid to initiate its epoxidation.[1864] In the case of 2-hydroxyethylphosphonate dioxygenase, however, the hydroxyl radical would participate in a colligation with the radical at carbon 2 of the 2-hydroxyethylphosphonate that, in this case, results from the abstraction of hydrogen from carbon 2 by superoxyiron(III), which becomes hydroperoxyiron(III).[1860]

There are a number of oxygenases that obtain the two electrons necessary for their oxygenations one at a time from a reduced Rieske [2Fe–2S] iron–sulfur cluster,[1865-1868] rather than from ascorbate, BH_4, or 2-oxoglutarate. The Rieske [2Fe–2S] iron–sulfur cluster is ultimately reduced one electron at a time by flavin. In naphthalene 1,2-dioxygenase

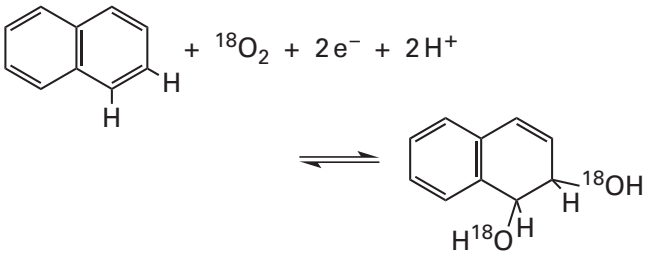

(2–290)

from *P. putida*, the prosthetic iron ion is coordinated by two imidazolyl groups from two histidines and two oxygens from the same bidentate carboxylato group of an aspartate (Figure 2–57E). The flavin that provides the electrons to the Rieske [2Fe–2S] iron–sulfur cluster is reduced by NADH.[1790] Naphthalene 1,2-dioxygenase with only a reduced nonheme Fe^{2+} and a reduced Rieske [2Fe–2S] iron–sulfur cluster catalyzes one dioxygenation of a naphthalene in the absence of any further source of electrons[1869] to give the diolate monoanion of the product tightly bound to the resulting Fe^{3+}.[1870] The diol, however, is released only upon reduction of the Fe^{3+}. These observations demonstrate that the actual oxygenation performed by the nonheme Fe^{2+} requires only one electron from the Rieske [2Fe–2S] iron–sulfur cluster and that the role of the second electron is to reduce the Fe^{3+} formed during oxygenation back to Fe^{2+}.

The first step in the reaction catalyzed by naphthalene 1,2-dioxygenase is the association of molecular oxygen with the prosthetic nonheme Fe^{2+}. In a crystallographic molecular model of fully reduced naphthalene 1,2-dioxygenase exposed to molecular oxygen, either a peroxide dianion or **molecular oxygen is bound sideways to the Fe^{2+}**, occupying both of its open positions (Figure 2–57E).[1790] Kinetic studies of the electron transfer from the prosthetic Rieske [2Fe–2S] iron–sulfur cluster during the dioxygenation of a series of reactants by benzoate 1,2-dioxygenase,[1868] a related enzyme (25% identity; 3.6 gap percent) also from *P. putida*, and during the monooxygenation of a series of reactants by the related enzyme, salicylate 5-hydroxylase[1871] from *Ralstonia* (23% identity;

3.3 gap percent), are consistent with an adduct forming between the reactant and the oxyiron(II) prior to transfer of an electron from the Rieske [2Fe–2S] iron–sulfur cluster, which would require that the distal oxygen of the equivalent of a superoxyiron(III) add to the phenyl ring of a reactant to form a pentadienyl radical within the ring. This conclusion would identify the complex observed in the crystallographic molecular model as the complex between molecular oxygen and Fe^{2+}. The products formed by naphthalene 1,2-dioxygenase when radical probes are used as reactants instead of naphthalene are consistent with a radical of the naphthalene[1872] being an intermediate in the enzymatic reaction.

The fact that fully oxidized benzoate 1,2-dioxygenase, in the absence of any reductant, catalyzes the same 1,2-dioxygenation of benzoate that it normally does when hydrogen peroxide is substituted for molecular oxygen[1873] and the fact that during this unnatural reaction a hydroperoxyiron(III) is an intermediate[1874] at first suggested that, following the association of molecular oxygen with Fe^{2+} in the active site, an electron is transferred from the reduced Rieske [2Fe–2S] iron–sulfur cluster to the complex and a peroxyiron(III) is formed, as would be formed directly from hydroperoxide ion and Fe^{3+}, and that peroxyiron(III) is the species accomplishing the rest of the reaction. It has been concluded, however, that this unnatural oxidation with hydrogen peroxide follows a different mechanism from the natural reaction up to a point at which the two mechanisms converge.[1874]

Once the radical of the substrate is formed by **radical addition of the superoxyiron(III) to the aromatic ring**, how the rest of the reaction proceeds is unclear. There are computations that favor a particular mechanism.[1874] In a model compound containing peroxyiron(III) in which the Fe^{3+} is coordinated with ligands homologous to the two imidazolyl groups and the carboxylato group, the carboxylato group ends up as a peroxy acid. Spectroscopic observations indicate that the distal oxygen of the peroxy acid and the acyl oxygen of the peroxy acid are ligands to an octahedral Fe^{3+}. This observation implies that a peroxy acid could be involved in the enzymatic reaction.[1418,1875]

There are also dinuclear clusters of prosthetic iron ions that bind molecular oxygen and use it to perform oxidations. Hemerythrin is an example of a dinuclear prosthetic iron cluster that binds molecular oxygen. One of the Fe^{2+} ions of its dinuclear cluster is coordinated by three histidines from the protein, and the other Fe^{2+} is coordinated by two histidines (Figure 2–57F).[1876-1878] Two of the other ligands to each of the Fe^{2+} ions are provided by the respective oxygens of the same aspartate and the same glutamate. Finally, the two Fe^{2+} ions are bridged by a μ-oxo group. A ***μ*-oxo group** is an oxide dianion or a hydroxide that coordinates simultaneously two metallic ions.[1879] The μ-oxo oxide or μ-hydroxo hydroxide in a ***μ*-oxo diiron cluster** or a μ-hydroxo diiron cluster couples the Fe^{2+} ions ferromagnetically in the inner sphere.

Hemerythrin, like hemoglobin, is responsible for binding molecular oxygen and transporting it in the circulation. In its deoxygenated, diferrous state, one Fe^{2+} is octahedrally and fully coordinated, but the other, although it is also octahedrally coordinated, has an open site. When molecular oxygen is bound by diferrous hemerythrin, it occupies this open site (Figure 2–57F) to saturate the octahedral coordination of this Fe^{2+}. When molecular oxygen is bound to the Fe^{2+} in the heme of a hemoprotein such as hemoglobin or myoglobin, the resulting complex has properties expected of both a complex between molecular oxygen and Fe^{2+} and a complex between superoxide radical anion and Fe^{3+} (Equation 2–246). When molecular oxygen is bound to the Fe^{2+} with the open site in diferrous hemerythrin, however, both iron ions are reversibly oxidized to Fe^{3+} ions.[1880,1881] The molecular oxygen in turn is reversibly reduced by the two electrons from the two Fe^{2+} ions and hydronated by the adjacent μ-hydroxo group on its distal oxygen through a hydrogen bond that remains in the final complex between the diferric cluster and a hydroperoxide ion (Figure 2–57F).[1882] This **ability of a dinuclear, diferrous cluster to convert molecular oxygen on an open Fe^{2+} spontaneously to a peroxyiron(III)**

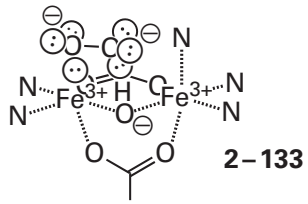

2 – 133

is one of the novel features of this type of prosthetic group. Hemerythrin performs no further chemistry with the peroxyiron(III), using it only as a stable form of molecular oxygen while carrying it from regions of high concentrations of molecular oxygen to regions of low concentrations of molecular oxygen.

In the μ-oxodiiron cluster (Figure 2–57G)[1883] of murine and human[1884] inositol oxygenase

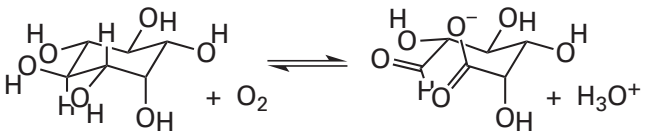

(2–291)

one of the iron ions is coordinated by the oxygen of a carboxylate and two nitrogens from imidazolyl groups and the other by two nitrogens from imidazolyl groups, and the iron ions are bridged by a μ-oxo group but only one carboxylato group. Because the other bridging carboxylato group is missing, one of the octahedral sites on the former iron ion (to the right in the drawing) is open, and two of the octahedral sites on the latter iron ion (to the left in the drawing) are open. The μ-oxodiiron cluster in inositol oxygenase oxidatively cleaves a carbon–carbon bond between two carbons, each with a hydroxy group trans to each other but equatorial (Equation 2–291). The distantly related[1885] 2-amino-1-hydroxyethylphosphonate dioxygenase (glycine-forming) from an unassigned species of bacterium has the same μ-oxodiiron cluster with the same ligands in the same orientation. It cleaves a bond between a carbon with a hydroxy group and a phosphorus with two hydroxy groups.[1886]

The active form of inositol oxygenase is not the diferrous state but a **mixed-valent state**[1887] in which one electron is delocalized between two Fe^{3+}. There is a completely symmetric, synthetic dinuclear cluster of prosthetic iron ions[1888] that is also able to support a similar mixed-valent state.[1889] Because this synthetic complex is symmetric, the two iron ions are in identical coordination, and the electron is delocalized equally between them.

myo-Inositol associates with the two open sites on the one iron ion in the active site of inositol oxygenase (Figure 2–57G), and upon its association, the affinity of the other iron ion for the molecule of water in its open, axial coordination site decreases measurably.[1890] This decrease in affinity for water suggests that this iron ion is now a localized Fe^{2+} while the other iron ion has become a localized Fe^{3+}. The decrease in affinity for water as the iron ion becomes a localized Fe^{2+} promotes the exchange of the molecule of water with a molecule of oxygen. The two hydroxy groups of the *myo*-inositol that have associated with the now Fe^{3+} are the two hydroxy groups between which the oxidative cleavage of the ring by the oxygenation catalyzed by the enzyme occurs (Equation 2–291 and Figure 2–57G), and the hydroxy group on carbon 1 and the hydroxy group on the phosphorus that associate with the iron ion in the active site of 2-amino-1-hydroxyethylphosphonate dioxygenase (glycine-forming) are the two hydroxy groups between which the oxidative cleavage occurs.[1886] The dioxygen of the oxyiron(II) at the iron ion to which the *myo*-inositol is not bound has the properties of a superoxide radical anion bound to Fe^{3+} and is in position to abstract the hydrogen from carbon 1 of the bound *myo*-inositol (Figure 2–57G).[1891] Following abstraction of the hydrogen atom, the oxyiron(II) has become a hydroperoxyiron(III), which is then converted into a species of high-valent iron that performs the oxygenation. No reductant is required in the stoichiometry reaction, so at the end for the oxygenation, the diiron cluster has necessarily returned to the mixed-valent state. Abstraction of the hydrogen on carbon 1 in 2-amino-1-hydroxyethylphosphonate also initiates the oxidative cleavage performed by 2-amino-1-hydroxyethylphosphonate dioxygenase (glycine-forming) from *Gimesia maris*.[1892]

In the μ-oxodiiron cluster (Figure 2–57H)[1893] of rubredoxin:oxygen oxidoreductase

$$4\ \text{rubredoxin}_{\text{red}} + 4\ H^+ + O_2 \rightleftharpoons 4\ \text{rubredoxin}_{\text{ox}} + 2\ H_2O \qquad (2\text{–}292)$$

from *D. gigas*, one of the iron ions is coordinated by the imidazolyl groups of two histidines and the carboxylato group of a glutamate and the other by the imidazolyl group of one histidine and the carboxylato group of an aspartate, and they are bridged by a μ-oxo group and the carboxylato group of another aspartate. The carboxylato group of the nonbridging aspartate forms a hydrogen bond with the μ-oxo hydroxide, as did one of the carboxylato groups of an aspartate in inositol oxygenase (Figure 2–57G).

In the first step in the four-electron reduction catalyzed by rubredoxin:oxygen oxidoreductase, molecular oxygen binds to the diiron(II) cluster in the resting enzyme at an open site on one of the two Fe^{2+} ions in the cluster (Figure 2–57H), and it is converted to hydroperoxydiiron(III). In 4-aminobenzoate *N*-oxygenase from *Streptomyces thioluteus*, which has the same distribution of ligands in its diiron cluster as rubredoxin:oxygen oxidoreductase, nuclear resonance vibrational spectra of this intermediate are consistent with an arrangement in

which each oxygen of the hydroperoxide is a ligand to a different iron ion in the cluster,[1894] and the hydron on the hydroperoxy group forms a hydrogen bond with the carboxylato group of the glutamate the carboxy group of which was a donor in the hydrogen bond with molecular oxygen (Figure 2–57H) and must have hydronated that oxygen. In the active site of rubredoxin:oxygen oxidoreductase, one of the oxygens of the hydroperoxydiiron(III), presumably the one already hydronated, becomes a molecule of water and and the other either becomes a higher-valent iron ion, which is then reduced to aquoiron(III) to complete the conversion of the molecular oxygen to two molecules of water, or it is reduced to aquoiron(III) in concert with the dissociation of the oxygen–oxygen bond. It is thought, however, that an oxoiron(IV) is formed during the dissociation of the oxygen–oxygen bond in 4-aminobenzoate *N*-oxygenase and that oxoiron(IV) is responsible for the oxygenation of the 4-amino group to the *N*-oxide as the first step in oxidizing it to the 4-nitro group.

In the μ-oxodiiron cluster in rubrerythrin from *D. vulgaris* in its diferric state, one Fe^{3+} is coordinated by the imidazolyl group of a histidine and by both oxygens of the carboxylato group of a glutamate and the other Fe^{3+} is coordinated by one of the oxygens of the carboxylato group of a glutamate and both oxygens of the carboxylato group of another glutamate. The carboxylato groups of two glutamates bridge the two Fe^{3+}, as do the aspartate and the glutamate in hemerythrin (Figure 2–57F), and there is one μ-oxo group.[1895] This coordination has the fewest imidazolyl groups and the most carboxylato groups and other oxyanions of any diiron cluster. Ruberythrin is a peroxidase (Equation 2–237) that uses two rubredoxins as the source of the necessary two electrons.[1896] The diferrous form of the prosthetic group binds hydrogen peroxide with one of its oxygens on each of the Fe^{2+} ions, reduces the hydrogen peroxide with the two electrons from the two Fe^{2+} ions to a molecule of water and a hydroxide that ends up as that μ-oxo group between the two now Fe^{3+} ions. The dinuclear cluster then releases the μ-oxo hydroxide as a molecule of water, but only after both Fe^{3+} ions have been reduced back to Fe^{2+} ions.[1897] As a result, the diferrous cluster has no μ-oxo group and each Fe^{2+} has an open site because the μ-oxo group of the diferric cluster has been released as the second molecule of water derived from the hydrogen peroxide. This sequence of events demonstrates that **a μ-oxo group is nothing more than an oxide ion,** which is the conjugate base of a hydroxide ion, which is the conjugate base of a molecule of water.

The **most common diiron cluster**,[1895,1898-1903] however, is one in which each of the two iron ions is coordinated by the imidazolyl group of a histidine and the carboxylato group of a glutamate, and they are bridged by a third carboxylato group from a glutamate (Figure 2–57I).[1904,1905] This arrangement of these five ligands is bilaterally pseudosymmetric rather than rotationally pseudosymmetric and hence the symmetry is serendipitous. The other participants coordinating the diferric cluster in methane monooxygenase (soluble) from *Methylococcus capsulatus* are a fourth carboxylato group from a glutamate (the upper glutamate in Figure 2–57I) and two μ-oxo groups.

In these clusters, **the coordination of the two irons varies noticeably between the diferric state and the diferrous state** and from one enzyme to the next. For example, in the diferric cluster in methane monooxygenase (soluble) from *M. capsulatus* (Figure 2–57I) there are two μ-oxo groups, one of which forms a hydrogen bond to the other oxygen of the carboxylato group of the upper glutamate in the drawing; but in the diferrous cluster in the same enzyme, there is only one μ-oxo group. The other μ-oxo group has been replaced completely by the now bidentate anionic oxygen of the carboxylato group of the upper glutamate, which swings in to replace the μ-oxo group and bridge the two Fe^{2+}.[1905] In its mixed-valent state, the diiron cluster in methane monooxygenase (soluble) has a structure intermediate between the diferrous and the diferric structures.[1906] In yet other enzymes in particular oxidation states, the carboxylato group of the glutamate in the front of the drawing bridges the two iron ions to form an arrangement like that of the two carboxylato groups in hemerythrin (Figure 2–57F) except that there is no μ-oxo group.[1907] In the diferrous state of the cluster in the active site of benzoyl-CoA 2,3-epoxidase from *Aromatoleum evansii*, only one oxygen from the carboxylato group of a glutamate coordinates one of the Fe^{2+} ions, in addition to the imidazolyl group of a histidine and the single oxygen from the carboxylato group of a glutamate coordinating each of the Fe^{2+} ions, respectively.[1908] In general, the diferric form of one of these diiron clusters has one or two μ-oxo groups as well as additional carboxylato oxygens coordinating the two Fe^{3+} ions while the diferrous form of the same cluster usually has no μ-oxo group or μ-hydroxo group bridging the Fe^{2+} ions or one μ-hydroxo group bridging them.[1905,1908-1910] The imidazolyl group and the

single carboxylato oxygen at each iron ion and the bridging carboxylato group, however, are the constant ligands from species to species, remain unchanged by reduction or oxidation, and form **the core of the dinuclear cluster**.

This most common μ-oxodiiron cluster performs **several different oxidation–reductions**. For example, the diferrous diiron cluster in toluene 4-monooxygenase[1911] catalyzes the hydroxylation of toluene at carbon 4 (the para position). Several intermediates in the monooxygenation catalyzed by toluene 4-monooxygenase from *Pseudomonas mendocina* have been observed crystallographically.[1912] In the initial complex between molecular oxygen and the dinuclear diiron(II) complex, one of the two oxygens is coordinated by both of the Fe^{2+} as if it were a μ-oxo group. In an intermediate 4-peroxytolyl complex and an unnatural complex between hydrogen peroxide and the prosthetic diiron(III) in the oxidized enzyme, the two oxygens of the peroxy group are both ligands to both of the iron ions. It was concluded from these observations that in the initial complex between toluene and oxydiiron(II), the superoxyiron(II)iron(III), which is a resonance hybrid of the oxydiiron(II), adds homolytically to carbon 4 of the toluene to form the 4-peroxytolyl radical, in which the other carbons in the ring are participants in a delocalized pentadienyl radical and the two oxygens of the peroxy group are both ligands to both of the iron ions

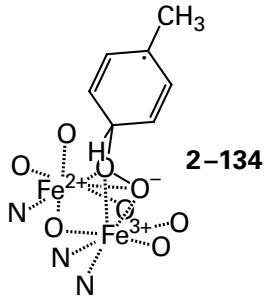

2–134

How this intermediate proceeds through the necessary aromatization and dissociation of the oxygen–oxygen bond of the peroxide is unclear. It does not, however, seem to proceed through a high-valent intermediate. A nearly quantitative hydride migration of the hydrogen from carbon 4 of the toluene to carbon 3 of the product 4-hydroxytoluene (see Equation 2–288) requires that the hydride migration be a step in the overall mechanism and consequently that the pentadienyl radical in the intermediate become a pentadienyl carbenium ion by losing its unpaired electron.[1913] This transformation of the radical to the carbenium ion would require an outer-sphere electron transfer because there is a saturated carbon between the pentadienyl radical and the rest of the complex that would act as an acceptor of the electron. The weakest bond in the intermediate is the oxygen–oxygen bond, but the point at which it dissociates has not been established. One possibility is that the electron is transferred, the hydride migrates, and the resulting carbenium ion withdraws the electrons in the oxygen-oxygen bond. The final step in the reaction is reduction of the two Fe^{3+} by two electrons to two Fe^{2+} and the release of the now loosely bound 4-hydroxytoluene and the μ-hydroxy group as a water.

The diferrous diiron cluster in stearoyl-[acyl-carrier-protein] 9-desaturase from *Ricinus communis*

$$2\,H^+ + 2\,e^- + \text{stearoyl-SACP} + O_2 \rightleftharpoons \text{oleoyl-SACP} + 2\,H_2O \qquad (2\text{–}293)$$

also has all the same ligands as the diferrous diiron cluster in methane monooxygenase (soluble). It performs the **conversion of an alkane to an alkene**. In the resting diferrous state, there are no μ-oxo groups and the two iron ions are bridged by the carboxylato groups of the two glutamates.[1910] There is one vacant position on each of the two Fe^{2+} ions. The diferrous cluster binds molecular oxygen, and during the association, the molecular oxygen is reduced by the two Fe^{2+} ions to a peroxide dianion that bridges the two now Fe^{3+} ions with one of its oxyanions bound by each of the irons[1914]

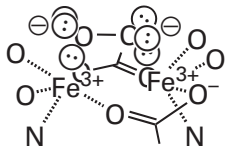

2–135

A **peroxydiiron(III)** with this structure has been chemically synthesized. This model compound, unlike the clusters in the various enzymes, is two-fold rotationally symmetric around the oxygen–oxygen bond, and the bonding between the one Fe^{3+}, the one oxygen, the other oxygen, and the other Fe^{3+}, Fe–O–O–Fe, is twisted so that the dihedral angle for the two Fe^{3+} down the oxygen–oxygen bond is 52° to accommodate, within the steric constraints, the usual 90° dihedral angle along the oxygen–oxygen bond in a peroxide.[1915] There is also a crystallographic molecular model of the peroxy-

diiron(III) intermediate in stearoyl-[acyl-carrier-protein] 9-desaturase.[1916] In this molecular model, the same dihedral angle for the four atoms, Fe–O–O–Fe, is only 30°, presumably because the crystallographic molecular model is not so accurate as that for the model compound and because there are different steric constraints.

In aldehyde oxygenase (deformylating) from *Nostoc punctiforme*, the peroxydiiron(III) itself is the species accomplishing the enzymatic reaction, in which the peroxyanion first adds as a nucleophile to the carbonyl of an aldehyde.[1917] In stearoyl-[acyl-carrier-protein] 9-desaturase, however, and most other enzymes that have this type of nonheme diiron(II) cluster, the peroxydiiron(III) (**2–135**), upon heterolysis, becomes a **high-valent intermediate**. In the active site of stearoyl-[acyl-carrier-protein] 9-desaturase, this high-valent intermediate is electrophilic enough to remove the formal equivalent of a hydride from the saturated alkane of the reactant to desaturate it.[1918] The two electrons supplied by two [2Fe–2S]-ferredoxins during this reaction (Equation 2–293) are required to convert the diiron(III) that is formed during the oxidation of the alkane to the alkene back to diiron(II). In the diiron(III) state, there is at least one μ-oxo group bridging the iron, which one might think comes from the molecular oxygen, but when the diiron(III) cluster is formed using $^{18}O_2$, there is no μ-oxo oxygen that is an oxygen-18,[1898] perhaps because it exchanges with water in the solution too rapidly to be observed.

The chemical **identity of the high-valent intermediate** formed from one of these peroxydiirons(III) (**2–135**) has been elucidated in methane monooxygenase (soluble) from bacteria such as *Methylosinus trichosporium* and *M. capsulatus*. The peroxydiiron(III) in one of these enzymes, which is the same whether it is formed from molecular oxygen bound to the diferrous cluster[1919] or hydrogen peroxide bound to the diferric cluster,[1920] is hydronated and cleaves heterolytically to produce a cyclic **2,4-dioxo-1,3-diiron(IV)***[1921-1924]

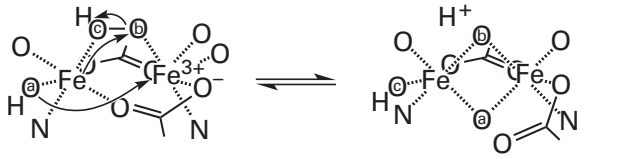

(2–294)

This cyclic 2,4-dioxo-1,3-diiron(IV), in which each iron is iron(IV), has solved the problem of the source of the electron that is usually transferred from a porphyrin, a tryptophan, a tyrosine, or an L-ascorbate to the oxoiron(V) formed by heterolysis of a hydroperoxyiron(III) by taking that electron from the other Fe^{3+}

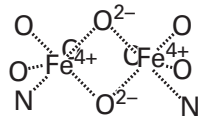

2–136

Its structure is homologous to a [2Fe–2S] iron–sulfur cluster, but the bonding is more ionic and the two iron ions are octahedrally rather than tetrahedrally coordinated because the ligands are oxygens instead of sulfurs. The more electronegative oxygens stabilize the Fe^{+4} oxidation states as opposed to the Fe^{+3} oxidation states of an oxidized [2Fe–2S] iron–sulfur cluster. A model compound containing this 2,4-dioxo-1,3-diiron(IV) has been synthesized. In the model compound, the lengths of the iron–oxygen bonds are 0.177 nm,[1925] similar to the iron–oxygen bond (0.172 nm) in the oxoiron(IV) porphyrin$^{\bullet+}$ of a hemoperoxidase. A mixed-valent, cyclic dioxoiron(IV)iron(III) has also been synthesized,[1926] and its crystallographic molecular model is also available.[1927]

In addition to being able to turn an alkyl group into an alkenyl group as it does in stearoyl-[acyl-carrier-protein] 9-desaturase, a cyclic 2,4-dioxo-1,3-diiron(IV) also can **hydroxylate methane** as it does in the reaction catalyzed by methane monooxygenase[1928,1929]

$$H^+ + NADH + CH_4 + O_2 \rightleftharpoons CH_3OH + NAD^+ + H_2O$$

(2–295)

The hydroxylation of methane is the most difficult hydroxylation of an alkane because methane has the greatest bond dissociation energy (440 kJ mol^{-1}) for its carbon–hydrogen bonds. Another synthetic

*The three oxygens involved in the rearrangement are labeled with the letters a, b, and c to distinguish them one from the others, and their disposition before and after the rearrangement has been determined experimentally with isotopes of oxygen.

version of cyclic 2,4-dioxo-1,3-diiron(IV) (**2–136**) is capable of hydroxylating a hydrocarbon.[1930]

As with the hydroxylations of alkyl carbons performed by enzymes containing hemes P450, which proceed by the same stoichiometry, the mechanism of these hydroxylations has not been settled.[1931-1933] Several aspects of the reaction catalyzed by methane monooxygenase (soluble), however, have been established. It is known that the oxygen of the hydroxy group of the methanol is one of the oxygen atoms that was in the molecular oxygen[1934,1935] and that, at the completion of the reaction catalyzed by methane monooxygenase from *M. capsulatus*, the oxygen of the methanol that is the product of the monooxygenation is in one of the μ-oxo positions in the cyclic di-μ-oxo-diiron(III) that is the product of the oxygenation performed by the cyclic 2,4-dioxo-1,3-diiron(IV).[1936] These results suggest that the 2,4-dioxo-1,3-diiron(IV) abstracts a hydrogen from the methane, and the resulting methyl radical colligates with the hydroxyl radical that is a μ-oxo group in the resulting hydroxyl-oxodiiron(III) to give methanol with its oxygen at that μ-oxo position.

Two electrons are required at the end of the hydroxylation to return the dioxodiiron(III) to the diiron(II) state, so the cluster is ready to go again, and also able to release the methanol. In methane monooxygenase (soluble) from *M. trichosporium*, these two electrons are ultimately from NADH reducing a flavin, and in the membrane-embedded methane monooxygenase (particulate) from *M. capsulatus*, these two electrons are from a quinol.

When the electrons are required in one of these reactions is in part determined by the reactants and the products. Because the stoichiometry of the reaction of molecular oxygen with *myo*-inositol to produce D-glucuronate (Equation 2–291) does not involve any electrons, none have to be supplied. When molecular oxygen and methane are turned into methanol and water (Equation 2–295), or molecular oxygen and stearoyl-[acyl-carrier protein] are turned into oleoyl-[acyl-carrier protein] (Equation 2–293), two electrons are required, but these are used only at the end of the reaction to regenerate the dioxo-diiron(II). When molecular oxygen is turned into water (Equation 2–292), however, four electrons are required and at least some of them must be supplied during the oxidation.

Although the cyclic 2,4-dioxo-1,3-diiron(IV) in methane monooxygenase (soluble) from *M. capsulatus* is required to hydroxylate methane, methyl groups adjacent to a functional group such as a cyano group or a nitro group, which can withdraw electron density effectively, can be hydroxylated by the initial peroxydiiron(III) (**2–135**). The rate of this hydroxylation decreases as the bond dissociation energy of the carbon–hydrogen bond in such substituted methyl groups increases,[1937] a result suggesting that the first step in such a hydroxylation is also the abstraction of a hydrogen atom. The same enzyme, however, hydroxylates a set of radical clocks without significant rearrangement,[1938] a result suggesting that a radical intermediate, which would result from the abstraction of a hydrogen atom, is not involved in these hydroxylations, The hydroxylations of these radical clocks, however, are probably accomplished by the 2,4-dioxo-1,3-diiron(IV) rather than the peroxydiiron(III) because these substrates are electron-rich rather than electron-poor. Significant rearrangement of 1,1-dimethylcyclopropane, however, which is another radical clock, occurs when it is hydroxylated by the methane monooxygenase (soluble) from *M. trichosporium*, but the products of the rearrangements that occur during this particular hydroxylation are consistent with the formation of both a methyl radical and a methyl carbenium ion.[1935]

In murine ribonucleoside-diphosphate reductase, a cyclic 2,4-dioxo-1,3-diiron(IV) formed in the usual way is first reduced by one electron,[1939] perhaps from a neighboring tryptophan.[1940] This reduction forms a mixed-valent species in which the ring in **2–136** has been broken and the iron(III) that is the product of the reduction has a hydroxide, which was a μ-oxo group, as a ligand but is still connected by the remaining μ-oxo group to the remaining iron(IV), which now has an open site, the site from which the hydroxide on the iron(III) left.[1941,1942] This species removes the formal equivalent of a hydrogen atom, perhaps as an electron and a hydron, from the hydroxy group of a tyrosine in the protein[1943] to **produce the neutral tyrosyl radical** required for the enzymatic reaction. The role of the diiron cluster is to create this tyrosyl radical initially, and presumably to maintain it over the lifetime of the enzyme, but the diiron cluster does not participate in the reduction of the ribonucleoside diphosphate that is the enzymatic reaction catalyzed by ribonucleoside-diphosphate reductase.

A diiron(II) cluster can also have **an oxide of nitrogen rather than an oxide of oxygen as its substrate**. Nitric oxide reductase [NAD(P)$^+$, nitrous oxide-forming] (Equation 2–258) from *Thermotoga maritima* has a diiron(II) cluster. Two molecules of nitric oxide, NO (**2–115**), bind to the cluster, one nitric oxide on each Fe^{2+}. The two Fe^{2+} ions provide the two

electrons needed for the production of one molecule of nitrous oxide, NNO (**2–106**), from the two nitric oxides in the process forming a double bond between the two nitrogens, and one of the oxygen atoms from one of the two nitric oxides leaves as a molecule of water.[1944] The resulting diiron(III) cluster is then reduced back to the diiron(II) cluster by a reduced flavin.

There are also oxygenases in which the non-heme metallic ion is a nickel ion rather than an iron ion. Acireductone dioxygenase (Ni^{2+}-requiring) from *K. pneumoniae* uses molecular oxygen to perform an oxidative cleavage

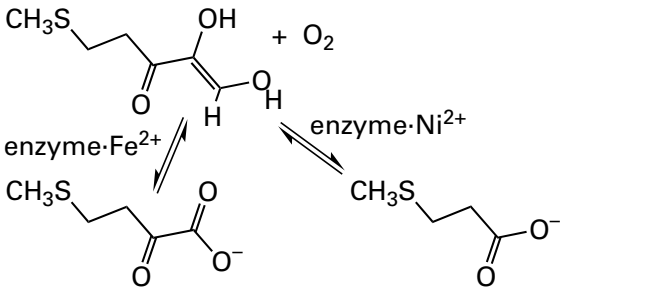

(2–296)

When acireductone dioxygenase from *K. pneumonia* is expressed in *E. coli*, it retains both Fe^{2+} and Ni^{2+} upon purification. Both metallic dications are in the respective high-spin states.[1945,1946] The enzyme with Fe^{2+} in the active site and the enzyme with Ni^{2+} in the active site can be separated and shown to produce, from the same reactant, 1,2-dihydroxy-5-thiomethylpent-1-ene-3-one, the product 2-oxo-4-thiomethylbutanoate in the former case and the product 3-thiomethylpropanoate in the latter.[1947] The difference in the products results from a difference in the electronic properties in the two metallic ions.[1948] There are also two different groups of hydrogenases, diiron hydrogenases and nickel–iron hydrogenases.

Unlike those in diiron oxygenases, the diiron clusters found in hydrogenases have two μ-sulfido groups instead of μ-oxo groups. A hydrogenase reduces the equivalent of two hydrons to form molecular hydrogen in one direction and oxidizes molecular hydrogen in the other

(2–297)

rather than reducing molecular oxygen. The two electrons participating in the reaction are provided or taken up, respectively, by various electron-transferring coenzymes, such as ferredoxins, cytochromes *c*, and menaquinones, depending on the species in which the hydrogenase is found. The cluster in the crystallographic molecular model of the diiron hydrogenase from *C. pasteurianum*

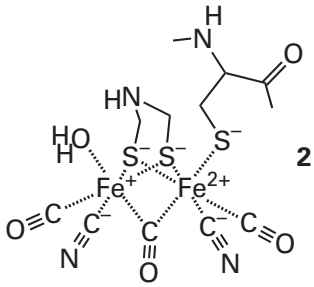

2–137

has only one ligand from the protein itself, the sulfido group of a cysteine,[1949] but it is surrounded and enclosed by the folded polypeptide. Two of the ligands to the iron ions are cyanide ions and three are isoelectronic, but neutral, carbon monoxides.[1950] In the resting state of the enzyme, one of the carbon monoxides bridges the two iron ions as a **μ-carbonmonoxy group**. There is some disagreement in the crystallographic molecular models as to whether or not the bridging carbon monoxide is present in all the diiron clusters, but Fourier-transform infrared spectra of diiron hydrogenases from *C. acetobutylicum*[1951] and *Chlamydomonas reinhardtii*[1952,1953] demonstrate that when the cluster is enzymatically active, the bridging carbon monoxide is present throughout the reaction. The two μ-sulfido groups are the two sulfido groups from the dithiodihemiaminal, 2-aza-1,3-disulfanylpropane,[1954-1957] which would not be a stable compound in free aqueous solution. The sulfido group of the lone cysteine is also one of the four cysteines that attach the four iron ions of a separate prosthetic [4Fe–4S] iron–sulfur cluster to the protein[1954,1958,1959]

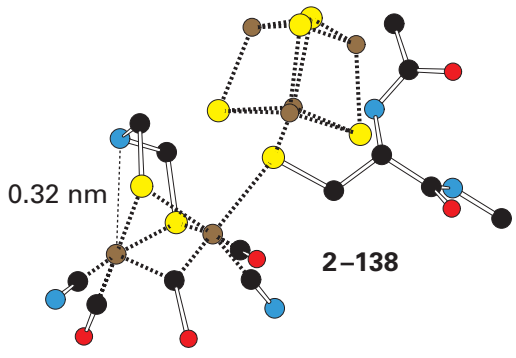

2–138

and thus the sulfido group of this cysteine electronically couples the two prosthetic groups, the diiron cluster **2–137** and the [4Fe–4S] iron–sulfur cluster, in the inner sphere. There are three other [4Fe–4S] iron–sulfur clusters in the diiron hydrogenase from *C. pasteurianum* to remove or provide electrons during the oxidation of molecular hydrogen or the reduction of hydrons, respectively.

There are also **hydrogenases with a nickel–iron dinuclear cluster**. These hydrogenases are apparently unrelated to the diiron hydrogenases.[591,1949] The cluster itself

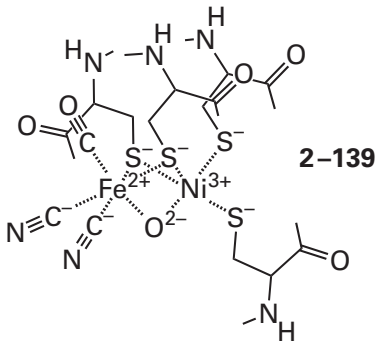

2–139

however, can be viewed as homologous to a diiron cluster in the family of diiron hydrogenases in which some of the ligands have been changed. First and foremost, the iron ion on the right in **2–137** is replaced by a nickel ion. There is no bridging carbon monoxide, and in its place in the fully oxidized but inactive nickel–iron hydrogenase from *A. vinosum* is a μ-oxo group,[1960] which dissociates as a hydroxide upon activation of the enzyme by reduction.[1961,1962] This dissociation leaves an open site on the iron ion and an open site on the nickel ion, both of which probably participate in the oxidation–reduction. The two bridging sulfido groups from the 2-aza-1,3-disulfanylpropane are replaced by the sulfido groups of two cysteines, the carbon monoxide on the iron ion is replaced by a cyanide, and the water on the iron ion is replaced by a carbon monoxide. The nickel ion has the sulfido group of a fourth cysteine and a open site instead of a carbon monoxide and a cyanide, respectively. The replacement of a carbon monoxide by a sulfido group makes sense because nickel is a softer metal than iron,[1963,1964] the bond dissociation energy of a nickel–sulfur bond ($+360 \pm 20$ kJ mol^{-1}) is greater than that of an iron–sulfur bond ($+340 \pm 20$ kJ mol^{-1}), and the bond dissociation energy of a nickel–carbonyl bond ($+100$ kJ mol^{-1}) is less than that of an iron–carbonyl bond ($+170$ kJ mol^{-1}).[1965]

In a subunit of nickel–iron hydrogenase from *A. vinosum*, in addition to the nickel–iron dinuclear cluster, there are three [4Fe–4S] iron–sulfur clusters evenly spaced in a chain leading away from the nickel–iron dinuclear cluster to remove electrons or provide electrons as needed.

The details of the **catalytic cycle of diiron hydrogenases** are well understood. Because the [4Fe–4S] iron–sulfur cluster is electronically coupled to the diiron cluster in its inner sphere, it is difficult to distinguish spectroscopic absorptions based on unpaired spins arising from an unpaired electron in the [4Fe–4S] iron–sulfur cluster from those arising from an unpaired electron in the diiron cluster. It has been found, however, that the distribution of electrons between the [4Fe–4S] iron–sulfur cluster and the diiron cluster can be distinguished by Fourier-transform infrared spectroscopy, and this has allowed potentiometric titrations of diiron hydrogenase from *C. reinhardtii* to be dissected.[1966] In the **oxidized paramagnetic resting state**, one of the iron ions in the diiron cluster is an Fe^{+} and the other is an Fe^{2+},[1967] and the [4Fe–4S] iron–sulfur cluster is in the $[(Fe^{2+})_2(Fe^{3+})_2\,(^{2-}S)_4(^{-}S-)_4]^{2-}$ state. After reduction by one electron, there is a pH-dependent electronic equilibrium[1966] between [iron(I)iron(II)]·$[(Fe^{2+})_3Fe^{3+}(^{2-}S)_4(^{-}S-)_4]^{3-}$ and [diiron(I)]·$[(Fe^{2+})_2(Fe^{3+})_2(^{2-}S)_4(^{-}S-)_4]^{2-}$. Below a p$K_a$ of 7.2, the equilibrium is between [iron(I)iron(II)]·$[(Fe^{2+})_3Fe^{3+}(^{2-}S)_4(^{-}S-)_4]^{3-}$ and [H^{+}diiron(I)]·$[(Fe^{2+})_2(Fe^{3+})_2(^{2-}S)_4(^{-}S-)_4]^{2-}$ with a reduction potential of greater than –250 mV.* Above the pK_a of 7.2, the equilibrium is between [iron(I)iron(II)]·$[(Fe^{2+})_3Fe^{3+}(^{2-}S)_4(^{-}S-)_4]^{3-}$ and [diiron(I)]·$[(Fe^{2+})_2(Fe^{3+})_2\,(^{2-}S)_4(^{-}S-)_4]^{2-}$ with a reduction potential of –530 mV. Consequently, as might be expected, hydronation of the diiron cluster makes it significantly easier for the [4Fe–4S] iron–sulfur cluster to reduce the diiron cluster to diiron(I). Because of the value of the pK_a, it has been concluded that the nitrogen in the 2-aza-1,3-disulfanylpropane is the acid–base responsible for easing the reduction when hydronated. The two Fe^{+} in either the [diiron(I)]·$[(Fe^{2+})_2(Fe^{3+})_2(^{2-}S)_4(^{-}S-)_4]^{2-}$ state or the [H^{+}diiron(I)]·$[(Fe^{2+})_2(Fe^{3+})_2(^{2-}S)_4(^{-}S-)_4]^{2-}$ state are able to reduce a hydron to a hydride.[1951,1953,1968-1970]

*The notation [H^{x}iron(X)iron(X)]·$[(Fe^{x+})_3Fe^{x+}(^{2-}S)_4(^{-}S\text{-})_4]^{3-}$ refers to the distribution of electrons in the complete cluster **2–138**. The two irons in the hydrogenase cluster are designated as iron rather than Fe to distinguish them from the four irons in the [4Fe–4S] iron–sulfur cluster.

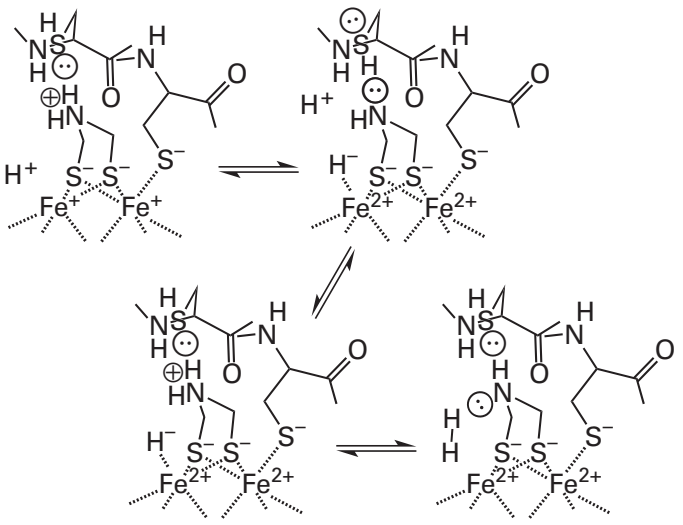

(2–298)

Nuclear magnetic resonance,[1971] Mössbauer,[1972] Fourier-transform infrared, and nuclear resonance vibrational[1973] spectra are those expected if the hydride ends up occupying the open site on the iron ion to the left in **2–137** as a terminal iron hydride. During reduction of the hydron, an electron is transferred from the other iron–sulfur clusters in the enzyme to the coupled [4Fe–4S] iron–sulfur cluster, so the final state of the active site is $[H^{-}\text{diiron(II)}]\cdot[(Fe^{2+})_3Fe^{3+}(^{2-}S)_4(^{-}S-)_4]^{3-}$. The conversion of $[H^{+}\text{diiron(I)}]\cdot[(Fe^{2+})_2(Fe^{3+})_2(^{2-}S)_4(^{-}S-)_4]^{2-}$ to $[H^{-}\text{diiron(II)}]\cdot[(Fe^{2+})_3Fe^{3+}(^{2-}S)_4(^{-}S-)_4]^{3-}$ can be followed by Fourier-transform infrared spectroscopy at cryogenic temperatures.[1951]

During reduction of the hydron to the hydride, because the diiron cluster ends up after reduction as diiron(II) rather than diiron(I), Fourier-transform infrared spectra gathered at cryogenic temperatures demonstrate that the hydron on the nitrogen in the 2-aza-1,3-disulfanylpropane has dissociated.[1953] Presumably, the increase in charge on the iron ions has lowered the pK_a for the nitrogen. In the active sites of diiron hydrogenases from *C. reinhardtii* and *Desulfovibrio desulfuricans,* the hydronation state of this nitrogen at this stage can be monitored by ^{57}Fe nuclear resonance vibrational spectroscopy.[1974] There is a hydrogen bond between the sulfanyl group of a cysteine in the active site and the amino nitrogen in the 2-aza-1,3-disulfanylpropane (Equation 2–298). Because the amino nitrogen and the iron ion on which the hydride is located are only 0.32 nm apart,[1950,1954] when the sulfanyl group is a donor to the amino nitrogen and the hydron on the amino nitrogen is pointed at the hydride, the two van der Waals circumferences of the hydrogen on the ammonium and the hydrogen in the iron hydride are only separated by around 0.05 nm. The sole hydron on the amino nitrogen, however, is not acidic enough to react with the hydride, but when there is a hydrogen bond between the lone pair of electrons on the sulfanyl group of the cysteine rather than the hydrogen and one of the hydrons on the hydronated ammonio group of the 2-aza-1,3-disulfanylpropane, the hydron pointed at the hydride has become acidic enough to hydronate the hydride.* This hydronation forms H_2, the product of the reaction, which probably dissociates immediately. The hydronation and the dissociation of the H_2 return the clusters to the resting oxidized $[\text{iron(I)iron(II)}]\cdot[(Fe^{2+})_2(Fe^{3+})_2(^{2-}S)_4(^{-}S-)_4]^{2-}$ state.

The **catalytic cycle of the nickel–iron hydrogenases** seems to differ significantly from that of the diiron hydrogenases. During the oxidation of molecular hydrogen, the nickel–iron cluster in the hydrogenase from *D. vulgaris* passes through three major intermediates, Ni-SI_a, Ni-R, and Ni-C, that have been identified spectroscopically.[1975] By microscopic reversibility it must pass through through the same three intermediates in the reverse direction when it is reducing two hydrons. In the resting, reduced, activated Ni-SI_a state, the metallic ions are Ni^{2+} and Fe^{2+}, and the two respective sites on the metallic ions that were coordinated by the μ-oxo group in the inactive, oxidized state **2–139** are open. Upon the association of molecular hydrogen from the solution to form the fully reduced Ni-R intermediate, a hydride, as a ***μ*-hydrido group**, bridges the two formerly open sites on the metallic ions

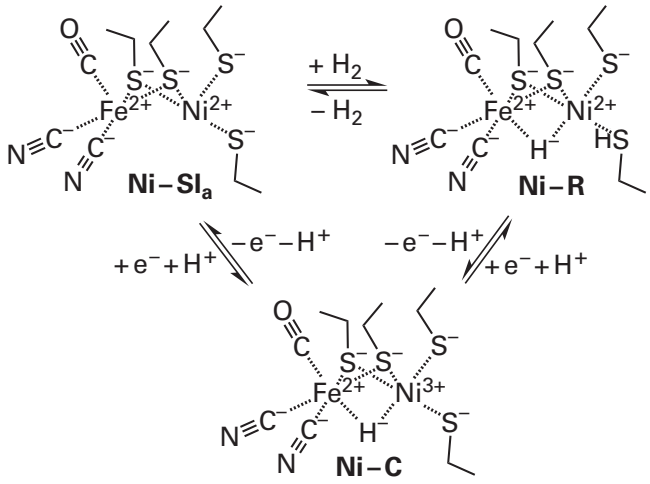

(2–299)

*One should recall that there is no such thing as a bare hydron in aqueous solution.

This Ni-R intermediate has been crystallized under an atmosphere of molecular hydrogen, and reflections from the resulting crystal could be collected to Bragg spacing of 0.089 nm. At this level of resolution, **hydrogen atoms could be observed** in the map of electron density.[1964] There was clear electron density for the μ-hydrido group between the Ni^{2+} and the Fe^{2+} as well as for a hydron on the sulfido group coordinating the nickel ion that is closest to the μ-hydrido group.[1976] The distance from the bridging hydride to this hydron is 0.245 nm, so the two are almost within van der Waals contact (0.23 nm). It has been concluded that a molecule of hydrogen from the solution has been dissociated heterolytically by the cluster into the μ-hydrido group and this hydron.

Because there is a channel[1977] from the solution to the Ni^{2+}, it has been suggested that the hydrogen associates first with it. Calculations of dissociation energies between Ni^{2+} and molecular hydrogen and between Fe^{2+} and molecular hydrogen are consistent with this conclusion.[1978] This conclusion is also consistent with the fact that the **hydron ends up on one of the sulfido groups** coordinating the Ni^{2+}. If the molecular hydrogen associates initially with the open site on the Ni^{2+}, this would bring the hydrogen that is to become the hydron immediately adjacent to the sulfido group.

The next intermediate in the direction of the oxidation of molecular hydrogen, the Ni-C state, is normally formed upon the transfer of an electron from the Ni-R intermediate (Equation 2–299). Spectra of this intermediate with a bridging atom of protium and a bridging atom of deuterium provided the first unambiguous evidence for the existence of an atom of hydrogen bridging the two metallic ions in the mechanism of the enzyme.[1979,1980] In the Ni-C state, which is one electron more oxidized than the Ni-R state in which a hydride bridged the two metallic ions, the two metallic ions are Ni^{3+} and Fe^{2+},[1975] so the atom of hydrogen bridging the two metallic ions that was observed spectroscopically in the Ni-C intermediate must still be a hydride. Because the nickel ion is so electropositive, the hydron has dissociated from the sulfanyl group.

Even though, in the usual steps that occur during the oxidation of molecular hydrogen, the Ni-C intermediate is produced by oxidizing the Ni-R intermediate by the removal of one electron, in the spectroscopic experiments, the Ni-C intermediate was formed by reducing the resting, activated Ni-SI_a state with an external reductant. It follows that the reductive conversion of the Ni-SI_a state to the Ni-C intermediate, which is the first step in the reduction of two hydrons (Equation 2–299), requires that the addition of an electron to the resting, activated Ni-SI_a state causes a hydron to be converted into a bridging μ-hydrido group, since no molecular hydrogen was present. Presumably, in the reverse direction, the removal of an electron from the intermediate Ni-C state state **oxidizes the bridging μ-hydrido group to a hydron** that dissociates during the oxidation returning the enzyme to the resting, activated Ni-SI_a state. One way to explain the oxidation in this step that occurs during the oxidation of molecular hydrogen is that during the transition from the Ni-C state with a bridging hydride to the resting Ni-SI_a state (Equation 2–299), an electron is removed from the Fe^{2+}, and the resulting Fe^{3+} and the Ni^{3+} then each remove an electron from the hydride to convert it into a hydron that is forced to dissociate immediately from the cluster. This step would resemble the reverse of the step in which a hydron is converted to a hydride by the transfer of one electron from each of the Fe^{+} in a diiron hydrogenase (Equation 2–298).

In Equation 2–299, the conversion of two hydrons and two electrons to molecular hydrogen proceeds in a counterclockwise direction; and the conversion of molecular hydrogen to two hydrons and two electrons, in a clockwise direction.

There are model compounds for intermediates in the oxidation–reduction catalyzed by the nickel–iron cluster in a hydrogenase. There are synthetic nickel–iron clusters in which a hydride bridges the two metallic ions.[1981-1983] A model compound that mimics the nickel–iron cluster in hydrogenase is hydronated by HBF_4 ($pK_a = -4.9$) preferentially on one of the alkanethiolates coordinating the nickel ion rather than an equivalent alkanethiolate coordinating the iron ion.[1984] In a different model compound in which there are only two μ-sulfido groups, the hydronation occurs on one of these sulfurs, but generation of molecular hydrogen from this hydronated complex requires the addition of both an electron and an external hydron.[1983] A mononuclear nickel(I) complex, in which one of the ligands to the nickel is a tertiary amine, is able to dissociate a molecule of hydrogen heterolytically; the hydride ends up on the nickel and the hydron ends up on the amino nitrogen.[1981,1982]

There are synthetic model compounds for the diiron cluster in a hydrogenase that have a carbon monoxide as well as two sulfido groups, bridging two Fe^{+} ions in their resting state. Kinetic and spectroscopic observations of these model diiron clusters

have led to the conclusion that a hydron, transferred from a nearby ammonio nitrogen, associates with an open site on one of these Fe^{+} ions. The resulting complex then rearranges by a concerted ligand exchange

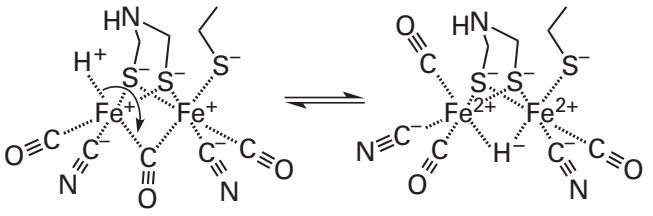

(2–300)

so that the hydron ends up as a bridging hydride[1985] between the two now Fe^{2+} ions and the carbon monoxide ends up at the position at which an open site was located before the rearrangement.[1986-1988] These four ligands are not attached covalently to the iron ion and are free to move across its surface. The result would be a bridging hydride in place of the former bridging carbon monoxide, which would become a nonbridging carbon monoxide. It is possible to accomplish such a ligand exchange in the active site of diiron hydrogenase from *C. reinhardtii*, the product of which has been identified as containing a bridging hydride by infrared spectroelectrochemistry. It was concluded, however, that this arrangement is not involved in the normal equilibration of two hydrons and two electrons with molecular hydrogen catalyzed by the enzyme.[1951,1952]

The diiron hydrogenases complete the **panoply of the oxidation states of iron, from iron(I) to iron(V)**, that are achieved in enzymatic reactions.

The ligands to the iron ions in a diiron hydrogenase and the ligands to the iron ion in a nickel–iron hydrogenase are cyanide ions and carbon monoxides. These diatomic ions and molecules are **isoelectronic with a molecule of nitrogen** (**2–140**)

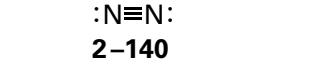

2–140

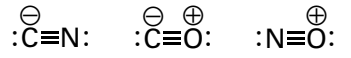

2–141 **2–142** **2–114**

The ten electrons in molecular nitrogen are distributed into the five molecular orbitals of a symmetric, diatomic molecular orbital system (**2–86**). The two pairs of electrons indicated in **2–140** and the pair of electrons in the σ bond are delocalized into the three cylindrically symmetric σ molecular orbitals—bonding σ_s, antibonding σ_s^*, and bonding σ_p—and there are two orthogonal π bonds, each occupied by two electrons.

When the nucleus of a nitrogen atom is replaced by the nucleus of a carbon atom, the same molecular orbital system remains in the resulting **cyanide** (**2–141**) with the following exceptions. The electric field of a carbon nucleus with only six protons is less than that of a nitrogen nucleus that has seven protons, so the atomic orbitals from carbon that are mixing are of higher energy than those from nitrogen. As a result, there is more mixing between the p_z orbital on nitrogen and the *s* orbital on carbon. The carbon atom, because its nucleus has one fewer proton, has a negative formal elementary charge.

When the nucleus of a nitrogen atom is replaced by the nucleus of an oxygen atom, the same molecular orbital system remains in the resulting **azanylidyneoxidanium ion** (**2–114**) with the following exceptions. The electric field of an oxygen nucleus with eight protons is greater than that of a nitrogen nucleus that has only seven protons, so the atomic orbitals from oxygen that are mixing are of lower energy than those from nitrogen. As a result, there is more mixing between the p_z orbital on oxygen and the *s* orbital on nitrogen. The oxygen atom, because its nucleus has one more proton, has a positive formal elementary charge.

In **carbon monoxide** (**2–142**), the difference in the energies of the atomic orbitals that are mixing is even more extreme, but for the same reasons, the carbon atom has a negative formal elementary charge and the oxygen has a positive formal elementary charge, which is the reverse of their differences in electronegativity. The negative formal elementary charges on the carbon atoms in the cyanide and carbon monoxide cause their lone pairs of electrons to be the ligands to a metallic ion rather than the lone pairs on the oxygens, which in most other Lewis bases would be the ligands to a metallic ion.

Certain anaerobic bacteria, such as *Carboxydothermus hydrogenoformans*, *M. thermoacetica*, *Methanosarcina barkeri*, and *M. thermophila*, convert carbon monoxide into carbon dioxide and use the reducing equivalents obtained from this oxidation as a source of energy as well as for reducing metabolites, much as carbon monoxide used to be burned in households for heat. These bacteria also convert carbon monoxide into acetyl-SCoA, from which they

can produce all the carbon in their metabolites[1989,1990] by the Wood–Ljungdahl metabolic pathway.[1991] In a sense this is a strategy similar to photosynthesis, in which reducing equivalents are obtained from light and all the fixed carbon is obtained from carbon dioxide. Any excess reducing equivalents that arise during metabolism in these bacteria are excreted as molecular hydrogen, which is produced by a ferredoxin hydrogenase with the usual nickel–iron cluster.

The enzyme responsible for oxidizing carbon monoxide to carbon dioxide is anaerobic carbon monoxide dehydrogenase

$$2\,H^+ + CO_2 + 2\,\text{reduced ferredoxin} \rightleftharpoons CO + H_2O + 2\,\text{oxidized ferredoxin} \qquad (2\text{–}301)$$

The standard reduction potential for the half-reaction[1992,1993]

$$CO_2(g) + 2\,e^- + 2\,H^+ \rightleftharpoons CO(g) + H_2O \qquad (2\text{–}302)$$

is –560 mV, which is why a [4Fe–4S] ferredoxin (Figure 2–19) is the carrier of electrons that has been matched with the enzyme, just as a [4Fe–4S] ferredoxin is matched with photosystem I.

Carbon dioxide, bound to the nickel ion in the crystallographic molecular model of the complex between carbon dioxide and the **[4Fe–4S–Ni] iron–sulfur–nickel cluster** in the active site of anaerobic carbon monoxide dehydrogenase from *C. hydrogenoformans*,[1994] can be superposed on the crystallographic molecular model of the complex between cyanide, hydroxide, and the [4Fe–4S–Ni] iron–sulfur–nickel cluster and its surrounding catalytic amino acids in active site of the enzyme from *M. thermoacetica*[1995]

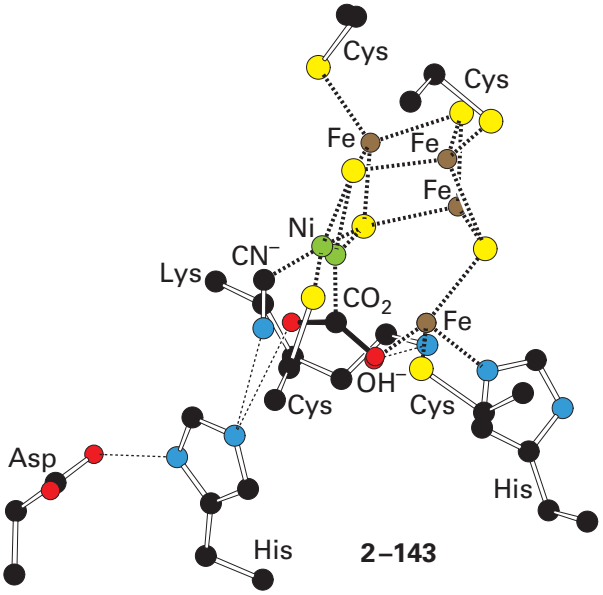

In the drawing, only the carbon dioxide and one of the nickel ions are from the former crystallographic molecular model while the cyanide and the hydroxide, as well as the entire cluster and the surrounding amino acids, are from the latter. Because the complex between carbon dioxide (CO_2) and the [4Fe–4S–Ni] iron–sulfur–nickel cluster in the former active site is assumed to be the complex between the cluster and the substrate carbon dioxide, the complex between a cyanide (CN^-), a hydroxide (OH^-), and the [4Fe–4S–Ni] iron–sulfur–nickel cluster is assumed to mimic the complex between the cluster and the substrates carbon monoxide and hydroxide ion in the latter active site. Electron-paramagnetic spectra of the [4Fe–4S–Ni] iron–sulfur–nickel clusters in the enzymes from *M. thermoacetica* and *M. thermophila* change as either carbon monoxide or carbon dioxide associates with the respective enzyme.[1996,1997]

In the anaerobic carbon monoxide dehydrogenases from both *C. hydrogenoformans* and *M. thermoacetica*, the [4Fe–4S–Ni] iron–sulfur–nickel cluster (**2–143**) is a [4Fe–4S] iron–sulfur cluster from which one of the iron ions has pulled away and its former location in the cluster has become occupied by a nickel ion. Both the nickel ion and the iron ion that has been pulled away are tetracoordinate. The iron ion that has pulled away is still coordinated by one of the sulfides in the cluster, the sulfido group of the usual cysteine, and the imidazolyl group of a histidine while the nickel ion is coordinated by two sulfides within the cluster (large light gray atoms) and the sulfido group of another cysteine. In both the complex with cyanide and hydroxide and the complex with carbon dioxide, the nickel ion is in a

slightly distorted square planar coordination, which is one of its usual dispositions, with the cyanide or the carbon of the carbon dioxide as its fourth ligand, and the detached iron ion is in a somewhat more distorted tetrahedral coordination with the oxygen of the hydroxide or an oxygen of the carbon dioxide as its fourth ligand.

In addition to this [4Fe–4S–Ni] iron–sulfur–nickel cluster, in each of these enzymes there is a standard [4Fe–4S] iron–sulfur cluster 1.1 nm away, and another standard [4Fe–4S] iron–sulfur cluster 1.0 nm further away.[1996-1999] These clusters **shuttle electrons** from the [4Fe–4S–Ni] iron–sulfur–nickel cluster to the oxidized ferredoxin that is a substrate for the enzyme and that carries each of the electrons away from the enzyme. In the reverse direction, these clusters shuttle electrons to the [4Fe–4S–Ni] iron–sulfur–nickel cluster from the reduced ferredoxin that brings each of the electrons to the enzyme.

In the crystallographic molecular model (**2–143**) of the complex between the cluster and carbon dioxide,[2000] the **bond length** between the nickel ion and the carbon of the carbon dioxide is 0.181 nm, and the three **bond angles** around the carbon are all within 5° of 120°. The bond length between nickel and carbon is quite short for a bond of this type.[2001] Both this short bond length and the bond angles suggest that this complex can be considered to be the **nickel ester of carbonic acid**. In fact, the carbon–oxygen bond lengths (0.130 ± 0.003 nm) are indistinguishable from those (0.128 nm) in a carbonate ion.[2002]

The biochemical standard reduction potential of the [4Fe–4S–Ni] iron–sulfur–nickel cluster in anaerobic carbon monoxide dehydrogenase from *M. thermoacetica*[2003,2004] is –530 mV, and this value is for a two-electron reduction. Because the biochemical standard reduction potential of a [3Fe–4S] iron–sulfur cluster is in the range of +65 to −400 mV (Figure 2–19), because the reduced form of a [3Fe–4S] iron–sulfur cluster is $[Fe^{2+}(Fe^{3+})_2(^{2-}S)_4(^{-}S-)_3]$ (Equation 2–171), and because the reduced [4Fe–4S–Ni] iron–sulfur–nickel cluster in anaerobic carbon monoxide dehydrogenase is paramagnetic, the most likely **form of the reduced** [4Fe–4S–Ni] **iron–sulfur–nickel cluster** is equivalent to $[(Fe^{2+})_2(Fe^{3+})_2Ni^{+}(^{2-}S)_4(^{-}S-)_2]$. The nickel ion in such an oxidation state would be Ni^{+1}, which is nucleophilic, and the peripheral iron ion could be Fe^{3+}, which is a strong Lewis acid. The reduced state of the [4Fe–4S–Ni] iron–sulfur–nickel cluster binds carbon dioxide,[2005] and the crystal of anaerobic carbon monoxide dehydrogenase from *C. hydrogenoformans* was poised in the reduced state before the carbon dioxide that formed the complex with the [4Fe–4S–Ni] iron–sulfur–nickel cluster (**2–143**) was diffused into the crystal.[1994]

From all these considerations, a reasonable mechanism for the reduction of carbon dioxide can be formulated.[2004] One of the oxygen atoms of the carbon dioxide associates with the peripheral Fe^{3+} as a coordinated ligand and forms a hydrogen bond to the ammonio group of a lysine, and the other oxygen forms a hydrogen bond with the imidazolyl group of a histidine. The **nucleophilic Ni^{+}** adds to the carbon atom to form the nickel analogue of an ester of carbonic acid observed in the one crystallographic molecular model (**2–143**). The ammonio group of the lysine hydronates the oxygen of the carbonate, the hydronated oxygen leaves the carbon as a ferric hydroxide,[2005] and the carbon of the resulting carbon monoxide rotates away from the hydroxide into the position of the carbon of the cyanide in the other crystallographic molecular model, while the hydrogen bond between the oxygen atom and the imidazolyl group remains intact. The cluster has been oxidized by the removal of two electrons during this transformation, and the carbon monoxide leaves the oxidized form of the cluster, which is the equivalent of $[Fe^{2+}(Fe^{3+})_3Ni^{2+}(^{2-}S)_4(^{-}S-)_2]$. Two ferredoxins bind in sequence and their single electrons are passed in the outer sphere through the [4Fe–4S] iron–sulfur clusters to rereduce the [4Fe–4S–Ni] iron–sulfur–nickel cluster.[2005] In the reverse reaction, as one or two electrons are removed from the carbon monoxide by the nickel and the iron ions of the $[Fe^{2+}(Fe^{3+})_3Ni^{2+}(^{2-}S)_4(^{-}S-)_2]$ cluster, the carbon of the carbon monoxide becomes electrophilic enough for the hydroxide on the adjacent iron ion in the cluster (**2–143**) to accomplish a nucleophilic addition to produce carbon dioxide.

It has been proposed,[2004] however, that the reduced state of the cluster is actually paramagnetic $[(Fe^{2+})_4Ni^{+}(^{2-}S)_4(^{-}S-)_2]$ rather than paramagnetic $[(Fe^{2+})_2(Fe^{3+})_2Ni^{+}(^{2-}S)_4(^{-}S-)_2]$, and the oxidized state is, therefore, $[(Fe^{2+})_3Fe^{3+}Ni^{2+}(^{2-}S)_4(^{-}S-)_2]$. If this is the case, the ferrous hydroxide rather than a ferric hydroxide is the leaving group, albeit a poorer one, during the reduction of carbon dioxide, but the nickel ion would still be nucleophilic because the cluster would have two additional electrons. The hydroxide, on an Fe^{2+}, would exchange more rapidly with the next molecule of CO_2, but in the oxidation

of carbon monoxide, the electron withdrawal from the carbon monoxide by the oxidized cluster would be significantly weaker, making it less electrophilic.

There are also mononuclear, prosthetic copper ions and dinuclear, trinuclear, and tetranuclear clusters of prosthetic copper ions that catalyze reactions in which the oxides of oxygen and the oxides of nitrogen are substrates. For example, quercetin 2,3-dioxygenase*

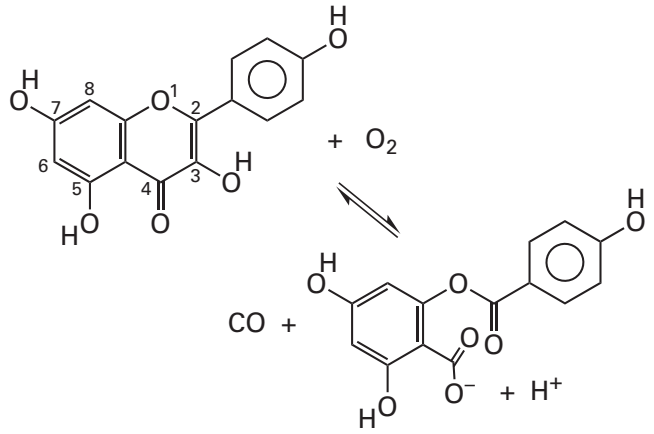

(2–303)

from *Aspergillus japonicus* oxidatively cleaves two adjacent carbon–carbon bonds, between carbons 2 and 3 and between carbons 3 and 4, while turning the central carbon into carbon monoxide. The prosthetic, **mononuclear Cu^{2+}** in its active site is coordinated by three imidazolyl groups from three histidines as well as the carboxylato group of a glutamate, which stabilizes the cupric state. In the crystallographic molecular model of the anaerobic complex between the reactant kaempferol (Equation 2–303), and this Cu^{2+} in the enzyme (Figure 2–58A),[2006] the 3-hydroxy group of the kaempferol, which will become the oxygen of the carbon monoxide (Equation 2–303), is coordinated[2007] to the Cu^{2+}. In this complex, the Cu^{2+} withdraws electron density from carbon 3 of the kaempferol (Equation 2–303) to create a partial radical cation at carbon 3. The positive elementary charge of the radical cation, which resides mostly on carbon 2, is stabilized by π electron donation from both the 4-hydroxyphenyl group and oxygen 1. Oxygen reacts with this partial radical as it does with the partial radical in protocatechuate 3,4-dioxygenase (Equation 2–275), and the resulting 3-hydroxy-3-peroxy intermediate rearranges to the products by a mechanism that has yet to be determined. The actual mechanism may involve[1775] a Baeyer–Villiger rearrangement similar to the one thought to occur in the mechanism for an extradiol dioxygenase (Equation 2–278).

The prosthetic, mononuclear copper ion in lytic chitin monooxygenase

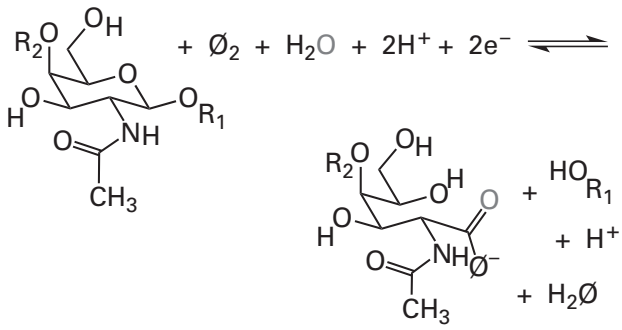

(2–304)

which is a polysaccharide monooxygenase from *Serratia marcescens*, oxidatively cleaves chitin, poly-(β1,4)-2-acetamido-2-deoxy-D-glucose. From isotopic distributions it has been determined that one of the oxygens in the new carboxylate comes from molecular oxygen (denoted Ø) and the other from water (denoted with a gray O).[2008] In a crystallographic molecular model of the related (45% identity; 2.0 gap percent) polysaccharide monooxygenase from *Bacillus amyloliquefaciens*, the copper ion is coordinated by the imidazolyl group of a histidine and both the imidazolyl group and the amino group of the amino-terminal histidine.[2009] In the crystallographic molecular model of the complex between molecular oxygen and the active site of the yet again related (29% identity; 3 gap percent) lytic chitin monooxygenase from *Jonesia denitrificans*, the oxygen associated with the prosthetic Cu^{+} is bound in a bent configuration to the now mononuclear Cu^{2+} and has been identified as a peroxide. In a crystallographic molecular model by neutron diffraction of the same complex, the amino-terminal amino group coordinating the Cu^{2+} has been observed to be the highly unusual anionic conjugate base of the amino group,[2010] which might stabilize a higher-valent form of the copper ion that could be responsible for the monooxygenation. Hydroxylation of carbon 1 of a 2-acetamido-2-deoxy-D-glucose (bond dissociation energy = 380 kJ mol^{-1}) would create a tetrahedral intermediate.

*In Equation 2–303, the enzyme is shown oxidizing kaempferol, 2-(4-hydroxyphenyl)-3,5,7-trihydroxy-4*H*-chromen-4-one, which is a close relative of quercetin, 2-(3,4-di-hydroxyphenyl)-3,5,7-trihydroxy-4*H*-chromen-4-one.

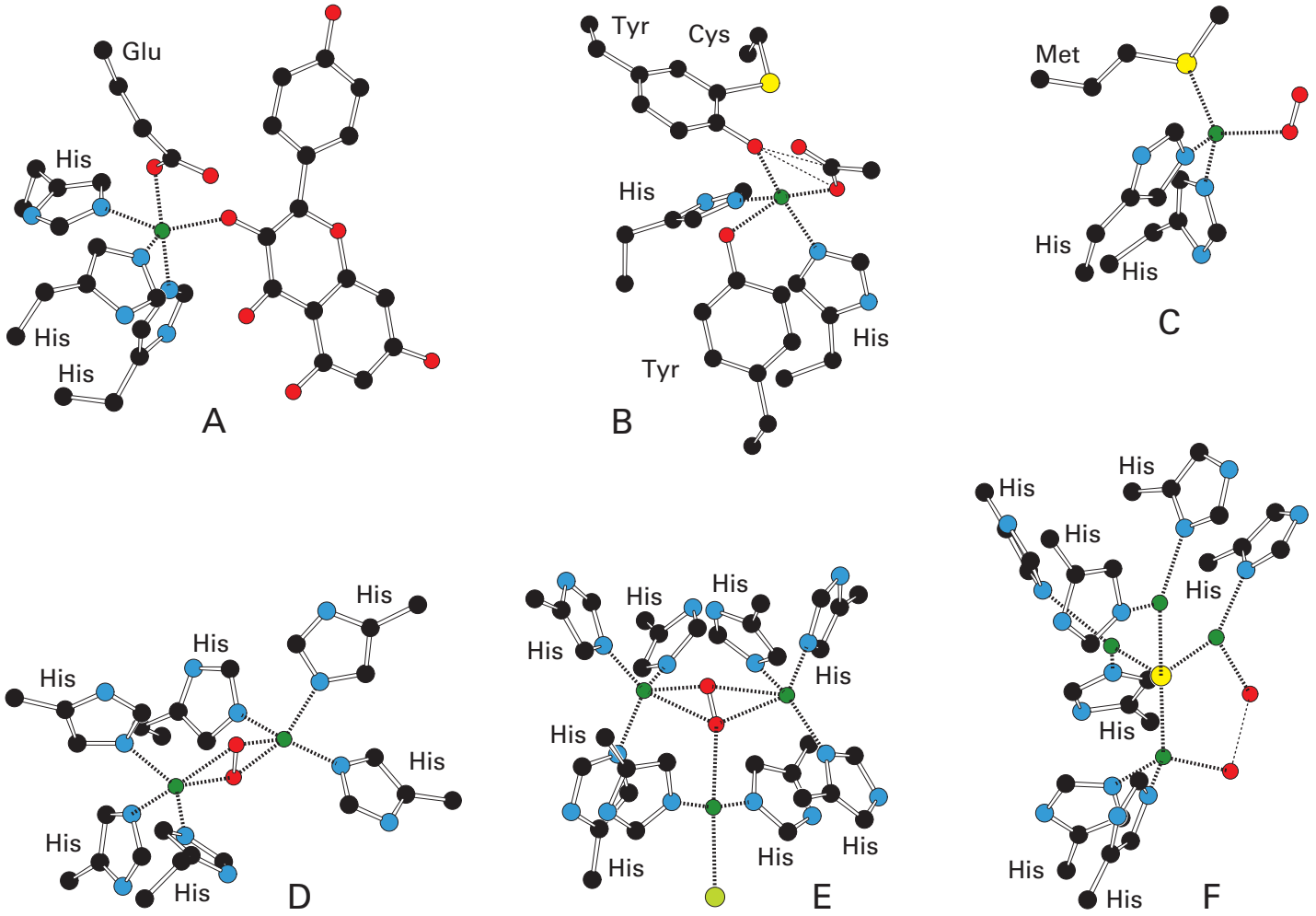

Figure 2–58: Drawings[50] of the ligands to prosthetic copper ions in the crystallographic molecular models of **(A)** quercetin 2,3-dioxygenase from *A. japonicus*,[2006] **(B)** galactose oxidase from *H. rosellus*,[1314,2013] **(C)** peptidylglycine monooxygenase from *R. norvegicus*,[2055] **(D)** hemocyanin from *L. polyphemus*,[2026,2027] **(E)** laccase from *M. albomyces*,[2065] and **(F)** nitrous-oxide reductase from *A. cycloclastes*.[2073] Black atoms are carbons, red atoms are oxygens, and blue atoms are nitrogens. Copper ions are the dark green spheres surrounded by their ligands. Each copper ion has three, four, or five ligands and, unlike in most inorganic copper complexes, there are no regular geometries to the arrangements of the ligands. The side chains acting as ligands are labeled. The open site on the copper in galactose oxidase in Panel B is occupied by a molecule of acetate. The two lone red spherical ligands in Panel F are molecules of water or hydroxide ions that form a hydrogen bond with each other. In Panel A, a molecule of kaempferol, a substrate for quercetin 2,3-dioxygenase, which was coordinated to the copper ion in the enzyme in the crystal submitted to diffraction, is drawn. In Panels C, D, and E, the complex between the respective enzyme and molecular oxygen was present in the crystal, and the molecule of oxygen is drawn. In peptidylglycine monooxygenase (C), the molecule of oxygen forms one bond to the copper ion. In hemocyanin (D) and laccase (E), however, the molecule of oxygen is found between two copper ions; one oxygen forms two bonds, one to each copper ion, and the other oxygen also forms two bonds, one to each copper ion. In laccase (E), one of the oxygens forms a third bond, to a third copper ion. This third copper ion has a chloride (lone, large, light green sphere at very bottom of the drawing) as its fourth ligand. The four copper ions in nitrous-oxide reductase (F) are each coordinated by a single central sulfide dianion (lone, large, light yellow sphere in the center of the drawing).

There is a methane monooxygenase (particulate) embedded in the plasma membranes of *Methylocystis, M. trichosporium*, and *M. capsulatus* that uses a copper ion, similarly coordinated to two imidazolyl groups and both the imidazolyl group and the amino group of the amino-terminal histidine, to hydroxylate methane (bond dissociation energy = 439 kJ mol^{-1}).[2011,2012]

In the active site of galactose oxidase

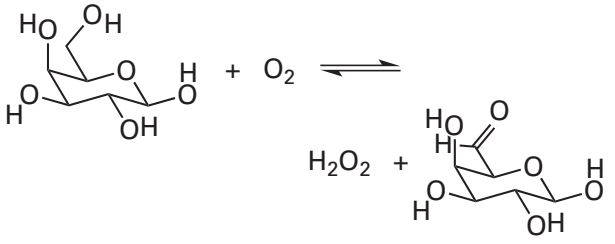

(2–305)

from *Hypomyces rosellus*, the mononuclear Cu^{2+} is coordinated by the imidazolyl groups of two histidines, the 4-oxidophenyl group of a tyrosine, and the 4-oxidophenyl group of the conjugate base of a 3-(*S*-cysteinyl)tyrosine (Figure 2–58B).[1314,2013] In the active form of the oxidized cupric galactose oxidase from *H. rosellus*, the 3-(*S*-cysteinyl)-4-oxidophenyl ion has been converted into the fairly stable, neutral **3-(*S*-cysteinyl)phen-4-oxi radical**

2–144

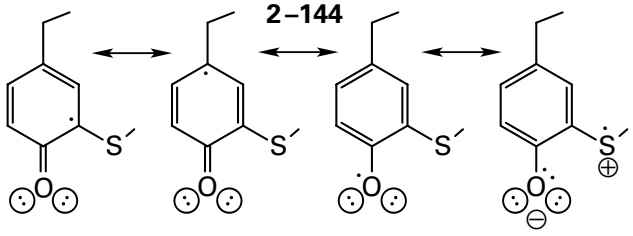

by removal of an electron.[1316,2014,2015] In this radical, the unpaired spin is distributed evenly among the oxygen, the sulfur, and carbons 1 and 3 of the phenyl group,[536] as expected from the resonance structures. To exploit the last resonance form that defines the delocalization of the unpaired electron onto the sulfur, the alkylsulfanyl group must be in an orientation that brings one of its lone pairs of electrons parallel to the π molecular orbital system of the phenyl group so that it can be conjugated with it. Aligning this lone pair of electrons decreases the standard reduction potential of the phenolato oxygen by as much as 150 mV.[2016]

The 6-hydroxy group of the D-galactose that is to be oxidized associates with the Cu^{2+} at its open site, which is occupied by a molecule of water in the resting state, located at the same ligand position as acetate in the crystallographic molecular model (Figure 2–58B). The hydron is removed from the 6-hydroxy group, and the equivalent of a hydride is removed from carbon 6 of the D-galactose to convert it to the product D-*galacto*-hexodialdose. The hydron and the two electrons equivalent to a hydride are removed in such a way that one of the electrons converts the Cu^{2+} to a Cu^{+} and the other electron converts 3-(*S*-cysteinyl)tyrosinyl radical to 3-(*S*-cysteinyl)tyrosine,[2017] which remains associated[2018] with the Cu^{+}. Following dissociation of the product, molecular oxygen associates with the Cu^{+}, an electron is transferred from the Cu^{+} to the molecular oxygen to produce the equivalent of superoxide radical anion coordinated to Cu^{2+}, and the cupric superoxide removes an electron from the 3-(*S*-cysteinyl)tyrosine and is hydronated to produce **cupric hydroperoxide**.[2019] The hydroperoxide ion dissociates from the now regenerated, oxidized, cupric resting state. The most likely candidate for the catalytic base that removes the two hydrons from D-galactose and adds the hydron to the superoxide radical anion is the 4-oxido group of the 3-(*S*-cysteinyl)tyrosine itself. In the crystallographic molecular model, the active site is occupied by acetate (an analogue of the reactant), various intermediates, and the product at carbon 6 as well as a stand-in for the superoxide radical anion. In this model, the acyl carbon of the acetate and the acyl oxygen of the acetate coordinating the copper ion are only 0.29 and 0.28 nm, respectively, from this 4-oxido group (thin dashed lines in Figure 2–58B).[1314]

Mononuclear copper ions also catalyze **reductions of nitrogen oxides** as well as oxygen oxides. Nitrite reductase (NO-forming) reduces nitrite ion, ONO^{-} (**2–113**), to nitric oxide, NO (**2–115**), and a molecule of water, a one-electron reduction. The prosthetic group in nitrite reductase (NO-forming) from *A. faecalis*[2020] and nitrite reductase (NO-forming) from *A. xylosoxidans*[703] is a copper ion coordinated by three imidazolyl groups from three histidines as ligands. The Cu^{+} provides the one electron needed for the reduction of the nitrite ion.[2021] The electron-transferring coenzyme that ultimately provides the electron is pseudoazurin. There is a second mononuclear, prosthetic copper ion in the enzyme—coordinated by a sulfanyl group, two imidazolyl groups, and a sulfide from a methionine (Figure 2–26D)—that relays the electron from the pseudoazurin to the catalytic copper ion. Nitrite ion reversibly associates with the reduced catalytic Cu^{+} as a fourth ligand.[1061,2020,2022] A model compound, in which a Cu^{+} is coordinated by the three nitrogens in 1,4,7-triisopropyl-1,4,7-triazacyclononane, with nitrite ion as its fourth ligand, is able to reduce the nitrite ion to nitrous oxide (**2–106**) upon addition of acetic acid.[2023] The acid is necessary for hydronation of the oxygen that leaves the nitrogen of the nitrite ion as a molecule of water during the reduction (see Equation 2–262). In the active site of nitrite reductase (NO-forming) from *A. xylosoxidans*, there

are both a carboxy group from an aspartic acid and an imidazolyl group from a histidine, properly positioned to supply together two hydrons to ensure that a molecule of water is the leaving group.[2024] When each of these amino acids in nitrite reductase (NO-forming) from *A. faecalis* is mutated in turn to an asparagine, the enzymatic activity decreases by factors of 100 and 1500, respectively.[2025] In the enzymatic reaction, following the reduction of nitrite ion to nitric oxide, the resulting Cu^{2+} is then reduced by an electron from a typical prosthetic copper, with two sulfurs from a cysteine and a methionine and two nitrogens from two histidines as ligands (Figure 2–26D),[703,711] which relays the electron[2021] from the Cu^{+} in the small dissociable electron-transferring coenzyme pseudoazurin or the heme in cytochrome c_{551}.[1168]

Enzymes that have oxides of oxygen and oxides of nitrogen as substrates also contain **dinuclear clusters of prosthetic copper ions** in their active sites. The paradigm of such a dinuclear cluster of prosthetic copper ions is the one in hemocyanin (Figure 2–58D).[2026,2027] The protein surrounding the dinuclear cluster in the crystallographic molecular model of hemocyanin from *Limulus polyphemus* is superposable on the protein surrounding the dinuclear cluster of prosthetic iron ions in the crystallographic molecular models of hemerythrins (Figure 2–57F),[2027] and this observation demonstrates that these two proteins, hemocyanin and hemerythrin, share a common ancestor. In a hemocyanin, histidines are found at positions both in the sequence of amino acids and in the crystallographic molecular model equivalent to those of Histidines 25, 54, 73, 77, and 106 in the hemerythrin from *Themiste hennahi*, and as they do to the iron ions in hemerythrin, they all provide ligands to the two copper ions. In the hemocyanins, however, Glutamate 58 and Aspartate 11, which are bidentate ligands to the iron ions in hemerythrin from *T. hennahi*, are replaced by a threonine and an asparagine, neither of which is coordinated to either copper ion.[2028] This change removes two negative elementary charges from the constellation around the metallic ions, consistent with the difference in charge number between two Fe^{2+} and two Cu^{+}. There is, however, one additional ligand in the hemocyanins to compensate partially for the loss of the four carboxylato oxygens. Phenylalanine 29 in the sequence of amino acids for the hemerythrin from *T. hennahi* is replaced by a histidine in the hemocyanins that provides a third ligand to the one copper ion. This replacement causes the two copper ions in hemocyanin to be equivalent in their coordination, as each has three imidazolyl groups from three histidines surrounding it arranged in roughly the same orientations (Figure 2–58D).

In the hemocyanins in the active deoxygenated state, the two copper ions are in the cuprous state. When molecular oxygen binds, they are both oxidized reversibly[2029] to Cu^{2+} and the dioxygen is reduced to the peroxide dianion, O_2^{2-}, just as it is in a hemerythrin, but it is then not hydronated. The **peroxide dianion is bound between the two Cu^{2+}** with each of its oxygens coordinated to each of them (Figure 2–58D).

For the hemocyanins, the oxygen–oxygen bond of the peroxide dianion remains intact in this reversible complex between the dinuclear cluster of copper ions and molecular oxygen.[2030] There are synthetic dinuclear clusters of cuprous ions, in each of which the Cu^{+} is also coordinated by three diazoles as in hemocyanin. These clusters bind molecular oxygen in a complex with the same spectroscopic signatures and the same structures as those for hemocyanins and in which the oxygen–oxygen bond of the bound peroxide dianion definitely remains intact.[2031-2033]

When, however, the ligands coordinating the two copper ions in a synthetic dinuclear cluster are more basic than diazoles, an equilibrium can be observed[2034,2035] in which the bond between the two oxygens is broken

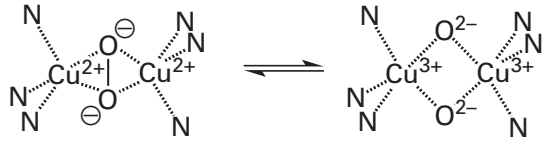

(2–306)

and a **cyclic 1,3-dioxo-2,4-dicopper(III)** is produced.[2036-2040] These synthetic, cyclic, high-valent oxocopper complexes are able to remove hydrogen atoms from aromatic rings,[2041] hydroxylate benzylic carbons,[2038,2040] oxidize a sulfide to a sulfoxide,[2040] perform a Baeyer–Villiger oxidation,[2040] and hydroxylate a *m*-dialkylphenyl group between its two alkyl substituents[2042] as well as **hydroxylate a phenol ortho to its hydroxy group**.[2043-2045]

This last reaction, performed by a synthetic, high-valent 1,3-dioxo-2,4-dicopper(III), is the same one catalyzed by monophenol monooxygenase*

*This enzyme is also widely referred to as "tyrosinase".

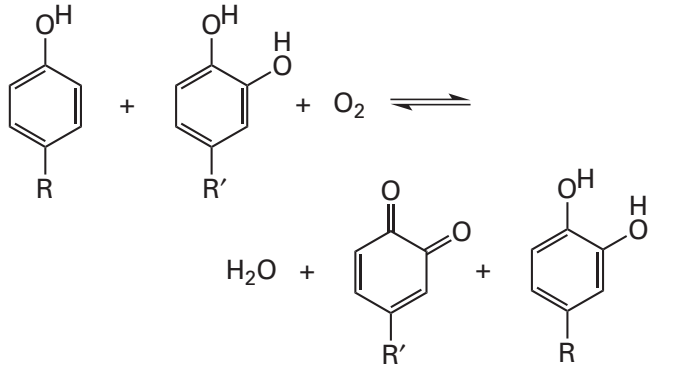

(2–307)

where R can be the same as R′. Monophenol monooxygenase from *Streptomyces castaneoglobisporus* has a dinuclear cluster of copper ions that is the same as that of hemocyanin within a protein structurally and functionally homologous to hemocyanin.[2046,2047] The most significant difference between monophenol monooxygenase and hemocyanin is that monophenol monooxygenase has the 4-hydroxy group of a tyrosine in a position from which it can form a hydrogen bond or transfer a hydron to one of the oxygen atoms of the molecular oxygen when it is bound as a peroxide dianion to the dinuclear cluster (Figure 2–58D). This catalytic acid may promote the cleavage of the oxygen–oxygen bond in the dicupric peroxide to produce cyclic 1,3-dioxo-2,4-dicopper(III) (Equation 2–306), in which one of the μ-oxo groups is a μ-hydroxo group. Such a cyclic 1-oxo-3-hydroxo-2,4-dicopper(III) may be responsible for the hydroxylation catalyzed by this enzyme. It is also possible, however, that the species responsible for the observed monooxygenation is the dicupric peroxide itself.[2048] The two electrons required to regenerate the dicuprous cluster from the dicupric cluster that remains after the hydroxylation has occurred are provided by the catechol that is a cosubstrate for the enzymatic reaction (follow R′ in Equation 2–307). This catechol acts as if it were a quinol. Once the remaining μ-oxo is hydronated and dissociates as a molecule of water, the dicuprous cluster is then ready to bind the next molecule of oxygen.

In catechol oxidase

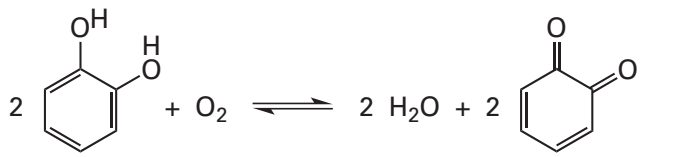

(2–308)

from *Ipomoea batatas*, which is also homologous to hemocyanin,[2046,2049] there is no catalytic base adjacent to the usual dicupric peroxide. Nor does the enzyme catalyze a hydroxylation, only an oxidation by electron transfer, so in this case, the **dicupric peroxide itself may be the oxidant** receiving the two pairs of electrons sequentially from the two catechols that are the reactants and that associate one after the other with the active site.[2049] The result, however, is the same: upon hydronation, the two μ-oxo groups between the two now cuprous copper ions become two molecules of water. In catechol oxidase, one of the six histidines coordinating the two copper ions (see Figure 2–58D) is a 2-(*S*-cysteinyl)histidine.

A cyclic 1,3-dioxo-2,4-dicopper(III) is homologous to the cyclic 2,4-dioxo-1,3-diiron(IV) that is the oxidant formed in the active site of methane monooxygenase (particulate) (**2-136**). In fact, methane monooxygenase (particulate) from *M. capsulatus* has a dinuclear cluster of prosthetic copper ions rather than a dinuclear cluster of prosthetic iron ions. In this cluster, one of the copper ions is coordinated by two imidazolyl groups from two histidines, and the other copper is coordinated by one imidazolyl group from the amino-terminal histidine and the free α-amino group of that histidine. There is a symmetric synthetic 1,3-dioxo-2,4-dicopper(III) in which each copper ion is coordinated by an imidazolyl group and a primary amine.[2050] Spectral properties of this synthetic 1,3-dioxo-2,4-dicopper(III) are similar to those of a high-valent intermediate in the reaction catalyzed by the methane monooxygenase (particulate) that uses copper ions as prosthetic groups.[2051]

Peptidylglycine monooxygenase performs the hydroxylation of the secondary α carbon of an amino-terminal glycine

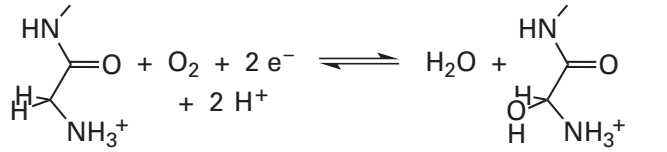

(2–309)

A related enzyme,[730] dopamine β-monooxygenase, hydroxylates the benzylic carbon in 4-(2-aminoethyl)benzene-1,2-diol. Both enzymes use L-ascorbate (Equation 2–163) as the source of the two electrons. In both enzymes there are two prosthetic copper ions in coordinations that are analogous to those of the two copper ions in nitrite reductase (NO-forming). One is coordinated by the imidazolyl

groups of two histidines and the sulfide of a methionine,[730] reminiscent of the widely distributed type of mononuclear copper ion in plastocyanin (Figure 2–26D) except that the usual cysteine is missing, which is not the case in nitrite reductase (NO-forming). This absence leaves an open site[536] on the Cu^+ in the active form of the enzyme. The other copper ion is trigonally coordinated by three imidazolyl groups, just as is the catalytic copper ion in nitrite reductase (NO-forming).

It was always thought that, just like the two mononuclear copper ions in nitrite reductase (NO-forming), the two prosthetic copper ions in peptidylglycine monooxygenase and dopamine β-monooxygenase operated independently, except that their roles were exchanged. The open site on the prosthetic copper ion coordinated by the two imidazolyl groups and the sulfide was the catalytic site in these two latter enzymes, and the copper ion coordinated by the three imidazolyl groups relayed the electrons consecutively from the two ascorbates.[535]

There is what may well be a critical difference, however, between nitrite reductase (NO-forming) and peptidylglycine monooxygenase. In the former case, the cysteine coordinating the one copper ion is from the cysteine that follows one of the histidines coordinating the other copper ion in the sequence of amino acids for the enzyme,[703,2022] so all the intervening atoms are rigidly holding the two copper ions apart. In peptidylglycine monooxygenase and dopamine β-monooxygenase the cysteine is no longer there, and although the two copper ions are 1.1 nm apart in the unoccupied enzymes,[730] as they are in nitrite reductase (NO-forming),[2020] there is nothing between them. In a crystallographic molecular model of human dopamine β-monooxygenase, there is a closed conformation in which two hinged domains, coordinating one of the copper ions, have closed upon each other to bring the two copper ions to within 0.5 nm of each other,[2052] in an orientation in which they can share either a molecule of oxygen or a hydroperoxide.[2053]

Consequently, peptidylglycine monooxygenase and dopamine β-monooxygenase and their relatives could well be considered to have a dinuclear cluster of prosthetic copper ions in their active sites. One hint that this may well be the case is that in the resting state of peptidylglycine monooxygenase the two copper ions have different reduction potentials (+270 and −15 mV), but upon association of a peptide that is a reactant for the enzyme the two copper ions have the same reduction potential (+80 mV) as if they were participants in an electronically coupled cluster.[535]

A complex forms between molecular oxygen and the Cu^+ that is coordinated by the two imidazolyl groups and the sulfide (Figure 2–58C),[2054,2055] but this occurs only when the active site is in a complex with a peptide substrate containing an amino-terminal glycine.[2054] Molecular oxygen binds at a location immediately adjacent to the hydrogen that is to be replaced by a hydroxy group (Equation 2–309). The **association of molecular oxygen with the Cu^+** is analogous to the binding of molecular oxygen to a prosthetic Fe^{2+} or ferroheme both because it ends up in a bent configuration (Figure 2–58C) and because carbon monoxide is able to associate[2056] with the Cu^+. The Cu^+ provides one of the electrons required by the reaction.

Following this initial association between molecular oxygen and the Cu^+, the mechanism of the monooxygenation is less clear. The initial complex is equivalent to a superoxycopper(II), which would be a weak oxidant.[2057-2060] It seems likely, however, that the active species is the dinuclear cluster of copper ions that forms when the domains close. In this case, the initial complex between Cu^+ and molecular oxygen could be first hydronated[2061] and then reduced by the second electron in the dinuclear cluster to the dicupric hydroperoxide,[2053] which could be either the active oxidant or a precursor to the active oxidant,[2057,2060] as is the case with a peroxyiron(III).

The multicopper oxidases are a family of related enzymes[695,696,706,2062-2064] that each contain a **trinuclear cluster of prosthetic copper ions**. A representative of these clusters is the trinuclear cluster in laccase from *M. albomyces* (Figure 2–58E).[2065] In a laccase, this cluster in its fully reduced tricuprous state reduces molecular oxygen to two molecules of water. The four electrons required for this reduction, depending on the laccase, are derived from the oxidation of four quinols, four catechols, four aminophenols, or four phenylenediamines that are oxidized, each by one electron, to their semiquinones. These one-electron oxidations are the purpose of the respective laccase.

Following the association of a molecule of oxygen with the trinuclear cluster of three Cu^+ in the active site of a laccase, the **molecular oxygen is reduced to two molecules of water**. The molecule of oxygen coordinates all three Cu^+ ions (Figure 2–58E). As the molecular oxygen associates with the trinuclear cluster, the molecule of oxygen is reduced to a peroxide dianion by two of the three Cu^+ among which

it is bound.[2066-2068] The peroxide dianion is then hydronated at one of its two oxygens by the carboxy group of an aspartic acid[2067] and reduced by one electron from the third Cu^+ as the oxygen–oxygen bond dissociates.[2069] Finally, an electron is transferred from a fourth, nearby (1.2 nm), mononuclear Cu^+ (Figure 2–26A) by outer-sphere electron transfer.

The product of the reductions and the heterolytic cleavage of the peroxide is a complex in which the hydroxide resulting from hydronation of one oxygen atom has become a μ-hydroxy group between two of the Cu^{2+} and the oxide dianion that was the other oxygen is now sitting in the plane of and equidistant from all three Cu^{2+}, coordinating all three of them[2070]

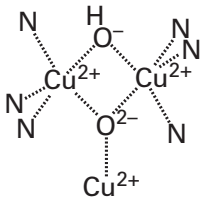

2–145

In this form of the cluster, all the copper ions have been oxidized, and in the active site of the laccase from *T. vernicifluum*, it is only after its formation that three successive electron transfers from the nearby mononuclear copper ion occur, passing the electrons one at a time from three of the aromatic coreactants to rereduce[2071] the three Cu^{2+}. Hydronations of the oxide dianion and the hydroxide, concerted with rereduction of the three Cu^{2+} to three Cu^+, are necessary to regenerate the fully reduced form of the cluster in the active site of laccase and two molecules of water.[2072] The electron removed from the fourth aromatic coreactant reduces the mononuclear copper itself to Cu^+ ready to provide the fourth electron needed to reduce the next molecular oxygen to water. As in cytochrome oxidase, all the electrons necessary to reduce molecular oxygen to the equivalent of two molecules of water are present in the enzyme itself so that no intermediates have a chance to dissociate into the solution.

The nearby mononuclear copper ion in one of these multicopper oxidases, of which laccase is an example, is reduced from Cu^{2+} to Cu^+ by removing an electron from the **particular reactant that is oxidized by that particular multicopper oxidase**. It has already been noted that the mononuclear copper ion in laccase (Figure 2–26A) consecutively removes one electron from each of four quinols, four catechols, four aminophenols, or four phenylenediamines to produce their semiquinones, and these four electrons consecutively reduce the completely cupric cluster (**2–145**) to the completely cuprous cluster as the μ-hydroxide and the μ-oxide dianion are hydronated and eventually leave the enzyme as hydroxide ions or molecules of water.

Each of the other enzymes in the family of multicopper oxidases has, in addition to the trinuclear cluster, a mononuclear cluster responsible for the consecutive oxidations of its particular reactants. For example, L-ascorbate oxidase uses a mononuclear copper ion, coordinated as is the one in plastocyanin (Figure 2–26D), to oxidize consecutively four molecules of L-ascorbate to four L-monodehydroascorbates by four separate outer-sphere electron transfers.[696] After rereduction of the enzyme, the tricuprous cluster is ready to bind the next molecule of oxygen (Figure 2–58E) and the cuprous mononuclear cluster is ready to provide the fourth electron. Because the reduction of oxygen to water oxidizes a particular multicopper oxidase, the mononuclear Cu^{2+} that it then uses to perform its particular oxidation is a **particularly strong oxidant**. The purpose of L-ascorbate oxidase, an enzyme that seems to oxidize a coenzyme that is only used as a reductant by converting molecular oxygen to water, is unknown.

Nitrous-oxide reductase

$$2\,H^+ + 2\,e^- + NNO \rightleftharpoons N_2 + H_2O \qquad (2\text{–}310)$$

contains a **tetranuclear cluster of prosthetic copper ions** (Figure 2–58F).[747,2073] In the crystallographic molecular models of nitrous-oxide reductase from *P. denitrificans*[2074] and from *Achromobacter cycloclastes*,[2073] three of the copper ions are coordinated by the imidazolyl groups of two histidines and one of them by the imidazolyl group of only one histidine, and each of the four copper ions forms a bond with the same tetrahedrally coordinated sulfide dianion in the center of the cluster.[2075,2076] This form of the cluster is responsible for the enzymatic activity.[2077,2078] The **nitrous oxide**, $N{\equiv}N^+{-}O^-$ (**2–106**), is thought to bind to the reduced tetracopper(I) cluster in the active site of the enzyme at the position occupied by the two molecules of water in the crystallographic molecular model of the oxidized enzyme (Figure 2–58F),[2079] with its peripheral nitrogen taking the place of one of the waters and its peripheral oxygen taking the place of the other[2080] to form

a six-membered ring composed of the two nitrogens and the oxygen of nitrous oxide, the two copper ions with open sites, and the sulfide dianion. The fully reduced tetracuprous cluster is responsible for the reduction,[2078,2080] and it performs successive inner-sphere transfers of the two electrons to the bound nitrous oxide while its oxygen is hydronated twice by a catalytic acid base.[2079] In the paramagnetic tricopper(I)copper(II) intermediate, there is an unpaired electron shared between the two copper ions coordinated by the resulting O-hydronated tautomer, $^{\bullet}$N=N–OH (**2–108**), of the radical (**2–107**) of nitrous amide (**2–109**).[2081] Transfer of the next electron and a hydron produces molecular nitrogen and a molecule of water. There is a CuA dinuclear cluster of copper ions (Figure 2–26F) 1.0 nm away from the tetranuclear cluster of prosthetic copper ions, and this CuA cluster is the point of entry for the electrons from the natural donor that rereduces the enzyme.[747] It is unclear why six Cu^{+} are needed for a two-electron reduction (Equation 2–310).

Manganese ions are also found in enzymes that perform oxidation–reductions of the oxides and hydrides of hydrogen, oxygen, nitrogen, carbon, and sulfur. In these enzymes, the prosthetic manganese ions can assume the oxidation states **Mn^{+2}, Mn^{+3}, Mn^{+4}, and possibly Mn^{+5}**.

There are several enzymes that have a prosthetic, **mononuclear manganese ion** in their active sites and use it to catalyze reactions similar to those catalyzed by mononuclear iron ions. For example, 3,4-dihydroxyphenylacetate 2,3-dioxygenase from *Arthrobacter globiformis* has a manganese ion in its active site even though it catalyzes the same reaction (Equation 2–277) passing through the same intermediates (Equation 2–278) as a 3,4-dihydroxyphenylacetate 2,3-dioxygenase that has a mononuclear iron ion in its active site.[2082] Toxoflavin lyase from *Paenibacillus polymyxa* has a mononuclear manganese ion in its active site that is coordinated by two carboxylato groups and an imidazolyl group,[2083] a coordination that ensures that the manganese ion remains Mn^{2+} during the reaction. The enzyme catalyzes a reaction analogous to a Baeyer–Villiger rearrangement[2084] like the one catalyzed by the Fe^{2+} in 3,4-dihydroxyphenylacetate 2,3-dioxygenase (Equation 2–278).

There are also enzymes that have mononuclear manganese ions in their active sites that are unlike enzymes with iron ions in their active sites. Oxalate decarboxylase

$$\text{oxalate} + H^{+} \rightleftharpoons CO_2 + \text{formate} \qquad (2\text{–}311)$$

from *B. subtilis*[2085] has a mononuclear Mn^{2+} in its active site octahedrally coordinated by three imidazolyl groups, a carboxylato group, and two molecules of water.[2086] Although it catalyzes a reaction that does not involve molecular oxygen, molecular oxygen must be present for the enzymatic reaction to occur. It is believed that the two open sites on the Mn^{2+} are occupied at the same time by oxalate and molecular oxygen, and that the molecular oxygen removes an electron from the carboxylato group of the oxalate that is a ligand to the Mn^{2+} and becomes a superoxide radical anion.[2085] The electron transfer produces the carboxy radical of oxalate ($^{-}OOCCOO^{\bullet}$) that decomposes into carbon dioxide and a formyl radical anion ($^{-}OOC^{\bullet}$). The existence of the formyl radical anion as an intermediate in the enzymatic reaction has been demonstrated by trapping it with *N-tert*-butyl-1-phenylmethanimine oxide, a stable radical that adds to the formyl radical anion released adventitiously into the solution as a side product by a mutant of the enzyme.[2087] In the unmutated enzyme this intermediate is presumably held tightly in the active site. Hydronation of the carbon of the formyl radical anion coincident with transfer of an electron from the superoxide radical anion back to the resulting formate radical completes the reaction and regenerates the molecular oxygen. In one sense, the molecular oxygen is an electron-transferring coenzyme, accepting an electron and then donating it back, much as the electron-transferring coenzyme for ribonucleoside-diphosphate reductase containing the stable tyrosyl radical removes an electron from the sulfido group in the active site and then donates it back at the end of the reaction.

The decomposition of the carboxy radical of oxalate is an example of the rapid and **spontaneous decarboxylation of any carboxy radical**. During decarboxylation, the carbon dioxide leaves behind the radical of the carbon to which it was attached

$$RCO_2^{\bullet} \longrightarrow R^{\bullet} + CO_2 \qquad (2\text{–}312)$$

In the case of oxalate decarboxylase, this is the formyl radical anion. The bond dissociation energies of most carbon–carbon bonds between a carboxy radical and an adjacent carbon are actually negative (–30 to –110 kJ mol^{-1}),[2088] unlike those for almost every other type of carbon–carbon bond, because

carbon dioxide is such a stable molecule. The first-order rate constants for the decarboxylations of most carboxy radicals[2089-2091] at 20 °C are in the range between 1 and 800 ns^{-1}. The decarboxylation of the carboxy radical formed upon dissociation of the oxygen–oxygen bond of the peroxy group in the *tert*-butyl peroxy ester of ethyl oxalate occurs so rapidly that it was concluded that it was indistinguishable from being concerted with dissociation of the oxygen–oxygen bond.[2092]

Oxalate oxidase

$$\text{oxalate} + O_2 + 2\,H^+ \rightleftharpoons 2\,CO_2 + H_2O_2 \qquad (2\text{–}313)$$

from *Hordeum vulgare* has a mononuclear manganese ion also coordinated by three imidazolyl groups and a carboxylato group.[1409] The manganese ion, however, must be Mn^{3+} or Mn^{4+} rather than Mn^{2+} for the enzyme to be active. In oxalate oxidase, the **Mn^{3+}**, rather than the complex between molecular oxygen and Mn^{2+}, **removes an electron** from the oxalate to produce carbon dioxide and the same formyl radical anion, which is then converted into carbon dioxide rather than formate when the molecular oxygen removes the unpaired electron from it. The resulting superoxide radical anion is hydronated, and transfer of a hydron from an acid and an electron from the Mn^{2+} to the hydroperoxy radical completes the reaction.[2093]

There is also a dinuclear cluster of prosthetic manganese ions in an oxidase in *S. thioluteus* that has a structure similar to those of dinuclear clusters of prosthetic iron ions (Figure 2–57F to 2–57I) in that it has two bidentate bridging carboxylato groups. One of the manganese ions is coordinated by two imidazolyl groups and a monodentate carboxylato group, and the other manganese ion is coordinated by an imidazolyl group and another monodentate carboxylato group. This dinuclear cluster of prosthetic manganese ions catalyzes the *N*-hydroxylation of arylamines.[2094]

Catalase from *L. plantarum* (Equation 2–242) has a **dinuclear cluster of prosthetic manganese ions**[2095,2096]

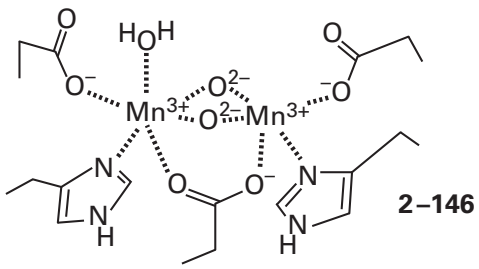

2–146

that resembles closely the dinuclear cluster of prosthetic iron ions (Figure 2–57I) in methane monooxygenase (soluble). The dinuclear cluster cycles between the $Mn^{+3}\,Mn^{+3}$ oxidation state and the $Mn^{+2}\,Mn^{+2}$ oxidation state.[2097,2098] The former oxidizes hydrogen peroxide to oxygen; the latter reduces hydrogen peroxide to water. It is thought that, in the oxidized cluster, hydrogen peroxide replaces water as a ligand on the exocyclic open site of one of the manganese ions in **2–146,** and after the reduction and the removal of the hydrons, the resulting molecular oxygen leaves from the resulting Mn^{2+}. In the reduced enzyme, however, hydrogen peroxide is able to replace a μ-hydroxy group, the conjugate acid of one of the μ-oxo groups in **2–146**, because it is not held that tightly by the Mn^{2+} ions.[2095]

There is a synthetic dinuclear cluster of manganese ions that is able to catalyze the same dismutation of hydrogen peroxide performed by the catalase, albeit at a much slower rate.[2099] It is possible to oxidize manganese catalase from *L. plantarum* to a superoxymanganese(IV)manganese(III)[2100] state, which is not an intermediate in the normal enzymatic reaction but displays some of the properties[2101] of the cluster of four manganese ions in photosytem II.

The prosthetic cluster of four manganese ions in photosytem II of green plants and cyanobacteria is responsible for producing molecular oxygen from two molecules of water. The random choice of water as the source of electrons for photosynthesis, and the production of molecular oxygen as a by-product of this choice, is one of the most influential events in the history of life on earth. The oxidation of water is performed by a pentanuclear cluster of four manganese ions, a calcium dication, and five μ-oxo ions.[1009,1028,2102,2103] During the conversion of two molecules of water to a molecule of oxygen, a four-electron oxidation, the four hydrons that are also products are released to the positive, acidic solution because electrons are transferred from the cluster that performs the oxidation to the hole in the special pair, which is on the positive, acidic side of the membrane (Figure 2–34).

In the crystallographic molecular model of photosystem II from *Thermosynechococcus vulcanus*, **each of the four manganese ions in the cluster is octahedrally coordinated** by six ligands (Figure 2–59).[1011,1012,2104-2106] The ligands are μ-oxo ions, carboxylato groups, molecules of water, and imidazolyl groups, typical ligands for manganese ions (see **2–146**). The calcium dication has seven oxygens, anionic and neutral, as ligands pushing and shoving around it, which is one of the typical coordinations for Ca^{2+}. Three of the seven external faces of the cluster have bidentate carboxylato groups coordinating the two metallic ions on that face. Each μ-oxo ion has four ligands. By convention the manganese ions, the μ-oxo groups, and the molecules of water in the vicinity are numbered as in the figure to ease discussion of their roles.

In a synthetic cubane of three Mn^{4+}, four μ-oxo groups, and a Ca^{2+}, for which a crystallographic molecular model of high resolution is available, all nine of the oxygen–manganese distance are between 0.183 and 0.192 nm.[2107,2108] Six of the distances between manganese ions and oxo groups in the crystallographic molecular model of the cluster in photosystem II from *T. vulcanus*[2106] are between 0.18 and 0.19 nm. The distance, however, between Oxo 5 and Manganese 1 is 0.27 nm and the distance between Oxo 5 and Manganese 4 is 0.22 nm, and these dispositions significantly widen the gap between Manganese 4 and Manganese 1. **Within this gap, the molecule of oxygen is produced** from two oxygen atoms that were originally in two molecules of water.[2109,2110] This widening is presumably a steric effect produced by the side chains of the amino acids that are ligands to these manganese ions, and it is essential to provide the room necessary for the oxidation. In response to this steric widening of the gap between Manganese 1 and Manganese 4, the distance between Manganese 3 and Oxo 3 increases to 0.23 nm, the distance between Manganese 3 and Oxo 5 increases to 0.21 nm, and the distance between Manganese 2 and Oxo 3 increases to 0.21 nm.

Because Ca^{2+} is incapable of being oxidized or reduced at normal biochemical potentials, the **manganese ions in the cluster provide four electrons**, one at a time in a sequence of steps, to the successive holes that develop in the special pair during the absorption of four successive quanta of light by the reaction center within photosystem II. As has already been noted, transfer of each of these four electrons from the cluster of manganese ions (Figure 2–59) to the hole in the special pair (Figure 2–35) passes through a tyrosine—Tyrosine 161 in the active site of photosystem II from *T. vulcanus* (Figure 2–59)—which donates an electron to the hole in the special pair to become the tyrosyl radical, which then removes an electron from the cluster.

The **four separate removals from the cluster, each of one electron,** by the special pair in the reaction center can be coordinated over a population of photosystems II by sitting a suspension of chloroplasts in the dark until the majority of the tetranuclear clusters of prosthetic manganese ions are reduced by endogenous reductants to the resting S_1 or $(Mn^{3+})_2(Mn^{4+})_2$ oxidation state, the state of the crystallographic molecular model in Figure 2–59, and then exposing them to a regular sequence of short flashes of light intense enough to excite almost all photosystems II in the sample on each flash.[2111-2113] The same result can be achieved by poising purified photosystem II electrochemically in the S_1 state and then exposing the preparation to successive flashes of light.

If it is intense enough, the **first flash** creates holes in almost all the special pairs, and each hole then accepts an electron through the tyrosine from its associated cluster to take the majority of the clusters to the S_2 or $\mathbf{Mn^{3+}(Mn^{4+})_3}$ oxidation state ($t_{½}$ = 100 μs).[2114-2116] The distribution of absorbances in the electron–nuclear double resonance spectrum for this S_2 oxidation state of photosystem II of *Thermosynechococcus elongatus* indicates that the electron, and hence the hole, is shared almost equally among the four manganese ions and that none of the manganese ions can be Mn^{2+}.[2117]

Up to this point, the two molecules of water or μ-oxo bridges within each cluster that will become the molecule of oxygen are still molecules of water, μ-hydroxy bridges, or μ-oxo bridges, and they exchange with molecules of water in the solution, albeit slowly.[2118-2120] Oxo 5 has been identified as one of these exchangeable oxygens by W-band oxygen-17 electron–electron double resonance-detected nuclear magnetic resonance spectra[2121] after rapid dilution of samples poised in the S_2 oxidation state into $H_2{}^{17}O$. This μ-oxo bridge is the most likely to be one of the two **oxygens destined to become molecular oxygen** because it is the only μ-oxo bridge that is coordinated by the Ca^{2+} and two of the four manganese ions, is adjacent to a third manganese ion, and sits in the widened gap between Manganese 1 and Manganese 4. Furthermore, the geometry of its coordination is strained because it is farther from

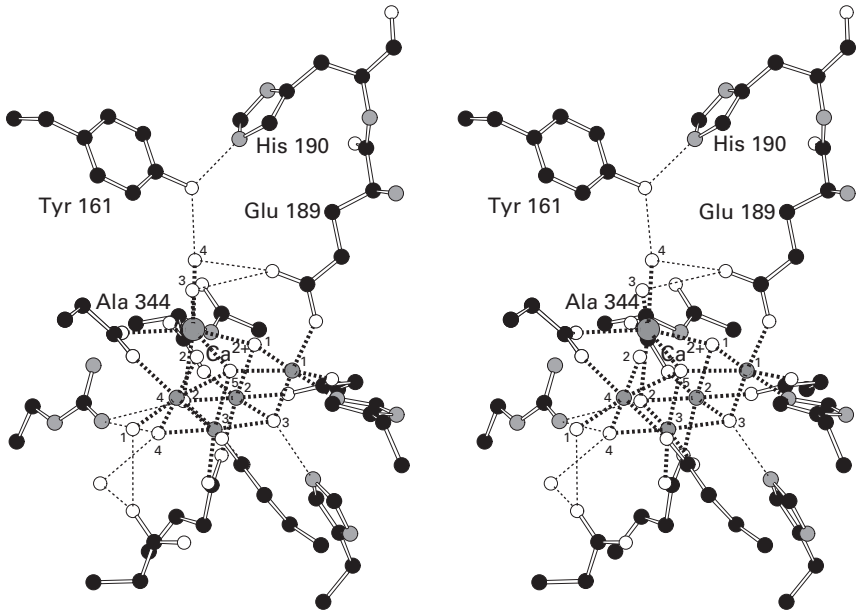

Figure 2–59: Stereodrawing[50] of the cluster of four manganese ions and a calcium dication responsible for the conversion of two molecules of water into a molecule of oxygen.[1011] Black atoms are carbons, white atoms are oxygens, and gray atoms are nitrogens. The calcium dication is the large labeled dark gray sphere, and the four manganese ions are the smaller dark gray spheres surrounded by their ligands. By convention, the manganese ions, the μ-oxo groups, and the molecules of water in the vicinity are numbered as in the figure to ease discussion of their roles. The μ-oxo groups among the metallic ions and several molecules of water are the small white spheres. Crude particles containing photosystem II were extracted from thylakoids of *T. vulcanus* with the detergent lauryldimethylamine *N*-oxide. These crude particles were dissolved in a solution of 2.0% *n*-dodecyl β-D-maltoside, 20 mM NaCl, and 25% glycerol at pH 6.0, and purified by stepwise elution from a chromatographic medium to which quaternary amines are covalently attached.[2105] The intact photosystem II with all its components still associated was then further purified by recrystallization with poly(ethylene glycol) from 40 mM $MgSO_4$, 20 mM $CaCl_2$, 20 mM NaCl, and 0.02% *n*-dodecyl β-D-maltoside at pH 6.5.[2104] The final crystals were submitted to X-ray crystallography, and data were collected to Bragg spacing of 0.19 nm.[1011] The cluster and the side chains of the aspartates, glutamates, histidines, and an arginine that attach it to the protein are drawn. The free carboxylate of the carboxy-terminal alanine (Alanine 344) of one of the folded polypeptides in the complex is also a bidentate ligand to the cluster.

tetrahedral than any of the other μ-oxo bridges in the cluster. There is evidence from crystallography performed with short pulses of X-rays that one of the bonds between this μ-oxo group and either Manganese 1 or Manganese 4 lengthens further during the transition between S_1 and S_2.[2123]

In the next step, the **second flash** takes the cluster to the S_3 oxidation state ($t_{½} = 250\ \mu s$).[2114] Magnetic resonance spectroscopy of this oxidation state[2124] and determinations of its spin state[2125] demonstrate that **all four of the manganese ions are Mn^{4+}**.

A crystallographic molecular model of the cluster in the S_3 oxidation state, derived from a data set with reflections to Bragg spacing of 0.215 nm that was assembled from reflections collected with short pulses of X-radiation (10 fs) impinged on the crystals after two flashes of light, clearly shows that **two oxo groups are now between Manganese 4 and Manganese 1**.[2110] The distances from Manganese 4 to the first oxo group, from the first oxo group to the second oxo group, and from the second oxo group to Manganese 1 are 0.22, 0.19, and 0.17 nm, and the distance between Manganese 4 and Manganese 1 has expanded from 0.49 nm in the S_1 oxidation state to 0.52 nm. This disposition of oxygen atoms is consistent with other crystallographic observations performed with short pulses of X-rays[2126] and extended X-ray absorption fine structure,[2127] which are consistent with a structure for the complex in which the bond between Oxo 5 and either Manganese 1 or Manganese 4 has been broken, and the open coordination site on that Mn^{4+} has become occupied by a hydroxide. The van der Waals radius of an oxygen atom is 0.15 nm, the oxygen–oxygen bond length in hydrogen peroxide is 0.149 nm, and the oxygen–oxygen bond length in a molecule of oxygen is 0.121 nm. Consequently, because the distance between the two oxo groups is 0.19 nm, the two oxo groups are forced into a disposition in which their van der Waals circumferences overlap significantly, but they are not yet either a hydroperoxide or a molecule of oxygen.

In the S_1 oxidation state, the distances from Manganese 4 to Oxo 5 and from Oxo 5 to Manganese 1 are 0.22 and 0.27 nm, so at first glance it seems as though an oxo group has been inserted between Oxo 5 and Manganese 1, but there is obviously no way to tell one of the oxo groups from the other crystallographically. The closest molecule of water to the bonds between Manganese 4, Oxo 5, and Manganese 1 at the S_1 oxidation state (Figure 2–59) is Water 3 on the Ca^{2+}, but it lies immediately adjacent to the bond between Manganese 4 and Oxo 5. If this molecule of water becomes the second oxo group, it probably inserts into the space between Manganese 4 and Oxo 1, and the two resulting oxo groups simply shift in location to the orientations of lowest energy. Studies of the effect of external pH on the rate lead to the conclusion that the transition from the S_2 to the S_3 oxidation state proceeds with the release of a hydron into the solution,[2128] perhaps one of the hydrons on the molecule of water or the hydroxide that is removed before it enters the gap. If indeed Water 3 has entered the gap, it is probably the carboxylato group of Glutamate 189 that removes the hydron.

There are a number of observations consistent with the conclusion that the molecule of water that becomes the second oxo group during the transition to the S_3 oxidation state is Water 5, the **closest molecule of water on the Ca^{2+}**. In the presence of ammonia, Water 1 and Water 2 on Manganese 4, respectively, are replaced by two molecules of ammonia, but ammonia has no effect on the ability of photosystem II to turn molecules of water into molecules of oxygen.[2129] Because these are the only other observed molecules of water near the space between Manganese 4 and Manganese 1, this observation supports the conclusion that the new oxo group between them in the S_3 oxidation state was Water 3 before it inserted. In addition, Fourier-transform infrared spectra of the molecule of water destined to enter the gap are significantly affected by the substitution of Ca^{2+} by Sr^{2+}, an observation that indicates that Water 3 is that molecule of water.[2130] There are also arguments,[2109,2131-2133] however, that the molecule of water that fills the gap is actually Water 2 on Manganese 4, but the fact that the replacement of this molecule of water by ammonia has no effect on the conversion of water to molecular oxygen would seem to rule out this possibility.

It is only after the **third flash**[2111] takes the cluster to the S_4 oxidation state by removing one more electron from it that four electrons in the two oxo groups in the gap between Manganese 1 and Manganese 4 are removed by the surrounding manganese ions and a molecule of oxygen is produced. The transfer is so rapid that no intermediates, not even S_4 itself, have been observed while the molecule of oxygen is being produced.[2111,2113,2134] During this transition between S_3 and S_4, the exchange of oxygens in the cluster destined to become molecular oxygen with molecules of water in the solution slows dramatically,[2134] a fact suggesting that at this point an

almost irreversible commitment to **forming an oxygen–oxygen bond** has been made. During this transition between S_3 and S_4, a transient intermediate has been observed that is produced by the dissociation of a hydron from the cluster, perhaps from a hydroxy group, before the four electrons are removed essentially simultaneously from the two oxo groups.[2135]

In S_3, all four manganese ions are Mn^{4+}, and the cluster itself contains an even number of electrons. The removal of an electron from the cluster in which the two oxo groups are in position between Manganese 1 and Manganese 4 initiates the immediate formation of molecular oxygen. Upon removal of the electron, the cluster has an odd number of electrons. Formally, because one electron has been removed from a cluster of four Mn^{4+}, one of the manganese ions on which an oxo group is located has become an **oxomanganese(V)**. Just as in S_2, however, the unpaired electron in the cluster in photosystem II could well be distributed over the entire complex, so it is not clear whether the formation of molecular oxygen is the expression of the capacity of an oxomanganese(V) or the expression of the capacity of the unpaired electron itself. Synthetic oxomanganese(V) complexes, however, have been proposed to be models of an oxomanganese(V) in the S_4 oxidation state.[2136]

In isolation, surrounded by singlet ligands such as nitrogens, oxygens, or sulfurs, an oxomanganese(V) has an even number of electrons and is a strong electrophile, which would be expected to react instantaneously with an immediately adjacent formal oxide or hydroxide. In fact, oxomanganese(V) in a binuclear dioxodimanganese(V) is known to be able to act as an electrophile in a nucleophilic addition of hydroxide to produce molecular oxygen[2137]

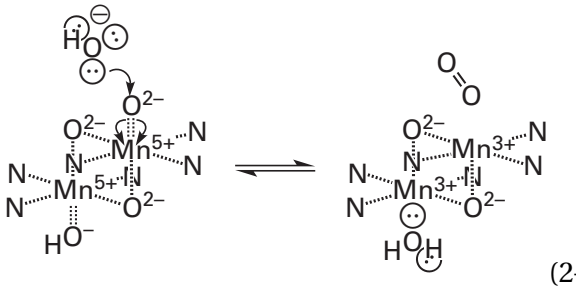

(2–314)

When, however, a mononuclear oxomanganese(V) in 5,10,15-tri(4-nitrophenyl)porphyrin was synthesized, it also reacted as an electrophile with hydroxide, but the product was peroxymanganese(III) rather than molecular oxygen.[2138] Consequently, the other oxomanganese(V) in the dinuclear complex (Equation 2–314), an excellent oxidant, is required to remove two electrons from the initial peroxymanganese(III) formed from the oxomanganese(V) to which the hydroxide added to produce the molecular oxygen. If there is a transient oxomanganese(V) in the cluster at the S_4 oxidation state, it must be formed from either Manganese 1 or Manganese 4 and the respective, adjacent oxo group in the space between them. The other oxo group would be equivalent to a hydroxide and would immediately add nucleophilically to the oxygen of the oxomanganese(V). It is possible that the other three Mn^{4+} in the cluster together would constitute a strong enough oxidant to convert the resulting hydroperoxymanganese(III) to molecular oxygen and Mn^{3+}, as well as a hydron.

If, however, the unpaired electron in S_4 is distributed over the cluster, including the oxygen atoms in the cluster, it is possible that the equivalent of an oxy radical initiates a sequence of radical intermediates in the production of molecular oxygen.[2120,2139] In one of the steps in this sequence, a single bond would be formed between the two oxo groups between Manganese 1 and Manganese 4 in the cluster to produce again a peroxide dianion shared by the two Mn^{4+}.

In both the mechanism involving a nucleophilic addition and the mechanism involving a colligation, a peroxide or hydroperoxide between two Mn^{4+} is an intermediate. A binuclear peroxydimanganese(IV)

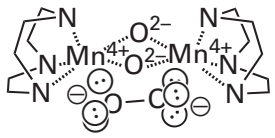

2–147

has been synthesized in which two Mn^{4+} are complexed with a bridging peroxide dianion. Upon acidification (pH 3) in 0.5 M NaCl, the peroxide is released as molecular oxygen[2140] and the manganese ions end up as the chlorides of Mn^{3+}. In this reaction, each manganese has oxidized each atom of oxygen in the final molecular oxygen by one electron.

There is also precedence, in a synthetic cluster of manganese ions that can convert water to molecular oxygen, for the oxygen to be produced from two μ-oxo oxides.[2141] In this case, however, both μ-oxo groups that combine to form oxygen are ligands to the same manganese ion. It has been proposed that such an intermediate could be involved in the

formation of molecular oxygen in the S_4 oxidation state,[2142] but it is hard to see how the two oxo groups between Manganese 1 and Manganese 4 could end up on just one manganese ion because both manganese ions are coordinated by five other ligands, and Mn^{4+} holds its ligands tightly. Another synthetic cluster of manganese ions can convert two molecules of water to molecular oxygen, but again, the two molecules of water must occupy two open sites on the single manganese ion in the cluster.[2137]

During the hidden formation of molecular oxygen in the S_4 oxidation state in photosystem II, four electrons are transferred to the manganese ions from the two oxygens that begin at the oxidation state of water and end up at the oxidation state of molecular oxygen. Consequently, the manganese ions that consumed the four electrons have been reduced to the S_0 or $(Mn^{3+})_3Mn^{4+}$ oxidation state.[2115] Magnetic multiresonance electron paramagnetic spectra[2122] following rapid dilution into $H_2{}^{17}O$ and surface-enhanced Raman infrared spectra[2143] of photosystem II poised electrochemically in the S_0 oxidation state identify a hydroxy group, presumably derived from a molecule of water that has filled the empty space between Manganese 4 and Manganese 1 left behind after dissociation of the molecular oxygen. This hydroxy group then becomes Oxo 5 in the S_1 oxidation state after the removal of an electron from the cluster at the S_0 oxidation state.[2122]

The **fourth flash** returns the majority of the photosystems II to the S_1 or $(Mn^{3+})_2(Mn^{4+})_2$ oxidation state, where we began.[2115] Consequently, four successive flashes, which provide four successive quanta of light to each photosystem II and which absorb one electron from the cluster for each quantum of light, complete the cycle.

At this point in the discussion, the role of the Ca^{2+} and why it is suitable to fill this role become obvious. Water 3 on the Ca^{2+} lies immediately adjacent to the gap between Manganese 4 and Manganese 1, and its role seems to be to feed molecules of water or hydroxide ions into the gap.[2144,2145] It is also immediately adjacent to Water 4 on the Ca^{2+} that participates in an extended cluster of molecules of water* that are held together by hydrogen bonds and that ultimately blend into the positive, acidic solution.[2110] The two oxo groups in the gap between Manganese 1 and Manganese 4 in the S_3 oxidation state immediately become a molecule of oxygen on reaching the S_4 oxidation state. The molecule of oxygen immediately dissociates because the Manganese 4 and Manganese 1 are both Mn^{3+}, neither of which has any affinity for molecular oxygen. The empty gap is filled by Water 3 in the S_0 oxidation state, Water 4 moves over to the position previously occupied by Water 3, and Water 4 is replaced by a molecule of water from the extended cluster of molecules of water. Upon again reaching the S_3 oxidation state, the single oxo group between Manganese 4 and Manganese 1 is shoved over to Manganese 1 as a molecule of water or a hydroxide is pulled into the gap, and Water 4 again moves over and is replaced by a molecule of water in the chain.

Water 3 and Water 4 seem to be at the center of the action (Figure 2–59). The 4-hydroxy group of Tyrosine 161, the tyrosine from which electrons are removed consecutively during photosynthesis, forms a hydrogen bond to Water 4. There is a hydrogen bond between the 4-hydroxy group of Tyrosine 161 and the imidazolyl group of Histidine 190, which along with the carboxy group of Glutamate 189 (a ligand to Manganese 1) can be a catalytic acid shuttling hydrons away from Water 3 and Water 4. The most reasonable path along which an electron can pass out of the cluster upon the successful capture of a photon would be through Histidine 190 and Glutamate 189. The carboxy group of Glutamate 189 can form a hydrogen bond with either Water 3 or Water 4, and there are crystallographic maps of difference electron density suggesting that this carboxy group is planted by one of its oxygens on Manganese 1 while its other oxygen pivots as the consecutive oxidations proceed.[2110,2144,2145] When Glutamate 189 is mutated to a serine or a glycine, the progression from the S_2 to the S_3 oxidation state is prevented.[2132]

Manganese(III) is the paradigmatic octahedrally coordinated transition metallic ion. Its ionic radius (0.075 nm) is quite small, and it is a hard metallic ion that holds its ligands tightly and closely because of the high field strength. As a result, the rate constant for the exchange of a molecule of water[2146] from a Mn^{3+} is in the range of 10 μs^{-1}. Calcium dication is an even harder metallic ion that is almost exclusively coordinated by oxygens from its ligands, but it has a large ionic radius (0.11 nm). As a result, it holds its ligands farther from its nucleus, and, because they are held farther away and its charge number is only +2, it holds its ligands less tightly. As a result, the rate constant for the exchange of a molecule of water from Ca^{2+} is 200 μs^{-1}. Because it

*There is also a chain of water molecules, albeit far less extensive, connecting the waters on Manganese 4 to the positive, acidic solution.[2110]

is so large and holds its ligands so loosely, its coordination is haphazard, varying from four oxygens to seven oxygens oriented unpredictably, presumably in a configuration dictated only by steric forces and electron repulsion within the ligands themselves. Consequently, molecules of water can move over the surface of a Ca^{2+} readily, the perfect situation for feeding molecules of water into the breach between Manganese 1 and Manganese 4 one after the other as molecules of oxygen are made and rapidly dissociate.

Molybdenum ions are used prosthetically in active sites to perform oxidation–reductions in which single atoms of oxygen are reduced or oxidized, while coreactants are oxidized or reduced. In these reactions the prosthetic molybdenum ion can assume the oxidation states **Mo^{4+}, Mo^{5+}, and Mo^{6+}**. A mononuclear, prosthetic molybdenum ion is almost always coordinated by one or two **molybdopterins**

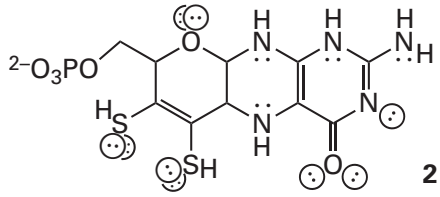

2–148

or one or two of its derivatives.[2147-2153] Eukaryotic molybdoenzymes usually contain the unmodified molybdopterin (**2–148**) while prokaryotic molybdoenzymes almost always contain modified molybdopterins that are dinucleotides in which a GMP, a CMP, an AMP, or an IMP is attached to the phosphate group of the molybdopterin* in a diphosphate linkage,[2154] but there is at least one bacterial molybdoenzyme in which the molybdenum ion is coordinated by two unmodified molybdopterins.[2155] Eukaryotic **molybdoenzymes** always have a molybdenum ion coordinated by only one unmodified molybdopterin while bacterial and archael molybdoenzymes can have molybdenum ion coordinated by one or two modified molybdopterins. The oxomolybdenum(VI) bismolybdopterin prosthetic group in respiratory dimethylsulfoxide reductase from *R. sphaeroides* (Figure 2–60)[2148,2156] is an example of a prosthetic molybdenum ion coordinated by two molybdopterins. In the figure, the 5′-guanidyl groups on the phospho groups of the two molybdopterins in this bacterial molybdoenzyme have been omitted.

Most, but not all,[2157] of the enzymes containing molybdenum ions coordinated by one or two molybdopterins **convert the oxygen atom in an oxo group or hydroxy group on a reactant into a molecule of water**, a conversion involving no oxidation or reduction of the atom of oxygen, coincident with the reduction of the reactant by two electrons supplied by an electron-transferring coenzyme. In the reverse direction, they convert the atom of oxygen in a molecule of water into an oxo group or hydroxy group on a reactant, again a conversion involving no oxidation or reduction of the atom of oxygen, coincident with the oxidation of the substrate by two electrons that are accepted by the same electron-transferring coenzyme. Examples of molybdoenzymes are respiratory dimethylsulfoxide reductase

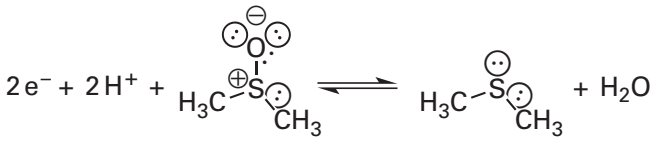

(2–315)

trimethylamine-*N*-oxide reductase[2149]

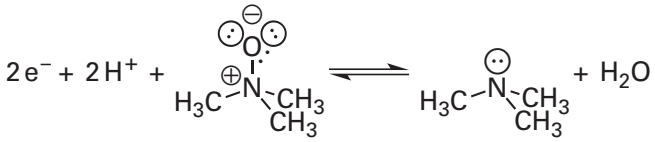

(2–316)

amidoxime reductase[2158,2159]

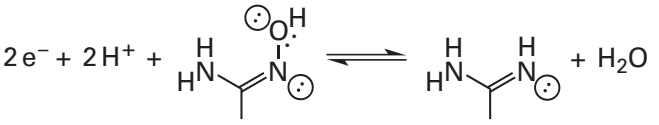

(2–317)

arsenate reductase (azurin)[2160]

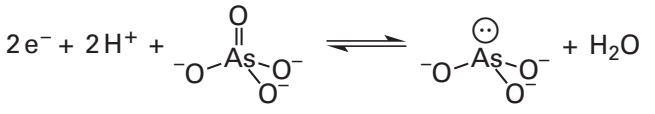

(2–318)

*From here on, no distinction will be made between molybdopterin itself and a molybdopterin to which a nucleotide is attached. They will both be called "molybdopterin".

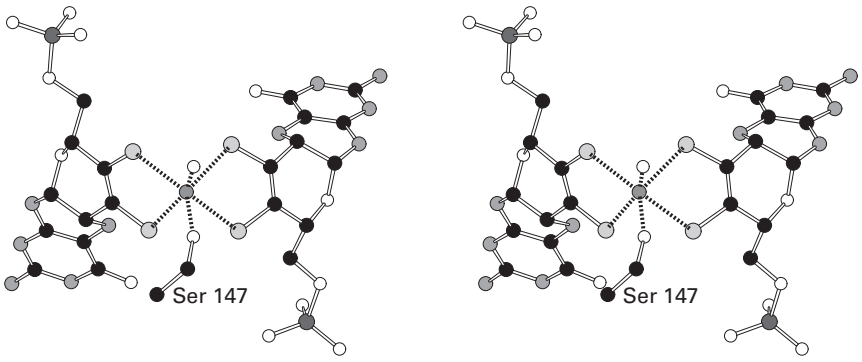

Figure 2–60: Stereodrawing[50] of the enzymatically active oxomolybdenum(VI) bismolybdopterin in the crystallographic molecular model of fully oxidized respiratory dimethylsulfoxide reductase from *R. sphaeroides*.[2156] Black atoms are carbons, white atoms are oxygens, and gray atoms are nitrogens. The molybdenum ion is the smaller dark gray sphere surrounded by its ligands in the center of the drawing. The two molybdopterins (**2–148**), to the right and to the left in the drawing, provide four sulfido groups as ligands to the Mo^{6+}. The two molybdopterins are related by a twofold rotational axis of pseudosymmetry passing through the molybdenum. The hydroxy group of Serine 147 provides a sixth ligand to the molybdenum ion. The axis of pseudosymmetry roughly bisects the angle between the oxo group and the hydroxy group.

nitrate reductase (quinone)[883]

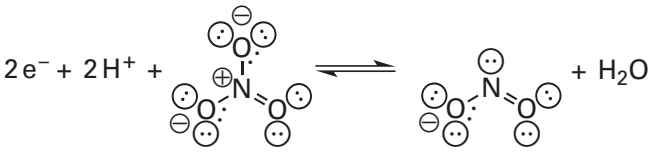

(2–319)

aerobic carbon monoxide dehydrogenase[2161,2162]

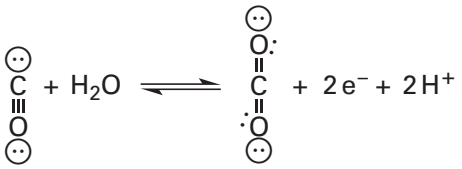

(2–320)

sulfite oxidase

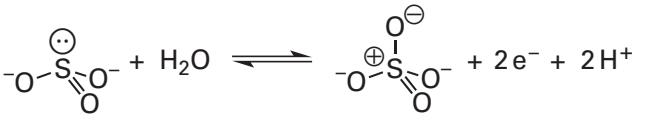

(2–321)

4-hydroxybenzoyl-CoA reductase[2163]

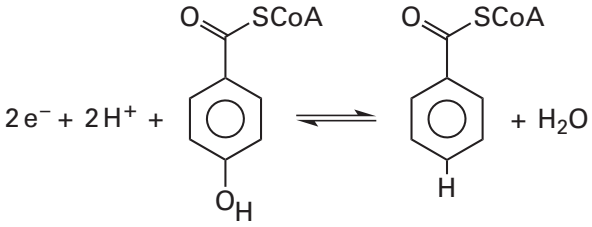

(2–322)

xanthine dehydrogenase[2164]

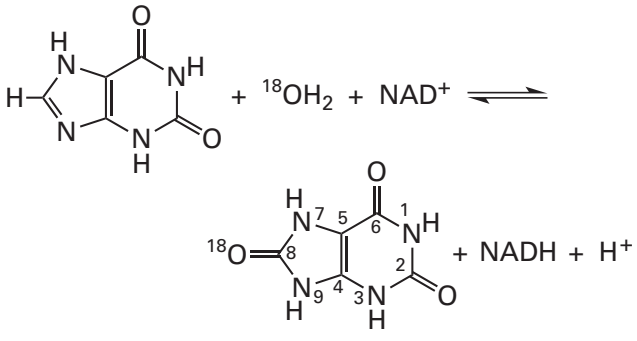

(2–323)

and aldehyde dehydrogenase (FAD-independent)

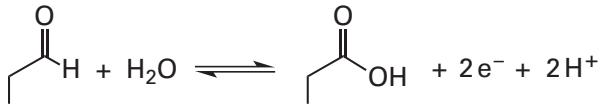

(2–324)

These examples illustrate the fact that these enzymes containing molybdenum ions coordinated by one or two molybdopterins are able to transfer an oxo group or hydroxy group to or remove an oxo group or a hydroxy group from an atom of sulfur, nitrogen, arsenic, or carbon. In the case of carbon, a hydrogen on the carbon is usually replaced by a hydroxy group or, in reverse, a hydroxy group is replaced by a hydrogen. These reactions at carbon, however, should be distinguished from the hydroxylations catalyzed by prosthetic groups such as oxoiron(IV) porphyrin$^{\bullet+}$ because the carbons hydroxylated are not aliphatic carbons.

In the crystallographic molecular model of the enzymatically active[2156,2165,2166] oxidized form of respiratory dimethylsulfoxide reductase from *R. sphaeroides*, the hexacoordinate molybdenum ion in the oxomolybdenum(VI) bismolybdopterin is **coordinated by the four sulfido groups from the two molybdopterins** and the oxido group of a serine in addition to an oxo group (Figure 2–60). In the oxomolybdenum(VI) bismolybdopterin in the enzyme, the molybdenum ion is stable in the **Mo^{+6} oxidation state** because at this level of oxidation it is isoelectronic with the noble gas krypton. The ion, however, because of its large positive charge number, must be coordinated by several ligands of nominally negative charge number, such as oxide ions and sulfido groups. Again, the degree of covalency between these ligands and the metallic ion is left to the preferences of the reader.

The first step in the enzymatic reaction of respiratory dimethylsulfoxide reductase in the direction of reduction is the **reduction of the oxomolybdenum(VI) bismolybdopterin to aquomolybdenum(IV) bismolybdopterin.** The oxomolybdenum(VI) bismolybdopterin in the active site of respiratory dimethylsulfoxide reductase from *E. coli*, which is embedded in the plasma membrane of the bacterium, is reduced by two successive electrons from two of the four prosthetic [4Fe–4S] iron–sulfur clusters situated in the enzyme.[2167] These [4Fe–4S] iron–sulfur clusters are in turn reduced by two molecules of menaquinol dissolved in the membrane that associate one after the other with the enzyme. The oxomolybdenum(VI) bismolybdopterin in the

active site of the soluble, cytoplasmic respiratory dimethylsulfoxide reductase from *R. sphaeroides* contains no prosthetic groups that transfer electrons, but it is reduced by two successive electrons[2168] from the reduced form of a single molecule of pentaheme cytochrome *c* that associates with the enzyme,[2169] so there are two electrons available at the same time to the oxomolybdenum(VI) bismolybdopterin in the reduced hemes of the cytochrome *c*. During the reduction, because the electrons are transferred from the [4Fe–4S] iron–sulfur clusters or the cytochrome one at a time, an intermediate oxomolybdenum(V) bismolybdopterin can be observed. For the enzyme from *R. sphaeroides*, the biochemical standard reduction potential for the redox couple of oxomolybdenum(VI) bismolybdopterin and oxomolybdenum(V) bismolybdopterin is +200 mV, and that for the redox couple of oxomolybdenum(V) bismolybdopterin and oxomolybdenum(IV) bismolybdopterin is +140 mV, which is appropriate for the biochemical standard reduction potential (+160 mV) for the redox couple dimethyl sulfoxide and dimethyl sulfide. The successive biochemical standard reduction potentials, however, for the enzyme from *E. coli* are –15 mV and –174 mV.[2170,2171]

In the respiratory dimethylsulfoxide reductase from *R. sphaeroides*, the molecule of water in the aquomolybdenum(IV) bismolybdopterin that was the oxo group is replaced by the oxygen of the dimethyl sulfoxide. In the next step, dimethyl sulfide dissociates, completing **transfer of the oxygen to the molybdenum ion**

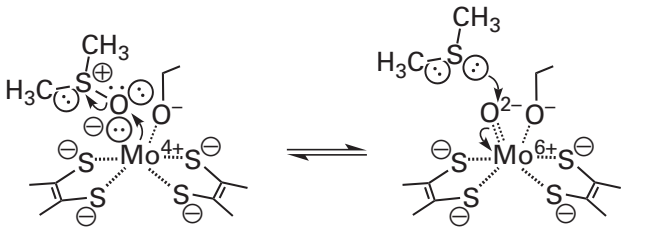

(2–325)

and in the process reoxidizing it from Mo^{4+} to Mo^{6+}. In a sense, the Mo^{4+} provides a nucleophilic pair of electrons that nucleophilically adds to the electrophilic oxygen of the dimethyl sulfoxide, and dimethyl sulfide is the leaving group in an associative nucleophilic substitution. The oxygen of the dimethyl sulfoxide becomes the oxygen of the now-regenerated oxomolybdenum(VI) bismolybdopterin.[2172]

The dissociation of dimethyl sulfide from the oxomolybdenum(VI) bismolybdopterin (Equation 2–325) in the enzyme from from *R. sphaeroides* is reversible (K_d = 120 μM), and if high concentrations of dimethyl sulfide are present, dimethyl sulfoxide bound to molybdenum(IV) bismolybdopterin becomes the dominant species of the enzyme,[2168,2173] inhibiting catalysis.

A **synthetic complex** of a molybdenum ion coordinated by two molecules of bis-(4-*tert*-butylphenyl)-2-pyridylmethanethiolate, which together provide two sulfido groups and two pyridinium nitrogens as ligands to the metallic ion, has in addition two identical oxo groups (molybdenum–oxygen bond lengths of 0.1696 nm) on the oxidized Mo^{+6} and one oxo group (bond length of 0.1681 nm) on its reduced Mo^{+4}. The reduced form of this synthetic complex can be transformed into the oxidized form by transfer of an oxygen atom from dimethyl sulfoxide or trimethylamine *N*-oxide to the molybdenum in reactions producing dimethyl sulfide or trimethylamine, respectively. Another synthetic complex of a molybdenum ion coordinated by a phenolate and two 2,3-disulfanylbut-2-enes, which mimics structurally the more elaborate complex of molybdenum, two molybdopterins, and a serine[2174] in respiratory dimethylsulfoxide reductase, is also able to reduce dimethyl sulfoxide to dimethyl sulfide[2175] and trimethylamine *N*-oxide to trimethylamine (Equation 2–319),[2176] but at much slower rates than the reductions catalyzed by the enzymes. In this nonenzymatic reaction, an intermediate complex between molybdenum(IV) and the oxygen of the sulfoxide (Equation 2–325) forms before the bond between sulfur and oxygen in the sulfoxide dissociates,[2177] just as it does in the enzymes. Neither of these synthetic complexes, however, can perform the reductions catalytically; the reactions that they catalyze are merely stoichiometric. There is, however, a synthetic complex of a molybdenum ion coordinated with two molecules of 2,2-diphenyl-2-sulfanylacetate, each of which coordinates the metallic ion with its sulfido group and its carboxylato group, that is able to catalyze the dehydration of nitrobenzene ($C_6H_5NO_2$) to nitrosobenzene (C_6H_5NO) and water using benzenethiol as a reducing agent.[2178]

Both trimethylamine-*N*-oxide reductases (Equation 2–316) and bacterial nitrate reductases (quinone) (Equation 2–319) share a common ancestor with respiratory dimethylsulfoxide reductases[2179] and presumably proceed by the same mechanism. In fact, in some organisms the same protein cata-

lyzes the activities of both respiratory dimethylsulfoxide reductase and trimethylamine-*N*-oxide reductase. Bacterial nitrate reductases (quinone), however, have variations on the coordination found in respiratory dimethylsulfoxide reductase. The oxidized form of nitrate reductase (quinone) from *E. coli* has, as usual, an oxomolybdenum(VI) bismolybdopterin, but it uses the carboxylate of an aspartate rather than the alkoxide of a serine as the sixth ligand to the oxomolybdenum(VI) bismolybdopterin.[883] Otherwise, reduction of nitrate ion, NO_3^- (**2–112**), to nitrite ion, ONO^- (**2–113**), proceeds as does the reduction of dimethyl sulfoxide by respiratory dimethylsulfoxide reductase. One of the oxygens in the nitrate ion exchanges with the molecule of water on the reduced aquomolybdenum(IV) bismolybdopterin, and the nitrite ion leaves to give the oxomolybdenum(VI) bismolybdopterin, which is then reduced by two electrons back to aquomolybdenum(IV) bismolybdopterin. The two necessary electrons are provided by a quinol acting as an electron-transferring coenzyme.

The resting oxidized forms of the nitrate reductases (quinone) from *D. desulfuricans* and *C. necator*, however, have a molybdenum(VI) bismolybdopterin, but they have thioxo groups instead of oxo groups and the serines have been replaced by cysteines.[2180,2181] Upon addition of nitrate, the sulfido group of the cysteine adds to the electrophilic thioxo group in a nucleophilic addition with molybdenum(IV) bismolybdopterin as a leaving group. The nucleophilic addition turns the sulfanyl group of the cysteine into a dithio group and coincidentally reduces the molybdenum(VI) bismolybdopterin to molybdenum(IV) bismolybdopterin. The site on molybdenum(IV) bismolybdopterin that was formerly occupied by the thioxo group is now open for the nitrate, and the resulting anionic dithio group of the modified cysteine, as a monodentate ligand, occupies the site on molybdenum(IV) bismolybdopterin formerly occupied by the sulfido group of the cysteine. The reduction of nitrate then proceeds, as does the reduction of dimethyl sulfoxide (Equation 2–325) and the reduction of the nitrate in the active site of nitrate reductase (quinone) from *E. coli*, with an oxomolybdenum(VI) bismolybdopterin intermediate alternating with an aquomolybdenum(IV) bismolybdopterin intermediate while the dithio group remains unchanged as a ligand to the molybdenum now uninvolved in the reduction of nitrate,[2182-2184] just as the oxido group of the serine remains uninvolved in the reduction of dimethyl sulfoxide. The nitrate reductases (quinone) from *D. desulfuricans* and *C. necator* obtain the necessary electrons from a cytochrome *c* that acts as an electron-transferring coenzyme.

In sulfite oxidase (Equation 2–321) from *G. gallus*, the molybdenum ion in the oxomolybdenum(VI) is pentacoordinate. It is **coordinated by only one molybdopterin**, and the remainder of the coordination of Mo^{6+} is completed by the sulfido group of a cysteine, a hydroxide, and an oxo group.[2151] Both in sulfite oxidase from *G. gallus* and in a synthetic model of its prosthetic group,[2185] the distribution of the ligands around the molybdenum is **square pyramidyl**, with the oxo group at the apex of the pyramid and the two sulfido groups of the molybdopterin, the sulfido group of the cysteine, and the hydroxide at the four equatorial positions at the base of the pyramid.

In sulfite oxidase from *G. gallus*, the **equatorial hydroxy group is the electrophile** (Equation 2–326),[2151,2186] not the apical oxo group as in respiratory dimethylsulfoxide reductase from *R. sphaeroides*. The oxomolybdenum(VI) bismolybdopterin in the active site of respiratory dimethylsulfoxide reductase from *R. sphaeroides* is electrophilic at its oxo oxygen, and the dimethyl sulfoxide is a nucleophile that adds to this electrophile (reverse of Equation 2–325). In sulfite oxidase (Equation 2–321) from *G. gallus*,[2151] in the direction of reduction, the oxygen of the sulfate exchanges with the equatorial hydroxy group (molybdenum–oxygen bond of 0.22 nm) in the oxohydroxymolybdenum(IV) molybdopterin rather than the oxo group (molybdenum–oxygen bonds of 0.17 nm). Consequently, in the reverse reaction, the sulfite must add to a hydroxymolybdenum(VI) molybdopterin rather than an oxomolybdenum(VI) molybdopterin

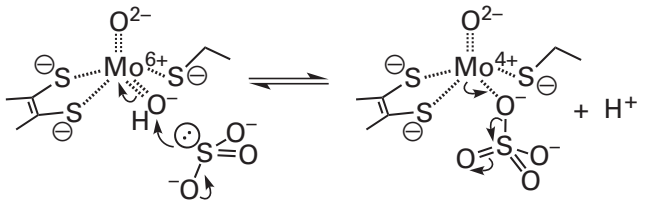

(2–326)

which seems counterintuitive.

Sulfite is definitely a nucleophile. In the addition to hydroxymolybdenum(VI) molybdopterin, as in the addition of a nucleophile such as methyl sulfide to a carbonyl carbon (previously**1–17**)

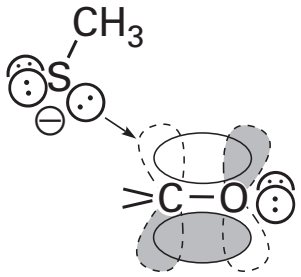

2–149

the σ lone pair of electrons on the sulfur in sulfite adds to the lowest unoccupied molecular orbital of the π molecular orbital system of the electrophile, in this case hydroxyoxomolybdenum(VI) molybdopterin. The main difference is that in a carbonyl group the more electronegative atom is the oxygen, and in a hydroxyoxomolybdenum(VI) molybdopterin it is the Mo^{6+}. It also turns out that, at least in the case of sulfite oxidase, the **lowest unoccupied π molecular orbital**, spread over the complete oxohydroxymolybdenum(VI) molybdopterin, is much more extensive over the hydroxy group than over the oxo group.[2186] Consequently, it seems to make sense that the enzyme has directed the nucleophile toward this oxygen, in addition to the fact that it is far easier for the sulfate to exchange with a hydroxide on hydroxyoxomolybdenum(VI) than an oxo group.

Following the addition of sulfite ion to the hydroxy group of the oxohydroxymolybdenum(VI) molybdopterin in sulfite oxidase from *A. thaliana* (Equation 2–326), the sulfate remains coordinated to oxomolybdenum(IV) molybdopterin for a while and can be trapped on the molybdenum by oxidizing it to oxomolybdenum(V) molybdopterin,[2187] which exchanges anions more slowly because of its higher positive charge.

Following dissociation of sulfate from the usual oxomolybdenum(IV) molybdopterin and its replacement by a molecule of water, **oxoaquomolybdenum(IV) molybdopterin is oxidized back to oxohydroxymolybdenum(VI) molybdopterin**. In sulfite oxidase from *A. thaliana*, two molecules of oxygen remove one electron at a time from the molybdenum ion as they are reduced to two superoxide radical anions, which then disproportionate, while in sulfite oxidase from *G. gallus*, in spite of its name, hemes in the enzyme shuttle electrons to and from cytochrome *c*.[2188]

In respiratory dimethylsulfoxide reductase, the oxomolybdenum(VI) bismolybdopterin produced by reduction of dimethyl sulfoxide (Equation 2–325) is rereduced by the addition of two electrons, and the oxygen of the resulting hydroxy group, which was the oxygen of the dimethyl sulfoxide, is hydronated and dissociates as a molecule of water,[2189] the other product of the reaction. In sulfite oxidase, aquooxomolybdenum(IV) molybdopterin, which forms upon the exchange of sulfate (Equation 2–326) with the molecule of water that is the other reactant in the oxidation of sulfite (Equation 2–321), is oxidized by the removal of two electrons with the concomitant dehydronation of the molecule of water to give a hydroxy group on Mo^{6+}. The equatorial hydroxy group of the resulting dioxohydroxymolybdenum(VI) molybdopterin, which was the molecule of water, becomes the oxygen in the next sulfate (Equation 2–326).

Xanthine dehydrogenase (Equation 2–323) is altered by oxidation upon purification and becomes a xanthine oxidase, but the enzyme in the cytoplasm, which has a reducing environment, is xanthine dehydrogenase.[2190] The alteration of the dehydrogenase to the oxidase can also be accomplished by digestion of the enzyme with endopeptidases.[2150] The two electrons removed from xanthine during its oxidation to urate at the prosthetic molybdenum ion in the active site pass one at a time through two [2Fe–2S] iron–sulfur clusters to a flavin adenine dinucleotide.[2191] In the unmodified enzyme in cytoplasm, the electrons are conjoined by the flavin and passed to NAD^+. In the enzyme after it is oxidized adventitiously during purification or altered by digestion, the flavin passes the two electrons to molecular oxygen in the usual way (Equations 2–207 and 2–208).

In the active site of bovine xanthine dehydrogenase, as in sulfite oxidase from *G. gallus* (Equation 2–326), the prosthetic molybdenum ion is coordinated by only one molybdopterin[2150]

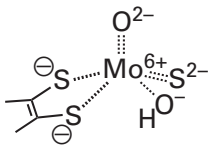

2–150

The ligands are again arrayed roughly at the vertices of a square pyramid (Figure 2–61).[2192-2194] The equatorial sulfido group of the cysteine in sulfite oxidase is replaced by an **equatorial thioxo group** in the fully oxidized enzyme. In this oxohydroxythioxomolybdenum(VI) molybdopterin, the length of the bond between the molybdenum and the sulfur identifies it as a formal double bond and identifies the sulfur as a thioxo group (**2–150**).[2195] An oxo group

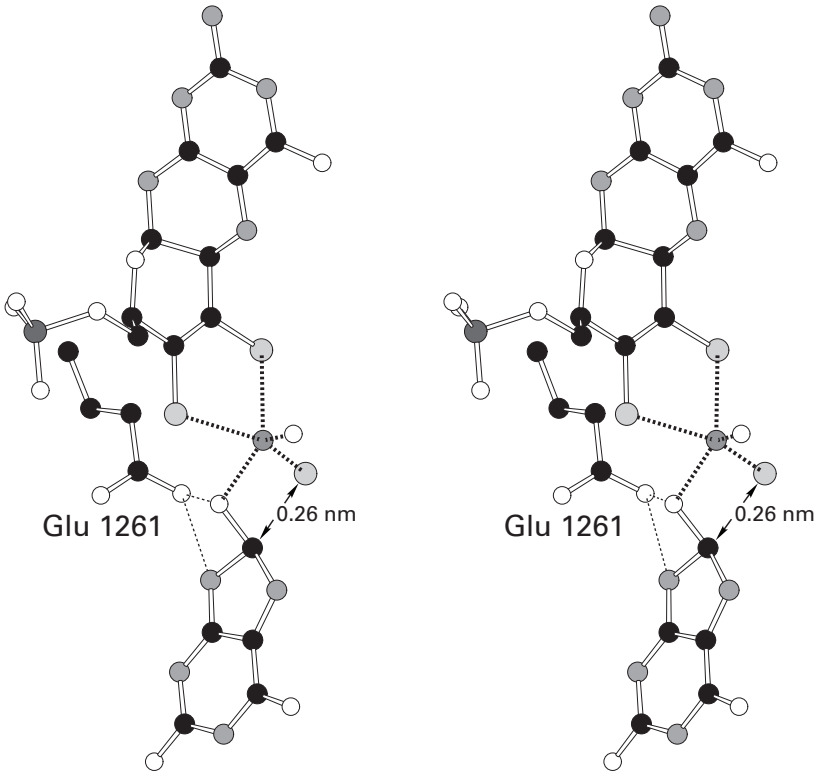

Figure 2–61: Stereodrawing[50] from the crystallographic molecular model of bovine xanthine dehydrogenase complexed with urate.[2194] Black atoms are carbons, white atoms are oxygens, and gray atoms are nitrogens. A crystal of bovine xanthine dehydrogenase was soaked in a large excess of NADH under strictly anaerobic conditions in order to reduce both flavin and the iron–sulfur clusters in the protein and to block any electron transfer from the molybdenum ion. Then the molybdenum ions in the crystal were fully reduced by soaking the crystal in 4 mM titanium citrate. The resulting crystal of fully reduced enzyme was then soaked in 250 μM urate. The molybdenum ion is the dark gray sphere in the right-center of the drawing surrounded by its ligands: the two sulfanyl groups of one molybdopterin (upper portion of the drawing), an oxo group (to the right of the molybdenum ion), the oxygen on carbon 2 of the urate (Equation 2–323), and a hydrosulfide (large light gray sphere to the lower right of the molybdenum). One of the oxygens of the carboxy group of Glutamate 1261 is equidistant (0.29 nm) from nitrogen 1 and the oxygen on carbon 2 of the urate. Carbon 2 of the urate is essentially tetrahedral. The place in the tetrahedron that would be occupied by a hydrogen points directly to the hydrosulfide, and carbon 2 is only 0.26 nm away from the sulfur.

again occupies the apical position, and a hydroxy group occupies one of the equatorial positions (oxygen–molybdenum bond lengths of 0.17 and 0.20 nm, respectively).[2195,2196]

The first transfer of an electron from the molybdenum ion takes the Mo^{4+} to Mo^{5+}, which can be monitored because it is paramagnetic,[2197] and the next transfer of an electron takes the Mo^{5+} to Mo^{6+}. In the active site of bovine xanthine oxidase these steps have biochemical standard reduction potentials of −410 and −380 mV, respectively.[2198] The **ability of molybdenum to assume the Mo^{+5} oxidation state**[2197] and flavin to form the semiquinone permits these transfers of single electrons through the iron–sulfur clusters connecting them.

In the crystallographic molecular model of the complex that forms between urate and the fully reduced prosthetic group in the active site of bovine xanthine dehydrogenase (Figure 2–61), the equatorial position occupied by the hydroxy group in the fully oxidized enzyme is occupied by the oxygen that is removed from urate during its reduction (reverse of Equation 2–323). Consequently, during the oxidation of xanthine, the **oxygen of the equatorial hydroxy group must be transferred to the xanthine** to become the oxygen of the urate, just as the equatorial hydroxy group in sulfite oxidase becomes the oxygen of the sulfate (Equation 2–326).

The **oxygen atom can be followed** over short intervals of time from a molecule of water in the solution to the hydroxy group on the molybdenum ion and then to the ureylene group in the urate by monitoring oxygen-18 by mass spectrometry and by following the effects of oxygen-17 on the electron paramagnetic spectrum of the molybdenum ion in oxohydroxythioxomolybdenum(V) in the active site of bovine xanthine oxidase.[2199-2202] These observations demonstrate that a molecule of water first occupies the open site on oxothioxomolybdenum(IV) molybdopterin; then becomes, upon the removal of two electrons through the iron–sulfur clusters to the flavin, the equatorial hydroxy group on oxohydroxythioxomolybdenum(VI) molybdopterin; and is then transferred to carbon 8 of the xanthine.

The equatorial hydroxy group in the fully oxidized oxohydroxythioxomolybdenum(VI) molybdopterin (**2–150**) of bovine xanthine oxidase has a pK_a somewhere above 8.5,[2195] but that of the equatorial thioxo group is much lower, as would be expected of a thioxo group in an environment identical to that of the hydroxy group, because sulfur is a less electronegative element than oxygen. Upon dehydronation of the hydroxy group by a glutamate in the active site (Figure 2–61) that acts as a catalytic base, the resulting **equatorial oxide adds nucleophilically** to carbon 8 of the xanthine,[2164,2193,2202] which is the carbon hydroxylated in the course of the enzymatic reaction

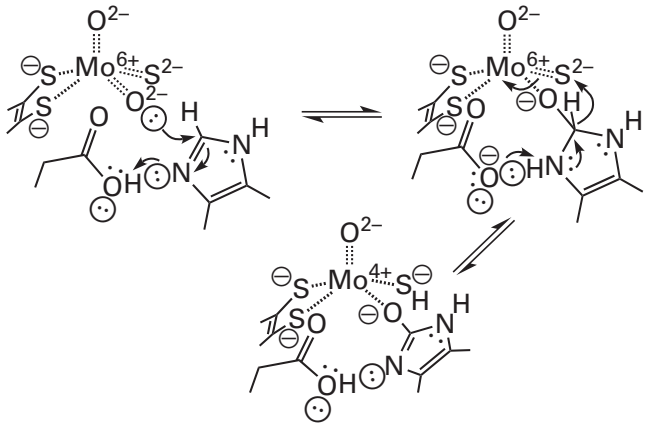

(2–327)

In two crystallographic molecular models, one of the complex between xanthine and bovine xanthine oxidase in which the thioxo group has been replaced by an oxo group[2203] and one of the complex between hypoxanthine and unadulterated bovine xanthine oxidase,[2204] carbon 8 of the xanthine and carbon 8 of the hypoxanthine, respectively, are in each case the closest atom (0.27 and 0.28 nm) and well within van der Waals contact (0.32 nm) with the equatorial hydroxy group that should be the nucleophile in the initial addition, and in each case this equatorial hydroxy group is the closest atom to carbon 8.

The now hydronated carboxy group of the glutamate **hydronates the nitrogen** of the xanthine (Equation 2–327), thereby increasing the electrophilicity of its aromatic ring and susceptibility to the nucleophilic aromatic addition of the oxide. In the crystallographic molecular model of the complex in the active site of bovine xanthine dehydrogenase (Figure 2–61)[2194] between the fully reduced enzyme and urate, one of the oxygens of this glutamate, Glutamate 1261, is equidistant (0.285 nm) from both the oxygen that was the hydroxy group on the molybdenum ion and nitrogen 1 of the urate.

A crystallographic molecular model of fully oxidized bovine xanthine oxidase has been obtained from crystals soaked in a solution containing 2-hydroxy-6-methylpurine, a slow substrate for the enzyme.[2205] In this molecular model, there is a bond (0.16 nm) between the oxygen of the equatorial hydroxy group of the oxohydroxythioxomolybdenum(VI) molybdopterin and carbon 8 of the

2-hydroxy-6-methylpurine, indicating that the hydroxy group has added nucleophilically to carbon 8 in the imidazolyl ring of the substrate (Equation 2–327). In the crystallographic molecular model of the complex between the conjugate base of urate and the fully reduced oxosulfidomolybdenum(IV) in the active site of bovine xanthine dehydrogenase (Figure 2–61),[2194] an almost identical complex is also observed with the oxygen on carbon 8 of the urate as a ligand to the molybdenum ion at the same location as that occupied by the hydroxy group in the unoccupied oxidized enzyme. Consequently, this particular complex can be formed between the oxidized enzyme and a reduced substrate and between the reduced enzyme and an oxidized substrate, a fact demonstrating that it represents a **central intermediate in the enzymatic reaction**.

In the crystallographic molecular model of the complex between the conjugate base of urate and the fully reduced oxosulfidomolybdenum(IV) molybdopterin, the length of the bond between the oxygen and the molybdenum ion is 0.22 nm, the usual length between a hydroxide and molybdenum. The length of the bond between the oxygen and the carbon is 0.14 nm, the usual length of a single carbon–oxygen bond, and the bond angle between these two bonds is 116°. Both the bond lengths and the bond angle are consistent with a simple **complex between a molybdenum ion and an alkoxy group** participating in a single bond with a carbon. The lengths of the bond between the molybdenum and the sulfur in this complex and the one in the complex between the oxidized enzyme and another slow unnatural substrate, 4-[5-pyri-din-4-yl-1*H*-[1,2,4]triazol-3-yl]pyridine-2-carbonitrile, are both 0.23 nm, a bond length consistent with coordination between a hydrosulfide ion and a molybdenum ion rather than a thioxo group.

The next step in the enzymatic reaction (second step in Equation 2–327) is **transfer of a hydride** from carbon 8 of the tetrahedral intermediate to the thioxo group on the molybdenum. In the crystallographic molecular model of the reduced enzyme and urate, carbon 2 of the urate has become essentially tetrahedral, and the position in the tetrahedron that would be occupied by a hydrogen is pointed directly at the sulfur (Figure 2–61) of what is apparently a hydrosulfide, based on the length of its bond to the molybdenum ion. The distance between this carbon and the sulfur is 0.26 nm, a distance significantly less than the sum (0.29 nm) of a carbon–hydrogen bond length (0.11 nm) and the van der Waals radius for sulfur (0.18 nm). This short distance and the orientation implies that there is an intimate association between this carbon and the sulfur. It is almost as if this complex is halfway between that in which the hydride has been removed by the thioxo group, which becomes a hydrosulfide as a result, and that in which the hydride is still on carbon 2 and the sulfur of the thioxo group has not yet removed it. This consideration implies that in the active site in the crystal there is an equilibrium between the two locations for the hydrogen atom, on sulfur and on carbon. In any case, the crystallographic structure is completely consistent with the participation of this transfer of the hydride in the enzymatic reaction, and in effect, the molecular model portrays the transfer of the hydride. When the protium on carbon 8 of the xanthine is replaced by a tritium, the enzymatic reaction decreases by a factor of 3.5, a fact demonstrating that transfer of the hydride is a slow and therefore difficult step in the reaction.[2206]

The crystallographic molecular model of the complex between the oxidized prosthetic group in the active site of bovine xanthine dehydrogenase and the slow unnatural substrate 4-[5-pyridin-4-yl-1*H*-[1,2,4]triazol-3-yl]pyridine-2-carbonitrile[2193] also manifests the features of this central intermediate in Equation 2–327. The reaction in the active site with this unnatural substrate proceeds to the step at which the bond between oxygen and carbon is formed (first step in Equation 2–327) but continues further only very slowly. Again, the carbon that has been attacked nucleophilically by the oxygen on the molybdenum is not planar as it will be in the product but slightly puckered, with the apex of its pucker again pointing toward the sulfur, which is only 0.35 nm from the carbon. The overall structure of the complex with the inhibitor in the crystallographic molecular model suggests again that the following equilibrium has been established in the active site

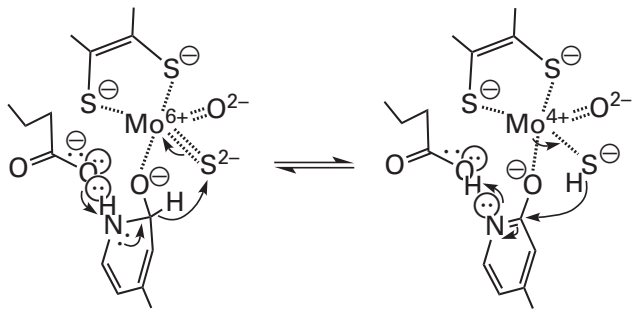

(2–328)

A **thioxo group on an oxothioxomolybdenum(VI) molybdopterin is electrophilic before the hydride is transferred** because it is the equivalent of the oxo group in an oxomolybdenum(VI) molybdopterin (Equation 2–326).[2195] In the active site of aldehyde dehydrogenase (FAD-independent) (Equation 2–324), an enzyme that shares a common ancestor with xanthine dehydrogenase,[2153] the basic equatorial oxide on its dioxothioxomolybdenum(VI) molybdopterin, also formed by dehydronation of the equatorial hydroxy group, adds nucleophilically to the electrophilic carbonyl carbon of an aldehyde, and the hydrogen of the aldehyde is transferred as a hydride to the thioxo group on its Mo^{6+}. The oxo oxygen of an oxomolybdenum(VI) bismolybdopterin in ethylbenzene dehydrogenase is also able to remove a hydride from a benzylic carbon to produce a benzylcarbenium ion,[2207] so there is nothing special about a thioxo group in this regard. In the active sites of the formate dehydrogenases from *E. coli*,[2208] *C. necator*,[2209] and *D. desulfuricans*,[2210] the thioxo group on the prosthetic thioxomolybdenum(VI) dimolybdopterin also accepts a hydride from a formate either bound noncovalently in the active site, immediately adjacent to the thioxo group, or coordinated to the molybdenum ion by its carboxylato group.

In the normal enzymatic reaction catalyzed by xanthine dehydrogenase (Equation 2–327), as well as the reaction with the unnatural substrate (Equation 2–328), even though neither of the final products is significantly aromatic in the respective locations, transfer of the formal equivalent of a hydride from carbon to the electrophilic thioxo group is driven by **restoration of the aromaticity** of the 2-oxidopyridyl group or of the 2-oxidoimidazolyl group in the conjugate base of the urate, respectively. In addition, the hydride is pushed off the carbon by the lone pairs of electrons on the three heteroatoms or the two heteroatoms, respectively, of the tetrahedral intermediate. Following this transfer of a hydride, the conjugate base of urate, the product of the reaction catalyzed by xanthine dehydrogenase and xanthine oxidase, ends up as a ligand to the Mo^{4+} and exchanges with a molecule of water to complete the cycle.

One of the more peculiar aspects of a hydroxymolybdenum(VI) molybdopterin, which is illustrated by the dramatic difference between its use in sulfite oxidase (Equation 2–326) and its use in xanthine dehydrogenase (Equation 2–327), is that in the former case it is used as an electrophile and in the latter case it is used as a nucleophile. One might argue that the difference is in its hydronation or dehydronation, but more likely it is whether the reactant is a nucleophile or an electrophile that determines its eventual role in the reaction.

There are aerobic carbon monoxide dehydrogenases (Equation 2–320) that use a molybdenum ion coordinated by a single molybdopterin rather than a nickel ion (**2–143**). In aerobic carbon monoxide dehydrogenase from *Afipia carboxidovorans*, the molybdenum ion is coordinated in equatorial positions by the two sulfido groups of the sole molybdopterin and a hydroxy group and in the axial position by an oxo group. When the molybdenum ion is Mo^{6+}, the remaining equatorial position is occupied by a thioxo group (0.23 nm) that becomes a sulfido group (0.29 nm) when it is Mo^{4+}. This thioxo group or sulfido group is also a ligand[2162,2211] for a prosthetic Cu^{+}. The Cu^{+} is in turn coordinated by the sulfido group of a cysteine and the nitrogen of one of the amido groups in the backbone of the polypeptide. At the open site on Cu^{+} in both oxidized and reduced active sites, there is a molecule of water that forms a hydrogen bond with the equatorial hydroxy group on the molybdenum ion. The function of the Cu^{+} is believed to be the provision of an open site at which the carbon of the carbon monoxide can associate

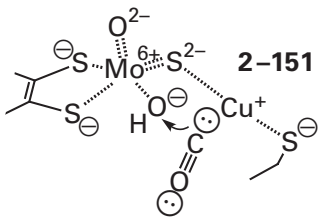

2–151

displacing this molecule of water. The distance between the Cu^{+} and the hydroxy group in the equatorial position on the Mo^{6+} is 0.34 nm, so the association of the carbon monoxide with the Cu^{+} would bring the carbon immediately adjacent to the hydroxy group on the molybdenum. Although there are several mechanisms that have been proposed to explain the remainder of the reaction,[2161,2211,2212] the simplest and the one most consistent with the usual mechanism of an active site containing a prosthetic molybdenum is one in which the carbon of the carbon monoxide, as a nucleophile, adds to the electrophilic hydroxide while the carboxylato group forming a hydrogen bond with the hydroxide removes the hydron. This nucleophilic addition would produce carbon dioxide directly, which would then dissociate from the cluster.[2213]

All the transition metallic ions of the fourth row from vanadium to zinc, with the possible exception of chromium, play enzymatic roles. Ironically, molybdenum, the transition metal below chromium, is the only one from the fifth row that does. It turns out that tungsten, the transition metal below molybdenum, is the only one in the sixth row that plays a role enzymatically, but almost exclusively as a congener of molybdenum. **Tungstoenzymes** contain one or two molybdopterins[2214-2216] that coordinate the respective tungsten ion in the same way that molybdenum is coordinated in molybdoenzymes,[2152] and the tungsten in these tungstoenzymes[2217] assumes the same oxidation states as molybdenum: W^{+4}, W^{+5}, and W^{+6}. In fact, when the molybdenum ion in respiratory dimethylsulfoxide reductase from *R. capsulatus* is replaced by a tungsten ion, the enzyme catalyzes the reduction of dimethyl sulfoxide even more rapidly.[2218] The tungsten ion in the active site of aldehyde ferredoxin oxidoreductase from *P. furiosus*, the surrounding side chains, and the site at which the substrates associate are superposable on those in the active site of the molybdoenzyme aldehyde ferredoxin oxidoreductase from *D. gigas*.[2219]

There are, however, tungstoenzymes that catalyze reactions that are unusual. In the active site of benzoyl-CoA reductase, a tungstoenzyme in *Geobacter metallireducens*, the reduced aquotungsten(IV) bismolybdopterin provides two electrons and perhaps a hydron to reduce the phenyl group in benzoyl-SCoA to a cyclohexa-1,5-dienyl group by the formal addition of two hydrogen atoms to carbon 3 and carbon 4 in a difficult reduction* that breaks the aromaticity of the phenyl ring.[2220,2221] In the active site of acetylene hydratase from *Pelobacter acetylenicus*, a tungsten ion coordinated by two molybdopterins and the sulfido group of a cysteine[2222] catalyzes the simple hydration of acetylene to acetaldehyde, a reaction that involves no formal oxidation or reduction.

It has been pointed out that, in the early anaerobic world, ionic tungsten was much more available to living organisms than ionic molybdenum.[2223] Consequently, the respective tungstoenzymes were probably the **ancestors of the present-day molybdoenzymes**. In *Methanothermobacter wolfeii* there are two formylmethanofuran dehydrogenases, one with a molybdenum ion in its active site and the other with a tungsten ion in its active site, that share a common ancestor but are only distantly related.[2224,2225] The enzyme containing a tungsten ion is constitutively active, but the enzyme containing molybdenum is only present when molybdenum ion is available in the environment. This fact and the fact that the tungsto version of respiratory dimethylsulfoxide reductase is more effective raise the question of why the tungstoenzymes became molybdoenzymes.[2223]

Nitrogenase catalyzes a reduction that converts molecular nitrogen to two ammonium ions (Figure 2–56). So far, the discussion has centered on reactions in which one or more oxygen atoms are participants. In the case of nitrogenase, there are no oxygen atoms involved as participants in the reduction performed by the prosthetic metallic ions.

Nitrogenase occurs in both aerobic bacteria and anaerobic bacteria, but the proteins catalyzing the reaction in each case are closely related and presumably all operate by the same mechanism. One of the two stoichiometric equations for the enzymatic reaction in the aerobic bacterium *A. vinelandii* is[2226,2227]

$$\begin{aligned} &8\ \text{reduced ferredoxin} + 16\ MgATP^{2-} + 16\ H_2O \\ &+ N_2 \rightleftharpoons H_2 + 2\ NH_4^+ + 6\ H^+ + \\ &8\ \text{oxidized ferredoxin} + 16\ MgADP^- + 16\ HOPO_3^{2-} \end{aligned} \qquad (2\text{–}329)$$

In the second stoichiometric reaction, the nitrogenase from *A. vinelandii* uses its indigenous flavodoxin rather than its indigenous ferredoxin as a source of the necessary electrons.[2228,2229] Nitrogenase is also able to reduce acetylene, the conjugate acid of carbide ($C{\equiv}C^{2-}$), to ethylene,[2230] a two-electron reduction, and hydrogen cyanide to methane and NH_4^+,[2231,2232] a six-electron reduction. The substrates in these two reductions are isoelectronic with N_2, and are presumably mistaken for it. Neither of these reductions, however, is as difficult as the reduction of N_2.

Two proteins together are responsible for reduction of N_2 to NH_4^+. They are dinitrogenase, the molybdenum–iron protein, in the active site of which the actual reduction

$$N_2 + 10\ H^+ + 8\ e^- \rightleftharpoons H_2 + 2\ NH_4^+ \qquad (2\text{–}330)$$

*In the Birch reduction, sodium metal is used as the reductant.

occurs and dinitrogenase reductase, the iron protein, that provides each of the electrons

$$\text{reduced ferredoxin} + 2\,\text{MgATP}^{2-} + 2\,H_2O \rightleftharpoons 2\,H^+ + e^- + \text{oxidized ferredoxin} + 2\,\text{MgADP}^- + 2\,HOPO_3^{2-} \quad (2\text{–}331)$$

required for the reduction of N_2. Dinitrogenase reductase is the electron-transferring coenzyme specific to dinitrogenase that in turn uses reduced ferredoxin as the source of the electron. No external reductant, regardless of its standard reduction potential, is able to substitute for dinitrogenase reductase in providing electrons to dinitrogenase for the reduction of N_2 nor is any other reductase or small electron-transferring coenzyme. The expression of nitrogenase activity requires both enzymes simultaneously, but they associate with and dissociate from each other at particular steps during the complete catalytic cycle.[2233]

Dinitrogenase, the molybdenum–iron protein, from *A. vinelandii* **contains a prosthetic [Mo–7Fe–9S–C] molybdenum–iron–sulfur–carbon cluster** that is responsible for the reduction of the N_2 to NH_4^+. This cluster has three local twofold rotational axes of pseudosymmetry, normal to a local threefold rotational axis of symmetry, and is also bilaterally pseudosymmetric (Figure 2–62).[2234] In the center of the cluster there is a mononuclear carbide ion (C^{4-}) that is surrounded by six iron ions.[2235-2237] This mononuclear carbide is derived from *S*-adenosyl-L-methionine[2238] and is a permanent feature of the cluster.[2239]

The bond angles and bond lengths in the central [6Fe–C] iron–carbon subcluster[2234] are almost identical to those in the [6Fe–C] iron–carbon subclusters found in cementite, an iron carbide (Fe_3C) in which each mononuclear carbide is coordinated by six iron ions and each iron ion is coordinated by two mononuclear carbides.[2240,2241] Cementite is a hard, brittle solid, and this property suggests that the [6Fe–C] iron–carbon subcluster might form a rigid central scaffold stabilizing the [Mo–7Fe–9S–C] cluster.[2242] This rigid scaffold allows the cluster to be unsupported by any cysteines over its entire length, unlike a normal iron–sulfur cluster.

The 322 (D_3) rotational symmetry of this central [6Fe–C] iron–carbon subcluster produces the rotational pseudosymmetry of the complete [Mo–7Fe–9S–C] cluster. The iron ion at one end of the cluster is coordinated by a cysteine from the protein, and the pseudosymmetrically related molybdenum at the other end is coordinated by the imidazolyl group of a histidine. In addition to the imidazolyl group and three of the sulfide dianions in the cluster, the remaining two octahedral positions around the molybdenum ion are occupied by one of the carboxylate oxygens and the central hydroxy oxygen of a molecule of homocitrate.

The mononuclear carbide must decrease the reduction potential of the cluster because as the iron ions are oxidized, a portion of the excess negative charge should shift from the carbon to the iron ions to compensate for their increase in charge number.[2243] In the resting state of the cluster, however, three of the iron ions—the one at the vertex and the two above the carboxylato group of the homocitrate that is a ligand to the molybdenum ion—are Fe^{2+} and the other four are Fe^{3+} (Figure 2–62),[2244] a ratio similar to the ratio of Fe^{2+} and Fe^{3+} in a typical [4Fe–4S] iron–sulfur cluster in which there is no mononuclear carbide. The molybdenum ion, however, is Mo^{3+}, a more reduced molybdenum ion than is usually found in the active sites of enzymes.[2245]

There is also a prosthetic **[8Fe–7S] iron–sulfur cluster** in dinitrogenase that has the following structure in the native, reduced enzyme

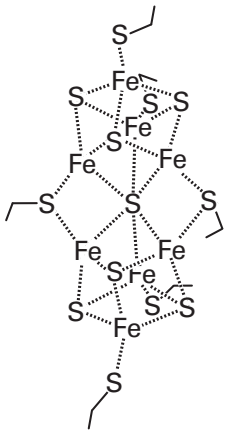

2–152

This [8Fe–7S] iron–sulfur cluster participates in transfer of each of the eight electrons between dinitrogenase reductase, the protein providing the electrons to dinitrogenase, and the [Mo–7Fe–9S–C] cluster at which the reduction of N_2 occurs. The closest iron ion in this cluster is 1.4 nm from the [Mo–7Fe–9S–C] cluster,[2246] so transfer of an electron from the one to the other is outer sphere through the protein itself.

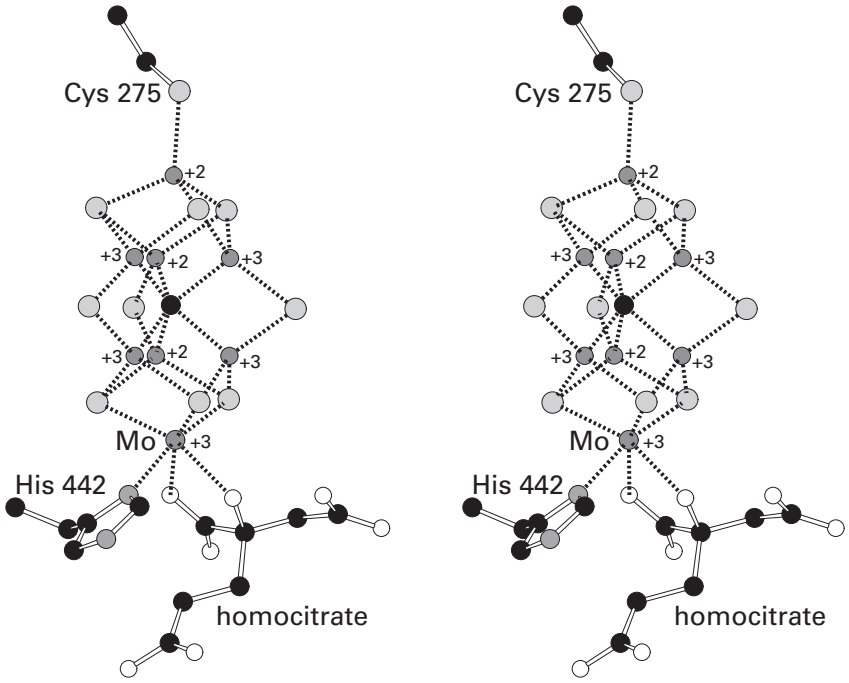

Figure 2–62: Stereodrawing[50] from the crystallographic molecular model of dinitrogenase, the molybdenum–iron protein of nitrogenase.[2234] Black atoms are carbons, white atoms are oxygens, and gray atoms are nitrogens. In the molybdenum–iron–sulfur–carbon cluster, large light gray spheres are sulfides, small dark gray spheres are iron ions, and the single molybdenum ion is labeled. The drawing includes the [Mo–7Fe–9S–C] molybdenum–iron–sulfur–carbon cluster in the active site as well as the sulfido group of Cysteine 275, coordinating one of the iron ions of the complex, and the imidazolyl group of Histidine 442, coordinating the molybdenum ion. A homocitrate completes the coordination of the molybdenum ion by providing one of its carboxylates and its central hydroxy group as ligands. The single carbon of the mononuclear carbide ion (C^{4-}) is the black sphere in the middle of the structure.

The resting, fully reduced [8Fe–7S] iron–sulfur cluster has the same disposition of iron ions as the [Mo–7Fe–9S–C] cluster with several exceptions. The molybdenum ion is replaced with an iron ion, and that iron is coordinated by a single cysteine rather than a histidine and a homocitrate. One of the central equatorial sulfide ions is missing, the other two are replaced by two sulfido groups from two cysteines, and the mononuclear carbide tetraion is replaced by a sulfide diion. The two iron ions that are not joined by the sulfido group of a cysteine (the two iron ions in the center rear of **2–152**), but are each coordinated by their own cysteines, move apart from each other, and as a result, one of the bonds from the central sulfide to one of these iron ions (the one in the lower rear) is abnormally long and, presumably, abnormally weak.

This [8Fe–7S] iron–sulfur cluster contains a standard [4Fe–4S] iron–sulfur subcluster (upper half of **2–152**). Depending on the oxidation state of the [8Fe–7S] iron–sulfur cluster, this standard [4Fe–4S] iron–sulfur subcluster is coupled through one of its sulfide dianions (the central sulfide in **2–152**) to three, two or one of the iron ions in a [4Fe–3S] iron–sulfur subcluster that forms the other half of the entire cluster (lower half of **2–152**).[647]

In the resting, reduced form of the [8Fe–7S] iron–sulfur cluster (**2–152**), the **sulfide dianion joins the two iron–sulfur subclusters** by acting as a ligand to six iron ions and as a result occupying simultaneously in two [4Fe–4S] iron–sulfur subclusters the respective positions normally occupied by one of their sulfides.[2247] The [8Fe–7S] iron–sulfur cluster **can be oxidized in two one-electron transfers** ($E^{\circ\prime}_1 = -310$ mV; $E^{\circ\prime}_2 = -270$ mV). In the cluster oxidized by the removal of one electron, the central sulfide has dissociated from the iron ion with which it was most loosely associated but remains associated with two of the iron ions in the [4Fe–3S] iron–sulfur subcluster, and in the cluster oxidized by the removal of two electrons, the sulfide is associated with only one of the iron ions in the [4Fe–3S] iron–sulfur subcluster.[647,2248] In the most oxidized, most dissociated state, in which the sulfide is associated with only one of the iron ions in the [4Fe–3S] iron–sulfur subcluster, the [4Fe–4S] iron–sulfur subcluster has the magnetic circular dichroic spectrum of a normal [4Fe–4S] iron–sulfur cluster.[2249] Neither of these oxidized forms of the [8Fe–7S] iron–sulfur cluster, however, participates in the reduction of N_2 to NH_4^+.

The reduced form of the cluster in the resting enzyme cannot be reduced further by any external reductant.[2250,2251] There is, however, no uncontroversial evidence that either of the observed oxidized states is involved in the normal transfer of the electron between dinitrogenase reductase and the [Mo–7Fe–9S–C] cluster that is mediated by this [8Fe–7S] iron–sulfur cluster. In fact, the biochemical standard reduction potentials associated with these two oxidations seem to be too positive to be involved in at least the first step in the reduction of N_2. It follows that there may be a further accessible reduced state, of significantly more negative reduction potential, that can only be accessed by dinitrogenase reductase, which is a most unusual reductant.

Dinitrogenase reductase, the iron protein, is a homodimeric protein that contains only one [4Fe–4S] iron–sulfur cluster.[2252,2253] This [4Fe–4S] iron–sulfur cluster is in the interface between the two subunits, bridges them, and is bisected by the twofold rotational axis of symmetry of the homodimer. Kinetic studies[2254,2255] and the results of site-directed mutation[2256] indicate that molecules of dinitrogenase reductase provide electrons from this [4Fe–4S] iron–sulfur cluster one at a time in the usual manner by associating with the dinitrogenase, transferring one electron, and then dissociating.[2233] The transfer of each electron from dinitrogenase reductase, however, is unusual because for every electron transferred, **two molecules of $MgATP^{2-}$ are hydrolyzed** by this electron-transferring coenzyme while it is associated with dinitrogenase.

Although no substitute for this coenzyme for the delivery of electrons to dinitrogenase during the reduction of N_2 has been discovered, Eu^{2+} coordinated by ethylenediaminetetraacetate ($E^{\circ\prime} = -1100$ mV) can provide the two electrons required for dinitrogenase from *A. vinelandii* to reduce hydrazine (**2–123**) to two NH_3 (**2–124**).[2257] It is also possible to deliver electrons photochemically to dinitrogenase from *A. vinelandii* in the absence of dinitrogenase reductase by attaching bis(2,2′-bipyridine)(phenanthroline)-ruthenium dication covalently to the enzyme. Upon illumination, with dithionite as the source of the electrons, this modified enzyme is able to photochemically reduce hydrogen cyanide to NH_4^+ and methane, a six-electron reduction.[2258] In both alternatives, all the complications of the reaction catalyzed by dinitrogenase reductase are avoided, but the most difficult step in the reduction of N_2, the addition of the first two electrons, can be accomplished at the moment only with electrons provided by dinitrogenase reductase.

The reduced form of dinitrogenase reductase binds two molecules of $MgATP^{2-}$, one on each of its identical subunits. The binding of the two $MgATP^{2-}$ to dinitrogenase reductase from *A. vinelandii* decreases the biochemical standard reduction potential of its [4Fe–4S] iron–sulfur cluster[2259] from –300 to –400 mV and alters the conformation of dinitrogenase reductase to permit its association with dinitrogenase.[2233,2260] This conformational change ensures that only dinitrogen reductases associated with two $MgATP^{2-}$ can associate with dinitrogenase. Upon the association of $(MgATP^{2-})_2$·dinitrogenase reductase with dinitrogenase, an electron is transferred from the [4Fe–4S] iron–sulfur cluster on dinitrogenase reductase (140 s^{-1} at 25 °C).[2233,2261] The [4Fe–4S] iron–sulfur cluster is thrust up against the surface of the dinitrogenase, and the electron passes through the [8Fe–7S] iron–sulfur cluster to the [Mo–7Fe–9S–C] cluster.[2253,2262] This transfer of the electron is followed immediately by hydrolysis (70 s^{-1} at 25 °C) of the two $MgATP^{2-}$ molecules to two $MgADP^{-}$ molecules and two phosphates,[2263] which induces a conformational change in the dinitrogenase reductase. This conformational change and the reduction of the now-oxidized [4Fe–4S] iron–sulfur cluster of dinitrogenase reductase from *A. vinelandii* by the flavodoxin[2228,2229,2264] that is one of its physiological reductants promote the dissociation of the complex between dinitrogenase and dinitrogenase reductase.[2233] The reduction of the [4Fe–4S] iron–sulfur cluster in dinitrogenase reductase also decreases the free energy of dissociation for the two molecules of $MgADP^{-}$ by –20 kJ mol^{-1}, which promotes their release and returns the system to the initial state.[2259]

This complex sequence of events, by coupling steps in the hydrolysis of $MgATP^{2-}$ to steps in transfer of the electron, is **a way to ensure that every time an electron is transferred from dinitrogenase reductase to dinitrogenase, two molecules of $MgATP^{2-}$ are hydrolyzed** and every time two molecules of $MgATP^{2-}$ are hydrolyzed by dinitrogenase reductase, an electron is transferred.[2265] This coupling has the effect of decreasing the biochemical standard reduction potential (–425 and –619 mV) of each electron delivered by the indigenous ferredoxin in *A. vinelandii*[2266,2267] by an additional –1100 mV, an amount equal to the free energy of hydrolysis (–100 kJ mol^{-1}) for two $MgATP^{2-}$ (Equation 2–331) at physiological concentrations of $MgATP^{2-}$, $MgADP^{-}$, and phosphate.[2268] This estimate of the decrease in the biochemical standard reduction potential provided by the hydrolysis of $MgATP^{2-}$ assumes that the system is at equilibrium. In the normal reduction of N_2, the system is not at equilibrium during turnover and the decreases in actual biochemical standard reduction potential may be less than these estimates.

In the benzoyl-CoA reductases from *A. evansii* and *T. aromatica*, there is a similar reductant the reduction potential of which is decreased by the hydrolysis of $MgATP^{2-}$ so that it is a strong enough reductant to break the aromaticity of benzoyl-SCoA during its conversion to cyclohexa-1,5-diene-1-carbonyl-SCoA.[2269]

When reductions are initiated by mixing dinitrogenase reductase and dinitrogenase from *K. pneumoniae* with $MgATP^{2-}$ in the presence of reductant and N_2 and quenched in acid at various times,[2270] the only products observed[2271] are H_2, hydrazine (N_2H_4), and NH_3 (Figure 2–56). By following the production of these three products as a function of time and the concentration of the reactants, N_2, $MgATP^{2-}$, and reductant, a kinetic mechanism could be formulated[2270] that is consistent with later observations. Consistent with this scheme, dinitrogenase reductase from *A. vinelandii* reduces the resting dinitrogenase from *A. vinelandii* in three **one-electron steps**, each involving the association and then the dissociation of a dinitrogenase reductase, before N_2 can associate with the [Mo–7Fe–9S–C] cluster, but N_2 can also associate after four electrons have been transferred.[2272-2275] Electron paramagnetic resonance and electron–nuclear double resonance spectra of dinitrogenase from *A. vinelandii* has identified two μ-hydrido groups, each of them between two of the iron ions, in this reduced form of the cluster.[2276-2280] The identity of the iron ions that participate is not known, but it is assumed that they are four of the iron ions that coordinate the mononuclear carbide on one of the faces of the triangular prism that surrounds it, that each hydride is bound by two adjacent iron ions, and that the two hydrides are forced to be immediately adjacent to each other by the hybridization around the iron ions.*

*Recall that the mononuclear carbide is well below the two hydrides in this diagram (see Figure 2–62).

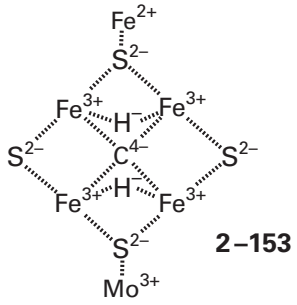

2–153

Calculations are consistent with this distribution of atoms.[2281] Because the four electrons have been added to two hydrons to produce the two μ-hydrido groups, the metals in the cluster remain at the oxidation state of the resting state,[2277] but they are not necessarily distributed as they are in the resting state. It is assumed,[2281] however, that the electrons are distributed so that the four iron ions to which the two hydrides are ligands are Fe^{3+}. In the absence of N_2, hydrons slowly associate with these μ-hydrido groups in a detrimental side reaction that continuously produces H_2, just as hydrons normally do in hydrogenase, and when the concentration of N_2 is not high enough, the ratio of H_2 to NH_3 in the products exceeds the stoichiometric equation (Equation 2–329) because of this side reaction.[2282-2285]

When N_2 binds to the [Mo–7Fe–9S–C] cluster, a molecule of H_2 is released from it, which is formed from the two μ-hydrido groups. The formation of a molecule of H_2 from two hydrides is a two-electron oxidation, so this reductive elimination has the effect of reducing the [Mo–7Fe–9S–C] cluster by two electrons, and this reduction is driven by formation of the bond between the two hydrides and dissociation of the H_2. This exchange of H_2 for N_2 is fully reversible,[2286] and the equilibrium constant is equal to 5 when the cluster has been reduced by three electrons and equal to 1 when the cluster has been reduced by four electrons.[2270] The rate constants for the steps in the overall reaction, however, are such that at high electron flux, the cluster reduced by four electrons is the predominant species with which N_2 associates.[2270,2285] At temperatures below 20 K it is possible to photolytically induce the dissociation of H_2 from the intermediate with the two μ-hydrido groups, and this hyperreduced cluster reassociates with the H_2 as the temperature is raised,[2287] a fact demonstrating that the dissociation of H_2 is also reversible in the absence of N_2.

The source of the two hydrons that become the two μ-hydrido groups, the hydrons that add to the two nitrogens in N_2 as it becomes N_2H_2, and the hydrons that eventually become the three hydrogens on the two NH_3 is unclear. There is a water channel from the solution into a location near the [Mo–7Fe–9S–C] cluster, but aside from the carboxy group on the homocitrate that is a ligand to the molybdenum ion, the acid–bases of the amino acid side chains in the vicinity of the [Mo–7Fe–9S–C] cluster are not conserved among the dinitrogenases from different species.[2288] In the different active sites, however, there is always a side chain in a location from which it could act as a donor in a hydrogen bond to N_2 after it associates with the cluster, an outcome that has been shown to weaken the triple bond in a molecule of N_2 that is a ligand to a metallic ion.[2289]

The [Mo–7Fe–9S–C] cluster that has been hyperreduced by the formation and dissociation of H_2 is a powerful enough reductant to reduce N_2 immediately by two electrons, which is the most difficult step in the reduction of N_2, without the need for any additional electrons. The product of the reduction of N_2 by two electrons and two hydrons is diazene, N_2H_2 (**2–122**). When the intermediate in the reaction with which the N_2H_2 is associated, however, is quenched with acid or base during the kinetic studies and the diazene is released into the solution, it rapidly disproportionates to N_2 (**2–121**) and hydrazine, N_2H_4 (**2–123**). This N_2H_4 is observed as one of the products in the kinetic studies, and it stands in for the diazene that is actually produced in the active site at this step.

Neither the hydronation state of the nitrogens at this level of reduction nor whether or not the nitrogen atoms are still covalently associated with each other, however, is known. There is a crystallographic molecular model of dinitrogenase from *A. vinelandii* in which molecules of either N_2 or N_2H_2, which cannot be distinguished crystallographically, are bound to the [Mo–7Fe–9S–C] cluster. In one asymmetric unit, however, each nitrogen atom in N_2 or N_2H_2 is a ligand to a different iron ion. In the other asymmetric unit, two molecules of N_2 or N_2H_2 are bound and in each case only one of the nitrogen atoms is a ligand to each of the two iron ions. Furthermore, the molecules are each bound to different iron ions in the respective active sites, so it is impossible to know which, if any, of these dispositions are relevant to the reduction of N_2. In each case, however, only one of the two nitrogen atoms is an acceptor in one or more hydrogen bonds from the protein surrounding the respective cluster.[2290]

Both **diazene, N_2H_2 (2–122)**,[2291] and **hydrazine, N_2H_4 (2–123)**,[2292] are substrates for the dinitrogenase, which, with the proper number of electrons, converts both into NH_4^+. Consequently, it is possible that the enzymatic reaction proceeds in three two-electron steps

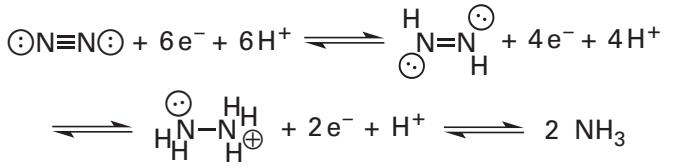

(2–332)

with N_2H_2 and N_2H_4 remaining tightly bound as ligands to one or more[2293] of the metallic ions in the [Mo–7Fe–9S–C] cluster. The bond order of the nitrogens at these oxidation states, however, is unknown. The kinetic mechanism has identified intermediate steps in the overall reduction[2270] and is consistent with the two NH_3 dissociating from the active site in different steps separated by two one-electron reductions,[2294] but this conclusion says nothing about when the two NH_3 are created in the active site. Several intermediate forms of nitrogen on the [Mo–7Fe–9S–C] cluster have been identified.[2272,2295] Single nitrogen atoms, unbonded to another nitrogen atom and reduced by the addition of either two or three hydrogen atoms, respectively, comprise two of the latter intermediates.[2296,2297] The precise structures of none of these intermediates, however, is known.[2295]

When the structure of the [Mo–7Fe–9S–C] cluster became available from crystallographic molecular models, it was not known that the central atom was a mononuclear carbide. At the time it was thought that the most unusual feature of the cluster in the active site of dinitrogenase was the molybdenum ion rather than the iron ions.[2298] This assumption led to an examination of **synthetic complexes of molybdenum ions** that were able to reduce N_2 to NH_3.[2299-2302] The recent discovery of a more reduced molybdenum ion in the [Mo–7Fe–9S–C] cluster than in any other enzymatic prosthetic group has reinvigorated some of the enthusiasm for the molybdenum ion to be involved directly in the reduction.[2245]

When it became known that the central ion was a mononuclear carbide, it also became obvious that the completely unprecedented feature of the [Mo–7Fe–9S–C] cluster was the [6Fe–3S–C] iron–sulfur–carbon subcluster at its core. In addition, the fact that there are nitrogenases that have [8Fe–9S–C] iron–sulfur–carbon clusters[2303] and [V–7Fe–9S–C] clusters rather than a [Mo–7Fe–9S–C] cluster[2304] belied the conclusion that the molybdenum ion plays a direct role in the reduction. For example, a nitrogenase that has a vanadium ion in place of the molybdenum ion[2242] has been purified from *Azotobacter chroococcum*.[2305] This vanadium nitrogenase is closely related to the molybdenum nitrogenase from *A. vinelandii* (31% identity; 1.7 gap percent), and the [V–7Fe–9S–C] cluster has an identical structure with the exception of the substitution of a vanadium ion for a molybdenum ion.[2306] In cells of *A. vinelandii*, three related (31% identity; 1.4 gap percent; 32% identity; 1.9 gap percent; and 54% identity; 0 gap percent) but definitely different dinitrogenases are present,[2307] one with a [Mo–7Fe–9S–C] cluster, one with an [8Fe–9S–C] cluster, and one with a [V–7Fe–9S–C] cluster in the respective active sites,[2308] and as expected, the mechanism by which the [8Fe–9S–C] cluster and the [V–7Fe–9S–C] cluster convert N_2 to NH_4^+ is the same as that of the [Mo–7Fe–9S–C] cluster.[2309] In cells of *R. capsulatus*, there is both an iron version and a molybdenum version of dinitrogenase.[2310] Further evidence that the molybdenum ion is not involved in the reduction of N_2 is that upon dissociation of H_2 from the [Mo–7Fe–9S–C] cluster in the active site of dinitrogenase from *A. vinelandii* as a result of the reductive elimination that leaves behind two electrons, the oxidation state of the Mo^{3+} is unchanged.[2280]

When it became clear that the iron ions in the core of the [Mo–7Fe–9S–C] cluster were in a [6Fe–3S–C] subcluster, synthetic complexes of iron ions were examined for their ability to reduce N_2 to NH_3. A synthetic complex between tri(2-diisopropylphosphinophenyl)borane and a single Fe^+ is able to catalyze the reduction of N_2 to NH_4^+ (as many as 7 equivalents of NH_4^+ from every iron ion) in diethyl ether at –70 °C, using as a reducing agent atomic potassium dispersed on graphite ($E^{\circ\prime} \geq -2900$ mV).[2311,2312] A mononuclear ion coordinated by three diisopropylphenylphosphines as equatorial ligands and either a triphenylsilane[2313] or a triphenylborane[2314] as the axial ligand, in which the iron is formally Fe^0, forms a complex with N_2 at the open site on the trigonal bipyramid. Upon addition of acid to either of these complexes,[2315,2316] the distal nitrogen becomes dihydronated, and the complex is now between a formally Fe^{4+} and $N_2H_2^{2-}$, the dianionic conjugate base of N_2H_4. The triphenylborane complex is able to convert N_2 into NH_3 catalytically,[2314] in a reduction in which, presumably, hydrazidoiron(IV) is an intermediate. The hydrazidoiron(IV), if reduced to

hydrazidoiron(III), would be the nitrogen analogue of hydroperoxyiron(III), the precursor of oxoiron(V). This analogy suggests that an azoiron(V) could be produced by hydronation of the distal nitrogen in a hydrazidoiron(III) and dissociation of NH_3 and that an azoiron(V) could be another intermediate in this reduction of N_2 to NH_3. Stable complexes containing azoiron(V) have been synthesized.[2317,2318]

The catalysis in the industrial **Haber–Bosch process** for converting N_2 to NH_4^+ occurs on surfaces of metallic iron in the catalyst.[2319] In this instance, the catalyst is produced from a dust of magnetite (Fe_2O_3) that has been partially reduced to form a layer of ferrous oxide surrounded by a layer of porous metallic iron. The first step in this surface catalysis is the chemisorption of a molecule of N_2 on a surface of the elemental iron. Following its association, the second step in the Haber–Bosch catalysis is the dissociation of nitrogen gas into individual nitrogen atoms spread over the metallic surface that are then reduced by H_2. The activation energy for the dissociation of N_2 by the surface is small, so the most difficult step is the chemisorption, after which the dissociation proceeds rapidly. These observations suggest that one step in the enzymatic reaction could be the initial dissociation of N_2 into two nitrogen atoms.

The biochemical standard reduction potential for the reduction catalyzed by dinitrogenase (Equation 2–330) is –310 mV,[2320] which appears to explain the fact that, in the absence of N_2 or at low electron flux,[2272,2273] the enzyme produces H_2 from two hydrons ($E^{\circ\prime} = -410$ mV). These rather normal standard reduction potentials, however, are misleading. Nonenzymatic electrochemical reductions of N_2 to NH_4^+ always requires voltages that are equal to or less than –1000 mV,[2321,2322] an overpotential necessitated by the fact that the first transfer of an electron to N_2 is significantly endergonic. Nonenzymatic reductions of N_2 to NH_4^+ by synthetic mononuclear molybdenum complexes require reductants with standard reduction potentials of around –1000 mV;[2299,2300] the nonenzymatic, catalytic reduction of N_2 to NH_4^+ by the synthetic mononuclear iron complex requires strong reductants such as potassium dispersed on graphite; and the standard reduction potential for converting N_2 to N_2H_4 is –750 mV. These observations explain why a rather strong reductant is needed in the enzymatic reaction.

The Haber–Bosch process and the reduction of N_2, both electrochemically and under catalysis by a mononuclear molybdenum ion or a mononuclear iron ion, in turn illustrate two of the most vexing problems with converting N_2 into NH_4^+. The first is the **difficulty in promoting the association of N_2 with the catalyst**. In the case of the metallic surfaces in a Haber–Bosch catalyst, only one in 10^6 to one in 10^8 collisions of N_2 with the surface results in successful chemisorption.[2319] How the active site of the enzyme solves this problem, if it does, is unknown. The second problem is the **high voltages needed to reduce N_2** because of the overpotential. This second problem has been solved by dinitrogenase reductase, which uses a stratagem to decrease dramatically the standard reduction potential of the electrons it delivers.[2254,2255,2260,2263]

In addition to the vanadium nitrogenases, there are chloride peroxidases

$$H_2O_2 + Cl^- + H^+ + RH \rightleftharpoons RCl + 2\,H_2O \qquad (2\text{–}333)$$

and bromide peroxidases that use vanadium as a mononuclear metallic ion in their active sites. The difference between a bromide peroxidase and a chloride peroxidase is that the former can only catalyze halogenations with the more nucleophilic bromide while the latter can catalyze halogenations with the less nucleophilic chloride as well as bromide. This difference suggests that the halides are acting as nucleophiles. Bromide peroxidase from *Ascophyllum nodosum* and chloride peroxidase from *Curvularia inaequalis* have superposable tertiary structures[2323] and, therefore, share a common ancestor. The carbon–hydrogen bonds that are converted into carbon–chlorine bonds or carbon–bromine bonds by the halogenations are at a wide array of aliphatic, alkenyl, and aryl positions in natural products.[2324-2326] The halogenations performed by bromide peroxidase from *A. nodosum* display a regiospecificity that differs from brominations that occur in solution. This fact requires that the substrates associate with the enzyme before they are brominated[2325] and that the brominations occur in the active site of the enzyme.

The first step in the enzymatic reaction is the **association of hydrogen peroxide** with the halogenase. Kinetic studies as a function of pH of the reactions catalyzed by bromide peroxidase from *A. nodosum*[2327] and chloride peroxidase from *C. inaequalis*[2328] are consistent with the conclusion that the hydroperoxy ion associates with the vanadium in the respective active sites. In the crystallographic

molecular model of the active site in chloride peroxidase from *C. inaequalis* with which a hydroperoxy ion has associated, the **hydroperoxy ion has become a ligand to the vanadium ion**[2329]

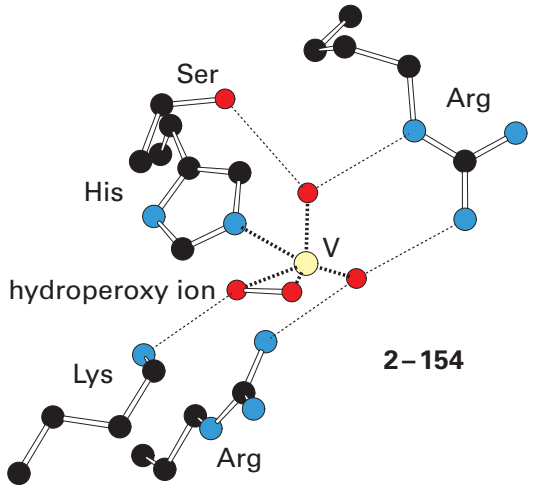

The hydroperoxy ion occupies two sites on the vanadium that are occupied by hydroxy groups in the unoccupied active site. That these two ligands in the unoccupied enzyme[2330] are hydroxy groups follows from the lengths of their vanadium–oxygen bonds: 0.195 and 0.169 nm.[2331] The lengths of the respective bonds to the two oxygens of the hydroperoxy group remain the same: 0.188 and 0.167 nm. The shorter bond is for the oxygen that forms a hydrogen bond to the ammonio group of the lysine. The oxygen that forms hydrogen bonds to the two arginines (the oxygen to the right in **2–154**) is also a hydroxy group (0.168 nm), and the oxygen that forms trigonal hydrogen bonds to the serine and the δ-imino group of the arginine (vertical bond in **2–154**) is an oxo group (0.154 nm). There is a strong interaction between the imidazolyl group of a histidine and the vanadium ion (0.20 nm) to complete the pentacoordination. The vanadium ion in the active site of bromide peroxidase from *A. nodosum* is also pentacoordinated, with the imidazolyl group of a histidine as again the only ligand from the protein to the vanadium ion, but the side chains forming hydrogen bonds to the oxo group and the three hydroxy groups on the vanadium, although they are the same, differ somewhat in their orientations.[2323]

When a vanadium ion is coordinated by two amino nitrogens and two phenolato oxygens by the ligand ethylenebis[(*o*-hydroxyphenyl)glycine], it can exist in solution as dioxovanadium(V), oxohydroxyvanadium(V), oxovanadium(V), and oxovanadium(IV)\as well as in the oxidation state V^{+3}, and the various oxidation statess can be readily interconverted.[2332] These results suggest that vanadium has the capability to remove or provide electrons in the reactions catalyzed by haloperoxidases. From electron paramagnetic resonance spectra, however, it was concluded that the vanadium ion in bromide peroxidase from *A. nodosum* **remains in the oxidation state V^{+5}** throughout the enzymatic reaction and is not required to remove or add electrons to either the substrates or the intermediates in the reaction.[2327] In effect, the oxovanadium(V) is simply a metallic ion on which nucleophilic substitutions can proceed.

From the situation of the peroxy ion in the active site (**2–154**), it has been concluded that, in both chloride peroxidase and bromide peroxidase, **the halide, as a nucleophile, adds to the adjacent oxygen** of the peroxy ion. The other oxygen, which is engaged in a hydrogen bond to the ammonio group of the lysine, is hydronated by that ammonio group to become the leaving group in the nucleophilic substitution, and it eventually leaves the active site as either a hydroxide or a molecule of water. That the former **oxygen is electrophilic** and susceptible to nucleophilic substitution is illustrated by the fact that it is transferred from the peroxy ion in the active site of bromide peroxidase from *A. nodosum* to methyl phenyl sulfide to produce methyl phenyl sulfoxide.[2333] A synthetic model compound, in which an oxovanadium(V) is coordinated by three phenolato oxygens and a tertiary amine, is able to catalyze both the oxidation of methyl phenyl sulfide to a mixture of methyl phenyl sulfoxide and methyl phenyl sulfone by hydrogen peroxide (900 turnovers) and the bromination of 1,3,5-trimethoxybenzene using hydrogen peroxide as the oxidant (200 turnovers).[2334]

The immediate product of the normal nucleophilic substitution that occurs in the active site of bromide peroxidase or chloride peroxidase—in which a bromide or a chloride, respectively, is the nucleophile and the bound hydroperoxide is the electrophile—should be hypobromite or hypochlorite bound as a ligand to the vanadium ion. The species that performs halogenations of the natural substrates has not been definitively established.[2324] That bromide peroxidase from *A. nodosum*, in the absence of a substrate that can be brominated, produces hypobromous acid as a product[2335] and chloride peroxidase from *C. inaequalis*, in the absence of a substrate that can be chlorinated, produces hypochlorous acid as a product,[2328] however, suggests that the **intermediate responsible for the brominations and chlorinations** is either hypo-

bromite or hypochlorite, respectively. If so, the hypobromite or the hypochlorite must remain bound as a ligand to the vanadium ion because kinetic studies of bromide peroxidase have shown that once hypobromous acid has dissociated as the conjugate acid from the vanadium, even though it is still bound to the enzyme, it is not the species brominating substrates.[2335]

Bromide peroxidase from *A. nodosum* brominates 2,3-dimethoxytoluene within the phenyl ring rather than at the methyl group and produces the same product as the electrophilic aromatic substitution performed by bromonium ion.[2336,2337] This result demonstrates that the species halogenating this unnatural substrate in the active site of the enzyme must be a bromonium ion or its equivalent rather than a bromine radical. Consequently, the **brominations catalyzed by the enzyme are heterolytic**. It is likely that the ammonio group of the lysine can hydronate the oxygen of the hypobromite or hypochlorite bound as a ligand to the vanadium ion to make that oxygen a better leaving group and make the bromine more electrophilic and more like a bromonium ion if not, after the oxygen leaves in the first step of a dissociative nucleophilic substitution, an actual bromonium ion. The intermediate responsible for the brominations catalyzed by bromide peroxidase is also able to oxidize hydrogen peroxide, which is a singlet molecule, to singlet molecular oxygen[2336,2338] in yet another **heterolytic reaction**. This latter oxidation permits the enzyme to be a catalase in the absence of a substrate it would otherwise brominate.

Suggested Reading

Branchaud, B. P., and Walsh, C. T. (1985) Functional group diversity in enzymatic oxygenation reactions catalyzed by bacterial flavin-containing cyclohexanone oxygenase, *J. Am. Chem. Soc. 107,* 2153–2161. https://doi.org/10.1021/ ja00293a054

Groves, J. T., Haushalter, R. C., Nakamura, M., Nemo, T. E., and Evans, B. J. (1981) High-valent iron-porphyrin complexes related to peroxidase and cytochrome P-450, *J. Am. Chem. Soc. 103,* 2884–2886. https://doi.org/10.1021/ja00400a075

Shu, L., Nesheim, J. C., Kauffmann, K., Munck, E., Lipscomb, J. D., and Que, L., Jr. (1997) An $Fe^{IV}_2O_2$ diamond core structure for the key intermediate Q of methane monooxygenase, *Science 275*, 515–518. https://doi.org/10.1126/science.275.5299.515

Suga, M., Akita, F., Yamashita, K., Nakajima, Y., Ueno, G., Li, H., Yamane, T., Hirata, K., Umena, Y., Yonekura, S., Yu, L. J., Murakami, H., Nomura, T., Kimura, T., Kubo, M., Baba, S., Kumasaka, T., Tono, K., Yabashi, M., Isobe, H., Yamaguchi, K., Yamamoto, M., Ago, H., and Shen, J. R. (2019) An oxyl/oxo mechanism for oxygen–oxygen coupling in PSII revealed by an X-ray free-electron laser, *Science 366*, 334–338. https://doi.org/10.1126/science.aax6998

Spatzal, T., Aksoyoglu, M., Zhang, L., Andrade, S. L., Schleicher, E., Weber, S., Rees, D. C., and Einsle, O. (2011) Evidence for interstitial carbon in nitrogenase FeMo cofactor, *Science 334*, 940. https://doi.org/10.1126/science.1214025

Problem 2–27: Anthranilate 3-monooxygenase (deaminating) is a flavoenzyme catalyzing the oxidation[1327]

$$\text{NADPH} + 2\,\text{H}^+ + \text{O}_2 + \text{anthranilate} \rightleftharpoons 2,3\text{-dihydroxybenzoate} + \text{NH}_4^+ + \text{NADP}^+$$

Write a mechanism for this reaction.

Problem 2–28: There is a flavoenzyme isolated from *Streptomyces lividans* that catalyzes the oxygenation[2339]

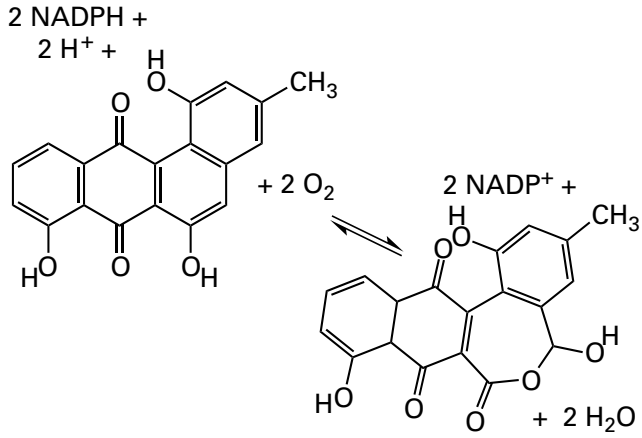

Write a mechanism for this reaction including all the different intermediates of the flavin.[1327]

Problem 2–29: Write a mechanism for the following dioxygenation catalyzed by dihydroxyacetanilide epoxidase from *Streptomyces*[2340]

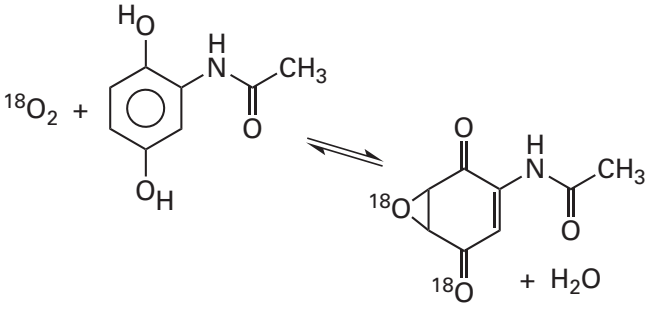

The incorporation of ^{18}O into the 4-oxo group is only 20%, a fact that your mechanism should explain.

Problem 2–30: The flavoenzyme 3-hydroxy-2-methylpyridinecarboxylate monooxygenase catalyzes the monooxygenation[2341]

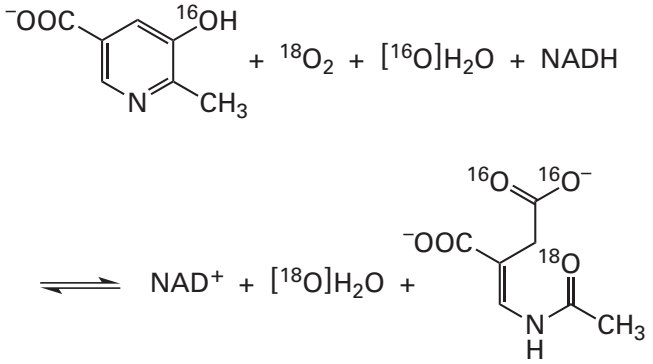

using a 4a-hydroperoxyflavin. Write a complete mechanism for the reaction beginning with oxidized flavin.

Problem 2–31: Factor-independent urate hydroxylase catalyzes the reaction

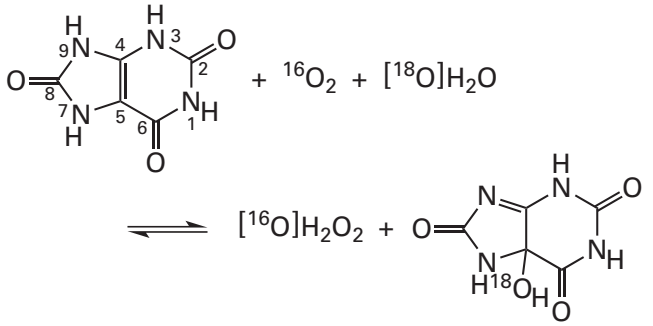

There are two intermediates, the urate 3,9-dianion and urate 5-hydroperoxide.[1375,2342] Write a mechanism for the enzymatic reaction.

Problem 2–32: Write a complete mechanism for reduction of nitrite ion

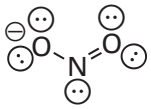

at the siroheme in ferredoxin—nitrite reductase.

Problem 2–33: Write a complete mechanism for cytochrome-*c* oxidase including the neutral phenol radical of the 3-(N^{τ}-histidinyl)tyrosine and the tryptophan radical.

Problem 2–34: Write a mechanism for the reaction catalyzed by 4-hydroxyphenylpyruvate dioxygenase[2343]

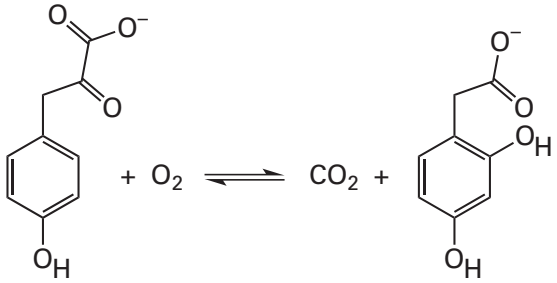

The enzyme contains a nonheme iron ion coordinated by two histidines and a glutamate (see Figure 2–57D for a similar coordination).[2344] If $^{18}O_2$ were used as a substrate, where would the two atoms of oxygen-18 end up?

Problem 2–35: Draw a detailed mechanism for the oxidation of carbon monoxide catalyzed by the prosthetic group **2–143**.

1,2-Benzoquinones

There are several different 1,2-benzoquinones that act as electrophiles in enzymatic reactions. In this sense, they are one of the prosthetic groups that make up for the fact that there are no electrophiles among the side chains of the amino acids. These 1,2-benzoquinones are the prosthetic group pyrroloquinoline quinone (**2–155**),[2345-2347] which is synthesized from a glutamate and a tyrosine in a short peptide,[2348,2349] and the posttranslational modifications 2,4,5-trihydroxyphenylalanylquinone (**2–156**),[7]

lysine tyrosylquinone (**2–157**),[2350] tryptophan tryptophylquinone (**2–158**),[2351,2352] and cysteine tryptophylquinone (**2–159**)[2353,2354]

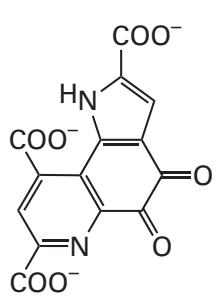

2–155

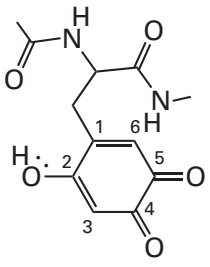

2–156

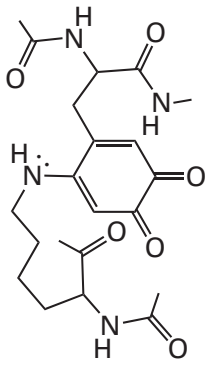

2–157

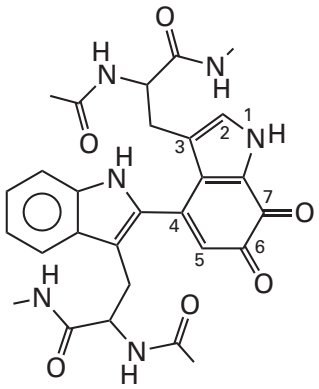

2–158

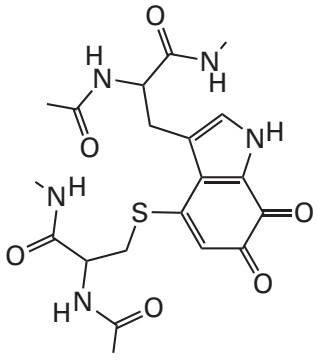

2–159

The 1,2-benzoquinones produced by the four post-translational modifications catalyze the oxidation of primary amines to aldehydes

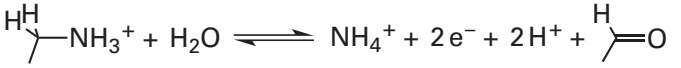

(2–334)

and pyrroloquinoline quinone (**2–155**) catalyzes the oxidation of primary and secondary alcohols to aldehydes and ketones

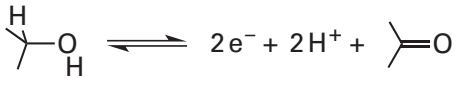

(2–335)

and *gem*-diols to carboxylic acids

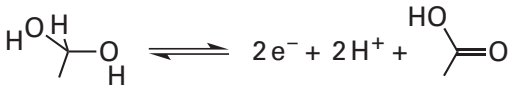

(2–336)

The **oxidation of primary amines to aldehydes by 2,4,5-trihydroxyphenylalanylquinone** in the active site of primary-amine oxidase (Equation 2–334) is an introduction to the capabilities of 1,2-benzoquinones. The two electrons resulting from the oxidation are transferred to molecular oxygen, reducing it to hydrogen peroxide. The enzyme also contains a prosthetic copper ion coordinated by three imidazolyl groups from three histidines. Either one or two molecules of water or the oxygen at carbon 4 of 2,4,5-trihydroxyphenylalanylquinone (**2–156**), depending on the situation,[2355-2360] completes the coordination of the copper ion. In the crystallographic molecular models of the primary-amine oxidases in which it is not a direct ligand to the copper ion, 2,4,5-trihydroxyphenylalanylquinone is either immediately adjacent to or forming a hydrogen bond through one of its oxygens to one of the molecules of water that is a ligand to the copper ion. In the resting state of the enzyme, the copper ion is in the oxidized cupric state.

The mechanism of oxidation of primary amines to aldehydes (Figure 2–63)[2361,2362] is homologous to the one for conversion of secondary amines to ketones catalyzed by pyridoxal 5′-phosphate. The primary amine forms **proximal imine 2–160**[2363,2364] with the carbonyl carbon 5 of 2,4,5-trihydroxyphenylalanylquinone.[2361,2365] This imine has been trapped as the stable amine by reduction with sodium cyanoborohydride.[2366] As in deaminations catalyzed by pyridoxal phosphate (Equation 2–4), the next step in the reaction catalyzed by primary-amine oxidase is the dehydronation of the secondary carbon immediately adjacent to the imino nitrogen in proximal imine **2–160**. When a series of benzylamines with different substituents in the phenyl ring were used as substrates for bovine primary-amine oxidase, the rate at which a hydrogen was removed from the benzyl carbon increased as the ability of the substituents to withdraw electron density from the benzyl carbon increased,[2367] as expected if a hydrogen is removed from the benzylic carbon as a hydron.

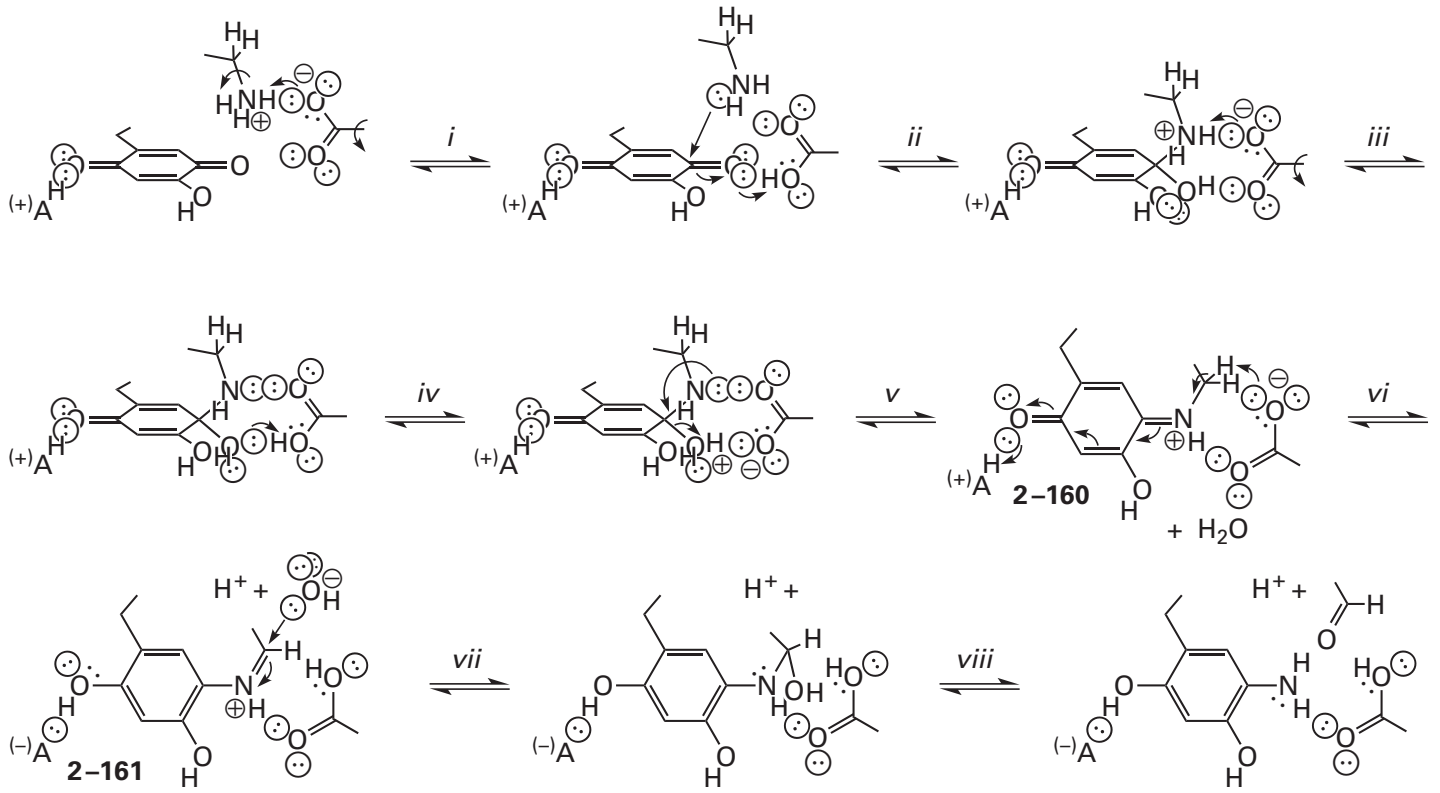

Figure 2–63: Mechanism for the conversion of a primary amine to an aldehyde by the 2,4,5-trihydroxyphenylalanylquinone in primary-amine oxidase.[2361,2362] The hydron of the primary amine is (*i*) removed by the carboxylate of an aspartate in the active site of the enzyme, and the resulting carboxy group (*ii*) hydronates the carbonyl oxygen at position 5 in the 2,4,5-trihydroxyphenylalanylquinone as the lone pair of electrons on the amine attacks the carbonyl carbon to form the conjugate acid of the internal hemiaminal. The carboxylate of the aspartate then (*iii*) transfers a hydron from the ammonium nitrogen to the hydroxy group of the hemiaminal, and the hydronated hydroxy group (*iv*) is pushed away as a leaving group by the lone pair of electrons on the adjacent amino group to produce the internal iminium ion. Both oxygens of the resulting 2,4-dihydroxy-5-amino-phenylalanylquinone (*v*) withdraw electrons through the π system of the quinone from the bond between the primary carbon of the former amine and one of its hydrogens when that bond is parallel to the π system. The carboxylate of the aspartate (*vi*) removes the hydron from the weakened bond, creating an *N*-(5-alkyl-2,4-dihydroxyphenyl)-imine. A hydroxide (*vii*) nucleophilically attacks the iminium carbon of this external *N*-hydronated imine to produce the external hemiaminal. The carboxy group of the aspartate is available (*viii*) to provide a hydron to the oxygen and remove a hydron from the nitrogen of the hemiaminal to promote the dissociation of 5-alkyl-2,4-dihydroxy-aniline and form the aldehyde. During all these transfers, a hydron is never required to enter or leave the active site, although hydrons probably do so.

The atoms in proximal imine **2–160** that **withdraw electron density from the this primary carbon–hydrogen bond** are the two oxygens at positions 2 and 4 rather than the pyridyl nitrogen in an external pyridoximine (Equation 2–4). These two oxygens are involved in a tautomeric equilibrium

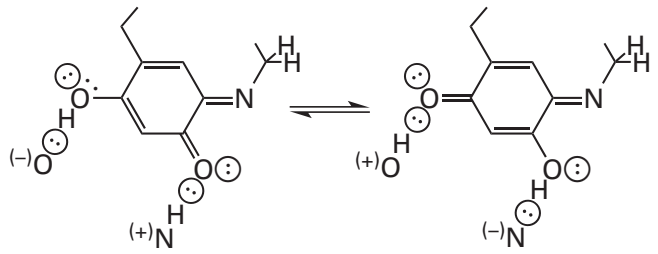

(2–337)

that interconverts each of them, respectively, between an oxo group and a hydroxy group. In primary-amine oxidase, acid–bases form hydrogen bonds to each of these two oxygens that give or take the respective hydrons as needed. For example, in primary-amine oxidase from several different species, the hydroxy group of a tyrosine ($pK_a \cong 9.8$)* forms a hydrogen bond to oxygen 4, and an acidic molecule of water ($pK_a \geq 7$) is coordinated to the prosthetic Cu^{2+} and forms a hydrogen bond to oxygen 2.[2356,2361,2365] In the primary-amine oxidase from *P. sativum*, the ammonio group of a lysine ($pK_a \cong 10.5$) forms a

*The values of pK_a are for an average tyrosine, lysinium ion, or aspartic acid in a protein.[2368] Acid–bases in active sites often have quite different acidities.

hydrogen bond at oxygen 4, and the carboxy group of an aspartic acid ($pK_a \cong 4.0$) forms a hydrogen bond at oxygen 2.[2355] Consequently, at any instant either oxygen 2 or oxygen 4 can be a carbonyl oxygen at the ortho or para position to the proximal imine, respectively, and can withdraw electron density from the carbon–hydrogen bond immediately adjacent to that imino nitrogen.

To permit this electron withdrawal by the oxo groups in the ring to occur, the acidic carbon–hydrogen bond in the proximal imine is held parallel to the π molecular orbital system (Equation 2–337) connecting the imino nitrogen to the carbonyl oxygens at positions 2 and 4[2361,2369] in proximal imine **2–160**. Removal of the hydron from the carbon produces **distal imine 2–161** and is coincident with the **aromatization** that produces a 2,4-dihydroxyphenyl group on the nitrogen of the distal imine (Figure 2–63). This aromatization provides significant favorable free energy of activation to the removal of the hydron from the carbon, usually a difficult reaction. After a **hydrolysis** that produces the aldehyde and its dissociation, the initial 1,2-benzoquinone has been reduced to the aminobenzoquinol 5-amino-2,4-dihydroxyphenylalanine.

In most of the primary-amine oxidases, the hydron is removed from the carbon adjacent to the imino nitrogen of proximal imine **2–160** by the **carboxylato group of an aspartate**.[2370] that is properly situated and aligned for the removal.[2361] This carboxylato group is also in the proper location to remove the hydron from the incoming amine, to add a hydron to the 5-oxido oxygen, to remove a second hydron from the amino group in the proximal hemiaminal, and to add a second hydron to the 5-hydroxy group of the hemiaminal to create the water that leaves (Figure 2–63), just as the oxygen of the phenoxylato group in the proximal pyridoximine catalyzes its transimination to the external pyridoximine (Figure 2–2). The conclusion that this is one of the roles played by this aspartate is supported by the fact that, in addition to the rate of the dehydronation of the secondary carbon in distal imine **2–161**, the rate for the formation of proximal imine **2–160** in the active site of primary-amine oxidase from *A. globiformis* is dramatically decreased (by a factor of 10^6) when this aspartate is mutated to alanine.[2361] In addition, this aspartic acid may act as an acid and then a base in the hydrolysis of the distal imine between 5-amino-2,4-dihydroxyphenylalanine and the aldehyde. It is also positioned so that it sterically pins the ring of 2,4,5-trihydroxyphenylalanylquinone in its proper orientation for catalysis. The plenipotency of this carboxy group is reminiscent of the plenipotency of the amino group of the lysine in enzymes using pyridoxal phosphate as a prosthetic group.

Several 2,4,5-trihydroxyphenylquinones that differ only in the substituents at carbon 1 have been synthesized. These **synthetic models** are able to catalyze, in solution nonenzymatically, the oxidation of primary amines to their aldehydes using molecular oxygen as the receptacle for the electrons,[2371,2372] just as a primary-amine oxidase is able to do. The proximal imine of the primary amine and the synthetic 2,4,5-trihydroxyphenylquinone, the distal imine of the product aldehyde and the synthetic aminodihydroxyphenylquinol, and the aminodihydroxyphenylquinol itself (see Figure 2–63) have all been identified under anaerobic conditions as intermediates in the deaminations that are accomplished by these synthetic models.[2371,2373,2374]

In the primary-amine oxidases as well as in bovine protein-lysine 6-oxidase, which uses lysine tyrosylquinone (**2–157**) as an electrophile,[2350,2375] 5-amino-2,4-dihydroxyphenylalanine and lysine tyrosylquinol, which are the reduced products of the respective prosthetic groups following the oxidations of amines to aldehydes, are reoxidized to 2,4,5-trihydroxyphenylalanylquinone (**2–156**) and lysine tyrosylquinone (**2–157**), respectively, by molecular oxygen, which is reduced by the two electrons to hydrogen peroxide. Although the precise **mechanism of the reoxidation by molecular oxygen** has not yet been established,[2376] there are several provocative observations.

Oxygen is only able to bind to a Cu^+, not a Cu^{2+}. In the reduced enzyme that must be reoxidized, however, the copper ion, because it does not participate as an oxidant in deamination of the substrate by the 2,4,5-trihydroxyphenylalanylquinone, remains the Cu^{2+} that it was in the resting enzyme. In fact, all the steps leading to the formation of 5-amino-2,4-dihydroxyphenylalanine and the release of the aldehyde are unaffected by the removal of the Cu^{2+} from the active site of primary-amine oxidase from *Lens culinaris*.[2377] Nevertheless, in the active site from which the Cu^{2+} has been removed, the enzymatic reaction cannot proceed beyond formation of the prosthetic 5-amino-2,4-dihydroxyphenylalanine in the presence of saturating concentrations of oxygen, so the **Cu^{2+} is required for the reoxidation**.

In several primary-amine oxidases that are in the reduced state after oxidizing an amine under anaerobic conditions, the 5-amino-2,4-dihydroxyphenylalanine in their active sites engages in an

electron transfer with the adjacent Cu^{2+} to produce a Cu^{+} and the semiquinone of 5-amino-2,4-dihydroxyphenylalanine (**2–162**)[2378,2379]

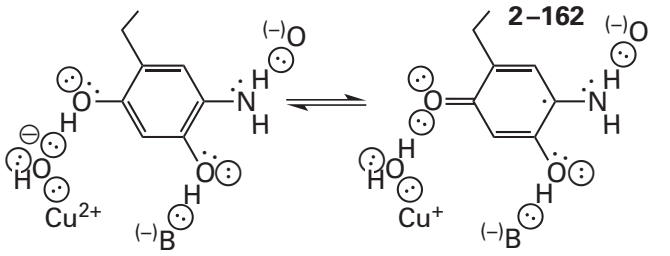

(2–338)

which was identified from the electron-spin resonance spectrum of its unpaired electron.[2380] In reduced primary-amine oxidase from *P. sativum*, in the absence of oxygen, this equilibrium is rapidly established.[2381] There is a crystallographic molecular model of the cuprous semiquinone in the active site of primary-amine oxidase from *Ogataea parapolymorpha* in which the anionic conjugate base of the 4-hydroxy group of the semiquinone has swung over to displace a molecule of water and become the fourth ligand to the copper ion.[2382] Such a ligation could represent an intermediate in this electron transfer, but it should not be necessary because the Cu^{2+} is coupled to the 5-amino-2,4-dihydroxyphenylalanine in the outer sphere through the molecule of water. Nevertheless, inner-sphere electron transfer is usually instantaneous.

The **biochemical standard reduction potential of 2,4,5-trihydroxyphenylalanylquinone**[2383] in free solution is +75 mV. This reduction is fully reversible but is a reduction by two electrons. No evidence for the presence of the semiquinone of 2,4,5-trihydroxyphenylalanine was seen in the voltammograms of this reduction in solution. Consequently, the biochemical standard reduction potential for the redox couple of the semiquinone and the fully reduced 2,4,5-trihydroxyphenylalanine should be significantly more positive than +75 mV, which is not surprising since the single ring is unable to delocalize the unpaired electron as well as it is delocalized, for example, in the semiquinone of a flavin or a pterin. The one-electron biochemical standard reduction potential of the semiquinone of 5-amino-2,4-dihydroxyphenylalanine (**2–162**), however, should be less positive than that for the semiquinone of 2,4,5-trihydroxyphenylalanine because the amino group is a stronger electron-releasing functional group. Dehydronation of the 2-hydroxy group by the cupric hydroxide should decrease the one-electron standard reduction potential even further. Cupric ions involved in electron transfer in proteins usually have biochemical standard reduction potentials greater than +80 mV (Figure 2–19), so a Cu^{2+} immediately adjacent to 5-amino-2,4-dihydroxyphenylalanine and connected to it in the inner sphere should be able to oxidize it by one electron, as is observed.

In a crystallographic molecular model of primary-amine oxidase from *E. coli*, **molecular oxygen is associated with cuprous semiquinone 2–162**,[2384] displacing the molecule of water that is a ligand to the copper ion and sitting between the copper ion and the 2-hydroxy group of the semiquinone of 5-amino-2,4-dihydroxyphenylalanine.[2385] This observation suggests that this complex between molecular oxygen and the cuprous semiquinone is an intermediate in reoxidation of the 5-amino-2,4-dihydroxyphenylalanine. The proposal can be divided into three steps. First, molecular oxygen associates with cuprous semiquinone **2–162** and is reduced by the Cu^{+} to superoxide radical anion. Second, the superoxide radical anion is then hydronated to form hydroperoxy radical that removes the electron from the semiquinone of 5-amino-2,4-dihydroxyphenylalanine. Third, the resulting hydroperoxy ion or, upon hydronation, the hydrogen peroxide then dissociates.[2386] The imine of the resulting 5-imino-2,4-dihydroxyphenylalanylquinone is then hydrolyzed to 2,4,5-trihydroxyphenylalanylquinone, returning the enzyme to the resting state.

In other primary-amine oxidases, however, the equilibrium between the cupric 5-amino-2,4-dihydroxyphenylalanine and the cuprous semiquinone (Equation 2–338) cannot be observed. This failure may simply indicate that the equilibrium constant is smaller in these instances, but when the Cu^{2+} in primary-amine oxidase from *S. cerevisiae*[2387] and the Cu^{2+} in primary-amine oxidase from *A. globiformis*[2388] were each **replaced with Co^{2+}**, with which this transfer of an electron does not occur, the respective enzyme nevertheless retained 100% or 2% of its activity at saturating concentrations of reactants. This result brings into question the importance of the rapid electron transfer and the role of the copper ion as a participant in the oxidation–reductions involved in the reoxidation of the 5-amino-2,4-dihydroxyphenylalanine.

Direct transfer of an electron between 5-amino-2,4-dihydroxyphenylalanine and molecular oxygen to form superoxide radical anion and the semiquinone of 5-amino-2,4-dihydroxyphenylalanine has been proposed as the first step in its reoxidation.[2389] Such a transfer of an electron is reminiscent of the

direct transfer of an electron from reduced flavin to molecular oxygen (Equation 2–207). Transfer of an electron from 5-amino-2,4-dihydroxyphenylalanine to molecular oxygen ($E^{\circ\prime}$ = –160 mV for 1 M O_2 and 1 M $O_2^{\bullet-}$), however, should be significantly endergonic, even when electron donation of the amino nitrogen and dehydronation of the 2-hydroxy group are considered. If such an electron transfer is actually the first step in reoxidation of 5-amino-2,4-dihydroxyphenylalanine by molecular oxygen, the superoxide radical anion that is being formed or that has been formed would be able to associate with the Cu^{2+} during or after the transfer, respectively, but not before, and this association would definitely stabilize the superoxide radical anion and facilitate the transfer. By both this mechanism and the mechanism involving the cuprous semiquinone, hydroperoxy copper(II) 5-amino-2,4-dihydroxyphenylalanyl semiquinone is a common intermediate even though the details of its formation differ.

The enzymes that oxidize primary amines to aldehydes with **tryptophan tryptophylquinone (2–158)** and **cysteine tryptophylquinone (2–159)** use the same mechanism for the oxidation as that used by 2,4,5-trihydroxyphenylalaninylquinone (Figure 2–63). The amine adds as a nucleophile to the 6-oxo carbon[2352] to form the proximal imine.[2390] There is a crystallographic molecular model of the proximal imine formed between the prosthetic cysteine tryptophylquinone and L-lysine in the active site of L-lysine 6-oxidase from *Marinomonas mediterranea*,[2354] and a stable proximal imine forms between the prosthetic cysteine tryptophylquinone and glycine in the active site of glycine oxidase from *Pseudoalteromonas luteoviolacea*[2391] that has been defined by its resonance Raman spectra and that has been observed in a crystallographic molecular model.[2392] In the active site of glycine oxidase from *P. luteoviolacea*, Aspartate 678 is responsible for catalyzing the transimination that forms the proximal imine and for the transimination of the distal imine. This conclusion follows from the facts that when it is mutated to an asparagine, the proximal imine cannot form, and when it is mutated to a glutamate, the distal imine accumulates.[2393]

The hydron on the carbon immediately adjacent to the nitrogen of the proximal imine in the active sites of the enzymes that use prosthetic tryptophan tryptophylquinone and cysteine tryptophylquinone is then removed, again by the carboxylate of an aspartate.[2352,2354,2394] Electron withdrawal by substituents within benzylamines that have formed proximal imines with the prosthetic tryptophan tryptophylquinone in the active site of aralkylamine dehydrogenase (azurin) from *A. faecalis* causes the rate constant for the removal of this hydron from carbon to increase, as expected.[2395]

Following hydrolysis of the resulting distal imine and release of the aldehyde that is the product, the tryptophan tryptophylquinone in the active site of methylamine dehydrogenase (amicyanin) from *P. denitrificans* has become an **aminoquinol, 6-amino-7-hydroxy-4-(2-tryptophyl)tryptophan**[2396]

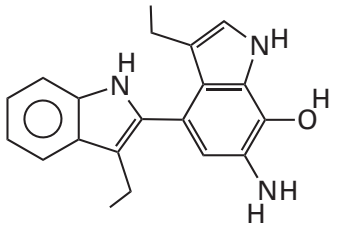

2–163

In a mutant in which Histidine 767 has been changed to alanine in glycine oxidase from *P. luteoviolacea*, the hemiaminal, which is an intermediate in hydrolysis of the distal imine that has formed between the glycine and the prosthetic cysteine tryptophylquinone, accumulates and can be observed in a crystallographic molecular model.[2397]

Unlike 5-amino-2,4-dihydroxyphenylalanine in the active site of a primary-amine oxidase, however, the aminoquinols of both tryptophan tryptophylquinone (**2–163**) and cysteine tryptophylquinone are usually **oxidized back to the respective quinones by two outer-sphere, one-electron transfers** to amicyanin, azurin, or a cytochrome, depending on the particular enzyme and the particular species.[2353,2398] 6-Amino-7-hydroxy-4-(2-tryptophyl)-tryptophan (**2–163**) in the active site of methylamine dehydrogenase (amicyanin) from *P. denitrificans* forms a stable, neutral radical upon transfer of the first electron and removal of a hydron. In this neutral radical the unpaired electron can be delocalized over four rings,[2399-2401] perhaps making this semiquinone even more stable relative to the quinol than the semiquinone of flavin is relative to reduced flavin. In the active site of glycine oxidase from *P. luteoviolacea*, however, in which the electron can delocalize only onto the sulfur of the cysteinyl group in the prosthetic cysteine tryptophylquinone, the biochemical standard reduction potential for the couple of the quinone and the semiquinone is +110 mV and that for the couple of the semiquinone and the quinol is +20 mV, so the semiquinone is again quite stable.[2402] In this latter instance, the ultimate receptacle for the two electrons is a molecule of oxygen, so the semiquinone is presumably

necessary to separate the unpaired electrons on the molecular oxygen in the first electron transfer, as in the case of flavin oxidases. The two-electron biochemical standard reduction potential of the cysteine tryptophylquinone in the active site of quinohemoprotein amine dehydrogenase from *P. denitrificans* is +40 mV, and the biochemical standard reduction potentials of the two hemes *c* within the enzyme, which pass in turn the two electrons to two cytochromes *c*-550, during the reoxidation of 6-amino-7-hydroxy-4-(*S*-cysteinyl)-tryptophan are +150 and +240 mV, respectively.[758] Even if the initial one-electron oxidation of 6-amino-7-hydroxy-4-(*S*-cysteinyl)tryptophan has a significantly higher biochemical standard reduction potential than +40 mV, it is clear that each transfer of an electron is probably exergonic.

The mechanisms for oxidations of alcohols catalyzed by enzymes that use pyrroloquinoline quinone (2–155) as a prosthetic group may or may not differ significantly from the mechanisms of the enzymes that use 2,4,5-trihydroxyphenylalanylquinone, lysine tyrosylquinone, tryptophan tryptophylquinone, and cysteine tryptophylquinone.

In methanolic solution under acidic conditions, the trimethyl ester of pyrroloquinoline quinone gives the dimethyl ketal at carbon 4[2403]

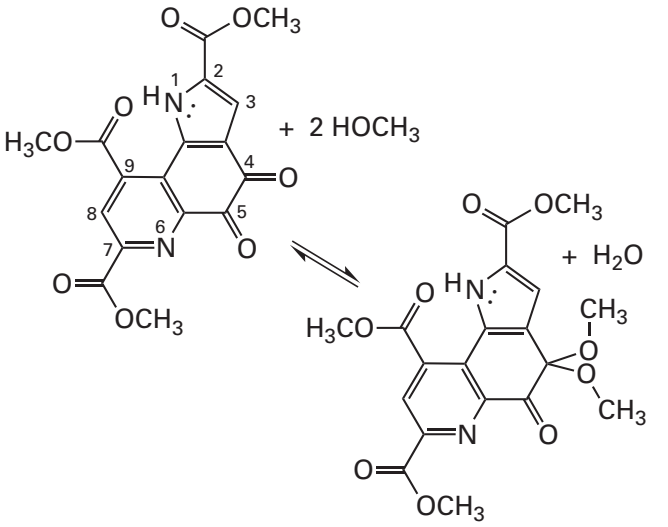

(2–339)

The required cationic intermediate in the formation of this ketal would be the vinylogous imidate at nitrogen 1, which delocalizes the positive formal elementary charge to nitrogen 1 from which the hydron can dissociate. The **more electrophilic carbonyl group** of the two in pyrroloquinoline quinone or its trimethyl ester, however, both in solution[2403,2404] and in an enzyme,[2405] is the carbonyl at **carbon 5**. In crystallographic molecular models, the structures for the active sites of enzymes using pyrroloquinoline quinone as a prosthetic group also suggest that the carbonyl at carbon 5 is the electrophile in the enzymatic reaction,[2347,2406] but an examination of the electronic structures of the hemiketals between the reactant alcohol and pyrroloquinoline quinone at oxocarbon 5[2347,2407] seem to afford no obvious way of directly improving the acidity of the primary carbon of the alcohol from which the hydrogen must be removed during the oxidation (Equations 2–335 and 2–336) because a saturated carbon sits between that hydron and the pyrroloquinolinyl group.

Nevertheless, in solution, the **methyl hemiacetal at carbon 5 of pyrroloquinoline quinone,** which was identified by its absorption spectrum,[2403] produces formaldehyde and pyrroloquinoline quinol upon treatment with strong base[2408]

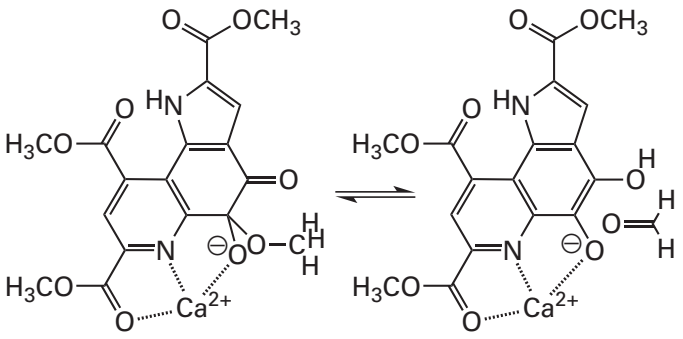

(2–340)

as long as there is a Ca^{2+} bound to the pyrroloquinoline quinone, as there is in the crystallographic molecular models of glucose 1-dehydrogenase (PQQ, quinone) from *Acinetobacter calcoaceticus*[2406]

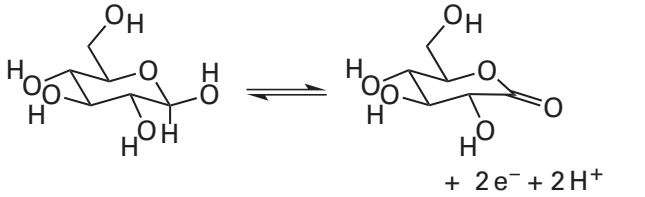

(2–341)

and the methanol dehydrogenases (cytochrome *c*) from *Methylophilus methylotrophus,*[2347] *Methylorubrum extorquens,*[2407,2409] and *M. capsulatus.*[2410]

These observations in solution suggest a mechanism for the observed oxidation of methanol under catalysis by pyrroloquinoline quinone, Ca^{2+},

and strong base (Figure 2–64)[2408] that proceeds through the hemiketal at carbon 5 of the pyrroloquinoline quinone and that is an analogue of the oxidation of amines by 1,2-benzoquinones (Figure 2–63). The methanol adds to carbon 5 to form the hemiacetal. The hydroxy group leaves as a hydroxide on Ca^{2+}, and the usual carbenium ion that is an intermediate in this dissociation of the leaving hydroxy group is delocalized to nitrogen 1 while the hydron on nitrogen 1 is removed by the adjacent carboxylato group to give the enol ether at carbon 5. Rehydronation of nitrogen 1 creates a widely delocalized proximal oxocarbenium ion on carbon 5. Removal of a hydron from the methyl group that creates the distal oxocarbenium ion aromatizes the entire pyrroloquinolinyl group. Aromatization provides the driving force for the dehydronation. The resulting distal oxocarbenium ion of formaldehyde hydrolyzes at the former methyl carbon of the methanol to produce pyrroloquinoline quinol and formaldehyde. Although not shown in the figure, the hydroxide on Ca^{2+} could be the nucleophile that hydrolyzes the distal oxocarbenium ion.

There are, however, problems with this mechanism. Oxygen is a more electronegative atom than nitrogen. Oxocarbenium ions have very short lifetimes. The dissociation of water from a hemiacetal has only been observed to occur under quite acidic conditions, never under basic conditions, but this is an unusual hemiketal. While the Ca^{2+} as a Lewis acid could satisfy this requirement for a hydron to add to the hydroxy group of the hemiketal, it seems unlikely since Ca^{2+} is a significantly weaker acid (10^{-14}) than a hydron.

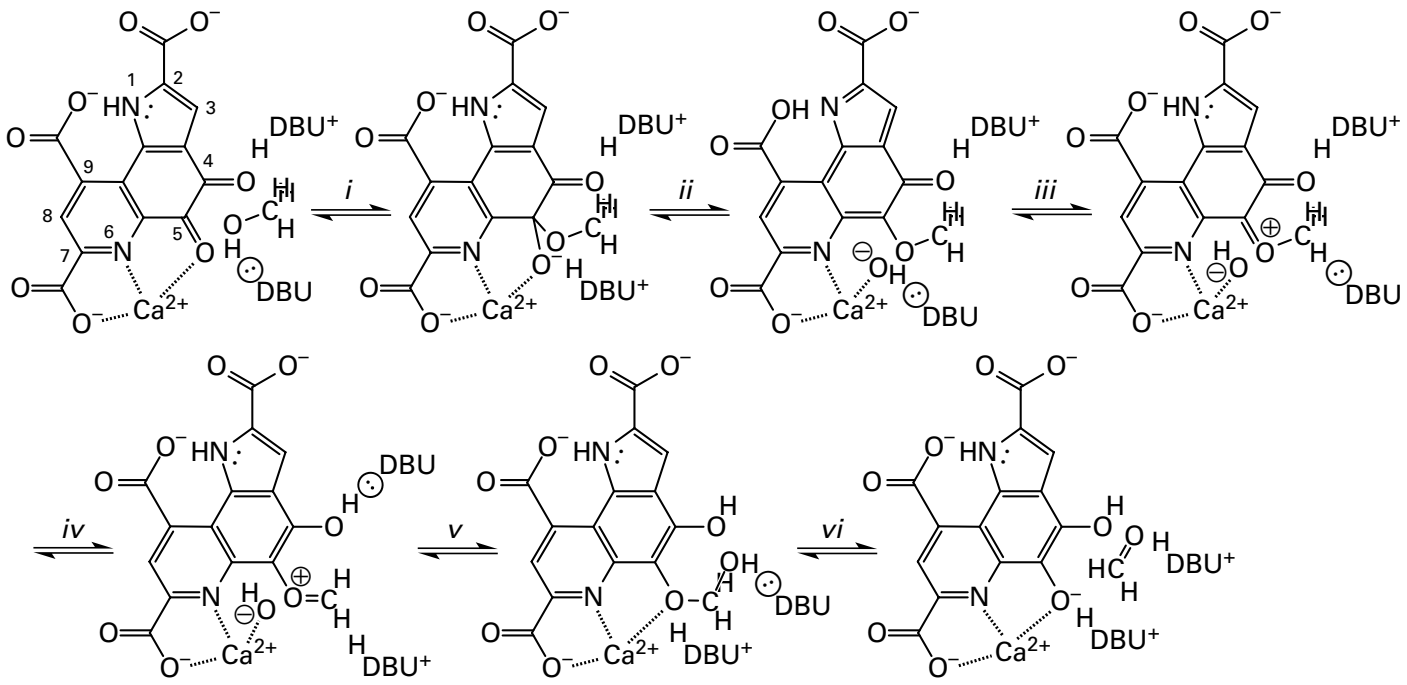

Figure 2–64: Mechanism for the nonenzymatic oxidation of methanol by pyrroloquinoline quinone that has been shown to proceed through the formation of a hemiketal at the carbonyl at carbon 5.[2408] The reaction is carried out in a solution of anhydrous acetonitrile to which has been added the nonnucleophilic base 1,8-diazabicyclo[5.4.0]undec-7-ene (DBU) and methanol. Methoxide (*i*) adds to carbon 5 to form the hemiketal. The Ca^{2+} facilitates this nucleophilic addition of the hydroxy group of methanol as the DBU removes its hydron. The lone pair of nitrogen 1, upon its dehydronation, is (*ii*) delocalized to provide the push to eliminate the hydroxy group of the hemiketal and form a vinylogous imido ester. The hydroxy group remains as a ligand to the Ca^{2+}, which has enhanced its ability as a leaving group. Rehydronation of nitrogen 1 (*iii*) promotes the formation of a delocalized proximal oxocarbenium ion that (*iv*) tautomerizes to the distal oxocarbenium ion. The aromatization of the prosthetic group promotes the tautomerization. A hydroxide, either the one on the calcium or one that has been released into the solution from another calcium, (*v*) adds to the distal oxocarbenium ion to form the hemiacetal. The oxygen on carbon 5 of the pyrroloquinoline quinol (*vi*) leaves the hemiacetal to give formaldehyde. This oxygen of the pyrroloquinoline quinol ($pK_a \cong 9$), especially as a ligand to a Ca^{2+}, is a good leaving group.

In the crystallographic molecular model of the complex between methanol and methanol dehydrogenase (cytochrome *c*) from *M. capsulatus*,[2410] the electron density for the molecule of methanol is situated immediately adjacent to carbon 5 of the pyrroloquinoline quinone and one of the atoms of methanol is only 0.21 nm from carbon 5, well within van der Waals contact.[2410] It is not possible, however, to distinguish whether this atom is the carbon or the hydroxy group of the methanol since they differ in electron density by only one electron. If, as the authors believe, it is the hydroxy group, this observation is consistent with formation of the hemiacetal at carbon 5 during the oxidation (Figure 2–64), but it is also possible that the atom intimately pushed up against carbon 5 is the methyl group of the methanol. This disposition would be consistent with the fact that the other atom in the electron density for the methanol is not far from the Ca^{2+} in the active site. If the methyl group is actually adjacent to carbon 5, then this regiochemistry would be consistent with a crystallographic molecular model of the complex between glucose 1-dehydrogenase (PQQ, quinone) (Equation 2–341) and D-glucopyranose.[2406] In the crystallographic molecular model of the complex, in which the pyrroloquinoline is the quinol rather than the quinone to prevent further reaction by pairing reduced substrate with reduced prosthetic group, the **carbon–hydrogen bond on carbon 1 of the D-glucopyranose is unmistakably pointed at carbon 5 of the pyrroloquinoline quinol.**

The **biochemical standard reduction potential of pyrroloquinoline quinone** in aqueous solution in a two-electron reduction, in which it takes up the equivalent of two hydrons and two electrons, is +70 mV,[2411] which is considerably more positive than that for NAD^+ (–310 mV), so it should be a better oxidant. In many dehydrogenases, the formal equivalent of a hydride is transferred from the carbon immediately adjacent to the hydroxy group of a simple, unadulterated alcohol (previously **1–76**)

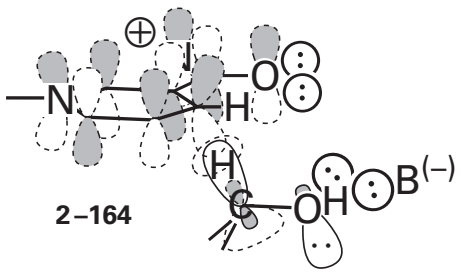

2–164

to NAD^+, which is a vinylogous iminium (previously **1–67**)

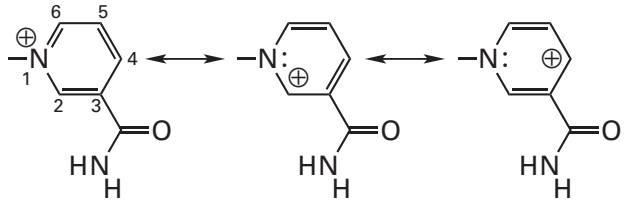

2–165

Consequently, it should also be possible for a hydride to be transferred from the carbon of an alcohol to carbon 5, a carbonyl rather than a vinylogous iminium, of pyrroloquinoline quinone

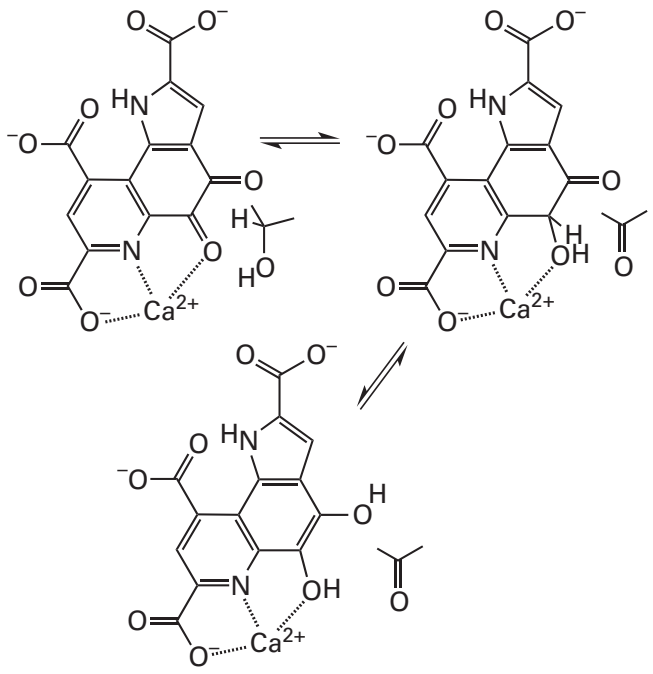

(2–342)

This **transfer of a hydride** should be facilitated by the Ca^{2+} that has the carbonyl oxygen on carbon 5 on the pyrroloquinoline quinone as one of its ligands in each of the crystallographic molecular models.[2347,2406,2407] This divalent cation would further increase both the electrophilicity and the standard reduction potential of carbon 5 of the pyrroloquinoline quinone, making it an even better acceptor of a hydride. Following transfer of the hydride, the hydrogen becomes a hydrogen on a carbon α to a carbonyl group, which would even nonenzymatically tautomerize to the fully aromatic pyrroloquinoline quinol.

The hydrogen on carbon 1 of D-glucopyranose, and perhaps one of the hydrogens on the methyl group

of methanol, would be removed by carbon 5 of the prosthetic pyrroloquinoline quinone (Equation 2–342) in the active sites of both glucose 1-dehydrogenase (PQQ, quinone) and methanol dehydrogenase (cytochrome *c*). In the crystallographic molecular model of glucose 1-dehydrogenase (PQQ, quinone), the distance between carbon 1 of D-glucopyranose and carbon 5 of pyrroloquinoline quinol (0.32 nm) is also well within van der Waals contact (0.40 nm),[2406] and in the complex between the quinone and the hemiketal, the distance should be even shorter because one fewer hydrogen would be in the gap. The oxygen of the hydroxy group on carbon 1 of D-glucopyranose, which would form the hemiacetal during an addition (Figure 2–64), is actually pointed in the other direction and is farther (0.36 nm) from carbon 5 of the pyrroloquinoline quinol than carbon 1. In the crystallographic molecular model, this hydroxy group at carbon 1 of D-glucopyranose, from which a hydron must be removed in either mechanism (Figure 2–64; Equation 2–342), forms a hydrogen bond to the imidazolyl group of a histidine, as occurs in alcohol dehydrogenase,[2412] which uses NAD^+ as the oxidant. All these structural features suggest that in the normal oxidation of D-glucopyranose catalyzed by pyrroloquinoline quinone, and if so in the oxidation of methanol, the formal transfer of a hydride occurs between carbon 1 of the D-glucopyranoside or the methyl group and carbon 5 of pyrroloquinoline quinone to produce the keto tautomer of pyrroloquinoline quinol (Equation 2–342) and the carbonyl group of the product. It appears that pyrroloquinoline quinone has a mechanism more similar to that of nicotinamideadenine dinucleotide than to that of the other 1,2-benzoquinones.

The pyrroloquinoline quinol formed in these enzymatic oxidations, regardless of mechanism, is reduced back to the quinol in two one-electron, outer-sphere transfers, which should be permitted because the semiquinone radical of pyrroloquinoline quinone is a stable species.[2413,2414] In the case of methanol dehydrogenase (cytochrome *c*) in *M. extorquens*, the outer-sphere transfers of single electrons are to successive cytochromes c_L, which have a biochemical standard reduction potential of +260 mV.[2415] The radical anion of a nearby cystine, identified both by its absorption spectrum and by electron paramagnetic resonance, in the active site of methanol dehydrogenase from *M. capsulatus*[2410] has been observed to exist in the active site in a steady-state concentration during the enzymatic reaction. This radical anion may be a relay station in the transfer of each electron to a cytochrome c_L.

Suggested Reading

Mure, M., and Klinman, J. P. (1995) Model studies of topaquinone-dependent amine oxidases: 1. Oxidation of benzylamine by topaquinone analogs. *J. Am. Chem. Soc. 117*, 8698–8706. https://doi.org/10.1021/ja00139a002

Nakamura, N., Moenne-Loccoz, P., Tanizawa, K., Mure, M., Suzuki, S., Klinman, J. P., and Sanders-Loehr, J. (1997) Topaquinone-dependent amine oxidases: Identification of reaction intermediates by Raman spectroscopy. *Biochemistry 36*, 11479–11486. https://doi.org/10.1021/bi9708139

Oubrie, A., Rozeboom, H. J., Kalk, K. H., Olsthoorn, A. J., Duine, J. A., and Dijkstra, B. W. (1999) Structure and mechanism of soluble quinoprotein glucose dehydrogenase. *EMBO J. 18*, 5187–5194. https://doi.org/10.1093/emboj/18.19.5187

Problem 2–36: Write three different mechanisms for the reoxidation of 5-amino-2,4-dihydroxyphenylalanine in primary-amine oxidase: one by molecular oxygen in which there are two successive electron transfers from the 5-amino-2,4-dihydroxyphenyl group to molecular oxygen; one in which transfer of an electron from the 5-amino-2,4-dihydroxyphenyl group to the Cu^{2+} precedes the association of molecular oxygen;[2376] and one in which Cu^{2+} is coordinated by the 4-hydroxy group of 5-amino-2,4-dihydroxyphenylalanine, a radical is formed at carbon 4 by electron withdrawal, as in protocatechuate 3,4-dioxygenase (Equation 2–275) and quercetin 2,3-dioxygenase (Equation 2–303), and oxygen adds to the radical at carbon 4. What could be the role of Cu^{2+} in the first mechanism?

Problem 2–37: The following concerted mechanism has been proposed for oxidation of an alcohol in an active site with a prosthetic pyrroloquinoline quinone

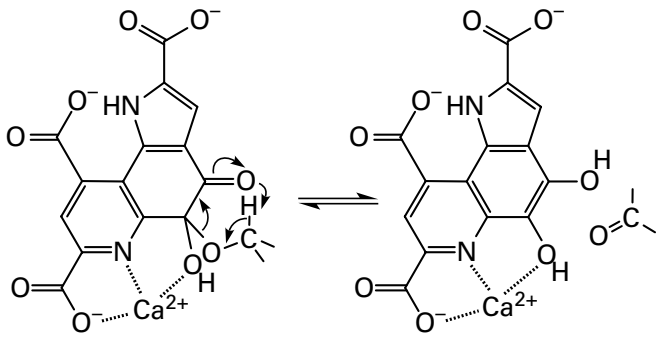

Build a ball-and-stick model of the reactant and rotate around the exocyclic bonds until the molecular orbitals participating in the concerted reaction as written are all aligned parallel to each other, as they must be, and criticize the proposal (see Chapter 1).

Selenocysteine

Selenium is found in several enzymes from diverse sources such as glycine reductase and some of the anaerobic carbon monoxide dehydrogenases, hydrogenases, and formate dehydrogenases from aerobic bacteria; the nicotinate dehydrogenases, 6-hydroxynicotinate dehydrogenases, hydrogenases, and formate dehydrogenases from some obligate and facultative anaerobic bacteria;[2416] and thioredoxin-disulfide reductase and glutathione peroxidase from mammals and birds.

The cysteines in certain prosthetic groups in particular enzymes are replaced with ***S*-selanylcysteines**

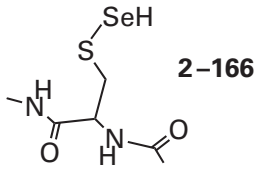

2–166

Anaerobic carbon monoxide dehydrogenase from *A. carboxidovorans* has an **oxomolybdenum(VI) molybdopterin** with two equatorial hydroxy groups, and the molybdenum ion is adjacent to but not coordinated to an *S*-selanylcysteine.[2417] Formate dehydrogenase (hydrogenase) from *E. coli* has a hydroxymolybdenum(VI) bismolybdopterin in its active site with the four sulfanyl groups of the molybdopterins as equatorial ligands and the selanyl group of a selenocysteine as the sixth ligand to the molybdenum ion adjacent to the hydroxy group.[2418,2419] In the active site of formate dehydrogenase from *D. gigas*, the central transition metal is a tungsten ion rather than a molybdenum ion,[2423] but all the other components, including the selanyl group of the selenocysteine, are the same as formate dehydrogenase (hydrogenase) from *E. coli*.[2424] Nicotinate dehydrogenase from *Eubacterium barkeri* has an oxomolybdenum(VI) molybdopterin in its active site that has a hydroxy group as a ligand at one of its equatorial positions and a **selenide** as a ligand at its other equatorial position instead of a sulfide (see Equation 2–327).[2420] In the active site of ferredoxin hydrogenase from *D. vulgaris*, one of the cysteines coordinating the nickel ion in the **nickel–iron dinuclear cluster 2–139** (the one on the lower right) has been replaced with a selenocysteine.[2421,2422]

Selenium is the element in group 16 below oxygen and sulfur on the periodic table, which themselves are abundant elements in living organisms. In most of the enzymes that have a selenium in their active sites, it is a selanyl group on a **selenocysteine**, as is the case with ferredoxin hydrogenase from *D. vulgaris* and the formate dehydrogenases. Selenocysteine is an amino acid homologous to serine and cysteine, in which a selenium replaces the oxygen or sulfur, respectively.[2425-2427] Rather than as a posttranslational modification, in those organisms that contain selenocysteine in one or more of their enzymes, the selenocysteine is inserted into their sequences of amino acids during the translation of their mRNA by redefining the UGA stop codon with a special transfer ribonucleic acid, $tRNA^{Sec}$.[2416] For this reason, selenocysteine is the "21st amino acid".

The selanyl group (–SeH) in a selenol such as selenocysteine offers several advantages over its closest relative, the sulfanyl group in a thiol such as cysteine, as well as a few disadvantages.[2428] Just as a thiolate is more nucleophilic but less basic [$pK_a(H_2S) = 7.0$; pK_a(L-cysteine) = 9.1] than an alcoholate [$pK_a(H_2O) = 15.7$; pK_a(L-serine) = 14], **a selenolate is more nucleophilic but less basic** [$pK_a(H_2Se) = 3.9$; pK_a(L-selenocysteine) = 5.4][2429] than a thiolate. Consequently, a selenol is fully ionized at pH 7 in addition to being more nucleophilic. When the two are surrounded by the same functional groups, a selenide is also **more electrophilic** than a sulfide. This electrophilicity has the disadvantage of making an organoselenium compound susceptible to **deselenation** proceeding through nucleophilic substitution at selenium, leading to the dissociation of the selenium–carbon bond with the carbanion as the leaving group. A selenolate is also a **better leaving group** than a thiolate. A disadvantage, however, of this enhanced ability of selenium as a leaving group is that selenols are more prone to elimination of

hydrogen selenide, to give the alkene, than are thiols to elimination of hydrogen sulfide. Because of its larger size and greater number of electrons, a selenium atom is easier to ionize than a sulfur atom, either by removing an electron or adding an electron.

Several of the advantages of selenium are illustrated by **selenol–diselenide exchange**

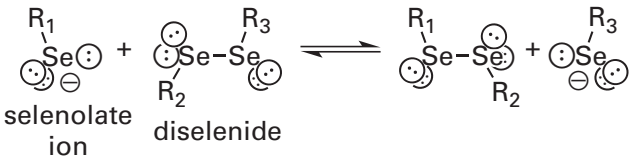

(2–343)

the homologue of thiol–disulfide exchange (see Equation 2–136). In solution, selenol–diselenide exchange is 10^7 times more rapid than thiol–disulfide exchange[2430] because the selenolate ion is a better nucleophile than a thiolate, a selenium is a better electrophile than a sulfur, and a selenolate is a better leaving group than a thiolate. The exchange that is more relevant for the active sites of selenoenzymes, however, is a selenol–disulfide exchange and thiol–sulfenoselenoate exchange

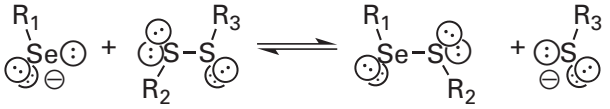

(2–344)

which is an equilibrium that is also more rapidly established than a thiol–disulfide exchange.

In the same surroundings, **the biochemical standard reduction potential of a diselenide** in a protein is more negative than that of a disulfide.[2431] When the two sulfanyl groups in glutaredoxin from *E. coli* that form the cystine in the active site that participates in thiol–disulfide exchange were in turn substituted with selanyl groups and then when both were substituted with selanyl groups, the biochemical standard reduction potential of the disulfide decreased from −194 mV to −260 and −275 mV and then to −309 mV, respectively.[2432]

At pH 7, hydrogen selenide ion (HSe^-; $pK_a = 11$) is less prone thermodynamically to **oxidation** ($E^{\circ\prime} = -70$ mV) to hydrogen selenite ($HSeO_3^-$; $pK_a = 8.3$) than is the equilibrium mixture of hydrogen sulfide ($pK_a = 7.0$) and its conjugate base to oxidation ($E^{\circ\prime} = -120$ mV) to the equilibrium mixture of hydrogen sulfite (HSO_3^-; $pK_a = 7.0$) and sulfite. This feature would tend to cause selanyl groups to be more stable to oxidation than sulfanyl groups, but because of their increased nucleophilicity, selenols are kinetically more reactive with oxidants than thiols.[2428] Selenium, however, has the advantage that it is much more difficult both kinetically and thermodynamically to oxidize the **selenino group** ($-SeO_2H$) in a **seleninic acid**, which is easy to reduce back to a selenol, to the **selenono group** ($-SeO_3H$) in a **selenonic acid** ($RSeO_3H$), which is difficult to reduce back to a selenol, than it is to oxidize a sulfinate (RSO_2^-) to a sulfonate (RSO_3^-). Consequently, selenocysteine is less prone to adventitious complete oxidation, and the consequent inactivation of an enzyme in which it is a catalyst, than is cysteine. Murine thioredoxin-disulfide reductase has a selenocysteine in its active site involved in the enzymatic reaction. It is significantly more stable to added oxidants than is the enzyme from *D. melanogaster* (46% identity; 1.3 gap percent), in the active site of which there is a cysteine instead of a selenocysteine. When the cysteine in thioredoxin-disulfide reductase from *D. melanogaster* is changed to a selenocysteine, the enzyme becomes as resistant to oxidation as the murine enzyme.[2433] Murine thioredoxin-disulfide reductase is inactivated by various electrophiles but can be reactivated by oxidation with hydrogen peroxide. When its selenocysteine, however, was mutated to a cysteine, the cysteinyl enzyme inactivated with electrophiles could not be reactivated.[2434]

Natural selection may have capitalized on these advantages of selenium relative to sulfur. It has been argued,[2435] however, that the lower values of pK_a, the more negative values of biochemical standard reduction potential, and the nucleophilicity of the selanyl group, each on its own, is probably not so advantageous as it seems. Active sites are able to efficiently lower the pK_a of the sulfanyl group of a cysteine. They are also able to significantly adjust biochemical standard reduction potentials of cystines. For example, just within the family of thioredoxins,[2436] the biochemical standard reduction potentials for their cystines span the range from −130 to −270 mV. Finally, the nucleophilicities of selenocysteine and cysteine, which are reflected in the rates of selanol–disulfide exchange and thiol–disulfide exchange, can also be adjusted by an active site. For example, the single selenocysteine in human thioredoxin–disulfide reductase, which is required for enzymatic activity, is replaced by a cysteine in the closely related (49% identity; 1.9 gap per cent) thioredoxin-disulfide reductase from *D. melanogaster*.

These enzymes rely on four successive selenol–disulfide exchanges and thiol–sulfenoselenoate exchanges or four successive thiol–disulfide exchanges, respectively, during each turnover, and yet the enzyme from *D. melanogaster* has an enzymatic activity that is somewhat greater than that of the human enzyme,[2437] and replacement of its cysteine with a selenocysteine does not improve the rate of its enzymatic reaction,[2438] even though the nucleophilicity of the cysteine in its active site can be changed by altering side chains surrounding it in the active site.[2438,2439] Thioredoxin reductase from *Plasmodium falciparum* is also related to the human enzyme (39% identity; 1.9 gap per cent), but replacing the cysteine that is in the homologous position in its sequence of amino acids with the selenocysteine that is in the human enzyme decreases the rate of its reaction at saturating concentrations of thioredoxin[2440] by a factor of 4.

When one considers these observations, the selective advantage of selenocysteine relative to cysteine is not so obvious. It may, however, be that the combination of all these advantages is so beneficial that natural selection has gone to all the trouble of selecting a way of inserting selenocysteine in some enzymes. Or it may be that there is another reason for the presence of selenocysteine. It is also possible that the use of selenocysteine is adventitious, but both the fact that the natural abundance of selenium in the seawater in which life evolved is 10^{-7} that of sulfur and the fact that a complicated mechanism for its insertion into sequences of amino acids has evolved suggest that there is some compelling selective pressure.

There is a formate dehydrogenase (hydrogenase) from *E. coli* that catalyzes the oxidation of formate

$$HCOO^- \rightleftharpoons CO_2 + H^+ + 2\,e^- \qquad (2\text{–}345)$$

In the hydroxymolybdenum(VI) bismolybdopterin in its active site,[2418,2419] a selenocysteine occupies the same position as the serine in the active site of respiratory dimethylsulfoxide reductase (Figure 2–60) and a hydroxide is the sixth ligand at the same position as the oxo group in respiratory dimethylsulfoxide reductase. Because the selenium in the selenocysteine is a direct ligand to the molybdenum in the oxidized, molybdenum(VI) form of the prosthetic group[2157,2419,2441] and because it is selenium rather than sulfur, it is electrophilic enough to remove a hydride from an immediately adjacent formate when one of the oxygens of the formate replaces the hydroxide and becomes the sixth ligand to the molybdenum.[2419] **Transfer of this hydride from the carbon of the formate to the selenium** turns the formate directly into carbon dioxide, with no incorporation of oxygen from the hydroxide that was coordinated to the molybdenum before it was displaced by the formate,[2442] which is the usual outcome with enzymes using molybdenum ions and molybdopterins. The hydride transferred to the electrophilic selenium of the molybdenum(VI) selenolate produces a molybdenum(IV) selenol, and the hydron is then removed from the resulting selenol by the adjacent imidazolyl group of a histidine[2419] to produce molybdenum(IV) bismolybdopterin selenolate,[2157] which is reoxidized to hydroxymolybdenum(VI) bismolybdopterin selenolate by two successive one-electron transfers in the outer sphere to a [4Fe–4S] iron–sulfur cluster.[2419,2443]

Human thioredoxin-disulfide reductase

$$NADP^+ + \text{thioredoxin dithiol} \rightleftharpoons NADPH + H^+ + \text{thioredoxin disulfide} \qquad (2\text{–}346)$$

contains a selenocysteine[2444] that is essential for its activity.[2445] It is the penultimate amino acid in the sequence of the protein. The amino acid on its carboxy-terminal side is the carboxy-terminal glycine of the protein, and the amino acid on its amino-terminal side is a cysteine. When the enzyme is oxidized, the **selenocysteine forms a vicinal sulfenoselenoate**

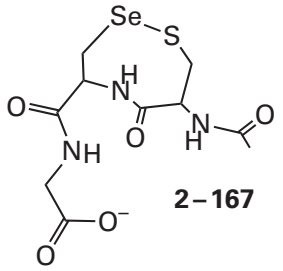

2–167

with that cysteine.[2446] The carboxy-terminal 12 amino acids, including this sulfenoselenoate, are only loosely incorporated in the structure and can be considered a **flexible arm**.[2447] The enzyme is a close relative of human glutathione-disulfide reductase (34% identity; 2 gap per cent), The structure of the active site is almost the same as that of glutathione-

disulfide reductase (Figure 2–11), and the mechanism of the enzyme is probably quite similar.

Consistent with the enhanced facility of selenol–disulfide exchange (Equation 2–344), a sulfenoselenoate such as **2–167** should be much more reactive than a disulfide. **Replacement of the selenocysteine with a cysteine** in human thioredoxin-disulfide reductase[2448] or thioredoxin-disulfide reductase from *R. norvegicus*[2445] decreases the enzymatic activity 10–100-fold, as would be expected if the enzyme is capitalizing on the more favorable electrophilicity and nucleophilicity of the selenium and the consequent increase in the rate of selenol–disulfide exchange. It has also been shown that, probably because of its larger size, the selenium atom makes the strained, vicinal sulfenoselenoate **2–167** more stable than the corresponding vicinal disulfide in the same location.[2446,2448] The following mechanism for thioredoxin-disulfide reductase involving **three successive sulfenoselenoates** and four consecutive selenol–disulfide and thiol–sulfenoselenoate exchanges[2449] is consistent with the observations that have been reported.

Starting with fully reduced human thioredoxin-disulfide reductase and oxidized thioredoxin, in which the disulfide is between Cysteine 32 and Cysteine 35, the selanyl group of the selenocysteine on the flexible arm in the reduced enzyme exchanges with the sulfanyl group of Cysteine 35 (Equation 2–344) and forms a sulfenoselenoate with Cysteine 32.[2450] This initial selenol–disulfide exchange takes advantage of the nucleophilicity of the selenido group. In the crystallographic molecular model of the complex between human thioredoxin and human thioredoxin-disulfide reductase in which the selenocysteine has been mutated to a cysteine, there is an intermolecular cystine between the mutant cysteine in the thioredoxin-disulfide reductase and Cysteine 32.[2451] This disulfide is the homologue of the normal sulfenoselenoate. The thiol of the cysteine adjacent in the sequence of amino acids to the selenocysteine in the native enzyme exchanges with the Cysteine 32 from thioredoxin in the native intermolecular sulfenoselenoate to form sulfenoselenoate **2–167** and release reduced thioredoxin. This thiol–sulfenoselenoate exchange takes advantage of the electrophilicity of the selenide.

The arm with this sulfenoselenoate then swings into the active site of the enzyme. There is a crystallographic molecular model of this conformation of human thioredoxin-disulfide reductase in which the arm is within the active site.[2447] The cysteine within the active site distal to the flavin (Figure 2–11) nucleophilically attacks the selenium in the sulfenoselenoate **2–167** in exchange for its cysteine (see reverse of Equation 2–136).[2452] The proximal cysteine at the flavin then nucleophilically attacks the resulting acyclic, intramolecular sulfenoselenoate, releasing the selenolate ion and forming a cystine adjacent to the flavin. This step takes advantage of the ability of the selenido group as a leaving group. The resulting disulfide, adjacent to nitrogen 5 and carbon 4a, is reduced in the normal fashion by the flavin, which in turn is reduced by NADPH.

Glutathione peroxidase serves as a paradigm for the **interaction of selenocysteine with oxides of oxygen.** The enzyme catalyzes the reaction

$$\mathrm{ROOH + 2\,GSH \rightleftharpoons ROH + H_2O + GSSG} \qquad (2\text{–}347)$$

where GSH is glutathione, and its purpose is to eliminate adventitious peroxides from the cytoplasm. There is a selenocysteine in the active site of the enzyme that participates in its catalysis. Although one might think that the enzyme is taking advantage of the superior nucleophilicity of selenocysteinate, human thioredoxin-dependent peroxiredoxin,[2453] a peroxidase that is distantly related to glutathione peroxidase[2454,2455] and in which a cysteine serves the same purpose as the selenocysteine in glutathione peroxidase, catalyzes the reduction of hydrogen peroxide at a rate[2453] comparable to that of bovine glutathione peroxidase,[2456] again belying the advantages of selenocysteine.

When bovine glutathione peroxidase has been reduced by reduced glutathione, the selenocysteine is the selenol (**2–168**)

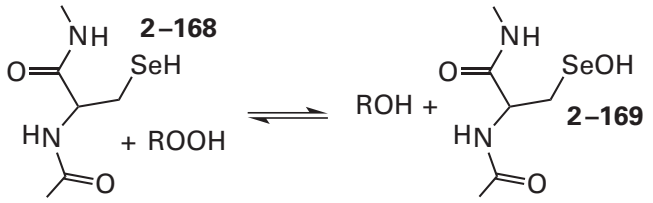

(2–348)

but when the enzyme is oxidized with a peroxide, the selenium is the **hydroxyselanyl group** (–SeOH) in a **selenenic acid** (**2–169**).[2457] From these observations, a plausible mechanism for the reduction of peroxides can be formulated (Figure 2–65),[2458] which is consistent with the kinetics of the enzymatic reaction.[2456,2459] The three exchanges—selenium for oxygen, sulfur for oxygen, and sulfur for selenium—

are all within group 16 and resemble the four exchanges that occur in the mechanism of thioredoxin-disulfide reductase.

The selenenic acid (RSeOH) has not been observed directly in glutathione peroxidase because in the crystals of the oxidized enzyme the selenol has become the seleninic acid ($RSeO_2H$).[2460] It is, however, possible to trap chemically a selenenic acid intermediate[2461] in the peroxidase reaction catalyzed by human selenoprotein S, and in a human peroxiredoxin, the sulfenic acid (RSOH) that is an intermediate in its peroxidase reaction has been observed in a crystallographic molecular model.[2454] A cysteinesulfenic acid has also been observed by nuclear magnetic resonance spectroscopy in yet another peroxidase in which it is an intermediate in the enzymatic reaction.[2462] Finally, there is a synthetic selenol that is able to catalyze the reduction of *tert*-butyl hydroperoxide by benzylsulfide in a mechanism equivalent to that drawn in Figure 2–65,[2463] and replacing the cysteine in the active site of the endopeptidase subtilisin with a selenocysteine converts it to a peroxidase.[2464,2465]

Glycine reductase from *Acetoanaerobium sticklandii* catalyzes the reaction

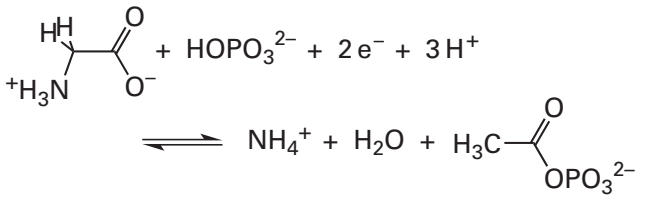

(2–349)

The enzyme catalyzes the reaction by a mechanism (Figure 2–66) that involves a selenocysteine and a posttranslation modification that has produced the modified amino-terminal amino acid, *N*-pyruvoylvaline (see Equation 2–45). There are three proteins participating in the catalysis.[2466] One contains the *N*-pyruvoyl group that catalyzes the **deamination**.[2467,2468] Another contains the selenocysteine[2425] as well as the cysteine that is the nucleophile accomplishing the deselenation and producing the sulfenoselenoate. The third protein contains the cysteine that forms the thioacyl intermediate in a **thioacylation** that is necessary for the stabilization of the enolate that leaves during the **deselenation**.[2467,2469] This last protein, by itself, then catalyzes the phosphorolysis of the resulting *S*-acetylcysteine that was formed at its active site to give acetyl phosphate.

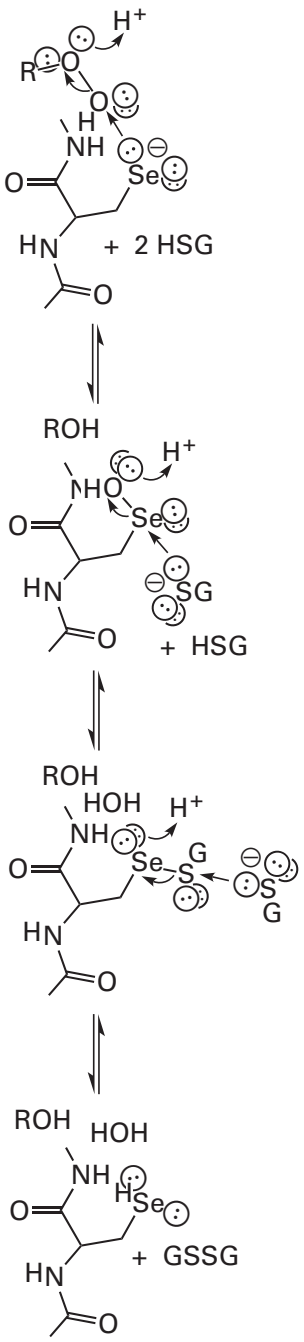

Figure 2–65: Mechanism for the reduction of peroxides catalyzed by glutathione peroxidase.[2458] The mechanism is a series of reactions, each analogous to selenol–diselenide exchange or thiol–disulfide exchange. The selenolate ion is used in the first step because it is a stronger nucleophile than sulfur and more able to cleave the oxygen–oxygen bond of the peroxide heterolytically. In the second step, the greater electrophilicity of selenium facilitates the nucleophilic attack of the sulfido group of glutathione upon the selenium, with water or hydroxide as the leaving group. In the last step, the sulfido group of glutathione performs a thiol–sulfenoselenoate exchange to regenerate the selenol and produce oxidized glutathione.

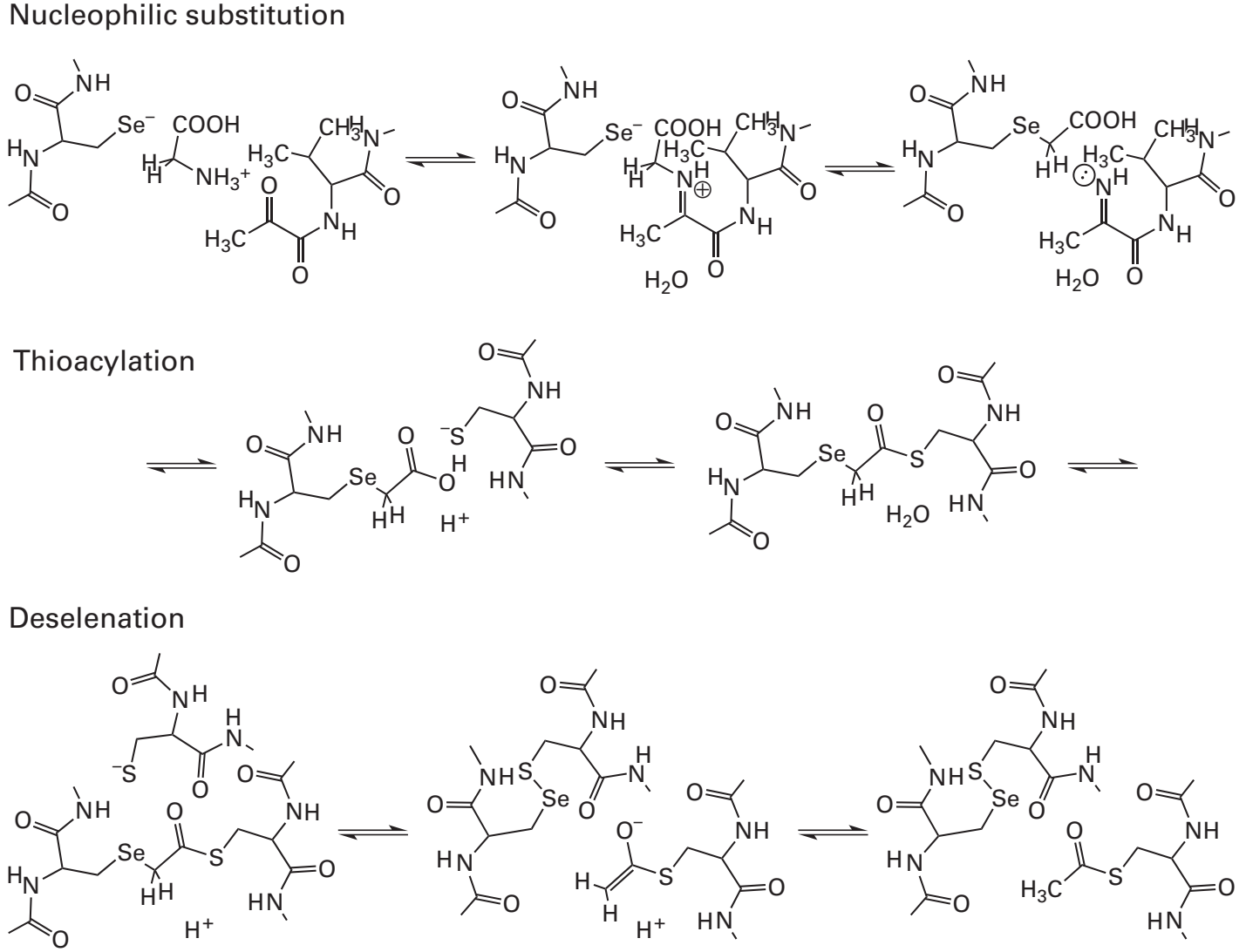

Figure 2–66: Mechanism for the reductive deamination of glycine catalyzed by glycine reductase.[2425,2466-2471] The overall mechanism can be divided into three transformations: nucleophilic substitution of a nitrogen with a selenium, thioacylation of a carboxy group, and deselenation of the α carbon of the thioester. During the nucleophilic substitution, glycine forms an imine with an *N*-pyruvoyl group at the amino terminus of one of the three proteins catalyzing the overall reaction. The imine ($pK_a \cong 8$) should be a better leaving group than ammonia ($pK_a = 9.2$), and the selenolate ion of a selenocysteine in the second protein catalyzing the reaction is the nucleophile. A selenoether is the product of the nucleophilic substitution of selenium for nitrogen at the primary carbon. The pyruvoyl imine hydrolyzes to produce ammonia, one of the products of the reaction, and to regenerate the *N*-pyruvoyl group (not shown). During thioacylation, a cysteine in the third protein catalyzing the overall reaction participates in a nucleophilic substitution at the unactivated carboxy group of *Se*-(carboxymethyl)selenol to produce the thioester, which activates the acyl group. During deselenation, the sulfido group of a cysteine from the second protein catalyzing the overall reaction, the same protein in which the selenocysteine is located, is the nucleophile in a nucleophilic substitution at selenium in which the enolate or enol of the thioacetyl group leaves and the intramolecular sulfenoselenoate is formed. The enolate is hydronated to form the thioacetyl group. The thioester is phosphorolyzed to produce acetyl phosphate (not shown), one of the products of the overall reaction, and to regenerate the unmodified cysteine. The sulfenoselenoate is reduced to regenerate the selenocysteine and the cysteine (not shown). Because four different amino acid side chains and three different proteins are involved in the overall reaction, only the side chains involved in the particular transformation are included in the respective drawing to avoid confusion. Only the hydrons needed are included in each transformation.

The *Se*-carboxymethylselenocysteine produced by the deamination[2470] in the active site of glycine reductase has been produced by direct alkylation of the selenocysteine by bromoacetate and shown to participate in the thioacetylation and the deselenation,[2471] and the intermediate sulfenoselenoate in the deselenation has been isolated.[2470] The third protein by itself catalyzes the exchange of [^{32}P]phosphate into acetyl phosphate, a reaction that relies on the protein establishing the equilibrium of the phosphorolysis of the *S*-acetylcysteine, and this third protein catalyzes the formation of *S*-acetyl-cysteine within itself upon the addition of acetyl phosphate.[2467]

Suggested Reading

Boyington, J. C., Gladyshev, V. N., Khangulov, S. V., Stadtman, T. C., and Sun, P. D. (1997) Crystal structure of formate dehydrogenase H: Catalysis involving Mo, molybdopterin, selenocysteine, and an Fe_4S_4 cluster. *Science 275*, 1305–1308. https://doi.org/10.1126/science.275.5304.1305

Back, T. G., and Dyck, B. P. (1997) A novel camphor-derived selenenamide that acts as a glutathione peroxidase mimetic. *J. Am. Chem. Soc. 119*, 2079–2083. https://doi.org/10.1021/ja963602k

Problem 2–38: Write out the mechanism of formate dehydrogenase.

Problem 2–39: Write out the exchanges among disulfides and sulfenoselenoates performed by thioredoxin-disulfide reductase..

Problem 2–40: For each step in the mechanism for glycine reductase in Figure 2–66 in which it is involved, state the advantage that selenocysteine has over cysteine.

Cobalamins

Cobalamin (**2–172**) is a prosthetic group that contains a cobalt ion

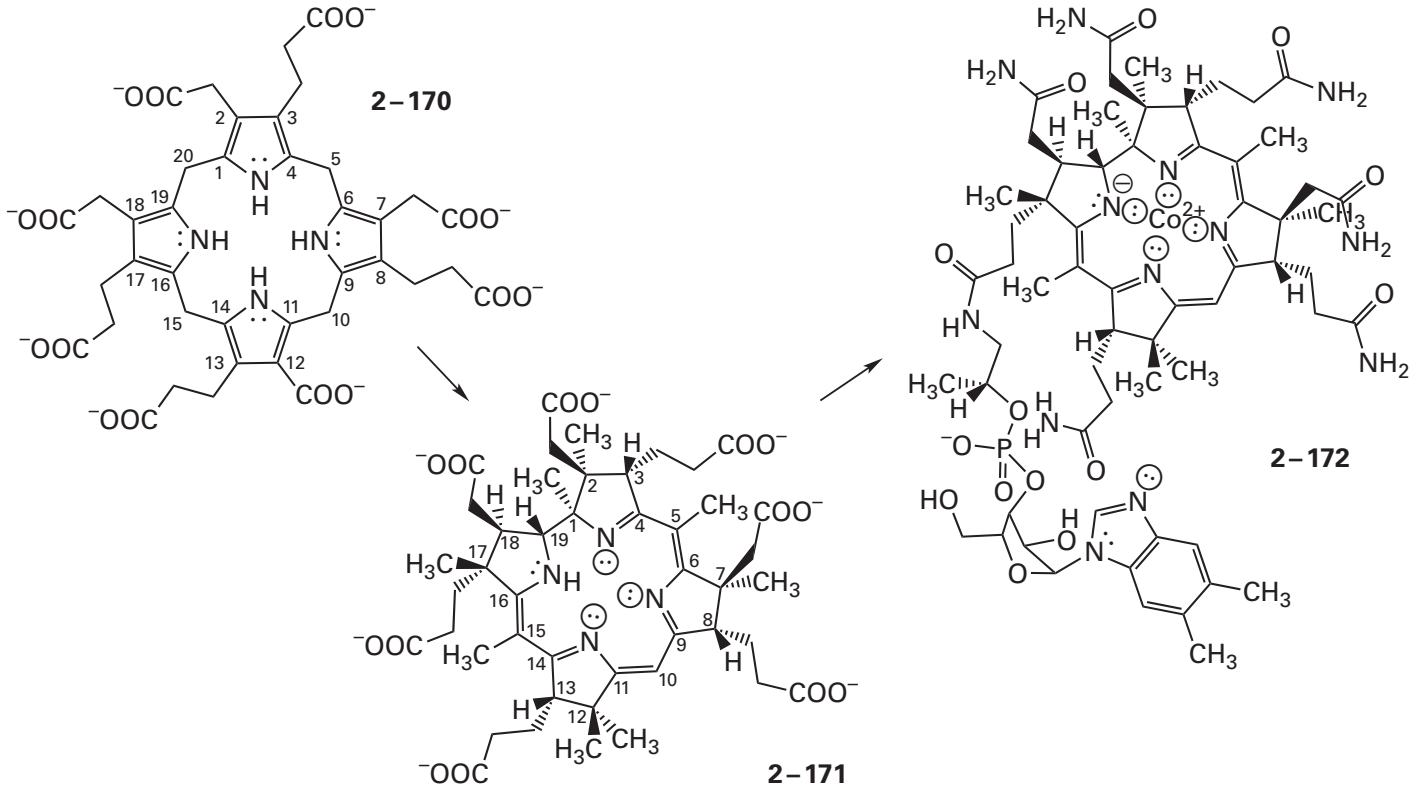

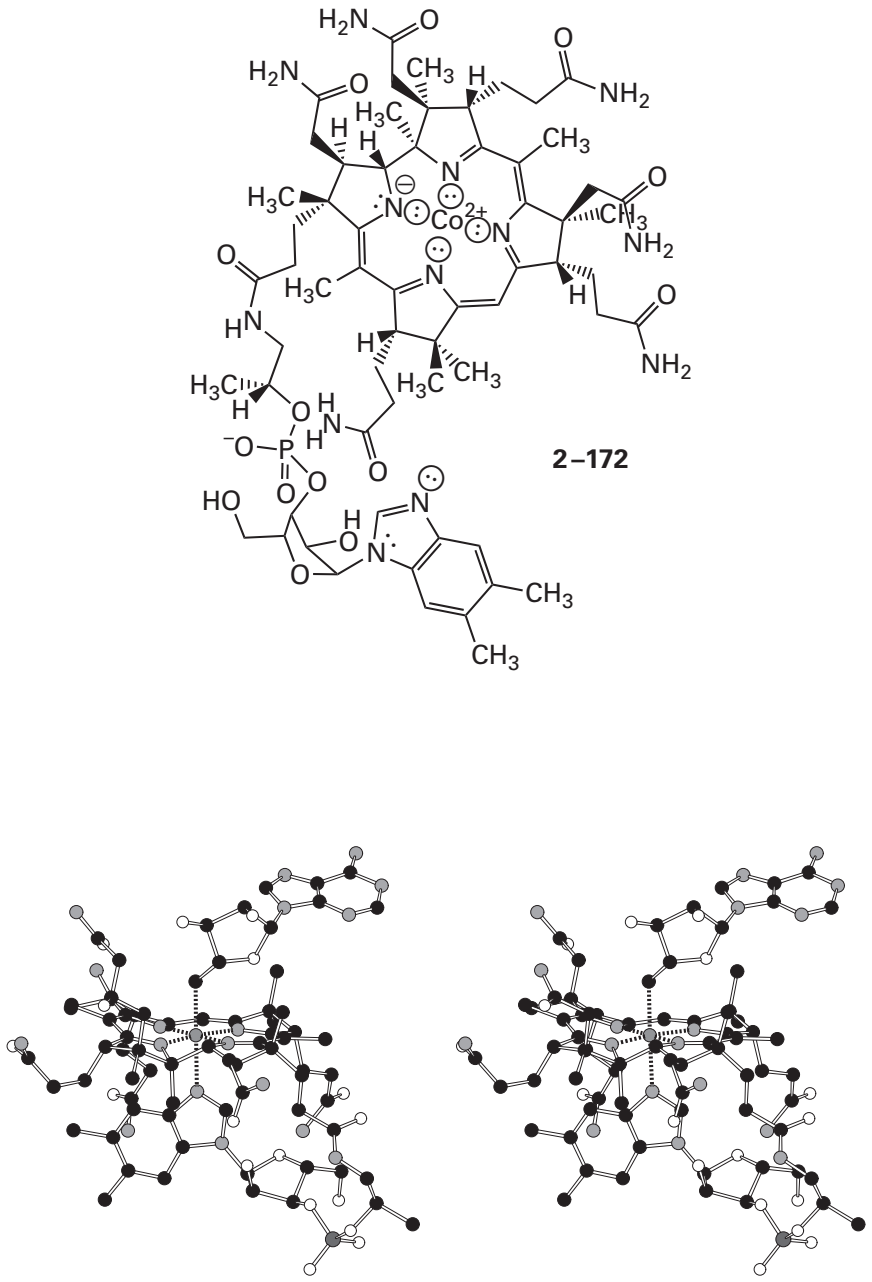

2–172

Figure 2–67: Crystallographic molecular model of adenosylcobalamin.[2472] Crystals were produced by slowly diffusing acetone into a concentrated solution of adenosylcobalamin in water. The drawing of the chemical structure of cobalamin (**2–172**), which is adenosylcobalamin without the adenosyl ligand, can be used as a guide to the stereodrawing[50] of the crystallographic molecular model built from maps of electron density derived from a crystallographic analysis. Black atoms are carbons, white atoms are oxygens, gray atoms are nitrogens, and the small gray sphere is the cobalt ion surrounded by its ligands.

Four of the ligands around the cobalt ion are lone pairs of electrons from the four central nitrogens in a **corrinoid**. The corrinoids are a group of compounds containing four reduced pyrrole rings joined into a macrocyclic ring by links between their α positions; three of these links are formed by one-carbon units and the other by a direct carbon–carbon bond. The tetrapyrrole that forms the core of a corrinoid, when it is completely unsubstituted and uncoordinated to a cobalt ion, is the heterocycle **corrin**.

As is the porphyrin in heme *b* or siroheme, the corrinoid that coordinates the cobalt ion in cobalamin is derived biosynthetically from the tetrapyrrole uroporphyrinogen III (**2–170**). One of the corrinoids along the aerobic biosynthetic pathway through which cobalamin is constructed is hydrogenobyrinic acid (**2–171**)

To form **cobyrinic acid,** a cobalt ion replaces the one acidic hydron of hydrogenobyrinic acid (**2–171**)

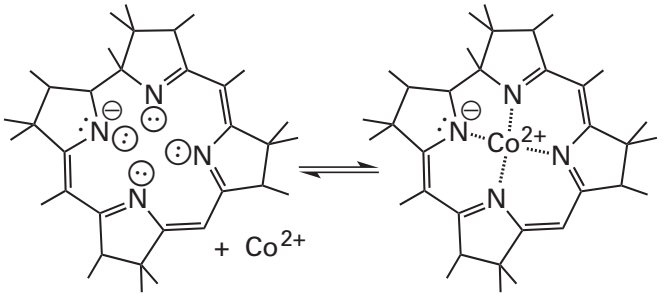

(2–350)

In the actual aerobic biosynthetic pathway, however, a Co^{2+} is not inserted into hydrogenobyrinic acid until it is modified by amidation of the carboxymethyl groups at positions 2 and 7. This insertion produces cob(II)byrinic acid *a*,*c*-diamide.

In cobalamin (**2–172** in Figure 2–67),[2472] six of the seven carboxylates of hydrogenobyrinic acid are **primary amides** and the seventh is an amide formed with (*R*)-1-amino-*O*-[1-(5,6-dimethylbenzimidazol-1-yl)-3-phospho-α-D-ribofuranosyl]propan-2-ol.* When the seventh amide is the one formed with only (*R*)-1-aminopropan-2-ol and there is no cobalt coordinated, the corrinoid is **cobinamide**.

A corrinoid, unlike a porphyrin, is **not aromatic** because saturation at several locations prevents it from having an unbroken ring of *p* orbitals. The tetrapyrrole ring is also one carbon smaller than a porphyrin because during its biosynthesis from uroporphyrinogen III (**2–170**), one of the methylene carbons connecting two of the pyrroles is removed, turning a porphyrin into a corrinoid. This ring contraction, however, would have no effect on the aromaticity. If the tetrapyrrole were still as unsaturated as it is in protoporphyrin, it would be aromatic.

The axial ligand in cobalamin (Figure 2–67)[2472] is a lone pair of electrons from nitrogen 3 of the intramolecular **5,6-dimethylbenzimidazolyl group**

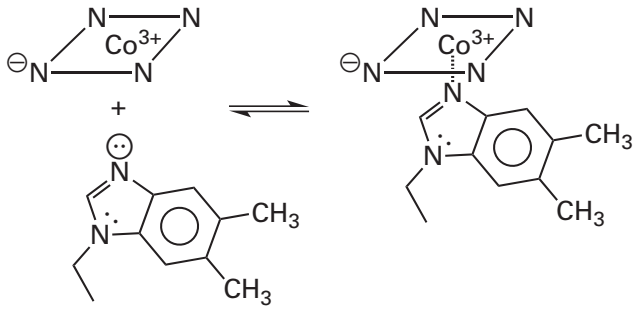

(2–351)

that is covalently attached to the cobinamido group in cobalamin in an α-N-glycosidic linkage to a ribose that is in turn attached through a phosphate diester to the hydroxy group of the (*R*)-1-aminopropan-2-ol.

When cobalamin is a prosthetic group in an enzyme, it is usually alkylated at the open axial position on its cobalt. An alkylcobalamin is an **organocobalt compound**, and the source of its reactivity is its carbon–cobalt bond. In **adenosylcobalamin** (Figure 2–67), the open axial position on the formal Co^{3+} is occupied by a formal 5′-deoxy-5′-adenosyl carbanion

*From here on, the corrinoid of cobalamin will be abbreviated, as was a porphyrin, by a square with four nitrogens at its vertices.

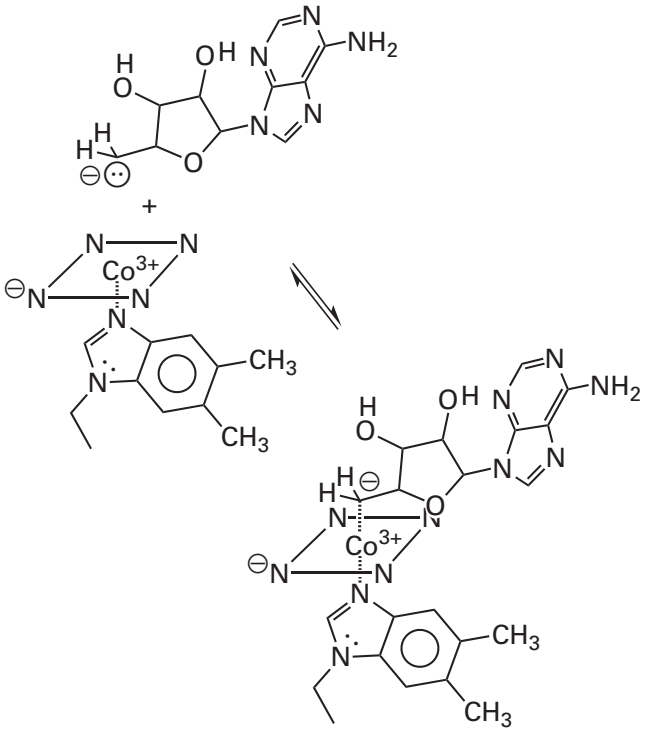

(2–352)

In **methylcobalamin**, a methyl group, formally a carbanion participating in a carbon–cobalt bond with the formal Co^{3+}, is the axial ligand to the cobalt in its cobalamin. Unlike the carbon in an organolithium compound or an organomagnesium compound, the carbon in an organocobalt compound such as adenosylcobalamin or methylcobalamin is much less carbanionic. When it is unalkylated, cobalamin coordinating a Co^{3+} can be **aquocobalamin** or **hydroxycobalamin**, in which the oxygen of a molecule of water or a hydroxide, respectively, is the axial ligand. Commercially, cobalamin is sold as the vitamin cyanocobalamin, in which cyanide is the axial ligand.

The cobalt in a cobalamin can be in the +3, +2, or +1 **oxidation state**, which is indicated as, for example, methylcob(III)alamin, cob(II)alamin, or cob(I)alamin, respectively. The standard reduction potential in solution for the reduction of aquocob(III)alamin to cob(II)alamin is +220 mV, and that for the reduction of cob(II)alamin to cob(I)alamin is –630 mV.[2473,2474] Upon the first reduction, the molecule of water dissociates, and upon the second reduction, which forms cob(I)alamin, the 5,6-dimethylbenzimidazolyl group dissociates from the cobalt, leaving both axial positions vacant. Cob(I)alamin is a strong reductant and may act as a one-electron donor in the microbial reduction of perchloroethylene to trichloroethylene,[2475] but usually cobalamins do not participate in productive oxidation–reduction reactions in biochemical situations. Cob(I)alamin, however, because of its susceptibility to oxidation, can be adventitiously oxidized to cob(II)alamin.

When adenosylcobalamin or methylcobalamin is incorporated as a tightly bound[2476] prosthetic group into the active site of an enzyme, the 5,6-dimethylbenzimidazolyl group usually, but not always,[2477,2478] swings well away from the cobalt as it does in solution upon reduction to cob(I)alamin, and is **replaced by the imidazolyl group of a histidine** in the protein (Figure 2–68).[2479-2486] In this way the enzyme is able to modulate the reactivity of the carbon–cobalt bond more effectively by controlling the environment around this histidine.[2487] When the cobalt is in the oxidation state of +1 (Co^{+}), the histidine can dissociate and swing away.[2488]

Many **organometallic compounds,** such as organolithium, organomagnesium, organocadmium, and organocopper compounds, react heterolytically. In these heterolytic reactions, the carbon participating in the carbon–metal bond acts as if it were a nucleophilic carbanion, and the dissociating metal ends up as its most stable cation. The reactivity of the carbanion in such situations is determined by the ionic character of the bond.[2489] In theory, a carbon–cobalt bond should have about the same ionic character as a carbon–copper bond. Were the carbon–cobalt in adenosylcobalamin to cleave heterolytically, the products would be 5′-deoxyadenosyl anion and cob(III)alamin.

In fact, alkylcobalamins such as methylcobalamin, unlike alkylmagnesium compounds such as methylmagnesium chloride, are electrophilic rather than nucleophilic at carbon. Methylcobalamin in solution reacts with 2-sulfanylethanol as an electrophilic methylating agent

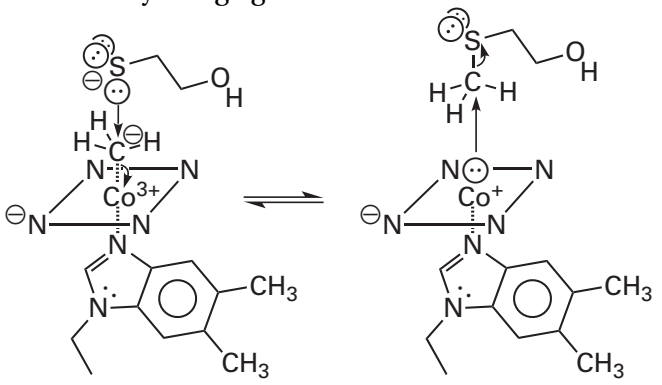

(2–353)

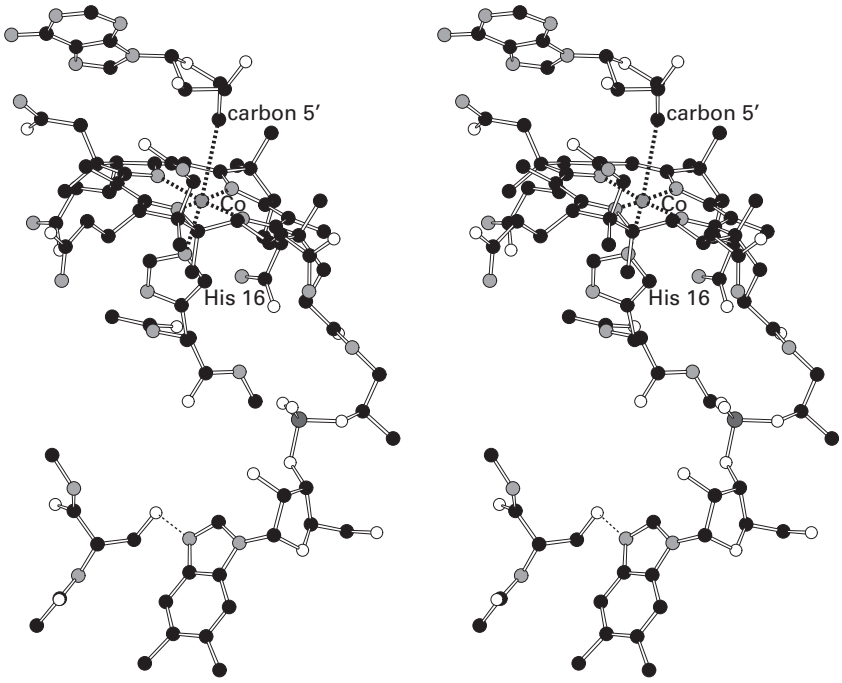

Figure 2–68: Stereodrawing[50] from the crystallographic molecular model of adenosylcobalamin in the active site of methylaspartate mutase from *C. cochlearium*.[2479,2483] Black atoms are carbons, white atoms are oxygens, gray atoms are nitrogens, and the small gray sphere is the cobalt ion surrounded by its ligands. The gene for the protein from *C. cochlearium* was expressed in *E. coli*, and the resulting enzyme was purified and crystallized. Data were gathered to Bragg spacing of 0.19 nm. The enzyme is an $\alpha_2\beta_2$ heterotetramer with two symmetrically positioned active sites in each tetramer. The crystallographic asymmetric unit is the heterotetramer. In the map of electron density, in each active site, two conformations of the adenosyl group can be discerned.[2479] The conformation in the drawing is the one in which carbon 5′ is closest to the cobalt ion (Co) and is an axial ligand. Upon association of adenosylcobalamin with the enzyme, the 5,6-dimethylbenzimidazolyl group swings out of coordination with the cobalt, and the imidazolyl group of Histidine 16 takes its place. Nitrogen 3 of the 5,6-dimethylbenzimidazolyl group forms a hydrogen bond with the hydroxy group of a serine (lower left) in the active site.

and the leaving group is cob(I)alamin.[2490] This nonenzymatic methylation is equivalent to the methylation of L-homocysteine performed enzymatically by the intermediate prosthetic methyl-cob(III)alamin in the active site of methionine synthase

5-methyltetrahydrofolate + L-homocysteine
⇌ tetrahydrofolate + L-methionine
(2–354)

In the active site of methionine synthase, the 5,6-dimethylbenzimidazolyl group of the prosthetic cobalamin has been replaced by the imidazolyl group of a histidine, and the sulfido group of the L-homocysteine upon its association with the active site is a ligand to a Zn^{2+}, which ensures that it remains unhydronated and nucleophilic.[2491] The enzymatic reaction is the simple direct, concerted nucleophilic substitution at the methyl group of the Co^{+} by the anionic conjugate base of the sulfanyl group of L-homocysteine (see Equation 2–353).

A dehalogenase from *Nitratireductor pacificus* reductively dehalogenates 2,2-dichloro- and 2,2-dibromophenols. The dehalogenation is a reduction because chloride or bromide, in each case the final product, is replaced at the ortho position by a hydron, a substitution that requires two electrons. The chlorine or bromine that is removed from the phenol ends up at first as a chlorocob(II)alamin or a bromocob(II)alamin, respectively. The chlorocob(II)alamin has been observed in a crystallographic molecular model of the enzyme.[2492] These observations suggest that in the formal electrophilic aromatic substitution of the halogen for a hydrogen that occurs ortho to the hydroxy group of the phenol, the actual leaving group is the **electrophilic chlorocob(III)alamin** or bromocob(III)alamin, which is then immediately reduced by one electron from an adjacent [4Fe–4S] iron–sulfur cluster to chlorocob(II)alamin or bromocob(II)alamin. The chlorocob(III)alamin or bromocob(III)alamin would dissociate from the intermediate 2,6-dichlorocyclo-hexa-2,4-dien-1-one or 2,6-dibromocyclohexa-2,4-di-en-1-one coordinated to the initial cob(I)alamin through the chlorine or bromine that is substituted. This intermediate 2,6-dihalo-2,4-cyclohexadien-1-one would be formed by hydronation of the reactant at the position from which the halogen is removed as in the usual electrophilic aromatic substitution. There is a second [4Fe–4S] iron–sulfur cluster in the enzyme, so the two electrons needed for reductive substitution of a chloride or bromide by a hydron can be supplied on site. The second electron reduces chlorocob(II)alamin or bromocob(II)alamin to the respective cob(I)alamin from which the halide dissociates.

Cob(I)alamin is a strong nucleophile. Cobalt(I) has an even number of electrons (8 valence electrons). In cob(I)alamin, there is a nucleophilic lone pair of electrons on the cobalt in the axial position. Cob(I)alamin reacts nucleophilically with primary alkyl halides[2493] and with secondary alkyl halides under acidic conditions[2494] to yield alkylcobalamins

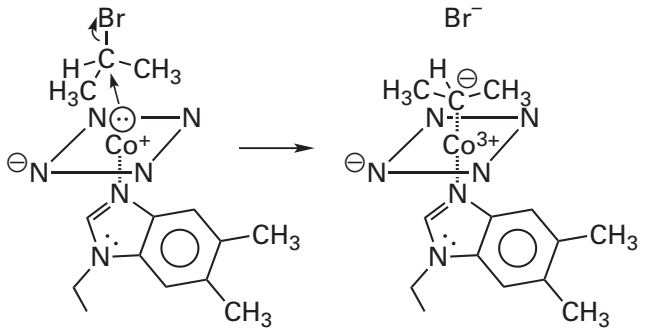

(2–355)

The cob(I)alamin produced upon methylation of L-homocysteine by methionine synthase (see Equations 2–353 and 2–354), or upon methylations catalyzed by other methyltransferases that use cobalamin as a prosthetic group, is the nucleophile in transfer of the methyl group of 5-methyltetrahydrofolate to the cobalt in a direct, concerted nucleophilic substitution

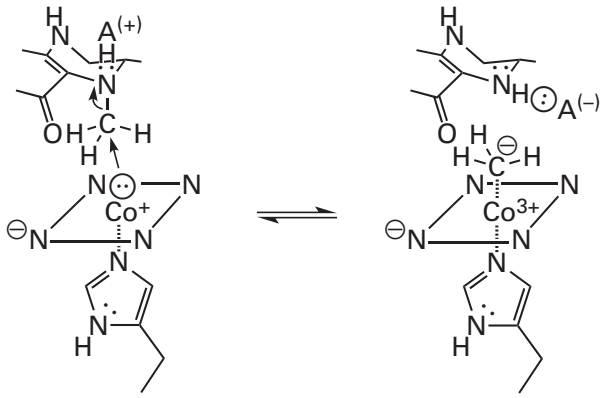

(2–356)

that regenerates the methylcobalamin.[2495,2496] The cob(I)alamin participating as the nucleophile in the direct, concerted nucleophilic substitutions performed by the enzymes is often adventitiously inactivated by oxidation to cob(II)alamin ($E^{\circ\prime} \cong -430$ mV on an enzyme), and there are strategies specific to each of

the enzymes for rereducing it[2497-2500] to retain enzymatic activity.

Adenosylcobalamin is synthesized biochemically by the direct, concerted nucleophilic attack of cob(I)alamin on carbon 5′ of $MgATP^{2-}$ in which magnesium triphosphate is the leaving group.[2501] In the active site of the enzyme that catalyzes this substitution, the side chains of a phenylalanine and a tryptophan at one of the axial positions of the cobalt ion exclude an axial ligand and raise its biochemical standard reduction potential so that it can be maintained in the nucleophilic Co^{+} oxidation state.[2502]

A cob(I)amide is the nucleophile that accepts the methyl group of methanol in one of the several steps in the **production of methane** in certain bacteria.[2503-2505] The cob(I)amide, with the imidazolyl group of a histidine replacing the benzimidazolyl group, nucleophilically attacks the carbon of methanol in a direct, concerted nucleophilic substitution

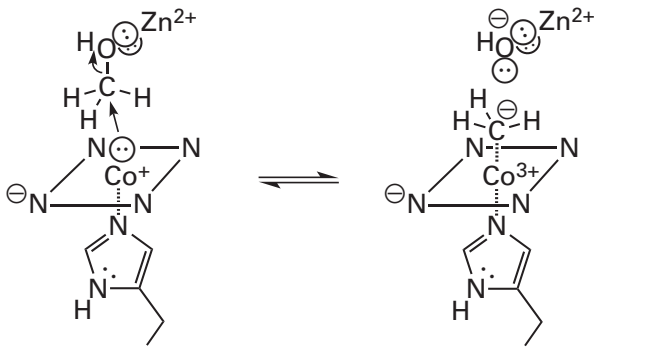

(2–357)

under Lewis acid catalysis by a Zn^{2+} in the active site that is coordinated by the hydroxy group of the methanol.[2485] The methyl group is then transferred in a second direct, concerted nucleophilic substitution (see Equation 2–353) to 2-sulfanylethanesulfonate, known as coenzyme M, abbreviated as HSCoM. The resulting 2-(methylsulfanyl)ethanesulfonate, methyl-SCoM

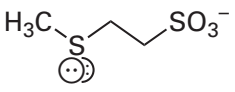

2–173

is the source of the methyl group converted to methane in all methanobacteria. Butyl-SCoM is converted by certain archaea into butane.[2506]

The enzyme catalyzing the actual production of methane is coenzyme-B sulfoethylthiotransferase

(2–358)

where coenzyme B, abbreviated as CoBSH, is *N*-(7-sulfanylheptanoyl)-L-threonine 3-*O*-phosphate

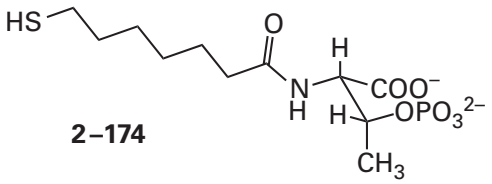

2–174

Kinetic isotopic effects indicate that the rate-limiting step in the production of methane by the enzyme is the breaking of the carbon–sulfur bond in methyl-SCoB for which the transition state involves a trigonal methyl group.[2511]

The nucleophilic prosthetic group in coenzyme-B sulfoethylthiotransferase is **coenzyme F_{430}**

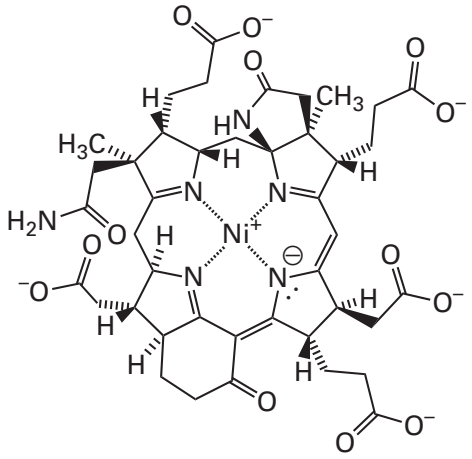

2–175

Coenzyme F_{430} is an extensively saturated, modified, nonaromatic porphyrin that contains **nickel(I) rather than cobalt(I)**. The porphyrin in coenzyme F_{430} is also derived from uroporphyrinogen III (**2–170**). As with cobalamin, the metallic ion replaces a single hydron from the conjugate acid of the porphyrin (see Equation 2–350).[2507,2508] The Ni^{+} in coenzyme F_{430} is poorly coordinated by water[2509] and is extremely nucleophilic,[2488] and when it is in the active site of coenzyme-B sulfoethylthiotransferase, it can react with methyl bromide to give a methylnickel(III).[2510,2511] Even though a methylnickel(III) can be formed in the active site when an analogue of coenzyme B, which is shorter by one methylene group, is used as a substrate for coenzyme-B sulfoethylthiotransferase

from *Methanothermobacter marburgensis*,[2513] this methylnickel(III) may not be an intermediate in the normal enzymatic reaction. This conclusion follows from the observation that an adduct between the nickel and a sulfur, rather than between nickel and a methyl group, has been identified by magnetic circular dichroism spectroscopy as an intermediate in the active site of the enzyme.[2512] Consequently, the reaction may involve a nucleophilic substitition at sulfur rather than carbon.

The majority of the enzymatic reactions in which adenosylcobalamin participates as a prosthetic group can be written as variations on a common enzymatic theme that is completely different from that of the direct, concerted nucleophilic substitutions in which methylcobalamin participates. Formally, a hydrogen atom in the reactant for the enzyme undergoes a **1,2 migration in concert with a reciprocal 2,1 migration** by one of the substituents on the carbon to which the hydrogen moves

(2–359)

where each pair of substituents, R_1 and R_2 or R_3 and R_4, can be two hydrogens, a hydrogen and an alkyl group, a hydrogen and a hydroxy group, or a hydrogen and a carboxy group. Consequently, the carbons between which the substituents migrate can be electron-donating or electron-withdrawing or neither. Either **inversion or retention of configuration** at each of the two carbon occurs, depending upon the particular enzyme,[2514] and this requires that the mechanism of the catalysis performed by adenosylcobalamin be consistent with either stereochemical outcome. One of the two participants migrating is always a hydrogen, but the other can be any one of a number of apparently unrelated functional groups (Table 2–3). An example of one of these reactions is that catalyzed by bovine methylaspartate mutase. This reaction proceeds with inversion of configuration at carbon 3[2514] when [3-^{2}H]-L-*threo*-3-methylaspartate is used as a reactant

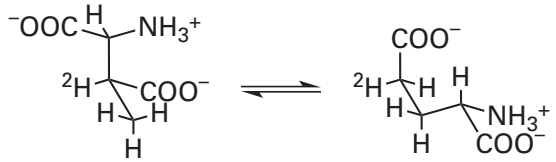

(2–360)

Table 2–3: Substituents Migrating in Reactions Catalyzed by Adenosylcobalamin

enzyme	X in Equation 2–359
ethanolamine ammonia-lyase[2515]	$-NH_3^+$
propanediol dehydratase[2516]	$-OH$
lysine 5,6-aminomutase[2517,2518]	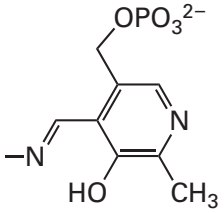
D-ornithine 4,5-aminomutase[2519]	
methylaspartate mutase[2520]	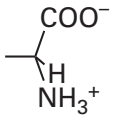
methylmalonyl-CoA mutase[2521]	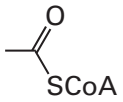
ethylmalonyl-CoA mutase[2522]	
2-hydroxyisobutanoyl-CoA mutase[2523]	
isobutyryl-CoA mutase[2521,2524,2525]	
2-methyleneglutarate mutase[2526]	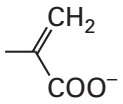

In reactions catalyzed by adenosylcobalamin as a prosthetic group, the hydrogen that formally migrates across the reactant (Equation 2–359) does not exchange with hydrons in the solvent.[2527] If, however, reactant labeled at this hydrogen is mixed with the appropriate enzyme, the hydrogens at carbon 5′ of the 5′-deoxy-5′-adenosyl group of the adenosylcobalamin become labeled; or if the 5′-deoxy-5′-adenosyl group is labeled on carbon 5, the hydrogens on the reactant become labeled,[2528,2529] as in

the isotopic exchange catalyzed by propanediol dehydratase from *Klebsiella aerogenes*

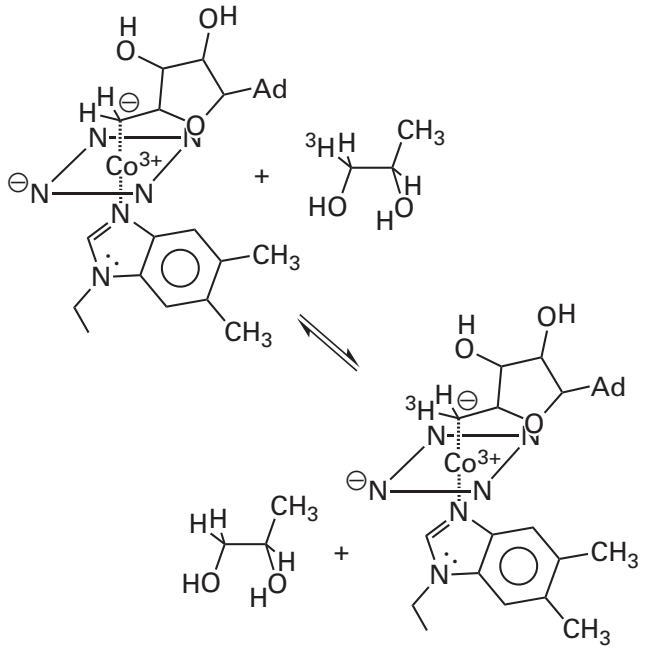

(2–361)

where Ad is an adenin-9-yl group. The **hydrogens equilibrating between substrates and carbon 5′ of the 5′-deoxy-5′-adenosyl group** of the prosthetic group do so in such a way that they occupy one of three equivalent locations when they enter carbon 5′ of the deoxyadenosine,[2527] so it must be the case that 5′-deoxyadenosine itself, which has a methyl group at the 5′ position, rather than adenosylcobalamin, is an intermediate.

All these observations are consistent with the existence of a step in the mechanism for the normal enzymatic reactions in which the carbon–cobalt bond of the adenosylcobalamin dissociates, **the hydrogen that is to migrate is transferred to the adenosyl group**, and the products of these two steps are 5′-deoxyadenosine and some form of the substrate lacking the hydrogen. When 2-aminopropanol, a slower (0.7%) substrate[2529] than the normal reactant 2-aminoethanol, is added to ethanolamine ammonia-lyase from *Clostridium*, the carbon–cobalt bond of adenosylcobalamin dissociates rapidly to produce 5′-deoxyadenosine and cob(II)alamin. This intermediate, containing the dissociated prosthetic group, is still fully active in the normal ethanolamine ammonia-lyase reaction,[2530] a fact consistent with the conclusion that this dissociated form of adenosylcobalamin is an intermediate in the normal enzymatic reaction. The 2-aminopropanol, because the isomerization that occurs in the next step of its enzymatic reaction is so slow that it becomes rate-limiting, causes the enzyme to accumulate in the intermediate state in which the carbon–cobalt bond has dissociated and the hydrogen on carbon 1 of 2-aminopropanol has been transferred to carbon 5′ of deoxyadenosine but the isomerization of the dehydro reactant has not yet occurred.

The form of the reactant in the intermediate state of an enzymatic reaction catalyzed by adenosylcobalamin, immediately after the carbon–cobalt bond has dissociated and the 5′-deoxyadenosine has been produced, could be the carbenium ion of the dehydro reactant and cob(I)alamin, the radical of the dehydro reactant and cob(II)alamin, or the carbanion of the dehydro reactant and cob(III)alamin. To produce one of these three outcomes, the initial step in the reaction would be dissociation of the carbon–cobalt bond of the adenosylcobalamin to produce a 5′-deoxy-5′-adenosyl carbenium ion, a 5′-deoxy-5′-adenosyl radical, or a 5′-deoxy-5′-adenosyl carbanion that then removes the appropriate hydride, hydrogen atom, or hydron, respectively, from the reactant for the enzyme. An intermediate 5′-deoxy-5′-adenosyl carbenium ion is unlikely, as it should rearrange immediately by an intramolecular 4′,5′-hydride migration to the more stable 5′-deoxy-4′-adenosyl carbenium ion. In fact, under basic conditions, 5′-deoxy-5′-adenosylcobaloxime dissociates heterolytically to give cob(I)aloxime and 4′,5′-dehydroadenosine, the conjugate base of the 5′-deoxy-4′-adenosyl carbenium ion.[2531] Both the 5′-deoxy-5′-adenosyl radical and the 5′-deoxy-5′-adenosyl carbanion, however, are so reactive that they should be able to remove a hydrogen atom or a hydron, respectively, from side chains of the amino acids surrounding them as readily as they would from the unactivated, often primary alkyl position of the reactant for the enzyme, a problem that has been solved by natural selection. In the intermediate state that accumulates when 2-aminopropanol is used as a reactant for ethanolamine ammonia-lyase,[2530] the cobalt is in oxidation state Co^{+2}. This observation is most consistent with an intermediate radical of the reactant, but it could also be consistent with a carbanionic intermediate if that carbanionic intermediate has at some point transferred an electron to the cob(III)alamin because of the wait resulting from using the slow reactant.

In the currently accepted mechanism, however, for the isomerizations catalyzed by adenosylcobalamin, the first step is homolytic cleavage of the carbon–cobalt bond of the adenosylcobalamin to yield 5′-deoxy-5′-adenosyl radical and cob(II)alamin*

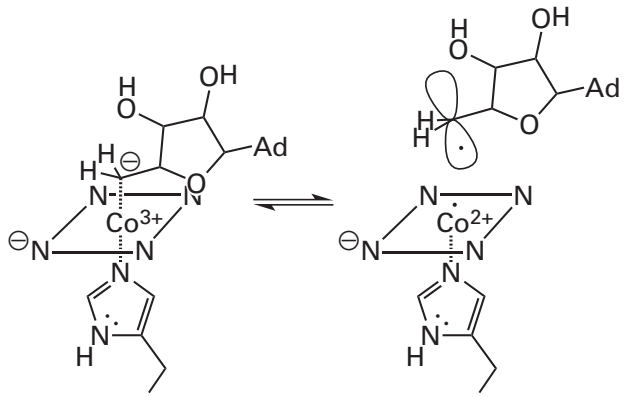

(2–362)

When ethanolamine ammonia-lyase from *Clostridium*,[2532] methylmalonyl-CoA mutase from *Propionibacterium freudenreichii*,[2533] methylaspartate mutase from *Clostridium tetanomorphum*,[2534] or D-ornithine 4,5-aminomutase from *A. sticklandii*,[2535] each containing its full complement of adenosylcobalamin, is mixed with its reactant, there is a rapid decrease in its absorbance at 525 nm and increase in its absorbance at 475 nm, as expected if the adenosylcobalamin has been converted into cob(II)alamin. This **appearance of cob(II)alamin** is rapid enough to be a step in the overall enzymatic reaction and accounts for 20–30% of the adenosylcobalamin on the enzyme at equililbrium. 5′-Deoxyadenosine is also formed in the active site of methylaspartate mutase from *C. tetanomorphum* rapidly with the same rate constant as that for the formation of cob(II)alamin.[2536] In crystallographic molecular models of active sites that are occupied by their substrates or by substrate analogues, the carbon–cobalt bond often has broken,[2482,2537-2539] but crystallography cannot distinguish whether the products are those of heterolytic or homolytic dissociation or what the products were in the first instant after dissociation of the carbon–cobalt bond.

Upon mixing propanediol dehydratase from *K. aerogenes* with 1,2-propanediol,[2540] methylaspartate mutase from *Clostridium cochlearium* with L-glutamate,[2541-2543] ethanolamine ammonia-lyase from *S. typhimurium* with ethanolamine,[2544-2546] or methylmalonyl-CoA mutase from *P. freudenreichii* subsp. *shermanii* with (*R*)-methylmalonyl-SCoA,[2547] a **neutral radical of the respective reactant** or a neutral radical of the already rearranged reactant, in which the localized unpaired electron occupies the carbon from which or to which the hydrogen migrates (Equation 2–359), respectively, also forms rapidly in 20–50% yield. The cob(II)alamin and the radical of the reactant are in an equilibrium with the ternary complex of reactant or product and undissociated adenosylcobalamin.[2548] These observations are consistent with homolytic cleavage of the carbon–cobalt bond of adenosylcobalamin (Equation 2–362) followed immediately by the removal of a hydrogen atom from the appropriate carbon of the reactant by the 5′-deoxy-5′-adenosyl radical. No 5′-deoxy-5′-adenosyl radical is detected, presumably because it is unstable relative to the observed participants in the equilibrium.

In the case of propanediol dehydratase, the neutral radical present at equilibrium has been identified by **electron paramagnetic resonance spectra** as the 1,2-dihydroxypropyl radical, produced by abstraction of a hydrogen from the hydoxymethyl carbon of the 1,2-propanediol.[2549] In the case of ethanolamine ammonia-lyase, the neutral radical present at equilibrium has also been identified by electron paramagnetic resonance spectra as the 1-hydroxy-2-aminoethyl radical, produced by the abstraction of a hydrogen from the hydoxymethyl carbon of the ethanolamine, because only when [1-^{13}C]ethanolamine is used as the reactant, and not [2-^{13}C]ethanolamine, is the absorbance of the radical split in two.[2550] No 1-amino-2-hydroxyethyl radical, the product of the normal isomerization leading to product, is observed during the enzymatic reaction because rearrangement of the 1-hydroxy-2-aminoethyl radical to the 1-amino-2-hydroxyethyl radical is the rate-limiting step in the overall reaction.[2551] As soon as the rearrangement produces 1-amino-2-hydroxyethyl radical, it immediately converts to the final product. The fact that the rearrangement is rate-limiting explains why the intermediate 1-hydroxy-2-aminoethyl radical can be observed in the first place. In the case of methylmalonyl-CoA mutase, however, the radical that accumulates during the enzymatic reaction has been identified by electron paramagnetic spectroscopy as that of the properly rearranged (*R*)-methylmalonyl-SCoA,[2547] so the rate-limiting step of this

*Cob(II)alamin has one unpaired electron and is a radical, as is the 5′-deoxy-5′-adenosyl radical.

reaction must be abstraction of the hydrogen from 5′-deoxyadenosine by this radical.

As was the case when 2-aminopropanol was used as an unnatural reactant for ethanolamine ammonia-lyase, the catalytic reaction of an enzyme using adenosylcobalamin as a prosthetic group can be stopped in its tracks by using an **appropriate unnatural analogue** of the reactant or an analogue of adenosylcobalamin, and in some of these instances **intermediates consistent with a homolytic mechanism accumulate**. In the case of 2-aminopropanol and ethanolamine ammonia-lyase, 2-amino-1-hydroxy-1-propyl radical accumulates in the active site, consistent with abstraction of the hydrogen from the carbon of the hydroxymethyl group of 2-aminopropanol, just as in the normal reaction the hydrogen would be abstracted from the carbon of the hydroxymethyl group of 2-aminoethanol.[2552,2553]

When ethanolamine ammonia-lyase from *S. typhimurium* is mixed with [1,1,2,2-$^2H_4$]-2-hydroxyethylhydrazine, another unnatural analogue of ethanolamine, cob(II)alamin, [5′-^{2}H]-5′-deoxyadenosine, [1,2,2-$^2H_3$]acetaldehyde, and the radical cation of hydrazine are formed rapidly on the enzyme.[2554,2555] [1,2,2-$^2H_3$]Acetaldehyde and the radical cation of hydrazine are the products expected from the decomposition of 1-hydroxy-2-hydrazino-1-ethyl radical **2–176**

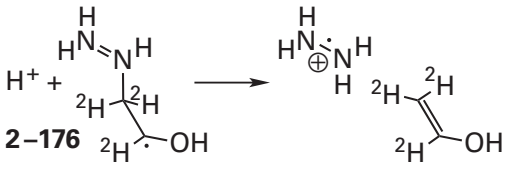

(2–363)

that is formed by abstraction of a hydrogen from the carbon of the hydroxymethyl group of 2-hydroxyethylhydrazine.

In the active site of D-ornithine 4,5-aminomutase from from *A. sticklandii*, it is actually the **pyridoximine** that forms between a prosthetic pyridoxal 5′-phosphate in the active site and the 5-amino group of the L-ornithine that migrates (Table 2–3). When D-ornithine 4,5-aminomutase is mixed with D-2,4-diaminobutyrate, an analogue one carbon shorter than D-ornithine, cob(II)alamin is formed rapidly on the enzyme.[2556] Electron paramagnetic resonance spectra identified a radical formed from the imine of D-2,4-diaminobutyrate and the prosthetic pyridoxal 5′-phosphate. In the enzymatic reaction catalyzed by lysine 5,6-aminomutase, the 6-amino group of L-lysine migrates to carbon 5

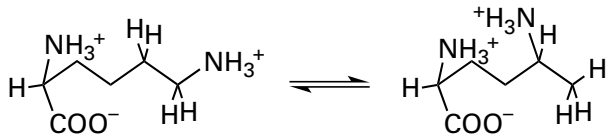

(2–364)

and again the pyridoximine forms between a prosthetic pyridoxal 5′-phosphate in the active site and the 6-amino group of the L-lysine that migrates (Table 2–3). When carbon 4 of L-lysine is replaced by a sulfur and the resulting unnatural analogue, 4-thia-L-lysine, is mixed with the enzyme from *Porphyromonas gingivalis*, one of the hydrogens on carbon 5 is abstracted by the adenosylcobalamin, and the resulting radical, which is the analogue of the radical that should be formed in the first step of the normal enzymatic reaction by abstraction of hydrogen from the pyridoximine, can be observed. The immediately adjacent sulfur at position 4 stabilizes the radical at carbon 5 by sharing the unpaired electron, and this stabilization prevents the migration of the 6-imino group.

When the hydrate of glycolaldehyde is used as an unnatural reactant for propanediol dehydratase from *K. aerogenes* (Table 2–3), the immediate product of the reaction is the stable 1-oxo-2-hydroxy-2-ethyl radical[2557,2558]

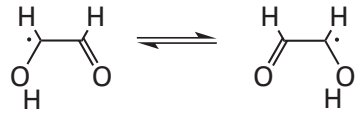

(2–365)

as expected from the removal of a hydrogen atom from the carbon of the hydroxymethyl group of the glycolaldehyde.

There are also **unnatural substrates that reveal the formation of a 5′-deoxy-5′-adenosyl radical**. When methylaspartate mutase from *C. tetanomorphum* (Table 2–3) is mixed with 2-methyleneglutarate, an analogue of the substrate L-glutamate, the carbon–cobalt bond of the adenosylcobalamin cleaves homolytically and the 5′-deoxy-5′-adenosyl radical adds to the double bond of the methylene group at the distal carbon to give a stable adduct in which the unpaired electron ends up on a tertiary carbon[2559]

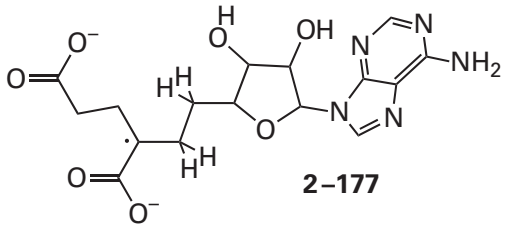

2–177

The same observation was made later with methylmalonyl-CoA mutase from *M. tuberculosis*. When methylmalonyl-CoA mutase is mixed with 2-methylenesuccinyl-SCoA, an analogue of the substrate succinyl-SCoA, the 5′-deoxy-5′-adenosyl radical generated in the active site again adds to the methylene group to give a stable adduct analogous to **2–177** with a succinyl-SCoA group rather than a glutaryl group covalently attached to the 5′-deoxy-5′-adenosyl group. In this instance, the adduct was stable enough that it could be identified unambiguously by crystallography.[2560] The 5′-deoxy-5′-adenosyl radical, however, as a radical at a primary carbon, is so unstable that when it dissociates from the adenosylcobalamin, it either abstracts a hydrogen immediately upon its formation or recolligates with cob(II)alamin, so it has not yet been observed directly in any enzyme with a prosthetic adenosylcobalamin.

Rather than an unnatural analogue of the reactant, an **unnatural analogue of adenosylcobalamin** can be incorporated into an enzyme. When adenosin-3′,4′-enylcobalamin[2561] is used as a prosthetic group in the active site of propanediol dehydratase from *K. aerogenes*, its carbon–cobalt bond cleaves upon the addition of 1,2-propanediol to the enzyme to produce a 5′-deoxyadenosin-4′,5′-en-3′-yl radical.[2562] The unpaired electron in this radical

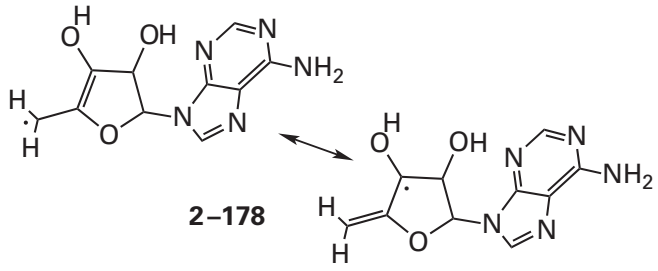

2–178

is delocalized over the immediately adjacent 4′,5′ double bond and stabilized captodatively by the 3′-hydroxy group, both effects that result in a stable intermediate insufficiently reactive to abstract a hydrogen from the 1,2-propanediol at anywhere near the rate at which the normal 5′-deoxy-5′-adenosyl radical does.[2563] Instead, the delocalized radical is reduced by the cob(II)alamin and hydrogenated to give the final product 3′,5′-dideoxyadenosin-4′,5′-ene, which registers the formation of radical **2–178**.

Several of these stable radicals that can be observed in the active site have been used to obtain estimates of the distances involved in the enzymatic reaction. These estimates are for the distances from the respective radical to either the cobalt ion in cob(II)alamin, from which the 5′-deoxy-5′-adenosyl radical dissociated, or to the methyl group of the 5′-deoxyadenosine produced during creation of the respective radical.

Analysis of the shapes of the lines in spectra from electron paramagnetic resonance,[2553,2564] spectra from X-band electron spin-echo electron paramagnetic resonance and spin-echo envelope modulation,[2565,2566] and spectra from pulsed electron–nuclear double resonance[2567] of either the radical of 2-aminopropanol or the radical of [$^2H_4$]-2-aminoethanol in the active site of ethanolamine ammonia-lyase from *S. typhimurium* all provide consistent estimates of the distance between the respective radicals and the cobalt ion in cob(II)alamin of 1.0 ± 0.1 nm. Spectra from X-band and Q-band electron paramagnetic resonance[2568] provide an estimate of distance between the radical on 4-thia-L-lysine and the cobalt ion in cob(II)alamin within the active site of lysine 5,6-aminomutase from *A. sticklandii* of 1.0 nm. In the crystallographic molecular model of the complex between (*S*)-1,2-propanediol and propanediol dehydratase from *Klebsiella oxytoca*,[2569] the distance from the cobalt of the prosthetic cobalamin to the carbons of the reactant between which the hydrogen migrates is 0.9 nm; in the crystallographic molecular model of the complex between methylaspartate mutase from *C. cochlearium* and an equilibrium mixture of L-glutamate and (2*S*,3*S*)-3-methylaspartate,[2479] the distance from the cobalt of the prosthetic cobalamin to the carbons of the substrates between which the hydrogen migrates is 0.7 nm; and in the crystallographic molecular model of the complex between methylmalonyl-CoA mutase from *P. freudenreichii* and the inhibitor *S*-2-carboxypropyl-SCoA,[2570] the distance from the cobalt of the prosthetic cobalamin to the carbons of the inhibitor between which the hydrogen would migrate in the substrates is 0.6 nm.

All these distances seem to require that, in each instance, the carbon–cobalt bond dissociates and the 5′-deoxy-5′-adenosyl radical swings over to the reactant from the cobalt ion it leaves behind before the hydrogen can be abstracted. While it is

swinging over to the reactant, it is a rather reactive 5′-deoxy-5′-adenosyl radical that can abstract a hydrogen from almost any carbon in the protein. There is, however, no such thing as empty space in a condensed solution, so the apparently empty space through which the 5′-deoxy-5′-adenosyl radical must swing between the cobalt and the reactant must be occupied by disordered molecules of water. In fact, in the crystallographic molecular model of the complex between methylmalonyl-CoA mutase from *P. freudenreichii* and *S*-2-carboxypropyl-SCoA, there are several fixed molecules of water between the cobalt ion of the cobalamin and the carbons in the inhibitor between which the hydrogen would migrate in the substrates. The reason for surrounding the 5′-deoxy-5′-adenosyl radical with molecules of water is that of all the hydrogens in the solution, the most difficult to abstract are the hydrogens on molecules of water (bond dissociation energy = 497 kJ mol^{-1}), none of which can be abstracted by a 5′-deoxy-5′-adenosyl radical (bond dissociation energy = 390 kJ mol^{-1}). In a sense, it is almost as if, during its lifetime in transit, the 5′-deoxy-5′-adenosyl radical were surrounded by vacuum as it swings over to the reactant.

The 5′-deoxyadenosine remains intimately associated with the radical of the reactant that it forms upon abstraction of the respective hydrogen. Spectra from electron spin-echo envelope modulation of the radical of [$^2H_4$]-2-aminoethanol,[2571] spectra from X-band electron spin-echo electron paramagnetic resonance and from electron spin-echo envelope modulation of the radical of 2-aminopropanol[2565] and the radical of [$^2H_4$]-2-aminoethanol,[2566] and spectra from pulsed electron–nuclear double resonance of the radical of 2-aminopropanol,[2572] each in the active site of ethanolamine ammonia-lyase from *S. typhimurium*, are consistent with all three hydrogens on the 5′-methyl group of the deoxyadenosine being located within 0.23–0.42 nm of the respective radical and the carbon of the 5′-methyl group being located 0.35 nm from the radical. If this is so, then the 5′-methyl carbon is within van der Waals contact with the carbon on which the unpaired electron resides.

When the hydrogen on the reactant that migrates during the reaction catalyzed by methyl-malonyl-CoA mutase from *P. freudenreichii* is converted to a deuterium, the rate constant for the appearance of cob(II)alamin decreases dramatically.[2533,2534] This observation suggests that **homolysis of the carbon–cobalt bond is concerted with abstraction of a hydrogen from the reactant**, which would require that the carbon of the reactant from which the hydrogen is abstracted be positioned by the enzyme immediately adjacent to carbon 5′ of the adenosyl group in the intact adenosylcobalamin. The distances observed by spectroscopy and crystallography rule out this possibility. It may simply be the case that the homolysis of the carbon–cobalt bond precedes abstraction of the hydrogen from the substrate[2573] and is not concerted with it but that the equilibrium constant for homolysis of the carbon–cobalt bond is significantly less than 1, as might be expected. Abstraction of the hydrogen from the reactant for the enzyme shifts the equilibrium by mass action, in favor of dissociation of the carbon–cobalt bond. This sequence of events would explain both the requirement that the hydrogen must be abstracted from the reactant as the cob(II)alamin is formed, as required by the kinetic isotope effect, and the fact that no 5′-deoxy-5′-adenosyl radical is ever observed as a transient intermediate in any of these enzymatic reactions.[2548] These considerations suggest that, **rather than being concerted, dissociation of the carbon–cobalt bond is coincident with abstraction of the hydrogen** simply because the equilibrium is shifted by subsequent abstraction of the hydrogen. In this way, the lifetime of the 5′-deoxy-5′-adenosyl radical is kept to a minimum.

Homolytic dissociation of the carbon–cobalt bond of adenosylcobalamin should be the most difficult step in the accepted mechanism, especially if it is not concerted with abstraction of the hydrogen from the reactant. The bond dissociation energy of a carbon–cobalt bond in an alkylcobalamin[2574] is around 100 kJ mol^{-1}, and that for the homolysis of adenosylcobalamin[2575] is 125 ± 10 kJ mol^{-1}. Even more remarkable is that the rate constant for uncatalyzed dissociation of the carbon–cobalt bond in adenosylcobalamin at 25 °C is 4×10^{-10} s^{-1}.

Nevertheless, the active site of an enzyme that uses adenosylcobalamin as a prosthetic group somehow **overcomes these formidable thermodynamic and kinetic barriers.** In the map of electron density within an active site of methylaspartate mutase from *C. cochlearium* unoccupied by substrates, two orientations of the 5′-deoxyadenosyl group can be discerned. The orientation in the drawing (Figure 2–68) is the one in which carbon 5′ is closest to the cobalt ion (Co). In the other orientation, which is not drawn, the carbon–cobalt coordination is broken; carbon 5′ is farther (0.45 nm) from the cobalt, well out of coordination; carbon 5′ is not in an axial position; and it is pointing instead toward the location in the active site in which substrates are

normally bound.[2479,2483] The conclusion that can be drawn in this instance is that there is an equilibrium established in the active site between the intact carbon–cobalt bond and the dissociated carbon–cobalt bond even in the absence of substrate. How the active site is able to change the equilibrium constant from the highly unfavorable value in solution to such an isoergonic one is puzzling but perhaps only because catalysis of homolytic reactions by the active sites of enzymes is not so well understood as is the catalysis of heterolytic reactions.

When the reactant binds to one of these enzymes with a prosthetic cobalamin in its active site, there is spectroscopic evidence that the carbon–cobalt bond of adenosylcobalamin, if it is not broken almost immediately,[2533] is distorted,[2576] and this distortion and other **steric effects**[2577,2578] may weaken the bond. These steric effects are probably not exerted on the corrin itself because it has virtually the same conformation in both adenosylcobalamin and cob(II)alamin.[2579] It is possible that the carbon–cobalt bond could be stretched by the active site. For example, the undissociated orientation of the carbon–cobalt bond of the adenosylcobalamin in the crystallographic molecular model of methylaspartate mutase from *C. cochlearium*, in which the carbon is closest to the cobalt ion (Figure 2–68), the distance between carbon and cobalt (0.32 nm) is significantly longer than the unstretched carbon–cobalt bond in free adenosylcobalamin (0.205 nm).[2472] When amino acids the side chains of which form hydrogen bonds to the ribosyl ring of the adenosyl group in the active site of methylaspartate mutase are mutated,[2580] the rate of dissociation of the carbon–cobalt bond upon addition of substrate decreased by a factor of 100–10,000. These hydrogen bonds could enforce a distortion or stretching of the carbon–cobalt bond. The carbon–cobalt bonds of adenosylcobalamins in the active sites of isobutyryl-CoA mutase from *Cupriavidus metallidurans*[2581] and human methyl-malonyl-CoA mutase,[2537] however, are of normal length (0.23 and 0.22 nm).

When adenosylcobalamin is bound to an enzyme and the benzimidazolyl group has been replaced by **the imidazolyl group of the histidine**, the carbon–cobalt bond loses only about 2% of its strength.[2582] Consistent with the small decrease in its strength observed upon its association with an enzyme and the exchange of its axial ligand, the exchange of the benzimidazolyl group in adenosylcobalamin with *N*-methylimidazole does increase the rate constant for homolytic dissociation of the carbon–cobalt bond in free solution but only by 8-fold. This exchange, however, also increases by 350-fold the heterolysis of the carbon–cobalt bond that produces the 5′-deoxy-5′-adenosyl carbanion and cob(III)alamin (Equation 2–352) to give this heterolytic dissociation the same rate constant as the homolytic dissociation.[2583] Another factor that may decrease the homolytic bond dissociation energy of the carbon–cobalt bond is that the unpaired electron in the 5′-deoxy-5′-adenosyl radical, during the majority of its short lifetime of around 1 ns,[2584] remains less than 0.5 nm from the cobalt in cob(II)alamin,[2577] presumably before it happens to move to its effective location.

If it is assumed that, following the required rearrangement (Equation 2–359), the radical of the dehydro product of the enzymatic reaction abstracts a hydrogen from the 5′-methyl group of deoxyadenosine to become the product and the 5′-deoxy-5′-adenosyl radical immediately recombines with cob(II)alamin to restore the adenosylcobalamin (reverse of Equation 2–362), then the only remaining question is **how the rearrangement of the radical of the reactant to the radical of the product occurs**. It has already been noted that in crystallographic molecular models of complexes between enzymes that use adenosylcobalamin as a prosthetic group and their substrates, the carbons from which the hydrogen is abstracted by the 5′-deoxy-5′-adenosyl radical are located 0.6–0.9 nm from the cobalt of cob(II)alamin.[2479,2569,2570] These observations seem to preclude a carbon–cobalt bond involving cob(II)alamin and either the dehydro radical of the reactant or the dehydro radical of the product, so model reactions that involve the rearrangements of organocobalt compounds that mimic those catalyzed by the enzyme but that require the rearrangement to occur on the metallic ion[2585] are probably irrelevant.

There are a number of nonenzymatic rearrangements that mimic the rearrangements that occur in the active sites containing prosthetic cobalamins.

There are nonenzymatic rearrangements that use **organocobalt compounds** as precursors to radicals, which then rearrange appropriately after their dissociation from the cobalt. For example, 1,2-dihydroxyethyl cobaloxime

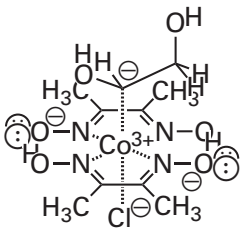

2–179

produces high yields of ethanal as a result of homolytic cleavage of its carbon–cobalt bond and subsequent rearrangement of the 1,2-dihydroxyethyl radical to the 2,2-hydroxyethyl radical

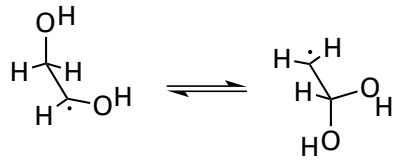

(2–366)

followed by abstraction of a hydrogen from the solvent.[2586] The other product of the reaction is cob(II)aloxime. This rearrangement mimics that performed by propanediol dehydratase (Table 2–3). Homolysis of 2,2,6-triethoxycarbonyl-6-(*S*-ethylthiocarboxy)-1-heptylcobalamin produces the 2,2,6-triethoxycarbonyl-6-(*S*-ethylthiocarboxy)heptyl radical that undergoes intramolecular transfer of a hydrogen and subsequent isomerization[2587]

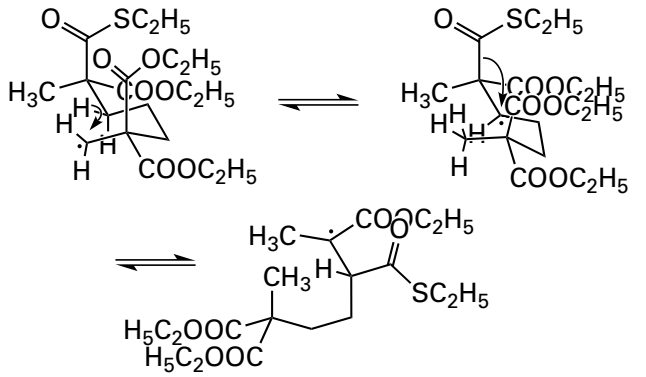

(2–367)

by a migration that resembles those catalyzed by methylmalonyl-CoA mutase and isobutyryl-CoA mutase (Table 2–3).

These reactions, however, that use the respective cobaloxime or cobalamin as the precursor for what is believed to be a neutral radical from a homolytic cleavage of the carbon–cobalt bond are **equivocal**. For example, in the rearrangement[2588]

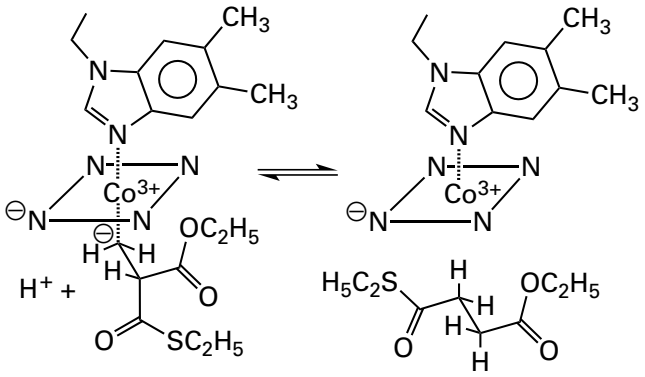

(2–368)

which is a model for methylmalonyl-CoA mutase (Table 2–3), it has been demonstrated with **radical clocks** and traps for radicals that the 2-ethoxycarbonyl-2-(*S*-ethylthiocarboxy)-1-propyl radical is not formed by a homolytic cleavage of the carbon–cobalt bond[2589,2590] and therefore is not the species rearranging.

It is also possible, however, to unambiguously **generate either chemically or photolytically appropriate radicals** that subsequently rearrange. For example, 2-ethoxycarbonyl-2-(*S*-ethylthiocarboxy)-propyl bromide, when treated with tri-(*n*-butyl)tin hydride, yields the 2-ethoxycarbonyl-2-(*S*-ethylthiocarboxy)propyl radical, which then rearranges to the 1-ethoxycarbonyl-1-methyl-2-(*S*-ethylthiocarboxy)-ethyl radical[2591]

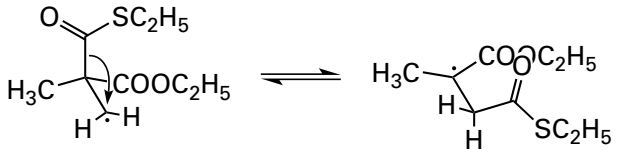

(2–369)

This isomerization is a model for the reaction catalyzed by methylmalonyl-CoA mutase. Phenylseleno groups (C_6H_6Se–) dissociate homolytically upon photolysis to yield the radical at the carbon to which they were attached, and these precursors have also been used to generate appropriate radicals for rearrangement.[2592,2593]

The **mechanisms by which the rearrangements of these various radicals proceed in solution,** which mimic the heterolytic rearrangements thought to occur in the active sites of enzymes, are either associative, dissociative, or concerted. As always, in an associative mechanism,[2591] a bond forms before another bond is broken; in a dissociative mechanism,[2594] a bond breaks before another bond is formed; and in a concerted mechanism, one bond is breaking as the other is forming. As in most cases

when there are associative, dissociative, and concerted alternatives for any reaction, the differences between them are not substantive; rather, they are differences in timing. In addition, it is probably the case that some rearrangements catalyzed by these enzymes are associative, others are dissociative, and others are concerted. Furthermore, the timing in solution may not be the same as that on an active site, even for the same rearrangement.

The rearrangement in solution of the 2-ethoxycarbonyl-2-(*S*-ethylthiocarboxy)propyl radical (Equation 2–369) has several kinetic properties consistent with **an associative mechanism** that has cyclopropyl radical **2–180** as an intermediate

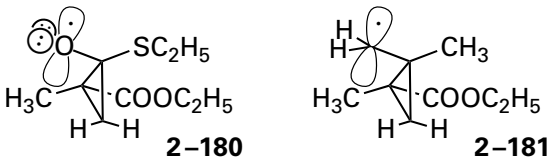

2–180 **2–181**

This **cyclopropyl radical** is formed by intramolecular cyclization of the radical of the reactant or, in the reverse reaction, the radical of the product, and it cleaves to form either the radical of the reactant or the radical of the product.[2591] The homologous associative rearrangement with the homologous intermediate cyclopropyl radical has also been proposed to occur in the active site of methylmalonyl-CoA mutase (Table 2–3).[2595]

Rearrangement of 2-ethoxycarbonyl-2-(1-methylethenyl)propyl radical

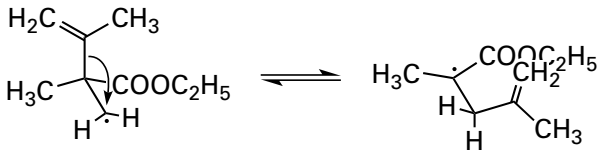

(2–370)

which is a model for the reaction catalyzed by 2-methyleneglutarate mutase (Table 2–3) and in which a 1-methylethenyl group [–C(CH$_3$)=CH$_2$)] replaces the *S*-ethylthiocarbonyl group [–C(SC$_2$H$_5$)=O] in Equation 2–369, is even more facile. The intermediate in this latter nonenzymatic reaction, cyclopropyl radical **2–181**, has been trapped and identified.[2593] When 2-[*E*-^{2}H$_1$]methyleneglutarate is mixed with 2-methyleneglutarate mutase from *E. coli*, the 2-[*E*-^{2}H$_1$]methyleneglutarate at equilibrium with 2-methylene-3-methylsuccinate, the product of the enzymatic reaction, gradually isomerizes, in a reaction catalyzed by the enzyme, to an equimolar mixture of 2-[*E*-^{2}H$_1$]methyleneglutarate and 2-[*Z*-^{2}H$_1$]methyleneglutarate.[2596] This result is consistent with the unesterified carboxylic acid of cyclopropyl radical **2–181** being an intermediate in the enzymatic reaction because rotation about the exocyclic carbon–carbon bond in the radical should be allowed while such a rotation forbidden in either the reactant or the product.

Rearrangement of the (2*S*,3*R*)-2-amino-3-carboxy-4-butanoate radical catalyzed by methylaspartate mutase (Table 2–3), however, cannot proceed by an associative mechanism because the carbon that is migrating is saturated. In the **dissociative isomerization** through which this rearrangement would have to proceed, a glycyl radical, stabilized by extensive delocalization, moves across the double bond in the conjugate base of acrylic acid[2597]

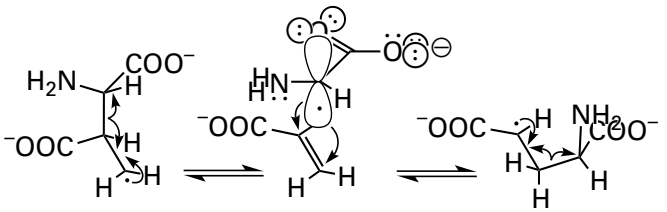

(2–371)

Both of these fragments, glycine and acrylate, have been shown to be formed during the rearrangement catalyzed by methylaspartate mutase from *C. cochlearium*,[2598] and spectroscopic evidence for the intermediacy of the glycyl radical in the enzymatic reaction has also been presented.[2543] When (2*S*,3*R*)-2-sulfanyl-3-carboxy-4-butanoate is used as a sulfanyl analogue of the usual amino reactant, (2*S*,3*R*)-2-amino-3-carboxy-4-butanoate, the even more stable 1-sulfanylcarboxymethyl radical forms in the active site rather than the glycyl radical (Equation 2–371). The thiyl radical was identified by its electron paramagnetic resonance spectrum, and zero-field splitting parameters suggested that the radical was the proper distance from the cobalt.[2599]

The reaction catalyzed by 2-methyleneglutarate mutase (Table 2–3) from *E. barkeri* is inhibited by two acrylate anions acting in concert but is not inhibited by 1-methylcyclopropane 1,2-dicarboxylate, an analogue of the cyclopropyl radical that would be the intermediate in an associative mechanism (see **2–180**).[2600] These observations suggest that a dissociative migration

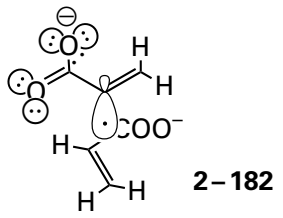

2–182

involving an acrylate anion and a 2-acrylate radical anion (**2–182**) occurs in this enzymatic reaction. The chemical evidence from nonenzymatic model reactions, however, suggest it should proceed by an associative mechanism.[2591] These contradictions throw the exact assignment of mechanism in doubt, but they could be resolved if the mechanism in the active site differs from that in solution.

For both the rearrangement of the 1,2-dihydroxypropyl radical to 1-methyl-2,2-dihydroxyethyl radical

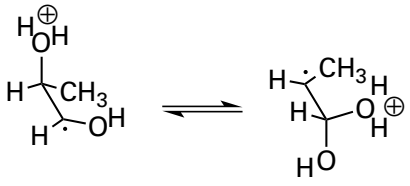

(2–372)

in the reaction catalyzed by propanediol dehydratase and the rearrangement of the homologous 1-hydroxy-2-aminoethyl radical to 2-hydroxy-2-aminoethyl radical

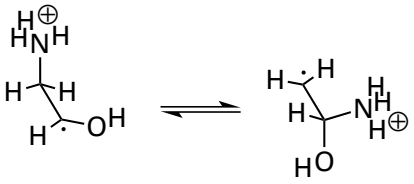

(2–373)

in the reaction catalyzed by ethanolamine ammonia-lyase, the hydroxy group that is migrating and the amino group that is migrating, respectively, are each **hydronated before the migration takes place**.[2601,2602] In the former rearrangement, the hydroxy group is hydronated by the conjugate acid of the imidazolyl group of a histidine in the active site,[2569] and in the latter rearrangement, the ammonio group that enters the active site is maintained in its hydronated state by a hydrogen bond to the carboxylato group of a glutamate.

In neither of these two reactions is either an associative mechanism or a dissociative mechanism realistic. An associative mechanism would require that either the migrating oxygen or the migrating nitrogen be pentavalent, which is impossible. A dissociative mechanism would require a hydronated hydroxyl radical cation or a hydronated amino radical cation, neither of which is realistic, to migrate across a double bond, or it would require a molecule of water or a molecule of ammonia to migrate across the radical cation of a double bond, which is also unrealistic. Consequently, it is believed that both reactions (Equations 2–372 and 2–373) are **concerted isomerizations** with the bond to the oxygen of the hydronated hydroxy group or the bond to the nitrogen of the ammonio group breaking as the other bond to the oxygen of the hydronated hydroxy group or the nitrogen of the ammonio group, respectively, is forming.[2601,2602] Each concerted isomerization would have a transition state with a π molecular orbital system that combines a p orbital from each of the two carbons and a p orbital from the planar sp^2 oxygen or the planar sp^2 nitrogen

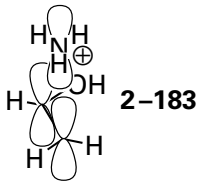

2–183

respectively. Each of these respective π molecular orbital systems, the one in which the oxygen is the third atom and the one in which nitrogen is the third atom (**2–183**), is occupied by three electrons.

In this transition state in the active site of ethanolamine ammonia-lyase from *E. coli*, a hydrogen bond between one of the nitrogen–hydrogens on the ammonio group on the conjugate acid of ethanolamine and a σ lone pair on one of the carboxylato oxygens of the glutamate that maintains the hydronation of the amino group during the migration guides the nitrogen from one carbon to the other. This pivoting carboxylato group is planted on the hydroxy group of the ethanolamine by a hydrogen bond to its other oxygen.[2602]

The large majority of the evidence at the moment suggests that the radical of the dehydro reactant isomerizes to the radical of the dehydro product in the rearrangements catalyzed by enzymes using adenosylcobalamin as a prosthetic group. Several isomerizations of carbanions, however, that resemble the carbanions of the dehydro reactants in the enzymatic reactions also mimic the rearrangements performed by the respective enzymes. When the rearrangement of bis(tetrahydro-*H*-pyran-2-yl) 2-methylcobalaminylitaconate

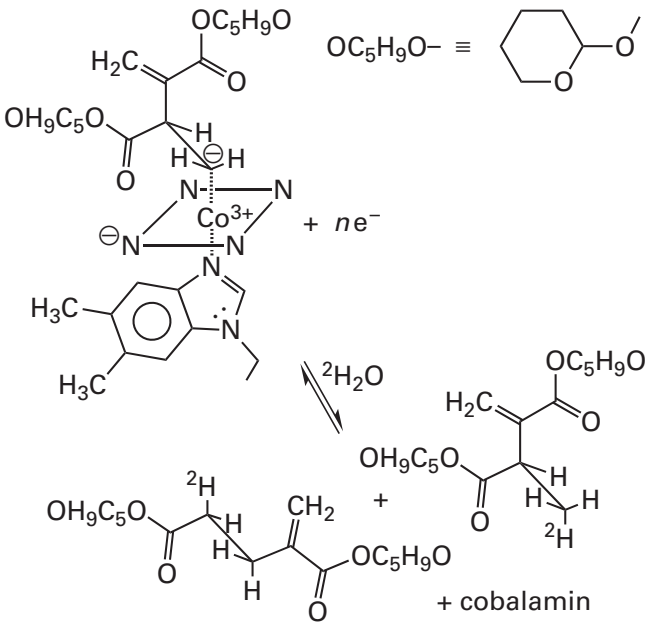

(2–374)

was performed in ^2H_2O in the absence of any enzyme, a deuterium atom was found in the products at the locations at which the hydrogen migrating during the reaction catalyzed by 2-methyleneglutarate mutase

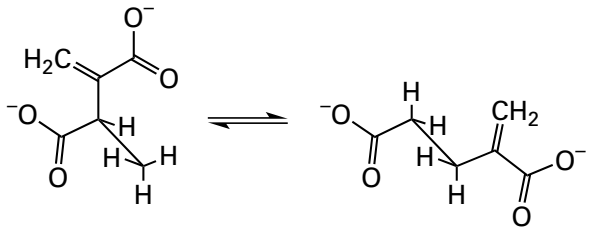

(2–375)

would have occupied.[2526,2603] Although water gives up a hydron readily, a hydrogen atom (bond dissociation energy = 497 kJ mol^{-1}) is abstracted from water only with great difficulty. This result and the requirement for coincident reduction of cobalt to yield rearranged products has led to the conclusion that these rearrangements occur within a carbanion released from the cobalt directly or upon reduction

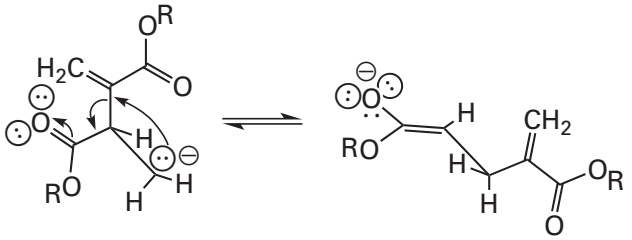

(2–376)

The carbanions released during these reactions would readily pick up a hydron from the solvent prior to or following their rearrangement.

Under similar reductive conditions, alkylcobalamin **2–184**

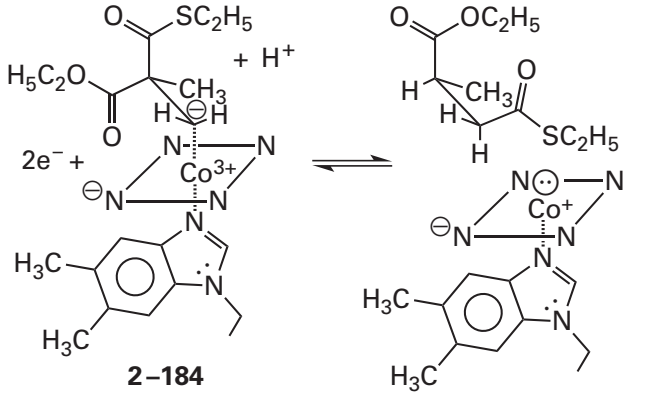

(2–377)

rearranges to produce high yields of the product, thioethyl 3-ethoxycarbonylbutanoate.[2604] This reaction serves as a model for the rearrangement catalyzed by methylmalonyl-CoA mutase (Table 2–3).

A radical of the dehydro reactant and cob(II)alamin is only the transfer of an electron away from a carbanion of the dehydro reactant and cob(III)alamin. Perhaps, just as the distinction between a concerted nucleophilic substitution and a dissociative nucleophilic substitution is ambiguous, the distinction between a homolytic rearrangement and a heterolytic rearrangement, at least in this context, is ambiguous. In the case of lysine 5,6-aminomutase from *A. sticklandii* (Table 2–3), however, the appearance of cob(III)alamin resulting from transfer of an electron from cob(II)alamin to an intermediate in the enzymatic reaction, as would be required if the reaction were some hybrid of homolytic and heterolytic, produces the irreversible inactivation of the enzyme.[2605] It may be the case that the radicals of reactant and product are held so far away from the cobalt ion to prevent just such a detrimental electron transfer.

Suggested Reading

Grate, J. H., Grate, J. W., and Schrauzer, G. N. (1982) Synthesis and reactions of organocobalamins relevant to the mechanism of the methylmalonyl-CoA–succinyl-CoA mutase enzyme, *J. Am. Chem. Soc. 104*, 1588–1594. https://doi.org/10.1021/ja00370a023

Marsh, E. N. G., and Ballou, D. P. (1998) Coupling of cobalt–carbon bond homolysis and hydrogen

atom abstraction in adenosylcobalamin-dependent glutamate mutase. *Biochemistry 37*, 11864–11872. https://doi.org/10.1021/bi980512e

Chih, H. W., and Marsh, E. N. G. (1999) Pre-steady-state kinetic investigation of intermediates in the reaction catalyzed by adenosylcobalamin-dependent glutamate mutase. *Biochemistry 38*, 13684–13691. https://doi.org/10.1021/bi991064t

Bothe, H., Darley, D. J., Albracht, S. P. J., Gerfen, G. J., Golding, B. T., and Buckel, W. (1998) Identification of the 4-glutamyl radical as an intermediate in the carbon skeleton rearrangement catalyzed by coenzyme B_{12}-dependent glutamate mutase from *Clostridium cochlearium*. *Biochemistry 37*, 4105–4113. https://doi.org/10.1021/bi971393q

Chih, H.-W., and Marsh, E. N. G. (2000) Mechanism of glutamate mutase: Identification and kinetic competence of acrylate and glycyl radical as intermediates in the rearrangement of glutamate to methylaspartate. *J. Am. Chem. Soc. 122*, 10732–10733. https://doi.org/10.1021/ja002488%2B

Problem 2–41: Write the mechanism for methionine synthase (Equation 2–354), which uses methylcobalamin as a prosthetic group.[2495]

Problem 2–42: Write a mechanism for the conversion

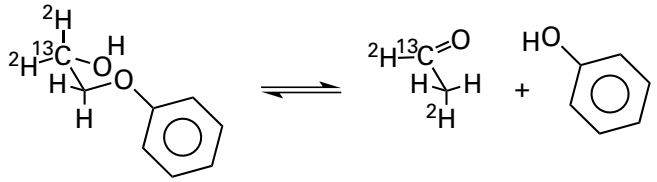

as it would be catalyzed by an enzyme using adenosylcobalamin as a prosthetic group and an intermediate radical.[2606]

Problem 2–43: Write associative and dissociative homolytic mechanisms for each of the reactions in Table 2-3.

(A) Write the overall equation for the reaction with the chemical structures of the reactant and the product, each drawn in the sawhorse projection with the orientation of the sawhorse in Equation 2–360. When necessary, make sure that the chirality of each of the two central carbons between which the hydrogen and the substituent are interchanged is correct.

(B) To write the mechanism, remove the hydrogen atom and produce the radical of the reactant as would be done on the enzyme by a 5′-deoxy-5′-adenosyl radical.

(C) Write the cyclopropyl radical for the associative mechanism and the radical of the product resulting from the dissociation of the proper bond in the cyclopropyl radical.

(D) Write the two fragments, one a radical and one an alkene, of the dissociative mechanism.

(E) Decide in each case which alternative—the associative, the dissociative, or a concerted mechanism—is the more likely for that particular rearrangement.

Problem 2–44: When 1,4-diethyl 2-(bromomethyl)-2-methyl-3-[*N*-benzylimino]succinate

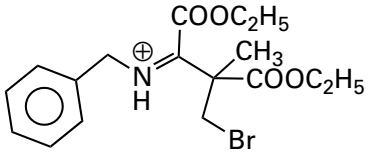

is treated with tri-(*n*-butyl)tin hydride, its neutral radical is formed. Draw the neutral radical and the product of its rearrangement that mimics the rearrangement catalyzed by methylaspartate mutase (Table 2–3).[2607]

Problem 2–45: Each of the following reactions is catalyzed by an enzyme that has a catalytic prosthetic group in its active site. What is the particular prosthetic group used in each of these reactions? Do not write mechanisms.

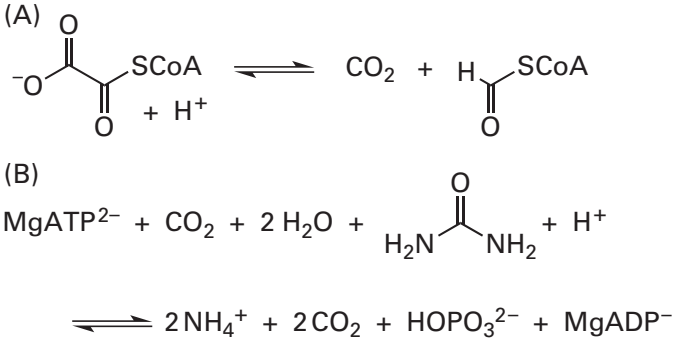

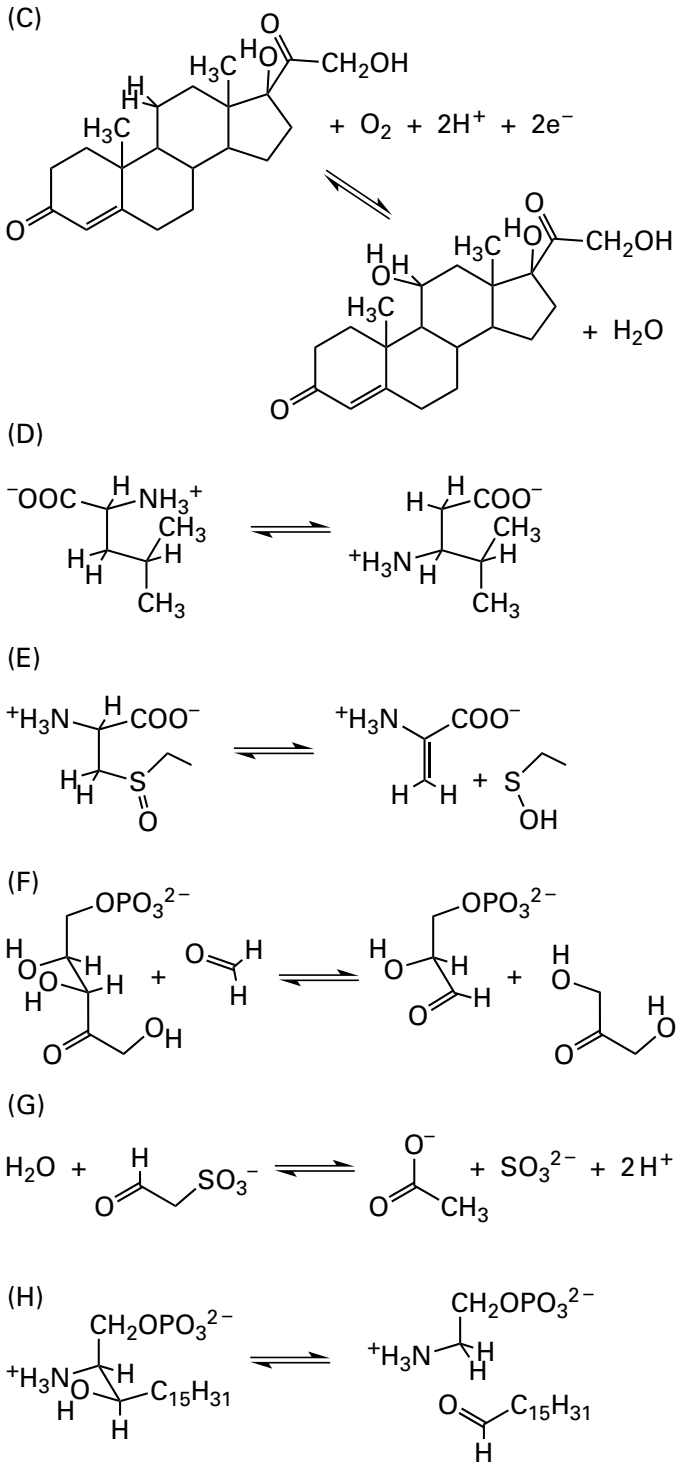

References

1. Willie, A., and Jorns, M. S. (1995) Discovery of a third coenzyme in sarcosine oxidase, *Biochemistry 34*, 16703–16707.
2. Larrabee, A. R., McDaniel, E. G., Bakerman, H. A., and Vagelos, P. R. (1965) Acyl carrier protein. V. Identification of 4′-phosphopantetheine bound to a mammalian fatty acid synthetase preparation, *Proc. Natl. Acad. Sci. U.S.A. 54*, 267–273.
3. Ehmann, D. E., Gehring, A. M., and Walsh, C. T. (1999) Lysine biosynthesis in *Saccharomyces cerevisiae*: Mechanism of α-aminoadipate reductase (Lys2) involves posttranslational phosphopantetheinylation by Lys5, *Biochemistry 38*, 6171–6177.
4. Scott, A. I., Roessner, C. A., Stolowich, N. J., Karuso, P., Williams, H. J., Grant, S. K., Gonzalez, M. D., and Hoshino, T. (1988) Site-directed mutagenesis and high-resolution NMR spectroscopy of the active site of porphobilinogen deaminase, *Biochemistry 27*, 7984–7990.
5. Jordan, P. M., and Warren, M. J. (1987) Evidence for a dipyrromethane cofactor at the catalytic site of *E. coli* porphobilinogen deaminase, *FEBS Lett. 225*, 87–92.
6. Hart, G. J., Miller, A. D., Leeper, F. J., and Battersby, A. R. (1987) Biosynthesis of the natural porphyrins: Proof that hydroxymethylbilane synthase (porphobilinogen deaminase) uses a novel binding group in its catalytic action, *J. Chem.Soc. Chem. Commun.*, 1762–1765.
7 Janes, S. M., Mu, D., Wemmer, D., Smith, A. J., Kaur, S., Maltby, D., Burlingame, A. L., and Klinman, J. P. (1990) A new redox cofactor in eukaryotic enzymes: 6-Hydroxydopa at the active site of bovine serum amine oxidase, *Science 248*, 981–987.
8. Schuster, B., and Retey, J. (1995) The mechanism of action of phenylalanine ammonia-lyase: The role of prosthetic dehydroalanine, *Proc. Natl. Acad. Sci. U.S.A. 92*, 8433–8437.
9. Schwede, T. F., Retey, J., and Schulz, G. E. (1999) Crystal structure of histidine ammonia-lyase revealing a novel polypeptide modification as the catalytic electrophile, *Biochemistry 38*, 5355–5361.
10. Ford, G. C., Eichele, G., and Jansonius, J. N. (1980) Three-dimensional structure of a pyridoxal-phosphate-dependent enzyme, mito-

chondrial aspartate aminotransferase, *Proc. Natl. Acad. Sci. U. S. A. 77*, 2559–2563.
11. Hughes, R. C., Jenkins, W. T., and Fischer, E. H. (1962) The site of binding of pyridoxal-5′-phosphate to heart glutamic-aspartic transaminase, *Proc. Natl. Acad. Sci. U.S.A. 48*, 1615–1618.
12. Jenkins, W. T., and Sizer, I. W. (1957) Glutamic-aspartic transaminase, *J. Am. Chem. Soc. 79*, 2655–2656.
13. Kyte, J. (2007) *Structure in Protein Chemistry: Second Edition*, p 21, Garland Science, New York.
14. Oliveira, E. F., Cerqueira, N. M. F. S. A., Fernandes, P. A., and Ramos, M. J. (2011) Mechanism of formation of the internal aldimine in pyridoxal 5′-phosphate-dependent enzymes, *J. Am. Chem. Soc. 133*, 15496–15505.
15. Bruice, T. C., and Benkovic, S. J. (1966) *Bioorganic Mechanisms*, pp 226–300, Benjamin, New York.
16. Jencks, W. P. (1969) *Catalysis in Chemistry and Enzymology*, pp 133–146, McGraw-Hill, New York.
17. Caulkins, B. G., Bastin, B., Yang, C., Neubauer, T. J., Young, R. P., Hilario, E., Huang, Y. M. M., Chang, C. E. A., Fan, L., Dunn, M. F., Marsella, M. J., and Mueller, L. J. (2014) Protonation states of the tryptophan synthase internal aldimine active site from solid-state NMR spectroscopy: Direct observation of the protonated Schiff base linkage to pyridoxal-5′-phosphate, *J. Am. Chem. Soc. 136*, 12824–12827.
18. Caulkins, B. G., Yang, C., Hilario, E., Fan, L., Dunn, M. F., and Mueller, L. J. (2015) Catalytic roles of βLys87 in tryptophan synthase: Solid state NMR studies, *Biochim. Biophys. Acta 1854*, 1194–1199.
19. Metzler, D. E. (1957) Equilibria between pyridoxal and amino acids and their imines, *J. Am. Chem. Soc. 79*, 485–490.
20. Barrett, A. N., and Palmer, R. A. (1969) Crystal and molecular structure of pyridoxal phosphate oxime, *Acta Crystallogr. B 25*, 688–695.
21. Inoue, Y., Kuramitsu, S., Inoue, K., Kagamiyama, H., Hiromi, K., Tanase, S., and Morino, Y. (1989) Substitution of a lysyl residue for arginine 386 of *Escherichia coli* aspartate aminotransferase, *J. Biol. Chem. 264*, 9673–9681.
22. Fasella, P., Giartosio, A., and Hammes, G. G. (1966) The interaction of aspartate aminotransferase with α-methylaspartic acid, *Biochemistry 5*, 197–202.
23. Metzler, C. M., and Metzler, D. E. (1987) Quantitative description of absorption spectra of a pyridoxal phosphate-dependent enzyme using lognormal distribution curves, *Anal. Biochem. 166*, 313–327.
24. Goldberg, J. M., Swanson, R. V., Goodman, H. S., and Kirsch, J. F. (1991) The tyrosine-225 to phenylalanine mutation of *Escherichia coli* aspartate aminotransferase results in an alkaline transition in the spectrophotometric and kinetic pK_a values and reduced values of both k_{cat} and K_m, *Biochemistry 30*, 305–312.
25. Goldberg, J. M., and Kirsch, J. F. (1996) The reaction catalyzed by *Escherichia coli* aspartate aminotransferase has multiple partially rate-determining steps, while that catalyzed by the Y225F mutant is dominated by ketimine hydrolysis, *Biochemistry 35*, 5280–5291.
26. Hayashi, H., and Kagamiyama, H. (1995) Reaction of aspartate aminotransferase with L-erythro-3-hydroxyaspartate: Involvement of Tyr70 in stabilization of the catalytic intermediates, *Biochemistry 34*, 9413–9423.
27. Kallen, R. G., Korpela, T., Martell, A. E., Matsushima, Y., Metzler, C. M., Metzler, D. E., Morozov, Y. V., Ralston, I. M., Savin, F. A., Torchinsky, Y. M., and Ueno, H. (1985) Chemical and spectroscopic properties of pyridoxal and pyridoxamine phosphates, In *Transaminases* (Christen, P., and Metzler, D. E., Eds.), pp 37–108, John Wiley and Sons, New York.
28. Chan-Huot, M., Dos, A., Zander, R., Sharif, S., Tolstoy, P. M., Compton, S., Fogle, E., Toney, M. D., Shenderovich, I., Denisov, G. S., and Limbach, H. H. (2013) NMR studies of protonation and hydrogen bond states of internal aldimines of pyridoxal 5′-phosphate acid–base in alanine racemase, aspartate aminotransferase, and poly-L-lysine, *J. Am. Chem. Soc. 135*, 18160–18175.
29. Rhee, S., Silva, M. M., Hyde, C. C., Rogers, P. H., Metzler, C. M., Metzler, D. E., and Arnone, A. (1997) Refinement and comparisons of the crystal structures of pig cytosolic aspartate aminotransferase and its complex with 2-methylaspartate, *J. Biol. Chem. 272*, 17293–17302.
30. Hayashi, H., Mizuguchi, H., and Kagamiyama, H. (1998) The imine-pyridine torsion of

the pyridoxal 5′-phosphate Schiff base of aspartate aminotransferase lowers its pK_a in the unliganded enzyme and is crucial for the successive increase in the pK_a during catalysis, *Biochemistry 37*, 15076–15085.
31. Hayashi, H., Mizuguchi, H., Miyahara, I., Islam, M. M., Ikushiro, H., Nakajima, Y., Hirotsu, K., and Kagamiyama, H. (2003) Strain and catalysis in aspartate aminotransferase, *Biochim. Biophys. Acta 1647*, 103–109.
32. Islam, M. M., Hayashi, H., Mizuguchi, H., and Kagamiyama, H. (2000) The substrate activation process in the catalytic reaction of *Escherichia coli* aromatic amino acid aminotransferase, *Biochemistry 39*, 15418–15428.
33. Gong, J., Hunter, G. A., and Ferreira, G. C. (1998) Aspartate-279 in aminolevulinate synthase affects enzyme catalysis through enhancing the function of the pyridoxal 5′-phosphate cofactor, *Biochemistry 37*, 3509–3517.
34. Tong, H., and Davis, L. (1995) 2-Amino-3-ketobutyrate-CoA ligase from beef liver mitochondria: An NMR spectroscopic study of low-barrier hydrogen bonds of a pyridoxal 5′-phosphate-dependent enzyme, *Biochemistry 34*, 3362–3367.
35. Rhee, S., Parris, K. D., Hyde, C. C., Ahmed, S. A., Miles, E. W., and Davies, D. R. (1997) Crystal structures of a mutant (βK87T) tryptophan synthase $\alpha_2\beta_2$ complex with ligands bound to the active sites of the α- and β-subunits reveal ligand-induced conformational changes, *Biochemistry 36*, 7664–7680.
36. Burkhard, P., Dominici, P., Borri-Voltattorni, C., Jansonius, J. N., and Malashkevich, V. N. (2001) Structural insight into Parkinson's disease treatment from drug-inhibited DOPA decarboxylase, *Nature Struct. Biol. 8*, 963–967.
37. Shaw, J. P., Petsko, G. A., and Ringe, D. (1997) Determination of the structure of alanine racemase from *Bacillus stearothermophilus* at 1.9 Å resolution, *Biochemistry 36*, 1329–1342.
38. Hogg, J. L., Jencks, D. A., and Jencks, W. P. (1977) Catalysis of transimination through trapping by acids and bases, *J. Am. Chem. Soc. 99*, 4772–4778.
39. Weng, S. H., and Leussing, D. L. (1983) Transimination kinetics of pyridoxal 5′-phosphate Schiff bases, *J. Am. Chem. Soc. 105*, 4082–4090.
40. Abbott, E. H., and Martell, A. E. (1971) Reaction of amines with pyridoxal azomethines. Transaldimation and its role in the mechanism of vitamin B_6 enzymes, *J. Am. Chem. Soc. 93*, 5852–5856.
41. Jackson, L. K., Baldwin, J., Akella, R., Goldsmith, E. J., and Phillips, M. A. (2004) Multiple active site conformations revealed by distant site mutation in ornithine decarboxylase, *Biochemistry 43*, 12990–12999.
42. Angelaccio, S., Pascarella, S., Fattori, E., Bossa, F., Strong, W., and Schirch, V. (1992) Serine hydroxymethyltransferase: Origin of substrate specificity, *Biochemistry 31*, 155–162.
43. Cook, P. D., and Holden, H. M. (2007) A structural study of GDP-4-keto-6-deoxy-D-mannose-3-dehydratase: Caught in the act of geminal diamine formation, *Biochemistry 46*, 14215–14224.
44. Karthikeyan, S., Zhou, Q., Zhao, Z., Kao, C.-L., Tao, Z., Robinson, H., Liu, H.-w., and Zhang, H. (2004) Structural analysis of *Pseudomonas* 1-aminocyclopropane-1-carboxylate deaminase complexes: Insight into the mechanism of a unique pyridoxal-5′-phosphate dependent cyclopropane ring-opening reaction, *Biochemistry 43*, 13328–13339.
45. Sivaraman, J., Li, Y., Larocque, R., Schrag, J. D., Cygler, M., and Matte, A. (2001) Crystal structure of histidinol phosphate aminotransferase (HisC) from *Escherichia coli*, and its covalent complex with pyridoxal-5′-phosphate and L-histidinol phosphate, *J. Mol. Biol. 311*, 761–776.
46. Cheong, C.-G., Escalante-Semerena, J. C., and Rayment, I. (2002) Structural studies of the L-threonine-*o*-3-phosphate decarboxylase (CobD) enzyme from *Salmonella enterica*: The apo, substrate, and product-aldimine complexes, *Biochemistry 41*, 9079–9089.
47. Hester, G., Stark, W., Moser, M., Kallen, J., Markovic-Housley, Z., and Jansonius, J. N. (1999) Crystal structure of phosphoserine amino-transferase from *Escherichia coli* at 2.3Å Resolution: Comparison of the unligated enzyme and a complex with α-methyl-L-glutamate, *J. Mol. Biol. 286*, 829–850.
48. Kielkopf, C. L., and Burley, S. K. (2002) X-ray structures of threonine aldolase complexes: Structural basis of substrate recognition, *Biochemistry 41*, 11711–11720.
49. Malashkevich, V. N., Strop, P., Keller, J. W., Jansonius, J. N., and Toney, M. D. (1999) Crystal structures of dialkylglycine decar-

boxylase inhibitor complexes, *J. Mol. Biol. 294*, 193–200.
50. Kraulis, P. J. (1991) Molscript: A program to produce both detailed and schematic plots of protein structures, *J.. Appl. Crystallogr. 24*, 946–950.
51. Schmidt, A., Sivaraman, J., Li, Y., Larocque, R., Barbosa, J. A., Smith, C., Matte, A., Schrag, J. D., and Cygler, M. (2001) Three-dimensional structure of 2-amino-3-ketobutyrate-CoA ligase from *Escherichia coli* complexed with a PLP-substrate intermediate: Inferred reaction mechanism, *Biochemistry 40*, 5151–5160.
52. Griswold, W. R., Castro, J. N., Fisher, A. J., and Toney, M. D. (2012) Ground-state electronic destabilization via hyperconjugation in aspartate aminotransferase, *J. Am. Chem. Soc. 134*, 8436–8438.
53. Okamoto, A., Higuchi, T., Hirotsu, K., Kuramitsu, S., and Kagamiyama, H. (1994) X-ray crystallographic study of pyridoxal 5′-phosphate-type aspartate aminotransferases from *Escherichia coli* in open and closed form, *J. Biochem. (Tokyo) 116*, 95–107.
54. Jung, M. J., and Metcalf, B. W. (1975) Catalytic inhibition of γ-aminobutyric acid-α-ketoglutarate transaminase of bacterial origin by 4-aminohex-5-ynoic acid, a substrate analog, *Biochem. Biophys. Res. Commun. 67*, 301–306.
55. Toth, K., and Richard, J. P. (2007) Covalent catalysis by pyridoxal: Evaluation of the effect of the cofactor on the carbon acidity of glycine, *J. Am. Chem. Soc. 129*, 3013–3021.
56. Crugeiras, J., Rios, A., Riveiros, E., Amyes, T. L., and Richard, J. P. (2008) Glycine enolates: The effect of formation of iminium ions to simple ketones on α-amino carbon acidity and a comparison with pyridoxal iminium ions, *J. Am. Chem. Soc. 130*, 2041–2050.
57. Crugeiras, J., Rios, A., Riveiros, E., and Richard, J. P. (2011) Substituent effects on electrophilic catalysis by the carbonyl group: Anatomy of the rate acceleration for PLP-catalyzed deprotonation of glycine, *J. Am. Chem. Soc. 133*, 3173–3183.
58. Griswold, W. R., Fisher, A. J., and Toney, M. D. (2011) Crystal structures of aspartate aminotransferase reconstituted with 1-deazapyridoxal 5′-phosphate: Internal aldimine and stable L-aspartate external aldimine, *Biochemistry 50*, 5918–5924.
59. Yoshikane, Y., Yokochi, N., Yamasaki, M., Mizutani, K., Ohnishi, K., Mikami, B., Hayashi, H., and Yagi, T. (2008) Crystal structure of pyridoxamine-pyruvate aminotransferase from *Mesorhizobium loti* maff303099, *J. Biol. Chem. 283*, 1120–1127.
60. Peisach, D., Chipman, D. M., Van Ophem, P. W., Manning, J. M., and Ringe, D. (1998) D-Cycloserine inactivation of D-amino acid aminotransferase leads to a stable noncovalent protein complex with an aromatic cycloserine-PLP derivative, *J. Am. Chem. Soc. 120*, 2268–2274.
61. Peisach, D., Chipman, D. M., Van Ophem, P. W., Manning, J. M., and Ringe, D. (1998) Crystallographic study of steps along the reaction pathway of D-amino acid aminotransferase, *Biochemistry 37*, 4958–4967.
62. Hur, O., Niks, D., Casino, P., and Dunn, M. F. (2002) Proton transfers in the β-reaction catalyzed by tryptophan synthase, *Biochemistry 41*, 9991–10001.
63. Scarsdale, J. N., Radaev, S., Kazanina, G., Schirch, V., and Wright, H. T. (2000) Crystal structure at 2.4.Å: Resolution of *E. coli* serine hydroxymethyltransferase in complex with glycine substrate and 5–formyl tetrahydrofolate, *J. Mol. Biol. 296*, 155–168.
64. Inoue, K., Kuramitsu, S., Okamoto, A., Hirotsu, K., Higuchi, T., Morino, Y., and Kagamiyama, H. (1991) Tyr225 in aspartate aminotransferase: Contribution of the hydrogen bond between Tyr225 and coenzyme to the catalytic reaction, *J. Biochem. (Tokyo) 109*, 570–576.
65. Schirch, D., Delle Fratte, S., Iurescia, S., Angelaccio, S., Contestabile, R., Bossa, F., and Schirch, V. (1993) Function of the active-site lysine in *Escherichia coli* serine hydroxymethyltransferase, *J. Biol. Chem. 268*, 23132–23138.
66. Toney, M. D., Hohenester, E., Keller, J. W., and Jansonius, J. N. (1995) Structural and mechanistic analysis of two refined crystal structures of the pyridoxal phosphate-dependent enzyme dialkylglycine decarboxylase, *J. Mol. Biol. 245*, 151–179.
67. Capitani, G., De Biase, D., Aurizi, C., Gut, H., Bossa, F., and Grutter, M. G. (2003) Crystal structure and functional analysis of *Escherichia coli* glutamate decarboxylase, *The EMBO journal 22*, 4027–4037.
68. Uhl, M. K., Oberdorfer, G., Steinkellner, G., Riegler-Berket, L., Mink, D., van Assema, F.,

Schurmann, M., and Gruber, K. (2015) The crystal structure of D-threonine aldolase from *Alcaligenes xylosoxidans* provides insight into a metal ion assisted PLP-dependent mechanism, *PLoS One 10*, e0124056.
69. Koh, J. T., Delaude, L., and Breslow, R. (1994) Geometric control of a pyridoxal-catalyzed aldol condensation, *J. Am. Chem. Soc. 116*, 11234–11240.
70. Seebeck, F. P., and Hilvert, D. (2003) Conversion of a PLP-dependent racemase into an aldolase by a single active site mutation, *J. Am. Chem. Soc. 125*, 10158–10159.
71. Zhang, J., and Ferreira, G. C. (2002) Transient state kinetic investigation of 5-aminolevulinate synthase reaction mechanism, *J. Biol. Chem. 277*, 44660–44669.
72. Laver, W. G., Neuberger, A., and Udenfriend, S. (1958) Initial stages in the biosynthesis of porphyrins. I. The formation of δ-aminolaevulic acid by particles obtained from chicken erythrocytes, *Biochem. J. 70*, 4–14.
73. Stojanovski, B. M., Hunter, G. A., Jahn, M., Jahn, D., and Ferreira, G. C. (2014) Unstable reaction intermediates and hysteresis during the catalytic cycle of 5-aminolevulinate synthase: Implications from using pseudo and alternate substrates and a promiscuous enzyme variant, *J. Biol. Chem. 289*, 22915–22925.
74. Dunathan, H. C. (1966) Conformation and reaction specificity in pyridoxal phosphate enzymes, *Proc. Natl. Acad. Sci. U. S. A. 55*, 712–716.
75. Sun, S., Zabinski, R. F., and Toney, M. D. (1998) Reactions of alternate substrates demonstrate stereoelectronic control of reactivity in dialkylglycine decarboxylase, *Biochemistry 37*, 3865–3875.
76. Trivedi, V., Gupta, A., Jala, V. R., Saravanan, P., Rao, G. S., Rao, N. A., Savithri, H. S., and Subramanya, H. S. (2002) Crystal structure of binary and ternary complexes of serine hydroxymethyltransferase from *Bacillus stearothermophilus*: Insights into the catalytic mechanism, *J. Biol. Chem. 277*, 17161–17169.
77. Szebenyi, D. M., Musayev, F. N., di Salvo, M. L., Safo, M. K., and Schirch, V. (2004) Serine hydroxymethyltransferase: Role of Glu75 and evidence that serine is cleaved by a retroaldol mechanism, *Biochemistry 43*, 6865–6876.
78. Metzler, D. E., and Snell, E. E. (1952) Some transamination reactions involving vitamin B_6, *J. Am. Chem. Soc. 74*, 979–983.
79. Snell, E. E. (1945) Vitamin B_6 group. V. The reversible interconversion of pyridoxal and pyridoxamine by transamination reactions, *J. Am. Chem. Soc. 67*, 194–197.
80. Thanassi, J. W., and Fruton, J. S. (1962) Aminomalonic decarboxylase, *Biochemistry 1*, 975–982.
81. Ito, T., Koga, K., Hemmi, H., and Yoshimura, T. (2012) Role of zinc ion for catalytic activity in D-serine dehydratase from *Saccharomyces cerevisiae*, *FEBS J. 279*, 612–624.
82. Griswold, W. R., and Toney, M. D. (2011) Role of the pyridine nitrogen in pyridoxal 5′-phosphate catalysis: Activity of three classes of PLP enzymes reconstituted with deazapyridoxal 5′-phosphate, *J. Am. Chem. Soc. 133*, 14823–14830.
83. Toney, M. D., and Kirsch, J. F. (1991) Kinetics and equilibria for the reactions of coenzymes with wild type and the Y70F mutant of *Escherichia coli* aspartate aminotransferase, *Biochemistry 30*, 7461–7466.
84. Yano, T., Kuramitsu, S., Tanase, S., Morino, Y., and Kagamiyama, H. (1992) Role of Asp222 in the catalytic mechanism of *Escherichia coli* aspartate aminotransferase: The amino acid residue which enhances the function of the enzyme-bound coenzyme pyridoxal 5′-phosphate, *Biochemistry 31*, 5878–5887.
85. Phillips, R. S., Sundararaju, B., and Koushik, S. V. (1998) The catalytic mechanism of kynureninase from *Pseudomonas fluorescens*: Evidence for transient quinonoid and ketImine intermediates from rapid-scanning stopped-flow spectrophotometry, *Biochemistry 37*, 8783–8789.
86. Furumo, N. C., and Kirsch, J. F. (1995) Accumulation of the quinonoid intermediate in the reaction catalyzed by aspartate aminotransferase with cysteine sulfinic acid, *Arch. Biochem. Biophys. 319*, 49–54.
87. Phillips, R. S., Demidkina, T. V., and Faleev, N. G. (2014) The role of substrate strain in the mechanism of the carbon–carbon lyases, *Bioorg. Chem. 57*, 198–205.
88. Milic, D., Demidkina, T. V., Faleev, N. G., Matkovic-Calogovic, D., and Antson, A. A. (2008) Insights into the catalytic mechanism of tyrosine phenol-lyase from X-ray struc-

tures of quinonoid intermediates, *J. Biol. Chem. 283*, 29206–29214.
89. Bhavani, S., Trivedi, V., Jala, V. R., Subramanya, H. S., Kaul, P., Prakash, V., Appaji Rao, N., and Savithri, H. S. (2005) Role of Lys-226 in the catalytic mechanism of *Bacillus stearothermophilus* serine hydroxymethyltransferase-Crystal structure and kinetic studies, *Biochemistry 44*, 6929–6937.
90. Phillips, R. S., and Harris, A. P. (2021) Structural basis of the stereochemistry of inhibition of tryptophan synthase by tryptophan and derivatives, *Biochemistry 60*, 231–244.
91. White, M. F., Vasquez, J., Yang, S. F., and Kirsch, J. F. (1994) Expression of apple 1-aminocyclopropane-1-carboxylate synthase in *Escherichia coli*: Kinetic characterization of wild-type and active-site mutant forms, *Proc. Natl. Acad. Sci. U.S.A. 91*, 12428–12432.
92. Capitani, G., McCarthy, D. L., Gut, H., Gruetter, M. G., and Kirsch, J. F. (2002) Apple 1-aminocyclopropane-1-carboxylate synthase in complex with the inhibitor L-aminoethoxyvinylglycine, *J. Biol. Chem. 277*, 49735–49742.
93. Ploux, O., and Marquet, A. (1992) The 8-amino-7-oxopelargonate synthase from *Bacillus sphaericus*: Purification and preliminary characterization of the cloned enzyme overproduced in *Escherichia coli*, *Biochem. J. 283 (Pt 2)*, 327–331.
94. Alexeev, D., Alexeeva, M., Baxter, R. L., Campopiano, D. J., Webster, S. P., and Sawyer, L. (1998) The crystal structure of 8-amino-7-oxononanoate synthase: A bacterial PLP-dependent, acyl-CoA-condensing enzyme, *J. Mol. Biol. 284*, 401–419.
95. Laghai, A., and Jordan, P. M. (1976) A partial reaction of δ-aminolaevulinate synthetase from *Rhodopseudomonas spheroides*, *Biochem. Soc. Trans. 4*, 52–53.
96. Ploux, O., and Marquet, A. (1996) Mechanistic studies on the 8-amino-7-oxopelargonate synthase, a pyridoxal-5′-phosphate-dependent enzyme involved in biotin biosynthesis, *Eur. J. Biochem. 236*, 301–308.
97. Hunter, G. A., and Ferreira, G. C. (2011) Molecular enzymology of 5-aminolevulinate synthase, the gatekeeper of heme biosynthesis, *Biochim. Biophys. Acta 1814*, 1467–1473.
98. Nandi, D. L. (1978) Studies on δ-aminolevulinic acid synthase of *Rhodopseudomonas spheroides*. Reversibility of the reaction, kinetic, spectral, and other studies related to the mechanism of action, *J. Biol. Chem. 253*, 8872–8877.
99. Kumagai, H., and Miles, E. W. (1971) The b protein of *Escherichia coli* tryptophan synthetase. II. New β-elimination and β-replacement reactions, *Biochem. Biophys. Res. Commun. 44*, 1271–1278.
100. Campanini, B., Schiaretti, F., Abbruzzetti, S., Kessler, D., and Mozzarelli, A. (2006) Sulfur mobilization in cyanobacteria: The catalytic mechanism of L-cystine C–S lyase (C-des) from *Synechocystis*, *J. Biol. Chem. 281*, 38769–38780.
101. Newton, W. A., Morino, Y., and Snell, E. E. (1965) Properties of crystalline tryptophanase, *J. Biol. Chem. 240*, 1211–1218.
102. Roy, M., Keblawi, S., and Dunn, M. F. (1988) Stereoelectronic control of bond formation in *Escherichia coli* tryptophan synthase: Substrate specificity and enzymatic synthesis of the novel amino acid dihydroisotryptophan, *Biochemistry 27*, 6698–6704.
103. Phillips, R. S., and Craig, S. (2018) Crystal structures of wild-type and F448A mutant *Citrobacter freundii* tyrosine phenol-lyase complexed with a substrate and inhibitors: Implications for the reaction mechanism, *Biochemistry 57*, 6166–6179.
104. Yamada, T., Komoto, J., Takata, Y., Ogawa, H., Pitot, H. C., and Takusagawa, F. (2003) Crystal structure of serine dehydratase from rat liver, *Biochemistry 42*, 12854–12865.
105. Cook, P. F., Hara, S., Nalabolu, S., and Schnackerz, K. D. (1992) pH Dependence of the absorbance and ^{31}P NMR spectra of *O*-acetylserine sulfhydrylase in the absence and presence of *O*-acetyl-L-serine, *Biochemistry 31*, 2298–2303.
106. Mothersole, R. G., and Wolthers, K. R. (2019) Structural and kinetic insight into the biosynthesis of H_2S and L-lanthionine from L-cysteine by a pyridoxal 5′-phosphate-dependent enzyme from *Fusobacterium nucleatum*, *Biochemistry 58*, 3592–3603.
107. Tu, Y., Kreinbring, C. A., Hill, M., Liu, C., Petsko, G. A., McCune, C. D., Berkowitz, D. B., Liu, D., and Ringe, D. (2018) Crystal structures of cystathionine β-synthase from *Saccharomyces cerevisiae*: One enzymatic step at a time, *Biochemistry 57*, 3134–3145.
108. Schneider, T. R., Gerhardt, E., Lee, M., Liang, P.-H., Anderson, K. S., and Schlichting, I.

(1998) Loop closure and intersubunit communication in tryptophan synthase, *Biochemistry 37*, 5394–5406.
109. McDowell, L. M., Lee, M., Schaefer, J., and Anderson, K. S. (1995) Observation of an aminoacrylate enzyme intermediate in the tryptophan synthase reaction by solid-state NMR, *J. Am. Chem. Soc. 117*, 12352–12353.
110. Shimon, L. J., Rabinkov, A., Shin, I., Miron, T., Mirelman, D., Wilchek, M., and Frolow, F. (2007) Two structures of alliinase from *Alliium sativum* l.: Apo form and ternary complex with aminoacrylate reaction intermediate covalently bound to the PLP cofactor, *J. Mol. Biol. 366*, 611–625.
111. Clausen, T., Huber, R., Laber, B., Pohlenz, H.-D., and Messerschmidt, A. (1996) Crystal structure of the pyridoxal-5′-phosphate dependent cystathionine β-lyase from *Escherichia coli* at 1.83 Å, *J. Mol. Biol. 262*, 202–224.
112. Oda, Y., Mino, K., Ishikawa, K., and Ataka, M. (2005) Three-dimensional structure of a new enzyme, *O*-phosphoserine sulfhydrylase, involved in L-cysteine biosynthesis by a hyperthermophilic archaeon, *Aeropyrum pernix* K1, at 2.0.Å. resolution, *J. Mol. Biol. 351*, 334–344.
113. Forchhammer, K., and Bock, A. (1991) Selenocysteine synthase from *Escherichia coli*. Analysis of the reaction sequence, *J. Biol. Chem. 266*, 6324–6328.
114. Rabeh, W. M., Alguindigue, S. S., and Cook, P. F. (2005) Mechanism of the addition half of the *O*-acetylserine sulfhydrylase-a reaction, *Biochemistry 44*, 5541–5550.
115. Malashkevich, V. N., Toney, M. D., and Jansonius, J. N. (1993) Crystal structures of true enzymatic reaction intermediates: Aspartate and glutamate ketimines in aspartate aminotransferase, *Biochemistry 32*, 13451–13462.
116. Cram, D. J., and Guthrie, R. D. (1965) Claim of a bimolecular mechanism of prototropy, *J. Am. Chem. Soc. 87*, 397–398.
117. Blake, M. I., Siegel, F. P., Katz, J. J., and Kilpatrick, M. (1963) Deuterium isotope effects in transamination: L-Alanine and pyridoxal, *J. Am. Chem. Soc. 85*, 294–297.
118. Zimmerman, S. C., Czarnik, A. W., and Breslow, R. (1983) Intramolecular general base-acid catalysis in transaminations catalyzed by pyridoxamine enzyme analogs, *J. Am. Chem. Soc. 105*, 1694–1695.
119. Yennawar, N. H., Conway, M. E., Yennawar, H. P., Farber, G. K., and Hutson, S. M. (2002) Crystal structures of human mitochondrial branched chain aminotransferase reaction intermediates: Ketimine and pyridoxamine phosphate forms, *Biochemistry 41*, 11592–11601.
120. Toney, M. D., and Kirsch, J. F. (1993) Lysine 258 in aspartate aminotransferase: Enforcer of the circe effect for amino acid substrates and general-base catalyst for the 1,3-prototropic shift, *Biochemistry 32*, 1471–1479.
121. Hagino, H., and Nakayama, K. (1968) Amino acid metabolism in microorganisms: 4. L-methionine decarboxylase produced by a *Streptomyces* strain, *Agr. Biol. Chem. Tokyo 32*, 727–733.
122. Stevenson, D. E., Akhtar, M., and Gani, D. (1990) L-Methionine decarboxylase from *Dryopteris filix-mas*: Purification, characterization, substrate specificity, abortive transamination of the coenzyme, and stereochemical courses of substrate decarboxylation and coenzyme transamination, *Biochemistry 29*, 7631–7647.
123. von Stosch, A. G. (1996) Aspartate aminotransferase complexed with erythro-β-hydroxyaspartate: Crystallographic and spectroscopic identification of the carbinolamine intermediate, *Biochemistry 35*, 15260–15268.
124. Longenecker, J. B., and Snell, E. E. (1956) On the mechanism and optical specificity of transamination reactions, *Proc. Natl. Acad. Sci. U. S. A. 42*, 221–227.
125. Posner, B. I., and Flavin, M. (1972) Cystathionine γ -synthase. Studies of hydrogen exchange reactions, *J. Biol. Chem. 247*, 6402–6411.
126. Phillips, R. S., and Dua, R. K. (1991) Stereochemistry and mechanism of aldol reactions catalyzed by kynureninase, *J. Am. Chem. Soc. 113*, 7385–7388.
127. Brzovic, P., Holbrook, E. L., Greene, R. C., and Dunn, M. F. (1990) Reaction mechanism of *Escherichia coli* cystathionine γ-synthase: Direct evidence for a pyridoxamine derivative of vinylgloxylate as a key intermediate in pyridoxal phosphate dependent γ-elimination and γ-replacement reactions, *Biochemistry 29*, 442–451.
128. Chen, M., Liu, C. T., and Tang, Y. (2020) Discovery and biocatalytic application of a

PLP-dependent amino acid γ-substitution enzyme that catalyzes C–C bond formation, *J. Am. Chem. Soc. 142*, 10506–10515.
129. Clausen, T., Wahl, M. C., Messerschmidt, A., Huber, R., Fuhrmann, J. C., Laber, B., Streber, W., and Steegborn, C. (1999) Cloning, purification and characterisation of cystathionine γ-synthase from *Nicotiana tabacum*, *Biol. Chem. 380*, 1237–1242.
130. Omi, R., Goto, M., Miyahara, I., Mizuguchi, H., Hayashi, H., Kagamiyama, H., and Hirotsu, K. (2003) Crystal structures of threonine synthase from *Thermus thermophilus* hb8: Conformational change, substrate recognition, and mechanism, *J. Biol. Chem. 278*, 46035–46045.
131. Covarrubias, A. S., Hogbom, M., Bergfors, T., Carroll, P., Mannerstedt, K., Oscarson, S., Parish, T., Jones, T. A., and Mowbray, S. L. (2008) Structural, biochemical, and *in vivo* investigations of the threonine synthase from *Mycobacterium tuberculosis*, *J. Mol. Biol. 381*, 622–633.
132. Fukumoto, M., Kudou, D., Murano, S., Shiba, T., Sato, D., Tamura, T., Harada, S., and Inagaki, K. (2012) The role of amino acid residues in the active site of L-methionine γ-lyase from *Pseudomonas putida*, *Biosci. Biotechnol. Biochem. 76*, 1275–1284.
133. Esaki, N., Nakayama, T., Sawada, S., Tanaka, H., and Soda, K. (1985) ^{1}H NMR studies of substrate hydrogen exchange reactions catalyzed by L-methionine γ-lyase, *Biochemistry 24*, 3857–3862.
134. Sato, D., Shiba, T., Karaki, T., Yamagata, W., Nozaki, T., Nakazawa, T., and Harada, S. (2017) X-Ray snapshots of a pyridoxal enzyme: A catalytic mechanism involving concerted [1,5]-hydrogen sigmatropy in methionine γ-lyase, *Sci Rep 7*, 4874.
135. Jencks, W. P. (1969) *Catalysis in chemistry and enzymology*, pp 136–137, McGraw-Hill, New York.
136. Gonzalez-Porque, P., and Strominger, J. L. (1972) Introduction of the 3-deoxy group in 3,6-dideoxyhexoses. Novel cofactor function for pyridoxamine-5′-phosphate, *Proc. Natl. Acad. Sci. U.S.A. 69*, 1625–1628.
137. Weigel, T. M., Liu, L. D., and Liu, H. W. (1992) Mechanistic studies of the biosynthesis of 3,6-dideoxyhexoses in *Yersinia pseudotuberculosis*: Purification and characterization of CDP-4-keto-6-deoxy-D-glucose-3-dehydrase, *Biochemistry 31*, 2129–2139.
138. Beyer, N., Alam, J., Hallis, T. M., Guo, Z., and Liu, H.-w. (2003) The biosynthesis of GDP-L-colitose: C-3 deoxygenation is catalyzed by a unique coenzyme B_6-dependent enzyme, *J. Am. Chem. Soc. 125*, 5584–5585.
139. Cook, P. D., and Holden, H. M. (2008) GDP-4-keto-6-deoxy-D-mannose 3-dehydratase, accommodating a sugar substrate in the active site, *J. Biol. Chem. 283*, 4295–4303.
140. Smith, P., Szu, P. H., Bui, C., Liu, H. W., and Tsai, S. C. (2008) Structure and mutagenic conversion of E1 dehydrase: At the crossroads of dehydration, amino transfer, and epimerization, *Biochemistry 47*, 6329–6341.
141. Johnson, D. A., Gassner, G. T., Bandarian, V., Ruzicka, F. J., Ballou, D. P., Reed, G. H., and Liu, H. W. (1996) Kinetic characterization of an organic radical in the ascarylose biosynthetic pathway, *Biochemistry 35*, 15846–15856.
142. Chang, C.-W. T., Johnson, D. A., Bandarian, V., Zhou, H., LoBrutto, R., Reed, G. H., and Liu, H.-W. (2000) Characterization of a unique coenzyme B_6 radical in the ascarylose biosynthetic pathway, *J. Am. Chem. Soc. 122*, 4239–4240.
143. Thorson, J. S., and Liu, H. W. (1993) Coenzyme B_6 as a redox cofactor: A new role for an old coenzyme?, *J. Am. Chem. Soc. 115*, 12177–12178.
144. Schoenhofen, I. C., Lunin, V. V., Julien, J. P., Li, Y., Ajamian, E., Matte, A., Cygler, M., Brisson, J. R., Aubry, A., Logan, S. M., Bhatia, S., Wakarchuk, W. W., and Young, N. M. (2006) Structural and functional characterization of PseC, an aminotransferase involved in the biosynthesis of pseudaminic acid, an essential flagellar modification in *Helicobacter pylori*, *J. Biol. Chem. 281*, 8907–8916.
145. Abell, L. M., and O'Leary, M. H. (1988) Isotope effect studies of the pyruvate-dependent histidine decarboxylase from *Lactobacillus* 30a, *Biochemistry 27*, 5933–5939.
146. Gallagher, T., Snell, E. E., and Hackert, M. L. (1989) Pyruvoyl-dependent histidine decarboxylase. Active site structure and mechanistic analysis, *J. Biol. Chem. 264*, 12737–12743.
147. Anton, D. L., and Kutny, R. (1987) Mechanism of substrate inactivation of *Escherichia*

coli S-adenosylmethionine decarboxylase, *Biochemistry 26*, 6444–6447.
148. Lee, B. I., and Suh, S. W. (2004) Crystal structure of the Schiff base intermediate prior to decarboxylation in the catalytic cycle of aspartate α-decarboxylase, *J. Mol. Biol. 340*, 1–7.
149. Miles, E. W. (1987) Stereochemistry and mechanism of a new single-turnover, half-transamination reaction catalyzed by the tryptophan synthase $\alpha 2\beta 2$ complex, *Biochemistry 26*, 597–603.
150. Yard, B. A., Carter, L. G., Johnson, K. A., Overton, I. M., Dorward, M., Liu, H., McMahon, S. A., Oke, M., Puech, D., Barton, G. J., Naismith, J. H., and Campopiano, D. J. (2007) The structure of serine palmitoyltransferase: Gateway to sphingolipid biosynthesis, *J. Mol. Biol. 370*, 870–886.
151. Rando, R. R., and Bangerter, F. W. (1976) The irreversible inhibition of mouse brain γ-aminobutyric acid (GABA)-α-ketoglutaric acid transaminase by gabaculine, *J. Am. Chem. Soc. 98*, 6762–6764.
152. Pugh, C. E., Harwood, J. L., and John, R. A. (1992) Mechanism of glutamate semialdehyde aminotransferase. Roles of diamino- and dioxo-intermediates in the synthesis of aminolevulinate, *J. Biol. Chem. 267*, 1584–1588.
153. Breslow, R. (1958) Mechanism of thiamine action. IV. Evidence from studies on model systems, *J. Am. Chem. Soc. 80*, 3719–3726.
154. Breslow, R. (1957) The mechanism of thiamine action. II. Rapid deuterium exchange in thiazolium salts, *J. Am. Chem. Soc. 79*, 1762–1763.
155. Suchy, J., Mieyal, J. J., Bantle, G., and Sable, H. Z. (1972) Coenzyme interactions. Vi. Properties of the pyrimidine moiety of thiamine, *J. Biol. Chem. 247*, 5905–5912.
156. Haake, P., Bausher, L. P., and Miller, W. B. (1969) Thiazolium ions and related heteroaromatic systems. III. Comparison of rates of hydrogen exchange with ^{13}C–H coupling constants. Evidence for stabilization of heterocyclic ylides by sulfur, *J. Am. Chem. Soc. 91*, 1113–1119.
157. Washabaugh, M. W., and Jencks, W. P. (1988) Thiazolium C2-proton exchange: Structure-reactivity correlations and the pK_a of thiamin C2-H revisited, *Biochemistry 27*, 5044–5053.
158. Bruice, T. C., and Benkovic, S. J. (1966) In *Bioorganic mechanisms*, pp 204–226, Benjamin, New York.
159. Bordwell, F. G., and Satish, A. V. (1991) Acidities of C2 hydrogen atoms in thiazolium cations and reactivities of their conjugate bases, *J. Am. Chem. Soc. 113*, 985–990.
160. Jordan, F. (1974) Semiempirical calculations on the electronic structure and preferred conformations of thiamine (vitamin B_1) and thiamine pyrophosphate (cocarboxylase), *J. Am. Chem. Soc. 96*, 3623–3630.
161. Gallo, A. A., and Sable, H. Z. (1974) Coenzyme interactions. VIII. Carbon-13 nuclear magnetic resonance studies of thiamine and related compounds. Electronic aspects of thiamine catalysis, *J. Biol. Chem. 249*, 1382–1389.
162. Lee, J. K., and Houk, K. N. (1997) A proficient enzyme revisited: The predicted mechanism for orotidine monophosphate decarboxylase, *Science 276*, 942–945.
163. Yount, R. G., and Metzler, D. E. (1959) Decarboxylation of pyruvate by thiamine analogues, *J. Biol. Chem. 234*, 738–741.
164. Nemeria, N., Korotchkina, L., McLeish, M. J., Kenyon, G. L., Patel, M. S., and Jordan, F. (2007) Elucidation of the chemistry of enzyme-bound thiamin diphosphate prior to substrate binding: Defining internal equilibria among tautomeric and ionization states, *Biochemistry 46*, 10739–10744.
165. Kern, D., Kern, G., Neef, H., Tittmann, K., Killenberg-Jabs, M., Wikner, C., and Schneider, G. (1997) How thiamine diphosphate is activated in enzymes, *Science 275*, 67–70.
166. Dyda, F., Furey, W., Swaminathan, S., Sax, M., Farrenkopf, B., and Jordan, F. (1993) Catalytic centers in the thiamin diphosphate dependent enzyme pyruvate decarboxylase at 2.4 Å resolution, *Biochemistry 32*, 6165–6170.
167. Muller, Y. A., Schumacher, G., Rudolph, R., and Schulz, G. E. (1994) The refined structures of a stabilized mutant and of wild-type pyruvate oxidase from *Lactobacillus plantarum*, *J. Mol. Biol. 237*, 315–335.
168. Lindqvist, Y., Schneider, G., Ermler, U., and Sundstrom, M. (1992) Three-dimensional structure of transketolase, a thiamine diphosphate dependent enzyme, at 2.5 Å resolution, *EMBO J. 11*, 2373–2379.

169. Nikkola, M., Lindqvist, Y., and Schneider, G. (1994) Refined structure of transketolase from *Saccharomyces cerevisiae* at 2.0 Å resolution, *J. Mol. Biol. 238*, 387–404.
170. Arjunan, P., Umland, T., Dyda, F., Swaminathan, S., Furey, W., Sax, M., Farrenkopf, B., Gao, Y., Zhang, D., and Jordan, F. (1996) Crystal structure of the thiamin diphosphate-dependent enzyme pyruvate decarboxylase from the yeast *Saccharomyces cerevisiae* at 2.3 Å resolution, *J. Mol. Biol. 256*, 590–600.
171. Hasson, M. S., Muscate, A., McLeish, M. J., Polovnikova, L. S., Gerlt, J. A., Kenyon, G. L., Petsko, G. A., and Ringe, D. (1998) The crystal structure of benzoylformate decarboxylase at 1.6 Å resolution: Diversity of catalytic residues in thiamin diphosphate-dependent enzymes, *Biochemistry 37*, 9918–9930.
172. Arjunan, P., Nemeria, N., Brunskill, A., Chandrasekhar, K., Sax, M., Yan, Y., Jordan, F., Guest, J. R., and Furey, W. (2002) Structure of the pyruvate dehydrogenase multienzyme complex E1 component from *Escherichia coli* at 1.85 Å resolution, *Biochemistry 41*, 5213–5221.
173. Mosbacher, T. G., Mueller, M., and Schulz, G. E. (2005) Structure and mechanism of the ThDP-dependent benzaldehyde lyase from *Pseudomonas fluorescens*, *FEBS J. 272*, 6067–6076.
174. Kaplun, A., Binshtein, E., Vyazmensky, M., Steinmetz, A., Barak, Z., Chipman, D. M., Tittmann, K., and Shaanan, B. (2008) Glyoxylate carboligase lacks the canonical active site glutamate of thiamine-dependent enzymes, *Nature Chem. Biol. 4*, 113–118.
175. Arjunan, P., Sax, M., Brunskill, A., Chandrasekhar, K., Nemeria, N., Zhang, S., Jordan, F., and Furey, W. (2006) A thiamin-bound, pre-decarboxylation reaction intermediate analogue in the pyruvate dehydrogenase E1 subunit induces large scale disorder-to-order transformations in the enzyme and reveals novel structural features in the covalently bound adduct, *J. Biol. Chem. 281*, 15296–15303.
176. Fiedler, E., Thorell, S., Sandalova, T., Golbik, R., Konig, S., and Schneider. (2002) Snapshot of a key intermediate in enzymatic thiamin catalysis: Crystal structure of the α-carbanion of (α,β-dihydroxyethyl)-thiamin diphosphate in the active site of transketolase from *Saccharomyces cerevisiae*, *Proc. Natl. Acad. Sci. U. S. A. 99*, 591–595.
177. Nemeria, N., Binshtein, E., Patel, H., Balakrishnan, A., Vered, I., Shaanan, B., Barak, Z., Chipman, D., and Jordan, F. (2012) Glyoxylate carboligase: A unique thiamin diphosphate-dependent enzyme that can cycle between the 4′-aminopyrimidinium and 1′,4′-iminopyrimidine tautomeric forms in the absence of the conserved glutamate, *Biochemistry 51*, 7940–7952.
178. Killenberg-Jabs, M., Konig, S., Eberhardt, I., Hohmann, S., and Hubner, G. (1997) Role of Glu51 for cofactor binding and catalytic activity in pyruvate decarboxylase from yeast studied by site-directed mutagenesis, *Biochemistry 36*, 1900–1905.
179. Guo, F., Zhang, D., Kahyaoglu, A., Farid, R. S., and Jordan, F. (1998) Is a hydrophobic amino acid required to maintain the reactive v conformation of thiamin at the active center of thiamin diphosphate-requiring enzymes? Experimental and computational studies of isoleucine 415 of yeast pyruvate decarboxylase, *Biochemistry 37*, 13379–13391.
180. Jordan, F., Nemeria, N. S., Zhang, S., Yan, Y., Arjunan, P., and Furey, W. (2003) Dual catalytic apparatus of the thiamin diphosphate coenzyme: Acid–base via the 1′,4′-iminopyrimidine tautomer along with its electrophilic role, *J. Am. Chem. Soc. 125*, 12732–12738.
181. Nemeria, N., Baykal, A., Joseph, E., Zhang, S., Yan, Y., Furey, W., and Jordan, F. (2004) Tetrahedral intermediates in thiamin diphosphate-dependent decarboxylations exist as a 1′,4′-imino tautomeric form of the coenzyme, unlike the Michaelis complex or the free coenzyme, *Biochemistry 43*, 6565–6575.
182. Jordan, F., Zhang, Z., and Sergienko, E. (2002) Spectroscopic evidence for participation of the 1′,4′-imino tautomer of thiamin diphosphate in catalysis by yeast pyruvate decarboxylase, *Bioorg. Chem. 30*, 188–198.
183. Baykal, A. T., Kakalis, L., and Jordan, F. (2006) Electronic and nuclear magnetic resonance spectroscopic features of the 1′,4′-iminopyrimidine tautomeric form of thiamin diphosphate, a novel intermediate on enzymes requiring this coenzyme, *Biochemistry 45*, 7522–7528.
184. Mitschke, L., Parthier, C., Schroder-Tittmann, K., Coy, J., Ludtke, S., and Tittmann, K. (2010) The crystal structure of human transketolase

and new insights into its mode of action, *J. Biol. Chem. 285*, 31559–31570.
185. Kyte, J. (2007) *Structure in protein chemistry: Second edition*, p 277, Garland Science, New York.
186. Chen, P. Y., DeColli, A. A., Freel Meyers, C. L., and Drennan, C. L. (2019) X-ray crystallography-based structural elucidation of enzyme-bound intermediates along the 1-deoxy-D-xylulose 5-phosphate synthase reaction coordinate, *J. Biol. Chem. 294*, 12405–12414.
187. Sax, M., Pulsinelli, P., and Pletcher, J. (1974) Stereochemistry of intermediates in thiamine catalysis. I. Crystal structures of 2-(α-hydroxyethyl)-3,4-dimethylthiazolium bromide and DL-2-(α-hydroxyethyl)thiamine chloride hydrochloride, *J. Am. Chem. Soc. 96*, 155–165.
188. Mieyal, J. J., Bantle, G., Votaw, R. G., Rosner, I. A., and Sable, H. Z. (1971) Coenzyme interactions. V. The second carbanion in reactions catalyzed by thiamine, *J. Biol. Chem. 246*, 5213–5219.
189. Barletta, G., Huskey, W. P., and Jordan, F. (1992) Observation of a 2-α-enamine from a 2-(methoxyphenylmethyl)-3,4-dimethylthiazolium salt in water: Implications for catalysis by thiamin diphosphate-dependent α-keto acid decarboxylases, *J. Am. Chem. Soc. 114*, 7607–7608.
190. Stivers, J. T., and Washabaugh, M. W. (1992) C_α-Proton transfer from thiazolium ions: Structure-reactivity correlations and the C_α–H pK_a of 2-(1-hydroxyethyl)thiamin, *Bioorg. Chem. 20*, 155–172.
191. Washabaugh, M. W., Stivers, J. T., and Hickey, K. A. (1994) C_α-Proton transfer from 2-(1-hydroxybenzyl)oxythiamin: The unit Brønsted slope overestimates the amount of bond formation to the base catalyst in the transition state, *J. Am. Chem. Soc. 116*, 7094–7097.
192. Crosby, J., Stone, R., and Lienhard, G. E. (1970) Mechanisms of thiamine-catalyzed reactions. Decarboxylation of 2-(1-carboxy-L-hydroxyethyl)-3,4-dimethylthiazolium chloride, *J. Am. Chem. Soc. 92*, 2891–2900.
193. Kluger, R., Chin, J., and Smyth, T. (1981) Thiamin-catalyzed decarboxylation of pyruvate. Synthesis and reactivity analysis of the central, elusive intermediate, α-lactylthiamin, *J. Am. Chem. Soc. 103*, 884–888.
194. Kluger, R., Karimian, K., and Kitamura, K. (1987) Chiral intermediates in thiamin catalysis. Stereochemical course of the decarboxylation step in the conversion of pyruvate to acetaldehyde, *J. Am. Chem. Soc. 109*, 6368–6371.
195. Crosby, J., and Lienhard, G. E. (1970) Mechanisms of thiamine-catalyzed reactions. A kinetic analysis of the decarboxylation of pyruvate by 3,4-dimethylthiazolium ion in water and ethanol, *J. Am. Chem. Soc. 92*, 5707–5716.
196. Marlier, J. F., and O'Leary, M. H. (1986) Solvent dependence of the carbon kinetic isotope effect on the decarboxylation of 4-pyridylacetic acid. A model for enzymatic decarboxylations, *J. Am. Chem. Soc. 108*, 4896–4899.
197. Washburn, L. A., Foley, B., Martinez, F., Lee, R. P., Pryor, K., Rimes, E., and Watanabe, C. M. H. (2019) Transketolase activity in the formation of the azinomycin azabicycle moiety, *Biochemistry 58*, 5255–5258.
198. Bunik, V. I., Denton, T. T., Xu, H., Thompson, C. M., Cooper, A. J., and Gibson, G. E. (2005) Phosphonate analogues of α-ketoglutarate inhibit the activity of the α-ketoglutarate dehydrogenase complex isolated from brain and in cultured cells, *Biochemistry 44*, 10552–10561.
199. Brandt, G. S., Nemeria, N., Chakraborty, S., McLeish, M. J., Yep, A., Kenyon, G. L., Petsko, G. A., Jordan, F., and Ringe, D. (2008) Probing the active center of benzaldehyde lyase with substitutions and the pseudosubstrate analogue benzoylphosphonic acid methyl ester, *Biochemistry 47*, 7734–7743.
200. Brandt, G. S., Kneen, M. M., Chakraborty, S., Baykal, A. T., Nemeria, N., Yep, A., Ruby, D. I., Petsko, G. A., Kenyon, G. L., McLeish, M. J., Jordan, F., and Ringe, D. (2009) Snapshot of a reaction intermediate: Analysis of benzoylformate decarboxylase in complex with a benzoylphosphonate inhibitor, *Biochemistry 48*, 3247–3257.
201. Jordan, F., Kudzin, Z. H., and Rios, C. B. (1987) Generation and physical properties of enamines related to the key intermediate in thiamin diphosphate-dependent enzymic pathways, *J. Am. Chem. Soc. 109*, 4415–4416.
202. Moore, I. F., and Kluger, R. (2002) Substituent effects in carbon–nitrogen cleavage of thiamin derivatives. Fragmentation pathways and enzymic avoidance of cofactor destruction, *J. Am. Chem. Soc. 124*, 1669–1673.

203. Hu, Q., and Kluger, R. (2004) Fragmentation of the conjugate base of 2-(1-hydroxybenzyl)thiamin: Does benzoylformate decarboxylase prevent orbital overlap to avoid it?, *J. Am. Chem. Soc. 126*, 68–69.
204. Chakraborty, S., Nemeria, N., Yep, A., McLeish, M. J., Kenyon, G. L., and Jordan, F. (2008) Mechanism of benzaldehyde lyase studied via thiamin diphosphate-bound intermediates and kinetic isotope effects, *Biochemistry 47*, 3800–3809.
205. Suzuki, R., Katayama, T., Kim, B. J., Wakagi, T., Shoun, H., Ashida, H., Yamamoto, K., and Fushinobu, S. (2010) Crystal structures of phosphoketolase: Thiamine diphosphate-dependent dehydration mechanism, *J. Biol. Chem. 285*, 34279–34287.
206. Meyer, D., Neumann, P., Koers, E., Sjuts, H., Ludtke, S., Sheldrick, G. M., Ficner, R., and Tittmann, K. (2012) Unexpected tautomeric equilibria of the carbanion-enamine intermediate in pyruvate oxidase highlight unrecognized chemical versatility of thiamin, *Proc. Natl. Acad. Sci. U.S.A. 109*, 10867–10872.
207. Sergienko, E. A., Wang, J., Polovnikova, L., Hasson, M. S., McLeish, M. J., Kenyon, G. L., and Jordan, F. (2000) Spectroscopic detection of transient thiamin diphosphate-bound intermediates on benzoylformate decarboxylase, *Biochemistry 39*, 13862–13869.
208. Barletta, G. L., Zou, Y., Huskey, W. P., and Jordan, F. (1997) Kinetics of C(2α)-proton abstraction from 2-benzylthiazolium salts leading to enamines relevant to catalysis by thiamin-dependent enzymes, *J. Am. Chem. Soc. 119*, 2356–2362.
209. Murry, J. A., Frantz, D. E., Soheili, A., Tillyer, R., Grabowski, E. J. J., and Reider, P. J. (2001) Synthesis of α-amido ketones via organic catalysis: Thiazolium-catalyzed cross-coupling of aldehydes with acylimines, *J. Am. Chem. Soc. 123*, 9696–9697.
210. Ibdah, M., Bar-Ilan, A., Livnah, O., Schloss, J. V., Barak, Z. e., and Chipman, D. M. (1996) Homology modeling of the structure of bacterial acetohydroxy acid synthase and examination of the active site by site-directed mutagenesis, *Biochemistry 35*, 16282–16291.
211. Bhasin, M., Billinsky, J. L., and Palmer, D. R. J. (2003) Steady-state kinetics and molecular evolution of *Escherichia coli* MenD [(1*R*,6*R*)-2-succinyl-6-hydroxy-2,4-cyclohexadiene-1-carboxylate synthase], an anomalous thiamin diphosphate-dependent decarboxylase-carboligase, *Biochemistry 42*, 13496–13504.
212. Dawson, A., Fyfe, P. K., and Hunter, W. N. (2008) Specificity and reactivity in menaquinone biosynthesis: The structure of *Escherichia coli* MenD (2-succinyl-5-enolpyruvyl-6-hydroxy-3-cyclohexadiene-1-carboxylate synthase), *J. Mol. Biol. 384*, 1353–1368.
213. Song, H., Dong, C., Qin, M., Chen, Y., Sun, Y., Liu, J., Chan, W., and Guo, Z. (2016) A thiamine-dependent enzyme utilizes an active tetrahedral intermediate in vitamin K biosynthesis, *J. Am. Chem. Soc. 138*, 7244–7247.
214. Holzer, H., Kattermann, R., and Busch, D. (1962) A thiamine pyrophosphate-glyco-aldehyde compound ("active glycolaldehyde") as intermediate in the transketolase reaction, *Biochem. Biophys. Res. Commun. 7*, 167–172.
215. Sprenger, G. A., Schorken, U., Wiegert, T., Grolle, S., de Graaf, A. A., Taylor, S. V., Begley, T. P., Bringer-Meyer, S., and Sahm, H. (1997) Identification of a thiamin-dependent synthase in *Escherichia coli* required for the formation of the 1-deoxy-D-xylulose 5-phosphate precursor to isoprenoids, thiamin, and pyridoxol, *Proc. Natl. Acad. Sci. U. S. A. 94*, 12857–12862.
216. Lange, B. M., Wildung, M. R., McCaskill, D., and Croteau, R. (1998) A family of transketolases that directs isoprenoid biosynthesis via a mevalonate-independent pathway, *Proc. Natl. Acad. Sci. U. S. A. 95*, 2100–2104.
217. Tittmann, K., Golbik, R., Uhlemann, K., Khailova, L., Schneider, G., Patel, M., Jordan, F., Chipman, D. M., Duggleby, R. G., and Hubner, G. (2003) NMR analysis of covalent intermediates in thiamin diphosphate enzymes, *Biochemistry 42*, 7885–7891.
218. Shin, W., and Kim, Y. C. (1986) Crystal structure of thiamine thiazolone: A possible transition-state analog with an intramolecular N–H...O hydrogen bond in the V form, *J. Am. Chem. Soc. 108*, 7078–7082.
219. Harris, T. K., and Washabaugh, M. W. (1995) Distribution of the thiamin diphosphate C2-proton during catalysis of acetaldehyde formation by brewers' yeast pyruvate decarboxylase, *Biochemistry 34*, 13994–14000.
220. Flournoy, D. S., and Frey, P. A. (1989) Inactivation of the pyruvate dehydrogenase com-

plex of *Escherichia coli* by fluoropyruvate, *Biochemistry 28*, 9594–9602.
221. Sun, S., Smith, G. S., O'Leary, M. H., and Schowen, R. L. (1997) The linkage of catalysis and regulation in enzyme action. Fluoropyruvate as a probe of regulation in pyruvate decarboxylases, *J. Am. Chem. Soc. 119*, 1507–1515.
222. Khaleeli, N., Li, R., and Townsend, C. A. (1999) Origin of the β-lactam carbons in clavulanic acid from an unusual thiamine pyrophosphate-mediated reaction, *J. Am. Chem. Soc. 121*, 9223–9224.
223. Merski, M., and Townsend, C. A. (2007) Observation of an acryloyl-thiamin diphosphate adduct in the first step of clavulanic acid biosynthesis, *J. Am. Chem. Soc. 129*, 15750–15751.
224. Chabriere, E., Charon, M. H., Volbeda, A., Pieulle, L., Hatchikian, E. C., and Fontecilla-Camps, J. C. (1999) Crystal structures of the key anaerobic enzyme pyruvate:ferredoxin oxidoreductase, free and in complex with pyruvate, *Nature Struct. Biol. 6*, 182–190.
225. Muller, Y. A., and Schulz, G. E. (1993) Structure of the thiamine- and flavin-dependent enzyme pyruvate oxidase, *Science 259*, 965–967.
226. Tittmann, K., Wille, G., Golbik, R., Weidner, A., Ghisla, S., and Hubner, G. (2005) Radical phosphate transfer mechanism for the thiamin diphosphate- and FAD-dependent pyruvate oxidase from *Lactobacillus plantarum*. Kinetic coupling of intercofactor electron transfer with phosphate transfer to acetyl-thiamin diphosphate via a transient FAD semiquinone/hydroxyethyl-ThDP radical pair, *Biochemistry 44*, 13291–13303.
227. Menon, S., and Ragsdale, S. W. (1997) Mechanism of the *Clostridium thermoaceticum* pyruvate:ferredoxin oxidoreductase: Evidence for the common catalytic intermediacy of the hydroxyethylthiamine pyropyrosphate radical, *Biochemistry 36*, 8484–8494.
228. Mansoorabadi, S. O., Seravalli, J., Furdui, C., Krymov, V., Gerfen, G. J., Begley, T. P., Melnick, J., Ragsdale, S. W., and Reed, G. H. (2006) EPR Spectroscopic and computational characterization of the hydroxyethylidene-thiamine pyrophosphate radical intermediate of pyruvate:ferredoxin oxidoreductase, *Biochemistry 45*, 7122–7131.
229. Chabriere, E., Vernede, X., Guigliarelli, B., Charon, M. H., Hatchikian, E. C., and Fontecilla-Camps, J. C. (2001) Crystal structure of the free radical intermediate of pyruvate:ferredoxin oxidoreductase, *Science 294*, 2559–2563.
230. Barletta, G., Chung, A. C., Rios, C. B., Jordan, F., and Schlegel, J. M. (1990) Electrochemical oxidation of enamines related to the key intermediate on thiamin diphosphate dependent enzymic pathways: Evidence for one-electron oxidation via a thiazolium cation radical, *J. Am. Chem. Soc. 112*, 8144–8149.
231. Chiu, C. C., Pan, K., and Jordan, F. (1995) Modeling an elementary step of the enzyme pyruvate oxidase: Oxidation of a thiamin diphosphate-bound enamine intermediate by a flavin analog, *J. Am. Chem. Soc. 117*, 7027–7028.
232. Gibson, M. I., Chen, P. Y. T., Johnson, A. C., Pierce, E., Can, M., Ragsdale, S. W., and Drennan, C. L. (2016) One-carbon chemistry of oxalate oxidoreductase captured by X-ray crystallography, *Proc. Natl. Acad. Sci. U.S.A. 113*, 320–325.
233. Rastetter, W. H., Adams, J., Frost, J. W., Nummy, L. J., Frommer, J. E., and Roberts, K. B. (1979) On the involvement of lipoic acid in α-keto acid dehydrogenase complexes, *J. Am. Chem. Soc. 101*, 2752–2753.
234. Das, M. L., Koike, M., and Reed, L. J. (1961) On the role of thiamine pyrophosphate in oxidative decarboxylation of α-keto acids, *Proc. Natl. Acad. Sci. U. S. A. 47*, 753–759.
235. Chiu, C. C., Chung, A., Barletta, G., and Jordan, F. (1996) Intramolecular model for the reductive acyl transfer catalyzed by α-keto acid dehydrogenases, *J. Am. Chem. Soc. 118*, 11026–11029.
236. Pan, K., and Jordan, F. (1998) D,L-*S*-Methyllipoic acid methyl ester, a kinetically viable model for *S*-protonated lipoic acid as the oxidizing agent in reductive acyl transfers catalyzed by the 2-oxoacid dehydrogenase multienzyme complexes, *Biochemistry 37*, 1357–1364.
237. Kyte, J. (2007) *Structure in protein chemistry: Second edition*, pp 122–125, Garland Science, New York.
238. Gruys, K. J., Datta, A., and Frey, P. A. (1989) 2-Acetylthiamin pyrophosphate (acetyl-TPP) pH-rate profile for hydrolysis of acetyl-TPP and isolation of acetyl-TPP as a transient

species in pyruvate dehydrogenase catalyzed reactions, *Biochemistry 28*, 9071–9080.
239. Nemeria, N. S., Ambrus, A., Patel, H., Gerfen, G., Adam-Vizi, V., Tretter, L., Zhou, J., Wang, J., and Jordan, F. (2014) Human 2-oxoglutarate dehydrogenase complex E1 component forms a thiamin-derived radical by aerobic oxidation of the enamine intermediate, *J. Biol. Chem. 289*, 29859–29873.
240. Asmus, K. D. (1983) Sulfur-centered free radicals, In *Radioprotectors and anticarcinogens* (Nygaard, O. F., and Simic, M. D., Eds.), pp 23–42, Academic Press, New York.
241. Favaudon, V., Tourbez, H., Houee-Levin, C., and Lhoste, J. M. (1990) CO_2-Radical induced cleavage of disulfide bonds in proteins. A γ-ray and pulse radiolysis mechanistic investigation, *Biochemistry 29*, 10978–10989.
242. Farver, O., Skov, L. K., Pascher, T., Karlsson, B. G., Nordling, M., Lundberg, L. G., Vangard, T., and Pecht, I. (1993) Intramolecular electron transfer in single-site-mutated azurins, *Biochemistry 32*, 7317–7322.
243. Faraggi, M., and Klapper, M. H. (1988) Intramolecular long-range electron transfer in the α-hemoglobin subunit, *J. Am. Chem. Soc. 110*, 5753–5756.
244. Lmoumene, C. E., Conte, D., Jacquot, J. P., and Houee-Levin, C. (2000) Redox properties of protein disulfide bond in oxidized thioredoxin and lysozyme: A pulse radiolysis study, *Biochemistry 39*, 9295–9301.
245. Flournoy, D. S., and Frey, P. A. (1986) Pyruvate dehydrogenase and 3-fluoropyruvate: Chemical competence of 2-acetylthiamin pyrophosphate as an acetyl group donor to dihydrolipoamide, *Biochemistry 25*, 6036–6043.
246. Gruys, K. J., Halkides, C. J., and Frey, P. A. (1987) Synthesis and properties of 2-acetylthiamin pyrophosphate: An enzymatic reaction intermediate, *Biochemistry 26*, 7575–7585.
247. Annan, N., Paris, R., and Jordan, F. (1989) (*E*)-4-(α-halo-*p*-tolyl)-2-oxo-3-butenoic acids inhibit yeast pyruvate decarboxylase by a diversity of mechanisms: Multiple fate for the thiamin-bound enamine intermediate, *J. Am. Chem. Soc. 111*, 8895–8901.
248. Zeng, X., Chung, A., Haran, M., and Jordan, F. (1991) Direct observation of the kinetic fate of a thiamin diphosphate bound enamine intermediate on brewers' yeast pyruvate decarboxylase. Kinetic and regiospecific consequences of allosteric activation, *J. Am. Chem. Soc. 113*, 5842–5849.
249. Fiedler, E., Golbik, R., Schneider, G., Tittmann, K., Neef, H., Konig, S., and Hubner, G. (2001) Examination of donor substrate conversion in yeast transketolase, *J. Biol. Chem. 276*, 16051–16058.
250. Calabrese, J. C., Jordan, D. B., Boodhoo, A., Sariaslani, S., and Vannelli, T. (2004) Crystal structure of phenylalanine ammonia lyase: Multiple helix dipoles implicated in catalysis, *Biochemistry 43*, 11403–11416.
251. Ritter, H., and Schulz, G. E. (2004) Structural basis for the entrance into the phenylpropanoid metabolism catalyzed by phenylalanine ammonia-lyase, *Plant Cell 16*, 3426–3436.
252. Louie, G. V., Bowman, M. E., Moffitt, M. C., Baiga, T. J., Moore, B. S., and Noel, J. P. (2006) Structural determinants and modulation of substrate specificity in phenylalanine-tyrosine ammonia-lyases, *Nature Chem. Biol. 13*, 1327–1338.
253. Wybenga, G. G., Szymanski, W., Wu, B., Feringa, B. L., Janssen, D. B., and Dijkstra, B. W. (2014) Structural investigations into the stereochemistry and activity of a phenylalanine-2,3-aminomutase from *Taxus chinensis*, *Biochemistry 53*, 3187–3198.
254. Strom, S., Wanninayake, U., Ratnayake, N. D., Walker, K. D., and Geiger, J. H. (2012) Insights into the mechanistic pathway of the *Pantoea agglomerans* phenylalanine aminomutase, *Angew. Chem., Int. Ed. Engl. 51*, 2898–2902.
255. Christenson, S. D., Wu, W., Spies, M. A., Shen, B., and Toney, M. D. (2003) Kinetic analysis of the 4-methylideneimidazole-5-one-containing tyrosine aminomutase in enediyne antitumor antibiotic c-1027 biosynthesis, *Biochemistry 42*, 12708–12718.
256. Christianson, C. V., Montavon, T. J., Van Lanen, S. G., Shen, B., and Bruner, S. D. (2007) The structure of L-tyrosine 2,3-aminomutase from the c-1027 enediyne antitumor antibiotic biosynthetic pathway, *Biochemistry 46*, 7205–7214.
257. Walker, K. D., Klettke, K., Akiyama, T., and Croteau, R. (2004) Cloning, heterologous expression, and characterization of a phenylalanine aminomutase involved in taxol biosynthesis, *J. Biol. Chem. 279*, 53947–53954.

258. Heberling, M. M., Masman, M. F., Bartsch, S., Wybenga, G. G., Dijkstra, B. W., Marrink, S. J., and Janssen, D. B. (2015) Ironing out their differences: Dissecting the structural determinants of a phenylalanine aminomutase and ammonia lyase, *Am. Chem. Soc. Chem. Biol 10*, 989–997.
259. Hanson, K. R., Wightman, R. H., Staunton, J., and Battersby, A. R. (1971) Stereochemical course of elimination catalysed by L-phenylalanine ammonia-lyase and configuration of 2-benzamidocinnamic azlactone, *J. Chem. Soc. Chem. Comm.*, 185–186.
260. Givot, I. L., Smith, T. A., and Abeles, R. H. (1969) Studies on the mechanism of action and the structure of the electrophilic center of histidine ammonia lyase, *J. Biol. Chem. 244*, 6341–6353.
261. Mutatu, W., Klettke, K. L., Foster, C., and Walker, K. D. (2007) Unusual mechanism for an aminomutase rearrangement: Retention of configuration at the migration termini, *Biochemistry 46*, 9785–9794.
262. Ratnayake, N. D., Wanninayake, U., Geiger, J. H., and Walker, K. D. (2011) Stereochemistry and mechanism of a microbial phenylalanine aminomutase, *J. Am. Chem. Soc. 133*, 8531–8533.
263. Cooke, H. A., and Bruner, S. D. (2010) Probing the active site of MIO-dependent aminomutases, key catalysts in the biosynthesis of β-amino acids incorporated in secondary metabolites, *Biopolymers 93*, 802–810.
264. Montavon, T. J., Christianson, C. V., Festin, G. M., Shen, B., and Bruner, S. D. (2008) Design and characterization of mechanism-based inhibitors for the tyrosine aminomutase SgTAM, *Bioorg. Med. Chem. Lett. 18*, 3099–3102.
265. Wang, L., Gamez, A., Archer, H., Abola, E. E., Sarkissian, C. N., Fitzpatrick, P., Wendt, D., Zhang, Y., Vellard, M., Bliesath, J., Bell, S. M., Lemontt, J. F., Scriver, C. R., and Stevens, R. C. (2008) Structural and biochemical characterization of the therapeutic *Anabaena variabilis* phenylalanine ammonia lyase, *J. Mol. Biol. 380*, 623–635.
266. Christianson, C. V., Montavon, T. J., Festin, G. M., Cooke, H. A., Shen, B., and Bruner, S. D. (2007) The mechanism of MIO-based aminomutases in β-amino acid biosynthesis, *J. Am. Chem. Soc. 129*, 15744–15745.
267. Langer, M., Reck, G., Reed, J., and Retey, J. (1994) Identification of serine-143 as the most likely precursor of dehydroalanine in the active site of histidine ammonia-lyase. A study of the overexpressed enzyme by site-directed mutagenesis, *Biochemistry 33*, 6462–6467.
268. Retey, J. (2003) Discovery and role of methylidene imidazolone, a highly electrophilic prosthetic group, *Biochim. Biophys. Acta 1647*, 179–184.
269. Consevage, M. W., and Phillips, A. T. (1985) Presence and quantity of dehydroalanine in histidine ammonia-lyase from *Pseudomonas putida*, *Biochemistry 24*, 301–308.
270. Langer, B., Rother, D., and Retey, J. (1997) Identification of essential amino acids in phenylalanine ammonia-lyase by site-directed mutagenesis, *Biochemistry 36*, 10867–10871.
271. Bordwell, F. G., Algrim, D., and Vanier, N. R. (1977) Acidities of anilines and toluenes, *J. Org. Chem. 42*, 1817–1819.
272. Langer, M., Pauling, A., and Retey, J. (1995) The role of dehydroalanine in catalysis by histidine ammonia-lyase, *Angewandte Chemie-International Edition in English 34*, 1464–1465.
273. Furuta, T., Takahashi, H., and Kasuya, Y. (1990) Evidence for a carbanion intermediate in the elimination of ammonia from L-histidine catalyzed by histidine ammonia-lyase, *J. Am. Chem. Soc. 112*, 3633–3636.
274. Baedeker, M., and Schulz, G. E. (2002) Structures of two histidine ammonia-lyase modifications and implications for the catalytic mechanism, *Eur. J. Biochem. 269*, 1790–1797.
275. Weise, N. J., Ahmed, S. T., Parmeggiani, F., Galman, J. L., Dunstan, M. S., Charnock, S. J., Leys, D., and Turner, N. J. (2017) Zymophore identification enables the discovery of novel phenylalanine ammonia lyase enzymes, *Sci Rep 7*, 13691.
276. Feng, L., Wanninayake, U., Strom, S., Geiger, J., and Walker, K. D. (2011) Mechanistic, mutational, and structural evaluation of a *Taxus* phenylalanine aminomutase, *Biochemistry 50*, 2919–2930.
277. Rettig, M., Sigrist, A., and Retey, J. (2000) Mimicking the reaction of phenylalanine ammonia lyase by a synthetic model, *Helv. Chim. Acta 83*, 2246–2265.
278. Louie, T. M., Xie, X. S., and Xun, L. (2003) Coordinated production and utilization of

$FADH_2$ by NAD(P)H-flavin oxidoreductase and 4-hydroxyphenylacetate 3-monooxygenase, *Biochemistry 42*, 7509–7517.
279. Galan, B., Diaz, E., Prieto, M. A., and Garcia, J. L. (2000) Functional analysis of the small component of the 4-hydroxyphenylacetate 3-monooxygenase of *Escherichia coli* W: A prototype of a new flavin:NAD(P)H reductase subfamily, *J. Bacteriol. 182*, 627–636.
280. Walker, W. H., and Singer, T. P. (1970) Identification of the covalently bound flavin of succinate dehydrogenase as 8-α-(histidyl) flavin adenine dinucleotide, *J. Biol. Chem. 245*, 4224–4225.
281. Walker, W. H., Kearney, E. B., Seng, R., and Singer, T. P. (1971) Sequence and structure of a cysteinyl flavin peptide from monoamine oxidase, *Biochem. Biophys. Res. Commun. 44*, 287–292.
282. Podzelinska, K., Latimer, R., Bhattacharya, A., Vining, L. C., Zechel, D. L., and Jia, Z. C. (2010) Chloramphenicol biosynthesis: The structure of CmIS, a flavin-dependent halogenase showing a covalent flavin-aspartate bond, *J. Mol. Biol. 397*, 316–331.
283. Walsh, C. (1980) Flavin coenzymes: At the crossroads of biological redox chemistry, *Accounts Chem Res 13*, 148–155.
284. Starbird, C. A., Maklashina, E., Sharma, P., Qualls-Histed, S., Cecchini, G., and Iverson, T. M. (2017) Structural and biochemical analyses reveal insights into covalent flavinylation of the *Escherichia coli* complex II homolog quinol:fumarate reductase, *J. Biol. Chem. 292*, 12921–12933.
285. Hassan-Abdallah, A., Zhao, G., and Jorns, M. S. (2006) Role of the covalent flavin linkage in monomeric sarcosine oxidase, *Biochemistry 45*, 9454–9462.
286. Eberlein, G., and Bruice, T. C. (1983) The chemistry of a 1,5-diblocked flavin. 2. Proton and electron transfer steps in the reaction of dihydroflavins with oxygen, *J. Am. Chem. Soc. 105*, 6685–6697.
287. Bruice, T. C. (1976) Models and flavin catalysis, *Prog. Bioorganic Chem. 4*, 1–87.
288. Draper, R. D., and Ingraham, L. L. (1968) A potentiometric study of the flavin semiquinone equilibrium, *Arch. Biochem. Biophys. 125*, 802–808.
289. Kemal, C., and Bruice, T. C. (1976) The chemistry of an N^5-methyl-1,5-dihydroflavin and its aminium cation radical, *J. Am. Chem. Soc. 98*, 3955–3964.
290. Macheroux, P. (1999) UV-Visible spectroscopy as a tool to study flavoproteins, *Methods Mol. Biol. 131*, 1–7.
291. Sucharitakul, J., Phongsak, T., Entsch, B., Svasti, J., Chaiyen, P., and Ballou, D. P. (2007) Kinetics of a two-component *p*-hydroxyphenylacetate hydroxylase explain how reduced flavin is transferred from the reductase to the oxygenase, *Biochemistry 46*, 8611–8623.
292. Song, S. H., Dick, B., and Penzkofer, A. (2007) Photo-induced reduction of flavin mononucleotide in aqueous solutions, *Chem. Phys. 332*, 55–65.
293. Massey, V., and Palmer, G. (1966) On the existence of spectrally distinct classes of flavoprotein semiquinones. A new method for quantitative production of flavoprotein semiquinones, *Biochemistry 5*, 3181–3189.
294. Shethna, Y. I., Wilson, P. W., and Beinert, H. (1966) Purification of a nonheme iron protein and other electron transport components from *Azotobacter* extracts, *Biochim. Biophys. Acta 113*, 225–234.
295. Garcia, J. I., Medina, M., Sancho, J., Alonso, P. J., Gomez-Moreno, C., Mayoral, J. A., and Martinez, J. I. (2002) Theoretical analysis of the electron spin density distribution of the flavin semiquinone isoalloxazine ring within model protein environments, *J. Phys. Chem. A 106*, 4729–4735.
296. Zheng, Y.-J., and Ornstein, R. L. (1996) A theoretical study of the structures of flavin in different oxidation and protonation states, *J. Am. Chem. Soc. 118*, 9402–9408.
297. Hall, L. H., Bowers, M. L., and Durfor, C. N. (1987) Further consideration of flavin coenzyme biochemistry afforded by geometry-optimized molecular orbital calculations, *Biochemistry 26*, 7401–7409.
298. Werner, P. E., and Ronnquist, O. (1970) Flavin derivatives. Crystal structure of 5-acetyl-9-bromo-1,3,7,8,10-pentamethyl-1,5-dihydroisoalloxazine, *Acta Chem. Scand. 24*, 997–1009.
299. Tauscher, L., Ghisla, S., and Hemmerich, P. (1973) NMR-study of nitrogen inversion and conformation of 1,5-dihydro-isoalloxazines ("reduced flavin"). Studies in the flavin series, xix, *Helv. Chim. Acta 56*, 630–644.
300. Bolognesi, M., Ghisla, S., and Incoccia, L. (1978) The crystal and molecular structure of

two models of catalytic flavo(co)enzyme intermediates, *Acta Crystallogr. B B34*, 821–828.
301. Moonen, C. T., Vervoort, J., and Muller, F. (1984) Reinvestigation of the structure of oxidized and reduced flavin: Carbon-13 and nitrogen-15 nuclear magnetic resonance study, *Biochemistry 23*, 4859–4867.
302. Kuo, M. C., Dunn, J. B. R., and Fritchie, C. J., Jr. (1974) Crystal structure of a flavine molecular complex 10-propylisoalloxazine-bis(naphthalene-2,3-diol), *Acta Crystallogr. B 30, Pt. 7*, 1766–1771.
303. Fritche, C. J., Jr., Trus, B. L., Wells, J. L., Johnstone, R. M., and Marsh, R. E. (1971) Crystal structure of the yellow 1:2 molecular complex lumiflavine-bis-2,3-naphthalene diol, *J. Chem.Soc. D*, 751–752.
304. Fritchie, C. J., Jr., and Johnston, R. M. (1975) Molecular complexes of flavines. Crystal structure of lumiflavin bis(naphthalene-2,3-diol) trihydrate, *Acta Crystallogr. B B31*, 454–461.
305. Ludwig, M. L., Schopfer, L. M., Metzger, A. L., Pattridge, K. A., and Massey, V. (1990) Structure and oxidation–reduction behavior of 1-deaza-FMN flavodoxins: Modulation of redox potentials in flavodoxins, *Biochemistry 29*, 10364–10375.
306. Karplus, P. A., and Schulz, G. E. (1989) Substrate binding and catalysis by glutathione reductase as derived from refined enzyme: Substrate crystal structures at 2 Å resolution, *J. Mol. Biol. 210*, 163–180.
307. Burnett, R. M., Darling, G. D., Kendall, D. S., LeQuesne, M. E., Mayhew, S. G., Smith, W. W., and Ludwig, M. L. (1974) The structure of the oxidized form of clostridial flavodoxin at 1.9 Å resolution, *J. Biol. Chem. 249*, 4383–4392.
308. Fukuyama, K., Matsubara, H., and Rogers, L. J. (1992) Crystal structure of oxidized flavodoxin from a red alga *Chondrus crispus* refined at 1.8 Å resolution. Description of the flavin mononucleotide binding site, *J. Mol. Biol. 225*, 775–789.
309. Kyte, J. (2007) *Structure in protein chemistry: Second edition*, pp 271–272, Garland Science, New York.
310. Berkholz, D. S., Faber, H. R., Savvides, S. N., and Karplus, P. A. (2008) Catalytic cycle of human glutathione reductase near 1 Å resolution, *J. Mol. Biol. 382*, 371–384.
311. Pai, E. F., and Schulz, G. E. (1983) The catalytic mechanism of glutathione reductase as derived from X-ray diffraction analyses of reaction intermediates, *J. Biol. Chem. 258*, 1752–1757.
312. Mattevi, A., Vanoni, M. A., Todone, F., Rizzi, M., Teplyakov, A., Coda, A., Bolognesi, M., and Curti, B. (1996) Crystal structure of D-amino acid oxidase: A case of active site mirror-image convergent evolution with flavocytochrome b_2, *Proc. Natl. Acad. Sci. U.S.A. 93*, 7496–7501.
313. Umhau, S., Pollegioni, L., Molla, G., Diederichs, K., Welte, W., Pilone, M. S., and Ghisla, S. (2000) The X-ray structure of D-amino acid oxidase at very high resolution identifies the chemical mechanism of flavin-dependent substrate dehydrogenation, *Proc. Natl. Acad. Sci. U. S. A. 97*, 12463–12468.
314. Vrielink, A., Lloyd, L. F., and Blow, D. M. (1991) Crystal structure of cholesterol oxidase from *Brevibacterium sterolicum* refined at 1.8 Å resolution, *J. Mol. Biol. 219*, 533–554.
315. Schreuder, H. A., Prick, P. A., Wierenga, R. K., Vriend, G., Wilson, K. S., Hol, W. G., and Drenth, J. (1989) Crystal structure of the *p*-hydroxybenzoate hydroxylase-substrate complex refined at 1.9 Å resolution. Analysis of the enzyme-substrate and enzyme-product complexes, *J. Mol. Biol. 208*, 679–696.
316. Kim, J. J., Wang, M., and Paschke, R. (1993) Crystal structures of medium-chain acyl-CoA dehydrogenase from pig liver mitochondria with and without substrate, *Proc. Natl. Acad. Sci. U. S. A. 90*, 7523–7527.
317. Fritz, G., Roth, A., Schiffer, A., Buchert, T., Bourenkov, G., Bartunik, H. D., Huber, H., Stetter, K. O., Kroneck, P. M., and Ermler, U. (2002) Structure of adenylylsulfate reductase from the hyperthermophilic *Archaeoglobus fulgidus* at 1.6 Å resolution, *Proc. Natl. Acad. Sci. U. S. A. 99*, 1836–1841.
318. Hecht, H. J., Kalisz, H. M., Hendle, J., Schmid, R. D., and Schomburg, D. (1993) Crystal structure of glucose oxidase from *Aspergillus niger* refined at 2.3 Å resolution, *J. Mol. Biol. 229*, 153–172.
319. Bruns, C. M., and Karplus, P. A. (1995) Refined crystal structure of spinach ferredoxin reductase at 1.7 Å resolution: Oxidized, reduced and 2′-phospho-5′-AMP bound states, *J. Mol. Biol. 247*, 125–145.

320. Conant, J. B., Kahn, H. M., Fieser, L. F., and Kurtz, S. S., Jr. (1922) Electrochemical study of the reversible reduction of organic compounds, *J. Am. Chem. Soc. 44*, 1382–1396.
321. Michaelis, L., Schubert, M. P., and Smythe, C. V. (1936) Potentiometric study of the flavins, *J. Biol. Chem. 116*, 587–607.
322. Saenger, A. K., Nguyen, T. V., Vockley, J., and Stankovich, M. T. (2005) Thermodynamic regulation of human short-chain acyl-CoA dehydrogenase by substrate and product binding, *Biochemistry 44*, 16043–16053.
323. Koder, R. L., Haynes, C. A., Rodgers, M. E., Rodgers, D. W., and Miller, A. F. (2002) Flavin thermodynamics explain the oxygen insensitivity of enteric nitroreductases, *Biochemistry 41*, 14197–14205.
324. Mancini-Samuelson, G. J., Kieweg, V., Sabaj, K. M., Ghisla, S., and Stankovich, M. T. (1998) Redox properties of human medium-chain acyl-CoA dehydrogenase, modulation by charged active-site amino acid residues, *Biochemistry 37*, 14605–14612.
325. Trimmer, E. E., Ballou, D. P., and Matthews, R. G. (2001) Methylenetetrahydrofolate reductase from *Escherichia coli*: Elucidation of the kinetic mechanism by steady-state and rapid-reaction studies, *Biochemistry 40*, 6205–6215.
326. Kyte, J. (2007) *Structure in protein chemistry: Second edition*, p 123, Garland Science, New York.
327. Einarsdottir, G. H., Stankovich, M. T., and Tu, S. C. (1988) Studies of electron-transfer properties of salicylate hydroxylase from *Pseudomonas cepacia* and effects of salicylate and benzoate binding, *Biochemistry 27*, 3277–3285.
328. Lennon, B. W., and Williams, C. H., Jr. (1996) Enzyme-monitored turnover of *Escherichia coli* thioredoxin reductase: Insights for catalysis, *Biochemistry 35*, 4704–4712.
329. Maeda-Yorita, K., Russell, G. C., Guest, J. R., Massey, V., and Williams, C. H., Jr. (1994) Modulation of the oxidation–reduction potential of the flavin in lipoamide dehydrogenase from *Escherichia coli* by alteration of a nearby charged residue, K53R, *Biochemistry 33*, 6213–6220.
330. Swenson, R. P., and Krey, G. D. (1994) Site-directed mutagenesis of tyrosine-98 in the flavodoxin from *Desulfovibrio vulgaris* (Hildenborough): Regulation of oxidation–reduction properties of the bound FMN cofactor by aromatic, solvent, and electrostatic interactions, *Biochemistry 33*, 8505–8514.
331. Hasford, J. J., and Rizzo, C. J. (1998) Linear free energy substituent effect on flavin redox chemistry, *J. Am. Chem. Soc. 120*, 2251–2255.
332. Raibekas, A. A., Ramsey, A. J., and Jorns, M. S. (1993) Properties of a high-potential flavin analogue and its use as an active site probe with clostridial flavodoxin, *Biochemistry 32*, 4420–4429.
333. Stankovich, M. T., and Soltysik, S. (1987) Regulation of the butyryl-CoA dehydrogenase by substrate and product binding, *Biochemistry 26*, 2627–2632.
334. Ghisla, S., and Massey, V. (1986) New flavins for old: Artificial flavins as active site probes of flavoproteins, *Biochem. J. 239*, 1–12.
335. Serre, L., Vellieux, F. M., Medina, M., Gomez-Moreno, C., Fontecilla-Camps, J. C., and Frey, M. (1996) X-ray structure of the ferredoxin:NADP$^+$ reductase from the cyanobacterium *Anabaena PCC* 7119 at 1.8 Å resolution, and crystallographic studies of NADP$^+$ binding at 2.25 Å resolution, *J. Mol. Biol. 263*, 20–39.
336. Ghanem, M., and Gadda, G. (2006) Effects of reversing the protein positive charge in the proximity of the flavin N1 locus of choline oxidase, *Biochemistry 45*, 3437–3447.
337. Hoover, D. M., Drennan, C. L., Metzger, A. L., Osborne, C., Weber, C. H., Pattridge, K. A., and Ludwig, M. L. (1999) Comparisons of wild-type and mutant flavodoxins from *Anacystis nidulans*. Structural determinants of the redox potentials, *J. Mol. Biol. 294*, 725–743.
338. Niemz, A., Imbriglio, J., and Rotello, V. M. (1997) Model systems for flavoenzyme activity: One- and two-electron reduction of flavins in aprotic hydrophobic environments, *J. Am. Chem. Soc. 119*, 887–892.
339. Kobayashi, K., Iyanagi, T., Ohara, H., and Hayashi, K. (1988) One-electron reduction of hepatic NADH-cytochrome b_5 reductase as studied by pulse radiolysis, *J. Biol. Chem. 263*, 7493–7499.
340. Muchmore, C. R., Krahn, J. M., Kim, J. H., Zalkin, H., and Smith, J. L. (1998) Crystal structure of glutamine phosphoribosylpyrophosphate amidotransferase from *Escherichia coli*, *Prot. Sci. 7*, 39–51.

341. Rostas, A., Einholz, C., Illarionov, B., Heidinger, L., Said, T. A., Bauss, A., Fischer, M., Bacher, A., Weber, S., and Schleicher, E. (2018) Long-lived hydrated FMN radicals: EPR characterization and implications for catalytic variability in flavoproteins, *J. Am. Chem. Soc. 140*, 16521–16527.
342. Coves, J., Zeghouf, M., Macherel, D., Guigliarelli, B., Asso, M., and Fontecave, M. (1997) Flavin mononucleotide-binding domain of the flavoprotein component of the sulfite reductase from *Escherichia coli*, *Biochemistry 36*, 5921–5928.
343. Job, V., Marcone, G. L., Pilone, M. S., and Pollegioni, L. (2002) Glycine oxidase from *Bacillus subtilis*. Characterization of a new flavoprotein, *J. Biol. Chem. 277*, 6985–6993.
344. Mayhew, S. G. (1971) Properties of two clostridial flavodoxins, *Biochim. Biophys. Acta 235*, 276–288.
345. Noble, M. A., Munro, A. W., Rivers, S. L., Robledo, L., Daff, S. N., Yellowlees, L. J., Shimizu, T., Sagami, I., Guillemette, J. G., and Chapman, S. K. (1999) Potentiometric analysis of the flavin cofactors of neuronal nitric oxide synthase, *Biochemistry 38*, 16413–16418.
346. Iyanagi, T., Makino, N., and Mason, H. S. (1974) Redox properties of the reduced nicotinamide adenine dinucleotide phosphate-cytochrome P-450 and reduced nicotinamide adenine dinucleotide-cytochrome b_5 reductases, *Biochemistry 13*, 1701–1710.
347. Muh, U., Cinkaya, I., Albracht, S. P., and Buckel, W. (1996) 4-Hydroxybutyryl-CoA dehydratase from *Clostridium aminobutyricum*: Characterization of FAD and iron–sulfur clusters involved in an overall non-redox reaction, *Biochemistry 35*, 11710–11718.
348. Kittleman, W., Thibodeaux, C. J., Liu, Y. N., Zhang, H., and Liu, H. W. (2007) Characterization and mechanistic studies of type II isopentenyl diphosphate:dimethylallyl diphosphate isomerase from *Staphylococcus aureus*, *Biochemistry 46*, 8401–8413.
349. Akiyama, T., Simeno, F., Murakami, M., and Yoneda, F. (1992) Flavin-6-carboxylic acids as novel and simple flavoenzyme models. Nonenzymatic stabilization of the flavin semiquinone radical and the 4a-hydroperoxyflavin by intramolecular hydrogen bonding, *J. Am. Chem. Soc. 114*, 6613–6620.
350. Chang, F. C., and Swenson, R. P. (1999) The midpoint potentials for the oxidized-semiquinone couple for Gly57 mutants of the *Clostridium beijerinckii* flavodoxin correlate with changes in the hydrogen-bonding interaction with the proton on N(5) of the reduced flavin mononucleotide cofactor as measured by NMR chemical shift temperature dependencies, *Biochemistry 38*, 7168–7176.
351. Yang, K. Y., and Swenson, R. P. (2007) Modulation of the redox properties of the flavin cofactor through hydrogen-bonding interactions with the N(5) atom: Role of αSer254 in the electron-transfer flavoprotein from the methylotrophic bacterium W3a1, *Biochemistry 46*, 2289–2297.
352. Lindqvist, Y., Branden, C. I., Mathews, F. S., and Lederer, F. (1991) Spinach glycolate oxidase and yeast flavocytochrome b_2 are structurally homologous and evolutionarily related enzymes with distinctly different function and flavin mononucleotide binding, *J. Biol. Chem. 266*, 3198–3207.
353. Francis, K., Russell, B., and Gadda, G. (2005) Involvement of a flavosemiquinone in the enzymatic oxidation of nitroalkanes catalyzed by 2-nitropropane dioxygenase, *J. Biol. Chem. 280*, 5195–5204.
354. Essenmacher, C., Kim, S. T., Atamian, M., Babcock, G. T., and Sancar, A. (1993) Tryptophan radical formation in DNA photolyase: Electron-spin polarization arising from photoexcitation of a doublet ground state, *J. Am. Chem. Soc. 115*, 1602–1603.
355. Ghanem, M., Fan, F., Francis, K., and Gadda, G. (2003) Spectroscopic and kinetic properties of recombinant choline oxidase from *Arthrobacter globiformis*, *Biochemistry 42*, 15179–15188.
356. Dewanti, A. R., Xu, Y., and Mitra, B. (2004) Role of glycine 81 in (*S*)-mandelate dehydrogenase from *Pseudomonas putida* in substrate specificity and oxidase activity, *Biochemistry 43*, 10692–10700.
357. Buey, R. M., Fernandez-Justel, D., de Pereda, J. M., Revuelta, J. L., Schurmann, P., Buchanan, B. B., and Balsera, M. (2018) Ferredoxin-linked flavoenzyme defines a family of pyridine nucleotide-independent thioredoxin reductases, *Proc. Natl. Acad. Sci. U. S. A. 115*, 12967–12972.

358. Nagai, T., Unno, H., Janczak, M. W., Yoshimura, T., Poulter, C. D., and Hemmi, H. (2011) Covalent modification of reduced flavin mononucleotide in type-2 isopentenyl diphosphate isomerase by active-site-directed inhibitors, *Proc. Natl. Acad. Sci. U.S.A. 108*, 20461–20466.
359. Thibodeaux, C. J., Chang, W. C., and Liu, H. W. (2010) Linear free energy relationships demonstrate a catalytic role for the flavin mononucleotide coenzyme of the type II isopentenyl diphosphate:dimethylallyl diphosphate isomerase, *J. Am. Chem. Soc. 132*, 9994–9996.
360. Thibodeaux, C. J., and Liu, H. W. (2017) The type II isopentenyl diphosphate:dimethylallyl diphosphate isomerase (IDI-2): A model for acid/base chemistry in flavoenzyme catalysis, *Arch. Biochem. Biophys. 632*, 47–58.
361. Mehra-Chaudhary, R., Dai, Y., Sobrado, P., and Tanner, J. J. (2016) In crystallo capture of a covalent intermediate in the UDP-galactopyranose mutase reaction, *Biochemistry 55*, 833–836.
362. Gruber, T. D., Westler, W. M., Kiessling, L. L., and Forest, K. T. (2009) X-ray crystallography reveals a reduced substrate complex of UDP-galactopyranose mutase poised for covalent catalysis by flavin, *Biochemistry 48*, 9171–9173.
363. Soltero-Higgin, M., Carlson, E. E., Gruber, T. D., and Kiessling, L. L. (2004) A unique catalytic mechanism for UDP-galactopyranose mutase, *Nat. Struct. Mol. Biol. 11*, 539–543.
364. Hamdane, D., Grosjean, H., and Fontecave, M. (2016) Flavin-dependent methylation of RNAs: Complex chemistry for a simple modification, *J. Mol. Biol. 428*, 4867–4881.
365. Mishanina, T. V., Yu, L., Karunaratne, K., Mondal, D., Corcoran, J. M., Choi, M. A., and Kohen, A. (2016) An unprecedented mechanism of nucleotide methylation in organisms containing thyX, *Science 351*, 507–510.
366. White, M. D., Payne, K. A., Fisher, K., Marshall, S. A., Parker, D., Rattray, N. J., Trivedi, D. K., Goodacre, R., Rigby, S. E., Scrutton, N. S., Hay, S., and Leys, D. (2015) UbiX is a flavin prenyltransferase required for bacterial ubiquinone biosynthesis, *Nature 522*, 502–506.
367. Binda, C., Hubalek, F., Li, M., Herzig, Y., Sterling, J., Edmondson, D. E., and Mattevi, A. (2004) Crystal structures of monoamine oxidase B in complex with four inhibitors of the *N*-propargylaminoindan class, *J Med Chem 47*, 1767–1774.
368. Nenci, S., Piano, V., Rosati, S., Aliverti, A., Pandini, V., Fraaije, M. W., Heck, A. J. R., Edmondson, D. E., and Mattevi, A. (2012) Precursor of ether phospholipids is synthesized by a flavoenzyme through covalent catalysis, *Proc. Natl. Acad. Sci. U.S.A. 109*, 18791–18796.
369. Payne, K. A., White, M. D., Fisher, K., Khara, B., Bailey, S. S., Parker, D., Rattray, N. J., Trivedi, D. K., Goodacre, R., Beveridge, R., Barran, P., Rigby, S. E., Scrutton, N. S., Hay, S., and Leys, D. (2015) New cofactor supports α,β-unsaturated acid decarboxylation via 1,3-dipolar cycloaddition, *Nature 522*, 497–501.
370. Ferguson, K. L., Eschweiler, J. D., Ruotolo, B. T., and Marsh, E. N. G. (2017) Evidence for a 1,3-dipolar cyclo-addition mechanism in the decarboxylation of phenylacrylic acids catalyzed by ferulic acid decarboxylase, *J. Am. Chem. Soc. 139*, 10972–10975.
371. Kaneshiro, A. K., Koebke, K. J., Zhao, C., Ferguson, K. L., Ballou, D. P., Palfey, B. A., Ruotolo, B. T., and Marsh, E. N. G. (2021) Kinetic analysis of transient intermediates in the mechanism of prenyl-flavin-dependent ferulic acid decarboxylase, *Biochemistry 60*, 125–134.
372. Pang, S. S., Duggleby, R. G., and Guddat, L. W. (2002) Crystal structure of yeast acetohydroxyacid synthase: A target for herbicidal inhibitors, *J. Mol. Biol. 317*, 249–262.
373. Muller, F., and Massey, V. (1969) Flavin-sulfite complexes and their structures, *J. Biol. Chem. 244*, 4007–4016.
374. Ghisla, S., Massey, V., Lhoste, J. M., and Mayhew, S. G. (1974) Fluorescence and optical characteristics of reduced flavines and flavoproteins, *Biochemistry 13*, 589–597.
375. Ghisla, S., Hartmann, U., Hemmerich, P., and Mueller, F. (1973) Flavine series. XVIII. Reductive alkylation of the flavine nucleus. Structure and reactivity of dihydroflavines, *Justus Liebigs Annalen der Chemie*, 1388–1415.
376. Fritz, G., Buchert, T., and Kroneck, P. M. (2002) The function of the [4Fe–4S] clusters and FAD in bacterial and archaeal adenylylsulfate reductases. Evidence for flavin-catalyzed reduction of adenosine 5′-phosphosulfate, *J. Biol. Chem. 277*, 26066–26073.

377. Schiffer, A., Fritz, G., Kroneck, P. M., and Ermler, U. (2006) Reaction mechanism of the iron–sulfur flavoenzyme adenosine-5′-phosphosulfate reductase based on the structural characterization of different enzymatic states, *Biochemistry 45*, 2960–2967.
378. Heroux, A., Bozinovski, D. M., Valley, M. P., Fitzpatrick, P. F., and Orville, A. M. (2009) Crystal structures of intermediates in the nitroalkane oxidase reaction, *Biochemistry 48*, 3407–3416.
379. Dudley, K. H., and Hemmerich, P. (1967) Flavins. 13. Rearrangement reactions of 1,3,10-trialkylflavinium salts, *J. Org. Chem. 32*, 3049–3054.
380. Hevesi, L., and Bruice, T. C. (1973) Reaction of sulfite with isoalloxazines, *Biochemistry 12*, 290–297.
381. Bruice, T. C., Hevesi, L., and Shinkai, S. (1973) Mechanisms of formation and equilibria of 4a and 5 adducts of an isoalloxazine. Reaction of 10-(2′,6′-dimethylphenyl)-3-methylisoalloxazine-6,8-disulfonate with sulfite in aqueous media, *Biochemistry 12*, 2083–2089.
382. Clerin, D., and Bruice, T. C. (1974) Kinetic study of the fate of a covalent intermediate of the type proposed to be involved in flavin catalysis, *J. Am. Chem. Soc. 96*, 5571–5573.
383. Chan, T. W., and Bruice, T. C. (1978) Importance of C4a- and N5-covalent adducts in the flavin oxidation of carbanions, *Biochemistry 17*, 4784–4793.
384. Venkataram, U. V., and Bruice, T. C. (1984) On the mechanism of flavin-catalyzed dehydrogenation α,β to an acyl function. The mechanism of 1,5-dihydroflavin reduction of maleimides, *J. Am. Chem. Soc. 106*, 5703–5709.
385. Kim, J. M., Bogdan, M. A., and Mariano, P. S. (1993) Mechanistic analysis of the 3-methyllumiflavin-promoted oxidative deamination of benzylamine. A potential model for monoamine oxidase catalysis, *J. Am. Chem. Soc. 115*, 10591–10595.
386. Loechler, E. L., and Hollocher, T. C. (1980) Reduction of flavins by thiols. 1. Reaction mechanism from the kinetics of the attack and breakdown steps, *J. Am. Chem. Soc. 102*, 7312–7321.
387. Schiering, N., Kabsch, W., Moore, M. J., Distefano, M. D., Walsh, C. T., and Pai, E. F. (1991) Structure of the detoxification catalyst mercuric ion reductase from *Bacillus* sp. Strain rc607, *Nature 352*, 168–172.
388. Mattevi, A., Schierbeek, A. J., and Hol, W. G. (1991) Refined crystal structure of lipoamide dehydrogenase from *Azotobacter vinelandii* at 2.2 Å resolution. A comparison with the structure of glutathione reductase, *J. Mol. Biol. 220*, 975–994.
389. Kuriyan, J., Krishna, T. S., Wong, L., Guenther, B., Pahler, A., Williams, C. H., Jr., and Model, P. (1991) Convergent evolution of similar function in two structurally divergent enzymes, *Nature 352*, 172–174.
390. Pandey, A. S., Nocek, B., Clark, D. D., Ensign, S. A., and Peters, J. W. (2006) Mechanistic implications of the structure of the mixed-disulfide intermediate of the disulfide oxidoreductase, 2-ketopropyl-coenzyme M oxidoreductase/carboxylase, *Biochemistry 45*, 113–120.
391. Stehle, T., Ahmed, S. A., Claiborne, A., and Schulz, G. E. (1991) Structure of NADH peroxidase from *Streptococcus faecalis* 10c1 refined at 2.16 Å resolution, *J. Mol. Biol. 221*, 1325–1344.
392. Yeh, J. I., Claiborne, A., and Hol, W. G. (1996) Structure of the native cysteine-sulfenic acid redox center of enterococcal NADH peroxidase refined at 2.8 Å resolution, *Biochemistry 35*, 9951–9957.
393. Waksman, G., Krishna, T. S., Williams, C. H., Jr., and Kuriyan, J. (1994) Crystal structure of *Escherichia coli* thioredoxin reductase refined at 2 Å resolution. Implications for a large conformational change during catalysis, *J. Mol. Biol. 236*, 800–816.
394. Nocek, B., Jang, S. B., Jeong, M. S., Clark, D. D., Ensign, S. A., and Peters, J. W. (2002) Structural basis for CO_2 fixation by a novel member of the disulfide oxidoreductase family of enzymes, 2-ketopropyl-coenzyme M oxidoreductase/carboxylase, *Biochemistry 41*, 12907–12913.
395. Gross, E., Sevier, C. S., Vala, A., Kaiser, C. A., and Fass, D. (2002) A new FAD-binding fold and intersubunit disulfide shuttle in the thiol oxidase Erv2p, *Nature Struct. Biol. 9*, 61–67.
396. Thorpe, C., and Williams, C. H., Jr. (1976) Spectral evidence for a flavin adduct in a monoalkylated derivative of pig heart lipoamide dehydrogenase, *J. Biol. Chem. 251*, 7726–7728.

397. O'Donnell, M. E., and Williams, C. H., Jr. (1984) Reconstitution of *Escherichia coli* thioredoxin reductase with 1-deazaFAD. Evidence for 1-deazaFAD C-4a adduct formation linked to the ionization of an active site base, *J. Biol. Chem. 259*, 2243–2251.
398. Prongay, A. J., and Williams, C. H., Jr. (1990) Evidence for direct interaction between cysteine 138 and the flavin in thioredoxin reductase. A study using flavin analogs, *J. Biol. Chem. 265*, 18968–18975.
399. Miller, S. M., Massey, V., Ballou, D., Williams, C. H., Jr., Distefano, M. D., Moore, M. J., and Walsh, C. T. (1990) Use of a site-directed triple mutant to trap intermediates: Demonstration that the flavin C(4a)-thiol adduct and reduced flavin are kinetically competent intermediates in mercuric ion reductase, *Biochemistry 29*, 2831–2841.
400. Arscott, L. D., Thorpe, C., and Williams, C. H., Jr. (1981) Glutathione reductase from yeast. Differential reactivity of the nascent thiols in two-electron reduced enzyme and properties of a monoalkylated derivative, *Biochemistry 20*, 1513–1520.
401. Hynson, R. M., Mathews, F. S., and Schuman Jorns, M. (2006) Identification of a stable flavin-thiolate adduct in heterotetrameric sarcosine oxidase, *J. Mol. Biol. 362*, 656–663.
402. Parsonage, D., and Claiborne, A. (1995) Analysis of the kinetic and redox properties of NADH peroxidase C42S and C42A mutants lacking the cysteine-sulfenic acid redox center, *Biochemistry 34*, 435–441.
403. Jencks, W. P. (1969) *Catalysis in chemistry and enzymology*, pp 437–462, McGraw-Hill, New York.
404. Hopkins, N., and Stanley, R. J. (2003) Measurement of the electronic properties of the flavoprotein old yellow enzyme (OYE) and the OYE:*p*-Cl phenol charge-transfer complex using Stark spectroscopy, *Biochemistry 42*, 991–999.
405. Ghisla, S., and Thorpe, C. (2004) Acyl-CoA dehydrogenases. A mechanistic overview, *Eur. J. Biochem. 271*, 494–508.
406. Gutierrez, A., Lian, L. Y., Wolf, C. R., Scrutton, N. S., and Roberts, G. C. (2001) Stopped-flow kinetic studies of flavin reduction in human cytochrome P450 reductase and its component domains, *Biochemistry 40*, 1964–1975.
407. Wilkinson, K. D., and Williams, C. H., Jr. (1979) Evidence for multiple electronic forms of two-electron-reduced lipoamide dehydrogenase from *Escherichia coli*, *J. Biol. Chem. 254*, 852–862.
408. Thorpe, C., and Williams, C. H., Jr. (1981) Lipoamide dehydrogenase from pig heart. Pyridine nucleotide induced changes in monoalkylated two-electron reduced enzyme, *Biochemistry 20*, 1507–1513.
409. Hopkins, N., and Williams, C. H., Jr. (1995) Characterization of lipoamide dehydrogenase from *Escherichia coli* lacking the redox active disulfide: C44S and C49S, *Biochemistry 34*, 11757–11765.
410. Miller, S. M., Ballou, D. P., Massey, V., Williams, C. H., Jr., and Walsh, C. T. (1986) Two-electron reduced mercuric reductase binds Hg(II) to the active site dithiol but does not catalyze Hg(II) reduction, *J. Biol. Chem. 261*, 8081–8084.
411. Harris, R. J., Meskys, R., Sutcliffe, M. J., and Scrutton, N. S. (2000) Kinetic studies of the mechanism of carbon-hydrogen bond breakage by the heterotetrameric sarcosine oxidase of *Arthrobacter* sp. 1-IN, *Biochemistry 39*, 1189–1198.
412. Zhao, G., and Jorns, M. S. (2002) Monomeric sarcosine oxidase: Evidence for an ionizable group in the E·S complex, *Biochemistry 41*, 9747–9750.
413. Basran, J., Bhanji, N., Basran, A., Nietlispach, D., Mistry, S., Meskys, R., and Scrutton, N. S. (2002) Mechanistic aspects of the covalent flavoprotein dimethylglycine oxidase of *Arthrobacter globiformis* studied by stopped-flow spectrophotometry, *Biochemistry 41*, 4733–4743.
414. Massey, V., and Gibson, Q. H. (1964) Role of semiquinones in flavoprotein catalysis, *Fed. Proc. 23*, 18–29.
415. Kubo, H., Watari, H., and Shiga, T. (1959) Study on an intermediate form in the oxidation–reduction of D-amino acid oxidase, *Bull. Soc. Chim. Biol. (Paris) 41*, 981–988.
416. Efimov, I., and McIntire, W. S. (2005) Relationship between charge-transfer interactions, redox potentials, and catalysis for different forms of the flavoprotein component of *p*-cresol methylhydroxylase, *J. Am. Chem. Soc. 127*, 732–741.
417. Bruice, T. C. (1980) Carbon acid oxidations and oxygen activation by flavins, In *Biomimetic chemistry* (Dolphin, D., McKenna, C., Murakami, Y., and Tabushi, I., Eds.), pp 89–

118, American Chemical Society, Washington, DC.
418. Walsh, C. T., Schonbrunn, A., and Abeles, R. H. (1971) Studies on the mechanism of action of D-amino acid oxidase. Evidence for removal of substrate-hydrogen as a proton, *J. Biol. Chem. 246*, 6855–6866.
419. Walsh, C., Lockridge, O., Massey, V., and Abeles, R. (1973) Studies on the mechanism of action of the flavoenzyme lactate oxidase. Oxidation and elimination with β-chlorolactate, *J. Biol. Chem. 248*, 7049–7054.
420. Baker-Malcolm, J. F., Haeffner-Gormley, L., Wang, L., Anders, M. W., and Thorpe, C. (1998) Elimination reactions in the medium-chain acyl-CoA dehydrogenase: Bioactivation of cytotoxic 4-thiaalkanoic acids, *Biochemistry 37*, 1383–1393.
421. Urban, P., and Lederer, F. (1984) Baker's yeast flavocytochrome b_2. A mechanistic study of the dehydrohalogenation reaction, *Eur. J. Biochem. 144*, 345–351.
422. Reid, G. A., White, S., Black, M. T., Lederer, F., Mathews, F. S., and Chapman, S. K. (1988) Probing the active site of flavocytochrome b_2 by site-directed mutagenesis, *Eur. J. Biochem. 178*, 329–333.
423. Tiffany, K. A., Roberts, D. L., Wang, M., Paschke, R., Mohsen, A. W., Vockley, J., and Kim, J. J. (1997) Structure of human isovaleryl-CoA dehydrogenase at 2.6 Å resolution: Structural basis for substrate specificity, *Biochemistry 36*, 8455–8464.
424. Mohsen, A. W., and Vockley, J. (1995) Identification of the active site catalytic residue in human isovaleryl-CoA dehydrogenase, *Biochemistry 34*, 10146–10152.
425. Battaile, K. P., Molin-Case, J., Paschke, R., Wang, M., Bennett, D., Vockley, J., and Kim, J. J. (2002) Crystal structure of rat short chain acyl-CoA dehydrogenase complexed with acetoacetyl-CoA: Comparison with other acyl-CoA dehydrogenases, *J. Biol. Chem. 277*, 12200–12207.
426. Battaile, K. P., Mohsen, A. W., and Vockley, J. (1996) Functional role of the active site glutamate-368 in rat short chain acyl-CoA dehydrogenase, *Biochemistry 35*, 15356–15363.
427. Gopalan, K. V., and Srivastava, D. K. (2002) Beyond the proton abstracting role of Glu-376 in medium chain acyl-CoA dehydrogenase: Influence of Glu-376-Gln substitution on ligand binding and catalysis, *Biochemistry 41*, 4638–4648.
428. Dewanti, A. R., and Mitra, B. (2003) A transient intermediate in the reaction catalyzed by (*S*)-mandelate dehydrogenase from *Pseudomonas putida*, *Biochemistry 42*, 12893–12901.
429. Dewanti, A. R., Xu, Y., and Mitra, B. (2004) Esters of mandelic acid as substrates for (*S*)-mandelate dehydrogenase from *Pseudomonas putida*: Implications for the reaction mechanism, *Biochemistry 43*, 1883–1890.
430. Beinert, H., and Page, E. (1957) On the mechanism of dehydrogenation of fatty acyl derivatives of coenzyme A. V. Oxidation–reductions of the flavoproteins, *J. Biol. Chem. 225*, 479–497.
431. Schopfer, L. M., Massey, V., Ghisla, S., and Thorpe, C. (1988) Oxidation–reduction of general acyl-CoA dehydrogenase by the butyryl-CoA/crotonyl-CoA couple. A new investigation of the rapid reaction kinetics, *Biochemistry 27*, 6599–6611.
432. Kumar, N. R., and Srivastava, D. K. (1995) Facile and restricted pathways for the dissociation of octenoyl-CoA from the medium-chain fatty acyl-CoA dehydrogenase (MCAD)-$FADH_2$-octenoyl-CoA charge-transfer complex: Energetics and mechanism of suppression of the enzyme's oxidase activity, *Biochemistry 34*, 9434–9443.
433. Lau, S. M., Brantley, R. K., and Thorpe, C. (1988) The reductive half-reaction in acyl-CoA dehydrogenase from pig kidney: Studies with thiaoctanoyl-CoA and oxaoctanoyl-CoA analogues, *Biochemistry 27*, 5089–5095.
434. Powell, P. J., and Thorpe, C. (1988) 2-Octynoyl coenzyme A is a mechanism-based inhibitor of pig kidney medium-chain acyl coenzyme A dehydrogenase: Isolation of the target peptide, *Biochemistry 27*, 8022–8028.
435. Vock, P., Engst, S., Eder, M., and Ghisla, S. (1998) Substrate activation by acyl-CoA dehydrogenases: Transition-state stabilization and p*K*s of involved functional groups, *Biochemistry 37*, 1848–1860.
436. Reinsch, J., Katz, A., Wean, J., Aprahamian, G., and McFarland, J. T. (1980) The deuterium isotope effect upon the reaction of fatty acyl-CoA dehydrogenase and butyryl-CoA, *J. Biol. Chem. 255*, 9093–9097.
437. Schmidt, J., Reinsch, J., and McFarland, J. T. (1981) Mechanistic studies on fatty acyl-CoA

dehydrogenase, *J. Biol. Chem. 256*, 11667–11670.
438. Strauss, E., Zhai, H., Brand, L. A., McLafferty, F. W., and Begley, T. P. (2004) Mechanistic studies on phosphopantothenoylcysteine decarboxylase: Trapping of an enethiolate intermediate with a mechanism-based inactivating agent, *Biochemistry 43*, 15520–15533.
439. Williams, R. F., and Bruice, T. C. (1976) The kinetics and mechanisms of 1,5-dihydroflavin reduction of carbonyl compounds and flavin oxidation of alcohols. 2. Ethyl pyruvate, pyruvamide, and pyruvic acid, *J. Am. Chem. Soc. 98*, 7752–7768.
440. Bruice, T. C., and Yano, Y. (1975) Radical mechanisms for 1,5-dihydro-5-methylflavine reduction of carbonyl compounds, *J. Am. Chem. Soc. 97*, 5263–5271.
441. Novak, M., and Bruice, T. C. (1980) Mechanistic investigation of the oxidation of the carbanion of methyl 2-methoxy-2-phenylacetate by an isoalloxazine, *J. Chem.Soc. Chem. Commun.*, 372–374.
442. Li, D., Zhou, H.-q., Dakoji, S., Shin, I., Oh, E., and Liu, H.-w. (1998) Spiropentylacetyl-CoA, a mechanism-based inactivator of acyl-CoA dehydrogenases, *J. Am. Chem. Soc. 120*, 2008–2017.
443. Silverman, R. B., Zhou, J. J. P., Ding, C. Z., and Lu, X. (1995) Monoamine oxidase-catalyzed oxidative decarboxylation of *cis*- and *trans*-5-aminomethyl-3-(4-methoxyphenyl)dihydrofuran-2(3H)-one. Evidence for the intermediacy of an α-radical, *J. Am. Chem. Soc. 117*, 12895–12896.
444. Kim, J.-M., Hoegy, S. E., and Mariano, P. S. (1995) Flavin chemical models for monoamine oxidase inactivation by cyclopropylamines, α-silylamines, and hydrazines, *J. Am. Chem. Soc. 117*, 100–105.
445. Miller, J. R., Edmondson, D. E., and Grissom, C. B. (1995) Mechanistic probes of monoamine oxidase B catalysis: Rapid-scan stopped flow and magnetic field independence of the reductive half-reaction, *J. Am. Chem. Soc. 117*, 7830–7831.
446. Eirich, L. D., Vogels, G. D., and Wolfe, R. S. (1978) Proposed structure for coenzyme F420 from *Methanobacterium*, *Biochemistry 17*, 4583–4593.
447. Fox, J. A., Livingston, D. J., Orme-Johnson, W. H., and Walsh, C. T. (1987) 8-hydroxy-5-deazaflavin-reducing hydrogenase from *Methanobacterium thermoautotrophicum*: 1. Purification and characterization, *Biochemistry 26*, 4219–4227.
448. te Brommelstroet, B. W., Hensgens, C. M., Keltjens, J. T., van der Drift, C., and Vogels, G. D. (1990) Purification and properties of 5,10-methylenetetrahydromethanopterin reductase, a coenzyme f420-dependent enzyme, from *Methanobacterium thermoautotrophicum* strain δ H, *J. Biol. Chem. 265*, 1852–1857.
449. Brustlein, M., and Bruice, T. C. (1972) Demonstration of a direct hydrogen transfer between NADH and a deazaflavin, *J. Am. Chem. Soc. 94*, 6548–6549.
450. Shinkai, S., and Bruice, T. C. (1973) Question of covalent intermediate formation in the flavine-catalyzed carbonyl to carbinol oxidation–reduction reaction, *J. Am. Chem. Soc. 95*, 7526–7528.
451. Hersh, L. B., and Jorns, M. S. (1975) Use of 5-deazaFAD to study hydrogen transfer in the D-amino acid oxidase reaction, *J. Biol. Chem. 250*, 8728–8734.
452. Jorns, M. S., and Hersh, L. B. (1974) Demonstration of enzymic hydrogen transfer from substrate to a flavine, *J. Am. Chem. Soc. 96*, 4012–4014.
453. Ghisla, S., Thorpe, C., and Massey, V. (1984) Mechanistic studies with general acyl-CoA dehydrogenase and butyryl-CoA dehydrogenase: Evidence for the transfer of the β-hydrogen to the flavin N^5-position as a hydride, *Biochemistry 23*, 3154–3161.
454. Sumner, J. S., and Matthews, R. G. (1992) Stereochemistry and mechanism of hydrogen transfer between NADPH and methylenetetrahydrofolate in the reaction catalyzed by methylenetetrahydrofolate reductase from pig liver, *J. Am. Chem. Soc. 114*, 6949–6956.
455. Benson, T. E., Marquardt, J. L., Marquardt, A. C., Etzkorn, F. A., and Walsh, C. T. (1993) Overexpression, purification, and mechanistic study of UDP-*N*-acetylenolpyruvyl-glucosamine reductase, *Biochemistry 32*, 2024–2030.
456. Taylor, P., Pealing, S. L., Reid, G. A., Chapman, S. K., and Walkinshaw, M. D. (1999) Structural and mechanistic mapping of a unique fumarate reductase, *Nature Struct. Biol. 6*, 1108–1112.
457. Leys, D., Tsapin, A. S., Nealson, K. H., Meyer, T. E., Cusanovich, M. A., and Van Beeumen,

J. J. (1999) Structure and mechanism of the flavocytochrome *c* fumarate reductase of *Shewanella putrefaciens* MR-1, *Nature Struct. Biol. 6*, 1113–1117.
458. Bossi, R. T., Negri, A., Tedeschi, G., and Mattevi, A. (2002) Structure of FAD-bound L-aspartate oxidase: Insight into substrate specificity and catalysis, *Biochemistry 41*, 3018–3024.
459. Steinbacher, S., Hernandez-Acosta, P., Bieseler, B., Blaesse, M., Huber, R., Culianez-Macia, F. A., and Kupke, T. (2003) Crystal structure of the plant PPC decarboxylase AtHAL3a complexed with an ene-thiol reaction intermediate, *J. Mol. Biol. 327*, 193–202.
460. Fu, Z., Wang, M., Paschke, R., Rao, K. S., Frerman, F. E., and Kim, J. J. (2004) Crystal structures of human glutaryl-CoA dehydrogenase with and without an alternate substrate: Structural bases of dehydrogenation and decarboxylation reactions, *Biochemistry 43*, 9674–9684.
461. Malito, E., Coda, A., Bilyeu, K. D., Fraaije, M. W., and Mattevi, A. (2004) Structures of michaelis and product complexes of plant cytokinin dehydrogenase: Implications for flavoenzyme catalysis, *J. Mol. Biol. 341*, 1237–1249.
462. Liavonchanka, A., Hornung, E., Feussner, I., and Rudolph, M. G. (2006) Structure and mechanism of the *Propionibacterium acnes* polyunsaturated fatty acid isomerase, *Proc. Natl. Acad. Sci. U. S. A. 103*, 2576–2581.
463. Faust, A., Niefind, K., Hummel, W., and Schomburg, D. (2007) The structure of a bacterial L-amino acid oxidase from *Rhodococcus opacus* gives new evidence for the hydride mechanism for dehydrogenation, *J. Mol. Biol. 367*, 234–248.
464. Forneris, F., Heuts, D. P., Delvecchio, M., Rovida, S., Fraaije, M. W., and Mattevi, A. (2008) Structural analysis of the catalytic mechanism and stereoselectivity in *Streptomyces coelicolor* alditol oxidase, *Biochemistry 47*, 978–985.
465. Inaoka, D. K., Sakamoto, K., Shimizu, H., Shiba, T., Kurisu, G., Nara, T., Aoki, T., Kita, K., and Harada, S. (2008) Structures of *Trypanosoma cruzi* dihydroorotate dehydrogenase complexed with substrates and products: Atomic resolution insights into mechanisms of dihydroorotate oxidation and fumarate reduction, *Biochemistry 47*, 10881–10891.
466. Kachalova, G. S., Bourenkov, G. P., Mengesdorf, T., Schenk, S., Maun, H. R., Burghammer, M., Riekel, C., Decker, K., and Bartunik, H. D. (2010) Crystal structure analysis of free and substrate-bound 6-hydroxyl-nicotine oxidase from *Arthrobacter nicotinovorans*, *J. Mol. Biol. 396*, 785–799.
467. Fu, G., Yuan, H., Li, C., Lu, C. D., Gadda, G., and Weber, I. T. (2010) Conformational changes and substrate recognition in *Pseudomonas aeruginosa* D-arginine dehydrogenase, *Biochemistry 49*, 8535–8545.
468. Tararina, M. A., Xue, S., Smith, L. C., Muellers, S. N., Miranda, P. O., Janda, K. D., and Allen, K. N. (2018) Crystallography coupled with kinetic analysis provides mechanistic underpinnings of a nicotine-degrading enzyme, *Biochemistry 57*, 3741–3751.
469. Harris, C. M., Molla, G., Pilone, M. S., and Pollegioni, L. (1999) Studies on the reaction mechanism of *Rhodotorula gracilis* D-amino-acid oxidase. Role of the highly conserved Tyr-223 on substrate binding and catalysis, *J. Biol. Chem. 274*, 36233–36240.
470. Binda, C., Newton-Vinson, P., Hubalek, F., Edmondson, D. E., and Mattevi, A. (2002) Structure of human monoamine oxidase B: A drug target for the treatment of neurological disorders, *Nature Struct. Biol. 9*, 22–26.
471. Nishina, Y., Sato, K., Shi, R., Setoyama, C., Miura, R., and Shiga, K. (2001) On the ligands in charge-transfer complexes of porcine kidney flavoenzyme D-amino acid oxidase in three redox states: A resonance raman study, *J. Biochem. (Tokyo) 130*, 637–647.
472. Fraaije, M. W., and Mattevi, A. (2000) Flavoenzymes: Diverse catalysts with recurrent features, *Trends Biochem. Sci. 25*, 126–132.
473. Jorns, M. S., Chen, Z. W., and Mathews, F. S. (2010) Structural characterization of mutations at the oxygen activation site in monomeric sarcosine oxidase, *Biochemistry 49*, 3631–3639.
474. Gaweska, H. M., Taylor, A. B., Hart, P. J., and Fitzpatrick, P. F. (2013) Structure of the flavoprotein tryptophan 2-monooxygenase, a key enzyme in the formation of galls in plants, *Biochemistry 52*, 2620–2626.
475. Schaller, R. A., Mohsen, A. W., Vockley, J., and Thorpe, C. (1997) Mechanism-based inhibitor discrimination in the acyl-CoA dehydrogenases, *Biochemistry 36*, 7761–7768.

476. Benson, T. E., Walsh, C. T., and Hogle, J. M. (1997) X-ray crystal structures of the S229A mutant and wild-type MurB in the presence of the substrate enolpyruvyl-UDP-*N*-acetylglucosamine at 1.8 Å resolution, *Biochemistry 36*, 806–811.
477. Lees, W. J., Benson, T. E., Hogle, J. M., and Walsh, C. T. (1996) (*E*)-Enolbutyryl-UDP-*N*-acetylglucosamine as a mechanistic probe of UDP-*N*-acetylenolpyruvylglucosamine reductase (MurB), *Biochemistry 35*, 1342–1351.
478. Dobritzsch, D., Ricagno, S., Schneider, G., Schnackerz, K. D., and Lindqvist, Y. (2002) Crystal structure of the productive ternary complex of dihydropyrimidine dehydrogenase with NADPH and 5-iodouracil. Implications for mechanism of inhibition and electron transfer, *J. Biol. Chem. 277*, 13155–13166.
479. Safo, M. K., Musayev, F. N., di Salvo, M. L., and Schirch, V. (2001) X-ray structure of *Escherichia coli* pyridoxine 5′-phosphate oxidase complexed with pyridoxal 5′-phosphate at 2.0 Å resolution, *J. Mol. Biol. 310*, 817–826.
480. Griese, J. J., Jacob, R, P., Schwarzinger, S., and Dobbek, H. (2006) Xenobiotic reductase A in the degradation of quinoline by *Pseudomonas putida* 86: Physiological function, structure and mechanism of 8-hydroxycoumarin reduction, *J. Mol. Biol. 361*, 140–152.
481. Sampathkumar, P., Turley, S., Ulmer, J. E., Rhie, H. G., Sibley, C. H., and Hol, W. G. (2005) Structure of the *Mycobacterium tuberculosis* flavin dependent thymidylate synthase (MtbThyX) at 2.0 Å resolution, *J. Mol. Biol. 352*, 1091–1104.
482. Barna, T. M., Khan, H., Bruce, N. C., Barsukov, I., Scrutton, N. S., and Moody, P. C. (2001) Crystal structure of pentaerythritol tetranitrate reductase: "Flipped" binding geometries for steroid substrates in different redox states of the enzyme, *J. Mol. Biol. 310*, 433–447.
483. Pejchal, R., Sargeant, R., and Ludwig, M. L. (2005) Structures of NADH and CH_3-H_4folate complexes of *Escherichia coli* methylenetetrahydrofolate reductase reveal a spartan strategy for a ping-pong reaction, *Biochemistry 44*, 11447–11457.
484. Senda, T., Yamada, T., Sakurai, N., Kubota, M., Nishizaki, T., Masai, E., and Fukuda, M. (2000) Crystal structure of NADH-dependent ferredoxin reductase component in biphenyl dioxygenase, *J. Mol. Biol. 304*, 397–410.
485. Deng, Z., Aliverti, A., Zanetti, G., Arakaki, A. K., Ottado, J., Orellano, E. G., Calcaterra, N. B., Ceccarelli, E. A., Carrillo, N., and Karplus, P. A. (1999) A productive $NADP^+$ binding mode of ferredoxin-$NADP^+$ reductase revealed by protein engineering and crystallographic studies, *Nature Struct. Biol. 6*, 847–853.
486. Bossi, R. T., Aliverti, A., Raimondi, D., Fischer, F., Zanetti, G., Ferrari, D., Tahallah, N., Maier, C. S., Heck, A. J., and Rizzi, M. (2002) A covalent modification of $NADP^+$ revealed by the atomic resolution structure of FprA, a *Mycobacterium tuberculosis* oxidoreductase, *Biochemistry 41*, 8807–8818.
487. Driggers, C. M., Dayal, P. V., Ellis, H. R., and Karplus, P. A. (2014) Crystal structure of *Escherichia coli* SsuE: Defining a general catalytic cycle for FMN reductases of the flavodoxin-like superfamily, *Biochemistry 53*, 3509–3519.
488. Lans, I., Medina, M., Rosta, E., Hummer, G., Garcia-Viloca, M., Lluch, J. M., and Gonzalez-Lafont, A. (2012) Theoretical study of the mechanism of the hydride transfer between ferredoxin-$NADP^+$ reductase and $NADP^+$: The role of Tyr303, *J. Am. Chem. Soc. 134*, 20544–20553.
489. Pudney, C. R., Hay, S., Sutcliffe, M. J., and Scrutton, N. S. (2006) α-Secondary isotope effects as probes of "tunneling-ready" configurations in enzymatic H-tunneling: Insight from environmentally coupled tunneling models, *J. Am. Chem. Soc. 128*, 14053–14058.
490. Sweet, W. L., and Blanchard, J. S. (1991) Human erythrocyte glutathione reductase: Chemical mechanism and structure of the transition state for hydride transfer, *Biochemistry 30*, 8702–8709.
491. Pudney, C. R., Hay, S., Pang, J., Costello, C., Leys, D., Sutcliffe, M. J., and Scrutton, N. S. (2007) Mutagenesis of morphinone reductase induces multiple reactive configurations and identifies potential ambiguity in kinetic analysis of enzyme tunneling mechanisms, *J. Am. Chem. Soc. 129*, 13949–13956.
492. Pang, J., Hay, S., Scrutton, N. S., and Sutcliffe, M. J. (2008) Deep tunneling dominates the biologically important hydride transfer reaction from NADH to FMN in morphinone reductase, *J. Am. Chem. Soc. 130*, 7092–7097.

493. Khan, H., Harris, R. J., Barna, T., Craig, D. H., Bruce, N. C., Munro, A. W., Moody, P. C., and Scrutton, N. S. (2002) Kinetic and structural basis of reactivity of pentaerythritol tetranitrate reductase with NADPH, 2-cyclohexenone, nitroesters, and nitroaromatic explosives, *J. Biol. Chem. 277*, 21906–21912.
494. Rietveld, P., Arscott, L. D., Berry, A., Scrutton, N. S., Deonarain, M. P., Perham, R. N., and Williams, C. H., Jr. (1994) Reductive and oxidative half-reactions of glutathione reductase from *Escherichia coli*, *Biochemistry 33*, 13888–13895.
495. Wolthers, K. R., and Scrutton, N. S. (2004) Electron transfer in human methionine synthase reductase studied by stopped-flow spectrophotometry, *Biochemistry 43*, 490–500.
496. Gassner, G., Wang, L., Batie, C., and Ballou, D. P. (1994) Reaction of phthalate dioxygenase reductase with NADH and NAD: Kinetic and spectral characterization of intermediates, *Biochemistry 33*, 12184–12193.
497. Schopfer, L. M., and Massey, V. (1979) Kinetic and mechanistic studies on the reduction of melilotate hydroxylase by reduced pyridine nucleotides, *J. Biol. Chem. 254*, 10634–10643.
498. Beaty, N. B., and Ballou, D. P. (1981) The reductive half-reaction of liver microsomal FAD-containing monooxygenase, *J. Biol. Chem. 256*, 4611–4618.
499. Argyrou, A., Blanchard, J. S., and Palfey, B. A. (2002) The lipoamide dehydrogenase from *Mycobacterium tuberculosis* permits the direct observation of flavin intermediates in catalysis, *Biochemistry 41*, 14580–14590.
500. Basran, J., Harris, R. J., Sutcliffe, M. J., and Scrutton, N. S. (2003) H-Tunneling in the multiple H-transfers of the catalytic cycle of morphinone reductase and in the reductive half-reaction of the homologous pentaerythritol tetranitrate reductase, *J. Biol. Chem. 278*, 43973–43982.
501. Lennon, B. W., and Williams, C. H., Jr. (1997) Reductive half-reaction of thioredoxin reductase from *Escherichia coli*, *Biochemistry 36*, 9464–9477.
502. Niviere, V., Vanoni, M. A., Zanetti, G., and Fontecave, M. (1998) Reaction of the NAD(P)H:flavin oxidoreductase from *Escherichia coli* with NADPH and riboflavin: Identification of intermediates, *Biochemistry 37*, 11879–11887.
503. Gassner, G. T., and Ballou, D. P. (1995) Preparation and characterization of a truncated form of phthalate dioxygenase reductase that lacks an iron–sulfur domain, *Biochemistry 34*, 13460–13471.
504. Maeda-Yorita, K., Russell, G. C., Guest, J. R., Massey, V., and Williams, C. H., Jr. (1991) Properties of lipoamide dehydrogenase altered by site-directed mutagenesis at a key residue (I184Y) in the pyridine nucleotide binding domain, *Biochemistry 30*, 11788–11795.
505. Ortiz-Maldonado, M., Entsch, B., and Ballou D. P. (2003) Conformational changes combined with charge-transfer interactions are essential for reduction in catalysis by *p*-hydroxybenzoate hydroxylase, *Biochemistry 42*, 11234–11242.
506. Shen, A. L., and Kasper, C. B. (1996) Role of Ser457 of NADPH-cytochrome P450 oxidoreductase in catalysis and control of FAD oxidation–reduction potential, *Biochemistry 35*, 9451–9459.
507. Rowland, P., Bjornberg, O., Nielsen, F. S., Jensen, K. F., and Larsen, S. (1998) The crystal structure of *Lactococcus lactis* dihydroorotate dehydrogenase A complexed with the enzyme reaction product throws light on its enzymatic function, *Prot. Sci. 7*, 1269–1279.
508. Bjornberg, O., Rowland, P., Larsen, S., and Jensen, K. F. (1997) Active site of dihydroorotate dehydrogenase A from *Lactococcus lactis* investigated by chemical modification and mutagenesis, *Biochemistry 36*, 16197–16205.
509. Fisher, J., and Walsh, C. (1974) Enzymatic reduction of 5-deazariboflavine from reduced nicotinamide adenine dinucleotide by direct hydrogen transfer, *J. Am. Chem. Soc. 96*, 4345–4346.
510. Ohashi, M., Jamieson, C. S., Cai, Y., Tan, D., Kanayama, D., Tang, M. C., Anthony, S. M., Chari, J. V., Barber, J. S., Picazo, E., Kakule, T. B., Cao, S., Garg, N. K., Zhou, J., Houk, K. N., and Tang, Y. (2020) An enzymatic alder-ene reaction, *Nature 586*, 64–69.
511. Ziegler, G. A., and Schulz, G. E. (2000) Crystal structures of adrenodoxin reductase in complex with $NADP^+$ and NADPH suggesting a mechanism for the electron transfer of an enzyme family, *Biochemistry 39*, 10986–10995.

512. Sucharitakul, J., Buckel, W., and Chaiyen, P. (2020) Rapid kinetics reveal surprising flavin chemistry in the bifurcating electron transfer flavoprotein from *Acidaminococcus fermentans*, *J. Biol. Chem.*
513. Jorns, M. S. (1985) Properties and catalytic function of the two nonequivalent flavins in sarcosine oxidase, *Biochemistry 24*, 3189–3194.
514. Pascal, R. A., Jr., Le Trang, N., Cerami, A., and Walsh, C. (1983) Purification and properties of dihydroorotate oxidase from *Crithidia fasciculata* and *Trypanosoma brucei*, *Biochemistry 22*, 171–178.
515. Chen, G. C., and Jordan, F. (1984) Brewers' yeast pyruvate decarboxylase produces acetoin from acetaldehyde: A novel tool to study the mechanism of steps subsequent to carbon dioxide loss, *Biochemistry 23*, 3576–3582.
516. Hosseinzadeh, P., Marshall, N. M., Chacon, K. N., Yu, Y., Nilges, M. J., New, S. Y., Tashkov, S. A., Blackburn, N. J., and Lu, Y. (2016) Design of a single protein that spans the entire 2-V range of physiological redox potentials, *Proc. Natl. Acad. Sci. U. S. A. 113*, 262–267.
517. Fajer, J., Fujita, I., Forman, A., Hanson, L. K., Craig, G. W., Goff, D. A., Kehres, L. A., and Smith, K. M. (1983) Anion radicals of bacteriochlorophylls *c*, *d*, and *e*. Likely electron acceptors in the primary photochemistry of green and brown photosynthetic bacteria, *J. Am. Chem. Soc. 105*, 3837–3843.
518. Morrison, L. E., Schelhorn, J. E., Cotton, T. M., Bering, C. L., and Loach, P. A. (1982) Electrochemical and spectral properties of ubiquinone and synthetic analogs: Relevance to bacterial photosynthesis, In *Function of quinones in energy conserving systems* (Trumpower, B. L., Ed.), pp 35–58, Academic Press, New York.
519. Takamiya, K. I., and Dutton, P. L. (1979) Ubiquinone in *Rhodopseudomonas sphaeroides*. Some thermodynamic properties, *Biochim. Biophys. Acta 546*, 1–16.
520. Urban, P. F., and Klingenberg, M. (1969) On the redox potentials of ubiquinone and cytochrome *b* in the respiratory chain, *Eur. J. Biochem. 9*, 519–525.
521. Okayama, S. (1976) Redox potential of plastoquinone *a* in spinach chloroplasts, *Biochim. Biophys. Acta 440*, 331–336.
522. Golbeck, J. H., and Kok, B. (1979) Redox titration of electron acceptor Q and the plastoquinone pool in photosystem II, *Biochim. Biophys. Acta 547*, 347–360.
523. Crane, F. L., and Barr, R. (1985) In *Coenzyme q: Biochemistry, bioenergetics and clinical applications of ubiquinone* (Lenaz, G., Ed.), pp 1–37, John Wiley and Sons, New York.
524. Liebl, U., Pezennec, S., Riedel, A., Kellner, E., and Nitschke, W. (1992) The Rieske FeS center from the gram-positive bacterium PS3 and its interaction with the menaquinone pool studied by EPR, *J. Biol. Chem. 267*, 14068–14072.
525. Land, E. J., and Swallow, A. J. (1970) One-electron reactions in biochemical systems as studied by pulse radiolysis. 3. Ubiquinone, *J. Biol. Chem. 245*, 1890–1894.
526. Maroti, P., and Wraight, C. A. (1988) Flash-induced proton binding by bacterial photosynthetic reaction centers: Influences of the redox states of the acceptor quinones and primary donor, *Biochim. Biophys. Acta 934*, 329–347.
527. McPherson, P. H., Okamura, M. Y., and Feher, G. (1988) Light-induced proton uptake by photosynthetic reaction centers from *Rhodobacter sphaeroides* R-26. I. Protonation of the one-electron states $D^+Q_A^-$, DQ_A^-, $D^+Q_AQ_B^-$, and DQ_AQ_B, *Biochim. Biophys. Acta 934*, 348–368.
528. Hauska, G., Hurt, E., Gabellini, N., and Lockau, W. (1983) Comparative aspects of quinol-cytochrome *c*/plastocyanin oxidoreductases, *Biochim. Biophys. Acta 726*, 97–133.
529. Kroger, A., and Unden, G. (1985) The function of menaquinone in bacterial electron transport, In *Coenzyme Q: Biochemistry, Bioenergetics and Clinical Applications of Ubiquinone* (Lenaz, G., Ed.), John Wiley and Son, New York.
530. Yu, C. A., Nagaoka, S., Yu, L., and King, T. (1978) Evidence for the existence of a ubiquinone protein and its radical in the cytochromes *b* and c_1 region in the mitochondrial electron transport chain, *Biochem. Biophys. Res. Commun. 82*, 1070–1078.
531. T'Sai A, L., and Palmer, G. (1983) Potentiometric studies on yeast complex III, *Biochim. Biophys. Acta 722*, 349–363.
532. Greaves, M. D., Niemz, A., and Rotello, V. M. (1999) Control of one- versus two-electron reduction of ubiquinone via redox-depen-

dent recognition, *J. Am. Chem. Soc. 121*, 266–267.
533. Horsefield, R., Yankovskaya, V., Sexton, G., Whittingham, W., Shiomi, K., Omura, S., Byrne, B., Cecchini, G., and Iwata, S. (2006) Structural and computational analysis of the quinone-binding site of complex II (succinate-ubiquinone oxidoreductase): A mechanism of electron transfer and proton conduction during ubiquinone reduction, *J. Biol. Chem. 281*, 7309–7316.
534. Eipper, B. A., Perkins, S. N., Husten, E. J., Johnson, R. C., Keutmann, H. T., and Mains, R. E. (1991) Peptidyl-α-hydroxyglycine α-amidating lyase. Purification, characterization, and expression, *J. Biol. Chem. 266*, 7827–7833.
535. Chauhan, S., Hosseinzadeh, P., Lu, Y., and Blackburn, N. J. (2016) Stopped-flow studies of the reduction of the copper centers suggest a bifurcated electron transfer pathway in peptidylglycine monooxygenase, *Biochemistry 55*, 2008–2021.
536. Chufan, E. E., Prigge, S. T., Siebert, X., Eipper, B. A., Mains, R. E., and Amzel, L. M. (2010) Differential reactivity between two copper sites in peptidylglycine α-hydroxylating monooxygenase, *J. Am. Chem. Soc. 132*, 15565–15572.
537. Williams, N. H., and Yandell, J. K. (1982) Outer-sphere electron-transfer reactions of ascorbate anions, *Australian J. Chem. 35*, 1133–1144.
538. Laroff, G. P., Fessenden, R., and Schuler, R. H. (1972) Electron spin resonance spectra of radical intermediates in the oxidation of ascorbic acid and related substances, *J. Am. Chem. Soc. 94*, 9062–9073.
539. Viehe, H. G., Janousek, Z., Merenyi, R., and Stella, L. (1985) The captodative effect, *Acc. Chem. Res. 18*, 148–154.
540. Everling, F. B., Weis, W., and Staudinger, H. (1969) Measurement of standard redox potential (pH 7.0) of L(+)-ascorbate/semidehydro-L(+)-ascorbic acid by non-enzymic reaction of L(+)-ascorbate/semidehydrol-L(+)-ascorbic acid with cytochrome b_5 (Fe^{2+})/cytochrome b_5 (Fe^{3+}), *Hoppe-Seyler's Z. Physiol. Chem. 350*, 886–888.
541. Ball, E. G. (1937) Studies on oxidation–reduction XXIII. Ascorbic acid, *J. Biol. Chem. 118*, 219–239.
542. Tu, Y. J., Njus, D., and Schlegel, H. B. (2017) A theoretical study of ascorbic acid oxidation and HOO /O_2^- radical scavenging, *Org Biomol Chem 15*, 4417–4431.
543. Wells, W. W., and Xu, D. P. (1994) Dehydroascorbate reduction, *J. Bioenerg. Biomembr. 26*, 369–377.
544. Tolbert, B. M., and Ward, J. B. (1982) Dehydroascorbic acid, In *Ascorbic acid: Chemistry, metabolism, and uses* (Seib, P. A., and Tolbert, B. M., Eds.), pp 101–123, American Chemistry Society, Washington, D. C.
545. Kassner, R. J. (1972) Effects of nonpolar environments on the redox potentials of heme complexes, *Proc. Natl. Acad. Sci. U.S.A. 69*, 2263–2267.
546. Agro, A. F., Cannella, C., Graziani, M. T., and Cavallini, D. (1971) A possible role for rhodanese: The formation of 'labile' sulfur from thiosulfate, *FEBS Lett. 16*, 172–174.
547. Horowitz, P. M., and Criscimagna, N. L. (1983) A study of the apolar interaction of the enzyme rhodanese with octyl substituted agarose gel, *Biochem. Biophys. Res. Commun. 111*, 595–601.
548. White, R. H. (1983) Origin of the labile sulfide in the iron–sulfur proteins of *Escherichia coli*, *Biochem. Biophys. Res. Commun. 112*, 66–72.
549. Archer, M., Huber, R., Tavares, P., Moura, I., Moura, J. J., Carrondo, M. A., Sieker, L. C., LeGall, J., and Romao, M. J. (1995) Crystal structure of desulforedoxin from *Desulfovibrio gigas* determined at 1.8 Å resolution: A novel nonheme iron protein structure, *J. Mol. Biol. 251*, 690–702.
550. Watenpaugh, K. D., Sieker, L. C., Herriott, J. R., and Jensen, L. H. (1973) Refinement of the model of a protein. Rubredoxin at 1.5 Å resolution, *Acta Crystallogr. B 29*, 943–956.
551. Adman, E. T., Sieker, L. C., and Jensen, L. H. (1991) Structure of rubredoxin from *Desulfovibrio vulgaris* at 1.5 Å Resolution, *J. Mol. Biol. 217*, 337–352.
552. Kummerle, R., Zhuang-Jackson, H., Gaillard, J., and Moulis, J. M. (1997) Site-directed mutagenesis of rubredoxin reveals the molecular basis of its electron transfer properties, *Biochemistry 36*, 15983–15991.
553. Bes, M. T., Parisini, E., Inda, L. A., Saraiva, L. M., Peleato, M. L., and Sheldrick, G. M. (1999) Crystal structure determination at 1.4 Å resolution of ferredoxin from the green alga *Chlorella fusca*, *Structure 7*, 1201–1211.
554. Muller, J. J., Muller, A., Rottmann, M., Bernhardt, R., and Heinemann, U. (1999) Verte-

brate-type and plant-type ferredoxins: Crystal structure comparison and electron transfer pathway modelling, *J. Mol. Biol. 294*, 501–513.
555. Kakuta, Y., Horio, T., Takahashi, Y., and Fukuyama, K. (2001) Crystal structure of *Escherichia coli* Fdx, an adrenodoxin-type ferredoxin involved in the assembly of iron–sulfur clusters, *Biochemistry 40*, 11007–11012.
556. Mayerle, J. J., Frankel, R. B., Holm, R. H., Ibers, J. A., Phillips, W. D., and Weiher, J. F. (1973) Synthetic analogs of the active sites of iron–sulfur proteins. Structure and properties of bis(*O*-xylyldithiolato-*m*-2-sulfidoferrate$_3$), an analog of the 2Fe–2S proteins, *Proc. Natl. Acad. Sci. U. S. A. 70*, 2429–2433.
557. Fee, J. A., and Palmer, G. (1971) The properties of parsley ferredoxin and its selenium-containing homolog, *Biochim. Biophys. Acta 245*, 175–195.
558. Batie, C. J., and Kamin, H. (1981) The relation of pH and oxidation–reduction potential to the association state of the ferredoxin·ferredoxin:NADP$^+$ reductase complex, *J. Biol. Chem. 256*, 7756–7763.
559. Tagawa, K., and Arnon, D. I. (1968) Oxidation–reduction potentials and stoichiometry of electron transfer in ferredoxins, *Biochim. Biophys. Acta 153*, 602–613.
560. Jacobson, B. L., Chae, Y. K., Markley, J. L., Rayment, I., and Holden, H. M. (1993) Molecular structure of the oxidized, recombinant, heterocyst [2Fe–2S] ferredoxin from *Anabaena* 7120 determined to 1.7 Å resolution, *Biochemistry 32*, 6788–6793.
561. Sazanov, L. A. (2007) Respiratory complex I: Mechanistic and structural insights provided by the crystal structure of the hydrophilic domain, *Biochemistry 46*, 2275–2288.
562. Ohnishi, T. (1998) Iron–sulfur clusters/semiquinones in complex I, *Biochim. Biophys. Acta 1364*, 186–206.
563. Yankovskaya, V., Horsefield, R., Tornroth, S., Luna-Chavez, C., Miyoshi, H., Leger, C., Byrne, B., Cecchini, G., and Iwata, S. (2003) Architecture of succinate dehydrogenase and reactive oxygen species generation, *Science 299*, 700–704.
564. Tsukihara, T., Fukuyama, K., Mizushima, M., Harioka, T., Kusunoki, M., Katsube, Y., Hase, T., and Matsubara, H. (1990) Structure of the [2Fe–2S] ferredoxin I from the blue-green alga *Aphanothece sacrum* at 2.2 Å resolution, *J. Mol. Biol. 216*, 399–410.
565. Sevrioukova, I. F., Garcia, C., Li, H., Bhaskar, B., and Poulos, T. L. (2003) Crystal structure of putidaredoxin, the [2Fe–2S] component of the P450$_{cam}$ monooxygenase system from *Pseudomonas putida*, *J. Mol. Biol. 333*, 377–392.
566. Vidakovic, M., Fraczkiewicz, G., Dave, B. C., Czernuszewicz, R. S., and Germanas, J. P. (1995) The environment of [2Fe–2S] clusters in ferredoxins: The role of residue 45 probed by site-directed mutagenesis, *Biochemistry 34*, 13906–13913.
567. Bak, D. W., and Elliott, S. J. (2014) Alternative FeS cluster ligands: Tuning redox potentials and chemistry, *Curr. Opin. Chem. Biol. 19*, 50–58.
568. Paddock, M. L., Wiley, S. E., Axelrod, H. L., Cohen, A. E., Roy, M., Abresch, E. C., Capraro, D., Murphy, A. N., Nechushtai, R., Dixon, J. E., and Jennings, P. A. (2007) MitoNEET is a uniquely folded 2Fe–2S outer mitochondrial membrane protein stabilized by pioglitazone, *Proc. Natl. Acad. Sci. U.S.A. 104*, 14342–14347.
569. Bonisch, H., Schmidt, C. L., Schafer, G., and Ladenstein, R. (2002) The structure of the soluble domain of an archaeal Rieske iron–sulfur protein at 1.1 Å resolution, *J. Mol. Biol. 319*, 791–805.
570. Gurbiel, R. J., Batie, C. J., Sivaraja, M., True, A. E., Fee, J. A., Hoffman, B. M., and Ballou, D. (1989) Electron–nuclear double resonance spectroscopy of ^{15}N-enriched phthalate dioxygenase from *Pseudomonas cepacia* proves that two histidines are coordinated to the [2Fe–2S] Rieske-type clusters, *Biochemistry 28*, 4861–4871.
571. Britt, R. D., Sauer, K., Klein, M. P., Knaff, D. B., Kriauciunas, A., Yu, C. A., Yu, L., and Malkin, R. (1991) Electron spin echo envelope modulation spectroscopy supports the suggested coordination of two histidine ligands to the Rieske [4Fe–4S] centers of the cytochrome b_6f complex of spinach and the cytochrome bc_1 complexes of *Rhodospirillum rubrum*, *Rhodobacter sphaeroides* R-26, and bovine heart mitochondria, *Biochemistry 30*, 1892–1901.
572. Berkovitch, F., Nicolet, Y., Wan, J. T., Jarrett, J. T., and Drennan, C. L. (2004) Crystal structure of biotin synthase, an *S*-adenosyl-meth-

ionine-dependent radical enzyme, *Science 303*, 76–79.
573. Zu, Y., Couture, M. M., Kolling, D. R., Crofts, A. R., Eltis, L. D., Fee, J. A., and Hirst, J. (2003) Reduction potentials of Rieske clusters: Importance of the coupling between oxidation state and histidine protonation state, *Biochemistry 42*, 12400–12408.
574. Hsueh, K. L., Westler, W. M., and Markley, J. L. (2010) NMR investigations of the Rieske protein from *Thermus thermophilus* support a coupled proton and electron transfer mechanism, *J. Am. Chem. Soc. 132*, 7908–7918.
575. Baymann, F., Robertson, D. E., Dutton, P. L., and Mantele, W. (1999) Electrochemical and spectroscopic investigations of the cytochrome bc_1 complex from *Rhodobacter capsulatus*, *Biochemistry 38*, 13188–13199.
576. Schroter, T., Hatzfeld, O. M., Gemeinhardt, S., Korn, M., Friedrich, T., Ludwig, B., and Link, T. A. (1998) Mutational analysis of residues forming hydrogen bonds in the Rieske [2Fe–2S] cluster of the cytochrome bc_1 complex in *Paracoccus denitrificans*, *Eur. J. Biochem. 255*, 100–106.
577. Denke, E., Merbitz-Zahradnik, T., Hatzfeld, O. M., Snyder, C. H., Link, T. A., and Trumpower, B. L. (1998) Alteration of the midpoint potential and catalytic activity of the Rieske iron–sulfur protein by changes of amino acids forming hydrogen bonds to the iron–sulfur cluster, *J. Biol. Chem. 273*, 9085–9093.
578. Guergova-Kuras, M., Kuras, R., Ugulava, N., Hadad, I., and Crofts, A. R. (2000) Specific mutagenesis of the Rieske iron–sulfur protein in *Rhodobacter sphaeroides* shows that both the thermodynamic gradient and the pK of the oxidized form determine the rate of quinol oxidation by the bc_1 complex, *Biochemistry 39*, 7436–7444.
579. Leggate, E. J., Bill, E., Essigke, T., Ullmann, G. M., and Hirst, J. (2004) Formation and characterization of an all-ferrous Rieske cluster and stabilization of the $[2Fe–2S]^0$ core by protonation, *Proc. Natl. Acad. Sci. U. S. A. 101*, 10913–10918.
580. Robertson, D. E., Ding, H., Chelminski, P. R., Slaughter, C., Hsu, J., Moomaw, C., Tokito, M., Daldal, F., and Dutton, P. L. (1993) Hydroubiquinone-cytochrome c_2 oxidoreductase from *Rhodobacter capsulatus*: Definition of a minimal, functional isolated preparation, *Biochemistry 32*, 1310–1317.
581. Andrews, K. M., Crofts, A. R., and Gennis, R. B. (1990) Large-scale purification and characterization of a highly active four-subunit cytochrome bc_1 complex from *Rhodobacter sphaeroides*, *Biochemistry 29*, 2645–2651.
582. Bak, D. W., Zuris, J. A., Paddock, M. L., Jennings, P. A., and Elliott, S. J. (2009) Redox characterization of the FeS protein mitoNEET and impact of thiazolidinedione drug binding, *Biochemistry 48*, 10193–10195.
583. Bergner, M., Dechert, S., Demeshko, S., Kupper, C., Mayer, J. M., and Meyer, F. (2017) Model of the mitoNEET [2Fe–2S] cluster shows proton coupled electron transfer, *J. Am. Chem. Soc. 139*, 701–707.
584. Albers, A., Demeshko, S., Dechert, S., Saouma, C. T., Mayer, J. M., and Meyer, F. (2014) Fast proton-coupled electron transfer observed for a high-fidelity structural and functional [2Fe–2S] Rieske model, *J. Am. Chem. Soc. 136*, 3946–3954.
585. Hunsicker-Wang, L. M., Heine, A., Chen, Y., Luna, E. P., Todaro, T., Zhang, Y. M., Williams, P. A., McRee, D. E., Hirst, J., Stout, C. D., and Fee, J. A. (2003) High-resolution structure of the soluble, respiratory-type Rieske protein from *Thermus thermophilus*: Analysis and comparison, *Biochemistry 42*, 7303–7317.
586. Elsen, N. L., Moe, L. A., McMartin, L. A., and Fox, B. G. (2007) Redox and functional analysis of the Rieske ferredoxin component of the toluene 4-monooxygenase, *Biochemistry 46*, 976–986.
587. Nojiri, H., Ashikawa, Y., Noguchi, H., Nam, J. W., Urata, M., Fujimoto, Z., Uchimura, H., Terada, T., Nakamura, S., Shimizu, K., Yoshida, T., Habe, H., and Omori, T. (2005) Structure of the terminal oxygenase component of angular dioxygenase, carbazole 1,9a-dioxygenase, *J. Mol. Biol. 351*, 355–370.
588. Dauter, Z., Wilson, K. S., Sieker, L. C., Meyer, J., and Moulis, J. M. (1997) Atomic resolution (0.94 Å) structure of *Clostridium acidurici* ferredoxin. Detailed geometry of [4Fe–4S] clusters in a protein, *Biochemistry 36*, 16065–16073.
589. Herskovitz, T., Averill, B. A., Holm, R. H., Ibers, J. A., Phillips, W. D., and Weiher, J. F. (1972) Structure and properties of a synthetic analogue of bacterial iron–sulfur proteins, *Proc. Natl. Acad. Sci. U. S. A. 69*, 2437–2441.

590. Fukuyama, K., Okada, T., Kakuta, Y., and Takahashi, Y. (2002) Atomic resolution structures of oxidized [4Fe–4S] ferredoxin from *Bacillus thermoproteolyticus* in two crystal forms: Systematic distortion of [4Fe–4S] cluster in the protein, *J. Mol. Biol. 315*, 1155–1166.
591. Volbeda, A., Charon, M. H., Piras, C., Hatchikian, E. C., Frey, M., and Fontecilla-Camps, J. C. (1995) Crystal structure of the nickel-iron hydrogenase from *Desulfovibrio gigas*, *Nature 373*, 580–587.
592. Evans, R. M., Brooke, E. J., Wehlin, S. A., Nomerotskaia, E., Sargent, F., Carr, S. B., Phillips, S. E., and Armstrong, F. A. (2016) Mechanism of hydrogen activation by [NiFe] hydrogenases, *Nat Chem Biol 12*, 46–50.
593. Gruner, I., Fradrich, C., Bottger, L. H., Trautwein, A. X., Jahn, D., and Hartig, E. (2011) Aspartate 141 is the fourth ligand of the oxygen-sensing $[4Fe–4S]^{2+}$ cluster of *Bacillus subtilis* transcriptional regulator Fnr, *J. Biol. Chem. 286*, 2017–2021.
594. Ohki, Y., Tanifuji, K., Yamada, N., Imada, M., Tajima, T., and Tatsumi, K. (2011) Synthetic analogues of $[Fe_4S_4(Cys)_3(His)]$ in hydrogenases and $[Fe_4S_4(Cys)_4]$ in HiPIP derived from all-ferric $[Fe_4S_4\{N(SiMe_3)_2\}_4]$, *Proc. Natl. Acad. Sci. U.S.A. 108*, 12635–12640.
595. Hinckley, G. T., and Frey, P. A. (2006) Cofactor dependence of reduction potentials for $[4Fe–4S]^{2+/1+}$ in lysine 2,3-aminomutase, *Biochemistry 45*, 3219–3225.
596. Jameson, G. N., Walters, E. M., Manieri, W., Schurmann, P., Johnson, M. K., and Huynh, B. H. (2003) Spectroscopic evidence for site specific chemistry at a unique iron site of the [4Fe–4S] cluster in ferredoxin:thioredoxin reductase, *J. Am. Chem. Soc. 125*, 1146–1147.
597. Walters, E. M., Garcia-Serres, R., Jameson, G. N., Glauser, D. A., Bourquin, F., Manieri, W., Schurmann, P., Johnson, M. K., and Huynh, B. H. (2005) Spectroscopic characterization of site-specific $[Fe_4S_4]$ cluster chemistry in ferredoxin:thioredoxin reductase: Implications for the catalytic mechanism, *J. Am. Chem. Soc. 127*, 9612–9624.
598. Carter, C. W., Jr., Kraut, J., Freer, S. T., Alden, R. A., Sieker, L. C., Adman, E., and Jensen, L. (1972) A comparison of Fe_4S_4 clusters in high-potential iron protein and in ferredoxin, *Proc. Natl. Acad. Sci. U. S. A. 69*, 3526–3529.
599. Watt, G. D., and Reddy, K. R. N. (1994) Formation of an all ferrous Fe_4S_4 cluster in the iron protein component of *Azotobacter vinelandii* nitrogenase, *J. Inorg. Biochem. 53*, 281–294.
600. Angove, H. C., Yoo, S. J., Munck, E., and Burgess, B. K. (1998) An all-ferrous state of the Fe protein of nitrogenase. Interaction with nucleotides and electron transfer to the Mo-Fe protein, *J. Biol. Chem. 273*, 26330–26337.
601. Deng, L., and Holm, R. H. (2008) Stabilization of fully reduced iron–sulfur clusters by carbene ligation: The $[Fe(n)F(n)]^0$ oxidation levels (n = 4, 8), *J. Am. Chem. Soc. 130*, 9878–9886.
602. Kyte, J. (2007) *Structure in protein chemistry: Second edition*, pp 645–650, Garland Science, New York.
603. Kyritsis, P., Kummerle, R., Huber, J. G., Gaillard, J., Guigliarelli, B., Popescu, C., and Munck, E. (1999) Unusual NMR, EPR, and Mössbauer properties of *Chromatium vinosum* 2[4Fe–4S] ferredoxin, *Biochemistry 38*, 6335–6345.
604. Middleton, P., Dickson, D. P., Johnson, C. E., and Rush, J. D. (1978) Interpretation of the Mössbauer spectra of the four-iron ferredoxin from *Bacillus stearothermophilus, Eur. J. Biochem. 88*, 135–141.
605. Green, A. J., Munro, A. W., Cheesman, M. R., Reid, G. A., von Wachenfeldt, C., and Chapman, S. K. (2003) Expression, purification and characterisation of a *Bacillus subtilis* ferredoxin: A potential electron transfer donor to cytochrome P450 BioI, *J Inorg Biochem 93*, 92–99.
606. Heering, H. A., Bulsink, B. M., Hagen, W. R., and Meyer, T. E. (1995) Influence of charge and polarity on the redox potentials of high-potential iron–sulfur proteins: Evidence for the existence of two groups, *Biochemistry 34*, 14675–14686.
607. Low, D. W., and Hill, M. G. (2000) Backbone-engineered high-potential iron proteins: Effects of active-site hydrogen bonding on reduction potential, *J. Am. Chem. Soc. 122*, 11039–11040.
608. Funk, M. A., Judd, E. T., Marsh, E. N., Elliott, S. J., and Drennan, C. L. (2014) Structures of benzylsuccinate synthase elucidate roles of accessory subunits in glycyl radical enzyme activation and activity, *Proc. Natl. Acad. Sci. U.S.A. 111*, 10161–10166.

609. Dai, S. D., Friemann, R., Glauser, D. A., Bourquin, F., Manieri, W., Schurmann, P., and Eklund, H. (2007) Structural snapshots along the reaction pathway of ferredoxin-thioredoxin reductase, *Nature 448*, 92–102.
610. Ishikita, H., and Knapp, E. W. (2003) Redox potential of quinones in both electron transfer branches of photosystem I, *J. Biol. Chem. 278*, 52002–52011.
611. Stombaugh, N. A., Sundquist, J. E., Burris, R. H., and Orme-Johnson, W. H. (1976) Oxidation–reduction properties of several low potential iron–sulfur proteins and of methylviologen, *Biochemistry 15*, 2633–2641.
612. Maiocco, S. J., Grove, T. L., Booker, S. J., and Elliott, S. J. (2015) Electrochemical resolution of the [4Fe–4S] centers of the AdoMet radical enzyme BtrN: Evidence of proton coupling and an unusual, low-potential auxiliary cluster, *J. Am. Chem. Soc. 137*, 8664–8667.
613. Hill, C. I., Renaud, J., Holm, R. H., and Mortenson, I. E. (1977) Synthetic analogues of the active sites of iron–sulfur proteins. 15. Comparative polarographic potentials of the $[Fe_4S_4(Sr)_4]^{2-,3-}$and *Clostridium pasteurianum* ferredoxin redox couples, *J. Am. Chem. Soc. 99*, 2549–2557.
614. Backes, G., Mino, Y., Loehr, T. M., Meyer, T. E., Cusanovich, M. A., Sweeney, W. V., Adman, E. T., and Sanders-Loehr, J. (1991) The environment of Fe_4S_4 clusters in ferredoxins and high-potential iron proteins. New information from X-ray crystallography and resonance Raman spectroscopy, *J. Am. Chem. Soc. 113*, 2055–2064.
615. Jang, S. B., Seefeldt, L. C., and Peters, J. W. (2000) Modulating the midpoint potential of the [4Fe–4S] cluster of the nitrogenase Fe protein, *Biochemistry 39*, 641–648.
616. Langen, R., Jensen, G. M., Jacob, U., Stephens, P. J., and Warshel, A. (1992) Protein control of iron–sulfur cluster redox potentials, *J. Biol. Chem. 267*, 25625–25627.
617. Strop, P., Takahara, P. M., Chiu, H., Angove, H. C., Burgess, B. K., and Rees, D. C. (2001) Crystal structure of the all-ferrous $[4Fe–4S]^0$ form of the nitrogenase iron protein from *Azotobacter vinelandii*, *Biochemistry 40*, 651–656.
618. Breiter, D. R., Meyer, T. E., Rayment, I., and Holden, H. M. (1991) The molecular structure of the high potential iron–sulfur protein isolated from *Ectothiorhodospira halophila* determined at 2.5 Å resolution, *J. Biol. Chem. 266*, 18660–18667.
619. Rayment, I., Wesenberg, G., Meyer, T. E., Cusanovich, M. A., and Holden, H. M. (1992) Three-dimensional structure of the high-potential iron–sulfur protein isolated from the purple phototrophic bacterium *Rhodocyclus tenuis* determined and refined at 1.5 Å resolution, *J. Mol. Biol. 228*, 672–686.
620. Benning, M. M., Meyer, T. E., Rayment, I., and Holden, H. M. (1994) Molecular structure of the oxidized high-potential iron–sulfur protein isolated from *Ectothiorhodospira vacuolata*, *Biochemistry 33*, 2476–2483.
621. Adamson, H., Robinson, M., Wright, J. J., Flanagan, L. A., Walton, J., Elton, D., Gavaghan, D. J., Bond, A. M., Roessler, M. M., and Parkin, A. (2017) Retuning the catalytic bias and overpotential of a [NiFe]-hydrogenase via a single amino acid exchange at the electron entry/exit site, *J. Am. Chem. Soc. 139*, 10677–10686.
622. Stout, G. H., Turley, S., Sieker, L. C., and Jensen, L. H. (1988) Structure of ferredoxin i from *Azotobacter vinelandii*, *Proc. Natl. Acad. Sci. U. S. A. 85*, 1020–1022.
623. Stout, C. D. (1989) Refinement of the 7 Fe ferredoxin from *Azotobacter vinelandii* at 1.9 Å resolution, *J. Mol. Biol. 205*, 545–555.
624. Kissinger, C. R., Adman, E. T., Sieker, L. C., and Jensen, L. H. (1988) Structure of the 3Fe–4S cluster in *Desulfovibrio gigas* ferredoxin II, *J. Am. Chem. Soc. 110*, 8721–8723.
625. Kent, T. A., Dreyer, J. L., Kennedy, M. C., Huynh, B. H., Emptage, M. H., Beinert, H., and Munck, E. (1982) Mössbauer studies of beef heart aconitase: Evidence for facile interconversions of iron–sulfur clusters, *Proc. Natl. Acad. Sci. U. S. A. 79*, 1096–1100.
626. Krebs, C., Henshaw, T. F., Cheek, J., Huynh, B. H., and Broderick, J. B. (2000) Conversion of [3Fe–4S] to [4Fe–4S] clusters in native pyruvate formate-lyase activating enzyme: Moessbauer characterization and implications for mechanism, *J. Am. Chem. Soc. 122*, 12497–12506.
627. Johnson, M. K., Bennett, D. E., Morningstar, J. E., Adams, M. W., and Mortenson, L. E. (1985) The iron–sulfur cluster composition of *Escherichia coli* nitrate reductase, *J. Biol. Chem. 260*, 5456–5463.
628. Manodori, A., Cecchini, G., Schroder, I., Gunsalus, R. P., Werth, M. T., and Johnson,

M. K. (1992) [3Fe–4S] to [4Fe–4S] cluster conversion in *Escherichia coli* fumarate reductase by site-directed mutagenesis, *Biochemistry 31*, 2703–2712.
629. Knaff, D. B., Hirasawa, M., Ameyibor, E., Fu, W., and Johnson, M. K. (1991) Spectroscopic evidence for a [3Fe–4S] cluster in spinach glutamate synthase, *J. Biol. Chem. 266*, 15080–15084.
630. Hagerhall, C. (1997) Succinate:quinone oxidoreductases. Variations on a conserved theme, *Biochim. Biophys. Acta 1320*, 107–141.
631. Johnson, M. K., Bennett, D. E., Fee, J. A., and Sweeney, W. V. (1987) Spectroscopic studies of the seven-iron-containing ferredoxins from *Azotobacter vinelandii* and *Thermus thermophilus*, *Biochim. Biophys. Acta 911*, 81–94.
632. Rousset, M., Montet, Y., Guigliarelli, B., Forget, N., Asso, M., Bertrand, P., Fontecilla-Camps, J. C., and Hatchikian, E. C. (1998) [3Fe–4S] to [4Fe–4S] cluster conversion in *Desulfovibrio fructosovorans* [NiFe] hydrogenase by site-directed mutagenesis, *Proc. Natl. Acad. Sci. U.S.A. 95*, 11625–11630.
633. Zhao, J., Li, N., Warren, P. V., Golbeck, J. H., and Bryant, D. A. (1992) Site-directed conversion of a cysteine to aspartate leads to the assembly of a [3Fe–4S]cluster in PsaC of photosystem I. The photoreduction of F_A is independent of F_B, *Biochemistry 31*, 5093–5099.
634. Schipke, C. G., Goodin, D. B., McRee, D. E., and Stout, C. D. (1999) Oxidized and reduced *Azotobacter vinelandii* ferredoxin I at 1.4 angstrom resolution: Conformational change of surface residues without significant change in the $[3Fe–4S]^{+/0}$ cluster, *Biochemistry 38*, 8228–8239.
635. Zhou, J., Hu, Z., Muenck, E., and Holm, R. H. (1996) The cuboidal Fe_3S_4 cluster: Synthesis, stability, and geometric and electronic structures in a non-protein environment, *J. Am. Chem. Soc. 118*, 1966–1980.
636. Sweeney, W. V., Rabinowitz, J. C., and Yoch, D. C. (1975) High and low reduction potential [4Fe–4S] clusters in *Azotobacter vinelandii* $[4Fe–4S]_2$ ferredoxin I. Influence of the polypeptide on the reduction potentials, *J. Biol. Chem. 250*, 7842–7847.
637. Shen, B., Martin, L. L., Butt, J. N., Armstrong, F. A., Stout, C. D., Jensen, G. M., Stephens, P. J., La Mar, G. N., Gorst, C. M., and Burgess, B. K. (1993) *Azotobacter vinelandii* ferredoxin I. Aspartate 15 facilitates proton transfer to the reduced [3Fe–4S]cluster, *J. Biol. Chem. 268*, 25928–25939.
638. Stephens, P. J., Jensen, G. M., Devlin, F. J., Morgan, T. V., Stout, C. D., Martin, A. E., and Burgess, B. K. (1991) Circular dichroism and magnetic circular dichroism of *Azotobacter vinelandii* ferredoxin I, *Biochemistry 30*, 3200–3209.
639. Ghosh, D., O'Donnell, S., Furey, W., Jr., Robbins, A. H., and Stout, C. D. (1982) Iron–sulfur clusters and protein structure of *Azotobacter* ferredoxin at 2.0 Å resolution, *J. Mol. Biol. 158*, 73–109.
640. Duff, J. L. C., Breton, J. L. J., Butt, J. N., Armstrong, F. A., and Thomson, A. J. (1996) Novel redox chemistry of [3Fe–4S]clusters: Electrochemical characterization of the all-Fe(II) form of the [3Fe–4S]cluster generated reversibly in various proteins and its spectroscopic investigation in *Sulfolobus acidocaldarius* ferredoxin, *J. Am. Chem. Soc. 118*, 8593–8603.
641. Kissinger, C. R., Sieker, L. C., Adman, E. T., and Jensen, L. H. (1991) Refined crystal structure of ferredoxin II from *Desulfovibrio gigas* at 1.7 Å, *J. Mol. Biol. 219*, 693–715.
642. Wagner, T., Koch, J., Ermler, U., and Shima, S. (2017) Methanogenic heterodisulfide reductase (HdrABC-MvhAGD) uses two noncubane [4Fe–4S] clusters for reduction, *Science 357*, 699–703.
643. Simianu, M., Murakami, E., Brewer, J. M., and Ragsdale, S. W. (1998) Purification and properties of the heme- and iron–sulfur-containing heterodisulfide reductase from *Methanosarcina thermophila*, *Biochemistry 37*, 10027–10039.
644. Fritsch, J., Scheerer, P., Frielingsdorf, S., Kroschinsky, S., Friedrich, B., Lenz, O., and Spahn, C. M. (2011) The crystal structure of an oxygen-tolerant hydrogenase uncovers a novel iron-sulphur centre, *Nature 479*, 249–252.
645. Shomura, Y., Yoon, K. S., Nishihara, H., and Higuchi, Y. (2011) Structural basis for a [4Fe–3S] cluster in the oxygen-tolerant membrane-bound [NiFe]-hydrogenase, *Nature 479*, 253–256.
646. Rees, D. C., and Howard, J. B. (2003) The interface between the biological and inorganic worlds: Iron–sulfur metalloclusters, *Science 300*, 929–931.

647. Peters, J. W., Stowell, M. H., Soltis, S. M., Finnegan, M. G., Johnson, M. K., and Rees, D. C. (1997) Redox-dependent structural changes in the nitrogenase P-cluster, *Biochemistry 36*, 1181–1187.
648. Vanoni, M. A., Edmondson, D. E., Zanetti, G., and Curti, B. (1992) Characterization of the flavins and the iron–sulfur centers of glutamate synthase from *Azospirillum brasilense* by absorption, circular dichroism, and electron paramagnetic resonance spectroscopies, *Biochemistry 31*, 4613–4623.
649. Petrouleas, V., Brand, J. J., Parrett, K. G., and Golbeck, J. H. (1989) A Mössbauer analysis of the low-potential iron–sulfur center in photosystem I: Spectroscopic evidence that Fx is a [4Fe–4S] cluster, *Biochemistry 28*, 8980–8983.
650. Busby, R. W., Schelvis, J. P. M., Yu, D. S., Babcock, G. T., and Marletta, M. A. (1999) Lipoic acid biosynthesis: LipA is an iron–sulfur protein, *J. Am. Chem. Soc. 121*, 4706–4707.
651. Sazanov, L. A., and Hinchliffe, P. (2006) Structure of the hydrophilic domain of respiratory complex I from *Thermus thermophilus*, *Science 311*, 1430–1436.
652. Wu, W., Chang, C. K., Varotsis, C., Babcock, G. T., Puustinen, A., and Wikstrom, M. (1992) Structure of the heme *o* prosthetic group from the terminal quinol oxidase of *Escherichia coli*, *J. Am. Chem. Soc. 114*, 1182–1187.
653. Murshudov, G. N., Grebenko, A. I., Barynin, V., Dauter, Z., Wilson, K. S., Vainshtein, B. K., Melik-Adamyan, W., Bravo, J., Ferran, J. M., Ferrer, J. C., Switala, J., Loewen, P. C., and Fita, I. (1996) Structure of the heme *d* of *Penicillium vitale* and *Escherichia coli* catalases, *J. Biol. Chem. 271*, 8863–8868.
654. Weeg-Aerssens, E., Wu, W. S., Ye, R. W., Tiedje, J. M., and Chang, C. K. (1991) Purification of cytochrome cd_1 nitrite reductase from *Pseudomonas stutzeri* jm300 and reconstitution with native and synthetic heme d_1, *J. Biol. Chem. 266*, 7496–7502.
655. Wu, W., and Chang, C. K. (1987) Structure of dioneheme. Total synthesis of the green heme prosthetic group in cytochrome cd_1 dissimilatory nitrite reductase, *J. Am. Chem. Soc. 109*, 3149–3150.
656. Takano, T., and Dickerson, R. E. (1981) Conformation change of cytochrome *c*. I. Ferrocytochrome *c* structure refined at 1.5 Å resolution, *J. Mol. Biol. 153*, 79–94.
657. Cedervall, P., Hooper, A. B., and Wilmot, C. M. (2013) Structural studies of hydroxylamine oxidoreductase reveal a unique heme cofactor and a previously unidentified interaction partner, *Biochemistry 52*, 6211–6218.
658. Smith, M. A., and Lancaster, K. M. (2018) The eponymous cofactors in cytochrome P460s from ammonia-oxidizing bacteria are iron porphyrinoids whose macrocycles are dibasic, *Biochemistry 57*, 334–343.
659. Pearson, A. R., Elmore, B. O., Yang, C., Ferrara, J. D., Hooper, A. B., and Wilmot, C. M. (2007) The crystal structure of cytochrome P460 of *Nitrosomonas europaea* reveals a novel cytochrome fold and heme-protein cross-link, *Biochemistry 46*, 8340–8349.
660. Mashiko, T., Marchon, J. C., Musser, D. T., Reed, C. A., Kastner, M. E., and Scheidt, W. R. (1979) Cytochrome *c* models, *J. Am. Chem. Soc. 101*, 3653–3655.
661. Crane, B. R., Siegel, L. M., and Getzoff, E. D. (1995) Sulfite reductase structure at 1.6 Å: Evolution and catalysis for reduction of inorganic anions, *Science 270*, 59–67.
662. Poulos, T. L., Finzel, B. C., and Howard, A. J. (1987) High-resolution crystal structure of cytochrome $P450_{cam}$, *J. Mol. Biol. 195*, 687–700.
663. Murthy, M. R., Reid, T. J., 3rd, Sicignano, A., Tanaka, N., and Rossmann, M. G. (1981) Structure of beef liver catalase, *J. Mol. Biol. 152*, 465–499.
664. Yun, C. H., Crofts, A. R., and Gennis, R. B. (1991) Assignment of the histidine axial ligands to the cytochrome b_H and cytochrome b_L components of the bc_1 complex from *Rhodobacter sphaeroides* by site-directed mutagenesis, *Biochemistry 30*, 6747–6754.
665. Xia, D., Yu, C. A., Kim, H., Xia, J. Z., Kachurin, A. M., Zhang, L., Yu, L., and Deisenhofer, J. (1997) Crystal structure of the cytochrome bc_1 complex from bovine heart mitochondria, *Science 277*, 60–66.
666. Martinez, S. E., Huang, D., Ponomarev, M., Cramer, W. A., and Smith, J. L. (1996) The heme redox center of chloroplast cytochrome *f* is linked to a buried five-water chain, *Prot. Sci. 5*, 1081–1092.
667. Martinez, S. E., Huang, D., Szczepaniak, A., Cramer, W. A., and Smith, J. L. (1994) Crystal structure of chloroplast cytochrome *f* reveals a novel cytochrome fold and unexpected heme ligation, *Structure 2*, 95–105.

668. Carrell, C. J., Schlarb, B. G., Bendall, D. S., Howe, C. J., Cramer, W. A., and Smith, J. L. (1999) Structure of the soluble domain of cytochrome *f* from the *Cyanobacterium phormidium* laminosum, *Biochemistry 38*, 9590–9599.
669. Chi, Y. I., Huang, L. S., Zhang, Z. L., Fernandez-Velasco, J. G., and Berry, E. A. (2000) X-ray structure of a truncated form of cytochrome *f* from *Chlamydomonas reinhardtii*, *Biochemistry 39*, 7689–7701.
670. McRee, D. E., Richardson, D. C., Richardson, J. S., and Siegel, L. M. (1986) The heme and Fe_4S_4 cluster in the crystallographic structure of *Escherichia coli* sulfite reductase, *J. Biol. Chem. 261*, 10277–10281.
671. Cai, L., and Holm, R. H. (1994) Synthesis and electron delocalization of $[Fe_4S_4]$-S-Fe(III) bridged assemblies related to the exchange-coupled catalytic site of sulfite reductases, *J. Am. Chem. Soc. 116*, 7177–7188.
672. Parey, K., Warkentin, E., Kroneck, P. M. H., and Ermler, U. (2010) Reaction cycle of the dissimilatory sulfite reductase from *Archaeoglobus fulgidus*, *Biochemistry 49*, 8912–8921.
673. Tsukihara, T., Aoyama, H., Yamashita, E., Tomizaki, T., Yamaguchi, H., Shinzawa-Itoh, K., Nakashima, R., Yaono, R., and Yoshikawa, S. (1995) Structures of metal sites of oxidized bovine heart cytochrome *c* oxidase at 2.8 Å, *Science 269*, 1069–1074.
674. Iverson, T. M., Arciero, D. M., Hsu, B. T., Logan, M. S., Hooper, A. B., and Rees, D. C. (1998) Heme packing motifs revealed by the crystal structure of the tetra-heme cytochrome c_{554} from *Nitrosomonas europaea*, *Nature Struct. Biol. 5*, 1005–1012.
675. Perutz, M. F. (1979) Regulation of oxygen affinity of hemoglobin: Influence of structure of the globin on the heme iron, *Annu. Rev. Biochem. 48*, 327–386.
676. Halcrow, M. A. (2016) The effect of ligand design on metal ion spin state: Lessons from spin crossover complexes, *Crystals 6*, 58.
677. Bruschi, M., Loutfi, M., Bianco, P., and Haladjian, J. (1984) Correlations studies between structural and redox properties of cytochromes c_3, *Biochem. Biophys. Res. Commun. 120*, 384–389.
678. Mizusawa, N., Yamashita, T., and Miyao, M. (1999) Restoration of the high-potential form of cytochrome b_{559} of photosystem II occurs via a two-step mechanism under illumination in the presence of manganese ions, *Biochim. Biophys. Acta 1410*, 273–286.
679. Ortega, J. M., Hervas, M., and Losada, M. (1988) Redox and acid–base characterization of cytochrome b_{559} in photosystem II particles, *Eur. J. Biochem. 171*, 449–455.
680. Reedy, C. J., Elvekrog, M. M., and Gibney, B. R. (2008) Development of a heme protein structure-electrochemical function database, *Nucleic Acids Res. 36*, D307–313.
681. Hendrich, M. P., Petasis, D., Arciero, D. M., and Hooper, A. B. (2001) Correlations of structure and electronic properties from EPR spectroscopy of hydroxylamine oxidoreductase, *J. Am. Chem. Soc. 123*, 2997–3005.
682. Falk, J. E. (1964) *Porphyrins and Metalloporphyrins: Their General, Physical and Coordination Chemistry, and Laboratory Methods.*, Elsevier Publishing Company, Amsterdam.
683. Moore, G. R., and Pettigrew, G. W. (1990) *Cytochromes c: Evolutionary, Structural, and Physicochemical Aspects*, p 21, Springer-Verlag, Berlin.
684. Kaysser, T. M., Ghaim, J. B., Georgiou, C., and Gennis, R. B. (1995) Methionine-393 is an axial ligand of the heme b_{558} component of the cytochrome *bd* ubiquinol oxidase from *Escherichia coli*, *Biochemistry 34*, 13491–13501.
685. Lorence, R. M., Green, G. N., and Gennis, R. B. (1984) Potentiometric analysis of the cytochromes of an *Escherichia coli* mutant strain lacking the cytochrome *d* terminal oxidase complex, *J. Bacteriol. 157*, 115–121.
686. Pettigrew, G. W., and Moore, G. R. (1987) *Cytochromes c: Biological Aspects*, Springer-Verlag, Berlin.
687. Pettigrew, G. W., and Moore, G. R. (1987) *Cytochromes c: Biological Aspects*, p 22, Springer-Verlag, Berlin.
688. Rivera, M., Seetharaman, R., Girdhar, D., Wirtz, M., Zhang, X., Wang, X., and White, S. (1998) The reduction potential of cytochrome b_5 is modulated by its exposed heme edge, *Biochemistry 37*, 1485–1494.
689. Rees, D. C., and Farrelly, D. (1990) Biological electron transfer, In *The Enzymes, Vol. 19* (Sigman, D. S., and Boyer, P., Eds.), pp 37–97, Elsevier, Burlington.
690. Moore, G. R., and Pettigrew, G. W. (1990) In *Cytochromes c: Evolutionary, Structural, and Physicochemical aspects*, pp 318–336, Springer-Verlag, Berlin.

691. Worrall, J. A., Schlarb-Ridley, B. G., Reda, T., Marcaida, M. J., Moorlen, R. J., Wastl, J., Hirst, J., Bendall, D. S., Luisi, B. F., and Howe, C. J. (2007) Modulation of heme redox potential in the cytochrome c_6 family, *J. Am. Chem. Soc. 129*, 9468–9475.
692. Olea, C., Kuriyan, J., and Marletta, M. A. (2010) Modulating heme redox potential through protein-induced porphyrin distortion, *J. Am. Chem. Soc. 132*, 12794–12795.
693. Santos, H., Moura, J. J., Moura, I., LeGall, J., and Xavier, A. V. (1984) NMR studies of electron transfer mechanisms in a protein with interacting redox centres: *Desulfovibrio gigas* cytochrome c_3, *Eur. J. Biochem. 141*, 283–296.
694. Li, H., Webb, S. P., Ivanic, J., and Jensen, J. H. (2004) Determinants of the relative reduction potentials of type-1 copper sites in proteins, *J. Am. Chem. Soc. 126*, 8010–8019.
695. Ducros, V., Brzozowski, A. M., Wilson, K. S., Ostergaard, P., Schneider, P., Svendson, A., and Davies, G. J. (2001) Structure of the laccase from *Coprinus cinereus* at 1.68 Å resolution: Evidence for different 'type 2 Cu-depleted' isoforms, *Acta Crystallogr. D 57*, 333–336.
696. Messerschmidt, A., Ladenstein, R., Huber, R., Bolognesi, M., Avigliano, L., Petruzzelli, R., Rossi, A., and Finazzi-Agro, A. (1992) Refined crystal structure of ascorbate oxidase at 1.9 Å resolution, *J. Mol. Biol. 224*, 179–205.
697. Machonkin, T. E., Zhang, H. H., Hedman, B., Hodgson, K. O., and Solomon, E. I. (1998) Spectroscopic and magnetic studies of human ceruloplasmin: Identification of a redox-inactive reduced type 1 copper site, *Biochemistry 37*, 9570–9578.
698. Holland, P. L., and Tolman, W. B. (1999) Three-coordinate Cu(II) complexes: Structural models of trigonal-planar type 1 copper protein active sites, *J. Am. Chem. Soc. 121*, 7270–7271.
699. Randall, D. W., DeBeer George, S., Holland, P. L., Hedman, B., Hodgson, K. O., Tolman, W. B., and Solomon, E. I. (2000) Spectroscopic and electronic structural studies of blue copper model complexes. 2. Comparison of three- and four-coordinate Cu(II)-thiolate complexes and fungal laccase, *J. Am. Chem. Soc. 122*, 11632–11648.
700. Romero, A., Nar, H., Huber, R., Messerschmidt, A., Kalverda, A. P., Canters, G. W., Durley, R., and Mathews, F. S. (1994) Crystal structure analysis and refinement at 2.15 Å resolution of amicyanin, a type I blue copper protein, from *Thiobacillus versutus*, *J. Mol. Biol. 236*, 1196–1211.
701. Petratos, K., Dauter, Z., and Wilson, K. S. (1988) Refinement of the structure of pseudoazurin from *Alcaligenes faecalis* S-6 at 1.55 Å resolution, *Acta Crystallogr B 44 (Pt 6)*, 628–636.
702. Barrett, M. L., Harvey, I., Sundararajan, M., Surendran, R., Hall, J. F., Ellis, M. J., Hough, M. A., Strange, R. W., Hillier, I. H., and Hasnain, S. S. (2006) Atomic resolution crystal structures, EXAFS, and quantum chemical studies of rusticyanin and its two mutants provide insight into its unusual properties, *Biochemistry 45*, 2927–2939.
703. Ellis, M. J., Dodd, F. E., Sawers, G., Eady, R. R., and Hasnain, S. S. (2003) Atomic resolution structures of native copper nitrite reductase from *Alcaligenes xylosoxidans* and the active site mutant Asp92Glu, *J. Mol. Biol. 328*, 429–438.
704. Einsle, O., Mehrabian, Z., Nalbandyan, R., and Messerschmidt, A. (2000) Crystal structure of plantacyanin, a basic blue cupredoxin from spinach, *J. Biol. Inorg. Chem. 5*, 666–672.
705. Bond, C. S., Blankenship, R. E., Freeman, H. C., Guss, J. M., Maher, M. J., Selvaraj, F. M., Wilce, M. C., and Willingham, K. M. (2001) Crystal structure of auracyanin, a "blue" copper protein from the green thermophilic photosynthetic bacterium *Chloroflexus aurantiacus*, *J. Mol. Biol. 306*, 47–67.
706. Roberts, S. A., Weichsel, A., Grass, G., Thakali, K., Hazzard, J. T., Tollin, G., Rensing, C., and Montfort, W. R. (2002) Crystal structure and electron transfer kinetics of CueO, a multicopper oxidase required for copper homeostasis in *Escherichia coli*, *Proc. Natl. Acad. Sci. U. S. A. 99*, 2766–2771.
707. Guss, J. M., Bartunik, H. D., and Freeman, H. C. (1992) Accuracy and precision in protein structure analysis: Restrained least-squares refinement of the structure of poplar plastocyanin at 1.33 Å resolution, *Acta Crystallogr B 48 (Pt 6)*, 790–811.
708. Inoue, T., Sugawara, H., Hamanaka, S., Tsukui, H., Suzuki, E., Kohzuma, T., and Kai, Y. (1999) Crystal structure determinations of oxidized and reduced plastocyanin from the

cyanobacterium *Synechococcus* sp. Pcc 7942, *Biochemistry 38*, 6063–6069.
709. Shibata, N., Inoue, T., Nagano, C., Nishio, N., Kohzuma, T., Onodera, K., Yoshizaki, F., Sugimura, Y., and Kai, Y. (1999) Novel insight into the copper-ligand geometry in the crystal structure of *Ulva pertusa* plastocyanin at 1.6 Å resolution. Structural basis for regulation of the copper site by residue 88, *J. Biol. Chem. 274*, 4225–4230.
710. Walter, R. L., Ealick, S. E., Friedman, A. M., Blake, R. C., 2nd, Proctor, P., and Shoham, M. (1996) Multiple wavelength anomalous diffraction (MAD) crystal structure of rusticyanin: A highly oxidizing cupredoxin with extreme acid stability, *J. Mol. Biol. 263*, 730–751.
711. Wijma, H. J., Macpherson, I., Alexandre, M., Diederix, R. E., Canters, G. W., Murphy, M. E., and Verbeet, M. P. (2006) A rearranging ligand enables allosteric control of catalytic activity in copper-containing nitrite reductase, *J. Mol. Biol. 358*, 1081–1093.
712. Ma, J. K., Mathews, F. S., and Davidson, V. L. (2007) Correlation of rhombic distortion of the type 1 copper site of M98Q amicyanin with increased electron transfer reorganization energy, *Biochemistry 46*, 8561–8568.
713. Garner, D. K., Vaughan, M. D., Hwang, H. J., Savelieff, M. G., Berry, S. M., Honek, J. F., and Lu, Y. (2006) Reduction potential tuning of the blue copper center in *Pseudomonas aeruginosa* azurin by the axial methionine as probed by unnatural amino acids, *J. Am. Chem. Soc. 128*, 15608–15617.
714. Choi, M., Sukumar, N., Liu, A., and Davidson, V. L. (2009) Defining the role of the axial ligand of the type 1 copper site in amicyanin by replacement of methionine with leucine, *Biochemistry 48*, 9174–9184.
715. Jeuken, L. J. C., van Vliet, P., Verbeet, M. P., Camba, R., McEvoy, J. P., Armstrong, F. A., and Canters, G. W. (2000) Role of the surface-exposed and copper-coordinating histidine in blue copper proteins: The electron-transfer and redox-coupled ligand binding properties of His117Gly azurin, *J. Am. Chem. Soc. 122*, 12186–12194.
716. Gray, H. B., Malmstrom, B. G., and Williams, R. J. (2000) Copper coordination in blue proteins, *J. Biol. Inorg. Chem. 5*, 551–559.
717. Niles McLeod, D. D., Freeman, H. C., Harvey, I., Lay, P. A., and Bond, A. M. (1996) Voltammetry of plastocyanin at a graphite electrode: Effects of structure, charge, and electrolyte, *Inorg. Chem. 35*, 7156–7165.
718. Battistuzzi, G., Bellei, M., Borsari, M., Canters, G. W., de Waal, E., Jeuken, L. J., Ranieri, A., and Sola, M. (2003) Control of metalloprotein reduction potential: Compensation phenomena in the reduction thermodynamics of blue copper proteins, *Biochemistry 42*, 9214–9220.
719. Gorman, D. S., and Levine, R. P. (1966) Photosynthetic electron transport chain of *Chlamydomonas reinhardi*. Iv. Purification and properties of plastocyanin, *Plant physiology 41*, 1637–1642.
720. Yoshizaki, F., Sugimura, Y., and Shimokoriyama, M. (1981) Purification, crystallization, and properties of plastocyanin from a green alga, *Enteromorpha prolifera*, *J. Biochem. (Tokyo) 89*, 1533–1539.
721. Rooney, M. B., Honeychurch, M. J., Selvaraj, F. M., Blankenship, R. E., Bond, A. M., and Freeman, H. C. (2003) A thin-film electrochemical study of the "blue" copper proteins, auracyanin A and auracyanin B, from the photosynthetic bacterium *Chloroflexus aurantiacus*: The reduction potential as a function of pH, *J. Biol. Inorg. Chem. 8*, 306–317.
722. Chen, Z. W., Barber, M. J., McIntire, W. S., and Mathews, F. S. (1998) Crystallographic study of azurin from *Pseudomonas putida*, *Acta Crystallogr. D 54*, 253–268.
723. Baker, E. N. (1988) Structure of azurin from *Alcaligenes denitrificans* refinement at 1.8 Å resolution and comparison of the two crystallographically independent molecules, *J. Mol. Biol. 203*, 1071–1095.
724. Matsushita, K., Yamashita, T., Aoki, N., Toyama, H., and Adachi, O. (1999) Electron transfer from quinohemoprotein alcohol dehydrogenase to blue copper protein azurin in the alcohol oxidase respiratory chain of *Pseudomonas putida* HK5, *Biochemistry 38*, 6111–6118.
725. Libeu, C. A., Kukimoto, M., Nishiyama, M., Horinouchi, S., and Adman, E. T. (1997) Site-directed mutants of pseudoazurin: Explanation of increased redox potentials from X-ray structures and from calculation of redox potential differences, *Biochemistry 36*, 13160–13179.
726. Battistuzzi, G., Bellei, M., Borsari, M., Canters, G. W., de Waal, E., Jeuken, L. J. C., Rani-

eri, A., and Sola, M. (2003) Control of metalloprotein reduction potential: Compensation phenomena in the reduction thermodynamics of blue copper proteins, *Biochemistry 42*, 9214–9220.
727. Guss, J. M., Merritt, E. A., Phizackerley, R. P., and Freeman, H. C. (1996) The structure of a phytocyanin, the basic blue protein from cucumber, refined at 1.8 Å resolution, *J. Mol. Biol. 262*, 686–705.
728. Collyer, C. A., Guss, J. M., Sugimura, Y., Yoshizaki, F., and Freeman, H. C. (1990) Crystal structure of plastocyanin from a green alga, *Enteromorpha prolifera*, *J. Mol. Biol. 211*, 617–632.
729. Marshall, N. M., Garner, D. K., Wilson, T. D., Gao, Y. G., Robinson, H., Nilges, M. J., and Lu, Y. (2009) Rationally tuning the reduction potential of a single cupredoxin beyond the natural range, *Nature 462*, 113–116.
730. Prigge, S. T., Kolhekar, A. S., Eipper, B. A., Mains, R. E., and Amzel, L. M. (1997) Amidation of bioactive peptides: The structure of peptidylglycine α-hydroxylating monooxygenase, *Science 278*, 1300–1305.
731. Solomon, E. I., and Lowery, M. D. (1993) Electronic structure contributions to function in bioinorganic chemistry, *Science 259*, 1575–1581.
732. Gewirth, A. A., and Solomon, E. I. (1988) Electronic structure of plastocyanin: Excited state spectral features, *J. Am. Chem. Soc. 110*, 3811–3819.
733. Dong, S., and Spiro, T. G. (1998) Ground- and excited-state mapping of plastocyanin from resonance Raman spectra of isotope-labeled proteins, *J. Am. Chem. Soc. 120*, 10434–10440.
734. Kallio, J. P., Auer, S., Janis, J., Andberg, M., Kruus, K., Rouvinen, J., Koivula, A., and Hakulinen, N. (2009) Structure-function studies of a *Melanocarpus albomyces* laccase suggest a pathway for oxidation of phenolic compounds, *J. Mol. Biol. 392*, 895–909.
735. Paraskevopoulos, K., Sundararajan, M., Surendran, R., Hough, M. A., Eady, R. R., Hillier, I. H., and Hasnain, S. S. (2006) Active site structures and the redox properties of blue copper proteins: Atomic resolution structure of azurin II and electronic structure calculations of azurin, plastocyanin and stellacyanin, *Dalton Trans.*, 3067–3076.
736. Nar, H., Messerschmidt, A., Huber, R., van de Kamp, M., and Canters, G. W. (1991) Crystal structure analysis of oxidized *Pseudomonas aeruginosa* azurin at pH 5.5 and pH 9.0. A pH-induced conformational transition involves a peptide bond flip, *J. Mol. Biol. 221*, 765–772.
737. Dennison, C., and Harrison, M. D. (2004) The active-site structure of umecyanin, the stellacyanin from horseradish roots, *J. Am. Chem. Soc. 126*, 2481–2489.
738. Koch, M., Velarde, M., Harrison, M. D., Echt, S., Fischer, M., Messerschmidt, A., and Dennison, C. (2005) Crystal structures of oxidized and reduced stellacyanin from horseradish roots, *J. Am. Chem. Soc. 127*, 158–166.
739. Xie, Y., Inoue, T., Miyamoto, Y., Matsumura, H., Kataoka, K., Yamaguchi, K., Nojini, M., Suzuki, S., and Kai, Y. (2005) Structural reorganization of the copper binding site involving Thr15 of mavicyanin from *Cucurbita pepo medullosa* (zucchini) upon reduction, *J. Biochem. (Tokyo) 137*, 455–461.
740. Hart, P. J., Nersissian, A. M., Herrmann, R. G., Nalbandyan, R. M., Valentine, J. S., and Eisenberg, D. (1996) A missing link in cupredoxins: Crystal structure of cucumber stellacyanin at 1.6 Å resolution, *Prot. Sci. 5*, 2175–2183.
741. Nersissian, A. M., Immoos, C., Hill, M. G., Hart, P. J., Williams, G., Herrmann, R. G., and Valentine, J. S. (1998) Uclacyanins, stellacyanins, and plantacyanins are distinct subfamilies of phytocyanins: Plant-specific mononuclear blue copper proteins, *Prot. Sci. 7*, 1915–1929.
742. Lieberman, R. L., Arciero, D. M., Hooper, A. B., and Rosenzweig, A. C. (2001) Crystal structure of a novel red copper protein from *Nitrosomonas europaea*, *Biochemistry 40*, 5674–5681.
743. Arciero, D. M., Pierce, B. S., Hendrich, M. P., and Hooper, A. B. (2002) Nitrosocyanin, a red cupredoxin-like protein from *Nitrosomonas europaea*, *Biochemistry 41*, 1703–1709.
744. Inoue, T., Nishio, N., Suzuki, S., Kataoka, K., Kohzuma, T., and Kai, Y. (1999) Crystal structure determinations of oxidized and reduced pseudoazurins from *Achromobacter cycloclastes*. Concerted movement of copper site in redox forms with the rearrangement of hydrogen bond at a remote histidine, *J. Biol. Chem. 274*, 17845–17852.
745. Zhu, Z., Cunane, L. M., Chen, Z., Durley, R. C., Mathews, F. S., and Davidson, V. L. (1998)

Molecular basis for interprotein complex-dependent effects on the redox properties of amicyanin, *Biochemistry 37*, 17128–17136.
746. Williams, P. A., Blackburn, N. J., Sanders, D., Bellamy, H., Stura, E. A., Fee, J. A., and McRee, D. E. (1999) The CuA domain of *Thermus thermophilus* ba_3-type cytochrome *c* oxidase at 1.6 Å resolution, *Nature Struct. Biol. 6*, 509–516.
747. Brown, K., Tegoni, M., Prudencio, M., Pereira, A. S., Besson, S., Moura, J. J., Moura, I., and Cambillau, C. (2000) A novel type of catalytic copper cluster in nitrous oxide reductase, *Nature Struct. Biol. 7*, 191–195.
748. Farrar, J. A., Neese, F., Lappalainen, P., Kroneck, P. M. H., Saraste, M., Zumft, W. G., and Thomson, A. J. (1996) The electronic structure of CuA: A novel mixed-valence dinuclear copper electron-transfer center, *J. Am. Chem. Soc. 118*, 11501–11514.
749. Immoos, C., Hill, M. G., Sanders, D., Fee, J. A., Slutter, S. E., Richards, J. H., and Gray, H. B. (1996) Electrochemistry of the CuA domain of *Thermus thermophilus* cytochrome ba_3, *JBIC, J. Biol. Inorganic Chem. 1*, 529–531.
750. Houser, R. P., Young, V. G., Jr, and Tolman, W. B. (1996) A thiolate-bridged, fully delocalized mixed-valence dicopper^{I,II} complex that models the CuA biological electron-transfer site, *J. Am. Chem. Soc. 118*, 2101–2102.
751. Rodkey, F. L., and Ball, E. G. (1950) Oxidation–reduction potentials of the cytochrome *c* system, *J. Biol. Chem. 182*, 17–28.
752. Takano, T., and Dickerson, R. E. (1981) Conformation change of cytochrome *c*. II. Ferricytochrome c refinement at 1.8 Å and comparison with the ferrocytochrome structure, *J. Mol. Biol. 153*, 95–115.
753. Dennison, C., Lawler, A. T., and Kohzuma, T. (2002) Unusual properties of plastocyanin from the fern *Dryopteris crassirhizoma*, *Biochemistry 41*, 552–560.
754. McDevitt, C. A., Hanson, G. R., Noble, C. J., Cheesman, M. R., and McEwan, A. G. (2002) Characterization of the redox centers in dimethyl sulfide dehydrogenase from *Rhodovulum sulfidophilum*, *Biochemistry 41*, 15234–15244.
755. Myer, Y. P., Saturno, A. F., Verma, B. C., and Pande, A. (1979) Horse heart cytochrome c. The oxidation–reduction potential and protein structures, *J. Biol. Chem. 254*, 11202–11207.
756. Berry, E. A., Huang, L. S., and DeRose, V. J. (1991) Ubiquinol-cytochrome *c* oxidoreductase of higher plants. Isolation and characterization of the bc_1 complex from potato tutuber mitochondria, *J. Biol. Chem. 266*, 9064–9077.
757. Takagi, K., Torimura, M., Kawaguchi, K., Kano, K., and Ikeda, T. (1999) Biochemical and electrochemical characterization of quinohemoprotein amine dehydrogenase from *Paracoccus denitrificans*, *Biochemistry 38*, 6935–6942.
758. Fujieda, N., Mori, M., Kano, K., and Ikeda, T. (2002) Spectroelectrochemical evaluation of redox potentials of cysteine tryptophylquinone and two hemes *c* in quinohemoprotein amine dehydrogenase from *Paracoccus denitrificans*, *Biochemistry 41*, 13736–13743.
759. Morais, J., Palma, P. N., Frazao, C., Caldeira, J., LeGall, J., Moura, I., Moura, J. J., and Carrondo, M. A. (1995) Structure of the tetraheme cytochrome from *Desulfovibrio desulfuricans* ATCC 27774: X-ray diffraction and electron paramagnetic resonance studies, *Biochemistry 34*, 12830–12841.
760. Fraser, D. M., and Lindahl, P. A. (1999) Stoichiometric CO reductive titrations of acetyl-CoA synthase (carbon monoxide dehydrogenase) from *Clostridium thermoaceticum*, *Biochemistry 38*, 15697–15705.
761. Artz, J. H., Mulder, D. W., Ratzloff, M. W., Lubner, C. E., Zadvornyy, O. A., LeVan, A. X., Williams, S. G., Adams, M. W. W., Jones, A. K., King, P. W., and Peters, J. W. (2017) Reduction potentials of [FeFe]-hydrogenase accessory iron–sulfur clusters provide insights into the energetics of proton reduction catalysis, *J. Am. Chem. Soc. 139*, 9544–9550.
762. Suzuki, S., Nakamura, N., Yamaguchi, K., Kataoka, K., Inoue, T., Nishio, N., Kai, Y., and Tobari, J. (1999) Spectroscopic and electrochemical properties of two azurins (az-iso1 and az-iso2) from the obligate methylotroph *Methylomonas* sp. Strain J and the structure of novel az-iso2, *J. Biol. Inorg. Chem. 4*, 749–758.
763. Randles, J. E. B. (1948) Cathode-ray polarograph. II. Current-voltage curves, *Trans. Faraday Soc. 44*, 327–338.
764. Sevcik, A. (1948) Oscillographic polarography with periodical triangular voltage, *Collection of Czechoslovak Chemical Communications 13*, 349–377.

765. Nicholson, R. S., and Shain, I. (1964) Theory of stationary electrode polarography. Single scan and cyclic methods applied to reversible, irreversible, and kinetic systems, *Anal. Chem. 36*, 706–723.
766. Ikeda, O., and Sakurai, T. (1994) Electron transfer reaction of stellacyanin at a bare glassy carbon electrode, *Eur. J. Biochem. 219*, 813–819.
767. Fox, S., Wang, Y., Silver, A., and Millar, M. (1990) Viability of the $[Ni^{III}(SR)_4]^-$ unit in classical coordination compounds and in the nickel-sulfur center of hydrogenases, *J. Am. Chem. Soc. 112*, 3218–3220.
768. Santucci, R., Faraoni, A., Campanella, L., Tranchida, G., and Brunori, M. (1991) Use of 'solid-state' promoters in the electrochemistry of cytochrome *c* at a gold electrode, *Biochem. J. 273 (Pt 3)*, 783–786.
769. Link, T. A., Hatzfeld, O. M., Unalkat, P., Shergill, J. K., Cammack, R., and Mason, J. R. (1996) Comparison of the "Rieske" [2Fe–2S] center in the bc_1 complex and in bacterial dioxygenases by circular dichroism spectroscopy and cyclic voltammetry, *Biochemistry 35*, 7546–7552.
770. Arciero, D. M., Collins, M. J., Haladjian, J., Bianco, P., and Hooper, A. B. (1991) Resolution of the four hemes of cytochrome c_{554} from *Nitrosomonas europaea* by redox potentiometry and optical spectroscopy, *Biochemistry 30*, 11459–11465.
771. Walker, L. M., Kincannon, W. M., Bandarian, V., and Elliott, S. J. (2018) Deconvoluting the reduction potentials for the three [4Fe–4S] clusters in an AdoMet radical SCIFF maturase, *Biochemistry 57*, 6050–6053.
772. Armstrong, F. A., Butt, J. N., and Sucheta, A. (1993) Voltammetric studies of redox-active centers in metalloproteins adsorbed on electrodes, *Methods Enzymol. 227*, 479–500.
773. Leger, C., and Bertrand, P. (2008) Direct electrochemistry of redox enzymes as a tool for mechanistic studies, *Chem. Rev. 108*, 2379–2438.
774. Fourmond, V., and Leger, C. (2016) Protein electrochemistry: Questions and answers, *Adv. Biochem. Eng. Biotechnol. 158*, 1–41.
775. Johnson, D. L., Maxwell, C. J., Losic, D., Shapter, J. G., and Martin, L. L. (2002) The influence of promoter and of electrode material on the cyclic voltammetry of *Pisum sativum* plastocyanin, *Bioelectrochemistry 58*, 137–147.
776. Hirst, J., Duff, J. L. C., Jameson, G. N. L., Kemper, M. A., Burgess, B. K., and Armstrong, F. A. (1998) Kinetics and mechanism of redox-coupled, long-range proton transfer in an iron–sulfur protein. Investigation by fast-scan protein-film voltammetry, *J. Am. Chem. Soc. 120*, 7085–7094.
777. Hirst, J., and Armstrong, F. A. (1998) Fast-scan cyclic voltammetry of protein films on pyrolytic graphite edge electrodes: Characteristics of electron exchange, *Anal. Chem. 70*, 5062–5071.
778. Elliott, S. J., McElhaney, A. E., Feng, C., Enemark, J. H., and Armstrong, F. A. (2002) A voltammetric study of interdomain electron transfer within sulfite oxidase, *J. Am. Chem. Soc. 124*, 11612–11613.
779. Leger, C., Heffron, K., Pershad, H. R., Maklashina, E., Luna-Chavez, C., Cecchini, G., Ackrell, B. A., and Armstrong, F. A. (2001) Enzyme electrokinetics: Energetics of succinate oxidation by fumarate reductase and succinate dehydrogenase, *Biochemistry 40*, 11234–11245.
780. Hoke, K. R., Cobb, N., Armstrong, F. A., and Hille, R. (2004) Electrochemical studies of arsenite oxidase: An unusual example of a highly cooperative two-electron molybdenum center, *Biochemistry 43*, 1667–1674.
781. Pulcu, G. S., Elmore, B. L., Arciero, D. M., Hooper, A. B., and Elliott, S. J. (2007) Direct electrochemistry of tetraheme cytochrome c_{554} from *Nitrosomonas europaea*: Redox cooperativity and gating, *J. Am. Chem. Soc. 129*, 1838–1839.
782. Kumar, S., and Bandyopadhyay, U. (2005) Free heme toxicity and its detoxification systems in human, *Toxicol Lett 157*, 175–188.
783. Allen, J. P., Feher, G., Yeates, T. O., Rees, D. C., Deisenhofer, J., Michel, H., and Huber, R. (1986) Structural homology of reaction centers from *Rhodopseudomonas sphaeroides* and *Rhodopseudomonas viridis* as determined by X-ray diffraction, *Proc. Natl. Acad. Sci. U. S. A. 83*, 8589–8593.
784. Walker, J. E., Arizmendi, J. M., Dupuis, A., Fearnley, I. M., Finel, M., Medd, S. M., Pilkington, S. J., Runswick, M. J., and Skehel, J. M. (1992) Sequences of 20 subunits of NADH:ubiquinone oxidoreductase from bovine heart mitochondria. Application of a novel strategy for sequencing proteins using

the polymerase chain reaction, *J. Mol. Biol. 226*, 1051–1072.
785. Roberts, D. L., Frerman, F. E., and Kim, J. J. (1996) Three-dimensional structure of human electron transfer flavoprotein to 2.1-Å resolution, *Proc. Natl. Acad. Sci. U. S. A. 93*, 14355–14360.
786. Watenpaugh, K. D., Sieker, L. C., and Jensen, L. H. (1973) The binding of riboflavin-5′-phosphate in a flavoprotein: Flavodoxin at 2.0 angstrom resolution, *Proc. Natl. Acad. Sci. U. S. A. 70*, 3857–3860.
787. Wakabayashi, S., Kimura, T., Fukuyama, K., Matsubara, H., and Rogers, L. J. (1989) The amino acid sequence of a flavodoxin from the eukaryotic red alga *Chondrus crispus*, *Biochem. J. 263*, 981–984.
788. Chen, D., and Swenson, R. P. (1994) Cloning, sequence analysis, and expression of the genes encoding the two subunits of the methylotrophic bacterium W3A1 electron transfer flavoprotein, *J. Biol. Chem. 269*, 32120–32130.
789. Meimberg, K., Lagoutte, B., Bottin, H., and Muhlenhoff, U. (1998) The PsaE subunit is required for complex formation between photosystem I and flavodoxin from the *Cyanobacterium synechocystis* sp. Pcc 6803, *Biochemistry 37*, 9759–9767.
790. Talfournier, F., Munro, A. W., Basran, J., Sutcliffe, M. J., Daff, S., Chapman, S. K., and Scrutton, N. S. (2001) α Arg-237 in *Methylophilus methylotrophus* (sp. W3a1) electron-transferring flavoprotein affords approximately 200 millivolt stabilization of the FAD anionic semiquinone and a kinetic block on full reduction to the dihydroquinone, *J. Biol. Chem. 276*, 20190–20196.
791. De Francesco, R., Edmondson, D. E., Moura, I., Moura, J. J., and LeGall, J. (1994) Kinetic studies on the electron-transfer reaction between cytochrome c_3 and flavodoxin from *Desulfovibrio vulgaris* strain Hildenborough, *Biochemistry 33*, 10386–10392.
792. Watenpaugh, K. D., Sieker, L. C., and Jensen, L. H. (1979) The structure of rubredoxin at 1.2 Å resolution, *J. Mol. Biol. 131*, 509–522.
793. Steigerwald, V. J., Pihl, T. D., and Reeve, J. N. (1992) Identification and isolation of the polyferredoxin from *Methanobacterium thermoautotrophicum* strain δH, *Proc. Natl. Acad. Sci. U. S. A. 89*, 6929–6933.
794. Hedderich, R., Albracht, S. P., Linder, D., Koch, J., and Thauer, R. K. (1992) Isolation and characterization of polyferredoxin from *Methanobacterium thermoautotrophicum*. The MvhB gene product of the methylviologen-reducing hydrogenase operon, *FEBS Lett. 298*, 65–68.
795. Fukuyama, K., Hase, T., Matsumoto, S., Tsukihara, T., Katsube, Y., Tanaka, N., Kakudo, M., Wada, K., and Matsubara, H. (1980) Structure of *S. platensis* [2Fe–2S] ferredoxin and evolution of chloroplast-type ferredoxins, *Nature 286*, 522–524.
796. Sieker, L. C., Adman, E., and Jensen, L. H. (1972) Structure of the Fe–S complex in a bacterial ferredoxin, *Nature 235*, 40–42.
797. Duee, E. D., Fanchon, E., Vicat, J., Sieker, L. C., Meyer, J., and Moulis, J. M. (1994) Refined crystal structure of the 2[4Fe–4S] ferredoxin from *Clostridium acidurici* at 1.84 Å resolution, *J. Mol. Biol. 243*, 683–695.
798. Sweeney, W. V., and McIntosh, B. A. (1979) Determination of cooperative interaction between clusters in *Clostridium pasteurianum* 2 [4Fe–4S] ferredoxin, *J. Biol. Chem. 254*, 4499–4501.
799. Lederer, F., Glatigny, A., Bethge, P. H., Bellamy, H. D., and Matthew, F. S. (1981) Improvement of the 2.5 Å resolution model of cytochrome b_{562} by redetermining the primary structure and using molecular graphics, *J. Mol. Biol. 148*, 427–448.
800. Weber, P. C., Bartsch, R. G., Cusanovich, M. A., Hamlin, R. C., Howard, A., Jordan, S. R., Kamen, M. D., Meyer, T. E., Weatherford, D. W., Nguyen huu, X., and Salemme, F. R. (1980) Structure of cytochrome *c′*: A dimeric, high-spin haem protein, *Nature 286*, 302–304.
801. Takano, T., Kallai, O. B., Swanson, R., and Dickerson, R. E. (1973) The structure of ferrocytochrome *c* at 2.45 Å resolution, *J. Biol. Chem. 248*, 5234–5255.
802. Bewley, K. D., Ellis, K. E., Firer-Sherwood, M. A., and Elliott, S. J. (2013) Multi-heme proteins: Nature's electronic multi-purpose tool, *Biochim. Biophys. Acta 1827*, 938–948.
803. Kadziola, A., and Larsen, S. (1997) Crystal structure of the dihaem cytochrome c_4 from *Pseudomonas stutzeri* determined at 2.2Å resolution, *Structure 5*, 203–216.
804. Assfalg, M., Bertini, I., Turano, P., Bruschi, M., Durand, M. C., Giudici-Orticoni, M. T.,

and Dolla, A. (2002) A quick solution structure determination of the fully oxidized double mutant K9-10A cytochrome c_7 from *Desulfuromonas acetoxidans* and mechanistic implications, *J. Biomol. NMR 22*, 107–122.
805. Pokkuluri, P. R., Londer, Y. Y., Duke, N. E., Long, W. C., and Schiffer, M. (2004) Family of cytochrome c_7-type proteins from *Geobacter sulfurreducens*: Structure of one cytochrome c_7 at 1.45 Å resolution, *Biochemistry 43*, 849–859.
806. Haser, R., Pierrot, M., Frey, M., Payan, F., Astier, J. P., Bruschi, M., and Le Gall, J. (1979) Structure and sequence of the multihaem cytochrome c_3, *Nature 282*, 806–810.
807. Czjzek, M., Payan, F., Guerlesquin, F., Bruschi, M., and Haser, R. (1994) Crystal structure of cytochrome c_3 from *Desulfovibrio desulfuricans* Norway at 1.7 Å resolution, *J. Mol. Biol. 243*, 653–667.
808. Deisenhofer, J., Epp, O., Miki, K., Huber, R., and Michel, H. (1985) Structure of the protein subunits in the photosynthetic reaction centre of *Rhodopseudomonas viridis* at 3Å resolution, *Nature 318*, 618–624.
809. Santos, H., Moura, J. J. G., Moura, I., LeGall, J., and Xavier, A. V. (1984) NMR studies of electron transfer mechanisms in a protein with interacting redox centers: *Desulfovibrio gigas* cytochrome c_3, *Eur. J. Biochem. 141*, 283–296.
810. Arciero David, M., Pierce Brad, S., Michael, H., and Hooper Alan, B. (2002) Nitrosocyanin, a red cupredoxin-like protein from *Nitrosomonas europaea*, *Biochemistry 41*, 1703–1709.
811. Borner, G. H., Lilley, K. S., Stevens, T. J., and Dupree, P. (2003) Identification of glycosylphosphatidylinositol-anchored proteins in *Arabidopsis*. A proteomic and genomic analysis, *Plant Physiol 132*, 568–577.
812. Chen, L., Durley, R. C., Mathews, F. S., and Davidson, V. L. (1994) Structure of an electron transfer complex: Methylamine dehydrogenase, amicyanin, and cytochrome c_{551i}, *Science 264*, 86–90.
813. Sato, K., and Dennison, C. (2002) Effect of histidine 6 protonation on the active site structure and electron-transfer capabilities of pseudoazurin from *Achromobacter cycloclastes*, *Biochemistry 41*, 120–130.
814. van de Kamp, M., Silvestrini, M. C., Brunori, M., Van Beeumen, J., Hali, F. C., and Canters, G. W. (1990) Involvement of the hydrophobic patch of azurin in the electron-transfer reactions with cytochrome c_{551} and nitrite reductase, *Eur. J. Biochem. 194*, 109–118.
815. Santabarbara, S., Heathcote, P., and Evans, M. C. (2005) Modelling of the electron transfer reactions in photosystem I by electron tunnelling theory: The phylloquinones bound to the PsaA and the PsaB reaction centre subunits of PS I are almost isoenergetic to the iron–sulfur cluster F(X), *Biochim. Biophys. Acta 1708*, 283–310.
816. Warren, P. V., Smart, L. B., McIntosh, L., and Golbeck, J. H. (1993) Site-directed conversion of Cysteine-565 to serine in PsaB of photosystem I results in the assembly of [3Fe–4S] and [4Fe–4S] clusters in F_X. A mixed-ligand [4Fe–4S] cluster is capable of electron transfer to F_A and F_B, *Biochemistry 32*, 4411–4419.
817. Xia, Z. X., and Mathews, F. S. (1990) Molecular structure of flavocytochrome b_2 at 2.4 Å resolution, *J. Mol. Biol. 212*, 837–863.
818. Daff, S., Ingledew, W. J., Reid, G. A., and Chapman, S. K. (1996) New insights into the catalytic cycle of flavocytochrome b_2, *Biochemistry 35*, 6345–6350.
819. Capeillere-Blandin, C. (1982) Transient kinetics of the one-electron transfer reaction between reduced flavocytochrome b_2 and oxidized cytochrome *c*. Evidence for the existence of a protein complex in the reaction, *Eur. J. Biochem. 128*, 533–542.
820. Schwalb, C., Chapman, S. K., and Reid, G. A. (2003) The tetraheme cytochrome CymA is required for anaerobic respiration with dimethyl sulfoxide and nitrite in *Shewanella oneidensis*, *Biochemistry 42*, 9491–9497.
821. Turner, K. L., Doherty, M. K., Heering, H. A., Armstrong, F. A., Reid, G. A., and Chapman, S. K. (1999) Redox properties of flavocytochrome c_3 from *Shewanella frigidimarina* NCIMB400, *Biochemistry 38*, 3302–3309.
822. Jones, A. K., Camba, R., Reid, G. A., Chapman, S. K., and Armstrong, F. A. (2000) Interruption and time-resolution of catalysis by a flavoenzyme using fast scan protein film voltammetry, *J. Am. Chem. Soc. 122*, 6494–6495.
823. Cameron, M. D., and Aust, S. D. (2000) Kinetics and reactivity of the flavin and heme cofactors of cellobiose dehydrogenase from *Phanerochaete chrysosporium*, *Biochemistry 39*, 13595–13601.

824. Kracher, D., Scheiblbrandner, S., Felice, A. K., Breslmayr, E., Preims, M., Ludwicka, K., Haltrich, D., Eijsink, V. G., and Ludwig, R. (2016) Extracellular electron transfer systems fuel cellulose oxidative degradation, *Science 352*, 1098–1101.
825. Phillips, C. M., Beeson, W. T., Cate, J. H., and Marletta, M. A. (2011) Cellobiose dehydrogenase and a copper-dependent polysaccharide monooxygenase potentiate cellulose degradation by *Neurospora crassa*, *Am. Chem. Soc. Chem. Biol 6*, 1399–1406.
826. Laurent, C., Breslmayr, E., Tunega, D., Ludwig, R., and Oostenbrink, C. (2019) Interaction between cellobiose dehydrogenase and lytic polysaccharide monooxygenase, *Biochemistry 58*, 1226–1235.
827. Keller, K. L., Rapp-Giles, B. J., Semkiw, E. S., Porat, I., Brown, S. D., and Wall, J. D. (2014) New model for electron flow for sulfate reduction in *Desulfovibrio alaskensis* g20, *Appl. Environ. Microbiol. 80*, 855–868.
828. Creevey, N. L., McEwan, A. G., Hanson, G. R., and Bernhardt, P. V. (2008) Thermodynamic characterization of the redox centers within dimethylsulfide dehydrogenase, *Biochemistry 47*, 3770–3776.
829. Mohsen, A. W., Rigby, S. E., Jensen, K. F., Munro, A. W., and Scrutton, N. S. (2004) Thermodynamic basis of electron transfer in dihydroorotate dehydrogenase B from *Lactococcus lactis*: Analysis by potentiometry, EPR spectroscopy, and ENDOR spectroscopy, *Biochemistry 43*, 6498–6510.
830. Rowland, P., Norager, S., Jensen, K. F., and Larsen, S. (2000) Structure of dihydroorotate dehydrogenase B: Electron transfer between two flavin groups bridged by an iron-sulphur cluster, *Structure 8*, 1227–1238.
831. Schnackerz, K. D., Dobritzsch, D., Lindqvist, Y., and Cook, P. F. (2004) Dihydropyrimidine dehydrogenase: A flavoprotein with four iron–sulfur clusters, *Biochim. Biophys. Acta 1701*, 61–74.
832. Huang, L., Rohlfs, R. J., and Hille, R. (1995) The reaction of trimethylamine dehydrogenase with electron transferring flavoprotein, *J. Biol. Chem. 270*, 23958–23965.
833. Astashkin, A. V., Seravalli, J., Mansoorabadi, S. O., Reed, G. H., and Ragsdale, S. W. (2006) Pulsed electron paramagnetic resonance experiments identify the paramagnetic intermediates in the pyruvate ferredoxin oxidoreductase catalytic cycle, *J. Am. Chem. Soc. 128*, 3888–3889.
834. Sanderson, D. G., Anderson, L. B., and Gross, E. L. (1986) Determination of the redox potential and diffusion coefficient of the protein plastocyanin using optically transparent filar electrodes, *Biochim. Biophys. Acta 852*, 269–278.
835. Taylor, M. K., Stevenson, D. E., Berlouis, L. E., Kennedy, A. R., and Reglinski, J. (2006) Modelling the impact of geometric parameters on the redox potential of blue copper proteins, *J Inorg Biochem 100*, 250–259.
836. Hatefi, Y., Haavik, A. G., and Griffiths, D. E. (1962) Studies on the electron transfer system. Xli. Reduced coenzyme Q (QH2)-cytochrome *c* reductase, *J. Biol. Chem. 237*, 1681–1685.
837. Rieske, J. S., Zaugg, W. S., and Hansen, R. E. (1964) Studies on the electron transfer system. LIX. Distribution of iron and of the component giving an electron paramagnetic resonance signal at g = 1.90 in subfractions of complex 3, *J. Biol. Chem. 239*, 3023–3030.
838. Hurt, E., and Hauska, G. (1981) A cytochrome f/b_6 complex of five polypeptides with plastoquinol-plastocyanin-oxidoreductase activity from spinach chloroplasts, *Eur. J. Biochem. 117*, 591–595.
839. Zhu, J., Vinothkumar, K. R., and Hirst, J. (2016) Structure of mammalian respiratory complex I, *Nature 536*, 354–358.
840. Fiedorczuk, K., Letts, J. A., Degliesposti, G., Kaszuba, K., Skehel, M., and Sazanov, L. A. (2016) Atomic structure of the entire mammalian mitochondrial complex I, *Nature 538*, 406–410.
841. Kampjut, D., and Sazanov, L. A. (2020) The coupling mechanism of mammalian respiratory complex I, *Science 370*, eabc4209.
842. Gonzalez-Halphen, D., Lindorfer, M. A., and Capaldi, R. A. (1988) Subunit arrangement in beef heart complex III, *Biochemistry 27*, 7021–7031.
843. Iwata, S., Lee, J. W., Okada, K., Lee, J. K., Iwata, M., Rasmussen, B., Link, T. A., Ramaswamy, S., and Jap, B. K. (1998) Complete structure of the 11-subunit bovine mitochondrial cytochrome bc_1 complex, *Science 281*, 64–71.
844. Kurisu, G., Zhang, H., Smith, J. L., and Cramer, W. A. (2003) Structure of the cytochrome b_6f complex of oxygenic photosyn-

thesis: Tuning the cavity, *Science 302*, 1009–1014.
845. Malone, L. A., Qian, P., Mayneord, G. E., Hitchcock, A., Farmer, D. A., Thompson, R. F., Swainsbury, D. J. K., Ranson, N. A., Hunter, C. N., and Johnson, M. P. (2019) Cryo-EM structure of the spinach cytochrome b_6 *f* complex at 3.6 Å resolution, *Nature 575*, 535–539.
846. Yun, C. H., Beci, R., Crofts, A. R., Kaplan, S., and Gennis, R. B. (1990) Cloning and DNA sequencing of the *fbc* operon encoding the cytochrome bc_1 complex from *Rhodobacter sphaeroides*. Characterization of *fbc* deletion mutants and complementation by a site-specific mutational variant, *Eur. J. Biochem. 194*, 399–411.
847. Rieske, J. S. (1976) Composition, structure, and function of complex III of the respiratory chain, *Biochim. Biophys. Acta 456*, 195–247.
848. Erecinska, M., Wilson, D. F., and Miyata, Y. (1976) Mitochondrial cytochrome *b*-*c* complex: Its oxidation–reduction components and their stoichiometry, *Arch. Biochem. Biophys. 177*, 133–143.
849. Gray, J. C. (1978) Purification and properties of monomeric cytochrome *f* from charlock, *Sinapis arvensis* L, *Eur. J. Biochem. 82*, 133–141.
850. Kim, C. H., and King, T. E. (1987) Preparation and properties of cardiac cytochrome c_1, *Biochemistry 26*, 1955–1961.
851. Li, Y., Leonard, K., and Weiss, H. (1981) Membrane-bound and water-soluble cytochrome c_1 from *Neurospora* mitochondria, *Eur. J. Biochem. 116*, 199–205.
852. Trumpower, B. L., and Edwards, C. A. (1979) Purification of a reconstitutively active iron–sulfur protein (oxidation factor) from succinate. Cytochrome *c* reductase complex of bovine heart mitochondria, *J. Biol. Chem. 254*, 8697–8706.
853. Weiss, H. (1976) Subunit composition and biogenesis of mitochondrial cytochrome *b*, *Biochim. Biophys. Acta 456*, 291–313.
854. T'Sai A, L., and Palmer, G. (1982) Purification and characterization of highly purified cytochrome *b* from complex III of baker's yeast, *Biochim. Biophys. Acta 681*, 484–495.
855. Karlsson, B., Hovmoller, S., Weiss, H., and Leonard, K. (1983) Structural studies of cytochrome reductase. Subunit topography determined by electron microscopy of membrane crystals of a subcomplex, *J. Mol. Biol. 165*, 287–302.
856. Yu, L., Yu, C., and King, T. E. (1977) Subunit structure of the reconstitutively active cytochrome *b*-c_1 complex. Determination of amino acids and molar distribution of subunit fractions from gel electrophoresis, *Biochim. Biophys. Acta 495*, 232–247.
857. Cramer, W. A., and Zhang, H. (2006) Consequences of the structure of the cytochrome b_6f complex for its charge transfer pathways, *Biochim. Biophys. Acta 1757*, 339–345.
858. Stroebel, D., Choquet, Y., Popot, J. L., and Picot, D. (2003) An atypical haem in the cytochrome b_6f complex, *Nature 426*, 413–418.
859. Mitchell, O. R. (1976) Effect of spatial frequency on the visibility of unstructured patterns, *J. Opt. Soc. Am. 66*, 327–332.
860. Crofts, A. R., and Meinhardt, S. W. (1982) A Q-cycle mechanism for the cyclic electron-transfer chain of *Rhodopseudomonas sphaeroides*, *Biochem. Soc. Trans. 10*, 201–203.
861. Huang, L. S., Cobessi, D., Tung, E. Y., and Berry, E. A. (2005) Binding of the respiratory chain inhibitor antimycin to the mitochondrial bc_1 complex: A new crystal structure reveals an altered intramolecular hydrogen-bonding pattern, *J. Mol. Biol. 351*, 573–597.
862. Kim, H., Xia, D., Yu, C. A., Xia, J. Z., Kachurin, A. M., Zhang, L., Yu, L., and Deisenhofer, J. (1998) Inhibitor binding changes domain mobility in the iron–sulfur protein of the mitochondrial bc_1 complex from bovine heart, *Proc. Natl. Acad. Sci. U. S. A. 95*, 8026–8033.
863. Crofts, A. R., Barquera, B., Gennis, R. B., Kuras, R., Guergova-Kuras, M., and Berry, E. A. (1999) Mechanism of ubiquinol oxidation by the bc_1 complex: Different domains of the quinol binding pocket and their role in the mechanism and binding of inhibitors, *Biochemistry 38*, 15807–15826.
864. Zhu, J., Egawa, T., Yeh, S. R., Yu, L., and Yu, C. A. (2007) Simultaneous reduction of iron–sulfur protein and cytochrome b_l during ubiquinol oxidation in cytochrome bc_1 complex, *Proc. Natl. Acad. Sci. U. S. A. 104*, 4864–4869.
865. Cape, J. L., Bowman, M. K., and Kramer, D. M. (2007) A semiquinone intermediate generated at the Q(o) site of the cytochrome bc_1, complex: Importance for the Q-cycle and superoxide production, *Proc. Natl. Acad. Sci. U.S.A. 104*, 7887–7892.

866. Zhang, Z., Huang, L., Shulmeister, V. M., Chi, Y. I., Kim, K. K., Hung, L. W., Crofts, A. R., Berry, E. A., and Kim, S. H. (1998) Electron transfer by domain movement in cytochrome bc_1, *Nature 392*, 677–684.
867. Brugna, M., Rodgers, S., Schricker, A., Montoya, G., Kazmeier, M., Nitschke, W., and Sinning, I. (2000) A spectroscopic method for observing the domain movement of the Rieske iron–sulfur protein, *Proc. Natl. Acad. Sci. U. S. A. 97*, 2069–2074.
868. Darrouzet, E., Valkova-Valchanova, M., Moser, C. C., Dutton, P. L., and Daldal, F. (2000) Uncovering the [2Fe2S] domain movement in cytochrome bc_1 and its implications for energy conversion, *Proc. Natl. Acad. Sci. U.S.A. 97*, 4567–4572.
869. Crofts, A. R., Hong, S., Zhang, Z., and Berry, E. A. (1999) Physicochemical aspects of the movement of the Rieske iron sulfur protein during quinol oxidation by the bc_1 complex from mitochondria and photosynthetic bacteria, *Biochemistry 38*, 15827–15839.
870. Esser, L., Gong, X., Yang, S., Yu, L., Yu, C. A., and Xia, D. (2006) Surface-modulated motion switch: Capture and release of iron–sulfur protein in the cytochrome bc_1 complex, *Proc. Natl. Acad. Sci. U. S. A. 103*, 13045–13050.
871. Snyder, C. H., Merbitz-Zahradnik, T., Link, T. A., and Trumpower, B. L. (1999) Role of the Rieske iron–sulfur protein midpoint potential in the protonmotive Q-cycle mechanism of the cytochrome bc_1 complex, *J. Bioenerg. Biomembr. 31*, 235–242.
872. Ding, H., Robertson, D. E., Daldal, F., and Dutton, P. L. (1992) Cytochrome bc_1 complex [2Fe–2S]cluster and its interaction with ubiquinone and ubihydroquinone at the Q_o site: A double-occupancy Q_o site model, *Biochemistry 31*, 3144–3158.
873. Baymann, F., Giusti, F., Picot, D., and Nitschke, W. (2007) The c_i/b_h moiety in the b_6f complex studied by EPR: A pair of strongly interacting hemes, *Proc. Natl. Acad. Sci. U.S.A. 104*, 519–524.
874. Yamashita, E., Zhang, H., and Cramer, W. A. (2007) Structure of the cytochrome b_6f complex: Quinone analogue inhibitors as ligands of heme c_n, *J. Mol. Biol. 370*, 39–52.
875. Hacker, B., Barquera, B., Crofts, A. R., and Gennis, R. B. (1993) Characterization of mutations in the cytochrome *b* subunit of the bc_1 complex of *Rhodobacter sphaeroides* that affect the quinone reductase site (Q_c), *Biochemistry 32*, 4403–4410.
876. Ohnishi, T., and Trumpower, B. L. (1980) Differential-effects of antimycin on ubisemiquinone bound in different environments in isolated succinate cytochrome-c reductase complex, *J. Biol. Chem. 255*, 3278–3284.
877. Devries, S., Berden, J. A., and Slater, E. C. (1980) Properties of a semi-quinone anion located in the Q_{h2}-cytochrome-*c* oxidoreductase segment of the mitochondrial respiratory-chain, *FEBS Lett. 122*, 143–148.
878. Covian, R., Zwicker, K., Rotsaert, F. A., and Trumpower, B. L. (2007) Asymmetric and redox-specific binding of quinone and quinol at center n of the dimeric yeast cytochrome bc_1 complex: Consequences for semiquinone stabilization, *J. Biol. Chem. 282*, 24198–24208.
879. Swierczek, M., Cieluch, E., Sarewicz, M., Borek, A., Moser, C. C., Dutton, P. L., and Osyczka, A. (2010) An electronic bus bar lies in the core of cytochrome bc_1, *Science 329*, 451–454.
880. Yang, X. H., and Trumpower, B. L. (1988) Protonmotive Q cycle pathway of electron transfer and energy transduction in the three-subunit ubiquinol-cytochrome *c* oxidoreductase complex of *Paracoccus denitrificans*, *J. Biol. Chem. 263*, 11962–11970.
881. Engel, W. D., Schagger, H., and von Jagow, G. (1980) Ubiquinol-cytochrome *c* reductase (EC 1.10.2.2). Isolation in Triton X-100 by hydroxyapatite and gel chromatography. Structural and functional properties, *Biochim. Biophys. Acta 592*, 211–222.
882. Rich, P. R., and Bendall, D. S. (1980) The redox potentials of the *b*-type cytochromes of higher plant chloroplasts, *Biochim. Biophys. Acta 591*, 153–161.
883. Bertero, M. G., Rothery, R. A., Palak, M., Hou, C., Lim, D., Blasco, F., Weiner, J. H., and Strynadka, N. C. (2003) Insights into the respiratory electron transfer pathway from the structure of nitrate reductase A, *Nature Struct. Biol. 10*, 681–687.
884. Ziegler, D. M., and Doeg, K. A. (1962) The electron transport system. XLIII. The isolation of a succinic-coenzyme Q reductase from beef heart mitochondria, *Arch. Biochem. Biophys. 97*, 41–50.

885. Baginsky, M. L., and Hatefi, Y. (1969) Reconstitution of succinate-coenzyme Q reductase (complex II) and succinate oxidase activities by a highly purified, reactivated succinate dehydrogenase, *J. Biol. Chem. 244*, 5313–5319.
886. Davis, K. A., and Hatefi, Y. (1971) Succinate dehydrogenase. I. Purification, molecular properties, and substructure, *Biochemistry 10*, 2509–2516.
887. Ohnishi, T., and Salerno, J. C. (1976) Thermodynamic and EPR characteristics of two ferredoxin-type iron–sulfur centers in the succinate-ubiquinone reductase segment of the respiratory chain, *J. Biol. Chem. 251*, 2094–2104.
888. Ohnishi, T., Lim, J., Winter, D. B., and King, T. E. (1976) Thermodynamic and EPR characteristics of a HiPIP-type iron–sulfur center in the succinate dehydrogenase of the respiratory chain, *J. Biol. Chem. 251*, 2105–2109.
889. Johnson, M. K., Morningstar, J. E., Bennett, D. E., Ackrell, B. A., and Kearney, E. B. (1985) Magnetic circular dichroism studies of succinate dehydrogenase. Evidence for [2Fe–2S], [3Fe–xS], and [4Fe–4S] centers in reconstitutively active enzyme, *J. Biol. Chem. 260*, 7368–7378.
890. Tran, Q. M., Rothery, R. A., Maklashina, E., Cecchini, G., and Weiner, J. H. (2007) *Escherichia coli* succinate dehydrogenase variant lacking the heme *b*, *Proc. Natl. Acad. Sci. U.S.A. 104*, 18007–18012.
891. Anderson, R. F., Shinde, S. S., Hille, R., Rothery, R. A., Weiner, J. H., Rajagukguk, S., Maldashina, E., and Cecchini, G. (2014) Electron-transfer pathways in the heme and quinone-binding domain of complex II (succinate dehydrogenase), *Biochemistry 53*, 1637–1646.
892. Lanciano, P., Magalon, A., Bertrand, P., Guigliarelli, B., and Grimaldi, S. (2007) High-stability semiquinone intermediate in nitrate reductase a (NarGHI) from *Escherichia coli* is located in a quinol oxidation site close to heme *bd*, *Biochemistry 46*, 5323–5329.
893. Jones, T. A., Zou, J. Y., Cowan, S. W., and Kjeldgaard, M. (1991) Improved methods for building protein models in electron density maps and the location of errors in these models, *Acta Crystallogr. A 47 (Pt 2)*, 110–119.
894. Iverson, T. M., Luna-Chavez, C., Cecchini, G., and Rees, D. C. (1999) Structure of the *Escherichia coli* fumarate reductase respiratory complex, *Science 284*, 1961–1966.
895. Iverson, T. M., Luna-Chavez, C., Croal, L. R., Cecchini, G., and Rees, D. C. (2002) Crystallographic studies of the *Escherichia coli* quinol-fumarate reductase with inhibitors bound to the quinol-binding site, *J. Biol. Chem. 277*, 16124–16130.
896. Madej, M. G., Nasiri, H. R., Hilgendorff, N. S., Schwalbe, H., and Lancaster, C. R. (2006) Evidence for transmembrane proton transfer in a dihaem-containing membrane protein complex, *EMBO J. 25*, 4963–4970.
897. Biel, S., Simon, J., Gross, R., Ruiz, T., Ruitenberg, M., and Kroger, A. (2002) Reconstitution of coupled fumarate respiration in liposomes by incorporating the electron transport enzymes isolated from *Wolinella succinogenes*, *Eur. J. Biochem. 269*, 1974–1983.
898. Haas, A. H., Sauer, U. S., Gross, R., Simon, J., Mantele, W., and Lancaster, C. R. (2005) FTIR difference spectra of *Wolinella succinogenes* quinol:fumarate reductase support a key role of Glu c180 within the "e-pathway hypothesis" of coupled transmembrane electron and proton transfer, *Biochemistry 44*, 13949–13961.
899. Beckmann, J. D., and Frerman, F. E. (1985) Electron-transfer flavoprotein-ubiquinone oxidoreductase from pig liver: Purification and molecular, redox, and catalytic properties, *Biochemistry 24*, 3913–3921.
900. Ruzicka, F. J., and Beinert, H. (1977) A new iron–sulfur flavoprotein of the respiratory chain. A component of the fatty acid β oxidation pathway, *J. Biol. Chem. 252*, 8440–8445.
901. Husain, M., Stankovich, M. T., and Fox, B. G. (1984) Measurement of the oxidation–reduction potentials for one-electron and two-electron reduction of electron-transfer flavoprotein from pig liver, *Biochem. J. 219*, 1043–1047.
902. Zhang, J., Frerman, F. E., and Kim, J. J. (2006) Structure of electron transfer flavoprotein-ubiquinone oxidoreductase and electron transfer to the mitochondrial ubiquinone pool, *Proc. Natl. Acad. Sci. U. S. A. 103*, 16212–16217.
903. Guenebaut, V., Schlitt, A., Weiss, H., Leonard, K., and Friedrich, T. (1998) Consistent structure between bacterial and mitochondrial NADH:ubiquinone oxidoreductase (complex I), *J. Mol. Biol. 276*, 105–112.

904. Carroll, J., Fearnley, I. M., Shannon, R. J., Hirst, J., and Walker, J. E. (2003) Analysis of the subunit composition of complex I from bovine heart mitochondria, *Mol Cell Proteomics 2*, 117–126.
905. Hatefi, Y., Haavik, A. G., and Griffiths, D. E. (1962) Studies on the electron transfer system. Xl. Preparation and properties of mitochondrial DPNH-coenzyme Q reductase, *J. Biol. Chem. 237*, 1676–1680.
906. Pilkington, S. J., Skehel, J. M., Gennis, R. B., and Walker, J. E. (1991) Relationship between mitochondrial NADH-ubiquinone reductase and a bacterial NAD-reducing hydrogenase, *Biochemistry 30*, 2166–2175.
907. Ragan, C. I., Galante, Y. M., and Hatefi, Y. (1982) Purification of three iron–sulfur proteins from the iron-protein fragment of mitochondrial NADH-ubiquinone oxidoreductase, *Biochemistry 21*, 2518–2524.
908. Ohnishi, T. (1975) Thermodynamic and EPR characterization of iron–sulfur centers in the NADH-ubiquinone segment of the mitochondrial respiratory chain in pigeon heart, *Biochim. Biophys. Acta 387*, 475–490.
909. Hinchliffe, P., Carroll, J., and Sazanov, L. A. (2006) Identification of a novel subunit of respiratory complex I from *Thermus thermophilus*, *Biochemistry 45*, 4413–4420.
910. Ohnishi, T., and Nakamaru-Ogiso, E. (2008) Were there any "misassignments" among iron–sulfur clusters N_4, N_5 and N_{6b} in NADH-quinone oxidoreductase (complex I)?, *Biochim. Biophys. Acta. 1777*, 703–710.
911. Paech, C., Reynolds, J. G., Singer, T. P., and Holm, R. H. (1981) Structural identification of iron–sulfur clusters of the respiratory chain-linked NADH dehydrogenase, *J. Biol. Chem. 256*, 3167–3170.
912. Albracht, S. P., and Subramanian, J. (1977) The number of Fe atoms in the iron-sulphur centers of the respiratory chain, *Biochim. Biophys. Acta 462*, 36–48.
913. Pohl, T., Bauer, T., Dorner, K., Stolpe, S., Sell, P., Zocher, G., and Friedrich, T. (2007) Iron–sulfur cluster N_7 of the NADH : Ubiquinone oxidoreductase (complex I) is essential for stability but not involved in electron transfer, *Biochemistry 46*, 6588–6596.
914. Ruprecht, J., Yankovskaya, V., Maklashina, E., Iwata, S., and Cecchini, G. (2009) Structure of *Escherichia coli* succinate:quinone oxidoreductase with an occupied and empty quinone-binding site, *J. Biol. Chem. 284*, 29836–29846.
915. Jones, A. J., Blaza, J. N., Varghese, F., and Hirst, J. (2017) Respiratory complex I in *Bos taurus* and *Paracoccus denitrificans* pumps four protons across the membrane for every NADH oxidized, *J. Biol. Chem. 292*, 4987–4995.
916. Belogrudov, G., and Hatefi, Y. (1994) Catalytic sector of complex I (NADH:ubiquinone oxidoreductase): Subunit stoichiometry and substrate-induced conformation changes, *Biochemistry 33*, 4571–4576.
917. Finel, M., Skehel, J. M., Albracht, S. P., Fearnley, I. M., and Walker, J. E. (1992) Resolution of NADH:ubiquinone oxidoreductase from bovine heart mitochondria into two subcomplexes, one of which contains the redox centers of the enzyme, *Biochemistry 31*, 11425–11434.
918. Sazanov, L. A., Peak-Chew, S. Y., Fearnley, I. M., and Walker, J. E. (2000) Resolution of the membrane domain of bovine complex I into subcomplexes: Implications for the structural organization of the enzyme, *Biochemistry 39*, 7229–7235.
919. Braun, M., Bungert, S., and Friedrich, T. (1998) Characterization of the overproduced NADH dehydrogenase fragment of the NADH:ubiquinone oxidoreductase (complex I) from *Escherichia coli*, *Biochemistry 37*, 1861–1867.
920. Baradaran, R., Berrisford, J. M., Minhas, G. S., and Sazanov, L. A. (2013) Crystal structure of the entire respiratory complex I, *Nature 494*, 443–448.
921. Efremov, R. G., and Sazanov, L. A. (2011) Structure of the membrane domain of respiratory complex I, *Nature 476*, 414–420.
922. Kroger, A., and Klingenberg, M. (1973) The kinetics of the redox reactions of ubiquinone related to the electron-transport activity in the respiratory chain, *Eur. J. Biochem. 34*, 358–368.
923. Kroger, A., and Klingenberg, M. (1973) Further evidence for the pool function of ubiquinone as derived from the inhibition of the electron transport by antimycin, *Eur. J. Biochem. 39*, 313–323.
924. Letts, J. A., Fiedorczuk, K., and Sazanov, L. A. (2016) The architecture of respiratory supercomplexes, *Nature 537*, 644–648.

925. Norling, B., Glazek, E., Nelson, B. D., and Ernster, L. (1974) Studies with ubiquinone-depleted submitochondrial particles. Quantitative incorporation of small amounts of ubiquinone and its effects on the NADH and succinate oxidase activities, *Eur. J. Biochem. 47*, 475–482.
926. Griffiths, D. E., and Wharton, D. C. (1961) Studies of the electron transport system. XXXV. Purification and properties of cytochrome oxidase, *J. Biol. Chem. 236*, 1850–1856.
927. Fowler, L. R., Richardson, S. H., and Hatefi, Y. (1962) A rapid method for the preparation of highly purified cytochrome oxidase, *Biochim. Biophys. Acta 64*, 170–173.
928. Wikstrom, M., and Krab, K. (1979) Mechanism and stoicheiometry of redox-linked proton translocation in mitochondria, *Biochem. Soc. Trans. 7*, 880–887.
929. Wikstrom, M. (2004) Cytochrome *c* oxidase: 25 years of the elusive proton pump, *Biochim. Biophys. Acta 1655*, 241–247.
930. Wharton, D. C., and Cusanovich, M. A. (1969) The oxidation–reduction potential of copper in cytochrome oxidase, *Biochem. Biophys. Res. Commun. 37*, 111–115.
931. Blair, D. F., Ellis, W. R., Jr., Wang, H., Gray, H. B., and Chan, S. I. (1986) Spectroelectrochemical study of cytochrome *c* oxidase: pH and temperature dependences of the cytochrome potentials. Characterization of site-site interactions, *J. Biol. Chem. 261*, 11524–11537.
932. Ostermeier, C., Harrenga, A., Ermler, U., and Michel, H. (1997) Structure at 2.7 Å resolution of the *Paracoccus denitrificans* two-subunit cytochrome *c* oxidase complexed with an antibody FV fragment, *Proc. Natl. Acad. Sci. U. S. A. 94*, 10547–10553.
933. Kita, K., Konishi, K., and Anraku, Y. (1984) Terminal oxidases of *Escherichia coli* aerobic respiratory chain. I. Purification and properties of cytochrome b_{562}-*o* complex from cells in the early exponential phase of aerobic growth, *J. Biol. Chem. 259*, 3368–3374.
934. Georgiou, C. D., and Webster, D. A. (1987) Purification and partial characterization of the membrane-bound cytochrome $o_{561,564}$ from *Vitreoscilla*, *Biochemistry 26*, 6521–6526.
935. Matsushita, K., Ebisuya, H., and Adachi, O. (1992) Homology in the structure and the prosthetic groups between two different terminal ubiquinol oxidases, cytochrome a_1 and cytochrome *o*, of *Acetobacter aceti*, *J. Biol. Chem. 267*, 24748–24753.
936. Chepuri, V., Lemieux, L., Au, D. C., and Gennis, R. B. (1990) The sequence of the cyo operon indicates substantial structural similarities between the cytochrome *o* ubiquinol oxidase of *Escherichia coli* and the aa_3-type family of cytochrome *c* oxidases, *J. Biol. Chem. 265*, 11185–11192.
937. Calhoun M. W., Thomas J. W., Hill J. J., Hosler J. P., Shapleigh J. P., Tecklenburg M. M., Ferguson-Miller S., Babcock G. T., Alben J. O., Gennis R. B. (1993) Identity of the axial ligand of the high-spin heme in cytochrome oxidase: Spectroscopic characterization of mutants in the *bo*-type oxidase of *Escherichia coli* and the aa_3-type oxidase of *Rhodobacter sphaeroides*, *Biochemistry. 32*, 10905–10911.
938. Puustinen, A., and Wikstrom, M. (1991) The heme groups of cytochrome *o* from *Escherichia coli*, *Proc. Natl. Acad. Sci. U. S. A. 88*, 6122–6126.
939. Saiki, K., Mogi, T., and Anraku, Y. (1992) Heme *o* biosynthesis in *Escherichia coli*: The cyoE gene in the cytochrome *bo* operon encodes a protoheme IX farnesyltransferase, *Biochem. Biophys. Res. Commun. 189*, 1491–1497.
940. Sato-Watanabe, M., Mogi, T., Ogura, T., Kitagawa, T., Miyoshi, H., Iwamura, H., and Anraku, Y. (1994) Identification of a novel quinone-binding site in the cytochrome *bo* complex from *Escherichia coli*, *J. Biol. Chem. 269*, 28908–28912.
941. Choi, S. K., Schurig-Briccio, L., Ding, Z., Hong, S., Sun, C., and Gennis, R. B. (2017) Location of the substrate binding site of the cytochrome bo_3 ubiquinol oxidase from *Escherichia coli*, *J. Am. Chem. Soc. 139*, 8346–8354.
942. Kobayashi, K., Tagawa, S., and Mogi, T. (2000) Transient formation of ubisemiquinone radical and subsequent electron transfer process in the *Escherichia coli* cytochrome *bo*, *Biochemistry 39*, 15620–15625.
943. Puustinen, A., Finel, M., Haltia, T., Gennis, R. B., and Wikstrom, M. (1991) Properties of the two terminal oxidases of *Escherichia coli*, *Biochemistry 30*, 3936–3942.
944. Erecinska, M., Vanderkooi, J. M., and Wilson, D. F. (1975) Cytochrome *c* interactions with

membranes. A photoaffinity-labeled cytochrome *c*, *Arch. Biochem. Biophys. 171*, 108–116.
945. Birchmeier, W., Kohler, C. E., and Schatz, G. (1976) Interaction of integral and peripheral membrane proteins: Affinity labeling of yeast cytochrome oxidase by modified yeast cytochrome *c*, *Proc. Natl. Acad. Sci. U. S. A. 73*, 4334–4338.
946. Lange, C., and Hunte, C. (2002) Crystal structure of the yeast cytochrome bc_1 complex with its bound substrate cytochrome *c*, *Proc. Natl. Acad. Sci. U. S. A. 99*, 2800–2805.
947. Konig, B. W., Wilms, J., and Van Gelder, B. F. (1981) The reaction between cytochrome c_1 and cytochrome *c*, *Biochim. Biophys. Acta 636*, 9–16.
948. Sarewicz, M., Borek, A., Daldal, F., Froncisz, W., and Osyczka, A. (2008) Demonstration of short-lived complexes of cytochrome *c* with cytochrome bc_1 by EPR spectroscopy: Implications for the mechanism of interprotein electron transfer, *J. Biol. Chem. 283*, 24826–24836.
949. Chiang, Y. L., Kaminsky, L. S., and King, T. E. (1976) A complex of cardiac cytochrome c_1 and cytochrome *c*, *J. Biol. Chem. 251*, 29–36.
950. Tsukihara, T., Aoyama, H., Yamashita, E., Tomizaki, T., Yamaguchi, H., Shinzawa-Itoh, K., Nakashima, R., Yaono, R., and Yoshikawa, S. (1996) The whole structure of the 13-sub-unit oxidized cytochrome *c* oxidase at 2.8 Å, *Science 272*, 1136–1144.
951. Hartley, A. M., Meunier, B., Pinotsis, N., and Marechal, A. (2020) Rcf2 revealed in cryo-EM structures of hypoxic isoforms of mature mitochondrial III-IV supercomplexes, *Proc. Natl. Acad. Sci. U. S. A. 117*, 9329–9337.
952. Kerfeld, C. A., Chan, C., Hirasawa, M., Kleis-SanFrancisco, S., Yeates, T. O., and Knaff, D. B. (1996) Isolation and characterization of soluble electron transfer proteins from *Chromatium purpuratum*, *Biochemistry 35*, 7812–7818.
953. Hochkoeppler, A., Zannoni, D., Ciurli, S., Meyer, T. E., Cusanovich, M. A., and Tollin, G. (1996) Kinetics of photo-induced electron transfer from high-potential iron–sulfur protein to the photosynthetic reaction center of the purple phototroph *Rhodoferax fermentans*, *Proc. Natl. Acad. Sci. U.S.A. 93*, 6998–7002.
954. Bonora, P., Principi, I. I., Monti, B., Ciurli, S., Zannoni, D., and Hochkoeppler, A. (1999) On the role of high-potential iron–sulfur proteins and cytochromes in the respiratory chain of two facultative phototrophs, *Biochim. Biophys. Acta 1410*, 51–60.
955. Stowell, M. H., McPhillips, T. M., Rees, D. C., Soltis, S. M., Abresch, E., and Feher, G. (1997) Light-induced structural changes in photosynthetic reaction center: Implications for mechanism of electron-proton transfer, *Science 276*, 812–816.
956. Allen, J. P., Feher, G., Yeates, T. O., Komiya, H., and Rees, D. C. (1987) Structure of the reaction center from *Rhodobacter sphaeroides* R-26: The cofactors, *Proc. Natl. Acad. Sci. U. S. A. 84*, 5730–5734.
957. Yeates, T. O., Komiya, H., Chirino, A., Rees, D. C., Allen, J. P., and Feher, G. (1988) Structure of the reaction center from *Rhodobacter sphaeroides* R-26 and 2.4.1: Protein-cofactor (bacteriochlorophyll, bacteriopheophytin, and carotenoid) interactions, *Proc. Natl. Acad. Sci. U. S. A. 85*, 7993–7997.
958. Norris, J. R., Uphaus, R. A., Crespi, H. L., and Katz, J. J. (1971) Electron spin resonance of chlorophyll and the origin of signal I in photosynthesis, *Proc. Natl. Acad. Sci. U. S. A. 68*, 625–628.
959. Deisenhofer, J., Epp, O., Miki, K., Huber, R., and Michel, H. (1984) X-Ray structure analysis of a membrane protein complex. Electron density map at 3 Å resolution and a model of the chromophores of the photosynthetic reaction center from *Rhodopseudomonas viridis*, *J. Mol. Biol. 180*, 385–398.
960. Deisenhofer, J., Epp, O., Sinning, I., and Michel, H. (1995) Crystallographic refinement at 2.3 Å resolution and refined model of the photosynthetic reaction centre from *Rhodopseudomonas viridis*, *J. Mol. Biol. 246*, 429–457.
961. Okamura, M. Y., Steiner, L. A., and Feher, G. (1974) Characterization of reaction centers from photosynthetic bacteria. I. Subunit structure of the protein mediating the primary photochemistry in *Rhodopseudomonas spheroides* R-26, *Biochemistry 13*, 1394–1403.
962. Williams, J. C., Steiner, L. A., Feher, G., and Simon, M. I. (1984) Primary structure of the L subunit of the reaction center from *Rhodopseudomonas sphaeroides*, *Proc. Natl. Acad. Sci. U. S. A. 81*, 7303–7307.

963. Deisenhofer, J., Epp, O., Miki, K., Huber, R., and Michel, H. (1986) Structure of the protein subunits in the photosynthetic reaction center of *Rhodopseudomonas viridis* at 3Å Resolution, *Nature 318*, 618–624.
964. Kyte, J. (1981) Molecular considerations relevant to the mechanism of active transport, *Nature 292*, 201–204.
965. Gisriel, C., Sarrou, I., Ferlez, B., Golbeck, J. H., Redding, K. E., and Fromme, R. (2017) Structure of a symmetric photosynthetic reaction center-photosystem, *Science 357*, 1021–1025.
966. Nogi, T., Fathir, I., Kobayashi, M., Nozawa, T., and Miki, K. (2000) Crystal structures of photosynthetic reaction center and high-potential iron–sulfur protein from *Thermochromatium tepidum*: Thermostability and electron transfer, *Proc. Natl. Acad. Sci. U.S.A. 97*, 13561–13566.
967. Camara-Artigas, A., and Allen, J. P. (2004) Comparative analyses of three-dimensional models of bacterial reaction centers, *Photosynth. Res. 81*, 227–237.
968. Kirmaier, C., and Holten, D. (1987) Primary photochemistry of reaction centers from the photosynthetic purple bacteria, *Photosynth. Res. 13*, 225–260.
969. Lieutaud, C., Alric, J., Bauzan, M., Nitschke, W., and Schoepp-Cothenet, B. (2005) Study of the high-potential iron sulfur protein in *Halorhodospira halophila* confirms that it is distinct from cytochrome *c* as electron carrier, *Proc. Natl. Acad. Sci. U. S. A. 102*, 3260–3265.
970. Huang, L. B., Ponomarenko, N., Wiederrecht, G. P., and Tiede, D. M. (2012) Cofactor-specific photochemical function resolved by ultrafast spectroscopy in photosynthetic reaction center crystals, *Proc. Natl. Acad. Sci. U.S.A. 109*, 4851–4856.
971. Dods, R., Bath, P., Morozov, D., Gagner, V. A., Arnlund, D., Luk, H. L., Kubel, J., Maj, M., Vallejos, A., Wickstrand, C., Bosman, R., Beyerlein, K. R., Nelson, G., Liang, M., Milathianaki, D., Robinson, J., Harimoorthy, R., Berntsen, P., Malmerberg, E., Johansson, L., Andersson, R., Carbajo, S., Claesson, E., Conrad, C. E., Dahl, P., Hammarin, G., Hunter, M. S., Li, C., Lisova, S., Royant, A., Safari, C., Sharma, A., Williams, G. J., Yefanov, O., Westenhoff, S., Davidsson, J., DePonte, D. P., Boutet, S., Barty, A., Katona, G., Groenhof, G., Branden, G., and Neutze, R. (2021) Ultrafast structural changes within a photosynthetic reaction centre, *Nature 589*, 310–314.
972. van Stokkum, I. H., Beekman, L. M., Jones, M. R., van Brederode, M. E., and van Grondelle, R. (1997) Primary electron transfer kinetics in membrane-bound *Rhodobacter sphaeroides* reaction centers: A global and target analysis, *Biochemistry 36*, 11360–11368.
973. Woodbury, N. W., Becker, M., Middendorf, D., and Parson, W. W. (1985) Picosecond kinetics of the initial photochemical electron-transfer reaction in bacterial photosynthetic reaction centers, *Biochemistry 24*, 7516–7521.
974. Holten, D., Windsor, M. W., Parson, W. W., and Thornber, J. P. (1978) Primary photochemical processes in isolated reaction centers of *Rhodopseudomonas viridis*, *Biochim. Biophys. Acta 501*, 112–126.
975. Kennis, J. T., Shkuropatov, A. Y., van Stokkum, I. H., Gast, P., Hoff, A. J., Shuvalov, V. A., and Aartsma, T. J. (1997) Formation of a long-lived $P^{+}BA^{-}$ state in plant pheophytin-exchanged reaction centers of *Rhodobacter sphaeroides* R26 at low temperature, *Biochemistry 36*, 16231–16238.
976. Fleming, G. R., Martin, J. L., and Breton, J. (1988) Rates of primary electron transfer in photosynthetic reaction centers and their mechanistic implications, *Nature 333*, 190–192.
977. Breton, J., Martin, J. L., Fleming, G. R., and Lambry, J. C. (1988) Low-temperature femtosecond spectroscopy of the initial step of electron transfer in reaction centers from photosynthetic purple bacteria, *Biochemistry 27*, 8276–8284.
978. McDowell, L. M., Gaul, D., Kirmaier, C., Holten, D., and Schenck, C. C. (1991) Investigation into the source of electron transfer asymmetry in bacterial reaction centers, *Biochemistry 30*, 8315–8322.
979. Chirino, A. J., Lous, E. J., Huber, M., Allen, J. P., Schenck, C. C., Paddock, M. L., Feher, G., and Rees, D. C. (1994) Crystallographic analyses of site-directed mutants of the photosynthetic reaction center from *Rhodobacter sphaeroides*, *Biochemistry 33*, 4584–4593.
980. Alden, R. G., Parson, W. W., Chu, Z. T., and Warshel, A. (1996) Orientation of the OH dipole of Tyrosine (M)210 and its effect on electrostatic energies in photosynthetic bac-

terial reaction centers, *J. Phys. Chem. 100*, 16761–16770.
981. Kirmaier, C., He, C., and Holten, D. (2001) Manipulating the direction of electron transfer in the bacterial reaction center by swapping Phe for Tyr near BChl (ML181) and Tyr for Phe near BChl(L) (M208), *Biochemistry 40*, 12132–12139.
982. Gunner, M. R., and Dutton, P. L. (1989) Temperature and $-\Delta G^{\circ}$ dependence of the electron transfer from $BPh^{\bullet -}$ to Q_A in reaction center protein from *Rhodobacter sphaeroides* with different quinones as Q_A, *J. Am. Chem. Soc. 111*, 3400–3412.
983. Kleinfeld, D., Okamura, M. Y., and Feher, G. (1984) Electron transfer in reaction centers of *Rhodopseudomonas sphaeroides*. I. Determination of the charge recombination pathway of $D^+ Q_A Q_B^-$ and free energy and kinetic relations between $Q_A^- Q_B$ and $Q_A Q_B^-$, *Biochim. Biophys. Acta 766*, 126–140.
984. Paddock, M. L., McPherson, P. H., Feher, G., and Okamura, M. Y. (1990) Pathway of proton transfer in bacterial reaction centers: Replacement of Serine-L223 by alanine inhibits electron and proton transfers associated with reduction of quinone to dihydroquinone, *Proc. Natl. Acad. Sci. U. S. A. 87*, 6803–6807.
985. Tetreault, M., Cusanovich, M., Meyer, T., Axelrod, H., and Okamura, M. Y. (2002) Double mutant studies identify electrostatic interactions that are important for docking cytochrome c_2 onto the bacterial reaction center, *Biochemistry 41*, 5807–5815.
986. Prince, R. C., Cogdell, R. J., and Crofts, A. R. (1974) The photo-oxidation of horse heart cytochrome *c* and native cytochrome c_2 by reaction centres from *Rhodopseudomonas spheroides* R26, *Biochim. Biophys. Acta 347*, 1–13.
987. Venturoli, G., Melandri, B. A., Gabellini, N., and Oesterhelt, D. (1990) Kinetics of photosynthetic electron transfer in artificial vesicles reconstituted with purified complexes from *Rhodobacter capsulatus*. I. The interaction of cytochrome c_2 with the reaction center, *Eur. J. Biochem. 189*, 105–112.
988. Myllykallio, H., Drepper, F., Mathis, P., and Daldal, F. (1998) Membrane-anchored cytochrome c_y mediated microsecond time range electron transfer from the cytochrome bc_1 complex to the reaction center in *Rhodobacter capsulatus*, *Biochemistry 37*, 5501–5510.
989. Jenney, F. E., Jr., Prince, R. C., and Daldal, F. (1994) Roles of the soluble cytochrome c_2 and membrane-associated cytochrome c_y of *Rhodobacter capsulatus* in photosynthetic electron transfer, *Biochemistry 33*, 2496–2502.
990. Oh-oka, H., Iwaki, M., and Itoh, S. (1998) Membrane-bound cytochrome c_z couples quinol oxidoreductase to the p840 reaction center complex in isolated membranes of the green sulfur bacterium *Chlorobium tepidum*, *Biochemistry 37*, 12293–12300.
991. Kimura, Y., Alric, J., Vermeglio, A., Masuda, S., Hagiwara, Y., Matsuura, K., Shimada, K., and Nagashima, K. V. P. (2007) A new membrane-bound cytochrome *c* works as an electron donor to the photosynthetic reaction center complex in the purple bacterium, *Rhodovulum sulfidophilum*, *J. Biol. Chem. 282*, 6463–6472.
992. Ke, B., Chaney, T. H., and Reed, D. W. (1970) The electrostatic interaction between the reaction-center bacteriochlorophyll derived from *Rhodopseudomonas spheroides* and mammalian cytochrome *c* and its effect on light-activated electron transport, *Biochim. Biophys. Acta 216*, 373–383.
993. Okamura, M. Y., Isaacson, R. A., and Feher, G. (1975) Primary acceptor in bacterial photosynthesis: Obligatory role of ubiquinone in photoactive reaction centers of *Rhodopseudomonas spheroides*, *Proc. Natl. Acad. Sci. U. S. A. 72*, 3491–3495.
994. Shopes, R. J., and Wraight, C. A. (1985) The acceptor quinone complex of *Rhodopseudomonas viridis* reaction centers, *Biochim. Biophys. Acta 806*, 348–356.
995. Wraight, C. A. (1979) Electron acceptors of bacterial photosynthetic reaction centers. II. H^+ binding coupled to secondary electron transfer in the quinone acceptor complex, *Biochim. Biophys. Acta 548*, 309–327.
996. Williams, J., Paddock, M. L., Feher, G., and Allen, J. P. (1991) Effects of iron ligand substitutions in reaction centers from *Rhodobacter sphaeroides*, *Biophys. J. 59*, 142a.
997. Debus, R. J., Feher, G., and Okamura, M. Y. (1986) Iron-depleted reaction centers from *Rhodopseudomonas sphaeroides* r-26.1: Characterization and reconstitution with

Fe^{2+}, Mn^{2+}, Co^{2+}, Ni^{2+}, Cu^{2+}, and Zn^{2+}, *Biochemistry 25*, 2276–2287.

998. Arata, H., and Parson, W. W. (1981) Delayed fluorescence from *Rhodopseudomonas sphaeroides* reaction centers: Enthalpy and free-energy changes accompanying electron-transfer from P-870 to quinones, *Biochim. Biophys. Acta 638*, 201–209.
999. Graige, M. S., Paddock, M. L., Bruce, J. M., Feher, G., and Okamura, M. Y. (1996) Mechanism of proton-coupled electron transfer for quinone Q_B reduction in reaction centers of *Rhodopseudomonas sphaeroides*, *J. Am. Chem. Soc. 118*, 9005–9016.
1000. Paddock, M. L., Feher, G., and Okamura, M. Y. (1995) Pathway of proton transfer in bacterial reaction centers: Further investigations on the role of Ser-L223 studied by site-directed mutagenesis, *Biochemistry 34*, 15742–15750.
1001. Paddock, M. L., Rongey, S. H., McPherson, P. H., Juth, A., Feher, G., and Okamura, M. Y. (1994) Pathway of proton transfer in bacterial reaction centers: Role of Aspartate-L213 in proton transfers associated with reduction of quinone to dihydroquinone, *Biochemistry 33*, 734–745.
1002. Remy, A., and Gerwert, K. (2003) Coupling of light-induced electron transfer to proton uptake in photosynthesis, *Nature Struct. Biol. 10*, 637–644.
1003. Vermeglio, A. (1977) Secondary electron transfer in reaction centers of *Rhodopseudomonas sphaeroides*. Out-of-phase periodicity of two for the formation of ubisemiquinone and fully reduced ubiquinone, *Biochim. Biophys. Acta 459*, 516–524.
1004. Wraight, C. A. (1977) Electron acceptors of photosynthetic bacterial reaction centers. Direct observation of oscillatory behaviour suggesting two closely equivalent ubiquinones, *Biochim. Biophys. Acta 459*, 525–531.
1005. McPherson, P. H., Schonfeld, M., Paddock, M. L., Okamura, M. Y., and Feher, G. (1994) Protonation and free energy changes associated with formation of Q_BH_2 in native and GluL212→Gln mutant reaction centers from *Rhodobacter sphaeroides*, *Biochemistry 33*, 1181–1193.
1006. Junge, W., and Auslaender, W. (1974) Electric generator in photosynthesis of green plants. I. Vectorial and protolytic properties of the electron transport chain, *Biochim. Biophys. Acta 333*, 59–70.
1007. Venturoli, G., Gabellini, N., Oesterhelt, D., and Melandri, B. A. (1990) Kinetics of photosynthetic electron-transfer in artificial vesicles reconstituted with purified complexes from *Rhodobacter capsulatus*. 2. Direct electron-transfer between the reaction center and the bc_1-complex and role of cytochrome c_2, *Eur. J. Biochem. 189*, 95–103.
1008. Zouni, A., Witt, H. T., Kern, J., Fromme, P., Krauss, N., Saenger, W., and Orth, P. (2001) Crystal structure of photosystem II from *Synechococcus elongatus* at 3.8 Å resolution, *Nature 409*, 739–743.
1009. Kamiya, N., and Shen, J. R. (2003) Crystal structure of oxygen-evolving photosystem II from *Thermosynechococcus vulcanus* at 3.7 Å resolution, *Proc. Natl. Acad. Sci. U. S. A. 100*, 98–103.
1010. Loll, B., Kern, J., Saenger, W., Zouni, A., and Biesiadka, J. (2005) Towards complete cofactor arrangement in the 3.0 Å resolution structure of photosystem II, *Nature 438*, 1040–1044.
1011. Umena, Y., Kawakami, K., Shen, J. R., and Kamiya, N. (2011) Crystal structure of oxygen-evolving photosystem II at a resolution of 1.9 Å, *Nature 473*, 55–60.
1012. Suga, M., Akita, F., Hirata, K., Ueno, G., Murakami, H., Nakajima, Y., Shimizu, T., Yamashita, K., Yamamoto, M., Ago, H., and Shen, J. R. (2015) Native structure of photosystem II at 1.95 Å resolution viewed by femtosecond X-ray pulses, *Nature 517*, 99–103.
1013. Ago, H., Adachi, H., Umena, Y., Tashiro, T., Kawakami, K., Kamiya, N., Tian, L., Han, G., Kuang, T., Liu, Z., Wang, F., Zou, H., Enami, I., Miyano, M., and Shen, J. R. (2016) Novel features of eukaryotic photosystem II revealed by its crystal structure analysis from a red alga, *J. Biol. Chem. 291*, 5676–5687.
1014. Krauss, N., Schubert, W. D., Klukas, O., Fromme, P., Witt, H. T., and Saenger, W. (1996) Photosystem I at 4 Å resolution represents the first structural model of a joint photosynthetic reaction centre and core antenna system, *Nature Struct. Biol. 3*, 965–973.
1015. Schubert, W. D., Klukas, O., Krauss, N., Saenger, W., Fromme, P., and Witt, H. T. (1997) Photosystem I of *Synechococcus elongatus* at 4 Å resolution: Comprehensive structure analysis, *J. Mol. Biol. 272*, 741–769.

1016. Jordan, P., Fromme, P., Witt, H. T., Klukas, O., Saenger, W., and Krauss, N. (2001) Three-dimensional structure of cyanobacterial photosystem I at 2.5 Å resolution, *Nature 411*, 909–917.
1017. Amunts, A., Drory, O., and Nelson, N. (2007) The structure of a plant photosystem I supercomplex at 3.4 Å resolution, *Nature 447*, 58–63.
1018. Mazor, Y., Borovikova, A., and Nelson, N. (2015) The structure of plant photosystem I supercomplex at 2.8 Å resolution, *Elife 4*, e07433.
1019. Ben-Shem, A., Frolow, F., and Nelson, N. (2003) Crystal structure of plant photosystem I, *Nature 426*, 630–635.
1020. Wasielewski, M. R., Johnson, D. G., Seibert, M., and Govindjee. (1989) Determination of the primary charge separation rate in isolated photosystem II reaction centers with 500-fs time resolution, *Proc. Natl. Acad. Sci. U. S. A. 86*, 524–528.
1021. Romero, E., van Stokkum, I. H. M., Novoderezhkin, V. I., Dekker, J. P., and van Grondelle, R. (2010) Two different charge separation pathways in photosystem II, *Biochemistry 49*, 4300–4307.
1022. van Mieghem, F., Brettel, K., Hillmann, B., Kamlowski, A., Rutherford, A. W., and Schlodder, E. (1995) Charge recombination reactions in photosystem II. I. Yields, recombination pathways, and kinetics of the primary pair, *Biochemistry 34*, 4798–4813.
1023. Sanakis, Y., Petasis, D., Petrouleas, V., and Hendrich, M. (1999) Simultaneous binding of fluoride and NO to the nonheme iron of photosystem II: Quantitative EPR evidence for a weak exchange interaction between the semiquinone Q_A^- and the iron-nitrosyl complex, *J. Am. Chem. Soc. 121*, 9155–9164.
1024. Kalman, L., LoBrutto, R., Allen, J. P., and Williams, J. C. (1999) Modified reaction centres oxidize tyrosine in reactions that mirror photosystem II, *Nature 402*, 696–699.
1025. Debus, R. J., Barry, B. A., Sithole, I., Babcock, G. T., and McIntosh, L. (1988) Directed mutagenesis indicates that the donor to P_{680}^+ in photosystem II is Tyrosine-161 of the D1 polypeptide, *Biochemistry 27*, 9071–9074.
1026. Barry, B. A., and Babcock, G. T. (1987) Tyrosine radicals are involved in the photosynthetic oxygen-evolving system, *Proc. Natl. Acad. Sci. U. S. A. 84*, 7099–7103.
1027. Boerner, R. J., and Barry, B. A. (1993) Isotopic labeling and EPR spectroscopy show that a tyrosine residue is the terminal electron donor, *Z*, in manganese-depleted photosystem II preparations, *J. Biol. Chem. 268*, 17151–17154.
1028. Yano, J., Kern, J., Sauer, K., Latimer, M. J., Pushkar, Y., Biesiadka, J., Loll, B., Saenger, W., Messinger, J., Zouni, A., and Yachandra, V. K. (2006) Where water is oxidized to dioxygen: Structure of the photosynthetic Mn_4Ca cluster, *Science 314*, 821–825.
1029. Di Donato, M., Stahl, A. D., van Stokkum, I. H. M., van Grondelle, R., and Groot, M. L. (2011) Cofactors involved in light-driven charge separation in photosystem I identified by subpicosecond infrared spectroscopy, *Biochemistry 50*, 480–490.
1030. Savikhin, S., Xu, W., Martinsson, P., Chitnis, P. R., and Struve, W. S. (2001) Kinetics of charge separation and $A_0 \rightarrow A_1$ electron transfer in photosystem I reaction centers, *Biochemistry 40*, 9282–9290.
1031. Drepper, F., Hippler, M., Nitschke, W., and Haehnel, W. (1996) Binding dynamics and electron transfer between plastocyanin and photosystem I, *Biochemistry 35*, 1282–1295.
1032. Danielsen, E., Scheller, H. V., Bauer, R., Hemmingsen, L., Bjerrum, M. J., and Hansson, O. (1999) Plastocyanin binding to photosystem I as a function of the charge state of the metal ion: Effect of metal site conformation, *Biochemistry 38*, 11531–11540.
1033. Luneberg, J., Fromme, P., Jekow, P., and Schlodder, E. (1994) Spectroscopic characterization of PS I core complexes from thermophilic *Synechococcus* sp.: Identical reoxidation kinetics of A_1^- before and after removal of the iron–sulfur–clusters F_A and F_B, *FEBS Lett. 338*, 197–202.
1034. Moenne-Loccoz, P., Heathcote, P., Maclachlan, D. J., Berry, M. C., Davis, I. H., and Evans, M. C. (1994) Path of electron transfer in photosystem I: Direct evidence of forward electron transfer from A_1 to Fe-Sx, *Biochemistry 33*, 10037–10042.
1035. Karyagina, I., Pushkar, Y., Stehlik, D., van der Est, A., Ishikita, H., Knapp, E. W., Jagannathan, B., Agalarov, R., and Golbeck, J. H. (2007) Contributions of the protein environment to the midpoint potentials of the A_1 phylloquinones and the Fx iron–sulfur cluster in photosystem I, *Biochemistry 46*, 10804–10816.

1036. Diaz-Quintana, A., Leibl, W., Bottin, H., and Setif, P. (1998) Electron transfer in photosystem I reaction centers follows a linear pathway in which iron–sulfur cluster F_b is the immediate electron donor to soluble ferredoxin, *Biochemistry 37*, 3429–3439.
1037. Laughlin, T. G., Bayne, A. N., Trempe, J. F., Savage, D. F., and Davies, K. M. (2019) Structure of the complex I-like molecule NDH of oxygenic photosynthesis, *Nature 566*, 411–414.
1038. Strand, D. D., Fisher, N., and Kramer, D. M. (2017) The higher plant plastid NAD(P)H dehydrogenase-like complex (NDH) is a high efficiency proton pump that increases ATP production by cyclic electron flow, *J. Biol. Chem. 292*, 11850–11860.
1039. Kramer, D. M., and Evans, J. R. (2011) The importance of energy balance in improving photosynthetic productivity, *Plant Physiol 155*, 70–78.
1040. Arnon, D. I. (1971) The light reactions of photosynthesis, *Proc. Natl. Acad. Sci. U. S. A. 68*, 2883–2892.
1041. Moser, C. C., Keske, J. M., Warncke, K., Farid, R. S., and Dutton, P. L. (1992) Nature of biological electron transfer, *Nature 355*, 796–802.
1042. Igarashi, N., Moriyama, H., Fujiwara, T., Fukumori, Y., and Tanaka, N. (1997) The 2.8 Å structure of hydroxylamine oxidoreductase from a nitrifying chemoautotrophic bacterium, *Nitrosomonas europaea*, *Nature Struct. Biol. 4*, 276–284.
1043. Hendrich, M. P., Upadhyay, A. K., Riga, J., Arciero, D. M., and Hooper, A. B. (2002) Spectroscopic characterization of the NO adduct of hydroxylamine oxidoreductase, *Biochemistry 41*, 4603–4611.
1044. Byrdin, M., Eker, A. P., Vos, M. H., and Brettel, K. (2003) Dissection of the triple tryptophan electron transfer chain in *Escherichia coli* DNA photolyase: Trp382 is the primary donor in photoactivation, *Proc. Natl. Acad. Sci. U. S. A. 100*, 8676–8681.
1045. Page, C. C., Moser, C. C., Chen, X., and Dutton, P. L. (1999) Natural engineering principles of electron tunnelling in biological oxidation–reduction, *Nature 402*, 47–52.
1046. Gray, H. B., and Winkler, J. R. (1996) Electron transfer in proteins, *Annu. Rev. Biochem. 65*, 537–561.
1047. Yoshikawa, S., Shinzawa-Itoh, K., Nakashima, R., Yaono, R., Yamashita, E., Inoue, N., Yao, M., Fei, M. J., Libeu, C. P., Mizushima, T., Yamaguchi, H., Tomizaki, T., and Tsukihara, T. (1998) Redox-coupled crystal structural changes in bovine heart cytochrome *c* oxidase, *Science 280*, 1723–1729.
1048. Karlsson, A., Beharry, Z. M., Eby, D. M., Coulter, E. D., Neidle, E. L., Kurtz, D. M., Eklund, H., and Ramaswamy, S. (2002) X-ray crystal structure of benzoate 1,2-dioxygenase reductase from *Acinetobacter* sp strain ADP1, *J. Mol. Biol. 318*, 261–272.
1049. Lim, L. W., Shamala, N., Mathews, F. S., Steenkamp, D. J., Hamlin, R., and Xuong, N. H. (1986) Three-dimensional structure of the iron–sulfur flavoprotein trimethylamine dehydrogenase at 2.4 Å resolution, *J. Biol. Chem. 261*, 15140–15146.
1050. Baker, S. C., Saunders, N. F., Willis, A. C., Ferguson, S. J., Hajdu, J., and Fulop, V. (1997) Cytochrome cd_1 structure: Unusual haem environments in a nitrite reductase and analysis of factors contributing to β-propeller folds, *J. Mol. Biol. 269*, 440–455.
1051. Dodd, F. E., Van Beeumen, J., Eady, R. R., and Hasnain, S. S. (1998) X-ray structure of a blue-copper nitrite reductase in two crystal forms. The nature of the copper sites, mode of substrate binding and recognition by redox partner, *J. Mol. Biol. 282*, 369–382.
1052. Wang, M., Roberts, D. L., Paschke, R., Shea, T. M., Masters, B. S., and Kim, J. J. (1997) Three-dimensional structure of NADPH-cytochrome P450 reductase: Prototype for FMN- and FAD-containing enzymes, *Proc. Natl. Acad. Sci. U. S. A. 94*, 8411–8416.
1053. Winkler, J. R., Nocera, D. G., Yocom, K. M., Bordignon, E., and Gray, H. (1982) Electron-transfer kinetics of pentaammineruthenium(III)(Histidine-33)-ferricytochrome *c*. Measurement of the rate of intramolecular electron transfer between redox centers separated by 15Å in a protein, *J. Am. Chem. Soc. 104*, 5798–5800.
1054. McGourty, J. L., Blough, N. V., and Hoffman, B. M. (1983) Electron transfer at crystallographically known long distances (25 Å) in [ZnII,FeIII] hybrid hemoglobin, *J. Am. Chem. Soc. 105*, 4470–4472.
1055. Lieber, C. M., Karas, J. L., and Gray, H. B. (1987) Reversible long-range electron trans-

fer in ruthenium-modified sperm whale myoglobin, *J. Am. Chem. Soc. 109*, 3778–3779.
1056. Farver, O., and Pecht, I. (1989) Long-range intramolecular electron transfer in azurins, *Proc. Natl. Acad. Sci. U. S. A. 86*, 6968–6972.
1057. Blough, N. V., Zemel, H., Hoffman, B. M., Lee, T. C. K., and Gibson, Q. H. (1980) Kinetics of carbon monoxide binding to manganese, zinc, and cobalt hybrid hemoglobins, *J. Am. Chem. Soc. 102*, 5683–5685.
1058. Zemel, H., and Hoffman, B. M. (1981) Long-range triplet-triplet energy transfer within metal-substituted hemoglobins, *J. Am. Chem. Soc. 103*, 1192–1201.
1059. Peterson-Kennedy, S. E., McGourty, J. L., and Hoffman, B. M. (1984) Temperature dependence of long-range electron transfer in [Zn,FeIII] hybrid hemoglobin, *J. Am. Chem. Soc. 106*, 5010–5012.
1060. Taube, H., Myers, H., and Rich, R. L. (1953) The mechanism of electron transfer in solution, *J. Am. Chem. Soc. 75*, 4118–4119.
1061. Tocheva, E. I., Rosell, F. I., Mauk, A. G., and Murphy, M. E. (2004) Side-on copper-nitrosyl coordination by nitrite reductase, *Science 304*, 867–870.
1062. Bassolo, F., and Pearson, R. G. (1967) *Mechanisms of Inorganic Reactions: A Study of Metal Complexes in Solution, Second Edition*, p. 152, Wiley, New York.
1063. Stengle, T. R., and Langford, C. H. (1967) Uses of nuclear magnetic resonance in the study of ligand substitution processes, *Coord. Chem. Rev. 2*, 349–370.
1064. Bassolo, F., and Pearson, R. G. (1967) *Mechanisms of Inorganic Reactions: A Study of Metal Complexes in Solution, Second Edition*, p. 198, Wiley, New York.
1065. Marcus, R. A. (1993) Electron-transfer reactions in chemistry: Theory and experiment (Nobel lecture), *Angew. Chem., Int. Ed. Engl. 32*, 1111–1121.
1066. Libby, W. F. (1952) Theory of electron exchange reactions in aqueous solution, *J. Phys. Chem. 56*, 863–866, discussion 866–868.
1067. Marcus, R. A., and Sutin, N. (1985) Electron transfers in chemistry and biology, *Biochim. Biophys. Acta 811*, 265–322.
1068. Winkler, J. R., and Gray, H. B. (2014) Long-range electron tunneling, *J. Am. Chem. Soc. 136*, 2930–2939.
1069. Closs, G. L., and Miller, J. R. (1988) Intramolecular long-distance electron transfer in organic molecules, *Science 240*, 440–447.
1070. Winkler, J. R., and Gray, H. B. (1992) Electron-transfer in ruthenium-modified proteins, *Chem. Rev. 92*, 369–379.
1071. Brooks, H. B., and Davidson, V. L. (1994) Kinetic and thermodynamic analysis of a physiological intermolecular electron-transfer reaction between methylamine dehydrogenase and amicyanin, *Biochemistry 33*, 5696–5701.
1072. Ma, J. K., Carrell, C. J., Mathews, F. S., and Davidson, V. L. (2006) Site-directed mutagenesis of proline 52 to glycine in amicyanin converts a true electron transfer reaction into one that is conformationally gated, *Biochemistry 45*, 8284–8293.
1073. Wasielewski, M. R., Niemczyk, M. P., Svec, W. A., and Pewitt, E. B. (1985) Dependence of rate constants for photoinduced charge separation and dark charge recombination on the free energy of reaction in restricted-distance porphyrin-quinone molecules, *J. Am. Chem. Soc. 107*, 1080–1082.
1074. Fox, L. S., Kozik, M., Winkler, J. R., and Gray, H. B. (1990) Gaussian free-energy dependence of electron-transfer rates in iridium complexes, *Science 247*, 1069–1071.
1075. Takeda, N., and Miller, J. R. (2020) Inverted region in bimolecular electron transfer in solution enabled by delocalization, *J. Am. Chem. Soc. 142*, 17997–18004.
1076. Scott, J. R., Willie, A., McLean, M., Stayton, P. S., Sligar, S. G., Durham, B., and Millett, F. (1993) Intramolecular electron transfer in cytochrome b_5 labeled with ruthenium(II) polypyridine complexes: Rate measurements in the marcus inverted region, *J. Am. Chem. Soc. 115*, 6820–6824.
1077. McLendon, G., and Miller, J. R. (1985) The dependence of biological electron transfer rates on exothermicity. The cytochrome *c*/cytochrome b_5 couple, *J. Am. Chem. Soc. 107*, 7811–7816.
1078. Lin, X., Williams, J. C., Allen, J. P., and Mathis, P. (1994) Relationship between rate and free energy difference for electron transfer from cytochrome c_2 to the reaction center in *Rhodobacter sphaeroides*, *Biochemistry 33*, 13517–13523.
1079. Zhou, J. S., and Rodgers, M. A. J. (1991) Driving force dependence of rate constants of elec-

tron-transfer within cytochrome-*c* and uroporphyrin complexes, *J. Am. Chem. Soc. 113*, 7728–7734.
1080. Mines, G. A., Bjerrum, M. J., Hill, M. G., Casimiro, D. R., Chang, I. J., Winkler, J. R., and Gray, H. B. (1996) Rates of heme oxidation and reduction in Ru(His33)cytochrome *c* at very high driving forces, *J. Am. Chem. Soc. 118*, 1961–1965.
1081. Sekretaryova, A., Jones, S. M., and Solomon, E. I. (2019) O_2 Reduction to water by high potential multicopper oxidases: Contributions of the T_1 copper site potential and the local environment of the trinuclear copper cluster, *J. Am. Chem. Soc. 141*, 11304–11314.
1082. Karas, J. L., Lieber, C. M., and Gray, H. B. (1988) Free energy dependence of the rate of long-range electron transfer in proteins. Reorganization energy in ruthenium-modified myoglobin, *J. Am. Chem. Soc. 110*, 599–600.
1083. Conklin, K. T., and McLendon, G. (1988) Free energy effects on biological electron transfer: Reactions of iron(IV) cytochrome *c* peroxidase (ES) with metallocytochromes *c*, *J. Am. Chem. Soc. 110*, 3345–3350.
1084. Elias, H., Chou, M. H., and Winkler, J. R. (1988) Electron-transfer kinetics of zinc-substituted cytochrome *c* and its $Ru(NH_3)_5$ (Histidine-33) derivative, *J. Am. Chem. Soc. 110*, 429–434.
1085. Wijma, H. J., MacPherson, I., Farver, O., Tocheva, E. I., Pecht, I., Verbeet, M. P., Murphy, M. E., and Canters, G. W. (2007) Effect of the methionine ligand on the reorganization energy of the type-1 copper site of nitrite reductase, *J. Am. Chem. Soc. 129*, 519–525.
1086. Davidson, V. L., and Jones, L. H. (1996) Electron transfer from copper to heme within the methylamine dehydrogenase–amicyanin–cytochrome c_{551i} complex, *Biochemistry 35*, 8120–8125.
1087. Piontek, K., Antorini, M., and Choinowski, T. (2002) Crystal structure of a laccase from the fungus *Trametes versicolor* at 1.90-Å resolution containing a full complement of coppers, *J. Biol. Chem. 277*, 37663–37669.
1088. Closs, G. L., Calcaterra, L. T., Green, N. J., Penfield, K. W., and Miller, J. R. (1986) Distance, stereoelectronic effects, and the Marcus inverted region in intramolecular electron-transfer in organic radical-anions, *J. Phys. Chem. 90*, 3673–3683.
1089. Oevering, H., Paddon-Row, M. N., Heppener, M., Oliver, A. M., Cotsaris, E., Verhoeven, J. W., and Hush, N. S. (1987) Long-range photoinduced through-bond electron transfer and radiative recombination via rigid nonconjugated bridges: Distance and solvent dependence, *J. Am. Chem. Soc. 109*, 3258–3269.
1090. Faraggi, M., DeFelippis, M. R., and Klapper, M. H. (1989) Long-range electron transfer between tyrosine and tryptophan in peptides, *J. Am. Chem. Soc. 111*, 5141–5145.
1091. Schanze, K. S., and Sauer, K. (1988) Photoinduced intramolecular electron transfer in peptide-bridged molecules, *J. Am. Chem. Soc. 110*, 1180–1186.
1092. Serron, S. A., Aldridge, W. S., Fleming, C. N., Danell, R. M., Baik, M.-H., Sykora, M., Dattelbaum, D. M., and Meyer, T. J. (2004) Evidence for through-space electron transfer in the distance dependence of normal and inverted electron transfer in oligoproline arrays, *J. Am. Chem. Soc. 126*, 14506–14514.
1093. Mishra, A. K., Chandrasekar, R., Faraggi, M., and Klapper, M. H. (1994) Long-range electron transfer in peptides. Tyrosine reduction of the indolyl radical: Reaction mechanism, modulation of reaction rate, and physiological considerations, *J. Am. Chem. Soc. 116*, 1414–1422.
1094. Ponce, A., Gray, H. B., and Winkler, J. R. (2000) Electron tunneling through water: Oxidative quenching of electronically excited $Ru(tpy)_2^{2+}$ (tpy = 2,2′:6,2″-terpyridine) by ferric ions in aqueous glasses at 77 K, *J. Am. Chem. Soc. 122*, 8187–8191.
1095. Langen, R., Chang, I. J., Germanas, J. P., Richards, J. H., Winkler, J. R., and Gray, H. B. (1995) Electron tunneling in proteins: Coupling through a β strand, *Science 268*, 1733–1735.
1096. Karpishin, T. B., Grinstaff, M. W., Komarpanicucci, S., Mclendon, G., and Gray, H. B. (1994) Electron-transfer in cytochrome-*c* depends upon the structure of the intervening medium, *Structure 2*, 415–422.
1097. Casimiro, D. R., Richards, J. H., Winkler, J. R., and Gray, H. B. (1993) Electron-transfer in ruthenium-modified cytochromes-*c*: σ-Tunneling pathways through aromatic residues, *J. Phys. Chem. 97*, 13073–13077.
1098. Wuttke, D. S., Bjerrum, M. J., Winkler, J. R., and Gray, H. B. (1992) Electron-tunneling

pathways in cytochrome *c*, *Science 256*, 1007–1009.
1099. Winkler, J. R., Di Bilio, A. J., Farrow, N. A., Richards, J. H., and Gray, H. B. (1999) Electron tunneling in biological molecules, *Pure and Applied Chemistry 71*, 1753–1764.
1100. Regan, J. J., Di Bilio, A. J., Langen, R., Skov, L. K., Winkler, J. R., Gray, H. B., and Onuchic, J. N. (1995) Electron tunneling in azurin: The coupling across a β-sheet, *Nature Chem. Biol. 2*, 489–496.
1101. Di Bilio, A. J., Hill, M. G., Bonander, N., Karlsson, B. G., Villahermosa, R. M., Malmstroem, B. G., Winkler, J. R., and Gray, H. B. (1997) Reorganization energy of blue copper: Effects of temperature and driving force on the rates of electron transfer in ruthenium- and osmium-modified azurins, *J. Am. Chem. Soc. 119*, 9921–9922.
1102. Langen, R., Colon, J. L., Casimiro, D. R., Karpishin, T. B., Winkler, J. R., and Gray, H. B. (1996) Electron tunneling in proteins: Role of the intervening medium, *J. Biol. Inorganic Chem. 1*, 221–225.
1103. Babini, E., Bertini, I., Borsari, M., Capozzi, F., Luchinat, C., Zhang, X. Y., Moura, G. L. C., Kurnikov, I. V., Beratan, D. N., Ponce, A., Di Bilio, A. J., Winkler, J. R., and Gray, H. B. (2000) Bond-mediated electron tunneling in ruthenium-modified high-potential iron–sulfur protein, *J. Am. Chem. Soc. 122*, 4532–4533.
1104. Chang, I. J., Gray, H. B., and Winkler, J. R. (1991) High-driving-force electron transfer in ferrocytochrome *c* by $Ru(2,2'\text{-bpy})_2(im)(His\text{-}33)^{3+}$, *J. Am. Chem. Soc. 113*, 7056–7057.
1105. Onuchic, J. N., and Beratan, D. N. (1990) A predictive theoretical model for electron tunneling pathways in proteins, *J. Chem. Phys. 92*, 722–733.
1106. Onuchic, J. N., De Andrade, P. C. P., and Beratan, D. N. (1991) Electron tunneling pathways in proteins: A method to compute tunneling matrix elements in very large systems, *J. Chem. Phys. 95*, 1131–1138.
1107. Skourtis, S. S., Regan, J. J., and Onuchic, J. N. (1994) Electron-transfer in proteins: A novel approach for the description of donor-acceptor coupling, *J. Phys. Chem. 98*, 3379–3388.
1108. de Rege, P. J., Williams, S. A., and Therien, M. J. (1995) Direct evaluation of electronic coupling mediated by hydrogen bonds: Implications for biological electron transfer, *Science 269*, 1409–1413.
1109. van Amsterdam, I. M., Ubbink, M., Einsle, O., Messerschmidt, A., Merli, A., Cavazzini, D., Rossi, G. L., and Canters, G. W. (2002) Dramatic modulation of electron transfer in protein complexes by crosslinking, *Nature Struct. Biol. 9*, 48–52.
1110. Francisco, W. A., Wille, G., Smith, A. J., Merkler, D. J., and Klinman, J. P. (2004) Investigation of the pathway for inter-copper electron transfer in peptidylglycine α-amidating monooxygenase, *J. Am. Chem. Soc. 126*, 13168–13169.
1111. de la Lande, A., Mart, S., Parisel, O., and Moliner, V. (2007) Long distance electron-transfer mechanism in peptidylglycine α-hydroxylating monooxygenase: A perfect fitting for a water bridge, *J. Am. Chem. Soc. 129*, 11700–11707.
1112. Antonyuk, S. V., Han, C., Eady, R. R., and Hasnain, S. S. (2013) Structures of protein-protein complexes involved in electron transfer, *Nature 496*, 123–126.
1113. Beratan, D. N., Betts, J. N., and Onuchic, J. N. (1991) Protein electron transfer rates set by the bridging secondary and tertiary structure, *Science 252*, 1285–1288.
1114. Bowler, B. E., Meade, T. J., Mayo, S. L., Richards, J. H., and Gray, H. B. (1989) Long-range electron transfer in structurally engineered pentaammineruthenium (histidine-62)cytochrome *c*, *J. Am. Chem. Soc. 111*, 8757–8759.
1115. Jacobs, B. A., Mauk, M. R., Funk, W. D., MacGillivray, R. T. A., Mauk, A. G., and Gray, H. B. (1991) Preparation, characterization, and intramolecular electron transfer in pentaammineruthenium Histidine-26 cytochrome b_5 derivatives: Role of the intervening medium in long-range donor-acceptor electronic coupling, *J. Am. Chem. Soc. 113*, 4390–4394.
1116. Prigge, S. T., Kolhekar, A. S., Eipper, B. A., Mains, R. E., and Amzel, L. M. (1999) Substrate-mediated electron transfer in peptidylglycine α-hydroxylating monooxygenase, *Nature Struct. Biol. 6*, 976–983.
1117. Arimura, T., Ide, S., Suga, Y., Nishioka, T., Murata, S., Tachiya, M., Nagamura, T., and Inoue, H. (2001) Electron transfer through-space or through-bonds? A novel system that permits a direct evaluation, *J. Am. Chem. Soc. 123*, 10744–10745.

1118. Napper, A. M., Head, N. J., Oliver, A. M., Shephard, M. J., Paddon-Row, M. N., Read, I., and Waldeck, D. H. (2002) Use of U-shaped donor-bridge-acceptor molecules to study electron tunneling through nonbonded contacts, *J. Am. Chem. Soc. 124*, 10171–10181.
1119. Napper, A. M., Read, I., Waldeck, D. H., Head, N. J., Oliver, A. M., and Paddon-Row, M. N. (2000) An unequivocal demonstration of the importance of nonbonded contacts in the electronic coupling between electron donor and acceptor units of donor-bridge-acceptor molecules, *J. Am. Chem. Soc. 122*, 5220–5221.
1120. Antonello, S., Formaggio, F., Moretto, A., Toniolo, C., and Maran, F. (2003) Anomalous distance dependence of electron transfer across peptide bridges, *J. Am. Chem. Soc. 125*, 2874–2875.
1121. Bollinger, J. M., Jr. (2008) Electron relay in proteins, *Science 320*, 1730–1731.
1122. Shih, C., Museth, A. K., Abrahamsson, M., Blanco-Rodriguez, A. M., Di Bilio, A. J., Sudhamsu, J., Crane, B. R., Ronayne, K. L., Towrie, M., Vlcek, A., Jr., Richards, J. H., Winkler, J. R., and Gray, H. B. (2008) Tryptophan-accelerated electron flow through proteins, *Science 320*, 1760–1762.
1123. Gray, H. B., and Winkler, J. R. (2010) Electron flow through metalloproteins, *Biochim. Biophys. Acta. 1797*, 1563–1572.
1124. Winkler, J. R., and Gray, H. B. (2014) Electron flow through metalloproteins, *Chem. Rev. 114*, 3369–3380.
1125. Liu, Z., Tan, C., Guo, X., Li, J., Wang, L., Sancar, A., and Zhong, D. (2013) Determining complete electron flow in the cofactor photoreduction of oxidized photolyase, *Proc. Natl. Acad. Sci. U. S. A. 110*, 12966–12971.
1126. Naik, G. H., Priyadarsini, K. I., and Mohan, H. (2002) One-electron reduction of some indole derivatives: Effect of 5-hydroxy substitution, *Phys. Chem. Chem. Phys. 4*, 5872–5877.
1127. Shen, X. H., Lind, J., and Merenyi, G. (1987) One-electron oxidation of indoles and acid–base properties of the indolyl radicals, *J. Phys. Chem. 91*, 4403–4406.
1128. Li, C., and Hoffman, M. Z. (1999) One-electron redox potentials of phenols in aqueous solution, *J. Phys. Chem. B 103*, 6653–6656.
1129. Ravichandran, K. R., Taguchi, A. T., Wei, Y., Tommos, C., Nocera, D. G., and Stubbe, J. (2016) A >200 meV uphill thermodynamic landscape for radical transport in *Escherichia coli* ribonucleotide reductase determined using fluorotyrosine-substituted enzymes, *J. Am. Chem. Soc. 138*, 13706–13716.
1130. Greene, B. L., Taguchi, A. T., Stubbe, J., and Nocera, D. G. (2017) Conformationally dynamic radical transfer within ribonucleotide reductase, *J. Am. Chem. Soc. 139*, 16657–16665.
1131. Park, H. W., Kim, S. T., Sancar, A., and Deisenhofer, J. (1995) Crystal structure of DNA photolyase from *Escherichia coli*, *Science 268*, 1866–1872.
1132. Uhlin, U., and Eklund, H. (1994) Structure of ribonucleotide reductase protein R1, *Nature 370*, 533–539.
1133. Stubbe, J., Nocera, D. G., Yee, C. S., and Chang, M. C. Y. (2003) Radical initiation in the class I ribonucleotide reductase: Long-range proton-coupled electron transfer?, *Chem. Rev. 103*, 2167–2201.
1134. Byrdin, M., Villette, S., Eker, A. P., and Brettel, K. (2007) Observation of an intermediate tryptophanyl radical in W306F mutant DNA photolyase from *Escherichia coli* supports electron hopping along the triple tryptophan chain, *Biochemistry 46*, 10072–10077.
1135. Lee, W., Kasanmascheff, M., Huynh, M., Quartararo, A., Costentin, C., Bejenke, I., Nocera, D. G., Bennati, M., Tommos, C., and Stubbe, J. (2018) Properties of site-specifically incorporated 3-aminotyrosine in proteins to study redox-active tyrosines: *Escherichia coli* ribonucleotide reductase as a paradigm, *Biochemistry 57*, 3402–3415.
1136. Madej, E., and Wardman, P. (2007) The oxidizing power of the glutathione thiyl radical as measured by its electrode potential at physiological pH, *Arch. Biochem. Biophys. 462*, 94–102.
1137. Seyedsayamdost, M. R., Xie, J., Chan, C. T., Schultz, P. G., and Stubbe, J. (2007) Site-specific insertion of 3-aminotyrosine into subunit $\alpha 2$ of *E. coli* ribonucleotide reductase: Direct evidence for involvement of Y730 and Y731 in radical propagation, *J. Am. Chem. Soc. 129*, 15060–15071.
1138. Ekberg, M., Sahlin, M., Eriksson, M., and Sjoberg, B. M. (1996) Two conserved tyrosine residues in protein R1 participate in an in-

termolecular electron transfer in ribonucleotide reductase, *J. Biol. Chem. 271*, 20655–20659.
1139. Osheroff, N., Brautigan, D. L., and Margoliash, E. (1980) Definition of enzymic interaction domains on cytochrome *c*. Purification and activity of singly substituted carboxydinitrophenyl-lysine 7, 25, 73, 86, and 99 cytochromes c, *J. Biol. Chem. 255*, 8245–8251.
1140. Roberts, V. A., and Pique, M. E. (1999) Definition of the interaction domain for cytochrome *c* on cytochrome *c* oxidase. III. Prediction of the docked complex by a complete, systematic search, *J. Biol. Chem. 274*, 38051–38060.
1141. Scharlau, M., Geren, L., Zhen, E. Y., Ma, L., Rajagukguk, R., Ferguson-Miller, S., Durham, B., and Millett, F. (2019) Definition of the interaction domain and electron transfer route between cytochrome *c* and cytochrome oxidase, *Biochemistry 58*, 4125–4135.
1142. Osborne, R. L., Zhu, H., Iavarone, A. T., Blackburn, N. J., and Klinman, J. P. (2013) Interdomain long-range electron transfer becomes rate-limiting in the Y216A variant of tyramine β-monooxygenase, *Biochemistry 52*, 1179–1191.
1143. Park, S. Y., Yamane, K., Adachi, S., Shiro, Y., Weiss, K. E., Maves, S. A., and Sligar, S. G. (2002) Thermophilic cytochrome P450 (CYP119) from *Sulfolobus solfataricus*: High resolution structure and functional properties, *J Inorg Biochem 91*, 491–501.
1144. Girvan, H. M., Seward, H. E., Toogood, H. S., Cheesman, M. R., Leys, D., and Munro, A. W. (2007) Structural and spectroscopic characterization of P450 BM3 mutants with unprecedented P450 heme iron ligand sets. New heme ligation states influence conformational equilibria in p450 BM3, *J. Biol. Chem. 282*, 564–572.
1145. Ener, M. E., Gray, H. B., and Winkler, J. R. (2017) Hole hopping through tryptophan in cytochrome P450, *Biochemistry 56*, 3531–3538.
1146. Warren, J. J., Herrera, N., Hill, M. G., Winkler, J. R., and Gray, H. B. (2013) Electron flow through nitrotyrosinate in *Pseudomonas aeruginosa* azurin, *J. Am. Chem. Soc. 135*, 11151–11158.
1147. Pilet, E., Jasaitis, A., Liebl, U., and Vos, M. H. (2004) Electron transfer between hemes in mammalian cytochrome *c* oxidase, *Proc. Natl. Acad. Sci. U. S. A. 101*, 16198–16203.
1148. Hazzard, J. T., McIntire, W. S., and Tollin, G. (1991) Laser flash photolysis study of intermolecular and intramolecular electron transfer in trimethylamine dehydrogenase, *Biochemistry 30*, 4559–4564.
1149. Kobayashi, K., Koppenhofer, A., Ferguson, S. J., and Tagawa, S. (1997) Pulse radiolysis studies on cytochrome cd_1 nitrite reductase from *Thiosphaera pantotropha*: Evidence for a fast intramolecular electron transfer from *c*-heme to d_1-heme, *Biochemistry 36*, 13611–13616.
1150. Chen, Z. W., Koh, M., Van Driessche, G., Van Beeumen, J. J., Bartsch, R. G., Meyer, T. E., Cusanovich, M. A., and Mathews, F. S. (1994) The structure of flavocytochrome *c* sulfide dehydrogenase from a purple phototrophic bacterium, *Science 266*, 430–432.
1151. Sharp, R. E., White, P., Chapman, S. K., and Reid, G. A. (1994) Role of the interdomain hinge of flavocytochrome b_2 in intra- and inter-protein electron transfer, *Biochemistry 33*, 5115–5120.
1152. Sevrioukova, I. F., Li, H., Zhang, H., Peterson, J. A., and Poulos, T. L. (1999) Structure of a cytochrome P450-redox partner electron-transfer complex, *Proc. Natl. Acad. Sci. U. S. A. 96*, 1863–1868.
1153. Sugishima, M., Sato, H., Higashimoto, Y., Harada, J., Wada, K., Fukuyama, K., and Noguchi, M. (2014) Structural basis for the electron transfer from an open form of NADPH-cytochrome P450 oxidoreductase to heme oxygenase, *Proc. Natl. Acad. Sci. U.S.A. 111*, 2524–2529.
1154. Qin, L., and Kostic, N. M. (1992) Electron-transfer reactions of cytochrome *f* with flavin semiquinones and with plastocyanin. Importance of protein-protein electrostatic interactions and of donor-acceptor coupling, *Biochemistry 31*, 5145–5150.
1155. Sevrioukova, I. F., Hazzard, J. T., Tollin, G., and Poulos, T. L. (2001) Laser flash induced electron transfer in $P450_{cam}$ monooxygenase: Putidaredoxin reductase-putidaredoxin interaction, *Biochemistry 40*, 10592–10600.
1156. Ma, J. K., Wang, Y., Carrell, C. J., Mathews, F. S., and Davidson, V. L. (2007) A single methionine residue dictates the kinetic mechanism of interprotein electron transfer from methylamine dehydrogenase to amicyanin, *Biochemistry 46*, 11137–11146.

1157. Pan, L. P., Hazzard, J. T., Lin, J., Tollin, G., and Chan, S. I. (1991) The electron input to cytochrome *c* oxidase from cytochrome *c*, *J. Am. Chem. Soc. 113*, 5908–5910.
1158. Pelletier, H., and Kraut, J. (1992) Crystal structure of a complex between electron transfer partners, cytochrome *c* peroxidase and cytochrome *c*, *Science 258*, 1748–1755.
1159. Chen, L., Durley, R., Poliks, B. J., Hamada, K., Chen, Z., Mathews, F. S., Davidson, V. L., Satow, Y., Huizinga, E., Vellieux, F. M., and Hol, W. G. J. (1992) Crystal structure of an electron-transfer complex between methylamine dehydrogenase and amicyanin, *Biochemistry 31*, 4959–4964.
1160. Meschi, F., Wiertz, F., Klauss, L., Cavalieri, C., Blok, A., Ludwig, B., Heering, H. A., Merli, A., Rossi, G. L., and Ubbink, M. (2010) Amicyanin transfers electrons from methylamine dehydrogenase to cytochrome c_{551i} via a ping-pong mechanism, not a ternary complex, *J. Am. Chem. Soc. 132*, 14537–14545.
1161. Kurisu, G., Kusunoki, M., Katoh, E., Yamazaki, T., Teshima, K., Onda, Y., Kimata-Ariga, Y., and Hase, T. (2001) Structure of the electron transfer complex between ferredoxin and ferredoxin-NADP(+) reductase, *Nature Struct. Biol. 8*, 117–121.
1162. Axelrod, H. L., Abresch, E. C., Okamura, M. Y., Yeh, A. P., Rees, D. C., and Feher, G. (2002) X-ray structure determination of the cytochrome c_2: Reaction center electron transfer complex from *Rhodobacter sphaeroides*, *J. Mol. Biol. 319*, 501–515.
1163. Toogood, H. S., van Thiel, A., Basran, J., Sutcliffe, M. J., Scrutton, N. S., and Leys, D. (2004) Extensive domain motion and electron transfer in the human electron transferring flavoprotein.Medium chain acyl-CoA dehydrogenase complex, *J. Biol. Chem. 279*, 32904–32912.
1164. Sukumar, N., Chen, Z. W., Ferrari, D., Merli, A., Rossi, G. L., Bellamy, H. D., Chistoserdov, A., Davidson, V. L., and Mathews, F. S. (2006) Crystal structure of an electron transfer complex between aromatic amine dehydrogenase and azurin from *Alcaligenes faecalis*, *Biochemistry 45*, 13500–13510.
1165. Ashikawa, Y., Fujimoto, Z., Noguchi, H., Habe, H., Omori, T., Yamane, H., and Nojiri, H. (2006) Electron transfer complex formation between oxygenase and ferredoxin components in Rieske nonheme iron oxygenase system, *Structure 14*, 1779–1789.
1166. Hagelueken, G., Wiehlmann, L., Adams, T. M., Kolmar, H., Heinz, D. W., Tummler, B., and Schubert, W. D. (2007) Crystal structure of the electron transfer complex rubredoxin rubredoxin–reductase of *Pseudomonas aeruginosa*, *Proc. Natl. Acad. Sci. U.S.A. 104*, 12276–12281.
1167. Senda, M., Kishigami, S., Kimura, S., Fukuda, M., Ishida, T., and Senda, T. (2007) Molecular mechanism of the redox-dependent interaction between NADH-dependent ferredoxin reductase and Rieske-type [2Fe–2S] ferredoxin, *J. Mol. Biol. 373*, 382–400.
1168. Nojiri, M., Koteishi, H., Nakagami, T., Kobayashi, K., Inoue, T., Yamaguchi, K., and Suzuki, S. (2009) Structural basis of interprotein electron transfer for nitrite reduction in denitrification, *Nature 462*, 117–120.
1169. Jensen, L. M., Sanishvili, R., Davidson, V. L., and Wilmot, C. M. (2010) In crystallo post-translational modification within a MauG/pre-methylamine dehydrogenase complex, *Science 327*, 1392–1394.
1170. Shin, S., Abu Tarboush, N., and Davidson, V. L. (2010) Long-range electron transfer reactions between hemes of MauG and different forms of tryptophan tryptophylquinone of methylamine dehydrogenase, *Biochemistry 49*, 5810–5816.
1171. Jasion, V. S., Doukov, T., Pineda, S. H., Li, H., and Poulos, T. L. (2012) Crystal structure of the *Leishmania major* peroxidase-cytochrome *c* complex, *Proc. Natl. Acad. Sci. U.S.A. 109*, 18390–18394.
1172. Hunte, C., Solmaz, S., and Lange, C. (2002) Electron transfer between yeast cytochrome bc_1 complex and cytochrome *c*: A structural analysis, *Biochim. Biophys. Acta 1555*, 21–28.
1173. Liu, R. Q., Miller, M. A., Han, G. W., Hahm, S., Geren, L., Hibdon, S., Kraut, J., Durham, B., and Millett, F. (1994) Role of methionine 230 in intramolecular electron transfer between the oxyferryl heme and tryptophan 191 in cytochrome *c* peroxidase compound II, *Biochemistry 33*, 8678–8685.
1174. Sivaraja, M., Goodin, D. B., Smith, M., and Hoffman, B. M. (1989) Identification by ENDOR of Trp191 as the free-radical site in cytochrome *c* peroxidase compound ES, *Science 245*, 738–740.

1175. Mauro, J. M., Fishel, L. A., Hazzard, J. T., Meyer, T. E., Tollin, G., Cusanovich, M. A., and Kraut, J. (1988) Tryptophan-191→phenylalanine, a proximal-side mutation in yeast cytochrome *c* peroxidase that strongly affects the kinetics of ferrocytochrome *c* oxidation, *Biochemistry 27*, 6243–6256.
1176. Wang, K., Mei, H., Geren, L., Miller, M. A., Saunders, A., Wang, X., Waldner, J. L., Pielak, G. J., Durham, B., and Millett, F. (1996) Design of a ruthenium-cytochrome *c* derivative to measure electron transfer to the radical cation and oxyferryl heme in cytochrome *c* peroxidase, *Biochemistry 35*, 15107–15119.
1177. Hahm, S., Miller, M. A., Geren, L., Kraut, J., Durham, B., and Millett, F. (1994) Reaction of horse cytochrome *c* with the radical and the oxyferryl heme in cytochrome *c* peroxidase compound I, *Biochemistry 33*, 1473–1480.
1178. Miller, M. A., Vitello, L., and Erman, J. E. (1995) Regulation of interprotein electron transfer by Trp 191 of cytochrome *c* peroxidase, *Biochemistry 34*, 12048–12058.
1179. Zhou, J. S., and Hoffman, B. M. (1994) Sternvolmer in reverse: 2:1 Stoichiometry of the cytochrome *c*-cytochrome *c* peroxidase electron-transfer complex, *Science 265*, 1693–1696.
1180. Zhou, J. S., Tran, S. T., McLendon, G., and Hoffman, B. M. (1997) Photoinduced electron transfer between cytochrome *c* peroxidase (D37K) and Zn-substituted cyto-chrome *c*: Probing the two-domain binding and reactivity of the peroxidase, *J. Am. Chem. Soc. 119*, 269–277.
1181. Mei, H., Wang, K., Peffer, N., Weatherly, G., Cohen, D. S., Miller, M., Pielak, G., Durham, B., and Millett, F. (1999) Role of configurational gating in intracomplex electron transfer from cytochrome *c* to the radical cation in cytochrome *c* peroxidase, *Biochemistry 38*, 6846–6854.
1182. Pappa, H. S., Tajbaksh, S., Saunders, A. J., Pielak, G. J., and Poulos, T. L. (1996) Probing the cytochrome *c* peroxidase-cytochrome *c* electron transfer reaction using site specific cross-linking, *Biochemistry 35*, 4837–4845.
1183. Guo, M., Bhaskar, B., Li, H., Barrows, T. P., and Poulos, T. L. (2004) Crystal structure and characterization of a cytochrome *c* peroxidase-cytochrome *c* site-specific cross-link, *Proc. Natl. Acad. Sci. U. S. A. 101*, 5940–5945.
1184. Jeng, M. F., Englander, S. W., Pardue, K., Rogalskyj, J. S., and McLendon, G. (1994) Structural dynamics in an electron-transfer comcomplex, *Nature Struct. Biol. 1*, 234–238.
1185. Tezcan, F. A., Crane, B. R., Winkler, J. R., and Gray, H. B. (2001) Electron tunneling in protein crystals, *Proc. Natl. Acad. Sci. U. S. A. 98*, 5002–5006.
1186. Miller, M. A., Geren, L., Han, G. W., Saunders, A., Beasley, J., Pielak, G. J., Durham, B., Millett, F., and Kraut, J. (1996) Identifying the physiological electron transfer site of cytochrome *c* peroxidase by structure-based engineering, *Biochemistry 35*, 667–673.
1187. Schram, B. L., and Kroes, H. H. (1971) Structure of phycocyanobilin, *Eur. J. Biochem. 19*, 581–594.
1188. Wedemayer, G. J., Kidd, D. G., Wemmer, D. E., and Glazer, A. N. (1992) Phycobilins of cryptophycean algae. Occurrence of dihydrobiliverdin and mesobiliverdin in cryptomonad biliproteins, *J. Biol. Chem. 267*, 7315–7331.
1189. Lagarias, J. C., Glazer, A. N., and Rapoport, H. (1979) Chromopeptides from C-phycocyanin: Structure and linkage of a phycocyanobilin bound to the β-subunit, *J. Am. Chem. Soc. 101*, 5030–5037.
1190. Glazer, A. N. (1984) Phycobilisome. A macromolecular complex optimized for light energy transfer, *Biochim. Biophys. Acta 768*, 29–51.
1191. Schoenleber, R. W., Leung, S. L., Lundell, D. J., Glazer, A. N., and Rapoport, H. (1983) Chromopeptides from phycoerythrins: Structure and linkage of a phycoerythrobilin tryptic tripeptide derived from a B-phycoerythrin, *J. Am. Chem. Soc. 105*, 4072–4076.
1192. Wilk, K. E., Harrop, S. J., Jankova, L., Edler, D., Keenan, G., Sharples, F., Hiller, R. G., and Curmi, P. M. (1999) Evolution of a light-harvesting protein by addition of new subunits and rearrangement of conserved elements: Crystal structure of a cryptophyte phycoerythrin at 1.63 Å resolution, *Proc. Natl. Acad. Sci. U. S. A. 96*, 8901–8906.
1193. Ficner, R., Lobeck, K., Schmidt, G., and Huber, R. (1992) Isolation, crystallization, crystal structure analysis and refinement of B-phycoerythrin from the red alga *Porphyridium sordidum* at 2.2 Å resolution, *J. Mol. Biol. 228*, 935–950.

1194. Collins, A. M., Wen, J., and Blankenship, R. E. (2012) Photosynthetic light-harvesting complexes, In *Molecular solar fuels* (Wydrzynski, T. J., and Hillier, W., Eds.), pp 85–106, Royal Society of Chemistry, Cambridge, U. K.
1195. Qin, X. C., Suga, M., Kuang, T. Y., and Shen, J. R. (2015) Structural basis for energy transfer pathways in the plant PSI-LHCI supercomplex, *Science 348*, 989–995.
1196. Liu, Z., Yan, H., Wang, K., Kuang, T., Zhang, J., Gui, L., An, X., and Chang, W. (2004) Crystal structure of spinach major light-harvesting complex at 2.72 Å resolution, *Nature 428*, 287–292.
1197. Kuhlbrandt, W., Wang, D. N., and Fujiyoshi, Y. (1994) Atomic model of plant light-harvesting complex by electron crystallography, *Nature 367*, 614–621.
1198. Schubert, A., Beenken, W. J., Stiel, H., Voigt, B., Leupold, D., and Lokstein, H. (2002) Excitonic coupling of chlorophylls in the plant light-harvesting complex LHC-II, *Biophys. J. 82*, 1030–1039.
1199. Amarnath, K., Bennett, D. I., Schneider, A. R., and Fleming, G. R. (2016) Multiscale model of light harvesting by photosystem II in plants, *Proc. Natl. Acad. Sci. U. S. A. 113*, 1156–1161.
1200. Wei, X., Su, X., Cao, P., Liu, X., Chang, W., Li, M., Zhang, X., and Liu, Z. (2016) Structure of spinach photosystem II-LHCII supercomplex at 3.2 Å resolution, *Nature 534*, 69–74.
1201. Su, X., Ma, J., Wei, X., Cao, P., Zhu, D., Chang, W., Liu, Z., Zhang, X., and Li, M. (2017) Structure and assembly mechanism of plant $C_2S_2M_2$-type PSII-LHCII supercomplex, *Science 357*, 815–820.
1202. Palsson, L. O., Flemming, C., Gobets, B., van Grondelle, R., Dekker, J. P., and Schlodder, E. (1998) Energy transfer and charge separation in photosystem I: P700 oxidation upon selective excitation of the long-wavelength antenna chlorophylls of *Synechococcus elongatus*, *Biophys. J. 74*, 2611–2622.
1203. Bryant, D. A., Guglielmi, G., Tandeaudemarsac, N., Castets, A. M., and Cohenbazire, G. (1979) The structure of cyanobacterial phycobilisomes: A model, *Arch. Microbiol. 123*, 113–127.
1204. Duerring, M., Schmidt, G. B., and Huber, R. (1991) Isolation, crystallization, crystal structure analysis and refinement of constitutive C-phycocyanin from the chromatically adapting cyanobacterium *Fremyella diplosiphon* at 1.66 Å resolution, *J. Mol. Biol. 217*, 577–592.
1205. Kyte, J. (2007) *Structure in protein chemistry: Second edition*, pp 472–473, Garland Science, New York.
1206. Brejc, K., Ficner, R., Huber, R., and Steinbacher, S. (1995) Isolation, crystallization, crystal structure analysis and refinement of allophycocyanin from the cyanobacterium *Spirulina platensis* at 2.3 Å resolution, *J. Mol. Biol. 249*, 424–440.
1207. Arteni, A. A., Ajlani, G., and Boekema, E. J. (2009) Structural organisation of phycobilisomes from *Synechocystis* sp. Strain pcc6803 and their interaction with the membrane, *Biochim. Biophys. Acta 1787*, 272–279.
1208. Arteni, A. A., Liu, L. N., Aartsma, T. J., Zhang, Y. Z., Zhou, B. C., and Boekema, E. J. (2008) Structure and organization of phycobilisomes on membranes of the red alga *Porphyridium cruentum*, *Photosynth. Res. 95*, 169–174.
1209. Gantt, E., and Lipschultz, C. A. (1980) Structure and phycobiliprotein composition of phycobilisomes from *Griffithsia pacifica* (rhodophyceae), *J Phycol 16*, 394–398.
1210. Guglielmi, G., Cohenbazire, G., and Bryant, D. A. (1981) The structure of *Gloeobacter violaceus* and its phycobilisomes, *Arch. Microbiol. 129*, 181–189.
1211. Liu, H. J., Zhang, H., Niedzwiedzki, D. M., Prado, M., He, G. N., Gross, M. L., and Blankenship, R. E. (2013) Phycobilisomes supply excitations to both photosystems in a megacomplex in cyanobacteria, *Science 342*, 1104–1107.
1212. Zhang, J., Ma, J., Liu, D., Qin, S., Sun, S., Zhao, J., and Sui, S. F. (2017) Structure of phycobilisome from the red alga *Griffithsia pacifica*, *Nature 551*, 57–63.
1213. Ma, J., You, X., Sun, S., Wang, X., Qin, S., and Sui, S. F. (2020) Structural basis of energy transfer in *Porphyridium purpureum* phycobilisome, *Nature 579*, 146–151.
1214. Yu, L. J., Suga, M., Wang-Otomo, Z. Y., and Shen, J. R. (2018) Structure of photosynthetic LH1-RC supercomplex at 1.9 Å resolution, *Nature 556*, 209–213.
1215. Roszak, A. W., Howard, T. D., Southall, J., Gardiner, A. T., Law, C. J., Isaacs, N. W., and Cogdell, R. J. (2003) Crystal structure of the

RC-LH1 core complex from *Rhodopseudomonas palustris*, *Science 302*, 1969–1972.
1216. McDermott, G., Prince, S. M., Freer, A. A., Hawthornthwaite-Lawless, A. M., Papiz, M. Z., Cogdell, R. J., and Isaacs, N. W. (1995) Crystal structure of an integral membrane light-harvesting complex from photosynthetic bacteria, *Nature 374*, 517–521.
1217. Sener, M. K., Olsen, J. D., Hunter, C. N., and Schulten, K. (2007) Atomic-level structural and functional model of a bacterial photosynthetic membrane vesicle, *Proc. Natl. Acad. Sci. U. S. A. 104*, 15723–15728.
1218. Nagarajan, V., and Parson, W. W. (1997) Excitation energy transfer between the B850 and B875 antenna complexes of *Rhodobacter sphaeroides*, *Biochemistry 36*, 2300–2306.
1219. Hunter, C. N., Bergstrom, H., van Grondelle, R., and Sundstrom, V. (1990) Energy-transfer dynamics in three light-harvesting mutants of *Rhodobacter sphaeroides*: A picosecond spectroscopy study, *Biochemistry 29*, 3203–3207.
1220. Engel, G. S., Calhoun, T. R., Read, E. L., Ahn, T. K., Mancal, T., Cheng, Y. C., Blankenship, R. E., and Fleming, G. R. (2007) Evidence for wavelike energy transfer through quantum coherence in photosynthetic systems, *Nature 446*, 782–786.
1221. Scholes, G. D., Fleming, G. R., Olaya-Castro, A., and van Grondelle, R. (2011) Lessons from nature about solar light harvesting, *Nature Chem. 3*, 763–774.
1222. Sener, M., Strumpfer, J., Hsin, J., Chandler, D., Scheuring, S., Hunter, C. N., and Schulten, K. (2011) Forster energy transfer theory as reflected in the structures of photosynthetic light-harvesting systems, *ChemPhysChem 12*, 518–531.
1223. Croce, R., and van Amerongen, H. (2014) Natural strategies for photosynthetic light harvesting, *Nature Chem. Biol. 10*, 492–501.
1224. Forster, T. (1948) Intermolecular energy transference and fluorescence, *Ann. Physik (Leipzig). 2*, 55–75.
1225. Kyte, J. (2007) *Structure in protein chemistry: Second edition*, pp 603–606, Garland Science, New York.
1226. Grabowski, J., and Gantt, E. (1978) Photophysical properties of phycobiliproteins from phycobilisomes: Fluorescence lifetimes, quantum yields, and polarization spectra, *Photochem. Photobiol. 28*, 39–45.
1227. Schirmer, T., Huber, R., Schneider, M., Bode, W., Miller, M., and Hackert, M. L. (1986) Crystal structure analysis and refinement at 2.5 Å of hexameric C-phycocyanin from the cyanobacterium *Agmenellum quadruplicatum*. The molecular model and its implications for light-harvesting, *J. Mol. Biol. 188*, 651–676.
1228. van Oijen, A. M., Ketelaars, M., Kohler, J., Aartsma, T. J., and Schmidt, J. (1999) Unraveling the electronic structure of individual photosynthetic pigment-protein complexes, *Science 285*, 400–402.
1229. Vulto, S. I. E., Kennis, J. T. M., Streltsov, A. M., Amesz, J., and Aartsma, T. J. (1999) Energy relaxation within the B850 absorption band of the isolated light-harvesting complex LH2 from *Rhodopseudomonas acidophila* at low temperature, *J. Phys. Chem. B 103*, 878–883.
1230. Cogdell, R. J., and Scheer, H. (1985) Circular dichroism of light-harvesting complexes from purple photosynthetic bacteria, *Photochem. Photobiol. 42*, 669–678.
1231. Hess, S., Visscher, K. J., Pullerits, T., Sundstrom, V., Fowler, G. J., and Hunter, C. N. (1994) Enhanced rates of subpicosecond energy transfer in blue-shifted light harvesting LH2 mutants of *Rhodobacter sphaeroides*, *Biochemistry 33*, 8300–8305.
1232. Trautman, J. K., Shreve, A. P., Violette, C. A., Frank, H. A., Owens, T. G., and Albrecht, A. C. (1990) Femtosecond dynamics of energy transfer in B800-850 light-harvesting complexes of *Rhodobacter sphaeroides*, *Proc. Natl. Acad. Sci. U. S. A. 87*, 215–219.
1233. Gardiner, A. T., Cogdell, R. J., and Takaichi, S. (1993) The effect of growth-conditions on the light-harvesting apparatus in *Rhodopseudomonas acidophila*, *Photosynth. Res. 38*, 159–167.
1234. Ramsey, A. J., Alderfer, J. L., and Jorns, M. S. (1992) Energy transduction during catalysis by *Escherichia coli* DNA photolyase, *Biochemistry 31*, 7134–7142.
1235. Eker, A. P., Kooiman, P., Hessels, J. K., and Yasui, A. (1990) DNA Photoreactivating enzyme from the cyanobacterium *Anacystis nidulans*, *J. Biol. Chem. 265*, 8009–8015.
1236. Ueda, T., Kato, A., Kuramitsu, S., Terasawa, H., and Shimada, I. (2005) Identification and characterization of a second chromophore of

DNA photolyase from *Thermus thermophilus* HB27, *J. Biol. Chem. 280*, 36237–36243.
1237. Fujihashi, M., Numoto, N., Kobayashi, Y., Mizushima, A., Tsujimura, M., Nakamura, A., Kawarabayasi, Y., and Miki, K. (2007) Crystal structure of archaeal photolyase from *Sulfolobus tokodaii* with two FAD molecules: Implication of a novel light-harvesting cofactor, *J. Mol. Biol. 365*, 903–910.
1238. Kavakli, I. H., and Sancar, A. (2004) Analysis of the role of intraprotein electron transfer in photoreactivation by DNA photolyase *in vivo*, *Biochemistry 43*, 15103–15110.
1239. Kodali, G., Siddiqui, S. U., and Stanley, R. J. (2009) Charge redistribution in oxidized and semiquinone *E. coli* DNA photolyase upon photoexcitation: Stark spectroscopy reveals a rationale for the position of Trp382, *J. Am. Chem. Soc. 131*, 4795–4807.
1240. Beale, S. I., and Cornejo, J. (1991) Biosynthesis of phycobilins. 3(*Z*)-phycoerythrobilin and 3(*Z*)-phycocyanobilin are intermediates in the formation of 3(*E*)-phycocyanobilin from biliverdin IX α, *J. Biol. Chem. 266*, 22333–22340.
1241. Gegiou, D., Muszkat, K. A., and Fischer, E. (1968) Temperature dependence of photoisomerization. VI. Viscosity effect, *J. Am. Chem. Soc. 90*, 12–18.
1242. Leitner, D. M., Levine, B., Quenneville, J., Martinez, T. J., and Wolynes, P. G. (2003) Quantum energy flow and *trans*-stilbene photoisomerization: An example of a non-RRKM reaction, *J. Phys. Chem. A 107*, 10706–10716.
1243. Quenneville, J., and Martinez, T. J. (2003) Ab initio study of cis-trans photoisomerization in stilbene and ethylene, *J. Phys. Chem. A 107*, 829–837.
1244. Ladanyl, B. M., and Evans, G. T. (1983) Kinetic models for stilbene photoisomerization: Comparison of theory and experiments, *J. Chem. Phys. 79*, 944–952.
1245. Hoff, W. D., Dux, P., Hard, K., Devreese, B., Nugteren-Roodzant, I. M., Crielaard, W., Boelens, R., Kaptein, R., van Beeumen, J., and Hellingwerf, K. J. (1994) Thiol ester-linked *p*-coumaric acid as a new photoactive prosthetic group in a protein with rhodopsin-like photochemistry, *Biochemistry 33*, 13959–13962.
1246. Hoff, W. D., Devreese, B., Fokkens, R., Nugteren-Roodzant, I. M., Van Beeumen, J., Nibbering, N., and Hellingwerf, K. J. (1996) Chemical reactivity and spectroscopy of the thiol ester-linked *p*-coumaric acid chromophore in the photoactive yellow protein from *Ectothiorhodospira halophila*, *Biochemistry 35*, 1274–1281.
1247. Meyer, T. E., Tollin, G., Hazzard, J. H., and Cusanovich, M. A. (1989) Photoactive yellow protein from the purple phototrophic bacterium, *Ectothiorhodospira halophila*. Quantum yield of photobleaching and effects of temperature, alcohols, glycerol, and sucrose on kinetics of photobleaching and recovery, *Biophys. J. 56*, 559–564.
1248. Pande, K., Hutchison, C. D., Groenhof, G., Aquila, A., Robinson, J. S., Tenboer, J., Basu, S., Boutet, S., DePonte, D. P., Liang, M., White, T. A., Zatsepin, N. A., Yefanov, O., Morozov, D., Oberthuer, D., Gati, C., Subramanian, G., James, D., Zhao, Y., Koralek, J., Brayshaw, J., Kupitz, C., Conrad, C., Roy-Chowdhury, S., Coe, J. D., Metz, M., Xavier, P. L., Grant, T. D., Koglin, J. E., Ketawala, G., Fromme, R., Srajer, V., Henning, R., Spence, J. C., Ourmazd, A., Schwander, P., Weierstall, U., Frank, M., Fromme, P., Barty, A., Chapman, H. N., Moffat, K., van Thor, J. J., and Schmidt, M. (2016) Femtosecond structural dynamics drives the *trans/cis* isomerization in photoactive yellow protein, *Science 352*, 725–729.
1249. Jung, Y. O., Lee, J. H., Kim, J., Schmidt, M., Moffat, K., Srajer, V., and Ihee, H. (2013) Volume-conserving *trans-cis* isomerization pathways in photoactive yellow protein visualized by picosecond X-ray crystallography, *Nat Chem 5*, 212–220.
1250. Schotte, F., Cho, H. S., Kaila, V. R., Kamikubo, H., Dashdorj, N., Henry, E. R., Graber, T. J., Henning, R., Wulff, M., Hummer, G., Kataoka, M., and Anfinrud, P. A. (2012) Watching a signaling protein function in real time via 100-ps time-resolved Laue crystallography, *Proc. Natl. Acad. Sci. U. S. A. 109*, 19256–19261.
1251. Ihee, H., Rajagopal, S., Srajer, V., Pahl, R., Anderson, S., Schmidt, M., Schotte, F., Anfinrud, P. A., Wulff, M., and Moffat, K. (2005) Visualizing reaction pathways in photoactive yellow protein from nanoseconds to seconds, *Proc. Natl. Acad. Sci. U. S. A. 102*, 7145–7150.
1252. Genick, U. K., Soltis, S. M., Kuhn, P., Canestrelli, I. L., and Getzoff, E. D. (1998) Structure

at 0.85 Å resolution of an early protein photocycle intermediate, *Nature 392*, 206–209.
1253. Imamoto, Y., Kamikubo, H., Harigai, M., Shimizu, N., and Kataoka, M. (2002) Light-induced global conformational change of photoactive yellow protein in solution, *Biochemistry 41*, 13595–13601.
1254. Sprenger, W. W., Hoff, W. D., Armitage, J. P., and Hellingwerf, K. J. (1993) The eubacterium *Ectothiorhodospira halophila* is negatively phototactic, with a wavelength dependence that fits the absorption spectrum of the photoactive yellow protein, *J. Bacteriol. 175*, 3096–3104.
1255. Meyer, T. E., Yakali, E., Cusanovich, M. A., and Tollin, G. (1987) Properties of a water-soluble, yellow protein isolated from a halophilic phototrophic bacterium that has photochemical activity analogous to sensory rhodopsin, *Biochemistry 26*, 418–423.
1256. Ruddat, A., Schmidt, P., Gatz, C., Braslavsky, S. E., Gartner, W., and Schaffner, K. (1997) Recombinant type A and B phytochromes from potato. Transient absorption spectroscopy, *Biochemistry 36*, 103–111.
1257. Rudiger, W., Thummler, F., Cmiel, E., and Schneider, S. (1983) Chromophore structure of the physiologically active form (P_{fr}) of phytochrome, *Proc. Natl. Acad. Sci. U. S. A. 80*, 6244–6248.
1258. Zhang, C. F., Farrens, D. L., Bjorling, S. C., Song, P. S., and Kliger, D. S. (1992) Time-resolved absorption studies of native etiolated oat phytochrome, *J. Am. Chem. Soc. 114*, 4569–4580.
1259. Briggs, W. R., and Olney, M. A. (2001) Photoreceptors in plant photomorphogenesis to date. Five phytochromes, two cryptochromes, one phototropin, and one superchrome, *Plant Physiol 125*, 85–88.
1260. Chen, E., Lapko, V. N., Lewis, J. W., Song, P. S., and Kliger, D. S. (1996) Mechanism of native oat phytochrome photoreversion: A time-resolved absorption investigation, *Biochemistry 35*, 843–850.
1261. Palczewski, K., Kumasaka, T., Hori, T., Behnke, C. A., Motoshima, H., Fox, B. A., Le Trong, I., Teller, D. C., Okada, T., Stenkamp, R. E., Yamamoto, M., and Miyano, M. (2000) Crystal structure of rhodopsin: A G protein-coupled receptor, *Science 289*, 739–745.
1262. Okada, T., Fujiyoshi, Y., Silow, M., Navarro, J., Landau, E. M., and Shichida, Y. (2002) Functional role of internal water molecules in rhodopsin revealed by X-ray crystallography, *Proc. Natl. Acad. Sci. U.S.A. 99*, 5982–5987.
1263. Okada, T., Sugihara, M., Bondar, A. N., Elstner, M., Entel, P., and Buss, V. (2004) The retinal conformation and its environment in rhodopsin in light of a new 2.2 Å crystal structure, *J. Mol. Biol. 342*, 571–583.
1264. Yan, M., Manor, D., Weng, G., Chao, H., Rothberg, L., Jedju, T. M., Alfano, R. R., and Callender, R. H. (1991) Ultrafast spectroscopy of the visual pigment rhodopsin, *Proc. Natl. Acad. Sci. U. S. A. 88*, 9809–9812.
1265. Schnedermann, C., Muders, V., Ehrenberg, D., Schlesinger, R., Kukura, P., and Heberle, J. (2016) Vibronic dynamics of the ultrafast all-*trans* to 13-*cis* photoisomerization of retinal in channelrhodopsin-1, *J. Am. Chem. Soc. 138*, 4757–4762.
1266. Kandori, H., Matuoka, S., Shichida, Y., Yoshizawa, T., Ito, M., Tsukida, K., Balogh-Nair, V., and Nakanishi, K. (1989) Mechanism of isomerization of rhodopsin studied by use of 11-*cis*-locked rhodopsin analogues excited with a picosecond laser pulse, *Biochemistry 28*, 6460–6467.
1267. Choe, H. W., Kim, Y. J., Park, J. H., Morizumi, T., Pai, E. F., Krauss, N., Hofmann, K. P., Scheerer, P., and Ernst, O. P. (2011) Crystal structure of metarhodopsin II, *Nature 471*, 651–655.
1268. Murakami, M., and Kouyama, T. (2011) Crystallographic analysis of the primary photochemical reaction of squid rhodopsin, *J. Mol. Biol. 413*, 615–627.
1269. Hubbard, R., and Kropf, A. (1958) The action of light on rhodopsin, *Proc. Natl. Acad. Sci. U. S. A. 44*, 130–139.
1270. Green, B. H., Monger, T. G., Alfano, R. R., Aton, B., and Callender, R. H. (1977) *Cis-trans* isomerisation in rhodopsin occurs in picoseconds, *Nature 269*, 179–180.
1271. Maiti, P., Kong, J., Kim, S. R., Sparrow, J. R., Allikmets, R., and Rando, R. R. (2006) Small molecule RPE65 antagonists limit the visual cycle and prevent lipofuscin formation, *Biochemistry 45*, 852–860.
1272. Kiser, P. D., Golczak, M., Lodowski, D. T., Chance, M. R., and Palczewski, K. (2009) Crystal structure of native RPE65, the retinoid isomerase of the visual cycle, *Proc. Natl. Acad. Sci. U.S.A. 106*, 17325–17330.

1273. Moiseyev, G., Chen, Y., Takahashi, Y., Wu, B. X., and Ma, J. X. (2005) RPE65 is the isomerohydrolase in the retinoid visual cycle, *Proc. Natl. Acad. Sci. U.S.A. 102*, 12413–12418.
1274. Jin, M., Li, S., Moghrabi, W. N., Sun, H., and Travis, G. H. (2005) RPE65 is the retinoid isomerase in bovine retinal pigment epithelium, *Cell 122*, 449–459.
1275. Redmond, T. M., Poliakov, E., Kuo, S., Chander, P., and Gentleman, S. (2010) RPE65, visual cycle retinol isomerase, is not inherently 11-*cis*-specific: Support for a carbocation mechanism of retinol isomerization, *J. Biol. Chem. 285*, 1919–1927.
1276. Pettei, M. J., Yudd, A. P., Nakanishi, K., Henselman, R., and Stoeckenius, W. (1977) Identification of retinal isomers isolated from bacteriorhodopsin, *Biochemistry 16*, 1955–1959.
1277. Smith, S. O., Myers, A. B., Pardoen, J. A., Winkel, C., Mulder, P. P., Lugtenburg, J., and Mathies, R. (1984) Determination of retinal Schiff base configuration in bacteriorhodopsin, *Proc. Natl. Acad. Sci. U. S. A. 81*, 2055–2059.
1278. Harbison, G. S., Smith, S. O., Pardoen, J. A., Winkel, C., Lugtenburg, J., Herzfeld, J., Mathies, R., and Griffin, R. G. (1984) Dark-adapted bacteriorhodopsin contains 13-*cis*, 15-*syn* and all-*trans*, 15-*anti* retinal Schiff bases, *Proc. Natl. Acad. Sci. U. S. A. 81*, 1706–1709.
1279. Schobert, B., Cupp-Vickery, J., Hornak, V., Smith, S., and Lanyi, J. (2002) Crystallographic structure of the K intermediate of bacteriorhodopsin: Conservation of free energy after photoisomerization of the retinal, *J. Mol. Biol. 321*, 715–726.
1280. Varo, G., and Lanyi, J. K. (1991) Thermodynamics and energy coupling in the bacteriorhodopsin photocycle, *Biochemistry 30*, 5016–5022.
1281. Luecke, H., Schobert, B., Richter, H. T., Cartailler, J. P., and Lanyi, J. K. (1999) Structure of bacteriorhodopsin at 1.55 Å resolution, *J. Mol. Biol. 291*, 899–911.
1282. Edman, K., Nollert, P., Royant, A., Belrhali, H., Pebay-Peyroula, E., Hajdu, J., Neutze, R., and Landau, E. M. (1999) High-resolution X-ray structure of an early intermediate in the bacteriorhodopsin photocycle, *Nature 401*, 822–826.
1283. Royant, A., Edman, K., Ursby, T., Pebay-Peyroula, E., Landau, E. M., and Neutze, R. (2000) Helix deformation is coupled to vectorial proton transport in the photocycle of bacteriorhodopsin, *Nature 406*, 645–648.
1284. Lanyi, J., K., and Schobert, B. (2003) Mechanism of proton transport in bacteriorhodopsin from crystallographic structures of the K, L, M_1, M_2, and M_2' intermediates of the photocycle, *J. Mol. Biol. 328*, 439–450.
1285. Lanyi, J. K., and Schobert, B. (2004) Local-global conformational coupling in a heptahelical membrane protein: Transport mechanism from crystal structures of the nine states in the bacteriorhodopsin photocycle, *Biochemistry 43*, 3–8.
1286. Schobert, B., Brown, L. S., and Lanyi, J. K. (2003) Crystallographic structures of the M and N intermediates of bacteriorhodopsin: Assembly of a hydrogen-bonded chain of water molecules between Asp-96 and the retinal Schiff base, *J. Mol. Biol. 330*, 553–570.
1287. Kouyama, T., Nishikawa, T., Tokuhisa, T., and Okumura, H. (2004) Crystal structure of the L intermediate of bacteriorhodopsin: Evidence for vertical translocation of a water molecule during the proton pumping cycle, *J. Mol. Biol. 335*, 531–546.
1288. Lanyi, J. K. (2004) What is the real crystallographic structure of the L photointermediate of bacteriorhodopsin?, *Biochim. Biophys. Acta 1658*, 14–22.
1289. Skopintsev, P., Ehrenberg, D., Weinert, T., James, D., Kar, R. K., Johnson, P. J. M., Ozerov, D., Furrer, A., Martiel, I., Dworkowski, F., Nass, K., Knopp, G., Cirelli, C., Arrell, C., Gashi, D., Mous, S., Wranik, M., Gruhl, T., Kekilli, D., Brunle, S., Deupi, X., Schertler, G. F. X., Benoit, R. M., Panneels, V., Nogly, P., Schapiro, I., Milne, C., Heberle, J., and Standfuss, J. (2020) Femtosecond-to-millisecond structural changes in a light-driven sodium pump, *Nature 583*, 314–318.
1290. Nango, E., Royant, A., Kubo, M., Nakane, T., Wickstrand, C., Kimura, T., Tanaka, T., Tono, K., Song, C., Tanaka, R., Arima, T., Yamashita, A., Kobayashi, J., Hosaka, T., Mizohata, E., Nogly, P., Sugahara, M., Nam, D., Nomura, T., Shimamura, T., Im, D., Fujiwara, T., Yamanaka, Y., Jeon, B., Nishizawa, T., Oda, K., Fukuda, M., Andersson, R., Bath, P., Dods, R., Davidsson, J., Matsuoka, S., Kawatake, S., Murata, M., Nureki, O., Owada, S., Kameshima, T., Hatsui, T., Joti, Y.,

Schertler, G., Yabashi, M., Bondar, A. N., Standfuss, J., Neutze, R., and Iwata, S. (2016) A three-dimensional movie of structural changes in bacteriorhodopsin, *Science 354*, 1552–1557.
1291. Ni, Q. Z., Can, T. V., Daviso, E., Belenky, M., Griffin, R. G., and Herzfeld, J. (2018) Primary transfer step in the light-driven ion pump bacteriorhodopsin: An irreversible U-turn revealed by dynamic nuclear polarization-enhanced magic angle spinning NMR, *J. Am. Chem. Soc. 140*, 4085–4091.
1292. Weinert, T., Skopintsev, P., James, D., Dworkowski, F., Panepucci, E., Kekilli, D., Furrer, A., Brunle, S., Mous, S., Ozerov, D., Nogly, P., Wang, M., and Standfuss, J. (2019) Proton uptake mechanism in bacteriorhodopsin captured by serial synchrotron crystallography, *Science 365*, 61–65.
1293. Bartberger, M. D., Fukuto, J. M., and Houk, K. N. (2001) On the acidity and reactivity of HNO in aqueous solution and biological systems, *Proc. Natl. Acad. Sci. U. S. A. 98*, 2194–2198.
1294. Goddard, W. A., and Olafson, B. D. (1979) Theoretical studies of the bonding of O_2 to hemoglobin: Implications for cooperativity, In *Biochemical and Clinical Aspects of Oxygen* (Caughey, W., Ed.), pp 87–123, Academic Press, New York.
1295. Ingraham, L. L., and Meyer, D.L. (1985) *Biochemistry of Dioxygen*, Plenum Press, New York.
1296. Lapidot, A., and Irving, C. S. (1974) The electronic structure of coordinated oxygen, In *Molecular Oxygen in Biology* (Hayaishi, O., Ed.), pp 33–80, North Holland Publishing, Amsterdam.
1297. Borden, W. T., Hoffmann, R., Stuyver, T., and Chen, B. (2017) Dioxygen: What makes this triplet diradical kinetically persistent?, *J. Am. Chem. Soc. 139*, 9010–9018.
1298. Kearns, D. R. (1971) Physical and chemical properties of singlet molecular oxygen, *Chem. Rev. 71*, 395–427.
1299. Ilan, Y. A., Czapski, G., and Meisel, D. (1976) The one-electron transfer redox potentials of free radicals. I. The oxygen/superoxide system, *Biochim. Biophys. Acta 430*, 209–224.
1300. Bertini, I., Gray, H. B., Stiefel, E. I., and Selverstone, J. (2007) *Biological Inorganic Chemistry : Structure and Reactivity*, University Science Books, Sausalito, California.
1301. Wood, P. M. (1974) Redox potential of the system oxygen-superoxide, *FEBS Lett. 44*, 22–24.
1302. Bielski, B. H. J. (1978) Reevaluation of the spectral and kinetic properties of hydroperoxo and superoxide anion free radicals, *Photochem. Photobiol. 28*, 645–649.
1303. George, P. (1965) The fitness of oxygen, In *Oxidases and Related Redox Systems* (King, T. E., Mason, H. S., and Morrison, M., Eds.), pp 1–36, John Wiley, New York.
1304. Ferreira, P., Hernandez-Ortega, A., Herguedas, B., Martinez, A. T., and Medina, M. (2009) Aryl-alcohol oxidase involved in lignin degradation: A mechanistic study based on steady and pre-steady state kinetics and primary and solvent isotope effects with two alcohol substrates, *J. Biol. Chem. 284*, 24840–24847.
1305. Shamsipur, M., and Tabrizi, M. A. (2014) Achieving direct electrochemistry of glucose oxidase by one step electrochemical reduction of graphene oxide and its use in glucose sensing, *Mater Sci Eng C Mater Biol Appl 45*, 103–108.
1306. Su, Q., and Klinman, J. P. (1999) Nature of oxygen activation in glucose oxidase from *Aspergillus niger*: The importance of electrostatic stabilization in superoxide formation, *Biochemistry 38*, 8572–8581.
1307. Roth, J. P., and Klinman, J. P. (2003) Catalysis of electron transfer during activation of O_2 by the flavoprotein glucose oxidase, *Proc. Natl. Acad. Sci. U. S. A. 100*, 62–67.
1308. Kemal, C., Chan, T. W., and Bruice, T. C. (1977) Reaction of $^3O_2$ with dihydroflavins. 1. $N^{3,5}$-dimethyl-1,5-dihydrolumiflavin and 1,5-dihydroisoalloxazines, *J. Am. Chem. Soc. 99*, 7272–7286.
1309. Wohlfahrt, G., Witt, S., Hendle, J., Schomburg, D., Kalisz, H. M., and Hecht, H. J. (1999) 1.8 and 1.9 Å resolution structures of the *Penicillium amagasakiense* and *Aspergillus niger* glucose oxidases as a basis for modelling substrate complexes, *Acta Crystallogr. D 55*, 969–977.
1310. Wang, R., and Thorpe, C. (1991) Reactivity of medium-chain acyl-CoA dehydrogenase toward molecular oxygen, *Biochemistry 30*, 7895–7901.
1311. Ballou, D., Palmer, G., and Massey, V. (1969) Direct demonstration of superoxide anion production during the oxidation of reduced

flavin and of its catalytic decomposition by erythrocuprein, *Biochem. Biophys. Res. Commun. 36*, 898–904.
1312. Porras, A. G., Olson, J. S., and Palmer, G. (1981) The reaction of reduced xanthine oxidase with oxygen. Kinetics of peroxide and superoxide formation, *J. Biol. Chem. 256*, 9096–9103.
1313. Pauling, L., and Coryell, C. D. (1936) The magnetic properties and structure of hemoglobin, oxyhemoglobin and carbonmonoxyhemoglobin, *Proc. Natl. Acad. Sci. U. S. A. 22*, 210–216.
1314. Ito, N., Phillips, S. E., Stevens, C., Ogel, Z. B., McPherson, M. J., Keen, J. N., Yadav, K. D., and Knowles, P. F. (1991) Novel thioether bond revealed by a 1.7 Å crystal structure of galactose oxidase, *Nature 350*, 87–90.
1315. Whittaker, M. M., and Whittaker, J. W. (1990) A tyrosine-derived free radical in apogalactose oxidase, *J. Biol. Chem. 265*, 9610–9613.
1316. Whittaker, M. M., and Whittaker, J. W. (1988) The active site of galactose oxidase, *J. Biol. Chem. 263*, 6074–6080.
1317. Strickland, S., and Massey, V. (1973) The mechanism of action of the flavoprotein melilotate hydroxylase, *J. Biol. Chem. 248*, 2953–2962.
1318. Entsch, B., Ballou, D. P., and Massey, V. (1976) Flavin-oxygen derivatives involved in hydroxylation by *p*-hydroxybenzoate hydroxylase, *J. Biol. Chem. 251*, 2550–2563.
1319. Branchaud, B. P., and Walsh, C. T. (1985) Functional group diversity in enzymic oxygenation reactions catalyzed by bacterial flavin-containing cyclohexanone oxygenase, *J. Am. Chem. Soc. 107*, 2153–2161.
1320. Nakamoto, K. D., Perkins, S. W., Campbell, R. G., Bauerle, M. R., Gerwig, T. J., Gerislioglu, S., Wesdemiotis, C., Anderson, M. A., Hicks, K. A., and Snider, M. J. (2019) Mechanism of 6-hydroxynicotinate 3-monooxygenase, a flavin-dependent decarboxylative hydroxylase involved in bacterial nicotinic acid degradation, *Biochemistry 58*, 1751–1763.
1321. Matsushita, T., Kishimoto, S., Hara, K., Hashimoto, H., and Watanabe, K. (2020) Structural and functional analyses of a spiro-carbon-forming, highly promiscuous epoxidase from fungal natural product biosynthesis, *Biochemistry 59*, 4787–4792.
1322. Feng, L., Wang, W., Cheng, J., Ren, Y., Zhao, G., Gao, C., Tang, Y., Liu, X., Han, W., Peng, X., Liu, R., and Wang, L. (2007) Genome and proteome of long-chain alkane degrading *Geobacillus thermodenitrificans* NG80-2 isolated from a deep-subsurface oil reservoir, *Proc. Natl. Acad. Sci. U.S.A. 104*, 5602–5607.
1323. Li, L., Liu, X., Yang, W., Xu, F., Wang, W., Feng, L., Bartlam, M., Wang, L., and Rao, Z. (2008) Crystal structure of long-chain alkane monooxygenase (LadA) in complex with coenzyme FMN: Unveiling the long-chain alkane hydroxylase, *J. Mol. Biol. 376*, 453–465.
1324. Entsch, B., and Ballou, D. P. (1989) Purification, properties, and oxygen reactivity of *p*-hydroxybenzoate hydroxylase from *Pseudomonas aeruginosa*, *Biochim. Biophys. Acta 999*, 313–322.
1325. Wessiak, A., and Bruice, T. C. (1983) Synthesis and study of a 6-amino-5-oxo-3H,5H-uracil and derivatives. The structure of an intermediate proposed in mechanisms of flavin and pterin oxygenases, *J. Am. Chem. Soc. 105*, 4809–4825.
1326. Ghisla, S., Hastings, J. W., Favaudon, V., and Lhoste, J. M. (1978) Structure of the oxygen adduct intermediate in the bacterial luciferase reaction: C nuclear magnetic resonance determination, *Proc. Natl. Acad. Sci. U. S. A. 75*, 5860–5863.
1327. Powlowski, J., Ballou, D. P., and Massey, V. (1990) Studies of the oxidative half-reaction of anthranilate hydroxylase (deaminating) with native and modified substrates, *J. Biol. Chem. 265*, 4969–4975.
1328. Nanni, E. J., Jr., Sawyer, D. T., Ball, S. S., and Bruice, T. C. (1981) Redox chemistry of N^5-ethyl-3-methyllumiflavinium cation and N^5-ethyl-4a-hydroperoxy-3-methyllumiflavin in dimethylformamide. Evidence for the formation of the N^5-ethyl-4a-hydroperoxy-3-methyllumiflavin anion via radical-radical coupling with superoxide ion, *J. Am. Chem. Soc. 103*, 2797–2802.
1329. Kemal, C., and Bruice, T. C. (1976) Simple synthesis of a 4a-hydroperoxy adduct of a 1,5-dihydroflavine: Preliminary studies of a model for bacterial luciferase, *Proc. Natl. Acad. Sci. U. S. A. 73*, 995–999.
1330. Sucharitakul, J., Prongjit, M., Haltrich, D., and Chaiyen, P. (2008) Detection of a C4a-hydroperoxyflavin intermediate in the reaction of a flavoprotein oxidase, *Biochemistry 47*, 8485–8490.

1331. Visitsatthawong, S., Chenprakhon, P., Chaiyen, P., and Surawatanawong, P. (2015) Mechanism of oxygen activation in a flavin-dependent monooxygenase: A nearly barrier less formation of C4a-hydroperoxyflavin via proton-coupled electron transfer, *J. Am. Chem. Soc. 137*, 9363–9374.
1332. Robinson, R., Badieyan, S., and Sobrado, P. (2013) C4a-Hydroperoxyflavin formation in *N*-hydroxylating flavin monooxygenases is mediated by the 2′-OH of the nicotinamide ribose of NADP(+), *Biochemistry 52*, 9089–9091.
1333. Franceschini, S., Fedkenheuer, M., Vogelaar, N. J., Robinson, H. H., Sobrado, P., and Mattevi, A. (2012) Structural insight into the mechanism of oxygen activation and substrate selectivity of flavin-dependent *N*-hydroxylating monooxygenases, *Biochemistry 51*, 7043–7045.
1334. Shoun, H., Higashi, N., Beppu, T., Nakamura, S., Hiromi, K., and Arima, K. (1979) Studies on the interaction of *p*-hydroxybenzoate hydroxylase with NADPH. Effects of pH and substrates on the enzyme·NADPH complex formation, *J. Biol. Chem. 254*, 10944–10951.
1335. Bruice, T. C., Noar, J. B., Ball, S. S., and Venkataram, U. V. (1983) Monooxygen donation potential of 4a-hydroperoxyflavins as compared with those of a percarboxylic acid and other hydroperoxides. Monooxygen donation to olefin, tertiary amine, alkyl sulfide, and iodide ion, *J. Am. Chem. Soc. 105*, 2452–2463.
1336. Murahashi, S., Oda, T., and Masui, Y. (1989) Flavin-catalyzed oxidation of amines and sulfur compounds with hydrogen peroxide, *J. Am. Chem. Soc. 111*, 5002–5003.
1337. Imada, Y., Iida, H., Ono, S., and Murahashi, S. (2003) Flavin catalyzed oxidations of sulfides and amines with molecular oxygen, *J. Am. Chem. Soc. 125*, 2868–2869.
1338. Ryerson, C. C., Ballou, D. P., and Walsh, C. (1982) Mechanistic studies on cyclohexanone oxygenase, *Biochemistry 21*, 2644–2655.
1339. Sheng, D., Ballou, D. P., and Massey, V. (2001) Mechanistic studies of cyclohexanone monooxygenase: Chemical properties of intermediates involved in catalysis, *Biochemistry 40*, 11156–11167.
1340. Ortiz-Maldonado, M., Ballou, D. P., and Massey, V. (1999) Use of free energy relationships to probe the individual steps of hydroxylation of *p*-hydroxybenzoate hydroxylase: Studies with a series of 8-substituted flavins, *Biochemistry 38*, 8124–8137.
1341. Hartmann, S., Hultschig, C., Eisenreich, W., Fuchs, G., Bacher, A., and Ghisla, S. (1999) NIH shift in flavin-dependent monooxygenation: Mechanistic studies with 2-aminobenzoyl-CoA monooxygenase/reductase, *Proc. Natl. Acad. Sci. U. S. A. 96*, 7831–7836.
1342. Alfieri, A., Fersini, F., Ruangchan, N., Prongjit, M., Chaiyen, P., and Mattevi, A. (2007) Structure of the monooxygenase component of a two-component flavoprotein monooxygenase, *Proc. Natl. Acad. Sci. U. S. A. 104*, 1177–1182.
1343. Wessiak, A., Schopfer, L. M., and Massey, V. (1984) pH Dependence of the reoxidation of *p*-hydroxybenzoate hydroxylase·2,4-dihydroxybenzoate complex, *J. Biol. Chem. 259*, 12547–12556.
1344. Schopfer, L. M., Wessiak, A., and Massey, V. (1991) Interpretation of the spectra observed during oxidation of *p*-hydroxybenzoate hydroxylase reconstituted with modified flavins, *J. Biol. Chem. 266*, 13080–13085.
1345. Detmer, K., and Massey, V. (1985) Effect of substrate and pH on the oxidative half-reaction of phenol hydroxylase, *J. Biol. Chem. 260*, 5998–6005.
1346. Anderson, R. F., Patel, K. B., and Stratford, M. R. (1987) Absorption spectra of radicals of substrates for *p*-hydroxybenzoate hydroxylase following electrophilic attack of the ˙OH radical in the 3 position, *J. Biol. Chem. 262*, 17475–17479.
1347. Anderson, R. F., Patel, K. B., and Stratford, M. R. (1990) Absorption spectra of the hydroxycyclohexadienyl radicals of substrates for phenol hydroxylase, *J. Biol. Chem. 265*, 1952–1957.
1348. Husain, M., Entsch, B., Ballou, D. P., Massey, V., and Chapman, P. J. (1980) Fluoride elimination from substrates in hydroxylation reactions catalyzed by *p*-hydroxybenzoate hydroxylase, *J. Biol. Chem. 255*, 4189–4197.
1349. Ridder, L., Mulholland, A. J., Vervoort, J., and Rietjens, I. M. C. M. (1998) Correlation of calculated activation energies with experimental rate constants for an enzyme catalyzed aromatic hydroxylation, *J. Am. Chem. Soc. 120*, 7641–7642.
1350. Hicks, K. A., Yuen, M. E., Zhen, W. F., Gerwig, T. J., Story, R. W., Kopp, M. C., and Snider, M.

J. (2016) Structural and biochemical characterization of 6-hydroxynicotinic acid 3-monooxygenase, a novel decarboxylative hydroxylase involved in aerobic nicotinate degradation, *Biochemistry 55*, 3432–3446.
1351. Schreuder, H. A., Hol, W. G., and Drenth, J. (1990) Analysis of the active site of the flavoprotein *p*-hydroxybenzoate hydroxylase and some ideas with respect to its reaction mechanism, *Biochemistry 29*, 3101–3108.
1352. Guroff, G., Daly, J. W., Jerina, D. M., Renson, J., Witkop, B., and Udenfriend, S. (1967) Hydroxylation-induced migration: The NIH shift. Recent experiments reveal an unexpected and general result of enzymatic hydroxylation of aromatic compounds, *Science 157*, 1524–1530.
1353. Fraley, A. E., Garcia-Borras, M., Tripathi, A., Khare, D., Mercado-Marin, E. V., Tran, H., Dan, Q., Webb, G. P., Watts, K. R., Crews, P., Sarpong, R., Williams, R. M., Smith, J. L., Houk, K. N., and Sherman, D. H. (2017) Function and structure of MalA/MalA′. Iterative halogenases for late-stage C–H functionalization of indole alkaloids, *J. Am. Chem. Soc. 139*, 12060–12068.
1354. Schwab, J. M., Li, W., and Thomas, L. P. (1983) Cyclohexanone oxygenase: Stereochemistry, enantioselectivity, and regioselectivity of an enzyme-catalyzed Baeyer–Villiger reaction, *J. Am. Chem. Soc. 105*, 4800–4808.
1355. Yachnin, B. J., Sprules, T., McEvoy, M. B., Lau, P. C., and Berghuis, A. M. (2012) The substrate-bound crystal structure of a Baeyer–Villiger monooxygenase exhibits a Criegee-like conformation, *J. Am. Chem. Soc. 134*, 7788–7795.
1356. Malito, E., Alfieri, A., Fraaije, M. W., and Mattevi, A. (2004) Crystal structure of a Baeyer–Villiger monooxygenase, *Proc. Natl. Acad. Sci. U. S. A. 101*, 13157–13162.
1357. Mukherjee, T., Zhang, Y., Abdelwahed, S., Ealick, S. E., and Begley, T. P. (2010) Catalysis of a flavoenzyme-mediated amide hydrolysis, *J. Am. Chem. Soc. 132*, 5550–5551.
1358. Adak, S., and Begley, T. P. (2017) RutA-Catalyzed oxidative cleavage of the uracil amide involves formation of a flavin-N^5-oxide, *Biochemistry 56*, 3708–3709.
1359. Anton, D. L., and Friedman, P. A. (1983) Fate of the activated γ-carbon–hydrogen bond in the uncoupled vitamin K-dependent γ-glutamyl carboxylation reaction, *J. Biol. Chem. 258*, 14084–14087.
1360. Tishler, M., Fieser, L. F., and Wendler, N. L. (1940) Hydro, oxido and other derivatives of vitamin K_1 and related compounds, *J. Am. Chem. Soc. 62*, 2866–2871.
1361. Larson, A. E., Friedman, P. A., and Suttie, J. W. (1981) Vitamin K-dependent carboxylase. Stoichiometry of carboxylation and vitamin K 2,3-epoxide formation, *J. Biol. Chem. 256*, 11032–11035.
1362. Wallin, R., and Suttie, J. W. (1982) Vitamin K-dependent carboxylase: Evidence for cofractionation of carboxylase and epoxidase activities, and for carboxylation of a high-molecular-weight microsomal protein, *Arch. Biochem. Biophys. 214*, 155–163.
1363. Ham, S. W., and Dowd, P. (1990) On the mechanism of action of vitamin K. A new nonenzymic model, *J. Am. Chem. Soc. 112*, 1660–1661.
1364. Dowd, P., Ham, S. W., and Geib, S. J. (1991) Mechanism of action of vitamin K, *J. Am. Chem. Soc. 113*, 7734–7743.
1365. Dowd, P., and Ham, S. W. (1991) On the intramolecularity of the vitamin K model oxidation, *J. Am. Chem. Soc. 113*, 9403–9404.
1366. Flowers, R. A., II, Naganathan, S., Dowd, P., Arnett, E. M., and Ham, S. W. (1993) Thermochemical investigation of the oxygenation of vitamin K, *J. Am. Chem. Soc. 115*, 9409–9416.
1367. Dowd, P., Hershline, R., Ham, S. W., and Naganathan, S. (1995) Vitamin K and energy transduction: A base strength amplification mechanism, *Science 269*, 1684–1691.
1368. Rishavy, M. A., Pudota, B. N., Hallgren, K. W., Qian, W., Yakubenko, A. V., Song, J. H., Runge, K. W., and Berkner, K. L. (2004) A new model for vitamin K-dependent carboxylation: The catalytic base that deprotonates vitamin K hydroquinone is not Cys but an activated amine, *Proc. Natl. Acad. Sci. U. S. A. 101*, 13732–13737.
1369. Naganathan, S., Hershline, R., Ham, S. W., and Dowd, P. (1993) Active site of vitamin K. Regiospecific oxygenation of vitamin K hydroquinone in its role as carboxylase cofactor, *J. Am. Chem. Soc. 115*, 5839–5840.
1370. Dowd, P., Ham, S. W., and Hershline, R. (1992) Role of oxygen in the vitamin K-dependent carboxylation reaction: Incorporation of a second atom of oxygen-18 from

molecular oxygen ($^{18}O_2$) into vitamin K oxide during carboxylase activity, *J. Am. Chem. Soc. 114*, 7613–7617.
1371. Kuliopulos, A., Hubbard, B. R., Lam, Z., Koski, I. J., Furie, B., Furie, B. C., and Walsh, C. T. (1992) Dioxygen transfer during vitamin K dependent carboxylase catalysis, *Biochemistry 31*, 7722–7728.
1372. Naganathan, S., Hershline, R., Ham, S. W., and Dowd, P. (1994) The active site of vitamin K and the role of the vitamin K-dependent carboxylase, *J. Am. Chem. Soc. 116*, 9831–9839.
1373. Ducrocq, C., Righini-Tapie, A., Azerad, R., Green, J. F., Friedman, P. A., Beaucourt, J. P., and Rousseau, B. (1986) Synthesis of L-glutamic acid stereospecifically labeled at C-4 with tritium: Stereochemistry of tritium release catalyzed by the vitamin K-dependent carboxylase in the absence of carboxylation, *J. Chem.Soc. Perkin Trans.*, 1323–1328.
1374. Li, S., Furie, B. C., Furie, B., and Walsh, C. T. (1997) The propeptide of the vitamin K-dependent carboxylase substrate accelerates formation of the γ-glutamyl carbanion intermediate, *Biochemistry 36*, 6384–6390.
1375. Kahn, K., and Tipton, P. A. (1998) Spectroscopic characterization of intermediates in the urate oxidase reaction, *Biochemistry 37*, 11651–11659.
1376. Truscoe, R., and Williams, V. (1965) Effect of inhibitors on activity of ox-kidney urate oxidase, *Biochim. Biophys. Acta 105*, 292–300.
1377. Frerichs-Deeken, U., Ranguelova, K., Kappl, R., Huttermann, J., and Fetzner, S. (2004) Dioxygenases without requirement for cofactors and their chemical model reaction: Compulsory order ternary complex mechanism of ^{1}H-3-hydroxy-4-oxoquinaldine 2,4-dioxygenase involving general base catalysis by histidine 251 and single-electron oxidation of the substrate dianion, *Biochemistry 43*, 14485–14499.
1378. Han, L., Vuksanovic, N., Oehm, S. A., Fenske, T. G., Schwabacher, A. W., and Silvaggi, N. R. (2018) *Streptomyces wadayamensis* MppP is a PLP-dependent oxidase, not an oxygenase, *Biochemistry 57*, 3252–3264.
1379. Yeh, A. P., Hu, Y., Jenney, F. E., Jr., Adams, M. W., and Rees, D. C. (2000) Structures of the superoxide reductase from *Pyrococcus furiosus* in the oxidized and reduced states, *Biochemistry 39*, 2499–2508.
1380. Emerson, J. P., Coulter, E. D., Cabelli, D. E., Phillips, R. S., and Kurtz, D. M., Jr. (2002) Kinetics and mechanism of superoxide reduction by two-iron superoxide reductase from *Desulfovibrio vulgaris*, *Biochemistry 41*, 4348–4357.
1381. Kitagawa, T., Dey, A., Lugo-Mas, P., Benedict, J. B., Kaminsky, W., Solomon, E., and Kovacs, J. A. (2006) A functional model for the cysteinate-ligated nonheme iron enzyme superoxide reductase (SOR), *J. Am. Chem. Soc. 128*, 14448–14449.
1382. McCord, J. M., and Fridovich, I. (1969) Superoxide dismutase. An enzymic function for erythrocuprein (hemocuprein), *J. Biol. Chem. 244*, 6049–6055.
1383. Youn, H. D., Kim, E. J., Roe, J. H., Hah, Y. C., and Kang, S. O. (1996) A novel nickel-containing superoxide dismutase from *Streptomyces* spp, *Biochem. J. 318 (Pt 3)*, 889–896.
1384. Keele, B. B., Jr., McCord, J. M., and Fridovich, I. (1970) Superoxide dismutase from *Escherichia coli* B. A new manganese-containing enzyme, *J. Biol. Chem. 245*, 6176–6181.
1385. Yost, F. J., Jr., and Fridovich, I. (1973) An iron-containing superoxide dismutase from *Escherichia coli*, *J. Biol. Chem. 248*, 4905–4908.
1386. Cooper, J. B., McIntyre, K., Badasso, M. O., Wood, S. P., Zhang, Y., Garbe, T. R., and Young, D. (1995) X-ray structure analysis of the iron-dependent superoxide dismutase from *Mycobacterium tuberculosis* at 2.0 angstroms resolution reveals novel dimer-dimer interactions, *J. Mol. Biol. 246*, 531–544.
1387. Wuerges, J., Lee, J. W., Yim, Y. I., Yim, H. S., Kang, S. O., and Djinovic Carugo, K. (2004) Crystal structure of nickel-containing superoxide dismutase reveals another type of active site, *Proc. Natl. Acad. Sci. U. S. A. 101*, 8569–8574.
1388. Tainer, J. A., Getzoff, E. D., Richardson, J. S., and Richardson, D. C. (1983) Structure and mechanism of copper, zinc superoxide dismutase, *Nature 306*, 284–287.
1389. Stallings, W. C., Pattridge, K. A., Strong, R. K., and Ludwig, M. L. (1985) The structure of manganese superoxide dismutase from *Thermus thermophilus* HB8 at 2.4 Å resolution, *J. Biol. Chem. 260*, 16424–16432.
1390. Carlioz, A., Ludwig, M. L., Stallings, W. C., Fee, J. A., Steinman, H. M., and Touati, D. (1988) Iron superoxide dismutase. Nucleo-

tide sequence of the gene from *Escherichia coli* K12 and correlations with crystal structures, *J. Biol. Chem. 263*, 1555–1562.
1391. Stoddard, B. L., Howell, P. L., Ringe, D., and Petsko, G. A. (1990) The 2.1 Å resolution structure of iron superoxide dismutase from *Pseudomonas ovalis*, *Biochemistry 29*, 8885–8893.
1392. Ludwig, M. L., Metzger, A. L., Pattridge, K. A., and Stallings, W. C. (1991) Manganese superoxide dismutase from *Thermus thermophilus*. A structural model refined at 1.8 Å resolution, *J. Mol. Biol. 219*, 335–358.
1393. Lah, M. S., Dixon, M. M., Pattridge, K. A., Stallings, W. C., Fee, J. A., and Ludwig, M. L. (1995) Structure-function in *Escherichia coli* iron superoxide dismutase: Comparisons with the manganese enzyme from *Thermus thermophilus*, *Biochemistry 34*, 1646–1660.
1394. Knapp, S., Kardinahl, S., Hellgren, N., Tibbelin, G., Schafer, G., and Ladenstein, R. (1999) Refined crystal structure of a superoxide dismutase from the hyperthermophilic archaeon *Sulfolobus acidocaldarius* at 2.2 Å resolution, *J. Mol. Biol. 285*, 689–702.
1395. Porta, J., Vahedi-Faridi, A., and Borgstahl, G. E. (2010) Structural analysis of peroxide-soaked MnSOD crystals reveals side-on binding of peroxide to active-site manganese, *J. Mol. Biol. 399*, 377–384.
1396. Ogihara, N. L., Parge, H. E., Hart, P. J., Weiss, M. S., Goto, J. J., Crane, B. R., Tsang, J., Slater, K., Roe, J. A., Valentine, J. S., Eisenberg, D., and Tainer, J. A. (1996) Unusual trigonal-planar copper configuration revealed in the atomic structure of yeast copper-zinc superoxide dismutase, *Biochemistry 35*, 2316–2321.
1397. Moss, T. H., and Fee, J. A. (1975) On the magnetic properties of cobalt substituted bovine superoxide dismutase derivatives, *Biochem. Biophys. Res. Commun. 66*, 799–808.
1398. Bailey, D. B., Ellis, P. D., and Fee, J. A. (1980) Cadmium-113 nuclear magnetic resonance studies of cadmium-substituted derivatives of bovine superoxide dismutase, *Biochemistry 19*, 591–596.
1399. Blackburn, N. J., Hasnain, S. S., Binsted, N., Diakun, G. P., Garner, C. D., and Knowles, P. F. (1984) An extended-X-ray-absorption-fine-structure study of bovine erythrocyte superoxide dismutase in aqueous solution. Direct evidence for three-coordinate Cu(I) in reduced enzyme, *Biochem. J. 219*, 985–990.
1400. Bertini, I., Luchinat, C., and Monnanni, R. (1985) Evidence of the breaking of the copper imidazolate bridge in copper cobalt-substituted superoxide-dismutase upon reduction of the copper(II) centers, *J. Am. Chem. Soc. 107*, 2178–2179.
1401. Hough, M. A., and Hasnain, S. S. (2003) Structure of fully reduced bovine copper zinc superoxide dismutase at 1.15 Å, *Structure 11*, 937–946.
1402. Hough, M. A., and Hasnain, S. S. (1999) Crystallographic structures of bovine copper-zinc superoxide dismutase reveal asymmetry in two subunits: Functionally important three and five coordinate copper sites captured in the same crystal, *J. Mol. Biol. 287*, 579–592.
1403. Verhagen, M. F., Meussen, E. T., and Hagen, W. R. (1995) On the reduction potentials of Fe and Cu-Zn containing superoxide dismutases, *Biochim. Biophys. Acta 1244*, 99–103.
1404. Vance, C. K., and Miller, A. F. (2001) Novel insights into the basis for *Escherichia coli* superoxide dismutase's metal ion specificity from Mn-substituted FeSOD and its very high E(m), *Biochemistry 40*, 13079–13087.
1405. Dai, Y., Pochapsky, T. C., and Abeles, R. H. (2001) Mechanistic studies of two dioxygenases in the methionine salvage pathway of *Klebsiella pneumoniae*, *Biochemistry 40*, 6379–6387.
1406. Pelmenschikov, V., and Siegbahn, P. E. M. (2005) Copper-zinc superoxide dismutase: Theoretical insights into the catalytic mechanism, *Inorg. Chem. 44*, 3311–3320.
1407. Smirnov, V. V., and Roth, J. P. (2006) Evidence for Cu-O_2 intermediates in superoxide oxidations by biomimetic copper(II) complexes, *J. Am. Chem. Soc. 128*, 3683–3695.
1408. Hart, P. J., Balbirnie, M. M., Ogihara, N. L., Nersissian, A. M., Weiss, M. S., Valentine, J. S., and Eisenberg, D. (1999) A structure-based mechanism for copper-zinc superoxide dismutase, *Biochemistry 38*, 2167–2178.
1409. Woo, E. J., Dunwell, J. M., Goodenough, P. W., Marvier, A. C., and Pickersgill, R. W. (2000) Germin is a manganese containing homohexamer with oxalate oxidase and superoxide dismutase activities, *Nature Struct. Biol. 7*, 1036–1040.
1410. Rohde, J. U., In, J. H., Lim, M. H., Brennessel, W. W., Bukowski, M. R., Stubna, A., Munck, E., Nam, W., and Que, L., Jr. (2003) Crystallo-

graphic and spectroscopic characterization of a nonheme Fe(IV)-O complex, *Science 299*, 1037–1039.
1411. Sastri, C. V., Lee, J., Oh, K., Lee, Y. J., Lee, J., Jackson, T. A., Ray, K., Hirao, H., Shin, W., Halfen, J. A., Kim, J., Que, L., Jr., Shaik, S., and Nam, W. (2007) Axial ligand tuning of a nonheme iron(IV)-oxo unit for hydrogen atom abstraction, *Proc. Natl. Acad. Sci. U. S. A. 104*, 19181–19186.
1412. Jensen, M. P., Costas, M., Ho, R. Y., Kaizer, J., Mairata i Payeras, A., Munck, E., Que, L., Jr., Rohde, J. U., and Stubna, A. (2005) High-valent nonheme iron. Two distinct iron(IV) species derived from a common iron(II) precursor, *J. Am. Chem. Soc. 127*, 10512–10525.
1413. Li, F. F., Meier, K. K., Cranswick, M. A., Chakrabarti, M., Van Heuvelen, K. M., Munck, E., and Que, L. (2011) Characterization of a high-spin nonheme Fe-III-O intermediate and its quantitative conversion to an Fe-IV=O complex, *J. Am. Chem. Soc. 133*, 7256–7259.
1414. Kass, D., Corona, T., Warm, K., Braun-Cula, B., Kuhlmann, U., Bill, E., Mebs, S., Swart, M., Dau, H., Haumann, M., Hildebrandt, P., and Ray, K. (2020) Stoichiometric formation of an oxoiron(IV) complex by a soluble methane monooxygenase type activation of O_2 at an iron(II)-cyclam center, *J. Am. Chem. Soc. 142*, 5924–5928.
1415. Tiago de Oliveira, F., Chanda, A., Banerjee, D., Shan, X., Mondal, S., Que, L., Jr., Bominaar, E. L., Munck, E., and Collins, T. J. (2007) Chemical and spectroscopic evidence for an FeV-oxo complex, *Science 315*, 835–838.
1416. Ghosh, M., Singh, K. K., Panda, C., Weitz, A., Hendrich, M. P., Collins, T. J., Dhar, B. B., and Sen Gupta, S. (2014) Formation of a room temperature stable Fe(V)(O) complex: Reactivity toward unactivated C–H bonds, *J. Am. Chem. Soc. 136*, 9524–9527.
1417. Martinez, J. L., Lutz, S. A., Yang, H., Xie, J., Telser, J., Hoffman, B. M., Carta, V., Pink, M., Losovyj, Y., and Smith, J. M. (2020) Structural and spectroscopic characterization of an Fe(VI) bis(imido) complex, *Science 370*, 356–359.
1418. Fan, R., Serrano-Plana, J., Oloo, W. N., Draksharapu, A., Delgado-Pinar, E., Company, A., Martin-Diaconescu, V., Borrell, M., Lloret-Fillol, J., Garcia-Espana, E., Guo, Y., Bominaar, E. L., Que, L., Jr., Costas, M., and Munck, E. (2018) Spectroscopic and DFT characterization of a highly reactive nonheme Fe(V)-oxo intermediate, *J. Am. Chem. Soc. 140*, 3916–3928.
1419. Dolphin, D., Forman, A., Borg, D. C., Fajer, J., and Felton, R. H. (1971) Compounds I of catalase and horse radish peroxidase: π-Cation radicals, *Proc. Natl. Acad. Sci. U. S. A. 68*, 614–618.
1420. Groves, J. T., Haushalter, R. C., Nakamura, M., Nemo, T. E., and Evans, B. (1981) High-valent iron-porphyrin complexes related to peroxidase and cytochrome P450, *J. Am. Chem. Soc. 103*, 2884–2886.
1421. Traylor, T. G., and Xu, F. (1990) Mechanisms of reactions of iron(III) porphyrins with hydrogen peroxide and hydroperoxides: Solvent and solvent isotope effects, *J. Am. Chem. Soc. 112*, 178–186.
1422. Nam, W., Han, H. J., Oh, S.-Y., Lee, Y. J., Choi, M.-H., Han, S.-Y., Kim, C., Woo, S. K., and Shin, W. (2000) New insights into the mechanisms of O-O bond cleavage of hydrogen peroxide and *tert*-alkyl hydroperoxides by iron(III) porphyrin complexes, *J. Am. Chem. Soc. 122*, 8677–8684.
1423. Traylor, T. G., Lee, W. A., and Stynes, D. V. (1984) Model compound studies related to peroxidases. Mechanisms of reactions of hemins with peracids, *J. Am. Chem. Soc. 106*, 755–764.
1424. Soper, J. D., Kryatov, S. V., Rybak-Akimova, E. V., and Nocera, D. G. (2007) Proton-directed redox control of O-O bond activation by heme hydroperoxidase models, *J. Am. Chem. Soc. 129*, 5069–5075.
1425. Groves, J. T., and Watanabe, Y. (1986) Oxygen activation by metalloporphyrins related to peroxidase and cytochrome P450. Direct observation of the oxygen-oxygen bond cleavage step, *J. Am. Chem. Soc. 108*, 7834–7836.
1426. Nam, W., Park, S. E., Lim, I. K., Lim, M. H., Hong, J., and Kim, J. (2003) First direct evidence for stereospecific olefin epoxidation and alkane hydroxylation by an oxoiron(IV) porphyrin complex, *J. Am. Chem. Soc. 125*, 14674–14675.
1427. Groves, J. T., and Watanabe, Y. (1988) Reactive iron porphyrin derivatives related to the catalytic cycles of cytochrome P450 and peroxidase. Studies of the mechanism of oxygen activation, *J. Am. Chem. Soc. 110*, 8443–8452.

1428. Zipplies, M. F., Lee, W. A., and Bruice, T. C. (1986) Influence of hydrogen ion activity and general acid–base catalysis on the rate of decomposition of hydrogen peroxide by a novel nonaggregating water-soluble iron(III) tetraphenylporphyrin derivative, *J. Am. Chem. Soc. 108*, 4433–4445.
1429. Lee, W. A., Yuan, L. C., and Bruice, T. C. (1988) Oxygen transfer from percarboxylic acids and alkyl hydroperoxides to (*meso*-tetraphenylporphinato)iron(III) and -chromium(III), *J. Am. Chem. Soc. 110*, 4277–4283.
1430. Alfonso-Prieto, M., Borovik, A., Carpena, X., Murshudov, G., Melik-Adamyan, W., Fita, I., Rovira, C., and Loewen, P. C. (2007) The structures and electronic configuration of compound I intermediates of *Helicobacter pylori* and *Penicillium vitale* catalases determined by X-ray crystallography and QM/MM density functional theory calculations, *J. Am. Chem. Soc. 129*, 4193–4205.
1431. Stephenson, N. A., and Bell, A. T. (2005) A study of the mechanism and kinetics of cyclooctene epoxidation catalyzed by iron(III) tetrakispentafluorophenyl porphyrin, *J. Am. Chem. Soc. 127*, 8635–8643.
1432. Traylor, T. G., and Xu, F. (1987) A biomimetic model for catalase: The mechanisms of reaction of hydrogen peroxide and hydroperoxides with iron(III) porphyrins, *J. Am. Chem. Soc. 109*, 6201–6202.
1433. Liu, L. V., Hong, S., Cho, J., Nam, W., and Solomon, E. I. (2013) Comparison of high-spin and low-spin nonheme Fe-III-OOH complexes in O-O bond homolysis and H-atom abstraction reactivities, *J. Am. Chem. Soc. 135*, 3286–3299.
1434. Yosca, T. H., Rittle, J., Krest, C. M., Onderko, E. L., Silakov, A., Calixto, J. C., Behan, R. K., and Green, M. T. (2013) Iron(IV)hydroxide pK_a and the role of thiolate ligation in C-H bond activation by cytochrome P450, *Science 342*, 825–829.
1435. Behan, R. K., and Green, M. T. (2006) On the status of ferryl protonation, *J. Inorg. Biochem. 100*, 448–459.
1436. Casadei, C. M., Gumiero, A., Metcalfe, C. L., Murphy, E. J., Basran, J., Concilio, M. G., Teixeira, S. C., Schrader, T. E., Fielding, A. J., Ostermann, A., Blakeley, M. P., Raven, E. L., and Moody, P. C. (2014) Heme enzymes. Neutron cryo-crystallography captures the protonation state of ferryl heme in a peroxidase, *Science 345*, 193–197.
1437. Wang, X., Ullrich, R., Hofrichter, M., and Groves, J. T. (2015) Heme-thiolate ferryl of aromatic peroxygenase is basic and reactive, *Proc. Natl. Acad. Sci. U.S.A. 112*, 3686–3691.
1438. Groves, J. T., and Watanabe, Y. (1986) The mechanism of olefin epoxidation by oxo-iron porphyrins. Direct observation of an intermediate, *J. Am. Chem. Soc. 108*, 507–508.
1439. Traylor, T. G., Nakano, T., Dunlap, B. E., Traylor, P. S., and Dolphin, D. (1986) Mechanisms of hemin-catalyzed alkene epoxidation. The effect of catalyst on the regiochemistry of epoxidation, *J. Am. Chem. Soc. 108*, 2782–2784.
1440. Traylor, T. G., Iamamoto, Y., and Nakano, T. (1986) Mechanisms of hemin-catalyzed oxidations: Rearrangements during the epoxidation of *trans*-cyclooctene, *J. Am. Chem. Soc. 108*, 3529–3531.
1441. Traylor, T. G., and Xu, F. (1988) Model reactions related to cytochrome P450. Effects of alkene structure on the rates of epoxide formation, *J. Am. Chem. Soc. 110*, 1953–1958.
1442. Groves, J. T., Gross, Z., and Stern, M. K. (1994) Preparation and reactivity of oxoiron(IV) porphyrins, *Inorg. Chem. 33*, 5065–5072.
1443. Nam, W., Lim, M. H., Moon, S. K., and Kim, C. (2000) Participation of two distinct hydroxylating intermediates in iron(III) porphyrin complex-catalyzed hydroxylation of alkanes, *J. Am. Chem. Soc. 122*, 10805–10809.
1444. Bell, S. R., and Groves, J. T. (2009) A highly reactive P450 model compound I, *J. Am. Chem. Soc. 131*, 9640–9641.
1445. Chang, C. K., and Kuo, M.-S. (1979) Reaction of iron(III) porphyrins and iodosoxylene. The active oxene complex of cytochrome P450, *J. Am. Chem. Soc. 101*, 3413–3415.
1446. Ehudin, M. A., Quist, D. A., and Karlin, K. D. (2019) Enhanced rates of C–H bond cleavage by a hydrogen-bonded synthetic heme high-valent iron(IV) oxo complex, *J. Am. Chem. Soc. 141*, 12558–12569.
1447. Harrison, J. E., and Schultz, J. (1976) Studies on the chlorinating activity of myeloperoxidase, *J. Biol. Chem. 251*, 1371–1374.
1448. Marquez, L. A., and Dunford, H. B. (1990) Reaction of compound III of myeloperoxidase with ascorbic acid, *J. Biol. Chem. 265*, 6074–6078.

1449. Paumann-Page, M., Katz, R. S., Bellei, M., Schwartz, I., Edenhofer, E., Sevcnikar, B., Soudi, M., Hofbauer, S., Battistuzzi, G., Furtmuller, P. G., and Obinger, C. (2017) Pre-steady-state kinetics reveal the substrate specificity and mechanism of halide oxidation of truncated human peroxidasin 1, *J. Biol. Chem. 292*, 4583–4592.
1450. Kunishima, N., Fukuyama, K., Matsubara, H., Hatanaka, H., Shibano, Y., and Amachi, T. (1994) Crystal structure of the fungal peroxidase from *Arthromyces ramosus* at 1.9 Å Resolution. Structural comparisons with the lignin and cytochrome *c* peroxidases, *J. Mol. Biol. 235*, 331–344.
1451. Poulos, T. L., Edwards, S. L., Wariishi, H., and Gold, M. H. (1993) Crystallographic refinement of lignin peroxidase at 2 Å, *J. Biol. Chem. 268*, 4429–4440.
1452. Erman, J. E., Vitello, L. B., Miller, M. A., and Kraut, J. (1992) Active-site mutations in cytochrome-*c* peroxidase: A critical role for Histidine-52 in the rate of formation of compound-I, *J. Am. Chem. Soc. 114*, 6592–6593.
1453. Erman, J. E., Vitello, L. B., Miller, M. A., Shaw, A., Brown, K. A., and Kraut, J. (1993) Histidine 52 is a critical residue for rapid formation of cytochrome *c* peroxidase compound I, *Biochemistry 32*, 9798–9806.
1454. Rodriguez-Lopez, J. N., Lowe, D. J., Hernandez-Ruiz, J., Hiner, A. N., Garcia-Canovas, F., and Thorneley, R. N. (2001) Mechanism of reaction of hydrogen peroxide with horseradish peroxidase: Identification of intermediates in the catalytic cycle, *J. Am. Chem. Soc. 123*, 11838–11847.
1455. Denisov, I. G., Makris, T. M., and Sligar, S. G. (2002) Formation and decay of hydroperoxoferric heme complex in horseradish peroxidase studied by cryoradiolysis, *J. Biol. Chem. 277*, 42706–42710.
1456. Davydov, R., Laryukhin, M., Ledbetter-Rogers, A., Sono, M., Dawson, J. H., and Hoffman, B. M. (2014) Electron paramagnetic resonance and electron–nuclear double resonance studies of the reactions of cryogenerated hydroperoxoferric-hemoprotein intermediates, *Biochemistry 53*, 4894–4903.
1457. Gouet, P., Jouve, H. M., Williams, P. A., Andersson, I., Andreoletti, P., Nussaume, L., and Hajdu, J. (1996) Ferryl intermediates of catalase captured by time-resolved Weissenberg crystallography and UV-vis spectroscopy, *Nature Struct. Biol. 3*, 951–956.
1458. Fita, I., and Rossmann, M. G. (1985) The active center of catalase, *J. Mol. Biol. 185*, 21–37.
1459. Poulos, T. L., and Kraut, J. (1980) The stereochemistry of peroxidase catalysis, *J. Biol. Chem. 255*, 8199–8205.
1460. Hashimoto, S., Tatsuno, Y., and Kitagawa, T. (1987) Observation of the FeIV=O stretching Raman band for a ferryl porphyrin π cation radical, *J. Am. Chem. Soc. 109*, 8096–8097.
1461. Czarnecki, K., Kincaid, J. R., and Fujii, H. (1999) Resonance Raman spectra of legitimate models for the ubiquitous compound I intermediates of oxidative heme enzymes, *J. Am. Chem. Soc. 121*, 7953–7954.
1462. Lee, A. Q., Streit, B. R., Zdilla, M. J., Abu-Omar, M. M., and DuBois, J. L. (2008) Mechanism of and exquisite selectivity for O-O bond formation by the heme-dependent chlorite dismutase, *Proc. Natl. Acad. Sci. U.S.A. 105*, 15654–15659.
1463. Huyett, J. E., Doan, P. E., Gurbiel, R., Houseman, A. L. P., Sivaraja, M., Goodin, D. B., and Hoffman, B. M. (1995) Compound ES of cytochrome *c* peroxidase contains a Trp π-cation radical: Characterization by continuous wave and pulsed Q-band external nuclear double resonance spectroscopy, *J. Am. Chem. Soc. 117*, 9033–9041.
1464. Fishel, L. A., Farnum, M. F., Mauro, J. M., Miller, M. A., Kraut, J., Liu, Y. J., Tan, X. L., and Scholes, C. P. (1991) Compound I radical in site-directed mutants of cytochrome *c* peroxidase as probed by electron paramagnetic resonance and electron–nuclear double resonance, *Biochemistry 30*, 1986–1996.
1465. Ruiz-Duenas, F. J., Pogni, R., Morales, M., Giansanti, S., Mate, M. J., Romero, A., Martinez, M. J., Basosi, R., and Martinez, A. T. (2009) Protein radicals in fungal versatile peroxidase: Catalytic tryptophan radical in both compound I and compound II and studies on W164Y, W164H, and W164S variants, *J. Biol. Chem. 284*, 7986–7994.
1466. Smith, A. T., Doyle, W. A., Dorlet, P., and Ivancich, A. (2009) Spectroscopic evidence for an engineered, catalytically active Trp radical that creates the unique reactivity of lignin peroxidase, *Proc. Natl. Acad. Sci. U.S.A. 106*, 16084–16089.

1467. Miller, M. A., Han, G. W., and Kraut, J. (1994) A cation binding motif stabilizes the compound I radical of cytochrome *c* peroxidase, *Proc. Natl. Acad. Sci. U.S.A. 91*, 11118–11122.
1468. Erman, J. E., Vitello, L. B., Mauro, J. M., and Kraut, J. (1989) Detection of an oxyferryl porphyrin π-cation-radical intermediate in the reaction between hydrogen peroxide and a mutant yeast cytochrome *c* peroxidase. Evidence for Tryptophan-191 involvement in the radical site of compound I, *Biochemistry 28*, 7992–7995.
1469. Saez-Jimenez, V., Baratto, M. C., Pogni, R., Rencoret, J., Gutierrez, A., Santos, J. I., Martinez, A. T., and Ruiz-Duenas, F. J. (2015) Demonstration of lignin-to-peroxidase direct electron transfer: A transient-state kinetics, directed mutagenesis, EPR, and NMR study, *J. Biol. Chem. 290*, 23201–23213.
1470. Patterson, W. R., Poulos, T. L., and Goodin, D. B. (1995) Identification of a porphyrin π cation radical in ascorbate peroxidase compound I, *Biochemistry 34*, 4342–4345.
1471. Ledray, A. P., Krest, C. M., Yosca, T. H., Mittra, K., and Green, M. T. (2020) Ascorbate peroxidase compound II is an iron(IV) oxo species, *J. Am. Chem. Soc. 142*, 20419–20425.
1472. Geng, J., Dornevil, K., Davidson, V. L., and Liu, A. (2013) Tryptophan-mediated charge-resonance stabilization in the bis-Fe(IV) redox state of MauG, *Proc. Natl. Acad. Sci. U.S.A. 110*, 9639–9644.
1473. Edwards, S. L., Kraut, J., and Poulos, T. L. (1988) Crystal structure of nitric oxide inhibited cytochrome *c* peroxidase, *Biochemistry 27*, 8074–8081.
1474. Miller, M. A., Shaw, A., and Kraut, J. (1994) 2.2 Å structure of oxy-peroxidase as a model for the transient enzyme:peroxide complex, *Nature Struct. Biol. 1*, 524–531.
1475. Savenkova, M. I., Kuo, J. M., and Ortiz de Montellano, P. R. (1998) Improvement of peroxygenase activity by relocation of a catalytic histidine within the active site of horseradish peroxidase, *Biochemistry 37*, 10828–10836.
1476. Edwards, S. L., Nguyen, H. X., Hamlin, R. C., and Kraut, J. (1987) Crystal structure of cytochrome *c* peroxidase compound I, *Biochemistry 26*, 1503–1511.
1477. Diaz, A., Horjales, E., Rudino-Pinera, E., Arreola, R., and Hansberg, W. (2004) Unusual Cys-Tyr covalent bond in a large catalase, *J. Mol. Biol. 342*, 971–985.
1478. Bravo, J., Fita, I., Ferrer, J. C., Ens, W., Hillar, A., Switala, J., and Loewen, P. C. (1997) Identification of a novel bond between a histidine and the essential tyrosine in catalase HPII of *Escherichia coli*, *Prot. Sci. 6*, 1016–1023.
1479. Green, M. T. (2001) The structure and spin coupling of catalase compound I: A study of noncovalent effects, *J. Am. Chem. Soc. 123*, 9218–9219.
1480. Ivancich, A., Jouve, H. M., and Gaillard, J. (1996) EPR Evidence for a tyrosyl radical intermediate in bovine liver catalase, *J. Am. Chem. Soc. 118*, 12852–12853.
1481. Njuma, O. J., Davis, I., Ndontsa, E. N., Krewall, J. R., Liu, A., and Goodwin, D. C. (2017) Mutual synergy between catalase and peroxidase activities of the bifunctional enzyme KatG is facilitated by electron hole-hopping within the enzyme, *J. Biol. Chem. 292*, 18408–18421.
1482. Meharenna, Y. T., Doukov, T., Li, H., Soltis, S. M., and Poulos, T. L. (2010) Crystallographic and single-crystal spectral analysis of the peroxidase ferryl intermediate, *Biochemistry 49*, 2984–2986.
1483. Sharp, K. H., Mewies, M., Moody, P. C., and Raven, E. L. (2003) Crystal structure of the ascorbate peroxidase-ascorbate complex, *Nature Struct. Biol. 10*, 303–307.
1484. Sundaramoorthy, M., Kishi, K., Gold, M. H., and Poulos, T. L. (1994) The crystal structure of manganese peroxidase from *Phanerochaete chrysosporium* at 2.06 Å resolution, *J. Biol. Chem. 269*, 32759–32767.
1485. Goto, Y., Watanabe, Y., Fukuzumi, S., Jones, J. P., and Dinnocenzo, J. P. (1998) Mechanisms of *N*-demethylations catalyzed by high-valent species of heme enzymes: Novel use of isotope effects and direct observation of intermediates, *J. Am. Chem. Soc. 120*, 10762–10763.
1486. Baciocchi, E., Lanzalunga, O., Malandrucco, S., Ioele, M., and Steenken, S. (1996) Oxidation of sulfides by peroxidases. Involvement of radical cations and the rate of the oxygen rebound step, *J. Am. Chem. Soc. 118*, 8973–8974.
1487. Stone, K. L., Behan, R. K., and Green, M. T. (2006) Resonance Raman spectroscopy of chloroperoxidase compound II provides direct evidence for the existence of an iron(IV)-

hydroxide, *Proc. Natl. Acad. Sci. U. S. A. 103*, 12307–12310.
1488. Green, M. T., Dawson, J. H., and Gray, H. B. (2004) Oxoiron(IV) in chloroperoxidase compound II is basic: Implications for P450 chemistry, *Science 304*, 1653–1656.
1489. Efimov, I., Papadopoulou, N. D., McLean, K. J., Badyal, S. K., Macdonald, I. K., Munro, A. W., Moody, P. C., and Raven, E. L. (2007) The redox properties of ascorbate peroxidase, *Biochemistry 46*, 8017–8023.
1490. Mondal, M. S., Fuller, H. A., and Armstrong, F. A. (1996) Direct measurement of the reduction potential of catalytically active cytochrome *c* peroxidase compound I: Voltammetric detection of a reversible, cooperative two-electron transfer reaction, *J. Am. Chem. Soc. 118*, 263–264.
1491. Wang, D., Zhang, M., Buhlmann, P., and Que, L. (2010) Redox potential and C–H bond cleaving properties of a nonheme Fe-IV=O complex in aqueous solution, *J. Am. Chem. Soc. 132*, 7638–7644.
1492. Gajhede, M., Schuller, D. J., Henriksen, A., Smith, A. T., and Poulos, T. L. (1997) Crystal structure of horseradish peroxidase *c* at 2.15 Å resolution, *Nature Struct. Biol. 4*, 1032–1038.
1493. DePillis, G. D., and Ortiz de Montellano, P. R. (1989) Substrate oxidation by the heme edge of fungal peroxidases. Reaction of *Coprinus macrorhizus* peroxidase with hydrazines and sodium azide, *Biochemistry 28*, 7947–7952.
1494. Yosca, T. H., Langston, M. C., Krest, C. M., Onderko, E. L., Grove, T. L., Livada, J., and Green, M. T. (2016) Spectroscopic investigations of catalase compound II: Characterization of an iron(IV) hydroxide intermediate in a non-thiolate-ligated heme enzyme, *J. Am. Chem. Soc. 138*, 16016–16023.
1495. Jarnagin, R. C., and Wang, J. H. (1958) Investigation of the catalytic mechanism of catalase and other ferric compounds with doubly ^{18}O-labeled hydrogen peroxide, *J. Am. Chem. Soc. 80*, 786–787.
1496. Khindaria, A., Nie, G., and Aust, S. D. (1997) Detection and characterization of the lignin peroxidase compound II-veratryl alcohol cation radical complex, *Biochemistry 36*, 14181–14185.
1497. Miki, K., Kondo, R., Renganathan, V., Mayfield, M. B., and Gold, M. H. (1988) Mechanism of aromatic ring cleavage of a β-biphenylyl ether dimer catalyzed by lignin peroxidase of *Phanerochaete chrysosporium*, *Biochemistry 27*, 4787–4794.
1498. Liu, Y., and Roth, J. P. (2016) A revised mechanism for human cyclooxygenase-2, *J. Biol. Chem. 291*, 948–958.
1499. Ruf, H. H., Raab-Brill, U., and Blau, C. (1993) A model for the catalytic mechanism of prostaglandin endoperoxide synthase, *Biochem. Soc. Trans. 21 (Pt 3)*, 739–744.
1500. Koshkin, V., and Dunford, H. B. (1999) Coupling of the peroxidase and cyclooxygenase reactions of prostaglandin H synthase, *Biochim. Biophys. Acta 1430*, 341–348.
1501. Osborne, R. L., Coggins, M. K., Raner, G. M., Walla, M., and Dawson, J. H. (2009) The mechanism of oxidative halophenol dehalogenation by *Amphitrite ornata* dehaloperoxidase is initiated by H_2O_2 binding and involves two consecutive one-electron steps: Role of ferryl intermediates, *Biochemistry 48*, 4231–4238.
1502. Rae, T. D., and Goff, H. M. (1998) The heme prosthetic group of lactoperoxidase. Structural characteristics of heme *l* and heme *l*-peptides, *J. Biol. Chem. 273*, 27968–27977.
1503. Fiedler, T. J., Davey, C. A., and Fenna, R. E. (2000) X-ray crystal structure and characterization of halide-binding sites of human myeloperoxidase at 1.8 Å resolution, *J. Biol. Chem. 275*, 11964–11971.
1504. Taylor, K. L., Strobel, F., Yue, K. T., Ram, P., Pohl, J., Woods, A. S., and Kinkade, J. M., Jr. (1995) Isolation and identification of a protoheme IX derivative released during autolytic cleavage of human myeloperoxidase, *Arch. Biochem. Biophys. 316*, 635–642.
1505. Ghiladi, R. A., Knudsen, G. M., Medzihradszky, K. F., and Ortiz de Montellano, P. R. (2005) The Met-Tyr-Trp cross-link in *Mycobacterium tuberculosis* catalase-peroxidase (KatG): Autocatalytic formation and effect on enzyme catalysis and spectroscopic properties, *J. Biol. Chem. 280*, 22651–22663.
1506. Yamada, Y., Fujiwara, T., Sato, T., Igarashi, N., and Tanaka, N. (2002) The 2.0 Å crystal structure of catalase-peroxidase from *Haloarcula marismortui*, *Nature Struct. Biol. 9*, 691–695.
1507. Ranguelova, K., Girotto, S., Gerfen, G. J., Yu, S., Suarez, J., Metlitsky, L., and Magliozzo, R. S. (2007) Radical sites in *Mycobacterium tuberculosis* KatG identified using electron paramagnetic resonance spectroscopy, the three-

dimensional crystal structure, and electron transfer couplings, *J. Biol. Chem. 282*, 6255–6264.
1508. Suarez, J., Ranguelova, K., Jarzecki, A. A., Manzerova, J., Krymov, V., Zhao, X., Yu, S., Metlitsky, L., Gerfen, G. J., and Magliozzo, R. S. (2009) An oxyferrous heme/protein-based radical intermediate is catalytically competent in the catalase reaction of *Mycobacterium tuberculosis* catalase-peroxidase (KatG), *J. Biol. Chem. 284*, 7017–7029.
1509. Zhao, X., Suarez, J., Khajo, A., Yu, S., Metlitsky, L., and Magliozzo, R. S. (2010) A radical on the Met-Tyr-Trp modification required for catalase activity in catalase-peroxidase is established by isotopic labeling and site-directed mutagenesis, *J. Am. Chem. Soc. 132*, 8268–8269.
1510. Zhang, H., He, S., and Mauk, A. G. (2002) Radical formation at Tyr39 and Tyr153 following reaction of yeast cytochrome *c* peroxidase with hydrogen peroxide, *Biochemistry 41*, 13507–13513.
1511. Celis, A. I., Gauss, G. H., Streit, B. R., Shisler, K., Moraski, G. C., Rodgers, K. R., Lukat-Rodgers, G. S., Peters, J. W., and DuBois, J. L. (2017) Structure-based mechanism for oxidative decarboxylation reactions mediated by amino acids and heme propionates in coproheme decarboxylase (HemQ), *J. Am. Chem. Soc. 139*, 1900–1911.
1512. Mylrajan, M., Valli, K., Wariishi, H., Gold, M. H., and Loehr, T. M. (1990) Resonance Raman spectroscopic characterization of compound III of lignin peroxidase, *Biochemistry 29*, 9617–9623.
1513. Feducia, J., Dumarieh, R., Gilvey, L. B., Smirnova, T., Franzen, S., and Ghiladi, R. A. (2009) Characterization of dehaloperoxidase compound ES and its reactivity with trihalophenols, *Biochemistry 48*, 995–1005.
1514. Jameson, G. B., Molinaro, F. S., Ibers, J. A., Collman, J. P., Brauman, J. I., Rose, E., and Suslick, K. (1980) Models for the active site of oxygen-binding hemoproteins. Dioxygen binding properties and the structures of (2-methylimidazole)-meso-tetra($\alpha,\alpha,\alpha,\alpha$-*O*-pivalamidophenyl)porphyrinatoiron(II)-ethanol and its dioxygen adduct, *J. Am. Chem. Soc. 102*, 3224–3237.
1515. Phillips, S. E. V. (1978) Structure of oxymyoglobin, *Nature 273*, 247–248.
1516. Phillips, S. E. (1980) Structure and refinement of oxymyoglobin at 1.6 Å resolution, *J. Mol. Biol. 142*, 531–554.
1517. Unno, M., Chen, H., Kusama, S., Shaik, S., and Ikeda-Saito, M. (2007) Structural characterization of the fleeting ferric peroxo species in myoglobin: Experiment and theory, *J. Am. Chem. Soc. 129*, 13394–13395.
1518. Vojtechovsky, J., Chu, K., Berendzen, J., Sweet, R. M., and Schlichting, I. (1999) Crystal structures of myoglobin-ligand complexes at near-atomic resolution, *Biophys. J. 77*, 2153–2174.
1519. Park, S. Y., Yokoyama, T., Shibayama, N., Shiro, Y., and Tame, J. R. (2006) 1.25 Å resolution crystal structures of human haemoglobin in the oxy, deoxy and carbonmonoxy forms, *J. Mol. Biol. 360*, 690–701.
1520. Gerothanassis, I. P., Momenteau, M., and Loock, B. (1989) Hydrogen-bond stabilization of dioxygen: Conformation excitation and autoxidation mechanism in hemoprotein models as revealed by oxygen-17 NMR spectroscopy, *J. Am. Chem. Soc. 111*, 7006–7012.
1521. Lukin, J. A., Simplaceanu, V., Zou, M., Ho, N. T., and Ho, C. (2000) NMR reveals hydrogen bonds between oxygen and distal histidines in oxyhemoglobin, *Proc. Natl. Acad. Sci. U. S. A. 97*, 10354–10358.
1522. Phillips, S. E., and Schoenborn, B. P. (1981) Neutron diffraction reveals oxygen-histidine hydrogen bond in oxymyoglobin, *Nature 292*, 81–82.
1523. Fermi, G., Perutz, M. F., Shaanan, B., and Fourme, R. (1984) The crystal structure of human deoxyhaemoglobin at 1.74 Å resolution, *J. Mol. Biol. 175*, 159–174.
1524. Shaanan, B. (1983) Structure of human oxyhaemoglobin at 2.1 Å resolution, *J. Mol. Biol. 171*, 31–59.
1525. Yang, J., Kloek, A. P., Goldberg, D. E., and Mathews, F. S. (1995) The structure of *Ascaris* hemoglobin domain I at 2.2 Å resolution: Molecular features of oxygen avidity, *Proc. Natl. Acad. Sci. U. S. A. 92*, 4224–4228.
1526. Traylor, T. G., White, D. K., Campbell, D. H., and Berzinis, A. P. (1981) Electronic effects on the binding of dioxygen and carbon monoxide to hemes, *J. Am. Chem. Soc. 103*, 4932–4936.

1527. Chang, C. K., and Traylor, T. G. (1973) Synthesis of the myoglobin active site, *Proc. Natl. Acad. Sci. U. S. A. 70*, 2647–2650.
1528. Traylor, T. G., Chang, C. K., Geibel, J., Berzinis, A., Mincey, T., and Cannon, J. (1979) Syntheses and NMR characterization of chelated heme models of hemoproteins, *J. Am. Chem. Soc. 101*, 6716–6731.
1529. Geibel, J., Cannon, J., Campbell, D., and Traylor, T. G. (1978) Model compounds for R-state and T-state hemoglobins, *J. Am. Chem. Soc. 100*, 3575–3585.
1530. Baldwin, J., and Chothia, C. (1979) Haemoglobin: The structural changes related to ligand binding and its allosteric mechanism, *J. Mol. Biol. 129*, 175–220.
1531. Louka, S., Barry, S. M., Heyes, D. J., Mubarak, M. Q. E., Ali, H. S., Alkhalaf, L. M., Munro, A. W., Scrutton, N. S., Challis, G. L., and de Visser, S. P. (2020) Catalytic mechanism of aromatic nitration by cytochrome P450 TxtE: Involvement of a ferric-peroxynitrite intermediate, *J. Am. Chem. Soc. 142*, 15764–15779.
1532. Hayaishi, O., and Nozaki, M. (1969) Nature and mechanisms of oxygenases, *Science 164*, 389–396.
1533. Hirata, F., Ohnishi, T., and Hayaishi, O. (1977) Indoleamine 2,3-dioxygenase. Characterization and properties of enzyme·O_2–complex, *J. Biol. Chem. 252*, 4637–4642.
1534. Forouhar, F., Anderson, J. L., Mowat, C. G., Vorobiev, S. M., Hussain, A., Abashidze, M., Bruckmann, C., Thackray, S. J., Seetharaman, J., Tucker, T., Xiao, R., Ma, L. C., Zhao, L., Acton, T. B., Montelione, G. T., Chapman, S. K., and Tong, L. (2007) Molecular insights into substrate recognition and catalysis by tryptophan 2,3-dioxygenase, *Proc. Natl. Acad. Sci. U. S. A. 104*, 473–478.
1535. Hayaishi, O., Rothberg, S., Mehler, A. H., and Saito, Y. (1957) Studies on oxygenases; enzymatic formation of kynurenine from tryptophan, *J. Biol. Chem. 229*, 889–896.
1536. Basran, J., Efimov, I., Chauhan, N., Thackray, S. J., Krupa, J. L., Eaton, G., Griffith, G. A., Mowat, C. G., Handa, S., and Raven, E. L. (2011) The mechanism of formation of *N*-formylkynurenine by heme dioxygenases, *J. Am. Chem. Soc. 133*, 16251–16257.
1537. Hirata, F., and Hayaishi, O. (1975) Studies on indoleamine 2,3-dioxygenase. I. Superoxide anion as substrate, *J. Biol. Chem. 250*, 5960–5966.
1538. Mondal, P., and Wijeratne, G. B. (2020) Modeling tryptophan/indoleamine 2,3-dioxygenase with heme superoxide mimics: Is ferryl the key intermediate?, *J. Am. Chem. Soc. 142*, 1846–1856.
1539. Lewis-Ballester, A., Forouhar, F., Kim, S. M., Lew, S., Wang, Y. Q., Karkashon, S., Seetharaman, J., Batabyal, D., Chiang, B. Y., Hussain, M., Correia, M. A., Yeh, S. R., and Tong, L. (2016) Molecular basis for catalysis and substrate-mediated cellular stabilization of human tryptophan 2,3-dioxygenase, *Sci. Rep. 6*, 35169.
1540. Chung, L. W., Li, X., Sugimoto, H., Shiro, Y., and Morokuma, K. (2008) Density functional theory study on a missing piece in understanding of heme chemistry: The reaction mechanism for indoleamine 2,3-dioxygenase and tryptophan 2,3-dioxygenase, *J. Am. Chem. Soc. 130*, 12299–12309.
1541. Lewis-Ballester, A., Batabyal, D., Egawa, T., Lu, C., Lin, Y., Marti, M. A., Capece, L., Estrin, D. A., and Yeh, S. R. (2009) Evidence for a ferryl intermediate in a heme-based dioxygenase, *Proc. Natl. Acad. Sci. U.S.A. 106*, 17371–17376.
1542. Makino, R., Obayashi, E., Hori, H., Iizuka, T., Mashima, K., Shiro, Y., and Ishimura, Y. (2015) Initial O_2 insertion step of the tryptophan dioxygenase reaction proposed by a heme-modification study, *Biochemistry 54*, 3604–3616.
1543. Zhang, Y., Zou, Y., Brock, N. L., Huang, T., Lan, Y., Wang, X., Deng, Z., Tang, Y., and Lin, S. (2017) Characterization of 2-oxindole forming heme enzyme MarE, expanding the functional diversity of the tryptophan dioxygenase superfamily, *J. Am. Chem. Soc. 139*, 11887–11894.
1544. White, R. E., and Coon, M. J. (1980) Oxygen activation by cytochrome P450, *Annu. Rev. Biochem. 49*, 315–356.
1545. Poulos, T. L., Finzel, B. C., Gunsalus, I. C., Wagner, G. C., and Kraut, J. (1985) The 2.6 Å crystal structure of *Pseudomonas putida* cytochrome P450, *J. Biol. Chem. 260*, 16122–16130.
1546. Tyson, C. A., Lipscomb, J. D., and Gunsalus, I. C. (1972) The role of putidaredoxin and $P450_{cam}$ in methylene hydroxylation, *J. Biol. Chem. 247*, 5777–5784.
1547. Baron, J., Taylor, W. E., and Masters, B. S. (1972) Immunochemical studies on electron transport chains involving cytochrome P450.

The role of the iron–sulfur protein, adrenodoxin, in mixed-function oxidation reactions, *Arch. Biochem. Biophys. 150*, 105–115.
1548. Yasukochi, Y., and Masters, B. S. (1976) Some properties of a detergent-solubilized NADPH-cytochrome *c*(cytochrome P450) reductase purified by biospecific affinity chromatography, *J. Biol. Chem. 251*, 5337–5344.
1549. Schlichting, I., Berendzen, J., Chu, K., Stock, A. M., Maves, S. A., Benson, D. E., Sweet, R. M., Ringe, D., Petsko, G. A., and Sligar, S. G. (2000) The catalytic pathway of cytochrome $P450_{cam}$ at atomic resolution, *Science 287*, 1615–1622.
1550. Nagano, S., and Poulos, T. L. (2005) Crystallographic study on the dioxygen complex of wild-type and mutant cytochrome $P450_{cam}$. Implications for the dioxygen activation mechanism, *J. Biol. Chem. 280*, 31659–31663.
1551. Ost, T. W., Clark, J., Mowat, C. G., Miles, C. S., Walkinshaw, M. D., Reid, G. A., Chapman, S. K., and Daff, S. (2003) Oxygen activation and electron transfer in flavocytochrome $P450_{bm3}$, *J. Am. Chem. Soc. 125*, 15010–15020.
1552. Lange, R., Larroque, C., and Anzenbacher, P. (1992) The cholesterol-side-chain-cleaving cytochrome P450 spin-state equilibrium. 1. Thermodynamic analysis, *Eur. J. Biochem. 207*, 69–73.
1553. Narasimhulu, S. (1993) Substrate-induced spin-state transition in cytochrome $P450_{lm2}$: A temperature-jump relaxation study, *Biochemistry 32*, 10344–10350.
1554. Denisov, I. G., Grinkova, Y. V., Baas, B. J., and Sligar, S. G. (2006) The ferrous-dioxygen intermediate in human cytochrome $P450_{3a4}$. Substrate dependence of formation and decay kinetics, *J. Biol. Chem. 281*, 23313–23318.
1555. Davydov, R., Makris, T. M., Kofman, V., Werst, D. E., Sligar, S. G., and Hoffman, B. M. (2001) Hydroxylation of camphor by reduced oxy-cytochrome $P450_{cam}$: Mechanistic implications of EPR and ENDOR studies of catalytic intermediates in native and mutant enzymes, *J. Am. Chem. Soc. 123*, 1403–1415.
1556. Raner, G. M., Chiang, E. W., Vaz, A. D., and Coon, M. J. (1997) Mechanism-based inactivation of cytochrome $P450_{2b4}$ by aldehydes: Relationship to aldehyde deformylation via a peroxyhemiacetal intermediate, *Biochemistry 36*, 4895–4902.
1557. Liu, J. G., Shimizu, Y., Ohta, T., and Naruta, Y. (2010) Formation of an end-on ferric peroxo intermediate upon one-electron reduction of a ferric superoxo heme, *J. Am. Chem. Soc. 132*, 3672–3673.
1558. Ogliaro, F., de Visser, S. P., Cohen, S., Sharma, P. K., and Shaik, S. (2002) Searching for the second oxidant in the catalytic cycle of cytochrome P450: A theoretical investigation of the iron(III)-hydroperoxo species and its epoxidation pathways, *J. Am. Chem. Soc. 124*, 2806–2817.
1559. Mak, P. J., Denisov, L. G., Victoria, D., Makris, T. M., Deng, T. J., Sligar, S. G., and Kincaid, J. R. (2007) Resonance Raman detection of the hydroperoxo intermediate in the cytochrome P450 enzymatic cycle, *J. Am. Chem. Soc. 129*, 6382–6383.
1560. Gerber, N. C., and Sligar, S. G. (1992) Catalytic mechanism of cytochrome P450: Evidence for a distal charge relay, *J. Am. Chem. Soc. 114*, 8742–8743.
1561. Newcomb, M., Zhang, R., Chandrasena, R. E., Halgrimson, J. A., Horner, J. H., Makris, T. M., and Sligar, S. G. (2006) Cytochrome P450 compound I, *J. Am. Chem. Soc. 128*, 4580–4581.
1562. Ogliaro, F., Cohen, S., de Visser, S. P., and Shaik, S. (2000) Medium polarization and hydrogen bonding effects on compound I of cytochrome P450: What kind of a radical is it really?, *J. Am. Chem. Soc. 122*, 12892–12893.
1563. Erdogan, H., Vandemeulebroucke, A., Nauser, T., Bounds, P. L., and Koppenol, W. H. (2017) Jumpstarting the cytochrome P450 catalytic cycle with a hydrated electron, *J. Biol. Chem. 292*, 21481–21489.
1564. Rutter, R., Hager, L. P., Dhonau, H., Hendrich, M., Valentine, M., and Debrunner, P. (1984) Chloroperoxidase compound I: Electron paramagnetic resonance and Mössbauer studies, *Biochemistry 23*, 6809–6816.
1565. Stone, K. L., Behan, R. K., and Green, M. T. (2005) X-ray absorption spectroscopy of chloroperoxidase compound I: Insight into the reactive intermediate of P450 chemistry, *Proc. Natl. Acad. Sci. U. S. A. 102*, 16563–16565.
1566. Wang, Q., Sheng, X., Horner, J. H., and Newcomb, M. (2009) Quantitative production of compound I from a cytochrome P450 enzyme at low temperatures. Kinetics, activation parameters, and kinetic isotope effects for oxidation of benzyl alcohol, *J. Am. Chem. Soc. 131*, 10629–10636.
1567. Rittle, J., and Green, M. T. (2010) Cytochrome P450 compound I: Capture, charac-

terization, and C–H bond activation kinetics, *Science 330*, 933–937.
1568. Newcomb, M., Halgrimson, J. A., Horner, J. H., Wasinger, E. C., Chen, L. X., and Sligar, S. G. (2008) X-ray absorption spectroscopic characterization of a cytochrome P450 compound II derivative, *Proc. Natl. Acad. Sci. U.S.A. 105*, 8179–8184.
1569. Lau, S. M., Harder, P. A., and O'Keefe, D. P. (1993) Low carbon monoxide affinity allene oxide synthase is the predominant cytochrome P450 in many plant tissues, *Biochemistry 32*, 1945–1950.
1570. Matsunaga, I., Yamada, A., Lee, D. S., Obayashi, E., Fujiwara, N., Kobayashi, K., Ogura, H., and Shiro, Y. (2002) Enzymatic reaction of hydrogen peroxide-dependent peroxygenase cytochrome P450s: Kinetic deuterium isotope effects and analyses by resonance Raman spectroscopy, *Biochemistry 41*, 1886–1892.
1571. Song, W. C., and Brash, A. R. (1991) Purification of an allene oxide synthase and identification of the enzyme as a cytochrome P450, *Science 253*, 781–784.
1572. Makino, M., Sugimoto, H., Shiro, Y., Asamizu, S., Onaka, H., and Nagano, S. (2007) Crystal structures and catalytic mechanism of cytochrome P450 StaP that produces the indolocarbazole skeleton, *Proc. Natl. Acad. Sci. U. S. A. 104*, 11591–11596.
1573. Wolff, T., Greim, H., Huang, M. T., Miwa, G. T., and Lu, A. Y. (1980) Aldrin epoxidation catalyzed by purified rat-liver cytochromes P450 and P448. High selectivity for cytochrome P450, *Eur. J. Biochem. 111*, 545–551.
1574. Ruettinger, R. T., and Fulco, A. J. (1981) Epoxidation of unsaturated fatty acids by a soluble cytochrome P450-dependent system from *Bacillus megaterium*, *J. Biol. Chem. 256*, 5728–5734.
1575. Karki, S. B., Dinnocenzo, J. P., Jones, J. P., and Korzekwa, K. R. (1995) Mechanism of oxidative amine dealkylation of substituted *N,N*-dimethylanilines by cytochrome P450: Application of isotope effect profiles, *J. Am. Chem. Soc. 117*, 3657–3664.
1576. Yoshimoto, F. K., and Guengerich, F. P. (2014) Mechanism of the third oxidative step in the conversion of androgens to estrogens by cytochrome P450 19A1 steroid aromatase, *J. Am. Chem. Soc. 136*, 15016–15025.
1577. Shaik, S., Kumar, D., de Visser, S. P., Altun, A., and Thiel, W. (2005) Theoretical perspective on the structure and mechanism of cytochrome P450 enzymes, *Chem. Rev. 105*, 2279–2328.
1578. Atkins, W. M., and Sligar, S. G. (1987) Metabolic switching in cytochrome $P450_{cam}$: Deuterium isotope effects on regiospecificity and the monooxygenase/oxidase ratio, *J. Am. Chem. Soc. 109*, 3754–3760.
1579. Groves, J. T., and McClusky, G. A. (1978) Aliphatic hydroxylation by highly purified liver microsomal cytochrome P450. Evidence for a carbon radical intermediate, *Biochem. Biophys. Res. Commun. 81*, 154–160.
1580. Grant, J. L., Mitchell, M. E., and Makris, T. M. (2016) Catalytic strategy for carbon-carbon bond scission by the cytochrome P450 OleT, *Proc. Natl. Acad. Sci. U. S. A. 113*, 10049–10054.
1581. Gelb, M. H., Heimbrook, D. C., Malkonen, P., and Sligar, S. G. (1982) Stereochemistry and deuterium isotope effects in camphor hydroxylation by the cytochrome $P450_{cam}$ monooxygenase system, *Biochemistry 21*, 370–377.
1582. Wang, X. S., Peter, S., Kinne, M., Hofrichter, M., and Groves, J. T. (2012) Detection and kinetic characterization of a highly reactive heme-thiolate peroxygenase compound I, *J. Am. Chem. Soc. 134*, 12897–12900.
1583. Davydov, R., Dawson, J. H., Perera, R., and Hoffman, B. M. (2013) The use of deuterated camphor as a substrate in H-1 ENDOR studies of hydroxylation by cryoreduced oxy $P450_{cam}$ provides new evidence of the involvement of compound I, *Biochemistry 52*, 667–671.
1584. Davydov, R., Gilep, A. A., Strushkevich, N. V., Usanov, S. A., and Hoffman, B. M. (2012) Compound I is the reactive intermediate in the first monooxygenation step during conversion of cholesterol to pregnenolone by cytochrome $P450_{scc}$: EPR/ENDOR/cryoreduction/annealing studies, *J. Am. Chem. Soc. 134*, 17149–17156.
1585. Ortiz de Montellano, P. R., and Stearns, R. A. (1987) Timing of the radical recombination step in cytochrome P450 catalysis with ring-strained probes, *J. Am. Chem. Soc. 109*, 3415–3420.
1586. Atkinson, J. K., Hollenberg, P. F., Ingold, K. U., Johnson, C. C., Letadic, M. H., Newcomb, M., and Putt, D. A. (1994) Cytochrome P450-

catalyzed hydroxylation of hydrocarbons: Kinetic deuterium-isotope effects for the hydroxylation of an ultrafast radical clock, *Biochemistry 33*, 10630–10637.
1587. Newcomb, M., Shen, R., Choi, S.-Y., Toy, P. H., Hollenberg, P. F., Vaz, A. D. N., and Coon, M. J. (2000) Cytochrome P450-catalyzed hydroxylation of mechanistic probes that distinguish between radicals and cations. Evidence for cationic but not for radical intermediates, *J. Am. Chem. Soc. 122*, 2677–2686.
1588. Toy, P. H., Newcomb, M., and Hollenberg, P. F. (1998) Hypersensitive mechanistic probe studies of cytochrome P450-catalyzed hydroxylation reactions. Implications for the cationic pathway, *J. Am. Chem. Soc. 120*, 7719–7729.
1589. Atkinson, J. K., and Ingold, K. U. (1993) Cytochrome P450 hydroxylation of hydrocarbons: Variation in the rate of oxygen rebound using cyclopropyl radical clocks including two new ultrafast probes, *Biochemistry 32*, 9209–9214.
1590. Bowry, V. W., and Ingold, K. U. (1991) A radical clock investigation of microsomal cytochrome P450 hydroxylation of hydrocarbons. Rate of oxygen rebound, *J. Am. Chem. Soc. 113*, 5699–5707.
1591. Auclair, K., Hu, Z., Little, D. M., Ortiz De Montellano, P. R., and Groves, J. T. (2002) Revisiting the mechanism of P450 enzymes with the radical clocks norcarane and spiro[2,5]octane, *J. Am. Chem. Soc. 124*, 6020–6027.
1592. Williams, P. A., Cosme, J., Ward, A., Angove, H. C., Matak Vinkovic, D., and Jhoti, H. (2003) Crystal structure of human cytochrome $P450_{2c9}$ with bound warfarin, *Nature 424*, 464–468.
1593. Newcomb, M., Le Tadic-Biadatti, M.-H., Chestney, D. L., Roberts, E. S., and Hollenberg, P. F. (1995) A nonsynchronous concerted mechanism for cytochrome P450 catalyzed hydroxylation, *J. Am. Chem. Soc. 117*, 12085–12091.
1594. Koo, L. S., Immoos, C. E., Cohen, M. S., Farmer, P. J., and Ortiz de Montellano, P. R. (2002) Enhanced electron transfer and lauric acid hydroxylation by site-directed mutagenesis of CYP119, *J. Am. Chem. Soc. 124*, 5684–5691.
1595. Wang, X., Peter, S., Kinne, M., Hofrichter, M., and Groves, J. T. (2012) Detection and kinetic characterization of a highly reactive heme-thiolate peroxygenase compound I, *J. Am. Chem. Soc. 134*, 12897–12900.
1596. Vaz, A. D., McGinnity, D. F., and Coon, M. J. (1998) Epoxidation of olefins by cytochrome P450: Evidence from site-specific mutagenesis for hydroperoxo-iron as an electrophilic oxidant, *Proc. Natl. Acad. Sci. U. S. A. 95*, 3555–3560.
1597. Jin, S., Makris, T. M., Bryson, T. A., Sligar, S. G., and Dawson, J. H. (2003) Epoxidation of olefins by hydroperoxo-ferric cytochrome P450, *J. Am. Chem. Soc. 125*, 3406–3407.
1598. Dowers, T. S., Rock, D. A., Rock, D. A., and Jones, J. P. (2004) Kinetic isotope effects implicate the iron-oxene as the sole oxidant in P450-catalyzed *N*-dealkylation, *J. Am. Chem. Soc. 126*, 8868–8869.
1599. Newcomb, M., Aebisher, D., Shen, R., Chandrasena, R. E., Hollenberg, P. F., and Coon, M. J. (2003) Kinetic isotope effects implicate two electrophilic oxidants in cytochrome P450-catalyzed hydroxylations, *J. Am. Chem. Soc. 125*, 6064–6065.
1600. Chandrasena, R. E., Vatsis, K. P., Coon, M. J., Hollenberg, P. F., and Newcomb, M. (2004) Hydroxylation by the hydroperoxy-iron species in cytochrome P450 enzymes, *J. Am. Chem. Soc. 126*, 115–126.
1601. Ullrich, R., and Hofrichter, M. (2007) Enzymatic hydroxylation of aromatic compounds, *Cell. Mol. Life Sci. 64*, 271–293.
1602. Kluge, M., Ullrich, R., Dolge, C., Scheibner, K., and Hofrichter, M. (2009) Hydroxylation of naphthalene by aromatic peroxygenase from *Agrocybe aegerita* proceeds via oxygen transfer from H_2O_2 and intermediary epoxidation, *Appl Microbiol Biotechnol 81*, 1071–1076.
1603. Asaka, M., and Fujii, H. (2016) Participation of electron transfer process in rate-limiting step of aromatic hydroxylation reactions by compound I models of heme enzymes, *J. Am. Chem. Soc. 138*, 8048–8051.
1604. Ramirez-Escudero, M., Molina-Espeja, P., Gomez de Santos, P., Hofrichter, M., Sanz-Aparicio, J., and Alcalde, M. (2018) Structural insights into the substrate promiscuity of a laboratory-evolved peroxygenase, *Am. Chem. Soc. Chem. Biol 13*, 3259–3268.
1605. Akhtar, M., Corina, D. L., Miller, S. L., Shyadehi, A. Z., and Wright, J. N. (1994) Incorporation of label from $^{18}O_2$ into acetate during side-chain cleavage catalyzed by cytochrome

P450(17-α) (17-α-hydroxylase-17,20-lyase), *J. Chem. Soc. Perkin Trans.*, 263–267.
1606. Lee-Robichaud, P., Shyadehi, A. Z., Wright, J. N., Akhtar, M. E., and Akhtar, M. (1995) Mechanistic kinship between hydroxylation and desaturation reactions: Acyl-carbon bond cleavage promoted by pig and human CYP17 ($P450_{17\alpha}$; 17α-hydroxylase-17,20-lyase), *Biochemistry 34*, 14104–14113.
1607. Watanabe, Y., and Ishimura, Y. (1989) A model study on aromatase cytochrome P450 reaction: Transformation of androstene-3,17,19-trione to 10β-hydroxyester-4-ene-3,17-dione, *J. Am. Chem. Soc. 111*, 8047–8049.
1608. Cole, P. A., and Robinson, C. H. (1988) Peroxide model reaction for placental aromatase, *J. Am. Chem. Soc. 110*, 1284–1285.
1609. Vaz, A. D., Pernecky, S. J., Raner, G. M., and Coon, M. J. (1996) Peroxo-iron and oxenoid-iron species as alternative oxygenating agents in cytochrome P450-catalyzed reactions: Switching by Threonine-302 to alanine mutagenesis of cytochrome $P450_{2b4}$, *Proc. Natl. Acad. Sci. U. S. A. 93*, 4644–4648.
1610. Mak, P. J., Gregory, M. C., Denisov, I. G., Sligar, S. G., and Kincaid, J. R. (2015) Unveiling the crucial intermediates in androgen production, *Proc. Natl. Acad. Sci. U.S.A. 112*, 15856–15861.
1611. Petrunak, E. M., DeVore, N. M., Porubsky, P. R., and Scott, E. E. (2014) Structures of human steroidogenic cytochrome $P450_{17\alpha1}$ with substrates, *J. Biol. Chem. 289*, 32952–32964.
1612. Yoshimoto, F. K., Gonzalez, E., Auchus, R. J., and Guengerich, F. P. (2016) Mechanism of 17α,20-lyase and new hydroxylation reactions of human cytochrome $P450_{17\alpha1}$: ^{18}O Labeling and oxygen surrogate evidence for a role of a perferryl oxygen, *J. Biol. Chem. 291*, 17143–17164.
1613. Akhtar, M., Corina, D., Miller, S., Shyadehi, A. Z., and Wright, J. N. (1994) Mechanism of the acyl-carbon cleavage and related reactions catalyzed by multifunctional P450s: Studies on cytochrome $P450_{17\alpha}$, *Biochemistry 33*, 4410–4418.
1614. Sivaramakrishnan, S., Ouellet, H., Matsumura, H., Guan, S. H., Moenne-Loccoz, P., Burlingame, A. L., and Ortiz de Montellano, P. R. (2012) Proximal ligand electron donation and reactivity of the cytochrome P450 ferric-peroxo anion, *J. Am. Chem. Soc. 134*, 6673–6684.
1615. Davydov, R., Strushkevich, N., Smil, D., Yantsevich, A., Gilep, A., Usanov, S., and Hoffman, B. M. (2015) Evidence that compound I is the active species in both the hydroxylase and lyase steps by which $P450_{scc}$ converts cholesterol to pregnenolone: EPR/ENDOR/cryoreduction/annealing studies, *Biochemistry 54*, 7089–7097.
1616. Strushkevich, N., MacKenzie, F., Cherkesova, T., Grabovec, I., Usanov, S., and Park, H. W. (2011) Structural basis for pregnenolone biosynthesis by the mitochondrial monooxygenase system, *Proc. Natl. Acad. Sci. U.S.A. 108*, 10139–10143.
1617. Garcia-Horsman, J. A., Barquera, B., Rumbley, J., Ma, J., and Gennis, R. B. (1994) The superfamily of heme-copper respiratory oxidases, *J. Bacteriol. 176*, 5587–5600.
1618. Tsukihara, T., Aoyama, H., Yamashita, E., Tomizaki, T., Yamaguchi, H., Shinzawa-Itoh, K., Nakashima, R., Yaono, R., and Yoshikawa, S. (1995) Structures of metal sites of oxidized bovine heart cytochrome *c* oxidase at 2.8 Å, *Science 269*, 1069–1074.
1619. Shapleigh, J. P., Hosler, J. P., Tecklenburg, M. M., Kim, Y., Babcock, G. T., Gennis, R. B., and Ferguson-Miller, S. (1992) Definition of the catalytic site of cytochrome *c* oxidase: Specific ligands of heme *a* and the heme a_3-CuB center, *Proc. Natl. Acad. Sci. U. S. A. 89*, 4786–4790.
1620. Wharton, D. C., and Gibson, Q. H. (1976) Stoichiometry of carbon monoxide binding by cytochrome *c* oxidase, *J. Biol. Chem. 251*, 2861–2862.
1621. Babcock, G. T., Vickery, L. E., and Palmer, G. (1976) Electronic state of heme in cytochrome oxidase. I. Magnetic circular dichroism of the isolated enzyme and its derivatives, *J. Biol. Chem. 251*, 7907–7919.
1622. Aoyama, H., Muramoto, K., Shinzawa-Itoh, K., Hirata, K., Yamashita, E., Tsukihara, T., Ogura, T., and Yoshikawa, S. (2009) A peroxide bridge between Fe and Cu ions in the O_2 reduction site of fully oxidized cytochrome *c* oxidase could suppress the proton pump, *Proc. Natl. Acad. Sci. U.S.A. 106*, 2165–2169.
1623. Mochizuki, M., Aoyama, H., Shinzawa-Itoh, K., Usui, T., Tsukihara, T., and Yoshikawa, S. (1999) Quantitative reevaluation of the redox active sites of crystalline bovine heart cytochrome *c* oxidase, *J. Biol. Chem. 274*, 33403–33411.

1624. Yoshikawa, S., Choc, M. G., O'Toole, M. C., and Caughey, W. S. (1977) An infrared study of CO binding to heart cytochrome *c* oxidase and hemoglobin a. Implications re O_2 reactions, *J. Biol. Chem. 252*, 5498–5508.
1625. Jancura, D., Antalik, M., Berka, V., Palmer, G., and Fabian, M. (2006) Filling the catalytic site of cytochrome *c* oxidase with electrons. Reduced CuB facilitates internal electron transfer to heme a_3, *J. Biol. Chem. 281*, 20003–20010.
1626. Adelroth, P., Brzezinski, P., and Malmstrom, B. G. (1995) Internal electron transfer in cytochrome *c* oxidase from *Rhodobacter sphaeroides*, *Biochemistry 34*, 2844–2849.
1627. Oliveberg, M., and Malmstrom, B. G. (1991) Internal electron transfer in cytochrome *c* oxidase: Evidence for a rapid equilibrium between cytochrome *a* and the bimetallic site, *Biochemistry 30*, 7053–7057.
1628. Morgan, J. E., Li, P. M., Jang, D. J., el-Sayed, M. A., and Chan, S. I. (1989) Electron transfer between cytochrome *a* and copper A in cytochrome *c* oxidase: A perturbed equilibrium study, *Biochemistry 28*, 6975–6983.
1629. Petty, R. H., Welch, B. R., Wilson, L. J., Bottomley, L. A., and Kadish, K. M. (1980) Cytochrome oxidase models. 2. μ-Bipyrimidyl mixed-metal complexes as synthetic models for the iron/copper binuclear active site of cytochrome oxidase, *J. Am. Chem. Soc. 102*, 611–620.
1630. Gorsky, L. D., Koop, D. R., and Coon, M. J. (1984) On the stoichiometry of the oxidase and monooxygenase reactions catalyzed by liver microsomal cytochrome P450. Products of oxygen reduction, *J. Biol. Chem. 259*, 6812–6817.
1631. Atkins, W. M., and Sligar, S. G. (1988) Deuterium isotope effects in norcamphor metabolism by cytochrome $P450_{cam}$: Kinetic evidence for the two-electron reduction of a high-valent iron-oxo intermediate, *Biochemistry 27*, 1610–1616.
1632. Aoyama, T., Korzekwa, K., Nagata, K., Gillette, J., Gelboin, H. V., and Gonzales, F. J. (1989) cDNA-Directed expression of rat testosterone 7α-hydroxylase using the modified vaccinia virus, T7-RNA-polymerase system and evidence for 6α-hydroxylation and Δ_6-testosterone formation, *Eur. J. Biochem. 181*, 331–336.
1633. Kumar, D., De Visser, S. P., and Shaik, S. (2004) Oxygen economy of cytochrome P450: What is the origin of the mixed functionality as a dehydrogenase-oxidase enzyme compared with its normal function?, *J. Am. Chem. Soc. 126*, 5072–5073.
1634. Verkhovsky, M. I., Morgan, J. E., Puustinen, A., and Wikstrom, M. (1996) The "ferrous-oxy" intermediate in the reaction of dioxygen with fully reduced cytochromes aa_3 and bo_3, *Biochemistry 35*, 16241–16246.
1635. Oliveberg, M., and Malmstrom, B. G. (1992) Reaction of dioxygen with cytochrome *c* oxidase reduced to different degrees: Indications of a transient dioxygen complex with copper-B, *Biochemistry 31*, 3560–3563.
1636. Boulatov, R., Collman, J. P., Shiryaeva, I. M., and Sunderland, C. J. (2002) Functional analogues of the dioxygen reduction site in cytochrome oxidase: Mechanistic aspects and possible effects of Cu_B, *J. Am. Chem. Soc. 124*, 11923–11935.
1637. Sigman, J. A., Kim, H. K., Zhao, X., Carey, J. R., and Lu, Y. (2003) The role of copper and protons in heme-copper oxidases: Kinetic study of an engineered heme-copper center in myoglobin, *Proc. Natl. Acad. Sci. U. S. A. 100*, 3629–3634.
1638. Ghiladi, R. A., Ju, T. D., Lee, D.-H., Moeenne-Loccoz, P., Kaderli, S., Neuhold, Y.-M., Zuberbuehler, A. D., Woods, A. S., Cotter, R. J., and Karlin, K. D. (1999) Formation and characterization of a high-spin heme-copper dioxygen (peroxo) complex, *J. Am. Chem. Soc. 121*, 9885–9886.
1639. Collman, J. P., Herrmann, P. C., Boitrel, B., Zhang, X., Eberspacher, T. A., Fu, L., Wang, J., Rousseau, D. L., and Williams, E. R. (1994) Synthetic analog for the oxygen binding site in cytochrome *c* oxidase, *J. Am. Chem. Soc. 116*, 9783–9784.
1640. Garcia-Bosch, I., Adam, S. M., Schaefer, A. W., Sharma, S. K., Peterson, R. L., Solomon, E. I., and Karlin, K. D. (2015) A "naked" Fe-III-(O_2^{2-})-Cu(II) species allows for structural and spectroscopic tuning of low-spin heme-peroxo-Cu complexes, *J. Am. Chem. Soc. 137*, 1032–1035.
1641. Wiertz, F. G., Richter, O. M., Ludwig, B., and de Vries, S. (2007) Kinetic resolution of a tryptophan-radical intermediate in the reaction cycle of *Paracoccus denitrificans* cytochrome *c* oxidase, *J. Biol. Chem. 282*, 31580–31591.

1642. Fabian, M., and Palmer, G. (1995) The interaction of cytochrome oxidase with hydrogen peroxide: The relationship of compounds P and F, *Biochemistry 34*, 13802–13810.
1643. Ogura, T., Takahashi, S., Hirota, S., Shinzawa-Itoh, K., Yoshikawa, S., Appelman, E. H., and Kitagawa, T. (1993) Time-resolved resonance Raman elucidation of the pathway for dioxygen reduction by cytochrome *c* oxidase, *J. Am. Chem. Soc. 115*, 8527–8536.
1644. Varotsis, C., Zhang, Y., Appelman, E. H., and Babcock, G. T. (1993) Resolution of the reaction sequence during the reduction of O_2 by cytochrome oxidase, *Proc. Natl. Acad. Sci. U. S. A. 90*, 237–241.
1645. Chance, B., Saronio, C., and Leigh, J. S., Jr. (1975) Functional intermediates in the reaction of membrane-bound cytochrome oxidase with oxygen, *J. Biol. Chem. 250*, 9226–9237.
1646. Van Eps, N., Szundi, I., and Einarsdottir, O. (2000) A new approach for studying fast biological reactions involving dioxygen: The reaction of fully reduced cytochrome *c* oxidase with O_2, *Biochemistry 39*, 14576–14582.
1647. Szundi, I., Liao, G. L., and Einarsdottir, O. (2001) Near-infrared time-resolved optical absorption studies of the reaction of fully reduced cytochrome *c* oxidase with dioxygen, *Biochemistry 40*, 2332–2339.
1648. Shimada, A., Etoh, Y., Kitoh-Fujisawa, R., Sasaki, A., Shinzawa-Itoh, K., Hiromoto, T., Yamashita, E., Muramoto, K., Tsukihara, T., and Yoshikawa, S. (2020) X-Ray structures of catalytic intermediates of cytochrome *c* oxidase provide insights into its O_2 activation and unidirectional proton-pump mechanisms, *J. Biol. Chem. 295*, 5818–5833.
1649. Kaila, V. R., Oksanen, E., Goldman, A., Bloch, D. A., Verkhovsky, M. I., Sundholm, D., and Wikstrom, M. (2011) A combined quantum chemical and crystallographic study on the oxidized binuclear center of cytochrome *c* oxidase, *Biochim. Biophys. Acta 1807*, 769–778.
1650. Yano, N., Muramoto, K., Shimada, A., Takemura, S., Baba, J., Fujisawa, H., Mochizuki, M., Shinzawa-Itoh, K., Yamashita, E., Tsukihara, T., and Yoshikawa, S. (2016) The Mg^{2+}-containing water cluster of mammalian cytochrome *c* oxidase collects four pumping proton equivalents in each catalytic cycle, *J. Biol. Chem. 291*, 23882–23894.
1651. Karpefors, M., Adelroth, P., Namslauer, A., Zhen, Y., and Brzezinski, P. (2000) Formation of the "peroxy" intermediate in cytochrome *c* oxidase is associated with internal proton/hydrogen transfer, *Biochemistry 39*, 14664–14669.
1652. Cappuccio, J. A., Ayala, I., Elliott, G. I., Szundi, I., Lewis, J., Konopelski, J. P., Barry, B. A., and Einarsdottir, O. (2002) Modeling the active site of cytochrome oxidase: Synthesis and characterization of a cross-linked histidine-phenol, *J. Am. Chem. Soc. 124*, 1750–1760.
1653. Gorbikova, E. A., Belevich, I., Wikstrom, M., and Verkhovsky, M. I. (2008) The proton donor for O-O bond scission by cytochrome *c* oxidase, *Proc. Natl. Acad. Sci. U.S.A. 105*, 10733–10737.
1654. Han, S., Ching, Y. C., and Rousseau, D. L. (1990) Ferryl and hydroxy intermediates in the reaction of oxygen with reduced cytochrome *c* oxidase, *Nature 348*, 89–90.
1655. Witt, S. N., and Chan, S. I. (1987) Evidence for a ferryl Ee_{a3} in oxygenated cytochrome *c* oxidase, *J. Biol. Chem. 262*, 1446–1448.
1656. Kumar, C., Naqui, A., Powers, L., Ching, Y. C., and Chance, B. (1988) Does the peroxide compound of cytochrome oxidase contain a ferryl iron?, *J. Biol. Chem. 263*, 7159–7163.
1657. Varotsis, C., and Babcock, G. T. (1990) Appearance of the $\nu(Fe^{IV}{=}O)$ vibration from a ferryl-oxo intermediate in the cytochrome oxidase/dioxygen reaction, *Biochemistry 29*, 7357–7362.
1658. Proshlyakov, D. A., Ogura, T., Shinzawa-Itoh, K., Yoshikawa, S., and Kitagawa, T. (1996) Microcirculating system for simultaneous determination of Raman and absorption spectra of enzymatic reaction intermediates and its application to the reaction of cytochrome *c* oxidase with hydrogen peroxide, *Biochemistry 35*, 76–82.
1659. Halime, Z., Kotani, H., Li, Y. Q., Fukuzumi, S., and Karlin, K. D. (2011) Homogeneous catalytic O_2 reduction to water by a cytochrome *c* oxidase model with trapping of intermediates and mechanistic insights, *Proc. Natl. Acad. Sci. U.S.A. 108*, 13990–13994.
1660. Sucheta, A., Szundi, I., and Einarsdottir, O. (1998) Intermediates in the reaction of fully reduced cytochrome *c* oxidase with dioxygen, *Biochemistry 37*, 17905–17914.

1661. Proshlyakov, D. A., Pressler, M. A., DeMaso, C., Leykam, J. F., DeWitt, D. L., and Babcock, G. T. (2000) Oxygen activation and reduction in respiration: Involvement of redox-active Tyrosine 244, *Science 290*, 1588–1591.
1662. MacMillan, F., Kannt, A., Behr, J., Prisner, T., and Michel, H. (1999) Direct evidence for a tyrosine radical in the reaction of cytochrome *c* oxidase with hydrogen peroxide, *Biochemistry 38*, 9179–9184.
1663. Yu, M. A., Egawa, T., Shinzawa-Itoh, K., Yoshikawa, S., Guallar, V., Yeh, S. R., Rousseau, D. L., and Gerfen, G. J. (2012) Two tyrosyl radicals stabilize high oxidation states in cytochrome *c* oxidase for efficient energy conservation and proton translocation, *J. Am. Chem. Soc. 134*, 4753–4761.
1664. Collman, J. P., Decreau, R. A., Yan, Y., Yoon, J., and Solomon, E. I. (2007) Intramolecular single-turnover reaction in a cytochrome *c* oxidase model bearing a Tyr244 mimic, *J. Am. Chem. Soc. 129*, 5794–5795.
1665. Collman, J. P., Devaraj, N. K., Decreau, R. A., Yang, Y., Yan, Y. L., Ebina, W., Eberspacher, T. A., and Chidsey, C. E. (2007) A cytochrome *c* oxidase model catalyzes oxygen to water reduction under rate-limiting electron flux, *Science 315*, 1565–1568.
1666. Schaefer, A. W., Kieber-Emmons, M. T., Adam, S. M., Karlin, K. D., and Solomon, E. I. (2017) Phenol-induced O-O bond cleavage in a low-spin heme-peroxo-copper complex: Implications for O_2 reduction in heme-copper oxidases, *J. Am. Chem. Soc. 139*, 7958–7973.
1667. Adam, S. M., Garcia-Bosch, I., Schaefer, A. W., Sharma, S. K., Siegler, M. A., Solomon, E. I., and Karlin, K. D. (2017) Critical aspects of heme-peroxo-Cu complex structure and nature of proton source dictate metal-O_{peroxo} breakage versus reductive O-O cleavage chemistry, *J. Am. Chem. Soc. 139*, 472–481.
1668. Zaslavsky, D., Sadoski, R. C., Wang, K., Durham, B., Gennis, R. B., and Millett, F. (1998) Single electron reduction of cytochrome *c* oxidase compound F: Resolution of partial steps by transient spectroscopy, *Biochemistry 37*, 14910–14916.
1669. Rigby, S. E., Junemann, S., Rich, P. R., and Heathcote, P. (2000) Reaction of bovine cytochrome *c* oxidase with hydrogen peroxide produces a tryptophan cation radical and a porphyrin cation radical, *Biochemistry 39*, 5921–5928.
1670. Fabian, M., Wong, W. W., Gennis, R. B., and Palmer, G. (1999) Mass spectrometric determination of dioxygen bond splitting in the "peroxy" intermediate of cytochrome *c* oxidase, *Proc. Natl. Acad. Sci. U. S. A. 96*, 13114–13117.
1671. Branden, M., Namslauer, A., Hansson, O., Aasa, R., and Brzezinski, P. (2003) Water-hydroxide exchange reactions at the catalytic site of heme-copper oxidases, *Biochemistry 42*, 13178–13184.
1672. Collman, J. P., Ghosh, S., Dey, A., Decreau, R. A., and Yang, Y. (2009) Catalytic reduction of O_2 by cytochrome *c* using a synthetic model of cytochrome *c* oxidase, *J. Am. Chem. Soc. 131*, 5034–5035.
1673. Harteck, P. (1933) Die darstellung von HNO bzw. $[HNO]_n$, *Berichte der Deutschen Chemischen Gesellschaft 66*, 423–426.
1674. So, S. P. (1990) Structures, relative stabilities, barriers to internal-rotation, and vibrational frequencies of isomeric HNOH and HPOH, *J. Phys. Chem. 94*, 2344–2347.
1675. Traylor, T. G., and Sharma, V. S. (1992) Why NO?, *Biochemistry 31*, 2847–2849.
1676. Suzuki, N., Higuchi, T., Urano, Y., Kikuchi, K., Uchida, T., Mukai, M., Kitagawa, T., and Nagano, T. (2000) First synthetic NO-heme-thiolate complex relevant to nitric oxide synthase and cytochrome $P450_{nor}$, *J. Am. Chem. Soc. 122*, 12059–12060.
1677. Abucayon, E. G., Khade, R. L., Powell, D. R., Zhang, Y., and Richter-Addo, G. B. (2016) Hydride attack on a coordinated ferric nitrosyl: Experimental and DFT evidence for the formation of a heme model-HNO derivative, *J. Am. Chem. Soc. 138*, 104–107.
1678. Park, S. Y., Shimizu, H., Adachi, S., Nakagawa, A., Tanaka, I., Nakahara, K., Shoun, H., Obayashi, E., Nakamura, H., Iizuka, T., and Shiro, Y. (1997) Crystal structure of nitric oxide reductase from denitrifying fungus *Fusarium oxysporum*, *Nature Struct. Biol. 4*, 827–832.
1679. Nakahara, K., Tanimoto, T., Hatano, K., Usuda, K., and Shoun, H. (1993) Cytochrome $P450_{55a1}$ ($P450_{dnir}$) acts as nitric oxide reductase employing NADH as the direct electron donor, *J. Biol. Chem. 268*, 8350–8355.
1680. Oshima, R., Fushinobu, S., Su, F., Zhang, L., Takaya, N., and Shoun, H. (2004) Structural evidence for direct hydride transfer from

NADH to cytochrome P450nor, *J. Mol. Biol. 342*, 207–217.
1681. Obayashi, E., Takahashi, S., and Shiro, Y. (1998) Electronic structure of reaction intermediate of cytochrome $P450_{nor}$ in its nitric oxide reduction, *J. Am. Chem. Soc. 120*, 12964–12965.
1682. Saraste, M., and Castresana, J. (1994) Cytochrome oxidase evolved by tinkering with denitrification enzymes, *FEBS Lett. 341*, 1–4.
1683. van der Oost, J., de Boer, A. P., de Gier, J. W., Zumft, W. G., Stouthamer, A. H., and van Spanning, R. J. (1994) The heme-copper oxidase family consists of three distinct types of terminal oxidases and is related to nitric oxide reductase, *FEMS Microbiol Lett 121*, 1–9.
1684. Hendriks, J., Warne, A., Gohlke, U., Haltia, T., Ludovici, C., Lubben, M., and Saraste, M. (1998) The active site of the bacterial nitric oxide reductase is a dinuclear iron center, *Biochemistry 37*, 13102–13109.
1685. Cheesman, M. R., Zumft, W. G., and Thomson, A. J. (1998) The MCD and EPR of the heme centers of nitric oxide reductase from *Pseudomonas stutzeri*: Evidence that the enzyme is structurally related to the heme-copper oxidases, *Biochemistry 37*, 3994–4000.
1686. Suharti, Strampraad, M. J., Schroder, I., and de Vries, S. (2001) A novel copper A containing menaquinol NO reductase from *Bacillus azotoformans*, *Biochemistry 40*, 2632–2639.
1687. Hendriks, J. H., Jasaitis, A., Saraste, M., and Verkhovsky, M. I. (2002) Proton and electron pathways in the bacterial nitric oxide reductase, *Biochemistry 41*, 2331–2340.
1688. Hino, T., Matsumoto, Y., Nagano, S., Sugimoto, H., Fukumori, Y., Murata, T., Iwata, S., and Shiro, Y. (2010) Structural basis of biological N_2O generation by bacterial nitric oxide reductase, *Science 330*, 1666–1670.
1689. Blomberg, M. R. (2017) Can reduction of NO to N_2O in cytochrome *c* dependent nitric oxide reductase proceed through a *trans*-mechanism?, *Biochemistry 56*, 120–131.
1690. Blomberg, M. R., and Siegbahn, P. E. (2012) Mechanism for N_2O generation in bacterial nitric oxide reductase: A quantum chemical study, *Biochemistry 51*, 5173–5186.
1691. Fulop, V., Moir, J. W. B., Ferguson, S. J., and Hajdu, J. (1995) The anatomy of a bifunctional enzyme: Structural basis for reduction of oxygen to water and synthesis of nitric-oxide by cytochrome cd_1, *Cell 81*, 369–377.
1692. Ranghino, G., Scorza, E., Sjogren, T., Williams, P. A., Ricci, M., and Hajdu, J. (2000) Quantum mechanical interpretation of nitrite reduction by cytochrome cd_1 nitrite reductase from *Paracoccus pantotrophus*, *Biochemistry 39*, 10958–10966.
1693. Wang, Y. N., and Averill, B. A. (1996) Direct observation by FTIR spectroscopy of the ferrous heme-NO^+ intermediate in reduction of nitrite by a dissimilatory heme cd_1 nitrite reductase, *J. Am. Chem. Soc. 118*, 3972–3973.
1694. Vega, J. M., and Kamin, H. (1977) Spinach nitrite reductase. Purification and properties of a siroheme-containing iron–sulfur enzyme, *J. Biol. Chem. 252*, 896–909.
1695. Swamy, U., Wang, M., Tripathy, J. N., Kim, S. K., Hirasawa, M., Knaff, D. B., and Allen, J. P. (2005) Structure of spinach nitrite reductase: Implications for multi-electron reactions by the iron–sulfur:siroheme cofactor, *Biochemistry 44*, 16054–16063.
1696. Hirasawa, M., Tollin, G., Salamon, Z., and Knaff, D. B. (1994) Transient kinetic and oxidation–reduction studies of spinach ferredoxin:nitrite oxidoreductase, *Biochim. Biophys. Acta 1185*, 336–345.
1697. Crane, B. R., Siegel, L. M., and Getzoff, E. D. (1997) Probing the catalytic mechanism of sulfite reductase by X-ray crystallography: Structures of the *Escherichia coli* hemoprotein in complex with substrates, inhibitors, intermediates, and products, *Biochemistry 36*, 12120–12137.
1698. Kuznetsova, S., Knaff, D. B., Hirasawa, M., Lagoutte, B., and Setif, P. (2004) Mechanism of spinach chloroplast ferredoxin-dependent nitrite reductase: Spectroscopic evidence for intermediate states, *Biochemistry 43*, 510–517.
1699. Lui, S. M., Soriano, A., and Cowan, J. A. (1993) Enzymic reduction of inorganic anions. Pre-steady-state kinetic analysis of the dissimilatory sulfite reductase (desulfoviridin) from *Desulfovibrio vulgaris* (Hildenborough). Mechanistic implications, *J. Am. Chem. Soc. 115*, 10483–10486.
1700. Ali, M., Stein, N., Mao, Y., Shahid, S., Schmidt, M., Bennett, B., and Pacheco, A. A. (2019) Trapping of a putative intermediate in the cytochrome *c* nitrite reductase (ccNiR)-catalyzed reduction of nitrite: Implications for the ccNiR reaction mechanism, *J. Am. Chem. Soc. 141*, 13358–13371.

1701. Einsle, O., Messerschmidt, A., Huber, R., Kroneck, P. M., and Neese, F. (2002) Mechanism of the six-electron reduction of nitrite to ammonia by cytochrome *c* nitrite reductase, *J. Am. Chem. Soc. 124*, 11737–11745.
1702. Matthews, J. C., Timkovich, R., Liu, M. Y., and Le Gall, J. (1995) Siroamide: A prosthetic group isolated from sulfite reductases in the genus *Desulfovibrio*, *Biochemistry 34*, 5248–5251.
1703. Ostrowski, J., Barber, M. J., Rueger, D. C., Miller, B. E., Siegel, L. M., and Kredich, N. M. (1989) Characterization of the flavoprotein moieties of NADPH-sulfite reductase from *Salmonella typhimurium* and *Escherichia coli*. Physicochemical and catalytic properties, amino acid sequence deduced from DNA sequence of CysJ, and comparison with NADPH-cytochrome P450 reductase, *J. Biol. Chem. 264*, 15796–15808.
1704. Einsle, O., Messerschmidt, A., Stach, P., Bourenkov, G. P., Bartunik, H. D., Huber, R., and Kroneck, P. M. (1999) Structure of cytochrome *c* nitrite reductase, *Nature 400*, 476–480.
1705. Bamford, V. A., Angove, H. C., Seward, H. E., Thomson, A. J., Cole, J. A., Butt, J. N., Hemmings, A. M., and Richardson, D. J. (2002) Structure and spectroscopy of the periplasmic cytochrome *c* nitrite reductase from *Escherichia coli*, *Biochemistry 41*, 2921–2931.
1706. Judd, E. T., Stein, N., Pacheco, A. A., and Elliott, S. J. (2014) Hydrogen bonding networks tune proton-coupled redox steps during the enzymatic six-electron conversion of nitrite to ammonia, *Biochemistry 53*, 5638–5646.
1707. Lukat, P., Rudolf, M., Stach, P., Messerschmidt, A., Kroneck, P. M., Simon, J., and Einsle, O. (2008) Binding and reduction of sulfite by cytochrome *c* nitrite reductase, *Biochemistry 47*, 2080–2086.
1708. Polyakov, K. M., Boyko, K. M., Tikhonova, T. V., Slutsky, A., Antipov, A. N., Zvyagilskaya, R. A., Popov, A. N., Bourenkov, G. P., Lamzin, V. S., and Popov, V. O. (2009) High-resolution structural analysis of a novel octaheme cytochrome *c* nitrite reductase from the haloalkaliphilic bacterium *Thioalkalivibrio nitratireducens*, *J. Mol. Biol. 389*, 846–862.
1709. Grabarczyk, D. B., Chappell, P. E., Eisel, B., Johnson, S., Lea, S. M., and Berks, B. C. (2015) Mechanism of thiosulfate oxidation in the SoxA family of cysteine-ligated cytochromes, *J. Biol. Chem. 290*, 9209–9221.
1710. White, K. A., and Marletta, M. A. (1992) Nitric oxide synthase is a cytochrome P450 type hemoprotein, *Biochemistry 31*, 6627–6631.
1711. McMillan, K., Bredt, D. S., Hirsch, D. J., Snyder, S. H., Clark, J. E., and Masters, B. S. (1992) Cloned, expressed rat cerebellar nitric oxide synthase contains stoichiometric amounts of heme, which binds carbon monoxide, *Proc. Natl. Acad. Sci. U. S. A. 89*, 11141–11145.
1712. Stuehr, D. J., Kwon, N. S., Nathan, C. F., Griffith, O. W., Feldman, P. L., and Wiseman, J. (1991) N^{ω}-Hydroxy-L-arginine is an intermediate in the biosynthesis of nitric oxide from L-arginine, *J. Biol. Chem. 266*, 6259–6263.
1713. Pufahl, R. A., Nanjappan, P. G., Woodard, R. W., and Marletta, M. A. (1992) Mechanistic probes of *N*-hydroxylation of L-arginine by the inducible nitric oxide synthase from murine macrophages, *Biochemistry 31*, 6822–6828.
1714. Kwon, N. S., Nathan, C. F., Gilker, C., Griffith, O. W., Matthews, D. E., and Stuehr, D. J. (1990) L-Citrulline production from L-arginine by macrophage nitric oxide synthase. The ureido oxygen derives from dioxygen, *J. Biol. Chem. 265*, 13442–13445.
1715. Leone, A. M., Palmer, R. M., Knowles, R. G., Francis, P. L., Ashton, D. S., and Moncada, S. (1991) Constitutive and inducible nitric oxide synthases incorporate molecular oxygen into both nitric oxide and citrulline, *J. Biol. Chem. 266*, 23790–23795.
1716. Abu-Soud, H. M., Presta, A., Mayer, B., and Stuehr, D. J. (1997) Analysis of neuronal NO synthase under single-turnover conditions: Conversion of N^{ω}-hydroxyarginine to nitric oxide and citrulline, *Biochemistry 36*, 10811–10816.
1717. Boggs, S., Huang, L., and Stuehr, D. J. (2000) Formation and reactions of the heme-dioxygen intermediate in the first and second steps of nitric oxide synthesis as studied by stopped-flow spectroscopy under single-turnover conditions, *Biochemistry 39*, 2332–2339.
1718. Clague, M. J., Wishnok, J. S., and Marletta, M. A. (1997) Formation of N^{δ}-cyanoornithine from N^{γ}-hydroxy-L-arginine and hydrogen peroxide by neuronal nitric oxide synthase:

Implications for mechanism, *Biochemistry 36*, 14465–14473.
1719. Pufahl, R. A., Wishnok, J. S., and Marletta, M. A. (1995) Hydrogen peroxide-supported oxidation of N^{γ}-hydroxy-L-arginine by nitric oxide synthase, *Biochemistry 34*, 1930–1941.
1720. Woodward, J. J., Chang, M. M., Martin, N. I., and Marletta, M. A. (2009) The second step of the nitric oxide synthase reaction: Evidence for ferric-peroxo as the active oxidant, *J. Am. Chem. Soc. 131*, 297–305.
1721. Mayer, B., John, M., Heinzel, B., Werner, E. R., Wachter, H., Schultz, G., and Bohme, E. (1991) Brain nitric oxide synthase is a biopterin- and flavin-containing multi-functional oxido-reductase, *FEBS Lett. 288*, 187–191.
1722. Hevel, J. M., and Marletta, M. A. (1992) Macrophage nitric oxide synthase: Relationship between enzyme-bound tetrahydrobiopterin and synthase activity, *Biochemistry 31*, 7160–7165.
1723. Schmidt, H. H., Smith, R. M., Nakane, M., and Murad, F. (1992) Ca^{2+}/Calmodulin-dependent NO synthase type I: A biopteroflavoprotein with Ca^{2+}/calmodulin-independent diaphorase and reductase activities, *Biochemistry 31*, 3243–3249.
1724. Hurshman, A. R., and Marletta, M. A. (2002) Reactions catalyzed by the heme domain of inducible nitric oxide synthase: Evidence for the involvement of tetrahydrobiopterin in electron transfer, *Biochemistry 41*, 3439–3456.
1725. Hurshman, A. R., Krebs, C., Edmondson, D. E., Huynh, B. H., and Marletta, M. A. (1999) Formation of a pterin radical in the reaction of the heme domain of inducible nitric oxide synthase with oxygen, *Biochemistry 38*, 15689–15696.
1726. Wei, C. C., Wang, Z. Q., Hemann, C., Hille, R., and Stuehr, D. J. (2003) A tetrahydrobiopterin radical forms and then becomes reduced during N^{ω}-hydroxyarginine oxidation by nitric-oxide synthase, *J. Biol. Chem. 278*, 46668–46673.
1727. Schmidt, P. P., Lange, R., Gorren, A. C. F., Werner, E. R., Mayer, B., and Andersson, K. K. (2001) Formation of a protonated trihydrobiopterin radical cation in the first reaction cycle of neuronal and endothelial nitric oxide synthase detected by electron paramagnetic resonance spectroscopy, *J. Biol. Inorganic Chem. 6*, 151–158.
1728. Crane, B. R., Arvai, A. S., Ghosh, D. K., Wu, C., Getzoff, E. D., Stuehr, D. J., and Tainer, J. A. (1998) Structure of nitric oxide synthase oxygenase dimer with pterin and substrate, *Science 279*, 2121–2126.
1729. Fischmann, T. O., Hruza, A., Niu, X. D., Fossetta, J. D., Lunn, C. A., Dolphin, E., Prongay, A. J., Reichert, P., Lundell, D. J., Narula, S. K., and Weber, P. C. (1999) Structural characterization of nitric oxide synthase isoforms reveals striking active-site conservation, *Nature Struct. Biol. 6*, 233–242.
1730. Ramasamy, S., Haque, M. M., Gangoda, M., and Stuehr, D. J. (2016) Tetrahydrobiopterin redox cycling in nitric oxide synthase: Evidence supports a through-heme electron delivery, *FEBS J. 283*, 4491–4501.
1731. Wei, C.-C., Wang, Z.-Q., Wang, Q., Meade, A. L., Hemann, C., Hille, R., and Stuehr, D. J. (2001) Rapid kinetic studies link tetrahydrobiopterin radical formation to heme-dioxy reduction and arginine hydroxylation in inducible nitric-oxide synthase, *J. Biol. Chem. 276*, 315–319.
1732. Wei, C.-C., Wang, Z.-Q., Durra, D., Hemann, C., Hille, R., Garcin, E. D., Getzoff, E. D., and Stuehr, D. J. (2005) The three nitric-oxide synthases differ in their kinetics of tetrahydrobiopterin radical formation, heme-dioxy reduction, and arginine hydroxylation, *J. Biol. Chem. 280*, 8929–8935.
1733. Adak, S., Wang, Q., and Stuehr, D. J. (2000) Arginine conversion to nitroxide by tetrahydrobiopterin-free neuronal nitric-oxide synthase. Implications for mechanism, *J. Biol. Chem. 275*, 33554–33561.
1734. Wei, C. C., Wang, Z. Q., Tejero, J., Yang, Y. P., Hemann, C., Hille, R., and Stuehr, D. J. (2008) Catalytic reduction of a tetrahydrobiopterin radical within nitric-oxide synthase, *J. Biol. Chem. 283*, 11734–11742.
1735. Tejero, J., Biswas, A., Wang, Z. Q., Page, R. C., Haque, M. M., Hemann, C., Zweier, J. L., Misra, S., and Stuehr, D. J. (2008) Stabilization and characterization of a heme-oxy reaction intermediate in inducible nitric-oxide synthase, *J. Biol. Chem. 283*, 33498–33507.
1736. Stuehr, D. J., and Ikeda-Saito, M. (1992) Spectral characterization of brain and macrophage nitric oxide synthases. Cytochrome P450-like hemeproteins that contain a flavin semiquinone radical, *J. Biol. Chem. 267*, 20547–20550.

1737. Tsutsui, Y., Kobayashi, K., Takeuchi, F., Tsubaki, M., and Kozawa, T. (2018) Reaction intermediates of nitric oxide synthase from *Deinococcus radiodurans* as revealed by pulse radiolysis: Evidence for intramolecular electron transfer from biopterin to Fe(II)- O_2 complex, *Biochemistry 57*, 1611–1619.
1738. Li, H., Raman, C. S., Martasek, P., Masters, B. S., and Poulos, T. L. (2001) Crystallographic studies on endothelial nitric oxide synthase complexed with nitric oxide and mechanism-based inhibitors, *Biochemistry 40*, 5399–5406.
1739. Pant, K., and Crane, B. R. (2006) Nitrosyl-heme structures of *Bacillus subtilis* nitric oxide synthase have implications for understanding substrate oxidation, *Biochemistry 45*, 2537–2544.
1740. Davydov, R., Ledbetter-Rogers, A., Martasek, P., Larukhin, M., Sono, M., Dawson, J. H., Masters, B. S., and Hoffman, B. M. (2002) EPR and ENDOR characterization of intermediates in the cryoreduced oxy-nitric oxide synthase heme domain with bound L-arginine or N^{γ}-hydroxyarginine, *Biochemistry 41*, 10375–10381.
1741. Huang, H., Hah, J. M., and Silverman, R. B. (2001) Mechanism of nitric oxide synthase. Evidence that direct hydrogen atom abstraction from the O–H bond of N^{γ}-hydroxyarginine is not relevant to the mechanism, *J. Am. Chem. Soc. 123*, 2674–2676.
1742. Doukov, T., Li, H. Y., Soltis, M., and Poulos, T. L. (2009) Single crystal structural and absorption spectral characterizations of nitric oxide synthase complexed with N^{ω}-hydroxy-L-arginine and diatomic ligands, *Biochemistry 48*, 10246–10254.
1743. Sabat, J., Egawa, T., Lu, C., Stuehr, D. J., Gerfen, G. J., Rousseau, D. L., and Yeh, S. R. (2013) Catalytic intermediates of inducible nitric-oxide synthase stabilized by the W188H mutation, *J. Biol. Chem. 288*, 6095–6106.
1744. Woodward, J. J., NejatyJahromy, Y., Britt, R. D., and Marletta, M. A. (2010) Pterin-centered radical as a mechanistic probe of the second step of nitric oxide synthase, *J. Am. Chem. Soc. 132*, 5105–5113.
1745. Rusche, K. M., Spiering, M. M., and Marletta, M. A. (1998) Reactions catalyzed by tetrahydrobiopterin-free nitric oxide synthase, *Biochemistry 37*, 15503–15512.
1746. Roberts, S. A., Weichsel, A., Qiu, Y., Shelnutt, J. A., Walker, F. A., and Montfort, W. R. (2001) Ligand-induced heme ruffling and bent NO geometry in ultra-high-resolution structures of nitrophorin 4, *Biochemistry 40*, 11327–11337.
1747. Kloer, D. P., Ruch, S., Al-Babili, S., Beyer, P., and Schulz, G. E. (2005) The structure of a retinal-forming carotenoid oxygenase, *Science 308*, 267–269.
1748. dela Sena, C., Riedl, K. M., Narayanasamy, S., Curley, R. W., Jr., Schwartz, S. J., and Harrison, E. H. (2014) The human enzyme that converts dietary provitamin A carotenoids to vitamin A is a dioxygenase, *J. Biol. Chem. 289*, 13661–13666.
1749. Sui, X., Weitz, A. C., Farquhar, E. R., Badiee, M., Banerjee, S., von Lintig, J., Tochtrop, G. P., Palczewski, K., Hendrich, M. P., and Kiser, P. D. (2017) Structure and spectroscopy of alkene-cleaving dioxygenases containing an atypically coordinated nonheme iron center, *Biochemistry 56*, 2836–2852.
1750. McCoy, J. G., Bailey, L. J., Bitto, E., Bingman, C. A., Aceti, D. J., Fox, B. G., and Phillips, G. N., Jr. (2006) Structure and mechanism of mouse cysteine dioxygenase, *Proc. Natl. Acad. Sci. U.S.A. 103*, 3084–3089.
1751. Simmons, C. R., Liu, Q., Huang, Q., Hao, Q., Begley, T. P., Karplus, P. A., and Stipanuk, M. H. (2006) Crystal structure of mammalian cysteine dioxygenase. A novel mononuclear iron center for cysteine thiol oxidation, *J. Biol. Chem. 281*, 18723–18733.
1752. Fernandez, R. L., Dillon, S. L., Stipanuk, M. H., Fox, B. G., and Brunold, T. C. (2020) Spectroscopic investigation of cysteamine dioxygenase, *Biochemistry 59*, 2450–2458.
1753. Ye, S., Wu, X., Wei, L., Tang, D., Sun, P., Bartlam, M., and Rao, Z. (2007) An insight into the mechanism of human cysteine dioxygenase. Key roles of the thioether-bonded tyrosine-cysteine cofactor, *J. Biol. Chem. 282*, 3391–3402.
1754. Gordon, J. B., McGale, J. P., Prendergast, J. R., Shirani-Sarmazeh, Z., Siegler, M. A., Jameson, G. N. L., and Goldberg, D. P. (2018) Structures, spectroscopic properties, and dioxygen reactivity of 5- and 6-coordinate nonheme iron(II) complexes: A combined enzyme/model study of thiol dioxygenases, *J. Am. Chem. Soc. 140*, 14807–14822.
1755. Crawford, J. A., Li, W., and Pierce, B. S. (2011) Single turnover of substrate-bound ferric cysteine dioxygenase with superoxide anion:

Enzymatic reactivation, product formation, and a transient intermediate, *Biochemistry 50*, 10241–10253.
1756. Simmons, C. R., Krishnamoorthy, K., Granett, S. L., Schuller, D. J., Dominy, J. E., Jr., Begley, T. P., Stipanuk, M. H., and Karplus, P. A. (2008) A putative Fe^{2+}-bound persulfenate intermediate in cysteine dioxygenase, *Biochemistry 47*, 11390–11392.
1757. Driggers, C. M., Cooley, R. B., Sankaran, B., Hirschberger, L. L., Stipanuk, M. H., and Karplus, P. A. (2013) Cysteine dioxygenase structures from pH 4 to 9: Consistent Cys-persulfenate formation at intermediate pH and a Cys-bound enzyme at higher pH, *J. Mol. Biol. 425*, 3121–3136.
1758. Ohlendorf, D. H., Orville, A. M., and Lipscomb, J. D. (1994) Structure of protocatechuate 3,4-dioxygenase from *Pseudomonas aeruginosa* at 2.15 Å resolution, *J. Mol. Biol. 244*, 586–608.
1759. Hayaishi, O., Katagiri, M., and Rothberg, S. (1955) Mechanism of the pyrocatechase reaction, *J. Am. Chem. Soc. 77*, 5450–5451.
1760. Vetting, M. W., D'Argenio, D. A., Ornston, L. N., and Ohlendorf, D. H. (2000) Structure of *Acinetobacter* strain ADP1 protocatechuate 3,4-dioxygenase at 2.2 Å resolution: Implications for the mechanism of an intradiol dioxygenase, *Biochemistry 39*, 7943–7955.
1761. Goudarzi, S., Babicz, J. T., Jr., Kabil, O., Banerjee, R., and Solomon, E. I. (2018) Spectroscopic and electronic structure study of ETHE1: Elucidating the factors influencing sulfur oxidation and oxygenation in mononuclear nonheme iron enzymes, *J. Am. Chem. Soc. 140*, 14887–14902.
1762. Pettinati, I., Brem, J., McDonough, M. A., and Schofield, C. J. (2015) Crystal structure of human persulfide dioxygenase: Structural basis of ethylmalonic encephalopathy, *Hum Mol Genet 24*, 2458–2469.
1763. Skrzypczak-Jankun, E., Bross, R. A., Carroll, R. T., Dunham, W. R., and Funk, M. O., Jr. (2001) Three-dimensional structure of a purple lipoxygenase, *J. Am. Chem. Soc. 123*, 10814–10820.
1764. Boyington, J. C., Gaffney, B. J., and Amzel, L. M. (1993) The three-dimensional structure of an arachidonic acid 15-lipoxygenase, *Science 260*, 1482–1486.
1765. Minor, W., Steczko, J., Stec, B., Otwinowski, Z., Bolin, J. T., Walter, R., and Axelrod, B. (1996) Crystal structure of soybean lipoxygenase L-1 at 1.4 Å resolution, *Biochemistry 35*, 10687–10701.
1766. Nelson, M. J., Seitz, S. P., and Cowling, R. A. (1990) Enzyme-bound pentadienyl and peroxyl radicals in purple lipoxygenase, *Biochemistry 29*, 6897–6903.
1767. Funk, M. O., Carroll, R. T., Thompson, J. F., Sands, R. H., and Dunham, W. R. (1990) Role of iron in lipoxygenase catalysis, *J. Am. Chem. Soc. 112*, 5375–5376.
1768. Schilstra, M. J., Veldink, G. A., and Vliegenthart, J. F. (1994) The dioxygenation rate in lipoxygenase catalysis is determined by the amount of iron(III) lipoxygenase in solution, *Biochemistry 33*, 3974–3979.
1769. Nelson, M. J., and Cowling, R. A. (1990) Observation of a peroxyl radical in samples of "purple" lipoxygenase, *J. Am. Chem. Soc. 112*, 2820–2821.
1770. Orville, A. M., Lipscomb, J. D., and Ohlendorf, D. H. (1997) Crystal structures of substrate and substrate analog complexes of protocatechuate 3,4-dioxygenase: Endogenous Fe^{3+} ligand displacement in response to substrate binding, *Biochemistry 36*, 10052–10066.
1771. Frazee, R. W., Orville, A. M., Dolbeare, K. B., Yu, H., Ohlendorf, D. H., and Lipscomb, J. D. (1998) The axial tyrosinate Fe^{3+} ligand in protocatechuate 3,4-dioxygenase influences substrate binding and product release: Evidence for new reaction cycle intermediates, *Biochemistry 37*, 2131–2144.
1772. Jang, H. G., Cox, D. D., and Que, L., Jr. (1991) A highly reactive functional model for the catechol dioxygenases. Structure and properties of [Fe(TPA)DBC]BPh_4,, *J. Am. Chem. Soc. 113*, 9200–9204.
1773. Cox, D. D., and Que, L., Jr. (1988) Functional models for catechol 1,2-dioxygenase. The role of the iron(III) center, *J. Am. Chem. Soc. 110*, 8085–8092.
1774. Pau, M. Y., Davis, M. I., Orville, A. M., Lipscomb, J. D., and Solomon, E. I. (2007) Spectroscopic and electronic structure study of the enzyme-substrate complex of intradiol dioxygenases: Substrate activation by a high-spin ferric nonheme iron site, *J. Am. Chem. Soc. 129*, 1944–1958.
1775. Pau, M. Y., Lipscomb, J. D., and Solomon, E. I. (2007) Substrate activation for O_2 reactions

by oxidized metal centers in biology, *Proc. Natl. Acad. Sci. U.S.A. 104*, 18355–18362.
1776. Que, L., Jr., Kolanczyk, R. C., and White, L. S. (1987) Functional models for catechol 1,2-dioxygenase. Structure, reactivity, and mechanism, *J. Am. Chem. Soc. 109*, 5373–5380.
1777. Mayer, R. J., and Que, L., Jr. (1984) ^{18}O Studies of pyrogallol cleavage by catechol 1,2-dioxygenase, *J. Biol. Chem. 259*, 13056–13060.
1778. Knoot, C. J., Purpero, V. M., and Lipscomb, J. D. (2015) Crystal structures of alkylperoxo and anhydride intermediates in an intradiol ring-cleaving dioxygenase, *Proc. Natl. Acad. Sci. U.S.A. 112*, 388–393.
1779. Windahl, M. S., Petersen, C. R., Christensen, H. E., and Harris, P. (2008) Crystal structure of tryptophan hydroxylase with bound amino acid substrate, *Biochemistry 47*, 12087–12094.
1780. Valegard, K., van Scheltinga, A. C., Lloyd, M. D., Hara, T., Ramaswamy, S., Perrakis, A., Thompson, A., Lee, H. J., Baldwin, J. E., Schofield, C. J., Hajdu, J., and Andersson, I. (1998) Structure of a cephalosporin synthase, *Nature 394*, 805–809.
1781. Miller, M. A., and Lipscomb, J. D. (1996) Homoprotocatechuate 2,3-dioxygenase from *Brevibacterium fuscum*. A dioxygenase with catalase activity, *J. Biol. Chem. 271*, 5524–5535.
1782. Han, S., Eltis, L. D., Timmis, K. N., Muchmore, S. W., and Bolin, J. T. (1995) Crystal structure of the biphenyl-cleaving extradiol dioxygenase from a PCB-degrading pseudomonad, *Science 270*, 976–980.
1783. Matera, I., Ferraroni, M., Burger, S., Scozzafava, A., Stolz, A., and Briganti, F. (2008) Salicylate 1,2-dioxygenase from *Pseudaminobacter salicylatoxidans*: Crystal structure of a peculiar ring-cleaving dioxygenase, *J. Mol. Biol. 380*, 856–868.
1784. Emerson, J. P., Kovaleva, E. G., Farquhar, E. R., Lipscomb, J. D., and Que, L., Jr. (2008) Swapping metals in Fe- and Mn-dependent dioxygenases: Evidence for oxygen activation without a change in metal redox state, *Proc. Natl. Acad. Sci. U.S.A. 105*, 7347–7352.
1785. Wang, Y., Shin, I., Fu, Y., Colabroy, K. L., and Liu, A. (2019) Crystal structures of L-DOPA dioxygenase from *Streptomyces sclerotialus*, *Biochemistry 58*, 5339–5350.
1786. Spence, E. L., Langley, G. J., and Bugg, T. D. H. (1996) *Cis-trans* isomerization of a cyclopropyl radical trap catalyzed by extradiol catechol dioxygenases: Evidence for a semiquinone intermediate, *J. Am. Chem. Soc. 118*, 8336–8343.
1787. Mbughuni, M. M., Chakrabarti, M., Hayden, J. A., Bominaar, E. L., Hendrich, M. P., Munck, E., and Lipscomb, J. D. (2010) Trapping and spectroscopic characterization of an FeIII-superoxo intermediate from a nonheme mononuclear iron-containing enzyme, *Proc. Natl. Acad. Sci. U.S.A. 107*, 16788–16793.
1788. Jeoung, J. H., Bommer, M., Lin, T. Y., and Dobbek, H. (2013) Visualizing the substrate-, superoxo-, alkylperoxo-, and product-bound states at the nonheme Fe(II) site of homogentisate dioxygenase, *Proc. Natl. Acad. Sci. U.S.A. 110*, 12625–12630.
1789. Kovaleva, E. G., and Lipscomb, J. D. (2007) Crystal structures of Fe^{2+} dioxygenase superoxo, alkylperoxo, and bound product intermediates, *Science 316*, 453–457.
1790. Karlsson, A., Parales, J. V., Parales, R. E., Gibson, D. T., Eklund, H., and Ramaswamy, S. (2003) Crystal structure of naphthalene dioxygenase: Side-on binding of dioxygen to iron, *Science 299*, 1039–1042.
1791. Bittner, M. M., Lindeman, S. V., and Fiedler, A. T. (2012) A synthetic model of the putative Fe(II)-iminobenzosemiquinonate intermediate in the catalytic cycle of *O*-aminophenol dioxygenases, *J. Am. Chem. Soc. 134*, 5460–5463.
1792. Kovaleva, E. G., and Lipscomb, J. D. (2008) Intermediate in the O-O bond cleavage reaction of an extradiol dioxygenase, *Biochemistry 47*, 11168–11170.
1793. Xin, M. T., and Bugg, T. D. H. (2008) Evidence from mechanistic probes for distinct hydroperoxide rearrangement mechanisms in the intradiol and extradiol catechol dioxygenases, *J. Am. Chem. Soc. 130*, 10422–10430.
1794. Kovaleva, E. G., and Lipscomb, J. D. (2012) Structural basis for the role of tyrosine 257 of homoprotocatechuate 2,3-dioxygenase in substrate and oxygen activation, *Biochemistry 51*, 8755–8763.
1795. Thrower, J. S., Blalock, R., 3rd, and Klinman, J. P. (2001) Steady-state kinetics of substrate binding and iron release in tomato ACC oxidase, *Biochemistry 40*, 9717–9724.

1796. Zhang, Z., Ren, J. S., Clifton, I. J., and Schofield, C. J. (2004) Crystal structure and mechanistic implications of 1-aminocyclopropane-1-carboxylic acid oxidase: The ethylene-forming enzyme, *Nature Chem. Biol. 11*, 1383–1394.
1797. Andersen, O. A., Flatmark, T., and Hough, E. (2001) High resolution crystal structures of the catalytic domain of human phenylalanine hydroxylase in its catalytically active Fe(II) form and binary complex with tetrahydrobiopterin, *J. Mol. Biol. 314*, 279–291.
1798. Goodwill, K. E., Sabatier, C., and Stevens, R. C. (1998) Crystal structure of tyrosine hydroxylase with bound cofactor analogue and iron at 2.3 Å resolution: Self-hydroxylation of Phe300 and the pterin-binding site, *Biochemistry 37*, 13437–13445.
1799. Zhang, Z., Ren, J., Stammers, D. K., Baldwin, J. E., Harlos, K., and Schofield, C. J. (2000) Structural origins of the selectivity of the trifunctional oxygenase clavaminic acid synthase, *Nature Struct. Biol. 7*, 127–133.
1800. Elkins, J. M., Ryle, M. J., Clifton, I. J., Dunning Hotopp, J. C., Lloyd, J. S., Burzlaff, N. I., Baldwin, J. E., Hausinger, R. P., and Roach, P. L. (2002) X-Ray crystal structure of *Escherichia coli* taurine/α-ketoglutarate dioxygenase complexed to ferrous iron and substrates, *Biochemistry 41*, 5185–5192.
1801. Dong, J. G., Fernandez-Maculet, J. C., and Yang, S. F. (1992) Purification and characterization of 1-aminocyclopropane-1-carboxylate oxidase from apple fruit, *Proc. Natl. Acad. Sci. U.S.A. 89*, 9789–9793.
1802. Bailey, S. W., Rebrin, I., Boerth, S. R., and Ayling, J. E. (1995) Synthesis of 4a-hydroxytetrahydropterins and the mechanism of their nonenzymic dehydration to quinoid dihydropterins, *J. Am. Chem. Soc. 117*, 10203–10211.
1803. Haavik, J., Doskeland, A. P., and Flatmark, T. (1986) Stereoselective effects in the interactions of pterin cofactors with rat-liver phenylalanine 4-monooxygenase, *Eur. J. Biochem. 160*, 1–8.
1804. Lazarus, R. A., DeBrosse, C. W., and Benkovic, S. J. (1982) Phenylalanine hydroxylase: Structural determination of the tetrahydropterin intermediates by carbon-13 NMR spectroscopy, *J. Am. Chem. Soc. 104*, 6869–6871.
1805. Rebrin, I., Bailey, S. W., Boerth, S. R., Ardell, M. D., and Ayling, J. E. (1995) Catalytic characterization of 4a-hydroxytetrahydropterin dehydratase, *Biochemistry 34*, 5801–5810.
1806. Cardinale, G. J., Rhoads, R. E., and Udenfriend, S. (1971) Simultaneous incorporation of ^{18}O into succinate and hydroxyproline catalyzed by collagen proline hydroxylase, *Biochem. Biophys. Res. Commun. 43*, 537–543.
1807. Mirica, L. M., and Klinman, J. P. (2008) The nature of O_2 activation by the ethylene-forming enzyme 1-aminocyclopropane-1-carboxylic acid oxidase, *Proc. Natl. Acad. Sci. U.S.A. 105*, 1814–1819.
1808. Zhou, J., Rocklin, A. M., Lipscomb, J. D., Que, L., Jr., and Solomon, E. I. (2002) Spectroscopic studies of 1-aminocyclopropane-1-carboxylic acid oxidase: Molecular mechanism and CO_2 activation in the biosynthesis of ethylene, *J. Am. Chem. Soc. 124*, 4602–4609.
1809. Zhou, J., Kelly, W. L., Bachmann, B. O., Gunsior, M., Townsend, C. A., and Solomon, E. I. (2001) Spectroscopic studies of substrate interactions with clavaminate synthase 2: A multifunctional α-KG-dependent nonheme iron enzyme: Correlation with mechanisms and reactivities, *J. Am. Chem. Soc. 123*, 7388–7398.
1810. Pember, S. O., Johnson, K. A., Villafranca, J. J., and Benkovic, S. J. (1989) Mechanistic studies on phenylalanine hydroxylase from *Chromobacterium violaceum*. Evidence for the formation of an enzyme-oxygen complex, *Biochemistry 28*, 2124–2130.
1811. Price, J. C., Barr, E. W., Hoffart, L. M., Krebs, C., and Bollinger, J. M., Jr. (2005) Kinetic dissection of the catalytic mechanism of taurine:α-ketoglutarate dioxygenase (TauD) from *Escherichia coli*, *Biochemistry 44*, 8138–8147.
1812. Pavon, J. A., Eser, B., Huynh, M. T., and Fitzpatrick, P. F. (2010) Single turnover kinetics of tryptophan hydroxylase: Evidence for a new intermediate in the reaction of the aromatic amino acid hydroxylases, *Biochemistry 49*, 7563–7571.
1813. Chang, W. C., Li, J., Lee, J. L., Cronican, A. A., and Guo, Y. (2016) Mechanistic investigation of a nonheme iron enzyme catalyzed epoxidation in (–)-4′-methoxycyclopenin biosynthesis, *J. Am. Chem. Soc. 138*, 10390–10393.
1814. Srnec, M., Iyer, S. R., Dassama, L. M. K., Park, K., Wong, S. D., Sutherlin, K. D., Yoda, Y., Kobayashi, Y., Kurokuzu, M., Saito, M., Seto,

M., Krebs, C., Bollinger, J. M., Jr., and Solomon, E. I. (2020) Nuclear resonance vibrational spectroscopic definition of the facial triad Fe^{IV}=O intermediate in taurine dioxygenase: Evaluation of structural contributions to hydrogen atom abstraction, *J. Am. Chem. Soc. 142*, 18886–18896.

1815. Andersen Ole, A., Flatmark, T., and Hough, E. (2002) Crystal structure of the ternary complex of the catalytic domain of human phenylalanine hydroxylase with tetrahydrobiopterin and 3-(2-thienyl)-L-alanine, and its implications for the mechanism of catalysis and substrate activation, *J. Mol. Biol. 320*, 1095–1108.
1816. Francisco, W. A., Tian, G., Fitzpatrick, P. F., and Klinman, J. P. (1998) Oxygen-18 kinetic isotope effect studies of the tyrosine hydroxylase reaction: Evidence of rate limiting oxygen activation, *J. Am. Chem. Soc. 120*, 4057–4062.
1817. Marota, J. J., and Shiman, R. (1984) Stoichiometric reduction of phenylalanine hydroxylase by its cofactor: A requirement for enzymatic activity, *Biochemistry 23*, 1303–1311.
1818. Pavel, E. G., Zhou, J., Busby, R. W., Gunsior, M., Townsend, C. A., and Solomon, E. I. (1998) Circular dichroism and magnetic circular dichroism spectroscopic studies of the nonheme ferrous active site in clavaminate synthase and its interaction with α-ketoglutarate cosubstrate, *J. Am. Chem. Soc. 120*, 743–753.
1819. Hoppner, A., Widderich, N., Lenders, M., Bremer, E., and Smits, S. H. (2014) Crystal structure of the ectoine hydroxylase, a snapshot of the active site, *J. Biol. Chem. 289*, 29570–29583.
1820. Martinez, S., and Hausinger, R. P. (2016) Biochemical and spectroscopic characterization of the nonheme Fe(II)- and 2-oxoglutarate-dependent ethylene-forming enzyme from *Pseudomonas syringae* pv. *phaseolicola* PK2, *Biochemistry 55*, 5989–5999.
1821. Mitchell, A. J., Dunham, N. P., Martinie, R. J., Bergman, J. A., Pollock, C. J., Hu, K., Allen, B. D., Chang, W. C., Silakov, A., Bollinger, J. M., Jr., Krebs, C., and Boal, A. K. (2017) Visualizing the reaction cycle in an iron(II)- and 2-(oxo)-glutarate-dependent hydroxylase, *J. Am. Chem. Soc. 139*, 13830–13836.
1822. Li, J., Liao, H. J., Tang, Y., Huang, J. L., Cha, L., Lin, T. S., Lee, J. L., Kurnikov, I. V., Kurnikova, M. G., Chang, W. C., Chan, N. L., and Guo, Y. (2020) Epoxidation catalyzed by the nonheme iron(II)- and 2-oxoglutarate-dependent oxygenase, AsqJ: Mechanistic elucidation of oxygen atom transfer by a ferryl intermediate, *J. Am. Chem. Soc. 142*, 6268–6284.
1823. Eser, B. E., Barr, E. W., Frantom, P. A., Saleh, L., Bollinger, J. M., Jr., Krebs, C., and Fitzpatrick, P. F. (2007) Direct spectroscopic evidence for a high-spin Fe(IV) intermediate in tyrosine hydroxylase, *J. Am. Chem. Soc. 129*, 11334–11335.
1824. Proshlyakov, D. A., Henshaw, T. F., Monterosso, G. R., Ryle, M. J., and Hausinger, R. P. (2004) Direct detection of oxygen intermediates in the nonheme Fe enzyme taurine/α-ketoglutarate dioxygenase, *J. Am. Chem. Soc. 126*, 1022–1023.
1825. Price, J. C., Barr, E. W., Tirupati, B., Bollinger, J. M., Jr., and Krebs, C. (2003) The first direct characterization of a high-valent iron intermediate in the reaction of an α-ketoglutarate-dependent dioxygenase: A high-spin FeIV complex in taurine/α-ketoglutarate dioxygenase (TauD) from *Escherichia coli*, *Biochemistry 42*, 7497–7508.
1826. Sinnecker, S., Svensen, N., Barr, E. W., Ye, S., Bollinger, J. M., Jr., Neese, F., and Krebs, C. (2007) Spectroscopic and computational evaluation of the structure of the high-spin Fe(IV)-oxo intermediates in taurine: α-ketoglutarate dioxygenase from *Escherichia coli* and its His99Ala ligand variant, *J. Am. Chem. Soc. 129*, 6168–6179.
1827. Hoffart, L. M., Barr, E. W., Guyer, R. B., Bollinger, J. M., Jr., and Krebs, C. (2006) Direct spectroscopic detection of a C–H-cleaving high-spin Fe(IV) complex in a prolyl-4-hydroxylase, *Proc. Natl. Acad. Sci. U. S. A. 103*, 14738–14743.
1828. Pavon, J. A., and Fitzpatrick, P. F. (2009) Demonstration of a peroxide shunt in the tetrahydropterin-dependent aromatic amino acid monooxygenases, *J. Am. Chem. Soc. 131*, 4582–4583.
1829. England, J., Guo, Y. S., Farquhar, E. R., Young, V. G., Munck, E., and Que, L. (2010) The crystal structure of a high-spin oxoiron(IV) complex and characterization of its

self-decay pathway, *J. Am. Chem. Soc. 132*, 8635–8644.
1830. Oloo, W. N., Fielding, A. J., and Que, L. (2013) Rate-determining water-assisted O-O bond cleavage of an Fe-III-OOH intermediate in a bio-inspired nonheme iron-catalyzed oxidation, *J. Am. Chem. Soc. 135*, 6438–6441.
1831. Eichhorn, E., van der Ploeg, J. R., Kertesz, M. A., and Leisinger, T. (1997) Characterization of α-ketoglutarate-dependent taurine dioxygenase from *Escherichia coli*, *J. Biol. Chem. 272*, 23031–23036.
1832. Ge, W., Wolf, A., Feng, T., Ho, C. H., Sekirnik, R., Zayer, A., Granatino, N., Cockman, M. E., Loenarz, C., Loik, N. D., Hardy, A. P., Claridge, T. D., Hamed, R. B., Chowdhury, R., Gong, L., Robinson, C. V., Trudgian, D. C., Jiang, M., Mackeen, M. M., McCullagh, J. S., Gordiyenko, Y., Thalhammer, A., Yamamoto, A., Yang, M., Liu-Yi, P., Zhang, Z., Schmidt-Zachmann, M., Kessler, B. M., Ratcliffe, P. J., Preston, G. M., Coleman, M. L., and Schofield, C. J. (2012) Oxygenase-catalyzed ribosome hydroxylation occurs in prokaryotes and humans, *Nature Chem. Biol. 8*, 960–962.
1833. Price, J. C., Barr, E. W., Glass, T. E., Krebs, C., and Bollinger, J. M., Jr. (2003) Evidence for hydrogen abstraction from C1 of taurine by the high-spin Fe(IV) intermediate detected during oxygen activation by taurine:α-Ketoglutarate dioxygenase (TauD), *J. Am. Chem. Soc. 125*, 13008–13009.
1834. Yi, C., Jia, G., Hou, G., Dai, Q., Zhang, W., Zheng, G., Jian, X., Yang, C. G., Cui, Q., and He, C. (2010) Iron-catalysed oxidation intermediates captured in a DNA repair dioxygenase, *Nature 468*, 330–333.
1835. Holme, E., Lindstedt, G., Lindstedt, S., and Tofft, M. (1971) ^{18}O Studies of the 2-ketoglutarate-dependent sequential oxygenation of thymine to 5-carboxyuracil, *J. Biol. Chem. 246*, 3314–3319.
1836. Copeland, R. A., Davis, K. M., Shoda, T. K. C., Blaesi, E. J., Boal, A. K., Krebs, C., and Bollinger, J. M., Jr. (2021) An iron(IV)-oxo intermediate initiating L-arginine oxidation but not ethylene production by the 2-oxoglutarate-dependent oxygenase, ethylene-forming enzyme, *J. Am. Chem. Soc. 143*, 2293–2303.
1837. Grzyska, P. K., Appelman, E. H., Hausinger, R. P., and Proshlyakov, D. A. (2010) Insight into the mechanism of an iron dioxygenase by resolution of steps following the Fe^{IV}=O species, *Proc. Natl. Acad. Sci. U.S.A. 107*, 3982–3987.
1838. Davis, K. M., Altmyer, M., Martinie, R. J., Schaperdoth, I., Krebs, C., Bollinger, J. M., Jr., and Boal, A. K. (2019) Structure of a ferryl mimic in the archetypal iron(II)- and 2-(oxo)-glutarate-dependent dioxygenase, TauD, *Biochemistry 58*, 4218–4223.
1839. Lee, H. J., Lloyd, M. D., Harlos, K., Clifton, I. J., Baldwin, J. E., and Schofield, C. J. (2001) Kinetic and crystallographic studies on deacetoxycephalosporin *c* synthase (DAOCS), *J. Mol. Biol. 308*, 937–948.
1840. Yan, W., Song, H., Song, F., Guo, Y., Wu, C. H., Sae Her, A., Pu, Y., Wang, S., Naowarojna, N., Weitz, A., Hendrich, M. P., Costello, C. E., Zhang, L., Liu, P., and Zhang, Y. J. (2015) Endoperoxide formation by an α-ketoglutarate-dependent mononuclear non-haem iron enzyme, *Nature 527*, 539–543.
1841. Matthews, M. L., Krest, C. M., Barr, E. W., Vaillancourt, F. H., Walsh, C. T., Green, M. T., Krebs, C., and Bollinger, J. M. (2009) Substrate-triggered formation and remarkable stability of the C–H bond-cleaving chloroferryl intermediate in the aliphatic halogenase, Syrb2, *Biochemistry 48*, 4331–4343.
1842. Yadav, V., Gordon, J. B., Siegler, M. A., and Goldberg, D. P. (2019) Dioxygen-derived nonheme mononuclear Fe^{III}(OH) complex and its reactivity with carbon radicals, *J. Am. Chem. Soc. 141*, 10148–10153.
1843. Moran, G. R., Derecskei-Kovacs, A., Hillas, P. J., and Fitzpatrick, P. F. (2000) On the catalytic mechanism of tryptophan hydroxylase, *J. Am. Chem. Soc. 122*, 4535–4541.
1844. Hillas, P. J., and Fitzpatrick, P. F. (1996) A mechanism for hydroxylation by tyrosine hydroxylase based on partitioning of substituted phenylalanines, *Biochemistry 35*, 6969–6975.
1845. Moran, G. R., Phillips, R. S., and Fitzpatrick, P. F. (1999) Influence of steric bulk and electrostatics on the hydroxylation regiospecificity of tryptophan hydroxylase: Characterization of methyltryptophans and azatryptophans as substrates, *Biochemistry 38*, 16283–16289.
1846. Tomaszewski, J. E., Jerina, D. M., and Daly, J. W. (1975) Deuterium isotope effects during formation of phenols by hepatic monooxy-

genases. Evidence for an alternative to arene oxide pathway, *Biochemistry 14*, 2024–2031.
1847. Daly, J. W., Jerina, D. M., and Witkop, B. (1972) Arene oxides and the NIH shift: The metabolism, toxicity and carcinogenicity of aromatic compounds, *Experientia 28*, 1129–1149.
1848. Vannelli, T., and Hooper, A. B. (1995) NIH shift in the hydroxylation of aromatic compounds by the ammonia-oxidizing bacterium *Nitrosomonas europaea*. Evidence against an arene oxide intermediate, *Biochemistry 34*, 11743–11749.
1849. Miller, R. J., and Benkovic, S. J. (1988) L-[2,5-H_2]Phenylalanine, an alternate substrate for rat liver phenylalanine hydroxylase, *Biochemistry 27*, 3658–3663.
1850. Salowe, S. P., Marsh, E. N., and Townsend, C. A. (1990) Purification and characterization of clavaminate synthase from *Streptomyces clavuligerus*: An unusual oxidative enzyme in natural product biosynthesis, *Biochemistry 29*, 6499–6508.
1851. Rocklin, A. M., Kato, K., Liu, H. W., Que, L., Jr., and Lipscomb, J. D. (2004) Mechanistic studies of 1-aminocyclopropane-1-carboxylic acid oxidase: Single turnover reaction, *J. Biol. Inorg. Chem. 9*, 171–182.
1852. Myllyla, R., Kuutti-Savolainen, E. R., and Kivirikko, K. I. (1978) The role of ascorbate in the prolyl hydroxylase reaction, *Biochem. Biophys. Res. Commun. 83*, 441–448.
1853. de Jong, L., Albracht, S. P., and Kemp, A. (1982) Prolyl 4-hydroxylase activity in relation to the oxidation state of enzyme-bound iron. The role of ascorbate in peptidyl proline hydroxylation, *Biochim. Biophys. Acta 704*, 326–332.
1854. Hayaishi, O. (1976) Properties and function of indoleamine 2,3-dioxygenase, *J. Biochem. (Tokyo) 79*, 13P–21P.
1855. Yan, F., Moon, S. J., Liu, P., Zhao, Z., Lipscomb, J. D., Liu, A., and Liu, H. W. (2007) Determination of the substrate binding mode to the active site iron of (*S*)-2-hydroxypropylphosphonic acid epoxidase using ^{17}O-enriched substrates and substrate analogues, *Biochemistry 46*, 12628–12638.
1856. Yun, D., Dey, M., Higgins, L. J., Yan, F., Liu, H. W., and Drennan, C. L. (2011) Structural basis of regiospecificity of a mononuclear iron enzyme in antibiotic fosfomycin biosynthesis, *J. Am. Chem. Soc. 133*, 11262–11269.
1857. Cicchillo, R. M., Zhang, H., Blodgett, J. A., Whitteck, J. T., Li, G., Nair, S. K., van der Donk, W. A., and Metcalf, W. W. (2009) An unusual carbon-carbon bond cleavage reaction during phosphinothricin biosynthesis, *Nature 459*, 871–874.
1858. Peck, S. C., Cooke, H. A., Cicchillo, R. M., Malova, P., Hammerschmidt, F., Nair, S. K., and van der Donk, W. A. (2011) Mechanism and substrate recognition of 2-hydroxyethyl-phosphonate dioxygenase, *Biochemistry 50*, 6598–6605.
1859. Peck, S. C., Chekan, J. R., Ulrich, E. C., Nair, S. K., and van der Donk, W. A. (2015) A common late-stage intermediate in catalysis by 2-hydroxyethyl-phosphonate dioxygenase and methylphosphonate synthase, *J. Am. Chem. Soc. 137*, 3217–3220.
1860. Zhu, H., Peck, S. C., Bonnot, F., van der Donk, W. A., and Klinman, J. P. (2015) Oxygen-18 kinetic isotope effects of nonheme iron enzymes HepD and MpnS support iron(III) superoxide as the hydrogen abstraction species, *J. Am. Chem. Soc. 137*, 10448–10451.
1861. Roach, P. L., Clifton, I. J., Fulop, V., Harlos, K., Barton, G. J., Hajdu, J., Andersson, I., Schofield, C. J., and Baldwin, J. E. (1995) Crystal structure of isopenicillin N synthase is the first from a new structural family of enzymes, *Nature 375*, 700–704.
1862. Howard-Jones, A. R., Elkins, J. M., Clifton, I. J., Roach, P. L., Adlington, R. M., Baldwin, J. E., and Rutledge, P. J. (2007) Interactions of isopenicillin N synthase with cyclopropyl-containing substrate analogues reveal new mechanistic insight, *Biochemistry 46*, 4755–4762.
1863. Peck, S. C., Wang, C., Dassama, L. M., Zhang, B., Guo, Y., Rajakovich, L. J., Bollinger, J. M., Jr., Krebs, C., and van der Donk, W. A. (2017) O–H Activation by an unexpected ferryl intermediate during catalysis by 2-hydroxyethylphosphonate dioxygenase, *J. Am. Chem. Soc. 139*, 2045–2052.
1864. Wang, B., Lu, J., Dubey, K. D., Dong, G., Lai, W., and Shaik, S. (2016) How do enzymes utilize reactive OH radicals? Lessons from nonheme HppE and Fenton systems, *J. Am. Chem. Soc. 138*, 8489–8496.
1865. Furusawa, Y., Nagarajan, V., Tanokura, M., Masai, E., Fukuda, M., and Senda, T. (2004) Crystal structure of the terminal oxygenase

component of biphenyl dioxygenase derived from *Rhodococcus* sp. strain RHA_1, *J. Mol. Biol. 342*, 1041–1052.
1866. Friemann, R., Ivkovic-Jensen, M. M., Lessner, D. J., Yu, C. L., Gibson, D. T., Parales, R. E., Eklund, H., and Ramaswamy, S. (2005) Structural insight into the dioxygenation of nitroarene compounds: The crystal structure of nitrobenzene dioxygenase, *J. Mol. Biol. 348*, 1139–1151.
1867. Dumitru, R., Jiang, W. Z., Weeks, D. P., and Wilson, M. A. (2009) Crystal structure of dicamba monooxygenase: A Rieske nonheme oxygenase that catalyzes oxidative demethylation, *J. Mol. Biol. 392*, 498–510.
1868. Rivard, B. S., Rogers, M. S., Marell, D. J., Neibergall, M. B., Chakrabarty, S., Cramer, C. J., and Lipscomb, J. D. (2015) Rate-determining attack on substrate precedes Rieske cluster oxidation during *cis*-dihydrox-ylation by benzoate dioxygenase, *Biochemistry 54*, 4652–4664.
1869. Wolfe, M. D., Parales, J. V., Gibson, D. T., and Lipscomb, J. D. (2001) Single turnover chemistry and regulation of O_2 activation by the oxygenase component of naphthalene 1,2-dioxygenase, *J. Biol. Chem. 276*, 1945–1953.
1870. Wolfe, M. D., and Lipscomb, J. D. (2003) Hydrogen peroxide-coupled *cis*-diol formation catalyzed by naphthalene 1,2-dioxygenase, *J. Biol. Chem. 278*, 829–835.
1871. Rogers, M. S., and Lipscomb, J. D. (2019) Salicylate 5-hydroxylase: Intermediates in aromatic hydroxylation by a Rieske monooxygenase, *Biochemistry 58*, 5305–5319.
1872. Chakrabarty, S., Austin, R. N., Deng, D., Groves, J. T., and Lipscomb, J. D. (2007) Radical intermediates in monooxygenase reactions of Rieske dioxygenases, *J. Am. Chem. Soc. 129*, 3514–3515.
1873. Neibergall, M. B., Stubna, A., Mekmouche, Y., Munck, E., and Lipscomb, J. D. (2007) Hydrogen peroxide dependent *cis*-dihydroxylation of benzoate by fully oxidized benzoate 1,2-dioxygenase, *Biochemistry 46*, 8004–8016.
1874. Sutherlin, K. D., Rivard, B. S., Bottger, L. H., Liu, L. V., Rogers, M. S., Srnec, M., Park, K., Yoda, Y., Kitao, S., Kobayashi, Y., Saito, M., Seto, M., Hu, M., Zhao, J., Lipscomb, J. D., and Solomon, E. I. (2018) NRVS studies of the peroxide shunt intermediate in a Rieske dioxygenase and its relation to the native Fe(II) O_2 reaction, *J. Am. Chem. Soc. 140*, 5544–5559.
1875. Oloo, W. N., Banerjee, R., Lipscomb, J. D., and Que, L., Jr. (2017) Equilibrating (L)Fe^{III}-OOAc and (L)Fe^{V}(O) species in hydrocarbon oxidations by bio-inspired nonheme iron catalysts using H_2O_2 and AcOH, *J. Am. Chem. Soc. 139*, 17313–17326.
1876. Holmes, M. A., Le Trong, I., Turley, S., Sieker, L. C., and Stenkamp, R. E. (1991) Structures of deoxy and oxy hemerythrin at 2.0 Å resolution, *J. Mol. Biol. 218*, 583–593.
1877. Sheriff, S., Hendrickson, W. A., and Smith, J. (1987) Structure of myohemerythrin in the azidomet state at 1.7/1.3 Å resolution, *J. Mol. Biol. 197*, 273–296.
1878. Stenkamp, R. E., Sieker, L. C., and Jensen, L. H. (1984) Binuclear iron complexes in methemerythrin and azidomethemerythrin at 2.0-Å Resolution, *J. Am. Chem. Soc. 106*, 618–622.
1879. Reem, R. C., and Solomon, E. I. (1987) Spectroscopic studies of the binuclear ferrous active site of deoxyhemerythrin: Coordination number and probable bridging ligands for the native and ligand-bound forms, *J. Am. Chem. Soc. 109*, 1216–1226.
1880. Stenkamp, R. E., Sieker, L. C., Jensen, L. H., McCallum, J. D., and Sanders-Loehr, J. (1985) Active site structures of deoxyhemerythrin and oxyhemerythrin, *Proc. Natl. Acad. Sci. U. S. A. 82*, 713–716.
1881. Klotz, I. M., and Klotz, T. A. (1955) Oxygen-carrying proteins: A comparison of the oxygenation reaction in hemocyanin and hemerythrin with that in hemoglobin, *Science 121*, 477–480.
1882. Brunold, T. C., and Solomon, E. I. (1999) Reversible dioxygen binding to hemerythrin. 1. Electronic structures of deoxy- and oxyhemerythrin, *J. Am. Chem. Soc. 121*, 8277–8287.
1883. Brown, P. M., Caradoc-Davies, T. T., Dickson, J. M. J., Cooper, G. J. S., Loomes, K. M., and Baker, E. N. (2006) Crystal structure of a substrate complex of *myo*-inositol oxygenase, a diiron oxygenase with a key role in inositol metabolism, *Proc. Natl. Acad. Sci. U.S.A. 103*, 15032–15037.
1884. Thorsell, A. G., Persson, C., Voevodskaya, N., Busam, R. D., Hammarstrom, M., Graslund, S., Graslund, A., and Hallberg, B. M. (2008) Structural and biophysical characterization

of human *myo*-inositol oxygenase, *J. Biol. Chem. 283*, 15209–15216.
1885. van Staalduinen, L. M., McSorley, F. R., Schiessl, K., Seguin, J., Wyatt, P. B., Hammerschmidt, F., Zechel, D. L., and Jia, Z. (2014) Crystal structure of PhnZ in complex with substrate reveals a diiron oxygenase mechanism for catabolism of organophosphonates, *Proc. Natl. Acad. Sci. U. S. A. 111*, 5171–5176.
1886. Worsdorfer, B., Lingaraju, M., Yennawar, N. H., Boal, A. K., Krebs, C., Bollinger, J. M., Jr., and Pandelia, M. E. (2013) Organophosphonate-degrading PhnZ reveals an emerging family of HD domain mixed-valent diiron oxygenases, *Proc. Natl. Acad. Sci. U. S. A. 110*, 18874–18879.
1887. Xing, G., Barr, E. W., Diao, Y., Hoffart, L. M., Prabhu, K. S., Arner, R. J., Reddy, C. C., Krebs, C., and Bollinger, J. M., Jr. (2006) Oxygen activation by a mixed-valent, diiron(II/III) cluster in the glycol cleavage reaction catalyzed by *myo*-inositol oxygenase, *Biochemistry 45*, 5402–5412.
1888. Murch, B. P., Bradley, F. C., and Que, L. (1986) A binuclear iron peroxide complex capable of olefin epoxidation, *J. Am. Chem. Soc. 108*, 5027–5028.
1889. Borovik, A. S., Murch, B. P., Que, L., Jr., Papaefthymiou, V., and Munck, E. (1987) Models for iron-oxo proteins: A mixed valence iron(II)-iron(III) complex, *J. Am. Chem. Soc. 109*, 7190–7191.
1890. Snyder, R. A., Bell, C. B., 3rd, Diao, Y., Krebs, C., Bollinger, J. M., Jr., and Solomon, E. I. (2013) Circular dichroism, magnetic circular dichroism, and variable temperature variable field magnetic circular dichroism studies of biferrous and mixed-valent *myo*-inositol oxygenase: Insights into substrate activation of O_2 reactivity, *J. Am. Chem. Soc. 135*, 15851–15863.
1891. Xing, G., Diao, Y., Hoffart, L. M., Barr, E. W., Prabhu, K. S., Arner, R. J., Reddy, C. C., Krebs, C., and Bollinger, J. M., Jr. (2006) Evidence for C–H cleavage by an iron-superoxide complex in the glycol cleavage reaction catalyzed by *myo*-inositol oxygenase, *Proc. Natl. Acad. Sci. U. S. A. 103*, 6130–6135.
1892. Gama, S. R., Lo, B. S. Y., Seguin, J., Pallitsch, K., Hammerschmidt, F., and Zechel, D. L. (2019) C–H Bond cleavage is rate-limiting for oxidative C–P bond cleavage by the mixed valence diiron-dependent oxygenase PhnZ, *Biochemistry 58*, 5271–5280.
1893. Frazao, C., Silva, G., Gomes, C. M., Matias, P., Coelho, R., Sieker, L., Macedo, S., Liu, M. Y., Oliveira, S., Teixeira, M., Xavier, A. V., Rodrigues-Pousada, C., Carrondo, M. A., and Le Gall, J. (2000) Structure of a dioxygen reduction enzyme from *Desulfovibrio gigas*, *Nature Struct. Biol. 7*, 1041–1045.
1894. Park, K., Li, N., Kwak, Y., Srnec, M., Bell, C. B., Liu, L. V., Wong, S. D., Yoda, Y., Kitao, S., Seto, M., Hu, M., Zhao, J., Krebs, C., Bollinger, J. M., Jr., and Solomon, E. I. (2017) Peroxide activation for electrophilic reactivity by the binuclear nonheme iron enzyme AurF, *J. Am. Chem. Soc. 139*, 7062–7070.
1895. deMare, F., Kurtz, D. M., Jr., and Nordlund, P. (1996) The structure of *Desulfovibrio vulgaris* rubrerythrin reveals a unique combination of rubredoxin-like FeS_4 and ferritin-like diiron domains, *Nature Struct. Biol. 3*, 539–546.
1896. Coulter, E. D., and Kurtz, D. M., Jr. (2001) A role for rubredoxin in oxidative stress protection in *Desulfovibrio vulgaris*: Catalytic electron transfer to rubrerythrin and two-iron superoxide reductase, *Arch. Biochem. Biophys. 394*, 76–86.
1897. Jin, S., Kurtz, D. M., Jr., Liu, Z. J., Rose, J., and Wang, B. C. (2002) X-Ray crystal structures of reduced rubrerythrin and its azide adduct: A structure-based mechanism for a nonheme diiron peroxidase, *J. Am. Chem. Soc. 124*, 9845–9855.
1898. Fox, B. G., Shanklin, J., Ai, J., Loehr, T. M., and Sanders-Loehr, J. (1994) Resonance Raman evidence for an Fe–O–Fe center in stearoyl-ACP desaturase. Primary sequence identity with other diiron-oxo proteins, *Biochemistry 33*, 12776–12786.
1899. Rosenzweig, A. C., Frederick, C. A., Lippard, S. J., and Nordlund, P. (1993) Crystal structure of a bacterial non-haem iron hydroxylase that catalyses the biological oxidation of methane, *Nature 366*, 537–543.
1900. Sazinsky, M. H., Bard, J., Di Donato, A., and Lippard, S. J. (2004) Crystal structure of the toluene/*o*-xylene monooxygenase hydroxylase from *Pseudomonas stutzeri* OX1. Insight into the substrate specificity, substrate channeling, and active site tuning of multicomponent monooxygenases, *J. Biol. Chem. 279*, 30600–30610.

1901. Nordlund, P., and Eklund, H. (1993) Structure and function of the *Escherichia coli* ribonucleotide reductase protein R2, *J. Mol. Biol. 232*, 123–164.
1902. Moche, M., Shanklin, J., Ghoshal, A., and Lindqvist, Y. (2003) Azide and acetate complexes plus two iron-depleted crystal structures of the di-iron enzyme Δ^9 stearoyl-acyl carrier protein desaturase. Implications for oxygen activation and catalytic intermediates, *J. Biol. Chem. 278*, 25072–25080.
1903. Nordlund, P., Dalton, H., and Eklund, H. (1992) The active site structure of methane monooxygenase is closely related to the binuclear iron center of ribonucleotide reductase, *FEBS Lett. 307*, 257–262.
1904. Rosenzweig, A. C., Brandstetter, H., Whittington, D. A., Nordlund, P., Lippard, S. J., and Frederick, C. A. (1997) Crystal structures of the methane monooxygenase hydroxylase from *Methylococcus capsulatus* (Bath): Implications for substrate gating and component interactions, *Proteins 29*, 141–152.
1905. Srinivas, V., Banerjee, R., Lebrette, H., Jones, J. C., Aurelius, O., Kim, I. S., Pham, C. C., Gul, S., Sutherlin, K. D., Bhowmick, A., John, J., Bozkurt, E., Fransson, T., Aller, P., Butryn, A., Bogacz, I., Simon, P., Keable, S., Britz, A., Tono, K., Kim, K. S., Park, S. Y., Lee, S. J., Park, J., Alonso-Mori, R., Fuller, F. D., Batyuk, A., Brewster, A. S., Bergmann, U., Sauter, N. K., Orville, A. M., Yachandra, V. K., Yano, J., Lipscomb, J. D., Kern, J., and Hogbom, M. (2020) High-resolution XFEL structure of the soluble methane monooxygenase hydroxylase complex with its regulatory component at ambient temperature in two oxidation states, *J. Am. Chem. Soc. 142*, 14249–14266.
1906. Whittington, D. A., and Lippard, S. J. (2001) Crystal structures of the soluble methane monooxygenase hydroxylase from *Methylococcus capsulatus* (Bath) demonstrating geometrical variability at the dinuclear iron active site, *J. Am. Chem. Soc. 123*, 827–838.
1907. Voegtli, W. C., Khidekel, N., Baldwin, J., Ley, B. A., Bollinger, J. M., Jr., and Rosenzweig, A. C. (2000) Crystal structure of the ribonucleotide reductase R2 mutant that accumulates a μ-1,2-peroxodiiron(III) intermediate during oxygen activation, *J. Am. Chem. Soc. 122*, 3255–3261.
1908. Rather, L. J., Weinert, T., Demmer, U., Bill, E., Ismail, W., Fuchs, G., and Ermler, U. (2011) Structure and mechanism of the diiron benzoyl-coenzyme A epoxidase BoxB, *J. Biol. Chem. 286*, 29241–29248.
1909. Rosenzweig, A. C., Nordlund, P., Takahara, P. M., Frederick, C. A., and Lippard, S. J. (1995) Geometry of the soluble methane monooxygenase catalytic diiron center in two oxidation states, *Nature Chem. Biol. 2*, 409–418.
1910. Lindqvist, Y., Huang, W., Schneider, G., and Shanklin, J. (1996) Crystal structure of Δ^9 stearoyl-acyl carrier protein desaturase from castor seed and its relationship to other diiron proteins, *The EMBO journal 15*, 4081–4092.
1911. Pikus, J. D., Studts, J. M., Achim, C., Kauffmann, K. E., Munck, E., Steffan, R. J., McClay, K., and Fox, B. G. (1996) Recombinant toluene-4-monooxygenase: Catalytic and Mössbauer studies of the purified diiron and Rieske components of a four-protein complex, *Biochemistry 35*, 9106–9119.
1912. Acheson, J. F., Bailey, L. J., Brunold, T. C., and Fox, B. G. (2017) In-crystal reaction cycle of a toluene-bound diiron hydroxylase, *Nature 544*, 191–195.
1913. Mitchell, K. H., Rogge, C. E., Gierahn, T., and Fox, B. G. (2003) Insight into the mechanism of aromatic hydroxylation by toluene 4-monooxygenase by use of specifically deuterated toluene and *p*-xylene, *Proc. Natl. Acad. Sci. U. S. A. 100*, 3784–3789.
1914. Broadwater, J. A., Achim, C., Munck, E., and Fox, B. G. (1999) Mössbauer studies of the formation and reactivity of a quasi-stable peroxo intermediate of stearoyl-acyl carrier protein Δ^9-desaturase, *Biochemistry 38*, 12197–12204.
1915. Kim, K., and Lippard, S. J. (1996) Structure and Mössbauer spectrum of a (μ-1,2-peroxo)bis(μ-carboxylato)diiron(III) model for the peroxo intermediate in the MMO hydroxylase reaction cycle, *J. Am. Chem. Soc. 118*, 4914–4915.
1916. Bailey, L. J., and Fox, B. G. (2009) Crystallographic and catalytic studies of the peroxide-shunt reaction in a diiron hydroxylase, *Biochemistry 48*, 8932–8939.
1917. Pandelia, M. E., Li, N., Norgaard, H., Warui, D. M., Rajakovich, L. J., Chang, W. C., Booker, S. J., Krebs, C., and Bollinger, J. M., Jr. (2013) Substrate-triggered addition of dioxygen to the diferrous cofactor of aldehyde-deformylating oxygenase to form a diferric-

peroxide intermediate, *J. Am. Chem. Soc. 135*, 15801–15812.
1918. Buist, P. H., and Behrouzian, B. (1998) Deciphering the cryptoregiochemistry of oleate Δ^{12} desaturase: A kinetic isotope effect study, *J. Am. Chem. Soc. 120*, 871–876.
1919. Banerjee, R., Meier, K. K., Munck, E., and Lipscomb, J. D. (2013) Intermediate P* from soluble methane monooxygenase contains a diferrous cluster, *Biochemistry 52*, 4331–4342.
1920. Andersson, K. K., Froland, W. A., Lee, S. K., and Lipscomb, J. D. (1991) Dioxygen independent oxygenation of hydrocarbons by methane monooxygenase hydroxylase component, *New J. Chem. 15*, 411–415.
1921. Valentine, A. M., Stahl, S. S., and Lippard, S. J. (1999) Mechanistic studies of the reaction of reduced methane monooxygenase hydroxylase with dioxygen and substrates, *J. Am. Chem. Soc. 121*, 3876–3887.
1922. Brazeau, B. J., and Lipscomb, J. D. (2000) Kinetics and activation thermodynamics of methane monooxygenase compound Q formation and reaction with substrates, *Biochemistry 39*, 13503–13515.
1923. Shu, L., Nesheim, J. C., Kauffmann, K., Munck, E., Lipscomb, J. D., and Que, L., Jr. (1997) An $Fe_2^{IV}O_2$ diamond core structure for the key intermediate Q of methane monooxygenase, *Science 275*, 515–518.
1924. Banerjee, R., Proshlyakov, Y., Lipscomb, J. D., and Proshlyakov, D. A. (2015) Structure of the key species in the enzymatic oxidation of methane to methanol, *Nature 518*, 431–434.
1925. Xue, G., Wang, D., De Hont, R., Fiedler, A. T., Shan, X., Munck, E., and Que, L., Jr. (2007) A synthetic precedent for the $[Fe^{IV}_2(\mu\text{-}O)_2]$ diamond core proposed for methane monooxygenase intermediate Q, *Proc. Natl. Acad. Sci. U. S. A. 104*, 20713–20718.
1926. Kim, C., Dong, Y., and Que, L., Jr. (1997) Modeling nonheme diiron enzymes: Hydrocarbon hydroxylation and desaturation by a high-valent Fe_2O_2 diamond core, *J. Am. Chem. Soc. 119*, 3635–3636.
1927. Wilkinson, E. C., Dong, Y., Zang, Y., Fujii, H., Fraczkiewicz, R., Fraczkiewicz, G., Czernuszewicz, R. S., and Que, L., Jr. (1998) Raman signature of the Fe_2O_2 "diamond" core, *J. Am. Chem. Soc. 120*, 955–962.
1928. Green, J., and Dalton, H. (1985) Protein B of soluble methane monooxygenase from *Methylococcus capsulatus* (Bath). A novel regulatory protein of enzyme activity, *J. Biol. Chem. 260*, 15795–15801.
1929. Fox, B. G., Froland, W. A., Dege, J. E., and Lipscomb, J. D. (1989) Methane monooxygenase from *Methylosinus trichosporium* Ob3B. Purification and properties of a three-component system with high specific activity from a type II methanotroph, *J. Biol. Chem. 264*, 10023–10033.
1930. Costas, M., Rohde, J. U., Stubna, A., Ho, R. Y., Quaroni, L., Munck, E., and Que, L., Jr. (2001) A synthetic model for the putative $Fe^{IV}_2O_2$ diamond core of methane monooxygenase intermediate Q, *J. Am. Chem. Soc. 123*, 12931–12932.
1931. Valentine, A. M., Wilkinson, B., Liu, K. E., Komar-Panicucci, S., Priestley, N. D., Williams, P. G., Morimoto, H., Floss, H. G., and Lippard, S. J. (1997) Tritiated chiral alkanes as substrates for soluble methane monooxygenase from *Methylococcus capsulatus* (Bath): Probes for the mechanism of hydroxylation, *J. Am. Chem. Soc. 119*, 1818–1827.
1932. Newcomb, M., Shen, R., Lu, Y., Coon, M. J., Hollenberg, P. F., Kopp, D. A., and Lippard, S. J. (2002) Evaluation of norcarane as a probe for radicals in cytochome P450- and soluble methane monooxygenase-catalyzed hydroxylation reactions, *J. Am. Chem. Soc. 124*, 6879–6886.
1933. Brazeau, B. J., Austin, R. N., Tarr, C., Groves, J. T., and Lipscomb, J. D. (2001) Intermediate Q from soluble methane monooxygenase hydroxylates the mechanistic substrate probe norcarane: Evidence for a stepwise reaction, *J. Am. Chem. Soc. 123*, 11831–11837.
1934. Higgins, I. J., and Quayle, J. R. (1970) Oxygenation of methane by methane-grown *Pseudomonas methanica* and *Methanomonas methanooxidans*, *Biochem. J. 118*, 201–208.
1935. Ruzicka, F., Huang, D. S., Donnelly, M. I., and Frey, P. A. (1990) Methane monooxygenase catalyzed oxygenation of 1,1-dimethylcyclopropane. Evidence for radical and carbocationic intermediates, *Biochemistry 29*, 1696–1700.
1936. Whittington, D. A., Sazinsky, M. H., and Lippard, S. J. (2001) X-Ray crystal structure of alcohol products bound at the active site of soluble methane monooxygenase hydroxylase, *J. Am. Chem. Soc. 123*, 1794–1795.
1937. Tinberg, C. E., and Lippard, S. J. (2010) Oxidation reactions performed by soluble me-

thane monooxygenase hydroxylase intermediates H-peroxo and Q proceed by distinct mechanisms, *Biochemistry 49*, 7902–7912.

1938. Liu, K. E., Johnson, C. C., Newcomb, M., and Lippard, S. J. (1993) Radical clock substrate probes and kinetic isotope effect studies of the hydroxylation of hydrocarbons by methane monooxygenase, *J. Am. Chem. Soc. 115*, 939–947.
1939. Yun, D., Krebs, C., Gupta, G. P., Iwig, D. F., Huynh, B. H., and Bollinger, J. M., Jr. (2002) Facile electron transfer during formation of cluster X and kinetic competence of X for tyrosyl radical production in protein R2 of ribonucleotide reductase from mouse, *Biochemistry 41*, 981–990.
1940. Baldwin, J., Krebs, C., Ley, B. A., Edmondson, D. E., Huynh, B. H., and Bollinger, J. M., Jr. (2000) Mechanism of rapid electron transfer during oxygen activation in the R2 subunit of *Escherichia coli* ribonucleotide reductase. 1. Evidence for a transient tryptophan radical, *J. Am. Chem. Soc. 122*, 12195–12206.
1941. Willems, J.-P., Lee, H.-I., Burdi, D., Doan, P. E., Stubbe, J., and Hoffman, B. M. (1997) Identification of the protonated oxygenic ligands of ribonucleotide reductase intermediate X by Q-band ^{1,2}H CW and pulsed ENDOR, *J. Am. Chem. Soc. 119*, 9816–9824.
1942. Andersson, M. E., Hoegbom, M., Rinaldo-Matthis, A., Andersson, K. K., Sjoeberg, B.-M., and Nordlund, P. (1999) The crystal structure of an azide complex of the diferrous R2 subunit of ribonucleotide reductase displays a novel carboxylate shift with important mechanistic implications for diiron-catalyzed oxygen activation, *J. Am. Chem. Soc. 121*, 2346–2352.
1943. Adrait, A., Ohrstrom, M., Barra, A. L., Thelander, L., and Graslund, A. (2002) EPR Studies on a stable sulfinyl radical observed in the iron–oxygen-reconstituted Y177F/I263C protein R2 double mutant of ribonucleotide reductase from mouse, *Biochemistry 41*, 6510–6516.
1944. Caranto, J. D., Weitz, A., Giri, N., Hendrich, M. P., and Kurtz, D. M., Jr. (2014) A diferrous-dinitrosyl intermediate in the N_2O-generating pathway of a deflavinated flavo-diiron protein, *Biochemistry 53*, 5631–5637.
1945. Kostic, M., Pochapsky, S. S., and Pochapsky, T. C. (2002) Rapid recycle ^{13}C′,^{15}N and ^{13}C,^{13}C′ heteronuclear and homonuclear multiple quantum coherence detection for resonance assignments in paramagnetic proteins: Example of Ni^{2+}-containing acireductone dioxygenase, *J. Am. Chem. Soc. 124*, 9054–9055.
1946. Mo, H., Dai, Y., Pochapsky, S. S., and Pochapsky, T. C. (1999) ^{1}H, ^{13}C and ^{15}N NMR assignments for a carbon monoxide generating metalloenzyme from *Klebsiella pneumoniae*, *J Biomol NMR 14*, 287–288.
1947. Dai, Y., Wensink, P. C., and Abeles, R. H. (1999) One protein, two enzymes, *J. Biol. Chem. 274*, 1193–1195.
1948. Sparta, M., Valdez, C. E., and Alexandrova, A. N. (2013) Metal-dependent activity of Fe and niacireductone dioxygenases: How two electrons reroute the catalytic pathway, *J. Mol. Biol. 425*, 3007–3018.
1949. Peters, J. W., Lanzilotta, W. N., Lemon, B. J., and Seefeldt, L. C. (1998) X-Ray crystal structure of the Fe-only hydrogenase (CpI) from *Clostridium pasteurianum* to 1.8 angstrom resolution, *Science 282*, 1853–1858.
1950. Pandey, A. S., Harris, T. V., Giles, L. J., Peters, J. W., and Szilagyi, R. K. (2008) Dithiomethylether as a ligand in the hydrogenase H-cluster, *J. Am. Chem. Soc. 130*, 4533–4540.
1951. Ratzloff, M. W., Artz, J. H., Mulder, D. W., Collins, R. T., Furtak, T. E., and King, P. W. (2018) Co-bridged H-cluster intermediates in the catalytic mechanism of [FeFe]-hydrogenase CaI, *J. Am. Chem. Soc. 140*, 7623–7628.
1952. Mebs, S., Senger, M., Duan, J., Wittkamp, F., Apfel, U. P., Happe, T., Winkler, M., Stripp, S. T., and Haumann, M. (2017) Bridging hydride at reduced H-cluster species in [FeFe]-hydrogenases revealed by infrared spectroscopy, isotope editing, and quantum chemistry, *J. Am. Chem. Soc. 139*, 12157–12160.
1953. Lorent, C., Katz, S., Duan, J., Kulka, C. J., Caserta, G., Teutloff, C., Yadav, S., Apfel, U. P., Winkler, M., Happe, T., Horch, M., and Zebger, I. (2020) Shedding light on proton and electron dynamics in [FeFe] hydrogenases, *J. Am. Chem. Soc. 142*, 5493–5497.
1954. Nicolet, Y., de Lacey, A. L., Vernede, X., Fernandez, V. M., Hatchikian, E. C., and Fontecilla-Camps, J. C. (2001) Crystallographic and FTIR spectroscopic evidence of changes in Fe coordination upon reduction of the active site of the Fe-only hydrogenase from

Desulfovibrio desulfuricans, *J. Am. Chem. Soc. 123*, 1596–1601.
1955. Silakov, A., Wenk, B., Reijerse, E., and Lubitz, W. (2009) ^{14}N HYSCORE investigation of the H-cluster of [FeFe] hydrogenase: Evidence for a nitrogen in the dithiol bridge, *Phys. Chem. Chem. Phys. 11*, 6592–6599.
1956. Erdem, O. F., Schwartz, L., Stein, M., Silakov, A., Kaur-Ghumaan, S., Huang, P., Ott, S., Reijerse, E. J., and Lubitz, W. (2011) A model of the [FeFe] hydrogenase active site with a biologically relevant azadithiolate bridge: A spectroscopic and theoretical investigation, *Angew. Chem., Int. Ed. Engl. 50*, 1439–1443.
1957. Siebel, J. F., Adamska-Venkatesh, A., Weber, K., Rumpel, S., Reijerse, E., and Lubitz, W. (2015) Hybrid [FeFe]-hydrogenases with modified active sites show remarkable residual enzymatic activity, *Biochemistry 54*, 1474–1483.
1958. Nicolet, Y., Piras, C., Legrand, P., Hatchikian, C. E., and Fontecilla-Camps, J. C. (1999) *Desulfovibrio desulfuricans* iron hydrogenase: The structure shows unusual coordination to an active site Fe binuclear center, *Structure 7*, 13–23.
1959. Esselborn, J., Muraki, N., Klein, K., Engelbrecht, V., Metzler-Nolte, N., Apfel, U. P., Hofmann, E., Kurisu, G., and Happe, T. (2016) A structural view of synthetic cofactor integration into [FeFe]-hydrogenases, *Chem Sci 7*, 959–968.
1960. Ogata, H., Kellers, P., and Lubitz, W. (2010) The crystal structure of the [NiFe] hydrogenase from the photosynthetic bacterium *Allochromatium vinosum*: Characterization of the oxidized enzyme (Ni-A state), *J. Mol. Biol. 402*, 428–444.
1961. Higuchi, Y., Ogata, H., Miki, K., Yasuoka, N., and Yagi, T. (1999) Removal of the bridging ligand atom at the Ni–Fe active site of [NiFe] hydrogenase upon reduction with H2, as revealed by X-ray structure analysis at 1.4 Å resolution, *Structure 7*, 549–556.
1962. Ogata, H., Mizoguchi, Y., Mizuno, N., Miki, K., Adachi, S., Yasuoka, N., Yagi, T., Yamauchi, O., Hirota, S., and Higuchi, Y. (2002) Structural studies of the carbon monoxide complex of [NiFe]hydrogenase from *Desulfovibrio vulgaris* Miyazaki F: Suggestion for the initial activation site for dihydrogen, *J. Am. Chem. Soc. 124*, 11628–11635.
1963. Higuchi, Y., Yagi, T., and Yasuoka, N. (1997) Unusual ligand structure in Ni–Fe active center and an additional Mg site in hydrogenase revealed by high resolution X-ray structure analysis, *Structure 5*, 1671–1680.
1964. Ogata, H., Nishikawa, K., and Lubitz, W. (2015) Hydrogens detected by subatomic resolution protein crystallography in a [NiFe] hydrogenase, *Nature 520*, 571–574.
1965. Skinner, H. A., and Connor, J. A. (1985) Metal-ligand bond-energies in organometallic compounds, *Pure and Applied Chemistry 57*, 79–88.
1966. Sommer, C., Adamska-Venkatesh, A., Pawlak, K., Birrell, J. A., Rudiger, O., Reijerse, E. J., and Lubitz, W. (2017) Proton coupled electronic rearrangement within the H-cluster as an essential step in the catalytic cycle of [FeFe] hydrogenases, *J. Am. Chem. Soc. 139*, 1440–1443.
1967. Mulder, D. W., Ratzloff, M. W., Shepard, E. M., Byer, A. S., Noone, S. M., Peters, J. W., Broderick, J. B., and King, P. W. (2013) EPR and FTIR analysis of the mechanism of H-2 activation by [FeFe]-hydrogenase HydA1 from *Chlamydomonas reinhardtii*, *J. Am. Chem. Soc. 135*, 6921–6929.
1968. van der Vlugt, J. I., Rauchfuss, T. B., Whaley, C. M., and Wilson, S. R. (2005) Characterization of a diferrous terminal hydride mechanistically relevant to the Fe-only hydrogenases, *J. Am. Chem. Soc. 127*, 16012–16013.
1969. Thomas, C. M., Darensbourg, M. Y., and Hall, M. B. (2007) Computational definition of a mixed valent Fe(II)Fe(I) model of the [FeFe]hydrogenase active site resting state, *J Inorg Biochem 101*, 1752–1757.
1970. Felton, G. A., Vannucci, A. K., Chen, J., Lockett, L. T., Okumura, N., Petro, B. J., Zakai, U. I., Evans, D. H., Glass, R. S., and Lichtenberger, D. L. (2007) Hydrogen generation from weak acids: Electrochemical and computational studies of a diiron hydrogenase mimic, *J. Am. Chem. Soc. 129*, 12521–12530.
1971. Rumpel, S., Sommer, C., Reijerse, E., Fares, C., and Lubitz, W. (2018) Direct detection of the terminal hydride intermediate in [FeFe] hydrogenase by NMR spectroscopy, *J. Am. Chem. Soc. 140*, 3863–3866.
1972. Mulder, D. W., Guo, Y., Ratzloff, M. W., and King, P. W. (2017) Identification of a catalytic iron-hydride at the H-cluster of [FeFe]-hydrogenase, *J. Am. Chem. Soc. 139*, 83–86.

1973. Reijerse, E. J., Pham, C. C., Pelmenschikov, V., Gilbert-Wilson, R., Adamska-Venkatesh, A., Siebel, J. F., Gee, L. B., Yoda, Y., Tamasaku, K., Lubitz, W., Rauchfuss, T. B., and Cramer, S. P. (2017) Direct observation of an iron-bound terminal hydride in [FeFe]-hydrogenase by nuclear resonance vibrational spectroscopy, *J. Am. Chem. Soc. 139*, 4306–4309.
1974. Pelmenschikov, V., Birrell, J. A., Pham, C. C., Mishra, N., Wang, H., Sommer, C., Reijerse, E., Richers, C. P., Tamasaku, K., Yoda, Y., Rauchfuss, T. B., Lubitz, W., and Cramer, S. P. (2017) Reaction coordinate leading to H_2 production in [FeFe]-hydrogenase identified by nuclear resonance vibrational spectroscopy and density functional theory, *J. Am. Chem. Soc. 139*, 16894–16902.
1975. Pandelia, M. E., Ogata, H., and Lubitz, W. (2010) Intermediates in the catalytic cycle of [NiFe]hydrogenase: Functional spectroscopy of the active site, *ChemPhysChem 11*, 1127–1140.
1976. Kampa, M., Pandelia, M. E., Lubitz, W., van Gastel, M., and Neese, F. (2013) A metal-metal bond in the light-induced state of [NiFe] hydrogenases with relevance to hydrogen evolution, *J. Am. Chem. Soc. 135*, 3915–3925.
1977. Montet, Y., Amara, P., Volbeda, A., Vernede, X., Hatchikian, E. C., Field, M. J., Frey, M., and Fontecilla-Camps, J. C. (1997) Gas access to the active site of Ni-Fe hydrogenases probed by X-ray crystallography and molecular dynamics, *Nature Struct. Biol. 4*, 523–526.
1978. Bruschi, M., Tiberti, M., Guerra, A., and De Gioia, L. (2014) Disclosure of key stereoelectronic factors for efficient H_2 binding and cleavage in the active site of [NiFe]-hydrogenases, *J. Am. Chem. Soc. 136*, 1803–1814.
1979. Brecht, M., van Gastel, M., Buhrke, T., Friedrich, B., and Lubitz, W. (2003) Direct detection of a hydrogen ligand in the [NiFe] center of the regulatory H_2-sensing hydrogenase from *Ralstonia eutropha* in its reduced state by HYSCORE and ENDOR spectroscopy, *J. Am. Chem. Soc. 125*, 13075–13083.
1980. Foerster, S., van Gastel, M., Brecht, M., and Lubitz, W. (2005) An orientation-selected ENDOR and HYSCORE study of the Ni–C active state of *Desulfovibrio vulgaris* Miyazaki F hydrogenase, *J. Biol. Inorganic Chem. 10*, 51–62.
1981. Barton, B. E., Whaley, C. M., Rauchfuss, T. B., and Gray, D. L. (2009) Nickel-iron dithiolato hydrides relevant to the [NiFe]-hydrogenase active site, *J. Am. Chem. Soc. 131*, 6942–6943.
1982. Barton, B. E., and Rauchfuss, T. B. (2010) Hydride-containing models for the active site of the nickel-iron hydrogenases, *J. Am. Chem. Soc. 132*, 14877–14885.
1983. Ulloa, O. A., Huynh, M. T., Richers, C. P., Bertke, J. A., Nilges, M. J., Hammes-Schiffer, S., and Rauchfuss, T. B. (2016) Mechanism of H_2 production by models for the [NiFe]-hydrogenases: Role of reduced hydrides, *J. Am. Chem. Soc. 138*, 9234–9245.
1984. Weber, K., Kramer, T., Shafaat, H. S., Weyhermuller, T., Bill, E., van Gastel, M., Neese, F., and Lubitz, W. (2012) A functional [NiFe]-hydrogenase model compound that undergoes biologically relevant reversible thiolate protonation, *J. Am. Chem. Soc. 134*, 20745–20755.
1985. Jablonskyte, A., Wright, J. A., Fairhurst, S. A., Peck, J. N. T., Ibrahim, S. K., Oganesyan, V. S., and Pickett, C. J. (2011) Paramagnetic bridging hydrides of relevance to catalytic hydrogen evolution at metallosulfur centers, *J. Am. Chem. Soc. 133*, 18606–18609.
1986. Barton, B. E., Olsen, M. T., and Rauchfuss, T. B. (2008) Aza- and oxadithiolates are probable proton relays in functional models for the [FeFe]-hydrogenases, *J. Am. Chem. Soc. 130*, 16834–16835.
1987. Camara, J. M., and Rauchfuss, T. B. (2011) Mild redox complementation enables H_2 activation by [FeFe]-hydrogenase models, *J. Am. Chem. Soc. 133*, 8098–8101.
1988. Wang, N., Wang, M., Wang, Y., Zheng, D. H., Han, H. X., Ahlquist, M. S. G., and Sun, L. C. (2013) Catalytic activation of H_2 under mild conditions by an [FeFe]-hydrogenase model via an active μ-hydride species, *J. Am. Chem. Soc. 135*, 13688–13691.
1989. Svetlichny, V. A., Sokolova, T. G., Gerhardt, M., Kostrikina, N. A., and Zavarzin, G. A. (1991) Anaerobic extremely thermophilic carboxydotrophic bacteria in hydrotherms of Kuril Islands, *Microb Ecol 21*, 1–10.
1990. Svetlitchnyi, V., Peschel, C., Acker, G., and Meyer, O. (2001) Two membrane-associated NiFeS-carbon monoxide dehydrogenases from the anaerobic carbon-monoxide-utilizing eubacterium *Carboxydothermus hydrogenoformans*, *J. Bacteriol. 183*, 5134–5144.

1991. Ljungdahl, L. G. (1986) The autotrophic pathway of acetate synthesis in acetogenic bacteria, *Annu Rev Microbiol 40*, 415–450.
1992. Pegis, M. L., Roberts, J. A. S., Wasylenko, D. J., Mader, E. A., Appel, A. M., and Mayer, J. M. (2015) Standard reduction potentials for oxygen and carbon dioxide couples in acetonitrile and *N,N*-dimethylformamide, *Inorg. Chem. 54*, 11883–11888.
1993. Grahame, D. A., and Demoll, E. (1995) Substrate and accessory protein-requirements and thermodynamics of acetyl-CoA synthesis and cleavage in *Methanosarcina-barkeri*, *Biochemistry 34*, 4617–4624.
1994. Jeoung, J. H., and Dobbek, H. (2007) Carbon dioxide activation at the Ni,Fe-cluster of anaerobic carbon monoxide dehydrogenase, *Science 318*, 1461–1464.
1995. Kung, Y., Doukov, T. I., Seravalli, J., Ragsdale, S. W., and Drennan, C. L. (2009) Crystallographic snapshots of cyanide- and water-bound C-clusters from bifunctional carbon monoxide dehydrogenase/acetyl-CoA synthase, *Biochemistry 48*, 7432–7440.
1996. Kumar, M., Lu, W. P., Liu, L. F., and Ragsdale, S. W. (1993) Kinetic evidence that carbon-monoxide dehydrogenase catalyzes the oxidation of carbon-monoxide and the synthesis of acetyl-CoA at separate metal centers, *J. Am. Chem. Soc. 115*, 11646–11647.
1997. Lu, W. P., Jablonski, P. E., Rasche, M., Ferry, J. G., and Ragsdale, S. W. (1994) Characterization of the metal centers of the Ni/Fe-S component of the carbon-monoxide dehydrogenase enzyme complex from *Methanosarcina thermophila*, *J. Biol. Chem. 269*, 9736–9742.
1998. Dobbek, H., Svetlitchnyi, V., Gremer, L., Huber, R., and Meyer, O. (2001) Crystal structure of a carbon monoxide dehydrogenase reveals a [Ni–4Fe–5S] cluster, *Science 293*, 1281–1285.
1999. Darnault, C., Volbeda, A., Kim, E. J., Legrand, P., Vernede, X., Lindahl, P. A., and Fontecilla-Camps, J. C. (2003) Ni–Zn–[Fe_4–S_4] and Ni–Ni–[Fe_4–S_4] clusters in closed and open subunits of acetyl-CoA synthase/carbon monoxide dehydrogenase, *Nature Struct. Biol. 10*, 271–279.
2000. Fesseler, J., Jeoung, J. H., and Dobbek, H. (2015) How the [$NiFe_4S_4$] cluster of CO dehydrogenase activates CO_2 and NCO^-, *Angew. Chem., Int. Ed. Engl. 54*, 8560–8564.
2001. Merschrod, E. F., Tang, S. H., and Hoffmann, R. (1998) Bonding in an unusual nickel carbide, *Z. Naturforsch. B 53*, 322–332.
2002. Bazzicalupi, C., Bencini, A., Bencini, A., Bianchi, A., Corana, F., Fusi, V., Giorgi, C., Paoli, P., Paoletti, P., Valtancoli, B., and Zanchini, C. (1996) CO_2 fixation by novel copper(II) and zinc(II) macrocyclic complexes. A solution and solid state study, *Inorg. Chem. 35*, 5540–5548.
2003. Lindahl, P. A., Munck, E., and Ragsdale, S. W. (1990) CO dehydrogenase from *Clostridium thermoaceticum*. EPR and electrochemical studies in CO_2 and argon atmospheres, *J. Biol. Chem. 265*, 3873–3879.
2004. Lindahl, P. A. (2002) The Ni-containing carbon monoxide dehydrogenase family: Light at the end of the tunnel?, *Biochemistry 41*, 2097–2105.
2005. Seravalli, J., Kumar, M., Lu, W. P., and Ragsdale, S. W. (1995) Mechanism of CO oxidation by carbon monoxide dehydrogenase from *Clostridium thermoaceticum* and its inhibition by anions, *Biochemistry 34*, 7879–7888.
2006. Steiner, R. A., Kalk, K. H., and Dijkstra, B. W. (2002) Anaerobic enzyme. Substrate structures provide insight into the reaction mechanism of the copper-dependent quercetin 2,3-dioxygenase, *Proc. Natl. Acad. Sci. U. S. A. 99*, 16625–16630.
2007. Steiner, R. A., Meyer-Klaucke, W., and Dijkstra, B. W. (2002) Functional analysis of the copper-dependent quercetin 2,3-dioxygenase. 2. X-Ray absorption studies of native enzyme and anaerobic complexes with the substrates quercetin and myricetin, *Biochemistry 41*, 7963–7968.
2008. Vaaje-Kolstad, G., Westereng, B., Horn, S. J., Liu, Z., Zhai, H., Sorlie, M., and Eijsink, V. G. (2010) An oxidative enzyme boosting the enzymatic conversion of recalcitrant polysaccharides, *Science 330*, 219–222.
2009. Hemsworth, G. R., Taylor, E. J., Kim, R. Q., Gregory, R. C., Lewis, S. J., Turkenburg, J. P., Parkin, A., Davies, G. J., and Walton, P. H. (2013) The copper active site of CBM33 polysaccharide oxygenases, *J. Am. Chem. Soc. 135*, 6069–6077.
2010. Bacik, J. P., Mekasha, S., Forsberg, Z., Kovalevsky, A. Y., Vaaje-Kolstad, G., Eijsink, V. G. H., Nix, J. C., Coates, L., Cuneo, M. J., Unkefer, C. J., and Chen, J. C. (2017) Neutron and atomic resolution X-ray structures of a

lytic polysaccharide monooxygenase reveal copper-mediated dioxygen binding and evidence for N-terminal deprotonation, *Biochemistry 56*, 2529–2532.
2011. Ross, M. O., MacMillan, F., Wang, J., Nisthal, A., Lawton, T. J., Olafson, B. D., Mayo, S. L., Rosenzweig, A. C., and Hoffman, B. M. (2019) Particulate methane monooxygenase contains only mononuclear copper centers, *Science 364*, 566–570.
2012. Smith, S. M., Rawat, S., Telser, J., Hoffman, B. M., Stemmler, T. L., and Rosenzweig, A. C. (2011) Crystal structure and characterization of particulate methane monooxygenase from *Methylocystis* species strain M, *Biochemistry 50*, 10231–10240.
2013. Ito, N., Phillips, S. E., Yadav, K. D., and Knowles, P. F. (1994) Crystal structure of a free radical enzyme, galactose oxidase, *J. Mol. Biol. 238*, 794–814.
2014. Whittaker, M. M., Chuang, Y. Y., and Whittaker, J. W. (1993) Models for the redox active site in galactose oxidase, *J. Am. Chem. Soc. 115*, 10029–10035.
2015. Halfen, J. A., Jazdzewski, B. A., Mahapatra, S., Berreau, L. M., Wilkinson, E. C., Que, L., Jr., and Tolman, W. B. (1997) Synthetic models of the inactive copper(II)-tyrosinate and active copper(II)-tyrosyl radical forms of galactose and glyoxal oxidases, *J. Am. Chem. Soc. 119*, 8217–8227.
2016. Verma, P., Pratt, R. C., Storr, T., Wasinger, E. C., and Stack, T. D. (2011) Sulfanyl stabilization of copper-bonded phenoxyls in model complexes and galactose oxidase, *Proc. Natl. Acad. Sci. U.S.A. 108*, 18600–18605.
2017. Wachter, R. M., Montague-Smith, M. P., and Branchaud, B. P. (1997) β-Haloethanol substrates as probes for radical mechanisms for galactose oxidase, *J. Am. Chem. Soc. 119*, 7743–7749.
2018. Rogers, M. S., Tyler, E. M., Akyumani, N., Kurtis, C. R., Spooner, R. K., Deacon, S. E., Tamber, S., Firbank, S. J., Mahmoud, K., Knowles, P. F., Phillips, S. E., McPherson, M. J., and Dooley, D. M. (2007) The stacking tryptophan of galactose oxidase: A second-coordination sphere residue that has profound effects on tyrosyl radical behavior and enzyme catalysis, *Biochemistry 46*, 4606–4618.
2019. Wachter, R. M., and Branchaud, B. P. (1996) Thiols as mechanistic probes for catalysis by the free radical enzyme galactose oxidase, *Biochemistry 35*, 14425–14435.
2020. Murphy, M. E., Turley, S., Kukimoto, M., Nishiyama, M., Horinouchi, S., Sasaki, H., Tanokura, M., and Adman, E. T. (1995) Structure of *Alcaligenes faecalis* nitrite reductase and a copper site mutant, M150E, that contains zinc, *Biochemistry 34*, 12107–12117.
2021. Kukimoto, M., Nishiyama, M., Murphy, M. E., Turley, S., Adman, E. T., Horinouchi, S., and Beppu, T. (1994) X-Ray structure and site-directed mutagenesis of a nitrite reductase from *Alcaligenes faecalis* s-6: Roles of two copper atoms in nitrite reduction, *Biochemistry 33*, 5246–5252.
2022. Murphy, M. E., Turley, S., and Adman, E. T. (1997) Structure of nitrite bound to copper-containing nitrite reductase from *Alcaligenes faecalis*. Mechanistic implications, *J. Biol. Chem. 272*, 28455–28460.
2023. Halfen, J. A., Mahapatra, S., Wilkinson, E. C., Gengenbach, A. J., Young, V. G., Que, L., and Tolman, W. B. (1996) Synthetic modeling of nitrite binding and activation by reduced copper proteins. Characterization of copper(I)-nitrite complexes that evolve nitric oxide, *J. Am. Chem. Soc. 118*, 763–776.
2024. Li, Y., Hodak, M., and Bernholc, J. (2015) Enzymatic mechanism of copper-containing nitrite reductase, *Biochemistry 54*, 1233–1242.
2025. Boulanger, M. J., Kukimoto, M., Nishiyama, M., Horinouchi, S., and Murphy, M. E. (2000) Catalytic roles for two water bridged residues (Asp-98 and His-255) in the active site of copper-containing nitrite reductase, *J. Biol. Chem. 275*, 23957–23964.
2026. Hazes, B., Magnus, K. A., Bonaventura, C., Bonaventura, J., Dauter, Z., Kalk, K. H., and Hol, W. G. (1993) Crystal structure of deoxygenated *Limulus polyphemus* subunit II hemocyanin at 2.18 Å resolution: Clues for a mechanism for allosteric regulation, *Prot. Sci. 2*, 597–619.
2027. Volbeda, A., and Hol, W. G. (1989) Pseudo 2-fold symmetry in the copper-binding domain of arthropodan haemocyanins. Possible implications for the evolution of oxygen transport proteins, *J. Mol. Biol. 206*, 531–546.
2028. Gaykema, W. P., Volbeda, A., and Hol, W. G. (1986) Structure determination of *Panulirus interruptus* haemocyanin at 3.2 Å resolution.

Successful phase extension by sixfold density averaging, *J. Mol. Biol. 187*, 255–275.
2029. Loehr, J. S., Freedman, T. B., and Loehr, T. M. (1974) Oxygen binding to hemocyanin: A resonance Raman spectroscopic study, *Biochem. Biophys. Res. Commun. 56*, 510–515.
2030. Ling, J., Nestor, L. P., Czernuszewicz, R. S., Spiro, T. G., Fraczkiewicz, R., Sharma, K. D., Loehr, T. M., and Sanders-Loehr, J. (1994) Common oxygen binding site in hemocyanins from arthropods and mollusks. Evidence from Raman spectroscopy and normal coordinate analysis, *J. Am. Chem. Soc. 116*, 7682–7691.
2031. Baldwin, M. J., Root, D. E., Pate, J. E., Fujisawa, K., Kitajima, N., and Solomon, E. I. (1992) Spectroscopic studies of side-on peroxide-bridged binuclear copper(II) model complexes of relevance to oxyhemocyanin and oxytyrosinase, *J. Am. Chem. Soc. 114*, 10421–10431.
2032. Hu, Z., Williams, R. D., Tran, D., Spiro, T. G., and Gorun, S. M. (2000) Re-engineering enzyme-model active sites: Reversible binding of dioxygen at ambient conditions by a bio-inspired copper complex, *J. Am. Chem. Soc. 122*, 3556–3557.
2033. Kitajima, N., Fujisawa, K., Morooka, Y., and Toriumi, K. (1989) μ-η^2:η^2-Peroxo binuclear copper complex, $[Cu(HB(3,5\text{-}iPr_2pz)_3)]_2(O_2)$, *J. Am. Chem. Soc. 111*, 8975–8976.
2034. Halfen, J. A., Mahapatra, S., Wilkinson, E. C., Kaderli, S., Young, V. G., Jr., Que, L., Jr., Zuberbuhler, A. D., and Tolman, W. B. (1996) Reversible cleavage and formation of the dioxygen O-O bond within a dicopper complex, *Science 271*, 1397–1400.
2035. Ottenwaelder, X., Rudd, D. J., Corbett, M. C., Hodgson, K. O., Hedman, B., and Stack, T. D. (2006) Reversible O-O bond cleavage in copper-dioxygen isomers: Impact of anion basicity, *J. Am. Chem. Soc. 128*, 9268–9269.
2036. Dubois, J. L., Mukherjee, P., Collier, A. M., Mayer, J. M., Solomon, E. I., Hedman, B., Stack, T. D. P., and Hodgson, K. O. (1997) Cu K-edge XAS study of the $[Cu_2(\mu\text{-}O)_2]$ core: Direct experimental evidence for the presence of Cu(III), *J. Am. Chem. Soc. 119*, 8578–8579.
2037. Company, A., Lamata, D., Poater, A., Sola, M., Rybak-Akimova, E. V., Que, L., Jr., Fontrodona, X., Parella, T., Llobet, A., and Costas, M. (2006) O_2 Chemistry of dicopper complexes with alkyltriamine ligands. Comparing synergistic effects on O_2 binding, *Inorg. Chem. 45*, 5239–5241.
2038. Itoh, S., Nakao, H., Berreau, L. M., Kondo, T., Komatsu, M., and Fukuzumi, S. (1998) Mechanistic studies of aliphatic ligand hydroxylation of a copper complex by dioxygen: A model reaction for copper monooxygenases, *J. Am. Chem. Soc. 120*, 2890–2899.
2039. Aboelella, N. W., Lewis, E. A., Reynolds, A. M., Brennessel, W. W., Cramer, C. J., and Tolman, W. B. (2002) Snapshots of dioxygen activation by copper: The structure of a 1:1 Cu/O_2 adduct and its use in syntheses of asymmetric bis(μ-oxo) complexes, *J. Am. Chem. Soc. 124*, 10660–10661.
2040. Feng, X., Song, Y., Chen, J. S., Xu, Z., Dunn, S. J., and Lin, W. (2021) Rational construction of an artificial binuclear copper monooxygenase in a metal-organic framework, *J. Am. Chem. Soc. 143*, 1107–1118.
2041. Obias, H. V., Lin, Y., Murthy, N. N., Pidcock, E., Solomon, E. I., Ralle, M., Blackburn, N. J., Neuhold, Y.-M., Zuberbuehler, A. D., and Karlin, K. D. (1998) Peroxo-, oxo-, and hydroxo-bridged dicopper complexes: Observation of exogenous hydrocarbon substrate oxidation, *J. Am. Chem. Soc. 120*, 12960–12961.
2042. Nasir, M. S., Cohen, B. I., and Karlin, K. D. (1992) Mechanism of aromatic hydroxylation in a copper monooxygenase model system. 1,2-Methyl migrations and the NIH shift in copper chemistry, *J. Am. Chem. Soc. 114*, 2482–2494.
2043. Mirica, L. M., Vance, M., Rudd, D. J., Hedman, B., Hodgson, K. O., Solomon, E. I., and Stack, T. D. (2005) Tyrosinase reactivity in a model complex: An alternative hydroxylation mechanism, *Science 308*, 1890–1892.
2044. Company, A., Palavicini, S., Garcia-Bosch, I., Mas-Balleste, R., Que, L., Jr., Rybak-Akimova, E. V., Casella, L., Ribas, X., and Costas, M. (2008) Tyrosinase-like reactivity in a $Cu(III)_2(\mu\text{-}O)_2$ species, *Chemistry 14*, 3535–3538.
2045. Holt, B. T. O., Vance, M. A., Mirica, L. M., Heppner, D. E., Stack, T. D. P., and Solomon, E. I. (2009) Reaction coordinate of a functional model of tyrosinase: Spectroscopic and computational characterization, *J. Am. Chem. Soc. 131*, 6421–6438.
2046. Matoba, Y., Kumagai, T., Yamamoto, A., Yoshitsu, H., and Sugiyama, M. (2006) Crystal-

lographic evidence that the dinuclear copper center of tyrosinase is flexible during catalysis, *J. Biol. Chem. 281*, 8981–8990.
2047. Rodriguez-Lopez, J. N., Fenoll, L. G., Garcia-Ruiz, P. A., Varon, R., Tudela, J., Thorneley, R. N., and Garcia-Canovas, F. (2000) Stopped-flow and steady-state study of the diphenolase activity of mushroom tyrosinase, *Biochemistry 39*, 10497–10506.
2048. Qayyum, M. F., Sarangi, R., Fujisawa, K., Stack, T. D. P., Karlin, K. D., Hodgson, K. O., Hedman, B., and Solomon, E. I. (2013) L-edge X-ray absorption spectroscopy and DFT calculations on Cu_2O_2 species: Direct electrophilic aromatic attack by side-on peroxo bridged dicopper(II) complexes, *J. Am. Chem. Soc. 135*, 17417–17431.
2049. Klabunde, T., Eicken, C., Sacchettini, J. C., and Krebs, B. (1998) Crystal structure of a plant catechol oxidase containing a dicopper center, *Nature Struct. Biol. 5*, 1084–1090.
2050. Citek, C., Gary, J. B., Wasinger, E. C., and Stack, T. D. (2015) Chemical plausibility of Cu(III) with biological ligation in pMMo, *J. Am. Chem. Soc. 137*, 6991–6994.
2051. Culpepper, M. A., Cutsail, G. E., 3rd, Hoffman, B. M., and Rosenzweig, A. C. (2012) Evidence for oxygen binding at the active site of particulate methane monooxygenase, *J. Am. Chem. Soc. 134*, 7640–7643.
2052. Vendelboe, T. V., Harris, P., Zhao, Y., Walter, T. S., Harlos, K., El Omari, K., and Christensen, H. E. (2016) The crystal structure of human dopamine β-hydroxylase at 2.9 Å resolution, *Sci Adv 2*, e1500980.
2053. Wu, P., Fan, F., Song, J., Peng, W., Liu, J., Li, C., Cao, Z., and Wang, B. (2019) Theory demonstrated a "coupled" mechanism for O_2 activation and substrate hydroxylation by binuclear copper monooxygenases, *J. Am. Chem. Soc. 141*, 19776–19789.
2054. Freeman, J. C., Villafranca, J. J., and Merkler, D. J. (1993) Redox cycling of enzyme-bound copper during peptide amidation, *J. Am. Chem. Soc. 115*, 4923–4924.
2055. Prigge, S. T., Eipper, B. A., Mains, R. E., and Amzel, L. M. (2004) Dioxygen binds end-on to mononuclear copper in a precatalytic enzyme complex, *Science 304*, 864–867.
2056. Jaron, S., and Blackburn, N. J. (1999) Does superoxide channel between the copper centers in peptidylglycine monooxygenase? A new mechanism based on carbon monoxide reactivity, *Biochemistry 38*, 15086–15096.
2057. Chen, P., Fujisawa, K., and Solomon, E. I. (2000) Spectroscopic and theoretical studies of mononuclear copper(II) alkyl- and hydroperoxo complexes: Electronic structure contributions to reactivity, *J. Am. Chem. Soc. 122*, 10177–10193.
2058. Chen, P., Root, D. E., Campochiaro, C., Fujisawa, K., and Solomon, E. I. (2003) Spectroscopic and electronic structure studies of the diamagnetic side-on Cu^{II}-superoxo complex $Cu(O_2)[HB(3\text{-}R\text{-}5\text{-}^{i}Prpz)_3]$: Antiferromagnetic coupling versus covalent delocalization, *J. Am. Chem. Soc. 125*, 466–474.
2059. Fujisawa, K., Tanaka, M., Morooka, Y., and Kitajima, N. (1994) A monomeric side-on superoxocopper(II) complex: $Cu(O_2)[HB(3\text{-}^{t}Bu\text{-}5\text{-}^{i}Prpz)_3]$, *J. Am. Chem. Soc. 116*, 12079–12080.
2060. Bauman, A. T., Yukl, E. T., Alkevich, K., McCormack, A. L., and Blackburn, N. J. (2006) The hydrogen peroxide reactivity of peptidylglycine monooxygenase supports a Cu(II)-superoxo catalytic intermediate, *J. Biol. Chem. 281*, 4190–4198.
2061. Peterson, R. L., Ginsbach, J. W., Cowley, R. E., Qayyum, M. F., Himes, R. A., Siegler, M. A., Moore, C. D., Hedman, B., Hodgson, K. O., Fukuzumi, S., Solomon, E. I., and Karlin, K. D. (2013) Stepwise protonation and electron-transfer reduction of a primary copper-dioxygen adduct, *J. Am. Chem. Soc. 135*, 16454–16467.
2062. Bertrand, T., Jolivalt, C., Briozzo, P., Caminade, E., Joly, N., Madzak, C., and Mougin, C. (2002) Crystal structure of a four-copper laccase complexed with an arylamine: Insights into substrate recognition and correlation with kinetics, *Biochemistry 41*, 7325–7333.
2063. Hakulinen, N., Kiiskinen, L. L., Kruus, K., Saloheimo, M., Paananen, A., Koivula, A., and Rouvinen, J. (2002) Crystal structure of a laccase from *Melanocarpus albomyces* with an intact trinuclear copper site, *Nature Struct. Biol. 9*, 601–605.
2064. Bento, I., Peixoto, C., Zaitsev, V. N., and Lindley, P. F. (2007) Ceruloplasmin revisited: Structural and functional roles of various metal cation-binding sites, *Acta Crystallogr. D 63*, 240–248.
2065. Hakulinen, N., Andberg, M., Kallio, J., Koivula, A., Kruus, K., and Rouvinen, J. (2008) A

near atomic resolution structure of a *Melanocarpus albomyces* laccase, *J. Struct. Biol. 162*, 29–39.
2066. Shin, W., Sundaram, U. M., Cole, J. L., Zhang, H. H., Hedman, B., Hodgson, K. O., and Solomon, E. I. (1996) Chemical and spectroscopic definition of the peroxide-level intermediate in the multicopper oxidases: Relevance to the catalytic mechanism of dioxygen reduction to water, *J. Am. Chem. Soc. 118*, 3202–3215.
2067. Quintanar, L., Stoj, C., Wang, T. P., Kosman, D. J., and Solomon, E. I. (2005) Role of aspartate 94 in the decay of the peroxide intermediate in the multicopper oxidase Fet3P, *Biochemistry 44*, 6081–6091.
2068. Ryde, U., Hsiao, Y. W., Rulisek, L., and Solomon, E. I. (2007) Identification of the peroxy adduct in multicopper oxidases by a combination of computational chemistry and extended X-ray absorption fine-structure measurements, *J. Am. Chem. Soc. 129*, 726–727.
2069. Andreasson, L. E., Branden, R., and Reinhammar, B. (1976) Kinetic studies of *Rhus vernicifera* laccase. Evidence for multielectron transfer and an oxygen intermediate in the reoxidation reaction, *Biochim. Biophys. Acta 438*, 370–379.
2070. Yoon, J., Liboiron, B. D., Sarangi, R., Hodgson, K. O., Hedman, B., and Solomon, E. I. (2007) The two oxidized forms of the trinuclear Cu cluster in the multicopper oxidases and mechanism for the decay of the native intermediate, *Proc. Natl. Acad. Sci. U. S. A. 104*, 13609–13614.
2071. Heppner, D. E., Kjaergaard, C. H., and Solomon, E. I. (2013) Molecular origin of rapid versus slow intramolecular electron transfer in the catalytic cycle of the multicopper oxidases, *J. Am. Chem. Soc. 135*, 12212–12215.
2072. Heppner, D. E., Kjaergaard, C. H., and Solomon, E. I. (2014) Mechanism of the reduction of the native intermediate in the multicopper oxidases: Insights into rapid intramolecular electron transfer in turnover, *J. Am. Chem. Soc. 136*, 17788–17801.
2073. Paraskevopoulos, K., Antonyuk, S. V., Sawers, R. G., Eady, R. R., and Hasnain, S. S. (2006) Insight into catalysis of nitrous oxide reductase from high-resolution structures of resting and inhibitor-bound enzyme from *Achromobacter cycloclastes*, *J. Mol. Biol. 362*, 55–65.
2074. Haltia, T., Brown, K., Tegoni, M., Cambillau, C., Saraste, M., Mattila, K., and Djinovic-Carugo, K. (2003) Crystal structure of nitrous oxide reductase from *Paracoccus denitrificans* at 1.6 Å resolution, *Biochem. J. 369*, 77–88.
2075. Alvarez, M. L., Ai, J., Zumft, W., Sanders-Loehr, J., and Dooley, D. M. (2001) Characterization of the copper–sulfur chromophores in nitrous oxide reductase by resonance Raman spectroscopy: Evidence for sulfur coordination in the catalytic cluster, *J. Am. Chem. Soc. 123*, 576–587.
2076. Rasmussen, T., Berks, B. C., Sanders-Loehr, J., Dooley, D. M., Zumft, W. G., and Thomson, A. J. (2000) The catalytic center in nitrous oxide reductase, Cu_z, is a copper–sulfide cluster, *Biochemistry 39*, 12753–12756.
2077. Pomowski, A., Zumft, W. G., Kroneck, P. M. H., and Einsle, O. (2011) N_2O Binding at a [4Cu:2S] copper–sulphur cluster in nitrous oxide reductase, *Nature 477*, 234–237.
2078. Johnston, E. M., Dell'Acqua, S., Ramos, S., Pauleta, S. R., Moura, I., and Solomon, E. I. (2014) Determination of the active form of the tetranuclear copper sulfur cluster in nitrous oxide reductase, *J. Am. Chem. Soc. 136*, 614–617.
2079. Tocheva, E. I., Eltis, L. D., and Murphy, M. E. (2008) Conserved active site residues limit inhibition of a copper-containing nitrite reductase by small molecules, *Biochemistry 47*, 4452–4460.
2080. Ghosh, S., Gorelsky, S. I., Chen, P., Cabrito, I., Moura, J. J., Moura, I., and Solomon, E. I. (2003) Activation of N_2O reduction by the fully reduced μ_4-sulfide bridged tetranuclear Cu_z cluster in nitrous oxide reductase, *J. Am. Chem. Soc. 125*, 15708–15709.
2081. Johnston, E. M., Carreira, C., Dell'Acqua, S., Dey, S. G., Pauleta, S. R., Moura, I., and Solomon, E. I. (2017) Spectroscopic definition of the Cu_z degrees intermediate in turnover of nitrous oxide reductase and molecular insight into the catalytic mechanism, *J. Am. Chem. Soc. 139*, 4462–4476.
2082. Gunderson, W. A., Zatsman, A. I., Emerson, J. P., Farquhar, E. R., Que, L., Jr., Lipscomb, J. D., and Hendrich, M. P. (2008) Electron paramagnetic resonance detection of intermediates in the enzymatic cycle of an extradiol dioxygenase, *J. Am. Chem. Soc. 130*, 14465–14467.

2083. Fenwick, M. K., Philmus, B., Begley, T. P., and Ealick, S. E. (2011) Toxoflavin lyase requires a novel 1-His-2-carboxylate facial triad, *Biochemistry 50*, 1091–1100.
2084. Philmus, B., Abdelwahed, S., Williams, H. J., Fenwick, M. K., Ealick, S. E., and Begley, T. P. (2012) Identification of the product of toxoflavin lyase: Degradation via a Baeyer–Villiger oxidation, *J. Am. Chem. Soc. 134*, 5326–5330.
2085. Tanner, A., Bowater, L., Fairhurst, S. A., and Bornemann, S. (2001) Oxalate decarboxylase requires manganese and dioxygen for activity. Overexpression and characterization of *Bacillus subtilis* YvrK and YoaN, *J. Biol. Chem. 276*, 43627–43634.
2086. Saylor, B. T., Reinhardt, L. A., Lu, Z., Shukla, M. S., Nguyen, L., Cleland, W. W., Angerhofer, A., Allen, K. N., and Richards, N. G. (2012) A structural element that facilitates proton-coupled electron transfer in oxalate decarboxylase, *Biochemistry 51*, 2911–2920.
2087. Imaram, W., Saylor, B. T., Centonze, C. P., Richards, N. G., and Angerhofer, A. (2011) EPR Spin trapping of an oxalate-derived free radical in the oxalate decarboxylase reaction, *Free Radic Biol Med 50*, 1009–1015.
2088. Luo, Y. R., and Holmes, J. L. (1994) Homolytic and heterolytic X–C bond-energies. 1. Homolytic bond-energies in common unsaturated organic-compounds, *J. Phys. Chem. 98*, 303–312.
2089. Falvey, D. E., and Schuster, G. B. (1986) Picosecond time scale dynamics of perester photodecomposition: Evidence for an acyloxy radical intermediate in the photolysis of *tert*-butyl 9-methylfluorene-9-percarboxylate, *J. Am. Chem. Soc. 108*, 7419–7420.
2090. Hilborn, J. W., and Pincock, J. A. (1991) Rates of decarboxylation of acyloxy radicals formed in the photocleavage of substituted 1-naphthylmethyl alkanoates, *J. Am. Chem. Soc. 113*, 2683–2686.
2091. Bockman, T. M., Hubig, S. M., and Kochi, J. K. (1997) Direct observation of ultrafast decarboxylation of acyloxy radicals via photoinduced electron transfer in carboxylate ion pairs, *J. Org. Chem. 62*, 2210–2221.
2092. Bartlett, P. D., and Pincock, R. E. (1960) Peresters: 6. Ethyl, benzyl, para-nitrobenzyl and para-methoxybenzyl *tert*-butyl-peroxyoxalates, *J. Am. Chem. Soc. 82*, 1769–1773.
2093. Whittaker, M. M., Pan, H. Y., Yukl, E. T., and Whittaker, J. W. (2007) Burst kinetics and redox transformations of the active site manganese ion in oxalate oxidase: Implications for the catalytic mechanism, *J. Biol. Chem. 282*, 7011–7023.
2094. Zocher, G., Winkler, R., Hertweck, C., and Schulz, G. E. (2007) Structure and action of the *N*-oxygenase AurF from *Streptomyces thioluteus*, *J. Mol. Biol. 373*, 65–74.
2095. Whittaker, M. M., Barynin, V. V., Antonyuk, S. V., and Whittaker, J. W. (1999) The oxidized (3,3) state of manganese catalase. Comparison of enzymes from *Thermus thermophilus* and *Lactobacillus plantarum*, *Biochemistry 38*, 9126–9136.
2096. Barynin, V. V., Whittaker, M. M., Antonyuk, S. V., Lamzin, V. S., Harrison, P. M., Artymiuk, P. J., and Whittaker, J. W. (2001) Crystal structure of manganese catalase from *Lactobacillus plantarum*, *Structure 9*, 725–738.
2097. Khangulov, S. V., Barynin, V. V., and Antonyuk-Barynina, S. V. (1990) Manganese-containing catalase from *Thermus thermophilus* peroxide-induced redox transformation of manganese ions in presence of specific inhibitors of catalase activity, *Biochim. Biophys. Acta 1020*, 25–33.
2098. Waldo, G. S., and Penner-Hahn, J. E. (1995) Mechanism of manganese catalase peroxide disproportionation: Determination of manganese oxidation states during turnover, *Biochemistry 34*, 1507–1512.
2099. Pessiki, P. J., and Dismukes, G. C. (1994) Structural and functional models of the dimanganese catalase enzymes. 3. Kinetics and mechanism of hydrogen peroxide dismutation, *J. Am. Chem. Soc. 116*, 898–903.
2100. Waldo, G. S., Yu, S. Y., and Penner-Hahn, J. E. (1992) Structural characterization of the binuclear Mn site in *Lactobacillus plantarum* manganese catalase, *J. Am. Chem. Soc. 114*, 5869–5870.
2101. Beal, N. J., and O'Malley, P. J. (2016) Manganese oxidation state assignment for manganese catalase, *J. Am. Chem. Soc. 138*, 4358–4361.
2102. Ferreira, K. N., Iverson, T. M., Maghlaoui, K., Barber, J., and Iwata, S. (2004) Architecture of the photosynthetic oxygen-evolving center, *Science 303*, 1831–1838.
2103. Pushkar, Y., Yano, J., Glatzel, P., Messinger, J., Lewis, A., Sauer, K., Bergmann, U., and Ya-

chandra, V. (2007) Structure and orientation of the Mn_4Ca cluster in plant photosystem II membranes studied by polarized range-extended X-ray absorption spectroscopy, *J. Biol. Chem. 282*, 7198–7208.
2104. Shen, J. R., and Kamiya, N. (2000) Crystallization and the crystal properties of the oxygen-evolving photosystem II from *Synechococcus vulcanus*, *Biochemistry 39*, 14739–14744.
2105. Shen, J. R., and Inoue, Y. (1993) Binding and functional properties of two new extrinsic components, cytochrome c_{550} and a 12-kda protein, in cyanobacterial photosystem II, *Biochemistry 32*, 1825–1832.
2106. Tanaka, A., Fukushima, Y., and Kamiya, N. (2017) Two different structures of the oxygen-evolving complex in the same polypeptide frameworks of photosystem II, *J. Am. Chem. Soc. 139*, 1718–1721.
2107. Kanady, J. S., Tsui, E. Y., Day, M. W., and Agapie, T. (2011) A synthetic model of the Mn_3Ca subsite of the oxygen-evolving complex in photosystem II, *Science 333*, 733–736.
2108. Kanady, J. S., Lin, P. H., Carsch, K. M., Nielsen, R. J., Takase, M. K., Goddard, W. A., 3rd, and Agapie, T. (2014) Toward models for the full oxygen-evolving complex of photosystem II by ligand coordination to lower the symmetry of the Mn_3CaO_4 cubane: Demonstration that electronic effects facilitate binding of a fifth metal, *J. Am. Chem. Soc. 136*, 14373–14376.
2109. Suga, M., Akita, F., Sugahara, M., Kubo, M., Nakajima, Y., Nakane, T., Yamashita, K., Umena, Y., Nakabayashi, M., Yamane, T., Nakano, T., Suzuki, M., Masuda, T., Inoue, S., Kimura, T., Nomura, T., Yonekura, S., Yu, L. J., Sakamoto, T., Motomura, T., Chen, J. H., Kato, Y., Noguchi, T., Tono, K., Joti, Y., Kameshima, T., Hatsui, T., Nango, E., Tanaka, R., Naitow, H., Matsuura, Y., Yamashita, A., Yamamoto, M., Nureki, O., Yabashi, M., Ishikawa, T., Iwata, S., and Shen, J. R. (2017) Light-induced structural changes and the site of O=O bond formation in PSII caught by XFEL, *Nature 543*, 131–135.
2110. Suga, M., Akita, F., Yamashita, K., Nakajima, Y., Ueno, G., Li, H., Yamane, T., Hirata, K., Umena, Y., Yonekura, S., Yu, L. J., Murakami, H., Nomura, T., Kimura, T., Kubo, M., Baba, S., Kumasaka, T., Tono, K., Yabashi, M., Isobe, H., Yamaguchi, K., Yamamoto, M., Ago, H., and Shen, J. R. (2019) An oxyl/oxo mechanism for oxygen–oxygen coupling in PSII revealed by an X-ray free-electron laser, *Science 366*, 334–338.
2111. Joliot, P., Barbieri, G., and Chabaud, R. (1969) Model of the system II photochemical centers, *Photochem. Photobiol. 10*, 309–329.
2112. Messinger, J., Seaton, G., Wydrzynski, T., Wacker, U., and Renger, G. (1997) S_{-3} state of the water oxidase in photosystem II, *Biochemistry 36*, 6862–6873.
2113. Kok, B., Forbush, B., and McGloin, M. (1970) Cooperation of charges in photosynthetic O_2 evolution. A linear four step mechanism, *Photochem. Photobiol. 11*, 457–475.
2114. Renger, G. (2001) Photosynthetic water oxidation to molecular oxygen: Apparatus and mechanism, *Biochim. Biophys. Acta 1503*, 210–228.
2115. Kulik, L. V., Epel, B., Lubitz, W., and Messinger, J. (2007) Electronic structure of the Mn_4O_xCa cluster in the S_0 and S_2 states of the oxygen-evolving complex of photosystem II based on pulse ^{55}Mn-ENDOR and EPR spectroscopy, *J. Am. Chem. Soc. 129*, 13421–13435.
2116. Krewald, V., Retegan, M., Cox, N., Messinger, J., Lubitz, W., DeBeer, S., Neese, F., and Pantazis, D. A. (2015) Metal oxidation states in biological water splitting, *Chem Sci 6*, 1676–1695.
2117. Cox, N., Pantazis, D. A., Neese, F., and Lubitz, W. (2013) Biological water oxidation, *Accounts Chem Res 46*, 1588–1596.
2118. Messinger, J., Badger, M., and Wydrzynski, T. (1995) Detection of one slowly exchanging substrate water molecule in the S_3 state of photosystem II, *Proc. Natl. Acad. Sci. U. S. A. 92*, 3209–3213.
2119. Hendry, G., and Wydrzynski, T. (2002) The two substrate-water molecules are already bound to the oxygen-evolving complex in the S_2 state of photosystem II, *Biochemistry 41*, 13328–13334.
2120. Cox, N., and Messinger, J. (2013) Reflections on substrate water and dioxygen formation, *Biochim. Biophys. Acta 1827*, 1020–1030.
2121. Rapatskiy, L., Cox, N., Savitsky, A., Ames, W. M., Sander, J., Nowaczyk, M. M., Rogner, M., Boussac, A., Neese, F., Messinger, J., and Lubitz, W. (2012) Detection of the water-binding sites of the oxygen-evolving complex of photosystem II using W-band ^{17}O electron–electron double resonance-detected

NMR spectroscopy, *J. Am. Chem. Soc. 134*, 16619–16634.
2122. Lohmiller, T., Krewald, V., Sedoud, A., Rutherford, A. W., Neese, F., Lubitz, W., Pantazis, D. A., and Cox, N. (2017) The first state in the catalytic cycle of the water-oxidizing enzyme: Identification of a water-derived μ-hydroxo bridge, *J. Am. Chem. Soc. 139*, 14412–14424.
2123. Askerka, M., Wang, J., Brudvig, G. W., and Batista, V. S. (2014) Structural changes in the oxygen-evolving complex of photosystem II induced by the S_1 to S_2 transition: A combined XrD and QM/MM study, *Biochemistry 53*, 6860–6862.
2124. Cox, N., Retegan, M., Neese, F., Pantazis, D. A., Boussac, A., and Lubitz, W. (2014) Photosynthesis. Electronic structure of the oxygen-evolving complex in photosystem II prior to O-O bond formation, *Science 345*, 804–808.
2125. Lee, H. B., Marchiori, D. A., Chatterjee, R., Oyala, P. H., Yano, J., Britt, R. D., and Agapie, T. (2020) S = 3 Ground state for a tetranuclear $Mn(IV)_4O_4$ complex mimicking the S3 state of the oxygen-evolving complex, *J. Am. Chem. Soc. 142*, 3753–3761.
2126. Kupitz, C., Basu, S., Grotjohann, I., Fromme, R., Zatsepin, N. A., Rendek, K. N., Hunter, M. S., Shoeman, R. L., White, T. A., Wang, D., James, D., Yang, J. H., Cobb, D. E., Reeder, B., Sierra, R. G., Liu, H., Barty, A., Aquila, A. L., Deponte, D., Kirian, R. A., Bari, S., Bergkamp, J. J., Beyerlein, K. R., Bogan, M. J., Caleman, C., Chao, T. C., Conrad, C. E., Davis, K. M., Fleckenstein, H., Galli, L., Hau-Riege, S. P., Kassemeyer, S., Laksmono, H., Liang, M., Lomb, L., Marchesini, S., Martin, A. V., Messerschmidt, M., Milathianaki, D., Nass, K., Ros, A., Roy-Chowdhury, S., Schmidt, K., Seibert, M., Steinbrener, J., Stellato, F., Yan, L., Yoon, C., Moore, T. A., Moore, A. L., Pushkar, Y., Williams, G. J., Boutet, S., Doak, R. B., Weierstall, U., Frank, M., Chapman, H. N., Spence, J. C., and Fromme, P. (2014) Serial time-resolved crystallography of photosystem II using a femtosecond X-ray laser, *Nature 513*, 261–265.
2127. Pushkar, Y., Yano, J., Sauer, K., Boussac, A., and Yachandra, V. K. (2008) Structural changes in the Mn_4Ca cluster and the mechanism of photosynthetic water splitting, *Proc. Natl. Acad. Sci. U.S.A. 105*, 1879–1884.
2128. Takemoto, H., Sugiura, M., and Noguchi, T. (2019) Proton release process during the S_2-to-S_3 transition of photosynthetic water oxidation as revealed by the pH dependence of kinetics monitored by time-resolved infrared spectroscopy, *Biochemistry 58*, 4276–4283.
2129. Young, I. D., Ibrahim, M., Chatterjee, R., Gul, S., Fuller, F., Koroidov, S., Brewster, A. S., Tran, R., Alonso-Mori, R., Kroll, T., Michels-Clark, T., Laksmono, H., Sierra, R. G., Stan, C. A., Hussein, R., Zhang, M., Douthit, L., Kubin, M., de Lichtenberg, C., Long Vo, P., Nilsson, H., Cheah, M. H., Shevela, D., Saracini, C., Bean, M. A., Seuffert, I., Sokaras, D., Weng, T. C., Pastor, E., Weninger, C., Fransson, T., Lassalle, L., Brauer, P., Aller, P., Docker, P. T., Andi, B., Orville, A. M., Glownia, J. M., Nelson, S., Sikorski, M., Zhu, D., Hunter, M. S., Lane, T. J., Aquila, A., Koglin, J. E., Robinson, J., Liang, M., Boutet, S., Lyubimov, A. Y., Uervirojnangkoorn, M., Moriarty, N. W., Liebschner, D., Afonine, P. V., Waterman, D. G., Evans, G., Wernet, P., Dobbek, H., Weis, W. I., Brunger, A. T., Zwart, P. H., Adams, P. D., Zouni, A., Messinger, J., Bergmann, U., Sauter, N. K., Kern, J., Yachandra, V. K., and Yano, J. (2016) Structure of photosystem II and substrate binding at room temperature, *Nature 540*, 453–457.
2130. Kim, C. J., and Debus, R. J. (2019) One of the substrate waters for O_2 formation in photosystem II is provided by the water-splitting Mn_4CaO_5 cluster's Ca^{2+} ion, *Biochemistry 58*, 3185–3192.
2131. Ghosh, I., Banerjee, G., Kim, C. J., Reiss, K., Batista, V. S., Debus, R. J., and Brudvig, G. W. (2019) D1-S169A substitution of photosystem II perturbs water oxidation, *Biochemistry 58*, 1379–1387.
2132. Kim, C. J., and Debus, R. J. (2020) Roles of D1-Glu189 and D1-Glu329 in O_2 formation by the water-splitting Mn_4Ca cluster in photosystem II, *Biochemistry 59*, 3902–3917.
2133. Askerka, M., Wang, J., Vinyard, D. J., Brudvig, G. W., and Batista, V. S. (2016) S_3 State of the O_2-evolving complex of photosystem II: Insights from QM/MM, EXAFS, and femtosecond X-ray diffraction, *Biochemistry 55*, 981–984.
2134. Nilsson, H., Rappaport, F., Boussac, A., and Messinger, J. (2014) Substrate-water ex-

change in photosystem II is arrested before dioxygen formation, *Nat Commun 5*, 4305.
2135. Haumann, M., Liebisch, P., Muller, C., Barra, M., Grabolle, M., and Dau, H. (2005) Photosynthetic O_2 formation tracked by time-resolved X-ray experiments, *Science 310*, 1019–1021.
2136. Hong, S., Lee, Y. M., Sankaralingam, M., Vardhaman, A. K., Park, Y. J., Cho, K. B., Ogura, T., Sarangi, R., Fukuzumi, S., and Nam, W. (2016) A manganese(V)-oxo complex: Synthesis by dioxygen activation and enhancement of its oxidizing power by binding scandium ion, *J. Am. Chem. Soc. 138*, 8523–8532.
2137. Limburg, J., Vrettos, J. S., Liable-Sands, L. M., Rheingold, A. L., Crabtree, R. H., and Brudvig, G. W. (1999) A functional model for O-O bond formation by the O_2-evolving complex in photosystem II, *Science 283*, 1524–1527.
2138. Gao, Y., Akermark, T., Liu, J., Sun, L., and Akermark, B. (2009) Nucleophilic attack of hydroxide on a Mn(V) oxo complex: A model of the O-O bond formation in the oxygen evolving complex of photosystem II, *J. Am. Chem. Soc. 131*, 8726–8727.
2139. Siegbahn, P. E. (2009) Structures and energetics for O_2 formation in photosystem II, *Accounts Chem Res 42*, 1871–1880.
2140. Bossek, U., Weyhermueller, T., Wieghardt, K., Nuber, B., and Weiss, J. (1990) $[L_2Mn_2(\mu\text{-}O)_2(\mu\text{-}O_2)](ClO_4)_2$. The first binuclear ($\mu$-peroxo) dimanganese(IV) complex (L = 1,4,7-trimethyl-1,4,7-triazacyclononane). A model for the $S_4 \rightarrow S_0$ transformation in the oxygen-evolving complex in photosynthesis, *J. Am. Chem. Soc. 112*, 6387–6388.
2141. Ruettinger, W., Yagi, M., Wolf, K., Bernasek, S., and Dismukes, G. C. (2000) O_2 Evolution from the manganese-oxo cubane core $Mn_4O_4^{6+}$: A molecular mimic of the photosynthetic water oxidation enzyme?, *J. Am. Chem. Soc. 122*, 10353–10357.
2142. Cox, N., Pantazis, D. A., Neese, F., and Lubitz, W. (2015) Artificial photosynthesis: Understanding water splitting in nature, *Interface Focus 5*, 20150009.
2143. Wilson, A. J., and Jain, P. K. (2018) Structural dynamics of the oxygen-evolving complex of photosystem II in water-splitting action, *J. Am. Chem. Soc. 140*, 5853–5859.
2144. Ibrahim, M., Fransson, T., Chatterjee, R., Cheah, M. H., Hussein, R., Lassalle, L., Sutherlin, K. D., Young, I. D., Fuller, F. D., Gul, S., Kim, I. S., Simon, P. S., de Lichtenberg, C., Chernev, P., Bogacz, I., Pham, C. C., Orville, A. M., Saichek, N., Northen, T., Batyuk, A., Carbajo, S., Alonso-Mori, R., Tono, K., Owada, S., Bhowmick, A., Bolotovsky, R., Mendez, D., Moriarty, N. W., Holton, J. M., Dobbek, H., Brewster, A. S., Adams, P. D., Sauter, N. K., Bergmann, U., Zouni, A., Messinger, J., Kern, J., Yachandra, V. K., and Yano, J. (2020) Untangling the sequence of events during the $S_2 \rightarrow S_3$ transition in photosystem II and implications for the water oxidation mechanism, *Proc. Natl. Acad. Sci. U. S. A. 117*, 12624–12635.
2145. Kern, J., Chatterjee, R., Young, I. D., Fuller, F. D., Lassalle, L., Ibrahim, M., Gul, S., Fransson, T., Brewster, A. S., Alonso-Mori, R., Hussein, R., Zhang, M., Douthit, L., de Lichtenberg, C., Cheah, M. H., Shevela, D., Wersig, J., Seuffert, I., Sokaras, D., Pastor, E., Weninger, C., Kroll, T., Sierra, R. G., Aller, P., Butryn, A., Orville, A. M., Liang, M., Batyuk, A., Koglin, J. E., Carbajo, S., Boutet, S., Moriarty, N. W., Holton, J. M., Dobbek, H., Adams, P. D., Bergmann, U., Sauter, N. K., Zouni, A., Messinger, J., Yano, J., and Yachandra, V. K. (2018) Structures of the intermediates of Kok's photosynthetic water oxidation clock, *Nature 563*, 421–425.
2146. Budimir, A., Jozsef, K., Istvan, F., Lente, G., Istvan, B., Batinic-Haberle, I., and Birus, M. (2010) Water exchange rates of water-soluble manganese(III) porphyrins of therapeutical potential, *Dalton Trans. 39*, 4405–4410.
2147. Kramer, S. P., Johnson, J. L., Ribeiro, A. A., Millington, D. S., and Rajagopalan, K. V. (1987) The structure of the molybdenum cofactor. Characterization of di-(carboxamidomethyl)molybdopterin from sulfite oxidase and xanthine oxidase, *J. Biol. Chem. 262*, 16357–16363.
2148. Schindelin, H., Kisker, C., Hilton, J., Rajagopalan, K. V., and Rees, D. C. (1996) Crystal structure of DMSO reductase: Redox-linked changes in molybdopterin coordination, *Science 272*, 1615–1621.
2149. Czjzek, M., Dos Santos, J. P., Pommier, J., Giordano, G., Mejean, V., and Haser, R. (1998) Crystal structure of oxidized trimethylamine *N*-oxide reductase from *Shewanella massilia* at 2.5 Å resolution, *J. Mol. Biol. 284*, 435–447.

2150. Enroth, C., Eger, B. T., Okamoto, K., Nishino, T., Nishino, T., and Pai, E. F. (2000) Crystal structures of bovine milk xanthine dehydrogenase and xanthine oxidase: Structure-based mechanism of conversion, *Proc. Natl. Acad. Sci. U. S. A. 97*, 10723–10728.
2151. Kisker, C., Schindelin, H., Pacheco, A., Wehbi, W. A., Garrett, R. M., Rajagopalan, K. V., Enemark, J. H., and Rees, D. C. (1997) Molecular basis of sulfite oxidase deficiency from the structure of sulfite oxidase, *Cell 91*, 973–983.
2152. Chan, M. K., Mukund, S., Kletzin, A., Adams, M. W., and Rees, D. C. (1995) Structure of a hyperthermophilic tungstopterin enzyme, aldehyde ferredoxin oxidoreductase, *Science 267*, 1463–1469.
2153. Romao, M. J., Archer, M., Moura, I., Moura, J. J., LeGall, J., Engh, R., Schneider, M., Hof, P., and Huber, R. (1995) Crystal structure of the xanthine oxidase-related aldehyde oxidoreductase from *D. gigas*, *Science 270*, 1170–1176.
2154. Johnson, J. L., Bastian, N. R., and Rajagopalan, K. V. (1990) Molybdopterin guanine dinucleotide: A modified form of molybdopterin identified in the molybdenum cofactor of dimethyl sulfoxide reductase from *Rhodobacter sphaeroides forma specialis denitrificans*, *Proc. Natl. Acad. Sci. U.S.A. 87*, 3190–3194.
2155. Reschke, S., Duffus, B. R., Schrapers, P., Mebs, S., Teutloff, C., Dau, H., Haumann, M., and Leimkuhler, S. (2019) Identification of YdhV as the first molybdoenzyme binding a bis-Mo-MPT cofactor in *Escherichia coli*, *Biochemistry 58*, 2228–2242.
2156. Li, H.-K., Temple, C., Rajagopalan, K. V., and Schindelin, H. (2000) The 1.3 Å Crystal structure of *Rhodobacter sphaeroides* dimethyl sulfoxide reductase reveals two distinct molybdenum coordination environments, *J. Am. Chem. Soc. 122*, 7673–7680.
2157. George, G. N., Costa, C., Moura, J. J. G., and Moura, I. (1999) Observation of ligand-based redox chemistry at the active site of a molybdenum enzyme, *J. Am. Chem. Soc. 121*, 2625–2626.
2158. Kubitza, C., Bittner, F., Ginsel, C., Havemeyer, A., Clement, B., and Scheidig, A. J. (2018) Crystal structure of human mARC1 reveals its exceptional position among eukaryotic molybdenum enzymes, *Proc. Natl. Acad. Sci. U. S. A. 115*, 11958–11963.
2159. Gruenewald, S., Wahl, B., Bittner, F., Hungeling, H., Kanzow, S., Kotthaus, J., Schwering, U., Mendel, R. R., and Clement, B. (2008) The fourth molybdenum containing enzyme mARC: Cloning and involvement in the activation of *N*-hydroxylated prodrugs, *J Med Chem 51*, 8173–8177.
2160. Anderson, G. L., Williams, J., and Hille, R. (1992) The purification and characterization of arsenite oxidase from *Alcaligenes faecalis*, a molybdenum-containing hydroxylase, *J. Biol. Chem. 267*, 23674–23682.
2161. Kaufmann, P., Duffus, B. R., Teutloff, C., and Leimkuhler, S. (2018) Functional studies on *Oligotropha carboxidovorans* molybdenum-copper CO dehydrogenase produced in *Escherichia coli*, *Biochemistry 57*, 2889–2901.
2162. Resch, M., Dobbek, H., and Meyer, O. (2005) Structural and functional reconstruction in situ of the [$CuSMoO_2$] active site of carbon monoxide dehydrogenase from the carbon monoxide oxidizing *Eubacterium oligotropha carboxidovorans*, *J. Biol. Inorg. Chem. 10*, 518–528.
2163. Boll, M., Fuchs, G., Meier, C., Trautwein, A., El Kasmi, A., Ragsdale, S. W., Buchanan, G., and Lowe, D. J. (2001) Redox centers of 4-hydroxybenzoyl-CoA reductase, a member of the xanthine oxidase family of molybdenum-containing enzymes, *J. Biol. Chem. 276*, 47853–47862.
2164. Stiefel, E. I. (1973) Proposed molecular mechanism for the action of molybdenum in enzymes: Coupled proton and electron transfer, *Proc. Natl. Acad. Sci. U. S. A. 70*, 988–992.
2165. Bell, A. F., He, X., Ridge, J. P., Hanson, G. R., McEwan, A. G., and Tonge, P. J. (2001) Active site heterogeneity in dimethyl sulfoxide reductase from *Rhodobacter capsulatus* revealed by Raman spectroscopy, *Biochemistry 40*, 440–448.
2166. Bray, R. C., Adams, B., Smith, A. T., Bennett, B., and Bailey, S. (2000) Reversible dissociation of thiolate ligands from molybdenum in an enzyme of the dimethyl sulfoxide reductase family, *Biochemistry 39*, 11258–11269.
2167. Heffron, K., Leger, C., Rothery, R. A., Weiner, J. H., and Armstrong, F. A. (2001) Determination of an optimal potential window for catalysis by *E. coli* dimethyl sulfoxide reductase

and hypothesis on the role of Mo(V) in the reaction pathway, *Biochemistry 40*, 3117–3126.
2168. Cobb, N., Conrads, T., and Hille, R. (2005) Mechanistic studies of *Rhodobacter sphaeroides* Me_2SO reductase, *J. Biol. Chem. 280*, 11007–11017.
2169. Shaw, A. L., Hochkoeppler, A., Bonora, P., Zannoni, D., Hanson, G. R., and McEwan, A. G. (1999) Characterization of DorC from *Rhodobacter capsulatus*, a *c*-type cytochrome involved in electron transfer to dimethyl sulfoxide reductase, *J. Biol. Chem. 274*, 9911–9914.
2170. Bastian, N. R., Kay, C. J., Barber, M. J., and Rajagopalan, K. V. (1991) Spectroscopic studies of the molybdenum-containing dimethyl sulfoxide reductase from *Rhodobacter sphaeroides* Sp. *denitrificans*, *J. Biol. Chem. 266*, 45–51.
2171. Trieber, C. A., Rothery, R. A., and Weiner, J. H. (1996) Consequences of removal of a molybdenum ligand (DmsA-Ser-176) of *Escherichia coli* dimethyl sulfoxide reductase, *J. Biol. Chem. 271*, 27339–27345.
2172. Schultz, B. E., Hille, R., and Holm, R. H. (1995) Direct oxygen atom transfer in the mechanism of action of *Rhodobacter sphaeroides* dimethyl sulfoxide reductase, *J. Am. Chem. Soc. 117*, 827–828.
2173. Bray, R. C., Adams, B., Smith, A. T., Richards, R. L., Lowe, D. J., and Bailey, S. (2001) Reactions of dimethylsulfoxide reductase in the presence of dimethyl sulfide and the structure of the dimethyl sulfide-modified enzyme, *Biochemistry 40*, 9810–9820.
2174. Webster, C. E., and Hall, M. B. (2001) The theoretical transition state structure of a model complex bears a striking resemblance to the active site structure of DMSO reductase, *J. Am. Chem. Soc. 123*, 5820–5821.
2175. Lim, B. S., Sung, K.-M., and Holm, R. H. (2000) Structural and functional bis(dithiolene)-molybdenum/tungsten active site analogues of the dimethylsulfoxide reductase enzyme family, *J. Am. Chem. Soc. 122*, 7410–7411.
2176. Lim, B. S., and Holm, R. H. (2001) Bis(dithiolene)molybdenum analogues relevant to the DMSO reductase enzyme family: Synthesis, structures, and oxygen atom transfer reactions and kinetics, *J. Am. Chem. Soc. 123*, 1920–1930.
2177. Sung, K. M., and Holm, R. H. (2002) Functional analogue reaction systems of the DMSO reductase isoenzyme family: Probable mechanism of *S*-oxide reduction in oxo transfer reactions mediated by bis(dithio-lene)-tungsten (IV,VI) complexes, *J. Am. Chem. Soc. 124*, 4312–4320.
2178. Cervilla, A., Corma, A., Fornes, V., Llopis, E., Perez, F., Rey, F., and Ribera, A. (1995) Model reactions of molybdo-reductase: A novel and highly efficient reduction of nitrobenzene to aniline catalyzed by a molybdenum-mediated oxygen-atom transfer-reaction, *J. Am. Chem. Soc. 117*, 6781–6782.
2179. Hille, R. (1996) The mononuclear molybdenum enzymes, *Chem. Rev. 96*, 2757–2816.
2180. Najmudin, S., Gonzalez, P. J., Trincao, J., Coelho, C., Mukhopadhyay, A., Cerqueira, N. M., Romao, C. C., Moura, I., Moura, J. J., Brondino, C. D., and Romao, M. J. (2008) Periplasmic nitrate reductase revisited: A sulfur atom completes the sixth coordination of the catalytic molybdenum, *J. Biol. Inorganic Chem. 13*, 737–753.
2181. Coelho, C., Gonzalez, P. J., Moura, J. G., Moura, I., Trincao, J., and Joao Romao, M. (2011) The crystal structure of *Cupriavidus necator* nitrate reductase in oxidized and partially reduced states, *J. Mol. Biol. 408*, 932–948.
2182. Cerqueira, N. M., Gonzalez, P. J., Brondino, C. D., Romao, M. J., Romao, C. C., Moura, I., and Moura, J. J. (2009) The effect of the sixth sulfur ligand in the catalytic mechanism of periplasmic nitrate reductase, *J. Comput. Chem. 30*, 2466–2484.
2183. Hofmann, M. (2009) Density functional theory study of model complexes for the revised nitrate reductase active site in *Desulfovibrio desulfuricans napa*, *J. Biol. Inorganic Chem. 14*, 1023–1035.
2184. Xie, H. J., and Cao, Z. X. (2010) Enzymatic reduction of nitrate to nitrite: Insight from density functional calculations, *Organometallics 29*, 436–441.
2185. Lim, B. S., Willer, M. W., Miao, M., and Holm, R. H. (2001) Monodithiolene molybdenum(V, VI) complexes: A structural analogue of the oxidized active site of the sulfite oxidase enzyme family, *J. Am. Chem. Soc. 123*, 8343–8349.
2186. Peariso, K., McNaughton, R. L., and Kirk, M. L. (2002) Active-site stereochemical control

of oxygen atom transfer reactivity in sulfite oxidase, *J. Am. Chem. Soc. 124*, 9006–9007.
2187. Astashkin, A. V., Johnson-Winters, K., Klein, E. L., Byrne, R. S., Hille, R., Raitsimring, A. M., and Enemark, J. H. (2007) Direct demonstration of the presence of coordinated sulfate in the reaction pathway of *Arabidopsis thaliana* sulfite oxidase using ^{33}S labeling and ESEEM spectroscopy, *J. Am. Chem. Soc. 129*, 14800–14810.
2188. Byrne, R. S., Hansch, R., Mendel, R. R., and Hille, R. (2009) Oxidative half-reaction of *Arabidopsis thaliana* sulfite oxidase: Generation of superoxide by a peroxisomal enzyme, *J. Biol. Chem. 284*, 35479–35484.
2189. Garton, S. D., Hilton, J., Oku, H., Crouse, B. R., Rajagopalan, K. V., and Johnson, M. K. (1997) Active site structures and catalytic mechanism of *Rhodobacter sphaeroides* dimethyl sulfoxide reductase as revealed by resonance Raman spectroscopy, *J. Am. Chem. Soc. 119*, 12906–12916.
2190. Corte, E. D., and Stirpe, F. (1972) The regulation of rat liver xanthine oxidase. Involvement of thiol groups in the conversion of the enzyme activity from dehydrogenase (type D) into oxidase (type O) and purification of the enzyme, *Biochem. J. 126*, 739–745.
2191. Barber, M. J., Salerno, J. C., and Siegel, L. M. (1982) Magnetic interactions in milk xanthine oxidase, *Biochemistry 21*, 1648–1656.
2192. Bonin, I., Martins, B. M., Purvanov, V., Fetzner, S., Huber, R., and Dobbek, H. (2004) Active site geometry and substrate recognition of the molybdenum hydroxylase quinoline 2-oxidoreductase, *Structure 12*, 1425–1435.
2193. Okamoto, K., Matsumoto, K., Hille, R., Eger, B. T., Pai, E. F., and Nishino, T. (2004) The crystal structure of xanthine oxidoreductase during catalysis: Implications for reaction mechanism and enzyme inhibition, *Proc. Natl. Acad. Sci. U. S. A. 101*, 7931–7936.
2194. Okamoto, K., Kawaguchi, Y., Eger, B. T., Pai, E. F., and Nishino, T. (2010) Crystal structures of urate bound form of xanthine oxidoreductase: Substrate orientation and structure of the key reaction intermediate, *J. Am. Chem. Soc. 132*, 17080–17083.
2195. Doonan, C. J., Stockert, A., Hille, R., and George, G. N. (2005) Nature of the catalytically labile oxygen at the active site of xanthine oxidase, *J. Am. Chem. Soc. 127*, 4518–4522.
2196. Cao, H., Hall, J., and Hille, R. (2014) Substrate orientation and specificity in xanthine oxidase: Crystal structures of the enzyme in complex with indole-3-acetaldehyde and guanine, *Biochemistry 53*, 533–541.
2197. Kim, J. H., and Hille, R. (1993) Reductive half-reaction of xanthine oxidase with xanthine. Observation of a spectral intermediate attributable to the molybdenum center in the reaction of enzyme with xanthine, *J. Biol. Chem. 268*, 44–51.
2198. Spence, J. T., Barber, M. J., and Siegel, L. M. (1982) Determination of the stoichiometry of electron uptake and the midpoint reduction potentials of milk xanthine oxidase at 25 °C by microcoulometry, *Biochemistry 21*, 1656–1661.
2199. Hille, R., and Sprecher, H. (1987) On the mechanism of action of xanthine oxidase. Evidence in support of an oxo transfer mechanism in the molybdenum-containing hydroxylases, *J. Biol. Chem. 262*, 10914–10917.
2200. Greenwood, R. J., Wilson, G. L., Pilbrow, J. R., and Wedd, A. G. (1993) Molybdenum(V) sites in xanthine-oxidase and relevant analog complexes: Comparison of ^{17}O hyperfine coupling, *J. Am. Chem. Soc. 115*, 5385–5392.
2201. Howes, B. D., Bray, R. C., Richards, R. L., Turner, N. A., Bennett, B., and Lowe, D. J. (1996) Evidence favoring molybdenum-carbon bond formation in xanthine oxidase action: ^{17}Q- and ^{13}C-ENDOR and kinetic studies, *Biochemistry 35*, 1432–1443.
2202. Xia, M., Dempski, R., and Hille, R. (1999) The reductive half-reaction of xanthine oxidase. Reaction with aldehyde substrates and identification of the catalytically labile oxygen, *J. Biol. Chem. 274*, 3323–3330.
2203. Pauff, J. M., Cao, H., and Hille, R. (2009) Substrate orientation and catalysis at the molybdenum site in xanthine oxidase: Crystal structures in complex with xanthine and lumazine, *J. Biol. Chem. 284*, 8760–8767.
2204. Cao, H., Pauff, J. M., and Hille, R. (2010) Substrate orientation and catalytic specificity in the action of xanthine oxidase: The sequential hydroxylation of hypoxanthine to uric acid, *J. Biol. Chem. 285*, 28044–28053.
2205. Pauff, J. M., Zhang, J., Bell, C. E., and Hille, R. (2008) Substrate orientation in xanthine oxidase: Crystal structure of enzyme in reaction

with 2-hydroxy-6-methylpurine, *J. Biol. Chem. 283*, 4818–4824.
2206. D'Ardenne, S. C., and Edmondson, D. E. (1990) Kinetic isotope effect studies on milk xanthine oxidase and on chicken liver xanthine dehydrogenase, *Biochemistry 29*, 9046–9052.
2207. Szaleniec, M., Hagel, C., Menke, M., Nowak, P., Witko, M., and Heider, J. (2007) Kinetics and mechanism of oxygen-independent hydrocarbon hydroxylation by ethylbenzene dehydrogenase, *Biochemistry 46*, 7637–7646.
2208. Robinson, W. E., Bassegoda, A., Reisner, E., and Hirst, J. (2017) Oxidation-state-dependent binding properties of the active site in a Mo-containing formate dehydrogenase, *J. Am. Chem. Soc. 139*, 9927–9936.
2209. Niks, D., Duvvuru, J., Escalona, M., and Hille, R. (2016) Spectroscopic and kinetic properties of the molybdenum-containing, NAD^+-dependent formate dehydrogenase from *Ralstonia eutropha*, *J. Biol. Chem. 291*, 1162–1174.
2210. Maia, L. B., Fonseca, L., Moura, I., and Moura, J. J. (2016) Reduction of carbon dioxide by a molybdenum-containing formate dehydrogenase: A kinetic and mechanistic study, *J. Am. Chem. Soc. 138*, 8834–8846.
2211. Dobbek, H., Gremer, L., Kiefersauer, R., Huber, R., and Meyer, O. (2002) Catalysis at a dinuclear [CuSMo(=O)OH] cluster in a CO dehydrogenase resolved at 1.1 Å resolution, *Proc. Natl. Acad. Sci. U. S. A. 99*, 15971–15976.
2212. Stein, B. W., and Kirk, M. L. (2014) Orbital contributions to CO oxidation in Mo–Cu carbon monoxide dehydrogenase, *Chem Commun (Camb) 50*, 1104–1106.
2213. Siegbahn, P. E., and Shestakov, A. F. (2005) Quantum chemical modeling of CO oxidation by the active site of molybdenum CO dehydrogenase, *J Comput Chem 26*, 888–898.
2214. Mukund, S., and Adams, M. W. (1991) The novel tungsten–iron–sulfur protein of the hyperthermophilic archaebacterium, *Pyrococcus furiosus*, is an aldehyde ferredoxin oxidoreductase. Evidence for its participation in a unique glycolytic pathway, *J. Biol. Chem. 266*, 14208–14216.
2215. Johnson, J. L., Rajagopalan, K. V., Mukund, S., and Adams, M. W. (1993) Identification of molybdopterin as the organic component of the tungsten cofactor in four enzymes from hyperthermophilic archaea, *J. Biol. Chem. 268*, 4848–4852.
2216. Almendra, M. J., Brondino, C. D., Gavel, O., Pereira, A. S., Tavares, P., Bursakov, S., Duarte, R., Caldeira, J., Moura, J. J., and Moura, I. (1999) Purification and characterization of a tungsten-containing formate dehydrogenase from *Desulfovibrio gigas*, *Biochemistry 38*, 16366–16372.
2217. Koehler, B. P., Mukund, S., Conover, R. C., Dhawan, I. K., Roy, R., Adams, M. W. W., and Johnson, M. K. (1996) Spectroscopic characterization of the tungsten and iron centers in aldehyde ferredoxin oxidoreductases from two hyperthermophilic archaea, *J. Am. Chem. Soc. 118*, 12391–12405.
2218. Stewart, L. J., Bailey, S., Bennett, B., Charnock, J. M., Garner, C. D., and McAlpine, A. S. (2000) Dimethylsulfoxide reductase: An enzyme capable of catalysis with either molybdenum or tungsten at the active site, *J. Mol. Biol. 299*, 593–600.
2219. Hu, Y., Faham, S., Roy, R., Adams, M. W., and Rees, D. C. (1999) Formaldehyde ferredoxin oxidoreductase from *Pyrococcus furiosus*: The 1.85 Å resolution crystal structure and its mechanistic implications, *J. Mol. Biol. 286*, 899–914.
2220. Culka, M., Huwiler, S. G., Boll, M., and Ullmann, G. M. (2017) Breaking benzene aromaticity: Computational insights into the mechanism of the tungsten-containing benzoyl-CoA reductase, *J. Am. Chem. Soc. 139*, 14488–14500.
2221. Weinert, T., Huwiler, S. G., Kung, J. W., Weidenweber, S., Hellwig, P., Stark, H. J., Biskup, T., Weber, S., Cotelesage, J. J., George, G. N., Ermler, U., and Boll, M. (2015) Structural basis of enzymatic benzene ring reduction, *Nature Chem. Biol. 11*, 586–591.
2222. Seiffert, G. B., Ullmann, G. M., Messerschmidt, A., Schink, B., Kroneck, P. M., and Einsle, O. (2007) Structure of the non-redox-active tungsten/[4Fe:4S] enzyme acetylene hydratase, *Proc. Natl. Acad. Sci. U.S.A. 104*, 3073–3077.
2223. Williams, R. J., and Frausto da Silva, J. J. (2002) The involvement of molybdenum in life, *Biochem. Biophys. Res. Commun. 292*, 293–299.
2224. Schmitz, R. A., Richter, M., Linder, D., and Thauer, R. K. (1992) A tungsten-containing active formylmethanofuran dehydrogenase

in the thermophilic archaeon *Methanobacterium wolfei*, *Eur. J. Biochem. 207*, 559–565.
2225. Hochheimer, A., Hedderich, R., and Thauer, R. K. (1998) The formylmethanofuran dehydrogenase isoenzymes in *Methanobacterium wolfei* and *Methanobacterium thermoautotrophicum*: Induction of the molybdenum isoenzyme by molybdate and constitutive synthesis of the tungsten isoenzyme, *Arch. Microbiol. 170*, 389–393.
2226. Yoch, D. C., Benemann, J. R., Valentine, R. C., and Arnon, D. I. (1969) The electron transport system in nitrogen fixation by *Azotobacter*. II. Isolation and function of a new type of ferredoxin, *Proc. Natl. Acad. Sci. U.S.A. 64*, 1404–1410.
2227. Simpson, F. B., and Burris, R. H. (1984) A nitrogen pressure of 50 atmospheres does not prevent evolution of hydrogen by nitrogenase, *Science 224*, 1095–1097.
2228. Deistung, J., Cannon, F. C., Cannon, M. C., Hill, S., and Thorneley, R. N. (1985) Electron transfer to nitrogenase in *Klebsiella pneumoniae*. NifF gene cloned and the gene product, a flavodoxin, purified, *Biochem. J. 231*, 743–753.
2229. Taylor, M. F., Boylan, M. H., and Edmondson, D. E. (1990) *Azotobacter vinelandii* flavodoxin: Purification and properties of the recombinant, dephospho form expressed in *Escherichia coli*, *Biochemistry 29*, 6911–6918.
2230. Dilworth, M. J. (1966) Acetylene reduction by nitrogen-fixing preparations from *Clostridium pasteurianum*, *Biochim. Biophys. Acta 127*, 285–294.
2231. Hardy, R. W., and Knight, E., Jr. (1967) ATP-Dependent reduction of azide and HCN by N_2-fixing enzymes of *Azotobacter vinelandii* and *Clostridium pasteurianum*, *Biochim. Biophys. Acta 139*, 69–90.
2232. Kelly, M. (1968) The kinetics of the reduction of isocyanides, acetylenes and the cyanide ion by nitrogenase preparation from *Azotobacter chroococcum* and the effects of inhibitors, *Biochem. J. 107*, 1–6.
2233. Thorneley, R. N., and Lowe, D. J. (1983) Nitrogenase of *Klebsiella pneumoniae*. Kinetics of the dissociation of oxidized iron protein from molybdenum–iron protein: Identification of the rate-limiting step for substrate reduction, *Biochem. J. 215*, 393–403.
2234. Einsle, O., Tezcan, F. A., Andrade, S. L., Schmid, B., Yoshida, M., Howard, J. B., and Rees, D. C. (2002) Nitrogenase MoFe-protein at 1.16 Å resolution: A central ligand in the FeMo-cofactor, *Science 297*, 1696–1700.
2235. Spatzal, T., Aksoyoglu, M., Zhang, L., Andrade, S. L., Schleicher, E., Weber, S., Rees, D. C., and Einsle, O. (2011) Evidence for interstitial carbon in nitrogenase FeMo cofactor, *Science 334*, 940.
2236. Lancaster, K. M., Roemelt, M., Ettenhuber, P., Hu, Y., Ribbe, M. W., Neese, F., Bergmann, U., and DeBeer, S. (2011) X-ray emission spectroscopy evidences a central carbon in the nitrogenase iron-molybdenum cofactor, *Science 334*, 974–977.
2237. Lancaster, K. M., Hu, Y., Bergmann, U., Ribbe, M. W., and DeBeer, S. (2013) X-ray spectroscopic observation of an interstitial carbide in NifEN-bound FeMoco precursor, *J. Am. Chem. Soc. 135*, 610–612.
2238. Wiig, J. A., Hu, Y., Lee, C. C., and Ribbe, M. W. (2012) Radical SAM-dependent carbon insertion into the nitrogenase M-cluster, *Science 337*, 1672–1675.
2239. Wiig, J. A., Lee, C. C., Hu, Y., and Ribbe, M. W. (2013) Tracing the interstitial carbide of the nitrogenase cofactor during substrate turnover, *J. Am. Chem. Soc. 135*, 4982–4983.
2240. Fasiska, E. J., and Jeffrey, G. A. (1965) On cementite structure, *Acta Crystallographica 19*, 463–471.
2241. Wood, I. G., Vocadlo, L., Knight, K. S., Dobson, D. P., Marshall, W. G., Price, G. D., and Brodholt, J. (2004) Thermal expansion and crystal structure of cementite, Fe_3C, between 4 and 600 K determined by time-of-flight neutron powder diffraction, *J.. Appl. Crystallogr. 37*, 82–90.
2242. Rees, J. A., Bjornsson, R., Kowalska, J. K., Lima, F. A., Schlesier, J., Sippel, D., Weyhermuller, T., Einsle, O., Kovacs, J. A., and DeBeer, S. (2017) Comparative electronic structures of nitrogenase FeMoco and Fe-Vco, *Dalton Trans. 46*, 2445–2455.
2243. Arnett, C. H., Bogacz, I., Chatterjee, R., Yano, J., Oyala, P. H., and Agapie, T. (2020) Mixed-valent diiron μ-carbyne, μ-hydride complexes: Implications for nitrogenase, *J. Am. Chem. Soc. 142*, 18795–18813.
2244. Spatzal, T., Schlesier, J., Burger, E. M., Sippel, D., Zhang, L., Andrade, S. L., Rees, D. C., and Einsle, O. (2016) Nitrogenase FeMoco investigated by spatially resolved anomalous dispersion refinement, *Nat. Commun. 7*, 10902.

2245. Bjornsson, R., Neese, F., Schrock, R. R., Einsle, O., and DeBeer, S. (2015) The discovery of Mo(III) in FeMoco: Reuniting enzyme and model chemistry, *J. Biol. Inorg. Chem. 20*, 447–460.
2246. Kim, J., and Rees, D. C. (1992) Structural models for the metal centers in the nitrogenase molybdenum–iron protein, *Science 257*, 1677–1682.
2247. Ohki, Y., Sunada, Y., Honda, M., Katada, M., and Tatsumi, K. (2003) Synthesis of the P-cluster inorganic core of nitrogenases, *J. Am. Chem. Soc. 125*, 4052–4053.
2248. Keable, S. M., Zadvornyy, O. A., Johnson, L. E., Ginovska, B., Rasmussen, A. J., Danyal, K., Eilers, B. J., Prussia, G. A., LeVan, A. X., Raugei, S., Seefeldt, L. C., and Peters, J. W. (2018) Structural characterization of the P^{1+} intermediate state of the P-cluster of nitrogenase, *J. Biol. Chem. 293*, 9629–9635.
2249. Rupnik, K., Hu, Y., Lee, C. C., Wiig, J. A., Ribbe, M. W., and Hales, B. J. (2012) P^{+} State of nitrogenase P-cluster exhibits electronic structure of a $[Fe_4S_4]^{+}$ cluster, *J. Am. Chem. Soc. 134*, 13749–13754.
2250. Pierik, A. J., Wassink, H., Haaker, H., and Hagen, W. R. (1993) Redox properties and EPR spectroscopy of the P clusters of *Azotobacter vinelandii* MofE protein, *Eur. J. Biochem. 212*, 51–61.
2251. Lanzilotta, W. N., Christiansen, J., Dean, D. R., and Seefeldt, L. C. (1998) Evidence for coupled electron and proton transfer in the [8Fe–7S] cluster of nitrogenase, *Biochemistry 37*, 11376–11384.
2252. Georgiadis, M. M., Komiya, H., Chakrabarti, P., Woo, D., Kornuc, J. J., and Rees, D. C. (1992) Crystallographic structure of the nitrogenase iron protein from *Azotobacter vinelandii*, *Science 257*, 1653–1659.
2253. Schindelin, H., Kisker, C., Schlessman, J. L., Howard, J. B., and Rees, D. C. (1997) Structure of ADP x AlF_4^{-}-stabilized nitrogenase complex and its implications for signal transduction, *Nature 387*, 370–376.
2254. Hageman, R. V., and Burris, R. H. (1978) Nitrogenase and nitrogenase reductase associate and dissociate with each catalytic cycle, *Proc. Natl. Acad. Sci. U. S. A. 75*, 2699–2702.
2255. Burgess, B. K., and Lowe, D. J. (1996) Mechanism of molybdenum nitrogenase, *Chem. Rev. 96*, 2983–3012.
2256. Owens, C. P., Katz, F. E., Carter, C. H., Luca, M. A., and Tezcan, F. A. (2015) Evidence for functionally relevant encounter complexes in nitrogenase catalysis, *J. Am. Chem. Soc. 137*, 12704–12712.
2257. Danyal, K., Inglet, B. S., Vincent, K. A., Barney, B. M., Hoffman, B. M., Armstrong, F. A., Dean, D. R., and Seefeldt, L. C. (2010) Uncoupling nitrogenase: Catalytic reduction of hydrazine to ammonia by a MoFe protein in the absence of Fe protein-ATP, *J. Am. Chem. Soc. 132*, 13197–13199.
2258. Roth, L. E., and Tezcan, F. A. (2012) ATP-Uncoupled, six-electron photoreduction of hydrogen cyanide to methane by the molybdenum–iron protein, *J. Am. Chem. Soc. 134*, 8416–8419.
2259. Watt, G. D., Wang, Z. C., and Knotts, R. R. (1986) Redox reactions of and nucleotide binding to the iron protein of *Azotobacter vinelandii*, *Biochemistry 25*, 8156–8162.
2260. Jang, S. B., Seefeldt, L. C., and Peters, J. W. (2000) Insights into nucleotide signal transduction in nitrogenase: Structure of an iron protein with MgADP bound, *Biochemistry 39*, 14745–14752.
2261. Duval, S., Danyal, K., Shaw, S., Lytle, A. K., Dean, D. R., Hoffman, B. M., Antony, E., and Seefeldt, L. C. (2013) Electron transfer precedes ATP hydrolysis during nitrogenase catalysis, *Proc. Natl. Acad. Sci. U.S.A. 110*, 16414–16419.
2262. Lanzilotta, W. N., and Seefeldt, L. C. (1996) Electron transfer from the nitrogenase iron protein to the [8Fe-(7/8)S] clusters of the molybdenum–iron protein, *Biochemistry 35*, 16770–16776.
2263. Duyvis, M. G., Wassink, H., and Haaker, H. (1998) Nitrogenase of *Azotobacter vinelandii*: Kinetic analysis of the Fe protein redox cycle, *Biochemistry 37*, 17345–17354.
2264. Watt, G. D. (1979) An electrochemical method for measuring redox potentials of low potential proteins by microcoulometry at controlled potentials, *Anal. Biochem. 99*, 399–407.
2265. Hageman, R. V., Orme-Johnson, W. H., and Burris, R. H. (1980) Role of magnesium adenosine 5′-triphosphate in the hydrogen evolution reaction catalyzed by nitrogenase from *Azotobacter vinelandii*, *Biochemistry 19*, 2333–2342.

2266. Iismaa, S. E., Vazquez, A. E., Jensen, G. M., Stephens, P. J., Butt, J. N., Armstrong, F. A., and Burgess, B. K. (1991) Site-directed mutagenesis of *Azotobacter vinelandii* ferredoxin I. Changes in [4Fe–4S] cluster reduction potential and reactivity, *J. Biol. Chem. 266*, 21563–21571.
2267. Chen, K., Jung, Y. S., Bonagura, C. A., Tilley, G. J., Prasad, G. S., Sridhar, V., Armstrong, F. A., Stout, C. D., and Burgess, B. K. (2002) *Azotobacter vinelandii* ferredoxin I: A sequence and structure comparison approach to alteration of $[4Fe–4S]^{2+/+}$ reduction potential, *J. Biol. Chem. 277*, 5603–5610.
2268. Nelson, D. L., and Cox, M. M. (2005) *Lehninger Principles of Biochemistry*, Fourth ed., W. H. Freeman.
2269. Schmid, G., Auerbach, H., Pierik, A. J., Schunemann, V., and Boll, M. (2016) ATP-Dependent electron activation module of benzoyl-coenzyme A reductase from the hyperthermophilic archaeon *Ferroglobus placidus*, *Biochemistry 55*, 5578–5586.
2270. Lowe, D. J., and Thorneley, R. N. (1984) The mechanism of *Klebsiella pneumoniae* nitrogenase action. Pre-steady-state kinetics of H_2 formation, *Biochem. J. 224*, 877–886.
2271. Thorneley, R. N. F., Eady, R. R., and Lowe, D. J. (1978) Biological nitrogen-fixation by way of an enzyme-bound dinitrogen-hydride intermediate, *Nature 272*, 557–558.
2272. Lukoyanov, D., Barney, B. M., Dean, D. R., Seefeldt, L. C., and Hoffman, B. M. (2007) Connecting nitrogenase intermediates with the kinetic scheme for N_2 reduction by a relaxation protocol and identification of the N_2 binding state, *Proc. Natl. Acad. Sci. U. S. A. 104*, 1451–1455.
2273. Orme-Johnson, W. H. (1985) Molecular basis of biological nitrogen fixation, *Annu. Rev. Biophys. Biophys. Chem. 14*, 419–459.
2274. Thorneley, R. N., and Lowe, D. J. (1985) Kinetics and mechanism of the nitrogenase enzyme system, In *Molybdenum enzymes* (Spiro, T. G., Ed.), pp 89–116, Wiley-Interscience, New York.
2275. Thorneley, R. N., and Lowe, D. J. (1984) The mechanism of *Klebsiella pneumoniae* nitrogenase action. Simulation of the dependences of H_2-evolution rate on component-protein concentration and ratio and sodium dithionite concentration, *Biochem. J. 224*, 903–909.
2276. Igarashi, R. Y., Laryukhin, M., Dos Santos, P. C., Lee, H. I., Dean, D. R., Seefeldt, L. C., and Hoffman, B. M. (2005) Trapping H^- bound to the nitrogenase FeMo-cofactor active site during H_2 evolution: Characterization by ENDOR spectroscopy, *J. Am. Chem. Soc. 127*, 6231–6241.
2277. Doan, P. E., Telser, J., Barney, B. M., Igarashi, R. Y., Dean, D. R., Seefeldt, L. C., and Hoffman, B. M. (2011) ^{57}Fe ENDOR spectroscopy and 'electron inventory' analysis of the nitrogenase E_4 intermediate suggest the metal-ion core of FeMo-cofactor cycles through only one redox couple, *J. Am. Chem. Soc. 133*, 17329–17340.
2278. Kinney, R. A., Saouma, C. T., Peters, J. C., and Hoffman, B. M. (2012) Modeling the signatures of hydrides in metalloenzymes: ENDOR analysis of a diiron Fe(μ-NH)(μ-H)Fe core, *J. Am. Chem. Soc. 134*, 12637–12647.
2279. Lukoyanov, D., Khadka, N., Yang, Z. Y., Dean, D. R., Seefeldt, L. C., and Hoffman, B. M. (2016) Reductive elimination of H_2 activates nitrogenase to reduce the N≡N triple bond: Characterization of the E_4(4H) janus intermediate in wild-type enzyme, *J. Am. Chem. Soc. 138*, 10674–10683.
2280. Lukoyanov, D. A., Yang, Z. Y., Dean, D. R., Seefeldt, L. C., Raugei, S., and Hoffman, B. M. (2020) Electron redistribution within the nitrogenase active site FeMo-cofactor during reductive elimination of H_2 to achieve N≡N triple-bond activation, *J. Am. Chem. Soc. 142*, 21679–21690.
2281. Raugei, S., Seefeldt, L. C., and Hoffman, B. M. (2018) Critical computational analysis illuminates the reductive-elimination mechanism that activates nitrogenase for N_2 reduction, *Proc. Natl. Acad. Sci. U. S. A. 115*, E10521–E10530.
2282. Guth, J. H., and Burris, R. H. (1983) Inhibition of nitrogenase-catalyzed NH_3 formation by H_2, *Biochemistry 22*, 5111–5122.
2283. Burgess, B. K., Wherland, S., Newton, W. E., and Stiefel, E. I. (1981) Nitrogenase reactivity: Insight into the nitrogen-fixing process through hydrogen-inhibition and HD-forming reactions, *Biochemistry 20*, 5140–5146.
2284. Rivera-Ortiz, J. M., and Burris, R. H. (1975) Interactions among substrates and inhibitors of nitrogenase, *J. Bacteriol. 123*, 537–545.
2285. Harris, D. F., Yang, Z. Y., Dean, D. R., Seefeldt, L. C., and Hoffman, B. M. (2018) Kinetic

understanding of N_2 reduction versus H_2 evolution at the E_4(4H) Janus state in the three nitrogenases, *Biochemistry 57*, 5706–5714.
2286. Lukoyanov, D., Yang, Z. Y., Khadka, N., Dean, D. R., Seefeldt, L. C., and Hoffman, B. M. (2015) Identification of a key catalytic intermediate demonstrates that nitrogenase is activated by the reversible exchange of N_2 for H_2, *J. Am. Chem. Soc. 137*, 3610–3615.
2287. Lukoyanov, D., Khadka, N., Yang, Z. Y., Dean, D. R., Seefeldt, L. C., and Hoffman, B. M. (2016) Reversible photoinduced reductive elimination of H_2 from the nitrogenase dihydride state, the E_4(4H) janus intermediate, *J. Am. Chem. Soc. 138*, 1320–1327.
2288. Morrison, C. N., Spatzal, T., and Rees, D. C. (2017) Reversible protonated resting state of the nitrogenase active site, *J. Am. Chem. Soc. 139*, 10856–10862.
2289. Shanahan, J. P., and Szymczak, N. K. (2019) Hydrogen bonding to a dinitrogen complex at room temperature: Impacts on N_2 activation, *J. Am. Chem. Soc. 141*, 8550–8556.
2290. Kang, W., Lee, C. C., Jasniewski, A. J., Ribbe, M. W., and Hu, Y. (2020) Structural evidence for a dynamic metallocofactor during N_2 reduction by Mo-nitrogenase, *Science 368*, 1381–1385.
2291. Barney, B. M., McClead, J., Lukoyanov, D., Laryukhin, M., Yang, T. C., Dean, D. R., Hoffman, B. M., and Seefeldt, L. C. (2007) Diazene (HN=NH) is a substrate for nitrogenase: Insights into the pathway of N_2 reduction, *Biochemistry 46*, 6784–6794.
2292. Davis, L. C. (1980) Hydrazine as a substrate and inhibitor of *Azotobacter vinelandii* nitrogenase, *Arch. Biochem. Biophys. 204*, 270–276.
2293. Durrant, M. C. (2002) An atomic-level mechanism for molybdenum nitrogenase. Part 1. Reduction of dinitrogen, *Biochemistry 41*, 13934–13945.
2294. Rohde, M., Sippel, D., Trncik, C., Andrade, S. L. A., and Einsle, O. (2018) The critical E_4 state of nitrogenase catalysis, *Biochemistry 57*, 5497–5504.
2295. Hoffman, B. M., Dean, D. R., and Seefeldt, L. C. (2009) Climbing nitrogenase: Toward a mechanism of enzymatic nitrogen fixation, *Accounts Chem Res 42*, 609–619.
2296. Lukoyanov, D., Yang, Z. Y., Barney, B. M., Dean, D. R., Seefeldt, L. C., and Hoffman, B. M. (2012) Unification of reaction pathway and kinetic scheme for N_2 reduction catalyzed by nitrogenase, *Proc. Natl. Acad. Sci. U.S.A. 109*, 5583–5587.
2297. Shaw, S., Lukoyanov, D., Danyal, K., Dean, D. R., Hoffman, B. M., and Seefeldt, L. C. (2014) Nitrite and hydroxylamine as nitrogenase substrates: Mechanistic implications for the pathway of N_2 reduction, *J. Am. Chem. Soc. 136*, 12776–12783.
2298. Seefeldt, L. C., Dance, I. G., and Dean, D. R. (2004) Substrate interactions with nitrogenase: Fe versus Mo, *Biochemistry 43*, 1401–1409.
2299. Yandulov, D. V., and Schrock, R. R. (2003) Catalytic reduction of dinitrogen to ammonia at a single molybdenum center, *Science 301*, 76–78.
2300. Pickett, C. J. (1996) The Chatt cycle and the mechanism of enzymic reduction of molecular nitrogen, *J. Biol. Inorganic Chem. 1*, 601–606.
2301. Chatt, J., Dilworth, J. R., and Richards, R. L. (1978) Recent advances in the chemistry of nitrogen fixation, *Chem. Rev. 78*, 589–625.
2302. Schrock, R. R. (2005) Catalytic reduction of dinitrogen to ammonia at well-defined single metal sites, *Philos. Trans. R. Soc. London A, 363*, 959–969.
2303. Harris, D. F., Lukoyanov, D. A., Shaw, S., Compton, P., Tokmina-Lukaszewska, M., Bothner, B., Kelleher, N., Dean, D. R., Hoffman, B. M., and Seefeldt, L. C. (2018) Mechanism of N_2 reduction catalyzed by Fe-nitrogenase involves reductive elimination of H_2, *Biochemistry 57*, 701–710.
2304. Eady, R. R. (1996) Structure–function relationships of alternative nitrogenases, *Chem. Rev. 96*, 3013–3030.
2305. Eady, R. R., Robson, R. L., Richardson, T. H., Miller, R. W., and Hawkins, M. (1987) The vanadium nitrogenase of *Azotobacter chroococcum*. Purification and properties of the VFe protein, *Biochem. J. 244*, 197–207.
2306. Rohde, M., Grunau, K., and Einsle, O. (2020) Co binding to the FeV cofactor of CO-reducing vanadium nitrogenase at atomic resolution, *Angew. Chem., Int. Ed. Engl. 59*, 23626–23630.
2307. Joerger, R. D., Jacobson, M. R., Premakumar, R., Wolfinger, E. D., and Bishop, P. E. (1989) Nucleotide sequence and mutational analysis of the structural genes (anfHDGK) for the

second alternative nitrogenase from *Azotobacter vinelandii*, *J. Bacteriol. 171*, 1075–1086.
2308. Pau, R. N., Eldridge, M. E., Lowe, D. J., Mitchenall, L. A., and Eady, R. R. (1993) Molybdenum-independent nitrogenases of *Azotobacter vinelandii*: A functional species of alternative nitrogenase-3 isolated from a molybdenum-tolerant strain contains an iron-molybdenum cofactor, *Biochem. J. 293 (Pt 1)*, 101–107.
2309. Harris, D. F., Lukoyanov, D. A., Kallas, H., Trncik, C., Yang, Z. Y., Compton, P., Kelleher, N., Einsle, O., Dean, D. R., Hoffman, B. M., and Seefeldt, L. C. (2019) Mo-, V-, and Fe-nitrogenases use a universal eight-electron reductive-elimination mechanism to achieve N_2 reduction, *Biochemistry 58*, 3293–3301.
2310. Krahn, E., Weiss, R., Krockel, M., Groppe, J., Henkel, G., Cramer, P., Trautwein, X., Schneider, K., and Muller, A. (2002) The Fe-only nitrogenase from *Rhodobacter capsulatus*: Identification of the cofactor, an unusual, high-nuclearity iron–sulfur cluster, by Fe K-edge EXAFS and ^{57}Fe Mössbauer spectroscopy, *J. Biol. Inorganic Chem. 7*, 37–45.
2311. Ebert, L. B., Mills, D. R., Garcia, A. R., and Scanlon, J. C. (1985) More on the reaction of graphite potassium with water, *Mater Res Bull 20*, 1453–1460.
2312. Weitz, A., and Rabinovitz, M. (1995) Reduction of polycyclic hydrocarbons with potassium-graphite intercalate KC8, *Synthetic Meth. 74*, 201–205.
2313. Lee, Y., Mankad, N. P., and Peters, J. C. (2010) Triggering N_2 uptake via redox-induced expulsion of coordinated NH_3 and N_2 silylation at trigonal bipyramidal iron, *Nat Chem 2*, 558–565.
2314. Anderson, J. S., Rittle, J., and Peters, J. C. (2013) Catalytic conversion of nitrogen to ammonia by an iron model complex, *Nature 501*, 84–87.
2315. Rittle, J., and Peters, J. C. (2016) An Fe-N_2 complex that generates hydrazine and ammonia via Fe=NNH_2: Demonstrating a hybrid distal-to-alternating pathway for N_2 reduction, *J. Am. Chem. Soc. 138*, 4243–4248.
2316. Anderson, J. S., Cutsail, G. E., 3rd, Rittle, J., Connor, B. A., Gunderson, W. A., Zhang, L., Hoffman, B. M., and Peters, J. C. (2015) Characterization of an Fe≡N–NH_2 intermediate relevant to catalytic N_2 reduction to NH_3, *J. Am. Chem. Soc. 137*, 7803–7809.
2317. Keilwerth, M., Grunwald, L., Mao, W., Heinemann, F. W., Sutter, J., Bill, E., and Meyer, K. (2021) Ligand tailoring toward an air-stable iron(V) nitrido complex, *J. Am. Chem. Soc. 143*, 1458–1465.
2318. Scepaniak, J. J., Vogel, C. S., Khusniyarov, M. M., Heinemann, F. W., Meyer, K., and Smith, J. M. (2011) Synthesis, structure, and reactivity of an iron(V) nitride, *Science 331*, 1049–1052.
2319. Ertl, G. (1983) Primary steps in catalytic synthesis of ammonia, *J. Vac. Sci. Technol. A 1*, 1247–1253.
2320. Charlot, G., Collumeau, A., and Marchon, M. J. C. (1971) *Selected Constants: Oxidation–reduction Potentials of Inorganic Substances in Aqueous Solution. International Union of Pure and Applied Chemistry. Commission of Electrochemical Data*, Butterworths, London.
2321. Pospisil, L., Bulickova, J., Hromadova, M., Gal, M., Civis, S., Cihelka, J., and Tarabek, J. (2007) Electrochemical conversion of dinitrogen to ammonia mediated by a complex of fullerene C60 and γ-cyclodextrin, *Chem. Commun.* 2270–2272.
2322. Kordali, V., Kyriacou, G., and Lambrou, C. (2000) Electrochemical synthesis of ammonia at atmospheric pressure and low temperature in a solid polymer electrolyte cell, *Chem.Comm.* 1673–1674.
2323. Weyand, M., Hecht, H., Kiess, M., Liaud, M., Vilter, H., and Schomburg, D. (1999) X-Ray structure determination of a vanadium-dependent haloperoxidase from *Ascophyllum nodosum* at 2.0 Å resolution, *J. Mol. Biol. 293*, 595–611.
2324. Butler, A. (1998) Vanadium haloperoxidases, *Curr. Opin. Chem. Biol. 2*, 279–285.
2325. Martinez, J. S., Carroll, G. L., Tschirret-Guth, R. A., Altenhoff, G., Little, R. D., and Butler, A. (2001) On the regiospecificity of vanadium bromoperoxidase, *J. Am. Chem. Soc. 123*, 3289–3294.
2326. Bernhardt, P., Okino, T., Winter, J. M., Miyanaga, A., and Moore, B. S. (2011) A stereoselective vanadium-dependent chloroperoxidase in bacterial antibiotic biosynthesis, *J. Am. Chem. Soc. 133*, 4268–4270.
2327. Deboer, E., Boon, K., and Wever, R. (1988) Electron-paramagnetic resonance studies on conformational states and metal-ion ex-

change properties of vanadium bromoperoxidase, *Biochemistry 27*, 1629–1635.
2328. Van Schijndel, J. W., Barnett, P., Roelse, J., Vollenbroek, E. G., and Wever, R. (1994) The stability and steady-state kinetics of vanadium chloroperoxidase from the fungus *Curvularia inaequalis*, *Eur. J. Biochem. 225*, 151–157.
2329. Messerschmidt, A., Prade, L., and Wever, R. (1997) Implications for the catalytic mechanism of the vanadium-containing enzyme chloroperoxidase from the fungus *Curvularia inaequalis* by X-ray structures of the native and peroxide form, *Biol. Chem. 378*, 309–315.
2330. Messerschmidt, A., and Wever, R. (1996) X-ray structure of a vanadium-containing enzyme: Chloroperoxidase from the fungus *Curvularia inaequalis*, *Proc. Natl. Acad. Sci. U.S.A. 93*, 392–396.
2331. Renirie, R., Charnock, J. M., Garner, C. D., and Wever, R. (2010) Vanadium K-edge XAS studies on the native and peroxo-forms of vanadium chloroperoxidase from *Curvularia inaequalis*, *J. Inorg. Biochem. 104*, 657–664.
2332. Bonadies, J. A., and Carrano, C. J. (1986) Vanadium phenolates as models for vanadium in biological-systems: 1. Synthesis, spectroscopy, and electrochemistry of vanadium complexes of ethylenebis[(*o*-hydroxy-phenyl)glycine] and its derivatives, *J. Am. Chem. Soc. 108*, 4088–4095.
2333. ten Brink, H. B., Schoemaker, H. E., and Wever, R. (2001) Sulfoxidation mechanism of vanadium bromoperoxidase from *Ascophyllum nodosum*. Evidence for direct oxygen transfer catalysis, *Eur. J. Biochem. 268*, 132–138.
2334. Mba, M., Pontini, M., Lovat, S., Zonta, C., Bernardinelli, G., Kundig, P. E., and Licini, G. (2008) C3 Vanadium(V) amine triphenolate complexes: Vanadium haloperoxidase structural and functional models, *Inorg. Chem. 47*, 8616–8618.
2335. de Boer, E., and Wever, R. (1988) The reaction mechanism of the novel vanadium-bromoperoxidase. A steady-state kinetic analysis, *J. Biol. Chem. 263*, 12326–12332.
2336. Soedjak, H. S., Walker, J. V., and Butler, A. (1995) Inhibition and inactivation of vanadium bromoperoxidase by the substrate hydrogen peroxide and further mechanistic studies, *Biochemistry 34*, 12689–12696.
2337. Clague, M. J., Keder, N. L., and Butler, A. (1993) Biomimics of vanadium bromoperoxidase: Vanadium(V)-Schiff base-catalyzed oxidation of bromide by hydrogen-peroxide, *Inorg. Chem. 32*, 4754–4761.
2338. Everett, R. R., Soedjak, H. S., and Butler, A. (1990) Mechanism of dioxygen formation catalyzed by vanadium bromoperoxidase. Steady state kinetic analysis and comparison to the mechanism of bromination, *J. Biol. Chem. 265*, 15671–15679.
2339. Tibrewal, N., Pahari, P., Wang, G., Kharel, M. K., Morris, C., Downey, T., Hou, Y., Bugni, T. S., and Rohr, J. (2012) Baeyer–Villiger C–C bond cleavage reaction in gilvocarcin and jadomycin biosynthesis, *J. Am. Chem. Soc. 134*, 18181–18184.
2340. Gould, S. J., Kirchmeier, M. J., and LaFever, R. E. (1996) Incorporation of two oxygens from $^{18}O_2$ in the epoxyquinone from the dihydroxyacetanilide epoxidase reaction: Evidence for a dioxygenase mechanism, *J. Am. Chem. Soc. 118*, 7663–7666.
2341. Chaiyen, P., Brissette, P., Ballou, D. P., and Massey, V. (1997) Unusual mechanism of oxygen atom transfer and product rearrangement in the catalytic reaction of 2-methyl-3-hydroxypyridine-5-carboxylic acid oxygenase, *Biochemistry 36*, 8060–8070.
2342. Sarma, A. D., and Tipton, P. A. (2000) Evidence for urate hydroperoxide as an intermediate in the urate oxidase reaction, *J. Am. Chem. Soc. 122*, 11252–11253.
2343. Gunsior, M., Ravel, J., Challis, G. L., and Townsend, C. A. (2004) Engineering *p*-hydroxyphenylpyruvate dioxygenase to a *p*-hydroxymandelate synthase and evidence for the proposed benzene oxide intermediate in homogentisate formation, *Biochemistry 43*, 663–674.
2344. Fritze, I. M., Linden, L., Freigang, J., Auerbach, G., Huber, R., and Steinbacher, S. (2004) The crystal structures of *Zea mays* and *Arabidopsis* 4-hydroxyphenylpyruvate dioxygenase, *Plant Physiol 134*, 1388–1400.
2345. Duine, J. A., Frank, J., and Verwiel, P. E. (1980) Structure and activity of the prosthetic group of methanol dehydrogenase, *Eur. J. Biochem. 108*, 187–192.
2346. Salisbury, S. A., Forrest, H. S., Cruse, W. B., and Kennard, O. (1979) A novel coenzyme from bacterial primary alcohol dehydrogenases, *Nature 280*, 843–844.

2347. Xia, Z. X., He, Y. N., Dai, W. W., White, S. A., Boyd, G. D., and Mathews, F. S. (1999) Detailed active site configuration of a new crystal form of methanol dehydrogenase from *Methylophilus* W3A1 at 1.9 Å resolution, *Biochemistry 38*, 1214–1220.
2348. Houck, D. R., Hanners, J. L., and Unkefer, C. J. (1991) Biosynthesis of pyrroloquinoline quinone: 2. Biosynthetic assembly from glutamate and tyrosine, *J. Am. Chem. Soc. 113*, 3162–3166.
2349. Bonnot, F., Iavarone, A. T., and Klinman, J. P. (2013) Multistep, eight-electron oxidation catalyzed by the cofactorless oxidase, PqqC: Identification of chemical intermediates and their dependence on molecular oxygen, *Biochemistry 52*, 4667–4675.
2350. Wang, S. X., Mure, M., Medzihradszky, K. F., Burlingame, A. L., Brown, D. E., Dooley, D. M., Smith, A. J., Kagan, H. M., and Klinman, J. P. (1996) A crosslinked cofactor in lysyl oxidase: Redox function for amino acid side chains, *Science 273*, 1078–1084.
2351. McIntire, W. S., Wemmer, D. E., Chistoserdov, A., and Lidstrom, M. E. (1991) A new cofactor in a prokaryotic enzyme: Tryptophan tryptophylquinone as the redox prosthetic group in methylamine dehydrogenase, *Science 252*, 817–824.
2352. Huizinga, E. G., van Zanten, B. A., Duine, J. A., Jongejan, J. A., Huitema, F., Wilson, K. S., and Hol, W. G. (1992) Active site structure of methylamine dehydrogenase: Hydrazines identify C6 as the reactive site of the tryptophan-derived quinone cofactor, *Biochemistry 31*, 9789–9795.
2353. Datta, S., Mori, Y., Takagi, K., Kawaguchi, K., Chen, Z. W., Okajima, T., Kuroda, S., Ikeda, T., Kano, K., Tanizawa, K., and Mathews, F. S. (2001) Structure of a quinohemoprotein amine dehydrogenase with an uncommon redox cofactor and highly unusual crosslinking, *Proc. Natl. Acad. Sci. U. S. A. 98*, 14268–14273.
2354. Okazaki, S., Nakano, S., Matsui, D., Akaji, S., Inagaki, K., and Asano, Y. (2013) X-Ray crystallographic evidence for the presence of the cysteine tryptophylquinone cofactor in L-lysine epsilon-oxidase from *Marinomonas mediterranea*, *J. Biochem. (Tokyo) 154*, 233–236.
2355. Kumar, V., Dooley, D. M., Freeman, H. C., Guss, J. M., Harvey, I., McGuirl, M. A., Wilce, M. C., and Zubak, V. M. (1996) Crystal structure of a eukaryotic (pea seedling) copper-containing amine oxidase at 2.2 Å resolution, *Structure 4*, 943–955.
2356. Li, R., Klinman, J. P., and Mathews, F. S. (1998) Copper amine oxidase from *Hansenula polymorpha*: The crystal structure determined at 2.4 Å resolution reveals the active conformation, *Structure 6*, 293–307.
2357. Parsons, M. R., Convery, M. A., Wilmot, C. M., Yadav, K. D., Blakeley, V., Corner, A. S., Phillips, S. E., McPherson, M. J., and Knowles, P. F. (1995) Crystal structure of a quinoenzyme: Copper amine oxidase of *Escherichia coli* at 2 Å resolution, *Structure 3*, 1171–1184.
2358. Duff, A. P., Cohen, A. E., Ellis, P. J., Kuchar, J. A., Langley, D. B., Shepard, E. M., Dooley, D. M., Freeman, H. C., and Guss, J. M. (2003) The crystal structure of *Pichia pastoris* lysyl oxidase, *Biochemistry 42*, 15148–15157.
2359. Chen, Z., Schwartz, B., Williams, N. K., Li, R., Klinman, J. P., and Mathews, F. S. (2000) Crystal structure at 2.5 Å resolution of zinc-substituted copper amine oxidase of *Hansenula polymorpha* expressed in *Escherichia coli*, *Biochemistry 39*, 9709–9717.
2360. Lunelli, M., Di Paolo, M. L., Biadene, M., Calderone, V., Battistutta, R., Scarpa, M., Rigo, A., and Zanotti, G. (2005) Crystal structure of amine oxidase from bovine serum, *J. Mol. Biol. 346*, 991–1004.
2361. Chiu, Y. C., Okajima, T., Murakawa, T., Uchida, M., Taki, M., Hirota, S., Kim, M., Yamaguchi, H., Kawano, Y., Kamiya, N., Kuroda, S., Hayashi, H., Yamamoto, Y., and Tanizawa, K. (2006) Kinetic and structural studies on the catalytic role of the aspartic acid residue conserved in copper amine oxidase, *Biochemistry 45*, 4105–4120.
2362. Mure, M., Mills, S. A., and Klinman, J. P. (2002) Catalytic mechanism of the TOPA quinone containing copper amine oxidases, *Biochemistry 41*, 9269–9278.
2363. Hartmann, C., Brzovic, P., and Klinman, J. P. (1993) Spectroscopic detection of chemical intermediates in the reaction of *para*-substituted benzylamines with bovine serum amine oxidase, *Biochemistry 32*, 2234–2241.
2364. Nakamura, N., Moenne-Loccoz, P., Tanizawa, K., Mure, M., Suzuki, S., Klinman, J. P., and Sanders-Loehr, J. (1997) Topaquinone-dependent amine oxidases: Identification of

reaction intermediates by Raman spectroscopy, *Biochemistry 36*, 11479–11486.
2365. Wilmot, C. M., Murray, J. M., Alton, G., Parsons, M. R., Convery, M. A., Blakeley, V., Corner, A. S., Palcic, M. M., Knowles, P. F., McPherson, M. J., and Phillips, S. E. (1997) Catalytic mechanism of the quinoenzyme amine oxidase from *Escherichia coli*: Exploring the reductive half-reaction, *Biochemistry 36*, 1608–1620.
2366. Hartmann, C., and Klinman, J. P. (1987) Reductive trapping of substrate to bovine plasma amine oxidase, *J. Biol. Chem. 262*, 962–965.
2367. Hartmann, C., and Klinman, J. P. (1991) Structure-function studies of substrate oxidation by bovine serum amine oxidase: Relationship to cofactor structure and mechanism, *Biochemistry 30*, 4605–4611.
2368. Kyte, J. (2007) *Structure in protein chemistry:Second edition*, p 75, Garland Science, New York.
2369. Taki, M., Murakawa, T., Nakamoto, T., Uchida, M., Hayashi, H., Tanizawa, K., Yamamoto, Y., and Okajima, T. (2008) Further insight into the mechanism of stereoselective proton abstraction by bacterial copper amine oxidase, *Biochemistry 47*, 7726–7733.
2370. Murray, J. M., Saysell, C. G., Wilmot, C. M., Tambyrajah, W. S., Jaeger, J., Knowles, P. F., Phillips, S. E., and McPherson, M. J. (1999) The active site base controls cofactor reactivity in *Escherichia coli* amine oxidase: X-Ray crystallographic studies with mutational variants, *Biochemistry 38*, 8217–8227.
2371. Mure, M., and Klinman, J. P. (1995) Model studies of topaquinone-dependent amine oxidases. 1. Oxidation of benzylamine by topaquinone analogs, *J. Am. Chem. Soc. 117*, 8698–8706.
2372. Lee, Y., and Sayre, L. M. (1995) Model reactions for the quinone-containing copper amine oxidases. Anaerobic reaction pathways and catalytic aerobic deamination of activated amines in buffered aqueous acetonitrile, *J. Am. Chem. Soc. 117*, 3096–3105.
2373. Mure, M., and Klinman, J. P. (1995) Model studies of topaquinone-dependent amine oxidases. 2. Characterization of reaction intermediates and mechanism, *J. Am. Chem. Soc. 117*, 8707–8718.
2374. Lee, Y., and Sayre, L. M. (1995) Model studies on the quinone-containing copper amine oxidases. Unambiguous demonstration of a transamination mechanism, *J. Am. Chem. Soc. 117*, 11823–11828.
2375. Shah, M. A., Scaman, C. H., Palcic, M. M., and Kagan, H. M. (1993) Kinetics and stereospecificity of the lysyl oxidase reaction, *J. Biol. Chem. 268*, 11573–11579.
2376. Welford, R. W., Lam, A., Mirica, L. M., and Klinman, J. P. (2007) Partial conversion of *Hansenula polymorpha* amine oxidase into a "plant" amine oxidase: Implications for copper chemistry and mechanism, *Biochemistry 46*, 10817–10827.
2377. Medda, R., Padiglia, A., Pedersen, J. Z., Rotilio, G., Finazzi Agro, A., and Floris, G. (1995) The reaction mechanism of copper amine oxidase: Detection of intermediates by the use of substrates and inhibitors, *Biochemistry 34*, 16375–16381.
2378. Dooley, D. M., McGuirl, M. A., Brown, D. E., Turowski, P. N., McIntire, W. S., and Knowles, P. F. (1991) A Cu(I)-semiquinone state in substrate-reduced amine oxidases, *Nature 349*, 262–264.
2379. Warncke, K., Babcock, G. T., Dooley, D. M., McGuirl, M. A., and McCracken, J. (1994) Structure of the TOPA-semiquinone catalytic intermediate of amine oxidase as revealed by magnetic interactions with exchangeable ^{2}H and ^{1}H nuclei, *J. Am. Chem. Soc. 116*, 4028–4037.
2380. Pedersen, J. Z., el-Sherbini, S., Finazzi-Agro, A., and Rotilio, G. (1992) A substrate-cofactor free radical intermediate in the reaction mechanism of copper amine oxidase, *Biochemistry 31*, 8–12.
2381. Turowski, P. N., McGuirl, M. A., and Dooley, D. M. (1993) Intramolecular electron transfer rate between active-site copper and TOPA quinone in pea seedling amine oxidase, *J. Biol. Chem. 268*, 17680–17682.
2382. Johnson, B. J., Yukl, E. T., Klema, V. J., Klinman, J. P., and Wilmot, C. M. (2013) Structural snapshots from the oxidative half-reaction of a copper amine oxidase: Implications for O_2 activation, *J. Biol. Chem. 288*, 28409–28417.
2383. Mure, M., and Klinman, J. P. (1993) Synthesis and spectroscopic characterization of model compounds for the active site cofactor in copper amine oxidases, *J. Am. Chem. Soc. 115*, 7117–7127.
2384. Hirota, S., Iwamoto, T., Tanizawa, K., Adachi, O., and Yamauchi, O. (1999) Spectroscopic

characterization of carbon monoxide complexes generated for copper/TOPA quinone-containing amine oxidases, *Biochemistry 38*, 14256–14263.
2385. Wilmot, C. M., Hajdu, J., McPherson, M. J., Knowles, P. F., and Phillips, S. E. (1999) Visualization of dioxygen bound to copper during enzyme catalysis, *Science 286*, 1724–1728.
2386. Mukherjee, A., Smirnov, V. V., Lanci, M. P., Brown, D. E., Shepard, E. M., Dooley, D. M., and Roth, J. P. (2008) Inner-sphere mechanism for molecular oxygen reduction catalyzed by copper amine oxidases, *J. Am. Chem. Soc. 130*, 9459–9473.
2387. Mills, S. A., and Klinman, J. P. (2000) Evidence against reduction of Cu^{2+} to Cu^{+} during dioxygen activation in a copper amine oxidase from yeast, *J. Am. Chem. Soc. 122*, 9897–9904.
2388. Kishishita, S., Okajima, T., Kim, M., Yamaguchi, H., Hirota, S., Suzuki, S., Kuroda, S., Tanizawa, K., and Mure, M. (2003) Role of copper ion in bacterial copper amine oxidase: Spectroscopic and crystallographic studies of metal-substituted enzymes, *J. Am. Chem. Soc. 125*, 1041–1055.
2389. Mills, S. A., Goto, Y., Su, Q., Plastino, J., and Klinman, J. P. (2002) Mechanistic comparison of the cobalt-substituted and wild-type copper amine oxidase from *Hansenula polymorpha*, *Biochemistry 41*, 10577–10584.
2390. Brooks, H. B., Jones, L. H., and Davidson, V. L. (1993) Deuterium kinetic isotope effect and stopped-flow kinetic studies of the quinoprotein methylamine dehydrogenase, *Biochemistry 32*, 2725–2729.
2391. Andreo-Vidal, A., Mamounis, K. J., Sehanobish, E., Avalos, D., Campillo-Brocal, J. C., Sanchez-Amat, A., Yukl, E. T., and Davidson, V. L. (2018) Structure and enzymatic properties of an unusual cysteine tryptophylquinone-dependent glycine oxidase from *Pseudoalteromonas luteoviolacea*, *Biochemistry 57*, 1155–1165.
2392. Avalos, D., Sabuncu, S., Mamounis, K. J., Davidson, V. L., Moenne-Loccoz, P., and Yukl, E. T. (2019) Structural and spectroscopic characterization of a product Schiff base intermediate in the reaction of the quinoprotein glycine oxidase, GoxA, *Biochemistry 58*, 706–713.
2393. Mamounis, K. J., Avalos, D., Yukl, E. T., and Davidson, V. L. (2019) Kinetic and structural evidence that Asp-678 plays multiple roles in catalysis by the quinoprotein glycine oxidase, *J. Biol. Chem. 294*, 17463–17470.
2394. Chen, L., Doi, M., Durley, R. C., Chistoserdov, A. Y., Lidstrom, M. E., Davidson, V. L., and Mathews, F. S. (1998) Refined crystal structure of methylamine dehydrogenase from *Paracoccus denitrificans* at 1.75 Å resolution, *J. Mol. Biol. 276*, 131–149.
2395. Hyun, Y. L., and Davidson, V. L. (1995) Mechanistic studies of aromatic amine dehydrogenase, a tryptophan tryptophylquinone enzyme, *Biochemistry 34*, 816–823.
2396. Bishop, G. R., Valente, E. J., Whitehead, T. L., Brown, K. L., Hicks, R. P., and Davidson, V. L. (1996) Direct detection by ^{15}N NMR of the tryptophan tryptophylquinone aminoquinol reaction intermediate of methylamine dehydrogenase, *J. Am. Chem. Soc. 118*, 12868–12869.
2397. Mamounis, K. J., Yukl, E. T., and Davidson, V. L. (2020) Roles of active-site residues in catalysis, substrate binding, cooperativity, and the reaction mechanism of the quinoprotein glycine oxidase, *J. Biol. Chem. 295*, 6472–6481.
2398. Hyun, Y. L., and Davidson, V. L. (1995) Electron transfer reactions between aromatic amine dehydrogenase and azurin, *Biochemistry 34*, 12249–12254.
2399. Bishop, G. R., and Davidson, V. L. (1998) Electron transfer from the aminosemiquinone reaction intermediate of methylamine dehydrogenase to amicyanin, *Biochemistry 37*, 11026–11032.
2400. Singh, V., Zhu, Z., Davidson, V. L., and McCracken, J. (2000) Characterization of the tryptophan tryptophyl-semiquinone catalytic intermediate of methylamine dehydrogenase by electron spin-echo envelope modulation spectroscopy, *J. Am. Chem. Soc. 122*, 931–938.
2401. Warncke, K., Brooks, H. B., Babcock, G. T., Davidson, V. L., and McCracken, J. (1993) The nitrogen atom of substrate methylamine is incorporated into the tryptophan tryptophyl-semiquinone catalytic intermediate in methylamine dehydrogenase, *J. Am. Chem. Soc. 115*, 6464–6465.
2402. Ma, Z., and Davidson, V. L. (2019) The redox properties of a cysteine tryptophylquinone-dependent glycine oxidase are distinct from

those of tryptophylquinone-dependent dehydrogenases, *Biochemistry 58*, 2243–2249.
2403. Itoh, S., Ogino, M., Fukui, Y., Murao, H., Komatsu, M., Ohshiro, Y., Inoue, T., Kai, Y., and Kasai, N. (1993) C-4 and C-5 Adducts of cofactor PQQ (pyrroloquinolinequinone). Model studies directed toward the action of quinoprotein methanol dehydrogenase, *J. Am. Chem. Soc. 115*, 9960–9967.
2404. Dekker, R. H., Duine, J. A., Frank, J., Verwiel, P. E., and Westerling, J. (1982) Covalent addition of H_2O, enzyme substrates and activators to pyrrolo-quinoline quinone, the coenzyme of quinoproteins, *Eur. J. Biochem. 125*, 69–73.
2405. Frank, J., Jr., van Krimpen, S. H., Verwiel, P. E., Jongejan, J. A., Mulder, A. C., and Duine, J. A. (1989) On the mechanism of inhibition of methanol dehydrogenase by cyclopropane-derived inhibitors, *Eur. J. Biochem. 184*, 187–195.
2406. Oubrie, A., Rozeboom, H. J., Kalk, K. H., Olsthoorn, A. J., Duine, J. A., and Dijkstra, B. W. (1999) Structure and mechanism of soluble quinoprotein glucose dehydrogenase, *EMBO J. 18*, 5187–5194.
2407. Afolabi, P. R., Mohammed, F., Amaratunga, K., Majekodunmi, O., Dales, S. L., Gill, R., Thompson, D., Cooper, J. B., Wood, S. P., Goodwin, P. M., and Anthony, C. (2001) Site-directed mutagenesis and X-ray crystallography of the PQQ-containing quinoprotein methanol dehydrogenase and its electron acceptor, cytochrome c_1, *Biochemistry 40*, 9799–9809.
2408. Itoh, S., Kawakami, H., and Fukuzumi, S. (1997) Modeling of the chemistry of quinoprotein methanol dehydrogenase. Oxidation of methanol by calcium complex of coenzyme PQQ via addition-elimination mechanism, *J. Am. Chem. Soc. 119*, 439–440.
2409. Ghosh, M., Anthony, C., Harlos, K., Goodwin, M. G., and Blake, C. (1995) The refined structure of the quinoprotein methanol dehydrogenase from *Methylobacterium extorquens* at 1.94 Å, *Structure 3*, 177–187.
2410. Chan, S. I., Chuankhayan, P., Reddy Nareddy, P. K., Tsai, I. K., Tsai, Y. F., Chen, K. H., Yu, S. S., and Chen, C. J. (2021) Mechanism of pyrroloquinoline quinone-dependent hydride transfer chemistry from spectroscopic and high-resolution X-ray structural studies of the methanol dehydrogenase from *Methylococcus capsulatus* (Bath), *J. Am. Chem. Soc. 143*, 3359–3372.
2411. Kano, K., Mori, K., Uno, B., Kubota, T., Ikeda, T., and Senda, M. (1990) Voltammetric determination of acid dissociation constants of pyrroloquinoline quinone and its reduced form under acidic conditions, *Bioelectrochem. and Bioenerg. 24*, 193–201.
2412. Grau, U. M., Trommer, W. E., and Rossmann, M. G. (1981) Structure of the active ternary complex of pig heart lactate dehydrogenase with *S*-lac-NAD at 2.7 Å resolution, *J. Mol. Biol. 151*, 289–307.
2413. Itoh, S., Kawakami, H., and Fukuzumi, S. (1998) Electrochemical behavior and characterization of semiquinone radical anion species of coenzyme PQQ in aprotic organic media, *J. Am. Chem. Soc. 120*, 7271–7277.
2414. Rodriguez, E. J., Bruice, T. C., and Edmondson, D. E. (1987) Studies on the radical species of 9-decarboxymethoxatin, *J. Am. Chem. Soc. 109*, 532–537.
2415. Williams, P., Coates, L., Mohammed, F., Gill, R., Erskine, P., Bourgeois, D., Wood, S. P., Anthony, C., and Cooper, J. B. (2006) The 1.6Å X-ray structure of the unusual *c*-type cytochrome, cytochrome c_1, from the methylotrophic bacterium *Methylobacterium extorquens*, *J. Mol. Biol. 357*, 151–162.
2416. Zinoni, F., Birkmann, A., Stadtman, T. C., and Bock, A. (1986) Nucleotide sequence and expression of the selenocysteine-containing polypeptide of formate dehydrogenase (formate-hydrogen-lyase-linked) from *Escherichia coli*, *Proc. Natl. Acad. Sci. U. S. A. 83*, 4650–4654.
2417. Dobbek, H., Gremer, L., Meyer, O., and Huber, R. (1999) Crystal structure and mechanism of CO dehydrogenase, a molybdo iron–sulfur flavoprotein containing *S*-selanylcysteine, *Proc. Natl. Acad. Sci. U.S.A. 96*, 8884–8889.
2418. Axley, M. J., Grahame, D. A., and Stadtman, T. C. (1990) *Escherichia coli* formate-hydrogen lyase. Purification and properties of the selenium-dependent formate dehydrogenase component, *J. Biol. Chem. 265*, 18213–18218.
2419. Boyington, J. C., Gladyshev, V. N., Khangulov, S. V., Stadtman, T. C., and Sun, P. D. (1997) Crystal structure of formate dehydrogenase H: Catalysis involving Mo, Molyb-

dopterin, selenocysteine, and an Fe_4S_4 cluster, *Science 275*, 1305–1308.
2420. Wagener, N., Pierik, A. J., Ibdah, A., Hille, R., and Dobbek, H. (2009) The Mo–Se active site of nicotinate dehydrogenase, *Proc. Natl. Acad. Sci. U.S.A. 106*, 11055–11060.
2421. Marques, M. C., Coelho, R., De Lacey, A. L., Pereira, I. A., and Matias, P. M. (2010) The three-dimensional structure of [NiFeSe] hydrogenase from *Desulfovibrio vulgaris hildenborough*: A hydrogenase without a bridging ligand in the active site in its oxidised, "as-isolated" state, *J. Mol. Biol. 396*, 893–907.
2422. Marques, M. C., Coelho, R., Pereira, I. A. C., and Matias, P. M. (2013) Redox state-dependent changes in the crystal structure of [NiFeSe] hydrogenase from *Desulfovibrio vulgaris* hildenborough, *Int. J Hydrogen Energ. 38*, 8664–8682.
2423. Yamamoto, I., Saiki, T., Liu, S. M., and Ljungdahl, L. G. (1983) Purification and properties of NADP-dependent formate dehydrogenase from *Clostridium thermoaceticum*, a tungsten–selenium–iron protein, *J. Biol. Chem. 258*, 1826–1832.
2424. Raaijmakers, H., Macieira, S., Dias, J. M., Teixeira, S., Bursakov, S., Huber, R., Moura, J. J., Moura, I., and Romao, M. J. (2002) Gene sequence and the 1.8 Å crystal structure of the tungsten-containing formate dehydrogenase from *Desulfovibrio gigas*, *Structure 10*, 1261–1272.
2425. Cone, J. E., del Rio, R. M., and Stadtman, T. C. (1977) Clostridial glycine reductase complex. Purification and characterization of the selenoprotein component, *J. Biol. Chem. 252*, 5337–5344.
2426. Zakowski, J. J., Forstrom, J. W., Condell, R. A., and Tappel, A. L. (1978) Attachment of selenocysteine in the catalytic site of glutathione peroxidase, *Biochem. Biophys. Res. Commun. 84*, 248–253.
2427. Jones, J. B., Dilworth, G. L., and Stadtman, T. C. (1979) Occurrence of selenocysteine in the selenium-dependent formate dehydrogenase of *Methanococcus vannielii*, *Arch. Biochem. Biophys. 195*, 255–260.
2428. Reich, H. J. (1979) Functional group manipulation using organoselenium reagents, *Acc. Chem. Res. 12*, 22–30.
2429. Arnold, A. P., Tan, K. S., and Rabenstein, D. L. (1986) Nuclear-magnetic-resonance studies of the solution chemistry of metal-complexes: 23. Complexation of methylmercury by selenohydryl-containing amino-acids and related molecules, *Inorg. Chem. 25*, 2433–2437.
2430. Pleasants, J. C., Guo, W., and Rabenstein, D. L. (1989) A comparative study of the kinetics of selenol/diselenide and thiol/disulfide exchange reactions, *J. Am. Chem. Soc. 111*, 6553–6558.
2431. Muller, S., Senn, H., Gsell, B., Vetter, W., Baron, C., and Bock, A. (1994) The formation of diselenide bridges in proteins by incorporation of selenocysteine residues: Biosynthesis and characterization of $(Se)_2$-thioredoxin, *Biochemistry 33*, 3404–3412.
2432. Metanis, N., Keinan, E., and Dawson, P. E. (2006) Synthetic seleno-glutaredoxin 3 analogues are highly reducing oxidoreductases with enhanced catalytic efficiency, *J. Am. Chem. Soc. 128*, 16684–16691.
2433. Snider, G. W., Ruggles, E., Khan, N., and Hondal, R. J. (2013) Selenocysteine confers resistance to inactivation by oxidation in thioredoxin reductase: Comparison of selenium and sulfur enzymes, *Biochemistry 52*, 5472–5481.
2434. Ste Marie, E. J., Wehrle, R. J., Haupt, D. J., Wood, N. B., van der Vliet, A., Previs, M. J., Masterson, D. S., and Hondal, R. J. (2020) Can selenoenzymes resist electrophilic modification? Evidence from thioredoxin reductase and a mutant containing α-methylselenocysteine, *Biochemistry 59*, 3300–3315.
2435. Arner, E. S. (2010) Selenoproteins–What unique properties can arise with selenocysteine in place of cysteine?, *Exp. Cell Res. 316*, 1296–1303.
2436. Aslund, F., Berndt, K. D., and Holmgren, A. (1997) Redox potentials of glutaredoxins and other thiol-disulfide oxidoreductases of the thioredoxin superfamily determined by direct protein-protein redox equilibria, *J. Biol. Chem. 272*, 30780–30786.
2437. Kanzok, S. M., Fechner, A., Bauer, H., Ulschmid, J. K., Muller, H. M., Botella-Munoz, J., Schneuwly, S., Schirmer, R., and Becker, K. (2001) Substitution of the thioredoxin system for glutathione reductase in *Drosophila melanogaster*, *Science 291*, 643–646.
2438. Gromer, S., Johansson, L., Bauer, H., Arscott, L. D., Rauch, S., Ballou, D. P., Williams, C. H.,

Jr., Schirmer, R. H., and Arner, E. S. (2003) Active sites of thioredoxin reductases: Why selenoproteins?, *Proc. Natl. Acad. Sci. U.S.A. 100*, 12618–12623.

2439. Lothrop, A. P., Snider, G. W., Flemer, S., Jr., Ruggles, E. L., Davidson, R. S., Lamb, A. L., and Hondal, R. J. (2014) Compensating for the absence of selenocysteine in high-molecular weight thioredoxin reductases: The electrophilic activation hypothesis, *Biochemistry 53*, 664–674.
2440. O'Keefe, J. P., Dustin, C. M., Barber, D., Snider, G. W., and Hondal, R. J. (2018) A "seleno effect" differentiates the roles of redox active cysteine residues in *Plasmodium falciparum* thioredoxin reductase, *Biochemistry 57*, 1767–1778.
2441. Gladyshev, V. N., Khangulov, S. V., Axley, M. J., and Stadtman, T. C. (1994) Coordination of selenium to molybdenum in formate dehydrogenase H from *Escherichia coli*, *Proc. Natl. Acad. Sci. U. S. A. 91*, 7708–7711.
2442. Khangulov, S. V., Gladyshev, V. N., Dismukes, G. C., and Stadtman, T. C. (1998) Selenium-containing formate dehydrogenase h from *Escherichia coli*: A molybdopterin enzyme that catalyzes formate oxidation without oxygen transfer, *Biochemistry 37*, 3518–3528.
2443. Jormakka, M., Tornroth, S., Byrne, B., and Iwata, S. (2002) Molecular basis of proton motive force generation: Structure of formate dehydrogenase-N, *Science 295*, 1863–1868.
2444. Gladyshev, V. N., Jeang, K. T., and Stadtman, T. C. (1996) Selenocysteine, identified as the penultimate C-terminal residue in human T-cell thioredoxin reductase, corresponds to TGA in the human placental gene, *Proc. Natl. Acad. Sci. U. S. A. 93*, 6146–6151.
2445. Zhong, L., and Holmgren, A. (2000) Essential role of selenium in the catalytic activities of mammalian thioredoxin reductase revealed by characterization of recombinant enzymes with selenocysteine mutations, *J. Biol. Chem. 275*, 18121–18128.
2446. Zhong, L., Arner, E. S., and Holmgren, A. (2000) Structure and mechanism of mammalian thioredoxin reductase: The active site is a redox-active selenolthiol/selenenylsulfide formed from the conserved cysteine-selenocysteine sequence, *Proc. Natl. Acad. Sci. U. S. A. 97*, 5854–5859.
2447. Fritz-Wolf, K., Urig, S., and Becker, K. (2007) The structure of human thioredoxin reductase 1 provides insights into C-terminal rearrangements during catalysis, *J. Mol. Biol. 370*, 116–127.
2448. Lee, S. R., Bar-Noy, S., Kwon, J., Levine, R. L., Stadtman, T. C., and Rhee, S. G. (2000) Mammalian thioredoxin reductase: Oxidation of the C-terminal cysteine/selenocysteine active site forms a thioselenide, and replacement of selenium with sulfur markedly reduces catalytic activity, *Proc. Natl. Acad. Sci. U. S. A. 97*, 2521–2526.
2449. Biterova, E. I., Turanov, A. A., Gladyshev, V. N., and Barycki, J. J. (2005) Crystal structures of oxidized and reduced mitochondrial thioredoxin reductase provide molecular details of the reaction mechanism, *Proc. Natl. Acad. Sci. U. S. A. 102*, 15018–15023.
2450. Brandes, H. K., Larimer, F. W., Geck, M. K., Stringer, C. D., Schurmann, P., and Hartman, F. C. (1993) Direct identification of the primary nucleophile of thioredoxin f, *J. Biol. Chem. 268*, 18411–18414.
2451. Fritz-Wolf, K., Kehr, S., Stumpf, M., Rahlfs, S., and Becker, K. (2011) Crystal structure of the human thioredoxin reductase-thioredoxin complex, *Nat Commun 2*, 383.
2452. Lothrop, A. P., Snider, G. W., Ruggles, E. L., Patel, A. S., Lees, W. J., and Hondal, R. J. (2014) Selenium as an electron acceptor during the catalytic mechanism of thioredoxin reductase, *Biochemistry 53*, 654–663.
2453. Manta, B., Hugo, M., Ortiz, C., Ferrer-Sueta, G., Trujillo, M., and Denicola, A. (2009) The peroxidase and peroxynitrite reductase activity of human erythrocyte peroxiredoxin 2, *Arch. Biochem. Biophys. 484*, 146–154.
2454. Choi, H. J., Kang, S. W., Yang, C. H., Rhee, S. G., and Ryu, S. E. (1998) Crystal structure of a novel human peroxidase enzyme at 2.0 Å resolution, *Nature Struct. Biol. 5*, 400–406.
2455. Declercq, J. P., Evrard, C., Clippe, A., Stricht, D. V., Bernard, A., and Knoops, B. (2001) Crystal structure of human peroxiredoxin 5, a novel type of mammalian peroxiredoxin at 1.5 Å resolution, *J. Mol. Biol. 311*, 751–759.
2456. Flohe, L., Loschen, G., Gunzler, W. A., and Eichele, E. (1972) Glutathione peroxidase: V. The kinetic mechanism, *Hoppe Seylers Z. Physiol. Chem. 353*, 987–999.
2457. Wendel, A., Pilz, W., Ladenstein, R., Sawatzki, G., and Weser, U. (1975) Substrate-induced

redox change of selenium in glutathione peroxidase studied by X-ray photoelectron spectroscopy, *Biochim. Biophys. Acta 377*, 211–215.
2458. Ladenstein, R., and Wendel, A. (1976) Crystallographic data of the selenoenzyme glutathione peroxidase, *J. Mol. Biol. 104*, 877–882.
2459. Ladenstein, R., Epp, O., Bartels, K., Jones, A., Huber, R., and Wendel, A. (1979) Structure analysis and molecular model of the selenoenzyme glutathione peroxidase at 2.8 Å resolution, *J. Mol. Biol. 134*, 199–218.
2460. Ren, B., Huang, W., Akesson, B., and Ladenstein, R. (1997) The crystal structure of seleno-glutathione peroxidase from human plasma at 2.9 Å resolution, *J. Mol. Biol. 268*, 869–885.
2461. Liu, J., and Rozovsky, S. (2013) Contribution of selenocysteine to the peroxidase activity of selenoprotein S, *Biochemistry 52*, 5514–5516.
2462. Crane, E. J., 3rd, Vervoort, J., and Claiborne, A. (1997) ^{13}C NMR Analysis of the cysteine-sulfenic acid redox center of enterococcal NADH peroxidase, *Biochemistry 36*, 8611–8618.
2463. Back, T. G., and Dyck, B. P. (1997) A novel camphor-derived selenenamide that acts as a glutathione peroxidase mimetic, *J. Am. Chem. Soc. 119*, 2079–2083.
2464. Wu, Z. P., and Hilvert, D. (1990) Selenosubtilisin as a glutathione peroxidase mimic, *J. Am. Chem. Soc. 112*, 5647–5648.
2465. Bell, I. M., and Hilvert, D. (1993) Peroxide dependence of the semisynthetic enzyme selenosubtilisin, *Biochemistry 32*, 13969–13973.
2466. Tanaka, H., and Stadtman, T. C. (1979) Selenium-dependent clostridial glycine reductase. Purification and characterization of the two membrane-associated protein components, *J. Biol. Chem. 254*, 447–452.
2467. Arkowitz, R. A., and Abeles, R. H. (1991) Mechanism of action of clostridial glycine reductase: Isolation and characterization of a covalent acetyl enzyme intermediate, *Biochemistry 30*, 4090–4097.
2468. Bednarski, B., Andreesen, J. R., and Pich, A. (2001) In vitro processing of the proproteins GrdE of protein B of glycine reductase and PrdA of D-proline reductase from *Clostridium sticklandii*: Formation of a pyruvoyl group from a cysteine residue, *Eur. J. Biochem. 268*, 3538–3544.
2469. Stadtman, T. C. (1989) Clostridial glycine reductase: Protein C, the acetyl group acceptor, catalyzes the arsenate-dependent dedecomposition of acetyl phosphate, *Proc. Natl. Acad. Sci. U. S. A. 86*, 7853–7856.
2470. Arkowitz, R. A., and Abeles, R. H. (1990) Isolation and characterization of a covalent selenocysteine intermediate in the glycine reductase system, *J. Am. Chem. Soc. 112*, 870–872.
2471. Stadtman, T. C., and Davis, J. N. (1991) Glycine reductase protein C. Properties and characterization of its role in the reductive cleavage of Se-carboxymethyl-selenoprotein A, *J. Biol. Chem. 266*, 22147–22153.
2472. Lenhert, P. G. (1968) Structure of vitamin B12. VII. X-Ray analysis of the vitamin B_{12} coenzyme, *Proc. R. Soc. London A 303*, 45–84.
2473. Rubinson, K. A., Parekh, H. V., Itabashi, E., and Mark, H. B., Jr. (1983) The chemistry of [Co]cobalamins: Equilibrium constants and energies of formation of species in aqueous solution, *Inorg. Chem. 22*, 458–463.
2474. Lexa, D., and Saveant, J. M. (1983) The electrochemistry of vitamin-B_{12}, *Accounts Chem. Res. 16*, 235–243.
2475. Shey, J., and van der Donk, W. A. (2000) Mechanistic studies on the vitamin B_{12}-catalyzed dechlorination of chlorinated alkenes, *J. Am. Chem. Soc. 122*, 12403–12404.
2476. Sauer, K., Harms, U., and Thauer, R. K. (1997) Methanol:Coenzyme M methyltransferase from *Methanosarcina barkeri*. Purification, properties and encoding genes of the corrinoid protein MT1, *Eur. J. Biochem. 243*, 670–677.
2477. Shibata, N., Masuda, J., Tobimatsu, T., Toraya, T., Suto, Morimoto, Y., and Yasuoka, N. (1999) A new mode of B_{12} binding and the direct participation of a potassium ion in enzyme catalysis: X-Ray structure of diol dehydratase, *Structure 7*, 997–1008.
2478. Yamanishi, M., Yamada, S., Muguruma, H., Murakami, Y., Tobimatsu, T., Ishida, A., Yamauchi, J., and Toraya, T. (1998) Evidence for axial coordination of 5,6-dimethyl-benzimidazole to the cobalt atom of adenosylcobalamin bound to diol dehydratase, *Biochemistry 37*, 4799–4803.
2479. Gruber, K., Reitzer, R., and Kratky, C. (2001) Radical shuttling in a protein: Ribose pseudorotation controls alkyl-radical transfer in the coenzyme B_{12} dependent enzyme gluta-

mate mutase, *Angew. Chem., Int. Ed. Engl. 40*, 3377–3380.
2480. Drennan, C. L., Huang, S., Drummond, J. T., Matthews, R. G., and Ludwig, M. L. (1994) How a protein binds B_{12}: A 3.0 Å X-Ray structure of B_{12}-binding domains of methionine synthase, *Science 266*, 1669–1674.
2481. Padmakumar, R., Taoka, S., Padmakumar, R., and Banerjee, R. (1995) Coenzyme B_{12} is coordinated by histidine and not dimethylbenzimidazole on methylmalonyl-CoA mutase, *J. Am. Chem. Soc. 117*, 7033–7034.
2482. Mancia, F., Keep, N. H., Nakagawa, A., Leadlay, P. F., McSweeney, S., Rasmussen, B., Bosecke, P., Diat, O., and Evans, P. R. (1996) How coenzyme B_{12} radicals are generated: The crystal structure of methylmalonyl-coenzyme A mutase at 2 Å resolution, *Structure 4*, 339–350.
2483. Reitzer, R., Gruber, K., Jogl, G., Wagner, U. G., Bothe, H., Buckel, W., and Kratky, C. (1999) Glutamate mutase from *Clostridium cochlearium*: The structure of a coenzyme B_{12}-dependent enzyme provides new mechanistic insights, *Structure 7*, 891–902.
2484. Berkovitch, F., Behshad, E., Tang, K. H., Enns, E. A., Frey, P. A., and Drennan, C. L. (2004) A locking mechanism preventing radical damage in the absence of substrate, as revealed by the X-ray structure of lysine 5,6-aminomutase, *Proc. Natl. Acad. Sci. U. S. A. 101*, 15870–15875.
2485. Hagemeier, C. H., Kruer, M., Thauer, R. K., Warkentin, E., and Ermler, U. (2006) Insight into the mechanism of biological methanol activation based on the crystal structure of the methanol-cobalamin methyltransferase complex, *Proc. Natl. Acad. Sci. U. S. A. 103*, 18917–18922.
2486. Svetlitchnaia, T., Svetlitchnyi, V., Meyer, O., and Dobbek, H. (2006) Structural insights into methyltransfer reactions of a corrinoid iron–sulfur protein involved in acetyl-CoA synthesis, *Proc. Natl. Acad. Sci. U. S. A. 103*, 14331–14336.
2487. Chen, H.-P., and Marsh, E. N. G. (1997) How enzymes control the reactivity of adenosylcobalamin: Effect on coenzyme binding and catalysis of mutations in the conserved histidine-aspartate pair of glutamate mutase, *Biochemistry 36*, 7884–7889.
2488. Datta, S., Koutmos, M., Pattridge, K. A., Ludwig, M. L., and Matthews, R. G. (2008) A disulfide-stabilized conformer of methionine synthase reveals an unexpected role for the histidine ligand of the cobalamin cofactor, *Proc. Natl. Acad. Sci. U.S.A. 105*, 4115–4120.
2489. Pauling, L. (1960) *The Nature of the Chemical Bond, Third Edition*, Cornell University Press, Ithaca, N. Y.
2490. Hogenkamp, H. P., Bratt, G. T., and Kotchevar, A. T. (1987) Reaction of alkylcobalamins with thiols, *Biochemistry 26*, 4723–4727.
2491. Koutmos, M., Pejchal, R., Bomer, T. M., Matthews, R. G., Smith, J. L., and Ludwig, M. L. (2008) Metal active site elasticity linked to activation of homocysteine in methionine synthases, *Proc. Natl. Acad. Sci. U.S.A. 105*, 3286–3291.
2492. Payne, K. A., Quezada, C. P., Fisher, K., Dunstan, M. S., Collins, F. A., Sjuts, H., Levy, C., Hay, S., Rigby, S. E., and Leys, D. (2015) Reductive dehalogenase structure suggests a mechanism for B_{12}-dependent dehalogenation, *Nature 517*, 513–516.
2493. Johnson, A. W., Mervyn, L., Shaw, N., and Smith, E. L. (1963) A partial synthesis of the vitamin B_{12} coenzyme and some of its analogs, *J. Chem.Soc.*, 4146–4156.
2494. Grate, J. H., and Schrauzer, G. N. (1979) Chemistry of cobalamins and related compounds. 48. Sterically induced, spontaneous dealkylation of secondary alkylcobalamins due to axial base coordination and conformational changes of the corrin ligand, *J. Am. Chem. Soc. 101*, 4601–4611.
2495. Frasca, V., Banerjee, R. V., Dunham, W. R., Sands, R. H., and Matthews, R. G. (1988) Cobalamin-dependent methionine synthase from *Escherichia coli* B: Electron paramagnetic resonance spectra of the inactive form and the active methylated form of the enzyme, *Biochemistry 27*, 8458–8465.
2496. Zhao, S., Roberts, D. L., and Ragsdale, S. W. (1995) Mechanistic studies of the methyltransferase from *Clostridium thermoaceticum*: Origin of the pH dependence of the methyl group transfer from methyltetrahydrofolate to the corrinoid/iron–sulfur protein, *Biochemistry 34*, 15075–15083.
2497. Grahame, D. A. (1993) Substrate and cofactor reactivity of a carbon monoxide dehydrogenase-corrinoid enzyme complex: Stepwise reduction of iron–sulfur and corrinoid centers, the corrinoid $Co^{2+/1+}$ redox midpoint

potential, and overall synthesis of acetyl-CoA, *Biochemistry 32*, 10786–10793.
2498. Jarrett, J. T., Hoover, D. M., Ludwig, M. L., and Matthews, R. G. (1998) The mechanism of adenosylmethionine-dependent activation of methionine synthase: A rapid kinetic analysis of intermediates in reductive methylation of cob(II)alamin enzyme, *Biochemistry 37*, 12649–12658.
2499. Menon, S., and Ragsdale, S. W. (1998) Role of the [4Fe–4S] cluster in reductive activation of the cobalt center of the corrinoid iron–sulfur protein from *Clostridium thermoaceticum* during acetate biosynthesis, *Biochemistry 37*, 5689–5698.
2500. Kung, Y., Ando, N., Doukov, T. I., Blasiak, L. C., Bender, G., Seravalli, J., Ragsdale, S. W., and Drennan, C. L. (2012) Visualizing molecular juggling within a B_{12}-dependent methyltransferase complex, *Nature 484*, 265–269.
2501. St Maurice, M., Mera, P., Park, K., Brunold, T. C., Escalante-Semerena, J. C., and Rayment, I. (2008) Structural characterization of a human-type corrinoid adenosyltransferase confirms that coenzyme B_{12} is synthesized through a four-coordinate intermediate, *Biochemistry 47*, 5755–5766.
2502. Pallares, I. G., Moore, T. C., Escalante-Semerena, J. C., and Brunold, T. C. (2014) Spectroscopic studies of the *Salmonella enterica* adenosyltransferase enzyme *Se*CobA: Molecular-level insight into the mechanism of substrate cob(II)alamin activation, *Biochemistry 53*, 7969–7982.
2503. Pol, A., van der Drift, C., and Vogels, G. D. (1982) Corrinoids from *Methanosarcina barkeri*: Structure of the α-ligand, *Biochem. Biophys. Res. Commun. 108*, 731–737.
2504. Wood, J. M., Moura, I., Moura, J. J., Santos, M. H., Xavier, A. V., LeGall, J., and Scandellari, M. (1982) Role of vitamin B_{12} in methyl transfer for methane biosynthesis by *Methanosarcina barkeri*, *Science 216*, 303–305.
2505. Sauer, K., and Thauer, R. K. (1997) Methanol:coenzyme M methyltransferase from *Methanosarcina barkeri*. Zinc dependence and thermodynamics of the methanol:cob(I)alamin methyltransferase reaction, *Eur. J. Biochem. 249*, 280–285.
2506. Laso-Perez, R., Wegener, G., Knittel, K., Widdel, F., Harding, K. J., Krukenberg, V., Meier, D. V., Richter, M., Tegetmeyer, H. E., Riedel, D., Richnow, H. H., Adrian, L., Reemtsma, T., Lechtenfeld, O. J., and Musat, F. (2016) Thermophilic archaea activate butane via alkyl-coenzyme m formation, *Nature 539*, 396–401.
2507. Pfaltz, A., Jaun, B., Faessler, A., Eschenmoser, A., Jaenchen, R., Gilles, H. H., Diekert, G., and Thauer, R. K. (1982) Factor F_{430} from methanogenic bacteria: Structure of the porphinoid ligand system, *Helv. Chem. Acta 65*, 828–865.
2508. Ermler, U., Grabarse, W., Shima, S., Goubeaud, M., and Thauer, R. K. (1997) Crystal structure of methyl-coenzyme M reductase: The key enzyme of biological methane formation, *Science 278*, 1457–1462.
2509. Holliger, C., Pierik, A. J., Reijerse, E. J., and Hagen, W. R. (1993) A spectroelectrochemical study of factor F_{430} nickel(II/I) from methanogenic bacteria in aqueous-solution, *J. Am. Chem. Soc. 115*, 5651–5656.
2510. Yang, N., Reiher, M., Wang, M., Harmer, J., and Duin, E. C. (2007) Formation of a nickel-methyl species in methyl-coenzyme M reductase, an enzyme catalyzing methane formation, *J. Am. Chem. Soc. 129*, 11028–11029.
2511. Scheller, S., Goenrich, M., Thauer, R. K., and Jaun, B. (2013) Methyl-coenzyme M reductase from methanogenic archaea: Isotope effects on the formation and anaerobic oxidation of methane, *J. Am. Chem. Soc. 135*, 14975–14984.
2512. Wongnate, T., Sliwa, D., Ginovska, B., Smith, D., Wolf, M. W., Lehnert, N., Raugei, S., and Ragsdale, S. W. (2016) The radical mechanism of biological methane synthesis by methyl-coenzyme M reductase, *Science 352*, 953–958..
2513. Dey, M., Li, X., Kunz, R. C., and Ragsdale, S. W. (2010) Detection of organometallic and radical intermediates in the catalytic mechanism of methyl-coenzyme M reductase using the natural substrate methyl-coenzyme M and a coenzyme B substrate analogue, *Biochemistry 49*, 10902–10911.
2514. Sprecher, M., Clark, M. J., and Sprinson, D. B. (1964) Absolute configuration of methylmalonyl coenzyme A (CoA) and stereochemistry of the methylmalonyl CoA mutase reaction, *Biochem. Biophys. Res. Commun. 15*, 581–587.
2515. Graves, S. W., Krouwer, J. S., and Babior, B. M. (1980) The mechanism of action of ethanolamine ammonia-lyase, an adenosylco-

balamin-dependent enzyme. Studies with isopropanolamine, a true substrate, *J. Biol. Chem. 255*, 7444–7448.
2516. Finlay, T. H., Valinsky, J., Mildvan, A. S., and Abeles, R. H. (1973) Electron spin resonance studies with dioldehydrase. Evidence for radical intermediates in reactions catalyzed by coenzyme B_{12}, *J. Biol. Chem. 248*, 1285–1290.
2517. Baker, J. J., van der Drift, C., and Stadtman, T. C. (1973) Purification and properties of β-lysine mutase, a pyridoxal phosphate and B_{12} coenzyme dependent enzyme, *Biochemistry 12*, 1054–1063.
2518. Tang, K. H., Harms, A., and Frey, P. A. (2002) Identification of a novel pyridoxal 5′-phosphate binding site in adenosylcobalamin-dependent lysine 5,6-aminomutase from *Porphyromonas gingivalis*, *Biochemistry 41*, 8767–8776.
2519. Somack, R., and Costilow, R. N. (1973) Purification and properties of a pyridoxal phosphate and coenzyme B_{12} dependent D-α-ornithine 5,4-aminomutase, *Biochemistry 12*, 2597–2604.
2520. Munch-Petersen, A., and Barker, H. A. (1958) The origin of the methyl group in mesaconate formed from glutamate by extracts of *Clostridium tetanomorphum*, *J. Biol. Chem. 230*, 649–653.
2521. Eggerer, H., Stadtmann, E. R., Overath, P., and Lynen, F. (1960) On the mechanism of the rearrangement of methylmalonyl CoA to succinyl CoA catalyzed by the cobalamine coenzyme, *Biochem. Z. 333*, 1–9.
2522. Erb, T. J., Retey, J., Fuchs, G., and Alber, B. E. (2008) Ethylmalonyl-CoA mutase from *Rhodobacter sphaeroides* defines a new subclade of coenzyme B_{12}-dependent acyl-CoA mutases, *J. Biol. Chem. 283*, 32283–32293.
2523. Yaneva, N., Schuster, J., Schafer, F., Lede, V., Przybylski, D., Paproth, T., Harms, H., Muller, R. H., and Rohwerder, T. (2012) Bacterial acyl-CoA mutase specifically catalyzes coenzyme B_{12}-dependent isomerization of 2-hydroxyisobutyryl-CoA and (*S*)-3-hydroxybutyryl-CoA, *J. Biol. Chem. 287*, 15502–15511.
2524. Cracan, V., and Banerjee, R. (2012) Novel coenzyme B_{12}-dependent interconversion of isovaleryl-CoA and pivalyl-CoA, *J. Biol. Chem. 287*, 3723–3732.
2525. Cracan, V., and Banerjee, R. (2012) Novel B_{12}-dependent acyl-CoA mutases and their biotechnological potential, *Biochemistry 51*, 6039–6046.
2526. Dowd, P., Trivedi, B. K., Shapiro, M., and Marwaha, L. K. (1976) Vitamin B_{12} model studies. Migration of the acrylate fragment in the carbon-skeleton rearrangement leading to α-methyleneglutaric acid, *J. Am. Chem. Soc. 98*, 7875–7877.
2527. Eagar, R. G., Jr., Herbst, M. M., Barker, H. A., and Richards, J. H. (1972) Mechanism of action of coenzyme B_{12}: Hydrogen transfer in the isomerization of β-methylaspartate to glutamate, *Biochemistry 11*, 253–264.
2528. Frey, P. A., and Abeles, R. H. (1966) The role of the B_{12} coenzyme in the conversion of 1,2-propanediol to propionaldehyde, *J. Biol. Chem. 241*, 2732–2733.
2529. Carty, T. J., Babior, B. M., and Abeles, R. H. (1974) The mechanism of action of ethanolamine ammonia-lyase, a B_{12}-dependent enzyme. Evidence for two intermediates in the catalytic process, *J. Biol. Chem. 249*, 1683–1688.
2530. Babior, B. M., Carty, T. J., and Abeles, R. H. (1974) The mechanism of action of ethanolamine ammonia-lyase, a B_{12}-dependent enzyme. The reversible formation of 5′-deoxy--adenosine from adenosylcobalamin during the catalytic process, *J. Biol. Chem. 249*, 1689–1695.
2531. Schrauzer, G. N., and Sibert, J. W. (1970) Coenzyme B_{12} and coenzyme B_{12} model compounds in the catalysis of the dehydration of glycols, *J. Am. Chem. Soc. 92*, 1022–1030.
2532. Hollaway, M. R., White, H. A., Joblin, K. N., Johnson, A. W., Lappert, M. F., and Wallis, O. C. (1978) A spectrophotometric rapid kinetic study of reactions catalysed by coenzyme-B_{12}-dependent ethanolamine ammonia-lyase, *Eur. J. Biochem. 82*, 143–154.
2533. Padmakumar, R., Padmakumar, R., and Banerjee, R. (1997) Evidence that cobalt–carbon bond homolysis is coupled to hydrogen atom abstraction from substrate in methylmalonyl-CoA mutase, *Biochemistry 36*, 3713–3718.
2534. Marsh, E. N., and Ballou, D. P. (1998) Coupling of cobalt–carbon bond homolysis and hydrogen atom abstraction in adenosylcobalamin-dependent glutamate mutase, *Biochemistry 37*, 11864–11872.
2535. Menon, B. R., Fisher, K., Rigby, S. E., Scrutton, N. S., and Leys, D. (2014) A conformational

sampling model for radical catalysis in pyridoxal phosphate- and cobalamin-dependent enzymes, *J. Biol. Chem. 289*, 34161–34174.
2536. Chih, H. W., and Marsh, E. N. (1999) Presteady-state kinetic investigation of intermediates in the reaction catalyzed by adenosylcobalamin-dependent glutamate mutase, *Biochemistry 38*, 13684–13691.
2537. Froese, D. S., Kochan, G., Muniz, J. R., Wu, X., Gileadi, C., Ugochukwu, E., Krysztofinska, E., Gravel, R. A., Oppermann, U., and Yue, W. W. (2010) Structures of the human GTPase MMAA and vitamin B_{12}-dependent methyl-0malonyl-CoA mutase and insight into their complex formation, *J. Biol. Chem. 285*, 38204–38213.
2538. Shibata, N., Higuchi, Y., and Toraya, T. (2011) How coenzyme B_{12}-dependent ethanolamine ammonia-lyase deals with both enantiomers of 2-amino-1-propanol as substrates: Structure-based rationalization, *Biochemistry 50*, 591–598.
2539. Kurteva-Yaneva, N., Zahn, M., Weichler, M. T., Starke, R., Harms, H., Muller, R. H., Strater, N., and Rohwerder, T. (2015) Structural basis of the stereospecificity of bacterial B_{12}-dependent 2-hydroxyisobutyryl-CoA mutase, *J. Biol. Chem. 290*, 9727–9737.
2540. Valinsky, J. E., Abeles, R. H., and Fee, J. A. (1974) Electron-spin resonance studies on diol dehydrase: 3. Rapid kinetic studies on rate of formation of radicals in reaction with propanediol, *J. Am. Chem. Soc. 96*, 4709–4710.
2541. Leutbecher, U., Albracht, S. P., and Buckel, W. (1992) Identification of a paramagnetic species as an early intermediate in the coenzyme B_{12}-dependent glutamate mutase reaction. A cob(II)amide?, *FEBS Lett. 307*, 144–146.
2542. Zelder, O., Beatrix, B., Leutbecher, U., and Buckel, W. (1994) Characterization of the coenzyme-B_{12}-dependent glutamate mutase from *Clostridium cochlearium* produced in *Escherichia coli*, *Eur. J. Biochem. 226*, 577–585.
2543. Bothe, H., Darley, D. J., Albracht, S. P., Gerfen, G. J., Golding, B. T., and Buckel, W. (1998) Identification of the 4-glutamyl radical as an intermediate in the carbon skeleton rearrangement catalyzed by coenzyme B_{12}-dependent glutamate mutase from *Clostridium cochlearium*, *Biochemistry 37*, 4105–4113.
2544. Ke, S.-C., and Warncke, K. (1999) Interactions of substrate and product radicals with CoII in cobalamin and with the active site in ethanolamine deaminase, characterized by ESE-EPR and ^{14}N ESEEM spectroscopies, *J. Am. Chem. Soc. 121*, 9922–9927.
2545. Warncke, K., Schmidt, J. C., and Ke, S.-C. (1999) Identification of a rearranged-substrate, product radical intermediate and the contribution of a product radical trap in vitamin B_{12} coenzyme-dependent ethanolamine deaminase catalysis, *J. Am. Chem. Soc. 121*, 10522–10528.
2546. Warncke, K., and Canfield, J. M. (2004) Direct determination of product radical structure reveals the radical rearrangement pathway in a coenzyme B_{12}-dependent enzyme, *J. Am. Chem. Soc. 126*, 5930–5931.
2547. Mansoorabadi, S. O., Padmakumar, R., Fazliddinova, N., Vlasie, M., Banerjee, R., and Reed, G. H. (2005) Characterization of a succinyl-CoA radical-cob(II)alamin spin triplet intermediate in the reaction catalyzed by adenosylcobalamin-dependent methylmalonyl-CoA mutase, *Biochemistry 44*, 3153–3158.
2548. Wang, M., and Warncke, K. (2008) Kinetic and thermodynamic characterization of Co(II)-substrate radical pair formation in coenzyme B_{12}-dependent ethanolamine ammonia-lyase in a cryosolvent system by using time-resolved, full-spectrum continuous-wave electron paramagnetic resonance spectroscopy, *J. Am. Chem. Soc. 130*, 4846–4858.
2549. Yamanishi, M., Ide, H., Murakami, Y., and Toraya, T. (2005) Identification of the 1,2-propanediol-1-yl radical as an intermediate in adenosylcobalamin-dependent diol dehydratase reaction, *Biochemistry 44*, 2113–2118.
2550. Bender, G., Poyner, R. R., and Reed, G. H. (2008) Identification of the substrate radical intermediate derived from ethanolamine during catalysis by ethanolamine ammonia-lyase, *Biochemistry 47*, 11360–11366.
2551. Zhu, C., and Warncke, K. (2010) Kinetic isolation and characterization of the radical rearrangement step in coenzyme B_{12}-dependent ethanolamine ammonia-lyase, *J. Am. Chem. Soc. 132*, 9610–9615.
2552. Babior, B. M., Moss, T. H., Orme-Johnson, W. H., and Beinert, H. (1974) The mechanism of

action of ethanolamine ammonia-lyase, a B_{12}-dependent enzyme. The participation of paramagnetic species in the catalytic deamination of 2-aminopropanol, *J. Biol. Chem. 249*, 4537–4544.
2553. Bandarian, V., and Reed, G. H. (2002) Analysis of the electron paramagnetic resonance spectrum of a radical intermediate in the coenzyme B_{12}-dependent ethanolamine ammonia-lyase catalyzed reaction of *S*-2-aminopropanol, *Biochemistry 41*, 8580–8588.
2554. Bandarian, V., and Reed, G. H. (1999) Hydrazine cation radical in the active site of ethanolamine ammonia-lyase: Mechanism-based inactivation by hydroxyethylhydrazine, *Biochemistry 38*, 12394–12402.
2555. Bandarian, V., Poyner, R. R., and Reed, G. H. (1999) Hydrogen atom exchange between 5′-deoxyadenosine and hydroxyethylhydrazine during the single turnover inactivation of ethanolamine ammonia-lyase, *Biochemistry 38*, 12403–12407.
2556. Wolthers, K. R., Rigby, S. E., and Scrutton, N. S. (2008) Mechanism of radical-based catalysis in the reaction catalyzed by adenosylcobalamin-dependent ornithine 4,5-aminomutase, *J. Biol. Chem. 283*, 34615–34625.
2557. Abend, A., Bandarian, V., Reed, G. H., and Frey, P. A. (2000) Identification of *cis*-ethanesemidione as the organic radical derived from glycolaldehyde in the suicide inactivation of dioldehydrase and of ethanolamine ammonia-lyase, *Biochemistry 39*, 6250–6257.
2558. Sandala, G. M., Smith, D. M., Coote, M. L., and Radom, L. (2004) Suicide inactivation of dioldehydratase by glycolaldehyde and chloroacetaldehyde: An examination of the reaction mechanism, *J. Am. Chem. Soc. 126*, 12206–12207.
2559. Huhta, M. S., Ciceri, D., Golding, B. T., and Marsh, E. N. (2002) A novel reaction between adenosylcobalamin and 2-methyleneglutarate catalyzed by glutamate mutase, *Biochemistry 41*, 3200–3206.
2560. Ruetz, M., Campanello, G. C., Purchal, M., Shen, H., McDevitt, L., Gouda, H., Wakabayashi, S., Zhu, J., Rubin, E. J., Warncke, K., Mootha, V. K., Koutmos, M., and Banerjee, R. (2019) Itaconyl-CoA forms a stable biradical in methylmalonyl-CoA mutase and derails its activity and repair, *Science 366*, 589–593.
2561. Magnusson, O. T., and Frey, P. A. (2000) Synthesis and characterization of 3′,4′-anhydroadenosylcobalamin: A coenzyme B_{12} analogue with unusual properties, *J. Am. Chem. Soc. 122*, 8807–8813.
2562. Mansoorabadi, S. O., Magnusson, O. T., Poyner, R. R., Frey, P. A., and Reed, G. H. (2006) Analysis of the cob(II)alamin-5′-deoxy-3′,4′-anhydroadenosyl radical triplet spin system in the active site of diol dehydrase, *Biochemistry 45*, 14362–14370.
2563. Magnusson, O. T., and Frey, P. A. (2002) Interactions of diol dehydrase and 3′,4′-anhydroadenosylcobalamin: Suicide inactivation by electron transfer, *Biochemistry 41*, 1695–1702.
2564. Boas, J. F., Hicks, P. R., Pilbrow, J. R., and Smith, T. D. (1978) Interpretation of electron spin resonance spectra due to some B_{12}-dependent enzyme reactions, *J. Chem. Soc. Faraday Trans. 74*, 417–431.
2565. Canfield, J. M., and Warncke, K. (2002) Geometry of reactant centers in the Co(II)-substrate radical pair state of coenzyme B_{12}-dependent ethanolamine deaminase determined by using orientation-selection-ESEEM spectroscopy, *J. Phys. Chem. B 106*, 8831–8841.
2566. Canfield, J. M., and Warncke, K. (2005) Active site reactant center geometry in the Co(II)-product radical pair state of coenzyme B_{12}-dependent ethanolamine deaminase determined by using orientation-selection electron spin-echo envelope modulation spectroscopy, *J Phys Chem B 109*, 3053–3064.
2567. LoBrutto, R., Bandarian, V., Magnusson, O. T., Chen, X., Schramm, V. L., and Reed, G. H. (2001) 5′-Deoxyadenosine contacts the substrate radical intermediate in the active site of ethanolamine ammonia-lyase: ^{2}H and ^{13}C Electron nuclear double resonance studies, *Biochemistry 40*, 9–14.
2568. Maity, A. N., Hsieh, C. P., Huang, M. H., Chen, Y. H., Tang, K. H., Behshad, E., Frey, P. A., and Ke, S. C. (2009) Evidence for conformational movement and radical mechanism in the reaction of 4-thia-L-lysine with lysine 5,6-aminomutase, *J Phys Chem B 113*, 12161–12163.
2569. Shibata, N., Nakanishi, Y., Fukuoka, M., Yamanishi, M., Yasuoka, N., and Toraya, T. (2003) Structural rationalization for the lack of stereospecificity in coenzyme B_{12}-depen-

dent diol dehydratase, *J. Biol. Chem. 278*, 22717–22725.
2570. Mancia, F., Smith, G. A., and Evans, P. R. (1999) Crystal structure of substrate complexes of methylmalonyl-CoA mutase, *Biochemistry 38*, 7999–8005.
2571. Warncke, K. (2005) Characterization of the product radical structure in the Co(II)-product radical pair state of coenzyme B_{12}-dependent ethanolamine deaminase by using three-pulse ^2H ESEEM spectroscopy, *Biochemistry 44*, 3184–3193.
2572. Warncke, K., and Utada, A. S. (2001) Interaction of the substrate radical and the 5′-deoxyadenosine-5′-methyl group in vitamin B_{12} coenzyme-dependent ethanolamine deaminase, *J. Am. Chem. Soc. 123*, 8564–8572.
2573. Wang, M., and Warncke, K. (2013) Entropic origin of cobalt-carbon bond cleavage catalysis in adenosylcobalamin-dependent ethanolamine ammonia-lyase, *J. Am. Chem. Soc. 135*, 15077–15084.
2574. Halpern, J., Ng, F. T. T., and Rempel, G. L. (1979) Metal-alkyl bond dissociation energies in organocobalt compounds related to vitamin B_{12} coenzymes, *J. Am. Chem. Soc. 101*, 7124–7126.
2575. Hay, B. P., and Finke, R. G. (1986) Thermolysis of the cobalt-carbon bond of adenosylcobalamin. 2. Products, kinetics, and cobalt-carbon bond dissociation energy in aqueous solution, *J. Am. Chem. Soc. 108*, 4820–4829.
2576. Dong, S., Padmakumar, R., Banerjee, R., and Spiro, T. G. (1999) Co-C Bond activation in B_{12}-dependent enzymes: Cryogenic resonance Raman studies of methylmalonyl-coenzyme A mutase, *J. Am. Chem. Soc. 121*, 7063–7070.
2577. Jensen, K. P., and Ryde, U. (2005) How the Co–C bond is cleaved in coenzyme B_{12} enzymes: A theoretical study, *J. Am. Chem. Soc. 127*, 9117–9128.
2578. Waddington, M. D., and Finke, R. G. (1993) Neopentylcobalamin (neopentyl B_{12}) cobalt–carbon bond thermolysis products, kinetics, activation parameters, and bond dissociation energy: A chemical model exhibiting 10^6 of the 10^{12} enzymic activation of coenzyme B_{12}'s cobalt–carbon bond, *J. Am. Chem. Soc. 115*, 4629–4640.
2579. Kraeutler, B., Keller, W., and Kratky, C. (1989) Coenzyme B_{12} chemistry: The crystal and molecular structure of cob(II)alamin, *J. Am. Chem. Soc. 111*, 8936–8938.
2580. Roman-Melendez, G. D., von Glehn, P., Harvey, J. N., Mulholland, A. J., and Marsh, E. N. (2014) Role of active site residues in promoting cobalt–carbon bond homolysis in adenosylcobalamin-dependent mutases revealed through experiment and computation, *Biochemistry 53*, 169–177.
2581. Jost, M., Born, D. A., Cracan, V., Banerjee, R., and Drennan, C. L. (2015) Structural basis for substrate specificity in adenosylcobalamin-dependent isobutyryl-CoA mutase and related acyl-CoA mutases, *J. Biol. Chem. 290*, 26882–26898.
2582. Dong, S., Padmakumar, R., Maiti, N., Banerjee, R., and Spiro, T. G. (1998) Resonance Raman spectra show that coenzyme B_{12} binding to methylmalonyl-coenzyme A mutase changes the corrin ring conformation but leaves the Co–C bond essentially unaffected, *J. Am. Chem. Soc. 120*, 9947–9948.
2583. Sirovatka, J. M., and Finke, R. G. (1997) Coenzyme B_{12} chemical precedent studies: Probing the role of the imidazole base-on motif found in B_{12}-dependent methylmalonyl-CoA mutase, *J. Am. Chem. Soc. 119*, 3057–3067.
2584. Cole, A. G., Yoder, L. M., Shiang, J. J., Anderson, N. A., Walker, L. A., 2nd, Banaszak Holl, M. M., and Sension, R. J. (2002) Time-resolved spectroscopic studies of B_{12} coenzymes: A comparison of the primary photolysis mechanism in methyl-, ethyl-, *n*-propyl-, and 5′-deoxyadenosylcobalamin, *J. Am. Chem. Soc. 124*, 434–441.
2585. Silverman, R. B., and Dolphin, D. (1976) Model studies for coenzyme B_{12} dependent enzyme-catalyzed rearrangements. Evidence for cobalt(III)-olefin π complexes, *J. Am. Chem. Soc. 98*, 4626–4633.
2586. Finke, R. G., and Schiraldi, D. A. (1983) Model studies of coenzyme B_{12} dependent diol dehydratase. 2. A kinetic and mechanistic study focusing upon the cobalt participation or nonparticipation question, *J. Am. Chem. Soc. 105*, 7605–7617.
2587. Dowd, P., Wilk, B., and Wilk, B. K. (1992) First hydrogen abstraction-rearrangement model for the coenzyme B_{12}-dependent methylmalonyl-CoA to succinyl-CoA carbon skeleton rearrangement reaction, *J. Am. Chem. Soc. 114*, 7949–7951.
2588. Scott, A. I., Karuso, P., Williams, H. J., Lally, J., Robinson, J., and Nayar, G. P. (1994) Inves-

tigation of a coenzyme B_{12} model reaction by ^{13}C NMR spectroscopy, *J. Am. Chem. Soc. 116*, 777–778.
2589. Choi, G. Y., Choi, S. C., Galan, A., Wilk, B., and Dowd, P. (1990) Vitamin B_{12s}-promoted model rearrangement of methylmalonate to succinate is not a free radical reaction, *Proc. Natl. Acad. Sci. U. S. A. 87*, 3174–3176.
2590. He, M., and Dowd, P. (1998) Mechanism of action of vitamin B_{12}. Ultrafast radical clocks provide no evidence for radical intermediates in cyclopropane models for the methylmalonyl-CoA to succinyl-CoA carbon skeleton rearrangement, *J. Am. Chem. Soc. 120*, 1133–1137.
2591. Wollowitz, S., and Halpern, J. (1988) 1,2-Migrations in free radicals related to coenzyme B_{12}-dependent rearrangements, *J. Am. Chem. Soc. 110*, 3112–3120.
2592. Daublain, P., Horner, J. H., Kuznetsov, A., and Newcomb, M. (2004) Solvent polarity effects and limited acid catalysis in rearrangements of model radicals for the methylmalonyl-CoA mutase- and isobutyryl-CoA mutase-catalyzed isomerization reactions, *J. Am. Chem. Soc. 126*, 5368–5369.
2593. Newcomb, M., and Miranda, N. (2003) Kinetic results implicating a polar radical reaction pathway in the rearrangement catalyzed by α-methyleneglutarate mutase, *J. Am. Chem. Soc. 125*, 4080–4086.
2594. Golding, B. T., and Radom, L. (1976) On the mechanism of action of adenosylcobalamin, *J. Am. Chem. Soc. 98*, 6331–6338.
2595. Smith, D. M., Golding, B. T., and Radom, L. (1999) Understanding the mechanism of B_{12}-dependent methylmalonyl-CoA mutase: Partial proton transfer in action, *J. Am. Chem. Soc. 121*, 9388–9399.
2596. Edwards, C. H., Golding, B. T., Kroll, F., Beatrix, B., Broker, G., and Buckel, W. (1996) Rotation of the exo-methylene group of 2-methyleneglutarate catalyzed by coenzyme B_{12}-dependent 2-methyleneglutarate mutase from *Clostridium barkeri*, *J. Am. Chem. Soc. 118*, 4192–4193.
2597. Rommel, J. B., and Kastner, J. (2011) The fragmentation-recombination mechanism of the enzyme glutamate mutase studied by QM/MM simulations, *J. Am. Chem. Soc. 133*, 10195–10203.
2598. Chih, H.-W., and Marsh, E. N. G. (2000) Mechanism of glutamate mutase: Identification and kinetic competence of acrylate and glycyl radical as intermediates in the rearrangement of glutamate to methylaspartate, *J. Am. Chem. Soc. 122*, 10732–10733.
2599. Yoon, M., Patwardhan, A., Qiao, C. H., Mansoorabadi, S. O., Menefee, A. L., Reed, G. H., and Marsh, E. N. G. (2006) Reaction of adenosylcobalamin-dependent glutamate mutase with 2-thiolglutarate, *Biochemistry 45*, 11650–11657.
2600. Beatrix, B., Zelder, O., Linder, D., and Buckel, W. (1994) Cloning, sequencing and expression of the gene encoding the coenzyme B_{12}-dependent 2-methyleneglutarate mutase from *Clostridium barkeri* in *Escherichia coli*, *Eur. J. Biochem. 221*, 101–109.
2601. Smith, D. M., Golding, B. T., and Radom, L. (2001) Understanding the mechanism of B_{12}-dependent diol dehydratase: A synergistic retro-push–pull proposal, *J. Am. Chem. Soc. 123*, 1664–1675.
2602. Mori, K., Oiwa, T., Kawaguchi, S., Kondo, K., Takahashi, Y., and Toraya, T. (2014) Catalytic roles of substrate-binding residues in coenzyme B_{12}-dependent ethanolamine ammonia-lyase, *Biochemistry 53*, 2661–2671.
2603. Grate, J. W., and Schrauzer, G. N. (1984) Studies of vitamin B_{12} and related compounds. 57. Organocobalamin reactions relevant to the mechanism of the α-methyleneglutarate mutase enzyme, *Z. Naturforsch. B 39B*, 821–823.
2604. Grate, J. H., Grate, J. W., and Schrauzer, G. N. (1982) Studies on vitamin B_{12} and related compounds. 53. Synthesis and reactions of organocobalamins relevant to the mechanism of the methylmalonyl-CoA-succi-nyl-CoA mutase enzyme, *J. Am. Chem. Soc. 104*, 1588–1594.
2605. Tang, K. H., Chang, C. H., and Frey, P. A. (2001) Electron transfer in the substrate-dependent suicide inactivation of lysine 5,6-aminomutase, *Biochemistry 40*, 5190–5199.
2606. Speranza, G., Mueller, B., Orlandi, M., Morelli, C. F., Manitto, P., and Schink, B. (2002) Mechanism of anaerobic ether cleavage: Conversion of 2-phenoxyethanol to phenol and acetaldehyde by *Acetobacterium* sp, *J. Biol. Chem. 277*, 11684–11690.
2607. Choi, S. C., and Dowd, P. (1989) Model for the coenzyme B_{12}-dependent glutamate-methylaspartate carbon skeleton rearrangement, *J. Am. Chem. Soc. 111*, 2313–2314.

2608. Hemmerich, P., Veeger, C., and Wood, H. C. S. (1965) Progress in chemistry and molecular biology of flavins and flavocoenzymes, *Angew. Chem., Int. Ed. Engl. 4*, 671–687.
2609. White, R. E., Miller, J. P., Favreau, L. V., and Bhattacharyya, A. (1986) Stereochemical dynamics of aliphatic hydroxylation by cytochrome P-450, *J. Am. Chem. Soc. 108*, 6024–6031.
2610. Kang, G., Taguchi, A. T., Stubbe, J., and Drennan, C. L. (2020) Structure of a trapped radical transfer pathway within a ribonucleotide reductase holocomplex, *Science (Washington, DC, U. S.) 368*, 424–427.

Chapter 3
Association of Substrates with the Active Site

The Reaction or Reactions Catalyzed

Before the mechanism of a particular enzyme can be studied kinetically, a stoichiometric and complete chemical equation must be established for the chemical reaction that it catalyzes. Although the stoichiometric equation seems clear in the cases of interconversions such as that between fumarate and malate catalyzed by fumarate hydratase (previously Equation 1–1)

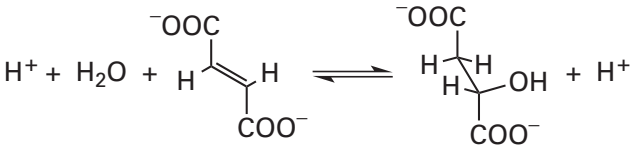

(3–1)

there are many instances in which it is obscured.

In many enzymatically catalyzed reactions, there are **substrates that are not explicit in the reaction** as it was originally identified. For example, fatty acids can be converted into the thioesters of coenzyme A in an acyl exchange reaction

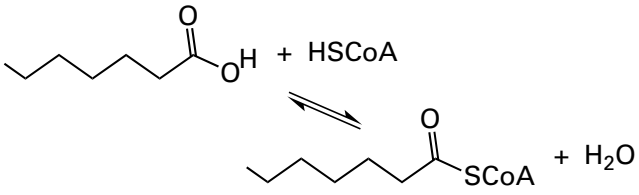

(3–2)

but the reaction as written is endergonic. Therefore, the actual reaction catalyzed by long-chain-fatty-acid–CoA ligase involves the coupled hydrolysis of a phosphodiester of $MgATP^{2-}$ as well[1]

$$MgATP^{2-} + \text{fatty acid} + HSCoA \rightleftharpoons \text{fatty acyl-SCoA} + 2\,H^+ + MgOPO_3PO_3^{2-} + AMP^{2-} \quad (3–3)$$

Procollagen-lysine 5-dioxygenase hydroxylates the carbons 5 of lysines in procollagen but only when stoichiometric amounts of 2-oxoglutarate are present to consume the other half of the molecular oxygen.[2]

$$\text{procollagen-lysine} + \text{2-oxoglutarate} + O_2 \rightleftharpoons \text{succinate} + CO_2 + \text{procollagen-5-hydroxylysine} \quad (3–4)$$

Unlike the examples just considered, sometimes the **additional substrates** are not part of the formal stoichiometric equation for the reaction catalyzed by the enzyme because they are **regenerated during the reaction**. Nevertheless, they must be present for the enzymatic reaction to occur. For example, the observed reaction[3] for glutamate-5-semialdehyde dehydrogenase from *Escherichia coli* is

$$NADP^+ + \text{L-glutamate 5-semialdehyde} \rightleftharpoons 2\,H^+ + \text{5-oxopyrrolidine-2-carboxylate} + NADPH \quad (3–5)$$

For enzymatic activity to be observed, however, phosphate must be present in the solution. There are several facts which lead to the conclusion that the reaction actually catalyzed by the enzyme is the production of L-glutamate 5-phosphate

$$NADP^+ + \text{L-glutamate 5-semialdehyde} + HOPO_3^{2-} \rightleftharpoons H^+ + \text{L-glutamate 5-phosphate} + NADPH \quad (3–6)$$

and the 5-oxopyrrolidine-2-carboxylate arises from a subsequent, nonenzymatic cyclization proceeding by nucleophilic substitution

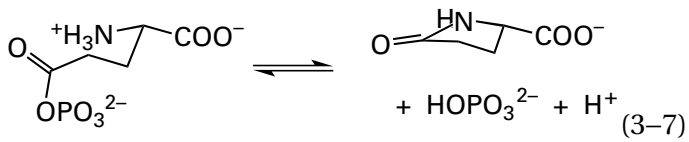

(3–7)

and regenerating the phosphate. Pyrogallol hydroxytransferase from *Pelobacter acidigallici* catalyzes the migration of a hydroxy group from carbon 2 of 1,2,3-trihydroxybenzene to carbon 5, producing 1,3,5-trihydroxybenzene, but the enzyme requires, as a second reactant, 1,2,3,5-tetrahydroxybenzene, which is also a product of the reaction, so it is not a participant in the stoichiometric equation for the enzymatic reaction.[4] The enzyme that catalyzes the transport of D-glucose 6-phosphate across the plasma membrane of *E. coli*, a reaction that is of physiological interest, is required to transport a phosphate ion in the opposite direction for every molecule of D-glucose 6-phosphate it transports.[5]

A related ambiguity arises when an enzyme, following its purification, is observed to catalyze a reaction that turns out to be an **incomplete version of its actual reaction in the cell** because a natural substrate has been overlooked. For example, purified sarcosine oxidase from *Corynebacterium* readily converts sarcosine and molecular oxygen to formaldehyde, glycine, and hydrogen peroxide. It was discovered, however, that tetrahydrofolate is a coenzyme for the enzyme under physiological conditions, and when it is present, the enzyme produces N^5,N^{10}-methylenetetrahydrofolate (previously **1–83**)

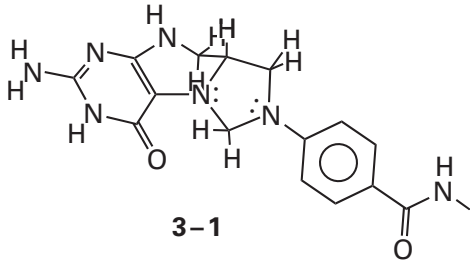

3–1

instead of formaldehyde, at the same rate.[6] An enzyme involved in oxidation–reduction is often purified by using an unnatural oxidant or reductant in the assay, and the natural oxidant or reductant may remain unknown for a considerable period.

Glutamate-5-semialdehyde dehydrogenase from *E. coli* (Equation 3–5) is an example of an enzyme catalyzing a reaction for which the ultimate product that is used by the next enzyme in a metabolic sequence, in its case 5-oxopyrrolidine-2-carboxylate, is formed by the **rapid nonenzymatic transformation of the actual product** produced by the enzyme, in its case L-glutamyl 5-phosphate.[7] When the nonenzymatic transformation of the actual product of an enzymatically catalyzed reaction is rapid enough,[8,9] there is no selective pressure to catalyze that transformation enzymatically. Usually the actual product of such an enzymatic reaction is the result of a simpler, more obvious transformation of the reactant, and a more complicated mechanism for the enzyme or the need for another enzyme is avoided by permitting the transformation of the actual product to remain uncatalyzed. For example, porcine D-amino-acid oxidase and L-amino-acid oxidase from *Crotalus adamanteus* release, as their respective actual products, the **imines** that are the products of a direct dehydrogenation of the respective reactants

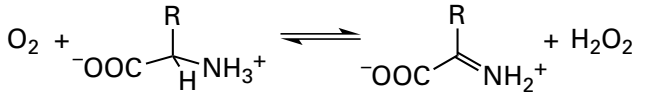

(3–8)

even though the α-oxo acids formed by the rapid nonenzymatic hydrolysis of the imines are the ultimate biochemical products,[10] and the equation written for the actual enzymatic reaction (Equation 3–8) must reflect this fact. Bovine monoamine oxidase also produces the imine of its reactant amine.[11]

Phosphoribosylanthranilate isomerase from *E. coli* catalyzes a simple elimination

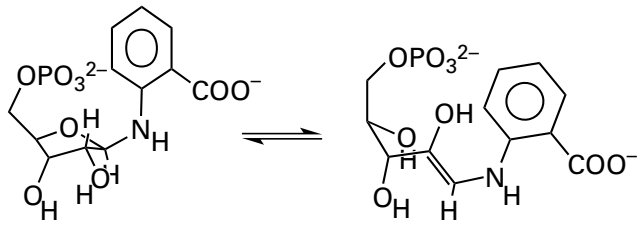

(3–9)

to produce an **enol** as its actual product. The enol then undergoes an enol–keto tautomerization, uncatalyzed by the enzyme, to produce 1-[(2-carboxyphenyl)amino]-1-deoxyribulose 5-phosphate, which has an oxo group at carbon 2 and is the ultimate biochemical product.[12] Other enzymes, however, catalyze final keto–enol tautomerizations before releasing the required tautomer for the next step in the metabolic sequence,[13] either because the uncatalyzed tautomerizations are too slow, because they are too nonspecific, or because they produce an undesired product.

Another nonenzymatic **cyclization** of the actual product, like the one that produces 5-oxopyrrolidine-2-carboxylate (Equation 3–7), is the cyclization and subsequent aromatization of the 2-amino-3-carboxymuconate semialdehyde

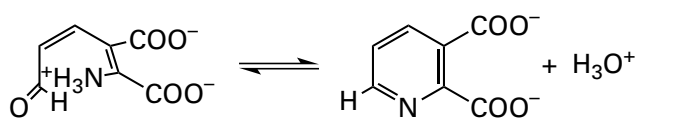

(3–10)

that is the actual product of the reaction of 3-hydroxyanthranilate 3,4-dioxygenase from *Cupriavidus metallidurans*.[14] An almost identical postenzymatic cyclization, however, to form (2*S*,4*S*)-4-hydroxy-2,3,4,5-tetrahydrodipicolinate from the 2-amino-4-hydroxy-6-oxopimelic acid produced from pyruvate and L-aspartate-4-semialdehyde from *E. coli* is catalyzed by the enzyme, 4-hydroxy-tetrahydrodipicolinate synthase, perhaps because it lacks the cis double bond approximating the nucleophile and the electrophile.[15]

The nonenzymatic conversion of the actual product of an enzymatic reaction into the metabolically required product sometimes requires that **another reactant not involved in the enzymatic reaction** be present in the cytoplasm or the extracellular solution. Acireductone synthase catalyzes the conversion of 2,3-dioxo-5-methylsulfanyl-1-phosphopentane to phosphate, formate, and 2-oxo-4-methylsulfanylbutanoate, but only in the presence of molecular oxygen. The actual products of the enzymatic reaction are phosphate and 1,2-dihydroxy-5-methylsulfanyl-3-oxo-1-pentene

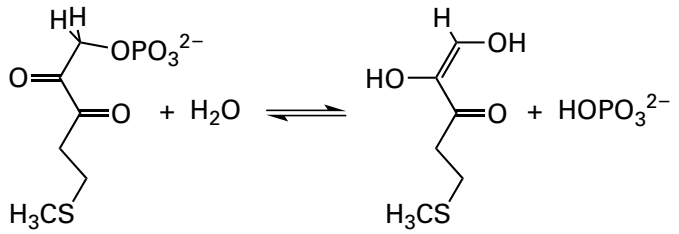

(3–11)

The latter is oxidized nonenzymatically by molecular oxygen to the ultimate products of the reaction, which is why the molecular oxygen appears to be a reactant.[16,17]

Just as the product of an enzymatic reaction may be nonenzymatically transformed after dissociating from the active site, the **actual reactant in an enzymatic reaction is often one formed nonenzymatically** from the compound originally thought to be the reactant. For example, dethiobiotin synthase from *E. coli* uses as its actual reactant the 7-carbamate formed nonenzymatically in solution from 7,8-diaminononanoic acid

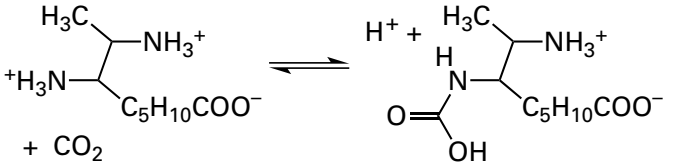

(3–12)

and carbon dioxide rather than 7,8-diaminononanoic acid itself.[18]

In many instances, a substrate in an enzymatic reaction exists in solution in several different forms in rapid equilibrium with each other, but the enzyme will recognize **only one of these several equilibrating forms**. Although only 3% of the D-glyceraldehyde 3-phosphate in solution is the unhydrated aldehyde, that is the only form of this substrate recognized by glyceraldehyde-3-phosphate dehydrogenase from *Homarus gammarus*.[19] In a solution of fructose 1,6-diphosphate, there is an equilibrium mixture containing 20% α anomer (**3–2**) and 80% β anomer (**3–3**) of the furanose[20]

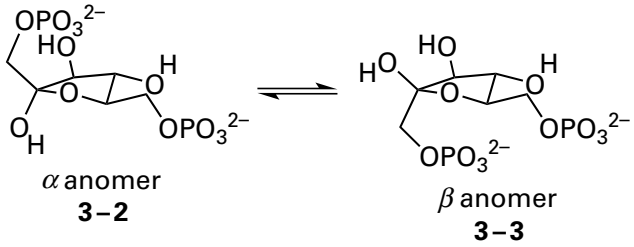

(3–13)

Although these are interconverted through the open ketone, less than 1% of either the open ketone or its hydrate is present in solution. The enzymes glucose-6-phosphate isomerase from *Saccharomyces cerevisiae*[21] and fructose-bisphosphatase from *Oryctolagus cuniculus*[22] act preferentially, but not exclusively, on the α anomer and catalyze the opening of the furanose ring to produce the ketone, which is required for the subsequent steps in the enzymatic reaction.[23] Human fructose-bisphosphate aldolase, however, acts preferentially on the β anomer[24] but also catalyzes the opening of the furanose ring.[25]

Carbon dioxide and carbonic acid are in equilibrium with each other, and it is difficult to distinguish which is the actual substrate in a given enzymatic reaction. By following the uptake of hydrons, it could demonstrated that the product of the reaction catalyzed by tartronate-semialdehyde synthase from *E. coli*, an enzyme containing thiamine diphosphate, is carbon dioxide[26]

$$H^+ + \text{2 glyoxylate} \rightleftharpoons \text{2-hydroxy-3-oxopropanoate} + CO_2 \quad (3\text{–}14)$$

Were carbonic acid the product, almost no hydrons would have been consumed. It could be shown, however, that β-ketoacyl-[acyl-carrier-protein] synthase I in the fatty-acid synthase system from *Rattus norvegicus* produces bicarbonate rather than CO_2 by following the production of bicarbonate in a continuous coupled assay.[27]

Many enzymes are able to **accept more than one reactant** and **produce more than one product**. For example, cytosine deaminase from *E. coli*, in addition to deaminating cytosine, also, and with even greater efficiency, deaminates isoguanine, a mutagenic purine that is produced during the repair of DNA and that would itself produce mutations if it were not eliminated effectively.[28] Transketolase can use either D-xylulose 5-phosphate or D-fructose 6-phosphate as the ketone in its reaction and, using thiamine diphosphate, transfers the same hydroxyacetyl group derived from either of these substrates, as the α-hydroxy enamine of thiamine diphosphate

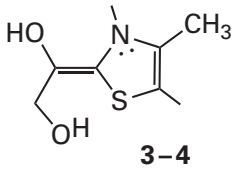

3–4

to ribose 5-phosphate[29]

D-xylulose 5-phosphate + D-ribose 5-phosphate $\rightleftharpoons$ sedoheptulose 7-phosphate + D-glyceraldehyde 3-phosphate (3–15)

D-fructose 6-phosphate + D-ribose 5-phosphate $\rightleftharpoons$ sedoheptulose 7-phosphate + D-erythrose 4-phosphate (3–16)

Likewise, 3-deoxy-7-phosphoheptulonate synthase from *Pyrococcus furiosus* is able to condense phospho*enol*pyruvate with any one of the aldehydes D-erythrose 4-phosphate, 2-deoxy-D-erythrose 4-phosphate, D-arabinose 5-phosphate, D-ribose 5-phosphate, or 2-deoxy-D-ribose 5-phosphate to produce the respective elongated product[30]

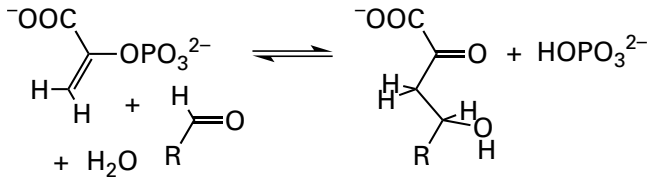

(3–17)

In these latter two examples, the respective enzyme either transfers the same fragment from two different ketones to the same aldehyde or condenses the same enolate with one of five different aldehydes, respectively, but in each case, the regiochemistry remains the same in the vicinity of the condensation. Ovine 3β,20α-hydroxysteroid oxidoreductase, however, catalyzes two reactions with **different regiochemistries**: the reduction of the 20-oxo group of progesterone to the 20-hydroxy group and the reduction of the 3-oxo group of 5α-dihydrotestosterone to the 3-hydroxy group.[31] These two different locations are on the opposite ends of the respective steroids.

There are also enzymes that catalyze two different reactions with the same regiochemistries but **different stereochemistries**. For example, 3-hydroxybutyryl-CoA epimerase from *E. coli* is able to dehydrate both the *R* and the *S* stereoisomers of 3-hydroxy-4-*trans*-decenoyl-CoA.[32] Alginate lyase from *Pseudomonas aeruginosa* cleaves disaccharides and trisaccharides of D-mannuronate and L-guluronate from the nonreducing end of the polysaccharide alginate. The active site is able to remove the disaccharide or the trisaccharide from the nonreducing end regardless of whether it is removed from either a D-mannuronate or an L-guluronate in the alginate, even though D-mannuronate and L-guluronate have the opposite chiralities at the carbon from which the enzyme is required to remove a hydron during the elimination that accomplishes the cleavage.[33] Both D-mannuronate and L-guluronate, from which the disaccharide and trisaccharide are respectively cleaved, are turned into a 4-deoxy-α-L-*erythro*-hex-4-enuronosyl group at the nonreducing end of the shortened polymer as a result of the elimination.[34]

There are enzymes that produce **different products from the same reactant**. For example, the fatty-acid synthase system produces a mixture of saturated fatty acids of variable chain length from the same two reactants, acetyl-SCoA and malonyl-SCoA. The composition of the mixture of products depends on the tissue and the species, and it can be varied by the presence of distinct [acyl-carrier-protein] hydrolases in a particular tissue.[35]

In addition to aphidicolan-16β-ol, aphidicolan-16β-ol synthase from *Neocamarosporium betae* produces aphidicol-15-ene and aphidicol-16-ene, which are the products of dehydration of aphidicolan-16β-ol. To solve the problem of this lack of specificity, all three products are converted by other enzymes to aphidicolin, the ultimate product of the metabolic pathway.[36]

There are many enzymes that are designed to perform the **same reaction on many different substrates**. For example, certain of the enzymes containing a heme P450 are designed to hydroxylate a large array of xenobiotics; aldehyde reductase is designed to reduce a large array of aldehydes, some of which are dangerously reactive, and at least one ketone[37] to the respective alcohols;[38] and phosphotriesterase is able to hydrolyze a variety of phosphate triesters.[39]

There are a number of proteins that can catalyze more than one enzymatic reaction because they have more than one active site within their structure, one dedicated to each of the different reactions, but there are also enzymes with only one active site that **perform different reactions depending on the identity of the reactant** they encounter. Palmitoyl-[glycerolipid] 7-desaturase from *Arabidopsis thaliana* desaturates palmityl groups in phospholipids

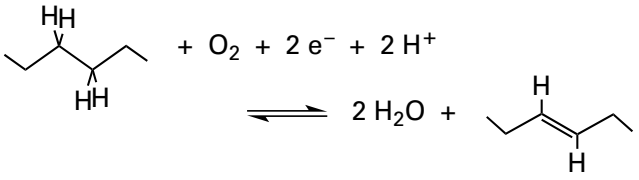

(3–18)

but the desaturation occurs between carbons 7 and 8 or between carbons 9 and 10 depending on the head group of the phospholipid that is the substrate.[40] Tartrate dehydrogenase from *Pseudomonas putida*, however, catalyzes significantly different reactions, not the same reaction with different regiochemistry, depending on the substrate. (*R,S)*-Tartrate is dehydrogenated to (*R)*-oxaloglycolate; D-malate is dehydrogenated and then decarboxylated to pyruvate; and *meso*-tartrate is dehydrogenated, decarboxylated, and dehydrogenated again to D-glycerate.[41] There are enzymes that can catalyze two reactions with substrates significantly more different from each other than (*R,S)*-tartrate is from D-malate. For example, *o*-succinylbenzoate synthase

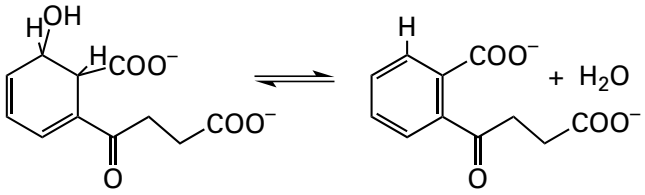

(3–19)

from *Amycolatopsis* can also catalyze the racemization of *N*-acylamino acids.[42,43] The fact, however, that an enzyme can catalyze the same reaction in both directions does not qualify as an example of the same active site catalyzing different reactions.[44]

When the same active site is able to catalyze different reactions or the same reaction with different substrates, this ability is often an important **clue as to its mechanism**. For example, the fact that glucose-6-phosphate isomerase from *O. cuniculus*, in addition to converting D-glucose 6-phosphate to D-fructose 6-phosphate, can convert D-glucose 6-phosphate to D-mannose 6-phosphate is evidence for an intermediate enediol in the enzymatic reaction.[45]

There is an enzyme in *Mycobacterium tuberculosis* that converts 7,8-dihydroneopterin into three products.[46] All three outcomes can be explained by a common intermediate enol. 6-(Hydroxymethyl)-7,8-dihydropterin is the product of a retroaldol cleavage of 7,8-dihydroneopterin followed by tautomerization of the intermediate enol, and glycolaldehyde is the other product. 7,8-Dihydromonapterin is the product of an epimerization of 7,8-dihydroneopterin that results from the same retroaldol cleavage followed by an aldol condensation of the intermediate enol with the glycolaldehyde. And 7,8-dihydroxanthopterin is the result of the same retroaldol cleavage followed by the oxidative cleavage of the intermediate enol.

There is an enzyme from mammalian erythrocytes that can catalyze three reactions:[47] phosphoglycerate mutase

2-phospho-D-glycerate $\rightleftharpoons$ 3-phospho-D-glycerate

(3–20)

bisphosphoglycerate mutase

H^+ + 2,3-bisphospho-D-glycerate $\rightleftharpoons$ 3-phospho-D-glyceroyl phosphate

(3–21)

and bisphosphoglycerate phosphatase

2,3-bisphospho-D-glycerate + H_2O ⇌
3-phospho-D-glycerate + $HOPO_3^{2-}$ (3–22)

The first two reactions are interrelated by the fact that the same **phosphorylated enzyme** is an intermediate in both. Equation 3–20 can be expanded to include the phosphorylated enzyme (E-OPO_3^{2-})

2-phospho-D-glycerate + E–OPO_3^{2-} ⇌
2,3-bisphospho-D-glycerate + EOH ⇌
3-phospho-D-glycerate + E–OPO_3^{2-} (3–23)

and Equation 3–21 can be expanded to include the phosphorylated enzyme

H^+ + 2,3-bisphospho-D-glycerate + EOH ⇌
H^+ + 3-phospho-D-glycerate + E–OPO_3^{2-} ⇌
3-phospho-D-glyceroyl phosphate + EOH (3–24)

Equation 3–22 is simply a result of the spontaneous hydrolysis of the phosphorylated enzyme. These expansions imply that if the enzyme added to the solution were completely dephosphorylated, the conversion of 2-phospho-D-glycerate to 3-phospho-D-glycerate would not be catalyzed; and if the enzyme added to the solution were completely and stably phosphorylated, the conversion of 2,3-bisphospho-D-glycerate to 3-phospho-D-glyceroyl phosphate would not be catalyzed. In the cell, however, phosphoenzyme is always being slowly dephosphorylated (Equation 3–22) and dephosphoenzyme is always being phosphorylated by 3-phospho-D-glyceroyl phosphate (reverse of second step in Equation 3–24) produced by glyceraldehyde-3-phosphate dehydrogenase (phosphorylating).

Just as the different reactions among natural metabolites that can be catalyzed by an enzyme provide insight into the mechanism of that enzyme, so too do the **transformations of unnatural substrates** catalyzed by the enzyme. Porcine fumarate hydratase, in addition to its normal reaction (Equation 3–1), can also catalyze the stereospecific hydration of *trans*-2,3-epoxysuccinate[48]

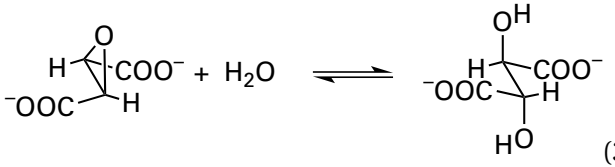
(3–25)

and any mechanism proposed for the natural reaction must explain this unnatural reaction. Because glyceraldehyde-3-phosphate dehydrogenase (phosphorylating) from *O. cuniculus* can catalyze the production of acetyl phosphate from acetaldehyde[49]

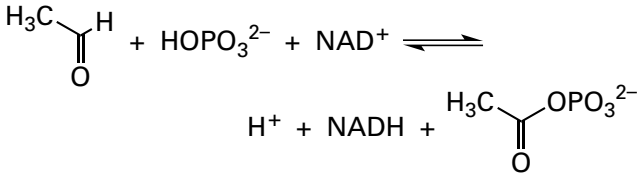
(3–26)

there is no portion of the normal substrate, D-glyceraldehyde 3-phosphate, other than the aldehyde, that is essential for the normal reaction.

Glyoxylate is not a natural substrate for L-lactate dehydrogenase, the enzyme that normally catalyzes the reaction

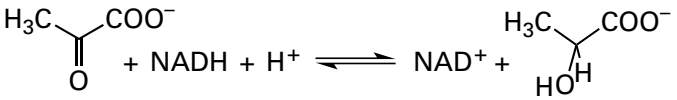
(3–27)

but the enzyme from *O. cuniculus* nevertheless reduces glyoxylate to glycolate[50]

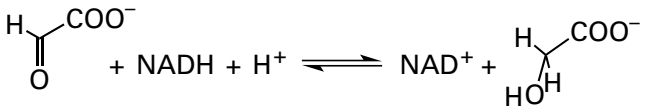
(3–28)

and reduces oxalate to glyoxylate.[51]

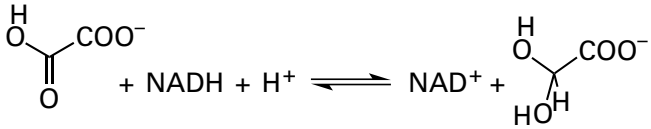
(3–29)

These results suggest that either a hydrogen or a hydroxy group, respectively, can be mistaken by the enzyme for a methyl group. Both of these functional groups are smaller than a methyl group and

would not be sterically excluded from substituting for it, but the hydroxy group is polar while the methyl group, with its three hydrogen–carbon bonds,[52] is nonpolar.

Often, one of the natural substrates for an enzyme cannot be used for kinetic experiments for some reason. For example, the product of the *oatA* gene in *Streptococcus pneumoniae* acetylates 6-hydroxy groups in the insoluble peptidoglycan forming the cell wall of the bacterium. Kinetic studies of the enzyme take advantage of the ability of the enzyme to acetylate an unnatural substrate, the soluble trisaccharide chitotriose.[53]

In many enzymatic reactions, in addition to those that use small electron carriers, a molecule of **another protein serves as a substrate**. For example, the reaction catalyzed by acetyl-CoA carboxylase from avian liver is

$$\text{acetyl-SCoA} + HCO_3^- + MgATP^{2-} \rightleftharpoons H^+ + HOPO_3^{2-} + MgADP^- + \text{malonyl-SCoA} \quad (3\text{–}30)$$

but the enzyme from *E. coli*[54] utilizes the carbamate of a biotin attached to a small protein (α_2; 2×210 aa), referred to as biotin carboxyl-carrier protein (BCCPNH)[55]

$$\text{acetyl-SCoA} + \text{BCCPN–}CO_2^- \rightleftharpoons \text{BCCPNH} + \text{malonyl-SCoA} \quad (3\text{–}31)$$

The biotin carboxyl-carrier protein is carboxylated in a separate reaction[56] that also requires the hydrolysis of $MgATP^{2-}$ (Figure 1–29). The enzyme from avian liver has a domain that is an intramolecular biotin carboxyl-carrier protein and another domain that is an intramolecular biotin carboxylase.[57]

In a few enzymatic reactions, the molar **concentration of active sites of the enzyme in the cytoplasm is equal to or greater than the concentrations of the substrates**. In such reactions, the enzyme must be considered as an explicit participant in the reaction. The enzyme glyceraldehyde-3-phosphate dehydrogenase (phosphorylating) catalyzes the reaction

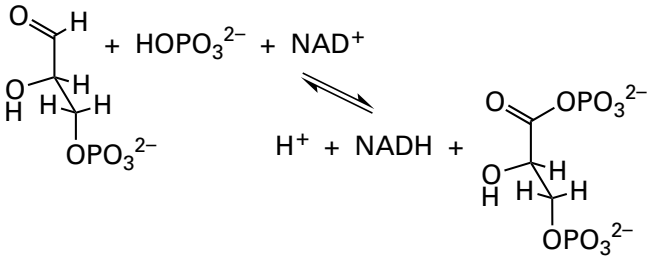

(3–32)

The substrate D-glyceraldehyde 3-phosphate is a reactive aldehyde that would be either bound as an imine to other proteins in the cell or present in solution as the hydrate,[19] and neither of these forms would be available to the enzyme, which can process only the unhydrated aldehyde.[19] The substrate 1,3-diphosphoglycerate is an acyl phosphate that is readily hydrolyzed. For both of these reasons, the strategy that seems to have evolved is to maintain the concentrations of these two substrates at low levels (<0.10 mM) in the cytoplasm but to have a high concentration of 3-phosphoglycerate bound at the active site of the enzyme as a thioester with a unique cysteine in the folded polypeptide.[58] For this reason, the molar concentration of the enzyme in the cytoplasm is abnormally high (1 mM). As a result, two of the reactions in glycolysis have glyceraldehyde-3-phosphate dehydrogenase (GAPDHSH) and its phosphorylated derivative, phosphoglyceryl glyceraldehyde-3-phosphate dehydrogenase, as reactants as well as catalysts

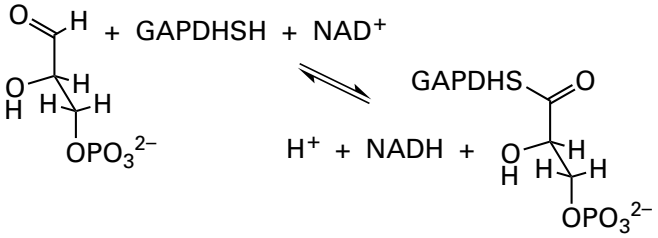

(3–33)

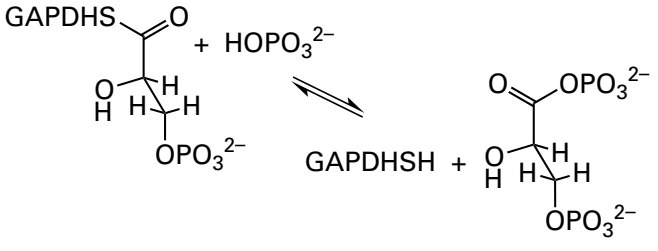

(3–34)

and the stoichiometric equations describing the enzymatic reactions that actually occur in the cyto-

plasm explicitly incorporate the concentrations of enzyme and phosphoglyceryl enzyme.

Lately, the publication of sequences of nucleic acids for genomes has provided sequences of amino acids for a large number of **proteins of unknown function** that can be shown to be evolutionarily related to known enzymes. These proteins often are able to catalyze the same types of reaction that are catalyzed by their relatives but with different substrates, often with several different substrates. For example, a protein encoded by the genome of *Salmonella typhimurium* that is related to glucarate dehydratase was shown to be able to dehydrate both L-talarate and galactarate,[59] and a protein encoded by the genome of *Dianthus caryophyllus* that is related to isocitrate lyase was shown to be able to cleave a number of 2-alkyl and 2,3-dialkyl-(2*R)*-malates as well as oxaloacetate at the carbon–carbon bonds between their respective carbons 2 and 3,[60] just as isocitrate lyase does to isocitrate. Once the ability of these enzymes to catalyze these reactions has been established, it is then necessary to discover which of these reactions are physiologically relevant.

Once the chemical reaction or reactions catalyzed by the enzyme have been unambiguously defined, the steps in the enzymatic reaction can be defined. The usual first step in this definition is to examine the steady-state kinetics of the reaction.

Suggested Reading

Rhoads, R. E., and Udenfriend, S. (1968) Decarboxylation of α-ketoglutarate coupled to collagen proline hydroxylase, *Proc. Natl. Acad. Sci. U.S.A. 60*, 1473–1478. https://doi.org/10.1073/pnas.60.4.147

Kahn, K., Serfozo, P., and Tipton, P. A. (1997) Identification of the true product of the urate oxidase reaction, *J. Am. Chem. Soc. 119*, 5435–5442. https://doi.org/10.1021/ja970375t

Problem 3–1: Show how all these conversions can be catalyzed by the same enzyme.

D-erythrose 4-phosphate ⇌ D-threose 4-phosphate

⇘ ⇗

D-erythrulose 4-phosphate

D-ribulose 5-phosphate ⇌ D-xylulose 5-phosphate

Why does the same enzyme not produce (*R,S*)-D-1,2,4,5-tetrahydroxy-3-oxopentane 5-phosphate?

Problem 3–2: Write a mechanism for the production of (2*S*,4*S*)-4-hydroxy-2,3,4,5-tetrahydrodipicolinate from pyruvate and L-aspartate-4-semialdehyde catalyzed by 4-hydroxy-tetrahydrodipicolinate synthase[15] and its subsequent nonenzymatic conversion to (*S*)-2,3-dihydrodipicolinate.

Problem 3–3: Write reactants, intermediates, and products for the three reactions catalyzed by tartrate dehydrogenase: (*R,S*)-tartrate to oxaloglycolate, D-malate to pyruvate, and *meso*-tartrate to D-glycerate.[41]

Problem 3–4: The active site of 3-hexulose-6-phosphate synthase catalyzes the two reactions[61]

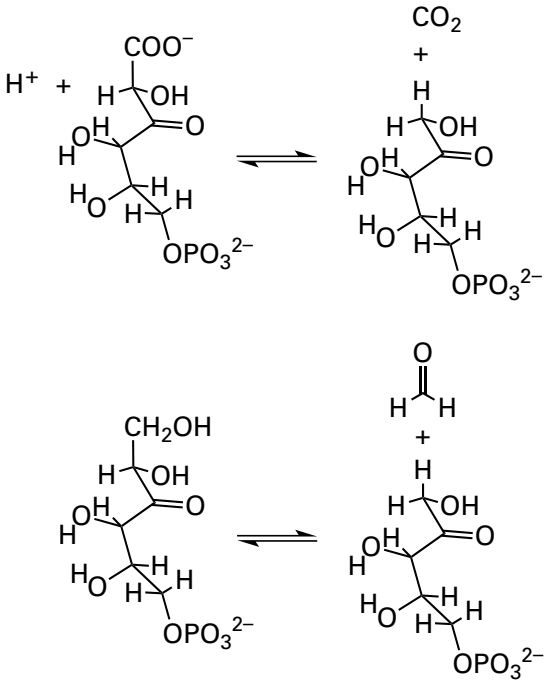

Write a mechanism for each reaction involving the same intermediate.

Steady-State Kinetics[62]

There are certain facts about the catalysis performed by an enzyme in an experimental situation and definitions of the parameters controlling the observations that are fundamental to a discussion of steady-state

kinetics. When an enzyme—for example, fumarate hydratase (Equation 3–1)—is added to a solution containing only the substrates appearing on one side of the stoichiometric chemical equation for the particular reaction for which it is responsible—for example, an aqueous solution of fumarate—all the substrates appearing on the other side of the equation—for example, malate—begin to appear in the solution. In this instance, the substrates present initially and decreasing in concentration as the reaction proceeds are necessarily the **reactants** in the chemical reaction being studied kinetically, and those appearing in the solution and increasing in concentration as the reaction proceeds are the **products**. Consequently, a **conscious decision** is made by the investigator as to the identity of the reactants and the identity of the products.

The **increase in the rate** of the designated reaction that is catalyzed by the enzyme is directly **proportional to its molar concentration** because the reaction is performed at an active site or several active sites present on each molecule of enzyme, and each molecule of enzyme is an independent actor. The reactants associate with an **active site** and are converted to products while they are there, and the products then dissociate from the active site.

Under normal circumstances, tens to thousands of substrate molecules are interconverted during each second by one molecule of enzyme. Therefore, only low molar concentrations of enzyme are almost always added to the solution to produce a measurable increase in the rate of the reaction. If too much enzyme is added, the reaction occurs so rapidly that rates at steady state cannot be measured leisurely. Because so many molecules of reactant are being processed in succession by the same molecule of enzyme, each molecule of enzyme, ready to process the next molecule of reactant, **must be regenerated** in exactly the same state at the end of each turnover. The enzyme, because it is usually present in the solution at a very small molar concentration and because it must be regenerated after each transformation, **cannot be a stoichiometric participant** in the chemical reaction, unlike the situation described for glyceraldehyde-3-phosphate dehydrogenase in the cytoplasm.

Because of **microscopic reversibility**, an enzymatically catalyzed reaction must pass through the same transition states but in opposite order in the forward and reverse directions. The enzyme accelerates the reaction by lowering the relative free energy of one or more of the transition states in this sequence. Therefore, it must **accelerate the reaction in both directions**. For this reason, enzymatically catalyzed reactions are approaches to equilibrium (as are all chemical reactions), and as the products begin to appear, the enzyme begins to catalyze the reaction in the reverse direction as it continues to catalyze it in the forward direction.

If a purified enzyme is added to a solution containing a mixture of all the substrates that appear on one side of the chemical equation for the reaction catalyzed by that enzyme

$$k\mathrm{A} + l\mathrm{B} + m\mathrm{C} + \ldots \rightleftharpoons \ldots + n\mathrm{X} + o\mathrm{Y} + p\mathrm{Z} \tag{3–35}$$

but missing one or more of the substrates that appear on the other side, the concentrations of the reactants will begin to decrease and the concentrations of the products will begin to increase. The **reactants** (A, B, C…) are the complete set of substrates from the one side of the chemical equation. The **products** (Z, Y, X…) are the incomplete or entirely absent set of substrates from the other side of the chemical equation. Again, in this artificial situation, what is a reactant and what is a product are defined by the investigator, who has purposely left out one or more of the products. The reaction will also proceed in one direction if all the products are present but purposely added at concentrations below their equilibrium levels. In this case, however, the initial rate of the reaction does not represent a unidirectional process. Unidirectional processes are easier to study.

The **progress of the reaction can be followed** by monitoring the concentration of one of the reactants or one of the products as a function of time because all changes in concentration are stoichiometrically related by the chemical equation for the reaction catalyzed

$$\frac{d[\mathrm{Z}]}{p\,dt} = \frac{d[\mathrm{Y}]}{o\,dt} = \frac{d[\mathrm{X}]}{n\,dt} = \ldots$$

$$\ldots = -\frac{d[\mathrm{C}]}{m\,dt} = -\frac{d[\mathrm{B}]}{l\,dt} = -\frac{d[\mathrm{A}]}{k\,dt} \tag{3–36}$$

where k, l, m, n, o, and p are integers that define the stoichiometry of the reaction.

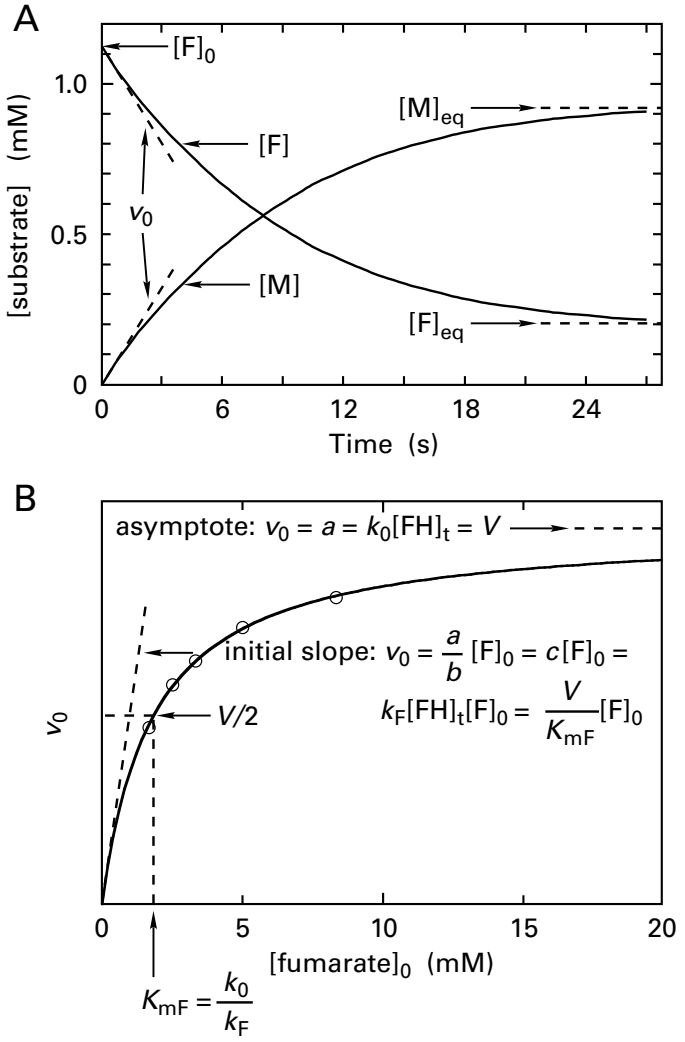

Figure 3–1: **(A)** Progress of the conversion of fumarate to (*S*)-malate catalyzed by the enzyme fumarate hydratase.[63] A solution of fumarate at pH 7 and 25 °C was added to the cuvette of a spectrophotometer. Each hydration was initiated by adding porcine fumarate hydratase (FH) to a final concentration of 15 μg mL^{-1}, and the initial concentration of fumarate was 1.13 mM. The decrease in the molar concentration of fumarate ([F]) was followed as a function of time by monitoring its absorbance at 270 nm. The increase in the concentration of (*S*)-malate ([M]) was estimated by difference. The concentrations of the two substrates (millimolar) are plotted as a function of time (seconds). At times greater than 1 min, the concentration of fumarate no longer decreased because it had reached its equilibrium level ($[F]_{eq}$). The initial slope of the decrease of fumarate as a function of time is the initial rate (v_0) in units of millimolar second^{-1}. **(B)** Behavior of the initial rates of the hydration catalyzed by fumarate hydratase as a function of the initial concentrations of fumarate.[1390] Equivalent amounts of fumarate hydratase were added to a series of mixtures at pH 6.4 and 23 °C that had various initial concentrations of fumarate. The decrease in absorbance at 295 nm was followed as a function of time for each mixture, and the initial slope of each progress curve was measured and converted to an initial rate. Initial rates (v_0 in unnoted units) are plotted as a function of the initial concentrations of fumarate (millimolar). The curve is the fit of the data to Equation 3–52, with x equal to $[\text{fumarate}]_0$ and y equal to v_0. Each of the two parameters, the catalytic constant $k_0[FH]_t$ and the limiting rate V, is the value for the initial rate at the horizontal asymptote (parameter a) of the rectangular hyperbola. The specificity constant for fumarate, $k_F[FH]_t$, is parameter c of the fit, and the Michaelis constant K_m is parameter b. The Michaelis constant is the value of $[F]_0$ when v_0 is $V/2$.

In the case of the reaction catalyzed by fumarate hydratase (Equation 3–1), if the purified porcine enzyme is added to a solution containing fumarate (F) from which malate (M) is absent, the concentration of fumarate will decrease as the concentration of malate increases until the equilibrium concentrations are reached. At this point, the reaction cannot proceed further (Figure 3–1).[63] Although no net change can occur at equilibrium, unidirectional changes are still taking place, albeit at rates somewhat less than the initial rates; it is just that the unidirectional rate of the reaction in the forward direction equals the unidirectional rate of the reaction in the reverse direction. At equilibrium, the enzyme is still catalyzing the reaction in both directions.

The curves describing the concentrations of fumarate and malate (Figure 3–1) describe the **complete kinetic course of the approach to equilibrium**. These curves can be simulated by using equations the form and parameters of which can be derived from simple kinetic mechanisms.[63-65] The strategy of fitting complete kinetic courses, however, is rarely applied because the form of the integrated rate equations is complicated: too many variables usually are changing at once, the enzyme may slowly inactivate with time, and the most characteristic changes occur late in the reaction, when the observations are most uncertain. In addition, in some instances the approach to equilibrium can pass beyond the point of equilibrium in an overshoot before returning to equilibrium,[66] behavior that further complicates a kinetic analysis. Instead, studies of initial rates of an enzymatic reaction are usually performed, and kinetic mechanisms consistent with these observations are formulated.

The **initial rate** (v_0 in Figure 3–1A) of an enzymatically catalyzed reaction is the rate of decrease in the concentration of reactant, A, or the rate of increase in the concentration of product, Z, observed immediately after initiating the reaction, either by adding the enzyme or by adding the final reactant necessary to complete the set of reac-

tants.[64] The initial rate is measured over a period of time so short that the rate remains constant rather than slowly decreasing with time. Over this short period of time, only small changes in the concentrations of substrates occur. If necessary, an extrapolation of the curve can be performed by numerical analysis to obtain the rate of the reaction at zero time. Consequently,

$$v_0 = \lim_{t \to 0} -\frac{d[\mathrm{A}]}{k\,dt} \tag{3–37}$$

or

$$v_0 = \lim_{t \to 0} \frac{d[\mathrm{Z}]}{p\,dt} \tag{3–38}$$

where the integers k and p are the molar stoichiometries of the overall reaction (Equation 3–35).

Because there are few enzymes that do not have unitary stoichiometries for all their reactants and products and because the decrease in the concentration of a reactant with unitary stoichiometry or the increase in a product with unitary stoichiometry is often followed in the few cases where there are substrates that do not have unitary stoichiometry, the **stoichiometry for the reactant or product** monitored (k in Equation 3–37 or p in Equation 3–38) in measuring an initial rate will be assumed to be one from here on.

If the initial rate of an enzymatic reaction measured by following the change in the concentration of a reactant or a product is, in fact, the desired limit, then the concentration of any reactant governing the initial rate must be the concentration initially present, or the initial concentration. For example, for reactant A, the initial concentration is designated as $[\mathrm{A}]_0$. The data collected in an experiment of this kind are the initial rates of the reaction at a systematic series of respective initial concentrations of reactants.

If there is only one reactant, for example, *N*-(5′-phosphoribosyl)anthranilate for the enzyme phosphoribosylanthranilate isomerase (Equation 3–9) from *S. cerevisiae* (Figure 3–2);[67] if the second reactant is water and hence always remains fixed in concentration, for example, during the hydrolysis of sucrose by β-fructofuranosidase*

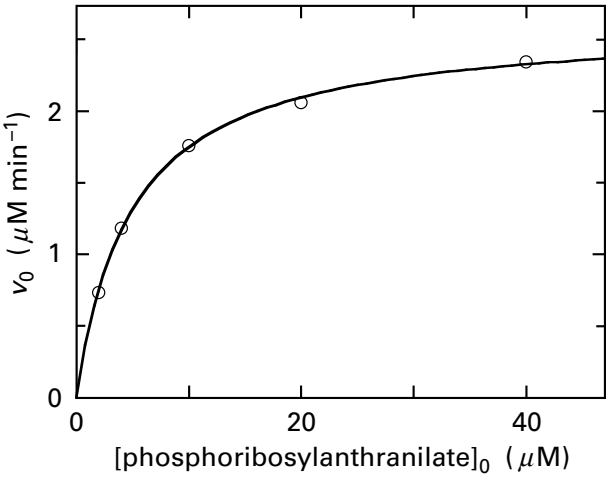

Figure 3–2: Kinetics for the isomerization of *N*-(5-phospho-β-D-ribosyl)anthranilate (Equation 3–9) by phosphoribosylanthranilate isomerase from *S. cerevisiae*.[67] Solutions were prepared that contained various concentrations of anthranilate and fixed concentrations of anthranilate phosphoribosyltransferase and magnesium 5-phospho-α-D-ribose 1-diphosphate sufficient to convert all the anthranilate to *N*-(5-phospho-β-D-ribosyl)anthranilate (phosphoribosylanthranilate) in less than 2 minutes. As soon as all the anthranilate in a solution had been converted to phosphoribosylanthranilate, which is unstable ($t_{½} \cong 10$ min), phosphoribosylanthranilate isomerase (PI) was added to initiate each isomerization, and the production of 1-(2-carboxyphenylamino)-1-deoxy-D-ribulose 5-phosphate was followed by monitoring the decrease in emission of fluorescence at 400 nm upon excitation at 310 nm. Each rate for the change in emission of fluorescence was converted to an initial rate for the production of 1-(2-carboxyphenylamino)-1-deoxy-D-ribulose 5-phosphate, v_0 (micromolar minute^{-1}). These initial rates are presented as a function of the initial concentrations of phosphoribosylanthranilate (micromolar). The curve is the fit of the data to Equation 3–52, with x equal to $[\text{phosphoribosylanthranilate}]_0$ and y equal to v_0. Parameter a for the fit is the catalytic constant, $k_0[\mathrm{PI}]_t$ (2.61 ± 0.03 μM min^{-1}), and parameter c is $k_{\mathrm{pRA}}[\mathrm{PI}]_t$, the specificity constant for phosphoribosylanthranilate [0.52 ± 0.02 μM min^{-1} (μM phosphoribosylanthranilate)$^{-1}$].

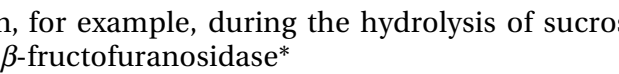

(3–39)

from *S. cerevisiae* (Figure 3–3A)[64,65] or the hydration

*For a discussion of kinetics, in either chemistry or enzymology, it is unnecessary to know either the structures of the reactants or products or the chemical mechanism of the reaction. All that one needs to know is the names of the reactants, intermediates, and products, and the only reason for knowing their names is to distinguish between them. Consequently, there is no need to try to figure out what is happening chemically when only kinetics are being examined.

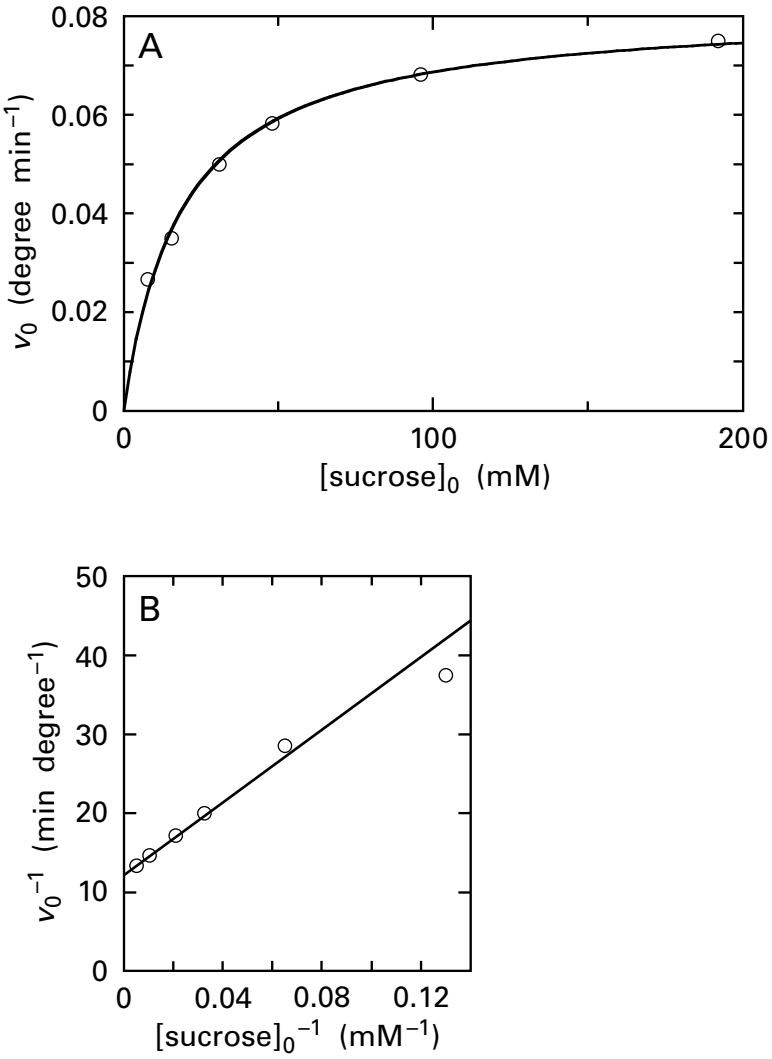

Figure 3–3: Kinetics for the hydrolysis of sucrose by β-fructofuranosidase.[64] Solutions were prepared with various concentrations of sucrose in 0.4 M sodium acetate at pH 4.7 and 25 °C. The hydrolysis of sucrose to D-glucose and D-fructose was monitored by the change in optical rotation of the solution at a wavelength of 589 nm. Each hydrolysis was initiated by adding an equal volume of an extract from cells of *S. cerevisiae* that contained β-fructofuranosidase (FF). The change in optical rotation of the solution (degrees) was followed as a function of time (minutes). **(A)** Initial rates of this change, v_0 (degrees minute^{-1}), are presented as a function of initial concentrations of sucrose (millimolar). The curve is the fit of the data to Equation 3–52, with x equal to $[\text{sucrose}]_0$ and y equal to v_0. Parameter a for the fit is the catalytic constant, $k_0[\text{FF}]_t$ (0.082 ± 0.002 degree min^{-1}), and parameter c is $k_{suc}[\text{FF}]_t$, the specificity constant for sucrose [4.3 ± 0.3 degrees min^{-1} (M sucrose)$^{-1}$]. **(B)** Reciprocals of the initial rates (minutes degree^{-1}) are presented as a function of reciprocals of the concentrations of sucrose (millimolar^{-1}). The line drawn in this panel is for the equation v_0^{-1} = 12.3 min degree^{-1} + 230 min degree^{-1} mM ($[\text{sucrose}]_0^{-1}$). The two parameters used in this equation are calculated from the numerical values for the two kinetic constants, $k_0[\text{FF}]_t$ and $k_{suc}[\text{FF}]_t$, obtained from the direct fit of the data to the equation for a hyperbola (Panel A).

of fumarate by porcine fumarate hydratase (Figure 3–1B);[68] or if the concentration of one of the reactants in a reaction with more than one reactant is varied while the concentrations of the other substrates are fixed (Figure 3–4A,E),[69] the **increase in the initial rate of the enzymatic reaction as a function of the initial concentration of the varied reactant** is described by the equation*

$$v_0 = \frac{[\text{E}]_t}{\dfrac{1}{k_A[\text{A}]_0} + \dfrac{1}{k_0}} = \frac{k_0 k_A [\text{E}]_t [\text{A}]_0}{k_0 + k_A[\text{A}]_0} \qquad (3\text{–}40)$$

where $[\text{E}]_t$* is the **total molar concentration of active sites** added to the solution, $[\text{A}]_0$ is the initial molar concentration of the varied reactant A, and k_0 and k_A are kinetic constants. The kinetic constant k_0 is the **catalytic constant**, and the kinetic constant k_A is the **specificity constant for reactant A**.[64,65]

The initial rate of an enzymatic reaction is almost always **directly proportional to the concentration of enzyme** in the solution at all values for the initial concentrations of substrates, as long as the enzyme is added at molar concentrations that are all at least an order of magnitude less than the change in the molar concentrations of reactants and products measured during the period of initial rate, and this fact is explicitly noted in Equation 3–40.

*As in the rest of this volume, the formalism chosen by the International Union of Biochemistry and Molecular Biology (http://www.chem.qmul.ac.uk/iubmb/kinetics/) will be used.

*The letter E has been used historically to designate the "enzyme concentration"[62,68] because the molar masses and oligomeric structures of enzymes were in doubt. Those doubts no longer exist in the age of sequences for genomes.

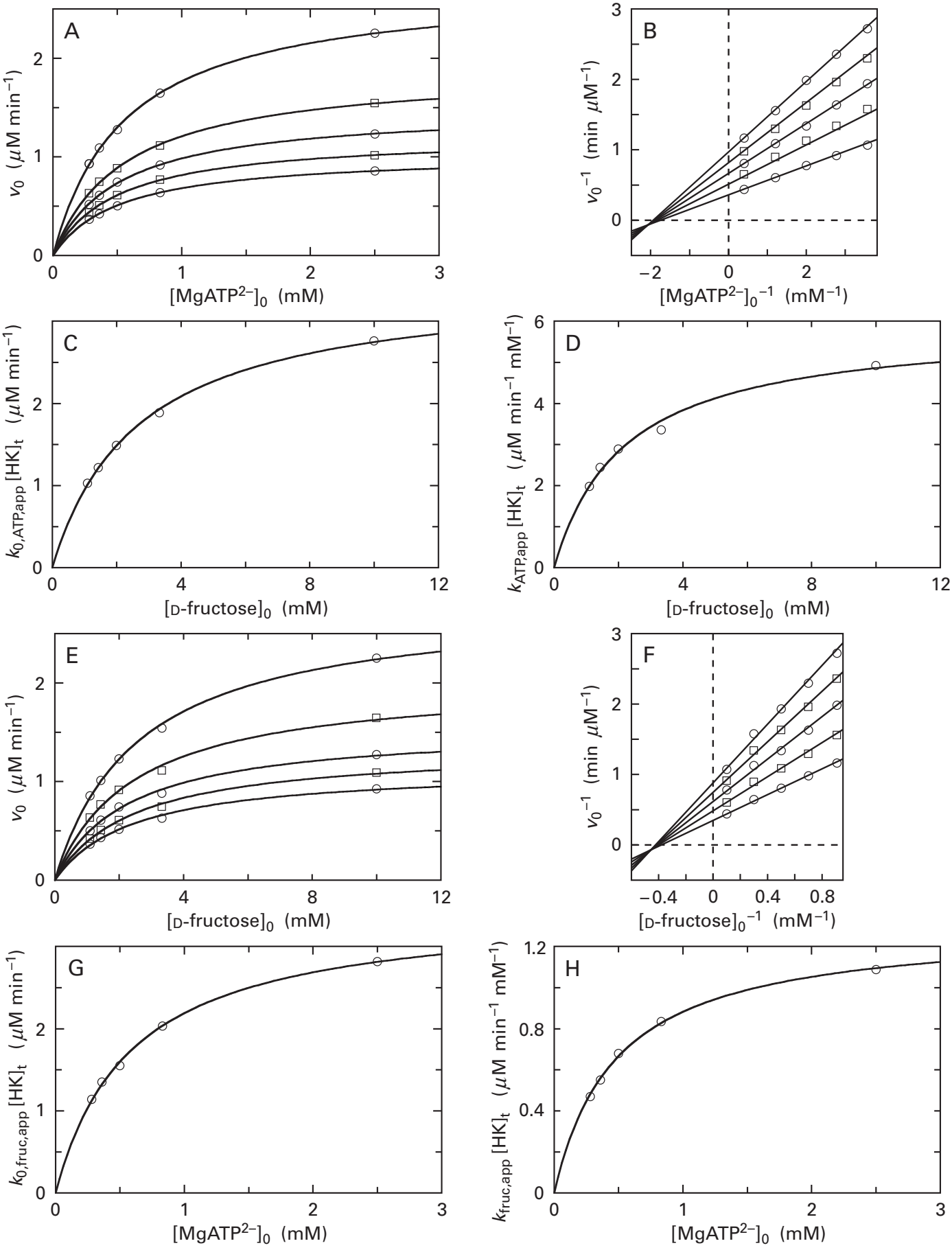
A
v_0 (μM min^{-1})
[MgATP^{2-}]$_0$ (mM)
B
v_0^{-1} (min μM^{-1})
[MgATP^{2-}]$_0^{-1}$ (mM^{-1})
C
$k_{0,ATP,app}$ [HK]$_t$ (μM min^{-1})
[D-fructose]$_0$ (mM)
D
$k_{ATP,app}$ [HK]$_t$ (μM min^{-1} mM^{-1})
[D-fructose]$_0$ (mM)
E
v_0 (μM min^{-1})
[D-fructose]$_0$ (mM)
F
v_0^{-1} (min μM^{-1})
[D-fructose]$_0^{-1}$ (mM^{-1})
G
$k_{0,fruc,app}$ [HK]$_t$ (μM min^{-1})
[MgATP^{2-}]$_0$ (mM)
H
$k_{fruc,app}$ [HK]$_t$ (μM min^{-1} mM^{-1})
[MgATP^{2-}]$_0$ (mM)

Figure 3–4: Kinetics for the phosphorylation of D-fructose catalyzed by hexokinase from the brain of *R. norvegicus*.[69] Solutions containing $MgATP^{2-}$ and D-fructose at various initial concentrations were prepared at pH 7.6 and 28 °C. The concentration of uncomplexed Mg^{2+} was fixed at 1.0 mM throughout by adding appropriate amounts of $MgCl_2$. Each phosphorylation was initiated by adding hexokinase (HK), and the production of D-fructose 6-phosphate was followed in a coupled assay with glucose-6-phosphate isomerase, glucose-6-phosphate dehydrogenase, and NAD^+ by monitoring the increase in A_{340} from the conversion of NAD^+ to NADH. Each initial rate of change in A_{340} was converted to an initial rate for the production of D-fructose 6-phosphate, v_0 (micromolar minute^{-1}). The initial concentrations of D-fructose chosen for the studies were 1.1, 1.43, 2.00, 3.33, and 10.00 mM, and the initial concentrations of $MgATP^{2-}$ were 0.28, 0.36, 0.50, 0.83, and 2.5 mM. The complete set of the 25 combinations of these initial concentrations was used to measure 25 separate initial rates. **(A)** Initial rates for production of D-fructose 6-phosphate are presented as a function of initial concentrations of $MgATP^{2-}$ (millimolar) at the five fixed initial concentrations of D-fructose. Each curve is for a higher fixed concentration of D-fructose than the one below it. The curves drawn are fits of Equation 3–52 to the data with x equal to $[MgATP^{2-}]_0$ and y equal to v_0. **(B)** Reciprocals of the initial rates (minutes micromolar^{-1}) are presented as a function of reciprocals of the initial concentrations of $MgATP^{2-}$ (millimolar^{-1}) at the five fixed initial concentrations of D-fructose. Each line fit to the data is for a higher fixed concentration of D-fructose than the one above it. **(C)** The five values for parameter a, the apparent catalytic constants for $MgATP^{2-}$, $k_{0,ATP,app}[HK]_t$ (micromolar minute^{-1}), for the five fits of Equation 3–52 to each of the five subsets of data in Panel A (the five curves on the graph), are presented as a function of the fixed initial concentrations of D-fructose corresponding to each value of $k_{0,ATP,app}[HK]_t$. The curve drawn is a fit of Equation 3–52 to the data with x equal to the respective fixed initial concentration of D-fructose and y equal to the respective $k_{0,ATP,app}[HK]_t$. Parameter a for this fit is the catalytic constant for the enzymatic reaction, $k_0[HK]_t$ (3.49 ± 0.05 μM D-fructose 6-phosphate min^{-1}), and parameter c is the specificity constant for D-fructose, $k_{fruc}[HK]_t$ [1.29 ± 0.03 μM D-fructose 6-phosphate min^{-1} (mM D-fructose)$^{-1}$]. **(D)** The five values for parameter c, the apparent specificity constants for $MgATP^{2-}$, $k_{ATP,app}[HK]_t$ (micromolar minute^{-1} millimolar^{-1}), for the five fits of Equation 3–52 to each of the five subsets of data in Panel A, are plotted as a function of the respective fixed initial concentrations of D-fructose. The curve drawn is a fit of Equation 3–52 to the data with x equal to the fixed initial concentration of D-fructose and y equal to $k_{ATP,app}[HK]_t$. Parameter a for this fit is the specificity constant for $MgATP^{2-}$, $k_{ATP}[HK]_t$ [5.9 ± 0.2 μM D-fructose 6-phosphate min^{-1} (mM $MgATP^{2-}$)$^{-1}$], and parameter c is $k_{ATP,fruc}[HK]_t$ [2.7 ± 0.2 μM D-fructose 6-phosphate min^{-1} (mM $MgATP^{2-}$)$^{-1}$ (mM fructose)$^{-1}$]. **(E)** Initial rates for production of D-fructose 6-phosphate are presented as a function of initial concentrations of D-fructose (millimolar) at the five fixed initial concentrations of $MgATP^{2-}$. Each curve is for a higher fixed concentration of $MgATP^{2-}$ than the one below it. The curves drawn are fits of Equation 3–52 to the data with x equal to $[D\text{-fructose}]_0$ and y equal to v_0. **(F)** Reciprocals of the initial rates (minutes micromolar^{-1}) are presented as a function of reciprocals of the initial concentrations of D-fructose (millimolar^{-1}) at the five fixed initial concentrations of $MgATP^{2-}$. Each line fit to the data is for a higher fixed concentration of $MgATP^{2-}$ than the one above it. **(G)** The five values for parameter a, the apparent catalytic constants for D-fructose, $k_{0,fruc,app}[HK]_t$ (micromolar minute^{-1}), for the five fits of Equation 3–52 to each of the five subsets of data in Panel E (the five curves on the graph), are presented as a function of the fixed initial concentrations of $MgATP^{2-}$ corresponding to each value of $k_{0,fruc,app}[HK]_t$. The curve drawn is a fit of Equation 3–52 to the data with x equal to the respective fixed initial concentration of $MgATP^{2-}$ and y equal to the respective $k_{0,fruc,app}[HK]_t$. Parameter a of this fit is the catalytic constant for the enzymatic reaction, $k_0[HK]_t$ (3.47 ± 0.06 μM D-fructose 6-phosphate min^{-1}), and parameter c is the specificity constant for $MgATP^{2-}$, $k_{ATP}[HK]_t$ [5.9 ± 0.2 μM fructose 6-P min^{-1} (mM $MgATP^{2-}$)$^{-1}$] **(H)** The five values for parameter c, the apparent specificity constants for D-fructose, $k_{fruc,app}[HK]_t$ (micromolar minute^{-1} millimolar^{-1}), for the five fits of Equation 3–52 to each of the five subsets of data in Panel A, are plotted as a function of the respective fixed initial concentrations of $MgATP^{2-}$. The curve drawn is a fit of Equation 3–52 to the data with x equal to the fixed initial concentration of $MgATP^{2-}$ and y equal to $k_{fruc,app}[HK]_t$. Parameter a of this fit is the specificity constant for D-fructose, $k_{fruc}[HK]_t$ [1.30 ± 0.02 μM fructose 6-P min^{-1} (mM fructose)$^{-1}$], and parameter c is $k_{ATP,fruc}[HK]_t$ [2.72 ± 0.07 μM fructose 6-P min^{-1} (mM fructose)$^{-1}$ (mM $MgATP^{2-}$)$^{-1}$]. Averages of these values for $k_0[HK]_t$, $k_{ATP}[HK]_t$, $k_{fruc}[HK]_t$, and $k_{ATP,fruc}[HK]_t$ were inserted into Equation 3–106 to obtain the lines in Panels B and F.

At the upper limit for Equation 3–40

$$\lim_{[A]_0 \to \infty} v_0 = k_0[E]_t \tag{3–41}$$

and at the lower limit

$$\lim_{[A]_0 \to 0} v_0 = k_A[E]_t[A]_0 \tag{3–42}$$

(Figure 3–1B). Consequently, in this formalism, the fundamental parameters defining the function, the rate constants $k_0[E]_t$ and $k_A[E]_t$, are its horizontal asymptote (Equation 3–41) and its initial slope (Equation 3–42). Recognizing these as the fundamental parameters allows Equation 3–40 to be rewritten as

$$v_0 = \frac{(k_0[E]_t)(k_A[E]_t)[A]_0}{k_0[E]_t + k_A[E]_t[A]_0} \tag{3–43}$$

Historically, however, the behavior of the initial rate of an enzymatic reaction as a function of the initial concentration of reactant has been defined by the equation[70]

$$v_0 = \frac{V[A]_0}{K_{mA} + [A]_0} \tag{3–44}$$

where the parameter V is referred to as the **limiting rate** and the parameter K_{mA} as the **Michaelis constant for reactant A**. With this formalism

$$\lim_{[A]_0 \to \infty} v_0 = V \tag{3–45}$$

but K_{mA} is not a limit. Instead, the Michaelis constant, K_{mA}, is equal to the initial concentration of the varied reactant, $[A]_0$, at which the initial rate of the reaction, v_0, has half its asymptotic value, V (Figure 3–1B). By comparing Equations 3–43 and 3–44, it can be seen that

$$k_0 [E]_t = V \tag{3–46}$$

$$\frac{k_0 [E]_t}{k_A [E]_t} = K_{mA} \tag{3–47}$$

from which it follows that

$$k_A [E]_t = \frac{V}{K_{mA}} \tag{3–48}$$

Equations 3–40 and 3–44 are equations defining a **rectangular hyperbola**. The equation

$$pq = -d^2 \tag{3–49}$$

is the accepted definition of a rectangular hyperbola within the fourth quadrant of the coordinate system (p,q). Because this rectangular hyperbola is entirely within the fourth quadrant, all the values of p are positive numbers and all the values of q are negative numbers. The original coordinate system for this rectangular hyperbola is translated to a new origin at a point on the curve (p_o, q_o) to create a new coordinate system (x, y). Since

$$p = x + p_o \tag{3–50}$$

$$q = y + q_o \tag{3–51}$$

and $q_o p_o$ is equal to $-d^2$, Equation 3–49, upon substitution and rearrangement, becomes

$$y = \frac{(-q_o)x}{\left[\frac{d^2}{(-q_o)}\right] + x} = \frac{ax}{b+x} = \frac{acx}{a+cx} \tag{3–52}$$

for the still rectangular hyperbola. Because the ordinate of the point (p_o, q_o) on the curve was in the fourth quadrant of the original coordinate system, the numerical value of q_o is negative (as are all numerical values of q), and a, b, and c are positive numbers. The horizontal asymptote of the translated rectangular hyperbola, which used to be the axis of the abscissa before the translation, is now $y = -q_o = a$. The slope of the rectangular hyperbola at the new origin is either $a\,b^{-1}$ or c, which are both equal to $q_o^2\ d^{-2}$. Consequently, the value for the horizontal asymptote is defined by the choice of the new origin, and the value for the initial slope is then defined by the parameter d^2. Equation 3–52 has the same form as Equations 3–43 and 3–44.

The most accurate values for the rate constants $k_A[E]_t$ and $k_0[E]_t$ in Equation 3–43 or the Michaelis constant K_{mA} and the limiting rate V in Equation 3–44 are obtained by **numerical analysis from experimental values for the initial rate v_0 as a function of the initial concentration of reactant A, $[A]_0$.** The data are a set of initial rates for the reaction, v_0, corresponding to a set of initial molar concentrations of reactant A. A sequence of initial concentrations of reactant A is chosen so that the values are evenly spaced over a range from a nearly saturating concentration to a concentration well below that equal to the Michaelis constant. Spacing the concentrations evenly ensures that values throughout the range of concentrations in which the initial rate is changing most rapidly with concentration, in particular the region around the Michaelis constant, are sampled. At the present time, the equation for a rectangular hyperbola (Equation 3–52) is fitted directly to the data (Figures 3–1B, 3–2, and 3–3A) by nonlinear least-squares analysis.[71] For the fit, y is the initial rate v_0, and x is the initial concentration $[A]_0$. Parameter a obtained from the fit is the rate constant $k_0[E]_t$ or the limiting rate V, parameter c obtained from the fit is the rate constant $k_A[E]_t$, and parameter b obtained from the fit is the Michaelis constant K_m. In the past, to determine values for the kinetic constants, the data were first converted to a linear form before the fitting was performed; but that practice, although it is still done occasionally, has been supplanted by the nonlinear numerical analysis made possible by digital computers, which

were not available when the habit of linearizing the data was universal.

Numerical values for the parameters $k_A[E]_t$ and $k_0[E]_t$ or the Michaelis constant K_{mA} and the limiting rate V and standard deviations of those numerical values are the numerical values obtained by the fitting procedure and are the **experimental observations**. Although K_{mA} and V are the parameters most often tabulated, the specificity constant k_A for reactant A and the catalytic constant k_0 are the two rate constants that have been found to vary independently of each other when pH, temperature, and concentrations of reactants, products, and inhibitors are varied. They also turn out to be the **most fundamental and informative numbers**.[72]

There is unequivocal evidence from crystallographic observations that enzymes have on their surfaces, or within their protein, active sites, at which reactants bind and are transformed into products. Most enzymes are rotationally symmetric oligomeric proteins. The **protomers of a rotationally symmetric oligomeric protein** are the identical, constituent complexes, between one or several folded polypeptides, each different from the others, that when combined in a fixed stoichiometry, form the oligomeric protein.[73] There is almost always one and only one active site that catalyzes a particular reaction for each protomer in an oligomeric protein that is an enzyme. These facts define the molar concentration of active sites in a given solution as being equal to the molar concentration of protomers.

If the total molar concentration of enzymatic active sites in the solution, $[E]_t$, is known from both the mass concentration of protein and the molar mass of its protomers, then explicit values for the catalytic constant k_0 and the specificity constant k_A for reactant A can be obtained from the observed values for $k_0[E]_t$ and $k_A[E]_t$ by simple division. The units on the observed values for $k_0[E]_t$ are molar concentration of product minute^{-1}. When $k_0[E]_t$ is divided by the molar concentration of active sites and the units of liter and the Avogadro constants in numerator and denomitor are canceled, the units on k_0 become molecules of product second^{-1} (molecule of active site)$^{-1}$; in other words, the number of molecules that active site turns into product every second. These units are always simplified to second^{-1} by canceling molecules of product by molecules of enzyme, essentially dividing apples by oranges. The units on the observed values for $k_A[E]_t$ are molar concentration of product minute^{-1} (molar concentration of reactant A)$^{-1}$. When $k_A[E]_t$ is divided by the molar concentration of active sites, the units on k_A become molar concentration of product minute^{-1} (molar concentration of reactant A)$^{-1}$ (molar concentration of active sites)$^{-1}$. Again, apples and oranges are divided, and the value becomes (molar concentration of reactant A)$^{-1}$ second^{-1}. This second-order rate constant (molar^{-1} second^{-1}) can be thought of, in the simplest instance, as the rate constant for the association of reactant A with the active site, but it will become clear that this is a simplistic interpretation. An example of these two conversions would be those applied to the kinetic observations of phosphoribosyl-anthranilate isomerase from *S. cerevisiae* (Figure 3–2). From the known concentrations of active sites added to the solution, the values of the catalytic constant k_0 and the specificity constant k_{pra} for phosphoribosylanthranilate are 40 ± 0.4 s^{-1} and 8.0 ± 0.2 μM^{-1} s^{-1}, respectively.[67]

In the case of kinetic observations of β-fructofuranosidase (FF) from *S. cerevisiae* (Figure 3–3), however, a partially purified cellular extract was used, so the total molar concentration of enzymatic active sites was unknown, and the extinction coefficient for the optical rotation that was used to follow the rates of the reaction was not provided either. As a result, only the rate constants $k_0[FF]_t$, 0.032 ± 0.002 degree min^{-1}, and $k_{suc}[FF]_t$, 4.3 ± 0.4 M^{-1} degrees min^{-1}, where k_{suc} is the specificity constant for sucrose, could be determined. Values, however, for the limiting rate V, which is equal to $k_0[FF]_t$, and the Michaelis constant for sucrose $K_{m,suc}$, 0.74 mM sucrose, could be tabulated in this instance. The fact that the value for the limiting rate V exists in the absence of knowledge of the concentration of active sites and the fact that **the value for the Michaelis constant K_{mA} is determined only by the initial free molar concentrations of reactant** in the different samples, which are almost always known quantities, are superficial advantages to using these parameters. These facts also explain why Equation 3–44 was used so frequently in the past, when the concentrations of active sites were unknown or poorly known.

While the tabulated values for the parameters $k_A[E]_t$ and $k_0[E]_t$ or K_{mA} and V should always be obtained by direct numerical analysis, the data themselves are often presented graphically in a linear form. The most widely used linear form is that based on the inverse of Equation 3–43 or Equation 3–44

$$\frac{1}{v_0} = \frac{1}{k_A [E]_t [A]_0} + \frac{1}{k_0 [E]_t} = \frac{K_{mA}}{V [A]_0} + \frac{1}{V} \qquad (3\text{–}53)$$

If the values for v_0^{-1} are plotted against the corresponding values for $[A]_0^{-1}$, the points should define a straight line the intercept of which at the axis of the ordinate is $(k_0[E]_t)^{-1}$ or V^{-1} , the slope of which is $(k_A[E]_t)^{-1}$ or $K_{mA}\,V^{-1}$, and the intercept of which at the axis of the abscissa is $-k_A\,(k_0)^{-1}$ or $-K_{mA}^{-1}$ (Figure 3–3B). Because this linear form, referred to as the double-reciprocal plot,[74] separates all the important parameters, $k_A[E]_t$ and $k_0[E]_t$ or V, K_{mA}, and $V\,K_m^{-1}$, it is perhaps the most useful presentation for a rapid visual evaluation of the data. For example, if water is disregarded, chymotrypsin catalyzes the hydrolysis of a single reactant, namely, any one in a series of phenyl hippurates

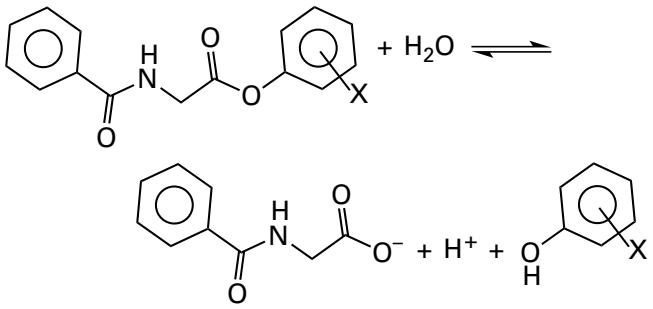

(3–54)

In this equation, X stands for a series of different substituents on the phenyl group. The behavior of v_0^{-1} as a function of $[\text{hippurate}]_0^{-1}$ for the hydrolysis of phenyl hippurates by chymotrypsin is linear with positive slope for the whole series of phenyl hippurates that were studied (Figure 3–5).[75] It is immediately obvious from visual inspection that the identity of the functional group X has its major, if not exclusive, effect on the value of the specificity constant k_{phh} for phenyl hippurate. Such visual inspections are the reason that linear presentations are often used.

To provide an explanation of the observed kinetic behavior and to give meaning to the two parameters—the specificity constant k_A for reactant A and the catalytic constant k_0, or the Michaelis constant K_{mA} for reactant A and the limiting rate V—a **kinetic mechanism is proposed**, and it is demonstrated mathematically that the kinetic mechanism predicts that the enzymatic reaction will display the observed behavior. In this exercise, however, it is

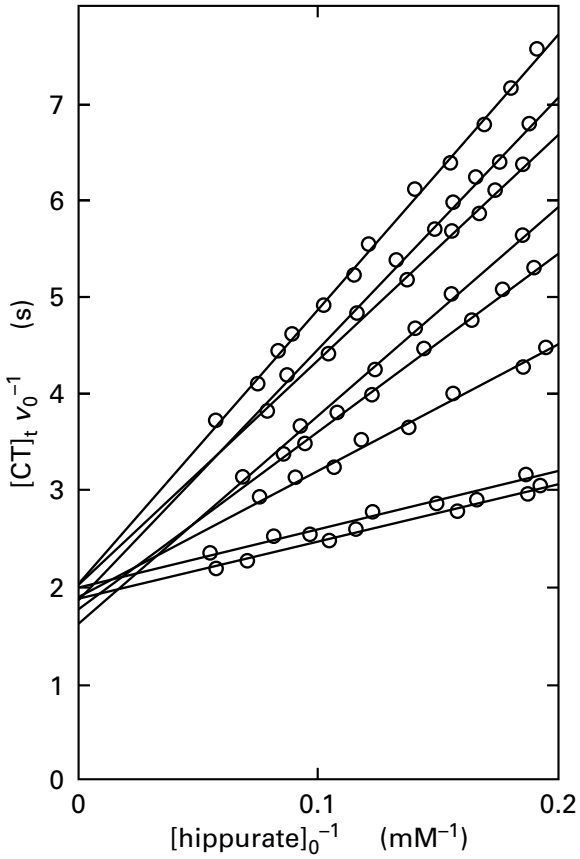

Figure 3–5: Kinetics for the hydrolysis of a series of phenyl hippurates by chymotrypsin.[75] Equivalent amounts of chymotrypsin (CT) were mixed with a series of solutions containing various concentrations of a particular phenyl hippurate at an ionic strength of 0.1 M, at pH 6.91 and 25 °C. The initial rate of release of the respective phenol was followed by its characteristic absorbance in the near-ultraviolet to provide a set of initial rates, v_0, corresponding to the set of concentrations of the respective phenyl hippurate. The reciprocal of each initial rate (seconds millimolar^{-1}) was multiplied by the total molar concentration for active sites of chymotrypsin ($[CT]_t$), and the resulting values ($[CT]_t\ v_0^{-1}$ in seconds) are plotted as a function of the reciprocals of the initial concentrations of the respective hippurate (millimolar) corresponding to those initial rates. The lines, in descending order, connect the data for the hydrolysis by chymotrypsin of the phenyl hippurates formed from phenol, 4-fluorophenol, 4-chlorophenol, 4-cresol, 4-methoxyphenol, 3-nitrophenol, 4-nitrophenol, and 4-acetophenol.

essential to maintain a separation between the observations and the kinetic mechanism proposed as an explanation for the observations. The reason for maintaining this separation is that the kinetic mechanism is **never an exclusive explanation** for the observations, only consistent with the observations.

Kinetic Mechanisms for One Reactant

Observation: In the case of an enzyme that has only one reactant and one product, such as phosphoribosylanthranilate isomerase from *S. cerevisiae* (Equation 3–9), the only observation to be explained is that the initial rate of an enzymatic reaction is usually a rectangularly hyperbolic function (Equation 3–40) of the initial concentration of the reactant (Figure 3–2).[67]

Explanation: A **kinetic mechanism**[76] that can explain the rectangularly hyperbolic behavior of the initial rate of the reaction as a function of the initial concentration of the lone reactant, $[A]_0$, is

$$E + A \underset{k_{-1}}{\overset{k_1}{\rightleftharpoons}} E{\cdot}A \xrightarrow{k_2} E + Z \qquad (3\text{–}55)$$

A complex, E·A, is formed reversibly between reactant A and the active site of enzyme E but does not involve the chemical transformation of reactant A. In the next step, the bound reactant A is converted to product Z, and product Z then dissociates from the enzyme. The very last step, the dissociation of Z, is an irreversible process because there is no product Z in the solution under the initial conditions. It should be emphasized that this kinetic mechanism was written by intuition rather than by deduction and is only a proposal to explain the kinetic behavior.

A **rate equation is then derived from the proposed kinetic mechanism**. A rate equation is a mathematical equation, derived from the written kinetic mechanism, that relates the observed initial rate, v_0, of the reaction to the initial concentrations of reactants, in this case, $[A]_0$, and the total concentration of the enzyme, $[E]_t$, all of which are known quantities

$$v_0 = f([E]_t, [A]_0) \qquad (3\text{–}56)$$

In a rate equation, the only parameters are rate constants, in this instance, k_1, k_{-1}, and k_2.

Because the only way that a product can be formed is through the step governed by k_2, it follows that

$$v_0 = \frac{d[Z]}{dt} = k_2[E{\cdot}A] \qquad (3\text{–}57)$$

But [E·A] is not a known concentration as are $[E]_t$ and $[A]_0$. The concentration of the complex between the active site and reactant A, [E·A], and the concentration of unoccupied active site, [E], are unknowns, and an expression for [E·A] only in terms of known quantities and rate constants must be obtained. To eliminate the unknown variable [E] and solve for the unknown variable [E·A], a set of **independent simultaneous equations** must be formulated such that there are as many independent simultaneous equations as there are unknown variables, as in any algebraic solution for multiple unknowns.

The first simultaneous equation in all derivations of steady-state rate equations for enzymatic catalysis is the **conservation of enzyme**, in analogy to an equation for the conservation of mass in an acid–base calculation. The total molar concentration of active sites, which is usually a known quantity, but that always remains constant throughout the reaction, must be equal to the sum of the concentrations of all forms of the active site. In the simple case of the kinetic mechanism in Equation 3–55

$$[E]_t = [E] + [E{\cdot}A] \qquad (3\text{–}58)$$

The next group of simultaneous equations are the **steady-state relations**. The approximation that is always made in derivations of this kind is that because the concentration of reactant is so much greater than the concentration of enzyme, after the first few molecules of reactant have been turned into product by each molecule of enzyme, the concentration of each species involving the enzyme has reached a constant, steady state. This approximation follows in the simple case of the kinetic mechanism of Equation 3–55 from the consideration that if [E·A] were increasing, [E] would be decreasing, and the rate of formation of E·A would be decreasing while its rate of decay would be increasing. At some point, the rate of formation and the rate of decay of E·A would become equal, and its concentration would remain constant. A similar argument can be made for the situation in which [E·A] is decreasing. As long as $[A]_0$ remains unchanged, which is the definition of an initial rate (Equation 3–37), the individual concentrations of all forms of the enzyme will remain constant once the steady state has been reached.

Direct measurements of the **rate of attainment of steady state** have shown that it is usually achieved within less than 1 s with most enzymes, but some enzymes reach steady state more slowly, in at least one instance taking as long as an hour.[77] In such peculiar circumstances, the initial rate of the reac-

tion is seen to increase with time rather than remaining constant or decreasing with time.

For the kinetic mechanism of Equation 3–55, the **steady-state approximation** is

$$\frac{d[\mathrm{E}]}{dt} = -\frac{d[\mathrm{E{\cdot}A}]}{dt} = 0 \tag{3–59}$$

Although this relation seems to define two equations, they turn out to be the same equation. The number of simultaneous, independent steady-state equations is always one less than the number of kinetically unique forms of the enzyme, the concentrations of which are the unknowns, and the shortfall is made up by the equation stating the conservation of enzyme (Equation 3–58). The single steady-state equation for the kinetic mechanism of Equation 3–55 is

$$\frac{d[\mathrm{E{\cdot}A}]}{dt} = k_1[\mathrm{E}][\mathrm{A}]_0 - \left(k_{-1} + k_2\right)[\mathrm{E{\cdot}A}] = 0 \tag{3–60}$$

Equation 3–60 states that the difference between the rate at which E·A is formed and the rate at which E·A is lost must be zero at steady state.

When the two independent simultaneous equations, Equations 3–58 and 3–60, are used to **solve algebraically** for [E·A] in terms of the known quantities, it is found that

$$[\mathrm{E{\cdot}A}] = \frac{k_1[\mathrm{E}]_t[\mathrm{A}]_0}{\left(k_{-1} + k_2\right) + k_1[\mathrm{A}]_0} \tag{3–61}$$

and that

$$v_0 = \frac{k_2 k_1[\mathrm{E}]_t[\mathrm{A}]_0}{\left(k_{-1} + k_2\right) + k_1[\mathrm{A}]_0} = \frac{k_2[\mathrm{E}]_t\left(\dfrac{k_2 k_1}{k_{-1} + k_2}\right)[\mathrm{E}]_t[\mathrm{A}]_0}{k_2[\mathrm{E}]_t + \left(\dfrac{k_2 k_1}{k_{-1} + k_2}\right)[\mathrm{E}]_t[\mathrm{A}]_0} = \frac{k_2[\mathrm{E}]_t[\mathrm{A}]_0}{\left(\dfrac{k_{-1} + k_2}{k_1}\right) + [\mathrm{A}]_0} \tag{3–62}$$

Taking the limits of Equation 3–40 and Equation 3–62

$$\lim_{[\mathrm{A}]_0 \to \infty} v_0 = k_0[\mathrm{E}]_t = k_2[\mathrm{E}]_t \tag{3–63}$$

$$\lim_{[\mathrm{A}]_0 \to 0} v_0 = k_\mathrm{A}[\mathrm{E}]_t[\mathrm{A}]_0 = \frac{k_1 k_2}{k_{-1} + k_2}[\mathrm{E}]_t[\mathrm{A}]_0 \tag{3–64}$$

Equation 3–62 is of the form of Equation 3–43 and Equation 3–44 and, therefore, provides an explanation of the observed behavior. It states that the measured value of the catalytic constant, k_0, is k_2, the measured value of V is $k_2[\mathrm{E}]_t$, the measured value of the specificity constant k_A for reactant A is $k_1k_2(k_{-1} + k_2)^{-1}$, and the measured value of the Michaelis constant for reactant A, K_{mA}, is $(k_2 + k_{-1})(k_1)^{-1}$, if the kinetic mechanism of Equation 3–55 is the actual kinetic mechanism applicable to the enzyme in question.

The point of the exercise is that the kinetic mechanism of Equation 3–55, which was formulated only by intuition and which did not follow by deduction from the observations, is nevertheless consistent with the behavior of the reaction as it is experimentally observed.

All present explanations of the catalytic activity of enzymes assume that the molecules of reactant associate with a molecule of the enzyme and are converted to products while they are bound, as they are in the kinetic mechanism of Equation 3–55. This hypothesis and kinetic mechanisms of the type represented by Equation 3–55 were originally intended to[64] and do provide an explanation for the universally observed fact that **the initial rate of an enzymatic reaction approaches a horizontal asymptote** as the initial concentrations of the reactants are increased. This explanation is that at high concentrations of the reactants, the enzyme is saturated and this saturation limits the rate of the overall reaction to the rate at which reactants can be converted to products while they are bound to the enzyme and those products can dissociate. Nonenzymatic catalysis can also display saturation for the same reasons.[78]

To understand what the kinetic constants in a kinetic mechanism and a rate equation represent, the difference between an elementary reaction and a composite reaction and the difference between elementary rate constants and composite rate constants must be understood. These differences are easiest to understand in the simplest possible kinetic mechanism, that of an enzymatic

reaction with only one reactant and one product. In the kinetic mechanism of Equation 3–55, the rate constant k_2 can have one of two quite different meanings, depending on the intentions of the author of the kinetic mechanism. If k_2 was intended to be an elementary rate constant, then the step immediately following the formation of the complex E·A has been designated the rate-limiting step in the reaction. As the kinetic mechanism is written, however, there must be at least two steps between the complex E·A and the dissociated enzyme E and product Z. These steps are the transformation of reactant A to product Z on the active site of the enzyme and the dissociation of product Z from the active site. If the author intended the rate constant k_2 to include the rate constants for these steps, then k_2 is a composite rate constant.

An **elementary reaction** is a reaction for which no reaction intermediates have been detected or need to be postulated to describe the chemical reaction on a molecular scale. An elementary reaction occurs in a single step and passes through only one transition state. An **elementary rate constant** is the rate constant for an elementary reaction. If a step in a kinetic mechanism is an elementary reaction, the respective rate constants for its two directions are elementary rate constants. The ultimate ideal of a kinetic investigation is to define explicitly the complete sequence of elementary steps in a reaction and to assign a numerical value to each elementary rate constant. In simple nonenzymatic reactions, the chemical mechanism usually involves only a few steps, and the individual events, such as bond-making, bond-breaking, hydronation, electron transfer, or noncovalent association, can be written as explicit steps, each of which seems to have only one transition state. Rate constants are then assigned systematically to these steps to define the elementary kinetics. In such situations, the measured rate constants are assumed to be elementary rate constants associated with the explicit chemical events.

If the author of the kinetic mechanism of Equation 3–55 intended k_2 to be an elementary rate constant, then k_2 cannot include the rate constant for the release of product because the release of product must involve a different transition state from the transition state that immediately follows the formation of the complex between enzyme and reactant. If the rate constant k_2 is intended to be the elementary rate constant only for the step immediately following the formation of the complex between enzyme and reactant, then the author of the kinetic mechanism has implicitly designated the step governed by the rate constant k_2 as the **rate-limiting step** of the overall reaction.[79] This designation follows from the fact that the author ignored the elementary rate constants for all the later steps.

Most students have been exposed to simple chemical kinetics before they encounter enzymatic kinetics and are trained to treat an unadorned rate constant as an elementary rate constant. This habit is always a simplification because even straightforward chemical reactions often involve more transition states, and hence more elementary steps, than have been defined. Even if there are several elementary steps between two points in a kinetic mechanism, however, there is a rate at which the reaction proceeds between those two points and a rate constant that can be assigned to the flux between those two points.

A **composite reaction** is a chemical reaction or a step in the kinetic mechanism for a reaction for which the expression for the rate of disappearance of a reactant or the rate of appearance of a product involves elementary rate constants of more than one elementary reaction. A composite reaction proceeds through more than one transition state and involves more than one elementary step. A **composite rate constant** is a rate constant for a composite reaction or a step in a kinetic mechanism that is a composite reaction. A composite rate constant can be expressed as a combination of several elementary rate constants for the several elementary steps between the two points. In the literature in which steady-state enzymatic kinetics are presented, composite rate constants are often called net rate constants.[80]

Suppose that k_2 is not a rate-limiting elementary rate constant in the kinetic mechanism of Equation 3–55 and that it is a composite rate constant for two steps: the transformation of reactant to product and the dissociation of product

$$\mathrm{E{\cdot}A} \underset{k_{-6}}{\overset{k_6}{\rightleftharpoons}} \mathrm{E{\cdot}Z} \xrightarrow{k_7} \mathrm{E} + \mathrm{Z} \qquad (3\text{–}65)$$

In this expansion of the second step in the kinetic mechanism of Equation 3–55, the dissociation of product, governed by the rate constant k_7, is written as an irreversible process, as was the second step in the kinetic mechanism of Equation 3–55, because there is no product in the solution under

the initial conditions. The rate at which product is produced

$$v_0 = \frac{d[Z]}{dt} = k_7[E{\cdot}Z] \tag{3–66}$$

If it is assumed that E·Z is in steady state, then

$$\frac{d[E{\cdot}Z]}{dt} = k_6[E{\cdot}A] - (k_{-6} + k_7)[E{\cdot}Z] = 0 \tag{3–67}$$

and

$$\frac{d[Z]}{dt} = \left(\frac{k_6 k_7}{k_{-6} + k_7}\right)[E{\cdot}A] \tag{3–68}$$

In the kinetic mechanism of Equation 3–55

$$\frac{d[Z]}{dt} = k_2[E{\cdot}A] \tag{3–69}$$

Therefore, if k_2 is a composite rate constant for the two steps in the expanded kinetic mechanism (Equation 3–65), then

$$k_2 = \frac{k_6 k_7}{k_{-6} + k_7} \tag{3–70}$$

If, however, k_6 is in fact the rate-limiting step of the reaction, then by definition[79] $k_7 >> k_{-6}$, k_2 equals k_6, and k_2 is the rate-limiting step.

Regardless of whether k_2 in the kinetic mechanism of Equation 3–55 is a rate-limiting elementary rate constant for the overall reaction or a composite rate constant including several steps, one of which is dissociation of the product, the transformation to which it refers, the conversion of reactant to product on the enzyme and the dissociation of the product from the enzyme, is kinetically irreversible. This property follows from the fact that the step governing the dissociation of the product must be irreversible because no product is present in the solution during the initial interval. The **creation of irreversibility by omitting one or more of the products** of a reaction is one purpose behind measuring its initial rates. In this way, the rate measured is a unidirectional rate and the equations are greatly simplified.

Formally, the rate constant k_1 in Equation 3–55 is the second-order rate constant for formation of the complex E·A, and the rate constant k_{-1} is the first-order rate constant for its dissociation. Although there is no necessity to assume it, the **rate constants k_1 and k_{-1} for formation of the complex preceeding the conversion of A to Z could also be composite rate constants**. In fact, they usually are. Suppose, for example, that there were three steps that preceded the conversion of reactant into product, one for association of the reactant with the enzyme and two involving isomerizations of the enzyme and reactant A, respectively

$$E + A \underset{k_{-3}}{\overset{k_3}{\rightleftharpoons}} E{\cdot}A \underset{k_{-4}}{\overset{k_4}{\rightleftharpoons}} E'{\cdot}A \underset{k_{-5}}{\overset{k_5}{\rightleftharpoons}} E'{\cdot}A' \tag{3–71}$$

The composite rate constant k_1 would then be the unidirectional rate constant for the conversion of E + A into E′·A′

$$E + A \underset{k_{-3}}{\overset{k_3}{\rightleftharpoons}} E{\cdot}A \underset{k_{-4}}{\overset{k_4}{\rightleftharpoons}} E'{\cdot}A \xrightarrow{k_5} E'{\cdot}A' \tag{3–72}$$

If it is assumed that [E·A] and [E′·A] are at steady state, then

$$k_3[E][A]_0 + k_{-4}[E'{\cdot}A] = (k_{-3} + k_4)[E{\cdot}A] \tag{3–73}$$

and

$$k_4[E{\cdot}A] = (k_{-4} + k_5)[E'{\cdot}A] \tag{3–74}$$

respectively. Solving for [E′·A]

$$[E'{\cdot}A] = \frac{k_3 k_4[E][A]_0}{k_{-3}k_{-4} + k_{-3}k_5 + k_4 k_5} \tag{3–75}$$

Because

$$\frac{d[E'{\cdot}A']}{dt} = k_5[E'{\cdot}A] = k_1[E][A]_0 \tag{3–76}$$

$$k_1 = \frac{k_3 k_4 k_5}{k_{-3}k_{-4} + k_{-3}k_5 + k_4 k_5} \tag{3–77}$$

The composite rate constant k_{-1} is the unidirectional rate constant for the conversion of E′·A′ into E + A

$$\mathrm{E'{\cdot}A'} \underset{k_5}{\overset{k_{-5}}{\rightleftharpoons}} \mathrm{E'{\cdot}A} \underset{k_4}{\overset{k_{-4}}{\rightleftharpoons}} \mathrm{E{\cdot}A} \xrightarrow{k_{-3}} \mathrm{E + A} \tag{3–78}$$

If it is assumed that [E′·A] and [E·A] are at steady state, then

$$k_4[\mathrm{E{\cdot}A}] + k_{-5}[\mathrm{E'{\cdot}A'}] = \left(k_{-4} + k_5\right)[\mathrm{E'{\cdot}A}] \tag{3–79}$$

and

$$k_{-4}[\mathrm{E'{\cdot}A}] = \left(k_{-3} + k_4\right)[\mathrm{E{\cdot}A}] \tag{3–80}$$

respectively. Solving for [E·A]

$$[\mathrm{E{\cdot}A}] = \frac{k_{-4}k_{-5}[\mathrm{E'{\cdot}A'}]}{k_{-3}k_5 + k_4k_5 + k_{-3}k_{-4}} \tag{3–81}$$

Because

$$\frac{d[\mathrm{E}]}{dt} = k_{-3}[\mathrm{E{\cdot}A}] = k_{-1}[\mathrm{E'{\cdot}A'}] \tag{3–82}$$

$$k_{-1} = \frac{k_{-3}k_{-4}k_{-5}}{k_{-3}k_{-4} + k_{-3}k_5 + k_4k_5} \tag{3–83}$$

The expressions for k_1, k_{-1}, and k_2, when they are the composite rate constants for the steps in the now **expanded kinetic mechanism**

$$\mathrm{E + A} \underset{k_{-3}}{\overset{k_3}{\rightleftharpoons}} \mathrm{E{\cdot}A} \underset{k_{-4}}{\overset{k_4}{\rightleftharpoons}} \mathrm{E'{\cdot}A} \underset{k_{-5}}{\overset{k_5}{\rightleftharpoons}} \mathrm{E'{\cdot}A'} \underset{k_{-6}}{\overset{k_6}{\rightleftharpoons}} \mathrm{E{\cdot}Z} \xrightarrow{k_7} \mathrm{E + Z} \tag{3–84}$$

contain only rate constants, regardless of whether they themselves are elementary rate constants or composite rate constants. Consequently, the form of the rate equations for the kinetic mechanisms of Equations 3–55 and 3–84 must be the same, and both of these kinetic mechanisms must be consistent with the experimental observation that the initial rate of an enzymatic reaction as a function of the initial concentration of the reactant is defined by Equation 3–40. **Steady-state kinetics cannot decide which kinetic mechanism is the complete kinetic mechanism**, or if either of them is, because further expansion of the kinetic mechanism is possible by supplying additional steps, and each expanded kinetic mechanism will also be consistent with the observations. The only facts are the observed behavior, and kinetic mechanisms are simply attempts by the authors to explain the facts.

The rate equations for such expanded kinetic mechanisms, however, are not simply Equation 3–62 with k_1, k_{-1}, and k_2 replaced by the respective composite rate constants. Equations such as Equation 3–61 define the **fraction of the total enzyme that is in a particular form**, in this instance the fraction of the total enzyme that is E·A. In the kinetic mechanism defined by Equation 3–84, [E·A] at steady state is no longer the same fraction of the total enzyme as that defined by Equation 3–61. There are now new forms of the enzyme, E′·A, E′·A′, and E·Z, in addition to E·A and E. Consequently, the expression for $[\mathrm{E}]_t$ (Equation 3–58) must be expanded to include these new forms, a new equation for [E·A] as a new fraction of the total enzyme must be derived to replace Equation 3–61, and that equation will not be the same as Equation 3–61.

For example, consider the **most reasonable kinetic mechanism for an enzyme with one substrate**

$$\mathrm{E + A} \underset{k_{-1}}{\overset{k_1}{\rightleftharpoons}} \mathrm{E{\cdot}A} \underset{k_{-6}}{\overset{k_6}{\rightleftharpoons}} \mathrm{E{\cdot}Z} \xrightarrow{k_7} \mathrm{E + Z} \tag{3–85}$$

If it is assumed that

$$v_0 = k_7[\mathrm{E{\cdot}Z}] \tag{3–86}$$

that

$$[\mathrm{E}]_t = [\mathrm{E}] + [\mathrm{E{\cdot}A}] + [\mathrm{E{\cdot}Z}] \tag{3–87}$$

that

$$\frac{d[\mathrm{E}]}{dt} = k_7[\mathrm{E{\cdot}Z}] + k_{-1}[\mathrm{E{\cdot}A}] - k_1[\mathrm{E}][\mathrm{A}] = 0 \tag{3–88}$$

and that Equation 3–67 supplies the required second steady-state relation, the rate equation that results from a standard derivation is

$$v_0 = \frac{\left(\frac{k_6 k_7 [\mathrm{E}]_t}{k_{-6} + k_6 + k_7}\right)\left(\frac{k_1 k_6 k_7 [\mathrm{E}]_t}{k_{-1}k_{-6} + k_{-1}k_7 + k_6 k_7}\right)[\mathrm{A}]_0}{\left(\frac{k_6 k_7 [\mathrm{E}]_t}{k_{-6} + k_6 + k_7}\right) + \left(\frac{k_1 k_6 k_7 [\mathrm{E}]_t}{k_{-1}k_{-6} + k_{-1}k_7 + k_6 k_7}\right)[\mathrm{A}]_0} \qquad (3\text{–}89)$$

Equations 3–67, 3–87, and 3–88 can be used to show that, for the kinetic mechanism proposed in Equation 3–85

$$[\mathrm{E{\cdot}A}] = \frac{(k_{-6} + k_7)k_1 [\mathrm{E}]_t [\mathrm{A}]_0}{(k_{-1}k_{-6} + k_{-1}k_7 + k_6 k_7) + (k_{-6} + k_6 + k_7)k_1 [\mathrm{A}]_0} \qquad (3\text{–}90)$$

If [E·A] defined by this equation is multiplied by the composite rate for formation of product from E·A (Equation 3–68), Equation 3–89 is again the result. Consequently, when a correct equation for the fraction of the total enzyme that is in a particular form is derived, this fraction and the appropriate composite rate constant can be combined to obtain the correct rate equation. This approach is a correct way of proceeding. If, however, k_2 in Equation 3–61 is simply replaced by the composite rate of Equation 3–68, Equation 3–90 is not the result, because Equation 3–61 does not give the correct value of [E·A] for the new kinetic mechanism. This approach is an incorrect way of proceeding. This exercise demonstrates that composite rate constants, which were used to show that expanded kinetic mechanisms give the same form of the rate equation and which will be used later for other purposes, can be misleading in deriving the rate equation from an explicit kinetic mechanism. It follows that the only infallible approach is to derive the rate equations for a proposed mechanism starting with the equation for conservation of enzyme and the steady-state equation.

An example of a kinetic mechanism for which it is known that there are **intermediates between the association of reactant and the production of product** bound in the active site, as in the first portion of Equation 3–84, would be that for the hydrolysis of phenyl hippurates by chymotrypsin (Equation 3–54). Chymotrypsin is an enzyme that hydrolyzes amides and esters by performing a nucleophilic substitution (Figure 1–10) that transfers the acyl group of the amide or ester to the hydroxy group of one of its serines, which acts as the nucleophile, to form an acyl intermediate (Figure 3–6).

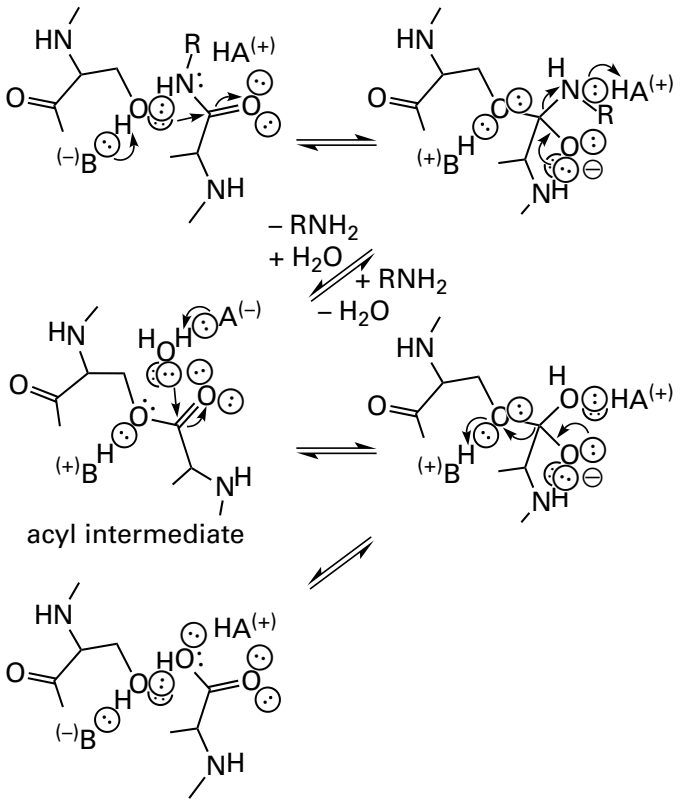

Figure 3–6: Mechanism by which serine endopeptidases catalyze the hydrolysis of a peptide bond. Attack of the hydroxy group of a serine in the active site, which is dehydronated as it adds to the acyl carbon of the amide of the peptide bond, produces the tetrahedral intermediate. The oxyanion of the tetrahedral intermediate pushes out the amine upon hydronation of its nitrogen to produce the acyl intermediate. A molecule of water replaces the amine in the active site. Attack of the molecule of water, which is dehydronated as it adds to the acyl carbon of the acyl intermediate, produces the second tetrahedral intermediate. The oxyanion pushes out the hydroxy group of the serine as it is being hydronated to produce the carboxylic acid. The hydrolysis requires a catalytic acid–base, $^{(-)}\mathrm{B}\odot$, at the hydroxy group of the serine and a catalytic acid–base, $\mathrm{HA}^{(+)}$, at the location occupied by the amino group and the molecule of water. These requirements are actually fulfilled by the same acid–base, usually a histidine, that pivots between the two positions.

A kinetic mechanism for hydrolysis of phenyl hippurates catalyzed by chymotrypsin, which ignores the details of the hydrolysis of the ester of the serine and release of the two products, could be

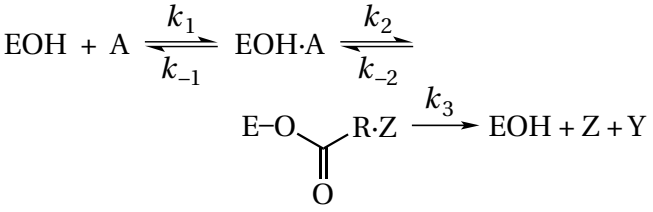

(3–91)

where A is the ester that is the reactant (Equation 3–54), E–OC(O)R is the seryl ester that is the acyl intermediate, Z is the phenol that is one product, and Y is the carboxylic acid that is the other. The rate equation for the kinetic mechanism as written is Equation 3–43, which has a catalytic constant

$$k_0 = \frac{k_2 k_3}{k_2 + k_{-2} + k_3} \tag{3–92}$$

and a specificity constant for a particular phenyl hippurate

$$k_{\text{phh}} = \frac{k_1 k_2 k_3}{k_{-1} k_{-2} + k_{-1} k_3 + k_2 k_3} \tag{3–93}$$

Because the nucleophilic substitution in Equation 3–54 is an alcohol for a phenol, $k_2 >> k_{-2}$ (Table 1–3).

When the reciprocals of the initial rates for the hydrolysis of several phenyl hippurates by chymotrypsin are plotted as a function of the initial concentrations of several phenyl hippurates, it can be seen that the catalytic constant is the same for all of them (Figure 3–5). It is unlikely that k_2 is the same for all the substituted phenols, so only if $k_2 >> k_3$ and $k_0 = k_3$ would k_0 be invariant. The specificity constants for the phenyl hippurates, however, register the effects of changes in the functional groups on the elementary rate constants k_2 and k_{-2}, but only indirectly.

Parenthetically, the effects of functional groups on the rate of hydrolysis of phenyl hippurates is an example of a **structure–activity correlation**. In this case, a correlation between the ability of the phenol as a leaving group and the specificity constants for phenyl hippurates was sought, but no systematic relation was observed. In the case of hydrolysis of a series of aryl β-D-glucosides and aryl β-D-cellobiosides by cellulose 1,4-β-cellobiosidase from *Cellulomonas fimi*, however, there was a clear correlation between the pK_a of the phenol that was the leaving group and the specificity constant for that reactant.[81]

It is often stated that kinetics cannot prove a kinetic mechanism and that **a kinetic mechanism can only be consistent with kinetic observations**. There are two levels of meaning to this statement. The first level of meaning is that kinetics cannot prove a kinetic mechanism because the possibility always exists that there is a significantly different kinetic mechanism with a different sequence of steps that is, nevertheless, also consistent with all the experimental observations. In this meaning, the kinetic method, because it proceeds inductively, must always suffer from this problem, which is common to all inductive reasoning. It follows that the most powerful use of kinetics is to disprove a proposed kinetic mechanism. One should never make the mistake, however, of assuming that since all the kinetic mechanisms you could imagine but one have been disproven, the one that has not been disproven has been proven. The second level of meaning is that even if a particular kinetic mechanism can be shown by independent experiments to be the correct kinetic mechanism, it may, nevertheless, be incomplete. **The complete kinetic mechanism for a chemical reaction includes explicitly every elementary step in that reaction**. A kinetic mechanism in which one or more of the steps are composite reactions or one or more of the rate constants are composite rate constants is an incomplete kinetic mechanism for the reaction even if it is not an incorrect kinetic mechanism. Because any of the rate constants in a kinetic mechanism can be composite rate constants and because the number of steps covered by a composite rate constant can be large, no kinetic mechanism can be proven to be complete. The rate constants in the kinetic mechanisms proposed for most enzymatic reactions are usually composite rate constants, and those kinetic mechanisms are incomplete.

Kinetic Mechanisms for Two Reactants: Converging Double Reciprocals

Observation: Most enzymes, even chymotrypsin, have two reactants and two products. When an enzyme has two reactants that can be varied independently, the procedure followed is to choose several initial concentrations of one reactant and several initial concentrations of the other reactant evenly spaced over ranges between a nearly saturating concentration and a concentration well below the apparent values for the Michaelis constant. Spacing the concentrations evenly ensures that concentrations above, below, and close to the apparent

Michaelis constant are chosen and that values throughout the range of concentrations in which the initial rate of the enzymatic reaction is changing most rapidly with concentration, in particular the region around the Michaelis constant, are sampled. A couple of points are usually chosen at high concentrations to establish saturation and the value for the apparent rate constant at saturation of the varied reactant. The initial rate of the reaction is then measured at every combination of these two sets of initial concentrations. The initial rates of the enzymatic reaction are plotted as a function of the initial concentrations of reactant A, the **varied reactant**, at a constant concentration of reactant B, the **fixed reactant**. The behavior of the initial rate is usually that defined by Equation 3–43, but the values of the specificity constant k_A for reactant A and the catalytic constant for reactant A, $k_{0,A}$, in the equation change as the concentration of reactant B, the fixed reactant, is changed. Because the parameters $k_A[E]_t$ and $k_0[E]_t$ in Equation 3–43 have become functions of the concentration of reactant B and vary as the concentration of reactant B is varied and vice versa, they are actually not constants; they are only **apparent rate constants** ($k_{0,A,app}[E]_t$ and $k_{A,app}[E]_t$) for a fixed concentration of reactant B.

The kinetics of hexokinase (HK) from *R. norvegicus*

$$\text{D-hexose} + \text{MgATP}^{2-} \rightleftharpoons \text{H}^+ + \text{MgADP}^- + \text{D-hexose 6-phosphate} \tag{3–94}$$

serve as an example of such observations. Either $MgATP^{2-}$ was chosen to be the varied reactant at several fixed initial concentrations of the hexose, in this case D-fructose, (Figure 3–4A),[69] or D-fructose was chosen to be the varied reactant at several fixed concentrations of $MgATP^{2-}$ (Figure 3–4E).[69] At each initial concentration of the fixed reactant, the observed values for the initial rate of hexokinase as a function of the initial concentration of the varied reactant could be fit by Equation 3–52. From these fits, in which y is the initial rate v_0 and x is the initial concentration of either $MgATP^{2-}$ or D-fructose, values for the rate constants $k_{0,ATP,app}[HK]_t$ (parameter a) and $k_{ATP,app}[HK]_t$ (parameter c) or $k_{0,fruc,app}[HK]_t$ (parameter a) and $k_{fruc,app}[HK]_t$ (parameter c) were obtained for each initial concentration of the fixed reactants fructose and $MgATP^{2-}$, respectively. When parameters a and c for $MgATP^{2-}$ are plotted against the initial concentration of D-fructose (Figure 3–4C,D) and when parameters a and c for D-fructose are plotted against the initial concentration of $MgATP^{2-}$ (Figure 3–4G,H), the data can again be fitted by Equation 3–52 when y is the respective rate constant being plotted and x is the initial concentration of D-fructose or $MgATP^{2-}$, respectively.

The **general empirical equation** defining this observed behavior is

$$v_0 = \frac{[E]_t}{\frac{1}{k_{AB}[A]_0[B]_0} + \frac{1}{k_B[B]_0} + \frac{1}{k_A[A]_0} + \frac{1}{k_0}} = \frac{k_0 k_A k_B k_{AB}[E]_t[A]_0[B]_0}{k_0 k_A k_B + k_0 k_A k_{AB}[A]_0 + k_0 k_B k_{AB}[B]_0 + k_A k_B k_{AB}[A]_0[B]_0} \tag{3–95}$$

for which

$$\lim_{[A]_0 \to \infty} v_0 = k_{0,A,app}[E]_t = \frac{k_0[E]_t k_B[E]_t[B]_0}{k_0[E]_t + k_B[E]_t[B]_0} \tag{3–96}$$

$$\lim_{[A]_0 \to 0} v_0 = k_{A,app}[E]_t[A]_0 = \left(\frac{k_A[E]_t k_{AB}[E]_t[B]_0}{k_A[E]_t + k_{AB}[E]_t[B]_0}\right)[A]_0 \tag{3–97}$$

$$\lim_{[B]_0 \to \infty} v_0 = k_{0,B,app}[E]_t = \frac{k_0[E]_t k_A[E]_t[A]_0}{k_0[E]_t + k_A[E]_t[A]_0} \tag{3–98}$$

and

$$\lim_{[B]_0 \to 0} v_0 = k_{B,app}[E]_t[B]_0 = \left(\frac{k_B[E]_t k_{AB}[E]_t[A]_0}{k_B[E]_t + k_{AB}[E]_t[A]_0}\right)[B]_0 \tag{3–99}$$

The four rate constants that define Equation 3–95 are each isolated in turn from the other three in the **double limits**

$$\lim_{\substack{[A]_0 \to \infty \\ [B]_0 \to \infty}} v_0 = k_0[E]_t \tag{3–100}$$

$$\lim_{\substack{[A]_0 \to \infty \\ [B]_0 \to 0}} v_0 = k_B[E]_t[B]_0 \tag{3–101}$$

$$\lim_{\substack{[A]_0 \to 0 \\ [B]_0 \to \infty}} v_0 = k_A[E]_t[A]_0 \tag{3–102}$$

$$\lim_{\substack{[A]_0 \to 0 \\ [B]_0 \to 0}} v_0 = k_{AB}[E]_t[A]_0[B]_0 \tag{3–103}$$

A key feature of the general equation (Equation 3–95) is that $[A]_0$ and $[B]_0$ are interchangeable, which must be the case because the behavior of the initial rate of an enzymatic reaction when A is the varied reactant and B is the fixed reactant (Figure 3–4, panels A–D) is the same as its behavior when B is the varied reactant and A is the fixed reactant (Figure 3–4, panels E–H), albeit with different numerical values for the parameters governing the respective situations.

The products of the concentration of active sites with the apparent catalytic constant, $k_{0,A,app}[E]_t$, as a function of the initial concentration $[B]_0$ (Equation 3–96); with the apparent specificity constant for reactant A, $k_{A,app}[E]_t$, as a function of the initial concentration $[B]_0$ (Equation 3–97); with the apparent catalytic constant, $k_{0,B,app}[E]_t$, as a function of the initial concentration $[A]_0$ (Equation 3–98); and with the apparent specificity constant, $k_{B,app}[E]_t$, as a function of the initial concentration $[A]_0$ (Equation 3–99) are all rectangular hyperbolae (Equation 3–52). From fits of Equation 3–52 to the various plots of the apparent rate constants as functions of the initial concentrations of the fixed reactants (Figure 3–4C, D, G, and H) and extrapolation to determine the four respective double limits (Equations 3–100 through 3–103), values for the **four fundamental rate constants** $k_0[E]_t$, $k_A[E]_t$, $k_B[E]_t$, and $k_{AB}[E]_t$ are obtained. These four fundamental rate constants govern all the kinetics and can be used to generate all the curves describing the observations.

Historically, the general empirical equation that was used and is still sometimes used to define the observed behavior of the initial rate of an enzymatic reaction is

$$v_0 = \frac{V[A]_0[B]_0}{K_{iA}K_{mB} + K_{mB}[A]_0 + K_{mA}[B]_0 + [A]_0[B]_0} \tag{3–104}$$

The symmetry of the equation is not so obvious, but it is the same equation as Equation 3–95 with the parameters given different notation.

The **double reciprocal** of Equation 3–95 is

$$\frac{1}{v_0} = \frac{1}{k_{AB}[E]_t[A]_0[B]_0} + \frac{1}{k_B[E]_t[B]_0} + \frac{1}{k_A[E]_t[A]_0} + \frac{1}{k_0[E]_t} \tag{3–105}$$

Consequently, when the reciprocals of the initial rates for an enzymatic reaction are plotted as a function of the reciprocals of the initial concentrations of the varied reactant at any constant initial concentration of the fixed reactant, the data can be fitted with a straight line (Figure 3–4B,F). Equation 3–105 separates the four kinetic constants into four separated terms.

When A is the varied reactant and B is the fixed reactant

$$\frac{1}{v_0} = \left(\frac{k_A[E]_t + k_{AB}[E]_t[B]_0}{k_A[E]_t k_{AB}[E]_t[B]_0}\right)\frac{1}{[A]_0} + \left(\frac{k_0[E]_t + k_B[E]_t[B]_0}{k_0[E]_t k_B[E]_t[B]_0}\right) \tag{3–106}$$

and both the slope of the straight line and its intercept with the axis of the ordinate should be functions of $[B]_0$ (Figure 3–4B,F). Because the slopes of the lines defining each of the individual double reciprocals when A is the varied reactant is a function of $[B]_0$, the initial concentration of the fixed reactant, the lines for the variable $[A]_0^{-1}$ at two different fixed $[B]_0$ will necessarily intersect at some point, just as any two lines with different slopes must intersect. Furthermore, it can be shown, by solving for the coordinates of the point of intersection, that all the lines defined by Equation 3–106 **intersect at the same point** (Figure 3–4B,F) where

$$\frac{1}{[A]_{0,int}} = -\frac{k_{AB}}{k_B} \tag{3–107}$$

and

$$\frac{1}{v_{0,\text{int}}} = \frac{k_A [E]_t k_B [E]_t - k_0 [E]_t k_{AB} [E]_t}{k_0 [E]_t k_B [E]_t k_A [E]_t} \quad (3\text{–}108)$$

where $[A]_{0,\text{int}}^{-1}$ and $v_{0,\text{int}}^{-1}$ are the coordinates of the common point of intersection. The points of intersection can be in the third quadrant (Figure 3–4B,F) or the second quadrant.

Explanation: If one assumes that both reactant A and reactant B add to the enzyme before any products dissociate, that all steps preceding the realization of the resulting **ternary complex** (E·A·B) are reversible, that reactant A binds first to the enzyme followed by reactant B, and that products Y and Z dissociate from the active site in that order, then

$$\begin{aligned} E + A + B &\underset{k_{-1}}{\overset{k_1}{\rightleftharpoons}} E{\cdot}A + B \underset{k_{-2}}{\overset{k_2}{\rightleftharpoons}} E{\cdot}A{\cdot}B \underset{k_{-3}}{\overset{k_3}{\rightleftharpoons}} \\ E{\cdot}Z{\cdot}Y &\xrightarrow{k_4} E{\cdot}Z + Y \xrightarrow{k_5} E + Y + Z \end{aligned} \quad (3\text{–}109)$$

The steps governed by rate constants k_4 and k_5 are formally irreversible because products Y and Z, respectively, dissociate during these steps and neither Y nor Z is present at initial times. The initial rate of the reaction is

$$v_0 = \frac{d[Z]}{dt} = \frac{d[Y]}{dt} = k_5 [E{\cdot}Z] \quad (3\text{–}110)$$

The principle of conservation of enzyme states that

$$[E]_t = [E] + [E{\cdot}A] + [E{\cdot}A{\cdot}B] + [E{\cdot}Z{\cdot}Y] + [E{\cdot}Z] \quad (3\text{–}111)$$

which is one of the simultaneous equations needed. As there are five unknowns, four other simultaneous equations are required. They are the four steady-state equations

$$k_1[E][A]_0 + k_{-2}[E{\cdot}A{\cdot}B] = (k_{-1} + k_2[B]_0)[E{\cdot}A] \quad (3\text{–}112)$$

$$k_2[E{\cdot}A][B]_0 + k_{-3}[E{\cdot}Z{\cdot}Y] = (k_{-2} + k_3)[E{\cdot}A{\cdot}B] \quad (3\text{–}113)$$

$$k_3[E{\cdot}A{\cdot}B] = (k_{-3} + k_4)[E{\cdot}Z{\cdot}Y] \quad (3\text{–}114)$$

and

$$k_4[E{\cdot}Z{\cdot}Y] = k_5[E{\cdot}Z] \quad (3\text{–}115)$$

Solving these five equations for [E·A·B] and entering that expression into Equation 3–110 gives a solution that has the form of Equation 3–95

$$v_0 = \frac{k_0 k_A k_B k_{AB} [E]_t [A]_0 [B]_0}{k_0 k_A k_B + k_0 k_A k_{AB} [A]_0 + k_0 k_B k_{AB} [B]_0 + k_A k_B k_{AB} [A]_0 [B]_0} \quad (3\text{–}116)$$

with*

$$k_0 = \frac{k_3 k_4 k_5}{k_3 k_4 + k_3 k_5 + k_{-3} k_5 + k_4 k_5} \quad (3\text{–}117)$$

$$k_B = \frac{k_2 k_3 k_4}{k_{-2} k_{-3} + k_{-2} k_4 + k_3 k_4} \quad (3\text{–}118)$$

$$k_A = k_1 \quad (3\text{–}119)$$

$$k_{AB} = \frac{k_1 k_2 k_3 k_4}{k_{-1}(k_{-2} k_{-3} + k_{-2} k_4 + k_3 k_4)} \quad (3\text{–}120)$$

Consequently, the kinetic mechanism in Equation 3–109 is consistent with the behavior that is observed.

Again, there is an array of **expanded kinetic mechanisms**, each of which is also consistent with the observed behavior. As before, the introduction of steps after both A and B have been bound to the active site but before the competent ternary complex E·A·B has been formed produces expanded kinetic mechanisms consistent with the observations. The introduction of reversible steps between the association of A with the active site and the association of B with the active site—or the introduction of reversible steps between the conversion of E·A·B to E·Z·Y and release of products from the active site—also produces expanded kinetic mechanisms consistent with the observations for the same reason:

*The following four empirical rate constants, k_0, k_A, k_B, and k_{AB}, are extracted by taking, in turn, the four double limits (Equations 3–100 to 3–103) of the complete equation derived from the five independent simultaneous equations (Equations 3–111 to 3–115).

namely, that composite rate constants are usually indistinguishable from elementary rate constants by simple steady-state kinetics. Because of this fact that composite rate constants for a series of steps, none of which involves the entry or exit of a substrate to or from the active site of the enzyme, are indistinguishable from elementary rate constants, **steady-state kinetics alone based on initial rates can provide information only about entry of substrates from the solution into the active site or exit of substrates to the solution from the active site**. If a reactant must associate with the active site of the enzyme during the reaction, experimental variation of the concentration of that reactant will usually affect the observed initial rate for an enzymatic reaction by the relation of Equation 3–40.

There are, however, substantively different kinetic mechanisms that are also consistent with the observations. In particular, **the order in which A and B add to the active site of the enzyme cannot be distinguished** by observation of initial rates for the enzymatic reaction in which only $[A]_0$ and $[B]_0$ are varied. This ambiguity is due to the fact that $[A]_0$ and $[B]_0$ appear interchangeably in Equation 3–95. Because Equation 3–95 is the only relation defined by the experimental observations, the experimental observations cannot distinguish which reactant, A or B, associates first with the enzyme.

It also happens that the rate equation has the form of Equation 3–95 if the **association of reactants A and B is random** and each association of a reactant is at equilibrium in an **equilibrium-random mechanism**

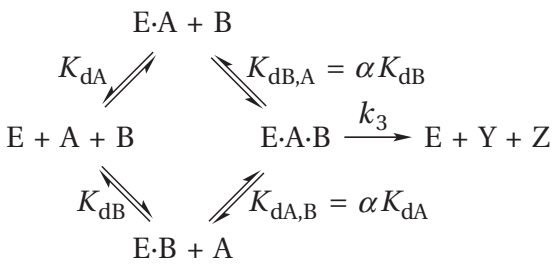

(3–121)

where K_{dA} and K_{dB} are the dissociation constants for reactant A and reactant B from the unoccupied enzyme, $K_{dA,B}$ is the dissociation constant for reactant A from the enzyme occupied by reactant B, and $K_{dB,A}$ is the dissociation constant for reactant B from the enzyme occupied by reactant A. This equation defines an equilibrium-random kinetic mechanism. It states that the rates of the associations and the dissociations of the reactants with the active site are all significantly greater than the conversion of reactants to products on the active site.

The equilibrium constants for Equation 3–121 are related to each other by the **linkage equations**

$$K_{dA} K_{dB,A} = K_{dB} K_{dA,B} \tag{3–122}$$

$$K_{dB,A} = \frac{K_{dA,B}}{K_{dA}} K_{dB} = \alpha K_{dB} \tag{3–123}$$

and

$$K_{dA,B} = \frac{K_{dA,B}}{K_{dA}} K_{dA} = \alpha K_{dA} \tag{3–124}$$

Consequently

$$[E] = \left(\frac{\alpha K_{dB} K_{dA}}{[A]_0 [B]_0}\right)[E{\cdot}A{\cdot}B] \tag{3–125}$$

$$[E{\cdot}A] = \left(\frac{\alpha K_{dB}}{[B]_0}\right)[E{\cdot}A{\cdot}B] \tag{3–126}$$

$$[E{\cdot}B] = \left(\frac{\alpha K_{dA}}{[A]_0}\right)[E{\cdot}A{\cdot}B] \tag{3–127}$$

and, from the conservation of enzyme

$$[E]_t = [E] + [E{\cdot}A] + [E{\cdot}B] + [E{\cdot}A{\cdot}B] \tag{3–128}$$

These four equations together give

$$v_0 = \frac{k_3 [E]_t [A]_0 [B]_0}{\alpha K_{dA} K_{dB} + \alpha K_{dB} [A]_0 + \alpha K_{dA} [B]_0 + [A]_0 [B]_0} \tag{3–129}$$

Taking the double limits of both Equation 3–95 and Equation 3–129

$$\lim_{\substack{[A]_0 \to \infty \\ [B]_0 \to \infty}} v_0 = k_0 [E]_t = k_3 [E]_t \tag{3–130}$$

$$\lim_{\substack{[A]_0 \to \infty \\ [B]_0 \to 0}} v_0 = k_B [E]_t [B]_0 = \frac{k_3 [E]_t [B]_0}{\alpha K_{dB}} \tag{3–131}$$

$$\lim_{\substack{[A]_0 \to 0 \\ [B]_0 \to \infty}} v_0 = k_A [E]_t [A]_0 = \frac{k_3 [E]_t [A]_0}{\alpha K_{dA}} \tag{3–132}$$

$$\lim_{\substack{[A]_0 \to 0 \\ [B]_0 \to 0}} v_0 = k_{AB} [E]_t [A]_0 [B]_0 = \frac{k_3 [E]_t [A]_0 [B]_0}{\alpha K_{dA} K_{dB}} \tag{3–133}$$

Because over the period of time in which initial rates are measured, the initial concentrations of the reactants are constant, any kinetic mechanism used to derive a rate equation for an initial rate of an enzymatic reaction can be treated as a sequence of steps, the individual rate constants of the forward and reverse reactions of which are both simple first-order rate constants and pseudo-first-order rate constants. This is the case regardless of which steps involve association of substrates with the active site of the enzyme or dissociation of substrates from the active site of the enzyme. For example, if the kinetic mechanism in Equation 3–109 is modified by two steps to add an isomerization of the enzyme and to make the dissociation of the first product the rate-limiting step, rather than the dissociation of the second, then

$$\begin{aligned} E \underset{k_{-3}}{\overset{k_3[A]_0}{\rightleftharpoons}} E{\cdot}A \underset{k_{-4}}{\overset{k_4[B]_0}{\rightleftharpoons}} E{\cdot}A{\cdot}B \underset{k_{-5}}{\overset{k_5}{\rightleftharpoons}} E'{\cdot}A{\cdot}B \\ \underset{k_{-6}}{\overset{k_6}{\rightleftharpoons}} E{\cdot}Z{\cdot}Y \xrightarrow{k_7} E + Y + Z \end{aligned} \tag{3–134}$$

If Equation 3–84 is rewritten in the same way, then

$$\begin{aligned} E \underset{k_{-3}}{\overset{k_3[A]_0}{\rightleftharpoons}} E{\cdot}A \underset{k_{-4}}{\overset{k_4}{\rightleftharpoons}} E'{\cdot}A \underset{k_{-5}}{\overset{k_5}{\rightleftharpoons}} E'{\cdot}A' \\ \underset{k_{-6}}{\overset{k_6}{\rightleftharpoons}} E{\cdot}Z \xrightarrow{k_7} E + Z \end{aligned} \tag{3–135}$$

Because the concentrations of reactants by definition remain constant at their initial values during the measurement of initial rates for an enzymatic reaction, the terms in these two kinetic mechanisms involving concentrations, such as $k_2[B]_0$ and $k_1[A]_0$, are pseudo-first-order rate constants that are formally equivalent to the normal first-order rate constants. In this sense, these two kinetic mechanisms are mathematically equivalent. Therefore, if reactant B is held at a fixed concentration, both should give equations for v_0 as a function of $[A]_0$ of the form of Equation 3–40.

This simplification that permits every kinetic mechanism for the initial rate of an enzymatic reaction to be written as a **series of first-order steps** has been exploited by King and Altman.[82,83] These investigators have formulated a series of rules by which an expression for v_0 can be obtained systematically from complicated kinetic mechanisms that have several reactants, several products, many steps, branching paths, coalescing paths, or several or all of these features. It is worth the time necessary to learn this system if one is required to derive rate equations for many long and complicated kinetic mechanisms. Most investigators, however, are only required to calculate initial rates for a few kinetic mechanisms, and these calculations can usually be performed without spending the time necessary to learn rather complicated general methods.

Because of Equations 3–121 and 3–129, one might imagine that the kinetic mechanism for the **steady-state random bimolecular association** of the two reactants

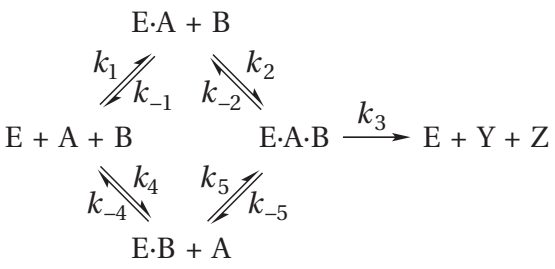

(3–136)

in which k_1 and k_5 are both first-order functions of $[A]_0$ and k_2 and k_4 are both first-order functions of $[B]_0$, would also give a kinetic rate equation consistent with Equation 3–95, but it does not. The rate equation for this kinetic mechanism, as derived by the method of King and Altman,[82] is

$$v_0 = \frac{a[\mathrm{A}]_0[\mathrm{B}]_0 + b[\mathrm{A}]_0[\mathrm{B}]_0^2 + c[\mathrm{A}]_0^2[\mathrm{B}]_0}{d + e[\mathrm{B}]_0 + f[\mathrm{B}]_0^2 + g[\mathrm{A}]_0 + h[\mathrm{A}]_0^2 + i[\mathrm{A}]_0[\mathrm{B}]_0 + j[\mathrm{A}]_0[\mathrm{B}]_0^2 + l[\mathrm{A}]_0^2[\mathrm{B}]_0} \quad (3\text{–}137)$$

where the parameters a through l are sums of the products of rate constants (Table 3–1).[84]

The reasons for the quadratic terms in Equation 3–137 are that the forms of the enzyme are not in rapid equilibrium with each other and that there are **two routes to the ternary complex** E·A·B. As the initial concentration of A is increased at a fixed initial concentration of B, the route in which A associates first with the enzyme becomes more dominant, and as the initial concentration of B is increased at a fixed initial concentration of A, the route in which B associates first with the enzyme becomes more dominant. At low initial concentrations of A and a fixed concentration of B, most of the flux goes on the path along which B binds first, and at high concentrations of A and the same fixed concentration of B, most of the flux goes on the path along which A associates first. The rate of flux on the two paths is almost always different, so increasing concentrations of A can cause the reaction to go either faster than the rate defined by Equation 3–95, leading to activation of the enzymatic rate by increasing concentrations of reactant A, or slower than the rate defined by Equation 3–95, leading to inhibition of the enzymatic rate by increasing concentrations of reactant A.[85]

Such **activation by a reactant or inhibition by a reactant** is observed frequently and may result from the consequences of this kinetic mechanism. It is probably often the case, however, that only one of the two routes in this kinetic mechanism dominates in the range of initial concentrations chosen, so the behavior observed is actually that of the kinetic mechanism of Equation 3–109. In fact, initial concentrations of reactants are often chosen to avoid activation or inhibition observed at higher concentrations of the reactants. The usual application of this habit suggests that the kinetic mechanism of Equation 3–136 may be more common than it seems to be. If it actually is fairly common, most of the conclusions drawn from inhibitors that are analogues of the reactants and from product inhibition that are about to be discussed may be misleading.

One should note that when k_{-3} is zero and k_4 and k_5 are both much larger than k_3 in the kinetic mechanism of Equation 3–109, it becomes a special case of the kinetic mechanism of Equation 3–136 in which the lower route actually is or has been assumed by the author to be kinetically nonexistent. When $k_4 = 0$ and $k_{-5} = 0$ in the kinetic mechanism of Equation 3–136 and when k_{-3} is zero and k_4 and k_5 are both much larger than k_3 in the kinetic mechanism of Equation 3–109, Equation 3–137 becomes Equation 3–95, as it must because, under these circumstances, the two kinetic mechanisms have become the same kinetic mechanism. This realization reinforces the point that it may be even more difficult to prove that all the flux in an enzymatic reaction proceeds through only one of the routes in the kinetic mechanism of Equation 3–136.

Table 3–1: Combinations of Rate Constants in Equation 3–136 that Define[82] the Parameters in Equation 3–137

$a = k_1k_2k_3k_{-4} + k_{-1}k_3k_4k_5$
$b = k_2k_3k_4k_5$
$c = k_1k_2k_3k_5$
$d = k_{-1}k_{-2}k_{-4} + k_{-1}k_{-4}k_{-5} + k_{-1}k_3k_{-4}$
$e = k_{-1}k_{-2}k_4 + k_{-1}k_4k_{-5} + k_{-1}k_3k_4 + k_2k_{-4}k_{-5} + k_2k_3k_{-4}$
$f = k_2k_4k_{-5} + k_2k_3k_4$
$g = k_1k_{-2}k_{-4} + k_1k_{-4}k_{-5} + k_1k_3k_{-4} + k_{-1}k_{-2}k_5 + k_{-1}k_3k_5$
$h = k_1k_{-2}k_5 + k_1k_3k_5$
$i = k_1k_2k_{-4} + k_{-1}k_4k_5 + k_1k_2k_{-5} + k_{-2}k_4k_5 + k_2k_3k_5$
$j = k_2k_4k_5$
$l = k_1k_2k_5$

Other than proving that the proposed kinetic mechanism is consistent with the observed behavior, the purpose of deriving a rate equation is to facilitate the **assignment of numerical values to the elementary rate constants and the composite rate constants** explicitly defined by that proposed kinetic mechanism. The complexity of the rate law (Equation 3–137 and Table 3–1) for Equation 3–136 indicates the difficulties of this endeavor for even as simple a kinetic mechanism as that for steady-state random bimolecular association. Theoretically, if each of the parameters a through l in Equation 3–137 could be obtained experimentally, one would have 11 equations (Table 3–1) with only 9 unknowns, the individual rate constants k_i, and numerical values for each of them could be calculated. This calculation, however, would require detailed measurements of the inhibition or activation that occurs at high concentrations of the reactants. Such systematic and detailed studies of the kinetics of any enzyme that proceeds by the kinetic mechanism of Equation 3–136 have probably not been performed. The difficulties of obtaining numerical values of the rate constants only increase for more complex steady-state kinetic mechanisms with more than two routes to the complex that produces products.

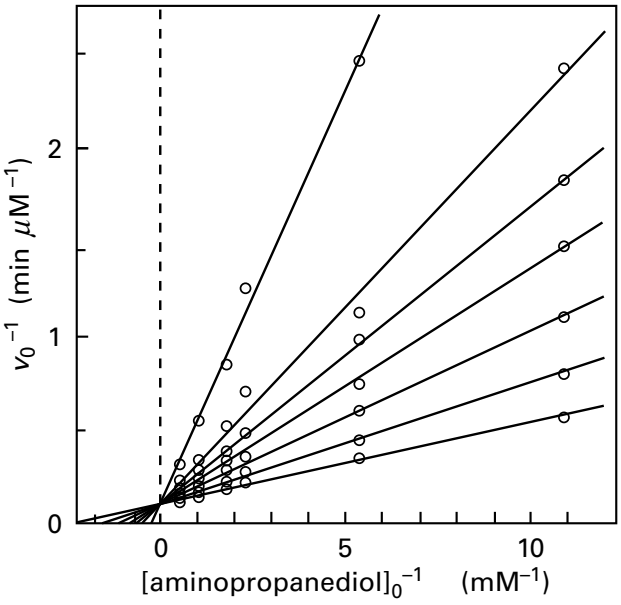

Figure 3–7: Kinetics for the phosphorylation of (*S*)-1-aminopropane-2,3-diol catalyzed by glycerol kinase from *C. mycoderma*.[86] Solutions were prepared that contained $MgATP^{2-}$ and (*S*)-1-aminopropane-2,3-diol at various concentrations at pH 9.4 and 25 °C. The concentration of uncomplexed Mg^{2+} was fixed at 7 mM throughout. Each phosphorylation was initiated by adding glycerol kinase, and the production of $MgADP^-$ was followed over the first few minutes in a coupled assay with phospho*enol*pyruvate, pyruvate kinase, dihydronicotinamide-adenine dinucleotide, and L-lactate dehydrogenase by monitoring the decrease in A_{340} from the conversion of NADH into NAD^+. Each initial rate of change in A_{340} was converted to an initial rate for the production of $MgADP^-$, v_0 (micromolar minute^{-1}). Reciprocals of the initial rates (minutes micromolar^{-1}) are presented as a function of reciprocals of the initial concentrations of (*S*)-1-aminopropane-2,3-diol (millimolar^{-1}) at fixed concentrations of $MgATP^{2-}$ (for the lines in descending order) of 0.13, 0.25, 0.37, 0.50, 0.76, 1.26, and 2.52 mM.

Kinetic Mechanisms for Two Reactants: Double Reciprocals Intersecting at the Axis of the Ordinate

Observation: An interesting and informative special case of Equation 3–95, which has been occasionally observed, is that in which the term $\boldsymbol{k_0 k_B k_{AB}[B]_0}$ **is missing from the denominator** and the empirical equation defining the behavior has become

$$v_0 = \frac{k_0 k_B k_{AB} [E]_t [A]_0 [B]_0}{k_0 k_B + k_0 k_{AB} [A]_0 + k_B k_{AB} [A]_0 [B]_0} \quad (3\text{–}138)$$

In this instance, unlike the more frequently encountered general case, the observations do distinguish between reactants A and B; the initial concentration of one of them does not have a term in the denominator. Because

$$\lim_{[B]_0 \to \infty} v_0 = k_0 [E]_t \quad (3\text{–}139)$$

has no terms in $[A]_0$, unlike the limit (Equation 3–98) for Equation 3–95, the curves for v_0 as a function of $[B]_0$ all converge to the same value for v_0 as $[B]_0$ is increased, regardless of the fixed concentration of reactant A. Consequently, the lines for the reciprocals of the initial rate as a function of the reciprocals of the initial concentrations of reactant B intersect at the axis of the ordinate because the term $(k_A[E]_t[A]_0)^{-1}$ is missing from Equation 3–105. This type of behavior is observed for the kinetics of glycerol kinase from *Candida norvegensis* (Figure 3–7)[86] when this enzyme phosphorylates (*S*)-1-aminopropane-2,3-diol

$$\begin{aligned}&(S)\text{-1-aminopropane-2,3-diol} + \\ &MgATP^{2-} \rightleftharpoons MgADP^- + \\ &\quad (S)\text{-}N\text{-phosphono-1-aminopropane-2,3-diol}\end{aligned} \quad (3\text{–}140)$$

Explanation: A simple kinetic mechanism consistent with this behavior is the **equilibrium-ordered mechanism with ordered association of reactants**

$$\begin{array}{l} \mathrm{E + A + B} \underset{K_{dA}}{\rightleftharpoons} \mathrm{E{\cdot}A + B} \underset{K_{dB,A}}{\rightleftharpoons} \mathrm{E{\cdot}A{\cdot}B} \\ \qquad\qquad\qquad\qquad\qquad\qquad\quad \Big\downarrow k_3 \\ \qquad\qquad\qquad\qquad\qquad\qquad\quad \mathrm{E + Y + Z} \end{array} \qquad (3\text{–}141)$$

where K_{dA} is the dissociation constant for reactant A from the unoccupied enzyme and $K_{dB,A}$ is the dissociation constant for reactant B from the enzyme occupied by reactant A. When the kinetic mechanism is written in this way, the author states that both the association of reactant A with the enzyme and the association of reactant B with the complex between enzyme and reactant A reach equilibrium so rapidly that the various complexes and free reactants are in equilibrium during the entire reaction. As before, in such an equilibrium kinetic mechanism, the steady-state approximations are unnecessary; the dissociation constants themselves provide the necessary relations

$$K_{dA} = \frac{[E][A]_0}{[E{\cdot}A]} \qquad (3\text{–}142)$$

$$K_{dB,A} = \frac{[E{\cdot}A][B]_0}{[E{\cdot}A{\cdot}B]} \qquad (3\text{–}143)$$

Upon rearrangement, these equilibria can be substituted into a shortened version of Equation 3–111 in which k_3 in the kinetic mechanism of Equation 3–109 is the rate-limiting step so that [E·Z·Y] and [E·Z] are zero. The resulting kinetic equation

$$v_0 = \frac{k_3[E]_t[A]_0[B]_0}{K_{dA}K_{dB,A} + K_{dB,A}[A]_0 + [A]_0[B]_0} \qquad (3\text{–}144)$$

has the same form as Equation 3–138. As before, taking the limits of Equation 3–138 and Equation 3–144

$$\lim_{\substack{[A]_0 \to \infty \\ [B]_0 \to \infty}} v_0 = k_0[E]_t = k_3[E]_t \qquad (3\text{–}145)$$

$$\lim_{\substack{[A]_0 \to \infty \\ [B]_0 \to 0}} v_0 = k_B[E]_t[B]_0 = \frac{k_3[E]_t[B]_0}{K_{dB,A}} \qquad (3\text{–}146)$$

$$\lim_{[A]_0 \to 0} v_0 = k_{AB}[E]_t[A]_0[B]_0 = \frac{k_3[E]_t[A]_0[B]_0}{K_{dA}K_{dB,A}} \qquad (3\text{–}147)$$

If glycerol kinase proceeds by the kinetic mechanism of Equation 3–141, $MgATP^{2-}$ must bind to the active site before (*S*)-1-aminopropane-2,3-diol.

Kinetic Mechanisms for Two Reactants: Double Reciprocals Parallel to Each Other

Observation: The observed kinetics of an enzyme with two reactants are defined by another special case of Equation 3–95, that in which the term $k_0k_Ak_B$ **is missing from the denominator** and the empirical equation has become

$$v_0 = \frac{k_0k_Ak_B[E]_t[A]_0[B]_0}{k_0k_A[A]_0 + k_0k_B[B]_0 + k_Ak_B[A]_0[B]_0} \qquad (3\text{–}148)$$

This relation is found, for example, with the kinetics of ovine 3-oxoacid CoA-transferase (Figure 3–8)[87-89]

$$\mathrm{acetoacetyl\text{-}SCoA + succinate} \rightleftharpoons \mathrm{acetoacetate + succinyl\text{-}SCoA} \qquad (3\text{–}149)$$

Two of the limits for Equation 3–148 are

$$\lim_{[A]_0 \to 0} v_0 = k_A[E]_t[A]_0 \qquad (3\text{–}150)$$

and

$$\lim_{[B]_0 \to 0} v_0 = k_B[E]_t[B]_0 \qquad (3\text{–}151)$$

Consequently, the **initial slopes** of the functions describing v_0 as a function of either $[A]_0$ or $[B]_0$ are no longer functions of $[B]_0$ or $[A]_0$, respectively, as they were before (Equations 3–97 and 3–99) and are now all the same for all concentrations of the fixed reactant, either $k_A[E]_t$ (Figure 3–8A) or $k_B[E]_t$ (Figure 3–8C).

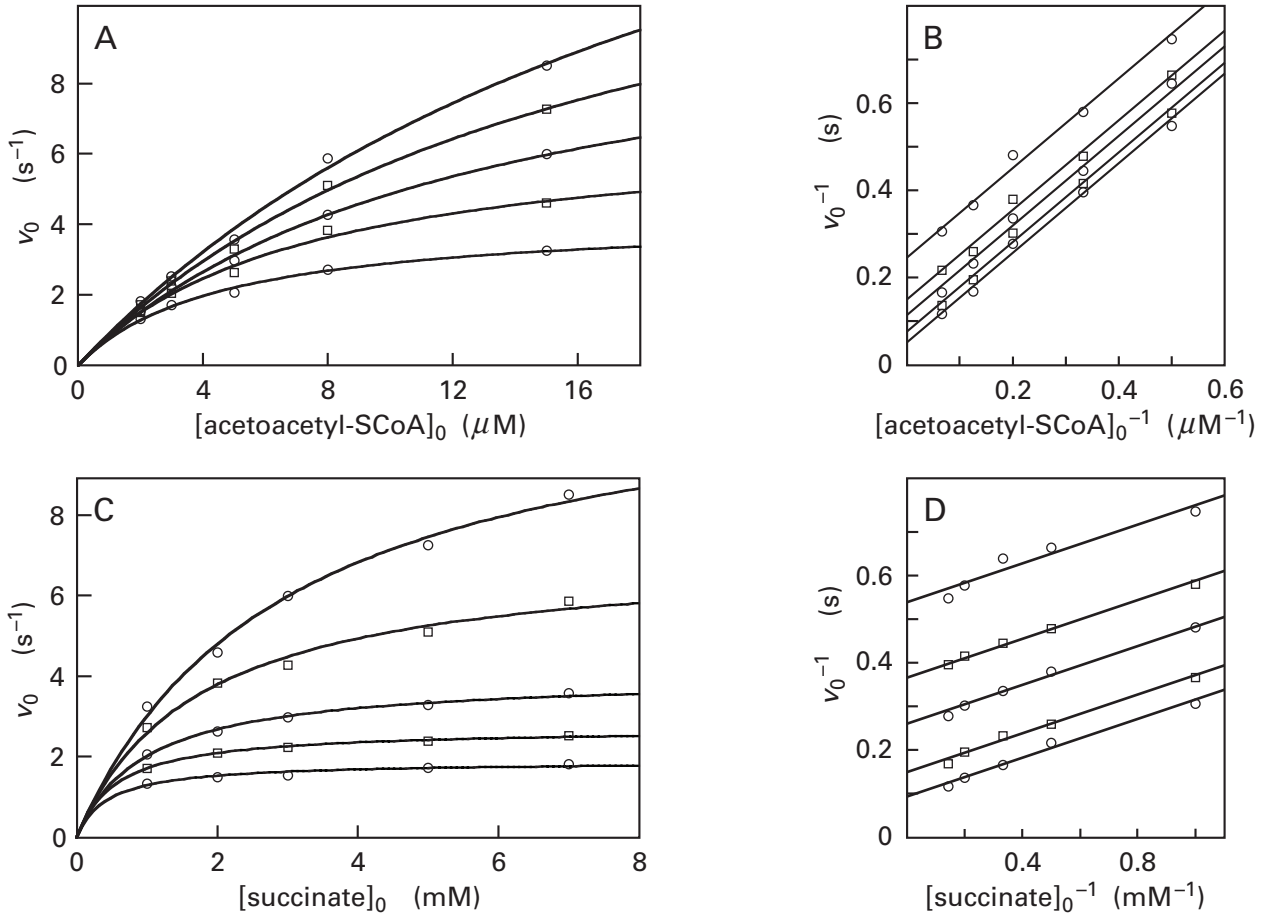

Figure 3–8: Kinetics for the transesterification catalyzed by 3-oxoacid CoA-transferase from ovine kidney.[87] Solutions containing 25 mM Mg^{2+} and various concentrations of acetoacetyl-SCoA and succinate were prepared at pH 8.1 and 30 °C. Each transesterification was initiated by adding purified 3-oxoacid CoA-transferase[88] to the mixture. The initial rate of each reaction was determined by monitoring the absorbance at 303 nm of the acetoacetyl-SCoA being lost as the transesterification proceeded. With the extinction coefficient for acetoacetyl-SCoA, the initial rate of each transesterification could be converted to micromoles of acetoacetyl-SCoA consumed $minute^{-1}$. With the molar mass of enzyme for each active site (51,000 g mol^{-1}),[89] the micromoles of acetoacetyl-SCoA $minute^{-1}$ (mg of enzyme)$^{-1}$ can be converted to the units of micromoles of acetoacetyl-SCoA $second^{-1}$ (micromole of 3-oxoacid CoA-transferase)$^{-1}$. The initial concentrations of acetoacetyl-SCoA chosen for the studies were 2, 3, 5, 8, and 15 μM, and the initial concentrations of succinate were 1, 2, 3, 5, and 7 mM. The complete set of the 25 combinations of these initial concentrations was used to measure 25 separate initial rates. **(A)** Initial rates ($second^{-1}$) are presented as a function of initial concentrations of acetoacetyl-SCoA at the five fixed concentrations of succinate, in order of ascent. The lines drawn are fits of Equation 3–52 to the data with x equal to [acetoacetyl-SCoA]$_0$ and y equal to v_0. The five values for parameter c of the fits (initial slopes of the five rectangular hyperbolae) deviated from each other at random, and the standard deviation of their mean was less than the standard deviations of each individual value. It was concluded that they all had the same value, 1.28 ± 0.05 s^{-1} (μM acetoacetyl-SCoA)$^{-1}$. **(B)** Reciprocals of the same initial rates (seconds) are plotted as a function of reciprocals of the initial concentrations of acetoacetyl-SCoA ($millimolar^{-1}$) at the five fixed initial concentrations of succinate. The slopes of the five lines fit separately to the data were the same within experimental error. Each line drawn in the figure has as its slope the mean of the five slopes of the individually fit lines. **(C)** Initial rates ($second^{-1}$) are presented as a function of initial concentrations of succinate at the five fixed concentrations of acetoacetyl-SCoA. The curves drawn are fits of Equation 3–52 to the data with x equal to [succinate]$_0$ and y equal to v_0. The initial slopes of the five rectangular hyperbolae (parameters c of the fits) were the same, 5.81 ± 0.37 s^{-1} (mM succinate)$^{-1}$, within experimental error. **(D)** Reciprocals of the same initial rates (seconds) are plotted as a function of reciprocals of the initial concentrations of succinate ($millimolar^{-1}$) at the five fixed initial concentrations of acetoacetyl-SCoA. The slopes of the five lines fit separately to the data were the same within experimental error. Each line drawn in the figure has as its slope the mean of the five slopes of the individually fit lines.

Because

$$\frac{1}{v_0} = \frac{1}{k_B[E]_t[B]_0} + \frac{1}{k_A[E]_t[A]_0} + \frac{1}{k_0[E]_t} \tag{3–152}$$

when A is the varied reactant and B is the fixed reactant

$$\frac{1}{v_0} = \left(\frac{1}{k_A[E]_t}\right)\frac{1}{[A]_0} + \left(\frac{k_0[E]_t + k_B[E]_t[B]_0}{k_0[E]_t k_B[E]_t[B]_0}\right) \tag{3–153}$$

and all the lines defining v_0^{-1} as a function of $[A]_0^{-1}$ have the same slope and are parallel (Figure 3–8B) Because of the symmetry of Equation 3–148, the same is true when B is the varied reactant and A is the fixed reactant (Figure 3–8D).

Explanation: A simple kinetic mechanism consistent with this behavior is

$$\begin{aligned} E + A + B &\underset{k_{-1}}{\overset{k_1}{\rightleftharpoons}} E{\cdot}A + B \xrightarrow{k_2} E'{\cdot}A + B \\ &\underset{k_{-3}}{\overset{k_3}{\rightleftharpoons}} E'{\cdot}A{\cdot}B \xrightarrow{k_4} E + Y + Z \end{aligned} \tag{3–154}$$

in which the second step is kinetically irreversible. A **kinetically irreversible step** is a step in which the rate of the back reaction is so slow that it can have no effect on the kinetics of the overall reaction. Because, at steady state, the flux through the two kinetically irreversible steps must be equal

$$v_0 = \frac{d[Z]}{dt} = k_2[E{\cdot}A] = k_4[E'{\cdot}A{\cdot}B] \tag{3–155}$$

Using this equation, the equation for conservation of enzyme, and two steady-state equations, it can be shown that

$$v_0 = \frac{k_1 k_2 k_3 k_4 [E]_t [A]_0 [B]_0}{k_1 k_2 (k_{-3} + k_4)[A]_0 + k_3 k_4 (k_{-1} + k_2)[B]_0 + k_1 k_3 (k_2 + k_4)[A]_0[B]_0} \tag{3–156}$$

which has the form of Equation 3–148 and thus explains the observations. Consequently, if there is a kinetically irreversible step between the association of the first reactant with the enzyme and the association of the second reactant with the enzyme, the kinetics of the enzyme will display this behavior. As before, taking the limits of Equation 3–148 and Equation 3–156

$$\lim_{\substack{[A]_0 \to \infty \\ [B]_0 \to \infty}} v_0 = k_0[E]_t = \frac{k_2 k_4}{k_2 + k_4}[E]_t \tag{3–157}$$

$$\lim_{\substack{[A]_0 \to \infty \\ [B]_0 \to 0}} v_0 = k_B[E]_t[B]_0 = \frac{k_3 k_4}{k_{-3} + k_4}[E]_t[B]_0 \tag{3–158}$$

$$\lim_{\substack{[A]_0 \to 0 \\ [B]_0 \to \infty}} v_0 = k_A[E]_t[A]_0 = \frac{k_1 k_2}{k_{-1} + k_2}[E]_t[A]_0 \tag{3–159}$$

This kinetic mechanism is called a **ping-pong mechanism** because the enzyme oscillates between two forms, E and E′·A, each separated from the other by a respective irreversible step, and each form has the same pattern of rate constants relating it to the other form. This symmetry of the ping-pong mechanism is reflected in the symmetry of the pattern in which the rate constants appear in Equations 3–156 through 3–159.

One particular explanation for the existence of a kinetically irreversible step between the association of reactant A with the enzyme and the association of reactant B with the enzyme is that **before reactant B associates, product Z dissociates** from the enzyme, leaving the remainder of reactant A, A′, bound to the enzyme

$$\begin{aligned} E + A + B &\underset{k_{-1}}{\overset{k_1}{\rightleftharpoons}} E{\cdot}A + B \xrightarrow{k_2} E{\cdot}A' + B + Z \\ &\underset{k_{-3}}{\overset{k_3}{\rightleftharpoons}} E{\cdot}A'{\cdot}B + Z \xrightarrow{k_4} E + Y + Z \end{aligned} \tag{3–160}$$

Because there is no product Z in the solution during the initial period, the step involving its release is necessarily kinetically irreversible.

It has been demonstrated by mass spectrometry that sulfate adenylyltransferase (ADP) from *Thiobacillus denitrificans*, which transfers an adenylyl group from sulfate to phosphate

$$\text{magnesium adenosine 5′-phosphosulfate} + HOPO_3^{2-} \rightleftharpoons H^+ + SO_4^{2-} + MgADP^- \quad (3\text{–}161)$$

reacts with adenosine-5′-phosphosulfate to form an covalent adduct between the adenylyl group and the enzyme, from which sulfate, one of the products of the enzymatic reaction, must dissociate before phosphate, one of the reactants, can associate. Presumably the phosphate associates with the same location in the active site from which the sulfate has dissociated, and this sequence of events explains the parallel lines in plots of the double reciprocals of initial rate as a function of either the initial concentration of adenosine-5′-phosphosulfate or the initial concentration of phosphate at fixed initial concentrations of the other reactant, respectively.[90]

If the kinetically irreversible step is the release of the first product (Equation 3–160), **the release of that product must occur before the second reactant can associate** with the enzyme for the double reciprocals to be parallel. For example, L-cysteine can associate with cystathionine γ-synthase from *S. cerevisiae*

$$\textit{O}\text{-succinyl-L-homoserine} + \text{L-cysteine} \rightleftharpoons H^+ + \text{succinate} + \text{L-cystathionine} \quad (3\text{–}162)$$

before succinate dissociates from the adduct between *O*-succinyl-L-homoserine and pyridoxal phosphate (see Equations 2–32 and 2–34)

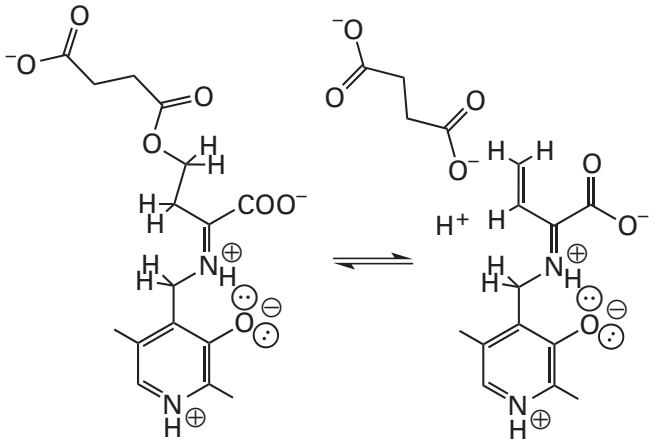

(3–163)

If the initial concentration of L-cysteine is low, however, the rate of its association is slower than the rate of dissociation of the succinate, and at low fixed initial concentrations of L-cysteine, the lines in a plot of the double reciprocals for the initial rates as a function of the initial concentrations of *O*-succinyl-L-homoserine are parallel. At higher concentrations of L-cysteine, its association becomes faster than the dissociation of succinate, and the double reciprocals at these higher concentrations intersect.[91] A similar switch from parallel double reciprocals to intersecting double reciprocals is observed in the kinetics of 1-deoxy-D-xylulose 5-phosphate synthase from *Rhodobacter capsulatus*.[92]

The dissociation of a product between the association of the first reactant and the association of the second reactant, however, is **not a necessary explanation for the existence of parallel double reciprocals**. Anything that causes the step between association of the first reactant and association of the second reactant to be kinetically irreversible will produce this behavior.

If there is a kinetically irreversible step between the association of reactant A and the association of reactant B, the lines in a plot of the double reciprocals are parallel to each other. If no products are present initially, the release of a product is, by definition of an initial rate, a kinetically irreversible step. Consequently, if the lines on a plot of the double reciprocals converge (Figure 3–4B,F), reactant A and reactant B must associate with the enzyme before any product dissociates. The complex between enzyme, unaltered reactant A, and unaltered reactant B (E·A·B) is a ternary complex, and **converging double reciprocals are considered to be evidence that a ternary complex is an intermediate** in the kinetic mechanism for the reaction.

There is another kinetic mechanism producing double reciprocals for the initial rates of an enzymatic reaction and the initial concentrations of a varied reactant that are parallel at various initial concentrations of a fixed reactant. This behavior is observed for the case in which reactant A is converted to product Z at one active site on the enzyme and the difference between A and Z—for example, an electron, a pair of electrons, or a carboxy group—is **transferred to another active site on the enzyme** to convert reactant B to product Y.[93] This mechanism is a fairly common one. For example, many enzymes engaged in electron transfer oxidize A to Z at one site, transfer the electron or electrons through a sequence of electron carriers, and then use those electrons to reduce B to Y. The enzyme methylmalonyl-CoA carboxytransferase removes a carboxy group from methylmalonyl-SCoA with biotin, transfers the carboxybiotin to another active site, and adds the carboxy group on that carboxybiotin to pyruvate. Both enzymes that transfer electrons between two active sites[94] and methylmalonyl-CoA carboxytransferase from *Propionibacterium freudenreichii* [93] have double reciprocals for which the lines, when one reactant is varied, are parallel at various fixed initial concentrations of the other reactant.

The kinetic constants governing the observed behavior of an enzymatic reaction in themselves have meaning. The catalytic constant k_0 is always a first-order rate constant (second^{-1}). The rate $k_0[E]_t$ is the product of a first-order rate constant and a concentration, and by definition it is the rate (molar second^{-1}) at which the enzymatic reaction proceeds at saturating concentrations of all the reactants at the particular concentration of enzyme. Depending on the kinetic mechanism thought to be consistent with the behavior of the enzymatic reaction, the catalytic constant k_0 can be a complex function of various rate constants for individual steps in that kinetic mechanism, but that complex function contains no terms in which any initial concentration appears. In all cases, the rate $k_0[E]_t$ is equal to the constant rate at which the enzymatic reaction proceeds as long as all reactants remain at saturation, and that rate is the fastest rate at which that particular concentration of enzyme can convert reactants to products. **The catalytic constant of the enzyme is the first-order rate constant for conversion of reactants free in solution to products free in solution** under conditions in which the enzymatic reaction is not limited by the rate of association of any of its reactants. It is not, however, necessarily the rate constant at which the assembled bound reactants are converted to assem-assembled bound products on the active site. There can be steps between the reactants free in solution and the unoccupied enzyme and this conversion, and there can be steps between this conversion and the complete dissociation of the products into the solution and the return of the enzyme to the unoccupied state prepared to associate with reactants.

When an enzyme converts a single reactant into one or more products, its observed initial rate is usually determined by only the catalytic constant k_0 and the specificity constant k_A for reactant A (Equation 3–40). The specificity constant k_A is a second-order rate constant with units of molar^{-1} second^{-1}. For the simplest kinetic mechanism (Equation 3–55), the specificity constant k_A is equal to $k_1[k_2(k_{-1} + k_2)^{-1}]$, which is the rate constant k_1 for the bimolecular association of E and A multiplied by a particular unitless fraction of rate constants, $k_2(k_2 + k_{-1})^{-1}$. This fraction is the fraction of the complex E·A that becomes product. Consequently, in this simple case, **the specificity constant is the rate constant for the formation of only those bimolecular associations between E and A that produce complexes that will be converted into product free in solution.** The specificity constant is the second-order "rate constant for the capture of…[reactant] into enzyme complexes that are destined to yield product…at some later time."[95]

It has been noted that the steps in the kinetic mechanism for an enzyme can be expanded indefinitely by adding steps that are not involved in the direct association of reactants and have no effect on the form of the rate law, only on the functions of the rate constants of the mechanism used to define the observed kinetic constants. For the expanded kinetic mechanism of Equation 3–84, the rate constants can be combined into the composite rate constants k_1 (Equation 3–77), k_{-1} (Equation 3–83), and k_2 (Equation 3–70). This combination reduces the expanded kinetic mechanism to that of Equation 3–55, for which the fraction of the complexes E′·A′ that becomes product is again $k_2(k_2 + k_{-1})^{-1}$, and

$$k_1\left(\frac{k_2}{k_{-1}+k_2}\right) = k_3\left(\frac{k_4k_5k_6k_7}{k_{-3}k_{-4}k_{-5}(k_{-6}+k_7)+k_5k_6k_7(k_{-3}+k_4)+k_{-3}k_{-4}k_6k_7}\right) \quad (3\text{–}164)$$

which is equal to the specificity constant k_A for reactant A in the rate equation for the kinetic mechanism of Equation 3–84. It follows that, regardless of the expansion performed to produce a kinetic mechanism, the specificity constant k_A will always be the product of the composite rate constant for the bimolecular association between enzyme and reactant A to produce the complex between enzyme and reactant A and the fraction of that complex destined to yield product.[72,95]

When an enzyme converts two reactants to one or more products, the initial rate of the reaction below saturation is determined by the catalytic constant k_0 and some combination of the specificity constants k_A, k_B,, and k_{AB} (Equation 3–95). For the ping-pong kinetic mechanism of Equation 3–154

$$k_A = k_1\left(\frac{k_2}{k_{-1}+k_2}\right) \quad (3\text{–}165)$$

which is again the rate constant for the bimolecular association of the unoccupied active site and reactant A multiplied by the fraction of the complex E·A that is destined to yield product. The same is true of k_B and reactant B. These simple expressions for the specificity constants k_A and k_B result from the fact that an irreversible step separates the association of reactant A and reactant B.

For the kinetic mechanism

$$\mathrm{E} + \mathrm{A} + \mathrm{B} \underset{k_{-1}}{\overset{k_1}{\rightleftharpoons}} \mathrm{E{\cdot}A} + \mathrm{B} \underset{k_{-2}}{\overset{k_2}{\rightleftharpoons}} \mathrm{E{\cdot}A{\cdot}B} \xrightarrow{k_3} \mathrm{E} + \mathrm{Y} + \mathrm{Z} \quad (3\text{–}166)$$

with the rate equation

$$v_0 = \frac{k_1k_2k_3[\mathrm{E}]_t[\mathrm{A}]_0[\mathrm{B}]_0}{k_{-1}(k_{-2}+k_3)+k_1(k_{-2}+k_3)[\mathrm{A}]_0+k_2k_3[\mathrm{B}]_0+k_1k_2[\mathrm{A}]_0[\mathrm{B}]_0} \quad (3\text{–}167)$$

the apparent specificity constant for reactant A

$$k_{A,app} = \frac{k_1k_2[\mathrm{B}]_0k_3}{k_{-1}(k_{-2}+k_3)+k_2[\mathrm{B}]_0k_3} \quad (3\text{–}168)$$

which is equal to $k_1'[\mathrm{B}]_0k_3(k_3+k_{-1}')^{-1}$, where $k_1'[\mathrm{B}]_0$ is the composite second-order rate constant for formation of E·A·B from E and A at the fixed concentration of reactant B and k_{-1}' is the composite rate constant for dissociation of E·A·B to E and A. The apparent specificity constant for reactant B

$$k_{B,app} = k_2\left(\frac{k_1[\mathrm{A}]_0}{k_{-1}+k_1[\mathrm{A}]_0}\right)\left(\frac{k_3}{k_{-2}+k_3}\right) \quad (3\text{–}169)$$

where $k_3(k_{-2}+k_3)^{-1}$ is the fraction of ternary complexes E·A·B that proceed to free product, k_2 is the second-order rate constant for association of B and E·A, and $k_1[\mathrm{A}]_0(k_1[\mathrm{A}]_0+k_{-1})^{-1}$ is the fraction of complexes E and E·A that are E·A. In each of these instances, the observed value for $k_{A,app}$ or $k_{B,app}$ is the product of the second-order rate constant for formation of ternary complex E·A·B from the free version of the respective reactant and the unoccupied active site and the fraction of ternary complexes that produce product free in solution.

The initial rate of an enzymatic reaction is decreased by the addition of particular compounds to the solution that inhibit its activity, and an examination of the effect of such inhibitors on the initial rate of the enzymatic reaction can provide useful information about the kinetic mechanism.[96] An **inhibitor** is any chemical substance that, when added to the solution, decreases the initial rate of an enzymatically catalyzed reaction. **Reversible inhibitors** exert their effect by associating noncovalently and reversibly with the enzyme and, when associated, decrease or eliminate its ability to catalyze the reaction. When a reversible inhibitor is removed from the solution, its effect on the enzymatic reaction disappears or is reversed. Almost always, reversible inhibitors are used in steady-state kinetic studies of enzymatic reactions.

In the presence of only reactants, a kinetic mechanism for ordered addition of reactants (Equation 3–109) is indistinguishable from one for random addition of reactants (Equation 3–121) by steady-state kinetics. A kinetic mechanism in which an irreversible step is due to dissociation of a product (Equation 3–160) is indistinguishable from one in which an irreversible step is not due to dissociation of a product (Equation 3–154) by steady-state kinetics. These are two particular cases of the more general fact that studies of initial rates of an enzymatic reaction in the presence of only reactants cannot, in most cases, define **the order for either association of reactants with the enzyme or dissociation of products from the enzyme**. This information, however, can usually be obtained from studies of inhibition caused by analogues for the reactants and from studies of inhibition by products and analogues of products. To understand these strategies, the effects of inhibitors of enzymatic reactions on steady-state kinetics must first be explained.

Inhibition of Enzymatic Reactions: Definition of Types

Observation: A **competitive reversible inhibitor with respect to reactant A** is any reversible inhibitor the addition of which to the solution decreases the observed values of the specificity constant for reactant A, k_A, or the apparent specificity constant for reactant A, $k_{A,app}$, while having no effect on the value of the catalytic constant, k_0, or the apparent catalytic constant for reactant A, $k_{0,A,app}$, respectively (Figure 3–9A). The competitive inhibition is **linear** if the factor by which k_A, $k_A[E]_t$, $k_{A,app}$, or $k_{A,app}[E]_t$ is decreased is $K_{icI}([I] + K_{icI})^{-1}$, where [I] is the molar concentration of inhibitor I (Figure 3–9G). The constant K_{icI} is the **inhibition constant for competitive inhibition** by inhibitor I. An inhibitor I that is competitive with respect to reactant A is not necessarily competitive with respect to the other reactants in the enzymatic reaction.

In the general case, where only the initial concentration of reactant A and the concentration of inhibitor I are varied and the initial concentrations of all other reactants are fixed, the **observed initial rate for an enzymatic reaction upon addition of a linear competitive inhibitor** with respect to reactant A is

$$v_0 = \frac{k_{0,A,app}[E]_t k_{A,app}[E]_t \left(\frac{K_{icI}}{[I] + K_{icI}}\right)[A]_0}{k_{0,A,app}[E]_t + k_{A,app}[E]_t \left(\frac{K_{icI}}{[I] + K_{icI}}\right)[A]_0}$$

$$= \frac{k_{0,A,app}[E]_t[A]_0}{K_{mA,app}\left(\frac{[I] + K_{icI}}{K_{icI}}\right) + [A]_0} \qquad (3–170)$$

As the concentration of inhibitor I is increased, the apparent value of $k_{A,app}[E]_t$ decreases by the factor $K_{icI}([I] + K_{icI})^{-1}$. Consequently, the initial slopes of the curves of v_0 as a function of $[A]_0$ decrease by the same factor. Regardless of the concentration of inhibitor I, however, the asymptotes of all the curves at saturating $[A]_0$ are the same, and $v_0 = k_{0,A,app}$.

The values for v_0 (y) as a function of $[A]_0$ (x) at a fixed concentration of I are plotted and fit with Equation 3–52. This fit is repeated for all values of I. When the values for $k_{A,I,app}[E]_t$ (parameter c of the fit) obtained from these fits are plotted as a function of the concentration of inhibitor I, [I], the data can be fit by the equation

$$u = u_0\left(\frac{h}{z + h}\right) \qquad (3–171)$$

where u is the value for $k_{A,I,app}[E]_t$ at a given concentration of inhibitor, z is [I], u_0 is the value of the apparent rate constant $k_{A,app}[E]_t$ in the absence of inhibitor, and h is K_{icI}.

In double-reciprocal form

$$\frac{1}{v_0} = \frac{1}{k_{A,app}[E]_t\left(\frac{K_{icI}}{[I] + K_{icI}}\right)[A]_0} + \frac{1}{k_{0,A,app}[E]_t} \qquad (3–172)$$

Upon taking the limit, it can be seen that, for competitive inhibition, the lines in a plot of v_0^{-1} as a function of $[A]_0^{-1}$ at different fixed concentrations of inhibitor I all intersect at the axis of the ordinate where $[A]_0^{-1}$ is zero (Figure 3–9B). **This intersection of the double reciprocals at the axis of the ordinate is the most obvious characteristic of competitive inhibition** and is usually used to identify competitive inhibition.

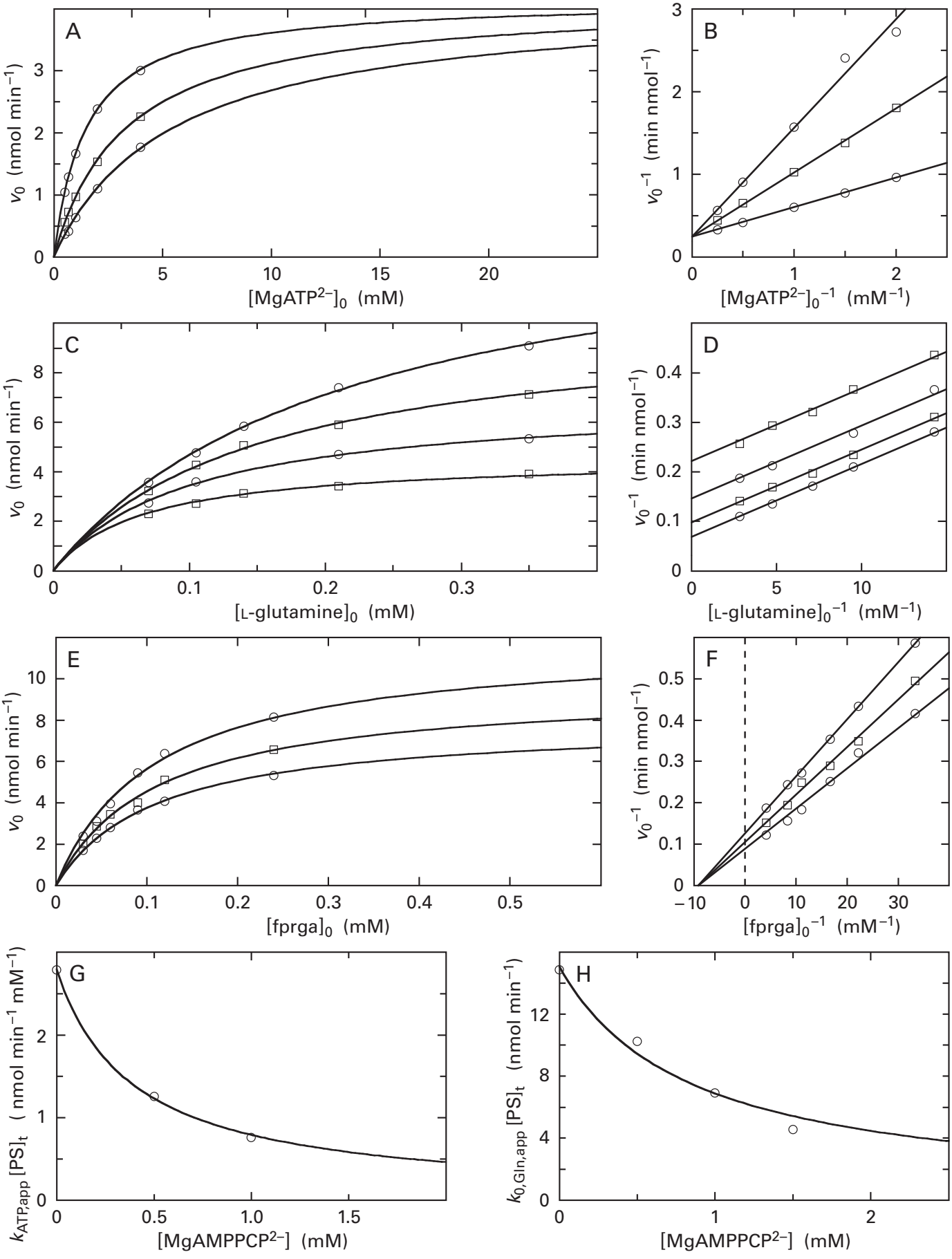
A
v_0 (nmol min^{-1})
[MgATP^{2-}]$_0$ (mM)
B
v_0^{-1} (min nmol^{-1})
[MgATP^{2-}]$_0^{-1}$ (mM^{-1})
C
v_0 (nmol min^{-1})
[L-glutamine]$_0$ (mM)
D
v_0^{-1} (min nmol^{-1})
[L-glutamine]$_0^{-1}$ (mM^{-1})
E
v_0 (nmol min^{-1})
[fprga]$_0$ (mM)
F
v_0^{-1} (min nmol^{-1})
[fprga]$_0^{-1}$ (mM^{-1})
G
$k_{ATP,app}$ [PS]$_t$ (nmol min^{-1} mM^{-1})
[MgAMPPCP^{2-}] (mM)
H
$k_{0,Gln,app}$ [PS]$_t$ (nmol min^{-1})
[MgAMPPCP^{2-}] (mM)

Figure 3–9: Kinetics for reversible inhibition of the transamidination catalyzed by phosphoribosylformylglycinamidine synthase from liver of *G. gallus*.[97] Solutions containing $MgATP^{2-}$, N^2-formyl-N^1-(5-phospho-D-ribosyl)glycinamide, and L-glutamine were prepared at pH 8.0 and 37 °C. The concentration of uncomplexed Mg^{2+} was fixed at 1 mM throughout. Each transamidination was initiated by adding phosphoribosylformylglycinamidine synthase (PS), and the production of L-glutamate was followed in a coupled assay with the 3-acetylpyridine analogue for NAD^+ and glutamate dehydrogenase by the increase in A_{363} upon reduction of the analogue. Each initial rate of the increase in A_{363} was converted to an initial rate for the production of L-glutamate, v_0 (micromolar minute^{-1}). **(A)** Initial rates (nanomoles minute^{-1}) and **(B)** reciprocals of the initial rates (minutes nanomole^{-1}) at 0.35 mM L-glutamine and 0.25 mM N^2-formyl-N^1-(5-phospho-D-ribosyl)glycinamide for different initial concentrations of $MgATP^{2-}$ (millimolar) and reciprocals of the different initial concentrations of $MgATP^{2-}$ (millimolar^{-1}), respectively, at 0, 0.5, and 1.0 mM $MgAMPPCP^{2-}$. The concentrations of inhibitor increase as the curves become lower in Panel A and as the lines become higher in Panel B. Equation 3–52, with x equal to $[MgATP^{2-}]_0$ and y equal to v_0, was fit to each set of data in Panel A. The three values for parameter a were equal to each other within their standard deviations. Consequently, they were set at the same value, 4.15 nmol of L-glutamate min^{-1}, and the data were refit to give the curves shown in the figure. The lines that were fit to the data in Panel B were forced to pass through 0.241 min (nmol of L-glutamate)$^{-1}$ at the axis of the ordinate. **(C)** Initial rates (nanomoles minute^{-1}) and **(D)** reciprocals of the initial rates (minutes nanomole^{-1}) at 2.0 mM $MgATP^{2-}$ and 0.25 mM N^2-formyl-N^1-(5-phospho-D-ribosyl)glycinamide for different initial concentrations of L-glutamine (millimolar) and reciprocals of the different initial concentrations of L-glutamine (millimolar^{-1}), respectively, at 0, 0.5, 1.0, and 1.5 mM $MgAMPPCP^{2-}$. The concentrations of inhibitor increase as the curves become lower in Panel C and as the lines become higher in Panel D. Equation 3–52, with x equal to $[\text{L-glutamine}]_0$ and y equal to v_0, was fit to each set of data in Panel C. The four values for parameter c, the initial slopes of the four curves, were equal to each other within their standard deviations. Consequently, they were set at the same value, 68 nmol of L-glutamate min^{-1} (mM L-glutamine)$^{-1}$, and the data were refit. These are the curves shown in the figure. The lines that were fit to the data in Panel D were forced to all have the slope of 0.0147 min (nmol of L-glutamate)$^{-1}$ mM L-glutamine. **(E)** Initial rates (nanomoles minute^{-1}) and **(F)** reciprocals of the initial rates (minutes nanomole^{-1}) at 0.35 mM L-glutamine and 2.0 mM $MgATP^{2-}$ for different initial concentrations of N^2-formyl-N^1-(5-phospho-D-ribosyl)glycinamide ($[\text{fprga}]_0$ in millimolar) and reciprocals of the different initial concentrations of N^2-formyl-N^1-(5-phospho-D-ribosyl)glycinamide ($[\text{fprga}]_0^{-1}$ in millimolar^{-1}), respectively, at 0, 0.5, and 1.0 mM $MgAMPPCP^{2-}$. The concentrations of inhibitor increase as the curves become lower in Panel E and as the lines become higher in Panel F. Equation 3–52, with x equal to $[\text{fprga}]_0$ and y equal to v_0, was fit to each set of data in Panel E. The three values for parameter b, the Michaelis constants K_m, from the fits for the three curves were equal to each other within their standard deviations. Consequently, they were set at the same value, 0.11 mM fprga, and the data were refit with this single parameter. These are the curves shown in the figure. The lines that were fit to the data in Panel F were forced to pass through –9.09 (mM fprga)$^{-1}$ at the axis of the abscissa. **(G)** The three values for parameter c for the curves in Panel A, the apparent specificity constants for $MgATP^{2-}$, $k_{ATP,app}[PS]_t$ (nanomoles minute^{-1} millimolar^{-1}), are plotted as a function of the concentrations of $MgAMPPCP^{2-}$ (millimolar). The data were fit by Equation 3–171 with u equal to these observed values and z equal to $[MgAMPPCP^{2-}]$. The value for $K_{icAMPPCP}$ (parameter h) obtained from the fit is 0.39 ± 0.01 mM. **(H)** The four values for parameter a from the fits in Panel C, the apparent catalytic constants for L-glutamine, $k_{0,Gln,app}[PS]_t$ (nanomoles minute^{-1}), are plotted as a function of the concentrations of $MgAMPPCP^{2-}$ (millimolar). The data were fit by Equation 3–171 with u equal to $k_{0,Gln,app}[PS]_t$ and z equal to $[MgAMPPCP^{2-}]$. The value for $K_{iuAMPPCP}$ obtained from the fit is 0.84 ± 0.14 mM $MgAMPPCP^{2-}$.

Phosphoribosylformylglycinamidine synthase (PS) from *Gallus gallus* catalyzes a reaction

$$N^2\text{-formyl-}N^1\text{-(5-phospho-D-ribosyl)glycinamide} + \text{L-glutamine} + MgATP^{2-} + H_2O \rightleftharpoons MgADP^- + HOPO_3^{2-} + \text{L-glutamate} + 2\,H^+ + 2\text{-(formamido)-}N^1\text{-(5-phospho-D-ribosyl)acetamidine} \quad (3\text{–}173)$$

that for kinetic purposes involves three reactants and four products. This enzymatic reaction is inhibited by magnesium 5′-adenylic methylenediphosphonic anhydride ($MgAMPPCP^{2-}$)

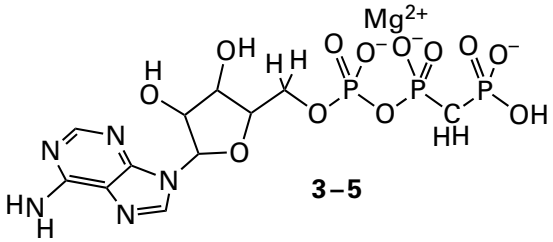

3–5

an inert analogue of $MgATP^{2-}$. When the initial concentrations of *N*-2-formyl-*N*-1-(5-phospho-D-ribosyl)-glycinamide and L-glutamine were fixed and $MgATP^{2-}$ was the varied reactant at several fixed concentrations of $MgAMPPCP^{2-}$, each curve describing a set of values for v_0 and $[MgATP]_0$ had the same value for the asymptote $k_{0,ATP,app}[PS]_t$, but the values for $k_{ATP,app}[PS]_t$, and

hence the initial slopes of the curves, decreased as the concentration of the inhibitor was increased (Figure 3–9A).[97] When the values for v_0^{-1} were plotted as a function of the respective values for $[MgATP]_0^{-1}$, the lines for the different fixed concentrations of the inhibitor all intersected at the axis of the ordinate (Figure 3–9B). Consequently, $MgAMPPCP^{2-}$ is a competitive inhibitor with respect to $MgATP^{2-}$ in the reaction catalyzed by phosphoribosylformylglycinamidine synthase.

When the various observed values for $k_{ATP,app}[PS]_t$ are plotted as a function of the respective concentrations of the inhibitor $MgAMPPCP^{2-}$ (Figure 3–9G), the plot is that for the function

$$k_{ATP,app,obs}[PS]_t = k_{ATP,app}[PS]_t\left(\frac{K_{icAMPPCP}}{[MgAMPPCP^{2-}] + K_{icAMPPCP}}\right) \quad (3–174)$$

with $K_{icAMPPCP} = 0.39 \pm 0.01$ mM, so the inhibition is linear. Magnesium 5′-adenylic methylenediphosphonic anhydride is also a linear competitive inhibitor with respect to $MgATP^{2-}$ in the reaction catalyzed by human Rho protein kinase (Figure 3–10A)[98] with an inhibition constant $K_{icAMPPCP}$ of 124 ± 1 μM (Figure 3–10B). *N*-Acetyl-D-glucosamine is a linear competitive inhibitor of hexokinase from *R. norvegicus* (Equation 3–94) with respect to hexose D-glucose (Figure 3–11A,B) with an inhibition constant K_{icNAG} of 70 ± 6 μM (Figure 3–11B).[99]

An **uncompetitive reversible inhibitor with respect to reactant A** is any reversible inhibitor the addition of which to the solution decreases the catalytic constant, k_0, or the apparent catalytic constant for reactant A, $k_{0,A,app}$, while having no effect on the value of the specificity constant for reactant A, k_A, or the apparent specificity constant for reactant A, $k_{A,app}$. Again, the uncompetitive inhibition is linear if the factor affecting k_0, $k_0[E]_t$, $k_{0,A,app}$ or $k_{0,A,app}[E]_t$ is $K_{iuI}([I] + K_{iuI})^{-1}$, where K_{iuI} is the **inhibition constant for the uncompetitive inhibition** produced by inhibitor I.

In the general case, where only the initial concentration of reactant A and the concentration of inhibitor I are varied and the initial concentrations of all other substrates are fixed, the **observed initial rate for an enzymatic reaction upon addition of a linear uncompetitive inhibitor** with respect to reactant A is

$$v_0 = \frac{k_{0,A,app}[E]_t\left(\frac{K_{iuI}}{[I] + K_{iuI}}\right)k_{A,app}[E]_t[A]_0}{k_{0,A,app}[E]_t\left(\frac{K_{iuI}}{[I] + K_{iuI}}\right) + k_{A,app}[E]_t[A]_0} \quad (3–175)$$

As the concentration of inhibitor I is increased, the apparent value for $k_0[E]_t$ in Equation 3–43, which is the kinetic constant observed in an experimental measurement, decreases by the factor $K_{iuI}([I] + K_{iuI})^{-1}$. Consequently, the asymptotes of the curves of v_0 as a function of $[A]_0$ at saturating $[A]_0$ decrease by the same factor. Regardless of the concentration of inhibitor I, however, the initial slopes of all the curves are the same because the apparent rate constant $k_{A,app}[E]_t$ is unaffected by the inhibitor.

In double-reciprocal form

$$\frac{1}{v_0} = \frac{1}{k_{A,app}[E]_t[A]_0} + \frac{1}{k_{0,A,app}[E]_t\left(\frac{K_{iuI}}{[I] + K_{iuI}}\right)} \quad (3–176)$$

For uncompetitive inhibition, the lines in a plot of v_0^{-1} as a function of $[A]_0^{-1}$ at several fixed concentrations of inhibitor I all have the same slope and are parallel to each other. **These parallel lines in the plots of the double reciprocals are the most obvious characteristic of uncompetitive inhibition.**

Magnesium 5′-adenylic methylenediphosphonic anhydride (**3–5**) is a linear uncompetitive inhibitor with respect to L-glutamine in the reaction (Equation 3–173) catalyzed by phosphoribosylformylglycinamidine synthase from *G. gallus* (Figure 3–9C,D) with an inhibition constant $K_{iuAMPPCP}$ of 0.84 ± 0.14 mM (Figure 3–9H). The chromium complex of ATP^{4-} ($CrATP^-$) is an uncompetitive inhibitor of glycerol kinase (Equation 3–140 with glycerol in place of (*S*)-1-aminopropane-2,3-diol) from *C. norvegensis* (Figure 3–12A)[100] with an inhibition constant $K_{iuCrATP}$ of 1.73 ± 0.02 μM (Figure 3–12B).

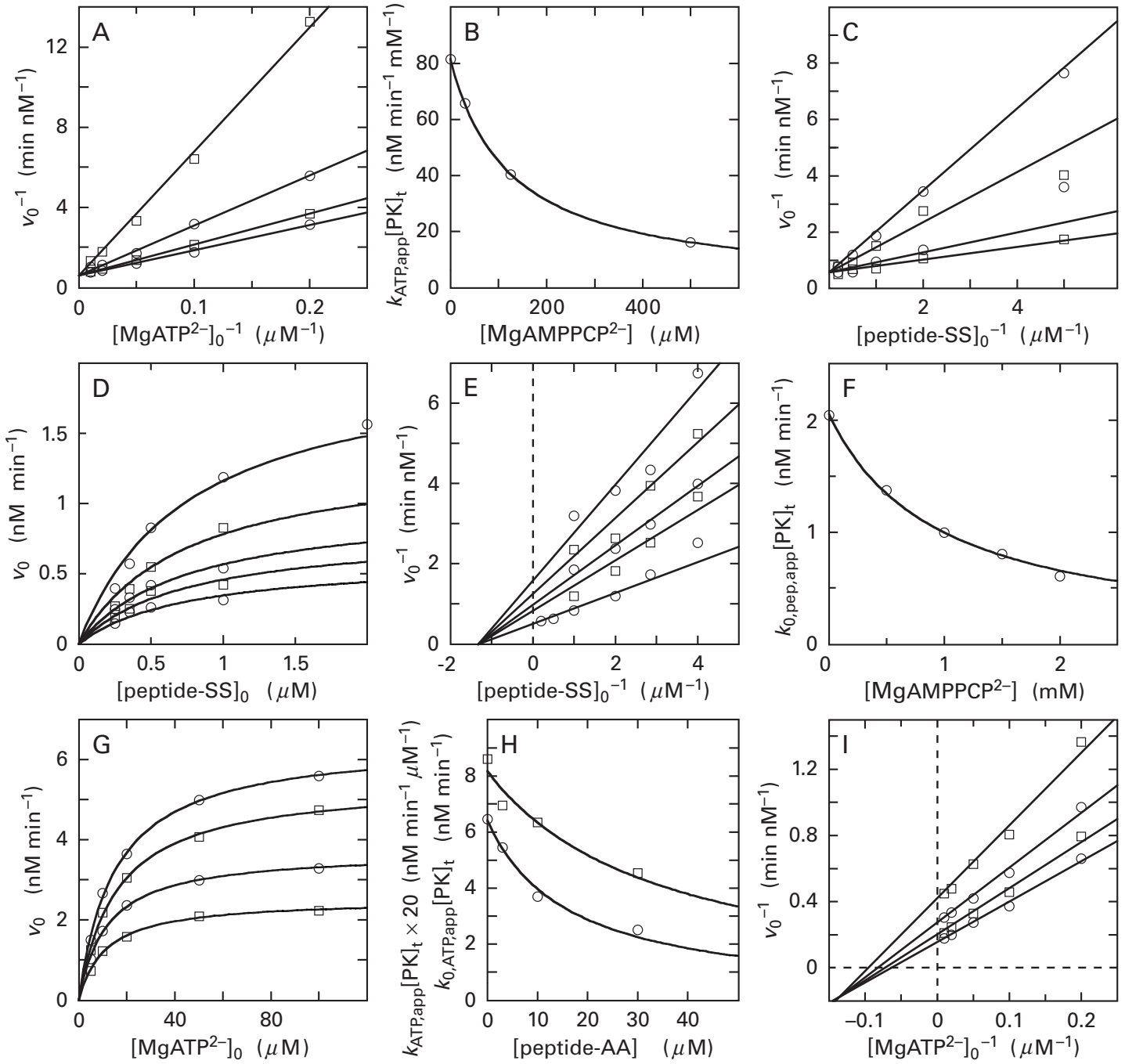

Figure 3–10: Kinetics for reversible inhibition of the phosphorylation catalyzed by the kinase domain (amino acids 1–543) of human Rho protein kinase.[98] The reactant used in place of one of the proteins that are physiological substrates for Rho protein kinase was the biotinylated peptide biotin-AKRRRLSSLRA-NH_2. This peptide contains a sequence of amino acids recognized by the enzyme that includes the two serines it phosphorylates. Solutions containing kinase domain (amino acids 1–543) of human Rho protein kinase (PK) and $MgATP^{2-}$ and [γ-^{32}P]$MgATP^{2-}$ or enzyme and biotin-AKRRRLSSLRA-NH_2 were prepared at pH 7.4 and 30 °C. The concentration of uncomplexed Mg^{2+} was fixed at 5 mM throughout. Each phosphorylation was initiated by adding biotin-AKRRRLSSLRA-NH_2 or $MgATP^{2-}$ and [γ-^{32}P]$MgATP^{2}$, Equation 3–52, with x equal to [peptide-SS]$_0$ and y equal to v_0, was fit to each set of data in Panel D. The five values for parameter b, the Michaelis constants, for the fits of the five curves varied unsystematically and were assumed to be equal to each other. Consequently, they were set at their average value, 0.75 μM biotin-AKRRRLSSLRA-NH_2, and the data were refit with this quotient. These are the curves shown in Panel D. The lines that were fit to the data in Panel E were forced to pass through –1.32 (μM biotin-AKRRRLSSLRA-NH_2)$^{-1}$ at the axis of the abscissa. (**F**) The five values for parameter a of the fits in Panel D, the observed values of the apparent catalytic constant for the peptide, biotin-AKRRRLSSLRA-NH_2, $k_{0,pep,app}$[PK]$_t$ (nanomolar minute^{-1}), are plotted as a function of the concentrations

respectively, and the rate of production of radioactively phosphorylated peptide was followed for 60 minutes by capturing the phosphopeptide through its covalently attached biotin with a membrane to which streptavidin had been covalently attached. Each initial rate of capture of phosphorus-32 was converted to an initial rate for the production of phosphorylated peptide, v_0 (micromolar minute^{-1}). **(A)** Reciprocals of the initial rates (minutes nanomolar^{-1}) at 2.5 μM biotin-AKRRRLSSLRA-NH_2 for reciprocals of different initial concentrations of $MgATP^{2-}$ (micromolar^{-1}) at 0, 30, 125, and 500 μM concentrations of the inhibitor $MgAMPPCP^{2-}$. The concentrations of inhibitor increase as the lines become higher. **(B)** Behavior of observed values for the apparent specificity constant for $MgATP^{2-}$, $k_{ATP,app}[PK]_t$ (nanomolar minute^{-1} millimolar^{-1}), which are reciprocals of the slopes of the lines fit to the data in Panel A, as a function of the concentrations of $MgAMPPCP^{2-}$ (micromolar). The data were fit by Equation 3–171 with u equal to the observed values for the apparent specificity constant and z equal to $[MgAMPPCP^{2-}]$, and the value for $K_{icAMPPCP}$ (parameter h of the fit) is 124 ± 0.4 μM. **(C)** Reciprocals of the initial rates (minutes nanomolar^{-1}) at 40 μM $MgATP^{2-}$ for reciprocals of different initial concentrations of biotin-AKRRRLSSLRA-NH_2 ($[peptide\text{-}SS]_0$; micromolar^{-1}) at 0, 2, 10, and 20 μM concentrations of the inhibitor acetyl-AKRRRLAALRA-NH_2, a peptide that lacks the serines phosphorylated by the enzyme. The concentrations of inhibitor increase as the lines become higher. **(D)** Initial rates (nanomolar minute^{-1}) and **(E)** reciprocals of the initial rates (minutes nanomolar^{-1}) at 40 μM $MgATP^{2-}$ for different initial concentrations of biotin-AKRRRLSSLRA-NH_2 (micromolar) and reciprocals of different initial concentrations of biotin-AKRRRLSSLRA-NH_2 (micromolar^{-1}), respectively, at 0, 0.5, 1.0, 1.5, and 2.0 mM concentrations of $MgAMPPCP^{2-}$. The concentrations of inhibitor increase as the curves become lower in Panel D and as the lines become higher in Panel E. **(F)** Reciprocals of the initial rates (minutes nanomolar^{-1}) at 2.5 μM biotin-AKRRRLSSLRA-NH_2 for reciprocals of different initial concentrations of $MgATP^{2-}$ (micromolar^{-1}) at 0, 3, 10, and 30 μM concentrations of the inhibitor $MgAMPPCP^{2-}$ (millimolar). The data were fit by Equation 3–171 with u equal to the observed values for the apparent catalytic constant and z equal to $[MgAMPPCP^{2-}]$. The value for $K_{inAMPPCP}$ (parameter h of the fit) is 0.94 ± 0.05 mM. **(G)** Initial rates (nanomolar minute^{-1}) at 2.5 μM biotin-AKRRRLSSLRA-NH_2 for different initial concentrations of $MgATP^{2-}$ (micromolar) at 0, 3, 10, and 30 μM concentrations of the inhibitor acetyl-AKRRRLAALRA-NH_2. The concentrations of inhibitor increase as the curves become lower. Equation 3–52, with x equal to $[MgATP^{2-}]_0$ and y equal to v_0, was fit to each set of data. **(H)** The four values for parameter c, the initial slopes of the four curves in Panel G, which are the observed values of the apparent specificity constant for $MgATP^{2-}$, $k_{ATP,app}[PK]_t$ (nanomolar minute^{-1} micromolar^{-1}; □) multiplied by 20, and the four values for parameter a, the asymptotes of the four curves, which are the observed values for the apparent catalytic constant for $MgATP^{2-}$, $k_{0,ATP,app}[PK]_t$ (nanomolar minute^{-1}; ○), are plotted against the concentrations of acetyl-AKRRRLAALRA-NH_2 ([peptide-AA] in micromolar). Equation 3–171, with z equal to [peptide-AA] and u equal to the respective observed rate constants, was fit to each set of data. The values for K_{icPAA} and K_{iuPAA} (parameters h from the respective fits) were 35 ± 9 μM and 16 ± 3 μM. **(I)** Reciprocals of the initial rates (minutes nanomolar^{-1}) at 2.5 μM biotin-AKRRRLSSLRA-NH_2 for reciprocals of the different initial concentrations of $MgATP^{2-}$ (micromolar^{-1}) at 0, 3, 10, and 30 μM concentrations of the inhibitor acetyl-AKRRRLAALRA-NH_2. The concentrations of inhibitor increase as the lines become higher. The values for K_{icPAA} and K_{iuPAA} and the values for $k_{0,ATP,app}$ and $k_{ATP,app}$ in the absence of inhibitor from the fits to the data in Panel H were used to calculate the theoretical point of intersection for the lines describing the double reciprocals for the observed mixed inhibition, and the four lines fit to the data in Panel I were forced to pass through that theoretical point of intersection.

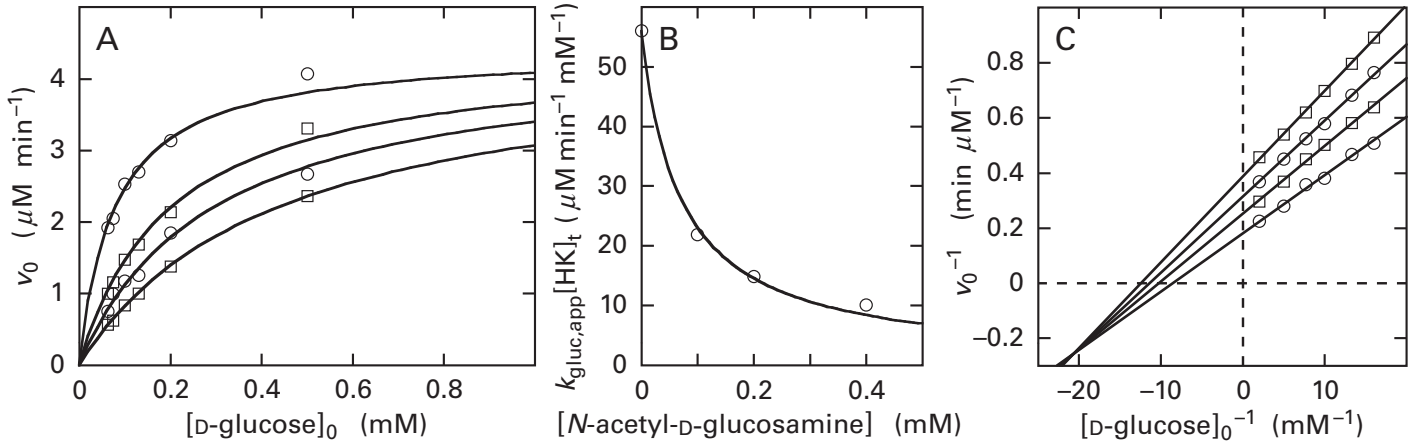

Figure 3–11: Kinetics for reversible inhibition of the phosphorylation catalyzed by partially purified hexokinase from skeletal muscle of *R. norvegicus*.[99] Solutions containing $MgATP^{2-}$ and D-glucose were prepared at pH 7.7 and 28 °C. Each phosphorylation was initiated by adding hexokinase (HK), and the production of D-glucose 6-phosphate was followed in a coupled assay with glucose-6-phosphate dehydrogenase and $NADP^+$ by monitoring the increase in A_{340} from the conversion of $NADP^+$ to constants for D-glucose, $k_{gluc,app}[HK]_t$, are plotted as a function of the concentrations of *N*-acetyl-D-glucosamine (millimolar). The data were fit by Equation 3–171 with u equal to the observed values for the apparent specificity constant and z equal to [*N*-acetyl-D-glucosamine]. The value for K_{icNAG} (parameter h of the fit) is 70 ± 6 μM. **(C)** Reciprocals of the initial rates (minutes micromolar^{-1}) at 0.25 mM $MgATP^{2-}$ for reciprocals of different initial concentrations of D-glucose (millimolar^{-1}) at 0, 0.5, 1.0,

NADPH (as in Figure 3–4). Each initial rate of change in A_{340} was converted to an initial rate for the production of D-glucose 6-phosphate, v_0 (micromolar D-glucose 6-phosphate minute^{-1}). **(A)** Initial rates (micromolar minute^{-1}) of hexokinase at 0.25 mM $MgATP^{2-}$ for different initial concentrations of D-glucose (millimolar) at 0, 0.1, 0.2, and 0.4 mM concentrations of the inhibitor *N*-acetyl-D-glucosamine. The concentrations of inhibitor increase as the curves become lower. Equation 3–52, with x equal to $[\text{D-glucose}]_0$ and y equal to v_0, was fit to each set of data. The four values for parameter a of the four fits, which are the observed values for $k_{0,\text{app,gluc}}[\text{HK}]_t$, were almost identical to each other within their standard deviations and did not vary systematically, a fact that defined the inhibition as competitive. Consequently, the four asymptotes were set at the same value, 4.4 μM D-glucose 6-phosphate min^{-1}, and the data were refit. These refits are the curves shown in the figure. **(B)** The four values for parameter c of the fits in Panel A, the apparent specificity constants for D-glucose, $k_{\text{gluc,app}}[\text{HK}]_t$, and the four values for parameter a, the apparent catalytic constants for D-glucose, $k_{0,\text{gluc,app}}[\text{HK}]_t$, were plotted against the concentrations of ATP^{4-}. The values for K_{icATP} and K_{iuATP} from the fits of these data to Equation 3–171 were 3.3 ± 0.5 mM and 1.4 ± 0.1 mM, respectively. The values for K_{icATP} and K_{iuATP} and the values for $k_{0,\text{app,gluc}}$ and $k_{\text{gluc,app}}$ in the absence of inhibitor from these fits to the data were used to calculate the theoretical point of intersection for the lines describing the double reciprocals for the observed mixed inhibition, and the four lines fit to the data in the figure were forced to pass through that calculated point of intersection.

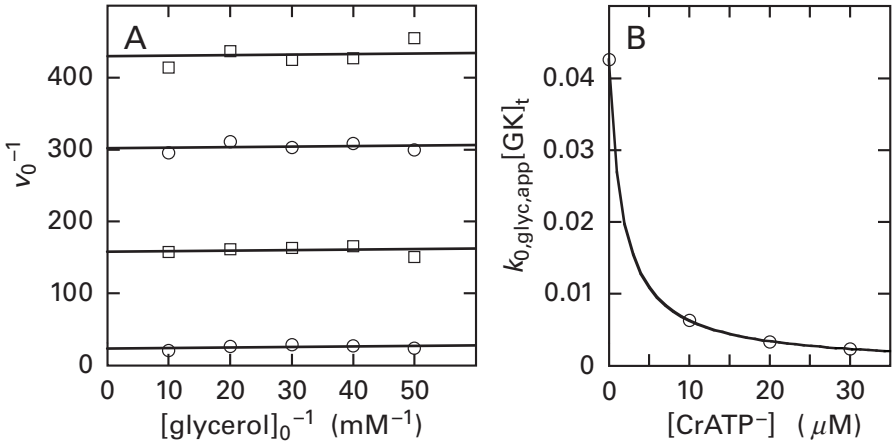

Figure 3–12: Kinetics for inhibition of glycerol kinase[100] from *C. norvegensis* by the chromium complex of ATP^{4-}. Solutions containing glycerol and $MgATP^{2-}$ were prepared at pH 7.0 and 25 °C. The concentration of uncomplexed Mg^{2+} was fixed at 3 mM throughout. Glycerol kinase (GK) was added to initiate the phosphorylation, and the production of $MgADP^-$ was monitored by coupling the production of $MgADP^-$ to the oxidation of NADH as in Figure 3–7. **(A)** Reciprocals of the initial rates for the production of $MgADP^-$ (in unreported units) at 20 μM $MgATP^{2-}$ for reciprocals of different initial concentrations of glycerol (millimolar^{-1}) at 0, 10, 20, and 30 μM $CrATP^-$. The concentrations of inhibitor increase as the lines become higher. The lines that were fit to the data were forced to be parallel to each other, as were the lines drawn by the authors, and to have the same slope as the lines drawn by the authors. **(B)** Reciprocals of the observed intersections of the lines fit to the data in Panel A with the axis of the abscissa, which are the observed values of the apparent catalytic constant for glycerol, $k_{0,\text{glyc,app}}[\text{GK}]_t$ (in unreported units), are plotted as a function of the concentration of $CrATP^-$ (micromolar). The data in this panel were fit by Equation 3–171 with u equal to the observed values for the apparent catalytic constant and z equal to $[CrATP^-]$, and the value for K_{iuCrATP} (parameter h of the fit) is 1.73 ± 0.02 μM.

A **noncompetitive reversible inhibitor with respect to reactant A** is any reversible inhibitor the addition of which to the solution decreases the specificity constant for reactant A, k_A , or the apparent specificity constant for reactant A, $k_{A,app}$, and the catalytic constant, k_0, or the apparent catalytic constant for reactant A, $k_{0,A,app}$ by the same factor. In this case, the inhibition is considered **linear** if the factor affecting each observed value of k_A, $k_A[E]_t$, $k_{A,app}$, or $k_{A,app}[E]_t$ and k_0, $k_0[E]_t$, $k_{0,A,app}$, or $k_{0,A,app}[E]_t$, is $K_{inI}([I] + K_{inI})^{-1}$, where K_{inI} is the inhibition constant for the noncompetitive inhibition produced by inhibitor I.

In the general case, where only the initial concentration of reactant A and the concentration of inhibitor I are varied and the initial concentrations of all other reactants are fixed, the **observed initial rate for an enzymatic reaction upon addition of a linear noncompetitive inhibitor** with respect to reactant A is

$$v_0 = \frac{k_{0,A,app}[E]_t\left(\frac{K_{inI}}{[I]+K_{inI}}\right)k_{A,app}[E]_t\left(\frac{K_{inI}}{[I]+K_{inI}}\right)[A]_0}{k_{0,A,app}[E]_t\left(\frac{K_{inI}}{[I]+K_{inI}}\right)+k_{A,app}[E]_t\left(\frac{K_{inI}}{[I]+K_{inI}}\right)[A]_0} = \left(\frac{k_{0,A,app}[E]_t k_{A,app}[E]_t[A]_0}{k_{0,A,app}[E]_t+k_{A,app}[E]_t[A]_0}\right)\left(\frac{K_{inI}}{[I]+K_{inI}}\right) \quad (3–177)$$

As indicated in the latter form of this equation, as the concentration of inhibitor I is increased, the value of v_0 at every $[A]_0$ for a fixed concentration of inhibitor I decreases by the same factor. Consequently, each successive curve shrinks in the vertical direction uniformly along its length. By combining Equations 3–43, 3–44, 3–46, and 3–177, it can be seen that

$$v_0 = \frac{k_{0,A,app}\left(\frac{K_{inI}}{[I]+K_{inI}}\right)[E]_t[A]_0}{K_{mA,app}+[A]_0} \quad (3–178)$$

From this equation, it can be concluded that two of the criteria for noncompetitive inhibition are that the apparent Michaelis constant is unaffected by the inhibitor, which also follows from the fact that every initial rate decreases by the same factor, and that the apparent catalytic constants decrease in proportion to the factor $K_{inI}([I]+K_{inI})^{-1}$.

In double-reciprocal form,

$$\frac{1}{v_0} = \frac{1}{k_{A,app}[E]_t\left(\frac{K_{inI}}{[I]+K_{inI}}\right)[A]_0} + \frac{1}{k_{0,A,app}[E]_t\left(\frac{K_{inI}}{[I]+K_{inI}}\right)} \quad (3–179)$$

By solving Equation 3–179 for the case in which v_0^{-1} is equal to zero, it can be seen that for noncompetitive inhibition, the lines in a plot of v_0^{-1} as a function of $[A]_0^{-1}$ at different fixed concentrations of I all intersect on the axis of the abscissa at the point $-k_{A,app}(k_{0,A,app})^{-1}$, as does the line for v_0^{-1} as a function of $[A]_0^{-1}$ in the absence of the inhibitor. **The intersection of the double reciprocals at the axis of the abscissa is the most obvious characteristic of noncompetitive inhibition.**

Magnesium 5′-adenylic methylenediphosphonic anhydride (**3–5**) is a noncompetitive inhibitor with respect to N^2-formyl-N^1-(5-phospho-D-ribosyl)-glycinamide in the reaction (Equation 3–173) catalyzed by phosphoribosylformylglycinamidine synthase from *G. gallus* (Figure 3–9E,F) with an inhibition constant of 1.1 mM. Rho protein kinase phosphorylates the two serines in the sequence –KRRRLSSLRA– in a protein that is a substrate using $MgATP^{2-}$ as the source of the phospho group. Magnesium 5′-adenylic methylenediphosphonic anhydride is a linear noncompetitive inhibitor of Rho protein kinase with respect to the synthetic peptide biotin-AKRRRLSSLRA-NH_2, when it is used as a reactant for the enzyme (Figure 3–10D,E),[98] with an inhibition constant $K_{inAMPPCP}$ of 0.94 ± 0.05 mM (Figure 3–10F).

A **mixed inhibitor with respect to reactant A** is any reversible inhibitor for which the inhibition constant K_{icI} that affects the specificity constant for reactant A, k_A, or the apparent specificity constant for reactant A, $k_{A,app}$, is different from the inhibition constant K_{iuI} that affects the catalytic constant, k_0, or the apparent catalytic constant for reactant A, $k_{0,A,app}$, and both inhibition constants are finite. As before, the mixed inhibition is **linear** if the factor affecting k_A, $k_A[E]_t$, $k_{A,app}$, or $k_{A,app}[E]_t$ is $K_{icI}([I]+K_{icI})^{-1}$ and the factor affecting k_0, $k_0[E]_t$, $k_{0,A,app}$, or $k_{0,A,app}[E]_t$ is $K_{iuI}([I]+K_{iuI})^{-1}$.

In the general case where only the initial concentration of reactant A and the concentration of inhibitor I are varied and the concentrations of all other reactants are fixed, **the observed initial rate for an enzymatic reaction upon addition of a linear mixed inhibitor** with respect to reactant A is

$$v_0 = \frac{k_{0,A,app}[E]_t\left(\frac{K_{iuI}}{[I]+K_{iuI}}\right)k_{A,app}[E]_t\left(\frac{K_{icI}}{[I]+K_{icI}}\right)[A]_0}{k_{0,A,app}[E]_t\left(\frac{K_{iuI}}{[I]+K_{iuI}}\right)+k_{A,app}[E]_t\left(\frac{K_{icI}}{[I]+K_{icI}}\right)[A]_0} \quad (3–180)$$

In double-reciprocal form

$$\frac{1}{v_0} = \frac{1}{k_{A,app}[E]_t\left(\frac{K_{icI}}{[I] + K_{icI}}\right)[A]_0} + \frac{1}{k_{0,A,app}[E]_t\left(\frac{K_{iuI}}{[I] + K_{iuI}}\right)} \quad (3\text{–}181)$$

Consequently, for **mixed inhibition**, the lines defined by a double-reciprocal plot of v_0^{-1} as a function of $[A]_0^{-1}$ at several fixed concentrations of the inhibitor do not intersect at the axis of the ordinate because K_{iuI} is not infinite, they do not intersect at the axis of the abscissa because $K_{uiI} \neq K_{icI}$, and they are not parallel to each other because K_{icI} is not infinite. Instead, **the double reciprocals intersect in the second or third quadrant**. If $K_{icI} < K_{iuI}$, they intersect in the second quadrant and the inhibition is **predominantly competitive**, and if $K_{icI} > K_{iuI}$, they intersect in the third quadrant and the inhibition is **predominantly uncompetitive**. Note that noncompetitive inhibition is a special case of mixed inhibition where $K_{icI} = K_{iuI} = K_{inI}$.

12-(Imidazolyl)dodecanoic acid (IDD) is a linear, predominantly competitive, mixed inhibitor with respect to laurate (Figure 3–13A,C)[101] in the reaction catalyzed by unspecific monooxygenase from *Bacillus megaterium*

$$\text{laurate} + O_2 + 2\,H^+ + 2\,e^- \rightleftharpoons H_2O + \text{12-hydroxylaurate} \quad (3\text{–}182)$$

which is an enzyme containing a heme P450. The inhibition constants are 1.6 ± 0.2 μM for K_{icIDD} and 7.0 ± 0.3 μM for K_{iuIDD} (Figure 3–13B) The synthetic peptide acetyl-AKRRRLAALRA-NH_2 (peptide-AA), in which the two serines phosphorylated by Rho protein kinase are replaced by alanines, is an inhibitor of the enzyme when it is phosphorylating the reactant biotin-AKRRRLSSLRA-NH_2 (peptide-SS).

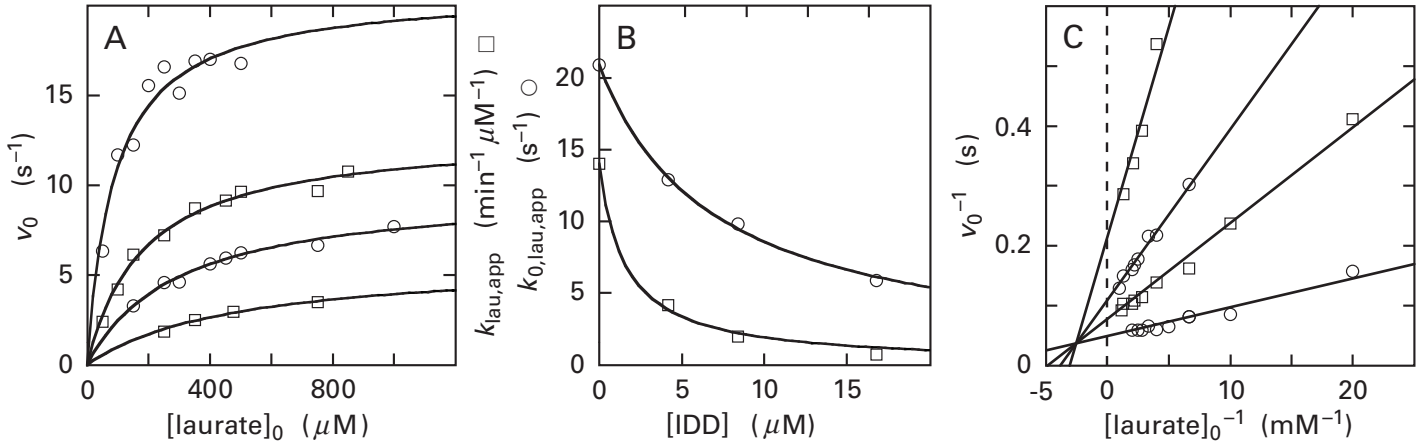

Figure 3–13: Kinetics for reversible inhibition of the oxidation of laurate catalyzed by unspecific monooxygenase (a cytochrome P450) from *B. megaterium*.[101] Buffered solutions containing ambient concentrations of molecular oxygen, various concentrations of laurate, and 0.2 mM NADPH were prepared at 30 °C. Unspecific monooxygenase was added to initiate each oxidation, and the production of $NADP^+$ was monitored by following the change in absorbance at 340 nm as NADPH was oxidized. Each initial rate of change in A_{340} was converted to an initial rate for the production of $NADP^+$ (micromoles minute^{-1}). The observed initial rates were divided by the molar concentration of active sites in the solution to give initial rates, v_0 (second^{-1}). **(A)** Initial rates for different initial concentrations of laurate (micromolar) at 0, 4.2, 8.4, and 16.8 μM concentrations of the inhibitor 12-(imidazolyl)dodecanoate. The concentrations of inhibitor increase as the curves become lower. Equation 3–52, with x equal to $[laurate]_0$ and y equal to v_0, was fit to each set of data. **(B)** The four values for parameter c of the four curves in Panel A, the specificity constants for laurate, $k_{lau,app}$ (minute^{-1} micromolar^{-1} ; □), and the four values for parameter a, the apparent catalytic constants for laurate, $k_{0,lau,app}$ (second^{-1}; ○), are plotted against the concentrations of the inhibitor 12-(imidazolyl)-dodecanoate ([IDD] in micromolar). Equation 3–171, with z equal to [IDD] and u equal to the observed values for $k_{lau,app}$ and $k_{0,lau,app}$, respectively, was fit to each set of data. The values for K_{icIDD} and K_{iuIDD}, respectively, were 1.6 ± 0.2 μM and 7.0 ± 0.3 μM. **(C)** Reciprocals of the initial rates (seconds) for reciprocals of the different initial concentrations of laurate (millimolar^{-1}) at 0, 4.2, 8.4, and 16.8 μM concentrations of the inhibitor 12-(imidazolyl)dodecanoate. The concentrations of inhibitor increase as the lines become higher. The values for K_{icIDD} and K_{iuIDD} and the values for $k_{lau,app}$ and $k_{0,lau,app}$ in the absence of inhibitor from the fits to the data in Panel B were used to calculate the theoretical point of intersection for the lines describing the double reciprocals for the observed mixed inhibition, and the four lines fit to the data in Panel C were forced to pass through that point of intersection.

Acetyl-AKRRRLAALRA-NH_2 is a linear, predominantly uncompetitive, mixed inhibitor of Rho protein kinase with respect to $MgATP^{2-}$ (Figure 3–10G,I)[98] with inhibition constants K_{icPAA} of $35 \pm 9\ \mu M$ and K_{iuPAA} of $16 \pm 3\ \mu M$ (Figure 3–10H).

The **decision as to what type of inhibition** is displayed by a particular inhibitor, I, with respect to a particular reactant, A, is usually made by examining graphical presentations of the experimental results gathered when all other substrates are at fixed concentrations. When the initial concentration of reactant A, $[A]_0$, is varied at a fixed concentration of inhibitor I and the experimentally determined values for the reciprocals of the initial rate, v_0^{-1}, are plotted against the respective values for $[A]_0^{-1}$, a linear relation between the two variables is usually observed. That relation is governed by Equation 3–53. If another fixed concentration of inhibitor I is then chosen and the experiment is repeated, a second line fitting the behavior of v_0^{-1} as a function of $[A]_0^{-1}$ will be generated and so forth. All the lines, each generated by a different fixed concentration of inhibitor I, will usually pass through the same point or be parallel to each other. If they intersect at the axis of the ordinate within the errors of the measurements, the inhibition is deemed competitive with respect to reactant A; if they intersect at the axis of the abscissa within the errors of the measurements, the inhibition is deemed noncompetitive with respect to reactant A; if they are parallel to each other within the errors of the measurements, the inhibition is deemed uncompetitive with respect to reactant A; and if they intersect in the second or third quadrant, the inhibition is mixed relative to reactant A.

A note of caution should be sounded, however. In two instances, uncompetitive inhibition and a ping-pong bisubstrate kinetic mechanism, sets of **parallel lines on such reciprocal plots** are considered to be diagnostic. If, however, concentrations of inhibitors and reactants are high enough, only a region of the field in which lines that are actually converging appear to be parallel may be being sampled. For example, in the case of 3-deoxy-7-phosphoheptulonate synthase from *S. typhimurium*, a set of apparently parallel lines generated by data at high concentrations of reactants became a set of clearly converging lines when much lower initial concentrations were employed to spread the data over a wider range.[102]

It should be emphasized that the definitions of competitive, uncompetitive, noncompetitive, and mixed inhibition and the designations of these types of inhibition are based entirely on observed behavior and do not involve any explanation of the observed behavior. There are, however, explanations.

Explanation: Suppose for the moment that the enzyme has only one reactant (Equation 3–55) and that inhibitor I can associate with both E and E·A

$$\begin{array}{ccccc} E + A & \underset{k_{-1}}{\overset{k_1}{\rightleftharpoons}} & E{\cdot}A & \xrightarrow{k_2} & E + Z \\ + & & + & & \\ I & & I & & \\ k_{i,1}\Big\downarrow\Big\uparrow k_{i,-1} & & k_{i,2}\Big\downarrow\Big\uparrow k_{i,-2} & & \\ E{\cdot}I & & E{\cdot}A{\cdot}I & & \end{array} \qquad (3\text{–}183)$$

In this kinetic mechanism, reversible inhibitor I associates with the enzyme whether or not reactant A is bound, and the inhibition is **dead-end inhibition** because the complex with the inhibitor is unable to engage in any further reaction while the inhibitor is bound. If the steady-state approximation is applied to the form [E·I]

$$k_{i,1}[E][I] = k_{i,-1}[E{\cdot}I] \qquad (3\text{–}184)$$

and the form [E·A·I]

$$k_{i,2}[E{\cdot}A][I] = k_{i,-2}[E{\cdot}A{\cdot}I] \qquad (3\text{–}185)$$

Because the concentration of I does not change during the reaction

$$\frac{[E][I]}{[E{\cdot}I]} = \frac{k_{i,-1}}{k_{i,1}} \qquad (3\text{–}186)$$

and

$$\frac{[E{\cdot}A][I]}{[E{\cdot}A{\cdot}I]} = \frac{k_{i,-2}}{k_{i,2}} \qquad (3\text{–}187)$$

The ratio $k_{i,-1}(k_{i,1})^{-1}$ is equal to the **dissociation constant**, K_{dI}, for the complex between the inhibitor and the unoccupied enzyme

$$K_{dI} = \frac{[E][I]}{[E{\cdot}I]} \qquad (3\text{–}188)$$

and the ratio $k_{i,-2}(k_{i,2})^{-1}$ is equal to the dissociation constant $K_{dI,A}$ for the inhibitor from the complex between enzyme, inhibitor I, and reactant A

$$K_{dI,A} = \frac{[E{\cdot}A][I]}{[E{\cdot}A{\cdot}I]} \tag{3–189}$$

Consequently

$$\begin{array}{ccccc} E + A & \underset{k_{-1}}{\overset{k_1}{\rightleftharpoons}} & E{\cdot}A & \xrightarrow{k_2} & E + Z \\ + & & + & & \\ I & & I & & \\ \Big\downarrow\uparrow K_{dI} & & \Big\downarrow\uparrow K_{dI,A} & & \\ E{\cdot}I & & E{\cdot}A{\cdot}I & & \end{array} \tag{3–190}$$

The existence of these complexes between enzyme and inhibitor expands the equation stating the **conservation of enzyme** (Equation 3–58)

$$[E]_t = [E] + [E{\cdot}I] + [E{\cdot}A] + [E{\cdot}A{\cdot}I] \tag{3–191}$$

and the number of unknowns, but it also provides two additional simultaneous equations, those for the two dissociation constants (Equation 3–188 and 3–189). It turns out that this is a trivial expansion because the unknowns [E·I] and [E·A·I] are eliminated immediately

$$\begin{aligned} [E]_t &= \left(1 + \frac{[I]}{K_{dI}}\right)[E] + \left(1 + \frac{[I]}{K_{dI,A}}\right)[E{\cdot}A] \\ &= \left(\frac{K_{dI} + [I]}{K_{dI}}\right)[E] + \left(\frac{K_{dI,A} + [I]}{K_{dI,A}}\right)[E{\cdot}A] \end{aligned} \tag{3–192}$$

Immediate eliminations of this type account for the appearance in expressions for v_0 of terms such as $(K_{dI} + [I])K_{dI}^{-1}$, $(K_a + [H^+])K_a^{-1}$, and $(K_{dL} + [L])K_{dL}^{-1}$, where K_a is an acid dissociation constant for the enzyme and K_{dL} is the dissociation constant for the complex of a ligand, L, and the enzyme. Because there are now only two unknowns in the equation for the conservation of enzyme (Equation 3–192), the only steady-state approximation needed is Equation 3–60, and

$$\begin{aligned} v_0 = & \\ & \frac{k_2[E]_t\left(\frac{K_{dI,A}}{[I] + K_{dI,A}}\right)\left(\frac{k_2k_1}{k_{-1} + k_2}\right)[E]_t\left(\frac{K_{dI}}{[I] + K_{dI}}\right)[A]_0}{k_2[E]_t\left(\frac{K_{dI,A}}{[I] + K_{dI,A}}\right) + \left(\frac{k_2k_1}{k_{-1} + k_2}\right)[E]_t\left(\frac{K_{dI}}{[I] + K_{dI}}\right)[A]_0} \\ & = \frac{k_0\left(\frac{K_{dI,A}}{[I] + K_{dI,A}}\right)[E]_t\, k_A\left(\frac{K_{dI}}{[I] + K_{dI}}\right)[E]_t\,[A]_0}{k_0\left(\frac{K_{dI,A}}{[I] + K_{dI,A}}\right)[E]_t + k_A\left(\frac{K_{dI}}{[I] + K_{dI}}\right)[E]_t\,[A]_0} \end{aligned} \tag{3–193}$$

Notice in this general case, the inhibition is linear because both the catalytic constant and the specificity constant are decreased by a term $K_I([I] + K_I)^{-1}$. **If the inhibition is in fact dead-end, kinetic measurements can be used to determine numerical values for the actual dissociation constants of the inhibitor.**

If $K_{dI,A} = \infty$ and I cannot associate with E·A, then Equation 3–193 has the form of Equation 3–170, and inhibitor I is competitive with respect to reactant A. Consequently, one explanation for the observation of reversible competitive inhibition is that, for whatever reason, a molecule of inhibitor I and a molecule of reactant A cannot associate simultaneously with the enzyme.

This explanation is often extended by the assumption that this exclusion results from the competition between the inhibitor and the reactant for the same location in an active site of the enzyme because the site with which inhibitor I associates includes a portion or all of the site with which reactant A associates so that the association of one precludes the association of the other. For example, it seems reasonable to assume that, since $MgAMPPCP^{2-}$ (**3–5**) is competitive with respect to $MgATP^{2-}$ in the reactions catalyzed by phosphoribosylformylglycinamidine synthase (Figure 3–9B) and Rho protein kinase (Figure 3–10A), $MgAMPPCP^{2-}$ and $MgATP^{2-}$, which differ from each other at only one atom in their structures, compete for association with the same location in the respective active site.

There is in general, however, no necessity to make this assumption of competition for the same site. For example, if reversible isomerizations of the enzyme occur between the dissociation of I and the

association of A, their existence will usually have no effect on the algebraic form of the final rate equation for v_0. There is one type of reversible isomerization, however, that can explain the ability of some enzymes to be inhibited competitively by inhibitors that do not resemble any of the reactants for the enzyme and do not compete with any of the reactants for the same location in the active site. If one isomer of the enzyme binds only inhibitor I and not reactant A and the other isomer of the enzyme binds only reactant A and not inhibitor I, inhibitor I will be competitive with respect to reactant A regardless of where it associates with the enzyme. Such competitive inhibition at a distance has been observed and will be discussed later.

The experimental observation that an inhibitor I is competitive with respect to reactant A (Figures 3–9A,B, 3–10A, and 3–11A,C) means that, regardless of the concentration of inhibitor I, increasing the concentration of reactant A can completely reverse the effect of inhibitor I on the initial rate for an enzymatic reaction.

In Equation 3–193, if $K_{dI} = \infty$ and I cannot associate with E, then the equation has the form of Equation 3–175, and inhibitor I is uncompetitive with respect to reactant A. Consequently, one explanation for uncompetitive inhibition with respect to reactant A is that the inhibitor for whatever reason is able to associate only with the complex between the enzyme and reactant A. Uncompetitive inhibition can result from the fact that the association of reactant A with the enzyme creates the site with which inhibitor I associates. Reactant A can accomplish this feat by participating structurally in the site with which inhibitor I associates or by stabilizing the isomer of the enzyme containing the site with which inhibitor I associates. For example, the fact that $MgAMPPCP^{2-}$ (**3–5**) is uncompetitive with respect to L-glutamine (Figure 3–9C,D) is consistent with the proposal that the association of L-glutamine with phosphoribosylformylglycinamidine synthase creates the site with which $MgATP^{2-}$ associates. At the least, L-glutamine must associate with the enzyme before $MgAMPPCP^{2-}$ can associate with it.

In Equation 3–193, if $K_{dI} = K_{dI,A}$, then the equation has the form of Equation 3–177, and inhibitor I is noncompetitive with respect to reactant A. Consequently, one explanation for the observation of reversible noncompetitive inhibition is that the inhibitor has the same dissociation constant for the enzyme whether or not reactant A has associated with it. This explanation is usually invoked when the inhibitor resembles neither reactant and is noncompetitive with respect to both reactants.

In Equation 3–193, if $\infty > K_{dI} \neq K_{dI,A} < \infty$, then the equation has the form expected for mixed inhibition (Equation 3–180). Consequently, one explanation for mixed inhibition is that the inhibitor is able to associate with the complex between enzyme and reactant A and with the unoccupied enzyme, but for some reason the dissociation constant for its complex with enzyme when it is occupied by reactant A is different from the dissociation constant for its complex with the enzyme when it is unoccupied. If K_{dI} is less than $K_{dI,A}$ and the inhibitor has a greater affinity for the enzyme when it is unoccupied than when it is occupied by reactant A, the lines will intersect in the second quadrant. Because the effect of the inhibitor is greater on $k_A[E]_t$ in Equation 3–40 than it is on $k_0[E]_t$, this type of mixed inhibition is predominantly competitive. If $K_{dI,A}$ is less than K_{dI} and the inhibitor has a greater affinity for the enzyme when it is occupied by reactant A than when it is unoccupied, the lines will intersect in the third quadrant. Because the effect of the inhibitor is greater on $k_0[E]_t$ in Equation 3–40 than it is on $k_A[E]_t$, this type of mixed inhibition is predominantly uncompetitive.

The patterns of inhibition of an enzymatic reaction that has two or more reactants can provide evidence for the order in which the reactants associate with the active site.

Consider the case of a kinetic mechanism for two reactants that proceeds by the ordered association of its reactants (Equation 3–109) and in which inhibitor I can associate only after reactant A associates and inhibitor I excludes the association of reactant B

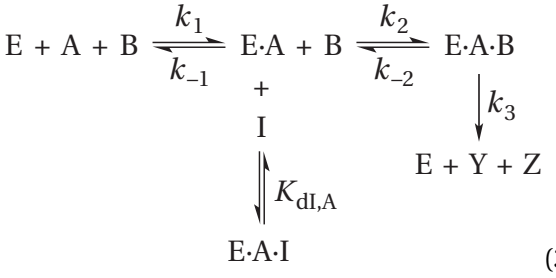

(3–194)

The rate equation for this kinetic mechanism is

$$v_0 = \frac{\left(\frac{k_1k_2k_3}{k_{-2}+k_3}\right)[\mathrm{E}]_t[\mathrm{A}]_0[\mathrm{B}]_0}{k_{-1}+k_1\left(\frac{[\mathrm{I}]+K_{\mathrm{dI,A}}}{K_{\mathrm{dI,A}}}\right)[\mathrm{A}]_0+\left(\frac{k_2k_3}{k_{-2}+k_3}\right)[\mathrm{B}]_0+\left(\frac{k_1k_2}{k_{-2}+k_3}\right)[\mathrm{A}]_0[\mathrm{B}]_0} \quad (3\text{–}195)$$

When $[A]_0$ is varied at several fixed concentrations of inhibitor I and at the same fixed concentration of $[B]_0$,

$$\lim_{[\mathrm{A}]_0\to\infty} v_0 = k_{0,\mathrm{A,app}}[\mathrm{E}]_t = \frac{\left(\frac{k_2k_3}{k_{-2}+k_3}\right)\left(\frac{K_{\mathrm{dI,A}}}{[\mathrm{I}]+K_{\mathrm{dI,A}}}\right)[\mathrm{E}]_t[\mathrm{B}]_0}{1+\left(\frac{k_2}{k_{-2}+k_3}\right)\left(\frac{K_{\mathrm{dI,A}}}{[\mathrm{I}]+K_{\mathrm{dI,A}}}\right)[\mathrm{B}]_0} = \left(\frac{K_{\mathrm{iuI,app}}}{[\mathrm{I}]+K_{\mathrm{iuI,app}}}\right)\frac{k_2k_3[\mathrm{E}]_t[\mathrm{B}]_0}{k_{-2}+k_3+k_2[\mathrm{B}]_0} \quad (3\text{–}196)$$

and

$$\lim_{[\mathrm{A}]_0\to 0} v_0 = k_{\mathrm{A,app}}[\mathrm{E}]_t[\mathrm{A}]_0 = \frac{\left(\frac{k_1k_2k_3}{k_{-2}+k_3}\right)[\mathrm{B}]_0[\mathrm{E}]_t[\mathrm{A}]_0}{k_{-1}+\left(\frac{k_2k_3}{k_{-2}+k_3}\right)[\mathrm{B}]_0} \quad (3\text{–}197)$$

Because [I] affects $k_{0,\mathrm{A,app}}[\mathrm{E}]_t$ but not $k_{\mathrm{A,app}}[\mathrm{E}]_t$, inhibitor I is uncompetitive with respect to reactant A at all $[B]_0$. The uncompetitive inhibition is linear with an apparent inhibition constant

$$K_{\mathrm{iuI,app}} = \left(\frac{k_{-2}+k_3+k_2[\mathrm{B}]_0}{k_{-2}+k_3}\right)K_{\mathrm{dI,A}} \quad (3\text{–}198)$$

The ratio $(k_{-2}+k_3)k_2^{-1}$ is the Michaelis constant, K_{mB}, for reactant B in the absence of inhibitor (Equation 3–104 and Equation 3–167). Only when the concentration of B is significantly less than its Michaelis constant is the apparent inhibition constant equal to the dissociation constant for the inhibitor.

If the inhibition is governed by Equation 3–195, when $[B]_0$ is varied at several fixed concentrations of inhibitor I, always at the same fixed concentration of $[A]_0$

$$\lim_{[\mathrm{B}]_0\to\infty} v_0 = k_{0,\mathrm{B,app}}[\mathrm{E}]_t = \frac{k_1k_3[\mathrm{E}]_t[\mathrm{A}]_0}{k_3 + k_1[\mathrm{A}]_0} \quad (3\text{–}199)$$

and

$$\lim_{[\mathrm{B}]_0\to 0} v_0 = k_{\mathrm{B,app}}[\mathrm{E}]_t[\mathrm{B}]_0 = \frac{\left(\frac{K_{\mathrm{dI,A}}}{[\mathrm{I}]+K_{\mathrm{dI,A}}}\right)\left(\frac{k_2k_3}{k_{-2}+k_3}\right)[\mathrm{A}]_0[\mathrm{E}]_t[\mathrm{B}]_0}{\left(\frac{K_{\mathrm{dI,A}}}{[\mathrm{I}]+K_{\mathrm{dI,A}}}\right)\left(\frac{k_{-1}}{k_1}\right)+[\mathrm{A}]_0} = \left(\frac{K_{\mathrm{icI,app}}}{[\mathrm{I}]+K_{\mathrm{icI,app}}}\right)\frac{k_1k_2k_3[\mathrm{A}]_0[\mathrm{E}]_t[\mathrm{B}]_0}{(k_{-2}+k_3)(k_{-1}+k_1[\mathrm{A}]_0)} \quad (3\text{–}200)$$

Because [I] affects $k_{\mathrm{B,app}}[\mathrm{E}]_t$ but not $k_{0,\mathrm{B,app}}[\mathrm{E}]_t$, inhibitor I is competitive with respect to reactant B at all $[A]_0$. The competitive inhibition is linear with an apparent inhibition constant

$$K_{\mathrm{icI,app}} = \left(\frac{k_{-1}+k_1[\mathrm{A}]_0}{k_1[\mathrm{A}]_0}\right)K_{\mathrm{dI,A}} \quad (3\text{–}201)$$

The ratio $k_{-1}\ k_1^{-1}$ is the dissociation constant, K_{dA}, for reactant A from the unoccupied active site. Only when the fixed concentration of reactant A is significantly greater than this dissociation constant will the apparent inhibition constant be equal to the dissociation constant for the inhibitor for the active site that is occupied by reactant A. This conclusion makes sense because the site for association of the inhibitor exists only when the active site is occupied by reactant A.

Consequently, **the facts that inhibitor I is uncompetitive with respect to reactant A and competitive with respect to reactant B are consistent with the conclusion that reactant A must associate with the enzyme before reactant B**. For example, the facts that N^2-(carboxymethyl)-L-arginine is competitive with respect to N^2-(carboxyethyl)-L-argi-

nine and uncompetitive with respect to $MgATP^{2-}$ are consistent with the conclusion that $MgATP^{2-}$ must associate with (carboxyethyl)arginine β-lactam-synthase from *Streptomyces clavuligerus*

$$\text{L-}N^2\text{-(2-carboxyethyl)arginine} + MgATP^{2-} \rightleftharpoons AMP^- + MgOPO_3PO_3^{2-} + \text{deoxyamidinoproclaviminate} \tag{3–202}$$

before N^2-(carboxyethyl)-L-arginine can associate with the enzyme.[103]

Regardless of the kinetic mechanism being tested, for any given enzymatic reaction, in the absence of any pertinent information, **either of the actual reactants can be reactant A or reactant B.** If there are more than two reactants, any one of them could be reactant A, reactant B, reactant C, and so forth. In the particular instance of (carboxyethyl)-arginine β-lactam-synthase, the fact that N^2-(carboxymethyl)-L-arginine is competitive with respect to N^2-(carboxyethyl)-L-arginine and uncompetitive with respect to $MgATP^{2-}$ is consistent with the conclusions that $MgATP^{2-}$ is actually reactant A and N^2-(carboxymethyl)-L-arginine is reactant B and that the addition of the two reactants to the active site is ordered.

Consider the case of a kinetic mechanism for two reactants that proceeds by the **random equilibrium association** of its reactants (Equation 3–121) and in which inhibitor I can associate with the active site only when reactant A is not bound

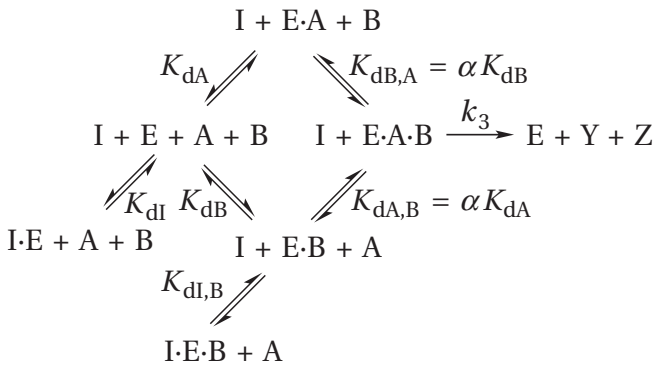

(3–203)

In this instance, the equation for conservation of enzyme becomes

$$[E]_t = [E] + [E{\cdot}I] + [E{\cdot}B] + [I{\cdot}E{\cdot}B] + [E{\cdot}A] + [E{\cdot}A{\cdot}B]$$
$$= \left(1 + \frac{[I]}{K_{dI}}\right)[E] + \left(1 + \frac{[I]}{K_{dI,B}}\right)[E{\cdot}B] + [E{\cdot}A] + [E{\cdot}A{\cdot}B] \tag{3–204}$$

Solving for the rate equation and taking the limits (see Equations 3–121 through 3–133)

$$\lim_{[A]_0 \to \infty} v_0 = k_{0,A,app}[E]_t = \frac{k_3[E]_t[B]_0}{\alpha K_{dB} + [B]_0} \tag{3–205}$$

$$\lim_{[A]_0 \to 0} v_0 = k_{A,app}[E]_t = \frac{k_3[E]_t[B]_0}{\left(\frac{[I] + K_{dI}}{K_{dI}}\right)\alpha K_{dA}K_{dB} + \left(\frac{[I] + K_{dI,B}}{K_{dI,B}}\right)\alpha K_{dA}[B]_0} \tag{3–206}$$

$$\lim_{[B]_0 \to \infty} v_0 = k_{0,B,app}[E]_t = \frac{k_3[E]_t[A]_0}{\left(\frac{[I] + K_{dI,B}}{K_{dI,B}}\right)\alpha K_{dA} + [A]_0} \tag{3–207}$$

$$\lim_{[B]_0 \to 0} v_0 = k_{B,app}[E]_t = \frac{k_3[E]_t[A]_0[B]_0}{\alpha K_{dB}\left\{\left(\frac{[I] + K_{dI}}{K_{dI}}\right)K_{dA} + [A]_0\right\}} \tag{3–208}$$

As expected, since the inhibitor cannot associate with the enzyme when the active site is occupied by A, the inhibitor is competitive with respect to reactant A at all concentrations of reactant B because there are no terms in Equation 3–205 involving the concentration of inhibitor I. If α is other than 1 and K_{dI} is not equal to $K_{dI,B}$, the inhibition is mixed with respect to reactant B, but if α is equal to 1 and K_{dI} is equal to $K_{dI,B}$, then the same factor involving the inhibitor decreases both $k_{0,B,app}$ and $k_{B,app}$, and the inhibition will be noncompetitive with respect to reactant B.

Consequently, **the facts that inhibitor I is competitive with respect to reactant A and noncompetitive with respect to reactant B are consistent**

with the conclusion that reactant A and reactant B associate with the enzyme at random. For example, the fact that MgAMPPCP^{2-} (**3–5**) is competitive with respect to MgATP^{2-} (Figure 3–9B) and noncompetitive with respect to N^2-formyl-N^1-(5-phospho-D-ribosyl)glycinamide (Figure 3–9E,F) is consistent with the conclusions that the association of N^2-formyl-N^1-(5-phospho-D-ribosyl)glycinamide with phosphoribosylformylglycinamidine synthase (Equation 3–173) from *G. gallus* does not affect the association of MgATP^{2-} with the enzyme and that N^2-formyl-N^1-(5-phospho-D-ribosyl)glycinamide and MgATP^{2-} add at random to the enzyme. The uncompetitive inhibition by MgAMPPCP^{2-} with respect to L-glutamine (Figure 3–9D) is consistent with the conclusion that neither MgATP^{2-} nor N^2-formyl-N^1-(5-phospho-D-ribosyl)-glycinamide can associate with the enzyme until L-glutamine has. A similar pattern of competitive, noncompetitive, and uncompetitive inhibition by L-phenyllactate with respect to phenylpyruvate, NH_4^+, and NADH, respectively, has been observed with phenylalanine dehydrogenase from *Rhodococcus*[104]

$$H^+ + \text{NADH} + \text{phenylpyruvate} + NH_4^+ \rightleftharpoons \text{L-phenylalanine} + H_2O + NAD^+ \quad (3\text{–}209)$$

In studies that use inhibitors resembling reactants to provide evidence that reactants add at random to the enzyme, **it is desirable to have inhibitors that exclude each of the reactants in turn**. The ability of each inhibitor to exclude one of the reactants is validated by showing that each inhibitor is competitive with respect to its respective congeneric reactant. Suppose that two inhibitors are available, inhibitors I and J, that closely resemble reactants A and B. The association of inhibitor I with the enzyme excludes reactant A but does not affect the association of reactant B, and the association of inhibitor J with the enzyme excludes reactant B but does not affect the association of reactant A. If reactants A and B bind at random to the active site, then inhibitor I will be competitive with respect to reactant A but noncompetitive with respect to reactant B, and inhibitor J will be competitive with respect to reactant B but noncompetitive with respect to reactant A.

For example, the synthetic peptide biotin-AKRRRLSSLRA-NH_2, which contains the two serines to be phosphorylated by the enzyme, can serve as a reactant for human Rho protein kinase, and acetyl-AKRRRLAALRA-NH_2, in which those two serines have been replaced with alanines, can serve as an inhibitor homologous to biotin-AKRRRLSSLRA-NH_2. Magnesium 5′-adenylic methylenediphosphonic anhydride (**3–5**) can serve as an inhibitor homologous to the other reactant, MgATP^{2-}. Magnesium 5′-adenylic methylenediphosphonic anhydride is competitive with respect to MgATP^{2-} (Figure 3–10A) and noncompetitive with respect to biotin-AKRRRLSSLRA-NH_2 (Figure 3–10E), and acetyl-AKRRRLAALRA-NH_2 is competitive with respect to biotin-AKRRRLSSLRA-NH_2 (Figure 3–10C) and almost noncompetitive with respect to MgATP^{2-} (Figure 3–10I).[98] This symmetric behavior of the two inhibitors is more convincing evidence for the conclusion that the two reactants, MgATP^{2-} and biotin-AKRRRLSSLRA-NH_2, can associate at random with the enzyme than if only one of these inhibitors was used because, in this case, each inhibitor, the structure of which is based closely on the respective chemical structure of one of the reactants, has the same or almost the same dissociation constant from the enzyme whether or not the other reactant is associated with it.

In the case of an ordered mechanism, however, inhibitors that exclude reactant A, the first reactant to associate with the active site, rather than reactant B, the second, can produce ambiguous results. Suppose that reactant A must associate with the enzyme before reactant B. As has already been demonstrated for the kinetic mechanism of Equation 3–194, inhibitor I, which may or may not be structurally related to reactant B but the association of which excludes the association of reactant B, should be competitive with respect to reactant B and uncompetitive with respect to reactant A (Equation 3–195). This behavior was observed with MgAMPPCP^{2-} in its inhibition of phosphoribosylformylglycinamidine synthase (Figure 3–9D) and with N^2-(carboxymethyl)-L-arginine in its inhibition of (carboxyethyl)arginine β-lactamsynthase (Equation 3–202). Suppose, for the same active site, one also has an **inhibitor J that may or may not be structurally related to reactant A but the association of which excludes reactant A from associating with the active site** and that forms a dead-end complex with the unoccupied active site

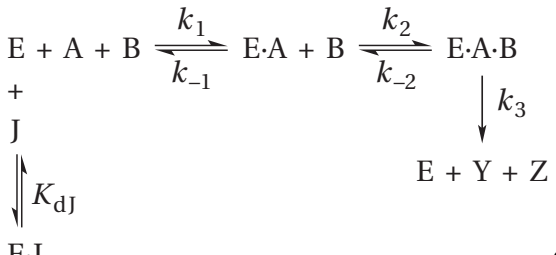

(3–210)

The rate equation for this kinetic mechanism is

$$v_0 = \frac{\left(\frac{k_1 k_2 k_3}{k_{-2} + k_3}\right)[\mathrm{E}]_t[\mathrm{A}]_0[\mathrm{B}]_0}{k_{-1}\left(\frac{[\mathrm{J}] + K_{\mathrm{dJ}}}{K_{\mathrm{dJ}}}\right) + k_1[\mathrm{A}]_0 + \left(\frac{k_2 k_3}{k_{-2} + k_3}\right)\left(\frac{[\mathrm{J}] + K_{\mathrm{dJ}}}{K_{\mathrm{dJ}}}\right)[\mathrm{B}]_0 + \left(\frac{k_1 k_2}{k_{-2} + k_3}\right)[\mathrm{A}]_0[\mathrm{B}]_0} \tag{3–211}$$

and

$$\lim_{[\mathrm{A}]_0 \to \infty} v_0 = k_{0,\mathrm{A,app}}[\mathrm{E}]_t = \frac{\left(\frac{k_2 k_3}{k_{-2} + k_3}\right)[\mathrm{B}]_0[\mathrm{E}]_t}{1 + \left(\frac{k_2}{k_{-2} + k_3}\right)[\mathrm{B}]_0} \tag{3–212}$$

$$\lim_{[\mathrm{A}]_0 \to 0} v_0 = k_{\mathrm{A,app}}[\mathrm{E}]_t[\mathrm{A}]_0 = \frac{\left(\frac{K_{\mathrm{dJ}}}{[\mathrm{J}] + K_{\mathrm{dJ}}}\right)\left(\frac{k_1 k_2 k_3}{k_{-2} + k_3}\right)[\mathrm{B}]_0[\mathrm{E}]_t[\mathrm{A}]_0}{k_{-1} + \left(\frac{k_2 k_3}{k_{-2} + k_3}\right)[\mathrm{B}]_0} \tag{3–213}$$

so inhibitor J is a linear competitive inhibitor with respect to reactant A at all values of $[\mathrm{B}]_0$.

The limits for the inhibition of inhibitor J with respect to reactant B are

$$\lim_{[\mathrm{B}]_0 \to \infty} v_0 = k_{0,\mathrm{B,app}}[\mathrm{E}]_t = \frac{\left(\frac{K_{\mathrm{dJ}}}{[\mathrm{J}] + K_{\mathrm{dJ}}}\right)k_3[\mathrm{A}]_0[\mathrm{E}]_t}{\left(\frac{k_3}{k_1}\right) + \left(\frac{K_{\mathrm{dJ}}}{[\mathrm{J}] + K_{\mathrm{dJ}}}\right)[\mathrm{A}]_0} = \left(\frac{K_{\mathrm{iuJ,app}}}{[\mathrm{J}] + K_{\mathrm{iuJ,app}}}\right)\frac{k_1 k_3[\mathrm{A}]_0[\mathrm{E}]_t}{k_3 + k_1[\mathrm{A}]_0} \tag{3–214}$$

where

$$K_{\mathrm{iuJ,app}} = \left(\frac{k_3 + k_1[\mathrm{A}]_0}{k_3}\right)K_{\mathrm{dJ}} \tag{3–215}$$

and

$$\lim_{[\mathrm{B}]_0 \to 0} v_0 = k_{\mathrm{B,app}}[\mathrm{E}]_t[\mathrm{B}]_0 = \frac{\left(\frac{K_{\mathrm{dJ}}}{[\mathrm{J}] + K_{\mathrm{dJ}}}\right)\left(\frac{k_2 k_3}{k_{-2} + k_3}\right)[\mathrm{A}]_0[\mathrm{E}]_t[\mathrm{B}]_0}{\left(\frac{k_{-1}}{k_1}\right) + \left(\frac{K_{\mathrm{dJ}}}{[\mathrm{J}] + K_{\mathrm{dJ}}}\right)[\mathrm{A}]_0} = \left(\frac{K_{\mathrm{icJ,app}}}{[\mathrm{J}] + K_{\mathrm{icJ,app}}}\right)\frac{k_1 k_2 k_3[\mathrm{A}]_0[\mathrm{E}]_t[\mathrm{B}]_0}{(k_{-2} + k_3)(k_{-1} + k_1[\mathrm{A}]_0)} \tag{3–216}$$

where

$$K_{\mathrm{icJ,app}} = \left(\frac{k_{-1} + k_1[\mathrm{A}]_0}{k_{-1}}\right)K_{\mathrm{dJ}} \tag{3–217}$$

It turns out that the value of the kinetic constants for this particular kinetic mechanism and the concentration of reactant A determine the type of inhibition displayed by inhibitor J with respect to reactant B. If both k_{-1} and k_3 are greater than $k_1[A]_0$, then both the apparent catalytic constant, $k_{0,B,app}$, and the apparent specificity constant, $k_{B,app}$ will be decreased by the same factor, and inhibitor J will be noncompetitive with respect to reactant B. The fact that the initial concentration of reactant A, however, appears in the expressions for the apparent inhibition constants means that there can be situations in which such noncompetitive inhibition will not be observed. Situations in which the inhibition with respect to reactant B are mixed are uninformative. If, however, $k_{-1} << k_3$, so that reactant A is a sticky reactant, then at high enough concentrations of reactant A, $K_{iuJ,app} << K_{icJ,app}$. When the concentrations of inhibitor J are all significantly less than $K_{icJ,app}$ but in the range of $K_{iuJ,app}$, the apparent specificity constant $k_{B,app}$ will be unaffected by the inhibitor while the apparent catalytic constant $k_{0,B,app}$ is decreasing significantly. In these circumstances, the inhibition observed will be uncompetitive with respect to reactant A rather than noncompetitive. An example of such behavior may be that for the inhibition of 4-hydroxy-tetrahydrodipicolinate synthase

$$\text{pyruvate} + \text{L-aspartate-4-semialdehyde} \rightleftharpoons (2S,4S)\text{-4-hydroxy-2,3,4,5-tetrahydrodipicolinate} + H^+ + H_2O \quad (3\text{–}218)$$

from *E. coli*. Both fluoropyruvate and 2-oxobutyrate are competitive inhibitors of the enzyme with respect to pyruvate at pH 8, but fluoropyruvate is noncompetitive with respect to L-aspartate-4-semialdehyde while 2-oxobutyrate is uncompetitive with respect to L-aspartate-4-semialdehyde.[105]

An **ambiguity** is raised by these considerations. It has already been stated that, because the letter designations can be interchanged, the facts that inhibitor I is uncompetitive with respect to reactant B and competitive with respect to reactant A are consistent with the conclusion that reactant B must associate with the enzyme before reactant A. It has just been demonstrated, however, that if an inhibitor I is competitive with respect to reactant A and uncompetitive with respect to reactant B, these observations are consistent with the conclusion that reactant A associates with the enzyme before reactant B. This contradiction is disconcerting. Dethiocoenzyme A, in which the sulfanyl group is replaced by a hydrogen,[106] is competitive with respect to acetyl-SCoA and uncompetitive with respect to glyoxylate in the reaction catalyzed by malate synthase

$$\text{glyoxylate} + \text{acetyl-SCoA} + H_2O \rightleftharpoons H^+ + \text{HSCoA} + (S)\text{-malate} \quad (3\text{–}219)$$

from *M. tuberculosis*. These facts are consistent with a kinetic mechanism in which glyoxylate must associate with the active site before acetyl-SCoA (Equations 3–194, 3–196, and 3–197), but they are also consistent with a kinetic mechanism in which acetyl-SCoA must associate with the active site before glyoxylate (Equations 3–210, 3–214, and 3–216). The fact, however, that the product malate is competitive with respect to glyoxylate and noncompetitive with respect to acetyl-SCoA is consistent only with the former kinetic mechanism[107] and resolves the ambiguity.

The situation can be summarized. Consider the two reactants, A and B. There are three possibilities: reactant A must associate with the active site before reactant B; reactant B must associate with the active site before reactant A; or reactant A and reactant B can associate with the active site at random.

If reactant A and reactant B add to the active site at random, an inhibitor that excludes the association of only reactant A will be competitive with respect to reactant A and noncompetitive with respect to reactant B, and an inhibitor that excludes only the association of reactant B will be competitive with respect to reactant B and noncompetitive with respect to reactant A. These four observations are unique and distinguish random addition from ordered addition of the reactants, but it is necessary to use both inhibitors to make the distinction.

If reactant A is required to associate with the active site before reactant B in an ordered kinetic mechanism, if inhibitor I can associate only after reactant A associates, and if inhibitor I excludes the association of reactant B (Equation 3–194), inhibitor I will be competitive with respect to reactant B and uncompetitive with respect to reactant A. If reactant A is required to associate with the active site before reactant B in an ordered kinetic mechanism, if inhibitor I can associate only with the empty active site, and if inhibitor I excludes the association of

reactant A (Equation 3–210), inhibitor I will be competitive with respect to reactant A and noncompetitive, mixed, or uncompetitive with respect to reactant B. Consequently, if one of the inhibitors is uncompetitive with respect to the reactant that is not its congener and the other is noncompetitive with respect to the reactant that is not its congener, then both results are consistent with an ordered addition of the former reactant before the latter. **If, however, the two inhibitors are competitive with respect to their respective congeners but both are uncompetitive with respect to the other reactant, these observations are consistent with an ordered addition of reactants but cannot distinguish which reactant associates first**.

An inhibitor that specifically excludes both reactants from associating with the enzyme can provide evidence that the two reactants must associate with an enzyme in a particular order. The inhibitor *N*-phosphonacetyl-L-aspartate (**3–6**)[108]

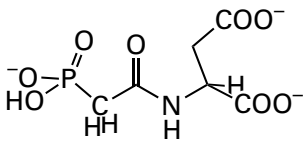

3–6

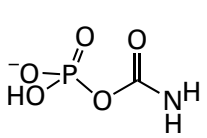

3–7

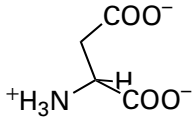

3–8

associates with aspartate carbamoyltransferase

$$\text{carbamoyl phosphate} + \text{L-aspartate} \rightleftharpoons \text{H}^+ + \textit{N}\text{-carbamoyl-L-aspartate} + \text{HOPO}_3^{2-} \quad (3\text{–}220)$$

from *E. coli* only when its active site is unoccupied. This exclusivity is due to the fact that *N*-phosphonacetyl-L-aspartate is a **bisubstrate analogue** composed of portions from both reactants for the enzyme, carbamoyl phosphate (**3–7**) and L-aspartate (**3–8**). If carbamoyl phosphate must associate with aspartate carbamoyltransferase before L-aspartate can associate, this behavior would be consistent with the observation that *N*-phosphonacetyl-L-aspartate is a competitive inhibitor with respect to carbamoyl phosphate but a noncompetitive inhibitor with respect to L-aspartate (Figure 3–14).[109,110] Had *N*-phosphonacetyl-L-aspartate, however, been competitive with respect to both reactants, then either reactant could have been bound by the unoccupied active site and the order of their addition in the enzymatic reaction would have been random. If inhibitor I can bind only to the completely unoccupied enzyme, every reactant with respect with which it is competitive should also be able to bind to the unoccupied active site, and the order of addition to the active site among that subset of reactants should be random.

In studies of the effect of inhibitors on steady-state kinetics, **the inhibitors do not have to resemble the reactants** so closely as the two used for Rho protein kinase or *N*-phosphonacetyl-L-aspartate; they need only associate with the enzyme in such a way as to exclude the association of one or the other reactant. For example, the inhibitor

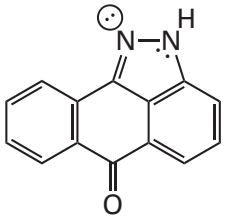

3–9

happens to associate with human c-Jun amino-terminal protein kinase so as to prevent $MgATP^{2-}$ from associating with the enzyme, and the peptide RPKRPTTLNLF, which does not even contain the sequence of the region of the protein c-Jun that is phosphorylated by the enzyme and is not itself phosphorylated, nevertheless associates with the enzyme so as to prevent the association of the protein c-Jun. Inhibitor **3–9** is competitive with respect to $MgATP^{2-}$ and noncompetitive with respect to a peptide that can be phosphorylated by the enzyme, and the peptide RPKRPTTLNLF is competitive with respect to the peptide that can be phosphorylated but noncompetitive with respect to $MgATP^{2-}$.[111] A conclusion consistent with these observations is that $MgATP^{2-}$ and the protein or peptide to be phosphorylated associate at random with the active site of the enzyme.

The observation of mixed inhibition is usually uninformative about the order of addition of reactants, but not always. In the case of the inhibition of Rho protein kinase, acetyl-AKRRRLAALRA-NH_2 is not quite noncompetitive with respect to $MgATP^{2-}$ (Figure 3–10G–I) because its apparent dissociation constant for the unoccupied enzyme (Equation 3–193; $K_{dPAA} = 35\ \mu M$) is somewhat greater than its

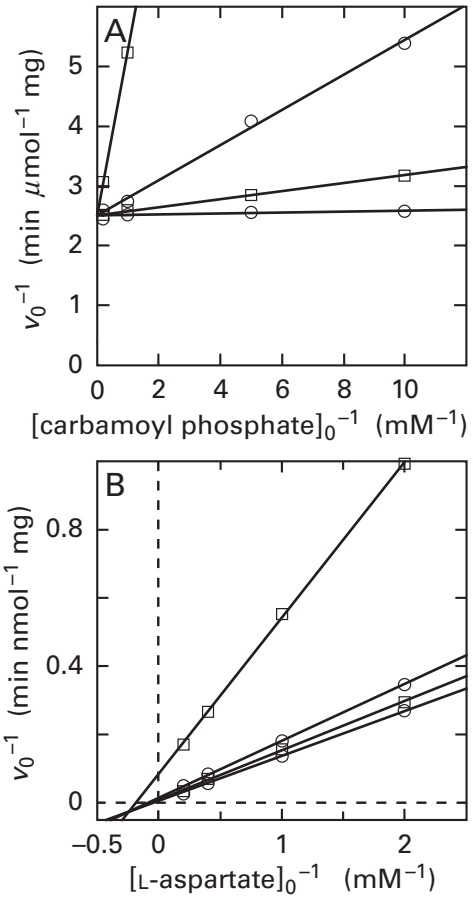

Figure 3–14: Kinetics for reversible inhibition of the carbamoyl transfer catalyzed by partially purified aspartate carbamoyltransferase from murine spleen by *N*-phosphonacetyl-L-aspartate.[110] Solutions containing L-aspartate and carbamoyl phosphate were prepared at pH 7.4 and 37 °C. Each carbamoyl transfer was initiated by adding enzyme. **(A)** The rate of production of *N*-carbamoyl-L-[^{14}C]aspartate (cAsp) was followed over several minutes to obtain each initial rate. For this assay, a small amount of L-[^{14}C]aspartate was added to a mixture, samples were withdrawn at appropriate intervals after addition of enzyme and quenched with acetic acid, and the *N*-carbamoyl-L-[^{14}C]aspartate was purified from each sample by cation-exchange chromatography. Reciprocals of initial rates for the production of *N*-carbamoyl-L-aspartate, v_0^{-1} [minutes micromole^{-1} (milligram of protein)] at 10 mM L-aspartate are presented as a function of the reciprocals of the initial concentrations of carbamoyl phosphate (millimolar^{-1}) at 0, 0.1, 1, and 10 μM *N*-phosphonacetyl-L-aspartate. The concentrations of inhibitor increase as the lines become steeper in slope. The initial rates were plotted directly as a function of the initial concentrations of carbamoyl phosphate (not shown), and the data were fit to Equation 3–52. The four values for parameter *a* of these fits were identical within their standard deviations, and a value of 0.40 μmol of *N*-carbamoyl-L-aspartate min^{-1} (mg of protein)$^{-1}$ was assigned to each of them. The lines in the drawing were forced to intersect at the axis of the ordinate at a value of 2.51 min (μmol of *N*-carbamoyl-L-aspartate)$^{-1}$ mg of protein. **(B)** The rate of production of *N*-[^{14}C]carbamoyl-L-aspartate was followed over several minutes to obtain each initial rate. For this assay, a small amount of [^{14}C]carbamoyl phosphate was added to a mixture, and samples were withdrawn at appropriate intervals after addition of enzyme and quenched with 10% perchloric acid. The strong acid hydrolyzed the [^{14}C]carbamoyl phosphate, but not the *N*-[^{14}C]carbamoyl-L-aspartate, to $^{14}CO_2$, and this radioactive CO_2 was flushed from each sample with unradioactive $^{12}CO_2$ to leave the enzymatically synthesized [^{14}C]carbamoyl-L-aspartate. Reciprocals of initial rates for the production of *N*-carbamoyl-L-aspartate, v_0^{-1} [minutes micromole^{-1} (milligram of protein)] at 20 mM carbamoyl phosphate are presented as a function of the reciprocals of the initial concentrations of L-aspartate (millimolar^{-1}) at 0.01, 0.05, 0.1, and 1 μM *N*-phosphonacetyl-L-aspartate. Lines were fit to the data, and average values for the ordinates and abscissas of the intersections of the line for 1 μM *N*-phosphonacetyl-L-aspartate and the other three lines were calculated. Lines forced to pass through this average point of intersection were then refit to the data, and these are the lines drawn in the figure.

apparent dissociation constant for the enzyme occupied by MgATP^{2-} (Equation 3–193; $K_{dPAA,ATP} = 16\,\mu M$). It comes as no surprise, however, that since the two reactants, MgATP^{2-} and biotin-AKRRRLSSLRA-NH_2, are to combine with each other while they are on the active site to produce products and hence must occupy adjacent subsites in the active site, the **association of one reactant can affect the affinity of the enzyme for an inhibitor mimicking the other**. In this case, the association of MgATP^{2-} increases the apparent affinity of the enzyme for the peptide inhibitor about 2-fold. If the association of MgATP^{2-} slightly improves the site on the enzyme with which the sequence –KRRRLAALRA– associates, then the observation that acetyl-AKRRRLAALRA-NH_2 is a competitive inhibitor relative to biotin and almost a noncompetitive inhibitor relative to MgATP^{2-} (Figure 3–10I) is still consistent with random association of reactants with the active site.

It is often difficult to distinguish uncompetitive inhibition, for which the double-reciprocal lines are parallel (Figure 3–9D) from mixed, predominantly uncompetitive inhibition, for which the double-reciprocal lines are almost parallel. This problem can be illustrated with a comparison of the inhibition of glycerol kinase from *C. norvegensis* by CrATP^{-} and the inhibition of hexokinase from *R. norvegicus* by unchelated ATP^{4-}.

If reactant A must associate with the enzyme before reactant B can associate, inhibitor I that excludes the association of reactant B will be competitive with respect to reactant B and uncompetitive with respect to reactant A. This proposal is an explanation for the behavior observed with glycerol kinase when the chromium complex of ATP^{4-}, CrATP^{-}, which closely resembles MgATP^{2-} but cannot engage in the enzymatic reaction, is used as an inhibitor (Figure 3–12).[100] The conclusion that MgATP^{2-} binds

to the enzyme only after glycerol binds to the enzyme would be consistent with these observations. It has already been noted, however, that when glycerol kinase phosphorylates (*S*)-1-aminopropane-2,3-diol, the observed kinetic behavior (Figure 3–7) is consistent with a kinetic mechanism in which $MgATP^{2-}$ binds to the enzyme before (*S*)-1-aminopropanol, an analogue for glycerol. Furthermore, glycerol kinase has a slow, but measurable, MgATPase activity in the absence of any cosubstrate, and this activity is another indication that $MgATP^{2-}$ can bind to the active site in the absence of glycerol.[86] Weak binding of $MgATP^{2-}$ to the unoccupied active site would allow it to precede (*S*)-1-aminopropanol onto the active site of glycerol kinase from *C. norvegensis*, even though it usually follows glycerol. Both of these observations seem to contradict the fact that $CrATP^{-}$ is an uncompetitive inhibitor with respect to glycerol. It could be the case, however, that either reactant can associate with the unoccupied active site but that the association of glycerol, rather than being required to precede the association of $MgATP^{2-}$ with the active site, simply decreases the dissociation constant for $MgATP^{2-}$ from the active site. This alteration does not have to involve a dramatic decrease in dissociation constant before the **converging double reciprocals for mixed, predominantly uncompetitive inhibition become indistinguishable from the parallel double reciprocals of uncompetitive inhibition**.

When unchelated ATP^{4-} is used as an inhibitor of hexokinase from *R. norvegicus*,[112] it is a mixed, predominantly uncompetitive inhibitor with respect to the reactant D-glucose (Figure 3–11C).[99] This observation and the fact that *N*-acetyl-D-glucosamine is a mixed, predominantly competitive inhibitor with respect to $MgATP^{2-}$ are consistent with the conclusion that D-glucose and $MgATP^{2-}$ associate with the enzyme at random. The lines in the double-reciprocal plot, however, are almost parallel when ATP^{4-} is the inhibitor with respect to D-glucose (Figure 3–11C). If they had been parallel, this pattern of inhibition would have indicated that the reactants must enter the active site of hexokinase in order, D-glucose before $MgATP^{2-}$.[113] If the association of D-glucose with hexokinase simply increases the affinity of the respective enzyme for $MgATP^{2-}$ by a significant factor, rather than being obligatory for the binding of $MgATP^{2-}$, then almost uncompetitive inhibition would be observed. If it is assumed, for the sake of argument, that K_{icATP} (3.3 mM) is the dissociation constant for unchelated ATP^{4-} from the unoccupied active site and K_{iuATP} (1.4 mM) is the dissociation constant for unchelated ATP^{4-} from the active site occupied by D-glucose, it would follow that a decrease in the dissociation constant of only a factor of 2.5 is sufficient to turn noncompetitive inhibition into almost uncompetitive inhibition. A significantly larger, but not dramatic, decrease in dissociation constant should accomplish this transformation. If this description is the explanation, $MgATP^{2-}$ should bind to the empty active site, albeit weakly.[86]

These considerations suggest that **all kinetic mechanisms in which the reactants are required to associate with an enzyme in a particular sequence are probably oversimplifications**. Reactants appear to associate in a particular order because the association of one reactant significantly, but not infinitely, decreases the dissociation constant of the other reactant from the enzyme.[86] In other words, the factor α in the kinetic mechanism of Equation 3–121 does not have to be that much smaller than 1 for random addition to become indistinguishable from ordered addition. An extreme example of this ambiguity is the fact that the apparent requirement for (4-hydroxyphenyl)-pyruvate to associate with human 4-hydroxyphenylpyruvate dioxygenase before molecular oxygen associates[114] is the result of a finite, albeit 3600-fold, increase in the rate at which oxygen associates with the enzyme caused by the association of (4-hydroxyphenyl)pyruvate.[115]

The association of a reactant frequently increases or decreases the affinity of the active site for an inhibitor, so mixed inhibition is often observed. In fact, the distinction between noncompetitive inhibition and mixed inhibition although formally justified, is in practice misleading.* It is usually assumed that the inhibition constants K_{icI} and K_{ucI} are the dissociation constants K_{dI} and $K_{dI,A}$ for inhibitor I from the active site unoccupied or occupied by reactant A, respectively (Equations 3–180 and 3–193). It is informative when the association of reactant A does not alter the dissociation constant of an inhibitor but not surprising when it does not. It is reasonable that the association of a reactant would change the affinity of the active site for

*The International Union of Biochemistry and Molecular Biology formally distinguishes noncompetitive inhibition from mixed inhibition. It seems that this distinction has been justified by the dramatic difference in form between Equations 3–177 and 3–180. In effect, the distinction is made at the level of observation. When, however, explanations for the various behaviors are considered, the distinction becomes ambiguous and is counterproductive.

the inhibitor because the complex between enzyme and reactant A is necessarily different from the enzyme when it is unoccupied by reactant A.

As a result of these considerations, it should never be assumed that inhibition by inhibitor I is formally noncompetitive and that K_{icI} and K_{ucI} are the same. The Michaelis constant for reactant A for the general case of mixed inhibition

$$K_{mA} = \frac{k_{0,A,app}\left(\frac{K_{iuI}}{[I] + K_{iuI}}\right)}{k_{A,app}\left(\frac{K_{icI}}{[I] + K_{icI}}\right)} \qquad (3\text{–}221)$$

Only when each curve is fit with Equation 3–52 to the values for the initial rate as a function of the initial concentration of reactant A at several concentrations of inhibitor I and the Michaelis constant, parameter *b* of the fits, remains the same within the standard deviations of the fits can it be concluded that K_{icI} and K_{ucI} are statistically the same and that the inhibition is formally noncompetitive.

In any case, it is reasonable to conclude that noncompetitive inhibition is actually a special case of mixed inhibition in which K_{iuI} and K_{icI} are the same. Traditionally, however, when a distinction between noncompetitive inhibition and mixed inhibition has purposely been avoided, the term noncompetitive inhibition has been used interchangeably for both situations.[96] This practice is both widely accepted and defensible. Semantically, noncompetitive inhibition encompasses any inhibition that is neither competitive nor uncompetitive, two special cases that do define mechanistically significant differences. Most publications describing enzymatic kinetics treat mixed inhibition and noncompetitive inhibition as the same thing and use the term noncompetitive inhibition for both of them. Consequently, when the actual data are not shown and it is simply stated that "noncompetitive inhibition was observed", there is no way to tell whether the inhibition was noncompetitive by the definition of the International Union of Biochemistry and Molecular Biology or just mixed inhibition. It follows that from here on it will be necessary to make no distinction between noncompetitive inhibition and mixed inhibition. In some cases, however, when the inhibition observed is mixed, that fact will be noted because it is usually informative to know whether the mixed inhibition is predominantly competitive or predominantly uncompetitive.

So far, the patterns of inhibition discussed have been for kinetic mechanisms in which reversible steps separate the associations of the reactants with the enzyme. Dead-end inhibition by reversible inhibitors homologous to reactants can also **provide information about kinetic mechanisms in which a kinetically irreversible step separates the association of the two reactants** for an enzymatic reaction. For example, in a ping-pong kinetic mechanism, the enzyme alternates symmetrically between two forms, each separated from the other by a respective irreversible step (Equation 3–154). An inhibitor I that excludes reactant A from the active site will be competitive with respect to reactant A and uncompetitive with respect to reactant B, and an inhibitor J that excludes reactant B from the active site will be competitive with respect to reactant B and uncompetitive with respect to reactant A.[116] Although they are consistent with the existence of an irreversible step between the association of reactant A and the association of reactant B and the existence of an irreversible step between the association of reactant B and the association of reactant A, such observations cannot determine whether the two irreversible steps are both due to the release of products of the reaction, only one is due to the dissociation of a product, or neither of them is due to the dissociation of a product. Product inhibition is used to make this determination.

The use of products of an enzymatic reaction as inhibitors can clarify the order in which reactants associate with an enzyme and are required to determine the order in which products dissociate from an enzyme. Because the products are directly derived from the reactants and relationships between reactants and products are more readily established, the inhibition displayed by a product is less equivocal than the inhibition displayed by an inhibitor that only resembles the reactant. By microscopic reversibility, **a product must be able to associate with the same location in the active site from which it dissociates** during the enzymatic reaction. This location is usually the same one with which one or more of the reactants associate. Consequently, **the association of a product with the enzyme necessarily prevents the association of a reactant that shares a portion of its structure with that product**. In the instance of product inhibition there is usually, but not always, little doubt that the

Table 3–2: Some Patterns of Product Inhibition[a]

mechanism		variable reactant			
		A		B	
	product inhibitor	unsaturated with B	saturated with B	unsaturated with A	saturated with A
A and B associate at random, Y and Z associate at random, and both complexes E·A·Y and E·Z·B can form[b]	Y	NC[c]	NI[d]	C[c]	C
	Z	C	C	NC	NI
A and B associate at random, Y and Z associate at random, B and Z share no common atoms, and B and Z can bind simultaneously to form E·Z·B, but the complex E·A·Y cannot form[b]	Y	C	NI	C	NI
	Z	C	C	NC	NI
A must associate before B, and Y and Z dissociate at random	Y	C	C	NC	
	Z	C	C	NC	
A must associate before B, and Y must dissociate before Z	Y	NC	UC[c]	NC	NC
	Z	C	C	NC	NI
A must associate before B, and X must dissociate before Y, which must dissociate before Z	X	NC	UC	NC	NC
	Y	UC	UC	UC	UC
	Z	C	C	NC	
Z dissociates after A associates but before B associates, and Y dissociates after B associates but before A associates[e]	Y	C	C	NC	NI
	Z	NC	NI	C	C
A and Z associate with one active site, B and Y associate with another active site, and the difference between A and Z is transferred from the first active site to the second[93]	Y	NC	NI	C	C
	Z	C	C	NC	NI

[a]These are patterns expected for product inhibition for an enzymatic reaction with formally two reactants and two or three products. For a more complete list see references 62 and 119, which are the sources for this table. [b]Reactants and products must associate and dissociate so rapidly that they are always at equilibrium with the active site. [c]Abbreviations: NC, noncompetitive (term includes mixed inhibition); C, competitive; UC, uncompetitive; [d]NI indicates that no inhibition occurs. In all these situations, in theory, the saturation of the active site with the indicated reactant would block access to the active site for the product that shares the same atoms and prevent it from being an inhibitor. In practice, the reactant, because its concentration cannot be infinite, simply increases the apparent dissociation constant for the inhibitory product by a finite factor. [e]Refers only to a mechanism confined to one active site, not cases where intermediates are moved between two or more different active sites as in the next mechanism.

association of the product as an inhibitor is with the active site of the enzyme and that its effect as an inhibitor is to sterically exclude one or more of the reactants. For example, when (*S*)-malate as a product associates with the active site of fumarate hydratase (Equation 3–1), fumarate as a reactant cannot also associate because (*S*)-malate and fumarate share the same carbon skeleton and associate at the same location in the active site.

Moreover, the hydroxy group of (*S*)-malate shares the same subsite in the active site as the other reactant, water, and when (*S*)-malate is bound to the active site, it should also prevent the association of that molecule of water. This latter consideration illustrates the fact that **at least one of the products of an enzymatic reaction that has two or more reactants usually contains atoms derived from two or more of the reactants** and will often exclude both or all of those reactants from the active site when it is bound there, depending upon how tightly the shared structures are bound. Therefore, the structures of the products and reactants and the structure of the active site will dictate which products exclude which reactants. In the following discussion, it will be assumed that product Z comes mainly from reactant A and product Y comes mainly from reactant B. This convention can be expanded to product X coming mainly from reactant C, product W coming mainly from reactant D, and so forth.

Because an active site must catalyze its reaction in both directions and because most of the reactions catalyzed by enzymes have fairly small changes in standard free energy associated with them, the products of an enzymatic reaction associate with the active site often as well as, if not more avidly than, the reactants do. In the occasional instance in which the change in standard free energy of an enzymatic reaction has a large negative value, it is possible, but not necessarily so, for the dissociation constant of a product to be so large that it does not associate with the active site at any achievable level of its concentration, and thus it cannot inhibit the enzymatic reaction. Usually, however, the dissociation constant of a product is within an achievable range of concentration, and in that range, the product will associate with the active site. **If it associates with the active site within an achievable range of concentration, a product will inhibit the conversion of reactants into products by enzymatic reaction.**

Inhibition of Enzymatic Reactions: Product Inhibition

Observation: An **example of the inhibition of an enzymatic reaction by its products** is the inhibition of pyruvate kinase from *O. cuniculus*

$$\text{phospho}\textit{enol}\text{pyruvate} + H^+ + \text{MgADP}^- \rightleftharpoons \text{MgATP}^{2-} + \text{pyruvate} \quad (3\text{–}222)$$

by the products pyruvate and $MgATP^{2-}$ when the reactants are chosen to be phospho*enol*pyruvate and $MgADP^-$ (Figure 3–15).[117,118] Pyruvate is a linear (Figure 3–15F) competitive (Figure 3–15A) inhibitor with respect to phospho*enol*pyruvate and a linear (Figure 3–15F) noncompetitive (Figure 3–15D) inhibitor with respect to $MgADP^-$, and $MgATP^{2-}$ is a linear (Figure 3–15E) competitive inhibitor with respect to both $MgADP^-$ (Figure 3–15B) and phospho*enol*pyruvate (Figure 3–15C).

Explanation: Rate equations for enzymatic reactions with two reactants and two products have been derived for kinetic mechanisms that differ one from the other in the order in which reactants and products enter and leave the active site.[62] These derivations include all steps involving association of the reactants with the active site and dissociation of each product that is chosen to act as the inhibitor in turn from the active site. From each of these rate equations, **the pattern in which each of the products should inhibit the reaction for a given kinetic mechanism could be established** (Table 3–2).[62,119]

Consider an **enzymatic reaction in which reactants A and B associate with the active site at random and products Y and Z dissociate at random**, and all complexes between substrates and enzyme are in rapid equilibrium relative to the rate of the conversion between E·A·B and E·Z·Y. Suppose that product Y excludes only reactant B and product Z excludes only reactant A, so complexes E·A·Y and E·Z·B can form. If product Y is present, so

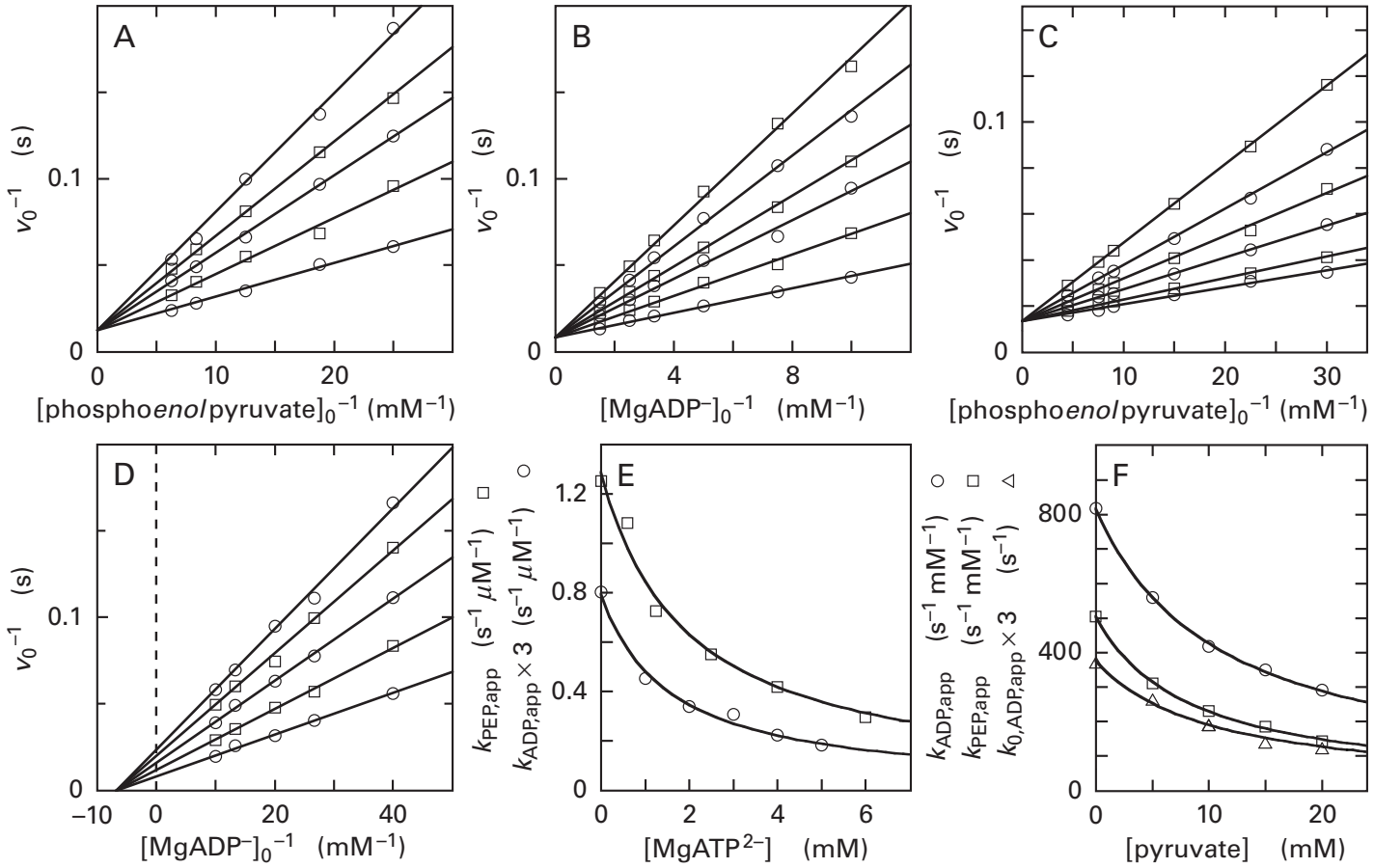

Figure 3–15: Kinetics for reversible inhibition by the products pyruvate and $MgATP^{2-}$ of the conversion of phospho*enol*pyruvate and $MgADP^-$ catalyzed by pyruvate kinase from *O. cuniculus*.[117] Solutions containing $MgADP^-$, phospho*enol*pyruvate , and $MgATP^{2-}$ or pyruvate, acting as product inhibitors, were prepared at pH 6.2. The concentration of uncomplexed Mg^{2+} was fixed at 10.0 mM and that of KCl at 0.10 M. Pyruvate kinase was added to initiate each phosphotransfer. When pyruvate was the inhibitor, production of $MgATP^{2-}$ was monitored by coupling it to the phosphorylation of 3-phospho-D-glycerate by phosphoglycerate kinase and the reduction of the resulting 3-phospho-D-glyceroyl phosphate by glyceraldehyde-3-phosphate dehydrogenase (phosphorylating). When $MgATP^{2-}$ was the inhibitor, production of pyruvate was followed by monitoring the oxidation of NADH by pyruvate catalyzed by L-lactate dehydrogenase. In each instance, the initial rate of decrease in A_{340} was used to calculate initial rates for the production of $MgATP^{2-}$ or pyruvate [micromoles minute^{-1} (microgram of enzyme)$^{-1}$]. The molar mass of a subunit of the enzyme (58,000 g mol^{-1}), which contains one independent active site,[118] was used to convert initial rates into units of second^{-1}. The concentrations of pyruvate or $MgATP^{2-}$ when one or the other is used as an inhibitor do not change significantly during the measurements of intial rates. **(A)** Reciprocals of the initial rates for the production of $MgATP^{2-}$, v_0^{-1} (seconds), as a function of reciprocals of the initial concentrations of phospho*enol*pyruvate (millimolar^{-1}). The concentrations of the product pyruvate were 0.0, 5.0, 10.0, 15.0, and 20.0 mM for the lines in ascending order. When the data were plotted directly (not shown) and fitted to Equation 3–52 with y equal to v_0 and x equal to the initial concentration of phospho*enol*pyruvate, the five values for parameter a of the fits, the apparent catalytic constants for phospho*enol*pyruvate, $k_{0,PEP,app}$, fluctuated unsystematically around a mean of 80 s^{-1}. Consequently, the five lines in this panel were forced to intersect the axis of the ordinate at 0.0125 s. **(B)** Reciprocals of the initial rates for the production of $MgATP^{2-}$, v_0^{-1} (second), as a function of reciprocals of the initial concentrations of phospho*enol*pyruvate (millimolar^{-1}). The concentrations of the product $MgATP^{2-}$ were 0.0, 0.6, 1.25, 2.5, 4.0, and 6.0 mM for the respective lines in ascending order. When the data were plotted directly and fit to Equation 3–52 (not shown) with y equal to v_0 and x equal to the initial concentration of phospho*enol*pyruvate, the values for parameter a of the fits, the apparent catalytic constants for phospho*enol*pyruvate, $k_{0,PEP,app}$, fluctuated unsystematically and were within a standard deviation of a mean of 73 s^{-1}. Consequently, the six lines in this panel were forced to intersect the axis of the ordinate at 0.0137 s. **(D)** Reciprocals of the initial rates for the production of $MgATP^{2-}$, v_0^{-1} (second), as a function of reciprocals of the initial concentrations of $MgADP^-$(millimolar^{-1}). The concentrations of pyruvate were 0.0, 5.0, 10.0, 15.0, and 20.0 mM for the respective lines in ascending order. When the data were plotted directly and fit to Equation 3–52 (not shown) with y equal to v_0 and x equal to the initial concentration of $MgADP^-$, the values for parameter b of the fits, the apparent Michaelis constants K_m, fluctuated unsystematically and were within a standard deviation of a mean of 0.148 mM. Consequently, the five lines in this panel were forced to intersect the axis of the abscissa at –6.8 mM^{-1}. **(E)** The observed values of the apparent specificity constant for phospho*enol*pyruvate, $k_{PEP,app}$ (second^{-1} micromolar^{-1}; □), from the direct plot and fit of the data in Panel C and the observed values of the apparent specificity constant for $MgADP^-$ $k_{ADP,app} \times 3$ (second^{-1} micromolar^{-1}; ○) from the direct plot and fit of the data in Panel B are plotted against the concentrations of $MgATP^{2-}$. The two values for parameter h, K_{ic}, in the fits of Equation 3–171 to the data, with y equal to $k_{PEP,app}$ or $k_{ADP,app}$ and x equal to [$MgATP^{2-}$], are 1.9 ± 0.3 mM and 1.55 ± 0.13 mM, respectively, which are identical within the errors of the measurements. **(F)** The observed values of the apparent specificity

rocals of the initial rates for the production of pyruvate, v_0^{-1} (second), as a function of reciprocals of the initial concentrations of $MgADP^-$ (millimolar^{-1}). The initial concentrations of product $MgATP^{2-}$ were 0.0, 1.0, 2.0, 3.0, 4.0, and 5.0 mM for the lines in ascending order. When the data were plotted directly and fit to Equation 3–52 (not shown) with y equal to v_0 and x equal to the initial concentration of $MgADP^-$, the six values for parameter a of the fits, the apparent catalytic constants for $MgADP^-$, $k_{0,ADP,app}$, fluctuated unsystematically around a mean of 120 s^{-1}. Consequently, the six lines in this panel were forced to intersect the axis of the ordinate at 0.0083 s. **(C)** Reciprocals of the initial rates for the production of pyruvate, v_0^{-1} constant for $MgADP^-$, $k_{ADP,app}$ (second^{-1} millimolar^{-1}; ○), from the direct plot and fit of the data in Panel D; the observed values of the apparent specificity constant for phospho*enol*pyruvate, $k_{PEP,app}$ (second^{-1} millimolar^{-1}; □) from the direct plot and fit of the data in Panel A; and the observed values of the apparent catalytic constant for $MgADP^-$, $k_{0,ADP,app} \times 3$ (second^{-1}; △) from the direct plot and fit of the data in Panel D are plotted against the concentrations of pyruvate (millimolar). The three values for K_i, parameters h in the fits of Equation 3–171 with $k_{ADP,app}$, $k_{PEP,app}$, and $k_{0,ADP,app}$ equal to u and [pyruvate] equal to z, are 10.9 ± 0.2 mM, 8.4 ± 0.3 mM, and 10.2 ± 0.8 mM, respectively, which are identical within the errors of the measurements.

that product inhibition can be observed, but product Z[120] is absent to prevent the reaction from running in reverse

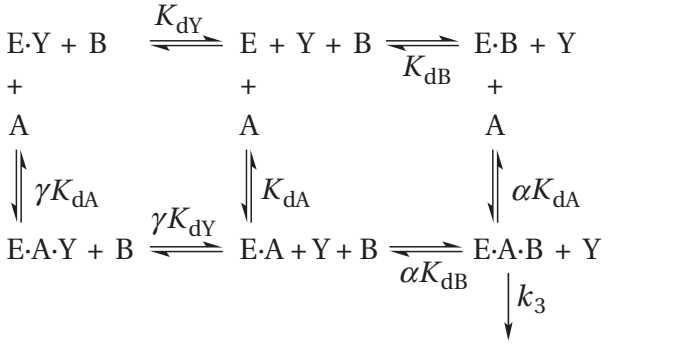

(3–223)

(see Equations 3–121 through 3–124), and

$$v_0 = \frac{k_3[E]_t[A]_0[B]_0}{\alpha K_{dA}K_{dB}\left(\frac{K_{dY} + [Y]}{K_{dY}}\right) + \alpha K_{dB}\left(\frac{\gamma K_{dY} + [Y]}{\gamma K_{dY}}\right)[A]_0 + \alpha K_{dA}[B]_0 + [A]_0[B]_0} \quad (3–224)$$

If $[B]_0$ is saturating, product Y cannot be an inhibitor with respect to reactant A. If $[B]_0$ is not saturating, product Y is noncompetitive with respect to reactant A. Product Y is competitive with respect to reactant B at all concentrations of reactant A. When product Z is used as an inhibitor, B and A are interchanged in Equations 3–223 and 3–224, as are Y and Z. Consequently, the pattern of the inhibitions by product Z is symmetrical to the pattern of the inhibitions by product Y (Table 3–2).

Human phosphoinositide-dependent protein kinase uses $MgATP^{2-}$ to phosphorylate serines and threonines in particular proteins

$$MgATP^{2-} + \text{protein} \rightleftharpoons H^+ + \text{phosphoprotein} + MgADP^- \quad (3–225)$$

The product $MgADP^-$ is a competitive inhibitor with respect to $MgATP^{2-}$ as a reactant and a noncompetitive inhibitor with respect to a peptide 39 amino acids long used as a reactant in place of a protein. The apparent dissociation constants for $MgADP^-$, K_{icADP} and K_{iuADP}, are the same. The phosphorylated peptide is a competitive inhibitor with respect to the unphosphorylated peptide as a reactant but a noncompetitive inhibitor relative to $MgATP^{2-}$ as a reactant. The apparent dissociation constants for the phosphorylated peptide (pp), K_{icpp} and K_{iupp}, are the same. These facts are consistent with the proposals that reactants and products associate with and dissociate from the enzyme at random (Table 3–2), association of the phosphorylated peptide has little or no effect on the association of $MgATP^{2-}$, and association of $MgADP^-$ has little or no effect on the association of the unphosphorylated peptide.[121]

This example illustrates the way in which patterns of product inhibition are collected and used to reach a conclusion concerning the order in which reactants associate with an enzyme and products dissociate from an enzyme. It should be empha-

sized that, as with all kinetic observations, **a given pattern of product inhibition is only consistent with a particular kinetic mechanism** in which a particular order of association and dissociation of substrates is postulated and cannot prove that this is the actual order.

If, as in the foregoing example, the reactants and products associate with and dissociate from the active site so rapidly that they are always in rapid equilibrium with it, and if they associate at random with the active site, then **the patterns of product inhibition usually incorporate a specific pair of competitive inhibitions**. If the substrates associate with the active site at random, any one of them—reactant A, reactant B, product Y, or product Z—can associate with the empty active site. If this is the case, the reactants and the products that share most of their structure with each other usually compete with each other for the same location in the empty active site, and a product that shares most of its structure with a given reactant will be a competitive inhibitor of the enzymatic reaction with respect to that reactant.

In this situation, two dead-end complexes often can form, one between reactant A and product Y that share only a few atoms with each other, such as $MgATP^{2-}$ and the phosphorylated peptide, and one between reactant B and product Z that share no atoms with each other, such as the unphosphorylated peptide and $MgADP^{-}$. If, however, a significant portion of one reactant is transferred to the other reactant during the reaction, **the product that has gained the portion transferred may be large enough to exclude the reactant that loses the portion transferred as well as the reactant that shares all its atoms with that product**.

In the case of pyruvate kinase (Figure 3–15),[117] the product pyruvate is a linear competitive inhibitor with respect to the reactant, phospho*enol*pyruvate (Figure 3–15A,F), and the product $MgATP^{2-}$ is a linear competitive inhibitor with respect to the reactant $MgADP^{-}$ (Figure 3–15B,E). These results are consistent with a kinetic mechanism in which $MgADP^{-}$ and phospho*enol*pyruvate associate with the active site of the enzyme at random and $MgATP^{2-}$ and pyruvate dissociate from the active site at random (Table 3–2). The other two product inhibitions that are observed are peculiar, but they make sense. Magnesium adenosine triphosphate as a product is a linear competitive inhibitor relative to phospho*enol*pyruvate as a reactant (Figure 3–15C,E) because $MgATP^{2-}$ carries the phospho group that is transferred between phospho*enol*pyruvate and $MgADP^{-}$, and phospho*enol*pyruvate, a small molecule, cannot occupy its location in the active site when $MgATP^{2-}$ is bound. Pyruvate, however, is a linear noncompetitive inhibitor with respect to $MgADP^{-}$ (Figure 3–15D,F), and the dissociation constants for pyruvate from the unoccupied enzyme and from the enzyme occupied by $MgADP^{-}$ appear to be the same. Because neither $MgADP^{-}$ nor pyruvate has the phospho group that is transferred, the association of pyruvate with the active site cannot sterically interfere with the association of $MgADP^{-}$. This lack of overlap would be consistent with the fact that only one dissociation constant is needed to explain the inhibition. A phospho group, even in situations in which it is not transferred but certainly in situations in which it is transferred, is usually surrounded extensively by an oriented array of donors of hydrogen bonds when it is bound to an active site, and as a result it is tightly associated. Consequently, it comes as no surprise that the association of $MgATP^{2-}$ appears to prevent the association of phospho*enol*pyruvate.

As was the case with phosphoinositide-dependent protein kinase (Equation 3–225), however, even though a portion of one reactant is transferred to the other reactant during an enzymatic reaction, **the product and the reactant that overlap may not exclude each other from the active site**. Even if the portion that overlaps is large, exclusion may not occur if both reactant and product are large molecules. For example, citrate (*Si*)-synthase from *R. norvegicus* catalyzes the reaction

$$H^+ + \text{HSCoA} + \text{citrate} \rightleftharpoons H_2O + \text{oxaloacetate} + \text{acetyl-SCoA} \qquad (3\text{–}226)$$

The reactants enter the active site at random, and the products leave the active site at random,[112] yet the product acetyl-SCoA is a mixed inhibitor with respect to the reactant citrate,[112] even though both of these substrates share the acetyl group that is transferred. Presumably, acetyl-SCoA is so large that it can associate with the enzyme even when its acetyl group is prevented from occupying its usual position in the active site by citrate, and this ability allows citrate and acetyl-SCoA to bind simultaneously to the enzyme. In fact, since the mixed inhibition is predominantly uncompetitive, acetyl-SCoA seems to increase the affinity of the active site for citrate rather than decreasing it by steric interference.

An assignment of a random order for the association and dissociation of substrates from the active site can often be made by **examining patterns of product inhibition in both directions** of the enzymatic reaction. For example, orotate phosphoribosyltransferase from *S. typhimurium* catalyzes the reaction

$$\begin{aligned}\text{magnesium 5-phospho-}\alpha\text{-D-ribose 1-diphosphate} \\ + \text{ orotate} \rightleftharpoons MgOPO_3PO_3^{2-} \\ + H^+ + \text{ orotidine 5}'\text{-phosphate}\end{aligned} \quad (3\text{–}227)$$

In the forward direction, the product orotidine 5′-phosphate is competitive with respect to both reactants, orotate and magnesium 5-phospho-α-D-ribose 1-diphosphate, and the product magnesium diphosphate is competitive with respect to the reactant magnesium 5-phospho-α-D-ribose 1-diphosphate and noncompetitive with respect to the reactant orotate. In the reverse direction, the product magnesium 5-phospho-α-D-ribose 1-diphosphate is competitive with respect to both reactants, magnesium diphosphate and orotidine 5′-phosphate, and the product orotate is competitive with respect to the reactant orotidine 5′-phosphate and noncompetitive with respect to the reactant magnesium diphosphate. The observations in each direction are consistent (Table 3–2) with the conclusion that all substrates associate with and dissociate from the enzyme at random.[122] The observations in each direction by themselves are consistent with this conclusion; that they are both consistent with the same conclusion is reassuring. It also makes sense that these results are consistent with the conclusion that the complex containing both orotidine 5′-phosphate and magnesium 5-phospho-α-D-ribose 1-diphosphate cannot form. In this case, the phosphoribosyl group transferred from magnesium diphosphate to orotate is so large and the groups between which the transfer takes place are so small that the two substrates containing the group that is transferred exclude each other from the active site.

In a few instances, the binding of either product to the active site seems to be sufficient to exclude either reactant. Glycine dehydrogenase (decarboxylating) from *G. gallus* is an enzyme containing pyridoxal phosphate and N^6-(lipoyl)lysine that catalyzes the reaction

$$\begin{aligned}H^+ + \text{glycine} + \text{H-protein-lipoyllysine} \rightleftharpoons CO_2 \\ + \text{H-protein-}S\text{-aminomethyldihydrolipoyllysine}\end{aligned} \quad (3\text{–}228)$$

Either product, CO_2 or *S*-aminomethyldihydrolipoyllysine, is competitive with respect to either reactant, glycine or oxidized H-protein-lipoyllysine.[123] This observation suggests that neither product can associate with the active site to form a dead-end complex when either reactant is bound, and this conclusion is supported by isotope exchange studies. An explanation consistent with the observation of these exclusions, which cannot be entirely steric, is that the enzyme itself undergoes a reversible isomerization between dissociation of products and association of reactants. In one conformation, the active site can bind only products, and in the other conformation, it can bind only reactants.

To this point, only mechanisms that involve the random addition of reactants and the random dissociation of products have been discussed. In such situations, the inhibitions by products can be treated as if they resulted from the formation of dead-end complexes. **Another property of a product, however, that affects its inhibition of an enzymatic reaction is its ability to reverse the reaction, rather than forming a simple dead-end complex.** This property of a product is not consequential with enzymatic reactions that proceed by the random dissociation of products, but it is consequential when enzymatic reactions proceed by the ordered dissociation of products.

Consider an **enzymatic reaction in which the reactants, A and B, associate with the active site of the enzyme in a particular order and the products, Y and Z, dissociate in a particular order**.* If all these substrates are present initially in the solution at subsaturating concentrations, none of the steps in the kinetic mechanism of the reaction

*Usually, for steric reasons, if there is an obligate order in the addition of the two reactants, the product that incorporates most of the atoms in the second reactant to add to the active site will be the product that dissociates first from the active site, and the product that incorporates most of the atoms in the first reactant will be the product that dissociates second from the active site.

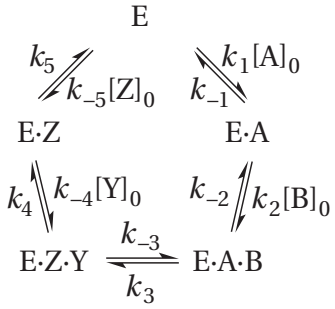

(3–229)

is formally irreversible because none of the substrates is missing. The **direction of net flux around the circle will be determined only by the standard free energy change of the reaction** and the concentration of the four substrates. If, however, one or both of the products are missing, the flux around the circle will always be clockwise because that **absence of a product converts a reversible step into an irreversible step**.

If the **substrate Y is not present initially**, the net flux must be in a clockwise direction because step 4 is forced by this choice to be formally irreversible in the other direction, and the kinetic mechanism becomes

$$\begin{aligned} \mathrm{E{\cdot}Z + A + B} &\underset{k_{-5}}{\overset{k_5}{\rightleftharpoons}} \mathrm{Z + E + A + B} \\ &\underset{k_{-1}}{\overset{k_1}{\rightleftharpoons}} \mathrm{Z + E{\cdot}A + B} \underset{k_{-2}}{\overset{k_2}{\rightleftharpoons}} \mathrm{Z + E{\cdot}A{\cdot}B} \\ &\underset{k_{-3}}{\overset{k_3}{\rightleftharpoons}} \mathrm{Z + E{\cdot}Z{\cdot}Y} \xrightarrow{k_4} \mathrm{Z + E{\cdot}Z + Y} \end{aligned} \tag{3–230}$$

Because k_3, k_{-3}, and k_4 do not involve entry of substrates into the active site, they can be combined as a composite rate constant, k_{34},* by considering the two steps

$$\mathrm{E{\cdot}A{\cdot}B} \underset{k_{-3}}{\overset{k_3}{\rightleftharpoons}} \mathrm{E{\cdot}Z{\cdot}Y} \xrightarrow{k_4} \mathrm{E{\cdot}Z + Y} \tag{3–231}$$

as one step

$$\mathrm{E{\cdot}A{\cdot}B} \xrightarrow{k_{34}} \mathrm{E{\cdot}Z + Y} \tag{3–232}$$

In analogy with Equation 3–70

$$k_{34} = \frac{k_3 k_4}{k_{-3} + k_4} \tag{3–233}$$

and the kinetic mechanism of Equation 3–230 becomes

$$\begin{aligned} &\mathrm{E{\cdot}Z + A + B} \underset{k_{-5}}{\overset{k_5}{\rightleftharpoons}} \mathrm{Z + E + A + B} \underset{k_{-1}}{\overset{k_1}{\rightleftharpoons}} \\ &\mathrm{Z + E{\cdot}A + B} \underset{k_{-2}}{\overset{k_2}{\rightleftharpoons}} \mathrm{Z + E{\cdot}A{\cdot}B} \xrightarrow{k_{34}} \mathrm{Z + E{\cdot}Z + Y} \end{aligned} \tag{3–234}$$

which is formally equivalent to the kinetic mechanism of Equation 3–210

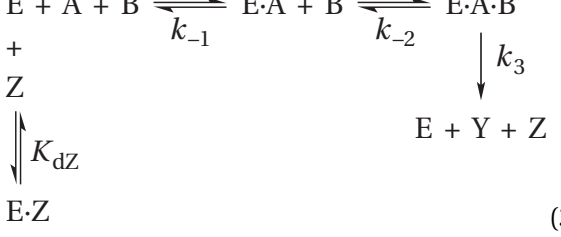

(3–235)

because, in the absence of product Y, **product Z does actually form a dead-end complex** with the enzyme, and the equation for its inhibition has the same form as Equation 3–211

*From here on, when the rate constants of two or more steps are purposely combined into a composite rate constant, the subscript on the composite rate constant will be the integer of the first forward rate constant and the integer of the last.

$$v_0 = \frac{k_0 k_A k_B k_{AB} [E]_t [A]_0 [B]_0}{k_0 k_A k_B \left(\frac{[Z] + K_{dZ}}{K_{dZ}}\right) + k_0 k_A k_{AB} [A]_0 + k_0 k_B k_{AB} \left(\frac{[Z] + K_{dZ}}{K_{dZ}}\right) [B]_0 + k_A k_B k_{AB} [A]_0 [B]_0} \quad (3–236)$$

and the dissociation constant of product Z from the active site ($K_{dZ} = k_{-5}\ k_5^{-1}$) is an explicit term in the equation.

From the conclusions drawn earlier from the kinetic mechanism of Equation 3–210, it follows that when product Z is added to the reaction, it will behave as a competitive inhibitor with respect to reactant A (Equation 3–170) and a noncompetitive or uncompetitive inhibitor with respect to reactant B. Therefore, if product Z is competitive with respect to reactant A and noncompetitive with respect to reactant B, then the conclusion that reactant A must bind to the enzyme before reactant B and product Y must be released by the enzyme before product Z is consistent with these observations (Table 3–2). If, however, it is not noncompetitive with respect to reactant B, the situation, as before, is indeterminate.

If, however, **product Z is not present initially** and product Y is present, product Y can convert the complex from which it dissociates back to a complex between the active site and both reactants, E·A·B, as well as the complex between the active site and both products, E·Z·Y. Consequently, **product Y does not form a dead-end complex** with the active site because it is able to reverse the enzymatic reaction if it associates with the active site before product Z dissociates. The general kinetic mechanism of Equation 3–229 becomes

$$\begin{aligned} E + A + B &\underset{k_{-1}}{\overset{k_1}{\rightleftharpoons}} E{\cdot}A + B \underset{k_{-2}}{\overset{k_2}{\rightleftharpoons}} E{\cdot}A{\cdot}B \\ &\underset{k_{-3}}{\overset{k_3}{\rightleftharpoons}} E{\cdot}Z{\cdot}Y \underset{k_{-4}}{\overset{k_4}{\rightleftharpoons}} E{\cdot}Z + Y \xrightarrow{k_5} E + Y + Z \end{aligned} \quad (3–237)$$

The rate equation for this kinetic mechanism has the form of Equation 3–116

$$v_0 = \frac{k_0 k_A k_B k_{AB} [E]_t [A]_0 [B]_0}{k_0 k_A k_B + k_0 k_A k_{AB} [A]_0 + k_0 k_B k_{AB} [B]_0 + k_A k_B k_{AB} [A]_0 [B]_0} \quad (3–238)$$

except that the catalytic constant k_0, the specificity constant k_B for reactant B, and the specificity constant k_{AB} are apparent rate constants, $k_{0,Y,app}$, $k_{B,Y,app}$, and $k_{AB,Y,app}$, respectively, because they contain terms that include the concentration of product Y

$$k_{0,Y,app} = \frac{k_3 k_4 k_5}{(k_3 k_4 + k_3 k_5 + k_{-3} k_5 + k_4 k_5) + k_{-4}(k_3 + k_{-3})[Y]} = \left(\frac{K_{iuY}}{[Y] + K_{iuY}}\right) \frac{k_3 k_4 k_5}{(k_3 k_4 + k_3 k_5 + k_{-3} k_5 + k_4 k_5)} \quad (3–239)$$

$$k_A = k_1 \quad (3–240)$$

$$k_{B,Y,app} = \frac{k_2 k_3 k_4 k_5}{k_5(k_{-2} k_{-3} + k_{-2} k_4 + k_3 k_4) + k_{-2} k_{-3} k_{-4}[Y]} = \left(\frac{K_{icY}}{[Y] + K_{icY}}\right) \frac{k_2 k_3 k_4}{k_{-2} k_{-3} + k_{-2} k_4 + k_3 k_4} \quad (3–241)$$

$$k_{AB,Y,app} = \frac{k_1 k_2 k_3 k_4 k_5}{k_{-1} k_5 (k_{-2} k_{-3} + k_{-2} k_4 + k_3 k_4) + k_{-1} k_{-2} k_{-3} k_{-4}[Y]} = \left(\frac{K_{icY}}{[Y] + K_{icY}}\right) \frac{k_1 k_2 k_3 k_4}{k_{-1}(k_{-2} k_{-3} + k_{-2} k_4 + k_3 k_4)} \quad (3–242)$$

where

$$K_{iuY} = \frac{(k_3 k_4 + k_3 k_5 + k_{-3} k_5 + k_4 k_5)}{k_{-4}(k_3 + k_{-3})} \quad (3–243)$$

$$K_{icY} = \frac{k_5(k_{-2}k_{-3} + k_{-2}k_4 + k_3k_4)}{k_{-2}k_{-3}k_{-4}} \quad (3\text{–}244)$$

Neither of the inhibition constants in this instance of product inhibition are dissociation constants. Notice that when [Y] is zero, Equations 3–239 through 3–242, which are no longer for apparent rate constants, become Equations 3–117 through 3–120, as they must.

Because, in the absence of product Y

$$k_{0,A,app} = \frac{k_{0,Y,app}\,k_{B,Y,app}[B]_0}{k_{0,Y,app} + k_{B,Y,app}[B]_0} \quad (3\text{–}245)$$

$$k_{A,app} = \frac{k_A k_{AB,Y,app}[B]_0}{k_A + k_{AB,Y,app}[B]_0} \quad (3\text{–}246)$$

$$k_{0,B,app} = \frac{k_{0,Y,app}\,k_A[A]_0}{k_{0,Y,app} + k_A[A]_0} \quad (3\text{–}247)$$

$$k_{B,app} = \frac{k_{B,Y,app}\,k_{AB,Y,app}[A]_0}{k_{B,Y,app} + k_{AB,Y,app}[A]_0} \quad (3\text{–}248)$$

(see Equations 3–96 through 3–99), product Y will be noncompetitive with respect to reactant B, uncompetitive with respect to reactant A when saturating initial concentrations of reactant B are present, and noncompetitive with respect to reactant A when reactant B is not at saturating concentrations (Table 3–2).[62]

D-Lactate dehydrogenase from *Streptomyces toyocaensis* catalyzes the reaction

$$\text{NADH} + \text{H}^+ + \text{pyruvate} \rightleftharpoons (R)\text{-lactate} + \text{NAD}^+ \quad (3\text{–}249)$$

As a product, NAD^+ is competitive with respect to NADH as a reactant and noncompetitive with respect to pyruvate as a reactant. (*R*)-Lactate as a product is noncompetitive with respect to pyruvate as a reactant, noncompetitive with respect to NADH as a reactant at concentrations of pyruvate below saturation, and uncompetitive with respect to NADH as a reactant at saturating concentrations of pyruvate.[124] These facts are consistent with an ordered kinetic mechanism in which NADH must associate with the enzyme before pyruvate can associate and D-lactate must dissociate before NAD^+ dissociates (Table 3–2). It follows that NADH and NAD^+, which are large, complex substrates, can associate with the enzyme in the absence of the other substrates. Historically, this fact has led to the distinction between an "apoenzyme" to which these two coenzymes are not bound in the active site and a "holoenzyme" to which one of these dinucleotides is bound, a distinction that has little practical use.

Coenzyme A as a product is a competitive inhibitor of histone acetyltransferase from *S. cerevisiae*

$$\text{acetyl-SCoA} + \text{histone} \rightleftharpoons \text{acetylhistone} + \text{HSCoA} \quad (3\text{–}250)$$

with respect to acetyl-SCoA as a reactant but does not inhibit the enzyme at saturating concentrations of acetyl-SCoA. Acetylhistone as a product is noncompetitive with respect to acetyl-SCoA as a reactant and noncompetitive with respect to histone as a reactant at concentrations of histone below saturation.[125] These facts are consistent with a kinetic mechanism in which acetyl-SCoA must associate with the active site of the enzyme before histone can associate and acetylhistone must dissociate before coenzyme A dissociates (Table 3–2).

Again, **if the reaction catalyzed by the enzyme can be assayed in both directions**, the patterns of inhibition by products in each direction reinforce a conclusion about kinetic mechanism. 5-Phospho-α-D-ribose 1-diphosphate as a product is competitive with respect to inosine 5′-phosphate as a reactant, and inosine 5′-phosphate as a product is competitive with respect to 5-phospho-α-D-ribose 1-diphosphate as a reactant in the reaction catalyzed by hypoxanthine phosphoribosyltransferase from *Tritrichomonas foetus*

$$\text{magnesium 5-phospho-}\alpha\text{-D-ribose 1-diphosphate} + \text{hypoxanthine} \rightleftharpoons \text{MgOPO}_3\text{PO}_3^{2-} + \text{inosine 5′-phosphate} + \text{H}^+ \quad (3\text{–}251)$$

Magnesium diphosphate as a product is noncompetitive with respect to both of the reactants hypoxanthine and magnesium 5-phospho-α-D-ribose 1-diphosphate in one direction, and magnesium 5-phospho-α-D-ribose 1-diphosphate as a product is noncompetitive with respect to magnesium diphosphate as a reactant in the other direction.[126]

These facts are consistent with a kinetic mechanism in which magnesium 5-phospho-α-D-ribose 1-diphosphate must associate with the enzyme before hypoxanthine and magnesium diphosphate must dissociate before inosine 5′-phosphate (Table 3–2).

Reactants also can associate in an obligate order and products can dissociate at random. Both magnesium uridine 5′-diphosphate and deoxycytidine 5′-phosphate as products are competitive with respect to magnesium uridine 5′-triphosphate as a reactant in the reaction catalyzed by human deoxycytidine kinase

$$\mathrm{MgUTP^{2-}} + \text{deoxycytidine} \rightleftharpoons \mathrm{H^+} + \text{deoxycytidine 5′-phosphate} + \mathrm{MgUDP^-} \quad (3\text{–}252)$$

while magnesium uridine 5′-diphosphate as a product is uncompetitive and deoxycytidine 5′-phosphate as a product is noncompetitive with respect to deoxycytidine at saturating magnesium uridine 5′-triphosphate.[127] These facts are consistent with a kinetic mechanism in which magnesium uridine 5′-triphosphate must associate with the enzyme before deoxycytidine can associate but deoxycytidine 5′-phosphate and magnesium uridine 5′-diphosphate dissociate at random (Table 3–2).

In the case of an enzyme displaying double reciprocals for the initial concentrations of each varied reactant that are parallel to each other at fixed concentrations of the other reactant (Figure 3–8), inhibition by products determines **whether the two irreversible steps in this ping-pong kinetic mechanism are each the result of the dissociation of a product or one or both of them is due to some other irreversible process**. For example, in the reaction catalyzed by ovine 3-oxoacid CoA-transferase (Equation 3–149)

$$\text{acetoacetate} + \text{succinyl-SCoA} \rightleftharpoons \text{acetoacetyl-SCoA} + \text{succinate} \quad (3\text{–}253)$$

the double reciprocals for the reactants succinyl-SCoA and acetoacetate when one is fixed and the other is varied are both sets of parallel lines.[87] Succinate (succ) as a product is competitive with respect to acetoacetate (acac) as a reactant, and acetoacetyl-SCoA (acac-SCoA) as a product is competitive with respect to succinyl-SCoA as a reactant. Succinate as a product is noncompetitive with respect to succinyl-SCoA (succ-SCoA) as a reactant, and acetoacetyl-SCoA as a product is noncompetitive with respect to acetoacetate as a reactant.[87] These facts are consistent with a kinetic mechanism

$$\begin{aligned} &\mathrm{E} + \text{succ-SCoA} + \text{acac} \rightleftharpoons \mathrm{E{\cdot}succ\text{-}SCoA} + \text{acac} \\ &\rightleftharpoons \mathrm{E(SCoA)} + \text{succ} + \text{acac} \rightleftharpoons \\ &\mathrm{E(SCoA){\cdot}acac} + \text{succ} \rightleftharpoons \mathrm{E{\cdot}acac\text{-}SCoA} + \text{succ} \\ &\rightleftharpoons \mathrm{E} + \text{acac-SCoA} + \text{succ} \end{aligned} \quad (3\text{–}254)$$

in which succinate dissociates from the enzyme in a step preceding the association of acetoacetate (acac) and acetoacetyl-SCoA dissociates from the enzyme in a step preceding the association of succinyl-SCoA (Table 3–2).

In this kinetic mechanism, the irreversible steps separating the associations of each of the two reactants, succinyl-SCoA and acetoacetate, both result from the dissociation of a product, acetoacetyl-SCoA and succinate, respectively. Succinate in the reverse direction and acetoacetate in the forward direction associate with the same form of the enzyme, E(SCoA), and compete with each other for that form (Equation 3–254). Acetoacetyl-SCoA and succinyl-SCoA associate with the same form of the enzyme, E, and compete with each other for that form (Equation 3–254). These two competitions are consistent with the conclusion that succinate and acetoacetate, in turn, occupy the same locations in the active site and that succinyl-SCoA and acetoacetyl-SCoA, in turn, occupy the same locations in the active site. The fact that, in this kinetic mechanism, succinate must dissociate from the enzyme before acetoacetate can associate requires that the coenzyme A portion of succinyl-SCoA remain associated with the active site in the undefined form E(SCoA) because, if it did not, the reaction would become a simple acyl-CoA hydrolase, and the free energy of hydrolysis of the thioester would be lost.

Patterns of product inhibition such as the one just described are not alone sufficient to define a ping-pong kinetic mechanism in which the dissociations of products provide the irreversible steps (compare the first entry and sixth entry in Table 3–2), but the behavior of the initial rates of the enzymatic reaction as a function of the reactants (Figure 3–8) and the product inhibitions (Table 3–2) together are sufficient.

There are enzymes that convert reactant A to product Z at one active site, transfer to another active

site the functional group that was subtracted from reactant A to make product Z, and add that functional group to reactant B at that other active site to convert reactant B into product Y. In such instances, the pattern of product inhibition is opposite[93] from that for the kinetic mechanism in which product A is released before reactant B can bind and product Y is released before product A can bind (Table 3–2) because the product and the reactant for each of the independent active sites compete with each other. This latter kinetic mechanism, however, also produces double reciprocals for the initial concentrations of each varied reactant that are parallel to each other at fixed concentrations of the other reactant, but it is distinguished from the former by the pattern of product inhibition.

In the foregoing discussion, rate equations for the effects of product inhibition on the various kinetic mechanisms—random addition and dissociation, ordered association and dissociation, and ping-pong association—were derived as an academic exercise. In general, if the behavior of the observed product inhibition is that described by one and only one of the entries in Table 3–2, there is no necessity to derive a rate equation because it has already been done for that situation. First, a full set of kinetic data is obtained by varying both the concentration of each reactant and the concentration of each product, in both the forward and the reverse direction, if possible. Second, the types of product inhibition are assigned by examining double-reciprocal presentations of the data. Third, each set of data is fit directly by the appropriate equations for the type of product inhibition observed to obtain numerical values for the observed rate constants. With all this information in hand, simple consultation of the table is usually sufficient to discover a particular kinetic mechanism consistent with the observations.[128]

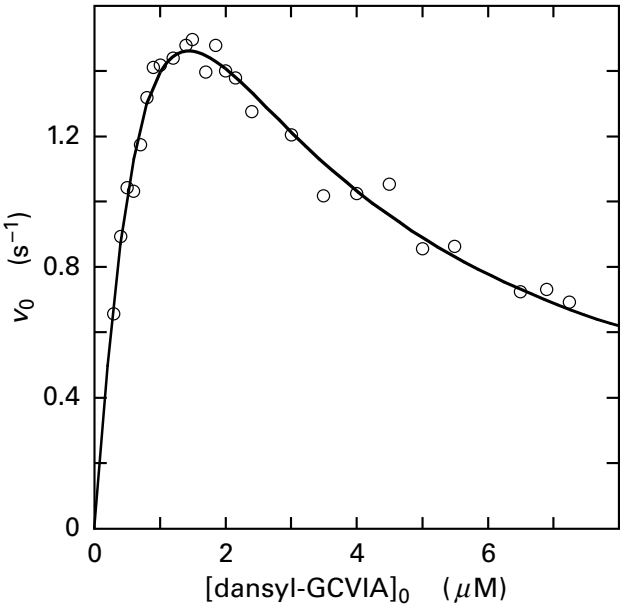

Figure 3–16: Behavior of the initial rates of the farnesylations catalyzed by protein farnesyltransferase as a function of the initial concentrations of the synthetic peptide GCVIA that has been modified at its amino terminus with 5-(dimethylamino)-naphthalene-1-sulfonyl chloride (dansyl chloride).[129] Equivalent amounts of protein farnesyltransferase were added to a series of reaction mixtures at pH 7.0 and 30 °C in which the concentration of magnesium (2*E*,6*E*)-farnesyl diphosphate was fixed at 5 μM and the concentrations of dansyl-GCVIA was varied between 0.3 and 7.25 μM. The increase in fluorescence of the dansyl group upon alkylation of the cysteine in the dansylated peptide was monitored continuously to obtain initial rates that were converted to the units of second^{-1} using an emission coefficient for dansyl-GC(farnesyl)VIA and the molar mass of protein for each mole of active sites. The initial rates (second^{-1}) are plotted as a function of the initial concentrations of dansyl-GCVIA (micromolar). The data were fit with Equation 3–257, and the values for the parameters of the fit were $k_0 = 5.5 \pm 0.9$ s^{-1}, $k_{pep} = 2.77 \pm 0.15$ s^{-1} μM^{-1}, and $K_{i,pep} = 1.05 \pm 0.21$ μM, where pep refers to the reactant dansyl-GCVIA and k_{pep} is the specificity constant for dansyl-GCVIA.

Inhibition of Enzymatic Reactions: Reactant Inhibition

Observation: When the initial concentration of a reactant in a reaction catalyzed by an enzyme is increased from zero, the initial rate of the reaction increases, passes through a maximum, and then begins to decrease. The synthetic peptide dansyl-GCVIA is a reactant in the farnesyl transfer catalyzed by protein farnesyltransferase from *S. cerevisiae*

$$\text{magnesium (2}E\text{,6}E\text{)-farnesyl diphosphate} + \text{–GCVIA–} \rightleftharpoons \text{–GC(}S\text{-farnesyl)VIA–} + H^+ + MgOPO_3PO_3^{2-} \quad (3\text{–}255)$$

where –GCVIA– is the segment of a protein containing a cysteine that is farnesylated by the enzyme. The fact that the synthetic peptide is a competent reactant suggests that the active site recognizes only this short sequence in the much larger proteins that are its natural substrates. When the initial concentration of dansyl-GCVIA is varied, the initial rate of the reaction increases and then decreases (Figure 3–16).[129]

The **decrease in the initial rate as the initial concentration of the reactant is increased beyond the maximum** is an inhibition of the enzymatic reaction by that reactant. In fact, in the seminal examination of enzymatic kinetics, that of the reaction catalyzed by β-fructofuranosidase (Figure 3–3),[64] the reaction was inhibited at 770 mM sucrose.

When reactant inhibition is observed, the initial rates for the enzymatic reaction at the various initial concentrations of reactant A, the reactant producing the inhibition, can usually be described by the equation

$$v_0 = \frac{k_0[\mathrm{E}]_t k_\mathrm{A}[\mathrm{E}]_t[\mathrm{A}]_0}{k_0[\mathrm{E}]_t + k_\mathrm{A}[\mathrm{E}]_t[\mathrm{A}]_0 + \left(\frac{k_\mathrm{A}[\mathrm{E}]_t}{K_\mathrm{iA}}\right)[\mathrm{A}]_0^2}$$

$$= \frac{k_0[\mathrm{E}]_t k_\mathrm{A}[\mathrm{E}]_t[\mathrm{A}]_0}{k_0[\mathrm{E}]_t + k_\mathrm{A}[\mathrm{E}]_t[\mathrm{A}]_0\left(\frac{K_\mathrm{iA} + [\mathrm{A}]_0}{K_\mathrm{iA}}\right)} \quad (3\text{–}256)$$

where K_iA is the **inhibition constant** for reactant A. In a reaction with two reactants, for which the catalytic constant for reactant A and the specificity constant for reactant A are apparent rate constants, the same equation will describe reactant inhibition by reactant A as reactant A is varied at fixed concentrations of reactant B. In cases of reactant inhibition, the data are fit with the equation

$$y = \frac{acx}{a + cx + \left(\frac{c}{d}\right)x^2} \quad (3\text{–}257)$$

where y is v_0, x is $[\mathrm{A}]_0$, a is $k_0[\mathrm{E}]_t$, c is $k_\mathrm{A}[\mathrm{E}]_t$, and d is K_iA. This equation is the one fit to the curve in Figure 3–16, for which $K_\mathrm{iGCVIA} = 1.05 \pm 0.21$ μM and the Michaelis constant = 2.0 ± 0.21 μM. Notice that when $K_\mathrm{iA} = \infty$, Equation 3–256 reduces to Equation 3–43 as it must.

Equation 3–256 states that the reactant A is uncompetitive with respect to itself because, if the respective limits are taken, it can be seen that the inhibitor only affects the catalytic constant but not the specificity constant for reactant A. This feature of the equation makes sense because reactant A cannot compete with itself.

The dissociation constant for a reactant acting as an inhibitor does not have to be in the range of the Michaelis constant, as it is when synthetic peptide GCVIA is a reactant for protein farnesyltransferase. L-Tryptophan is a reactant which is also an inhibitor of the reaction catalyzed by human indoleamine 2,3-dioxygenase (previously Equation 2–248)

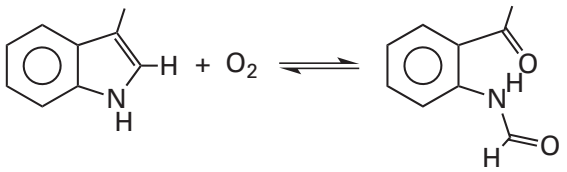

(3–258)

Its Michaelis constant is 15 μM and its inhibition constant is 170 μM.[130]

Explanation: Consider the kinetic mechanism of Equation 3–190 for an enzymatic reaction with only one reactant but with **reactant A as the inhibitor instead of inhibitor I**

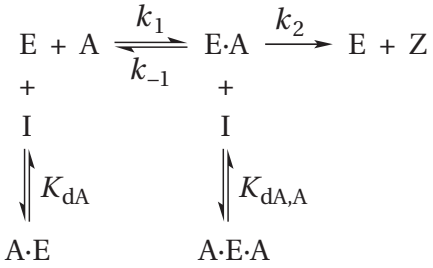

(3–259)

If K_dI is replaced by K_dA, $K_\mathrm{dI,A}$ is replaced by $K_\mathrm{dA,A}$, and [I] is replaced by $[\mathrm{A}]_0$, Equation 3–193 can be rearranged to

$$v_0 = \frac{\left\{\dfrac{k_1k_2K_{dA}[E]_t}{(k_{-1}+k_2)+k_1K_{dA}}\right\}\left\{\dfrac{k_1k_2[E]_t}{k_{-1}+k_2}\right\}[A]_0}{\dfrac{k_1k_2K_{dA}[E]_t}{(k_{-1}+k_2)+k_1K_{dA}} + \left(\dfrac{k_1k_2[E]_t}{k_{-1}+k_2}\right)[A]_0 + \dfrac{\left(\dfrac{k_1k_2[E]_t}{k_{-1}+k_2}\right)}{\left(\dfrac{k_{-1}+k_2}{k_1}\right)\left(\dfrac{K_{dA,A}}{K_{dA}}\right)+K_{dA,A}}[A]_0^2} \quad (3\text{–}260)$$

which has the form of Equation 3–256. For the kinetic mechanism of Equation 3–55, which is that for Equation 3–259 in the absence of any reactant inhibition, K_m is $(k_2 + k_{-1})\,k_1^{-1}$, so in Equation 3–256

$$K_{iA} = \frac{K_mK_{dA,A}}{K_{dA}} + K_{dA,A} \quad (3\text{–}261)$$

Therefore, in the abstract, if reactant A can associate with a site that is distinct from the active site with which it associates productively, and if that association produces a dead-end complex,[131] Equation 3–256 should describe that inhibition. It has been concluded that, in the case of human indoleamine 2,3-dioxygenase, the L-tryptophan associates with a site other than the active site when it is acting as an inhibitor.[130] If $K_{dA} = K_{dA,A} > K_m$, the measured value of K_{iA} is K_{dA}, the dissociation constant for reactant A from the site at which it inhibits the enzyme.

One site with which reactant A can associate to produce a fully inhibited, dead-end complex is **the site with which reactant B associates** in an enzyme that has two reactants. For example, the inhibition by the reactant phospho*enol*pyruvate of the reaction catalyzed by 3-phosphoshikimate 1-carboxyvinyltransferase from *E. coli*

$$\text{phospho}\textit{enol}\text{pyruvate} + \text{3-phosphoshikimate} \rightleftharpoons \text{phosphate} + \text{5-}O\text{-(1-carboxyvinyl)-3-phosphoshikimate} \quad (3\text{–}262)$$

is thought to result from the dead-end association of phospho*enol*pyruvate with the site with which 3-phosphoshikimate associates because increasing the initial concentration of 3-phosphoshikimate increases the inhibition constant K_{iPEP} for phospho*enol*pyruvate as an inhibitor.[132] Likewise, the inhibition by the reactant L-homocysteine of the reaction catalyzed by cystathionine β-synthase from *S. cerevisiae*

$$\text{L-homocysteine} + \text{L-serine} \rightleftharpoons H_2O + \text{L-cystathionine} \quad (3\text{–}263)$$

is thought to result from its dead-end association with the site with which L-serine must associate during the enzymatic reaction.[133] This conclusion makes sense because both of the reactants are L-amino acids.

Suppose that, in an enzymatic reaction with two reactants, the **two reactants must associate with the enzyme in a particular order** for a productive ternary complex between the enzyme and the reactants to be produced (Equation 3–109). If the reactant required to be second (reactant B) associates before the reactant required to be first (reactant A), a dead-end complex that cannot participate in the enzymatic reaction could form. For example, in the reaction catalyzed by protein farnesyltransferase from *S. cerevisiae* (Equation 3–255), there is kinetic evidence consistent with the conclusion that (2*E*,6*E*)-farnesyl diphosphate (reactant A) must associate with the active site before the protein to be farnesylated (reactant B) associates to produce a productive ternary complex. Consequently, the reactant inhibition observed with dansyl-GCVIA (Figure 3–16) is thought to result from the formation of a binary, unproductive, dead-end complex between the enzyme and the peptide (E·B) associating in its usual location in the active site and that this complex is unproductive because it prevents association of (2*E*,6*E*)-farnesyl diphosphate.[129] In the case of the reactant inhibition of human tryptophan 5-monooxygenase by L-tryptophan, it was concluded that the reactant inhibition was due to the association of L-tryptophan in its usual location in the active site but in the wrong order so that the association of the reactant 5,6,7,8-tetrahydropteridine is prevented. To form a productive ternary

complex, the reactant 5,6,7,8-tetrahydropteridine must associate before L-tryptophan. This conclusion that the inhibition is the result of L-tryptophan associating with the active site in its usual location was based on examinations of crystallographic molecular models of the occupied enzyme as well the fact that 5,6,7,8-tetrahydropteridine competes with L-tryptophan for the form of the enzyme with which L-tryptophan associates as an reactant inhibitor.[134]

A kinetic mechanism in which reactants are required to associate in a particular order (Equation 3–109) is a special case of the kinetic mechanism of Equation 3–136 in which only one of the two paths is productive. Suppose that only the upper path in the kinetic mechanism of Equation 3–136 is productive. If, however, only the first step in the lower path can occur—namely, the association of reactant B in the wrong order—this association would result in a dead-end complex and inhibition by that reactant, but the lower path can also produce a productive ternary complex E·A·B, albeit at a significantly slower rate than the upper.[135] In this case, reactant B, by shunting the reaction onto the lower path, would be an inhibitor of the reaction at high concentration, but it would not be a dead-end inhibitor. In this situation, there will still be a finite rate to the catalytic reaction at an infinite concentration of reactant B, which is possible for Equation 3–137, rather than a zero rate as required by Equation 3–256. Consequently, reactant inhibition that shows the behavior of Equation 3–137, with a finite rate at saturating initial concentrations of the reactant, is consistent with the steady-state kinetic mechanism of Equation 3–136. Again, however, perhaps because the kinetic equations are so complex (Table 3–1), few if any kinetic studies have concluded that the kinetic mechanism of an enzyme is that of Equation 3–136.

In addition to dead-end inhibition, product inhibition, and reactant inhibition, the trapping of a radioisotopically labeled reactant provides another observation in a determination of the order in which reactants associate with an enzyme.

When orotate phosphoribosyltransferase from *S. typhimurium* (Equation 3–227) at a high concentration (40 μM) was equilibrated with a saturating concentration (40 μM) of magnesium 5-phospho-α-D-ribose 1-[β-^{32}P]diphosphate in 10 μL of solution and then rapidly diluted into a large volume (800 μL) of a second solution containing 10 mM nonradioactive magnesium 5-phospho-α-D-ribose 1-diphosphate and 2.5 mM orotate, an amount of magnesium [^{32}P]diphosphate equivalent to 88% of the active sites present in the first solution was produced in the first few seconds of the enzymatic reaction that commenced in the second solution.[136] This observation demonstrates that magnesium 5-phospho-α-D-ribose 1-diphosphate must be able to associate with the enzyme in the absence of orotate. If it had to wait for orotate, no radiolabeled magnesium 5-phospho-α-D-ribose 1-diphosphate could have associated with the enzyme before the dilution, only insignificantly radiolabeled magnesium 5-phospho-α-D-ribose 1-diphosphate could have associated after the dilution, and no radiolabeled diphosphate would have been produced. It also demonstrates that this magnesium 5-phospho-α-D-ribose 1-diphosphate that associates with the unoccupied active site is capable of participating in the reaction. When enzyme (150 μM) and [2-^{14}C]orotate (180 μM) in 10 μL of solution were diluted into 800 μL of a solution containing 1.9 mM nonradioactive orotate and 2 mM magnesium 5-phospho-α-D-ribose 1-diphosphate, an amount of [2-^{14}C]orotidine 5′-phosphate equal to 55% of the active sites present was produced in the first few seconds.[136] Consequently, both magnesium 5-phospho-α-D-ribose 1-diphosphate and orotidine must be able associate productively with the unoccupied active site, and consequently they must be able to associate at random during the normal enzymatic reaction.

Squalene synthase from *S. cerevisiae* is unusual in that it converts two molecules of the same reactant, (2*E*,6*E*)-farnesyl diphosphate, into an intermediate in the active site that is then reduced by NADPH to give the product squalene. If the enzyme is mixed first with a saturating concentration of [^{14}C]-(2*E*,6*E*)-farnesyl diphosphate and then mixed with solution containing a saturating concentration of [4-^{3}H]NADPH and unlabeled (2*E*,6*E*)-farnesyl diphosphate in significant excess over the initial [^{14}C]-(2*E*,6*E*)-farnesyl diphosphate, the ratio between carbon-14 and tritium in the product after the first turnover of the reaction could be estimated by extrapolation of the ratio observed over time. The results clearly demonstrated that two molecules of [^{14}C]-(2*E*,6*E*)-farnesyl diphosphate were trapped on the active site by the association of the [4-^{3}H]NADPH. It could be concluded that two molecules of (2*E*,6*E*)-farnesyl diphosphate can associate with the unoccupied active site in the absence of NADPH and presumably form the intermediate that is then reduced after the dilution when the NADPH was present.[137]

Unfortunately, the results expected from trapping of isotopically labeled reactants in the case of their ordered addition to the enzyme are often ambiguous. For example, in the case of 2-*C*-methyl-D-erythritol 4-phosphate cytidylyltransferase

$$\mathrm{MgCTP^{2-}} + \text{2-}C\text{-methyl-D-erythritol 4-phosphate} \rightleftharpoons \mathrm{MgOPO_3PO_3^{2-}} + \text{4-(cytidine 5′-diphospho)-2-}C\text{-methyl-D-erythritol} \quad (3\text{–}264)$$

from *E. coli*, Mg[2-^{14}C]CTP^{2-} associated with the unoccupied active site is trapped in the product upon addition of 2-*C*-methyl-D-erythritol 4-phosphate, but [2-^{14}C]2-*C*-methyl-D-erythritol 4-phosphate is not trapped in the product[138] upon addition of MgCTP^{2-}. This result is consistent with a kinetic mechanism in which MgCTP^{2-} must associate with the enzyme before 2-*C*-methyl-D-erythritol 4-phosphate, but it is also consistent with a kinetic mechanism in which reactants can associate at random but the dissociation of 2-*C*-methyl-D-erythritol 4-phosphate from the enzyme is much more rapid than the conversion of the two reactants to the products once they are in the active site. In other words, for such observations to be consistent with an ordered addition of reactants, both reactants, MgCTP^{2-} and 2-*C*-methyl-D-erythritol 4-phosphate, once they are in the active site, must dissociate from the active site more slowly than they are converted to the products free in solution.[139] Likewise, the failure to trap $^{18}O_2$ preequilibrated with unoccupied active site in the product 5-hydroxyisourate can mean, in the absence of other observations, either that urate must associate with urate oxidase from *Glycine max* before O_2 can associate or that O_2 equilibrates with the enzyme much more rapidly than urate can be turned into 5-hydroxyisourate on the active site,[140] which seems reasonable when the structures of the two reactants are considered. Such measurements, however, can be used to provide further evidence consistent with the existence of an ordered addition, along with other kinetic measurements.

In the case of the reaction catalyzed by bovine cAMP-dependent protein kinase

$$\mathrm{H^+ + MgADP^- + LRRAS(PO_3^{2-})LG} \rightleftharpoons \mathrm{LRRASLG + MgATP^{2-}} \quad (3\text{–}265)$$

where LRRASLG is the peptide of this sequence, the failure of the peptide to trap Mg[2-^{3}H]ADP$^-$ preequilibrated with the unoccupied active site in the product MgATP^{2-} was attributed to the rapid equilibration of MgADP$^-$ with the enzyme relative to the conversion of reactants to products on the active site rather than a requirement that LRRAS(PO$_3^{2-}$)LG must associate before MgADP$^-$ does.[141]

The kinetics of any enzymatic reaction in which there are more than two reactants can be simplified to the kinetics of a reaction with two reactants by adding saturating concentrations of the other reactants to the solution. This stratagem, however, has consequences that depend on the order in which reactants associate with the enzyme.

If the reactants must associate with the enzyme in a particular order, A, B, C, …, then the **place in that sequence of each reactant that is set in turn at saturation** determines the patterns of bireactant kinetics observed. When any one of the reactants is held at saturation, this choice of conditions has the effect of converting the step in which this reactant associates with the enzyme into a **kinetically irreversible step**.

Consider an enzyme with three reactants, A, B, and C, that must add in the order reactant A before reactant B before reactant C. When reactant C is held at saturation, its association with the enzyme becomes a formally and kinetically irreversible step and is **incorporated into the kinetically silent processes** of the conversion of reactants to products on the active site and the release of products. The bireactant kinetics for variation in the initial concentrations of reactant A and reactant B, the effects of dead-end inhibitors, and the inhibitions by products are those for two reactants that must associate with the enzyme in the order reactant A before reactant B.

When reactant A is held at saturation, the unoccupied active site is converted entirely to the complex E·A, and a kinetically irreversible step has been formally created between the dissociation of products and the association of reactant B. The bireactant kinetics for variations in the initial concentrations of reactant B and reactant C and the effects of dead-end inhibitors are those for two reactants that must associate with the enzyme in the order reactant B before reactant C, and the patterns of product inhibition are those for a kinetic mechanism in which a kinetically irreversible step exists between the dissociation of products and the association of the first reactant, reactant B.

When reactant B is held at saturation, however, the association of reactant B with the complex E·A to form the complex E·A·B becomes formally and kinetically irreversible. This situation places a kinetically irreversible step between the association of reactant A and the association of reactant C. When one of these two reactants, A or C, is varied at several fixed concentrations of the other, **the bireactant kinetics are those in which the double reciprocals are parallel lines**. For example, when the initial concentration of carbon dioxide was varied at several fixed concentrations of NADH, the double reciprocals of the initial rates for the reaction catalyzed by homoisocitrate dehydrogenase from *S. cerevisiae*

$$\text{NADH} + \text{2-oxoadipate} + \text{CO}_2 \rightleftharpoons \text{NAD}^+ + (1R,2S)\text{-1-hydroxybutane-1,2,4-tricarboxylate} \quad (3\text{–}266)$$

were parallel lines if a saturating concentration of 2-oxoadipate was present. This observation is consistent with a kinetic mechanism in which NADH must associate with the enzyme before 2-oxoadipate, which must associate with the enzyme before CO_2.[142]

The observation of parallel double reciprocals when one reactant is varied at several fixed concentrations of the other while a third reactant is held at saturation, however, is not alone indicative of a fully ordered kinetic mechanism. For example, when the initial concentration of tetrahydrobiopterin was varied at several fixed initial concentrations of molecular oxygen, the double reciprocals of the initial rates for the reaction catalyzed by phenylalanine 4-monooxygenase from *Chromobacterium violaceum*

$$\text{O}_2 + \text{L-phenylalanine} + \text{tetrahydrobiopterin} \rightleftharpoons \text{L-tyrosine} + \text{4a-hydroxytetrahydrobiopterin} \quad (3\text{–}267)$$

at saturating concentrations of L-phenylalanine were parallel.[143] In this case, however, other observations indicated that the kinetic mechanism for the enzyme is one in which molecular oxygen must associate first and then L-phenylalanine and tetrahydrobiopterin associate at random. When the concentration of L-phenylalanine is at saturation, it associates immediately and irreversibly with the active site after molecular oxygen has associated, and its kinetically irreversible association separates the association of oxygen and the association of tetrahydrobiopterin, resulting in the parallel double reciprocals. In this case, the reason for the parallel double reciprocals is the same; namely, that the saturation with one reactant creates a kinetically irreversible step between the association of the other two, but the kinetic mechanism of the reaction is not fully ordered.

The kinetics of phosphopantothenate—cysteine ligase (CTP)

$$\text{Mg CTP}^{2-} + (R)\text{-4′-phosphopantothenate} + \text{L-cysteine} \rightleftharpoons 2\,\text{H}^+ + \text{MgOPO}_3\text{PO}_3^{2-} + \text{CMP}^{2-} + N\text{-[(}R\text{)-4′-phosphopantothenoyl]-L-cysteine} \quad (3\text{–}268)$$

from *Enterococcus faecalis* illustrate the complexity that can be encountered when an enzyme has three reactants and three products.

When the initial concentration of $MgCTP^{2-}$ is varied at saturating concentrations of L-cysteine and several fixed concentrations of (*R*)-4′-phosphopantothenate, the double reciprocals are a set of lines that intersect in the second quadrant. When, however, the initial concentration of L-cysteine is varied at several fixed concentrations of either $MgCTP^{2-}$ or (*R*)-4′-phospho-pantothenate while the other reactant is held at saturating concentrations, the double reciprocals in each case are a set of parallel lines. These observations are consistent with a kinetic mechanism in which a kinetically irreversible step exists between the association of $MgCTP^{2-}$ and (*R*)-4′-phospho-pantothenate and the association of L-cysteine with the active site.

The product CMP^- is competitive with respect to the reactant $MgCTP^{2-}$ and noncompetitive with respect to the reactant (*R*)-4′-phosphopantothenate when both L-cysteine and the third reactant, (*R*)-4′-phosphopantothenate or $MgCTP^{2-}$, are held at saturating concentrations. These observations are consistent with a requirement that $MgCTP^{2-}$ must to add to the unoccupied active site before (*R*)-4′-phosphopantothenate, and CMP^- can be the last product to dissociate from the active site.

The product CMP^- is uncompetitive with respect to the reactant L-cysteine when both $MgCTP^{2-}$ and (*R*)-4′-phosphopantothenate (PPA) are held at saturating concentrations. This observation can be shown to be consistent with the following kinetic mechanism

$$\begin{aligned}
\text{E}{\cdot}\text{CMP} + \text{CTP} + \text{PPA} + \text{Cys} &\xrightleftharpoons{K_{\text{d,CMP}}} \\
\text{CMP} + \text{E} + \text{CTP} + \text{PPA} + \text{Cys} &\xrightarrow{k_1} \\
\text{CMP} + \text{E}' + \text{Cys} + \text{PP}_\text{i} &\underset{k_{-2}}{\overset{k_2}{\rightleftharpoons}} \\
\text{CMP} + \text{E}'{\cdot}\text{Cys} + \text{PP}_\text{i} &\xrightarrow{k_3} \\
\text{CMP} + \text{E} + \text{PPCys} + \text{CMP} + \text{PP}_\text{i}
\end{aligned} \tag{3–269}$$

The irreversible step between the unoccupied enzyme, E, and a form of the enzyme with an altered active site, E′, which is governed by the rate constant k_1, includes the association of $MgCTP^{2-}$ and the association of (*R*)-4′-phosphopantothenate, which are both at saturating concentrations, and the dissociation of diphosphate (PP_i), one of the products of the enzymatic reaction, which is absent from the solution. The irreversible step between the complex E′·Cys and the unoccupied enzyme E, which is governed by the rate constant k_3, includes the dissociation of *N*-[(*R*)-4′-phosphopantothenoyl]-L-cysteine (PPCys), one of the products of the enzymatic reaction, which is absent from the solution. The dissociation of the product CMP^- cannot be an irreversible step because it is present in the solution as a product inhibitor. The rate equation for the kinetic mechanism of Equation 3–269

$$v_0 = \frac{k_1 k_2 k_3 [\text{E}]_t [\text{Cys}]_0}{\left\{k_1 k_2 + k_2 k_3 \left(\frac{[\text{CMP}] + K_{\text{d,CMP}}}{K_{\text{d,CMP}}}\right)\right\}[\text{Cys}]_0 + k_1(k_{-2} + k_3)} \tag{3–270}$$

requires that CMP^- be an uncompetitive inhibitor, which it is. Because both $MgCTP^{2-}$ and (*R*)-4′-phosphopantothenate are held at saturating concentrations, this fact alone makes the step governed by the rate constant k_1 irreversible, so there is no requirement that the dissociation of a product occur during that step governed. It may be the case that diphosphate dissociates after L-cysteine has associated rather than before.

All these kinetic observations are consistent with a kinetic mechanism in which $MgCTP^{2-}$ associates first with the unoccupied active site, followed by (*R*)-4′-phosphopantothenate. These two bound reactants undergo a kinetically irreversible transformation after which L-cysteine associates. Following a further chemical transformation, *N*-[(*R*)-4′-phosphopantothenoyl]-L-cysteine dissociates from the active site before CMP^-, or the two dissociate from the active site at random.[144] If the kinetically irreversible step governed by rate constant k_1 is the dissociation of diphosphate, then diphosphate should be competitive with respect to L-cysteine, an experiment that was not performed.

The same kinetic mechanism has been proposed for the reaction catalyzed by EntE, the protein encoded by the *entE* gene

$$\begin{aligned}
\text{2,3-dihydroxybenzoate} + \text{MgATP}^{2-} + \text{HSEntB} &\rightleftharpoons \text{MgOPO}_3\text{PO}_3^{2-} + \text{H}^+ + \text{AMP}^{2-} \\
&\quad + \text{2,3-dihydroxybenzoyl-SEntB}
\end{aligned} \tag{3–271}$$

in *E. coli*, where HSEntB is the protein encoded by the *entB* gene and 2,3-dihydroxybenzoyl-SEntB is HSEntB that has had a 2,3-dihydroxybenzoyl group esterified onto the sulfanyl group of its covalently attached phosphopantetheinyl group to produce a thioester. In this instance, the kinetic mechanism that is consistent with the results is one in which 2,3-dihydroxybenzoate associates first with the unoccupied active site, followed by $MgATP^{2-}$. These two bound reactants undergo a transformation after which magnesium diphosphate dissociates from the active site and then HSEntB associates. Following a further chemical transformation, 2,3-dihydroxybenzoyl-SEntB dissociates from the active site before AMP^-. This order is consistent with the facts that when the initial concentration of 2,3-dihydroxybenzoate is varied at saturating concentrations of a truncated form of HSEntB that acts as a reactant and several fixed concentrations of $MgATP^{2-}$, the double reciprocals are a set of lines that intersect in the second quadrant. When, however, the initial concentration of either 2,3-dihydroxybenzoate or the initial concentration $MgATP^{2-}$ is varied at several fixed concentrations of the truncated form of HSEntB, when the other reactant is held at saturating concentrations the double reciprocals in each case are a set of parallel lines. That the dissociation of magnesium diphosphate is the only irreversible step separating the association of 2,3-dihydroxybenzoate and $MgATP^{2-}$ and the association of the truncated form of HSEntB, and is therefore responsible for these parallel double reciprocals, was demonstrated by showing that when magnesium diphosphate is

included in the solution, the double reciprocals become a set of intersecting lines.[145]

In both the reaction catalyzed by phosphopantothenate—cysteine ligase (CTP) and the reaction catalyzed by the product of the *entE* gene, a nucleoside triphosphate and a reactant with a carboxy group associate with the active site, and diphosphate dissociates before the third reactant associates. These kinetic observations in each case suggest that a covalent intermediate, an anhydride between the carboxy group and either a cytidylate or an adenylate, is formed on the active site by a nucleophilic substitution at the α phosphorus of the respective nucleoside triphosphate with the respective carboxylato group as the nucleophile and diphosphate as the leaving group. This intermediate anhydride, which is electrophilic and susceptible to nonenzymatic hydrolysis because the cytidylate or the adenylate is a good leaving group, is tightly held in the active site awaiting the association of the respective thiol to which the carboxy group is to be transferred in a second nucleophilic substitution.

If the reactants associate at random with the enzyme, then the patterns of the bireactant kinetics observed when any two are varied and the others are held at saturation will all be the same because all the reactants are equivalent as far as their association with the active site is concerned. For example, if there are four reactants (A, B, C, and D) and reactant C and reactant D are held at saturation, the unoccupied active site is converted completely into the complex E·C·D. A kinetically irreversible step is placed between the release of products and the association of reactant A and reactant B, but since at least one of the products must be absent, the dissociation of that product is already an irreversible step. The bireactant kinetics for variation in the initial concentrations of reactant A and reactant B and the effects of dead-end inhibitors will be those for the random addition of A and B to the enzyme. The same kinetic patterns will be observed when reactant A and reactant B are held at saturation and reactant C and reactant D are varied and so forth.

For example, for the reaction catalyzed by phosphoribosylaminoimidazolesuccinocarboxamide synthase from *E. coli*

$$\begin{aligned}&\text{5-amino-1-(5-phospho-D-ribosyl)imidazole-4-carboxylate} + \text{MgATP}^{2-} + \text{L-aspartate} \rightleftharpoons \\ &\text{MgADP}^{-} + \text{H}_2\text{OPO}_3^{-} + \\ &\text{(}S\text{)-2-[5-amino-1-(5-phospho-D-ribosyl)imidazole-4-carboxamido]succinate}\end{aligned} \tag{3–272}$$

when each of the reactants in turn was held at saturation, the initial rates as a function of the initial concentrations of the other two all showed intersecting patterns for the double reciprocals. The patterns of dead-end inhibition for each bireactant combination at saturation with the third were those expected for a kinetic mechanism in which the two reactants associate at random with the active site on the enzyme.[146] Consequently, all the observations together were consistent with a kinetic mechanism in which all three of the reactants combined with the enzyme at random.

When there are three or more products for an enzymatic reaction, **patterns of product inhibition** will suggest the order in which they dissociate (Table 3–2). For example, *S*-adenosylmethionine:tRNA ribosyltransferase-isomerase from *E. coli* catalyzes a reaction with two reactants and three products. It modifies 7-(aminomethyl)-7-deazaguanosine in a transfer RNA (preQ_1-tRNA) to produce epoxyqueuosine at that site in the transfer RNA (oQ-tRNA) in the reaction

$$\begin{aligned}&\text{preQ}_1\text{-tRNA} + \textit{S}\text{-adenosyl-L-methionine} \\ &\rightleftharpoons \text{adenine} + \text{L-methionine} + \text{oQ-tRNA}\end{aligned} \tag{3–273}$$

The patterns of product inhibition (Table 3–3) are consistent with a kinetic mechanism in which preQ_1-tRNA must associate with the enzyme before *S*-adenosyl-L-methionine, and adenine must dissociate before L-methionine, which must dissociate before oQ-tRNA. Were the association of reactants at random and the dissociation of products at random, each product the structure of which overlapped significantly the structure of one of the reactants would be competitive with respect to that reactant, which is not observed to be the case.

Table 3–3: Pattern of Product Inhibitions of *S*-Adenosylmethionine:tRNA Ribosyltransferase Isomerase from *E. coli*[147]

product inhibitor	varied reactant	status of fixed reactant	pattern of inhibition
adenine	preQ$_1$-tRNA	unsaturating	noncompetitive
	preQ$_1$-tRNA	saturating	uncompetitive
	S-adenosylmethionine	unsaturating	noncompetitive
methionine	preQ$_1$-tRNA	unsaturating	uncompetitive
	S-adenosylmethionine	unsaturating	noncompetitive
	S-adenosylmethionine	saturating	uncompetitive
oQ-tRNA	preQ$_1$-tRNA	unsaturating	competitive
	S-adenosylmethionine	unsaturating	noncompetitive

The foregoing discussion has substantiated two features of steady-state kinetics. First, any step in the kinetic mechanism of the enzymatic reaction that involves the association of a substrate with the enzyme, or the dissociation of a substrate from the enzyme, is ultimately responsible for the variations in initial rate that are observed when the initial concentration of that substrate is varied. Because of this fact, **steady-state kinetics elucidate details of only the association and dissociation of substrates**. Second, any step following the assembly of all the reactants on the active site and preceding the release of the first product from the active site cannot be studied in isolation by steady-state kinetics because the rate constants for these steps are accumulated into composite rate constants and do not affect the form of the rate equation for the initial rate or the patterns of any inhibitions.

For such kinetically silent steps, steady-state kinetics provide only a value for a composite rate constant. The catalytic constant k_0 is usually such a composite rate constant and registers the overall rate of transformation of reactants into products, usually through several elementary steps, and the rates of dissociation of the products because the reaction is not limited by the rates at which the reactants associate with the active site. This property of the catalytic constant results from the fact that, at saturation, the initial concentrations of reactants are so high that their association with the active site is more rapid than those steps that do not involve their association.

Once these two aspects of steady-state kinetics have been understood, a **notation that is used to represent the only conclusion of a kinetic study** can be appreciated. A horizontal line is drawn that represents the progress of the enzymatic reaction. Vertical arrows above the horizontal line and joined to it connect each substrate to the horizontal line. An arrow entering the line indicates a reactant associating with the active site; an arrow exiting the line indicates a product dissociating from the active site. The order in which the arrows are drawn indicates the order in which substrates associate with or dissociate from the enzyme. For example, for the D-lactate dehydrogenase from *S. toyocaensis* (Equation 3–249), the notation would be

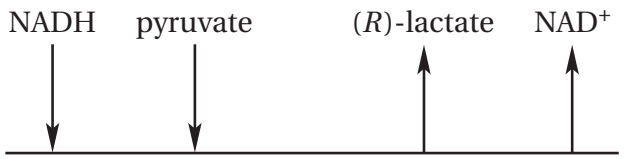

(3–274)

and for ovine 3-oxoacid CoA-transferase (Equation 3–149) the notation would be

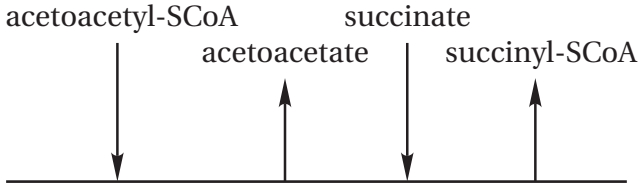

(3–275)

If the order is random, the horizontal line is bifurcated. For example, for human phosphoinositide-dependent protein kinase (Equation 3–225) the notation would be

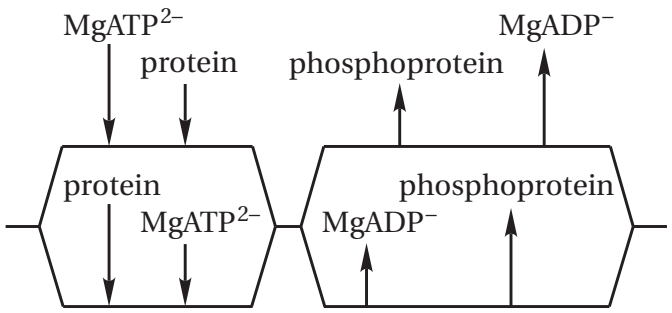

(3–276)

By microscopic reversibility, it must be the case that, in the reverse direction, the arrows are simply reversed, and the relative order of events must be the exact opposite of that in the forward direction.

In addition, however, to determining the order in which reactants associate with the active site and products dissociate from the active site, steady-state kinetics also **provide numerical values for the catalytic constant, the various specificity constants, and hence the various Michaelis constants**. These kinetic constants are **fundamental constants** describing a particular enzymatic reaction, and they are relied upon for, among others, comparisons of various reactants, comparisons of various site-directed mutants, and comparisons of the same enzyme from different species. For example, the fact that the catalytic constant and the specificity constant for a mismatched pair of nucleotide bases between the template and the 2′-deoxynucleoside triphosphate that is adding to the elongating strand of DNA are 0.02 s^{-1} mM^{-1} and 0.14 s^{-1}, respectively, while the catalytic constant and specificity constant for a matched pair are 15,000 s^{-1} mM^{-1} and 300 s^{-1}, respectively, dramatically demonstrates the fidelity of the active site of DNA-directed DNA polymerase from Escherichia phage T7 while it is replicating DNA.[148]

Suggested Reading

Cleland, W. W. (1963) The kinetics of enzyme-catalyzed reactions with two or more substrates or products: I. Nomenclature and rate equations, *Biochim. Biophys. Acta 67*, 104–137. https://doi.org/10.1016/0926-6569(63)90211-6

Munagala, N. R., Chin, M. S., and Wang, C. C. (1998) Steady-state kinetics of the hypoxanthine-guanine-xanthine phosphoribosyltransferase from *Tritrichomonas foetus*: the role of Threonine-47, *Biochemistry 37*, 4045–4051. https://doi.org/10.1021/bi972515h

Niu, L., Chang, K. C., Wilson, S., Tran, P., Zuo, F., and Swinney, D. C. (2007) Kinetic characterization of human JNK2α2 reaction mechanism using substrate competitive inhibitors, *Biochemistry 46*, 4775–4784. https://doi.org/10.1021/bi602423e

Eddershaw, A. R., Stubbs, C. J., Edwardes, L. V., Underwood, E., Hamm, G. R., Davey, P. R. J., Clarkson, P. N., and Syson, K. (2020) Characterization of the kinetic mechanism of human protein arginine methyltransferase 5, *Biochemistry 59*, 4775–4786. https://doi.org/10.1021/acs.biochem.0c00554

Problem 3–5: Porcine fumarate hydratase (FH) catalyzes the hydration of fumarate to L-malate (Equation 3–1). The following data were obtained when fumarate was used as the reactant and the initial rate of the hydration reaction was measured at pH 6.2 and 25 °C, and a concentration of active sites of 8 μM.

fumarate (mM)	rate of formation of malate (mmol L^{-1} min^{-1})
2.0	2.5
3.3	3.1
5.0	3.6
10.0	4.2

When the same reaction was studied in a buffer containing 0.06 M phosphate, at the same pH and concentration of enzyme, the following data were obtained.

fumarate (mM)	rate of formation of malate (mmol L^{-1} min^{-1})
2.0	4.0
3.3	5.0
5.0	5.8
10.0	6.6

(A) Determine the value of the observed catalytic constant, $k_{0,F}$, and the observed specificity constant for fumarate, k_F, for the two conditions listed. Analyze and discuss briefly any significant differences.

The Haldane equation for an enzymatically catalyzed reaction with a single reactant A and a single product Z relates the specificity constant k_A and the specificity constant k_Z for the forward and the reverse reaction, respectively, to the equilibrium constant for the reaction K_{eq}

$$K_{eq} = \frac{k_A}{k_Z}$$

The initial rates of the hydration reaction catalyzed by fumarate hydratase at 25 °C were measured as a function of pH and for various initial concentrations of fumarate and an enzyme concentration of 2×10^{-6} M. The values obtained, expressed as millimoles of malate $liter^{-1}$ $minute^{-1}$, were as follows.

	concentration of fumarate (mM)			
pH	10	5	2.5	1.25
5	0.92	0.81	0.66	0.48
6	4.00	3.28	2.42	1.60
7	5.40	4.30	3.08	1.96
8	2.67	2.40	1.99	1.53
9	0.21	0.17	0.16	0.12

The values of the limiting rate for the dehydration of L-malate ($k_{0,M}[FH]_t$), catalyzed by fumarate hydratase under the same conditions, had the following dependence on pH.

pH	$k_{0,M}[FH]_t$ for malate (mmol L^{-1} min^{-1})
5	0.068
6	0.044
7	3.00
8	5.88
9	2.00

The overall equilibrium constant for the reaction, K_{eq}, is independent of pH over the range from pH 5 to 9 and has a value of 4.7.

(B) Determine values for the observed catalytic constant, $k_{0,F}$, and the observed specificity constant for fumarate, k_F, for the hydration reaction at each value of pH.

(C) Calculate the values of the observed specificity constant for malate, k_M, for the dehydration reaction at each value of pH.

The decrease in the concentration of fumarate due to its hydration to D,L-malate was measured at pH 5.7 and 25 °C in the absence of enzyme.

fumarate (mM)	time (h)
20.0	0
19.1	20
18.3	40
17.5	60
16.7	80

(D) Compare the initial rate constant for this reaction with the catalytic constant for the catalyzed reaction and calculate the factor by which the rate of the hydration reaction is increased when the reactants are bound to the active site of the enzyme.

Problem 3–6: Derive the rate equations for the kinetic mechanisms in Equations 3–55, 3–84, 3–85, 3–91, 3–109, 3–121, 3–134, 3–141, 3–154, 3–183, 3–194, 3–210, 3–223, and 3–237.

Problem 3–7: Derive the rate equation for the kinetic mechanism

$$\mathrm{E + A + B} \underset{k_{-1}}{\overset{k_1}{\rightleftharpoons}} \mathrm{E{\cdot}A + B} \underset{k_{-2}}{\overset{k_2}{\rightleftharpoons}} \mathrm{E{\cdot}A{\cdot}B} \underset{k_{-3}}{\overset{k_3}{\rightleftharpoons}} \mathrm{E{\cdot}Z{\cdot}Y} \xrightarrow{k_4} \mathrm{E + Y + Z}$$

Problem 3–8: Hexokinase (HK) catalyzes the reaction in Equation 3–94. Magnesium ion, Mg^{2+}, is required for the enzymatic reaction. Magnesium dication forms complexes with the various conjugate bases of ATP

$$\mathrm{Mg^{2+} + H}_n\mathrm{ATP}^{(4-n)-} \rightleftharpoons \mathrm{MgH}_m\mathrm{ATP}^{(2-m)-} + (n-m)\mathrm{H^+}$$

where H_n and H_m are the numbers of hydrons on the free phosphotriester of ATP and the chelated phosphotriester, respectively. The values for these numbers depend on the pH. The values for the dissociation constants of these various complexes have been measured as a function of pH. At a particular pH, at any total concentration of Mg^{2+} in all its complexes, and at any total concentration of ATP in all its complexes, the following concentrations can be calculated: the total molar concentration of MgATP, $[MgATP]_t$, which is the total concentration of ATP in all hydronation states that is complexed with Mg^{2+}, and the total molar concentration of ATP, $[ATP]_t$, which is the total concentration of ATP in all hydronation states that is not complexed with Mg^{2+}. In this way the molar concentrations of MgATP and ATP can be varied independently. When $[ATP]_t$ was fixed and $[MgATP]_t$ was varied systematically, v_0^{-1} was a linear function of $[MgATP]_t^{-1}$. When $[ATP]_t$ was changed to a higher fixed level, the initial rate v_0 of hexokinase from *R. norvegicus* decreased at every $[MgATP]_t$, but the limiting rate, $k_0[HK]_t$, for $[MgATP]_t$ was unchanged (Figure 3–11A). How do these results define what is the actual reactant and what is an inhibitor of the enzymatic reaction? What type of inhibitor is it?

Problem 3–9: Procollagen-lysine 5-dioxygenase catalyzes the reaction

$$\text{lysyl peptide} + \text{2-oxoglutarate} + \mathrm{O_2} \rightleftharpoons (2S,5R)\text{-5-hydroxylysyl peptide} + \text{succinate} + \mathrm{CO_2}$$

Although it is not a participant in the stoichiometric reaction, ascorbate (Equation 2–163) and Fe^{2+} are required to maintain the iron in the enzyme in the ferrous form. When the concentration of ascorbate is varied at a fixed concentration of any one of the three stoichiometric reactants and saturating concentrations of the other two, the reciprocal of the initial rate, v_0^{-1}, for the enzyme from *G. gallus* is a linear function of $[\text{ascorbate}]_0^{-1}$. If the fixed substrate is set at other concentrations, the lines defined by the data are all parallel.[149] For example, if lysyl peptide is the fixed substrate and oxygen and 2-oxoglutarate are always saturating

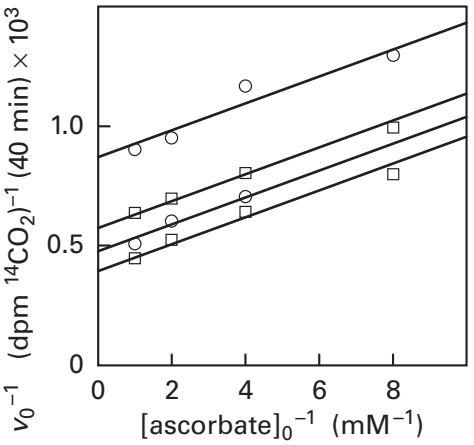

Behavior of the initial rate of the reaction catalyzed by procollagen-lysine 5-dioxygenase from *G. gallus* as a function of the initial concentrations of ascorbate and a peptide oxidized by the enzyme. The enzymatic reaction was assayed by using 2-oxo-[1-^{14}C]glutarate as a reactant and following the production of $^{14}CO_2$. The initial rates are the disintegrations per minute of $^{14}CO_2$ produced over 40 min at 37 °C. The reciprocals of the initial rates of the reaction, v_0^{-1}, are plotted as a function of the reciprocals of the initial concentrations of ascorbate (millimolar^{-1}) at different fixed concentrations of the peptide substrate.[149] The concentrations of the lysyl peptide were 0.1, 0.15, 0.2, and 0.75 mg mL^{-1} for the lines in descending order. The concentration of Fe^{2+} was 0.05 mM, and that of 2-oxo-[1-^{14}C]glutarate was 0.1 mM.

(A) What do these kinetic observations say about the relation between the lysyl peptide and ascorbate?
(B) Because the same type of behavior is observed between each of the other two stoichiometric reactants and ascorbate, what do these kinetic observations say about the relation between each of these other reactants and ascorbate?
(C) Explain this kinetic behavior on the basis of the role of ascorbate in the enzymatic reaction.
(D) Write a kinetic mechanism based on this explanation.

Problem 3–10: Derive the rate equation for the following kinetic mechanism.

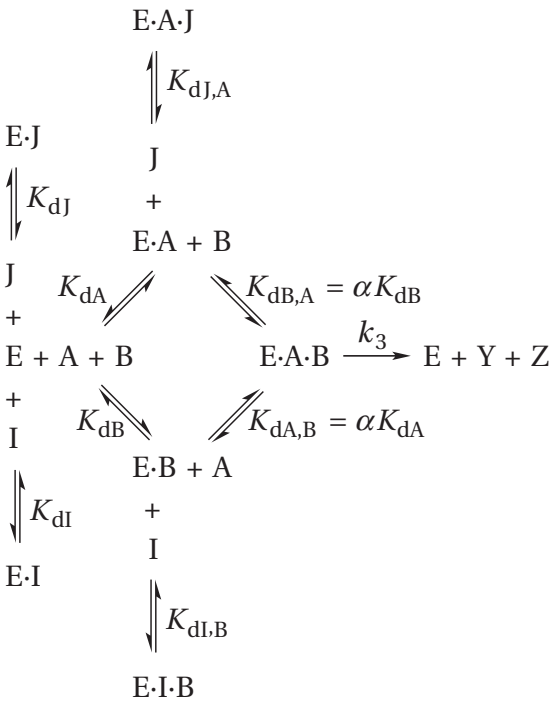

Note that all the reactions preceding the reaction governed by k_3 are at equilibrium. Inhibitor I prevents reactant A from binding to the enzyme, and inhibitor J prevents reactant B from binding to the enzyme.

(A) What type of inhibition does inhibitor I display with respect to reactant A, and what type does it display with respect to reactant B?
(B) What type of inhibition does inhibitor J display with respect to reactant A, and what type does it display with respect to reactant B?

Problem 3–11: Suppose there is an enzyme that catalyzes the reaction A + B $\rightleftharpoons$ Y + Z. Suppose reactant A has to bind to the active site before reactant B can bind, and reactant B has to bind before products are formed. Suppose there were an inhibitor I that, like reactant B, could bind to the active site only after reactant A was bound.

(A) Write a kinetic mechanism describing both the enzymatic reaction and its inhibition by the inhibitor I.
(B) Show that the rate equation for the initial rate for this kinetic mechanism is

$$v_0 = \frac{k_0 k_A k_B k_{AB} [E]_t [A]_0 [B]_0}{k_0 k_A k_B + k_0 k_A k_{AB} \left(\frac{[I] + K_i}{K_i} \right) [A]_0 + k_0 k_B k_{AB} [B]_0 + k_A k_B k_{AB} [A]_0 [B]_0}$$

where K_i is an inhibition constant.

(C) If this were the kinetic mechanism, what would k_0, k_A, k_B, and k_{AB} be equal to in terms of the rate constants in your kinetic mechanism in (A)?
(D) If this mechanism were the actual kinetic mechanism, what dissociation constant would K_i be equal to in terms of your kinetic mechanism in (A)?
(E) What would plots of v_0^{-1} against $[A]_0^{-1}$ at constant $[B]_0$ and several fixed [I] look like?
(F) What would plots of v_0^{-1} against $[B]_0^{-1}$ at constant $[A]_0$ and several fixed [I] look like?

Glycerol kinase catalyzes the reaction

$$\text{glycerol} + \text{MgATP}^{2-} \rightleftharpoons \text{MgADP}^{-} + \textit{sn}\text{-glycerol 3-phosphate}$$

(G) Write a chemical mechanism for this reaction.

The chromium complex of ATP, $CrATP^{-}$, cannot be used by the enzyme as a reactant in the glycerol kinase reaction because the chromium–oxygen bonds are too strong, but it is a potent inhibitor of the enzyme.

Examine Figure 3–12 and the following figure.

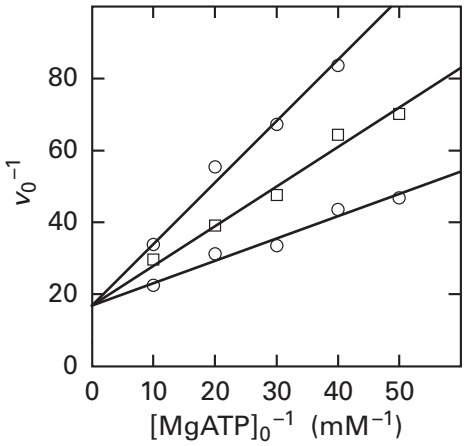

Inhibition of the reciprocal of the initial rate v_0^{-1} for glycerol kinase from *C. norvegensis* by $CrATP^{-}$ as a function of the initial concentration of $MgATP^{2-}$. The concentration of glycerol was held constant at 5 mM throughout.[100] The concentrations of $CrATP^{-}$ were 0, 5, and 10 μM for the lines in ascending order.

(H) On the basis of these results, which of the reactants for glycerol kinase binds first to the active site?

Problem 3–12: 1-Deoxy-D-xylulose-5-phosphate synthase catalyzes the thiamine diphosphate-dependent reaction

$$H^+ + \text{pyruvate} + \text{D-glyceraldehyde 3-phosphate} \rightleftharpoons \text{1-deoxy-D-xylulose 5-phosphate} + CO_2$$

3-Fluoropyruvate is a competitive inhibitor of the enzyme from *R. capsulatus* with respect to pyruvate and an uncompetitive inhibitor with respect to D-glyceraldehyde 3-phosphate.[92] What do these results suggest about the order in which the reactants associate with the enzyme?

Problem 3–13: Pyruvate, phosphate dikinase catalyzes the reaction

$$\text{phospho}\textit{enol}\text{pyruvate} + MgOPO_3PO_3^{2-} + H^+ + AMP^{2-} \rightleftharpoons MgATP^{2-} + HOPO_3^{2-} + \text{pyruvate}$$

The following results were observed for inhibition of the enzyme from *Clostridium symbiosum* by the dead-end inhibitors adenosine 5′-monophosphorothioate ($AMPS^{2-}$) and magnesium imidodiphosphate ($MgOPO_2NHPO_3H^-$; MgPNP) when each of the respective unnamed reactants were held at saturation.

inhibitor	varied reactant	type of inhibition
AMPS	MgAMP	competitive
AMPS	$MgOPO_3PO_3^{2-}$	mixed
AMPS	phospho*enol*pyruvate	uncompetitive
PNP	$MgOPO_3PO_3^{2-}$	competitive
PNP	phospho*enol*pyruvate	uncompetitive
PNP	MgAMP	uncompetitive

(A) With what order of association for the three reactants is this pattern of dead-end inhibition consistent?

When initial rates for the reaction were measured at saturating concentrations of phospho*enol*pyruvate, the initial concentration of AMP^{2-} was varied at several fixed initial concentrations of $MgOPO_3PO_3^{2-}$, and the initial concentration of $MgOPO_3PO_3^{2-}$ was varied at several fixed initial concentrations of AMP^{2-}; in both cases, the double reciprocals were intersecting. When the initial rates were measured at saturating concentrations of AMP^{2-}, the initial concentration of $MgOPO_3PO_3^{2-}$ was varied at several fixed initial concentrations of phospho*enol*pyruvate, and the initial concentration of phospho*enol*pyruvate was varied at several fixed initial concentrations of $MgOPO_3PO_3^{2-}$; in both cases, the double reciprocals were parallel. When the initial rates were measured at a fixed subsaturating concentration of $MgOPO_3PO_3^{2-}$, the initial concentration of phospho*enol*pyruvate was varied at several fixed concentrations of AMP^{2-}, and the initial concentration of AMP^{2-} was varied at several fixed concentrations of phospho-*enol*-pyruvate; in both cases, the lines fitting the double reciprocals were parallel.[150]

(B) What do these results say about the steps between the associations of the three reactants?

(C) What observation, which would resolve an ambiguity about one of the steps between the associations of two of the reactants, is missing?

Problem 3–14: The flavoenzyme thymidylate synthase (FAD) from *Chlamydia trachomatis* catalyzes the reaction

$$\begin{aligned}&\text{5,10-methylenetetrahydrofolate} + \\ &\quad \text{NADPH} + \text{H}^+ + \text{dUMP}^{2-} \rightleftharpoons \\ &\qquad \text{dTMP}^{2-} + \text{tetrahydrofolate} + \text{NADP}^+\end{aligned}$$

When NADPH is held at saturating concentration and deoxyuridine 5′-phosphate is varied at several fixed concentrations of 5,10-methylenetetrahydrofolate, the double reciprocals of the initial rates are parallel lines. When NADPH is saturating, deoxythymidine 5′-phosphate is noncompetitive with respect to deoxyuridine 5′-phosphate and competitive with respect to 5,10-methylenetetrahydrofolate, and tetrahydrofolate is noncompetitive with respect to 5,10-methylenetetrahydrofolate and competitive with respect to deoxyuridine 5′-phosphate.[151] Write a kinetic mechanism for the enzyme that is consistent with these observations.

Problem 3–15: The enzyme adenine phosphoribosyltransferase catalyzes the reaction

$$\begin{aligned}&\text{magnesium 5-phospho-}\alpha\text{-D-ribose 1-diphosphate} \\ &\quad + \text{adenine} \rightleftharpoons \text{AMP}^{2-} + \\ &\quad \text{H}^+ + \text{magnesium diphosphate}\end{aligned}$$

The double-reciprocal plots of v_0^{-1} as a function of either $[\text{adenine}]_0^{-1}$ or $[\text{5-phospho-}\alpha\text{-D-ribose 1-diphosphate}]_0^{-1}$ at several fixed initial concentrations of either magnesium 5-phospho-α-D-ribose 1-diphosphate or adenine were sets of parallel lines as in Figure 3–8.

(A) Show that these data can be fit by the function

$$v_0 = \frac{k_0 k_{\text{Ad}} k_{\text{PRPP}} [\text{E}]_t [\text{Ad}]_0 [\text{PRPP}]_0}{k_0 k_{\text{PRPP}} [\text{PRPP}]_0 + k_0 k_{\text{Ad}} [\text{Ad}]_0 + k_{\text{Ad}} k_{\text{PRPP}} [\text{Ad}]_0 [\text{PRPP}]_0}$$

where $[\text{Ad}]_0$ is the initial molar concentration of adenine and $[\text{PRPP}]_0$ is the initial molar concentration of magnesium 5-phospho-α-D-ribose 1-diphosphate.

(B) Write the kinetic mechanism usually associated with this rate equation.

(C) For this kinetic mechanism to be correct, what type of inhibition must adenosine 5′-phosphate display toward magnesium 5-phospho-α-D-ribose 1-diphosphate?

(D) For this kinetic mechanism to be correct, what type of inhibition must magnesium diphosphate display toward adenine?

(E) Adenosine 5′-phosphate is a competitive inhibitor relative to magnesium 5-phospho-α-D-ribose 1-diphosphate, and magnesium diphosphate is a noncompetitive inhibitor relative to adenine.[152] Do these observations match your expectations?

(F) Derive the initial rate equation for the following kinetic mechanism

$$\begin{aligned}&\text{E} + \text{PRPP} + \text{Ad} \underset{k_{-1}}{\overset{k_1}{\rightleftharpoons}} \text{E·PRPP} + \text{Ad} \underset{k_{-2}}{\overset{k_2}{\rightleftharpoons}} \\ &\qquad \text{E·PRPP·Ad} \xrightarrow{k_3} \text{E} + \text{AMP} + \text{PP}\end{aligned}$$

where PP is magnesium diphosphate.

(G) Show how this equation can assume the form of the rate equation in part A if two reasonable inequalities hold.

Problem 3–16: When methylmalonyl-CoA mutase (Table 2–3), which contains [5′-^{3}H]adenosylcobalamin as a prosthetic group, is mixed with methylmalonyl-SCoA and the reaction is allowed to proceed for 5 s, all the tritium is washed out of adenosylcobalamin and is transferred to methylmalonyl-SCoA and succinyl-SCoA in a ratio of 1 to 3. When methylmalonyl-CoA mutase that contains [5′-^{3}H]adenosylcobalamine is mixed with succinyl-SCoA and the reaction allowed to proceed for 5 s, all the tritium is again washed out of the adenosylcobalamin and is transferred to methylmalonyl-SCoA and succinyl-SCoA in the same ratio of 1:3.[153] Explain these results in terms of the simplest kinetic mechanism consistent with them and the rate-limiting steps and an intermediate equilibrium common to both of these reactions.

Problem 3–17: The fatty-acid synthase system, a multienzymatic complex, catalyzes the reaction

$$\begin{aligned}&\text{acetyl-SCoA} + n\text{-malonyl-SCoA} + 2n\,\text{NADPH} \\ &\quad + (3n-1)\,\text{H}^+ \rightleftharpoons 2n\,\text{NADP}^+ + n\,\text{CO}_2 + \\ &\quad (n+1)\,\text{HSCoA} + \text{CH}_3(\text{CH}_2\text{CH}_2)_n\text{COO}^-\end{aligned}$$

When the initial rate of the reaction at fixed concentrations of malonyl-SCoA and NADPH was fol-

lowed as a function of the concentration of acetyl-SCoA for the enzyme from *Columba livia*, the following behavior was observed.[154]

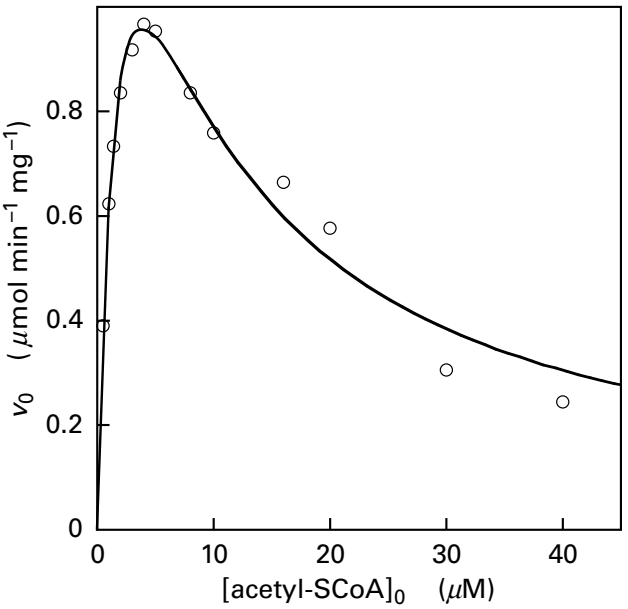

Initial rate of fatty acid synthesis v_0, in units of micromoles of NADPH oxidized minute^{-1} (milligram of protein)$^{-1}$, as a function of the initial concentration of acetyl-SCoA (micromolar). The reactions were run in 0.2 M phosphate buffer at pH 7.0. The concentrations of the other reactants were 10 μM malonyl-SCoA and 30 μM NADPH. Rates were followed spectrophotometrically with a 5 cm cell.

The inhibition observed at high concentrations of acetyl-SCoA decreases as the concentration of malonyl-SCoA is raised. Explain both the observed behavior of the initial rate as a function of the initial concentration of acetyl-SCoA and the decrease in inhibition as the concentration of malonyl-SCoA is raised. Why is this explanation reasonable?

Binding

Historically, it was the analysis of steady-state kinetics that led to the conclusion that reactants are assembled at an active site on an enzyme before they are transformed into products. It is now abundantly clear that reactants associate with the enzyme within an active site on the surface or in the interior of a protomer of the enzyme prior to the chemical interconversion between reactants and products within that active site and the subsequent dissociation of the products. If the association or dissociation of each substrate can be treated as a discrete step in an enzymatic reaction, then each of these steps involving only association and dissociation should be no different from the **association and dissociation that accomplishes reversible binding** of any small molecule, or ligand, to a particular site on a molecule of protein. Only what follows the association or precedes the dissociation makes the difference between the complex of a ligand with a site that is not an active site and the complex of a substrate with an active site.

A **ligand** is any molecule that binds to but is not chemically transformed by a protein. The lack of chemical transformation distinguishes a ligand from a substrate. An **agonist** is a ligand, either one that is endogenous to the organism in which the protein is found or a synthetic compound, that binds to a protein and, upon binding, produces a measurable change in the characteristic physiological function of that protein and accomplishes the normal response of that protein to the endogenous agonist. An **antagonist** is a ligand that binds to a protein, does not elicit this characteristic change in its function that is normally produced by an agonist, but blocks the ability of an agonist to effect that change. An **inhibitor** or an **activator** is a ligand that binds to an enzyme and forms a dead-end complex with a rate of catalysis that is smaller or larger, respectively. An inhibitor or an activator can form a complex either within the active site of an enzyme or at sites other than its active site. Inorganic anions, inorganic cations, and hydrophobic molecules that bind adventitiously to a protein are also examples of ligands.

Usually, one molecule of a ligand will associate specifically with a particular constellation of amino acids on the surface or in the interior of a protein, and because of symmetry, the number of those sites for binding that ligand on the protein will be equal to the number of protomers it contains. Usually, each of the symmetrically arrayed sites in a homooligomer will bind the ligand independently. In this situation, **the molar concentration of sites in a particular solution is equal to the molar concentration of native, properly folded protomers**. If, however, the site for the ligand is on an axis of symmetry and involves side chains of amino acids from two protomers, there will be half as many sites as protomers because there will be only one site for every dimer of protomers.

The binding of a ligand, L, to a site, ST, on a protein to form a specific complex, ST·L, is quantitatively described by a **dissociation constant**

$$K_{dL} = \frac{a_{ST}\, a_L}{a_{ST\cdot L}} \qquad (3\text{–}277)$$

where a_i is the activity of component i at equilibrium. In terms of molar concentrations

$$K_{dL} = \left(\frac{\gamma_{ST}\, \gamma_L}{\gamma_{ST\cdot L}}\right)\left(\frac{[ST]_{eq}\,[L]_{eq}}{[ST\cdot L]_{eq}}\right) \qquad (3\text{–}278)$$

where γ_i is the activity coefficient of component i, the subscript eq refers to molar concentrations at equilibrium, and $[L]_{eq}$ is the concentration of free, unbound ligand at equilibrium. If the actual molar concentrations of the various participants are low when the measurement is made, which is usually the case with biochemical measurements, and if the solution has an ionic strength of 0.1 M or greater, which is usually the case with experimental measurements, then the ratio of the activity coefficients is usually close enough to unity to be ignored. The dissociation constant, because it is an equilibrium constant, is **directly related to the standard free energy change for the dissociation** of the ligand from the protein. As an equilibrium constant, it must be distinguished from a kinetic parameter such as the Michaelis constant, K_m, which is rarely related directly to a thermodynamic variable.

The dissociation constant for the binding between a ligand and a site on a molecule of protein can be **determined directly from experimental observations**. In any solution in which the population of sites for the ligand is homogeneous, the dissociation is governed by the simple equation

$$K_{dL} = \frac{[ST]_{eq}\,[L]_{eq}}{[ST\cdot L]_{eq}} \qquad (3\text{–}279)$$

If all the sites are functional, the concentration of bound ligand at equilibrium is equal to

$$[ST\cdot L]_{eq} = \frac{[ST]_t\,[L]_{eq}}{K_{dL} + [L]_{eq}} \qquad (3\text{–}280)$$

where $[ST]_t$ is the total molar concentration of sites, both occupied and unoccupied. This equation has the form of the function defining a rectangular hyperbola with a horizontal asymptote (Equation 3–52) if the **concentration of protein**, and hence $[ST]_t$, **is fixed** at a constant value during the experimental measurements.

It is often not possible, however, to fix the concentration of sites at a constant value because unavoidable changes in volume occur during the experimental procedure[155] or because the experimental protocol itself requires the concentration of sites to be varied. It can be assumed, however, that for a given set of sites

$$C_{prot} = \frac{[ST]_t}{\kappa} \qquad (3\text{–}281)$$

where C_{prot} **is the concentration of protein expressed in any known units and** κ **is a constant of proportionality**. If the concentration of protein in each sample is known in grams liter^{-1}, the units of the constant of proportionality κ are moles of sites (gram of protein)$^{-1}$. To learn this number is often one of the goals of the experiment. If the concentration of protein in each sample is known in moles of protomer liter^{-1}, the constant of proportionality κ is unitless and equal to the fraction of the protomers in the solution that are competent to bind the ligand, which is also informative.

If the **concentration of protein is varied** as the measurements are made, then Equation 3–280 can be rewritten

$$\frac{[ST\cdot L]_{eq}}{C_{prot}} = \frac{\kappa\,[L]_{eq}}{K_{dL} + [L]_{eq}} \qquad (3\text{–}282)$$

This equation defines a rectangular hyperbola (Equation 3–52) in the free concentration of ligand, $[L]_{eq}$, regardless of the variations in the concentration of protein, C_{prot}. The parameters of that rectangular hyperbola are the constant of proportionality, κ, and K_{dL}. Regardless of the total concentration of sites and the total concentration of ligand, if values for $[L]_{eq}$ and $[ST\cdot L]_{eq}\,(C_{prot})^{-1}$ are known, they define the same rectangular hyperbola. For example, the binding of 5-phospho-α-D-ribose 1-[β-^{32}P]diphosphate to orotate phosphoribosyltransferase (Equation 3–227) from *S. typhimurium* can be followed by adding increasing amounts of phosphoribosyl [β-^{32}P]diphosphate to a series of samples each containing the same concentration of orotate phosphoribosyltransferase. Following equilibration, the free concentration of 5-phospho-α-D-ribose 1-[β-^{32}P]diphosphate in each sample, $[PRPP]_{eq}$, can be assessed

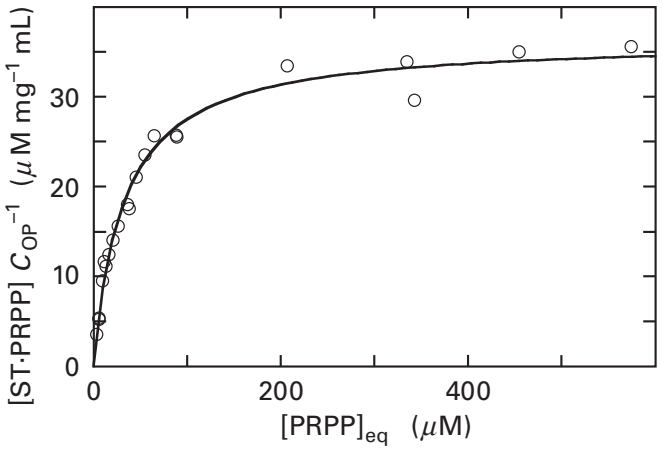

Figure 3–17: Binding of 5-phospho-α-D-ribose 1-[β-^{32}P]diphosphate to orotate phosphoribosyltransferase from *S. typhimurium*.[136] Various amounts of 5-phospho-α-D-ribose 1-[β-^{32}P]diphosphate (PRPP) were added to solutions of orotate phosphoribosyltransferase (OP) in 5 mM $MgCl_2$ and 80 mM 2-amino-2-(hydroxymethyl)propane-1,3-diol chloride at pH 8.0. After 10 min, the samples were added to Centricon centrifugation tubes. The tubes were submitted to centrifugation until 50–100 μL of fluid had emerged from each of them. The protein remained entirely in the tube, so the fluid that emerged contained only free 5-phospho-α-D-ribose 1-[β-^{32}P]diphosphate at the same concentration as the free concentration in the tube at equilibrium. Its concentration was determined by scintillation counting. The amount of bound 5-phospho-α-D-ribose 1-[β-^{32}P]diphosphate ([ST·PRPP]) was calculated by subtracting the free concentration from the total concentration of 5-phospho-α-D-ribose 1-[β-^{32}P]diphosphate in the tube. The nominal molar concentration of the dimeric enzyme was varied in the range from 3 to 150 μM to ensure that the free concentration of substrate and the bound concentration of substrate would always be of the same order of magnitude so that a statistically significant difference between the two measurements could be obtained. The concentration of bound phosphoribose diphosphate (micromolar) divided by the concentration of enzyme (milligrams of protein milliliter^{-1}) is presented as a function of the concentration of 5-phospho-α-D-ribose 1-diphosphate (micromolar). The curves drawn are fits of Equation 3–52 to the data with x equal to [PRPP]$_{eq}$ and y equal to [ST·PRPP] C_{OP}^{-1}. The dissociation constant for 5-phospho-α-D-ribose diphosphate (parameter b in Equation 3–52) is 32 ± 2 μM, and the micromoles of sites (gram of protein)$^{-1}$ (parameter a in Equation 3–52) is 36.4 ± 0.8 μM mg^{-1} mL, which is equivalent to 28 g of protein (mmol of sites)$^{-1}$. The molar mass of a subunit of the dimeric protein is 23.45 g mmol^{-1}.

by ultrafiltration, and the concentration of 5-phospho-α-D-ribose 1-[β-^{32}P]diphosphate bound by the sites on the protein in each sample, [ST·PRPP]$_{eq}$, can be assessed by the difference between the total concentration and the free concentration of the ligand

$$[ST{\cdot}L]_{eq} = [L]_t - [L]_{eq} \qquad (3–283)$$

The molar concentration of bound 5-phospho-α-D-ribose 1-[β-^{32}P]diphosphate divided by the concentration of enzyme as function of the molar concentration of free 5-phospho-α-D-ribose 1-[β-^{32}P]diphosphate at equilibrium in the solution before ultrafiltration (Figure 3–17)[136] satisfies Equation 3–282.

To perform a direct determination of the binding of a ligand to a protein, simultaneous measurements at equilibrium must be made of the molar concentration of bound ligand, [ST·L]$_{eq}$, and the molar concentration of free ligand, [L]$_{eq}$, in several samples of known protein concentration, C_{prot}, at a number of different concentrations of free ligand (Figure 3–17). There are several ways to accomplish this feat.

Semipermeable membranes are polymer films that have pores large enough to permit small ligands to pass through them but too small to permit the passage of macromolecules such as proteins, polysaccharides, or nucleic acids. There are a number of ways to use these membranes to measure the binding of a ligand to a protein.

In one approach, the protein is placed on one side of a semipermeable membrane separating two compartments, ligand is added to both compartments, and the system is allowed to reach equilibrium. At equilibrium, in the absence of ionic imbalances because the ionic strength of the solutions is appropriate, the molar concentration of the ligand in the compartment without the protein will be equal to [L]$_{eq}$, and the total molar concentration, [L]$_t$, of the ligand in the compartment containing the protein will be [L]$_{eq}$ + [ST·L]$_{eq}$ (Figure 3–18).[156] The final concentration of protein in its compartment at equilibrium is measured independently.[155] This technique is referred to as **equilibrium dialysis**.[157,158]

In the next approach, a known concentration of protein, C_{prot}, and a known concentration of ligand, [L]$_t$, are placed in a compartment on one side of a semipermeable membrane, and the compartment on the other side is flushed continuously with a solution that does not contain the protein or the ligand. The unidirectional rate at which the ligand passes through the semipermeable membrane is directly proportional to its free concentration, [L]$_{eq}$, on the side from which it is leaving.[159] This **rate of dialysis** is measured by monitoring the amount of ligand appearing in the flushing solution as a function of time. If the chamber and the dialysis membrane are calibrated with known concentrations of

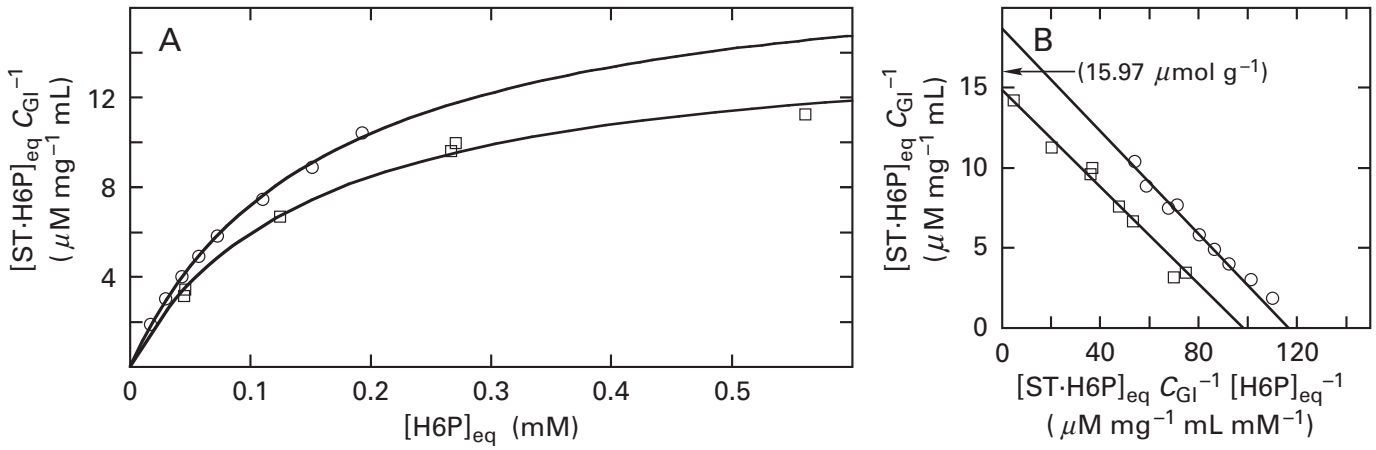

Figure 3–18: Measurement of the binding of an equilibrium mixture of [U-^{14}C]-D-glucose 6-phosphate and [U-^{14}C]-D-fructose 6-phosphate to glucose-6-phosphate isomerase from rabbit muscle by equilibrium dialysis and rate of dialysis.[156] For the measurements by equilibrium dialysis, a series of apparatuses separating two chambers by a dialysis membrane was used. In one chamber of each apparatus, D-glucose-6-phosphate isomerase (10.0 mg mL^{-1}) was present; in the other, buffer alone. [U-^{14}C]-D-Glucose 6-phosphate was added to both sides and allowed to reach equilibrium with fructose 6-phosphate as well as reach equilibrium across the membrane. The concentration of hexose 6-phosphate in the side lacking enzyme is the free concentration of the substrates in both chambers; the concentration of hexose 6-phosphate in the side containing the protein is the sum of free and bound concentrations of the substrates. For the measurements by rate dialysis, an apparatus separating two chambers by a dialysis membrane was used. The enzyme (6.6 mg mL^{-1}) in a buffer at pH 8.0 and 22 °C was in the upper chamber (1 mL). The lower chamber was a spiral groove, in contact with the membrane, through which solution was pumped at a steady rate (4 mL min^{-1}). [U-^{14}C]-D-Glucose 6-phosphate was added at a low concentration to the upper chamber, and the rate at which carbon-14 appeared in the lower chamber was determined by submitting the constantly flowing solution to scintillation counting. When equilibrium had been reached, the concentration of [U-^{14}C]-D-glucose 6-phosphate in the upper chamber was increased, and so forth. By calibrating the apparatus in the absence of protein, the rate of appearance of counts per minute (cpm) of carbon-14 in the lower fluid could be converted to the free concentration of [U-^{14}C]hexose 6-phosphate in the upper solution. From the known total concentration of hexose 6-phosphate in the upper solution, the concentration of bound substrates could be calculated by difference. **(A)** Direct presentation of the measurements. The variable $[ST{\cdot}H6P]_{eq}\ C_{GI}^{-1}$ (micromolar milligram^{-1} milliliter)—where ST is an active site of glucose-6-phosphate isomerase (GI), H6P is hexose 6-phosphate, and C_{GI} is the concentration of glucose-6-phosphate isomerase (milligrams milliliter^{-1})—is plotted as a function of the concentration of hexose 6-phosphate (millimolar). Data from measurements by equilibrium dialysis (□) and measurements by rate dialysis (○) are plotted. Equation 3–52 was fit to each set of data with y equal to $[ST{\cdot}H6P]_{eq}\ C_{GI}^{-1}$ and x equal to [H6P]. The apparent dissociation constants for the substrates (values for parameter b in Equation 3–52) are 0.15 ± 0.01 and 0.16 ± 0.01 mM, respectively, and the micromoles of sites (gram of protein)$^{-1}$ (values for parameter a in Equation 3–52) are 18.7 ± 0.7 and 14.8 ± 0.3 μM mg^{-1} mL, respectively, for the two different measurements. Because the molar mass of a protomer of glucose-6-phosphate isomerase is 62,630 g mol^{-1}, there are, in theory, 15.97 μmol of active sites on glucose-6-phosphate isomerase for every gram of protein. **(B)** Linear presentation of the measurements. The data from measurements by equilibrium dialysis (□) and by rate dialysis (○) are plotted in the linear form of $[ST{\cdot}H6P]_{eq}\ C_{GI}^{-1}$ (micromolar milligram^{-1} milliliter) as a function of $[ST{\cdot}H6P]_{eq}\ C_{GI}^{-1}\ [H6P]_{eq}^{-1}$ (micromolar milligram^{-1} milliliter millimolar^{-1}), where $[H6P]_{eq}$ is the concentration (millimolar) of hexose 6-phosphate at equilibrium. The lines are those calculated for the dissociation constants and the micromoles of sites (gram of protein)$^{-1}$ from the fits of the data in Panel A. The theoretical intercept of 15.97 micromoles of sites (gram of protein)$^{-1}$ is noted.

ligand, the rate of dialysis can be converted directly into a value for the free concentration of ligand, $[L]_{eq}$, in the compartment, and the concentration of bound ligand, $[ST{\cdot}L]_{eq}$, can be calculated by difference (Figure 3–18) from the known total concentration of ligand in the compartment with the protein, $[L]_t$, and the concentration of free ligand.

In yet another approach, the protein and the ligand are allowed to equilibrate in a solution, and then a portion of the solution is forced under pressure through a semipermeable membrane.[160] This process is referred to as **ultrafiltration**. The concentration of ligand in the ultrafiltrate will be the free concentration, $[L]_{eq}$, in the original solution, and the known total concentration of ligand in the original solution, $[L]_t$, will be the sum of that free concentration and the bound concentration, $[ST{\cdot}L]_{eq}$ (Figure 3–17).[136]

Chromatography by size exclusion takes place on a column of beaded, tightly crosslinked dextran that excludes the protein from the interior of the beads, that includes the free ligand in the interior of the beads, and that can been equilibrated with a solution containing a fixed concentration of ligand. If a sample of protein is run on such a size-exclusion column, the protein, which exits the column in the

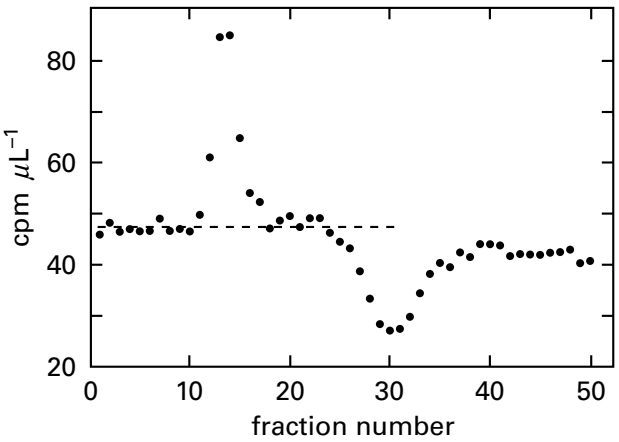

Figure 3–19: Determination of the concentration of histidinol bound to histidinol dehydrogenase by molecular exclusion.[161] A column (0.5 cm × 7.5 cm) of beaded, crosslinked dextran (Sephadex G-50) was equilibrated with buffer containing 0.5 mM $MnCl_2$, 1 mM potassium phosphate, 1.0×10^5 counts per minute mL^{-1} [^{32}P]phosphate, 10 μM [^{3}H]histidinol (4.7×10^6 counts per minute μmol^{-1}) and 50 mM sodium glycinate at pH 9.05. A sample of histidinol dehydrogenase dissolved in 100 μL of the buffer used to equilibrate the column was applied, and the column was eluted with 2.8 mL of the buffer. Each fraction from the column was one drop of effluent (48–53 μL). To determine the counts per minute (cpm) of [^{3}H]histidinol for every microliter of solution in each fraction, the exact volume of each drop was determined from the counts per minute of [^{32}P]phosphate, and the counts per minute of [^{3}H]histidinol in each fraction was divided by that volume. The counts per minute of [^{3}H]histidinol in each microliter of effluent (cpm μL^{-1}) is presented as a function of the fraction number. The free concentration of histidinol is represented by the counts per minute $microliter^{-1}$ in the effluent before and after the excluded volume of the column (fractions 11–17), as indicated by the dashed line. The counts per minute in excess of those representing the free concentration of [^{3}H]histidinol in each fraction were summed over the excluded volume and converted to nanomoles of bound histidinol.

excluded volume, will bind ligand as it passes through the beaded dextran until the binding reaches equilibrium. The concentration of the excess ligand eluting with the protein should be ligand that is bound to the protein. If the protein has moved far enough to leave behind the deficit it created by binding the ligand, and the deficit is separated completely from the fractions containing the protein, which is ascertained by locating the deficit in the included volume (Figure 3–19),[161] the concentration of free ligand, $[L]_{eq}$, in fractions from the excluded volume, at which the protein elutes, should be the molar concentration of ligand with which the column was initially equilibrated.[162,163] It is usually assumed that the amount of protein eluting in the excluded volume is equal to the amount added to the column, but that should be verified independently. A similar procedure uses electrophoresis on a gel of poly(acrylamide) cast in a solution containing ligand at a particular concentration to ascertain the concentration of ligand bound to sites, $[ST{\cdot}L]_{eq}$, at that free concentration of ligand, $[L]_{eq}$.[164]

In each of the five methods just described for direct determination of the concentration of sites and the dissociation constant for the ligand, the concentration of bound ligand, $[ST{\cdot}L]_{eq}$, is determined by assessing the difference between the total concentration of the ligand in the solution, $[L]_t$, and the free concentration of the ligand, $[L]_{eq}$

$$[ST{\cdot}L]_{eq} = [L]_t - [L]_{eq} \qquad (3\text{–}284)$$

Consequently, **the concentration of bound ligand must always be a significant fraction of the total concentration of ligand**. Since the binding is a hyperbolic function of the free concentration of ligand, the concentration of protein must usually be increased as the concentration of ligand is increased. This requirement, however, is an advantage. If the measured values for $[L]_{eq}$ satisfy Equation 3–282 as $[L]_t$ and C_{prot} are varied independently, there is increased confidence that an uncomplicated dissociation constant is being measured (Figure 3–17).

In all of the many different procedures that have been developed to follow directly the binding of a ligand to a protein, **three variables are simultaneously measured**: the free concentration of the ligand, $[L]_{eq}$; the total concentration of protein, C_p; and the concentration of the complex between protein and ligand, $[ST{\cdot}L]_{eq}$. Each one of a set of solutions whose molar concentrations of protein and ligand are systematically varied is allowed to reach equilibrium, and these three concentrations are then measured by techniques that can assess what their values were in the solution when it was at equilibrium. As in the case of an analysis of results from studies of enzymatic kinetics, the data from a study of the binding of a ligand are submitted to numerical analysis. In this case, the data are a set of measured values for $[ST{\cdot}L]_{eq}\ C_{prot}^{-1}$ corresponding to a set of equilibrium molar concentrations for the free ligand $[L]_{eq}$. Again, as in the case of enzymatic kinetics, it is now customary to fit a rectangular hyperbola (Equation 3–52), where y is $[ST{\cdot}L]_{eq}\ C_{prot}^{-1}$ and x is $[L]_{eq}$, to the data by nonlinear least-squares analysis.[136,165] The two parameters, a and b, and their standard deviations, provided by the fitting procedure, are κ and K_{dL} (Equation 3–282). Such nonlinear numerical analysis can be extended to situa-

tions where several different sites, at different relative concentrations, are binding the same ligand, and each site has its own unique dissociation constant.[166] In either case, the experimental results obtained from such analyses are the individual values for the dissociation constant, K_{dL}, and the individual values for κ, which can be the inverse of the grams of protein (mole of sites)$^{-1}$. If the protein is pure and the molar mass of a protomer is known, the fraction of the protomers capable of binding the ligand can be determined.

The techniques for measuring the equilibrium concentrations in two compartments separated by a semipermeable membrane, for measuring the rate at which ligand passes through a semipermeable membrane, and for measuring the total concentration of ligand in the excluded volume of a column of crosslinked dextran, respectively, were applied separately to the binding at pH 8.0 and 22 °C of the competitive inhibitor 6-phosphogluconate (PGN) to glucose-6-phosphate isomerase from *O. cuniculus*. Values for $K_{d,PGN}$ were 0.08, 0.04, and 0.03 mM, respectively, and values for the inverse of the constant of proportionality κ were 66,000, 66,000, and 63,000 g (mol of sites)$^{-1}$, respectively.[156] These latter values are only slightly larger than the molar mass of one protomer of this enzyme, 62,747 g mol^{-1}. Larger values are expected if the preparation of enzyme was not absolutely pure or if some of the enzyme in the preparation was defunct. At pH 8 and 30 °C, the dissociation constant, determined kinetically for 6-phosphogluconate as a competitive inhibitor of glucose-6-phosphate isomerase, is 0.03 mM,[167] which agrees satisfactorily with the values obtained for its dissociation constant when measured directly.

In kinetic equations derived as explanations of the dead-end inhibition of initial rates for an enzymatic reaction, the **inhibition constants**, K_i, are dissociation constants for the inhibitor. It is gratifying to find that one of them actually is a dissociation constant. In the absence of proof that it is,[168] an inhibition constant, K_i, is, nevertheless, usually assumed to be the dissociation constant of the inhibitor from the enzyme.[169,170]

In the past, the data for the binding of a ligand to a protein were first **converted to a linear form**[157] before the fitting was performed, but this mode of analysis is rarely done anymore because digital computers permit nonlinear numerical analysis to be performed readily. Mainly for historical reasons, however, when the data are presented graphically for the reader's evaluation, they are often presented in a linear form. Equation 3–282 can be cast in a linear form either by inversion[157]

$$\frac{C_{prot}}{[ST{\cdot}L]_{eq}} = \frac{1}{\kappa} + \frac{K_{dL}}{\kappa}\left(\frac{1}{[L]_{eq}}\right) \tag{3–285}$$

or by the rearrangement[171]

$$\frac{[ST{\cdot}L]_{eq}}{C_{prot}} = \kappa - K_{dL}\left(\frac{[ST{\cdot}L]_{eq}}{C_{prot}\,[L]_{eq}}\right) \tag{3–286}$$

Because it was pointed out by Professor Scatchard that the use of Equation 3–285 "gives undue weight to that portion of … [the] data which is poorest in experimental precision,"[157] Equation 3–286, that for a **Scatchard plot**, is usually used as the linear form of the function. This method of analysis is in contradistinction to the common use of Equation 3–53 as the linear form of the function for initial rate of an enzymatic reaction.

The **Donnan effect** is one potential drawback of all the techniques described so far. In each instance, a solution containing the protein and the ligand is physically separated from a solution containing only the ligand but remains in equilibrium with it. The protein is almost always charged at the pH at which the measurements are made. Even during chromatography by size exclusion, the dimensions of the two compartments, that containing the protein surrounding the beads and that lacking the protein in the interior of the beads, are greater than the thickness of the ionic double layer around the protein.[172] If the ligand is also charged, it will act as any other electrolyte in the diffuse layer of dissolved counterions around the protein. It will either be depleted in the layer if it is of the same charge as the protein or enriched in the layer if it is of opposite charge. This depletion has the effect of decreasing or increasing, respectively, the measured concentration of bound ligand in the compartment containing the protein. This source of error can be minimized by performing the binding experiments at a **concentration of supporting electrolyte high enough** to eliminate the contribution of the ligand itself to the layer of mobile counterions. This elimination can be seen in the following way.

Suppose that the solution of protein contains impermeant macromolecules, including the molecules of protein themselves, that have a net charge at the pH chosen for the measurements. In the sys-

tem there are two compartments: the compartment α containing the charged macromolecules and the compartment β lacking them. Assume that the only permeant electrolytes are the ligand, potassium, and chloride, and also assume that the solution of protein contains no binding sites for ligand L. By electroneutrality

$$[\text{charge}]_\alpha = [K^+]_\beta - [K^+]_\alpha + [Cl^-]_\alpha - [Cl^-]_\beta + z_L\left([L]_\beta - [L]_\alpha\right) \quad (3\text{–}287)$$

where $[\text{charge}]_\alpha$ is the net molar concentration of all impermeant elementary charge in compartment α (in equivalents liter^{-1}) which can have either a positive or a negative value), z_L is the charge number on ligand L, and the subscripts on the concentrations indicate the respective compartment. This equation defines the contribution of each ion to the maintenance of electroneutrality. A quantity $f_{\text{charge,L}}$ can be defined, which is the fraction of the charge compensation contributed by the ligand L

$$f_{\text{charge,L}} = \frac{z_L\left([L]_\beta - [L]_\alpha\right)}{[K^+]_\beta - [K^+]_\alpha + [Cl^-]_\alpha - [Cl^-]_\beta + z_L\left([L]_\beta - [L]_\alpha\right)} \quad (3\text{–}288)$$

If $|z_L| = 1$ and $[\text{charge}]_\alpha$ is much less than the sum of the concentrations of the permeant electrolytes, it can be shown[173] that

$$z_L\left([L]_\beta - [L]_\alpha\right) \cong \frac{[\text{charge}]_\alpha\,[L]}{\left([K^+] + [Cl^-]\right) + [L]} \quad (3\text{–}289)$$

This relation states that even if the solution of protein contains no sites for ligand L, it will **appear to contain binding sites for ligand L** if the charge of ligand L is opposite that of the nondiffusible charge on the macromolecules. The apparent dissociation constant measured for ligand L will be $[K^+] + [Cl^-]$.

If the Donnan effect is the only reason for the excess ligand in the compartment containing the protein, the apparent dissociation constant should be directly proportional to the concentration of supporting electrolyte. If, however, **a molar concentration of supporting electrolyte is purposely chosen so that it is always much greater than the molar concentration of ligand and the net concentration of impermeant elementary charge**, the amount of ligand retained or excluded from compartment β due to the Donnan effect, $[L]_\beta - [L]_\alpha$, as opposed to that due to legitimate binding, will be negligible (Equation 3–289). The Donnan effect, however, is difficult to eliminate if the macromolecule to which binding is being measured is nucleic acid instead of protein because nucleic acid is so negatively charged.

If the net charge of ligand L is the same as that of the nondiffusible macromolecules, the concentration of ligand L will be decreased in the compartment containing the protein, and if the net charge of ligand L is opposite that of the nondiffusible macromolecules, the concentration of ligand L will be increased in the compartment containing the protein. If there are legitimate sites for ligand L on the protein, the apparent binding to those sites will be less than the actual binding in the former case and greater in the latter case. The magnitude of these effects, however, decreases as the concentration of the supporting electrolyte is increased. Consequently, **dependence on ionic strength of any apparent binding** should be discounted until it is demonstrated that this dependence does not result simply from the Donnan effect.

There are also methods to **determine $[L]_{eq}$ and $[ST{\cdot}L]_{eq}$ by indirection**. In such an approach, the fraction of the population of molecules of ligand that is occupied by sites on the molecules of protein is still measured; and from the known total concentration of ligand in solution, $[L]_t$, the desired concentration of $[ST{\cdot}L]_{eq}$ and $[L]_{eq}$ can be calculated. For example, solutions each containing the same known concentration of an end-labeled fragment of DNA can be mixed with various concentrations, C_{prot}, of a protein that binds to a particular site on that fragment. After equilibrium is achieved, a small volume of deoxyribonuclease is added to the solution while the protein is still in equilibrium with the site on the DNA with which it associates. The amount of deoxyribonuclease added is small enough that it digests the DNA partially and at random. After a period of digestion, the DNA is submitted to electrophoresis, and the end-labeled fragments produced by deoxyribonuclease are quantified. When the protein is bound at its specific site, that site is protected from digestion by the deoxyribonuclease. As the digestion proceeds, the protein is associating and dissociating from its specific sites, but because of the equilibrium, the fraction of the sites protected ($[ST{\cdot}L]_{eq}\,[ST]_t^{-1}$) at any given instant remains constant during the digestion. As a result, fragments resulting from that particular cleavage decrease in amount in direct proportion to the frac-

tion of the sites occupied by the protein at equilibrium.[174,175] From the fraction of the sites occupied and the known molar concentration of the fragment of DNA in the initial solution, the concentrations $[ST{\cdot}L]_{eq}$ and $[L]_{eq}$ can be calculated. This method has the advantage that it can independently assess the binding of the protein to two or more sites on the same fragment of DNA.[176] This procedure is not immune from the Donnan effect because immediately adjacent to the DNA, which is a densely charged polyelectrolyte, the free concentration of protein can be significantly increased or decreased, depending upon its net charge and the ionic strength of the solution, and its occupation of the sites can be artifactually increased or decreased, respectively.[177]

Any physical or chemical property of the protein or of the ligand that changes upon the formation of a complex between a site and a ligand can be used to determine a value for the dissociation constant of the ligand. Examples of these properties would be the absorbance of the protein itself;[178] the absorbance of a prosthetic group in the protein, such as flavin,[179] heme,[101] or pyridoxal phosphate;[180] the absorbance of the ligand;[181] the fluorescence of the protein itself;[182-184] the fluorescence of a fluorophore that has been covalently attached to the protein;[185] the fluorescence of the natural ligand itself;[186] the fluorescence of a fluorescent derivative of the natural ligand;[187,188] the anisotropy of the fluorescence of a ligand;[189-191] the lifetime of the fluorescence of the protein[183] or the ligand; the chemical shift of a nuclear magnetic absorption of the ligand;[192] the absorption or emission of heat measured by a microcalorimeter;[193,194] or the rate of the covalent reaction of a particular amino acid in the protein with a particular chemical reagent.

For example, *N*-methylnicotinamide binds to lysozyme from *G. gallus* to form a complex that absorbs light at 350 nm, a wavelength at which both the ligand and the protein are transparent.[195] The **absorbance observed at a certain wavelength**, A_λ, of a particular complex between the ligand and the protein—in this instance the absorbance at 350 nm of the complex between *N*-methylnicotinamide and lysozyme—should be directly proportional to the molar concentration of the complex between the ligand, *N*-methylnicotinamide, and the protein, lysozyme, on which the site (ST) for binding is located

$$A_\lambda = \varepsilon_\lambda [ST{\cdot}L]_{eq} \qquad (3\text{–}290)$$

where ε_λ is the extinction coefficient of the complex at the wavelength chosen to monitor its formation, which in the case of *N*-methylnicotinamide binding to lysozyme was 350 nm. When Equation 3–290 is combined with Equation 3–282

$$\frac{A_\lambda}{C_{prot}} = \frac{\varepsilon_\lambda \kappa [L]_{eq}}{K_{dL} + [L]_{eq}} \qquad (3\text{–}291)$$

which defines a rectangular hyperbola. In the case of *N*-methylnicotinamide (NMN) binding to lysozyme, when C_{prot} is expressed in molarity, $[lysozyme]_t$

$$\frac{A_{350}}{[lysozyme]_t} = \frac{\varepsilon_{350}\, \kappa\, [NMN]_{eq}}{K_{dNMN} + [NMN]_{eq}} \qquad (3\text{–}292)$$

A plot (Figure 3–20)[195] of $A_{350}\,[lysozyme]_t^{-1}$ (y) as a function of $[NMN]_{eq}$ (x) is a rectangular hyperbola (Equation 3–52) with a equal to $\varepsilon_{350}\kappa$ and b equal to K_{dNMN}. If it is assumed that there is one site on each molecule of lysozyme, then κ is 1 and the horizontal asymptote a is the extinction coefficient, ε_{350}, for the complex, which in the case of the complex between *N*-methylnicotinamide and lysozyme is $1040 \pm 12\ M^{-1}$, and the dissociation constant for *N*-methylnicotinamide from lysozyme is 304 ± 9 mM.

The example just described, in which neither the protein nor the ligand itself absorbs nor fluoresces at the wavelength at which the complex absorbs or fluoresces, is rarely encountered. Usually, either the protein or the ligand, or both, absorbs or fluoresces over the entire range of wavelengths in which significant changes in absorption or fluorescence occur, and a **difference in absorption or fluorescence upon formation of the complex** is monitored. For example, when a series of solutions of various concentrations of the inhibitor D-malate between 1 and 50 mM was prepared, each with the same concentration (75 μM) of protomers of aspartate carbamoyltransferase (Equation 3–220), the absorbance of the solution at 290 nm increased as the concentration of D-malate increased.[178] Since D-malate is transparent at 290 nm, the absorbance of one or more tryptophans in the protomer of aspartate carbamoyltransferase is increasing. From this increase in the absorbance of the solution, the dissociation constant for D-malate can be determined.

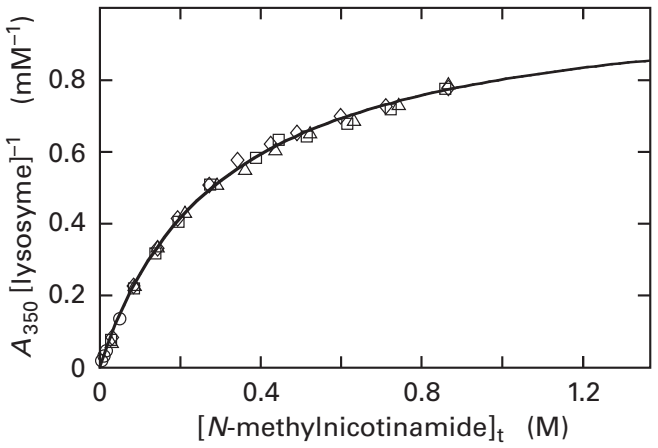

Figure 3–20: Binding of *N*-methylnicotinamide to lysozyme,[195] followed by the increase in absorbance of the solution at 350 nm. Crystalline lysozyme was dissolved at pH 5 and 22 °C to a final concentration of 10.0 mg mL^{-1} in a volume of 2.00 mL, which was assumed to be a concentration of 0.35 mM. Successive additions of solid *N*-methylnicotinamide (final concentrations between 5 and 890 mM) were made. After each addition, the absorbance of the solution at 350 nm was measured in a spectrophotometer, and the new concentration of protein resulting from the dilution caused by adding the solid was calculated. Because the concentration of *N*-methylnicotinamide was always in significant excess over the molar concentration of protein (8-fold to 1500-fold), it can be assumed that the total concentration of *N*-methylnicotinamide (molar) was equal to its free concentration. The quotient A_{350} [lysozyme]$_t^{-1}$ (millimolar^{-1}) is presented as a function of the concentration of *N*-methylnicotinamide. The different symbols refer to statistically independent measurements. The curve is the fit of Equation 3–52 to all the points with y equal to A_{350} [lysozyme]$_t^{-1}$ and x equal to [*N*-methylnicotinamide]$_t$. The dissociation constant for *N*-methylnicotinamide from lysozyme (parameter b) is 304 ± 9 mM, and the molar extinction coefficient (parameter a) is 1044 ± 12 M^{-1}.

For the dissociation of a ligand from a site on the protomer of a protein, Equation 3–280 usually applies and a **quantity *Y*, the fraction of the sites in the solution that are occupied by ligand**, can be defined

$$Y \equiv \frac{[\mathrm{ST{\cdot}L}]_{eq}}{[\mathrm{ST}]_t} = \frac{[\mathrm{L}]_{eq}}{K_{dL} + [\mathrm{L}]_{eq}} \qquad (3\text{–}293)$$

If the absorbance of the protein changes as a ligand that is transparent at the wavelength monitored associates with it, then

$$A_{obs} = \varepsilon_{uo}[\mathrm{ST}]_t(1 - Y) + \varepsilon_{occ}[\mathrm{ST}]_t Y \qquad (3\text{–}294)$$

where A_{obs} is the observed absorbance of a solution of the protein at a particular free concentration of ligand, ε_{uo} is the extinction coefficient of the protomers unoccupied by ligand, and ε_{occ} is the extinction coefficient of protomers occupied by ligand. The absorbance of a solution of the same concentration of protein in the absence of ligand

$$A_{uo} = \varepsilon_{uo}[\mathrm{ST}]_t \qquad (3\text{–}295)$$

and the absorbance of a solution of the same concentration of protein at saturating concentrations of ligand

$$A_{sat} = \varepsilon_{occ}[\mathrm{ST}]_t \qquad (3\text{–}296)$$

From Equations 3–293 through 3–296 it follows that

$$Y = \frac{A_{obs} - A_{uo}}{A_{sat} - A_{uo}} = \frac{\Delta A}{\Delta A_t} = \frac{[\mathrm{L}]_{eq}}{K_{dL} + [\mathrm{L}]_{eq}} \qquad (3\text{–}297)$$

and

$$\Delta A = \frac{\Delta A_t [\mathrm{L}]_{eq}}{K_{dL} + [\mathrm{L}]_{eq}} \qquad (3\text{–}298)$$

Consequently if the quantity ΔA (y) is plotted as a function of $[\mathrm{L}]_{eq}$ (x), the data should describe a rectangular hyperbola (Equation 3–52) with $a = \Delta A_t$ and $b = K_{dL}$. For the binding of D-malate to aspartate carbamoyltransferase, such hyperbolic behavior was observed for the increase in absorbance with a dissociation constant of 4.9 ± 0.2 mM.[178]

If the protein contains a **prosthetic group**, which will usually be within its active site, and that prosthetic group absorbs light of a particular wavelength, that absorption will often change upon the association of a ligand. For example, the absorbance of the heme in a mutant of unspecific monooxygenase BM3 from *B. megaterium* in which Phenylalanine 87 has been replaced with tyrosine shifts from a maximum at 419 nm to a maximum at 424 nm when the inhibitor 10-(imidazolyl)decanoate associates with the enzyme. This shift produces a characteristic difference spectrum (Figure 3–21A).[101] The greatest difference in absorbance between the active site occupied by 10-(imidazolyl)decanoate and the unoccupied active site is the difference in absorbance between that at 433 nm and that at 410 nm.

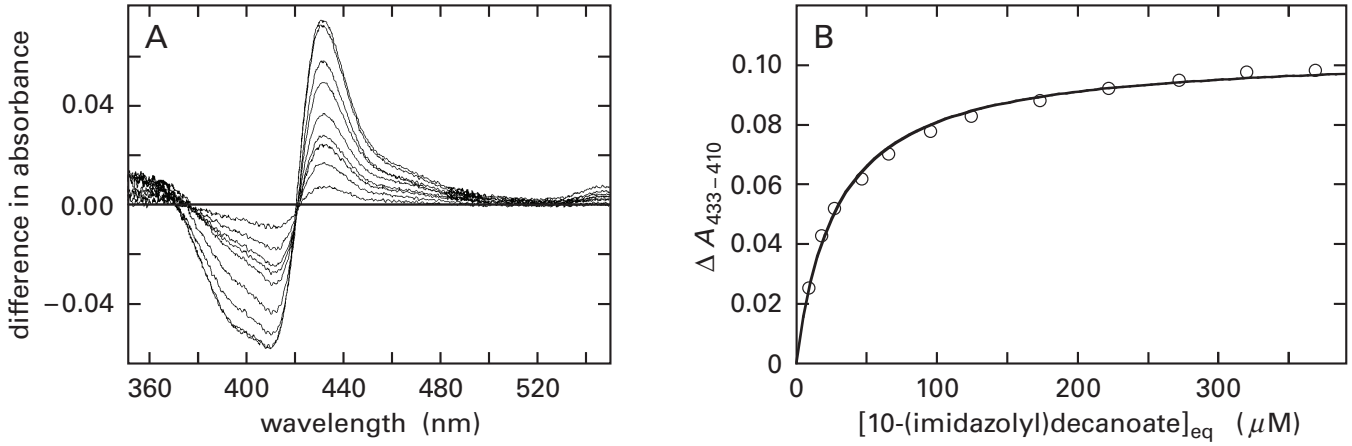

Figure 3–21: Binding of 10-(imidazolyl)decanoate to unspecific monooxygenase BM3 from *B. megaterium*, followed by the difference between absorbance of its heme at 433 nm and at 410 nm.[101] **(A)** Difference spectra resulting from addition of the ligand to the enzyme. A solution of the purified enzyme (5 μM) was prepared in 100 mM KCl and 20 mM 3-(*N*-morpholino)-propanesulfonic acid at pH 7.4. The absorption spectrum of this solution served as the reference spectrum for all difference spectra. Small amounts of a concentrated solution of 10-(imidazolyl)decanoic acid in dimethyl sulfoxide/methanol (1:1 v/v) were added to the solution of enzyme, and the reference spectrum was subtracted from the spectrum observed after the addition of the ligand. The final total concentrations of 10-(imidazolyl)decanoate for the difference spectra were 9.1, 18.3, 27.4, 36.5, 45.6, 63.8, 82.0, 119, and 228 μM, in order of increasing magnitude of difference. Notice that as the absorbance at 433 nm increases, the absorbance at 410 nm decreases, reflecting the shift in wavelength of maximum absorption from 419 to 424 nm. **(B)** Binding of 10-(imidazolyl)decanoate to a mutant of unspecific monooxygenase BM3 from *B. megaterium* in which Phenylalanine 87 has been replaced by a tyrosine. A solution of the mutant enzyme at a concentration of 3.1 μM in 100 mM KCl and 20 mM 3-(*N*-morpholino)propanesulfonic acid at pH 7.4 was titrated with increasing concentrations of 10-(imidazolyl)decanoate. The difference in absorbance between that at 433 nm and that at 410 nm ($\Delta A_{433-410}$) is plotted as a function of the equilibrium concentration of 10-(imidazolyl)-decanoate (micromolar). The differences in absorbance have been corrected for the effects of dilution on the spectra, and the total concentrations of 10-(imidazolyl)decanoate have been corrected for the amount of 10-(imidazolyl)decanoate bound to the enzyme. For this correction, it was assumed that one mole of enzyme binds one mole of ligand at saturation and that the observed difference in absorbance divided by the difference in absorbance at saturation is equal to the fraction of the sites that are occupied (Equation 3–297). The data were fitted with Equation 3–52 with y equal to $\Delta A_{433-410}$ and x equal to $[10\text{-(imidazolyl)decanoate}]_{eq}$. Parameter b is the dissociation constant for 10-(imidazolyl)decanoate from the enzyme, 29.2 ± 1.5 μM, and parameter a is the difference in absorbance at saturation, 0.104 ± 0.001. Adapted with permission from reference 101. Copyright 1998 American Chemical Society. https://doi.org/10.1021/bi980462d

Because the absorbance A_λ at every wavelength conforms to Equations 3–295 and 3–296, the **difference in absorbance between two wavelengths** $\Delta A_{\lambda_1-\lambda_2}$ must also conform to Equations 3–295 and 3–296, and consequently to Equations 3–297 and 3–298

$$\Delta A_{\lambda_1-\lambda_2} = \frac{\Delta A_{\lambda_1-\lambda_2,t}[L]_{eq}}{K_{dL} + [L]_{eq}} \qquad (3\text{–}299)$$

where $\Delta A_{\lambda_1-\lambda_2,t}$ is the difference in absorbance between the two wavelengths at saturating concentrations of ligand. In the case of the binding of 10-(imidazolyl)decanoate to the mutant of unspecific monooxygenase, the difference in absorbance between that at 433 nm and that at 410 nm, $\Delta A_{433-410}$, describes a rectangular hyperbola with parameter b (Equation 3–52) equal to the dissociation constant for 10-(imidazolyl)decanoate, $K_{d10D} = 29.2 \pm 1.5$ μM (Figure 3–21B).

In this instance, unlike the observations with aspartate carbamoyltransferase, the total concentrations of 10-(imidazolyl)decanoate used in the titration are only about 10-fold greater than the concentrations of occupied sites at the lower concentrations of ligand, and each total concentration of 10-(imidazolyl)decanoate had to be **corrected for the concentration of bound ligand** (Equation 3–283), on the assumption that there is only one site for ligand on each protomer, to give the equilibrium concentration of free ligand at each total concentration of ligand.

The same type of analysis can be performed upon a **change in the fluorescence of a protein**. For example, when 6-phosphofructokinase

$$\text{D-fructose 6-phosphate} + \text{MgATP}^{2-} \rightleftharpoons \text{H}^+ + \text{MgADP}^- + \text{D-fructose 1,6-bisphosphate} \quad (3\text{–}300)$$

from *E. coli* binds its substrate D-fructose 6-phosphate, the intrinsic fluorescence of its tryptophans decreases; and when it binds its substrate $MgATP^{2-}$, the intrinsic fluorescence of its tryptophans increases. Both the decrease in fluorescence and the increase in fluorescence are rectangularly hyperbolic functions of the free concentrations of the respective ligands with dissociation constants of 7 μM and 25 nM, respectively.[183] It is also possible to modify a protein with a fluorescent reagent to increase its fluorescence and use changes in the fluorescence of the inserted fluorophore to determine a dissociation constant.[185]

In Equation 3–279, the molar concentration of sites and the molar concentration of ligand are formally equivalent. Consequently, in the analogous arrangement to that producing Equation 3–280, the concentration of the complex between ligand and site at equilibrium

$$[\text{ST}\cdot\text{L}]_{eq} = \frac{[\text{L}]_t[\text{ST}]_{eq}}{K_{dL} + [\text{ST}]_{eq}} \quad (3\text{–}301)$$

A quantity Y_{lig}, the **fraction of the molecules of ligand in the solution that are occupied by sites**, can be defined

$$Y_{lig} \equiv \frac{[\text{ST}\cdot\text{L}]_{eq}}{[\text{L}]_t} = \frac{[\text{ST}]_{eq}}{K_{dL} + [\text{ST}]_{eq}} \quad (3\text{–}302)$$

Assume that the fluorescence of a protein is not elicited by a wavelength used to produce the fluorescence of a ligand. If the fluorescence of the ligand changes when a site on the protein associates with it, then in a derivation analogous to that for Equation 3–297

$$Y_{lig} = \frac{F_{obs} - F_{uo}}{F_{sat} - F_{uo}} = \frac{\Delta F}{\Delta F_t} = \frac{[\text{ST}]_{eq}}{K_{dL} + [\text{ST}]_{eq}} \quad (3\text{–}303)$$

where F_{obs} is the observed fluorescence of a solution of the ligand at a particular free concentration of sites, F_{uo} is the fluorescence of a solution of the same concentration of ligand in the absence of sites, ΔF is the difference between the two, F_{sat} is the fluorescence of a solution of the same concentration of ligand at a saturating concentration of sites, and ΔF_t is the total change in fluorescence observed when the concentration of ligand is at saturation. It follows that

$$\Delta F = \frac{\Delta F_t[\text{ST}]_{eq}}{K_{dL} + [\text{ST}]_{eq}} \quad (3\text{–}304)$$

and that when ΔF is plotted as a function of the free concentration of empty sites at equilibrium, the data should define a rectangular hyperbola. For example, a series of solutions, each with the same concentration (0.5 μM) of the peptide SIESDV, the amino terminus of which had been modified by a fluorescent 5-(dimethylamino)naphthalene-1-sulfonyl group, was prepared containing increasing concentrations of the PDZ domain from murine α-1-syntrophin (1–40 μM). As the concentration of the PDZ domain increased, the increase in the fluorescence of the solution was a hyperbolic function of the free concentration of PDZ domain, $[\text{ST}]_{eq}$, from which a dissociation constant of 1.93 ± 0.04 μM could be calculated (Figure 3–22).[188] Again, the concentration of sites has been corrected for the small concentration of sites that are occupied at each concentration of ligand to obtain the much larger values for the concentration of sites unoccupied by ligand.

In practice, however, these two formally equivalent participants, **site and ligand, are not actually equivalent**. It is often difficult if not impossible to ascertain the molar concentration of active, functional protomers but relatively easy to determine the concentration of ligand. It is often difficult or expensive to prepare solutions of protomers at molar concentrations in the range of the dissociation constant, an ability that is required to produce the hyperbolic curves necessary to assess the dissociation constant. Consequently, **the concentration of sites is usually held constant** at a level below the dissociation constant and the concentration of ligand that is varied in the range of the dissociation constant. This common practice is only for economy, not because the ligand and the site are not formally equivalent participants in the association.

As has been already mentioned, there are several **physical properties other than absorbance and fluorescence** that can monitor the formation of a complex between a ligand and a site on a protein.

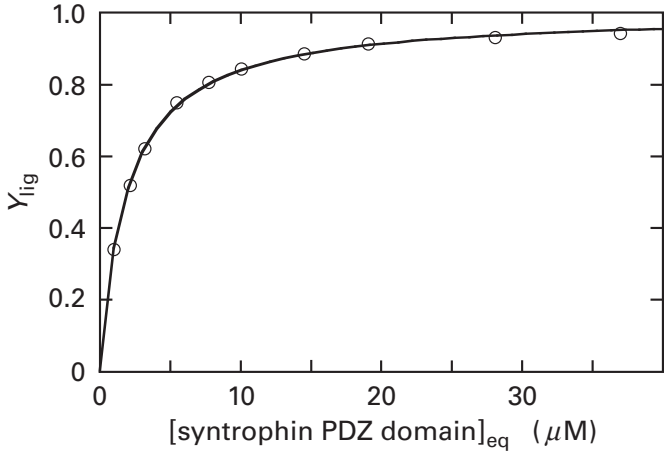

Figure 3–22: Binding of the PDZ domain (amino acids 77 through 171) of murine α-1-syntrophin to the fluorescently labeled hexapeptide *N*-[5-(dimethylamino)naphthalene-1-sulfonyl]serylisoleucylglutamylserylaspartylvaline (dansyl-SIESDV), followed by the change in fluorescence upon the association.[188] To a solution containing 0.5 μM dansyl-SIESDV (1.25 mL) in a continuously stirred cuvette in a fluorometer, small samples (2–5 μL) of a concentrated solution of the PDZ domain were added. After each addition, the fluorescence (excitation at 330 nm; emission at 540 nm) was monitored. The measured values of the fluorescence were corrected for any dilution that occurred upon addition of the concentrated solution, and the total concentrations of PDZ domain in the final solution were corrected by subtracting the concentration of bound PDZ domain to obtain the free concentration at equilibrium, [syntrophin PDZ domain]$_{eq}$. The concentration of bound PDZ domain was assumed to be equal to the fraction of dansyl-SIESDV bound, Y_{lig}, at each total concentration (Equation 3–303) times the concentration of dansyl-SIESDV (0.5 μM). The data were fitted with Equation 3–52 with y equal to $F_{obs} - F_{uo}$ and x equal to [syntrophin PDZ domain]$_{eq}$ (a rearranged form of Equation 3–303). Parameter a is $F_{sat} - F_{uo}$, and parameter b is K_{dPDZ} (1.93 ± 0.04 μM). By using the value of F_{sat} obtained from this fit, the fractional saturation, Y_{lig}, could be calculated (Equation 3–303). The fractional saturation (unitless) is presented as a function of the free concentration of PDZ domain at equilibrium ([syntrophin PDZ domain]$_{eq}$ in micromolar).

The increase or decrease in the fluorescence of a ligand or a protein observed when a complex forms is often accompanied by a change in the lifetime of the fluorescence, and the fraction of the fluorophore displaying the free lifetime and the fraction of the fluorophore displaying the bound lifetime can often be resolved so that Y or Y_{lig} can be measured directly.[183] When a large rotationally immobile molecule of protein, such as bovine pancreatic ribonuclease, associates with a small rotationally mobile ligand, such as the tetranucleotide dAdUdAdA that has been modified with fluorescein, the rotational mobility of the ligand bound to the active site decreases dramatically and the anisotropy of its fluorescence increases.[191] The chemical shift of a nucleus in a ligand in a nuclear magnetic resonance spectrum, such as the phosphorus-31 in [4-^{31}P]phosphatidylinositol 4,5-bisphosphate, can change upon association with a protein, such as a pleckstrin homology domain.[192] When a protein, such as gentamicin 2″-nucleotidyltransferase from *P. aeruginosa*, associates with a ligand, such as tobramycin, heat is either emitted or absorbed, and that heat can be measured in a microcalorimeter.[193]

Each of these latter changes—the increase in anisotropy, the change in chemical shift, or the emission or absorption of heat—is **directly proportional to the concentration of the complex** that is formed, and the same strategies and equations (Equations 3–297 and 3–303) can be used to evaluate the data, with the respective physical property, be it anisotropy, chemical shift, or heat emitted or absorbed, in place of absorbance or fluorescence. When the dissociation constant for binding of the inhibitor *N*-(phosphonomethyl)glycine to the complex ren shikimate 3-phosphate and 3-phosphoshikimate 1-carboxyvinyltransferase from *E. coli* was determined by following the heat emitted upon formation of the ternary complex, its value (0.15 ± 0.03 μM) agreed closely with its dissociation constant obtained by following changes in fluorescence (0.16 ± 0.02 μM) and its inhibition constant (0.16 μM) for the enzymatic reaction.[168]

In the measurements described so far, the concentration of the component that displays the physical property that changes during formation of the complex was held constant—for example, the concentration of aspartate carbamoyltransferase—and the concentration of the component that does not display that behavior was varied—for example, the concentration of D-malate. The latter concentration, however, can also be held constant and the former varied. For the moment, the physical property used in the following discussion will be fluorescence, but the equations and the conclusions are the same for any physical property.

The coenzyme NADPH displays fluorescence at 450 nm when it is excited by light at a wavelength of 290 nm. Its fluorescence is enhanced about 25-fold when it is bound at the active site of homoserine dehydrogenase from *E. coli*. The effect of an enhancement or diminution in fluorescence when a ligand associates with a protein—for example, in the case of homoserine dehydrogenase, the enhancement of the fluorescence of NADPH—can

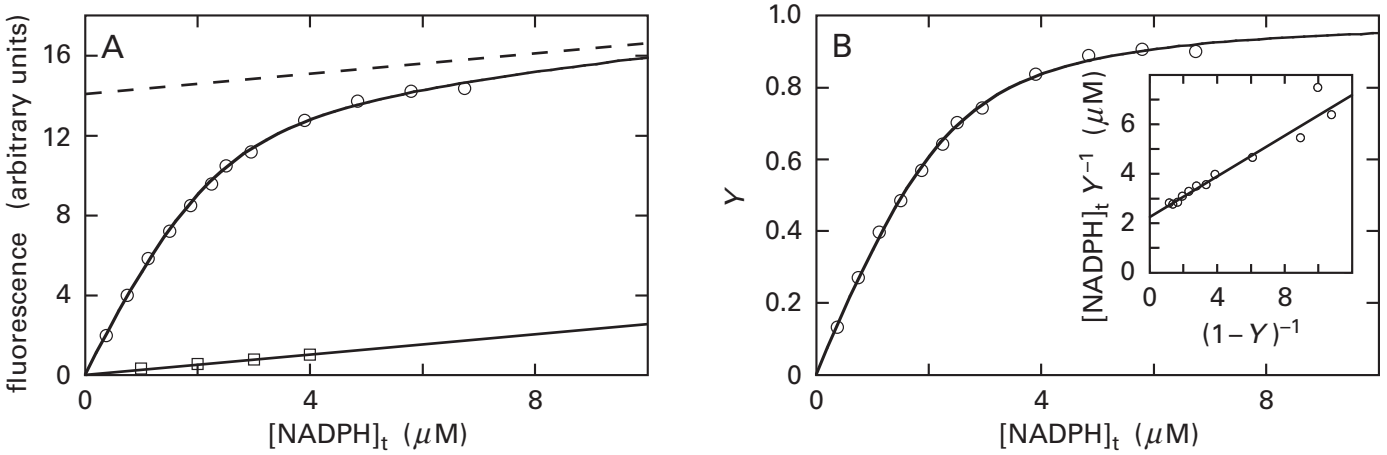

Figure 3–23: Binding of NADPH to homoserine dehydrogenase from *E. coli*, followed by the enhancement of the fluorescence of NADPH.[186] To a cuvette containing either a solution of 0.25 mg mL^{-1} homoserine dehydrogenase (HS) or buffer alone, successive additions of concentrated solutions of NADPH were made to produce the noted final, total concentrations of ligand. Between each addition, the fluorescence of the solution was determined ($\lambda_{excitation}$ = 285 nm; $\lambda_{emission}$ = 350 nm). **(A)** Fluorescence (in arbitrary units) as a function of the total concentration of NADPH (micromolar). Data for the fluorescence in the absence of enzyme (□) as a function of [NADPH]$_t$ were fitted with a line of direct proportionality to obtain a value for the constant of proportionality α (0.262 ± 0.006 μM^{-1}). Data for the fluorescence in the presence of enzyme (○) were then fitted with Equation 3–322, in which y is F_{obs}, x is [L]$_t$, parameter a is K_{dNADPH} (0.41 ± 0.08 μM), parameter b is [HS]$_t$ (2.2 ± 0.1 μM), and parameter c is the constant of proportionality, β (6.5 ± 0.4 μM^{-1}). The fit of Equation 3–322 to the data was then used to calculate the horizontal asymptote for the function (dashed line). **(B)** Fractional saturation of sites for NADPH on homoserine dehydrogenase, Y, as a function of the total concentration of NADPH (micromolar). Values for the constants of proportionality, α (0.262 μM^{-1}) and β (6.5 μM^{-1}), and the total molar concentration of sites, [HS]$_t$ (2.2 μM), were used in Equation 3–309 to convert each value for F_{obs} to the respective fractional saturation (Y, which is dimensionless). The curve drawn is that defined by Equation 3–322 into which were inserted the values for K_{dNADPH} (0.41 μM) and [HS]$_t$ (2.2 μM) obtained in the fit to the data in Panel A. (Inset to Panel B) The variable [NADPH]$_t$ Y^{-1}, where [NADPH]$_t$ is the total concentration of the ligand (in micromolar), is presented as a function of the dimensionless quantity $(1 - Y)^{-1}$. The line drawn is that for Equation 3–323 with the value of the dissociation constant K_{dNADPH} (0.41 μM) obtained from the fit in Panel A for its slope and the molar concentration of sites, [HS]$_t$ (2.2 μM), obtained from the fit in Panel A for its intercept with the axis of the ordinate.

be monitored. The values for the fluorescence are measured for a series of solutions in which **the total concentration of the participant in the complex that is responsible for the fluorescence is increased in increments**—for example, in the case of homoserine dehydrogenase when the total concentration of NADPH is increased incrementally at a fixed concentration of sites (Figure 3–23A).[186]

In the absence of sites, the fluorescence of the solution increases in direct proportion to the concentration of the fluorescent ligand, as in the case of NADPH (lower line in Figure 3–23A) as well as most fluorophores at low concentration, and the fluorescence observed, F_{free}, is due entirely to free ligand, unbound to any sites because there are no sites present in the solution. In this situation,

$$F_{free} = \xi_f [L]_t \qquad (3–305)$$

where ξ_f is a constant of proportionality for the free ligand. If, however, a fixed concentration of sites—for example, active sites on homoserine dehydrogenase that associate with NADPH—is present in the solution, then the fluorescence increases either less steeply or more steeply when increments of the ligand are added—as when NADPH is added to the solution containing homoserine dehydrogenase. The change in the incremental increase occurs because the fluorescence, F_{bound}, of the complex between ligand and protein, ST·L, is either less than or greater than, respectively, that of free ligand. The fluorescence of the bound fluorophore

$$F_{bound} = \xi_b [ST·L]_{eq} \qquad (3–306)$$

where ξ_b is also a constant of proportionality. The association of the ligand with the site either **enhances** its fluorescence ($\xi_b > \xi_f$) or **quenches** its fluorescence ($\xi_b < \xi_f$).

If [L]$_t$ is the total concentration of ligand, both bound and free, for each experimental point, and Y is, as before, defined as the fraction of the sites

occupied (Equation 3–293), then the fluorescence observed, F_{obs}, at any total concentration of ligand, $[L]_t$, will be

$$F_{obs} = F_{free} + F_{bound} \tag{3–307}$$

and

$$F_{obs} = \xi_f([L]_t - [ST]_t Y) + \xi_b [ST]_t Y \tag{3–308}$$

After rearrangement

$$Y = \frac{F_{obs} - \xi_f [L]_t}{(\xi_b - \xi_f)[ST]_t} \tag{3–309}$$

At saturation ($Y = 1$)

$$F_{obs} = \xi_f [L]_t + (\xi_b - \xi_f)[ST]_t \tag{3–310}$$

This equation defines the asymptote (dashed line in Figure 3–23A) of the curve observed in the presence of sites. This **asymptote** will be a line the slope of which is the same as the slope of the line in the absence of protein (ξ_f) and the intercept of which at the axis of the ordinate will be $(\xi_b - \xi_f)[ST]_t$. In the case of association of NADPH with homoserine dehydrogenase (HD), the intercept of the asymptote with the axis of the ordinate has a positive value. If association of the ligand with the protein quenches the fluorescence of the ligand, the intercept of the asymptote with the axis of the ordinate is at a negative value. By using the value for $(\xi_b - \xi_f)[HD]_t$ determined from this intercept and the value for ξ_f obtained from the slopes of both the asymptote and the linear increase in fluorescence in the absence of sites, values of Y can be obtained for each value of $[NADPH]_t$ (Equation 3–309) and can be plotted as a function of $[NADPH]_t$ (Figure 3–23B).

This approach is a general one for any physical property the magnitude of which is directly proportional to the concentration of ligand free in solution and also directly proportional to the concentration of ligand bound to sites and has significantly different constants of proportionality for free ligand (ξ_f) and bound ligand (ξ_b), respectively. The value for ξ_b can be greater than the value for ξ_f or it can be smaller; these two constants of proportionality just must differ enough to observe statistically significant differences between measurements in the presence of protein and measurements in its absence.

The values of Y obtained in the particular measurements just described for homoserine dehydrogenase and NADPH do not describe a rectangular hyperbola, although they seem to do so (Figure 3–23B). To understand why they do not, one must examine the behavior of Y as a function of the total concentration of sites

$$[ST]_t = [ST]_{eq} + [ST{\cdot}L]_{eq} \tag{3–311}$$

and the total concentration of ligand

$$[L]_t = [L]_{eq} + [ST{\cdot}L]_{eq} \tag{3–312}$$

There are three regimes in which the binding of a ligand can be quantified by monitoring a physical property. These three regimes can be understood by examining three quadratic equations.

To understand the **first regime**, Equations 3–279, 3–311, and 3–312 can be combined and rearranged to give the quadratic equation*

$$K_{dL}[L]_t - (K_{dL} + [ST]_t - [L]_t)[L]_{eq} - [L]_{eq}^2 = 0 \tag{3–313}$$

When measurements are made in the first regime, **either the fixed concentration of sites or the fixed concentration of ligand in the samples is purposely set at a value that is much lower than the dissociation constant**. If, for example, $[ST]_t << K_{dL}$ and the concentration of ligand is in the range of the dissociation constant, then because $[ST]_t << [L]_t$, Equation 3–313 can be factored

$$(K_{dL} + [L]_{eq})([L]_t - [L]_{eq}) \cong 0 \tag{3–314}$$

and

$$[L]_{eq} \cong [L]_t \tag{3–315}$$

This approach is the one that was chosen for measurements of the dissociation constant for *N*-methylnicotinamide from lysozyme (Figure 3–20; $[ST]_t$ = 0.35 mM, K_d = 300 mM) and for the dissociation constant for D-malate from aspartate carbamoyltrans-

*It should be noted in passing that this quadratic equation, because it can be solved for the free concentration of ligand, as opposed to the total concentration, if K_{dL} is known, is useful in its own right.[155]

ferase ($[ST]_t = 75\ \mu M$, $K_{d,mal} = 4900\ \mu M$). In the first regime, only the dissociation constant for the ligand can be ascertained.

If the concentration of sites is too close to the dissociation constant, then the concentration of free ligand $[L]_{eq}$ will not be approximately equal to the total molar concentration of ligand $[L]_t$, and the molar concentration of sites in which ligand is bound, $[ST{\cdot}L]_{eq}$, if at all possible, must be deducted from the total concentration of ligand originally added to the solution, $[L]_t$, to obtain the free concentration of ligand. In the case of the dissociation constant for 10-(imidazolyl)decanoate from unspecific monooxygenase (Figure 3–21B; $[ST]_t = 3\ \mu M$, $K_{dL} = 29\ \mu M$), which approaches the upper boundary of the first regime, the total concentrations of ligand could be **corrected for the amounts bound** to obtain the free concentration of ligand plotted in the graph. It should always be remembered that the concentration of ligand, $[L]_{eq}$, and the concentration of sites, $[ST]_{eq}$, in all the equations are the free concentrations, respectively, which are often unknown, not the total concentrations, which are usually known.

Because $[ST]_{eq}$ and $[L]_{eq}$ are mathematically equivalent in Equation 3–279, **the quadratic equation equivalent to Equation 3–313 can be derived for $[ST]_{eq}$**, and when the concentration of ligand is held constant at levels well below the dissociation constant ($[L]_t < K_{dL}$) and the concentration of sites is varied in the range of the dissociation constant, the concentration of total sites will be close to the concentration of free sites ($[ST]_t \cong [ST]_{eq}$) because $[L]_t < [ST]_t$. For titration of the fluorescently modified peptide SIESDV with the PDZ domain from murine α-1-syntrophin (Figure 3–22),[188] the concentration of ligand chosen, $0.5\ \mu M$, was significantly less than the dissociation constant, $1.9\ \mu M$. Nevertheless, the fixed concentration of the ligand was close enough to the dissociation constant that the free concentrations of the PDZ domain from murine α-1-syntrophin unoccupied by the peptide were ascertained by subtracting from the total concentration of sites the concentration of PDZ domain from murine α-1-syntrophin that was occupied by the fluorescent peptide. In this instance, the correction was easily done because the total concentration of ligand was known.

In this first regime, when a dissociation constant is measured by following a change in a physical property, **no independent estimate of the total concentration of sites** can be made from the results.

To understand the **second regime**, Equations 3–279, 3–311, and 3–312 can be combined and rearranged to give the quadratic equation

$$[ST]_t[L]_t - \left(K_{dL} + [ST]_t + [L]_t\right)[ST{\cdot}L]_{eq} + [ST{\cdot}L]_{eq}^{\,2} = 0 \qquad (3\text{–}316)$$

When measurements are made in the second regime, **the total concentration of sites and the total concentration of ligand are purposely set at values that are much higher than the dissociation constant**. Under these circumstances, because K_{dL} is much less than either concentration, Equation 3–316 can be factored

$$\left([ST]_t - [ST{\cdot}L]_{eq}\right)\left([L]_t - [ST{\cdot}L]_{eq}\right) \cong 0 \qquad (3\text{–}317)$$

Either the total concentration of ligand or the total concentration of sites is varied while the total concentration of the other is held constant. If the total concentration of ligand is varied, when $[ST{\cdot}L]_{eq} < [ST]_t$

$$[ST{\cdot}L]_{eq} \cong [L]_t \qquad (3\text{–}318)$$

Each mole of ligand added to the solution will be bound stoichiometrically by a site until all the sites are occupied. Beyond saturation, where $[ST{\cdot}L]_{eq} = [ST]_t$, further addition of ligand will simply be equivalent to the addition of ligand to a solution lacking the protein. In the second regime, a plot of the physical property responding to the binding of the ligand as a function of the total concentration of ligand provides an **estimate of the total concentration of sites** in the solution.

When either NADH or NADPH binds to bovine glutamate dehydrogenase [NAD(P)$^+$]

$$\text{L-glutamate} + H_2O + NAD(P)^+ \rightleftharpoons H^+ + \text{2-oxoglutarate} + NH_4^+ + NAD(P)H \qquad (3\text{–}319)$$

in the absence of 2-oxoglutarate and NH_4^+, the absorbance of the respective nucleotide at 320 nm decreases by about 25%. If the concentration of enzyme is fixed at $5.3\ mg\ mL^{-1}$ and increasing concentrations of either NADH or NADPH are added, the rate of increase in the absorbance of the solution is significantly lower than the rate of increase when

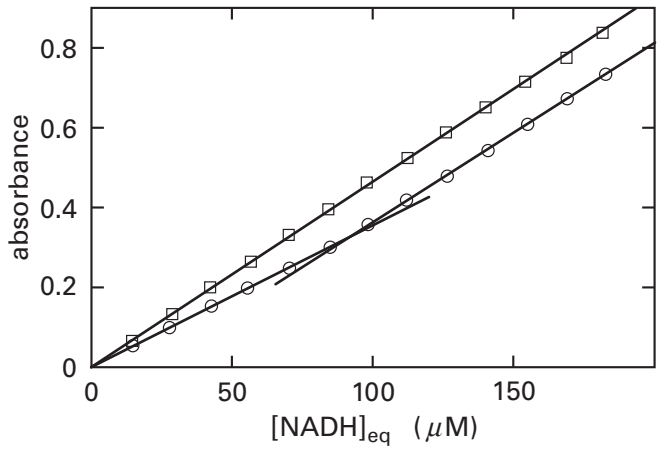

Figure 3–24: Spectrophotometric titration[181] of the sites on bovine glutamate dehydrogenase [NAD(P)+] for the binding of NADH. Crystalline glutamate dehydrogenase [NAD(P)+] was dissolved in a solution (3.00 mL) of 0.17 M glutamate at pH 7.0. The final concentration of enzyme in each solution was 5.30 mg of protein mL^{-1} based on an extinction coefficient determined by dry weight analysis. Successive additions (5 μL) of a standard solution of NADH were made to the solution to establish the noted final concentrations. An otherwise identical 3.00 mL solution of 0.17 M L-glutamate at pH 7.0, to which no enzyme had been added, served as the control. The same successive additions (5 μL) of NADH were made to the control. After each successive addition, the absorbance of each solution was measured. The absorbances of the several solutions (dimensionless) are presented as a function of the final equilibrium concentrations of NADH (micromolar). The intersection of the two lines is at 92 μM NADH, which gives a value of 57.5 mg of protein (μmol of sites)$^{-1}$. There are 55.726 mg of bovine glutamate dehydrogenase [NAD(P)+] for every micromole of active sites.

the enzyme is not present; but, beyond a concentration of ligand equal to that of the concentration of sites, the rate of increase in absorbance discontinuously assumes the value observed in the absence of enzyme (Figure 3–24).[181] At the point of inflection, the total concentration of ligand must equal the total concentration of sites. The concentration of sites in the 5.3 mg mL^{-1} solutions of glutamate dehydrogenase [NAD(P)+] was estimated in this way to be 93 μM; and consequently, there is one mole of sites for binding NADH or NADPH for every 57,000 g of protein. The molar mass of a protomer of bovine glutamate dehydrogenase [NAD(P)+] is 55,726 g. This exact molar mass was not known at the time the measurements were made, but if it had been, these results would have demonstrated that the number of active sites was equal to the number of protomers and that the preparation of the enzyme was 98% pure and active.

An experiment of this type is a **spectrophotometric titration** of the concentration of sites for binding of the ligand.[184] Properly, such a determination should be made at several different concentrations of protein because, as the concentration of protein is increased, the point of inflection must shift proportionally to the right if the total concentration of sites is actually greater than the dissociation constant. This shift should be demonstrated directly. Again, the same type of measurement can be performed by fixing the concentration of ligand at a level much greater than the dissociation constant and varying the concentration of protein.

The concentration of sites in a solution can also be determined by a kinetic titration performed in this second regime. A **kinetic titration** is a titration of the sites for an activator, substrate, or inhibitor of an enzyme that is followed by its effect on the kinetics of the enzymatic reaction. For example, when in the second regime, an inhibitor of the enzymatic activity that has a small enough dissociation constant is stoichiometrically bound by the enzyme if both the concentration of sites and the concentration of inhibitor are in excess of the dissociation constant for the inhibitor from the site. In this situation, the decreases in initial rate of the enzymatic reaction observed at several different concentrations of the inhibitor are directly proportional to the concentration of bound inhibitor, which is equal to the known total concentration of the inhibitor.[196] The molar concentration of inhibitor required to inhibit the enzyme completely is equal to the molar concentration of sites for the inhibitor. When the concentration of enzyme needed to exceed the dissociation constant of a ligand is so high that it is greater than that at which initial rates can be measured, a single turnover of the enzyme can often be followed. For example, the ligand can be a tightly bound substrate for the enzyme. A kinetic titration performed by increasing the concentration of the enzyme and following the increase in the initial rate of single turnovers can be used to estimate the molar concentration of sites for the substrate in a solution of the enzyme.[197] When the unknown concentration of active sites equals the known concentration of substrate, the rate of single turnovers no longer increases but discontinuously levels out.

In this second regime, when the concentration of sites is measured by following a change in a physical property or the kinetics of the enzymatic reaction, **no estimate of the dissociation constant can be made**.

To understand the **third regime**, Equations 3–279, 3–293, 3–311, and 3–312 can be combined and rearranged to give the quadratic equation

$$[ST]_t Y^2 - \left(K_{dL} + [ST]_t + [L]_t\right)Y + [L]_t = 0 \quad (3\text{–}320)$$

The relevant of the two roots of this quadratic equation is the one in which

$$Y = \frac{K_{dL} + [ST]_t + [L]_t - \sqrt{\left(K_{dL} + [ST]_t + [L]_t\right)^2 - 4[ST]_t[L]_t}}{2[ST]_t} \quad (3\text{–}321)$$

When measurements are made in the third regime, **the concentration of sites is purposely set at a value that is in the same range as the dissociation constant**, $[ST]_t \cong K_{dL}$. Under these circumstances, Y, the fraction of sites occupied by ligand L, is a function of the total concentration of ligand $[L]_t$, the dissociation constant K_{dL}, and the total concentration of sites $[ST]_t$ (Equation 3–321). As a result, in this range, both the total concentration of sites and the dissociation constant become parameters of the measurement.

For example, if fluorescence is being monitored, Equations 3–309 and 3–321 can be combined and

$$y = \left\{\frac{a + b + x - \sqrt{(a + b + x)^2 - 4bx}}{2}\right\}(c - \xi_f) + \xi_f x \quad (3\text{–}322)$$

where y is F_{obs} and x is $[L]_t$ and the parameters of the fit are a, b, and c. The value for ξ_f is known from the behavior of fluorescence in the absence of protein (lower line in Figure 3–23A). Parameter a from the fit is K_{dL}, parameter b is $[ST]_t$, and parameter c is ξ_b. Equation 3–322 can be fit by nonlinear least-squares analysis to the behavior of the observed fluorescence as a function of the total concentration of ligand L. In the example of homoserine dehydrogenase, the constant of proportionality from the slope of the line in the absence of the enzyme, ξ_f, is $0.262 \pm 0.006\ \mu M^{-1}$, and when Equation 3–322 is fit to the data directly (Figure 3–23A), the dissociation constant K_{dNADPH} is $0.41 \pm 0.08\ \mu M$, the molar concentration of sites is $2.26 \pm 0.11\ \mu M$, and the constant of proportionality ξ_b is $6.5 \pm 0.4\ \mu M^{-1}$. In an experiment of this type, once the values for K_{dL} and $[ST]_t$ have been estimated in preliminary experiments, $[ST]_t$ can be purposely chosen to be of the same magnitude as K_{dL}, as in the experiments with homoserine dehydrogenase. Because K_{dL} and $[ST]_t$ are of approximately equivalent weight in Equation 3–321, the most ideal situation is one in which they are approximately equal in magnitude.*

Equations 3–309, 3–321, and 3–322 **can be applied to any physical property** that, like fluorescence, is proportional to the concentration of free ligand and to the concentration of bound ligand and for which the two constants of proportionality, ξ_f and ξ_b, differ significantly simply by replacing F_{obs} by the symbol for the physical property being measured.[184,187,198] The fit of Equation 3–322 to the data provides the most accurate asymptote for the curve (dashed line in Figure 3–23A), and this asymptote can be used to convert the observed values for the physical property being measured (Equations 3–309 and 3–310) into values for the fractional saturation Y as a function of the total concentration of ligand so that they can be plotted (Figure 3–23B).

Equation 3–320 can be **rearranged to the linear form**

$$\frac{[L]_t}{Y} = \frac{K_{dL}}{1 - Y} + [ST]_t \quad (3\text{–}323)$$

When $[L]_t\ Y^{-1}$ is plotted as a function of $(1-Y)^{-1}$, a straight line[180] with a slope of K_{dL} and an intercept with the axis of the ordinate of $[ST]_t$ is observed (inset to Figure 3–23B). Equation 3–323 and its graphical representation define the information available in the three regimes. Because $0 < 1 - Y < 1$, when $[ST]_t << K_{dL}$, the intercept of the line will be indistinguishable from zero and only the dissociation constant can be measured, which is still the slope of the line. When $[ST]_t >> K_{dL}$, the slope of the line will be indistinguishable from zero and only $[ST]_t$ can be measured, which is still the intercept with the axis of the ordinate. It is only when the total concentration of sites is in the range of the dissociation constant that the line has both a slope other than zero and an intercept other than zero, and both of the terms can be measured.

A kinetic titration can also be carried out in the third regime. For example, a small protein, calmodulin, activates Ca^{2+}-transporting ATPase from human erythrocyte membranes.[199,200] If the initial rate of this enzymatic reaction is followed as a function of the concentration of calmodulin at saturation with Ca^{2+} and $MgATP^{2-}$, a monotonic increase in the initial rate, Δv_0, is observed that reaches a maximum, ΔV, at high concentrations of calmodulin. It can be

*This conclusion is supported by the almost equivalent standard deviations on these two parameters from the fit in Figure 3-23B.

shown[155] that $[CM]_{t,0.5}$, the total concentration of calmodulin producing an increase in the initial rate, Δv_0, equal to half the maximum increase, ΔV, is related to the total molar concentration of sites with which calmodulin associates by the equation

$$[CM]_{t,0.5} = K_{dCM,app} + \frac{[CM]_t}{2} \tag{3–324}$$

where $K_{dCM,app}$ is the apparent dissociation constant for the binding of calmodulin to Ca^{2+}-transporting ATPase. When Equation 3–324 is combined with Equation 3–281

$$[CM]_{t,0.5} = K_{dCM,app} + \frac{\kappa C_{CM}}{2} \tag{3–325}$$

If the concentration of protein (grams liter^{-1}) can be adjusted so that the concentration of sites has a value in the range of the value for the apparent dissociation constant and Equation 3–325 has a discernable slope, and if initial rates for the enzymatic reaction can be measured at these concentrations, a plot of $[CM]_{t,0.5}$ as a function of the concentration of the protein (in grams liter^{-1}) will have a slope of $(\kappa/2)$. In this instance, the parameter κ is the moles of sites (gram of protein)$^{-1}$. A simple way to understand Equation 3–324 is to consider that the free concentration of calmodulin is less than the total concentration by the amount bound to the enzyme. To effect the same fractional activation as the concentration of enzyme is increased, the total concentration of calmodulin must be increased to adjust for the increase in the bound calmodulin, and the additional calmodulin needed is directly proportional to half the concentration of sites.

When experimental studies of binding are performed, **a clear distinction among these three regimes must be made** from the start. If $[ST]_t$ is actually much less than K_{dL}, changing the concentration of protein will have no effect on the apparent dissociation constant measured with the assumption that $[L]_t = [L]_{eq}$. If $[ST]_t$ is actually in the range of K_{dL}, changing the concentration of protein will change the apparent dissociation constant measured with the assumption that $[L]_t = [L]_{eq}$. If $[ST]_t$ is actually much greater than K_{dL}, a titration with an inflection will be observed, and the point of inflection will shift proportionally as the concentration of protein is varied.

The dissociation constant for ligand L, the physical properties of which are unaffected by its association with a site ST, can be still be determined if it competes for site ST with ligand M, the physical properties of which are affected by its association with site ST. If the two ligands compete with each other for the same site on a protomer of a molecule of protein, then ligand M and ligand L cannot both bind to the site simultaneously, and the complex M·ST·L cannot form. It follows that

$$M{\cdot}ST + L \underset{}{\overset{K_{dM}}{\rightleftharpoons}} M + ST + L \underset{K_{dL}}{\rightleftharpoons} M + ST{\cdot}L \tag{3–326}$$

where

$$K_{dM} = \frac{[ST]_{eq}[M]_{eq}}{[M{\cdot}ST]_{eq}} \tag{3–327}$$

and

$$K_{dL} = \frac{[ST]_{eq}[L]_{eq}}{[ST{\cdot}L]_{eq}} \tag{3–328}$$

If, because of the competition

$$[ST]_t = [ST]_{eq} + [M{\cdot}ST]_{eq} + [ST{\cdot}L]_{eq} \tag{3–329}$$

and

$$[M]_t = [M]_{eq} + [M{\cdot}ST]_{eq} \tag{3–330}$$

and

$$[L]_t = [L]_{eq} + [ST{\cdot}L]_{eq} \tag{3–331}$$

it follows that

$$\left(K_{dL} - K_{dM}\right)[M{\cdot}ST]_{eq}^{3} + \left(K_{dM}^{2} - K_{dM}K_{dL} + K_{dM}[M]_t - 2K_{dL}[M]_t - K_{dM}[L]_t - K_{dL}[ST]_t + K_{dM}[ST]_t\right)[M{\cdot}ST]_{eq}^{2}$$
$$+ \left(K_{dL}K_{dM}[M]_t + K_{dL}[M]_t^{2} + K_{dM}[L]_t[M]_t - K_{dM}[ST]_t[M]_t + 2K_{dL}[ST]_t[M]_t\right)[M{\cdot}ST]_{eq} - K_{dL}[ST]_t[M]_t^{2} = 0 \quad (3\text{–}332)$$

which is a cubic equation in the molar concentration of the complex between ligand M and site ST on the protein.

In the absence of any information about the equilibrium constants, the appropriate **cubic root** of Equation 3–332 provides an equation for the value of the observed physical property for ligand M as a function of the total concentration of ligand L. When the total concentrations of ligand M and sites are in the proper range, this equation can be fit to the data to obtain values for K_{dM}, K_{dL}, and $[ST]_t$. If the experiment is designed properly so that certain terms in Equation 3–332 become negligible, the cubic equation can be simplified to a quadratic equation. From the appropriate root of this **quadratic equation**, an equation can be derived for the value of the observed physical property of ligand M as a function of the total concentration of ligand L when the concentrations of protein and ligand M are held constant, and this equation can be fit to the data to obtain values of K_{dM}, K_{dL}, and $[ST]_t$.[188,201]

If, however, the moles of sites (gram of protein)$^{-1}$ is known, so that the total concentration of sites in a particular solution is known, and if the dissociation constant for ligand M, K_{dM}, is also known, then a value of K_{dL}, the only missing parameter, can be obtained from the data without having to fit a cubic root or a quadratic root. Titrations can be performed in the usual manner, in the absence of ligand L, by following the physical property to obtain values for the dissociation constant of ligand M and the constant of proportionality κ, the moles of sites (gram of protein)$^{-1}$, so that the molar concentration of sites can be known for a given concentration of protein.

If a physical property Q of ligand M is affected by its association with site ST, then from Equations 3–293 and 3–297

$$Y_M = \frac{[M{\cdot}ST]_{eq}}{[ST]_t} = \frac{Q_{obs} - Q_M}{Q_{M{\cdot}ST} - Q_M} \quad (3\text{–}333)$$

where Q_{obs} is the observed value for the physical property at particular fixed concentrations of ligand M and site ST, Q_M is the value of that physical property at the same fixed concentration of ligand M in the absence of sites ST, and $Q_{M{\cdot}P}$ is the value of that physical property at the same fixed concentration of ligand M when ligand M is fully saturated with sites ST. If a series of solutions, each with the same fixed molar concentrations of ligand M and site ST, so that $Y_M > 0.5$, are titrated with different concentrations of ligand L, the bound concentration of ligand M, $[M{\cdot}ST]_{eq}$, will decrease as a result of the competition of ligand L for site ST, and Y_M will also decrease. The total concentration of ligand L, $[L]_{t,0.5}$, that brings Y_M to 0.5, which is where

$$Q_{obs} = 0.5\left(Q_{M{\cdot}ST} + Q_M\right) \quad (3\text{–}334)$$

can be measured in this titration. When $Y_M = 0.5$, regardless of the presence of ligand L, $[M]_{eq} = K_{dM}$ (Equation 3–293), and

$$K_{dL} = \frac{2K_{dM}^{2} + 2K_{dM}[L]_{t,0.5} + K_{dM}[M]_t - 2K_{dM}[ST]_t}{2[ST]_t - [M]_t - 2K_{dM}} \quad (3\text{–}335)$$

All the terms in the quotient on the right are known quantities. The measurements can be repeated with several different molar concentrations of sites, $[ST]_t$, and ligand M, $[M]_t$, each measurement beginning at levels where $Y_M > 0.5$, to show that K_{dL} is always the same.

There are many situations in which the concentration of sites for binding a ligand present in a biological preparation is too low for the methods described so far to be applied. Most of the experimental results and procedures examined so far require that the **molar concentration of binding sites** be fairly high. For example, in all the procedures where the bound concentration of the ligand is determined by the difference between the free concentration and the sum of bound and free concentrations, the bound concentration of the ligand must be of the same order of magnitude as the free concentra-

tion.[202] In experiments in which either the absorbance of the protein (Figure 3–21) or the absorbance of the protein in a complex between the ligand and the protein (Figure 3–20) is monitored, the concentration of the protein must be high enough and the protein must be pure enough to produce measurable changes in absorbance. Where differences in the fluorescence of a ligand are being followed (Figure 3–23), unless the increase in quantum yield is quite large, the concentrations of bound and free ligand must also be within the same range; and, since

$$\frac{[\mathrm{ST{\cdot}L}]_{eq}}{[\mathrm{L}]_{eq}} = \frac{[\mathrm{ST}]_{eq}}{K_{dL}} \qquad (3\text{–}336)$$

it follows that the concentration of sites must be of the same order of magnitude as the dissociation constant. Likewise, when the concentration of protein is varied to determine the dissociation constant (Figure 3–22), the concentration of sites must cover a range including the dissociation constant. In the titration of glutamate dehydrogenase by NADH (Figure 3–24), the concentration of sites had to be in excess of the dissociation constant. None of these requirements are prohibitive when the protein in question is abundant, soluble, and pure because molar concentrations as high as 1–10 mM in sites can be achieved under these circumstances. In other instances, however—particularly in situations where the protein on which the sites reside is only a small fraction of the protein present—it may not be possible to produce high enough concentrations of sites.

Many examples of this problem are encountered in the large group of proteins known as receptors. As the name implies, in many cases these proteins are identified only on the basis of their ability to bind a ligand. For example, the insulin receptor is defined as a protein in the plasma membrane of cells that binds insulin. Although one of the first receptors to be identified was identified by equilibrium dialysis,[202] often, for technical reasons, receptors are too impure, insoluble, and available only in small quantities. In such instances, the procedures described so far do not work.

When such problems arise, usually the binding is followed by **using radiolabeled ligands and rapidly separating the large quantities of unbound ligand from the small amount of bound ligand**. For example, the binding of insulin to the insulin receptor from *R. norvegicus*[203] that had been dissolved and purified in solutions of detergent was followed through the purification by using ^{125}I-labeled insulin of high specific radioactivity (1.7×10^{18} cpm mol^{-1}) and separating the small amount of bound insulin from the unbound insulin by precipitating the protein at 0 °C with poly(ethylene glycol) and rapidly capturing and washing the precipitate with buffer at 0 °C to complete the removal of free ligand.[204] The binding of epidermal growth factor to the human epidermal growth factor receptor in purified plasma membranes has been followed by using ^{125}I-labeled epidermal growth factor of high specific radioactivity (1.8×10^{17} cpm mol^{-1}) and separating the small amount of bound ^{125}I-labeled epidermal growth factor (usually <5% of the total) from the large amount of unbound ^{125}I-labeled epidermal growth factor by filtering the membranes directly.[205]

With the exception of these last examples, in all the methods for measuring binding discussed so far, the sites at which the ligand is bound remain in a solution in which the free concentration of ligand is unaltered by the procedure, and the ligand and the site remain at equilibrium. The measurements of the binding of ^{125}I-labeled insulin to insulin receptor or ^{125}I-labeled epidermal growth factor to epidermal growth factor receptor, however, are examples of procedures in which sites with their **bound ligands have to be separated completely from free ligand** to monitor the bound ligand.[204] Free ligand can also be completely separated from bound ligand by electrophoresis.[206-208] If the sites are attached to fragments of membrane or cells, the free ligand can be rapidly removed by centrifugation or filtration without the need to precipitate the protein.[204,209]

In all these instances, the concentration of **bound ligand begins to decrease from its level at equilibrium as soon as the free concentration of ligand begins to decrease**. In the extreme, no ligand will be left with the protein because it has all dissociated and then been washed away. If free ligand is removed abruptly and completely in some way, then an accurate estimate of the dissociation at equilibrium can still be made even if significant dissociation has occurred during the separation because the dissociation of ligand is a first-order reaction. Consequently, the same percentage of the initially bound ligand will be present in each washed sample, and the hyperbola defining the concentration of bound ligand as a function of the concentration of the ligand will decrease by the same fraction at each point. The concentration of bound ligand at saturation, however, will be less, often by a significant fraction, than its concentration at equilibrium before free ligand was removed, so the concentration of sites cannot be accurately

assessed by these procedures unless the binding is so tight that little if any dissociation occurs during the separation. If the removal of free ligand is gradual rather than abrupt, the dissociation constant determined will also be inaccurate.

In all these experiments examining the binding of ligands to receptors, two **controls** are usually run. First, it must be shown that the method used to separate physically the bound ligand and the unbound ligand is rapid enough that only manageable amounts of the ligand dissociate from the site during the procedure. Second, a control for nonspecific binding is also usually performed. In most cases, this control involves addition of a high concentration of nonradioactive ligand to see if this eliminates binding of the radioactive ligand. A better control, however, is to add a different ligand, known from independent experiments to block completely the binding of the ligand being tested. For example, specific binding of α-cobratoxin from *Naja siamensis* to murine acetylcholine receptor could be defined as the binding that was blocked by a high concentration of carbamoyl choline,[210] a structurally different ligand for acetylcholine receptor that competes with α-cobratoxin for binding.

There is a direct connection between a dissociation constant K_{dL} and the rate constants governing the kinetics of association of the ligand, k_1, and dissociation of the complex, k_{-1}. At equilibrium, Equation 3–279 applies as well as

$$k_1[ST]_{eq}[L]_{eq} = k_{-1}[ST{\cdot}L]_{eq} \qquad (3–337)$$

from which it follows that

$$K_{dL} = \frac{k_{-1}}{k_1} \qquad (3–338)$$

Equation 3–338, because it contains no concentrations, must be true under any set of circumstances. In particular, even in a situation in which an enzyme and its substrates exist in a steady state, which is not to be confused with existing at equilibrium, Equation 3–338 is valid. If a set of kinetic measurements, made in any situation, provides an unambiguous numerical value for the ratio of the two individual rate constants, k_{-1} $(k_1)^{-1}$, then the numerical value for this ratio is the numerical value of K_{dL}.

Under certain circumstances, the easiest way to measure a dissociation constant is to measure these **rate constants for the association and dissociation of the ligand.**[211] One of these circumstances is that in which the dissociation constant is so small that it cannot be measured directly. For example, at 25 °C the rate constant for the association of cyanocobalamin with haptocorrin from *G. gallus* is 0.24 nM^{-1} s^{-1} and the rate constant for its dissociation is 4×10^{-9} s^{-1}, from which an immeasurably small dissociation constant of 2×10^{-8} nM can be calculated.[212] Another circumstance is one in which equilibrium is established so slowly that it is easier to measure the rates at which the ligand associates and dissociates than it is to ensure that equilibrium has been established before a direct measurement is made.[213] In another instance, a measurement of the dissociation constant for tetrodotoxin from sodium channels from canine heart at –50 mV was made by assessing its rate constants of association and dissociation because a vanishingly small amount of protein was present in the membrane on which the difference in electric potential was imposed.[214] The dissociation constant (14 ± 2 μM) calculated from the rate constants for association (0.167 ± 0.003 μM^{-1} s^{-1}) of chorismate with the active site and dissociation (2.3 ± 0.1 s^{-1}) of chorismate from the active site in an inactive mutant of isochorismatase from *P. aeruginosa* was in good agreement with the dissociation constant (19 ± 2 μM) measured directly from changes in fluorescence.[198]

Up to this point, the binding between a site on a molecule of protein and a ligand has been discussed with the **assumption that the complex formed, ST·L, is a dead-end complex**. Because a dead-end complex is one in which the ligand is not transformed but dissociates from the complex in its original form, dead-end complexes are defined by a simple dissociation constant. Before they are interconverted, **reactants and products associate with and dissociate from the active sites** of enzymes as if they were ligands, but their transformation on the active site complicates the picture. Measurement of the dissociation constant for a dead-end complex is a thermodynamic measurement; that for a complex between an enzyme and its substrate is usually a kinetic measurement. One way to avoid the kinetic complication of turnover of the reactant by an enzyme is to examine the binding of that reactant to a mutant form of the enzyme that still binds the reactant but cannot convert it to product.[198] This strategy, however, is not so unambiguous as a measurement of the dissociation constant for the complex between the reactant and the unaltered enzyme.

There is significant confusion between the Michaelis constant for reactant A in an enzymatic reaction, K_{mA}, and the dissociation constant for the binding of reactant A to the active site, K_{dA}. This confusion arises from the provocative appeal of Equation 3–55, the simplest possible kinetic mechanism for an enzymatically catalyzed reaction. In the rate equation (Equation 3–62) for v_0 derived from the kinetic mechanism of Equation 3–55

$$K_{mA} = \frac{k_{-1} + k_2}{k_1} > \frac{k_{-1}}{k_1} = K_{dA} \qquad (3–339)$$

The assumption is that the step governed by the rate constant k_2, in which covalent bonds are made and broken, should be much slower than the step governed by the rate constant k_{-1}, in which only noncovalent bonds are broken and made, as would be the case in most uncatalyzed chemical reactions in which an encounter complex forms between two reactants many times before there is the proper orientation and kinetic energy of collision to achieve reaction. If $k_2 << k_{-1}$, then

$$K_{mA} \cong K_{dA} \qquad (3–340)$$

If all enzymatic reactions had kinetic mechanisms as simple as that of Equation 3–55, and if, in all cases, the chemical transformations of the reactants were slower than the rate constants for their dissociation from the active site, this approximation would be valid.

Unfortunately, **most enzymatic reactions have much more complicated kinetic mechanisms** involving multiple steps, and the expression for K_m is more complicated and more distant from the simple expression for a dissociation constant.* Even if the kinetic mechanism were as simple as the one in Equation 3–55, many enzymes have become so efficient that they are able to perform the transformations of the covalent bonds more rapidly than the bound reactants are able to dissociate from the active site. For both of these reasons, Equation 3–340 is seldom valid. An example of this ambiguity is that when two amino acids, Lysine 116 and Glutamate 135, which form hydrogen bonds with the α-phospho group of the reactant $MgATP^{2-}$ in the active site of cAMP-dependent protein kinase from *S. cerevisiae*,[215,216] are mutated in turn to alanines, the Michaelis constant for the peptide that is the other reactant for the enzyme increases by factors of 25 and 50, respectively, while the Michaelis constant for $MgATP^{2-}$ increases by factors of only 6 and 3.[217]

If it is desired that the observed Michaelis constant be approximately equal to the actual dissociation constant of the reactant from the active site, **that desire in that particular instance must be established experimentally**.

The common desire to treat a Michaelis constant as if it were a dissociation constant[218-223] arises from the fact that it is often difficult to measure the binding of a substrate to an enzyme because the enzyme transforms the substrate while the measurements are being attempted. Often, therefore, kinetic measurements are the only measurements available for determining the dissociation constants between an enzyme and its substrates.

In some instances, **the steady-state kinetics can be dissected** to isolate a dissociation constant. Acetylcholinesterase (AE) catalyzes the reaction

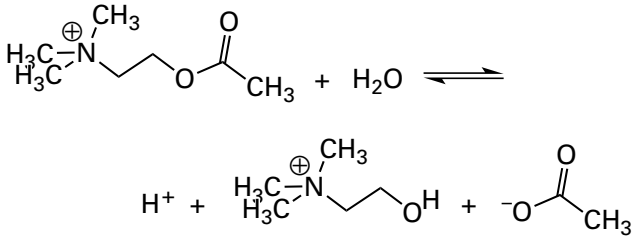

(3–341)

The enzyme also catalyzes the hydrolysis of a number of related acetyl esters. The binding of acetyl esters to acetylcholinesterase cannot be assessed in the absence of water, the other reactant in the reaction catalyzed by the enzyme, so a series of acetyl esters has been used to study the properties of the active site in the enzyme from *Electrophorus electricus* involved in binding these reactants by following the steady-state kinetics of the enzyme.[224]

It had been shown in earlier studies that the kinetic mechanism

*It was the realization that, during most enzymatic reactions, the association of a reactant with the active site is not at equilibrium that led Briggs and Haldane[76] to propose that the steps in an enzymatic reaction, including the associations of reactants, should be treated as being in a steady state rather than at equilibrium, as had been proposed by Michaelis and Menten.[64]

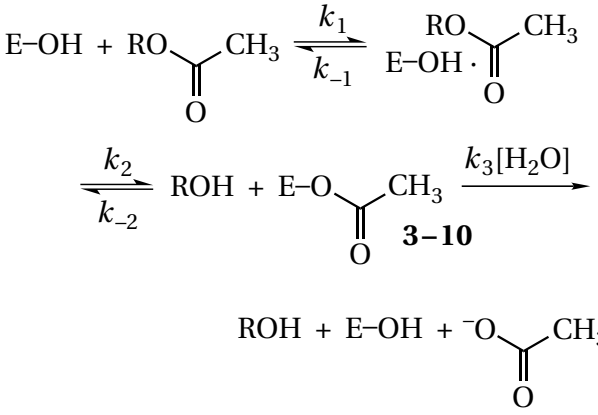

(3–342)

where E–OH is a serine in the active site, was consistent with all the kinetic observations that had been made with acetylcholinesterase. In this mechanism, the term $k_3[H_2O]$ had the same value for all the reactants used in the study because the reactants were all acetyl esters producing the same acetyl enzyme (**3–10**), and the value for the term $k_3[H_2O]$ had already been determined accurately. The catalytic constant, k_0, for the kinetic mechanism (Equation 3–342), when the initial concentration of the product alcohol, $[ROH]_0$, is zero is

$$k_0 = \frac{k_2 k_3 [H_2O]}{k_2 + k_3 [H_2O]} \qquad (3–343)$$

Consequently, from the observed values of the rate constant k_0 for each reactant and the known values for $k_3[H_2O]$ and $[AE]_t$, values of the rate constant k_2 could be calculated for each reactant.

For the kinetic mechanism (Equation 3–342)

$$k_A = \frac{k_2}{\left(\frac{k_{-1} + k_2}{k_1}\right)} \qquad (3–344)$$

With this equation, the observed values of the specificity constant k_A for reactant A, and the calculated values of k_2, values of $(k_{-1} + k_2)\ k_1^{-1}$ could be calculated for each reactant. From comparing measured values of k_2 to estimated values of k_{-1}, it was concluded that, for every reactant except acetylcholine, $k_{-1} >> k_2$ and $(k_{-1} + k_2)\ k_1^{-1}$ was an accurate estimate of the dissociation constant (Equation 3–339) for the binding of each reactant to the active site.[224]

Numerical values of the dissociation constants measured for complexes between enzymes and substrates, between enzymes and competitive inhibitors, or between proteins and ligands have a number of uses. Because they are directly related to changes in standard free energy, they are often related to the types of noncovalent interactions between the site and the ligand. In this way, these dissociation constants are often used to probe the structure of the binding site or the active site.

In the case of acetylcholinesterase, the dissociation constants for a series of *N*-methylated 2-aminoethyl acetates [$H_3N^+C_2H_4$–, $(CH_3)H_2N^+C_2H_4$–, $(CH_3)_2HN^+C_2H_4$–, and $(CH_3)_3N^+C_2H_4$–] were compared, respectively, with a series of corresponding alkyl acetates in which nitrogen has been replaced by carbon [$H_3CC_2H_4$–, $(CH_3)H_2CC_2H_4$–, $(CH_3)_2HCC_2H_4$–, and $(CH_3)_3CC_2H_4$–]. All these acetate esters, both the cations and the alkanes, were reactants in hydrolyses catalyzed by the enzyme (Table 3–4). The fact that little if any difference was observed between the estimated dissociation constants for pairs of substrates having or lacking the cationic elementary charge demonstrates that this feature of the structure of the physiologically relevant substrate, acetylcholine, does not contribute significantly to the favorable change in standard free energy accompanying its association with the active site. The fact that substrates with the same number of hydrogen–carbon bonds, regardless of their net charge, had about the same dissociation constants and the fact that the dissociation constants decrease as the number of hydrogen–carbon bonds increase suggest that it is mainly a hydrophobic effect that drives this association.

In the crystallographic molecular models of complexes between acetylcholinesterase from *Tetronarce californica*[225] and several inhibitors, each containing a trimethylammonium group, that group is found to be pushed up against the side chain of a tryptophan with two of its methyl groups in direct contact with the aromatic π system of the indolyl group, which isolates the hydrogen–carbon bonds from contact with the water of the solution. One of these methyl groups was also in direct contact with the aromatic π system of the phenyl group of a phenylalanine, and three molecules of water form a partial shell of hydration around the third otherwise unoccupied methyl group.[226,227] The fact that this third methyl group has no direct interaction with the active site may explain why the dissociation

Table 3–4: Dissociation Constants[224] for the Binding of Reactants to Acetylcholinesterase[a]

reactant	dissociation constant (mM)
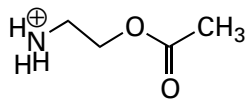	27
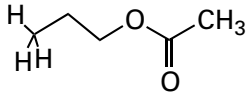	33
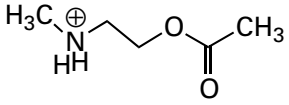	22
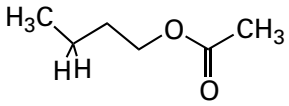	13
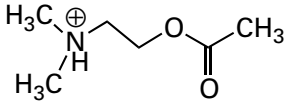	1.4
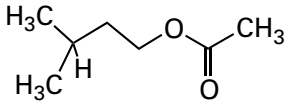	2.8
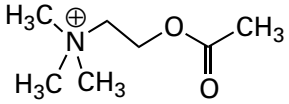	1.2
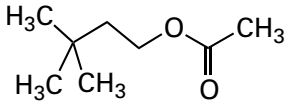	3.1

[a]Dissociation constants were estimated from steady-state kinetics at pH 7.8, 25 °C, and ionic strength of 0.18 M.

constants for the trimethyl reactants are essentially same as those for the dimethyl reactants (Table 3–4). In one of the complexes, a glutamate is 0.35 nm from one of the two methyl groups pushed up against theindolyl group. Site-directed mutations of the tryptophan,[228,229] the phenylalanine,[230] and the glutamate,[170] however, suggest that the π system of the indolyl group of the tryptophan provides the majority of the standard free energy stabilizing the complex between the enzyme and the quaternary ammonium ion. The quadrupole moment of the aromatic π sys-tems surrounding the cation permits the trimethyl-ammonium group to be tolerated in a nonpolar pocket and to bind with the same affinity as a *tert*-butyl group.[231]

In the instance of acetylcholinesterase, a cationic functional group interacts mainly with nonpolar, aromatic π molecular orbital systems, while in a crystallographic molecular model of exo-α-sialidase from influenza virus, the nonpolar methyl group contributing significantly to the potency of an inhibitor is surrounded by three carboxy groups from the side chains of two glutamates and an aspartate.[232] These examples indicate that the structures of the **binding sites for ligands on proteins are often counterintuitive**.

Hexokinase from *S. cerevisiae* associates with its reactants[233,234] with a preference for D-glucose to associate before $MgATP^{2-}$. Because the reactants associate and dissociate rapidly relative to their turnover and because D-glucose is usually the first substrate to bind in this rapid-equilibrium random kinetic mechanism, the Michaelis constant $K_{m,gluc}$ for D-glucose has been shown to be approximately equal to the dissociation constant for its binding to the open active site. Kinetic values for K_m were used as estimates of the dissociation constants for the binding of various analogues for D-glucose to the active site (Table 3–5).[235,236] As is D-glucose, most of these derivatives of D-glucose are phosphorylated at the 6-hydroxy group in a reaction

It is possible **to get a feeling for the structure of the active site** of hexokinase from the changes in K_m caused by various replacements. The active site of the enzyme seems to be open and unrestrictive at carbon 2 of D-glucose because epimerization or replacement of the OH with smaller (hydrogen or fluorine) or larger (chloro or acetamido) groups has little effect on the Michaelis constant. At both carbons 3 and 4, however, epimerization eliminates the ability of the monosaccharide to participate in the reaction. This result suggests that there are either amino acids or polypeptide on the side of the ring opposite the 3-hydroxy group and on the side of the ring opposite the 4-hydroxy group, and anything larger than a hydrogen is sterically excluded. This steric effect must also apply adjacent to the hydroxy group on carbon 3 because methylation at this oxygen produces a substrate that cannot participate in the reaction. A more subtle effect is seen when either the 3-hydroxy group or the 4-hydroxy group is replaced by a fluorine. The 550-fold increase in the Michaelis constant ($\Delta\Delta G^\circ = +15$ kJ mol^{-1}) suggests that in each case a noncovalent interaction, such as a hydrogen bond, directed toward the hydroxy group

Table 3-5: Michaelis Constants[235,236] for Derivatives of D-Glucose[a] as Reactants for Hexokinase[b]

derivative of glucose	Michaelis constant (mM)
D-glucose	0.14
2*S* epimer (D-mannose)	0.05
2-deoxy	0.30
2-deoxy-(2*R*)-acetamido	1.0
2-deoxy-(2*R*)-fluoro	0.19
2-deoxy-(2*S*)-fluoro	0.14
2-deoxy-(2*R*)-chloro	2.1
3*R* epimer (D-allose)	>100
3-deoxy-(3*S*)-fluoro	70
3-*O*-methyl	>100
4*S* epimer (D-galactose)	>50
4-deoxy-(4*R*)-fluoro	84
5-dehydroxymethyl (D-xylose)	10[c]
6-deoxy-6-fluoro	8[c]

[a](2*R*,3*S*,4*R*,5R)-2,3,4,5-Tetrahydroxy-5-(hydroxymethyl)-pentanal. [b]30 °C, pH 7–8.5. [c]Competitive inhibitor, K_i listed.

in particular has been prevented from occurring. A similar although 10-fold less dramatic change is seen when either the 6-hydroxy group is replaced by a fluorine or carbon 6 is eliminated entirely (xylose). All these intuitions about the active site that were derived from the values for these dissociation constants are consistent with the structure of the complex between D-glucose and the active site of the enzyme in a crystallographic molecular model that was constructed much later.[237]

The substitution of a hydrogen on a ligand with a halogen, as was just described in the case of hexokinase, can be used to probe the structure of the site for that ligand on a protein in the vicinity of that hydrogen. If the dissociation constant for the ligand decreases in the sequence –F,–H,–Cl,–Br,–I, this observation indicates that the vicinity is nonpolar.[238] If it decreases and then increases over the same sequence, this observation indicates that the vicinity is sterically hindered because the larger halogens are not tolerated.[239]

The **disposition of subsites** within a particular binding site can be probed systematically. For example, when the distance between a guanidinio group and a phosphate in a series of inhibitors for human purine-nucleoside phosphorylase was varied synthetically, a minimum in the values for the inhibition constant was observed at a distance of 1.1 nm,[240] which suggests that the subsites for these functional groups on the nucleotides that are the normal substrates for the enzyme are located at this distance from each other, as they should be.

In the studies just described, changes are made synthetically in the ligand to probe the structure of the site on the protein or its subsites, but often they are made in pharmaceutical research for the purpose of **improving systematically the affinity of the ligand** for the protein. The specificity of a site on a protein for a ligand can also be changed by directed evolution.[241-243] The protein is randomly mutated, the mutants are screened to discover those with altered affinity in the desired direction, and the best candidates are mutated again and rescreened.

Measurements of the binding of a substrate to an enzyme in the absence of its cosubstrates are often used to confirm or to reject kinetic mechanisms that propose a particular order in which the reactants bind to that active site during enzymatic catalysis.

Most enzymes operate on two or more reactants, and if only one of the two or more reactants is present, it will usually not be transformed by the enzyme. If the enzyme associates with its reactants at random or if the reactant of interest is the first one to associate with the active site, then in the absence of any coreactants, **a reactant will form a meaningful, dead-end complex** with the enzyme, the dissociation constant of which can be measured. For example, NADPH, in the absence of L-homoserine, forms a dead-end complex ($K_{dNADPH} = 0.41 \pm 0.08\ \mu M$) with homoserine dehydrogenase (Figure 3–23); NADH, in the absence of 2-oxoglutarate and ammonia, forms a dead-end complex with glutamate dehydrogenase (Figure 3–24); orotidine 5′-phosphate, in the absence of diphosphate, forms a dead-end complex ($K_{dOMP} = 3.1 \pm 0.3\ \mu M$) with orotate phosphoribosyltransferase; and 2′-deoxyuridine 5′-phosphate, in the absence of (6*R*)-5,10-methylenetetrahydrofolate, forms a dead-end complex ($K_{d,dUMP} = 5\ \mu M$) with thymidylate synthase from *E. coli*.[184]

There are sometimes **ambiguities** in measurements of this kind. For example, the kinetic behavior of the inhibition of aspartate carbamoyltransferase (Equation 3–220) from *E. coli* by *N*-(phosphonacetyl)-L-aspartate (Figure 3–14) and studies of product inhibition of the enzyme,[244] as well as the fact that

addition of carbamoyl phosphate to a solution of aspartate carbamoyltransferase produces a major change in the conformation of the protein while addition of L-aspartate does not,[108,245] are all consistent with the conclusion that carbamoyl phosphate must associate with the active site before L-aspartate can associate with the active site in the reaction leading to products. Aspartate, however, can bind to the unoccupied enzyme, presumably at a site unrelated to the active site, with a dissociation constant even smaller than its dissociation constant when it is productively associating with the active site occupied by carbamoyl phosphate.[178] The substrate fructose 6-phosphate can bind to six sites on each protomer of ovine 6-phosphofructokinase (Equation 3–300), but the addition of phosphate, which eliminates the nonspecific binding attributable to the phospho group on fructose 6-phosphate, decreases the number of sites to one for each subunit.[246] Presumably, this one remaining site is the active site. Analogues for ATP bind to three sites on every protomer of 6-phosphofructokinase from *O. cuniculus*. One of these is a site at which fructose 1,6-bisphosphate also binds,[247] which cannot be the site for productive association of $MgATP^{2-}$.

When reactants enter the active site at random, either reactant must be able to bind to the enzyme in the absence of the other. For example, the observation that both $MgATP^{2-}$ and fructose 6-phosphate by themselves can associate with 6-phosphofructokinase from *E. coli* to form the respective dead-end complexes was presented as further evidence that these two reactants normally associate at random with the active site of the enzyme.[183]

If **the kinetic mechanism is rapid-equilibrium random** (Equation 3–121) so that $K_{mA} = \alpha K_{dA}$ and $K_{mB} = \alpha K_{dB}$ (Equations 3–104 and 3–129) and if those two reactants associate with the enzyme independently of each other ($\alpha = 1$), then the two Michaelis constants, K_{mA} and K_{mB}, should equal the dissociation constants for the respective reactants. Both quinolate alone ($K_{dQA} = 20\ \mu M$) and 5-phospho-α-D-ribose 1-phosphate alone ($K_{dPRPP} = 50\ \mu M$) bind to nicotinate-nucleotide diphosphorylase (carboxylating) from *S. typhimurium* and, in the absence of the other reactant, form dead-end complexes with the enzyme. The similarity between these two dissociation constants and the respective Michaelis constants ($K_{mQA} = 25\ \mu M$ and $K_{mPRPP} = 30\ \mu M$) was presented as evidence that the enzyme has a rapid-equilibrium, random kinetic mechanism.[163] The dissociation constants for either NAD^+ (300 μM) or UDP-glucose (40 μM) when either binds to bovine UDP-glucose dehydrogenase in the absence of the other[248] are of the same order of magnitude as the values for their Michaelis constants (500 μM and 10 μM, respectively),[249,250] which were measured under significantly different conditions, and these observations were presented as evidence for a kinetic mechanism in which the two reactants bind at random and at equilibrium in the first steps of the reaction catalyzed by this enzyme. The directly measured dissociation constants for either L-isoleucine (25 μM) or $MgATP^{2-}$ (150 μM) when either binds in the absence of the other[251] to isoleucine-tRNA ligase from *E. coli* are close to the values estimated for their dissociation constants calculated from kinetic measurements (4 μM and 150 μM, respectively).[252]

When **reactants must associate with the active site in a particular order**, only the first should be able to bind to the unoccupied enzyme. The fact that thymidine kinase from herpes simplex virus forms a dead-end complex with thymidine in the absence of $MgATP^{2-}$ but associates with H_2ATP^{2-}, an unreactive analogue of $MgATP^{2-}$, only in the presence of thymidine suggests[253] that, in the normal enzymatic reaction, thymidine must associate with the enzyme before $MgATP^{2-}$. Likewise, the facts that isocitrate forms a dead-end complex with isocitrate dehydrogenase (NAD^+)

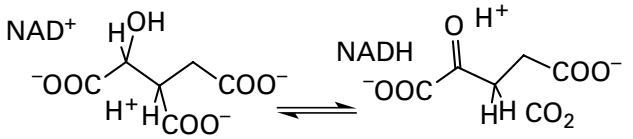

(3–345)

from *S. cerevisiae* in the absence of NAD^+, with a dissociation constant equal to its Michaelis constant, but that NAD^+ does not bind to the enzyme in the absence of isocitrate[254] are consistent with a kinetic mechanism in which isocitrate is required to enter the active site before NAD^+.* The facts that D-glucose binds to hexokinase from *S. cerevisiae*, in the absence of $MgATP^{2-}$, with a dissociation constant equal to its Michaelis constant but that $MgATP^{2-}$ binds much less strongly to the enzyme in the absence of a monosaccharide[234] confirms a kinetic mechanism in which D-glucose usually binds first to the active site.

*This behavior is an example of an active site that does not form a "holoenzyme" with a nicotinamide coenzyme in the absence of its nominal substrate.

In theory, in the situation when one reactant is required to associate with the enzyme before another, the association of the first reactant must decrease the dissociation constant for the second reactant from infinity to a finite value. This shift would be an extreme example of an increase in the affinity of a protein for one ligand caused by the binding of another. Usually, as one might expect, **one ligand increases the affinity of a protein for another** by less than an infinite factor. For example, the association of $MgGDP^-$ increases the affinity of amidophosphoribosyltransferase from *Bacillus subtilis* for $MgADP^-$ by only a factor of 200.[255] In the case of the binding of nitrate, creatine, and $MgADP^-$ to creatine kinase from *O. cuniculus*, any two of the ligands bind independently of each other, but for all possible combinations, the association of two of the ligands decreases the dissociation constant of the third by a factor of 10.[256] In reality, the conclusion that one reactant must associate with an active site before the other is actually a conclusion that the association of the first reactant simply increases the affinity of the active site for the second.

As already noted, the increase in the affinity of a protein for one ligand in the presence of another is best described by a linkage relation (Equation 3–122). For example, the inhibitor *N*-(phosphonomethyl)-glycine (PMG)

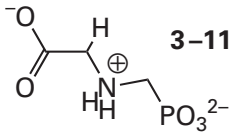

has a dissociation constant for 3-phosphoshikimate 1-carboxyvinyltransferase (Equation 3–262) from *S. pneumoniae* that is 1700 times smaller when the enzyme is occupied its substrate shikimate 3-phosphate ($K_{dPMG,S3P} = 0.25\ \mu M$) than when its active site is vacant ($K_{dPMG} = 420\ \mu M$).[257,258] The linkage relation defining this increase in affinity is

$$\begin{array}{ccc} E + S3P + PMG & \underset{K_{dS3P}}{\rightleftharpoons} & E{\cdot}S3P + PMG \\ \Big\Updownarrow K_{dPMG} & & \Big\Updownarrow K_{dPMG,S3P} \\ E{\cdot}PMG + S3P & \underset{K_{dS3P,PMG}}{\rightleftharpoons} & E{\cdot}S3P{\cdot}PMG \end{array} \qquad (3\text{–}346)$$

where E is the enzyme and S3P is shikimate 3-phosphate. In a clockwise direction around the cycle, $K_{dS3P}^{-1}\, K_{dPMG,S3P}^{-1}\, K_{dS3P,PMG}\, K_{dPMG} = 1$. If this linkage relation describes the situation, the observed dissociation constant for shikimate 3-phosphate from enzyme occupied by *N*-phosphonomethyl-glycine ($K_{dS3P,PMG} = 0.50\ \mu M$) should also be 1700 times smaller than that for the unoccupied enzyme ($K_{dS3P} = 770\ \mu M$), which it is. The independent measurement of the four dissociation constants in this particular cycle establishes the linkage relation.[257]

Suggested Reading

Hasan, F. B., Cohen, S. G., and Cohen, J. B. (1980) Hydrolysis by acetylcholinesterase: Apparent molal volumes and trimethyl and methyl subsites, *J. Biol. Chem. 255*, 3898–3904. https:// www.jbc.org/article/S0021-9258(19)85610-7/pdf

Anderson, K. S., Sikorski, J. A., and Johnson, K. A. (1988) Evaluation of 5-enolpyruvoylshikimate-3-phosphate synthase substrate and inhibitor binding by stopped-flow and equilibrium fluorescence measurements, *Biochemistry 27*, 1604–1610. https://doi.org/10.1021/bi00405a032

Harris, B. Z., Hillier, B. J., and Lim, W. A. (2001) Energetic determinants of internal motif recognition by PDZ domains, *Biochemistry 40*, 5921–5930. https://doi.org/10.1021/bi010142l

Problem 3–18: Show that Equations 3–343 and 3–344 follow from the kinetic mechanism in Equation 3–342.

Problem 3–19: When D-glucose 6-phosphate (G6P) or D-fructose 6-phosphate (F6P) is added to glucose-6-phosphate isomerase from *O. cuniculus*, the enzyme converts either one to an equilibrium mixture of both (hexose 6-phosphate, H6P). The sum of their concentrations, [H6P], can be measured by beginning the experiment with versions of either that are uniformly labeled with carbon-14. The following observations[156] were made by equilibrium dialysis at pH 8.0 and 30 °C. The concentration of protein was 10.0 g L^{-1}.

$[H6P]_{free}$ (mM)	$[H6P]_{bound}$ (mM)
46	35
45	32
125	67
266	96
270	100
561	113
3010	142

(A) Plot these data directly.
(B) Use a fitting program to fit these data to a rectangular hyperbola, or plot the data on a Scatchard plot.
(C) Determine the apparent dissociation constant for hexose 6-phosphate and the grams of protein (mole of sites)$^{-1}$ at saturation.
(D) The molar mass of glucose-6-phosphate isomerase from *O. cuniculus* calculated from the sequences of amino acids for its subunits is 125,230 g mol^{-1}. How many protomers does each oligomer contain?

Each measurement is made at equilibrium. At equilibrium, each step in the kinetic mechanism of the enzyme has come to equilibrium, as well as the concentrations of D-glucose 6-phosphate and D-fructose 6-phosphate.

(E) Write an equilibrium mechanism for the enzymatic reaction that takes into account the binding of substrates to the active site and the interconversion of the substrates on the active site. Your expression should be a set of four linked equilibria.
(F) What is the expression for the apparent dissociation constant

$$K_{dGP,app} = \frac{[E]_{eq}\left([F6P]_{eq} + [G6P]_{eq}\right)}{\left([E{\cdot}F6P]_{eq} + [E{\cdot}G6P]_{eq}\right)}$$

of the equilibrium mixture of substrates from the active site in terms of only equilibrium constants from your linked equilibria.

Problem 3–20: Using Equations 3–326 through 3–331, derive the cubic equation in $[M{\cdot}ST]_{eq}$ (Equation 3–332) and then the cubic equations in Y_M (Equation 3–333) and in Q_{obs} (Equation 3–334).

Problem 3–21: A group of proteins, the selectins, which are found on the surfaces of particular cells, are mammalian lectins that are distinguishable by their ability to recognize and bind unique oligosaccharides. When the specific selectins on the surface of one cell bind to the oligosaccharides on the surface of another cell, the first cell adheres to the second cell. The extracellular portion of E-selectin is a fragment of the intact molecule of E-selectin that lacks the membrane-spanning portions of the protein, is freely soluble, and contains one binding site for its particular ligands, one of which is the sialyl Lewis *x* oligosaccharide *N*AcNeu*p*-(β2,3)-D-Gal*p*-(β1,4)-[L-Fuc*p*-(α1,3)]-D-Glc, where *N*AcNeu is the pyranose of *N*-acetylneuraminic acid, β-D-Gal*p* is β-D-galactopyranose linked at the 4-hydroxy group of D-glucopyranose, α-L-Fuc*p* is α-L-fucopyranose linked at the 4-hydroxy group of the same D-glucopyranose, and D-Glc is D-glucose.[259] A fluoresceinyl group was attached synthetically to the hydroxy group of the hemiacetal of the D-glucose in this oligosaccharide, and the product is designated sLe^x[Glc]-Fl. When sLe^x[Glc]-Fl is bound by the extracellular portion of human E-selectin (E1), the anisotropy of the fluorescence from its fluoresceinyl group increases because it becomes less mobile. When samples containing 1.0 μM or 0.2 μM sLe^x[Glc]-Fl were mixed with various concentrations of E1, the following values for anisotropy of fluorescence were observed.[190]

	anisotropy of fluorescence (r)	
[E1] (μM)	1.0 μM sLe^x[Glc]-Fl	0.2 μM sLe^x[Glc]-Fl
173	0.172	0.184
140	0.159	0.164
53	0.130	0.133
41	0.121	0.120
34	0.115	0.115
25	0.108	0.110
23	0.105	
15	0.095	0.095
0	0.075	0.075

where the concentrations of E1 and sLe^x[Glc]-Fl are all total concentrations.

(A) Plot Δr against $[E1]_{eq}$ (Equation 3–303).
(B) Use a fitting program to fit these data to a rectangular hyperbola, or plot the data on a Scatchard plot.
(C) Determine the dissociation constant for sLe^x[Glc]-Fl from E1 and r_{sat}, the anisotropy of the fluorescence at saturation.
(D) Why were two different concentrations of sLe^x[Glc]-Fl used in the measurements?

Problem 3–22: Adenine phosphoribosyltransferase catalyzes the reaction

magnesium 5-phospho-α-D-ribose 1-diphosphate + adenine $\rightleftharpoons$ AMP^{2-} + magnesium diphosphate

Various phosphates have been found to be inhibitors of adenine phosphoribosyltransferase.[260] Values for the dissociation constants (determined as inhibition constants, K_i) between various inhibitors and the enzyme are shown in the table, and some are plotted in the figure on a common logarithmic scale.

compound	K_d (mM)
Mg 5-phospho-α-D-ribose 1-diphosphate	0.0002
D-ribose	>50
α-D-ribose 1-phosphate	>50
D-ribose 5-phosphate	3.3
D-fructose 6-phosphate	5.1
D-glucose 6-phosphate	5.1
α-D-ribose 1,5-bisphosphate	0.12
D-ribulose 1,5-bisphosphate	0.41
D-fructose 1,6-bisphosphate	0.20
α-D-glucose 1,6-bisphosphate	0.42
ethylene glycol bisphosphate	24
propane-1,3-diol bisphosphate	1.2
butane-1,4-diol bisphosphate	0.45
pentane-1,5-diol bisphosphate	0.39
hexane-1,6-diol bisphosphate	0.38

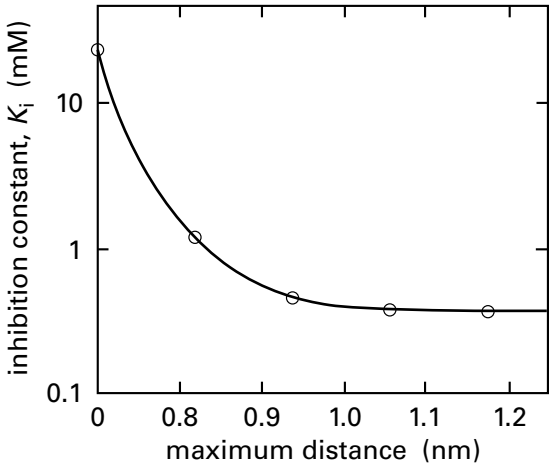

(A) Explain the dissociation constants listed in the table. Why were the other monosaccharide phosphates and bisphosphates included?
(B) Explain the dissociation constants plotted in the figure.
(C) What is the difference in free energy of binding between a diol bisphosphate that fits the active site well and α-D-ribose 1,5-bisphosphate?
(D) Assume that the main difference between a diol bisphosphate and D-ribose 1,5-bisphosphate is the hydroxy groups of the ribose, and discuss this difference of free energy in terms of the enthalpies of formation of the hydrogen bonds. Recall that the active site is constructed for a ribose.

Molecularity and Approximation

During an elementary chemical reaction or during one of the elementary steps of a composite reaction, **the nuclei of the atoms involved in the reaction change their mean positions relative to each other**. The relative positions of the atomic nuclei in the reactants are different from their relative positions in the products. If there are n nuclei in the reactants, and therefore n nuclei in the products, $3n-6$ coordinates are required to define the relative positions of these nuclei in space when they are close enough together to participate in the reaction. Assigning a numerical value to each of these $3n-6$ coordinates defines a relative distribution of the nuclei in space. It can be assumed that the electrons redistribute in response to the motion of the nuclei so rapidly that the positions of the nuclei are all that is needed to define the system.[261] This particular distribution of nuclei and electrons has a specific potential energy, E_p, associated with it. The atomic coordinates and the associated potential

energies together create a surface of potential energy in $(3n-5)$-dimensional space.

The initial state for an **intramolecular, unimolecular reaction** in which a bond will be formed between two atoms in the reactant is any conformation of a molecule of the reactant in which the two atoms to be joined are separated sufficiently that the behavior of each is not significantly affected by the motion of the other but are approaching each other on a trajectory that will lead to intramolecular collision and formation of the bond. The final state for such a reaction is the product containing the new bond in its ground state. The initial state for an intramolecular, unimolecular reaction in which a bond will be broken is the ground state of the molecule containing the susceptible bond. The final state for such a reaction is the molecules of product in which the two atoms previously bonded have separated from each other sufficiently that the behavior of each is not significantly affected by the motion of the other. The initial state for an **intermolecular, bimolecular reaction** is the separated molecules of the reactants, too distant from each other to affect their individual free energies but on trajectories that will lead to a productive collision. The final state is the separated molecules of product departing from the productive collision. In any given reaction, the initial state and the final state can be assigned to broad minima on the surface of potential energy describing that reaction.

Any reaction that converts reactants into products must **follow a path on the surface of potential energy** between the region occupied by the reactants and the region occupied by the products. Each path must pass through a point that has the highest potential energy for that particular path. Within the set of the infinite number of paths between reactant and product, there will be a col. The **col** is the highest point on a subset of these paths that has a lower potential energy than the highest points on all the other paths. This col is analogous to the pass of lowest altitude through a range of mountains separating two geographical points. Because this col represents the lowest barrier of potential energy between reactants and products, a chemical reaction connecting reactants and products usually will proceed on a path through or near this col. For a given reaction, if a local minimum of potential energy is encountered along the paths leading through a col so that all the paths have two cols, or two maxima of potential energy, then the reaction is a composite reaction that proceeds through

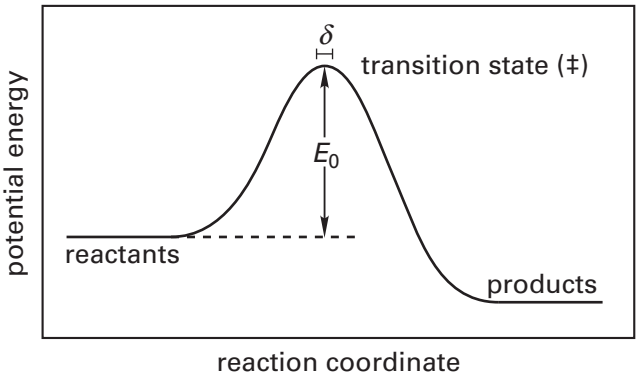

Figure 3–25: Variation in potential energy, E_p, as function of the distance along a reaction coordinate.[262] The plateaus on the two sides are the potential energies of separated reactants and separated products, far enough apart that they have no interaction with each other. The potential energy at the peak is the potential energy of the transition state (‡). The width, δ, is the portion of the reaction coordinate occupied by the transition state. The height, E_0, is the difference in potential energy between reactants and transition state.

an intermediate. In this instance, the reaction is divided into two steps, and each step is an elementary reaction. Consequently, a path between reactants and products, between reactants and an intermediate, between one intermediate and another intermediate, or between an intermediate and products on the surface of potential energy through the col for that particular step has only one maximum of potential energy, which is the col itself. **A reaction coordinate is a path through a col**.

A reaction coordinate is presented figuratively (Figure 3–25)[262] as a curve beginning on a plateau the potential energy of which is that of the separated reactants and ending on a plateau the potential energy of which is that of the separated products for a particular step in a reaction. The abscissa is the distance along the reaction coordinate over the surface of potential energy, and the ordinate is the potential energy associated with a given distance along the reaction coordinate. Each point on the reaction coordinate defines a distribution of atomic nuclei in space. As the reaction progresses along the reaction coordinate, the nuclei participating in the reaction are changing their relative positions as reactants are transformed into products.

The relative positions of the nuclei in space at the col, the point of highest potential energy, comprise the transition state. The transition state, as for any stable molecule, is a collection of nuclei distributed in space in association with a particular number of electrons, which are confined to the atomic and

molecular orbitals dictated by that distribution of nuclei. The only difference between a transition state for an elementary reaction and the reactants or products for that elementary reaction is that the transition state is directly unstable with respect to both. If the transition state were at rest at the highest point of the col, it would be immediately transformed with equal probability into either reactants or products.

For reactants to be transformed into products in an elementary reaction, **sufficient energy must be available** for the reactants to reach the potential energy of the transition state. This energy is usually provided by the kinetic energy of the collision in a multimolecular reaction or by fluctuations in internal energy in a unimolecular reaction, but any other source of energy is also acceptable.

According to **transition state theory**,[262,263] the rate constant of a chemical reaction, k_r, is

$$k_r = \kappa_T \frac{k_B T}{h} {}^{\ddagger}K' \tag{3–347}$$

where κ_T is the transmission coefficient, k_B is the Boltzmann constant, and h is the Planck constant. The transmission coefficient is the fraction of the transition states that have been successfully reached by the reactants and then decompose into products, and it is thought to be close to unity under normal circumstances because the motion along the reaction coordinate is usually in the direction of products.[263] The constant ${}^{\ddagger}K'$ is defined as

$${}^{\ddagger}K' = \frac{{}^{\ddagger}Q^{0\prime}}{Q^0_A Q^0_B \cdots} e^{-E_0/RT} \tag{3–348}$$

where ${}^{\ddagger}Q^{0\prime}$ is the **partition function of the transition state** calculated from all degrees of freedom available to the transition state except motion along the reaction coordinate, $Q^0{}_i$ is the partition function of reactant i, and E_0 is the difference in potential energy between the reactants and the transition state (Figure 3–25). The zeroes as superscripts denote partition functions for the same standard volume.

Although ${}^{\ddagger}K'$ is formally determined only by partition functions and potential energies, it is mathematically indistinguishable from the statistical mechanical expression for an equilibrium constant, and it is possible to define a **standard free energy of activation $\Delta^{\ddagger}G^{\circ\prime}$** for an elementary reaction by the equation

$$\Delta^{\ddagger}G^{\circ\prime} \equiv -RT \ln {}^{\ddagger}K' = -RT \ln\left(\frac{h k_r}{\kappa_T k_B T}\right) \tag{3–349}$$

It should be noted that this equation is a definition of $\Delta^{\ddagger}G^{\circ\prime}$ only in terms of the observed rate constant for the elementary reaction, k_r. While values for $\Delta^{\ddagger}G^{\circ\prime}$ can be estimated by calculation, at the moment, tabulated experimental values for $\Delta^{\ddagger}G^{\circ\prime}$ are nothing more than tabulations of values obtained with Equation 3–349 from particular observed rate constants, usually with the unacknowledged assumption that $\kappa_T = 1.0$.

In transition state theory, ${}^{\ddagger}Q^{0\prime}$ is the quotient of the actual partition function for the transition state, ${}^{\ddagger}Q^0$, and the factor $[\delta(2\pi {}^{\ddagger}m k_B T)^{1/2}]\ h^{-1}$, where ${}^{\ddagger}m$ is the mass of the transition state and δ is the distance along the reaction coordinate occupied by the transition state (Figure 3–25). This factor is **the partition function for translation of the transition state along the reaction coordinate**. Therefore

$$k_r = \frac{\kappa_T}{\delta}\left(\frac{k_B T}{2\pi {}^{\ddagger}m}\right)^{1/2}\left(\frac{{}^{\ddagger}Q^0}{Q^0_A Q^0_B \cdots}\right) e^{-E_0/RT} \tag{3–350}$$

The same reaction can be performed at the same temperature but under two separate situations. For example, it could be performed in solution and on the active site of an enzyme, or on the respective active sites of the same enzymes from two different species, or on the wild type and a mutant form of the same enzyme. If it is assumed that κ_T, δ, and ${}^{\ddagger}m$ are about the same in the two situations, then, because

$$\mu^{\circ}{}_i = -RT \ln Q^0{}_i \tag{3–351}$$

where $\mu^{\circ}{}_i$ is the standard chemical potential of species i

$$-RT \ln\left(\frac{k_1}{k_2}\right) = \Delta E_0 + \left({}^{\ddagger}\mu^{\circ}{}_1 - {}^{\ddagger}\mu^{\circ}{}_2\right) - \left(\mu^{\circ}{}_{A1} - \mu^{\circ}{}_{A2}\right) - \left(\mu^{\circ}{}_{B1} - \mu^{\circ}{}_{B2}\right) - \cdots \tag{3–352}$$

and

$$-RT \ln\left(\frac{k_1}{k_2}\right) = \Delta\Delta^{\ddagger}G^{\circ} \tag{3–353}$$

In Equation 3–353 the **difference in standard free energies of activation, $\Delta\Delta^{\ddagger}G^{\circ}$**, is the difference in the actual standard free energies of activation for the reactions under the two circumstances. The actual standard free energies of activation themselves, $\Delta^{\ddagger}G^{\circ}_{i}$, are the differences between the standard chemical potentials of the reactants and the standard chemical potentials of the respective transition states. Therefore, any difference between the two situations that increases the standard chemical potential of the reactants or decreases the standard chemical potential of the transition state in the second situation, or does both, will cause the reaction to have a greater rate in the second situation than in the first. The observed difference in rate between the two situations can be used to calculate the numerical value for the change in standard chemical potential of the transition state relative to that of the reactants. The three assumptions made in deriving Equation 3–353, however, should not be forgotten.

One of the more remarkable advantages of enzymatically catalyzed reactions is the increase in rate accomplished by the enzyme. Comparisons of enzymatically catalyzed rates of reaction and uncatalyzed rates of reaction are usually made with the catalytic constant of the enzyme, k_0, and the rate constant for the same reaction in aqueous solution at neutral pH, at the same temperature, and in the absence of catalysis. It has already been noted that increases of as much as 10^{20} and 10^{23} M in rate have been observed.[264,265] In discussions of enzymatic catalysis, these dramatic accelerations are usually emphasized.

The catalytic constant of an enzymatic reaction is the rate constant for that reaction as it occurs on the active site after all reactants have been assembled by their association with the active site. Rates of association of the reactants with the active site have been eliminated from consideration by adding saturating concentrations of all reactants to achieve the conditions producing a rate governed only by k_0. Therefore, **a catalytic constant is always the rate constant for an intramolecular reaction**.

Intramolecular, nonenzymatic chemical reactions often occur at rates much greater than those of equivalent intermolecular reactions. In almost all cases, the intramolecular reactions involved in the comparisons are for a molecule containing two reactive centers that combine in a transition state. In the following discussion, bimolecular reactions between two separate reactants will be compared with intramolecular reactions between the same reactive centers. An example of such a comparison is that between the intramolecular attack of the hydroxy group in the intramolecular nucleophilic substitution[266]

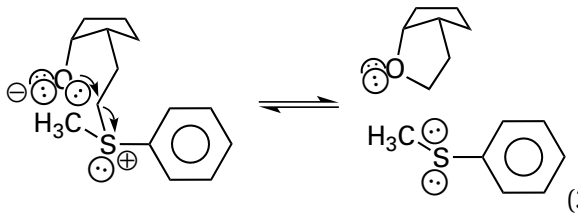

(3–354)

for which the rate constant at 25 °C is 5×10^{-6} s^{-1} while the rate constant for the attack of water on 4-nitrophenyldimethylsulfonium at 25 °C is approximately 10^{-11} M^{-1} s^{-1}.

The rate constant for transfer of the acetyl group between the adjacent 2′- and 3′-hydroxy groups of the ribose in *O*-acetyluridine

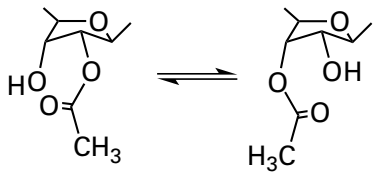

(3–355)

is 0.01 s, and the rate constant for hydrolysis of *O*-acetyluridine by the water that surrounds it is 3×10^{-7} M^{-1} s^{-1}, in each case at neutral pH and 20 °C.[267,268]

At neutral pH and 50 °C, the rate constant (2×10^{-3} s^{-1}) for hydrolysis of the dianion of bis(salicylyl) phosphodiester **3–12**

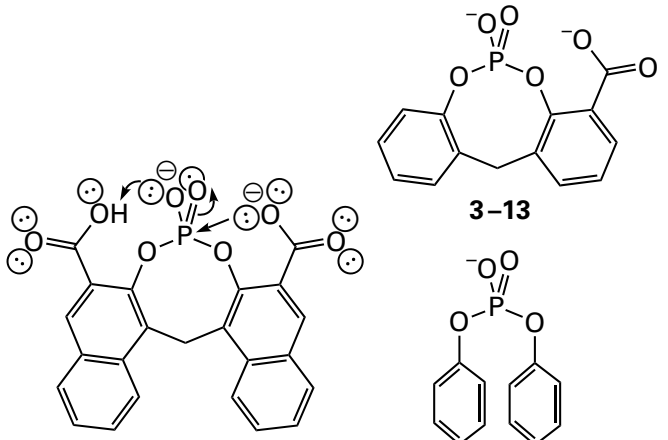

3–13 **3–12** **3–14**

is 7×10^{4} times faster than the rate constant (3×10^{-8} s^{-1}) for hydrolysis of the phosphomonoanion

of *o*-carboxylatobisphenyl phosphodiester **3–13**, and the rate constant estimated for hydrolysis of the monoanion of diphenyl phosphate **3–14** is $1 \times 10^{-13}\ M^{-1}\ s^{-1}$. Hydrolysis of the bis(salicylyl) phosphodiester **3–12** results from rate-limiting intramolecular nucleophilic attack on phosphorus of one of the *o*-carboxy groups under intramolecular general acid catalysis by the other *o*-carboxy group.[269] Many other examples of intramolecular accelerations of rates have been reported.[270,271]

At one time it was fashionable to refer to these accelerations in rate as due to an increase in the **effective molarity** of one of the reactants brought about by attaching it covalently to the other. As more exaggerated examples of this phenomenon were reported, however, the unreality of discussing concentrations such as 5×10^5 M, as in the case of the intramolecular nucleophilic substitution of Equation 3–354, became apparent,[272] and a more sophisticated view of the situation was required.

In all instances in which the rate constant for an intramolecular reaction is compared to the rate constant for an intermolecular reaction, the difference observed in the two rate constants, k_{intra} and k_{inter}, is due in large part to the fact that the standard entropy of molecularity is missing from the standard free energy of activation for the intramolecular reaction. In the case of an intermolecular reaction, the **standard entropy of molecularity**, $\Delta^{\ddagger}S^{\circ}_{molec}$, is the change in standard entropy due solely to bringing two separate reactants together into the same solvent cage in an encounter complex. The formation within a solvent shell of a complex between the two molecules requires that two or more independent molecules become the equivalent of one molecule, and this combination of the two molecules involves a considerable decrease in standard entropy. The standard entropy of molecularity is a negative number because the intrinsic entropy of two separate reactants diffusing independently through solution is greater than that of a complex within a solvent cage into which the two reactants have entered that is also diffusing through the same solution. This decrease in standard entropy is a major, unavoidable, unfavorable term in the standard free energy of activation in any bimolecular intermolecular reaction. In an intramolecular reaction, however, this decrease due to the standard entropy of molecularity does not occur, because the one molecule containing the two reactants is already in a solvent cage diffusing through solution. This fact has the effect of increasing dramatically the standard entropy of activation for the intramolecular reaction relative to the intermolecular reaction. Because the standard entropy of molecularity is missing from the standard entropy of activation for the intramolecular reaction, owing to the fact that approximation has already been accomplished synthetically, the standard entropy of activation for the intramolecular reaction is necessarily greater than that for the intermolecular reaction.

These considerations can be expressed in equations. If the same reaction with the same changes in standard enthalpy and standard entropy were occurring once the reactants have entered the solvent shell, then the standard entropy of activation, $\Delta^{\ddagger}S^{\circ}_{intra}$, of the intramolecular reaction would be related to the standard entropy of activation, $\Delta^{\ddagger}S^{\circ}_{inter}$, of the intermolecular reaction by

$$\Delta^{\ddagger}S^{\circ}_{inter} = \Delta^{\ddagger}S^{\circ}_{intra} + \Delta^{\ddagger}S^{\circ}_{molec} \qquad (3\text{–}356)$$

Consequently

$$R\ln\left(\frac{k_{intra}}{k_{inter}}\right) = \Delta^{\ddagger}S^{\circ}_{intra} - \Delta^{\ddagger}S^{\circ}_{inter} = -\Delta^{\ddagger}S^{\circ}_{molec} \qquad (3\text{–}357)$$

Because $\Delta^{\ddagger}S^{\circ}_{molec} < 0$, $k_{intra} > k_{inter}$. Once the encounter complex has formed in the intermolecular reaction, however, the achievement of the transition state is quite different from that in the intramolecular reaction.

There is a standard entropy of rotational restraint affiliated with both an intramolecular reaction and an encounter complex of two molecules in a solvent shell. The **standard entropy of rotational restraint** is the decrease in standard entropy that is required to constrain a portion of the rotational motions within a solvent cage during the formation of a transition state to achieve the proper orientation of the atoms participating directly in the reaction. In the intermolecular reaction, the two reactants in the solvent cage are unattached and free to rotate independently. In the intramolecular reaction, where the two reactants are attached together, the standard entropy of rotational restraint arises from the fact that formation of the transition state during an intramolecular reaction requires that a portion of the internal rotational entropy in the molecule be eliminated because only a fraction, often only a small fraction, of the accessible rotational isomers can participate in the reaction productively. In both cases, a decrease in entropy is required to bring

these rotational motions into the conformation required for the transition state to form.

The **standard entropy of approximation** is the decrease in standard entropy that results when two reactants that are either free in solution or in covalent association are within a solvent cage with the alignments required to form the transition state for the reaction in which they participate. It is necessarily a negative number. The magnitude of the standard entropy of approximation is the sum of the standard entropy of molecularity and the standard entropy of rotational restraint[272]

$$\Delta^{\ddagger}S^{\circ}_{\text{approx}} = \Delta^{\ddagger}S^{\circ}_{\text{molec}} + \Delta^{\ddagger}S^{\circ}_{\text{rot}} \qquad (3\text{–}358)$$

The **magnitudes of each of these terms** can be discussed in turn.

The standard entropy of molecularity is the decrease in standard entropy that should accompany the change of an intermolecular reaction to an intramolecular reaction.[272] In the specific case of a bimolecular reaction in free solution, the two independent reactants have six translational and six external rotational degrees of freedom when moving through the solution, but the one encounter complex formed by the association of the two reactants should have only three translational and three external rotational degrees of freedom. The **change in standard entropy associated with the loss of just the three translational and three external rotational degrees of freedom** during this inescapable association, calculated for the situation in which the two reactants and the transition state or product are dissolved in a solution at 25 °C with a standard state of 1 M in solutes, has been estimated[272] to be between –160 and –210 J K^{-1} mol^{-1}.

It has also been estimated[272] that –190 to –220 J K^{-1} mol^{-1} is an adequate estimate for $\Delta^{\ddagger}S^{\circ}_{\text{approx}}$, the maximum decrease in standard entropy change expected from converting an intermolecular, bimolecular reaction into an encounter complex with the proper orientations to achieve the transition state, when molarities are used as units of concentration for **standard states**. This estimate can be compared to the standard entropy change observed for a simple bimolecular reaction between two rigid molecules to form a single rigid molecule entropically resembling a transition state, such as the dimerization of cyclopentadiene in the liquid phase, for which the standard entropy change is –130 to –170 J K^{-1} mol^{-1} with the same choice of standard state. The difference between the calculated and the observed standard entropy change in the particular instance of cyclopentadiene can be accounted for by the presence of low-frequency **vibrations** in the dimer that could not be present in the two monomers because of their smaller size. If corrected volume fractions[273,274] are used as units of concentration for standard states and the partial molar volumes of the reactants were 0.1 L mol^{-1}, which is about the volume of a normal small molecule, then the range expected for standard entropy of approximation for a bimolecular reaction would be –160 to –190 J K^{-1} mol^{-1}.

As the example of the dimerization of cyclopentadiene illustrates, an intramolecular reaction, because it usually involves a larger and more flexible molecule than any of the reactants in the intermolecular reaction with which it is being compared, can never realize all of this favorable standard entropy of approximation. Major factors in decreasing the portion of the standard entropy of approximation that an intramolecular reaction will enjoy are the internal rotations about the covalent bonds within the intramolecular reactant itself. These rotations decrease the probability that the necessary juxtaposition of reactive centers will occur. For example, in the case of the sulfonium ion in Equation 3–354, if its cyclopentane is for the moment assumed to be rigid, then the rotational orientation around two carbon–carbon bonds must be appropriate if the hydroxy oxygen is to be placed adjacent to the electrophilic carbon. It has been estimated[272] from the results of thermodynamic and kinetic measurements from a number of intramolecular reactions that the standard entropy of rotational restraint decreases by about 20 J K^{-1} mol^{-1} for every bond that lies between the two atoms participating directly in the reaction and about which free rotation can occur. This value is for reactions in which a covalent bond is formed between the two participants. Nevertheless, measurements of the effect of increasing the number of bonds between donor and acceptor on the standard free energy of formation of an intramolecular hydrogen bond between a hydroxy group and an acyl oxygen in $CDCl_3$ led to the conclusion that the standard entropy of rotational restraint also decreased by about 20 J K^{-1} mol^{-1} for every bond that lies between the two atoms participating directly in the hydrogen bond and about which free rotation can occur.[275]

The effect of approximation on the rate constant for an intramolecular reaction is usually significant only when the two central atoms that participate in the reaction become involved in a **five-membered or six-membered ring** in the transition state. A

four-membered ring is usually too strained, because of the normal bond angles of commonly encountered organic molecules, to provide any favorable approximation. A seven-membered ring, if there is free rotation about every bond, has too negative a value of $\Delta^{\ddagger}S^{\circ}_{\text{rot}}$ to exhibit a $\Delta^{\ddagger}S^{\circ}_{\text{approx}}$ negative enough to have a noticeable effect on rates. For example, even in the intramolecular nucleophilic catalysis of phenyl ester hydrolysis by a carboxy group,[271,276] a series of reactions unusually prone to intramolecular catalysis, phenyl adipate would show a rate of phenolate release due to nucleophilic catalysis only 4-fold greater than that for the same reaction of phenyl acetate in 1.0 M sodium acetate. Large, rigid molecules in which the two atoms that must react are more than five covalent bonds apart yet close enough to collide are difficult to synthesize, with the relevant exception of two reactants held in the proper orientation within the active site of a molecule of protein.

There are also **steric effects** that arise in an intramolecular reaction that are absent in the corresponding intermolecular reaction and that result from the structure of the covalent scaffold that connects the two reactive centers. These steric effects increase the standard free energy of activation and decrease the ratio between the rate constants for the intramolecular reaction and the intermolecular reaction. In the case of an enzyme, however, the two reactants are not covalently attached by a scaffold but juxtaposed by noncovalent forces, a situation in which disadvantageous steric effects may well be at a minimum as a result of natural selection.

If the magnitude of $\Delta\Delta^{\ddagger}S^{\circ}$, the actual difference between the standard entropies of activation, must be less than the magnitude of $\Delta^{\ddagger}S^{\circ}_{\text{approx}}$, then

$$T\Delta^{\ddagger}S^{\circ}_{\text{approx}} < -RT\ln\left(\frac{k_{\text{intra}}}{k_{\text{inter}}}\right) - \Delta\Delta^{\ddagger}H^{\circ} \qquad (3\text{–}359)$$

where k_{intra} and k_{inter} are the intramolecular and intermolecular rate constants. If the differences in the actual standard enthalpies of activation, $\Delta\Delta^{\ddagger}H^{\circ}$, are assumed to be zero, for the sake of argument, then the experimentally estimated **standard entropy of approximation is always an upper limit for the actual standard entropy of approximation**.

At least **three points can be drawn from the foregoing exercise**. First, the largest intramolecular increases in rate yet measured—with the educational exceptions of cases involving severe enthalpic,[277,278] compressive,[279] steric effects in the transition states engendered by methyl groups, such as during the intramolecular lactonization of

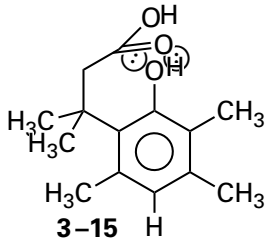

3–15

are of a magnitude significantly less than that expected simply for the transformation of an intermolecular reaction into an intramolecular reaction. Second, the larger the number of bonds about which rotation can occur between the atoms that must collide during an intramolecular reaction, the smaller will be the decrease in standard free energy of activation when an intermolecular reaction becomes an intramolecular reaction. Third, the maximum decrease in the standard free energy of activation to be expected when a bimolecular, intermolecular reaction is turned into a unimolecular, intramolecular reaction is –60 kJ mol^{-1} at 25 °C, which would produce a rate enhancement of 10^{10} M.

Both entropy of molecularity and entropy of rotational restraint are major contributors to the acceleration achieved by an enzyme.

The best way to understand the **effect of the standard entropy of molecularity on the rate of an enzymatic reaction** is to consider the equilibrium constant for formation of the encounter complex in a bimolecular reaction. If the standard entropy of molecularity[272] is assumed to be –180 J K^{-1} mol^{-1} and if the enthalpy change for formation of an encounter complex is ignored for the moment, then the equilibrium constant of association for formation of an encounter complex should be 10^{-9} M^{-1}. The rate constant for dissociation of an encounter complex should the quotient of the rate constant for its formation and its equilibrium constant of association. If the encounter-controlled rate constant for the collision of two reactants is 10^{10} M^{-1} s^{-1}, then the rate of dissociation for an encounter complex, the formation of which involves no change in standard enthalpy, should be 10^{19} s^{-1}, an unimaginably rapid rate. The reason that so few reactions are encounter-controlled is that an encounter complex has a vanishingly small lifetime. The few encounter complexes that have been observed directly

are charge-transfer complexes,[1391] which have significant standard enthalpies of formation. The fact that most encounter complexes have such short lifetimes is also why termolecular rates usually, if not always, involve preassociation of two of the reactants. The encounter complex between two previously unassociated reactants does not exist long enough for a third reactant to collide. The lifetime of a complex between an enzyme and its substrates, however, is on the order of milliseconds to seconds. Catalytic groups on amino acids and prosthetic groups are also assembled in this complex automatically so that, in the abstract, the complex is of an order greater than termolecular. Consequently, from the standpoint of entropy of molecularity, the acceleration achieved by an enzyme should be greater than what is observed.

The best way to consider the **effect of standard entropy of rotational restraint on the rate of an enzymatic reaction** is to consider what occurs in an encounter complex in a nonenzymatic reaction. For a reaction to occur in an encounter complex, the reactants themselves and the sites of reaction within those reactants must rotate from their random orientations in the initial encounter complex to the orientations necessary to accomplish the reaction. In almost every encounter, there is simply not enough time for this to occur. In the complex between an enzyme and its catalytic groups and substrates, as revealed by crystallography, the proper orientations of substrates and catalytic groups required for reaction are achieved by the simple act of association of the substrates with the active site, because the complex is designed to grasp the substrates in the proper orientation. Consequently, from the standpoint of standard entropy of rotational restraint, the acceleration achieved by an enzyme is not in the least surprising.

If the reaction catalyzed by an enzyme involves two or more reactants, as almost all enzymatic reactions do when catalytic acid–bases are included, then the standard entropy of approximation realized as the reactants associate with the active site decreases the intrinsic standard entropy of the reactants and brings the standard free energy of the reactants closer to that of the consecutive transition states for the reaction.[280] As a result, it is misleading to compare the catalytic constant of an enzymatic reaction and the rate constant of the respective intermolecular reaction, in spite of the apparently amazing aspects of the comparison. If the comparison were to be a valid one, then the change in standard free energy attributable to this standard entropy of approximation would have to be accounted for to obtain the **difference in the standard free energy of activation, $\Delta\Delta^{\ddagger}G^{\circ}$, that the active site is able to achieve by strategies other than simply juxtaposing the two reactants and the catalytic groups in the proper orientation**. If the apparent difference in standard free energy of activation, $\Delta\Delta^{\ddagger}G^{\circ}_{\text{app}}$, is that calculated from the difference between the rates of the uncatalyzed and enzymatically catalyzed reactions

$$-RT\ln\left(\frac{k_0}{k_{\text{uncat}}}\right) = \Delta\Delta^{\ddagger}G^{\circ}_{\text{app}} \tag{3–360}$$

and

$$\Delta\Delta^{\ddagger}G^{\circ} - \Delta\Delta^{\ddagger}G^{\circ}_{\text{approx}} = \Delta\Delta^{\ddagger}G^{\circ}_{\text{app}} \tag{3–361}$$

then

$$\Delta\Delta^{\ddagger}G^{\circ} = \Delta\Delta^{\ddagger}G^{\circ}_{\text{app}} - T\Delta^{\ddagger}S^{\circ}_{\text{approx}} \tag{3–362}$$

The conclusion from this equation is that the assistance that an active site provides to catalyze the reaction once the reactants are bound is far less than one might assume simply from comparing the rate of the uncatalyzed reaction to that of the enzymatically catalyzed reaction.

Enzymes usually **hold their substrates within the active site in a remarkably firm grip** that orients them rigidly and freezes internal rotation. There is experimental evidence supporting the conclusion that enzymatic active sites are able to hold substrates so tightly as to achieve alignments that are fixed in orientation to within 10 pm.[281] As a result of such a firm grip, rotational degrees of freedom within the substrates themselves, which would detrimentally increase the entropy of approximation accomplished by the enzyme, are inaccessible, just as rotational degrees of freedom for the side chains of amino acids in the interior of a molecule of protein are usually inaccessible. Consequently, an enzyme, in theory, should be able to realize the full acceleration in rate available in the standard entropy of approximation simply by binding its reactants.

The **theoretical acceleration expected from simply bringing the two reactants in a bimolecular reaction together on an active site** and holding them tightly in the proper orientation is a factor of

10^{10} M if, as is usually the case, the rate of the bimolecular reaction is expressed in units of molar^{-1} second^{-1} and the standard entropy of approximation is –200 J K^{-1} mol^{-1} with this standard state. In addition, the active sites of enzymes gather together catalytic side chains of their amino acids to replace the freely diffusing acids and bases in an aqueous solution, and standard entropies of approximation should apply also to these catalysts. Consequently, the question seems to be why the increases in rate are not larger. When it is examined from the other direction, this question becomes "Why are reactions in solution so slow?" The answer to this question seems far more obvious, but it is the same question.

The almost exclusive contributor to the acceleration in rate accomplished by an enzyme is its ability to assemble reactants, prosthetic groups, and catalytic acids and bases within its active site firmly in the proper orientation. Consequently, the question of acceleration becomes moot. It follows that an active site, to the best of its abilities, must avoid hindering the reaction. The importance of this conclusion, which has been intentionally discussed before any other conclusions about an active site, cannot be overstated. There are, however, other strategies beyond approximation that can be employed and other requirements that must be satisfied by an active site to achieve effective catalysis.

The only observation that seems to contradict this obvious conclusion is the puzzling fact that the decrease in standard free energy of activation achieved by an enzyme results mainly from an apparent decrease in the standard enthalpy of activation for the reaction.[282,283] This apparent contradiction probably results from the fact that increases in entropy resulting from changes in solvation accompanying the association of reactants mask the entropy of approximation. The significant increase in entropy accompanying the hydrophobic effect that drives the association of reactants and that must mask the entropy of approximation is probably the most important contributor to the increase in entropy resulting from changes in solvation.

The standard entropy of approximation is overcome during the association of reactants with the active site. This decrease in the standard entropy of the substrates, which is caused by the disappearance of their respective translational and external rotational degrees of freedom relative to each other, represents an increase in intrinsic standard free energy that is paid for by favorable noncovalent interactions between each reactant and the active site. The consequent elimination of the standard entropy of approximation brings the standard free energies of the reactants closer to the standard free energies of the successive transition states through which the enzymatic reaction passes once the reactants have been assembled. For such a strategy to work, the associations between the enzyme and the reactants must be fast enough that they do not become excessively rate-affecting,* or even rate-limiting, even though a considerable decrease in translational and rotational entropy is occurring during these associations. Consequently, the concentrations of the reactants in the cytoplasm and their bimolecular rate constants of association must be high enough to prevent their associations from being close to rate-limiting. The association rate constants between active sites and substrates are usually quite large [$(0.01–10) \times 10^8$ M^{-1} s^{-1}],[263] and they often approach values expected for the encounter-controlled limit.[284] Such rapid rates of association, achieved by natural selection, are actually more remarkable than the enhanced rates of the chemical reactions once the substrates are bound.

These considerations can be summarized diagrammatically (Figure 3–26). In the absence of the enzyme (Figure 3–26A), reactant A collides with reactant B to produce a transition state of high standard free energy relative to the standard free energy of the reactants. The standard free energy of the transition state is higher than the standard free energy of the separated reactants by the standard free energy of activation of the uncatalyzed reaction, $\Delta^{\ddagger}G^{\circ}_{u}$, necessarily a positive number. If the enzyme were catalyzing the reaction only by approximation, the two steps encompassing association of the reactants, both proceeding rapidly with small standard free energies of activation, would bring the reactants into juxtaposition and proper alignment. The standard free energy of activation for the chemical transformation on the active site of the

*Although the term "rate-limiting step" has been unambiguously defined,[79] there is no accepted term for an elementary rate constant that simply appears in the kinetic equation governing a particular reaction and thus affects the rate of the reaction rather than being rate-limiting. From here on in this text, the term "**rate-affecting step**" will be used to describe any step in a kinetic mechanism the elementary rate constant of which appears in the equation governing the rate of a reaction other than the rate-limiting rate constant for that reaction. The terms "rate-controlling" and "rate-determining" have been used in various contexts, but at the present time these terms are considered to be synonymous with the term "rate-limiting", and hence cannot be used to convey what is here defined as "rate-affecting".

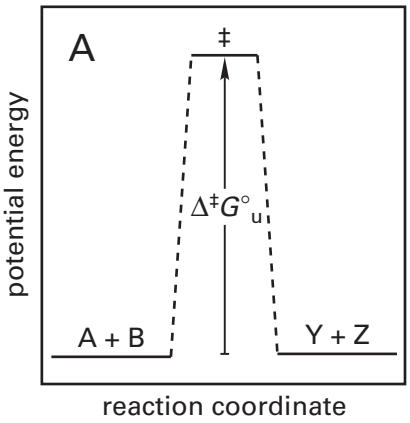

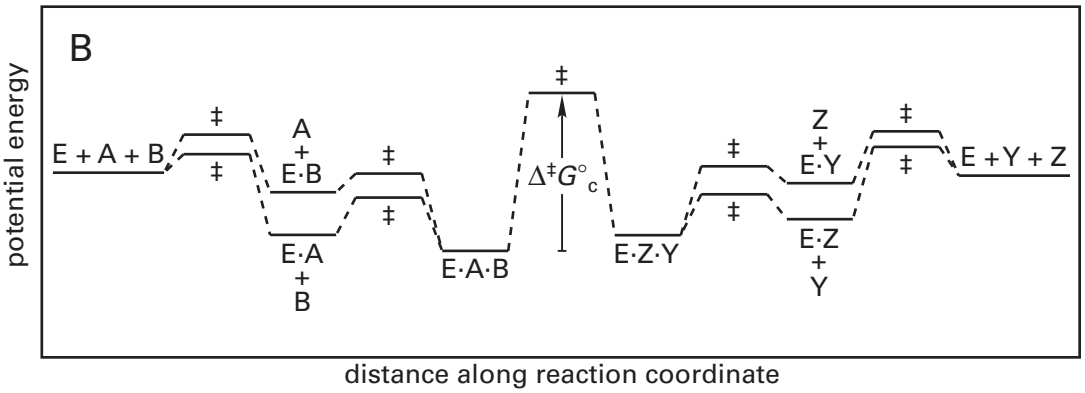

Figure 3–26: Diagrammatic representations of the difference in standard free energy of activation between a simple single-step reaction and the steps involved when that reaction occurs at the active site of an enzyme. **(A)** The steps involved in the reaction at the active site of the enzyme are the binding of the first reactant to the active site followed by the binding of the second to form the ternary complex, E·A·B; the conversion ($\Delta^{\ddagger}G^{\circ}_{c}$) of the ternary complex with the reactants and the active site into the ternary complex with the products and the active site, E·Z·Y; and the dissociation of the first product from the active site followed by the dissociation of the second. Each step has its own transition state, indicated by ‡. **(B)** In the respective bimolecular reaction uncatalyzed by the enzyme, the reactants pass through only one transition state ($\Delta^{\ddagger}G^{\circ}_{u}$) rather than the five transition states for the enzymatically catalyzed reaction.

enzyme, $\Delta^{\ddagger}G^{\circ}_{c}$, again a positive number, would be decreased relative to that of the bimolecular reaction (Figure 3-26B) because of the consequent elimination of the standard entropy of approximation, necessarily a negative number

$$\Delta^{\ddagger}G^{\circ}_{c} = \Delta^{\ddagger}G^{\circ}_{u} + T\Delta^{\ddagger}S^{\circ}_{approx} \qquad (3–363)$$

This decrease in the standard free energy of activation results from the fact that the standard chemical potential of the reactants has increased because a certain fraction of the standard free energy of noncovalent interaction between reactant and active site has been expended to compensate for loss of the translational and rotational entropy of the free reactants.

Weakening the grip of the active site on its reactants can cause decreases in the catalytic constant. The active site of an enzyme has evolved to associate with its specific substrates. The result of this evolution by natural selection is that it usually holds those particular molecules firmly. This firm grip permits the active site to perform the advantageous orientations of substrates, prosthetic groups, and catalytic side chains to enforce the maximum entropy of approximation.

Altering the structures of the reactants at locations distant from the atoms at which the reaction occurs can cause the rate of the enzymatic reaction to decrease. For example, if acetyl-SCoA instead of acetoacetyl-SCoA is used as a substrate for porcine 3-oxoacid CoA-transferase

$$\text{3-oxoacyl-SCoA} + \text{succinate} + H^{+} \rightleftharpoons \text{3-oxocarboxylic acid} + \text{succinyl-SCoA} \qquad (3–364)$$

the specificity constant for the enzymatic reaction decreases by a factor of 600. It is easy to imagine that the active site would have a difficult time gripping an acetyl group tightly when it has evolved to grip a 3-oxoacyl group. In addition, the enzyme shows no detectable activity with either acetoacetylpantetheine or *S*-acetoacetyl-*N*-acetylcysteamine, each of which contains only a proximal fragment of coenzyme A. One possible explanation for this latter result is that the active site must extend its grip over the

entire acetoacetyl-SCoA molecule to align the substrate properly in the active site.[285] In the crystallographic molecular model of coenzyme A bound to the active site of the enzyme, the majority of the noncovalent interactions with coenzyme A are to the adenosine diphosphophosphate group and a portion of the pantetheinyl group,[286] a fact that is consistent with this conclusion.

Cytidine deaminase

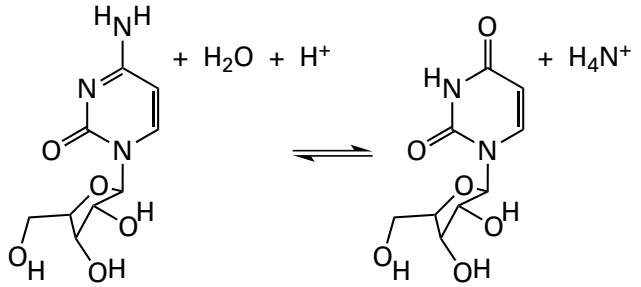

3–16

(3–365)

catalyzes a reaction that occurs entirely within the pyrimidine base of its reactant, yet the removal of the 3′-hydroxy group from the ribosyl group of cytidine (**3–16**) decreases the catalytic constant of the enzyme from *E. coli*[287] by a factor of 370. The most reasonable explanation for this result is that removal of the 3′-hydroxy group deteriorates the fit between the active site and the reactant, loosens the grip of the active site on the reactant, and decreases the ability of the active site to orient the reactant productively within the complex.

These decreases in catalytic constant can be expressed as increases in the entropy of approximation. For example, when the nucleotide portion of coenzyme A is removed, the decrease in the catalytic constant of porcine 3-oxoacid CoA-transferase that results[288] is equivalent to an increase in the entropy of approximation achieved by the enzyme of +90 J K^{-1} mol^{-1} (Equation 3–357).

The active site does not have to fit the reactant tightly to observe changes in the turnover of an enzyme that result from alterations in the structure of the reactant distant from the site of catalysis. Thermolysin is an endopeptidase from *Bacillus thermoproteolyticus* that is required to hydrolyze peptide bonds between a glycine and a leucine in a broad array of different sequences. Consequently, it cannot fit its reactants too tightly beyond the peptide bond itself. Nevertheless, when a series of peptides was synthesized in which the substituents on either side of a central glycylleucine peptide bond were altered, the catalytic constant for hydrolysis of that glycylleucine peptide bond by the enzyme varied by a factor of 1000 while the K_m varied only by a factor of 21 (Table 3–6). If the three peptides with the smallest K_m are removed from consideration, K_m varies by only a factor of 2 while the catalytic constant still varies by a factor of 1000.[289] These observations are consistent with the conclusion that each of these distant alterations had its own particular effect on the rigidity, geometry, and orientation of the reactant in the immediate vicinity of the peptide bond being cleaved by the enzyme, and each of these effects was registered mainly in the catalytic constant.

Table 3-6: Effect of Changes in the Structure of the Reactant on the Kinetic Parameters[289] of Thermolysin[a]

peptide[b]	K_m[c] (mM)	k_0[d] (s^{-1})
Cbz[e]-Gly-Leu-D-Ala	16	5
Cbz-Gly-Leu-Gly-D-Ala	13	25
Cbz-Gly-Leu-Gly	11	65
Cbz-Gly-Leu-amide	21	105
Cbz-Gly-Leu-Phe	2.4	120
Cbz-Gly-Leu-Gly-Phe	11	130
Cbz-Gly-Leu-Leu	2.6	370
Cbz-Gly-Leu-Gly-Ala	14	420
Cbz-Phe-Gly-Leu-Ala	1.0	450
Cbz-Gly-Leu-Ala	11	780
Cbz-Ala-Gly-Leu-Ala	9	5200
↑ point of cleavage		

[a]Determined at 40 °C, pH 7.0 from measurements of initial rates of hydrolysis followed by colorimetric assay for the α-amino group produced in the reaction. [b]Peptide used as reactant. [c]From linear fits to double reciprocals. [d]$V[E]_t^{-1}$. [e]Cbz, benzyloxycarbonyl, which was historically given the name carbobenzoxy.

Mutating side chains of amino acids in the active site that are known to form contacts with a reactant distant from the atoms participating in the reaction also can decrease the catalytic constant of an enzyme.[290] For example, Aspartate 296 in murine adenosine deaminase forms a hydrogen bond with

nitrogen 7 of an analogue of adenosine in a crystallographic molecular model of the complex of the analogue with the enzyme, and presumably with nitrogen 7 of adenosine in the normal reaction of the enzyme.[291] When Aspartate 296 is mutated to alanine, the K_m for the enzymatic reaction increases by only 10-fold while the catalytic constant decreases more than 1000-fold. Aspartate 37 of orotidine-5′-phosphate decarboxylase

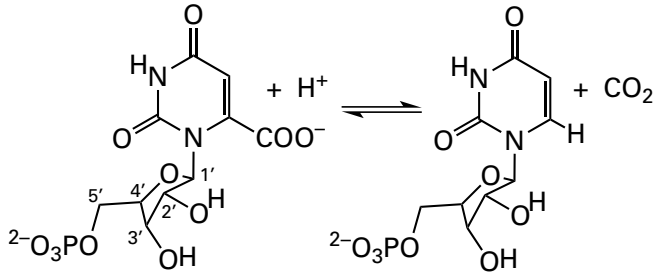

3–17

(3–366)

from *S. cerevisiae*, which forms a hydrogen bond to the 3′-hydroxy group of the 5′-phosphoribosyl group of orotidine 5′-phosphate (**3–17**) when it is in the active site and which is even farther from the location within the active site at which catalysis occurs, is mutated to alanine, the catalytic constant of the enzyme[292] decreases by a factor of 50. When Glutamate 91 of cytidine deaminase from *E. coli*, which forms a hydrogen bond to the 3′-hydroxy group group of cytidine (**3–16**) when it is in the active site, is mutated to alanine, the catalytic constant of the enzyme[287] decreases by a factor of 30. When Arginine 235 of orotidine-5′-phosphate decarboxylase from *S. cerevisiae*, which forms two hydrogen bonds to the 5′-phospho group of orotidine 5′-phosphate, is mutated to alanine, the catalytic constant of the enzyme[293] decreases by a factor of 100. Often the effect of such a mutation at a location distant from the site of catalysis is expressed exclusively as a decrease in catalytic constant.[294] Again, these decreases in catalytic constant can be explained as the result of a loosening of the grip of the enzyme on its reactant caused by the mutation.

The ability of an enzyme to hold its reactant in a firm grip and orient the reactants is often used to prevent undesirable side reactions from occurring. In this way, the reaction is directed exclusively to the desired product. For example, when the reaction catalyzed by chorismate mutase

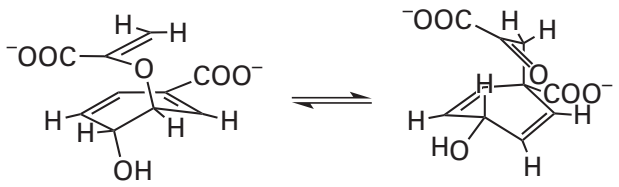

chorismate prephenate

(3–367)

is performed nonenzymatically in a solvent of 2:1 methanol/water, 33% of the product is 4-hydroxybenzoic acid and pyruvate.[295] In both this elimination and the desired electrocyclic rearrangement, there is considerable cleavage of the carbon–oxygen bond, but in the former reaction, no formation of the carbon–carbon bond occurs. One way in which the enzyme prevents the elimination is to position carbon 2 of the 1-carboxyvinyl group immediately adjacent to carbon 1 of chorismate to increase the yield of the formation of this bond.

The intermediate (+)-presqualene diphosphate is formed on the active site of squalene synthase from the allyl carbenium ion that results from the dissociation of diphosphate from one molecule of (2*E*,6*E*)-farnesyl diphosphate (see Figure 1–26) and that then adds to the double bond between carbons 2 and 3 of another (2*E*,6*E*)-farnesyl diphosphate in an electrophilic addition that produces a cyclopropyl group. The carbenium ion **3–18**, resulting from the dissociation of (+)-presqualene diphosphate, is converted to squalene by squalene synthase through the rearrangement of the successive carbenium ions

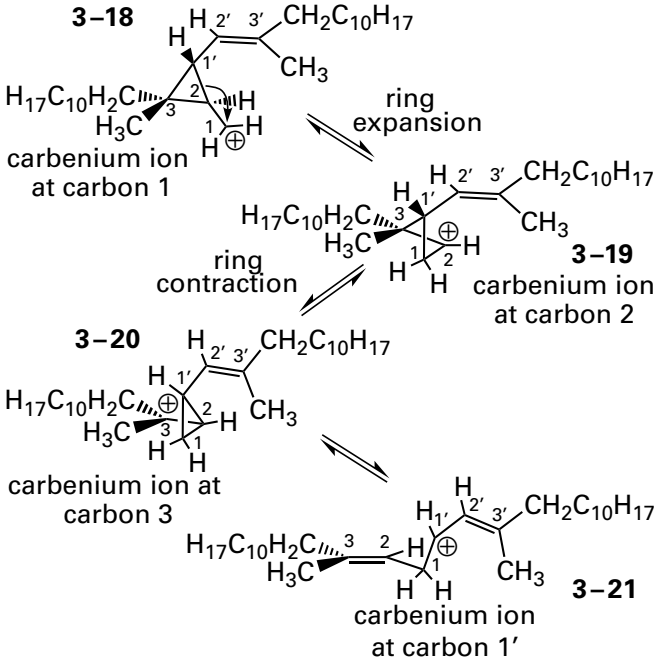

(3–368)

where the numbering of the intermediates is that of the two constituent farnesyl groups and $C_{10}H_{17}$ is a geranyl group

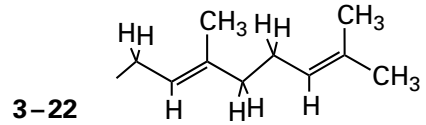

When initial carbenium ion **3–18** is produced nonenzymatically in aqueous solution,[296] only 0.02% of the product results from the desired rearrangement to carbenium ion **3–19** because the carbenium ion **3–18** strongly prefers to rearrange (99%) to a carbenium ion at carbon 1′ in conjugation with the exocyclic double bond between carbons 2′ and 3′ or rearrange (1%) to a tertiary carbenium ion at carbon 3, the more saturated position in the cyclopropyl group. In the former rearrangement, the electrons in the bond between carbons 1′ and 2 swing away from carbon 1′ to form a double bond between carbons 1 and 2 rather than participating in a ring expansion, and in the latter rearrangement, the electrons in the bond between carbons 3 and 2 swing away from carbon 3 also to form a double bond between carbons 1 and 2. In fact, on the active site of botryococcene synthase from *Botryococcus braunii*, an enzyme related (45% identity; 1.3 gap percent) to squalene synthase, carbenium ion **3–18** does rearrange by the former, most favorable route on the way to its normal product, botryococcene.[297] Somehow the active site of squalene synthase has to prevent these unfavorable rearrangements from occurring.

The favored rearrangement in solution to the carbenium ion at carbon 1′ (99% yield) would be a rather devastating side reaction in the sequence of rearrangements (Equation 3–368) that must be catalyzed by the active site of squalene synthase during its production of squalene. This side reaction can be prevented by holding the π system of the exocyclic carbon–carbon bond between carbons 2′ and 3′ orthogonal to the *p* orbital of the potential carbenium ion at carbon 1′ to prevent its conjugation. In the crystallographic molecular model of the complex between (+)-presqualene diphosphate and the active site of human squalene synthase in which Tyrosine 73 was mutated to an alanine to decrease the enzymatic activity and Mn^{2+} was used as the required metallic dication to produce the proper conformation of the (+)-presqualene diphosphate,[298] the bond between carbons 1′ and 2 of the cyclopropyl ring is almost parallel to the plane of the carbon–carbon double bond between carbons 2′ and 3′ (23° out of plane). Consequently, the π system of this exocyclic double bond should end up almost fully orthogonal to the *p* orbital of a carbenium ion at carbon 1′ were the bond between carbons 1′ and 2 to dissociate from carbon 1′ rather than from carbon 2. The ability of the enzyme to grip its reactants tightly permits it to enforce this orientation and prevent the unfortunate rearrangement.

In the crystallographic molecular model, however, between (+)-presqualene diphosphate and 4,4′-diapophytoene synthase from *Staphylococcus aureus* in which Tyrosine 129 has been mutated to alanine to decrease its activity,[299] the bond between carbons 1′ and 2 of the cyclopropyl ring is almost perpendicular to the plane of the carbon–carbon double bond between carbons 2′ and 3′ (72° out of plane). This active site is required to perform the same rearrangements as the active site of squalene synthase (Equation 3–368). This orientation would favor the conjugation of the carbon–carbon double bond between carbons 2′ and 3′ with a developing *p* orbital of a carbenium ion at carbon 1′. Consequently this orientation significantly favors the side reaction. If this crystallographic molecular model actually replicates the normal conformation of the (+)-presqualene diphosphate in the active site, it seems hard to believe that the side reaction does not occur most of the time. The resulting allyl carbenium ion at carbon 1′, however, may well be a dead end, and eventually the proper carbenium ion at carbon 2

forms and the reaction proceeds. The allyl carbenium ion at carbon 1′ would be a dead end if the active site prevents any nucleophile from adding to it because there is no adjacent hydron that can depart to produce a stable neutral product. Nevertheless, the situation in the active site of 4,4′-diapophytoene synthase is not so clear as that in the active site of squalene synthase.

The other side reaction that is favored in solution (1% yield) and that would be detrimental to the proper reaction is the formation of the tertiary carbenium ion at carbon 3. In fact, in both crystallographic models, that for the complex of (+)-presqualene diphosphate with the active site of squalene synthase and that for the complex of (+)-presqualene diphosphate with the active site of 4,4′-diapophytoene synthase, this rearrangement seems to be favored. In both cases, the carbon–carbon bond between carbons 2 and 3 is more in-line (122° and 146°, respectively) with the carbon–oxygen bond between carbon 1 and the oxygen of the leaving diphosphate than the carbon–carbon bond between carbons 1′ and 2 (58° and 76°, respectively). If these two conformations of the (+)-presqualene diphosphate replicate the active conformation, it is hard to see how formation of the carbenium ion at carbon 3 is prevented by the active site. This rearrangement has the potential to be even more damaging because there is a hydron adjacent to this carbenium ion that can depart to give a remarkably stable side product with a double bond between carbons 3 and 1′. It would take a tight grip indeed to prevent carbon 3 from flattening to the trigonal configuration required of a carbenium ion.

Once these difficulties are somehow surmounted, the rearrangement of carbenium ion **3–20** produces allyl carbenium ion **3–21**, so all the active site has to do is not hinder the formation of this last intermediate by ensuring that the double bond is not hindered from becoming oriented parallel to the *p* orbital of the carbenium ion.

When the cycloaddition catalyzed by prosolanapyrone-III cycloisomerase

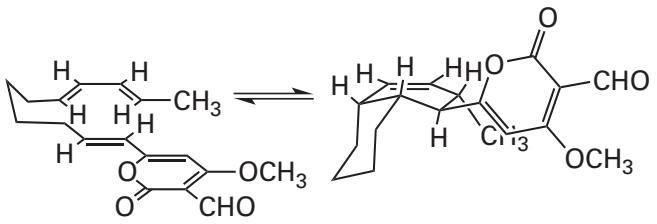

(3–369)

is performed in the absence of the enzyme, the product from exo addition

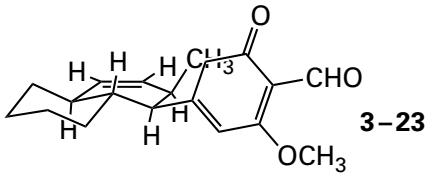

3–23

which is the more stable isomer from the more stable transition state, predominates (87%).[300] When the purified enzyme from *Alternaria solani* catalyzes the reaction, however, enantiomerically pure solanapyrone A, resulting from endo addition (Equation 3–369), is the product.[301] This reversal of the stereochemistry performed by the enzyme results from the ability of the active site to align atoms in the reactant in such a way that only the endo transition state can form. This conclusion from the crystallographic molecular model is the most convincing evidence that the active site itself catalyzes this cycloaddition.[302]

Suggested Reading

Page, M. I., and Jencks, W. P. (1971) Entropic contributions to rate accelerations in enzymic and intramolecular reactions and the chelate effect, *Proc. Natl. Acad. Sci. U.S.A. 68*, 1678–1683. https://doi.org/10.1073/pnas.68.8.1678

Poulter, C. D., Marsh, L. L., Hughes, J. M., Argyle, J. C., Satterwhite, D. M., Goodfellow, R. J., and Moesinger, S. G. (1977) Model studies of the biosynthesis of non-head-to-tail terpenes: Rearrangements of the chrysanthemyl system, *J. Am. Chem. Soc. 99*, 3816–3823. https://doi.org/10.1021/ja00453a050

Sigala, P. A., Kraut, D. A., Caaveiro, J. M. M., Pybus, B., Ruben, E. A., Ringe, D., Petsko, G. A., and Herschlag, D. (2008) Testing geometrical discrimination within an enzyme active site: Constrained hydrogen bonding in the ketosteroid isomerase oxyanion hole, *J. Am. Chem. Soc. 130*, 13696–13708. https://doi.org/10.1021/ja803928m

Problem 3–23: The rate constant for the reaction between trimethylamine and phenyl acetate to produce the *N,N,N*-trimethylacetamide ion $[(CH_3)_3{}^+NCOCH_3]$ and phenoxide is 8×10^{-3} M^{-1} min^{-1} at 20 °C. The rate constant for the intramolecular aminolysis of phenyl 4-(*N,N*-dimethylamino)butyrate to yield *N,N*-dimethyl-2-oxopyrrolidinium and phenoxide is 10 min^{-1} at 20 °C.

(A) Calculate the "effective molarity" of trimethylamine that would be required for the rate of the intermolecular reaction to equal the rate of the intramolecular reaction.
(B) Calculate an upper limit for $\Delta^{\ddagger}S^{\circ}_{approx}$ for the intramolecular reaction on the assumptions that the solvent for both of these reactions is water and that the standard enthalpies of activation are the same for the two reactions. First use molarity as the units for the second-order rate constant, and then use corrected volume fraction.

Strain

The examples of chorismate mutase (Equation 3–367), squalene synthase (Equation 3–368), and prosolanapyrone-III cycloisomerase (Equation 3–369) illustrate the ability of an active site to juxtapose particular atoms in a reactant to increase dramatically the probability that these locations will collide and to guarantee that the proper product results from the catalysis. To ensure that prephenate is the product of the reaction catalyzed by chorismate mutase (Equation 3–367), the distal carbon of the double bond of the *enol*pyruvyl group must collide with carbon 4 of the cyclohexadienyl group (Figure 1–30). To ensure that these two atoms are juxtaposed when the chorismate is bound in the active site, however, in addition to selecting the proper rotamer, the active site must also force the cyclohexadienyl group of chorismate to assume the conformation placing the oxygen of the *enol*pyruvyl group in an axial orientation.[303,304] The active site is constructed so that the axial conformer is the only one that can associate with it.[305,306] In this instance, the active site is sterically forcing the reactant to assume a less stable conformation. This steric enforcement is an example of the **ability of an active site to strain a substrate in the interest of catalysis**.

The equilibrium constant[307] for isomerization between the equatorial and axial conformers of the hexadienyl group in chorismate is 0.14 at 25 °C in aqueous solution. Consequently, as a result of forcing the hexadienyl group to assume the less stable conformer, an apparent acceleration of around 10-fold should be observed when the catalytic constant of the enzyme is compared to the rate constant of the uncatalyzed reaction. Between these two locations are two bonds about which full rotation can occur. Elimination of the entropy of internal rotation about these two bonds would translate into a modest 100-fold increase in the rate of the reaction.[272] The catalytic constant of the enzymatically catalyzed reaction is 2×10^6 times that of the nonenzymatic reaction in water at pH 7.5 and 37 °C. Together, freezing of internal rotations and enforcement of the axial conformation by the configuration of the active site should provide an acceleration of 10^3. This acceleration, however, can be achieved by the active site of the enzyme only if it is able to enforce both of these restrictions with high efficiency. If not, the full acceleration cannot be realized. If the full acceleration is actually achieved, a factor of only 10^3 remains unaccounted for.

To catalyze the decarboxylation of the carboxylato group at carbon 6 of (3*E*)-2-oxohex-3-enedioate, the active site of 2-oxo-3-hexenedioate decarboxylase has to hold the bond between carbons 5 and 6 parallel to the π molecular orbital system encompassing the carboxylato group at carbon 1, the carbonyl group at carbon 2, and the double bond between carbons 3 and 4

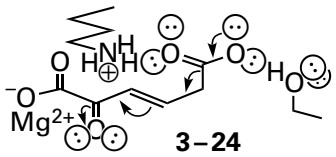

3–24

so that this π molecular orbital system can withdraw electron density from it. In the crystallographic molecular model of the active site of the enzyme from *P. putida* occupied by 2-oxohexanedioate,[308] an analogue of the substrate, 2-oxohex-3-enedioate, both steric effects and hydrogen bonds to a lysine and a serine perform this orientation with precision and rigidity.

The ability to constrain a reactant in a conformation more similar to the transition state than the ground state is not an exclusive property of enzymes. There are also **synthetic examples of catalysts** that are able to do so. For example, there is a tetrahedral complex of four gallium atoms held at the vertices of a tetrahedron by six *N*,*N*′-bis(2,3-dihydroxybenzoyl)-1,5-diaminonaphthalenes, which form the limbs of the tetrahedron. This complex has a sizeable enclosed, nonpolar cavity at its center, and it can catalyze the cyclization

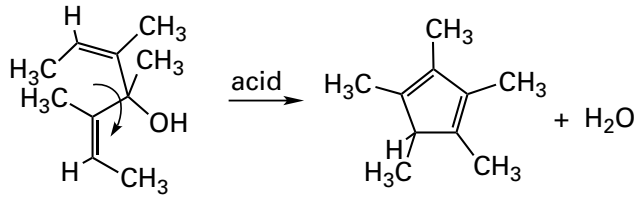

(3–370)

that results from rearrangement of a carbenium ion formed when the hydronated hydroxy group on carbon 4 of the reactant leaves. The bond that forms to produce the cyclohexadiene is a bond between carbons 2 and 6 of the diene that is the reactant. Consequently, there have to be rotations around the bonds between carbons 4 and 5 and between carbons 3 and 4 to bring carbons 2 and 6 close enough together for the bond to form. In addition, because the two double bonds in the reactant are both cis, the methyl groups of carbons 1 and 7 run into each other as carbons 2 and 6 approach each other and sterically hinder the molecule from assuming the proper conformation for the transition state.

The association of the reactant with the complex of the four galliums and the six *N,N′*-bis(2,3-dihydroxybenzoyl)-1,5-diaminonaphthalenes increases the rate of the reaction significantly.[309] One explanation for this observation is that the reactant binds within the nonpolar cavity in the catalyst and can fit in the cavity only when it has assumed the compact, globular conformation that brings carbons 2 and 6 next to each other on the way to the transition state. The catalyzed reaction has the same steady-state kinetics as an enzymatic reaction with a specificity constant of 0.4 M^{-1} s^{-1} and a catalytic constant of 0.016 s^{-1}. Because the rate constant for the uncatalyzed reaction is 8×10^{-9} s^{-1}, the acceleration observed is 2×10^6 or a decrease in $\Delta^{\ddagger}G^{\circ}$ of –36 kJ M^{-1}. This decrease is much larger than that expected for the freezing of two rotational degrees of freedom and suggests that some compression by the cavity of the compact conformer in the direction of the transition state is also occurring.

If, during the association of substrates with the active site on an enzyme, they are not only oriented properly to achieve a configuration appropriate to the transition state but also **contorted physically by the active site** of the enzyme into that configuration, then **catalysis by strain** results. In this situation, an additional fraction of the standard free energy of dissociation, beyond that used to overcome the entropy of approximation, is used to provide the energy necessary to contort the substrates toward the transition state. Catalysis by strain does not account for a large portion of the decrease in standard free energy of activation accomplished by an active site,[310] but it can contribute significantly to the decrease.

Catalysis by strain was originally defined in detail by Pauling in 1948 in the following credo:[311]

> I believe that an enzyme has a structure closely similar to that found for antibodies, but with one important difference, namely, that the surface configuration of the enzyme is not so closely contemporary [sic] to its specific substrate as is that of an antibody to its homologous antigen, but is instead complementary to an unstable molecule with only transient existence—namely, the "activated complex" [transition state] for the reaction that is catalyzed by the enzyme. The mode of action of an enzyme would then be the following: the enzyme would show a small power of attraction for the substrate molecule or molecules, which would become attached to it in its active surface region [its active site]. This substrate molecule, or these molecules, would then be strained by the forces of attraction to the enzyme, which would tend to deform it into the configuration of the activated complex, for which the power of attraction by the enzyme is the greatest. The activated complex would then, under the influence of ordinary thermal agitation, either reassume the configuration corresponding to the reactants, or assume the configuration corresponding to the products. The assumption made above that the enzyme has a configuration complementary to the activated complex, and accordingly has the strongest power of attraction for the activated complex, means that the activation energy for the reaction is less in the presence of the enzyme that in its absence, and accordingly that the reaction would be speeded up by the enzyme. My colleague Professor Carl Niemann and I are carrying out experiments on inhibition of enzyme activity designed to test this postulate, by the search for inhibitors that have a greater power of combination with the enzyme than have the substrate molecules themselves.

The crystallographic molecular models of lysozyme and other glycosidases provided early experimental evidence consistent with this hypothesis. Lysozyme is a glycosidase that normally catalyzes

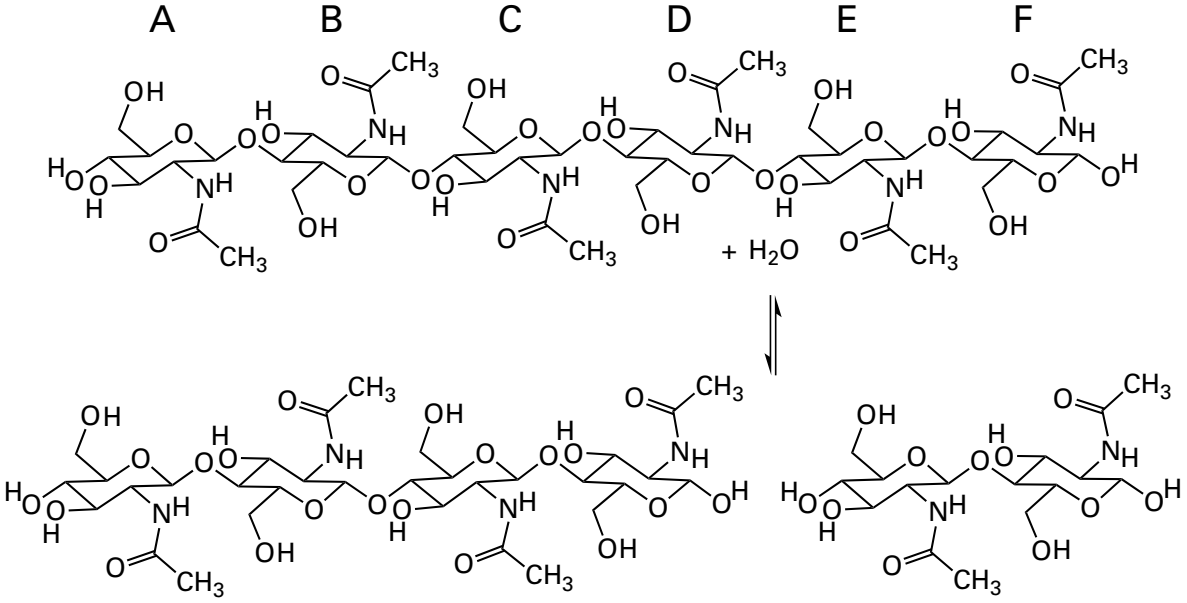

Figure 3–27: Hydrolysis of (β1,4)-hexa-*N*-acetylglucosaminopyranose to a molecule of (β1,4)-di-*N*-acetylglucosaminopyranose and a molecule of (β1,4)-tetra-*N*-acetylglucosaminopyranose, a reaction catalyzed by lysozyme from *G. gallus*.[312]

the hydrolysis of polysaccharides in bacterial outer membranes. It also catalyzes the hydrolysis of the hexasaccharide (β1,4)-hexa-*N*-acetylglucosaminopyranose (Figure 3–27).[312] Within the hexasaccharide, the cleavage occurs at monosaccharide D between the fourth and the fifth *N*-acetyl-D-glucosamines.[313] When lysozyme from *G. gallus* was crystallized with the trisaccharide (β1,4)-tri-*N*-acetylglucosaminopyranose occupying the active site and a map of difference electron density was computed, a crystallographic molecular model incorporating reasonable hydrogen bonds and lack of steric hindrance could be constructed for the complex between the trisaccharide and three subsites (A, B, and C) in the active site.[314] Three additional molecular models of the proper monosaccharides were added to the reducing end of the molecular model of the trisaccharide in the complex to produce the hexasaccharide. These last three monosaccharides could be placed in subsites D, E, and F in the active site. They could be linked in a similar array of hydrogen bonds and inserted without steric clashes[315] in these subsites only if the entire molecular model of the hexa-*N*-acetylglucosaminopyranose was **contorted from the all-chair conformation** shown in Figure 3–27. The contortion required to fit the last three monosaccharides into the active site required a flattening of monosaccharide D into the sofa configuration in which carbon 4, carbon 5, oxygen 5, carbon 1, and carbon 2 of monosaccharide D are all in the same plane[314,316]

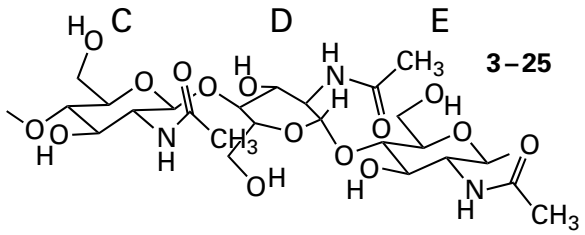

3–25

On the basis of this rather primitive model-building, the crystallographers proposed that one way lysozyme catalyzes the hydrolysis is to use the energy of its association to contort the monosaccharide D into a form that accommodates the planar oxocarbenium ion that would be an intermediate in this acetal hydrolysis.[317]

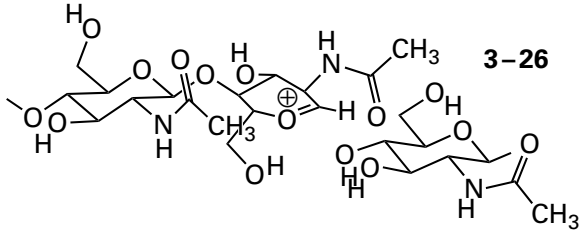

3–26

The most stable conformation for this oxocarbenium ion is one in which carbon 5, oxygen 5, carbon 1, and carbon 2 of the pyranose are all in the same plane. Such an oxocarbenium ion can be an intermediate of high energy in the hydrolysis of acetals and ketals. By the **Hammond postulate**,[318] the transition state between a reactant or reactants and

an intermediate of high energy should resemble the intermediate more closely than the reactant or reactants. Therefore, the conclusion was reached that lysozyme was catalyzing the reaction by **contorting the substrate in the direction of the transition state**.

Since this original conjecture, several crystallographic molecular models of complexes between lysozyme from *G. gallus* and various oligosaccharides have been reported in which the monosaccharide at the reducing end is actually located in the D site.[312,319] In each of these models, the monosaccharide in the D site has been distorted by the active site into a conformation in which carbon 5, oxygen 5, carbon 1, and carbon 2 are all in almost the same plane (Figure 3–28)[319] as required for the most stable conformation of oxocarbenium ion **3–26**.

A distortion of a monosaccharide at the reducing end of an oligosaccharide in the crystallographic molecular model of another endoglycosidase, cellulase from *Acetivibrio thermocellus,* also puts carbon 5, oxygen 5, carbon 1, and carbon 2 of the monosaccharide in the hydrolytic location in the same plane,[320] and an analogous distortion to achieve planarity also occurs in the crystallographic molecular model of a complex between the active site of exo-α-sialidase from *S. typhimurium* and 4-acetamido-2,4-dideoxy-D-*glycero*-D-*galacto*-α-octopyranosylphosphonic acid, an analogue of the *N*-acetyl-D-neuraminic acid in an α-glycosidic linkage in a sialylglycoside that is normally a substrate for the enzyme.[321] In several other crystallographic molecular models of endoglycosidases, however, the distortions observed do not put these four atoms in the same plane.[322,323]

When a decasaccharide that has (3*S*,4*S*,5*S*,6*R*)-3-amino-4,5,6-hydroxy-1-(hydroxymethyl)cyclohexenyl group

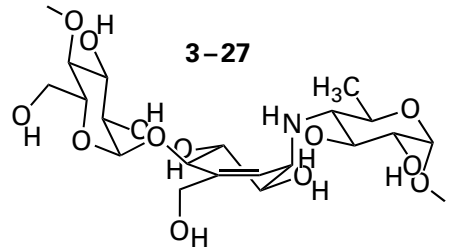

3–27

at two internal positions associates with a bacterial α-amylase, the planar carbon–carbon double bond in one of these rigid rings, in which four of the carbons are in the same plane, ends up, presumably by design, at the location in the active site at which hydrolysis of the oligosaccharide is usually catalyzed.[324]

It may[317,325,326] or may not[327] be the case that there is an oxocarbenium ion as an intermediate in the reaction catalyzed by these enzymes. One of the arguments routinely used to dismiss the existence of a glycosyl oxocarbenium ion as an intermediate in these active sites is that the lifetime of a glycosyl oxocarbenium ion in aqueous solution[328] has been estimated to be only 10^{-12} s. What is usually omitted in these dismissals is the statement that the carbenium ion has "short but significant lifetime in aqueous solution".[328] In other words, it is not that glycosyl oxocarbenium ion cannot exist but only that its existence is short. It was also emphasized when the estimate of the lifetime was presented that the lifetime is short in aqueous solution because when it is formed, there is always a molecule of water immediately adjacent to it with which it almost immediately reacts. In the active site of an enzyme, however, there would be no molecule of water adjacent to an oxocarbenium ion, so its lifetime could be prolonged indefinitely. None of these arguments either prove or disprove the existence of a glycosyl oxocarbenium ion as an intermediate in these enzymatic nucleophilic substitutions. Nevertheless, the alternative transition state in which a concerted nucleophilic substitution by a carboxylato group in the active site on the carbonyl carbon of the glycosyl group still requires the coplanarity of carbon 5, oxygen 5, carbon 1, and carbon 2.

Coincidently, the act of distorting the pyranose or the furanose of a glycoside into a planar conformation around an incipient oxocarbenium ion (Figure 3–28) performed by the active site of a glycosidase or a glycosylase also causes the cis lone pair of electrons on the oxygen to become parallel to the σ bond of the leaving group

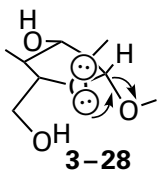

3–28

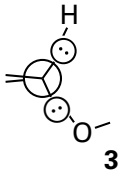

3–29

and consequently increases the overlap between the two. This overlap provides **push ejecting the leaving group**.[329,330]

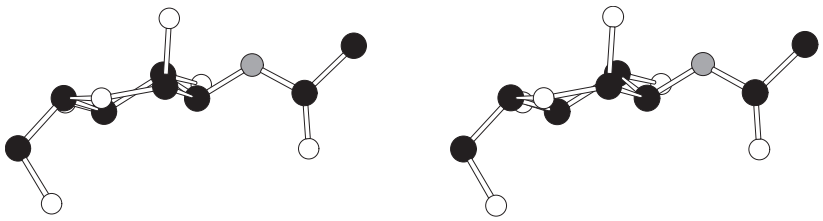

Figure 3–28: Crystallographic molecular model of the *N*-acetyl-D-glucosaminyl group at the reducing end of the tetrasaccharide (β1,4)-tetra-*N*-acetylglucosaminopyranose bound in the active site of a mutant of lysozyme from *G. gallus* in which the catalytic amino acid Aspartate 52 had been mutated to a serine.[319] Black atoms are carbons, white atoms are oxygens, and the small gray atom is a nitrogen. The mutant of lysozyme with an equimolar ratio of the hexasaccharide (β1,4)-hexa–*N*-acetylglucosaminopyranose and the enzyme was crystallized from the mixture over a period of 14 days at 16 °C. During that time, the almost inactive mutant enzyme nevertheless hydrolyzed the hexasaccharide to disaccharide and tetrasaccharide. A data set was collected from these crystals to a Bragg spacing of 0.2 nm. In the map of electron density calculated from this data set, electron density corresponding to the tetrasaccharide (β1,4)-tetra-*N*-acetylglucosaminopyranose was observed in the active site of the enzyme. A molecular model of the tetrasaccharide in the all-chair configuration was inserted into this electron density, and the entire molecular model was submitted to refinement. During the refinement, the *N*-acetylglucosaminyl group at the reducing end of the tetrasaccharide, which was located in the D subsite of the active site, gradually assumed the conformation shown in the drawing. The conformation the *N*-acetylglucosaminyl group assumed during the refinement was almost a perfect sofa conformation, in which carbons 1, 2, 4, and 5 and oxygen 5 all would have been in the same plane. The α isomer of the *N*-acetylglucosaminyl group was clearly designated by the electron density, and the oxygen of its 1-hydroxy group was axial in the final refined conformation.

Another example of an active site built to enforce a usually unstable conformation of a substrate is that of scytalone dehydratase from *Magnaporthe grisea*. From observations of the effect of site-directed mutations on the relative activities of the enzyme for three different substrates, it was concluded that the active site enforces boat conformations of each of the substrates, conformations causing the bonds to the hydroxy group that leaves as a molecule of water and the adjacent hydrogen that is removed as a hydron during the dehydration resulting from a *syn* elimination to be parallel to each other.[331]

In the nucleophilic substitution catalyzed by orotate phosphoribosyltransferase

$$\begin{gathered}H^+ + \text{ orotidine 5′-phosphate } + \\ MgOPO_3PO_3^{2-} \rightleftharpoons \text{ orotate } + \\ \text{magnesium 5-phospho-}\alpha\text{-D-ribose 1-diphosphate}\end{gathered} \qquad (3\text{–}371)$$

with magnesium diphosphate as the nucleophile and orotate as the leaving group from carbon 1′ of the orotidine 5′-phosphate, the transition state is thought to be somewhere between the tight pentavalent intermediate of a concerted nucleophilic substitution and the intermediate oxocarbenium ion of a dissociative nucleophilic substitution. In either case, carbon 1′ of the intermediate is in the same plane as carbon 2′, the oxygen of the furanose ring, and the hydrogen on carbon 1′. Isotope effects on the association of [1′-^{3}H]orotidine 5′-phosphate with the active site of human orotate phosphoribosyltransferase are consistent with a distortion of this substrate by the active site as it associates that **flattens carbon 1′ in the direction of its planar conformation** in the transition state.[332]

A distortion such as the ones that occur in the active sites of chorismate mutase and lysozyme, in which **dihedral angles along covalent bonds are forcefully altered,** is one example of strain in catalysis.

Enzymatic active sites also seem to pull on covalent bonds to decrease their strength. For example, the homolytic dissociation of the carbon–cobalt bond of adenosylcobalamin

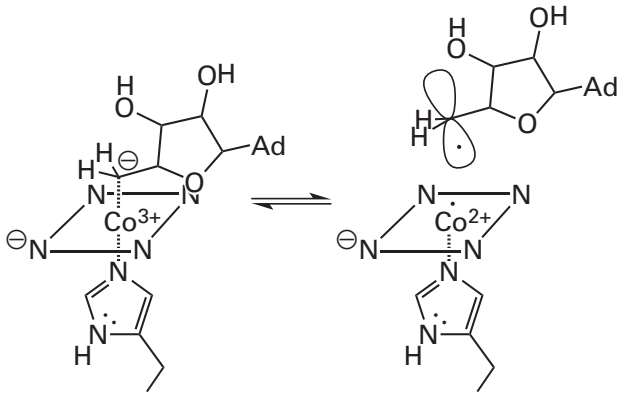

(3–372)

is catalyzed by both the active site of methylmalonyl-CoA mutase and the active site of glutamate mutase. In the crystallographic molecular model of cobalamin in the active site of methylmalonyl-CoA mutase from *P. freudenreichii*, the imidazolyl group of the histidine that is the axial ligand on the opposite side of the cobalt in the adenosylcobalamin is constrained sterically to be at a greater distance from the plane of the ring than it would be in an unconstrained situation. This displacement, exerted by the active site, in turn pulls the cobalt out of the plane of the corrin in the direction of the imidazolyl group and must lengthen and weaken the carbon–cobalt bond to the adenosyl group on the other side of the corrin in the prosthetic adenosylcobalamin.[333] Quantum mechanical calculations of the dissociation of the carbon–cobalt bond of adenosylcobalamin in the active site of glutamate mutase from *Clostridium cochlearium* lead to the conclusion that as the carbon–cobalt bond dissociates within the active site and the two incipient products of the dissociation, the 5′-adenosyl radical and the cob(II)alamin, move farther apart, they each are bound more and more tightly. In other words, the active site is constructed so that a long carbon–cobalt bond allows both the adenosyl group and the cobalaminyl group to be bound by the active site more effectively. In this way, the enzyme promotes the lengthening of the carbon–cobalt bond that pulls it apart homolytically.[334]

A carbon–cobalt bond is a weak covalent bond. Its bond dissociation energy (110 ± 10 kJ mol^{-1})[335] is only about 30% that of a carbon–carbon bond (370 kJ mol^{-1}). Because, however, it is still a covalent bond, when the active site pulls, it does not lengthen significantly enough to be registered in a crystallographic molecular model, but it is weakened nevertheless by the tug.

The process of distorting a dihedral angle, such as that occurring in lysozyme, or stretching a bond,

such as that occurring in glutamate mutase, **can be viewed dynamically**.[311] As the nuclei around the bond to be broken move by thermal motion in the direction of the configuration they must assume in the transition state, the hexa-*N*-acetyl-D-glucosamine or the adenosylcobalamin fits the respective active site more effectively, and the sum of the standard free energies of formation for noncovalent forces between hexasaccharide or adenosylcobalamin and the active site decreases accordingly. As the nuclei move by thermal motion away from the configuration they must assume in the transition state, each substrate fits the respective active site less effectively, and the standard free energy of formation for noncovalent forces increases accordingly. Both the active site and the substrate are rearranging at random as a result of thermal motion, but as the ensemble of conformations moves in the direction of the transition state, the sum of the standard free energy of noncovalent interactions decreases. Because the standard free energy of formation for the noncovalent forces decreases continuously as the respective reactant moves along the reaction coordinate toward the transition state, the standard free energy of activation is less than it would have been if the reaction were occurring in free solution, and the rate of the reaction is greater. The consequence of this process is that the standard chemical potential of the transition state is decreased by the additional standard free energy of noncovalent interaction realized along the trajectory.

An active site is also able to bend a covalent bond as well as stretch one. For example, the decarboxylation of 5-carboxy-4-hydroxy-3-methoxybenzoate (5-carboxyvanillate) by 5-carboxyvanillate decarboxylase from *Sphingomonas paucimobilis* is formally an electrophilic aromatic substitution of the 5-carboxylato group with a hydron. In the crystallographic molecular model of the enzyme in a complex with the unreactive analogue 4-hydroxy-3-methoxy-5-nitrobenzoate, in which an isosteric nitro group replaces the carboxylato group that is the electrophile that leaves as carbon dioxide in the normal substitution, the nitro group is bent out of the plane of the phenyl ring by 23°, even though the nitro group in free 4-hydroxy-3-methoxy-5-nitrobenzoic acid is coplanar with the ring.[336] Presumably, the 5-carboxylato on the reactant 5-carboxy-4-hydroxy-3-methoxybenzoate is also bent out of the plane by the active site, a conformation that favors the hydronation of carbon 5 to form 1,5-carboxy-3-methoxy-4-oxocyclohexa-2,6-diene, which is the intermediate in the electrophilic aromatic substitution. In this intermediate, carbon 5 is tetrahedral as a result of the hydronation, so bending the carboxylato group in the direction of tetrahedrality from trigonality promotes the hydronation and hence the substitution.

In the crystallographic molecular model of the adduct between the prosthetic thiamine diphosphate in the active site of transketolase from *E. coli* and the ketose, xylulose 5-phosphate,[337] the bond between carbon 2 of the thiazole ring and the α carbon of the adduct is **pulled out of the plane of the thiazole ring** so that the angle between it and the plane of the thiazole is 25°. The pull seems to be exerted on the portion of the xylulose 5-phosphate beyond carbon 2 by noncovalent interactions between this portion of the substrate and the active site, most notably the phospho group. Because carbon 2 in the adduct, which is participating in the aromatic thiazole ring, is sp^2-hybridized, the bond between carbon 2 and the α carbon would normally be in the plane of the ring. The bond between carbons 2 and 3 breaks in the next step of the enzymatic reaction

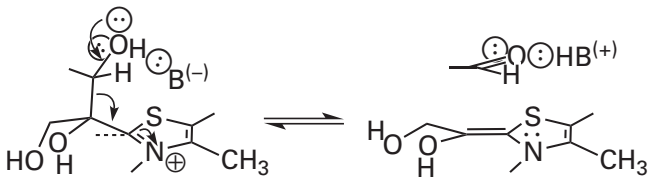

(3–373)

In the drawing, the dashed line represents the position of the bond were it in the plane of the thiazole ring. The fact that the active site is pulling on this bond vigorously enough to distort carbon 2 should also weaken it and make it easier to break.

Orotidine-5′-phosphate decarboxylase (Equation 3–366) catalyzes an electrophilic substitution in which a carboxylato group, which leaves from carbon 6 of orotidine 5′-phosphate as carbon dioxide (an electrophile), is replaced by a hydron (also an electrophile).* In this electrophilic substitution, there is no reasonable anionic intermediate. For the lack of a reasonable intermediate, an unreasonable intermediate, in which carbon 6 is a carbanion with a σ lone pair of undelocalized electrons in the plane of the ring and jutting out from it, seems inescapable. Strangely enough, the active site also catalyzes the nucleophilic substitution of a hydroxide for the 6-cyano group in 6-cyanouridine 5′-phosphate, which leaves as a cyanide. When 6-cyanouridine

*This substitution is not an electrophilic aromatic substitution.

5′-phosphate is bound in the active site of orotidine-5′-phosphate decarboxylase from *Methanothermobacter thermautotrophicus*,[338] the cyano group is bent out of the plane of the pyrimidine ring by an angle of 30°, a distortion that should be required by a nucleophilic substitution. This bending accomplished by the active site is estimated to require about +30 kJ mol^{-1} of standard free energy. The 6-carboxylato group on orotidine 5′-phosphate should also be bent out of the plane of the ring upon its association with the active site, and this contortion should weaken the bond between carbon 6 and the carbon of the carboxylato group and increase the withdrawal of electron density in this bond by the acyl oxygen at carbon 4. A similar distortion is observed in a crystallographic molecular model of the active site occupied by orotidine 5′-phosphate in a mutant of orotidine-5′-phosphate decarboxylase from *M. thermautotrophicus* in which Aspartate 70 has been mutated to an alanine,[339] so the distortion does not seem to be accomplished by a steric interaction with this immediately adjacent side chain.[340] The distortion is not confined to molecules that are substrates for the enzyme. When 6-methyluridine 5′-phosphate occupies the active site,[341] the methyl group is bent out of the plane of the pyrimidine ring by 15°.

In the normal reaction catalyzed by orotidine-5′-phosphate decarboxylase, the carbanionic intermediate is hydronated by the ammonio group of Lysine 72. In a crystallographic molecular model of the complex between orotidine-5′-phosphate decarboxylase from *M. thermautotrophicus* and the substrate uridine 5′-phosphate,[342] carbon 6 in the uracil is also bent by the active site out of the plane of the ring by 0.01 nm by the 6-amino group of Lysine 72. When Lysine 72 is mutated to an alanine, the dissociation constant for uridine 5′-phosphate decreases by a factor of 10^5, a result consistent with Lysine 72 being responsible for the steric distortion of carbon 6 of the uridine 5′-phosphate. During catalysis, this distortion would result from the compression of one of the hydrogens on the ammonio group of Lysine 72 against carbon 6. In a crystallographic molecular model of the active site of the same mutant occupied by 6-cyanouridine 5′-phosphate, however, the cyano group is still bent out of the plane of the ring to the same degree as it is in the wild type by two fixed molecules of water occupying the same location as the lysine does in the wild-type active site.[338]

During the electrophilic aromatic substitution catalyzed by tyrosine phenol-lyase

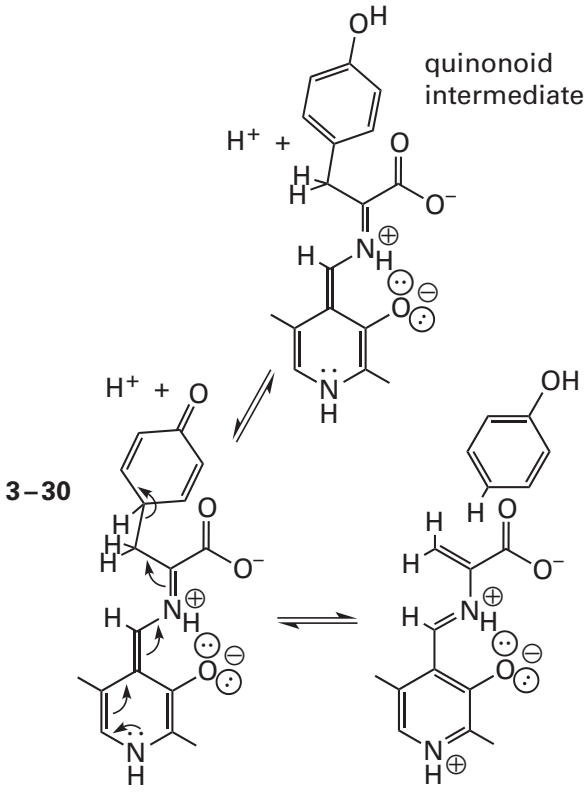

(3–374)

carbon 1 of the 4-hydroxyphenyl group, upon its hydronation, changes its hybridization from sp^2 to sp^3, from trigonal planar to tetrahedral. In the crystallographic molecular model of the quinonoid intermediate of L-tyrosine in the active site of a mutant of tyrosine phenol-lyase from *Citrobacter freundii*,[343] the active site has pushed on the 4-hydroxyphenyl group, so carbon 1, although it remains trigonal, is no longer planar. In the active site, as a result of this push, the angle between the still planar, aromatic phenyl ring and the bond between carbon 1 and the β carbon has decreased from 180° to around 158°, on its way to the 125° that it has in hydronated intermediate **3–30**.

2′-Deoxypseudouridine is an inactive analogue of uridine, which is the natural substrate for the active site of uracil-DNA glycosylase. In the crystallographic molecular model of the active site of human uracil-DNA glycosylase occupied by 2′-deoxypseudouridine, which has swung out from the double-helical DNA in which it was incorporated, the 2′-deoxypseudouracil in the 2′-deoxypseudouridine has been twisted and the ring bent over so that it is almost coplanar with the ring of the ribose.[344] This bending of the 2′-deoxypseudouracil at the bond of the hemiaminal that connects the ribose and the nucleotide base brings the π molecular orbital system of the 2′-deoxypseudouracil almost parallel with the

σ bond between the 2′-deoxypseudouracil and the ribose, allowing the π molecular orbital system of the 2′-deoxypseudouracil to withdraw electron density from the σ bond and promote the heterolytic dissociation of this bond, which is the first step in the dissociative nucleophilic substitution of the 2′-deoxypseudouracil with a hydroxy group.

Active sites also force two atoms between which a covalent bond is to be formed into closer proximity than the sum of their van der Waals radii. This ability explains the compression of the ammonio group on Lysine 72 in orotidine-5′-phosphate decarboxylase against carbon 6 of the orotidine.

The first intermediate in the reaction catalyzed by the active site of porcine 3-oxoacid CoA-transferase (Equation 3–364) is a mixed anhydride[285,345,346] between Glutamate 305[347] and the 3-oxoacyl group of the 3-oxoacyl-SCoA resulting from a nucleophilic substitution at the acyl carbon of the 3-oxoacyl-SCoA of the carboxylato group of the glutamate for the sulfanyl group of coenzyme A. There is a crystallographic molecular model of a complex between a mutant of acetate CoA-transferase from *Acetobacter aceti*, in which the glutamate equivalent to Glutamate 305 in 3-oxoacid CoA-transferase is replaced with an alanine, and dethiaacetyl-CoA, an inert analogue of coenzyme A in which the sulfur of the thioacetyl group is replaced by a carbon.[346] When dethiaacetyl-CoA is superposed on a crystallographic molecular model of the wild-type enzyme, the carbonyl carbon of the dethiaacetyl-CoA, which is the analogue of the acyl carbon of acetyl-SCoA, is only 0.2 nm from the nearest oxygen of the carboxylato group of Glutamate 305, well within van der Waals contact. The new bond will be formed between this carbon and this oxygen. This compression, if it actually occurs in the active site during the normal reaction, would explain the fact that all the noncovalent interactions between acetoacetyl-SCoA and the active site of porcine 3-oxoacid CoA-transferase (Equation 3–364) are needed for it to perform its catalysis. This compression would validate the prediction that "the thiol ester group of the bound acyl-CoA is then clamped against the enzyme carboxylate group in a viselike grip that causes an increase in rate by decreasing the low frequency motions and entropy that must be lost to form a new covalent bond, and by destabilizing the bound thiol ester group relative to the transition state."[285] In the transition state for formation of the tetrahedral intermediate in anhydride formation, the distance between the oxygen of the glutamate and the acyl carbon of acetoacetyl-SCoA should be about 0.2 nm.

Alkaline phosphatase from *E. coli* catalyzes the hydrolysis of a large variety of phosphate monoesters. The promiscuity results from the fact that the enzyme associates only with the four oxygens of the phospho group and does not associate with the remainder of the alcohol taking part in the phosphoester. The enzyme uses the alkoxide of a serine in the active site, which is stabilized by a prosthetic Zn^{2+}, as a nucleophile in a nucleophilic substitution at phosphorus, with the alcohol as the leaving group, to form a phosphoserine as an intermediate in the reaction. A hydroxide from solution, which is stabilized by another prosthetic Zn^{2+}, then replaces the oxygen of the leaving alcohol and participates in a second nucleophilic substitution at phosphorus, in which the alkoxide of the serine is the leaving group and the product is phosphate. In the reverse direction, phosphate should associate with the active site, and a phospho group should be transferred to the alkoxide of the serine. The dissociation constant for the trianion of phosphate from the active site when serine is the nucleophilic alkoxide is $\geq 1 \times 10^{-7}$ M. When the serine is mutated to a glycine, the dissociation constant of the trianion of phosphate from the active site[348] is approximately 1×10^{-15} M. It was concluded that a portion (<-24 kJ mol^{-1}) of the dramatically large standard free energy of dissociation for the trianion of phosphate for the active site, which is revealed when the serine has been mutated to a glycine, has been used to push the phosphorus atom of the phosphate trianion up against the lone pair of electrons on the alkoxide of the serine. This alkoxide adds to the phosphorus atom during the formation of the phosphorane that is the intermediate in the nucleophilic substitution of the alkoxide of the serine for the hydroxide that is the leaving group in the reverse direction. The dissociation constant for the dianion of phosphate from the active site in which the serine is the alkoxide, however, which is the model for a phosphate ester, the ground state, increases only by a factor of 46 (4.4 kJ mol^{-1}) when the serine is replaced by a glycine.

Forcing of one atom of a reactant up against an atom of another reactant between which a covalent bond is to be formed can lead to **reactant antagonism**. Reactant antagonism occurs when one reactant decreases the dissociation constant for another reactant and vice versa. For example, the dissociation constant for 3-phospho-D-glyceroyl phosphate from human phosphoglycerate kinase

$$MgADP^- + \text{3-phospho-D-glyceroyl phosphate} \rightleftharpoons \text{3-phospho-D-glycerate} + MgATP^{2-} \quad (3\text{–}375)$$

increases from 0.03 μM when the active site is unoccupied to 0.9 μM when the active site is occupied by $MgADP^-$, and the dissociation constant for $MgADP^-$ increases from 8 μM when the active site is unoccupied to 100 μM when the active site is occupied by 3-phospho-D-glyceroyl phosphate.[349] One explanation for these observations is that the active site pushes the oxygen of the $MgADP^-$, to which the 1-phospho group of 3-phospho-D-glyceroyl phosphate is to be transferred, up against the phosphorus atom to catalyze the transfer and that this push is manifested in a steric effect that increases the respective dissociation constants.

Active sites also **force a base and a carbon from which a hydron is to be removed or an acid and a carbon to which a hydron is to be added into closer proximity** than the sum of their van der Waals radii. In effect, this property is a corollary to forcing together two atoms between which a covalent bond is to be formed. In a crystallographic molecular model between the active site of a mutant of steroid Δ-isomerase

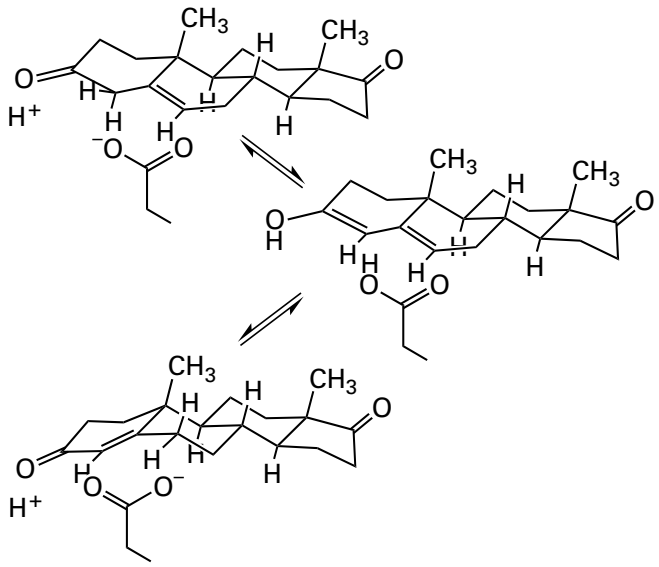

(3–376)

from *Comamonas testosteroni* and its substrate androst-4-ene-3,17-dione (the product in Equation 3–376), the carboxylato oxygen of Aspartate 38, the catalytic base, is forced up against carbon 4 (0.27 nm) and carbon 6 (0.33 nm), the two carbons between which it transfers a hydron, closer than the sum (0.38 nm) of the van der Waals radii of a hydrogen (0.115 nm) and an oxygen (0.15 nm) and the length of a carbon–hydrogen bond (0.11 nm). When Proline 38, which is immediately adjacent to Aspartate 38, is mutated to a glycine, the side chain of Aspartate 38 is able to swing away from carbons 4 and 6 of androst-4-ene-3,17-dione, and the strain is relieved. This relief is manifest in the decrease of the dissociation constant for androst-4-ene-3,17-dione from the active site from 60 μM in the wild type to 1.1 μM for the mutant in which the proline has been replaced with glycine.[350] This difference in the standard free energy of dissociation for the substrate is presumed to be approximately equal to the standard free energy of dissociation for androst-4-ene-3,17-dione, which is used by the active site to force the carboxylato oxygen up against the two carbons.

The standard free energy that accomplishes strain within an active site is provided by noncovalent interactions between the active site and the reactants. The **hydrophobic effect** accompanying the association of reactants with the active site results from the removal of hydrogen–carbon bonds both on the reactant and within the active site itself from contact with water.[52] In many active sites, a few of the hydrogen–carbon bonds on the reactant and within the active site may still be exposed to the water of the surrounding solution, but those that have been sequestered produce the favorable, negative standard free energy of the hydrophobic effect that accompanies the association. The hydrophobic effect is the main contributor to the standard free energy of dissociation and as such is responsible for assembling the reactants on the active site. The reactant and the active site of an enzyme almost always have complementary donors and acceptors for hydrogen bonds. There is little net standard enthalpy change when these **hydrogen bonds** form, however, because the donors and acceptors were participating in hydrogen bonds with the water before the complex between reactant and active site is formed, and there is usually no net change in the number of hydrogen bonds in the solution.[351] If, however, the donors and acceptors from water were not replaced by acceptors and donors in the active site, there would be an increase in standard free energy upon the association of a substrate with an active site. Once they are within the active site, the reactants engage in **van der Waals forces** with the functional groups within the active site. Again, there is little net standard enthalpy change resulting

from these interactions because both the functional groups in the active site and those on the reactants were engaged in van der Waals forces with the water of the solution before the reactants entered the active site.[352] After it has been occupied by the reactant, the active site also has associated with it a particular **electric potential energy** that arises from the disposition of the formal elementary charges and the orientation of the dipoles that it contains.

Because all or almost all of the hydrophobic effect is realized simply upon the dehydration of hydrogen–carbon bonds on the reactant and those in the active site, only the standard free energies of the hydrogen bonds, the van der Waals forces, and the electric potential change as the conformation of the occupied active site progresses from the ground state to the transition state. These interactions, in dramatic contradistinction to the hydrophobic effect, are critically dependent on the orientation and position of the participants.[351,352] When all three noncovalent interactions between the reactant and the active site are accomplished as favorably as possible, the maximum standard free energy of dissociation, ΔG°_{t}, which is composed of the **total available standard free energy of the noncovalent interactions and the electric potential** and which is always a positive number, is achieved.

These effects can be represented on **free energy diagrams** (Figure 3–29).[353] Suppose that the enzyme catalyzing the reaction had an active site constructed so that all these interactions that are subject to change—namely the hydrogen bonds, the van der Waals forces, and the electric potential—were completely engaged and the electric potential energy was at a minimum, and hence the sum of the standard free energies resulting from these interactions was **at the absolute minimum, when the ground states of the reactants were bound**. This situation would cause the reactants to be bound tightly, and its standard free energy of dissociation, $\Delta G^{\circ\prime}_{A}$, would equal $\Delta G^{\circ\prime}_{t}$, the maximum standard free energy of dissociation for the optimally aligned noncovalent interactions and the minimum of electric potential in this situation. The sum of the standard free energies for the formation of hydrogen bonds, the formation of van der Waals forces, and the electric potential would be at an absolute minimum when the reactants are bound. During the approach to the transition state, however, the standard free energy of these interactions would have to increase as the nuclei changed their configuration from the one they had in the ground states of the reactants. In this situation, the standard free energy of activation, $\Delta^{\ddagger}G^{\circ\prime}_{E}$, for the reaction on the active site of the enzyme would be increased relative to the standard free energy of activation for the uncatalyzed reaction, $\Delta^{\ddagger}G^{\circ}_{u}$ (corrected for entropy of approximation and changes in solvation between the water in the solution and the active site), by an amount of standard free energy, $\Delta^{\ddagger}G^{\circ\prime}_{nci}$ (in this case a positive number), equal in magnitude to the standard free energy of formation for the noncovalent interactions lost during the progress along the reaction coordinate. Under these circumstances, the enzyme would decrease the rate of the reaction after approximation has been accomplished.

Suppose, however, that the enzyme catalyzing the reaction has an active site constructed so that all these interactions that are subject to change—namely the hydrogen bonds, and the van der Waals forces—are completely engaged and the electric potential energy is at a minimum, and hence the sum of the standard free energies resulting from these interactions is **at the absolute minimum, only when the transition state is bound**. In this situation, the transition state is bound tightly, and its standard free energy of dissociation, $\Delta G^{\ddagger\circ}_{t}$, is equal to ΔG°_{t}, the maximum standard free energy of dissociation for the optimally aligned noncovalent interactions and the minimum of electric potential in this situation. The sum of the standard free energies for the formation of hydrogen bonds, the formation of van der Waals forces, and the electric potential are at an absolute minimum only when the transition state is achieved. During the approach to the transition state, however, the standard free energy for these interactions decreases as the nuclei change their configuration from the one they had in the ground states of the reactants. In this situation, the standard free energy of activation, $\Delta^{\ddagger}G^{\circ}_{E}$, for the reaction on the active site of the enzyme is decreased relative to the standard free energy of activation for the uncatalyzed reaction, $\Delta^{\ddagger}G^{\circ}_{u}$ (corrected for entropy of approximation and changes in solvation), by an amount of standard free energy, $\Delta^{\ddagger}G^{\circ}_{nci}$ (in this case a negative number), equal in magnitude to the standard free energy of formation gained and the decrease in the electric potential during the progress along the reaction coordinate. The sum of the standard free energies arising from all these interactions that change as the conformation of the occupied active site changes is at a minimum only when the transition state is reached. Under these circumstances, the enzyme increases the rate of the reaction after approximation has been accomplished.

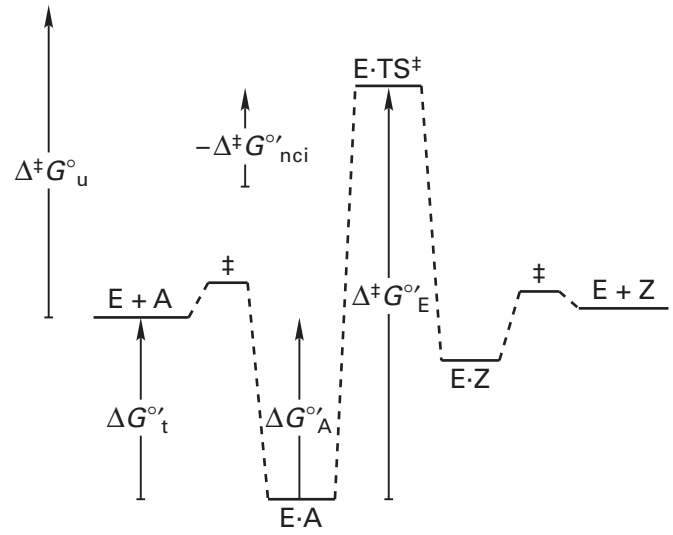

enzyme that binds reactant efficiently

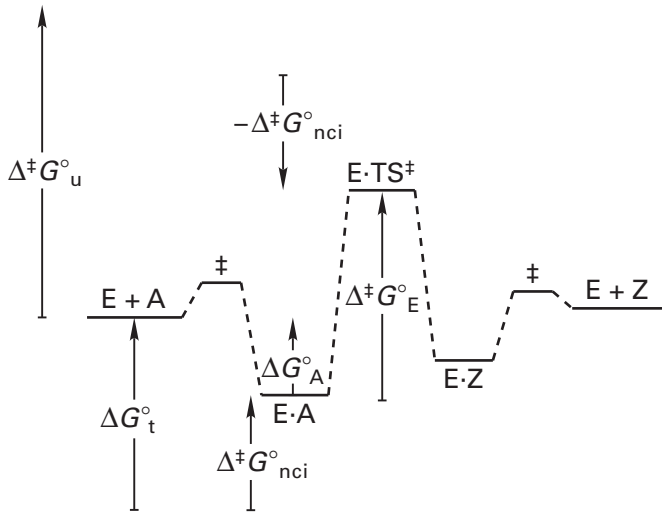

enzyme that binds transition state efficiently

Figure 3–29: Diagrammatic representation of the effect of binding the transition state more efficiently than the ground state on the standard free energy of activation for an enzymatic reaction. The free energy of activation for the uncatalyzed reaction, $\Delta^{\ddagger}G^{\circ}_{u}$, is for the uncatalyzed reaction once any free energy of approximation has been subtracted so that one can focus only on events that occur after association of reactant A with the active site. **(A)** An enzyme the active site of which binds the reactant most efficiently will have a large positive standard free energy of dissociation ($\Delta G^{\circ\prime}_{A} >> 0$) for the reactant, but it will bind the transition state poorly because standard free energies of dissociation for some of the noncovalent interactions are lost ($\Delta^{\ddagger}G^{\circ\prime}_{nci} < 0$) as the reactant is transformed to the transition state. It has been assumed that, without the loss of noncovalent interactions, the standard free energy of activation on the active site would be the same as the standard free energy of activation of the uncatalyzed reaction ($\Delta^{\ddagger}G^{\circ}_{u}$), corrected for standard free energy of approximation. Raising of the standard free energy of the E·TS‡ complex because some noncovalent interactions are lost causes the standard free energy of activation on the active site ($\Delta^{\ddagger}G^{\circ\prime}_{E}$) to be larger than the standard free energy of activation of the uncatalyzed reaction ($\Delta^{\ddagger}G^{\circ}_{u}$), after correcting for the standard free energy of approximation. **(B)** An enzyme the active site of which binds the transition state most effectively will still have a positive standard free energy of dissociation ($\Delta G_{A}^{\circ} > 0$) for the reactant, but it will bind the transition state strongly because standard free energies of dissociation for some of the noncovalent interactions are gained ($\Delta^{\ddagger}G^{\circ}_{nci} > 0$) as the reactant is transformed to the transition state. Lowering of the standard free energy of the E·TS‡ complex causes the standard free energy of activation on the active site ($\Delta^{\ddagger}G^{\circ}_{E}$) to be smaller than the standard free energy of activation of the uncatalyzed reaction ($\Delta^{\ddagger}G^{\circ}_{u}$), after correcting for the standard free energy of approximation.

Regardless of whether strain is occurring, the large increase in the rate of reaction that results simply from assembling and orienting the reactants on the active site would still apply. In one case, however, this increased rate would be decreased by the loss of noncovalent interactions on approach to the transition state. In the other case, it is increased by the gain in noncovalent interactions on approach to the transition state. Considered in this way, it seems almost to be a necessity that the full effect of noncovalent interactions not be exerted until the transition state is reached.

Another way to present the effects of binding upon the rate of an enzymatic reaction is a more general approach not confined simply to a consideration of noncovalent forces. In this approach, all the consequences associated with the binding of the transition state to the active site of an enzyme are included.[354,355] In the case of an enzyme that operates on two reactants, the following linkage box can be constructed[355]

$$\begin{array}{ccccc} \mathrm{E + A + B} & \overset{^{\ddagger}K_{u}}{\rightleftharpoons} & \mathrm{E + A{\cdot}B^{\ddagger}} & \xrightarrow{\dfrac{\kappa_{T,u}}{\delta_{u}}\left(\dfrac{k_{B}T}{2\pi^{\ddagger}m_{u}}\right)^{1/2}} & \mathrm{E + Z{\cdot}Y} \\ \Big\downarrow\Big\uparrow K_{dA} & & \Big\Vert\Big\Vert\, {}^{\ddagger}K_{d} & & \\ \mathrm{E{\cdot}A + B} & & & & \\ \Big\downarrow\Big\uparrow K_{dB} & & & & \\ \mathrm{E{\cdot}A{\cdot}B} & \overset{^{\ddagger}K_{E}}{\rightleftharpoons} & \mathrm{E{\cdot}A{\cdot}B^{\ddagger}} & \xrightarrow{\dfrac{\kappa_{T,E}}{\delta_{E}}\left(\dfrac{k_{B}T}{2\pi^{\ddagger}m_{E}}\right)^{1/2}} & \mathrm{E{\cdot}Z{\cdot}Y} \end{array} \qquad (3\text{–}377)$$

where K_{dA}, K_{dB}, and ${}^{\ddagger}K_{d}$ are the dissociation constants from the active site for reactant A, reactant B, and the transition state, respectively; $A{\cdot}B^{\ddagger}$ is the

transition state; $\kappa_{T,u}$, δ_u, and ${}^{\ddagger}m_u$ and $\kappa_{T,E}$, δ_E, and ${}^{\ddagger}m_E$ are transmission coefficients, lengths of the reaction coordinate at the transition state, and masses of the transition state for the uncatalyzed and enzymatically catalyzed reactions, respectively; and ${}^{\ddagger}K_u$ and ${}^{\ddagger}K_E$ are the equilibrium constants between the respective reactants and transition states.

Assume for the moment that expressions containing transmission coefficients, lengths of the reaction coordinates at the transition state, and masses of the transition states for the uncatalyzed and enzymatically catalyzed reactions are approximately equal.* Because

$$k_i = \frac{\kappa_{T,i}}{\delta_i}\left(\frac{k_B T}{2\pi {}^{\ddagger}m_i}\right)^{1/2} {}^{\ddagger}K_i \qquad (3\text{–}378)$$

it follows that

$$\frac{K_{dA}K_{dB}}{{}^{\ddagger}K_d} \cong \frac{k_0}{k_u} \qquad (3\text{–}379)$$

This expression states that, given all the rather bold assumptions that have been made, the quotient of the product of dissociation constants for the reactants and the dissociation constant for the transition state determines the ratio between the catalytic constant for the enzymatically catalyzed reaction and the rate constant for the uncatalyzed reaction. Therefore, to catalyze a reaction, **an enzyme must bind the transition state more tightly than the reactants**, and the degree of preference it displays for the transition state relative to the reactants determines entirely the increase in rate that is realized.

This statement alone, however—that an active site must bind the transition state more tightly than the reactants—although indisputable,[263] is uninformative. The informative observations are **the details of the explicit strategies** used by the active site to bind the transition state preferentially. One strategy is to design an active site in which noncovalent forces increase in strength and electric potential decreases as the configuration of the atoms in the reactants moves toward that of the transition state. In the transition state, covalent bonds are partially formed and partially broken between the reactants themselves, and the active site must associate with these shortened or elongated distances between particular atoms in the transition state more effectively than it does with the same atoms in the reactants. Another strategy is to provide appropriately located acids and bases. The transition states in most biochemical reactions involve hydrons in transit. A bare hydron leaving a shrinking lone pair of electrons in a reactant or a bare hydron being attracted to an enlarging lone pair of electrons in a reactant are hydrons in transit. They are structural features of the transition state that must be bound by the enzyme if the transition state is to be bound more tightly than the reactants, in which these peculiar situations do not exist. To stabilize and provide these hydrons in transit, acids and bases must be located appropriately within the active site but also compressed against the corresponding bases and acids in the reactants to approach the respective distances between the nuclei in the transition state. Finally, in many instances, prosthetic groups or metallic ions are incorporated in the active site to provide capabilities unavailable in a simple aqueous solution. All these features, and any others that apply to the interaction between the active site and the transition state, produce the difference in standard free energy of dissociation for the reactants in their ground state from the active site and the standard free energy of dissociation for the transition state from the active site.

It has been a widely accepted custom to quantify the catalytic proficiency of an enzyme[356] as the rate constant $k_0\,(K_{mA}K_{mB}\ldots)^{-1}$. The ratio $k_0\,(K_{mA}K_{mB}\ldots)^{-1}$, however, is a rate constant that is only indirectly related to the actual catalytic proficiency of the enzyme. The rate constant actually quantifying the catalytic proficiency of the enzyme is $k_0\,(K_{dA}K_{dB}\ldots)^{-1}$, a number that should be proportional to the association constant between the transition state and the active site (Equation 3–379) if several related enzymatically catalyzed reactions are compared for which the rate of the uncatalyzed reaction is the same—always with the caveat that all of the foregoing assumptions are valid. It is significantly more difficult, however, to measure the dissociation constant for a reactant than to measure its Michaelis constant. Consequently, the unmentioned assumption made to avoid this labor is that the Michaelis constant for a reactant is approxi-

*It is difficult to decide what the mass of the transition state is when the reaction is occurring within an active site because an indeterminate portion of that active site is actively in motion as the transition state is being approached. When the reaction occurs in solution, however, a significant portion of the solvation shell is also actively in motion as the transition state is being approached. It can be assumed, merely for the sake of the argument, that roughly the same mass of the active site is in motion as the mass of the solvation shell that is in motion.

mately the same as its dissociation constant, a rather tenuous assumption. It has also been decided that it is more gratifying to use a number indirectly related to the association constant for the transition state, ${}^{\ddagger}K_{\mathrm{d}}^{-1}$, rather than a number more directly related to the dissociation constant because it is always a number greater than 1 and therefore seems to indicate that the enzyme is increasing the rate of the reaction. Regardless of all these caveats, the custom of tabulating the rate constants $k_0\,(K_{\mathrm{mA}}K_{\mathrm{mB}}\ldots)^{-1}$ has become universal. One is forced to consider these ratios as more or less the same as the intended rate constants $k_0\,(K_{\mathrm{dA}}K_{\mathrm{dB}}\ldots)^{-1}$.

The rate constant $k_0\,K_{\mathrm{mA}_i}{}^{-1}$ can be used to obtain **information about the structure of the transition state in a particular enzymatic reaction from a series of reactants $\mathbf{A}_i$,** each of which can participate in the reaction catalyzed by the enzyme.[357,358] If a series of reactants A_i for an enzyme is examined in which all the rate constants for the uncatalyzed reaction are the same; if the reaction is being catalyzed only by the increase in standard free energy of dissociation of the transition state; and if the dissociation constants for the other reactants in the enzymatic reaction do not change as the identity of reactant A is changed, then the quantities $K_{\mathrm{dA}_i}\,k_0{}^{-1}$ will be proportional to the dissociation constants for the respective transition states from the active site (Equation 3–379). The rate constant $k_0\,K_{\mathrm{mA}_i}{}^{-1}$ may also be proportional to the association constants for the respective transition states from the active site. For example, a series of alkyl phosphates and a series of phenyl phosphates that differed in the $\mathrm{p}K_{\mathrm{a}}$ of the leaving groups in each case were used as reactants for alkaline phosphatase

$$\mathrm{ROPO_3^{2-}} + \mathrm{HOH} \rightleftharpoons \mathrm{ROH} + {}^{2-}\mathrm{O_3POH} \qquad (3\text{–}380)$$

from *E. coli*, an enzyme in which the portion of the reactant beyond the phospho group hangs out into the solution. The values for the common logarithms of $k_0\,K_{\mathrm{m,phos}}{}^{-1}$ were plotted against the respective values of $\mathrm{p}K_{\mathrm{a}}$ for the leaving groups. The Brønsted coefficient for the phenyl phosphates was -0.77 ± 0.1, and that for the alkyl phosphates was -0.85 ± 0.1. From these values it was concluded that, in the transition states for the rate-limiting nucleophilic substitutions at phosphorus, the bond between oxygen and phosphorus is mostly dissociated.[359]

The rate constant $k_0\,K_{\mathrm{m}}{}^{-1}$ can be used to obtain information about the apparent change in the standard free energy of the dissociation constant for the transition state relative to the dissociation constant for the reactant from the active sites in **a series of site-directed mutations**. For example, the values of $k_0\,K_{\mathrm{m}}{}^{-1}$ for four mutations of orotidine-5′-phosphate decarboxylase from *S. cerevisiae*, both alone and in all fifteen combinations, were used to estimate the changes in standard free energies of activation for the enzymatic reaction produced by each mutation, and hence the contributions of the side chains of those amino acids to stabilization of the transition state relative to the ground state.[360]

One misunderstanding of the statement that the enzyme must bind the transition state more tightly than the reactants is the impression it leaves that the enzyme actually binds transition states present in the solution and that this ability would explain its catalysis. An enzyme binds otherwise unassociated and unactivated reactants, and the transition states are achieved within the active site. If an enzyme preferentially bound only transition states formed in solution, it could only decrease the rate of the reaction because, by definition, a transition state decomposes to products instantaneously. That the enzyme must bind the transition state more strongly than the ground state is only a thermodynamic argument, not something that actually occurs.

If a transition state has to be bound more tightly to an active site than the substrates, it should be possible, as proposed by Pauling in the credo cited above,[311] to design molecules the structures of which resemble the structures of the respective transition states and to demonstrate that they bind to the enzyme far more tightly than do the substrates. In most instances, transition states involve bond lengths and bond angles that cannot be reproduced in a stable molecule. By the **Hammond postulate**,[318] however, an intermediate of high energy encountered along a reaction coordinate, which by definition does have normal bond lengths and bond angles, resembles in its structure the transition states on either side of its well of potential energy more closely than do either the immediate reactant or the immediate product. Because one is rarely able to synthesize analogues for transition states, **analogues for intermediates of high energy** have been synthesized and shown to be potent inhibitors of enzymes, as predicted. In spite of the inaccuracy of the phrase, analogues for intermediates of high energy are often referred to as "transition-state analogues".

The trisaccharide *N*-acetylglucosaminopyranosyl-(β1,4)-*N*-acetylmuramopyranosyl-(β1,4)-*N*-acetyl-D-glucosamine binds to the active site of lysozyme from *G. gallus* in subsites A, B, and C (Figure 3–27) with a dissociation constant of 4 μM, while the tetrasaccharide *N*-acetylglucosaminopyranosyl-(β1,4)-*N*-acetylmuramopyranosyl-(β1,4)-*N*-acetylglucosaminopyranosyl-(β1,4)-*N*-acetylmuramate binds with a dissociation constant of 500 μM.[361] This increase in the dissociation constant for the tetrasaccharide relative to the trisaccharide is thought to be due to the fact that the more stable chair conformation of the pyranose of the additional *N*-acetylmuramate in the fourth position of the tetrasaccharide cannot fit into the subsite for the D-pyranose in the active site of the enzyme without being distorted into a half-chair conformation (Figure 3–28),[319] and this distortion increases the dissociation constant. The δ-lactone of (β1,4)-tri-*N*-acetylglucosaminopyranosyl-2-acetamido-2-deoxygluconate

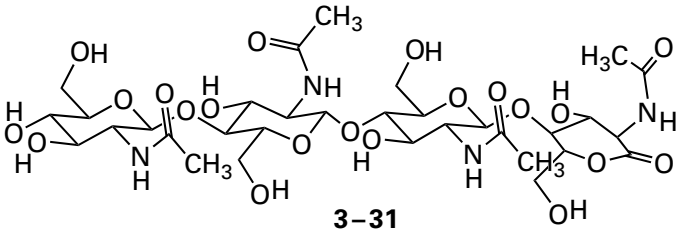

3–31

however, binds to the active site of lysozyme with a dissociation constant of 0.2 μM.[362] All these results are consistent with the conclusion that at the reducing end of a tetrasaccharide that occupies the active site of lysozyme, rather than the chair conformation of a pyranose, a planar conformation at carbon 5, oxygen 5, carbon 1, and carbon 2, which is the case with the lactone, is the structure that fits in subsite D. On the basis of these observations, it was proposed that the δ-lactone resembles oxocarbenium ion **3–26**, an intermediate of high energy, or the planar arrangement at these atoms in the transition state of a concerted nucleophilic substitution by a carboxylato group that the active site has evolved to stabilize.

In the crystallographic molecular model obtained from a crystal of lysozyme in which the active site was occupied by tetrasaccharide **3–31**, the lactone was found to occupy the subsite in the active site for the D pyranose at the reducing end of the tetrasaccharide, and it was bound in the planar, sofa conformation, which is its usual unhindered conformation in solution.[316] Because the terminal δ-lactone definitely occupies this subsite when tetrasaccharide **3–31** is bound even though a pyranose in the chair conformation at this position in a tetrasaccharide might not occupy the same subsite, only an upper limit to the difference in the standard free energy of dissociation between a lactone and a pyranose from the D subsite can be calculated. This upper limit for $\Delta\Delta G^\circ$ is 20 kJ mol^{-1}.

A few **analogues for transition states** and many other **analogues for intermediates of high energy** have been synthesized and shown to have dissociation constants from the enzyme for which each was designed that are significantly smaller than those for the respective reactants (Table 3–7). For example, the inhibition constant K_i—which in general is assumed to be a dissociation constant—for the bicyclic dicarboxylate **3–33** (100 nM) is 100 times smaller than the Michaelis constant $K_{m,chr}$ for chorismate,[364] which in the absence of a dissociation constant for chorismate was assumed to be an approximation of its dissociation constant. Analogues for the respective transition states in an electrocyclic reaction (**3–32**), a 1,2-methyl migration (**3–34**), the dissociation of a nucleophile (**3–36**), and a dissociative nucleophilic substitution at phosphorus (**3–39**) have been reported. Analogues for intermediates of high energy such as carbenium ions (**3–41** and **3–43**), oxocarbenium ions (**3–45**, **3–47**, and **3–50**), enolates (**3–52**, **3–54**, **3–56**, **3–58**, and **3–60**), phosphoranes (**3–62**), unstable ketals (**3–64**), hemiaminals,[448,449] and tetrahedral intermediates (**3–66**) have also been reported. In the special case of tetrahedral intermediates in nucleophilic substitutions, sulfoximines (**3–67**), hemiaminals (**3–68**), boronates (**3–69**), hemiacetals and hemiketals (**3–70**), phosphonamidates (**3–71**), sulfonamides (**3–72**), phosphonates (**3–73**), phosphinates,[450-452] and phosphates[453] have been used as analogues.

Table 3-7: Analogues for Transition States and Intermediates of High Energy[a]

transition state	analogue[a]	references	intermediate	analogue	references
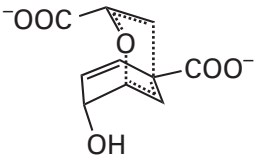 **3–32**	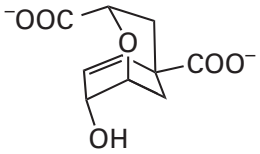 **3–33** K_i = 150 nM	303, 363-365	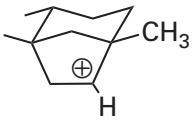 **3–41**	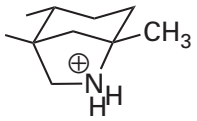 **3–42** K_i = 4 nM	366
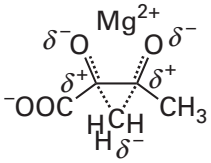 **3–34**	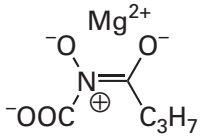 **3–35** K_i = 22 pM	367	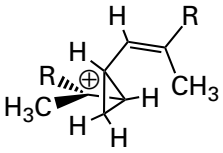 R = $C_{11}H_{19}$ **3–43**	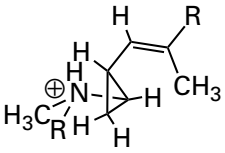 R = $C_{11}H_{19}$ **3–44** K_i = 3 μM	368
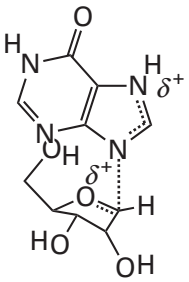 **3–36**	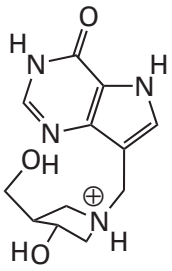 **3–37** K_i = 42 pM	369-371	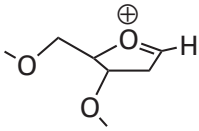 **3–45**	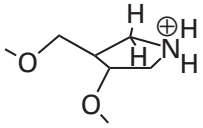 **3–46** K_i = 110 pM	211,376
	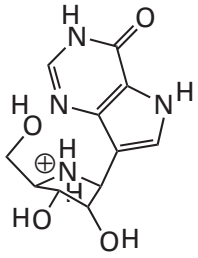 **3–38** K_i = 20 pM	372-375	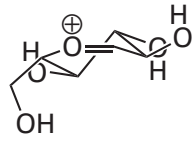 **3–47**	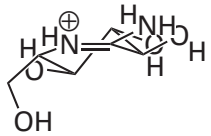 **3–48** K_i = 10 μM	377-379
				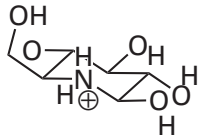 **3–49** K_i = 20 μM	377-380
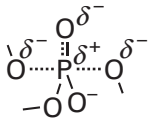 **3–39**	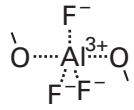 **3–40**	381-385	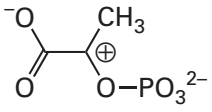 **3–50**	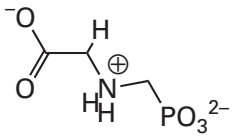 **3–51** K_i = 1 μM	386,387

intermediate	analogue	references	intermediate	analogue	references
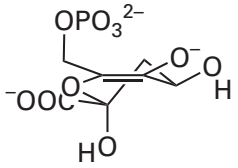 **3–52**	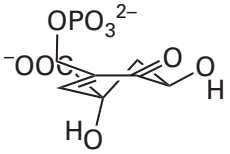 **3–53** K_i = 120 pM	388	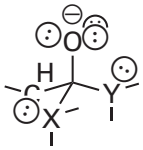 **3–66** X = O, N Y = O, N, S	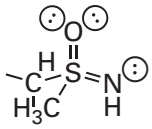 **3–67** K_i = 150 μM	389-391
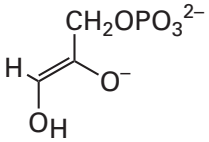 **3–54**	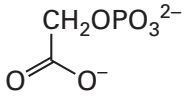 **3–55** K_i = 7 μM	354,355,392,393		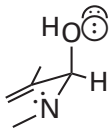 **3–68** K_i = 0.16 pM	354,394-400
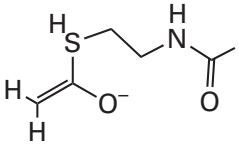 **3–56**	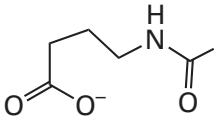 **3–57** K_i = 16 nM	401		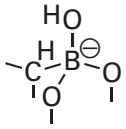 **3–69** K_i = 40 pM	402-412
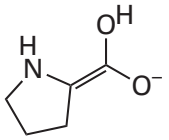 **3–58**	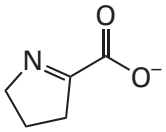 **3–59**	413-417		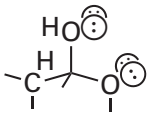 **3–70** K_i = 60 μM	418,419
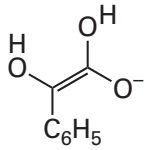 **3–60**	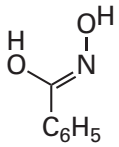 **3–61** K_i = 12 μM	420		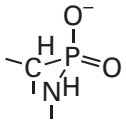 **3–71** K_i = 1 pM	421-427
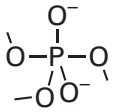 **3–62**	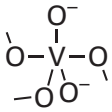 **3–63** K_i = 10 pM	428-437		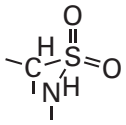 **3–72** K_i = 4 μM	390,438
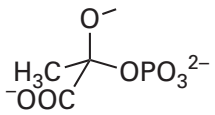 **3–64**	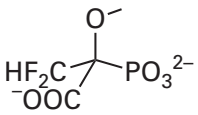 **3–65** K_i = 4 nM	439-441		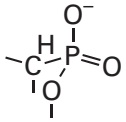 **3–73** K_i = 10 fM	213,390, 442-447

[a]The noted inhibition constant is for inhibition of only one of the enzymes inhibited by the analogue and is usually the smallest of the values observed when several enzymes or several different conditions were tested.

One peculiar property of a few of these analogues for intermediates of high energy, especially those that bind with the smallest dissociation constants, is that their **rates of association are quite slow** compared to those at which other ligands bind to the same active site.[454-456] For example, the analogue

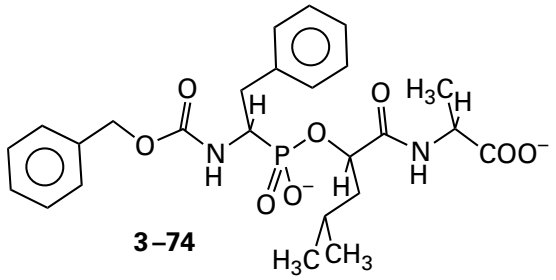

3–74

for the tetrahedral intermediate in the hydrolysis of peptides catalyzed by thermolysin from *B. thermoproteolyticus* (Table 3–6) has a rate of association of only $470\ M^{-1}\ s^{-1}$ but a dissociation constant of 45 nM.[427] It may be that, in these peculiar instances, the active site in its ground state has evolved to associate rapidly with the reactants, yet the respective intermediate of high energy differs enough in structure and conformation from the ground state that a molecule mimicking it cannot associate efficiently.[455] In the case of analogue **3–74** of the tetrahedral intermediate in the active site of thermolysin, because it does not resemble the reactant, it binds slowly. This behavior should be distinguished from the situation in which an inhibitor associates with a normal, rapid second-order rate constant but appears to associate slowly because the approach to equilibrium is governed by its slow rate of dissociation[457] or the situation in which an inhibitor associates slowly because it forms a covalent adduct with the enzyme.[458]

Such analogues for intermediates of high energy **should be distinguished from bisubstrate analogues.**[109,280] A bisubstrate analogue is a compound in which two of the substrates of an enzymatic reaction have been attached together synthetically. For example, *N*-(phosphonacetyl)-L-aspartate (**3–6**), a competitive inhibitor of aspartate carbamoyltransferase, combines the structures of carbamoylphosphate (**3–7**) and L-aspartate (**3–8**). The dissociation constant for carbamoyl phosphate from the empty active site of aspartate carbamoyltransferase from *E. coli* is 27 μM, and the dissociation constant for L-aspartate from the empty active site is 11 mM.[178] The respective standard free energies of dissociation, based on a standard state of corrected volume fraction,[273,274] are +33 and +18 kJ mol^{-1}. The inhibition constant K_i for *N*-(phosphonacetyl)-L-aspartate, when it is acting as a competitive inhibitor binding to the empty active site of aspartate carbamoyltransferase, is 30 nM, from which a standard free energy of dissociation of +48 kJ mol^{-1} can be calculated. The standard free energy of dissociation for the bisubstrate analogue is almost equal to the sum of the free energies of dissociation for the two substrates. Consequently, it cannot be an analogue of an intermediate of high energy. It is simply an example of free energy of approximation.

An inhibitor of phosphoribosylglycinamide formyltransferase from *E. coli* in which the substrates 10-formyltetrahydrofolate and N^1-(5-phospho-D-ribosyl)glycinamide have been joined together synthetically with a simple methylene[459] has a standard free energy of dissociation (+57 kJ mol^{-1}) that is almost equal to or less than the sum of the standard free energies of dissociation of 10-formyltetrahydrofolate (≥27 kJ mol^{-1}) and N^1-(5-phospho-D-ribosylglycinamide (≥34 kJ mol^{-1}).[460]

An analogue in which the 5′-hydroxy group of adenosine is covalently attached to the carbamoyl nitrogen of L-cysteinamide by a sulfonyl group is a strong inhibitor (K_i = 300 nM; K_d = 100 nM) of the nucleophilic substitution at phosphorus catalyzed by L-cysteine:1D-*myo*-inositol 2-amino-2-deoxy-α-D-glucopyranoside ligase from *Mycolicibacterium smegmatis*. Even though the analogue is isosteric with *O*-adenylyl-L-cysteine, a proposed intermediate of high energy in the enzymatic reaction; even though the dissociation constants for AMP and L-cysteine were not measured; and even though the Michaelis constants for $MgATP^{2-}$ and L-cysteine suggest that it may well be an analogue of that intermediate of high energy, the authors have decided that the analogue is simply a "bisubstrate analogue".[461,462] Such caution should probably be applied to all analogues in which portions of two substrates are combined.

The standard free energy of dissociation defines the difference between a bisubstrate analogue and an analogue of an intermediate of high energy. The standard free energies of dissociation for *N*-(phosphonacetyl)-L-aspartate and the inhibitor of phosphoribosylglycinamide formyltransferase, although they are large, are almost equal to but nevertheless less than the **sum of the standard free energies of dissociation** for their respective parts. Consequently, they are bisubstrate analogues and not analogues for intermediates of high energy. In fact, their designs were not intended to mimic a transition state or an intermediate of high energy.

The standard free energy of dissociation for an analogue of a transition state or an intermediate of high energy that coincidentally combines two substrates for the enzyme must be greater than the sum of the standard free energies of dissociation for each separate substrate. For example, an analogue for a proposed tetrahedral intermediate

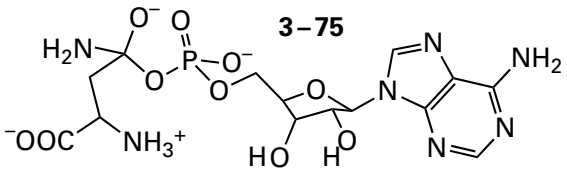

in the reaction catalyzed by aspartate—ammonia ligase from *E. coli*

$$\text{MgATP}^{2-} + \text{L-aspartate} + \text{NH}_4^+ \rightleftharpoons \text{AMP}^{2-} + \text{MgOPO}_3\text{PO}_3^{2-} + \text{L-asparagine} + 2\,\text{H}^+ \quad (3\text{–}381)$$

was synthesized using a sulfoximine (**3–67**) to substitute for the tetrahedral intermediate. This inhibitor has an inhibition constant of 70 nM,[456] which is impressive, but its standard free energy of dissociation (+44 kJ mol^{-1}) is not significantly greater than, and may be less than, the sum of the standard free energies of dissociation for L-aspartate (≥23 kJ mol^{-1}) and MgATP^{2-} (≥20 kJ mol^{-1}) from the enzyme. This comparison is ambiguous because the dissociation constant for AMP^{2-} was not measured. If AMP^{2-} binds weakly to the active site, the sulfoximine may well be an analogue of an intermediate of high energy. Nevertheless, the claim that an inhibitor is an analogue of an intermediate of high energy should require a demonstration that it is not merely a bisubstrate analogue.

This caveat, however, does not mean that **useful information** cannot be obtained from a bisubstrate analogue. For example, the bisubstrate analogue

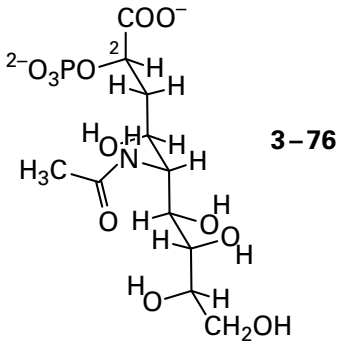

covalently attaches the properly positioned phospho group and carboxy group of phospho*enol*pyruvate, one substrate, and *N*-acetyl-D-mannosamine, the other substrate for *N*-acetylneuraminate synthase from *Neisseria meningitidis*. The fact that only the *R* isomer at carbon 2 of the analogue associates with the active site is consistent with a tetrahedral intermediate in the enzymatic reaction that has a particular sterochemistry. This intermediate, which forms between the carbon–carbon double bond of phospho*enol*pyruvate as a nucleophile, the carbonyl group of the *N*-acetyl-D-mannosamine as the electrophile, and a molecule of water as the second nucleophile, must have the *R* configuration at its carbon 2. Consequently, a crystallographic molecular model of the 2*R* analogue in the active site should reveal the orientation of the catalytic groups that occur around the actual tetrahedral intermediate.[463]

In several instances, a **bisubstrate analogue has been produced on the active site** of an enzyme rather than synthetically from one of the substrates that happens to be a nucleophile and an analogue for another substrate that incorporates an electrophilic carbon in the proper location[464] or from one of the substrates that happens to be an electrophile and an analogue for another substrate that incorporates a nucleophilic carbon in the proper location.[465]

The existence of a particular inhibitor that binds tightly and noncovalently to a particular enzyme is often used as an argument in favor of a transition state or a particular intermediate in the mechanism of the enzyme. For example, to provide evidence for the existence of the anionic intermediate **3–77** in the reaction catalyzed by protocatechuate 3,4-dioxygenase from *P. aeruginosa*

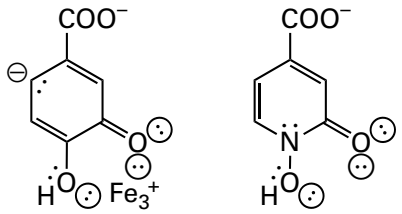

the hydroxamate **3–78** was synthesized.[466] The inhibition constant K_i for this inhibitor (100 nM)[467] is 300 times smaller* than the Michaelis constant (30 μM) for protocatechuate.[468]

*The problem of whether or not the inhibitor is a bisubstrate analogue does not arise with an enzyme that has only one reactant.

The inhibition effected by analogues for intermediates of high energy has also been used to distinguish between alternatives for the **conformation of the transition state** in a particular enzymatic reaction. For example, the transition state in the reaction catalyzed by chorismate mutase (Equation 3–367) could proceed through either an all-chair conformer of the transition state or a chair–boat conformer. The fact that *exo*-6-hydroxybicyclo[3.3.1]nonane-1,*exo*-3-dicarboxylate (**3–79**) was a reasonable competitive inhibitor of chorismate mutase from *E. coli* (K_i = 400 μM) while *exo*-6-hydroxybicyclo[3.3.1]nonane-1,*endo*-3-dicarboxylate (**3–80**) was not (K_i >10 mM)

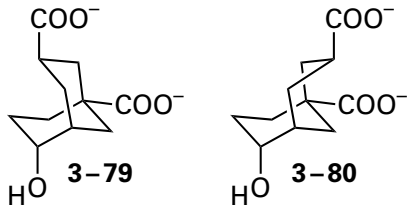

3–79 **3–80**

has been used as an argument that the transition state in the enzymatic reaction is in the all-chair conformation.[363]

A compound thought to be the actual intermediate of high energy in an enzymatic reaction can sometimes be synthesized. If it binds tightly to the enzyme, this tight binding is presented as evidence for its participation in the reaction. For example, the phosphorylated hemiketal **3–81**

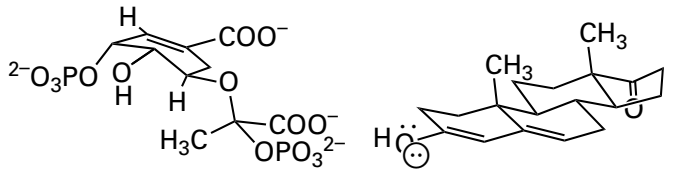

3–81 **3–82**

has a dissociation constant of less than 1 nM from 3-phosphoshikimate 1-carboxyvinyltransferase (Equation 3–262) from *E. coli*,[469] and the dienol **3–82** has a dissociation constant of 6 nM from a mutant of steroid Δ-isomerase from *C. testosteroni*.[470] These small dissociation constants are presented as evidence that these compounds are intermediates in these reactions.

Correlations between the dissociation constants of analogues for intermediates of high energy and the rate constants $K_m\ k_0^{-1}$ can provide information about both analogues and intermediates in the enzymatic reaction. Thermolysin hydrolyzes peptide bonds in polypeptides amino-terminal to hydrophobic side chains (Table 3–6) through a tetrahedral intermediate

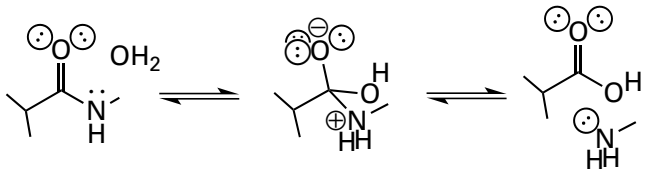

(3–382)

Analogues for six of the peptides in Table 3–6 were synthesized that incorporate a phosphonamidate (**3–71**) in place of a peptide bond. For example, the phosphonamidate

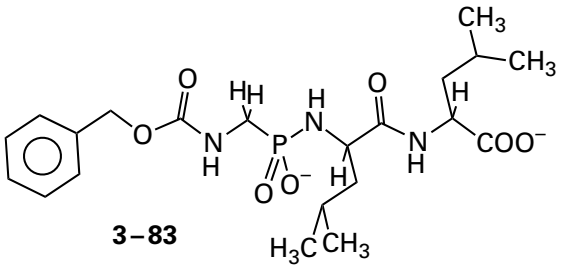

3–83

is identical to the peptide Cbz-Gly-Leu-Leu (Table 3–6) with the exception that one of the acyl carbons has been replaced by the phosphorus and oxygen of the phosphonamidate. This compound inhibits thermolysin strongly as a competitive inhibitor (K_i = 9 nM).[426] Each of the six respective phosphonamidates was shown to be a potent competitive inhibitor of the hydrolytic reactions catalyzed by the enzyme.

If these phosphonamidates are bound to the active site of thermolysin as if they were the respective tetrahedral intermediates in the normal catalytic mechanism (Equation 3–382 and Table 3–7), then they should be bound with much of the standard free energy of the available interactions between the active site and transition state. The values of the competitive inhibition constants $K_{ic,phn}$ **for each competitive inhibitor in the series should be directly proportional to** $^{\ddagger}K_d$ **for the corresponding transition state** (Equation 3–377). If this is the case and k_u, the rate constant for the uncatalyzed hydrolysis of each peptide, is approximately the same for all the peptides in the series, the values for $K_{i,phn}$ should be proportional to the values for the product $K_{d,pep}\ k_0^{-1}$ (Equation 3–379). The values for the common logarithms of $K_{i,phn}$ should be a linear function for the respective values of the common logarithms for $K_{d,pep}\ k_0^{-1}$ with a slope equal to 1. When these values of the

common logarithms for $K_{i,phn}$ were plotted as a function of the common logarithms for $K_{m,pep}\ k_0^{-1}$, the slope of the line fit to the data was 0.87 ± 0.15 over a range for K_i from 9 to 1700 nM.[426] Such a correlation simultaneously provides evidence, in the case of thermolysin, for the existence of the tetrahedral intermediate in the enzymatic reaction, for the diversion of standard free energy of dissociation to lower the standard free energy of activation, and for the ability of a phosphonamidate to mimic the tetrahedral intermediate (Figure 1–10).

A similar, though more extensive, series of 14 tripeptides and tetrapeptides were synthesized in which a phosphonate (**3–73**) rather than a phosphonamidate replaced the peptide bond between their two carboxy-terminal alanines. These analogues for the respective tetrahedral intermediates were found to be competitive inhibitors of bovine carboxypeptidase A, an exopeptidase that hydrolyzes the peptide bond between the carboxy-terminal amino acid of a protein and its penultimate amino acid. Over three orders of magnitude, their competitive inhibition constants $K_{ic,pho}$ were proportional to the values of $K_{m,pep}\ k_0^{-1}$ for the respective peptides as reactants for the enzyme because the slope of the line fit to a plot of the common logarithms of $K_{ic,pho}$ as a function of the common logarithms of $K_{m,pep}\ k_0^{-1}$ is indistiguishable from 1 (Figure 3–30A).[213,471,472] In this instance, each of the 14 inhibitors had an inhibition constant $K_{i,pho}$ that was at least 1000 times smaller than the value for the corresponding Michaelis constant $K_{m,pep}$. Again, in addition to the conclusion that a portion of the standard free energy of dissociation of the respective reactants is used by the active site to distort the reactants in the direction of the transition state, this correlation provides evidence that the intermediate in the reaction catalyzed by carboxypeptidase A is a tetrahedral intermediate.

A **proportionality between K_i and $K_m\ k_0^{-1}$** (Figure 3–30A) is used as an argument that each member of a particular series of inhibitors resembles an intermediate of high energy or a transition state in the enzymatic reaction.[473] If the series of inhibitors fails this test, however, it cannot be concluded that its members are not analogues for intermediates or transition states[474,475] because the Michaelis constant K_{mA} is often uncorrelated with the dissociation constant for a particular reactant.

The same type of correlation can be made between the dissociation constants for the same analogue of an intermediate in an enzymatic reaction and the **values of $K_m\ k_0^{-1}$ for a series of mutants** of the enzyme of decreasing catalytic efficiency. For example, tungstate associates with the active site of alkaline phosphatase from *E. coli* and forms an adduct with the serine responsible for nucleophilically catalyzing the hydrolysis of phosphate esters. The fact that the dissociation constants for tungstate from the active sites of several site-directed mutants of the enzyme are almost proportional to the values of $K_m\ k_0^{-1}$ for the hydrolysis of methyl 4-nitrophenyl phosphate by the respective mutants (Figure 3–30B) is evidence for the conclusion that the adduct of tungstate is mimicking an actual intermediate of high energy in the enzymatic reaction. The crystallographic molecular model of that adduct demonstrates that it is a pentavalent, trigonal bipyramid isosteric with a phosphorane.[476] Consequently, these results are consistent with a phosphorane being an intermediate in the enzymatic reaction, which is reasonable because the nucleophile is a strong one and the leaving group is a poor one.

The structure of the active site of bovine carboxypeptidase A was also varied. Some of the aforementioned phosphonates were used as inhibitors of three mutants of carboxypeptidase A, with significantly different values of $K_{m,pep}\ k_0^{-1}$ from the wild type, to obtain 15 different values of $K_{i,pho}$ and $K_{m,pep}\ k_0^{-1}$ for the various combinations of inhibitors and mutant enzymes. Again, the common logarithms of the values of $K_{i,pho}$ were proportional (slope 1.03) to the common logarithms of $K_{m,pep}\ k_0^{-1}$ for the respective mutants hydrolyzing the respective peptides.[477]

Endo-1,4-β-xylanase from *C. fimi* hydrolyzes (β1,4)-D-xylosidic linkages in xylans. Three derivatives of D-xylosyl-(β1,4)-D-xyloside that place a planar lactam oxime, a planar imidazolyl group, and a lactam in the location of carbon 1 and the pyranose oxygen at the reducing end of this disaccharide are potent inhibitors (inhibition constants of 0.37 μM, 0.16 μM, and 0.33 μM, respectively) of the enzyme. When each is used as an inhibitor of a series of mutants of the enzyme, the common logarithms of the inhibition constants of each inhibitor were linearly related (slopes of 1.18, 1.20, and 1.31, respectively) to the values for the common logarithms of $K_m\ k_0^{-1}$ for

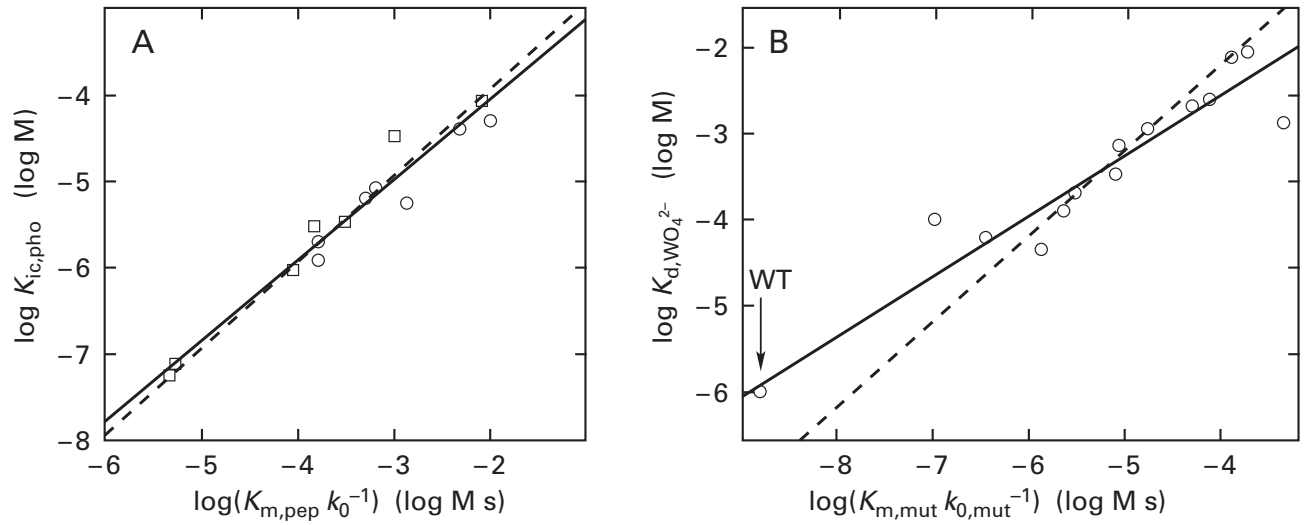

Figure 3–30: **(A)** Correlation between the dissociation constants, $K_{ic,pho}$, for a set of phosphonates from the active site of bovine carboxypeptidase A and the values of the steady-state rate constants, $K_{m,pep}$ k_0^{-1}, for the homologous reactants.[213] The reactants, listed in order of increasing values for $K_{m,pep}$ k_0^{-1}, were the peptides Cbz-Phe-Ala-Ala, Cbz-Ala-Ala-Ala, Cbz-D-Ala-Ala-Ala, Cbz-Leu-Ala-Ala-Ala, Cbz-Phe-Ala-Ala-Ala, Cbz-Gly-Ala-Ala, Pp-Ala-Ala-Ala, Pp-Ala-Ala-Ala-Ala, Cbz-Ala-Ala-Ala-Ala, Ac-Ala-Ala-Ala-Ala, Ac-Ala-Ala-Ala, Cbz-Ala-D-Ala-Ala-Ala, Ac-Ala-D-Ala-Ala-Ala, and Ac-D-Ala-Ala-Ala, where Cbz is benzyloxycarbonyl, Pp is 3-phenylpropanoyl, and Ac is acetyl. In each case, the peptide is cleaved by the enzyme at the peptide bond in the carboxy-terminal alanylalanine. An analogue of each peptide was synthesized in which a phosphonate (**3–73**) replaced the peptide bond between the carboxy-terminal alanylalanine as the phosphonamidate replaces the peptide bond in analogue **3–83**. Each analogue was assayed for its ability to inhibit carboxypeptidase A at pH 7.6, 27 °C, and an ionic strength of 0.5 M with the fluorescent reactant *N*-[3-(2-furyl)-acryloyl]-L-phenylalanyl-L-phenylalanine. The analogues were all competitive inhibitors of the enzyme. The common logarithms of the competitive inhibition constants, $K_{ic,pho}$ (molar), for tripeptides (□) and tetrapeptides (○) are plotted as a function of the common logarithms of their respective steady-state rate constants, $K_{m,pep}$ k_0^{-1} (molar second), determined previously at pH 7.6 and 27 °C.[471,472] The solid line is a least-squares linear fit to the data with a slope of 0.93 (r = 0.975), and the dashed line is a least-squares fit of a line of slope 1 to the data (r = 0.973). **(B)** Correlation between the dissociation constants, $K_{ic,WO_4^{2-}}$, for tungstate from the active sites of a set of mutants of alkaline phosphatase from *E. coli* and the values of the steady-state rate constants, K_m k_0^{-1}, for the hydrolysis of methyl 4-nitrophenyl phosphate at pH 8.0 by the respective mutant.[476] The mutants, listed in order of increasing values for K_m k_0^{-1}, were the wild type (WT), D101A, D153A, K328A, D153A/K328A, D101A, R166S/K328A, D101A/R166S, D101A/R166S/D153A, D153A/R166S, E322Y, D101A/D153A/R166S/K328A, and D153A/E322Y. The dissociation constants for tungstate from the various mutants were the values of the inhibition constant for competitive inhibition of each mutant by tungstate. The common logarithms of these inhibition constants, $K_{ic,WO_4^{2-}}$ (molar), are plotted as a function of the common logarithms of their respective steady-state rate constants, K_m k_0^{-1} (molar second). The solid line is a least-squares linear fit to the data with a slope of 0.7 (root mean square deviation = 0.28), and the dashed line is a least-squares fit of a line of slope 1 to the data (root mean square deviation = 0.41).

each mutant. The similarity of the slopes, the fact that the data span three orders of magnitude, and the quality of the correlations are arguments in favor of these three inhibitors being analogues of an intermediate or a transition state in the enzymatic reaction.[478] The lactam oxime and the imidazolyl group have carbon 2, carbon 1, the pyranosyl oxygen and carbon 5 in the same plane as would an oxocarbenium ion, and the lactam has carbon 2, carbon 1, and the pyranosyl oxygen in the same plane. These facts are consistent with an oxocarbenium ion as an intermediate in the reaction or an expanded, concerted nucleophilic substitution.

Such correlations can also be evidence that the standard free energies of dissociation for particular functional groups on substrates, even those distant from the site of catalysis, are being used by an active site to lower the standard free energy of the transition state relative to that of the ground state. For example, steroid Δ-isomerase from *P. putida* (Equation 3–376) also catalyzes the alternative isomerization

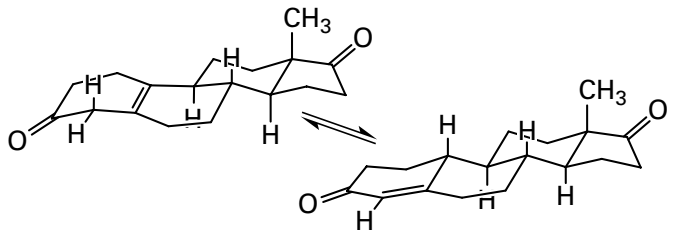

(3–383)

of estr-5(10)-ene-3,17-dione (ed). Cyclohex-3-en-1-one (co) is an analogue of the single ring in which the isomerization occurs. The value for $k_0\,K_{m,ed}^{-1}$ is 27,000 times greater than $k_0\,K_{m,co}^{-1}$. One interpretation of this large difference is that a portion of the standard free energy of dissociation for the rest of the estr-5(10)-ene-3,17-dione has been used to lower the standard free energy of the transition state for one or more rate-affecting steps in the enzymatic reaction.[479]

Two related enzymes (25% identity; 2.3 gap percent), 2-dehydro-3-deoxy-phosphogluconate/2-dehydro-3-deoxy-6-phosphogalactonate aldolase from *Saccharolobus solfataricus* and 2-dehydro-3-deoxy-phosphogluconate aldolase from *Picrophilus torridus*, each perform a retroaldol reaction on 2-dehydro-3-deoxy-6-phospho-D-gluconate (KDPG), but the value of $k_0\,K_{m,KDPG}^{-1}$ for the former enzyme is 2000 times greater than that for the latter. The enzyme from *S. solfataricus* has a cluster of amino acid side chains responsible for binding the 6-phospho group of 2-dehydro-3-deoxy-6-phospho-D-gluconate that is missing in the enzyme from *P. torridus*. It has been proposed that this difference permits the increased free energy of dissociation, exerted at a significant distance from the point at which the retroaldol cleavage occurs, to be used to lower the standard free energy of the transition state. This decrease in standard free energy increases catalytic activity of the former enzyme.[480]

When the phospho group distant from the site of the substitution catalyzed by human orotidine-5′-phosphate decarboxylase (Equation 3–366) is removed from orotidine 5′-phosphate (**3–17**), the catalytic constant decreases[481] by a factor of 10^5. (1-β-D-Erythrofuranosyl)orotic acid (EO) is an analogue of orotidine 5′-phosphate with not just the phospho group but the entire phosphohydroxymethyl group at carbon 4′ replaced by a hydrogen. When it is used as a substrate for orotidine-5′-phosphate decarboxylase (Equation 3–366) from *S. cerevisiae*, the specificity constant $k_0\,K_{mEO}^{-1}$ at pH 7 and 25 °C is 0.02 $M^{-1}\,s^{-1}$, which is 4×10^8 times smaller than the specificity constant $k_0\,K_{mOMP}^{-1}$ ($1\times10^7\ M^{-1}\,s^{-1}$) for the natural substrate, orotidine 5′-phosphate (OMP). This observation is consistent with a decrease in the standard free energy of dissociation for the transition state relative to that of the ground state of –49 kJ mol^{-1}, as a result eliminating the phosphohydroxymethyl group (Equation 3–379).[482] When orotate (O) alone is used as a substrate for orotidine-5′-phosphate decarboxylase (Equation 3–366) from *S. cerevisiae*, the specificity constant $k_0\,K_{mO}^{-1}$ at pH 7 and 25 °C is $3\times10^{-10}\ M^{-1}\,s^{-1}$, which is 7×10^7 times smaller than the specificity constant $k_0\,K_{mEO}^{-1}$. This observation is consistent with a further decrease in the standard free energy of dissociation for the transition state relative to that of the ground state of –45 kJ mol^{-1} as a result of eliminating the β-D-erythrofuranosyl group. These apparent decreases in the standard free energy of dissociation for the transition state are, in turn, consistent with the conclusion that the free energy of dissociation for some or all of the noncovalent interactions of both the phosphohydroxymethyl group at carbon 4′ of orotidine 5′-phosphate and the ribose of orotidine 5′-phosphate is used by the active site to increase the standard free energy of dissociation for the transition state relative to that of the ground state by +94 kJ mol^{-1} and thereby lower the free energy of activation by –94 kJ mol^{-1} (Figure 3–29).[483]

When phosphite, HPO_3^{2-} (PHI), is present at saturation, however, the specificity constant $k_0\,K_{mEO}^{-1}\,K_{dPHI}^{-1}$ (Equation 3–379) is 1600 $M^{-1}\,s^{-1}$, where K_{dPHI} is the dissociation constant from the active site for the cosubstrate phosphite. This specificity constant is consistent with a restoration by the phosphite of +28 kJ mol^{-1} to the standard free energy of dissociation of the transition state relative to that of the ground state[482] and a consequent decrease of –28 kJ mol^{-1} in the standard free energy of activation for the reaction (Figure 3–29). Phosphite substitutes in part for the missing phosphohydroxymethyl group. Because, however, phosphite is not connected covalently to carbon 4′ of (1-β-D-erythrofuranosyl)orotic acid, the active site, by gripping it, cannot be decreasing the entropy of approximation at the site of catalysis. Both the large decrease in the standard free energy of dissociation for the transition state relative to the ground state when the phosphohydroxymethyl group is removed and the subsequent significant increase in the standard free energy of dissociation for the transition state relative to that of the ground state when a portion of that phosphohydroxymethyl group is restored are consistent with the association of the 4′-phosphohydroxymethyl group of orotidine 5′-phosphate,

which is distant from the site of the decarboxylation, nevertheless providing standard free energy to lower the standard free energy of activation.

A series of site-directed mutants of orotidine-5′-phosphate decarboxylase (Equation 3–366) from *S. cerevisiae* with different values for $k_0\,K_{mOMP}^{-1}$ were constructed. When the common logarithms of the rate constants $k_0\,K_{mEO}^{-1}\,K_{dPHI}^{-1}$ were plotted against the common logarithms of the respective rate constants $k_0\,K_{mOMP}^{-1}$, there was a linear correlation between the two, over five orders of magnitude, with a slope of 1.05 ± 0.08. This correlation is further validation of the conclusion that association of the phosphohydroxymethyl group at carbon 4′ of orotidine 5′-phosphate provides standard free energy used to lower the standard free energy of the transition state relative to that of the ground state for the reaction catalyzed by orotidine-5′-phosphate decarboxylase.[484]

A similar correlation (slope = 1.04 ± 0.3) was observed for the reactions catalyzed by a series of site-directed mutants of triose-phosphate isomerase

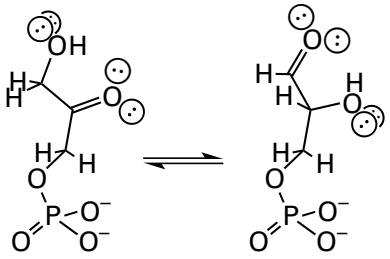

(3–384)

from *Trypanosoma brucei* between the common logarithms of $k_0\,K_{mGAP}^{-1}$, where the Michaelis constant is for D-glyceraldehyde 3-phosphate (GAP), and the common logarithms of $k_0\,K_{mGAP}^{-1}\,K_{dPHI}^{-1}$, where the Michaelis constant is for glycolaldehyde (GA), a truncated version of D-glyceraldehyde 3-phosphate in which the 2-phosphohydroxymethyl group is replaced by a hydrogen, and the dissociation constant is for phosphite (PHI). Again the conclusion is that standard free energy of dissociation for the phosphohydroxymethyl group of D-glyceraldehyde 3-phosphate is used to lower the standard free energy of the transition state relative to that of the ground state for the isomerization catalyzed by the enzyme.[485]

A decrease in the apparent standard free energy of dissociation for the transition state relative to that of the ground state (-35 kJ mol^{-1}) is observed for the reaction catalyzed by 1-deoxy-D-xylulose-5-phosphate reductoisomerase from *M. tuberculosis* when 1-deoxy-L-erythrulose (1-deoxy-D-xylulose-5-phosphate missing its phosphohydroxymethyl group) is used as a substrate, and a portion of the standard free energy of dissociation for the transition state relative to that of the ground state (+13 kJ mol^{-1}) can be restored when phosphite associates with the active site along with 1-deoxy-L-erythrulose.[486]

Thermolysin and carboxypeptidase A catalyze the hydrolysis of a peptide bond by activating water and catalyzing its direct addition to the amide. Another whole group of endopeptidases and esterases, such as trypsin, chymotrypsin, elastase, and acetylcholinesterase, catalyze hydrolyses of acyl compounds by forming covalent intermediates between serines in their active sites and the acyl carbons of the reactants (Figure 3–6). In the case of acetylcholinesterase, the covalent intermediate is an ester formed between a serine in the active site and the acetyl moiety of the reactant

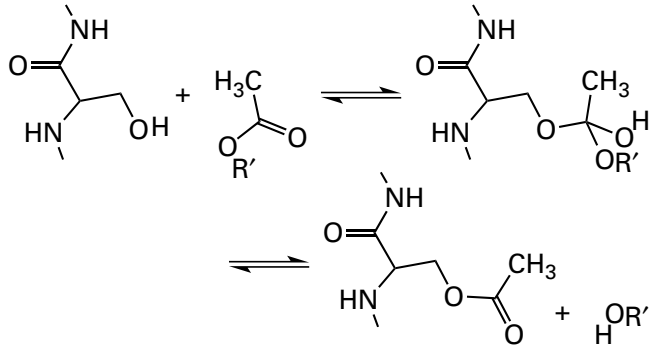

(3–385)

Several trifluoromethyl ketones were synthesized to act as precursors to the respective hemiacetals formed from the serine in the active site[487]

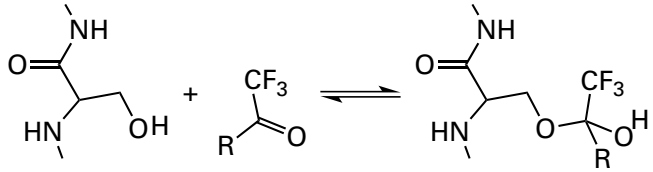

(3–386)

These hemiacetals, because they mimic the tetrahedral intermediate of the nucleophilic substitution catalyzed by acetylcholinesterase (Equation 3–385), are examples of analogues for intermediates of high energy **formed on the active site of the enzyme itself from a precursor**.[488] Because they can form such adducts, trifluoromethyl ketones are potent inhibitors of the enzymatic reaction. For example, the trifluoromethyl ketone that is an analogue for acetylcholine [R = $-(CH_2)_3N^+(CH_3)_3$] has an inhibition

constant, K_i, of 0.06 nM for acetylcholinesterase from *E. electricus*.[487]

It has been pointed out by Jencks,[489] and implied by Pauling,[311] that if an active site catalyzes a reaction by binding the transition state or an intermediate of high energy more tightly than it does the substrates,[311] an immunoglobulin raised against an analogue for either a transition state or an intermediate of high energy, because it would bind the corresponding transition state or intermediate of high energy tightly, should catalyze the corresponding reaction. Such **catalytic immunoglobulins** have been produced. For example, monoclonal immunoglobulins were raised against an analogue[364]

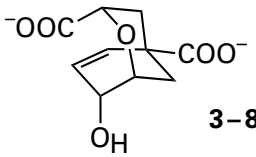

3–84

of the transition state in the chorismate mutase reaction ($K_i = 0.1\ \mu M$) that had been attached as a hapten to a protein carrier through a tyrosine[490]

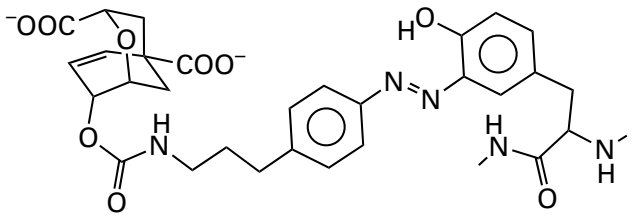

3–85

One of the monoclonal immunoglobulins produced was able to catalyze the chorismate mutase reaction enzymatically ($k_0 = 2.7\ min^{-1}$, $K_m = 260\ \mu M$ at 10 °C). Although this monoclonal immunoglobulin was not so efficient as chorismate mutase itself ($k_0 = 820\ min^{-1}$, $K_m = 290\ \mu M$ at 10 °C), its catalytic constant was 10^4 times that of the first-order, uncatalyzed reaction under the same conditions. It has already been noted that freezing rotation around the two exocyclic bonds of chorismate and forcing the exocyclic carbon–carbon double bond into the axial position could accelerate the reaction by a factor of 10^3. The same analogue for the transition state was used in other experiments[491] and a similar monoclonal antibody was isolated.

A number of these catalytic immunoglobulins have been produced. None has yet duplicated the acceleration of rate achieved by an enzyme. For example, the largest catalytic constants observed so far are in the range 20–100 min^{-1} at 25 °C[492-495] while enzymes usually have catalytic constants[264] between 10 and $10^6\ s^{-1}$. The advantage of such catalytic immunoglobulins, however, is that they can be designed to catalyze reactions not catalyzed by extant enzymes.[492,496-500]

The standard free energy of dissociation of the substrates can be exploited by an enzyme to alter the difference in standard free energy between reactants and products while they are bound at the active site. The equilibrium constant for the reaction catalyzed by L-lactate dehydrogenase (Equation 3–27) at pH 7, in the direction of reducing pyruvate to lactate and converting NADH to NAD^+ in free solution, is 2.5×10^4 in favor of NAD^+ and lactate because of the gain in aromaticity of the nicotinamide and the conversion of a π bond to a σ bond. When all the substrates, however, are within the active site of the porcine enzyme, the equilibrium constant for the same reaction is only 4.[501] This represents a shift in the standard free energy change for the reaction as written of +22 kJ mol^{-1} when it takes place on the active site. This shift can be explained with the following linkage box

$$\begin{array}{ccc} \mathrm{E + NAD^+ + lactate} & \underset{\Delta G^\circ_1}{\rightleftharpoons} & \mathrm{E + NADH + H^+ + pyruvate} \\ \Big\updownarrow \Delta G^\circ_2 & & \Big\updownarrow \Delta G^\circ_4 \\ \mathrm{E{\cdot}NAD^+{\cdot}lactate} & \underset{\Delta G^\circ_3}{\rightleftharpoons} & \mathrm{EH^+{\cdot}NADH{\cdot}pyruvate} \end{array} \qquad (3\text{–}387)$$

By observation

$$\Delta G^\circ_1 + 22\ \mathrm{kJ\ mol^{-1}} = \Delta G^\circ_3 \qquad (3\text{–}388)$$

It necessarily follows that

$$\Delta G^\circ_2 = \Delta G^\circ_4 + 22\ \mathrm{kJ\ mol^{-1}} \qquad (3\text{–}389)$$

and that pyruvate and NADH dissociate from the enzyme less readily, by +22 kJ mol^{-1}, than lactate and NAD^+. A standard free energy change of +22 kJ mol^{-1} must occur in the noncovalent forces holding the substrates in the active site as pyruvate and NADH are turned into lactate and NAD^+.

A similar effect is observed with isoleucine—tRNA ligase

$$MgATP^{2-} + \text{L-isoleucine} + tRNA^{Ile} \rightleftharpoons AMP^{2-} + H^+ + MgOPO_3PO_3^{2-} + \text{L-isoleucyl-}tRNA^{Ile} \quad (3\text{–}390)$$

from *E. coli*. When the substrates are on the active site,[502] the standard free energy change is +5 kJ mol^{-1} to form the amino acid adenylate that is the intermediate in the reaction; but, in solution,[502,503] the standard free energy change for the same reaction has been estimated to be between +20 and +40 kJ mol^{-1}.

Such shifts in the standard free energy change for an enzymatically catalyzed reaction, brought about by the **preferential association of reactants or the preferential association of products** to the active site, may be advantageous. It has been argued that when the standard free energy change for the reaction catalyzed by an enzyme is shifted sufficiently so that it has a value of 0 within the active site, the enzyme can catalyze the reaction with the highest efficiency.[504] This property is supposed to be essential when the role of that reaction in metabolism is to perform the net transformation of substrates either in one direction or in the other direction, depending on the demands of the moment, and to accomplish this feat, the enzyme must maintain its substrates at their equilibrium concentrations in the cytoplasm.[505] Several enzymes, such as arginine kinase from *Homarus vulgaris*, creatine kinase from *O. cuniculus*, phosphopyruvate hydratase from *S. cerevisiae*, glutamine synthetase from *E. coli*, phosophoglucomutase from *O. cuniculus*, and phosphoglycerate kinase (Equation 3–375) from *S. cerevisiae*,[506] all maintain their substrates at equilibrium in the cytoplasm and all shift the equilibrium constants on the active site to values close or considerably closer to 1.[507] The generality, however, of the conclusion that a perfect enzyme will maintain the equilibrium constant between reactants and products on its active site near a value of 1 has been questioned.[508]

Suggested Reading

Jencks, W. P. (1975) Binding energy, specificity, and enzymic catalysis, *Adv. Enzymol. Relat. Areas Mol. Biol. 43,* 219–410. https://doi.org/10.1002/9780470122884.ch4

Hanson, J. E., Kaplan, A. P., and Bartlett, P. A. (1989) Phosphonate analogues of carboxypeptidase A substrates are potent transition-state analogue inhibitors, *Biochemistry 28*, 6294–6305. https://doi.org/10.1021/bi00441a022

Vladimirova, A., Patskovsky, Y., Fedorov, A. A., Bonanno, J. B., Fedorov, E. V., Toro, R., Hillerich, B., Seidel, R. D., Richards, N. G. J., Almo, S. C., and Raushel, F. M. (2016) Substrate distortion and the catalytic reaction mechanism of 5-carboxyvanillate decarboxylase, *J. Am. Chem. Soc. 138*, 826–836. https://doi.org/10.1021/jacs.5b08251

Problem 3–24: The catalytic subunit of aspartate carbamoyltransferase contains the active site that catalyzes the reaction of Equation 3–220.

(A) Write a mechanism for this reaction, involving a tetrahedral intermediate, as it would occur in the active site of the enzyme. Indicate the removals and additions of hydrons by acids and bases in the active site.

(B) Succinate is an inhibitor of the enzyme that competes with L-aspartate for the same corner of the active site. Draw the structures of succinate and aspartate side by side in the same orientation. What is the difference between the two?

When the catalytic subunit of aspartate carbamoyltransferase from *E. coli* is mixed with saturating concentrations of carbamoyl phosphate and succinate, a significant conformational change occurs in the enzyme that is associated with increased absorbance of the protein at 290 nm[178] and a 1.8% increase in the sedimentation coefficient.[509] Neither carbamoyl phosphate nor succinate alone causes this change in conformation; nor does it occur when the carbamoyl phosphate corner of the active site is occupied by $HOPO_3^{2-}$ and either L-aspartate or succinate occupies its corner. The following are dissociation constants for succinate and L-aspartate from the enzyme when it is saturated with either phosphate or carbamoyl phosphate.[178]

ligand	phosphate	carbamoyl phosphate
aspartate	6.7 mM	>20 mM
succinate	33 mM	0.74 mM

The conclusion that can be drawn from these measurements is that carbamoyl phosphate increases the affinity of the enzyme for succinate 50-fold but decreases the affinity of the enzyme for L-aspartate greater than 3-fold.

(C) Examine closely your mechanism for the enzymatic reaction and the structural difference between L-aspartate and succinate and explain values of the tabulated dissociation constants in terms of strain.

(D) Assume that the same noncovalent forces are involved in the binding of either L-aspartate or succinate to the enzyme and that the available noncovalent free energy for L-aspartate changes by the same amount as that for succinate when carbamoyl phosphate is substituted for phosphate. If these assumptions apply, how much free energy of association is apparently used by the enzyme to lower the free energy of activation for the reaction?

Problem 3–25:

(A) Write the chemical mechanism for the hydrolysis of a peptide bond, RCONHR′, when it is not catalyzed by an enzyme. Include all transfers of hydrons explicitly. Draw the reactants, all intermediates, and the products with proper stereochemistry.

A series of inhibitors has been synthesized for thermolysin from *B. thermoproteolyticus*[426]

inhibitor	K_i (nM)
CbzNHCH$_2$PO$_2$-L-Leu-D-Ala	1700
CbzNHCH$_2$PO$_2$-L-Leu-amide	760
CbzNHCH$_2$PO$_2$-L-Leu-Gly	270
CbzNHCH$_2$PO$_2$-L-Leu-L-Phe	78
CbzNHCH$_2$PO$_2$-L-Leu-L-Ala	78
CbzNHCH$_2$PO$_2$-L-Leu-L-Leu	9.1

where Cbz is benzyloxycarbonyl.

(B) By drawing the appropriate structures, explain why these inhibitors (see Table 3–7) bind so much more tightly to the enzyme than their analogous substrates (Table 3–6).

(C) What is the central intermediate in the peptide hydrolysis catalyzed by thermolysin?

One way to write the mechanism of the reaction catalyzed by thermolysin and compare it to the mechanism of the nonenzymatic reaction is

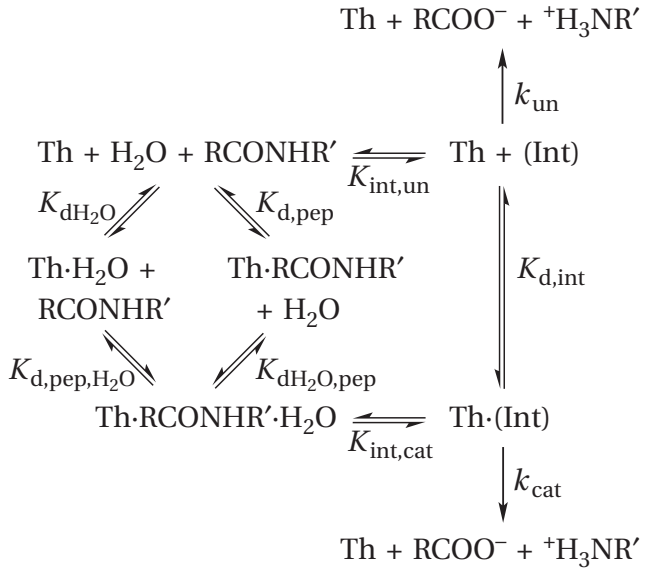

where (Int) is the central intermediate in peptide hydrolysis, k_{un} and k_{cat} are rate constants for the dissociation of the intermediate into the two products in free solution or on the active site of the enzyme, Th is thermolysin

$$K_{int,un} = \frac{[(Int)]}{[RCONHR'][H_2O]}$$

$$K_{int,cat} = \frac{[Th\cdot(Int)]}{[Th\cdot RCONHR'\cdot H_2O]}$$

and all the other constants are dissociation constants.

It has been shown that the values of K_m (Table 3–6) for the reactants analogous to these inhibitors are approximately equal to their dissociation constants from the active site. These tabulated values are presumed to be apparent dissociation constants.

$$K_{d,pep,app} = \frac{([Th] + [Th\cdot H_2O])[RCONHR']}{[Th\cdot RCONHR'] + [Th\cdot RCONHR'\cdot H_2O]}$$

(D) Show that

$$K_{d,pep,app} = \frac{K_{d,pep,H_2O}\left(1 + \frac{K_{dH_2O}}{[H_2O]}\right)}{\left(1 + \frac{K_{dH_2O,pep}}{[H_2O]}\right)}$$

(E) Show that

$$K_{d,int} = \frac{K_{dH_2O}\, K_{int,un}\, K_{d,pep,app}\left(1 + \frac{K_{dH_2O,pep}}{[H_2O]}\right)}{K_{int,cat}\left(1 + \frac{K_{dH_2O}}{[H_2O]}\right)}$$

(F) Show that there should be a correlation among the values of inhibition constants, K_i, for the six inhibitors and the values of the dissociation constant, $K_{d,pep}$, and the catalytic constant, k_0, for the respective peptide if the following reasonable assumptions are made.

(a) The initial rate $v_0 = k_0[\text{Th}\cdot\text{RCONHR}'\cdot H_2O] = k_{cat}[\text{Th(Int)}]$ so that $k_0 = k_{cat}K_{int,cat}$.

(b) The rate constant, k_{cat}, is the same for all substrates.

(c) Both the enzymatic reaction and the uncatalyzed reaction proceed through the same central intermediate.

(d) The equilibrium constant, $K_{int,un}$, is the same for all the substrates because the differences among them are distant from the point of hydrolysis.

(e) The concentration of the reactant water is at saturation so that it is greater than the two dissociation constants, K_{dH_2O} and $K_{dH_2O,pep}$.

(f) The equilibrium constants, K_i and $K_{d,int}$, vary in direct proportion to each other as the substrates and their analogous inhibitors are varied in structure.

(G) Show that the results display this correlation.

Problem 3–26: The enzyme inorganic diphosphatase catalyzes the reaction

$$MgO_3POPO_3^{2-} + H_2O \rightleftharpoons MgO_3PO^- + HOPO_3^{2-} + H^+$$

where $MgO_3POPO_3^{2-}$ is the magnesium complex of inorganic diphosphate, $HOPO_3^{2-}$ is phosphate, and MgO_3PO^- is the magnesium complex of phosphate. From the following equilibrium constants[510]

$$\frac{[HOPO_3^{2-}]^2}{[H_2O_3POPO_3^{2-}]} = 2.7\times10^4\ \text{M}$$

$$\frac{[Mg^{2+}][HOPO_3^{2-}]}{[MgO_3PO^-]} = 5\times10^{-2}\ \text{M}$$

$$\frac{[Mg^{2+}][H_2O_3POPO_3^{2-}]}{[MgO_3POPO_3^{2-}]} = 2.7\times10^{-4}\ \text{M}$$

for the species at pH 7, calculate the equilibrium constant for this reaction as written. On the active site of the enzyme from *S. cerevisiae*, the equilibrium constant at pH 7 for the reaction catalyzed by the enzyme is 5. The ionization state of the reactants and products in the active site is unknown. Compare the two equilibrium constants, the one in solution with the one on the active site. Discuss their relative magnitudes in terms of approximation and strain.

Problem 3–27: These competitive inhibitors were designed as analogues for intermediates of high energy for the respective enzymes. Draw the inhibitor next to the intermediate of high energy in the reaction that it was designed to mimic in the same orientation as the drawing of the compound.

enzyme	inhibitor	K_{ic}
aconitate hydratase[511]	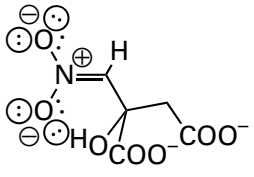	60 nM
isocitrate lyase[512]	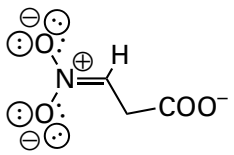	<20 nM

orotidine-5′-phosphate decarboxylase[513]	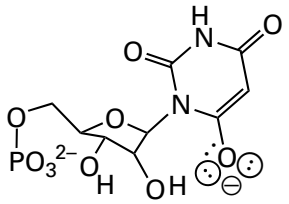	10 pM
adenosine deaminase[514]	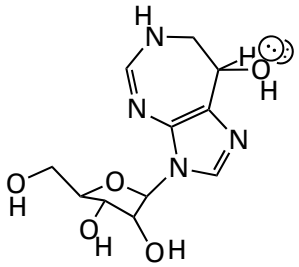	3 pM
acetylcholinesterase[515]	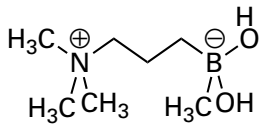	30 nM
glucose-6-phosphate isomerase[516]	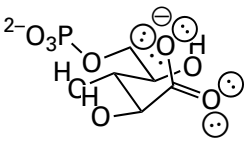	0.3 μM
phosphopyruvate hydratase[517]	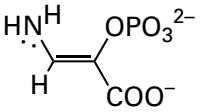	0.1 μM
adenosine deaminase (3.5.4.4)[400]	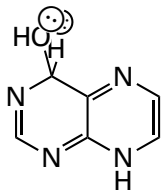	25 μM

The reactions catalyzed by these enzymes can be learned at https://www.enzyme-database.org/.

Problem 3–28: Is the magnesium complex of *P*(1),*P*(5)-bis(5′-adenosyl) pentaphosphate a bisubstrate analogue or an analogue for an intermediate of high energy for adenylate kinase from *O. cuniculus*

$$AMP^{2-} + MgATP^{2-} \rightleftharpoons ADP^{3-} + MgADP^{-}$$

if its dissociation constant as a competitive inhibitor[518] is 3 nM while the dissociation constants from the active site for AMP^{-} and $MgATP^{2-}$ are 0.1 and 0.6 mM?

Problem 3–29: L-Methionine (*S*)-sulfoximine *N*-phosphate

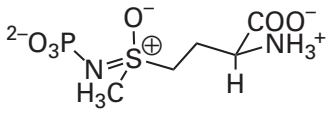

forms a tight complex with ovine glutamine synthetase.[391,519] What does this fact suggest about the mechanism of the enzyme?

Crystallographic Studies of Active Sites

The initial step in a crystallographic study of the active site of an enzyme is to construct a **refined crystallographic molecular model of the enzyme in one of its forms** by the usual procedures of crystallization, diffraction of X-rays, collection of a data set, calculation of a map of electron density, construction of a molecular model, and refinement. For a protein that has just been crystallized and to which these methods are being applied, molecular replacement is always the first resort for calculating a map of electron density.

There are now so many crystallographic molecular models of so many proteins that one is often already available of a protein that is known from its sequence of amino acids to be homologous to the enzyme of interest.* In addition, methods of artificial intelligence can use the large and ever-growing collection of established crystallographic molecular models to learn how to construct a molecular model from the sequence of amino acids for a protein.[520] Either or both of these approaches can be used to create a hypothetical molecular model† for the purposes of molecular replacement of a protein that has been crystallized but for which a crystallographic molecular model is unavailable.

*It is now the case that the sequence of amino acids for any protein that has been purified and crystallized is almost always available from genomic sequencing.

†It should be pointed out that these methods provide a hypothetical molecular model of only the unoccupied protein and are as yet unable to provide a hypothetical molecular model of a form of the enzyme in which the active site is occupied by any ligand. Hence, crystallography is still required to examine the mechanism of an enzyme. It should also be kept in mind that these methods, because they do not rely on any understanding of the forces involved in protein folding, which are at best poorly understood, cannot provide any information about why a protein has a certain structure.

The crystallographic molecular model of a related protein or a hypothetical molecular model created by artificial intelligence is used as a starting point to apply molecular replacement to the observed reflections from a crystal of the enzyme of interest. **Molecular replacement** allows the crystallographer to initiate refinement without the need for the arduous tasks of discovering isomorphous replacements, locating the positions of the heavy atoms in those isomorphous replacements, and phasing the initial data set of observed reflections. Consequently, molecular replacement has had a significant impact on crystallography.

Molecular replacement uses **Patterson maps** to score its trials and errors. A Patterson map is calculated by the usual Fourier transform from squares of the amplitudes of reflections in an observed data set, but the phases for the reflections are all set at zero. A Patterson map provides a map of all the vectors between all the atoms in the unit cell rather than a map of electron density. Nevertheless, a Patterson map is indirectly related to the actual electron density within the unit cell.

If a known molecular model of a homologous protein is used as a starting point, a molecular model of the actual protein in the crystal with which to initiate refinement is then built from the molecular model of the homologous protein by placing each of its amino acids in the location of the homologous amino acid in the protein used to initiate the molecular replacement. When a hypothetical molecular model derived from artificial intelligence is used to initiate molecular replacement, it already has the correct sequence of amino acids.

Methods are available to **rotate and translate the homologous or hypothetical molecular model** of the protein within the unit cell of the crystal of the protein of interest for which a molecular model is not available.* The homologous or hypothetical crystallographic molecular model is rotated and translated until the calculated Patterson map of the rotated and translated molecular model in the unit cell containing the protein of interest has the highest correlation with the Patterson map calculated from the amplitudes of the reflections observed directly from the new crystal. When the best correlation is achieved, it is assumed that the orientation and position of the homologous or hypothetical crystallographic molecular model is as close as possible to the orientation and position of the actual molecule of the protein of interest in the unit cell of the crystal.

Once the molecular model in which the amino acids of the homologous protein have been replaced or the hypothetical molecular model has been positioned and oriented in the unit cell of the new crystal, a data set of reflections, F_c, and a data set of phases, α_c, is calculated from that oriented molecular model. These two data sets are used to initiate a refinement of the structure against the data set of the observed amplitudes of the reflections, F_o, from the crystal, again the only actual observations.

Gradually, under the influence of the observed data set, the map of electron density shifts from that of the initial molecular model to one for the actual molecule in the crystal. At first, the set of atoms that were present in the initial crystallographic molecular model positioned by the molecular replacement are continuously repositioned in the maps of electron density calculated during initial rounds of refinement as accurately as possible. When further adjustments of these atoms are no longer required, the positive electron density for any prosthetic groups in the active site or molecules of water or other ligands that are at any location in the protein in the crystal and that were not present in the anhydrous molecular model used to initiate the refinement will be at their most accurate resolution, and molecular models of these prosthetic groups, molecules of water, and ligands are placed within their respective electron densities. The more complete structure is then submitted to further refinement against the observed amplitudes, and molecules of water are added as they appear in the map of electron density.

In the initial crystallographic molecular model of the enzyme, the active site is usually unoccupied by substrates or inhibitors because neither substrates nor inhibitors were present in the solution from which the enzyme was crystallized. In many instances, however, **a form of the enzyme occupied by a substrate or an inhibitor** is the form chosen for the initial crystals, often because it crystallizes more readily. Such a salutary effect of a ligand on the crystallization is thought to be due to the rigidification of the active site produced by its association. Just as is done with molecules of water or prosthetic groups, as soon as the electron density of that substrate or inhibitor becomes definitive in one of the intermediate maps of difference electron density calculated during the refinement, a molecular model of it is

*Most unit cells have more than one molecule of protein within them. Each molecule of protein, however, is usually related to every other molecule of protein by the symmetry operations of the space group. As a result, rotation of the known crystallographic molecular model of the protein can be continuously coupled to rotation of other copies of that same known crystallographic molecular model within the new unit cell by these symmetry operations so that all copies rotate at the same time.

positioned within that electron density, and that molecular model of the ligand simply becomes a part of the overall molecular model of the enzyme submitted to further refinement.

In some instances, a protein, thought to be unoccupied, has been found to have a ligand bound to it other than any of the components in the solution used to crystallize the protein. When such unexpected features appear in its map of electron density, the unexpected ligand should then be identified by chemical analysis rather than just by guessing what it is.[521-523]

The initial crystals of the enzyme, either occupied or unoccupied; the data sets for the observed amplitudes of the reflections, F_o, the calculated amplitudes of the reflections, F_c, and the calculated phases for the reflections,* both α_o and α_c; the refined maps of electron density; and the fully refined crystallographic molecular model itself comprise the starting point in a study of the active site of a particular enzyme.

Although molecular models of substrates and inhibitors are often **docked computationally** with an empty active site to produce imaginary complexes, this practice is usually unreliable,[524] while crystallographic molecular models of actual complexes are definitive pictures of actual events.

Crystals of an enzyme, the active site of which is occupied by one or more substrates or inhibitors of interest that were not present in the initial crystals, can be prepared in at least two ways. The initial crystals of the enzyme with an unoccupied or otherwise occupied active site can be transferred to a solution containing one or more of these ligands of interest, which diffuse into the crystal and occupy the active sites. Often this **soaking** causes the crystals to shatter as adjustments in the structure of the protein occur in response to the occupation of the active site. Sometimes this shattering can be prevented by crosslinking the crystals, but this procedure can often prevent a conformational change required to produce the active conformation of the active site or even prevent the added ligands from occupying the active site. Preferably, **the ligands of interest can be present during crystallization** at concentrations adequate to saturate the active sites and become directly incorporated into the crystal while on the active site of the enzyme. This strategy, however, can lead to crystals that are not isomorphous with the original crystals and have a different space group from the original crystals simply because the enzyme is a different molecule when one or more ligands are bound than when no ligand or another ligand is bound. For example, while the unliganded α_2 dimer of equine alcohol dehydrogenase crystallizes in the $C222_1$ space group with a single protomer as the asymmetric unit, the form of the enzyme in which the active site is occupied by NADH crystallizes in the $P1$ space group with the entire α_2 dimer necessarily comprising the asymmetric unit.[525]

If crystals of the enzyme occupied with the substrate or inhibitor of interest have a **different space group from the initial crystals** of the unoccupied or otherwise occupied enzyme, they necessarily present an entirely new crystallographic problem. In almost all cases, however, this new problem can again be solved rapidly by molecular replacement using the initial molecular model of the protein of interest as a starting point.

If one is lucky and **the new crystals of the liganded enzyme are isomorphous** with the crystals that produced the initial crystallographic molecular model, a map of electron density can be calculated using the set of calculated phases, α_c, from the initial refined crystallographic molecular model and the observed data set of amplitudes for the reflections, F_o, collected from the new crystals. Were the phases of all the reflections from the new crystals the same as the phases of the reflections from the initial crystals, an unambiguous map of electron density could be calculated from this data set immediately, but they are not the same because the presence of new ligands has produced a different set of reflections with different phases from those collected from the initial crystals. Although the electron density for the polypeptide itself is almost the same as it was in the earlier refined map of electron density of the otherwise occupied or unoccupied enzyme, there are often differences, especially in the vicinity of the active site, resulting from changes in the conformation of the polypeptide elicited by the binding of substrates or inhibitors that now occupy the enzyme, and these changes must be incorporated during refinement. The alterations in electron density resulting from these changes in conformation become more definitive as the refinement against the data set of observed

*It is worth reminding the reader that the only observed data are the reflections from particular crystals and their amplitudes, which are tabulated both in the several data sets that are needed to calculate the phases and in the data sets F_o used with the phases to calculate maps of electron density. All the remaining data sets are for calculated data, including the euphemistically designated "observed phases", α_o, as well as the data sets for the phases, α_c, and the reflections, F_c, calculated from the various interim crystallographic molecular models built by the crystallographer in the computer during the cycles of refinement.

amplitudes progresses, and these alterations guide the necessary adjustments of the polypeptide. Again, the atoms present in the initial model are positioned in the new model as accurately as possible first, and then, either initially or as the refinement proceeds, molecular models of the novel ligand or ligands are inserted in the respective features of positive electron density.

There are, however, **problems with isomorphous crystals**. Isomorphous crystals may not have the enzyme in the proper conformation for catalysis. For example, when $MgATP^{2-}$ is diffused into crystals of a domain of myosin II from *Dictyostelium discoideum*, it is unhydrolyzed in the map of electron density calculated from the observed data set even though the domain would have rapidly hydrolyzed the $MgATP^{2-}$ were it in solution.[526] When Mg^{2+} is diffused into crystals of a complex between the *Eco*RV endonuclease from *E. coli* and a fragment of DNA, the DNA remains unhydrolyzed even though the Mg^{2+} associates in the active site adjacent to the phosphodiester that is normally hydrolyzed by the enzyme in the presence of Mg^{2+} when it is in solution.[527] Another disadvantage of trying to avoid molecular replacement by using isomorphous crystals is that it is difficult to eliminate bias toward the initial, unliganded structure. Often molecular replacement is still used to obtain an initial map of electron density from an isomorphous crystal to avoid these biases.

A refined crystallographic molecular model of **a complex between a protein that is not an enzyme and a ligand** that binds to that protein can also be obtained by these procedures. Strategically, this approach is a simpler problem than that of a complex between an enzyme and its substrates because a protein that simply binds a ligand does not alter the ligand covalently in a catalytic reaction. Examples of crystallographic molecular models for such naturally static complexes are those for hormone receptors and their hormones,[528] immunoglobulins and their antigens,[529] binding proteins that deliver metabolites to proteins catalyzing transport and their metabolites,[530-532] lectins and their oligosaccharides,[533,534] agglutinins and their oligosaccharides,[535,536] lipid-binding proteins and their lipids,[537-539] and histocompatibility antigens and their peptidic ligands.[540-542]

When the refinement of a crystallographic molecular model of the liganded enzyme is complete, an **omit map of difference electron density** is calculated**.** For the calculation of this omit map, the molecular model of a substrate, ligand, or inhibitor is omitted from a crystallographic molecular model, a data set is calculated from this molecular model, and refinement against the observed reflections is initiated and continued until the positive electron density for these omitted participants in the maps no longer changes This omit map of difference electron density and the value of R_{free} for the omit map are presented as validation and a measure of the accuracy, respectively, of the final orientations of all these essential groups (Figure 3–31).[543] In many instances, any prosthetic groups, molecules of water, and amino acid side chains judged to be essential to catalysis are omitted and consequently become features in the map. It is always the final omit map of difference electron density that provides the most accurate picture of the actual occupancy of the active site.

An active site or binding site that is unoccupied by substrates or ligands is filled with molecules of water. This observation is almost universal because empty space is always minimized in a condensed phase. Because a molecule of protein in its crystal is still entirely dissolved in water, and therefore still in a condensed phase, empty spaces larger than a molecule of water will usually be automatically filled with molecules of water. An active site is required to orient substrates so they can act as participants in the reaction catalyzed by the enzyme. The noncovalent interactions usually employed to perform this orientation are hydrogen bonds formed between the active site and the substrates. The donors and acceptors for those hydrogen bonds in the active site when it is unoccupied by substrates form hydrogen bonds with more or less rigidly held molecules of water.[511] In the map of electron density for the unoccupied active site, these fixed molecules of water appear as spheres of electron density. There are, however, in the map of electron density many apparently vacant areas, especially the spaces between the molecules of protein but those within the molecules of protein as well. Because nature abhors a vacuum, these apparent vacancies are areas in the actual crystal that are almost always filled with **molecules of disordered water**.

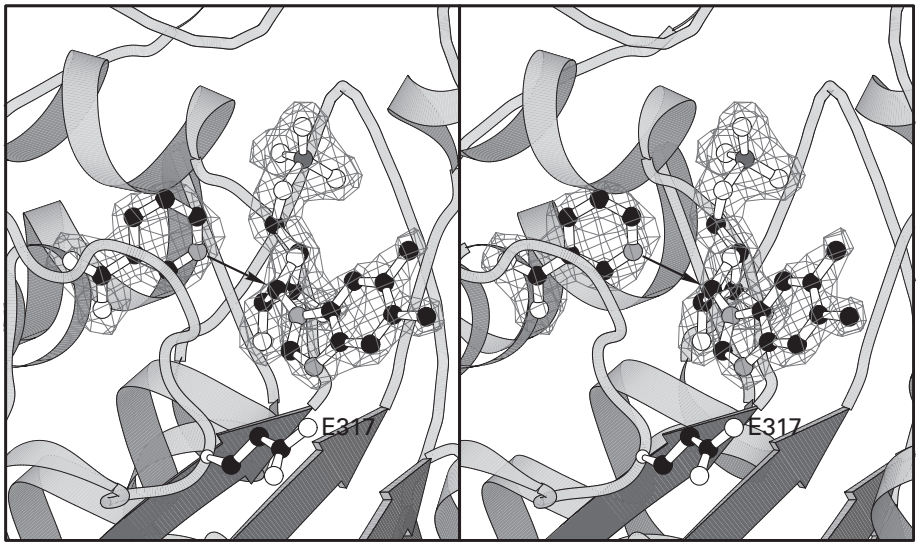

Figure 3–31: Map of difference electron density between nicotinate-nucleotide—dimethylbenzimidazole phosphoribosyltransferase from *S. typhimurium* with a vacant active site and the enzyme with its active site occupied by α-ribazole 5′-phosphate and nicotinate.[543] Black atoms are carbons, white atoms are oxygens, small gray atoms are nitrogens, and the large dark gray atom is phosphorus. Nicotinate-nucleotide—dimethylbenzimidazole phosphoribosyltransferase from *S. typhimurium* was crystallized in a buffer of ammonium phosphate containing the substrate 5,6-dimethylbenzimidazole. A refined crystallographic molecular model of the complex between the enzyme and 5,6-dimethylbenzimidazole was constructed from a data set gathered to Bragg spacing of 0.19 nm from crystals of this complex and several isomorphous replacements. Samples of these crystals were soaked in a solution of the substrate β-nicotinate D-ribonucleotide, and a new data set was gathered, again to Bragg spacing of 0.19 nm. A map of difference electron density was calculated from amplitudes of the reflections of this new data set and amplitudes and phases of the reflections calculated from the original refined crystallographic molecular model of the complex between the enzyme and 5,6-dimethylbenzimidazole from which the molecular models of the 5,6-dimethylbenzimidazoles, all the waters, and all the phosphate ions had been removed to completely empty the active sites. The map of electron density that resulted (features of isoelectronic density in the drawing) clearly demonstrated that β-nicotinate D-ribonucleotide and 5,6-dimethylbenzimidazole had been converted by the enzyme within its active site to nicotinate (to the left) and α-ribazole 5′-phosphate (to the right). Molecular models of these two substrates were inserted into the respective features of electron density, and their exact positions were determined by refinement. A ribbon drawing of the crystallographic molecular model of the protein surrounding the active site is included in the figure. Nitrogen 1 of the nicotinate can displace the 5,6-dimethylbenzimidazole of the α-ribazole 5′-phosphate in the nucleophilic substitution catalyzed by the enzyme (arrow) to produce β-nicotinate D-ribonucleotide, but the equilibrium within the active site favors the observed substrates nicotinate and α-ribazole 5′-phosphate. Glutamate 317 hydronates nitrogen 3 of the 5,6-dimethylbenzimidazole in α-ribazole 5′-phosphate to make it a better leaving group in the reaction catalyzed by the enzyme. Adapted with permission from reference 543. Copyright 1999 American Chemical Society. https://doi.org/10.1021/bi991752c

In building the initial crystallographic molecular model of the enzyme, **fixed molecules of water*** are added to the molecular model as its refinement progresses, and they become obvious features of electron density. Consequently, the fully refined initial crystallographic molecular model, which forms the basis for calculating the maps of electron density for the various forms of the enzyme occupied by the various ligands, contains many molecules of water. This initial molecular model is to be the starting point for either molecular replacement or for calculating a new map of electron density from an isomorphous crystal. For these calculations, under the assumption that occupation of the active site changes the position and occupation of these sites for fixed molecules of water, even at distant locations, **all the molecules of water in the initial crystallographic molecular model are routinely discarded** before it is used as a starting point in the rotation and translation operations of molecular replacement and refinement. As the subsequent refinement of the liganded molecular model progresses, fixed molecules of water appear, not necessarily in the same places as the ones that were discarded, and they are added to the new structure during its refinement. If the active site in the initial model is occupied by any other ligand, that ligand is also removed before the set of phases used to initiate the refinement is calculated from the initial model properly positioned in the unit cell. An exception to this procedure is a tightly bound prosthetic group, which is usually retained in the active site under all conditions and is consequently retained in the stripped initial molecular model.

When a substrate, inhibitor, or ligand associates with an active site or a binding site, **it displaces the molecules of water that occupied the active site** in its absence. Because an active site often has a significant constellation of donors and acceptors ready to form hydrogen bonds with its substrates, there are usually quite a few fixed molecules of water within the active site in a crystallographic molecular model of the unoccupied enzyme. The displacement of these fixed molecules of water can be followed by examining crystallographic molecular models. For example, in the active site of streptogrisin A from *Streptomyces griseus*, there are 15 fixed molecules of water that are displaced when the competitive inhibitor chymostatin binds to the active site (Figure 3–32).[544] In the absence of the inhibitor 1-deoxynojirimycin, the donors and acceptors that will form hydrogen bonds to the four hydroxy groups of the 1-deoxynojirimycin when it occupies the active site of glucoamylase from *Aspergillus awamori* are occupied by four fixed molecules of water, which assume the same positions that the hydroxy groups of the inhibitor do.[545]

Large nonpolar pockets intended for purely hydrophobic portions of the substrates, even though they themselves are lined by hydrophobic amino acids, do not remain empty in the absence of substrates but are occupied by molecules of water, often fixed molecules of water. For example, when a molecule of oleate associates with the binding site for fatty acids in the intestinal fatty acid binding protein from *R. norvegicus*, its alkane displaces at least nine fixed molecules of water occupying that hydrophobic site in its absence.[546] As a ligand binds to the active site by occupying the donors and acceptors for hydrogen bonds and nonpolar pockets, the molecules of water that were occupying these locations must dissociate before the ligand can settle in.

Aside from occupying donors and acceptors for hydrogen bonds in an active site that will ultimately by occupied by acceptors and donors on a substrate and filling otherwise empty space that will be filled by atoms of the substrate, **a fixed molecule of water in the empty active site can itself wind up being a substrate for the enzyme.** For example, in the crystallographic molecular model of the empty active site of β-lactamase from *S. aureus*, there is a molecule of water fixed by hydrogen bonds to Glutamate 166 and Asparagine 170.[547] During the hydrolysis of β-lactams catalyzed by the enzyme, the acyl group of the lactam participates in a nucleophilic substitution in which the hydroxy group of Serine 70 replaces the amino group of the lactam to produce an intermediate ester. The molecule of water fixed by these two hydrogen bonds is positioned in the empty active site at a location where it can participate in a second nucleophilic substitution, replacing the hydroxy group of Serine 70 in this intermediate ester and releasing the hydrolyzed lactam. When Asparagine 170 is replaced with a glutamine, this water in the empty active site is displaced,[548] and the hydrolysis of the intermediate ester with Serine 70 is decreased by a factor of 800.

*As before, a fixed molecule of water is a molecule of water that has a fixed location in a map of electron density. This usage is not meant to imply that the same molecule of water occupies this location for any appreciable length of time; rather, these molecules of water are exchanging rapidly with molecules of water in the solvent. At any given instant, however, the site is occupied by a molecule of water.

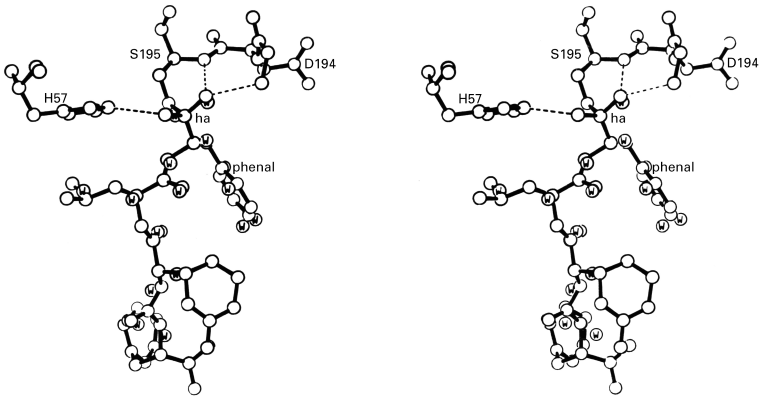

Figure 3–32: Crystallographic molecular model of the inhibitor chymostatin bound within the active site of streptogrisin A from *S. griseus*, including the molecules of water displaced from the active site by the inhibitor.[544] Streptogrisin A was crystallized (space group $P4_2$) from 1.3 M sodium phosphate at pH 4.1. A data set, F_{nat}, was collected to Bragg spacing of 0.18 nm. The phases of these reflections were estimated from four isomorphous replacements, and the initial crystallographic molecular model was refined to an *R*-factor of 0.14. This refined crystallographic molecular model contained 200 molecules of water. Crystals were soaked in mother liquor containing chymostatin, and a new data set, F_{chym0}, was then collected. The map of difference electron density ($F_{chym0} - F_{nat}$) was then calculated to locate the position of chymostatin in the unit cell. The inhibitor was found to overlap 18 of the molecules of water in the refined crystallographic molecular model of the unoccupied enzyme. These molecules of water were removed from the crystallographic molecular model, and a data set, F_c, was then calculated from it. The difference map of electron density ($F_{chym0} - F_c$) was then used to position the chymostatin as accurately as possible. This resulting molecular model was then refined against the data set F_{chym0}. The stereo drawing presents the final configuration of the chymostatin (P1–P4) and three of the amino acids in the active site (H57, S195, and D194). The aldehyde of the carboxy-terminal phenylalaninal (phenal) of the chymostatin has formed a hemiacetal (ha) with the hydroxy group of Serine 195. Fourteen of the 15 waters located within the active site of the unliganded crystallographic molecular model of streptogrisin A at locations overlapping that of the chymostatin, which are displaced by the chymostatin as it associates with the active site, are indicated as W. Reprinted with permission from reference 544. Copyright 1985 Academic Press. https://doi.org/10.1016/0022-2836(85)90283-9

The final crystallographic molecular model of the occupied active site, in which the protein is positioned by the refinement itself and the substrates, inhibitors, or other ligands are positioned by the omit map, is used to draw conclusions about the mechanism of the enzymatic reaction. The crystallographic molecular model of an enzyme with its active site occupied by the full complement of substrates presents a challenging problem because an enzyme, by definition, catalytically interconverts its substrates. Consequently, most crystallographic studies of enzymatic active sites are performed in the absence of a full complement of substrates. The crystallographic molecular model of the active site of an enzyme occupied by one or more substrates or inhibitors, in which the entire complement of substrates is not present, is a static structure. Because it is a static structure rather than an active catalyst, the information gained about the catalytic mechanism of the enzyme from such a crystallographic molecular model **depends entirely upon the ligands that are chosen to occupy in the active site.**

The simplest information gained from a crystallographic molecular model is the **location of the active site** in its structure. If the enzyme happens to contain a tightly bound prosthetic group involved in the catalytic mechanism, it will identify the location of the active site.[549] If an enzyme has only one reactant and one product or if one of the two reactants is water itself, which cannot be left out of the crystal, then **competitive inhibitors are often used to locate the active site**.[550,551] For example, 2-benzylsuccinate dianion is a competitive inhibitor of carboxypeptidase C from *S. cerevisiae* and is found in the crystallographic molecular model of its complex with the enzyme. The 1-carboxy group of the inhibitor forms hydrogen bonds to the side chains of Glutamate 145, Histidine 397, and Asparagine 51 and the amido group of Glycine 52, and its phenyl group is inserted into an adjacent nonpolar pocket. These donors and acceptors for hydrogen bonds and this nonpolar pocket together constitute the subsite within the active site at which the carboxy-terminal amino acid of a normal reactant for the enzyme is thought to bind.[552]

Crystallographic molecular models of the active sites of enzymes occupied by **inhibitors of pharmaceutical interest** can be used to design even more potent inhibitors that have even smaller dissociation constants.[553-555] For example, an examination of the crystallographic molecular model of the complex between exo-α-sialidase from influenza virus and the inhibitor 2-deoxy-2,3-dehydro-D-*N*-acetylneuraminic acid ($K_i = 1\ \mu M$) suggested that substitution of the 4-hydroxy group of the inhibitor with a guanidinio group would take advantage of four properly oriented acceptors in the protein for four of the five new donors for hydrogen bonds in the guanidinio group. The 4-guanidinio derivative was a far more tightly bound inhibitor ($K_i = 0.1$ nM), and its guanidinio group did occupy the acceptors as predicted.[556]

Examination of the crystallographic molecular model of an acyl intermediate between penicillanic acid and the active site of TEM-1β-lactamase, which hydrolyzes penicillins, suggested that adding a hydroxymethyl group to carbon 6 of the penicillanic acid would displace the water necessary to hydrolyze that acyl enzyme intermediate, just as mutation of the asparagine in the active site of β-lactamase from *S. aureus* to a glutamine displaced a molecule of water responsible for hydrolyzing the acyl enzyme intermediate in its enzymatic reaction.

6α-(Hydroxymethyl)penicillanic acid

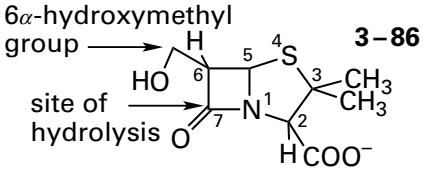

3–86

was found to form a long-lived, inactive, covalent complex with the enzyme in which its hydroxy group does displace the hydrolytic water.[557] Crystallographic molecular models can also be used to locate binding sites on enzymes for inhibitors of pharmaceutical interest that do not mimic the substrates of the enzyme.[558-560]

Competitive inhibitors that are much closer **analogues for substrates** of the enzyme are usually used to define the complex between an enzyme and a lone substrate. For example, D-glucitol 6-phosphate, in which the 2-oxo group of the substrate D-fructose 6-phosphate has been reduced to the secondary alcohol, locates the active site in the crystallographic molecular model of its complex with D-psicose-6-phosphate 3-epimerase

D-psicose 6-phosphate $\rightleftharpoons$ D-fructose 6-phosphate (3–391)

from *E. coli*. In addition to identifying the active site, this crystallographic molecular model also defines the coordination of the actual substrate D-fructose 6-phosphate with a prosthetic Mg^{2+} and reveals a

pocket with a lining of amido groups from the backbone of the polypeptide and hydroxy groups from side chains that together form five hydrogen bonds to the three nonbridging oxygens of the 6-phospho group.[561]

Most enzymes catalyze reactions involving two or more reactants and two or more products. In such a situation, the active site and the subsite within the active site for a substrate can be located by **occupying it with only one of the two reactants or products**.[562-566] For example, a crystallographic molecular model of (2*E*,6*E*)-farnesyl diphosphate bound to protein farnesyltransferase from *R. norvegicus*, in the absence of its other reactant, a protein to which the enzyme transfers the (2*E*,6*E*)-farnesyl group, locates the active site on the enzyme and defines the snug nonpolar pocket into which the farnesyl group inserts.[567] Likewise, the crystallographic molecular model of UDP-galactose bound to bovine *β*-*N*-acetylglucosaminyl-glycopeptide *β*-1,4-galactosyltransferase in the absence of its other reactant, an oligosaccharide with *β*-*N*-acetyl-D-glucosamine at its nonreducing end, locates the subsite within the active site with which UDP-galactose associates and also defines the significant conformational change that occurs in the polypeptide surrounding the active site and that creates the site to which the oligosaccharide that is the other reactant binds after the UDP-galactose has associated.[568] The complex between the substrate uridine 5′-phosphate and the active site of orotidine-5′-phosphate decarboxylase (Equation 3–366) from *B. subtilis* in the absence of CO_2 **identifies the catalytic side chains surrounding the site** of the carboxylation.[569] Orotidine 5′-phosphate, the reactant corresponding to the product uridine 5′-phosphate, would be immediately decarboxylated if it were mixed with the enzyme.

Both $MgADP^-$ and $MgATP^{2-}$ were bound in separate experiments at the active site of crystalline equine phosphoglycerate kinase (Equation 3–375) by soaking crystals in solutions of the respective ligand. Both of these substrates, one a reactant and the other the respective product, were bound at the same location and in the same orientation in a pocket on the surface of the enzyme, and this observation both located the active site and **defined the noncovalent interactions** between the active site and an adenine nucleotide.[570] There are crystallographic molecular models of much higher accuracy and resolution[571] of $MgADP^-$ and $MgATP^{2-}$, respectively, occupying the active site of 5-(carboxyamino)imidazole ribonucleotide synthase from *Aspergillus clavatus*, in which the precise conformation of the nucleotides, their ligation by two Mg^{2+} ions, and the donors and acceptors for hydrogen bonds ensnaring them in the active site are clearly observed.

Many of the dehydrogenases using nicotinamide-adenine dinucleotides as coenzymes have been crystallized with either NAD^+, NADH, $NADP^+$, and NADPH occupying their active sites,[525,572-574] the so-called "holoenzyme", in the absence of the other respective nominal reactant or in the presence of an inhibitor that is competitive with the nominal reactant. In most instances, crystallographic molecular models of such "holoenzymes" have permitted the description of the extensive networks of hydrogen bonds that form between amino acids of the active site and NAD^+, NADH, $NADP^+$ or NADPH (Figure 3–33),[575,576] which are large molecules.

In a strategy similar to using just one of two reactants, for an enzyme that has three reactants, using **two of the three reactants** will often form a static complex. The crystallographic molecular model of this complex will not only locate the subsites in the active site for each of the two reactants but will also reveal the relative orientation of the reactants and allow one to imagine the corresponding orientation of the third reactant.[577]

The practice of using just one of two reactants or two of three reactants, however, can be misleading. For example, crystals of unliganded citrate (*Si*)-synthase (Equation 3–226) were soaked in solutions of citrate, and isomorphous crystals of the enzyme to which citrate is bound were obtained. When crystals were formed from enzyme to which both citrate and coenzyme A had been bound, however, the enzyme changed its conformation, causing the active site to rearrange and the details of the interactions between citrate and the amino acids around it to change significantly.[578]

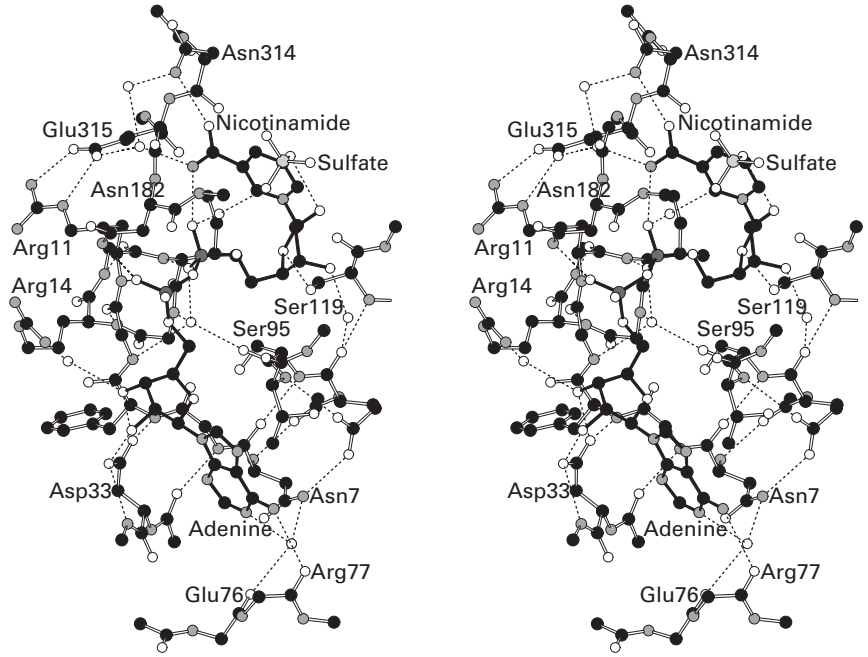

Figure 3–33: Stereodrawing[576] of the network of hydrogen bonds between NAD^+ and side chains of amino acids in the polypeptide surrounding the active site in the crystallographic molecular model of the complex between NAD^+ and glyceraldehyde-3-phosphate dehydrogenase from *G. stearothermophilus*.[575] Black atoms are carbons, white atoms are oxygens, small gray atoms are nitrogens, the two large dark gray atoms are atoms of phosphorus, and the large light gray atom is a sulfur. The complex between glyceraldehyde-3-phosphate dehydrogenase and NAD^+ was crystallized from a phosphate buffer containing 1 mM NAD^+. In the final crystallographic molecular model from a data set gathered to Bragg spacing of 0.18 nm and data sets of several isomorphous replacements, the adenine ring (Adenine) of the NAD^+ in the active site participates in hydrogen bonds with the peptidic oxygen of Arginine 77 from the protein and a fixed molecule of water (white sphere). The O2′ and O3′ groups on the adenylyl ribose participate in hydrogen bonds with the carboxy group of Aspartate 33 and the latter with a molecule of water (white sphere). The two phospho groups participate in hydrogen bonds to the peptidic amido nitrogens of Arginine 11 and Isoleucine 12 and the amido nitrogen in the side chain of Asparagine 182 as well as several molecules of water (white spheres). The O4′ oxygen of the ribose of the nicotinamide nucleotide participates in a hydrogen bond with the hydroxy group of Serine 119. The O2′ and O3′ oxygens of the ribose of the nicotinamide nucleotide participate in hydrogen bonds to a sulfate and a molecule of water (white sphere). The nicotinamide participates in hydrogen bonds to the amido nitrogen in the side chain of Asparagine 314 and a molecule of water (white sphere). There is also an intramolecular hydrogen bond within the NAD^+ between the amido nitrogen of the nicotinamide and its phospho group.

One way to occupy simultaneously both of the subsites on the active site of an enzyme and avoid the difficulty of these subsequent rearrangements when a second reactant associates is to effect these changes in conformation relevant to the enzymatic reaction by using a **bisubstrate analogue** as a ligand. For example, the bisubstrate analogue **3–87***

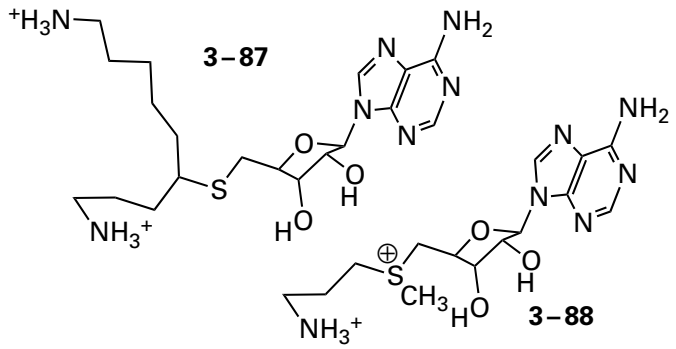

which combines the structural features of *S*-adenosyl-3-(methylthio)propylamine (**3–88**) and putrescine (1,4-diaminobutane), locates the subsites for these two reactants in the active site in the crystallographic molecular model[579] of its complex with spermidine synthase

S-adenosyl-3-(methylsulfanyl)propylamine + putrescine ⇌ spermidine + H^+ + *S*-methyl-5′-thioadenosine (3–392)

from *Thermotoga maritima*. Likewise, *N*-phosphonacetyl-L-aspartate (**3–6**), a bisubstrate analogue that combines the structural features of carbamoyl phosphate and L-aspartate, has been used to locate the active site and the catalytic side chains in a crystallographic molecular model of aspartate carbamoyltransferase (Equation 3–220) from *E. coli*.[580]

In a number of enzymatic reactions, **a small portion of one reactant is transferred to the other reactant**. In such cases, the reactant to which the group is transferred and the product from which the group has been transferred will often form an inactive dead-end complex defining the subsites for these substrates and the orientation in which the two substrates between which the group is transferred are held by the enzyme. For example, the **enzymatically inactive complex** between IMP dehydrogenase from *T. foetus* and the reactant xanthosine 5′-phosphate and the product NAD^+ lacks the hydride transferred from NADH to xanthosine 5′-phosphate during the enzymatic reaction, and the crystallographic molecular model of this complex defines the noncovalent interactions recognizing and orienting the two substrates as well as a significant conformational change in the enzyme that occurs upon the binding of substrates.[581]

The crystallographic molecular model of the enzymatically inactive complex (Figure 3–34)[582] between the active site of guanidinoacetate *N*-methyltransferase from *R. norvegicus* and the reactant guanidinoacetate (GuanAc) and the product *S*-adenosyl-L-homocysteine (SAHC) is missing the methyl group that is transferred by the active site back and forth from *S*-adenosyl-L-methionine to guanidinoacetate and from the resulting creatine to *S*-adenosyl-L-homocysteine, but the alignment of guanidinoacetate and *S*-adenosyl-L-homocysteine by the enzyme places the sulfur and the nitrogen between which the methyl group is transferred immediately adjacent to each other at a distance of 0.39 nm, in perfect orientation for a concerted nucleophilic substitution, and reveals the basic strategy employed by the active site.

A similar disposition of *S*-adenosyl-L-homocysteine and geranyl *S*-thiolodiphosphate, an analogue of geranyl diphosphate, is observed in a crystallographic molecular model of the active site of geranyl diphosphate 2-*C*-methyltransferase from *Streptomyces coelicolor*. In this instance, the distance between the carbon that would be methylated in geranyl diphosphate and the sulfur of the *S*-adenosyl-L-homocysteine is 0.55 nm. This enzyme catalyzes a concerted nucleophilic substitution that transfers the methyl group from *S*-adenosyl-L-methionine to carbon 2 in the nucleophilic carbon–carbon double bond between carbons 2 and 3 of geranyl diphosphate rather than to a guanidino nitrogen. In this latter molecular model, the π electrons on one side of the carbon–carbon double bond are pointed at the sulfur of the L-homocysteine just as the nucleophilic lone pair of electrons of the guanidino nitrogen is pointed at the sulfur in the active site of guanidinoacetate *N*-methyltransferase (Figure 3–34).

*From here on in this text, whenever possible, in drawings of chemical structures and in chemical equations, the substrates, analogues of substrates, analogues for intermediates of high energy, inhibitors, and side chains of amino acids participating in the respective enzymatic reactions will be drawn in the conformations and relative orientations they assume within their respective active sites in crystallographic molecular models. In these instances, molecular drawings have been chosen rather than drawings of the actual crystallographic molecular models to permit detailed explanations of the chemistry of the respective reactions.

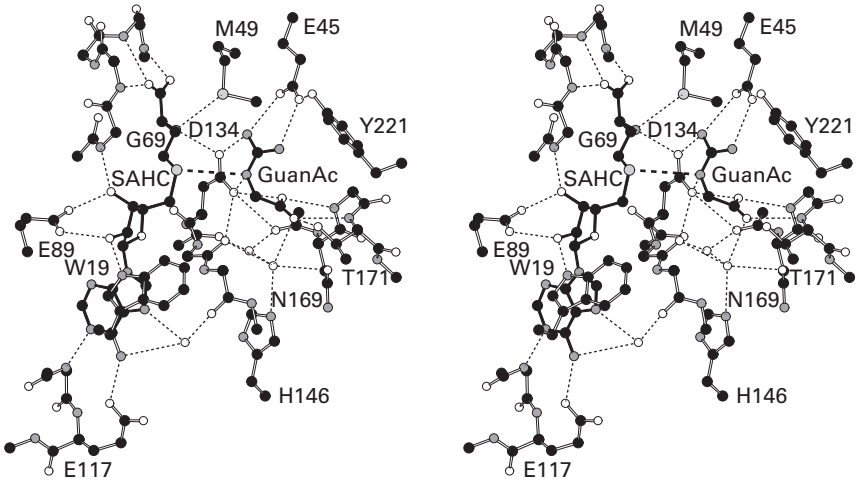

Figure 3–34: Stereodrawing[576] of the occupied active site in the crystallographic molecular model for the complex of guanidinoacetate *N*-methyltransferase from *R. norvegicus* and the reactant guanidinoacetate and the product *S*-adenosylhomocysteine.[582] Black atoms are carbons, white atoms are oxygens, small gray atoms are nitrogens, and large light gray atoms are sulfurs. Crystals of the enzyme were grown from a solution containing 1 mM *S*-adenosylhomocysteine and 2 mM guanidinoacetate. A data set was gathered at Bragg spacing of 0.20 nm, and a map of electron density was produced by molecular replacement using an earlier crystallographic molecular model of a complex between the enzyme and *S*-adenosylhomocysteine. Features in the initial map of electron density into which *S*-adenosylhomocysteine (SAHC) and guanidinoacetate (GuanAc) could be satisfactorily inserted were found in the region already assigned as the active site. Following the insertion, the crystallographic molecular model was submitted to refinement. A portion of the final refined molecular model is drawn. In a nucleophilic substitution, the enzyme transfers a methyl group back and forth between the sulfur in *S*-adenosylhomocysteine and the imido nitrogen of guanidinoacetate, which are connected by a thick dashed line in the drawing. The methyl group itself is missing in the crystallographic molecular model but can be imagined on the fly. There are a number of hydrogen bonds between donors and acceptors in the substrates, the polypeptide, and molecules of water (white spheres) orienting the two substrates in the active site. Tryptophan 19 stacks upon the adenine of the *S*-adenosylhomocysteine.

In both crystallographic molecular models, the line of centers between the nucleophile and the sulfur of *S*-adenosyl-L-homocysteine passes through one of the vertices of the tetrahedral sulfur, the location that would be occupied by the methyl group on the tetrahedral sulfonium ion were the *S*-adenosyl-L-homocysteine actually *S*-adenosyl-L-methionine. The alignment between the sulfur in the L-homocysteine and the As^{3+}, the methyl acceptor, is less ideal in the crystallographic molecular model of the occupied active site of arsenite methyltransferase from *Cyanidioschyzon*,[583] but it can be inferred that steric effects on the methyl group itself would complete the alignment.

An enzymatically inactive complex forms on the active site of rhamnulokinase from *E. coli* between the product $MgADP^-$ and the reactant β-L-fructofuranose, an alternative to the nominal reactant L-rhamnofuranose. This complex is missing the phospho group normally transferred from $MgATP^{2-}$ to the 1-hydroxy group of β-L-fructofuranose, but its crystallographic molecular model defines an extensive conformational change that occurs upon binding of substrates and shows how the reactants are oriented by the enzyme to achieve the phospho transfer.[584] One can readily imagine the missing phospho group on the fly between the oxygen of $MgADP^-$ and the oxygen of β-L-fructofuranose.

At times, one of the substrates in a formally unimolecular reaction is used as a ligand in crystallographic studies even though it is continuously transformed in the crystal by the enzyme. Usually, under these circumstances, only one of the two substrates, reactant or product, is observed in the active site, but occasionally the equilibrium constant for the reaction in the active site close enough to 1 that **both reactant and product, in equilibrium with each other, can be observed simultaneously in a crystallographic molecular model of the active site**. For example, the substrates in the reaction catalyzed by phosphopyruvate hydratase from *O. cuniculus*, 2-phospho-D-glycerate and phospho*enol*pyruvate and a molecule of water

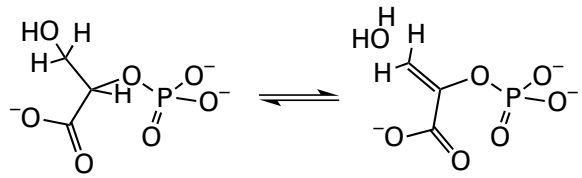

(3–393)

are present in an almost equimolar mixture when they are in the active site.[507] Crystals of phosphopyruvate hydratase from *S. cerevisiae* were grown from a solution containing phospho*enol*pyruvate and the Mg^{2+} needed for catalysis, and a feature of

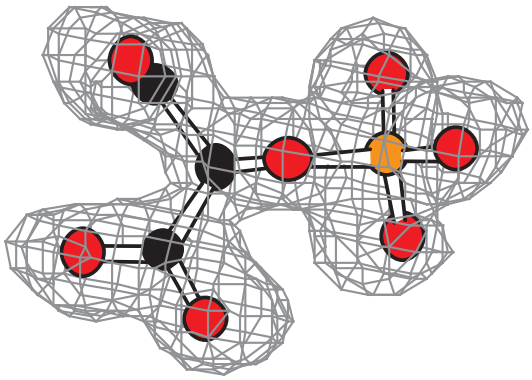

Figure 3–35: Equilibrium mixture of 2-phospho-D-glycerate and phospho*enol*pyruvate and a molecule of water (Equation 3–393) in the active site of phosphopyruvate hydratase from *S. cerevisiae*.[585] Black atoms are carbons, red atoms are oxygens, and the orange atom is a phosphorus. The purified enzyme was dissolved in a solution containing 2 mM phospho*enol*-pyruvate, 2 mM $MgCl_2$, 0.25 M KCl, and 50 mM 3-[4-(2-hydroxyethyl)piperazin-1-yl]propane-1-sulfonic acid at pH 8.0. The enzyme was crystallized from this solution, and a map of electron density was calculated from diffracted X-rays to Bragg spacing of 0.18 nm. In the active site of the enzyme, there was a feature of electron density that resembled either 2-phospho-D-glycerate or phospho*enol*pyruvate and a molecule of water. The substrates were intentionally omitted during the refinement, and the final omit map of electron density is presented as a cage of light gray lines. A molecule of 2-phospho-D-glycerate has been inserted into this map of electron density, but it is clear from the protrusion in the upper left-hand corner of the map that a molecule of phospho*enol*pyruvate and a molecule of water could just as easily been inserted. Reprinted with permission from reference 585. Copyright 1996 American Chemical Society. https://doi.org/ 10.1021/bi952859c

electron density was observed in the map that resembled a substrate. A refined omit map of difference electron density (Figure 3–35) has a continuous feature of electron density into which either 2-phospho-D-glycerate or phospho*enol*pyruvate and a molecule of water can be inserted,[585] consistent with the expectation that the substrates are both present in equilibrium with each other. An omit map of electron density within the active site of a complex between L-fucose and L-fucose mutarotase from *E. coli* demonstrates unequivocally that both reactant, α-L-fucopyranose, and product, β-L-fucopyranose, are present in an almost equimolar mixture,[586] presumably in equilibrium with each other. In the active site of UDP-glucuronic acid 4-epimerase from *Bacillus cereus*, both UDP-D-glucuronic acid and UDP-D-galacturonic acid, the reactant and product of the enzymatic reaction, are present in an equilibrium mixture.[587]

Phosphopyruvate hydratase from *S. cerevisiae* also crystallizes in a different space group in which the complete dimer is in the asymmetric unit. The **different environments** in this other crystal for the two subunits of the homodimer of the enzyme, which is symmetric in solution, **have altered the conformations of the two active sites** in such a way that the equilibrium constants between 2-phospho-D-glycerate and phospho*enol*pyruvate and a molecule of water are shifted in opposite directions. In the unit cell of this other crystal, in one of the active sites of the dimer, electron density for only 2-phospho-D-glycerate is observed, and in the other active site, electron density for only phospho*enol*pyruvate and a molecule of water is observed.[588] The same situation occurs in a crystal of dihydroorotase

(*S*)-dihydroorotate + H_2O $\rightleftharpoons$ H^+ + *N*-carbamoyl-L-aspartate (3–394)

from *E. coli*. The dimeric enzyme crystallizes in the space group $P2_12_12_1$ with the dimer as the asymmetric unit. The environments of the two subunits in the crystal are different enough that one subunit stabilizes (*S*)-dihydroorotate and water in its active site and the other subunit stabilizes *N*-carbamoyl-L-aspartate in its active site.[589]

The equilibrium mixture of substrates in the active site of an enzyme that has two reactants and two products and catalyzes a bimolecular reaction can also be observed crystallographically. For example, cytidine deaminase catalyzes the hydrolysis of cytidine to uridine

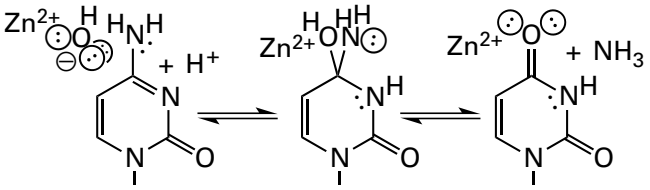

(3–395)

A hydroxide on a Zn^{2+} in the active site is the nucleophile in a nucleophilic substitution at the acyl carbon of the amidine. The nucleophilic substitution passes through the usual tetrahedral intermediate. The omit map of electron density for the complex between murine cytidine deaminase and cytidine had a feature of electron density that was clearly a hybrid of a cytidine and a water (Figure 3–36A) and a uridine and an ammonia (Figure 3–36B) in an equilibrium ratio of 3:1.[590]

(3*S*)-5-(3-Carboxy-3-hydroxypropyl)nicotinamide-adenine dinucleotide (previously **1–78**)

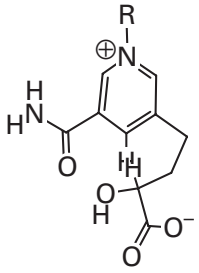

3–89

R ≡ 5′-(adenosine-5′-diphosphoryl)ribosyl

is a bisubstrate analogue for L-lactate dehydrogenase (Equation 3–27). When this bisubstrate analogue is added to a solution of L-lactate dehydrogenase, the hydride is transferred back and forth intramolecularly between carbon 3 of the 3-carboxy-3-hydroxypropyl group and carbon 4 of the nicotinamide while it is in the active site, an observation demonstrating that one analogue effectively mimics two substrates. A crystallographic molecular model of the bisubstrate analogue occupying the active site of porcine L-lactate dehydrogenase, in crystals within which the hydride is presumably being transferred back and forth continuously, identifies the groups responsible for catalysis, in particular the imidazolyl group of Histidine 195 that is responsible for removing the hydron from the 3-hydroxy group during its oxidation to the 3-oxo group.[591]

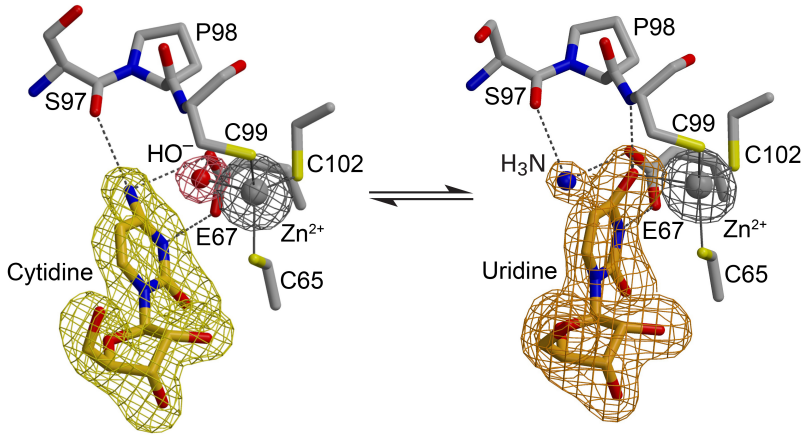

Figure 3–36: Omit maps of electron density for substrates bound in the active sites in crystallographic molecular models for **(A)** the complex of murine cytidine deaminase and the substrates cytidine and water and **(B)** the complex of murine cytidine deaminase and the substrates uridine and ammonia.[590] Crystals of the enzyme were grown from a solution containing 5 mM cytidine. A data set was gathered at Bragg spacing of 0.207 nm, and a map of electron density was produced by molecular replacement using an earlier crystallographic molecular model of human cytidine deaminase.[599] In the initial map of electron density, there were features in the active site that could be explained by the superposition of molecules of cytidine and water and molecules of uridine and ammonia with a ratio of occupancy of about 3:1. Three quarters of a molecule of cytidine, three quarters of a hydroxide, one quarter of a molecule of uridine, and one quarter of a molecule of ammonia were inserted into these hybrid features of electron density, and the resulting molecular model of these substrates at their respective partial occupancies and the enzyme were submitted to refinement. Following the refinement, omit maps of electron density (features of electron density in Panels A and B, respectively) were prepared for each pair of substrates by omitting their respective partial molecules and the equivalent fraction of a Zn^{2+} from the final crystallographic molecular model. Portions of the final crystallographic molecular model are drawn including, on the one hand (Panel A), the final positions of the molecules of cytidine and hydroxide (OH) and, on the other hand (Panel B), the final positions of the molecules of uridine and ammonia (N), as well as portions of the protein providing donors and acceptors of hydrogen bonds to the substrates and ligands for the Zn^{2+}. Arrows indicate the nucleophilic attack of hydroxide (Panel A) coordinated to Zn^{2+} on the cytosine of the cytidine and the nucleophilic attack of ammonia (Panel B) on the uracil of the uridine. One of the hydrogens on the ammonia participates in a hydrogen bond with the peptidic oxygen of Serine 97. The upper oxygen of the carboxy group of Glutamate 67 (which is behind the water in panel A and behind the molecule of ammonia in panel B) is close enough to the amido nitrogen on carbon 4 of the cytidine (0.30 nm) and the hydroxide on the Zn^{2+} (0.28 nm) in Panel A, and also close enough to the acyl oxygen on carbon 4 of the uridine (0.30 nm) and the ammonia (0.29 nm) in Panel B, to form hydrogen bonds with both functional groups and both nucleophiles. The lower oxygen of Glutamate 67 forms a hydrogen bond with nitrogen 3 of both the cytosine (0.29 nm) and the uridine (0.27 nm), facts which suggest that it is planted as the other oxygen pivots around it. Reprinted with permission from reference 590. Copyright 2006 American Chemical Society. https://doi.org/10.1021/bi060345f

The fact that **most crystals are frozen before a data set is collected may shift an equilibrium** one way or the other. For example, the equilibrium constant within the active site[136] at 30 °C for the reaction catalyzed by orotate phosphoribosyltransferase from *S. typhimurium* is 2 in favor of the products, orotidine 5′-phosphate and diphosphate. Nevertheless, the omit map of electron density within its occupied active site, from a data set gathered at –178 °C, is consistent with the presence of only the reactants, orotate and 5-phospho-α-D-ribose 1-diphosphate, with no indication of the presence of orotidine 5′-phosphate or diphosphate.[592] It must be the case that the equilibrium is shifted in favor of orotidine 5′-phosphate and diphosphate at the lower temperature. Even though the equilibrium constant in solution at 25 °C for the reaction catalyzed by isochorismate synthase is 0.84 in favor of the reactant chorismate,[593] the map of electron density calculated from a data set gathered from crystals of the enzyme from *E. coli* at cryogenic temperatures is consistent with the presence of only the product isochorismate in the active site.[594]

As is the case with orotate phosphoribosyltransferase and isochorismate synthase at cryogenic temperatures, for the majority, if not almost all, of the equilibria between substrates when they are in their respective active sites and when the enzymes are either in solution or in a crystal, **the equilibrium constant within the active site favors one of the outcomes**, often the outcome favored by the overall equilibrium for the reaction being catalyzed. If the equilibrium constant for the reaction within the active site is such that less than 10% of the substrates on one side of the equation for the enzymatic reaction are present, the electron density for the minor participants cannot be resolved from the electron density of the major participants. One reason for the presence of the substrates on only one side of the equilibrium, as was observed with the two different conformations of the subunits of phosphopyruvate hydratase and the two different conformations of the subunits of dihydroorotase in the respective crystals, can be that the conformation of the enzyme that has crystallized favors the substrates on only that side of the equation even though there may be other conformations in the solution favoring the substrates on the other side of the equation.

Complexes between an active site and a full complement of the substrates favored by the equilibrium existing in the active site in the crystal under the conditions at which the data set is gathered (often referred to ambiguously as a "complex with the products of the enzymatic reaction") can be crystallized.[595,596] The resulting complex will usually show no feature of electron density suggesting that the substrates unfavored by the equilibrium are also present in the active site even though they must be present at a ratio dictated by the equilibrium constant for the reaction as it occurs in the active site under the conditions of data collection. For example, within the active site of triose-phosphate isomerase (Equation 3–384) from *S. cerevisiae*, as in solution, the equilibrium favors glycerone phosphate.[597] In the map of electron density for the complex between glycerone phosphate and the enzyme (Figure 3–37),[598,599] there is a feature within the active site into which only a molecule of glycerone phosphate can be inserted.

Lanosterol synthase catalyzes an equilibrium

$$\text{(3}S\text{)-2,3-epoxy-2,3-dihydrosqualene} \rightleftharpoons \text{lanosterol} \qquad (3\text{–}396)$$

that in solution is heavily in favor of lanosterol. In the map of difference electron density from crystals of the complex between the human enzyme and lanosterol, there is no evidence for electron density arising from (3*S*)-2,3-epoxy-2,3-dihydrosqualene, only a clear feature of electron density for lanosterol.[600] Likewise, in the case of the complex between nicotinate-nucleotide—dimethylbenzimidazole phosphoribosyltransferase from *S. typhimurium*

$$\beta\text{-nicotinate D-ribonucleotide} + \text{5,6-dimethylbenzimidazole} \rightleftharpoons \text{H}^+ + \text{nicotinate} + \alpha\text{-ribazole 5′-phosphate} \qquad (3\text{–}397)$$

and its two substrates nicotinate and α-ribazole 5′-phosphate, there is no indication in the difference map of electron density for the presence of any β-nicotinate D-ribonucleotide or 5,6-dimethylbenzimidazole, but the orientation of the two substrates favored by the equilibrium positions them perfectly for the phosphoribosyl transfer catalyzed by the enzyme (Figure 3–31).[543] In the case of glutathione transferase, when it catalyzes the condensation of glutathione and phenanthrene 9,10-oxide, there are two reactants but only one product, 9-(*S*-glutathionyl)-10-hydroxy-9,10-dihydrophenanthrene. The reaction heavily favors this substrate, and the complex between it and the enzyme from *R. norvegicus* could be crystallized.[601]

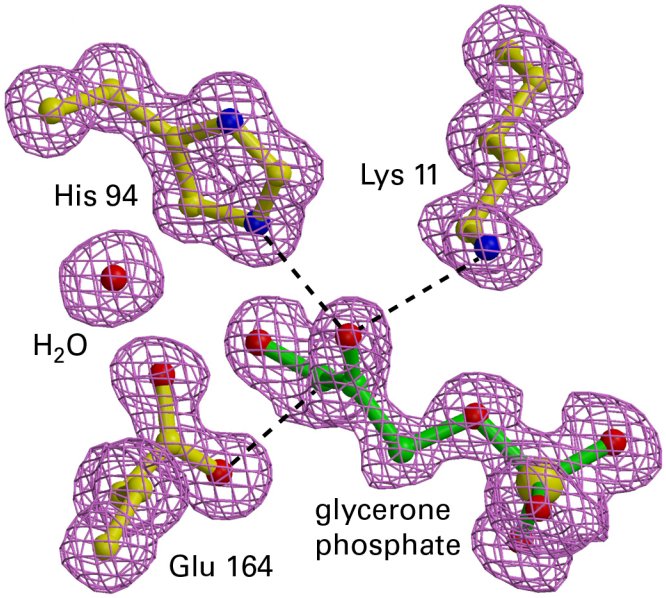

Figure 3–37: Omit maps of electron density for three catalytic side chains and glycerone phosphate bound in the active site of triose-phosphate isomerase from *S. cerevisiae*.[598] Crystals of a fully active double mutant of the enzyme in which Tryptophan 90 was mutated to a tyrosine and Tryptophan 157 to a phenylalanine were soaked in a solution of glycerone phosphate. The crystals gradually disappeared and new crystals gradually appeared that were monoclinic and of space group $P2_1$. A data set was gathered from these monoclinic crystals at Bragg spacing of 0.12 nm, and a map of electron density was produced by molecular replacement using an earlier crystallographic molecular model of the enzyme.[599] In the refined map of electron density, there was a feature of electron density into which a molecular model of glycerone phosphate could be inserted. Following the refinement, omit maps of electron density were prepared by omitting glycerone phosphate and the side chains of Lysine 11, Histidine 94, and Glutamate 164. The drawing is of the electron density in that omit map filled with molecular models of glycerone phosphate and the side chains. Dashed lines for Lysine 11 and Histidine 94 are for hydrogen bonds that they form with the carbonyl oxygen of the glycerone phosphate. The dashed line from one of the carboxylato oxygens of Glutamate 164 to carbon 3 of the glycerone phosphate indicates its role as a base that removes a hydron from that carbon in the enzymatic reaction. Reprinted with permission from reference 598. Copyright 2003 National Academy of Sciences, U.S.A. https://doi.org/10.1073/pnas.0233793100

When neither a complex between an enzyme and an equilibrium mixture of substrates nor one between the enzyme and the set of substrates favored by the equilibrium as it occurs on the active site can be crystallized, it is often possible to produce a complex closely resembling the natural complex by using an almost identical but inactive analogue in place of one of the substrates.[602]

Isoprene synthase catalyzes the dissociation of diphosphate from 3,3-dimethylallyl diphosphate to produce the 3,3-dimethylallyl carbenium ion (**1–99** in Figure 1–26) as an intermediate in the reaction. The transfer of a hydron from one of the methyl groups of the dimethylallyl carbenium ion produces isoprene, 2-methylbuta-1,3-diene, which is the product of the enzymatic reaction. 3,3-Dimethylallyl *S*-thiolo diphosphate

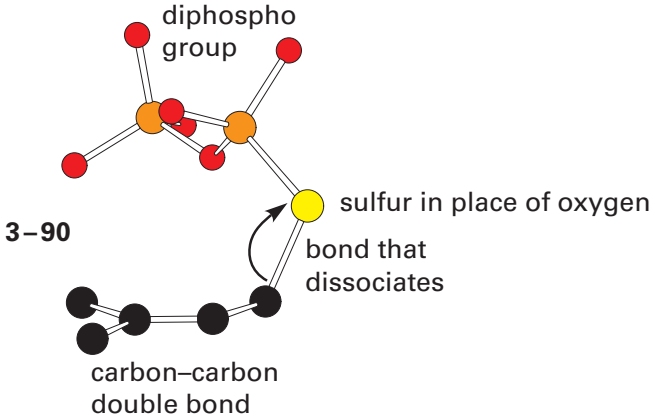

is an inactive analogue of dimethylallyl diphosphate in which the oxygen between the dimethylallyl group and the diphospho group, which would leave the dimethylallyl group in the normal reaction

catalyzed by the enzyme, has been replaced with a sulfur. In a crystallographic molecular model of the active site of isoprene synthase from *Populus canescens*,[603] the analogue is forced by the active site to assume a conformation in which the bond between carbon and sulfur, which would be the bond that dissociates in 3,3-dimethylallyl diphosphate (**1–99** in Figure 1–26), is parallel to the *p* orbitals that form the π molecular orbital system of the carbon–carbon double bond of dimethylallyl diphosphate (as in **3–90**). Consequently, the two electrons in the occupied π molecular orbital of the carbon–carbon bond can push on the carbon–oxygen bond of the substrate and enhance the dissociation. One of the oxygens of the distal phospho group is also positioned by the active site to remove the hydron from the cis methyl group of the dimethylallyl carbenium ion to produce the isoprene. This oxygen is oriented by the active site so that it is on a line with the carbon of the methyl group that is perpendicular to the plane of the carbon–carbon double bond. In this orientation, it is able to remove the hydron in a carbon–hydrogen bond on the methyl group when that bond is parallel to the π molecular orbital system of the allyl carbenium ion, which withdraws the two electrons in that bond into itself.

Hypoxanthine phosphoribosyltransferase, which is able to catalyze the nucleophilic substitution at the carbon of the hemiaminal in the ribose of the alternative substrate, guanosine 5′-phosphate

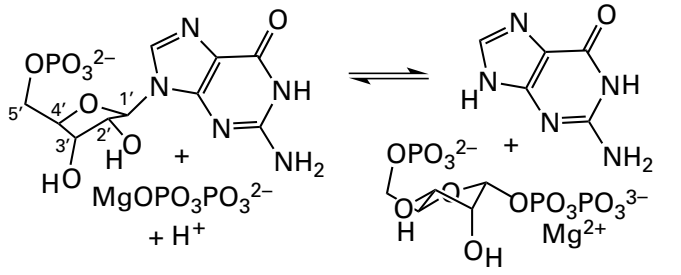

(3–398)

is inhibited by the pyrrolidinium ion

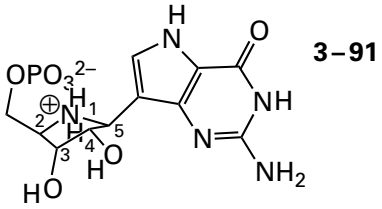

3–91

In a crystallographic molecular model of a complex between the human enzyme and magnesium diphosphate, Mg^{2+}, and pyrrolidinium **3–91** (Figure 3–38),[604,605] the Mg^{2+} of the magnesium diphosphate has two of the nonbridging oxygens as ligands. The other Mg^{2+} in the active site has two other nonbridging oxygens of the diphosphate and the 3-hydroxy group and the 4-hydroxy group of pyrrolidinium **3–91** as ligands. This network of ligation creates a rigid structure of two five-membered rings and two six-membered rings that holds the oxygen of the diphosphate that is the acceptor of the phosphoribosyl group in the nucleophilic substitution catalyzed by the enzyme immediately adjacent to carbon 2 of the pyrrolidinium **3–91** (Figure 3–38). Carbon 2 is the homologue of the electrophilic carbon 1′ of the ribose in the guanosine 5′-phosphate (Equation 3–398). The crystallographic molecular model demonstrates that hydronation of nitrogen 9 of the guanine in guanosine 5′-phosphate increases the electrophilicity of carbon 1′ by improving the leaving group in the nucleophilic substitution. In the transition state of the enzymatic reaction, the nonbridging oxygen of the diphosphate that is immediately below (dotted line in the figure) the oxygen in the intermediate oxocarbenium ion of the ribosyl group, represented in the analogue by the ammonio nitrogen, stabilizes its positive elementary charge.[606]

In a similar complex with a similar inhibitor in the active site of purine-nucleoside phosphorylase from *E. coli*, the phosphate that normally attacks carbon 1′ of ribose in the nucleoside is held in position by hydrogen bonds from the six ω nitrogen–hydrogens of three guanidinio groups from three arginines instead of two Mg^{2+}, but these hydrogen bonds also form a network of rigid five-membered rings.[607]

In the case of enzymes that have two identical reactants, such as porphobilinogen synthase from *P. aeruginosa*, which condenses two 5-aminolevulinates, the same enzymatically inactive analogue of these two reactants can be used to occupy each of the two respective subsites in the active site.[608]

Complexes between **two substrates and an analogue of the third substrate** and an enzyme catalyzing a reaction with three reactants and three products have also been crystallized, and the alignment of the three ligands defines the orientation of the three substrates in the normal reaction.[609]

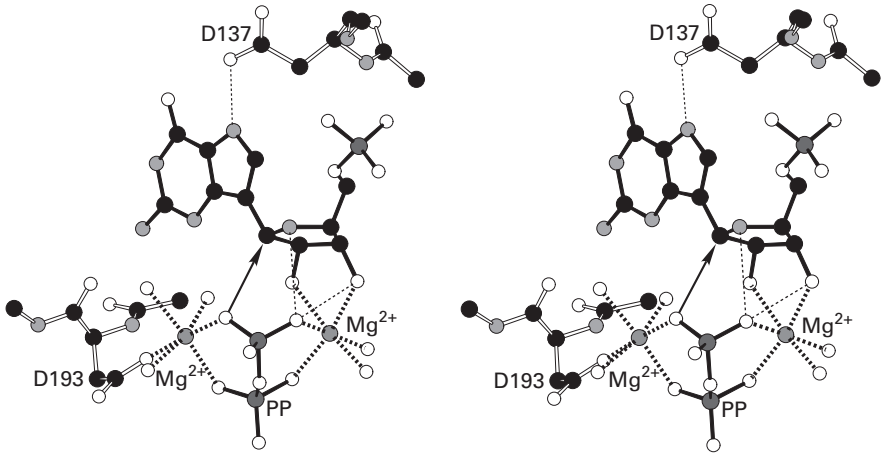

Figure 3–38: Stereodrawing[576] of the crystallographic molecular model of the active site in the complex of human hypoxanthine phosphoribosyltransferase, its substrate magnesium diphosphate, and the pyrrolidinium **3–91**, which is an inhibitor of the enzyme.[604] Black atoms are carbons, white atoms are oxygens, small gray atoms are nitrogens, large dark gray atoms are atoms of phosphorus, and the two small dark gray spheres are magnesium ions. The enzyme was crystallized from a solution containing an equimolar concentration of pyrrolidinium **3–91** and an excess of magnesium diphosphate. A data set was gathered from the crystals at Bragg spacing of 0.20 nm, and a map of electron density was produced by molecular replacement using an earlier crystallographic molecular model of hypoxanthine phosphoribosyltransferase from *T. gondii*.[605] In the initial map of electron density, there were features in the active site into which molecular models of molecules of magnesium diphosphate and pyrrolidinium **3–91** could be unambiguously inserted. The molecular models of the pyrrolidinium, Mg^{2+}, and the diphosphate (PP) in the final refined crystallographic molecular model are drawn. The arrow indicates the nucleophilic attack of the closest oxyanion in the magnesium diphosphate that would occur during the reaction catalyzed at the active site on carbon 1 of guanosine 5′-phosphate, the normal substrate for the enzyme, which is represented by carbon 5 of the inhibitor. The nearly vertical, thin dashed line indicates a hydrogen bond between the quaternary ammonium of the pyrrolidinium and another oxyanion of the diphosphate. This hydrogen bond represents an ionic interaction between the oxygen atom of the normal oxocarbenium ion intermediate and this oxyanion in the nucleophilic substitution catalyzed by the enzyme. The second Mg^{2+}, in addition to the one brought into the active site on the diphosphate, is also coordinated by the diphosphate. In addition to five molecules of water (white spheres) and ligands from the diphosphate and the two hydroxy groups on pyrrolidinium **3–91** that provide ligands to the two Mg^{2+}, Aspartate 193 from the enzyme provides a ligand to one of the magnesium ions.

Magnesium 5′-adenylic methylenediphosphonic anhydride (**3–5**), in which the bridging oxygen to the γ-phospho group of $MgATP^{2-}$ has been changed to a methylene group; magnesium 5′-adenylic imidodiphosphonic anhydride ($MgAMPPNP^{2-}$), in which the bridging oxygen to the γ-phospho group of $MgATP^{2-}$ has been changed to an imino group; and magnesium adenosine 5′-(3-thiotriphosphate), in which one of the nonbridging oxygens on the γ-phospho group of $MgATP^{2-}$ has been changed to sulfur, are **analogues often used in place of $MgATP^{2-}$**. These analogues are widely used because there are so many enzymes that have $MgATP^{2-}$ as a substrate. They cannot participate in the enzymatic reaction, yet they often form ternary complexes with an active site and the substrate to which and from which the γ-phospho group of $MgATP^{2-}$ is transferred during the normal nucleophilic substitution at phosphorus catalyzed by an enzyme that has $MgATP^{2-}$ as a substrate. Examples of cosubstrates to which γ-phospho groups are transferred from $MgATP^{2-}$ in such active sites are shikimate,[610] adenosine,[611] uridine 5′-phosphate,[612] formylglycinamide ribonucleotide,[613] flavin mononucleotide,[614] the hydroxy group of serine in a peptide,[615] and fructose 6-phosphate (Figure 3–39).[616] In crystallographic molecular models of ternary complexes with the respective active sites for each substrate, as in that for human 6-phosphofructo-2-kinase (Figure 3–39), the oxygen of the cosubstrate to be phosphorylated is nestled against the γ phosphorus of the analogue of $MgATP^{2-}$ and surrounded by the three terminal nonbridging oxygens and aligned for an in-line nucleophilic substitution at the γ phosphorus of $MgATP^{2-}$. In this orientation, there is considerable electron repulsion between the lone pairs of electrons on the oxygen receiving the phospho group and the lone pairs of electrons on three nonbridging oxygens, and this electron repulsion must be overcome by pushing the oxygen against the phosphorus.

An enzymatically inactive ternary complex that mimics the complex between the actual substrates in an active site can be produced between **an analogue that lacks a nucleophilic heteroatom and the other substrate** participating in a nucleophilic substitution. For example, for an enzyme catalyzing a phospho transfer to and from $MgATP^{2-}$, an analogue of the cosubstrate that is missing just the oxygen to and from which the phospho group is transferred can be used to produce a complex in a crystallographic molecular model of the active site of an enzyme. The inactive complex mimics the actual complex in which the nucleophilic substitution at phosphorus takes place.[215,216,617] It was possible to crystallize a complex between a galactosyl transferase from *N. meningitidis* and UDP-galactose and an analogue of the oligosaccharide that would normally accept the galactosyl group but that is missing the hydroxy group to which the galactosyl group is transferred, and a crystallographic molecular model of this complex could be obtained.[618]

Succinate, which is an analogue of L-aspartate missing the α-amino group to which a carbamoyl group is transferred from carbamoyl phosphate by aspartate carbamoyltransferase (Equation 3–220), can be used to form an inactive complex with the enzyme and carbamoyl phosphate. The succinate and the carbamoyl phosphate are tightly held and oriented by the active site in the crystallographic molecular model of the complex (Figure 3–40).[580,619] When L-aspartate is superposed on the succinate in the crystallographic molecular model, its amino nitrogen ends up 0.21 nm from the carbamoyl carbon of the carbamoyl phosphate, well within van der Waals contact (0.33 nm) and in an orientation placing it in the location of the large central lobe in the lowest unoccupied molecular orbital of the π system of the carbamoyl group. Considering how short this distance is, it is easy to imagine the amino group of the L-aspartate forcefully pushed up against the carbamoyl carbon of the carbamoyl phosphate by the active site to promote the reaction.

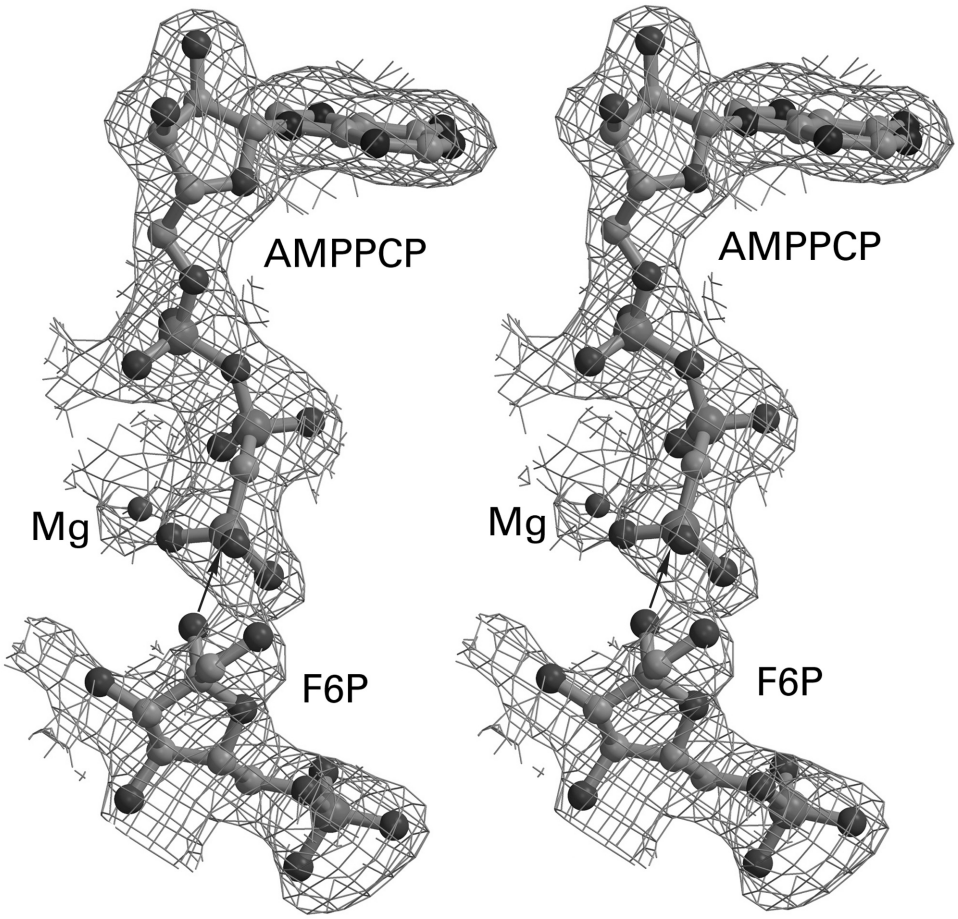

Figure 3–39: Omit map of electron density for the ligands bound in the active site in a crystallographic molecular model for the complex of human 6-phosphofructo-2-kinase, its substrate β-D-fructose 6-phosphate, and the inhibitor $MgAMPPCP^{2-}$ (**3–5**).[616] Crystals of the enzyme were transferred to a solution containing 0.2 mM β-D-fructose 6-phosphate, and 0.2 mM $MgAMPPCP^{2-}$. After one hour, a data set was gathered from the crystals at Bragg spacing of 0.27 nm, and a map of electron density was produced by molecular replacement using an earlier crystallographic molecular model of human 6-phosphofructo-2-kinase from which all ligands and molecules of water had been stripped. In the initial map of electron density, there were features in the active site into which molecular models of molecules of β-D-fructose 6-phosphate and $MgAMPPCP^{2-}$ could be unambiguously inserted. Following refinement, an omit map of electron density (features of electron density in the drawing) was prepared by omitting the molecules of β-D-fructose 6-phosphate and $MgAMPPCP^{2-}$. The molecular models of the molecules of β-D-fructose 6-phosphate (F6P), and $MgAMPPCP^{2-}$ in the final crystallographic molecular model are drawn. The arrow indicates the nucleophilic attack of the 2-hydroxy group of β-D-fructose 6-phosphate on what would be the γ-phospho group of $MgATP^{2-}$ in the normal reaction catalyzed by the enzyme. Reprinted from reference 616 with permission from Elsevier. https://doi.org/10.1016/j.jmb.2007.03.038

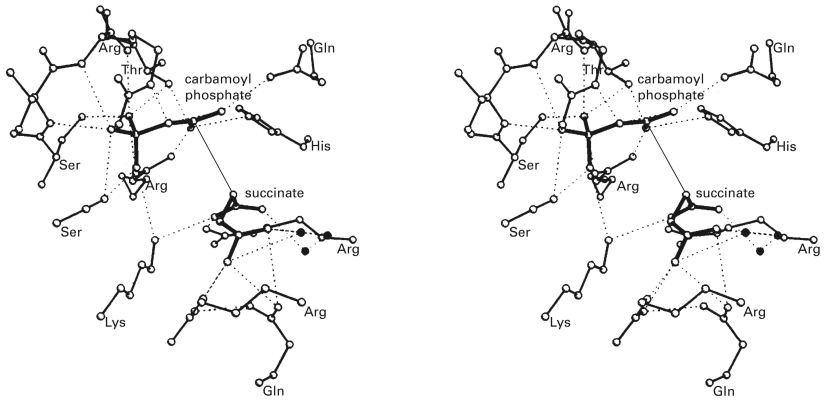

Figure 3–40: Crystallographic molecular model of the active site in the complex between aspartate carbamoyltransferase from *E. coli* and succinate and carbamoyl phosphate.[619] Crystals of the enzyme, in which the active sites had been occupied with *N*-phosphonacetyl-L-aspartate (**3–6**) to promote crystallization of the enzyme in its active conformation, were soaked for 60 h in a solution of 20 mM carbamoyl phosphate and 30 mM succinate at pH 5.9 and 20 °C. A data set was gathered from the resulting crystals to Bragg spacing of 0.26 nm. The molecular model used to initiate refinement was a crystallographic molecular model of the enzyme, determined from crystals in which the active site was occupied by *N*-phosphonacetyl-L-aspartate.[580] This provisional molecular model had water and *N*-phosphonacetyl-L-aspartates removed from it before it was inserted into the unit cell. A map of electron density was produced by using the data set of the phases calculated from this provisional model in the unit cell and the data set of observed phases gathered from the crystals in which the active site was occupied by succinate and carbamoyl phosphate. As the refinement of this initial model progressed, features appeared in the map of electron density within the known active site and became more distinct. Eventually, molecular models of succinate and carbamoyl phosphate could be unambiguously inserted into these features and the refinement was continued. The drawing is of the succinate and the carbamoyl phosphate in the final refined crystallographic molecular model. The dashed lines, as usual, indicate hydrogen bonds, and a thin solid line has been drawn from carbon 2 of the succinate, the carbon on which the amino group would be located on (2*S*)-2-aminosuccinate (L-aspartate), and the carbamoyl carbon of the carbamoyl phosphate. This line would intersect with the nitrogen atom in (2*S*)-2-aminosuccinate were it occupying the active site and is at an acceptable angle with respect to the plane of the carbamoyl group for nucleophilic addition to its π system. The hole for the oxyanion of the tetrahedral intermediate in the nucleophilic substitution at the carbamoyl carbon can be identified in the crystallographic molecular model of the complex between the enzyme and *N*-phosphonacetyl-L-aspartate.[580] The oxyanion hole is for the oxygen atom at the back of the drawing of carbamoyl phosphate in the figure. This oxyanion hole is formed by the hydrogen on the hydroxy group of threonine, the guanidino group of arginine, and the hydronated imidazolyl group of histidine.

A similar way to form an enzymatically inactive complex that closely resembles the catalytically active complex between substrates and the active site is available if the enzyme catalyzes electron transfer. In this instance, instead of removing a functional group, an electron is added or subtracted. If an **incorrect oxidation state of the active site and the substrates** is chosen, the electron transfer cannot proceed. For example, when the heme in camphor 5-monooxygenase from *P. putida* is in the ferric form rather than the ferrous form, the enzyme is unable to hydroxylate camphor, and a crystallographic molecular model of the complex between camphor and the enzyme shows the orientation of the camphor accomplished by the active site, with its carbon 5 the distance of one oxygen atom away from the iron and at an angle appropriate for hydrogen abstraction by the oxoiron(IV) porphyrin$^{\bullet+}$ (previously Equation 2–252)

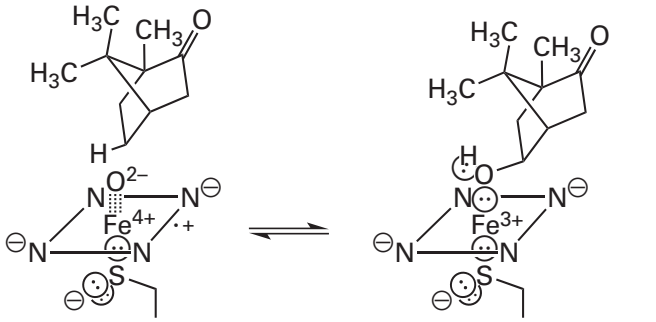

(3–399)

that is the normal intermediate in the active form of the enzyme.[620]

An almost identical, inactive form of an enzyme can also be obtained by **mutating one of the side chains of the amino acids shown to be in the active site** in an earlier crystallographic molecular model of the enzyme.[621-625] For example, in the crystallographic molecular model of a complex between the substrates pyruvate and succinate and an inactive (<1% activity) mutant of methylisocitrate lyase from *E. coli*

succinate + pyruvate $\rightleftharpoons$ (2*S*,3*R*)-3-hydroxybutane-1,2,3-tricarboxylate (3–400)

in which Cysteine 123 had been mutated to serine,[626] the hydroxy group of the serine is immediately adjacent to carbon 2 of the succinate, from which the cysteinate would normally remove a hydron to form the enolate, and the carbonyl carbon of the pyruvate is immediately adjacent to the other side of carbon 2 of succinate, oriented perfectly to participate in a nucleophilic addition with the resulting enolate of succinate

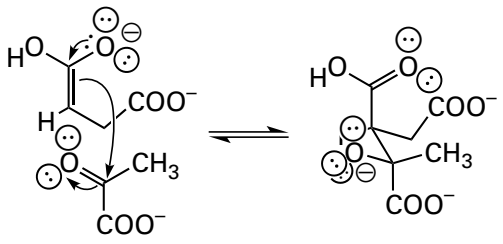

(3–401)

to produce (2*S*,3*R*)-3-hydroxybutane-1,2,3-tricarboxylate in the normal enzymatic reaction.

Mutating one or another of the amino acids in the active site often enables a crystallographic molecular model of the **active site occupied by an intermediate** that would otherwise be evanescent and unable to be observed.[571] For example, when Glutamate 166 in the active site of β-lactamase from *M. tuberculosis* is mutated to an alanine, the transient acyl intermediate in the enzymatic reaction can no longer be hydrolyzed and becomes stable, and the acyl intermediate of the substrate cefamandole can be observed in a crystallographic molecular model of the active site.[627]

A mutant of the enzyme can also **reveal a Michaelis complex** between the reactant and the active site that would otherwise be rapidly converted to product. When Lysine 73 in the active site of β-lactamase from *M. tuberculosis* is mutated to an alanine, the initial Michaelis complex in the enzymatic reaction between the active site and unaltered cefamandole, a reactant for the enzyme, becomes stable and can also be observed crystallographically.[627] A mutant of nicotinamidase from *S. pneumoniae* stabilizes the acyl intermediate in its reaction, and another mutant stabilizes the Michaelis complex with its substrate nicotinamide so that crystallographic molecular models could be constructed of these complexes.[628] Mutating Histidine 187 in the active site of mannuronate-specific alginate lyase from *Defluviitalea phaphyphila* prevented the normal cleavage of alginate and permitted a complex to be formed in the crystal in which all five of the D-mannurates of intact [(α1,4)-D-mannuronate]$_5$ are bound in the active site, and this Michaelis complex spans the location in the active site at which the cleavage of the oligomer would normally occur. When the same substrate was bound in the active site of the native alginate lyase in the crystal, the [(α1,4)-D-mannuronate]$_5$ is cleaved, only three

of the sites are occupied, and the nonreducing end of the trimer sits at the point of cleavage,[629] as was the case in the original crystallographic molecular model of the occupied active site of lysozyme.

Unquestionably, the most informative ligands that can be chosen for crystallographic studies of the active site of an enzyme are analogues of transition states or analogues for intermediates of high energy.[316] For example, a crystallographic molecular model of a complex between analogue **3–84** for the transition state of chorismate mutase (previously Equation 3–167)

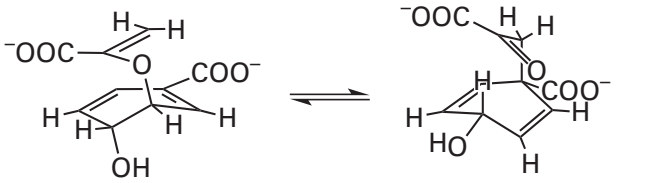

(3–402)

from *B. subtilis* and the enzyme identifies the amino acids creating the active site and confining the transition state to the proper geometry for the electrocyclic reaction.[365]

Crystallographic molecular models of complexes between **analogues for intermediates of high energy** are more numerous than those for analogues of transition states. **Nitrate** (NO_3^-) is isosteric and isoionic with monomeric metaphosphate anion*

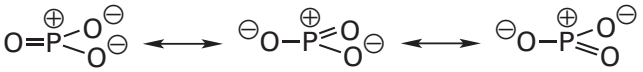

3–92

In the omit map of electron density generated from crystals of the complex between arginine kinase

$$\text{L-arginine} + MgATP^{2-} \rightleftharpoons H^+ + MgADP^- + \text{L-arginine phosphate} \quad (3–403)$$

from *Limulus polyphemus* and L-arginine, $MgADP^-$, and nitrate, the electron density for nitrate is clearly observed (Figure 3–41).[630] The plane of nitrate is normal to a line drawn between one of the nonbridging β-oxygens of $MgADP^-$ and one of the ε amido nitrogens of L-arginine with the nitrogen of nitrate on the line. This orientation of the nitrate mimics monomeric phosphate as an intermediate in the reaction on the fly between these two atoms in the nucleophilic substitution at phosphorus normally catalyzed by the enzyme. In this instance, because both L-arginine phosphate and $MgATP^{2-}$ are phosphate esters of high energy, the nucleophilic substitution should be dissociative, and monomeric metaphosphate should be mimicking an intermediate instead of a transition state. The orientation of the guanidino group of L-arginine, the nucleophile, suggests that the nucleophilic electrons that participate in the reaction are those in the highest occupied molecular orbital of its π molecular orbital system.

Another **analogue of monomeric metaphosphate**, which resembles it in planarity and charge number, is MgF_3^-. It has already been noted that MgF_3^- was used in a crystallographic description of the steps in the mechanism of cAMP-dependent protein kinase,[631] where it was located in a crystallographic molecular model on the line of centers between the hydroxy group of the serine normally phosphorylated by the enzyme and one of the nonbridging β-oxygens of $MgADP^-$, just as nitrate is located in the crystallographic molecular model of the active site of arginine kinase on the line of centers between the two atoms to and from which the phospho group is transferred (Figure 3–41). In a crystallographic molecular model[632] of a complex between the active site of β-phosphoglucomutase from *Lactococcus lactis* and β-D-glucose 6-phosphate and MgF_3^-, the atom of magnesium is located on the line of centers between the 1-hydroxy group of β-D-glucose 6-phosphate and the carboxy oxygen of an aspartate in the active site. In the reaction catalyzed by the enzyme, a phospho group is transferred back and forth between these two oxygens.

One of the **phosphonamido inhibitors** of thermolysin, phosphonamidate **3–83**, is based on the reactant Cbz-Gly-Leu-Leu (Table 3–6). Crystals of thermolysin from *B. thermoproteolyticus* soaked in a solution of phosphonamidate **3–83** were used to generate a refined crystallographic molecular model of the active site occupied by this analogue for the tetrahedral intermediate in the enzymatic reaction (Figure 3–42).[633] Aside from identifying all the important catalytic side chains, the crystallographic molecular model defines the noncovalent interactions holding the analogue in the active site along its entire length.

*Recall that phosphorus is immediately below nitrogen on the periodic table.

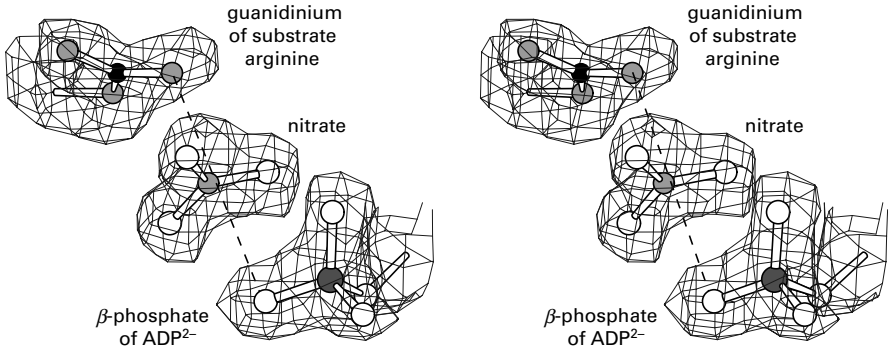

Figure 3–41: Omit map of electron density for the ligands bound in the active site in a crystallographic molecular model of the complex formed from arginine kinase from *L. polyphemus*, its substrates L-arginine and $MgADP^-$, and nitrate.[630] White atoms are oxygens, small gray atoms are nitrogens, and the large dark gray atom is a phosphorus. The enzyme was crystallized from a solution containing 53 mM $MgCl_2$, 2 mM ADP^{2-}, 25 mM KNO_3, and 10 mM L-arginine. A data set was gathered from the crystals at Bragg spacing of 0.186 nm, and a map of electron density was produced using phases estimated by a combination of molecular replacement and isomorphous replacement. In the initial map of electron density, there were features in the active site into which molecular models of molecules of ADP^{2-}, NO_3^- (nitrate), and L-arginine could be unambiguously inserted. Following refinement, an omit map of electron density (features of electron density in the drawing) was prepared by omitting these three ligands. The molecular models of NO_3^- and portions of the molecules of ADP^{2-} and L-arginine in the final crystallographic molecular model are drawn. The dashed line indicates the axis of the nucleophilic substitution at phosphorus that would occur in the normal reaction, in which monomeric metaphosphate takes the place of nitrate. Reprinted with permission from reference 630. Copyright 1998 National Academy of Sciences, U.S.A. https://doi.org/10.1073/pnas.95.15.8449

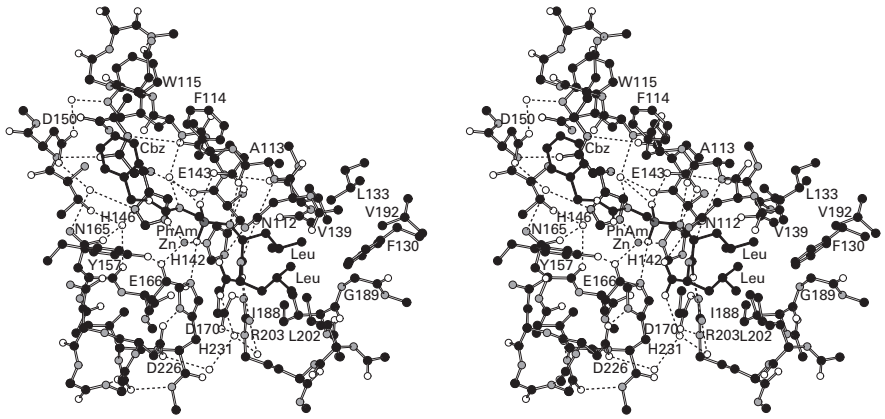

Figure 3–42: Stereodrawing[576] of the occupied active site in the crystallographic molecular model of the complex between thermolysin from *B. thermoproteolyticus* and phosphonamidate **3–83**.[633] Black atoms are carbons, white atoms are oxygens, small gray atoms are nitrogens, the large dark gray atom is a phosphorus, and the small dark gray sphere is a zinc ion. A data set from crystals of unliganded thermolysin was gathered to Bragg spacing of 0.16 nm, and a crystallographic molecular model refined against this data set served as the starting point of the study. Crystals of thermolysin were soaked in a 10 mM solution of the phosphonamidate for several days. A data set, $|F_{\text{complex}}|$, was gathered to Bragg spacing of 0.16 nm from these crystals. From maps of difference electron density, the general location occupied by the phosphonamidate in the active site could be defined. All molecules of water overlapping this location in the refined crystallographic molecular model were removed, and a data set, $|F_{\text{nat,calcd}}|$, and a set of phases, $a_{\text{nat,calcd}}$, were calculated from this dehydrated model to Bragg spacing of 0.16 nm. A map of difference electron density ($F_{\text{complex}} - F_{\text{nat,calcd}}$) was calculated from these two data sets and the set of phases. A molecular model of the phosphon-amidate was inserted into the large feature of positive electron density found in the active site. The initial crystallographic molecular model of phosphonamidate in the active site was refined against the observed data set $|F_{\text{complex}}|$, and a drawing of the phosphonamidate (PhAm; black bonds) in the active site (white bonds) in the final refined crystallographic molecular model is presented. The carbobenzoxy group (Cbz) of the phosphonamidate is labeled to orient the drawing.The Zn^{2+} of the metalloenzyme is included in the drawing. Molecules of water (white spheres) involved in the network of hydrogen bonds in the active site are included.

The hydrate of pyrimidin-2-one ribonucleoside (**3–93**)

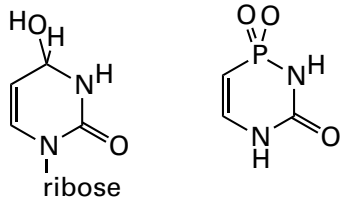

3–93 **3–94**

is an analogue for the tetrahedral intermediate in the reaction catalyzed by cytidine deaminase (Equation 3–395). The same arrangement of catalytic groups and Zn^{2+} around analogue **3–93** is observed in a crystallographic molecular model of the active site of cytidine deaminase from *E. coli*[634] as is observed (Figure 3–36) for the equilibrium mixture cytidine and uridine in the active site of murine cytidine deaminase (28% identity; 2.7 gap percent). Phosphonocytosine (**3–94**) is an analogue for the tetrahedral intermediate in the reaction catalyzed by cytosine deaminase, an enzyme apparently evolutionarily unrelated to cytidine deaminase. In the crystallographic molecular model of phosphonocytosine in the active site of cytosine deaminase from *E. coli*, a similar but distinct distribution of catalytic functional groups around the analogue is observed.[635] A hydroxide on Zn^{2+} is still the nucleophile, but an aspartate takes the place of the glutamate in the active site of cytidine deaminase. The cytosine is flipped over relative to the cytosine ring in the active site of cytidine deaminase (Figure 3–36), so a second carboxy group is required to hydronate nitrogen 3. Finally, the hydrogen bond to the acyl oxygen is provided by a histidine rather than the amido nitrogen–hydrogen of Cysteine 99.

The trialkylammonium **3–95**

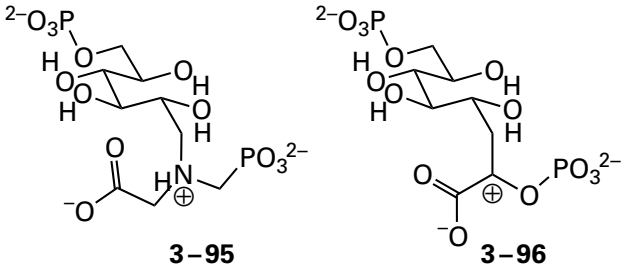

3–95 **3–96**

is an **analogue of carbenium ion 3–96**, another intermediate of high energy. Carbenium ion **3–96** is the initial intermediate in the condensation between phospho*enol*pyruvate and D-arabinose 5-phosphate catalyzed by 3-deoxy-8-phosphooctulonate synthase. Crystallographic molecular models of the complexes between trialkylammonium **3–95** and the 3-deoxy-8-phosphooctulonate synthases from *E. coli* and *Aquifex aeolicus* identify the side chains of the amino acids that orient the two reactants within the respective active sites.[636,637] The relative orientation of the groups that mimic D-arabinose 5-phosphate on the one end and phospho*enol*pyruvate on the other end of the analogue explains the stereochemistry determined previously for the condensation.[637]

It has been proposed that the reaction catalyzed by isopentenyl-diphosphate Δ-isomerase from *S. cerevisiae* proceeds through a tertiary carbenium ion resulting from the hydronation of either substrate on carbon

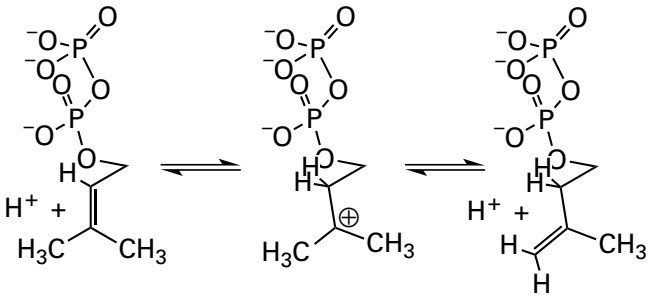

(3–404)

This proposal is based on the fact that the enzyme is inhibited by 2-(dimethylamino)ethyl diphosphate, a tertiary ammonium analogue of this carbenium ion, in which the ammonio nitrogen replaces the carbon of the carbenium ion.[638] In crystallographic molecular models of a complex between isopentenyl-diphosphate Δ-isomerase from *E. coli* and 2-(dimethylamino)ethyl diphosphate[551] and a complex of human isopentenyl-diphosphate Δ-isomerase (26% identity; 3.3 gap percent) and 2-amino-1-ethyl diphosphate,[639] the candidates for the respective catalytic acids performing these hydronations can be identified.

Analogues for intermediates of high energy can also be **formed on the active site of an enzyme** and observed in a crystallographic molecular model. For example, glutamine synthetase from *M. tuberculosis*

$$\text{L-glutamate} + NH_3 + MgATP^{2-} \rightleftharpoons MgADP^- + HOPO_3^{2-} + \text{L-glutamine} \quad (3\text{–}405)$$

was mixed with the sulfoximine (**3–67**) of L-methionine and $MgATP^{2-}$ and then crystallized. In the crystallographic molecular model, the adduct **3–97**

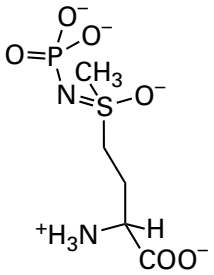

3–97

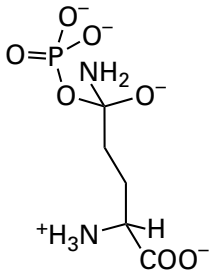

3–98

was observed occupying the active site[640] along with $MgADP^-$. Adduct **3–97** is an analogue of the tetrahedral intermediate **3–98**, which forms on the active site when ammonia attacks the 5-phospho-L-glutamate produced by the phosphorylation of the carboxylato group of L-glutamate by $MgATP^{2-}$ during the step in the mechanism in which there is a nucleophilic substitution of the phospho group for an amido group catalyzed by the active site. The position of the methyl group of adduct **3–97** occupies the site at which ammonia normally binds,[641] the sulfoximido oxygen identifies the guanidinio group of an arginine that is the donor in a hydrogen bond stabilizing the oxyanion of intermediate **3–98**, the $MgADP^-$ assumes an orientation appropriate for the initial transfer of the phospho group to the carboxylato group of L-glutamate, and the three Mg^{2+} ions that orient the three phospho groups and the carboxylato group of the L-glutamate that is phosphorylated are clearly defined in the crystallographic molecular model.

An enzyme catalyzing a **nucleophilic substitution at the phosphorus in a monoester of phosphoric acid** is the phosphatase encoded by the BT4131 gene of *Bacteroides thetaiotaomicron*. This enzyme first performs a nucleophilic substitution at a phosphate monoester in which the alcohol of the phosphoester is the leaving group and the magnesium carboxylato group of Aspartate 8 in the active site is the nucleophile. The enzyme then catalyzes a second nucleophilic substitution at the same phosphate group in which the magnesium carboxylato group of Aspartate 8 is the leaving group and water, under general base catalysis by Aspartate 10, is the nucleophile (Figure 3–43).[643] Vanadate (Table 3–7) forms, with the carboxylato group of Aspartate 8, an analogue (**3–99**) for the phosphorane (**3–100**) formed during the normal reaction in the active site

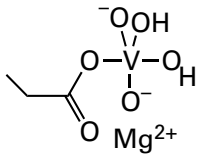

3–99

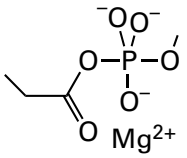

3–100

This phosphorane is an intermediate in the nucleophilic substitution of the magnesium carboxylato group of this Aspartate 8 with a hydroxy group from water catalyzed by the enzyme.[642] In the crystallographic molecular model of the complex between the enzyme and vanadate, a hydrogen bond between the carboxylato group of Aspartate 10 and the axial hydroxy group of the vanadate identifies Aspartate 10 as the catalytic base that removes a hydron from the molecule of water.

The goal of the approaches discussed so far is to obtain experimentally a single accurate crystallographic molecular model in which details of the catalytic mechanism are unveiled.

There are also computational approaches to creating a molecular model of the fully occupied active site. These approaches are not so satisfying as having a single informative crystallographic molecular model, but they can be provocative nevertheless.

A molecular model of the complex between the active site of an enzyme and its several reactants can be computed by **superposing separate crystallographic molecular models** of complexes between the enzyme and each reactant by itself.[644,645] For example, the crystallographic molecular model of a complex between the active site of human galactosylgalactosylxylosylprotein 3-β-glucuronosyltransferase and $MgUDP^-$ and the trisaccharide 3-β-D-galactosyl-4-β-D-galactosyl-*O*-β-xylose was superposed on a crystallographic molecular model of a complex between the active site and UDP-glucuronate. In the superposition, the 3-hydroxy group of the terminal D-galactose of the trisaccharide, to which the glucuronosyl group is transferred during the enzymatic

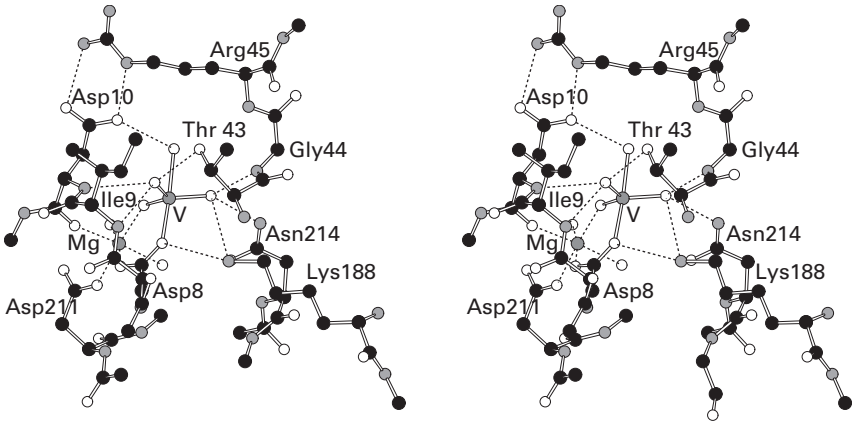

Figure 3–43: Stereodrawing[576] of the occupied active site in the crystallographic molecular model of the complex between the phosphatase encoded by the BT4131 gene of *B. thetaiotaomicron* and a vanadate.[642] Black atoms are carbons, white atoms are oxygens, small gray atoms are nitrogens, and the small dark gray sphere is a magnesium ion. Crystals of the enzyme were grown from a solution containing 10 mM $MgCl_2$ and 5 mM sodium orthovanadate. A data set was gathered at Bragg spacing of 0.1 nm, and a map of electron density was produced by molecular replacement using an earlier crystallographic molecular model of the phosphatase from which all the ligands and molecules of water had been stripped. A feature of electron density was found in the active site immediately adjacent to the electron density for one of the oxygens in the carboxy group of Aspartate 8. An atom of vanadium and four atoms of oxygen could be inserted into this trigonal pyramidal distribution of electron density, and a bond was made between vanadium and the oxygen of Aspartate 8. A sphere of electron density consistent with a Mg^{2+} was found adjacent to the electron density assigned to the vanadate, and a magnesium atom was inserted in this sphere. The initial molecular model with these insertions was submitted to refinement. The drawing of the final refined structure includes the vanadyl group centered on the atom of vanadium (V), the Mg^{2+}, and most of the amino acids in the surrounding polypeptide providing hydrogen bonds to vanadate and amino acids and the molecules of water (white spheres) providing ligands to Mg^{2+}.

reaction, ends up on the opposite side of carbon 1 of the glucuronosyl group of UDP-glucuronate from the phosphate group of $MgUDP^-$ that leaves during the nucleophilic substitution catalyzed by the enzyme[646]

3–101

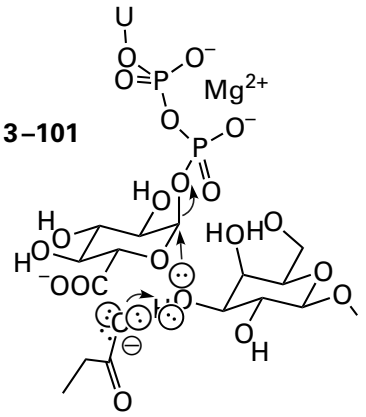

in line for the nucleophilic substitution.

When the crystallographic molecular model of the complex between shikimate kinase from *M. tuberculosis* and shikimate 3-phosphate and $MgADP^-$ is superposed on the crystallographic molecular model of the complex between the enzyme and $MgATP^{2-}$, the three nonbridging oxygens of the phosphate on shikimate phosphate superpose on the three nonbridging oxygens of the γ-phospho group of $MgATP^{2-}$, and the in-line nucleophilic substitution with inversion of configuration at the phosphorus that transfers the phospho group from $MgATP^{2-}$ to the hydroxy group of shikimate is easily imagined.[647]

(2*E*,6*E*)-Farnesyl diphosphate synthase

magnesium isopentenyl diphosphate +
magnesium geranyl diphosphate $\rightleftharpoons$
$MgOPO_3PO_3^{2-}$ + H^+ +
magnesium (2*E*,6*E*)-farnesyl diphosphate
(3–406)

catalyzes the alkylation of the isopentenyl alkene by the same mechanism as that of dimethylallyl-*trans*transferase (Figure 1–26), in which the allyl carbenium ion formed from geranyl diphosphate, instead of 3,3-dimethylallyl diphosphate, adds to the carbon–carbon double bond in isopentenyl diphosphate. Two crystallographic molecular models were superposed. One was a model of the complex between (2*E*,6*E*)-farnesyl diphosphate synthase from *E. coli*[648] and isopentenyl diphosphate and *S*-diphospho-1-sulfanyl-3-methyl-2-butene, an inactive analogue of the substrate geranyl diphosphate. The other was a model of a complex of the closely related (42% identity; 1.3 gap percent) enzyme farnesyl*trans*transferase

magnesium isopentenyl diphosphate +
magnesium (2*E*,6*E*)-farnesyl diphosphate
$\rightleftharpoons$ $MgOPO_3PO_3^{2-}$ + H^+ +
magnesium geranylgeranyl diphosphate
(3–407)

from *Sinapis alba* with geranylgeranyl diphosphate, which is the product of its reaction as written and which is homologous to (2*E*,6*E*)-farnesyl diphosphate.

The superposition of these two crystallographic molecular models (Figure 3–44)[648,649] clearly shows how the atoms involved in the reaction move as reactants are converted to products in the respective, mechanistically identical reactions catalyzed by these two different enzymes. The steps of the alkylation are indicated by the numbers. First, the bond between the allylic carbon 1 of the respective polyisoprenoid and the oxygen of trimagnesium diphosphate dissociates heterolytically to produce the allyl carbenium ion. Second, the double bond of the isopentenyl diphosphate, the alkene, acting as a nucleophile in the alkylation, reacts with the carbenium ion to form the new carbon–carbon bond in the adduct. Third, the hydron at carbon 2 of the former isopentenyl diphosphate immediately adjacent to the carbenium ion at carbon 3 of the former isopentenyl diphosphate is removed by one of the oxygens of trimagnesium diphosphate, which is the product of the dissociation that occurred in the first step, to produce the double bond between carbons 2 and 3 in the product.

If a crystallographic molecular model of the active site of an enzyme occupied by one of the substrates and an inactive, competitive inhibitor of the other substrate that happens to contains the other substrate as part of its structure has been constructed, the actual substrate can be inserted in place of the portion of the inhibitor that is in common and the resulting **hypothetical molecular model can be submitted to energy minimization**. For example, there is a crystallographic molecular model of the active site of malate dehydrogenase from *E. coli* occupied by NAD^+ and citrate, which is an inactive inhibitor of the enzyme that contains all the atoms of the normal substrate, (*S*)-malate, except the hydride that would be transferred to NAD^+ in the normal reaction.

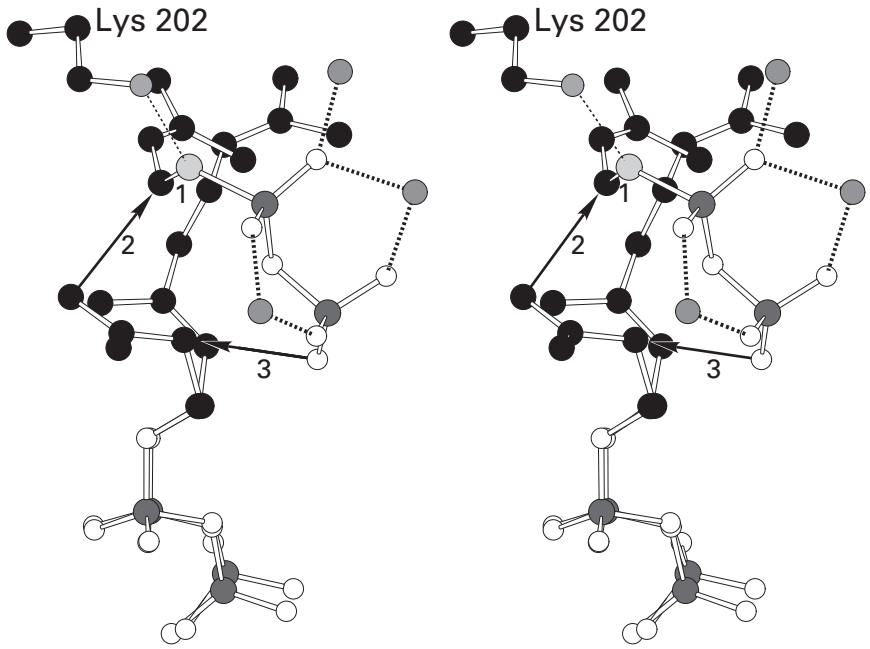

Figure 3–44: Superposition of the molecular models of isopentenyl diphosphate and *S*-diphospho-1-sulfanyl-3-methylbut-2-ene in the active site of the crystallographic molecular model of their complex with (2*E*,6*E*)-farnesyl diphosphate synthase from *E. coli*[648] upon the molecular model of geranylgeranyl diphosphate in the active site of the crystallographic molecular model of its complex with farnesyl*trans*transferase from *Sinapsis alba*.[649] Black atoms are carbons, white atoms are oxygens, gray atoms are nitrogens, the large light gray atom is a sulfur, the large dark gray atoms are atoms of phosphorus, and the three small dark gray spheres are magnesium ions that are ligands to the diphospho group of the geranylgeranyl diphosphate. The *S*-diphospho-1-sulfanyl-3-methylbut-2-ene in the former crystallographic molecular model is an inactive analogue of the first five carbons of the normal substrate, geranyl diphosphate. The superposition describes the conversion of the two respective reactants into the two respective products catalyzed by each of these enzymes, which are closely related and catalyze alkylations that have identical mechanisms (see Figure 1–26).

A molecular model of (*S*)-malate was inserted into the electron density for the citrate, and the resulting molecular model of the occupied active site was submitted to energy minimization. The **computed structure** places electrophilic carbon 4 of the NAD^+ 0.35 nm from carbon 2 of the malate, from which it would normally abstract a hydride in the reaction catalyzed by the enzyme, and in a favorable orientation for such an abstraction.[650]

A series of crystallographic molecular models of strategically designed complexes between an enzyme and various ligands can represent the complete sequence of events in its catalytic cycle.[651-653] For example, DNA (cytosine-5-)-methyltransferase is responsible for using *S*-adenosyl-L-methionine to methylate carbons 5 in cytosines

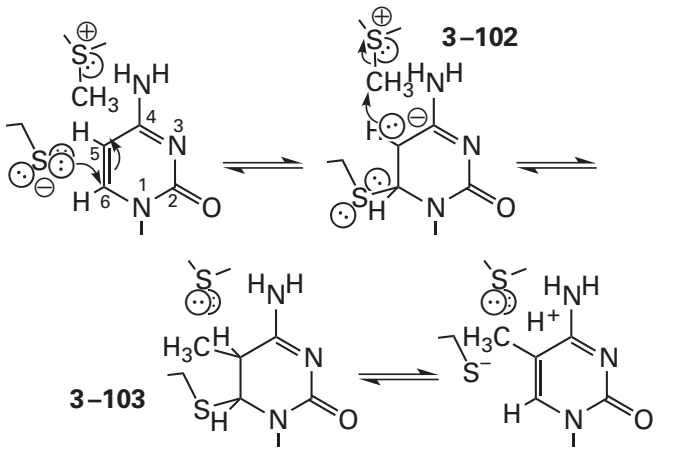

(3–408)

at particular positions in the double-stranded DNA of a bacterium to protect it from its own restriction endonucleases.

Three crystallographic molecular models represent the three steps in the enzymatic reaction. The crystallographic molecular model of a complex between the enzyme from *Haemophilus parahaemolyticus* and *S*-adenosyl-L-homocysteine, which is *S*-adenosyl-L-methionine missing the methyl group, and a segment of DNA containing a deoxycytidine that can be methylated by the enzyme illustrates the first step in the reaction, in which the deoxycytidine is flipped out of the double helix into the active site of the enzyme. When a segment of DNA containing the deoxycytidine to be methylated, which has been modified by fluorination at carbon 5, is mixed with the enzyme and *S*-adenosyl-L-methionine, the active site methylates carbon 5 of this 5-fluorodeoxycytidine, but there is a fluorine in place of the hydrogen at carbon 5 in the equivalent of adduct **3–103,** so the reaction cannot proceed to the next step. The crystallographic molecular model of this stalled complex and *S*-adenosyl-L-homocysteine occupying the active site[654] identifies the 5-fluorinated form of adduct **3–103**. Unfluorinated adduct **3–103** in the normal reaction results from the methylation at carbon 5 of carbanion **3–102** that in turn is produced by the nucleophilic addition of the sulfido group of Cysteine 81 in the active site to carbon 6 of the flipped-out deoxycytidine. The crystallographic molecular model of the complex between the products *S*-adenosyl-L-homocysteine and the segment of DNA containing the methylated deoxycytidine represents the final step in the reaction.[655]

cAMP-Dependent protein kinase catalyzes a nucleophilic substitution at phosphorus during which a phospho group is transferred from $MgATP^{2-}$ to the hydroxy group of a serine in one of its protein substrates to form a phosphomonoester. The molecular details of the steps in the reaction that occurs in its active site can be followed in crystallographic molecular models of the active sites of the enzymes from *Mus musculus* and *O. cuniculus* in three complexes: a complex with $CaATP^{2-}$ and a peptide in which the serine that is usually phosphorylated has been replaced by a cysteine; a complex of $MgADP^-$, the unmodified seryl peptide, and MgF_3^-, a trigonal mimic of monomeric metaphosphate (see the homologous complex **3–40** with aluminum); and a complex of $MgADP^-$ and the phosphorylated seryl peptide.[631]

In the case of inorganic diphosphatase from *S. cerevisiae*, complexes of wild-type enzyme and two mutants with phosphate, diphosphate, and various divalent metallic ions provide crystallographic molecular models for the reactants and products of six steps in the enzymatic reaction that comprise the complete catalytic cycle.[656]

A data set suitable for calculating a map of electron density can also be gathered over intervals as short as picoseconds by using intense short flashes of X-rays. As already noted, this procedure has been used to follow events in the active sites of bacteriorhodopsin,[657,658] photosystem II,[659-661] and photoactive yellow protein.[662-664] In each case, the reaction within the active site could be initiated by a strong flash of light of the proper wavelength, and the changes in the active site could then be followed by the flashes of X-rays at appropriate intervals. This procedure has seldom been applied to enzymatic reactions because in the active sites of most enzymes, few ways have been developed to initiate the reaction in a crystal in such a way that all the

active sites proceed in concert through the reaction. In the case of haloacetate dehalogenase from *Rhodopseudomonas palustris*, however, this problem was solved by soaking the crystals of the enzyme in a solution of 2-(4-hydroxyphenyl)-2-oxoethyl 2-fluoroacetate, which upon photolysis rapidly releases 2-fluoroacetate, a reactant for the enzyme. The photolytically released 2-fluoroacetate immediately associates with a significant proportion of the active sites in the crystal, and the dehalogenation then proceeds. Data sets could be collected at intervals from 30 ms to 30 s following the initiation of the reaction to follow the steps in the catalytic mechanism.[665]

The structure of the active site itself; the conformations, orientations, and positions of the substrates, analogues of substrates, and analogues of transition states and intermediates of high energy within an active site; and the distances among their atoms and atoms of the active site are the only facts revealed by a crystallographic molecular model. Each of these purely stereochemical features in this static structure is the consequence of noncovalent interactions. It follows that the information provided by the crystallographic molecular model also defines these noncovalent interactions. They are hydrogen bonding,[351] electric fields that arise from both ionic and dipolar forces, the hydrophobic effect,[666] and van der Waals forces.[352]

Most of the hydrogen bonds that are formed between an enzyme and its substrates and other ligands occupying the active site are participants in networks of hydrogen bonds that ensnare those substrates and ligands (Figures 3–33, 3–34, 3–40, and 3–42). These networks of hydrogen bonds are revealed in a crystallographic molecular model in which the active site is occupied by substrates, analogues of substrates, or analogues of transition states or intermediates of high energy. The networks of hydrogen bonds between substrates and ligands and an active site or a binding site, as with the networks of hydrogen bonds within the protein itself, have been **the most compelling features of crystallographic molecular models** from the beginning of their revelation, no doubt because of the emphasis on hydrogen bonding in the early models of the α helix and β structure that were published[667,668] before any crystallographic molecular models of proteins had been revealed. The fact that hydrogen bonds are blatant in crystallographic molecular models has led to the mistaken impression that they provide standard free energy of association for a substrate or a ligand during its association with an active site or a binding site. As has already been discussed, however, because of the properties of liquid water in which the substrates, the ligands, and the active site are dissolved before they associate, the only noncovalent interaction that can provide significant, favorable standard free energy of association is the hydrophobic effect.

One of the more paradigmatic examples of hydrogen bonding between a ligand and its site is found in the crystallographic molecular model of the complex between β-D-galactose and the periplasmic D-glucose/D-galactose-binding protein from *E. coli* (Figure 3–45).[669-671] Of the 17 donors and acceptors for hydrogen bonds on the β-D-galactose, 11 are occupied by acceptors and donors from the amino acids surrounding the site and two are occupied by the acceptors of a tightly bound molecule of water. Every donor for a hydrogen bond on the D-galactose is associated with an acceptor.

Not all the hydrogen bonds in these networks are provided by the folded polypeptide. As the complex between β-D-galactose and the periplasmic D-glucose/D-galactose-binding protein illustrates, **molecules of water fixed by hydrogen bonds** within the active site or within a binding site often provide donors and acceptors for hydrogen bonds to the substrates or ligands when they are bound (Figures 3–33, 3–34, and 3–42).[464,672] For example, in the crystallographic molecular model of the complex between asparagine—tRNA ligase from *Pyrococcus horikoshii* and the intermediate asparaginyl-adenylate, a molecule of water provides an acceptor for a hydrogen bond with the primary carbamoyl nitrogen–hydrogen of the side chain of the asparaginyl group that was the substrate L-asparagine, and another molecule of water provides a donor for a hydrogen bond to the acyl oxygen of the carbamoyl group[673]

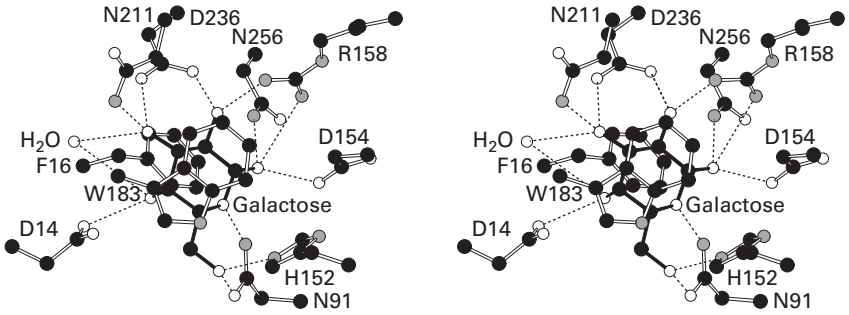

Figure 3–45: Stereodrawing[576] of the networks of hydrogen bonds formed between β-D-galactose and the various donors and acceptors surrounding it in the binding site within the crystallographic molecular model of the complex between β-D-galactose and the periplasmic D-glucose/D-galactose-binding protein from *E. coli*.[669,670] Black atoms are carbons, white atoms are oxygens, and gray atoms are nitrogens. The tightly associated β-D-glucose that is bound to the binding site in the protein in the cell and that copurifies with it was replaced by β-D-galactose,[671] and the complex was then crystallized. A data set was gathered to Bragg spacing of 0.2 nm, and a map of electron density was calculated using phases calculated from an earlier crystallographic molecular model of the protein to which β-D-glucose was bound and from which the molecular models of β-D-glucose and the waters had been removed. In an initial map of difference electron density, a feature that could be unambiguously identified as that of a molecule of β-D-galactose in the binding site was observed. The side chains of each amino acid that forms hydrogen bonds to β-D-galactose in the refined crystallographic molecular model are drawn, as well as a fixed molecule of water that provides two hydrogen bonds. The side chains of Tryptophan 183 and Phenylalanine 16 sandwich the two hydrophobic faces of β-D-galactose.

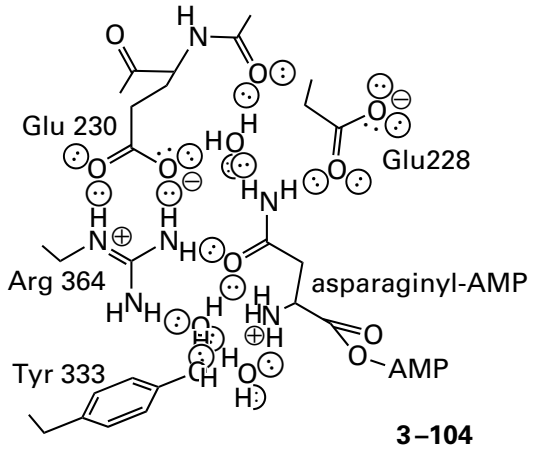

3–104

To ensure that the former molecule of water provides only an acceptor, its two donors are occupied with hydrogen bonds to the peptidyl acyl oxygen of Leucine 229 and the carboxylato group of Glutamate 230. These two molecules of water are responsible in part for identifying the L-asparagine that is the substrate for the enzyme, a role that is critical to avoiding rather catastrophic misacylation of the transfer RNA.

In a crystallographic molecular model of the active site of DNA-directed DNA polymerase from Escherichia phage RB69 occupied by a synthetic fragment of DNA that is a substrate for the enzyme, a cluster of five fixed molecules of water is used to provide donors and acceptors for hydrogen bonds for the acceptors and donors in the minor groove of the double-helical portion of the DNA.[674] The buried molecules of water in this crystallographic molecular model calculated from a data set to Bragg spacing of 0.18 nm are tetrahedrally aligned with each other as in the iceIh lattice, and the hydrogen bonds to the acceptors and donors in the minor groove are also tetrahedrally arrayed around each molecule of water.

In the binding site of sialic acid-binding periplasmic protein SiaP from *Haemophilus influenzae*, a cluster of five fixed molecules of water provides three donors of hydrogen bonds that recognize a molecule of the substrate sialic acid. When this cluster is disrupted by mutating a nearby alanine to an asparagine, the dissociation constant for sialic acid decreases[675] by a factor of 1400.

The crystallographic molecular model of the enzymatically inactive complex between human glutathione-disulfide reductase and its oxidized substrates glutathione disulfide and $NADP^+$ represents an extreme example of the participation of fixed molecules of water in identifying the substrate for an enzyme. There are 13 molecules of water that are fixed by 17 donors and acceptors for hydrogen bonds from the protein and that in turn provide 17 donors and acceptors to just the bound glutathione disulfide.[676]

In the case of D-glucose/D-galactose-binding protein (Figure 3–45), the binding site completely surrounds its ligand, preventing any contact with the bulk solution that surrounds the protein. An active site or a binding site on a protein, however, is often merely a depression or a crevice on its surface. In such a site, several of the donors and acceptors for hydrogen bonds on a bound substrate or a bound ligand can remain occupied by fixed molecules of water that occupied those donors and acceptors for hydrogen bonds when they were free in solution, and those **fixed molecules of water can still be in contact with molecules of water in the bulk solution.**

In almost all instances, the formation of a hydrogen bond between an acceptor or a donor on a functional group from the active site and a donor or an acceptor on a ligand, respectively, should be **an almost isenthalpic reaction**[677,678] because the concentration of hydrogen bonds in the solution does not increase significantly during the reaction.[351,679] This conclusion results from the fact that when the active site is unoccupied and the substrates are free in solution before they associate with the active site, a donor or an acceptor for a hydrogen bond in the active site or on a substrate is occupied most of the time with an acceptor or a donor from a molecule of water. When the substrates associate with the active site, if these donors and acceptors that were participating in hydrogen bonds with molecules of water do not find partners in the occupied active site, the number of hydrogen bonds in the solution decreases. When they do find partners, the number of hydrogen bonds in the solution does not change significantly, so the standard enthalpy of the solution remains approximately the same. Consequently, it is not because hydrogen bonds in an active site have favorable standard free energies of formation that there are so many of them; but it is because **whenever a donor or an acceptor for a hydrogen bond leaves water it must find an acceptor or the change in standard free energy is positive and unfavorable**.

Even though the formation of a hydrogen bond in an active site is almost isenthalpic, it so happens that, as in the case of the occupied site on D-glucose/D-galactose-binding protein (Figure 3–45), there is an imbalance between the occupation of donors and the occupation of acceptors for hydrogen bonds in a fully occupied active site. Although accep-

tors often do not find donors, **all or almost all of the donors for hydrogen bonds usually participate in hydrogen bonds** with acceptors in an occupied active site. This feature of the association of substrates, coenzymes, and prosthetic groups with an active site results from a historical fact. In a concentrated solution of protein, such as the cytoplasm in which most enzymes have evolved, acceptors always outnumber donors for hydrogen bonds because the polypeptide backbones of the proteins in that solution have two acceptors for hydrogen bonds on each acyl oxygen but only one donor on each amido nitrogen.[680] A donor for a hydrogen bond on a ligand or on the surface of the active site, when they are dissolved in cytoplasm, will always be occupied by an acceptor on a molecule of water in free solution. Whenever that donor is vacated by that molecule of water upon association of the ligand with an active site and does not participate in a hydrogen bond with an acceptor from the active site or another ligand or within the ligand itself, there is an inescapable positive change in the standard enthalpy of the solution as a whole because a net of one hydrogen bond is lost. In cytoplasm, however, this loss does not occur for an acceptor. If an acceptor for a hydrogen bond is not occupied by a donor following association of the ligand, there is no change in the number of hydrogen bonds in the solution because the donor on the molecule of water that dissociates from the acceptor can always find another unoccupied acceptor. It follows that during the association of substrates, coenzymes, and prosthetic groups with the active site on an enzyme, which has evolved over its entire history under these conditions, the maximum possible number of hydrogen bonds will form with donors, both on the ligands and on functional groups from the active site.*

A hydrogen bond between a donor and an acceptor in free aqueous solution always has a positive standard free energy of formation because of the competition of molecules of water for the donor and the acceptor,[678] but the formation of a hydrogen bond between an acceptor or a donor on an otherwise rigidly held ligand and a rigidly fixed donor or acceptor on a functional group from the active site involves significant **standard entropy of approximation**. Consequently, its formation in fact might display a negative standard free energy of formation. Nevertheless, if there are rigidly oriented hydrogen bonds in active sites that do have a negative free energies of formation, those standard free energies are probably not greatly negative.

There have been **many experiments that have been designed to discover a hydrogen bond in an occupied active site that has a negative standard free energy of formation**. In most of these experiments, rather small differences in thermodynamic state functions form the basis of the argument. It turns out, however, that it is difficult if not impossible to derive the standard free energy of formation of the hydrogen bond in question from these small, indirect effects. Perhaps it is educational to examine one of the more rigorous attempts to do so.

Two series of analogues for the tetrahedral intermediate in the hydrolytic reaction catalyzed by thermolysin from *B. thermoproteolyticus* have been synthesized. The various analogues in the first series were phosphonates (**3–73**), and the various analogues in the second series were the corresponding phosphonamidates (**3–71**). Each phosphonate was homologous to one of the phosphonamidates, each phosphonamidate was homologous to one of the phosphonates, and each pair of homologues was homologous to one of the peptides in a series of reactants for the enzyme (see **3–83** and Table 3–6). When the dissociation constants (K_i) for each phosphonamidate and its corresponding phosphonate, all acting as competitive inhibitors of thermolysin, were compared, a consistent difference, equivalent to a difference in free energy of dissociation of +16.7 ± 0.4 kJ mol^{-1}, was observed.[681] Each phosphonamidate had the larger free energy of dissociation (a smaller dissociation constant) relative to the corresponding phosphonate.

Between the refined crystallographic molecular models of the complex between a phosphonate and the enzyme and the complex between the corresponding phosphonamidate and the enzyme, no difference in the orientations or the positions of the two respective inhibitors or amino acids within the

*In a dilute solution of protein and a reasonably concentrated solution of reactants, such as the situation when steady-state kinetics or equilibrium binding is assessed experimentally, the solutes will determine whether donors or acceptors are in excess in the solution. If acceptors are in excess, as in cytoplasm, whenever a hydrogen bond between a donor and an acceptor on a molecule of water dissociates because the donor has lost contact with the water in the solution, there will be a net loss of one hydrogen bond if the donor fails to find an acceptor in the active site because the acceptor on the molecule of water released will not find an unoccupied donor. If, however, donors are in excess, whenever a hydrogen bond between a donor and an acceptor on a molecule of water dissociates because the donor has lost contact with the water, there will be no net loss of a hydrogen bond if the donor fails to find an acceptor in the active site because the molecule of water released will find another donor. These considerations, however, are irrelevant to natural selection, which has always operated in a cytoplasm with excess acceptors.

active site could be observed.[682] In the model of the phosphonamidate bound in the active site, the nitrogen of the nitrogen–hydrogen bond of the phosphonamidate is 0.30 nm from the acyl oxygen of the peptide bond of Alanine 113 with a reasonable orientation for a hydrogen bond (Figure 3–42). One difference between the complex of a phosphonate with the active site and the complex of the corresponding phosphonamidate with the active site is the existence of this hydrogen bond. If this hydrogen bond were the only difference, the free energy of formation of this rigidly oriented hydrogen bond, relative to the hydrogen bond between the same nitrogen–hydrogen and a molecule of water when it was free in solution, would be –17 kJ mol^{-1}, which could be attributed to the entropy of approximation. There are, however, at least two other differences.

First, the ester oxygen of each phosphonate is forced to reside next to the acyl oxygen of Alanine 113 in the complex between a phosphonate and the active site, and this juxtaposition should engender an electron repulsion. To test this possibility, two competitive inhibitors of thermolysin, both of which were phosphonates

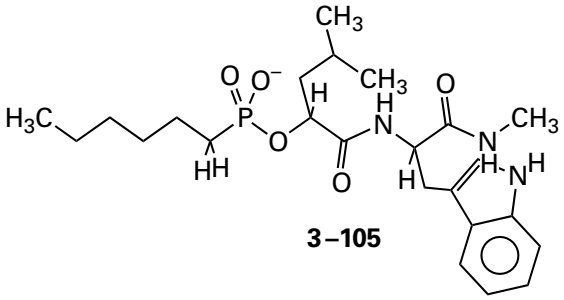

3–105

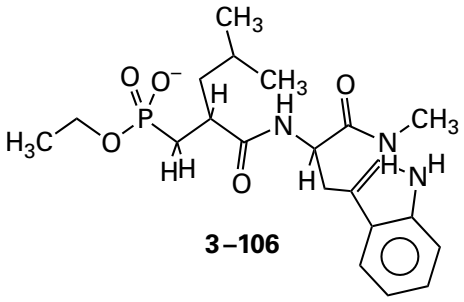

3–106

were synthesized.[683] The difference between the two was that the oxygen and the carbon of the phosphonate were interchanged. At the active site, this interchange would have replaced the oxygen with a carbon and a hydrogen, yet no difference in dissociation constant between these two competitive inhibitors was observed. The advantage of this experiment was that solvation of the two inhibitors in free solution should have been the same around the phosphorus, but in the active site, the oxygen would be replaced by the methylene. This result seems to suggest that electron repulsion is insignificant, but it would be surprising if there were not steric repulsion in the case of the methylene at least equivalent in magnitude to the electron repulsion of the oxygen because the distance that should exist between the carbon of the methylene and the oxygen of the peptide bond (0.30 nm) is well within the sum of the van der Waals radii of a hydrogen (0.115 nm) and an oxygen (0.15 nm) and the length of a carbon–hydrogen bond (0.11 nm), so this result is also inconclusive.

Second, the two free, nonbridging anionic oxygens of a phosphonate are less basic than the analogous anionic oxygens of a phosphonamidate and should bind less strongly to the zinc in the active site (Figure 3–42). This difference in pK_a could account for some or all of the difference in free energy of dissociation that was observed. To test this possibility, two sets of phosphonamidates (**3–71** and **3–83**), phosphonates (**3–73**), and phosphinates (**3–107**)

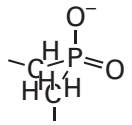

3–107

were synthesized, where each set is analogous to a peptide cleaved by thermolysin.[683] The phosphinates had the same pK_a as the phosphonamidates, but the values of pK_a for the analogous phosphonates were about 1.65 units lower. When the dissociation constants of the phosphonamidates and phosphinates were compared, the free energies of dissociation differed by only +6 kJ mol^{-1}, while the free energies of dissociation between phosphonamidates and phosphonates differed, as before, by +17 kJ mol^{-1}. When comparisons between phosphinates and phosphonamidates were made with the same series of peptide analogues used in the original comparisons between phosphonamidates and phosphonates,[684] the difference in free energy of dissociation between phosphonamidates and phosphinates was even less, +0.5 kJ mol^{-1}. From these observations, it might be concluded that the majority of the difference in free energy of dissociation between phosphonamidate and phosphonate is due not to the hydrogen bond but to the difference in basicity, which causes the oxygens of the phosphonamidate to bind more tightly to the zinc. When a series of arylphosphonate inhibitors of thermolysin that differed in the basicity of the phosphonate were examined, however, no

differences in dissociation constant were observed.[684] Again the observations are inconclusive.

From comparisons of the dissociation constants of all these phosphonamidates, phosphonates, and phosphinates, it can be concluded that the various differences in observed free energies of dissociation resulted from some combination of several factors: (1) the difference in hydrogen bonding in free solution between water and the nitrogen–hydrogen of the phosphonamidate or the oxygen of the phosphonate; (2) the difference in hydrophobic effect of the methylene in the phosphinates, the oxygen of the phosphonates, or the nitrogen–hydrogen of the phosphonamidates; (3) the difference in electron repulsion or steric repulsion between the acyl oxygen of Alanine 113 and the oxygen of the phosphonates or the methylene of the phosphinates; (4) the difference in basicity between the phosphinates, the phosphonamidates, and the phosphonates; and (5) the hydrogen bond itself. These experiments, at face value so simple, illustrate the difficulty of dissecting the various contributions of standard free energy to observed dissociation constants.

The most optimistic assessment of the results of these experiments is that the difference in standard free energy of formation between the hydrogen bond in the complex of a phosphonamidate with the active site of thermolysin and the hydrogen bond of the same phosphonamidate with water in free solution is greater than –17 kJ mol^{-1}; the most pessimistic is that it is in the neighborhood of 0 kJ mol^{-1}. The two states that differ by these amounts of free energy of formation are the nitrogen–hydrogen bond of the phosphonamidate in a hydrogen bond as a donor intramolecularly to the acyl oxygen of Alanine 113 and the nitrogen–hydrogen bond of the phosphonamidate as a donor intermolecularly to water. As the values of pK_a for the hydronated oxygen of water and the hydronated acyl oxygen of a peptide bond are essentially the same, no difference in enthalpy should exist between these two states. The lone pair of electrons on the peptide oxygen fixed and oriented adjacent to the nitrogen–hydrogen of the bound phosphonamidate, however, acts as if its entropy of approximation is no more negative than –50 J K^{-1} mol^{-1} relative to the entropy of approximation associated with the one mole fraction of water surrounding the unbound inhibitor and is probably much less negative.

In other, more equivocal experiments, the free energies of formation of single hydrogen bonds between amino acids in the active site of tyrosine-tRNA ligase from *Geobacillus stearothermophilus* and donors and acceptors on a bound substrate was estimated[679] to be about –4 kJ mol^{-1}. In these experiments, amino acids in the active site were replaced systematically by site-directed mutation, a procedure that involves significant and unpredictable steric effects. Similar results have been reported in other site-directed mutations.[685]

In any case, there seems to be agreement among those who have examined this question in detail that **it is possible for entropy of approximation to be of sufficient magnitude** to overcome the competition by water and provide a small favorable free energy of formation to one or more, but usually not the majority, of the hydrogen bonds in a complex between a ligand and a site on a protein. It should be kept in mind, however, that the entropy of approximation had to be paid for by the hydrophobic effect, so even if formally the formation of the hydrogen bond on the active site were to have a negative standard free energy of formation, a greater amount of negative standard free energy would have to be provided by the hydrophobic effect during the association of the substrate with the active site to accomplish the approximation. There is no doubt that when a donor or an acceptor for a hydrogen bond on a substrate cannot find an acceptor or a donor, respectively, in the active site, the standard free energy of formation between that donor or acceptor and a molecule of water is lost[678] and has to be paid for somehow.

Rather than to provide standard free energy of dissociation, the critical role of the hydrogen bonds that form between a substrate and an active site on an enzyme is to **orient the substrates relative to each other, to orient the substrates relative to the catalytic groups and prosthetic groups that perform the catalysis, and to recognize the substrates and ligands in the first place**. One important way that an enzyme or a protein that binds a particular substrate or ligand recognizes that substrate or that ligand is by providing donors and acceptors for hydrogen bonds positioned in space to complement the acceptors and donors, respectively, on the substrate or the ligand (Figures 3–33, 3–34, 3–36, 3–38, 3–40, and 3–42). One of the more unusual examples of such hydrogen bonding is that between the active site of haloacetate dehalogenase from *R. palustris* and its substrate.[686] This enzyme has a catalytic constant for hydrolyzing fluoroacetate that is 5 times larger than that for chloroacetate even though the bond dissociation energy of a carbon–fluorine bond is 1.35 times that of a carbon–chlorine bond. In the crystallographic molecular model of the

complex between an inactive mutant of the enzyme and fluoroactetate, the fluorine atom of the fluoroacetate is the acceptor for three hydrogen bonds, from Tyrosine 219, Histidine 155, and Tryptophan 156. These hydrogen bonds are all of reasonable length (0.30-0.33 nm), and they position the carbon on which the fluorine resides in the optimal alignment with the carboxylato group on Aspartate 110 that acts as a nucleophile in the nucleophilic substitution of the fluorine for one of the carboxylato oxygens. When chloroacetate occupies the active site, the larger radius of the chlorine atom causes it to fit improperly in this pocket, and it is pushed over, twisting the carbon–chlorine bond out of proper alignment and causing the catalytic constant for chloroacetate to be 5 times smaller than that for fluoroacetate. When the histidine is mutated to an asparagine, increasing the size of the pocket but retaining the donor for a hydrogen bond, the enzyme has a catalytic constant for chloroactetate that is 8 times larger than that for fluoroacetate.

Of even more importance than recognizing the proper substrate, however, is **the requirement that the arrangement of donors and acceptors for hydrogen bonds in the active site not complement the arrangement of acceptors and donors on closely related metabolites** in the cytoplasm or the environment that are not substrates or ligands for the enzyme or the protein. When an incorrect metabolite associates with an active site or a binding site, some of its acceptors and donors lose the donors and acceptors for hydrogen bonds provided by molecules of water when it is in solution and remain vacant while they are on the site, and some of the donors and acceptors in the active site or the binding site also lose the acceptors and donors provided by molecules of water in the empty active site and remain vacant in the complex. For each hydrogen bond lost in the overall solution, there will be an increase in standard free energy. For example, double-stranded uracil-DNA glycosylase from herpes simplex virus type 1 must distinguish a uracil from a cytosine. The active site focuses on the amido oxygen at carbon 4 of the uracil. At carbon 4 of cytosine, there is an amido group rather than an acyl oxygen. The active site provides two amido nitrogen–hydrogens, one from the side chain of an asparagine and the other from the polypeptide backbone, to form hydrogen bonds with the acyl oxygen of uracil.[687] Were cytosine to occupy the same location in the active site, the amido group at carbon 4 would lose its hydrogen bonds to two molecules of water, its amido group would displace the waters providing hydrogen bonds to the two amido nitrogen–hydrogens of the active site, no compensating hydrogen bonds would be formed, and four donors for hydrogen bonds in the overall solution would be vacated. The loss of the hydrogen bonds between these donors and molecules of water provides the positive standard free energy excluding cytosine from the active site, in addition to the steric overlaps of the four hydrogens in the incorrect complex. In this instance, the two donors are from amido groups, the values of pK_a (17) for which prevents them from dehydronating and becoming acceptors.

In the active site of thymidylate synthase from *Lactobacillus casei*, the side chain of an asparagine recognizes the acyl oxygen at position 4 of the 2′-deoxyuridine monophosphate (dUMP) that is its substrate with one of its carbamoyl nitrogen–hydrogens, and it recognizes the amido nitrogen–hydrogen of dUMP with its carbamoyl oxygen (**3–108**)

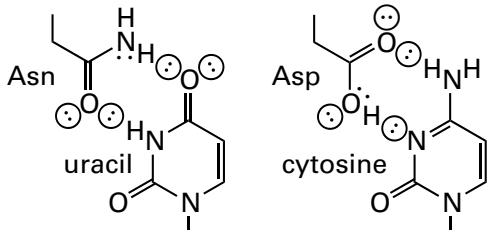

3–108 **3–109**

When the asparagine is mutated to an aspartic acid so that a donor for a hydrogen bond is converted into an acceptor (**3–109**), the mutant enzyme, unlike the wild-type enzyme, is able to methylate 2′-deoxycytidine monophosphate (dCMP) with a catalytic constant 0.06 times that of the catalytic constant for the wild-type enzyme when it is methylating dUMP.[688,689] Mutating the histidine that normally forms a hydrogen bond to the other lone pair of electrons on the acyl oxygen on carbon 4 of dUMP, which would sterically clash with the nitrogen–hydrogen bond on that side of the amido group on dCMP and assist in excluding it from the active site, increased the catalytic constant for the methylation[690] of dCMP by the aspartyl mutant by a further factor of 5.

Asparagine-tRNA ligase must distinguish aspartyl-AMP, the incorrect substrate, from asparaginyl-AMP, the correct substrate. The only difference between them is that an asparaginyl group has two donors and two acceptors for hydrogen bonds on its carbamoyl group, and an aspartyl group has at most only one donor and at least three acceptors in its β-carboxy group. The active site of the enzyme

from *P. horikoshii* provides two acceptors and two donors for hydrogen bonds

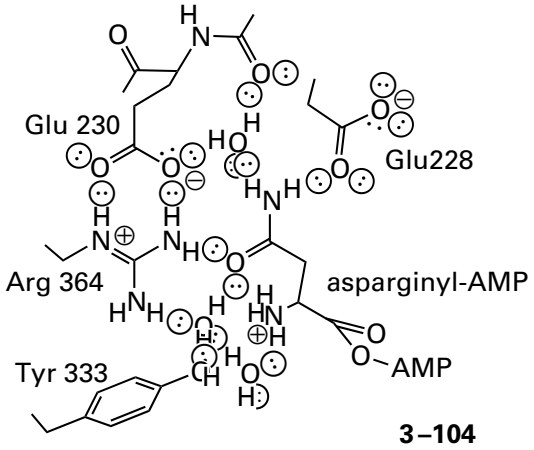

3–104

at the proper locations to complement the carbamoyl group of asparaginyl-AMP.[673] If the aspartyl group in aspartyl-AMP, rather than an asparaginyl-AMP, were to bind as the unhydronated β-carboxylato group, both Glutamate 228 and Glutamate 230 in the active site would have to be hydronated for the four acceptors on the β-carboxylato group to find four donors for hydrogen bonds properly positioned in the site. If, however, the aspartyl group in aspartyl-AMP were to bind as the hydronated β-carboxy group, then only one of the two glutamates in the active site would have to be hydronated for the single donor and the three acceptors for hydrogen bonds on the β-carboxy group to find one acceptor and three donors properly positioned in the site. The sum of the positive standard free energies for one or the other of these two unfavorable states of hydronation permits the enzyme, in part, to distinguish between aspartyl-AMP and asparaginyl-AMP.

A phospho group is usually recognized in an active site by a cuplike structure lined with an array of as many as ten donors for hydrogen bonds positioned to chelate its three nonbridging oxygens.[691] Each of the three formal oxyanions in the phospho group bound in the cup can be coordinated by as many as four donors for hydrogen bonds.[692] Usually there are three donors for hydrogen bonds for two of the oxyanions, and these donors are arranged roughly at three of the vertices of a tetrahedron, with a bond between phosphorus and the oxygen at the fourth vertex (see two of the vanadyl oxygens in Figure 3–43). The third oxyanion participates in only two or even one hydrogen bond.[692] Remarkably, this arrangement is contrary to the orientation of donors to oxyanions of phospho groups in crystallographic structures of small molecules,[693] in which the donors are arranged trigonally around each oxygen.* In the absence of a phospho group, the cup is filled with molecules of water. If any other ligand displaces even one of these waters without providing acceptors for any donors for hydrogen bonds vacated, there is a positive change in standard free energy that excludes that other ligand. The large number of properly positioned donors for hydrogen bonds in the cup are arrayed to fit the acceptors on a phospho group rather than the acceptors on any possible cluster of molecules of water. In the unoccupied state, some of these donors must be vacant, but they become occupied when the phospho group associates. Furthermore, there must be significant entropy of approximation favoring the association of the phospho group because so many properly aligned hydrogen bonds form at once. Consequently, a phospho group associates tightly with this array by extensive chelation and strongly anchors within an active site or a binding site the rest of the substrate or the ligand to which it is attached. The strength of this interaction explains why phosphate or other phosphorylated compounds at high concentration often act as inhibitors of enzymes that catalyze reactions involving phosphorylated substrates and consequently have one of these cups. The strength of these interactions may also be a reason, in addition to the ability of a phospho group to confine the metabolite to the cytoplasm, that phosphorylated substrates have been selected by evolution for most of the reactions in glycolysis.

The crystallographic molecular model of the phosphatase encoded by the BT4131 gene of *B. thetaiotaomicron* (Figure 3–43) introduces the oxyanion hole, one of the frequently encountered features of an active site that can be revealed in a crystallographic molecular model by an analogue of an intermediate of high energy. The three equatorial oxygens of the vanadate are three equatorial oxyanions in the intermediate phosphorane. Two of these three oxygens form hydrogen bonds to the α-amido groups of Isoleucine 9, Aspartate 10, and Glycine 44, the hydroxy group of Threonine 43, the 6-amino group of Lysine 188, and the γ-amido group of Asparagine 214. These six donors for hydrogen bonds stabilize the single negative elementary charges on the two oxyanions and consequently the phosphorane itself. It is remarkable that the donors are arranged

*In some of these cups, there are trigonal arrays of donors around one of the oxygens.[694] Either arrangement is consistent with the requirement that the molecular orbitals of the phospho group have its overall symmetry.

tetrahedrally* around each oxygen, as the three lone pairs of electrons on each of them would be if they actually are hybridized sp^3.

An **oxyanion hole is an arrangement of donors for hydrogen bonds that associates with an oxyanion in a substrate or intermediate** in an enzymatic reaction, but usually it stabilizes an oxyanion in an intermediate.[412] In addition to stabilizing oxyanions in a phosphorane, an intermediate of high energy, oxyanion holes are usually found in enzymes that hydrolyze peptide bonds through oxyanionic tetrahedral intermediates (Figures 1–10B and 3–6). The single oxyanion holes in subtilisin,[412] chymotrypsin,[695] streptogrisin A (Figure 3–32),[544] carboxypeptidase D from *Triticum aestivum*,[696] and bovine thrombin,[697] which in each enzyme is formed from two **α-amido groups of the polypeptide backbone**, can be identified in crystallographic molecular models of the complexes between the enzymes and the respective analogues for the tetrahedral intermediates.[412] Each analogue places an oxygen at the position of the oxyanion in the actual intermediate (Figure 3–32). In many of these structures, one of the two donors for hydrogen bonds is part of a stable six-membered ring that incorporates a nucleophilic serine and the tetrahedral intermediate (Figure 3–32).†

There are a number of other active sites that catalyze reactions other than a nucleophilic substitution at phosphorus or the hydrolysis of a peptide bond and yet use two α-amido groups from the polypeptide to form an oxyanion hole. For example, β-lactamase from *Enterobacter cloacae* hydrolyzes an amide through an oxyanionic tetrahedral intermediate,[698] and acetylcholinesterase from *T. californica* hydrolyzes an ester through an oxyanionic tetrahedral intermediate,[227] and the active site in each enzyme has an oxyanion hole formed from two α-amido groups from the polypeptide. β-Ketoacyl-[acyl-carrier-protein] synthase III from *M. tuberculosis* transfers an acyl group from the sulfanyl group of coenzyme A to the sulfanyl group of a cysteine in the protein and then transfers the acyl group from the cysteine to the enolate of acetyl-SCoA (previously Equation 1–118)

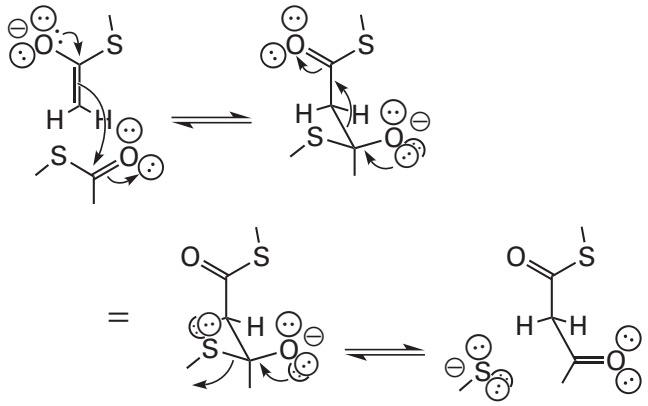

(3–409)

that is formed by the decarboxylation of malonyl-SCoA. Each of the two nucleophilic substitutions transferring the acyl group from the respective sulfanyl group proceeds through a tetrahedral intermediate at the acyl carbon, and the oxyanion of this tetrahedral intermediate is accommodated in an oxyanion hole formed by two α-amido groups from the polypeptide.[621] In the nucleophilic aromatic substitution catalyzed by 4-chlorobenzoyl-CoA dehalogenase from *Pseudomonas*, the oxyanion of the usual intermediate

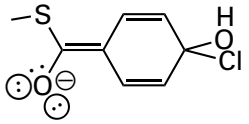

3–110

in such a substitution in a thiobenzoate sits in an oxyanion hole formed from two α-amido groups from the polypeptide.[699]

There are other oxyanion holes, however, that are **not formed from two α-amido groups**. In the active site of aspartate carbamoyltransferase (Figure 3–40), the oxyanion hole for the tetrahedral intermediate at the carbamoyl carbon is formed by the hydroxy group of a threonine, the guanidinio group of an arginine, and the hydronated imidazolyl group of a histidine. In the active site of thermolysin (Figure 3–42), the oxyanion hole for the tetrahedral intermediate is formed by the carboxy group of a glutamic acid and a molecule of water. In acetyl-CoA *C*-acetyltransferase from *Zoogloea ramigera*, which catalyzes almost the same reaction as that catalyzed by β-ketoacyl-[acyl-carrier-protein] synthase III (Equation 3–409), one of the oxyanion holes is formed instead by the imidazolio group of a histidine and a molecule of water.[700]

In the active site of acetyl-CoA *C*-acetyltransferase from *Z. ramigera* there are **two oxyanion holes**. The

*It is also the case, however, that a tetrahedral arrangment minimizes the steric interactions among the donors of the hydrogen bonds.

†The six-membered ring in Figure 3–32 is formed by the amido nitrogen of Serine 195, its α and β carbons, its γ oxygen, the carbon of the hemiacetal (ha), and the oxygen of the hemiacetal that forms the hydrogen bond with the amido nitrogen of Serine 195.

enzyme performs a Claisen condensation (Equation 3–409) in which the enolate of an acetyl group on a cysteine in the active site is condensed with an acyl-SCoA. The oxyanion hole for the oxyanion of the enolate is provided by the fixed molecule of water and the imidazolio group of a histidine, and the oxyanion hole for the oxyanion in the tetrahedral intermediate in the nucleophilic substitution is provided by two amido nitrogen–hydrogen bonds from the backbone of the polypeptide.[701]

When amino acids that provide donors for hydrogen bonds in oxyanion holes are mutated, the rate constants for the enzymatic reaction usually decrease.[702] For example, in the active site of carboxypeptidase A from *R. norvegicus*, which hydrolyzes a peptide bond through an oxyanionic tetrahedral intermediate, the *ω*-guanidinio group of Arginine 127 and a Zn^{2+} form the oxyanion hole.[703] When Arginine 127 is mutated to a methionine, the specificity constant of the enzyme for its substrate decreases by a factor of 9000.[704]

It has been pointed out that when a reaction that is catalyzed by an enzyme in which an oxyanion is formed as an intermediate occurs in aqueous solution, water invariably provides donors for the oxyanion. That water is required to provide these donors can be inferred from the fact[705] that when the catalytic base that removes the hydron during the enolization of acetone is bulky enough to bump off one of the molecules of water solvating the carbonyl oxygen that becomes the oxyanion of the enolate, the rate of enolization decreases by a factor of 10. Consequently, if the reaction is brought into an active site, the active site has to provide the donors for hydrogen bonds that water provides outside or it will actually decrease the rate of the reaction. Nevertheless, there may be advantages to providing **fixed donors for hydrogen bonds in the proper orientation**. In most of the situations in which an oxyanion forms during the enzymatic reaction, the oxygen begins as a trigonal acyl or carbonyl oxygen on a trigonal carbon and becomes a tetrahedral oxyanion on a tetrahedral carbon as the intermediate forms. This rehybridization usually perfects the fit of the oxygen within the oxyanion hole. To the extent that the hydrogen bonds in the occupied oxyanion hole come into existence or become more stable during this rehybridization, the increase in standard free energy of formation they experience must **lower the standard free energy of activation for the reaction**. When amino acids around the oxyanion hole in steroid Δ-isomerase from *P. putida* were mutated so that there was enough room in the active site for disorganized molecules of water to solvate the oxyanion rather than the fixed donors for hydrogen bonds provided normally by the enzyme,[706] the rate of the reaction decreased by a factor of 1000. Consequently, the hydrogen bonds achieved by the donors from the active site in an occupied oxyanion hole may be examples of hydrogen bonds that, during their formation or their increase in stability as the transition state is achieved, lower the standard free energy of activation of the reaction catalyzed by the enzyme.

The role of ionic interactions in the formation of complexes between substrates and active sites is difficult to assess. In part, this difficulty results from the fact that water solvates elementary charges so effectively. The change in standard enthalpy when two opposite elementary charges that were in free solution are juxtaposed in an active site during the association of a substrate is probably always positive because this solvation is lost in the process.[707] This endergonic change is the reason that ion pairs are usually unstable relative to the separated, independent ions in aqueous solution, and it forms the basis for the ionic theory of solution.

The main reason it is difficult to evaluate the importance of ionic interactions is that there are almost never fixed elementary charges in biochemical metabolites. The **charged molecules in biochemistry are almost always cationic acids or anionic bases** that can be neutralized in acid–base reactions and that have multiple donors and acceptors for hydrogen bonds. It is difficult to distinguish a hydrogen bond between a donor and an acceptor that just happen to be oppositely charged from an interaction due solely to ionic attraction. An example of this difficulty is the **charged hydrogen bonds** in the crystallographic molecular models of the adducts between the prosthetic pyridoxal phosphate and either aspartate or glutamate in the active site of aspartate transaminase (previously Equation 2–29)

$$\text{L-aspartate} + \text{2-oxoglutarate} \rightleftharpoons \text{oxaloacetate} + \text{L-glutamate} \qquad (3\text{–}410)$$

from *G. gallus*.[708,709] Each pair of charged hydrogen bonds between a guanidinio group and a carboxylato group is canonical

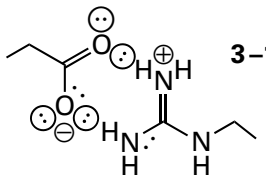

Are these hydrogen bonds or ionic interactions? When a fatty acid is bound to intestinal fatty acid binding protein from *R. norvegicus*, its carboxylato group forms two hydrogen bonds to two guanidinio nitrogen–hydrogens of an arginine side chain, but the geometry of the hydrogen bonding in the crystallographic molecular model seems more important than the balance of elementary charges.[710]

In the one instance that had always been presented as a purely ionic interaction,[711] that between the trimethylammonio group in acetylcholine and acetylcholinesterase, it has now been concluded that the noncovalent interaction that causes the quaternary ammonium to associate with the active site arises from the hydrophobic effect as well as electric forces (cation–π interactions) between the π molecular orbital system of uncharged aromatic side chains and the fixed cation.[226,229] A similar combination of the hydrophobic effect and cation–π interactions with two phenylalanines is involved in recognizing the sulfonium ion of *S*-adenosyl-L-methionine in the active site of human adenosylmethionine decarboxylase.[712] In this instance, the positively charged sulfur atom is covalently surrounded in the *S*-adenosyl-L-methionine itself by a methyl group, the β- and γ-methylenes of the L-methionine, and the methylene of carbon 5 of the ribosyl group, all of which insulate it. Contrariwise, in the case of the SH2 domain of the non-specific protein-tyrosine kinase from avian leukosis virus RSA, the phenyl ring of the phospho-L-tyrosine that is a ligand for the binding site in this domain is sandwiched between the guanidinio nitrogen of an arginine and the 6-ammonio group of a lysine in the crystallographic molecular model in what also appear to be cation–π interactions rather than ionic interactions.[713]

In the instance of the positively charged guanidinio group of an arginine involved in binding or catalysis, it has been proposed that ionic interactions can be dissected from hydrogen bonding by **mutating an arginine to a citrulline**. For example, in the crystallographic molecular model of the complex between the active site of chorismate mutase (Equation 3–402) from *B. subtilis* and analogue **3–84** for the transition state in the electrocyclic rearrangement catalyzed by the enzyme, one of the ω-amido nitrogen–hydrogens in the positively charged guanidinio group of Arginine 90 engages in a hydrogen bond with the ether oxygen of the analogue. This oxygen in the analogue is the homologue of the ether oxygen in chorismate that becomes the carbonyl of the prephenate.[365] When Arginine 90 is mutated to a citrulline, in effect replacing one of the ω-amido groups with a carbonyl oxygen as well as eliminating the single positive elementary charge that was on the guanidinio group of the arginine, the specificity constant for chorismate decreases by a factor of 20,000. This observation was presented as evidence that the positive elementary charge on the guanidinio group in the unmutated active site stabilizes the actual transition state in the reaction.[714] This conclusion was consistent with the fact that only mutants of the enzyme that have the guanidinio group of an arginine or the ammonio group of a lysine in the immediate vicinity of the ether oxygen in chorismate are enzymatically active.[715] In another instance, where the substitution of each of the two arginines in an active site with citrullines has been performed, there is no crystallographic evidence of the disposition of these arginines in a complex between the active site and either a substrate or an analogue, so it is difficult to evaluate the decreases of greater than 5000 in the catalytic constant that are observed when both arginines are mutated to citrullines. Nevertheless, the decrease was attributed to the loss of the positive elementary charges.[716]

During the substitution of citrulline for arginine, in addition to elimination of the charge, two nitrogen–hydrogens on an amido group are converted to two lone pairs of electrons; as a result, two donors for hydrogen bonds are converted to two acceptors. There are at least two problems with this substitution. First, the ω-carbamoyl nitrogen of the arginine in the unmutated active site that does not form the hydrogen bonds to the substrate that are the focus of attention may not actually end up in the occupied active site as the ureido oxygen of the citrulline, as is desired. If it does not, then the ω-carbamoyl nitrogen that does provide the hydrogen bond will be replaced by the ureido oxygen that cannot provide a hydrogen bond but would direct a lone pair of electrons at the lone pair of electrons in the acceptor of the substrate. For example, in the particular case of chorismate mutase, in the complex between the active site and the analogue of the transition state, the nitrogen atom of the other ω-amido group of the arginine that does not form the hydrogen bond with the oxygen of the substrate is sandwiched

between one of the carboxylato oxygens of Glutamate 78 (0.32 nm), and the sulfanyl group of Cysteine 88 (0.32 nm).[365] It is entirely possible that this intimate interaction is exclusive for a carbamoyl group and that in the mutated enzyme the acyl oxygen, rather than being sandwiched between these two atoms as is desired, is directed toward the oxygen of the substrate, which would certainly disrupt the reaction. Second, in most instances the amido group that does not form a hydrogen bond with the substrate engages with other side chains in the active site, and the mutation must interfere with these interactions, disrupting the alignment of the ureido group of the citrulline. This interference could well explain much if not all of the decrease in a specificity constant.

Most substrates of enzymatic reactions or ligands for binding proteins bear elementary charges at neutral pH and probably enter an active site or a binding site as charged molecules. In crystallographic molecular models of the resulting complexes, however, there is no obvious pattern in which each formal elementary charge on the substrate or ligand is exactly balanced by an amino acid bearing the opposite elementary charge in the site. Rather, the **distributions of elementary charges over occupied active sites or binding sites are far more disorganized and unpredictable** (Figures 3–33, 3–34, 3–40, 3–42, and 3–45). An example of an active site in which no cationic amino acid is located adjacent to a negative elementary charge on a substrate is found with tryptophan synthase. In the crystallographic molecular model of the active site of the enzyme from *S. typhimurium* occupied by the competitive inhibitor propane phosphate, the negatively charged phosphate is surrounded only by uncharged donors and acceptors for hydrogen bonds.[717] In the case of the phospho group of deoxyuridine phosphate, however, when it is bound in the active site of thymidylate synthase from *L. casei*, there are four arginines forming hydrogen bonds with its oxygens, so its maximum of two negative elementary charges is surrounded by four positive elementary charges.[718] The orientation by the active site of the seven donors for these hydrogen bonds creates the cup into which the three nonbridging oxygens of the phospho group fit perfectly.

There is another example of a complex of a positively charged substrate with a negatively charged amino acid in an active site that has been cited as a simple ionic interaction. Trypsin is an endopeptidase that cleaves peptide bonds (Figure 3–6) to the carboxy-terminal side of lysines and arginines exclusively. The enzyme was thought to be confined to cleave at these locations because, in the region of its active site where the side chain of the amino acid to the amino-terminal side of the susceptible bond is bound, there is a strategically placed aspartate,[719] Aspartate 171 in bovine α-trypsin, that would provide a compensating elementary charge. Before refined crystallographic molecular models (Figure 3–46)[720] of complexes between inhibitors and bovine trypsinogen, the precursor of bovine trypsin, were available, the interaction between trypsin and the lysines or arginines on its reactants was thought to be ionic. It turns out, however, that at least in this instance, it is **difficult if not impossible to distinguish the importance of hydrogen bonding from the importance of ionic interaction.**

In crystallographic models of complexes between trypsinogen and small inhibitory proteins in which either lysine or arginine in the respective protein occupies the pocket for the targeted amino acid in the reaction catalyzed by the enzyme, it is clear that either the lysine or the arginine, in turn, participates in a complex network of hydrogen bonds rather than participating only in an ionic interaction. This observation is remarkable because the arrangement of the donors for hydrogen bonds in lysine and the donors for hydrogen bonds in arginine are so different. Nevertheless, acceptors for hydrogen bonds are arranged within the binding site with great precision so as to accommodate either side chain. When lysine is bound, the three tetrahedrally arrayed donors on its ammonio group find three tetrahedrally arrayed acceptors for hydrogen bonds: Water 416, Water 414, and the peptidic acyl oxygen of Serine 172 within the polypeptide (Figure 3–46). The carboxy group of Aspartate 171 is not directly bound to lysine because its side chain is too short, but it forms a hydrogen bond to one of the actual ligands, Water 414. Arginine, however, is longer, by one atom, than lysine, and arginine forms a canonical bis-hydrogen bond (**3–111**) with Aspartate 171 directly. The other three donors of the planar guanidinio group in the arginine form hydrogen bonds with the acyl oxygen of Glycine 196, Water 416, and Water 403. Only one of these five acceptors for hydrogen bonds, Water 416, is also used in the complex with lysine. When arginine is bound, Water 414 is displaced and the acceptor for a hydrogen bond on the acyl oxygen of Serine 172 is vacant. When lysine is bound, the acceptor on Water 403 and the lone pair on Aspartate 171 are vacant.

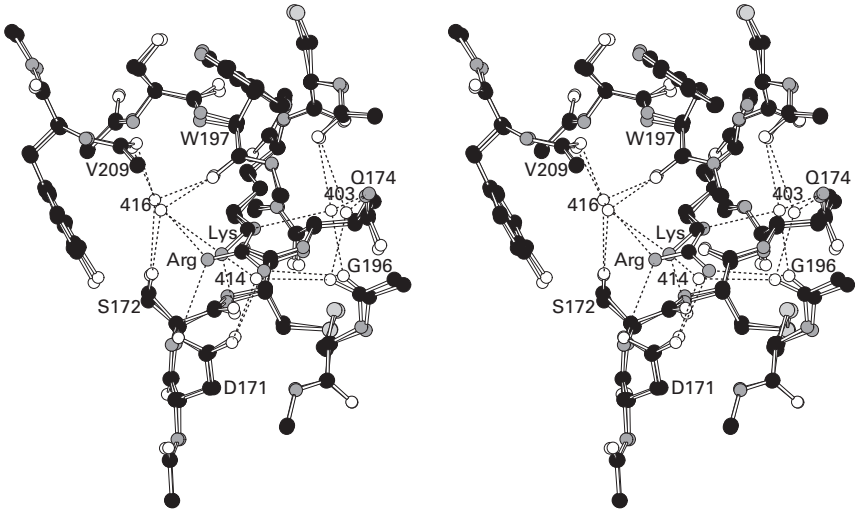

Figure 3–46: Superposed stereodrawings[576] of crystallographic molecular models of the binding of either lysine or arginine to the portion of the active site of trypsin, the specificity pocket, that determines its specificity for lysines and arginines.[720] Black atoms are carbons, white atoms are oxygens, small gray atoms are nitrogens, and large light gray atoms are sulfurs. The two crystallographic molecular models are superposed to show that the same conformation of the specificity pocket accommodates both side chains and that the side chains themselves superpose closely at each of their common atoms. The two crystallographic molecular models from which these regions come are those of the complex between native bovine pancreatic trypsin inhibitor (58 aa) and bovine trypsinogen, the precursor to bovine trypsin, in which a Lysine 15 of the inhibitor occupies the specificity pocket, and the complex between bovine trypsinogen and bovine pancreatic trypsin inhibitor, in which Lysine 15 has been replaced with an arginine. In the models, the side chain of the lysine occupies exactly the same location as that of arginine, with the 6-amino group of the lysine occupying the location of the guanidino carbon of the arginine. Water 414, Water 416, and the acyl oxygen of Serine 172 form a triangular array of hydrogen-bond acceptors for the three donors on the lysine. Aspartate 171, Water 403, Water 416, and the acyl oxygen of Glycine 196 form a planar array of hydrogen-bond acceptors for the five donors on the arginine.

In these two instances, the vacant acceptors in a given complex that are used to bind the other reactant in the other complex are enthalpically inconsequential in the wild. It is noteworthy, however, that every donor for a hydrogen bond on the respective side chain ends up in a hydrogen bond when it is bound at the active site.

The complexity of the hydrogen bonding in this subsite within the active site of trypsin when it is associating with a lysyl or an arginyl side chain in a substrate clearly reveals the naiveté of the expectation that changing Aspartate 171 to lysine would reverse the specificity of trypsin from peptide bonds carboxy-terminal to lysines and arginines to peptide bonds carboxy-terminal to aspartates and glutamates.[721] In the case of the active site of aspartate transaminase from *E. coli*, however, L-aspartate, the exclusive substrate for the enzyme, seems to be recognized mainly by the canonical pair of hydrogen bonds (**3–111**) between its γ-carboxylato group and Arginine 292. Mutating Arginine 292 to an aspartate did reverse the specificity of the transaminase from L-aspartate (7×10^5) in the native enzyme to L-arginine (7) in the mutant, but the specificity constant of the mutant for L-arginine was only 2×10^{-5} that of the wild type for L-aspartate.[722] The specificity was reversed, but the activity of the mutant for L-arginine was minuscule. Similar changes in specificity and activity were observed when an attempt was made to change the specificity of trypsin from *R. norvegicus* from hydrolyzing peptide bonds carboxy-terminal to arginines and lysines to the preference shown by the related enzyme chymotrypsin (38% identity; 2.8 gap percent) for aromatic side chains by mutating Aspartate 171 to the serine found at that location in chymotrypsin.[723]

The manifestation of the hydrophobic effect in a crystallographic molecular model is less apparent than the hydrogen bonds and ionic interactions. Nevertheless, because it is directly proportional to the number of hydrogen–carbon bonds removed from contact with the solution,[52] the magnitude of the hydrophobic effect affiliated with the association of ligand with an active site can be estimated by counting up the number of hydrogen–carbon bonds that are exposed to the solution in the unbound substrates, in the unbound coenzymes, and in the empty active site itself in the crystallographic molecular model of the unoccupied enzyme and then counting up the number of those same hydrogen–carbon bonds that remain in contact with the solution in the crystallographic molecular model of the fully occupied active site. The difference between these two tallies is an indication of the strength of the hydrophobic effect elicited by the association.

A crystallographic molecular model, however, leaves one with the false impression that where a particular hydrogen–carbon bond ends up once a substrate associates with an active site is somehow consequential to the hydrophobic effect. The only significant contribution to the hydrophobic effect is the behavior of the water that occurs after the hydrogen–carbon bond leaves. No interaction that occurs between that hydrogen–carbon bond and the environment that surrounds it in the active site is of importance.[352] It follows that observing the situation of a particular hydrogen–carbon bond within the active site provides no information about the magnitude of the hydrophobic effect in which it has participated.

Hydrogen–carbon bonds that have been removed from contact with water are always observed in a crystallographic molecular model of a substrate or a ligand bound in an active site or a binding site, and hydrogen–carbon bonds on functional groups from the active site that have been removed from contact with water upon the association of a substrate or a ligand are also always observed. For example, the hydrogen–carbon bonds of the three methylenes, of the ribosyl group, and of the adenine ring are all removed from contact with water upon formation of the complex between the active site of guanidinoacetate *N*-methyltransferase and *S*-adenosyl-L-homocysteine (Figure 3–34). In the crystallographic molecular model of the complex between porcine L-lactate dehydrogenase (Equation 3–27) and NAD^+, the planar π system of the adenine ring of NAD^+ is sandwiched between an alanine, an isoleucine, a valine, and a glycine on one side and two valines and a leucine on the other,[591] and the hydrogen–carbon bonds on these side chains that sandwich the adenine ring are removed from contact with water after intimately contacting the π molecular orbital system of the adenine upon formation of the complex.

In the case of side chains in the active site, the situation is somewhat ambiguous. The hydrophobic effect is the negative standard free energy change that occurs when a hydrogen–carbon bond is removed from bulk water. Because of the coordinated behavior of molecules of water in bulk, the magnitude of the hydrophobic effect may well depend on the behavior of the molecules of water beyond those immediately in contact with the hydrogen–carbon bond. In the active site of an enzyme, the hydrogen–carbon

side chains of the amino acids that are in contact with water before a substrate binds are usually in contact with molecules of water that are more or less isolated from the bulk phase, so the hydrophobic effect arising from their dehydration may be significantly less than the hydrophobic effect of removing a hydrogen–carbon bond from the bulk solution.

In most instances, the hydrophobic side chains in an unoccupied active site are surrounded by molecules of water because there is usually little vacant space in a condensed phase. In maps of electron density for the unoccupied active site of thermolysin from *B. thermoproteolyticus*, when those maps are calibrated to absolute electron density, there is no detectable electron density in the hydrophobic pocket formed from Phenylalanine 130, Leucine 133, Valine 139, Isoleucine 188, Valine 192, Leucine 202, and the π faces of the amides in the polypeptide backbone between positions 138 and 140, 188 and 189, and 112 and 113. This pocket is occupied by the leucine adjacent to the site of hydrolysis in the crystallographic molecular model in Figure 3–42. Consequently, there is no water adjacent to the hydrophobic side chains that form this empty hole in the unoccupied active site, and the situation is not complicated by the ambiguity accompanying the dehydration of those side chains. A series of otherwise identical phosphonamidates (see **3–71** in Table 3–7), which are analogues of the tetrahedral intermediate in the enzymatic reaction, were synthesized that place a methyl group, an isopropyl group, or an isobutyl group in this vacant subsite, and their free energies of association were measured.[724] The free energies of association for these three inhibitors decrease with a slope of -2.35 ± 0.03 kJ (mol of hydrogen–carbon bonds)$^{-1}$. This value is quite close to the value of -1.9 ± 0.2 kJ (mol of hydrogen–carbon bonds)$^{-1}$ that is the standard free energy for the removal of a hydrogen–carbon bond from water into a condensed phase of alkane based on units of molarity.[52] The small difference in the two values may result from the fact that during transfer between two isotropic condensed phases, which is the standard measure of the hydrophobic effect, a hole has to be made in the nonpolar phase, a process with a positive change in standard free energy. In the case of inhibitors associating with the active site of thermolysin, however, the hole is already there. In any case, this result for the association of these inhibitors with thermolysin is a rather unambiguous demonstration of the favorable standard free energy that is gained from the hydrophobic effect during the removal of hydrogen–carbon bonds from contact with water when a substrate enters the active site of an enzyme.

Although this fact is seldom emphasized, as is the case for the four hydrogens in the ring of the ribosyl group in *S*-adenosyl-L-homocysteine, **monosaccharides have two hydrophobic axial surfaces** opposite each other on the ring, each containing two to five hydrogen–carbon bonds.[725] For example, cyclodextrins, which are cyclic, cylindrical rings of D-glucosyl groups, have structures that turn an axial face of each monosaccharide, in which there are two hydrogen–carbon bonds, toward the axis of the cylinder, and together they form a significantly hydrophobic pocket.

In the refined crystallographic molecular model of the complex between β-D-galactose and the D-glucose/D-galactose-binding protein from *E. coli*, the β-pyranose of β-D-galactose is flush against the π molecular orbital system of a tryptophan on its axial face containing five hydrogen–carbon bonds, and one of the two hydrogen–carbon bonds on its other axial face is flush against the π molecular orbital system of a phenylalanine (Figure 3–45). The monosaccharide bound in the B subsite in lysozyme has one of its axial faces, containing three hydrogen–carbon bonds, flush against the π molecular orbital system of Tryptophan 62.[314] In the crystallographic molecular model of the complex between chitinase from *Ostrinia furnacalis* and the two products of the hydrolysis of $[(\beta 1,4)$-*N*-acetyl-D-glucosamine$]_7$, four of the five *N*-acetylglucosaminyl groups encompassing the site of hydrolysis each have one of their hydrophobic faces flush against the indolyl group of a tryptophan.[726,727] In the crystallographic molecular model of the complex between the maltodextrin-binding protein from *E. coli* and maltose, one of the glucosyl groups in the maltose is sandwiched between the π molecular orbital systems of a tyrosine and a tryptophan on one axial face and the π molecular orbital system of another tryptophan on the other axial face, and the other glucosyl group of the maltose is sandwiched between the edge of the indolyl group of a tryptophan on one side and the π molecular orbital system of another tryptophan on the other side.[728] In each instance, all the hydrogen–carbon bonds on the axial surfaces of the monosaccharides are removed from contact with the solution when the respective complex is formed. The π molecular orbital systems in these instances provide convenient flat surfaces to cover up the hydrogen–carbon bonds without also sequestering donors for hydrogen bonds in the process.

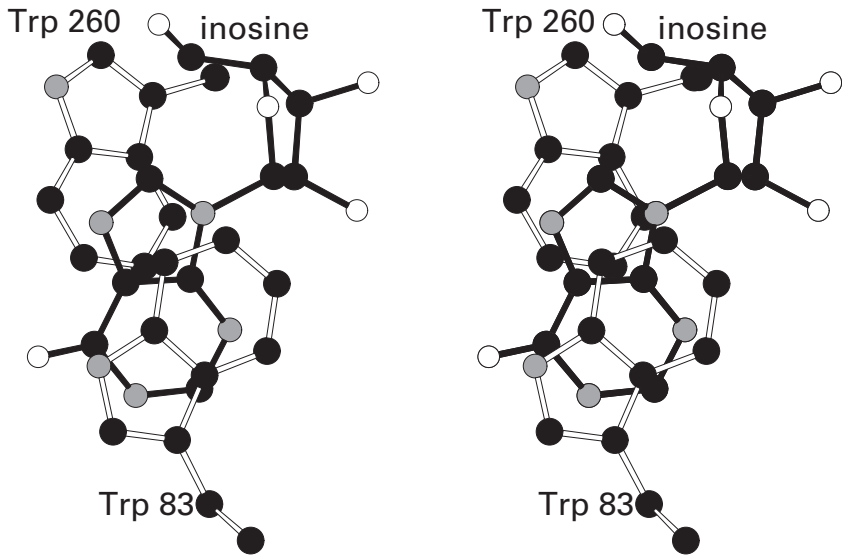

Figure 3–47: Stereodrawing[576] of hypoxanthine sandwiched between two tryptophans in the crystallographic molecular model of the complex between the active site of a mutant of purine nucleosidase from *T. vivax* and inosine, a substrate for the enzyme.[729] Black atoms are carbons, white atoms are oxygens, and gray atoms are nitrogens. To produce the mutant, Aspartate 10 in the active site was mutated to an alanine. The mutant enzyme is virtually inactive, which allowed a data set to be gathered before the inosine in the active site was hydrolyzed. Crystals of the mutant enzyme were soaked in a solution containing 50 mM inosine at pH 7.5 for 3 min and then frozen. A data set was gathered from the frozen crystals to Bragg spacing of 0.16 nm. The refinement of the crystallographic molecular model was initiated by using the amplitudes of the reflections in this data set and a data set of phases calculated from a crystallographic molecular model of the native enzyme in a complex with the inhibitor 3-deazaadenosine, from which all ligands, in particular the 3-deazaadenosine, and molecules of water had been removed. The crystal from which this initial crystallographic molecular model was solved was isomorphous with the crystal of the mutant in complex with the normal substrate, inosine. As the refinement progressed, electron density consistent with a molecule of inosine appeared in maps of electron density in the same location at which 3-deazaadenosine was found in the initial crystallographic molecular model. The drawing contains only the molecule of inosine that was inserted into this electron density and the side chains of the two tryptophans between which the inosine is sandwiched.

Because of the high frequency with which hydrophobic amino acids and the hydrophobic portions of hydrophilic amino acids line the surfaces of enzymatic active sites in crystallographic molecular models, **a significant hydrophobic effect must be involved in the association of any ligand**, other than an inorganic ion, with the active site of an enzyme.

There are many examples of **π molecular orbital systems within substrates and ligands for enzymes and proteins ending up sandwiched between π molecular orbital systems or stacked upon π molecular orbital systems of amino acids** forming the sites for those substrates and ligands. For example, in the crystallographic molecular model of the complex between a mutant of purine nucleosidase from *Trypanosoma vivax* and inosine, the hypoxanthine ring is sandwiched between two tryptophans (Figure 3–47).[729,730] In the complex between dihydrolipoyllysine-residue acetyltransferase from *Azotobacter vinelandii* and its substrate coenzyme A, however, the π molecular orbital system of the adenine ring is stacked upon the π molecular orbital system of the peptide bond between Glycine 561 and Histidine 562.[731] Because surfaces created by π molecular orbital systems do not display a hydrophobic effect when they are removed from water,[52] if such stacking is energetically advantageous rather than simply sterically advantageous, it must involve favorable van der Waals forces arising from the polarizability of the π molecular orbital systems.[732]

In the case of the complex between purine nucleosidase from *T. vivax* and inosine (Figure 3–47), it has been argued that the stacking of the two tryptophans above and below the inosine serves the purpose of raising the pK_a of the hydron on nitrogen 7 in the imidazolio group of the conjugate acid of the hypoxanthine and consequently promoting its hydronation during the enzymatic reaction. This hydronation would increases the capacity of the hypoxanthine to be a leaving group in the reaction.[730] If this is the case, in this instance the stacking has a **catalytic purpose** beyond possibly providing standard free energy of association.

In the crystallographic molecular model of a complex between an enzyme and its substrates or inhibitors, distortions of a reactant by the active site in the direction of the transition state (Figure 3–28) can often be observed.[733] For example, in the crystallographic molecular model of the complex between creatinase from *P. putida* and its substrate creatine, the planar guanidinio group of the creatine has been twisted by the active site so that the lone pair of electrons on the nitrogen that is the leaving group in the reaction

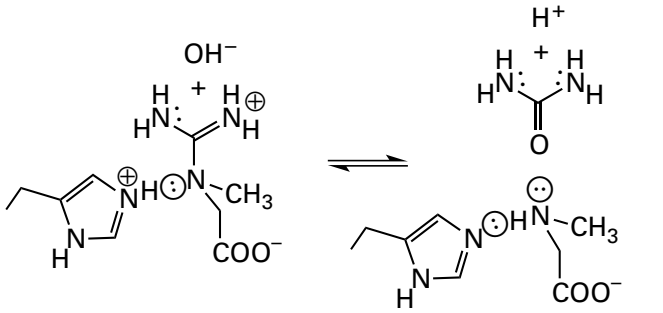

(3–411)

is almost orthogonal to and no longer conjugated to the amidino π molecular orbital system. Because it is now a basic σ lone pair of electrons rather than a delocalized π lone pair of electrons, it can be readily hydronated by an adjacent imidazolium from a histidine to enhance its ability to leave.[734] In the crystallographic molecular model of the complex between 3-deoxy-7-phosphoheptulonate synthase from *E. coli* and the substrate phospho*enol*pyruvate, the normally coplanar phospho*enol* group is twisted by the active site 30° with respect to the plane of the carboxylato group to prevent conjugation between the intermediate enolate and the carboxylato group, which would destabilize the enolate.[735] Although many of the distortions such as these are assisted by the appropriate orientation of donors and acceptors so that they complement acceptors and donors for hydrogen bonds in the distorted conformation of the reactant, the major force accomplishing such a distortion is often a steric effect.

Far and away the most reliable way to control a chemical reaction is to use a steric effect, and this fact has not been overlooked in the evolution of active sites. A steric effect is accomplished when a portion of the structure of the protein in the active site occupies the same location that some portion of the reactant in its most stable conformation would occupy when it associates with the site, and the conformation of the reactant must change to accommodate the obstacle.

There are five similar enzymes that bind to double-helical DNA substrates: DNA (cytosine-5-)-methyltransferase from *H. parahaemolyticus*,[654,655] human thymine-DNA glycosylase,[736] human uracil-DNA glycosylase,[737,738] human methylated-DNA—[protein]-cysteine *S*-methyltransferase,[739] and human DNA-(apurinic or apyrimidinic site) lyase.[740,741] In

each crystallographic molecular model of the complexes between these enzymes and their double-helical DNA substrates,* a base—cytosine, thymine, uracil, *O*-alkylguanine, or 8-oxo-7,8-dihydroguanine, respectively—has swung out of the stack of base pairs into the catalytic region of the active site. The positions in the double-helical DNA that were occupied by each of the flipped bases are now occupied by one or two amino acid side chains from the active site—glutamine and serine, arginine, leucine, arginine, and asparagine and arginine, respectively.

There are two ways to interpret these observations. As the double-helical DNA associates with the active site, the amino acid side chains are unavoidable obstacles in part responsible for pushing the flipped bases out of the double helix. Alternatively, as the bases flip out of the double helix by simple thermal agitation, the amino acid side chains swing into the slot vacated by the respective base and sterically prevent the substrate from leaving the active site and the base pair from reentering the double helix. The actual sequence of events is probably some combination of these scenarios.

Steric effects are also the most **dependable way to exclude the incorrect reactant** from the active site of an enzyme. For example, editing is the process by which a tRNA that has been aminoacylated by an incorrect amino acid is recognized and the incorrect amino acid is removed by hydrolysis.[742] Editing ensures that no misacylated tRNA arrives at a ribosome. When site-directed mutations are made in the active site for hydrolyzing misacylated L-valyl-tRNA^{Ile} in isoleucine-tRNA ligase from *E. coli*, the rate of hydrolysis of L-valyl-tRNA^{Ile} decreases dramatically and the amount of L-valyl-tRNA^{Ile} produced by the enzyme increases dramatically.[743] The nonpolar pocket in the active site for editing in isoleucine-tRNA ligase from *Thermus thermophilus*, which recognizes a misacylated L-valine so it can be excised, is just large enough for the isopropyl group of the L-valine but too small for the 2-butyl group of a correctly acylated L-isoleucine.[744] The 2-butyl group, and hence the properly acylated L-isoleucyl-tRNA^{Ile}, is successfully excluded from the active site responsible for editing and not subject to the hydrolysis performed by this site. In many of the tRNA ligases, the most reliable way to ensure that the correct amino acid is aminoacylated to a tRNA is to use steric effects. Amino acids larger than the correct one, such as L-methionine in the case of isoleucine-tRNA ligase, are excluded from the site for aminoacylation by steric effects; amino acids smaller than the correct one, such as L-valine, are removed by hydrolysis at the site for editing; and the correct amino acid is excluded from the site for editing by steric effects.

DNA-Directed DNA polymerase from *Escherichia* phage RB69 shows a greater than 10,000-fold preference for 2′-deoxyribonucleoside triphosphates over ribonucleoside triphosphates. In the crystallographic molecular model of the active site of the enzyme occupied by a template and magnesium 2′-deoxycytidine triphosphate, the π system on one surface of the 4-hydroxyphenyl group of Tyrosine 216 is flush against carbon 2′, the deoxy carbon.[674] If there were a hydroxy group on carbon 2′, as there is in cytidine triphosphate, it would overlap the 4-hydroxyphenyl ring of the tyrosine. The dissociation constant for magnesium cytidine triphosphate from the active site decreases from 16 to 0.52 mM and the catalytic constant for its incorporation into DNA increases from 0.74 to 8.6 s^{-1} when this tyrosine is mutated to an alanine. In contrast, the dissociation constant for the normal substrate, magnesium 2′-deoxycytidine triphosphate, from the active site remains 0.07 mM and the catalytic constant for its incorporation into DNA decreases from 200 to 22 s^{-1}. These two facts are consistent with the conclusion that the 4-hydroxyphenyl ring provides a steric effect that excludes ribonucleoside triphosphates from the active site.[745]

In the crystallographic molecular model of a complex between proline dehydrogenase from *E. coli* and tetrahydrofuran-2-carboxylic acid,[746] which is an analogue of the substrate L-proline, Tyrosine 540 is fixed in a location that would sterically overlap the hydroxy group of *trans*-4-hydroxy-L-proline, a metabolite present in the cytoplasm of the cell. This steric effect should prevent *trans*-4-hydroxy-L-proline from associating with the enzyme, just as Tyrosine 216 in DNA-directed DNA polymerase from *Escherichia* phage RB69 prevents ribonucleoside triphosphates from associating with its active site. Mutation of Tyrosine 540 to an alanine[747] decreases the ratio of the specificity constants for L-proline and *trans*-4-hydroxy-L-proline by a factor of 50.

A steric effect can also be used experimentally to **modify the reaction catalyzed by an enzyme**. When Asparagine 170 in the active site of β-lactamase from *S. aureus* is mutated to a glutamine, the resulting steric effect pushes the molecule of water responsible

*In the case of DNA (cytosine-5-)-methyltransferase, the double-helical substrate was fluorinated.

for the hydrolysis catalyzed by the enzyme away from the acyl group it must attack, and the rate of hydrolysis decreases more than 800-fold.[548]

One way to consider the steric effects exerted by an active site is to imagine that the active site is a more or less rigid mold into which a substrate must insert by adopting a conformation complementary to the mold. For example, when creatine binds to creatinase (Equation 3–411) from *P. putida*,[734] its methyl group fits into a nonpolar pocket; its amidino group fits into a pocket formed by the edge of a histidine, a valine, and two glutamates and two molecules of water that provide acceptors for the donors for hydrogen bonds on the amidino group; and its carboxymethyl group fits into a pocket formed by an isoleucine, the π molecular orbital system of another histidine, and two arginines that provide donors for the acyl oxygen. A creatine will fit into the mold created by these three pockets only if its central nitrogen is tetrahedral and twisted so that its lone pair of electrons is in the plane of the amidino group that is now unconjugated to it.

Many of these molds can be quite rigid. The **rigidity of the mold** formed by the active site of steroid Δ-isomerase from *P. putida* prevents the hydrogen bonds between its oxyanion hole and a phenolate from shortening as it should when 2,6-difluorophenolate is the ligand instead of phenolate.[281]

The mold is also able to **hold functional groups apart from each other** to prevent unfavorable reactions from occurring. For example, the 6-ammonium of a lysine in β-ketoacyl-[acyl-carrier-protein] synthase must be held close enough to the acetyl enolate formed during the decarboxylation of malonyl acyl-carrier protein to stabilize it but far enough away from it to prevent it from hydronating the enolate.[748]

The mold can also hold functional **groups in the reactant near the site of catalysis** in conformations that favor the catalysis. For example, there are three conformations of the hydroxymethyl group at carbon 5 of a pyranose

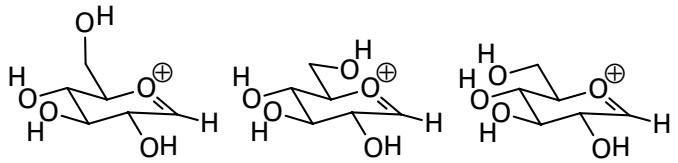

gauche,gauche **3–112** *gauche,trans* **3–113** *trans,gauche* **3–114**

Studies of the hydrolysis of fused rings that lock carbon 6 in one or the other of these conformations have demonstrated that gauche,gauche D-glucosyl glycosides hydrolyze 1.5 times more rapidly than gauche,trans D-glucosyl glycosides and 3.5 times more rapidly than trans,gauche D-glucosyl glycosides because in the gauche,gauche conformation at carbon 6, the carbon–oxygen bond is parallel to the π molecular orbital system of the intermediate oxocarbenium ion that is an intermediate and can donate electron density to it. Although these differences are quite small, nevertheless, in crystallographic molecular models of the occupied active sites of most glucosidases (94%), the mold holds the hydroxymethyl groups in the *gauche,gauche* conformation.[749] If this orientation is the result of natural selection, it illustrates the fact that natural selection operating for two billion years over the surface of the earth can respond to even small increases in enzymatic rate.

The mold can force a functional group in the reactant into an **environment that promotes catalysis**. For example, it has already been noted that decarboxylations occur far more rapidly in nonpolar solvents than in water.[750,751] In the active site of methylmalonyl-CoA decarboxylase from *E. coli*, the mold forces the polar carboxylato group of methylmalonyl-SCoA into a nonpolar pocket lined by three leucines, a valine, an edge of the phenyl ring of a tyrosine, a glycine, and a proline.[752]

The mold formed by an active site can **determine the specificity of the enzyme for its reactant** as well as **preventing the enzyme from converting the incorrect reactant**. For example, the deep nonpolar pocket in protein farnesyltransferase from *R. norvegicus* should be able to bind several different shorter isoprenoid diphosphates, but only when the (2*E*,6*E*)-farnesyl group of (2*E*,6*E*)-farnesyl diphosphate snugly fills the pocket is carbon 1 of the isoprenoid diphosphate properly positioned for the nucleophilic substitution catalyzed by the enzyme that takes place at this carbon.[567] Shorter isoprenoid diphosphates descend into the hole so far that their carbons 1 are improperly located relative to the catalytic groups; longer isoprenoid diphosphates spill out of the active site.

In a crystallographic molecular model of (2*E*,6*E*)-farnesyl diphosphate synthase from *G. gallus*,[753] there is a nonpolar pocket that snugly fits the geranyl group of a molecular model of the substrate geranyl diphosphate. The active site produces a geranyl carbenium ion and then alkylates it with isopentenyl diphosphate (see Figure 1–26). The

enzyme is specific for the geranyl group of geranyl diphosphate ($k_{gpp} = 5\ \mu M^{-1}\ s^{-1}$) and only reluctantly adds isopentenyl diphosphate to the farnesyl carbenium ion of farnesyl diphosphate ($k_{fpp} = 0.001\ \mu M^{-1}\ s^{-1}$), presumably because the longer farnesyl chain cannot fit in the pocket. Phenylalanine 112 and Phenylalanine 113 form the floor of the pocket. When they are mutated to an alanine and a serine, respectively, the specificity constant for farnesyl diphosphate, k_{fpp}, increases to $4.5\ \mu M^{-1}\ s^{-1}$, indistinguishable from that for geranyl diphosphate for the native enzyme.[754] Although the specificity constant of the mutant for geranyl diphosphate remains the same ($k_{gpp} = 3\ \mu M^{-1}\ s^{-1}$), the catalytic constant decreases by a factor of 20, presumably because the geranyl diphosphate no longer fits snugly in the pocket. Furthermore, in addition to producing the tetraisoprenoid geranylgeranyl diphosphate from farnesyl diphosphate and isopentenyl diphosphate, the enzyme now produces pentaisoprenoids, hexaisoprenoids, heptaisoprenoids, and octaisoprenoids because there is now no bottom to the nonpolar pocket, which has become a long nonpolar tube.

If the mold dictates the reactant for the enzymatic reaction, then it necessarily follows that the structure of the mold **determines what product is formed** in the enzymatic reaction because a reactant in one direction is a product in the other. For example, nonspecific monooxygenase 4B1 from *O. cuniculus* is an enzyme containing a heme P450 that preferentially hydroxylates carbon 1 of octane (90%) rather than carbon 2 (10%), which should be significantly more reactive to hydrogen abstraction. In the active site of the enzyme, there is a long hydrophobic tube into which octane fits snugly. Because the free energy of association is maximized when the entire octane molecule associates with the tube, only carbon 1 is accessible at the end of the tube where the oxoiron(IV) porphyrin$^{\bullet+}$ that performs the hydroxylation is located. Consequently, oxoiron(IV) porphyrin$^{\bullet+}$ usually removes a hydrogen from carbon 1 to initiate the hydroxylation rather than carbon 2.[755] In this instance, the mold **determines the regioselectivity of the reaction**. The chemistry of the reaction is the same, it is only where on the reactant the chemistry occurs that is controlled.

There is a family of enzymes that catalyze the prenylation of the indolyl group in either L-tryptophan or derivatives of L-tryptophan modified at its α-amino or α-carboxy group or both of them. Each reaction catalyzed by these enzymes is initiated by the dissociation of 3,3-dimethylallyl diphosphate (Figure 1–26) to produce dimethylallyl carbenium ion (previously **1–99**)

3–115

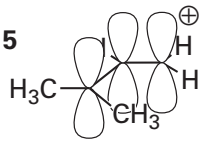

the primary carbon of which or the tertiary carbon of which then adds to either nitrogen 1 or to carbon 2, 3, 4, 5, 6, or 7 of the respective indolyl group.[756,757] Consequently, in theory, there are 14 possible products. An example of one specific regioselectivity would be the electrophilic aromatic substitution at carbon 4 catalyzed by 4-dimethylallyltryptophan synthase (previously Equation 1–155)

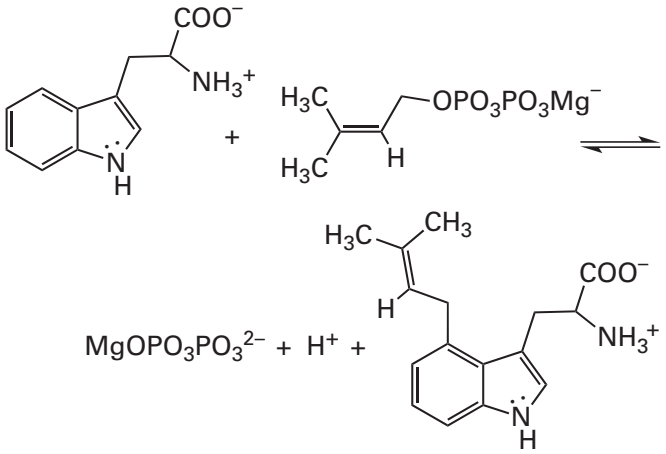

(3–412)

In this instance, the primary carbon of dimethylallyl carbenium ion **3–115**, the least reactive carbon, adds to the indolyl group. Each enzyme in this set catalyzes the electrophilic aromatic substitution or the electrophilic aromatic addition of only one of the two possible carbenium centers at only the nitrogen or only one of the six carbons with strict regiochemistry. All the enzymes in this set are homologous to each other, their sequences of amino acids can be aligned, and the same catalytic amino acids are found in the aligned sequences, in particular a glutamate the carboxylato group of which is the acceptor for a hydrogen bond from the indolyl nitrogen–hydrogen, a tyrosine that is responsible for hydronating the leaving oxygen of the diphosphate during the dissociation that produces dimethylallyl carbenium ion **3-115,** and several invariant amino acids that provide donors for hydrogen bonds to the diphosphate,[757] yet the regioselectivity of each active site is unique. The mold of the particular active site accomplishes the regioselectivity.

N^1-(1,1-Dimethylprop-2-enyl)tryptophan synthase from *Salinispora arenicola* adds the carbenium center situated on the tertiary carbon of the dimethylallyl carbenium ion **3–115** to nitrogen 1 of the indolyl group. In a crystallographic molecular model of the active site occupied by L-tryptophan and dimethylallyl *S*-thiolodiphosphate, which is an analogue of dimethylallyl diphosphate in which the leaving oxygen is replaced by a sulfur, the planar 3-methylprop-1-enyl group of the dimethylallyl diphosphate is sandwiched between the indolyl group of the L-tryptophan to which the tertiary carbon of dimethylallyl carbenium ion **3–115** adds and the indolyl group of Tryptophan 148, which is not modified during the reaction.[757] All the other enzymes in the set have either a tryptophan or a tyrosine at the position homologous to that of Tryptophan 148, so they all presumably form an analogous sandwich in which the three planes are parallel to each other. The tertiary carbon of the dimethylallyl *S*-thiolodiphosphate and the indolyl nitrogen of the L-tryptophan sit 0.34 nm apart on a line almost normal (104°) to the planes of the sandwich. In other words, the active site determines the regiochemistry of the reaction by placing the carbenium ion on the tertiary carbon of dimethylallyl carbenium ion **3–115** immediately adjacent to the atom in the L-tryptophan to which it is supposed to add and in the proper orientation for the electrophilic addition. The regiochemistry of all the other prenyltransferases in this set of enzymes is presumably determined in the same way; the active site positions carbon 1 or carbon 3 in the dimethylallyl diphosphate immediately adjacent to and on a line with the atom in the indolyl group to which it is to add, normal to the planes of the sandwich, to give the product produced by that particular enzyme. The active site of each enzyme sterically shifts the dimethylallyl diphosphate within the sandwich so that the proper orientation is achieved.

Enzymes in this family that add the carbenium ion to nitrogen 1, carbon 2, or carbon 3 of the indolyl group add either the tertiary carbon or the primary carbon of dimethylallyl carbenium ion **3–115**, but enzymes in this set that add the carbenium ion to carbons 4, 5, 6, or 7, always add the primary carbon of the allylic carbenium ion to the respective carbons of the indolyl group. This general regiochemistry can be explained by the fact that, in the crystallographic molecular model of N^1-(1,1-dimethylprop-2-enyl)tryptophan synthase, carbon 1 of the dimethylallyl *S*-thiolodiphosphate, which will become the primary carbon, sits against the phenyl ring of the indolyl group and carbon 3, which will become the tertiary carbenium ion, sits against the pyrrolyl group.

There are two related (25% identity; 3.2% gap percent) enzymes, 2-amino-4-deoxychorismate synthase from *Burkholderia lata* and anthranilate synthase from *Serratia marcescens*, that both convert chorismate to (2*S*)-2-amino-4-deoxychorismate

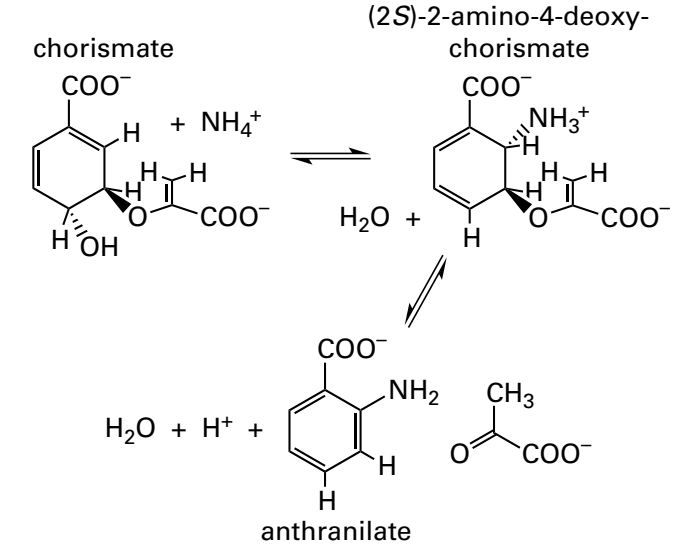

(3–413)

in an elimination followed by an addition. In the active site of anthranilate synthase, (2*S*)-2-amino-4-deoxychorismate undergoes the further elimination of an *eno*lpyruvate anion and a hydron to form anthranilate, the nominal product of its reaction. In the active site of 2-amino-4-deoxychorismate synthase, this elimination does not occur and 2-amino-4-deoxychorismate, the nominal product of its reaction, dissociates from the active site.

There are crystallographic molecular models of each active site occupied in both cases by benzoate, Mg^{2+}, and pyruvate. When the molecular models of benzoate and pyruvate in each active site are replaced by a molecular model of 2-amino-4-deoxychorismate and the resulting structures are submitted to energy minimization, it can be seen that the molds created by the two active sites differ in one significant way. The mold formed by the active site of 2-amino-4-deoxychorismate synthase sterically forces 2-amino-4-deoxychorismate into a conformation in which the hydron at carbon 2, the amino carbon, is locked into an equatorial position, preventing its overlap with the neighboring π molecular orbital system of the cyclohexadiene. Forcing the hydrogen to adopt an equatorial position prevents the elimination, which requires it to be in an axial position, and also

tilts it away from the amino group of the lysine homologous to the lysine that removes the hydron in anthranilate synthase. In the mold formed by the active site of anthranilate synthase, however, the molecular model of 2-amino-4-deoxychorismate assumes a conformation that places the hydrogen on carbon 2 in an axial position, ensuring both its overlap with the neighboring π molecular orbital system and its juxtaposition with the amino group of the lysine responsible for its removal as a hydron.[758] Again, the final product of an enzymatic reaction is dictated by the conformation that the mold of the active site forces the substrates or intermediates to assume.

In the crystallographic molecular model of stearoyl-SCoA occupying the active site of murine stearoyl-CoA 9-desaturase, the octadecanoyl group of the stearoyl-SCoA snugly occupies a mold just long enough to contain it. The mold, when it is fully occupied, places carbons 9 and 10 of the octadecanoyl group immediately adjacent to the diferrous diiron cluster that is also in the active site.[759] These two nonheme Fe^{2+}, along with a molecule of oxygen, produce the peroxydiiron(III) (previously **2–135**)

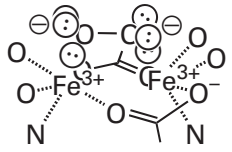

3–116

This structure is the precursor to the high-valent oxoiron intermediate that performs the actual desaturation, producing the double bond between carbons 9 and 10. The mold itself is bent into an acute angle so that when the octadecanoyl group occupies the mold, it is bent by the mold at both carbon 9 and carbon 10, forcing the bond between them into a less stable gauche conformation that is closer to the geometry of the cis double bond in the product than the more stable trans conformation. Consequently, in addition to determining the specificity of the enzymatic reaction for a stearoyl-SCoA, the rigid mold in stearoyl-CoA 9-desaturase also ensures that the desaturation occurs between carbons 9 and 10 and that the product contains a cis double bond rather than the more stable trans double bond.

A kink, albeit on a much larger scale, occurs in the crystallographic molecular model of human DNA ligase (ATP) in complex with a double helix containing 20 base pairs that is nicked on one strand in the middle. The 5′ end in the nick in this double helix has been adenylylphosphorylated on the 5′-hydroxy group to mimic exactly the adenylylphospho intermediate in the enzymatic reaction, but the 3′ end is lacking the 3′-hydroxy group, so the intermediate cannot proceed further in the normal ligation. The mold formed by the active site, which completely surrounds the double helix over nine of its base pairs, physically distorts the double helix, unwinding it to produce a kink that offsets the helical axis on one side of the kink by 0.5 nm from the helical axis on the other side. This kink opens up the double helix around the nick to allow the catalytic side chains in the active site to approach the phospho group at which the nucleophilic substitution at its phosphorus occurs as well as the 3′-hydroxy group that is the nucleophile and the adenylyl leaving group.[760] The product of the nucleophilic substitution is the repaired, intact double helix. In this instance, **the mold formed by the active site distorts the reactant to provide access to the site of the reaction.**

Rather than kink double-helical DNA at a site at which a base has been removed by a DNA glycosylase that recognizes damaged bases, the mold of the active site of human exodeoxyribonuclease III physically bends the DNA at the site of the apurinic or apyrimidinic deoxyribosyl group. The bend is quite abrupt, and the axes of the double helix at the two sides of the bend are at an angle of 35° to each other and are also displaced from each other by 0.5 nm. This bend extrudes the deoxyribosyl group from the double helix and permits both the deoxyribosyl group and the phospho groups at its 5′ and its 3′ end to enter the site at which the hydrolysis of these two phosphodiesters occurs, excising the apurinic or apyrimidinic deoxyribose.[761] The bend produced by the mold of the active site in double-helical DNA by the active site of type II site-specific deoxyribonuclease from *E. coli* is much smoother and less abrupt, but again the catalytic portion of the active site responsible for the hydrolysis is at the center of the bend. The major groove in the DNA is on the convex side of the bend, and at the center of the bend, the major groove is occupied by a loop of polypeptide. The seven side chains in this loop are responsible for recognizing the sequence of nucleotides in the DNA in the center of which the hydrolysis is to occur by reading the donors and acceptors for hydrogen bonds and the shapes of the base pairs along the major groove.[527] Again, in both of these instances, the mold provides access of the portion of the substrate to be hydrolyzed, rather than ligated, to the site of the hydrolysis.

Enzymes such as the fatty-acid synthase system

$$\text{acetyl-SCoA} + n\text{-malonyl-SCoA} + 2n\,\text{NADPH} + (3n-1)\,H^+ \rightleftharpoons 2n\,\text{NADP}^+ + n\,CO_2 + (n+1)\,\text{HSCoA} + CH_3(CH_2CH_2)_nCOO^- \quad (3\text{–}414)$$

or the polyketide synthases condense enolates of acetyl-SCoA formed by the decarboxylation of malonyl-SCoA, one after the other, to produce an elongating sequence of products. The ultimate length of **the final product is dictated by the volume of the mold in a portion of the active site** in which the elongating portion of the intermediate is situated. For example, chalcone synthase from *Medicago sativa* adds three acetyl units from three malonyl-SCoA, in equivalent Claisen condensations, one after the other, to 4-coumaryl-SCoA (analogous to the acetyl-SCoA in Equation 3–414) to produce naringenin. The volume of the portion of the active site in which the elongating polyketide ends up[762] causes the reaction to cease at three acetyl units when that volume has been filled. If the volume of that portion of the active site is decreased by mutating a glycine to a leucine, the enzyme produces bis-noryangonin, which results from the condensation of only two acetyl groups instead of three.[763]

Changing the shape of the mold by mutation can also change the identity of the product more significantly. For example, cyclohexanone monooxygenase from *Thermocrispum municipale* performs a Baeyer–Villiger oxidation (Figure 2–47) of the unnatural reactant 4-phenyl-2-butanone, for which the product is 2–phenylethyl acetate (<99%). When a leucine, phenylalanine, threonine, and leucine in the active site are mutated to glycine, glycine, phenylalanine, and threonine, respectively, the regiochemistry of the reaction is reversed, and the product of the oxidation of 4-phenyl-2-butanone is ethyl phenylacetate (98%).[764] The ester oxygen ends up on the other side of the original carbonyl group.

The role of the mold in determining the product of the reaction is **exploited most dramatically in the family of terpene cyclases.** Terpene cyclases are enzymes that cyclize geranyl diphosphate (two isoprene units), (2*E*,6*E*)-farnesyl diphosphate (three isoprene units), or geranylgeranyl diphosphate (four isoprene units) to produce monoterpenes, sesquiterpenes, or diterpenes, respectively. Each terpene cyclase cyclizes the particular isoprenoid diphosphate that is its substrate to form its particular unique terpene or its characteristic distribution of two or three terpenes. These enzymes as a group produce a vast array of terpenes from only the three respective isoprenoid diphosphates. The set of sesquiterpene synthases alone, the structurally related enzymes that use only (2*E*,6*E*)-farnesyl diphosphate as a substrate, produces over 300 different products, each from the same precursor.[765] Each active site in a terpene cyclase contains a mold that guides the reaction to the terpene or the two or three terpenes the enzyme is designed to produce.[765-768] The portion of a terpene controlled by the mold in a terpene cyclase is its polyisoprenyl group, which is entirely hydrocarbon. Consequently, hydrogen bonding is irrelevant and only the mold itself is guiding the reaction as it progresses.

The reaction of each of the hundreds of terpene cyclases begins with the heterolytic dissociation of the diphosphate from geranyl diphosphate, (2*E*,6*E*)-farnesyl diphosphate, or geranylgeranyl diphosphate to produce an **allylic carbenium ion**. In the active site of several if not most of the sesquiterpene synthases[765,769,770] and monoterpene synthases,[770,771] the diphospho group on the (2*E*,6*E*)-farnesyl diphosphate that enters the active site with at least one Mg^{2+} as a ligand is further liganded with two more Mg^{2+}. The result of such ligation is that it becomes a trimagnesium diphospho group with a cumulative charge number in its completely unhydronated state of +3. This excess positive elementary charge makes the trimagnesium diphospho group an excellent leaving group, but the trimagnesium diphosphate dication that results from its leaving should be inert to further participation in the reaction as either an acid or a base. The allylic carbenium ion of the geranyl group, the (2*E*,6*E*)-farnesyl group, or the geranylgeranyl group that results from the dissociation of the trimagnesium diphosphate then rearranges through a sequence of steps involving **carbon–carbon bond formation by intramolecular alkylation** (see Figure 1–26), leading to cyclization and the usual rearrangements of carbenium ions such as **hydride migrations and 1,2-methyl migrations**. The culmination of this sequence of reactions is usually the loss of a hydron to give a cyclic hydrocarbon, the terpene, that is the product of the reaction. A paradigmatic example of such a sequence of events is the one that proceeds in the active site of aristolochene synthase during the conversion of (2*E*,6*E*)-farnesyl diphosphate into (+)-aristolochene (Figure 3–48).[770,772-775]

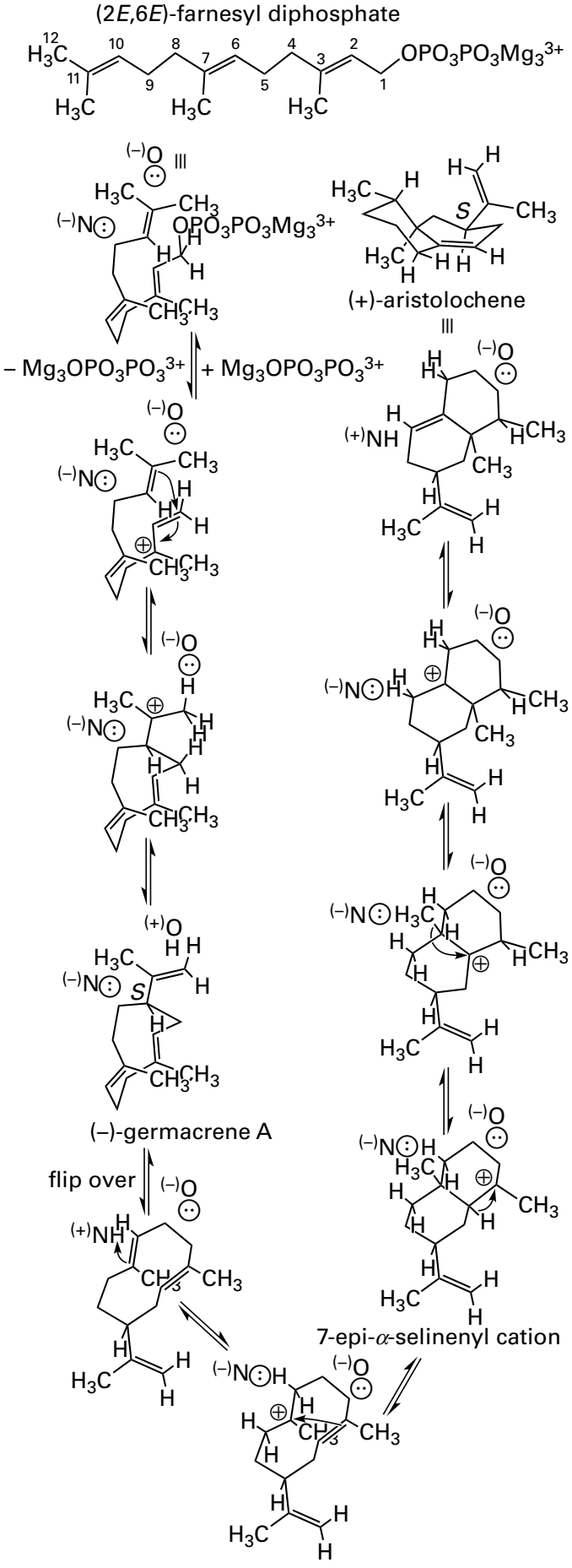

Figure 3–48: Mechanism of the conversion of magnesium (2*E*,6*E*)-farnesyl diphosphate into (+)-aristolochene, a sesquiterpene, catalyzed by aristolochene synthase.[772,773] In the active site of the enzyme, there are two Mg^{2+} ions that are ligands to the diphospho group in addition to the Mg^{2+} that enters the active site with (2*E*,6*E*)-farnesyl diphosphate.[775] The first step is the dissociation of trimagnesium diphosphate as a leaving group, which produces an allyl carbenium ion, the predominant resonance form of which is drawn. The predominance of this resonance form, which fixes the configuration at carbon 1, as well as the immediate alkylation in the next step explains the fact that the reaction proceeds with inversion of configuration at that carbon[774] even though it is a dissociative nucleophilic substitution (see the orientation in Figure 3–49A). The fact that this resonance form predominates explains how rotation about the bond between carbons 2 and 3 of the allylic carbenium ion can occur, as required, in certain terpene cyclases.[770] The double bond between carbons 10 and 11 as a nucleophile adds to the electrophilic carbon 1 of the allylic carbenium ion, forming a single bond between carbon 1 and carbon 10. During this cyclic alkylation, the carbocation ends up at carbon 11, as a tertiary carbenium ion. A base, $^{(-)}O\odot$, then removes a hydron from one of the methyl groups on carbon 11 to produce the neutral molecule (–)-germacrene A, (1*E*,5*E*,8*S*)-1,5-dimethyl-8-prop-1-en-2-yl-cyclodeca-1,5-diene, as an intermediate. The (–)-germacrene A then flips over in the active site to assume the orientation defined in Figure 3–49B. The double bond that was originally between carbons 6 and 7 of (2*E*,6*E*)-farnesyl diphosphate is then hydronated by a strong acid, $^{(+)}NH$, to produce the tertiary carbenium ion at original carbon 7. The double bond between the original carbons 2 and 3 then adds to this electrophilic carbenium ion, and the resulting cyclic alkylation produces the tertiary 7-*epi*-α-selinenyl cation in which the original carbon 2 forms a bond with the original carbon 7. The hydrogen that was on the original carbon 2 then migrates to the tertiary carbenium carbon of the 7-*epi*-α-selinenyl cation from its anterior position, as drawn, to produce the *S*-configuration at the original carbon 3. The methyl group that was on the original carbon 7 then migrates to the resulting tertiary carbenium carbon from the posterior position, as drawn, to produce the *R*-configuration of a quaternary carbon at the original carbon 2. The removal of a hydron by a base, $^{(-)}N\odot$, from the original carbon 8 produces the product (+)-aristolochene.

The inhibitor (2*E*,6*E*)-farnesyl *S*-thiolodiphosphate is an analogue of the substrate (2*E*,6*E*)-farnesyl diphosphate that cannot participate in the reaction because the oxygen in the trimagnesium diphospho group that leaves carbon 1 of (2*E*,6*E*)-farnesyl diphosphate has been replaced synthetically with a sulfur. This difference is the only one between the two molecules. In a crystallographic molecular model of the active site of aristolochene synthase from *Aspergillus terreus* occupied by magnesium (2*E*,6*E*)-farnesyl *S*-thiolodiphosphate (Figure 3–49A),[775] the mold into which the farnesyl group of the analogue has inserted causes it to assume a conformation favorable to the reaction that the enzyme

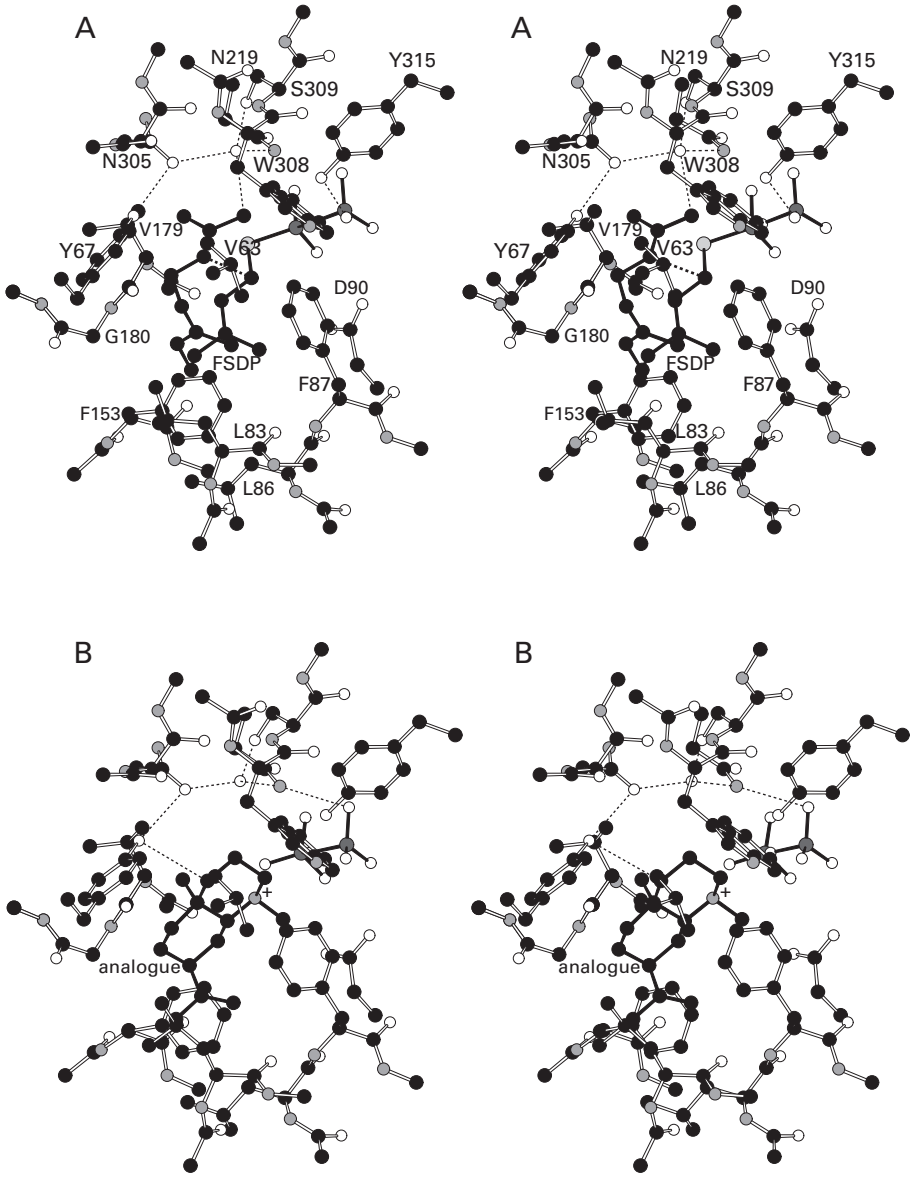

Figure 3–49: Stereodrawing[576] of the mold for the farnesyl group of (2*E*,6*E*)-farnesyl diphosphate created by side chains of the amino acids and the polypeptide backbone within the active site of aristolochene synthase from *A. terreus* that ensures the production of (+)-aristolochene.[775] Black atoms are carbons, white atoms are oxygens, small gray atoms are nitrogens, large light gray atoms are sulfurs, and large dark gray atoms are atoms of phosphorus. **(A)** Initial Michaelis complex between the active site and magnesium (2*E*,6*E*)-farnesyl diphosphate. Crystals were grown from a solution containing 0.15 mM active sites of aristolochene synthase, 1.0 mM $MgCl_2$, 60 mM NaCl, 0.8 mM sodium diphosphate, and 0.75 mM (2*E*,6*E*)-farnesyl-*S*-thiolodiphosphate at pH 6.5. In the map of electron density calculated from a data set to Bragg spacing of 0.19 nm, there was a feature of electron density located in the active site into which a molecular model of (2*E*,6*E*)-farnesyl-*S*-thiolodiphosphate (FSDP) could be confidently inserted, and there were three features of electron density consistent with three Mg^{2+} ions coordinated by the diphospho group. The mold into which the farnesyl group of the inactive analogue of the substrate (2*E*,6*E*)-farnesyl diphosphate inserts, and presumably the substrate itself, is featured in the drawing. It is formed by two phenylalanines, two tyrosines, a tryptophan, two leucines, two valines, a glycine, and an asparagine, as well as portions of the polypeptide backbone. The farnesyl group of the inactive analogue folds into this mold with carbon 1 only 0.40 nm from carbon 10 (dashed line). **(B)** Complex between the active site and the 7-*epi*-α-selinenyl cation. Crystals were grown from a solution containing 0.15 mM active sites of aristolochene synthase, 1.0 mM $MgCl_2$, 60 mM NaCl, 0.8 mM sodium diphosphate, and 1.5 mM (1*R*,4a*S*,7*S*,8a*R*)-1,4a-dimethyl-7-(prop-1-en-2-yl)decahydroquinolinium at pH 6.5. (1*R*,4a*S*,7*S*,8a*R*)-1,4a-Dimethyl-7-(prop-1-en-2-yl)decahydroquinolinium is an analogue of the 7-*epi*-α-selinenyl cation that is an intermediate in the enzymatic reaction in which the carbenium carbon has been replaced by a tertiary ammonium ion. In the map of electron density calculated from a data set to Bragg spacing of 0.19 nm, there were two features of electron density located in the active site into which a molecular model of (1*R*,4a*S*,7*S*,8a*R*)-1,4a-di-methyl-7-(prop-1-en-2-yl)-decahydroquinolinium and a molecular model of a diphosphate could be confidently inserted, and there were three features of electron density consistent with three Mg^{2+} ions coordinated by the diphospho group. The drawing is in the same orientation as that in Panel A and is composed of the same side chains and strands of polypeptide.

catalyzes. The distance between carbons 1 and 10 of (2*E*,6*E*)-farnesyl *S*-thiolodiphosphate, the atoms between which the first carbon–carbon bond would be formed in (2*E*,6*E*)-farnesyl diphosphate (Figure 3–48), is 0.40 nm, which is close to the distance expected of van der Waals contact (0.42 nm).

Intramolecular alkylations other than this first one, however, must be prevented by the mold. The carbenium ion at carbon 3 must be prevented from adding to carbon 10, and the distance between these two carbons is 0.47 nm, and they are held in an unfavorable orientation. The allyl carbenium ion that is formed in the first step must also be prevented from adding to the double bond between carbons 6 and 7, which would be the more favorable cyclization in solution. In the conformation in which the farnesyl group is held by the active site, the distance between carbons 3 and 6 is 0.30 nm, the distance between carbons 1 and 6 is 0.46 nm, and the distance between carbons 3 and 7 is 0.35 nm. Even though they are immediately adjacent to each other, if carbon 3 were to add to carbon 6, an unfavorable four-membered ring would form, an outcome ruling out this cyclization. The pair of carbons 1 and 6 and the pair of carbons 3 and 7, both suitable candidates for alkylation, are oriented by the mold in conformations unsuitable for addition.

The inhibitor (1*R*,4a*S*,7*S*,8a*R*)-1,4a-dimethyl-7-(prop-1-en-2-yl)decahydroquinolinium ion is an analogue of the 7-*epi*-α-selinenyl cation that is an intermediate in the enzymatic reaction (Figure 3–48). It is identical in structure to the 7-*epi*-α-selinenyl cation with the exception that the positively charged carbon of the carbenium ion is replaced by a positively charged ammonio nitrogen. In a crystallographic molecular model of the active site of aristolochene synthase from *A. terreus* occupied by (1*R*,4a*S*,7*S*,8a*R*)-1,4a-dimethyl-7-(prop-1-en-2-yl)decahydroquinolinium ion and magnesium diphosphate (Figure 3–49B),[775] it can be seen that the **intermediate has flipped over** in the active site relative to the initial orientation of the (2*E*,6*E*)-farnesyl group. One might ask why this should be the case.

The most difficult step in the reaction catalyzed by the active site of aristolochene synthase is the **hydronation of the carbon–carbon double bond** in (–)-germacrene A (Figure 3–48). Such a hydronation requires a strong acid, and an acid that is strong enough is hard to come by in the active site of an enzyme. The hydron that departs from original carbon 12 of the (2*E*,6*E*)-farnesyl diphosphate in the third step of the mechanism, as with any hydron that departs from a carbon adjacent to a carbenium ion, is a strong acid. The feat is to **somehow transfer that strongly acidic hydron** from original carbon 12 to original carbon 6 without losing its acidity.

This acidic hydron is removed from original carbon 12 by a molecule of water held tightly in position by Asparagine 219 (0.28 nm), Asparagine 305 (0.28 nm), and Serine 309 (0.27 nm). These three tetrahedrally arrayed hydrogen bonds force a lone pair of electrons on the molecule of water against carbon 12 of (2*E*,6*E*)-farnesyl *S*-thiolodiphosphate at a distance of 0.31 nm, well within van der Waals contact (0.38 nm), and in precisely the orientation required for removing a hydron in a hydrogen–carbon bond parallel to the vacant *p* orbital on an adjacent carbenium ion on original carbon 11.

An acidic hydron is added to original carbon 6 in (–)-germacrene A, after it has flipped over in the active site, by the 4-hydroxy group of Tyrosine 67. In the complex between the active site and (1*R*,4a*S*,7*S*,8a*R*)-1,4a-dimethyl-7-(prop-1-en-2-yl)decahydroquinolinium ion (Figure 3–49B), the equatorial hydrogen on the carbon of the analogue of the 7-*epi*-α-selinenyl cation equivalent to original carbon 6 lies on the line of centers between the oxygen of this 4-hydroxy group and the carbon, and the distance between oxygen and carbon is 0.36 nm, within the sum (0.38 nm) of the van der Waals radii for hydrogen and oxygen and the length of a carbon–hydrogen bond. The distances and orientations leave little doubt that these two acid–bases, the molecule of water and the 4-hydroxy group of the tyrosine, are responsible for the respective dehydronation and hydronation.

Connecting the fixed molecule of water that acts as a base and the 4-hydroxy group of Tyrosine 67 that acts as an acid in each crystallographic molecular model is a network of oxygens participating in hydrogen bonds. The hydroxy group of Serine 309, the molecule of water, the acyl oxygen of Asparagine 305, and the phenolic 4-hydroxy group of Tyrosine 67 comprise this network. The values of pK_a for the hydronated forms of these four oxygens are –3, 0, –0.5, and –6, respectively. Each oxygen becomes a strong acid, in turn, when it is hydronated, and as judged from the individual values of pK_a, each is capable of **conserving the acidity of the hydron** removed by the molecule of water from original carbon 12 adjacent to the carbenium ion on original carbon 11. A hydron can be readily distributed among them through the hydrogen bonds creating the network. None of these participants, however, is able to hydronate the double bond between original carbons 6 and 7 in the initial con-

formation of the (2*E*,6*E*)-farnesyl diphosphate as it folds into the active site (Figure 3–48). Only after the neutral molecule of (–)-germacrene A, which is a stable intermediate and not evanescent as are the various carbenium ions, flips over in the active site is the carbon–carbon bond positioned for hydronation by the hydronated, cationic 4-hydroxy group of Tyrosine 67 ($pK_a = -6$) bearing the relayed, strongly acidic hydron. The fact that the plane of the phenyl ring is normal to the line of centers between the oxygen and the carbon is not consequential because hydronation of the 4-hydroxy group to produce an acid strong enough to hydronate the carbon–carbon bond would unconjugate the oxygen from the π system of the ring.*

Site-directed mutations reinforce the conclusion that these amino acids are involved in the hydron transfers that produce, in turn, the (–)-germacrene A and the 7-*epi*-α-selinenyl cation. When the homologue of Tyrosine 67 in aristolochene synthase from *Penicillium roqueforti* is mutated to a phenylalanine[777] or an alanine[778], the specificity constant for (2*E*,6*E*)-farnesyl diphosphate decreases by a factor of 1000, and 44% or 100%, respectively, of the terpenes produced by the active site are those expected if the reaction cannot proceed beyond (–)-germacrene A. When Serine 309 is mutated to an alanine, although the specificity constant for the production of (+)-aristolochene is unaffected, the mutant produces (–)-germacrene A as a product (10%), a fact suggesting that the hydronation of the (–)-germacrene A in the active site has been hampered because the molecule of water is no longer so rigidly fixed. When Asparagine 305 is mutated to alanine, the specificity constant for production of (+)-aristolochene decreases by a factor of 20, and half of the product produced is now (–)-germacrene A, again indicating a failure to hydronate the (–)-germacrene A while it is in the active site. When both Serine 309 and Asparagine 305 are mutated to alanines, the specificity constant for production of (+)-aristolochene decreases by a factor of 400, and 95% of the product is a mixture of (–)-germacrene A and (2*E*,6*E*)-farnesol, and (*E*)-nerlolidol.[776] These are products expected from an almost complete failure to hydronate (–)-germacrene A in the active site and either its release into the solution or the hydration of precursors to it, respectively. This last result is consistent with the rigidly oriented network of hydrogen bonds being replaced by a more disorganized collection of molecules of water in the empty space that is created by the two mutations to alanine and that is much less efficient at retaining the strongly acidic hydron and transferring it from one carbon to the other. In addition to indicating that the network of hydrogen bonds is responsible for the dehydronation to form the (–)-germacrene A and its subsequent hydronation, all these results are also consistent with the intermediate dehydronation and hydronation becoming the rate-limiting step of the reaction in the mutants rather than the dissociation of the trimagnesium diphosphate.

A comparison of the two crystallographic molecular models (Figure 3–49) suggests that **the mold formed by the active site is not completely rigid and has a degree of plasticity**. For example, the side chains of Leucine 83, Leucine 86, and Phenylalanine 87 have assumed different conformations in the two molecular models in which the unflipped and flipped orientations of the intermediate are observed. This observation suggests that the ability of the mold to change shape in certain locations in a certain way is also critical to determining the product of a specific cyclase.

All these observations, albeit made on only one of the terpene cyclases, lead to the following view of the mechanism common to the enzymes in this family. The first step in the reaction catalyzed by the active site of a terpene cyclase is the dissociation of diphosphate from the linear isoprenoid diphosphate to produce an allylic carbenium ion. Following the production of the allylic carbenium ion, the mold in which it finds itself determines which cyclizations, alkylations, rearrangements, hydronations, and dehydronations of the carbenium ion occur. During these processes, it is unlikely that the evolving carbenium ion reorients in the mold because it is so evanescent, but a stable intermediate terpene can reorient in the mold. Consequently, the mold must be plastic enough to tolerate not only the changes in shape of the evolving carbenium ion but

*Despite the desire that it be so,[776] it is unlikely that the trimagnesium diphosphate that is the leaving group in the first step of the reaction participates as an acid or a base in any of the hydronations or dehydronations that occur during the enzymatic mechanism of aristolochene synthase. First, it would be almost impossible to hydronate any of the oxygens of the trimagnesium phosphate because in its completely unhydronated state it has a formal charge number of +2. Second, the only connection between the water that removes a hydron from original carbon 12 and the hydronated 4-hydroxy group that hydronates (–)-germacrene A is two hydrogen bonds to the amido group of Asparagine 219. An amido group is a very poor base that cannot be hydronated in the orientation in which it is firmly fixed in both crystallographic molecular models. This amido group is responsible for rigidly fixing the molecule of water rather than any hydron transfers.

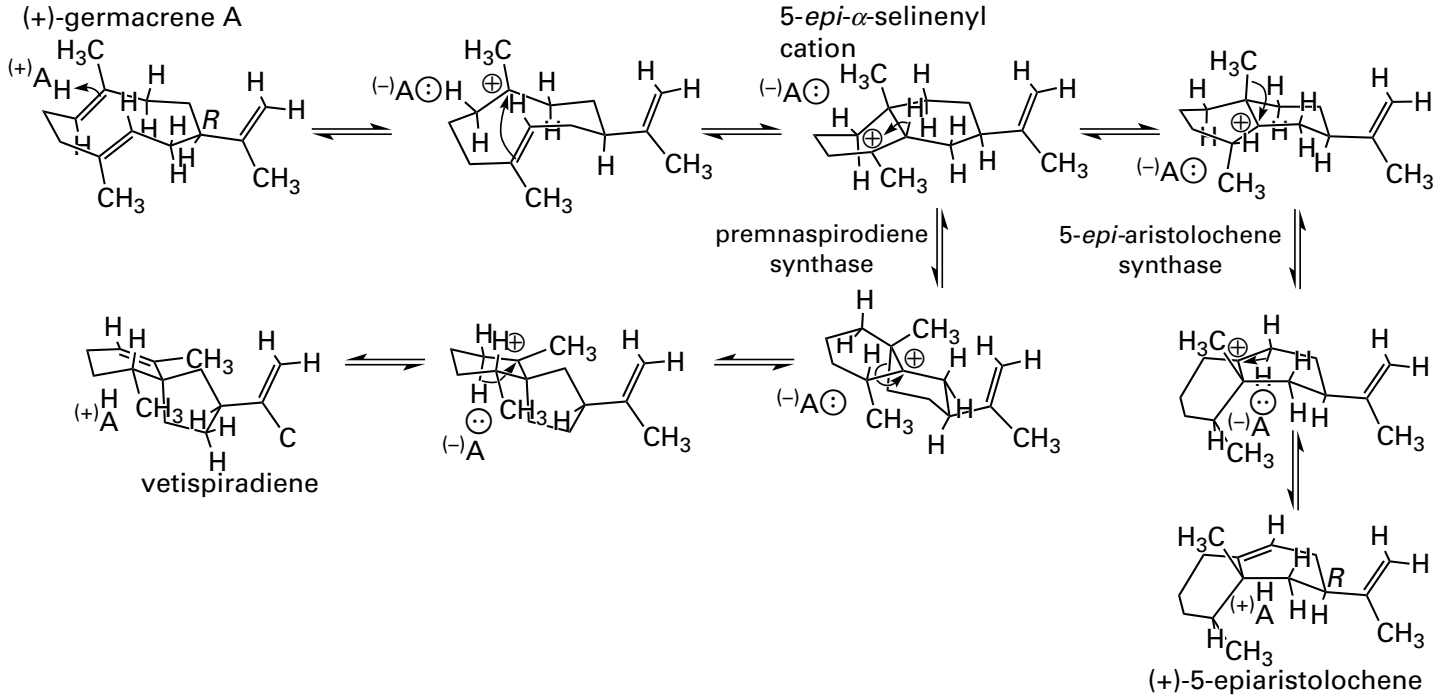

Figure 3–50: Enforcing the conformations of (+)-germacrene A that lead to 5-*epi*-aristolochene and vetispiradiene. These conversions proceed to completion within the active sites of 5-*epi*-aristolochene synthase and vetispiradiene synthase, respectively, and each passes through the same two intermediates, the sesquiterpene (+)-germacrene A and the 5-*epi*-α-selinenyl cation, which is produced in both active sites by hydronation of (+)-germacrene A and carbon–carbon bond formation across the center of the ring. The reactions diverge at the point where migration occurs across the central bond in the 5-*epi*-α-selinenyl cation. One way to control this migration conformationally is to control whether the methyl group or the carbon–carbon bond is parallel to the *p* orbital of the carbenium ion in the 5-*epi*-α-selinenyl cation. This conformational difference is prefigured in the angle enforced by the mold of the respective active site between the two endocyclic double bonds in (+)-germacrene A. If they are held in a conformation in which they are parallel, the methyl group will eventually end up parallel to the cation; if they are held in a conformation in which they are inclined at 60° to each other, the carbon–carbon bond will eventually end up parallel to the cation. It is also possible that bulky groups in the active sites of 5-*epi*-aristolochene synthase and vetispiradiene synthase sterically prevent the migration of the carbon–carbon bond and the methyl group, respectively, of the 5-*epi*-α-selinenyl cation.

also the reorientation of a stable intermediate. The shape of the active site and the plasticity that is inherent in the composition of the amino acids forming it determine the ultimate product or products of the reaction. In this way, basically the same chemical reaction can lead to the terpene, or the small number of terpenes, particular to that enzyme while the family of terpene cyclases, each with its own particular mold, can produce hundreds of different terpenes.

Site-directed mutation of amino acid side chains within the mold formed by the active site can change the product of the reaction catalyzed by one of these terpene cyclases. For example, nine different amino acids in the active site of *epi*-isozizaene synthase from *S. coelicolor* were mutated to create a set of 26 different mutants. Ten different sesquiterpenes that are not produced by the wild-type enzyme were produced by one or more of these mutants. Three different sesquiterpenes that were produced as minor products by the wild type were major products produced by one or more of the mutants.[779] When a single phenylalanine in the active site was mutated to seven different amino acids, each mutant produced one of five different sesquiterpenes, all different from *epi*-isozizaene.[780]

5-*Epi*-aristolochene synthase converts the farnesyl allylic carbenium ion, formed when trimagnesium diphosphate dissociates from trimagnesium (2E,6E)-farnesyl diphosphate, to the sesquiterpene 5-*epi*-aristolochene (Figure 3–50). It has a 5-*epi*-α-selinenyl cation as an intermediate, rather than a 7-*epi*-α-selinenyl cation, because the intermediate that is hydronated in its active site is (+)-germacrene A rather than (–)-germacrene A.[781] The reaction proceeds through an intramolecular, electrophilic alkylation that forms a carbon–carbon bond followed

by the transfer of a hydron, just as in the first steps of the mechanism of aristolochene synthase (Figure 3–48), but the mold in 5-*epi*-aristolochene synthase dictates the formation of an *R* configuration at original carbon 10 instead of an *S* configuration. The resulting stable intermediate, (+)-germacrene A, is also locked in the mold in a conformation that causes the two carbon–carbon double bonds within its ring to assume opposite orientations instead of the same orientation as they do in the active site of aristolochene synthase (Figure 3–49A) so that a 5-*epi*-α-selinenyl cation is formed as an intermediate. A hydride migration, a 1,2-methyl migration, and a dehydronation produces (+)-5-*epi*-aristolochene rather than (+)-5-aristolochene. A crystallographic molecular model of a complex between the enzyme from *Nicotiana tabacum* and magnesium 2-fluoro-(2*E*,6*E*)-farnesyl diphosphate, an inactive analogue of magnesium (2*E*,6*E*)-farnesyl diphosphate, has been reported.[766,769]

There is a terpene cyclase closely related to 5-*epi*-aristolochene synthase from *N. tabacum*, vetispiradiene synthase from *Hyoscyamus muticus* (75% identity; 0.9 gap per cent), that converts (2*E*,6*E*)-farnesyl diphosphate to vetispiradiene (97%) rather than (+)-5-*epi*-aristolochene, also through an intermediate 5-*epi*-α-selinenyl cation (Figure 3–50). When the nine amino acids that form the mold enforcing the rearrangement of (2*E*,6*E*)-farnesyl diphosphate to (+)-5-*epi*-aristolochene (in 90% yield) in the active site of 5-*epi*-aristolochene synthase are mutated to the amino acids occupying those locations in vetispiradiene synthase, to create a mold dictating the production of vetispiradiene, the mutant 5-*epi*-aristolochene synthase produces vetispiradiene (in 75% yield) instead of (+)-5-*epi*-aristolochene (in 3% yield).[782] A mutant in which only two of the nine amino acids have been mutated has a mold that dictates yet another sesquiterpene, *epi*-eremorphilene (70%). These observations demonstrate that, on the same superstructure, **the mold can be remachined by natural selection to change the products** of the enzymatic reaction, and they also further explain the raft of products produced by the various terpene cyclases.

The triterpene cyclase cycloartenol synthase from *A. thaliana*

(*S*)-2,3-epoxysqualene $\rightleftharpoons$ cycloartenol (3–415)

was mutated at random rather than at specific positions in its sequence of amino acids, and the mutants were selected for their ability to produce another triterpene, lanosterol, from (3*S*)-2,3-epoxy-2,3-dihydrosqualene. It was found that either the mutation of an amino acid in the lining of the mold or the **mutation of an amino acid in the protein outside the mold** in this enzyme could change the shape of the mold sufficiently to cause it to dictate the production of lanosterol instead of cycloartenol.[783,784] In the case of two related (54% identity; 0.6 gap percent) triterpene synthases, lupeol synthase from *Olea europaea* and β-amyrin synthase from *Panax genseng*, the mutation of leucine to tryptophan or the mutation of tryptophan to leucine at the respective homologous positions in the sequences of amino acids caused the lupeol synthase to produce β-amyrin (>99%) and the β-amyrin synthase to produce lupeol (66%).[785]

The terpene cyclizations described in detail in Figures 3–48 and 3–50 leave the impression that the intermediate carbenium ions in such cyclizations are always allyl or tertiary carbenium ions and that the mold cannot overcome the significant instability of **secondary carbenium ions** relative to allyl or tertiary carbenium ions. In the majority of terpene cyclizations, the intermediates are either allyl or tertiary carbenium ions, a realistic preference, but there are terpene cyclases in which the mold is able to dictate that a secondary carbenium ion be an intermediate. For example, in the initial cyclization in the active site of pentalenene synthase, a secondary carbenium ion is the intermediate

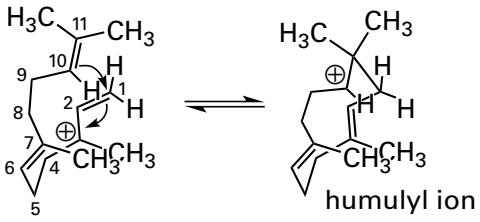

(3–416)

in an intramolecular alkylation of an alkene that is analogous to the first step in the alkylation catalyzed by aristolochene synthase (Figure 3–48), except for its regioselectivity. The mold of the active site dictates that the allyl carbenium ion cyclize to a humulyl ion, which is a secondary carbenium ion, rather than the tertiary germacradienyl ion. In the active site of pentalenene synthase from *Streptomyces exfoliatus* in a complex with 12,13-difluorofarnesyl diphosphate, an inactive analogue of farnesyl diphosphate, the mold holds carbon 1 of farnesyl diphos-

phate 0.03 nm closer to carbon 11 than to carbon 10, and one face of the π molecular orbital system of the phenyl group of a phenylalanine is pushed up against carbon 10 and the hydrogen on carbon 9. This phenyl group should be able to stabilize the secondary carbenium ion on carbon 10 by a cation–π interaction and orient the carbon–hydrogen bond on carbon 9 so that it is parallel to the vacant *p* orbital on the carbenium ion to provide hyperconjugation.[786] These features of the mold are thought to overcome the instability of the secondary carbenium ion.

There is a synthetic cavity that is able to enclose various derivatives of (*E*)-geraniol that have been activated by attaching leaving groups competent to form the geranyl carbenium ion. The resulting enclosed carbenium ion rearranges to produce one of a set of various monoterpenes. In this instance, the cavity remains the same; the distribution of monoterpenes produced depends on steric effects resulting from the different sizes of the appended leaving groups but also the time during which the rearrangement takes place.[787]

It is also possible to reconfigure the mold in an active site by mutation so that it will accept a chemical compound that is not present in the biological collection of metabolites and thereby use an enzyme, evolved for a different substrate, to perform a nonbiochemical reaction desired by a synthetic organic chemist.[779]

So far, the rigidity of the mold and its ability to grip substrates and intermediates in fixed orientations to select the proper reactant and determine the proper product have been stressed. In at least one instance, however, it was demonstrated that changing the structure of a fatty acyl group in the reactant for a monooxygenase, by changing one of its methylene carbons to an oxygen, caused the fatty acyl group to slide over in the active site so that the oxygenation occurred at the carbon adjacent to the one normally oxygenated.[788,789] This observation suggests that functional groups of substrates, especially alkanes, **are not always held that immovably** in their subsites.

The orientation of substrates and intermediates accomplished by the more or less rigid mold comprising an active site is the exploitation by natural selection of the principle of least nuclear motion. The principle of least nuclear motion[790] is that those elementary reactions will be favored that involve the least change in atomic position.[791] A corollary of this principle is that the less change in atomic position a reaction involves, the lower will be the standard free energy of activation and the faster will the reaction proceed.

Active sites follow this corollary by providing a mold that not only is complementary to the transition state or the transition states in a reaction but also **positions reactants and products such that their atoms are as close as possible to the positions occupied by respective atoms in the transition state**. This aspect of a mechanism proceeding in the active site of a particular enzyme can be appreciated by superposing crystallographic molecular models representing complexes between the active site and reactants, intermediates, and products.[792] For example, superposition of crystallographic molecular models of complexes between L-methionine adenosyltransferase from *E. coli*

$$\begin{aligned} MgATP^{2-} + \text{L-methionine} + \\ H_2O \rightleftharpoons \textit{S}\text{-adenosyl-L-methionine} + \\ MgOPO_3PO_3^{2-} + HOPO_3^{2-} + H^+ \end{aligned} \qquad (3\text{–}417)$$

and magnesium 5′-adenylic imidodiphosphonic anhydride ($MgAMPPNP^{2-}$) and L-methionine, on the one hand, and *S*-adenosyl-L-methionine and magnesium phosphoric imidodiphosphonic anhydride, on the other, shows that the atoms in the reactants move less than 0.1 nm during the transition to products (Figure 3–51).[793] The omit map of electron density (Figure 3–35) for the equilibrium mixture of 2-phospho-D-glycerate and phospho*enol*pyruvate and the molecule of water in the active site of phosphopyruvate hydratase illustrates how small the movements are in the positions of the atoms when reactant is converted to product.

The superposition of crystallographic molecular models of complexes between human double-stranded uracil-DNA glycosylase and an analogue of the reactant, an analogue for the intermediate oxocarbenium ion, and the products of the reaction show that the only atom that moves more than 0.1 nm during the reaction is the 1′-glycosidic carbon of the ribose in the uridylyl group.[794] An identical conclusion was reached about the respective 1′-glycosidic carbons and the other atoms in the substrates from crystallographic molecular models

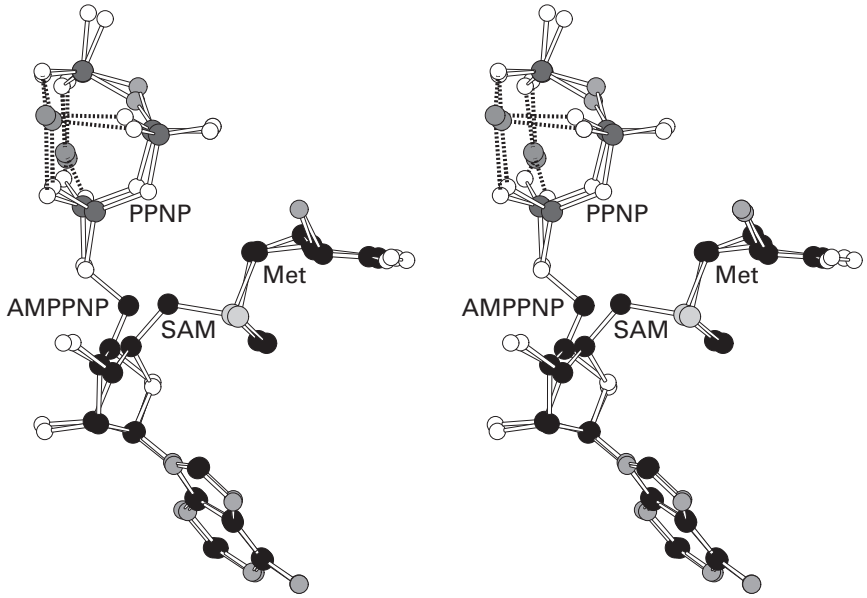

Figure 3–51: Superposition of stereodrawings[576] of molecular models of ligands in the active site in two crystallographic molecular models of complexes of methionine adenosyltransferase from *E. coli*. One molecular model is for the complex of the enzyme with its substrate L-methionine and the inhibitor $MgAMPPNP^{2-}$, and the other molecular model is for the complex of the enzyme with its substrate *S*-adenosyl-L-methionine (SAM) and the inhibitor magnesium phosphoric imidodiphosphonic anhydride (PPNP).[793] Black atoms are carbons, white atoms are oxygens, small gray atoms are nitrogens, large light gray atoms are sulfurs, and large dark gray atoms are atoms of phosphorus. The enzyme was dissolved in a solution containing 5 mM $MgAMPPNP^{2-}$, 10 mM L-methionine, and 5 mM $MgCl_2$ at pH 8.0. After 60 min at 37 °C, the protein was crystallized. In the map of electron density calculated from a data set to Bragg spacing of 0.25 nm and calculated by imposing noncrystallographic 222(D_2) symmetry on the tetramer of the enzyme, the resulting feature of electron density located in the active site could be shown to be the sum of electron density arising from molecules of L-methionine and $MgAMPPNP^{2-}$ and electron density arising from molecules of *S*-adenosyl-L-methionine and magnesium phosphoric imidodiphosphonic anhydride. The latter pair of molecules arose from the nucleophilic transfer of an adenylyl group from $MgAMPPNP^{2-}$ to L-methionine catalyzed at the active site by the enzyme. Consequently, the molecular models of the former pair of molecules and the latter pair of molecules were each inserted into this feature of electron density at half occupancy, and the resulting molecular model was submitted to refinement. The final refined positions of the two pairs of substrates are superposed in the drawing. Two features of electron density consistent with Mg^{2+} were found to be coordinated by 5′-adenylic imidodiphosphonic anhydride, and phosphoric imidodiphosphonic anhydride, and those two Mg^{2+} (gray spheres) are included in the drawing. The 5′-carbon of the ribosyl group in the adenylyl group, at which the nucleophilic substitution catalyzed by the enzyme occurs, moves 0.13 nm during the substitution, and the 4′-carbon moves 0.06 nm.

for complexes of bovine purine-nucleoside phosphorylase,[795] uridine phosphorylase from *E. coli*,[796] and adenine phosphoribosyl transferase from *Giardia intestinalis*.[797] All these observations emphasize that enzymes are usually designed to minimize changes in atomic position as their reactions proceed.

The active site must also accommodate both the reactants and the products of the enzymatic reaction. In cases in which the reaction requires only minimal alterations in the reactants during their conversion to products, the principle of least nuclear motion can be satisfied during the conversion. In more complicated reactions, however, rather significant shifts, such as the flipping over of (–)-germacrene A (Figure 3–48), have to occur in the bound substrates and intermediates for the reaction to proceed successfully from reactants to products. For example, in the reaction catalyzed by aldehyde dehydrogenase (NAD^+)

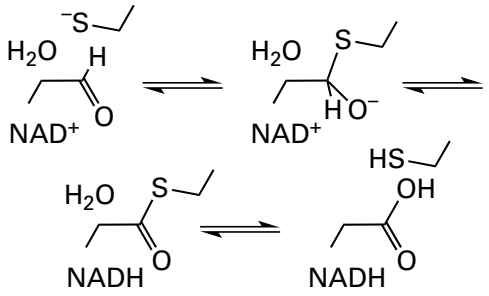

(3–418)

there are three consecutive steps with quite different chemistry: nucleophilic addition of the sulfanyl group of a cysteine in the active site to the carbonyl, dehydrogenation of the resulting thiohemiacetal by NAD^+, and hydrolysis of the resulting thioester. In the crystallographic molecular model of the active site of human aldehyde dehydrogenase (NAD^+) occupied by NAD^+, the nicotinamide ring of NAD^+ is in the location expected for removal of the hydride from the thiohemiacetal, but when the active site is occupied by NADH, the nicotinamide ring has withdrawn from its former location. The adenosyl group remains fixed in place as the reduced nicotinamide and its ribosyl group are displaced by about 0.4 nm from their position in the complex with NAD^+. It has been proposed that the purpose of this withdrawal of the nicotinamide ring performed by the active site is to provide room for the hydrolysis to proceed.[798] At the beginning of the reaction, the NAD^+ assumes the former conformation as it associates with the active site, and at the end of the reaction, the NADH is in the latter conformation, having shifted as the reaction progresses.

In the active site of **photoactive yellow protein** from *Halorhodospira halophila,* when the chromophore, (*E*)-4-hydroxycinnamic acid, photoisomerizes to (*Z*)-4-hydroxycinnamic acid, which is the photochemical product, hydrogen bonds to the chromophore break initially, but within 100 ps the rigidity of the active site causes them to re-form. Nevertheless, the active site is flexible enough to accommodate the *Z* carbon–carbon double bond, an accommodation that requires shifts in the mold of up to 0.1 nm.[664]

As the example of the subsite in trypsin responsible for its specificity has illustrated (Figure 3–46), the mold provided by the active site must sometimes be designed so that a subsite within it is able to recognize two different reactants. This accommodation can be accomplished by having a mold either large enough or flexible enough to achieve it. There are many other examples of **subsites within active sites that must recognize more than one functional group**. For example, unlike double-stranded uracil-DNA glycosylase from herpes simplex virus type 1, which must exclude cytosine from the active site, cytidylate kinase from *D. discoideum* must phosphorylate both cytidine phosphate and uridine phosphate, so the active site must be able to accommodate both substrates. The active site uses a molecule of water that is not controlled by other donors and acceptors, as is the one in double-stranded uracil-DNA glycosylase, to act as a donor for a hydrogen bond to the acyl oxygen at position 4 of the uracil and as an acceptor for a hydrogen bond from the carbamoyl nitrogen–hydrogen at position 4 of the cytosine.[799]

A significantly greater requirement for accommodation is satisfied by the active site of branched-chain-amino-acid transaminase from *E. coli*

L-leucine + 2-oxoglutarate ⇌
4-methyl-2-oxopentanoate + L-glutamate

(3–419)

The same subsite in the active site must recognize both the polar side chain of glutamate and the nonpolar side chain of leucine as well as those of isoleucine and valine. The subsite is a hydrophobic tube into which the isobutyl, 2-butyl, and isopropyl groups of leucine, isoleucine, and valine, respectively, can insert, as well as the two methylenes of the glutamate, and the tube has four donors at its

end that form hydrogen bonds with the carboxylato group of the glutamate when it is in the subsite or among themselves and molecules of water when it is not.[800]

Thermolysin catalyzes the hydrolysis of peptide bonds to the amino-terminal side of hydrophobic amino acids such as alanine, valine, leucine, isoleucine, and phenylalanine almost exclusively.[801,802] The reliability of this specificity results from the expandable, exclusively hydrophobic pocket observed in the crystallographic molecular model at the location in the active site where the side chain on a reactant associates on the carboxy-terminal side of the point of cleavage (Figure 3–42). Phospholipase A_2 from *Naja atra* must recognize phospholipids that have the usual heterogeneous mixture of fatty acyl substituents at oxygens 2 and 3 of the glycero group. Consequently, it has a deep, flexible pocket lined entirely by hydrophobic side chains to accommodate indiscriminately the long alkyl and alkenyl chains.[447]

The **transaminases** that use pyridoxal phosphate as a prosthetic group are particularly good examples of active sites that must recognize two substrates at the same subsite of the complete mold. During transamination, an amino group is transferred from an amine to a 2-oxo acid, usually 2-oxoglutarate. The 2-oxo acid becomes an α-amino acid, usually L-glutamate, and the amine becomes the respective ketone, in which the oxygen of a carbonyl group replaces the amino group, just as the amino group replaced the oxygen of a carbonyl on the 2-oxo acid. The order of the steps in the forward reaction is mechanistically the same as the order of the steps in the reverse reaction. Because of this symmetry, a subsite within the active site has to accommodate equivalently both ketones and both amines and their respective adducts with pyridoxal phosphate. For example, LL-diaminopimelate aminotransferase transfers an amino group from LL-2,6-diaminoheptanedioate to 2-oxoglutarate to produce L-glutamate, which is L-2-aminopentanedioate, and L-2-oxo-6-aminoheptanedioate. The reaction takes place in LL-2,6-diaminoheptanedioate and L-glutamate at the 2-amino groups and in the respective ketones at the 2-oxo groups, but the functional groups attached to the carbons 2, a 4-amino-4-carboxybutyl group and a 2-carboxyethyl group, respectively, differ significantly in length and substitution. Nevertheless, they must be accommodated by the same subsite in the active site.

In contrast to the subtle arrangement of acceptors for hydrogen bonds necessary to recognize both arginines and lysines in the specificity pocket of trypsin, the arrangement of donors for hydrogen bonds necessary to recognize both L-glutamate and LL-2,6-diaminoheptanedioate in the specificity pocket of LL-diaminopimelate aminotransferase from *A. thaliana*[803] is more straightforward. The 6-carboxylato group in the substrate LL-2,6-diaminoheptanedioate and its various adducts with pyridoxal phosphate is two methylenes further away from its carbon 2 than the 4-carboxylato group in the substrate L-glutamate is from its carbon 2, and there is the additional ammonio group in the former. Nevertheless, the same donors to the 6-carboxylato group in LL-2,6-diaminoheptanedioate and its adducts, two tyrosines and a lysine, are used in the same roles to the 4-carboxylato group of L-glutamate and its adducts. The two extra methylenes in LL-2,6-diaminoheptanedioate are accommodated by kinking the longer alkane. The additional 6-ammonio group in LL-2,6-diaminoheptanedioate, immediately adjacent to the 6-carboxylato group, occupies a pocket that is occupied by disordered molecules of water when L-glutamate is in the active site. Two of these disordered molecules of water become fixed as acceptors for hydrogen bonds from the ammonio group, and the third nitrogen–hydrogen of the ammonio group forms a hydrogen bond with the carbamoyl group in the side chain of an asparagine. This carbamoyl group was hydrated in the complex with L-glutamate by the disordered molecule of water taking the place of the ammonio group in LL-2,6-diaminoheptanedioate.

In a much less dramatic example, the same arginine, with the same canonical hydrogen bonds (**3–111**), recognizes both the β-carboxylato group of L-aspartate and its adducts and the γ-carboxylato group of L-glutamate and its adducts in the active site of aspartate transaminase (Equation 3–410).[709]

Because it transfers the amino group from L-histidinol phosphate (**3–117**) to 2-oxoglutarate to produce 3-(imidazol-4-yl)-2-oxopropyl phosphate and L-glutamate (**3–118**)

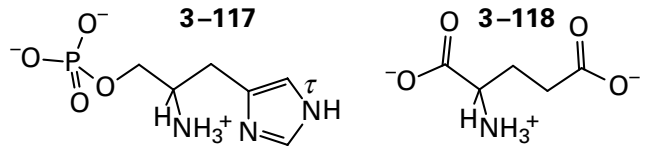

histidinol-phosphate transaminase has to accommodate both the substrate L-histidinol phosphate and its adducts, as well as L-glutamate and its adducts. In the active site of the enzyme from *E. coli*, the guanidinio group of Arginine 386 forms canonical hydrogen bonds (**3–111**) with the α-carboxylato

group of L-glutamate and donates the same nitrogen–hydrogens to two of the oxyanions of the phospho group in L-histidinol phosphate. An amido nitrogen–hydrogen from the carbamoyl group of Asparagine 194 donates a second hydrogen bond to one of the oxyanions of the α-carboxylato group of L-glutamate and donates a second hydrogen bond to the oxyanion of the phospho group of L-histidinol phosphate that ends up in the same location. A molecule of water fixed in position by Aspartate 109 acts as a donor in a hydrogen bond with the 4-carboxylato group of L-glutamate, and Aspartate 109 by itself acts as an acceptor to the τ-nitrogen of the imidazolyl group of L-histidinol phosphate. Because L-histidinol phosphate has more donors and acceptors for hydrogen bonds than L-glutamate, the remainder of the donors and acceptors to L-histidinol phosphate and its adducts are unique. A reasonable cup for the phospho group, with two donors for each oxyanion, and two acceptors for the two donors on the imidazolio group are provided by the active site.[804]

In the case of transaminases, because two different amines or amino acids have to engage in the same nucleophilic addition to the internal pyridoximine, the subsite that recognizes one of the substrates must recognize the other substrate but also exclude other amines and amino acids. The active sites in these enzymes have evolved to employ a strategy where the prosthetic pyridoxal phosphate remains in a fixed location in the active site while the different substrates add to it from within the same subsite. If, however, the substrates that are required to participate in reactions with a prosthetic group are dramatically different in structure, the active site may be constructed in such a way that **the prosthetic group moves between two subsites** for the substrates, rather than the two substrates occupying the same subsite. For example, the reduced prosthetic flavin in the active site of L-ornithine N^5-monooxygenase (NADPH)

$$\text{L-ornithine} + O_2 + \text{NADPH} \rightleftharpoons N^5\text{-hydroxy-L-ornithine} + H_2O + \text{NADP}^+ \quad (3\text{–}420)$$

becomes oxidized during the hydroxylation of L-ornithine and must be rereduced by NADPH, two substrates that differ considerably in structure. In crystallographic molecular models of the active site of the enzyme from *Kutzneria* occupied by various substrates, a significant movement of 0.6 nm within the active site of the 7,8-dimethylisoalloxazine of the prosthetic flavin adenine dinucleotide was observed that shifts it back and forth between the subsite with which NADPH associates and the subsite with which L-ornithine associates.[805]

As is illustrated by the active site of aristolochene synthase (Figure 3–49), there are also **subsites within certain active sites that must accommodate two orientations of the same intermediate**. For example, in the crystallographic molecular model of phosphoglycerate mutase from *Leishmania mexicana*, the active site is occupied by an equilibrium mixture of the sole reactant 3-phospho-D-glycerate and the sole product 2-phospho-D-glycerate. In this equilibrium mixture within the active site, the reactant and the product differ in their conformation and orientation only by a 120° rotation around the bond between carbons 1 and 2 while the carboxylato group remains fixed in position. The rotation is accompanied by a tilt that nevertheless retains the position of the two carboxylato oxygens

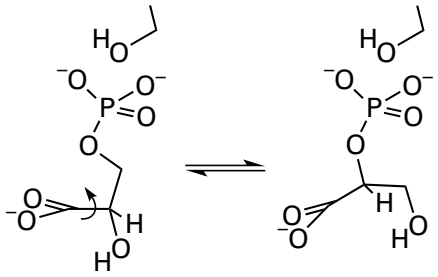

3-phospho-D-glycerate 2-phospho-D-glycerate (3–421)

but brings the phospho group on carbon 2 of 2-phospho-D-glycerate into the same position it occupies on carbon 3 of 3-phospho-D-glycerate.[806] In the enzymatic reaction, the phosphate is transferred from oxygen 3 to Serine 75 to give the intermediate D-glycerate, the rotation and the tilt of the intermediate D-glycerate take place, and the phospho group is then transferred to oxygen 2 from Serine 75.

In the active site of UDP-glucose 4-epimerase (previously Equation 1–88)

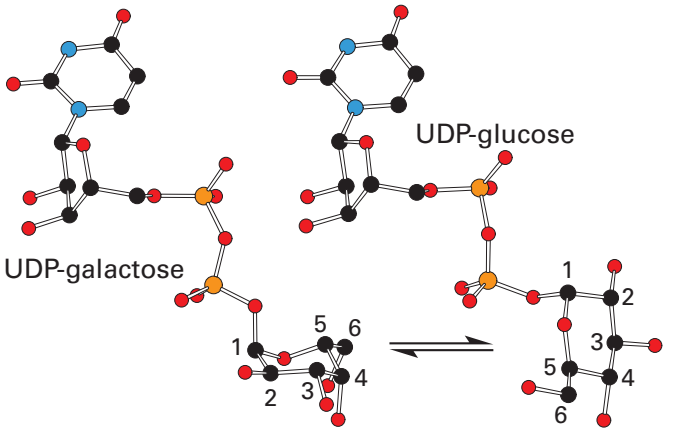

(3–422)

a hydride is removed from carbon 4 of UDP-galactose by the prosthetic NAD^+ in the active site, and the resulting 4-oxoglucopyranosyl group of UDP-4-dehydroglucose pivots so that the hydride can be added by the stationary NADH to the side of the 4-oxo group opposite the side from which it was removed to produce UDP-glucose.* Carbon 4 of the hexose and its hydroxy group are held in exactly the same orientation and position by the active site in both UDP-galactose and UDP-glucose (Equation 3–422). This reorientation of the intermediate 4-oxopyranose is defined by crystallographic molecular models of complexes between an inactive mutant of the enzyme from *E. coli* and either UDP-galactose or UDP-glucose (Equation 3–422).[807] In a related (28% identity; 3.0 gap percent) enzyme, UDP-glucuronic acid 4-epimerase from *B. cereus*, when crystallographic molecular models of the active site occupied by the reactant and product, UDP-D-glucuronic acid and UDP-D-galacturonic acid, which in the active site in the crystal are in equilibrium with each other, are superposed, the epimeric carbons 4 in the two substrates occupy identical positions even though the two pyranoses have flipped over.[587]

In a crystallographic molecular model (Figure 3–52)[808] of the complex between porcine aconitate hydratase

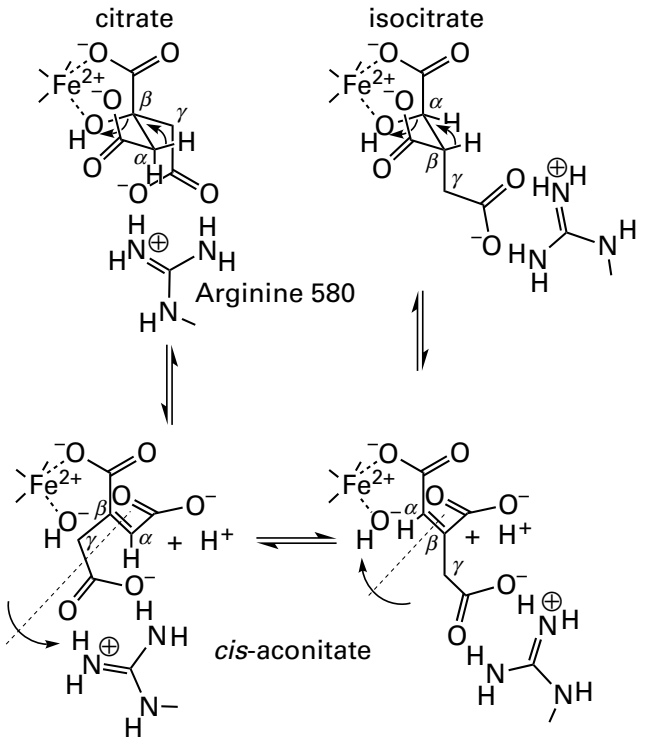

(3–423)

and isocitrate, the isocitrate coordinates only one of the iron ions, a Fe^{2+},[809] in a prosthetic [4Fe–4S] iron–sulfur cluster with its α-hydroxy group and one of the oxygens* in its α-carboxylato group (upper right structure in Equation 3–423).[810] In the crystallographic molecular model between citrate and an inactive mutant of bovine aconitate hydratase in which Serine 642† has been changed to alanine, one of the oxygens of the β-carboxylato group and the β-hydroxy group of the citrate occupy the same two coordination sites on the Fe^{2+}.[811] In each case, the hydroxy group that is bound to Fe^{2+} is the one that leaves as ferrous hydroxide from both isocitrate and citrate, respectively, to produce *cis*-aconitate.

The *cis*-aconitate then must reorient in the active site, switching its coordination from its α-carboxy group to its β-carboxy group or vice versa (lower equilibrium in Equation 3–423). During this change in ligation, the *cis*-aconitate, when it is unliganded to the iron, pivots on the two σ bonds between the carbon–carbon double bond and the γ-carboxylato group while the γ-carboxylato group remains fixed

*Convince yourself that, in the drawing of UDP-galactose and UDP-glucose in Equation 3–422, the hydrogen on carbon 4 has the opposite stereochemistry even though it is pointed in the same direction, namely, the direction of the nicotinamide.

*This coordination resembles the coordination of the molybdenum ion in the [Mo–7Fe–9S–C] cluster of dinitrogenase by homocitrate (Figure 2–62).

†The hydroxy group of Serine 642 is equidistant (0.34–0.36 nm) from one oxygen in each of the three carboxy groups of isocitrate (Figure 3–52) but does not seem to form a hydrogen bond with any of them.

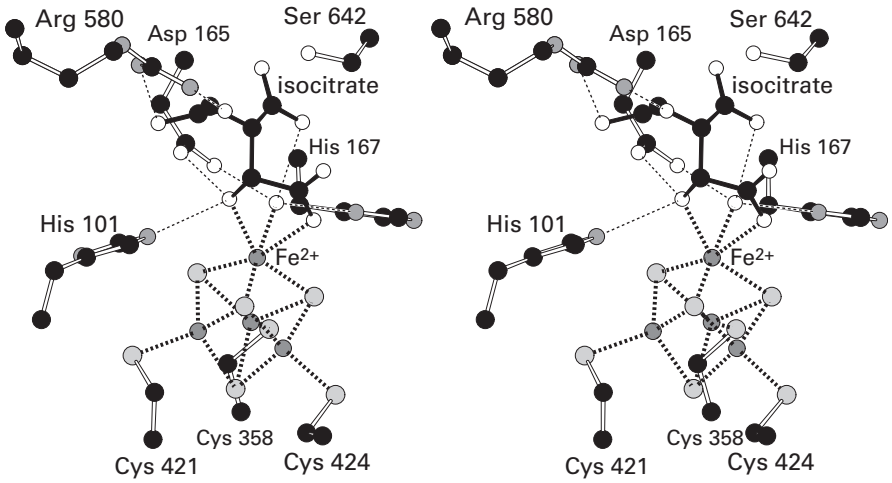

Figure 3–52: Stereodrawing[576] of the crystallographic molecular model of the active site of unmodified, enzymatically active porcine aconitate hydratase occupied by the substrate isocitrate.[808] Black atoms are carbons, white atoms are oxygens, small gray atoms are nitrogens, and large light gray atoms are sulfurs. In the iron–sulfur clusters, large light gray spheres are sulfides and small dark gray spheres are iron ions.The enzyme was purified from porcine heart, activated with 2 mM ferrous ammonium sulfate and 2 mM sodium dithionite, and crystallized in 2.4 M ammonium sulfate, 15 mM 1,2,3-tricarboxypropane, 20 mM citrate, and 60 mM 2-amino-2-(hydroxymethyl)propane-1,3-diol at pH 7.8. A data set to Bragg spacing of 0.20 nm was collected. Electron density consistent only with isocitrate was observed in the active site even though the enzyme was crystallized in the presence of only citrate. The isocitrate was a ligand to the iron ion in the [4Fe–4S] iron–sulfur cluster that lacks a cysteine as a fourth tetrahedral ligand (iron at top corner) while all the other iron ions have a cysteine as their fourth ligands. This iron ion is hexacoordinate rather than tetrahedral as the others are, and it is a ferrous ion.[809] Three of its open coordination sites are filled by the three sulfides of the cluster. The isocitrate provides two ligands to the hexacoordinate Fe^{2+}: its 2-hydroxy group and its 1-carboxylato group. The final ligand to the Fe^{2+} is a molecule of water that acts as a Brønsted acid that hydronates the 3-carboxylato group of the isocitrate by relaying the acidity of Aspartate 166 or Histidine 167. *cis*-Aconitate performs a pivot in the active site so that its 1-carboxylato group (the α-carboxylato group in Equation 3–423) is replaced as a ligand to the hexacoordinate Fe^{2+} by its 3-carboxylato group (the β-carboxylato group in Equation 3–423). Following the pivot, the 1-carboxylato group of *cis*-aconitate that left the Fe^{2+} ends up with its two oxygens in the same pocket that was occupied by the two oxygens of the 3-carboxylato group that is now on the Fe^{2+}. This retention of position can be visualized by moving in your imagination the carboxymethyl group from carbon 2 of the isocitrate to carbon 3, thus creating citrate, and rotating the carboxymethyl group until its two oxygens end up in the same place that they were before you moved the carboxymethyl group.

by the two canonical hydrogen bonds between its two oxygens and the two ω-amido nitrogens of Arginine 580 as well as four other donors. After the pivot, the hydroxy group of the ferrous hydroxide can be added to the other end of the carbon–carbon double bond so that isocitrate can be turned into citrate or citrate can be turned into isocitrate. Both before and after the pivot, the two oxygens of the α-carboxylato group in citrate and the two oxygens of the β-carboxylato group in isocitrate, respectively—in each case the carboxylato group that is neither a ligand to the Fe^{2+} nor the acceptor for the hydrogen bonds from Arginine 580—end up in the same pocket in the active site. In this pocket, the two oxygens of the α-carboxylato group before the pivot or the β-carboxylato group after the pivot are acceptors in six hydrogen bonds. While it is pivoting and neither of these carboxylato groups is associated with this pocket or with the Fe^{2+}, the loosely held *cis*-aconitate often leaves the active site, so there is always a significant concentration of *cis*-aconitate in the solution or the cytoplasm, and it enters and leaves the active site while the net conversion of citrate to isocitrate or the net conversion of isocitrate to citrate is proceeding.

The crystallographic molecular models of complexes between an enzyme and its substrates, prosthetic groups, or inhibitors define the boundary of the active site within which the reactants associate and at which they are converted to products. This active site will usually be a crevice, closed box, or tubular hole[812] deep enough, wide enough, and long enough to accommodate all the reactants when they are bound to the enzyme simultaneously. Its walls—from which protrude the functional groups that recognize the substrates, provide free energy of association, and catalyze the reaction—are formed from strands of the polypeptide comprising the protein. Although there are multienzymatic complexes that have active sites for more than one catalytic activity,[813] such as the multienzymatic complexes for fatty acid synthesis, the active sites of most enzymes are constructed to catalyze only one reaction or two or more closely related reactions.

In a monomeric enzyme, each molecule of the protein has an active site at a unique location on its surface or in its interior. Almost all enzymes, however, are oligomers formed from two or more protomers. In an oligomeric enzyme, each molecule of **the oligomer almost always contains as many active sites as there are protomers**. Usually, the active sites are all identical to each other, they are formed from strands of polypeptide that are all from the same protomer, and they are distributed over the surface or the interior of the oligomer by the same symmetry operations that govern the arrangements of the protomers themselves.[814] There are, however, many examples in which an active site in an oligomeric protein is constructed from strands of polypeptide from more than one of the protomers. In most of these instances, strands of polypeptide from two protomers form the active site, but in rare cases, an active site is constructed from strands of polypeptide from three protomers,[815-817] and in at least one instance, an active site is formed from strands of polypeptide from four of its protomers.[818,819] In such situations, the active site, by definition, lies within an interface or interfaces in the oligomer.

When an **active site is formed from strands of polypeptide from more than one protomer**, there can be two outcomes. The two or three protomers that form the interface or interfaces within which the active site is located are almost always related to each other by a twofold rotational axis of symmetry[820] or a threefold rotational axis of symmetry,[821] respectively. If the rotational axis of symmetry runs through the active site, it necessarily follows that the same amino acids from each protomer form the active site, and therefore there can only be one active site that is formed by the two or three protomers. In such a situation, the number of active sites in the oligomer will be equal to half or a third the number of protomers, respectively. If, however, the active site is formed from strands of polypeptide from only two of the protomers in the oligomer and the twofold rotational axis of symmetry relating them is far enough from the active site that all the strands of polypeptide forming an active site are unique, then there will be two active sites in the interface between the two protomers related by the axis of symmetry. In this instance, the number of active sites in the oligomer will be equal to the number of protomers. This equivalence is the usual case because an active site with an axis of symmetry running through it has difficulties associating with asymmetric substrates.

Ribulose-bisphosphate carboxylase[812]

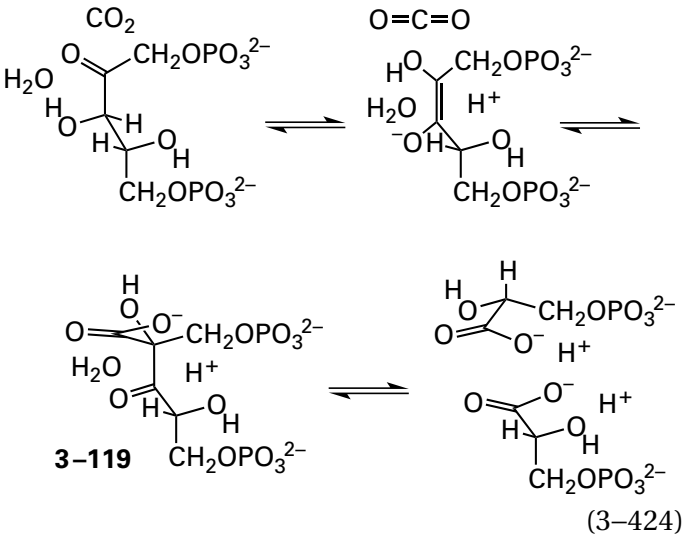

(3–424)

from *Spinacia oleracea* is composed of eight copies of a folded α polypeptide (475 aa) and eight copies of a folded β polypeptide (123 aa). The octamer contains four α_2 dimers arranged around a fourfold rotational axis of symmetry, and the two twofold rotational axes of symmetry relating the subunits within the α_2 dimers are both normal to, and intersect perpendicularly at, the fourfold rotational axis of symmetry. Only the β subunits link the four α_2 dimers together around the fourfold axis of symmetry, so each α_2 dimer is an independent unit of the higher structure. Each α_2 dimer of ribulose-bisphosphate carboxylase contains **two active sites symmetrically displayed on opposite sides of the twofold rotational axis of symmetry** of that α_2 dimer. These two identical and symmetrically related active sites both lie within the interface between the two α subunits. The amino acids that form each of the two active sites (Figure 3–53)[812] are Threonine 171, Lysine 173, Lysine 175, Threonine 198, Aspartate 200, Glutamate 202, Histidine 292, Arginine 293, Histidine 325, Lysine 332, Leucine 333, Serine 377, Glycine 378, Glycine 379, Glycine 401, and Glycine 402 from one subunit (designated A in the figure) and Glutamate 58, Threonine 63, Tryptophan 64, and Asparagine 121 from the adjacent subunit across the interface (designated B in the figure). In no case is the same amino acid from both subunits present in the same active site, so there can be two active sites in each α_2 dimer.

This catalogue of the amino acids forming the active site of ribulose-bisphosphate carboxylase illustrates the fact that an active site is formed from **a cluster of neighboring amino acids in the structure of the protein, regardless of their covalent affiliation.** The only purpose for which the polypeptide has folded to form a globular structure and for which this globular structure has been created by natural selection is to gather these amino acids in proper alignment to catalyze the enzymatic reaction. Because the polypeptide folds into a complexly ordered, globular structure, amino acids distant in the sequence of amino acids or from different polypeptides are brought together opportunistically to form an active site.[822]

If it is unknown, but suspected for some reason, that an active site is composed of amino acids from two different subunits, this suspicion can be examined by **complementation**. An oligomer of an enzyme that has been mutated at one amino acid so that it is enzymatically inactive is mixed, under conditions where the subunits or the oligomer can interchange, with an inactive oligomer of the same enzyme that has been mutated at a different amino acid. If the enzymatic activity returns, one explanation is that the unmutated amino acid on the one subunit has joined the unmutated amino acid on the other in a now unmutated active site. For example, when Histidine 68 in the active site of adenylosuccinate lyase from *B. subtilis* is mutated to a glutamine or Histidine 141 is mutated to an alanine, the resulting mutants are each enzymatically inactive. When equal amounts of the two inactive mutants are mixed together in 20 mM NaCl at pH 7 and 25 °C for 12 h, enzymatic activity returns. The final level of reconstituted activity is equal to 15% of the level expected for the concentration of active sites present. If Histidine 68 from one subunit and Histidine 141 from an adjacent subunit are part of the same active site at the interface between the two subunits in adenylosuccinate lyase, the probability that unmutated Histidine 68 from one subunit and unmutated Histidine 141 from the other subunit end up in the same active site, if the subunits interchanged completely and at random, should be 25%, close to the observed value.[823] A yield of 25% has been observed in another complementation.[824]

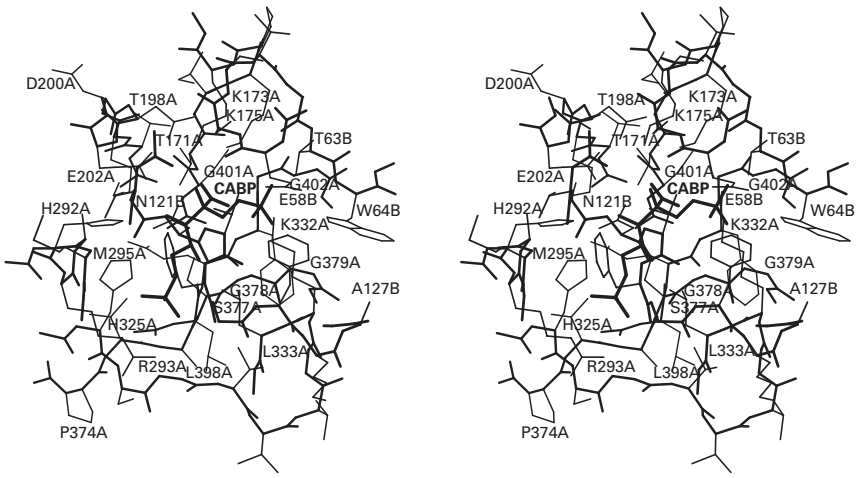

Figure 3–53: Stereodrawing[576] of the crystallographic molecular model of the active site of ribulose-bisphosphate carboxylase from *S. oleracea* occupied with 2-carboxy-D-arabinitol 1,5-bisphosphate, an analogue for intermediate **3–119** in the enzymatic reaction (Equation 3–424).[812] The complex between ribulose-bisphosphate carboxylase and 2-carboxy-D-arabinitol 1,5-bisphosphate was crystallized from a solution of ammonium sulfate. The phases of the reflections were determined by multiple isomorphous replacement with three derivatives. A model of the polypeptide was inserted into the initial map of electron density, and the resulting molecular model was used to initiate refinement. After several cycles of refinement, a molecular model of 2-carboxy-D-arabinitol 1,5-bisphosphate (CABP) was inserted into the difference map of electron density within a feature of positive electron density that was unmistakably the correct size and shape. Refinement then proceeded to a final *R*-factor of 0.24. The view is of the analogue (in thick lines) surrounded by segments of the polypeptide creating the active site. The polypeptide backbone is drawn with lines of intermediate width, and the side chains are drawn with thin lines. In the final crystallographic molecular model, the active site is a blind tube, open at one end to the solution, into which the 2-carboxy-D-arabinitol 1,5-bisphosphate has inserted. It is formed from eight strands of polypeptide, six from one subunit (designated A) and two from an adjacent, identical subunit related to the first by a twofold rotational axis of symmetry (designated B).

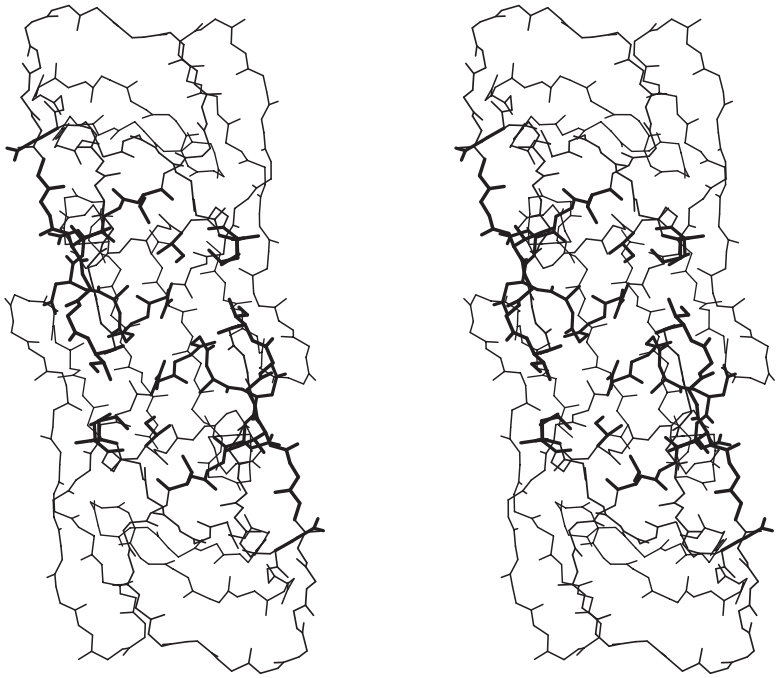

Figure 3–54: Stereodrawing[576] of the crystallographic molecular model of the α_2 dimer of aspartic endopeptidase from human immunodeficiency virus type 1 group M subtype B (isolate BH10).[825-828] The viral enzyme was expressed in *E. coli* and crystallized. The space group of the crystals was $P4_12_12$ with a single folded polypeptide in the asymmetric unit and related to an immediately adjacent asymmetric unit by an exact crystallographic twofold rotational axis of symmetry. Together these two folded, symmetrically related polypeptides form one molecule of the enzyme. The phases of the reflections to 0.3 nm were determined by molecular replacement using a previous crystallographic molecular model of the protein, and the resulting crystallographic molecular model was refined against a data set with Bragg spacing to 0.14 nm. The drawing is of the polypeptide backbones (thin lines) of the two folded polypeptides in the refined crystallographic molecular model of the complete molecule of the enzyme. The exact twofold rotational axis of symmetry of the molecule is normal to the plane of the page. Those portions of the polypeptide backbones and those side chains of the amino acids that make contact with peptide in complexes between the enzyme and substrates or peptidic inhibitors[829,830] are highlighted by thicker lines. The active site that is defined by these thicker lines runs diagonally across the enzyme as drawn from top left to bottom right. The active site makes contact with as many as ten amino acids in the polypeptide that it cleaves, which stretches in an elongated conformation across the active site. Two symmetrically displayed flaps of polypeptide form two symmetric arches enclosing the active site and the substrate.

One of the more unusual active sites is that in the aspartic endopeptidase from human immunodeficiency virus type 1 (Figure 3–54).[822,825-830] The protein is an α_2 dimer composed of two identical polypeptides (99 aa). It is a member of a family of aspartic endopeptidases that includes the pepsins from animals. Most of the other members of the family, however, are composed of folded polypeptides at least twice as long. These larger proteins all have an internal duplication that resulted from a gene duplication, and the two internally repeating domains, each of which is superposable on a single subunit of the dimeric viral enzyme, are arranged around a twofold rotational axis of pseudosymmetry that passes through the one protomer. In the large aspartic endopeptidases, this axis of pseudosymmetry passes through the one active site formed by the single folded polypeptide. In the viral aspartic endopeptidase, however, each of the two identically folded polypeptides assume the same position as one of the two domains in a larger aspartic endopeptidase, the protein is an α_2 dimer containing only one active site, the two folded polypeptides are arranged around a twofold rotational axis of symmetry, and **the twofold rotational axis of symmetry in the α_2 dimer passes through the center of the single active site** (Figure 3–54).

The peculiar aspect of this situation is that although the active site of the viral aspartic endopeptidase is symmetric in the unoccupied enzyme, its reactant, a strand of polypeptide that it is designed to cleave, is completely asymmetric, a fact that presents the difficulty already noted. When the reactant associates with the active site, the conformation of each subunit changes to complement the distinct sequence of five amino acids with which it associates on its side of the point of cleavage, so in the complex the conformations of the two protomers have become different from each other.[829,830] This plasticity within the active site contrasts with the rigidity of the active site in a terpene synthase but is a common feature of an endopeptidase that must accept many different sequences of amino acids. The symmetry of the unoccupied active site, however, can be exploited in designing inhibitors for a viral aspartic endopeptidase. A twofold rotationally symmetric inhibitor was synthesized that was bound tightly ($K_i = 5$ nM) to the aspartic endopeptidase from human immunodeficiency virus type 1.[831]

The larger, internally duplicated aspartic endopeptidases are examples of one of the **outcomes that can result from gene duplication**. As with these endopeptidases, the active site of diaminopimelate epimerase from *H. influenzae* also sits at the twofold rotational axis of pseudosymmetry in a monomeric protein that has two internally repeating domains.[832] Lactoylglutathione lyase from *S. cerevisiae*, however, has two internally repeating domains, each of which forms its own active site, so there are two functional active sites on each monomer of this enzyme, each catalyzing the same reaction.[833] Some of the internally duplicated hexokinases have one functional active site on each of the two internally repeating domains, two for each folded polypeptide, while in others, one of the active sites has become defunct.[834]

Suggested Reading

Gouaux, J. E., and Lipscomb, W. N. (1988) Three-dimensional structure of carbamoyl phosphate and succinate bound to aspartate carbamoyltransferase, *Proc. Natl. Acad. Sci. U. S. A. 85*, 4205–4208. https://doi.org/10.1073/pnas. 85.12.4205

Cheong, C.-G., Escalante-Semerena, J. C., and Rayment, I. (1999) The three-dimensional structures of nicotinate mononucleotide:5,6-dimethylbenzimidazole phosphoribosyltransferase (CobT) from *Salmonella typhimurium* complexed with 5,6-dimethybenzimidazole and its reaction products determined to 1.9 Å resolution, *Biochemistry 38*, 16125–16135.https://doi.org/10.1021/bi991752c

Teh, A.-H., Kimura, M., Yamamoto, M., Tanaka, N., Yamaguchi, I., and Kumasaka, T. (2006) The 1.48 Å resolution crystal structure of the homotetrameric cytidine deaminase from mouse, *Biochemistry 45*, 7825–7833. https://doi.org/10.1021/bi060345f

Matos, J. O., Kumar, R. P., Ma, A. C., Patterson, M., Krauss, I. J., and Oprian, D. D. (2020) Mechanism underlying anti-Markovnikov addition in the reaction of pentalenene synthase, *Biochemistry 59*, 3271–3283. https://doi.org/10.1021/acs.biochem.0c00518

Problem 3–30: Methotrexate

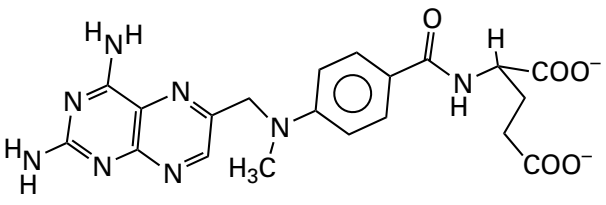

is a strong inhibitor of dihydrofolate reductase that is competitive with respect to dihydrofolate, which it closely resembles. A view of a portion of the crystallographic molecular model of the complex between methotrexate and the active site of dihydrofolate reductase from *L. casei* is presented in the following figure. There are six hydrogen bonds, indicated with dashed lines, between the pteridinyl group of the inhibitor and the active site.

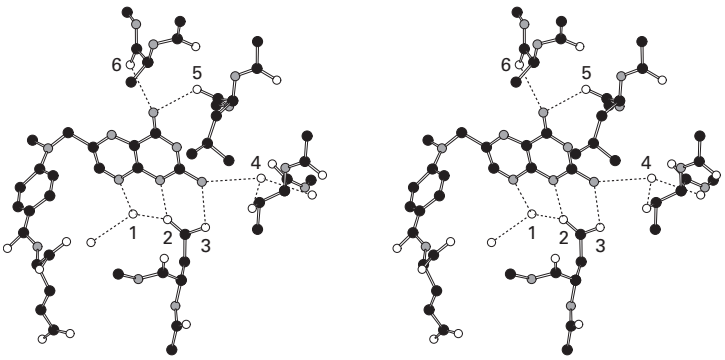

(A) Identify by their numbers the donor or acceptor to the methotrexate in each of the six hydrogen bonds. Identify the amino acid side chain by naming the amino acid, identify an atom from the peptide backbone by naming the functional group, and identify any other donor or acceptor by its name.

(B) Draw the σ structure of only the pteridinyl group of methotrexate. Include all σ lone pairs of electrons and acidic hydrons in their proper orientations. As an afterthought, to make your drawing more familiar, add π electrons distributed as they would be in one of the resonance structures.

(C) Around the pteridine ring in your drawing, place the functional groups that form the hydrogen bonds seen in the figure. Draw each functional group fully enough so that it is clear what it is. Draw each functional group with the proper size to match your drawing of the pteridine ring. Orient each functional group so that an ideal hydrogen bond is formed in each instance. Put σ lone pairs on the acceptors for hydrogen bonds in the proper orientations. Put acidic hydrogens on the donors for hydrogen bonds in the proper orientations. Choose one of the resonance hybrids of the functional groups.

(D) Two of the hydrogen bonds as they are formed in the crystallographic molecular model are not in the ideal configuration. Which two are they and why are they not ideal? Why does it not matter?

The following figure is a view of the active site in the crystallographic molecular model of bovine chymotrypsin.[835] The narrow dashed lines are supposed to indicate hydrogen bonds.

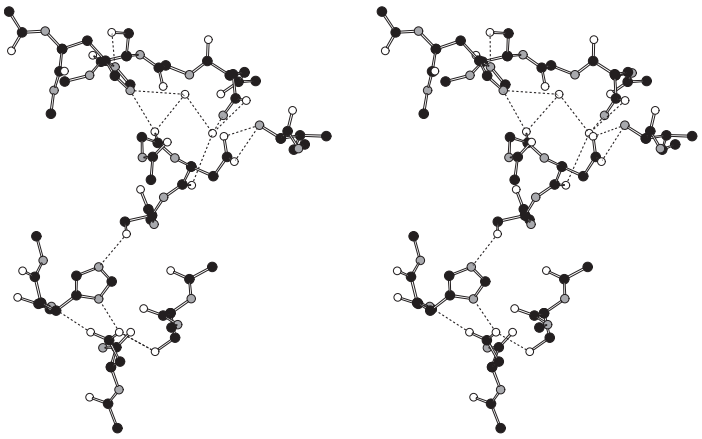

(E) Make a list identifying both the donor and the acceptor in each of the 14 hydrogen bonds. Identify the amino acid side chain by naming the amino acid, identify an atom from the peptide backbone by naming the functional group, and identify any other donor or acceptor by its name.

(F) Attempt to draw out each hydrogen bond with the care you exercised in your answer to part B.

(G) If you have done your work carefully enough, you will have found at least three hydrogen bonds indicated in the figure that are formally impossible for electronic or steric reasons. Identify each formally impossible hydrogen bond and describe why each is impossible.

(H) Assume that the crystallographer knew these were impossible as written and meant to indicate a different arrangement from single hydrogen bonds. Provide a reasonable explanation for what may be happening at each formally impossible location.

Problem 3–31: What information would be obtained from the crystallographic molecular model of the complex between *P*1,*P*5-bis(5′-adenosyl) pentaphosphate and adenylate kinase?[836]

Problem 3–32: What information can be gained from a crystallographic molecular model of the complex between deoxyuridine 5′-diphosphate and dUTP diphosphatase?[837]

$$MgdUTP^{2-} + H_2O \rightleftharpoons dUMP^{-} + MgOPO_3PO_3^{2-} + H^+$$

Problem 3–33: Draw the structures of the two reactants that the bisubstrate analogue **3–87** for spermidine synthase combines into one molecule. Draw them next to a drawing of bisubstrate analogue **3–87** so that it is clear which parts of the analogue mimic which reactant.

Problem 3–34: (1*S*)-1-Diphospho-(2*R*,3*R*)-dihydroxy-(4*S*)-4-(phosphoryloxymethyl)cyclopentane[838] forms inactive complexes with phosphoribosyl transferases and the acceptor to which the phosphoribosyl group is transferred. These complexes can be crystallized, and in the crystallographic molecular models the alignment of the acceptor and the analogue producing the phosphoribosyl transfer can be observed.[839] Why is this analogue inactive in the enzymatic reaction?

Problem 3–35: Tartrate dehydrogenase catalyzes three different reactions:[41]

$$(R,R)\text{-tartrate} + NAD^+ \rightleftharpoons (R)\text{-oxaloglycolate} + NADH + H^+$$

$$(R,S)\text{-tartrate} + NAD^+ + H^+ \rightleftharpoons CO_2 + (R)\text{-glycerate} + NAD^+$$

$$(R)\text{-malate} + NAD^+ \rightleftharpoons CO_2 + \text{pyruvate} + NADH$$

The enzyme has a Mn^{2+} as a prosthetic group in its active site.

(A) Draw each reactant in a sawhorse representation, with the *R* carbon of each reactant in front and in the same orientation. Draw the carbon in back of your structures of (*R*,*R*)-tartrate and (*R*,*S*)-tartrate with the hydroxy group in the orientation in which it can share the Mn^{2+} in the active site with the carboxy group on the front carbon in a metallocyle with six atoms.

(B) Explain the results of the three reactions in terms of these three structures that you just drew by making your mechanisms as similar as possible, aligning orbitals to permit the required overlap, and completing each reaction with least nuclear motion.

Problem 3–36: One way to verify that an active site is formed from strands of polypeptide from two different protomers in an oligomer is to perform a hybridization of mutants to assess complementation.[840-843] Suppose that Tyrosine 85 from one protomer and Lysine 273 from another protomer in an oligomeric enzyme participate in the same active site. Tyrosine 85 can be mutated to alanine (Y85A) and Lysine 273 can be mutated to alanine (K273A), and oligomers with only Y85A protomers and oligomers with only K273A protomers are both completely inactive.

(A) If equimolar amounts of each mutant oligomer are mixed together, the oligomers dissociate into monomers, and the monomers then reassociate into oligomers at random. What are the four different types of active sites that would result from the hybridization?

(B) In what ratio would these four different active sites be present in the final hybrids?

(C) What would be the enzymatic activity of this final mixture of hybrids relative to that of the unmutated, wild-type enzyme?

(D) Suppose a constant concentration of Y85A homooligomer is mixed with increasing concentrations of K273A homooligomer, the oligomers dissociate, and the monomers reassociate at random. Derive an equation for the fraction of Y85A protomers that would be associated with K273A homooligomers in the final mixture of hybrids.[844]

(E) In the experiment described in part D, what would be the enzymatic activity for each mole of Y85A protomer relative to the enzymatic activity for each protomer in the wild-type enzyme at infinite concentration of K273A?

Physical Measurements of Complexes between Enzymes and Ligands

The **same stable complexes between enzymes and substrates and inhibitors** that can be studied crystallographically and that were just discussed at length can also be probed by physical measurements. The most commonly used physical methods for this purpose are infrared spectroscopy, ultraviolet and visible spectroscopy, and nuclear magnetic resonance spectroscopy.

Infrared spectroscopy is used to monitor changes in vibrational modes in a substrate or the analogue of a substrate when it associates with an active site. Although other molecular vibrational modes, such as those of the phosphorus–oxygen bonds in nucleotides and other substrates with phosphate groups,[845,846] can be followed, the strong, characteristic stretching frequency of the carbon–oxygen double bond of a carbonyl group or an acyl group in a substrate or an inhibitor bound in an active site is most often monitored by infrared spectroscopy. When a substrate or an inhibitor is bound in the active site, its infrared vibrational modes overlap those of the protein, so either Fourier transform infrared spectroscopy or Raman infrared spectroscopy, in both of which peaks of absorbance are significantly narrowed, is used for measurements. In addition, in both instances a difference spectrum between a solution of the enzyme alone and a solution of the same concentration of enzyme with the active site occupied by the substrate or inhibitor is used to isolate the vibrational modes of the ligand.

When glycerone phosphate associates with triosephosphate isomerase (Equation 3–384) from *G. gallus*, the stretching frequency of its carbonyl group[847] in a **difference Fourier transform infrared spectrum** between a solution of the enzyme alone and a solution of the enzyme with the active site occupied by glycerone phosphate has a maximum of absorbance at 1713 cm^{-1}. This stretching vibration has been assigned to the carbonyl group of glycerone phosphate when it occupies the active site in its productive orientation. In free solution, the same absorption has a maximum of absorbance at 1732 cm^{-1}. Consequently, there is a shift of –19 cm^{-1} in this absorption upon association of glycerone phosphate with the active site. By site-directed mutation, this shift could be shown to result from the presence of the imidazolyl group of the histidine in the active site[848] that is immediately adjacent to, and that forms a hydrogen bond with, the carbonyl oxygen of glycerone phosphate in the crystallographic molecular model of the occupied active site (Figure 3–37).

19-Nortestosterone is an enone

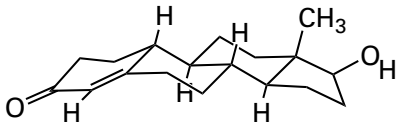

3–120

that is a competitive inhibitor of steroid Δ-isomerase

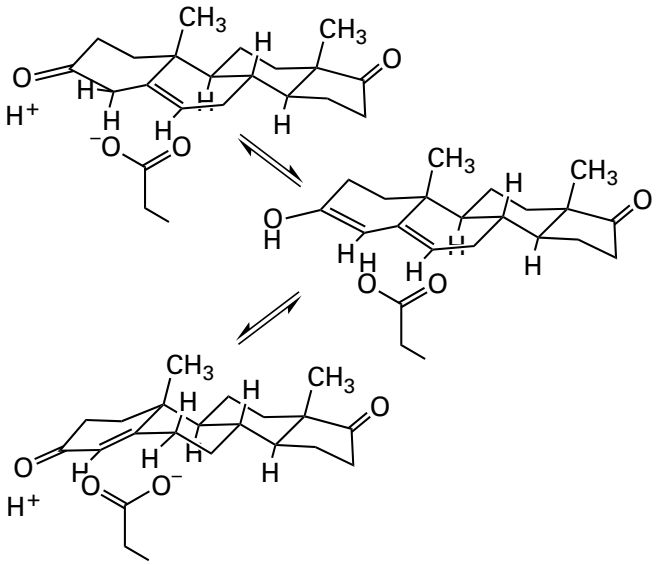

(3–425)

with respect to the substrate androst-5-ene-3,17-dione.[849] A difference Fourier transform infrared spectrum was recorded for 19-nortestosterone when it is occupying the active site of steroid Δ-isomerase from *P. putida*.[850] Upon association of the inhibitor with the active site from the solution, the maximum of absorbance for the stretching frequency of its carbonyl group shifts –46 cm^{-1}, from 1634 to 1588 cm^{-1}.

In a low-resolution structure of the active site of steroid Δ-isomerase from *C. testosteroni* occupied by the succinyl ester of nortestosterone, obtained by two-dimensional nuclear magnetic resonance spectroscopy, both the carboxy group of Aspartate 99 and the hydroxy group of Tyrosine 14 are immediately adjacent to the carbonyl oxygen of the inhibitor.[851] In a high-resolution crystallographic molecular model of the same active site occupied by equilenin, an inhibitor with the same carbon skeleton as 19-nortestosterone in which the two rings to the left in the drawing of **3–120** are aromatic, one of the carboxy oxygens of Aspartate 99 and the hydroxy

group of Tyrosine 14 form compressed (0.26 nm) hydrogen bonds with the hydroxy group that takes the place of the carbonyl carbon of 19-nortestosterone.[852] One of the oxygens of the homologous carboxy group in Aspartate 103 and the homologous hydroxy group in Tyrosine 16 in the active site of the enzyme from *P. putida* form short (0.26 nm) hydrogen bonds with the carbonyl oxygen of 19-nortestosterone (**3–120**) in the crystallographic molecular model of its occupied active site.[853]

When Aspartate 103 of the enzyme from *P. putida* is mutated to a leucine, the maximum of absorbance for the stretching frequency of 19-nortestosterone in the active site shifts +32 cm^{-1} to 1626 cm^{-1}. When Tyrosine 16 is mutated to a phenylalanine,[850] the maximum of absorbance for the stretching frequency shifts +61 cm^{-1} to 1649 cm^{-1}, a value larger than that of the stretching vibration of 19-nortestosterone in solution but not so large as its value in hexane (1690 nm). Both of these results suggest that the red shift observed when 19-nortestosterone associates with the enzyme is **due to both of these hydrogen bonds** and also that the 19-nortestosterone is in a nonpolar environment.

Isotopic editing can be used to assign absorptions in difference Fourier transform infrared spectra. For example, replacing a carbon-12 in a molecule, either synthetically or biosynthetically, with a carbon-13 increases the mass of that atom. The force constants of the bond remain the same, but the increase in mass causes the vibrational modes in which that carbon atom participates to shift to a lower frequency. These shifts in frequency can then be used to identify the absorptions that arise from the vibrational modes in which this carbon participates. For example, when [2-^{12}C]pyruvate is bound in the active site of the complex between NADH and porcine L-lactate dehydrogenase

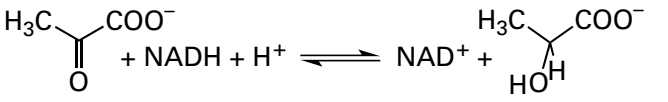

(3–426)

there is a maximum of absorbance in the difference Fourier transform infrared spectrum[854] of the resulting ternary complex at 1679 cm^{-1}. When [2-^{13}C]pyruvate associates with the same complex, the absorption with a maximum of absorbance at 1679 cm^{-1} is no longer present in the difference spectrum and is replaced with an absorption with a maximum of absorbance at 1640 cm^{-1}. The magnitude of the shift to lower frequency is that expected for the shift of the stretching vibration of a carbonyl group as a result of the increase of 1.00 g mol^{-1} in the molar mass of the carbon. Consequently, the maximum of absorbance at 1679 cm^{-1} was assigned to the stretching frequency of the carbonyl group in the [2-^{12}C]pyruvate occupying the active site. The frequency of the maximum of absorbance for the stretching vibration of the carbonyl in [2-^{12}C]pyruvate, which was assigned by isotopic editing, shifts –31 cm^{-1}, from 1710 to 1679 cm^{-1}, when the pyruvate enters the active site from the solution.

By recording a complete difference spectrum between the ternary complex of [2-^{12}C]pyruvate and that of [2-^{13}C]pyruvate with the active site occupied by NADH, **other vibrational modes in which this carbon participates** could also be identified, including a complex vibrational mode in which atoms from both pyruvate and the nicotinamide of NADH participate. This latter result is consistent with the obvious fact that pyruvate and NADH are intimately associated with each other in the active site.

Isotopic editing was also used to identify the stretching vibration of the ureido carbon–oxygen double bond at carbon 2 of orotidine 5′-monophosphate and the stretching vibration of the acyl carbon–oxygen double bond at carbon 4 of orotidine 5′-monophosphate when this substrate occupies the active site of orotate phosphoribosyltransferase

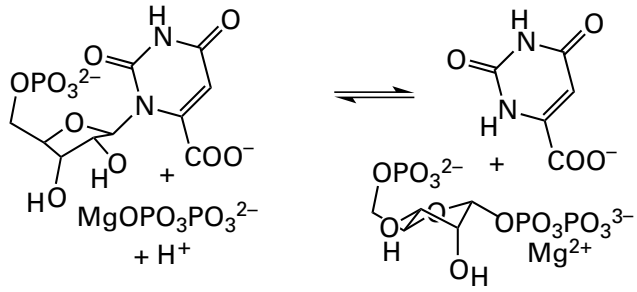

(3–427)

from *Plasmodium falciparum* in the absence of magnesium diphosphate. On the basis of these identifications, it could be unambiguously demonstrated that the frequencies of the maxima of absorbance for both absorptions shift to lower values by –20 cm^{-1} when orotidine 5′-monophosphate associates with the active site. In the crystallographic molecular model of the complex between the enzyme from *S. cerevisiae* and orotidine 5′-monophosphate, the oxygen at carbon 4 participates in two **short (0.26 nm) in-plane hydrogen bonds, trigonal at the oxygen**, with the nitrogen–hydrogen of an ω-guanidinio nitrogen of an arginine and an amido nitrogen–

hydrogen from the polypeptide, and the oxygen on carbon 2 participates in two out-of-plane hydrogen bonds with two fixed molecules of water.[855] Isotopic editing can also be used to identify absorptions from vibrational modes in phospho groups.[846]

Difference Raman infrared spectroscopy can be used to monitor the stretching frequency of the carbon–oxygen double bond of a carbonyl group or an acyl group in a substrate when it is bound in the active site of an enzyme. Again, the difference spectrum is between the spectrum of the unoccupied enzyme and the spectrum of the enzyme occupied by a substrate or an inhibitor. When pyruvate associates with the active sites of L-lactate dehydrogenases (Equation 3–426) from *G. stearothermophilus*, *Squalus acanthias*, and *Sus scrofa*,[856,857] each of which is already occupied by NAD^+, the stretching vibration of its carbonyl group in a difference Raman infrared spectrum decreases by $-42\ cm^{-1}$, from 1710 to $1668\ cm^{-1}$. Isotopic editing was used in this instance to validate the assignment of the absorptions. In the crystallographic molecular model of the complex between the active site of porcine L-lactate dehydrogenase and (3*S*)-5-(3-carboxy-3-hydroxypropyl)-nicotinamide-adenine dinucleotide (**3–89**), there are hydrogen bonds from the hydronated imidazolyl group of Histidine 195 and one of the ω-guanidinio nitrogens of Arginine 109 to the oxygen that is analogous to the carbonyl oxygen of pyruvate.[591]

Within a set of nine seryl-acyl enzyme intermediates (Equation 3–91) for three different serine endopeptidases, the common logarithm of the rate constant for the step in which the acyl intermediate is hydrolyzed (k_3 in Equation 3–91) was a linear function of the observed stretching frequencies (centimeters^{-1}) in the difference resonance Raman infrared spectra for the acyl carbon–oxygen double bond within the active site. As the stretching frequency of the substrate in the active site decreased, the common logarithm of the rate constant increased.[858,859] Each active site has an **oxyanion hole** into which the acyl oxygen in these acyl intermediates fits in the tetrahedral intermediates preceding and following the respective acyl intermediates. The correlation suggests that as the ability of an oxyanion hole to withdraw electron density from the carbon–oxygen double bond increases and the electrophilicity of the carbon increases, the rate of the hydrolysis of the acyl enzyme increases.

An advantage of difference Raman spectroscopy is that **many other infrared absorptions** can be observed in addition to the strong absorption of a carbon–oxygen double bond. For example, the absorptions in a difference Raman spectrum with absorbance maxima at 1650 and $1675\ cm^{-1}$ have been assigned to the stretching vibrations for the bond between unhydronated nitrogen 5 and carbon 6 of the pteridine ring in dihydrofolate and hydronated nitrogen 5 and carbon 6, respectively

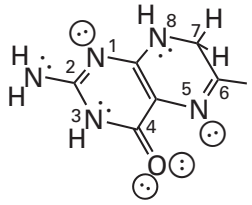

3–121

These absorptions shift reciprocally in relative absorbance with pH when dihydrofolate is in the active site of dihydrofolate reductase (previously Equation 1–89)

$$\text{NADPH} + \text{7,8-dihydrofolate} + H^+ \rightleftharpoons \text{5,6,7,8-tetrahydrofolate} + NADP^+ \quad (3\text{–}428)$$

from *E. coli*, and these reciprocal shifts in absorbance can be used to measure the pK_a of nitrogen 5 when the folate is in the active site.[860]

In the case of the stable ternary complex between equine alcohol dehydrogenase, an enzyme with a prosthetic Zn^{2+} in its active site, and NADH and 4-dimethylaminobenzaldehyde

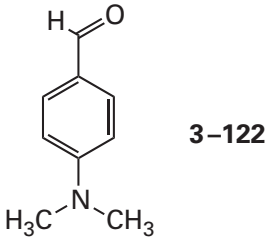

3–122

which is a substrate for the enzyme, a complete difference Raman spectrum for the bound 4-dimethylaminobenzaldehyde could be collected from 300 to $1700\ cm^{-1}$ in which the 16 absorptions create a fingerprint for the substrate. This fingerprint was almost identical to that for the complex between Zn^{2+} and 4-dimethylaminobenzaldehyde in dichloromethane, which was proposed to mimic the situation of the substrate in the active site.[861]

A **resonance Raman infrared spectrum** is observed when a chromophore in the active site is excited by passing a beam of light with a wavelength that is absorbed by that chromophore through the sample perpendicular to the beam from

the laser that is registering the Raman spectrum. The excitation of the chromophore by this perpendicular beam of light enhances the intensity of the absorptions from oscillators in the vicinity of the excited chromophore. For example, there is an oxidized, inactive form of murine cysteine dioxygenase

$$\text{L-cysteine} + O_2 \rightleftharpoons \text{3-sulfino-L-alanine} + H^+ \qquad (3\text{–}429)$$

that has mononuclear, nonheme Fe^{3+} in its active site rather than the Fe^{2+} present in the active enzyme. The complex between the substrate L-cysteine and the oxidized active site has a blue color resulting from an absorption with a maximum of absorbance at 640 nm. When this stable, inactive complex is excited by a perpendicular beam of light from a laser at a wavelength of 647 nm, two absorptions, with maxima of absorbance at 340 and 292 cm^{-1}, are enhanced sufficiently that they dominate the Raman spectrum in a region containing many overlapping unenhanced absorptions.[862] These enhanced absorptions were assigned to a stretching vibration of the bond between the Fe^{3+} and the sulfur of L-cysteine, which has become one of its ligands in the active site, and a bending vibration at the β carbon of that L-cysteine.

When the guanine (λ_{max} = 253 nm) in guanosine monophosphate

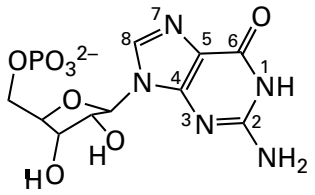

3–123

bound in the active site of human hypoxanthine phosphoribosyltransferase (Equation 3–398) is excited with a laser emitting light of wavelength 263 nm, eight vibrational modes in the guanine are enhanced and dominate the Raman infrared spectrum. Most of these vibrational modes are shifted relative to their positions in the infrared spectrum of guanosine monophosphate in free solution.[863] The maximum of absorbance for the stretching vibration at 1682 cm^{-1} of the acyl carbon–oxygen double bond at carbon 6 decreases in frequency by –40 cm^{-1}, and maxima of absorbance for two complex vibrational modes at 1538 and 1577 cm^{-1}, each involving both the nitrogen–hydrogen bond at nitrogen 1 and the amido group at carbon 2 in the guanidino group of the guanine, decrease in frequency by –11 cm^{-1}. In the crystallographic molecular model of the active site of human hypoxanthine phosphoribosyltransferase occupied by guanosine monophosphate,[864] Lysine 165 forms a hydrogen bond to the acyl carbon–oxygen bond at carbon 6 of the guanosine monophosphate, the acyl oxygen of the peptide bond of Valine 187 forms hydrogen bonds with the nitrogen–hydrogen bond of nitrogen 1 and one of the amido nitrogen–hydrogen bonds in the amido group on carbon 2, and the acyl oxygen of the peptide bond of Aspartate 193 forms a hydrogen bond with the other nitrogen–hydrogen bond of the amido group on carbon 2.

The absorption of the bending vibration at 1468 cm^{-1} of the nitrogen–hydrogen bond at nitrogen 1 of inosine monophosphate, observed in the resonance Raman infrared spectrum resulting from excitation at 260 nm, shifts by +5 cm when inosine monophosphate associates with the active site of adenylosuccinate synthase from *Methanocaldococcus jannaschii*.[865] This shift is consistent with a shift in the equilibrium between hydronated and unhydronated nitrogen 1 of the inosine monophosphate, the pK_a of which in solution is 12.5. The first step in the enzymatic reaction is the phosphorylation of the adjacent acyl oxygen in the amido group that includes nitrogen 1 by $MgATP^{2-}$. The dehydronation of nitrogen 1 by the carboxylato group of the aspartate with which it forms a hydrogen bond in the crystallographic molecular model[866] of murine adenylosuccinate synthase (26% identity; 1.8 gap percent) should be required to make the acyl oxygen sufficiently nucleophilic to engage in the nucleophilic substitution at phosphorus, even at the γphosphorus of $MgATP^{2-}$, and the shift in the absorption is consistent with this expectation.

Most authors of the foregoing infrared spectroscopic observations of the stretching vibrations of a carbon–oxygen double bond have proposed that the decreases in frequency for absorptions of the vibrational modes for carbon–oxygen double bonds that were observed upon association of the substrates or inhibitors with the respective active sites resulted from a weakening of those double bonds by the hydrogen bonds that are formed between the oxygen and the donors observed in the respective crystallographic molecular models. This weakening of the double bond would be brought about by a shifting of the electron density in the occupied π molecular orbital of the carbon–oxygen double bond toward the oxygen and thus in the direction of a configuration represented by the usually unfavored resonance

structure in which the oxygen bears a full negative formal charge, the carbon bears a full positive formal charge, and the double bond is broken. Consequently, in this view, the function of the donors for hydrogen bonds aligned by the active site would be to destabilize the ground state of the substrate relative to the immediate transition state by causing this shift in electron density.

This explanation of the shifts in the maxima of absorbance, however, is probably mistaken. First, the oxygen of each carbon–oxygen double bond accepts hydrogen bonds from molecules of water when it is free in solution, so the replacement of these hydrogen bonds by hydrogen bonds in the active site should be relatively inconsequential. Second, there are calculations suggesting that quite large local electric fields, larger than those that can be created by an active site, are required to produce significant shifts in electron density in the occupied π molecular orbital of a carbon–oxygen double bond.[850,867] Finally, it has been shown that **similar red shifts in the maximum of absorbance for a carbon–oxygen double bond do not result from decreases in its force constant**, as would be required if the active site were actually polarizing the occupied π molecular orbital significantly.

When acetophenone

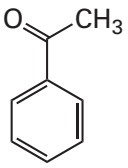

3–124

is dissolved in nine different solvents, the frequency of the stretching vibration of the double bond of its carbonyl group shifts over a similar range (30 cm^{-1}) to the shifts observed in active sites, albeit increasing from water to hexane, from polar to nonpolar solvent, rather than decreasing as usually occurs when the carbonyls already discussed associate with the respective active sites from an aqueous solution. Nevertheless, similar shifts in infrared spectra of the stretching vibrations of carbon–oxygen double bonds in carbonyl and acyl groups upon changing solvent have often been invoked as a model for the shifts observed upon the association of a substrate with an active site. It has been demonstrated experimentally that the shifts in the observed frequency for the maximum of absorbance for the stretching vibration for the carbonyl group in acetophenone in these several solvents are not due to changes in the force constant of the bond, and hence its weakening, because the anharmonicity of the stretching vibration does not shift in concert with the shift in frequency of the absorption, as it must if the shift were due to a change in force constant, but remains unaltered within the resolution of the measurement.[868]

When a carbon–oxygen double bond is free in solution, **its fixed dipole induces an electric field in the solvent** surrounding it. The magnitude of this induced electric field can be estimated from known properties of the solvent.[869] When the shifts in the infrared absorptions of acetophenone in the same set of solvents used for the measurements of anharmonicity are plotted as a function of these calculated induced electric fields, a linear correlation is observed.[868,870] A similar linear correlation between the calculated values of the induced electric fields and the shift in infrared absorptions for 19-nortestosterone (**3–120**) was observed for the same set of solvents.[850]

The **sign on the component of an electric field at a carbon–oxygen bond and parallel to it** has been chosen so that the fixed electric field of the dipole of the carbon–oxygen bond in the ground state is positive, with oxygen at the negative end and carbon at the positive end. Since the induced electric field in water and the other solvents is, by definition, in the direction opposite to the fixed electric field of the dipole of the carbonyl group, the induced field has a negative sign.[871] As the induced local electric field becomes more negative, the stretching frequency of the carbon–oxygen double bond decreases. This convention for the sign of a local electric field in the vicinity of a carbon–oxygen double bond, based on the direction of its dipole, will be used from here on. A field with a negative sign is one that would be created by fixed positive formal charge in the surroundings that is closer to the oxygen than it is to the carbon or by a dipole oriented so that its positive charge is closer to the oxygen than it is to the carbon.

On the basis of the correlations between the induced local electric field in the adjacent solvent and the frequency for the maximum of absorbance, it has been proposed that the shifts in the maxima of absorbance for the stretching vibrations of carbon–oxygen bonds observed in the different solvents are the result of a vibrational Stark effect, rather than any change in the force constant or strength of the carbon–oxygen double bond.[870]

A **vibrational Stark effect** is a shift in the frequency of the maximum of absorbance for a vibrational mode produced by an electric field, either applied

externally to the entire solution or existing only in the immediate vicinity of the atoms participating in that vibrational mode.[871] It results from the fact that the lengths of the bonds participating in a particular vibrational mode increase in the excited state. Because the bond lengths increase, their dipoles increase, and the effect of the local electric field in their vicinity is greater in the excited state than in the ground state. In the particular case of the stretching vibration of a carbon–oxygen double bond in a carbonyl or acyl group, the dipole moment of the bond is large because of the difference in electronegativity between oxygen and carbon, and as a result, the difference in dipole moment between the ground state and the excited state is also significant. The local electric field, depending on its direction, may stabilize the excited state relative to the ground state and produce a red shift of the frequency of the maximum of absorbance to lower wavenumbers (lower energy), or it may destabilize the excited state relative to the ground state and produce a blue shift of the frequency of the maximum of absorbance to higher wavenumbers (higher energy). The important point in this description is that a vibrational Stark effect arises from a difference between the effect of the electric field on the excited state and its effect on the ground state and is a **property of only the spectroscopy and not a property of the bonds participating in the vibrational mode in the ground state** of the molecule. In other words, the force constants, and hence the strengths of the bonds themselves that are participating in the vibrational mode, can be unaffected by the electric field induced in the surroundings, but the presence of the field will nevertheless shift the frequency of the maximum of absorbance.

If the shifts in the stretching frequencies of the maxima of absorbance that are observed for its carbon–oxygen double bond when a carbonyl or acyl group enters an active site arise from the same physical process as these shifts in frequency in the various solvents, then they also should result from a vibrational Stark effect. Consequently, in practice, **the frequency of the maximum of absorbance in an infrared spectrum for the stretching vibration of a carbon–oxygen bond on a substrate or an inhibitor within an active site is a monitor of the local static electric field at the location of the carbon–oxygen bond created by the active site itself**.

There are a couple of **problems with using this shift in the frequency of the maximum of absorbance quantitatively to assess the local electric field in an active site**.[850,870,871] First, the slopes of the lines relating the shifts in frequency of the maximum of absorbance for both acetophenone (**3–124**)[868,870] and 19-nortestosterone (**3–120**)[850] and the calculated induced, microscopic electric fields in the various solvents, 0.41 and 0.70 cm^{-1} $(MV\,cm^{-1})^{-1}$, are considerably smaller than the slopes of the lines for the shifts in frequency for the maxima of absorbance in a fixed, applied, macroscopic electric field, 1.1 and 1.4 cm^{-1} $(MV\,cm^{-1})^{-1}$, respectively. It is unclear which of these coefficients should be used to estimate the fixed, microscopic electric field in an active site from shifts observed in infrared absorptions. Second, a carbon–oxygen double bond does not monitor the magnitude of the actual net local electric field, E_{loc}, at its position in the active site; it monitors only the component of the local electric field, $E_{loc}\cos\theta$, parallel to its fixed dipole, where θ is the angle between the net local electric field and the fixed dipole. Consequently, the actual electric field in its vicinity could be significantly larger than what it reports and not necessarily aligned with the carbon–oxygen double bond.* For both reasons, these measurements should be evaluated qualitatively.

Although reliable estimates of the absolute magnitude and direction of the electric field at the location of a carbon–oxygen double bond in a substrate or an inhibitor within an active site cannot be made by vibrational Stark effects, it nevertheless seems to be the case that **the shift in the frequency of its maximum of absorbance is linearly related to the magnitude of the component of the electric field parallel to the dipole of that carbon–oxygen bond**. A series of mutants of steroid Δ-isomerase (Equation 3–425) from *P. putida* were made in which Aspartate 103 was mutated to leucine or asparagine; Tyrosine 16 was mutated to phenylalanine, serine, or 3-chlorotyrosine; and Tyrosine 57 and Tyrosine 32, which participate in a network of hydrogen bonds with Tyrosine 16, were mutated to 3-chlorotyrosines. The frequencies of the maxima of absorbance of 19-nortestosterone (**3–120**) in the active sites of eight of these single and double mutants were linearly related to the common logarithm of their catalytic constants for the substrate androst-5-ene-3,17-dione.[850,853] As the frequency of the maximum of absorbance increases, and hence the red shift experienced when 19-nortestosterone enters the active site decreases, the common logarithm of the catalytic constant decreases. This linear

*In the case of steroid Δ-isomerase, however, calculations suggest that the static local electric field of the active site is aligned with the carbon–oxygen double bond.[872]

correlation is the one expected from the effect of an electric field on a particular standard free energy.

As the reaction catalyzed by steroid Δ-isomerase approaches its transition state, the electron density in the occupied π molecular orbital of the carbon–oxygen double bond is shifting onto the oxygen to become one of the lone pairs of electrons on the hydroxy group of the γ,δ-unsaturated enol that is the immediate intermediate (Equation 3–425). This shift in electron density is the result of the unfolding reaction, not a shift in the ground state prior to the onset of the reaction. This inescapable **shift in electron density onto the oxygen in the transition state** causes the negative elementary charge on the oxygen to increase, and this increase in negative charge in the transition state is favored by the component of the fixed, local negative electric field created by the distribution of formal charge and dipoles within the active site parallel to the dipole of the initial carbon–oxygen bond. A decrease in this component of the field, which results in a directly proportional decrease in the electric potential energy experienced by the transition state, should be linearly related to the standard free energy of activation, as is observed, because electric fields exert their influence on standard free energies in direct proportion. It has already been noted that a similar correlation exists between the frequencies of maximum absorption of the carbon–oxygen double bond in a series of seryl-acyl enzyme intermediates in the active sites of three endopeptidases and the common logarithms of the rate constants for their hydrolysis. Each result suggests that **the local electric field established by the active site can participate directly in catalyzing an enzymatic reaction.**

As is the case with the active site of steroid Δ-isomerase, in almost all the other examples of carbon–oxygen double bonds discussed earlier, because they involve red shifts when the substrate or inhibitor enters the active site, the local, fixed electric fields created by the respective active sites and experienced by the carbon–oxygen bonds upon their association with the active site must be more negative than the local electric fields induced by these same carbonyl and acyl groups when they are in water. In the active sites of triose-phosphate isomerase, L-lactate dehydrogenase, and serine endopeptidases, the negative elementary charge on the oxygen of the carbon–oxygen double bond increases in the respective transition state in the reaction. Consequently, a fixed, negative electric field existing in the ground state along the respective carbon–oxygen bond that is greater than the negative electric field induced in the surrounding water when the reactant is in solution provides greater stabilization of the transition state than does water and favors catalysis. In the active sites of orotate phosphoribosyltransferase and hypoxanthine phosphoribosyltransferase, either orotate or guanine is the **leaving group in the nucleophilic substitution**, so local negative electric fields at the respective carbon–oxygen bonds should stabilize excess negative charge accumulating on the oxygens in the transition state as orotate or guanine is leaving.

Mutation of an amino acid acting as a donor in a hydrogen bond with the oxygen of a carbon–oxygen double bond in a crystallographic molecular model of an occupied active site causes the frequency of the maximum of absorbance for its stretching vibration to increase by +20 to +60 cm^{-1}. In fact, the +61 cm^{-1} shift that occurs upon mutation of Tyrosine 16 in the active site of steroid Δ-isomerase[850] shifts the frequency of the maximum of absorbance of the carbon–oxygen bond by +20 cm^{-1} relative to its value in water. These results suggest that **the major contributors in an active site to the negative electric field along the axis of a carbon–oxygen bond in the ground state are the donors for hydrogen bonds to the oxygen**.[871] This conclusion seems reasonable. Each donor has a dipole moment that is positive at the hydrogen in the hydrogen bond and negative at the respective heteroatom on which the hydrogen is located. Each dipole producing these dipole moments is as intimate to the oxygen of the carbon–oxygen bond as possible because a hydrogen bond always brings the atoms participating much closer together than the sum of their van der Waals radii and covalent bonds.

Even though the oxygen of the carbon–oxygen bond is an acceptor for hydrogen bonds from water when it is in solution, the relative permittivity of an aqueous solution (80) is large while the relative permittivity of an occupied active site is much smaller. The strength of the electric field created by a fixed dipole is inversely proportional to the relative permittivity of the surroundings, so a smaller relative permittivity increases the strength of the electric field produced by each donor for a hydrogen bond even if their dipole moments are the same as that of a molecule of water. There may also be a contribution to the electric field that results from the donors being rigidly oriented by the active site. In any case, the donors for hydrogen bonds, although they probably do not significantly shift the electron density of the carbon–oxygen bonds in the ground state, do provide the electric field that stabilizes the

shift of electron density onto the oxygen that occurs in the respective transition states. In effect, the explanation of the effect is quite different even though the origin of the effect, the hydrogen bonds, is the same.

The frequency of the maximum of absorbance for a carbon–oxygen bond can also demonstrate a **blue shift** relative to the frequency for the maximum of its absorbance in water. When an phenacyl group, spectrally equivalent to acetophenone, is substituted synthetically for Phenylalanine 8 in bovine ribonuclease S, the frequency of the maximum of absorbance for the stretching frequency of its carbonyl group (1688 cm^{-1}) experiences a blue shift of +19 cm^{-1} relative to that for the same phenacyl group in water (1669 cm^{-1}).[870] In the crystallographic molecular model of bovine ribonuclease S,[873] Phenylalanine 8 is in a nonpolar pocket, but its π molecular orbital system is in van der Waals contact with the imidazolyl group of Histidine 12. Consequently, the blue shift in the maximum of absorbance for the phenacyl group is not so large as the one observed when it is transferred from water to hexane, +27 cm^{-1}, which represents a completely nonpolar environment. The blue shift (+11 cm^{-1}), however, observed in the frequency of the maximum of absorbance for the stretching vibration for the carbonyl of pyruvate bound in the active site of L-lactate dehydrogenase when it is occupied by NADH, relative to the active site when it is occupied by NAD^+. This blue shift results from the fact that the positive elementary charge on NAD^+, because it is immediately adjacent to the carbon of the carbon–oxygen bond rather than the oxygen, causes the local electric field experienced by the carbon–oxygen bond to be more negative.

Ultraviolet and visible absorption spectra are also used to examine the environment of chromophores on substrates or inhibitors when they are bound to active sites. For example, when 19-nortestosterone (**3–120**) is bound to steroid Δ-isomerase from *C. testosteroni*, the maximum of absorbance for the enone in the ultraviolet absorption spectrum shifts[849] from 248 to 260 nm. When 19-nortestosterone ($pK_{a,C=OH^+} = -2.3$) is dissolved in 10 M sulfuric acid, almost the same shift, from 248 to 258 nm, is observed.[874] The compressed hydrogen bonds (0.26 nm)[853] formed between the carbonyl oxygen of 19-nortestosterone and Aspartate 99 and Tyrosine 14 in the active site of the enzyme from *C. testosteroni* may mimic the hydronation that occurs in 10 M sulfuric acid.

Neither of these donors for hydrogen bonds, however, is anywhere near so strong an acid as a hydronium. The shift observed may in part be the result of the local electric field caused by the dipoles of these two donors that was detected by the Stark effect on infrared spectra of 19-nortestosterone when it is bound to the active site of steroid Δ-isomerase (Equation 3–425) from *P. putida*. It has been shown that a shift of the same magnitude in the ultraviolet spectrum of steroids closely related to 19-nortestosterone can be produced in a nonpolar environment by the dipole of an adjacent hydroxy group that is incapable of forming a hydrogen bond with the oxygen.[875] If the delocalized electrons in the π molecular orbital system are shifted toward the oxygen by the local electric field of the oxygen–hydrogen bond in the carboxy group of Aspartate 99 and the hydroxy group of Tyrosine 14, which are participating in hydrogen bonds with the oxygen, more than they are by the donors for hydrogen bonds from molecules of water in the solution, there should be a greater separation of charge in the molecule than it has in solution. Zwitterionic molecules, such as a pyridoximine of pyridoxal phosphate, in which the two opposite formal charges are on atoms that are conjugated to each other by a π molecular orbital system, have absorbances that are red-shifted relative to their conjugate acids and conjugate bases (Figure 2–1)[876] or to nonzwitterionic analogues with an isoelectronic π molecular orbital system. There must also be a contribution to the red shift observed in the wavelength for the maximum of absorbance from the decrease in relative permittivity experienced when the enone leaves the solution and enters the active site. The wavelength for the maximum of absorbance for an unconjugated carbonyl group shifts to higher wavelength as the relative permittivity of the solvent in which it is dissolved decreases, and the range of wavelengths over which this red shift occurs (about 10 nm) in mixed solvents from water to dioxane[877] is the same as the red shift that is observed when 19-nortestosterone associates with the active site.

A larger red shift in the maximum of absorbance, from 368 to 408 nm, is observed in the ultraviolet spectrum of 1-hydroxy-2-naphthoyl-SCoA, an analogue of the product 1,4-dihydroxy-2-naphthoyl-SCoA

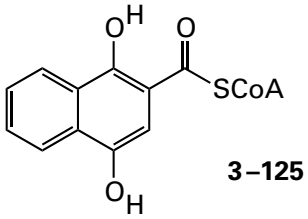

3–125

when it associates with the active site of 1,4-dihydroxy-2-naphthoyl-CoA synthase from *E. coli*. In this instance, however, the shift was attributed to dehydronation of the 1-hydroxy group by a base on the active site.[878] The dehydronation increases the conjugation of the oxygen of the thiocarboxy group on carbon 2 with the naphthoyl group, resulting in a shift of its maximum of absorbance to longer wavelengths, the same reason that dehydronation of a tyrosine in a protein shifts its maximum of absorbance from 275 to 293 nm.[879]

Nuclear magnetic resonance spectroscopy is used to examine the environment experienced by a nucleus of nonzero spin such as carbon-13, nitrogen-15, or fluorine-19* that has been incorporated into a substrate or inhibitor when it is bound to an active site. For example, deoxyuridine monophosphate labeled with **carbon-13** at carbon 2 or at carbon 4 both register the dehydronation of nitrogen 3 ($pK_a = 9.2$), which sits between them, by a downfield shift in their absorptions in a nuclear magnetic resonance spectrum of 8 parts per million (ppm). When either isotopically labeled deoxyuridine monophosphate is in solution, nitrogen 3 is hydronated, but after each of them has associated with the active site of thymidylate synthase (FAD) from *T. maritima*, nitrogen 3 is unhydronated. Site-directed mutation identifies the guanidinio group of Arginine 174 as the functional group in the active site responsible for the fact that deoxyuridine monophosphate is unhydronated following its association.[880] Whether the active site preferentially associates with the conjugate base or is itself responsible for the dehydronation is not clear, but it is possible to observe the dissociation of the hydron that occurs upon the association with an indicator of pH.

Labeling of indolene and L-serine with both carbon-13 and **nitrogen-15** at the locations marked with asterisks has been used to assign the tautomeric equilibrium in the quinonoid intermediate

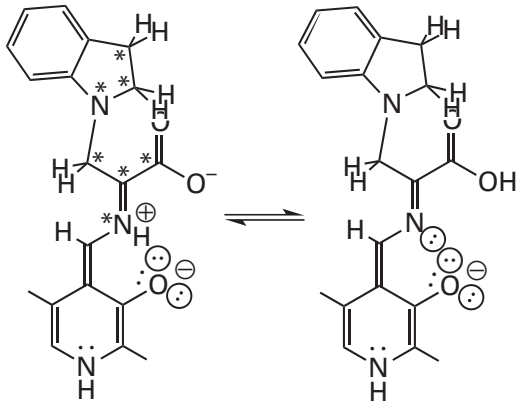

(3–430)

that indolene forms on the active site for tryptophan synthase (indole-salvaging) within tryptophan synthase from *S. typhimurium*. This saturated quinonoid intermediate results from addition of the anilino nitrogen of the indolene ($pK_a \cong 29$) to the external pyridoximine of 2-aminoacrylate rather than the aromatic π electrons of unsaturated, aromatic indole. This adduct is an analogue of the quinonoid intermediate formed by electrophilic aromatic substitution on the indole by the electrophilic external pyridoximine of 2-aminoacrylate produced from L-serine in the normal enzymatic reaction

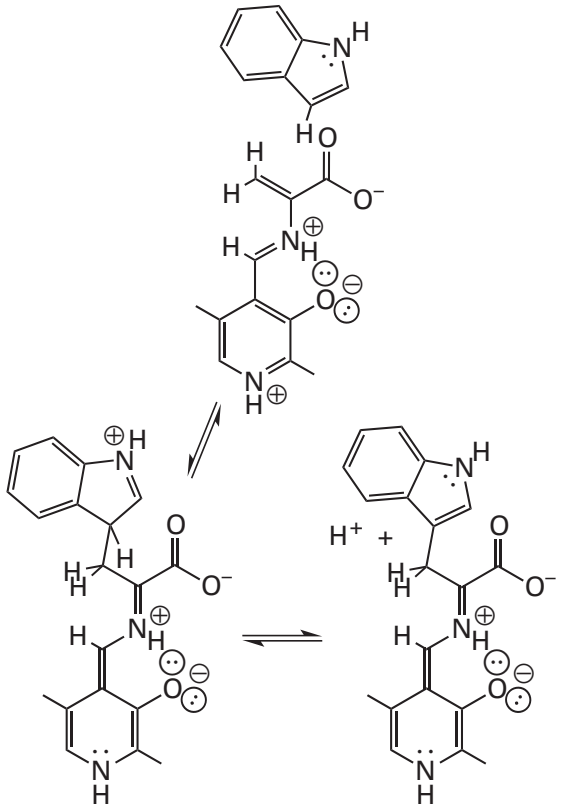

(3–431)

In this instance, an equilibrium between two different molecules (Equation 3–430) is being monitored by the physical method.

*Carbon-13 (1.1%) and nitrogen-15 (0.4%) are rare isotopes of carbon and nitrogen, but fluorine-19 is the naturally abundant isotope (100%) of fluorine.

The three **fluorine-19** atoms in MgF_3^-, an analogue of monomeric metaphosphate, when it associates with the complex between the active site of unphosphorylated β-phosphoglucomutase from *L. lactis* and the substrate β-D-glucose 6-phosphate, each have unique maxima of absorbance at −147, −152, and −159 ppm, respectively. Each peak reflects the **shielding** or **deshielding** that the unique electric field in the vicinity of its fluorine nucleus produces. There is no $[^{19}F]MgF_3^-$ in the solution in the absence of enzyme because it only forms on the active site, which is constructed to bind PO_3^- tightly, but if there were, its three fluorines would all be identical.

There are certain alterations in double-stranded DNA that convert a cytosine into a thymine with the result that a thymine is paired with a guanine, a mispairing that can lead to mutations. Thymine-DNA glycosylase recognizes these mispairings and hydrolyzes the hemiaminal between ribose and thymine. As has already been mentioned, in the first step in this hydrolysis, the thymine swings out of the stack of bases into the catalytic portion of the active site. The absorption of 2′-fluoro-*arabino*-deoxythymidine, which has been incorporated into duplex DNA so that its thymine is mispaired with a guanine, shifts upfield by −7 to −11 ppm from its absorption at −115 ppm in the stacked conformation, which predominates in solution, when it associates with the active site of human thymine-DNA glycosylase and flips out of the stack. The equilibrium constants between stacked and flipped conformations when the DNA is in the active site of the enzyme for four different double-stranded DNAs is proportional to the catalytic constant for the hydrolysis of hemiaminal in the active site.[881]

Nuclear magnetic resonance spectroscopy can also be used to obtain information about the electric field created by the active site and experienced by a **carbon–oxygen double bond** in a substrate or an inhibitor. The substrate or inhibitor can be synthesized, either chemically or enzymatically, in such a way that the carbon in the carbon–oxygen double bond is carbon-13 rather than carbon-12 while all the other carbons are normal carbon-12. A complex can then be formed with the modified substrate or inhibitor, and the carbon-13 nuclear magnetic resonance spectrum can be taken. For example, in a solution of 3 mM active sites of porcine citrate (*Si*)-synthase

$$\text{oxaloacetate} + \text{acetyl-SCoA} + H_2O \rightleftharpoons H^+ + \text{HSCoA} + \text{citrate} \qquad (3\text{–}432)$$

containing 3 mM carboxymethyl-SCoA, an analogue of the enolate of acetyl-SCoA,* and 3 mM [2-^{13}C]oxaloacetate, the active sites are saturated with carboxymethyl-SCoA and [2-^{13}C]oxaloacetate, and very little of either ligand remains free in solution. In the carbon-13 nuclear magnetic resonance spectrum, the carbon-13 at the carbonyl carbon in [2-^{13}C]oxaloacetate has a maximum of absorbance at 206.6 ppm, shifted downfield +7 ppm from its maximum of absorbance in free solution (199.9 ppm).[882] In the crystallographic molecular model of the same complex, the imidazolyl group of Histidine 320 and one of the ω-nitrogen–hydrogens of the guanidinio group of Arginine 329 are donors for two in-plane, trigonally arrayed hydrogen bonds (0.29 and 0.26 nm, respectively) to the carbonyl oxygen of the oxaloacetate.[883] When Histidine 320 is mutated to a glycine,[884] the maximum of absorbance for carbon-13 is at 200.7 ppm, only +1 ppm from its maximum of absorbance in free solution.

Cinnamoyl-SCoA, a substrate for the addition to a carbon–carbon double bond catalyzed by enoyl-CoA hydratase

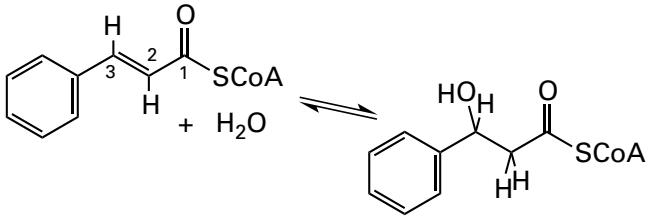

(3–433)

can be synthesized in three isotopically labeled forms: [1-^{13}C]cinnamoyl-SCoA, [2-^{13}C,2-^{2}H]cinnamoyl-SCoA, and [3-^{13}C,3-^{2}H]cinnamoyl-SCoA. Carbon-13 nuclear magnetic resonance spectra of complexes between the active site of bovine enoyl-CoA hydratase and each labeled substrate in turn were obtained. The chemical shift of the maximum of absorbance for carbon 1 (201.0 ppm) was situated downfield by +5.1 ppm relative to its chemical shift in solution (195.9 ppm); that of carbon 2 (126.1 ppm) was situated upfield by −0.8 ppm relative to its chemical shift in solution (126.98 ppm); and that of carbon 3 (147.2 ppm) was

*The enolate is an intermediate in the enzymatic reaction. It is the nucleophile in the nucleophilic addition to the carbonyl group of oxaloacetate (see Equation 3–409) catalyzed by the enzyme.

situated downfield by +3.2 ppm relative to its chemical shift in solution (144.0 ppm).[885] In the crystallographic molecular model of enoyl-CoA hydratase from *R. norvegicus* occupied by 4-dimethylaminocinnamoyl-SCoA,[886] there are two amido groups from the polypeptide forming an oxyanion hole for the acyl oxygen of the cinnamoyl group, one at a location normal to the plane of the cinnamoyl group and the other near a tetrahedral position around the oxygen relative to the first.

The downfield shifts experienced by the [^{13}C]carbonyl carbons in oxaloacetate and cinnamoyl-SCoA result from **deshielding of the respective carbons**. As such, they indicate that electron density has shifted away from the carbon-13 of the carbonyl group. In oxaloacetate, this shift in electron density must be onto the oxygen of the carbonyl. In the extended π molecular orbital system of the cinnamoyl group, there is no necessity that it should be so, but it has been calculated that the shift of electron density from the carbon is also onto the oxygen.

These more or less unambiguous conclusions that **electron density in the respective π molecular orbital systems shifts from carbon to oxygen in the ground state** appear to contradict the proposal that electron density in the highest occupied π molecular orbitals of a carbon–oxygen double bond in a carbonyl or acyl group, when it enters an active site, is not displaced sufficiently in the direction of the oxygen to change the force constant of the carbon–oxygen bond. That the deshielding observed in the nuclear magnetic resonance spectrum of cinnamoyl-SCoA must result from a shift in electron density in the highest occupied π molecular orbital follows from the fact that the deshielding is also experienced by carbon 3, which has a lobe over it in the highest occupied π molecular orbital, but not by carbon 2, which has a node at its location. In the case of cinnamoyl-SCoA, however, it has been estimated that a shift in electron density at carbon 1 in the cinnamoyl group onto the oxygen atom equal to only about 0.02–0.05 of an elementary charge can account for the deshielding of +5.1 ppm, or about 1–2% of the electron density in the highest occupied molecular orbital. Since the deshielding is about the same (+7 ppm) at carbon 2 in [2-^{13}C]oxaloacetate, in the active site of citrate (*Si*)-synthase, the shift in electron density should also be about the same.[887] These shifts are fairly small and could well not measurably affect the force constant for the stretching frequency of a carbon–oxygen double bond yet cause an easily measurable increase in chemical shift.

The shift of electron density onto the oxygen in both oxaloacetate and cinnamoyl-SCoA that is registered by the deshielding results from the component of the local electric field along the carbon–oxygen bond created by the donors for hydrogen bonds to the respective oxygens. This component of the electric field in each case must have a negative sign to explain the deshielding. In the transition states of both enzymatic reactions, negative charge increases on these oxygens. Consequently, these local electric fields will stabilize the respective transition states relative to the ground states and contribute favorably to the catalysis.

By examining the two- and three-dimensional spectra of an unbound substrate or inhibitor in the solution surrounding an enzyme, it is possible to observe the residua of **nuclear Overhauser effects** between two hydrogen-1 atoms, a proton on the enzyme, substrate, or inhibitor and another proton on the substrate or inhibitor. These nuclear Overhauser effects were initiated while the substrate or inhibitor was associated with the active site of an enzyme, and they persist after its dissociation. The **transfer of saturation between two protons** that is accomplished while a substrate or inhibitor is bound to the active site of an enzyme persists for an interval long enough for the substrate or inhibitor to dissociate because relaxation is slow in nuclear magnetic resonance spectroscopy. If the substrate or inhibitor usually dissociates from the active site before relaxation has occurred, then the population of unbound ligand in the solution will contain a significant subpopulation of recently released individuals that retain the transfer of saturation that they gained while they were bound, and this subpopulation of unbound ligands will experience a nuclear Overhauser effect in the absorption of each proton to which saturation was transferred. This nuclear Overhauser effect will be manifested in the nuclear magnetic resonance spectrum of the entire population of unbound ligands at the chemical shift that the proton has when it is on the unbound ligand free in solution. It follows that, to observe such **transferred nuclear Overhauser effects**, the substrate or inhibitor must be in rapid exchange between the site and the solution, with a rate constant for dissociation from the site greater than the rate constant for the relaxation of its saturation.

Transferred nuclear Overhauser effects[888] can be produced by transfer of saturation either between a proton on a side chain in the active site and a proton on a substrate or inhibitor[889,890] or between two protons on the substrate or inhibitor while it is

bound in a particular conformation in the active site.[891] Saturation transfer produces negative nuclear Overhauser effects; a population of protons to which saturation has been transferred does not absorb so strongly as an equivalent population to which saturation has not been transferred. Because negative nuclear Overhauser effects are usually not observed between protons in a rapidly rotating small molecule in free solution, negative nuclear Overhauser effects observed for peaks of absorption of protons in a substrate or inhibitor in rapid equilibrium with an active site can be confidently assigned to saturation transfer that occurs when the substrate or inhibitor is bound to the site, and these negative nuclear Overhauser effects indicate that the two protons, one that has been saturated and one to which this saturation has been transferred, were close to each other in the conformation of the ligand bound to the site.

In several instances, the proximities between protons producing transferred nuclear Overhauser effects have been checked against crystallographic molecular models of the respective complexes and found to be consistent.[891-893] For example, the seven negative, transferred nuclear Overhauser effects observed in two-dimensional nuclear magnetic spectra of the hexapeptide Thr-Pro-norVal-*N*-methyl-Leu-Tyr-Thr, when it is in solution with porcine elastase and rapidly entering and leaving the active site, arise from pairs of protons on the peptide that are 0.2–0.4 nm apart in the crystallographic molecular model of the complex between this inhibitor and the enzyme.[894]

The **agreement of observed transferred nuclear Overhauser effects between protons with the proximities of the hydrons in crystallographic molecular models** of appropriate complexes provides reassurance that transferred nuclear Overhauser effects are informative in situations for which crystallographic molecular models are not available. For example, transferred nuclear Overhauser effects for acetylcholine in complex with acetylcholine receptor from *T. californica*[895] and for micellar 1-(hexylthio)-2-(nonanoylamino)-1,2-dideoxy-*sn*-glycero-3-phosphocholine in complex with phospholipase A_2 from *N. atra*[896] have been used to define the conformations adopted by this ligand and this inhibitor, respectively, when they are bound by their respective sites. Crystallographic molecular models were unavailable at the time for either complex.

Nuclear magnetic resonance spectroscopy can provide other **information that cannot be obtained by crystallography**. For example, the hydronation state of amino acid side chains in a crystallographic molecular model, which usually can be determined only by neutron diffraction, can be established from two-dimensional nuclear magnetic resonance spectra of the same complex between the enzyme and the particular ligand of interest.[897] The tautomeric state of the neutral imidazolyl group of a particular histidine in the active site of an enzyme can be established by nuclear magnetic resonance spectroscopy.[898] If it is in the range of rate constants for relaxation of excited states in nuclear magnetic resonance spectroscopy, the rate constant for the dissociation of a substrate or inhibitor from an active site can be estimated.[899] In the case of enzymes in which a substrate or intermediate must be bound in two different orientations at different steps in the enzymatic reaction, the observation of two distinct maxima of absorption in a nuclear magnetic resonance spectrum from the same nucleus originally in a substrate or inhibitor when the substrate or inhibitor is within the active site provides evidence for the existence of the two orientations. Such an observation has been made with the inhibitor 6-deoxy-6-fluoro-α-D-glucopyranosyl phosphate when it is bound in the active site of phosphoglucomutase from *O. cuniculus*,[900] an active site that must accommodate two orientations of the intermediate α-D-glucose 1,6-bisphosphate during the enzymatic reaction, just as the active site of phosphoglycerate mutase (Equation 3–421) must accommodate two orientations of the intermediate in its reaction.

Nuclear magnetic resonance spectroscopy can be used, just as crystallography is used, to obtain a **molecular model of the complex between an enzyme and a substrate or inhibitor**.[851,901] These nuclear magnetic molecular models are obtained by the usual procedures of assigning all the proton absorptions from the complex in two- and three-dimensional nuclear magnetic resonance spectra and then tabulating all nuclear Overhauser effects between them. The problem with such molecular models when active sites are examined is their low resolution. For example, in the molecular model of 19-nortestosterone (**3–120**) occupying the active site of steroid Δ-isomerase from *C. testosteroni* built from 1647 nuclear Overhauser effects (an average of 13.2 effects for each amino acid in the enzyme), it could not be determined unequivocally whether or not the carboxy group of Aspartate 99 and the hydroxy group of Tyrosine 14 form hydrogen bonds with the carbonyl oxygen of the inhibitor.[851] Crystallographic molecular models, however, because of their higher resolution,

unequivocally establish that they do, and they provide a measurement of the lengths of the hydrogen bonds.[852,853]

Originally, it was thought that molecular models derived from nuclear magnetic resonance spectra had the advantage that the molecules of enzyme were in solution, but this claim ignored the fact that molecules of enzyme in a crystal are still in solution. Molecular models from nuclear magnetic resonance spectroscopy, however, do have the advantage that different conformations of an enzyme in solution can be observed in equilibrium with each other rather than in separate crystals. There is also the advantage that a molecular model of a molecule of protein that has not yet been crystallized can be constructed from cross peaks in two-dimensional nuclear magnetic resonance spectra of that protein in solution, if the protein is small enough.

4-Chlorobenzoyl-CoA dehalogenase from *Pseudomonas* catalyzes the hydrolysis of 4-chlorobenzoyl-SCoA in a nucleophilic aromatic substitution

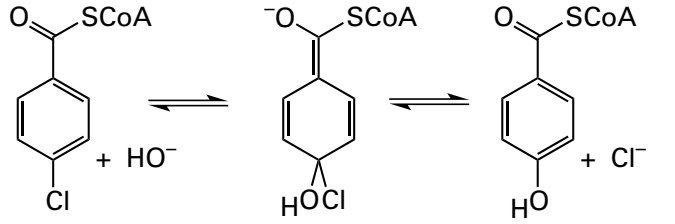

(3–434)

The stable complex between its active site and its substrate 4-hydroxybenzoyl-SCoA has been **examined by nuclear magnetic resonance spectroscopy, infrared spectroscopy, and ultraviolet spectroscopy**.[902] When the labeled substrate [^{13}C=O]4-hydroxybenzoyl-SCoA associates with the active site, the maximum of absorbance for the carbon-13 in the acyl group in a nuclear magnetic resonance spectrum shifts downfield +2.8 ppm, from 193.2 to 196.0 ppm. When the unlabeled substrate, 4-hydroxybenzoyl-SCoA, associates with the active site, the frequency of the maximum of absorbance for the stretching vibration of its acyl carbon–oxygen bond in the difference Raman infrared spectrum shifts −12 cm^{-1}, from 1609 to 1597 cm^{-1}, and the maximum of absorbance for its benzoyl group in the ultraviolet spectrum shifts to the red from 292 to 373 nm.

Both the deshielding of the carbon in the carbon–oxygen double bond and a vibrational Stark effect on the frequency of the maximum of absorbance for its stretching vibration are consistent with the existence of a significant component of an electric field, of negative sign, produced by the active site along the axis of the carbon–oxygen double bond of 4-hydroxybenzoyl-SCoA. In the crystallographic molecular model of the active site of the complex between the enzyme and 4-hydroxybenzoyl-SCoA, there is an oxyanion hole for the carbon–oxygen double bond that consists of two amido groups from the polypeptide, one normal to the plane of the benzoyl ring and the other near a tetrahedral location relative to the first.[699] This oxyanion hole should provide an electric field with a component along the axis of the carbon–oxygen double bond of negative sign. In the transition states leading to the tetrahedral intermediate in the nucleophilic aromatic substitution, in either direction, negative charge is greater on the oxygen than in the ground state because a negatively charged nucleophile has been added to carbon 4, and the acyl oxygen ends up with the majority of that negative charge in the pentadienyl intermediate of the nucleophilic aromatic substitution. This increase in negative charge, and hence the transition state, is stabilized by such an electric field.

The electric field detected by nuclear magnetic resonance spectroscopy and infrared absorption would cause a polarization of the highest occupied π molecular orbital system of the 4-hydroxybenzoyl group in 4-hydroxybenzoyl-SCoA, and the separation of charge produced by this polarization could be responsible in part for the red shift in the maximum absorption in the ultraviolet spectrum. The red shift observed, however, seems too large for such an effect to be responsible for it. In this instance, the change in relative permittivity between the solution and the active site should not be consequential, because the ultraviolet absorption spectrum of benzaldehyde actually displays a small blue shift upon transfer from water to cyclohexane.[903] It has been suggested that the red shift observed is in large part the result of a dehydronation of the 4-hydroxy group on 4-hydroxybenzoyl-SCoA by the carboxylato group of an aspartate that forms a hydrogen bond to it in the crystallographic molecular model.[699] In support of this possibility is the fact that the wavelength of the maximum of absorbance for 4-hydroxymethylbenzoyl-SCoA only shifts from 292 to 323 nm when it associates with the active site. The dehydronation of the oxygen following the initial addition of hydroxide to carbon 4 would provide push during the dissociation of the chloride.

Suggested Reading

Belasco, J. G., and Knowles, J. R. (1980) Direct observation of substrate distortion by triosephosphate isomerase using Fourier transform infrared spectroscopy, *Biochemistry 19*, 472–477. https://doi.org/10.1021/bi00544a012

Lin, Y., and Nageswara Rao, B. D. (2000) Structural characterization of adenine nucleotides bound to *Escherichia coli* adenylate kinase: 1. Adenosine conformations by proton two-dimensional transferred nuclear Overhauser effect spectroscopy, *Biochemistry 39*, 3636–3646. https://doi.org/10.1021/bi991921t

Wu, Y., and Boxer, S. G. (2016) A critical test of the electrostatic contribution to catalysis with noncanonical amino acids in ketosteroid isomerase, *J. Am. Chem. Soc. 138*, 11890–11895. https://doi.org/10.1021/jacs.6b06843

Problem 3–37: Histidine 159 is a catalytic base within the active site in crystallographic molecular models of papain from *Carica papaya*.[904] The peak of absorption from the hydron on carbon 2 of Histidine 159 has been identified in the nuclear magnetic resonance spectrum of papain. The following are its chemical shifts ($\delta_{H159,CH2}$) as a function of pH.[905]

pH	$\delta_{H159,CH2}$
6.18	8.55
6.93	8.48
7.24	8.48
7.89	8.38
8.14	8.29
8.38	8.23
8.59	8.14
8.96	8.00
9.07	7.94
9.37	7.89
9.95	7.73
10.58	7.75

(A) Plot ($\delta_{H159,CH2}$) as a function of pH.
(B) What information does this plot contain?
(C) What is the numerical value of this equilibrium constant?
(D) Is this equilibrium constant a macroscopic or an elementary equilibrium constant?

Induced Fit

From crystallographic molecular models, it has become apparent that the active sites of enzymes display a spectrum of structural responses to the association of substrates. At one end of the spectrum are active sites the structures of which are affected very little when a substrate binds.[906] An example is ribonuclease T_1 from *Aspergillus oryzae*. The crystallographic molecular models of the polypeptide surrounding the active site of this enzyme display only a few reorientations of the side chains of amino acids surrounding and creating the active site upon association of an analogue for the substrate in the enzymatic reaction.[907-909] At the other end of the spectrum are active sites that close around the substrates as they bind so that the amino acids forming the active site and responsible for catalysis are assembled and properly oriented only after the substrates have associated. An example is hexokinase from *S. cerevisiae*.[910] When D-glucose associates with the enzyme, its structure changes so significantly that the unliganded enzyme and the liganded enzyme form crystals that are not isomorphous.[911] This difference in structure results from a rigid-body movement of 12° about an axis between two independently shifting domains within the same subunit. This movement closes the active site, which lies in the crevice between the domains, around the bound substrates (Figure 3–55).[910,912] Between the extremes represented by ribonuclease T_1 and hexokinase, examples of a variety of intermediate structural responses can be found.

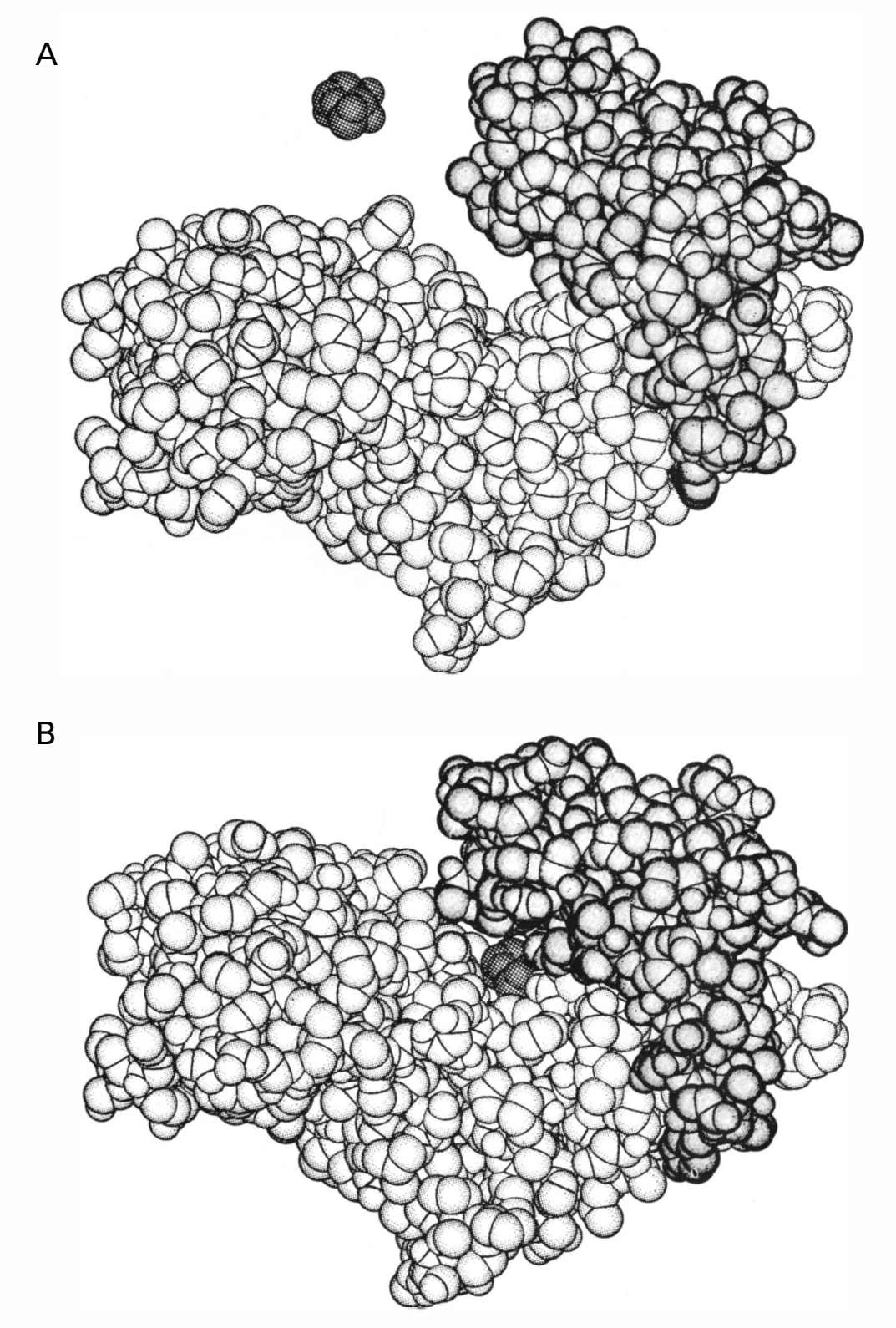
A
B

Figure 3–55: Space-filling model of the two conformations of a subunit of hexokinase from *S. cerevisiae*: (**A**) the form in which the active site is open and (**B**) the form in which the active site is occupied by D-glucose and the protein has closed around the substrate.[912] The crystallographic molecular model of the open form was constructed from a map of electron density calculated from the reflections of a crystal of hexokinase with space group $P2_12_12_1$. The phases were determined by isomorphous replacement. The crystallographic molecular model of the closed form was obtained from crystals of the enzyme complexed with D-glucose. Although these crystals were, by chance, also of the space group $P2_12_12_1$, the dimensions of the unit cell and the packing of the protein were completely different. The phases of the reflections from this nonisomorphous crystal were also determined by multiple isomorphous replacement independently of the previous crystallographic study of the open form. The active site lies in the deep cleft between the two lobes of the open form (Panel A). When D-glucose is bound in this cleft, the lobes close around the active site to enclose the molecule of D-glucose (atoms highlighted with speckled pattern). Reprinted from reference 912 Copyright 1980 with permission from Elsevier. https://doi.org/10.1016/0022-2836(80)90103-5

Reorientations of the side chains of amino acids in the active site upon the association of substrates, such as those observed for phosphoserine phosphatase from *Methanococcus jannaschii* (Figure 3–56),[913] are probably universal. A particularly striking example is the rotation of –160° around the bond between the α carbon and β carbon of Tyrosine 248 in bovine carboxypeptidase, with no change in the position of these two carbon atoms, that brings the 4-hydroxy group of the side chain into a hydrogen bond with the carboxy-terminal carboxylato group of its substrate.[914,915]

Occasionally, a **prosthetic group shifts its position** rather dramatically during the association of a substrate. In a crystallographic molecular model of the active site of 4-hydroxybenzoate 3-monooxygenase

$$\text{4-hydroxybenzoate} + \text{NADPH} + \text{H}^+ + \text{O}_2 \rightleftharpoons \text{3,4-dihydroxybenzoate} + \text{NADP}^+ + \text{H}_2\text{O} \qquad (3\text{–}435)$$

from *P. aeruginosa*, in which the substrate 4-hydroxybenzoate is bound, the isoalloxazine of the prosthetic flavin in the enzyme sits between the bound 4-hydroxybenzoate and the solution. In a crystallographic molecular model of another conformation of the enzyme, however, the isoalloxazine has slid aside, providing unhindered access to the site with which the 4-hydroxybenzoate associates.[916] It was concluded that, following association of 4-hydroxybenzoate with this open version of the subsite, the isoalloxazine slides over it, isolating it from the solution. In crystallographic molecular models of the active site of the flavoenzyme L-ornithine N^5-monooxygenase [NAD(P)H] from *Neosartorya fumigata*, the adenylate and the phosphoribose to which the isoalloxazine of the prosthetic flavin adenine dinucleotide is attached are firmly anchored within the protein, but the isoalloxazine can swing into and out of the active site by pivoting on the stationary single bond between carbons 1′ and 2′ of the phosphoribosyl group. In the unoccupied active site, the flavin has swung out of the active site, but when the active site is occupied by either the substrate L-ornithine or the substrate NAD^+ or both of them, the flavin has swung in to leave room for them to bind.[917]

Another change in the conformation of an enzyme that is often observed when crystallographic molecular models of liganded and unliganded versions are compared is a **tightening of the structure** of the protein surrounding the active site. Segments of secondary structure around the active site often shift perceptibly in the direction of a bound inhibitor or substrate as if closing around it (Figure 3–57).[918-922] When crystallographic molecular models of unoccupied enzyme and enzyme occupied by substrates or inhibitors are compared, this tightening is also manifested as significant decreases in the crystallographic *B*-factors of segments of the polypeptide surrounding the active site[923] or increases in the order parameters for relaxation of the excitation of amido hydrons in the polypeptide backbone surrounding the active site in nuclear magnetic resonance spectra.[924,925] In small proteins with large substrates, this tightening often occurs over the entire structure of the protein.

In enzymes with two reactants, in which association of the reactants with the active site is ordered, association of the first reactant can cause **conformational changes that create the subsite for the second reactant**. For example, when aspartate carbamoyltransferase (Equation 3–220) from *E. coli* binds carbamoyl phosphate, which is the first reactant to associate with the enzyme (Figure 3–14), there are small but significant changes in the conformations of the side chains that surround the carbamoyl phosphate as well as shifts in the polypeptide backbone that together create the subsite for L-aspartate, the second reactant to bind to the active site.[926]

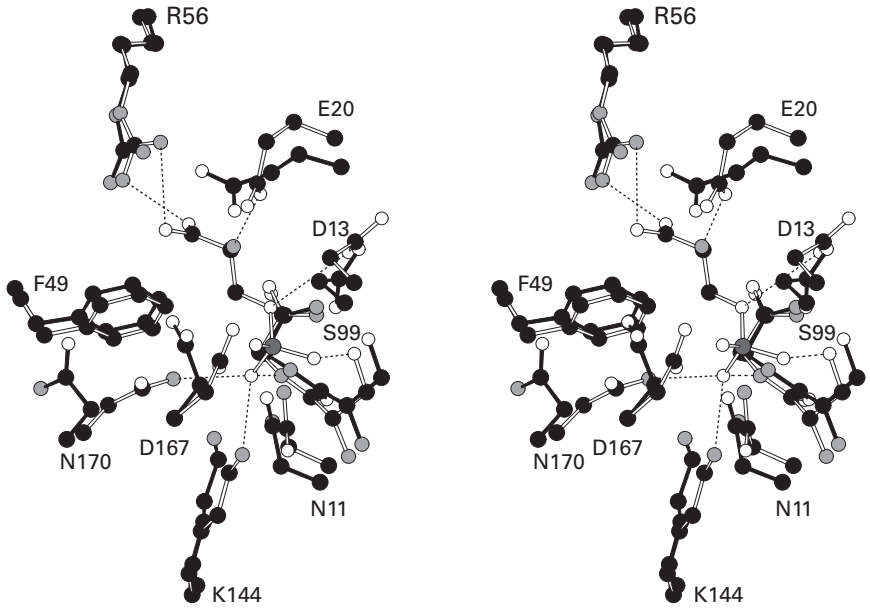

Figure 3–56: Superposed stereodrawings[576] showing the small shifts in side chains and a portion of the polypeptide backbone in the active site of phosphoserine phosphatase from *M. jannaschii* accompanying the association of the reactant *O*-phospho-L-serine.[913] Black atoms are carbons, white atoms are oxygens, small gray atoms are nitrogens, and the large dark gray atom is a phosphorus. An enzymatically inactive mutant of the enzyme in which Aspartate 11 had been mutated to an asparagine was crystallized in 5 mM $MgCl_2$ and a buffer at pH 7.4, either alone or in the presence of *O*-phospho-L-serine. The resulting crystallographic molecular models were superposed. The drawing is the superposition of the empty active site (black bonds) and the active site occupied by *O*-phospho-L-serine (white bonds). The side chains of several amino acids surrounding the active site are included in the drawing as well as a short segment of polypeptide. Hydrogen bonds (dashed lines) between donors and acceptors in the side chains or polypeptide and acceptors and donors in the *O*-phospho-L-serine are also drawn.

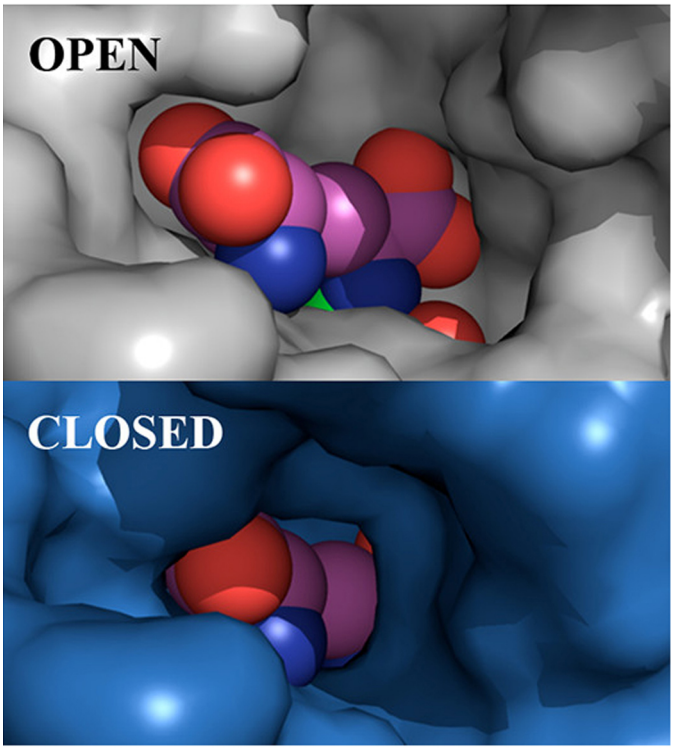

Figure 3–57: Tightening of the active site of cysteine synthase from *Fusobacterium nucleatum* around the external pyridoximine of L-lanthionine.[918] The central intermediate in the reaction catalyzed by cysteine synthase is the external pyridoximine of 2-aminoacrylate (Equation 2–13), which in the usual reaction is formed in one direction from *O*-acetyl-L-serine and formed in the other direction from L-cysteine. The enzyme, however, is promiscuous about the nucleophile that adds to the pyridoximine of 2-aminoacrylate. The sulfido group of L-cysteine is one of the nucleophiles that can add, and it gives L-lanthionine as the final product. The open active site is observed in the crystallographic molecular model of the internal pyridoximine in the otherwise unoccupied enzyme, and the closed active site is observed in the crystallographic molecular model of the external pyridoximine of L-lanthionine.[919] The molecular model of the L-lanthionine in the external pyridoximine from the latter model was inserted into the former model to provide a picture of the complex that forms between the open active site and the substrate L-lanthionine. Lavender atoms are carbons, red atoms are oxygens, and blue atoms are nitrogens The resulting superposition is presented as the OPEN conformation in space-filling format, and the crystallographic molecular model of the active site occupied by the external pyridoxime of L-lanthionine is presented as the CLOSED conformation. The view of the open conformation contains, from left to right, the α-carboxy group, the α-carbon, and the α-amino group from the L-cysteine that added to the pyridoximine of 2-aminoacrylate as well as carbon 3, the 2-amino group, and the carboxy group formerly in 2-amino-acrylate. Two segments of the polypeptide, each consisting of two amino acids, move toward each other to close over the occupied active site. Serine 224 in one of the segments provides both a donor, the amido oxygen of its peptide bond, and an acceptor, its hydroxy group, for hydrogen bonds to the α-carboxy group of L-lanthionine. Reprinted with permission from reference 918. Copyright 2020 American Chemical Society. https://doi.org/10.1021/acs.biochem.0c00683

The reorientation of side chains and prosthetic groups and the small shifts of secondary structures that close and tighten the structure of the protein around a substrate result in only **small changes in the relative positions of the α carbons** of the folded polypeptide that constitutes the enzyme. When crystallographic molecular models of the unliganded conformations and the respective liganded conformations in a large collection of crystallographic molecular models were compared, most of these enzymes (75–80%) showed only small changes (<0.1 nm) in the mean positions of their α carbons, consistent with only minor adjustments to a preexisting active site upon the association of substrates.[908,927] The minority (20–25%), however, show more significant conformational changes of the polypeptide upon the association of substrates and inhibitors.

A common example of these more significant conformational changes is the **closing of a loop of polypeptide over the substrates** or inhibitors after they have associated. For example, after glycerone phosphate[1] or an analogue of the *cis*-enediol intermediate in the enzymatic reaction[928] associates with the active site of triose-phosphate isomerase (Equation 3–384), a short loop of polypeptide, comprising amino acids 165–175 in the enzyme from *S. cerevisiae*,[929] closes over the substrate or inhibitor to lock it in the active site (Figure 3–58).[928,930,931] The closing of this lid embeds the phospho group of the substrate within a mold of amino acids[932] that prevents it from moving during the reaction. Because the phospho group is held in the plane of the *cis*-enediol that is an intermediate in the reaction (Figure 3–58), orthogonal to its π system, and because it binds to the enzyme as the dianion,[2] the elimination of phosphate from the intermediate *cis*-enediol that would produce methyl glyoxal

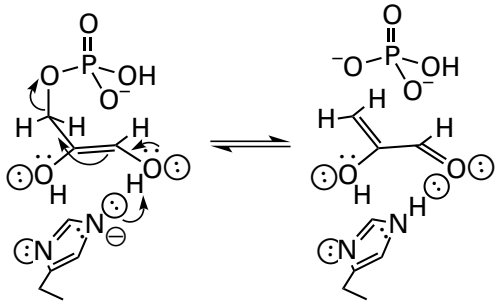

(3–436)

an undesired side product, is prevented. This elimination requires that the phospho group be normal

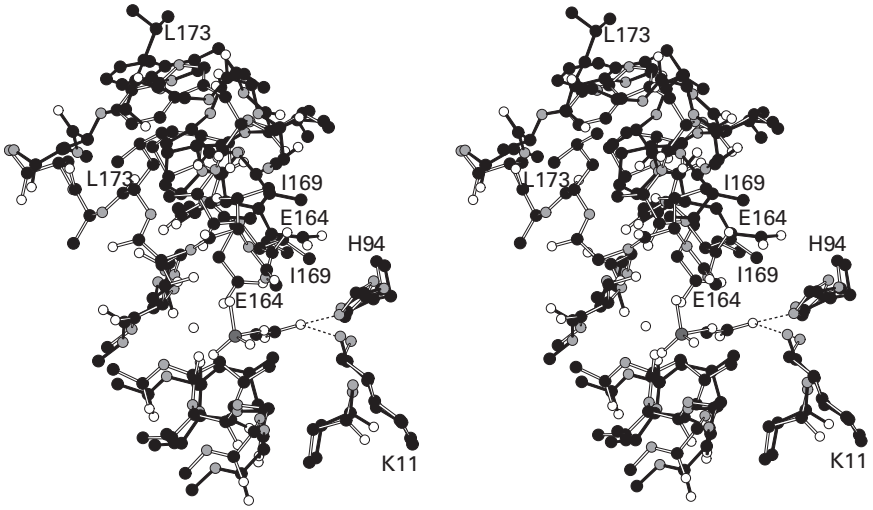

Figure 3–58: Superposed stereodrawings[576] showing the closing of the lid over the active site of triose-phosphate isomerase from *S. cerevisiae*.[930,931] Black atoms are carbons, white atoms are oxygens, small gray atoms are nitrogens, and the large dark gray atom is a phosphorus. The crystallographic molecular model of the enzyme with an empty active site (black filled bonds) was superposed onto the crystallographic molecular model of the enzyme with its active site occupied by phosphoglycerate (white open bonds), an analogue of the *cis*-enediol intermediate in the enzymatic reaction. The analogue of the intermediate occupies the active site and also causes the loop of polypeptide from Tryptophan 167 to Alanine 174 to drop over the active site, clamping down on the phospho group of phosphoglycerate. The movement can be appreciated by following the translation of Isoleucine 169 and Leucine 173 and the polypeptide between them. While Leucine 173 drops down with the lid, the side chain of Isoleucine 169, because it is at the edge of the lid, slides into place as the lid closes. The side chain of Glutamate 164 swings into the active site as the lid closes. The twisting of the polypeptide allowing this motion can be appreciated by observing the motion of Proline 165. The twist causes the side chain of Proline 165 to move up rather than down. The hydrogen bonds between the side chains of Histidine 94 (Figure 3–37) and Lysine 11 and the oxygen of the inhibitor that mimics the oxygens on carbons 2 of the substrates D-glyceraldehyde 3-phosphate and glycerone phosphate are drawn.

to the plane of the *cis*-enediol and that it be at least the monoanion. The unrelated enzyme methylglyoxal synthase from *E. coli*, the purpose of which is to produce methylglyoxal from glycerone phosphate, binds the glycerone phosphate so that its phospho group is normal to the plane of the *cis*-enediol, an orientation ideal for elimination.[393]

When the loop in triose-phosphate isomerase from *G. gallus* is shortened by four amino acids by site-directed mutation, the mutant enzyme, in addition to having a specificity constant for glyceraldehyde 3-phosphate that is 8×10^5 smaller than the wild type, produces significant quantities of methylglyoxal (as much as 95% of the product from glyceraldehyde 3-phosphate)[933] because the active site is still able to produce the *cis*-enediol intermediate but it dissociates and decomposes in solution,[934] presumably because the loop is not long enough to retain it until the isomerization has been completed. When only Valine 166 and Tryptophan 167 in one of the hinges for the loop, however, are mutated to proline and glutamate, respectively,[933] the specificity constant for glyceraldehyde 3-phosphate is still dramatically smaller (2×10^4) than that of the wild type, but the percentage of the product that is methylglyoxal decreases to 20%, presumably because the loop is long enough to prevent a larger fraction of the *cis*-enediol from escaping into the solution.

There is a loop that closes over the active site of ribulose-bisphosphate carboxylase (Equation 3–424) after the association of 2-carboxy-D-arabinitol 1,5-bisphosphate, an analogue for intermediate **3–119** in the enzymatic reaction (Figure 3–53). When the entire loop in the enzyme from *Rhodospirillum rubrum* was replaced by two glycines by site-directed mutation, the active site still catalyzed the enolization of D-ribulose 1,5-bisphosphate, which is the first step in the overall enzymatic mechanism, just as the active site of triose-phosphate isomerase was still able to catalyze the enolization of glyceraldehyde 3-phosphate. In the absence of the loop, however, the active site of ribulose-bisphosphate carboxylase was unable to carboxylate the enolate to complete the reaction.[935]

Loops that fold over the active site to enclose the substrates can be as short as four to six amino acids[936-938] or as long as 32 amino acids.[939]

So far, only the closing of a loop over the active site of enzymes with a single reactant have been considered. In an **enzyme with two reactants**, a loop of polypeptide can close over the active site once both of the reactants have associated to occlude them from the solution. There is a loop of polypeptide (53 aa) composed of three α helices on the surface of hydroxymethylglutaryl-CoA reductase from *S. pneumoniae* that swings as a rigid body in a rotation of 180° on a hinge of two strands of random meander* to close over the active site. In a crystallographic molecular model of the open conformation,[940] the loop adheres to the surface of the enzyme on one side of the hinge. In a crystallographic molecular model[941] of hydroxymethylglutaryl-CoA reductase from *Pseudomonas mevalonii* (40% identity; 0.4 gap percent) in the conformation in which the loop has enclosed the two oxidized substrates, 3-hydroxy-3-methylglutaryl-SCoA and NAD^+, the loop is adhering to the surface of the enzyme on the other side of the hinge and closing the active site. In the crystallographic molecular model[942] of hydroxymethylglutaryl-CoA reductase from *S. pneumoniae*, however, in which the active site is occupied by only one of the reactants, 3-hydroxy-3-methylglutaryl-SCoA, the loop has only partially closed, and the 3-hydroxy-3-methylglutaryl-SCoA has been enclosed; but the immediately adjacent subsite for the other reactant, NADPH, is still open to permit its association. In the enzymatic reaction, 3-hydroxy-3-methylglutaryl-SCoA is reduced by four electrons, so this partial closure permits the first molecule of NAD^+ to dissociate and the second molecule of NADH to associate while the partially reduced 3-hydroxy-3-methylglutaryl-SCoA remains enclosed.

Although the closing of a loop over an active site is often emphasized because it seems to have more catalytic advantages, **loops can also move over to open an active site** to its reactant and remain in this shifted conformation after the reactant associates. In a comparison of crystallographic molecular models of the unoccupied active site of cholesterol oxidase from *Brevibacterium sterolicum* and the active site occupied by the substrate dehydroisoandrosterone, it can be seen that a loop comprising amino acids 75–85 moves over, and this motion opens the active site rather than closing it.[943]

When a loop closes over an active site, **an amino acid participating in the catalysis is often brought into the active site by the closure of the loop**.[944-946] For example, Glutamate 140 in endoglucanase CelC

*A distinction is made between **random meander**, which is the fixed, randomly meandering path the polypeptide follows in the folded structure of a protein and which, aside from molecular vibration, does not change significantly with time, and a **random coil**, which is an expanded unfolded polypeptide in solution that is constantly changing its entire structure as a result of random rotations around its single bonds.

from *A. thermocellus*, which is the catalytic acid that hydronates the leaving group in the hydrolysis catalyzed by this enzyme, is brought into the active site when the loop containing amino acids 138–141 closes around the reactant.[936] In the active site of triose-phosphate isomerase (Equation 3–384) from *S. cerevisiae*, the catalytic carboxylato group of Glutamate 164 (Figure 3–37) enters the active site as the loop containing amino acids 164–175 closes over a reactant (Figure 3–58).

The loops that close over a substrate always assume a particular conformation in the crystallographic molecular model of the **closed conformation** of the active site, but they can have a particular conformation,[929,947] can have two conformations,[948] can be disordered and lack electron density,[949,950] or can be partially disordered[951] in the crystallographic molecular models of the **open conformation,** or the several open conformations, of the active site. Because the loop is often disordered or at least more exposed in the open conformation while it is ordered in the closed conformation, its availability to digestion by an endopeptidase when the enzyme is in solution can be used to determine when the active site is open and when it is closed.[952]

In some cases, the transition from the open to the closed conformation is accompanied by a **change in the secondary structure of a loop**. For example, the closing of a loop can cause a new α helix to form within it[953,954] or extend an already existing α helix.[955] In the case of purine-nucleoside phosphorylase from *E. coli*, an α helix of 14 amino acids that exists in the open conformation breaks in two, and one half shifts over to close the active site.[956] A loop in dihydrofolate reductase from *E. coli* has an irregular structure in the crystallographic molecular model of the open conformation, but when the loop is closed over the active site, it has become a hairpin of β structure.[957]

In contrast to these examples of changes in the secondary structure within a loop as it closes over the active site, the secondary structure of the loop, as was the case with hydroxymethylglutaryl-CoA reductase, can remain unchanged after it has closed. For example, the loop of fifteen amino acids that closes over the intermediate analogue ethyl *n*-hexylphosphonate, in crystallographic molecular models of the unoccupied and occupied conformations of triacylglycerol lipase from *Rhizomucor miehei* contains an α helix of seven amino acids that **moves as a rigid body** during the closure, which is accomplished by hinges at the two ends of the loop.[958]

In some cases, **two,**[959,960] **three**[949,961] **or as many as six**[962] **loops close over the active site**, almost as if they were short fingers closing as a fist over an object. Sometimes the **carboxy terminus**[963] or the **amino terminus**,[949] rather than an internal loop, closes over the substrates after they have associated with the active site. In one instance, however, the amino-terminal strand of the protein can block access to the active site in an unliganded conformation of the enzyme and must swing away to make the active site available to substrates.[964]

The ultimate solution to closing an active site around the substrate is to **bring together two independently shifting domains**, as does hexokinase from *S. cerevisiae* (Figure 3–55) or porcine citrate (*Si*)-synthase.[578] The motion of the two domains relative to each other can be described by comparing crystallographic molecular models of the enzyme in the open and closed conformations. In the transition from an open to a closed conformation, amino acids participating in catalysis and those recognizing substrates by noncovalent interactions are considerably reoriented to form a functional active site in the closed conformation where only a portion existed in the open conformation. In isocitrate dehydrogenase ($NADP^+$) from *Aeropyrum pernix* (Equation 3–345), one reactant, $NADP^+$, is bound to one domain in the crystallographic molecular model of the open conformation, and the other reactant, isocitrate, is bound to the other domain in the open conformation; and the closure of the two domains upon each other, in addition to creating the active site, moves the two substrates closer together by 0.5 nm so they can react with each other.[965] The two domains that close upon each other are usually domains in the same polypeptide, but the reorientation can also be between two heterologous subunits of the enzyme,[966] which in the future may become two domains of the same polypeptide as a result of gene fusion. Usually the reorientation of the domains occurs upon association of the reactants, but it can also occur between intermediate steps in the reaction.[967,968]

As was the case with the closing of the loop in hydroxymethylglutaryl-CoA reductase, in the closing of domains, there can be a **partially open conformation** in addition to the open and closed conformations. 4-Phytase from *Bifidobacterium longum* hydrolyzes the 4-phospho group from *myo*-inositol hexakisphosphate to give phosphate and 1D-*myo*-inositol 1,2,3,5,6-pentakisphosphate as products.

The open conformation is observed in the crystallographic molecular model of the unoccupied enzyme and the closed conformation in the crystallographic molecular model of the complex between the enzyme and *myo*-inositol hexakissulfate, an analogue of the reactant. When the active site, however, is occupied only by phosphate, one of the products, the site is partially open, with the angle between the two domains about half of the full angle through which the two independently shifting domains swing to fully close.[969]

As was the case with the closing of loops over the active site, but more so, **the closing of domains almost always gathers the functional groups on amino acids that participate in catalysis into the closed active site and orients them for catalysis**. This occlusion is often accomplished simply by the **closing of the jaws**. For example, when the two independently shifting domains of isocitrate dehydrogenase ($NADP^+$) from *E. coli* in the crystallographic molecular models of the open and closed forms are superposed, it can be seen that the amino acids responsible for catalysis on the two domains "move as rigid bodies during domain closure".[970] In other instances, there can be significant conformational changes that occur in the side chains of catalytic amino acids coordinated with the closing of the domains. For example, in the crystallographic molecular model of the open conformation of *β*-phosphoglucomutase from *L. lactis*, the carboxy group of Aspartic Acid 10 is swung out of the active site, forming a hydrogen bond with the amido group of Threonine 16 in the polypeptide backbone. In the crystallographic molecular model of the two domains closed around the substrate D-glucose 6-phosphate, however, the carboxy group has swung over to form a hydrogen bond with the oxygen on carbon 6 of D-glucose 6-phosphate, which is the leaving group in the phosphotransfer catalyzed by the enzyme.[971]

Often **closure of the domains causes the substrates to become completely surrounded by protein** and to be no longer in contact with the solution. Even substrates as large as NADH can be encased in protein in this way, as in the closed conformation of formate dehydrogenase from *Pseudomonas*.[972] Because the closure of the domains usually sequesters side chains of the amino acids as well as substrates from access to the solution, the rate of reaction for a side chain that is known to be sequestered with a reagent that modifies it, such as the reaction between a lysine and 2,4-dinitrophenyl acetate,[973] can be used to monitor the closure when the enzyme is in solution.

Other local changes in conformation often accompany the closure of the two domains. For example, during the closing of the two domains in adenosine kinase from *Toxoplasma gondii* around the substrate adenosine and the analogue $MgAMPPCP^{2-}$ (**3–5**), the *α*-helical segment composed of amino acids 312–316 in the open conformation becomes a random coil that creates an oxyanion hole, and the segment of random coil composed of amino acids 307–310 in the open conformation becomes a 3_{10} helix.[611] Often, segments of polypeptide that are disordered and lack electron density in models of the open conformation of the enzyme become ordered and display well-defined electron density when the domains close around a substrate.[974]

As might be expected, the closure of domains around the substrates decreases the number of amido hydrogens in the polypeptide backbone that can exchange with hydrons in the solution. As the domains close, the **amido nitrogen–hydrogen bonds become buried** and inaccessible. For example, there is a large cleft between two independently shifting domains in phosphoglycerate kinase (Equation 3–375) in the absence of substrates. From the crystallographic molecular model[975] of the ternary complex between phosphoglycerate kinase from *T. brucei* and the reactant 3-phospho-D-glycerate and the product $MgADP^-$, as well as measurements of the scattering of X-radiation[976] from solutions of the ternary complex between phosphoglycerate kinase from *S. cerevisiae* (44% identity; 1.9 gap percent) and 3-phospho-D-glycerate and $MgADP^-$, it has been concluded that these two domains have closed around the ligands. When the rates of exchange for the amido hydrons in the polypeptide backbone of phosphoglycerate kinase from *G. stearothermophilus* (45% identity; 1.2 gap percent) were measured, it was observed that the number of amido groups that had rates of exchange 10^8 times slower than those they would have in the unfolded polypeptide increased from 17 to 40 when either 3-phospho-D-glycerate or $MgADP^-$ was bound in the active site. The number then further increased to 59 when 3-phospho-D-glycerate, AlF_4^-, and $MgADP^-$ were all bound in the active site.[977] The latter combination forms within the active site either an analogue of the transition state or an analogue of the intermediate monomeric metaphosphate in the phosphotransfer catalyzed by the enzyme. These

increases in the slowly exchanging amido hydrons monitor their exclusion from the solution as the domains close.

A closure of domains that sequesters both substrates and side chains of amino acids from the solution also involves **changes in the hydration of the protein**. The water hydrating the two surfaces in the open conformation is mostly gone in the closed conformation after they have closed upon each other. Consequently, the closed conformation is dehydrated relative to the open conformation, causing dissociation constants for substrates[978] and enzymatic rate constants[979] to become functions of the concentration of water. For example, from changes in the dissociation constant for D-glucose from hexokinase from *S. cerevisiae* as a function of the concentration of water, it has been estimated[978] that about 60 molecules of water of hydration are lost upon closure of the active site (Figure 3–55).

Usually the two domains that close upon each other are about the same size, but sometimes one is considerably smaller than the other.[973,980,981] In most cases, as with hexokinase (Figure 3–55), the **two domains move as rigid bodies** because they are large enough to retain their stable tertiary structures during the conformational change. In some instances, however, usually when one of the domains is small, there can be changes in the tertiary structure of the smaller domain during the closure,[982] or one of the domains in the open conformation can be disordered in the crystal.[941] When one of the domains is small enough, it is simply a more or less structured loop that closes over the active site.[947]

The closure of the domains[983] can be a simple **hinged bending** as in hexokinase (Figure 3–55), a twisting motion that slides one domain over the surface of the other,[984] or a ball-and-socket motion that rotates one domain within a shallow cup on the surface of the other.[968,980] When the motion closing the domains is a hinged bending, two to as many as seven strands of polypeptide form the hinge upon which the two domains swing.[983] These strands are usually random meander and hence flexible enough to bend by the necessary angle. The two domains in aspartate transaminase from *G. gallus* are joined by two strands of polypeptide. One strand is a random meander in both the open and closed conformations, but the other strand in the open conformation is a long continuous rod of α helix, half in one domain and half in the other, that kinks in its center by 12° in the closed conformation to accommodate the closing of the domains.[985,986] In one instance where the closure results from a twisting motion, there are only two flexible strands connecting the two domains on either side of the axis of the twist.[984] In the case of 5′-nucleotidase from *E. coli*, in which a ball-and-socket motion closes the active site, the rotation of the ball unwinds a turn of α helix in the lone segment polypeptide connecting the two domains.[987]

Sometimes a screw axis, which is an operation capable of describing any reorientation of two rigid bodies, must be used to describe the motion.[912] Usually, however, **the motion of the two domains as rigid bodies can be described as a relative motion about a rotational axis** (Table 3–8).

Enzymes that have **nucleic acids** as their substrates usually have the most dramatic induced fits as they associate with their respective reactants because nucleic acids are also macromolecules, and they are of a size equal to the enzymes themselves. For example, it has already been noted that human DNA ligase (ATP) completely surrounds nine of the base pairs in the nicked double-stranded DNA that is its reactant.[760] The induced fit required to accomplish this enclosure has been described in crystallographic molecular models of DNA ligase (NAD^+) from *E. coli* both in the absence of DNA[995] and after it has surrounded a segment of DNA.[996] In the crystallographic molecular model of the unliganded conformation, the enzyme contains four independently shifting domains that form an arc of roughly 160° that is open on its concave side. As the DNA is surrounded during formation of the complex, the arc contracts into an almost complete circle. During this contraction, the four domains twist and flip with respect to each other as they contact the surface of the DNA so that surfaces on three of them that were not on the concave side of the arc end up on the concave surface of the final structure.

Type II site-specific deoxyribonuclease from *B. subtilis* hydrolyzes foreign, double-stranded DNA at restriction sites that have not been modified by the bacterium. The enzyme is a homodimer of two subunits (233 aa) that is rotationally symmetric in the crystallographic molecular models of both the free enzyme[997] and the complex with double-helical DNA.[998] The sequence of nucleotides in the double-stranded DNA is palindromic, and in the complex the rotational axis of symmetry of the protein coincides with the rotational axis of symmetry of the palindrome. During the transition from the unliganded to the liganded conformation, the two

Table 3-8: Rotations of Domains about an Axis during Closure of Active Sites

enzyme	rotation
formate dehydrogenase from *Pseudomonas*[972]	7.5°
2*S* epimer (D-mannose) from *S. cerevisiae*[912]	12°
orotidine-5′-phosphate decarboxylase from *E. coli*[988]	12°
3-dehydroquinate synthase from *Aspergillus nidulans*[972,989]	12°
glycogen synthase from *E. coli*[990]	15°
thermolysin from *B. thermoproteolyticus*[991]	16°
porcine citrate (*Si*)-synthase[578]	18°
isocitrate dehydrogenase ($NADP^+$) from *A. pernix*[965]	19°
phospho*enol*pyruvate carboxykinase (ATP) from *E. coli*[992]	20°
pyruvate kinase from *O. cuniculus*[993]	41°
human lactotransferrin[994]	53°
periplasmic dipeptide transport protein from *E. coli*[993]	55°

dimers pivot with respect to each other by 100° about an axis that passes through the interface between the two subunits and that intersects and is normal to the rotational axis of symmetry, just as the two blades of a scissors, which are related to each other by a rotational axis of symmetry, pivot around the pin that holds them together and that is perpendicular to that rotational axis of symmetry. Within the interface, the two faces rotate relative to each other about this axis so that the noncovalent interactions creating the interface are almost completely different in the complex than what they were in the unliganded conformation, even though there is still a rotational axis of symmetry running through the interface. This pivot allows the two subunits to close around the DNA and surround a 250° sector of the cylinder of DNA. The enclosure is completed by two loops of polypeptide from each subunit that were disordered in the unliganded conformation but become ordered as they embrace the DNA.

Unlike DNA ligase and type II site-specific deoxyribonuclease, which must find a specific nick or a specific sequence of nucleic acids in the long DNA of the chromosome, DNA-directed DNA polymerase is responsible for elongating any segment of DNA of any sequence. On one side of the active site in its substrate, there is a double-stranded DNA duplex in which one strand ends at the catalytic site with a 3′-hydroxy group. On the other side of the active site, the other strand of the DNA is a continuous single strand forming the template on which the elongation is to occur. On the surface of a large (604 aa) truncated version of DNA-directed DNA polymerase I from *E. coli*, in the crystallographic of molecular model of the unliganded conformation,[999] there is a deep groove, the width of double-stranded DNA, on one side of the active site. On the other side of the active site, there is a narrower groove on the surface of the protein at an angle of 130° to the wider groove. In the crystallographic molecular model of the liganded conformation,[1000] associatied with a molecule of DNA that is a complex between a single strand representing the template and a primer the 3′ end of which represents the point of elongation, the double-stranded portion of the DNA is sitting in the wide groove and the short single-stranded portion of the DNA is sitting at the entrance to the narrow groove, presumably representing the single strand of a much longer template on its way into the active site. An independently shifting domain of the protein (100 aa), known as the "thumb", has closed over the catalytic portion of the active site in an induced fit that isolates it from the solution. Presumably, the wide groove has no preference for the sequence of nucleotides in the double-stranded DNA, and likewise, the narrow groove has no preference for the sequence of nucleotides in the single-stranded DNA.

The open form of DNA-directed DNA polymerase I from *E. coli* with the thumb swung away from the catalytic site is susceptible to digestion by trypsin while the closed form is not. Using susceptibility of the intact polypeptide to tryptic digestion, as well as using selective templates in which a short single strand of DNA is annealed to a longer strand so that the identity of the next nucleotide to be added to the elongating strand is known, it could be shown that the thumb closes over the catalytic site only when the nucleoside triphosphate of the correct, complementary base has associated with the active site and presumably the template.[1001,1002] The subsequent opening of the active site following the catalytic step permits release of the diphosphate that is the product of elongation of the primer by one nucleotide and permits association of the next, correct nucleoside triphosphate. The active site then closes around that correct nucleotide and the DNA. Consequently, both the opening and the closing must happen at each step in elongation. For the structurally related DNA-directed DNA polymerase from Escherichia phage T7,[1003] both the rate constant at which the active site opens to release the diphosphate as a product ($1.2\ ms^{-1}$) and the rate constant at which the active site closes over the DNA and the correct magnesium deoxyribonucleoside triphosphate in the next step of the elongation ($0.3\ ms^{-1}$) have been measured.[1004] These rate constants are fast enough to accomplish the opening and closing of the active site at each step in the elongation, just as the active site of hexokinase opens and closes during each turnover.

In the much shorter (335 aa), but nevertheless structurally related[1005] DNA-directed DNA polymerase β from *R. norvegicus*, the grooves are missing and only the portion the enzyme containing the active site remains. In the crystallographic molecular model of the unliganded enzyme,[1005] the active site is wide open to a molecule the size of a molecule of DNA that is a duplex up to the 3′-hydroxy group and a single strand beyond the point of elongation. In the crystallographic molecular model of the closed conformation,[1006] a rather long rodlike, independently shifting domain (80 aa), composed of six short α helices, has closed over the single-stranded and double-stranded DNA by an almost rigid-body motion through an angle of 80° about a hinge composed of two short α helices. The movement of this domain again isolates the active site from the solution and creates the catalytic center.

Tightening of the protein around the substrates, closure of a loop or several loops over the substrates, or enclosure of the substrates brought about by the reorientation of domains are **not exclusive possibilities**. Tightening of the active site can accompany closure of a loop,[1007,1008] and closure of two domains can be accompanied by closure of one or more loops.[947,986,1009,1010] When aspartate—tRNA ligase associates with its substrate $tRNA^{Asp}$, two of its three independently shifting domains rotate with respect to the third, each about its own axis, to form contact with $tRNA^{Asp}$, which is a large substrate. In the single sites on each domain that make contact, as well as in the catalytic site that associates with L-aspartyl acyl adenylate and $tRNA^{Asp}$, the only conformational changes from the respective unliganded conformations are rotations of side chains to adjust to the substrates.[1011] The sum of all the structural changes characteristic of a particular enzyme defines the difference between open and closed conformations.

In a certain sense, many of the rotations, pivots, reorientations, and closings of hinges observed in the respective pairs of crystallographic molecular models may be illusory. Although the closed conformation is most likely the conformation the protein assumes in solution upon association of the substrate or substrates, the particular open conformation observed in a crystallographic molecular model may be more a result of the crystallization than any inherent structure. **In solution, the two domains in the open conformation may be constantly reorienting** relative to each other rather that being rigidly held at some particular angle. In several crystallographic studies, more than one structure has been observed for the open conformation of an enzyme.[1012,1013] In other instances, the angle between the two domains in the open conformation fluctuates widely.[1014,1015] In the case of triose-phosphate isomerase, calculations suggest that the loop in the open conformation is in fact highly flexible and samples many different conformations,[1016] so the picture of a rigid-body motion (Figure 3–58), although educational, is probably incorrect.

There are other observations, however, suggesting that **the structures observed in static crystallographic molecular models of the unoccupied, open conformations are often realistic**. For example, in five different, nonisomorphous crystalline forms, aspartate transaminase from *G. gallus* exists in only two conformations, either open or closed.[1017] There are spectroscopic observations with a modified form of the enzyme in which a fluorescent functional group has been incorporated that are consistent with only two conformations of the enzyme existing

in solution.[985] The conclusion that there are only two conformations in this instance seems reasonable since the open conformation has a long, rigid α helix spanning the two domains.

When arginine kinase from *L. polyphemus* is in solution in the absence of substrates or inhibitors, nuclear magnetic resonance spectra are consistent with an equilibrium existing between open and closed conformations that are observed crystallographically and that differ from each other by the opening and closing of two independently shifting domains.[1018] These observations correlate the motions in solution to the conformational change defined in these static structures.

The behavior of the absorbances of 27 amido nitrogens-15 and their amido hydrogens in a two-dimensional (^{1}H–^{15}N) correlated nuclear magnetic resonance spectrum of adenylate kinase from *E. coli*, which shift in concert under perturbation, are also consistent with only two conformations, open and closed, being present in the solution.[962]

Any change in the conformation of an enzyme that is thermodynamically linked to the association of its substrates is an induced fit. That such alterations in the structure of a protein could occur in response to the binding of a reactant or reactants was proposed before any such changes were observed crystallographically.[1019] Assume for the moment that the sequence of amino acids for the polypeptide that folds to form the native structure for a protomer of the enzyme contains the information necessary to specify two distinct native structures, which are **two distinct conformations** of the enzyme. These two conformations could be, for example, the open conformation (E_o) and the closed conformation (E_c) observed in crystallographic molecular models. Assume also that, in the absence of reactant A, the open conformation is more stable than the closed, but that when reactant A is bound, the closed conformation is more stable than the open. The equilibria describing this situation are

$$\begin{array}{ccc} E_o + A & \underset{\Delta G_4^\circ}{\rightleftharpoons} & E_o{\cdot}A \\ \Big\Updownarrow \Delta G_2^\circ & & \Big\Updownarrow \Delta G_3^\circ \\ E_c + A & \underset{\Delta G_1^\circ}{\rightleftharpoons} & E_c{\cdot}A \end{array} \qquad (3\text{–}437)$$

The standard free energy changes for binding of reactant A to the two conformations of the enzyme are for the directions of dissociation, from right to left, and those for the conformational changes are for the directions from closed to open, upward. The free energies for all four limbs of such a **linkage relation** have been measured for the association of nucleotides with tryptophan—tRNA ligase from *G. stearothermophilus*,[1020]

Because free energy is a state function and independent of path

$$\Delta G_1^\circ + \Delta G_2^\circ = \Delta G_3^\circ + \Delta G_4^\circ \qquad (3\text{–}438)$$

Because the enzyme is open in the absence of reactants and closed in the presence of reactant A, $\Delta G^\circ_2 < 0$, and $\Delta G^\circ_3 > 0$, from which it follows that

$$\Delta G_1^\circ >> \Delta G_4^\circ \qquad (3\text{–}439)$$

These linkage relations state that if and only if reactant A binds more tightly to the closed conformation than the open conformation, as is reasonable, will the binding of reactant A be able to invert the equilibrium between the open and closed conformations of the enzyme. This difference in the standard free energies of dissociation tips the balance and closes the active site around the reactant.

The linkage relation of Equation 3–437, for the sake of simplicity, assumes that the enzyme can exist in only two conformations, open and closed. When domains or loops in the open conformation fluctuate among many different orientations, which may be the more common situation, the ensemble of the conformations can be treated thermodynamically as the single open conformation in Equation 3–437 by assigning to the ensemble a mean standard free energy.

Although a thermodynamic distinction between the two is irrelevant, a kinetic distinction can be made between the two directions around the linkage square (Equation 3–437). The path on which the ligand associates before the conformational change occurs, designated as **induced fit**,[1019] can be distinguished kinetically from a path on which the conformational change occurs before the ligand can associate with the active site, designated as **conformational selection**.[1021,1022] The difference is between a thermodynamic statement that free energy is independent of path and a kinetic mechanism describing the actual events of the association. In the former instance, a site with which a reactant can associate must exist in the open conformation. Certainly, in the instances in which the active site

closes around that substrate and its cosubstrates, occluding them from the solution, it must be the case that a site exists on the open conformation since there is no access of any ligand to the active site in the closed conformation. In the latter kinetic mechanism, the actual association of the reactant or reactants is preceded by a pre-equilibrium that does not involve the reactants. That many kinetic mechanisms not involving enzymes proceed through preequilibria is well-known and uncontroversial. There is no reason to doubt that there may be instances in which an active site is both open to the solution in the closed conformation and unable to associate with the reactants in the open conformation. Although such a situation may be involved in the control of enzymatic activity, if such control is not occurring, the main consequence of such a kinetic mechanism is to decrease the concentration of active enzyme in the solution and decrease the efficiency of catalysis, an outcome that seems contrary to natural selection.

The original proposal for the existence of induced fit was provided as an **explanation for the specificity that certain enzymes displayed toward certain reactants**. For example, bovine 5′-nucleotidase catalyzes the hydrolysis of the phosphate ester of adenosine 5′-phosphate 100-fold more rapidly than it does that of ribose 5-phosphate.[1019] One explanation for this kinetic preference was that the larger reactant causes an induced fit to occur more effectively.* If the active site is able to catalyze the reaction only in the closed conformation, then any reactant that is more effective at inducing closure of the active site will be more effectively transformed by the enzyme. Consequently, in this explanation, induced fit is a strategy to enhance the specificity of the enzyme for its reactant relative to portions of its reactant or other related reactants if only the proper reactant is able to elicit the induced fit, which in turn brings the catalytic groups into proper locations and orientations for catalysis.

Induced fit can be used to improve the specificity of an enzyme only at the expense of its catalytic efficiency.[1023] This conclusion follows from the fact that a portion of the negative change in free energy accompanying the association of the reactant must be expended to shift the equilibrium between the inactive, open conformation and the active, closed conformation of the enzyme rather than being used to hasten the reaction. If almost all the unoccupied enzyme is in the open conformation to begin with, the total change in standard free energy for dissociation of reactant A from the catalytically active complex, E_c·A, is either $\Delta G^\circ_1 + \Delta G^\circ_2$ or $\Delta G^\circ_3 + \Delta G^\circ_4$, but either sum is always more negative than ΔG°_1, the standard free energy of dissociation of reactant A from the closed form. Therefore, reactant A binds less tightly to the enzyme than it would if only the closed conformation were present from the beginning. Therefore, tight binding is sacrificed to perform the conformational change.

Because the active site assembles only after the proper reactant or all the proper reactants are present, and therefore catalysis can proceed only after the active site closes, the enzyme avoids catalyzing a reaction for which it was not intended. It has been shown, for example, that the open active site of 5′-nucleotidase from *E. coli* is unable to catalyze the enzymatic reaction.[1024] If the enzyme were always present in the closed conformation and reactant A were able to bind to the closed conformation, reactant A would bind more tightly, and the enzyme could be a better catalyst. Nothing, however, would prevent molecules that contained only a portion of reactant A from binding and participating in the normal reaction mechanism. For example, the specificity constant for oxaloacetate, which is 3-carboxylatopyruvate, in the reaction catalyzed by porcine malate dehydrogenase, which normally reduces oxaloacetate to (*S*)-malate with NADH, is 10^6 times greater than the specificity constant for the reduction of pyruvate to lactate in the same active site. This discrimination in favor of 3-carboxylatopyruvate and against pyruvate can be explained by the fact that there is an induced fit upon the binding of 3-carboxylatopyruvate, which has been demonstrated crystallographically.[392] This conformational change, which assembles the catalytic groups, seems to require the presence of the 3-carboxylato group on oxaloacetate.

The **smaller molecule of most concern is water,** and the reaction catalyzed by hexokinase from *S. cerevisiae* (Figure 3–55) illustrates this problem most graphically. Hexokinase transfers the γ-phospho group from $MgATP^{2-}$ to the primary alcohol on carbon 6 of D-glucose. Water is also a primary alcohol and occupies the same location in the active site occupied by the primary alcohol of D-glucose in its absence. If the active site in hexokinase were properly configured for catalysis in the absence of D-glucose, $MgATP^{2-}$ could bind, water would be

*The conformational change accompanying the induced fit linked to the association of a nucleotide accomplished by 5′-nucleotidase from *E. coli* was subsequently shown to exist.[980]

present at the site for the primary alcohol, and the γ-phospho group would be transferred to water. In this instance, hexokinase would catalyze the hydrolysis of $MgATP^{2-}$, an unfortunate outcome.

Hexokinase from *S. cerevisiae* does catalyze the hydrolysis of $MgATP^{2-}$ in the absence of D-glucose, but the Michaelis constant for $MgATP^{2-}$ (4 mM) and the catalytic constant ($4\ s^{-1}$) are higher and lower, respectively, than the Michaelis constant for $MgATP^{2-}$ (0.2 mM) and the catalytic constant ($140\ s^{-1}$) for the transfer of phosphate to the primary 6-hydroxy group of D-glucose. From what is known about the conformational changes in which hexokinase from *S. cerevisiae* engages (Figure 3–55), one explanation for this counterproductive hydrolytic activity would be that occasionally the active site closes when $MgATP^{2-}$ is bound but D-glucose is not bound. Because water is occupying the location in the active site at which the primary hydroxy group at carbon 6 of D-glucose would normally be located, the hydrolysis of $MgATP^{2-}$ would result as soon as the proper active site was assembled.

If this is the explanation for the observed hydrolysis of $MgATP^{2-}$, it should be possible to amplify the error by including a **ligand missing a portion of the normal substrate**. D-Mannose is also a substrate for hexokinase. When D-lyxose

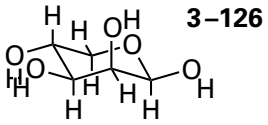
3–126

which is the five-carbon analogue missing carbon 6 of D-mannose, is added at a concentration of 0.1 M ($K_{m,lyx}$ = 5 mM), the hydrolysis of $MgATP^{2-}$ is remarkably accelerated to levels approaching the normal levels of hexokinase activity [$K_{m,ATP}$ = 0.1 mM and $k_0 = 60\ s^{-1}$].[1025] D-Xylose, the five-carbon analogue for D-glucose, also accelerates the hydrolysis of $MgATP^{2-}$. Because both D-mannose and D-glucose are excellent substrates for hexokinase (Table 3–5) these results suggest that D-lyxose or D-xylose, instead of D-mannose or D-glucose, respectively, induces the closing of the active site when $MgATP^{2-}$ is also bound but that a molecule of water is trapped at the position usually occupied by the hydroxymethyl group on the respective hexose and acts as the acceptor.

In a similar set of experiments, it could be shown that 3-phosphoshikimate 1-carboxyvinyltransferase (Equation 3–262) from *E. coli* would catalyze hydrogen exchange at carbon 3 of phospho*enol*pyruvate only when 4,5-dideoxyshikimate 3-phosphate was present.[1026] This analogue is missing the 5-hydroxy group to which the enzyme normally transfers the carboxyvinyl group of phospho*enol*pyruvate, but its ability to activate the catalysis of one of the partial reactions catalyzed by the enzyme indicates that it can nevertheless induce the active site to close.

Under certain circumstances, the process of induced fit would **not be able to accomplish the increase in specificity** that has just been described. Consider the closed conformation of an enzyme (E_c in Equation 3–437). Suppose that both the proper reactant, for example, D-glucose in the case of hexokinase, and an improper reactant, for example, water in the case of hexokinase, could equilibrate so rapidly with the active site in its closed conformation that the association and dissociation of each reactant with and from the closed conformation were all faster than the turnover of the enzyme and the rate at which the active site could open. If this were the case, adding the ability of the enzyme to open and close would not change the ratio of the rates for participation of the two reactants in the enzymatic reaction. As soon as the enzyme closed, these two competing reactants would equilibrate on the active site, and the fact that the enzyme had just closed would be irrelevant unless the opening of the enzyme when the improper reactant is bound were much faster than the catalytic constant of the closed enzyme to which the improper reactant was bound. Therefore, if the proper and improper reactant were able to enter and leave the closed conformation of the enzyme rapidly, induced fit would not improve the specificity of the enzyme. Induced fit can increase the specificity of an enzyme only if the active site closes so tightly on the proper reactant that it cannot dissociate or be displaced by an improper reactant before turnover occurs. This secure enclosure seems to be the case with hexokinase (Figure 3–55). It is unlikely that a molecule of D-glucose upon which the enzyme has closed would be able to dissociate from the closed conformation. This consideration suggests that induced fit will usually involve the closing of the active site around a reactant, as it does in hexokinase and triose-phosphate isomerase (Figure 3–58), and that seldom will the unoccupied active site in the closed conformation be able to associate with its substrate.

The foregoing considerations suggest that, in most cases in which the association of substrates induces the enzyme to close, the loops of polypeptide or the clefts between the two hinged domains should close sufficiently that entry and exit of substrates from the closed conformation should be

very difficult if not impossible. If so, the closed conformation cannot by itself be a more efficient enzyme. Even though, in theory, substrates bind more tightly to the closed form, their entry into it and exit from it should be kinetically too slow for it to be an effective catalyst. Consequently, **induced fit can be viewed as a way to create an active site that surrounds the substrates on all sides but that can nevertheless bind and release reactants and products rapidly**. The ability to surround substrates completely seems to be a reasonable advantage for catalysis.

When the closing of the active site sequesters the reactants so effectively from the solution that they are unable to enter the closed conformation, it must necessarily follow that the reactants are able to associate with the open conformation rapidly and with a large enough free energy of dissociation so that most of the time, when reactants are present at saturating concentrations, they are occupying the active site when it closes.[1027]

So far it has been assumed that the enzyme is active only in the closed conformation, but this assumption is not necessary for induced fit to be beneficial. When equine alcohol dehydrogenase is locked artificially in the open conformation, its catalytic constant is actually somewhat greater than when it can assume both open and closed conformations as it does naturally. The Michaelis constant for an alcohol, however, decreases by a factor of 100–1000 when the enzyme is able to close around it.[1028] Consequently, the enzyme can catalyze the reaction more effectively at low concentrations of reactant, when the induced fit is functioning, but not when the reactant is present at high enough concentrations to saturate the active site in the open conformation.

When the **two reactants of a bimolecular reaction** catalyzed by an enzyme together induce the closing of the active site around themselves, each individual dissociation constant is affected by the presence of the other reactant.[1029] The reason for this interaction is most easily understood by examining the **linkage cube** for this reaction

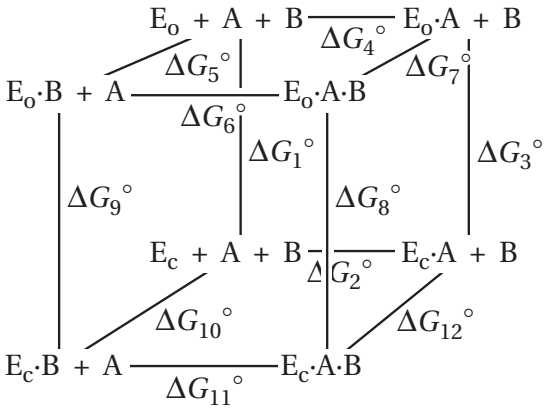

(3–440)

In this representation, the changes in standard free energies ΔG°_2, ΔG°_4, ΔG°_5, ΔG°_6 ΔG°_7, ΔG°_{10} ΔG°_{11}, and ΔG°_{12} are standard free energies of dissociation and ΔG°_1, ΔG°_3, ΔG°_8, and ΔG°_9 are standard free energies of isomerization in the direction from closed to open, as in Equation 3–437. Double arrows are replaced with lines for simplicity. If it is assumed, to simplify matters, that each of the two reactants, A and B, binds with the same affinity to the open conformation of the enzyme whether the other is bound or not, then $\Delta G^\circ_5 = \Delta G^\circ_7$ and $\Delta G^\circ_4 = \Delta G^\circ_6$. If it is assumed that the enzyme does not close until both reactants are present, then $\Delta G^\circ_1 < 0$, $\Delta G^\circ_3 < 0$, and $\Delta G^\circ_9 < 0$. When both reactants are bound, the conformational change takes place, and therefore $\Delta G^\circ_8 > 0$. When reactant A binds to the enzyme in the absence of reactant B to form E_o·A, the standard free energy of dissociation is ΔG°_4. When reactant A binds to the enzyme after reactant B has been bound to form E_c·A·B, the standard free energy of dissociation is $\Delta G^\circ_6 + \Delta G^\circ_8$ or $\Delta G^\circ_9 + \Delta G^\circ_{11}$, both of which must be more positive than ΔG°_4. When reactant B binds to the enzyme in the absence of reactant A to form E_o·B, the standard free energy of dissociation is ΔG°_5. When reactant B binds to the enzyme after reactant A has been bound to form E_c·A·B, the standard free energy of dissociation is $\Delta G^\circ_7 + \Delta G^\circ_8$ or $\Delta G^\circ_3 + \Delta G^\circ_{12}$, both of which must be more positive than ΔG°_5. Therefore, each reactant will bind more tightly when the other is already bound.

This linkage can be observed in the binding of reactants to hexokinase from *S. cerevisiae*. The dissociation constant for the binding of $MgATP^{2-}$ in the absence of monosaccharide to the empty, open active site is 4 mM. When D-lyxose binds along with $MgATP^{2-}$, the Michaelis constant for $MgATP^{2-}$ is 0.1 mM, and when D-mannose binds along with

$MgATP^{2-}$, the Michaelis constant for $MgATP^{2-}$ is 28 μM.[1029]

The linkage box and the linkage cube (Equations 3–437 and 3–440) imply that, in the absence of substrate, **open and closed conformations of the unoccupied enzyme are both present** and that, when substrates occupy the active site, closed and open conformations of the enzyme are also both present. Both open and closed conformations of the loop in triose-phosphate isomerase from *O. cuniculus* have been observed in the absence of ligands;[1030] both open and closed conformations of the loop in triose-phosphate isomerase from *P. falciparum* have been observed when the active site of the enzyme is occupied by phosphoglycolate, an analogue of the *cis*-enediol intermediate in the reaction;[1031] and both open and closed conformations of the loop in triose-phosphate isomerase from *S. cerevisiae* have been observed in the unoccupied enzyme, the enzyme occupied by substrates, and the enzyme occupied by phosphoglycolate.[1032]

The loop that closes over the substrates when they associate with the active site of human phosphoribosylglycinamide formyltransferase also closes over the empty active site when the pH of the solution for crystallization is 4, and this closure blocks access of the substrates. When the pH of the solution for crystallization is 8, however, the loop is in the open conformation with the active site ready for association.[1033] At intermediate values of pH, both the open and closed forms must be in equilibrium with each other because the catalytic constant of the enzyme declines smoothly as the pH is lowered as a consequence of the shift in the equilibrium between the open accessible active site and the closed inaccessible active site.

When arginine kinase from *L. polyphemus* is in solution in the absence of substrates or inhibitors, nuclear magnetic resonance spectra are consistent with an equilibrium existing between the open and closed conformations that are observed crystallographically.[1018]

In solution, nuclear magnetic resonance spectra of adenylate kinase from *E. coli* to which $MgATP^{2-}$ has bound are consistent with the existence of an equilibrium mixture in which its two domains are in closed and open conformations.[1034] When the equilibrium for the unoccupied enzyme is shifted toward the open conformation by mutation, the catalytic constant of the enzyme increases, and when the equilibrium is shifted in favor of the closed conformation by decreasing the concentration of water in the solution, the catalytic constant decreases,[962] as expected if the substrates can associate only with the open conformation of the enzyme.

It is the case, however, that the linkage box and the linkage cube (Equations 3–437 and 3–440) only imply that, in the absence of substrate, open and closed conformations of the unoccupied enzyme are both present, not that they are required to be. It has already been noted that even if the open conformation observed in crystallographic molecular models is only one member of an array of states, the entire ensemble can be assigned a standard free energy. Even if the closed conformation does exist only in vanishingly small concentration in the absence of substrate or substrates, nevertheless it would have a standard free energy.

In solution, the closing of a loop of polypeptide or the closing of domains over an active site is a dynamic process, and particular rate constants govern these conformational changes. In triose-phosphate isomerase from *S. cerevisiae*, the rate constant at 25 °C for closing the loop over either the unoccupied or the occupied active site is 40 ms^{-1}, and the rate constant at which it swings open is 3 ms^{-1}.[1032,1035] These rates are in the same range as the catalytic constant of the enzyme (3–10 ms^{-1}), and this fact suggests that either the closing or the opening of the loop is the rate-limiting step in catalysis or at least a significant rate-affecting step.

In the crystallographic molecular model of the complex between arginine kinase from *L. polyphemus* and L-arginine, $MgADP^{-}$, and nitrate (Figure 3–41), in addition to the two domains that have closed around the substrates, there is a loop of polypeptide from Isoleucine 182 to Glycine 209 that has folded over the substrates and the nitrate. Arginine 309, Threonine 311, and Glutamate 314 in this loop form hydrogen bonds to the substrates.[630] In the crystallographic molecular model of the unliganded enzyme, this loop has swung away from the active site, and the portion of the loop from Threonine 311 to Glutamate 319 is disordered and lacks electron density in the map.[1018] Transverse relaxation optimized spectra of nitrogen-15 nuclei in this loop in arginine kinase can be used to estimate the rate at which this loop closes over the active site. The rate of its closure in the unoccupied enzyme (40 s^{-1}) is slower than the catalytic constant (110 s^{-1}), but the activation energy for its closure (35 ± 10 kJ mol^{-1}) is the same as that for the catalytic constant.[1036] These measurements suggest that the rate-limiting step in

the nucleophilic substitution at phosphorus catalyzed by arginine kinase is the closure of this loop.

The dynamic opening and closing of the cleft between the domains in unoccupied phosphoglycerate kinase[1037] also seems to correlate with the turnover of the enzyme,[1038] and the rate constant for a global conformation change in unoccupied bovine pancreatic ribonuclease ($1.7\ ms^{-1}$) agrees closely with the catalytic constant of the enzyme ($1.9\ ms^{-1}$) under the same conditions.[1039,1040] All these results suggest that, in at least some enzymes, the rates of the conformational changes required for the active site to close around the reactants or for the active site to open to release products are rate-limiting steps in the rate of the reaction catalyzed by the enzyme.

In the case of dihydrofolate reductase from *E. coli*, however, conformational fluctuations associated with catalysis are observed after substrates have associated with the active site, it has already closed around them, and catalysis is taking place.[1041] Intrinsic fluctuations in the closed, occupied active site of the same enzyme that are detected by nuclear magnetic resonance spectroscopy are dramatically reduced in two different mutants of the enzyme, and in active sites of these rigid mutants, the rate of hydride transfer is 20-fold less than in the wild type.[1042] These results suggest that conformational fluctuations in an active site can continue to play a role in catalysis even after that active site has closed around the reactants.

Suggested Reading

DelaFuente, G., Lagunas, R., and Sols, A. (1970) Induced fit in yeast hexokinase, *Eur. J. Biochem. 16,* 226–233. https://doi.org/10.1111/j.1432-1033.1970.tb01075.x

Knöfel, T., and Sträter, N. (2001) Mechanism of hydrolysis of phosphate esters by the dimetal center of 5′-nucleotidase based on crystal structures, *J. Mol. Biol. 309*, 239–254.https://doi.org/10.1006/jmbi.2001.4656

Gutteridge, A., and Thornton, J. (2005) Conformational changes observed in enzyme crystal structures upon substrate binding, *J. Mol. Biol. 346*, 21–28. https://doi.org/10.1016/j.jmb.2004.11.013

Association of Reactants and Dissociation of Products

Both associations of the reactants with the active site and usually their respective dissociations from the active site as reactants, as well as dissociations of the products of the enzymatic reaction, are inescapable steps in the kinetic mechanism of an enzymatic reaction, and they can be rate-affecting or even rate-limiting. Although most active sites are open to the solution and immediately accessible to their reactants or open and accessible before they close around their assembled reactants by an induced fit, there are a number of **molecular and structural aspects** that influence the events involved in this association in addition to its rate. For example, in a crystallographic molecular model of the ternary complex of $NADP^+$, cyclohexanone, and the flavoenzyme cyclohexanone monooxygenase

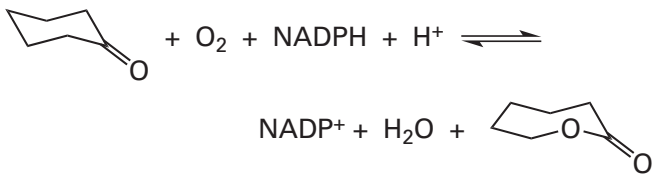

(3–441)

from *Rhodococcus*, the cyclohexanone occupies the same position as the nicotinamide ring does in the binary complex between the enzyme and $NADP^+$. This observation suggests that the nicotinamide ring in the ternary complex has swung out of its position in the binary complex. It was concluded that the oxidized nicotinamide ring, after it has reduced the flavin, has to swing away from the flavin before the cyclohexanone can associate.[1043]

When a reactant associates with an active site, it must always displace molecules of water that occupy the active site in its absence. It has been pointed out that, because the active site has been designed by natural selection to associate with its reactants and not those molecules of water, the molecules of water that will be displaced by the reactant are poorly coordinated relative to their coordination in the bulk solution. As a result, they are more easily displaced during the association.[1044] The rate at which they are displaced may have been enhanced by natural selection.

The **reactant in one direction of an enzymatically catalyzed reaction is a product in the other direction**. Consequently, the molecular aspects of the process of association of a particular reactant apply in reverse to its dissociation as a product and

vice versa. For example, the steps in the dissociation of CO_2 as a product from the active site of human carbonic anhydrase and its replacement by two fixed molecules of water can be followed crystallographically,[1045] and these steps must apply in reverse to its association as a reactant.

Often **access to an active site can be a compromise** mediated by natural selection. In the active site of myohemerythrin from *Phascolopsis gouldii*, a carrier of molecular oxygen, there is an invariant leucine. Mutating the leucine to a phenylalanine decreases the rate of association of oxygen with the iron ions by a factor of more than 100 because of steric hindrance by the larger side chain, but mutating it to valine, which has a smaller side chain, increased 3-fold the rate of autoxidation of the heme, an unfortunate side reaction.[1046] Mutating Alanine 68 in myoglobin from *Physeter catodon* to large amino acids also decreased the rate of association of oxygen with the heme.[1047]

In other instances, access of a reactant to the active site has been altered by natural selection to create new opportunities. In the common mechanism of a set of closely related lipoxygenases, each with different regiochemistry or stereochemistry, a molecule of oxygen adds to a pentadienyl radical

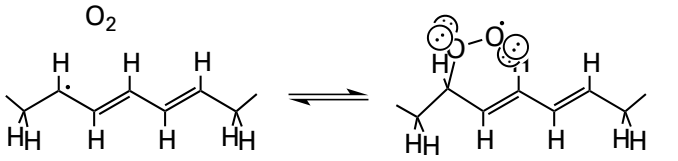

(3–442)

formed during the enzymatic reaction within the respective polyunsaturated fatty acid that is a reactant for the enzyme. The presence of a glycine at a particular location in the active site of two enzymes in this family permits the oxygen to associate and react at a carbon of the pentadienyl radical immediately adjacent to the glycine to produce the products specific to these enzymes. The presence of an alanine, however, at the same location in the active sites of two other members of the family prevents access to this carbon, and the oxygen adds instead to the other end of the pentadienyl radical to produce the products specific to these other enzymes.[1048]

It has already been noted that association of a nucleic acid with an enzyme is challenging because of its size. In the case of aspartate—tRNA ligase from *S. cerevisiae*, the initial nucleophilic substitution at the γ-phospho group of $MgATP^{2-}$ and the subsequent nucleophilic substitution at the α-carboxy group of L-aspartate catalyzed by the active site occurs at the 3′-hydroxy group of the ribose at the 3′ end of the $tRNA^{Asp}$; the four nucleotides at the 3′ end are not paired in the acceptor stem of the $tRNA^{Asp}$ and are freely moiling in solution;[1049] and the active site at which the nucleophilic substitutions occur is a shallow depression on the surface of enzyme with which only the cytidine and the adenine at the very 3′ end have any contact.[1050] Consequently, one might think that there would be no problem with the association of the reactant $tRNA^{Asp}$ with the active site of the enzyme. Aspartate—tRNA ligase, however, must recognize the transfer RNA as $tRNA^{Asp}$ unerringly. If it were to esterify L-aspartate to any other transfer RNA, a mutation would occur in the elongating protein to which L-aspartate is subsequently added. Aspartate—tRNA ligase from *S. cerevisiae* is a rigid homodimer (2×556 aa) of the same dimensions as $tRNA^{Asp}$ from *S. cerevisiae*, and following the association of $tRNA^{Asp}$ with the enzyme, an interface has formed along the whole length of the enzyme and the whole length of the $tRNA^{Asp}$ that brings them into intimate contact.[1050,1051] At one end of the interface, the cytidine and adenine at the 3′ end of the $tRNA^{Asp}$ have entered the active site of aspartate—tRNA ligase. Seven nanometers from the active site at the other end of the interface, which is at the other end of $tRNA^{Asp}$ at the tip of the anticodon arm, the guanosine, uridine, and cytidine of the anticodon associate intimately with a binding site on the surface of aspartate—tRNA ligase. In this instance, recognition of the actual anticodon ensures that the correct transfer RNA with the correct anticodon has been selected. In contrast, in the complex between $tRNA^{Leu}$ and leucine—tRNA ligase from *T. thermophilus*, although the anticodon stem is held firmly by the homologous domain on the ligase, the anticodon loop itself does not contact the ligase.[1052] In the middle of the interface, between the active site and the anticodon in aspartate—tRNA ligase from *S. cerevisiae*, there is another binding site on the surface of the protein into which the D loop of $tRNA^{Asp}$ inserts to provide further insurance. During the association of $tRNA^{Asp}$ with aspartate—tRNA ligase, there are various loops of polypeptide that reorient in induced fits, but these reorientations, although they may perform other purposes, are not so consequential to the correct association of the enzyme with its reactant.

Provocative descriptions of the **intermediate steps in the association or dissociation** of a substrate can be provided by calculations, and those descriptions can then be assessed experimentally.[1053]

Occasionally, as was the case with carbonic anhydrase, intermediates in the association and dissociation of a substrate can be observed crystallographically. For example, in a crystallographic molecular model of the active site of aspartate carbamoyltransferase (Equation 3–220) from *E. coli*, crystallized in the presence of the substrate phosphate, there are two phosphate ions occupying the site, one at the location occupied by the phospho group of the substrate carbamoyl phosphate in the crystallographic molecular model of its complex with the active site, and the other in an adjacent location.[1054] It has been proposed that the second phosphate is occupying a way station for a phosphate on its way out of or into the active site.

Separate crystals of human indoleamine 2,3-dioxygenase (previously Equation 2–248)

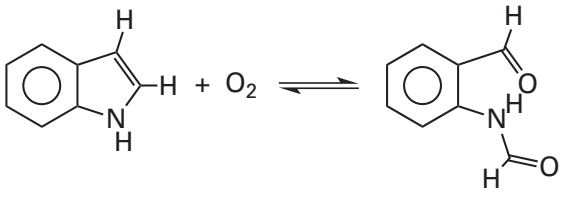

(3–443)

that had been soaked for different times in a solution of the inhibitor *N*-(4-chlorophenyl)-4-(6-fluoro-4-quinolyl)-α-methyl-*cis*-(αR)-cyclohexaneacetamide could be selected. In three different crystallographic molecular models obtained from these selected crystals, the inhibitor occupied three different locations in the tunnel leading to the active site. In each model, only one inhibitor was in the tunnel, in each case in its unique location. It was proposed that these three different locations represented intermediate way stations in the passage of inhibitor to its final location as a ligand to the iron ion in the heme at the end of the tunnel.[1055]

As with indoleamine 2,3-dioxygenase, there are a number of enzymes in which the active site is deeply buried in the protein, and access for substrates is afforded by a tunnel passing into the protein from the solution. For example, the iron ion of the heme in catalase from *Bos taurus* or *S. cerevisiae* is at the blind end of a straight tunnel 3 nm long and 1.5 nm wide at its opening to the solution on the surface of the protein. The tunnel gradually narrows to a width of 0.6–0.9 nm just above the iron ion and is lined by nonpolar side chains (Figure 3–59).[1056-1058] The substrates H_2O_2, H_2O, and O_2 pass through this tunnel while associating with and dissociating from the iron. When they are not occupied by substrates, locations along one of these tunnels in a catalase are occupied by molecules of water except at its narrow, innermost end. The tunnel for substrates into the imino carbon of the internal pyridoximine in the active site of diaminopropionate ammonia-lyase from *E. coli* is 1.2 nm long. It narrows slightly as the imino carbon is approached and the intruder has to be identified as one of the substrates: 2,3-diaminopropanoate, pyruvate, or ammonia.[1059]

The tunnel into the heme in the active site of bovine cholesterol monooxygenase (side-chain-cleaving) is also a long one. When 22*R*-hydroxycholesterol, an intermediate in the reaction, is in position to be oxidized, it fills two-thirds of the tunnel because it is so large.[1060] This situation is in contrast to the tunnel to the heme in catalase and the tunnel to the pyridoximine in diaminopropionate ammonia-lyase, which are both enzymes with small substrates. In cholesterol monooxygenase, the tunnel not only serves as access to the heme but probably has a role in specifically selecting the cholesterol that is the substrate for the reaction.

There is a long convoluted tunnel from the surface of the protein into the diiron cluster (see Figure 2–57I) in the active site of methane monooxygenase (soluble) from *Methylosinus trichosporium* that is remarkably uniform in width. It is wide enough to allow the passage of the substrates O_2 and CH_4 from the solution into the active site but narrow enough to hinder the access of larger hydrocarbons, a fact that would explain the preference of the enzyme for methane. The enzyme is activated by a smaller protein, the association of which with the enzyme increases the bimolecular rate of association of O_2 with the cluster by a factor of more than 1000. In the absence of this activator, the tunnel is almost completely constricted about halfway along its length; the conformational change of the enzyme produced by the activator eliminates the constriction and opens the channel.[1061] Site-directed mutation of Valine 41 at the opening of the tunnel on the surface of the protein, which is well removed from the active site, to an arginine decreases the rate of association of O_2 with the cluster in the center of the protein by a factor greater than 25,000.

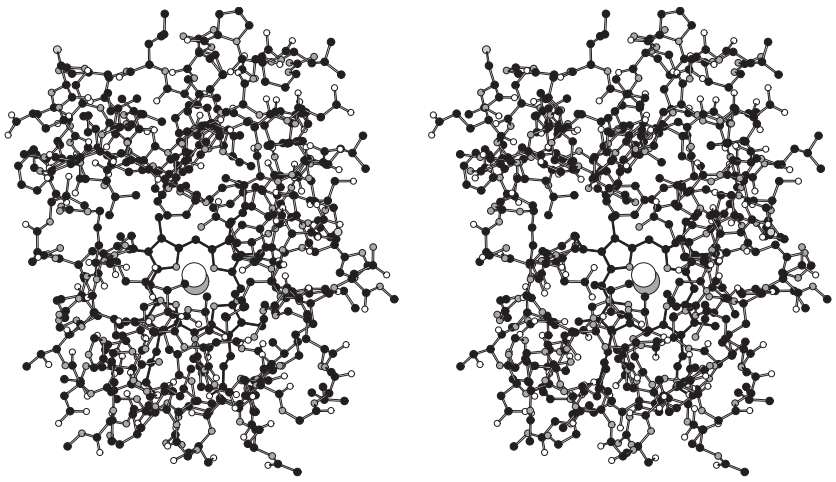

Figure 3–59: Stereodrawing[576] of the tunnel into the active site in the crystallographic molecular model of bovine catalase.[1058] Black atoms are carbons, white atoms are oxygens, small gray atoms are nitrogens, and large light gray atoms are sulfurs. Bovine catalase was purchased and further purified by size-exclusion chromatography. To the pooled and concentrated solution of catalase, NH_4OH was added to adjust the pH, and an equal volume of 50 mM magnesium formate was then added. The protein was then crystallized in this solution. The crystals were suspended and mixed with 1-(*N*,*N*-diethylamino)diazen-1-ium-1,2-diolate, which releases nitric oxide when dissolved in water, and the nitric oxide generated was then bound as a ligand to the iron in the heme. The crystals diffracted X-rays to Bragg spacing of 0.188 nm. A map of electron density was calculated by molecular replacement using the known structure of bovine catalase,[1056] and the molecular model was submitted to refinement. The drawing is of six segments of polypeptide in the molecular model that line the tunnel into the active site. The heme (black bonds) can be seen at the end of the tunnel. The nitric oxide on the iron ion in the center of the heme, which is hidden by the nitric oxide, is drawn in space-filling representation to illustrate the sizes of molecular oxygen, hydrogen peroxide, and water, which are the substrates for the enzyme and each must pass through the tunnel to and away from the heme.

One of the longest tunnels (16 nm) that has been found to date is the tunnel into the active site of the exosome from *S. cerevisiae*, a large enzyme (4000 aa) responsible for the hydrolysis of single-stranded RNA. This tunnel accommodates about 25 nucleotides of single-stranded RNA.[1062] The enzyme is composed of 11 different subunits, some structurally related and others structurally unrelated to each other, and the tunnel passes through the center of the protein among and within the subunits. The active site at the end of the long tunnel is an exoribonuclease II, catalyzing the hydrolysis of 5′-nucleotides from the unphosphorylated 3′ end of the single-stranded RNA threading through the tunnel. As each 5′-nucleotide is disconnected from the RNA by hydrolysis, it dissociates from the active site into the solution.

An acyl-SCoA is a long molecule. At one end of the molecule is a 3′-phosphoadenosyl group, and between its 5′-oxygen and the sulfur of the coenzyme A, there is a linear chain of 15 atoms, none of which is excessively substituted. Attached to the sulfur of the coenzyme A is an acyl group, which in the case of the reaction catalyzed by acyl-CoA:acyl-CoA alkyltransferase from *Xanthomonas campestris* is at least 14 carbons long, which makes the entire linear portion of the molecule at least 31 atoms long. There is a tunnel from the surface of the enzyme into the active site, which is in the center of the protein (338 aa). The linear portion of an acyl-SCoA that is a reactant for the enzyme threads through the tunnel, with the fatty acyl group in the lead, and it continues threading beyond the catalytic subsite into a blind tunnel lined with nonpolar side chains while the linear portion of coenzyme A ends up filling the tunnel with the adenylyl group sitting on the outside end of the tunnel acting as a stop to the threading. When the threading is halted by this stop, the thioester of the acyl-SCoA ends up adjacent to the catalytic subsite. When the thioester arrives at the catalytic subsite, its acyl group is transferred to the sulfanyl group of a cysteine to form a thioester of the cysteine. Then, the first product of the overall reaction, the coenzyme A that was a portion of the first acyl-SCoA, dissociates from the tunnel, leaving behind the thioester of the acyl group. A second acyl-SCoA threads into the tunnel. Its acyl group threads into a second blind tunnel leading away from the catalytic subsite in the opposite direction to the first. The enolate of the second acyl-SCoA then adds in a Claisen condensation to the thioester of the initial acyl group on the sulfanyl group of the cysteine to form the ketone containing both alkyl chains that is the product of the enzymatic reaction.[1063]

The active site of cellulose synthase (UDP-forming) adds D-glucosyl groups from UDP-glucose to an elongating polymer of cellulose, $[(\beta 1,4)$-D-glucosyl$]_n$.* In the crystallographic molecular model of the enzyme from *Cereibacter sphaeroides*, the active site at which the glucosyl groups are added to the elongating polymer could be identified by the UDP-glucose with which it is occupied. The active site is located in the cytoplasmic domain of the enzyme, which spans the plasma membrane of the cell. UDP-Glucose enters the active site from the cytoplasmic solution in which it is made, but the elongating polymer emerges from the enzyme across the membrane into the extracytoplasmic solution. In the crystallographic molecular model, there is a polymer of cellulose, 18 $(\beta 1,4)$-D-glucosyl groups long, located in a tunnel 0.8 nm wide and 6 nm long that leads out of the active site across the membrane into the extracytoplasmic solution.[1064] As each $(\beta 1,4)$-D-glucosyl group is added to the elongating chain of cellulose, it slides along the tunnel. In theory, an infinitely long polymer of cellulose could be continuously secreted into the extracytoplasmic solution by the enzyme. The distantly related (according to alignment of amino acids in the active site) cellulose synthase from *Populus tremula* is a rotationally symmetric trimer, rather than being a monomer, with a threefold rotational axis of symmetry normal to the plane of the membrane. The three tunnels in its membrane-spanning portion converge on a common point of exit on the threefold rotational axis of symmetry. The product that emerges from this common point of exit is a protofibril of cellulose, which is a trimeric strand of cellulose monomers.[1065]

Tunnels that connect a buried active site with the solution are often not so straight and direct as they are in catalase, diaminopropionate ammonia-lyase, cellulose synthase (UDP-forming), superoxide dismutase from *E. coli*,[1066] and ascorbate oxidase from *Cucurbita pepo*.[1067] Tunnels can be **tortuous** and of irregular width[1068] and contain **abrupt changes of direction**.[1069] They sometimes bifurcate and have **two openings** to the solution.[1070] The tunnel into the active site in 3-hydroxybenzoate 4-monooxygenase from *C. testosteroni* has two openings to the solution, one hydrophilic and the

*Amylose, which is the primary source of energy for humans, is $[(\alpha 1,4)$-D-glucosyl$]_n$, which is readily digested. Cellulose, $[(\beta 1,4)$-D-glucosyl$]_n$, unfortunately, cannot be digested by humans.

other hydrophobic, that provide access to a large internal chamber adjacent to the prosthetic flavin.[1071] In some instances, as was the case with the tunnel into the active site in the unactivated form of methane monooxygenase (soluble), the tunnels seem to be interrupted by side chains that act as gates along the way, swinging into the tunnel or out of it.[1072]

As was the case for association of the inhibitor with indoleamine 2,3-dioxygenase, as reactants move into and products move out of the active site through these tunnels, there are **way stations along the course** with which substrates have been observed to associate in crystallographic molecular models.[1071,1073] These way stations may assist in the selection of the correct reactant and thereby increase the rate of the enzymatic reaction at low concentrations of reactant, but the association of a reactant with one of these way stations may cause reactant inhibition by blocking the dissociation of product at high concentrations of reactant.[1074]

Tunnels into active sites are usually identified by applying algorithms that calculate the surface of the anhydrous crystallographic molecular model to molecules of water and then search for **regions of continuous empty space** wide enough to permit passage of small molecules.[1075,1076] Tunnels can also be recognized in a crystallographic molecular model by the continuous distribution of actual, fixed molecules of water that usually occupy them.[1044] Those tunnels that are lined with hydrophobic amino acids can be traced in a crystallographic molecular model by filling them with xenon (van der Waals radius = 0.21 nm), an electron-dense (54 electrons atom^{-1}), hydrophobic noble gas applied to the crystal at high pressure while the data are collected.[1068,1070,1077,1078]

Aside from permitting sensitive prosthetic groups such as hemes, internal pyridoximines, flavins, and clusters of metallic ions to be **isolated within the protection provided by the protein** and yet still gain access to the substrates they must transform, tunnels into the active site can accomplish other purposes. The mouth of the hydrophobic tunnel in ovine prostaglandin-endoperoxide synthase is placed against the surface of a lipid bilayer when the enzyme is bound at a cellular membrane, and the arachidonic acid that is its reactant can slither up the tunnel out of the membrane into the active site.[1079] The narrow tunnel along the sevenfold rotational axis of symmetry of the eicosaoctamer into the large central cavity of the proteosome, in which the active sites for its endopeptidases are located[1080] and which is ungated in the prokaryotic enzymes but gated in the eukaryotic enzymes,[1081] is narrow enough to ensure that the protein to be digested by the proteosome enters as the unfolded polypeptide,[1082] which threads through the tunnel on its way to its hydrolysis.[1083]

When there are several tunnels from the solution to the active site, the question arises as to **which tunnel or tunnels are used by the substrates.** The cluster of four manganese ions, five μ-oxo ions, and a Ca^{2+} (Figure 2–59) in the crystallographic molecular model of photosystem II from *Thermosynechococcus vulcanus* is responsible for the oxidation of two molecules of water to a molecule of oxygen. This cluster is well buried within the protein. There are three tunnels from the solution to the cluster that are occupied by fixed molecules of water, and each is a candidate for the tunnel through which the molecules of water that are substrates for the enzyme could queue.[1076] Only one of the three tunnels leads from the solution to a molecule of water that is a ligand to the Ca^{2+} in the cluster. Results from Fourier transform infrared spectroscopy identify this molecule of water as contributing one of the oxygen atoms in the molecule of oxygen produced by the cluster.[1084] The μ-oxo ion that contributes the other oxygen atom is also a ligand to the Ca^{2+}, as well as to three manganese ions. In the coordination sphere of the Ca^{2+}, that μ-oxo ion is immediately adjacent to the molecule of water at the end of the tunnel. As the cluster produces molecules of oxygen, molecules of water destined to become oxygen move along the tunnel from the solution to the cluster.

In each crystallographic molecular model from three different species, five tunnels from the solution to various locations around the [Mo–7Fe–9S–C] cluster buried in dinitrogenase can be identified.[1085] In this instance, since it is still unclear with what position in the cluster molecular nitrogen associates, the tunnel or tunnels through which it usually approaches the active site cannot yet be assigned.

Pharmaceutical agents can exert their effects by **blocking a tunnel**. Aspirin, 2-acetyloxybenzoic acid, achieves its anti-inflammatory effect by acetylating a serine lining the tunnel[1079] into the active site of ovine prostaglandin-endoperoxide synthase and blocking the slither of the arachidonic acid from a membrane into the active site.[1086] Ibuprofen, 2-[4-(2-methylpropyl)phenyl]propanoic acid, blocks the same tunnel by binding tightly within it.[1079]

Because there is no such thing as a bare hydron in solution, for enzymes that have a hydron as one of their stoichiometric reactants or products, there must be one or several lone pairs of electrons responsible for shuttling a hydron into or out of the active site. When a hydron is a reactant, that hydron could occupy a lone pair of electrons on another reactant as it enters the active site, but then the active site would have to associate with the conjugate acid of that reactant, which may be present at lower concentration in the solution than the conjugate base. When a hydron is a product, that hydron could leave the active site on a lone pair of electrons on another product, but there may be no basic lone pair of electrons on that other product that is accessible to the hydron when the other product and the hydron are produced in the active site. For example, a hydron is a reactant in the reaction catalyzed by 3-oxoacyl-[acyl-carrier-protein] reductase

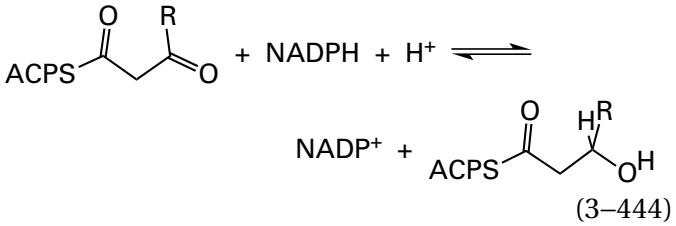

(3–444)

where ACPSH is acyl-carrier protein. This hydron does not enter the active site on its ultimate receptacle, the 3-oxo oxygen of the 3-oxoacyl-[acyl-carrier-protein], because this oxygen is not basic ($pK_a < -7$).

In many instances, an active site is exposed sufficiently to the bulk solvent to permit the delivery of a hydronium, or there is a water-filled channel connecting it to the bulk solvent that would permit a hydronium to enter it. In the crystallographic molecular model of the complex between 3-oxoacyl-[acyl-carrier-protein] reductase from *E. coli* and $NADP^+$, however, a tyrosine, which forms a hydrogen bond with the carbonyl oxygens of the respective substrates in crystallographic molecular models of the complexes of homologous enzymes with their substrates and which hydronates each of these oxygens during those reactions, is not in direct contact with the solution but is connected to it by a network of hydrogen bonds (Figure 3–60)[1087,1088] that can act as a hydron wire during the association of the hydron that is a stoichiometric reactant.

A **hydron wire** is a chain of hydrogen bonds into one end of which a hydron enters and out of the other end of which a hydron emerges[1089] or out of one end of which a hydron is removed and into the other end of which a hydron enters.[1090] The distinction between these two processes is that, as the hydrons are transferred between donors and acceptors for hydrogen bonds within the wire, either a sequence of conjugate acids or a sequence of conjugate bases, respectively, is the intermediate. In one case a hydron on sequential hydroniums is transported, and in the other case a basic lone pair of electrons on sequential hydroxides is transported. The distinction is a kinetic one based on whether the acid at one end initiates the transfer by adding a hydron to the hydron wire or the base at the other end initiates the transfer by removing a hydron from the hydron wire. In the case of 3-oxo-acyl-[acyl-carrier-protein] reductase from *E. coli*, the two processes would be distinguished as a hydronium at one end of the hydron wire that adds a hydron to the wire and a hydron emerging from the wire onto the oxygen of the carbonyl of 3-oxoacyl-[acyl-carrier-protein] (Figure 3–60) or the oxygen of the carbonyl oxygen that removes a hydron from the wire and a molecule of water at the other end that adds a hydron to the wire and becomes a hydroxide. Considering the pK_a of the carbonyl group ($pK_a < -7$) the overwhelmingly most likely sequence of events is the former.

When 7-hydroxyquinoline, which is the neutral tautomer in solution at pH 7

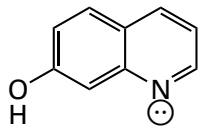

3–127

absorbs a photon, the pK_a of the hydroxy group in the resulting excited state becomes 0.4 and the pK_a of the conjugate acid of the quinolyl nitrogen becomes 11.1 while the values of pK_a are 8.7 and 5.6, respectively, for these functional groups in the ground state. Consequently, in water or methanol, a hydron dissociates from the hydroxy group and a hydron is added to the nitrogen when neutral 7-hydroxyquinoline enters the excited state. In this instance, the removal of a hydron from a molecule of water or methanol by the quinolyl nitrogen initiates the transfer, rather than the addition of a hydron from the hydroxy group to a molecule of water or methanol, and, contrary to the probable situation in 3-oxoacyl-[acyl-carrier-protein] reductase, the transfer through a hydron wire of water molecules between the two functional groups is hydroxide or methoxide transfer.[1090]

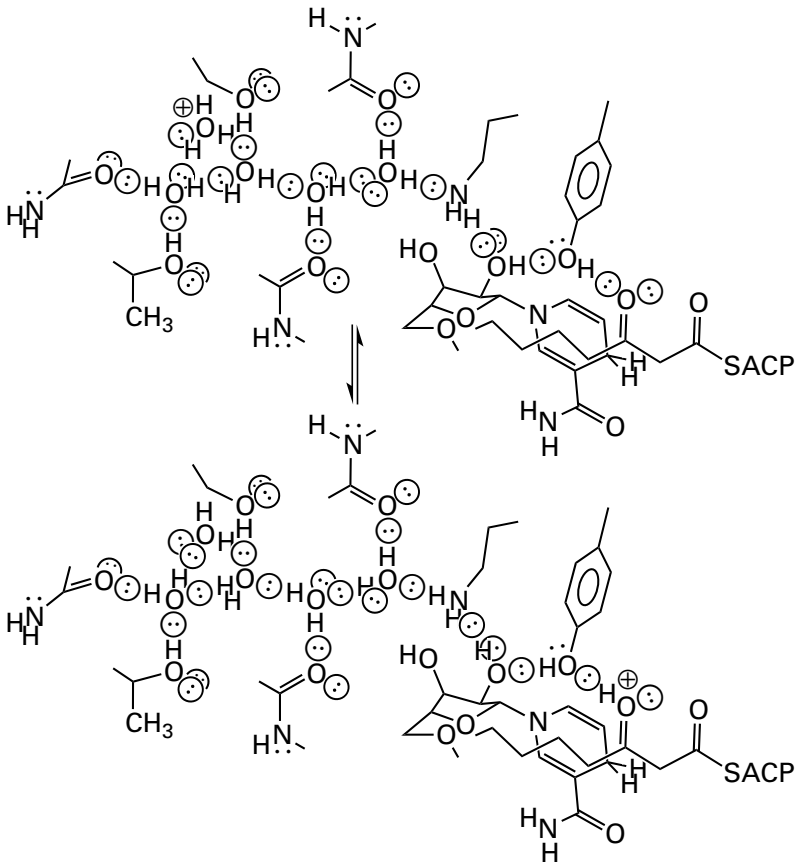

Figure 3–60: The hydron wire in the crystallographic molecular model of 3-oxoacyl-[acyl-carrier-protein] reductase from *E. coli*. The hydron wire does not form until the coenzyme $NADP^+$ or NADPH associates with the active site and induces a conformational change. The crystallographic molecular models on which the drawing is based are those of the binary complexes of the enzyme with either $NADP^+$ or NADPH. The hydrogen bond between the tyrosine and the carbonyl oxygen is inferred from crystallographic molecular models of complexes between substrates and inhibitors or other homologous short-chain dehydrogenases and reductases that reduce β-oxoacids in which the homologous tyrosine forms a hydrogen bond with the carbonyl carbon of the substrate. In the hydron wire illustrated here, a string of four molecules of water is held in fixed location by hydrogen bonds to the side chains of asparagine, threonine, and serine and the acyl oxygens of two amido groups of the polypeptide backbone. The wire then runs through the side chain of lysine, the 2-hydroxy group of NADPH, and the side chain of tyrosine before ending on the carbonyl oxygen of 3-oxoacyl-[acyl-carrier-protein]. Acyl-carrier protein is abbreviated ACPSH. A hydronium is shown donating a hydron to the first water in the wire.

In enzymatic reactions, although it can be decided with some certainty in cases such as 3-oxoacyl-[acyl-carrier-protein], it is usually unknown whether the transfer of a hydron through a hydron wire is the result of the transport of a hydron on sequential hydroniums or the transport of a lone pair of electrons on sequential hydroxides. From here on, for the sake of simplicity, it will be assumed that transport of a hydron is occurring.

In at least one set of enzymes, the carbonic anhydrases

$$CO_2 + H_2O \rightleftharpoons HCO_3^- + H^+ \qquad (3–445)$$

it has been shown that, in the hydrations catalyzed by these enzymes, the **rate-limiting step is the transit of the hydron** that is the stoichiometric product through a hydron wire consisting of the imidazolyl group of a histidine and a chain of two fixed molecules of water.[1091] One of the hydrons on a molecule of water on the Zn^{2+} in the active site enters the hydron wire connecting the active site with the solution. This hydron is transferred through the hydron wire to a general base or a molecule of water in the solution.[1092-1096] The distribution of hydrons in this hydron wire can be defined by **neutron diffraction**.[1097] The molecule of water that will accept the hydron is neutral and is the acceptor in a hydrogen bond to the molecule of water on

the Zn^{2+} from which the hydron is to be removed. One of its hydrogens is the donor in a hydrogen bond to the next molecule of water, and one of the hydrons on this molecule of water is a donor to the lone pair of electrons on the nitrogen of the imidazolyl group from which a hydron is to depart into the solution.*

Changes in the hydronation state within a hydron wire resulting from changes in the active site can be assessed by examining difference spectra from **Fourier transform infrared spectroscopy**. The wire for the two hydrons that are substrates for ferredoxin hydrogenase from *Chlamydomonas reinhardtii* runs from the solution through the guanidinio group of an arginine, the carboxy group of a glutamate, the hydroxy group of a serine, the carboxy group of a glutamate, a fixed molecule of water, and the sulfanyl group of a cysteine to the secondary amino group in a diiron cluster (previously **2–137**)

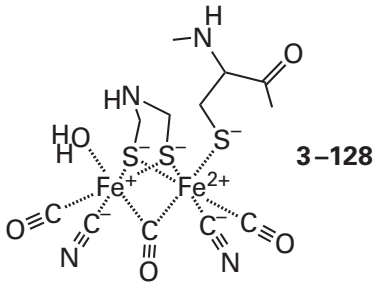

3–128

in the active site.[1098] The same hydron wire is also conserved in the related ferredoxin hydrogenase from *Clostridium pasteurianum* (37% identity; 1.6 gap percent)[1099] The cluster can be photoreduced, and differences in peaks of absorbance in Fourier transform infrared spectra between the oxidized state and the photoreduced state are observed upon photoreduction. These differences could be assigned by successive site-directed mutation to changes in the absorption of side chains of the amino acids in the hydron wire resulting from changes in their state of hydronation upon photoreduction.[1100]

A hydron wire can be as short as a molecule of water and the hydroxy group of a threonine,[1101] but in the hydron wire in 3-oxoacyl-[acyl-carrier-protein] reductase (Figure 3–60), there are four fixed molecules of water at one end, then an unhydronated lysine, the 2′-hydroxy group of the NADPH, and the tyrosine, with the carbonyl oxygen of the bound reactant at the other end. The hydron wire in thymidylate kinase from *M. tuberculosis* runs from the solution through the carboxy group of a glutamic acid, the hydroxy group of a serine, the guanidinio group of an arginine, and the carboxy group of an aspartic acid to the phospho group that is transferred by the enzyme.[1102] The hydron wire that connects the oxygen of sorbose that must be hydronated during the reaction catalyzed by sorbose reductase from *Gluconobacter frateurii* runs from the solution through two fixed molecules of water, the 6-amino group of a lysine, the 2′-hydroxy group of the nicotinamide ribose in NADPH, and the 4-hydroxyphenyl group of a tyrosine.[1103] The hydron wire out of the active site of betaine-aldehyde dehydrogenase from *P. aeruginosa* runs through two carboxy groups of two glutamates into the solution.[1104] The hydron wire in nitrite reductase (NO-forming) from *Alcaligenes xylosoxidans* runs from the solution through the imidazolyl group of a histidine, two fixed molecules of water, and the carboxy group of an aspartic acid to the nitrite being reduced by the enzyme. [1105]

While one of their oxygens alone can function as if it were a simple hydroxy group, albeit with a far more negative pK_a, **carboxy groups**, such as the two in the hydron wire of betaine-aldehyde dehydrogenase, are able to span a greater distance

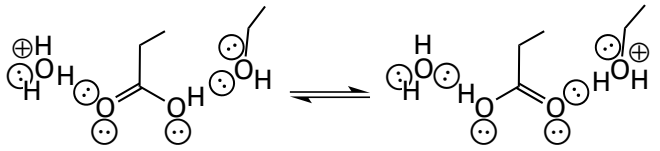

(3–446)

than a molecule of water, a hydroxy group, or an amino group. The two nitrogens in a stationary **imidazolyl group** are able to span the same distance as the two oxygens in a carboxyl group

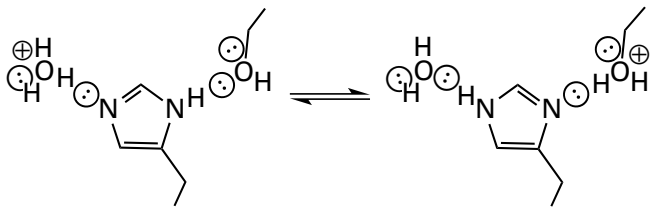

(3–447)

but in the hydron wire in human carbonic anhydrase 2,[1092] the imidazolyl group on Histidine 64 covers an even greater distance by swinging 0.35 nm about the pivot of the bond between its α and β carbons. It assumes two different conformations

*In this instance, it seems more likely that a hydroxide ion in the solution removes a hydron from the imidazolyl group to initiate the transfer of the hydron.

while shuttling the hydron, one in contact with the solution and the other in contact with a fixed molecule of water in the hydron wire leading from the active site.[1091]

For many hydron wires, only the hydron that is a stoichiometric reactant or product has to be transferred into or out of the active site, respectively, for each turnover, and the arrangement of hydrogen bonds in the wire can be **reset between turnovers**. In the case of the hydron wire in 4-hydroxy-tetrahydrodipicolinate synthase from *E. coli*, however, three hydrons are passed along it into the active site during a single turnover.[1106]

To accomplish the **transfer of more than one hydron**, which is always required for multiple turnovers of an enzyme that has only one hydron as a stoichiometric substrate, each participant in a hydron wire has to rotate after the first hydron has been moved to reestablish the initial distribution of hydrons in the wire. For example, the distribution of hydrons in the wire in 4-hydroxy-tetrahydrodipicolinate synthase[1106] after the transfer of the first hydron

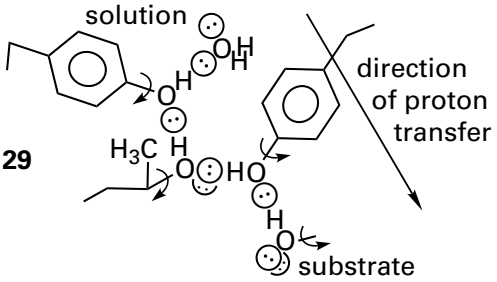

3–129

can be converted to the distribution required for the second transfer by rotations of the hydroxy groups on tyrosine, threonine, tyrosine, and the substrate of 180°, 120°, 180°, and 120°, respectively. A rotation of 180° in a carboxyl group (Equation 3–446) reestablishes the initial distribution, but an imidazolyl group (Equation 3–447) cannot rotate to reestablish the initial distribution because its two nitrogens are not symmetrically disposed. Consequently, as in carbonic anhydrase and nitrite reductase (NO-forming), the imidazolyl groups in a hydron wire are usually at the interface with the solution where a symmetric rotation is not required.

Bacteriorhodopsin from *Halobacterium salinarium* is an enzyme that catalyzes the reaction[1107]

$$2\ h\nu_{575} + H_i^+ \rightleftharpoons H_o^+ \qquad (3\text{–}448)$$

where H_i^+ is a hydron inside the cell and H_o^+ is a hydron outside the cell. The absorption of a photon produces a photoisomerization of the retinal that is a prosthetic group in the active site, and for every two photons absorbed, the photoisomerization succeeds in moving one hydron in the proper direction. The hydron wire from the solution on one side of the membrane into the active site and the hydron wire from the active site into the solution on the other side of the membrane together **have to transfer hydrons over a considerable distance** (3.5–4.0 nm).[1108,1109]

The hydron wire from the cytoplasmic solution into the active site is composed of a carboxy group from an aspartic acid and four molecules of water, and it is reconstructed from different molecules of water from the solution during each turnover so that no rotation of its participants is required between turnovers.[1110] Mutation of the aspartic acid in this hydron wire to asparagine slows the uptake of hydrons by the enzyme by 20-fold.[1111,1112]

The hydron wire out of the active site into the extracytoplasmic solution is composed of a molecule of water, the oxygen of a carboxyl group, a molecule of water, and the guanidinio group of an arginine.[1113,1114] The guanidinio group changes its position during each turnover from one in which it is forming a hydrogen bond to the interior molecule of water in the hydron wire to one in which it can form hydrogen bonds with molecules of water in the solution.[1115] Mutation of the aspartate in this hydron wire decreases the quantum yield of hydron transport 20-fold without affecting hydron uptake,[1112] and mutation of the arginine eliminates rapid hydron release into the extracytoplasmic solution.[1116]

Many hydron wires in enzymes contain two or more fixed molecules of water. The hydron wire into the active site in bacteriorhodopsin is composed in part of four **fixed molecules of water in a chain of hydrogen bonds**. In liquid water, such evanescent chains of molecules of water, through which the net of one hydron can be rapidly transferred, are thought to be responsible for the anomalously high mobility of hydrons in this solvent. In this explanation, a hydron would associate with a molecule of water at one end of the chain, and then there would be an almost instantaneous, concerted shift of hydrons within the hydrogen bonds of the chain that results in the molecule of water at the other end of the chain becoming a hydronium.* The net result would be the formal transfer of a hydron from one end of the chain to the other.[1089] Such hydron jumping probably

*The description of this process is usually attributed to Theodor Grotthus.[1117]

occurs in a hydron wire in enzymes where there are molecules of water in a chain of hydrogen bonds and hydroxy groups.[1118] There are also a number of synthetic materials that incorporate continuous, isolated chains of water molecules,[1119,1120] and there are calculations leading to the conclusion that hydron transfer through such single-file chains of water molecules can be as much as 40 times faster than hydron transfer in bulk water.[1121,1122]

As was the case with bacteriorhodopsin, a decrease in the rate of an enzymatic reaction resulting from the **mutation of an amino acid** participating in a chain of hydrogen bonds that is a candidate for a hydron wire is often used as evidence for the participation of that hydron wire in transferring hydrons into or out of the active site.[1101,1123] For example, mutation of two histidines on the way from the solution into the active site of the reaction center from *C. sphaeroides* decreases the rate of the first hydron transfer into the active site by a factor of 10 and the second hydron transfer by a factor of 4.[1124] Mutation of a histidine on the way from the active site of aryl-alcohol dehydrogenase from *P. putida* into the solution[1028] to glutamine decreases the specificity constant of the enzymatic reaction for benzyl alcohol by a factor of 125, and the effects of amines added to the solution are consistent with this decrease in rate arising from a decrease in the rate of transfer of the stoichiometric hydron in the overall reaction out of the active site.[1125] The fact that the participants in a hydron wire are conserved in a large number of species in which the enzyme is found is another indication of their importance to the enzymatic reaction.[1099]

While in some instances the rate constant of association of a reactant is so fast that it is equal to that expected for encounter control,[1126] the second-order rate constants for associations of reactants with the active site of an enzyme usually have values that are less than the rate constant predicted for an encounter-controlled reaction between a small molecule and a macromolecule by 1–3 orders of magnitude. At 25 °C, the rate of a encounter-controlled reaction is about $10^9\ M^{-1}\ s^{-1}$, depending on the diffusion constant for the substrate.[284,1127,1128] The concentrations of most substrates in the cytoplasm, however, are usually less than 1 mM, which means that the pseudo-first-order rate constants of association between reactants and most enzymes at physiologically relevant concentrations are usually significantly less than $10^5\ s^{-1}$. With this in mind, it should come as no surprise that some enzymes have catalytic constants that are equal to or greater than the pseudo-first-order rate constants with which the reactants, when present at physiological concentrations rather than at saturation, associate with the active site. Consequently, it is possible for the association of the reactants with the active site, rather than the subsequent turnover of the bound reactants, to be the rate-limiting step in an enzymatic reaction when those reactants are at their physiological concentrations.

The association of the reactants when they are present at physiological concentrations can be rate-limiting, however, only if those reactants are sticky.[1129] A **sticky reactant** is a reactant that is converted to products free in solution faster than it can dissociate from the active site once it has associated with it. For example, in the simple kinetic mechanism

$$\mathrm{E} + \mathrm{A} \underset{k_{-1}}{\overset{k_1}{\rightleftharpoons}} \mathrm{E{\cdot}A} \underset{k_{-2}}{\overset{k_2}{\rightleftharpoons}} \mathrm{E{\cdot}Z} \xrightarrow{k_3} \mathrm{E} + \mathrm{Z} \qquad (3\text{–}449)$$

if k_2 and k_3 are much greater than k_{-1}, then reactant A is converted to product Z free in solution much faster than it can dissociate back into the solution, and reactant A is a sticky reactant. If a reactant is sticky, almost every molecule of that sticky reactant that associates with the enzyme is converted to a molecule of product free in the solution.

If the reactants are not sticky and dissociate from the active site faster than they can be converted into products that have dissociated from the enzyme—for example if k_{-1} in Equation 3–449 is much greater than either k_2 or k_3—then a rapid pre-equilibrium is established between the enzyme and the reactants, and either chemical turnover or the release of the products must be the rate-limiting step, not association of the reactant.[1129] Pyruvate is a sticky reactant in the reaction catalyzed by acetolactate synthase from *E. coli*

$$2\ \text{pyruvate} + \mathrm{H^+} \rightleftharpoons \mathrm{CO_2} + \text{2-acetolactate} \qquad (3\text{–}450)$$

The enzyme associates in a kinetically irreversible step with the first pyruvate, the sticky reactant, and the second pyruvate then associates with the enzyme in a reversible pre-equilibrium preceding the chemical conversion and the release of acetolactate.[1130]

If a reactant in a particular enzymatic reaction is sticky, then two situations can be distinguished.

If the concentrations of the reactants in the enzymatic reaction are all at saturation, then as each active site releases products, it is immediately filled with reactants, and the rate-limiting step of the reaction must be a step that does not involve association of reactants, usually turnover of the bound reactants or the dissociation of the products. If the concentration of one reactant is so low that the rate of its association with the active site becomes less than the rates of turnover, dissociation of the products, and any other step affecting the overall rate of the reaction; if that reactant is sticky so that almost every molecule is converted to product free in solution once it associates with the active site; and if the concentrations of the other reactants remain at saturation, then the rate-limiting step in the reaction will become the association of that sticky reactant with the active site. It follows that **when one of the reactants in an enzymatically catalyzed reaction is sticky, a change in rate-limiting step must occur when the concentration of that reactant is decreased below a certain level**.

Coincident with this change in rate-limiting step for the sticky reactant is a **change in reaction order**. At high concentrations of the sticky reactant that is being varied, its turnover, the dissociation of products, or some other first-order process not involving its association is rate-limiting; at low concentrations of the reactant, its association, a second-order process, is rate-limiting. As a result, the behavior observed is an increase in the initial rate of the enzymatic reaction that is proportional to the concentration of reactant at low concentrations, followed by an approach to a horizontal asymptote at higher concentrations of reactant as the rate-limiting step changes from association to turnover. This change in rate-limiting step is observed as apparent saturation. This **apparent saturation**, however, is not caused by saturation of the active site but by the change in rate-limiting step. This behavior will be indistinguishable by steady-state kinetics from the behavior of an enzyme that does not have sticky reactants. In each instance, the initial rate of the enzymatic reaction is a rectangularly hyperbolic function of the concentration of reactant.

These general conclusions, however, have significant consequences for natural selection. To understand these consequences, consider the simplest kinetic mechanism

$$\mathrm{E} + \mathrm{A} \underset{k_{-1}}{\overset{k_1}{\rightleftharpoons}} \mathrm{E{\cdot}A} \xrightarrow{k_2} \mathrm{E} + \mathrm{Z} \qquad (3\text{–}451)$$

In all cases, at concentrations of reactants that saturate an enzyme, none of the pseudo-first-order rate constants for association between an enzyme and its reactants can be rate-limiting because the concentrations of reactants—and consequently their pseudo-first-order rate constants of association, which can be increased until no more reactant will dissolve in the solution—have been purposely increased by the investigator to a level at which no further increases in the rate of the enzymatic reaction are observed. When saturation is reached, the first-order rates at which bound reactant is converted to product and product dissociates from the enzyme limit any further increase in the initial rate of the reaction.

If, on the one hand, $k_{-1} << k_2$ so that the reactant is sticky, then Equation 3–62 becomes

$$v_0 = \frac{k_2[\mathrm{E}]_t k_1[\mathrm{E}]_t[\mathrm{A}]_0}{k_2[\mathrm{E}]_t + k_1[\mathrm{E}]_t[\mathrm{A}]_0} \qquad (3\text{–}452)$$

the specificity constant $k_A = k_1$, and the catalytic constant $k_0 = k_2$. At low concentration of reactant

$$v_0 \cong k_1[\mathrm{E}]_t[\mathrm{A}]_0 \qquad (3\text{–}453)$$

and the enzymatic reaction is limited by the rate of the second-order association of enzyme with reactant. At high concentration of reactant

$$v_0 \cong k_2[\mathrm{E}]_t \qquad (3\text{–}454)$$

and the rate of the reaction is limited by the rate of the first-order conversion of reactant to product and dissociation of the product. In this situation the Michaelis constant K_{mA} for the reaction is $k_2\, k_1^{-1}$, which is not even remotely connected to the dissociation constant K_{dA} for reactant A from the active site.

If, on the other hand, $k_{-1} >> k_2$ so that the reactant is not at all sticky, then Equation 3–62 becomes

$$v_0 = \frac{k_2[\mathrm{E}]_t[\mathrm{A}]_0}{\left(\frac{k_{-1}}{k_1}\right) + [\mathrm{A}]_0} \qquad (3\text{–}455)$$

At high saturating concentrations of reactant A, Equation 3–454 still applies, $k_0 = k_2$, and the rate of the reaction is limited by the rate of the first-order conversion of reactant to product and dissociation

of the product, but the Michaelis constant is equal to the dissociation constant for reactant A from the active site

$$K_{mA} = \frac{k_{-1}}{k_1} = K_{dA} \tag{3–456}$$

The consequential aspect of this situation is that, at concentrations of reactant A significantly less than the Michaelis constant

$$v_0 = \frac{k_2[E]_t[A]_0}{K_{dA}} \tag{3–457}$$

the rate of the reaction is not limited by the rate of association of reactant with the enzyme. At this low concentration of the reactant, the rate of the reaction should increase as the dissociation constant for reactant A decreases. If the physiological concentration of reactant A is less than the Michaelis constant and reactant A is not sticky, natural selection can increase the rate of the enzymatic reaction, and hence its efficiency, by selecting for decreases in the dissociation constant of reactant A.

If, however, reactant A is sticky and its physiological concentration is less than the Michaelis constant for the enzyme, then the rate of diffusion of sticky reactant A to the active site is rate-limiting at its physiological concentrations; the initial rate for the enzymatic reaction at the physiological concentration of reactant A will be proportional to its concentration; and the constant of that proportionality, by definition the observed specificity constant k_A for reactant A, will be equal to the second-order rate constant for its association with the enzyme, k_1. If the catalytic constant of an enzyme is so fast that the rate of association of one or more sticky reactants, when they are at their physiological concentrations, is the rate-limiting step in the reaction, then the enzyme will have evolved to a state where an increase in its catalytic constant cannot increase the rate of the enzymatic reaction as it occurs in the cytoplasm, and natural selection can no longer operate upon the catalytic constant. At this stage, if it is not possible to increase the rate of diffusion of that reactant or those reactants to the active site, short of increasing their cellular concentrations, the enzyme will have become a **perfect catalyst.**[284,1131] Natural selection, however, might still select for an increase in the rate at which the reactant associates with the active site once it has collided with the enzyme.

As most substrates for enzymes bear a net charge at physiological pH, the possibility that rates of association can be increased by providing elementary charges around the active site that are opposite to the charge of the reactant has been rather enthusiastically considered as one way in which natural selection could increase the rate of association. For example, the rate of association of NADH, which has a charge number of –1 above pH 7, decreases by a factor of 10 as the net elementary charge on equine liver alcohol dehydrogenase is changed from +16 to –24 by increasing the pH, but only when the ionic strength of the solution is 0.01 M.[1132] As with most such purely electric effects, enhancements in the rate of association observed when the vicinity of the active site is oppositely charged from its substrate decrease dramatically, in the case of alcohol dehydrogenase to less than a factor of 2, at physiological levels of ionic strength. In the case of acetylcholine receptor, mutation of an aspartate or glutamate in the region surrounding its channel for the transport of potassium ions to a neutral amino acid decreases its conductance by a factor of around 2 at an ionic strength of 0.10 M, a change thought to result from an electric effect on the rate of association of K^+ with the channel in the enzyme,[1133] a rather small effect. Although there are other reasons for the fact that all cytoplasm has this level of ionic strength, one reason may be to minimize electric effects between charged reactants and charged proteins.

Electric effects on rates of association at physiological levels of ionic strength appear to be significant in cases in which a small protein acting as a carrier of an electron associates with an enzyme.[1134,1135] In this instance the net elementary charges on the participants can be large. For example, at physiological pH, the net charge number on equine ferricytochrome *c* is +7 and that on a tryptic fragment of cytochrome b_5 is –9, and it seems that the large difference in the elementary charge on these two proteins increases the rates at which they associate by a factor of around 20 at physiological ionic strength.[1136] In these cases, natural selection would be able to operate successfully on electric effects.

The rate of dissociation of a product from the active site is often slow enough to be the rate-limiting step in an enzymatically catalyzed reaction. Because the dissociation constants of substrates from enzymes are often in the range of 10^{-6} M and

the respective second-order rate constants for their association are usually less than $10^8\ M^{-1}\ s^{-1}$, it follows that rates of dissociation of the substrates, and hence the products, of an enzymatic reaction can be less than $100\ s^{-1}$. Many enzymatic reactions in which the dissociations of the products are rate-limiting have been identified. Therefore, the rate of release of products from the active site can be an important factor in the overall rate of the enzymatic reaction.

A **sticky product** is a product that dissociates slowly from the active site relative to the rate of either the back reaction to bound reactant or the forward reaction from bound reactant to bound product. In other words, for the simple kinetic mechanism of Equation 3–449, a sticky product would be the product in the enzymatic reaction for which $k_3 << k_{-2}$ or $k_3 << k_2$ or both of these inequalities occur, regardless of whether k_3, k_2, or k_{-2} themselves are microscopic or composite rate constants. Under these circumstances, the dissociation of a sticky product (k_3), not the chemical transformation of reactant and product (k_2), determines the catalytic constant of the enzymatic reaction. For example, the rate at which acyl-CoA dehydrogenase

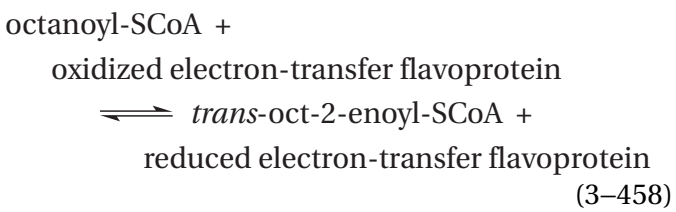

(3–458)

from *E. coli* oxidizes octanoyl-SCoA on its active site at 25 °C is $400\ s^{-1}$, but the rate at which the resulting large, sticky *trans*-oct-2-enoyl-SCoA dissociates from the enzyme is only $13\ s^{-1}$, which determines the catalytic constant for the enzyme of $15\ s^{-1}$. When the enzyme is mutated so that oxidation of octanoyl-SCoA decreases from $400\ s^{-1}$ to $0.5\ s^{-1}$, this rate of $0.5\ s^{-1}$ determines the catalytic constant of $0.7\ s^{-1}$, not the dissociation of the no longer sticky product, which is $8\ s^{-1}$ in the mutant.[1137] The catalytic constant of equine alcohol dehydrogenase is equal to the rate constant at which the large, sticky product NADH dissociates from the enzyme, and a mutation that increases this rate of dissociation by a factor of 7 increases the catalytic constant of the enzyme by a factor of 6.[1138]

Even the smallest substrate, a hydron, however, can be a sticky product. For example, the dissociation of the hydron that is a product of the dehydration catalyzed by fumarate hydratase (Equation 3–1) from *E. coli* is slower than both the dehydration itself and the dissociation of fumarate.[1139]

In the case of nucleophilic aromatic substitution of the sulfanyl group of glutathione for the chloro group in 1-chloro-2,4-dinitrobenzene catalyzed by isoenzyme M1-1 of glutathione transferase from *R. norvegicus*, the dissociation of the product is 60-fold slower than the actual nucleophilic substitution because a conformational change in the enzyme must precede the dissociation.[1140,1141] The dissociation of the product nitric oxide from nitric-oxide synthase (flavodoxin) from *G. stearothermophilus*, however, is slow not because of a conformational change but because an isoleucine and a histidine on the way out of the active site sterically hinder its release into the solution.[1142]

In an enzymatic reaction in which **both product and reactant are sticky**, the chemical transformation converting reactant and product has time to reach equilibrium while the reactant and product remain on the enzyme.

The effects of microviscosity of the solution on the observed steady-state catalytic constant k_0 and the specificity constant k_A for reactant A can be used to distinguish microscopic rate constants for the association and dissociation of reactant A and for the dissociation of product Z in the underlying kinetic mechanism from those rate constants for the chemical transformations that occur within the active site.[1143] If the rate constant for the association of substrate A with the active site of enzyme E[1143] and the rate constant for the dissociation of substrate A from the active site of enzyme E[1144] are each directly proportional to the sum of the diffusion coefficient of substrate A, D_A, and the diffusion coefficient of enzyme E, D_E, in the solution, then

$$k_i = \xi_i (D_A + D_E) = \xi_i \frac{k_B T}{6\pi\eta}\left(\frac{1}{r_A} + \frac{1}{r_E}\right) \qquad (3–459)$$

where k_i is a rate constant for either association or dissociation, ξ_i is a constant of proportionality unique to that rate constant, k_B is the Boltzmann constant, T is the temperature, η is the microviscosity of the solution, and r_A and r_E are the Stokes radii of substrate A and enzyme E, respectively. It follows that

$$\frac{k_i}{k_{i\eta}} = \frac{\eta}{\eta_0} = \eta_{rel} \qquad (3–460)$$

where k_i is the rate constant in a reference solution of microviscosity η_0, usually chosen to be the aqueous solution containing the enzyme at the pH and ionic strength at which the initial rates of its reaction have been studied, and $k_{i\eta}$ is the rate constant in the reference solution to which a microviscogen such as glycerol, sucrose, or trehalose has been added to produce a microviscosity η,* which is greater than η_0.

Suppose the enzyme has one reactant A and one product Z. If the dissociation of product Z is explicitly included, the kinetic mechanism of the reaction is that of Equation 3–449 and the rate equation (see Equation 3–89) for this kinetic mechanism is

$$v_0 = \frac{\left(\frac{k_2k_3[\mathrm{E}]_t}{k_{-2}+k_2+k_3}\right)\left(\frac{k_1k_2k_3[\mathrm{E}]_t}{k_{-1}k_{-2}+k_{-1}k_3+k_2k_3}\right)[\mathrm{A}]_0}{\left(\frac{k_2k_3[\mathrm{E}]_t}{k_{-2}+k_2+k_3}\right)+\left(\frac{k_1k_2k_3[\mathrm{E}]_t}{k_{-1}k_{-2}+k_{-1}k_3+k_2k_3}\right)[\mathrm{A}]_0} \tag{3–461}$$

from which it follows that

$$k_0 = \frac{k_2k_3}{k_{-2}+k_2+k_3} \tag{3–462}$$

and

$$k_\mathrm{A} = \frac{k_1k_2k_3}{k_{-1}k_{-2}+k_{-1}k_3+k_2k_3} \tag{3–463}$$

If only the rate constants governing association and dissociation of substrates with and from the active site are affected by the microviscosity of the solution and k_1, k_{-1}, and k_3 behave according to Equation 3–460, it follows that the ratio

$$\frac{k_0}{k_{0\eta}} = \frac{(k_{-2}+k_2)\eta_\mathrm{rel}+k_3}{k_{-2}+k_2+k_3} \tag{3–464}$$

where k_0 and $k_{0\eta}$ are the catalytic constants observed in the absence and presence of microviscogen, respectively. It also follows that the ratio

$$\frac{k_\mathrm{A}}{k_{\mathrm{A}\eta}} = \frac{(k_{-1}k_{-6}+k_6k_7)\eta_\mathrm{rel}+k_{-1}k_7}{k_{-1}k_{-6}+k_6k_7+k_{-1}k_7} \tag{3–465}$$

The ratio $k_0\,k_{0\eta}^{-1}$ as a function of η_rel defines a line with a slope

$$\mathrm{slope}_{0\eta} = \frac{k_{-2}+k_2}{k_{-2}+k_2+k_3} \tag{3–466}$$

and a value of 1 when $\eta_\mathrm{rel} = 1$. The ratio $k_\mathrm{A}\,k_{\mathrm{A}\eta}^{-1}$ as a function of η_rel defines a line with a slope

$$\mathrm{slope}_{\mathrm{A}\eta} = \frac{k_{-1}k_{-2}+k_2k_3}{k_{-1}k_{-2}+k_2k_3+k_{-1}k_3} \tag{3–467}$$

and a value of 1 when $\eta_\mathrm{rel} = 1$. Consequently, the slopes of these plots provide information in addition to the only observed rate constants, k_0 and k_A, obtained from steady-state kinetics.[1143]

Consider first the situation in which the slope of the line for the ratio $k_0\,k_{0\eta}^{-1}$ as a function of η_rel (Equation 3–464) is indistinguishable from 0 and the slope of the line for the ratio $k_\mathrm{A}\,k_{\mathrm{A}\eta}^{-1}$ as a function of η_rel (Equation 3–465) is indistinguishable from 1, as is the case for bovine adenosine deaminase (Figure 3–61A)[283,455] and bovine alkaline phosphatase at pH 6.[1144] From the former observation it follows that $k_3 >> k_2$ and $k_3 >> k_{-2}$, and from the latter observation it follows that $k_{-1} << k_2$. Therefore, if the kinetic mechanism of Equation 3–85 describes the reaction, reactant A—for example, adenosine in the case of adenosine deaminase or a phosphate monoester in the case of alkaline phosphatase—is a sticky reactant, the respective product is not sticky, the specificity constant k_A for reactant A (Equation 3–463) is equal to the bimolecular rate constant k_1 for association of reactant A with the enzyme,[1144] the Michaelis constant K_mA is unrelated to the dissociation constant for reactant A from the active site, and the observed catalytic constant k_0 is equal to k_2.

*The **microviscosity** of the solution, the viscosity experienced by a molecule, is distinguished from the **macroviscosity** of the solution, the viscosity measured by a viscometer. Small viscogens such as glycerol, sucrose, or trehalose affect both the microviscosity and the macroviscosity equivalently. In these instances, the microviscosity is the viscosity measured by a viscometer. Macromolecular viscogens such as long, flexible, hydrophilic polymers can affect the macroviscosity more than they do the microviscosity.[1145] The lack of an effect of a macromolecular viscogen on the rate constants for an enzymatic reaction demonstrates that it is actually the microviscosity that is affecting those rates.[1146]

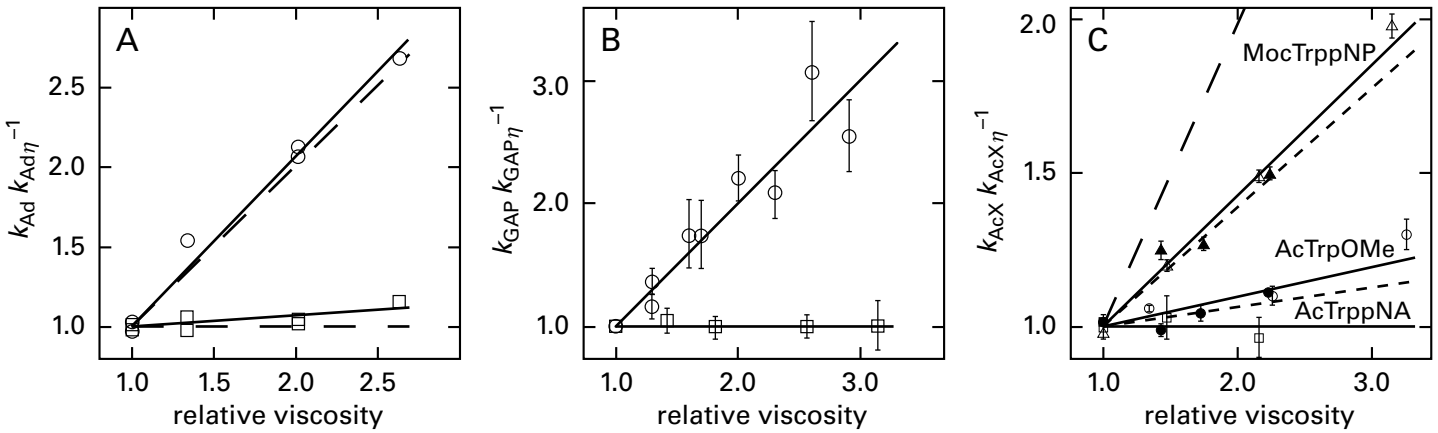

Figure 3–61: Effect of microviscosity of the solution on rate constants for the reactions catalyzed by bovine adenosine deaminase,[455] triose-phosphate isomerase from *G. gallus*,[284] and bovine chymotrypsin.[1143] **(A)** Steady-state catalytic constant k_0 and specificity constant k_{Ad} for adenosine for the conversion of adenosine (Ad) to inosine catalyzed by adenosine deaminase were determined by fitting full time courses for approaches to equilibrium (see Figure 3–1A) at an ionic strength of 0.15 M, pH 7.0, and 20 °C, and in solutions containing various concentrations of sucrose to increase the microviscosity. The ratios of the steady-state rate constants $k_{Ad}\ k_{Ad\eta}^{-1}$ (○) and $k_0\ k_{0\eta}^{-1}$ (□), where k_{Ad} and k_0 refer to values for the rate constants in the absence of microviscogen and $k_{Ad\eta}$ and $k_{0\eta}$ refer to values for the rate constants at a particular relative microviscosity, are plotted as a function of relative microviscosity η_{rel}, which is the microviscosity of the particular solution, η, divided by the microviscosity of the same solution in the absence of sucrose, η_0. The solid lines are linear, least-squares fits to the data, and the dashed lines are lines of slope 1 and slope 0, respectively. **(B)** Initial rates of conversion of D-glyceraldehyde 3-phosphate to glycerone phosphate, catalyzed by wild-type triose-phosphate isomerase (○) or a mutant in which Glutamate 164 had been changed to aspartate (□), were measured at pH 7.6 and 30 °C in solutions containing various concentrations of D-glyceraldehyde 3-phosphate (GAP) and various concentrations of glycerol to increase the microviscosity. The initial rates were used to determine the specificity constant k_{GAP} for D-glyceraldehyde 3-phosphate in the absence of glycerol and the specificity constants $k_{GAP\eta}$ at particular relative viscosities, and the data are presented as in Panel A. The solid lines are lines of slope 1 and slope 0. **(C)** Initial rates of hydrolysis catalyzed by chymotrypsin were measured for various concentrations of several acyl derivatives (AcX) that are reactants for the enzyme—the 4-nitroanilide (□, AcTrppNA) and the methyl ester (○, ●, AcTrpOMe) of *N*-acetyl-L-tryptophan and the 4-nitrophenyl ester of *N*-(methoxycarbonyl)-L-tryptophan (△, ▲, MocTrppNP)—at an ionic strength of 0.5 M, pH 8.0, and 25 °C. Initial rates were also measured in solutions containing various concentrations of sucrose (□, ○, △) to increase the microviscosity or Ficoll (●, ▲) to increase the macroviscosity. The initial rates were used to determine the specificity constant k_{AcX} for the various reactants in the absence of microviscogen and the specificity constants $k_{AcX\eta}$ at particular relative viscosities for each of the reactants, and the data are presented as in Panel A. The solid lines are fits to the data for sucrose as microviscogen, and the lines with shorter dashes are fits to the data for Ficoll as the macroviscogen. The line with longer dashes is a line of slope 1.

The only reason the initial rate of the reaction decreases below V as the concentration of adenosineis decreased is that a change in rate-limiting step occurs from turnover, at high concentrations, to the unidirectional association of adenosine, at low concentrations.

That these conclusions are reasonable in a particular instance is strengthened by the observation that when turnover of the reactant is decreased significantly—either by site-directed mutation (Figure 3–61B),[284,840,1147,1148] by using a reactant that is turned over more slowly,[1143] or by changing the pH[1145]—the slope of the line for $k_A\ k_{A\eta}^{-1}$ as a function of η_{rel} goes to 0 because the reactant is no longer sticky.

If the slope of the line for $k_A\ k_{A\eta}^{-1}$ as a function of η_{rel} is 0, as is the case for cytidine deaminase from *E. coli* with no alterations,[283] then $k_2 << k_{-1}$ and the reactant is not at all sticky; a pre-equilibrium between reactant A, the enzyme, and a complex of reactant A with the enzyme precedes the chemical step transforming reactant to product within the active site; and in the simplest case, the Michaelis constant is the dissociation constant for reactant A from the active site (Equation 3–455).

Consider the situation in which the slope of the line for the ratio $k_0\ k_{0\eta}^{-1}$ as a function of η_{rel} (Equation 3–464) is indistinguishable from 1 and the slope of the line for the ratio $k_A\ k_{A\eta}^{-1}$ as a function of η_{rel} (Equation 3–465) is indistinguishable from 0. It follows from both of these observations together that $k_{-2} << k_3$, $k_3 << k_2$, and $k_2 << k_{-1}$. Therefore, if the kinetic mechanism of Equation 3–449 describes the reaction, the product is sticky, all steps before the release of product reach equilibrium, and the rate-limiting step of the reaction is

the release of product Z. For example, in the case of murine cyclic-AMP-dependent non-specific serine/threonine protein kinase, the slope of the line for $k_0\ k_{0\eta}^{-1}$ as a function of η_{rel} is indistinguishable from 1 and the slope of the line for $k_{pep}\ k_{pep\eta}^{-1}$ as a function of η_{rel} is close to 0 for the peptide LRRASLG as a reactant. It could be concluded that the rate-limiting step in the reaction is the dissociation of the product; that k_3, the rate constant for dissociation of product, is equal to the observed catalytic constant k_0 (22 s^{-1});[1149] and that the association of the peptide with the active site is at equilibrium. Even though the association of the reactant is at equilibrium, because

$$K_{mA} = \frac{k_0}{k_A} = \frac{k_{-1}k_{-2} + k_{-1}k_3 + k_2k_3}{k_1k_{-2} + k_1k_2 + k_1k_3} \cong \frac{k_{-1}k_3}{k_1k_2} \qquad (3\text{–}468)$$

the Michaelis constant is not equal to the dissociation constant for the reactant. If it is the case for this enzyme, as seems reasonable, that $k_{-2} << k_2$ because the chemical step is the transfer of a phospho group from a phosphoric anhydride to an aliphatic hydroxy group, it can concluded that product piles up on the active site waiting to dissociate.

If the slope of either the line for behavior of the ratio $k_0\ k_{0\eta}^{-1}$ as a function of η_{rel} (Equation 3–464) or the line for behavior of the ratio $k_A\ k_{A\eta}^{-1}$ as a function of η_{rel} (Equation 3–465) is significantly different from either 1 or 0, then the rate of association of reactant A at low concentration cannot be rate-limiting. Nevertheless, the rate of association for the reactant must be affecting the overall rate of the reaction, and in such circumstances, the slope of one or the other of these lines can be used to obtain **estimates of the values for underlying rate constants in the kinetic mechanism** of Equation 3–449.[1143,1150]

For example, the lines describing the effect of relative microviscosity of the solution on the ratio of the specificity constants, $k_{ester}\ k_{ester,\eta}^{-1}$, for hydrolysis of *N*-(methoxycarbonyl)-L-tryptophan 4-nitrophenyl ester and *N*-acetyl-L-tryptophan methyl ester by bovine chymotrypsin (Figure 3–61C)[1143] have slopes of 0.4 ± 0.1 and 0.1, respectively. Over the same ranges, the respective values for the catalytic constants k_0 actually increased by about 10% rather than decreasing as the microviscosity of the solution was increased. Consequently, the rate constant k_3 in the kinetic mechanism for chymotrypsin

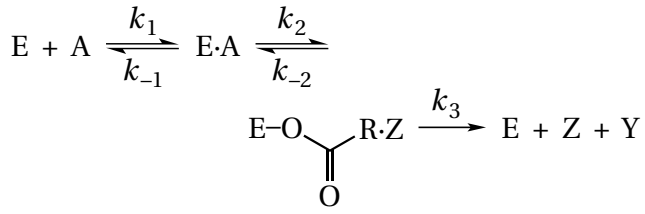

(3–469)

for both reactants cannot be affected by the rate constant for the dissociation of either product. It is also known that, for the two reactants used in these experiments, the second step in the kinetic mechanism is irreversible because the respective product Z, 4-nitrophenol or methanol, dissociates rapidly and immediately after the acyl enzyme is formed, so the value of the rate constant k_{-2} is formally 0. It follows (Equation 3–467) that

$$\text{slope}_{ester,\eta} = \frac{k_2}{k_{-1} + k_2} \qquad (3\text{–}470)$$

From the slopes of the lines for *N*-(methoxycarbonyl)-L-tryptophan 4-nitrophenyl ester and *N*-acetyl-L-tryptophan methyl ester, values for the ratio $k_{-1}\ k_2^{-1}$ of 1.5 and 11, respectively, could be calculated (Equation 3–470). Since the values for k_{ester} in the absence of microviscogen are 35 and 0.81 $\mu M^{-1}\ s^{-1}$, respectively, the values estimated for k_1 are 90 and 10 $\mu M^{-1}\ s^{-1}$.

The slope of the line for the effect of microviscosity on the catalytic constant for the decarboxylation of orotidine 5′-phosphate by orotidine-5′-phosphate decarboxylase (Equation 3–366) from *M. thermautotrophicus* is 0.02 ± 0.03, so dissociation of the product, uridine monophosphate, cannot be the rate-limiting step in the enzymatic reaction. The slope of the line for the effect of microviscosity on the specificity constant for the reactant,[1146] orotidine 5′-phosphate, however, is 0.6 ± 0.1, so the association of orotidine 5′-phosphate must be a rate-affecting step. From the value of the slope, it could be calculated that the rate constant k_1 for its association is 4 $\mu M^{-1}\ s^{-1}$.

In theory, if the slopes of both the line for $k_0\ k_{0\eta}^{-1}$ and the line for $k_A\ k_{A\eta}^{-1}$ as a function of the relative microviscosity are between 0 and 1, and one of the rate constants in the mechanism of Equation 3–449 has been assigned a value by some other observation, the remaining four underlying rate constants can be estimated from these slopes and from the observed values of the specificity constant k_A for reactant A and the catalytic constant k_0. In practice,

however, the rate constants k_{-1}, k_2, and k_3 are seldom, if ever, close enough to each other in numerical value that both slopes fall between and are significantly different from 1 and 0.

In the preceding discussion, it has been assumed that the only effects of relative microviscosity on the observed rate constants for the enzymatic reaction are on the rates of association and dissociation of substrates with the enzyme. There are, however, several situations in which it has been concluded that the **observed effects of the relative microviscosity result from changes in the rates of conformational changes**, such as an induced fit (Figure 3–55) that the enzyme undergoes during catalysis.[1151-1153] These observations suggest that the effects of relative viscosity on observed kinetic constants may be more ambiguous than they are often assumed to be and that effects of microviscosity on conformational changes must be ruled out before the assumption that the effects of microviscosity are only on rates of association and dissociation is made. The observation that an increase in relative microviscosity affects only the observed specificity constant k_A for reactant A and not the observed catalytic constant k_0 is the least ambiguous result and usually means that the effect of microviscosity is only on association and dissociation of reactant A. For example, the 10% increase in the catalytic constant for chymotrypsin observed at high concentrations of microviscogens was used as an argument that the only effect of microviscogens was on the association of reactant with the enzyme.[1143]

Now that you are familiar with the molecular details of noncovalent interactions between substrates and active sites, it becomes possible for you to imagine the steps in the dissociation of a product. Because almost every substrate is held in the active site of an enzyme by many localized interactions and because covalent bonds about which free rotation can occur are located between these individual points of contact within most substrates, the release of a product can be viewed as the culmination of a series of steps taken in a random order.[1154] A molecule of a given product can be divided into segments connected by one or more covalent bonds about which free rotation can occur. Even though the configurational flexibility of a bound or partially bound product is likely to be much less than what it displays in solution, it is possible to imagine each segment independently detaching from the active site momentarily as the subset of noncovalent interactions holding that segment in the active site breaks and rotation, albeit hindered, occurs around the covalent bonds connecting that segment to the rest of the substrate. Just as quickly, however, that segment reestablishes its connection with the active site before the neighboring segments can break theirs. These local dissociations and reassociations from subsites of the active site occur randomly over the molecule of product. Eventually, at some instant, all the local contacts are broken at the same time, and the molecule of product departs. For example, a mutant of streptavidin from *Streptomyces avidinii* in which Aspartate 128 has been changed to alanine is unable to form the usual hydrogen bond between one of the ureido nitrogen–hydrogens of the biotin that is the normal ligand of the protein because the acyl oxygen in the carboxy group of the aspartate is no longer there. In a crystallographic molecular model of the complex between biotin and the mutant, the rigid, bicyclic 2-oxohexahydro-1*H*-thieno-[3,4*d*]imidazol-4-yl group of the biotin has pulled away from its normal position into a configuration believed to represent one of the **individual detachments** leading to the eventual dissociation of biotin from streptavidin.[1155]

Another example of such a process may occur within the active site of phosphoglycerate kinase (Equation 3–375) from *S. cerevisiae*.[1154] At high concentrations, sulfate is a competitive inhibitor with respect to $MgATP^{2-}$ in the forward reaction and with respect to 3-phospho-D-glyceroyl phosphate, but not with respect to $MgADP^{-}$, in the reverse reaction.[1154] These results suggest that sulfate can bind to the same location as the phospho group that is transferred from the phosphoanhydride of $MgATP^{2-}$ to the carboxylato group of 3-phospho-D-glyceroyl phosphate. At low concentrations, however, sulfate and several other polyanions activate the enzymatic reaction (Figure 3–62).[1156]

One explanation for both **the activation and the competitive inhibition observed in the respective ranges of concentration** is that, during the instant that the 1-phosphate group on the carboxy carbon of the product 3-phospho-D-glyceroyl phosphate has momentarily detached from its cup of both donors for hydrogen bonds and the Mg^{2+} and rotated away and before it can reattach, sulfate can associate with the cup that the phospho group normally occupies (Figure 3–63).[644,1156-1159] The sulfate prevents reassociation of the 1-phospho group, and 3-phospho-D-glyceroyl phosphate is forced to depart as soon as the 3-phospho group breaks away from its

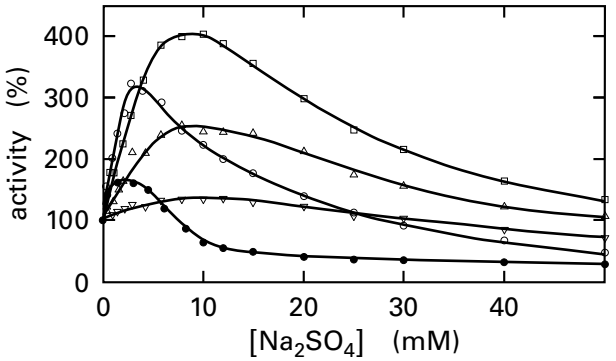

Figure 3–62: Effect of sulfate on the enzymatic activity of yeast phosphoglycerate kinase.[1156] Samples were prepared that contained phosphoglycerate kinase in 5 μM (●), 50 μM (○), 0.5 mM (□), 1.5 mM (△), or 5.0 mM (▽) $MgATP^{2-}$ and 1.0 mM free Mg^{2+}, 50 mM 3-phosphoglycerate, and various concentrations of Na_2SO_4. The initial rate of production of 1,3-bisphosphoglycerate was monitored by the decrease in concentration of NADH in a coupled assay involving glyceraldehyde-3-phosphate dehydrogenase, creatine kinase, creatine phosphate, and triose-phosphate isomerase. Initial rates of decrease in the fluorescence of NADH were measured continuously for each sample. The activity of the enzyme (percent of the initial rate in the absence of phosphate) is presented as a function of the concentration of Na_2SO_4 (millimolar).

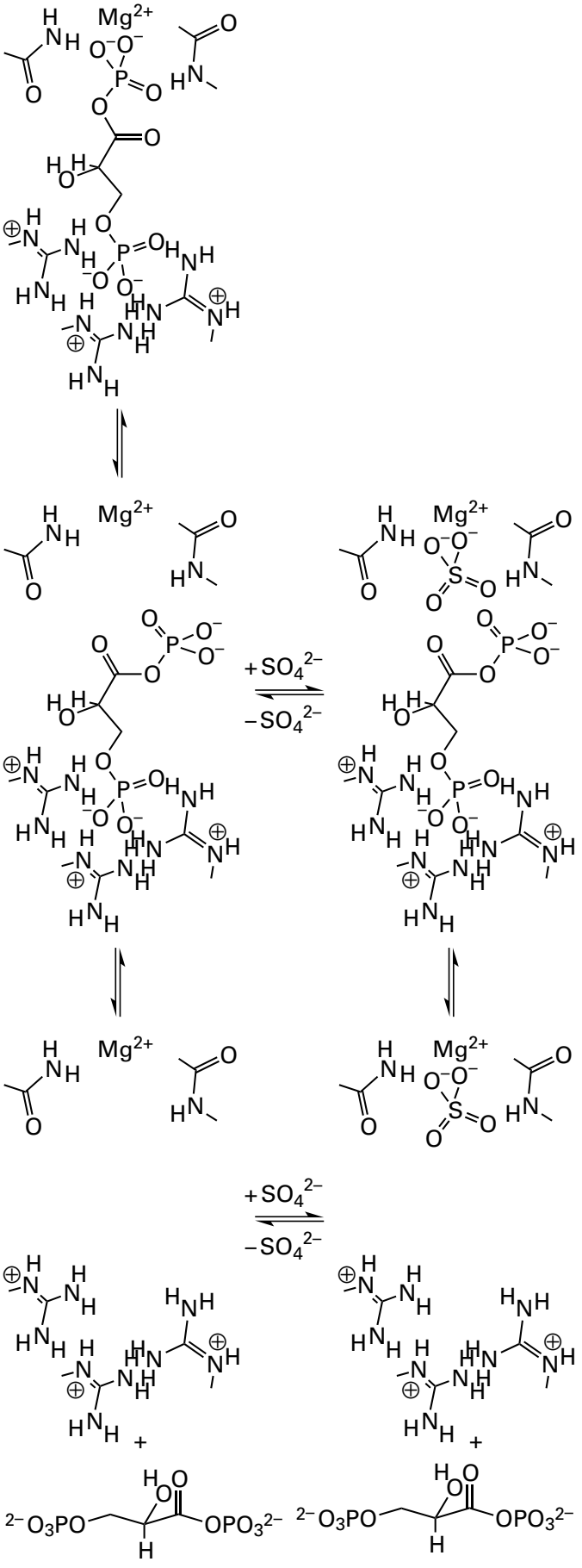

Figure 3–63: Schematic representation of the possibility that sulfate may accelerate the dissociation of 3-phospho-D-glyceroyl phosphate from the active site of phosphoglycerate kinase from *S. cerevisiae* by associating with one of the two subsites that bind its phospho groups.[644,1156-1158] Dissociation of 3-phospho-D-glyceroyl phosphate from the active site can be considered to occur in at least two steps: release of the 1-phospho group and release of the 3-phospho group (left side of drawing). These dissociations can occur in either order, but either dissociation probably coincides with an induced widening of the active site.[1159] In the drawing, the 1-phospho group is the first to dissociate. During its dissociation, the bond between carbons 1 and 2 has rotated to remove the 3-phospho group from the vicinity of its subsite. It is possible that sulfate occupies the subsite for either the 1-phospho group, as is drawn, or the 3-phospho group (right side of drawing), preventing its reassociation and the reclosing of the active site and hastening the dissociation of the complete molecule of 3-phospho-D-glyceroyl phosphate. The sulfate is drawn as occupying the subsite for the 1-phospho group because sulfate appears to compete with $MgATP^{2-}$ for its association with the enzyme (Figure 3–62), perhaps because it occupies the same subsite occupied by both the 1-phospho group of 3-phospho-D-glyceroyl phosphate and the γ-phospho group of $MgATP^{2-}$.

cup of donors for hydrogen bonds. In this view of the process of dissociation, the 3-phospho group in the absence of sulfate would usually break away from its cup after the 1-phosphate group had already reassociated with its cup, and the 3-phospho group would have to detach many times before it happened to detach at the same time that the 1-phosphate group was also unattached. The sulfate, however, at concentrations high enough to occupy the active site effectively but not high enough to occupy the active site continuously and block the association of the γ-phospho group of $MgATP^{2-}$, would block the reassociation of the 1-phosphate group, and activation rather than inhibition would result. For this explanation to be the correct one, dissociation of the product must be a rate-limiting step in the enzymatic reaction.

Phosphoglycerate kinase serves as an example not only of stepwise dissociation of a product but also of a mechanism by which **reactants or other ligands could accelerate the dissociation of a product** from the active site. The individual sites of noncovalent interaction distributed over the reactants in an enzymatic reaction are usually found distributed over the products, albeit in a different order. For example, the γ-phospho group of $MgATP^{2-}$ is the 1-phospho group of 3-phospho-D-glyceroyl phosphate in the reaction catalyzed by phosphoglycerate kinase, but the 3-phospho group of 3-phosphoglycerate is the 3-phospho group of 3-phospho-D-glyceroyl phosphate. It follows that reactants usually have substituents that can occupy the regions of the active site occupied by the respective substituents on products. In this view, a molecule of reactant that contains a functional group that ends up in a product should always have the potential to hasten dissociation of the molecule of that product that immediately precedes association of that reactant with the active site. In the particular case of phosphoglycerate kinase, the γ-phospho group of $MgATP^{2-}$ is an anion that can bind at the site for the 1-phospho group of 3-phospho-D-glyceroyl phosphate and should be able to accelerate the dissociation of 3-phospho-D-glyceroyl phosphate just as sulfate was able to do. As it turns out, $MgATP^{2-}$ does display reactant activation,[1156] consistent with an ability to perform this acceleration of the reaction by displacement of the product 3-phospho-D-glyceroyl phosphate.

Reactant activation in steady-state kinetics is the acceleration of an enzymatic reaction by a reactant as its concentration is increased, beyond the usual increase in rate resulting only from its association with the active site. One way in which reactant activation can occur is the **acceleration of dissociation of the product from the active site** by association of the reactant with the active site.

Consider an enzyme the product of which, C–D, is bound at the active site by separate subsets of noncovalent interactions to segments C and D, respectively. Assume that these separate subsites are beyond the immediate vicinity of the chemical transformation and that the reactant, A–B, is bound by the same subsets of noncovalent interactions to segments A and B, which are identical to segments C and D, respectively. Under conditions of initial rate, in which the concentration of product C–D is 0, the replacement of product C–D by reactant A–B during the kinetic mechanism could occur in the following sequence

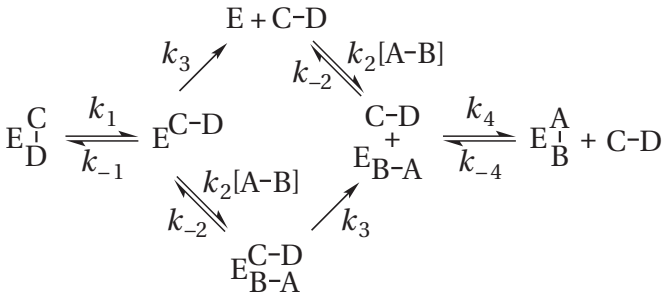

(3–471)

In this scheme, the binding of segment B of the reactant blocks the rebinding of segment D of the product. The rate of dissociation of product C–D from the complex between enzyme and product is

$$\frac{d[\text{C-D}]}{dt} = k_3\left(\left[\text{E}^{\text{C-D}}\right] + \left[\text{E}^{\text{C-D}}_{\text{B-A}}\right]\right) \tag{3–472}$$

where [C–D] is the concentration of fully dissociated C–D. From the various steady-state relations it follows that

$$\frac{d[\text{C-D}]}{dt} = k_{1,\text{app}}\left[\text{E}^{\text{C}}_{\text{D}}\right] \tag{3–473}$$

where the apparent rate of dissociation of the product C–D

$$k_{1,\text{app}} = k_1\frac{k_3(k_{-2}+k_3) + k_2k_3[\text{A-B}]}{(k_{-1}+k_3)(k_{-2}+k_3) + k_2k_3[\text{A-B}]} \tag{3–474}$$

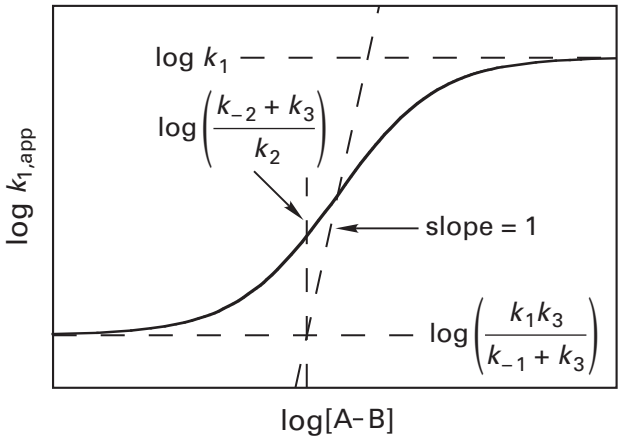

Figure 3–64: Graphical representation of the common logarithm of the function defined by Equation 3–474. The horizontal asymptotes of the curve are fixed by the values for log $[k_1k_3(k_{-1}+k_3)^{-1}]$ and log k_1, and the intersection of a line of slope 1 passing through the midpoint of the curve and the lower horizontal asymptote is fixed at a value of log[A–B] equal to log $[(k_{-2}+k_3)\ k_2^{-1}]$. These are the points that position the curve on the axes.

The common logarithm of the apparent first-order dissociation rate constant $k_{1,app}$ can be plotted as a function of the common logarithm of the concentration of reactant, [A–B] (Figure 3–64). Because $k_1k_3\ (k_3+k_{-1})^{-1}$ is always less than k_1, the addition of reactant A–B will always accelerate the dissociation of product C–D.

Equation 3–471 is for a **branched mechanism** and contains two paths from the fully intact complex between the enzyme and product C–D to the fully intact complex between the enzyme and reactant A–B, and the fluxes on the two paths shift in relative magnitude as the concentration of A–B is increased. Such a branched mechanism is known to produce reactant activation.[1160]

Many instances of reactant activation might result from the process of reactants displacing products. For example, in the steady-state kinetics of human dihydrofolate reductase (Equation 3–428), NADPH displays reactant activation.[1161] This activation results from the fact that the product tetrahydrofolate dissociates from the enzyme 5 times more rapidly when the site for nicotinamide-adenine dinucleotide is occupied by the reactant NADPH than when it is occupied by the product $NADP^+$. A reasonable explanation of this fact is that the hydride on carbon 4 of NADPH, after the hydronicotinamide ring slips into its subsite following the momentary departure of the 2-amino-4-oxo-5,6,7,8-tetrahydro-1*H*-pteridinyl group from its subsite, blocks the reattachment of the pteridinyl group. This block permits the 4-aminobenzoyl group and the L-glutamyl group, which comprise the remainder of tetrahydrofolate, to dissociate without the complication of the pteridinyl group reassociating.

If this explanation is correct for human dihydrofolate reductase, this reactant activation is a particularly striking example of the power of a steric effect because NADPH differs from $NADP^+$ by only a hydrogen. In the case of dihydrofolate reductase from *E. coli* (25% identity; 3.9 gap percent), the association of NADPH enhances the dissociation of tetrahydrofolate by a factor of 350.[1162] Results from both crystallography and relaxation dispersion of hydrogen-1 in nuclear magnetic resonance spectra[1162,1163] are consistent with the adenylyl portion of NADPH initially associating on the surface of the complex between the enzyme and tetrahydrofolate and the nicotinamide portion then swinging into the active site at a rate of 21 s^{-1} before tetrahydrofolate dissociates into the solution with a rate constant of 1000 s^{-1}. The relaxation dispersion spectra also suggest that, in concert with the nicotinamide swinging into the active site, the 2-amino-4-oxo-5,6,7,8-tetrahydro-1*H*-pteridinyl group is displaced from its original position, coincident with a conformational change in the active site, but that even though it is displaced, the pteridinyl group remains associated with the active site for a short time until the entire molecule of tetrahydrofolate fully dissociates. Whether the conformational change or the extra hydrogen is responsible for the initial displacement was not determined. In the case of dihydrofolate reductase from *M. tuberculosis* (23% identity; 2.2 gap percent), the association of NADPH accelerates the dissociation of tetrahydrofolate by a factor of 2, but there is a conformational change in the active site prior to dissociation of the products that prevents this acceleration from increasing the overall rate of the reaction.[1164]

The displacement of products by reactants at the active site seems so unavoidable that it may occur far more often than the frequency with which obvious reactant activation is observed in steady-state kinetics. A kinetic mechanism in which dissociation of a product is accelerated by association of a reactant can apply even when obvious deviations from the usual rectangularly hyperbolic kinetic behavior are not observed. For example, mutation of Phenylalanine 31 in human dihydrofolate reductase to leucine produces an enzyme in which the reactant NADPH no longer displays reactant activation in steady-state kinetics. Nevertheless, it could

be shown that the association of NADPH still accelerated the dissociation of tetrahydrofolate by directly measuring rates of dissociation for the product tetrahydrofolate from the active site in the presence and absence of NADPH. The reason that reactant activation is no longer observed in steady-state kinetics of the mutant is that, following the transfer of a hydride from NADPH to 7,8-dihydrofolate (H_2F), the dissociation of 5,6,7,8-tetrahydrofolate (H_4F) from enzyme in which $NADP^+$ occupies the site for nicotinamide-adenine dinucleotide has become 30 times slower than when it is occupied by NADPH rather than only 5 times slower, so the reaction proceeds almost exclusively on the path in which NADPH associates before tetrahydrofolate dissociates

$$\begin{aligned} &\text{E·NADPH} \underset{k_{-1}}{\overset{k_1[\text{H}_2\text{F}]}{\rightleftharpoons}} \text{E·NADPH·H}_2\text{F} \underset{k_{-2}}{\overset{k_2}{\rightleftharpoons}} \\ &\text{E·NADP}^+\text{·H}_4\text{F} \xrightarrow{k_3} \text{E·H}_4\text{F} \underset{k_{-4}}{\overset{k_4[\text{NADPH}]}{\rightleftharpoons}} \\ &\text{E·NADPH·H}_4\text{F} \xrightarrow{k_5} \text{E·NADPH} + \text{H}_4\text{F} \end{aligned} \qquad (3\text{–}475)$$

a kinetic mechanism that displays normal rectangularly hyperbolic behavior because there are no longer two kinetically significant paths for dissociation of product.[1165] For dihydrofolate reductase from *E. coli*, however, mutation of Leucine 54 to isoleucine accelerates the dissociation of tetrahydrofolate so that its rate becomes the same whether NADPH or $NADP^+$ is bound. The reactant activation is also lost,[1166] but for the opposite reason: namely, that dissociation of tetrahydrofolate has increased so much that association of NADPH no longer makes a difference and the reaction proceeds almost exclusively on the path in which tetrahydrofolate dissociates before NADPH can associate.

Porcine aconitate hydratase (see Equation 3–423),[1167] which catalyzes the three reactions

$$\begin{array}{ccc} \text{citrate} & \rightleftharpoons & \text{isocitrate} \\ & \rightleftharpoons & \\ \textit{cis}\text{-aconitate} + \text{H}_2\text{O} & & \end{array} \qquad (3\text{–}476)$$

is another example of such a **direct measurement of the rate of dissociation of a product**. The enzyme displays linear and uncomplicated initial rates with each of its three substrates as reactants.[1168] The unassisted release of [^{14}C]citrate from the active site of bovine aconitate hydratase in the absence of any other substrates is far too slow, however, for it to be a step in the conversion of *cis*-aconitate to citrate. If the release of [^{14}C]citrate is measured in the presence of unlabeled citrate, however, its release becomes fast enough. In addition, the effects of pH on the rate of the enzymatically catalyzed reaction are inconsistent with the effects of pH on the inhibition shown by analogues for the substrates. It has been concluded that as any one of the three carboxylato arms of a molecule of any one of the three products bound at the active site of aconitate hydratase momentarily pulls away from its subsite on the active site, either that carboxylato group can be trapped by a hydron or the subsite can be seized by the respective carboxylato arm of a molecule of the respective reactant entering the active site from the solution. Either event would prevent the carboxylato arm of the product from reassociating and would hasten the rate of dissociation of the product. If this is the case, aconitate hydratase would be an example of another enzyme the kinetics of which are unremarkable but that nevertheless uses reactants to displace products.

In other situations, the requirement for one of the reactants to associate before one of the products dissociates has been demonstrated in other ways. For example, protein farnesyltransferase from *R. norvegicus* catalyzes the reaction

$$\begin{aligned} &(2E,6E)\text{-farnesyl diphosphate} + \text{CVIM} \rightleftharpoons \\ &\qquad (2E,6E)\text{-farnesyl-CVIM} + \text{diphosphate} \end{aligned} \qquad (3\text{–}477)$$

where (2*E*,6*E*)-farnesyl-CVIM is the tetrapeptide CVIM farnesylated on the sulfanyl group of its cysteine. In a crystallographic molecular model of a complex between the enzyme and both the reactant (2*E*,6*E*)-farnesyl diphosphate and the product (2*E*,6*E*)-farnesyl-CVIM, the (2*E*,6*E*)-farnesyl group of the reactant has displaced the (2*E*,6*E*)-farnesyl group of the product from the farnesyl subsite while the tetrapeptide portion of the product remains bound at its subsite. This observation suggests that the reactant (2*E*,6*E*)-farnesyl diphosphate must associate with the active site before the product (2*E*,6*E*)-farnesyl-CVIM can dissociate,[562] even though (2*E*,6*E*)-farnesyl diphosphate does not display reactant activation.[1169]

There are **several factors that would limit the effectiveness of such mechanisms** for acceleration of the dissociation of product and hence the rate of the enzymatic reaction. First, in the conformation in which only a portion of the product has dissociated, there will likely remain considerable steric hindrance to the approach of the displacing ligand. This steric hindrance will be particularly acute if the displacing ligand is large and can associate with the momentarily exposed portion of the active site in only one particular conformation. In the case of protein farnesyltransferase, however, even though reactant and product are large, the entire (2*E*,6*E*)-farnesyl group in the farnesylated peptide that is its product can swing out of the active site while its tetrapeptide remains bound so that the (2*E*,6*E*)-farnesyl diphosphate that is its reactant can associate unhindered. Second, a rigid molecule like the pyranose of D-glucose acting as a reactant may be able to associate with an active site in only one specific orientation that could not be accommodated if any portion of the product was still bound. Third, not only such steric effects but also charge repulsion could prevent a molecule of the displacing ligand from associating even partially before the entire molecule of product has dissociated. Fourth, if the mechanism of the enzyme involves induced fit, the active site may be continuously changing its conformation as the product dissociates, and this plasticity might preclude the association of any other ligand until the active site was completely vacated. Finally, ligand-promoted dissociations of products are often observed only at high, unphysiological concentrations of the displacing ligand, and such examples could be irrelevant biologically. In spite of these difficulties, promotion of the dissociation of a molecule of product from the active site by a molecule of reactant or another ligand may still be a common feature of enzymatically catalyzed reactions.

The product of an enzymatic reaction in one direction is a reactant in the other direction, and by the principle of microscopic reversibility, if the dissociation of a product proceeds through multiple, reversible detachments, the **association of that same substrate as a reactant must proceed through multiple, reversible attachments.** In solution, most reactants for enzymes have internal rotational degrees of freedom around their single bonds and randomly assume many different conformations. When reactants are bound to an active site, however, only one of those conformations that can be achieved in solution is usually assumed on the site. While it is unlikely, a particular active site may pick only that one conformation out of the solution. It seems more reasonable, however, that an active site is able to **associate partially with the incorrect conformers of its reactant and promote the conformational change to the correct conformer**. In this strategy, following the association of only a portion of the reactant in a subsite of the active site, the sequential, reversible formation of the multiple attachments that are precisely positioned by that active site would cause any one of the many conformations of the reactant existing in solution to assume gradually the specific conformation it adopts when it is completely pinned down. As each attachment is formed and rotation about intervening single bonds then aligns the next set of noncovalent donors and acceptors, the next noncovalent interaction is completed, and so forth until all the attachments have formed, and the reactant has assumed the unique, bound conformation. For example, a small protein that has no detectable secondary structure in solution is a physiological inhibitor of aspartic endopeptidase A from *S. cerevisiae*. In a crystallographic molecular model of the inhibitor bound to the enzyme, the portion of the inhibitor occupying the active site is an α helix.[1170] One can imagine a sequence of properly aligned, noncovalent interactions, completed in a random order, that would guide the structureless inhibitor gradually into an α helix as opposed to the active site binding only the vanishingly small concentration of α helix in the solution.*

A similar issue arises in situations in which **a particular ionization state of a reactant is required for an enzymatic reaction**. For example, Arginine 381 forms a hydrogen bond with the phenoxy oxygen of the L-tyrosine that is a reactant for tyrosine phenol-lyase

$$\text{L-tyrosine} + H_2O \rightleftharpoons \text{phenol} + \text{pyruvate} + NH_4^+ \qquad (3\text{–}478)$$

from *C. freundii*, which uses pyridoxal 5′-phosphate as a prosthetic group. This hydrogen bond stabilizes the phenolate that is required in the elimination of the 1-oxo-2,5-cyclohexadien-4-yl group catalyzed by the enzyme.[1171] Does the enzyme associate only with the conjugate base of the 4-hydroxyphenyl

*It should be recalled that an isolated α helix is always unstable in solution, again because of the competition of molecules of water for the donors and acceptors of hydrogen bonds.

group of L-tyrosine, the phenolate, which is present in the solution at a low concentration relative to the conjugate acid, the phenol? Or does the 4-hydroxyphenyl group of L-tyrosine associate with the active site and does its hydron dissociate as the hydrogen bond forms with this arginine? The increase in the observed specificity constant for L-tyrosine, k_{tyr}, with increasing pH, from 65 M^{-1} s^{-1} at pH 6.6 to 1.3×10^4 M^{-1} s^{-1} at pH 8.4, suggests that the actual reactant for tyrosine phenol-lyase is the phenolate.

As do substrates, active sites change conformations during association and dissociation of substrates. It is usually assumed that the conformation of the enzyme from which the products dissociate is the same conformation with which the next set of reactants associate. There are instances, however, in which this is not the case.[1172,1173] In such an instance, **the conformation of the active site from which the product dissociates is different from the conformation with which the reactant associates**. For example, the conformation of triose-phosphate isomerase from *G. gallus* (Equation 3–384) from which glycerone phosphate has just dissociated as a product or with which glycerone phosphate must associate as a reactant is different from the conformation with which glyceraldehyde 3-phosphate must associate as a reactant or from which it has just dissociated as a product.[1174] In the case of proline racemase from *Clostridium stricklandii*

$$\text{L-proline} \rightleftharpoons \text{D-proline} \qquad (3\text{–}479)$$

the two forms of the enzyme, one specific for L-proline and the other for D-proline, are not different conformations but different tautomers in which the hydron just removed from the reactant still sits on the base that removed it and the conjugate base of the acid that just added a hydron to the reactant remains unhydronated.[1175] The hydron must be removed from the former and another hydron added to the latter before the next reactant can associate with the enzyme for the next catalytic cycle. The two forms of fumarate hydratase (Equation 3–1) from *S. cerevisiae*, however, are tautomers that also differ in conformation.[1176]

The simplest kinetic mechanism for these enzymes is

$$\mathrm{E} + \mathrm{A} \underset{k_{-1}}{\overset{k_1}{\rightleftharpoons}} \mathrm{E{\cdot}A} \underset{k_{-2}}{\overset{k_2}{\rightleftharpoons}} \mathrm{E'{\cdot}Z} \xrightarrow{k_3} \mathrm{E'} + \mathrm{Z} \underset{k_{-4}}{\overset{k_4}{\rightleftharpoons}} \mathrm{E} + \mathrm{Z} \qquad (3\text{–}480)$$

In most cases, the conversion between the two conformations or two tautomers of the unliganded enzyme (E and E′) is so fast (0.1–10 μs^{-1})[1174] that it does not limit the catalytic constant of the enzyme, but a rate-affecting conversion can be detected by measuring flux ratios[1177] with isotopic tracers.[1172]

A large number of enzymes have substrates that are not solutes in free solution in an aqueous phase. One major group of such enzymes is those that catalyze reactions in which the substrates are **lipids**. Lipids such as fats, oils, polyisoprenoids, phospholipids, and sphingolipids are almost always dissolved in a separate amphipathic phase composed of either the lipid itself or a mixture of the lipid with other fats, oils, polyisoprenoids, phospholipids, or sphingolipids. These separate amphipathic phases can be fat droplets, lipoproteins, micelles, or membranes. There are some enzymes that are embedded permanently in one or the other of these separate amphipathic phases with their active sites immersed in that nonpolar phase, so their reactants can enter the active site from that phase and their products leave the active site into that phase by simple diffusion, just as reactants enter an active site from the aqueous solution by simple diffusion. Examples of such enzymes are bovine quinol—cytochrome-*c* reductase (Figure 2–32), an enzyme spanning the inner mitochondrial membrane that oxidizes ubiquinol, and the two related enzymes found in membranes of the endoplasmic reticulum: diacylglycerol *O*-acyltransferase,[1178] the enzyme responsible for the synthesis of triacylglycerols, and sterol *O*-acyltransferase,[1179] the enzyme responsible for acylating the 3-hydroxy group of cholesterol. Many enzymes that have substrates sequestered in a separate amphipathic phase, however, remain in the aqueous phase almost completely surrounded by water, but nevertheless their substrates in the amphipathic phase must associate with and dissociate from their active sites.

Phospholipase A_2 catalyzes the hydrolysis of phosphatidylcholine, which is 1,2-diacyl-*sn*-glycero-3-phosphocholine

1,2-diacyl-*sn*-glycero-3-phosphocholine
+ H_2O $\rightleftharpoons$ a carboxylic acid
+ 1-acyl-*sn*-glycero-3-phosphocholine
(3–481)

As was originally demonstrated with porcine triacylglycerol lipase,[1180] although phospholipase A_2 free in solution will hydrolyze soluble, unaggregated short-chain 1,2-diacyl-*sn*-glycero-3-phosphocholine, its activity increases dramatically when a particular 1,2-diacyl-*sn*-glycero-3-phosphocholine aggregates into micelles or bilayers[1181] or is dispersed into micelles of detergent.[1182] These observations demonstrate that the enzyme is most efficient when **operating at an interface** between the aqueous phase and a separate **amphipathic phase** in which the reactant is dissolved.

Phospholipase A_2 accomplishes its catalysis of the hydrolysis of its reactant phosphatidylcholine by associating with the surface of the amphipathic phase in which phosphatidylcholine is dissolved and, **while remaining bound to the surface, hydrolyzing many molecules of phosphatidylcholine** by diffusing in two dimensions or scooting over the surface to reach them one after the other.[1183] Such two-dimensional diffusion on a surface is the equivalent of the three-dimensional diffusion of the usual enzyme through the cytoplasm. Phospholipase A_2 from *N. atra* associates firmly with the surface of the amphipathic phase, in part through hydrophobic interactions between that surface and a ring of hydrophobic amino acids on the surface of the enzyme surrounding its active site,[1184] but human 1-alkyl-2-acetylglycerophosphocholine esterase, which also acts as a phospholipase on the surface of the amphipathic phase of a lipoprotein, has an amphipathic α helix 11 amino acids long that associates with the lipids and holds the enzyme on the surface.[1185] A molecule of phosphatidylcholine, when it is encountered by either of these scooting enzymes, rises by simple diffusion out of the surface into the active site.[1184] A similar ring of hydrophobic amino acids surrounds the active site of triacylglycerol lipase,[958,1186] which hydrolyzes triacylglycerides by a similar interfacial mechanism. The hydrophobic patch on the surface of human sphingomyelin phosphodiesterase, however, that mediates its association with a membrane does not surround the active site but is adjacent to it.[1187] In addition to the ring of hydrophobic amino acids that associate nonspecifically with the surface of the amphipathic phase, there is a separate site on phospholipase A_2 for binding tightly to the head groups of anionic phospholipids such as phosphatidic acid and phosphatidylserine in a biological membrane.[1188] This other site provides selection for biological membranes, which usually contain one of these anionic phospholipids, rather than any other amphipathic phase.

There are several observations consistent with this **scooting mechanism**. The initial rate of hydrolysis of phosphatidylcholine catalyzed by phospholipase A_2 increases as a rectangularly hyperbolic function of the concentration of micelles of phosphatidylcholine[1189] or the concentration of micelles of detergent containing a particular molar ratio of phosphatidylcholine.[1190] These results are consistent with the reversible association between the enzyme and a micelle and the dissociation constant being greater than 0. When the concentration of micelles of detergent is held at saturation so that all the phospholipase A_2 from *Naja naja* is bound to micelles at a given instant, the initial rate of hydrolysis increases as a rectangularly hyperbolic function of the mole fraction of phosphatidylcholine in the micelles.[1191,1192] This result is consistent with a normal enzymatic reaction proceeding through the collision and association of reactant with the active site as a result of diffusion of enzyme and phosphatidylcholine over the surface of each occupied micelle. When porcine phospholipase A_2 hydrolyzes 1,2-ditetradecanoyl-*sn*-glycero-3-phosphomethanol in the form of an aqueous suspension of small bilayer vesicles, the amount of hydrolysis achieved at the completion of the reaction increases nonlinearly with the concentration of phospholipase A_2.[1193] This result is consistent with a situation in which each molecule of enzyme, under these circumstances, participates in a kinetically irreversible association with a vesicle so that it can hydrolyze the phospholipid only by scooting over the surface of that one vesicle during the course of the reaction. If these small vesicles are fused into larger vesicles after the reaction has ceased, hydrolysis resumes as each molecule of enzyme encounters unhydrolyzed reactant that has fused with the vesicle to which it is bound. When the mole fraction of the diester 1,2-ditetradecanoyl-*sn*-glycero-3-phosphomethanol is increased in vesicles of the inert diether 1,2-ditetradecyl-*sn*-glycero-3-phosphomethanol, the initial rate of hydrolysis of the diester by porcine phospholipase A_2 increases.[1194] This result is again consistent with a normal enzymatic reaction proceeding through the collision and association of reactant with the active site as a

result of diffusion of enzyme and reactant over the surface of the vesicle.

Cellulose is a **solid** that is secreted by the cells of plants and bacteria. Individual long molecules of $[(\beta 1,4)\text{-D-glucose}]_n$ are the strands of polymer that comprise the solid. Each type of cellulose consists of a particular distribution of amorphous cellulose, in which the strands are randomly arrayed, and crystalline cellulose, in which the strands are aligned parallel to each other in a crystalline array. Crystalline cellulose is an impenetrable solid, so cellulases, the purpose of which is to hydrolyze cellulose, must operate on the surface of the solid. The holoenzyme of cellulose 1,4-β-cellobiosidase (reducing end) Cbh1, a cellulase from *Hypocrea jecorina*, associates with the surface of solid crystalline cellulose from *Cladophora* and diffuses over the surface at random at a rate of 30 nm s^{-1} until it encounters the reducing end of a strand of $[(\beta 1,4)\text{-D-glucose}]_n$ protruding from the surface. If it successfully associates with the end of the strand, it then digests the strand at a rate of 9 nm s^{-1}, successively releasing molecules of the disaccharide cellobiose, (β1,4)-D-glucosyl-D-glucose, from the reducing end of the polymer. The cellulase spends, on average, about 8 s digesting the polymer of $[(\beta 1,4)\text{-D-glucose}]_n$ with which it is associated before it dissociates, releasing over the interval about 70 molecules of cellobiose.[1195]

Some reactants are incorporated into linear polymers rather than separate phases with two-dimensional interfaces such as biological membranes. In such instances, enzymes searching the polymer for a specific reactant are often able to **diffuse along the polymer in one dimension**. As is the case with diffusion in solution or diffusion of an enzyme over a surface, diffusion of a protein along a linear polymer is usually an unbiased random walk in which motion in either direction has an equal probability, and the molecule of protein moves back and forth at random. A fibril of collagen is a linear cable formed by polymerization of individual collagen monomers.[1196] Interstitial collagenase cleaves fibrils of collagen into fragments by hydrolyzing a specific peptide bond in each collagen monomer in the fibril. This single peptide bond is the reactant that the enzyme has to find in the linear polymer. To accomplish this goal, a molecule of interstitial collagenase diffuses back and forth in a random walk along a collagen fibril, cleaving monomers at the specific peptide bond as it encounters each site of hydrolysis.[1197]

Double-stranded and single-stranded DNA are also linear polymers. A number of enzymes are able to diffuse along a strand of DNA searching for a particular reactant within the polymer.[1198] Examples of such proteins are *lac* repressor from *E. coli*,[1199] type II site-specific deoxyribonuclease BamHI from *Bacillus amyloliquefaciens*,[1200] DNA-(apurinic or apyrimidinic site) lyase V encoded by Escherichia phage T4,[1201] DNA (cytosine-5-)-methyltransferase from *E. coli*,[1202,1203] late enhancer complex for DNA-directed DNA polymerase encoded by Escherichia phage T4,[1204] and RNA-directed DNA polymerase encoded by human immunodeficiency virus.[1205]

The paradigm for diffusing along duplex DNA is type II site-specific deoxyribonuclease EcoRI from *E. coli*.[1206] The enzyme cleaves double-stranded DNA at the restriction site with the palindromic sequence GAATTC that is unmethylated on the two cytosines. The enzyme must find this sequence of nucleotides in long stretches of DNA before it cleaves it between guanine and adenine on each strand. To find the reactant, the enzyme associates with duplex DNA and diffuses along the DNA until it encounters the palindrome. When two fragments of duplex DNA, one 4316 base pairs long and the other 34 base pairs long, each with a restriction site approximately in their center, are mixed at equimolar concentrations, type II site-specific deoxyribonuclease is added for various times, and the rates at which the two fragments are cleaved at the respective restriction site are assessed, the apparent association of the enzyme with the longer fragment is about 7 times more rapid than with the shorter.[1206] The explanation is that, even though the molar concentration of the two restriction sites is the same, the likelihood of the enzyme encountering a portion of the longer DNA, associating with it, and diffusing to the restriction site is far greater than the likelihood of it encountering a portion of the shorter DNA and associating with it. Once it encounters any portion of duplex DNA, the enzyme associates and then diffuses along the duplex in a random walk to the restriction site.

When a fragment of 1027 base pairs containing two restriction sites in the middle separated by 51 base pairs was mixed at 100-fold molar excess with type II site-specific deoxyribonuclease from *E. coli* at an ionic strength of 0.13 M, the initial rate at which two cleavages were made in the fragment exceeds the initial rate at which only a single cleavage was made[1207] by a factor of 1.7. This observation suggests that the enzyme can associate with the duplex DNA, diffuse along it, and most times, but not always, make two consecutive cleavages before

dissociating. If the enzyme always cleaved the second restriction site once it had cleaved the first, no fragments that had been cleaved at only one site would have been observed. Six separate fragments of duplex DNA were then constructed in which two restriction sites were placed at distances from each other of 42, 134, 234, 335, 482, and 605 base pairs while on each side of each of the six pairs the length of DNA was the same. When each fragment was mixed in 400-fold molar excess with type II site-specific deoxyribonuclease at an ionic strength of 0.07 M, the ratio between the initial rate at which two cleavages were made by the enzyme in a fragment and the initial rate at which only a single cleavage was made declined as the distance between the two restriction sites was increased. From the ratio of these rates, it could be calculated that the first-order rate constant for diffusive movement of the enzyme from one base pair to an adjacent base pair in a random walk is 300,000 times greater than the first-order rate constant for dissociation of the enzyme from the DNA.[1208] Even for the two fragments in which the two restriction sites are separated by the shortest distances (42 base pairs and 135 base pairs), however, the rate constant at which a second cleavage occurs after the first is only 1.5 times the rate constant at which the first cleavage occurs. The fact that, on average, the protein walks at random from one base pair to one next door 300,000 times before it dissociates and yet often does not cover such short linear distances before it dissociates is simply a consequence of diffusing between two points in an unbiased random walk along a linear polymer.

One solution to this drawback of a random walk is to bias the diffusion. Biasing diffusion, however, requires an expenditure of standard free energy. DNA Helicase is an enzyme that unwinds duplex DNA into its component single strands. The energy necessary to perform the unwinding catalyzed by DNA helicase is provided by the hydrolysis of $MgATP^{2-}$. When it unwinds DNA the enzyme is a homodimer, but the monomer is able to diffuse along single-stranded DNA with a bias in the direction from the 3′ end to the 5′ end, and this bias is also established by hydrolyzing $MgATP^{2-}$. A molecule of $MgATP^{2-}$ is hydrolyzed each time DNA helicase PcrA from *G. stearothermophilus*[1209,1210] or the related (42% identity; 1.1 gap percent) DNA helicase UvrD from *E. coli*[1211] moves from one nucleotide in a single strand of DNA to the nucleotide on its 5′ side. A fragment of single-stranded DNA covalently labeled at its 5′ end with a fluorescent dye was preincubated at a 2-fold molar excess with monomers of DNA helicase UvrD from *E. coli*. After a monomer associated at random on a fragment of single-stranded DNA, its diffusion was initiated by adding $MgATP^{2-}$, and quenching of the fluorescence of the dye as a function of time was measured.[1212] If it is assumed that each monomer associated at random with the single-stranded DNA and then began to move toward the 5′ end when the $MgATP^{2-}$ was added, from the time course of the quenching, it could be calculated that the rate at which the monomer slides in one direction is 200 nucleotides s^{-1} at 25 °C. No movement of the protein could be detected in the absence of $MgATP^{2-}$.

In this instance, the stepping of the enzyme from one nucleotide to the one on its 5′ side, coincident with the hydrolysis of one molecule of $MgATP^{2-}$, can be considered to be a catalytic turnover of the monomer acting as an enzyme. In this view, the nucleotide in the active site, the nucleotide to its 5′ side, $MgATP^{2-}$, $MgADP^{-}$, and phosphate are the substrates for the enzyme, and the enzymatic reaction is the transfer of the active site from the nucleotide to the nucleotide to its 5′ side, or in other words, the transfer of the nucleotide on the 5′ side into the active site upon dissociation of the nucleotide on the 3′ side.

Suggested Reading

Scopes, R. K. (1978) Binding of substrates and other anions to yeast phosphoglycerate kinase, *Eur. J. Biochem. 91,* 119–129. https://doi.org/10.1111/j.1432-1033. 1978.tb20944.x

Caldwell, S. R., Newcomb, J. R., Schlecht, K. A., and Raushel, F. M. (1991) Limits of diffusion in the hydrolysis of substrates by the phosphotriesterase from *Pseudomonas diminuta*, *Biochemistry 30*, 7438–7444. https://doi.org/10.1021/bi00244a010

Problem 3–38: Draw the hydron wire in 4-hydroxytetrahydrodipicolinate synthase in the reset configuration by making the rotations indicated in **3–129** while replacing the water in the solution with a hydronium and rotating the hydroxy group on the substrate to offer a lone pair of electrons to the hydron wire. Then draw the configuration after the hydron is transferred as in Figure 3–60.

Problem 3–39: Nonspecific protein-tyrosine kinase v-Fps from Fujinami sarcoma virus catalyzes the transfer of the γ-phospho group from $MgATP^{2-}$ to a tyrosine in another protein. Its steady-state rate constants were measured in solutions containing various concentrations of glycerol or sucrose to produce different relative viscosities.[1213] The slope of the line for the ratio of its specificity constants as a function of the relative microviscosity of the solution, $k_{pep}\ k_{pep,\eta}^{-1}$, where pep refers to a tyrosyl-peptide used as a reactant for the enzyme in place of one of the proteins that are the natural reactants for the enzyme, is indistinguishable from 0 when measurements of the rate constant k_{pep} are made at saturating concentrations of $MgATP^{2-}$. Because $MgATP^{2-}$ can associate with the enzyme in the absence of the peptide, because $MgATP^{2-}$ is at saturation, and because the change in standard free energy for the overall reaction is significantly exergonic, it has been assumed that this observation of the effect of microviscosity means that the kinetic mechanism for the reaction is

$$\text{E·MgATP} + \text{pep} \underset{K_{d,pep,ATP}}{\rightleftharpoons} \text{E·MgATP·pep} \xrightarrow{k_6} \text{E·MgADP·Ppep} \xrightarrow[+\,\text{MgATP}]{k_7} \text{E·MgATP} + \text{MgADP} + \text{Ppep}$$

where Ppep is the peptide phosphorylated on its tyrosine.

(A) Why was it assumed that the association of the peptide with the enzyme can be described by a simple dissociation constant?

(B) Show that the rate equation for this mechanism is

$$v_0 = \frac{\left(\frac{k_6 k_7}{k_6 + k_7}\right)\left(\frac{k_6}{K_{d,pep,ATP}}\right)[E]_t[pep]_0}{\frac{k_6 k_7}{k_6 + k_7} + \left(\frac{k_6}{K_{d,pep,ATP}}\right)[pep]_0} = \frac{k_0\, k_{pep}[E]_t[pep]_0}{k_0 + k_{pep}[pep]_0}$$

(see Equation 3–40).

The observed slope of the line for the ratio of catalytic constants, $k_0\ k_{0\eta}^{-1}$, as a function of the relative microviscosity is 0.63 ± 0.072. In the absence of microviscogens, when the relative microviscosity of the solution is 1 by definition, the steady-state rate constant $k_{pep} = 35 \pm 7\ mM^{-1}\ s^{-1}$ and the catalytic constant $k_0 = 14 \pm 1\ s^{-1}$.

(C) Derive an expression for the slope of the line for $k_0\ k_{0\eta}^{-1}$ as a function of the relative microviscosity based on the assumed kinetic mechanism and rate equation. Assume that $k_7\ k_{7\eta}^{-1}$ is equal to η_{rel} (Equation 3–460) and that k_6 is unaffected by the microviscosity of the solution.

(D) What are the values of $K_{d,pep,ATP}$, k_6, and k_7 in the assumed mechanism?

Problem 3–40: Show that the mechanism in Equation 3–475 gives the rate equation

$$v_0 = \frac{k_0\, k_{NPH}\, k_{H_2F}[E]_t[NPH]_0[H_2F]_0}{k_0\, k_{NPH}[NPH]_0 + k_0\, k_{H_2F}[H_2F]_0 + k_{NPH}\, k_{H_2F}[NPH]_0[H_2F]_0}$$

where NPH is NADPH and H_2F is dihydrofolate.

(A) Show how this rate equation requires hyperbolic behavior when v_0 is measured as a function of $[NPH]_0$ at a fixed concentration of dihydrofolate.

(B) If v_0^{-1} is plotted as a function of $[NPH]_0^{-1}$ at several fixed concentrations of dihydrofolate, what should be observed if the enzymatic reaction has the kinetic mechanism of Equation 3–475?

Transfer of Substrates among Active Sites

In most reactions that occur sequentially within a metabolic pathway, the product of the preceding reaction in the pathway is released into the cytoplasm from the active site of one enzyme; it diffuses freely and randomly; and upon fortuitous collision, it associates with the active site on the next enzyme. There are, however, situations in which the active sites for two or more different, consecutive reactions in a metabolic pathway are assembled into a **multienzymatic complex**.

In many multienzymatic complexes, substrates or portions of substrates are transferred as covalent adducts between active sites on the same multienzymatic complex without being released into the cytoplasm as free solutes.

A family of **small, independently folding, detachable domains**[1214,1215] is responsible for transferring either an *N*-carboxybiotinyl group

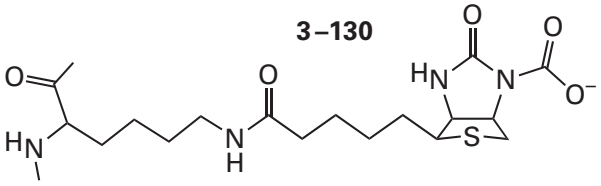

or the corresponding uncarboxylated biotinyl group or an S^8-acyldihydrolipoyl group

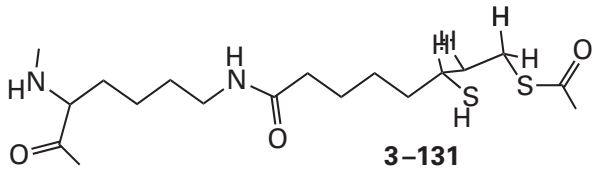

or the corresponding lipoyl group

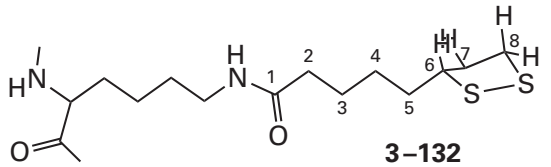

among the active sites of certain multienzymatic complexes. The *N*-carboxybiotinyl, biotinyl,[1216] S^8-acyldihydrolipoyl, and lipoyl groups[1217] are each covalently incorporated into their respective domains through an amide formed between their carboxy groups and nitrogen 6 of a lysine within the respective sequence of amino acids.* These domains, known as **biotin carboxyl-carrier domains and lipoyl acyl-carrier domains**, respectively, are all about 70 amino acids long, at the lower limit of the number of amino acids necessary to produce a stable folded globular structure in the absence of internal disulfides. Biotin carboxyl-carrier domains and lipoyl acyl-carrier domains are all evolutionarily related to each other (20–25% identity and less than 1 gap percent) and have superposable structures composed of a core of six roughly parallel β strands and often, but not always, a couple of peripheral β strands.[1214,1215,1218] The particular lysines to which the respective biotinyl groups or lipoyl groups are attached are at the same position in the respective sequences of amino acids when they are aligned with each other.

In the α_2 homodimer of **acetyl-CoA carboxylase**

$$\mathrm{MgATP^{2-} + HOCO_2^- + acetyl\text{-}SCoA \rightleftharpoons MgADP^- + HOPO_3^{2-} + H^+ + malonyl\text{-}SCoA} \quad (3\text{–}482)$$

from *S. cerevisiae*, the biotin carboxyl-carrier domain (BCCD) is located between positions 701 and 769 in the middle of the polypeptide (2233 aa) that folds to form each of the two identical subunits in the homodimer.[57] Acetyl-CoA carboxylase is a multienzymatic complex because each subunit contains two **enzymatic domains**. The active site of the amino-terminal enzymatic domain in each subunit catalyzes biotin carboxylase

$$\mathrm{MgATP^{2-} + HOCO_2^- + [BCCD]\text{-}N^6\text{-biotinyl-L-lysine} \rightleftharpoons [BCCD]\text{-}N^6\text{-carboxybiotinyl-L-lysine} + MgADP^- + H^+ + HOPO_3^{2-}} \quad (3\text{–}483)$$

and the active site of the carboxy-terminal enzymatic domain in each subunit catalyzes acetyl-CoA carboxytransferase

$$\mathrm{[BCCD]\text{-}N^6\text{-carboxybiotinyl-L-lysine} + acetyl\text{-}SCoA \rightleftharpoons malonyl\text{-}SCoA + [BCCD]\text{-}N^6\text{-biotinyl-L-lysine}} \quad (3\text{–}484)$$

The biotin carboxyl-carrier domain, which is between these two enzymatic domains in the polypeptide, is responsible for transferring the carboxy group that is covalently attached to nitrogen 6 of biotin (**3–130**) from the active site of biotin carboxylase, where it is added to biotin, to the enolate of acetyl-SCoA within the active site of acetyl-CoA carboxytransferase, where it is added to the enolate.

In the crystallographic molecular model of the complex between acetyl-CoA carboxylase from *S. cerevisiae* and coenzyme A (Figure 3–65),[57] the active site for acetyl-CoA carboxytransferase could be located by inspection because it is occupied by both coenzyme A and the biotinyl group. In this active site, nitrogen 1 of the biotinyl group is 0.43 nm from the sulfur of coenzyme A, an appropriate distance for carboxylation of the enolate of an acetyl group, if it were on the sulfur of the coenzyme A, by a carboxy group, if it were on nitrogen 1 of the biotinyl group.

*Note that the distal sulfur in each prosthetic group is six atoms from the amide and the acyl oxygen in each prosthetic group is 10 atoms from the amide.

Figure 3–65: Stereodrawing[576] of the crystallographic molecular model of one of the two subunits in the homodimer of the complex between acetyl-CoA carboxylase from *S. cerevisiae* and coenzyme A.[57] The enzyme is a dimer of two folded polypeptides, each 2233 amino acids long. A number of disordered segments of polypeptide in the crystal account for gaps in the molecular model. The biotin carboxyl-carrier domain (center right in the drawing), the biotinyl group (BTN) attached to the biotinylated carboxyl-carrier domain through an amide to Lysine 735 (**3–130**), and the molecule of coenzyme A are drawn with thicker lines. The label BTN is adjacent to the bicyclic *N,N′*-dialkylurea of the biotin, and the label CoA is adjacent to the sulfanyl group of coenzyme A. Coenzyme A occupies the active site for acetyl-SCoA, and the biotinyl group is docked in this active site as well. Because it is in the middle of the sequence of amino acids for the polypeptide, the biotinylated carboxyl-carrier domain is attached to the rest of the protein by two leashes. One is a short segment of extended polypeptide, within which are nine single bonds about which rotation of the polypeptide can occur. The other is a long stretch of polypeptide in which there is a disordered region between Proline 772 and Alanine 778 (dashed line in the center of the drawing) for which there is no electron density. The active site of biotin carboxylase (BC) was identified by superposing upon the enzymatic domain for biotin carboxylase the crystallographic molecular model of the ternary complex between $MgADP^-$ and biotin and the homologous (33% identity; 1.6 gap percent) biotin carboxylase from *E. coli*, which is a single enzyme and not part of a multienzymatic complex.

Although the domain in the crystallographic molecular model of acetyl-CoA carboxylase responsible for catalyzing biotin carboxylase could be readily identified by comparison with other biotin carboxylases, the active site within this domain in the crystallographic molecular model was unoccupied by any ligand. Therefore, the active site for biotin carboxylase in this domain was located by superposing on it the crystallographic molecular model of biotin carboxylase from *E. coli* in which the active site was occupied by biotin and $MgADP^-$.

The two active sites in the two enzymatic domains of one subunit of acetyl-CoA carboxylase are 8.0 nm apart. The biotinyl group is attached covalently to the biotin carboxyl-carrier domain by a tether (**3–130**) that, if fully extended, as it essentially is in the crystallographic molecular model (Figure 3–65), has a length of 1.4 nm. The biotin carboxyl-carrier domain is attached covalently to the rest of the subunit at its amino-terminal end by an extended disordered segment of polypeptide with the sequence ENDP and at its carboxy-terminal end by a long disordered leash of polypeptide (dashed line in Figure 3–65) with the sequence DDPSKVKHALPFEGMLPDFGSPVIEGTK. Even though the two active sites are so far apart, it can be seen that the biotinyl group should be able to withdraw from the active site of acetyl-CoA carboxytransferase, the biotin carboxyl-carrier domain should be able to **pivot on the amino-terminal connector while the long disordered carboxy-terminal connector winds around the pivot, and the biotinyl group should then be able t**o associate with the active site of biotin carboxylase. In this instance, it has been concluded that the biotin in the biotinylated carboxyl-carrier domain moves back and forth between the two enzymatic domains on the same subunit in the homodimer.

Pyruvate carboxylase

$$MgATP^{2-} + HOCO_2^- + \text{pyruvate} \rightleftharpoons MgADP^- + HOPO_3^{2-} + H^+ + \text{oxaloacetate} \quad (3\text{–}485)$$

is also a multienzymatic complex. The two enzymatic domains on each subunit in the complex catalyze two reactions analogous to those catalyzed by acetyl-CoA carboxylase: biotin carboxylase (Equation 3–483) and pyruvate carboxytransferase

$$[\text{BCCD}]\text{-}N^6\text{-carboxybiotinyl-L-lysine} + \text{pyruvate} \rightleftharpoons \text{oxaloacetate} + [\text{BCCD}]\text{-}N^6\text{-biotinyl-L-lysine} \quad (3\text{–}486)$$

Pyruvate carboxylase from *Rhizobium etli* is an α_4 homotetramer, and each folded polypeptide contains an amino-terminal enzymatic domain for biotin carboxylase and an enzymatic domain in the middle of the polypeptide for pyruvate carboxytransferase.

Unlike the biotin carboxyl-carrier domain in acetyl-CoA carboxylase from *S. cerevisiae*, which is in the middle of its polypeptide, the biotin carboxyl-carrier domain in pyruvate carboxylase from *R. etli* is at the carboxy-terminal end of its polypeptide. In the crystallographic molecular model,[1219] each of the four biotinylated carboxyl-carrier domains in the rotationally symmetric α_4 homotetramer is connected to the carboxy terminus of the rest of its folded polypeptide by a **structureless leash of polypeptide** with the sequence GATGAAVRRKAEPGNAA.

Unlike the biotinylated carboxyl-carrier domain in acetyl-CoA carboxylase, which transfers the carboxy group between two active sites on the same folded polypeptide in which the biotinylated carboxyl-carrier domain itself is located (Figure 3–65), a biotinylated carboxyl-carrier domain in pyruvate carboxylase on the end of a folded polypeptide in the homotetramer transfers the carboxy group between the active site of biotin carboxylase on another folded polypeptide in the complex and the active site of pyruvate transcarboxylase on yet another of the folded polypeptides. These two active sites, one on the second subunit and the other on the third subunit, are 6.5 nm apart, so the leash has to be long enough to accomplish this feat while remaining attached covalently to the first subunit. Because of the $222(D_2)$ symmetry of the α_4 homotetramer, there are four symmetrically distributed units of biotin carboxylase, pyruvate transcarboxylase, and biotinylated carboxyl-carrier domain in each molecule of the enzyme even though the three domains are each in three different subunits.

The **pyruvate dehydrogenase complex** is responsible for the overall reaction

$$\text{pyruvate} + HSCoA + NAD^+ \rightleftharpoons CO_2 + \text{acetyl-SCoA} + NADH \quad (3\text{–}487)$$

a reaction central to metabolism that connects glycolysis with the citric acid cycle. The homotetracosameric core of the complex from *E. coli* is a symmetric octahedral oligomeric protein[1220] composed of 24 identical, folded polypeptides 630 amino acids long arrayed around six twofold, four threefold, and three fourfold axes of symmetry.[1221] Consequently, the 24 subunits are symmetrically equivalent to each other. By taking advantage of the octahedral symmetry of the protein, a map of scattering density has been produced by reconstructive summation of electron microscopic images of the protein embedded in amorphous ice at a resolution sufficient to insert the 24 polypeptides and construct a molecular model of this homotetracosameric core.[1222]

The 316 amino-terminal amino acids in each of the 24 core polypeptides[1223] comprise **three lipoyl acyl-carrier domains**, each homologous to a biotin carboxyl-carrier domain. As is the case with biotinylated carboxyl-carrier domains, these lipoyl acyl-carrier domains are around 70 amino acids long and folded into a globular structure.[1224,1225] Because all three of the lipoyl acyl-carrier domains in each amino-terminal segment are homologous to each other, they are **internally repeating domains**. Because the three consecutive lipoyl acyl-carrier domains in each subunit of the pyruvate dehydrogenase complex are at the amino-terminal end of the polypeptide forming that subunit, the biotinylated carboxyl-carrier domain in acetyl-CoA carboxylase is found in the middle of its polypeptide, and the biotinylated carboxyl-carrier domain in pyruvate carboxylase is found at the carboxy-terminal end of its polypeptide, these homologous domains are also **evolutionarily shifting domains**.*

In the pyruvate dehydrogenase complex, the acyl group being transferred among the active sites by the lipoyl acyl-carrier domain is an acetyl group. Depending on its place in the catalytic cycle at a given instant, each lipoyl acyl-carrier domain on the homotetracosameric core contains a covalently attached lipoyl group (**3–132**), an S^8-acetyldihydrolipoyl group (**3–131**),[1217] or a dihydrolipoyl group (**3–131** with the acetyl group replaced by a hydron) extending out from its surface the same length as the biotinyl group extends out from the surface in a biotin carboxyl-carrier domain (Figure 3–65). Between the first and second internally repeating domains on each folded polypeptide in the pyruvate dehydrogenase complex from *E. coli* is the sequence ADGAADAAPAQAEEKKEAAPAAAPAAAAAKDVA; between the second and third internally repeating domains is the sequence GEAGAAAPAAKQEAAPAAA-PAPAAG; and between the third internally repeating domain and the rest of the folded polypeptide is the sequence GAAPAAAPAKQEAAAPAPAAKAEAPAAAP-AAKAEG.

The inescapable conclusion from an examination of their sequences alone, in particular considering the high fraction of alanines and prolines, is that each segment is completely disordered and acts as a **flexible leash of random coil**. Consequently, the three consecutive globular lipoyl acyl-carrier domains and their attached N^6-(lipoyl)lysine form **a flexible, triply jointed arm** extending out from each of the 24 protomers in the core.[1226] The purpose of this flexibility is to permit each N^6-(lipoyl)lysine on the arms to gain access consecutively to the three unique active sites in the multienzymatic complex. The individual leashes connecting the domains, if fully extended, are between 10 and 13 nm long, and when the arm is fully extended, it should cover a distance of about 40 nm. In the molecular model from electron microscopy, only the third of these three domains from each subunit, the one closest to the core, is present, presumably because the other two have been frozen in many different locations and orientations and are consequently absent from the reconstruction.[1222] The lipoyl acyl-carrier domain closest to the core seems to assume only one orientation because its lipoyl lysine is inserted into the active site on its subunit and thereby fixed in location.

The pyruvate dehydrogenase complex from *E. coli* can be dissociated and resolved into three separate, discrete proteins: the core and two other proteins.[1227] Each protein carries an active site responsible for one of the three steps in the overall reaction catalyzed by the complex (Equation 3–487). Each of the **three separate enzymes is composed of copies of its own distinct folded polypeptide**, and they are not connected covalently to each other, as are the enzymatic domains in acetyl-CoA carboxylase and pyruvate carboxylase, but associated noncovalently. The core forms the center of the complex. The other two proteins are attached through interfaces between them and the core in the intact complex, but when separated from the core, they are homodimers with the usual twofold rotational axes of symmetry relating

*Evolutionarily shifting domains are domains that are homologous, either in amino acid sequence or because their crystallographic molecular models are superposable, and that appear at different locations in the polypeptides of apparently unrelated proteins. The inference is that natural selection caused them to be inserted adventitiously into already existing proteins.

their respective subunits.[1228,1229] Images of molecules of the entire complex embedded in amorphous ice have also been submitted to reconstruction, but because of the size of the complex, the resulting molecular model is not of sufficient resolution to insert any of the constituent polypeptides. Nevertheless, large globular structures formed from the other two subunits situated on twofold rotational axes of the octahedral core can be observed in the molecular model.[1222]

Pyruvate dehydrogenase (acetyl-transferring)[1229]

$$\text{pyruvate} + \text{protein } N^6\text{-(lipoyl)lysine} + H^+ \rightleftharpoons CO_2 + \text{protein } N^6\text{-(}S\text{-acetyldihydrolipoyl)lysine} \quad (3\text{–}488)$$

is a homodimeric protein (2×887 aa) bound noncovalently to the homotetracosameric core of the pyruvate dehydrogenase complex. Each identical and symmetrically arrayed active site of pyruvate dehydrogenase (acetyl-transferring) uses thiamine diphosphate as a prosthetic group to decarboxylate pyruvate, creating 2-(1-hydroxyethylidene)thiamine diphosphate (Figure 2–6), and then transfers the hydroxyethylidene group of the decarboxylated pyruvate (Figure 2–7) as an acetyl group to an N^6-(lipoyl)lysine (**3–132**) on one of the lipoyl acyl-carrier domains on one of the jointed, flexible arms that happens to be bound to its active site.

The flexible arm then swings around randomly until the resulting N^6-(*S*-acetyldihydrolipoyl)lysine can associate with one of the 24 identical, symmetrically arrayed active sites of dihydrolipoyllysine-residue acetyltransferase

$$\text{protein } N^6\text{-(}S\text{-acetyldihydrolipoyl)lysine} + \text{HSCoA} \rightleftharpoons \text{acetyl-SCoA} + \text{protein } N^6\text{-(dihydrolipoyl)lysine} \quad (3\text{–}489)$$

This enzyme is the homotetracosameric core itself, and the acetyl group arriving on the sulfanyl group in the dihydrolipoyl group of the lipoyl acyl-carrier domain is transferred by the active site to the sulfanyl group of coenzyme A.

The long flexible arm then swings around randomly until the N^6-(dihydrolipoyl)lysine (**3–131**, with the acetyl group replaced by a hydron) on the lipoyl acyl-carrier domain that is the product of the second acetyl transfer can associate with one of the two identical, symmetrically displayed active sites of dihydrolipoyl dehydrogenase[1228]

$$\text{protein } N^6\text{-(dihydrolipoyl)lysine} + NAD^+ \rightleftharpoons NADH + H^+ + \text{protein } N^6\text{-(lipoyl)lysine} \quad (3\text{–}490)$$

another dimeric protein (2×474 aa) bound noncovalently to the homotetracosameric core, and the N^6-(dihydrolipoyl)lysine is oxidized to N^6-(lipoyl)lysine (**3–132**). The long flexible arm then swings around randomly until the N^6-(lipoyl)lysine that is the product of dehydrogenation can associate with an active site for pyruvate dehydrogenase (acetyl-transferring) (Equation 3–488), and the cycle begins again.

In this description, the impression is left that the pyruvate dehydrogenase complex can be divided into 24 independent sectors, each of which is serviced by one of the 24 triply jointed arms and in which these cycles proceed in isolation, much as acetyl-CoA carboxylase seems to be divided into two independent sectors and pyruvate carboxylase can be divided into four independent sectors. It has been demonstrated, however, that the **arms on which the lipoyl acyl-carrier domains are situated are so long and so flexible that a significant fraction of the active sites within a given complex are chemically interconnected**.

A set of pyruvate dehydrogenase complexes from *E. coli*, containing decreasing ratios of the active site for the first enzyme in the sequence, pyruvate dehydrogenase (acetyl-transferring), can be produced either by reconstituting the complex with less than stoichiometric amounts of this particular protein[1230,1231] or by adding an inhibitor of such high affinity that it binds stoichiometrically to a portion of these active sites.[1231] The overall enzymatic activity decreases in direct proportion to the loss of these active sites, and the rate at which N^6-(lipoyl)lysine is acetylated by [2-^{14}C]pyruvate in the absence of coenzyme A and NADH also decreases in direct proportion to the loss of these active sites (Figure 3–66).[1232] All the N^6-(lipoyl)lysines on the lipoyl acyl-carrier domains in the complex, however, still become acetylated in a simple first-order reaction (Figure 3–66), even when as few as five competent active sites for pyruvate dehydrogenase (acetyl-transferring) are present for every homotetracosameric core of dihydrolipoyllysine-residue acetyltransferase.[1231] When, however, fewer than two competent

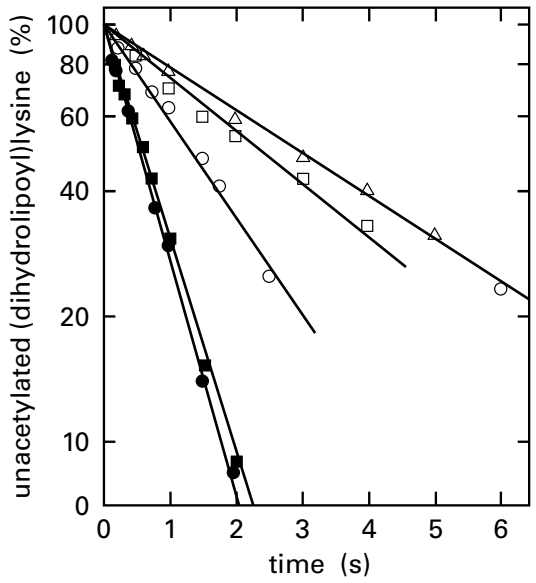

Figure 3–66: Incorporation of [2-^{14}C]pyruvate into a series of partly assembled pyruvate dehydrogenase complexes.[1232] The pyruvate dehydrogenase complexes were reassembled from purified pyruvate decarboxylase and a purified form of the complex between dehydrolipoamide transacetylase and dihydrolipoyl dehydrogenase with a stoichiometry of 0.88 polypeptide of dehydrogenase for every polypeptide of transacetylase. Various ratios of these two purified proteins were mixed and allowed to reassemble, and the products were purified. This procedure produced complexes with 0.21 (△), 0.39 (□), 0.71 (○), and 1.29 (●) polypeptides of decarboxylase for every polypeptide of transacetylase. The native protein (■) has 1.24 polypeptides of decarboxylase for every polypeptide of transacetylase. Transfer of the acetyl moiety from [2-^{14}C]pyruvate (18 μM) to the N^6-(lipoyl)lysines of the transacetylase was monitored as a function of time at 0.7 mM thiamine diphosphate, 10 mM $MgCl_2$, and 1.0 mM NAD^+ at pH 7.0 and 25 °C. The reaction was quenched at various times by mixing with trichloroacetic acid, and the radioactivity bound to protein was assayed. The common logarithm of the percent N^6-(dihydrolipoyl)lysine not acetylated is presented as a function of time (seconds). Notice that the N^6-(lipoyl)lysines became acetylated in each case in a simple first-order reaction.

active sites for pyruvate dehydrogenase (acetyl-transferring) are present for every homotetracosameric core of dihydrolipoyllysine-residue acetyltransferase, the acetylation of N^6-(lipoyl)lysines is incomplete, From the final levels of acetylation reached at these low molar ratios of active sites for pyruvate dehydrogenase (acetyl-transferring), it was concluded that each active site in these more incomplete complexes can accomplish the acetylation of only a third to a half of the N^6-(lipoyl)lysines on the homotetracosameric core.[1230,1233]

For steric reasons, a third to a half of the 72 N^6-(lipoyl)lysines on all 72 lipoyl acyl-carrier domains covalently attached to the homotetracosameric core are unable to associate with the same active site on a particular homodimer of pyruvate dehydrogenase (acetyl-transferring). In fact, in the molecular model of the complex, because each globular structure containing dihydrolipoyl dehydrogenase and pyruvate dehydrogenase (acetyl-transferring) sits on one of the twofold axes,[1222] each well removed from the others, the pyruvate dehydrogenase complex can be divided into 12 independent sectors. It must be the case that although the N^6-(lipoyl)lysines on several lipoyl acyl-carrier domains can be acetylated in succession by the same active site of pyruvate dehydrogenase (acetyl-transferring), most of the distribution of acetyl groups over the surface of the homotetracosamer among the 24–36 N^6-(lipoyl)-lysines that can be eventually acetylated by a single active site results from rapid, uncatalyzed exchange of both sulfanyl groups and acetyl groups between sulfanyl groups

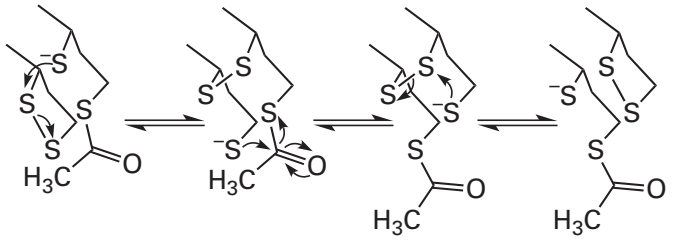

(3–491)

Therefore, acetyl groups are transferred not only among active sites in the complex but also among the N^6-(dihydrolipoyl)lysines attached to the core of the complex. As a result, complexes that are missing up to 80% of their pyruvate dehydrogenase (acetyl-transferring) subunits are still able to function efficiently. This rapid transfer of acetyl groups among all the N^6-(dihydrolipoyl)lysines can still occur unabated in a deletion mutant in which the two amino-terminal lipoyl acyl-carrier domains have been removed, but shortening the leash that is rich in alanines and prolines between the remaining lipoyl acyl-carrier domain and the rest of the protein from 36 amino acids to fewer than 20 amino acids pulls the remaining lipoyl acyl-carrier domain into the central homotetracosamer and decreases its extent significantly.[1234]

An examination of Equation 3–491 leads to the conclusion that a pyruvate dehydrogenase complex, which, for any reason, is deficient in functional active sites for dihydrolipoyl dehydrogenase, should be able to equilibrate dithio groups among all of its 72 lipoyl acyl-carrier domains just as it equilibrates acetyl groups.

The animal fatty-acid synthase system is a multienzymatic complex that is an α_2 homodimer, in which each of the two identical folded polypeptides contains six globular enzymatic domains and an **acyl-carrier domain** (ACD). The entire length of a constituent human polypeptide is 2511 amino acids. In prokaryotes and plants, the six enzymes that together accomplish the synthesis of fatty acids are six unassociated, separate proteins. The **acyl-carrier protein** that carries the elongating fatty acyl group among them as they diffuse at random through the cytoplasm is also a small separate protein. Several of the six enzymatic domains and the acyl-carrier domain in animal fatty acid synthases are homologous in their sequences of amino acids to the respective proteins of plants and bacteria. All the enzymatic domains can be delineated in the complete sequences of amino acids for the multienzymatic complexes from *G. gallus* and *R. norvegicus* by alignment of these two homologous sequences with those of the plant and bacterial enzymes and the position of peptides within these complete sequences that have been identified as participating in particular active sites of intact animal fatty-acid synthase systems.[1235,1236]

The six enzymatic domains of the animal fatty-acid synthase system catalyze eight reactions[1237]

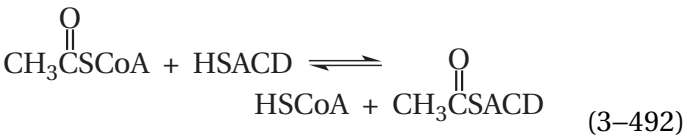

(3–492)

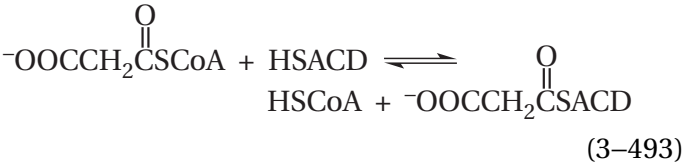

(3–493)

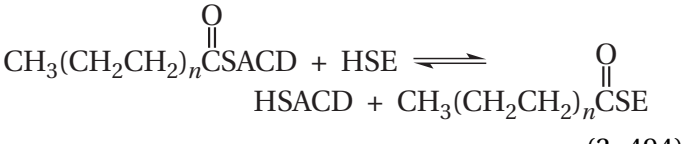

(3–494)

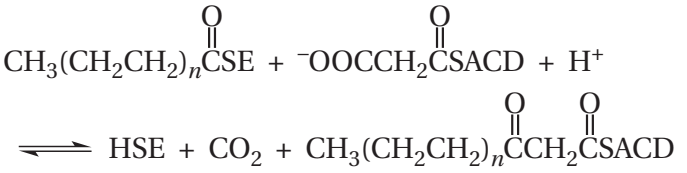

(3–495)

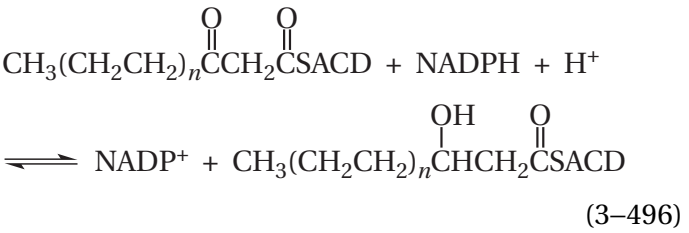

(3–496)

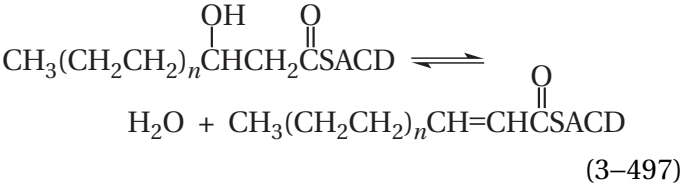

(3–497)

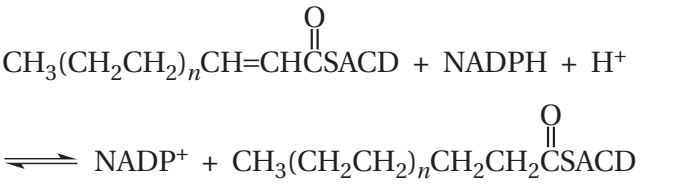

(3–498)

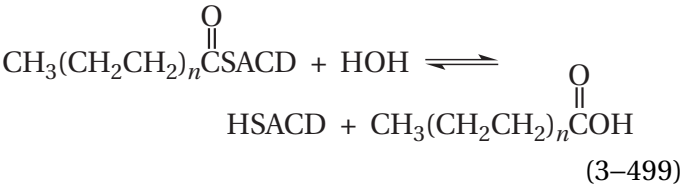

(3–499)

where HSACD is a sulfanyl group on the phosphopantotheinyl group attached as a phosphodiester to a serine in the acyl-carrier domain and HSE is a sulfanyl group on a cysteine in the active site in the domain responsible for β-ketoacyl-[acyl-carrier-protein] synthase I.

The first two reactions, [acyl-carrier-protein] *S*-acetyltransferase (acetyltransferase; Equation 3–492) and [acyl-carrier-protein] *S*-malonyltransferase (malonyltransferase; Equation 3–493), are nucleophilic substitutions of the sulfanyl group of an acyl-carrier domain in the enzyme for the sulfanyl group of coenzyme A at the respective acyl carbon. Both nucleophilic substitutions are catalyzed by the same active site in acyltransferase, one of the enzymatic domains. β-Ketoacyl-[acyl-carrier-protein] synthase I (oxoacyl synthase; sum of Equations 3–494 and 3–495), is carried out by an active site on one of the other enzymatic domains. The final four reactions —3-oxoacyl-[acyl-carrier-protein] reductase (oxoacyl reductase; Equation 3–496), 3-hydroxyacyl-[acyl-carrier-protein] dehydratase (hydroxyacyl dehydratase; Equation 3–497), enoyl-[acyl-carrier-protein] reductase (NADPH, *Re*-specific) (enoyl reductase; Equation 3–498), and oleoyl-[acyl-carrier-protein]

hydrolase (oleoyl hydrolase; Equation 3–499)—are each carried out by one of the other four enzymatic domains in the intact enzyme. The acyl-carrier domain is responsible for carrying the elongating fatty acyl group among the active sites on four of the six enzymatic domains, those catalyzing the reactions of Equations 3–494 through 3–498. When the elongating fatty acid is the proper length, oleoyl hydrolase hydrolyzes it from the sulfanyl on the acyl-carrier domain, and it dissociates into the cytoplasm as a fatty acid.

The acyl-carrier domains, although the same size as the biotinylated carboxyl-carrier domains and the lipoyl acyl-carrier domains, are unrelated to them.* They are instead globular, independently folding, detachable domains that are composed of only α helixes, with no β structure. Each of the two small, globular acyl-carrier domains (70 aa) in an animal fatty-acid synthase system[1238,1239] sits between the five amino-terminal enzymatic domains and a sixth carboxy-terminal enzymatic domain in the sequence of amino acids for each of the two polypeptides that constitute the homodimeric multienzymatic complex.[1237] Consequently, each acyl-carrier domain is in theory attached to the protein by two strands of polypeptide, just as is the biotin carboxyl-carrier domain in acetyl-CoA carboxylase (Figure 3–65). It turns out, however, that the carboxy-terminal enzymatic domain, which is oleoyl hydrolase (Equation 3–499) responsible for only the final step in the synthesis of a fatty acid, is not associated with the large structure formed from the five amino-terminal enzymatic domains (Figure 3–67).[1240] Instead it is a free-floating globular domain[1241,1242] attached to the carboxy terminus of the acyl-carrier domain by a long flexible strand of polypeptide 25 amino acids long.

The portion of the fatty-acid synthase system resolved in the crystallographic molecular model of the porcine enzyme is formed from the two sets of five amino-terminal enzymatic domains from the two identical folded polypeptides of the α_2 homodimer. In this resolved portion of the complete homodimer, there are two identical, symmetrically arrayed **open bays** on either side of the complete protein that are each formed by and surrounded by two peninsulas (Figure 3–67).[1240] The upper peninsula in the drawing is formed of three globular enzymatic domains from the carboxy-terminal 1699 amino acids of the resolved portion of one folded polypeptide in the homodimer. The lower peninsula is formed of two globular enzymatic domains from the amino-terminal 414 amino acids of the resolved portion of the other folded polypeptide in the homodimer.

The acyl-carrier domain is carboxy-terminal to the fifth enzymatic domain, which is the domain responsible for oxoacyl reductase (OR). It is in the same folded polypeptide chain as this enzymatic domain, and it is **attached to this fifth domain by a leash** (LSH in Figure 3–67) The leash contains no hydrophobic amino acids that would be necessary for it to have any stable structure. Consequently, it is a flexible, protean, random coil. The leash in the porcine fatty-acid synthase system, –KKAAAPRDGSS–, if fully extended, would be around 4 nm long. The carboxy-terminal serine of the leash is attached to the acyl-carrier domain on the side opposite the phosphopantotheinyl group, and the point of connection is 1.7 nm from that sulfanyl group. These dimensions give the sulfanyl group a range of 5.7 nm from its point of attachment.

The flexibility of the leash permits the acyl-carrier domain to wander randomly around the open bay, in a manner similar to the biotinylated carboxyl-carrier domain wandering back and forth between the two domains in acetyl-CoA carboxylase (Figure 3–65). It picks up an acetyl group at the active site on acyl transferase (AT) that catalyzes both acetyltransferase and malonyltransferase; swings over to the active site of oxoacyl synthase (OS) and drops off that acetyl group on a sulfanyl group in its active site; swings back to the active site of the former enzymatic domain to pick up a malonyl group; swings back over to the active site of oxoacyl synthase, which condenses that malonyl group with the acetyl group, or in later cycles an elongating fatty acid, on the sulfanyl group in its the active site. The 3-oxoacyl group from the condensation ends up on the sulfanyl group of the acyl-carrier domain, which then swings from there to the active sites for oxoacyl reductase (OR), hydroxyacyl dehydratase (DH), and enoyl reductase (ER) before swinging back to the active site for oxoacyl synthase to deposit the longer fatty acyl group on the same sulfanyl group in its active site. When the fatty acyl group becomes the proper length, its transfer to the sulfanyl group in the active site of oxoacyl synthase slows down so dramatically[1243] that the freely floating, carboxy-terminal oleoyl hydrolase (Equation 3–499)

*It is possible that these unrelated domains are the same size because natural selection has pared them both down to the minimum size for the folding of a polypeptide.

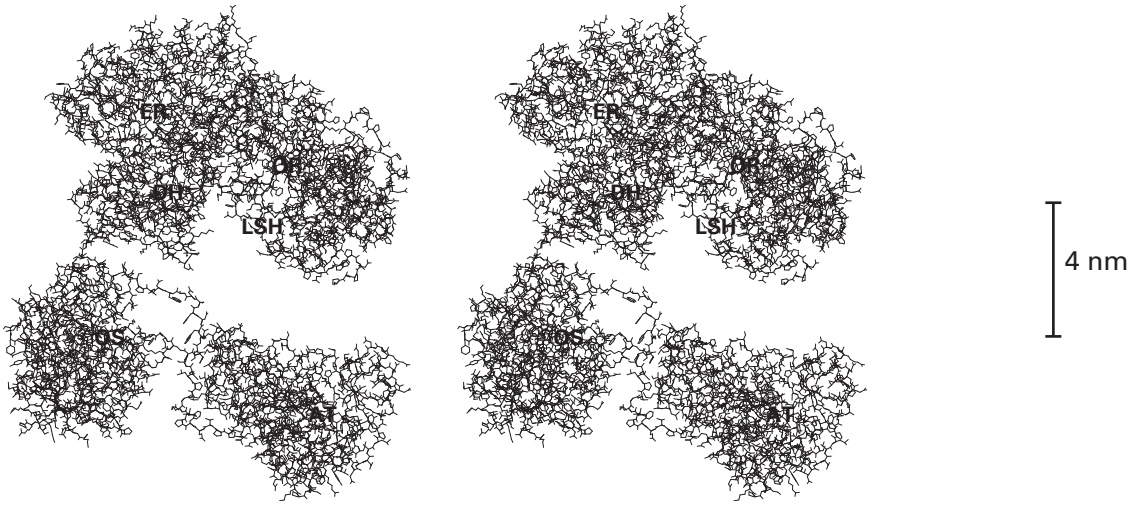

Figure 3–67: Stereodrawing[576] of the crystallographic molecular model of enzymatic domains of the porcine fatty-acid synthase system that form two peninsulas surrounding and creating the open bay around the shoreline of which the acyl-carrier domain ferries the elongating fatty acyl group from active site to active site.[1240] The enzyme is a dimer of two folded polypeptides, each 2512 amino acids long. Because, however, the acyl-carrier domain and the enzymatic domain catalyzing oleoyl hydrolase, which are attached to the carboxy terminus of the fifth enzymatic domain from the amino terminus, are on intentionally flexible leashes, their locations fluctuate dramatically within the crystal and no electron density is observed for either. Consequently, the folded polypeptide in the crystallographic molecular model ends at Glutamate 2113 even though the remaining 399 amino acids are present. The flexible leash, on the end of which is the acyl-carrier domain, is attached at this location in the model, designated as LSH. The leash is about 4 nm long, and the scale provided to the right is that length. The two folded polypeptides that comprise the dimer in the crystallographic molecular model are arrayed around a twofold rotational axis of pseudosymmetry. The relation of the two folded polypeptides is pseudosymmetric because there is a flexible neck connecting the upper peninsula in the drawing to the lower peninpeninsula. This neck is composed of a single strand from each of the two folded polypeptides. There is also a flexible link between the two enzymatic domains on the lower peninsula. Consequently, when the entire molecule crystallizes, the rotational axis is bent at the neck by crystal packing. The axis of pseudosymmetry is vertical and on the left-hand edge of the drawing. Only one half of the entire crystallographic molecular model is drawn. The active sites for acyltransferase (AT), oxoacyl synthase (OS), oxoacyl reductase (OR), hydroxyacyl dehydratase (DH), and enoyl reductase (ER) are labeled. The upper peninsula of the bay is formed from three compact enzymatic domains (ER, OR, and DH), and the lower penninsula is formed from two compact enzymatic domains (OS and AT).

on the longer leash has the time to find it and hydrolyze it from the acyl-carrier domain to give the fatty acid that is the product of the sequence of condensations and reductions.

Unlike the biotinylated carboxyl-carrier domain, which is clearly resolved in the crystallographic molecular model of acetyl-CoA carboxylase from *S. cerevisiae* (Figure 3–65) because its biotinyl group is firmly associated with the active site of the acetyl-CoA carboxytransferase, neither the acyl-carrier protein domain nor the enzymatic domain that catalyzes oleoyl hydrolase is resolved in the crystallographic molecular model of the porcine fatty-acid synthase system. The panthotheinyl groups on the acyl-carrier domains in the crystal, in the absence of the active production of fatty acids, must not associate with any active site, and they are wandering aimlessly around in their respective bays in the molecules of enzyme in the crystal.

In one molecular model produced from reconstructive summation of electron microscopic images of the fatty-acid synthase system from *S. cerevisiae*, separate features of scattering density of the proper size for its acyl-carrier domain are observed in the immediate vicinity of the active sites for acyl transferase, oxoacyl synthase, oxoacyl reductase, and enoyl reductase. The scattering densities observed are consistent with the unacylated acyl-carrier domain in this enzyme, in the absence of reactants, spending 30%, 30%, 10%, and 30% of its time associated with the respective active site.[1244] In another molecular model, however, also produced from reconstructive summation of electron microscopic images of the fatty-acid synthase system from *S. cerevisiae*, the acyl-carrier domain can be resolved, and it is associated with the active site of acyl transferase.[1245] In a crystallographic molecular model of the same enzyme, the acyl-carrier domain is also resolved but not associated with any of the active sites.[1246] The fatty-acid synthase system from *S. cerevisiae* is an $\alpha_6\beta_6$ heterododecamer in which six $\alpha\beta$ heterodimers are arranged with 322(D_3) symmetry, and the order in which the different active sites are arranged around each of the six bays in the molecule differs from their order in the mammalian fatty-acid synthase system.

Unlike a biotinylated carboxyl-carrier domain, a lipoyl acyl-carrier domain, or an acyl-carrier domain, the small, globular phosphoryl-carrier domain (99 aa) in pyruvate, phosphate dikinase (Problem 3–13)

$$\text{phospho}\textit{enol}\text{pyruvate} + MgOPO_3PO_3^{2-} + 2\,H^+ + AMP^{2-} \rightleftharpoons MgATP^{2-} + HOPO_3^{2-} + \text{pyruvate} \quad (3\text{–}500)$$

from *C. symbiosum*, which transfers a phospho group between the two active sites on its two respective enzymatic domains, is not on a leash of flexible polypeptide or on a flexible, jointed arm. It performs the transfer by rotating 100° back and forth around a fixed axis that lies between two adjacent strands of extended, flexible polypeptide connecting the phosphoryl-carrier domain to two enzymatic domains (340 aa), one amino-terminal and one carboxy-terminal to it.[1247-1249] These two strands act as a **stationary spindle on which the phosphoryl-carrier domain revolves**. The imidazolyl group of the histidine that is to carry the phospho group between the two enzymatic domains is phosphorylated by phospho*enol*pyruvate at the active site in the carboxy-terminal enzymatic domain

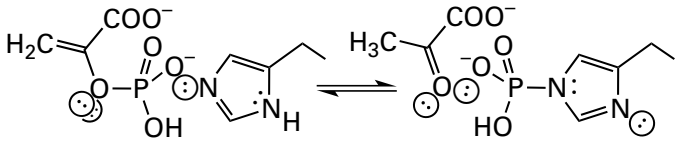

(3–501)

and the phospho group on the imidazolyl group rides on the surface of the rotor to the active site in the amino-terminal enzymatic domain where it is phosphorylated by magnesium diphosphate

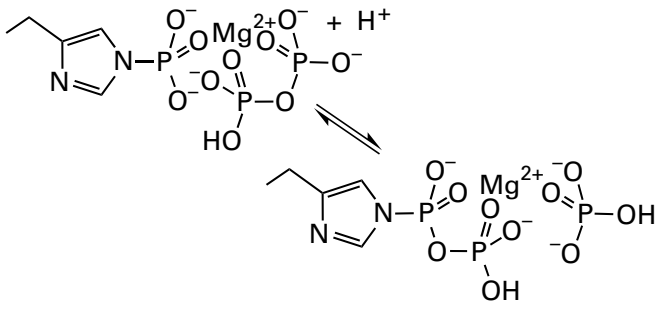

(3–502)

and then transfers the resulting magnesium diphospho group[1250] from the imidazolyl group of the histidine to AMP^{2-} to form $MgATP^{2-}$

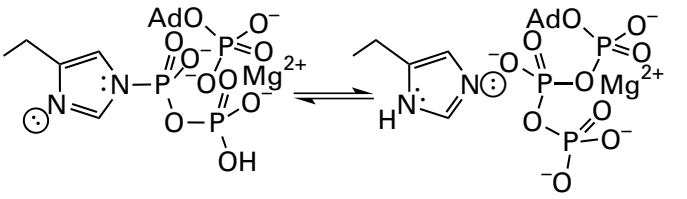

(3–503)

where Ad is an adenosyl group.

Methionine synthase from *E. coli* is an α_2 homodimer composed of two polypeptides 1226 amino acids long. The two globular **cob(I)alamin methyl-carrier domains** (235 aa) in each folded polypeptide contain the cob(I)alamin that in turn transfers a methyl group among three larger, globular enzymatic domains (325, 261, and 324 aa). Each cob(I)alamin methyl-carrier domain is located between the second and third domains in the sequence of amino acids for the complete polypeptide. In this instance, unlike biotinylated carboxyl-carrier domains, lipoyl acyl-carrier domains, or acyl-carrier domains, which are flexibly anchored domains attached to larger globular structures, the two cob(I)alamin methyl-carrier domains in the homodimer of methionine synthase can be considered the core of the structure because the only interface holding the two intact folded polypeptides together to form the homodimer is between these two methyl-carrier domains. As such, these two domains together form a relatively large, compact dimeric globular structure. Within the interface in this globular structure between these two identical cob(I)alamin methyl-carrier domains is a twofold rotational axis of symmetry relating only these two domains.[1251]

The three enzymatic domains of methionine synthase, listed from the amino terminus of each folded polypeptide to its carboxy terminus, catalyze the respective reactions

$$\text{Co(III)CH}_3 + \text{L-homocysteine} \rightleftharpoons \text{L-methionine} + \text{Co(I)} + \text{H}^+ \quad (3\text{–}504)$$

$$\text{Co(I)} + \text{5-methyltetrahydrofolate} + \text{H}^+ \rightleftharpoons \text{tetrahydrofolate} + \text{Co(III)CH}_3 \quad (3\text{–}505)$$

$$\text{Co(II)} + \text{flavodoxin}_{\text{red}} + \textit{S}\text{-adenosylmethionine} \rightleftharpoons \text{flavodoxin}_{\text{ox}} + \textit{S}\text{-adenosylhomocysteine} + \text{Co(III)CH}_3 \quad (3\text{–}506)$$

where Co(III) is methyl cob(III)alamin, Co(I) is cob(I)alamin, and Co(II) is cob(II)alamin. The first two reactions sustain the overall chain reaction synthesizing L-methionine from L-homocysteine and 5-methyltetrahydrofolate, and the third reaction performs the housekeeping that repropagates the chain when it has been terminated adventitiously by the oxidation of the cob(I)alamin.

The two enzymatic domains catalyzing transfer of the methyl group from methyl cob(III)alamin to L-homocysteine (Equation 3–504) and transfer of the methyl group from 5-methyltetrahydrofolate to cob(I)alamin (Equation 3–505) are composed of the amino-terminal 616 amino acids of each polypeptide in the multienzymatic complex. They are associated with each other by an asymmetric interdomain interface and together form a compact globular structure.[1252] The globular enzymatic domain catalyzing transfer of the methyl group from *S*-adenosyl-L-methionine to cob(II)alamin (Equation 3–506) is composed of the carboxy-terminal 324 amino acids.[1253] These three domains are not associated with their twins in the other half of the homodimer, and they freely diffuse at random while attached to the dimeric cob(I)alamin methyl-carrier domain.

Each amino-terminal enzymatic domain is connected to one of the domains in the central, symmetric homodimeric cob(I)alamin methyl-carrier domain by a **leash that is a random coil** with the sequence EDVILNRRDDGTERLLELAEKYRGSKTDDTANAQQAEWRSWEVNK. These two leashes emerge from the dimeric central globular domain, composed of two cobalamin-carrier domains with the two cobalamins on opposite sides of its surface. The active sites in the two amino-terminal domains are 5.0 nm apart.[1252] Nevertheless, each leash is long enough to permit the active site in the amino-terminal domain responsible for the nucleophilic substitution in Equation 3–504 to associate with methylcob(III)alamin in a cobalamin methyl-carrier domain and transfer a methyl group between methylcob(III)alamin and L-homocysteine (previously Equation 2–353)

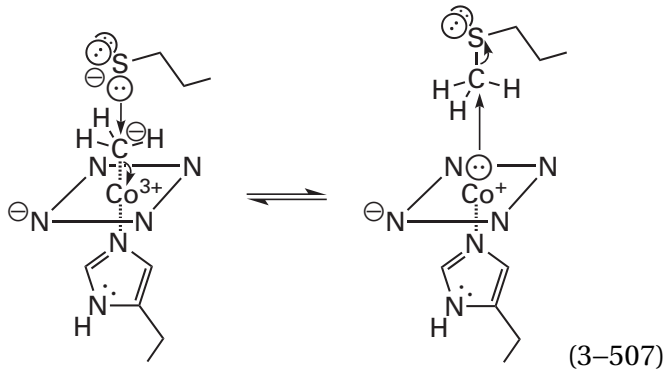

(3–507)

Each leash is also long enough to permit the active site in the amino-terminal domain responsible for the nucleophilic substitution in Equation 3–505 to associate with cob(I)alamin in a cobalamin methyl-carrier domain and transfer a methyl group between 5-methyltetrahydofolate and cob(I)alamin (previously Equation 2–356)

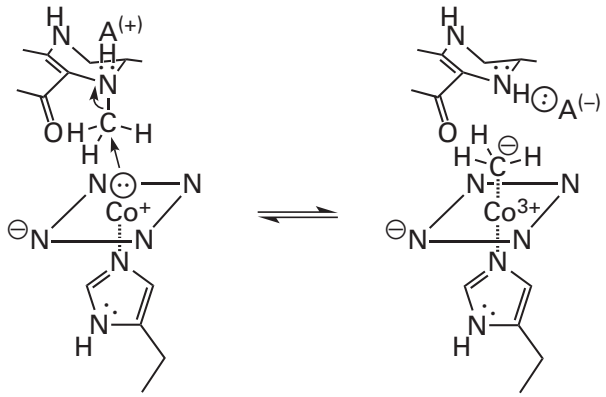

(3–508)

Each carboxy-terminal enzymatic domain that catalyzes the regeneration of cob(I)alamin is attached to the central homodimeric cobalamin methyl-carrier domain by a shorter leash with the sequence KKPRTPP. These two leashes emerge from the central homodimeric domain at locations on its surface that are immediately adjacent to each other. When the leashes are constricted artificially by mutationally inserting a disulfide into them[1253] or by mutating the histidine that provides the axial ligand to the cobalamin,[1255] the carboxy-terminal domain forms a stable complex between its active site and the cobalamin in the cobalamin methyl-carrier domain to which it is attached, a consquence that hinders the overall reaction.

The leash between the globular structure containing the two amino-terminal enzymatic domains and the central cobalamin methyl-carrier domain is so long and so flexible, and the two are so loosely attached to each other, that each cobalamin in the central homodimeric domain probably services at random all four active sites in the two identical amino-terminal globular structures that are unattached to each other and flail independently of each other. The leash is also long enough, however, and contains enough bonds about which free rotation can occur that the amino-terminal globular domain containing the two respective active sites can be considered a free agent that is just as likely to associate with cobalamins on other homodimers of methionine synthase as with cobalamins on the molecule of protein in which it happens to be located, with **little distinction between intramolecular association and intermolecular association**.

The possibility that the transfer of methyl groups among the active sites on the amino-terminal enzymatic domains of methionine synthase is intermolecular rather than intramolecular has been examined by using site-directed mutation to cleave the multienzymatic complex at the Alanines 649 in the middle of the two long leashes between the amino-terminal enzymatic domains and the central homodimeric cobalamin methyl-transfer domain. When the resulting monomeric globular portion containing the two enzymatic domains is mixed in equimolar proportion with the dimeric portion containing the two cob(I)alamin methyl-carrier domains, the observed initial rates of methionine synthesis at 37 °C and saturating concentrations of L-homocysteine and 5-methyltetrahydrofolate are, as might be expected from a bimolecular reaction, directly proportional to the square of the common molar concentration of the two halves from 30 to 300 nM.[1256] Over the same range of concentrations for the intact enzyme, the initial rates are directly proportional to only the concentration of enzyme.* The catalytic constant for the two halves at equimolar concentrations of 270 nM is 11 s^{-1} while that for the intact enzyme[1257,1258] is 30 s^{-1} at all concentrations in the same range. These two observations rule out significant rates of intermolecular transfer of the methyl group by the cobalamin methyl-transfer domain for the intact enzyme at concentrations less than 200 nM. If, however, the concentration of intact enzyme is greater than 1 μM, because the initial rates of the mixture of the dissociated halves increase as the square of their common concentration, most of the methyl transfer by the cobalamin methyl-transfer domain among the enzymatic domains for the intact enzyme must occur intermolecularly.

*Rowena Matthews, personal communication.

It has already been noted that, when a tRNA ligase is aminoacylating the correct tRNA with the correct amino acid, the complex between the tRNA ligase and the transfer RNA, two macromolecules of similar dimensions, is held together by an extensive interface that includes both the anticodon stem at one end of the transfer RNA and the unpaired nucleotides at the 3′ end of the transfer RNA in the acceptor stem at the other end.[1011,1050,1052,1259,1260] These unpaired nucleotides protruding from the acceptor stem must associate with the active site for the aminoacylation catalyzed by the enzyme in such a way that the 3′-hydroxy group at the 3′ end if the transfer RNA can be aminoacylated. In a sense, although the complex is transient, while it is in existence, it is similar to an intact macromolecule composed of two subunits, the transfer RNA and the ligase. It has also been noted that, to ensure that the correct amino acid has been aminoacylated, the active site for aminoacylation is as specific as possible, but the accuracy of the aminoacylation is often double-checked by editing at another active site within the enzyme that hydrolyzes any misacylated 3′-hydroxy group at the 3′ end before the complex dissociates. Consequently, transfer of the aminoacylated 3′-hydroxy group of the transfer RNA between the site for aminoacylation and the site for editing is an example of the transfer of a covalent intermediate between two active sites.

In the crystallographic molecular model of the complex between $tRNA^{Ile}$ and isoleucine—tRNA ligase from *S. aureus*, the unpaired ACCA at the 3′ end of the transfer RNA is located in the site for editing,[1260] the selectivity of which has also already been discussed. The active site for editing and the active site for aminoacylation are 3.4 nm apart, but the space between them is a bay empty of protein and filled with water, similar to the bay in fatty acid synthase (Figure 3–67) but much smaller. In the crystallographic molecular model of the complex between glutamine—tRNA ligase from *E. coli* and $tRNA^{Gln}$, the 3′-hydroxy group of the transfer RNA is inserted into the active site for aminoacylation rather than the site for editing.[1259] By comparing the two structures, it can be seen how the completely flexible, single-stranded tail at the 3′ end of the acceptor stem of a tRNA can swing from the active site for aminoacylation to the active site for hydrolytic editing, easily spanning the 3.4 nm between them,[1260] just as the small carrier domains attached to multienzymatic complexes swing among active sites.

Most multienzymatic complexes do not transfer a substrate or a portion of a substrate between their active sites in the form of a covalent adduct, as do acetyl-CoA carboxylase, pyruvate carboxylase, pyruvate dehydrogenase complex, animal fatty-acid synthase system, pyruvate, phosphate dikinase, and methionine synthase. In these other multienzymatic complexes, the substrate or substrates transferred between the series of active sites responsible for the sequential reactions catalyzed by the multienzymatic complex are freely diffusing, independent molecules. In each multienzymatic complex, the **intermediate substrates** are the products of the reactions catalyzed by each active site in the complex except the last one in the sequence, the **initial reactants** are the reactants that enter the active site for the first reaction in the sequence, and the **final products** are the products that dissociate from the active site for the last reaction in the sequence.

In many of these multienzymatic complexes, if not most of them, even though all the active sites for the complete overall reaction resulting from the sequence of individual reactions are on the same molecule of protein, the intermediate substrates are not transferred preferentially between active sites in the same complex but instead are **transferred by free diffusion through the solution between active sites that are usually on different molecules of the same multienzymatic complex**. When an intermediate substrate dissociates into the solution from the active site catalyzing one of the reactions in the sequence of reactions for which the multienzymatic complex is responsible, it is immediately in free diffusion and has no obligation to associate with the active site catalyzing the next reaction in the sequence on the same molecule of the multienzymatic complex from which it just dissociated. Consequently, there is no catalytic advantage in such circumstances to having the enzymatic domains attached together in the same multienzymatic complex. The active sites in these cases are gathered into the multienzymatic complex to coordinate the biosynthesis of the proteins at the level of expression of the protein, not for the purpose of catalytic cooperation.

Chorismate mutase–prephenate dehydratase from *E. coli* is a multienzymatic complex catalyzing two sequential reactions in the biosynthetic pathway for phenylalanine: the reaction catalyzed by chorismate mutase (previously Equation 3–402)

$$\text{chorismate} \rightleftharpoons \text{prephenate} \qquad (3\text{–}509)$$

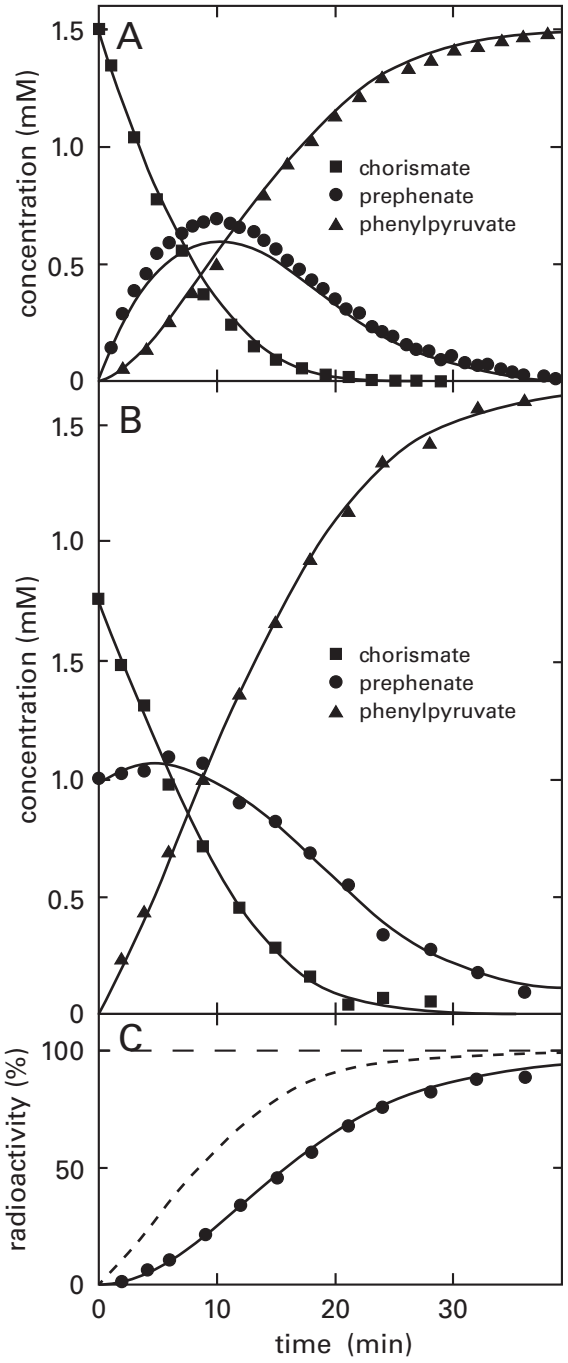

Figure 3–68: Changes in the concentrations of substrates with time in solutions containing *E. coli* chorismate mutase–prephenate dehydratase.[1261] **(A)** Chorismate mutase–prephenate dehydratase was mixed with 1.5 mM chorismate at pH 7.5 and 37 °C. At the noted times (in minutes), samples were removed and assayed for chorismate (■), prephenate (●), and phenylpyruvate (▲). The three smooth curves are for theoretical functions derived from the kinetic constants (K_m and V) for the two active sites and from the assumption that all products and reactants dissociate into the solution and associate from the solution. Any preferential intramolecular channeling between active sites on the same protein would have caused the observed concentrations of prephenate to be less than the theoretical function. **(B)** Chorismate mutase–prephenate dehydratase was mixed under the same conditions with 1.76 mM [U-^{14}C]chorismate (12,000 cpm μmol^{-1}) and 1.0 mM prephenate, and the concentrations of the three substrates, disregarding the radioactivity, were again monitored as a function of time. The curves are calculated with the same assumptions and the same functions as were used for the curves in Panel A. **(C)** In each sample from the experiment in Panel B, the percent of the total carbon-14 radioactivity in phenylpyruvate was determined as a function of time (minutes), disregarding the total molar concentration of phenylpyruvate. The solid line represents the predictions of the functions used in Panels A and B that were derived on the assumption that no channeling occurs. The dashed line is for a function derived on the assumption that prephenate is completely channeled between the active sites.

and the reaction catalyzed by prephenate dehydratase

$$\text{prephenate} + H^+ \rightleftharpoons \text{phenylpyruvate} + CO_2 + H_2O \qquad (3\text{–}510)$$

These two reactions are catalyzed by two distinct active sites[1261] in enzymatic domains that are on the same folded polypeptide.[1262,1263] Prephenate, the intermediate substrate, is the exclusive product of the first reaction and the exclusive reactant in the second reaction. The progress of the overall reaction can be followed by assaying for the concentrations of chorismate, prephenate, and phenylpyruvate as a function of time (Figure 3–68A).[1261] As the reaction progresses, the concentration of prephenate in the solution increases, reaches a maximum, and declines as all the substrates are converted to phenylpyruvate. The important question is whether all the prephenate passes through the solution in going from an active site catalyzing the first reaction to an active site catalyzing the second or if some of it is transferred intramolecularly between the active sites on the same molecule of enzyme without leaving it.

One way to answer the question of whether or not chorismate mutase–prephenate dehydratase transfers prephenate intramolecularly between its two active sites is to evaluate the behavior of the concentrations of the reactant chorismate, the intermediate substrate prephenate, and the final product phenylpyruvate as a function of time after adding enzyme to a solution of chorismate (Figure 3–68A). The fact that **the intermediate substrate appears in solution, builds to a maximum, and then declines** indicates that at least a portion of the prephenate passes through the solution. Both the fact that **the concen-**

tration of the final product shows a distinct lag and the fact that the amount of prephenate observed as a function of time is that predicted from the values of $k_{\text{chorismate}}$ and k_0 for chorismate mutase and the values of $k_{\text{prephenate}}$ and k_0 for prephenate dehydratase (smooth curve in Figure 3–68A) suggest that most if not all the prephenate passes through the solution.

Such **a kinetic argument is often used to rule out intramolecular transfer**.[1264-1267] Another approach is to examine the **effect of adding the intermediate substrate** on the kinetics (Figure 3–68B). Finally, when [^{14}C]chorismate and nonradioactive prephenate were mixed with the enzyme and the production of [^{14}C]phenylpyruvate was monitored (Figure 3–68C), the production of [^{14}C]phenylpyruvate followed the calculated curve (solid line in Figure 3–68C) expected if all the prephenate produced at the active site of chorismate mutase had to pass through the solution to reach the active site of prephenate dehydratase. If all the prephenate produced at the first active site had been transferred to the second active site without leaving the enzyme, the production of [^{14}C]phenylpyruvate would have begun at a steady rate (dashed line in Figure 3–68C). If, however, all the [^{14}C]prephenate enters the solution before it enters the second active site, it should be diluted by the nonradioactive prephenate, and there should be a lag in its production as [^{14}C]prephenate builds up, as was observed.

Suppose that there are **two mutants of a multienzymatic complex**, one in which the active site for the first reaction it catalyzes is inactive and one in which the active site for the second reaction is inactive. If these two mutants are mixed in equimolar concentration and the conversion of reactants of the first reaction into products of the second reaction occurs at the same rate as the rate observed with the same molar concentration of unmutated multienzymatic complex, it can be concluded that intramolecular transfer is not required for the reactions to proceed.

For example, there is a multienzymatic complex in the cytoplasm of *H. influenzae* that has two enzymatic domains: one with an active site catalyzing ribitol-5-phosphate 2-dehydrogenase ($NADP^+$)

$$\text{D-ribulose 5-phosphate} + \text{NADPH} + \text{H}^+ \rightleftharpoons \text{D-ribitol 5-phosphate} + \text{NADP}^+ \quad (3\text{–}511)$$

and the other with an active site catalyzing D-ribitol-5-phosphate cytidylyltransferase

$$\text{D-ribitol 5-phosphate} + \text{MgCTP}^{2-} \rightleftharpoons \text{MgOPO}_3\text{PO}_3^{2-} + \text{CDP-ribitol} \quad (3\text{–}512)$$

A mutant of the multienzymatic complex in which Lysine 386 has been mutated to an alanine in the active site for the former reaction lacks significant activity for the dehydrogenase but has normal activity for the cytidyltransferase, and a mutant in which Arginine 18 has been mutated to an alanine in the active site for the latter reaction lacks significant activity for the cytidylyltransferase but has normal activity for the dehydrogenase. When equimolar amounts of the two mutants are mixed together,[1267] the catalytic constant for the overall reaction, based on the molar concentration of unmutated active sites, is 6 s^{-1} while the catalytic constant for the unmutated intact multienzymatic complex, based on the molar concentration of active sites, is 12 s^{-1}. If the intermediate D-ribitol 5-phosphate were being transferred only intramolecularly between active sites on the same molecule of the multienzymatic complex, the mixture of mutants should have no enzymatic activity because the reactant for the second reaction produced by the former mutant could not be transformed into the product for the second reaction by the latter mutant.

Another way to test whether or not an intermediate is being transferred intramolecularly between active sites is to **add the active site for the second reaction** to a solution of the intact multienzymatic complex while it is catalyzing the overall reaction. Either a mutant that is unable to catalyze the first reaction but can catalyze the second or a fragment of the multienzymatic complex containing only the intact active site for the second reaction can be used. If either protein lacking the first active site is added to the solution and formation of the products of the second reaction increases in rate and the lag in the rate of their formation (see Figure 3–68) decreases, then intramolecular transfer cannot be a necessary step in the reaction.

For example, there is a multienzymatic complex from *E. coli* that contains an enzymatic domain catalyzing glucosamine-1-phosphate *N*-acetyltransferase and an enzymatic domain catalyzing UDP-*N*-acetylglucosamine diphosphorylase. This multienzymatic complex catalyzes the overall reaction that equilibrates $MgUTP^{2-}$, acetyl-SCoA, and D-glucosamine 1-phosphate with $MgUDP^-$, diphosphate, HSCoA, and UDP-*N*-acetyl-α-D-glucosamine. When an amino-terminal fragment of the multienzymatic complex, containing only the active site for UDP-

N-acetylglucosamine diphosphorylase, is added (to a final concentration of 1 μM) to a solution containing 0.013 μM intact multienzymatic complex, the catalytic constant for production of diphosphate from $MgUTP^{2-}$, acetyl-SCoA, and D-glucosamine 1-phosphate increases[1268] from 16 to 44 s^{-1}. In this experiment, the choice of the reactants has made the reaction catalyzed by UDP-*N*-acetylglucosamine diphosphorylase the second reaction in the sequence.

There are **enzymes that catalyze several successive reactions at the same active site** rather than at several different active sites. These enzymes convert a reactant into a product through one or more intermediate substrates. One example of such an enzyme would be aristolochene synthase (Figure 3–48), in which (–)-germacrene A is a tightly held intermediate substrate. The same criteria can be used to decide whether or not the intermediate substrates in such a sequence of reactions dissociate from the lone active site.

For example, human aromatase contains a heme P450 that converts androst-4-ene-3,17-dione into estrone in three successive hydroxylations using successive oxoiron(IV) porphyrins$^{\bullet+}$ formed at the same heme from three successive molecules of oxygen. The two intermediates in the reaction, produced by the first two successive, individual hydroxylations, are 19-hydroxyandrost-4-ene-3,17-dione and 19-oxoandrost-4-ene-3,17-dione, respectively. In this instance, the question is whether the intermediates remain bound on the active site or are released into the solution and then bound again at the same or another active site for the next hydroxylation. Because the concentrations of the two intermediate substrates build up and then decrease at levels predicted for their complete dissociation from and reassociation with the active sites between each successive reaction (see Figure 3–68A) and because the addition of either nonradioactive intermediate dramatically decreases the yield of [1,2,6,7-$^3H_4$]estrone produced from [1,2,6,7-$^3H_4$]androst-4-ene-3,17-dione, it was concluded that the intermediate substrates freely dissociate and reassociate with the active sites in the solution between successive hydroxylations rather than remaining in the same active site for all three hydroxylations,[1269] unlike the situation with (–)-germacrene A in the active site of aristolochene synthase.

There are many multienzymatic complexes, albeit probably the minority, in which intermediate substrates are channeled within the protein between active sites in the complex. A molecule of a multienzymatic complex channels an intermediate substrate between two of its active sites if that substrate passes between them intramolecularly through the molecule of the enzyme without dissociating into the solution and without being covalently attached to the protein. As mentioned previously, intermediate substrates cannot be channeled if they dissociate from any of the active sites in the complex into the solution.

Cavities or tunnels that connect separate active sites are usually observed in crystallographic molecular models of multienzymatic complexes for which evidence of the channeling of an intermediate substrate has been presented. A cavity or a tunnel can connect active sites on two or more separate enzymatic domains in the same folded polypeptide or on two or more separate subunits, each a different folded polypeptide. As in the case of tunnels leading from solution into a single active site, these tunnels connecting active sites can be traced by filling them with atoms of xenon (Figure 3–69).[1270-1272] Usually, however, they are identified as cavities or long tunnels, filled with water or apparently empty, running through the crystallographic molecular model of the protein.

It should be kept in mind, however, that crystallography is always unable to determine whether or not an intermediate substrate actually does pass through a tunnel that is observed. Consequently, kinetic observations, such as the ones described for multienzymatic complexes that do not channel their intermediate substrates, are always essential to conclude that an intermediate substrate is channeled. Several different kinds of observations have been used as **evidence that an intermediate substrate actually is channeled** by a multienzymatic complex between two of its active sites.

A characteristic feature of a multienzymatic complex that is unable to channel intermediate substrates between its active sites is a pronounced lag in the production of the final product in the sequence (Figure 3–68A). This lag results from the requirement that the intermediate substrate—in the case of chorismate mutase–prephenate dehydratase, the prephenate—must accumulate in the solution to a concentration high enough to sustain a steady-state rate for production of the final product—in the case of chorismate mutase–prephenate dehydratase, the phenylpyruvate. The **lack of a lag** in the production of a final product from the initial reactants can be used as evidence that the intermediate substrates do not have to accumulate in the solution

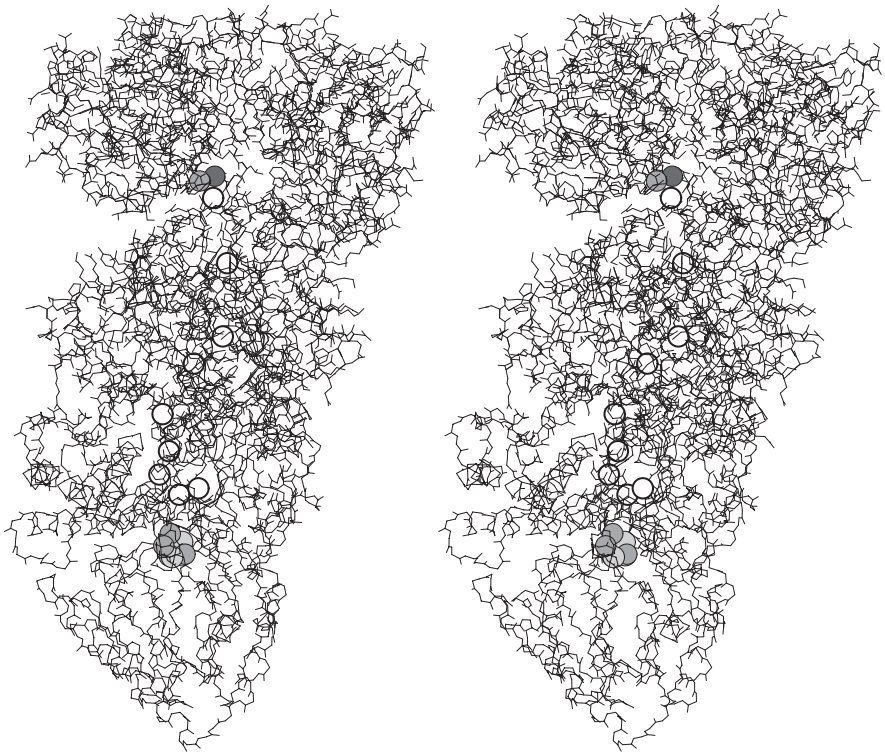

Figure 3–69: Stereodrawing[576] of the tunnel connecting the active sites for anaerobic carbon monoxide dehydrogenase (Equation 3–521) and CO-methylating acetyl-CoA synthase (Equation 3–522) in the multienzymatic complex from *M. thermoacetica*.[1271] The enzyme was purified from a homogenate of bacterial cells under strictly anaerobic conditions.[1270] Crystals were grown from a solution of 200 mM calcium acetate and 20% glycerol at pH 7 with poly(ethylene glycol) as a precipitant, again under anaerobic conditions.[1272] The crystals were exposed to 14 atm of xenon gas for 60 s, and then a data set was collected to Bragg spacing of 0.25 nm. In the resulting map of electron density, nine electron-dense xenon atoms (131 electrons) could be observed in the center of an $\alpha\beta$ heteromonomer of the symmetric $(\alpha\beta)_2$ homodimer, distributed within a tunnel connecting the active site for anaerobic carbon monoxide dehydrogenase, which was identified by its [4Fe–4S–Ni] cluster (**3–133**), and the active site for CO-methylating acetyl-CoA synthase, which was identified by its dinuclear cluster of a nickel ion and a copper ion. The two active sites are located in the two different subunits, α and β, of the $\alpha\beta$ heteromonomer. The nine xenon atoms (represented by open circles) serve to trace the rather tortuous tunnel. The [4Fe–4S–Ni] cluster is drawn in space-filling representation in the lower half of the drawing, and the dinuclear cluster of a nickel ion and a copper ion is also drawn in space-filling representation in the upper half of the drawing. The CO is produced at the active site of the dehydrogenase and then travels up through the tunnel to the active site of the synthase, where it is turned into acetyl-SCoA. Side chains of the amino acids are included in the upper subunit, which contains the active site for CO-methylating acetyl-CoA synthase, to delineate more clearly the wall of the tunnel in this location, but side chains are not included in the lower subunit, which contains the active site for anaerobic carbon monoxide dehydrogenase, because they obscured the tunnel through this subunit.

because they are channeled within the molecule of each multienzymatic complex from one active site to the other intramolecularly.[1273-1278]

For example, a multienzymatic complex from *Bradyrhizobium japonicum* is an α_4 homotetramer, with each subunit composed of a single folded polypeptide that contains two enzymatic domains.[1262,1263] One enzymatic domain has an active site for proline dehydrogenase

$$\text{L-proline} + \text{ubiquinone} + H^+ \rightleftharpoons (S)\text{-1-pyrroline-5-carboxylate} + \text{ubiquinol} \quad (3\text{–}513)$$

and the other has an active site for glutamate-5-semialdehyde dehydrogenase

$$\text{L-glutamate 5-semialdehyde} + NAD^+ + H_2O \rightleftharpoons \text{L-glutamate} + NADH + 2H^+ \quad (3\text{–}514)$$

The intermediate substrate (*S*)-1-pyrroline-5-carboxylate hydrolyzes rapidly and spontaneously to the intermediate substrate L-glutamate 5-semialdehyde during its transfer. The overall reaction catalyzed is a four-electron oxidation of L-proline to L-glutamate using a quinone and NAD^+ as the two respective two-electron oxidants. The production of L-glutamate from L-proline, ubiquinone, and NAD^+ by the multienzymatic complex commences with only a short lag of less than 15 s (upper solid line in Figure 3–70).[1279,1280]

That the short lag observed is not the result of a requirement for L-glutamate 5-semialdehyde to accumulate in the solution could be shown by performing an identical assay to which the same molar amounts of two mutants of the complex were added in place of the unmutated complex. The active site for proline dehydrogenase had been inactivated in one of the mutants and the active site for glutamate-5-semialdehyde dehydrogenase had been inactivated in the other so that the intermediate substrate L-glutamate 5-semialdehyde was required to pass through the solution from an active site for proline dehydrogenase to the active site for glutamate-5-semialdehyde dehydrogenase. In this case, a much longer lag was observed (○ in Figure 3–70), which could be explained quantitatively as a requirement for the accumulation of L-glutamate 5-semialdehyde in the solution (lower solid line in Figure 3–70). Following the lag, the steady-state rate of this reaction (dashed line in Figure 3–70) catalyzed by the two mutants working in concert was the same as that for the unmutated multienzymatic complex. This fact suggests that once adequate concentrations of L-glutamate 5-semialdehyde have accumulated at these concentrations of the active sites, the rate of the overall reaction is determined not by steps that involve L-glutamate 5-semialdehyde in solution associating with the active site for glutamate-5-semialdehyde dehydrogenase but by the rates of steps common to both intramolecular and intermolecular reactions.

In the crystallographic molecular model of this multienzymatic complex in which the site for NAD^+ is occupied,[1279] there is a **large cavity surrounded almost completely by protein** within each of the four subunits. The cavity is filled with disordered molecules of water. The flavin adenine dinucleotide in the active site of proline dehydrogenase is exposed at one end of the cavity, and the NAD^+ in the active site of glutamate-5-semialdehyde dehydrogenase is exposed at the other end of this cavity. It seems reasonable to assume that a molecule of (*S*)-1-pyrroline-5-carboxylate, which is produced by the oxidized flavin from a molecule of L-proline, dissociates from that active site into the cavity and is hydrolyzed to L-glutamate 5-semialdehyde while trapped in the cavity. The resulting L-glutamate 5-semialdehyde is then oxidized by the NAD^+ to L-glutamate at the other end of the cavity before it can escape into the solution. In this way, the intermediate L-glutamate 5-semialdehyde is channeled from one active site to the other within the same molecule of the multienzymatic complex. There are two small openings to the solution in the walls of the cavity through which the reactants L-proline, ubiquinone, and NAD^+ must enter the cavity and through which the products L-glutamate, ubiquinol, and NADH must exit the cavity.* In addition to the absence of a lag, no intermediate substrate in the sequence of reactions catalyzed by a multienzymatic complex accumulates to levels predicted by the steady-state

*When the multienzymatic complex for proline dehydrogenase and glutamate-5-semialdehyde dehydrogenase, in which the flavin is oxidized, is mixed with L-proline and NAD^+, so that only one turnover can occur, the rate at which NADH is produced has no lag (<1 s).[1280] Consequently, the short lag observed in the steady-state assay (Figure 3–70) is a delay required to establish a steady-state rate of flavin oxidation rather than to establish a steady-state rate for the hydrolysis of (*S*)-1-pyrroline-5-carboxylate to L-glutamate 5-semialdehyde or the diffusion of either of these intermediate substrates through the cavity between the active sites.

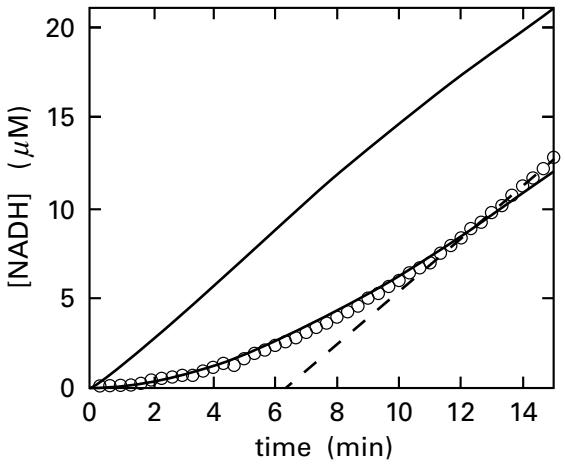

Figure 3–70: Channeling between active sites in the multienzymatic complex from *B. japonicum* that converts L-proline into L-glutamate in the sequential reactions catalyzed by the active sites for proline dehydrogenase and glutamate-5-semialdehyde dehydrogenase, respectively.[1279] The intact multienzymatic complex (0.2 nmol) was assayed at 23 °C in 25 mM NaCl, 10 mM $MgCl_2$, and 50 mM potassium phosphate at pH 7.5, by following continuously at 340 nm the production of NADH as L-proline (40 mM) is oxidized to L-glutamate by the two sequential two-electron oxidations. The first oxidation, at the first active site, is with the oxidant ubiquinone (0.1 mM), and the second oxidation, at the second active site, is with the oxidant NAD^+ (0.2 mM). The concentration of NADH produced during the second reaction as the assay progressed (upper solid line) is plotted as a function of time (minutes). Identical assays were performed with 0.2 nmol of each of two monofunctional mutants of the multienzymatic complex rather than 0.2 nmol of the native multienzymatic complex. The mutant in which Arginine 456 is converted to a methionine has undetectable activity for proline dehydrogenase but has the same specificity constant for L-glutamate 5-semialdehyde and catalytic constant for glutamate-5-semialdehyde dehydrogenase as the intact multienzymatic complex. The mutant in which Cysteine 792 is converted to an alanine has the same specificity constant for proline and catalytic constant for proline dehydrogenase as the intact multienzymatic complex but undetectable activity for glutamate-5-semialdehyde dehydrogenase. The concentration of NADH (○) produced in the same two sequential reactions by this equimolar mixture of mutants is plotted as a function of time (minutes). The solid line through these points is a function calculated from the catalytic constants and the specificity constants for each site under two assumptions: first, that the (*S*)-1-pyrroline-5-carboxylate produced by an active site for proline dehydrogenase dissociates from that active site into the solution and rapidly hydrolyzes to L-glutamate 5-semialdehyde, and second, that the L-glutamate 5-semialdehyde freely diffusing through the solution associates with an active site of glutamate-5-semialdehyde dehydrogenase and is converted into L-glutamate. The reduction of NAD^+ increases in rate as the concentration of L-glutamate 5-semialdehyde builds up in the solution to reach eventually a linear, steady-state rate (dashed asymptote).

rate constants of the individual active sites (as does prephenate in Figure 3–68A). This **lack of accumulation of the intermediate substrates in the solution** is evidence for channeling of the intermediate substrates.[1277,1278,1281] For example, a porcine multienzymatic complex is an α_8 homooctamer,[1282] with each subunit composed of a single folded polypeptide that contains enzymatic domains for glutamate formimidoyltransferase

$$\begin{gathered}\text{tetrahydropteroylpentaglutamate} + \\ \textit{N}\text{-formimidoyl-L-glutamate} \rightleftharpoons \text{L-glutamate} + \\ \text{5-formimidoyltetrahydropteroylpentaglutamate}\end{gathered} \tag{3–515}$$

and formimidoyltetrahydrofolate cyclodeaminase

$$\begin{gathered}\text{5-formimidoyltetrahydropteroylpentaglutamate} \\ + 2\,H^+ \rightleftharpoons NH_4^+ + \\ \text{5,10-methenyltetrahydropteroylpentaglutamate}\end{gathered} \tag{3–516}$$

The fact that no 5-formimidoyltetrahydropteroylpentaglutamate accumulates in the solution when the porcine multienzymatic complex converts tetrahydropteroylpentaglutamate and *N*-formimidoyl-L-glutamate into 5,10-methenyltetrahydropteroylpentaglutamate, L-glutamate, and ammonia has been presented as evidence that the sole intermediate substrate, 5-formimidoyltetrahydropteroylpentaglutamate, is channeled between the two active sites.[1277,1278]

In the two multienzymatic complexes just discussed, the two active sites are on two enzymatic domains of a single folded polypeptide. There are also examples of **intramolecular channeling of an intermediate substrate between two active sites within a noncovalent complex between two separate enzymes**, each composed of its own folded polypeptide with its own active site that catalyzes only one of the two sequential metabolic reactions. In fact, there are a number of organisms in which separate proteins catalyze proline dehydrogenase (Equation 3–513) and glutamate-5-semialdehyde dehydrogenase (Equation 3–514) rather than a single folded polypeptide containing two enzymatic domains responsible for each reaction. For example, in *T. thermophilus* there are two independent enzymes, each homologous (26%, 4.2 gap percent and 33%, 1.9 gap percent) to the respective enzymatic domains in the multienzymatic complex of *B. japonicum*. These two independent enzymes form a noncova-

lent complex with a dissociation constant of 3 μM, and steady-state measurements of the conversion of L-proline to L-glutamate are consistent with intramolecular channeling of the intermediate substrates (*S*)-1-pyrroline-5-carboxylate and L-glutamate 5-semialdehyde within this noncovalent complex,[1283] just as they are channeled in the multienzymatic complex from *B. japonicum*.

There is a multienzymatic complex that has active sites for acetaldehyde dehydrogenase (acetylating)

$$\text{acetyl-SCoA} + \text{NADH} + \text{H}^+ \rightleftharpoons \text{acetaldehyde} + \text{NAD}^+ + \text{HSCoA} \quad (3\text{–}517)$$

and 4-hydroxy-2-oxovalerate aldolase

$$\text{acetaldehyde} + \text{pyruvate} \rightleftharpoons (S)\text{-4-hydroxy-2-oxopentanoate} \quad (3\text{–}518)$$

Together these active sites convert acetyl-SCoA, NADH, and pyruvate to NAD^+, coenzyme A, and (*S*)-4-hydroxy-2-oxopentanoate, as well as converting (*S*)-4-hydroxy-2-oxopentanoate, coenzyme A, and NAD^+ to pyruvate, NADH, and acetyl-SCoA. The multienzymatic complex in bacteria is a $\beta\alpha_2\beta$ heterotetramer. In crystallographic molecular models of the heterotetramers from *Pseudomonas*[1284] and *M. tuberculosis*,[1285] the two active sites for 4-hydroxy-2-oxovalerate aldolase are symmetrically displayed at the two ends of a rotationally symmetric α_2 homodimer that forms the core of the complex, and the two monomeric β subunits, each of which contains an active site for acetaldehyde dehydrogenase (acetylating), are noncovalently and symmetrically associated at the two ends of the central α_2 homodimer. Running between each active site on an α_2 dimer for 4-hydroxy-2-oxovalerate aldolase and an active site for acetaldehyde dehydrogenase (acetylating) on the adjacent β subunit is a tunnel. A number of observations support the conclusion that, in the multienzymatic complex for 4-hydroxy-2-oxovalerate aldolase and acetaldehyde dehydrogenase (acetylating) from *Paraburkholderia xenovorans*, which is homologous (54% identity; 0.6 gap percent) to that from *Pseudomonas*, the sole intermediate substrate for the sequential reactions, acetaldehyde, diffuses back and forth through this tunnel between the active sites at its two ends.[1286] This arrangement makes sense because acetaldehyde is a reactive molecule from which the cytoplasm should be protected.

In the case of two independent enzymes, amidophosphoribosyltransferase and phosphoribosylamine—glycine ligase, from *E. coli*, the intermediate substrate, 5-phospho-β-D-ribosylamine, is the product of the first enzymatic reaction that is used as a reactant in the second. The half life of 5-phospho-β-D-ribosylamine under the conditions in the cytoplasm of the bacterium is only 5 s, a fact that seems to demand channeling. In a solution containing both enzymes, the rate of production of the final product, N^1-(5-phospho-D-ribosyl)glycinamide, from the initial reactants chosen for the experiment, L-glutamine and 5-phospho-α-D-ribose 1-diphosphate, occurs without a lag. The small amount of 5-phospho-β-D-ribosylamine accumulated in the solution was significantly less than the amount necessary to explain the rate of the overall reaction.[1273] Both results are consistent with intramolecular channeling within a complex of the two enzymes, but no complex of the two could be observed under any circumstances. The results suggest that a transient complex forms during the enzymatic reaction to permit what seems to be a required channeling. In this instance, the intermediate substrate, 5-phospho-β-D-ribosylamine, is not harmful, but its hydrolysis is wasteful.

In addition to the lack of a lag in production of the ultimate product of a set of sequential reactions catalyzed by a multienzymatic complex and the lack of significant accumulation of intermediate substrates, **the lack of competition between two different intermediate substrates** is also evidence that channeling is involved in the mechanism. When a multienzymatic complex is able to turn two different reactants into two different products, the opportunity arises of using the two respective intermediate substrates to compete with each other for the second active site in the sequence of reactions.

For example, the multienzymatic complex for 4-hydroxy-2-oxovalerate aldolase and acetaldehyde dehydrogenase (acetylating) from *P. xenovorans*, in addition to being able to turn (*S*)-4-hydroxy-2-oxopentanoate into pyruvate and acetyl-SCoA (sum of Equations 3–518 and 3–517), is also able to turn (*S*)-4-hydroxy-2-oxohexanoate into pyruvate and propionyl-SCoA. With the former reactant, acetaldehyde is the intermediate substrate, and with the latter reactant, propionaldehyde is the intermediate substrate. When the reaction mixture contained the multienzymatic complex and 0.1 mM (*S*)-4-hydroxy-2-oxopentanoate and 1 mM propion-

aldehyde, in addition to coenzyme A and NAD^+, 95% of the product was acetyl-SCoA. When the reaction mixture contained 0.1 mM (*S*)-4-hydroxy-2-oxohexanoate and 1 mM acetaldehyde, 99% of the product was propionyl-SCoA.[1286] Clearly, the particular product of the active site for 4-hydroxy-2-oxovalerate aldolase, acetaldehyde in the former instance or propionaldehyde in the latter instance, is preferentially converted by the active site of acetaldehyde dehydrogenase (acetylating) into the respective acyl-SCoA. The best explanation for this observation is that the respective intermediate substrate is transferred through the tunnel observed crystallographically from one active site to the next while the alternative intermediate substrate in the solution, propionaldehyde or acetaldehyde, respectively, is almost entirely excluded from the tunnel and the active site for acetaldehyde dehydrogenase (acetylating).

It is also possible to conclude that channeling occurs by examining **the effect of a later reaction in the sequence on the first reaction in the sequence**. For example, for the multienzymatic complex for 4-hydroxy-2-oxovalerate aldolase and acetaldehyde dehydrogenase (acetylating) from *P. xenovorans*, the rate for the production of pyruvate, which normally dissociates into the solution from the active site for 4-hydroxy-2-oxovalerate aldolase (Equation 3–518) while the acetaldehyde is channeled, increases by a factor of 15 when NAD^+ and coenzyme A are added to an assay containing only (*S*)-4-hydroxy-2-oxopentanoate.[1286] The explanation for this observed increase in rate is that when NAD^+ and coenzyme A, the substrates for acetaldehyde dehydrogenase (acetylating), are missing, the acetaldehyde produced by the active site of 4-hydroxy-2-oxovalerate aldolase from (*S*)-4-hydroxy-2-oxopentanoate (Equation 3–518) piles up in the tunnel and, as a product, inhibits the turnover of the aldolase, so the rate-limiting step in the enzymatic reaction becomes the rate at which acetaldehyde leaks from the tunnel into the solution. Again, this result is consistent with the tunnel being quite effective at containing the acetaldehyde.

The **channeling efficiency** for an intermediate substrate or substrates being channeled through one of these cavities or tunnels among the active sites is the percentage of the initial reactant that is converted to the final product intramolecularly within the same multienzymatic complex relative to the total amount of initial reactant converted to final product both intramolecularly, by passing from one active site to the next within a molecule of the complex, and intermolecularly, by passing through the solution between active sites on different molecules of the complex.

The channeling efficiency for acetaldehyde through the tunnel in the multienzymatic complex from *P. xenovorans* has been assessed.[1287] In the presence of only acetyl-SCoA, pyruvate, and NADH, the reactants acetyl-SCoA and pyruvate are converted in one direction to (*S*)-4-hydroxy-2-oxopentanoate (sum of Equations 3–517 and 3–518). During this conversion, those molecules of acetaldehyde that are transferred intramolecularly through the tunnel between the two active sites never enter the solution because they are occluded from it by the tunnel. Those molecules of acetaldehyde, however, that leak out of the tunnel in one molecule of the multienzymatic complex enter the solution and, because they are free solutes, can be converted to ethanol by alcohol dehydrogenase

$$\text{acetaldehyde} + \text{NADH} + \text{H}^+ \rightleftharpoons \text{ethanol} + \text{NAD}^+ \quad (3\text{–}519)$$

from *S. cerevisiae* that has been added to the solution.

The initial rates observed in the two assays can be used to estimate the efficiency of channeling. The initial rate at which NADH is oxidized in the presence of the multienzymatic complex, pyruvate, and acetyl-SCoA and in the absence of alcohol dehydrogenase is a measure of the total amount of acetyl-SCoA converted to acetaldehyde at the active site for acetaldehyde dehydrogenase (acetylating) (Equation 3–517), the first step in the overall sequence. The initial rate at which NADH is oxidized in the presence of both the multienzymatic complex and alcohol dehydrogenase is a measure of that same rate of conversion of acetyl-SCoA to acetaldehyde in the active site for acetaldehyde dehydrogenase (acetylating) plus the rate at which acetaldehyde leaks into the solution and is immediately reduced by NADH to ethanol at the active site of alcohol dehydrogenase. The channeling rate is the difference between the initial rate at which acetaldehyde is produced from acetyl-SCoA at the active site of acetaldehyde dehydrogenase (acetylating) and the initial rate at which acetaldehyde leaks out of the multienzymatic complex and is converted to ethanol. The channeling efficiency is the channeling rate divided by the total rate at which acetaldehyde is produced. In this instance, the channeling efficiency was 84%.

The **channeling efficiency in the reverse reaction** has been estimated for the multienzymatic complex from *P. xenovorans* and the homologous (52% identity; 0.6 gap percent) multienzymatic complex from *T. thermophilus*.[1288] The assay contained (*S*)-4-hydroxy-2-oxopentanoate, coenzyme A, and NAD^+ in the presence of aldehyde dehydrogenase (NAD)

$$\text{acetaldehyde} + NAD^+ + H_2O \rightleftharpoons \text{acetate ion} + NADH + 2\,H^+ \quad (3\text{–}520)$$

from *S. cerevisiae* to convert any acetaldehyde leaking into the solution to acetic acid by oxidizing it with the NAD^+ already in the solution. Under these conditions, the initial rate at which acetaldehyde is produced from (*S*)-4-hydroxy-2-oxopentanoate at the active site of 4-hydroxy-2-oxovalerate aldolase (Equation 3–518) is the initial rate at which NAD^+ is oxidized in the presence of both the multienzymatic complex and aldehyde dehydrogenase (NAD) (Equation 3–517) because the acetaldehyde either passes through the tunnel and is converted to acetyl-SCoA at the active site for acetaldehyde dehydrogenase (acetylating) or leaks out of the multienzymatic complex into the solution and is converted to acetate. The initial rate at which the final product, acetyl-SCoA, was produced in the same assay was assessed by measuring acetyl-SCoA in the solution at the completion of the assay. The quotient between the initial rate for production of acetyl-SCoA and the initial rate for reduction of NAD^+ is the channeling efficiency. For the reverse reactions catalyzed by the multienzymatic complexes from *P. xenovorans* and *T. thermophilus*, the channeling efficiencies were 95% and 94%, respectively.

In the measurements of channeling efficiency for the multienzymatic complex of acetaldehyde dehydrogenase (acetylating) and 4-hydroxy-2-oxovalerate aldolase, alcohol dehydrogenase and aldehyde dehydrogenase (NAD) were used as scavengers for acetaldehyde. The **lack of an effect of a scavenger for the intermediate substrate** on the rate of the overall reaction catalyzed by a multienzymatic complex is consistent with channeling of the intermediate substrate out of contact with the solution. For example, a multienzymatic complex from *Moorella thermoacetica* has active sites catalyzing, respectively, anaerobic carbon monoxide dehydrogenase

$$CO_2 + 2\,H^+ + 2\,\text{ferredoxin}_{red} \rightleftharpoons 2\,\text{ferredoxin}_{ox} + H_2O + CO \quad (3\text{–}521)$$

and CO-methylating acetyl-CoA synthase

$$CO + \text{methylcorrinoid protein} + HSCoA \rightleftharpoons \text{corrinoid protein} + \text{acetyl-SCoA} + H^+ \quad (3\text{–}522)$$

Each active site is on a different subunit in the multienzymatic complex,[1289,1290] and they are far apart from each other. Carbon monoxide is the intermediate substrate in this sequence of consecutive reactions. When hemoglobin, which binds CO tightly, is added to the solution, there is no decrease in the rate at which acetyl-SCoA is produced from CO_2.[1274]

Another observation consistent with channeling of an intermediate substrate is the **lack of isotopic dilution**. If the addition of unlabeled intermediate substrate to the solution has little or no effect on the rate of incorporation of radioactive atoms from an initial reactant into a final product, when those radioactive atoms are confined to the portion of the initial reactant that produces the intermediate substrate, this lack of isotopic dilution from the solution is consistent with channeling of the intermediate substrate.[1291-1293] For example, unlabeled CO in solution has no effect on the rate at which carbon-14 from $[^{14}C]CO_2$ is incorporated into acetyl-SCoA by the multienzymatic complex from *M. thermoacetica* (Equations 3–521 and 3–522) or on the specific radioactivity of that acetyl-SCoA.[1292] This observation is consistent with an inability of CO to penetrate the tunnel.

Both the effect of the scavenger and the lack of isotopic dilution are consistent with transfer of CO from one active site to the other within the multienzymatic complex from *M. thermoacetica* rather than through the solution. The active site of anaerobic carbon monoxide dehydrogenase contains a [4Fe–4S–Ni] iron–sulfur–nickel cluster (previously **2–143**)

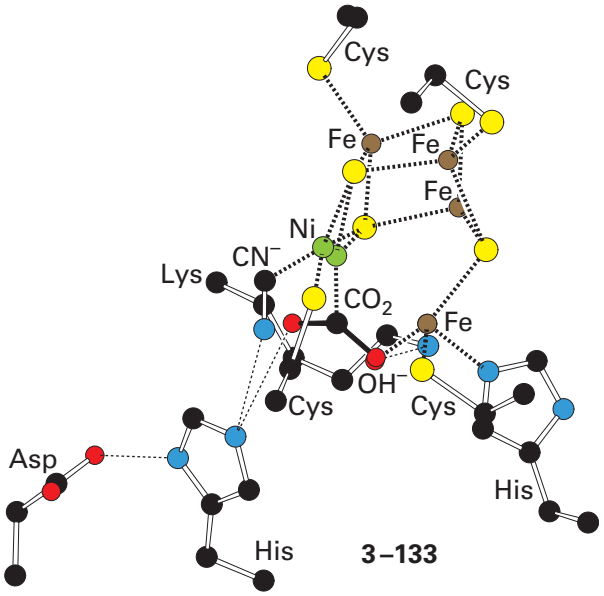

3–133

and the active site for CO-methylating acetyl-CoA synthase contains a dinuclear cluster of a copper ion and a nickel ion. Consequently, the two active sites are readily identified in a crystallographic molecular model. In the crystallographic molecular model of the multienzymatic complex,[1294] there is a tunnel 7.0 nm long that has been traced with xenon (Figure 3–69),[1271] through which it is believed that CO, produced from CO_2 in the active site of anaerobic carbon monoxide dehydrogenase, passes to the active site of CO-methylating acetyl-CoA synthase. The tunnel can be seen to wind its way through the center of the protein and also passes from one subunit to the other across the interface between them.

If the rate at which the final products are produced from the initial reactants for the first active site is considerably faster than the rate at which they are produced from the intermediate substrate when it is free in solution, this **preference for the intermediate substrate produced at the first active site** is consistent with channeling of the intermediate substrate.[1274,1284]

Tryptophan synthase is another multienzymatic complex in which the intermediate substrate does not have to enter the solution to be transferred between its two active sites. Tryptophan synthase is an $\alpha\beta_2\alpha$ heterotetramer.[717] The intact heterotetramer catalyzes the reaction

1-*C*-(indol-3-yl)glycerol 3-phosphate + L-serine $\rightleftharpoons$ L-tryptophan + D-glyceraldehyde 3-phosphate + H_2O

(3–523)

The isolated α subunit has an active site that catalyzes indole-3-glycerol-phosphate lyase (previously Equation 1–156)[1295]

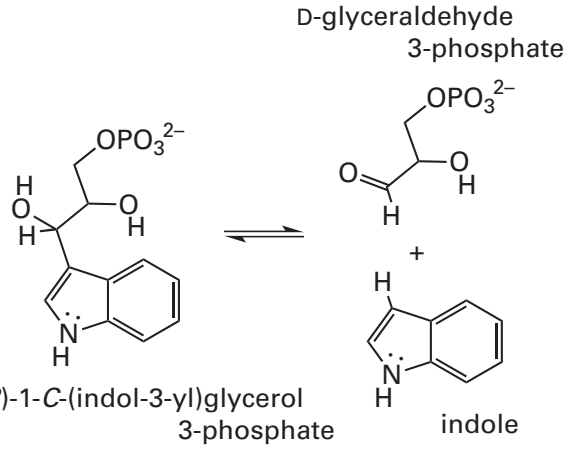

(3–524)

and the isolated β_2 homodimer has an active site that catalyzes tryptophan synthase (indole-salvaging) (previously Equation 2–20)[1295]

L-serine + indole $\rightleftharpoons$ H_2O + L-tryptophan

(3–525)

In the crystallographic molecular model of the $\alpha\beta_2\alpha$ heterotetramer from *S. typhimurium*,[717] the two monomeric α subunits are noncovalently and symmetrically associated, one at each end of the central, rotationally symmetric β_2 homodimer, in the same arrangement as the $\beta\alpha_2\beta$ heterotetramer of the multienzymatic complex for acetaldehyde dehydrogenase (acetylating) and 4-hydroxy-2-oxovalerate aldolase. In the crystallographic molecular model of the intact multienzymatic complex, the active site for indole-3-glycerol-phosphate lyase (Equation 3–524) has been located on the α subunit by soaking crystals in a solution of the competitive inhibitor 3-(indol-3-yl)propanol phosphate, and the active site for tryptophan synthase (indole-salvaging) (Equation 3–525) has been located on the β subunits by locating the pyridoxal phosphates present in the enzyme as prosthetic groups. The distance in the crystallographic molecular model between an active site on an α subunit and the closest active site on a β_2 homodimer is 2.5–3.0 nm.

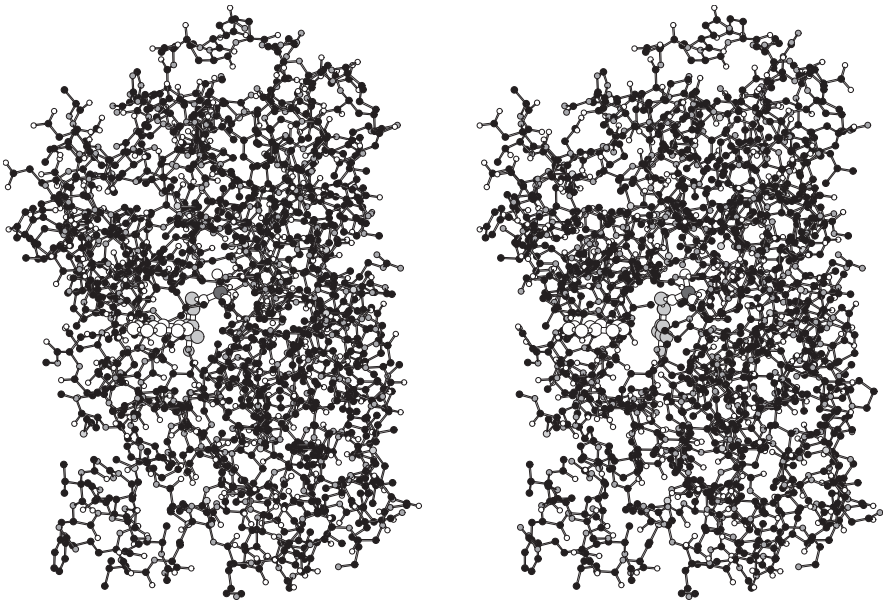

Figure 3–71: Stereodrawing[576] of one of the tunnels connecting the active sites for indole-3-glycerol-phosphate lyase (Equation 3–524) and tryptophan synthase (indole-salvaging) (Equation 3–525) in multimeric tryptophan synthase complex from *S. typhimurium*.[1296] Black atoms are carbons, white atoms are oxygens, small gray atoms are nitrogens, and large light gray atoms are sulfurs. The crystallographic molecular model from which the drawing was made is for crystals of the conformation that tryptophan synthase assumes in the presence of K^+, which should be the conformation that exists in the cytoplasm. Indole is released at the active site for indole-3-glycerol-phosphate lyase, and the location at which it is released has been located in the α subunit in the crystallographic molecular model of the complex between tryptophan synthase and the inhibitor 3-(indol-3-yl)propanol phosphate.[717] A molecule of indole (white atoms and white bonds at the top of the tunnel) has been drawn occupying the location of the indolyl group in that model. At the bottom of the tunnel is the pyridoxal phosphate (gray atoms and gray bonds that can be located by its phospho group) occupying the active site for tryptophan synthase (indole-salvaging) in the β subunit of the model of the potassium conformation from which the rest of the drawing is made. The indole has to slide under a proline at the top of the tunnel and also has to push aside the side chain of a leucine near the top. From there on, the tunnel is open, leading straight to the pyridoxal phosphate. The active site for indole-3-glycerol-phosphate lyase is in the α subunit at the interface with the β subunit, and most of the tunnel passes from the interface through the middle of the β subunit.

In the crystallographic molecular model, two symmetrically arrayed tunnels pass through the protein. Each tunnel is 2.5 nm long and connects the active site for indole-3-glycerol-phosphate lyase on an α subunit with an active site for tryptophan synthase (indole-salvaging) on a β subunit (Figure 3–71).[717,1296] Each tunnel is enclosed along its length on all sides by protein and is wide enough to permit molecules of the intermediate substrate indole to pass through. These tunnels are much shorter and straighter than the tunnel in the multienzymatic complex for anaerobic carbon monoxide dehydrogenase and CO-methylating acetyl-CoA synthase (Figure 3–69). In the crystallographic molecular model of tryptophan synthase with the inhibitor 3-indolylpropanol phosphate occupying the active sites for indole-3-glycerol-phosphate lyase in the α subunits, the indolyl group is in the bottom of each active site, as far from the solution as possible, and sitting at the opening of the tunnel for that active site. Upon cleavage of the normal initial reactant, 1-*C*-(indol-3-yl)glycerol 3-phosphate, the indole would be released at this location in the active site, and it would be hindered from being released into the solution but not from entering the adjacent tunnel. These details suggest that the indole feeding the active site on a β subunit during the overall reaction (Equation 3–523) is transferred between the two active sites through this tunnel. There are a number of observations verifying the proposal that each of the two tunnels is a **tunnel for indole**.

In the absence of L-serine, intact tryptophan synthase from *Neurospora crassa* produces indole from 1-(indol-3-yl)glycerol 3-phosphate, but the rate at which indole appears in solution is 50 times slower than the rate at which L-tryptophan is produced by the intact multienzymatic complex from 1-(indol-3-yl)glycerol 3-phosphate and L-serine under the same circumstances.[1297,1298] When L-serine is present, indole is no longer produced by the multienzymatic complex from 1-(indol-3-yl)glycerol 3-phosphate. During a reaction in which 100 nmol of L-tryptophan was produced from 1-(indol-3-yl)glycerol 3-phosphate and L-serine, no indole was released into the solution (<2 nmol). An explanation for these kinetic observations is that when L-serine is absent and an active site for tryptophan synthase (indole-salvaging) is not operating, indole piles up in the tunnels and acts as a product inhibitor of indole-3-glycerol-phosphate lyase. Indole can escape from a tunnel into the solution, but only slowly, and this escape is the rate-limiting step in its production in the absence of L-serine. When L-serine is present, all the channeled indole is immediately transformed into L-tryptophan. Indole does not pile up in the tunnels, and it does not have time to leak out of them before it is converted into L-tryptophan.

If indole is transferred between the two active sites through the affiliated tunnel, the **mutation of an amino acid in the wall of the tunnel that sterically blocks it** should prevent the transfer. Under normal circumstances, when 1-*C*-([^{14}C]indol-3-yl)-glycerol 3-phosphate and L-serine are converted in a single turnover to L-[^{14}C]tryptophan by a molar excess of tryptophan synthase, no [^{14}C]indole can be detected (<1%). If Cysteine 170 in the β subunit of tryptophan synthase, which is in the wall of the tunnel, is mutated to a tryptophan, the rate of synthesis of L-[^{14}C]tryptophan from 1-*C*-([^{14}C]indol-3-yl)-glycerol 3-phosphate and L-serine during a single turnover decreases by a factor of 30, and [^{14}C]indole can be detected (10%).[1299] In addition, the rate of synthesis of L-tryptophan from L-serine and indole, rather than 1-*C*-(indol-3-yl)glycerol 3-phosphate, is decreased 20-fold in the mutant, a result that is consistent with indole entering the enzyme from solution only from the end of a tunnel (Figure 3–71) at the active site on an α subunit, which is the location where indole is normally produced (Equation 3–524).

If indole is able to **enter a tunnel only through an active site** on an α subunit and from there pass through the tunnel and enter the active site on the β subunit (Equation 3–525) at the end if the tunnel, this requirement would explain an observation that might seem inconsistent with the channeling of indole between the two active sites. When 1-*C*-([2-^{14}C]indol-3-yl)glycerol 3-phosphate is used as a reactant in the presence of L-serine, L-[2-^{14}C]tryptophan is produced by tryptophan synthase, and no [2-^{14}C]indole is released into the solution.[1300] If, however, a large enough concentration of nonradioactive indole is added to the solution, the rate of production of L-[2-^{14}C]tryptophan decreases remarkably, and significant amounts of [2-^{14}C]indole are released into the solution. As the concentration of nonradioactive indole is increased, the rate of production of L-[2-^{14}C]tryptophan decreases, and the rate of production of [2-^{14}C]indole in solution increases. One explanation for this observation would be that as a tunnel becomes filled with indole that has entered it from solution through the active site on an α subunit while that active site was temporarily empty, the [2-^{14}C]indole produced at that active site by the reaction in Equation 3–524 will dissociate into the solution because it is unable to move

through the overcrowded tunnel. Consistent with this explanation is the fact that, in the intact enzyme, indole from the solution is able to react rapidly with the α-aminoacrylate intermediate (previously Equation 2–14)

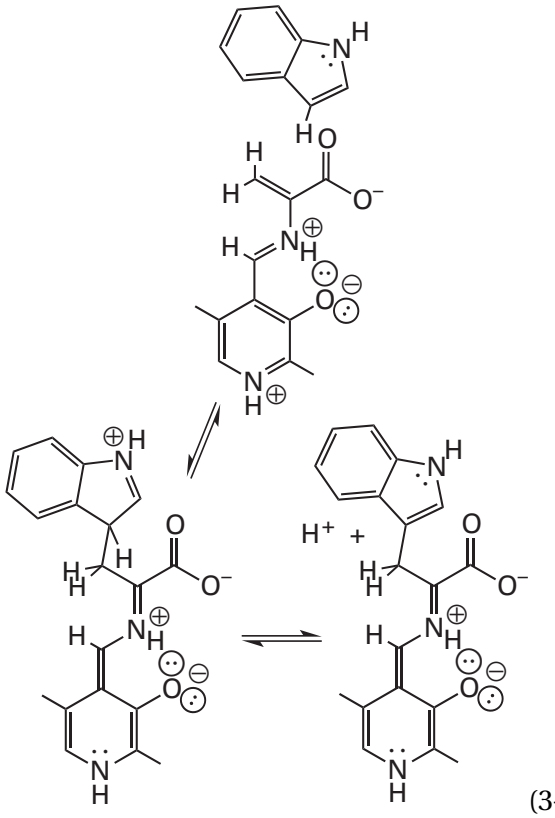

(3–526)

formed in the active site on a β subunit (200 s^{-1} at saturation). When, however, glyceraldehyde 3-phosphate is bound at the active sites on the α subunits, blocking the indole from entering the tunnel between the active sites, the rate of this reaction with indole is dramatically inhibited (10 s^{-1}).[1301]

Ammonia is a toxic metabolite, but it is necessary for a large number of biosynthetic reactions. This conflict is resolved by converting ammonia to L-glutamine in the reaction catalyzed in the cytoplasm of all cells by glutamine synthetase

$$NH_4^+ + MgATP^{2-} + \text{L-glutamate} \rightleftharpoons MgADP^- + H_2PO_4^- + \text{L-glutamine} \quad (3\text{–}527)$$

and then releasing the ammonia at the locations where it is needed in a hydrolysis catalyzed by glutaminase

$$\text{L-glutamine} + H_2O \rightleftharpoons \text{L-glutamate} + NH_4^+ \quad (3\text{–}528)$$

Because these two enzymes, when functioning consecutively, would catalyze the hydrolysis of $MgATP^{2-}$, the ammonia produced by glutaminase cannot be released into the cytoplasm, or it would create an ATPase that consumes energy but accomplishes nothing. Consequently, there are a large number of multienzymatic complexes in which an active site for glutaminase is combined with an active site for a particular biosynthetic reaction that has ammonia as one of its reactants. For example, the active site for

$$\text{D-fructose 6-phosphate} + NH_3 \rightleftharpoons H_2O + \text{D-glucosamine 6-phosphate} \quad (3\text{–}529)$$

is combined with an active site for glutaminase in the multienzymatic complex glutamine—fructose-6-phosphate transaminase (isomerizing), which catalyzes the overall reaction

$$\text{D-fructose 6-phosphate} + \text{L-glutamine} \rightleftharpoons \text{L-glutamate} + \text{D-glucosamine 6-phosphate} \quad (3\text{–}530)$$

In the biosynthetic reaction, an acceptor for the ammonia, such as D-fructose 6-phosphate, is the nominal substrate, as in glutamine-fructose-6-phosphate transaminase (isomerizing). In these multienzymatic complexes, the two active sites are connected by a **tunnel through which ammonia is transferred** between them.[954,1302-1308] These tunnels for ammonia vary in length from 1.5 to 4.5 nm.[1302]

Because ammonia rarely, if ever, enters or escapes from the tunnel before it is incorporated into the final product, the two reactions are tightly coupled. For example, glutamine-fructose-6-phosphate transaminase (isomerizing), both from *E. coli* and from *R. norvegicus*, catalyzes, within the error of the measurement,[1309] a **completely stoichiometric reaction** (Equation 3–530). If ammonia were to escape from the tunnel, the reaction would not be stoichiometric. The overall reaction is the sum of Equations 3–528 and 3–529, and these two reactions are catalyzed at two distinct active sites on the multienzymatic complex.[1302] Ammonia cannot substitute for L-glutamine.[1309] If ammonia cannot leak

out of the tunnel, by microscopic reversibility, it cannot leak in.

In several amidotransferases, the tunnel for ammonia is formed by a conformational change in the enzyme that is coupled to association of the acceptor for ammonia at its active site or coupled to simultaneous association of glutamine at the active site of glutaminase and association of the acceptor for ammonia at its active site.[953,954,1305,1310-1312] This **induced fit** presumably serves the usual purpose of ensuring that none of the dangerous steps in the reaction, such as the glutaminase reaction (Equation 3–528) or a step activating the acceptor for ammonia, is able to occur until **all the reactants are bound to their respective active sites**.

Such induced fits are common features of multienzymatic complexes that transfer intermediate substrates through tunnels between distant active sites. For example, in tryptophan synthase, the association of 1-*C*-(indol-3-yl)glycerol 3-phosphate with the active site on an α subunit (Equation 3–524) induces a conformational change that **opens the active site** on the affiliated β subunit so that L-serine can associate.[1313] Subsequent formation of the aminoacrylate at the pyridoxal phosphate from L-serine in the active site on a β subunit (Equations 3–525 and 3–526) then induces a conformational change that enhances cleavage of 1-*C*-(indol-3-yl)glycerol 3-phosphate at the active sites on the affiliated α subunit by a factor of 30.[1314,1315]

Carbamoyl-phosphate synthase (glutamine-hydrolysing) is a multienzymatic complex composed of two subunits. The smaller of the two (382 aa) is glutaminase, which hydrolyzes L-glutamine to produce the ammonia that is an intermediate substrate

$$H_2O + \text{L-glutamine} \rightleftharpoons \text{L-glutamate} + NH_3 + H^+ \quad (3\text{–}531)$$

The larger subunit (1073 aa) contains the two active sites

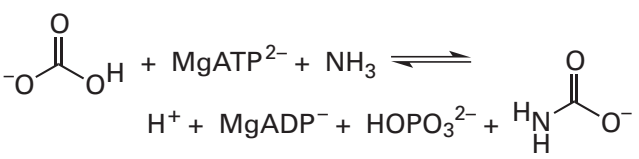

(3–532)

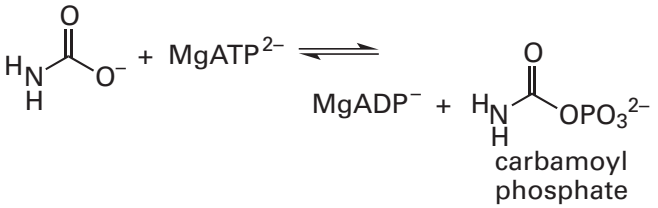

(3–533)

on two separate structural domains that are responsible for the synthesis of carbamoyl phosphate from that ammonia.[1316,1317] [^{14}N]Ammonia produced at the glutaminase within the multienzymatic complex from *E. coli*, rather than the [^{15}N]ammonium added to the solution, is the almost exclusive (>95%) reactant for the second reaction,[1291] so it must be channeled. The half life for hydrolysis of carbamate at 25 °C is 28 ms,[1318] so it cannot come into contact with surrounding solution. Because the stoichiometry of the overall reaction

$$HCO_3^- + \text{L-glutamine} + 2\,MgATP^{2-} + H_2O \rightleftharpoons \text{L-glutamate} + 2\,MgADP^- + HOPO_3^{2-} + H_2NCOOPO_3^{2-} + 2\,H^+ \quad (3\text{–}534)$$

catalyzed by the multienzymatic complex is precise, within the error of measurement,[1319] ammonia must be channeled without loss between the first two active sites (Equations 3–531 and 3–532) and carbamate must be channeled, without being hydrolyzed, back and forth between the second and third active sites (Equations 3–532 and 3–533).

In the crystallographic molecular model of the enzyme from *E. coli*, a tunnel runs between the active site for the glutaminase (Equation 3–531) on a smaller subunit and the active site in the adjacent larger subunit at which carbamate is synthesized (Equation 3–532). These two active sites are 4.5 nm apart. The tunnel then continues on to the active site at which carbamoyl phosphate is synthesized (Equation 3–533), which is another 3.5 nm away.[1320] Even though it is longer (9.6 nm) because it has to service three active sites, this tunnel resembles the tunnel (7.0 nm) in the multienzymatic complex containing the active sites for anaerobic carbon monoxide dehydrogenase and CO-methylating acetyl-CoA synthase in its bends and changes of direction (Figure 3–69) and in the fact that it also passes through an interface between two subunits. As a measure of its tortuosity, each tunnel is about 20% longer than the linear distance between the active sites that it services. The tunnel in carbamoyl-

phosphate synthase (glutamine-hydrolysing) is, however, somewhat more deeply buried in the center of the protein.

The results of site-directed mutation confirm that the intermediate substrates for carbamoyl-phosphate synthase (glutamine-hydrolysing) do move through the tunnel in the enzyme. When the tunnel for ammonia is blocked within the smaller subunit of the enzyme by mutating Glycine 359 on its wall to phenylalanine, the catalytic constant for synthesis of carbamoyl phosphate from L-glutamine decreases 70-fold.[1321,1322] When the tunnel for ammonia is blocked within the larger subunit by mutating Cysteine 232, Alanine 251, and Alanine 314 on its wall to valines, the catalytic constant for synthesis of carbamoyl phosphate from L-glutamine decreases more than 500-fold.[1323] When a hole to the solution is made in the tunnel for ammonia by mutating Proline 360 and Histidine 361 in the smaller subunit and Arginine 265 in the larger subunit to alanines, the catalytic constant for synthesis of carbamoyl phosphate from L-glutamine decreases 300-fold.[1324] And when the **tunnel for carbamate** within the larger subunit is blocked at its two narrowest points by mutating Alanine 23 to phenylalanine, Glycine 575 to phenylalanine,[1325] or both Alanine 23 and Glycine 575 in its wall to leucines,[1326] the catalytic constant for synthesis of carbamoyl phosphate decreases by 60-fold, 25-fold, and more than 500-fold, respectively.

The possibility that channeling of an intermediate substrate between two distant active sites across the surface of a multienzymatic complex could occur by **entrapment of the substrate in the ionic double layer*** surrounding the protein, rather than in a tunnel, has been proposed to explain the channeling observed in multienzymatic complexes from *Leishmania tropica* and *T. gondii*, which both contain active sites for thymidylate synthase

$$\text{5,10-methylenetetrahydrofolate} + \text{dUMP} \rightleftharpoons \text{dTMP} + \text{7,8-dihydrofolate} \quad (3\text{–}535)$$

and dihydrofolate reductase

$$\text{NADPH} + \text{7,8-dihydrofolate} + \text{H}^+ \rightleftharpoons \text{5,6,7,8-tetrahydrofolate} + \text{NADP}^+ \quad (3\text{–}536)$$

for which the intermediate substrate is 7,8-dihydrofolate. There is no lag in production of $NADP^+$ in the latter reaction when 7,8-dihydrofolate is produced at the former active site from 5,10-methylenetetrahydrofolate,[1328,1329] and there is no accumulation of tritium-labeled intermediate substrate 7,8-dihydrofolate when tritium-labeled 5,10-methylenetetrahydrofolate is converted to tritium-labeled 5,6,7,8-tetrahydrofolate by the two active sites[1329,1330] operating consecutively. These two facts are consistent with tightly coupled channeling. There is, however, no obvious tunnel between the two active sites, which are 4.0 nm apart in crystallographic molecular models of the multienzymatic complexes.[1329,1331]

The fixed ionic layer of charged side chains of amino acids on the surface of the multienzymatic complex between the active sites for thymidylate synthase and dihydrofolate reductase in the crystallographic molecular model is dramatically enriched in positively charged side chains, which would produce an ionic double layer in which the outer ionic layer is enriched in mobile negative ions. Consequently, dihydrofolate, a dianion, could be confined within the double layer and be transferred through the double layer between the active sites. The experiment in which apparent channeling was observed was performed in a solution of 25 mM $MgCl_2$ (I = 75 mM). Unfortunately, the effect of increasing ionic strength on the channeling efficiency was not assessed. An increase in ionic strength should eliminate channeling within the double layer.[1332] Mutating six of the arginines and lysines between the two active sites, however, to neutral amino acids did not decrease the channeling efficiency,[1333] a result inconsistent with channeling through the double layer. Consequently, the mechanism by which channeling occurs in this multienzymatic complex is unknown.

Many enzymes catalyze reactions that have homopolymers as their reactants, and some of these enzymes have active sites that perform successive reactions on successive segments of the polymer without dissociating from it.[1334] In such an enzyme, the active site is transferred from one monomer of the polymer to the next monomer of that polymer rather than a monomer of the polymer

*The layer of fixed charges on a macromolecule induces counterions of the opposite charge, such as a channeled substrate that is oppositely charged, to become concentrated in the layer of solution surrounding the macromolecule. These two layers, the layer of fixed charges and the layer of mobile charges of the opposite sign, comprise the ionic double layer.[1327]

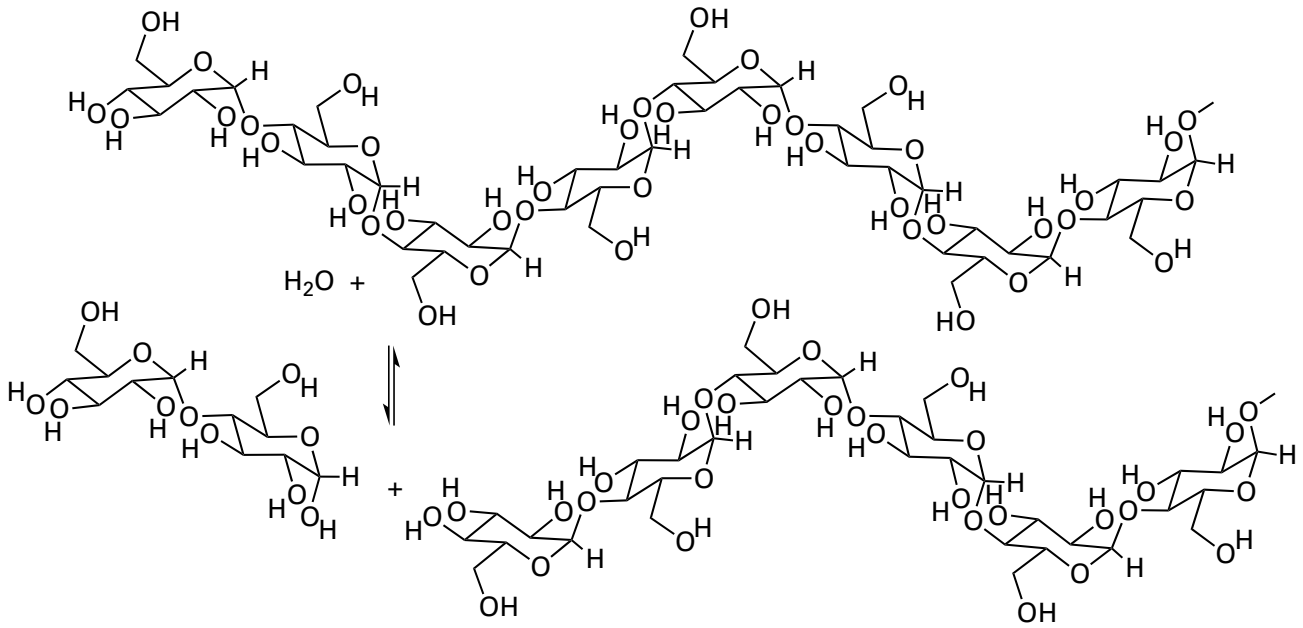

Figure 3–72: Hydrolysis of $(\alpha 1,4)$-glucose$_n$ by β-amylase.

being transferred from one active site to the next active site. For example, β-amylase from *G. max* is an exoglycosidase that hydrolyzes the linear polymer $[(\alpha 1,4)$-D-glucose$]_n$ from the nonreducing end at every other glycosidic linkage to release molecules of maltose (Figure 3–72).[1335] About half the time, the enzyme remains associated with the same molecule of $[(\alpha 1,4)$-D-glucose$]_n$ from which it just released a maltose and releases the next maltose from that same molecule.[1336]

DNA-Directed DNA polymerase catalyzes the alignment with the template of the next 2′-deoxyribonucleoside 5′-triphosphate to be added to an elongating strand of DNA, ensures that the proper base pair is formed between it and the next nucleotide in the template,[1337] and then catalyzes the nucleophilic substitution at phosphorus that attaches the next nucleotide to the elongating strand. The enzyme adds a number of nucleotides to the elongating strand before it dissociates from a particular elongating segment of DNA. The steps in the reaction are association and alignment of the correct 2′-deoxyribonucleoside 5′-triphosphate, nucleophilic substitution at phosphorus, and shifting of the duplex of template and elongating strand by a distance of one base pair to bring the 3′-hydroxy group of the added nucleotide into the position where the 3′-hydroxy group of the initial reactant was located to initiate the next round of elongation. The kinetics of these three steps have been assessed with the DNA-directed DNA polymerase encoded by Escherichia phage T7 at 20 °C. Following association of the 2′-deoxyribonucleoside 5′-triphosphate, there is a slow (0.3 ms^{-1}) conformational change preceding the chemical step, thought to ensure that the correct 2′-deoxyribonucleoside 5′-triphosphate has been properly aligned.[1338] The next step is rapid (>9 ms^{-1}) nucleophilic substitution at phosphorus followed by shifting of the product of elongation in the active site (1.2 ms^{-1}) to position the 3′-hydroxy group that will be the reactant for the next cycle.[1004]

In a **processive reaction**, the active site of an enzyme[1334] catalyzes a reaction within a particular segment of a linear homopolymer and then moves, without dissociating, to the adjacent segment of that homopolymer to catalyze the same reaction within the next segment. If the **processive enzyme** removes segments from one end of the polymer, it moves to the newly created end to remove the next segment and so forth, as in the case of β-amylase (Figure 3–72). If the processive enzyme adds segments to one end of the polymer, it moves to the new end and adds a new segment to the new end and so forth, as in the case of DNA-directed DNA polymerase.

The **processivity** of a reaction catalyzed by a processive enzyme is the ratio between the rate at which the active site moves to the next segment of the polymer and completes its catalysis of the reaction at that location and the rate at which the polymer dissociates from the enzyme. The processivity of the enzyme can be determined by measuring directly the rate at which the enzyme catalyzes the

reaction while bound to the polymer and the rate at which it dissociates from the polymer.[1339] It can also be determined by assessing the distribution of lengths in the final product as a function of the degree to which the reaction has proceeded.[1336] The processivity of β-amylase from *G. max* is 0.55,[1336] that for DNA-directed DNA polymerase β from *R. norvegicus* is 30,[1339] and that for DNA-directed DNA polymerase from Escherichia phage T7 is 1500.[1004] The distribution of products as a function of time can be fit to equations simulating that distribution as a function of the numerical value for the processivity.[1340] The best fit provides an estimate of the processivity.

In the case of the DNA-directed DNA polymerases, the processivity depends on conditions of the assay such as concentration of Mg^{2+}, the temperature, or the presence of polyamines normally present in cytoplasm.[1341] Because DNA and RNA bear significant net negative charge and because associations of proteins with nucleic acids often involve ionic interactions, when either DNA or RNA is the polymer on which the enzyme acts, the processivity of depolymerization or polymerization is often a function of the ionic strength of the solution. Uracil-DNA glycosylase from *E. coli* was perfectly processive at low ionic strength (<30 mM), but when the ionic strength was increased into the cytoplasmic range, the enzyme was significantly less processive.[1342] The processivity of many other processive enzymes probably depends on the conditions of the assay as well. Consequently, the actual processivity of a given enzyme in the cytoplasm of the cell may be considerably different from that measured in an artificial assay.

In addition to measuring the numerical value for the processivity, a test for determining whether or not an enzyme is processive is to add a form of the polymer that can be experimentally distinguished from the polymer on which the enzyme has initiated its reaction and assess whether or not the addition of the competitor changes the rate of the reaction on the original substrate by drawing enzyme away from the polymer on which it is processing.[1343] This approach is analogous to the addition of a scavenger to assess channeling.

A **nonprocessive enzyme** catalyzes a distributive reaction. In a **distributive reaction,** an active site catalyzes a reaction within a particular segment of a linear homopolymer—be it a cleavage of the polymer beyond that segment, the addition of a new segment to that segment, or simply a chemical alteration of that segment— by associating from solution before and dissociating into the solution after the catalytic event within that segment. The dissociated products, either one monomer shorter, one monomer longer, or altered in the one position, become indistinguishable from all the other polymers in solution, and the enzyme then associates at random with another polymer. If the enzyme is nonprocessive, there is no transfer of the active site from one position in the polymer to the next position.

A **perfectly processive enzyme** shortens, elongates or otherwise modifies a polymer without dissociating from it. When, however, a perfectly processive enzyme is operating in a finite environment, as is always the case, the numerical value for its processivity can never be infinity. Because the mean length of a polymer that is being depolymerized is finite, if an enzyme depolymerizing that polymer is perfectly processive, the numerical value for the processivity is equal to the mean length of the polymer. The enzyme can only shorten the polymer until it reaches its end. Because the concentration of the monomer being polymerized is finite, if an enzyme polymerizing a polymer is perfectly processive, the numerical value for the processivity is equal to the concentration of monomeric precursor in solution divided by the concentration of enzyme. The enzyme can only elongate the polymer until the monomers in solution run out.

During a perfectly processive depolymerization, polymers in the solution that are unassociated with a molecule of enzyme remain unaltered until polymers being shortened by the enzyme are completely depolymerized and molecules of the enzyme become available to shorten other polymers. For example, a molecule of exoribonuclease II from *E. coli* rapidly hydrolyzes a molecule of polyadenylic acid exonucleolytically from its 3′ end with complete processivity down to a small oligonucleotide from which the enzyme slowly dissociates, and then it associates with another molecule of polyadenylic acid and processively hydrolyzes it. As the reaction progresses, only intact, undegraded polyadenylic acid, adenosine monophosphate, and these small oligonucleotides are present at significant concentrations in the solution in addition to the enzyme.[1334,1344] The exosome from *S. cerevisiae* is also a perfectly processive exoribonuclease II. When single-stranded RNA labeled with a [^{32}P]phospho group at its 5′ end is mixed with the enzyme, the intact polymer gradually disappears and the only product that can be observed while the polymer is disappearing is the free [^{32}P]mononucleotide that was once on the 5′ end. It can be concluded from this observation that the

rate-limiting step in the processive hydrolysis of single-stranded RNA is its threading through the long tunnel that passes through the center of the protein. Once its 3′ end reaches the active site at the end of the tunnel, the enzyme processively hydrolyzes all the nucleotides in the RNA, one after the other from the 3′ end to the 5′ end, so rapidly that no shorter single-stranded ribonucleic acids can be observed.[1345]

During a perfectly processive polymerization, a molar concentration of polymer equal to the molar concentration of enzyme is continuously elongated until the reactant in the solution providing the monomers runs out while the remainder of the polymer in solution remains unaltered. In the case of nucleic acid polymerases, however, when they are elongating a strand of nucleic acid on a template, as long as there are sufficient nucleoside triphosphates in the solution, a perfectly processive enzyme continues to polymerize until a termination site is reached, at which point the completed polymer dissociates from the active site, leaving the enzyme free to initiate polymerization on another template.

Following a completed depolymerization or polymerization, a perfectly processive enzyme can remain associated for a significant interval with a final product. When DNA helicase I from *E. coli* is mixed with a duplex DNA 343 nucleotides long that is present in molar excess over the concentration of enzyme, the percentage of DNA unwound at the completion of the reaction is directly proportional to the concentration of enzyme.[1346] If the helicase dissociated from the unwound DNA, all the DNA would be unwound by the end of the reaction.

In most enzymes that catalyze processive reactions, at least five monomers in the intact polymer occupy consecutive subsites adjacent to the catalytic site within the active site at which the specific addition or subtraction of a monomer is catalyzed. These successive subsites can be in a groove on the surface of the protein, but usually they are within a tunnel into or out of the active site. For example, cellulose 1,4-β-cellobiosidase (reducing end) Cbh1, a cellulase from *H. jecorina*, hydrolyzes a strand of cellulose, $[(\beta 1,4)$-D-glucose$]_n$, releasing the disaccharide cellobiose from the reducing end of the polymer. Once it associates with the reducing end of a strand of $[(\beta 1,4)$-D-glucose$]_n$ protruding from the surface of solid crystalline cellulose from *Cladophora*, the enzyme proceeds down the polymeric strand[1195] with a processivity of 70 ± 40. In the crystallographic molecular model of the enzyme,[1347,1348] there is a tunnel occupied by the reducing end of the polymer of $[(\beta 1,4)$-D-glucose$]_n$ as it is being hydrolyzed. In this tunnel, there are nine subsites for the association of D-glucosyl monomers in the polymer. Two of these subsites are to the reducing side of the point of hydrolysis. Rapid diffusion of the reducing end of the polymer up the tunnel into these two subsites, after the cellobiose from the previous hydrolysis has dissociated as a product from them and before the next hydrolysis can occur, causes the enzyme to release cellobiose instead of individual molecules of D-glucose. In the case of β-amylase, there are also two subsites beyond the location at which the glycosidic hydrolysis is catalyzed, so two glucosyl groups on the nonreducing end of the $[(\alpha 1,4)$-D-glucose$]_n$ produced in the previous hydrolysis diffuse rapidly into those sites as the disaccharide maltose, the product of the previous hydrolysis (Figure 3–72), dissociates from them, and this movement aligns the next glycosidic linkage in the proper position.[1336]

At the entrance to the tunnel in cellulose 1,4-β-cellobiosidase (reducing end) Cbh1 from *H. jecorin*, distant from the active site, there are two tryptophans in the sequence –ANWRWTHA– that stack upon the hydrophobic faces of the first and fourth D-glucosyl groups in from the opening of the tunnel (see Figure 3–45). When one of these tryptophans is mutated to alanine,[1348] the rate at which the enzyme hydrolyzes 4-methylumbelliferyl-D-lactoside, a monomeric substrate, is unaffected, but the rate at which it hydrolyzes crystalline cellulose when it is associated with the surface of this solid decreases by a factor of 7. This result suggests that the two tryptophans that stack upon the two respective D-glucosyl groups at the entrance of the tunnel are involved in recruiting individual substrate chains into the tunnel to initiate processive hydrolysis, or facilitating movement of the polymer through the tunnel by providing flat surfaces on which $[(\beta 1,4)$-D-glucose$]_n$ can slide, or both of these effects. A completely unrelated enzyme that catalyzes the same processive reaction, cellulose 1,4-β-cellobiosidase (reducing end) CelCCF from *Ruminiclostridium cellulolyticum*,[1349,1350] also has two tryptophans in the unrelated sequence –STWSWII– at the entrance of its tunnel for $[(\beta 1,4)$-D-glucose$]_n$ stacked upon the first and the third D-glucosyl monomers in the polymer occupying the tunnel.[1349,1350]

The **tunnels into or out of an active site are significant factors in ensuring the processivity** of the depolymerization or polymerization catalyzed by an enzyme. For example, consider the long tunnel

(16 nm) of the exosome, a perfectly processive enzyme, that can accommodate 25 nucleotides in the RNA that is its reactant.[1062] If single-stranded RNA is able to thread through the tunnel to the active site, by microscopic reversibility, it must be able to unthread from the tunnel. Suppose that the active site has just hydrolyzed the 5′-phosphodiester of the nucleotide at the 3′ end of a strand of RNA in the tunnel and disconnected it from the rest of the reactant. As the nucleoside 5′-phosphate is dissociating as a product from the active site, the single-stranded RNA in the tunnel is undergoing **linear diffusion in a one-dimensional random walk up and down the tunnel**, but it is highly unlikely that it will unthread all the way out of the tunnel before the nucleotide on the new 3′ end diffuses during its random walk into the now-empty active site and is hydrolyzed, and so forth. In other words, the **tunnel is so long that its length alone traps the polymer** and prevents it from leaving the tunnel before the next monomer can be processed by the active site, even though it is free to diffuse in a random walk up and down the tunnel.

A polymer of cellulose, the product of a polymerization, also threads its way through a long tunnel (6 nm) away from the active site in cellulose synthase.[1064] Suppose that the active site has just transferred the next D-glucopyranose from a molecule of UDP-α-D-glucose to the 4-hydroxy group at the end of the elongating $[(1\rightarrow4)$-β-D-glucosyl$]_n$. The now-elongated cellulose diffuses linearly in a one-dimensional random walk up and down the tunnel. While the D-glucose at the nonreducing end of the elongated strand of cellulose has vacated the active site as a result of this random walk, it is replaced by the D-glucopyranose from another molecule of UDP-α-D-glucose, but it is highly unlikely that the strand of cellulose, which is free to leave, will unthread all the way out of the tunnel before its nonreducing end stumbles in its random walk into the active site now occupied by the UDP-α-D-glucose, and the next D-glucose is added to it, and so forth.

Exodeoxyribonuclease (lambda-induced) from Escherichia phage lambda performs the hydrolysis from the 5′ end of a shorter strand of DNA in a duplex with a much longer strand of DNA that extends beyond the 5′ end of a shorter strand. The enzyme is perfectly processive, completely hydrolyzing the shorter strand to its 3′ end.[1351] The enzyme is a rotationally symmetric trimer with a tunnel that runs along the threefold rotational axis of symmetry and is large enough to accommodate a double-stranded duplex at one end and a single strand of DNA at the other end.[1352] In the crystallographic molecular model of the complex between an inactive mutant of the enzyme and a double-stranded DNA in which the longer strand continues two nucleotides beyond the 5′ end of the shorter strand, nine base pairs in the double-stranded portion of the DNA occupy the larger end of the tunnel, and the two nucleotides at the 3′ end of the longer strand are on their way out of the narrower end of the tunnel.[1353] The tunnel for the double-stranded DNA does not seem long enough to ensure perfect processivity, but in this instance, because the unhydrolyzed single strand of DNA exits the tunnel as the enzyme hydrolyzes the other strand, the enzyme would **remain attached to this single strand** even if the nine base pairs of double-stranded DNA were to diffuse away from the wider portion of the tunnel. The random walk of the single strand would eventually bring the 3′ end of the double strand back to the active site for the next hydrolysis.

In the proteosome from *S. cerevisiae*, there is not a tunnel leading to the active site. In this instance, the ubiquinylated polypeptide being degraded processively feeds into a large central cavity surrounded by the active sites for the peptidases that hydrolyze it.[1354] In this instance, in addition to the random walk of monomers in the polymer in and out of the entrance to the cavity, the length of the polymer that has already entered allows the random walk at the door to continue without dissociation, a situation resembling that of exodeoxyribonuclease (lambda-induced).

Another significant factor, which is often cited, in promoting processivity is **whether or not the reaction is exergonic**. Consider, for example, a DNA-directed DNA polymerase. As each magnesium 2′-deoxyribonucleoside 5′-triphosphate enters the active site and its base pairs with the complementary base on the template, its 2′-deoxyribonucleotide is added to the elongating strand in a simple nucleophilic substitution at phosphorus in which the 3′-hydroxy group on the elongating strand as a nucleophile replaces magnesium diphosphate as the leaving group. In this substitution, a phosphate anhydride is replaced by a phosphate ester, a reaction that is significantly exergonic. It is unlikely that this nucleophilic substitution will be significantly reversible, so the elongation is not complicated by the back reaction. Consequently, the new nucleotide is locked onto the elongating polymer, and the resulting favorable change in free energy could cause the processivity to be unidirectional. The problem with such an exergonic argument, however, is illustrated

by the fact that the processivity of the elongation catalyzed by DNA-directed DNA polymerase β from *R. norvegicus* is only 30 while the processivity for DNA-directed DNA polymerase from Escherichia phage T7 is 1500, even though they catalyze the same nucleophilic substitution at phosphorus, and DNA-directed RNA polymerase, which also catalyzes the same nucleophilic substitution, is perfectly processive. One would suppose, if the change in standard free energy of the reaction were consequential, that the processivity of these three elongations would be more similar.

The problem that a polymerase has to solve is **preventing the dissociation of the elongating strand and the template to which it is attached** from the active site, and it is difficult to see how the change in standard free energy of the reaction that the enzyme catalyzes can contribute to a solution of this problem. There are many nonprocessive enzymes the active sites of which catalyze significantly exergonic reactions and from which all the products of the exergonic reaction rapidly dissociate after each turnover. There are also many processive enzymes that catalyze reactions that are almost isoergonic. For example, the hydrolysis catalyzed by an exosome is the nucleophilic substitution at phosphorus of the hydroxy group on a molecule of water for the 3′-hydroxy group of the RNA. In the active site of an enzyme, this substitution should be isoergonic. In spite of its appeal, whether a reaction catalyzed by the active site is exergonic or isoergonic cannot be so consequential in ensuring processivity, if it is consequential at all, as the long tunnels. The explanation for the differences in processivity among polymerases is the differences in the degree to which they surround their products and prevent their dissociation.

There are **processive enzymes that bias their processivity by hydrolyzing $MgATP^{2-}$** even though the hydrolysis does not participate in the chemical reaction catalyzed by the enzyme. An example of such a processive enzyme is DNA helicase PcrA from *G. stearothermophilus*.[1355] In the cell, the enzyme catalyzes the unwinding of a double-helical DNA. For the enzyme to unwind DNA, it must hydrolyze $MgATP^{2-}$. The unwinding of double-stranded, duplex DNA is endergonic. If it were not endergonic, linear double-stranded DNA would spontaneously unwind from its two ends, which it does not. The hydrolysis of $MgATP^{2-}$ provides the free energy required to unwind the DNA.

It has already been noted that DNA helicase PcrA displays a heavily, if not exclusively, biased diffusion in the 3′ to 5′ direction on single-stranded DNA and that the bias is accomplished by the hydrolysis of one molecule of $MgATP^{2-}$ for each nucleotide traversed.[1209,1210] In a crystallographic molecular model of the enzyme in a complex with magnesium 5′-adenylic imidodiphosphonic anhydride ($MgAMPPNP^{2-}$) and a short double helix of DNA of ten base pairs, one strand of which has a 3′ extension of seven nucleotides beyond the duplex, the double helix is partially unwound by four base pairs.[1356] The resulting four 5′ nucleotide bases of the shorter strand are protruding out into the solution, but the resulting single strand with the 3′ extension can be seen entering a tunnel into the enzyme. The tunnel contains four nucleotides of the 3′ extension, and two nucleotides at the 3′ end have entered the solution and are disordered and not observed in the map of electron density. Presumably, the tunnel is responsible for performing the biased diffusion of the single strand in the 3′ to 5′ direction, and this biased diffusion accomplished by the hydrolysis of $MgATP^{2-}$ simply pulls the single strand away from the unwinding DNA while the other strand enters the solution. It has been shown that the closely related DNA helicase UvrD from *E. coli* (42% identity; 1.1 gap percent) unwinds DNA in discrete steps of four base pairs,[1357] and in the crystallographic molecular model of DNA helicase PcrA, the DNA has been unwound by four base pairs. It seems as though the double-stranded DNA resists unwinding, but when enough pull is exerted, it suddenly unwinds cooperatively in a burst of four base pairs. The cooperativity of this burst may involve the association of the unwound double-stranded DNA with the surface of the helicase.[1358,1359] Once the slack of four nucleotides rapidly moves through the tunnel, it pulls on the DNA again.

In the crystallographic molecular model of DNA helicase PcrA, the closest atom of $MgAMPPNP^{2-}$ in the site for the hydrolysis of $MgATP^{2-}$, which is one of the nonbridging oxygens on the γphosphorus, is 1.5 nm from the closest atom in the single-stranded DNA in the tunnel, so there can be no chemical reaction that involves the two substrates. Rather, there must be a cycle of conformational changes in the enzyme to accomplish the conformational coupling of hydrolysis of the $MgATP^{2-}$ to unidirectional movement of the strand of DNA through the tunnel so that every time a molecule of $MgATP^{2-}$ is hydrolyzed, the single strand moves down the tunnel a distance of one nucleotide.[1356]

One might suppose that the bias of the movement of the polymer through the active site prevents it from dissociating from the enzyme. If, however, the active site were simply a depression or groove in the protein, there would be nothing to prevent the unwinding DNA from dissociating into the solution after one of the steps in movement of the single strand away from the duplex. Again, as with exodeoxyribonuclease (lambda-induced), although the tunnel is short, the unwound single strand extends out from the tunnel into solution, preventing the unwinding DNA from dissociating from the enzyme as the unwinding proceeds.

RecBCD exodeoxyribonuclease V from *E. coli* finds single-stranded breaks in DNA and unwinds as a helicase the double-helical DNA that was to the 3′ side of the break in the 5′ direction. As it unwinds the DNA, it hydrolyzes the broken strand from its 3′ end until it reaches a hot spot for recombination. It then dissociates, leaving the other single strand, which was (and is still) unbroken, intact and the double-stranded DNA, which was originally to the 5' side of the break, also intact.[1360] As it unwinds the double-stranded DNA as a helicase away from the original break and hydrolyzes the unwinding single strand as an exonuclease, the enzyme hydrolyzes two $MgATP^{2-}$ for every base pair unwound.[1361] It unwinds about 350 base pairs $second^{-1}$ at 25 °C.

In a crystallographic molecular model of RecBCD exodeoxyribonuclease V from *E. coli* in a complex with a completely complementary hairpin of double-stranded DNA,[1360] the open end of the hairpin has unwound into two single strands, each four nucleotides long. The strand with a 3′ end is entering a tunnel that leads to a domain in the enzyme that is structurally homologous to the domain in DNA helicase PcrA responsible for the biased diffusion along the single strand of its substrates. From there, another tunnel leads to the active site of exodeoxyribonuclease V. The strand with a 5′ end is entering a tunnel that leads to another domain that is also structurally homologous to the domain in DNA helicase PcrA and that may catalyze a biased diffusion along this strand as well but in the 5′ to 3′ direction.

In DNA helicase PcrA, the DNA seems to unwind in the solution on the surface of the protein.[1358,1359] The surface of the protein itself provides a steric obstruction, as the one single strand is pulled into the protein away from the other that wanders off into the solution. In the crystallographic molecular model of RecBCD exodeoxyribonuclease V,[1360] however, the stack of as yet unwound base pairs sits on top of a pin that sterically splits the double helix as each single strand beyond the split is fed into a separate tunnel in the enzyme. The pin that splits the double helix is formed from a loop of six amino acids. It is at the carboxy-terminal end of one of the long (17 aa) α helices in the enzyme that is well anchored in the protein, and it is at the amino-terminal end of a randomly meandering segment of polypeptide (4 aa) followed by a shorter α helix (6 aa) that is also anchored in the protein. The loop of six amino acids forming the pin has two bulky methionines at its tip. The pin seems to act as a steric obstruction around which the double helix splits in two as it is pulled forward by biased diffusion of one or both unwinding single strands into their tunnels, powered by the hydrolysis of $MgATP^{2-}$.

The transcription of DNA into RNA is accomplished by DNA-directed RNA polymerases. These enzymes perform a sequence of induced fits and processive transfers of reactants within their active sites that represent perhaps the most complicated example of reactants associating with and products dissociating from the active site of an enzyme. In addition, the ultimate description of their mechanism involves the use of an elaborate analogue of the central intermediate in the catalysis performed by one of these enzymes.

DNA-Directed RNA polymerase is required to locate a promoter designating a location within a continuous duplex of DNA at the 3′ end of a sequence of nucleotides, the coding sequence, in one of the strands of deoxyribonucleotides in the duplex, the template, that encodes the sequence of ribonucleotides in the messenger RNA that the enzyme will produce. Once the promoter is located, the enzyme unwinds the DNA to form a bubble of two single strands of DNA, which exposes the 3′ end of the coding sequence on the template encoding the messenger RNA, and the enzyme then places the end of the coding sequence within the catalytic site. The catalytic site initiates the synthesis of a single strand of messenger RNA, starting from its 5′ end, by adding ribonucleotides one at a time in the direction 5′ to 3′. Once initiation is accomplished and a short strand of RNA, forming a heteroduplex with the coding strand of the DNA, has been synthesized, that short strand of RNA is then elongated, again in the direction 5′ to 3′, by incorporating one ribonucleotide at time to produce a messenger RNA complementary to the coding sequence of the DNA. As the strand of messenger RNA is elongated, it must be unwound from the coding strand of the DNA because the messenger RNA that is the final

product is a single strand of nucleic acid. As the bubble of DNA moves through the active site from its upstream end to its downstream end, the downstream end must be unwound to expose the next bases in the template and the upstream end must rewind. Then, when the process is finished and the messenger RNA has dissociated, the bubble can also dissociate and rapidly rewind spontaneously to a complete unaltered duplex of DNA.

DNA-Directed RNA polymerases from different classes of organism differ significantly in their complexity. The simplest is DNA-directed RNA polymerase from Escherichia phage T7,[1362,1363] which is a single folded polypeptide (883 aa). The functional complex for DNA-directed RNA polymerase from bacteria such as *E. coli*, *T. thermophilus*, and *Thermus aquaticus* is an $\alpha_2\beta\beta'\sigma\omega$ heterohexamer (3800 aa).[1364-1367] The core portion of DNA-directed RNA polymerase from eukaryotes such as *S. cerevisiae*, containing the machinery for initiation and elongation, is an even larger protein (4500 aa) of twelve different subunits ranging in length from 1700 to 70 amino acids,[1368,1369] but to accomplish all the necessary functions of messenger RNA production, it requires the cooperation of other proteins. Each enzyme has several independently shifting domains, and the latter two domains have independently shifting subunits. In each case, the various domains and subunits have been given names to indicate similarities among the different enzymes.[1369]

A sequence of nucleotides in double-stranded DNA that identifies a point at which transcription is to occur, a **promoter sequence**, has to be located by DNA-directed RNA polymerase. The A1 promoter from the genomic DNA of Escherichia phage T7 is a strong promoter that is recognized by DNA-directed RNA polymerase from its host, *E. coli*. When the sequence of deoxyribonucleotides downstream from an A1 promoter is extended from 72 to 300 nucleotides, the occupancy of the promoter after 10 min doubles.[1370] The result is reminiscent of the effect of increasing the length of a double-stranded DNA substrate on the rate of its cleavage by type II site-specific deoxyribonuclease EcoRI from *E. coli*. That result was presented as evidence that the deoxyribonuclease associates at random with duplex DNA and then diffuses by a random walk to its restriction site. Consequently, it was concluded that DNA-directed RNA polymerase also **associates at random and diffuses along the DNA** to a promoter. DNA-Directed RNA polymerase from Escherichia phage T7 binds, with dissociation constants in the range of several nanomolar, to DNA from Escherichia phage T7 at many sites along the DNA that are not within promoters. This binding is consistent with this DNA-directed RNA polymerase also associating at random with DNA before it diffuses to a promoter.[1371]

This diffusion can be observed. A large spherical bead, to which a small fluorescent sphere had been affixed, was attached at the end of a molecule of DNA (1300 nucleotides). These labeled molecules of DNA were added to a chamber with a coverslip to which molecules of DNA-directed RNA polymerase from *E. coli* had been firmly attached. Some of these molecules of DNA, each attached to a sphere, were bound by molecules of the polymerase on the coverslip. By following the fluorescence of the smaller sphere asymmetrically bound to the larger bead, it could be seen that the larger bead rotated. It was concluded that the DNA-directed RNA polymerase diffused along the helical DNA in one of its grooves, causing the molecule of DNA, and hence the bead, to rotate. The diffusion was not biased, as would be expected because no source of energy was available, but the properties of the rotation were consistent with **diffusion of the protein along the groove in a random walk**.[1372] By this random walk, the DNA-directed RNA polymerase scans the groove of the DNA searching for a promoter.

In the crystallographic molecular model of a complex between DNA-directed RNA polymerase from Escherichia phage T7 and a short segment of DNA containing a promoter for the polymerase, there are two hairpins of polypeptide: one of β structure in the major groove and one of random meander at the ends of two α helices in the minor groove of the double-helical DNA.[1363] These two hairpins are presumably the structures that **slide along within the grooves of the DNA** and read the sequence of the bases in the grooves. The sliding of these hairpins along the grooves causes the DNA to rotate as the enzyme scans for a promoter sequence during its one-dimensional diffusion. In the molecular model containing the enzyme from Escherichia phage T7, the two hairpins have found a promoter.

In a crystallographic molecular model of the complex between DNA-directed RNA polymerase from *T. aquaticus* and a longer segment (30 nucleotides) of double-stranded DNA containing a promoter, the intact, rigid, linear double-helical DNA runs along the surface of the protein and makes intimate contact with the surface over a length of 25 nucleotides.[1373] The promoter is entirely within the portion of the DNA participating in the intimate contact, and presumably it is within this contact that the reading of the sequence of bases in both the minor

and major grooves takes place as the protein diffuses along the DNA. In this particular complex, the promoter has also been found.

Once the promoter is located, transcription of the coding strand of the DNA into RNA commences. The first step is **unwinding of the double helix of DNA**. The second step is pairing of the correct ribonucleoside triphosphate with the first base on the template strand of DNA at the site at which sequential formation of the phosphodiesters begins. The third step is correct pairing of the second ribonucleoside triphosphate on the second base in the template. The fourth step is formation of the first phosphodiester by nucleophilic substitution at phosphorus. At this point, the successive addition of ribonucleotides commences.

No external source of standard free energy is available to unwind the DNA because the double helix has to be unwound over a significant length before the synthesis of messenger RNA can begin. The synthesis of the messenger RNA, however, once begun, provides significant standard free energy because the addition of each nucleotide is a nucleophilic substitution at phosphorus where a phosphate anhydride is replaced by a phosphate ester. Nevertheless, the initial unwinding must be driven by noncovalent forces between the protein and the single strands of DNA that are formed as the double helix unwinds. In a crystallographic molecular model of DNA-directed RNA polymerase from Escherichia phage T7 and the promoter segment of DNA,[1363] and in a crystallographic molecular model of DNA-directed RNA polymerase from Escherichia phage T7 and the promoter sequence on which the first three ribonucleotides of the messenger RNA have been synthesized,[1374] four or five, respectively, of the nucleotides of the double helix have been unwound, and the two single strands are firmly held by noncovalent forces between their functional groups and side chains from the protein.

In a molecular model produced by reconstructive summation of electron microscopic images of complexes between DNA-directed RNA polymerase from *M. tuberculosis* and a long (90 nucleotides) segment of double-helical DNA containing a promoter in its middle, the DNA has been unwound to form a **"bubble" of two single strands**, each 12–14 nucleotides long, while the duplex DNA has remained doubly helical to each side of the bubble.[1375] The catalytic site responsible for nucleophilic substitution at phosphorus can be identified by the Mg^{2+} within it. The deoxycytidine in the coding strand of DNA at which initiation is to occur is located within the catalytic site in position to identify the complementary guanosine 5′-triphosphate with which the messenger RNA is to commence. In the bubble, this deoxycytidine is 3 nm from the deoxyguanosine in the other, noncoding strand of the bubble with which it was in a base pair in the original double-helical DNA. This much space is more than sufficient both for the guanosine 5′-triphosphate to associate with the cytosine of this deoxycytidine and for the next nucleoside 5′-triphosphate to associate so that the first nucleophilic substitution can occur between the 3′-hydroxy group of the guanosine 5′-triphosphate and the α-phospho group on the 5′-hydroxy group of the second ribonucleoside triphosphate.

A candidate for an intermediate state in the formation of the bubble has been trapped by adding an inhibitor that associates with the active site between the DNA and the catalytic site. In this complex, the bubble has only opened halfway, and the deoxycytidine that is to initiate the synthesis of messenger RNA is still paired with its complementary deoxyguanosine in the unwound portion of the DNA.[1375] One can imagine, by paraphrasing Pauling,[311] that as molecular motions cause the bubble to open at the site where it first opens and the single strands of DNA fit into their subsites, the standard free energy of dissociation for the DNA from the enzyme increases. As the subsequent base pairs unpair as a result of molecular motion and each of them fits into its subsite, the standard free energy of dissociation again increases until the whole segment is unwound.

It has been possible to follow the various **induced fits** that occur between the situation in which the promoter in the rigid, linear double-helical DNA has been recognized and is still bound only on the surface of bacterial DNA-directed RNA polymerase and the situation in which the DNA has entered the active site of the enzyme and the bubble has formed. The initial point is the crystallographic molecular model of the complex of the promoter with DNA-directed RNA polymerase from *T. aquaticus*,[1373] and the final point is the molecular model produced by reconstructive summation of electron microscopic images of complexes between DNA-directed RNA polymerase from *M. tuberculosis* (44% identity; 1.1 gap percent) and the two forms of bubbled DNA.[1375] The process of conversion between these two states was followed by the changes with time of emissions in spectra of fluorescent reporters covalently attached to strategic locations in either DNA-directed RNA polymerase from *M. tuberculosis*

or the long segment of DNA containing the promoter in its middle, and various inhibitors were used to block the process at several of its steps.[1376] In the case of DNA-directed RNA polymerase from *S. cerevisiae*, the induced fits involved in forming the complex with DNA in which the first six bases of the messenger RNA have been synthesized have been defined by comparing crystallographic molecular models of that complex[1377] and the unoccupied enzyme.[1368] In this case, another protein, transcription initiation factor IIB, in addition to the heterododecamer of the eukaryotic DNA-directed RNA polymerase, is required to form the complex accomplishing initiation, and it is present in the crystallographic molecular model of the former complex.

During the initiation phase, in most instances, the active site and the unwound DNA are still open to the solution to allow addition of the first few ribonucleotides, but at a certain point **initiation changes to elongation**. For DNA-directed RNA polymerase from Escherichia phage T7, this transition seems to occur after about seven ribonucleotides have been added to the elongating strand of messenger RNA. At this point, the number of transcripts that dissociate from the active site rather than being elongated decreases significantly.[1378]

In crystallographic molecular models of DNA-directed RNA polymerase from Escherichia phage T7 in complexes with unwound DNA on which seven and eight ribonucleotides have been polymerized, gradual induced fits of the enzyme relative to the complex early in initiation can be observed, which indicates that the enzyme is adjusting to the elongating strand of messenger RNA.[1379] In a comparison of another crystallographic molecular model of the enzyme in which a complex with unwound DNA on which seventeen ribonucleotides have been polymerized[1380] with crystallographic molecular models of complexes with unwound DNA on which only three[1374] or eight[1381] ribonucleotides have been polymerized, the full **induced fit resulting from the transition between initiation and elongation** can be observed. A major rearrangement of the amino-terminal domain in the enzyme has caused it to close over the catalytic site, burying it in an internal cavity, and the conformational change has also created a tunnel through which the elongating RNA emerges. In the active site, the messenger RNA peels away from the template strand of the DNA into the tunnel so that as the elongation proceeds, there is always a heteroduplex of eight base pairs between the elongating messenger RNA and the template strand of the DNA.[1380] All these induced fits explain the decrease in dissociation of the transcript.

In the crystallographic molecular model of the complex of DNA-directed RNA polymerase from Escherichia phage T7 with unwound DNA on which seventeen ribonucleotides have been polymerized, the bubble of DNA can be observed. At the downstream end of the bubble where the DNA is being unwound as elongation proceeds, an α helix "is wedged in the fork where the template and nontemplate strands separate from the downstream duplex" and "serves to divert the direction of the nontemplate strand, promoting its separation from the template" as transcription proceeds.[1380] This diversion by the α helix is a steric effect. Another α helix in the active site performs the same steric role in **splitting the RNA from the template strand** of the DNA after eight base pairs have formed in the heteroduplex. In the case of bacterial DNA-directed RNA polymerase, deletion mutants of the enzyme from *T. aquaticus* indicate that a loop of 14 amino acids protruding into the tunnel of the active site is responsible for splitting the RNA from the template strand of DNA.[1382] In the active site of eukaryotic DNA-directed RNA polymerase, there are also **steric hindrances** at strategic positions in the active site that seem to be involved in unwinding the homoduplex of the DNA and the heteroduplex of the template and the elongating messenger RNA.[1383]

During elongation, **DNA-directed RNA polymerase is required to be perfectly processive**. If the elongating complex of RNA and DNA within the bubble were to dissociate from the enzyme, its structure would be so peculiar that it would be unlikely to survive long enough to associate with another molecule of RNA polymerase. The incompletely elongated messenger RNA associated in a short heteroduplex with the template would dissociate and become a free, incomplete strand of RNA in the cytoplasm, and the DNA would rewind to a complete double helix. The best that could happen to the strand of RNA is that it would be quickly digested rather than translated. Even in this best case, the standard free energy expended at each step in its elongation, which on a total molar basis is considerable, would be wasted. In the crystallographic molecular model of the complex between DNA-directed RNA polymerase from Escherichia phage T7 and the elongating messenger RNA and the bubble of DNA, the burial of the active site, the strand of RNA passing through the tunnel and emerging from the other side into the solution, and the heteroduplex of eight base pairs connecting the

RNA with the template strand of DNA,[1380] acting together, firmly hold both the messenger RNA and the DNA, precluding the dissociation of either of these substrates and ensuring perfect processivity.

The **enclosure of the bubble of DNA and the heteroduplex** between the elongating messenger RNA and the template strand of DNA is even more complete during elongation catalyzed by eukaryotic DNA-directed RNA polymerase. An artificial substrate was constructed for which two single strands of DNA, each 48 deoxyribonucleotides long, were synthesized. A duplex could be formed between the two strands with the 11 mispaired bases creating an artificial bubble of 11 deoxyribonucleotides in the middle, on either side of which all the bases were paired so that the bubble would be firmly anchored in the otherwise double-helical DNA. An RNA that was 30 nucleotides long was also synthesized, in which the first nine ribonucleotides from the 3′ end were complementary to nine of the deoxyribonucleotides in one strand of DNA in the bubble, but the remaining 21 ribonucleotides were not complementary to any sequence of nucleotides in the DNA. A heterotriplex was then formed with the two strands of DNA containing the bubble and the strand of RNA that mimicked an elongating RNA in a bubble of DNA (Figure 3–73A).[1384,1385] This elaborate **analogue of the usual intermediate** in the elongation of messenger RNA was then bound to the heterododecameric DNA-directed RNA polymerase from *Komagataella phaffii* in the absence of the full complement of ribonucleoside 5′-triphosphates that would promote elongation. Three of the ancillary proteins normally required for elongation were added to ensure that the complete complex was formed.

In the molecular model produced by reconstructive summation of electron microscopic images of the final complex of fifteen proteins and the artificial heterotriplex (Figure 3–73B),[1384] the enzyme has closed around the analogue of the intermediate with the heteroduplex between eight of the nine complementary bases of RNA in the bubble of the otherwise double-helical DNA and its 3′ end in the catalytic site. The double-helical DNA on either side of the artificial bubble, upstream and downstream, and the emerging single strand of RNA mimicking the elongating messenger RNA are each now **enclosed in their respective tunnels of protein**. There is little doubt that such an extensive enclosure ensures that the transcription is perfectly processive.

The elongation of messenger RNA by DNA-directed RNA polymerase from *E. coli* is a **remarkably constant process**. A poly(styrene) bead 0.5 μm in diameter was attached to the downstream end of a strand of double-helical DNA containing a promoter and a long coding sequence for the synthesis of messenger RNA. This DNA was introduced into a chamber, one wall of which was a coverslip coated with DNA-directed RNA polymerase from *E. coli* and within which there was a solution with all the ingredients needed for the synthesis of messenger RNA. Once in the chamber, the DNA was bound by the enzyme, transcription was initiated, and elongation proceeded, pulling the bead toward the enzyme as the DNA was transcribed. The bead was then locked in an optical trap in such a way that the DNA was stretched taut by a constant force of 4 pN applied by the optical trap. The chamber was mechanically translated so that while the DNA shortened as the downstream end entered the enzyme, the bead remained in the trap. Under the applied force, the rate at which elongation proceeded (12 ± 2 nucleotides s^{-1}) was remarkably constant over stretches of 1000 nucleotides.[1386]

The diffusion of a molecule of DNA-directed RNA polymerase along double-helical DNA while it is searching for a promoter must be an unbiased random walk[1372] because no standard free energy is provided at this stage. As the messenger RNA is elongated, however, a phosphate anhydride becomes a phosphate ester at each addition of a ribonucleotide. The resulting negative difference in standard free energy creates mechanical work pulling the transcript through the active site. Force can be applied to a poly(styrene) bead, 0.5 μm in diameter, in an optical trap attached to the downstream end of a strand of double-helical DNA that contains a promoter and is bound to DNA-directed RNA polymerase from *E. coli*.[1387] As the force on the bead is increased, rather than being caused to remain constant by moving the chamber, the rate of elongation remains constant until a force equal to around 10 pN is applied, after which it declines to 0 over a range of applied forces from 10 to 20 pN.[1388,1389] This result demonstrates that as the RNA is elongated, mechanical work is being applied by the enzyme to move the bubble and the elongating messenger RNA in the downstream direction.

A

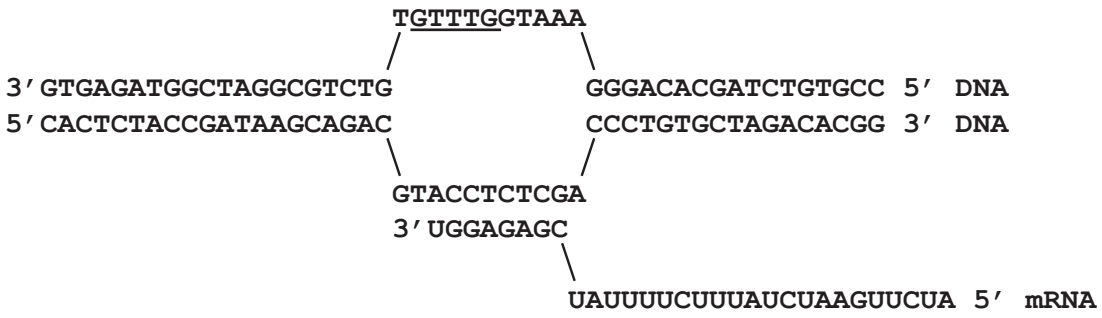
TGTTTGGTAAA
3′GTGAGATGGCTAGGCGTCTG
GGGACACGATCTGTGCC 5′ DNA
5′CACTCTACCGATAAGCAGAC
CCCTGTGCTAGACACGG 3′ DNA
GTACCTCTCGA
3′UGGAGAGC
UAUUUUCUUUAUCUAAGUUCUA 5′ mRNA

B

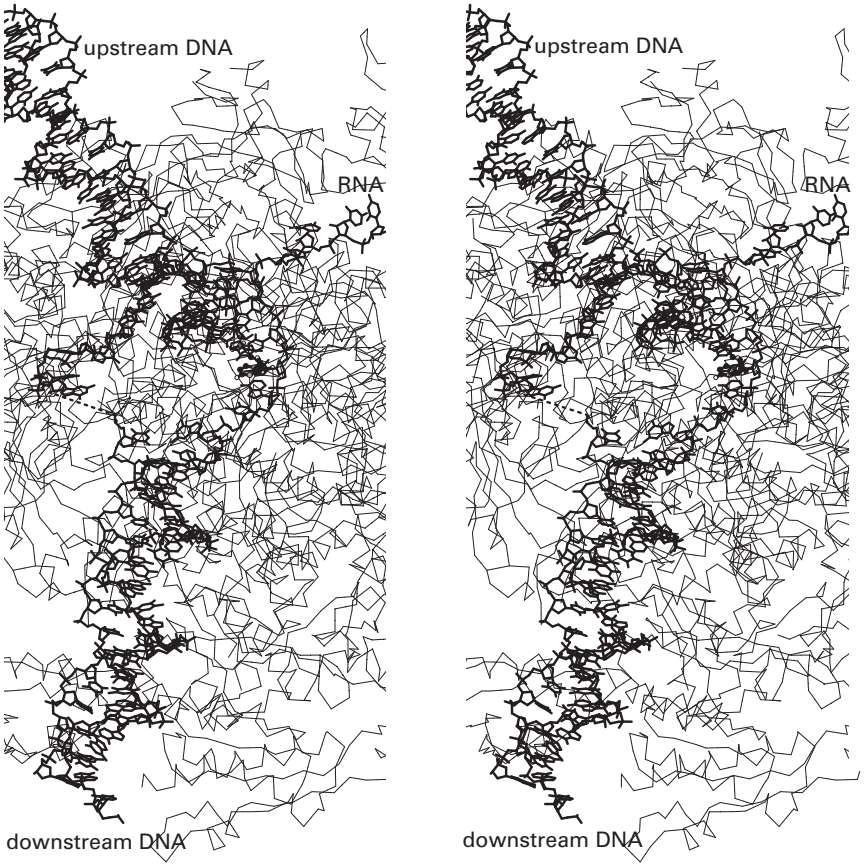
upstream DNA
RNA
downstream DNA
upstream DNA
RNA
downstream DNA

Figure 3–73: Stereodrawing[576] of a portion of the molecular model produced by reconstructive summation of electron microscopic images of DNA-directed RNA polymerase II from *K. phaffii* the active site of which has enclosed a heterotriplex of two strands of DNA and one strand of RNA.[1384] The complete heterododecameric complex that forms the core of DNA-directed RNA polymerase II from *K. phaffii*, which had been genetically tagged by altering the DNA of the fungus encoding the protein to facilitate purification, was purified in high yield from cells of *K. phaffii*. All twelve subunits were present in the final complex in equimolar amounts.[1385] Transcription elongation factors Elf1, TFIIS, and Spt5 from *K. phaffii* were expressed in and purified from cells of *E. coli*. Two segments of single-stranded DNA and a single segment of RNA were prepared synthetically. The three segments of nucleic acid were hybridized to form a heterotriplex (Panel **A**) by mixing them in equimolar amounts in 4 mM magnesium acetate, 20 mM 2-amino-2-(hydroxymethyl)propane-1,3-diol, and 150 mM potassium acetate at pH 7.5, heating to 60 °C for 2 min, and gradually cooling the mixture. The purified heterododecameric core of DNA-directed RNA polymerase, the elongation factors Spt5 and Elf1, and the annealed heterotriplex of DNA and RNA were mixed together at pH 7.5 and then passed over a molecular exclusion column to remove any uncomplexed heterotriplex, Spt5, and Elf1. The resulting complex was then mixed with elongation factor TFIIS and subjected to chemical crosslinking to stabilize the then-complete complex and purified a second time by molecular exclusion. A solution of the final purified complex in 0.1 mM tris(2-carboxyethyl)-phosphine, 1 μM zinc acetate, 20 mM 2-amino-2-(hydroxymethyl)propane-1,3-diol, and 150 mM potassium acetate, pH 7.5, was spread on a grid for electron microscopy, the film of solution was vitrified to form a solid of amorphous ice, and the vitrified sample was viewed by electron microscopy. A large collection of images of individual molecules of the complex (682,749) were each assigned orientations, and the images of the particles and their assigned orientation were the data set used to reconstruct a three-dimensional map of scattering density for the complex. This map was of high enough resolution to insert the polypeptides of the various subunits and elongation factors as well as the heterotriplex of DNA and RNA into the map and obtain a molecular model of the complete complex. A portion of that molecular model has been drawn and is presented in Panel **B**. Several of the subunits and elongation factors in the complete molecular model that were not near the heterotriplex of DNA and RNA are omitted from the drawing to increase its clarity, but all the portions of polypeptide adjacent to the DNA and RNA are included. The heterotriplex of DNA and RNA (thick lines) is presented in a line drawing of all its atoms. The dashed line connects two nucleotides in the noncoding strand of DNA in the bubble between which there was no scattering density. This missing sequence of five nucleotides is underlined in Panel **A**. The polypeptide (thin lines) is represented by line segments connecting the α carbons in the sequences of amino acids. An animation of this complex can be downloaded at https://www.science.org/doi/full/10.1126/science.aan8552

The free energy required to create this **mechanical work** must come from the successive nucleophilic substitutions at phosphorus. Unlike in the case of DNA helicase PcrA, however, the creation of the mechanical work that permits the biased translation is not the result of a sequence of conformational changes tightly coupled to the hydrolysis of $MgATP^{2-}$ elsewhere in the protein; rather, it is occurring in the catalytic site each time a phosphate anhydride is replaced by a phosphate ester. Consider the situation just after a phosphodiester has formed in a kinetically irreversible nucleophilic substitution at phosphorus. The heterotriplex can now move in either direction, downstream or upstream. If it moves downstream (the undesired direction), a base pair between the messenger RNA and the template several base pairs upstream from the catalytic site, which had been broken during the process of splitting the messenger RNA from the template, re-forms; a base pair between the two strands of the upstream DNA, which had been re-formed during the process of re-forming the upstream duplex, is broken; and a base pair between the two strands of the downstream DNA, which were broken during the propagation of the bubble, re-forms. The sum of these three changes should be a negative change in standard free energy. If, however, the heterotriplex moves upstream (the desired direction), a base pair between the messenger RNA and the template is broken; a base pair between the two strands of the upstream DNA re-forms; and a base pair between the two strands of the downstream DNA breaks, but the next nucleotide can then be added to the elongating messenger RNA in a nucleophilic substitution at phosphorus that liberates considerable standard free energy. The sum of these four changes should be a even greater negative change in standard free energy than occurs in a movement downstream and should create a ratchet that generates the observed mechanical work.

It should be noted, however, that this ratchet in no way guarantees processivity, which, as has been discussed, results from only prevention of the product of each nucleophilic substitution from dissociating from the active site. From the behavior of the bead when the force has stopped transcription, it was concluded that the excess applied force pulls the DNA out of the entry tunnel on the DNA-directed RNA polymerase by about five to ten base pairs,[1389] but even this rather remarkable distortion has not caused the DNA to dissociate from the enzyme.

Suggested Reading

De Moss, J. A. (1962) Studies on the mechanism of the tryptophan synthetase reaction, *Biochim. Biophys. Acta 62,* 279–293. https://doi.org/10.1016/0006-3002(62)90041-0

Maier, T., Leibundgut, M., and Ban, N. (2008) The crystal structure of a mammalian fatty acid synthase, *Science 321*, 1315–1322. https://doi.org/10.1126/science.1161269

Baker, P., Pan, D., Carere, J., Rossi, A., Wang, W., and Seah, S. Y. K. (2009) Characterization of an aldolase-dehydrogenase complex that exhibits substrate channeling in the polychlorinated biphenyls degradation pathway, *Biochemistry 48*, 6551–6558. https://doi.org/10.1021/bi9006644

References

1. Samuel, D., Estroumza, J., and Ailhaud, G. (1970) Partial purification and properties of acyl-CoA synthetase of *Escherichia coli*, *Eur. J. Biochem. 12*, 576–582.
2. Kivirikko, K. I., Shudo, K., Sakakibara, S., and Prockop, D. J. (1972) Studies on protocollagen lysine hydroxylase: Hydroxylation of synthetic peptides and the stoichiometric decarboxylation of α-ketoglutarate, *Biochemistry 11*, 122–129.
3. Hayzer, D. J., and Leisinger, T. (1981) Proline biosynthesis in *Escherichia coli*: Stoichiometry and end-product identification of the reaction catalysed by glutamate semialdehyde dehydrogenase, *Biochem. J. 197*, 269–274.
4. Reichenbecher, W., and Schink, B. (1999) Towards the reaction mechanism of pyrogallol-phloroglucinol transhydroxylase of *Pelobacter acidigallici*, *Biochim. Biophys. Acta 1430*, 245–253.
5. Sonna, L. A., Ambudkar, S. V., and Maloney, P. C. (1988) The mechanism of glucose 6-phosphate transport by *Escherichia coli*, *J. Biol. Chem. 263*, 6625–6630.
6. Kvalnes-Krick, K., and Jorns, M. S. (1987) Interaction of tetrahydrofolate and other folate derivatives with bacterial sarcosine oxidase, *Biochemistry 26*, 7391–7395.
7. Kahn, K., Serfozo, P., and Tipton, P. A. (1997) Identification of the true product of the urate oxidase reaction, *J. Am. Chem. Soc. 119*, 5435–5442.
8. Bartlett, P. A., and Satake, K. (1988) Does dehydroquinate synthase synthesize dehydroquinate?, *J. Am. Chem. Soc. 110*, 1628–1630.
9. Brash, A. R., Baertschi, S. W., Ingram, C. D., and Harris, T. M. (1988) Isolation and characterization of natural allene oxides: Unstable intermediates in the metabolism of lipid hydroperoxides, *Proc. Natl. Acad. Sci. U. S. A. 85*, 3382–3386.
10. Hafner, E. W., and Wellner, D. (1971) Demonstration of imino acids as products of the reactions catalyzed by D- and L-amino acid oxidases, *Proc. Natl. Acad. Sci. U. S. A. 68*, 987–991.
11. Woo, J. C. G., and Silverman, R. B. (1995) Monoamine oxidase B catalysis in low aqueous medium: Direct evidence for an imine product, *J. Am. Chem. Soc. 117*, 1663–1664.
12. Hommel, U., Eberhard, M., and Kirschner, K. (1995) Phosphoribosyl anthranilate isomerase catalyzes a reversible Amadori reaction, *Biochemistry 34*, 5429–5439.
13. Johnson, W. H., Jr., Hajipour, G., and Whitman, C. P. (1995) Stereochemical studies of 5-(carboxymethyl)-2-hydroxymuconate isomerase and 5-(carboxymethyl)-2-oxo-3-hexene-1,6-dioate decarboxylase from *Escherichia coli c*: Mechanistic and evolutionary implications, *J. Am. Chem. Soc. 117*, 8719–8726.
14. Colabroy, K. L., and Begley, T. P. (2005) The pyridine ring of NAD is formed by a nonenzymatic pericyclic reaction, *J. Am. Chem. Soc. 127*, 840–841.
15. Blickling, S., Renner, C., Laber, B., Pohlenz, H. D., Holak, T. A., and Huber, R. (1997) Reaction mechanism of *Escherichia coli* dihydrodipicolinate synthase investigated by X-ray crystallography and NMR spectroscopy, *Biochemistry 36*, 24–33.
16. Myers, R. W., Wray, J. W., Fish, S., and Abeles, R. H. (1993) Purification and characterization of an enzyme involved in oxidative carbon–carbon bond cleavage reactions in the methionine salvage pathway of *Klebsiella pneumoniae*, *J. Biol. Chem. 268*, 24785–24791.
17. Wang, H., Pang, H., Bartlam, M., and Rao, Z. (2005) Crystal structure of human E1 enzyme and its complex with a substrate analog reveals the mechanism of its phosphatase/enolase activity, *J. Mol. Biol. 348*, 917–926.

18. Gibson, K. J., Lorimer, G. H., Rendina, A. R., Taylor, W. S., Cohen, G., Gatenby, A. A., Payne, W. G., Roe, D. C., Lockett, B. A., Nudelman, A., Marcovici, D., Nachum, A., Wexler, B. A., Marsilii, E. L., Turner, I.M., Howe, L. D., Kalbach, C. E., and Chi, H. (1995) Dethiobiotin synthetase: The carbonylation of 7,8-diaminononanoic acid proceeds regiospecifically via the N7-carbamate, *Biochemistry 34*, 10976–10984.
19. Trentham, D. R., McMurray, C. H., and Pogson, C. I. (1969) The active chemical state of D-glyceraldehyde 3-phosphate in its reactions with D-glyceraldehyde 3-phosphate dehydrogenase, aldolase and triose phosphate isomerase, *Biochem. J. 114*, 19–24.
20. Koerner, T. A., Jr., Cary, L. W., Bhacca, N. S., and Younathan, E. S. (1973) Tautomeric composition of D-fructose phosphates in solution by Fourier transform carbon-13 nuclear magnetic resonance, *Biochem. Biophys. Res. Commun. 51*, 543–550.
21. Schray, K. J., Benkovic, S. J., Benkovic, P. A., and Rose, I. A. (1973) Catalytic reactions of phosphoglucose isomerase with cyclic forms of glucose 6-phosphate and fructose 6-phosphate, *J. Biol. Chem. 248*, 2219–2224.
22. Benkovic, P. A., Bullard, W. P., De Maine, M., Fishbein, R., Schray, K. J., Steffens, J. J., and Benkovic, S. J. (1974) Anomeric specificity of the alkaline form of fructose 1,6-diphosphatase from rabbit liver, *J. Biol. Chem. 249*, 930–931.
23. Lee, J. H., Chang, K. Z., Patel, V., and Jeffery, C. J. (2001) Crystal structure of rabbit phosphoglucose isomerase complexed with its substrate D-fructose 6-phosphate, *Biochemistry 40*, 7799–7805.
24. Choi, K. H., and Tolan, D. R. (2004) Presteady-state kinetic evidence for a ring-opening activity in fructose-1,6-(bis)phosphate aldolase, *J. Am. Chem. Soc. 126*, 3402–3403.
25. Lorentzen, E., Siebers, B., Hensel, R., and Pohl, E. (2005) Mechanism of the Schiff base forming fructose-1,6-bisphosphate aldolase: Structural analysis of reaction intermediates, *Biochemistry 44*, 4222–4229.
26. Hall, R. L., Vennesland, B., and Kezdy, F. J. (1969) Glyoxylate carboligase of *Escherichia coli*. Identification of carbon dioxide as the primary reaction product, *J. Biol. Chem. 244*, 3991–3998.
27. Witkowski, A., Joshi, A. K., and Smith, S. (2002) Mechanism of the β-ketoacyl synthase reaction catalyzed by the animal fatty acid synthase, *Biochemistry 41*, 10877–10887.
28. Hitchcock, D. S., Fedorov, A. A., Fedorov, E. V., Dangott, L. J., Almo, S. C., and Raushel, F. M. (2011) Rescue of the orphan enzyme isoguanine deaminase, *Biochemistry 50*, 5555–5557.
29. Paoletti, F. (1983) Purification and properties of transketolase from fresh rat liver, *Arch. Biochem. Biophys. 222*, 489–496.
30. Schofield, L. R., Anderson, B. F., Patchett, M. L., Norris, G. E., Jameson, G. B., and Parker, E. J. (2005) Substrate ambiguity and crystal structure of *Pyrococcus furiosus* 3-deoxy-D-arabino-heptulosonate-7-phosphate synthase: An ancestral 3-deoxyald-2-ulosonate-phosphate synthase?, *Biochemistry 44*, 11950–11962.
31. Chen, Q. X., Rosik, L. O., Nancarrow, C. D., and Sweet, F. (1989) Fetal lamb 3 β,20-α-hydroxysteroid oxidoreductase: Dual activity at the same active site examined by affinity labeling with 16 α-(bromo[2′-^{14}C]acetoxy)progesterone, *Biochemistry 28*, 8856–8863.
32. Smeland, T. E., Cuebas, D., and Schulz, H. (1991) Epimerization of 3-hydroxy-4-*trans*-decenoyl coenzyme A by a dehydration/-hydration mechanism catalyzed by the multienzyme complex of fatty acid oxidation from *Escherichia coli*, *J. Biol. Chem. 266*, 23904–23908.
33. Farrell, E. K., and Tipton, P. A. (2012) Functional characterization of AlgL, an alginate lyase from *Pseudomonas aeruginosa*, *Biochemistry 51*, 10259–10266.
34. Yamasaki, M., Ogura, K., Hashimoto, W., Mikami, B., and Murata, K. (2005) A structural basis for depolymerization of alginate by polysaccharide lyase family-7, *J. Mol. Biol. 352*, 11–21.
35. Libertini, L. J., and Smith, S. (1978) Purification and properties of a thioesterase from lactating rat mammary gland which modifies the product specificity of fatty acid synthetase, *J. Biol. Chem. 253*, 1393–1401.
36. Oikawa, H., Toyomasu, T., Toshima, H., Ohashi, S., Kawaide, H., Kamiya, Y., Ohtsuka, M., Shinoda, S., Mitsuhashi, W., and Sassa, T. (2001) Cloning and functional expression of cDNA encoding aphidicolan-16 β-ol synthase: A key enzyme responsible for formation of an unusual diterpene skeleton in

biosynthesis of aphidicolin, *J. Am. Chem. Soc. 123*, 5154–5155.
37. Warren, J. C., Murdock, G. L., Ma, Y., Goodman, S. R., and Zimmer, W. E. (1993) Molecular cloning of testicular 20 α-hydroxysteroid dehydrogenase: Identity with aldose reductase, *Biochemistry 32*, 1401–1406.
38. Srivastava, S., Watowich, S. J., Petrash, J. M., Srivastava, S. K., and Bhatnagar, A. (1999) Structural and kinetic determinants of aldehyde reduction by aldose reductase, *Biochemistry 38*, 42–54.
39. Hong, S. B., and Raushel, F. M. (1996) Metal-substrate interactions facilitate the catalytic activity of the bacterial phosphotriesterase, *Biochemistry 35*, 10904–10912.
40. Heilmann, I., Pidkowich, M. S., Girke, T., and Shanklin, J. (2004) Switching desaturase enzyme specificity by alternate subcellular targeting, *Proc. Natl. Acad. Sci. U. S. A. 101*, 10266–10271.
41. Tipton, P. A., and Peisach, J. (1990) Characterization of the multiple catalytic activities of tartrate dehydrogenase, *Biochemistry 29*, 1749–1756.
42. Palmer, D. R., Garrett, J. B., Sharma, V., Meganathan, R., Babbitt, P. C., and Gerlt, J. A. (1999) Unexpected divergence of enzyme function and sequence: "*N*-acylamino acid racemase" is *o*-succinylbenzoate synthase, *Biochemistry 38*, 4252–4258.
43. Taylor Ringia, E. A., Garrett, J. B., Thoden, J. B., Holden, H. M., Rayment, I., and Gerlt, J. A. (2004) Evolution of enzymatic activity in the enolase superfamily: Functional studies of the promiscuous *o*-succinylbenzoate synthase from *Amycolatopsis*, *Biochemistry 43*, 224–229.
44. Darbyshire, A. L., Mothersole, R. G., and Wolthers, K. R. (2021) A fold type II PLP-dependent enzyme from *Fusobacterium nucleatum* functions as a serine synthase and cysteine synthase, *Biochemistry 60*, 524–536.
45. Seeholzer, S. H. (1993) Phosphoglucose isomerase: A ketol isomerase with aldol C2-epimerase activity, *Proc. Natl. Acad. Sci. U. S. A. 90*, 1237–1241.
46. Czekster, C. M., and Blanchard, J. S. (2012) One substrate, five products: Reactions catalyzed by the dihydroneopterin aldolase from *Mycobacterium tuberculosis*, *J. Am. Chem. Soc. 134*, 19758–19771.
47. Sasaki, R., Ikura, K., Sugimoto, E., and Chiba, H. (1975) Purification of bisphosphoglyceromutase, 2,3-bisphosphoglycerate phosphatase and phosphoglyceromutase from human erythrocytes. Three enzyme activities in one protein, *Eur. J. Biochem. 50*, 581–593.
48. Albright, F., and Schroepfer, G. J., Jr. (1970) L-*trans*-2,3-epoxysuccinate: A new substrate for fumarase, *Biochem. Biophys. Res. Commun. 40*, 661–666.
49. Harting, J., and Velick, S. F. (1954) Acetyl phosphate formation catalyzed by glyceraldehyde-3-phosphate dehydrogenase, *J. Biol. Chem. 207*, 857–865.
50. Duncan, R. J., and Tipton, K. F. (1969) The oxidation and reduction of glyoxylate by lactic dehydrogenase, *Eur. J. Biochem. 11*, 58–61.
51. Sawaki, S., Hattori, H., and Yamada, K. (1967) Glyoxylate dehydrogenase activity of lactate dehydrogenase, *J. Biochem. (Tokyo) 62*, 263–268.
52. Kyte, J. (2003) The basis of the hydrophobic effect, *Biophys. Chem. 100*, 193–203.
53. Sychantha, D., and Clarke, A. J. (2018) Peptidoglycan modification by the catalytic domain of *Streptococcus pneumoniae oata* follows a ping-pong bi-bi mechanism of action, *Biochemistry 57*, 2394–2401.
54. Alberts, A. W., and Vagelos, P. R. (1968) Acetyl CoA carboxylase. I. Requirement for two protein fractions, *Proc. Natl. Acad. Sci. U. S. A. 59*, 561–568.
55. Fall, R. R., and Vagelos, P. R. (1972) Acetyl coenzyme A carboxylase. Molecular forms and subunit composition of biotin carboxyl carrier protein, *J. Biol. Chem. 247*, 8005–8015.
56. Alberts, A. W., Gordon, S. G., and Vagelos, P. R. (1971) Acetyl CoA carboxylase: The purified transcarboxylase component, *Proc. Natl. Acad. Sci. U. S. A. 68*, 1259–1263.
57. Wei, J., and Tong, L. (2015) Crystal structure of the 500-kda yeast acetyl-CoA carboxylase holoenzyme dimer, *Nature 526*, 723–727.
58. Bloch, W., MacQuarrie, R. A., and Bernhard, S. A. (1971) The nucleotide and acyl group content of native rabbit muscle glyceraldehyde 3-phosphate dehydrogenase, *J. Biol. Chem. 246*, 780–790.
59. Yew, W. S., Fedorov, A. A., Fedorov, E. V., Almo, S. C., and Gerlt, J. A. (2007) Evolution of enzymatic activities in the enolase superfamily: L-Talarate/galactarate dehydratase from

Salmonella typhimurium Lt2, *Biochemistry 46*, 9564–9577.
60. Lu, Z., Feng, X., Song, L., Han, Y., Kim, A., Herzberg, O., Woodson, W., R., Martin, B. M., Mariano, P. S., and Dunaway-Mariano, D. (2005) Diversity of function in the isocitrate lyase enzyme superfamily: The *Dianthus caryophyllus* petal death protein cleaves α-keto and α-hydroxycarboxylic acids, *Biochemistry 44*, 16365–16376.
61. Yew, W. S., Akana, J., Wise, E. L., Rayment, I., and Gerlt, J. A. (2005) Evolution of enzymatic activities in the orotidine 5′-monophosphate decarboxylase suprafamily: Enhancing the promiscuous D-arabino-hex-3-ulose 6-phosphate synthase reaction catalyzed by 3-keto-L-gulonate 6-phosphate decarboxylase, *Biochemistry 44*, 1807–1815.
62. Cleland, W. W. (1963) The kinetics of enzyme-catalyzed reactions with two or more substrates or products: I. Nomenclature and rate equations, *Biochim. Biophys. Acta 67*, 104–137.
63. Bates, D. J., and Frieden, C. (1973) Treatment of enzyme kinetic data: 3. The use of the full time course of a reaction, as examined by computer simulation, in defining enzyme mechanisms, *J. Biol. Chem. 248*, 7878–7884.
64. Michaelis, L., and Menten, M. L. (1913) Kinetics of invertase action, *Biochem. Z. 49*, 333–369.
65. Johnson, K. A., and Goody, R. S. (2011) The original Michaelis constant: Translation of the 1913 Michaelis-Menten paper, *Biochemistry 50*, 8264–8269.
66. Spies, M. A., Woodward, J. J., Watnik, M. R., and Toney, M. D. (2004) Alanine racemase free energy profiles from global analyses of progress curves, *J. Am. Chem. Soc. 126*, 7464–7475.
67. Hommel, U., Lustig, A., and Kirschner, K. (1989) Purification and characterization of yeast anthranilate phosphoribosyltransferase, *Eur. J. Biochem. 180*, 33–40.
68. Alberty, R. A., and Bock, R. M. (1953) Alteration of the kinetic properties of an enzyme by the binding of buffer, inhibitor, or substrate, *Proc. Natl. Acad. Sci. U. S. A. 39*, 895–900.
69. Purich, D. L., and Fromm, H. J. (1971) The kinetics and regulation of rat brain hexokinase, *J. Biol. Chem. 246*, 3456–3463.
70. Briggs, G. E. (1931) The significance of the Michaelis constant for saccharase, *Biochem. J. 25*, 1801–1806.
71. Cleland, W. W. (1979) Statistical analysis of enzyme kinetic data, *Methods Enzymol. 63*, 103–138.
72. Northrop, D. B. (1998) On the meaning of K_m and V/K in enzyme kinetics, *J. Chem. Educ. 75*, 1153–1157.
73. Monod, J., Wyman, J., and Changeux, J. P. (1965) On the nature of allosteric transitions: A plausible model, *J. Mol. Biol. 12*, 88–118.
74. Lineweaver, H., and Burk, D. (1934) The determination of enzyme dissociation constants, *J. Am. Chem. Soc. 56*, 658–666.
75. Williams, A. (1970) Chymotrypsin-catalyzed phenyl ester hydrolysis. Evidence for electrophilic assistance on carbonyl oxygen, *Biochemistry 9*, 3383–3390.
76. Briggs, G. E., and Haldane, J. B. S. (1925) A note on the kinetics of enzyme action., *Biochem. J. 19*, 338–339.
77. Flynn, J., Glickman, J. F., and Reich, N. O. (1996) Murine DNA cytosine-C5 methyltransferase: Pre-steady- and steady-state kinetic analysis with regulatory DNA sequences, *Biochemistry 35*, 7308–7315.
78. Pirrung, M. C., Liu, H., and Morehead, A. T., Jr. (2002) Rhodium chemzymes: Michaelis-Menten kinetics in dirhodium(II) carboxylate-catalyzed carbenoid reactions, *J. Am. Chem. Soc. 124*, 1014–1023.
79. Rocek, J., Schreiber, J., Moldovan.L, Eschenmoser, A., and Westheimer, F. H. (1962) Chromsaureester als zwischenprodukte bei der oxydation von alkoholen - geschwindigkeits-limitierende veresterung eines sterisch gehinderten alkohols, *Helv. Chim. Acta 45*, 2554–2567.
80. Cleland, W. W. (1975) Partition analysis and the concept of net rate constants as tools in enzyme kinetics, *Biochemistry 14*, 3220–3224.
81. Tull, D., and Withers, S. G. (1994) Mechanisms of cellulases and xylanases: A detailed kinetic study of the *exo*-β-1,4-glycanase from *Cellulomonas fimi*, *Biochemistry 33*, 6363–6370.
82. King, E. L., and Altman, C. (1956) A schematic method of deriving the rate laws for enzyme-catalyzed reactions, *J. Phys. Chem. 60*, 1375–1378.
83. Segel, I. H. (1975) *Enzyme kinetics: Behavior and analysis of rapid equilibrium and steady*

state enzyme systems, pp 506–523, Wiley, New York.
84. Segel, I. H. (1975) *Enzyme kinetics: Behavior and analysis of rapid equilibrium and steady state enzyme systems*, pp 646–647, Wiley, New York.
85. Cook, P. F., and Cleland, W. W. (2007) *Enzyme kinetics and mechanism*, Garland Science, New York.
86. Knight, W. B., and Cleland, W. W. (1989) Thiol and amino analogues as alternate substrates for glycerokinase from *Candida mycoderma*, *Biochemistry 28*, 5728–5734.
87. Sharp, J. A., and Edwards, M. R. (1983) Initial-velocity kinetics of succinoyl-coenzyme A-3-oxo acid coenzyme A-transferase from sheep kidney, *Biochem. J. 213*, 179–185.
88. Sharp, J. A., and Edwards, M. R. (1978) Purification and properties of succinyl-coenzyme A-3-oxo acid coenzyme A-transferase from sheep kidney, *Biochem. J. 173*, 759–765.
89. Bateman, K. S., Brownie, E. R., Wolodko, W. T., and Fraser, M. E. (2002) Structure of the mammalian CoA transferase from pig heart, *Biochemistry 41*, 14455–14462.
90. Bruser, T., Selmer, T., and Dahl, C. (2000) "ADP sulfurylase" from *Thiobacillus denitrificans* is an adenylylsulfate:Phosphate adenylyltransferase and belongs to a new family of nucleotidyltransferases, *J. Biol. Chem. 275*, 1691–1698.
91. Aitken, S. M., Kim, D. H., and Kirsch, J. F. (2003) *Escherichia coli* cystathionine γ-synthase does not obey ping-pong kinetics: Novel continuous assays for the elimination and substitution reactions, *Biochemistry 42*, 11297–11306.
92. Eubanks, L. M., and Poulter, C. D. (2003) *Rhodobacter capsulatus* 1-deoxy-D-xylulose 5--phosphate synthase: Steady-state kinetics and substrate binding, *Biochemistry 42*, 1140–1149.
93. Northrop, D. B. (1969) Transcarboxylase. VI: Kinetic analysis of the reaction mechanism, *J. Biol. Chem. 244*, 5808–5819.
94. Hines, V., and Johnston, M. (1989) Analysis of the kinetic mechanism of the bovine liver mitochondrial dihydroorotate dehydrogenase, *Biochemistry 28*, 1222–1226.
95. Northrop, D. B. (1999) Rethinking fundamentals of enzyme action, In *Advances in enzymology and related areas of molecular biology: Mechanism of enzyme action, part a* (Purich, D. L., Ed.), pp 25–55, John Wiley and Sons, Hoboken, NJ.
96. Cleland, W. W. (1963) The kinetics of enzyme-catalyzed reactions with two or more substrates or products: II. Inhibition: Nomenclature and theory, *Biochim. Biophys. Acta 67*, 173–187.
97. Li, H. C., and Buchanan, J. M. (1971) Biosynthesis of the purines: XXXIV. Initial rate studies of formylglycinamide ribonucleotide amidotransferase with competitive and product inhibitors, *J. Biol. Chem. 246*, 4720–4726.
98. Trauger, J. W., Lin, F. F., Turner, M. S., Stephens, J., and LoGrasso, P. V. (2002) Kinetic mechanism for human Rho-kinase II (Rock-II), *Biochemistry 41*, 8948–8953.
99. Lueck, J. D., and Fromm, H. J. (1974) Kinetics, mechanism, and regulation of rat skeletal muscle hexokinase, *J. Biol. Chem. 249*, 1341–1347.
100. Janson, C. A., and Cleland, W. W. (1974) The kinetic mechanism of glycerokinase, *J. Biol. Chem. 249*, 2562–2566.
101. Noble, M. A., Quaroni, L., Chumanov, G. D., Turner, K. L., Chapman, S. K., Hanzlik, R. P., and Munro, A. W. (1998) Imidazolyl carboxylic acids as mechanistic probes of flavocytochrome P-450 BM3, *Biochemistry 37*, 15799–15807.
102. DeLeo, A. B., Dayan, J., and Sprinson, D. B. (1973) Purification and kinetics of tyrosine-sensitive 3-deoxy-D-*arabino*-heptulosonic acid 7-phosphate synthetase from *Salmonella*, *J. Biol. Chem. 248*, 2344–2353.
103. Bachmann, B. O., and Townsend, C. A. (2000) Kinetic mechanism of the β-lactam synthetase of *Streptomyces clavuligerus*, *Biochemistry 39*, 11187–11193.
104. Brunhuber, N. M., Thoden, J. B., Blanchard, J. S., and Vanhooke, J. L. (2000) *Rhodococcus* L-phenylalanine dehydrogenase: Kinetics, mechanism, and structural basis for catalytic specificit, *Biochemistry 39*, 9174–9187.
105. Karsten, W. E. (1997) Dihydrodipicolinate synthase from *Escherichia coli*: pH Dependent changes in the kinetic mechanism and kinetic mechanism of allosteric inhibition by L-lysine, *Biochemistry 36*, 1730–1739.
106. Chase, J. F., Middleton, B., and Tubbs, P. K. (1966) A coenzyme A analogue, desulpho-CoA; preparation and effects on various enzymes, *Biochem. Biophys. Res. Commun. 23*, 208–213.

107. Quartararo, C. E., and Blanchard, J. S. (2011) Kinetic and chemical mechanism of malate synthase from *Mycobacterium tuberculosis*, *Biochemistry 50*, 6879–6887.
108. Collins, K. D., and Stark, G. R. (1971) Aspartate transcarbamylase. Interaction with the transition state analogue *N*-(phosphonacetyl)-L-aspartate, *J. Biol. Chem. 246*, 6599–6605.
109. Yu, M., Magalhaes, M. L., Cook, P. F., and Blanchard, J. S. (2006) Bisubstrate inhibition: Theory and application to *N*-acetyltransferases, *Biochemistry 45*, 14788–14794.
110. Hoogenraad, N. J. (1974) Reaction mechanism of aspartate transcarbamylase from mouse spleen, *Arch. Biochem. Biophys. 161*, 76–82.
111. Niu, L., Chang, K. C., Wilson, S., Tran, P., Zuo, F., and Swinney, D. C. (2007) Kinetic characterization of human JNK2α2 reaction mechanism using substrate competitive inhibitors, *Biochemistry 46*, 4775–4784.
112. Matsuoka, Y., and Srere, P. A. (1973) Kinetic studies of citrate synthase from rat kidney and rat brain, *J. Biol. Chem. 248*, 8022–8030.
113. Noat, G., Ricard, J., Borel, M., and Got, C. (1970) Kinetic study of yeast hexokinase. Inhibition of the reaction by magnesium and ATP, *Eur. J. Biochem. 13*, 347–363.
114. Rundgren, M. (1977) Steady state kinetics of 4-hydroxyphenylpyruvate dioxygenase from human liver (III), *J. Biol. Chem. 252*, 5094–5099.
115. Johnson-Winters, K., Purpero, V. M., Kavana, M., Nelson, T., and Moran, G. R. (2003) (4-Hydroxyphenyl)pyruvate dioxygenase from *Streptomyces avermitilis*: The basis for ordered substrate addition, *Biochemistry 42*, 2072–2080.
116. Leu, L. S., and Cook, P. F. (1994) Kinetic mechanism of serine transacetylase from *Salmonella typhimurium*, *Biochemistry 33*, 2667–2671.
117. Ainsworth, S., and MacFarlane, N. (1973) A kinetic study of rabbit muscle pyruvate kinase, *Biochem. J. 131*, 223–236.
118. Larsen, T. M., Laughlin, L. T., Holden, H. M., Rayment, I., and Reed, G. H. (1994) Structure of rabbit muscle pyruvate kinase complexed with Mn^{2+}, K^+, and pyruvate, *Biochemistry 33*, 6301–6309.
119. Segel, I. H. (1975) *Enzyme kinetics: Behavior and analysis of rapid equilibrium and steady state enzyme systems*, pp 653–656, Wiley, New York.
120. Segel, I. H. (1975) *Enzyme kinetics: Behavior and analysis of rapid equilibrium and steady state enzyme systems*, p 304, Wiley, New York.
121. Gao, X., and Harris, T. K. (2006) Steady-state kinetic mechanism of PDK1, *J. Biol. Chem. 281*, 21670–21681.
122. Bhatia, M. B., Vinitsky, A., and Grubmeyer, C. (1990) Kinetic mechanism of orotate phosphoribosyltransferase from *Salmonella typhimurium*, *Biochemistry 29*, 10480–10487.
123. Fujiwara, K., and Motokawa, Y. (1983) Mechanism of the glycine cleavage reaction. Steady state kinetic studies of the P-protein-catalyzed reaction, *J. Biol. Chem. 258*, 8156–8162.
124. Marshall, C. G., Zolli, M., and Wright, G. D. (1999) Molecular mechanism of VanHst, an α-ketoacid dehydrogenase required for glycopeptide antibiotic resistance from a glycopeptide producing organism, *Biochemistry 38*, 8485–8491.
125. Tanner, K. G., Langer, M. R., Kim, Y., and Denu, J. M. (2000) Kinetic mechanism of the histone acetyltransferase GCN5 from yeast, *J. Biol. Chem. 275*, 22048–22055.
126. Munagala, N. R., Chin, M. S., and Wang, C. C. (1998) Steady-state kinetics of the hypoxanthine-guanine-xanthine phosphoribosyltransferase from *Tritrichomonas foetus*: The role of threonine-47, *Biochemistry 37*, 4045–4051.
127. Hughes, T. L., Hahn, T. M., Reynolds, K. K., and Shewach, D. S. (1997) Kinetic analysis of human deoxycytidine kinase with the true phosphate donor uridine triphosphate, *Biochemistry 36*, 7540–7547.
128. Eddershaw, A. R., Stubbs, C. J., Edwardes, L. V., Underwood, E., Hamm, G. R., Davey, P. R. J., Clarkson, P. N., and Syson, K. (2020) Characterization of the kinetic mechanism of human protein arginine methyltransferase 5, *Biochemistry 59*, 4775–4786.
129. Dolence, J. M., Cassidy, P. B., Mathis, J. R., and Poulter, C. D. (1995) Yeast protein farnesyltransferase: Steady-state kinetic studies of substrate binding, *Biochemistry 34*, 16687–16694.
130. Lu, C., Lin, Y., and Yeh, S. R. (2009) Inhibitory substrate binding site of human indoleamine 2,3-dioxygenase, *J. Am. Chem. Soc. 131*, 12866–12867.

131. Hampele, I. C., D'Arcy, A., Dale, G. E., Kostrewa, D., Nielsen, J., Oefner, C., Page, M. G., Schonfeld, H. J., Stuber, D., and Then, R. L. (1997) Structure and function of the dihydropteroate synthase from *Staphylococcus aureus*, *J. Mol. Biol. 268*, 21–30.
132. Gruys, K. J., Walker, M. C., and Sikorski, J. A. (1992) Substrate synergism and the steady-state kinetic reaction mechanism for EPSP synthase from *Escherichia coli*, *Biochemistry 31*, 5534–5544.
133. Aitken, S. M., and Kirsch, J. F. (2003) Kinetics of the yeast cystathionine *β*-synthase forward and reverse reactions: Continuous assays and the equilibrium constant for the reaction, *Biochemistry 42*, 571–578.
134. Tidemand, K. D., Peters, G. H., Harris, P., Stensgaard, E., and Christensen, H. E. M. (2017) Isoform-specific substrate inhibition mechanism of human tryptophan hydroxylase, *Biochemistry 56*, 6155–6164.
135. Dalziel, K. (1962) Kinetic studies of liver alcohol dehydrogenase, *Biochem. J. 84*, 244–254.
136. Wang, G. P., Lundegaard, C., Jensen, K. F., and Grubmeyer, C. (1999) Kinetic mechanism of OMP synthase: A slow physical step following group transfer limits catalytic rate, *Biochemistry 38*, 275–283.
137. Radisky, E. S., and Poulter, C. D. (2000) Squalene synthase: Steady-state, pre-steady-state, and isotope-trapping studies, *Biochemistry 39*, 1748–1760.
138. Richard, S. B., Lillo, A. M., Tetzlaff, C. N., Bowman, M. E., Noel, J. P., and Cane, D. E. (2004) Kinetic analysis of *Escherichia coli* 2-C-methyl-D-erythritol-4-phosphate cytidyltransferase, wild-type and mutants, reveals roles of active site amino acids, *Biochemistry 43*, 12189–12197.
139. Mathis, J. R., and Poulter, C. D. (1997) Yeast protein farnesyltransferase: A pre-steady-state kinetic analysis, *Biochemistry 36*, 6367–6376.
140. Kahn, K., and Tipton, P. A. (1997) Kinetic mechanism and cofactor content of soybean root nodule urate oxidase, *Biochemistry 36*, 4731–4738.
141. Kong, C. T., and Cook, P. F. (1988) Isotope partitioning in the adenosine 3′,5′-monophosphate dependent protein kinase reaction indicates a steady-state random kinetic mechanism, *Biochemistry 27*, 4795–4799.
142. Lin, Y., Alguindigue, S. S., Volkman, J., Nicholas, K. M., West, A. H., and Cook, P. F. (2007) Complete kinetic mechanism of homoisocitrate dehydrogenase from *Saccharomyces cerevisiae*, *Biochemistry 46*, 890–898.
143. Pember, S. O., Johnson, K. A., Villafranca, J. J., and Benkovic, S. J. (1989) Mechanistic studies on phenylalanine hydroxylase from *Chromobacterium violaceum*. Evidence for the formation of an enzyme-oxygen complex, *Biochemistry 28*, 2124–2130.
144. Yao, J., Patrone, J. D., and Dotson, G. D. (2009) Characterization and kinetics of phosphopantothenoylcysteine synthetase from *Enterococcus faecalis*, *Biochemistry 48*, 2799–2806.
145. Sikora, A. L., Wilson, D. J., Aldrich, C. C., and Blanchard, J. S. (2010) Kinetic and inhibition studies of dihydroxybenzoate-AMP ligase from *Escherichia coli*, *Biochemistry 49*, 3648–3657.
146. Nelson, S. W., Binkowski, D. J., Honzatko, R. B., and Fromm, H. J. (2005) Mechanism of action of *Escherichia coli* phosphoribosylaminoimidazolesuccinocarboxamide synthetase, *Biochemistry 44*, 766–774.
147. Van Lanen, S. G., and Iwata-Reuyl, D. (2003) Kinetic mechanism of the tRNA-modifying enzyme *S*-adenosylmethionine:tRNA ribosyltransferase-isomerase (QueA), *Biochemistry 42*, 5312–5320.
148. Wong, I., Patel, S. S., and Johnson, K. A. (1991) An induced-fit kinetic mechanism for DNA replication fidelity: Direct measurement by single-turnover kinetics, *Biochemistry 30*, 526–537.
149. Puistola, U., Turpeenniemi-Hujanen, T. M., Myllyla, R., and Kivirikko, K. I. (1980) Studies on the lysyl hydroxylase reaction. I. Initial velocity kinetics and related aspects, *Biochim. Biophys. Acta 611*, 40–50.
150. Wang, H. C., Ciskanik, L., Dunaway-Mariano, D., von der Saal, W., and Villafranca, J. J. (1988) Investigations of the partial reactions catalyzed by pyruvate phosphate dikinase, *Biochemistry 27*, 625–633.
151. Griffin, J., Roshick, C., Iliffe-Lee, E., and McClarty, G. (2005) Catalytic mechanism of *Chlamydia trachomatis* flavin-dependent thymidylate synthase, *J. Biol. Chem. 280*, 5456–5467.
152. Gadd, R. E., and Henderson, J. F. (1969) Inhibition of adenine phosphoriboxyltransferase

by pyrophosphate, *Biochim. Biophys. Acta 191*, 735–737.
153. Meier, T. W., Thoma, N. H., and Leadlay, P. F. (1996) Tritium isotope effects in adenosylcobalamin-dependent methylmalonyl-CoA mutase, *Biochemistry 35*, 11791–11796.
154. Katiyar, S. S., and Porter, J. W. (1974) Substrate inhibition of pigeon liver fatty acid synthetase and optimum assay conditions for over-all synthetase activity, *Arch. Biochem. Biophys. 163*, 324–331.
155. Jarrett, H. W., and Kyte, J. (1979) Human erythrocyte calmodulin. Further chemical characterization and the site of its interaction with the membrane, *J. Biol. Chem. 254*, 8237–8244.
156. Bruch, P., Schnackerz, K. D., Chirgwin, J. M., and Noltmann, E. A. (1973) Binding studies on rabbit-muscle phosphoglucose isomerase, *Eur. J. Biochem. 36*, 564–568.
157. Klotz, I. M., Walker, F. M., and Pivan, R. B. (1946) The binding of organic ions by proteins, *J. Am. Chem. Soc. 68*, 1486–1490.
158. Teresi, J. D., and Luck, J. M. (1948) The combination of organic anions with serum albumin; Quantitative studies by equilibrium dialysis, *J. Biol. Chem. 174*, 653–661.
159. Colowick, S. P., and Womack, F. C. (1969) Binding of diffusible molecules by macromolecules: Rapid measurement by rate of dialysis, *J. Biol. Chem. 244*, 774–777.
160. Stitt, B. L. (1988) *Escherichia coli* transcription termination protein rho has three hydrolytic sites for ATP, *J. Biol. Chem. 263*, 11130–11137.
161. Grubmeyer, C. T., Chu, K. W., and Insinga, S. (1987) Kinetic mechanism of histidinol dehydrogenase: Histidinol binding and exchange reactions, *Biochemistry 26*, 3369–3373.
162. Hummel, J. P., and Dreyer, W. J. (1962) Measurement of protein-binding phenomena by gel filtration, *Biochim. Biophys. Acta 63*, 530–532.
163. Cao, H., Pietrak, B. L., and Grubmeyer, C. (2002) Quinolinate phosphoribosyltransferase: Kinetic mechanism for a type II PRTase, *Biochemistry 41*, 3520–3528.
164. Chu, Y. H., Lees, W. J., Stassinopoulos, A., and Walsh, C. T. (1994) Using affinity capillary electrophoresis to determine binding stoichiometries of protein-ligand interactions, *Biochemistry 33*, 10616–10621.
165. DeLean, A., Munson, P. J., and Rodbard, D. (1978) Simultaneous analysis of families of sigmoidal curves: Application to bioassay, radioligand assay, and physiological dose-response curves, *Am J Physiol 235*, E97–102.
166. Munson, P. J., and Rodbard, D. (1980) Ligand: A versatile computerized approach for characterization of ligand-binding systems, *Anal. Biochem. 107*, 220–239.
167. Dyson, J. E., and Noltmann, E. A. (1968) The effect of pH and temperature on the kinetic parameters of phosphoglucose isomerase. Participation of histidine and lysine in a proposed dual function mechanism, *J. Biol. Chem. 243*, 1401–1414.
168. Ream, J. E., Yuen, H. K., Frazier, R. B., and Sikorski, J. A. (1992) EPSP Synthase: Binding studies using isothermal titration microcalorimetry and equilibrium dialysis and their implications for ligand recognition and kinetic mechanism, *Biochemistry 31*, 5528–5534.
169. Etzkorn, F. A., Guo, T., Lipton, M. A., Goldberg, S. D., and Bartlett, P. A. (1994) Cyclic hexapeptides and chimeric peptides as mimics of tendamistat, *J. Am. Chem. Soc. 116*, 10412–10425.
170. Radic, Z., Gibney, G., Kawamoto, S., MacPhee-Quigley, K., Bongiorno, C., and Taylor, P. (1992) Expression of recombinant acetylcholinesterase in a baculovirus system: Kinetic properties of glutamate 199 mutants, *Biochemistry 31*, 9760–9767.
171. Scatchard, G. (1949) The attraction of proteins for small molecules and ions, *Ann. N.Y. Acad. Sci. 51*, 660–672.
172. Kyte, J. (2007) *Structure in protein chemistry: Second edition*, pp 38–39, Garland Science, New York.
173. Kyte, J. (1995) *Mechanism in protein chemistry*, p 178, Garland Science, New York.
174. Galas, D. J., and Schmitz, A. (1978) DNAse footprinting: A simple method for the detection of protein-DNA binding specificity, *Nucleic Acids Res. 5*, 3157–3170.
175. Brenowitz, M., Senear, D. F., Shea, M. A., and Ackers, G. K. (1986) "Footprint" titrations yield valid thermodynamic isotherms, *Proc. Natl. Acad. Sci. U. S. A. 83*, 8462–8466.
176. Senear, D. F., Brenowitz, M., Shea, M. A., and Ackers, G. K. (1986) Energetics of cooperative protein-DNA interactions: Comparison between quantitative deoxyribonuclease foot-

print titration and filter binding, *Biochemistry 25*, 7344–7354.
177. Senear, D. F., and Batey, R. (1991) Comparison of operator-specific and nonspecific DNA binding of the λ cI repressor: [KCl] and pH effects, *Biochemistry 30*, 6677–6688.
178. Collins, K. D., and Stark, G. R. (1969) Aspartate transcarbamylase. Studies of the catalytic subunit by ultraviolet difference spectroscopy, *J. Biol. Chem. 244*, 1869–1877.
179. Schuman, M., and Massey, V. (1971) Purification and characterization of glycolic acid oxidase from pig liver, *Biochim. Biophys. Acta 227*, 500–520.
180. Huang, T., Wang, C., Maras, B., Barra, D., and Schirch, V. (1998) Thermodynamic analysis of the binding of the polyglutamate chain of 5-formyltetrahydropteroylpolyglutamates to serine hydroxymethyltransferase, *Biochemistry 37*, 13536–13542.
181. Egan, R. R., and Dalziel, K. (1971) Active centre equivalent weight of glutamate dehydrogenase from dry weight determinations and spectrophotometric titrations of abortive complexes, *Biochim. Biophys. Acta 250*, 47–50.
182. Lundback, T., Zilliacus, J., Gustafsson, J. A., Carlstedt-Duke, J., and Hard, T. (1994) Thermodynamics of sequence-specific glucocorticoid receptor-DNA interactions, *Biochemistry 33*, 5955–5965.
183. Johnson, J. L., and Reinhart, G. D. (1992) MgATP and fructose 6-phosphate interactions with phosphofructokinase from *Escherichia coli*, *Biochemistry 31*, 11510–11518.
184. Spencer, H. T., Villafranca, J. E., and Appleman, J. R. (1997) Kinetic scheme for thymidylate synthase from *Escherichia coli*: Determination from measurements of ligand binding, primary and secondary isotope effects, and pre-steady-state catalysis, *Biochemistry 36*, 4212–4222.
185. Rajagopalan, P. T., Zhang, Z., McCourt, L., Dwyer, M., Benkovic, S. J., and Hammes, G. G. (2002) Interaction of dihydrofolate reductase with methotrexate: Ensemble and single-molecule kinetics, *Proc. Natl. Acad. Sci. U. S. A. 99*, 13481–13486.
186. Janin, J., van Rapenbusch, R., Truffa-Bachi, P., and Cohen, G. N. (1969) The threonine-sensitive homoserine dehydrogenase and aspartokinase activities of *Escherichia coli* K12: Binding of threonine and of pyridine nucleotides: Stoichiometry and optical effects, *Eur. J. Biochem. 8*, 128–138.
187. Li, Y., Wu, Y., Blaszczyk, J., Ji, X., and Yan, H. (2003) Catalytic roles of arginine residues 82 and 92 of *Escherichia coli* 6-hydroxymethyl-7,8-dihydropterin pyrophosphokinase: Site-directed mutagenesis and biochemical studies, *Biochemistry 42*, 1581–1588.
188. Harris, B. Z., Hillier, B. J., and Lim, W. A. (2001) Energetic determinants of internal motif recognition by PDZ domains, *Biochemistry 40*, 5921–5930.
189. Kelemen, B. R., Schultz, L. W., Sweeney, R. Y., and Raines, R. T. (2000) Excavating an active site: The nucleobase specificity of ribonuclease A, *Biochemistry 39*, 14487–14494.
190. Jacob, G. S., Kirmaier, C., Abbas, S. Z., Howard, S. C., Steininger, C. N., Welply, J. K., and Scudder, P. (1995) Binding of sialyl lewis X to E-selectin as measured by fluorescence polarization, *Biochemistry 34*, 1210–1217.
191. Fisher, B. M., Ha, J. H., and Raines, R. T. (1998) Coulombic forces in protein-RNA interactions: Binding and cleavage by ribonuclease A and variants at Lys7, Arg10, and Lys66, *Biochemistry 37*, 12121–12132.
192. Harlan, J. E., Yoon, H. S., Hajduk, P. J., and Fesik, S. W. (1995) Structural characterization of the interaction between a pleckstrin homology domain and phosphatidylinositol 4,5-bisphosphate, *Biochemistry 34*, 9859–9864.
193. Wright, E., and Serpersu, E. H. (2005) Enzyme-substrate interactions with an antibiotic resistance enzyme: Aminoglycoside nucleotidyltransferase(2″)-Ia characterized by kinetic and thermodynamic methods, *Biochemistry 44*, 11581–11591.
194. Barratt, E., Bingham, R. J., Warner, D. J., Laughton, C. A., Phillips, S. E., and Homans, S. W. (2005) van der Waals interactions dominate ligand-protein association in a protein binding site occluded from solvent water, *J. Am. Chem. Soc. 127*, 11827–11834.
195. Deranleau, D. A., Bradshaw, R. A., and Schwyzer, R. (1969) The use of *N*-methylnicotinamide chloride as a conformational probe for chicken egg-white lysozyme, *Proc. Natl. Acad. Sci. U. S. A. 63*, 885–889.
196. Kyte, J. (1972) The titration of the cardiac glycoside binding site of the $(Na^+ + K^+)$-adenosine triphosphatase, *J. Biol. Chem. 247*, 7634–7641.

197. Meighen, E. A., and Hastings, J. W. (1971) Binding site determination from kinetic data. Reduced flavin mononucleotide binding to bacterial luciferase, *J. Biol. Chem. 246*, 7666–7674.
198. Parsons, J. F., Calabrese, K., Eisenstein, E., and Ladner, J. E. (2003) Structure and mechanism of *Pseudomonas aeruginosa* PhzD, an isochorismatase from the phenazine biosynthetic pathway, *Biochemistry 42*, 5684–5693.
199. Gopinath, R. M., and Vincenzi, F. F. (1977) Phosphodiesterase protein activator mimics red blood cell cytoplasmic activator of (Ca^{2+}-Mg^{2+})ATPase, *Biochem. Biophys. Res. Commun. 77*, 1203–1209.
200. Jarrett, H. W., and Penniston, J. T. (1977) Partial purification of the Ca^{2+}-Mg^{2+} ATPase activator from human erythrocytes: Its similarity to the activator of 3′:5′-cyclic nucleotide phosphodiesterase, *Biochem. Biophys. Res. Commun. 77*, 1210–1216.
201. Jagath, J. R., Rodnina, M. V., Lentzen, G., and Wintermeyer, W. (1998) Interaction of guanine nucleotides with the signal recognition particle from *Escherichia coli*, *Biochemistry 37*, 15408–15413.
202. Gilbert, W., and Muller-Hill, B. (1966) Isolation of the lac repressor, *Proc. Natl. Acad. Sci. U. S. A. 56*, 1891–1898.
203. Maturo, J. M., 3rd, and Hollenberg, M. D. (1978) Insulin receptor: Interaction with nonreceptor glycoprotein from liver cell membranes, *Proc. Natl. Acad. Sci. U. S. A. 75*, 3070–3074.
204. Cuatrecasas, P., and Hollenberg, M. D. (1976) Membrane receptors and hormone action, *Adv. Protein Chem. 30*, 251–451.
205. Carpenter, G., King, L., Jr., and Cohen, S. (1979) Rapid enhancement of protein phosphorylation in A-431 cell membrane preparations by epidermal growth factor, *J. Biol. Chem. 254*, 4884–4891.
206. Fried, M. G., and Crothers, D. M. (1983) CAP and RNA polymerase interactions with the lac promoter: Binding stoichiometry and long range effects, *Nucleic Acids Res. 11*, 141–158.
207. Tao, X., Boyd, J., and Murphy, J. R. (1992) Specific binding of the diphtheria tox regulatory element DtxR to the tox operator requires divalent heavy metal ions and a 9-base-pair interrupted palindromic sequence, *Proc. Natl. Acad. Sci. U. S. A. 89*, 5897–5901.
208. Chen, C. S., White, A., Love, J., Murphy, J. R., and Ringe, D. (2000) Methyl groups of thymine bases are important for nucleic acid recognition by DtxR, *Biochemistry 39*, 10397–10407.
209. Roche, P. A., and Pizzo, S. V. (1987) Characterization of $\alpha 2$-macroglobulin-plasmin complexes: Complete subunit cleavage alters receptor recognition *in vivo* and in *vitro*, *Biochemistry 26*, 486–491.
210. Sine, S. M., and Taylor, P. (1980) The relationship between agonist occupation and the permeability response of the cholinergic receptor revealed by bound cobra α-toxin, *J. Biol. Chem. 255*, 10144–10156.
211. Jiang, Y. L., Ichikawa, Y., and Stivers, J. T. (2002) Inhibition of uracil DNA glycosylase by an oxacarbenium ion mimic, *Biochemistry 41*, 7116–7124.
212. Marchaj, A., Jacobsen, D. W., Savon, S. R., and Brown, K. L. (1995) Kinetics and thermodynamics of the interaction of cyanocobalamin (vitamin B12) with haptocorrin: Measurement of the highest protein-ligand binding constant yet reported, *J. Am. Chem. Soc. 117*, 11640–11646.
213. Hanson, J. E., Kaplan, A. P., and Bartlett, P. A. (1989) Phosphonate analogues of carboxypeptidase A substrates are potent transition-state analogue inhibitors, *Biochemistry 28*, 6294–6305.
214. Guo, X. T., Uehara, A., Ravindran, A., Bryant, S. H., Hall, S., and Moczydlowski, E. (1987) Kinetic basis for insensitivity to tetrodotoxin and saxitoxin in sodium channels of canine heart and denervated rat skeletal muscle, *Biochemistry 26*, 7546–7556.
215. Knighton, D. R., Zheng, J. H., Ten Eyck, L. F., Xuong, N. H., Taylor, S. S., and Sowadski, J. M. (1991) Structure of a peptide inhibitor bound to the catalytic subunit of cyclic adenosine monophosphate-dependent protein kinase, *Science 253*, 414–420.
216. Zheng, J., Knighton, D. R., ten Eyck, L. F., Karlsson, R., Xuong, N., Taylor, S. S., and Sowadski, J. M. (1993) Crystal structure of the catalytic subunit of cAMP-dependent protein kinase complexed with MgATP and peptide inhibitor, *Biochemistry 32*, 2154–2161.
217. Gibbs, C. S., and Zoller, M. J. (1991) Rational scanning mutagenesis of a protein kinase identifies functional regions involved in ca-

talysis and substrate interactions, *J. Biol. Chem 266*, 8923–8931.
218. Stuible, H. P., and Kombrink, E. (2001) Identification of the substrate specificity-conferring amino acid residues of 4-coumarate:Coenzyme A ligase allows the rational design of mutant enzymes with new catalytic properties, *J. Biol. Chem. 276*, 26893–26897.
219. Wang, X., and Kemp, R. G. (1999) Identification of residues of *Escherichia coli* phosphofructokinase that contribute to nucleotide binding and specificity, *Biochemistry 38*, 4313–4318.
220. McGinnis, K., Ku, G. M., VanDusen, W. J., Fu, J., Garsky, V., Stern, A. M., and Friedman, P. A. (1996) Site-directed mutagenesis of residues in a conserved region of bovine aspartyl (asparaginyl) β-hydroxylase: Evidence that histidine 675 has a role in binding Fe^{2+}, *Biochemistry 35*, 3957–3962.
221. Zhu, Z., Sun, D., and Davidson, V. L. (2000) Conversion of methylamine dehydrogenase to a long-chain amine dehydrogenase by mutagenesis of a single residue, *Biochemistry 39*, 11184–11186.
222. Sem, D. S., and Kasper, C. B. (1993) Interaction with arginine 597 of NADPH-cytochrome p-450 oxidoreductase is a primary source of the uniform binding energy used to discriminate between NADPH and NADH, *Biochemistry 32*, 11548–11558.
223. Metanis, N., Keinan, E., and Dawson, P. E. (2005) A designed synthetic analogue of 4-OT is specific for a non-natural substrate, *J. Am. Chem. Soc. 127*, 5862–5868.
224. Hasan, F. B., Cohen, S. G., and Cohen, J. B. (1980) Hydrolysis by acetylcholinesterase. Apparent molal volumes and trimethyl and methyl subsites, *J. Biol. Chem. 255*, 3898–3904.
225. Sussman, J. L., Harel, M., Frolow, F., Oefner, C., Goldman, A., Toker, L., and Silman, I. (1991) Atomic structure of acetylcholinesterase from *Torpedo californica*: A prototypic acetylcholine-binding protein, *Science 253*, 872–879.
226. Harel, M., Schalk, I., Ehret-Sabatier, L., Bouet, F., Goeldner, M., Hirth, C., Axelsen, P. H., Silman, I., and Sussman, J. L. (1993) Quaternary ligand binding to aromatic residues in the active-site gorge of acetylcholinesterase, *Proc. Natl. Acad. Sci. U. S. A. 90*, 9031–9035.
227. Harel, M., Quinn, D. M., Nair, H. K., Silman, I., and Sussman, J. L. (1996) The X-ray structure of a transition state analog complex reveals the molecular origins of the catalytic power and substrate specificity of acetylcholinesterase, *J. Am. Chem. Soc. 118*, 2340–2346.
228. Ordentlich, A., Barak, D., Kronman, C., Flashner, Y., Leitner, M., Segall, Y., Ariel, N., Cohen, S., Velan, B., and Shafferman, A. (1993) Dissection of the human acetylcholinesterase active center determinants of substrate specificity: Identification of residues constituting the anionic site, the hydrophobic site, and the acyl pocket, *J. Biol. Chem. 268*, 17083–17095.
229. Quinn, D. M., Feaster, S. R., Nair, H. K., Baker, N. A., Radic, Z., and Taylor, P. (2000) Delineation and decomposition of energies involved in quaternary ammonium binding in the active site of acetylcholinesterase, *J. Am. Chem. Soc. 122*, 2975–2980.
230. Radic, Z., Pickering, N. A., Vellom, D. C., Camp, S., and Taylor, P. (1993) Three distinct domains in the cholinesterase molecule confer selectivity for acetyl- and butyrylcholinesterase inhibitors, *Biochemistry 32*, 12074–12084.
231. Dougherty, D. A. (1996) Cation-π interactions in chemistry and biology: A new view of benzene, Phe, Tyr, and Trp, *Science 271*, 163–168.
232. Stoll, V., Stewart, K. D., Maring, C. J., Muchmore, S., Giranda, V., Gu, Y. G., Wang, G., Chen, Y., Sun, M., Zhao, C., Kennedy, A. L., Madigan, D. L., Xu, Y., Saldivar, A., Kati, W., Laver, G., Sowin, T., Sham, H. L., Greer, J., and Kempf, D. (2003) Influenza neuraminidase inhibitors: Structure-based design of a novel inhibitor series, *Biochemistry 42*, 718–727.
233. Rudolph, F. B., and Fromm, H. J. (1971) Computer simulation studies with yeast hexokinase and additional evidence for the random Bi Bi mechanism, *J. Biol. Chem. 246*, 6611–6619.
234. Colowick, S. P., Womack, F. C., and Nielsen, J. (1969) In *The Role of Nucleotides for the Function and Conformation of Enzymes* (Kalckar, H. M., Klenow, H., Munch-Petersen, A., Ottensen, M., and Thaysen, J. H., Ed.), pp 15–43, Academic Press, New York.
235. Bessell, E. M., Foster, A. B., and Westwood, J. H. (1972) The use of deoxyfluoro-D-glucopyranoses and related compounds in a study

of yeast hexokinase specificity, *Biochem. J. 128*, 199–204.
236. Sols, A., De La Fuente, G., Villarpalasi, C., and Asensio, C. (1958) Substrate specificity and some other properties of baker's yeast hexokinase, *Biochim. Biophys. Acta 30*, 92–101.
237. Aleshin, A. E., Zeng, C., Bourenkov, G. P., Bartunik, H. D., Fromm, H. J., and Honzatko, R. B. (1998) The mechanism of regulation of hexokinase: New insights from the crystal structure of recombinant human brain hexokinase complexed with glucose and glucose-6-phosphate, *Structure 6*, 39–50.
238. Cullis, P. M., Lewendon, A., Shaw, W. V., and Williams, J. A. (1991) Ligand interaction energies and molecular recognition by chloramphenicol acetyltransferase, *Biochemistry 30*, 3758–3762.
239. Kim, T. W., Delaney, J. C., Essigmann, J. M., and Kool, E. T. (2005) Probing the active site tightness of DNA polymerase in subangstrom increments, *Proc. Natl. Acad. Sci. U. S. A. 102*, 15803–15808.
240. Krenitsky, T. A., Tuttle, J. V., Miller, W. H., Moorman, A. R., Orr, G. F., and Beauchamp, L. (1990) Nucleotide analogue inhibitors of purine nucleoside phosphorylase, *J. Biol. Chem. 265*, 3066–3069.
241. Chen, K., and Arnold, F. H. (1993) Tuning the activity of an enzyme for unusual environments: Sequential random mutagenesis of subtilisin E for catalysis in dimethylformamide, *Proc. Natl. Acad. Sci. U. S. A. 90*, 5618–5622.
242. Stemmer, W. P. (1994) DNA shuffling by random fragmentation and reassembly: In vitro recombination for molecular evolution, *Proc. Natl. Acad. Sci. U. S. A. 91*, 10747–10751.
243. Fasan, R., Meharenna, Y. T., Snow, C. D., Poulos, T. L., and Arnold, F. H. (2008) Evolutionary history of a specialized P450 propane monooxygenase, *J. Mol. Biol. 383*, 1069–1080.
244. Porter, R. W., Modebe, M. O., and Stark, G. R. (1969) Aspartate transcarbamylase. Kinetic studies of the catalytic subunit, *J. Biol. Chem. 244*, 1846–1859.
245. Howlett, G. J., and Schachman, H. K. (1977) Allosteric regulation of aspartate transcarbamoylase: Changes in the sedimentation coefficient promoted by the bisubstrate analogue N-(phosphonacetyl)-L-aspartate, *Biochemistry 16*, 5077–5083.
246. Lorenson, M. Y., and Mansour, T. E. (1969) Studies on heart phosphofructokinase. Binding properties of native enzyme and of enzyme desensitized to allosteric control, *J. Bi-Biol. Chem. 244*, 6420–6431.
247. Liou, R. S., and Anderson, S. R. (1978) Binding of ATP and of 1,N^6-ethenoadenosine triphosphate to rabbit muscle phosphofructokinase, *Biochemistry 17*, 999–1004.
248. Franzen, J. S., Kuo, I., Eichler, A. J., and Feingold, D. S. (1973) UDP-glucose dehydrogenase: Substrate binding stoichiometry and affinity, *Biochem. Biophys. Res. Commun. 50*, 517–523.
249. Kalckar, H. M., Maxwell, E. S., and Strominger, J. L. (1956) Some properties of uridine diphosphoglucose dehydrogenase, *Arch. Biochem. Biophys. 65*, 2–10.
250. Salitis, G., and Oliver, I. T. (1964) Inhibition of uridine diphosphate glucose (UDPG) dehydrogenase by metabolic intermediates of galactose, *Biochim. Biophys. Acta 81*, 55–60.
251. Penzer, G. R., Bennett, E. L., and Calvin, M. (1971) Isoleucyl-tRNA synthetase. A fluorescence study of the binding properties of the synthetase from *Escherichia coli*, *Eur. J. Biochem. 20*, 1–13.
252. Cole, F. X., and Schimmel, P. R. (1970) On the rate law and mechanism of the adenosine triphosphate--pyrophosphate isotope exchange reaction of amino acyl transfer ribonucleic acid synthetases, *Biochemistry 9*, 480–489.
253. Perozzo, R., Jelesarov, I., Bosshard, H. R., Folkers, G., and Scapozza, L. (2000) Compulsory order of substrate binding to herpes simplex virus type 1 thymidine kinase. A calorimetric study, *J. Biol. Chem. 275*, 16139–16145.
254. Kuehn, G. D., Barnes, L. D., and Atkinson, D. E. (1971) Yeast diphosphopyridine nucleotide specific isocitrate dehydrogenase. Binding of ligands, *Biochemistry 10*, 3945–3951.
255. Chen, S., Tomchick, D. R., Wolle, D., Hu, P., Smith, J. L., Switzer, R. L., and Zalkin, H. (1997) Mechanism of the synergistic end-product regulation of *Bacillus subtilis* glutamine phosphoribosylpyrophosphate amidotransferase by nucleotides, *Biochemistry 36*, 10718–10726.
256. Borders, C. L., Jr., Snider, M. J., Wolfenden, R., and Edmiston, P. L. (2002) Determination of the affinity of each component of a com-

posite quaternary transition-state analogue complex of creatine kinase, *Biochemistry 41*, 6995–7000.
257. Du, W., Liu, W. S., Payne, D. J., and Doyle, M. L. (2000) Synergistic inhibitor binding to *Streptococcus pneumoniae* 5-enolpyruvylshikimate-3-phosphate synthase with both monovalent cations and substrate, *Biochemistry 39*, 10140–10146.
258. Anderson, K. S., Sikorski, J. A., and Johnson, K. A. (1988) Evaluation of 5-enolpyruvoylshikimate-3-phosphate synthase substrate and inhibitor binding by stopped-flow and equilibrium fluorescence measurements, *Biochemistry 27*, 1604–1610.
259. Miller, K. E., Mukhopadhyay, C., Cagas, P., and Bush, C. A. (1992) Solution structure of the Lewis x oligosaccharide determined by NMR spectroscopy and molecular dynamics simulations, *Biochemistry 31*, 6703–6709.
260. Gadd, R. E., and Henderson, J. F. (1970) Studies of the binding of phosphoribosyl pyrophosphate to adenine phosphoribosyltransferase, *J. Biol. Chem. 245*, 2979–2984.
261. Born, M., and Oppenheimer, J. R. (1927) Zur Quantentheorie der Molekeln, *Ann, Phys. 389*, 457–484.
262. Frost, A. A., and Pearson, R. G. (1961) *Kinetics and mechanism: A study of homogeneous chemical reactions*, John Wiley and Sons, New York.
263. Kraut, J. (1988) How do enzymes work?, *Science 242*, 533–540.
264. Wolfenden, R., and Snider, M. J. (2001) The depth of chemical time and the power of enzymes as catalysts, *Accounts Chem. Res. 34*, 938–945.
265. Lad, C., Williams, N. H., and Wolfenden, R. (2003) The rate of hydrolysis of phosphomonoester dianions and the exceptional catalytic proficiencies of protein and inositol phosphatases, *Proc. Natl. Acad. Sci. U. S. A. 100*, 5607–5610.
266. Coward, J. K., Lok, R., and Takagi, O. (1976) General base catalysis in nucleophilic attack at sp^3 carbon of methylase model compounds, *J. Am. Chem. Soc. 98*, 1057–1059.
267. Jencks, W. P. (1969) *Catalysis in chemistry and enzymology*, pp 9–10, McGraw-Hill, New York.
268. Griffin, B. E., Jarman, M., Reese, C. B., Sulston, J. E., and Trentham, D. R. (1966) Acyl mobility in aminoacyl soluble ribonucleic acids, *Biochemistry 5*, 3638–3649.
269. Bruice, T. C., Blasko, A., Arasasingham, R. D., and Kim, J.-S. (1995) Participation of two carboxyl groups in phosphodiester hydrolysis. 2. A kinetic, isotopic, and ^{31}P NMR study of the hydrolysis of a phosphodiester with carboxyl groups fixed in an attack conformation, *J. Am. Chem. Soc. 117*, 12070–12077.
270. Jencks, W. P. (1969) *Catalysis in chemistry and enzymology*, pp 8–30, McGraw-Hill, New York.
271. Bruice, T. C. (1970) Proximity effects and enzyme catalysis, In *The Enzymes: Kinetics and Mechanism, Vol. II, 3rd Edition* (Boyer, P. D., Ed.) 3rd ed., pp 217–279, Academic Press, New York.
272. Page, M. I., and Jencks, W. P. (1971) Entropic contributions to rate accelerations in enzymic and intramolecular reactions and the chelate effect, *Proc. Natl. Acad. Sci. U. S. A. 68*, 1678–1683.
273. Sharp, K. A., Nicholls, A., Friedman, R., and Honig, B. (1991) Extracting hydrophobic free energies from experimental data: Relationship to protein folding and theoretical models, *Biochemistry 30*, 9686–9697.
274. Kyte, J. (2007) *Structure in protein chemistry: Second edition*, pp 196–199, Garland Science, New York.
275. Hubbard, T. A., Brown, A. J., Bell, I. A., and Cockroft, S. L. (2016) The limit of intramolecular H-bonding, *J. Am. Chem. Soc. 138*, 15114–15117.
276. Bruice, T. C., and Pandit, U. K. (1960) The effect of geminal substitution, ring size, and rotamer distribution on the intramolecular nucleophilic catalysis of the hydrolysis of monophenyl esters of dibasic acids and the solvolysis of the intermediate anhydrides, *J. Am. Chem. Soc. 82*, 5858–5865.
277. Taylor, R., Kennard, O., and Versichel, W. (1984) Geometry of the N-H···O=C hydrogen bond. 2. Three-center ("bifurcated") and four-center ("trifurcated") bonds, *J. Am. Chem. Soc. 106*, 244–248.
278. Higuchi, T., Eberson, L., and Herd, A. K. (1966) The intramolecular facilitated hydrolytic rates of methyl-substituted succinanilic acids, *J. Am. Chem. Soc. 88*, 3805–3808.
279. Milstien, S., and Cohen, L. A. (1972) Stereopopulation control. I. Rate enhancement in

the lactonizations of o-hydroxyhydrocinnamic acids, *J. Am. Chem. Soc. 94*, 9158–9165.
280. Jencks, W. P. (1975) Binding energy, specificity, and enzymic catalysis: The circe effect, *Adv. Enzymol. Relat. Areas Mol. Biol. 43*, 219–410.
281. Sigala, P. A., Kraut, D. A., Caaveiro, J. M. M., Pybus, B., Ruben, E. A., Ringe, D., Petsko, G. A., and Herschlag, D. (2008) Testing geometrical discrimination within an enzyme active site: Constrained hydrogen bonding in the ketosteroid isomerase oxyanion hole, *J. Am. Chem. Soc. 130*, 13696–13708.
282. Wolfenden, R., Snider, M., Ridgway, C., and Miller, B. (1999) The temperature dependence of enzyme rate enhancements, *J. Am. Chem. Soc. 121*, 7419–7420.
283. Snider, M. J., Gaunitz, S., Ridgway, C., Short, S. A., and Wolfenden, R. (2000) Temperature effects on the catalytic efficiency, rate enhancement, and transition state affinity of cytidine deaminase, and the thermodynamic consequences for catalysis of removing a substrate "anchor", *Biochemistry 39*, 9746–9753.
284. Blacklow, S. C., Raines, R. T., Lim, W. A., Zamore, P. D., and Knowles, J. R. (1988) Triosephosphate isomerase catalysis is diffusion controlled. Appendix: Analysis of triose phosphate equilibria in aqueous solution by ^{31}P NMR, *Biochemistry 27*, 1158–1167.
285. White, H., and Jencks, W. P. (1976) Mechanism and specificity of succinyl-CoA:3-ketoacid coenzyme A transferase, *J. Biol. Chem 251*, 1688–1699.
286. Fraser, M. E., Hayakawa, K., and Brown, W. D. (2010) Catalytic role of the conformational change in succinyl-CoA:3-oxoacid CoA transferase on binding CoA, *Biochemistry 49*, 10319–10328.
287. Carlow, D. C., Short, S. A., and Wolfenden, R. (1998) Complementary truncations of a hydrogen bond to ribose involved in transition-state stabilization by cytidine deaminase, *Biochemistry 37*, 1199–1203.
288. Whitty, A., Fierke, C. A., and Jencks, W. P. (1995) Role of binding energy with coenzyme A in catalysis by 3-oxoacid coenzyme A transferase, *Biochemistry 34*, 11678–11689.
289. Morihara, K., and Tsuzuki, H. (1970) Thermolysin: Kinetic study with oligopeptides, *Eur. J. Biochem. 15*, 374–380.
290. Steyaert, J., Haikal, A. F., Wyns, L., and Stanssens, P. (1991) Subsite interactions of ribonuclease T_1: Asn36 and Asn98 accelerate GpN transesterification through interactions with the leaving nucleoside N, *Biochemistry 30*, 8666–8670.
291. Sideraki, V., Mohamedali, K. A., Wilson, D. K., Chang, Z., Kellems, R. E., Quiocho, F. A., and Rudolph, F. B. (1996) Probing the functional role of two conserved active site aspartates in mouse adenosine deaminase, *Biochemistry 35*, 7862–7872.
292. Miller, B. G., Butterfoss, G. L., Short, S. A., and Wolfenden, R. (2001) Role of enzyme-ribofuranosyl contacts in the ground state and transition state for orotidine 5′-phosphate decarboxylase: A role for substrate destabilization?, *Biochemistry 40*, 6227–6232.
293. Miller, B. G., Snider, M. J., Short, S. A., and Wolfenden, R. (2000) Contribution of enzyme-phosphoribosyl contacts to catalysis by orotidine 5′-phosphate decarboxylase, *Biochemistry 39*, 8113–8118.
294. Brosius, J. L., and Colman, R. F. (2000) A key role in catalysis for His89 of adenylosuccinate lyase of *Bacillus subtilis*, *Biochemistry 39*, 13336–13343.
295. Gajewski, J. J., Jurayj, J., Kimbrough, D. R., Gande, M. E., Ganem, B., and Carpenter, B. K. (1987) The mechanism of rearrangement of chorismic acid and related compounds, *J. Am. Chem. Soc. 109*, 1170–1186.
296. Poulter, C. D., Marsh, L. L., Hughes, J. M., Argyle, J. C., Satterwhite, D. M., Goodfellow, R. J., and Moesinger, S. G. (1977) Model studies of the biosynthesis of non-head-to-tail terpenes. Rearrangements of the chrysanthemyl system, *J. Am. Chem. Soc. 99*, 3816–3823.
297. Bell, S. A., Niehaus, T. D., Nybo, S. E., and Chappell, J. (2014) Structure-function mapping of key determinants for hydrocarbon biosynthesis by squalene and squalene synthase-like enzymes from the green alga *Botryococcus braunii* race B, *Biochemistry 53*, 7570–7581.
298. Liu, C. I., Jeng, W. Y., Chang, W. J., Shih, M. F., Ko, T. P., and Wang, A. H. (2014) Structural insights into the catalytic mechanism of human squalene synthase, *Acta Crystallogr. D 70*, 231–241.
299. Lin, F. Y., Liu, C. I., Liu, Y. L., Zhang, Y., Wang, K., Jeng, W. Y., Ko, T. P., Cao, R., Wang, A. H., and Oldfield, E. (2010) Mecha-

nism of action and inhibition of dehydrosqualene synthase, *Proc. Natl. Acad. Sci. U.S.A. 107*, 21337–21342.
300. Oikawa, H., Katayama, K., Suzuki, Y., and Ichihara, A. (1995) Enzymatic-activity catalyzing exo-selective Diels-Alder reaction in solanapyrone biosynthesis, *J. Chem. Soc. Chem. Comm.*, 1321–1322.
301. Kasahara, K., Miyamoto, T., Fujimoto, T., Oguri, H., Tokiwano, T., Oikawa, H., Ebizuka, Y., and Fujii, I. (2010) Solanapyrone synthase, a possible Diels-Alderase and iterative type I polyketide synthase encoded in a biosynthetic gene cluster from *Alternaria solani*, *ChemBioChem 11*, 1245–1252.
302. Klas, K., Tsukamoto, S., Sherman, D. H., and Williams, R. M. (2015) Natural Diels-Alderases: Elusive and irresistable, *J. Org. Chem. 80*, 11672–11685.
303. Okvist, M., Dey, R., Sasso, S., Grahn, E., Kast, P., and Krengel, U. (2006) 1.6 Å Crystal structure of the secreted chorismate mutase from *Mycobacterium tuberculosis*: Novel fold topology revealed, *J. Mol. Biol. 357*, 1483–1499.
304. Andrews, P. R., Smith, G. D., and Young, I. G. (1973) Transition-state stabilization and enzymic catalysis. Kinetic and molecular orbital studies of the rearrangement of chorismate to prephenate, *Biochemistry 12*, 3492–3498.
305. Guo, H., Cui, Q., Lipscomb, W. N., and Karplus, M. (2001) Substrate conformational transitions in the active site of chorismate mutase: Their role in the catalytic mechanism, *Proc. Natl. Acad. Sci. U. S. A. 98*, 9032–9037.
306. Hur, S., and Bruice, T. C. (2003) The near attack conformation approach to the study of the chorismate to prephenate reaction, *Proc. Natl. Acad. Sci. U. S. A. 100*, 12015–12020.
307. Copley, S. D., and Knowles, J. R. (1987) The conformational equilibrium of chorismate in solution: Implications for the mechanism of the non-enzymic and the enzyme-catalyzed rearrangement of chorismate to prephenate, *J. Am. Chem. Soc. 109*, 5008–5013.
308. Guimaraes, S. L., Coitinho, J. B., Costa, D. M., Araujo, S. S., Whitman, C. P., and Nagem, R. A. (2016) Crystal structures of apo and liganded 4-oxalocrotonate decarboxylase uncover a structural basis for the metal-assisted decarboxylation of a vinylogous β-keto acid, *Biochemistry 55*, 2632–2645.
309. Hastings, C. J., Pluth, M. D., Bergman, R. G., and Raymond, K. N. (2010) Enzymelike catalysis of the Nazarov cyclization by supramolecular encapsulation, *J. Am. Chem. Soc. 132*, 6938–6940.
310. Amyes, T. L., and Richard, J. P. (2013) Specificity in transition state binding: The Pauling model revisited, *Biochemistry 52*, 2021–2035.
311. Pauling, L. (1948) Chemical achievement and hope for the future, *Am Sci 36*, 51–58.
312. Strynadka, N. C., and James, M. N. (1991) Lysozyme revisited: Crystallographic evidence for distortion of an *N*-acetylmuramic acid residue bound in site D, *J. Mol. Biol. 220*, 401–424.
313. Rupley, J. A. (1967) The binding and cleavage by lysozyme of *N*-acetylglucosamine oligosaccharides, *Proc. R. Soc. London, B 167*, 416–428.
314. Blake, C. C., Johnson, L. N., Mair, G. A., North, A. C., Phillips, D. C., and Sarma, V. R. (1967) Crystallographic studies of the activity of hen egg-white lysozyme, *Proc. R. Soc. London, B 167*, 378–388.
315. Leung, A. K., Duewel, H. S., Honek, J. F., and Berghuis, A. M. (2001) Crystal structure of the lytic transglycosylase from bacteriophage lambda in complex with hexa-*N*-acetylchitohexaose, *Biochemistry 40*, 5665–5673.
316. Ford, L. O., Johnson, L. N., Machin, P. A., Phillips, D. C., and Tjian, R. (1974) Crystal structure of a lysozyme-tetrasaccharide lactone complex, *J. Mol. Biol. 88*, 349–371.
317. Amyes, T. L., and Jencks, W. P. (1989) Concerted bimolecular substitution-reactions of acetal derivatives of propionaldehyde and benzaldehyde, *J. Am. Chem. Soc. 111*, 7900–7909.
318. Hammond, G. S. (1955) A correlation of reaction rates, *J. Am. Chem. Soc. 77*, 334–338.
319. Hadfield, A. T., Harvey, D. J., Archer, D. B., MacKenzie, D. A., Jeenes, D. J., Radford, S. E., Lowe, G., Dobson, C. M., and Johnson, L. N. (1994) Crystal structure of the mutant D52S hen egg white lysozyme with an oligosaccharide product, *J. Mol. Biol. 243*, 856–872.
320. Guerin, D. M., Lascombe, M. B., Costabel, M., Souchon, H., Lamzin, V., Beguin, P., and Alzari, P. M. (2002) Atomic (0.94 Å) resolution structure of an inverting glycosidase in complex with substrate, *J. Mol. Biol. 316*, 1061–1069.

321. Crennell, S. J., Garman, E. F., Philippon, C., Vasella, A., Laver, W. G., Vimr, E. R., and Taylor, G. L. (1996) The structures of *Salmonella typhimurium* Lt2 neuraminidase and its complexes with three inhibitors at high resolution, *J. Mol. Biol. 259*, 264–280.
322. Larsson, A. M., Bergfors, T., Dultz, E., Irwin, D. C., Roos, A., Driguez, H., Wilson, D. B., and Jones, T. A. (2005) Crystal structure of *Thermobifida fusca* endoglucanase Cel6A in complex with substrate and inhibitor: The role of tyrosine Y73 in substrate ring distortion, *Biochemistry 44*, 12915–12922.
323. Davies, G. J., Mackenzie, L., Varrot, A., Dauter, M., Brzozowski, A. M., Schulein, M., and Withers, S. G. (1998) Snapshots along an enzymatic reaction coordinate: Analysis of a retaining β-glycoside hydrolase, *Biochemistry 37*, 11707–11713.
324. Brzozowski, A. M., Lawson, D. M., Turkenburg, J. P., Bisgaard-Frantzen, H., Svendsen, A., Borchert, T. V., Dauter, Z., Wilson, K. S., and Davies, G. J. (2000) Structural analysis of a chimeric bacterial α-amylase. High-resolution analysis of native and ligand complexes, *Biochemistry 39*, 9099–9107.
325. Watson, J. N., Dookhun, V., Borgford, T. J., and Bennet, A. J. (2003) Mutagenesis of the conserved active-site tyrosine changes a retaining sialidase into an inverting sialidase, *Biochemistry 42*, 12682–12690.
326. Thomas, A., Jourand, D., Bret, C., Amara, P., and Field, M. J. (1999) Is there a covalent intermediate in the viral neuraminidase reaction? A hybrid potential free-energy study, *J. Am. Chem. Soc. 121*, 9693–9702.
327. Vocadlo, D. J., Davies, G. J., Laine, R., and Withers, S. G. (2001) Catalysis by hen egg-white lysozyme proceeds via a covalent intermediate, *Nature 412*, 835–838.
328. Amyes, T. L., and Jencks, W. P. (1989) Lifetimes of oxocarbenium ions in aqueous-solution from common ion inhibition of the solvolysis of α-azido ethers by added azide ion, *J. Am. Chem. Soc. 111*, 7888–7900.
329. Parikh, S. S., Walcher, G., Jones, G. D., Slupphaug, G., Krokan, H. E., Blackburn, G. M., and Tainer, J. A. (2000) Uracil-DNA glycosylase-DNA substrate and product structures: Conformational strain promotes catalytic efficiency by coupled stereoelectronic effects, *Proc. Natl. Acad. Sci. U. S. A. 97*, 5083–5088.
330. Sulzenbacher, G., Driguez, H., Henrissat, B., Schulein, M., and Davies, G. J. (1996) Structure of the *Fusarium oxysporum* endoglucanase I with a nonhydrolyzable substrate analogue: Substrate distortion gives rise to the preferred axial orientation for the leaving group, *Biochemistry 35*, 15280–15287.
331. Zheng, Y. J., Basarab, G. S., and Jordan, D. B. (2002) Roles of substrate distortion and intramolecular hydrogen bonding in enzymatic catalysis by scytalone dehydratase, *Biochemistry 41*, 820–826.
332. Zhang, Y., and Schramm, V. L. (2011) Ground-state destabilization in orotate phosphoribosyltransferases by binding isotope effects, *Biochemistry 50*, 4813–4818.
333. Mancia, F., Keep, N. H., Nakagawa, A., Leadlay, P. F., McSweeney, S., Rasmussen, B., Bosecke, P., Diat, O., and Evans, P. R. (1996) How coenzyme B_{12} radicals are generated: The crystal structure of methylmalonyl-coenzyme A mutase at 2 Å resolution, *Structure 4*, 339–350.
334. Jensen, K. P., and Ryde, U. (2005) How the Co-C bond is cleaved in coenzyme B_{12} enzymes: A theoretical study, *J. Am. Chem. Soc. 127*, 9117–9128.
335. Halpern, J., Kim, S. H., and Leung, T. W. (1984) Cobalt carbon bond-dissociation energy of coenzyme-B_{12}, *J. Am. Chem. Soc. 106*, 8317–8319.
336. Vladimirova, A., Patskovsky, Y., Fedorov, A. A., Bonanno, J. B., Fedorov, E. V., Toro, R., Hillerich, B., Seidel, R. D., Richards, N. G. J., Almo, S. C., and Raushel, F. M. (2016) Substrate distortion and the catalytic reaction mechanism of 5-carboxyvanillate decarboxylase, *J. Am. Chem. Soc. 138*, 826–836.
337. Asztalos, P., Parthier, C., Golbik, R., Kleinschmidt, M., Hubner, G., Weiss, M. S., Friedemann, R., Wille, G., and Tittmann, K. (2007) Strain and near attack conformers in enzymic thiamin catalysis: X-Ray crystallographic snapshots of bacterial transketolase in covalent complex with donor ketoses xylulose 5-phosphate and fructose 6-phosphate, and in noncovalent complex with acceptor aldose ribose 5-phosphate, *Biochemistry 46*, 12037–12052.
338. Fujihashi, M., Wei, L., Kotra, L. P., and Pai, E. F. (2009) Structural characterization of the molecular events during a slow substrate-product transition in orotidine 5′-monophos-

phate decarboxylase, *J. Mol. Biol. 387*, 1199–1210.
339. Chan, K. K., Wood, B. M., Fedorov, A. A., Fedorov, E. V., Imker, H. J., Amyes, T. L., Richard, J. P., Almo, S. C., and Gerlt, J. A. (2009) Mechanism of the orotidine 5′-monophosphate decarboxylase-catalyzed reaction: Evidence for substrate destabilization, *Biochemistry 48*, 5518–5531.
340. Van Vleet, J. L., Reinhardt, L. A., Miller, B. G., Sievers, A., and Cleland, W. W. (2008) Carbon isotope effect study on orotidine 5′-monophosphate decarboxylase: Support for an anionic intermediate, *Biochemistry 47*, 798–803.
341. Fujihashi, M., Ishida, T., Kuroda, S., Kotra, L. P., Pai, E. F., and Miki, K. (2013) Substrate distortion contributes to the catalysis of orotidine 5′-monophosphate decarboxylase, *J. Am. Chem. Soc. 135*, 17432–17443.
342. Fujihashi, M., Mito, K., Pai, E. F., and Miki, K. (2013) Atomic resolution structure of the orotidine 5′-monophosphate decarboxylase product complex combined with surface plasmon resonance analysis: Implications for the catalytic mechanism, *J. Biol. Chem 288*, 9011–9016.
343. Milic, D., Demidkina, T. V., Faleev, N. G., Phillips, R. S., Matkovic-Calogovic, D., and Antson, A. A. (2011) Crystallographic snapshots of tyrosine phenol-lyase show that substrate strain plays a role in C-C bond cleavage, *J. Am. Chem. Soc. 133*, 16468–16476.
344. Lakomek, K., Dickmanns, A., Ciirdaeva, E., Schomacher, L., and Ficner, R. (2010) Crystal structure analysis of DNA uridine endonuclease Mth212 bound to DNA, *J. Mol. Biol. 399*, 604–617.
345. Pickart, C. M., and Jencks, W. P. (1979) Formation of stable anhydrides from CoA transferase and hydroxamic acids, *J. Biol. Chem 254*, 9120–9129.
346. Mullins, E. A., and Kappock, T. J. (2012) Crystal structures of *Acetobacter aceti* succinyl-coenzyme A (CoA):acetate CoA-transferase reveal specificity determinants and illustrate the mechanism used by class I CoA-transferases, *Biochemistry 51*, 8422–8434.
347. Rochet, J. C., and Bridger, W. A. (1994) Identification of glutamate 344 as the catalytic residue in the active site of pig heart CoA transferase, *Prot. Sci. 3*, 975–981.
348. Andrews, L. D., Fenn, T. D., and Herschlag, D. (2013) Ground state destabilization by anionic nucleophiles contributes to the activity of phosphoryl transfer enzymes, *PLoS Biol. 11*, e1001599.
349. Lallemand, P., Chaloin, L., Roy, B., Barman, T., Bowler, M. W., and Lionne, C. (2011) Interaction of human 3-phosphoglycerate kinase with its two substrates: Is substrate antagonism a kinetic advantage?, *J. Mol. Biol. 409*, 742–757.
350. Ruben, E. A., Schwans, J. P., Sonnett, M., Natarajan, A., Gonzalez, A., Tsai, Y., and Herschlag, D. (2013) Ground state destabilization from a positioned general base in the ketosteroid isomerase active site, *Biochemistry 52*, 1074–1081.
351. Kyte, J. (2007) *Structure in protein chemistry: Second edition*, pp 204–220, Garland Science, New York.
352. Jencks, W. P. (1987) *Catalysis in chemistry and enzymology*, pp 411–417, Dover Publications, Mineola, New York.
353. Jencks, W. P. (1969) *Catalysis in chemistry and enzymology*, pp 605–614, McGraw-Hill, New York.
354. Wolfenden, R. (1969) Transition state analogues for enzyme catalysis, *Nature 223*, 704–705.
355. Lienhard, G. E. (1973) Enzymatic catalysis and transition-state theory, *Science 180*, 149–154.
356. Radzicka, A., and Wolfenden, R. (1995) A proficient enzyme, *Science 267*, 90–93.
357. Sampson, J. R., Behlen, L. S., DiRenzo, A. B., and Uhlenbeck, O. C. (1992) Recognition of yeast $tRNA^{phe}$ by its cognate yeast phenylalanyl-tRNA synthetase: An analysis of specificity, *Biochemistry 31*, 4161–4167.
358. Quirk, S., and Seley, K. L. (2005) Substrate discrimination by the human GTP fucose pyrophosphorylase, *Biochemistry 44*, 10854–10863.
359. O'Brien, P. J., and Herschlag, D. (2002) Alkaline phosphatase revisited: Hydrolysis of alkyl phosphates, *Biochemistry 41*, 3207–3225.
360. Reyes, A. C., Plache, D. C., Koudelka, A. P., Amyes, T. L., Gerlt, J. A., and Richard, J. P. (2018) Enzyme architecture: Breaking down the catalytic cage that activates orotidine 5′-monophosphate decarboxylase for catalysis, *J. Am. Chem. Soc. 140*, 17580–17590.

361. Chipman, D. M., Grisaro, V., and Sharon, N. (1967) The binding of oligosaccharides containing *N*-acetylglucosamine and *N*-acetylmuramic acid to lysozyme. The specificity of binding subsites, *J. Biol. Chem. 242*, 4388–4394.
362. Secemski, I. I, Lehrer, S. S., and Lienhard, G. E. (1972) A transition state analog for lysozyme, *J. Biol. Chem. 247*, 4740–4748.
363. Andrews, P. R., Cain, E. N., Rizzardo, E., and Smith, G. D. (1977) Rearrangement of chorismate to prephenate. Use of chorismate mutase inhibitors to define the transition state structure, *Biochemistry 16*, 4848–4852.
364. Bartlett, P. A., and Johnson, C. R. (1985) An inhibitor of chorismate mutase resembling the transition-state conformation, *J. Am. Chem. Soc. 107*, 7792–7793.
365. Chook, Y. M., Gray, J. V., Ke, H., and Lipscomb, W. N. (1994) The monofunctional chorismate mutase from *Bacillus subtilis*. Structure determination of chorismate mutase and its complexes with a transition state analog and prephenate, and implications for the mechanism of the enzymatic reaction, *J. Mol. Biol. 240*, 476–500.
366. Roy, A., Roberts, F. G., Wilderman, P. R., Zhou, K., Peters, R. J., and Coates, R. M. (2007) 16-aza-*ent*-beyerane and 16-aza-*ent*-trachylobane: Potent mechanism-based inhibitors of recombinant *ent*-kaurene synthase from *Arabidopsis thaliana*, *J. Am. Chem. Soc. 129*, 12453–12460.
367. Aulabaugh, A., and Schloss, J. V. (1990) Oxalyl hydroxamates as reaction-intermediate analogues for ketol-acid reductoisomerase, *Biochemistry 29*, 2824–2830.
368. Poulter, C. D., Capson, T. L., Thompson, M. D., and Bard, R. S. (1989) Squalene synthetase. Inhibition by ammonium analogs of carbocationic intermediates in the conversion of presqualene diphosphate to squalene, *J. Am. Chem. Soc. 111*, 3734–3739.
369. Lewandowicz, A., Shi, W., Evans, G. B., Tyler, P. C., Furneaux, R. H., Basso, L. A., Santos, D. S., Almo, S. C., and Schramm, V. L. (2003) Over-the-barrier transition state analogues and crystal structure with *Mycobacterium tuberculosis* purine nucleoside phosphorylase, *Biochemistry 42*, 6057–6066.
370. Singh, V., Evans, G. B., Lenz, D. H., Mason, J. M., Clinch, K., Mee, S., Painter, G. F., Tyler, P. C., Furneaux, R. H., Lee, J. E., Howell, P. L., and Schramm, V. L. (2005) Femtomolar transition state analogue inhibitors of 5′-methylthioadenosine/*S*-adenosylhomocysteine nucleosidase from *Escherichia coli*, *J. Biol. Chem. 280*, 18265–18273.
371. Taylor, E. A., Rinaldo-Matthis, A., Li, L., Ghanem, M., Hazleton, K. Z., Cassera, M. B., Almo, S. C., and Schramm, V. L. (2007) *Anopheles gambiae* purine nucleoside phosphorylase: Catalysis, structure, and inhibition, *Biochemistry 46*, 12405–12415.
372. Miles, R. W., Tyler, P. C., Evans, G. B., Furneaux, R. H., Parkin, D. W., and Schramm, V. L. (1999) Iminoribitol transition state analogue inhibitors of protozoan nucleoside hydrolases, *Biochemistry 38*, 13147–13154.
373. Miles, R. W., Tyler, P. C., Furneaux, R. H., Bagdassarian, C. K., and Schramm, V. L. (1998) One-third-the-sites transition-state inhibitors for purine nucleoside phosphorylase, *Biochemistry 37*, 8615–8621.
374. Sauve, A. A., Cahill, S. M., Zech, S. G., Basso, L. A., Lewandowicz, A., Santos, D. S., Grubmeyer, C., Evans, G. B., Furneaux, R. H., Tyler, P. C., McDermott, A., Girvin, M. E., and Schramm, V. L. (2003) Ionic states of substrates and transition state analogues at the catalytic sites of *N*-ribosyltransferases, *Biochemistry 42*, 5694–5705.
375. Deng, H., Lewandowicz, A., Schramm, V. L., and Callender, R. (2004) Activating the phosphate nucleophile at the catalytic site of purine nucleoside phosphorylase: A vibrational spectroscopic study, *J. Am. Chem. Soc. 126*, 9516–9517.
376. Jiang, Y. L., Drohat, A. C., Ichikawa, Y., and Stivers, J. T. (2002) Probing the limits of electrostatic catalysis by uracil DNA glycosylase using transition state mimicry and mutagenesis, *J. Biol. Chem. 277*, 15385–15392.
377. Gloster, T. M., Meloncelli, P., Stick, R. V., Zechel, D., Vasella, A., and Davies, G. J. (2007) Glycosidase inhibition: An assessment of the binding of 18 putative transition-state mimics, *J. Am. Chem. Soc. 129*, 2345–2354.
378. Papandreou, G., Tong, M. K., and Ganem, B. (1993) Amidine, amidrazone, and amidoxime derivatives of monosaccharide aldonolactams: Synthesis and evaluation as glycosidase inhibitors, *J. Am. Chem. Soc. 115*, 11682–11690.
379. Tong, M. K., Papandreou, G., and Ganem, B. (1990) Potent, broad-spectrum inhibition of

glycosidases by an amidine derivative of D-glucose, *J. Am. Chem. Soc. 112*, 6137–6139.
380. Mitchell, E. P., Withers, S. G., Ermert, P., Vasella, A. T., Garman, E. F., Oikonomakos, N. G., and Johnson, L. N. (1996) Ternary complex crystal structures of glycogen phosphorylase with the transition state analogue nojirimycin tetrazole and phosphate in the T and R states, *Biochemistry 35*, 7341–7355.
381. Gil-Ortiz, F., Ramon-Maiques, S., Fita, I., and Rubio, V. (2003) The course of phosphorus in the reaction of *N*-acetyl-L-glutamate kinase, determined from the structures of crystalline complexes, including a complex with an AlF_4^- transition state mimic, *J. Mol. Biol. 331*, 231–244.
382. Sudom, A. M., Prasad, L., Goldie, H., and Delbaere, L. T. (2001) The phosphoryl-transfer mechanism of *Escherichia coli* phospho*enol*pyruvate carboxykinase from the use of AlF_3, *J. Mol. Biol. 314*, 83–92.
383. Miles, R. D., Gorrell, A., and Ferry, J. G. (2002) Evidence for a transition state analog, MgADP-aluminum fluoride-acetate, in acetate kinase from *Methanosarcina thermophila*, *J. Biol. Chem. 277*, 22547–22552.
384. Schlichting, I., and Reinstein, J. (1999) pH Influences fluoride coordination number of the AlF_x phosphoryl transfer transition state analog, *Nature Struct. Biol. 6*, 721–723.
385. Lunardi, J., Dupuis, A., Garin, J., Issartel, J. P., Michel, L., Chabre, M., and Vignais, P. V. (1988) Inhibition of H^+-transporting ATPase by formation of a tight nucleoside diphosphate-fluoroaluminate complex at the catalytic site, *Proc. Natl. Acad. Sci. U. S. A. 85*, 8958–8962.
386. Steinrucken, H. C., and Amrhein, N. (1984) 5-Enolpyruvylshikimate-3-phosphate synthase of *Klebsiella pneumoniae* 2. Inhibition by glyphosate [*N*-(phosphonomethyl)glycine], *Eur. J. Biochem. 143*, 351–357.
387. Schonbrunn, E., Eschenburg, S., Shuttleworth, W. A., Schloss, J. V., Amrhein, N., Evans, J. N., and Kabsch, W. (2001) Interaction of the herbicide glyphosate with its target enzyme 5-enolpyruvylshikimate 3-phosphate synthase in atomic detail, *Proc. Natl. Acad. Sci. U. S. A. 98*, 1376–1380.
388. Montchamp, J. L., and Frost, J. W. (1997) Cyclohexenyl and cyclohexylidene inhibitors of 3-dehydroquinate synthase: Active site interactions relevant to enzyme mechanism and inhibitor design, *J. Am. Chem. Soc. 119*, 7645–7653.
389. Pace, J., and Mc, D. E. (1952) Methionine sulphoximine and some enzyme systems in volving glutamine, *Nature 169*, 415–416.
390. Masters, D. S., Jr., and Meister, A. (1982) Inhibition of homocysteine sulfonamide of glutamate synthase purified from *Saccharomyces cerevisiae*, *J. Biol. Chem. 257*, 8711–8715.
391. Manning, J. M., Moore, S., Rowe, W. B., and Meister, A. (1969) Identification of L-methionine *S*-sulfoximine as the diastereoisomer of L-methionine *SR*-sulfoximine that inhibits glutamine synthetase, *Biochemistry 8*, 2681–2685.
392. Chapman, A. D., Cortes, A., Dafforn, T. R., Clarke, A. R., and Brady, R. L. (1999) Structural basis of substrate specificity in malate dehydrogenases: Crystal structure of a ternary complex of porcine cytoplasmic malate dehydrogenase, α-ketomalonate and tetrahydroNAD, *J. Mol. Biol. 285*, 703–712.
393. Saadat, D., and Harrison, D. H. (2000) Mirroring perfection: The structure of methylglyoxal synthase complexed with the competitive inhibitor 2-phosphoglycolate, *Biochemistry 39*, 2950–2960.
394. Wilson, D. K., and Quiocho, F. A. (1994) Crystallographic observation of a trapped tetrahedral intermediate in a metalloenzyme, *Nature Struct. Biol. 1*, 691–694.
395. Frick, L., Yang, C., Marquez, V. E., and Wolfenden, R. (1989) Binding of pyrimidin-2-one ribonucleoside by cytidine deaminase as the transition-state analogue 3,4-dihydrouridine and the contribution of the 4-hydroxyl group to its binding affinity, *Biochemistry 28*, 9423–9430.
396. Guo, H., Rao, N., Xu, Q., and Guo, H. (2005) Origin of tight binding of a near-perfect transition-state analogue by cytidine deaminase: Implications for enzyme catalysis, *J. Am. Chem. Soc. 127*, 3191–3197.
397. Carlow, D. C., Smith, A. A., Yang, C. C., Short, S. A., and Wolfenden, R. (1995) Major contribution of a carboxymethyl group to transition-state stabilization by cytidine deaminase: Mutation and rescue, *Biochemistry 34*, 4220–4224.
398. Kati, W. M., and Wolfenden, R. (1989) Major enhancement of the affinity of an enzyme for a transition-state analog by a single hydroxyl group, *Science 243*, 1591–1593.

399. Evans, B. E., Mitchell, G. N., and Wolfenden, R. (1975) The action of bacterial cytidine deaminase on 5,6-dihydrocytidine, *Biochemistry 14*, 621–624.
400. Evans, B. E., and Wolfenden, R. V. (1973) Catalysis of the covalent hydration of pteridine by adenosine aminohydrolase, *Biochemistry 12*, 392–398.
401. Martin, D. P., Bibart, R. T., and Drueckhammer, D. G. (1994) Synthesis of novel analogs of acetyl-coenzyme A: Mimics of enzyme reaction intermediates, *J. Am. Chem. Soc. 116*, 4660–4668.
402. Baggio, R., Elbaum, D., Kanyo, Z. F., Carroll, P. J., Cavalli, R. C., Ash, D. E., and Christianson, D. W. (1997) Inhibition of $(Mn^{2+})_2$-arginase by borate leads to the design of a transition state analogue inhibitor, 2(*S*)-amino-6-boronohexanoic acid, *J. Am. Chem. Soc. 119*, 8107–8108.
403. Di Costanzo, L., Sabio, G., Mora, A., Rodriguez, P. C., Ochoa, A. C., Centeno, F., and Christianson, D. W. (2005) Crystal structure of human arginase I at 1.29-Å resolution and exploration of inhibition in the immune response, *Proc. Natl. Acad. Sci. U. S. A. 102*, 13058–13063.
404. Chen, Y., Minasov, G., Roth, T. A., Prati, F., and Shoichet, B. K. (2006) The deacylation mechanism of AmpC β-lactamase at ultrahigh resolution, *J. Am. Chem. Soc. 128*, 2970–2976.
405. Stein, R. L., DeCicco, C., Nelson, D., and Thomas, B. (2001) Slow-binding inhibition of γ-glutamyl transpeptidase by γ-boroGlu, *Biochemistry 40*, 5804–5811.
406. Pechenov, A., Stefanova, M. E., Nicholas, R. A., Peddi, S., and Gutheil, W. G. (2003) Potential transition state analogue inhibitors for the penicillin-binding proteins, *Biochemistry 42*, 579–588.
407. Nicola, G., Peddi, S., Stefanova, M., Nicholas, R. A., Gutheil, W. G., and Davies, C. (2005) Crystal structure of *Escherichia coli* penicillin-binding protein 5 bound to a tripeptide boronic acid inhibitor: A role for Ser-110 in deacylation, *Biochemistry 44*, 8207–8217.
408. Benini, S., Rypniewski, W. R., Wilson, K. S., Mangani, S., and Ciurli, S. (2004) Molecular details of urease inhibition by boric acid: Insights into the catalytic mechanism, *J. Am. Chem. Soc. 126*, 3714–3715.
409. Kim, N. N., Cox, J. D., Baggio, R. F., Emig, F. A., Mistry, S. K., Harper, S. L., Speicher, D. W., Morris, S. M., Jr., Ash, D. E., Traish, A., and Christianson, D. W. (2001) Probing erectile funcfunction: *S*-(2-Boronoethyl)-L-cysteine binds to arginase as a transition state analogue and enhances smooth muscle relaxation in human penile corpus cavernosum, *Biochemistry 40*, 2678–2688.
410. Kettner, C., Mersinger, L., and Knabb, R. (1990) The selective inhibition of thrombin by peptides of boroarginine, *J. Biol. Chem. 265*, 18289–18297.
411. Koehler, K. A., and Lienhard, G. E. (1971) 2-Phenylethaneboronic acid, a possible transition-state analog for chymotrypsin, *Biochemistry 10*, 2477–2483.
412. Matthews, D. A., Alden, R. A., Birktoft, J. J., Freer, S. T., and Kraut, J. (1975) X-Ray crystallographic study of boronic acid adducts with subtilisin BPN′ (Novo). A model for the catalytic transition state, *J. Biol. Chem. 250*, 7120–7126.
413. Jencks, W. P. (1966) In *Current aspects of biochemical energetics* (Kaplan, N. O., and Kennedy, E. P., Eds.), pp 273–298, Academic Press, New York.
414. Rudnick, G., and Abeles, R. H. (1975) Reaction mechanism and structure of the active site of proline racemase, *Biochemistry 14*, 4515–4522.
415. Keenan, M. V., and Alworth, W. L. (1974) The inhibition of proline racemase by a transition state analogue: Δ-L-Pyrroline-2-carboxylate, *Biochem. Biophys. Res. Commun. 57*, 500–504.
416. Cardinale, G. J., and Abeles, R. H. (1968) Purification and mechanism of action of proline racemase, *Biochemistry 7*, 3970–3978.
417. Buschiazzo, A., Goytia, M., Schaeffer, F., Degrave, W., Shepard, W., Gregoire, C., Chamond, N., Cosson, A., Berneman, A., Coatnoan, N., Alzari, P. M., and Minoprio, P. (2006) Crystal structure, catalytic mechanism, and mitogenic properties of *Trypanosoma cruzi* proline racemase, *Proc. Natl. Acad. Sci. U. S. A. 103*, 1705–1710.
418. Shin, H., Cama, E., and Christianson, D. W. (2004) Design of amino acid aldehydes as transition-state analogue inhibitors of arginase, *J. Am. Chem. Soc. 126*, 10278–10284.
419. Poulos, T. L., Alden, R. A., Freer, S. T., Birktoft, J. J., and Kraut, J. (1976) Polypeptide

halomethyl ketones bind to serine proteases as analogs of the tetrahedral intermediate. X-Ray crystallographic comparison of lysine- and phenylalanine-polypeptide chloromethyl ketone-inhibited subtilisin, *J. Biol. Chem. 251*, 1097–1103.
420. St Maurice, M., and Bearne, S. L. (2004) Hydrophobic nature of the active site of mandelate racemase, *Biochemistry 43*, 2524–2532.
421. Hall, R. S., Brown, S., Fedorov, A. A., Fedorov, E. V., Xu, C., Babbitt, P. C., Almo, S. C., and Raushel, F. M. (2007) Structural diversity within the mononuclear and binuclear active sites of *N*-acetyl-D-glucosamine-6-phosphate deacetylase, *Biochemistry 46*, 7953–7962.
422. Morgan, B. P., Holland, D. R., Matthews, B. W., and Bartlett, P. A. (1994) Structure-based design of an inhibitor of the zinc peptidase thermolysin, *J. Am. Chem. Soc. 116*, 3251–3260.
423. Langley, D. B., Templeton, M. D., Fields, B. A., Mitchell, R. E., and Collyer, C. A. (2000) Mechanism of inactivation of ornithine transcarbamoylase by N^{δ}-(*N*′-sulfodiaminophosphinyl)-L-ornithine, a true transition state analogue? Crystal structure and implications for catalytic mechanism, *J. Biol. Chem. 275*, 20012–20019.
424. Tronrud, D. E., Monzingo, A. F., and Matthews, B. W. (1986) Crystallographic structural analysis of phosphoramidates as inhibitors and transition-state analogs of thermolysin, *Eur. J. Biochem. 157*, 261–268.
425. Kam, C. M., Nishino, N., and Powers, J. C. (1979) Inhibition of thermolysin and carboxypeptidase A by phosphoramidates, *Biochemistry 18*, 3032–3038.
426. Bartlett, P. A., and Marlowe, C. K. (1983) Phosphonamidates as transition-state analogue inhibitors of thermolysin, *Biochemistry 22*, 4618–4624.
427. Bartlett, P. A., and Marlowe, C. K. (1987) Possible role for water dissociation in the slow binding of phosphorus-containing transition-state-analogue inhibitors of thermolysin, *Biochemistry 26*, 8553–8561.
428. Lee, J. Y., Kwak, J. E., Moon, J., Eom, S. H., Liong, E. C., Pedelacq, J. D., Berendzen, J., and Suh, S. W. (2001) Crystal structure and functional analysis of the SurE protein identify a novel phosphatase family, *Nature Struct. Biol. 8*, 789–794.
429. Zhang, M., Zhou, M., Van Etten, R. L., and Stauffacher, C. V. (1997) Crystal structure of bovine low molecular weight phosphotyrosyl phosphatase complexed with the transition state analog vanadate, *Biochemistry 36*, 15–23.
430. Zalatan, J. G., Fenn, T. D., Brunger, A. T., and Herschlag, D. (2006) Structural and functional comparisons of nucleotide pyrophosphatase/phosphodiesterase and alkaline phosphatase: Implications for mechanism and evolution, *Biochemistry 45*, 9788–9803.
431. Ray, W. J., Jr., and Puvathingal, J. M. (1990) Characterization of a vanadate-based transition-state-analogue complex of phosphoglucomutase by kinetic and equilibrium binding studies: Mechanistic implications, *Biochemistry 29*, 2790–2801.
432. Liu, S., Gresser, M. J., and Tracey, A. S. (1992) ^{1}H and ^{51}V NMR Studies of the interaction of vanadate and 2-vanadio-3-phosphoglycerate with phosphoglycerate mutase, *Biochemistry 31*, 2677–2685.
433. Cantley, L. C., Jr., Josephson, L., Warner, R., Yanagisawa, M., Lechene, C., and Guidotti, G. (1977) Vanadate is a potent (Na,K)-ATPase inhibitor found in ATP derived from muscle, *J. Biol. Chem. 252*, 7421–7423.
434. Alber, T., Gilbert, W. A., Ponzi, D. R., and Petsko G., A. (1983) The role of mobility in the substrate binding and catalytic machinery of enzymes, *Ciba Foundation Symp. 93*, 4–24.
435. Lindquist, R. N., Lynn, J. L., Jr., and Lienhard, G. E. (1973) Possible transition-state analogs for ribonuclease. The complexes of uridine with oxovanadium(IV) ion and vanadium(V) ion, *J. Am. Chem. Soc. 95*, 8762–8768.
436. Cantley, L. C., Jr., Cantley, L. G., and Josephson, L. (1978) A characterization of vanadate interactions with the (Na,K)-ATPase. Mechanistic and regulatory implications, *J. Biol. Chem. 253*, 7361–7368.
437. Wlodawer, A., Miller, M., and Sjolin, L. (1983) Active site of RNAse: Neutron diffraction study of a complex with uridine vanadate, a transition-state analog, *Proc. Natl. Acad. Sci. U. S. A. 80*, 3628–3631.
438. Cama, E., Shin, H., and Christianson, D. W. (2003) Design of amino acid sulfonamides as transition-state analogue inhibitors of arginase, *J. Am. Chem. Soc. 125*, 13052–13057.

439. Funke, T., Healy-Fried, M. L., Han, H., Alberg, D. G., Bartlett, P. A., and Schonbrunn, E. (2007) Differential inhibition of class I and class II 5-enolpyruvylshikimate-3-phosphate synthases by tetrahedral reaction intermediate analogues, *Biochemistry 46*, 13344–13351.
440. Alberg, D. G., Lauhon, C. T., Nyfeler, R., Fassler, A., and Bartlett, P. A. (1992) Inhibition of EPSP synthase by analogs of the tetrahedral intermediate and of EPSP, *J. Am. Chem. Soc. 114*, 3535–3546.
441. Priestman, M. A., Healy, M. L., Becker, A., Alberg, D. G., Bartlett, P. A., Lushington, G. H., and Schonbrunn, E. (2005) Interaction of phosphonate analogues of the tetrahedral reaction intermediate with 5-enolpyruvylshikimate-3-phosphate synthase in atomic detail, *Biochemistry 44*, 3241–3248.
442. Kim, H., and Lipscomb, W. N. (1991) Comparison of the structures of three carboxypeptidase A-phosphonate complexes determined by X-ray crystallography, *Biochemistry 30*, 8171–8180.
443. Yu, L., and Dennis, E. A. (1991) Critical role of a hydrogen bond in the interaction of phospholipase A_2 with transition-state and substrate analogues, *Proc. Natl. Acad. Sci. U. S. A. 88*, 9325–9329.
444. Yu, L., and Dennis, E. A. (1993) Effect of polar head groups on the interactions of phospholipase A_2 with phosphonate transition-state analogues, *Biochemistry 32*, 10185–10192.
445. Skordalakes, E., Dodson, G. G., Green, D. S., Goodwin, C. A., Scully, M. F., Hudson, H. R., Kakkar, V. V., and Deadman, J. J. (2001) Inhibition of human α-thrombin by a phosphonate tripeptide proceeds via a metastable pentacoordinated phosphorus intermediate, *J. Mol. Biol. 311*, 549–555.
446. Kaplan, A. P., and Bartlett, P. A. (1991) Synthesis and evaluation of an inhibitor of carboxypeptidase A with a K_i value in the femtomolar range, *Biochemistry 30*, 8165–8170.
447. White, S. P., Scott, D. L., Otwinowski, Z., Gelb, M. H., and Sigler, P. B. (1990) Crystal structure of cobra-venom phospholipase A_2 in a complex with a transition-state analogue, *Science 250*, 1560–1563.
448. Kulik, V., Hartmann, E., Weyand, M., Frey, M., Gierl, A., Niks, D., Dunn, M. F., and Schlichting, I. (2005) On the structural basis of the catalytic mechanism and the regulation of the alpha subunit of tryptophan synthase from *Salmonella typhimurium* and BX1 from maize, two evolutionarily related enzymes, *J. Mol. Biol. 352*, 608–620.
449. Bearne, S. L., and Blouin, C. (2000) Inhibition of *Escherichia coli* glucosamine-6-phosphate synthase by reactive intermediate analogues. The role of the 2-amino function in catalysis, *J. Biol. Chem. 275*, 135–140.
450. Coates, L., Erskine, P. T., Crump, M. P., Wood, S. P., and Cooper, J. B. (2002) Five atomic resolution structures of endothiapepsin inhibitor complexes: Implications for the aspartic proteinase mechanism, *J. Mol. Biol. 318*, 1405–1415.
451. McDermott, A. E., Creuzet, F., Griffin, R. G., Zawadzke, L. E., Ye, Q. Z., and Walsh, C. T. (1990) Rotational resonance determination of the structure of an enzyme-inhibitor complex: Phosphorylation of an (aminoalkyl)phosphinate inhibitor of D-alanyl-D-alanine ligase by ATP, *Biochemistry 29*, 5767–5775.
452. Hiratake, J., Kato, H., and Oda, J. i. (1994) Mechanism-based inactivation of glutathione synthetase by phosphinic acid transition-state analog, *J. Am. Chem. Soc. 116*, 12059–12060.
453. Hansen, J. L., Schmeing, T. M., Moore, P. B., and Steitz, T. A. (2002) Structural insights into peptide bond formation, *Proc. Natl. Acad. Sci. U. S. A. 99*, 11670–11675.
454. Frieden, C., Kurz, L. C., and Gilbert, H. R. (1980) Adenosine deaminase and adenylate deaminase: Comparative kinetic studies with transition state and ground state analogue inhibitors, *Biochemistry 19*, 5303–5309.
455. Kurz, L. C., Weitkamp, E., and Frieden, C. (1987) Adenosine deaminase: Viscosity studies and the mechanism of binding of substrate and of ground- and transition-state analogue inhibitors, *Biochemistry 26*, 3027–3032.
456. Koizumi, M., Hiratake, J., Nakatsu, T., Kato, H., and Oda, J. i. (1999) A potent transition-state analogue inhibitor of *Escherichia coli* asparagine synthetase A, *J. Am. Chem. Soc. 121*, 5799–5800.
457. Dharmasena, S. P., Wimalasena, D. S., and Wimalasena, K. (2002) A slow-tight binding inhibitor of dopamine β-monooxygenase: A transition state analogue for the product release step, *Biochemistry 41*, 12414–12420.

458. Schonbrunn-Hanebeck, E., Laber, B., and Amrhein, N. (1990) Slow-binding inhibition of the *Escherichia coli* pyruvate dehydrogenase multienzyme complex by acetylphosphinate, *Biochemistry 29*, 4880–4885.
459. Inglese, J., Blatchly, R. A., and Benkovic, S. J. (1989) A multisubstrate adduct inhibitor of a purine biosynthetic enzyme with a picomolar dissociation constant, *J. Med. Chem. 32*, 937–940.
460. Klein, C., Chen, P., Arevalo, J. H., Stura, E. A., Marolewski, A., Warren, M. S., Benkovic, S. J., and Wilson, I. A. (1995) Towards structure-based drug design: Crystal structure of a multisubstrate adduct complex of glycinamide ribonucleotide transformylase at 1.96 Å resolution, *J. Mol. Biol. 249*, 153–175.
461. Tremblay, L. W., Fan, F., Vetting, M. W., and Blanchard, J. S. (2008) The 1.6 Å crystal structure of *Mycobacterium smegmatis* MshC: The penultimate enzyme in the mycothiol biosynthetic pathway, *Biochemistry 47*, 13326–13335.
462. Fan, F., and Blanchard, J. S. (2009) Toward the catalytic mechanism of a cysteine ligase (MshC) from *Mycobacterium smegmatis*: An enzyme involved in the biosynthetic pathway of mycothiol, *Biochemistry 48*, 7150–7159.
463. Liu, F., Lee, H. J., Strynadka, N. C., and Tanner, M. E. (2009) Inhibition of *Neisseria meningitidis* sialic acid synthase by a tetrahedral intermediate analogue, *Biochemistry 48*, 9194–9201.
464. Greasley, S. E., Marsilje, T. H., Cai, H., Baker, S., Benkovic, S. J., Boger, D. L., and Wilson, I. A. (2001) Unexpected formation of an epoxide-derived multisubstrate adduct inhibitor on the active site of GAR transformylase, *Biochemistry 40*, 13538–13547.
465. Bull, H. G., Garcia-Calvo, M., Andersson, S., Baginsky, W. F., Chan, H. K., Ellsworth, D. E., Miller, R. R., Stearns, R. A., Bakshi, R. K., Rasmusson, G. H., Tolman, R. L., Myers, R. W., Kozarich, J. W., and Harris, G. S. (1996) Mechanism-based inhibition of human steroid 5α-reductase by finasteride: Enzyme-catalyzed formation of NADP-dihydrofinasteride, a potent bisubstrate analog inhibitor, *J. Am. Chem. Soc. 118*, 2359–2365.
466. May, S. W., Oldham, C. D., Mueller, P. W., Padgette, S. R., and Sowell, A. L. (1982) Protocatechuate 3,4-dioxygenase. Mechanistic implications of inhibition by the transition state analog, 2-hydroxyisonicotinic acid N-oxide, *J. Biol. Chem. 257*, 12746–12751.
467. Whittaker, J. W., and Lipscomb, J. D. (1984) Transition state analogs for protocatechuate 3,4-dioxygenase. Spectroscopic and kinetic studies of the binding reactions of ketonized substrate analogs, *J. Biol. Chem. 259*, 4476–4486.
468. Fujisawa, H., and Hayaishi, O. (1968) Protocatechuate 3,4-dioxygenase. I. Crystallization and characterization, *J. Biol. Chem. 243*, 2673–2681.
469. Anderson, K. S., and Johnson, K. A. (1990) "Kinetic competence" of the 5-enolpyruvoylshikimate-3-phosphate synthase tetrahedral intermediate, *J. Biol. Chem. 265*, 5567–5572.
470. Hawkinson, D. C., Pollack, R. M., and Ambulos, N. P., Jr. (1994) Evaluation of the internal equilibrium constant for 3-oxo-Δ^5-steroid isomerase using the D38E and D38N mutants: The energetic basis for catalysis, *Biochemistry 33*, 12172–12183.
471. Abramowitz-Kurn, N., and Schechter, I. (1974) Mapping the active site of carboxypeptidase A: A proposed scheme for substrate binding at the active site, *Israel J. Chem. 12*, 543–555.
472. Abramowitz, N., Schechter, I., and Berger, A. (1967) On the size of the active site in proteases. II. Carboxypeptidase-A, *Biochem. Biophys. Res. Commun. 29*, 862–867.
473. Whitworth, G. E., Macauley, M. S., Stubbs, K. A., Dennis, R. J., Taylor, E. J., Davies, G. J., Greig, I. R., and Vocadlo, D. J. (2007) Analysis of PUGNAc and NAG-thiazoline as transition state analogues for human O-GlcNAcase: Mechanistic and structural insights into inhibitor selectivity and transition state poise, *J. Am. Chem. Soc. 129*, 635–644.
474. Deng, H., Callender, R., Huang, Z., and Zhang, Z. Y. (2002) Is the PTPase-vanadate complex a true transition state analogue?, *Biochemistry 41*, 5865–5872.
475. Messmore, J. M., and Raines, R. T. (2000) Pentavalent organo-vanadates as transition state analogues for phosphoryl transfer reactions, *J. Am. Chem. Soc. 122*, 9911–9916.
476. Peck, A., Sunden, F., Andrews, L. D., Pande, V. S., and Herschlag, D. (2016) Tungstate as a transition state analog for catalysis by alkaline phosphatase, *J. Mol. Biol. 428*, 2758–2768.

477. Phillips, M. A., Kaplan, A. P., Rutter, W. J., and Bartlett, P. A. (1992) Transition-state characterization: A new approach combining inhibitor analogues and variation in enzyme structure, *Biochemistry 31*, 959–963.
478. Wicki, J., Williams, S. J., and Withers, S. G. (2007) Transition-state mimicry by glycosidase inhibitors: A critical kinetic analysis, *J. Am. Chem. Soc. 129*, 4530–4531.
479. Schwans, J. P., Kraut, D. A., and Herschlag, D. (2009) Determining the catalytic role of remote substrate binding interactions in ketosteroid isomerase, *Proc. Natl. Acad. Sci. U. S. A. 106*, 14271–14275.
480. Zaitsev, V., Johnsen, U., Reher, M., Ortjohann, M., Taylor, G. L., Danson, M. J., Schonheit, P., and Crennell, S. J. (2018) Insights into the substrate specificity of archaeal Entner-Doudoroff aldolases: The structures of *Picrophilus torridus* 2-keto-3-deoxygluconate aldolase and *Sulfolobus solfataricus* 2-keto-3-deoxy-6-phosphogluconate aldolase in complex with 2-keto-3-deoxy-6-phosphogluconate, *Biochemistry 57*, 3797–3806.
481. Miller, B. G., Traut, T. W., and Wolfenden, R. (1998) Effects of substrate binding determinants in the transition state for orotidine 5′-monophosphate decarboxylase, *Bioorg. Chem. 26*, 283–288.
482. Amyes, T. L., Richard, J. P., and Tait, J. J. (2005) Activation of orotidine 5′-monophosphate decarboxylase by phosphite dianion: The whole substrate is the sum of two parts, *J. Am. Chem. Soc. 127*, 15708–15709.
483. Reyes, A. C., Amyes, T. L., and Richard, J. P. (2017) Enzyme architecture: Erection of active orotidine 5′-monophosphate decarboxylase by substrate-induced conformational changes, *J. Am. Chem. Soc. 139*, 16048–16051.
484. Goldman, L. M., Amyes, T. L., Goryanova, B., Gerlt, J. A., and Richard, J. P. (2014) Enzyme architecture: Deconstruction of the enzyme-activating phosphodianion interactions of orotidine 5′-monophosphate decarboxylase, *J. Am. Chem. Soc. 136*, 10156–10165.
485. Zhai, X., Amyes, T. L., and Richard, J. P. (2014) Enzyme architecture: Remarkably similar transition states for triosephosphate isomerase-catalyzed reactions of the whole substrate and the substrate in pieces, *J. Am. Chem. Soc. 136*, 4145–4148.
486. Kholodar, S. A., and Murkin, A. S. (2013) DXP reductoisomerase: Reaction of the substrate in pieces reveals a catalytic role for the non-reacting phosphodianion group, *Biochemistry 52*, 2302–2308.
487. Allen, K. N., and Abeles, R. H. (1989) Inhibition kinetics of acetylcholinesterase with fluoromethyl ketones, *Biochemistry 28*, 8466–8473.
488. Westerik, J. O., and Wolfenden, R. (1972) Aldehydes as inhibitors of papain, *J. Biol. Chem. 247*, 8195–8197.
489. Jencks, W. P. (1969) *Catalysis in chemistry and enzymology*, p 288, McGraw-Hill, New York.
490. Jackson, D. Y., Jacobs, J. W., Sugasawara, R., Reich, S. H., Bartlett, P. A., and Schultz, P. G. (1988) An antibody-catalyzed Claisen rearrangement, *J. Am. Chem. Soc. 110*, 4841–4842.
491. Hilvert, D., Carpenter, S. H., Nared, K. D., and Auditor, M. T. (1988) Catalysis of concerted reactions by antibodies: The Claisen rearrangement, *Proc. Natl. Acad. Sci. U. S. A. 85*, 4953–4955.
492. Braisted, A. C., and Schultz, P. G. (1990) An antibody-catalyzed bimolecular Diels-Alder reaction, *J. Am. Chem. Soc. 112*, 7430–7431.
493. Cochran, A. G., Pham, T., Sugasawara, R., and Schultz, P. G. (1991) Antibody-catalyzed bimolecular imine formation, *J. Am. Chem. Soc. 113*, 6670–6672.
494. Wade, H., and Scanlan, T. S. (1996) P1-S1 Interactions control the enantioselectivity and hydrolytic activity of catalytic antibody 17E8, *J. Am. Chem. Soc. 118*, 6510–6511.
495. Lo, C.-H. L., Wentworth, P., Jr., Jung, K. W., Yoon, J., Ashley, J. A., and Janda, K. D. (1997) Reactive immunization strategy generates antibodies with high catalytic proficiencies, *J. Am. Chem. Soc. 119*, 10251–10252.
496. Napper, A. D., Benkovic, S. J., Tramontano, A., and Lerner, R. A. (1987) A stereospecific cyclization catalyzed by an antibody, *Science 237*, 1041–1043.
497. Ulrich, H. D., Mundorff, E., Santarsiero, B. D., Driggers, E. M., Stevens, R. C., and Schultz, P. G. (1997) The interplay between binding energy and catalysis in the evolution of a catalytic antibody, *Nature 389*, 271–275.
498. Ma, L., Sweet, E. H., and Schultz, P. G. (1999) Selective antibody-catalyzed solvolysis of *endo*-2-norbornyl mesylate, *J. Am. Chem. Soc. 121*, 10227–10228.

499. Yoon, S. S., Oei, Y., Sweet, E., and Schultz, P. G. (1996) An antibody-catalyzed [2,3]-elimination reaction, *J. Am. Chem. Soc. 118*, 11686–11687.
500. Flanagan, M. E., Jacobsen, J. R., Sweet, E., and Schultz, P. G. (1996) Antibody-catalyzed retro-aldol reaction, *J. Am. Chem. Soc. 118*, 6078–6079.
501. Gutfreund, H., and Trentham, D. R. (1975) Energy changes during the formation and interconversion of enzyme-substrate complexes, In *Energy transformation in biological systems; Ciba foundation symposium 31* (Wolstenholme, G. E. W., and Fitzsimons, D. W., Eds.), pp 69–86, Elsevier, Amsterdam.
502. Holler, E., and Calvin, M. (1972) Isoleucyl transfer ribonucleic acid synthetase of *Escherichia coli* B. A rapid kinetic investigation of the L-isoleucine-activating reaction, *Biochemistry 11*, 3741–3752.
503. Wells, T. N., and Fersht, A. R. (1986) Use of binding energy in catalysis analyzed by mutagenesis of the tyrosyl-tRNA synthetase, *Biochemistry 25*, 1881–1886.
504. Knowles, J. R. (1980) Enzyme-catalyzed phosphoryl transfer reactions, *Annu. Rev. Biochem. 49*, 877–919.
505. Burbaum, J. J., Raines, R. T., Albery, W. J., and Knowles, J. R. (1989) Evolutionary optimization of the catalytic effectiveness of an enzyme, *Biochemistry 28*, 9293–9305.
506. Schmidt, P. P., Travers, F., and Barman, T. (1995) Transient and equilibrium kinetic studies on yeast 3-phosphoglycerate kinase. Evidence that an intermediate containing 1,3-bisphosphoglycerate accumulates in the steady state, *Biochemistry 34*, 824-832.
507. Burbaum, J. J., and Knowles, J. R. (1989) Internal thermodynamics of enzymes determined by equilibrium quench: Values of K_{int} for enolase and creatine kinase, *Biochemistry 28*, 9306–9317.
508. Chin, J. (1983) Perfect enzymes: Is the equilibrium constant between the enzyme's bound species unity?, *J. Am. Chem. Soc. 105*, 6502–6503.
509. Gerhart, J. C., and Schachman, H. K. (1968) Allosteric interactions in aspartate transcarbamylase: II. Evidence for different conformational states of the protein in the presence and absence of specific ligands, *Biochemistry 7*, 538–552.
510. Springs, B., Welsh, K. M., and Cooperman, B. S. (1981) Thermodynamics, kinetics, and mechanism in yeast inorganic pyrophosphatase catalysis of inorganic pyrophosphate: Inorganic phosphate equilibration, *Biochemistry 20*, 6384–6391.
511. Schloss, J. V., Porter, D. J., Bright, H. J., and Cleland, W. W. (1980) Nitro analogues of citrate and isocitrate as transition-state analogues for aconitase, *Biochemistry 19*, 2358–2362.
512. Schloss, J. V., and Cleland, W. W. (1982) Inhibition of isocitrate lyase by 3-nitropropionate, a reaction-intermediate analogue, *Biochemistry 21*, 4420–4427.
513. Levine, H. L., Brody, R. S., and Westheimer, F. H. (1980) Inhibition of orotidine-5′-phosphate decarboxylase by 1-(5′-phospho-β-D-ribofuranosyl)barbituric acid, 6-azauridine 5′-phosphate, and uridine 5′-phosphate, *Biochemistry 19*, 4993–4999.
514. Frick, L., Wolfenden, R., Smal, E., and Baker, D. C. (1986) Transition-state stabilization by adenosine deaminase: Structural studies of its inhibitory complex with deoxycoformycin, *Biochemistry 25*, 1616–1621.
515. Koehler, K. A., and Hess, G. P. (1974) A new, specific and reversible bifunctional alkylborinic acid inhibitor of acetylcholinesterase, *Biochemistry 13*, 5345–5350.
516. Chirgwin, J. M., and Noltmann, E. A. (1975) The enediolate analogue 5-phosphoarabinonate as a mechanistic probe for phosphoglucose isomerase, *J. Biol. Chem 250*, 7272–7276.
517. Spring, T. G., and Wold, F. (1971) Studies on two high-affinity enolase inhibitors. Reaction with enolases, *Biochemistry 10*, 4655–4660.
518. Lienhard, G. E., and Secemski, I, I. (1973) P^1,P^5-Di(adenosine-5′)pentaphosphate, a potent multisubstrate inhibitor of adenylate kinase, *J. Biol. Chem. 248*, 1121–1123.
519. Rowe, W. B., Ronzio, R. A., and Meister, A. (1969) Inhibition of glutamine synthetase by methionine sulfoximine. Studies on methionine sulfoximine phosphate, *Biochemistry 8*, 2674–2680.
520. Jumper, J., Evans, R., Pritzel, A., Green, T., Figurnov, M., Ronneberger, O., Tunyasuvunakool, K., Bates, R., Zidek, A., Potapenko, A., Bridgland, A., Meyer, C., Kohl, S. A. A., Ballard, A. J., Cowie, A., Romera-Paredes, B., Nikolov, S., Jain, R., Adler, J., Back, T., Petersen,

S., Reiman, D., Clancy, E., Zielinski, M., Steinegger, M., Pacholska, M., Berghammer, T., Bodenstein, S., Silver, D., Vinyals, O., Senior, A. W., Kavukcuoglu, K., Kohli, P., and Hassabis, D. (2021) Highly accurate protein structure prediction with AlphaFold, *Nature 596*, 583–589.

521. Saper, M. A., Bjorkman, P. J., and Wiley, D. C. (1991) Refined structure of the human histocompatibility antigen HLA-A2 at 2.6 Å resolution, *J. Mol. Biol. 219*, 277–319.
522. Falk, K., Rotzschke, O., Stevanovic, S., Jung, G., and Rammensee, H. G. (1991) Allele-specific motifs revealed by sequencing of self-peptides eluted from MHC molecules, *Nature 351*, 290–296.
523. Buetow, L., Smith, T. K., Dawson, A., Fyffe, S., and Hunter, W. N. (2007) Structure and reactivity of LpxD, the *N*-acyltransferase of lipid A biosynthesis, *Proc. Natl. Acad. Sci. U. S. A. 104*, 4321–4326.
524. Leonidas, D. D., Shapiro, R., Irons, L. I., Russo, N., and Acharya, K. R. (1997) Crystal structures of ribonuclease A complexes with 5′-diphosphoadenosine 3′-phosphate and 5′-diphosphoadenosine 2′-phosphate at 1.7 Å resolution, *Biochemistry 36*, 5578–5588.
525. Eklund, H., Samama, J. P., and Jones, T. A. (1984) Crystallographic investigations of nicotinamide adenine dinucleotide binding to horse liver alcohol dehydrogenase, *Biochemistry 23*, 5982–5996.
526. Bauer, C. B., Holden, H. M., Thoden, J. B., Smith, R., and Rayment, I. (2000) X-Ray structures of the apo and MgATP-bound states of *Dictyostelium discoideum* myosin motor domain, *J. Biol. Chem. 275*, 38494–38499.
527. Kostrewa, D., and Winkler, F. K. (1995) Mg^{2+} Binding to the active site of EcoRV endonuclease: A crystallographic study of complexes with substrate and product DNA at 2 Å resolution, *Biochemistry 34*, 683–696.
528. Wagner, R. L., Apriletti, J. W., McGrath, M. E., West, B. L., Baxter, J. D., and Fletterick, R. J. (1995) A structural role for hormone in the thyroid hormone receptor, *Nature 378*, 690–697.
529. Arevalo, J. H., Stura, E. A., Taussig, M. J., and Wilson, I. A. (1993) Three-dimensional structure of an anti-steroid Fab′ and progesterone-Fab′ complex, *J. Mol. Biol. 231*, 103–118.
530. Pflugrath, J. W., and Quiocho, F. A. (1988) The 2 Å resolution structure of the sulfate-binding protein involved in active transport in *Salmonella typhimurium*, *J. Mol. Biol. 200*, 163–180.
531. Sun, Y. J., Rose, J., Wang, B. C., and Hsiao, C. D. (1998) The structure of glutamine-binding protein complexed with glutamine at 1.94 Å resolution: Comparisons with other amino acid binding proteins, *J. Mol. Biol. 278*, 219–229.
532. Duan, X., and Quiocho, F. A. (2002) Structural evidence for a dominant role of nonpolar interactions in the binding of a transport/chemosensory receptor to its highly polar ligands, *Biochemistry 41*, 706–712.
533. Bourne, Y., Rouge, P., and Cambillau, C. (1992) X-Ray structure of a biantennary octasaccharide-lectin complex refined at 2.3-Å resolution, *J. Biol. Chem. 267*, 197–203.
534. Weis, W. I., Drickamer, K., and Hendrickson, W. A. (1992) Structure of a C-type mannose-binding protein complexed with an oligosaccharide, *Nature 360*, 127–134.
535. Harata, K., and Muraki, M. (2000) Crystal structures of *Urtica dioica* agglutinin and its complex with tri-*N*-acetylchitotriose, *J. Mol. Biol. 297*, 673–681.
536. Weis, W., Brown, J. H., Cusack, S., Paulson, J. C., Skehel, J. J., and Wiley, D. C. (1988) Structure of the influenza virus haemagglutinin complexed with its receptor, sialic acid, *Nature 333*, 426–431.
537. Cowan, S. W., Newcomer, M. E., and Jones, T. A. (1993) Crystallographic studies on a family of cellular lipophilic transport proteins. Refinement of P2 myelin protein and the structure determination and refinement of cellular retinol-binding protein in complex with all-*trans*-retinol, *J. Mol. Biol. 230*, 1225–1246.
538. Benning, M. M., Smith, A. F., Wells, M. A., and Holden, H. M. (1992) Crystallization, structure determination and least-squares refinement to 1.75 Å resolution of the fatty-acid-binding protein isolated from *Manduca sexta* L, *J. Mol. Biol. 228*, 208–219.
539. Curry, S., Mandelkow, H., Brick, P., and Franks, N. (1998) Crystal structure of human serum albumin complexed with fatty acid reveals an asymmetric distribution of binding sites, *Nature Struct. Biol. 5*, 827–835.

540. Stern, L. J., Brown, J. H., Jardetzky, T. S., Gorga, J. C., Urban, R. G., Strominger, J. L., and Wiley, D. C. (1994) Crystal structure of the human class II MHC protein HLA-DR1 complexed with an influenza virus peptide, *Nature 368*, 215–221.
541. Garrett, T. P., Saper, M. A., Bjorkman, P. J., Strominger, J. L., and Wiley, D. C. (1989) Specificity pockets for the side chains of peptide antigens in HLA-AW68, *Nature 342*, 692–696.
542. Silver, M. L., Guo, H. C., Strominger, J. L., and Wiley, D. C. (1992) Atomic structure of a human MHC molecule presenting an influenza virus peptide, *Nature 360*, 367–369.
543. Cheong, C. G., Escalante-Semerena, J. C., and Rayment, I. (1999) The three-dimensional structures of nicotinate mononucleotide:5,6- dimethylbenzimidazole phosphoribosyltransferase (CobT) from *Salmonella typhimurium* complexed with 5,6-dimethybenzimidazole and its reaction products determined to 1.9 Å resolution, *Biochemistry 38*, 16125–16135.
544. Delbaere, L. T., and Brayer, G. D. (1985) The 1.8 Å structure of the complex between chymostatin and *Streptomyces griseus* protease A. A model for serine protease catalytic tetrahedral intermediates, *J. Mol. Biol. 183*, 89–103.
545. Harris, E. M., Aleshin, A. E., Firsov, L. M., and Honzatko, R. B. (1993) Refined structure for the complex of 1-deoxynojirimycin with glucoamylase from *Aspergillus awamori* var. X100 to 2.4 Å resolution, *Biochemistry 32*, 1618–1626.
546. Sacchettini, J. C., Scapin, G., Gopaul, D., and Gordon, J. I. (1992) Refinement of the structure of *Escherichia coli*-derived rat intestinal fatty acid binding protein with bound oleate to 1.75 Å resolution. Correlation with the structures of the apoprotein and the protein with bound palmitate, *J. Biol. Chem. 267*, 23534–23545.
547. Herzberg, O. (1991) Refined crystal structure of β-lactamase from *Staphylococcus aureus* PC1 at 2.0 Å resolution, *J. Mol. Biol. 217*, 701–719.
548. Zawadzke, L. E., Chen, C. C., Banerjee, S., Li, Z., Wasch, S., Kapadia, G., Moult, J., and Herzberg, O. (1996) Elimination of the hydrolytic water molecule in a class A β-lactamase mutant: Crystal structure and kinetics, *Biochemistry 35*, 16475–16482.
549. Clausen, T., Huber, R., Laber, B., Pohlenz, H. D., and Messerschmidt, A. (1996) Crystal structure of the pyridoxal-5′-phosphate dependent cystathionine β-lyase from *Escherichia coli* at 1.83 Å, *J. Mol. Biol. 262*, 202–224.
550. Zou, Y., Zhang, H., Brunzelle, J. S., Johannes, T. W., Woodyer, R., Hung, J. E., Nair, N., van der Donk, W. A., Zhao, H., and Nair, S. K. (2012) Crystal structures of phosphite dehydrogenase provide insights into nicotinamide cofactor regeneration, *Biochemistry 51*, 4263–4270.
551. Wouters, J., Oudjama, Y., Barkley, S. J., Tricot, C., Stalon, V., Droogmans, L., and Poulter, C. D. (2003) Catalytic mechanism of *Escherichia coli* isopentenyl diphosphate isomerase involves Cys-67, Glu-116, and Tyr-104 as suggested by crystal structures of complexes with transition state analogues and irreversible inhibitors, *J. Biol. Chem 278*, 11903–11908.
552. Endrizzi, J. A., Breddam, K., and Remington, S. J. (1994) 2.8-Å Structure of yeast serine carboxypeptidase, *Biochemistry 33*, 11106–11120.
553. Ealick, S. E., Babu, Y. S., Bugg, C. E., Erion, M. D., Guida, W. C., Montgomery, J. A., and Secrist, J. A., 3rd. (1991) Application of crystallographic and modeling methods in the design of purine nucleoside phosphorylase inhibitors, *Proc. Natl. Acad. Sci. U. S. A. 88*, 11540–11544.
554. Erion, M. D., Dang, Q., Reddy, M. R., Kasibhatla, S. R., Huang, J., Lipscomb, W. N., and van Poelje, P. D. (2007) Structure-guided design of AMP mimics that inhibit fructose-1,6-bisphosphatase with high affinity and specificity, *J. Am. Chem. Soc. 129*, 15480–15490.
555. Strynadka, N. C., Martin, R., Jensen, S. E., Gold, M., and Jones, J. B. (1996) Structure-based design of a potent transition state analogue for TEM-1 β-lactamase, *Nature Struct. Biol. 3*, 688–695.
556. von Itzstein, M., Wu, W. Y., Kok, G. B., Pegg, M. S., Dyason, J. C., Jin, B., Van Phan, T., Smythe, M. L., White, H. F., Oliver, S. W., Colman, P. M., Varghese, J. N., Ryan D. M., Woods, J. M., Bethell R. C., Hotham V. J., Cameron, J. M., and Penn, C. R. (1993) Rational design of potent sialidase-based inhib-

itors of influenza virus replication, *Nature 363*, 418–423.
557. Miyashita, K., Massova, I., Taibi, P., and Mobashery, S. (1995) Design, synthesis, and evaluation of a potent mechanism-based inhibitor for the TEM β-lactamase with implications for the enzyme mechanism, *J. Am. Chem. Soc. 117*, 11055–11059.
558. Kurumbail, R. G., Stevens, A. M., Gierse, J. K., McDonald, J. J., Stegeman, R. A., Pak, J. Y., Gildehaus, D., Miyashiro, J. M., Penning, T. D., Seibert, K., Isakson, P. C., and Stallings, W. C. (1996) Structural basis for selective inhibition of cyclooxygenase-2 by anti-inflammatory agents, *Nature 384*, 644–648.
559. Finnin, M. S., Donigian, J. R., Cohen, A., Richon, V. M., Rifkind, R. A., Marks, P. A., Breslow, R., and Pavletich, N. P. (1999) Structures of a histone deacetylase homologue bound to the TSA and SAHA inhibitors, *Nature 401*, 188–193.
560. Istvan, E. S., and Deisenhofer, J. (2001) Structural mechanism for statin inhibition of HMG-CoA reductase, *Science 292*, 1160–1164.
561. Chan, K. K., Fedorov, A. A., Fedorov, E. V., Almo, S. C., and Gerlt, J. A. (2008) Structural basis for substrate specificity in phosphate binding $(\beta/\alpha)_8$-barrels: D-Allulose 6-phosphate 3-epimerase from *Escherichia coli* k-12, *Biochemistry 47*, 9608–9617.
562. Long, S. B., Casey, P. J., and Beese, L. S. (2002) Reaction path of protein farnesyltransferase at atomic resolution, *Nature 419*, 645–650.
563. Meining, W., Eberhardt, S., Bacher, A., and Ladenstein, R. (2003) The structure of the *N*-terminal domain of riboflavin synthase in complex with riboflavin at 2.6 Å resolution, *J. Mol. Biol. 331*, 1053–1063.
564. Todone, F., Vanoni, M. A., Mozzarelli, A., Bolognesi, M., Coda, A., Curti, B., and Mattevi, A. (1997) Active site plasticity in D-amino acid oxidase: A crystallographic analysis, *Biochemistry 36*, 5853–5860.
565. Zhang, M., Van Etten, R. L., and Stauffacher, C. V. (1994) Crystal structure of bovine heart phosphotyrosyl phosphatase at 2.2 Å resolution, *Biochemistry 33*, 11097–11105.
566. Lee, J., Johnson, J., Ding, Z., Paetzel, M., and Cornell, R. B. (2009) Crystal structure of a mammalian CTP: Phosphocholine cytidylyltransferase catalytic domain reveals novel active site residues within a highly conserved nucleotidyltransferase fold, *J. Biol. Chem 284*, 33535–33548.
567. Long, S. B., Casey, P. J., and Beese, L. S. (1998) Cocrystal structure of protein farnesyltransferase complexed with a farnesyl diphosphate substrate, *Biochemistry 37*, 9612–9618.
568. Ramakrishnan, B., Balaji, P. V., and Qasba, P. K. (2002) Crystal structure of β1,4-galactosyltransferase complex with UDP-Gal reveals an oligosaccharide acceptor binding site, *J. Mol. Biol. 318*, 491–502.
569. Appleby, T. C., Kinsland, C., Begley, T. P., and Ealick, S. E. (2000) The crystal structure and mechanism of orotidine 5′-monophosphate decarboxylase, *Proc. Natl. Acad. Sci. U. S. A. 97*, 2005–2010.
570. Blake, C. C., and Evans, P. R. (1974) Structure of horse muscle phosphoglycerate kinase. Some results on the chain conformation, substrate binding and evolution of the molecule from a 3 Å Fourier map, *J. Mol. Biol. 84*, 585–601.
571. Thoden, J. B., Holden, H. M., Paritala, H., and Firestine, S. M. (2010) Structural and functional studies of *Aspergillus clavatus* N^5-carboxyaminoimidazole ribonucleotide synthetase, *Biochemistry 49*, 752–760.
572. Hill, E., Tsernoglou, D., Webb, L., and Banaszak, L. J. (1972) Polypeptide conformation of cytoplasmic malate dehydrogenase from an electron density map at 3.0 Å resolution, *J. Mol. Biol. 72*, 577–589.
573. Charron, C., Talfournier, F., Isupov, M. N., Littlechild, J. A., Branlant, G., Vitoux, B., and Aubry, A. (2000) The crystal structure of D-glyceraldehyde-3-phosphate dehydrogenase from the hyperthermophilic archaeon *Methanothermus fervidus* in the presence of $NADP^+$ at 2.1 Å resolution, *J. Mol. Biol. 297*, 481–500.
574. Birktoft, J. J., Fernley, R. T., Bradshaw, R. A., and Banaszak, L. J. (1982) The interactions of NAD and NADH with 2-hydroxyacid dehydrogenase, In *Molecular structure and biological activity* (Harker, D., Griffin, J. F., and Duax, W. L., Eds.), pp 37–55, Elsevier Biomedical, New York.
575. Skarzynski, T., Moody, P. C., and Wonacott, A. J. (1987) Structure of holo-glyceraldehyde-3-phosphate dehydrogenase from *Bacillus*

stearothermophilus at 1.8 Å resolution, *J. Mol. Biol. 193*, 171–187.
576. Kraulis, P. J. (1991) Molscript, a program to produce both detailed and schematic plots of protein structures, *J. Appl. Crystallogr. 24*, 946–950.
577. Zhang, Y., White, R. H., and Ealick, S. E. (2008) Crystal structure and function of 5-formaminoimidazole-4-carboxamide ribonucleotide synthetase from *Methanocaldococcus jannaschii*, *Biochemistry 47*, 205–217.
578. Remington, S., Wiegand, G., and Huber, R. (1982) Crystallographic refinement and atomic models of two different forms of citrate synthase at 2.7 and 1.7 Å resolution, *J. Mol. Biol. 158*, 111–152.
579. Korolev, S., Ikeguchi, Y., Skarina, T., Beasley, S., Arrowsmith, C., Edwards, A., Joachimiak, A., Pegg, A. E., and Savchenko, A. (2002) The crystal structure of spermidine synthase with a multisubstrate adduct inhibitor, *Nature Struct. Biol. 9*, 27–31.
580. Krause, K. L., Volz, K. W., and Lipscomb, W. N. (1987) 2.5 Å Structure of aspartate carbamoyltransferase complexed with the bisubstrate analog *N*-(phosphonacetyl)–L-aspartate, *J. Mol. Biol. 193*, 527–553.
581. Prosise, G. L., and Luecke, H. (2003) Crystal structures of *Tritrichomonas foetus* inosine monophosphate dehydrogenase in complex with substrate, cofactor and analogs: A structural basis for the random-in ordered-out kinetic mechanism, *J. Mol. Biol. 326*, 517–527.
582. Komoto, J., Yamada, T., Takata, Y., Konishi, K., Ogawa, H., Gomi, T., Fujioka, M., and Takusagawa, F. (2004) Catalytic mechanism of guanidinoacetate methyltransferase: Crystal structures of guanidinoacetate methyltransferase ternary complexes, *Biochemistry 43*, 14385–14394.
583. Packianathan, C., Kandavelu, P., and Rosen, B. P. (2018) The structure of an As(III) *S*-adenosylmethionine methyltransferase with 3-coordinately bound As(III) depicts the first step in catalysis, *Biochemistry 57*, 4083–4092.
584. Grueninger, D., and Schulz, G. E. (2006) Structure and reaction mechanism of L-rhamnulose kinase from *Escherichia coli*, *J. Mol. Biol. 359*, 787–797.
585. Larsen, T. M., Wedekind, J. E., Rayment, I., and Reed, G. H. (1996) A carboxylate oxygen of the substrate bridges the magnesium ions at the active site of enolase: Structure of the yeast enzyme complexed with the equilibrium mixture of 2-phosphoglycerate and phospho*enol*pyruvate at 1.8 Å resolution, *Biochemistry 35*, 4349–4358.
586. Lee, K. H., Ryu, K. S., Kim, M. S., Suh, H. Y., Ku, B., Song, Y. L., Ko, S., Lee, W., and Oh, B. H. (2009) Crystal structures and enzyme mechanisms of a dual fucose mutarotase/ribose pyranase, *J. Mol. Biol. 391*, 178–191.
587. Iacovino, L. G., Savino, S., Borg, A. J. E., Binda, C., Nidetzky, B., and Mattevi, A. (2020) Crystallographic snapshots of UDP-glucuronic acid 4-epimerase ligand binding, rotation, and reduction, *J. Biol. Chem. 295*, 12461–12473.
588. Zhang, E., Brewer, J. M., Minor, W., Carreira, L. A., and Lebioda, L. (1997) Mechanism of enolase: The crystal structure of asymmetric dimer enolase-2-phospho-D-glycerate/enolase-phospho*enol*pyruvate at 2.0 Å resolution, *Biochemistry 36*, 12526–12534.
589. Thoden, J. B., Phillips, G. N., Jr., Neal, T. M., Raushel, F. M., and Holden, H. M. (2001) Molecular structure of dihydroorotase: A paradigm for catalysis through the use of a binuclear metal center, *Biochemistry 40*, 6989–6997.
590. Teh, A. H., Kimura, M., Yamamoto, M., Tanaka, N., Yamaguchi, I., and Kumasaka, T. (2006) The 1.48 Å resolution crystal structure of the homotetrameric cytidine deaminase from mouse, *Biochemistry 45*, 7825–7833.
591. Grau, U. M., Trommer, W. E., and Rossmann, M. G. (1981) Structure of the active ternary complex of pig heart lactate dehydrogenase with *S*-lac-NAD at 2.7 Å resolution, *J. Mol. Biol. 151*, 289–307.
592. Grubmeyer, C., Hansen, M. R., Fedorov, A. A., and Almo, S. C. (2012) Structure of *Salmonella typhimurium* OMP synthase in a complete substrate complex, *Biochemistry 51*, 4397–4405.
593. Tewari, Y. B., Davis, A. M., Reddy, P., and Goldberg, R. N. (2000) A thermodynamic study of the conversion of chorismate to isochorismate, *J. Chem. Thermodyn. 32*, 1057–1070.
594. Sridharan, S., Howard, N., Kerbarh, O., Blaszczyk, M., Abell, C., and Blundell, T. L. (2010) Crystal structure of *Escherichia coli*

enterobactin-specific isochorismate synthase (EntC) bound to its reaction product isochorismate: Implications for the enzyme mechanism and differential activity of chorismate-utilizing enzymes, *J. Mol. Biol. 397*, 290–300.
595. Kavran, J. M., Gundllapalli, S., O'Donoghue, P., Englert, M., Soll, D., and Steitz, T. A. (2007) Structure of pyrrolysyl-tRNA synthetase, an archaeal enzyme for genetic code innovation, *Proc. Natl. Acad. Sci. U. S. A. 104*, 11268–11273.
596. McCulloch, K. M., Kinsland, C., Begley, T. P., and Ealick, S. E. (2008) Structural studies of thiamin monophosphate kinase in complex with substrates and products, *Biochemistry 47*, 3810–3821.
597. Rozovsky, S., and McDermott, A. E. (2007) Substrate product equilibrium on a reversible enzyme, triosephosphate isomerase, *Proc. Natl. Acad. Sci. U. S. A. 104*, 2080–2085.
598. Jogl, G., Rozovsky, S., McDermott, A. E., and Tong, L. (2003) Optimal alignment for enzymatic proton transfer: Structure of the Michaelis complex of triosephosphate isomerase at 1.2-Å resolution, *Proc. Natl. Acad. Sci. U. S. A. 100*, 50–55.
599. Chung, S. J., Fromme, J. C., and Verdine, G. L. (2005) Structure of human cytidine deaminase bound to a potent inhibitor, *J. Med. Chem. 48*, 658–660.
600. Thoma, R., Schulz-Gasch, T., D'Arcy, B., Benz, J., Aebi, J., Dehmlow, H., Hennig, M., Stihle, M., and Ruf, A. (2004) Insight into steroid scaffold formation from the structure of human oxidosqualene cyclase, *Nature 432*, 118–122.
601. Ji, X., Johnson, W. W., Sesay, M. A., Dickert, L., Prasad, S. M., Ammon, H. L., Armstrong, R. N., and Gilliland, G. L. (1994) Structure and function of the xenobiotic substrate binding site of a glutathione *S*-transferase as revealed by X-ray crystallographic analysis of product complexes with the diastereomers of 9-(*S*-glutathionyl)-10-hydroxy-9,10-dihydrophenanthrene, *Biochemistry 33*, 1043–1052.
602. Heyes, D. J., Levy, C., Lafite, P., Roberts, I. S., Goldrick, M., Stachulski, A. V., Rossington, S. B., Stanford, D., Rigby, S. E., Scrutton, N. S., and Leys, D. (2009) Structure-based mechanism of CMP-2-keto-3-deoxymannooctulonic acid synthetase: Convergent evolution of a sugar-activating enzyme with DNA/RNA polymerases, *J. Biol. Chem 284*, 35514–35523.
603. Koksal, M., Zimmer, I., Schnitzler, J. P., and Christianson, D. W. (2010) Structure of isoprene synthase illuminates the chemical mechanism of teragram atmospheric carbon emission, *J. Mol. Biol. 402*, 363–373.
604. Shi, W., Li, C. M., Tyler, P. C., Furneaux, R. H., Grubmeyer, C., Schramm, V. L., and Almo, S. C. (1999) The 2.0 Å structure of human hypoxanthine-guanine phosphoribosyltransferase in complex with a transition-state analog inhibitor, *Nature Struct. Biol. 6*, 588–593.
605. Schumacher, M. A., Carter, D., Scott, D. M., Roos, D. S., Ullman, B., and Brennan, R. G. (1998) Crystal structures of *Toxoplasma gondii* uracil phosphoribosyltransferase reveal the atomic basis of pyrimidine discrimination and prodrug binding, *EMBO J. 17*, 3219–3232.
606. Shi, W., Munagala, N. R., Wang, C. C., Li, C. M., Tyler, P. C., Furneaux, R. H., Grubmeyer, C., Schramm, V. L., and Almo, S. C. (2000) Crystal structures of *Giardia lamblia* guanine phosphoribosyltransferase at 1.75 Å, *Biochemistry 39*, 6781–6790.
607. Koellner, G., Luic, M., Shugar, D., Saenger, W., and Bzowska, A. (1998) Crystal structure of the ternary complex of *E. coli* purine nucleoside phosphorylase with formycin B, a structural analogue of the substrate inosine, and phosphate (sulphate) at 2.1 Å resolution, *J. Mol. Biol. 280*, 153–166.
608. Frere, F., Schubert, W.-D., Stauffer, F., Frankenberg, N., Neier, R., Jahn, D., and Heinz Dirk, W. (2002) Structure of porphobilinogen synthase from *Pseudomonas aeruginosa* in complex with 5-fluorolevulinic acid suggests a double Schiff base mechanism, *J. Mol. Biol. 320*, 237–247.
609. Hara, T., Kato, H., Katsube, Y., and Oda, J. (1996) A pseudo-Michaelis quaternary complex in the reverse reaction of a ligase: Structure of *Escherichia coli* B glutathione synthetase complexed with ADP, glutathione, and sulfate at 2.0 Å resolution, *Biochemistry 35*, 11967–11974.
610. Gan, J., Gu, Y., Li, Y., Yan, H., and Ji, X. (2006) Crystal structure of *Mycobacterium tuberculosis* shikimate kinase in complex with shikimic acid and an ATP analogue, *Biochemistry 45*, 8539–8545.

611. Schumacher, M. A., Scott, D. M., Mathews, II, Ealick, S. E., Roos, D. S., Ullman, B., and Brennan, R. G. (2000) Crystal structures of *Toxoplasma gondii* adenosine kinase reveal a novel catalytic mechanism and prodrug binding, *J. Mol. Biol. 296*, 549–567.
612. Marco-Marin, C., Gil-Ortiz, F., and Rubio, V. (2005) The crystal structure of *Pyrococcus furiosus* UMP kinase provides insight into catalysis and regulation in microbial pyrimidine nucleotide biosynthesis, *J. Mol. Biol. 352*, 438–454.
613. Morar, M., Anand, R., Hoskins, A. A., Stubbe, J., and Ealick, S. E. (2006) Complexed structures of formylglycinamide ribonucleotide amidotransferase from *Thermotoga maritima* describe a novel ATP binding protein superfamily, *Biochemistry 45*, 14880–14895.
614. Huerta, C., Borek, D., Machius, M., Grishin, N. V., and Zhang, H. (2009) Structure and mechanism of a eukaryotic FMN adenylyltransferase, *J. Mol. Biol. 389*, 388–400.
615. Bastidas, A. C., Deal, M. S., Steichen, J. M., Guo, Y., Wu, J., and Taylor, S. S. (2013) Phosphoryl transfer by protein kinase A is captured in a crystal lattice, *J. Am. Chem. Soc. 135*, 4788–4798.
616. Kim, S. G., Cavalier, M., El-Maghrabi, M. R., and Lee, Y. H. (2007) A direct substrate-substrate interaction found in the kinase domain of the bifunctional enzyme, 6-phosphofructo-2-kinase/fructose-2,6-bisphosphatase, *J. Mol. Biol. 370*, 14–26.
617. Bossemeyer, D., Engh, R. A., Kinzel, V., Ponstingl, H., and Huber, R. (1993) Phosphotransferase and substrate binding mechanism of the cAMP-dependent protein kinase catalytic subunit from porcine heart as deduced from the 2.0 Å structure of the complex with Mn^{2+} adenylyl imidodiphosphate and inhibitor peptide PKI(5-24), *EMBO J. 12*, 849–859.
618. Persson, K., Ly, H. D., Dieckelmann, M., Wakarchuk, W. W., Withers, S. G., and Strynadka, N. C. (2001) Crystal structure of the retaining galactosyltransferase LgtC from *Neisseria meningitidis* in complex with donor and acceptor sugar analogs, *Nature Struct. Biol. 8*, 166–175.
619. Gouaux, J. E., and Lipscomb, W. N. (1988) Three-dimensional structure of carbamoyl phosphate and succinate bound to aspartate carbamoyltransferase, *Proc. Natl. Acad. Sci. U. S. A. 85*, 4205–4208.
620. Poulos, T. L., Finzel, B. C., and Howard, A. J. (1987) High-resolution crystal structure of cytochrome P450cam, *J. Mol. Biol. 195*, 687–700.
621. Musayev, F., Sachdeva, S., Scarsdale, J. N., Reynolds, K. A., and Wright, H. T. (2005) Crystal structure of a substrate complex of *Mycobacterium tuberculosis* β-ketoacyl-acyl carrier protein synthase III (FabH) with lauroyl-coenzyme A, *J. Mol. Biol. 346*, 1313–1321.
622. Yew, W. S., Fedorov, A. A., Fedorov, E. V., Wood, B. M., Almo, S. C., and Gerlt, J. A. (2006) Evolution of enzymatic activities in the enolase superfamily: D-Tartrate dehydratase from *Bradyrhizobium japonicum*, *Biochemistry 45*, 14598–14608.
623. Didierjean, C., Corbier, C., Fatih, M., Favier, F., Boschi-Muller, S., Branlant, G., and Aubry, A. (2003) Crystal structure of two ternary complexes of phosphorylating glyceraldehyde-3-phosphate dehydrogenase from *Bacillus stearothermophilus* with NAD and D-glyceraldehyde 3-phosphate, *J. Biol. Chem. 278*, 12968–12976.
624. Jensen, M. H., Otten, H., Christensen, U., Borchert, T. V., Christensen, L. L., Larsen, S., and Leggio, L. L. (2010) Structural and biochemical studies elucidate the mechanism of rhamnogalacturonan lyase from *Aspergillus aculeatus*, *J. Mol. Biol. 404*, 100–111.
625. Kuznetsova, E., Xu, L., Singer, A., Brown, G., Dong, A., Flick, R., Cui, H., Cuff, M., Joachimiak, A., Savchenko, A., and Yakunin, A. F. (2010) Structure and activity of the metal-independent fructose-1,6-bisphosphatase YK23 from *Saccharomyces cerevisiae*, *J. Biol. Chem 285*, 21049–21059.
626. Liu, S., Lu, Z., Han, Y., Melamud, E., Dunaway-Mariano, D., and Herzberg, O. (2005) Crystal structures of 2-methylisocitrate lyase in complex with product and with isocitrate inhibitor provide insight into lyase substrate specificity, catalysis and evolution, *Biochemistry 44*, 2949–2962.
627. Tremblay, L. W., Xu, H., and Blanchard, J. S. (2010) Structures of the Michaelis complex (1.2 a) and the covalent acyl intermediate (2.0 Å) of cefamandole bound in the active sites of the *Mycobacterium tuberculosis* β-lactamase K73A and E166A mutants, *Biochemistry 49*, 9685–9687.

628. French, J. B., Cen, Y., Sauve, A. A., and Ealick, S. E. (2010) High-resolution crystal structures of *Streptococcus pneumoniae* nicotinamidase with trapped intermediates provide insights into the catalytic mechanism and inhibition by aldehydes, *Biochemistry 49*, 8803–8812.
629. Ji, S., Dix, S. R., Aziz, A. A., Sedelnikova, S. E., Baker, P. J., Rafferty, J. B., Bullough, P. A., Tzokov, S. B., Agirre, J., Li, F. L., and Rice, D. W. (2019) The molecular basis of endolytic activity of a multidomain alginate lyase from *Defluviitalea phaphyphila*, a representative of a new lyase family, PL39, *J. Biol. Chem. 294*, 18077–18091.
630. Zhou, G., Somasundaram, T., Blanc, E., Parthasarathy, G., Ellington, W. R., and Chapman, M. S. (1998) Transition state structure of arginine kinase: Implications for catalysis of bimolecular reactions, *Proc. Natl. Acad. Sci. U. S. A. 95*, 8449–8454.
631. Gerlits, O., Tian, J., Das, A., Langan, P., Heller, W. T., and Kovalevsky, A. (2015) Phosphoryl transfer reaction snapshots in crystals: Insights into the mechanism of protein kinase A catalytic subunit, *J. Biol. Chem 290*, 15538–15548.
632. Baxter, N. J., Hounslow, A. M., Bowler, M. W., Williams, N. H., Blackburn, G. M., and Waltho, J. P. (2009) MgF_3^- and α-galactose 1-phosphate in the active site of β-phosphoglucomutase form a transition state analogue of phosphoryl transfer, *J. Am. Chem. Soc. 131*, 16334–16335.
633. Holden, H. M., Tronrud, D. E., Monzingo, A. F., Weaver, L. H., and Matthews, B. W. (1987) Slow- and fast-binding inhibitors of thermolysin display different modes of binding: Crystallographic analysis of extended phosphonamidate transition-state analogues, *Biochemistry 26*, 8542–8553.
634. Betts, L., Xiang, S., Short, S. A., Wolfenden, R., and Carter, C. W., Jr. (1994) Cytidine deaminase. The 2.3 Å crystal structure of an enzyme:transition-state analog complex, *J. Mol. Biol. 235*, 635–656.
635. Hall, R. S., Fedorov, A. A., Xu, C., Fedorov, E. V., Almo, S. C., and Raushel, F. M. (2011) Three-dimensional structure and catalytic mechanism of cytosine deaminase, *Biochemistry 50*, 5077–5085.
636. Wang, J., Duewel, H. S., Woodard, R. W., and Gatti, D. L. (2001) Structures of *Aquifex aeolicus* KDO8P synthase in complex with R5P and PEP, and with a bisubstrate inhibitor: Role of active site water in catalysis, *Biochemistry 40*, 15676–15683.
637. Asojo, O., Friedman, J., Adir, N., Belakhov, V., Shoham, Y., and Baasov, T. (2001) Crystal structures of KDOP synthase in its binary complexes with the substrate phospho*enol*-pyruvate and with a mechanism-based inhibitor, *Biochemistry 40*, 6326–6334.
638. Reardon, J. E., and Abeles, R. H. (1986) Mechanism of action of isopentenyl pyrophosphate isomerase: Evidence for a carbonium ion intermediate, *Biochemistry 25*, 5609–5616.
639. Zhang, C., Liu, L., Xu, H., Wei, Z., Wang, Y., Lin, Y., and Gong, W. (2007) Crystal structures of human IPP isomerase: New insights into the catalytic mechanism, *J. Mol. Biol. 366*, 1437–1446.
640. Krajewski, W. W., Jones, T. A., and Mowbray, S. L. (2005) Structure of *Mycobacterium tuberculosis* glutamine synthetase in complex with a transition-state mimic provides functional insights, *Proc. Natl. Acad. Sci. U. S. A. 102*, 10499–10504.
641. Liaw, S. H., Kuo, I., and Eisenberg, D. (1995) Discovery of the ammonium substrate site on glutamine synthetase: A third cation binding site, *Prot. Sci. 4*, 2358–2365.
642. Lu, Z., Dunaway-Mariano, D., and Allen, K. N. (2005) HAD superfamily phosphotransferase substrate diversification: Structure and function analysis of HAD subclass IIB sugar phosphatase BT4131, *Biochemistry 44*, 8684–8696.
643. Lu, Z., Dunaway-Mariano, D., and Allen, K. N. (2008) The catalytic scaffold of the haloalkanoic acid dehalogenase enzyme superfamily acts as a mold for the trigonal bipyramidal transition state, *Proc. Natl. Acad. Sci. U. S. A. 105*, 5687–5692.
644. Bernstein, B. E., and Hol, W. G. (1998) Crystal structures of substrates and products bound to the phosphoglycerate kinase active site reveal the catalytic mechanism, *Biochemistry 37*, 4429–4436.
645. Ajees, A. A., Marapakala, K., Packianathan, C., Sankaran, B., and Rosen, B. P. (2012) Structure of an As(III) *S*-adenosylmethionine methyltransferase: Insights into the mechanism of arsenic biotransformation, *Biochemistry 51*, 5476–5485.

646. Pedersen, L. C., Darden, T. A., and Negishi, M. (2002) Crystal structure of β 1,3-glucuronyltransferase I in complex with active donor substrate UDP-GlcUA, *J. Biol. Chem. 277*, 21869–21873.
647. Hartmann, M. D., Bourenkov, G. P., Oberschall, A., Strizhov, N., and Bartunik, H. D. (2006) Mechanism of phosphoryl transfer catalyzed by shikimate kinase from *Mycobacterium tuberculosis*, *J. Mol. Biol. 364*, 411–423.
648. Hosfield, D. J., Zhang, Y., Dougan, D. R., Broun, A., Tari, L. W., Swanson, R. V., and Finn, J. (2004) Structural basis for bisphosphonate-mediated inhibition of isoprenoid biosynthesis, *J. Biol. Chem. 279*, 8526–8529.
649. Kloer, D. P., Welsch, R., Beyer, P., and Schulz, G. E. (2006) Structure and reaction geometry of geranylgeranyl diphosphate synthase from *Sinapis alba*, *Biochemistry 45*, 15197–15204.
650. Hall, M. D., and Banaszak, L. J. (1993) Crystal structure of a ternary complex of *Escherichia coli* malate dehydrogenase citrate and NAD at 1.9 Å resolution, *J. Mol. Biol. 232*, 213–222.
651. Tomita, K., Ishitani, R., Fukai, S., and Nureki, O. (2006) Complete crystallographic analysis of the dynamics of CCA sequence addition, *Nature 443*, 956–960.
652. Parey, K., Warkentin, E., Kroneck, P. M., and Ermler, U. (2010) Reaction cycle of the dissimilatory sulfite reductase from *Archaeoglobus fulgidus*, *Biochemistry 49*, 8912–8921.
653. Nakamura, T., Zhao, Y., Yamagata, Y., Hua, Y. J., and Yang, W. (2012) Watching DNA polymerase η make a phosphodiester bond, *Nature 487*, 196–201.
654. Klimasauskas, S., Kumar, S., Roberts, R. J., and Cheng, X. (1994) HhaI methyltransferase flips its target base out of the DNA helix, *Cell 76*, 357–369.
655. O'Gara, M., Klimasauskas, S., Roberts, R. J., and Cheng, X. (1996) Enzymatic C5-cytosine methylation of DNA: Mechanistic implications of new crystal structures for HhaI methyltransferase-DNA-AdoHcy complexes, *J. Mol. Biol. 261*, 634–645.
656. Oksanen, E., Ahonen, A. K., Tuominen, H., Tuominen, V., Lahti, R., Goldman, A., and Heikinheimo, P. (2007) A complete structural description of the catalytic cycle of yeast pyrophosphatase, *Biochemistry 46*, 1228–1239.
657. Nango, E., Royant, A., Kubo, M., Nakane, T., Wickstrand, C., Kimura, T., Tanaka, T., Tono, K., Song, C., Tanaka, R., Arima, T., Yamashita, A., Kobayashi, J., Hosaka, T., Mizohata, E., Nogly, P., Sugahara, M., Nam, D., Nomura, T., Shimamura, T., Im, D., Fujiwara, T., Yamanaka, Y., Jeon, B., Nishizawa, T., Oda, K., Fukuda, M., Andersson, R., Bath, P., Dods, R., Davidsson, J., Matsuoka, S., Kawatake, S., Murata, M., Nureki, O., Owada, S., Kameshima, T., Hatsui, T., Joti, Y., Schertler, G., Yabashi, M., Bondar, A. N., Standfuss, J., Neutze, R., and Iwata, S. (2016) A three-dimensional movie of structural changes in bacteriorhodopsin, *Science 354*, 1552–1557.
658. Skopintsev, P., Ehrenberg, D., Weinert, T., James, D., Kar, R. K., Johnson, P. J. M., Ozerov, D., Furrer, A., Martiel, I., Dworkowski, F., Nass, K., Knopp, G., Cirelli, C., Arrell, C., Gashi, D., Mous, S., Wranik, M., Gruhl, T., Kekilli, D., Brunle, S., Deupi, X., Schertler, G. F. X., Benoit, R. M., Panneels, V., Nogly, P., Schapiro, I., Milne, C., Heberle, J., and Standfuss, J. (2020) Femtosecond-to-millisecond structural changes in a light-driven sodium pump, *Nature 583*, 314–318.
659. Suga, M., Akita, F., Sugahara, M., Kubo, M., Nakajima, Y., Nakane, T., Yamashita, K., Umena, Y., Nakabayashi, M., Yamane, T., Nakano, T., Suzuki, M., Masuda, T., Inoue, S., Kimura, T., Nomura, T., Yonekura, S., Yu, L. J., Sakamoto, T., Motomura, T., Chen, J. H., Kato, Y., Noguchi, T., Tono, K., Joti, Y., Kameshima, T., Hatsui, T., Nango, E., Tanaka, R., Naitow, H., Matsuura, Y., Yamashita, A., Yamamoto, M., Nureki, O., Yabashi, M., Ishikawa, T., Iwata, S., and Shen, J. R. (2017) Light-induced structural changes and the site of O=O bond formation in PSII caught by XFEL, *Nature 543*, 131–135.
660. Kupitz, C., Basu, S., Grotjohann, I., Fromme, R., Zatsepin, N. A., Rendek, K. N., Hunter, M. S., Shoeman, R. L., White, T. A., Wang, D., James, D., Yang, J. H., Cobb, D. E., Reeder, B., Sierra, R. G., Liu, H., Barty, A., Aquila, A. L., Deponte, D., Kirian, R. A., Bari, S., Bergkamp, J. J., Beyerlein, K. R., Bogan, M. J., Caleman, C., Chao, T. C., Conrad, C. E., Davis, K. M., Fleckenstein, H., Galli, L., Hau-Riege, S. P., Kassemeyer, S., Laksmono, H., Liang, M., Lomb, L., Marchesini, S., Martin, A. V., Messerschmidt, M., Milathianaki, D., Nass, K., Ros, A., Roy-Chowdhury, S., Schmidt, K., Seibert, M., Steinbrener, J., Stellato, F., Yan, L., Yoon, C., Moore, T. A., Moore, A. L., Push-

kar, Y., Williams, G. J., Boutet, S., Doak, R. B., Weierstall, U., Frank, M., Chapman, H. N., Spence, J. C., and Fromme, P. (2014) Serial time-resolved crystallography of photosystem II using a femtosecond X-ray laser, *Nature 513*, 261–265.

661. Suga, M., Akita, F., Yamashita, K., Nakajima, Y., Ueno, G., Li, H., Yamane, T., Hirata, K., Umena, Y., Yonekura, S., Yu, L. J., Murakami, H., Nomura, T., Kimura, T., Kubo, M., Baba, S., Kumasaka, T., Tono, K., Yabashi, M., Isobe, H., Yamaguchi, K., Yamamoto, M., Ago, H., and Shen, J. R. (2019) An oxyl/oxo mechanism for oxygen–oxygen coupling in PSII revealed by an X-ray free-electron laser, *Science 366*, 334–338.
662. Schotte, F., Cho, H. S., Kaila, V. R., Kamikubo, H., Dashdorj, N., Henry, E. R., Graber, T. J., Henning, R., Wulff, M., Hummer, G., Kataoka, M., and Anfinrud, P. A. (2012) Watching a signaling protein function in real time via 100-ps time-resolved Laue crystallography, *Proc. Natl. Acad. Sci. U. S. A. 109*, 19256–19261.
663. Ihee, H., Rajagopal, S., Srajer, V., Pahl, R., Anderson, S., Schmidt, M., Schotte, F., Anfinrud, P. A., Wulff, M., and Moffat, K. (2005) Visualizing reaction pathways in photoactive yellow protein from nanoseconds to seconds, *Proc. Natl. Acad. Sci. U. S. A. 102*, 7145–7150.
664. Pande, K., Hutchison, C. D., Groenhof, G., Aquila, A., Robinson, J. S., Tenboer, J., Basu, S., Boutet, S., DePonte, D. P., Liang, M., White, T. A., Zatsepin, N. A., Yefanov, O., Morozov, D., Oberthuer, D., Gati, C., Subramanian, G., James, D., Zhao, Y., Koralek, J., Brayshaw, J., Kupitz, C., Conrad, C., Roy-Chowdhury, S., Coe, J. D., Metz, M., Xavier, P. L., Grant, T. D., Koglin, J. E., Ketawala, G., Fromme, R., Srajer, V., Henning, R., Spence, J. C., Ourmazd, A., Schwander, P., Weierstall, U., Frank, M., Fromme, P., Barty, A., Chapman, H. N., Moffat, K., van Thor, J. J., and Schmidt, M. (2016) Femtosecond structural dynamics drives the trans/cis isomerization in photoactive yellow protein, *Science 352*, 725–729.
665. Mehrabi, P., Schulz, E. C., Dsouza, R., Muller-Werkmeister, H. M., Tellkamp, F., Miller, R. J. D., and Pai, E. F. (2019) Time-resolved crystallography reveals allosteric communication aligned with molecular breathing, *Science 365*, 1167–1170.
666. Kyte, J. (2007) *Structure in protein chemistry: Second edition*, pp 230–241, Garland Science, New York.
667. Pauling, L., Corey, R. B., and Branson, H. R. (1951) The structure of proteins: Two hydrogen-bonded helical configurations of the polypeptide chain, *Proc. Natl. Acad. Sci. U.S.A. 37*, 205–211.
668. Pauling, L., and Corey, R. B. (1951) Configurations of polypeptide chains with favored orientations around single bonds: Two new pleated sheets, *Proc. Natl. Acad. Sci. U.S.A. 37*, 729–740.
669. Vyas, N. K., Vyas, M. N., and Quiocho, F. A. (1991) Comparison of the periplasmic receptors for L-arabinose, D-glucose/D-galactose, and D-ribose. Structural and functional similarity, *J. Biol. Chem. 266*, 5226–5237.
670. Vyas, N. K., Vyas, M. N., and Quiocho, F. A. (1988) Sugar and signal-transducer binding sites of the *Escherichia coli* galactose chemoreceptor protein, *Science 242*, 1290–1295.
671. Vyas, M. N., Vyas, N. K., and Quiocho, F. A. (1994) Crystallographic analysis of the epimeric and anomeric specificity of the periplasmic transport/chemosensory protein receptor for D-glucose and D-galactose, *Biochemistry 33*, 4762–4768.
672. Shaltiel, S., Cox, S., and Taylor, S. S. (1998) Conserved water molecules contribute to the extensive network of interactions at the active site of protein kinase A, *Proc. Natl. Acad. Sci. U. S. A. 95*, 484–491.
673. Iwasaki, W., Sekine, S., Kuroishi, C., Kuramitsu, S., Shirouzu, M., and Yokoyama, S. (2006) Structural basis of the water-assisted asparagine recognition by asparaginyl-tRNA synthetase, *J. Mol. Biol. 360*, 329–342.
674. Wang, M., Xia, S., Blaha, G., Steitz, T. A., Konigsberg, W. H., and Wang, J. (2011) Insights into base selectivity from the 1.8 Å resolution structure of an RB69 DNA polymerase ternary complex, *Biochemistry 50*, 581–590.
675. Darby, J. F., Hopkins, A. P., Shimizu, S., Roberts, S. M., Brannigan, J. A., Turkenburg, J. P., Thomas, G. H., Hubbard, R. E., and Fischer, M. (2019) Water networks can determine the affinity of ligand binding to proteins, *J. Am. Chem. Soc. 141*, 15818–15826.
676. Karplus, P. A., and Schulz, G. E. (1989) Substrate binding and catalysis by glutathione

reductase as derived from refined enzyme: substrate crystal structures at 2 Å resolution, *J. Mol. Biol. 210*, 163–180.
677. Hine, J. (1972) Structural effects on rates and equilibriums. XV. Hydrogen-bonded intermediates and stepwise mechanisms for proton-exchange reactions between oxygen atoms in hydroxylic solvents, *J. Am. Chem. Soc. 94*, 5766–5771.
678. Stahl, N., and Jencks, W. P. (1986) Hydrogen bonding between solutes in aqueous solution, *J. Am. Chem. Soc. 108*, 4196–4205.
679. Fersht, A. R., Shi, J. P., Knill-Jones, J., Lowe, D. M., Wilkinson, A. J., Blow, D. M., Brick, P., Carter, P., Waye, M. M., and Winter, G. (1985) Hydrogen bonding and biological specificity analysed by protein engineering, *Nature 314*, 235–238.
680. Kyte, J. (2007) *Structure in protein chemistry: Second edition*, pp 306–309, Garland Science, New York.
681. Bartlett, P. A., and Marlowe, C. K. (1987) Evaluation of intrinsic binding energy from a hydrogen bonding group in an enzyme inhibitor, *Science 235*, 569–571.
682. Tronrud, D. E., Holden, H. M., and Matthews, B. W. (1987) Structures of two thermolysin-inhibitor complexes that differ by a single hydrogen bond, *Science 235*, 571–574.
683. Grobelny, D., Goli, U. B., and Galardy, R. E. (1989) Binding energetics of phosphorus-containing inhibitors of thermolysin, *Biochemistry 28*, 4948–4951.
684. Morgan, B. P., Scholtz, J. M., Ballinger, M. D., Zipkin, I. D., and Bartlett, P. A. (1991) Differential binding energy: A detailed evaluation of the influence of hydrogen-bonding and hydrophobic groups on the inhibition of thermolysin by phosphorus-containing inhibitors, *J. Am. Chem. Soc. 113*, 297–307.
685. Moran, G. R., Entsch, B., Palfey, B. A., and Ballou, D. P. (1999) Mechanistic insights into p-hydroxybenzoate hydroxylase from studies of the mutant Ser212Ala, *Biochemistry 38*, 6292–6299.
686. Chan, P. W., Yakunin, A. F., Edwards, E. A., and Pai, E. F. (2011) Mapping the reaction coordinates of enzymatic defluorination, *J. Am. Chem. Soc. 133*, 7461–7468.
687. Savva, R., McAuley-Hecht, K., Brown, T., and Pearl, L. (1995) The structural basis of specific base-excision repair by uracil-DNA glycosylase, *Nature 373*, 487–493.
688. Liu, L., and Santi, D. V. (1992) Mutation of asparagine 229 to aspartate in thymidylate synthase converts the enzyme to a deoxycytidylate methylase, *Biochemistry 31*, 5100–5104.
689. Finer-Moore, J. S., Liu, L., Schafmeister, C. E., Birdsall, D. L., Mau, T., Santi, D. V., and Stroud, R. M. (1996) Partitioning roles of side chains in affinity, orientation, and catalysis with structures for mutant complexes: Asparagine-229 in thymidylate synthase, *Biochemistry 35*, 5125–5136.
690. Agarwalla, S., LaPorte, S., Liu, L., Finer-Moore, J., Stroud, R. M., and Santi, D. V. (1997) A novel dCMP methylase by engineering thymidylate synthase, *Biochemistry 36*, 15909–15917.
691. Denesyuk, A. I., Denessiouk, K. A., Korpela, T., and Johnson, M. S. (2002) Functional attributes of the phosphate group binding cup of pyridoxal phosphate-dependent enzymes, *J. Mol. Biol. 316*, 155–172.
692. Xu, W., and Kantrowitz, E. R. (1991) Function of serine-52 and serine-80 in the catalytic mechanism of *Escherichia coli* aspartate transcarbamoylase, *Biochemistry 30*, 2535–2542.
693. Hay, B. P., Dixon, D. A., Bryan, J. C., and Moyer, B. A. (2002) Crystallographic evidence for oxygen acceptor directionality in oxyanion hydrogen bonds, *J. Am. Chem. Soc. 124*, 182–183.
694. Reynolds, R. A., Yem, A. W., Wolfe, C. L., Deibel, M. R., Jr., Chidester, C. G., and Watenpaugh, K. D. (1999) Crystal structure of the catalytic subunit of Cdc25B required for G2/M phase transition of the cell cycle, *J. Mol. Biol. 293*, 559–568.
695. Henderson, R. (1970) Structure of crystalline α-chymotrypsin. IV. The structure of indoleacryloyl- α-chyotrypsin and its relevance to the hydrolytic mechanism of the enzyme, *J. Mol. Biol. 54*, 341–354.
696. Bullock, T. L., Breddam, K., and Remington, S. J. (1996) Peptide aldehyde complexes with wheat serine carboxypeptidase II: Implications for the catalytic mechanism and substrate specificity, *J. Mol. Biol. 255*, 714–725.
697. Martin, P. D., Malkowski, M. G., DiMaio, J., Konishi, Y., Ni, F., and Edwards, B. F. (1996) Bovine thrombin complexed with an uncleavable analog of residues 7-19 of fibrinogen Aα: Geometry of the catalytic triad and

interactions of the P1′, P2′, and P3′ substrate residues, *Biochemistry 35*, 13030–13039.
698. Lobkovsky, E., Billings, E. M., Moews, P. C., Rahil, J., Pratt, R. F., and Knox, J. R. (1994) Crystallographic structure of a phosphonate derivative of the *Enterobacter cloacae* p99 cephalosporinase: Mechanistic interpretation of a β-lactamase transition-state analog, *Biochemistry 33*, 6762–6772.
699. Benning, M. M., Taylor, K. L., Liu, R. Q., Yang, G., Xiang, H., Wesenberg, G., Dunaway-Mariano, D., and Holden, H. M. (1996) Structure of 4-chlorobenzoyl coenzyme A dehalogenase determined to 1.8 Å resolution: An enzyme catalyst generated via adaptive mutation, *Biochemistry 35*, 8103–8109.
700. Kursula, P., Ojala, J., Lambeir, A. M., and Wierenga, R. K. (2002) The catalytic cycle of biosynthetic thiolase: A conformational journey of an acetyl group through four binding modes and two oxyanion holes, *Biochemistry 41*, 15543–15556.
701. Merilainen, G., Poikela, V., Kursula, P., and Wierenga, R. K. (2009) The thiolase reaction mechanism: The importance of Asn316 and His348 for stabilizing the enolate intermediate of the Claisen condensation, *Biochemistry 48*, 11011–11025.
702. Menard, R., Carriere, J., Laflamme, P., Plouffe, C., Khouri, H. E., Vernet, T., Tessier, D. C., Thomas, D. Y., and Storer, A. C. (1991) Contribution of the glutamine 19 side chain to transition-state stabilization in the oxyanion hole of papain, *Biochemistry 30*, 8924–8928.
703. Kim, H., and Lipscomb, W. N. (1990) Crystal structure of the complex of carboxypeptidase A with a strongly bound phosphonate in a new crystalline form: Comparison with structures of other complexes, *Biochemistry 29*, 5546–5555.
704. Phillips, M. A., Fletterick, R., and Rutter, W. J. (1990) Arginine 127 stabilizes the transition state in carboxypeptidase, *J. Biol. Chem. 265*, 20692–20698.
705. Mundle, S. O., Howe, G. W., and Kluger, R. (2012) Origins of steric effects in general-base-catalyzed enolization: Solvation and electrostatic attraction, *J. Am. Chem. Soc. 134*, 1066–1070.
706. Schwans, J. P., Sunden, F., Gonzalez, A., Tsai, Y., and Herschlag, D. (2011) Evaluating the catalytic contribution from the oxyanion hole in ketosteroid isomerase, *J. Am. Chem. Soc. 133*, 20052–20055.
707. Kyte, J. (2007) *Structure in protein chemistry: Second edition*, pp 199–204, Garland Science, New York.
708. Kirsch, J. F., Eichele, G., Ford, G. C., Vincent, M. G., Jansonius, J. N., Gehring, H., and Christen, P. (1984) Mechanism of action of aspartate aminotransferase proposed on the basis of its spatial structure, *J. Mol. Biol. 174*, 497–525.
709. Malashkevich, V. N., Toney, M. D., and Jansonius, J. N. (1993) Crystal structures of true enzymatic reaction intermediates: Aspartate and glutamate ketimines in aspartate aminotransferase, *Biochemistry 32*, 13451–13462.
710. Sacchettini, J. C., Gordon, J. I., and Banaszak, L. J. (1989) Crystal structure of rat intestinal fatty-acid-binding protein: Refinement and analysis of the *Escherichia coli*-derived protein with bound palmitate, *J. Mol. Biol. 208*, 327–339.
711. Wilson, I. B., and Bergmann, F. (1950) Studies on cholinesterase. VII. The active surface of acetylcholine esterase derived from effects of pH on inhibitors, *J. Biol. Chem. 185*, 479–489.
712. Bale, S., Brooks, W., Hanes, J. W., Mahesan, A. M., Guida, W. C., and Ealick, S. E. (2009) Role of the sulfonium center in determining the ligand specificity of human *S*-adenosylmethionine decarboxylase, *Biochemistry 48*, 6423–6430.
713. Waksman, G., Kominos, D., Robertson, S. C., Pant, N., Baltimore, D., Birge, R. B., Cowburn, D., Hanafusa, H., Mayer, B. J., Overduin, M., Resh M. D., Rios C. B., Silverman, L., and Kuriyan, J. (1992) Crystal structure of the phosphotyrosine recognition domain SH2 of v-src complexed with tyrosine-phosphorylated peptides, *Nature 358*, 646–653.
714. Kienhofer, A., Kast, P., and Hilvert, D. (2003) Selective stabilization of the chorismate mutase transition state by a positively charged hydrogen bond donor, *J. Am. Chem. Soc. 125*, 3206–3207.
715. Kast, P., Asif-Ullah, M., Jiang, N., and Hilvert, D. (1996) Exploring the active site of chorismate mutase by combinatorial mutagenesis and selection: The importance of electrostatic catalysis, *Proc. Natl. Acad. Sci. U.S.A. 93*, 5043–5048.

716. Metanis, N., Brik, A., Dawson, P. E., and Keinan, E. (2004) Electrostatic interactions dominate the catalytic contribution of Arg39 in 4-oxalocrotonate tautomerase, *J. Am. Chem. Soc. 126*, 12726–12727.
717. Hyde, C. C., Ahmed, S. A., Padlan, E. A., Miles, E. W., and Davies, D. R. (1988) Three-dimensional structure of the tryptophan synthase $\alpha_2\beta_2$ multienzyme complex from *Salmonella typhimurium*, *J. Biol. Chem. 263*, 17857–17871.
718. Morse, R. J., Kawase, S., Santi, D. V., Finer-Moore, J., and Stroud, R. M. (2000) Energetic contributions of four arginines to phosphate-binding in thymidylate synthase are more than additive and depend on optimization of "effective charge balance", *Biochemistry 39*, 1011–1020.
719. Steitz, T. A., Henderson, R., and Blow, D. M. (1969) Structure of crystalline α-chymotrypsin. 3. Crystallographic studies of substrates and inhibitors bound to the active site of α-chymotrypsin, *J. Mol. Biol. 46*, 337–348.
720. Bode, W., Walter, J., Huber, R., Wenzel, H. R., and Tschesche, H. (1984) The refined 2.2-Å (0.22-nm) X-ray crystal structure of the ternary complex formed by bovine trypsinogen, valine-valine and the Arg15 analogue of bovine pancreatic trypsin inhibitor, *Eur. J. Biochem. 144*, 185–190.
721. Graf, L., Craik, C. S., Patthy, A., Roczniak, S., Fletterick, R. J., and Rutter, W. J. (1987) Selective alteration of substrate specificity by replacement of aspartic acid-189 with lysine in the binding pocket of trypsin, *Biochemistry 26*, 2616–2623.
722. Cronin, C. N., and Kirsch, J. F. (1988) Role of arginine-292 in the substrate specificity of aspartate aminotransferase as examined by site-directed mutagenesis, *Biochemistry 27*, 4572–4579.
723. Graf, L., Jancso, A., Szilagyi, L., Hegyi, G., Pinter, K., Naray-Szabo, G., Hepp, J., Medzihradszky, K., and Rutter, W. J. (1988) Electrostatic complementarity within the substrate-binding pocket of trypsin, *Proc. Natl. Acad. Sci. U.S.A. 85*, 4961–4965.
724. Krimmer, S. G., Cramer, J., Schiebel, J., Heine, A., and Klebe, G. (2017) How nothing boosts affinity: Hydrophobic ligand binding to the virtually vacated S1′ pocket of thermolysin, *J. Am. Chem. Soc. 139*, 10419–10431.
725. Jencks, W. P. (1969) *Catalysis in chemistry and enzymology*, pp 409–411, McGraw-Hill, New York.
726. Liu, T., Chen, L., Zhou, Y., Jiang, X., Duan, Y., and Yang, Q. (2017) Structure, catalysis, and inhibition of *Of*Chi-h, the lepidoptera-exclusive insect chitinase, *J. Biol. Chem. 292*, 2080–2088.
727. Chen, W., Qu, M., Zhou, Y., and Yang, Q. (2018) Structural analysis of group II chitinase (chtII) catalysis completes the puzzle of chitin hydrolysis in insects, *J. Biol. Chem. 293*, 2652–2660.
728. Spurlino, J. C., Lu, G. Y., and Quiocho, F. A. (1991) The 2.3-Å resolution structure of the maltose- or maltodextrin-binding protein, a primary receptor of bacterial active transport and chemotaxis, *J. Biol. Chem. 266*, 5202–5219.
729. Versees, W., Decanniere, K., Van Holsbeke, E., Devroede, N., and Steyaert, J. (2002) Enzyme-substrate interactions in the purine-specific nucleoside hydrolase from *Trypanosoma vivax*, *J. Biol. Chem 277*, 15938–15946.
730. Versees, W., Loverix, S., Vandemeulebroucke, A., Geerlings, P., and Steyaert, J. (2004) Leaving group activation by aromatic stacking: An alternative to general acid catalysis, *J. Mol. Biol. 338*, 1–6.
731. Mattevi, A., Obmolova, G., Kalk, K. H., Teplyakov, A., and Hol, W. G. (1993) Crystallographic analysis of substrate binding and catalysis in dihydrolipoyl transacetylase (E2P), *Biochemistry 32*, 3887–3901.
732. Devoe, H., and Tinoco, I., Jr. (1962) The stability of helical polynucleotides: Base contributions, *J. Mol. Biol. 4*, 500–517.
733. Wu, N., Mo, Y., Gao, J., and Pai, E. F. (2000) Electrostatic stress in catalysis: Structure and mechanism of the enzyme orotidine monophosphate decarboxylase, *Proc. Natl. Acad. Sci. U. S. A. 97*, 2017–2022.
734. Coll, M., Knof, S. H., Ohga, Y., Messerschmidt, A., Huber, R., Moellering, H., Russmann, L., and Schumacher, G. (1990) Enzymatic mechanism of creatine amidinohydrolase as deduced from crystal structures, *J. Mol. Biol. 214*, 597–610.
735. Shumilin, I. A., Bauerle, R., and Kretsinger, R. H. (2003) The high-resolution structure of 3-deoxy-D-*arabino*-heptulosonate-7-phosphate synthase reveals a twist in the

plane of bound phospho*enol*pyruvate, *Biochemistry 42*, 3766–3776.
736. Maiti, A., Morgan, M. T., Pozharski, E., and Drohat, A. C. (2008) Crystal structure of human thymine DNA glycosylase bound to DNA elucidates sequence-specific mismatch recognition, *Proc. Natl. Acad. Sci. U. S. A. 105*, 8890–8895.
737. Slupphaug, G., Mol, C. D., Kavli, B., Arvai, A. S., Krokan, H. E., and Tainer, J. A. (1996) A nucleotide-flipping mechanism from the structure of human uracil-DNA glycosylase bound to DNA, *Nature 384*, 87–92.
738. Parikh, S. S., Mol, C. D., Slupphaug, G., Bharati, S., Krokan, H. E., and Tainer, J. A. (1998) Base excision repair initiation revealed by crystal structures and binding kinetics of human uracil-DNA glycosylase with DNA, *EMBO J. 17*, 5214–5226.
739. Daniels, D. S., Woo, T. T., Luu, K. X., Noll, D. M., Clarke, N. D., Pegg, A. E., and Tainer, J. A. (2004) DNA binding and nucleotide flipping by the human DNA repair protein AGT, *Nature Struct. Biol. 11*, 714–720.
740. Bruner, S. D., Norman, D. P., and Verdine, G. L. (2000) Structural basis for recognition and repair of the endogenous mutagen 8-oxoguanine in DNA, *Nature 403*, 859–866.
741. Bjoras, M., Seeberg, E., Luna, L., Pearl, L. H., and Barrett, T. E. (2002) Reciprocal "flipping" underlies substrate recognition and catalytic activation by the human 8-oxo-guanine DNA glycosylase, *J. Mol. Biol. 317*, 171–177.
742. Fersht, A. R., and Dingwall, C. (1979) Evidence for the double-sieve editing mechanism in protein synthesis. Steric exclusion of isoleucine by valyl-tRNA synthetases, *Biochemistry 18*, 2627–2631.
743. Hendrickson, T. L., Nomanbhoy, T. K., and Schimmel, P. (2000) Errors from selective disruption of the editing center in a tRNA synthetase, *Biochemistry 39*, 8180–8186.
744. Nureki, O., Vassylyev, D. G., Tateno, M., Shimada, A., Nakama, T., Fukai, S., Konno, M., Hendrickson, T. L., Schimmel, P., and Yokoyama, S. (1998) Enzyme structure with two catalytic sites for double-sieve selection of substrate, *Science 280*, 578–582.
745. Yang, G., Franklin, M., Li, J., Lin, T. C., and Konigsberg, W. (2002) A conserved Tyr residue is required for sugar selectivity in a pol α DNA polymerase, *Biochemistry 41*, 10256–10261.
746. Zhang, M., White, T. A., Schuermann, J. P., Baban, B. A., Becker, D. F., and Tanner, J. J. (2004) Structures of the *Escherichia coli* PutA proline dehydrogenase domain in complex with competitive inhibitors, *Biochemistry 43*, 12539–12548.
747. Ostrander, E. L., Larson, J. D., Schuermann, J. P., and Tanner, J. J. (2009) A conserved active site tyrosine residue of proline dehydrogenase helps enforce the preference for proline over hydroxyproline as the substrate, *Biochemistry 48*, 951–959.
748. Dewar, M. J., and Dieter, K. M. (1988) Mechanism of the chain extension step in the biosynthesis of fatty acids, *Biochemistry 27*, 3302–3308.
749. Quirke, J. C. K., and Crich, D. (2020) Glycoside hydrolases restrict the side chain conformation of their substrates to gain additional transition state stabilization, *J. Am. Chem. Soc. 142*, 16965–16973.
750. Crosby, J., Stone, R., and Lienhard, G. E. (1970) Mechanisms of thiamine-catalyzed reactions. Decarboxylation of 2-(1-carboxy-L-hydroxyethyl)-3,4-dimethylthiazolium chloride, *J. Am. Chem. Soc. 92*, 2891–2900.
751. Lewis, C. A., Jr., and Wolfenden, R. (2009) Orotic acid decarboxylation in water and nonpolar solvents: A potential role for desolvation in the action of OMP decarboxylase, *Biochemistry 48*, 8738–8745.
752. Stunkard, L. M., Dixon, A. D., Huth, T. J., and Lohman, J. R. (2019) Sulfonate/nitro bearing methylmalonyl-thioester isosteres applied to methylmalonyl-CoA decarboxylase structure-function studies, *J. Am. Chem. Soc. 141*, 5121–5124.
753. Tarshis, L. C., Yan, M., Poulter, C. D., and Sacchettini, J. C. (1994) Crystal structure of recombinant farnesyl diphosphate synthase at 2.6 Å resolution, *Biochemistry 33*, 10871–10877.
754. Tarshis, L. C., Proteau, P. J., Kellogg, B. A., Sacchettini, J. C., and Poulter, C. D. (1996) Regulation of product chain length by isoprenyl diphosphate synthases, *Proc. Natl. Acad. Sci. U.S.A. 93*, 15018–15023.
755. Hsu, M. H., Baer, B. R., Rettie, A. E., and Johnson, E. F. (2017) The crystal structure of cytochrome P450 4B1 (CYP4B1) monooxygenase complexed with octane discloses several structural adaptations for ω-hydroxylation, *J. Biol. Chem. 292*, 5610–5621.

756. Yu, X., Liu, Y., Xie, X., Zheng, X. D., and Li, S. M. (2012) Biochemical characterization of indole prenyltransferases: Filling the last gap of prenylation positions by a 5-dimethylallyltryptophan synthase from *Aspergillus clavatus*, *J. Biol. Chem. 287*, 1371–1380.
757. Roose, B. W., and Christianson, D. W. (2019) Structural basis of tryptophan reverse *N*-prenylation catalyzed by CymD, *Biochemistry 58*, 3232–3242.
758. Culbertson, J. E., Chung, D., Ziebart, K. T., Espiritu, E., and Toney, M. D. (2015) Conversion of aminodeoxychorismate synthase into anthranilate synthase with Janus mutations: Mechanism of pyruvate elimination catalyzed by chorismate enzymes, *Biochemistry 54*, 2372–2384.
759. Bai, Y., McCoy, J. G., Levin, E. J., Sobrado, P., Rajashankar, K. R., Fox, B. G., and Zhou, M. (2015) X-Ray structure of a mammalian stearoyl-CoA desaturase, *Nature 524*, 252–256.
760. Pascal, J. M., O'Brien, P. J., Tomkinson, A. E., and Ellenberger, T. (2004) Human DNA ligase I completely encircles and partially unwinds nicked DNA, *Nature 432*, 473–478.
761. Mol, C. D., Izumi, T., Mitra, S., and Tainer, J. A. (2000) DNA-Bound structures and mutants reveal abasic DNA binding by APE1 and DNA repair coordination [corrected], *Nature 403*, 451–456.
762. Ferrer, J. L., Jez, J. M., Bowman, M. E., Dixon, R. A., and Noel, J. P. (1999) Structure of chalcone synthase and the molecular basis of plant polyketide biosynthesis, *Nature Struct. Biol. 6*, 775–784.
763. Jez, J. M., Bowman, M. E., and Noel, J. P. (2001) Structure-guided programming of polyketide chain-length determination in chalcone synthase, *Biochemistry 40*, 14829–14838.
764. Li, G., Garcia-Borras, M., Furst, M., Ilie, A., Fraaije, M. W., Houk, K. N., and Reetz, M. T. (2018) Overriding traditional electronic effects in biocatalytic Baeyer–Villiger reactions by directed evolution, *J. Am. Chem. Soc. 140*, 10464–10472.
765. Rynkiewicz, M. J., Cane, D. E., and Christianson, D. W. (2001) Structure of trichodiene synthase from *Fusarium sporotrichioides* provides mechanistic inferences on the terpene cyclization cascade, *Proc. Natl. Acad. Sci. U. S. A. 98*, 13543–13548.
766. Starks, C. M., Back, K., Chappell, J., and Noel, J. P. (1997) Structural basis for cyclic terpene biosynthesis by tobacco 5-*epi*-aristolochene synthase, *Science 277*, 1815–1820.
767. Whittington, D. A., Wise, M. L., Urbansky, M., Coates, R. M., Croteau, R. B., and Christianson, D. W. (2002) Bornyl diphosphate synthase: Structure and strategy for carbocation manipulation by a terpenoid cyclase, *Proc. Natl. Acad. Sci. U. S. A. 99*, 15375–15380.
768. Shishova, E. Y., Di Costanzo, L., Cane, D. E., and Christianson, D. W. (2007) X-Ray crystal structure of aristolochene synthase from *Aspergillus terreus* and evolution of templates for the cyclization of farnesyl diphosphate, *Biochemistry 46*, 1941–1951.
769. Noel, J. P., Dellas, N., Faraldos, J. A., Zhao, M., Hess, B. A., Jr., Smentek, L., Coates, R. M., and O'Maille, P. E. (2010) Structural elucidation of cisoid and transoid cyclization pathways of a sesquiterpene synthase using 2-fluorofarnesyl diphosphates, *ACS Chem. Biol. 5*, 377–392.
770. Koksal, M., Chou, W. K., Cane, D. E., and Christianson, D. W. (2013) Unexpected reactivity of 2-fluorolinalyl diphosphate in the active site of crystalline 2-methylisoborneol synthase, *Biochemistry 52*, 5247–5255.
771. Kumar, R. P., Morehouse, B. R., Matos, J. O., Malik, K., Lin, H., Krauss, I. J., and Oprian, D. D. (2017) Structural characterization of early Michaelis complexes in the reaction catalyzed by (+)-limonene synthase from *Citrus sinensis* using fluorinated substrate analogues, *Biochemistry 56*, 1716–1725.
772. Shishova, E. Y., Yu, F., Miller, D. J., Faraldos, J. A., Zhao, Y., Coates, R. M., Allemann, R. K., Cane, D. E., and Christianson, D. W. (2008) X-Ray crystallographic studies of substrate binding to aristolochene synthase suggest a metal ion binding sequence for catalysis, *J. Biol. Chem 283*, 15431–15439.
773. Felicetti, B., and Cane, D. E. (2004) Aristolochene synthase: Mechanistic analysis of active site residues by site-directed mutagenesis, *J. Am. Chem. Soc. 126*, 7212–7221.
774. Cane, D. E., Prabhakaran, P. C., Salaski, E. J., Harrison, P. H. M., Noguchi, H., and Rawlings, B. J. (1989) Aristolochene biosynthesis and enzymatic cyclization of farnesyl pyrophosphate, *J. Am. Chem. Soc. 111*, 8914–8916.
775. Chen, M., Al-lami, N., Janvier, M., D'Antonio, E. L., Faraldos, J. A., Cane, D. E., Allemann, R.

K., and Christianson, D. W. (2013) Mechanistic insights from the binding of substrate and carbocation intermediate analogues to aristolochene synthase, *Biochemistry 52*, 5441–5453.
776. Chen, M., Chou, W. K., Al-Lami, N., Faraldos, J. A., Allemann, R. K., Cane, D. E., and Christianson, D. W. (2016) Probing the role of active site water in the sesquiterpene cyclization reaction catalyzed by aristolochene synthase, *Biochemistry 55*, 2864–2874.
777. Calvert, M. J., Ashton, P. R., and Allemann, R. K. (2002) Germacrene a is a product of the aristolochene synthase-mediated conversion of farnesylpyrophosphate to aristolochene, *J. Am. Chem. Soc. 124*, 11636–11641.
778. Deligeorgopoulou, A., and Allemann, R. K. (2003) Evidence for differential folding of farnesyl pyrophosphate in the active site of aristolochene synthase: A single-point mutation converts aristolochene synthase into an (*E*)- β-farnesene synthase, *Biochemistry 42*, 7741–7747.
779. Li, R., Chou, W. K., Himmelberger, J. A., Litwin, K. M., Harris, G. G., Cane, D. E., and Christianson, D. W. (2014) Reprogramming the chemodiversity of terpenoid cyclization by remolding the active site contour of *epi*-isozizaene synthase, *Biochemistry 53*, 1155–1168.
780. Blank, P. N., Barrow, G. H., Chou, W. K. W., Duan, L., Cane, D. E., and Christianson, D. W. (2017) Substitution of aromatic residues with polar residues in the active site pocket of *epi*-isozizaene synthase leads to the generation of new cyclic sesquiterpenes, *Biochemistry 56*, 5798–5811.
781. Rising, K. A., Starks, C. M., Noel, J. P., and Chappell, J. (2000) Demonstration of germacrene a as an intermediate in 5-*epi*-aristolochene synthase catalysis, *J. Am. Chem. Soc. 122*, 1861–1866.
782. Greenhagen, B. T., O'Maille, P. E., Noel, J. P., and Chappell, J. (2006) Identifying and manipulating structural determinates linking catalytic specificities in terpene synthases, *Proc. Natl. Acad. Sci. U. S. A. 103*, 9826–9831.
783. Herrera, J. B. R., Wilson, W. K., and Matsuda, S. P. T. (2000) A tyrosine-to-threonine mutation converts cycloartenol synthase to an oxidosqualene cyclase that forms lanosterol as its major product, *J. Am. Chem. Soc. 122*, 6765–6766.
784. Wu, T. K., and Griffin, J. H. (2002) Conversion of a plant oxidosqualene-cycloartenol synthase to an oxidosqualene-lanosterol cyclase by random mutagenesis, *Biochemistry 41*, 8238–8244.
785. Kushiro, T., Shibuya, M., Masuda, K., and Ebizuka, Y. (2000) Mutational studies on triterpene synthases: Engineering lupeol synthase into β-amyrin synthase, *J. Am. Chem. Soc. 122*, 6816–6824.
786. Matos, J. O., Kumar, R. P., Ma, A. C., Patterson, M., Krauss, I. J., and Oprian, D. D. (2020) Mechanism underlying anti-Markovnikov addition in the reaction of pentalenene synthase, *Biochemistry 59*, 3271–3283.
787. Zhang, Q., Catti, L., Pleiss, J., and Tiefenbacher, K. (2017) Terpene cyclizations inside a supramolecular catalyst: Leaving-group-controlled product selectivity and mechanistic studies, *J. Am. Chem. Soc. 139*, 11482–11492.
788. Behrouzian, B., Savile, C. K., Dawson, B., Buist, P. H., and Shanklin, J. (2002) Exploring the hydroxylation-dehydrogenation connection: Novel catalytic activity of castor stearoyl-ACP delta(9) desaturase, *J. Am. Chem. Soc. 124*, 3277–3283.
789. Rogge, C. E., and Fox, B. G. (2002) Desaturation, chain scission, and register-shift of oxygen-substituted fatty acids during reaction with stearoyl-ACP desaturase, *Biochemistry 41*, 10141–10148.
790. Hine, J. (1977) The principle of least nuclear motion, *Adv. Phys. Org. Chem. 15*, 1–61.
791. Rice, F. O., and Teller, E. (1938) The role of free radicals in elementary organic reactions, *J. Chem. Phys. 6*, 489–496.
792. Bruning, M., Berheide, M., Meyer, D., Golbik, R., Bartunik, H., Liese, A., and Tittmann, K. (2009) Structural and kinetic studies on native intermediates and an intermediate analogue in benzoylformate decarboxylase reveal a least motion mechanism with an unprecedented short-lived predecarboxylation intermediate, *Biochemistry 48*, 3258–3268.
793. Komoto, J., Yamada, T., Takata, Y., Markham, G. D., and Takusagawa, F. (2004) Crystal structure of the *S*-adenosylmethionine synthetase ternary complex: A novel catalytic mechanism of *S*-adenosylmethionine synthesis from ATP and Met, *Biochemistry 43*, 1821–1831.

794. Bianchet, M. A., Seiple, L. A., Jiang, Y. L., Ichikawa, Y., Amzel, L. M., and Stivers, J. T. (2003) Electrostatic guidance of glycosyl cation migration along the reaction coordinate of uracil DNA glycosylase, *Biochemistry 42*, 12455–12460.
795. Fedorov, A., Shi, W., Kicska, G., Fedorov, E., Tyler, P. C., Furneaux, R. H., Hanson, J. C., Gainsford, G. J., Larese, J. Z., Schramm, V. L., and Almo, S. C. (2001) Transition state structure of purine nucleoside phosphorylase and principles of atomic motion in enzymatic catalysis, *Biochemistry 40*, 853–860.
796. Caradoc-Davies, T. T., Cutfield, S. M., Lamont, I. L., and Cutfield, J. F. (2004) Crystal structures of *Escherichia coli* uridine phosphorylase in two native and three complexed forms reveal basis of substrate specificity, induced conformational changes and influence of potassium, *J. Mol. Biol. 337*, 337–354.
797. Shi, W., Sarver, A. E., Wang, C. C., Tanaka, K. S., Almo, S. C., and Schramm, V. L. (2002) Closed site complexes of adenine phosphoribosyltransferase from *Giardia lamblia* reveal a mechanism of ribosyl migration, *J. Biol. Chem. 277*, 39981–39988.
798. Perez-Miller, S. J., and Hurley, T. D. (2003) Coenzyme isomerization is integral to catalysis in aldehyde dehydrogenase, *Biochemistry 42*, 7100–7109.
799. Scheffzek, K., Kliche, W., Wiesmuller, L., and Reinstein, J. (1996) Crystal structure of the complex of UMP/CMP kinase from *Dictyostelium discoideum* and the bisubstrate inhibitor P^1-(5′-adenosyl) P^5-(5′-uridyl) pentaphosphate (UP_5A) and Mg^{2+} at 2.2 Å: Implications for water-mediated specificity, *Biochemistry 35*, 9716–9727.
800. Goto, M., Miyahara, I., Hayashi, H., Kagamiyama, H., and Hirotsu, K. (2003) Crystal structures of branched-chain amino acid aminotransferase complexed with glutamate and glutarate: True reaction intermediate and double substrate recognition of the enzyme, *Biochemistry 42*, 3725-3733.
801. Grant, J. A., Sanders, B., and Hood, L. (1971) Partial amino acid sequences of chicken and turkey immunoglobulin light chains. Homology with mammalian lambda chains, *Biochemistry 10*, 3123–3132.
802. Matsubara, H., Singer, A., Sasaki, R., and Jukes, T. H. (1965) Observations on the specificity of a thermostable bacterial protease "thermolysin", *Biochem. Biophys. Res. Commun. 21*, 242–247.
803. Watanabe, N., Clay, M. D., van Belkum, M. J., Cherney, M. M., Vederas, J. C., and James, M. N. (2008) Mechanism of substrate recognition and PLP-induced conformational changes in LL-diaminopimelate aminotransferase from *Arabidopsis thaliana*, *J. Mol. Biol. 384*, 1314–1329.
804. Haruyama, K., Nakai, T., Miyahara, I., Hirotsu, K., Mizuguchi, H., Hayashi, H., and Kagamiyama, H. (2001) Structures of *Escherichia coli* histidinol-phosphate aminotransferase and its complexes with histidinol-phosphate and *N*-(5′-phosphopyridoxyl)-L-glutamate: Double substrate recognition of the enzyme, *Biochemistry 40*, 4633–4644.
805. Setser, J. W., Heemstra, J. R., Jr., Walsh, C. T., and Drennan, C. L. (2014) Crystallographic evidence of drastic conformational changes in the active site of a flavin-dependent *N*-hydroxylase, *Biochemistry 53*, 6063–6077.
806. Nowicki, M. W., Kuaprasert, B., McNae, I. W., Morgan, H. P., Harding, M. M., Michels, P. A., Fothergill-Gilmore, L. A., and Walkinshaw, M. D. (2009) Crystal structures of *Leishmania mexicana* phosphoglycerate mutase suggest a one-metal mechanism and a new enzyme subclass, *J. Mol. Biol. 394*, 535–543.
807. Thoden, J. B., and Holden, H. M. (1998) Dramatic differences in the binding of UDP-galactose and UDP-glucose to UDP-galactose 4-epimerase from *Escherichia coli*, *Biochemistry 37*, 11469–11477.
808. Lauble, H., Kennedy, M. C., Beinert, H., and Stout, C. D. (1992) Crystal structures of aconitase with isocitrate and nitroisocitrate bound, *Biochemistry 31*, 2735–2748.
809. Kent, T. A., Emptage, M. H., Merkle, H., Kennedy, M. C., Beinert, H., and Munck, E. (1985) Mössbauer studies of aconitase. Substrate and inhibitor binding, reaction intermediates, and hyperfine interactions of reduced 3Fe and 4Fe clusters, *J. Biol. Chem. 260*, 6871–6881.
810. Lauble, H., Kennedy, M. C., Beinert, H., and Stout, C. D. (1994) Crystal structures of aconitase with *trans*-aconitate and nitrocitrate bound, *J. Mol. Biol. 237*, 437–451.
811. Lloyd, S. J., Lauble, H., Prasad, G. S., and Stout, C. D. (1999) The mechanism of aconitase: 1.8 Å resolution crystal structure of

the S642A:Citrate complex, *Prot. Sci. 8*, 2655–2662.
812. Knight, S., Andersson, I., and Branden, C. I. (1990) Crystallographic analysis of ribulose 1,5-bisphosphate carboxylase from spinach at 2.4 Å resolution. Subunit interactions and active site, *J. Mol. Biol. 215*, 113–160.
813. Xu, Q., Teplow, D., Lee, T. D., and Abelson, J. (1990) Domain structure in yeast tRNA ligase, *Biochemistry 29*, 6132–6138.
814. Kyte, J. (2007) *Structure in protein chemistry: Second edition*, pp 451–499, Garland Science, New York.
815. Weaver, T. M., Levitt, D. G., Donnelly, M. I., Stevens, P. P., and Banaszak, L. J. (1995) The multisubunit active site of fumarase C from *Escherichia coli*, *Nature Struct. Biol. 2*, 654–662.
816. Turner, M. A., Simpson, A., McInnes, R. R., and Howell, P. L. (1997) Human argininosuccinate lyase: A structural basis for intragenic complementation, *Proc. Natl. Acad. Sci. U. S. A. 94*, 9063–9068.
817. Brosius, J. L., and Colman, R. F. (2002) Three subunits contribute amino acids to the active site of tetrameric adenylosuccinate lyase: Lys268 and Glu275 are required, *Biochemistry 41*, 2217–2226.
818. Narayana, N., Matthews, D. A., Howell, E. E., and Nguyen-huu, X. (1995) A plasmid-encoded dihydrofolate reductase from trimethoprim-resistant bacteria has a novel D2-symmetric active site, *Nature Struct. Biol. 2*, 1018–1025.
819. Smiley, R. D., Stinnett, L. G., Saxton, A. M., and Howell, E. E. (2002) Breaking symmetry: Mutations engineered into R67 dihydrofolate reductase, a D2 symmetric homotetramer possessing a single active site pore, *Biochemistry 41*, 15664–15675.
820. Lindqvist, Y., Schneider, G., Ermler, U., and Sundstrom, M. (1992) Three-dimensional structure of transketolase, a thiamine diphosphate dependent enzyme, at 2.5 Å resolution, *EMBO J. 11*, 2373–2379.
821. Beaman, T. W., Blanchard, J. S., and Roderick, S. L. (1998) The conformational change and active site structure of tetrahydrodipicolinate *N*-succinyltransferase, *Biochemistry 37*, 10363–10369.
822. Jaskolski, M., Miller, M., Rao, J. K., Leis, J., and Wlodawer, A. (1990) Structure of the aspartic protease from Rous sarcoma retrovirus refined at 2 Å resolution, *Biochemistry 29*, 5889–5898.
823. Lee, T. T., Worby, C., Bao, Z. Q., Dixon, J. E., and Colman, R. F. (1999) His68 and His141 are critical contributors to the intersubunit catalytic site of adenylosuccinate lyase of *Bacillus subtilis*, *Biochemistry 38*, 22–32.
824. Segall, M. L., and Colman, R. F. (2004) Gln212, Asn270, and Arg301 are critical for catalysis by adenylosuccinate lyase from *Bacillus subtilis*, *Biochemistry 43*, 7391–7402.
825. Heaslet, H., Rosenfeld, R., Giffin, M., Lin, Y. C., Tam, K., Torbett, B. E., Elder, J. H., McRee, D. E., and Stout, C. D. (2007) Conformational flexibility in the flap domains of ligand-free HIV protease, *Acta Crystallogr. D 63*, 866–875.
826. Wlodawer, A., Miller, M., Jaskolski, M., Sathyanarayana, B. K., Baldwin, E., Weber, I. T., Selk, L. M., Clawson, L., Schneider, J., and Kent, S. B. (1989) Conserved folding in retroviral proteases: Crystal structure of a synthetic HIV-1 protease, *Science 245*, 616–621.
827. Lapatto, R., Blundell, T., Hemmings, A., Overington, J., Wilderspin, A., Wood, S., Merson, J. R., Whittle, P. J., Danley, D. E., Geoghegan, K. F., Hawrylik, S. J., Lee, S. E., Scheld, K. G., & Hobart, P. M. (1989) X-Ray analysis of HIV-1 proteinase at 2.7 Å resolution confirms structural homology among retroviral enzymes, *Nature 342*, 299–302.
828. Navia, M. A., Fitzgerald, P. M., McKeever, B. M., Leu, C. T., Heimbach, J. C., Herber, W. K., Sigal, I. S., Darke, P. L., and Springer, J. P. (1989) Three-dimensional structure of aspartyl protease from human immunodeficiency virus HIV-1, *Nature 337*, 615–620.
829. Miller, M., Schneider, J., Sathyanarayana, B. K., Toth, M. V., Marshall, G. R., Clawson, L., Selk, L., Kent, S. B., and Wlodawer, A. (1989) Structure of complex of synthetic HIV-1 protease with a substrate-based inhibitor at 2.3 Å resolution, *Science 246*, 1149–1152.
830. Prabu-Jeyabalan, M., Nalivaika, E., and Schiffer, C. A. (2000) How does a symmetric dimer recognize an asymmetric substrate? A substrate complex of HIV-1 protease, *J. Mol. Biol. 301*, 1207–1220.
831. Erickson, J., Neidhart, D. J., VanDrie, J., Kempf, D. J., Wang, X. C., Norbeck, D. W., Plattner, J. J., Rittenhouse, J. W., Turon, M., Wideburg, N., Kohlbrenner, W. E., Simmer, R., Helfrich, R., Paul, D. A., and Knigge, M.

(1990) Design, activity, and 2.8 Å crystal structure of a C2 symmetric inhibitor complexed to HIV-1 protease, *Science 249*, 527–533.
832. Cirilli, M., Zheng, R., Scapin, G., and Blanchard, J. S. (1998) Structural symmetry: The three-dimensional structure of *Haemophilus influenzae* diaminopimelate epimerase, *Biochemistry 37*, 16452–16458.
833. Frickel, E. M., Jemth, P., Widersten, M., and Mannervik, B. (2001) Yeast glyoxalase I is a monomeric enzyme with two active sites, *J. Biol. Chem. 276*, 1845–1849.
834. Aleshin, A. E., Kirby, C., Liu, X., Bourenkov, G. P., Bartunik, H. D., Fromm, H. J., and Honzatko, R. B. (2000) Crystal structures of mutant monomeric hexokinase I reveal multiple ADP binding sites and conformational changes relevant to allosteric regulation, *J. Mol. Biol. 296*, 1001–1015.
835. Birktoft, J. J., Kraut, J., and Freer, S. T. (1976) A detailed structural comparison between the charge relay system in chymotrypsinogen and in α-chymotrypsin, *Biochemistry 15*, 4481–4485.
836. Muller, C. W., and Schulz, G. E. (1992) Structure of the complex between adenylate kinase from *Escherichia coli* and the inhibitor AP_5A refined at 1.9 Å resolution. A model for a catalytic transition state, *J. Mol. Biol. 224*, 159–177.
837. Larsson, G., Svensson, L. A., and Nyman, P. O. (1996) Crystal structure of the *Escherichia coli* dUTPase in complex with a substrate analogue (dUDP), *Nature Struct. Biol. 3*, 532–538.
838. Parry, R. J., Burns, M. R., Jiralerspong, S., and Alemany, L. (1997) Synthesis of (+)-(1*S*)-1-pyrophosphoryl-(2*R*,3*R*)-2,3-dihydroxy-(4*S*)-4-(phosphoryloxymethyl)cyclopentane: A stable, optically-active carbocyclic analog of 5-phosphoribosyl-1-pyrophosphate (PRPP), *Tetrahedron 53*, 7077–7088.
839. Vos, S., Parry, R. J., Burns, M. R., de Jersey, J., and Martin, J. L. (1998) Structures of free and complexed forms of *Escherichia coli* xanthine-guanine phosphoribosyltransferase, *J. Mol. Biol. 282*, 875–889.
840. Li, Y., Feng, L., and Kirsch, J. F. (1997) Kinetic and spectroscopic investigations of wild-type and mutant forms of apple 1-aminocyclopropane-1-carboxylate synthase, *Biochemistry 36*, 15477–15488.
841. Distefano, M. D., Moore, M. J., and Walsh, C. T. (1990) Active site of mercuric reductase resides at the subunit interface and requires Cys135 and Cys140 from one subunit and Cys558 and Cys559 from the adjacent subunit: Evidence from in vivo and in vitro heterodimer formation, *Biochemistry 29*, 2703–2713.
842. Ozturk, D. H., Dorfman, R. H., Scapin, G., Sacchettini, J. C., and Grubmeyer, C. (1995) Structure and function of *Salmonella typhimurium* orotate phosphoribosyltransferase: Protein complementation reveals shared active sites, *Biochemistry 34*, 10764–10770.
843. Tobias, K. E., and Kahana, C. (1993) Intersubunit location of the active site of mammalian ornithine decarboxylase as determined by hybridization of site-directed mutants, *Biochemistry 32*, 5842–5847.
844. Pookanjanatavip, M., Yuthavong, Y., Greene, P. J., and Santi, D. V. (1992) Subunit complementation of thymidylate synthase, *Biochemistry 31*, 10303–10309.
845. Allin, C., and Gerwert, K. (2001) Ras catalyzes GTP hydrolysis by shifting negative charges from γ- to β-phosphate as revealed by time-resolved FTIR difference spectroscopy, *Biochemistry 40*, 3037–3046.
846. Deng, H., Callender, R., Schramm, V. L., and Grubmeyer, C. (2010) Pyrophosphate activation in hypoxanthine--guanine phosphoribosyltransferase with transition state analogue, *Biochemistry 49*, 2705–2714.
847. Belasco, J. G., and Knowles, J. R. (1980) Direct observation of substrate distortion by triosephosphate isomerase using Fourier transform infrared spectroscopy, *Biochemistry 19*, 472–477.
848. Komives, E. A., Chang, L. C., Lolis, E., Tilton, R. F., Petsko, G. A., and Knowles, J. R. (1991) Electrophilic catalysis in triosephosphate isomerase: The role of histidine-95, *Biochemistry 30*, 3011–3019.
849. Wang, S.-F., Kawahara, F. S., and Talalay, P. (1963) The mechanism of the Δ^5-3-keto steroid isomerase reaction: Absorption and fluorescence spectra of enzyme-steroid complexes, *J. Biol. Chem. 238*, 576–585.
850. Fried, S. D., Bagchi, S., and Boxer, S. G. (2014) Extreme electric fields power catalysis in the active site of ketosteroid isomerase, *Science 346*, 1510–1514.

851. Massiah, M. A., Abeygunawardana, C., Gittis, A. G., and Mildvan, A. S. (1998) Solution structure of Δ^5-3-ketosteroid isomerase complexed with the steroid 19-nortestosterone hemisuccinate, *Biochemistry 37*, 14701–14712.
852. Cho, H. S., Ha, N. C., Choi, G., Kim, H. J., Lee, D., Oh, K. S., Kim, K. S., Lee, W., Choi, K. Y., and Oh, B. H. (1999) Crystal structure of Δ^5-3-ketosteroid isomerase from *Pseudomonas testosteroni* in complex with equilenin settles the correct hydrogen bonding scheme for transition state stabilization, *J. Biol. Chem 274*, 32863–32868.
853. Wu, Y., and Boxer, S. G. (2016) A critical test of the electrostatic contribution to catalysis with noncanonical amino acids in ketosteroid isomerase, *J. Am. Chem. Soc. 138*, 11890–11895.
854. Peng, H. L., Deng, H., Dyer, R. B., and Callender, R. (2014) Energy landscape of the Michaelis complex of lactate dehydrogenase: Relationship to catalytic mechanism, *Biochemistry 53*, 1849–1857.
855. Gonzalez-Segura, L., Witte, J. F., McClard, R. W., and Hurley, T. D. (2007) Ternary complex formation and induced asymmetry in orotate phosphoribosyltransferase, *Biochemistry 46*, 14075–14086.
856. Deng, H., Zheng, J., Burgner, J., and Callender, R. (1989) Molecular properties of pyruvate bound to lactate dehydrogenase: A Raman spectroscopic study, *Proc. Natl. Acad. Sci. U.S.A. 86*, 4484–4488.
857. Deng, H., Zheng, J., Clarke, A., Holbrook, J. J., Callender, R., and Burgner, J. W., 2nd. (1994) Source of catalysis in the lactate dehydrogenase system. Ground-state interactions in the enzyme-substrate complex, *Biochemistry 33*, 2297–2305.
858. Tonge, P. J., and Carey, P. R. (1992) Forces, bond lengths, and reactivity: Fundamental insight into the mechanism of enzyme catalysis, *Biochemistry 31*, 9122–9125.
859. Whiting, A. K., and Peticolas, W. L. (1994) Details of the acyl-enzyme intermediate and the oxyanion hole in serine protease catalysis, *Biochemistry 33*, 552–561.
860. Chen, Y. Q., Kraut, J., Blakley, R. L., and Callender, R. (1994) Determination by Raman spectroscopy of the pK_a of N5 of dihydrofolate bound to dihydrofolate reductase: Mechanistic implications, *Biochemistry 33*, 7021–7026.
861. Callender, R., Chen, D., Lugtenburg, J., Martin, C., Rhee, K. W., Sloan, D., Vandersteen, R., and Yue, K. T. (1988) Molecular properties of *p*-(dimethylamino)benzaldehyde bound to liver alcohol dehydrogenase: A Raman spectroscopic study, *Biochemistry 27*, 3672–3681.
862. Gardner, J. D., Pierce, B. S., Fox, B. G., and Brunold, T. C. (2010) Spectroscopic and computational characterization of substrate-bound mouse cysteine dioxygenase: Nature of the ferrous and ferric cysteine adducts and mechanistic implications, *Biochemistry 49*, 6033–6041.
863. Gogia, S., Balaram, H., and Puranik, M. (2011) Hypoxanthine guanine phosphoribosyltransferase distorts the purine ring of nucleotide substrates and perturbs the pK_a of bound xanthosine monophosphate, *Biochemistry 50*, 4184–4193.
864. Eads, J. C., Scapin, G., Xu, Y., Grubmeyer, C., and Sacchettini, J. C. (1994) The crystal structure of human hypoxanthine-guanine phosphoribosyltransferase with bound GMP, *Cell 78*, 325–334.
865. Karnawat, V., Mehrotra, S., Balaram, H., and Puranik, M. (2016) Exquisite modulation of the active site of *Methanocaldococcus jannaschii* adenylosuccinate synthetase in forward reaction complexes, *Biochemistry 55*, 2491–2499.
866. Iancu, C. V., Borza, T., Fromm, H. J., and Honzatko, R. B. (2002) IMP, GTP, and 6-phosphoryl-IMP complexes of recombinant mouse muscle adenylosuccinate synthetase, *J. Biol. Chem. 277*, 26779–26787.
867. Dalosto, S. D., Vanderkooi, J. M., and Sharp, K. A. (2004) Vibrational Stark effects on carbonyl, nitrile, and nitrosyl compounds including heme ligands, CO, CN^-, and NO, studied with density functional theory, *J. Phys. Chem. B 108*, 6450–6457.
868. Schneider, S. H., Kratochvil, H. T., Zanni, M. T., and Boxer, S. G. (2017) Solvent-independent anharmonicity for carbonyl oscillators, *J. Phys. Chem. B 121*, 2331–2338.
869. Choi, J.-H., and Cho, M. (2011) Vibrational solvatochromism and electrochromism of infrared probe molecules containing C=O, C=N, C=O, or C-F vibrational chromophore, *J. Chem. Phys. 134*, 154513-1–154513-12.
870. Fried, S. D., Bagchi, S., and Boxer, S. G. (2013) Measuring electrostatic fields in both

hydrogen-bonding and non-hydrogen-bonding environments using carbonyl vibrational probes, *J. Am. Chem. Soc. 135*, 11181–11192.
871. Fried, S. D., and Boxer, S. G. (2015) Measuring electric fields and noncovalent interactions using the vibrational Stark effect, *Accounts Chem. Res. 48*, 998–1006.
872. Wu, Y., Fried, S. D., and Boxer, S. G. (2020) A preorganized electric field leads to minimal geometrical reorientation in the catalytic reaction of ketosteroid isomerase, *J. Am. Chem. Soc. 142*, 9993–9998.
873. Kim, E. E., Varadarajan, R., Wyckoff, H. W., and Richards, F. M. (1992) Refinement of the crystal structure of ribonuclease S. Comparison with and between the various ribonuclease A structures, *Biochemistry 31*, 12304–12314.
874. Kuliopulos, A., Mildvan, A. S., Shortle, D., and Talalay, P. (1989) Kinetic and ultraviolet spectroscopic studies of active-site mutants of Δ^5-3-ketosteroid isomerase, *Biochemistry 28*, 149–159.
875. Zhao, Q., Mildvan, A. S., and Talalay, P. (1995) Enzymatic and nonenzymatic polarizations of α,β-unsaturated ketosteroids and phenolic steroids. Implications for the roles of hydrogen bonding in the catalytic mechanism of Δ^5-3-ketosteroid isomerase, *Biochemistry 34*, 426–434.
876. Lunn, A. K., and Morton, R. A. (1952) Ultraviolet absorption spectra of pyridoxine and related compounds, *Analyst 77*, 718–731.
877. Mariella, R. P., Raube, R. R., Budde, J., and Moore, C. E. (1954) The effect of the dielectric constant of the solvent on the ultraviolet absorption spectra of some nonaromatic ketones, *J. Org. Chem. 19*, 678–682.
878. Chen, M., Jiang, M., Sun, Y., Guo, Z. F., and Guo, Z. (2011) Stabilization of the second oxyanion intermediate by 1,4-dihydroxy-2-naphthoyl-coenzyme A synthase of the menaquinone pathway: Spectroscopic evidence of the involvement of a conserved aspartic acid, *Biochemistry 50*, 5893–5904.
879. Wetlaufer, D. B., Edsall, J. T., and Hollingworth, B. R. (1958) Ultraviolet difference spectra of tyrosine groups in proteins and amino acids, *J. Biol. Chem 233*, 1421–1428.
880. Stull, F. W., Bernard, S. M., Sapra, A., Smith, J. L., Zuiderweg, E. R., and Palfey, B. A. (2016) Deprotonations in the reaction of flavin-dependent thymidylate synthase, *Biochemistry 55*, 3261–3269.
881. Dow, B. J., Malik, S. S., and Drohat, A. C. (2019) Defining the role of nucleotide flipping in enzyme specificity using ^{19}F NMR, *J. Am. Chem. Soc. 141*, 4952–4962.
882. Kurz, L. C., Shah, S., Crane, B. R., Donald, L. J., Duckworth, H. W., and Drysdale, G. R. (1992) Proton uptake accompanies formation of the ternary complex of citrate synthase, oxaloacetate, and the transition-state analog inhibitor, carboxymethyl-CoA. Evidence that a neutral enol is the activated form of acetyl-CoA in the citrate synthase reaction, *Biochemistry 31*, 7899–7907.
883. Karpusas, M., Branchaud, B., and Remington, S. J. (1990) Proposed mechanism for the condensation reaction of citrate synthase: 1.9 Å structure of the ternary complex with oxaloacetate and carboxymethyl coenzyme A, *Biochemistry 29*, 2213–2219.
884. Kurz, L. C., Shah, S., Frieden, C., Nakra, T., Stein, R. E., Drysdale, G. R., Evans, C. T., and Srere, P. A. (1995) Catalytic strategy of citrate synthase: Subunit interactions revealed as a consequence of a single amino acid change in the oxaloacetate binding site, *Biochemistry 34*, 13278–13288.
885. D'Ordine, R. L., Pawlak, J., Bahnson, B. J., and Anderson, V. E. (2002) Polarization of cinnamoyl-CoA substrates bound to enoyl-CoA hydratase: Correlation of ^{13}C NMR with quantum mechanical calculations and calculation of electronic strain energy, *Biochemistry 41*, 2630–2640.
886. Bahnson, B. J., Anderson, V. E., and Petsko, G. A. (2002) Structural mechanism of enoyl-CoA hydratase: Three atoms from a single water are added in either an E1cb stepwise or concerted fashion, *Biochemistry 41*, 2621–2629.
887. Spiesecke, H., and Schneider, W. G. (1961) Determination of π-electron densities in azulene from C13 and H1 nuclear resonance shifts, *Tetrahedron Lett.*, 468–472.
888. Clore, G. M., and Gronenborn, A. M. (1982) Theory and applications of the transferred nuclear Overhauser effect to the study of the conformations of small ligands bound to proteins, *J. Magn. Reson. 48*, 402–417.
889. Balaram, P., Bothner-By, A. A., and Dadok, J. (1972) Negative nuclear Overhauser effects as probes of macromolecular structure, *J. Am. Chem. Soc. 94*, 4015–4017.

890. Balaram, P., Bothner-By, A. A., and Breslow, E. (1972) Localization of tyrosine at the binding site of neurophysin II by negative nuclear Overhauser effects, *J. Am. Chem. Soc. 94*, 4017–4018.
891. Cayley, P. J., Albrand, J. P., Feeney, J., Roberts, G. C., Piper, E. A., and Burgen, A. S. (1979) Nuclear magnetic resonance studies of the binding of trimethoprim to dihydrofolate reductase, *Biochemistry 18*, 3886–3895.
892. Derrick, J. P., Lian, L. Y., Roberts, G. C., and Shaw, W. V. (1992) Analysis of the binding of 1,3-diacetylchloramphenicol to chloramphenicol acetyltransferase by isotope-edited ^{1}H NMR and site-directed mutagenesis, *Biochemistry 31*, 8191–8195.
893. Lin, Y., and Nageswara Rao, B. D. (2000) Structural characterization of adenine nucleotides bound to *Escherichia coli* adenylate kinase: 1. Adenosine conformations by proton two-dimensional transferred nuclear Overhauser effect spectroscopy, *Biochemistry 39*, 3636–3646.
894. Meyer, E. F., Jr., Clore, G. M., Gronenborn, A. M., and Hansen, H. A. (1988) Analysis of an enzyme-substrate complex by X-ray crystallography and transferred nuclear Overhauser enhancement measurements: Porcine pancreatic elastase and a hexapeptide, *Biochemistry 27*, 725–730.
895. Behling, R. W., Yamane, T., Navon, G., and Jelinski, L. W. (1988) Conformation of acetylcholine bound to the nicotinic acetylcholine receptor, *Proc. Natl. Acad. Sci. U. S. A. 85*, 6721–6725.
896. Plesniak, L. A., Yu, L., and Dennis, E. A. (1995) Conformation of micellar phospholipid bound to the active site of phospholipase A2, *Biochemistry 34*, 4943–4951.
897. Poon, D. K., Schubert, M., Au, J., Okon, M., Withers, S. G., and McIntosh, L. P. (2006) Unambiguous determination of the ionization state of a glycoside hydrolase active site lysine by ^{1}H-^{15}N heteronuclear correlation spectroscopy, *J. Am. Chem. Soc. 128*, 15388–15389.
898. Okar, D. A., Live, D. H., Devany, M. H., and Lange, A. J. (2000) Mechanism of the bisphosphatase reaction of 6-phosphofructo-2-kinase/fructose-2,6-bisphosphatase probed by ^{1}H-^{15}N NMR spectroscopy, *Biochemistry 39*, 9754–9762.
899. Kurz, L. C., and Frieden, C. (1987) Adenosine deaminase converts purine riboside into an analogue of a reactive intermediate: A ^{13}C NMR and kinetic study, *Biochemistry 26*, 8450–8457.
900. Percival, M. D., and Withers, S. G. (1992) ^{19}F NMR Investigations of the catalytic mechanism of phosphoglucomutase using fluorinated substrates and inhibitors, *Biochemistry 31*, 505–512.
901. Byeon, I. J., Yongkiettrakul, S., and Tsai, M. D. (2001) Solution structure of the yeast Rad53 FHA2 complexed with a phosphothreonine peptide pTXXL: Comparison with the structures of FHA2-pYXL and FHA1-pTXXD complexes, *J. Mol. Biol. 314*, 577–588.
902. Taylor, K. L., Liu, R. Q., Liang, P. H., Price, J., Dunaway-Mariano, D., Tonge, P. J., Clarkson, J., and Carey, P. R. (1995) Evidence for electrophilic catalysis in the 4-chlorobenzoyl-CoA dehalogenase reaction: UV, Raman, and ^{13}C-NMR spectral studies of dehalogenase complexes of benzoyl-CoA adducts, *Biochemistry 34*, 13881–13888.
903. Dearden, J. C., and Forbes, W. F. (1958) Light absorption studies. XII. Ultraviolet absorption spectra of benzaldehydes, *Can. J. Chem. 36*, 1362–1370.
904. Drenth, J., Kalk, K. H., and Swen, H. M. (1976) Binding of chloromethyl ketone substrate analogues to crystalline papain, *Biochemistry 15*, 3731–3738.
905. Lewis, S. D., Johnson, F. A., and Shafer, J. A. (1981) Effect of cysteine-25 on the ionization of histidine-159 in papain as determined by proton nuclear magnetic resonance spectroscopy. Evidence for a His-159–Cys-25 ion pair and its possible role in catalysis, *Biochemistry 20*, 48–51.
906. Malashkevich, V. N., Strop, P., Keller, J. W., Jansonius, J. N., and Toney, M. D. (1999) Crystal structures of dialkylglycine decarboxylase inhibitor complexes, *J. Mol. Biol. 294*, 193–200.
907. Martinez-Oyanedel, J., Choe, H. W., Heinemann, U., and Saenger, W. (1991) Ribonuclease T1 with free recognition and catalytic site: Crystal structure analysis at 1.5 Å resolution, *J. Mol. Biol. 222*, 335–352.
908. Koike, R., Amemiya, T., Ota, M., and Kidera, A. (2008) Protein structural change upon lig-

and binding correlates with enzymatic reaction mechanism, *J. Mol. Biol. 379*, 397–401.
909. Koepke, J., Maslowska, M., Heinemann, U., and Saenger, W. (1989) Three-dimensional structure of ribonuclease T1 complexed with guanylyl-2′,5′-guanosine at 1.8 Å resolution, *J. Mol. Biol. 206*, 475–488.
910. Anderson, C. M., Zucker, F. H., and Steitz, T. A. (1979) Space-filling models of kinase clefts and conformation changes, *Science 204*, 375–380.
911. Bennett, W. S., Jr., and Steitz, T. A. (1980) Structure of a complex between yeast hexokinase A and glucose. I. Structure determination and refinement at 3.5 Å resolution, *J. Mol. Biol. 140*, 183–209.
912. Bennett, W. S., Jr., and Steitz, T. A. (1980) Structure of a complex between yeast hexokinase A and glucose. II. Detailed comparisons of conformation and active site configuration with the native hexokinase B monomer and dimer, *J. Mol. Biol. 140*, 211–230.
913. Wang, W., Cho, H. S., Kim, R., Jancarik, J., Yokota, H., Nguyen, H. H., Grigoriev, I. V., Wemmer, D. E., and Kim, S. H. (2002) Structural characterization of the reaction pathway in phosphoserine phosphatase: Crystallographic "snapshots" of intermediate states, *J. Mol. Biol. 319*, 421–431.
914. Bukrinsky, J. T., Bjerrum, M. J., and Kadziola, A. (1998) Native carboxypeptidase A in a new crystal environment reveals a different conformation of the important tyrosine 248, *Biochemistry 37*, 16555–16564.
915. Rees, D. C., and Lipscomb, W. N. (1981) Binding of ligands to the active site of carboxypeptidase A, *Proc. Natl. Acad. Sci. U. S. A. 78*, 5455–5459.
916. Gatti, D. L., Palfey, B. A., Lah, M. S., Entsch, B., Massey, V., Ballou, D. P., and Ludwig, M. L. (1994) The mobile flavin of 4-OH benzoate hydroxylase, *Science 266*, 110–114.
917. Campbell, A. C., Stiers, K. M., Martin Del Campo, J. S., Mehra-Chaudhary, R., Sobrado, P., and Tanner, J. J. (2020) Trapping conformational states of a flavin-dependent *N*-monooxygenase *in crystallo* reveals protein and flavin dynamics, *J. Biol. Chem. 295*, 13239–13249.
918. Mothersole, R. G., Billett, C. R., Saini, G., Mothersole, M. K., Darbyshire, A. L., and Wolthers, K. R. (2020) S224 Presents a catalytic trade-off in PLP-dependent L-lanthionine synthase from *Fusobacterium nucleatum*, *Biochemistry 59*, 4250–4261.
919. Kezuka, Y., Ishida, T., Yoshida, Y., and Nonaka, T. (2018) Structural insights into the catalytic mechanism of cysteine (hydroxyl) lyase from the hydrogen sulfide-producing oral pathogen, *Fusobacterium nucleatum*, *Biochem. J. 475*, 733–748.
920. Bystroff, C., and Kraut, J. (1991) Crystal structure of unliganded *Escherichia coli* dihydrofolate reductase. Ligand-induced conformational changes and cooperativity in binding, *Biochemistry 30*, 2227–2239.
921. Joyce, M. A., Fraser, M. E., James, M. N., Bridger, W. A., and Wolodko, W. T. (2000) ADP-binding site of *Escherichia coli* succinyl-CoA synthetase revealed by X-ray crystallography, *Biochemistry 39*, 17–25.
922. Cherfils, J., Morera, S., Lascu, I., Veron, M., and Janin, J. (1994) X-Ray structure of nucleoside diphosphate kinase complexed with thymidine diphosphate and Mg^{2+} at 2 Å resolution, *Biochemistry 33*, 9062–9069.
923. Jamaluddin, H., Tumbale, P., Withers, S. G., Acharya, K. R., and Brew, K. (2007) Conformational changes induced by binding UDP-2F-galactose to α-1,3 galactosyltransferase—Implications for catalysis, *J. Mol. Biol. 369*, 1270–1281.
924. Shapiro, Y. E., Sinev, M. A., Sineva, E. V., Tugarinov, V., and Meirovitch, E. (2000) Backbone dynamics of *Escherichia coli* adenylate kinase at the extreme stages of the catalytic cycle studied by ^{15}N NMR relaxation, *Biochemistry 39*, 6634–6644.
925. Krishnamurthy, H., Munro, K., Yan, H., and Vieille, C. (2009) Dynamics in *Thermotoga neapolitana* adenylate kinase: ^{15}N Relaxation and hydrogen-deuterium exchange studies of a hyperthermophilic enzyme highly active at 30 °C, *Biochemistry 48*, 2723–2739.
926. Wang, J., Stieglitz, K. A., Cardia, J. P., and Kantrowitz, E. R. (2005) Structural basis for ordered substrate binding and cooperativity in aspartate transcarbamoylase, *Proc. Natl. Acad. Sci. U.S.A. 102*, 8881–8886.
927. Gutteridge, A., and Thornton, J. (2005) Conformational changes observed in enzyme crystal structures upon substrate binding, *J. Mol. Biol. 346*, 21–28.
928. Davenport, R. C., Bash, P. A., Seaton, B. A., Karplus, M., Petsko, G. A., and Ringe, D.

(1991) Structure of the triosephosphate isomerase-phosphoglycolohydroxamate complex: An analogue of the intermediate on the reaction pathway, *Biochemistry 30*, 5821–5826.
929. Joseph, D., Petsko, G. A., and Karplus, M. (1990) Anatomy of a conformational change: Hinged "lid" motion of the triosephosphate isomerase loop, *Science 249*, 1425–1428.
930. Lolis, E., Alber, T., Davenport, R. C., Rose, D., Hartman, F. C., and Petsko, G. A. (1990) Structure of yeast triosephosphate isomerase at 1.9 Å resolution, *Biochemistry 29*, 6609–6618.
931. Lolis, E., and Petsko, G. A. (1990) Crystallographic analysis of the complex between triosephosphate isomerase and 2-phosphoglycolate at 2.5 Å resolution: Implications for catalysis, *Biochemistry 29*, 6619–6625.
932. Wierenga, R. K., Noble, M. E., and Davenport, R. C. (1992) Comparison of the refined crystal structures of liganded and unliganded chicken, yeast and trypanosomal triosephosphate isomerase, *J. Mol. Biol. 224*, 1115–1126.
933. Zhai, X., Go, M. K., O'Donoghue, A. C., Amyes, T. L., Pegan, S. D., Wang, Y., Loria, J. P., Mesecar, A. D., and Richard, J. P. (2014) Enzyme architecture: The effect of replacement and deletion mutations of loop 6 on catalysis by triosephosphate isomerase, *Biochemistry 53*, 3486–3501.
934. Pompliano, D. L., Peyman, A., and Knowles, J. R. (1990) Stabilization of a reaction intermediate as a catalytic device: Definition of the functional role of the flexible loop in triosephosphate isomerase, *Biochemistry 29*, 3186–3194.
935. Larson, E. M., Larimer, F. W., and Hartman, F. C. (1995) Mechanistic insights provided by deletion of a flexible loop at the active site of ribulose-1,5-bisphosphate carboxylase/oxygenase, *Biochemistry 34*, 4531–4537.
936. Dominguez, R., Souchon, H., Lascombe, M., and Alzari, P. M. (1996) The crystal structure of a family 5 endoglucanase mutant in complexed and uncomplexed forms reveals an induced fit activation mechanism, *J. Mol. Biol. 257*, 1042–1051.
937. McMillan, F. M., Cahoon, M., White, A., Hedstrom, L., Petsko, G. A., and Ringe, D. (2000) Crystal structure at 2.4 Å resolution of *Borrelia burgdorferi* inosine 5′-monophosphate dehydrogenase: Evidence of a substrate-induced hinged-lid motion by loop 6, *Biochemistry 39*, 4533–4542.
938. Yoon, H. J., Kim, H. L., Mikami, B., and Suh, S. W. (2005) Crystal structure of nicotinic acid mononucleotide adenylyltransferase from *Pseudomonas aeruginosa* in its apo and substrate-complexed forms reveals a fully open conformation, *J. Mol. Biol. 351*, 258–265.
939. Gu, Y., Reshetnikova, L., Li, Y., Wu, Y., Yan, H., Singh, S., and Ji, X. (2002) Crystal structure of shikimate kinase from *Mycobacterium tuberculosis* reveals the dynamic role of the lid domain in catalysis, *J. Mol. Biol. 319*, 779–789.
940. Zhang, L., Feng, L., Zhou, L., Gui, J., Wan, J., and Hu, X. (2010) Purification, crystallization and preliminary X-ray analysis of 3-hydroxy-3-methylglutaryl-coenzyme A reductase of *Streptococcus pneumoniae*, *Acta Crystallogr. F 66*, 1500–1502.
941. Tabernero, L., Bochar, D. A., Rodwell, V. W., and Stauffacher, C. V. (1999) Substrate-induced closure of the flap domain in the ternary complex structures provides insights into the mechanism of catalysis by 3-hydroxy-3-methylglutaryl-CoA reductase, *Proc. Natl. Acad. Sci. U. S. A. 96*, 7167–7171.
942. Miller, B. R., and Kung, Y. (2018) Structural features and domain movements controlling substrate binding and cofactor specificity in class II HMG-CoA reductase, *Biochemistry 57*, 654–662.
943. Li, J., Vrielink, A., Brick, P., and Blow, D. M. (1993) Crystal structure of cholesterol oxidase complexed with a steroid substrate: Implications for flavin adenine dinucleotide dependent alcohol oxidases, *Biochemistry 32*, 11507–11515.
944. Muller-Dieckmann, H. J., and Schulz, G. E. (1995) Substrate specificity and assembly of the catalytic center derived from two structures of ligated uridylate kinase, *J. Mol. Biol. 246*, 522–530.
945. Zou, Y., Li, C., Brunzelle, J. S., and Nair, S. K. (2007) Molecular basis for substrate selectivity and specificity by an LPS biosynthetic enzyme, *Biochemistry 46*, 4294–4304.
946. Beynon, J. D., MacRae, I. J., Huston, S. L., Nelson, D. C., Segel, I. H., and Fisher, A. J. (2001) Crystal structure of ATP sulfurylase from the bacterial symbiont of the hydro-

thermal vent tubeworm *Riftia pachyptila*, *Biochemistry 40*, 14509–14517.
947. Blaszczyk, J., Li, Y., Yan, H., and Ji, X. (2001) Crystal structure of unligated guanylate kinase from yeast reveals GMP-induced conformational changes, *J. Mol. Biol. 307*, 247–257.
948. Cupp-Vickery, J. R., Urbina, H., and Vickery, L. E. (2003) Crystal structure of IscS, a cysteine desulfurase from *Escherichia coli*, *J. Mol. Biol. 330*, 1049–1059.
949. Schreuder, H. A., Knight, S., Curmi, P. M., Andersson, I., Cascio, D., Branden, C. I., and Eisenberg, D. (1993) Formation of the active site of ribulose-1,5-bisphosphate carboxylase/oxygenase by a disorder-order transition from the unactivated to the activated form, *Proc. Natl. Acad. Sci. U. S. A. 90*, 9968–9972.
950. Godsey, M. H., Ort, S., Sabini, E., Konrad, M., and Lavie, A. (2006) Structural basis for the preference of UTP over ATP in human deoxycytidine kinase: Illuminating the role of main-chain reorganization, *Biochemistry 45*, 452–461.
951. Liu, S., Lu, Z., Han, Y., Jia, Y., Howard, A., Dunaway-Mariano, D., and Herzberg, O. (2004) Conformational flexibility of PEP mutase, *Biochemistry 43*, 4447–4453.
952. Tanaka, T., Kato, H., Nishioka, T., and Oda, J. (1992) Mutational and proteolytic studies on a flexible loop in glutathione synthetase from *Escherichia coli* B: The loop and arginine 233 are critical for the catalytic reaction, *Biochemistry 31*, 2259–2265.
953. Chen, S., Burgner, J. W., Krahn, J. M., Smith, J. L., and Zalkin, H. (1999) Tryptophan fluorescence monitors multiple conformational changes required for glutamine phosphoribosylpyrophosphate amidotransferase interdomain signaling and catalysis, *Biochemistry 38*, 11659–11669.
954. Krahn, J. M., Kim, J. H., Burns, M. R., Parry, R. J., Zalkin, H., and Smith, J. L. (1997) Coupled formation of an amidotransferase interdomain ammonia channel and a phosphoribosyltransferase active site, *Biochemistry 36*, 11061–11068.
955. Barbosa, J. A., Smith, B. J., DeGori, R., Ooi, H. C., Marcuccio, S. M., Campi, E. M., Jackson, W. R., Brossmer, R., Sommer, M., and Lawrence, M. C. (2000) Active site modulation in the *N*-acetylneuraminate lyase sub-family as revealed by the structure of the inhibitor-complexed *Haemophilus influenzae* enzyme, *J. Mol. Biol. 303*, 405–421.
956. Koellner, G., Bzowska, A., Wielgus-Kutrowska, B., Luic, M., Steiner, T., Saenger, W., and Stepinski, J. (2002) Open and closed conformation of the *E. coli* purine nucleoside phosphorylase active center and implications for the catalytic mechanism, *J. Mol. Biol. 315*, 351–371.
957. Sawaya, M. R., and Kraut, J. (1997) Loop and subdomain movements in the mechanism of *Escherichia coli* dihydrofolate reductase: Crystallographic evidence, *Biochemistry 36*, 586–603.
958. Derewenda, U., Brzozowski, A. M., Lawson, D. M., and Derewenda, Z. S. (1992) Catalysis at the interface: The anatomy of a conformational change in a triglyceride lipase, *Biochemistry 31*, 1532–1541.
959. Li, G., Felczak, K., Shi, G., and Yan, H. (2006) Mechanism of the conformational transitions in 6-hydroxymethyl-7,8-dihydropterin pyrophosphokinase as revealed by NMR spectroscopy, *Biochemistry 45*, 12573–12581.
960. Stammers, D. K., Achari, A., Somers, D. O., Bryant, P. K., Rosemond, J., Scott, D. L., and Champness, J. N. (1999) 2.0 Å X-Ray structure of the ternary complex of 7,8-dihydro-6-hydroxymethylpterinpyrophosphokinase from *Escherichia coli* with ATP and a substrate analogue, *FEBS Lett. 456*, 49–53.
961. Arsenieva, D., and Jeffery, C. J. (2002) Conformational changes in phosphoglucose isomerase induced by ligand binding, *J. Mol. Biol. 323*, 77–84.
962. Aden, J., Verma, A., Schug, A., and Wolf-Watz, M. (2012) Modulation of a pre-existing conformational equilibrium tunes adenylate kinase activity, *J. Am. Chem. Soc. 134*, 16562–16570.
963. Chang, A. K., Nixon, P. F., and Duggleby, R. G. (2000) Effects of deletions at the carboxyl terminus of *Zymomonas mobilis* pyruvate decarboxylase on the kinetic properties and substrate specificity, *Biochemistry 39*, 9430–9437.
964. Lee, A. Y., Gulnik, S. V., and Erickson, J. W. (1998) Conformational switching in an aspartic proteinase, *Nature Struct. Biol. 5*, 866–871.
965. Karlstrom, M., Stokke, R., Steen, I. H., Birkeland, N. K., and Ladenstein, R. (2005) Iso-

citrate dehydrogenase from the hyperthermophile *Aeropyrum pernix*: X-Ray structure analysis of a ternary enzyme-substrate complex and thermal stability, *J. Mol. Biol. 345*, 559–577.
966. Shibata, N., Masuda, J., Morimoto, Y., Yasuoka, N., and Toraya, T. (2002) Substrate-induced conformational change of a coenzyme B_{12}-dependent enzyme: Crystal structure of the substrate-free form of diol dehydratase, *Biochemistry 41*, 12607–12617.
967. Jogl, G., and Tong, L. (2004) Crystal structure of yeast acetyl-coenzyme A synthetase in complex with AMP, *Biochemistry 43*, 1425–1431.
968. Lennon, B. W., Williams, C. H., Jr., and Ludwig, M. L. (2000) Twists in catalysis: Alternating conformations of *Escherichia coli* thioredoxin reductase, *Science 289*, 1190–1194.
969. Acquistapace, I. M., Zi Etek, M. A., Li, A. W. H., Salmon, M., Kuhn, I., Bedford, M. R., Brearley, C. A., and Hemmings, A. M. (2020) Snapshots during the catalytic cycle of a histidine acid phytase reveal an induced-fit structural mechanism, *J. Biol. Chem. 295*, 17724–17737.
970. Goncalves, S., Miller, S. P., Carrondo, M. A., Dean, A. M., and Matias, P. M. (2012) Induced fit and the catalytic mechanism of isocitrate dehydrogenase, *Biochemistry 51*, 7098–7115.
971. Dai, J., Finci, L., Zhang, C., Lahiri, S., Zhang, G., Peisach, E., Allen, K. N., and Dunaway-Mariano, D. (2009) Analysis of the structural determinants underlying discrimination between substrate and solvent in β-phosphoglucomutase catalysis, *Biochemistry 48*, 1984–1995.
972. Lamzin, V. S., Dauter, Z., Popov, V. O., Harutyunyan, E. H., and Wilson, K. S. (1994) High resolution structures of holo and apo formate dehydrogenase, *J. Mol. Biol. 236*, 759–785.
973. Zhang, G., Mazurkie, A. S., Dunaway-Mariano, D., and Allen, K. N. (2002) Kinetic evidence for a substrate-induced fit in phosphonoacetaldehyde hydrolase catalysis, *Biochemistry 41*, 13370–13377.
974. Satoh, A., Konishi, S., Tamura, H., Stickland, H. G., Whitney, H. M., Smith, A. G., Matsumura, H., and Inoue, T. (2010) Substrate-induced closing of the active site revealed by the crystal structure of pantothenate synthetase from *Staphylococcus aureus*, *Biochemistry 49*, 6400–6410.
975. Bernstein, B. E., Michels, P. A., and Hol, W. G. (1997) Synergistic effects of substrate-induced conformational changes in phosphoglycerate kinase activation, *Nature 385*, 275–278.
976. Pickover, C. A., McKay, D. B., Engelman, D. M., and Steitz, T. A. (1979) Substrate binding closes the cleft between the domains of yeast phosphoglycerate kinase, *J. Biol. Chem 254*, 11323–11329.
977. Marston, J. P., Cliff, M. J., Reed, M. A., Blackburn, G. M., Hounslow, A. M., Craven, C. J., and Waltho, J. P. (2010) Structural tightening and interdomain communication in the catalytic cycle of phosphoglycerate kinase, *J. Mol. Biol. 396*, 345–360.
978. Rand, R. P., Fuller, N. L., Butko, P., Francis, G., and Nicholls, P. (1993) Measured change in protein solvation with substrate binding and turnover, *Biochemistry 32*, 5925–5929.
979. Dzingeleski, G. D., and Wolfenden, R. (1993) Hypersensitivity of an enzyme reaction to solvent water, *Biochemistry 32*, 9143–9147.
980. Knofel, T., and Strater, N. (2001) *E. coli* 5′-nucleotidase undergoes a hinge-bending domain rotation resembling a ball-and-socket motion, *J. Mol. Biol. 309*, 255–266.
981. Wu, R., Cao, J., Lu, X., Reger, A. S., Gulick, A. M., and Dunaway-Mariano, D. (2008) Mechanism of 4-chlorobenzoate: Coenzyme A ligase catalysis, *Biochemistry 47*, 8026–8039.
982. Pugmire, M. J., Cook, W. J., Jasanoff, A., Walter, M. R., and Ealick, S. E. (1998) Structural and theoretical studies suggest domain movement produces an active conformation of thymidine phosphorylase, *J. Mol. Biol. 281*, 285–299.
983. Hayward, S. (1999) Structural principles governing domain motions in proteins, *Proteins 36*, 425–435.
984. Sali, A., Veerapandian, B., Cooper, J. B., Foundling, S. I., Hoover, D. J., and Blundell, T. L. (1989) High-resolution X-ray diffraction study of the complex between endothiapepsin and an oligopeptide inhibitor: The analysis of the inhibitor binding and description of the rigid body shift in the enzyme, *EMBO J. 8*, 2179–2188.
985. Picot, D., Sandmeier, E., Thaller, C., Vincent, M. G., Christen, P., and Jansonius, J. N.

(1991) The open/closed conformational equilibrium of aspartate aminotransferase. Studies in the crystalline state and with a fluorescent probe in solution, *Eur. J. Biochem. 196*, 329–341.
986. McPhalen, C. A., Vincent, M. G., Picot, D., Jansonius, J. N., Lesk, A. M., and Chothia, C. (1992) Domain closure in mitochondrial aspartate aminotransferase, *J. Mol. Biol. 227*, 197–213.
987. Knofel, T., and Strater, N. (2001) Mechanism of hydrolysis of phosphate esters by the dimetal center of 5′-nucleotidase based on crystal structures, *J. Mol. Biol. 309*, 239–254.
988. Harris, P., Poulsen, J. C., Jensen, K. F., and Larsen, S. (2002) Substrate binding induces domain movements in orotidine 5′-monophosphate decarboxylase, *J. Mol. Biol. 318*, 1019–1029.
989. Nichols, C. E., Ren, J., Lamb, H. K., Hawkins, A. R., and Stammers, D. K. (2003) Ligand-induced conformational changes and a mechanism for domain closure in *Aspergillus nidulans* dehydroquinate synthase, *J. Mol. Biol. 327*, 129–144.
990. Sheng, F., Jia, X., Yep, A., Preiss, J., and Geiger, J. H. (2009) The crystal structures of the open and catalytically competent closed conformation of *Escherichia coli* glycogen synthase, *J. Biol. Chem 284*, 17796–17807.
991. Holland, D. R., Tronrud, D. E., Pley, H. W., Flaherty, K. M., Stark, W., Jansonius, J. N., McKay, D. B., and Matthews, B. W. (1992) Structural comparison suggests that thermolysin and related neutral proteases undergo hinge-bending motion during catalysis, *Biochemistry 31*, 11310–11316.
992. Tari, L. W., Matte, A., Pugazhenthi, U., Goldie, H., and Delbaere, L. T. (1996) Snapshot of an enzyme reaction intermediate in the structure of the ATP-Mg^{2+}-oxalate ternary complex of *Escherichia coli* PEP carboxykinase, *Nature Struct. Biol. 3*, 355–363.
993. Larsen, T. M., Benning, M. M., Rayment, I., and Reed, G. H. (1998) Structure of the bis(Mg^{2+})-ATP-oxalate complex of the rabbit muscle pyruvate kinase at 2.1 Å resolution: ATP binding over a barrel, *Biochemistry 37*, 6247–6255.
994. Anderson, B. F., Baker, H. M., Norris, G. E., Rumball, S. V., and Baker, E. N. (1990) Apolactoferrin structure demonstrates ligand-induced conformational change in transferrins, *Nature 344*, 784–787.
995. Unciuleac, M. C., Goldgur, Y., and Shuman, S. (2017) Two-metal versus one-metal mechanisms of lysine adenylylation by ATP-dependent and NAD^+-dependent polynucleotide ligases, *Proc. Natl. Acad. Sci. U. S. A. 114*, 2592–2597.
996. Nandakumar, J., Nair, P. A., and Shuman, S. (2007) Last stop on the road to repair: Structure of *E. coli* DNA ligase bound to nicked DNA-adenylate, *Mol Cell 26*, 257–271.
997. Lukacs, C. M., Kucera, R., Schildkraut, I., and Aggarwal, A. K. (2001) Structure of free BglII reveals an unprecedented scissor-like motion for opening an endonuclease, *Nature Struct. Biol. 8*, 126–130.
998. Lukacs, C. M., Kucera, R., Schildkraut, I., and Aggarwal, A. K. (2000) Understanding the immutability of restriction enzymes: Crystal structure of BglII and its DNA substrate at 1.5 Å resolution, *Nature Struct. Biol. 7*, 134–140.
999. Ollis, D. L., Brick, P., Hamlin, R., Xuong, N. G., and Steitz, T. A. (1985) Structure of large fragment of *Escherichia coli* DNA polymerase I complexed with dTMP, *Nature 313*, 762–766.
1000. Beese, L. S., Derbyshire, V., and Steitz, T. A. (1993) Structure of DNA polymerase I Klenow fragment bound to duplex DNA, *Science 260*, 352–355.
1001. Dzantiev, L., Alekseyev, Y. O., Morales, J. C., Kool, E. T., and Romano, L. J. (2001) Significance of nucleobase shape complementarity and hydrogen bonding in the formation and stability of the closed polymerase-DNA complex, *Biochemistry 40*, 3215–3221.
1002. Dzantiev, L., and Romano, L. J. (2000) A conformational change in *E. coli* DNA polymerase I (Klenow fragment) is induced in the presence of a dNTP complementary to the template base in the active site, *Biochemistry 39*, 356–361.
1003. Doublie, S., Tabor, S., Long, A. M., Richardson, C. C., and Ellenberger, T. (1998) Crystal structure of a bacteriophage T7 DNA replication complex at 2.2 Å resolution, *Nature 391*, 251–258.
1004. Patel, S. S., Wong, I., and Johnson, K. A. (1991) Pre-steady-state kinetic analysis of processive DNA replication including com-

plete characterization of an exonuclease-deficient mutant, *Biochemistry 30*, 511–525.
1005. Sawaya, M. R., Pelletier, H., Kumar, A., Wilson, S. H., and Kraut, J. (1994) Crystal structure of rat DNA polymerase β: Evidence for a common polymerase mechanism, *Science 264*, 1930–1935.
1006. Pelletier, H., Sawaya, M. R., Kumar, A., Wilson, S. H., and Kraut, J. (1994) Structures of ternary complexes of rat DNA polymerase β, a DNA template-primer, and ddCTP, *Science 264*, 1891–1903.
1007. Andersen, O. A., Stokka, A. J., Flatmark, T., and Hough, E. (2003) 2.0 Å Resolution crystal structures of the ternary complexes of human phenylalanine hydroxylase catalytic domain with tetrahydrobiopterin and 3-(2-thienyl)-L-alanine or L-norleucine: Substrate specificity and molecular motions related to substrate binding, *J. Mol. Biol. 333*, 747–757.
1008. Pai, E. F., Sachsenheimer, W., Schirmer, R. H., and Schulz, G. E. (1977) Substrate positions and induced-fit in crystalline adenylate kinase, *J. Mol. Biol. 114*, 37–45.
1009. Duff, A. P., Andrews, T. J., and Curmi, P. M. (2000) The transition between the open and closed states of Rubisco is triggered by the inter-phosphate distance of the bound bisphosphate, *J. Mol. Biol. 298*, 903–916.
1010. Kochan, G., Pilka, E. S., von Delft, F., Oppermann, U., and Yue, W. W. (2009) Structural snapshots for the conformation-dependent catalysis by human medium-chain acyl-coenzyme A synthetase ACSM2A, *J. Mol. Biol. 388*, 997–1008.
1011. Rees, B., Webster, G., Delarue, M., Boeglin, M., and Moras, D. (2000) Aspartyl tRNA-synthetase from *Escherichia coli*: Flexibility and adaptability to the substrates, *J. Mol. Biol. 299*, 1157–1164.
1012. Bertrand, J. A., Fanchon, E., Martin, L., Chantalat, L., Auger, G., Blanot, D., van Heijenoort, J., and Dideberg, O. (2000) "Open" structures of MurD: Domain movements and structural similarities with folylpolyglutamate synthetase, *J. Mol. Biol. 301*, 1257–1266.
1013. Henzler-Wildman, K. A., Thai, V., Lei, M., Ott, M., Wolf-Watz, M., Fenn, T., Pozharski, E., Wilson, M. A., Petsko, G. A., Karplus, M., Hubner, C. G., and Kern, D. (2007) Intrinsic motions along an enzymatic reaction trajectory, *Nature 450*, 838–844.
1014. Nakasako, M., Fujisawa, T., Adachi, S., Kudo, T., and Higuchi, S. (2001) Large-scale domain movements and hydration structure changes in the active-site cleft of unligated glutamate dehydrogenase from *Thermococcus profundus* studied by cryogenic X-ray crystal structure analysis and small-angle X-ray scattering, *Biochemistry 40*, 3069–3079.
1015. Yoshida, T., Uchiyama, S., Nakano, H., Kashimori, H., Kijima, H., Ohshima, T., Saihara, Y., Ishino, T., Shimahara, H., Yoshida, T., Yokose, K., Ohkubo, T., Kaji, A., and Kobayashi, Y. (2001) Solution structure of the ribosome recycling factor from *Aquifex aeolicus*, *Biochemistry 40*, 2387–2396.
1016. Liao, Q., Kulkarni, Y., Sengupta, U., Petrovic, D., Mulholland, A. J., van der Kamp, M. W., Strodel, B., and Kamerlin, S. C. L. (2018) Loop motion in triosephosphate isomerase is not a simple open and shut case, *J. Am. Chem. Soc. 140*, 15889–15903.
1017. Hohenester, E., and Jansonius, J. N. (1994) Crystalline mitochondrial aspartate aminotransferase exists in only two conformations, *J. Mol. Biol. 236*, 963–968.
1018. Niu, X., Bruschweiler-Li, L., Davulcu, O., Skalicky, J. J., Bruschweiler, R., and Chapman, M. S. (2011) Arginine kinase: Joint crystallographic and NMR RDC analyses link substrate-associated motions to intrinsic flexibility, *J. Mol. Biol. 405*, 479–496.
1019. Koshland, D. E. (1958) Application of a theory of enzyme specificity to protein synthesis, *Proc. Natl. Acad. Sci. U. S. A. 44*, 98–104.
1020. Retailleau, P., Weinreb, V., Hu, M., and Carter, C. W., Jr. (2007) Crystal structure of tryptophanyl-tRNA synthetase complexed with adenosine-5′ tetraphosphate: Evidence for distributed use of catalytic binding energy in amino acid activation by class I aminoacyl-tRNA synthetases, *J. Mol. Biol. 369*, 108–128.
1021. Boehr, D. D., Nussinov, R., and Wright, P. E. (2009) The role of dynamic conformational ensembles in biomolecular recognition, *Nature Chem. Biol. 5*, 789–796.
1022. Vogt, A. D., and Di Cera, E. (2013) Conformational selection is a dominant mechanism of ligand binding, *Biochemistry 52*, 5723–5729.
1023. Jencks, W. P. (1969) *Catalysis in chemistry and enzymology*, pp 282–320, McGraw-Hill, New York.

1024. Schultz-Heienbrok, R., Maier, T., and Strater, N. (2005) A large hinge bending domain rotation is necessary for the catalytic function of *Escherichia coli* 5′-nucleotidase, *Biochemistry 44*, 2244–2252.
1025. DelaFuente, G., Lagunas, R., and Sols, A. (1970) Induced fit in yeast hexokinase, *Eur. J. Biochem. 16*, 226–233.
1026. Anton, D. L., Hedstrom, L., Fish, S. M., and Abeles, R. H. (1983) Mechanism of *enol*pyruvylshikimate-3-phosphate synthase exchange of phospho*enol*pyruvate with solvent protons, *Biochemistry 22*, 5903–5908.
1027. Sullivan, S. M., and Holyoak, T. (2008) Enzymes with lid-gated active sites must operate by an induced fit mechanism instead of conformational selection, *Proc. Natl. Acad. Sci. U. S. A. 105*, 13829–13834.
1028. Ramaswamy, S., Park, D. H., and Plapp, B. V. (1999) Substitutions in a flexible loop of horse liver alcohol dehydrogenase hinder the conformational change and unmask hydrogen transfer, *Biochemistry 38*, 13951–13959.
1029. Viola, R. E., Raushel, F. M., Rendina, A. R., and Cleland, W. W. (1982) Substrate synergism and the kinetic mechanism of yeast hexokinase, *Biochemistry 21*, 1295–1302.
1030. Aparicio, R., Ferreira, S. T., and Polikarpov, I. (2003) Closed conformation of the active site loop of rabbit muscle triosephosphate isomerase in the absence of substrate: Evidence of conformational heterogeneity, *J. Mol. Biol. 334*, 1023–1041.
1031. Parthasarathy, S., Ravindra, G., Balaram, H., Balaram, P., and Murthy, M. R. (2002) Structure of the *Plasmodium falciparum* triosephosphate isomerase-phosphoglycolate complex in two crystal forms: Characterization of catalytic loop open and closed conformations in the ligand-bound state, *Biochemistry 41*, 13178–13188.
1032. Williams, J. C., and McDermott, A. E. (1995) Dynamics of the flexible loop of triosephosphate isomerase: The loop motion is not ligand gated, *Biochemistry 34*, 8309–8319.
1033. Zhang, Y., Desharnais, J., Greasley, S. E., Beardsley, G. P., Boger, D. L., and Wilson, I. A. (2002) Crystal structures of human GAR Tfase at low and high pH and with substrate β-GAR, *Biochemistry 41*, 14206–14215.
1034. Aden, J., and Wolf-Watz, M. (2007) NMR Identification of transient complexes critical to adenylate kinase catalysis, *J. Am. Chem. Soc. 129*, 14003–14012.
1035. Desamero, R., Rozovsky, S., Zhadin, N., McDermott, A., and Callender, R. (2003) Active site loop motion in triosephosphate isomerase: T-Jump relaxation spectroscopy of thermal activation, *Biochemistry 42*, 2941–2951.
1036. Davulcu, O., Skalicky, J. J., and Chapman, M. S. (2011) Rate-limiting domain and loop motions in arginine kinase, *Biochemistry 50*, 4011–4018.
1037. Cliff, M. J., Bowler, M. W., Varga, A., Marston, J. P., Szabo, J., Hounslow, A. M., Baxter, N. J., Blackburn, G. M., Vas, M., and Waltho, J. P. (2010) Transition state analogue structures of human phosphoglycerate kinase establish the importance of charge balance in catalysis, *J. Am. Chem. Soc. 132*, 6507–6516.
1038. Varley, P. G., and Pain, R. H. (1991) Relation between stability, dynamics and enzyme activity in 3-phosphoglycerate kinases from yeast and *Thermus thermophilus*, *J. Mol. Biol. 220*, 531–538.
1039. Watt, E. D., Shimada, H., Kovrigin, E. L., and Loria, J. P. (2007) The mechanism of rate-limiting motions in enzyme function, *Proc. Natl. Acad. Sci. U. S. A. 104*, 11981–11986.
1040. Cole, R., and Loria, J. P. (2002) Evidence for flexibility in the function of ribonuclease A, *Biochemistry 41*, 6072–6081.
1041. Antikainen, N. M., Smiley, R. D., Benkovic, S. J., and Hammes, G. G. (2005) Conformation coupled enzyme catalysis: Single-molecule and transient kinetics investigation of dihydrofolate reductase, *Biochemistry 44*, 16835–16843.
1042. Bhabha, G., Lee, J., Ekiert, D. C., Gam, J., Wilson, I. A., Dyson, H. J., Benkovic, S. J., and Wright, P. E. (2011) A dynamic knockout reveals that conformational fluctuations influence the chemical step of enzyme catalysis, *Science 332*, 234–238.
1043. Yachnin, B. J., Sprules, T., McEvoy, M. B., Lau, P. C., and Berghuis, A. M. (2012) The substrate-bound crystal structure of a Baeyer–Villiger monooxygenase exhibits a Criegee-like conformation, *J. Am. Chem. Soc. 134*, 7788–7795.
1044. Koellner, G., Kryger, G., Millard, C. B., Silman, I., Sussman, J. L., and Steiner, T. (2000) Active-site gorge and buried water molecules in crystal structures of acetylcholinesterase

from *Torpedo californica*, *J. Mol. Biol. 296*, 713–735.
1045. Kim, C. U., Song, H., Avvaru, B. S., Gruner, S. M., Park, S., and McKenna, R. (2016) Tracking solvent and protein movement during CO_2 release in carbonic anhydrase II crystals, *Proc. Natl. Acad. Sci. U. S. A. 113*, 5257–5262.
1046. Xiong, J., Phillips, R. S., Kurtz, D. M., Jr., Jin, S., Ai, J., and Sanders-Loehr, J. (2000) The O binding pocket of myohemerythrin: Role of a conserved leucine, *Biochemistry 39*, 8526–8536.
1047. Egeberg, K. D., Springer, B. A., Sligar, S. G., Carver, T. E., Rohlfs, R. J., and Olson, J. S. (1990) The role of Val68(E11) in ligand binding to sperm whale myoglobin. Site-directed mutagenesis of a synthetic gene, *J. Biol. Chem. 265*, 11788–11795.
1048. Coffa, G., and Brash, A. R. (2004) A single active site residue directs oxygenation stereospecificity in lipoxygenases: Stereocontrol is linked to the position of oxygenation, *Proc. Natl. Acad. Sci. U. S. A. 101*, 15579–15584.
1049. Westhof, E., Dumas, P., and Moras, D. (1985) Crystallographic refinement of yeast aspartic acid transfer RNA, *J. Mol. Biol. 184*, 119–145.
1050. Cavarelli, J., Eriani, G., Rees, B., Ruff, M., Boeglin, M., Mitschler, A., Martin, F., Gangloff, J., Thierry, J. C., and Moras, D. (1994) The active site of yeast aspartyl-tRNA synthetase: Structural and functional aspects of the aminoacylation reaction, *EMBO J. 13*, 327–337.
1051. Sauter, C., Lorber, B., Cavarelli, J., Moras, D., and Giege, R. (2000) The free yeast aspartyl-tRNA synthetase differs from the $tRNA^{asp}$-complexed enzyme by structural changes in the catalytic site, hinge region, and anticodon-binding domain, *J. Mol. Biol. 299*, 1313–1324.
1052. Tukalo, M., Yaremchuk, A., Fukunaga, R., Yokoyama, S., and Cusack, S. (2005) The crystal structure of leucyl-tRNA synthetase complexed with $tRNA^{leu}$ in the post-transfer-editing conformation, *Nature Struct. Biol. 12*, 923–930.
1053. Li, L., Martinis, S. A., and Luthey-Schulten, Z. (2013) Capture and quality control mechanisms for adenosine-5′-triphosphate binding, *J. Am. Chem. Soc. 135*, 6047–6055.
1054. Mendes, K. R., and Kantrowitz, E. R. (2010) The pathway of product release from the R state of aspartate transcarbamoylase, *J. Mol. Biol. 401*, 940–948.
1055. Pham, K. N., and Yeh, S. R. (2018) Mapping the binding trajectory of a suicide inhibitor in human indoleamine 2,3-dioxygenase 1, *J. Am. Chem. Soc. 140*, 14538–14541.
1056. Murthy, M. R., Reid, T. J., 3rd, Sicignano, A., Tanaka, N., and Rossmann, M. G. (1981) Structure of beef liver catalase, *J. Mol. Biol. 152*, 465–499.
1057. Mate, M. J., Zamocky, M., Nykyri, L. M., Herzog, C., Alzari, P. M., Betzel, C., Koller, F., and Fita, I. (1999) Structure of catalase-A from *Saccharomyces cerevisiae*, *J. Mol. Biol. 286*, 135–149.
1058. Purwar, N., McGarry, J. M., Kostera, J., Pacheco, A. A., and Schmidt, M. (2011) Interaction of nitric oxide with catalase: Structural and kinetic analysis, *Biochemistry 50*, 4491–4503.
1059. Bisht, S., Rajaram, V., Bharath, S. R., Kalyani, J. N., Khan, F., Rao, A. N., Savithri, H. S., and Murthy, M. R. (2012) Crystal structure of *Escherichia coli* diaminopropionate ammonia-lyase reveals mechanism of enzyme activation and catalysis, *J. Biol. Chem. 287*, 20369–20381.
1060. Mast, N., Annalora, A. J., Lodowski, D. T., Palczewski, K., Stout, C. D., and Pikuleva, I. A. (2011) Structural basis for three-step sequential catalysis by the cholesterol side chain cleavage enzyme CYP11A1, *J. Biol. Chem. 286*, 5607–5613.
1061. Jones, J. C., Banerjee, R., Shi, K., Aihara, H., and Lipscomb, J. D. (2020) Structural studies of the *Methylosinus trichosporium* Ob3B soluble methane monooxygenase hydroxylase and regulatory component complex reveal a transient substrate tunnel, *Biochemistry 59*, 2946–2961.
1062. Makino, D. L., Baumgartner, M., and Conti, E. (2013) Crystal structure of an RNA-bound 11-subunit eukaryotic exosome complex, *Nature 495*, 70–75.
1063. Goblirsch, B. R., Jensen, M. R., Mohamed, F. A., Wackett, L. P., and Wilmot, C. M. (2016) Substrate trapping in crystals of the thiolase OleA identifies three channels that enable long chain olefin biosynthesis, *J. Biol. Chem. 291*, 26698–26706.
1064. Morgan, J. L., Strumillo, J., and Zimmer, J. (2013) Crystallographic snapshot of cellulose synthesis and membrane translocation, *Nature 493*, 181–186.

1065. Purushotham, P., Ho, R., and Zimmer, J. (2020) Architecture of a catalytically active homotrimeric plant cellulose synthase complex, *Science 369*, 1089–1094.
1066. Lah, M. S., Dixon, M. M., Pattridge, K. A., Stallings, W. C., Fee, J. A., and Ludwig, M. L. (1995) Structure-function in *Escherichia coli* iron superoxide dismutase: Comparisons with the manganese enzyme from *Thermus thermophilus*, *Biochemistry 34*, 1646–1660.
1067. Messerschmidt, A., Ladenstein, R., Huber, R., Bolognesi, M., Avigliano, L., Petruzzelli, R., Rossi, A., and Finazzi-Agro, A. (1992) Refined crystal structure of ascorbate oxidase at 1.9 Å resolution, *J. Mol. Biol. 224*, 179–205.
1068. Montet, Y., Amara, P., Volbeda, A., Vernede, X., Hatchikian, E. C., Field, M. J., Frey, M., and Fontecilla-Camps, J. C. (1997) Gas access to the active site of Ni-Fe hydrogenases probed by X-ray crystallography and molecular dynamics, *Nature Struct. Biol. 4*, 523–526.
1069. Cunane, L. M., Chen, Z. W., Shamala, N., Mathews, F. S., Cronin, C. N., and McIntire, W. S. (2000) Structures of the flavocytochrome *p*-cresol methylhydroxylase and its enzyme-substrate complex: Gated substrate entry and proton relays support the proposed catalytic mechanism, *J. Mol. Biol. 295*, 357–374.
1070. Luna, V. M., Chen, Y., Fee, J. A., and Stout, C. D. (2008) Crystallographic studies of Xe and Kr binding within the large internal cavity of cytochrome ba_3 from *Thermus thermophilus*: Structural analysis and role of oxygen transport channels in the heme-Cu oxidases, *Biochemistry 47*, 4657–4665.
1071. Hiromoto, T., Fujiwara, S., Hosokawa, K., and Yamaguchi, H. (2006) Crystal structure of 3-hydroxybenzoate hydroxylase from *Comamonas testosteroni* has a large tunnel for substrate and oxygen access to the active site, *J. Mol. Biol. 364*, 878–896.
1072. Lario, P. I., Sampson, N., and Vrielink, A. (2003) Sub-atomic resolution crystal structure of cholesterol oxidase: What atomic resolution crystallography reveals about enzyme mechanism and the role of the FAD cofactor in redox activity, *J. Mol. Biol. 326*, 1635–1650.
1073. Birdsall, D. L., Finer-Moore, J., and Stroud, R. M. (1996) Entropy in bi-substrate enzymes: Proposed role of an alternate site in chaperoning substrate into, and products out of, thymidylate synthase, *J. Mol. Biol. 255*, 522–535.
1074. Mallender, W. D., Szegletes, T., and Rosenberry, T. L. (2000) Acetylthiocholine binds to Asp74 at the peripheral site of human acetylcholinesterase as the first step in the catalytic pathway, *Biochemistry 39*, 7753–7763.
1075. Barford, D., Schwabe, J. W., Oikonomakos, N. G., Acharya, K. R., Hajdu, J., Papageorgiou, A. C., Martin, J. L., Knott, J. C., Vasella, A., and Johnson, L. N. (1988) Channels at the catalytic site of glycogen phosphorylase B: Binding and kinetic studies with the β-glycosidase inhibitor D-gluconohydroximo-1,5-lactone *N*-phenylurethane, *Biochemistry 27*, 6733–6741.
1076. Sakashita, N., Watanabe, H. C., Ikeda, T., Saito, K., and Ishikita, H. (2017) Origins of water molecules in the photosystem II crystal structure, *Biochemistry 56*, 3049–3057.
1077. McCormick, M. S., and Lippard, S. J. (2011) Analysis of substrate access to active sites in bacterial multicomponent monooxygenase hydroxylases: X-Ray crystal structure of xenon-pressurized phenol hydroxylase from *Pseudomonas* sp. Ox1, *Biochemistry 50*, 11058–11069.
1078. Funatogawa, C., Li, Y., Chen, Y., McDonald, W., Szundi, I., Fee, J. A., Stout, C. D., and Einarsdottir, O. (2017) Role of the conserved valine 236 in access of ligands to the active site of *Thermus thermophilus* ba_3 cytochrome oxidase, *Biochemistry 56*, 107–119.
1079. Picot, D., Loll, P. J., and Garavito, R. M. (1994) The X-ray crystal structure of the membrane protein prostaglandin H2 synthase-1, *Nature 367*, 243–249.
1080. Lowe, J., Stock, D., Jap, B., Zwickl, P., Baumeister, W., and Huber, R. (1995) Crystal structure of the 20S proteasome from the archaeon *T. acidophilum* at 3.4 Å resolution, *Science 268*, 533–539.
1081. Groll, M., Bajorek, M., Kohler, A., Moroder, L., Rubin, D. M., Huber, R., Glickman, M. H., and Finley, D. (2000) A gated channel into the proteasome core particle, *Nature Struct. Biol. 7*, 1062–1067.
1082. Wenzel, T., and Baumeister, W. (1995) Conformational constraints in protein degradation by the 20S proteasome, *Nature Struct. Biol. 2*, 199–204.
1083. Whitby, F. G., Masters, E. I., Kramer, L., Knowlton, J. R., Yao, Y., Wang, C. C., and Hill,

C. P. (2000) Structural basis for the activation of 20S proteasomes by 11S regulators, *Nature 408*, 115–120.
1084. Kim, C. J., and Debus, R. J. (2017) Evidence from FTIR difference spectroscopy that a substrate H_2O molecule for O_2 formation in photosystem II is provided by the Ca ion of the catalytic Mn_4CaO_5 cluster, *Biochemistry 56*, 2558–2570.
1085. Morrison, C. N., Hoy, J. A., Zhang, L., Einsle, O., and Rees, D. C. (2015) Substrate pathways in the nitrogenase MoFe protein by experimental identification of small molecule binding sites, *Biochemistry 54*, 2052–2060.
1086. Loll, P. J., Picot, D., and Garavito, R. M. (1995) The structural basis of aspirin activity inferred from the crystal structure of inactivated prostaglandin H2 synthase, *Nature Struct. Biol. 2*, 637–643.
1087. Price, A. C., Zhang, Y. M., Rock, C. O., and White, S. W. (2004) Cofactor-induced conformational rearrangements establish a catalytically competent active site and a proton relay conduit in FabG, *Structure 12*, 417–428.
1088. Korman, T. P., Hill, J. A., Vu, T. N., and Tsai, S. C. (2004) Structural analysis of actinorhodin polyketide ketoreductase: Cofactor binding and substrate specificity, *Biochemistry 43*, 14529–14538.
1089. Agmon, N. (1995) The Grotthuss mechanism, *Chem. Phys. Lett. 244*, 456–462.
1090. Ekimova, M., Hoffmann, F., Bekcioglu-Neff, G., Rafferty, A., Kornilov, O., Nibbering, E. T. J., and Sebastiani, D. (2019) Ultrafast proton transport between a hydroxy acid and a nitrogen base along solvent bridges governed by the hydroxide/methoxide transfer mechanism, *J. Am. Chem. Soc. 141*, 14581–14592.
1091. Fisher, S. Z., Maupin, C. M., Budayova-Spano, M., Govindasamy, L., Tu, C., Agbandje-McKenna, M., Silverman, D. N., Voth, G. A., and McKenna, R. (2007) Atomic crystal and molecular dynamics simulation structures of human carbonic anhydrase II: Insights into the proton transfer mechanism, *Biochemistry 46*, 2930–2937.
1092. Venkatasubban, K. S., and Silverman, D. N. (1980) Carbon dioxide hydration activity of carbonic anhydrase in mixtures of water and deuterium oxide, *Biochemistry 19*, 4984–4989.
1093. Fisher, Z., Hernandez Prada, J. A., Tu, C., Duda, D., Yoshioka, C., An, H., Govindasamy, L., Silverman, D. N., and McKenna, R. (2005) Structural and kinetic characterization of active-site histidine as a proton shuttle in catalysis by human carbonic anhydrase II, *Bio-Biochemistry 44*, 1097–1105.
1094. Jewell, D. A., Tu, C. K., Paranawithana, S. R., Tanhauser, S. M., LoGrasso, P. V., Laipis, P. J., and Silverman, D. N. (1991) Enhancement of the catalytic properties of human carbonic anhydrase III by site-directed mutagenesis, *Biochemistry 30*, 1484–1490.
1095. Heck, R. W., Boriack-Sjodin, P. A., Qian, M., Tu, C., Christianson, D. W., Laipis, P. J., and Silverman, D. N. (1996) Structure-based design of an intramolecular proton transfer site in murine carbonic anhydrase V, *Biochemistry 35*, 11605–11611.
1096. Qian, M., Tu, C., Earnhardt, J. N., Laipis, P. J., and Silverman, D. N. (1997) Glutamate and aspartate as proton shuttles in mutants of carbonic anhydrase, *Biochemistry 36*, 15758–15764.
1097. Mikulski, R., West, D., Sippel, K. H., Avvaru, B. S., Aggarwal, M., Tu, C., McKenna, R., and Silverman, D. N. (2013) Water networks in fast proton transfer during catalysis by human carbonic anhydrase II, *Biochemistry 52*, 125–131.
1098. Mulder, D. W., Boyd, E. S., Sarma, R., Lange, R. K., Endrizzi, J. A., Broderick, J. B., and Peters, J. W. (2010) Stepwise [FeFe]-hydrogenase H-cluster assembly revealed in the structure of $Hyda^{\Delta EFG}$, *Nature 465*, 248–251.
1099. Cornish, A. J., Gartner, K., Yang, H., Peters, J. W., and Hegg, E. L. (2011) Mechanism of proton transfer in [FeFe]-hydrogenase from *Clostridium pasteurianum*, *J. Biol. Chem. 286*, 38341–38347.
1100. Senger, M., Eichmann, V., Laun, K., Duan, J., Wittkamp, F., Knor, G., Apfel, U. P., Happe, T., Winkler, M., Heberle, J., and Stripp, S. T. (2019) How [FeFe]-hydrogenase facilitates bidirectional proton transfer, *J. Am. Chem. Soc. 141*, 17394–17403.
1101. Kow, R. L., Whicher, J. R., McDonald, C. A., Palfey, B. A., and Fagan, R. L. (2009) Disruption of the proton relay network in the class 2 dihydroorotate dehydrogenase from *Escherichia coli*, *Biochemistry 48*, 9801–9809.
1102. Haouz, A., Vanheusden, V., Munier-Lehmann, H., Froeyen, M., Herdewijn, P., Van Calenbergh, S., and Delarue, M. (2003) Enzymatic and structural analysis of inhibitors designed against *Mycobacterium tuberculosis* thymi-

dylate kinase. New insights into the phosphoryl transfer mechanism, *J. Biol. Chem. 278*, 4963–4971.
1103. Kubota, K., Nagata, K., Okai, M., Miyazono, K., Soemphol, W., Ohtsuka, J., Yamamura, A., Saichana, N., Toyama, H., Matsushita, K., and Tanokura, M. (2011) The crystal structure of L-sorbose reductase from *Gluconobacter frateurii* complexed with NADPH and L-sorbose, *J. Mol. Biol. 407*, 543–555.
1104. Gonzalez-Segura, L., Rudino-Pinera, E., Munoz-Clares, R. A., and Horjales, E. (2009) The crystal structure of a ternary complex of betaine aldehyde dehydrogenase from *Pseudomonas aeruginosa* provides new insight into the reaction mechanism and shows a novel binding mode of the 2′-phosphate of $NADP^+$ and a novel cation binding site, *J. Mol. Biol. 385*, 542–557.
1105. Ellis, M. J., Prudencio, M., Dodd, F. E., Strange, R. W., Sawers, G., Eady, R. R., and Hasnain, S. S. (2002) Biochemical and crystallographic studies of the Met144Ala, Asp92Asn and His254Phe mutants of the nitrite reductase from *Alcaligenes xylosoxidans* provide insight into the enzyme mechanism, *J. Mol. Biol. 316*, 51–64.
1106. Dobson, R. C., Valegard, K., and Gerrard, J. A. (2004) The crystal structure of three site-directed mutants of *Escherichia coli* dihydrodipicolinate synthase: Further evidence for a catalytic triad, *J. Mol. Biol. 338*, 329–339.
1107. Bogomolni, R. A., Baker, R. A., Lozier, R. H., and Stoeckenius, W. (1980) Action spectrum and quantum efficiency for proton pumping in *Halobacterium halobium*, *Biochemistry 19*, 2152–2159.
1108. Grigorieff, N., Ceska, T. A., Downing, K. H., Baldwin, J. M., and Henderson, R. (1996) Electron-crystallographic refinement of the structure of bacteriorhodopsin, *J. Mol. Biol. 259*, 393–421.
1109. Pebay-Peyroula, E., Rummel, G., Rosenbusch, J. P., and Landau, E. M. (1997) X-Ray structure of bacteriorhodopsin at 2.5 Å from microcrystals grown in lipidic cubic phases, *Science 277*, 1676–1681.
1110. Schobert, B., Brown, L. S., and Lanyi, J. K. (2003) Crystallographic structures of the M and N intermediates of bacteriorhodopsin: Assembly of a hydrogen-bonded chain of water molecules between Asp-96 and the retinal Schiff base, *J. Mol. Biol. 330*, 553–570.
1111. Gerwert, K., Hess, B., Soppa, J., and Oesterhelt, D. (1989) Role of aspartate-96 in proton translocation by bacteriorhodopsin, *Proc. Natl. Acad. Sci. U. S. A. 86*, 4943–4947.
1112. Marinetti, T., Subramaniam, S., Mogi, T., Marti, T., and Khorana, H. G. (1989) Replacement of aspartic residues 85, 96, 115, or 212 affects the quantum yield and kinetics of proton release and uptake by bacteriorhodopsin, *Proc. Natl. Acad. Sci. U. S. A. 86*, 529–533.
1113. Belrhali, H., Nollert, P., Royant, A., Menzel, C., Rosenbusch, J. P., Landau, E. M., and Pebay-Peyroula, E. (1999) Protein, lipid and water organization in bacteriorhodopsin crystals: A molecular view of the purple membrane at 1.9 Å resolution, *Structure 7*, 909–917.
1114. Lanyi, J. K., and Schobert, B. (2007) Structural changes in the L photointermediate of bacteriorhodopsin, *J. Mol. Biol. 365*, 1379–1392.
1115. Lanyi, J. K., and Schobert, B. (2003) Mechanism of proton transport in bacteriorhodopsin from crystallographic structures of the K, L, M1, M2, and M2′ intermediates of the photocycle, *J. Mol. Biol. 328*, 439–450.
1116. Otto, H., Marti, T., Holz, M., Mogi, T., Stern, L. J., Engel, F., Khorana, H. G., and Heyn, M. P. (1990) Substitution of amino acids Asp-85, Asp-212, and Arg-82 in bacteriorhodopsin affects the proton release phase of the pump and the p*K* of the Schiff base, *Proc. Natl. Acad. Sci. U. S. A. 87*, 1018–1022.
1117. de Grotthuss, C. J. T. (1806) Sur la décomposition do l'eau et des corps qu'ell tient en dissolution à l'aide de l'électricité galvanique, *Ann. Chim. 58*, 54–73.
1118. Efimov, I., Badyal, S. K., Metcalfe, C. L., Macdonald, I., Gumiero, A., Raven, E. L., and Moody, P. C. (2011) Proton delivery to ferryl heme in a heme peroxidase: Enzymatic use of the Grotthuss mechanism, *J. Am. Chem. Soc. 133*, 15376–15383.
1119. Stoyanov, E. S., Stoyanova, I. V., Tham, F. S., and Reed, C. A. (2009) H_{aq}^+ Structures in proton wires inside nanotubes, *J. Am. Chem. Soc. 131*, 17540–17541.
1120. Raghavender, U. S., Aravinda, S., Shamala, N., Kantharaju, Rai, R., and Balaram, P. (2009) Characterization of water wires inside hydrophobic tubular peptide structures, *J. Am. Chem. Soc. 131*, 15130–15132.

1121. Pomes, R., and Roux, B. (1998) Free energy profiles for H^+ conduction along hydrogen-bonded chains of water molecules, *Biophys. J. 75*, 33–40.
1122. Brewer, M. L., Schmitt, U. W., and Voth, G. A. (2001) The formation and dynamics of proton wires in channel environments, *Biophys. J. 80*, 1691–1702.
1123. Scolnick, L. R., and Christianson, D. W. (1996) X-Ray crystallographic studies of alanine-65 variants of carbonic anhydrase II reveal the structural basis of compromised proton transfer in catalysis, *Biochemistry 35*, 16429–16434.
1124. Adelroth, P., Paddock, M. L., Tehrani, A., Beatty, J. T., Feher, G., and Okamura, M. Y. (2001) Identification of the proton pathway in bacterial reaction centers: Decrease of proton transfer rate by mutation of surface histidines at H126 and H128 and chemical rescue by imidazole identifies the initial proton donors, *Biochemistry 40*, 14538–14546.
1125. Inoue, J., Tomioka, N., Itai, A., and Harayama, S. (1998) Proton transfer in benzyl alcohol dehydrogenase during catalysis: Alternate proton-relay routes, *Biochemistry 37*, 3305–3311.
1126. Lombard, M., Houee-Levin, C., Touati, D., Fontecave, M., and Niviere, V. (2001) Superoxide reductase from *Desulfoarculus baarsii*: Reaction mechanism and role of glutamate 47 and lysine 48 in catalysis, *Biochemistry 40*, 5032–5040.
1127. Eigen, M., and Hammes, G. G. (1963) Elementary steps in enzyme reactions (as studied by relaxation spectrometry), *Adv. Enzymol. Relat. Areas Mol. Biol. 25*, 1–38.
1128. Hammes, G. G., and Schimmel, P. (1970) Rapid reactions and transient states, In *The enzymes, volume II* (Boyer, P. D., Ed.) Third Edition, pp 67–114, Academic Press, New York.
1129. Rocek, J., Westheimer, F. H., Eschenmoser, A., Moldovanyi, L., and Schreiber, J. (1962) Chromic acid esters as intermediates in the oxidation of alcohols. Rate-limiting esterification of a sterically hindered alcohol, *Helv. Chim. Acta 45*, 2554–2567.
1130. Gollop, N., Damri, B., Barak, Z., and Chipman, D. M. (1989) Kinetics and mechanism of acetohydroxy acid synthase isozyme III from *Escherichia coli*, *Biochemistry 28*, 6310–6317.
1131. Albery, W. J., and Knowles, J. R. (1976) Evolution of enzyme function and the development of catalytic efficiency, *Biochemistry 15*, 5631–5640.
1132. Lively, C. R., Feinberg, B. A., and McFarland, J. T. (1987) Electrostatic effect upon association of reduced nicotinamide adenine dinucleotide and equine liver alcohol dehydrogenase, *Biochemistry 26*, 5719–5725.
1133. Imoto, K., Busch, C., Sakmann, B., Mishina, M., Konno, T., Nakai, J., Bujo, H., Mori, Y., Fukuda, K., and Numa, S. (1988) Rings of negatively charged amino acids determine the acetylcholine receptor channel conductance, *Nature 335*, 645–648.
1134. Sakurai, T. (1992) Kinetics of electron transfer between cytochrome *c* and laccase, *Biochemistry 31*, 9844–9847.
1135. Medina, M., Gomez-Moreno, C., and Tollin, G. (1992) Effects of chemical modification of *Anabaena* flavodoxin and ferredoxin-$NADP^+$ reductase on the kinetics of interprotein electron transfer reactions, *Eur. J. Biochem. 210*, 577–583.
1136. Eltis, L. D., Herbert, R. G., Barker, P. D., Mauk, A. G., and Northrup, S. H. (1991) Reduction of horse heart ferricytochrome *c* by bovine liver ferrocytochrome b_5. Experimental and theoretical analysis, *Biochemistry 30*, 3663–3674.
1137. Peterson, K. L., Galitz, D. S., and Srivastava, D. K. (1998) Influence of excision of a methylene group from Glu-376 (Glu376→Asp mutation) in the medium chain acyl-CoA dehydrogenase-catalyzed reaction, *Biochemistry 37*, 1697–1705.
1138. Fan, F., and Plapp, B. V. (1995) Substitutions of isoleucine residues at the adenine binding site activate horse liver alcohol dehydrogenase, *Biochemistry 34*, 4709–4713.
1139. Flint, D. H., and McKay, R. G. (1994) *Escherichia coli* fumarase A catalyzed transfer of ^{18}O from C-2 and ^{2}H from C-3 of malate to acetylene dicarboxylate to form ^{18}O and ^{2}H labeled oxalacetate, *J. Am. Chem. Soc. 116*, 5534–5539.
1140. Johnson, W. W., Liu, S., Ji, X., Gilliland, G. L., and Armstrong, R. N. (1993) Tyrosine 115 participates both in chemical and physical steps of the catalytic mechanism of a glutathione *S*-transferase, *J. Biol. Chem. 268*, 11508–11511.

1141. Codreanu, S. G., Ladner, J. E., Xiao, G., Stourman, N. V., Hachey, D. L., Gilliland, G. L., and Armstrong, R. N. (2002) Local protein dynamics and catalysis: Detection of segmental motion associated with rate-limiting product release by a glutathione transferase, *Biochemistry 41*, 15161–15172.
1142. Whited, C. A., Warren, J. J., Lavoie, K. D., Weinert, E. E., Agapie, T., Winkler, J. R., and Gray, H. B. (2012) Gating NO release from nitric oxide synthase, *J. Am. Chem. Soc. 134*, 27–30.
1143. Brouwer, A. C., and Kirsch, J. F. (1982) Investigation of diffusion-limited rates of chymotrypsin reactions by viscosity variation, *Biochemistry 21*, 1302–1307.
1144. Simopoulos, T. T., and Jencks, W. P. (1994) Alkaline phosphatase is an almost perfect enzyme, *Biochemistry 33*, 10375–10380.
1145. Caldwell, S. R., Newcomb, J. R., Schlecht, K. A., and Raushel, F. M. (1991) Limits of diffusion in the hydrolysis of substrates by the phosphotriesterase from *Pseudomonas diminuta*, *Biochemistry 30*, 7438–7444.
1146. Wood, B. M., Chan, K. K., Amyes, T. L., Richard, J. P., and Gerlt, J. A. (2009) Mechanism of the orotidine 5′-monophosphate decarboxylase-catalyzed reaction: Effect of solvent viscosity on kinetic constants, *Biochemistry 48*, 5510–5517.
1147. St Maurice, M., and Bearne, S. L. (2002) Kinetics and thermodynamics of mandelate racemase catalysis, *Biochemistry 41*, 4048–4058.
1148. Adams, J. A., McGlone, M. L., Gibson, R., and Taylor, S. S. (1995) Phosphorylation modulates catalytic function and regulation in the cAMP-dependent protein kinase, *Biochemistry 34*, 2447–2454.
1149. Adams, J. A., and Taylor, S. S. (1992) Energetic limits of phosphotransfer in the catalytic subunit of cAMP-dependent protein kinase as measured by viscosity experiments, *Biochemistry 31*, 8516–8522.
1150. Guha, M. K., Vander Jagt, D. L., and Creighton, D. J. (1988) Diffusion-dependent rates for the hydrolysis reaction catalyzed by glyoxalase II from rat erythrocytes, *Biochemistry 27*, 8818–8822.
1151. Sampson, N. S., and Knowles, J. R. (1992) Segmental motion in catalysis: Investigation of a hydrogen bond critical for loop closure in the reaction of triosephosphate isomerase, *Biochemistry 31*, 8488–8494.
1152. Taylor, J. C., Takusagawa, F., and Markham, G. D. (2002) The active site loop of *S*-adenosylmethionine synthetase modulates catalytic efficiency, *Biochemistry 41*, 9358–9369.
1153. Pocker, Y., and Janjic, N. (1988) Origin of viscosity effects in carbonic anhydrase catalysis. Kinetic studies with bulky buffers at limiting concentrations, *Biochemistry 27*, 4114–4120.
1154. Scopes, R. K. (1978) Binding of substrates and other anions to yeast phosphoglycerate kinase, *Eur. J. Biochem. 91*, 119–129.
1155. Freitag, S., Chu, V., Penzotti, J. E., Klumb, L. A., To, R., Hyre, D., Le Trong, I., Lybrand, T. P., Stenkamp, R. E., and Stayton, P. S. (1999) A structural snapshot of an intermediate on the streptavidin-biotin dissociation pathway, *Proc. Natl. Acad. Sci. U. S. A. 96*, 8384–8389.
1156. Scopes, R. K. (1978) The steady-state kinetics of yeast phosphoglycerate kinase. Anomalous kinetic plots and the effects of salts on activity, *Eur. J. Biochem. 85*, 503–516.
1157. Harlos, K., Vas, M., and Blake, C. F. (1992) Crystal structure of the binary complex of pig muscle phosphoglycerate kinase and its substrate 3-phospho-D-glycerate, *Proteins 12*, 133–144.
1158. McPhillips, T. M., Hsu, B. T., Sherman, M. A., Mas, M. T., and Rees, D. C. (1996) Structure of the r65q mutant of yeast 3-phosphoglycerate kinase complexed with Mg-AMP-PNP and 3-phospho-D-glycerate, *Biochemistry 35*, 4118–4127.
1159. Zerrad, L., Merli, A., Schroder, G. F., Varga, A., Graczer, E., Pernot, P., Round, A., Vas, M., and Bowler, M. W. (2011) A spring-loaded release mechanism regulates domain movement and catalysis in phosphoglycerate kinase, *J. Biol. Chem. 286*, 14040–14048.
1160. Moczydlowski, E. G., and Fortes, P. A. (1981) Characterization of 2′,3′-*O*-(2,4,6-trinitrocyclohexadienylidine)adenosine 5′-triphosphate as a fluorescent probe of the ATP site of sodium and potassium transport adenosine triphosphatase. Determination of nucleotide binding stoichiometry and ion-induced changes in affinity for ATP, *J. Biol. Chem. 256*, 2346–2356.
1161. Appleman, J. R., Beard, W. A., Delcamp, T. J., Prendergast, N. J., Freisheim, J. H., and Blakley, R. L. (1990) Unusual transient- and steady-state kinetic behavior is predicted by

the kinetic scheme operational for recombinant human dihydrofolate reductase, *J. Biol. Chem. 265*, 2740–2748.

1162. Oyen, D., Fenwick, R. B., Stanfield, R. L., Dyson, H. J., and Wright, P. E. (2015) Cofactor-mediated conformational dynamics promote product release from *Escherichia coli* dihydrofolate reductase via an allosteric pathway, *J. Am. Chem. Soc. 137*, 9459–9468.
1163. Oyen, D., Fenwick, R. B., Aoto, P. C., Stanfield, R. L., Wilson, I. A., Dyson, H. J., and Wright, P. E. (2017) Defining the structural basis for allosteric product release from *E. coli* dihydrofolate reductase using NMR relaxation dispersion, *J. Am. Chem. Soc. 139*, 11233–11240.
1164. Czekster, C. M., Vandemeulebroucke, A., and Blanchard, J. S. (2011) Two parallel pathways in the kinetic sequence of the dihydrofolate reductase from *Mycobacterium tuberculosis*, *Biochemistry 50*, 7045–7056.
1165. Tsay, J. T., Appleman, J. R., Beard, W. A., Prendergast, N. J., Delcamp, T. J., Freisheim, J. H., and Blakley, R. L. (1990) Kinetic investigation of the functional role of phenylalanine-31 of recombinant human dihydrofolate reductase, *Biochemistry 29*, 6428–6436.
1166. Murphy, D. J., and Benkovic, S. J. (1989) Hydrophobic interactions via mutants of *Escherichia coli* dihydrofolate reductase: Separation of binding and catalysis, *Biochemistry 28*, 3025–3031.
1167. Rose, I. A., and O'Connell, E. L. (1967) Mechanism of aconitase action: I. The hydrogen transfer reaction, *J. Biol. Chem. 242*, 1870–1879.
1168. Schloss, J. V., Emptage, M. H., and Cleland, W. W. (1984) pH Profiles and isotope effects for aconitases from *Saccharomycopsis lipolytica*, beef heart, and beef liver: α-Methyl-*cis*-aconitate and *threo*-D_s-α-methylisocitrate as substrates, *Biochemistry 23*, 4572–4580.
1169. Furfine, E. S., Leban, J. J., Landavazo, A., Moomaw, J. F., and Casey, P. J. (1995) Protein farnesyltransferase: Kinetics of farnesyl pyrophosphate binding and product release, *Biochemistry 34*, 6857–6862.
1170. Li, M., Phylip, L. H., Lees, W. E., Winther, J. R., Dunn, B. M., Wlodawer, A., Kay, J., and Gustchina, A. (2000) The aspartic proteinase from *Saccharomyces cerevisiae* folds its own inhibitor into α helix, *Nature Struct. Biol. 7*, 113–117.
1171. Sundararaju, B., Antson, A. A., Phillips, R. S., Demidkina, T. V., Barbolina, M. V., Gollnick, P., Dodson, G. G., and Wilson, K. S. (1997) The crystal structure of *Citrobacter freundii* tyrosine phenol-lyase complexed with 3-(4′-hydroxyphenyl)propionic acid, together with site-directed mutagenesis and kinetic analysis, demonstrates that arginine 381 is required for substrate specificity, *Biochemistry 36*, 6502–6510.
1172. Britton, H. G., and Clarke, J. B. (1968) The mechanism of the phosphoglucomutase reaction. Studies on rabbit muscle phosphoglucomutase with flux techniques, *Biochem. J. 110*, 161–180.
1173. Britton, H. G., and Clarke, J. B. (1972) Mechanism of the 2,3-diphosphoglycerate-dependent phosphoglycerate mutase from rabbit muscle, *Biochem. J. 130*, 397–410.
1174. Raines, R. T., and Knowles, J. R. (1987) Enzyme relaxation in the reaction catalyzed by triosephosphate isomerase: Detection and kinetic characterization of two unliganded forms of the enzyme, *Biochemistry 26*, 7014–7020.
1175. Fisher, L. M., Albery, W. J., and Knowles, J. R. (1986) Energetics of proline racemase: Racemization of unlabeled proline in the unsaturated, saturated, and oversaturated regimes, *Biochemistry 25*, 2529–2537.
1176. Rose, I. A. (1998) How fumarase recycles after the malate→fumarate reaction. Insights into the reaction mechanism, *Biochemistry 37*, 17651–17658.
1177. Britton, H. G. (1966) The concept and use of flux measurements in enzyme studies: A theoretical analysis, *Arch. Biochem. Biophys. 117*, 167–183.
1178. Sui, X., Wang, K., Gluchowski, N. L., Elliott, S. D., Liao, M., Walther, T. C., and Farese, R. V., Jr. (2020) Structure and catalytic mechanism of a human triacylglycerol-synthesis enzyme, *Nature 581*, 323–328.
1179. Qian, H., Zhao, X., Yan, R., Yao, X., Gao, S., Sun, X., Du, X., Yang, H., Wong, C. C. L., and Yan, N. (2020) Structural basis for catalysis and substrate specificity of human ACAT1, *Nature 581*, 333–338.
1180. Sarda, L., and Desnuelle, P. (1958) Action de la lipase pancréatique sur les esters en émulsion, *Biochim. Biophys. Acta 30*, 513–521.
1181. Pieterson, W. A., Vidal, J. C., Volwerk, J. J., and de Haas, G. H. (1974) Zymogen-catalyzed

hydrolysis of monomeric substrates and the presence of a recognition site for lipid-water interfaces in phospholipase A_2, *Biochemistry 13*, 1455–1460.
1182. Dennis, E. A. (1973) Kinetic dependence of phospholipase A_2 activity on the detergent Triton X-100, *J. Lipid Res. 14*, 152–159.
1183. Verger, R., Mieras, M. C., and de Haas, G. H. (1973) Action of phospholipase A at interfaces, *J. Biol. Chem. 248*, 4023–4034.
1184. Scott, D. L., White, S. P., Otwinowski, Z., Yuan, W., Gelb, M. H., and Sigler, P. B. (1990) Interfacial catalysis: The mechanism of phospholipase A_2, *Science 250*, 1541–1546.
1185. Cao, J., Hsu, Y. H., Li, S., Woods, V. L., and Dennis, E. A. (2011) Lipoprotein-associated phospholipase A_2 interacts with phospholipid vesicles via a surface-disposed hydrophobic α-helix, *Biochemistry 50*, 5314–5321.
1186. Brzozowski, A. M., Derewenda, U., Derewenda, Z. S., Dodson, G. G., Lawson, D. M., Turkenburg, J. P., Bjorkling, F., Huge-Jensen, B., Patkar, S. A., and Thim, L. (1991) A model for interfacial activation in lipases from the structure of a fungal lipase-inhibitor complex, *Nature 351*, 491–494.
1187. Xiong, Z. J., Huang, J., Poda, G., Pomes, R., and Prive, G. G. (2016) Structure of human acid sphingomyelinase reveals the role of the saposin domain in activating substrate hydrolysis, *J. Mol. Biol. 428*, 3026–3042.
1188. Ghomashchi, F., Yu, B. Z., Berg, O., Jain, M. K., and Gelb, M. H. (1991) Interfacial catalysis by phospholipase A_2: Substrate specificity in vesicles, *Biochemistry 30*, 7318–7329.
1189. de Haas, G. H., Bonsen, P. P., Pieterson, W. A., and van Deenen, L. L. (1971) Studies on phospholipase A and its zymogen from porcine pancreas: 3. Action of the enzyme on short-chain lecithins, *Biochim. Biophys. Acta 239*, 252–266.
1190. Dennis, E. A. (1973) Phospholipase A_2 activity towards phosphatidylcholine in mixed micelles: Surface dilution kinetics and the effect of thermotropic phase transitions, *Arch. Biochem. Biophys. 158*, 485–493.
1191. Deems, R. A., Eaton, B. R., and Dennis, E. A. (1975) Kinetic analysis of phospholipase A_2 activity toward mixed micelles and its implications for the study of lipolytic enzymes, *J. Biol. Chem. 250*, 9013–9020.
1192. Lin, Y. P., and Carman, G. M. (1990) Kinetic analysis of yeast phosphatidate phosphatase toward Triton X-100/phosphatidate mixed micelles, *J. Biol. Chem. 265*, 166–170.
1193. Jain, M. K., Rogers, J., Jahagirdar, D. V., Marecek, J. F., and Ramirez, F. (1986) Kinetics of interfacial catalysis by phospholipase A_2 in intravesicle scooting mode, and heterofusion of anionic and zwitterionic vesicles, *Biochim. Biophys. Acta 860*, 435–447.
1194. Jain, M. K., DeHaas, G. H., Marecek, J. F., and Ramirez, F. (1986) The affinity of phospholipase A_2 for the interface of the substrate and analogs, *Biochim. Biophys. Acta 860*, 475–483.
1195. Nakamura, A., Tasaki, T., Ishiwata, D., Yamamoto, M., Okuni, Y., Visootsat, A., Maximilien, M., Noji, H., Uchiyama, T., Samejima, M., Igarashi, K., and Iino, R. (2016) Single-molecule imaging analysis of binding, processive movement, and dissociation of cellobiohydrolase *Trichoderma reesei* Cel6A and its domains on crystalline cellulose, *J. Biol. Chem. 291*, 22404–22413.
1196. Kyte, J. (2007) *Structure in protein chemistry: Second edition*, pp 503–506, Garland Science, New York.
1197. Saffarian, S., Collier, I. E., Marmer, B. L., Elson, E. L., and Goldberg, G. (2004) Interstitial collagenase is a Brownian ratchet driven by proteolysis of collagen, *Science 306*, 108–111.
1198. Berg, O. G., Winter, R. B., and von Hippel, P. H. (1981) Diffusion-driven mechanisms of protein translocation on nucleic acids. 1. Models and theory, *Biochemistry 20*, 6929–6948.
1199. Winter, R. B., Berg, O. G., and von Hippel, P. H. (1981) Diffusion-driven mechanisms of protein translocation on nucleic acids. 3. The *Escherichia coli* lac repressor--operator interaction: Kinetic measurements and conclusions, *Biochemistry 20*, 6961–6977.
1200. Nardone, G., George, J., and Chirikjian, J. G. (1986) Differences in the kinetic properties of BamHI endonuclease and methylase with linear DNA substrates, *J. Biol. Chem. 261*, 12128–12133.
1201. Dowd, D. R., and Lloyd, R. S. (1990) Biological significance of facilitated diffusion in protein-DNA interactions. Applications to T4 endonuclease V-initiated DNA repair, *J. Biol. Chem. 265*, 3424–3431.
1202. Surby, M. A., and Reich, N. O. (1996) Contribution of facilitated diffusion and processive catalysis to enzyme efficiency: Implications

for the EcoRI restriction-modification system, *Biochemistry 35*, 2201–2208.
1203. Surby, M. A., and Reich, N. O. (1996) Facilitated diffusion of the EcoRI DNA methyltransferase is described by a novel mechamechanism, *Biochemistry 35*, 2209–2217.
1204. Herendeen, D. R., Kassavetis, G. A., and Geiduschek, E. P. (1992) A transcriptional enhancer whose function imposes a requirement that proteins track along DNA, *Science 256*, 1298–1303.
1205. Liu, S., Abbondanzieri, E. A., Rausch, J. W., Le Grice, S. F., and Zhuang, X. (2008) Slide into action: Dynamic shuttling of HIV reverse transcriptase on nucleic acid substrates, *Science 322*, 1092–1097.
1206. Jack, W. E., Terry, B. J., and Modrich, P. (1982) Involvement of outside DNA sequences in the major kinetic path by which EcoRI endonuclease locates and leaves its recognition sequence, *Proc. Natl. Acad. Sci. U. S. A. 79*, 4010–4014.
1207. Terry, B. J., Jack, W. E., and Modrich, P. (1985) Facilitated diffusion during catalysis by EcoRI endonuclease. Nonspecific interactions in EcoRI catalysis, *J. Biol. Chem. 260*, 13130–13137.
1208. Pollak, A. J., Chin, A. T., and Reich, N. O. (2014) Distinct facilitated diffusion mechanisms by *E. coli* type II restriction endonucleases, *Biochemistry 53*, 7028–7037.
1209. Dillingham, M. S., Wigley, D. B., and Webb, M. R. (2000) Demonstration of unidirectional single-stranded DNA translocation by PcrA helicase: Measurement of step size and translocation speed, *Biochemistry 39*, 205–212.
1210. Dillingham, M. S., Wigley, D. B., and Webb, M. R. (2002) Direct measurement of single-stranded DNA translocation by PcrA helicase using the fluorescent base analogue 2-aminopurine, *Biochemistry 41*, 643–651.
1211. Tomko, E. J., Fischer, C. J., and Lohman, T. M. (2012) Single-stranded DNA translocation of *E. coli* UvrD monomer is tightly coupled to ATP hydrolysis, *J. Mol. Biol. 418*, 32–46.
1212. Fischer, C. J., Maluf, N. K., and Lohman, T. M. (2004) Mechanism of ATP-dependent translocation of *E. coli* UvrD monomers along single-stranded DNA, *J. Mol. Biol. 344*, 1287–1309.
1213. Wang, C., Lee, T. R., Lawrence, D. S., and Adams, J. A. (1996) Rate-determining steps for tyrosine phosphorylation by the kinase domain of v-fps, *Biochemistry 35*, 1533–1539.
1214. Athappilly, F. K., and Hendrickson, W. A. (1995) Structure of the biotinyl domain of acetyl-coenzyme A carboxylase determined by MAD phasing, *Structure 3*, 1407–1419.
1215. Roberts, E. L., Shu, N., Howard, M. J., Broadhurst, R. W., Chapman-Smith, A., Wallace, J. C., Morris, T., Cronan, J. E., Jr., and Perham, R. N. (1999) Solution structures of apo and holo biotinyl domains from acetyl coenzyme A carboxylase of *Escherichia coli* determined by triple-resonance nuclear magnetic resonance spectroscopy, *Biochemistry 38*, 5045–5053.
1216. Sutton, M. R., Fall, R. R., Nervi, A. M., Alberts, A. W., Vagelos, P. R., and Bradshaw, R. A. (1977) Amino acid sequence of *Escherichia coli* biotin carboxyl carrier protein (9100), *J. Biol. Chem. 252*, 3934–3940.
1217. Daigo, K., and Reed, L. J. (1962) The amino acid sequence around the N^{ε}-lipoyllysine residue in α-oxo acid dehydrogenation complexes, *J. Am. Chem. Soc. 84*, 666–671.
1218. Reddy, D. V., Rothemund, S., Shenoy, B. C., Carey, P. R., and Sonnichsen, F. D. (1998) Structural characterization of the entire 1.3S subunit of transcarboxylase from *Propionibacterium shermanii*, *Prot. Sci. 7*, 2156–2163.
1219. St Maurice, M., Reinhardt, L., Surinya, K. H., Attwood, P. V., Wallace, J. C., Cleland, W. W., and Rayment, I. (2007) Domain architecture of pyruvate carboxylase, a biotin-dependent multifunctional enzyme, *Science 317*, 1076–1079.
1220. Reed, L. J. (1974) Multienzyme complexes, *Accounts Chem. Res. 7*, 40–46.
1221. Kyte, J. (2007) *Structure in protein chemistry: Second edition*, pp 486–488, Garland Science, New York.
1222. Skerlova, J., Berndtsson, J., Nolte, H., Ott, M., and Stenmark, P. (2021) Structure of the native pyruvate dehydrogenase complex reveals the mechanism of substrate insertion, *Nat Commun 12*, 5277.
1223. Stephens, P. E., Darlison, M. G., Lewis, H. M., and Guest, J. R. (1983) The pyruvate dehydrogenase complex of *Escherichia coli* K12. Nucleotide sequence encoding the dihydrolipoamide acetyltransferase component, *Eur. J. Biochem. 133*, 481–489.
1224. Ricaud, P. M., Howard, M. J., Roberts, E. L., Broadhurst, R. W., and Perham, R. N. (1996)

Three-dimensional structure of the lipoyl domain from the dihydrolipoyl succinyltransferase component of the 2-oxoglutarate dehydrogenase multienzyme complex of *Escherichia coli*, *J. Mol. Biol. 264*, 179–190.
1225. Green, J. D., Laue, E. D., Perham, R. N., Ali, S. T., and Guest, J. R. (1995) Three-dimensional structure of a lipoyl domain from the dihydrolipoyl acetyltransferase component of the pyruvate dehydrogenase multienzyme complex of *Escherichia coli*, *J. Mol. Biol. 248*, 328–343.
1226. Mande, S. S., Sarfaty, S., Allen, M. D., Perham, R. N., and Hol, W. G. (1996) Protein-protein interactions in the pyruvate dehydrogenase multienzyme complex: Dihydrolipoamide dehydrogenase complexed with the binding domain of dihydrolipoamide acetyltransferase, *Structure 4*, 277–286.
1227. Koike, M., Reed, L. J., and Carroll, W. R. (1963) α-Keto acid dehydrogenation complexes. IV. Resolution and reconstitution of the *Escherichia coli* pyruvate dehydrogenation complex, *J. Biol. Chem. 238*, 30–39.
1228. Chandrasekhar, K., Wang, J., Arjunan, P., Sax, M., Park, Y. H., Nemeria, N. S., Kumaran, S., Song, J., Jordan, F., and Furey, W. (2013) Insight to the interaction of the dihydrolipoamide acetyltransferase (E2) core with the peripheral components in the *Escherichia coli* pyruvate dehydrogenase complex via multifaceted structural approaches, *J. Biol. Chem. 288*, 15402–15417.
1229. Arjunan, P., Nemeria, N., Brunskill, A., Chandrasekhar, K., Sax, M., Yan, Y., Jordan, F., Guest, J. R., and Furey, W. (2002) Structure of the pyruvate dehydrogenase multienzyme complex E1 component from *Escherichia coli* at 1.85 Å resolution, *Biochemistry 41*, 5213–5221.
1230. Bates, D. L., Danson, M. J., Hale, G., Hooper, E. A., and Perham, R. N. (1977) Self-assembly and catalytic activity of the pyruvate dehydrogenase multienzyme complex of *Escherichia coli*, *Nature 268*, 313–316.
1231. Collins, J. H., and Reed, L. J. (1977) Acyl group and electron pair relay system: A network of interacting lipoyl moieties in the pyruvate and α-ketoglutarate dehydrogenase complexes from *Escherichia coli*, *Proc. Natl. Acad. Sci. U. S. A. 74*, 4223–4227.
1232. Danson, M. J., Fersht, A. R., and Perham, R. N. (1978) Rapid intramolecular coupling of active sites in the pyruvate dehydrogenase complex of *Escherichia coli*: Mechanism for rate enhancement in a multimeric structure, *Proc. Natl. Acad. Sci. U. S. A. 75*, 5386–5390.
1233. Danson, M. J., Hooper, E. A., and Perham, R. N. (1978) Intramolecular coupling of active sites in the pyruvate dehydrogenase multienzyme complex of *Escherichia coli*, *Biochem. J. 175*, 193–198.
1234. Miles, J. S., Guest, J. R., Radford, S. E., and Perham, R. N. (1988) Investigation of the mechanism of active site coupling in the pyruvate dehydrogenase multienzyme complex of *Escherichia coli* by protein engineering, *J. Mol. Biol. 202*, 97–106.
1235. Holzer, K. P., Liu, W., and Hammes, G. G. (1989) Molecular cloning and sequencing of chicken liver fatty acid synthase cDNA, *Proc. Natl. Acad. Sci. U. S. A. 86*, 4387–4391.
1236. Amy, C. M., Witkowski, A., Naggert, J., Williams, B., Randhawa, Z., and Smith, S. (1989) Molecular cloning and sequencing of cDNAs encoding the entire rat fatty acid synthase, *Proc. Natl. Acad. Sci. U. S. A. 86*, 3114–3118.
1237. Wakil, S. J. (1989) Fatty acid synthase, a proficient multifunctional enzyme, *Biochemistry 28*, 4523–4530.
1238. Ploskon, E., Arthur, C. J., Evans, S. E., Williams, C., Crosby, J., Simpson, T. J., and Crump, M. P. (2008) A mammalian type I fatty acid synthase acyl carrier protein domain does not sequester acyl chains, *J. Biol. Chem. 283*, 518–528.
1239. Bunkoczi, G., Pasta, S., Joshi, A., Wu, X., Kavanagh, K. L., Smith, S., and Oppermann, U. (2007) Mechanism and substrate recognition of human holo ACP synthase, *Chem. Biol. 14*, 1243–1253.
1240. Maier, T., Leibundgut, M., and Ban, N. (2008) The crystal structure of a mammalian fatty acid synthase, *Science 321*, 1315–1322.
1241. Chakravarty, B., Gu, Z., Chirala, S. S., Wakil, S. J., and Quiocho, F. A. (2004) Human fatty acid synthase: Structure and substrate selectivity of the thioesterase domain, *Proc. Natl. Acad. Sci. U. S. A. 101*, 15567–15572.
1242. Pemble, C. W. t., Johnson, L. C., Kridel, S. J., and Lowther, W. T. (2007) Crystal structure of the thioesterase domain of human fatty acid synthase inhibited by Orlistat, *Nature Struct. Biol. 14*, 704–709.
1243. Witkowski, A., Joshi, A. K., and Smith, S. (1997) Characterization of the interthiol acyl-

transferase reaction catalyzed by the β-ketoacyl synthase domain of the animal fatty acid synthase, *Biochemistry 36*, 16338–16344.
1244. Gipson, P., Mills, D. J., Wouts, R., Grininger, M., Vonck, J., and Kuhlbrandt, W. (2010) Direct structural insight into the substrate-shuttling mechanism of yeast fatty acid synthase by electron cryomicroscopy, *Proc. Natl. Acad. Sci. U. S. A. 107*, 9164–9169.
1245. Qiu, S., Liu, S., Zaoti, Z. F., Wang, X., and Cai, G. (2019) Modulation of fatty acid synthase by ATR checkpoint kinase Rad3, *J. Mol. Cell Biol. 11*, 1098–1100.
1246. Lomakin, I. B., Xiong, Y., and Steitz, T. A. (2007) The crystal structure of yeast fatty acid synthase, a cellular machine with eight active sites working together, *Cell 129*, 319–332.
1247. Herzberg, O., Chen, C. C., Kapadia, G., McGuire, M., Carroll, L. J., Noh, S. J., and Dunaway-Mariano, D. (1996) Swiveling-domain mechanism for enzymatic phosphotransfer between remote reaction sites, *Proc. Natl. Acad. Sci. U. S. A. 93*, 2652–2657.
1248. Nakanishi, T., Nakatsu, T., Matsuoka, M., Sakata, K., and Kato, H. (2005) Crystal structures of pyruvate phosphate dikinase from maize revealed an alternative conformation in the swiveling-domain motion, *Biochemistry 44*, 1136–1144.
1249. Lim, K., Read, R. J., Chen, C. C., Tempczyk, A., Wei, M., Ye, D., Wu, C., Dunaway-Mariano, D., and Herzberg, O. (2007) Swiveling domain mechanism in pyruvate phosphate dikinase, *Biochemistry 46*, 14845–14853.
1250. Xu, Y., McGuire, M., Dunaway-Mariano, D., and Martin, B. M. (1995) Separate site catalysis by pyruvate phosphate dikinase as revealed by deletion mutants, *Biochemistry 34*, 2195–2202.
1251. Drennan, C. L., Huang, S., Drummond, J. T., Matthews, R. G., and Lidwig, M. L. (1994) How a protein binds B_{12}: A 3.0 Å X-ray structure of B_{12}-binding domains of methionine synthase, *Science 266*, 1669–1674.
1252. Evans, J. C., Huddler, D. P., Hilgers, M. T., Romanchuk, G., Matthews, R. G., and Ludwig, M. L. (2004) Structures of the N-terminal modules imply large domain motions during catalysis by methionine synthase, *Proc. Natl. Acad. Sci. U. S. A. 101*, 3729–3736.
1253. Datta, S., Koutmos, M., Pattridge, K. A., Ludwig, M. L., and Matthews, R. G. (2008) A disulfide-stabilized conformer of methionine synthase reveals an unexpected role for the histidine ligand of the cobalamin cofactor, *Proc. Natl. Acad. Sci. U. S. A. 105*, 4115–4120.
1254. Goulding, C. W., Postigo, D., and Matthews, R. G. (1997) Cobalamin-dependent methionine synthase is a modular protein with distinct regions for binding homocysteine, methyltetrahydrofolate, cobalamin, and adenosylmethionine, *Biochemistry 36*, 8082–8091.
1255. Bandarian, V., Pattridge, K. A., Lennon, B. W., Huddler, D. P., Matthews, R. G., and Ludwig, M. L. (2002) Domain alternation switches B_{12}-dependent methionine synthase to the activation conformation, *Nature Struct. Biol. 9*, 53–56.
1256. Bandarian, V., and Matthews, R. G. (2001) Quantitation of rate enhancements attained by the binding of cobalamin to methionine synthase, *Biochemistry 40*, 5056–5064.
1257. Frasca, V., Banerjee, R. V., Dunham, W. R., Sands, R. H., and Matthews, R. G. (1988) Cobalamin-dependent methionine synthase from *Escherichia coli* B: Electron paramagnetic resonance spectra of the inactive form and the active methylated form of the enzyme, *Biochemistry 27*, 8458–8465.
1258. Banerjee, R. V., Frasca, V., Ballou, D. P., and Matthews, R. G. (1990) Participation of cob(I)alamin in the reaction catalyzed by methionine synthase from *Escherichia coli*: A steady-state and rapid reaction kinetic analysis, *Biochemistry 29*, 11101–11109.
1259. Rould, M. A., Perona, J. J., Soll, D., and Steitz, T. A. (1989) Structure of *E. coli* glutaminyl-tRNA synthetase complexed with $tRNA^{gln}$ and ATP at 2.8 Å resolution, *Science 246*, 1135–1142.
1260. Silvian, L. F., Wang, J., and Steitz, T. A. (1999) Insights into editing from an Ile-tRNA synthetase structure with $tRNA^{ile}$ and mupirocin, *Science 285*, 1074–1077.
1261. Duggleby, R. G., Sneddon, M. K., and Morrison, J. F. (1978) Chorismate mutase-prephenate dehydratase from *Escherichia coli*: Active sites of a bifunctional enzyme, *Biochemistry 17*, 1548–1554.
1262. Gething, M. J., and Davidson, B. E. (1976) Chorismate mutase/prephenate dehydratase from *Escherichia coli* K12. 2. Evidence for identical subunits catalysing the two activities, *Eur. J. Biochem. 71*, 327–336.
1263. Chiu, H. J., Abdubek, P., Astakhova, T., Axelrod, H. L., Carlton, D., Clayton, T., Das, D.,

Deller, M. C., Duan, L., Feuerhelm, J., Grant, J. C., Grzechnik, A., Han, G. W., Jaroszewski, L., Jin, K. K., Klock, H. E., Knuth, M. W., Kozbial, P., Krishna, S. S., Kumar, A., Marciano, D., McMullan, D., Miller, M. D., Morse, A. T., Nigoghossian, E., Okach, L., Reyes, R., Tien, H. J., Trame, C. B., van den Bedem, H., Weekes, D., Xu, Q., Hodgson, K. O., Wooley, J., Elsliger, M. A., Deacon, A. M., Godzik, A., Lesley, S. A., and Wilson, I. A. (2010) The structure of *Haemophilus influenzae* prephenate dehydrogenase suggests unique features of bifunctional TyrA enzymes, *Acta Crystallogr. F 66*, 1317–1325.

1264. McClard, R. W., and Shokat, K. M. (1987) Does the bifunctional uridylate synthase channel orotidine 5′-phosphate? Kinetics of orotate phosphoribosyltransferase and orotidylate decarboxylase activities fit a noninteracting sites model, *Biochemistry 26*, 3378–3384.
1265. Pereira, M. P., and Brown, E. D. (2004) Bifunctional catalysis by CDP-ribitol synthase: Convergent recruitment of reductase and cytidylyltransferase activities in *Haemophilus influenzae* and *Staphylococcus aureus*, *Biochemistry 43*, 11802–11812.
1266. Bulock, K. G., Beardsley, G. P., and Anderson, K. S. (2002) The kinetic mechanism of the human bifunctional enzyme ATIC (5-amino-4-imidazolecarboxamide ribonucleotide transformylase/inosine 5′-monophosphate cyclohydrolase). A surprising lack of substrate channeling, *J. Biol. Chem. 277*, 22168–22174.
1267. Zolli, M., Kobric, D. J., and Brown, E. D. (2001) Reduction precedes cytidylyl transfer without substrate channeling in distinct active sites of the bifunctional CDP-ribitol synthase from *Haemophilus influenzae*, *Biochemistry 40*, 5041–5048.
1268. Gehring, A. M., Lees, W. J., Mindiola, D. J., Walsh, C. T., and Brown, E. D. (1996) Acetyltransfer precedes uridylyltransfer in the formation of UDP-*N*-acetylglucosamine in separable active sites of the bifunctional GlmU protein of *Escherichia coli*, *Biochemistry 35*, 579–585.
1269. Sohl, C. D., and Guengerich, F. P. (2010) Kinetic analysis of the three-step steroid aromatase reaction of human cytochrome P450 19a1, *J. Biol. Chem. 285*, 17734–17743.
1270. Ragsdale, S. W., Clark, J. E., Ljungdahl, L. G., Lundie, L. L., and Drake, H. L. (1983) Properties of purified carbon monoxide dehydrogenase from *Clostridium thermoaceticum*, a nickel, iron–sulfur protein, *J. Biol. Chem. 258*, 2364–2369.
1271. Doukov, T. I., Blasiak, L. C., Seravalli, J., Ragsdale, S. W., and Drennan, C. L. (2008) Xenon in and at the end of the tunnel of bifunctional carbon monoxide dehydrogenase/acetyl-CoA synthase, *Biochemistry 47*, 3474–3483.
1272. Doukov, T. I., Iverson, T. M., Seravalli, J., Ragsdale, S. W., and Drennan, C. L. (2002) A Ni-Fe-Cu center in a bifunctional carbon monoxide dehydrogenase/acetyl-CoA synthase, *Science 298*, 567–572.
1273. Rudolph, J., and Stubbe, J. (1995) Investigation of the mechanism of phosphoribosylamine transfer from glutamine phosphoribosylpyrophosphate amidotransferase to glycinamide ribonucleotide synthetase, *Biochemistry 34*, 2241–2250.
1274. Maynard, E. L., and Lindahl, P. A. (1999) Evidence of a molecular tunnel connecting the active sites for CO_2 reduction and acetyl-CoA synthesis in acetyl-CoA synthase from *Clostridium thermoaceticum*, *J. Am. Chem. Soc. 121*, 9221–9222.
1275. Belkaid, M., Penverne, B., and Herve, G. (1988) In situ behavior of the pyrimidine pathway enzymes in *Saccharomyces cerevisiae*: 3. Catalytic and regulatory properties of carbamylphosphate synthetase: Channeling of carbamylphosphate to aspartate transcarbamylase, *Arch. Biochem. Biophys. 262*, 171–180.
1276. Penverne, B., Belkaid, M., and Herve, G. (1994) *In situ* behavior of the pyrimidine pathway enzymes in *Saccharomyces cerevisiae*. 4. The channeling of carbamylphosphate to aspartate transcarbamylase and its partition in the pyrimidine and arginine pathways, *Arch. Biochem. Biophys. 309*, 85–93.
1277. Mackenzie, R. E., and Baugh, C. M. (1980) Tetrahydropterolypolyglutamate derivatives as substrates of two multifunctional proteins with folate-dependent enzyme activities, *Biochim. Biophys. Acta 611*, 187–195.
1278. Paquin, J., Baugh, C. M., and MacKenzie, R. E. (1985) Channeling between the active sites of formiminotransferase-cyclodeaminase: Binding and kinetic studies, *J. Biol. Chem. 260*, 14925–14931.

1279. Srivastava, D., Schuermann, J. P., White, T. A., Krishnan, N., Sanyal, N., Hura, G. L., Tan, A., Henzl, M. T., Becker, D. F., and Tanner, J. J. (2010) Crystal structure of the bifunctional proline utilization a flavoenzyme from *Bradyrhizobium japonicum*, *Proc. Natl. Acad. Sci. U. S. A. 107*, 2878–2883.
1280. Moxley, M. A., Sanyal, N., Krishnan, N., Tanner, J. J., and Becker, D. F. (2014) Evidence for hysteretic substrate channeling in the proline dehydrogenase and Δ^1-pyrroline-5-carboxylate dehydrogenase coupled reaction of proline utilization A (PutA), *J. Biol. Chem. 289*, 3639–3651.
1281. Rakus, D., Pasek, M., Krotkiewski, H., and Dzugaj, A. (2004) Interaction between muscle aldolase and muscle fructose 1,6-bisphosphatase results in the substrate channeling, *Biochemistry 43*, 14948–14957.
1282. MacKenzie, R. E., Aldridge, M., and Paquin, J. (1980) The bifunctional enzyme formiminotransferase-cyclodeaminase is a tetramer of dimers, *J. Biol. Chem. 255*, 9474–9478.
1283. Sanyal, N., Arentson, B. W., Luo, M., Tanner, J. J., and Becker, D. F. (2015) First evidence for substrate channeling between proline catabolic enzymes: A validation of domain fusion analysis for predicting protein-protein interactions, *J. Biol. Chem. 290*, 2225–2234.
1284. Manjasetty, B. A., Powlowski, J., and Vrielink, A. (2003) Crystal structure of a bifunctional aldolase-dehydrogenase: Sequestering a reactive and volatile intermediate, *Proc. Natl. Acad. Sci. U. S. A. 100*, 6992–6997.
1285. Carere, J., McKenna, S. E., Kimber, M. S., and Seah, S. Y. (2013) Characterization of an aldolase-dehydrogenase complex from the cholesterol degradation pathway of *Mycobacterium tuberculosis*, *Biochemistry 52*, 3502–3511.
1286. Baker, P., Pan, D., Carere, J., Rossi, A., Wang, W., and Seah, S. Y. (2009) Characterization of an aldolase-dehydrogenase complex that exhibits substrate channeling in the polychlorinated biphenyls degradation pathway, *Biochemistry 48*, 6551–6558.
1287. Wang, W., Baker, P., and Seah, S. Y. (2010) Comparison of two metal-dependent pyruvate aldolases related by convergent evolution: Substrate specificity, kinetic mechanism, and substrate channeling, *Biochemistry 49*, 3774–3782.
1288. Baker, P., Hillis, C., Carere, J., and Seah, S. Y. (2012) Protein-protein interactions and substrate channeling in orthologous and chimeric aldolase-dehydrogenase complexes, *Biochemistry 51*, 1942–1952.
1289. Lu, W. P., Jablonski, P. E., Rasche, M., Ferry, J. G., and Ragsdale, S. W. (1994) Characterization of the metal centers of the Ni/Fe-S component of the carbon-monoxide dehydrogenase enzyme complex from *Methanosarcina thermophila*, *J. Biol. Chem. 269*, 9736–9742.
1290. Kumar, M., Lu, W. P., Liu, L. F., and Ragsdale, S. W. (1993) Kinetic evidence that carbon-monoxide dehydrogenase catalyzes the oxidation of carbon-monoxide and the synthesis of acetyl-CoA at separate metal centers, *J. Am. Chem. Soc. 115*, 11646–11647.
1291. Mullins, L. S., and Raushel, F. M. (1999) Channeling of ammonia through the intermolecular tunnel contained within carbamoyl phosphate synthetase, *J. Am. Chem. Soc. 121*, 3803–3804.
1292. Seravalli, J., and Ragsdale, S. W. (2000) Channeling of carbon monoxide during anaerobic carbon dioxide fixation, *Biochemistry 39*, 1274–1277.
1293. Serre, V., Guy, H., Liu, X., Penverne, B., Herve, G., and Evans, D. (1998) Allosteric regulation and substrate channeling in multifunctional pyrimidine biosynthetic complexes: Analysis of isolated domains and yeast-mammalian chimeric proteins, *J. Mol. Biol. 281*, 363–377.
1294. Darnault, C., Volbeda, A., Kim, E. J., Legrand, P., Vernede, X., Lindahl, P. A., and Fontecilla-Camps, J. C. (2003) Ni-Zn-[Fe_4-S_4] and Ni-Ni-[Fe_4-S_4] clusters in closed and open subunits of acetyl-CoA synthase/carbon monoxide dehydrogenase, *Nature Struct. Biol. 10*, 271–279.
1295. Creighton, T. E. (1970) A steady-state kinetic investigation of the reaction mechanism of the tryptophan synthetase of *Escherichia coli*, *Eur. J. Biochem. 13*, 1–10.
1296. Rhee, S., Parris, K. D., Ahmed, S. A., Miles, E. W., and Davies, D. R. (1996) Exchange of K^+ or Cs^+ for Na^+ induces local and long-range changes in the three-dimensional structure of the tryptophan synthase $\alpha_2\beta_2$ complex, *Biochemistry 35*, 4211–4221.

1297. Demoss, J. A. (1962) Studies on the mechanism of the tryptophan synthetase reaction, *Biochim. Biophys. Acta 62*, 279–293.
1298. Yanofsky, C., and Rachmeler, M. (1958) The exclusion of free indole as an intermediate in the biosynthesis of tryptophan in *Neurospora crassa*, *Biochim. Biophys. Acta 28*, 640–641.
1299. Anderson, K. S., Kim, A. Y., Quillen, J. M., Sayers, E., Yang, X. J., and Miles, E. W. (1995) Kinetic characterization of channel impaired mutants of tryptophan synthase, *J. Biol. Chem. 270*, 29936–29944.
1300. Matchett, W. H. (1974) Indole channeling by tryptophan synthase of *Neurospora*, *J. Biol. Chem. 249*, 4041–4049.
1301. Dunn, M. F., Aguilar, V., Brzovic, P., Drewe, W. F., Jr., Houben, K. F., Leja, C. A., and Roy, M. (1990) The tryptophan synthase bienzyme complex transfers indole between the α- and β-sites via a 25-30 Å long tunnel, *Biochemistry 29*, 8598–8607.
1302. Teplyakov, A., Obmolova, G., Badet, B., and Badet-Denisot, M. A. (2001) Channeling of ammonia in glucosamine-6-phosphate synthase, *J. Mol. Biol. 313*, 1093–1102.
1303. Larsen, T. M., Boehlein, S. K., Schuster, S. M., Richards, N. G., Thoden, J. B., Holden, H. M., and Rayment, I. (1999) Three-dimensional structure of *Escherichia coli* asparagine synthetase B: A short journey from substrate to product, *Biochemistry 38*, 16146–16157.
1304. Endrizzi, J. A., Kim, H., Anderson, P. M., and Baldwin, E. P. (2004) Crystal structure of *Escherichia coli* cytidine triphosphate synthetase, a nucleotide-regulated glutamine amidotransferase/ATP-dependent amidoligase fusion protein and homologue of anticancer and antiparasitic drug targets, *Biochemistry 43*, 6447–6463.
1305. Anand, R., Hoskins, A. A., Stubbe, J., and Ealick, S. E. (2004) Domain organization of *Salmonella typhimurium* formylglycinamide ribonucleotide amidotransferase revealed by X-ray crystallography, *Biochemistry 43*, 10328–10342.
1306. Tesmer, J. J., Klem, T. J., Deras, M. L., Davisson, V. J., and Smith, J. L. (1996) The crystal structure of GMP synthetase reveals a novel catalytic triad and is a structural paradigm for two enzyme families, *Nature Struct. Biol. 3*, 74–86.
1307. Wu, J., Bu, W., Sheppard, K., Kitabatake, M., Kwon, S. T., Soll, D., and Smith, J. L. (2009) Insights into tRNA-dependent amidotransferase evolution and catalysis from the structure of the *Aquifex aeolicus* enzyme, *J. Mol. Biol. 391*, 703–716.
1308. Nakamura, A., Yao, M., Chimnaronk, S., Sakai, N., and Tanaka, I. (2006) Ammonia channel couples glutaminase with transamidase reactions in GatCAB, *Science 312*, 1954–1958.
1309. Ghosh, S., Blumenthal, H. J., Davidson, E., and Roseman, S. (1960) Glucosamine metabolism. V. Enzymatic synthesis of glucosamine 6-phosphate, *J. Biol. Chem. 235*, 1265–1273.
1310. Knochel, T., Ivens, A., Hester, G., Gonzalez, A., Bauerle, R., Wilmanns, M., Kirschner, K., and Jansonius, J. N. (1999) The crystal structure of anthranilate synthase from *Sulfolobus solfataricus*: Functional implications, *Proc. Natl. Acad. Sci. U. S. A. 96*, 9479–9484.
1311. Myers, R. S., Amaro, R. E., Luthey-Schulten, Z. A., and Davisson, V. J. (2005) Reaction coupling through interdomain contacts in imidazole glycerol phosphate synthase, *Biochemistry 44*, 11974–11985.
1312. Mouilleron, S., Badet-Denisot, M. A., and Golinelli-Pimpaneau, B. (2008) Ordering of C-terminal loop and glutaminase domains of glucosamine-6-phosphate synthase promotes sugar ring opening and formation of the ammonia channel, *J. Mol. Biol. 377*, 1174–1185.
1313. Weyand, M., and Schlichting, I. (1999) Crystal structure of wild-type tryptophan synthase complexed with the natural substrate indole-3-glycerol phosphate, *Biochemistry 38*, 16469–16480.
1314. Anderson, K. S., Miles, E. W., and Johnson, K. A. (1991) Serine modulates substrate channeling in tryptophan synthase. A novel intersubunit triggering mechanism, *J. Biol. Chem. 266*, 8020–8033.
1315. Leja, C. A., Woehl, E. U., and Dunn, M. F. (1995) Allosteric linkages between β-site covalent transformations and α-site activation and deactivation in the tryptophan synthase bienzyme complex, *Biochemistry 34*, 6552–6561.
1316. Thoden, J. B., Huang, X., Kim, J., Raushel, F. M., and Holden, H. M. (2004) Long-range allosteric transitions in carbamoyl phosphate synthetase, *Prot. Sci. 13*, 2398–2405.

1317. Post, L. E., Post, D. J., and Raushel, F. M. (1990) Dissection of the functional domains of *Escherichia coli* carbamoyl phosphate synthetase by site-directed mutagenesis, *J. Biol. Chem. 265*, 7742–7747.
1318. Wang, T. T., Bishop, S. H., and Himoe, A. (1972) Detection of carbamate as a product of the carbamate kinase-catalyzed reaction by stopped flow spectrophotometry, *J. Biol. Chem. 247*, 4437–4440.
1319. Anderson, P. M., and Meister, A. (1965) Evidence for an activated form of carbon dioxide in the reaction catalyzed by *Escherichia coli* carbamyl phosphate synthetase, *Biochemistry 4*, 2803–2809.
1320. Thoden, J. B., Holden, H. M., Wesenberg, G., Raushel, F. M., and Rayment, I. (1997) Structure of carbamoyl phosphate synthetase: A journey of 96 Å from substrate to product, *Biochemistry 36*, 6305–6316.
1321. Huang, X., and Raushel, F. M. (2000) An engineered blockage within the ammonia tunnel of carbamoyl phosphate synthetase prevents the use of glutamine as a substrate but not ammonia, *Biochemistry 39*, 3240–3247.
1322. Huang, X., and Raushel, F. M. (2000) Restricted passage of reaction intermediates through the ammonia tunnel of carbamoyl phosphate synthetase, *J. Biol. Chem. 275*, 26233–26240.
1323. Fan, Y., Lund, L., Shao, Q., Gao, Y.-Q., and Raushel F. M. (2009) A combined theoretical and experimental study of the ammonia tunnel in carbamoyl phosphate synthetase, *J. Am. Chem. Soc. 131*, 10211–10219.
1324. Kim, J., and Raushel, F. M. (2004) Perforation of the tunnel wall in carbamoyl phosphate synthetase derails the passage of ammonia between sequential active sites, *Biochemistry 43*, 5334–5340.
1325. Lund, L., Fan, Y., Shao, Q., Gao, Y. Q., and Raushel, F. M. (2010) Carbamate transport in carbamoyl phosphate synthetase: A theoretical and experimental investigation, *J. Am. Chem. Soc. 132*, 3870–3878.
1326. Kim, J., Howell, S., Huang, X., and Raushel, F. M. (2002) Structural defects within the carbamate tunnel of carbamoyl phosphate synthetase, *Biochemistry 41*, 12575–12581.
1327. Kyte, J. (2007) *Structure in protein chemistry: Second edition*, pp 38–40, Garland Science, New York.
1328. Meek, T. D., Garvey, E. P., and Santi, D. V. (1985) Purification and characterization of the bifunctional thymidylate synthetase-dihydrofolate reductase from methotrexate-resistant *Leishmania tropica*, *Biochemistry 24*, 678–686.
1329. Sharma, H., Landau, M. J., Vargo, M. A., Spasov, K. A., and Anderson, K. S. (2013) First three-dimensional structure of *Toxoplasma gondii* thymidylate synthase-dihydrofolate reductase: Insights for catalysis, interdomain interactions, and substrate channeling, *Biochemistry 52*, 7305–7317.
1330. Liang, P. H., and Anderson, K. S. (1998) Substrate channeling and domain-domain interactions in bifunctional thymidylate synthase-dihydrofolate reductase, *Biochemistry 37*, 12195–12205.
1331. Knighton, D. R., Kan, C. C., Howland, E., Janson, C. A., Hostomska, Z., Welsh, K. M., and Matthews, D. A. (1994) Structure of and kinetic channelling in bifunctional dihydrofolate reductase-thymidylate synthase, *Nature Struct. Biol. 1*, 186–194.
1332. Shatalin, K., Lebreton, S., Rault-Leonardon, M., Velot, C., and Srere, P. A. (1999) Electrostatic channeling of oxaloacetate in a fusion protein of porcine citrate synthase and porcine mitochondrial malate dehydrogenase, *Biochemistry 38*, 881–889.
1333. Atreya, C. E., Johnson, E. F., Williamson, J., Chang, S. Y., Liang, P. H., and Anderson, K. S. (2003) Probing electrostatic channeling in protozoal bifunctional thymidylate synthase-dihydrofolate reductase using site-directed mutagenesis, *J. Biol. Chem. 278*, 28901–28911.
1334. Nossal, N. G., and Singer, M. F. (1968) The processive degradation of individual polyribonucleotide chains. I. *Escherichia coli* ribonuclease II, *J. Biol. Chem. 243*, 913–922.
1335. Mikami, B., Degano, M., Hehre, E. J., and Sacchettini, J. C. (1994) Crystal structures of soybean β-amylase reacted with β-maltose and maltal: Active site components and their apparent roles in catalysis, *Biochemistry 33*, 7779–7787.
1336. Ishikawa, K., Nakatani, H., Katsuya, Y., and Fukazawa, C. (2007) Kinetic and structural analysis of enzyme sliding on a substrate: Multiple attack in β-amylase, *Biochemistry 46*, 792–798.

1337. Johnson, S. J., Taylor, J. S., and Beese, L. S. (2003) Processive DNA synthesis observed in a polymerase crystal suggests a mechanism for the prevention of frameshift mutations, *Proc. Natl. Acad. Sci. U. S. A. 100*, 3895–3900.
1338. Kuchta, R. D., Mizrahi, V., Benkovic, P. A., Johnson, K. A., and Benkovic, S. J. (1987) Kinetic mechanism of DNA polymerase I (Klenow), *Biochemistry 26*, 8410–8417.
1339. Werneburg, B. G., Ahn, J., Zhong, X., Hondal, R. J., Kraynov, V. S., and Tsai, M. D. (1996) DNA polymerase β: Pre-steady-state kinetic analysis and roles of arginine-283 in catalysis and fidelity, *Biochemistry 35*, 7041–7050.
1340. Nakatani, H. (1997) Monte Carlo simulation of multiple attack mechanism of β-amylase-catalyzed reaction, *Biopolymers 42*, 831–836.
1341. Hohn, K. T., and Grosse, F. (1987) Processivity of the DNA polymerase α-primase complex from calf thymus, *Biochemistry 26*, 2870–2878.
1342. Bennett, S. E., Sanderson, R. J., and Mosbaugh, D. W. (1995) Processivity of *Escherichia coli* and rat liver mitochondrial uracil-DNA glycosylase is affected by NaCl concentration, *Biochemistry 34*, 6109–6119.
1343. Stenina, O., Pudota, B. N., McNally, B. A., Hommema, E. L., and Berkner, K. L. (2001) Tethered processivity of the vitamin K-dependent carboxylase: Factor IX is efficiently modified in a mechanism which distinguishes Gla's from Glu's and which accounts for comprehensive carboxylation *in vivo*, *Biochemistry 40*, 10301–10309.
1344. Cannistraro, V. J., and Kennell, D. (1994) The processive reaction mechanism of ribonuclease II, *J. Mol. Biol. 243*, 930–943.
1345. Mitchell, P., Petfalski, E., Shevchenko, A., Mann, M., and Tollervey, D. (1997) The exosome: A conserved eukaryotic RNA processing complex containing multiple 3′→5′ exoribonucleases, *Cell 91*, 457–466.
1346. Lahue, E. E., and Matson, S. W. (1988) *Escherichia coli* DNA helicase I catalyzes a unidirectional and highly processive unwinding reaction, *J. Biol. Chem. 263*, 3208–3215.
1347. Divne, C., Stahlberg, J., Teeri, T. T., and Jones, T. A. (1998) High-resolution crystal structures reveal how a cellulose chain is bound in the 50 Å long tunnel of cellobiohydrolase I from *Trichoderma reesei*, *J. Mol. Biol. 275*, 309–325.
1348. Nakamura, A., Tsukada, T., Auer, S., Furuta, T., Wada, M., Koivula, A., Igarashi, K., and Samejima, M. (2013) The tryptophan residue at the active site tunnel entrance of *Trichoderma reesei* cellobiohydrolase Cel7A is important for initiation of degradation of crystalline cellulose, *J. Biol. Chem. 288*, 13503–13510.
1349. Parsiegla, G., Reverbel-Leroy, C., Tardif, C., Belaich, J. P., Driguez, H., and Haser, R. (2000) Crystal structures of the cellulase Cel48F in complex with inhibitors and substrates give insights into its processive action, *Biochemistry 39*, 11238–11246.
1350. Parsiegla, G., Reverbel, C., Tardif, C., Driguez, H., and Haser, R. (2008) Structures of mutants of cellulase Cel48F of *Clostridium cellulolyticum* in complex with long hemithiocellooligosaccharides give rise to a new view of the substrate pathway during processive action, *J. Mol. Biol. 375*, 499–510.
1351. Carter, D. M., and Radding, C. M. (1971) The role of exonuclease and β protein of phage λ in genetic recombination. II. Substrate specificity and the mode of action of λ exonuclease, *J. Biol. Chem. 246*, 2502–2512.
1352. Kovall, R., and Matthews, B. W. (1997) Toroidal structure of λ-exonuclease, *Science 277*, 1824–1827.
1353. Zhang, J., McCabe, K. A., and Bell, C. E. (2011) Crystal structures of λ exonuclease in complex with DNA suggest an electrostatic ratchet mechanism for processivity, *Proc. Natl. Acad. Sci. U. S. A. 108*, 11872–11877.
1354. Groll, M., Ditzel, L., Lowe, J., Stock, D., Bochtler, M., Bartunik, H. D., and Huber, R. (1997) Structure of 20S proteasome from yeast at 2.4 Å resolution, *Nature 386*, 463–471.
1355. Bird, L. E., Brannigan, J. A., Subramanya, H. S., and Wigley, D. B. (1998) Characterisation of *Bacillus stearothermophilus* PcrA helicase: Evidence against an active rolling mechanism, *Nucleic Acids Res. 26*, 2686–2693.
1356. Velankar, S. S., Soultanas, P., Dillingham, M. S., Subramanya, H. S., and Wigley, D. B. (1999) Crystal structures of complexes of PcrA DNA helicase with a DNA substrate indicate an inchworm mechanism, *Cell 97*, 75–84.
1357. Ali, J. A., and Lohman, T. M. (1997) Kinetic measurement of the step size of DNA un-

winding by *Escherichia coli* UvrD helicase, *Science 275*, 377–380.
1358. Soultanas, P., Dillingham, M. S., Wiley, P., Webb, M. R., and Wigley, D. B. (2000) Uncoupling DNA translocation and helicase activity in PcrA: Direct evidence for an active mechanism, *EMBO J. 19*, 3799–3810.
1359. Lee, J. Y., and Yang, W. (2006) UvrD helicase unwinds DNA one base pair at a time by a two-part power stroke, *Cell 127*, 1349–1360.
1360. Singleton, M. R., Dillingham, M. S., Gaudier, M., Kowalczykowski, S. C., and Wigley, D. B. (2004) Crystal structure of RecBCD enzyme reveals a machine for processing DNA breaks, *Nature 432*, 187–193.
1361. Roman, L. J., and Kowalczykowski, S. C. (1989) Characterization of the helicase activity of the *Escherichia coli* RecBCD enzyme using a novel helicase assay, *Biochemistry 28*, 2863–2873.
1362. Chamberlin, M., McGrath, J., and Waskell, L. (1970) New RNA polymerase from *Escherichia coli* infected with bacteriophage T7, *Nature 228*, 227–231.
1363. Cheetham, G. M., Jeruzalmi, D., and Steitz, T. A. (1999) Structural basis for initiation of transcription from an RNA polymerase-promoter complex, *Nature 399*, 80–83.
1364. Burgess, R. R. (1969) Separation and characterization of the subunits of ribonucleic acid polymerase, *J. Biol. Chem. 244*, 6168–6176.
1365. Burgess, R. R., Travers, A. A., Dunn, J. J., and Bautz, E. K. (1969) Factor stimulating transcription by RNA polymerase, *Nature 221*, 43–46.
1366. Walter, G., Seifert, W., and Zillig, W. (1968) Modified DNA-dependent RNA polymerase from *E. coli* infected with bacteriophage T4, *Biochem. Biophys. Res. Commun. 30*, 240–247.
1367. Vassylyev, D. G., Sekine, S., Laptenko, O., Lee, J., Vassylyeva, M. N., Borukhov, S., and Yokoyama, S. (2002) Crystal structure of a bacterial RNA polymerase holoenzyme at 2.6 Å resolution, *Nature 417*, 712–719.
1368. Cramer, P., Bushnell, D. A., Fu, J., Gnatt, A. L., Maier-Davis, B., Thompson, N. E., Burgess, R. R., Edwards, A. M., David, P. R., and Kornberg, R. D. (2000) Architecture of RNA polymerase II and implications for the transcription mechanism, *Science 288*, 640–649.
1369. Cramer, P., Bushnell, D. A., and Kornberg, R. D. (2001) Structural basis of transcription: RNA Polymerase II at 2.8 Å resolution, *Science 292*, 1863–1876.
1370. Ricchetti, M., Metzger, W., and Heumann, H. (1988) One-dimensional diffusion of *Escherichia coli* DNA-dependent RNA polymerase: A mechanism to facilitate promoter location, *Proc. Natl. Acad. Sci. U. S. A. 85*, 4610–4614.
1371. Hinkle, D. C., and Chamberlin, M. J. (1972) Studies of the binding of *Escherichia coli* RNA polymerase to DNA. I. The role of σ subunit in site selection, *J. Mol. Biol. 70*, 157–185.
1372. Sakata-Sogawa, K., and Shimamoto, N. (2004) RNA polymerase can track a DNA groove during promoter search, *Proc. Natl. Acad. Sci. U. S. A. 101*, 14731–14735.
1373. Murakami, K. S., Masuda, S., Campbell, E. A., Muzzin, O., and Darst, S. A. (2002) Structural basis of transcription initiation: An RNA polymerase holoenzyme-DNA complex, *Science 296*, 1285–1290.
1374. Cheetham, G. M., and Steitz, T. A. (1999) Structure of a transcribing T7 RNA polymerase initiation complex, *Science 286*, 2305–2309.
1375. Boyaci, H., Chen, J., Jansen, R., Darst, S. A., and Campbell, E. A. (2019) Structures of an RNA polymerase promoter melting intermediate elucidate DNA unwinding, *Nature 565*, 382–385.
1376. Feklistov, A., Bae, B., Hauver, J., Lass-Napiorkowska, A., Kalesse, M., Glaus, F., Altmann, K. H., Heyduk, T., Landick, R., and Darst, S. A. (2017) RNA Polymerase motions during promoter melting, *Science 356*, 863–866.
1377. Sainsbury, S., Niesser, J., and Cramer, P. (2013) Structure and function of the initially transcribing RNA polymerase II-TFIIB complex, *Nature 493*, 437–440.
1378. Martin, C. T., Muller, D. K., and Coleman, J. E. (1988) Processivity in early stages of transcription by T7 RNA polymerase, *Biochemistry 27*, 3966–3974.
1379. Durniak, K. J., Bailey, S., and Steitz, T. A. (2008) The structure of a transcribing T7 RNA polymerase in transition from initiation to elongation, *Science 322*, 553–557.
1380. Yin, Y. W., and Steitz, T. A. (2002) Structural basis for the transition from initiation to elongation transcription in T7 RNA polymerase, *Science 298*, 1387–1395.
1381. Tahirov, T. H., Temiakov, D., Anikin, M., Patlan, V., McAllister, W. T., Vassylyev, D. G.,

and Yokoyama, S. (2002) Structure of a T7 RNA polymerase elongation complex at 2.9 Å resolution, *Nature 420*, 43–50.
1382. Naryshkina, T., Kuznedelov, K., and Severinov, K. (2006) The role of the largest RNA polymerase subunit lid element in preventing the formation of extended RNA-DNA hybrid, *J. Mol. Biol. 361*, 634–643.
1383. Gnatt, A. L., Cramer, P., Fu, J., Bushnell, D. A., and Kornberg, R. D. (2001) Structural basis of transcription: An RNA polymerase II elongation complex at 3.3 Å resolution, *Science 292*, 1876–1882.
1384. Ehara, H., Yokoyama, T., Shigematsu, H., Yokoyama, S., Shirouzu, M., and Sekine, S. I. (2017) Structure of the complete elongation complex of RNA polymerase II with basal factors, *Science 357*, 921–924.
1385. Higo, T., Suka, N., Ehara, H., Wakamori, M., Sato, S., Maeda, H., Sekine, S., Umehara, T., and Yokoyama, S. (2014) Development of a hexahistidine-3× FLAG-tandem affinity purification method for endogenous protein complexes in *Pichia pastoris*, *J. Struct. Funct. Genomics 15*, 191–199.
1386. Adelman, K., La Porta, A., Santangelo, T. J., Lis, J. T., Roberts, J. W., and Wang, M. D. (2002) Single molecule analysis of RNA polymerase elongation reveals uniform kinetic behavior, *Proc. Natl. Acad. Sci. U. S. A. 99*, 13538–13543.
1387. Schafer, D. A., Gelles, J., Sheetz, M. P., and Landick, R. (1991) Transcription by single molecules of RNA polymerase observed by light microscopy, *Nature 352*, 444–448.
1388. Yin, H., Wang, M. D., Svoboda, K., Landick, R., Block, S. M., and Gelles, J. (1995) Transcription against an applied force, *Science 270*, 1653–1657.
1389. Wang, M. D., Schnitzer, M. J., Yin, H., Landick, R., Gelles, J., and Block, S. M. (1998) Force and velocity measured for single molecules of RNA polymerase, *Science 282*, 902–907.
1390. Massey, V. (1953) Studies on fumarase: II. The effects of inorganic anions on fumarase activity, *Biochem. J. 53*, 67–71.
1391 Rathore, R., Hubig S. M., and Kochi.J. K. (1997) Direct Observation and Structural Characterization of the Encounter Complex in Bimolecular Electron Transfers with Photoactivated Acceptors *J. Am. Chem. Soc.* 119, 11468-11480

Chapter 4
Transfer of Hydrons

Hydron transfers are involved in almost all biochemical reactions, and reactions homologous to those that occur in particular active sites can often be studied in free, aqueous solution. Hydron transfers are also involved in these homologous reactions when they proceed in solution. Water is chosen for the solvent because it is the solvent in which enzymes are usually dissolved and the solvent in which life has evolved. When a reaction that is the same as one that occurs in a particular class of active sites is studied in free solution, homologues of the metabolites normally participating in the enzymatic reaction are chosen because the actual metabolites usually have too many reactive functional groups elsewhere in their structure. In an active site, the chemical reaction catalyzed by the enzyme is confined by the structure of the active site to only those functional groups directly involved in the mechanism. In free solution, however, functional groups that are not involved in the mechanism when the metabolite is in the active site would be involved in the reaction that is being observed as well as in undesired side reactions. The requirements for hydron transfers in such a homologous reaction are established and quantified systematically.

General Acid Catalysis and General Base Catalysis

The chemical mechanism for a reaction in free solution homologous to one catalyzed in an active site usually requires that one or more hydrons be provided for one or more existing or incipient lone pairs of electrons and that one or more hydrons be removed from one or more pairs of electrons. Although mechanistic shorthand permits hydrons to be written as H^+, there is no such thing in aqueous solution as a bare hydron. A hydron in aqueous solution either occupies one pair of electrons or is in the process of being transferred intimately and essentially instantaneously between two pairs of electrons. If a hydron is provided to a reactant, it is provided residing upon a pair of electrons in an acid. Most of the time, the acid, immediately before the transfer occurs, is the donor in a hydrogen bond to a lone pair of electrons that is the base receiving the hydron in that reactant. If a hydron is removed from a reactant, it is removed by being transferred to the lone pair of electrons of a base. Most of the time, the lone pair of electrons on the base, immediately before the transfer occurs, is the acceptor for a hydrogen bond from the acid giving up the hydron in that reactant. The requirements for these acids and bases that participate in one of these reactions are demonstrated by studying systematically changes in rate of the reaction as a function of the pH of the solution and as a function of the concentrations of added acids and bases.

As the pH of a solution is decreased, the concentration of hydronium, an acid, increases. If the observed rate constant for a reaction proceeding in solution increases as the pH of the solution is decreased, in the absence of significant concentrations of other added acids or bases, it is usually assumed that only the increase in the concentration of hydronium is responsible for the increase in rate because the only changes occurring in solution are the increase in the concentration of hydronium and a corresponding decrease in the concentration of hydroxide. **Specific acid catalysis** is the increase in the rate of a reaction due only to an increase in the concentration of hydronium. If the increase in rate is a linear function of the concentration of hydronium, the equation describing the behavior of the observed rate constant as a function of pH will contain the term $k_{H^+}[H^+]$ to account for this catalysis.

The existence of specific acid catalysis is established by measuring the rate constant for the reaction at a series of different values of pH. Although one can use a device known as a pH stat to maintain a fixed pH as the reaction proceeds, the pH of the solution is usually held constant for each individual rate measurement by adding a buffer of sufficient strength to prevent any change in pH due to the reaction itself. If, however, the pH of the solution is maintained with a buffer, one must be aware that the buffer itself, because it is necessarily composed of an acid and its conjugate base, often affects the rate of the reaction (Figure 4–1).[1] To **correct for the effect of the buffer on the observed rate**, the concentration of buffer is varied at constant pH, which

is established only by the ratio of the acid to the conjugate base in the buffer, and the value for the observed rate constant in the absence of buffer is obtained by extrapolation to zero concentration. For example, the observed pseudo-first-order rate constant k_{EE}

$$-\frac{d[\mathrm{EE}]}{dt} = k_{\mathrm{EE}}[\mathrm{EE}] \qquad (4\text{–}1)$$

for hydrolysis of methyl enol ether **4–1** (EE)

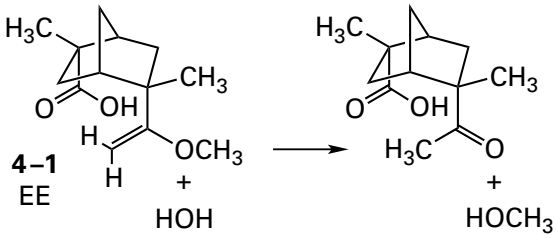

(4–2)

was measured at several values of pH and varying concentrations of the buffer potassium phosphate to estimate, by extrapolation, the behavior of the observed rate constant as a function of pH in the absence of any phosphate (Figure 4–1). Because the pseudo-first-order rate constants in the absence of buffer (intersections of the lines with the ordinate) increase as the pH decreases, specific acid catalysis is occurring.

As the pH of a solution is increased, the concentration of hydroxide, a base, increases. If the observed rate constant for a reaction proceeding in solution increases as the pH of the solution is increased, in the absence of significant concentrations of other added acids or bases, it is usually assumed that only the increase in the concentration of hydroxide is responsible for the increase in rate because the only changes occurring in the solution are the increase in the concentration of hydroxide and the corresponding decrease in the concentration of hydronium. **Specific base catalysis** is the increase in the rate of a reaction due only to an increase in the concentration of hydroxide ions. If the increase in rate is a linear function of the concentration of hydroxide, the equation describing the behavior of the observed rate constant as a function of pH will contain the term $k_{OH^-}[OH^-]$ to account for this catalysis. Although this term in an equation for an observed rate constant is mathematically symmetrical to the term $k_{H^+}[H^+]$, hydronium and hydroxide are chemically distinct. While a hydronium can only donate a hydron to a lone pair of electrons or an incipient lone pair of electrons, a hydroxide can either remove a hydron from a pair of electrons or participate in the reaction directly as a nucleophile.

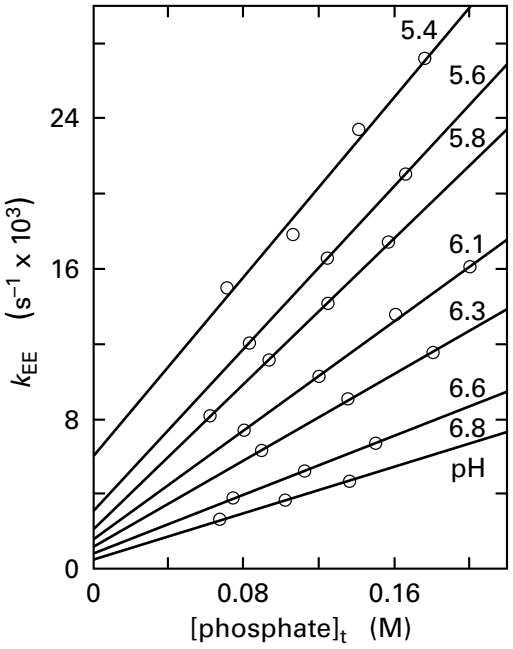

Figure 4-1: Catalysis of the hydrolysis of methyl enol ether 4-1 by phosphate anion at various values of pH.1 Solutions (0.4 mM) of the methyl enol ether 4-1 (EE) were prepared in 5% ethanol and 1 M KCl, with the noted concentrations of total phosphate as the potassium salts at the noted pH and 25 °C. Hydrolysis of the methyl enol ether (Equation 4-1) was followed spectrophotometrically by the decrease in absorbance at 230 nm from the vinyl ether and the increase in absorbance at 280 nm from the ketone. In all instances, the hydrolysis was first-order with respect to the total concentration of methyl enol ether. The pseudo-first-order rate constant was obtained from each kinetic run by nonlinear least-squares analysis of the curves. These pseudo-first-order rate constants, k_{EE} (second$^{-1} \times 10^3$), are plotted as a function of the total concentration of phosphate (molar) at a series of values for pH (noted to the right and above each respective line).

A **pH–rate profile** is a plot of the observed rate constants for a reaction, each of which has been estimated by extrapolation to zero concentration of buffer, as a function of pH at constant temperature and ionic strength in the absence of significant concentrations of other added acids and bases besides the species of the buffer. A pH–rate profile is usually presented as the common logarithms of the observed rate constant for the reaction as a function of pH, which is the negative common logarithm of the concentration of hydronium. The pH–rate profile for hydrolysis of 4-nitrophenyl β-D-*N*-acetyl-neuraminide

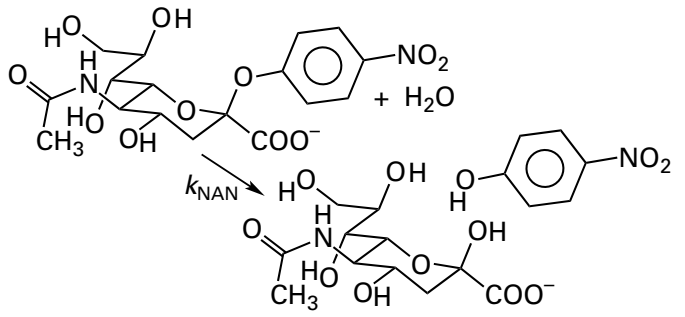

(4–3)

shows specific acid catalysis at low pH, specific base catalysis at high pH, and a region between these extremes in which the rate of the reaction is catalyzed by neither hydronium nor hydroxide (Figure 4–2).[2] The rate equation that describes this observed behavior is

$$-\frac{d[\mathrm{NAN}]}{dt} = k_{\mathrm{NAN}}[\mathrm{NAN}] \tag{4–4}$$

where [NAN] is the concentration of 4-nitrophenyl β-D-*N*-acetylneuraminide, and the equation for the observed rate constant is

$$k_{\mathrm{NAN}} = k_{\mathrm{H^+}}[\mathrm{H^+}] + k_{\mathrm{non}} + k_{\mathrm{OH^-}}[\mathrm{OH^-}] \tag{4–5}$$

where k_{non} is the rate constant for the rate of the uncatalyzed reaction, the reaction catalyzed by neither hydronium nor hydroxide. At low pH, $k_{\mathrm{NAN}} = k_{\mathrm{H^+}}[\mathrm{H^+}]$ and the common logarithm of the observed rate constant as a function of pH has a slope of –1. At high pH, $k_{\mathrm{NAN}} = k_{\mathrm{OH^-}}[\mathrm{OH^-}] = k_{\mathrm{OH^-}}K_{\mathrm{w}}[\mathrm{H^+}]^{-1}$, and the common logarithm of the observed rate constant as a function of pH has a slope of +1. At intermediate pH, $k_{\mathrm{NAN}} = k_{\mathrm{non}}$, and the common logarithm of the observed rate constant as a function of pH has a slope of 0. The meaning of the uncatalyzed rate is usually unknown. One possibility, which is usually in the back of the investigator's mind, is that the rate is the result of catalysis by molecules of water, the concentration of which remains constant throughout the measurements, but this does not need to be the case.

Often, a pH–rate profile is **complicated by an acid dissociation of one of the reactants**. For example, unlike the rates of hydrolysis for acetals formed from aldehydes that have no acid–bases within themselves, which are directly proportional to the concentration of hydronium and a function of only the concentration of hydronium at all values of pH,[3]

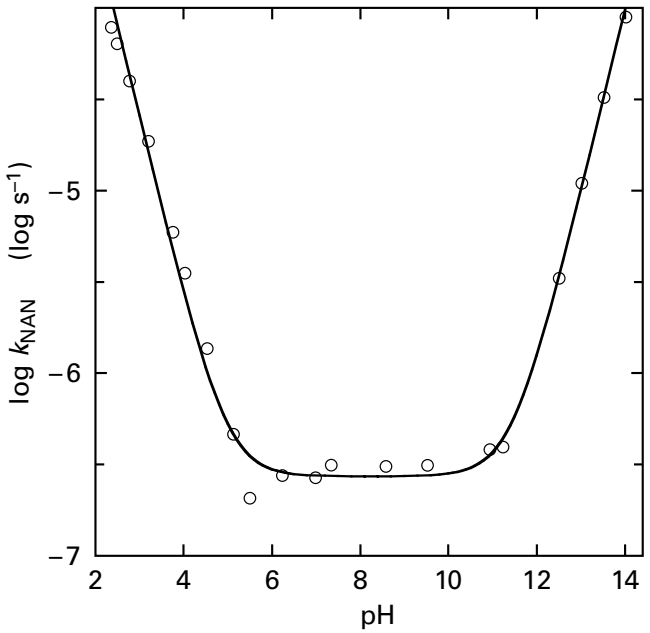

Figure 4–2: pH–Rate profile for the hydrolysis of 4-nitrophenyl β-D-*N*-acetylneuraminide (Equation 4–3) at an ionic strength of 0.3 M and 50 °C.[2] Hydrolysis of 4-nitrophenyl β-D-*N*-acetylneuraminide (NAN) was monitored by following the appearance of 4-nitrophenol at a wavelength of 340 or 408 nm, depending on the pH of the solution. The buffers used, in the noted ranges of pH, were malonic acid, 2.10–3.19; succinic acid, 3.76–4.02; acetic acid, 4.46–5.36; 2-(*N*-morpholino)ethanesulfonate, 5.50–6.30; 3-{[1,3-dihydroxy-2-(hydroxymethyl)propan-2-yl]amino}propane-1-sulfonate, 7.00–8.20; and 3-(cyclohexylamino)propane-1-sulfonate, 10.00–11.13. The pseudo-first-order increases in absorbance were fit by a nonlinear least-squares program to obtain values for the pseudo-first-order rate constants. The common logarithms of these rate constants, k_{NAN} (second^{-1}), are plotted as a function of pH. The solid curve is the common logarithm of Equation 4–5 with $k_{\mathrm{H^+}} = 0.025\ \mathrm{M^{-1}\,s^{-1}}$, $k_{\mathrm{non}} = 2.7\times10^{-7}\ \mathrm{s^{-1}}$, and $k_{\mathrm{OH^-}} = 9.7\times10^{-5}\ \mathrm{M^{-1}\,s^{-1}}$.

hydrolysis of the acetal of *cis*-cyclohexane-1,2-dioland 4-(dimethylamino)benzaldehyde is independent of the concentration of hydronium as long as the 4-dimethylamino group on the 4-(dimethylamino)benzaldehyde participating in the acetal is hydronated and positively charged. As the pH is increased, however, and the 4-dimethylamino group becomes dehydronated, hydrolysis of the neutral acetal becomes directly proportional to the concentration of hydronium and a function of only the concentration of hydronium[4] at all values of pH greater than its pK_{a}. As long as the 4-dimethylamino group is hydronated, its positive elementary charge, relayed to the aldehyde carbon through the π molecular orbital system of the 4-(dimethylamino)-phenyl group, prevents hydronation of one oxygen on that carbon in the acetal, a hydronation that is indispensable to the hydrolysis.

The pH–rate profile of observed pseudo-first-order rate constants for hydrolysis of *N*-acetylimidazole (AcIm)

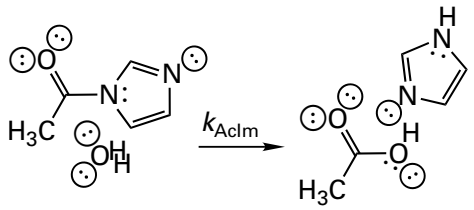

(4–6)

estimated by extrapolations to zero buffer concentration, has regions in which the observed rate constant increases with decreases in pH, regions in which it increases with increases in pH, and regions in which it is invariant with pH (Figure 4–3).[5] The reactant itself is not catalyzing the reaction, because at all values of pH the rate of the reaction is first-order in concentration

$$-\frac{d[\mathrm{AcIm}]_t}{dt} = k_{\mathrm{AcIm}}[\mathrm{AcIm}]_t \tag{4–7}$$

where $[\mathrm{AcIm}]_t$ is the total concentration of *N*-acetylimidazole in all its forms at any time during the reaction.

The behavior of observed pseudo-first-order rate constants, k_{AcIm}, for hydrolysis of *N*-acetylimidazole as a function of pH can be fully explained by the equation[5]

$$k_{\mathrm{AcIm}} = \left(k_{\mathrm{H^+}}[\mathrm{H^+}] + k_{\mathrm{non}} + k_{\mathrm{OH^-}}[\mathrm{OH^-}]\right)\left(\frac{K_{\mathrm{aAcIm}}}{K_{\mathrm{aAcIm}} + [\mathrm{H^+}]}\right) \tag{4–8}$$

where K_{aAcIm} is the acid dissociation constant of *N*-acetylimidazole ($pK_{\mathrm{aAcIm}} = 3.6$)

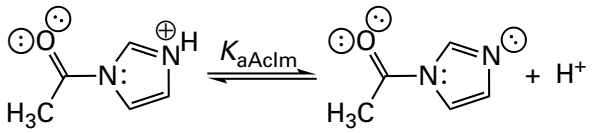

(4–9)

Because

$$[\mathrm{AcIm}] = \left(\frac{K_{\mathrm{aAcIm}}}{K_{\mathrm{aAcIm}} + [\mathrm{H^+}]}\right)[\mathrm{AcIm}]_t \tag{4–10}$$

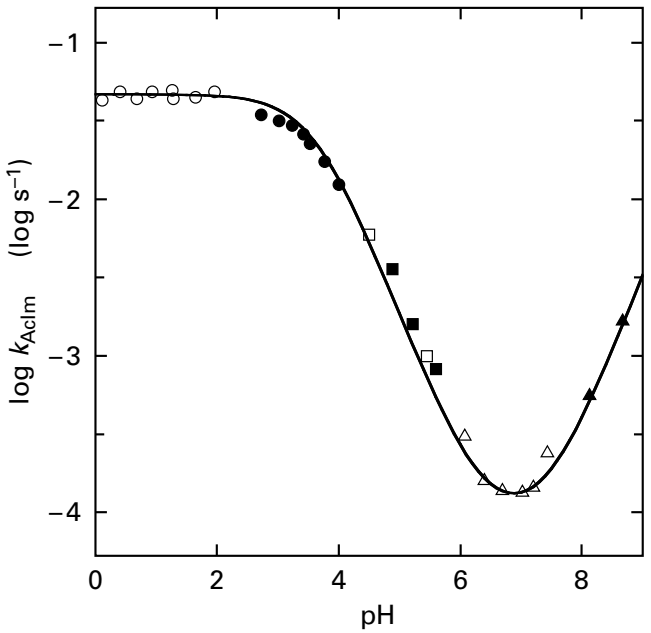

Figure 4–3: pH–Rate profile for the hydrolysis of *N*-acetylimidazole[5] at an ionic strength of 0.2 M and 25 °C. *N*-Acetylimidazole was added to a series of solutions adjusted to the noted values of pH with HCl (○) or buffered at the noted values of pH with sodium formate (●), sodium acetate (□), sodium succinate (■), imidazolium chloride (△), or 2-ammonio-2-(hydroxymethyl)propane-1,3-diol chloride (▲). The ionic strength was maintained by adding the appropriate concentration of sodium chloride. The progress of each reaction was followed by the decrease in absorbance at 245 nm resulting from the loss of *N*-acetylimidazole. All reactions were first-order in *N*-acetylimidazole, and pseudo-first-order rate constants were obtained by plotting the common logarithm of the extent of the reaction as a function of time. The values for the pseudo-first-order rate constants at each pH were extrapolated to zero buffer concentration. The common logarithms of the estimated pseudo-first-order rate constants in the absence of buffer, k_{AcIm} (second^{-1}), are plotted as a function of the pH. The solid curve is the common logarithm of Equation 4–8 with $k_{\mathrm{H^+}} = 186\ \mathrm{M^{-1}\ s^{-1}}$, $k_{\mathrm{non}} = 0.000083\ \mathrm{s^{-1}}$, $k_{\mathrm{OH^-}} = 317\ \mathrm{M^{-1}\ s^{-1}}$, and $K_{\mathrm{aAcIm}} = 10^{-3.6}$ M.

$$-\frac{d[\mathrm{AcIm}]_t}{dt} = \left(k_{\mathrm{H^+}}[\mathrm{H^+}] + k_{\mathrm{non}} + k_{\mathrm{OH^-}}[\mathrm{OH^-}]\right)[\mathrm{AcIm}] \tag{4–11}$$

where [AcIm] is the concentration of the conjugate base of *N*-acetylimidazole (Equation 4–9).

In the case of enolization of mandelic acid (MAH)

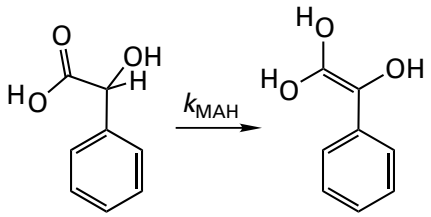

(4–12)

the rate of the reaction is also first-order in the concentration of reactant

$$-\frac{d[\mathrm{MAH}]_t}{dt} = k_{\mathrm{MAH}}[\mathrm{MAH}]_t \tag{4–13}$$

The equation that describes the behavior of the rate constant for enolization as a function of pH is[6]

$$k_{\mathrm{MAH}} = \left(k_{\mathrm{H^+}}[\mathrm{H^+}] + k_{\mathrm{OH^-}}[\mathrm{OH^-}] + k_{\mathrm{2OH^-}}[\mathrm{OH^-}]^2\right)\left(\frac{[\mathrm{H^+}]}{[\mathrm{H^+}] + K_{\mathrm{aMAH}}}\right) \tag{4–14}$$

where K_{aMAH} is the acid dissociation constant for the carboxy group of mandelic acid

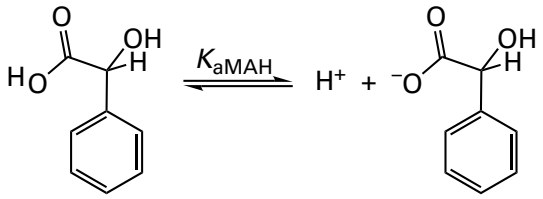

(4–15)

Because the concentration of the neutral conjugate acid of mandelic acid

$$[\mathrm{MAH}] = \left(\frac{[\mathrm{H^+}]}{K_{\mathrm{aMAH}} + [\mathrm{H^+}]}\right)[\mathrm{MAH}]_t \tag{4–16}$$

where $[\mathrm{MAH}]_t$ is the total concentration of unenolized mandelic acid, which is the sum of the concentrations of neutral conjugate acid, [MAH], and carboxylate anion, $[\mathrm{MA^-}]$

$$-\frac{d[\mathrm{MAH}]_t}{dt} = \left(k_{\mathrm{H^+}}[\mathrm{H^+}] + k_{\mathrm{OH^-}}[\mathrm{OH^-}] + k_{\mathrm{2OH^-}}[\mathrm{OH^-}]^2\right)[\mathrm{MAH}] \tag{4–17}$$

In this instance, only the concentration of the conjugate acid of the reactant appears in the rate equation, rather than only the concentration of the conjugate base of the reactant, as in the case of *N*-acetylimidazole (Equation 4–11).

The equation that describes the behavior of the rate for hydrolysis of the enol ether 2-methoxyacrylic acid

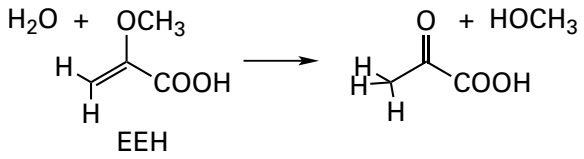

(4–18)

as a function of pH is

$$-\frac{d[\mathrm{EE}]_t}{dt} = k_{\mathrm{EE}}[\mathrm{EE}]_t = \left(k_{\mathrm{H^+}}[\mathrm{H^+}] + k_{\mathrm{non}}\right)\left(\frac{[\mathrm{H^+}]}{[\mathrm{H^+}] + K_{\mathrm{aEEH}}}\right)[\mathrm{EE}]_t = \left(k_{\mathrm{H^+}}[\mathrm{H^+}] + k_{\mathrm{non}}\right)[\mathrm{EEH}] \tag{4–19}$$

where $[\mathrm{EE}]_t$ is the total concentration of 2-methoxyacrylic acid, both its conjugate acid and its conjugate base, and K_{aEEH} is the acid dissociation constant for 2-methoxyacrylic acid ($pK_a = 3.39$).[7] Again, only the concentration of the conjugate acid appears in the rate equation.

It is often observed that addition of an acid–base to the solution, such as dihydrogen phosphate monoanion and its conjugate base, hydrogen phosphate dianion (Figure 4–1), increases the rate constant of a reaction. **General acid–base catalysis** is the increase in the rate of a reaction due only to an increase in the concentration of an added acid–base to the solution.

Because it is impossible to add an acid to water without simultaneously producing its conjugate base or to add a base without simultaneously producing its conjugate acid, it must be established which of the two forms is responsible for the acceleration observed. This decision is reached by using **the conjugate acid and conjugate base in constant ratio as the buffer**. As the total concentration of the acid–base is increased at constant ratio of conjugate acid to conjugate base and consequently at constant pH, the pseudo-first-order rate constant for the reaction increases (Figures 4–1 and 4–4)[1,8,9] if general acid–base catalysis is occurring.

If the rate constant for the reaction increases linearly with the concentration of buffer at constant pH, the behavior can be described by the equation for the observed rate constant at a particular pH and concentration of buffer

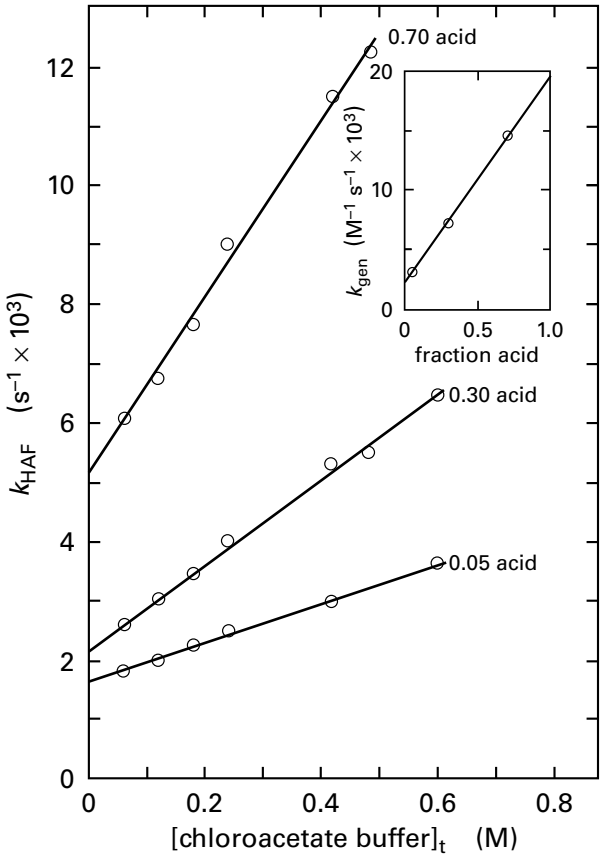

Figure 4–4: Determination of the rate constants for general acid and general base catalysis of the hydrolysis of formaldehyde ethyl hemiacetal (Equation 4–23) by chloroacetate buffers at an ionic strength of 1.0 M and 25 °C.[8] The ethyl hemiacetal of formaldehyde (HAF) was formed by mixing formaldehyde with anhydrous ethyl alcohol and allowing the mixture to stand for 3 h before use. Formaldehyde ethyl hemiacetal was added to a final concentration of 0.1 mM to solutions of 1.00 M KCl containing the noted total concentration of chloroacetic acid and potassium chloroacetate mixed in the ratios 70:30, 30:70, and 5:95 to give the fractions of acid in the buffer noted to the right of each line. Hydrolysis of the ethyl hemiacetal of formaldehyde was followed by trapping the formaldehyde produced with thiosemicarbazide (0.01 M). The increase in absorbance at 275 nm due to formation of the thiosemicarbazone was followed with time. For each individual run, pseudo-first-order rate constants were obtained from the slopes of plots of ln ($A_{275} - A_{\infty 275}$) against time. The pseudo-first-order rate constants, k_{HAF} (second$^{-1} \times 10^3$), are plotted as a function of the total molar concentration of chloroacetate anion plus chloroacetic acid (molar). The slopes of these lines, k_{gen} (molar^{-1} second$^{-1} \times 10^3$; Equation 4–20), are plotted (Equation 4–21) in the inset as a function of the fraction of total chloroacetate that was chloroacetic acid (fraction acid).

$$k_{obs} = k_{pH} + k_{gen}[\text{buffer}]_t \qquad (4\text{–}20)$$

where k_{pH} is a macroscopic rate constant containing the terms for specific acid catalysis, no catalysis, and specific base catalysis (Equation 4–5) and k_{gen} is the **macroscopic rate constant for general acid–base catalysis** reflecting the effects of the added acid and its conjugate base. Its kinetic order is one greater than that of the observed rate constant. This linear behavior states that the term $k_{gen}[\text{buffer}]_t$ producing an increase in the rate constant results from a reaction the transition state of which is composed of the reactant and the conjugate acid of the buffer or from a reaction the transition state of which is composed of the reactant and the conjugate base of the buffer or from both of these reactions proceeding simultaneously. In other words, the acid or the base or both of them, when they participate directly in the reaction, cause it to proceed more rapidly.

If the ratio between the acid and the base in the buffer is changed, and inescapably the pH as well, and the experiment is repeated, the **slope of the line** will usually change (Figures 4–1 and 4–4). If the slope of the line, and hence the rate constant k_{gen}, increases as the ratio between acid and base is increased, the conjugate acid of the buffer is a more important participant in catalysis (Figures 4–1 and 4–4) than its conjugate base. If the slope of the line decreases, the conjugate base of the buffer is a more important participant than its conjugate acid.

The term $k_{gen}[\text{buffer}]_t$ is itself often a sum of two separate terms

$$k_{gen}[\text{buffer}]_t = k_{ga}[HN^{(+)}] + k_{gb}[\odot N^{(-)}] \qquad (4\text{–}21)$$

where $HN^{(+)}$ is the conjugate acid and $\odot N^{(-)}$ is the conjugate base of the buffer. Numerical values for the two rate constants in this equation are obtained by extrapolation. If k_{gen} is plotted as a function of the fraction of the total buffer that is the conjugate acid, the extrapolated value of the rate constant for the point at which all the buffer is the conjugate acid, $[\text{buffer}]_t = [HN^{(+)}]$ and $[\odot N^{(-)}] = 0$, is the rate constant k_{ga} and the extrapolated value of the rate constant for the point at which all the buffer is the conjugate base, $[\text{buffer}]_t = [\odot N^{(-)}]$ and $[HN^{(+)}] = 0$, is the rate constant k_{gb} (inset to Figure 4–4). If reactants, other than the general acid–base of the buffer, contain no acid–bases themselves with values of pK_a within the range of pH studied (see Equations 4–8 and 4–14), then Equations 4–5, 4–20, and 4–21

can be combined to obtain a **general expression for acid–base catalysis**

$$k_{obs} = k_{H^+}[H^+] + k_{non} + k_{OH^-}[OH^-] + k_{ga}[HN^{(+)}] + k_{gb}[\odot N^{(-)}] \quad (4\text{–}22)$$

In each particular reaction, the two terms in Equation 4–22 governing the particular general acid–base catalyst have **relative degrees of importance reflected in numerical values for the respective rate constants**. Decomposition of the ethyl hemiacetal of formaldehyde (EHF)

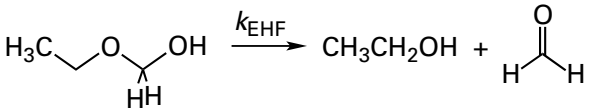

(4–23)

in a solution buffered with potassium chloroacetate at 25 °C (Figure 4–4)[8] has an observed pseudo-first-order rate constant k_{EHF}, the equation for which

$$k_{EHF} = k_{pH} + k_{ga}[ClCH_2COOH] + k_{gb}[ClCH_2COO^-] \quad (4\text{–}24)$$

contains two terms of similar magnitude, one directly proportional to the concentration of chloroacetic acid, $[ClCH_2COOH]$ ($k_{ga} = 20 \times 10^{-3}\ M^{-1}\ s^{-1}$), and the other directly proportional to the concentration of chloroacetate anion, $[ClCH_2COO^-]$ ($k_{gb} = 2 \times 10^{-3}\ M^{-1}\ s^{-1}$). Similar results were observed for catalysis of the dehydration of acetaldehyde hydrate by potassium acetate buffers at 25 °C ($k_{ga} = 290 \times 10^{-3}\ M^{-1}\ s^{-1}$, $k_{gb} = 50 \times 10^{-3}\ M^{-1}\ s^{-1}$).[9] Hydrolysis of methyl enol ether **4–1** (Equation 4–2), however, has a pseudo-first-order rate constant the equation for which, within experimental error, contains no term that is directly proportional to the concentration of the conjugate base of the phosphate buffer, $[HOPO_3^{2-}]$, even though it contains a term that is directly proportional to the concentration of the conjugate acid of the phosphate buffer, $[HOPO_3H^-]$ (Figure 4–1). Hydrolysis of *N*-acetylimidazole (Equation 4–6), in a solution buffered with imidazole, has a pseudo-first-order rate constant the equation for which, within experimental error, has no term directly proportional to the concentration of the cationic conjugate acid of imidazole, $[H_2Im^+]$, even though it contains a significant term directly proportional to the concentration of the neutral free base of imidazole, [HIm].[10]

The term $k_{gen}[buffer]_t$ can also be the sum of three terms[11]

$$k_{gen}[buffer]_t = k_{ga}[HN^{(+)}] + k_{gb}[\odot N^{(-)}] + k_{gab}[HN^{(+)}][\odot N^{(-)}] \quad (4\text{–}25)$$

instead of two (Equation 4–21), so that the general expression becomes

$$k_{obs} = k_{H^+}[H^+] + k_{non} + k_{OH^-}[OH^-] + k_{ga}[HN^{(+)}] + k_{gb}[\odot N^{(-)}] + k_{gab}[HN^{(+)}][\odot N^{(-)}] \quad (4\text{–}26)$$

In this case, the observed rate constant is a nonlinear function of the total concentration of buffer. Because the term $k_{gab}[HN^{(+)}][\odot N^{(-)}]$ is directly proportional to the square of the total concentration of buffer, Equation 4–26 is **quadratic in the total concentration of buffer** and the curves are parabolic. The three individual general acid–base rate constants are obtained by fitting the data for several different buffer ratios with Equation 4–26 by nonlinear least squares analysis.

Each term in the equation for the observed rate constant (Equation 4–22 or 4–26), because it appears as the participant in a sum, refers to an **independent route between reactants and products through a different transition state**. If it has been observed that a term in the observed rate constant proportional to the concentration of the conjugate acid of the buffer, or the conjugate acid of any other added acid–base, $k_{ga}[HN^{(+)}]$, is significant, then the path represented by this term is referred to as **general acid catalysis.** If it has been observed that the term in the observed rate constant proportional to the concentration of the conjugate base of the buffer, or the conjugate base any other added acid–base, $k_{gb}[\odot N^{(-)}]$, is significant, then the path represented by this term is referred to as **general base catalysis.**

So far, only unimolecular reactions have been discussed. If the reaction is a **bimolecular reaction**

$$A + B \longrightarrow Y + Z \quad (4\text{–}27)$$

for which the rate is directly proportional to concentrations of reactant A and reactant B and if the reaction is susceptible to specific acid, specific base, general acid, and general base catalysis, then the equation for the rate of the reaction is defined by the relation

$$-\frac{d[\mathrm{A}]}{dt} = -\frac{d[\mathrm{B}]}{dt} = k_{\mathrm{H^+}}[\mathrm{H^+}][\mathrm{A}][\mathrm{B}] + k_{\mathrm{non}}[\mathrm{A}][\mathrm{B}] + k_{\mathrm{OH^-}}[\mathrm{OH^-}][\mathrm{A}][\mathrm{B}] + k_{\mathrm{ga}}[\mathrm{HN^{(+)}}][\mathrm{A}][\mathrm{B}] + k_{\mathrm{gb}}[\odot\mathrm{N^{(-)}}][\mathrm{A}][\mathrm{B}] \quad (4\text{–}28)$$

This equation contains a termolecular term involving the concentration of the general acid and a termolecular term involving the concentration of the general base. **A termolecular collision is almost never involved in the mechanism of a chemical reaction.** Consequently, in a bimolecular reaction, in which two molecules must collide to form product, it is probably never the case that those two molecules and a general acid or a general base that is catalyzing the reaction collide simultaneously. A bimolecular reaction is catalyzed by a general acid or a general base because the conjugate base of one of the two reactants participating in the reaction is already pre-associated with the acceptor for a hydrogen bond from that general acid or the conjugate acid of one of the two reactants participating in the reaction is already pre-associated with the donor of a hydrogen bond to that general base, respectively, before two molecules of reactant collide. The rate of the reaction is directly proportional to the molar concentration of a general acid or general base that is catalyzing it because the concentration of the hydrogen bond in the **pre-association** between the one molecule and the general acid or base is directly proportional to the molar concentration of the acid or base. It is these complexes that participate in a productive collision and the resulting transition state that is responsible for that rate constant.

There are many reactions that seem to display neither general acid catalysis nor general base catalysis even though their rates are functions of the pH of the solution. For example, the pseudo-first-order rate constant, k_{FA}, for hydrolysis of formaldehyde acetal **4–2** (FA)

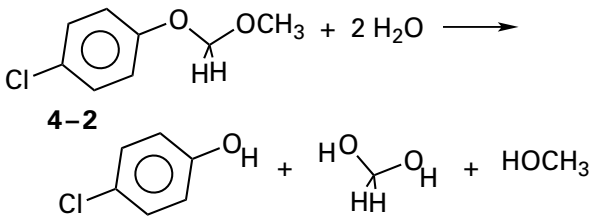

(4–29)

was unaffected by the concentration of buffer (sodium formate), but the pseudo-first-order rate constant was directly proportional to the concentration of hydronium.[12] The relation at 56 °C at an ionic strength of 1.0 M in H_2O is

$$k_{\mathrm{FA}} = 0.018\ \mathrm{M^{-1}\ s^{-1}}[\mathrm{H^+}] \quad (4\text{–}30)$$

In this case, as in the hydrolysis of most acetals and ketals, the rate constant for the reaction is a function only of the concentration of hydronium, it remains proportional to the concentration of hydronium even at relatively high values of pH, and it is unaffected by addition of any other acids or bases to the solution.[3]

As such, hydrolysis of an acetal serves as an example of a reaction that displays specific acid catalysis. **Specific acid catalysis** is the increase in the rate of a reaction produced by decreasing the pH when no general acid catalysis can be observed. **Specific base catalysis** is the increase in the rate of a reaction produced by increasing the pH when no general base catalysis can be observed. The fact that these terms have negative definitions makes them always equivocal. It is always possible that general acid–base catalysis, although it exists, has simply not yet been observed.

The observed behavior of the rate of a particular reaction as a function of pH and the concentration of general acids and bases is the basis for descriptions of the participation of hydron transfers in the mechanism of that reaction. Although the point was not made at the outset, it should be emphasized now that, as with any set of kinetic measurements, **observations must be clearly distinguished from interpretation of those observations**. All the dissection discussed so far is concerned with fitting the data to phenomenological equations that simply organize what has been measured without any attempt to explain what is observed. Rate equations that have been presented are formal descriptions of the observed behavior of the rate of a reaction as a function of pH and concentrations of general acids

and general bases, and they have intentionally avoided any implication of mechanisms that can explain these observations. Even though no mechanisms were proposed, nevertheless one's intuition intrudes. For example, one might think that general acid catalysis must involve the conjugate acid of the buffer pair and general base catalysis the conjugate base. Such intuitions can often be misleading and should be suppressed.

Kinetics are able to rule out mechanisms that are inconsistent with the observations, but kinetics can never prove a mechanism. As was the case with steady-state kinetics, all that can be concluded is that a mechanism proposed by the investigator is consistent with the observations. What follows describes how **mechanistic proposals are shown to be consistent with the observations**.

In the case of **pH–rate behavior in the absence of general acids and general bases**, mechanistic inferences are made by **rearranging each term that appears in the rate equation describing the observed behavior.** In the rearrangements, each term in the observed rate equation is converted into a form in which appear explicitly the concentrations of each species proposed by the investigator to be participating in an encounter complex. The investigator, on the basis of her intuition as to what is responsible for the catalysis observed or other observations that do not rely on kinetics, formulates a molecular description of the mechanism of the reaction that involves a certain collection and orientation of particular participants in the transition state for the rate-limiting step in the reaction. An **encounter complex** is a complex of all the necessary molecular participants in the transition state for the production of an intermediate or product, which have been assembled together at an encounter-controlled rate. Most of the time, the participants dissociate before a transition state forms, except in the case of an encounter-controlled reaction. The fact that a rearrangement of one term in the observed rate equation can be made so that it involves all these participants and only those participants in the encounter complex demonstrates that the proposed transition state for the reaction governed by that term is consistent with the observations.

For example, in the case of ketonization of vinyl alcohol (VA)

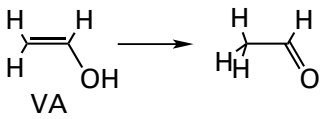

(4–31)

for which the pH–rate profile is defined by Equation 4–5,[13] the term $k_{OH^-}[OH^-][VA]$ in the observed rate equation is consistent with the existence of hydrogen-bonded encounter complex **4–3**

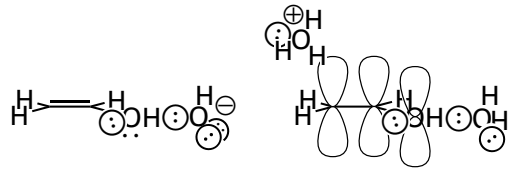

4–3 **4–4**

on the trajectory to a transition state in which a hydron is being removed from the hydroxy group of the vinyl alcohol ($pK_a = 10.5$; Figure 1–23) by a hydroxide to form the enolate. The term $k_{H^+}[H^+]$ in Equation 4–5 is equal to the term $k'_{H^+}[H^+][H_2O]$ because **the concentration of water was constant** during the measurements. This latter term is consistent with the encounter complex **4–4** on the trajectory to a transition state in which a hydron is being added to the π molecular orbital system of the vinyl alcohol while a molecule of water forming a hydrogen bond to the hydroxy group is accepting its hydron. The term $k_{non}[VA]$ can be rearranged to

$$k_{non}[VA] = \left(\frac{k_{non}}{K_w}\right)[H^+][OH^-][VA] \tag{4–32}$$

where K_w is the water constant. This rearrangement of this term in the rate equation is consistent with an encounter complex on the trajectory to a transition state in which a hydron from a hydronium is being added while a hydron is being removed from the vinyl alcohol

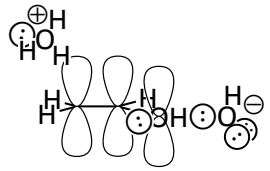

4–5

by a hydroxide. Each rearrangement of the terms demonstrates only that the respective proposed encounter complex is consistent with the observed behavior.

For the mechanism of enolization of mandelic acid (Equation 4–12), the rate equation (Equation 4–17) can be rearranged to

$$-\frac{d[\mathrm{MAH}]_t}{dt} = k'_{H^+}[H^+][H_2O][MAH] + k'_{OH^-}[H_2O][OH^-][MAH] + \left(\frac{k'_{2OH^-}K_w}{K_{aMAH}}\right)[H_2O][OH^-][MA^-] \quad (4\text{–}33)$$

where $k'_{H^+} = k_{H^+}[H_2O]^{-1}$, $k'_{OH^-} = k_{OH^-}[H_2O]^{-1}$, and $k'_{2OH^-} = k_{2OH^-}[H_2O]^{-1}$, which are constants as long as the concentration of water is unchanged. These rearrangements are consistent with the existence of three encounter complexes

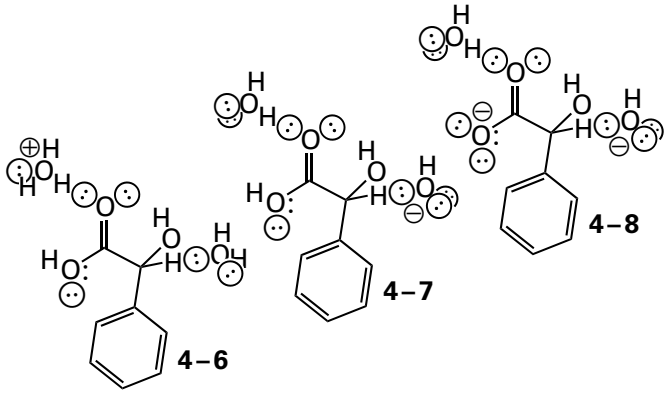

in three respective mechanisms, each on a trajectory to a unique transition state for the enolization. Each trajectory would dominate in a different region of pH.

Another aspect of the importance of distinguishing clearly between observation and explanation is the fact that **there are almost always several explanations** for the observation of specific acid catalysis, specific base catalysis, general acid catalysis, or general base catalysis. For example, the terms in the rate equation for the kinetic mechanism for hydrolysis of *N*-acetylimidazole (Equation 4–11) can be rearranged as the analogous terms were in Equation 4–33, and the rearranged rate equation

$$-\frac{d[\mathrm{AcIm}]_t}{dt} = k'_{H^+}[H^+][H_2O][AcIm] + \left(\frac{k_{non}}{K_w}\right)[H^+][OH^-][AcIm] + k'_{OH^-}[H_2O][OH^-][AcIm] \quad (4\text{–}34)$$

is consistent with the existence of three encounter complexes

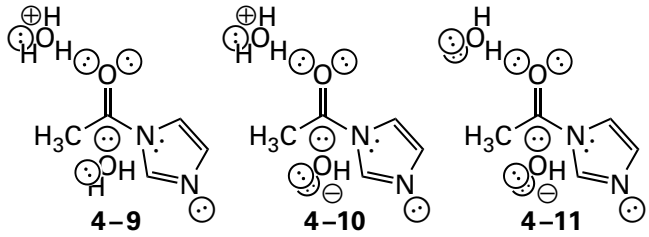

on the trajectories to three respective transition states. The first two encounter complexes themselves, however, can also be rearranged so that, in each case, the hydronium is hydronating nitrogen 3 of the imidazolyl group rather than the acyl oxygen. These two additional encounter complexes are also consistent with the observations.

The rate equation (Equation 4–11), however, can also be rearranged to

$$-\frac{d[\mathrm{AcIm}]_t}{dt} = k''_{H^+}K_{aAcIm}[H_2O]^2[AcImH^+] + \left(\frac{k_{non}K_{aAcIm}}{K_w}\right)[OH^-][AcImH^+] + k'_{OH^-}[H_2O][OH^-][AcIm] \quad (4\text{–}35)$$

where $k''_{H^+} = k_{H^+}[H_2O]^{-2}$. The first two terms in this latter rearrangement are consistent with the existence of the encounter complexes

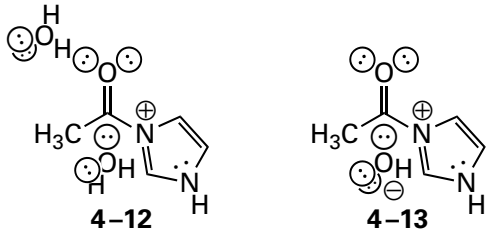

on the respective trajectories to different transition states. The fact that all these encounter complexes are consistent with the observations illustrates that a mechanism cannot be proven by a rate equation alone. In addition, as all the foregoing examples illustrate, any number of molecules of water can be added to the encounter complexes.

The terms in rate **equations for general acid–base catalysis can also be rearranged** to show that a proposed encounter complex is consistent with the observations. For example, the hydrolysis of ethyl

dichloroacetate, $C_2H_5OCOCHCl_2$, in a solution buffered by 2-amino-2-(hydroxymethyl)propane-1,3-diol (Tris) has a pseudo-first-order rate constant that, within experimental error, has no term proportional to the concentration of the conjugate acid of 2-amino-2-(hydroxymethyl)propane-1,3-diol ($TrisH^+$) even though it has a term proportional to the concentration of free base[14] In the rate equation for the reaction, however, this term containing the concentration of free base can be rearranged in two equivalent ways

$$k_{gb}[\text{Tris}][C_2H_5OCOCHCl_2] =$$

$$k'_{gb}[H_2O][\text{Tris}][C_2H_5OCOCHCl_2] =$$

$$\left(\frac{k'_{gb}K_{a\text{TrisH}^+}}{K_{aH_2O}}\right)[OH^-][\text{TrisH}^+][C_2H_5OCOCHCl_2] \qquad (4\text{–}36)$$

where k'_{gb} is $k_{gb}[H_2O]^{-1}$, $K_{a\text{TrisH}^+}$ is the acid dissociation constant of the conjugate acid $TrisH^+$ ($K_{a\text{TrisH}^+} = 8.1$), and K_{aH_2O} is the acid dissociation constant of water ($pK_{aH_2O} = 15.74$). The first rearrangement in Equation 4–36 implies that the free base of the catalyst, a molecule of the ester, and a molecule of water form the encounter complex on the trajectory to the transition state. The second rearrangement in Equation 4–36 implies that a molecule of the cationic conjugate acid of the catalyst, a molecule of the ester, and a hydroxide form an encounter complex on the trajectory to the transition state. At least three different arrangements of constituents

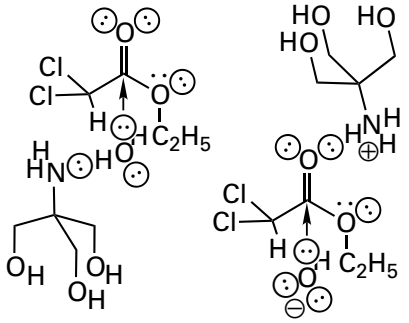

4–14 **4–15** **4–16**

within the encounter complex are consistent with the two rearrangements in Equation 4–36.[14] In each case, the encounter complex is formed in a bimolecular reaction because two reactants participate in a preexisting hydrogen bond.

To decide among the various alternatives for both the observed pH–rate behavior in the absence of general acid–base catalysis and any general acid–base catalysis, **other independent experiments** must be performed. For example, from the results of more extensive studies, it was concluded[8] that the term directly proportional to the concentration of the general acid catalyst chloroacetic acid, $[ClCH_2COOH]$, in the pseudo-first-order rate constant (Equation 4–24) for decomposition of the ethyl hemiacetal of formaldehyde (Equation 4–23) arose from the encounter complex **4–17**

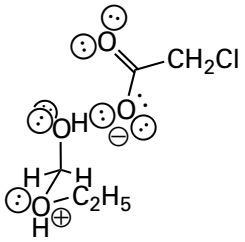

4–17 $k_{ga}[ClCH_2COOH]$

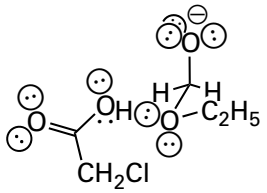

4–18 $k_{gb}[ClCH_2COO^-]$

while the term directly proportional to the concentration of the general base catalyst chloroacetate anion, $[ClCH_2COO^-]$, arose from the encounter complex **4–18**. Ironically, in this instance, contrary to one's immediate intuition, it was concluded that neither term referred to the most straightforward possibility.

The rate equation for hydrolysis of 2-methoxyacrylic acid (Equation 4–19) can be rearranged to

$$-\frac{d[\text{EE}]_t}{dt} = k_{H^+}[H^+][\text{EEH}] + k_{non}\left(\frac{[H^+]}{K_{a\text{EEH}}}\right)[\text{EE}^-] \qquad (4\text{–}37)$$

where, as before, EEH is the conjugate acid 2-methoxyacrylic acid and EE^- is the conjugate base. The two terms in this rearrangement are consistent with the existence of the respective encounter complexes

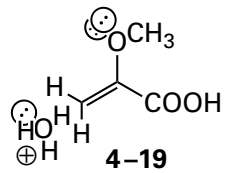

4–19

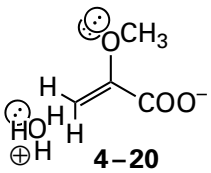

4–20

That these two encounter complexes account for all the hydrolysis is consistent with other observations. Encounter complex **4–19** is that of a hydron with the

neutral enol ether, and encounter complex **4–20** is that of a hydron with the anionic conjugate base of the enol ether.

The pH–rate profile for hydrolysis of 2-methoxyacrylic acid[7] decreases rapidly as the pH of the solution decreases until it levels out to a plateau above pH 0. The rate of hydrolysis is then independent of pH until the pH is increased above the pK_a for the carboxy group (pK_a = 3.39), when it then decreases by a factor of 10 for every increase of one unit of pH. Encounter complex **4–20** is essentially a tautomer of the neutral conjugate acid of the enol ether, EEH, and a molecule of water. The equilibrium between any two tautomers is always independent of pH, so in the range of pH from 0 to 3, where the rate of hydrolysis is independent of pH, this tautomer accomplishes it, and above a pH of 3.39, the decrease in rate is the direct result of the decrease in the concentration of this encounter complex. It follows that at all values of pH greater than 0, encounter complex **4–20** accounts for all the hydrolysis. In this range of pH, it was concluded that the mechanism of hydrolysis is

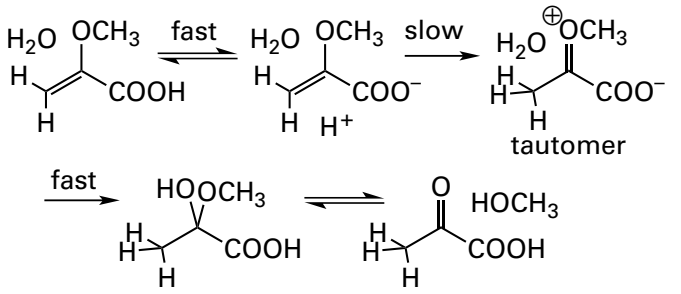

(4–38)

Hydronation of the conjugate base of 2-methoxyacrylic acid (the second step), because it is a hydronation of carbon, is the slow, rate-limiting step in the reaction and forms an actual, zwitterionic tautomer of the neutral conjugate acid. This mechanism is the relevant version of the established mechanism for hydrolysis of enol ethers,[15] in which distal hydronation of the carbon–carbon bond initiates hydrolysis.

The two encounter complexes **4–19** and **4–20** differ from each other only in the state of hydronation of their carboxy groups. Because the rate of the reaction remains the same from pH 0 to pH 3, it must be the case that the rate constant for hydronation of the anionic conjugate base of 2-methoxyacrylic acid at carbon 3 is much greater than the rate constant for hydronation of the neutral conjugate acid. From the pH–rate profile, it could be calculated that these two rate constants differ by a factor of 1300. This difference is reasonable. The carbon of a neutral carboxy group bears significant positive charge because of electron withdrawal by the two oxygens, and this positive charge would destabilize the oxocarbenium ion that is the intermediate in both hydronations, while the carbon of a carboxylato group bears far less positive charge because it is anionic.

All hydrons present in the species the concentrations of which participate in one of the original or rearranged terms in the rate equation are present in the actual encounter complex that gives rise to that term. As was the case with the encounter complex for hydrolysis of 2-methoxyacrylic acid, however, all other tautomers of each encounter complex in which **all these hydrons are present but are in different locations** is also consistent with the same term in the observed rate equation. This ambiguity arises from the simple fact that tautomeric equilibria are independent of pH. Consequently, the observed rate equation can make no distinction among the tautomers of a particular encounter complex, so every tautomer of every encounter complex consistent with a term in the rate equation is a valid candidate for the actual encounter complex.

The term for **concerted general acid–base catalysis**, $k_{gab}[HN^{(+)}][\odot N^{(-)}]$, that appears in some rate equations (see Equations 4–25 and 4–26) for the observed rate constant as a function of the concentration of buffer can also be used to support a particular mechanism. For example, the observed rate equation for the enolization of cyclohexanone, CyH, in buffers of sodium acetate at 25 °C and an ionic strength of 2.0 M has a term 4.8×10^{-7} M^{-2} s^{-1} [HOAc][OAc^-][CyH],[11] where HOAC is acetic acid and OAc^- is acetate. This term is believed to represent the encounter complex

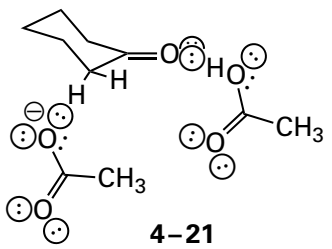

4–21

on the trajectory to a transition state in which a hydron is being added to the carbonyl oxygen of cyclohexanone while a hydron is being removed from its α carbon. In this instance, because a hydrogen bond probably cannot form between a carbon–hydrogen bond and a base, the hydrogen bond that preexists the encounter complex is that between the acetic acid and the carbonyl oxygen.

The distinction between observation and explanation is also critical when considering **specific acid or specific base catalysis** because there are always two different kinetic mechanisms that can explain these observations. A **pre-equilibrium** may occur that involves association of a hydron with or dissociation of a hydron from one of the reactants in a normal acid dissociation followed by a rate-limiting step involving bond-breaking or bond-making. Alternatively, **hydronium may participate as a general acid or hydroxide may participate as a general base** within the encounter complex. In many reactions, only the conjugate base or only the conjugate acid of one of the reactants participates significantly. Because acid–base reactions are so rapid, the equilibrium between the actual reactive species and its unreactive conjugate acid or its unreactive conjugate base can be established rapidly prior to a rate-limiting step that does not involve any hydron transfers in the transition state.

For example, one explanation for the observation of specific acid catalysis in the hydrolysis of formaldehyde acetal **4–2** would be that hydronation of one acetal oxygen in a rapid, normal acid–base equilibrium necessarily precedes the rate-limiting breaking of the bond between the carbonyl carbon and that oxygen, resulting in the departure of the consequently improved leaving group

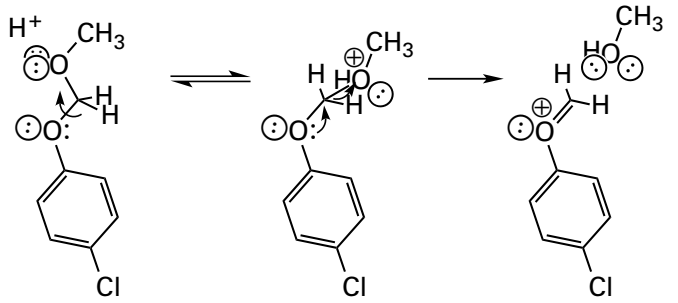

(4–39)

Because the concentration of the hydronated acetal should be directly proportional to the concentration of hydronium at values of pH significantly greater than the pK_a for the oxygen, which should be less than –3, this mechanism involving a pre-equilibrium rather than specific acid catalysis is nevertheless consistent with the observation of specific acid catalysis (Equation 4–30).

Originally, it was hoped that the distinction between general acid–base catalysis and specific acid–base catalysis could be used to **distinguish a mechanism with a pre-equilibrium from a mechanism in which a hydron must be transferred to or from a reactant in the transition state** of the rate-limiting step. It was supposed that if general acid–base catalysis could not be observed but the reaction displayed specific acid catalysis or specific base catalysis, then the mechanism must involve a pre-equilibrium. Unfortunately, an alternative explanation that is also consistent with the observation of specific acid catalysis or specific base catalysis is that the encounter complex for the rate-limiting step does contain either a hydronium or a hydroxide, respectively, that donate or remove a hydron in the transition state of the rate-limiting step in the role of a general acid or a general base, but that general acid catalysis performed by hydronium inescapably present in the solution or general base catalysis performed by the hydroxide inescapably present in the solution is simply so much more effective that catalysis by other acids and bases cannot be observed. In this alternative explanation, the reaction is in fact susceptible to general acid–base catalysis, but it simply cannot be detected at the concentrations of general acids and bases usually examined. An understanding of this imbalance between hydronium and other general acids or between hydroxide and other general bases requires an understanding of the relevant Brønsted relations.

Another issue related to the decision between a acid–base pre-equilibrium and general acid catalysis by hydronium or general base catalysis by hydroxide is that of the relative magnitudes of the observed rates of general acid or general base catalysis and the rate of the same reaction in the absence of any added acid or base. Even when general acid–base catalysis is observed, it rarely results in increases in rate of more than about a factor of 10 at concentrations of buffer less than 1.0 M (Figures 4–1 and 4–4). Specific acid–base catalysis can simply be viewed as the extreme where the magnitude of general acid–base catalysis is so small that it cannot be detected experimentally above the rate of the reaction in the absence of added acid–bases. Because **general acid–base catalysis is usually unremarkable**, and may often be undetectable, the impression might be left that such catalysis may be expendable in enzymatically catalyzed reactions. To understand the fallacy of this impression as well as the conundrum of the alternative kinetic explanations for the observation of specific acid–base catalysis, the reasons that general acid–base catalysis is so unremarkable when reactions are performed in aqueous solution must be appreciated. Again, the basis of this appreciation is a Brønsted relation.

The Brønsted relation for general acid–base catalysis is a function that relates the rate constants or common logarithms of the rate constants for general acid catalysis to the acid dissociation constants or values of pK_a for the catalysts or that relates the rate constants or common logarithms of the rate constants for general base catalysis to the acid dissociation constants or values of pK_a for the conjugate acids of the catalysts.

Suppose that a term in the rate equation for a particular reaction has been designated as the result of **general acid catalysis** because that term is directly proportional to the concentration of the conjugate acid of the buffer in the expression for the observed rate constant, and a series of acids, all with the same type of atom with the same formal elementary charge on which the acidic hydron or hydrons are situated, is chosen for buffering. The Brønsted relation usually observed is

$$\log\left(\frac{k_{ga}}{p}\right) = \log G_A + \alpha\log\left(\frac{qK_a}{p}\right) \qquad (4\text{–}40)$$

where k_{ga} is the observed rate constant for that term, p and q are integers, and $\log G_A$ is a parameter. The other parameter, α, is the **Brønsted coefficient** for general acid catalysis. The term k_{ga}/p is the observed general acid rate constant divided by the number of equivalent hydrons, p, on the general acid. This division yields the rate constant in terms of the molar concentration of acidic hydrons rather than the molar concentration of the general acid itself. The term qK_a/p is the acid dissociation constant of the respective general acid, K_a, **corrected statistically**[16] for the number of equivalent hydrons on the general acid, p, and the number of equivalent lone pairs on its conjugate base, q. After this correction, the dissociation constant of the respective buffer is expressed in terms of the molar concentrations of individual hydrons on the conjugate acid and on the conjugate base.

If $\log(k_{ga}/p)$ is plotted as a function of pK_a + $\log(p/q)$, a linear relation is usually observed with a slope of $-\alpha$. For example, when a series of acids were chosen as general acid catalysts for the cleavage of *N*-(4-nitrophenyl)carbamate

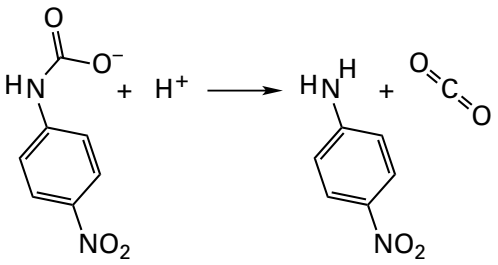

(4–41)

rate constants of the respective terms for general acid catalysis observed for the several catalysts were related to values of pK_a for the acids by a Brønsted relation (Equation 4–40) with $\alpha = 0.84$ (Figure 4–5A).[17] The points for oxygen acids, in which the formal charge number on the oxygen bearing the hydron was 0, and the points for nitrogen acids, in which the formal charge number on the nitrogen bearing the hydron was +1, defined two distinguishable lines of the same slope, a fact demonstrating that **acids with the same atom to which the hydron is attached and which bears the same formal elementary charge usually should be chosen** as the buffers.

Likewise, suppose that a term in the rate equation for a particular reaction has been designated as the result of **general base catalysis** because that term is directly proportional to the concentration of the conjugate base of the buffer in the expression for the observed rate constant, and a series of bases all with the same type of atom with the same formal elementary charge on which the basic lone pair or the basic lone pairs of electrons are situated is chosen for buffering. The Brønsted relation usually observed is

$$\log\left(\frac{k_{gb}}{q}\right) = \log G_B - \beta\log\left(\frac{qK_a}{p}\right) \qquad (4\text{–}42)$$

where k_{gb} is the observed rate constant for that term, $\log G_B$ is a parameter, and K_a is the acid dissociation constant of the conjugate acid of the catalytic general base comprising the buffer. The other parameter, β, is also referred to as a Brønsted coefficient. The integers p and q serve the same purpose as before. The rate constant for general base catalysis is divided by the numbers of equivalent lone pairs q to yield the rate constant in terms of the molar concentration of those lone pairs rather than the molar concentration of the general base. General base catalysis by a series of oxygen bases of the dissociation of 4-methoxyacetophenone bisulfite

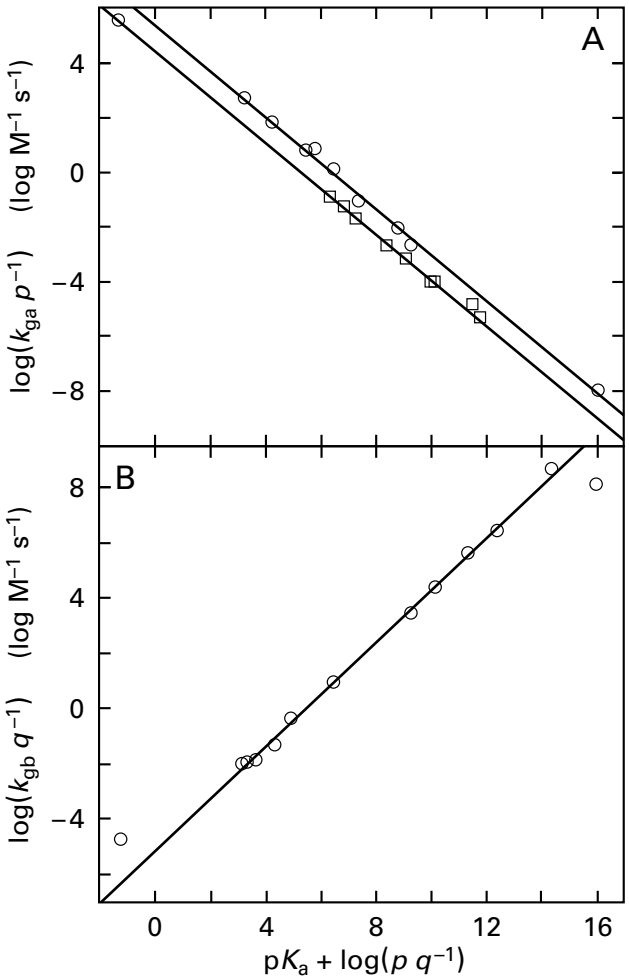

Figure 4–5: Brønsted plots for general acid catalysis and general base catalysis. (**A**) General acid catalysis for the decarboxylation of *N*-(4-nitrophenyl)carbamate (Equation 4–41).[17] Solutions of *N*-(4-nitrophenyl)carbamate were prepared at 1.0 M ionic strength (maintained with KCl) and 25 °C. The solutions were buffered with the respective general acid catalyst and its conjugate base. The decarboxylation was followed spectrophotometrically at 405 nm, the absorption maximum of the product 4-nitrophenylaniline. Rate constants for general acid catalysis, k_{ga}, were determined from the slopes of the lines relating the observed rate constants and the concentration of the respective buffer. The common logarithms of their statistically corrected values, $k_{ga}\ p^{-1}$ (molar^{-1} second^{-1}), are plotted as a function of the negative common logarithms of the statistically corrected values of the acid dissociation constant for each catalyst, $K_a\ q\ p^{-1}$ (molar). Oxygen acids (○), in order of increasing corrected pK_a, were hydronium, glycinium cation, acetic acid, β-glycerophosphate monoanion, cacodylic acid, phosphate monoanion, ethylphosphonate monoanion, boric acid, bicarbonate, and water. Nitrogen acids (□) are plotted separately; they were, in order of increasing corrected pK_a, trifluorethylammonium, imidazolium, 3-quinuclidonium, cyanoethylammonium, morpholinium, 3-hydroxyquinuclidinium, ammonium, quinuclidinium, and pyrrolidinium. (**B**) General base catalysis for the dissociation of 4-methoxyacetophenone bisulfite (Equation 4–43).[18] Solutions of 4-methoxyacetophenone bisulfite were prepared at 1.0 M ionic strength and 25 °C. The solutions were buffered with the general base catalyst and its conjugate acid. The dissociation was followed spectrophotometrically at 285 nm, the absorption maximum of the product 4-methoxyacetophenone. Rate constants for general base catalysis, k_{gb}, were determined from the slopes of the lines relating the observed rate constants and the concentration of the respective buffer. The common logarithms of their statistically corrected values, $k_{gb}\ q^{-1}$ (molar^{-1} second^{-1}), are plotted as a function of the negative common logarithms for the statistically corrected values of the acid dissociation constant for the conjugate acid of each catalyst, $K_a\ q\ p^{-1}$ (molar). The general bases, in order of increasing corrected pK_a for their conjugate acid, were water, formate, glycolate, chloroacetate, acetate, the anion of hexafluoroacetone hydrate, hexafluoro-2-propanolate, ammonia, ethylamine, trifluoroethanolate, guanidine, and hydroxide.

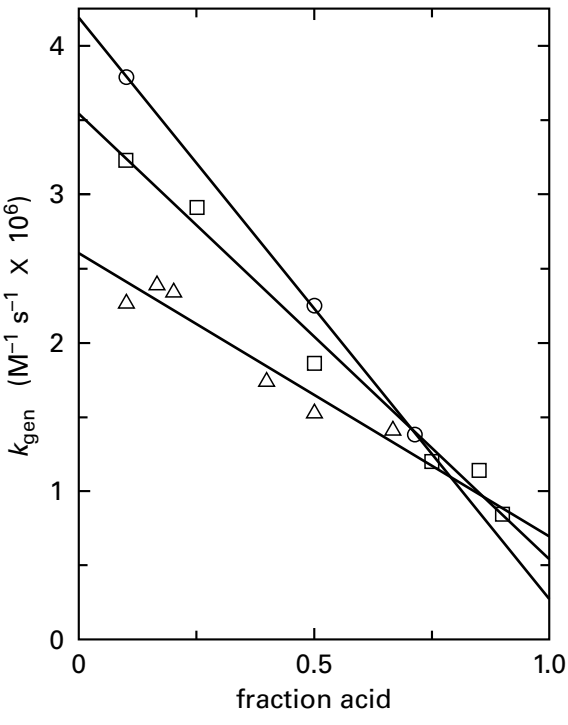

Figure 4–6: Behavior of rate constants for the hydrolysis of α-D-glucopyranosyl fluoride (Equation 4–44) at an ionic strength of 2.0 M and 30 °C as a function of the fraction of the buffer present as the conjugate acid.[19] The progress of the hydrolysis was monitored by polarimetry or nuclear magnetic resonance. The pseudo-first-order rate constants were obtained from linear semilogarithmic plots of the data. The respective rate constants, k_{gen} (molar^{-1} second^{-1} × 10^6; Equation 4–20), for hydrolysis under catalysis by a buffer of ethylphosphonate (○), a buffer of phosphate (□), and a buffer of (trichloro-methyl)phosphonate (△) are plotted as a function of the fraction of the buffer present as the monoanionic conjugate acid. The lines are linear fits of the data.

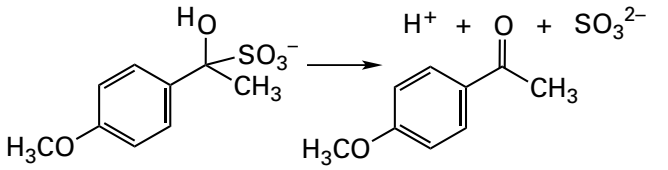

(4–43)

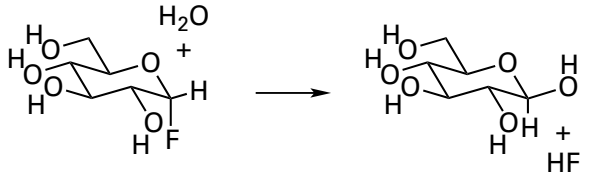

(4–44)

follows a Brønsted relation with $\beta = 0.94$ (Figure 4–5B).[18] As is the case for general acid catalysis, bases with the same atom on which the lone pairs are located and bearing the same formal elementary charge usually should be chosen as the buffers to be examined as general acid–base catalysts.

In **a reaction that is catalyzed by both general acids and general bases**, the lines that describe the behavior of the rate constant k_{gen} as a function of the fraction of acid and base in the buffer for a series of general acid–base catalysts always cross each other (Figure 4–6).[19] This crossing occurs because, as a result of the Brønsted relation, rate constants for general acid catalysis increase with decreases in pK_a for the conjugate acid of the buffer while rate constants for general base catalysis increase with increases in the pK_a for the conjugate acid of the conjugate base of the buffer.

The Brønsted relations demonstrate that **the acidity of the general acid or the basicity of the general base determines the effect of the catalyst** on the rate of the reaction. As might be expected, the more acidic the general acid, the greater will be the rate constant for general acid catalysis. The more basic the general base, the greater will be the rate constant for general base catalysis. The magnitude of values for α and β, however, will determine the strength of these effects. If the value for α or β is small, the acidity or basicity of the catalyst has only a small effect on the respective rate constant, but if α or β is near 1, the acidity or basicity of the catalyst will have a large effect.

If the mechanism of a reaction involves a general acid as the donor of a hydron in the transition state, it is generally assumed that a **small value for the Brønsted coefficient α indicates that the bond between the general acid and its hydron is only marginally broken at the transition state**. Likewise, if the mechanism involves the general base as the acceptor for a hydron in the transition state, a small value for β indicates that the bond between the general base and the hydron is only marginally formed at the transition state. For example, the hydrolysis of α-D-glucopyranosyl fluoride is catalyzed by several phosphates and phosphonates with different values of pK_a. Catalysis by the conjugate acids has a Brønsted coefficient $\alpha = 0.15$, and catalysis by the conjugate bases has a Brønsted coefficient $\beta = 0.06$.[19] Consequently, the hydron from the general acid is only marginally transferred to one of the reactants in the transition state for general acid catalysis, and the hydron from one of the reactants is only marginally transferred to the general base in the transition state for general base catalysis. It was concluded from other observations that the general acid forms a hydrogen bond to the fluoride ion (p$K_{aHF} = 3.2$), leaving the glucoside in the one transition state, and the general base forms a hydrogen bond with a hydron on the nucleophilic molecule of water in the other transition state. Each hydrogen bond, which involves only a small amount of hydron transfer, stabilizes the respective transition state, and the respective reaction is accelerated. When a Brønsted coefficient has a value near 0, any source of a hydron or any lone pair, respectively, will be as effective as any other.

If a general acid acts as a donor of a hydron in the transition state, it is generally assumed that a **value for α near 1.0 indicates that the bond between the general acid and its hydron is largely broken at the transition state**. Likewise, if a general base acts as a hydron acceptor in the transition state, a value for β near 1.0 indicates that the bond between the general base and the hydron is largely formed in the transition state. For example, for removal of the α-hydron from sulfonium cation **4–22**

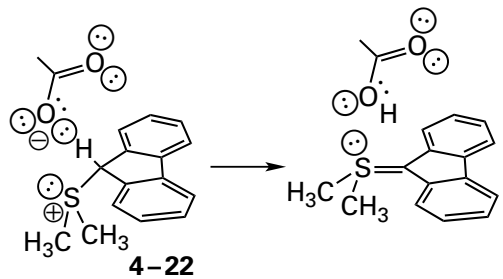

4 – 22

(4–45)

the Brønsted coefficient β for a series of carboxylates, the conjugate acids of which vary in pK_a, was 1.0. Sufficient evidence was provided that this Brønsted

coefficient should be corrected for the effects of solvation to a value of $\beta_{corr} = 0.8$; nevertheless, its magnitude was believed to indicate that the bond between the carbon and the hydron was mostly broken in the transition state.[20] This nonenzymatic reaction is an example of the ability of a carboxylate to remove a hydron from carbon, as Glutamate 164 does in the active site of triose-phosphate isomerase (previously Equation 3–384)

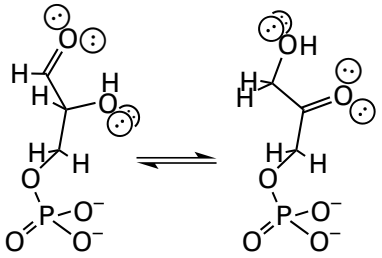

(4–46)

from *Saccharomyces cerevisiae* (Figure 3–37). When a Brønsted coefficient has a value near 1.0, the strength of the acid or the base, respectively, should be fully manifested in the transition state, and the identity of the acid or the base, respectively, is of significant consequence.

In many instances, the value for a **Brønsted coefficient changes as one of the substituents on a reactant is changed**. For example, in a series of acetaldehyde hemiacetals undergoing decomposition

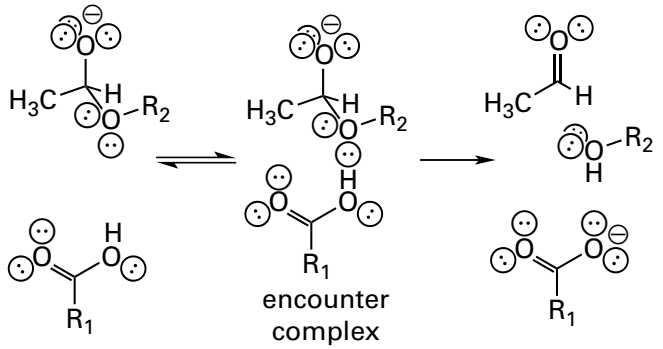

(4–47)

under apparent general base catalysis by a series of carboxylate anions (R_1COO^-), the Brønsted coefficient β increased as the pK_a for the alcohol (R_2OH) that is the product decreased. From other observations, it was concluded that the conjugate acid of the carboxylate actually catalyzed the breakdown of the oxyanionic conjugate base of the hemiacetal (Equation 4–47) so that the Brønsted coefficient for these catalysts, the carboxylic acids, decreased as the alcohol became a better leaving group. As the leaving group improves, the transition state is reached earlier along the reaction coordinate, where the bond between the oxygen of the carboxy group and the hydron in the carboxylic acid is less dissociated.[21] When the Brønsted coefficients (themselves the slopes of lines produced by the values of pK_a for other participants in the reaction) was plotted as a function of the values of pK_a for the leaving groups, a linear relation was observed, the slope of which is the **interaction coefficient**. In this instance, the interaction coefficient quantifies the coupling between dissociation of the carbon–oxygen bond and transfer of the hydron to the oxygen of the leaving group.

As already noted, if a reaction has a mechanism requiring that the transfer of a hydron occur in a step before the rate-limiting step, and if that transfer of a hydron is so rapid as to be at equilibrium, and if no further acid–base catalysis is occurring, then specific acid–base catalysis should be observed. It is also possible, however, that a reaction displays specific acid–base catalysis because the magnitude of the general acid–base catalysis, which in this particular instance does exist, is nevertheless too small to be observed. **The Brønsted relations explain why general acid or general base catalysis is usually weak or sometimes immeasurable**.

Consider a reaction susceptible to general acid catalysis. Assume for the moment that the hydronium, H_3O^+, behaves as a typical general acid in the set of catalytic acids. From the Brønsted relation for the reaction of interest (Equation 4–40)

$$k_{ga,HN^{(+)}} = k_{ga,H_3O^+}\left(\frac{q_{\odot N^{(-)}}}{2}\right)^{\alpha}\left(\frac{p_{HN^{(+)}}}{3}\right)^{1-\alpha}\left(\frac{K_{aNH}}{K_{aH_3O^+}}\right)^{\alpha} \tag{4–48}$$

where NH is any general acid in the series tested as catalysts and the integers 3 and 2 are, respectively, the number of acidic hydrons on a hydronium and the number of basic lone pairs on a molecule of water, its conjugate base. If it is also assumed that terms involving $q_{N^{(-)}}$, 2, $p_{NH^{(+)}}$, and 3 are together nearly equal to 1, then

$$k_{ga,HN^{(+)}} \cong \left(\frac{K_{aNH}}{K_{aH_3O^+}}\right)^{\alpha} k_{ga,H_3O^+} \tag{4–49}$$

If only acid catalysis is kinetically significant, then

$$k_{obs} = k_{non} + k_{H^+}[H^+] + k_{ga,NH}[HN^{(+)}] \quad (4–50)$$

If

$$k_{H^+}[H^+] = k_{ga,H_3O^+}[H_3O^+] \quad (4–51)$$

then

$$k_{obs} \cong k_{non} + k_{H^+}[H^+] + k_{H^+}[HN^{(+)}]\left(\frac{K_{aNH}}{K_{aH_3O^+}}\right)^{\alpha} \quad (4–52)$$

$$k_{obs} \cong k_{non} + k_{H^+}[H^+] + k_{H^+}[HN^{(+)}]\left(\frac{[\odot N^{(-)}][H^+]}{[H_2O][HN^{(+)}]}\right)^{\alpha} \quad (4–53)$$

$$k_{obs} \cong k_{non} + k_{H^+}[H^+] + k_{H^+}[HN^{(+)}]\left(\frac{[\odot N^{(-)}]}{[H_2O]}\right)^{\alpha}\left(\frac{[HN^{(+)}]}{[H^+]}\right)^{1-\alpha} \quad (4–54)$$

Because $[\odot N^{(-)}] << [H_2O]$ under all usual circumstances, the term $([HN^{(+)}]/[H^+])^{1-\alpha}$ must be sufficiently large to counteract the resulting, inescapable effect of the term $([\odot N^{(-)}]/[H_2O])^{\alpha}$ on the rate equation for general acid catalysis to be significant.

In particular, if α is near a value of 1.0, the disparity between the concentration of water, which is the conjugate base of the hydronium, and the concentration of the conjugate base of any general acid other than hydronium will dominate in the third term of Equation 4–54. In this instance, because hydronium is present inescapably in the solution, general acid catalysis by the added acid will not be observed even though general acid catalysis is occurring robustly with hydronium as the general acid and also occurring with the added acid but at an insignificant rate. If, however, α is sufficiently small and the added acid is sufficiently weak so that the chosen concentrations of its conjugate acid are much greater than the concentration of hydronium that can be achieved, then general acid catalysis will be significant.

A similar explanation can be formulated for the competition between specific base catalysis and general base catalysis. In this instance, when β is near a value of 1.0, general base catalysis by added bases will not be observed because general base catalysis by the hydroxide present inescapably in the solution will again dominate.

From all these considerations, it is clear that **the reason both general acid catalysis and general base catalysis are so unremarkable in any aqueous solution is that water is always the acid–base present at the highest concentration**. Because the concentration of water is so high relative to the concentration of any added acid or base, the concentrations of its conjugate acid, hydronium, or its conjugate base, hydroxide, are anomalously high relative to the concentration of any added acid or base, respectively. Because of these biases in concentration, hydronium or hydroxide acts preferentially when a general acid or a general base is required in the reaction. Another way of looking at the situation is that H_3O^+ is such a strong acid and OH^- is such a strong base that, even when their concentrations are small relative to an added general acid or general base, respectively, they can compete successfully, as long as the relevant Brønsted coefficient is large enough.

Nevertheless, most reactions homologous to those that occur in particular active sites have an absolute, inescapable requirement for catalytic acids or bases or both. The observation of specific acid–base catalysis and general acid–base catalysis demonstrates this requirement. The fact that the inescapable presence of hydroniums, hydroxides, and molecules of water in solution causes general acid–base catalysis to be so unimpressive leads to the misconception that acid–base catalysis in general is unimpressive. Nothing could be farther from the truth. In fact, **in almost all the reactions catalyzed by enzymes, acid–base catalysis is an essential requirement.**

There is a big difference, however, between a reaction requiring transfers of hydrons when it occurs in aqueous solution and that same reaction when it occurs in the active site of an enzyme. The two situations differ dramatically because a reactant in an active site can no longer diffuse through the solution encountering hydroniums, hydroxides, and molecules of water. Consequently, **the reaction must rely on the acids and bases within the active site**, and usually it must rely on them alone. As a result, whenever a hydron must be added to or removed from an atom in a substrate or an inter-

mediate, there will be a catalytic acid–base in the active site immediately adjacent to that atom. These catalytic acid–bases are usually side chains of the amino acids that comprise the active site. Nor is this requirement exclusive to the active sites of enzymes. Ribosomes use the bases of nucleotides in the nucleic acid that forms their active sites, all of which have hydrons and lone pairs of electrons with reasonable values of pK_a, as catalytic acid–bases for all the same reasons.[22]

A common feature of enzymatic active sites is that donors and acceptors for hydrogen bonds to a reactant often become catalytic acids and catalytic bases, respectively, as the reaction progresses. The active site of an enzyme binds substrates specifically and in the proper orientation in part because aligned hydrogen bonds form between donors and acceptors on the amino acids lining the active site and acceptors and donors on substrates. These donors and acceptors for hydrogen bonds involved in the recognition of substrates (Figures 3–33, 3–34, 3–40, and 3–42) can automatically become catalytic acid–bases when required by the reaction. For example, in the active site of triose-phosphate isomerase (Equation 4–46) from *S. cerevisiae*, the carbonyl oxygen of glycerone phosphate is recognized by participating in a hydrogen bond with the imidazolyl group on Histidine 94 and the ammonio group on Lysine 11 (Figure 3–37), and the hydroxy group on carbon 3 of glycerone phosphate is recognized by participating in a hydrogen bond (0.32 nm) with the amido group in the side chain of Asparagine 9.[23,24] Because the imidazolyl group of Histidine 94 is in its neutral form in the complex,[25] which is a poor acid (pK_a = 14), the ammonio group of Lysine 11 (pK_a = 10.5) is the catalytic acid–base that adds the hydron to and removes the hydron from the oxygen on carbon 2 to catalyze the enolization of glycerone phosphate.[26] Consistent with this conclusion, it is the amino group on Lysine 11 that is responsible for removing a hydron from the hydroxy oxygen on the *cis*-enediol intermediate.[27] While the ammonio group of Lysine 11 hydronates the carbonyl oxygen of glycerone phosphate, the carboxylato group of Glutamate 164 removes the hydron from carbon 3 to form the *cis*-enediol intermediate

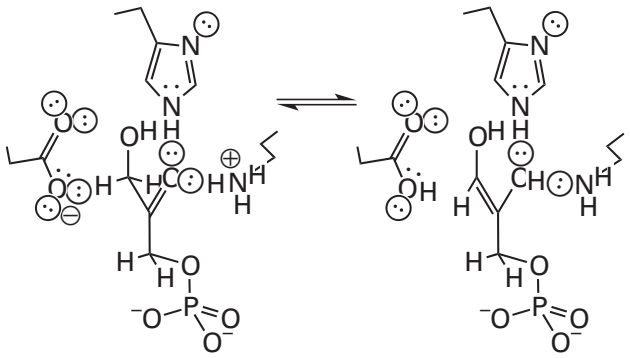

(4–55)

In the reverse direction, while the amino group of Lysine 11 dehydronates the hydroxy group of the *cis*-enediol, the carboxy group of Glutamate 164 adds the hydron to carbon 3 to form glycerone phosphate. In the next step, the imidazolyl group of Histidine 94 hydronates oxygen 2 of the *cis*-enediol simultaneously with the transfer of the hydron already on oxygen 2 back to the amino group of Lysine 11, and then the resulting anionic imidazo group of Histidine 94 swings over to remove the hydron from oxygen 1 of the *cis*-enediol[28] as the carboxy group on Glutamate 164 adds its hydron to carbon 2 to produce D-glyceraldehyde 3-phosphate. In reverse, the imidazolyl group of Histidine 94 adds the hydron to oxygen 1 D-glyceraldehyde 3-phosphate as the carboxylato group on Glutamate 164 removes the hydron from carbon 2 and then the imidazo group swings over to the oxygen on carbon 1 to dehydronate it as the ammonio group on Lysine 11 hydronates it to form the *cis*-enediol.*

The case of triose-phosphate isomerase (Equations 4–46 and 4–55 and Figure 3–37) illustrates the fact that catalytic acid–bases must be provided by an active site, or the reaction will not proceed. If an acid–base were not provided to add or remove a hydron from carbon, the enzymatic reaction would not occur. If an acid–base were not provided to hydronate and dehydronate the carbonyl oxygen of

*The imidazolyl group of Histidine 94 does not seem to move detectably during catalysis because the *B* factors of its atoms are the smallest of the atoms involved in catalysis (Figure 3-37).[23] This apparent immobility is probably due to two facts. First, as soon as it removes the hydron from oxygen 1 of the *cis*-enediol in the forward direction, oxygen 1 becomes a carbonyl oxygen (pK_a = –5) and the imidazolyl returns immediately to the stronger base, the hydroxyl (pK_a = –2) on oxygen 2. Second, in the reverse direction, as soon as the neutral imidazolyl group adds a hydron to oxygen 1 of D-glyceraldehyde 3-phosphate and becomes the anionic imidazolio group, it must immediately return to oxygen 2 to pick up a hydron relayed by oxygen 2 from the ammonio group of Lysine 11. Consequently, it seldom participates in a hydrogen bond to oxygen 1 and almost always participates in a hydrogen bond to oxygen 2.

glycerone phosphate, the rate of the enzymatic reaction would decrease dramatically.[26]

After reactants have bound and, in the process, have displaced waters of hydration within the empty site, the active site has become, by and large, anhydrous. In anhydrous benzene, the anomerization of 2,3,4,6-tetramethyl-D-glucose (TMG)

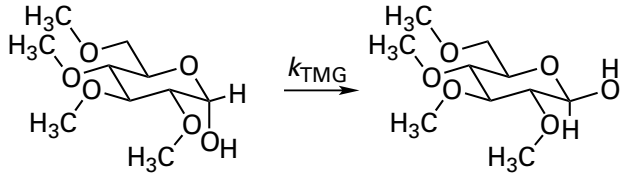

(4–56)

is very slow and variable in rate, suggesting that what little reaction is observed has an absolute requirement for traces of general acids or general bases contaminating the solvent even though it was rigorously purified.[29] When pyridine (Pyr) is added as a catalyst, the rate law contains, in addition to the negligible term for the uncatalyzed reaction, a term of the form $k_{Pyr,TMG}[Pyr][TMG]^2$. When both pyridine and phenol (PhOH) are added, the rate law contains an additional term of the form $k_{Pyr,PhOH,TMG}[Pyr][PhOH][TMG]$.

In these two instances of general acid–base catalysis, the individual terms are termolecular, and it was originally concluded[29] that, in benzene, the anomerization of tetramethyl-D-glucose has an absolute requirement for a general acid and a general base simultaneously

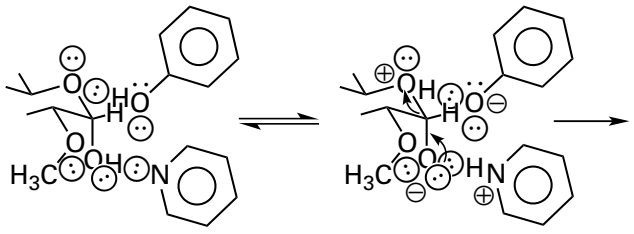

(4–57)

whereas for anomerization in the absence of phenol, the hydroxy group of another 2,3,4,6-tetramethyl-D-glucose would act as the general acid catalyst. It has since been shown that some of the catalysis observed, if not all of it, is due to general base catalysis by either glucosate anion or phenoxide anion acting alone at the hydroxy group on carbon 1 of 2,3,4,6-tetramethyl-D-glucose[30]

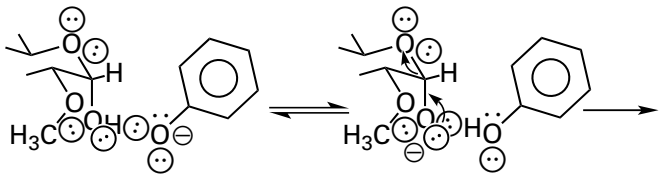

(4–58)

Values of pK_a of 9.9 for phenol and 14.4 for one of the hydroxy groups on 2,3,4,6-tetramethyl-D-glucose in aqueous solution should be significantly higher in benzene. Consequently, the molar concentrations of these strongly basic anions responsible for the catalysis are directly proportional either to [Pyr][TMG] or to [Pyr][PhOH], respectively, because pyridine is the strongest base in the solution and hence will be responsible for removing a hydron from either phenol or a hydroxy group in the absence of water. General base catalysis by other strong bases, acting alone, also is sufficient[30] for mutarotation. Nevertheless, all the results agree on the absolute necessity for at least one added catalyst when the anomerization is performed in anhydrous benzene.

One of the most effective catalysts of the mutarotation of 2,3,4,6-tetramethyl-D-glucose in benzene is 2-hydroxypyridine[31]

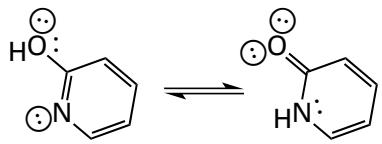

4–23

(4–59)

a compound chosen on the assumption that it would be a bifunctional catalyst

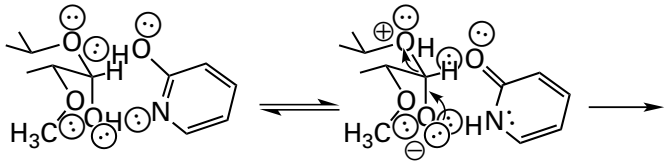

(4–60)

At a concentration of 0.05 M in benzene, 2-hydroxypyridine catalyzes the anomerization of tetramethyl-D-glucose 200 times more rapidly than 0.05 M phenol and 0.05 M pyridine.

In aqueous solution, however, the mutarotation of D-glucose is not significantly catalyzed by addition of 0.1 M 2-hydroxypyridine because the unavoidably present hydronium and hydroxide are even more efficient catalysts than 2-hydroxypyridine. Again, the implication of these observations is that

in an active site, in which bound reactants are no longer diffusing through the aqueous solution, the catalytic acids and catalytic bases provided by the active site become essential to catalysis even if, in the guise of general acid–bases, these same catalytic acid–bases are unnecessary when the reactants are dissolved in water.

Another feature of an anhydrous or mostly anhydrous active site in the Michaelis complex with a reactant immediately preceding a transition state is that the **relative permittivity of the active site is much less than the relative permittivity of water**. Acid dissociation constants tabulated for the side chains of the amino acids (aspartic acid, 4.0; glutamic acid, 4.3; histidinium, 6.6; cysteine, 8.7; tyrosine, 9.8; and lysinium, 10.5)[32] are for these acids in a randomly coiled polypeptide when they are fully exposed to the aqueous phase. As reactants and the protein close around a catalytic acid or catalytic base in the side chain of an amino acid in the active site during formation of the catalytically competent Michaelis complex between reactants and enzyme, the contact of the catalytic acid or catalytic base with the aqueous phase diminishes significantly or is completely lost, coincident with a significant decrease in the relative permittivity in its vicinity.

The relative permittivity surrounding an acid **affects its dissociation constant.** According to the Born approximation,[33,34] the standard free energy of solvation for an ion is

$$-\Delta G^{\circ}_{\text{ion}} = -\frac{Q^2}{2r}\left(1 - \frac{1}{\varepsilon_{\text{r}}}\right) \tag{4–61}$$

where Q is the electric charge (in coulombs) of the ion, ε_{r} is the relative permittivity of the surroundings, and r is the radius of the cavity produced by the ion.[35] In the simplest situation, when an acid or a base in an active site is dehydronated or hydronated, respectively, and the hydron dissociating enters the solution or the hydron associating enters the active site from the solution, then the shift in the pK_{a} for acid dissociation of the acid or the conjugate acid of the base will be determined only by the change in the electric charge of the acid–base during that dissociation or association[36]

$$\Delta \text{p}K_{\text{a}} = -\frac{(2z-1)e^2 N_{\text{A}}}{4.606\,RTr}\left(\frac{1}{\varepsilon_{\text{r,as}}} - \frac{1}{\varepsilon_{\text{r,H}_2\text{O}}}\right) \tag{4–62}$$

where z is the charge number on the acid or on the conjugate acid, $\varepsilon_{\text{r,as}}$ is the relative permittivity of the active site, and $\varepsilon_{\text{r,H}_2\text{O}}$ is the relative permittivity of water. For example, the α-imino group on the amino-terminal proline of 2-hydroxymuconate tautomerase from *Pseudomonas putida* has a pK_{a} of 6.4. This pK_{a} is 3 units lower than the pK_{a} for a fully solvated amino-terminal proline in aqueous solution. The shift in pK_{a} experienced by this imino group could be explained if the relative permittivity of the active site in which it is located is 15.[36] This value would be for the active site unoccupied by any substrate for the enzyme, so when it becomes occupied, the relative permittivity and the pK_{a} for the imino nitrogen should decrease even further.

When a carboxy group dissociates in solution

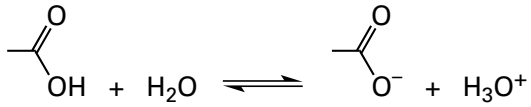

(4–63)

a positive ion and a negative ion are created. Consequently, as the relative permittivity of the solution decreases, and hence the ability of the surroundings to solvate charge, the acid dissociation constant of a carboxy group decreases, the pK_{a} for the carboxy group increases, and the basicity of the carboxylato group increases. In measurements in mixed solvents of alcohols and water or dioxane and water, values of pK_{a} for the carboxylic acids increase by one unit for every decrease of about 15–20 units in relative permittivity.[37-39] Since the relative permittivity of water is 79 at 25 °C, the limit to a shift in pK_{a} due to a decrease in relative permittivity should be around 4 or 5 units. The increase in pK_{a} with decreasing relative permittivity, however, seems to be magnified in aprotic solvents.[38,40] For example, the pK_{a} for acetic acid, which is 4.76 in water, is 11.1 in dimethylformamide ($\varepsilon_{\text{r}} = 38$) and 11.4 in dimethyl sulfoxide ($\varepsilon_{\text{r}} = 47$).[41] These observations may explain why a carboxylato group is among the most common catalytic bases in active sites. In the unoccupied active site, the pK_{a} of its conjugate acid would be fairly low, causing it to be present mostly as the carboxylato group. Upon occupation of the active site by a reactant, however, in particular a reactant that placed an acidic hydrogen on carbon immediately adjacent to it, the pK_{a} for its conjugate acid, and hence its basicity, should increase significantly.

The magnitude of the effect of decreasing the relative permittivity on the pK_{a} for an acid will also **depend on the degree of delocalization of charge** in

the charged species involved. The relative permittivity of the surroundings affects the dissociation constants for acids in which the negative elementary charge created upon dissociation is localized more than when that charge is delocalized. For example, the localized elementary charge on a sulfido group should be destabilized more by a decrease in relative permittivity than the delocalized elementary charge on a phenolate. When the location of the hydron in hydrogen bonds between various phenolates and various carboxylic acids was determined by nuclear magnetic resonance spectroscopy, it was observed that the hydron was on the phenolate oxygen in solvents of high relative permittivity but on the carboxylate oxygen in solvents of low relative permittivity.[42] The conclusion from these observations was that the increase in acid dissociation constant caused by the decrease in the relative permittivity was greater for the carboxy group than the 4-hydroxyphenyl group because the negative elementary charge of the conjugate base is more delocalized in a 4-oxidophenyl group than in a carboxylato group, and consequently a carboxylato group can become more basic than a 4-oxidophenyl group at low relative permittivity.

In more complicated situations, the magnitude of the effect of relative permittivity of an active site on the change in standard free energy of an acid dissociation depends on **the molecular details of the acid dissociation that is occurring**. In free solution, both a carboxylate and the hydronium produced by dissociation of a carboxy group experience low relative permittivity. Under ideal circumstances within a closed active site, in which the hydron is transferred to a neutral acceptor so that its positive elementary charge remains in the active site, the pK_a for a glutamyl or aspartyl side chain could shift from around 4 to around 10, so that the carboxylate anion would become a strong base. If, however, the hydron upon dissociation enters the solution where it will experience high relative permittivity, only the carboxylato group will experience low permittivity and the pK_a will shift by a smaller amount.

Nevertheless, burying an acid–base inside a protein, both by removing it from water, a protic solvent, and transferring it into an aprotic region of lower relative permittivity, causes significant shifts in its pK_a. For example, when 22 interior positions in the folded polypeptide of micrococcal nuclease from *Staphylococcus aureus*, chosen at random, were each in turn mutated to lysine, the pK_a for those buried lysines varied from an unperturbed value of 10.4 (5 substitutions) to values below 7.5 (6 substitutions).[43]

The actual shift that occurs in a pK_a, however, depends strongly on the type of hydron transfer in which the acid–base in an active site participates. If the transfer results in no net change in elementary charge, such as the transfer of a hydron from a carbon α to a carbonyl to a carboxylate

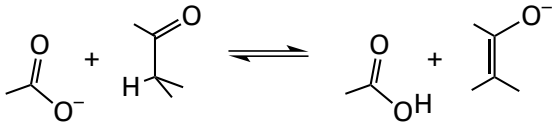

(4–64)

the relative permittivity of the surroundings, as long as they are reasonably uniform, will have much less effect. If, however, the alkylammonium cation of a lysine simultaneously hydronates the enolate oxygen (Equation 4–55), a positive elementary charge and a negative elementary charge disappear during the reaction, and low relative permittivity would decrease the standard free energy of hydron transfer significantly and improve catalysis dramatically.

When a cationic acid dissociates in solution

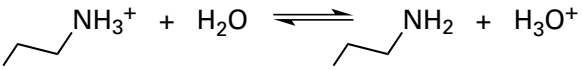

(4–65)

there is no change in the number of elementary charges in that solution. Consequently, the relative permittivity of the solution has only a small effect on the pK_a for the acid. For example, the changes in the apparent pK_a for *n*-butylammonium cation in the solvents methanol, acetone, and acetonitrile seem to be due almost completely to differences in values of the pK_a for the conjugate acids of the solvents themselves, the respective oxygens of which must act as the acceptor of the hydron, as does the water in Equation 4–65, rather than to any differences caused by relative permittivity.[44,45] Again, however, the effect of the relative permittivity of the surroundings will depend on the type of hydron transfer. For example, in the reaction

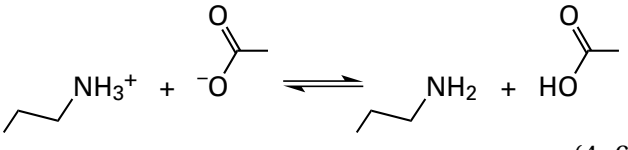

(4–66)

in which a positive elementary charge and a negative elementary charge are disappearing, the relative permittivity of the surroundings will have a significant effect.[46,47]

Another feature of the transfer of a hydron between a substrate and a catalytic acid–base in an active site is its intramolecularity. In the active site of an enzyme, the reaction between the bound substrate and a catalytic acid or catalytic base is an intramolecular reaction, and the **entropy of approximation** gained by converting what would be an intermolecular reaction in solution into an intramolecular reaction in the active site dramatically increases the efficiency of the catalytic acid–base. For example, it is estimated, from the results of site-directed mutation and from rate constants for intermolecular general acid catalysis in aqueous solution, that the general base catalysis in the enolization of mandelate anion (see Equation 4–12) achieved by the imidazolyl group in the active site of mandelate racemase from *P. putida* is 3×10^3 times more effective than that achieved in solution by 1 M imidazole.[6] Again, as before with other similar increases, the use of effective molarity to describe this increase is patently unrealistic.

There are many **examples of nonenzymatic, intramolecular general acid catalysis**. For example, the hydrolysis of acetals (Equation 4–29) is normally an example of pure specific acid catalysis with no evidence of general acid–base catalysis.[3] It is possible, however, to provide an intramolecular general acid catalyst in the form of the 2-carboxy group on phenyl methyl acetal **4–24**

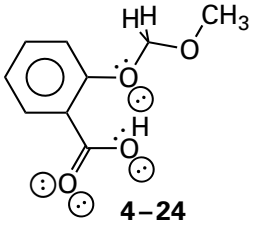

4–24

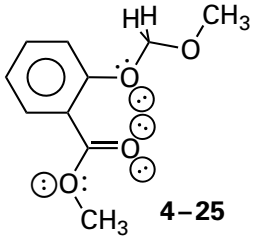

4–25

The methyl ester **4–25** of acetal **4–24** serves as a control that incorporates the electronic structure without the ability to provide a hydron. The pH–rate profiles for hydrolysis of acetal **4–24** and acetal **4–25** differ remarkably (Figure 4–7).[12] Hydrolysis of acetal **4–25,** as with other acetals, displays only specific acid catalysis. Hydrolysis of acetal **4–24,** however, displays a plateau in its pH–rate profile between pH 1 and 4 such that at values of pH greater than 5, in the neutral range of pH, the rate

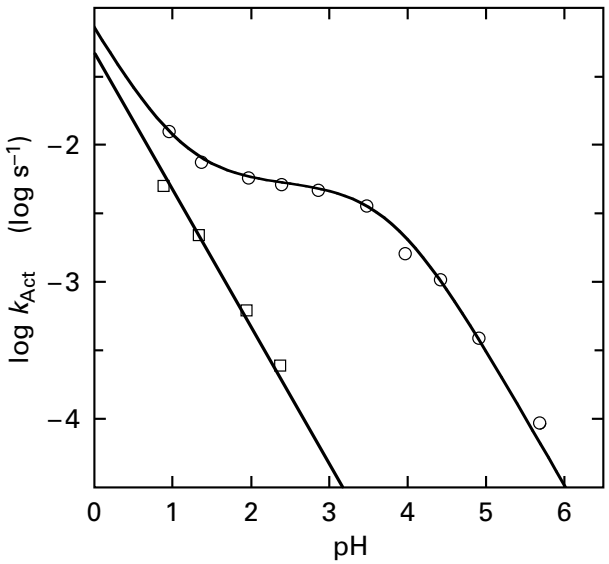

Figure 4–7: Intramolecular general acid catalysis of the hydrolysis of the 2-carboxyphenyl methyl acetal of formaldehyde.[12] Solutions of either 2-carboxyphenyl methyl formaldehyde acetal **4–24** (○) or 2-(methoxycarbonyl)phenyl methyl formaldehyde acetal **4–25** (□) were prepared at an ionic strength of 1.0 M (maintained with KCl) and 56 °C. Solutions were either unbuffered or buffered with sodium formate or potassium acetate. All values for observed rate constants were those obtained by extrapolation to eliminate any effect of buffer on the rate. In most instances, the buffer had no significant effect on the rate of the reaction. The release of the respective phenol as a product of hydrolysis was followed by the increase in absorbance at 302 nm, and pseudo-first-order rate constants, k_{Act}, for each acetal (Act) were obtained from the slopes of plots of the common logarithms of the absorbances as a function of time at the different values of pH. The pH–rate profiles presented are the common logarithms of tabulated pseudo-first-order rate constants for the hydrolysis of the respective acetals, k_{Act} (second^{-1}), plotted as functions of pH.

of its hydrolysis is 270-fold greater than the rate of hydrolysis of the methyl ester. The 2-carboxy group, because it able to hydronate the leaving oxygen intramolecularly in a cyclic transition state in which the hydron is on an oxygen four atoms away, increases the rate of hydrolysis by a factor large enough that general acid catalysis of a reaction in which it was not observed with intermolecular catalysts can now be observed.

Another instance of intramolecular general acid catalysis is hydrolysis of a methyl acetal of formaldehyde within a significantly more complicated scaffold.[48] In this other nucleophilic substitution, the acidic oxygen–hydrogen of the catalytic carboxy group is five atoms from the oxygen of the acetal rather than four as it is in **4–24**, the oxygen of the

acetal is not conjugated to the carboxy group as it is in **4–24**, and the scaffold holding the groups adjacent to each other is tricyclic, rather than monocyclic as it is in **4–24**. The pH–rate profile for this hydrolysis is almost identical to that in Figure 4–7, and the acceleration at higher values of pH is 100-fold greater than the rate of catalysis by hydronium.

The behavior of hydrolysis of acetal **4–24** (Act) as a function of pH (Figure 4–7) can be explained satisfactorily in the following way.[12] Below pH 1, the concentration of hydronium is so high that specific acid catalysis dominates, and

$$k_{\text{Act}} = k_{\text{H}^+}[\text{H}^+] \tag{4–67}$$

Above pH 1, the concentration of hydronium becomes small enough that intramolecular general acid catalysis dominates

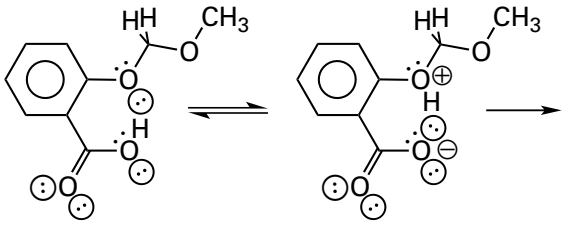

(4–68)

Until the pK_a for the 2-carboxylic acid is reached, the rate of the reaction is invariant with pH. At values of pH in excess of the pK_a for the 2-carboxy group (pK_a = 3.7), the concentration of the carboxylic acid—the species in which intramolecular catalysis can occur—and, consequently, the rate constants decrease by a factor of 10 for every increase of 1 unit in the pH.

The dianionic phosphomonoester **4–26**

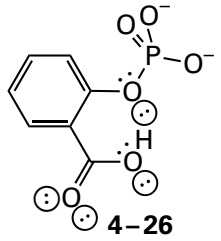

4–26

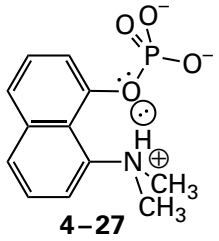

4–27

which is a phosphoric analogue of acetal **4–24**, also displays intramolecular general acid catalysis of its hydrolysis. This catalysis also results from hydronation of the leaving group by the carboxy group.[49] The intramolecular general acid catalysis observed for the zwitterionic dimethylaminonaphthyl phosphomonoester **4–27** results from hydronation of the leaving group by the ammonium.[50]

The observed pH–rate profile for hydrolysis of methyl enol ether **4–1** (Equation 4–2) also displays a plateau similar to that observed in Figure 4–7. The existence of this plateau is consistent with the *endo*-carboxylic acid acting as a general acid that intramolecularly hydronates the peripheral carbon of the enol to form the oxocarbenium ion[1]

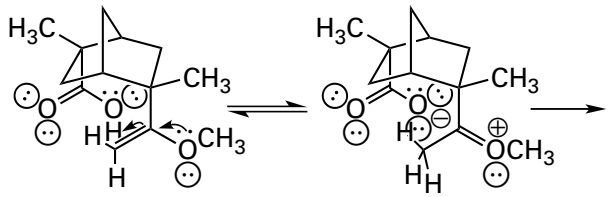

(4–69)

homologous to the oxocarbenium ion that is the intermediate in hydrolysis of 2-methoxyacrylic acid (Equation 4–38). This oxocarbenium ion then reacts with water at its now dramatically electrophilic carbon. This nonenzymatic reaction is an example of a carboxylic acid that hydronates carbon as Glutamatic Acid 164 does in the active site of triosephosphate isomerase from *S. cerevisiae* (Equations 4–46 and 4–55 and Figure 3–37).

The pH–rate profile (Figure 4–8)[51,52] for the intramolecular nucleophilic substitution of one phenoxy group by the *N*-methylimidazolyl group on the other phenoxy group within the symmetric phosphodiester **4–28**

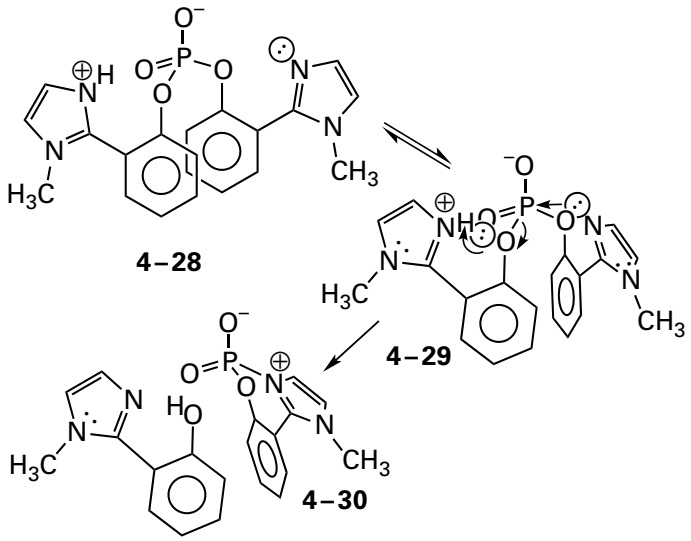

4–28

4–29

4–30

(4–70)

to give the cyclic *O*-aryl phosphoramidate **4–30**, displays a narrow maximum approached on the two sides by lines of slope +1 and slope –1, respectively.

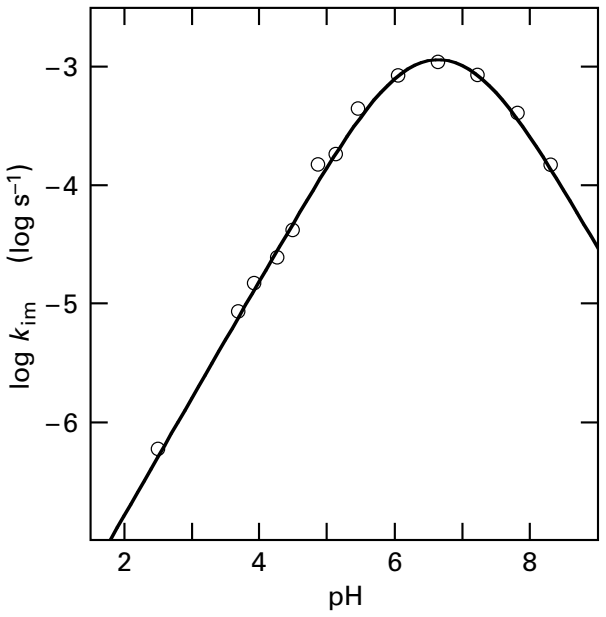

Figure 4–8: Simultaneous intramolecular general acid catalysis and general base catalysis of the hydrolysis of a phosphodiester by two imidazolyl groups.[51,52] The appearance of 2-(1-methyl-1*H*-imidazolyl)phenol resulting from the hydrolysis (Equation 4–70) of bis[2-(1-methyl-1*H*-imidazolyl)phenyl] phosphate (**4–28**) was followed by its absorbance at 290 nm at 60 °C. The rates of appearance of the phenol were first-order. From these rates, rate constants for the hydrolysis were determined at different values of pH. The common logarithms of the rate constants (second^{-1}) for the hydrolysis, k_{im}, are plotted as a function of pH. The solid line is the common logarithm of Equation 4–71 with $k_{im} = 2 \times 10^{-3}$ s^{-1}, pK_{a1} = 6.1, and pK_{a2} = 7.2.

The pH–rate profile is consistent with a rate law of the form

$$-\frac{d[\mathrm{PDE}]_t}{dt} = k_{im}\alpha_{zw}[\mathrm{PDE}]_t = k_{im}\left(\frac{[H^+]}{K_{a1}} + 1 + \frac{K_{a2}}{[H^+]}\right)[\mathrm{PDE}]_t \qquad (4\text{–}71)$$

where $[\mathrm{PDE}]_t$ is the total concentration of phosphodiester **4–28**, k_{im} is a first-order rate constant, and α_{zw} is the fraction of the total phosphodiester that is the zwitterion in which one *N*-methylimidazolyl group is hydronated on nitrogen and the other is unhydronated. Acid dissociation constant K_{a1} is the macroscopic acid dissociation constant for the first hydron from the cation in which both imidazolyl groups are dihydronated and the phospho group is monoanionic, and K_{a2} is the macroscopic acid dissociation constant for the hydron from the cationic imidazolyl group in the zwitterion. The fact that all rates measured in the pH–rate profile (Figure 4–8) are 10^6 times greater than the rate constant for uncatalyzed hydrolysis of diphenylphosphates[53] with leaving groups of the same pK_a is consistent with the absence of any indication of uncatalyzed hydrolysis in the measurements. The fit to the data in the figure is for Equation 4–71 with $k_{im} = 2 \times 10^{-3}$ s^{-1}, pK_{a1} = 6.1, and pK_{a2} = 7.2 at 60 °C. Directly measured values of pK_{a1} and pK_{a2} are 6.2 and 7.8 at 25 °C. This behavior is consistent with encounter complex **4–29** preceding the transition state. In the transition state, the imidazolyl group on the leaving phenoxy group is an intramolecular general acid catalyst of the intramolecular nucleophilic substitution. The concentration of this encounter complex should reach a maximum at the maximum concentration of the zwitterionic species.

It is also possible to **design molecules so that an intramolecular general acid catalyst is brought into an encounter complex as a result of formation of a covalent complex from two separate reactants**. For example, the distorted bicyclic anilide **4–31**

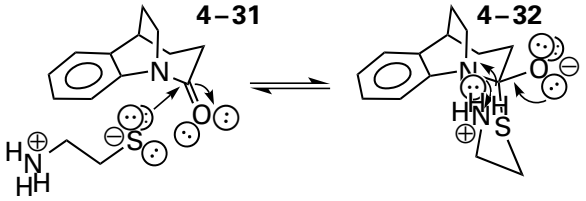

(4–72)

participates in a nucleophilic substitution with thiols to produce the respective monocyclic thioester. When the thiol has been constructed so that it contains a general acid, such as an ammonium, properly positioned in its structure, it brings that general acid into the tetrahedral intermediate (Equation 4–72). If the acidic hydron is four atoms from the sulfur, a cyclic encounter complex can be formed (**4–32**), and the nucleophilic substitution at the acyl group is accelerated by intramolecular general acid catalysis resulting from hydronation of the leaving anilino nitrogen, which is incapable of leaving without being hydronated one way or another. A pendant ammonium (as shown in the equation), acting as the general acid, increases the rate of nucleophilic substitution by a factor of more than 5000; a pendent imidazolium, by a factor of more than 5000; and a pendant carboxylic acid, by a factor of more than 200,000.[54,55]

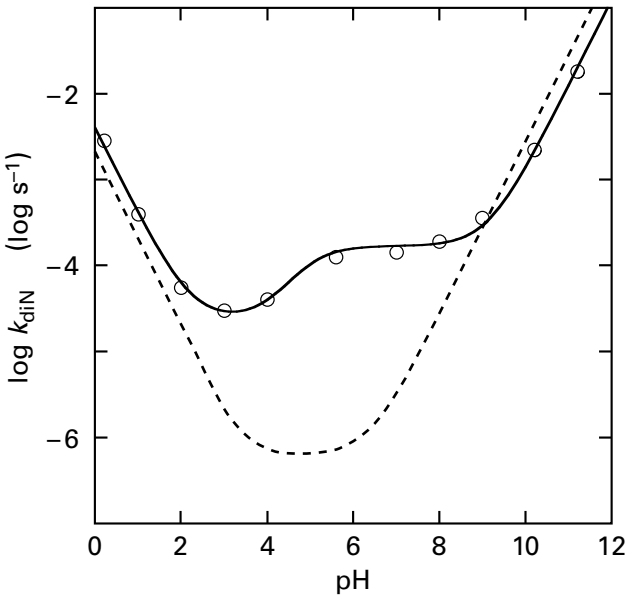

Figure 4–9: Intramolecular general acid catalysis by an ammonio group in the hydrolysis of a phosphodiester.[56] Solutions of either dinucleotide **4–33** (○; solid line) or its homologue in which the 2′-amino group is replaced with a methoxy group (dashed line) were prepared at an ionic strength of 0.1 M (maintained with NaCl) and 90 °C. The pH of the solutions was adjusted with hydrogen chloride or sodium hydroxide or buffered with formate, acetate, 2-[4-(2-hydroxyethyl)piperazin-1-yl]ethanesulfonate, or glycine. Low concentrations of buffers were used, and no buffer catalysis was observed. The progress of the reaction was followed by separating the reactants and products chromatographically. The common logarithms of the pseudo-first-order rate constants, k_{diN} (second^{-1}), for the hydrolysis of each dinucleotide (diN) to produce either 2′-aminouridine or 2′-methoxyuridine, respectively, and 2′,3′-cyclic guanidylic acid (Equation 4–73) are plotted as a function of pH.

There are also many **examples of nonenzymatic intramolecular general base catalysis**. For example, the amino group in the pseudosymmetric dinucleotide **4–33,** where G is guanine and U is uracil, acts as a formal intramolecular general base catalyst for the intramolecular nucleophilic substitution that results in its cleavage

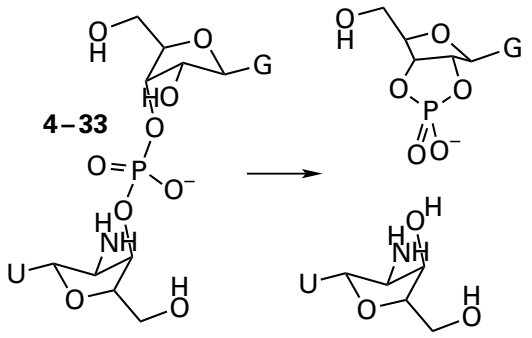

(4–73)

This conclusion follows from the fact that there is a plateau in the pH–rate profile that is not seen when the 2′-amino group is replaced with a methoxy group (Figure 4–9).[56] At values of pH greater than 9, the reaction displays specific base catalysis. Between pH 5 and 9, in the plateau, the reaction is invariant with pH because the amino group, which is unhydronated in this range of pH, is formally acting as an intramolecular general base catalyst. Below the pK_a for the amino group (pK_a = 5), the rate of the reaction decreases as the amino group becomes hydronated until specific acid catalysis takes over below pH 3. Formal intramolecular general base catalysis in this instance, however, actually results from intramolecular general acid catalysis of the reaction by the ammonio group in the tautomeric encounter complex **4–34**

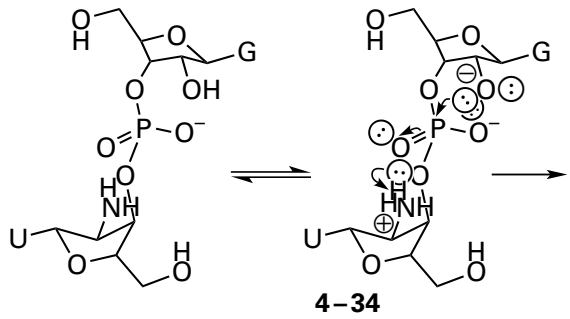

(4–74)

The *endo*-imidazolyl group in norbornyl ester **4–35**, however, acts as an actual rather than a formal intramolecular general base catalyzing the hydrolysis of the ester[57]

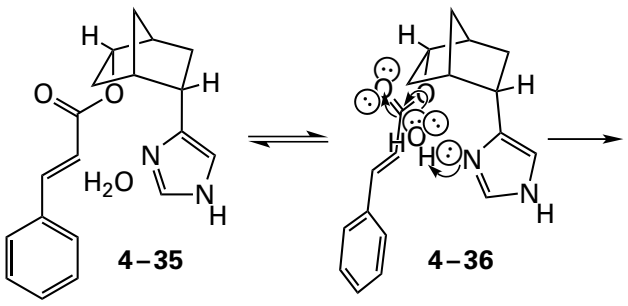

(4–75)

As the pH of the solution is decreased, the pH–rate profile for hydrolysis of norbornyl ester **4–35** displays a plateau consistent with a change in mechanism from specific base catalysis to intramolecular general base catalysis,[57] analogous to the behavior observed in Figure 4–9. Consistent with this conclusion that the imidazolyl group is acting as an internal general base is the observation that the exo isomer of norbornyl ester **4–35** displays no plateau. Encounter

complex **4–36**, which is unavailable to the exo isomer, would be consistent with these observations. At values of pH less than the pK_a for the imidazolyl group, however, the reaction involving intramolecular general base catalysis is only 6 times faster than the reaction involving only specific base catalysis, so the plateau observed for the intramolecular nucleophilic substitution in dinucleotide **4–33** (Figure 4–9) has become simply an inflection in the pH rate profile for this hydrolysis.

An intramolecular general base catalyst can also be brought into an encounter complex as a result of formation **of a covalent complex** from two separate reactants. For example, the observed rate equation for the aminolysis of *N*-acetylimidazole, AcIm, by aliphatic amines, RNH_2

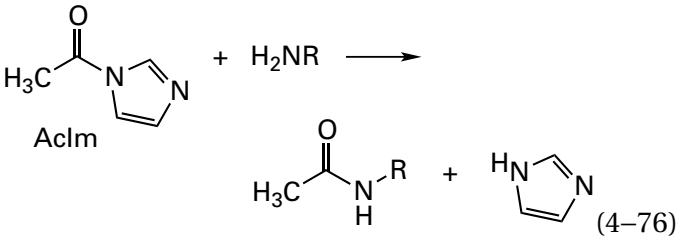

(4–76)

has a term, $k_B[RNH_2][AcIm]$, that is assumed to describe the attack of the unhydronated amine on the acyl carbon of unhydronated *N*-acetylimidazole.[58] The rate constant, k_B, for neutral unhydronated 1,3-diaminopropane is 75 times greater than the respective rate constant for neutral 1-aminopropane even though the conjugate monoacids of each compound have similar values (pK_a = 10.6 and 10.5, respectively) for their acid dissociation constants. This acceleration is believed to be due to the ability of the second amino group of 1,3-diaminopropane to remove intramolecularly a hydron from the tetrahedral intermediate

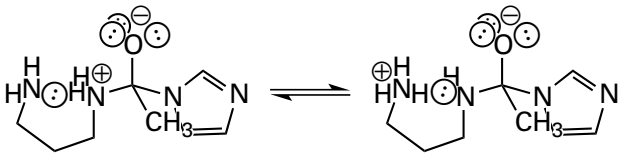

(4–77)

and thereby lock the distal nitrogen onto the acyl carbon. Intermolecular general base catalysis of the reaction between monoamines and *N*-acetylimidazole is also readily observed, and 1,3-diaminopropane participating as an intramolecular general base (Equation 4–77) is only as efficient as a 1 M concentration of a second molecule of 1-aminopropane acting as an unattached general base catalyst of its own aminolysis of *N*-acetylimidazole. Therefore, the entropy of approximation exerted in this reaction is not dramatic.

Another aspect of the entropy of approximation achieved by an enzymatic active site is that it should **enhance acid and base catalysis synergistically.** It has been observed that nonenzymatic intramolecular general acid–base reactions are more susceptible to intermolecular general acid–base catalysis in the same encounter complex than their entirely intermolecular counterparts. This observation and theoretical considerations suggest that the fewer degrees of freedom that are available to a transition state, the more susceptible it will be to catalysis by external general acids and general bases.[59]

Suggested Reading

Jencks, W. P., and Carriuolo, J. (1961) General base catalysis of ester hydrolysis, *J. Am. Chem. Soc. 83*, 1743–1750. https://doi.org/10.1021/ja01468a044

Sorensen, P. E., and Jencks, W. P. (1987) Acid- and base-catalyzed decomposition of acetaldehyde hydrate and hemiacetals in aqueous solution, *J. Am. Chem. Soc. 109*, 4675–4690. https://doi.org/10.1021/ja00249a034

Orth, E. S., Brandão, T. A., Souza, B. S., Pliego, J. R., Vaz, B. G., Eberlin, M. N., Kirby, A. J., and Nome, F. (2010) Intramolecular catalysis of phosphodiester hydrolysis by two imidazoles, *J. Am. Chem. Soc. 132*, 8513–8523. https://doi.org/10.1021/ja1034733

Problem 4–1: The observed rate constants

$$-\frac{d[\mathrm{GV}]}{dt} = k_{\mathrm{GV}}[\mathrm{GV}]$$

for hydrolysis of the amide between glycine and D-valine in *N*-(phenylacetyl)glycyl-D-valine (GV) at 37 °C as a function of pH, in the absence of added acid or base, are as follows.[60]

pH	k_{GV} (s^{-1})
0	1.0×10^{-6}
1	3.3×10^{-7}
3	1.3×10^{-9}
5	1.5×10^{-10}
7	2.7×10^{-11}
9	2.3×10^{-10}
11	9.9×10^{-10}
13	6.2×10^{-8}
14	2.4×10^{-6}

(A) Plot the common logarithms of the rate constants as a function of pH.
(B) Draw lines with slopes –1, 0, and +1 through the data.
(C) From these lines, estimate values for the rate constants k_{H^+}, k_{non}, and k_{OH^-}.
(D) Draw the most likely hydrogen-bonded encounter complexes immediately preceding the transition states for the three reactions governed by each rate constant in the form of **4–6**, **4–7**, and **4–8**.

Problem 4–2: Suppose that the kinetic mechanism for the following aldol condensation is[61]

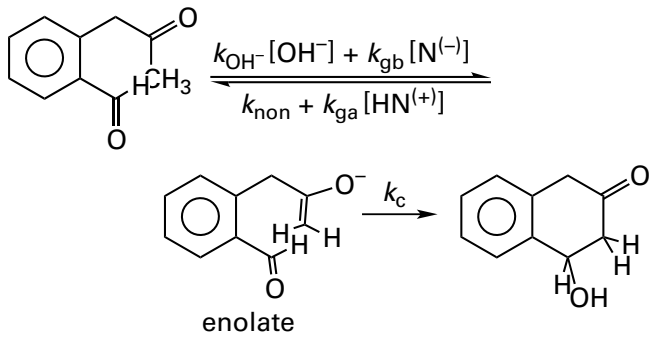

(A) Using the steady-state assumption that, during the course of measurement of the rate

$$\frac{d[\text{enolate}]}{dt} = 0$$

derive a rate equation for the reaction.

(B) What kinetic mechanism in Chapter 3 does this mechanism resemble closely?
(C) What type of behavior should the observed rate constant display as a function of the total concentration of buffer?

Problem 4–3: Hydrolysis of the methyl enol ether of cyclohexanone in water is catalyzed by general acids; the rate-limiting step is hydronation at the α position of the enol ether

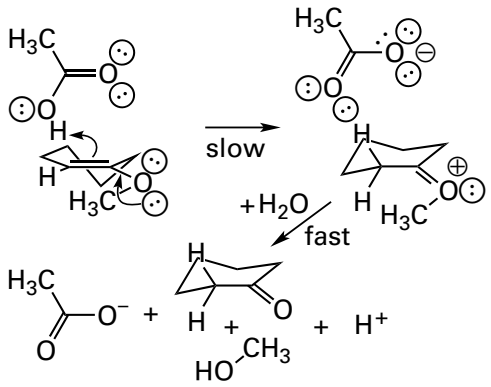

The Brønsted plot of rate constants, k_{ga}, for general acid catalysis by carboxylic acids, where

$$-\frac{d[\text{enol ether}]}{dt} = \left(k_{pH} + k_{ga}[\text{RCOOH}] + k_{gb}[\text{RCOO}^-]\right)[\text{enol ether}]$$

is strictly linear, except for the deviation of pivalic acid, $(CH_3)_3CCOOH$[62]

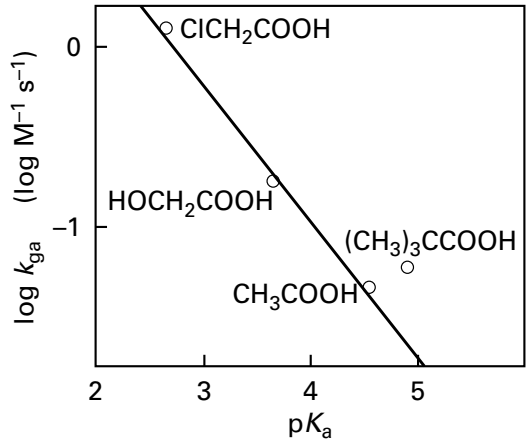

Suggest a hypothesis to explain this deviation of pivalic acid. How could you test your hypothesis?*

*G. E. Lienhard, Department of Biochemistry, Dartmouth School of Medicine, formulated these problems.

Problem 4–4: The tautomerization of certain imines related to pyridoximines

$$R_1R_2C{=}NCHR_3R_4 \longrightarrow R_1R_2CHN{=}CR_3R_4$$

is catalyzed by imidazole buffers.[63] This tautomerization (see Equation 2–22) is homologous with the tautomerization of a pyridoximine to an *N*-pyridoxylimine. There is a term, k_{gab}[Im][ImH$^+$][imine], in the rate equation where Im is the free base of imidazole and ImH$^+$ is the conjugate acid. Draw an encounter complex consistent with this term.*

Problem 4–5: The hydration of 1,3-dichloroacetone is catalyzed by imidazole buffers. The rate equation for the reaction contains a term, k_{gb}[Im]^2[H_2O][$ClCH_2COCH_2Cl$], where Im is the free base of imidazole. Write a mechanism consistent with this term that does not involve addition of imidazole to the carbonyl group of 1,3-dichloroacetone.*

Problem 4–6:

(A) Write a step-by-step mechanism for the following reaction.

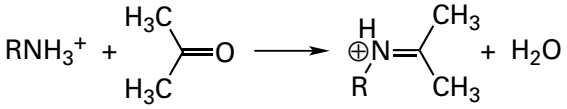

Hydroxylamine reacts with the iminium cation to yield the hydroxamate very rapidly, but it reacts only very slowly with acetone. Therefore, it is possible to follow the rate at which the iminium cation is formed when acetone is mixed with various amines by discharging the iminium cation with hydroxylamine as it is formed. It has been shown that the reaction in the direction written, that of formation of the iminium cation, is catalyzed by general acids.

(B) Choose the step in your overall mechanism where a general acid would participate directly and draw a picture of the general acid, NH$^{(+)}$, donating its hydron to the lone pair on the intermediate compound present at that step. Remember, you are considering only the reaction proceeding from left to right. The reverse reaction, hydrolysis of the iminium cation, has been prevented by trapping the iminium cation as it is formed.

Rates at which each of several primary amines, RCH_2NH_2, react with acetone to form the iminium cation were determined at a series of pH values. In addition, values of pK_a for each amino nitrogen in each reactant were determined. With the respective pK_a, the amount of every form of a particular primary amine present at a given pH could be calculated, as well as the pK_a for a primary amino group in a diamine when the other amino group is either neutral or hydronated. From the behavior of the rate constants as a function of pH and a knowledge of the concentrations of the various hydronated species at each pH, the pH-independent rate constants (k_{imn}) for the reaction of each form of a given amine with acetone could be calculated.[64]

amine	pK_a	10^3 k_{imn} (M^{-1} s^{-1})
n-$C_4H_9NH_2$	10.33	94.7
$CH_3O(CH_2)_2NH_2$	9.09	15.8
$CH_3O(CH_2)_3NH_2$	9.82	47.8
$(CH_3)_3N^+(CH_2)_2NH_2$	6.7	0.9
$(CH_3)_2HN^+(CH_2)_2NH_2$	6.71	797
$(CH_3)_2N(CH_2)_2NH_2$	9.27	21
$(CH_3)_2HN^+(CH_2)_3NH_2$	8.50	108
$(CH_3)_2N(CH_2)_3NH_2$	9.75	51.5
$(CH_3)_2HN^+(CH_2)_4NH_2$	9.23	69.4
$(CH_3)_2N(CH_2)_4NH_2$	10.00	66.7
$(CH_3)_2HN^+(CH_2)_5NH_2$	10.06	159
$(CH3)_2N(CH_2)_5NH_2$	10.34	84.4
$(CH_3)_2HN^+CH_2C_5H_8NH_2$[a]	8.33	388
$(CH_3)_2NCH_2C_5H_8NH_2$[a]	9.61	19

[a]These are the tertiary hydronated and unhydronated forms of *trans*-2-[(dimethylamino)methyl]cyclopentylamine.

The second-order rate constant for the reaction between acetone and the particular primary amine is noted in the right-hand column. The pK_a listed in the table is for the conjugate acid of the amino group in each primary amine. The primary amine must be unhydronated to add to the ketone, but a diamine can be hydronated or unhydronated at the other nitrogen.

(C) Make a Brønsted plot of all the experimental results. Draw a line through values for all the neutral compounds and the only quaternary ammonium cation, and determine the slope of the line.

All the cationic compounds, except the quaternary ammonium, deviate in their behavior from that expected from the values of pK_a for their primary amino groups.

(D) Explain this deviation in terms of intramolecular general acid catalysis in formation of the iminium cation by drawing several structures, one for each cationic primary amine, that explicitly incorporate this catalytic step and that show the hydron transfer unambiguously.

(E) Explain the two pH–rate profiles displayed in the following figure.[64] First explain the behavior of *n*-butylamine, and then provide a detailed explanation of the increase in rate, followed by the plateau, followed by the decrease in the curve for 2-(dimethylamino)ethylamine as the pH is decreased.

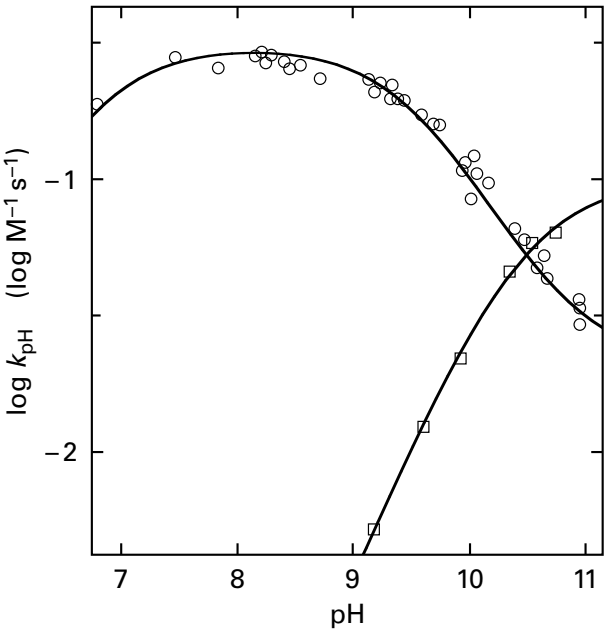

Plot of log (k_{pH}) against pH for formation of the iminium from acetone and either 2-(dimethylamino)ethylamine (○) or *n*-butylamine (□). The rate constant k_{pH} is the observed second-order rate constant at a given pH for formation of the iminium based on the total concentration of primary amine in all forms.

The difference in standard free energy of activation between two reactions is related to the rate constants by

$$\Delta\Delta G^{\circ\ddagger} = -RT\ln(k_1/k_2)$$

(F) Use k_{imn}, the rate of reaction of 5-(*N*,*N*-dimethylammonium)pentylamine, $Me_2N^+H(CH_2)_5NH_2$, as the example of the reaction showing the least intramolecular general acid catalysis. With the Brønsted relation, correct the rate constants of all the other reactions showing intramolecular general acid catalysis for the differences in values of pK_a for their primary amino groups from that of $(CH_3)_2N^+H(CH_2)_5NH_2$ so that they can be compared directly to the rate constant for $(CH_3)_2N^+H(CH_2)_5NH_2$. Calculate $\Delta\Delta^{\ddagger}G^{\circ}_{corr}$ for each corrected value relative to $(CH_3)_2N^+H(CH_2)_5NH_2$. Assume that entropy of approximation is responsible for all this corrected difference in free energy of activation, $\Delta\Delta^{\ddagger}G^{\circ}_{corr} = -T\Delta\Delta^{\ddagger}S^{\circ}_{approx}$, and determine $\Delta\Delta^{\ddagger}S^{\circ}_{approx}$ for $(CH_3)_2N^+H(CH_2)_5NH_2$, $(CH_3)_2N^+H(CH_2)_4NH_2$, $(CH_3)_2N^+H(CH_2)_3NH_2$, *trans*-$(CH_3)_2HN^+CH_2C_5H_8NH_2$, and $(CH_3)_2N^+H(CH_2)_2NH_2$.

(G) Comment on the trend in $\Delta\Delta^{\ddagger}S^{\circ}_{approx}$.

Problem 4–7: Write a mechanism for the enolization of 2-oxo-3-methylpentane to 2-hydroxy-3-methyl-2-pentene.

The rate equation for enolization of the amino-ketone

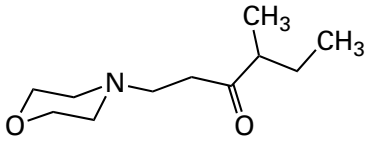

contains the term $k_{OH^-}[OH^-][^+HNKet]$.[65] Explain this term as the result of intramolecular general acid catalysis.

Enzymatic pH–Rate Profiles

Rates of most enzymatic reactions are functions of pH. The effects of pH on the activity of an enzyme, measured in the standard assay used to purify the enzyme, are theoretically meaningless, and the pH–activity relations that are often encountered have only practical value.[66] If, however, the **effects of pH on underlying parameters that govern the initial rate** for an enzymatic reaction—namely, the catalytic constant and the specificity constants—are assessed, the observed behavior is often informative.

In such experiments, the pH is usually established and maintained by using a buffer. There are two problems that can lead to **artifacts caused by buffers**.[67] First, as the pH is altered, the ionic strength contributed by the buffer changes. To avoid effects of **variation in ionic strength**, a neutral electrolyte, such as potassium chloride, is usually added to maintain a constant ionic strength. It is also possible to use a mix of ionic buffers that both buffer the pH over a large range and maintain ionic strength at the same time.[68] Second, either the conjugate acid or the conjugate base of the buffer chosen to maintain the pH or the neutral electrolyte chosen to maintain the ionic strength can be **inhibitors or activators** of the enzyme. Consequently, the concentrations of the buffer and of the electrolyte are varied independently at constant pH to make sure that they have no effect on enzymatic activity.[69] Often different buffers overlapping each other in the pH ranges examined are used to check whether or not the enzymatic activities are the same at the same pH when it is maintained with different buffers.

A simple example of the effect of pH on one of the steady-state rate constants is a situation in which the **catalytic constant** for the enzymatic reaction **decreases as the pH is decreased** (Figure 4–10A).[70] In such a situation, the decrease in the catalytic constant usually fits the equation for titration of a catalytic base.[71-73] The fraction of any monoprotic acid–base OH that is in the form of its conjugate base, $\alpha(\odot O^{(-)})$, is defined by the relation

$$\alpha\left(\odot O^{(-)}\right) = \frac{\left[\odot O^{(-)}\right]}{\left[OH\right]_t} = \frac{K_{aOH}}{[H^+] + K_{aOH}} \tag{4–78}$$

where $[\odot O^{(-)}]$ is the concentration of the conjugate base, $[OH]_t$ is the total concentration of the acid–base in both forms, and K_{aOH} is its acid dissociation constant. The behavior of the observed catalytic constant, $k_{0,app}$, of triose-phosphate isomerase (Equation 4–46) from *Gallus gallus* as a function of pH (Figure 4–10A) when glycerone phosphate is the reactant can be described by the function

$$k_{0,app} = k_0\left(\frac{K_a}{[H^+] + K_a}\right) \tag{4–79}$$

where k_0 is the value for the observed catalytic constant where it is invariant with pH and it is at its maximum value, and K_a is an acid dissociation constant. From the fit of the equation to the data (curve in Figure 4–10A), $pK_a = 6.0$ and $k_0 = 480\ s^{-1}$.

It is usually more informative, however, to present the **common logarithm of a rate constant as a function of pH** (Figure 4–10B).[74] This convention allows the behavior of the rate constant to be examined over a larger range of pH and reveals whether or not titration of additional acid–bases might be governing the rate constant. Taking the common logarithms of the terms in Equation 4–79

$$\log k_{0,app} = \log k_0 + \log\left(\frac{K_a}{[H^+] + K_a}\right) \tag{4–80}$$

When $pH < pK_a$ so that $[H^+] > K_a$

$$\log k_{0,app} \cong \log k_0 - pK_a + pH \tag{4–81}$$

(dashed line in Figure 4–10B with slope +1), and when $pH > pK_a$ so that $[H^+] < K_a$

$$\log k_{0,app} \cong \log k_0 \tag{4–82}$$

(dashed line in Figure 4–10B with slope 0). The **two asymptotes intersect when pH = pK_a.** Within the range in which observations were made, the behavior of the observed catalytic constant of choline oxidase from *Arthrobacter globiformis* can be fit with Equation 4–80 (curve in Figure 4–10B) and the parameters $pK_a = 6.5$ and $k_0 = 18\ s^{-1}$.

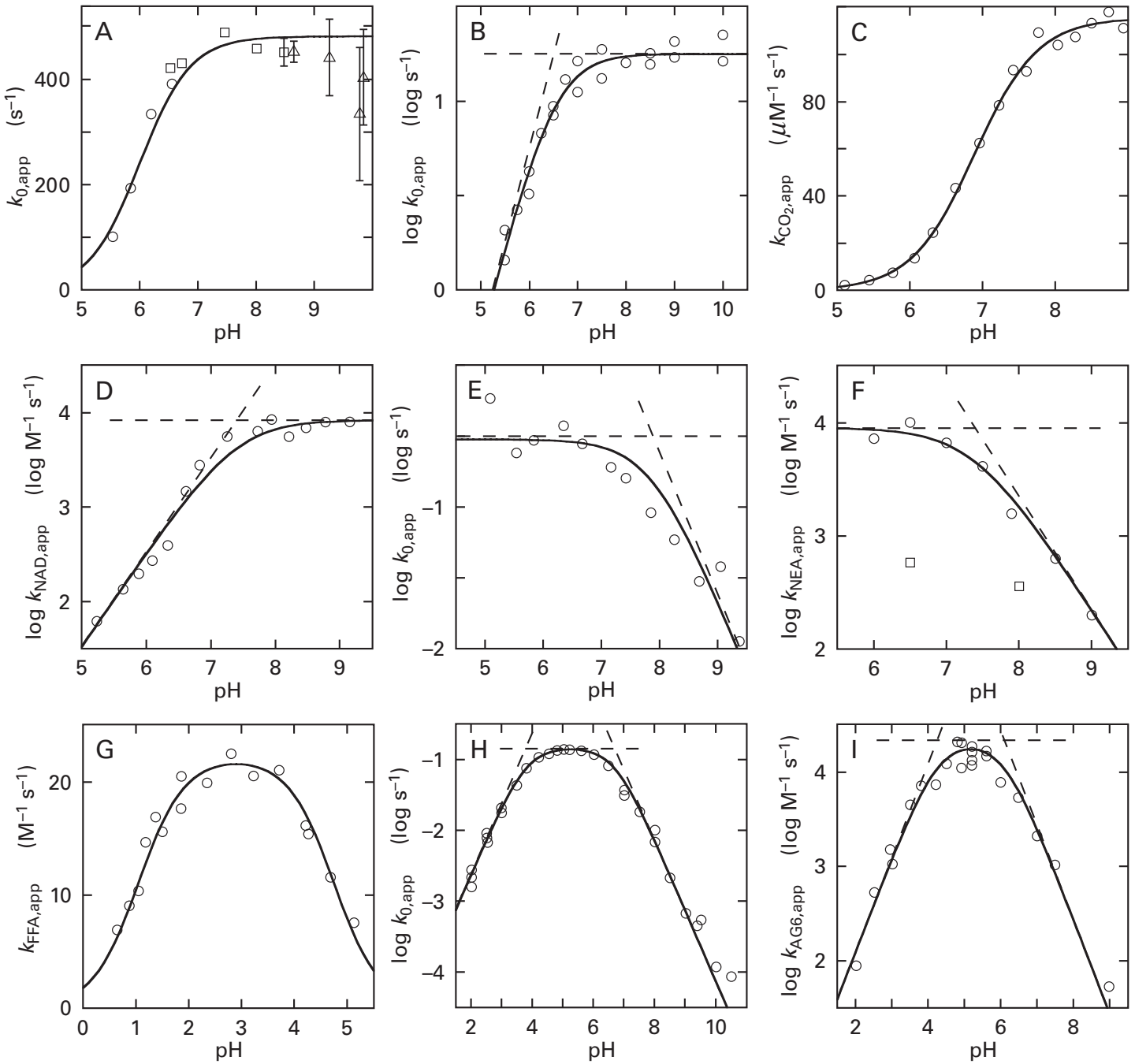

Figure 4–10: pH–Rate profiles for catalytic constants and specificity constants. (**A**) pH–Rate profile for the catalytic constant of triose-phosphate isomerase from *G. gallus* for glycerone phosphate at an ionic strength of 0.1 M and 30 °C.[70] The pH was buffered with 3,3-dimethylglutarate (○), triethanolamine (□), or carbonate (△). The observed catalytic constants, $k_{0,app}$ (second^{-1}), are plotted as a function of pH. (**B**) pH–Rate profile for the catalytic constant of choline oxidase from *A. globiformis* for choline at 25 °C.[74] The pH was buffered with 50 mM potassium phosphate between pH 6 and 8 and with 50 mM sodium phosphate between pH 5 and 6 and between pH 8 and 10. The common logarithms of the observed catalytic constants, $k_{0,app}$ (second^{-1}), are plotted as a function of pH. (**C**) pH–Rate profile for the steady-state specificity constant, k_{CO_2}, of human carbonic anhydrase 2 for CO_2 at an ionic strength of 0.2 M and 25 °C.[75] The pH was buffered only by the enzyme and the substrates. The observed steady-state rate constants, $k_{CO_2,app}$ (micromolar^{-1} oxidase from *F. oxysporum*, in which Aspartate 402 has been changed to a glutamate, for nitroethane anion (NEA) at 30 °C.[78] The pH was maintained by 0.5 M 2-(*N*-morpholino)-ethanesulfonate from pH 6 to 6.5, 0.5 M 2-[4-(2-hydroxyethyl)piperazin-1-yl]ethanesulfonate from pH 7 to 8.1, and 0.5 M 2-amino-2-(hydroxymethyl)propane-1,3-diol from pH 7.9 to 9. The common logarithms of the observed steady-state specificity constants, $k_{NEA,app}$ (molar^{-1} second^{-1}), are plotted as a function of pH. The unassociated data points (□) are for a mutant of the enzyme in which Aspartate 402 has been mutated to alanine. (**G**) pH–Rate profile for the steady-state specificity constant, k_{FFA}, of porcine pepsin for *N*-acetyl-L-phenylalanyl-L-phenylalanine amide (FFA) at 37 °C.[79] The pH and the ionic strength were established by buffers of 0.1 M sodium citrate. The observed steady-state specificity constants, $k_{FFA,app}$ (molar^{-1} second^{-1}), are plotted as a function of pH. (**H**) pH–Rate profile for the catalytic constant of lysozyme from *G. gallus* for (β1,4)-hexa-*N*-acetyl-

second^{-1}), are plotted as a function of pH. (**D**) pH–Rate profile for the steady-state specificity constant, k_{NAD}, of saccharopine dehydrogenase (NAD$^+$, L-lysine-forming) from *S. cerevisiae* for NAD$^+$ at 25 °C.[76] The pH was maintained by using the following buffers at ≥100 mM concentration: 2-(*N*-morpholino)ethanesulfonate from pH 5.5 to 6.8, 2-[4-(2-hydroxyethyl)piperazin-1-yl]ethanesulfonate from pH 6.8 to 8.2 and 2-(cyclohexylamino)ethanesulfonate from pH 8.2 to 10.0. The common logarithms of the observed steady-state specificity constants, $k_{NAD,app}$ (molar^{-1} second^{-1}), are plotted as a function of pH. (**E**) pH–Rate profile for the catalytic constant of human hypoxanthine phosphoribosyltransferase for inosine monophosphate and diphosphate at 23 °C.[77] A mixed buffer consisting of 30 mM 2-(*N*-morpholino)ethanesulfonate, 30 mM 2-amino-2-(hydroxymethyl)propane-1,3-diol, and 30 mM glycine was adjusted to the noted pH with either HCl or NaOH. The common logarithms of the observed catalytic constants, $k_{0,app}$ (second^{-1}), are plotted as a function of pH. (**F**) pH–Rate profile for the steady-state specificity constant, k_{NEA}, of a mutant of nitroethane glucosaminopyranose at an ionic strength of 0.1 M and 40 °C.[80] The pH was controlled in the range 3–9 with 0.01 M sodium acetate, phosphate, or carbonate. No buffer was used below pH 3. The common logarithms of the observed catalytic constants, $k_{0,app}$ (second^{-1}), are plotted as a function of pH. (**I**) pH–Rate profile for the steady-state specificity constants, k_{AG6}, of lysozyme from *G. gallus* for (β1,4)-hexa-*N*-acetylglucosaminopyranose (AG6) from the same kinetic measurements used to obtain the catalytic constants of Panel H.[80] The common logarithms of the steady-state specificity constants, $k_{AG6,app}$ (molar^{-1} second^{-1}), are plotted as a function of pH. In each panel in which common logarithms are plotted, dashed lines of slope +1 or −1 or both are included as asymptotes to the curves that are fit to the data below or above, respectively, or both below and above the values of pK_a indicated by the results. Dashed lines of slope 0 are placed in the same panels at values for the pH-independent catalytic constants, k_0, or steady-state specificity constants.

The **specificity constant** k_A for reactant A* can also **decrease as the pH decreases**. For example, the observed behavior (Figure 4–10C)[75] of the specificity constant for CO_2, $k_{CO_2,app}$, for human carbonic anhydrase 2 (previously Equation 3–445)

$$CO_2 + H_2O \rightleftharpoons HCO_3^- + H^+ \tag{4–83}$$

can be fit (curve in Figure 4–10C) with the equation

$$k_{CO_2,app} = k_{CO_2}\left(\frac{K_a}{[H^+] + K_a}\right) \tag{4–84}$$

and the parameters pK_a = 6.9 and k_{CO_2} = 116 μM^{-1} s^{-1}. The observed behavior (Figure 4–10D)[76] of the common logarithm of the specificity constant for NAD$^+$, $k_{NAD,app}$, in the reaction catalyzed by saccharopine dehydrogenase (NAD$^+$, L-lysine-forming)

$$\begin{aligned}&NAD^+ + N^6\text{-(L-1,3-dicarboxypropyl)-L-lysine} + H_2O\\ &\rightleftharpoons H^+ + \text{2-oxoglutarate} + \text{L-lysine} + NADH\end{aligned} \tag{4–85}$$

from *S. cerevisiae* can be fit (curve in Figure 4–10D) with the equation

$$\log k_{NAD,app} = \log k_{NAD} + \log\left(\frac{K_a}{[H^+] + K_a}\right) \tag{4–86}$$

and the parameters pK_a = 7.4 and k_{NAD} = 8.4 mM^{-1} s^{-1}.

The **catalytic constant** for an enzymatic reaction can **decrease as the pH is increased**. In this situation, the decrease in the catalytic constant as a function of pH usually fits the equation for titration of an acid.[71-73] The fraction of a monoprotic acid–base NH that is in the form of its conjugate acid, $\alpha(NH^{(+)})$, is defined by the relation

$$\alpha(NH^{(+)}) = \frac{[NH^{(+)}]}{[NH]_t} = \frac{[H^+]}{[H^+] + K_{aNH}} \tag{4–87}$$

where $[NH^{(+)}]$ is the concentration of the conjugate acid, $[NH]_t$ is the total concentration of the acid–base in both forms, and K_{aNH} is its acid dissociation constant. The behavior (Figure 4–10E)[77] of the observed catalytic constant, $k_{0,app}$, of human hypoxanthine phosphoribosyltransferase (previously Equation 3–251)

$$\begin{aligned}&\text{magnesium 5-phospho-}\alpha\text{-D-ribose 1-diphosphate}\\ &+ \text{hypoxanthine} \rightleftharpoons \text{magnesium diphosphate}\\ &+ \text{inosine 5′-phosphate}\end{aligned} \tag{4–88}$$

with hypoxanthine as a reactant can be fit (curve in Figure 4–10E) with the function

*In most publications, alternatives for the specificity constant, the limiting rate divided by the Michaelis constant ($V K_m^{-1}$) or the catalytic constant divided by the Michaelis constant ($k_0 K_m^{-1}$), are commonly used. The latter is the specificity constant.

$$\log k_{0,app} = \log k_0 + \log\left(\frac{[H^+]}{[H^+] + K_a}\right) \quad (4–89)$$

and the parameters $pK_a = 7.9$ and $k_0 = 0.32\ s^{-1}$. When $pH < pK_a$ so that $[H^+] > K_a$

$$\log k_{0,app} \cong \log k_0 + pK_a - pH \quad (4–90)$$

(dashed line in Figure 4–10E with slope of 0) and when $pH > pK_a$ so that $[H^+] < K_a$

$$\log k_{0,app} \cong \log k_0 + pK_a - pH \quad (4–91)$$

(dashed line in Figure 4–10E with slope of –1). The two asymptotes intersect when $pH = pK_a$.

The **specificity constant** k_A for reactant A can also **decrease as the pH is increased**. For example, the observed behavior (Figure 4–10F)[78] of the specificity constant $k_{NEA,app}$ for nitroethane anion (NEA) in the reaction catalyzed by a mutant of nitroalkane oxidase

$$\text{nitroethane} + H_2O + O_2 \rightleftharpoons H^+ + \text{nitrite} + \text{acetaldehyde} + H_2O_2 \quad (4–92)$$

from *Fusarium oxysporum*, in which Aspartate 402 has been changed to glutamate, can be fit (curve in Figure 4–10F) with the function

$$\log k_{NEA,app} = \log k_{NEA} + \log\left(\frac{[H^+]}{[H^+] + K_a}\right) \quad (4–93)$$

and the parameters $pK_a = 7.4$ and $k_{NEA} = 9\ mM^{-1}\ s^{-1}$.

In many instances, either the catalytic constant or one or more of the specificity constants **decrease from a maximum both as the pH is decreased and as the pH is increased** (Figure 4–10G).[79] In the simplest case, the behavior is that expected for a reaction that requires an acid–base HN to be in the form of its conjugate acid $HN^{(+)}$ and an acid–base OH to be in the form of its conjugate base $⊙O^{(–)}$.

Define a species $X(HN^{(+)},⊙O^{(–)})$ in which acid–base NH is present only as its conjugate acid, $HN^{(+)}$, and acid–base OH is present only as its conjugate base, $⊙O^{(–)}$. If acid–bases HN and OH titrate independently of each other, it follows from Equations 4–78 and 4–87 that the fraction, $\alpha(HN^{(+)},⊙O^{(–)})$, of the total concentration of X, $[X]_t$, in all four tautomers and states of ionization, that is the tautomer $X(HN^{(+)},⊙O^{(–)})$

$$\alpha\left(HN^{(+)},⊙O^{(–)}\right) = \frac{\left[X\left(HN^{(+)},⊙O^{(–)}\right)\right]}{[X]_t} = \alpha\left(HN^{(+)}\right)\alpha\left(⊙O^{(–)}\right) = \left(\frac{[H^+]}{[H^+] + K_{aNH}}\right)\left(\frac{K_{aOH}}{[H^+] + K_{aOH}}\right) \quad (4–94)$$

where pK_{aNH} is the pK_a of acid–base NH and pK_{aOH} is the pK_a of acid–base OH.

The behavior of the observed specificity constant $k_{FFA,app}$ as a function of pH for the peptide *N*-acetyl-L-phenylalanyl-L-phenylalanine amide (FFA) when it is hydrolyzed by porcine pepsin A, an endopeptidase active at low pH, can be fit (curve in Figure 4–10G) with the function

$$k_{FFA,app} = k_{FFA}\left(\frac{K_{a1}}{[H^+] + K_{a1}}\right)\left(\frac{[H^+]}{[H^+] + K_{a2}}\right) \quad (4–95)$$

and the parameters $pK_{a1} = 1.05$, $pK_{a2} = 4.75$, and $k_{FFA} = 22\ M^{-1}\ s^{-1}$.* The observed behavior (Figure 4–10H)[80] of the catalytic constant $k_{0,app}$ for hydrolysis of (β1,4)-hexa-*N*-acetylglucosaminopyranose (Figure 3–27) by lysozyme from *G. gallus* displays behavior as a function of pH that can be fit (curve in Figure 4–10H) with the function

$$\log k_{0,app} = \log k_0 + \log\left\{\left(\frac{K_{a1}}{[H^+] + K_{a1}}\right)\left(\frac{[H^+]}{[H^+] + K_{a2}}\right)\right\} \quad (4–96)$$

and the parameters $pK_{a1} = 3.8$, $pK_{a2} = 6.7$, and $k_0 = 0.15\ s^{-1}$. Its observed specificity constant $k_{AG6,app}$ for the reactant (β1,4)-hexa-*N*-acetylglucosaminopyranose (AG6) displays behavior (Figure 4–10I)[80] as a function of pH that can be fit (curve in Figure 4–10I) with the function

*It is the accepted convention to distinguish observed values of pK_a by numerical subscripts that increase in number as the observed values of pK_a increase in magnitude.

$$\log k_{AG6,app} = \log k_{AG6} + \log\left\{\left(\frac{K_{a3}}{[H^+] + K_{a3}}\right)\left(\frac{[H^+]}{[H^+] + K_{a4}}\right)\right\} \quad (4–97)$$

and the parameters $pK_{a3} = 4.25$, $pK_{a4} = 6.1$, and $k_{AG6} = 22\ mM^{-1}\ s^{-1}$.

When an **enzyme has two or more reactants**, the pH–rate profile for each specificity constant is usually measured by varying the reactant for the specificity constant at a particular pH to discover the specificity constant for that pH and then repeating the observations at the next pH. All these measurements are made at saturating concentrations of the other reactants. When there are two or more reactants, **each specificity constant will often have its own particular** pH–rate **profile** with its own particular values of pK_a below or above which it decreases. For example, the specificity constant $k_{ch,app}$ for choline (ch) in the reaction of choline oxidase

$$\text{choline} + 2\,O_2 + H_2O \rightleftharpoons \text{betaine} + 2\,H_2O_2 \quad (4–98)$$

from *A. globiformis*[74] decreases below a pK_a of 7.3 when the pH is lowered, but the specificity constant k_{O_2} for molecular oxygen (O_2) is invariant with pH from pH 6 to 10.

For equations of the form

$$\log k_{i,app} = \log k_i + \log\left(\frac{K_{a1}[H^+]}{[H^+]^2 + (K_{a1} + K_{a2})[H^+] + K_{a1}K_{a2}}\right) \quad (4–99)$$

as are Equations 4–96 and 4–97, when $[H^+]^2 > (K_{a1} + K_{a2})^2 > K_{a1}K_{a2}$

$$\log k_{i,app} \cong \log k_i - pK_{a1} + pH \quad (4–100)$$

(dashed line in Figure 4–10H with slope of +1), and when $[H^+] < K_{a1}K_{a2}\,(K_{a1} + K_{a2})^{-1}$

$$\log k_{i,app} \cong \log k_i + pK_{a2} - pH \quad (4–101)$$

(dashed line in Figure 4–10H with slope of –1). If $K_{a1} > K_{a2}$ and the inequalities $K_{a1} + K_{a2} > [H^+] > K_{a1}K_{a2}\,(K_{a1} + K_{a2})^{-1}$ hold over a range of pH, then there is a plateau at the maximum of the curve, as in Figures 4–10G and 4–10H, and

$$\log k_{i,app} \cong \log k_i \quad (4–102)$$

(dashed line in Figure 4–10H with slope of 0). For all values of K_{a1} and K_{a2}, however, the intersection of the lines defined by Equations 4–100 (the line of slope +1) and 4–101 (the line of slope –1) occurs at

$$pH = \frac{pK_{a1} + pK_{a2}}{2} \quad (4–103)$$

which is the **mean of the two values of pK_a.** The maximum value for $\log k_{i,app}$ also occurs when the pH is the mean of the two values of pK_a, a fact that can be verified by setting the derivative of the function in Equation 4–99 at 0.

When values of pK_a are within less than one unit of each other, the two values of pK_a are less well-defined by fitting the data to the appropriate equation. Regardless of how well these values are defined, however, their mean (Equation 4–103) is always well-defined by the intersection of the lines of slope +1 (Equation 4–100) and slope –1 (Equation 4–101).

It can also be observed that when the common logarithm of a steady-state rate constant is plotted as a function of pH, one or both of the lines describing a decrease in the common logarithm of the rate constant as a function of pH, either as the pH is lowered or as it is raised, can have a **slope of +2 or –2** rather than +1 or –1, respectively. For example, when the common logarithm of the specificity constant $k_{cCP,app}$ for hydrolysis of cytidine 2′,3′-cyclic phosphate (cCP) catalyzed by bovine pancreatic ribonuclease

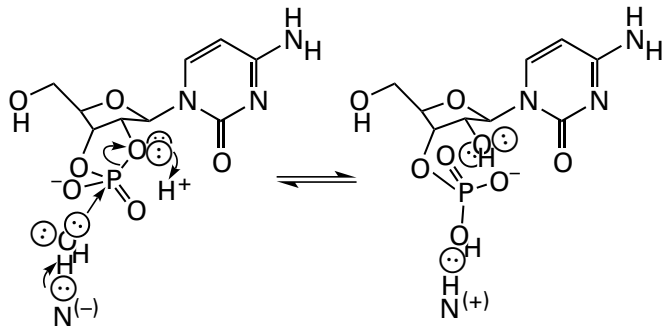

(4–104)

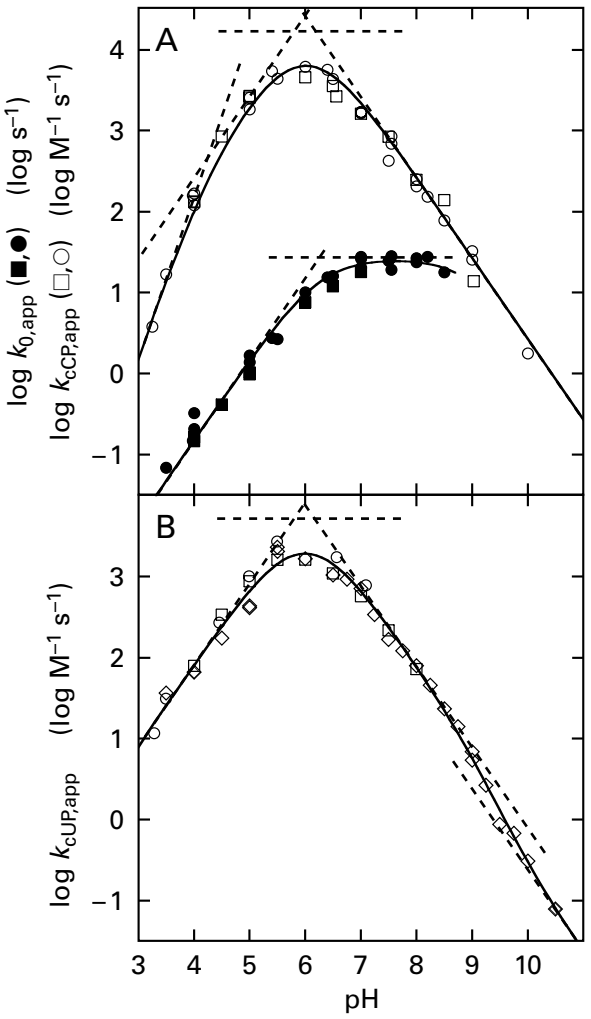

Figure 4–11: pH–Rate profiles for the hydrolyses of 2′,3′-cyclic nucleotide phosphates catalyzed by bovine pancreatic ribonuclease.[84] (**A**) pH–Rate profiles for the steady-state rate constants k_{cCP} (○, □) and the catalytic constant k_0 (●, ■) of bovine pancreatic ribonuclease for cytidine 2′,3′-cyclic phosphate at an ionic strength of 0.2 M and 25 °C. Rate constants were obtained by Eftink and Biltonen[81] (○, ●) with a spectrophotometric assay, a manual calorimetric assay, and a continuous gradient calorimetric assay in solutions buffered with sodium acetate, sodium cacodylate, imidazolium chloride, 2-ammonio-2-(hydroxymethyl)propane-1,3-diol chloride, or sodium glycinate. Rate constants were obtained by Herries, Mathias, and Rabin[84] (□, ■) with both a pH-stat and a spectrophotometric assay in solutions buffered with sodium formate, sodium acetate, sodium malonate, disodium 3,3-dicarboxypentane, imidazolium chloride, *N*-ethylmorpholinium chloride, or sodium borate. In both cases, the steady-state rate constants k_{cCP} and the catalytic constants were derived for each value of pH from the initial rates at several concentrations of cytidine 2′,3′-cyclic phosphate. The common logarithms of the observed steady-state rate constants, $k_{cCP,app}$ (molar^{-1} second^{-1}), and the common logarithms of the observed catalytic constants, $k_{0,app}$ (second^{-1}), respectively, are plotted as a function of pH. Dashed lines of slope +2 and +1 or of slope +1 and −1 are included as asymptotes to the curves that are fit to the data below and above the values of pK_a indicated by the results. Dashed lines of slope 0 are placed at values for the pH-independent steady-state rate constant k_{cCP} (17 mM^{-1} s^{-1}) and catalytic constant k_0 (27 s^{-1}). (**B**) pH–Rate profile for the steady-state rate constants k_{cUP} of pancreatic ribonuclease for uridine 2′,3′-cyclic phosphate at an ionic strength of 0.2 M and 25 °C. Rate constants were obtained by Eftink and Biltonen[81] (○) as described in Panel A. Rate constants were obtained by del Rosario and Hammes[82] (□) with a spectrophotometric assay in solutions buffered with 2-ammonio-2-(hydroxymethyl)propane-1,3-diol acetate. Rate constants were obtained by Machuga and Klapper[83] (◊) with a spectrophotometric assay in solutions buffered with sodium citrate (3.5–4.0), sodium acetate (4.0–6.0), 2-ammonio-2-(hydroxymethyl)propane-1,3-diol cacodylate (5.0–9.0), or sodium glycinate (8.75–10.0). In all cases, the steady-state rate constants k_{cUP} and the catalytic constants were derived for each value of pH from the initial rates at several concentrations of cytidine 2′,3′-cyclic phosphate. The common logarithms of the observed steady-state rate constants, $k_{cUP,app}$ (molar^{-1} second^{-1}), are plotted as a function of pH. A dashed line of slope +1 and two dashed lines of slope −1 are included as asymptotes to the curves that are fit to the data below and above the values of pK_a indicated by the results. A dashed line of slope 0 is placed at the value for the pH-independent steady-state rate constant k_{cUP} (4.5 mM^{-1} s^{-1}).

is plotted as a function of pH, its decrease at high pH defines a line of slope −1, but its decrease at low pH defines a line of slope +1 that becomes a line of slope +2 below pH 4 (Figure 4–11A).[81-84]

This behavior is that expected of a system in which there are three acid–bases involved in the reaction, NH, OH, and SH, and **the tautomer of the system** X(HN$^{(+)}$,⊙O$^{(-)}$,⊙S$^{(-)}$) is the only active species. This tautomer is the one with monoprotic acid–base HN as its conjugate acid, HN$^{(+)}$; monoprotic acid–base HO as its conjugate base, ⊙O$^{(-)}$; and monoprotic acid–base HS as its conjugate base, ⊙S$^{(-)}$. By extension, in such a situation, if each acid–base titrates independently of the other

$$\alpha\left(HN^{(+)},\odot O^{(-)},\odot S^{(-)}\right) = \left(\frac{[H^+]}{[H^+]+K_{aNH}}\right)\left(\frac{K_{aOH}}{[H^+]+K_{aOH}}\right)\left(\frac{K_{aSH}}{[H^+]+K_{aSH}}\right) \quad (4\text{–}105)$$

where pK_{aSH} is the pK_a for acid–base SH. For bovine pancreatic ribonuclease hydrolyzing cytidine 2′,3′-cyclic phosphate

$$\log k_{cCP,app} = \log k_{cCP} + \log\left\{\left(\frac{K_{a1}}{[H^+]+K_{a1}}\right)\left(\frac{K_{a2}}{[H^+]+K_{a2}}\right)\left(\frac{[H^+]}{[H^+]+K_{a3}}\right)\right\} \quad (4\text{–}106)$$

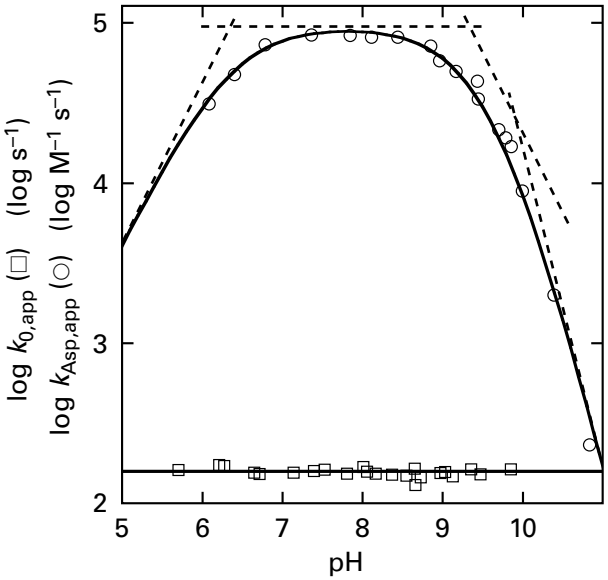

Figure 4–12: pH–Rate profiles for the transamination of aspartate catalyzed by aspartate transaminase.[85] Solutions of L-aspartate and 2-oxoglutarate at various concentrations were prepared at values of pH buffered with 1,4-bis(2-hydroxyethyl)piperazine, 2-(*N*-morpholino)ethanesulfonate, 2-[4-(2-hydroxyethyl)piperazin-1-yl]ethanesulfonate, 3-[[tris(hydroxymethyl)methylamino]-propane-1-sulfonate, 2-(cyclohexylamino)ethanesulfonate, or 3-(cyclohexylamino)propane-1-sulfonate and 25 °C. The reaction was initiated by adding enzyme, and the initial rates were monitored by coupling the production of oxaloacetate to the oxidation of NADH (decrease in A_{340}) with malate dehydrogenase. From the set of initial rates at a given pH as a function of the concentrations of both L-aspartate and 2-oxoglutarate and from a knowledge of the molar concentration of the enzyme, values of the catalytic constant and the specificity constant, k_{Asp}, for L-aspartate could be ascertained. The common logarithms for the observed values of the apparent specificity constant for aspartate, $k_{Asp,app}$ (○, molar^{-1} second^{-1}), are plotted as a function of pH, and the common logarithms of the observed values for the apparent catalytic constant, $k_{0,app}$ (□, second^{-1}), are plotted as a function of pH. The dashed lines are the asymptotes of the curve fit to the data (Equation 4–109) for common logarithms of the observed values for the apparent specificity constants for aspartate, $k_{Asp,app}$, below pK_{a1} (slope +1), between pK_{a1} and pK_{a2} (slope 0), between pK_{a2} and pK_{a3} (slope –1), and above pK_{a3} (slope –2).

When pH < pK_{a1} < pK_{a2} < pK_{a3}

$$\log k_{cCP,app} \cong \log k_{cCP} - pK_{a1} - pK_{a2} + 2\,pH \tag{4–107}$$

which defines a line of slope +2. The line of slope +1 intersects the line of slope +2 when pH = pK_{a1}. The curve fit to the data for $k_{cCP,app}$ (Figure 4–11A) has pK_{a1} = 4.2, pK_{a2} = 5.8, pK_{a3} = 6.2, and k_{cCP} = 17 mM^{-1} s^{-1}.

In the case of porcine aspartate transaminase (previously Equation 2–29)

L-aspartate + 2-oxoglutarate
$\rightleftharpoons$ oxaloacetate + L-glutamate (4–108)

when the common logarithm of the specificity constant $k_{Asp,app}$ for L-aspartate is plotted as a function of pH, its decrease at high pH defines a line of slope –1 that becomes a line of slope –2 above pH 10 (Figure 4–12).[85] This behavior is that expected for a situation in which the tautomer of the system X(HN$^{(+)}$,HO$^{(+)}$,⊙S$^{(-)}$) is the only active species. This tautomer is the one with monoprotic acid–base HN as its conjugate acid, HN$^{(+)}$; monoprotic acid–base HO as its conjugate acid, HO$^{(+)}$; and monoprotic acid–base HS as its conjugate base, ⊙S$^{(-)}$. For aspartate transaminase, the behavior of the common logarithm of $k_{Asp,app}$ as a function of pH can be fit (curve in Figure 4–12) with the function

$$\log k_{Asp,app} = \log k_{Asp} + \log\left\{\left(\frac{K_{a1}}{[H^+] + K_{a1}}\right)\left(\frac{[H^+]}{[H^+] + K_{a2}}\right)\left(\frac{[H^+]}{[H^+] + K_{a3}}\right)\right\} \tag{4–109}$$

and the parameters pK_{a1} = 6.35, pK_{a2} = 9.4, pK_{a3} = 9.9, and k_{Asp} = 95 mM^{-1} s^{-1}. When pH > pK_{a3} > pK_{a2} > pK_{a1}

$$\log k_{Asp,app} \cong \log k_{Asp} + pK_{a2} + pK_{a3} - 2\,pH \tag{4–110}$$

which defines a line of slope –2.*

Other examples in which a common logarithmic line of slope +1 is followed by one of slope +2 as the pH is decreased, so that the two values of pK_a on the one side of the maximum are clearly distinguished, are the behavior of the common logarithm of the catalytic constant $k_{0,app}$ below pH 7 for the retroaldol cleavage of (2*R*)-ethyl-(3*S*)-methylmalate by isocitrate lyase from *Dianthus caryophyllus*[86] and the behavior of the specificity constant $k_{Tyr,app}$ for L-tyrosine below pH 7 in the electrophilic aromatic substitution catalyzed by tyrosine phenol-lyase from *Pantoea agglomerans*.[87] In other instances, the two values of pK_a are too close together to obtain individual estimates for each of them when fitting the data

*Although not pertinent to the present discussion, which is concerned only with fitting curves to observations, the pK_a of 9.4 observed in the fit has been shown to be due to pH-dependent inhibition of the enzymatic reaction by the buffer used in the measurements.[67]

because the transition to a line with a slope of +2 on the acidic side of the maximum or a slope of –2 on the basic side of the maximum is too abrupt to observe the transition from a line of slope +1 or –1, respectively. In these instances, only an average of the two values of pK_a can be ascertained on either the acidic side[88-90] or the basic side[88,89,91,92] of the maximum, respectively. It is also possible to have a line of slope +3 or –3, identifying three different acid–bases on one side of the maximum.[90]

Another observation identifying the involvement of an additional acid–base is that of an inflection in the curve describing the behavior of a kinetic constant as a function of pH. Such an inflection is observed at around pH 9 in the behavior of the specificity constant $k_{cUP,app}$ for hydrolysis of uridine 2′,3′-cyclic phosphate (cUP) by bovine pancreatic ribonuclease (Figure 4–11B). This inflection can be fit (solid curve in the figure) with the equation

$$k_{cUP,app} = k_{cUP}\left\{\left(\frac{K_{a1}}{[H^+] + K_{a1}}\right)\left(\frac{[H^+]}{[H^+] + K_{a2}}\right)\left(\frac{[H^+]}{[H^+] + K_{a3}}\right)\right\} + k'_{cUP}\left\{\left(\frac{K_{a1}}{[H^+] + K_{a1}}\right)\left(\frac{[H^+]}{[H^+] + K_{a2}}\right)\left(\frac{K_{a3}}{[H^+] + K_{a3}}\right)\right\} \quad (4–111)$$

and the parameters pK_{a1} = 5.8, pK_{a2} = 6.2, pK_{a3} = 9.2, k_{cUP} = 4.5 mM^{-1} s^{-1}, and k'_{cUP} = 1.4 mM^{-1} s^{-1}. This behavior is that expected if the tautomer of the system X(⊙$S^{(-)}$,$NH^{(+)}$,$OH^{(+)}$) is enzymatically active and has a steady-state rate constant k_{cUP}, the tautomer of the system X(⊙$S^{(-)}$,$NH^{(+)}$,⊙$O^{(-)}$) is enzymatically active and has a steady-state rate constant k'_{cUP} less than k_{cUP}, and the other six tautomers and states of ionization of the system have negligible activity.

As with all kinetic measurements, the observations, the mathematical equations used to describe those observations, and the curves fit to the data with these equations must be clearly distinguished from chemical explanations of the behavior and the kinetic mechanisms derived from those explanations. Again, kinetics can only disprove a proposed mechanism; kinetics cannot prove a mechanism. A mechanism can be shown only to be consistent with the observations. From here on, examples of chemical explanations and kinetic mechanisms derived from those explanations and their consistency with the observations will be discussed.

If it is assumed that the enzyme remains in its native conformations and has not unfolded at either high or low values of pH in the range selected for the measurements, several **general conclusions** can be reached from an examination of observations of the behavior of the steady-state kinetic constants as a function of pH.

If the value for the observed catalytic constant or an observed specificity constant decreases as the pH is decreased, there **must be a catalytic base** that participates directly in the enzymatic reaction or the titration of which causes the polypeptide forming the active site to shift into an inactive conformation. In either case, when the conjugate acid of that base is formed by addition of a hydron, the enzymatic reaction cannot proceed effectively. The region of the pH–rate profile where the value for the observed rate constant decreases by a factor of 10 for every increase in the hydron concentration of a factor of 10 must occur at **values of pH less than the pK_a for the conjugate acid of this catalytic base**. This is the region in which the common logarithm of the rate constant as a function of pH has a slope of +1. The catalytic base is responsible for this decrease in the catalytic constant as the pH is decreased.

If the value for the observed catalytic constant or an observed specificity constant decreases as the pH is increased, there **must be a catalytic acid** that participates directly in the enzymatic reaction or the titration of which causes the polypeptide forming the active site to shift into an inactive conformation. In either case, when the conjugate base of that acid is formed by removal of a hydron, the enzymatic reaction cannot proceed effectively. The region in which the value for the parameter decreases by a factor of 10 for every decrease in the hydron concentration of a factor of 10 must occur at **values of pH greater than the value of pK_a for this catalytic acid**. This is the region in which the common logarithm of the rate constant as a function of pH has a slope of –1. The catalytic acid is responsible for this decrease in the catalytic constant as the pH is decreased.

As was discussed in detail earlier, other than the numerical values for rate constants, which are often informative, the conclusions drawn from steady-state kinetics measured at a constant pH rely entirely on the behavior of the rate of the enzymatic reaction as the concentrations of reactants are varied. Therefore, the kinetic mechanisms shown to be consistent with the observations describe only the entry and the exit of substrates from the active site, not what occurs after reactants are assembled in the active site or what occurs before products dissociate from

the active site. When variation of the steady-state rate constants of the enzymatic reaction with pH is observed, **the concentration of a catalytic acid is decreased** as the pH is raised or **the concentration of a catalytic base is decreased as the pH is lowered**, just as the concentrations of reactants and products are varied in normal steady-state measurements. Consequently, the kinetic mechanisms shown to be consistent with the observations describe the role of the catalytic acid or the catalytic base, respectively, in the reaction within the active site and the step or steps in the kinetic mechanism at which it is acts as an acid or as a base.

There are several possible explanations for a situation in which changes in the slope of the curve for the common logarithm of the catalytic constant occur at different values of pH than changes in the slope of the curve for the common logarithm of a specificity constant (Figures 4–10H, 4–10I, 4–11, and 4–12). Either the acids and bases involved in controlling these rate constants are different, or values of pK_a for the same acids and bases have changed as the reaction has progressed through its several steps, or the effects of these acids and bases on these parameters differ in their magnitude, or these changes in slope result from changes in the rate-limiting step of the enzymatic reaction that manifest themselves at different values of pH.

With these general facts in mind, specific kinetic mechanisms can be examined. Assume that the kinetic mechanism of a particular enzyme is **the simplest kinetic mechanism** for an active site catalyzing a conversion of reactant A

$$E + A \underset{k_{-1}}{\overset{k_1}{\rightleftharpoons}} E{\cdot}A \xrightarrow{k_2} E + Z \qquad (4\text{–}112)$$

to which many enzymatic mechanisms can be reduced by using saturating concentrations of all the reactants other than reactant A. In this instance, system X consists of both reactant A in all its tautomers and states of ionization and the collection of all the consequential catalytic acids and bases in the active site in all possible tautomers and states of ionization. Suppose, however, that titration of only four monoprotic acid–bases (NH, OH, PH, and SH) in system X affect the enzymatic activity, that titration of each is independent of titration of the others, and that hydronations and dehydronations of these four acid–bases are so rapid that they are always at equilibrium with the pH of the solution.

Suppose also that acid–bases NH and OH are both in the active site or both on reactant A, or one is in the active site and one is on the reactant. Suppose also that acid–base NH, wherever it is located, must be present as its conjugate acid, $NH^{(+)}$, and acid–base OH, wherever it is located, must be present as its conjugate base, $\odot O^{(-)}$, **before the active site can associate productively with reactant A** to form the Michaelis complex E·A. In this case, there is a set of active tautomers of the active site uncomplexed with reactant A, E_{act}, and a set of active tautomers of reactant A, A_{act}, in which together the two relevant acid–bases, again regardless of where they are located, are in their required states of ionization, and

$$[E_{act}][A_{act}] = \alpha_{E,A}(NH^{(+)})\,\alpha_{E,A}(\odot O^{(-)})[E][A] \qquad (4\text{–}113)$$

where [E] is the concentration of all tautomers and states of ionization of all forms of the active site uncomplexed with reactant A, [A] is the concentration of all tautomers and states of ionization of free reactant A, $\alpha_{E,A}(NH^{(+)})$ is the fraction of uncomplexed active site or free reactant in which acid–base NH is present as its conjugate acid, and $\alpha_{E,A}(\odot O^{(-)})$ is the fraction of uncomplexed active site or free reactant A in which acid–base OH is present as its conjugate base.

Suppose that acid–bases PH and SH, situated either on the active site or on the reactants, are both within the Michaelis complex E·A between the active site and reactant A. Suppose also that acid–base PH must be present as its conjugate acid, $PH^{(+)}$, and acid–base SH must be present as its conjugate base, $\odot S^{(-)}$, **before the Michaelis complex between the active site and reactant A can be converted to products** free in solution. In other words, "there is only one state of ionization of the active site that is capable of catalyzing the interconversion of [reactant] and product."[66] Assume also for the moment that k_2, the rate constant for the rate-limiting step in the reaction converting the Michaelis complex to products free in solution, is a microscopic rate constant produced by a single transition state in which both the conjugate acid of acid–base PH and the conjugate base of acid–base SH accomplish their catalysis. In this case, there is only one active tautomer of the Michaelis complex, $(E{\cdot}A)_{act}$, between active site and reactant A that can precede that transition state, much as an encounter complex precedes its transition state, and in which

the two relevant acid–bases are in their required states of hydronation so that

$$\left[(\mathrm{E{\cdot}A})_{\mathrm{act}}\right] = \alpha_{\mathrm{E{\cdot}A}}(\mathrm{PH}^{(+)})\,\alpha_{\mathrm{E{\cdot}A}}(\odot\mathrm{S}^{(-)})\left[\mathrm{E{\cdot}A}\right] \tag{4–114}$$

where [E·A] is the concentration of all tautomers and states of ionization of the Michaelis complex between active site and reactant A, $\alpha_{\mathrm{E{\cdot}A}}(\mathrm{PH}^{(+)})$ is the fraction of these complexes in which acid–base PH is present as its conjugate acid, and $\alpha_{\mathrm{E{\cdot}A}}(\odot\mathrm{S}^{(-)})$ is the fraction of these complexes in which acid–base SH is present as its conjugate base.

If

$$[\mathrm{E}]_{\mathrm{t}} = [\mathrm{E}] + [\mathrm{E{\cdot}A}] \tag{4–115}$$

where $[\mathrm{E}]_{\mathrm{t}}$ is the total concentration of all tautomers and states of ionization of all forms of the active site, and the relevant steady-state assumption is

$$k_1\left[\mathrm{E}_{\mathrm{act}}\right]\left[\mathrm{A}_{\mathrm{act}}\right] = (k_{-1} + k_2)\left[(\mathrm{E{\cdot}A})_{\mathrm{act}}\right] \tag{4–116}$$

it follows that

$$v_0 = \frac{k_{0,\mathrm{app}}k_{\mathrm{A,app}}[\mathrm{E}]_{\mathrm{t}}[\mathrm{A}]_0}{k_{0,\mathrm{app}} + k_{\mathrm{A,app}}[\mathrm{A}]_0} \tag{4–117}$$

where

$$k_{\mathrm{A,app}} = \left(\frac{k_1k_2}{k_{-1} + k_2}\right)\alpha_{\mathrm{E,A}}(\odot\mathrm{O}^{(-)})\,\alpha_{\mathrm{E,A}}(\mathrm{NH}^{(+)})$$

$$= \left(\frac{k_1k_2}{k_{-1} + k_2}\right)\left(\frac{K_{\mathrm{aOH}}}{[\mathrm{H}^+] + K_{\mathrm{aOH}}}\right)\left(\frac{[\mathrm{H}^+]}{[\mathrm{H}^+] + K_{\mathrm{aNH}}}\right) \tag{4–118}$$

and

$$k_{0,\mathrm{app}} = k_2\alpha_{\mathrm{E{\cdot}A}}(\odot\mathrm{S}^{(-)})\,\alpha_{\mathrm{E{\cdot}A}}(\mathrm{PH}^{(+)})$$

$$= k_2\left(\frac{K_{\mathrm{aSH}}}{[\mathrm{H}^+] + K_{\mathrm{aSH}}}\right)\left(\frac{[\mathrm{H}^+]}{[\mathrm{H}^+] + K_{\mathrm{aPH}}}\right) \tag{4–119}$$

If all the foregoing assumptions, which are many, are met, then values of the acid dissociation constants for acid–base NH and acid–base OH, each present in either the active site unassociated with reactant A or free reactant A, can be obtained from the behavior of the specificity constant k_{A} as a function of pH. Values of acid dissociation constants for the acid–bases SH and PH, present in the Michaelis complex between active site and reactant A, can be obtained from the behavior of the catalytic constant k_0 as a function of pH.

This derivation is the basis for **the usual, often unsupported, assumption** that values of $\mathrm{p}K_{\mathrm{a}}$ affecting the catalytic constant k_0 are those for Michaelis complexes between the active site and reactant A and that values of $\mathrm{p}K_{\mathrm{a}}$ affecting the specificity constant k_{A} for reactant A are those for the form of the active site with which reactant A associates or those for the form of reactant A itself that associates. The likelihood, however, that all the assumptions will apply to a particular enzymatic reaction is probably low.

There are **two special cases** of this general behavior that should be considered.

For many enzymes, the value of the **catalytic constant is invariant with pH** while the value of the specificity constant for reactant A is a function of pH. Suppose that rate constant k_2 in Equation 4–112 is invariant with pH because there is no essential catalytic acid in the Michaelis complex that can be dehydronated and there is no essential catalytic base in the Michaelis complex that can be hydronated in the range of pH over which the enzyme remains folded. If these are the circumstances, then $k_{0,\mathrm{app}} = k_2$ and the catalytic constant will be invariant with pH while the specificity constant k_{A} can be any function of pH. The Michaelis constant

$$K_{\mathrm{mA}} = \frac{k_{0,\mathrm{app}}}{k_{\mathrm{A,app}}} = \frac{k_2}{k_{\mathrm{A,app}}} \tag{4–120}$$

will be a function of pH reciprocal to that of the specificity constant. This situation, however, would also be consistent with an active site that closes over reactants so tightly that hydrons cannot enter the active site from the solution or leave the active site into the solution, regardless of the values for $\mathrm{p}K_{\mathrm{a}}$ of the catalytic acid–bases.

For many enzymes, the value for **the Michaelis constant, K_{m}, is invariant with pH** while the catalytic constant decreases below a $\mathrm{p}K_{\mathrm{a}}$ or decreases above a $\mathrm{p}K_{\mathrm{a}}$ or both. For example, the Michaelis constant for nitrile hydratase from *Comamonas testosteroni* is invariant with pH from pH 4 to 10 while both

the catalytic constant and the specificity constant, $k_{AC,app}$, for acrylonitrile (AC), the only reactant for the enzyme other than water, the concentration of which cannot be varied, decrease as the pH is lowered below a pK_a of 6.1 and decrease as the pH is raised above a pK_a of 9.2.[93] This behavior can be understood, if the simplest kinetic mechanism (Equation 4–112) applies, by making several assumptions. First, catalytic acid $NH^{(+)}$ is identical to catalytic acid $PH^{(+)}$ and catalytic base $\odot O^{(-)}$ is identical to catalytic base $\odot S^{(-)}$. Second, association of the reactant with the active site is unaffected by the state of ionization of either of these acid–bases or any others so that the dissociation constant for a reactant from the enzyme is invariant with pH. Third, rate constant k_{-1} is greater than rate constant k_2 at all values of pH. By factoring the equation for the apparent specificity constant

$$k_{A,app} = \left(\frac{k_1}{k_{-1}}\right)\left[k_2\left(\frac{K_{aSH}}{[H^+] + K_{aSH}}\right)\left(\frac{[H^+]}{[H^+] + K_{aPH}}\right)\right]$$

$$= \left(\frac{k_1}{k_{-1}}\right) k_{2,app} = \left(\frac{k_1}{k_{-1}}\right) k_{0,app} \qquad (4–121)$$

This equation explains why the same values of pK_a apply to both the catalytic constant and the specificity constant k_A for reactant A. From Equations 4–119 and 4–121, the Michaelis constant

$$K_{mA} = \frac{k_{0,app}[E]_t}{k_{A,app}[E]_t} = \frac{k_{-1}}{k_1} \qquad (4–122)$$

and is invariant with pH.

The fact that the individual rate constants appear in different factors in Equation 4–121 implies that **catalytic acids and catalytic bases can affect the underlying kinetic constants**, in this instance rate constant k_2, rather than just the forms of the enzyme present and the observed steady-state kinetic constants. For example, for a series of peptides (pep) that are reactants for bovine α-chymotrypsin, it was possible to determine independently the pH–rate profiles of rate constant k_2 and rate constant k_3 in the kinetic mechanism (previously Equation 3–91)

$$EOH + A \underset{k_{-1}}{\overset{k_1}{\rightleftharpoons}} EOH{\cdot}A \underset{k_{-2}}{\overset{k_2}{\rightleftharpoons}} E{-}O\underset{\underset{O}{\|}}{\overset{}{\diagdown}}R{\cdot}Z \xrightarrow{k_3} EOH + Z + Y \qquad (4–123)$$

for the enzymatic reaction.[94] As might be expected, because the chemistries of the two steps are quite different, the two rate constants had significantly different pH–rate profiles.

As noted above, when an enzyme has more than one reactant, the form of the enzyme with which reactant A, B, or C associates in a kinetic experiment is usually the **enzyme present at saturating concentrations of the other reactants**. This form of the enzyme, therefore, is usually one in which the active site is already occupied by one or more of the other reactants. For example, when the specificity constant k_{NAD} for NAD^+ was measured for saccharopine dehydrogenase (NAD^+, L-lysine forming) from *S. cerevisiae* (Equation 4–85), the other reactant, N^6-(L-1,3-dicarboxypropyl)-L-lysine (saccharopine, sac), was at saturation; and when the specificity constant k_{sac} for N^6-(L-1,3-dicarboxypropyl)-L-lysine was measured, NAD^+ was at saturation. Because this particular enzyme has been shown to associate with each reactant in the absence of the other, when the specificity constant k_{NAD} was measured, the form of the enzyme with which NAD^+ was associating was the complex between enzyme and saccharopine, E·sac, and when the specificity constant k_{sac} was measured, the form of the enzyme with which saccharopine was associating was the complex between enzyme and NAD^+, E·NAD^+. Consequently, it is not surprising that the specificity constants k_{NAD} and k_{sac} are governed by different values of pK_a. It has already been noted that the specificity constant k_{NAD} decreases when the pH is lowered below a pK_a of 7.4 (Figure 4–10D). The specificity constant k_{sac} decreases when the pH is lowered below a pK_{a1} of 6.2 and decreases when the pH is raised above a pK_{a2} of 7.2.[76] Neither reactant has a pK_a in this range, so it must be acid–bases with different values of pK_a in the complexes E·sac and E·NAD^+, respectively, that are responsible for these differences.

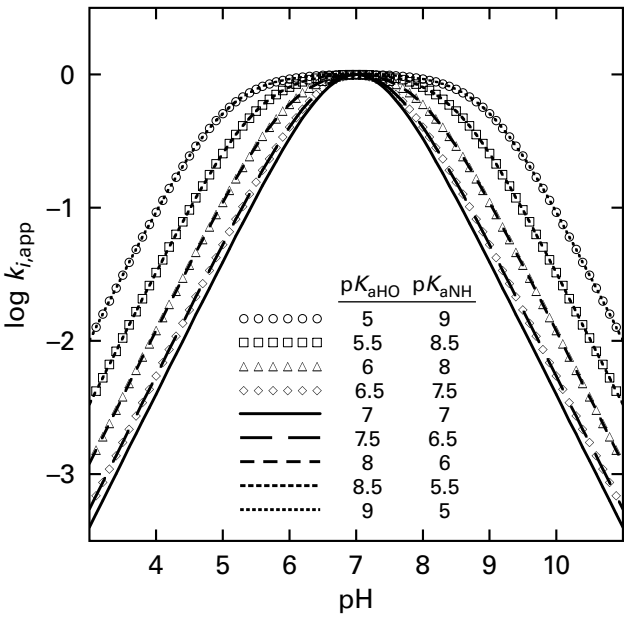

Figure 4–13: Shapes of the pH–rate profiles for an active site in which a general acid–base, HO, must be the conjugate base ⊙O$^{(-)}$ and a general acid–base, NH, must be the conjugate acid $^{(+)}$NH for the enzyme to be active. pH–Rate profiles defined by Equation 4–124 for different values of pK_{aHO} and pK_{aNH} are plotted. The values of pK_{aHO} and pK_{aNH} for each curve are given in the central table. The pH-independent rate constant k_i in Equation 4–124 was adjusted in each case to the respective value that gave a maximum value for log $k_{i,app}$ of 0 for each curve so that only the shapes of each curve could be compared. In the descending order of the table, these values for k_i are 1.02, 1.06, 1.21, 1.73, 4.00, 17.3, 121, 1060, and 10,200. The common logarithms of $k_{i,app}$ are plotted as a function of pH.

The ambiguity of reverse hydronation must be taken into account before the assignment of particular acid–bases to the observed values of pK_a and the assignment of their roles in the enzymatic reaction can be designated. For equations of the form

$$\log k_{i,app} = \log(k_i K_{a1}) + \log\left\{\frac{[H^+]}{[H^+]^2 + (K_{a1} + K_{a2})[H^+] + K_{a1}K_{a2}}\right\} \quad (4\text{–}124)$$

as are Equations 4–118 and 4–119, the argument of the first common logarithm to the right of the equal sign is a constant, and the argument of the second common logarithm is **symmetric in K_{a1} and K_{a2}.** At the moment, values of pK_{a1} and pK_{a2} are observed values of pK_a of unknown origin in the absence of independent assignment. Consider Equation 4–118, the equation for the specificity constant $k_{A,app}$, while realizing that the same argument can be made for Equation 4–119, the equation for the catalytic constant. The curve for the specificity constant can be defined by a situation in which pK_{aOH} = pK_{a1} (the lower of two observed values of pK_a) and pK_{aNH} = pK_{a2} (the higher of two observed values of pK_a). The curve can also be defined by the reverse situation, in which pK_{aOH} = pK_{a2} and pK_{aNH} = pK_{a1}. Because of the symmetry of Equation 4–124, the shapes of these two curves are identical (Figure 4–13). The only observed values are those for the pH at which two changes in slope occur on the curve and a rate constant that cannot be assigned to any function of the underlying fundamental rate constants, so there is no way to decide which observed pK_a goes with the catalytic acid and which goes with the catalytic base. Usually, in the absence of any observations to the contrary, it is simply assumed that pK_{aOH}, the pK_a for the catalytic base, is actually pK_{a1} and that pK_{aNH}, the pK_a for the catalytic acid, is actually pK_{a2}. This assumption seems reasonable because it gives the smaller value for k_i (Equation 4–124), which one might believe to be the easier value of this rate constant for natural selection to achieve.

There is, however, also the possibility that pK_{aOH}, the pK_a for the catalytic base, is actually pK_{a2} and that pK_{aNH}, the pK_a for the catalytic acid, is actually pK_{a1}. In this case, a minor tautomer of either the unoccupied active site or the reactant or both is enzymatically active. The tautomer with the stronger conjugate base (⊙O$^{(-)}$) and the stronger conjugate acid (NH$^{(+)}$) is the active species because, if by convention pK_{a1} < pK_{a2}, then pK_{aNH} < pK_{aOH}. In the case of the equation for the catalytic constant (Equation 4–119), if pK_{aSH}, the pK_a for the catalytic base, is actually pK_{a2} and pK_{aPH}, the pK_a for the catalytic acid, is actually pK_{a1}, then pK_{aPH} < pK_{aSH}, and a minor tautomer of the Michaelis complex is the actual active tautomer.

Reverse hydronation is the situation in which a minor tautomer of either unassociated reactant or unassociated active site, rather than the respective major tautomer, or a minor tautomer of the Michaelis complex of the two, rather than the major tautomer, is the active form of the active site.[95,96] In each case, the observations cannot distinguish which of the two tautomers, the major one or the minor one, is the one that is active and which is inactive. Nor can they distinguish which observed value of pK_a, pK_{a1} or pK_{a2}, belongs to the catalytic base and which to the catalytic acid for the simple reason that the ratio between any two tautomers of the system

$$\frac{\alpha(\odot O^{(-)}, NH^{(+)})}{\alpha(HO^{(+)}, \odot N^{(-)})} = \frac{K_{aOH}}{K_{aNH}} \qquad (4\text{–}125)$$

is invariant with pH. For example, if the simplest kinetic mechanism (Equation 4–112) applies to the catalytic constant of lysozyme and $pK_{a1} = pK_{aOH} = 3.8$, where $\odot O^{(-)}$ is the catalytic base, and $pK_{a2} = pK_{aNH} = 6.7$, where $NH^{(+)}$ is the catalytic acid (Figure 4–10H), then $k_2 = 0.15\ s^{-1}$ (Equation 4–119). If, however, $pK_{a1} = pK_{aNH} = 3.8$ and $pK_{a2} = pK_{aOH} = 6.7$, which gives an identical fit to the data because of the symmetry of Equation 4–124, then $k_2 = 120\ s^{-1}$.

On the one hand, the fact that, for example, rate constant k_2 is greater in a case of reverse hydronation means that natural selection has had the burden of making the enzyme more efficient. On the other hand, **a stronger base and a stronger acid are made available**, which might make it easier for natural selection to make the enzyme more efficient, if the Brønsted coefficients for the reaction catalyzed by the enzyme are large enough.

Consider, for the sake of argument, a catalytic base being used in the active site of an enzyme. If the pH of the cytoplasm is less than the pK_a for the conjugate acid of that base, only a fraction of the enzyme will be in the active ionization state at that pH. The higher the pK_a for the acid–base being used as a catalytic base, the stronger will be that catalytic base, but the smaller will be the fraction of enzyme that is active at the pH of the cytoplasm. If the Brønsted coefficient for the base in its catalysis of the reaction catalyzed by the enzyme were 1, then the increased rate of the reaction catalyzed by the proper tautomer of the system that would be brought about by increasing the basicity of the catalyst would cancel the decreased rate of the enzymatic reaction at the pH of the cytoplasm resulting from the decreased concentration of the proper tautomer of the system. For example, the hydroxide bound to a zinc ion in human carbonic anhydrase 3 (see Equation 4–83) acts as a catalytic base in the enzymatic reaction, and the pK_a for its conjugate acid is the pK_a that governs the behavior of the specificity constant $k_{CO_2,app}$ for CO_2 in the hydration catalyzed by the enzyme. When the pK_a for the water bound to the zinc is increased experimentally, the value for k_{CO_2}, which is the value for $k_{CO_2,app}$ at high pH (Equation 4–84), increases with a Brønsted coefficient of 0.9 in response to the increase in its basicity.[97] In this case, the increase in the maximum specificity constant k_{CO_2} almost compensates for the decrease in the apparent specificity constant $k_{CO_2,app}$ at low pH caused by the increased pK_a for the water bound to the Zn^{2+}. The Brønsted coefficients for most reactions, however, are usually significantly less than 1.

The reverse hydronation that occurs with mandelate racemase

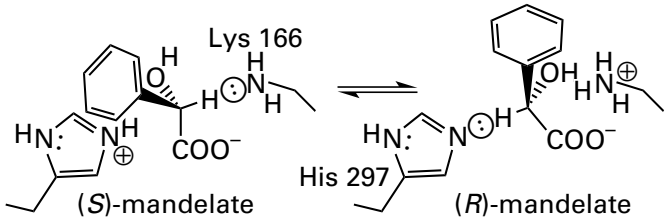

(4–126)

from *P. putida,* although its explanation jumps ahead in the overall argument, summarizes the various aspects of reverse hydronation in explicit terms. The standard free energy of (*S*)-mandelate (*S*-man) in free solution must be the same as the standard free energy of (*R*)-mandelate (*R*-man) in free solution because water is not a chiral molecule. Consequently, the equilibrium constant for the reaction must be 1, and the active site must catalyze the reaction in one direction as readily as in the other. The steady-state kinetic constants[98] in the two directions, *S* to *R* (*SR*) and *R* to *S* (*RS*) at pH 7.4, $k_{0SR} = 490 \pm 10\ s^{-1}$, $k_{0RS} = 650 \pm 60\ s^{-1}$, $k_{S\text{-man}} = 6.1 \pm 0.6\ M^{-1}\ s^{-1}$, and $k_{R\text{-man}} = 6.4 \pm 0.6\ M^{-1}\ s^{-1}$, confirm that requirement and satisfy the **Haldane equation**

$$K_{eq} = 1 = \frac{k_{S\text{-man}}}{k_{R\text{-man}}} \qquad (4\text{–}127)$$

which relates the steady-state kinetic constants to the equilibrium constant of the reaction in the solution.[99]

In the active site of a crystallographic molecular model for the complex between the enzyme from *P. putida* and 2-hydroxy-2-(4-iodophenyl)acetic acid, carbon 2 of this analogue of mandelate, 2-hydroxy-2-phenylacetic acid, sits between the side chain of Lysine 166 and the side chain of Histidine 297.[100] Lysine 166 is positioned to remove the hydron from (*S*)-mandelate, and Histidine 297 is positioned to remove the hydron from (*R*)-mandelate (Equation 4–126). When Histidine 297 is mutated to asparagine, the enzyme no longer racemizes mandelate, but it is able to exchange the hydron on (*S*)-mandelate for a deuteron in the solution but not the hydron on (*R*)-mandelate.[101] This result is that expected from the crystallographic molecular model of the complex.

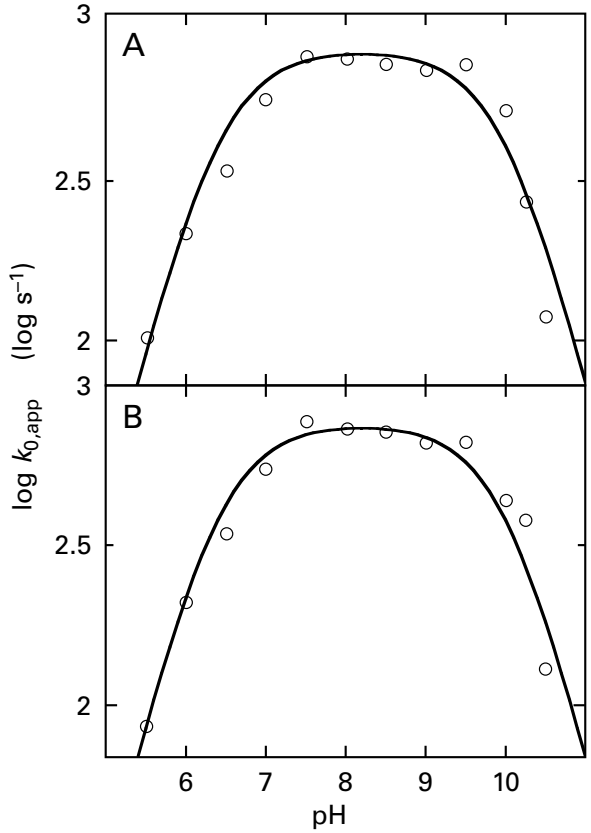

Figure 4–14: pH–Rate profiles for the catalytic constant of mandelate racemase from *P. putida* for (*R*)-mandelate (**A**) and (*S*)-mandelate (**B**) at 25 °C.[101] The buffers, all at 0.1 M, were 2-(*N*-morpholino)ethanesulfonate, pH 5.5, 6.0, and 6.5; 1,4-piperazinediethanesulfonate, pH 6.5, 7.0, and 7.5; 2-[4-(2-hydroxyethyl)piperazin-1-yl]ethanesulfonate, pH 7.5, 8.0, and 8.5; 3-[[tris(hydroxymethyl)methyl]amino]propane-1-sulfonate, pH 8.5 and 9.0; 2-(cyclohexylamino)ethanesulfonate, pH 9.0, 9.5, 9.75, and 10.0; 3-(cyclohexylamino)propane-1-sulfonate, pH 10.0, 10.25, and 10.5. The common logarithms of the observed catalytic constants $k_{0,app}$ (second^{-1}) are plotted as a function of pH. The data in each panel are fit with Equation 4–96, in both cases with values of pK_{a1} = 6.4 and pK_{a2} = 10.0.

Suppose that, in the encounter complex preceding the transition state for one step in an enzymatic reaction, one side chain in the active site acts as a catalytic acid and another acts as a catalytic base. Also suppose that, in the transition state, the hydron is being transferred from that catalytic acid to the substrate and a hydron is being transferred from the substrate to that catalytic base. If these conditions are met, it necessarily follows inescapably from the principle of microscopic reversibility that **in the encounter complex preceding that same transition state when the reaction is proceeding in the reverse direction, the conjugate base of the catalytic acid in the forward direction must be acting as a catalytic base, and the conjugate acid of the catalytic base in the forward direction must be acting as a catalytic acid.** For example, in the reaction catalyzed by mandelate racemase, for a single transition state in which the hydrons are being transferred simultaneously, in the encounter complex for the racemization of (*S*)-mandelate, the amino group of Lysine 166 acts as a catalytic base and the imidazolio group of Histidine 297 acts as a catalytic acid. In the encounter complex for the racemization of (*R*)-mandelate, the imidazolyl group of Histidine 166 acts as a catalytic base and the ammonio group of Lysine 166 acts as a catalytic acid. In a reaction such as that catalyzed by mandelate racemase, where there is probably only one rate-limiting transition state, in this case the transition state for removal of a hydron from carbon, accompanied by hydronation of that same carbon at its opposite face, the pH–rate profile for the catalytic constant should be governed by the pK_a for the side chain acting as a catalytic base (Lysine 166 in one direction and Histidine 297 in the other) as well as the pK_a for the side chain acting as a catalytic acid (Histidine 297 in one direction and Lysine 166 in the other). It follows that if values for pK_a for the two conjugate acids in any such enzymatic reaction are far enough apart that they cannot possibly shift enough to change their order, **reverse hydronation must occur in one, but only one, of the directions**.

The observed acid dissociation constants (pK_{a1} = 6.4 and pK_{a2} = 10.0) governing the pH–rate profile for the catalytic constant when (*R*)-mandelate is the reactant (Figure 4–14A) are identical within experimental error to those governing the pH–rate profile for the catalytic constant when (*S*)-mandelate is the reactant (Figure 4–14B).[101] Because these two values of pK_a are so different from each other, each acid–base governing these pH–rate profiles, if these are actually values of pK_a for acid–bases, must be titrating independently of the other. Because the two enantiomers of mandelate are indistinguishable in an achiral solution, the equilibrium constant for the reaction must be 1 not only at one pH but at all values of pH. Therefore, it follows from the Haldane equation that $k_{S\text{-man}}$ must equal $k_{R\text{-man}}$ at all values of pH. Because the apparent values of pK_a for the catalytic constant in each direction are identical, either the Michaelis constants in the two directions are invariant with pK_a or their variation with pH must have the same apparent values of pK_a as each other and as those for the catalytic constants.

From all the arguments just presented, it can be concluded that if the tautomer of the Michaelis

complex $^{+}$HHEK⊙·(*S*)-mandelate is responsible for racemization of (*S*)-mandelate, then the tautomer of the Michaelis complex ⊙HEKH^{+}·(*R*)-mandelate is responsible for the racemization of (*R*)-mandelate (Equation 4–126). In these two complexes, $^{+}$HH is the conjugate acid of Histidine 297, ⊙H is the conjugate base of Histidine 297, KH^{+} is the conjugate acid of Lysine 166, and K⊙ is the conjugate base of Lysine 166. Because of the symmetry of Equation 4–99, if association of (*S*)-mandelate with the enzyme has the same effect on the acid dissociations of acid–bases $^{+}$HHE and KH^{+} as does that of (*R*)-mandelate, which seems reasonable, the pH–rate profile for the catalytic constant of tautomer $^{+}$HHEK⊙·(*S*)-mandelate must be governed by the same two values of pK_a as the pH–rate profile for the catalytic constant of tautomer ⊙HEKH^{+}·(*R*)-mandelate (Figure 4–13), as is observed (Figure 4–14). This conclusion would follow from the fact that the ratio for concentrations of the two tautomers, [$^{+}$HHEK⊙·(*S*)-mandelate] and [⊙HEKH^{+}·(*R*)-mandelate], must be invariant with pH.

The pK_a of 6.4 has been assigned to the conjugate acid of Lysine 166 because the catalytic constant of the exchange of the hydron in (*S*)-mandelate for a deuteron in the solution catalyzed by Lysine 166 (Equation 4–126), in the mutant in which Histidine 297 has been changed to asparagine, has a pH–rate profile governed by a pK_a of 6.4 for a catalytic base.[101] The pK_a of 6.4 is significantly less than the pK_a for a fully solvated lysine on the surface of a protein exposed to the aqueous phase (10.5), but this decrease in pK_a can be explained by the fact that, in the complex between enzyme and substrate,[100] the cationic conjugate acid of the side chain of Lysine 166 is unsolvated by water and immediately adjacent (0.37 nm) to a Mg^{2+}. The pK_a of 10.0 can then be assigned to Histidine 297, which is significantly greater than the pK_a for a fully exposed histidine on the surface of a protein (6.6), but this increase in pK_a can be explained by the facts that the π nitrogen of its imidazolyl group, opposite from the catalytic τ nitrogen, forms a hydrogen bond with the carboxylato group of Aspartate 270 and that the negatively charged carboxylato group of Glutamate 317 is nearby.

Consequently, when (*S*)-mandelate is racemized by the major tautomer, $^{+}$HHEK⊙, the conjugate acid of the catalytic base, the amino group of Lysine 166, has a lower pK_a than the catalytic acid, the imidazolium of Histidine 297. In this instance, although the concentration of the active tautomer $^{+}$HHEK⊙ is far greater than that of the minor tautomer ⊙HEKH^{+}, it contains a weaker acid, the imidazolio group, and a weaker base, the amino group. When (*R*)-mandelate is racemized by the minor tautomer ⊙HEKH^{+}, the catalytic base, the imidazolyl group of Histidine 297, has a conjugate acid with a higher pK_a than the catalytic acid, the ammonio group of Lysine 166. In this instance, although the concentration of this active tautomer is far less than that of the major tautomer $^{+}$HHEK⊙, it contains a stronger acid and a stronger base, and reverse hydronation is operating. It should, however, be noted that the designation of which hydronation is reverse hydronation is based only on the convention that it is due to hydronation performed by the minor tautomer. Either hydronation could have been called "reverse hydronation".

In a twist on this usual **trade-off between basicity and the concentration of a base** at a pH less than the pK_a for its conjugate acid, a neighboring imidazolium cation in the active site of papain from *Carica papaya* lowers the pK_a for the sulfanyl group of a cysteine, increasing the concentration of the tautomers and states of ionization in which it is the conjugate base at neutral pH without decreasing its nucleophilicity in the reaction catalyzed by the enzyme.[102]

The most straightforward acid dissociation constants in a pH−rate profile to assign are acid dissociation constants of the free reactants. In such a case, one acid dissociation constant affecting the **specificity constant** k_A is an acid dissociation constant of reactant A. For example, when bovine pancreatic ribonuclease hydrolyzes cytidine 2′,3′-cyclic phosphate, there is a pK_a of 4.2 (change in slope in Figure 4–11A) that affects the specificity constant $k_{cCP,app}$ for cytidine 2′,3′-cyclic phosphate. When the same enzyme, however, hydrolyzes uridine 2′,3′-cyclic phosphate, there is a pK_a of 9.2 (inflection in Figure 4–11B) that affects its specificity constant $k_{cUP,app}$. These are the respective values of pK_a for the conjugate acids of the cytosine in cytidine 2′,3′-cyclic phosphate and the uracil in uridine 2′,3′-cyclic phosphate. The pK_a of 4.2 is not observed when the enzyme hydrolyzes uridine 2′,3′-cyclic phosphate, and the pK_a of 9.2 is not observed when the enzyme hydrolyzes cytidine 2′,3′-cyclic phosphate (Figure 4–11). The respective absences of these values of pK_a, in addition to the coincidence of the values of pK_a, are consistent with the conclusion that the acid–bases with these values of pK_a are on the two respective reactants and not on the enzyme. It follows that cytidine 2′,3′-cyclic phosphate must have a

neutral cytosine, not its cationic conjugate acid, to associate productively with pancreatic ribonuclease, but uridine 2′,3′-cyclic phosphate can have either a neutral or a monoanionic uracil and still associate productively with pancreatic ribonuclease. The latter form, however, has a specificity constant k_{cUP} that is 3.2 times smaller than that of the former.

The pH–rate profile for the specificity constant k_{Cth} for the reactant L-cystathionine (Cth) for cystathionine β-synthase from *S. cerevisiae* decreases as the pH is raised above a pK_a of 8.6. This pK_a has been assigned to the acid dissociation constant of one of the ammonio groups in the zwitterion of L-cystathionine (pK_a = 8.5). The pH–rate profile for the Michaelis constant $K_{m,pep}$ for the reactant *N*-(*N*-furylacryloyl-L-phenylalanyl)glycine for carboxypeptidase C from *S. cerevisiae* decreases as the pH is lowered below a pK_a of 3.58 ± 0.14. This pK_a has been assigned to the acid dissociation constant of the carboxy-terminal carboxy group of the reactant (pK_a = 3.44 ± 0.01). This assignment leads to the conclusion that *N*-(*N*-furylacryloyl-L-phenylalanyl)-glycine must be anionic to associate with the active site.[103]

In the case of porcine aspartate transaminase (Equation 4–108), the pK_a of 9.9 governing the behavior of the specificity constant $k_{Asp,app}$ for L-aspartate (Figure 4–12) is indistinguishable from that of the microscopic pK_a for the α-amino group of L-aspartate (9.85).[104] When L-cysteine sulfinate (CS) is used as a reactant for aspartate transaminase from *Escherichia coli*, the pK_a governing the decrease in its specificity constant $k_{CS,app}$ at high pH is 9.0, which is the pK_a for the α-amino group of L-cysteine sulfinate, but when L-aspartate is used as a reactant with the enzyme from *E. coli*, the pK_a governing the decrease in the specificity constant $k_{Asp,app}$ is 9.6,[67] which is the same, within experimental error, as that for the porcine enzyme. This shift in observed values of pK_a for the enzyme from *E. coli* clearly identifies each observed value of pK_a as that for the α-amino group of the respective reactant.

A pK_a of 6.0 governs the behavior of the specificity constant $k_{GAP,app}$ for glyceraldehyde 3-phosphate (GAP) in the reaction catalyzed by triose-phosphate isomerase (Equation 4–46) from *G. gallus*. Acid dissociation of the phospho group of glyceraldehyde 3-phosphate has a pK_a of 6.3. 2-Hydroxy-4-phosphonobutyraldehyde

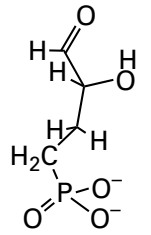

4–37

is also a substrate for triose-phosphate isomerase, but the pK_a for the phosphonate is 7.6 rather than 6.3 for the phosphate. The pK_a governing the specificity constant $k_{HPB,app}$ for 2-hydroxy-4-phosphonobutyraldehyde (HPB) is 7.5 rather than 6.0.[105] Because the apparent pK_a governing the kinetics shifts as expected when one reactant is substituted with the other, it must be the case in each instance that the pK_a in the pH–rate profile is that for the reactant.

In the cases of the human nonspecific tyrosine kinase Csk,[106] alkaline phosphatase from *E. coli*,[107] and chalcone isomerase from *Medicago sativa*,[108] sets of four or five different reactants were used for each enzyme. In each case, reactants in each set differed in pK_a over ranges of 1–2 units of pH. Each pK_a governing the variation of the specificity constants for the respective reactants as a function of pH agreed with the pK_a for that particular reactant. The fact that in each instance **the pK_a observed in the behavior of the specificity constant matched the pK_a for the reactant itself** clearly indicated that each pK_a observed kinetically was that of the respective reactant free in solution before it associated with the enzyme and that only one particular state of ionization of the reactant could associate efficiently and productively with the enzyme.

One way to treat these acid dissociations of a reactant is to **eliminate them from consideration**. If acid dissociation constants for the reactant are known and the form of the reactant that binds to the enzyme can be determined independently, the concentration of reactant in the appropriate form, α_A, can be calculated for each pH and total concentration of reactant, and a corrected specificity constant, $k'_{A,app}$, for just the concentration of the active tautomer and state of ionization of that reactant can be determined for each pH. This correction eliminates acid dissociation constants of the reactant from the data and leaves only acid dissociation constants of the enzyme. Because the effect of its acid dissociation constants is only on the free concentration of the competent form of the reactant, this correction is not mechanism-dependent. For example, from the kinetic behavior of the reaction, it was concluded that only zwitterionic L-ornithine

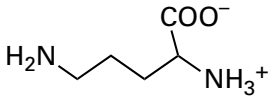

4–38

was a substrate for ornithine carbamoyltransferase from *E. coli*. Total concentrations of L-ornithine were corrected with an equation for α_{orn} so that a corrected value for the specificity constant, $k'_{orn,app}$, could be tabulated at each pH.[109]

The assignment of a pK_a in the pH–rate profile for a specificity constant to the pK_a for that reactant is straightforward because the pK_a for the reactant in the solution is the relevant value, but the pH–rate profile for the **catalytic constant** is governed by values of pK_a for the participants in the Michaelis complex. Usually, the pK_a for an acid–base on a reactant changes, often significantly, when it associates with the active site. For example, by following the nuclear magnetic resonance spectra as a function of pH for the fluorine-19 in 4-fluoro-3-hydroxybenzoate, both in solution and when it was bound to 3-hydroxybenzoate 6-monooxygenase from *Rhodococcus jostii*, it could be shown that the pK_a for its 3-hydroxy group decreased from 8.7 to 7.1 upon association with the active site.[110]

Consequently, if a **reactant within its complex with the active site** participates in an acid dissociation that affects the enzymatic reaction a measurement, such as the one for 4-fluoro-3-hydroxybenzoate, a measurement must be made of reactant within the active site to assign its pK_a to the pK_a in the pH–rate profile for the catalytic constant. For example, the catalytic constant for dehydration of 2-phospho-D-glycerate catalyzed by phosphopyruvate hydratase (previously Equation 3–393)

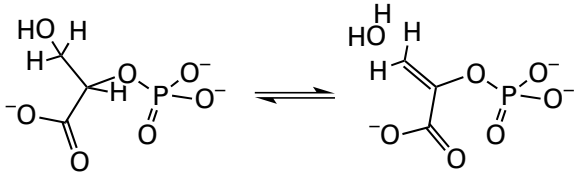

(4–128)

from *S. cerevisiae* decreases as the pH is decreased. The observed pK_a governing this decrease is 5.9 ± 0.1. This pK_a is within experimental error of the pK_a for the phospho group of 2-phospho-D-glycerate (5.82 ± 0.05) when it is bound to the active site of the enzyme.[111] This independent measurement of the pK_a was made from phosphorus-31 nuclear magnetic resonance spectra of the complex between enzyme and 2-phospho-D-glycerate at different values of pH.

When the reactant does not have an acid dissociation constant equal to an apparent acid dissociation constant governing the behavior of its specificity constant, it is usually assumed that the observed acid dissociation constant in a pH–rate profile is that for an acid–base in the active site of the enzyme. The assignment of a particular acid–base to a particular pK_a in the observed pH–rate profile is least ambiguous when there is an **independent measurement of the pK_a for a particular acid–base in the active site** that gives a value indistinguishable from that observed in the kinetic experiments. For example, dissociation of the hydron from the aldimine nitrogen on the internal lysylpyridoximine (previously Equation 2–2)

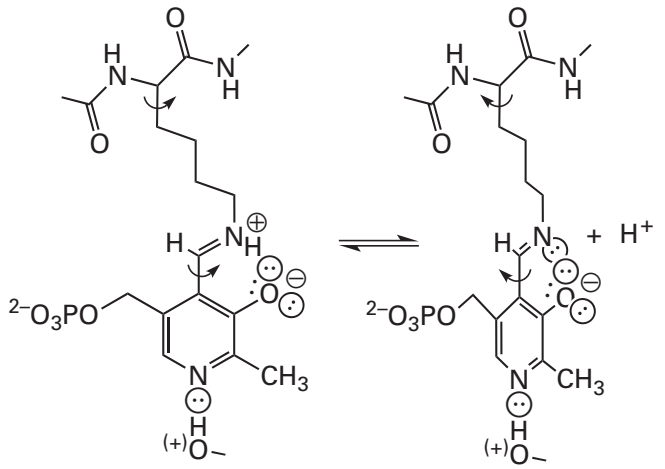

(4–129)

in the active site of porcine aspartate transaminase (Equation 4–108) can be assessed by following the absorbance of the enzyme, which shifts to shorter wavelengths as the dipolar π system is shortened upon dissociation of the hydron.[112] The pK_a for this acid dissociation at 25 °C is 6.3. In the steady-state kinetics of the enzyme,[85] the specificity constant $k_{Asp,app}$ for L-aspartate decreases as the pH decreases below a pK_a of 6.35 (Figure 4–12). This pK_a has been assigned to acid dissociation of the lysylpyridoximine on the basis of indistinguishable numerical values of pK_a. If this assignment is correct, then it is consistent with the conclusion that when the conjugate acid of the lysylpyridoximine is present, the active site cannot bind reactant productively, but when the conjugate base is present, it can. A chemical explanation for this conclusion[85] would be that because L-aspartate enters the active site with its α-amino group hydronated, the first step in the reaction would be for the phenolate oxyanion of the lysyl-

pyridoximine (Equation 4–129) to remove that hydron (Figure 2–2). This explanation would require that the oxygen of the phenolate be free of the hydrogen bond to the iminium nitrogen and available to act as a base. It is also possible, however, that the active tautomer of the system is that in which the α-amino group of the aspartate is unhydrated in solution, and thus a base, and the lysylpyridoximine is hydronated already, which would produce the same result by reverse hydronation and may make more chemical sense.

The visible spectrum of the prosthetic nicotinamide-adenine dinucleotide in UDP-glucose 4-epimerase

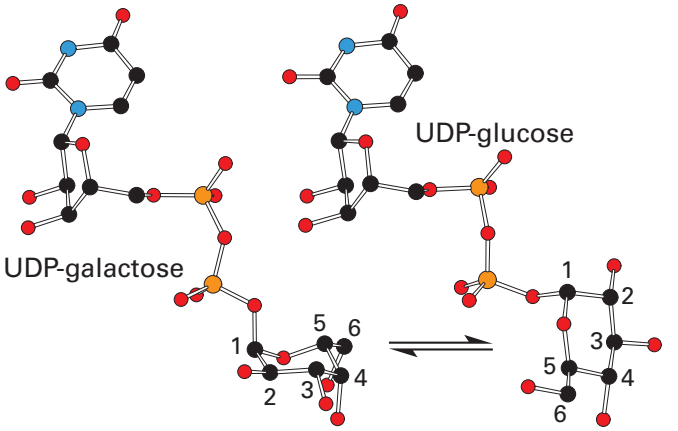

(4–130)

from *E. coli* has an absorption in a visible spectrum arising from charge transfer between the nicotinamide and the 4-oxidophenyl group of Tyrosine 149.[113] This charge-transfer band decreases in intensity below a pK_a of 6.1 as the 4-oxidophenyl group becomes hydronated in a mutant of the enzyme in which Serine 124 has been replaced with alanine. The pH–rate profile of the specificity constant $k_{Uga,app}$ for the reactant UDP-D-galactose (Uga) for this mutant also decreases as the pH is decreased below a pK_a of 6.1, which, consequently, has been assigned to Tyrosine 149.[114] It is assumed that Tyrosine 149 must be the unhydronated anion for the UDP-D-galactose to associate with the active site.

In the cases of aspartate transaminase and UDP-glucose 4-epimerase, the facts that the prosthetic groups, lysylpyridoximine (Equation 4–129) and NAD^+, are in the respective active sites is obvious. In most other instances, however, the amino acid side chains that are candidates for acid–bases with acid dissociation constants governing the behavior of the steady-state rate constants are usually identified by **examining the locations of the various acid–bases in a crystallographic molecular model of the active site of the enzyme.** For example, in the model of 2-hydroxymuconate tautomerase from *Pseudomonas*,[115] the amino-terminal proline of the enzyme is located in a pocket that was assumed to be the active site. The pK_a for the imino group of this proline was determined to be 6.4 ± 0.2 by following the nuclear magnetic resonance spectrum of its nitrogen, which had been enriched in nitrogen-15.[116] This acid dissociation constant agreed with the pK_a (6.2 ± 0.3) that governs a decrease in the specificity constant $k_{HPD,app}$ for tautomerization of the reactant 2-hydroxy-2*Z*,4-pentadienoate (HDP)

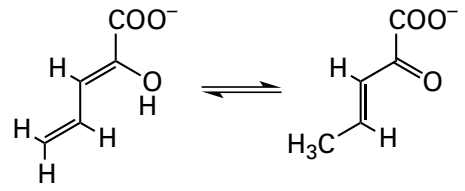

(4–131)

as the pH of the solution is decreased. It was concluded that the amino-terminal proline must be in the unhydronated neutral state of ionization for 2-hydroxy-2*Z*,4-pentadienoate to associate with the active site and that the imino nitrogen of the proline acts as a catalytic base in the reaction. This conclusion was also consistent with later crystallographic observations.[117]

In the crystallographic molecular model of a complex of D-glucose 6-phosphate and an inactive mutant of glucose-6-phosphate dehydrogenase [$NAD(P)^+$] from *Leuconostoc mesenteroides*,[118] Histidine 240 forms a hydrogen bond to the hydroxy group on carbon 1 of the β-pyranose of D-glucose 6-phosphate from which a hydron is removed during the reaction. The pK_a for the imidazolyl group of this histidine was determined to be 6.4 by following the chemical shift of the hydron on carbon 2 in nuclear magnetic resonance spectra as a function of pH.[119] This **independently determined acid dissociation constant agreed with the pK_a (6.3) that was observed in the behavior as a function of pH** of the catalytic constant k_0 for dehydrogenation of D-glucose 6-phosphate.

In the crystallographic molecular models of complexes between peptide deformylase from *E. coli*, the enzyme responsible for hydrolytically removing the formyl group from *N*-formylmethionyl proteins, and two inhibitors that mimic an *N*-formylated peptide[120] and a tripeptide with methionine at its amino terminus that mimics the product of hydrolysis,[121] Glutamate 133 is positioned properly to be a catalytic acid. A mutant in which Glutamate 133

has been replaced by aspartate is still enzymatically active, and the pK_a of Aspartate 133 in the mutant has been determined to be 10.1 by following the decrease in the infrared absorption of the C=O stretch (1740 cm^{-1}) of its carboxy group as a function of pH.[122] The observed value of this pK_a and the behavior of several mutants have been used to assign to Aspartate 133 the pK_a (10.1) above which the catalytic constant for the enzymatic reaction of the mutant decreases as the pH is raised and to assign it a role as a catalytic acid in the enzymatic reaction. If this assignment is correct, it is a rather dramatic example of a shift in pK_a for a carboxy group brought about by an active site.

In the crystallographic molecular model of a complex between (β1,4)-xylotetraose and an inactive mutant of endo-1,4-β-xylanase from *Bacillus circulans*, the position at which a xylan is normally hydrolyzed by the enzyme is immediately adjacent to both Glutamate 172 and Glutamate 78 within the active site of the enzyme,[123] in keeping with the usual arrangement of catalytic acid–bases in the active sites of glycosidases. The pK_a of Glutamate 78 (4.6 ± 0.1) and the pK_a of Glutamate 172 (6.7 ± 0.2) were determined from carbon-13 nuclear magnetic resonance spectra of the enzyme from bacteria grown on [δ-^{13}C]glutamate.[124] These values of pK_a agreed with those governing the behavior of the specificity constant $k_{NPX,app}$ for hydrolysis of 9-nitrophenyl β-xylobioside (NPX) catalyzed by the enzyme. The value of the specificity constant decreases below the pK_a of 4.6 as the pH is decreased, and it decreases below the pK_a of 6.7 as the pH is increased.

At first glance, it seems that assigning Glutamate 78 as the catalytic base and Glutamate 172 as the catalytic acid would be reasonable. Because, however, reverse hydronation cannot be ruled out by a pH–rate profile alone, the situation in which Glutamate 78 is the catalytic base and Glutamate 172 is the catalytic acid cannot be distinguished from the situation in which Glutamate 78 is the catalytic acid and Glutamate 172 is the catalytic base from these results alone. On the basis of crystallographic molecular models and identification of a covalent intermediate in the enzymatic reaction, it has been determined that Glutamate 78 is actually the catalytic base in the direction of hydrolysis and Glutamate 172 is the catalytic acid.[125]

Although there is some disagreement on this point, one way to determine the pK_a for a particular amino acid in a protein is to **monitor, as a function of pH, the rate of its modification by a reagent that can react with only one of its states of ionization**.[126] Normally, an electrophilic reagent is used to modify the amino acid so that only the conjugate base of the amino acid, a nucleophile, will react. For example, the lysine in the active site of acetoacetate decarboxylase from *Clostridium acetobutylicum* can be propionylated with 2,4-dinitrophenyl propionate

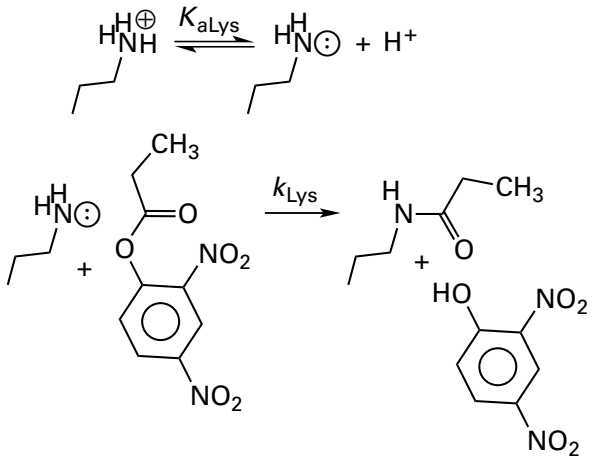

(4–132)

The rate of propionylation as a function of pH provides a pK_a for this lysine of 5.9 (Figure 4–15).[127]

The pK_a observed in such a chemical modification of the active site of an enzyme can often be correlated with the value of a pK_a observed in a kinetic measurement. For example, the active site of phospho*enol*pyruvate carboxykinase (GTP) from *G. gallus* contains a cysteine and a histidine. The enzyme is inactivated by iodoacetamide, a reagent that modifies cysteines preferentially, in a reaction governed by a pK_a of 8.2 ± 0.1.[92] The enzyme is also inactivated by diethyl dicarbonate, a reagent that modifies histidines almost exclusively, in a reaction governed by a pK_a of 6.7.[128] These inactivations were assumed to result from the modification of the cysteine and the histidine in the active site of the enzyme. On the basis of these two measured values of pK_a, the pK_a (8.15 ± 0.09) governing the specificity constant $k_{IDP,app}$ for $MgIDP^-$ and the pK_a (6.7 ± 0.3) governing the catalytic constant k_0 of the enzyme were assigned, respectively, to the cysteine and the histidine modified in these reactions.[92]

One drawback of determining the pK_a for a particular functional group on an amino acid in an active site by the rate of its alkylation with a nonspecific electrophile is the possibility that the **electrophile associates with the active site before modifying** it. Cysteine 645 is the nucleophilic catalyst in human arginine deiminase

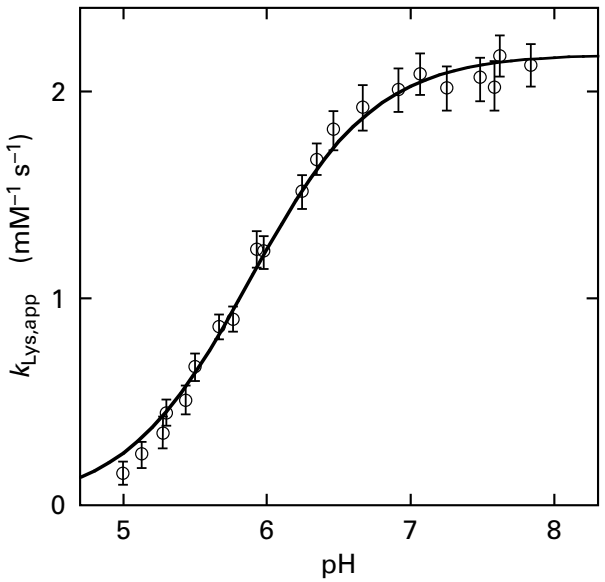

Figure 4–15: pH–Rate profile for the reaction of 2,4-dinitrophenyl propionate with acetoacetate decarboxylase.[127] Solutions of 2,4-dinitrophenyl propionate were prepared at various values of pH buffered with lutidine sulfate, *N,N,N′,N′*-tetramethyl-1,2-ethanediammonium sulfate, or 4-[(2-dimethylamino)ethyl]-morpholinium sulfate at 30 °C. The spontaneous rate of hydrolysis was recorded, and then a sample of acetoacetate decarboxylase was added. This addition caused a burst of 2,4-dinitrophenol production. The small rate of spontaneous hydrolysis of 2,4-dinitrophenol in the absence of enzyme was subtracted from the rate of this burst, and a pseudo-first-order rate constant was calculated from the rate at which the enzyme reacted with 2,4-dinitrophenyl propionate for each sample. These pseudo-first-order rate constants were divided by the respective concentrations of 2,4-dinitrophenyl propionate to obtain the observed second-order rate constant, $k_{Lys,app}$ (millimolar^{-1} second^{-1}), for the reaction of acetoacetate decarboxylase with 2,4-dinitrophenyl propionate, and these rate constants are plotted as a function of pH. In separate experiments, it was shown that the amplitude, in molarity, of the entire corrected burst of 2,4-dinitrophenol was equal to the molar concentration of active sites; that after the burst was complete, the enzyme had lost greater than 98% of its activity; that the loss of activity was coincident with the burst; that enzyme acetylated at the lysine within its active site showed no burst; and that occupation of the active site with acetopyruvate also eliminated the burst. The curve drawn through the points is that for an acid–base titration (Equation 4–79) with a pK_a of 5.88 and a value for the pH-independent rate constant at high pH of 2.18 mM^{-1} s^{-1}.

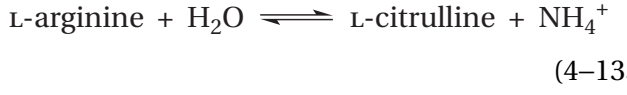

(4–133)

that adds to the guanidinio group of the reactant L-arginine in a nucleophilic substitution in which ammonia is the leaving group to form an (*N,S*-dialkyl)-thiourea as an intermediate in the enzymatic reaction. The pK_a of the sulfanyl group of Cysteine 645 (8.3 ± 0.07) was determined by its rate of reaction with iodoacetamide. The fact that the pK_a determined by its reaction with 2-chloroacetamidine (7.9 ± 0.16), which is more likely to form a complex with the active site because of its resemblance to the portion of the L-arginine at which the nucleophilic substitution occurs, was almost the same as that determined by iodoacetamide was presented as evidence that the former reaction was a simple bimolecular nucleophilic substitution providing an accurate measure of the pK_a and did not involve binding of the reagent to the active site. The pH–rate profile of the specificity constant for L-arginine in the enzymatic reaction decreases above a pK_a of 8.2 as the pH is increased, and it decreases below a pK_a of 7.3 as the pH is decreased. The pK_a of 8.2 was assigned to the sulfanyl group of Cysteine 645. Because its sulfanyl group must be unhydronated for it to act as a nucleophile, it was concluded that the pH–rate profile is recording a reverse hydronation in which the acid–base with the pK_a of 7.3 is acting as an acid while the unhydronated sulfanyl group of Cysteine 645 is acting as a nucleophile.[129]

In the crystallographic molecular model of bovine chymotrypsin,[130] Histidine 57 is located in the active site adjacent to Serine 195, which bears the hydroxy group at which the acyl intermediate in the enzymatic reaction is formed (Figure 3–6, Equation 4–123).[131] The pK_a of Histidine 57 in the unoccupied enzyme has been assigned as 6.8 on the basis of the rate of its arylation with 1-fluoro-2,4-dinitrobenzene, which decreases below this value of pK_a.[132] This measured value of the pK_a could be in error if the reaction of Histidine 57 with 1-fluoro-2,4-dinitrobenzene involves a step in which 1-fluoro-2,4-dinitrobenzene binds to the active site before the arylation. The imidazolio group in an equivalent complex formed from a histidine, a serine, and an aspartate in the active site of phospholipase C from *Bacillus cereus* has a pK_a, determined by nuclear magnetic resonance spectroscopy,[133] of 6.0, which gives an estimate for the pK_a for an imidazolyl group in such a situation.

It is known from crystallographic molecular models that the lone pair on the τ nitrogen of the

conjugate base of the imidazolyl group in the histidine in chymotrypsin accepts a hydrogen bond from the hydroxy group of Serine 195 (see the stereodrawing[134] for chymotrypsin in Problem 3–30)[130]

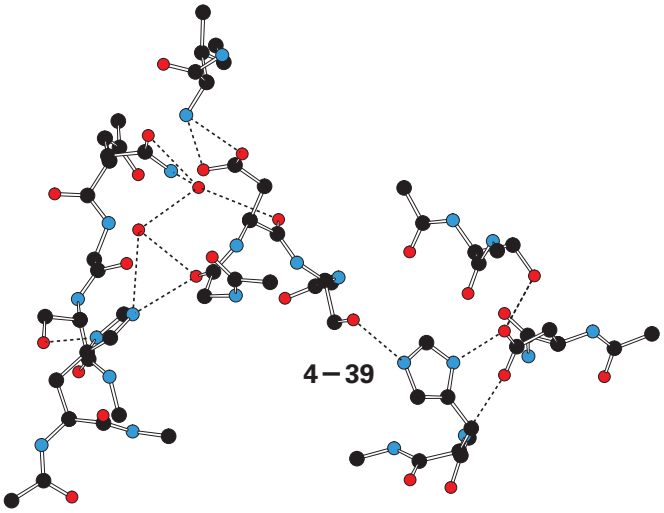

It is also known from neutron diffraction that the nitrogen–hydrogen bond on the π nitrogen in the cationic conjugate acid of the imidazolyl group is the donor in a hydrogen bond with the anionic carboxylato group of Aspartate 102 acting as an acceptor.[135] Therefore, the microscopic pK_a of 6.8 for dissociation of a hydron from Histidine 57, measured by the arylation, should be for

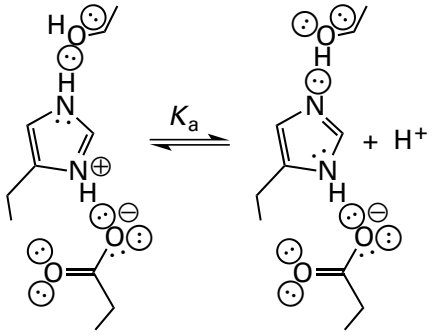

(4–134)

It has been determined by nuclear magnetic resonance spectroscopy[136] that the pK_a of Aspartate 102 is less than 1.5, presumably because it is engaged in this hydrogen bond with the imidazolio group of Histidine 57 at low pH, as well as additional hydrogen bonds. The pK_a for the hydroxy group of the serine should be considerably greater than 6.8, so in the acidic tautomer of the complex, the imidazolyl group should be the dihydronated conjugate acid as drawn.

In this instance, the pK_a for the carboxylato group is so low that no tautomer of the complex in which it is hydronated exists in the normal ranges of pH. Consequently, the carboxylato group mainly serves to orient the imidazolyl group by providing an acceptor for the hydrogen bond. In the active site of histone deacetylase from *Danio rerio*, the imidazolyl group of Histidine 137, which hydronates the amino group that leaves from the tetrahedral intermediate, is oriented by a hydrogen bond from the carbamoyl group of Glutamine 179, which is neither a reasonable acid nor reasonable base.[137]

The rate constant at saturating concentration of reactant for the acylation of Serine 195 in the active site of bovine chymotrypsin by nitrophenyl esters, the first chemical step in the kinetic mechanism (Equation 4–123) for hydrolysis of these esters catalyzed by the enzyme (Figure 3–6), is a function of pH and decreases as the pH is decreased below a pK_a of 6.7.[138] The coincidence of this pK_a with that observed directly for Histidine 57 by following the rate of its arylation suggests that the pK_a governing the pH–rate profile of the catalytic constant of the acylation reaction is that of Histidine 57. If this is the case, then the pK_a for this histidine in the Michaelis complex between enzyme and nitrophenyl ester must be same as in free enzyme, and it must be the conjugate base (Equation 4–134) for the active site to be capable of catalyzing the acylation. Because a hydron must be removed from Serine 195 either before or while the tetrahedral intermediate is formed in the acylation, the role of the imidazolyl group of Histidine 57 in the conjugate base of the hydrogen-bonded complex must be to act as the necessary catalytic base (Figure 3–6). The role of Aspartate 102, however, seems to be simply to provide the acceptor for a hydrogen bond from the imidazolyl group. Consistent with this conclusion is the fact that when the homologous aspartate in subtilisin from *Bacillus amyloliquefaciens* was mutated to cysteine,[139] the value of $k_0\,K_{m,pep}^{-1}$ for hydrolysis of a peptide (pep) that is a reactant for the enzyme decreased by only a factor of 10.

A similar hydrogen-bonded complex responsible for removing a hydron from a nucleophilic serine in the active site of β-lactamase from *Mycobacterium tuberculosis* is formed by the ammonio group of Lysine 73 and the carboxylato group of Glutamate 166.[140] In this instance, unlike the imidazolyl group in the active site of chymotrypsin, the pK_a for the ammonio group of Lysine 73 should be significantly closer to that of the hydroxy group of the serine, so the conjugate base should be more able to remove the hydron from the hydroxy group. Nevertheless, the hydron probably remains on the hydroxy group when the ammonio group dissociates and becomes

an amino group because, if it were to transfer to the imidazolyl group, the complex would be the zwitterion.

There is a similar hydrogen-bonded complex between the ammonio group of Lysine 165 and the carboxylato group of Aspartate 169 in the active site of phosphoribulokinase from *R. sphaeroides*, which uses $MgATP^{2-}$ to phosphorylate D-ribulose 5-phosphate (pr). When Aspartate 169 is mutated to alanine,[141] $k_0\,(K_{m,pr}K_{mATP})^{-1}$ decreases by a factor of 1.2×10^5, and when Lysine 166 is mutated to alanine,[142] $k_0\,(K_{m,pr}K_{mATP})^{-1}$ decreases by a factor of 2.3×10^6. These values are consistent with the two participants in the hydrogen-bonded complex acting in concert rather than the situation in chymotrypsin in which the carboxylato group only provides an acceptor for a hydrogen bond, the elimination of which is not so dramatic.

Independent determination of the pK_a for the side chain of an amino acid in the active site of an enzyme can also **rule out its assignment to a particular pK_a**. For example, the pK_a of Lysine 73 in the active site of β-lactamase from plasmid TEM-1 has been estimated to be 10.0 from the rate of its modification by 2,4,6-trinitrobenzenesulfonate.[143] This pK_a, if it is an accurate estimate, does not agree with either of the two values of pK_a (5. 6 and 7.8) that govern the behavior of the specificity constant $k_{BPC,app}$ for hydrolysis of benzylpenicillin (BPC) catalyzed by the enzyme.[144]

Contrary to the assumption that was made earlier to simplify the discussion of pH–rate profiles, the acid–bases in an active site often do not titrate independently of each other. If two or more of the acid–bases are close enough together within the active site, titration of one of them can shift the value or values of pK_a for the others. In such a case, **a tautomeric linkage governs microscopic values of pK_a**. The participants in a tautomeric linkage involving only two acid–bases are a linked pair.

The situation in the active site of lysozyme is an illustration of a **linked pair** participating in a tautomeric linkage.[145] In the crystallographic molecular model of lysozyme from *G. gallus*,[146] Glutamate 35 and Aspartate 52 are immediately adjacent to the site at which hydrolysis of a poly-(β1,4)-*N*-acetylglucosaminopyranose (Figure 3–27) occurs in the nucleophilic substitution catalyzed by the enzyme. Microscopic acid dissociation constants for these two carboxy groups have been estimated from the difference between the direct acid–base titrations of the enzyme and a derivative of the enzyme in which Aspartate 52 had been ethyl-esterified.[147] From fits of this difference titration curve and the direct titration curve of the unesterified enzyme to the appropriate equations, microscopic acid dissociation constants for these two carboxy groups

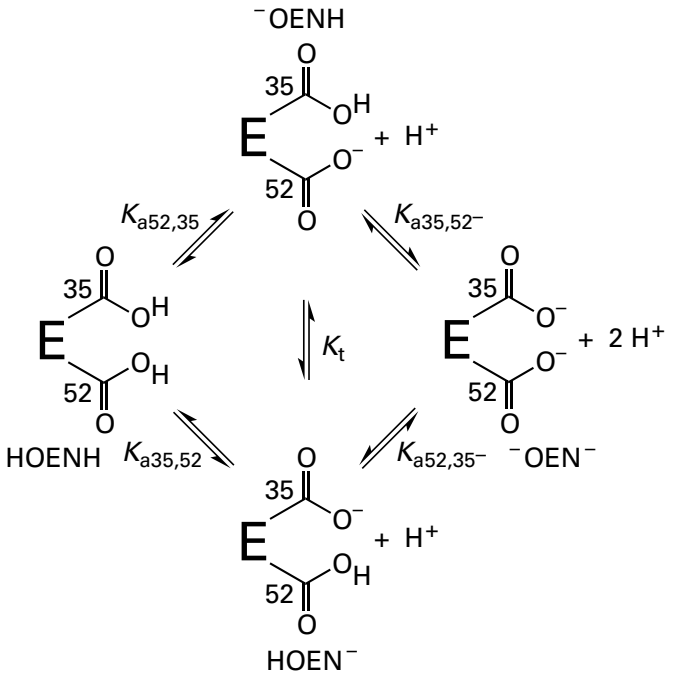

(4–135)

at 25 °C in 0.15 M KCl were estimated to be $pK_{a52,35} = 4.4$, $pK_{a52,35^-} = 5.2$, $pK_{a35,52} = 5.2$, and $pK_{a35,52^-} = 6.0$. As required by the linkage of the four equilibria among the tautomers and states of ionization

$$pK_{a52,35} + pK_{a35,52^-} = pK_{a35,52} + pK_{a52,35^-} \qquad (4\text{–}136)$$

Because these two carboxy groups are adjacent to each other in the active site, the anionization of either one raises the microscopic pK_a of the other one by 0.8 unit. It is also possible to estimate, in a similar fashion, the **four values of microscopic pK_a for two catalytic acid–bases** in the unoccupied active site of an enzyme from differences between the pH–rate profiles for the specificity constant $k_{A,app}$ of the unmutated enzyme and that of a mutant in which one of the two acid–bases has been eliminated.[148]

In Equation 4–135, there are two tautomers of the state of ionization of the dicarboxylic acid that contain only one hydron: one in which the hydron is on Glutamate 35 and one in which the hydron is

on Aspartate 52.* It is always the case that only one of the **two tautomers** in such a situation is enzymatically active in a particular direction of the reaction, and the fraction of the active sites that exist in this tautomer will determine the ultimate apparent catalytic constants in that direction at a given pH. Reverse hydronation is a corollary of this rule.

No pH–rate profile can distinguish between these two tautomers because the equilibrium constant, K_T, relating the two tautomers cannot be a function of pH (Equation 4–125), so the ratio between the two tautomers does not vary with pH. To decide on the role of each catalytic group in such a situation requires **information other than a pH–rate profile**. For example, it was proposed by the crystallographers that, from their locations in the active site, Aspartate 52 would act as the anionic conjugate base and Glutamic Acid 35 would act as a catalytic acid in hydrolysis of poly-(β1,4)-*N*-acetylglucosaminopyranose catalyzed by lysozyme.[146] It was, however, only serendipitous that these roles assigned by the crystallographer from an examination of the molecular model agree with one's intuition because the concentration of the other tautomer, in which Aspartate 52 is the catalytic acid and Glutamate 35 is the catalytic base, must increase and decrease in parallel with the concentration of the tautomer in which Aspartate 52 is the catalytic base and Glutamate 35 is the catalytic acid, and its increase and decrease must be governed by the same apparent values of pK_a. Consequently, if this situation were an example of reverse hydronation, the same pH–rate profile would have been observed.

Histidine 12 and Histidine 119 are located immediately adjacent to each other in the active site of bovine pancreatic ribonuclease,[149-151] and each is adjacent to the phosphodiester at which the nucleophilic substitution catalyzed by the enzyme occurs after it has associated with the active site. From an examination of a crystallographic molecular model of a complex between enzyme and uridyl vanadate (**4–40**)

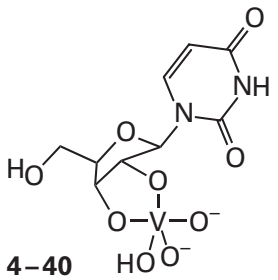

4–40

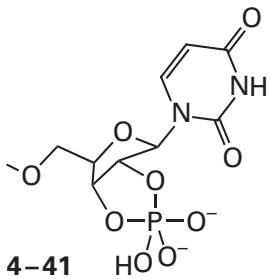

4–41

an analogue of phosphorane **4–41** that is an intermediate in the enzymatic reaction, it was concluded that Histidine 119 acts as a catalytic base and Histidine 12 acts as a catalytic acid in the enzymatic reaction.[152]

pH–Titration curves for these two adjacent imidazolyl groups have been followed by nuclear magnetic resonance spectroscopy.[153-155] Each titration curve has been fit with the equation[156]

$$\delta_{\mathrm{CHobs},i} = \delta_{\mathrm{CH^+},i} + \Delta\delta_{\mathrm{CH},i}\left\{\frac{K_{\mathrm{a}i,j^+}[\mathrm{H^+}] + K_{\mathrm{a}i,j}K_{\mathrm{a}j,i^+}}{[\mathrm{H^+}]^2 + (K_{\mathrm{a}i,j^+} + K_{\mathrm{a}j,i^+})[\mathrm{H^+}] + K_{\mathrm{a}i,j}K_{\mathrm{a}j,i^+}}\right\} \quad (4\text{–}137)$$

where $\delta_{\mathrm{CHobs},i}$ is the observed chemical shift for a proton on carbon 2 of the neutral imidazolyl group *i* at a given pH, δ_{CH,i^+} is the observed chemical shift for the proton on carbon 2 of imidazolyl group *i* when it is hydronated and cationic, $\Delta\delta_{\mathrm{CH},i}$ is the change in chemical shift for the proton on carbon 2 of imidazolyl group *i* upon its dehydronation, $K_{\mathrm{a}i,j^+}$ is the acid dissociation constant for imidazolyl group *i* when imidazolyl group *j* is hydronated and cationic, $K_{\mathrm{a}i,j}$ is the acid dissociation constant for imidazolyl group *i* when imidazolyl group *j* is unhydronated and neutral, and $K_{\mathrm{a}j,i^+}$ is the acid dissociation constant for imidazolyl group *j* when imidazolyl group *i* is hydronated and cationic. This equation defines the observed titration of a proton on carbon 2 of imidazolyl group *i*, and the same equation with the subscripts *i* and *j* switched defines titration of the proton on carbon 2 of imidazolyl group *j*. Parenthetically, Equation 4–137 is valid for any physical property that detects state of hydronation and any types of acid–bases, and it can be used to estimate relevant microscopic acid dissociation constants in such situations. From the fits of this equation to titration curves at 0.3 M NaCl and 30 °C, p$K_{\mathrm{a}119,12^+}$ = 6.01 ± 0.02, p$K_{\mathrm{a}119,12}$ = 6.29 ± 0.02, p$K_{\mathrm{a}12,119^+}$ = 5.80 ± 0.03, and p$K_{\mathrm{a}12,119}$ = 6.08 ± 0.04. Because these imidazolyl groups are adjacent to each other in the active site,

*It should be noted that, as is the case with most tautomers, the hydron is not transferred between the two carboxy groups because they are too far apart, but a hydron associates with each one from the solution and dissociates from each one into the solution.

the cationization of one lowers the pK_a for the other by 0.28 ± 0.05 unit.

In a crystallographic molecular model of the unoccupied active site of endo-1,4-β-xylanase from *B. circulans*, each of the two carboxy groups that are the catalytic acid–bases, those on Glutamate 78 and Glutamate 172, participates in a hydrogen bond with the same molecule of fixed water.[157] From observations of their nuclear magnetic resonance spectra, it was concluded that their ionizations are linked. The values obtained were p$K_{a78,172}$ = 4.6, p$K_{a78,172^-}$ = 5.8, p$K_{a172,78}$ = 5.5, and p$K_{a172,78^-}$ = 6.7. Consequently, the ionization of either one increases the pK_a for the other by 1.2. When the pK_a of Glutamate 78 is lowered by synthetically replacing it in turn with 4-fluoroglutamate and 4,4-difluoroglutamate, the pK_a below which the specificity constant decreases shifts from 4.7 to 3.4 and 3.0, as expected because this pK_a has been assigned to Glutamate 78. The pK_a above which the specificity constant decreases, however, which was assigned to Glutamate 172, also shifts from 7.1 to 6.0 and 6.0 upon the respective modification.[158] Because the specificity constant should reflect values of pK_a for the unoccupied enzyme, even though Glutamate 172 is unmodified, its apparent values for pK_a in the unoccupied active site nevertheless seem to be affected by modification of Glutamate 78, which is not a requirement of the linkage (Equation 4–136).

The carboxy groups in the active sites of lysozyme and endo-1,4-β-xylanase and the imidazolyl groups in the active site of bovine pancreatic ribonuclease are examples of acid–bases that are close enough to affect each other's acid dissociations. As a result of such an interaction, **a single pK_a cannot be assigned to either of these carboxy groups or either of these imidazolyl groups**.

These examples can be used to illustrate **what it means in practice for two acid–bases in an active site to titrate independently of each other**. Glutamatic Acid 78 (p$K_{a78,172}$ = 4.6) in endo-1,4-β-xylanase is more acidic than Glutamic Acid 172 (p$K_{a172,78}$ = 5.5). If Glutamic Acid 78 were even more acidic, then, as the pH of the solution was raised, it would be almost completely unhydronated and anionic before Glutamic Acid 172 began to ionize significantly. In this case, the anionization of Glutamatic Acid 78, because it would almost completely precede the anionization of Glutamic Acid 172, would not affect the titration of Glutamic Acid 172, and the anionization of Glutamic Acid 172, because it would almost completely follow the anionization of Glutamic Acid 78 would not affect the titration of Glutamic Acid 78. As a result, these two carboxy groups would titrate independently of each other, even though the interaction between them would remain just as strong. In other words, in the situation in which their ionizations were independent of each other, the only consequential acid dissociations during the titration would be p$K_{a78,172}$ for Glutamic Acid 78 when Glutamic Acid 172 was un-ionized and p$K_{a172,78^-}$ for Glutamic Acid 172 when Glutamic Acid 78 was anionized.

It has already been noted that the value for the specificity constant decreases below the pK_a of 4.6 as the pH is decreased and decreases below the pK_a of 6.7 as the pH is increased. These values agree with p$K_{a78,172}$ (4.6) and p$K_{a172,\,78^-}$ (6.7) and are consistent with the conclusion that only these two values of pK_a are consequential. So in practice, Glutamic Acid 78 and Glutamic Acid 172 titrate independently of each other because their acidities are different enough.

The acidities of Histidine 119 (p$K_{a119,12^+}$ = 6 .01) and Histidine 12 (p$K_{a12,119^+}$ = 5.80), however, are much closer together, but the interaction energy between them (ΔpK_a = 0.28) is much smaller than the interaction energy between the two carboxy groups (ΔpK_a = 1.2) in the active site of endo-1,4-β-xylanase. If there were insignificant interaction between them, for example, because they were more distant from each other, they would, by definition, titrate independently of each other, each with its own single unambiguous microscopic pK_a, unaffected by the state of ionization of the other, even though their values of pK_a are almost the same.

Consequently, **either large differences in pK_a or insignificant energies of interaction lead to independent titration of two acid–bases in an active site.**

In the case of lysozyme, the difference in pK_a between the carboxy groups is also large enough, and hence the equilibrium constant between the tautomers is small enough, that the pH–rate profile (Figure 4–10I) for specificity constant $k_{AG6,app}$ at an ionic strength of 0.1 M and 40 °C can be fit with Equation 4–97 to give pK_{a1} = 4.25 and pK_{a2} = 6.1, which are indistinguishable, within the error of measurement, from p$K_{a52,35}$ (4.4) and p$K_{a35,52^-}$ (6.0).

By **incorporating tautomeric linkage into the kinetic mechanism** chosen to explain an observed pH–rate profile, it can be seen that the resulting rate equation automatically incorporates reverse hydronation. Consider the interacting acid dissociation constants

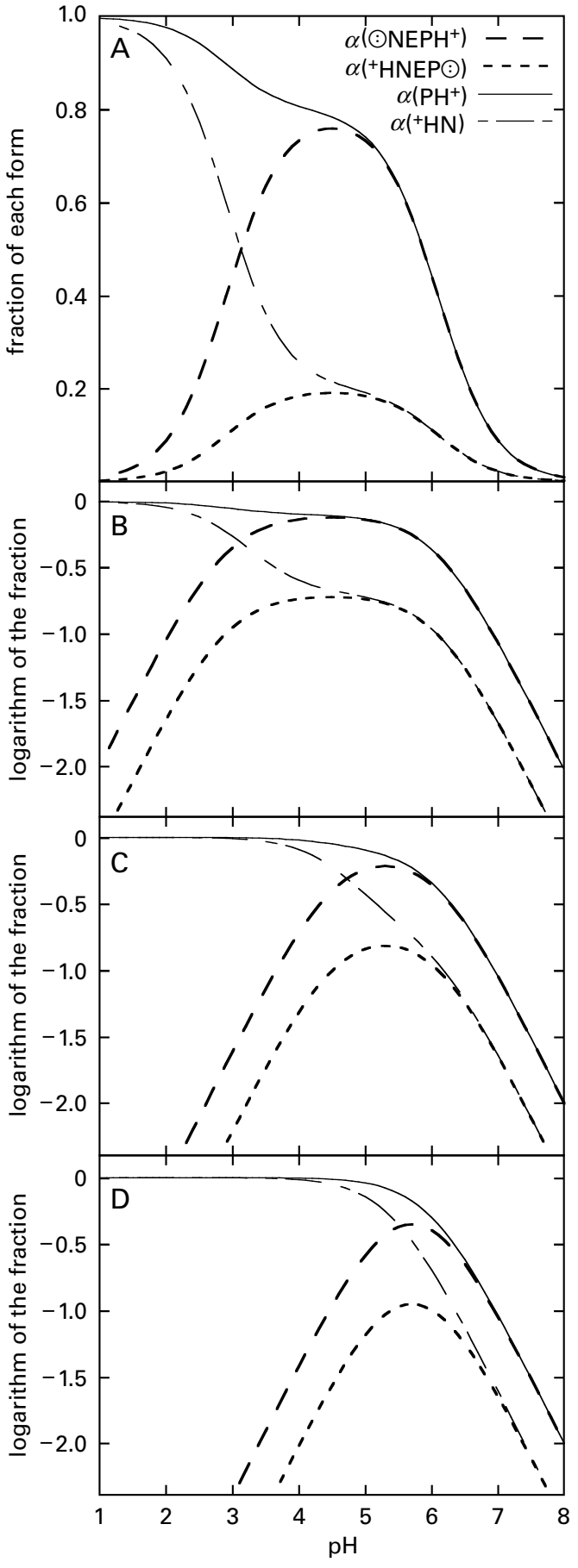

Figure 4–16: Fractions of either a particular tautomer of two acid–bases or the hydronated ionization states of two tautomerically linked acids as a function of the pH of the solution. The plots are for α(⊙NEPH$^+$) (Equation 4–140), α($^+$HNEP⊙) (Equation 4–141), α(PH$^+$) (Equation 4–146), or α($^+$HN) (see Equation 4–146 and switch NH$^+$ and PH$^+$) or for the common logarithms of these fractions. (**A**) Direct plots for pK_{aNH^+,PH^+} = 3.0, pK_{aPH^+,NH^+} = 3.6, p$K_{aNH^+,P\odot}$ = 5.4, and p$K_{aPH^+,N\odot}$ = 6.0. (**B**) Plots of the common logarithms for pK_{aNH^+,PH^+} = 3.0, pK_{aPH^+,NH^+} = 3.6, p$K_{aNH^+,P\odot}$ = 5.4, and p$K_{aPH^+,N\odot}$ = 6.0. (**C**) Plots of the common logarithms for pK_{aNH^+,PH^+} = 4.6, pK_{aPH^+,NH^+} = 5.2, p$K_{aNH^+,P\odot}$ = 5.4, and p$K_{aPH^+,N\odot}$ = 6.0. (**D**) Plots of the common logarithms for pK_{aNH^+,PH^+} = 5.4, pK_{aPH^+,NH^+} = 6.0, p$K_{aNH^+,P\odot}$ = 5.4, and p$K_{aPH^+,N\odot}$ = 6.0. In this last situation, the dissociations of the two acids are unlinked.

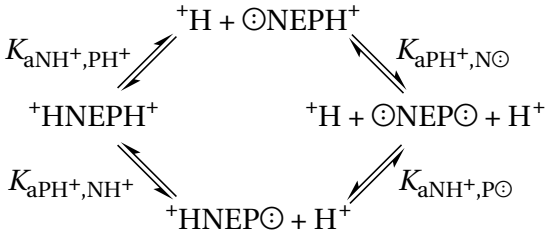

(4–138)

where NH$^+$ and PH$^+$ are cationic catalytic acids in the active site, K_{aNH^+,PH^+} is the dissociation constant of acid NH$^+$ when acid PH$^+$ is hydronated and cationic, $K_{aNH^+,P\odot}$ is the dissociation constant of acid NH$^+$ when acid PH$^+$ is the unhydronated conjugate base and uncharged, K_{aPH^+,NH^+} is the dissociation constant of acid PH$^+$ when acid NH$^+$ is hydronated and cationic, and $K_{aPH^+,N\odot}$ is the dissociation constant of acid PH$^+$ when acid NH$^+$ is the unhydronated conjugate base and uncharged. Mathematically, this linkage is identical to that of Equation 4–135 because the only difference is the identity of the four species and the names for the acid dissociation constants; the hydrons dissociating in each step are identical. Consequently, the result of the following derivation would be the same for Equation 4–135 or any other pair of linked acid dissociations.

If

$$\alpha(\odot\mathrm{NEPH}^+) = \frac{[\odot\mathrm{NEPH}^+]}{[^+\mathrm{HNEPH}^+] + [^+\mathrm{HNEP}\odot] + [\odot\mathrm{NEPH}^+] + [\odot\mathrm{NEP}\odot]} \tag{4–139}$$

it follows that

$$\alpha(\odot\mathrm{NEPH}^+) = \frac{K_{\mathrm{aNH}^+,\mathrm{PH}^+}[\mathrm{H}^+]}{[\mathrm{H}^+]^2 + (K_{\mathrm{aNH}^+,\mathrm{PH}^+} + K_{\mathrm{aPH}^+,\mathrm{NH}^+})[\mathrm{H}^+] + K_{\mathrm{aNH}^+,\mathrm{PH}^+}K_{\mathrm{aPH}^+,\mathrm{N}\odot}} \quad (4\text{–}140)$$

and by the equivalent derivation that

$$\alpha({}^+\mathrm{HNEP}\odot) = \frac{K_{\mathrm{aPH}^+,\mathrm{NH}^+}[\mathrm{H}^+]}{[\mathrm{H}^+]^2 + (K_{\mathrm{aNH}^+,\mathrm{PH}^+} + K_{\mathrm{aPH}^+,\mathrm{NH}^+})[\mathrm{H}^+] + K_{\mathrm{aNH}^+,\mathrm{P}\odot}K_{\mathrm{aPH}^+,\mathrm{NH}^+}} \quad (4\text{–}141)$$

Because $K_{\mathrm{aNH}^+,\mathrm{PH}^+}K_{\mathrm{aPH}^+,\mathrm{N}\odot} = K_{\mathrm{aNH}^+,\mathrm{P}\odot}K_{\mathrm{aPH}^+,\mathrm{NH}^+}$, the denominator is identical for both $\alpha(\odot\mathrm{NEPH}^+)$ and $\alpha({}^+\mathrm{HNEP}\odot)$.* Plots of Equations 4–140 and 4–141 (Figure 4–16) are indistinguishable from plots of kinetic equations for an enzymatic reaction catalyzed by an acid and a base that titrate independently of each other (Figures 4–10G, 4–10H, 4–12, and 4–14) rather than being tautomerically linked. The only term that differs between Equations 4–140 and 4–141 is the acid dissociation constant in the respective numerators, so as equations describing the observed behavior, they are indistinguishable. When there is no interaction between acid NH^+ and acid PH^+, $K_{\mathrm{aNH}^+,\mathrm{PH}^+} = K_{\mathrm{aNH}^+,\mathrm{P}\odot}$ and $K_{\mathrm{aPH}^+,\mathrm{NH}^+} = K_{\mathrm{aPH}^+,\mathrm{N}\odot}$ and Equation 4–140 becomes Equation 4–94.

If one steady-state rate constant is directly proportional to the fraction of the enzyme in the tautomer $\odot\mathrm{NEPH}^+$, then

$$k_{i,\mathrm{app}} = \frac{k_i K_{\mathrm{aNH}^+,\mathrm{PH}^+}[\mathrm{H}^+]}{[\mathrm{H}^+]^2 + (K_{\mathrm{aNH}^+,\mathrm{PH}^+} + K_{\mathrm{aPH}^+,\mathrm{NH}^+})[\mathrm{H}^+] + K_{\mathrm{aNH}^+,\mathrm{PH}^+}K_{\mathrm{aPH}^+,\mathrm{N}\odot}} \quad (4\text{–}142)$$

If one steady-state rate constant is directly proportional to the fraction of the enzyme in the form ${}^+\mathrm{HNEP}\odot$, then

$$k_{i,\mathrm{app}} = \frac{k_i K_{\mathrm{aPH,NH}^+}[\mathrm{H}^+]}{[\mathrm{H}^+]^2 + (K_{\mathrm{aNH}^+,\mathrm{PH}^+} + K_{\mathrm{aPH}^+,\mathrm{NH}^+})[\mathrm{H}^+] + K_{\mathrm{aNH}^+,\mathrm{P}\odot}K_{\mathrm{aPH}^+,\mathrm{NH}^+}} \quad (4\text{–}143)$$

Equations 4–142 and 4–143 have the same form as Equation 4–99. The observed acid dissociation constants, K_{a1} and K_{a2} in Equation 4–99, are simply the two roots of the quadratic term in the denominator of Equations 4–142 and 4–143.

Consequently, the data can be fit as successfully with either Equation 4–99, Equation 4–142, or Equation 4–143, and the pH–rate profiles alone can never distinguish whether the situation described by Equation 4–99, Equation 4–142, or Equation 4–143 applies. Nor is there any reason to expect consequential interaction between the acid–bases governing the behavior, regardless of observed values of $\mathrm{p}K_{\mathrm{a}}$, from the pH–rate profile alone. It follows that **any pH–rate profile is always consistent with either the catalytic acid–bases titrating independently of each other or one of the tautomers of a tautomeric linkage being the active tautomer**.

If, for bovine pancreatic ribonuclease, Histidine 119 is the catalytic base $\mathrm{N}\odot$ and Histidine 12 is the catalytic acid PH^+, as concluded from the crystallographic molecular model, then from nuclear magnetic resonance spectroscopy, $\mathrm{p}K_{\mathrm{aNH}^+,\mathrm{PH}^+} = \mathrm{p}K_{\mathrm{a119,12}^+} = 6.01$, $K_{\mathrm{aPH}^+,\mathrm{NH}^+} = \mathrm{p}K_{\mathrm{a12,119}^+} = 5.80$, and $K_{\mathrm{aPH}^+,\mathrm{N}\odot} = \mathrm{p}K_{\mathrm{a12,119}} = 6.08$. These values can be corrected for the difference in temperature between the measurements by nuclear magnetic resonance spectroscopy (30 °C) and those for the pH–rate profile (25 °C) with the relation

$$\frac{d\ln K_{\mathrm{a}}}{d(T^{-1})} = -\frac{\Delta H^\circ}{R} \quad (4\text{–}144)$$

where ΔH° is the heat of ionization of an imidazolyl group (37 kJ mol^{-1}).[159] When the corrected values are used as parameters in Equation 4–142, the resulting curves that are generated fit the measurements of $k_{\mathrm{cCP,app}}$ (Figure 4–11A) and $k_{\mathrm{cUP,app}}$ (Figure 4–11B). The data can also be fit with Equation 4–95 and the parameters $\mathrm{p}K_{\mathrm{a1}} = 5.8$ and $\mathrm{p}K_{\mathrm{a2}} = 6.2$, which are the respective roots of the quadratic equation in the denominator of Equation 4–142. In this interpretation, in which Histidine 119 is the catalytic base and Histidine 12 is the catalytic acid governing the pH–rate profile, based solely on the assignments of

*Note the similarity of Equations 4–140 and 4–141 to the factor in the second term on the right in Equation 4–137.

the crystallographic molecular model, catalysis performed by these catalytic acid–bases in the direction of hydrolysis would be an example of reverse hydronation because the pK_a of the conjugate acid of the imidazolyl group of Histidine 119 is greater than the pK_a for the imidazolium group of Histidine 12.

Consistent with the assignment of the observed pK_a of 5.8 to Histidine 12 and the observed pK_a of 6.2 to Histidine 119 is the fact that, when the imidazolyl group of Histidine 12 is replaced synthetically by a 4-fluoroimidazolyl group, the observed pK_a of 5.8 shifts to an observed pK_a of 3.4, and when the imidazolyl groups of both Histidine 12 and Histidine 119 are replaced by 4-fluoroimidazolyl groups, the observed pK_a of 6.2 shifts to an observed pK_a of 4.6.[160]

To this point it has been assumed that only one tautomer of a singly hydronated, linked pair of acid–bases is the catalytically active form of the active site because one linked pair of acid–bases would be acting as a catalytic base and the other as a catalytic acid in one direction and switching roles in the opposite direction, as was extensively described for mandelate racemase. It is also possible, however, that two acid–bases in the active site participate in a tautomeric linkage but that **only one of the two acts as a catalytic base or a catalytic acid and the other, the spectator acid–base, merely perturbs the acid dissociation constant of that catalytic acid or base**. For example, suppose that acid PH^+ in the previous tautomeric equilibrium (Equation 4–138) acts as a catalytic acid but the other acid, NH^+, although it is tautomerically linked to acid PH^+, is a spectator that has no role in catalysis. Suppose also that the spectator acid NH^+ is positively charged when it is hydronated and decreases the pK_a of the catalytic acid, PH^+, when it, the catalytic acid, is hydronated. In that case, catalysis should depend only on the fraction, $\alpha(PH^+)$, of the acid–base PH that is in the hydronated ionization state. Because

$$\alpha(PH^+) = \frac{[^+HNEPH^+] + [\odot NEPH^+]}{[^+HNEPH^+] + [^+HNEP\odot] + [\odot NEPH^+] + [\odot NEP\odot]} \quad (4\text{–}145)$$

it follows that

$$\alpha(PH^+) = \frac{K_{aNH,PH^+}[H^+] + [H^+]^2}{[H^+]^2 + (K_{aNH^+,PH^+} + K_{aPH^+,NH^+})[H^+] + K_{aNH^+,PH^+}K_{aPH^+,N\odot}} \quad (4\text{–}146)$$

Titration curves (Figure 4–16) of the catalytic acid, $\alpha(PH^+)$, and the spectator acid, $\alpha(NH^+)$, are quite different from titration curves of the two tautomers, $\alpha(\odot NEPH^+)$ and $\alpha(^+HNEP\odot)$. Suppose the value of pK_a for each of the two acids is shifted significantly enough by dehydronation of the other—for example, in Figure 4–16A,B, where the values are $pK_{aPH^+,NH^+} = 3.6$ and $pK_{aPH^+,N\odot} = 6.0$ and $pK_{aNH^+,PH^+} = 3.0$ and $pK_{aNH^+,P\odot} = 5.4$. Suppose also that the values of pK_a for the two acids when the other is unhydronated are close enough together that the concentrations of the two tautomers are of equal magnitude, again as they are in Figure 4–16A,B. Under these conditions, the titration curve for the catalytic acid has an unmistakable inflection, as does that of the spectator acid, and the pH–rate profile for catalysis should also display such an inflection. In fact, titration curves for Aspartate 10 and Aspartate 70 in the active site of ribonuclease H from *E. coli*,[161] determined by nuclear magnetic resonance spectroscopy, show inflections that are quite similar to those seen in Figure 4–16. As the shift of the one pK_a caused by dehydronation of the one acid decreases in magnitude, however, the inflections become less obvious (Figure 4–16C) before they disappear completely when there is no linkage between the two acid–bases (Figure 4–16D).

Values of pK_a for the plots in Figure 4–16A,B were intentionally chosen to exaggerate the inflections. In most cases, values of pK_a in a situation where a spectator acid–base shifts the pK_a for a catalytic acid–base, which is probably quite common, are usually not so extreme, either because the shifts produced by the one upon the other are not so large, as in the case of ribonuclease, or because values of pK_a for the acid–bases when the other is neutral are much larger so the equilibrium constant relating the concentrations of the tautomers is far from 1, as in the case of mandelate racemase. In either situation, the inflections are not noticed because the data are almost never extensive enough to define them. The inflection in Figure 4–11B is obvious only because the data are of exceptional quality.

It seems that most active sites perturb values of pK_a for their catalytic acid–bases. Therefore, the shifts in pK_a for the catalytic acid–bases caused by the surroundings that occur in the active sites of ribonuclease T_1 from *Aspergillus oryzae*, enoyl-CoA hydratase from *R. norvegicus*, lysozyme from *G. gallus*, bovine pancreatic ribonuclease, and mandelate racemase from *Pseudomonas putida*, which have already been described, are not unusual. These shifts in pK_a can be dramatic. For example, the pK_a of 7.0 below which the catalytic constant for IMP dehydrogenase from *Tritrichomonas foetus* decreases as the pH is lowered has been assigned to Arginine 418,[162,163] which would represent a shift in pK_a of around 6 units caused by the active site. In the active site of human medium-chain acyl-CoA dehydrogenase occupied by an acyl-SCoA eight carbons long,[164] the pK_a of Glutamate 376 is 9.2, which would represent a shift in pK_a of around 5 units.

Even though the reasons for these shifts in pK_a are usually obscure, and they have occurred over time for reasons usually understood only by natural selection, the temptation to rationalize them has not been resisted by observers as well as this author. For example, the pK_a for the ammonio group in Lysine 115 in acetoacetate decarboxylase from *C. acetobutylicum* is 5.9 (Figure 4–15),[127] even lower than the pK_a for Lysine 166 in mandelate racemase. In the crystallographic molecular model of the active site of this enzyme, Lysine 115 is found in a nonpolar funnel,[165] and it has been proposed that this nonpolar environment prevents solvation of the ammonio group and lowers its pK_a by lowering the relative permittivity of its surroundings (Equation 4–62).

It has been pointed out, however, that ad hoc explanations such as the one just given for the shift in pK_a for the ammonio group of the Lysine 115 may well be too simplistic. When 30 mutations—either single mutations, double mutations, or triple mutations—were made in amino acids surrounding Tyrosine 57 in the active site of steroid Δ-isomerase from *P. putida* and the pK_a of Tyrosine 57 was assessed for each mutant, many of the shifts caused by the mutations seemed counterintuitive. The conclusion reached[166] was that the "perturbations are more complex than suggested by visual inspection."

In cases where the value of a pK_a governing the catalytic constant is for the acid dissociation constant of the same group responsible for the value of pK_a governing the specificity constants, those **values of pK_a usually shift when reactant binds**, and the structure, identity of the various hydrogen bonds, and relative permittivity of the active site all change, **causing observed values of pK_a for specificity constants and the catalytic constant to differ**.[167] For example, in human acyl-CoA dehydrogenase (previously Equation 2–114)

$$\begin{aligned}&\text{octanoyl-SCoA} + \\ &\quad \text{oxidized electron-transfer flavoprotein} \\ &\qquad \rightleftharpoons \textit{trans}\text{-oct-2-enoyl-SCoA} + \\ &\qquad\quad \text{reduced electron-transfer flavoprotein}\end{aligned} \tag{4–147}$$

the pK_a of Glutamate 376, which is the catalytic base that removes a hydron from carbon 2 of acyl-SCoA during the reaction to form the enolate, shifts from 4.3 in the free enzyme to 9.3 when 4-thiaoctenoyl-SCoA, an analogue of the reactant octanoyl-SCoA, associates with the active site. This shift may explain the pK_a of 8.3 observed in the pH–rate profile for the catalytic constant of the enzyme with the actual reactant, octanoyl-SCoA.[164,168]

If Aspartate 52 and Glutamate 35 are responsible for the two observed values of pK_a governing the catalytic constant k_0 of lysozyme (3.8 and 6.7; Figure 4–10H), then the microscopic values of pK_a for Aspartate 52 in the free enzyme (4.4 and 5.2) have shifted to a lower value, and they have coalesced because they are no longer linked to the ionization of Glutamate 35. Likewise, the microscopic values of pK_a for Glutamate 35 in the free enzyme (5.2 and 6.0) have shifted to a higher value, and they have coalesced because they are no longer linked to the ionization of Aspartate 52. The linkage is probably eliminated because the substrate now sits between the two and their values of pK_a shift in opposite directions. The latter can be explained as a shift caused by the hydrogen bond Glutamic Acid 35 forms with the oxygen of the leaving group in the hydrolysis (Figure 3–27), which should raise its pK_a. If the lower pK_a, however, is still that of Aspartate 52, then the decrease in the pK_a for its side chain, which does not form a hydrogen bond with a reactant in the Michaelis complex and which finds itself in less polar surroundings in the complex, has no obvious explanation.

An active site can also **shift the pK_a for a substrate** upon its association. For example, the pK_a of nitrogen 1 of uracil in the complex between uracil-DNA glycosylase from *E. coli* and its substrates (uracil and a double-helical DNA fragment of 11 base pairs from which the enzyme has removed the uracil) has been determined by nuclear magnetic

resonance spectroscopy[169] to be 6.3 while the pK_a of uracil is free solution is 9.5. This shift in pK_a is caused by a hydrogen bond between the imidazolium of Histidine 187 and the acyl oxygen on carbon 2 of uracil,[170] and the shift may increase the ability of the uracil to leave during the nucleophilic substitution catalyzed by the active site.

Reasons other than a shift in pK_a, however, can explain the difference in the effects of pH on a specificity constant and a catalytic constant. In the case of porcine aspartate transaminase (Equation 4–108), where two values of pK_a govern the behavior of the specificity constant $k_{Asp,app}$ for L-aspartate, the catalytic constant of the enzyme is unaffected by pH (Figure 4–12). The pK_a of 6.35, assigned to the lysylpyridoximine (Equation 4–129) in the unoccupied active site, and the pK_a of 9.9, assigned to the α-amino group of the reactant L-aspartate, should become irrelevant once the first of the many hydron transfers in the mechanism have occurred (Figure 2–2), well before the rate-limiting step of the reaction, which is independent of pH.

An appealing explanation for the observation that **a catalytic constant is unaffected by pH** would be that once reactant has bound and the active site has closed around it, the acid–bases in the active site are no longer accessible to the solution and as a result cannot participate in acid dissociations. In the case of hexokinase from *S. cerevisiae*, however, which closes rather completely around its reactants (Figure 3–55), the catalytic constant nevertheless decreases as the pH is lowered below an apparent pK_a of 5.0.[171,172]

Because the pH–rate profiles for mandelate racemase (Figure 4–14) are for its catalytic constants in the two respective directions, the values of pK_a observed, 6.4 and 10.0, should be those for Lysine 166 and Histidine 297 in the complex between enzyme and the respective reactant (Equation 4–119). If this assignment is correct, which seems reasonable for an enzyme with such a simple mechanism, in which the rate-limiting step is the difficult removal of the hydron from the carbon,[101] then Lysine 166 and Histidine 297 in the Michaelis complex between enzyme and substrate are accessible enough to the solution to participate readily in acid dissociations.

The **shift caused by a hydrogen bond**, for example, when reactant binds to lysozyme, is an example of a common reason for the shift in pK_a of a catalytic acid–base upon formation of a Michaelis complex. If the catalytic lone pair of electrons on a catalytic base in the active site participates as an acceptor in a hydrogen bond with reactant, the pK_a for the conjugate acid of that catalytic base will decrease upon formation of the hydrogen bond in the complex between enzyme and reactant; and if the catalytic hydron on a catalytic acid in the active site participates as a donor in a hydrogen bond to the reactant, the pK_a for that catalytic acid will increase upon formation of the hydrogen bond. For example, in the crystallographic molecular model of the complex between androstenedione and the active site of human aromatase, the carboxy group of Aspartic Acid 309 is the donor in a hydrogen bond with the carbonyl group at carbon 3 of androstenedione. The pK_a for the carboxy group of this aspartic acid in the complex between the active site and androstenedione, measured by ultraviolet difference spectroscopy of the complex,[173] is 8.2, considerably greater than the pK_a (4.0) for aspartic acid on the surface of a protein. The pK_a of Glutamatic Acid 167 in the active site of triose-phosphate isomerase from *Trypanosoma brucei* shifts from around 4 in the unoccupied active site to a pK_a of around 10 when the active site associates with phosphoglycolate,[174] an analogue of the *cis*-1,2-enediolate intermediate in the enzymatic reaction. In the crystallographic molecular model of the complex between phosphoglycolate and the active site of triose-phosphate isomerase from *S. cerevisiae*, the carboxy group of Glutamic Acid 165 (the homologue of Glutamic Acid 167 in the enzyme from *T. brucei*) is a donor in a hydrogen bond to one carboxylato oxygen in phosphoglycolate.

In the case of bovine pancreatic ribonuclease, if the observed pK_a of 9.0 governing the behavior of the catalytic constant of the enzyme for the hydrolysis of cytidine 2′,3′-cyclic phosphate (Figure 4–11A) is that of Histidine 12, then its pK_a has increased from 5.8 in part because it acts as a donor in a hydrogen bond with the anionic phospho oxygen of the reactant. If the observed pK_a of 6.25 governing the behavior of the catalytic constant of the enzyme (Figure 4–11A), however, were that of Histidine 119, then its pK_a would not have shifted from an observed pK_{a2} of 6.2 for the unoccupied enzyme, even though one anionic oxygen of the phosphate in the reactant has slid in between Histidine 119 and the hydronated cationic Histidine 12.[152] This consideration seems to require that the pK_a of 6.25 governing the behavior of the catalytic constant is not that of Histidine 119 and that its pK_a has shifted out of the range of measurement.

Formation of a hydrogen bond can also affect the pK_a for an amino acid in the unoccupied active

site of an enzyme. For example, in the examination of the large array of mutants of steroid Δ-isomerase from *P. putida*, the authors[166] concluded that in the unmutated native enzyme, three donors of hydrogen bonds to the hydroxy group on Tyrosine 57, acting together within a cluster of hydrogen bonds that dictates what is a donor and what is an acceptor, are responsible for lowering the pK_a of Tyrosine 57 to 6.3.

Apparent values of pK_a observed in a pH–rate profile of a steady-state rate constant are often not registering the pK_a of any acid–base in the active site. To this point, it has been assumed that values of pK_a observed in the pH–rate profiles of steady-state rate constants are actual values of pK_a for specific acid–bases in the active site of the enzyme. When, however, a pK_a that appears to govern a steady-state rate constant cannot be confidently assigned by another observation to a reactant or a particular amino acid known crystallographically to be in the active site of the enzyme, **the likelihood that the kinetically observed pK_a is not an actual pK_a** must be considered.

Whether or not it is explicitly stated by the investigator, treating values of pK_a observed in a pH–rate profile of a catalytic constant or the specificity constant for reactant A as actual values of pK_a assumes that the kinetic mechanism for the reaction is as simple as that of Equation 4–112 or its equivalent for reactant A. It has been pointed out, however, that **the kinetic mechanism of Equation 4–112 is too simple to describe the kinetic mechanisms of most if not all enzymes**.[66] Any increase in the complexity of the mechanism can cause the catalytic constant or the specificity constant for reactant A, or both of them, no longer to be simple products of the fractions of free enzyme, free reactant, and their various complexes that are the proper tautomers for catalysis (Equations 4–118 and 4–119).[127] Therefore, in many if not most cases, the intersections of the asymptotes (Figures 4–10, 4–11, 4–12, and 4–14) are not values of pK_a for particular side chains in the active site. Any statement that they are must be accompanied by independent evidence of this claim, as has been done so far in this discussion in describing the identity of the acid–base responsible for particular situations.

The situation, however, is nothing more serious than an instance of what is true of all kinetic mechanisms: they may be consistent with the observations but cannot be proven by the observations. If, however, the kinetic mechanism of a particular enzymatic reaction with a particular reactant has been established independently and it differs from the kinetic mechanism in Equation 4–112, then **the meaning of the intersections of asymptotes** can be stated explicitly because an equation for the initial rate of the enzymatic reaction can be derived by the usual formalism, and it becomes clearer whether or not any of these intersections define acid dissociation constants of amino acids in the active site.[127]

To illustrate the fact that there is **no requirement for apparent values of pK_a to be actual values of pK_a** for amino acids in the active site or on the reactants, a simple example of a situation in which an apparent pK_a is not an actual pK_a can be formulated.[175] Suppose that an enzymatic reaction has two steps following association of all its reactants: a slow step independent of pH, followed by a step that requires a particular hydronated acid–base in the active site acting as a catalytic acid. Suppose also that reactants are all present at saturation so that the catalytic constant of the enzymatic reaction is being followed as a function of pH. Finally, suppose that at low pH, well below the pK_a of the catalytic acid in the complex, the second step, the one requiring the catalytic acid, is much faster than the first and that the first step is the rate-limiting step of the overall reaction. As the pH is raised, steady-state flux through the two steps, and hence the catalytic constant, will remain constant even as the pH rises above the actual pK_a for the acid–base in the complex because the second step would still remain faster than the first. Above a certain value of pH, however, there would be a **change in the rate-limiting step** as the concentration of hydronated catalytic acid–base in the complex becomes so small that the rate of the second step necessarily has become slower than the first. Above this value of pH, the catalytic constant of the enzyme, now limited by the second step rather than the first, would decrease by a factor of 10 for every increase of 1 unit in pH. Therefore, the pH at which the change in the rate-limiting step occurs only appears to define an acid dissociation constant of the occupied active site; the actual value of the pK_a for the catalytic conjugate acid of the acid–base controlling the rate of the second step is smaller than the pH at which the asymptotes in the common logarithmic pH–rate profile of the catalytic constant intersect.

A similar argument can be made for a situation in which the second step requires a particular unhydronated catalytic acid–base in the active site. In this instance, the change in rate-limiting step defined by the intersection of the asymptotes in the

common logarithmic pH–rate profile of the catalytic constant at the apparent pK_a, which seems to define the pK_a of the conjugate acid of the catalytic base, would actually occur at a pH less than the pK_a of the conjugate acid of the catalytic base, at the point at which the concentration of the required, unhydronated catalytic acid–base becomes small enough that the second step becomes slow enough to be rate-limiting.

The decrease in the common logarithm of the catalytic constant k_0 as a function of pH with a slope of –1 above the pH of the intersection in the first case (as in Figure 4–10E) and the decrease in the common logarithm of the catalytic constant k_0 as a function of pH with a slope of +1 below the pH of the intersection in the second case (as in Figure 4–10B) still result from the decrease in the concentration of the catalytic acid or the catalytic base, respectively, of a factor of 10 for every unit of pH. The intersections of the asymptotes, however, are no longer values of pK_a for the respective catalytic acid–base governing the behavior. In the former case, the actual pK_a for the catalytic acid is less than the pH at the intersection of the asymptotes; in the latter case, the actual pK_a for the conjugate acid of the catalytic base is greater than the pH at intersection; and in each case, the **intersection of the asymptotes defines only the pH at which the rate-limiting step changes**. Consequently, if the pK_a for a candidate for a catalytic acid in the enzymatic reaction is measured independently and found to be less than the apparent pK_a governing a pH–rate profile, or if the pK_a for the conjugate acid of a candidate for a catalytic base in the enzymatic reaction is measured independently and found to be greater than the apparent pK_a governing a pH–rate profile,[176] this discordance cannot be used as an argument ruling out the involvement of either acid–base as a catalyst in the mechanism of the enzyme. Nevertheless, the decrease in rate constant above or below a particular pH does indicate that there is an acid–base that must be hydronated or an acid–base that must be unhydronated for the enzymatic reaction to proceed.

A change in rate-limiting step can involve **dissociation of a product** as one step. For example, the catalytic constant k_0 of the reaction catalyzed by dihydrofolate reductase from *E. coli* (previously Equation 3–428)

$$\text{NADPH} + \text{7,8-dihydrofolate} + \text{H}^+ \rightleftharpoons \text{5,6,7,8-tetrahydrofolate} + \text{NADP}^+ \quad (4\text{–}148)$$

is determined both by the rate for hydride transfer from NADPH to 7,8-dihydrofolate and by the rate for dissociation of the product $NADP^+$ from the active site.[177] The rate constant for hydride transfer, k_{HT}, measured directly, is dependent on pH, decreasing above a pK_a of 6.5 from a maximum at 25 °C of 950 s^{-1} as a catalytic acid is titrated. The rate constant, k_{diss}, for dissociation of $NADP^+$ is independent of pH and has a value of 15 s^{-1}. At low pH, dissociation of the product $NADP^+$ is the rate-limiting step for turnover because the catalytic acid is stoichiometrically hydronated. As the pH is increased, however, there is a change in rate-limiting step at pH 8.3, which is identified by an intersection of asymptotes for the catalytic constant (Figure 4–17).[177,178] At high pH, hydride transfer is the rate-limiting step for turnover. If the rate of dissociation of $NADP^+$ is accelerated by using a different folate[179] or the rate of hydride transfer is decreased by mutating the enzyme,[180] the pH–rate profile of the catalytic constant k_0 is governed by the intrinsic pK_{aNH} of 6.5 of the catalytic acid required for hydride transfer. This situation is an example in which the actual pK_a for the catalytic acid is less than the pH at which the asymptotes intersect.

In the case of micrococcal nuclease from *S. aureus*, however, the dependence on pH of the catalytic constant of the enzyme for hydrolysis of single-stranded DNA decreases below an apparent pK_a of 7.3 as the pH is lowered. At this pH, the rate-limiting step changes from dissociation of the product at high pH to hydrolysis of the phosphodiester at low pH. This change in rate-limiting step was demonstrated by examining the effect of viscosity of the solution on the catalytic constant as a function of pH.[181] In this instance, the intrinsic pK_a for the acid–base below which the rate constant for hydrolysis decreases, leading eventually to the change in rate-limiting step at pH 7.3, is 8.7. This situation is an example in which the actual pK_a for the catalytic base is greater than the pH at which the asymptotes intersect.

Stickiness of a reactant can cause a change in rate-limiting step. A reactant is sticky if its rate of dissociation from the active site is slower than its conversion to product free in solution. In the simplest kinetic mechanism (previously Equations 3–55 and 3–62)

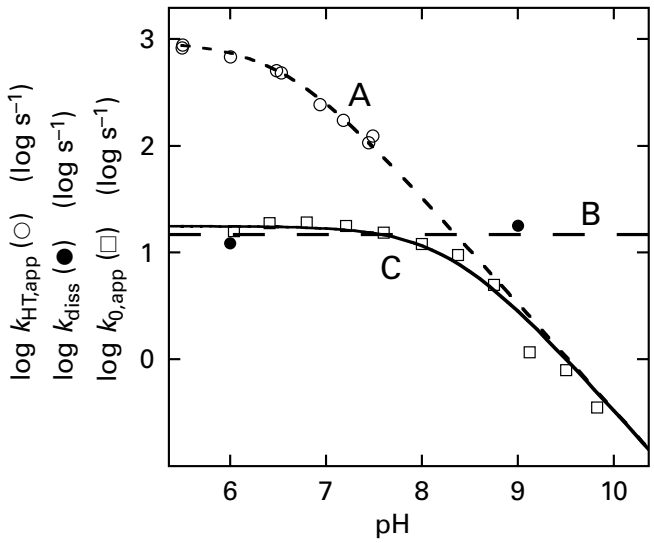

Figure 4–17: Change in rate-limiting step as a function of pH for the catalytic constant of dihydrofolate reductase from *E. coli* for NADPH and 7,8-dihydrofolate.[177] (**A**) The rate for transfer of the hydride from NADPH to 7,8-dihydrofolate on the active site was monitored at 25 °C as a decrease in fluorescence of NADPH following rapid mixing of the two reactants at saturating concentrations with the enzyme (as in Figure 4–18). The buffer contained 50 mM 2-(*N*-morpholino)ethanesulfonate, 25 mM 2-amino-2-(hydroxymethyl)propane-1,3-diol, 25 mM ethanolamine, and 100 mM sodium chloride. Over the pH range used, the ionic strength of this buffer remains constant. The common logarithms of the observed rate constants for transfer of the hydride, $k_{HT,app}$ (○, second^{-1}), are plotted as a function of pH. The dashed curve is for Equation 4–89 with $k_{HT} = 950$ s^{-1} and p$K_a = 6.55$. (**B**) The rate for the dissociation of the product 5,6,7,8-tetrahydrofolate from the active site was monitored at 25 °C as a decrease in fluorescence at 340 nm after rapid mixing of the preformed complex between the enzyme, 5,6,7,8-tetrahydrofolate, and NADPH with a solution of methotrexate, which immediately associates with the active site following dissociation of 5,6,7,8-tetrahydrofolate to prevent its rebinding. The common logarithms of the observed rate constants for the dissociation, k_{diss} (●, second^{-1}), are plotted. The dissociation was measured at pH 6 and 9 and found to be the same within the error of measurement. The horizontal dashed line is placed at the mean of these two measurements. (**C**) The initial rates for conversion of NADPH and 7,8-dihydrofolate to 5,6,7,8-tetrahydrofolate and NADP$^+$ catalyzed by the enzyme were measured at 30 °C by following the decrease in absorbance of NADPH at 340 nm.[178] The same buffer described above was used to establish the pH. The common logarithms of the observed catalytic constants of the enzyme, $k_{0,app}$ (□, second^{-1}), are plotted as a function of pH. Even though the behavior observed is due to a change in rate-limiting step, Equation 4–89 with $k_0 = 18$ s^{-1} and p$K_a = 8.3$ (solid curve) fits the data satisfactorily.

$$E + A \underset{k_{-1}}{\overset{k_1}{\rightleftharpoons}} E{\cdot}A \xrightarrow{k_2} E + Z \tag{4–149}$$

$$v_0 = \frac{k_2[E]_t\left(\frac{k_2k_1}{k_{-1}+k_2}\right)[E]_t[A]_0}{k_2[E]_t + \left(\frac{k_2k_1}{k_{-1}+k_2}\right)[E]_t[A]_0} \tag{4–150}$$

the specificity constant k_A is $k_1k_2(k_2 + k_{-1})$, and if the reactant in this simple mechanism is sticky, $k_{-1} < k_2$. In the case of murine cyclic AMP-dependent non-specific serine/threonine protein kinase, the specificity constant $k_{pep,app}$ for phosphorylation of the peptide LRRASLG (pep) decreases with pH above an apparent pK_a of 9.3. This behavior was shown, by studies of the effects of viscosity, to result from a change in rate-limiting step from association of the reactant at low pH, where the reactant was sticky ($k_{-1} < k_2$), to turnover of reactant at high pH.[182] In this instance, as the pH is increased, the rate constant for association of the reactant, k_{-1}, remains constant, but the microscopic rate constant for a step following association of the reactant depends on a catalytic acid. The concentration of this catalytic acid, and hence k_2, decreases as the pH is raised above its pK_a, until the rate-limiting step is no longer association of the reactant but some step following association. This decrease in the rate constant k_2 eventually causes the reactant no longer to be sticky because k_2 eventually becomes less than k_{-1}.

It is also possible for a change in rate-limiting step to occur in a situation in which **each of two acid–bases in the active site accomplishes its catalysis in a different step** of the mechanism. Consider the kinetic mechanism

$$E + A \underset{k_{-1}}{\overset{k_1}{\rightleftharpoons}} E{\cdot}A \underset{k_{-6}}{\overset{k_6}{\rightleftharpoons}} E{\cdot}A' \xrightarrow{k_7} E + Z \tag{4–151}$$

where A′ is an intermediate in the transformation of A to Z. If the step governed by rate constant k_6 is catalyzed by a catalytic base, $\odot O^{(-)}$, in the active site and the step governed by rate constant k_7 is catalyzed by a catalytic acid, $NH^{(+)}$, and

$$k_{6,app} = k_6\left(\frac{K_{aOH}}{[H^+] + K_{aOH}}\right) \quad (4–152)$$

and

$$k_{7,app} = k_7\left(\frac{[H^+]}{[H^+] + K_{aNH}}\right) \quad (4–153)$$

then by microscopic reversibility

$$k_{-6,app} = k_{-6}\left(\frac{[H^+]}{[H^+] + K'_{aOH}}\right) \quad (4–154)$$

where K_{aOH} is the acid dissociation constant of acid–base OH when A occupies the active site and K'_{aOH} is its acid dissociation constant when A′ occupies the active site. Solving the steady-state rate equation with the pH-dependent forms of the rate constants gives the catalytic constant

$$k_0 = \frac{k_{6,app}k_{7,app}}{k_{-6,app} + k_{7,app}} = \frac{K_{aOH}([H^+] + K'_{aOH})k_6k_7}{\{k_{-6}([H^+] + K_{aNH}) + k_7([H^+] + K'_{aOH})\}([H^+] + K_{aOH})} \quad (4–155)$$

At low pH (below pK_{aOH}, pK'_{aOH}, and pK_{aNH}) the rate of the step governed by k_6 (Equation 4–152) is so slow that it is rate-limiting. As the pH is raised within this low range, the catalytic constant increases by a factor of 10 for each increase in pH of 1 unit. At high pH (above pK_{aOH}, pK'_{aOH}, and pK_{aNH}) the catalytic constant does not decrease with pH but remains constant because $k_{-6,app}$ is decreasing as the pH is increasing in parallel with $k_{7,app}$, so the partition of E·A′ forward through the step governed by k_7 and backward through the step governed by k_{-6} remains constant.

In the intermediate range of pH, outcomes involving inflections as well as changes in slope in the pH–rate profiles are possible, depending on the values of rate constants and acid dissociation constants. If, however, pK_{aOH} = pK'_{aOH}, there are no intermediate inflections, and the curves all have only a single change in slope from +1 to 0 at a p$K_{a,app}$. This outcome can be explained by making $K_{aOH} = K'_{aOH}$ in Equation 4–155. In this case it reduces to a form

$$k_{0,app} = k_0\left(\frac{K_{a,app}}{[H^+] + K_{a,app}}\right) \quad (4–156)$$

for which

$$K_{a,app} = \frac{k_{-6}K_{aNH} + k_7K_{aOH}}{k_{-6} + k_7} \quad (4–157)$$

Consequently, the value of the observed p$K_{a,app}$ can take on any value between pK_{aHA} and pK_{aNH} depending on the values of k_{-6} and k_7, which determine the pH at which a change in rate-limiting step from the step governed by k_6 to the step governed by k_7 occurs. Again, a simple change in slope with an apparent pK_a is not the result of an actual pK_a but instead the result of a change in rate-limiting step.

Up to this point, with the exception of this most recent instance, one constraint that has been placed on explanations of pH–rate profiles of the catalytic constant when two acid–bases are acting catalytically is that they both accomplish their catalysis in the same transition state. The reason for this requirement is clear after considering the behavior defined by this most recent derivation (Equation 4–155), in which each of the two acid–bases accomplishes its catalysis in a different transition state. Because of microscopic reversibility, the step governed by k_{-6} must be catalyzed by the conjugate acid of the catalytic base or the conjugate base of the catalytic acid that catalyzes the step governed by k_6. Consequently, at infinite pH, the catalytic constant has become invariant with increasing pH rather than decreasing with a slope of –1 when a base catalyzes the step governed by k_6 and an acid catalyes the step governed by k_7. When an acid catalyzes the step governed by k_6 and a base catalyzes the step governed by k_7, the catalytic constant becomes invariant with pH at infinitely low pH rather than decreasing with a slope of +1. Whether or not a change in slope is observed in the range of pH chosen for the observations, either from +1 to 0 or from 0 to –1, will depend on the values of rate constants k_6, k_{-6}, and k_7. Peculiar inflections can occur at intermediate ranges of pH in each instance if the pK_a for the acid–base involved in the step governed

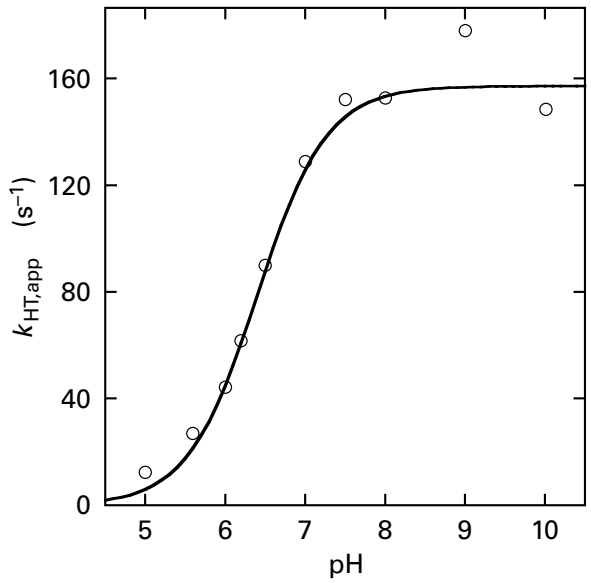

Figure 4–18: pH–Rate profile for transfer of a hydride from ethanol to NAD^+ (Equation 4–158) at the active site of liver alcohol dehydrogenase.[185] Solutions of 200 mM ethanol and 4 mM NAD^+ were prepared at various values of pH buffered with sodium phosphate or sodium glycinium phosphate at an ionic strength of 0.1 M and 25 °C. Each solution was mixed in turn with an equal volume of alcohol dehydrogenase at a 30 mM concentration of active sites. The mixing was performed in a stopped-flow apparatus, and the change in absorbance at 340 nm was monitored by an oscilloscope. A rapid increase of absorbance at 340 nm was observed, corresponding in magnitude to a single hydride transfer for each active site. The pseudo-first-order rate constant for this burst of absorbance was measured from each kinetic trace. The values of this rate constant, $k_{HT,app}$ (second^{-1}), for transfer of the hydride (HT) are plotted as a function of pH. The line drawn is for an acid–base titration with a pK_a of 6.4 and a pH-independent rate constant, k_{HT}, of 155 s^{-1}.

by k_6 and k_{-6} changes its pK_a during the step. It follows that when each of the two acid–bases accomplishes its catalysis in a different transition state, a significantly more complex pH–rate profile results that often if not usually defies explanation.

A change in rate-limiting step combined with hydronation of a catalytic base or dehydronation of a catalytic acid can also cause an inflection in the pH–rate profile of the catalytic constant as the pH is lowered below the pK_a for the catalytic base or raised above the pK_a for the catalytic acid.[183]

When a pH–rate profile for a steady-state rate constant is governed by observed, apparent values of pK_a to which no catalytic acid–bases can be assigned unambiguously—for example, in a situation when an observed pK_a is actually the pH at which a change in rate-limiting step occurs in a reaction—**a kinetic procedure that measures the pH–rate profile for the rate of only one step** in the kinetic mechanism can provide the pK_a for a catalytic acid or catalytic base in the active site. For example, the rate-limiting step in the reaction catalyzed by equine alcohol dehydrogenase

$$NAD^+ + \text{ethanol} \rightleftharpoons \text{acetaldehyde} + NADH + H^+ \qquad (4\text{–}158)$$

is release of NADH,[184] so the behavior of the steady-state rate constants as a function of pH when ethanol and NAD^+ are reactants does not reveal any values of pK_a for catalytic acids and bases in the active site. Because the absorbance of NAD^+ at 340 nm increases significantly at the instant it accepts a hydride while it is within the active site, monitoring an enzymatic reaction involving this coenzyme at this wavelength follows only this one explicit chemical step. Ethanol and NAD^+ can be added rapidly to a solution containing equine alcohol dehydrogenase, and the change in absorbance at 340 nm for only the transfer of a hydride can be monitored. If the concentrations of these two reactants are high enough, all the active sites in the solution will be filled much faster than the rate for hydride transfer[184]

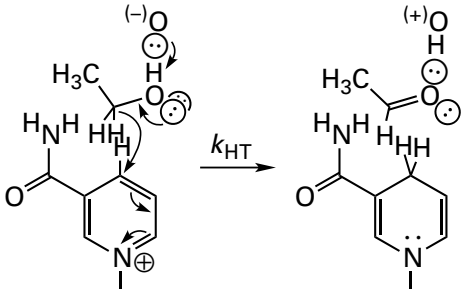

(4–159)

and only this one step should contribute to the observed rate constant. Under these circumstances, the observed rate constant k_{HT} for transfer of hydride decreases below a pK_a of 6.4 when the pH is lowered (Figure 4–18).[185] Because only a single pK_a appears to be controlling the behavior, it was assumed to be the microscopic pK_a for a single catalytic base in the active site. This assumption is valid only if all acid–base reactions and the two respective associations of reactants are so much faster than hydride transfer that they all reach equilibrium before any hydride transfer can occur and if all the other steps in the enzymatic mechanism preceding hydride transfer, if there are any, are rapid. Presumably this pK_a is for the catalytic base that removes the hydron from the hydroxy group of the ethanol. In the crystallographic molecular model of the complex of the

enzyme with trifluoroethanol,[186] this catalytic base is the hydroxy group of Serine 48, which relays the basicity of the sulfido group of Cysteine 46.

The state of hydronation of acid–bases in a site on a protein with which a ligand associates will usually affect the observed dissociation constant for that ligand. If this is the case, then when the protein binds an inhibitor, activator, drug, reactant, product, or any other ligand at a particular site, the apparent dissociation constant that is measured will usually be a function of pH. Consider the simplest situation in which only a form of the site containing an acid, $STH^{(+)}$, and a form of the site containing its conjugate base, $\odot ST^{(-)}$, exist in significant concentration within the range of pH covered. The ligand, L, can bind to either form of the site, and hydrons can enter or leave the occupied site

$$\begin{array}{ccc} L + STH^{(+)} & \underset{K_{dL1}}{\rightleftharpoons} & L{\cdot}STH^{(+)} \\ \Big\Updownarrow K_{aST} & & \Big\Updownarrow K_{aST\cdot L} \\ L + ST\odot^{(-)} + H^+ & \underset{K_{dL2}}{\rightleftharpoons} & L{\cdot}ST\odot^{(-)} + H^+ \end{array} \qquad (4\text{–}160)$$

In this mechanism, the equilibrium constants K_{aST} and $K_{aST\cdot L}$ are acid dissociation constants and the equilibrium constants K_{dL1} and K_{dL2} are dissociation constants for the ligand from the two states of hydronation for the site. It can be shown by inspection that

$$K_{aST}K_{dL1} = K_{aST\cdot L}K_{dL2} \qquad (4\text{–}161)$$

If the apparent dissociation constant for ligand L is defined as

$$K_{dL,app} = \frac{([STH^{(+)}] + [\odot ST^{(-)}])[L]}{[L{\cdot}STH^{(+)}] + [L{\cdot}\odot ST^{(-)}]} \qquad (4\text{–}162)$$

then it follows that

$$K_{dL,app} = \frac{\left(\dfrac{K_{aST\cdot L}}{[H^+] + K_{aST\cdot L}}\right)}{\left(\dfrac{K_{aST}}{[H^+] + K_{aST}}\right)} K_{dL2} \qquad (4\text{–}163)$$

and

$$\log K_{dL,app} = \log K_{dL2} + \log\left(\frac{K_{aST\cdot L}}{[H^+] + K_{aST\cdot L}}\right) - \log\left(\frac{K_{aST}}{[H^+] + K_{aST}}\right) \qquad (4\text{–}164)$$

For the moment, assume that the ligand binds more tightly to the site containing the acid than the site containing its conjugate base ($K_{dL1} < K_{dL2}$). Then, because of Equation 4–161, $K_{aST} > K_{aST\cdot L}$. When $[H^+] > K_{aST} > K_{aST\cdot L}$

$$\log K_{dL,app} \cong \log K_{dL2} - pK_{aST\cdot L} + pK_{aST} = \log K_{dL1} \qquad (4\text{–}165)$$

which is invariant with pH. When $K_{aST} > [H^+] > K_{aST\cdot L}$

$$\log K_{dL,app} \cong \log K_{dL2} - pK_{aST\cdot L} + pH \qquad (4\text{–}166)$$

which increases as pH is increased. When $K_{aST} > K_{aST\cdot L} > [H^+]$

$$\log K_{dL,app} \cong \log K_{dL2} \qquad (4\text{–}167)$$

which is invariant with pH. When the common logarithm of the apparent dissociation constant is plotted as a function of pH, the horizontal asymptote defined by Equation 4–165 is at the value for $-\log K_{dL1}$; the horizontal asymptote defined by Equation 4–167 is at the value for $-K_{dL2}$; the intersection of the horizontal asymptote defined by Equation 4–165 and the asymptote of slope +1 defined by Equation 4–166 occurs when $pH = pK_{aST}$; and the intersection of the horizontal asymptote defined by Equations 4–167 and the asymptote of slope +1 defined by Equation 4–166 occurs when $pH = pK_{aST\cdot L}$.

Examination of the mechanism of Equation 4–160 reveals that, as with any pH–rate profile for an enzymatic reaction, no distinction can be made between an ionization of the site and an ionization of the ligand from only the pH–dissociation behavior. Were the ligand and the site in the equation switched so that the mechanism was actually

$$\begin{array}{ccc} ST + LH^{(+)} & \underset{K_{dL1}}{\rightleftharpoons} & ST{\cdot}LH^{(+)} \\ \Big\Updownarrow K_{aL} & & \Big\Updownarrow K_{aST\cdot L} \\ ST + L\odot^{(-)} + H^+ & \underset{K_{dL2}}{\rightleftharpoons} & ST{\cdot}L\odot^{(-)} + H^+ \end{array} \qquad (4\text{–}168)$$

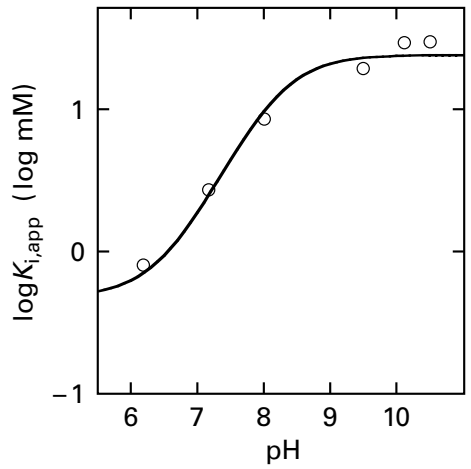

Figure 4–19: Dependence on pH of competitive substrate inhibition by 2-oxoglutarate of the transamination catalyzed by aspartate transaminase from L-aspartate and 2-oxoglutarate.[85] Solutions containing various concentrations of L-aspartate and 2-oxoglutarate at various values of pH (see Figure 4–10) were prepared at 25 °C. The reaction was initiated by adding aspartate transaminase, and the production of oxaloacetate was followed by coupling it to the oxidation of NADH with malate dehydrogenase. The decrease in A_{340} with time was used to measure initial rates. Both 2-oxoglutarate and L-aspartate are reactants in the reaction catalyzed by aspartate transaminase under these circumstances. Each of them, however, at high concentration, higher than that necessary to obtain their respective maximum rates, becomes an inhibitor of the enzyme. Each is a competitive inhibitor with respect to the other. From the competitive inhibition observed at high concentrations of 2-oxoglutarate (OG) at each pH, a value for the inhibition constant, K_{iOG}, was calculated. The common logarithms of these observed dissociation constants (millimolar) are plotted as a function of pH. The curves drawn are fits of Equation 4–164 to the data.

and the ligand was the acid–base rather than the site, the same equations would be derived for the behavior of the observed dissociation constant as a function of pH, except that the meaning of the values of pK_a observed would also be switched. This consideration illustrates the fact that the behavior of a dissociation constant as a function of pH indicates only whether a hydron is taken up from the solution as the complex is formed or a hydron is released to the solution as it forms.

The reaction catalyzed by porcine aspartate transaminase (Equation 4–108) can be divided into two steps

$$\begin{aligned}\text{(Lysyl 258)pyridoxamine 5′-phosphate} &+ H_2O \\ + \text{ L-aspartate} &\rightleftharpoons \text{oxaloacetate} + \\ \text{pyridoxamine 5′-phosphate} &+ \text{Lysine 258}\end{aligned} \qquad (4\text{–}169)$$

and

$$\begin{aligned}\text{Lysine 258} &+ \text{pyridoxamine 5′-phosphate} + \\ \text{2-oxoglutarate} &\rightleftharpoons \text{L-glutamate} + H_2O + \\ &\text{(Lysyl 258)pyridoximine 5′-phosphate}\end{aligned} \qquad (4\text{–}170)$$

where Lysine 258 is the lysyl side chain from the enzyme that forms the internal pyridoximine 5′-phosphate (Equation 4–129).[187] If 2-oxoglutarate (OG) enters the active site when the prosthetic group is lysylpyridoximine 5′-phosphate, no further reaction can occur. Therefore, 2-oxoglutarate is a competitive inhibitor with respect to L-aspartate. The observed inhibition constant for 2-oxoglutarate is a function of pH and obeys Equation 4–164 (Figure 4–19).[85] By fitting Equation 4–164 to the data, it was found that $K_{dOG,1} = 0.5$ mM, $K_{dOG,2} = 24$ mM, p$K_{aST} = 6.5$, and p$K_{aST\cdot OG} = 8.2$. Because, however, the site and the ligand are indistinguishable, these values are the same as values of $K_{dOG,1} = 0.5$ mM, $K_{dOG,2} = 24$ mM, p$K_{aL} = 6.5$, and p$K_{aL\cdot OG} = 8.2$.

These values state either that 2-oxoglutarate binds more tightly to the more hydronated, more cationic form of the active site or that the conjugate acid of 2-oxoglutarate binds more tightly to the active site than its conjugate base. These values also state that, after 2-oxoglutarate has associated with the active site, it either raises the pK_a of the acid in the active site, the acid dissociation of which is linked to its binding, or the pK_a of 2-oxoglutarate itself increases. In either case, in the midrange, a hydron is taken up as the ligand associates. Again, a decision between these two possibilities must be made from observations other than the behavior of a dissociation constant as a function of pH. The two values of pK_a for 3-oxoglutarate are 2.5 and 4.7. These values do not agree with pK_{aL}, but the pK_{aST} of 6.5 does agree with the pK_a for the iminium nitrogen of the internal lysylpyridoximine (Equation 4–129). If 2-oxoglutarate, a dianion, binds adjacent to this imine, it should bind more tightly when the imine is positive rather than zwitterionic, and the presence of the 2-oxoglutarate should cause the iminium nitrogen to be a weaker acid than it is in the absence of 2-oxoglutarate.

In this example of the association of 2-oxoglutarate with aspartate transaminase, the pK_a of the site increases because the ligand is anionic, and the same behavior would have been observed were the ligand the acid–base and the site anionic. Had the ligand been a cation or had the site been cationic, the pK_a of the site or the ligand, respectively, would have decreased upon association. In situations in

which the pK_a of the site or the ligand decreases upon association, the common logarithm of the dissociation constant begins with a plateau but then decreases in the midrange before reaching a second lower plateau.

The behavior of the inhibition constant for 2-oxoglutarate as a function of pH is unusual in that the full course of the effect of linkage between association of a hydron and association of the inhibitor with enzyme is observed. In most instances, only a portion of the entire linkage is observed within the range of pH chosen for the measurements. For example, the common logarithm of the inhibition constant of the inhibitor phosphoglycolate from the active site of triose-phosphate isomerase from *S. cerevisiae* increases with pH, with a slope of +1 over the range from pH 4 to 10. This observation is consistent with the two conclusions that, at all values of pH, a hydron is taken up by the complex when it forms and the titration is in the midrange between the plateaus. When Tyrosine 208 is mutated to phenylalanine, however, the common logarithm of the inhibition constant decreases with a slope of –1 only below a pK_a of 6.3; above the pK_a of 6.3, it is invariant with pH in a plateau.[188] Consequently, because the ligand is the same and the enzyme has changed, the mutation has shifted the pK_a of the site from above 10 to 6.3.

To explain the observed behavior of the dissociation constant for an inhibitor, K_i, as a function of pH, it is often assumed, by analogy with the explanation of pH behavior in steady-state rate constants, that, unlike 2-oxoglutarate, the inhibitor can bind to only one form of the enzyme. For example, this explanation would be equivalent to making the assumption in Equation 4–160 not only that K_{dL2} was greater than K_{dL1} but also that K_{dL2} was infinitely large. For Equation 4–161 to hold in the limit, as it must, this explanation would require that K_{aLST} be 0 if K_{dL1} and K_{aST} are to remain finite. Therefore, if the ligand can bind only to the hydronated state, $STH^{(+)}$, of the site, it necessarily follows that in the occupied site the hydronated acid can no longer dissociate. This example could lead to the conclusion that if the ligand can bind only to one state of ionization of the site, then the acid–bases within the site cannot participate in hydron exchanges with the solution once the site is occupied. This latter statement seems unlikely in most instances, but when the active site of HIV-1 retropepsin from human immunodeficiency virus is occupied by the inhibitor pepstatin, the carboxy group on one of the two catalytic aspartates in the active site remains hydronated and the carboxylato group on the other remains unhydronated[189] in nuclear magnetic resonance spectra collected in the range of pH from 2.7 to 6.2. Nevertheless, this range is not from minus infinity to infinity.

It is usually assumed that the dissociation constant, K_i, observed for an inhibitor of an enzymatic reaction from steady-state kinetic measurements is a simple equilibrium constant between the active site and the inhibitor. If the inhibitor is a close enough analogue of the reactant, the effect of pH on its constant should be an accurate reflection of the effect of pH on only the step in the kinetic mechanism of the enzyme in which the normal reactant associates with the active site. In particular, values of pK_a measured for the dissociation constant of an inhibitor can **support the conclusion that a pK_a observed in a steady-state pH–rate profile is actually for acid dissociation of a catalytic acid–base** rather than, for example, due to a change in rate-limiting step. The apparent dissociation constant for 2,4-diamino-6,7-dimethylpteridine, acting as a competitive inhibitor of dihydrofolate reductase (Equation 4–148) from *E. coli*, varies with pH.[178] It increases below an apparent pK_a of 5.9 and increases above an apparent pK_a of 7.9.* The specificity constant k_{DHF} for 7,8-dihydrofolate (DHF) for the reaction catalyzed by dihydrofolate reductase decreases above a pK_a of 8.1. Because 2,4-diamino-6,7-dimethylpteridine resembles 7,8-dihydrofolate and is a competitive inhibitor with respect to 7,8-dihydrofolate, the coincidence of these two apparent values for pK_a (pK_a = 7.9 and pK_a = 8.1), each of which should be for free enzyme, suggests that they reflect the same acid dissociation. The pK_a for the apparent dissociation constant of the inhibitor, because it governs an equilibrium between a protein and a ligand rather than a steady state, should be associated with a simple acid dissociation constant for free enzyme rather than a complex kinetic parameter. Therefore, the apparent pK_a observed in the behavior of k_{DHF} should also be a simple pK_a for a side chain in the free enzyme.

Azide anion ($N{=}N{=}N^-$), although a linear triatomic monoanion, is a competitive inhibitor of formate dehydrogenase

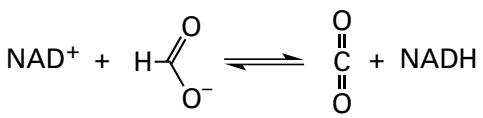

(4–171)

*Recall that as a dissociation constant increases, the affinity of the site for the ligand decreases.

from *S. cerevisiae* with respect to formate, a bent tetraatomic monoanion. The inhibition constant for azide[190] increases as the pH is lowered below a pK_a of 6.4, and it increases as the pH is increased above a pK_a of 8.3. If the inhibition constant for azide is detecting only acid dissociation constants for side chains in the free enzyme and if the specificity constant k_{FRM} for formate (FRM) is also governed only by the same acid dissociation constants for free enzyme, then the respective values of pK_a should coincide. For the reaction catalyzed by formate dehydrogenase, the specificity constant k_{FRM} decreases below a pK_a of 6.1 and decreases above a pK_a of 8.5. The pK_a of 8.5 could be that of Histidine 325, which is immediately adjacent to the azide and should be cationic for the azide to bind.[191]

Suggested Reading

Kiick, D. M., and Cook, P. F. (1983) pH Studies toward the elucidation of the auxiliary catalyst for pig heart aspartate aminotransferase, *Biochemistry 22*, 375–382. https://doi.org/10.1021/bi00271a022

McIntosh, L. P., Hand, G., Johnson, P. E., Joshi, M. D., Körner, M., Plesniak, L. A., Ziser, L., Wakarchuk, W. W., and Withers, S. G. (1996) The pK_a of the general acid/base carboxyl group of a glycosidase cycles during catalysis: a ^{13}C-NMR study of *Bacillus circulans* xylanase. *Biochemistry 35*, 9958–9966. https://doi.org/10.1021/bi9613234

Pitsawong, W., Chenprakhon, P., Dhammaraj, T., Medhanavyn, D., Sucharitakul, J., Tongsook, C., van Berkel, W. J. H., Chaiyen, P., and Miller, A.-F. (2020) Tuning of pK_a values activates substrates in flavin-dependent aromatic hydroxylases, *J. Biol. Chem. 295*, 3965–3981. https://doi.org/10.1074/jbc.RA119.011884

Problem 4–8:

(A) Show that the kinetic mechanism

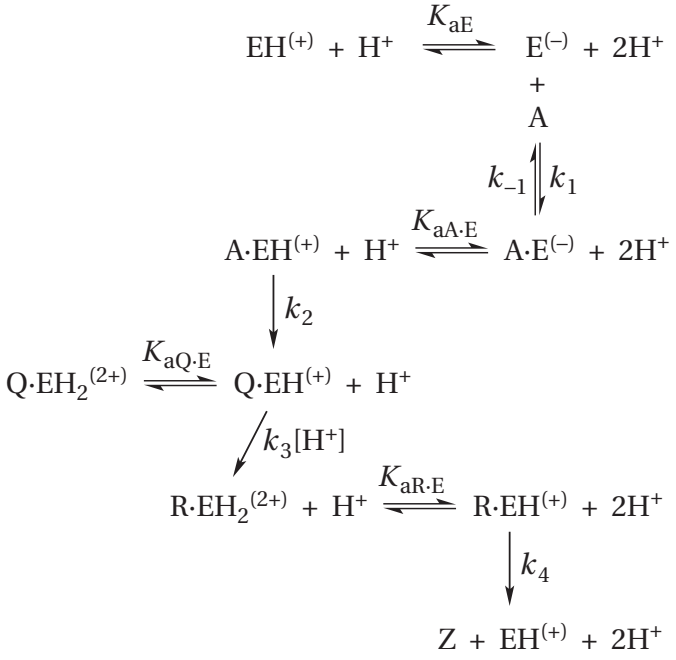

gives a rate equation of the form

$$v_0 = \frac{k_{0,app}\, k_{A,app}\, [E]_t\, [A]_0}{k_{0,app} + k_{A,app}\, [A]_0}$$

where

$$k_{0,app} = k_0 \left(\frac{K_{a1}}{[H^+] + K_{a1}} \right) \left(\frac{[H^+]}{[H^+] + K_{a2}} \right)$$

and

$$k_{A,app} = k_A \left(\frac{K_{a3}}{[H^+] + K_{a3}} \right) \left(\frac{[H^+]}{[H^+] + K_{a4}} \right)$$

(B) Write the expressions defining the four observed apparent acid dissociation constants, K_{a1}, K_{a2}, K_{a3}, and K_{a4}. Are any of them actually acid dissociation constants?

Problem 4–9: Acid dissociations of most substrates are equilibria established so rapidly that they are always fully at equilibrium at times longer than a millisecond. The equilibration of nitroethane and nitroethane anion, however, is so slow that one or the other can be used as a reactant for nitroalkane oxidase from *F. oxysporum*.

(A) Write the acid dissociation of nitroethane, drawing the conjugate acid and conjugate base with all lone pairs of electrons in proper hybridization and each in its most stable resonance hybrid.

When nitroethane anion is used as a reactant with the enzyme, the behavior of log $k_{NEA,app}$ as a function of pH displays behavior consistent with the existence of an acid–base with a pK_a of 7.4 ± 0.1 (Figure 4–10F).

(B) Is this behavior consistent with the participation of a catalytic acid or a catalytic base in the enzymatic reaction?

When neutral nitroethane (NE) is used as a reactant, the following measurements were made for the steady-state rate constant k_{NE}.[78]

pH	$k_{NE,app}$ (M^{-1} s^{-1})
6.0	230
6.5	1360
7.0	2930
7.5	4320
7.9	5350
8.1	6140
8.3	4490
8.5	7880
8.7	7590
8.8	7130
9.0	8930

(C) What is the pK_a for the acid–base that could be responsible for this behavior?
(D) Would it participate as a catalytic acid or a catalytic base in the reaction?
(E) What suggests that the acid–base in both reactions might be the same one?

When Aspartate 402 in the enzyme is mutated to alanine, the acid–base responsible for the decrease in $k_{NEA,app}$ at high pH seems to be lost (□, Figure 4–10F).

(F) What might the side chain of Aspartate 402 be responsible for in the enzymatic reaction?

Problem 4–10: Show that Equation 4–163 follows from Equation 4–162.

Site-Directed Mutation

Site-directed mutation is another method that can be used to assign a particular amino acid to a pK_a governing a pH–rate profile. When a catalytic acid or catalytic base in the side chain of an amino acid in the active site of an enzyme that has been definitively assigned crystallographically[192-197] to the role of adding a hydron to, or removing a hydron from, a reactant during the reaction catalyzed by an enzyme is mutated to a side chain incapable of performing that role, the common logarithm of the steady-state rate constant traditionally used for the catalytic proficiency of a particular enzyme, $\log[k_0\,(K_{mA}K_{mB}\ldots)^{-1}]$, at the optimum pH for catalysis, decreases by 4.2 ± 1.2 units.[113,197-239] The range of this **decrease in the common logarithm of rate constant $k_0\,(K_{mA}K_{mB}\ldots)^{-1}$** for the set of enzymes* chosen is 2.5–8.7.

The **upper limit to the range of decreases in rate constant $k_0\,(K_{mA}K_{mB}\ldots)^{-1}$ due to mutation** of a catalytic acid–base, observed in studies where that decrease for the mutant could be accurately measured,[240] is a factor of 10^9. There are also many instances in which no enzymatic activity could be measured for a mutant, but in most of these instances, lower limits for the levels of detection[231,241-244] unfortunately were not reported. From the results presented in these studies, however, it can be inferred that the actual lower limits of detection, which determine the upper limits on rate constant $k_0\,(K_{mA}K_{mB}\ldots)^{-1}$ of the mutants, are usually much greater than a decrease of 10^9 would have produced. Consequently, these observations, in which no enzymatic activities were observed, are all consistent with decreases of less than a factor of 10^9 in the value of rate constant $k_0\,(K_{mA}K_{mB}\ldots)^{-1}$. When decreases of 10^5 or greater in rate constant $k_0\,(K_{mA}K_{mB}\ldots)^{-1}$ are observed, the possibility that the residual activity results from misincorporation of the wild-type amino acid at the point of mutation should be considered.[209] If misincorporation is occurring, the decrease in catalytic proficiency upon mutation is actually greater than that observed.

*This mean and standard deviation are for 50 side chains known to participate as general acids and bases in the reactions catalyzed by 37 enzymes (9 of which had two reactants) chosen at random.

It is also possible that the rate-limiting step in the normal enzymatic reaction is not the chemical step requiring acid–base catalysis in which the mutated amino acid participates. If the step in which a particular amino acid participates as a catalytic acid–base is not the rate-limiting step, the decrease in steady-state rate constant $k_0\,(K_{mA}K_{mB}\ldots)^{-1}$ observed when that amino acid is mutated will be **less than the actual decrease in the rate constant for that step** in the enzymatic mechanism, and the decrease in the rate constant for that step could be much greater than the kinetic observations suggest. For example, when Tyrosine 146 in thymidylate synthase from *Lactobacillus casei* was replaced by aspartate, the value of $k_0\,(K_{mTHF}K_{m,dU})^{-1}$ for the reactants 5,10-methylenetetrahydrofolate (THF) and deoxyuridine monophosphate (dU) decreased by a factor of 1×10^5. The rate-limiting step of the enzymatic reaction, however, shifts from formation of a covalent intermediate between the active site and deoxyuridine monophosphate to the conversion of that covalent intermediate into the product deoxythymidine monophosphate,[245] so the effect of the mutant on the value of the rate constant for the step in which that covalent intermediate is converted into product must be greater than 1×10^5. Nevertheless, in those instances in which there is clear crystallographic evidence for the involvement of the amino acid as an acid–base in the reaction, several of which may well be involved in steps that are not rate-limiting, mutation of that amino acid almost always results in a decrease in the steady-state rate constant $k_0\,(K_{mA}K_{mB}\ldots)^{-1}$ of greater than a factor of 1000.

Consequently, it can be concluded that **if the mutation of a particular amino acid in an enzyme causes a decrease of less than a factor of 1000 in the value for rate constant $k_0\,(K_{mA}K_{mB}\ldots)^{-1}$, its side chain is probably not participating in the enzymatic reaction as a catalytic base or a catalytic acid.** In particular, when a crystallographic molecular model of a complex between the enzyme and one or more of its substrates or an analogue of its substrate is not available, any claim that a particular side chain the mutation of which results in a decrease of less then 1000 in rate constant $k_0\,(K_{mA}K_{mB}\ldots)^{-1}$ is a catalytic acid or catalytic base involved in the reaction catalyzed by that enzyme should be considered with suspicion. In fact, one of the most convincing ways to rule out the participation of an amino acid as a catalytic acid or catalytic base in the mechanism is to show that its mutation has little effect on catalysis.[193,210,246-256] Occasionally, an increase in rate of catalysis is observed upon mutation of a particular amino acid.[257,258] Amusingly, it has also been observed that a catalytically inactive mutant of the enzyme, by binding reactant tightly and occluding it from the solvent, can decrease the rate of the nonenzymatic reaction that would otherwise occur when reactant is free in solution.[208]

All these observations emphasize **the importance of the active site providing acid–bases that were not required in solution,** where reactants have access to hydroniums, molecules of water, and hydroxides.

The conclusion that a decrease of less than 1000 should be treated with suspicion does not mean that a role for the side chain as a catalytic acid–base has been ruled out completely. For example, from crystallographic molecular models of complexes of bovine carboxypeptidase A

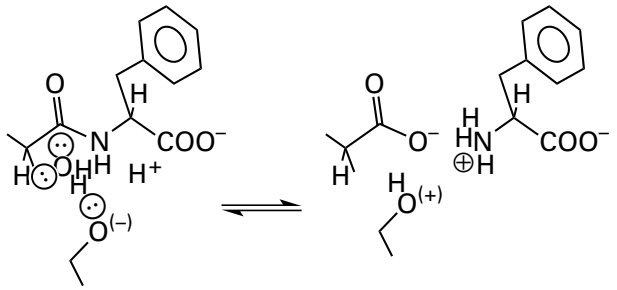

(4–172)

with several analogues of the tetrahedral intermediate in the enzymatic reaction,[259] it is clear that the hydroxy of Tyrosine 248 can swing into the active site[260] to hydronate the nitrogen (0.32 nm) that leaves from the intermediate during hydrolysis of the peptide bond catalyzed by this enzyme. When this tyrosine is mutated to phenylalanine,[261] the value of $k_0\,K_{mA}^{-1}$ decreases by only a factor of about 10. In this instance, the missing tyrosine is no longer able to swing over to cover the substrate, and the nitrogen that must be hydronated, which is a relatively strong base, remains exposed to the solution, which readily provides the hydron. Nevertheless, the tyrosine does improve catalysis relative to that performed by the solution. There is little question that the amino-terminal proline in the active site of 2-hydroxymuconate tautomerase from *P. putida* is responsible for removing one of the hydrons from carbon 5 of (2*Z*,4*E*)-2-hydroxyhexa-2,4-dienedioate (muc),[262] yet when it is mutated to either alanine or glycine,[263] the value of $k_0\,K_{m,muc}^{-1}$ decreases by only a factor of 20. In this case, however, each mutation simply replaces one amino group with another amino group in the same location, so the effects are minimal.

Even when large decreases in activity are observed upon mutation of an amino acid, that observation provides no information about the role of that amino acid in catalysis or even whether or not it has a role. There are many instances in which the mutation of an amino acid outside the active site nevertheless causes significant decreases in the catalytic proficiency of the enzyme. Consequently, **a crystallographic molecular model of the active site occupied by some ligand that can identify candidates for catalytic roles is still required**, not only to decide which amino acids to mutate but also to have any understanding of the observed effects of the mutations on catalysis. There is no reason to mutate an amino acid in a protein unless the question that the mutation will be able to answer is clearly stated and will provide useful information.

If a hydron must be removed from or added to a reactant during a reaction, that **reaction cannot occur on the active site of an enzyme unless the active site provides a basic lone pair of electrons or an acidic hydron**, respectively, immediately adjacent to the immobilized reactant, or unless the position from which the hydron must be removed or added remains accessible to the solution, as in the mutant of carboxypeptidase A. When a side chain providing the required lone pair of electrons or acidic hydron is removed from the active site by mutation, another lone pair of electrons or acidic hydron must have steped in if the enzyme retains any activity. In some instances, that lone pair of electrons or that hydron may be provided fortuitously by another side chain in the active site. An example is triose-phosphate isomerase from *S. cerevisiae*, in which the histidine acting as a catalytic acid–base (Equations 4–46 and 4–55 and Figure 3–37) has been mutated and its role is filled, albeit considerably less ably, by Glutamate 164.[28]

In most instances, however, it is probably a **molecule of water**, occupying the location in the active site of the mutant usually occupied by the now-missing heteroatom of the acid–base[118,264,265] that steps in as the catalytic acid or catalytic base. For example, when Aspartate 222, the catalytic acid–base in porcine aspartate transaminase, is mutated to threonine, a molecule of water that occupies the identical location to the catalytic oxygen in the carboxy group of the aspartate steps in to cause the mutant to retain 5% of the value of $k_0\ K_{m,Asp}^{-1}$ for the substrate L-aspartate;[266] and when the catalytic acid–base Histidine 143 is mutated to leucine, a molecule of water that occupies the identical location to the catalytic nitrogen in the imidazolyl group of the histidine steps in to cause the mutant to retain 50% of the value of $k_0\ K_{m,Asp}^{-1}$. The aspartate and the histidine participate in a hydrogen bond and together form the acid responsible for hydronation of nitrogen 1 of the prosthetic pyridoxal 5′-phosphate, a hydronation that is required by the enzymatic reaction.

The molecule of water that steps in to take the place of the catalytic acid–base is probably a molecule of water occupying the empty active site before reactant associates (Figure 3–32), and it remains in place rather than being displaced as in the wild-type enzyme by the normal juxtaposition of reactant and unmutated catalytic side chain. There are four problems with this subtitution that cause the rate constant for its removal or addition of the hydron to be slow. First, this molecule of water is usually either a **weaker base or a weaker acid** than the normal catalytic side chain. Second, this molecule of water **cannot be precisely aligned** by the active site, which would normally align the now-missing side chain that was mutated. An exception to this problem is the mutation of carboxypeptidase, where the base that must be hydronated, the amino group of the tetrahedral intermediate, is a strong one and is exposed to the molecules of water in the solution as a result of the mutation. Third, the effectiveness of the molecule of water that has stepped in **depends on the Brønsted coefficient** for the transfer of the hydron. Fourth, there is the problem of whether or not the rate of the step catalyzed by the unmutated acid–base was the rate-limiting step of the reaction. The wide variation in decreases in rate observed upon mutation reflects the wide variation in the severity of these four problems.

In some instances, it is possible to **supply a more satisfactory acid–base to the mutant** than a molecule of water and **rescue the enzymatic activity**. For example, the conjugate base of any one of several primary amines can replace the catalytic primary amine lost when Lysine 258 in aspartate transaminase from *E. coli* (Equation 4–108) is replaced by alanine.[267] The exogenous primary amine can rescue some of the enzymatic activity. In this instance, the **exogenous amines** participate in a simple bimolecular reaction with the active site and do not display saturation in their ability to rescue the catalytic activity. Consequently, they act from the solution in a bimolecular collision with the Michaelis complex, and the rate constant of the rescued reaction is a linear function of the concentration of amine. A concentration of 1 M methylamine allows the mutant to display 12% of the enzymatic activity of the wild

type. This result demonstrates that, in this instance, a primary amine entering the active site from solution, and presumably occupying transiently the location that is occupied by the amino group of the lysine in the unmutated enzyme, is a more effective acid–base than the molecule of water that most certainly catalyzes the enzymatic reaction in the active site of the mutant in the absence of the amino group of the lysine. The fact that a small portion of the enzymatic activity can be rescued in many instances provides a paradigm for the rescue that molecules of water perform in the absence of general acid–bases added to the solution.

In the case of rescue of a mutant of ribulose-bisphosphate carboxylase (previously Equation 3–424)

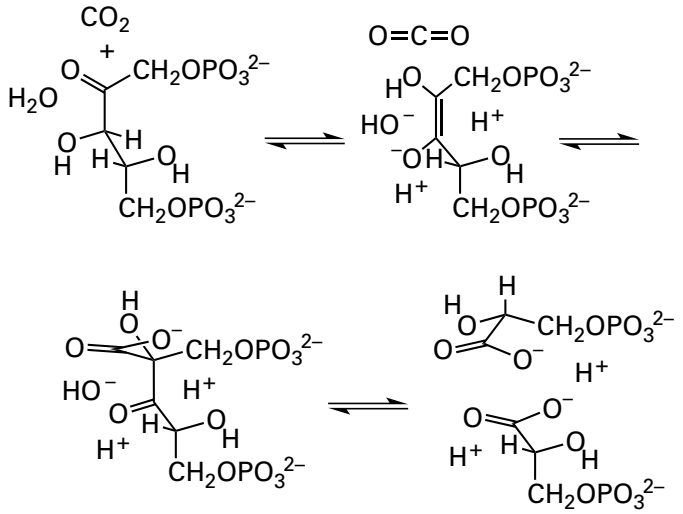

(4–173)

from *Rhodospirillum rubrum* in which Lysine 329 (corresponding to K332A in Figure 3–53) was converted to alanine, ethylamine displayed saturation with an apparent dissociation constant of 0.13 M in its ability to rescue the enzymatic activity. At saturation, ethylamine was able to achieve an increase in the limiting rate for the enzymatic reaction of a factor of 80 relative to that of the mutant and accomplished a limiting rate that was 2% of the activity of the wild type.[268]

Imidazole, when present at saturation, can rescue 0.1% of the enzymatic activity of a mutant of nucleoside-diphosphate kinase from *Dictyostelium* in which Histidine 122 has been replaced by glycine,[269] and it can rescue 0.1% of the enzymatic activity of a mutant of (*S*)-mandelate dehydrogenase from *P. putida* in which Histidine 274 has been replaced by glycine.[270]

Guanidinium, when present at saturation, can rescue 10% of the enzymatic activity in a mutant of ornithine carbamoyltransferase from *E. coli* in which Arginine 57 has been replaced by alanine,[271] and it can rescue 7% of the enzymatic activity in a mutant of IMP dehydrogenase from *T. foetus* in which Arginine 418 has been replaced by alanine.[162]

Formate can rescue the enzymatic activity of cytidine deaminase from *E. coli*. When Glutamate 104 is mutated to alanine, $k_0\,K_{mCyt}^{-1}$ for the reactant cytidine (Cyt) decreases by a factor of 4×10^6 and the catalytic constant decreases by a factor of 1×10^8 to a value of 2.6×10^{-6} s^{-1}. Formate occupies the vacancy in the active site caused by eliminating the carboxymethyl group of the glutamate by converting it to an alanine, and the enzymatic activity at saturation with cytidine becomes a linear function of the concentration of formate[199] with a rate constant of 3.6×10^{-5} M^{-1} s^{-1}. Consequently, at 2 M formate, the catalytic constant of the mutant increases by a factor of 30, but it is still less than the catalytic constant of the wild type by a factor of 4×10^6. A mutant of steroid Δ-isomerase from *P. putida* in which Aspartate 38 has been mutated to glycine has a catalytic constant 2.4×10^4 times smaller than that of the wild type (36 s^{-1}), and the enzymatic activity has become a linear function of the concentration of formate with a rate constant of 0.12 M^{-1} s^{-1}. At 2 M formate, the rate constant for the enzymatic reaction (0.24 s^{-1}) is only a factor of 150 smaller than that of the wild-type enzyme.[272]

An exogenous substitute can also rescue a mutant defective in **a site used to recognize a reactant**. Acetate can rescue 100% of the hydrolytic activity toward tosylglycyl-L-prolyl-L-arginine amide of a mutant of anionic trypsin from *R. norvegicus* in which Aspartate 171, which sits in the subsite recognizing the side chain of L-arginine in the substrate (Figure 3–46), has been mutated to serine.[273]

α-L-Fucosidase from *Saccharolobus solfataricus* hydrolyzes an α-glycosidic bond between an L-fucosyl group and the rest of an oligosaccharide. The reaction proceeds with retention of configuration at the glycosidic carbon of L-fucose. It is believed that the first step in the reaction is a nucleophilic substitution between one oxygen on the carboxylato group of Aspartate 242, followed by hydrolysis of this covalent intermediate. When this aspartate is mutated to glycine, the enzymatic activity toward 4-nitrophenyl-α-L-fucoside is lost. If, however, azide is added to the assay[274] at a concentration of 2 M, a small amount (0.5%) of the cleavage of glycoside catalyzed by the enzyme is rescued, the product is the β-L-fucosyl azide instead of α-L-fucose.[244] The

azide has replaced the carboxylato group of Aspartate 242, rescuing the enzymatic activity, and its nucleophilic substitution for the 4-nitrophenoxy group in the reactant produces a stable product, which, because it is no longer covalently attached to the enzyme, dissociates from the active site.[274]

There seems to be at least one **naturally occurring example** of the rescue of enzymatic activity. In 1,4-dihydroxy-2-naphthoyl-CoA synthases from mycobacteria, there is an aspartate that is a catalytic acid–base responsible for removing an acidic hydron from a carbon α to the thioester in the reactant 4-(2-carboxyphenyl)-4-oxobutanoyl-SCoA to form the enolate. This enolate initiates an intramolecular Claisen condensation and aromatization that yields 1,4-dihydroxy-2-naphthoyl-SCoA. In the homologous 1,4-dihydroxy-2-naphthoyl-CoA synthase from *E. coli* (44% identity; 0.17 gap percent) and other bacteria, that catalytic aspartate is replaced by glycine. These latter enzymes, unlike those from mycobacteria, require bicarbonate for enzymatic activity. In a crystallographic molecular model of the enzyme from *E. coli*, it can be seen that the bicarbonate occupies the same location as the carboxylato group of the aspartate in the crystallographic molecular model of the enzyme from *M. tuberculosis* and rescues the enzymatic activity by providing its carboxylato group.[275]

The ability to rescue the enzymatic activity of a mutant missing a side chain by adding an appropriate acid–base to the solution can be exploited for **Brønsted analysis**. Acid–bases with a series of different values of pK_a are used to rescue the mutant, and a plot of the common logarithms of the second-order rate constants for their ability to restore activity against their values of pK_a gives an estimate for the Brønsted coefficient for the catalysis performed by the side chain that was mutated.[267] For example, eight amines with different values of pK_a were used to rescue a mutant of human peptidyl-glutamate 4-carboxylase in which Lysine 217 had been replaced by alanine. The Brønsted coefficient for their ability to rescue the mutant was 0.7. This result suggests that the hydron removed from the hydroxy group of the *gem*-diol of the epoxide of vitamin K (**2–103** in Figure 2–49) is mostly transferred to the amino group of the lysine in the transition state for that step in the reaction.[276]

It is also possible to attach the acid–base that is rescuing the mutant covalently to the position that has been mutated, precluding the need to add it to the solution.[277] For example, when Lysine 166 (corresponding to K175A in Figure 3–53) in the active site of ribulose-bisphosphate carboxylase from *R. rubrum* was mutated to cysteine, no enzymatic activity could be detected, but when the sulfanyl group of that cysteine was alkylated with aziridine to covalently restore the amino group in the same location in the active site, 45% of the enzymatic activity was restored.[278] This example is not so much a rescue as mutation of lysine to 3-thialysine.[279]

Although the following description is certainly simplistic, the **effects of site-directed mutations on the pH–rate profiles** for the catalytic constant and the specificity constants of an enzyme are most readily understood graphically (Figure 4–20). Consider the situation in which one side chain, HO, in the active site acts as a catalytic base, $O\odot^{(-)}$, and another side chain, NH, in the active site acts as a catalytic acid, $NH^{(+)}$, in the catalysis accomplished by the enzyme. The acid and the base titrate independently of each other; both accomplish their catalysis in the same transition state; and in the absence of both the catalytic base and the catalytic acid when both have been removed by site-directed mutation, the enzyme would catalyze the reaction with a basal catalytic constant, k_0, or specificity constant, k_A, for reactant A of a certain value independent of the pH (indicated by the horizontal line labeled E in Figure 4–20).

If only catalytic base $O\odot^{(-)}$ is present in the active site, when only the amino acid NH providing the catalytic acid has been mutated, the increase in the catalytic constant, $k_{0,app}$, or the specificity constant for reactant A, $k_{A,app}$, caused by the presence of HO at a particular pH is equal to the increase it provides when acid–base HO is fully unhydronated times the fraction that is unhydronated, $\alpha(\odot O^{(-)})$ (Equation 4–78). The pH–rate profile for this situation is the curve labeled HOE in Figure 4–20.

If only catalytic acid–base NH is present in the active site, when only the amino acid providing HO has been mutated, the increase in the catalytic constant, $k_{0,app}$, or the specificity constant for reactant A, $k_{A,app}$, caused by the presence of NH at a particular pH is equal to the increase it provides when acid–base NH is fully hydronated times the fraction that is hydronated, $\alpha(NH^{(+)})$ (Equation 4–87) The pH–rate profile for this situation is the curve labeled ENH in Figure 4–20.

When both HO and NH are present in the active site, which is the case in the native enzyme, the increase in the catalytic constant, $k_{0,app}$, or the specificity constant for reactant A, $k_{A,app}$, caused by their presence at a particular pH would be equal to the product of the increases that they each provide when

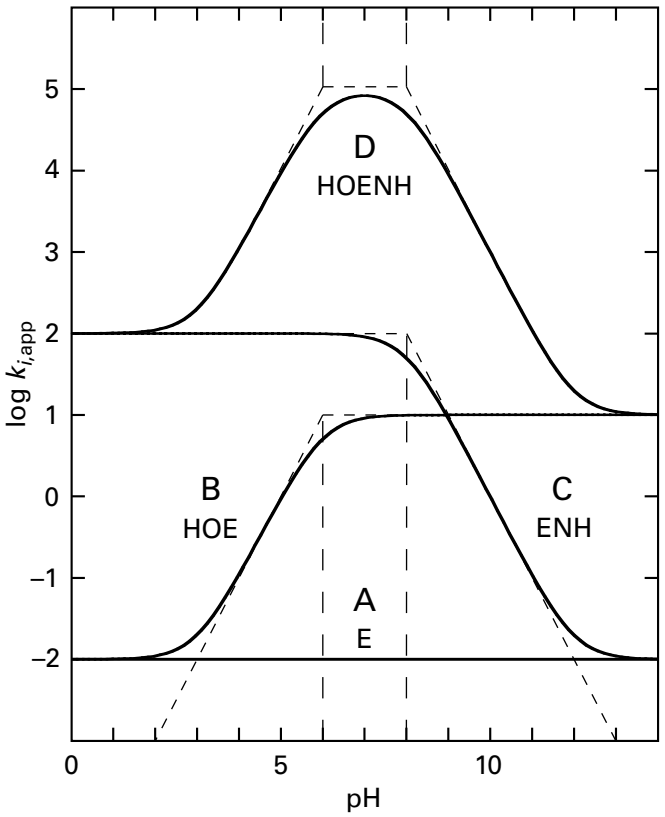

Figure 4–20: Theoretical pH–rate profiles for enzymatic reactions catalyzed by a catalytic base alone, a catalytic acid alone, and a catalytic base and a catalytic acid together in the active site of an enzyme. The explanation is the same for the pH–rate profiles of the steady-state rate constants k_A, k_B, and k_C and the catalytic constant k_0, so a generic steady-state rate constant k_i will be considered. The only differences among the behaviors of the rate constants are the complexes between enzyme and reactants to which the respective values of the pK_a refer. (**A**) In the absence of both the catalytic base and the catalytic acid, when the enzyme E is in the appropriate complex with reactants, the rate constants $k_{i,app}$ have low but finite basal values (horizontal line labeled E) that will be invariant with pH within the normal range because there is neither a catalytic acid nor a catalytic base in the active site. (**B**) If the enzyme has only a catalytic base, $^{(-)}\odot$O–, in its active site, the conjugate acid of which has a pK_a in the normal range for the appropriate complex with reactants, then the rate constants $k_{i,app}$ (curve labeled HOE) will be at the basal value at low pH when the unhydronated catalytic base is present at too low a level to catalyze the reaction. As the pH increases, however, the rate constants will begin to increase as the concentration of the unhydronated catalytic base increases, and they will finally reach a higher level (chosen to be 1000-fold the basal rate) when the catalytic base is fully unhydronated above its pK_a (chosen to be 6) and fully committed to the enzymatic reaction. When the curve over the range of pH in which the rate constants are increasing most rapidly is fit to an asymptote of slope +1 (dashed line) and the curve at high pH is fit to a horizontal asymptote (dashed line), the intersection of these two asymptotes is an estimate of the pK_a for the conjugate acid of the catalytic base in the appropriate complex with reactants. (**C**) If the enzyme has only a catalytic acid, –NH$^{(+)}$, in its active site, with a pK_a in the normal range for the appropriate complex with reactants, the rate constants $k_{i,app}$ (curve labeled ENH) will be at the basal value at high pH when the hydronated catalytic acid is present at too low a level to catalyze the reaction. As the pH decreases, however, the rate constants will begin to increase as the concentration of the hydronated catalytic acid increases, and they will finally reach a higher level (chosen to be 10,000-fold the basal rate) when the catalytic acid is fully hydronated below its pK_a (chosen to be 8) and fully committed to the enzymatic reaction. When the curve over the range of pH in which the rate constants are increasing most rapidly is fit to an asymptote of slope –1 (dashed line) and the curve at low pH is fit to a horizontal asymptote (dashed line), the intersection of these two asymptotes is an estimate of the pK_a for the catalytic acid in the appropriate complex with reactants. (**D**) If the enzyme has only one catalytic base, $^{(-)}\odot$O–, and only one catalytic acid, –NH$^{(+)}$, in its active site, with values of pK_a in the normal range for the appropriate complex with reactants, the rate constants $k_{i,app}$ (curve labeled HOENH) will be at the values for the reaction catalyzed only by the catalytic base at high pH when the hydronated catalytic acid is present at low levels, and they will be at the values for the reaction catalyzed only by the catalytic acid at low pH when the unhydronated catalytic base is present at low levels. As the pH, however, respectively increases or decreases, the rate constant will begin to increase and almost reach the highest possible level (10^7-fold the basal rate), which would be reached if the catalytic base could be fully unhydronated while the catalytic acid is fully hydronated at a pH between the two values of pK_a. When the curve over the range of pH in which the rate constant is increasing most rapidly at low pH is fit to an asymptote of slope +1 (dashed line), the curve over the range of pH in which it is increasing most rapidly at high pH is fit to an asymptote of slope –1 (dashed line), and a horizontal line is drawn at the rate constant that would be reached if the catalytic base could be fully unhydronated while the catalytic acid is fully hydronated, the intersection of these three asymptotes is an estimate for the two values of pK_a.

fully unhydronated and hydronated, respectively, times $\alpha(NH^{(+)},\odot O^{(-)})$ (Equation 4–94). The pH–rate profile for this situation is the curve labeled HOENH in Figure 4–20.

Each of these three types of pH–rate profiles has been observed in various native enzymes (Figure 4–10), but **an experimental paradigm of the theoretical effects of mutation** has been reported for protein-tyrosine-phosphatase from *Yersinia entereocolitica*. The effects of mutation of Glutamate 290 to glutamine, mutation of Aspartate 356 to asparagine, and mutation of both amino acids at the same time on the catalytic constant of this enzyme (Figure 4–21)[280] mimic the expected behavior. The pK_a of 4.7 governing the decrease in the pH–rate profile of the catalytic constant for the wild type (○) as the pH is decreased is lost in the mutant of Glutamate 290 (●), but the pK_a of 5.2 governing the decrease in the pH–rate profile as the pH is increased remains. The pK_a of 5.2 observed in the pH–rate profile of the catalytic constant for the wild type is lost in the mutant of Aspartate 356 (□), but the pK_a of 4.7 remains. When both amino acids are mutated, the remaining enzymatic activity has a catalytic constant that is independent of pH (■). Consequently, the pK_a of 4.7 governing the pH–rate

behavior of the unmutated enzyme must be that of Glutamate 290, and the pK_a of 5.2 must be that of Aspartate 356. In this instance, the fact that the acid–base catalysis provided by Glutamate 290 and the acid–base catalysis provided by Aspartate 356 are each relatively small (factors of around 100 and 10, respctively) has allowed the entire consequence of their catalysis to be observed.

There are many paradigmatic examples of a decrease in a steady-state rate constant above an apparent pK_a or a decrease in a steady-state rate constant below an apparent pK_a being lost upon mutation of a catalytic acid or a catalytic base, respectively, in the active site of an enzyme. In each case, the loss of the apparent pK_a is accompanied by a large overall decrease in that rate constant as expected (Figure 4–20). In most of the following examples, the respective rate constants for the unmutated enzymes decrease either above (ENH in Figure 4–20) or below a particular pK_a (HOE in Figure 4–20), while the same rate constants for the mutated enzymes do not (E in Figure 4–20). The greatest decrease observed in each rate constant upon mutation occurs at the optimum pH for the unmutated enzyme, either below (difference between ENH and E below pH 8 in Figure 4–20) or above (difference between EOH and E above pH 6 in Figure 4–20) the pK_a at which the rate constant for the unmutated enzyme begins to decrease while the rate constant for the mutated enzyme does not. When Histidine 40 is mutated to glutamine, the catalytic constant of glucose-6-phosphate dehydrogenase (coenzyme F_{420}) from *M. tuberculosis* at the respective optima of pH decreases by a factor of 1000, and the pK_a of 8.0, above which the catalytic constant decreases as the pH is increased, is lost. These facts are consistent with the conjugate acid of Histidine 40 playing the role of a catalytic acid in the enzymatic reaction.[281] When Glutamate 73 is mutated to alanine, the catalytic constant for the deacetylase LpxC from *Aquifex aeolicus* at the respective optima of pH decreases by a factor of 700, and the pK_a of 6.1, below which the catalytic constant decreases as the pH is decreased, is lost. These facts are consistent with Glutamate 73 playing the role of a catalytic base in the enzymatic reaction.[282] When Histidine 104 is mutated to glutamine, the specificity constant $k_{\alpha Gal}$ for the mutarotation of α-D-galactose (αGal) by aldose 1-epimerase from *E. coli* at the respective optima of pH decreases by a factor of 5000, and the pK_a of 7.6, above which the specificity constant decreases as the pH is increased, is lost.

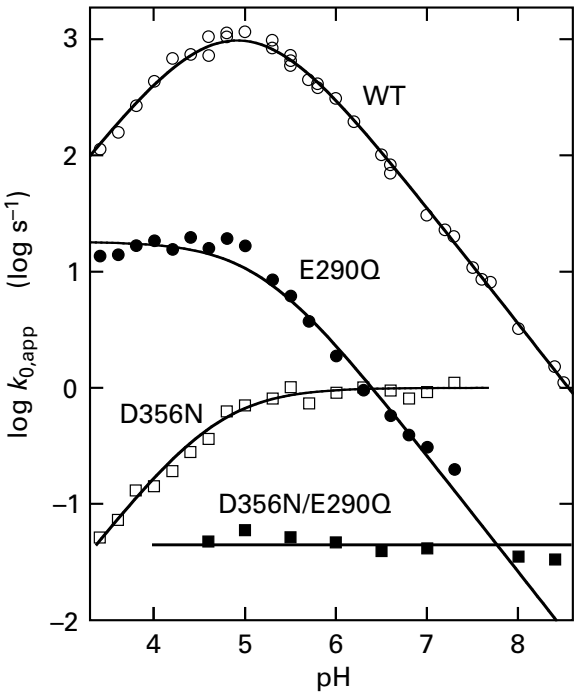

Figure 4–21: pH–Rate profiles for the hydrolysis of 4-nitrophenyl phosphate catalyzed by mutants of protein-tyrosine-phosphatase from *Y. entereocolitica*.[280] Initial rates for the hydrolysis were measured with a spectrophotometric assay at an ionic strength of 0.15 M and 30 °C for several concentrations of 4-nitrophenyl phosphate at each of the chosen values of pH, and catalytic constants were obtained from these initial rates. The pH was maintained with the following buffers: pH 3.4–3.8, 100 mM sodium formate; pH 4.0–5.7, 100 mM sodium acetate; pH 5.8–6.5, 50 mM sodium succinate; pH 6.6–7.3, 50 mM sodium 3,3-dimethylglutarate; pH 7.5–8.7, 100 mM sodium glycinamide. The common logarithms of the values of the catalytic constant $k_{0,app}$ for a portion (amino acids 219–462) of the wild-type protein-tyrosine-phosphatase containing the complete active site (WT, ○), a mutant of that same portion in which Glutamate 290 had been mutated to glutamine (E290Q, ●), a mutant of that same portion in which Aspartate 356 had been mutated to asparagine (D356N, □), and a double mutant of that same portion in which both mutations had been made (D356N/E290Q, ■) are plotted as a function of pH. The curve for the unmutated enzyme was fit to the data with pK_{a1} = 4.63 ± 0.07 and pK_{a2} = 5.20 ± 0.06. The curve for the mutant D356N was fit to the data with pK_a = 4.70 ± 0.04. The curve for the mutant E290Q was fit to the data with pK_a = 5.16 ± 0.06.

These facts are consistent with Histidine 104 playing the role of a catalytic acid in the enzymatic reaction.[283] When Histidine 52 is mutated to leucine, the bimolecular rate constant for association of hydrogen peroxide with the active site of cytochrome-*c* peroxidase from *S. cerevisiae* at the respective optima of pH decreases by a factor of 10^5, and the pK_a of 5.4, below which the rate constant decreases as the pH is lowered, is lost. These facts are consistent with Histidine 52 playing the role of a catalytic base in the enzymatic reaction.[284] When Histidine 464 is mutated to glutamine, the catalytic constant of

thioredoxin-disulfide reductase from *Drosophila melanogaster* at the respective optima of pH decreases by a factor of 50, and the pK_a of 9.3, above which the catalytic constant decreases as the pH is increased, is lost. These facts are consistent with the conjugate acid of Histidine 464 playing the role of a catalytic acid in the enzymatic reaction.[255]

The curves labeled HOE, ENH, and HOENH in Figure 4–20 are drawn so that the observed rate constant, $k_{i,app}$, which can be either a catalytic constant or a specificity constant, decreases at values of pH below the value of the respective pK_a, decreases at values of pH above the value of the respective pK_a, or decreases at values of pH below and above the respective values of the pK_a only to the level that the rate constant would be in the absence of the catalytic base or catalytic acid that is titrating. The assumption is that **when the fraction of the catalytic base or catalytic acid in the required state of ionization becomes so small** that the rate constant for the reaction catalyzed by that catalytic base or catalytic acid becomes smaller than the rate constant that the enzyme would display in its absence, the rate constant of the enzymatic reaction becomes the rate constant that it has in the absence of that acid or base.

The changes in slope at these points in the theoretical curves producing rate constants that become invariant with pH result from a change in mechanism. The mechanism catalyzed by the catalytic base or catalytic acid is replaced by a mechanism not involving that catalytic base or catalytic acid. In theory, this mechanism would be the one that the enzyme uses when that catalytic acid or catalytic base has been eliminated by mutation.

Data for the effects of pH on rate constants for an enzymatic reaction catalyzed by an unmutated enzyme have rarely if ever been gathered over the range necessary to observe these changes in slope at low pH and at high pH, if they indeed exist. There is a hint of such a change in slope in Figure 4–10H at high values of pH. It is also possible that the inactive, hydronated catalytic base or the inactive, unhydronated catalytic acid, respectively, interferes with the mechanism with the lower rate constant that is observed when that base or acid is removed by site-directed mutation, which probably represents catalysis by water. If the inactive hydronated base or the inactive unhydronated acid sterically blocks access of a molecule of water that could provide the necessary catalysis, the curve for the common logarithm of the rate constant would not level out at this lower level. It would continue to drop with a slope of +1 or −1 indefinitely because the mechanism observed with the respective mutant is precluded in the wild type by this interference with the access of water into a proper location and orientation, and a hydron cannot disappear or appear magically. Consequently, the lack of any indication of a plateau at low pH or high pH in the pH–rate profiles of native enzymes could be yet another indication of the absolute necessity for a catalytic acid or catalytic base, which in the complete absence of the usual catalytic acid–base would be supplied by a molecule of water. Most pH–rate profiles, however, unlike that for ribonuclease (Figure 4–11), are not determined over sufficiently wide ranges to conclude that such plateaus do not exist.

If the pH–rate profile for the common logarithm of one of the steady-state rate constants of an enzyme is a straightforward sum of the contributions of the catalytic acid–bases catalyzing a reaction within the active site of the native enzyme (Figure 4–20), then the contribution of a particular catalytic acid–base to that pH–rate profile should be represented by the difference between the pH–rate profiles for the wild type and for a mutant in which that catalytic acid–base has been removed (Figure 4–22). The simplest possible example is represented by the pH–rate profile for the catalytic constant, k_0, of β-glucosidase from *Agrobacterium faecalis*, which for the native enzyme is governed by a single pK_a of 7.8 (○; Figure 4–22A).[285] When Glutamate 470 is mutated to glycine, the catalytic constant of the mutant, which is 1800 times less than that of the wild type at its maximum, is invariant with pH. The **difference pH–rate profile**, which represents the contribution of Glutamate 470 to the catalysis of the unmutated wild-type enzyme relative to that of the mutant, demonstrates that Glutamate 470 is the catalytic acid responsible for the decrease in the catalytic constant above an apparent pK_a of 7.8.

In contradistinction to the change just described, the pH–rate profile for the catalytic constant of mRNA interferase toxin RelE from *E. coli* for hydrolysis of messenger RNA after its translation on the ribosome has been initiated is invariant with pH. When, however, Arginine 81 in the enzyme is mutated to alanine, the catalytic constant decreases by a factor of 80,000, and the pH–rate profile for the catalytic constant of the mutant is pH-dependent, decreasing below a pH of greater than 9. In the difference pH–rate profile, which defines the contribution of Arginine 81 to catalysis, the catalytic constant decreases by a factor of 10 for every increase

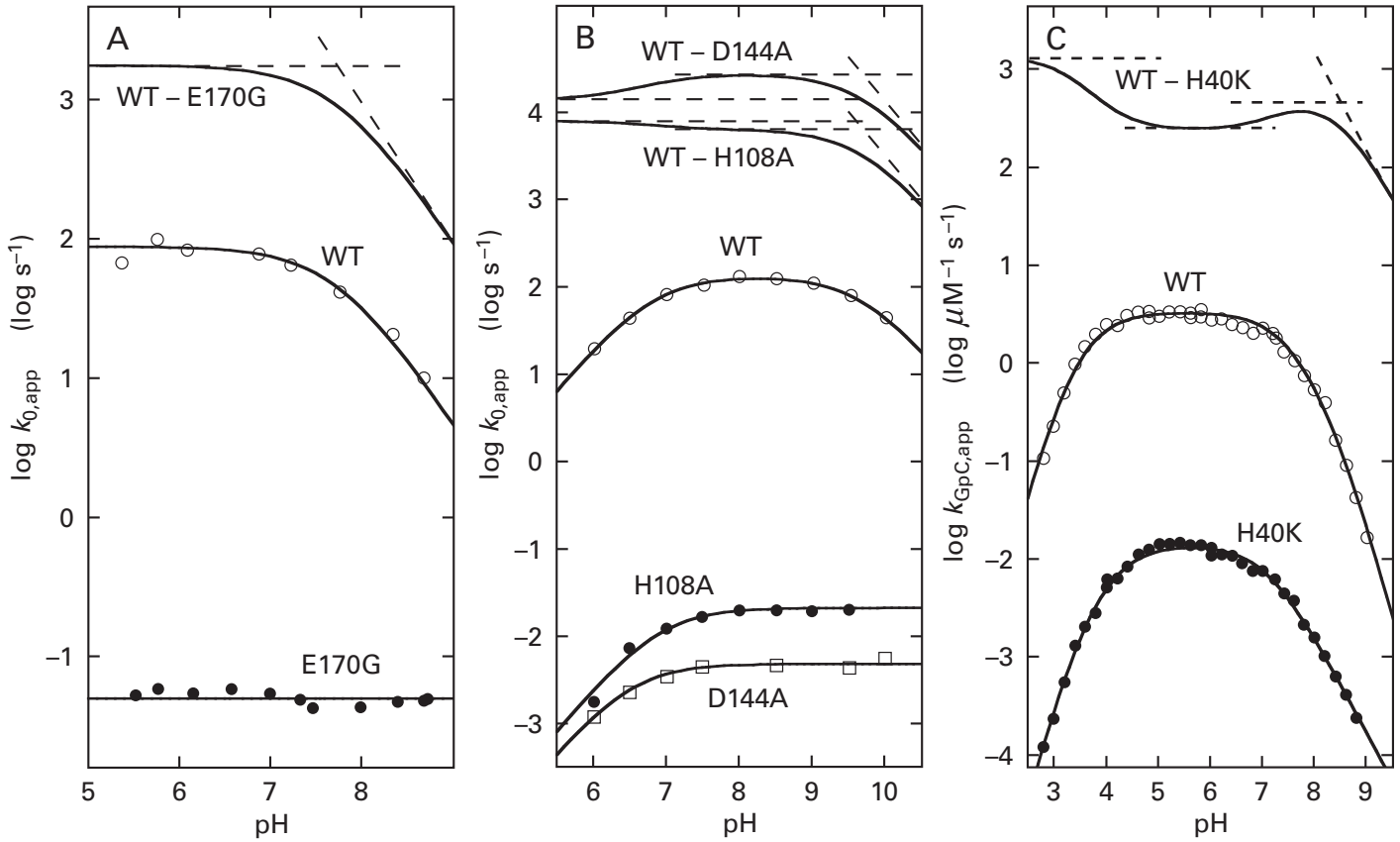

Figure 4–22: Difference pH–rate profiles for site-directed mutants. (**A**) pH–Rate profiles for the catalytic constant of β-glucosidase from *A. faecalis* for 2′,4′-dinitrophenyl β-D-glucopyranoside at an ionic strength of 0.2 M and 37 °C.[285] The common logarithms of the observed catalytic constants $k_{0,app}$ (second^{-1}) are plotted as a function of pH for the wild-type enzyme (WT, ○) and for a site-directed mutant in which Glutamate 170 had been converted to glycine (E170G, ●). The two sets of data were fit with Equation 4–89 or a horizontal line, respectively. The top curve, the difference pH–rate profile, is the difference between the pH–rate profiles fit to data for the wild type and data for the mutant. (**B**) pH–Rate profiles for the catalytic constant of phosphoribosylglycinamide formyltransferase from *E. coli* for 10-formyl-5,8-dideazafolate and N^1-(5-phospho-D-ribosyl)glycinamide at an ionic strength of 0.15 M and 25 °C.[218] The common logarithms of the observed catalytic constants $k_{0,app}$ (second^{-1}) are plotted as a function of pH for the wild-type enzyme (WT, ○), for a site-directed mutant in which Histidine 108 had been converted to alanine (H108A, ●), and for a site-directed mutant in which Aspartate 144 had been converted to alanine (D144A, □). The three sets of data were fit with Equations 4–96, 4–80, and 4–80, respectively. The top two curves are the respective differences between the pH–rate profile fit to the data for the wild type and the pH–rate profiles fit to the data for each mutant. (**C**) pH–Rate profiles for the steady-state rate constant k_{GpC} of ribonuclease T_1 from *A. oryzae* for the dinucleotide guanylyl-(3′-5′)cytidine (GpC) at an ionic strength of 0.1 M and 35 °C.[219] The common logarithms of the observed steady-state rate constants k_{GpC} (micromolar^{-1} second^{-1}) are plotted as a function of pH for the wild-type enzyme (WT, ○) and for a site-directed mutant in which Histidine 40 had been converted to lysine (H40K, ●). The two sets of data were fit with Equations 4–109 and 4–97, respectively. The top curve, the difference pH–rate profile, is the difference between the pH–rate profiles fit to data for the wild type and data for the mutant. In each panel (A–C), dashed lines of slope +1, 0, or –1 are included as asymptotes to the functions defining the difference pH–rate profiles.

of a unit of pH over the range of the measurements, with no indication of a pH below which it becomes invariant.[286] Consequently, it was concluded that the pH–rate profile of the wild type is invariant with pH because, in the range of the measurements, catalysis by a base of unknown identity in the mutant was increasing by a factor of 10 for every increase of one unit of pH while catalysis by the cationic conjugate acid of the guanidinio group of Arginine 81 is decreasing by a factor of 10 for every increase of one unit of pH. These two factors, necessarily represented by lines of slope –1 and +1, multiply to create the invariance of the catalytic constant for the wild type with pH. In this instance, the mutation has revealed acid–base catalysis where none seemed to be occurring rather than eliminating acid–base catalysis that is observed with the native enzyme. The reason for the invariance of the catalytic constant for the wild type is that the pK_a for the catalytic acid and the pK_a for the catalytic base in the Michaelis

complex are outside the values of pH chosen for the measurements. The results also suggest that the pK_a of Arginine 81, if it is acting as the catalytic acid in the Michaelis complex, as the authors have concluded, is less than 5, a rather startling proposal since the pK_a for an arginine in a protein, when fully exposed to the solution, is 13.

In more complicated instances, a difference pH–rate profile is a simple way of **isolating the various contributions of the particular acid–base** that has been mutated. For example, the pH–rate profile for the catalytic constant of phosphoribosylglycinamide formyltransferase from *E. coli* decreases above a pK_a of 9.7 (Figure 4–22B).[218] In a crystallographic molecular model of the active site of the enzyme, the carboxy group of Aspartate 144 and the imidazolyl group of Histidine 108 form a hydrogen bond.[287] When either Aspartate 144 or Histidine 108 is mutated, the difference pH–rate profile between either mutant and the wild type shows that both side chains together are responsible for the single pK_a of 9.7, just as the ammonio group of Lysine 165 and the carboxylato group of Aspartate 169 appear to be equally responsible for the acid–base catalysis in the active site of phosphoribulokinase from *Rhodobacter sphaeroides*. Consequently, this pK_a is for dissociation of a hydron from the hydrogen-bonded complex of Aspartate 144 and Histidine 108, and the observation is consistent with the conclusion that, in this instance, this complex is a composite acid–base that acts as a catalytic acid in the enzymatic reaction.

A **composite acid–base** is formed by the combination of more than one simple acid–base. The participating acid–bases are all part of a hydrogen-bonded network from which a hydron can dissociate from a peripheral acidic position or with which a hydron can associate at a peripheral lone pair. These dissociations and associations are often accompanied by shifts in the hydrons in the hydrogen bonds of the network. Within each level of ionization, the hydrogen-bonded network will have more than one tautomer. For example, in the case of a hydrogen-bonded complex between a carboxy group and a imidazolyl group (Equation 4–134), as in the case of the composite acid–base formed from Aspartate 144 and Histidine 108 in the active site of phosphoribosylglycinamide formyltransferase (Figure 4–22B), there are three reasonable tautomers: one in which the two hydrons are on the imidazolyl group (Equation 4–134), one in which the hydron of the hydrogen bond has transferred to the carboxy group and a neutral imidazolyl group is the acceptor for a hydrogen bond from the neutral carboxy group, and one in which the hydron other than the one in the hydrogen bond is on the carboxy group rather than the imidazolyl group and the neutral imidazolyl group is the donor in the hydrogen bond to the other, now acyl, oxygen of the carboxy group. When the hydrogen-bonded complex is the conjugate acid of a cationic imidazolio group and an anionic carboxylato group (Equation 4–134), its conjugate base is the hydrogen-bonded complex of a neutral imidazolyl group and a carboxylato group. At this level of ionization, when a hydron dissociates from the conjugate acid or associates with the conjugate base, the hydrogen bond remains intact and the complex remains an intact composite acid–base. Dissociation of a hydron from or association of a hydron with a composite acid–base, however, can disrupt the hydrogen bonding. For example, dissociation of a hydron from a composite acid between a neutral imidazolyl group and a carboxylato group would eliminate the hydrogen bond between them because there would no longer be a hydron between them with which a hydrogen bond could form.

The difference pH–rate profile in Figure 4–22B also shows that Aspartate 144 shifts the pK_a of yet another catalytic acid–base in the active site from 6.5 in its absence to 6.8 in its presence (inflection in the difference pH–rate profile around pH 6.7) while Histidine 108 shifts the pK_a of the same group from 6.9 to 6.8 (inflection in the difference pH–rate profile around pH 6.9). These effects are those that would be expected from an anion, the carboxylate of Aspartate 144, and a cation, the imidazolium of Histidine 108, which, on the basis of these observations, should be the tautomer of the composite acid–base present in the greatest concentration at this level of ionization (Equation 4–134).

In the case of ribonuclease T_1 from *A. oryzae*, the pH–rate profile for the specificity constant $k_{GpC,app}$ for transesterification of the dinucleotide guanylyl(3′-5′)cytidine (GpC) is governed by values of pK_a of 3.4, 3.4, 7.5, and 8.5 (Figure 4–22C).[219] The difference pH–rate profile for the mutant in which Histidine 40 in the active site[288] has been mutated to lysine demonstrates that Histidine 40 is responsible for the pK_a of 8.5. This observation is consistent with the cationic imidazolio group acting as a catalytic acid in the enzymatic reaction. In addition, Histidine 40 shifts the pK_a of another catalytic acid–base, probably the carboxy group of Glutamate 58, from 4.1 to 3.4 (inflection in the difference pH–rate profile around pH 3.8), as expected for a cationic imidazolium. It also seems, however, to shift the

pK_a of yet another catalytic acid–base from 7.1 to 7.5 (inflection in the difference pH–rate profile around pH 7.3), which cannot be explained as the effect of a cationic side chain. This shift can be explained, however, as the result of the new lysine that takes the place of Histidine 40 in the mutant. The ammonio group of this lysine could very well end up adjacent to Histidine 92 in the active site and shift its pK_a from 7.5 in the wild type to 7.1 in the mutant. The pK_a of Histidine 92 in the wild-type enzyme has been estimated by nuclear magnetic resonance spectroscopy to be 7.2.[219]

The difference pH–rate profile for the specificity constant k_{dpc} for 3′-dephosphocrotonyl-SCoA (dpc) for enoyl-CoA hydratase from *Rattus norvegicus*, in which Glutamate 144 has been mutated to glutamine, has an inflection below pH 7 resembling the inflection below pH 5 in the difference pH–rate profile for the mutant of ribonuclease T_1 (upper curve in Figure 4–22C), but this inflection does not begin to plateau as the pH is decreased as does the curve for the mutant of ribonuclease T_1.[289] It was concluded that the pK_a for a catalytic base, which was assigned as the pK_a for the carboxylato group of Glutamate 164 by examination of crystallographic molecular models, has a pK_a of less than 5 in the native enzyme and that its pK_a has shifted to a value of 6.8 in the mutant in which the carboxylato group of Glutamate 144 is missing. In other words, the carboxylato group of Glutamate 144 in the native enzyme causes the pK_a of that carboxy group of Glutamate 164 to shift from 6.8 to less than 5.

The proposal that the lysine inserted in place of Histidine 40 in the active site of ribonuclease T_1 shifts the pK_a of the carboxy group of Glutamate 58 is an example of the fact that the **identity of the amino acid that replaces the catalytic amino acid in the active site often has a significant effect** on the outcome of the site-directed mutation. For example, Tyrosine 146 in thymidylate synthase from *L. casei* was replaced in turn by 15 other amino acids,[245] and values of $k_0\,(K_{mTHF}K_{m,dU})^{-1}$ for the reactants 5,10-methylenetetrahydrofolate (THF) and deoxyuridine monophosphate (dU) decreased by various factors between 500 and 1.5×10^5, and the differences have no obvious explanation. When Histidine 238 in the active site of murine adenosine deaminase is replaced by glutamate, rate constant $k_0\,K_{m,Ad}^{-1}$, where $K_{m,Ad}$ is the Michaelis constant for adenosine (Ad), decreases 275,000-fold. When, however, Histidine 238 is replaced by arginine, the decrease in the steady-state rate constant $k_0\,K_{m,Ad}^{-1}$ is only a factor of 50.[290] Aspartate 326 in human creatine kinase is more than 0.7 nm away from any atom in the creatine or $MgATP^{2-}$ participating in the transfer of the phospho group between them.[291] When Aspartate 326 is replaced by glutamate, the steady-state rate constant $k_0\,K_{m,cycr}^{-1}$, where $K_{m,cycr}$ is the Michaelis constant for cyclocreatine (cycr), decreases by a factor of only 3, and when it is replaced by asparagine, $k_0\,K_{m,cycr}^{-1}$ decreases by a factor of only 7. When, however, Aspartate 326 is replaced by alanine, $k_0\,K_{m,cycr}^{-1}$ decreases by a factor of 200.[193] From the first two factors, the correct conclusion, that Aspartate 326 is not a catalytic acid–base, would be drawn, but the last factor of 200 is ambiguous. Consequently, a conclusion that an amino acid in the active site is a catalytic acid–base, based solely on the order of magnitude of the decrease in a kinetic constant upon its mutation, can be seen to be even more tenuous.

Tyrosine 16 forms a hydrogen bond with the carbonyl group at carbon 3 in the reactant estr-5(10)-ene-3,17-dione (ed), which is the carbonyl group α to the hydron removed during catalysis to form the enolate while estr-5(10)-ene-3,17-dione is in the active site of steroid Δ-isomerase from *P. putida*. When Tyrosine 16 is replaced by phenylalanine, the steady-state rate constant $k_0\,K_{m,ed}^{-1}$ decreases by a factor of 70,000. When, however, Tyrosine 16 is replaced by alanine, glycine, serine, or threonine, the decrease in the steady-state rate constant $k_0\,K_m^{-1}$ is only a factor of 280 ± 70.[290] In this case it seems that the phenylalanine precludes formation of a hydrogen bond to the carbonyl group by a molecule of water, while smaller replacements do not.

When Histidine 281 in the active site of benzoylformate decarboxylase from *P. putida* is replaced by alanine, the steady-state rate constant $k_0\,K_{m,bf}^{-1}$, where bf is the reactant benzoylformate, decreases 700-fold, which is on the borderline of suggesting that it is a catalytic acid–base in the enzymatic reaction. When, however, Histidine 281 is replaced by threonine, asparagine, tyrosine, glutamine, or tryptophan, the decrease in rate constant $k_0\,K_m^{-1}$ is less and less, and when it is replaced by phenylalanine, the decrease is only a factor of 10, which is insignificant.[292] One can conclude that Histidine 281 is not a catalytic acid–base in the enzymatic reaction, while the opposite conclusion might have been reached if only the substitution of alanine had been made.

The different mutants of benzoylformate decarboxylase just described were almost all cases in which an acid–base was replaced with a side chain that is not an acid base in the normal range of pH.

It is also possible, however, to **replace a catalytic acid–base with other side chains that are acid–bases** of different size and strength to assess their ability to assume the role of the normal catalytic side chain,[293] but conclusions drawn from these results, in the absence of crystallographic molecular models of the mutant active sites occupied by substrates or analogues of substrates, are ambiguous because of steric differences that accompany the differences in pK_a among the limited set of amino acids that are available to take the place of the one mutated.

In an enzyme in which a metallic hydroxide acts as a catalytic base, the **metallic cation can be mutated** by replacing it with another one, and the effect of that mutation on the pH–rate profile can identify the hydroxide on the metal as a catalytic acid–base responsible for one of the observed acid dissociation constants. For example, when the prosthetic metallic cation in the active site of human histone deacetylase is changed from the natural Zn^{2+} to Co^{2+}, a pK_a in the pH–rate profile, above which the specificity constant for a fluorescent unnatural reactant for the enzyme decreases, shifts from 9.1 to 10. This is the shift expected if zinc hydroxide (pK_a in water = 9.0) has been replaced by cobalt hydroxide (pK_a in water = 9.6).

A **reactant for the enzyme can also be mutated** to identify the role of a catalytic acid–base in the catalytic mechanism of an enzyme. For example, when hypoxanthine (**4–42**)

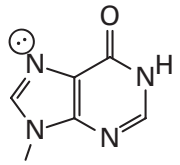

4–42

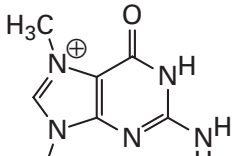

4–43

in a trinucleotide that is a reactant for human DNA-3-methyladenine glycosylase II was replaced with 7-methylguanine (**4–43**), the decrease in the pH–rate profile for the catalytic constant of the enzyme above a pK_a of 6.4 was no longer observed.[294] This result identified the side chain with this pK_a as a catalytic acid responsible for hydronating nitrogen 7 of the hypoxanthine to make it cationic and a better leaving group during hydrolysis of the N-glycosidic linkage. This hydronation is not necessary for nitrogen 7 in 7-methylguanine because it is methylated and already cationic.

Suggested Reading

Beebe, J. A., Arabshahi, A., Clifton, J. G., Ringe, D., Petsko, G. A., and Frey, P. A. (2003) Galactose mutarotase: pH Dependence of enzymatic mutarotation, *Biochemistry 42*, 4414–4420. https://doi.org/10.1021/bi020639a

Thoden, J. B., and Holden, H. M. (2002) High resolution X-ray structure of galactose mutarotase from *Lactococcus lactis*, *J. Biol. Chem. 277*, 20854–20861. https://doi.org/10.1074/jbc.M201415200

Problem 4–11: The following table lists the catalytic constants for human protein-tyrosine-phosphatase (WT) and a mutant of the enzyme in which Aspartate 92 has been changed to asparagine (D92N) for hydrolysis of 4-nitrophenyl phosphate as a function of pH.[295]

pH	$k_{0WT,app}$ (s^{-1})	pH	$k_{0A92N,app}$ (s^{-1})
4.50	0.60	4.80	0.018
4.55	0.82	4.90	0.027
4.55	1.34	5.00	0.034
4.75	2.64	5.25	0.042
5.00	3.17	5.50	0.054
5.25	4.24	6.00	0.058
5.50	5.26	6.40	0.056
5.55	4.51	7.00	0.061
6.00	5.18	7.50	0.062
6.40	5.42	7.70	0.056
7.00	3.70	8.50	0.061
7.50	2.13	9.00	0.053
8.00	0.84		
9.00	0.12		

(A) Plot the common logarithm of k_0 as a function of pH for the wild type and the mutant.
(B) Draw asymptotes and estimate values of pK_a governing these two pH–rate profiles.
(C) Plot the difference between these two pH–rate profiles.
(D) Which pK_a is that of Aspartate 92?

Kinetic Isotope Effects

Reactions in which a **hydron, hydrogen atom, or hydride is transferred in a rate-affecting step** proceed more slowly when the protium on the reactant is replaced by deuterium. For example, removal of deuterium (^{2}H) as a deuteron from 4-(4-nitrophenoxy)-[3,3-$^2H_2$]butan-2-one by phenoxide anion acting as a general base in aqueous solution

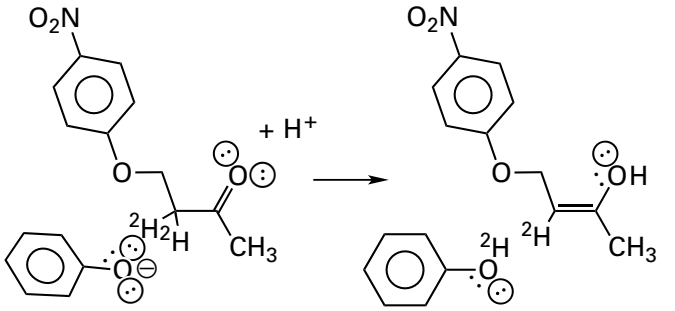

(4–174)

occurs 6.1 times more slowly than removal of that hydrogen as a proton from the same position by the same base.[296] This decrease in rate produced by replacing protium with deuterium is an example of a kinetic isotope effect.

A kinetic isotope effect is a change in a rate constant produced by substitution of the isotope of one or more atoms in a reactant for another isotope. A **primary kinetic isotope effect** is a kinetic isotope effect for a reaction in which the bond between the one atom that has been isotopically substituted and an atom to which it is covalently attached is broken or in which such a bond is formed. A **primary deuterium kinetic isotope effect** is a primary kinetic isotope effect produced by substitution of a deuterium for a protium in a reactant. Undeuterated reactant has a hydrogen at the substituted position, but since the relative natural abundance of deuterium is 0.0156%, the vast majority of hydrogen is protium, so substitution of a hydrogen at natural abundance by a deuterium is essentially substitution of protium with deuterium.

If a step in the mechanism of a reaction is **rate-affecting**, an increase or decrease in its forward rate constant, its rate constant in reverse, or both of them will cause a change in an observed rate constant of the overall reaction, but this change will not necessarily be of the same magnitude as the increase or decrease in the microscopic rates of that rate-affecting step. Because of the definition of a rate-limiting step,[297] a rate-affecting step must be or must precede the rate-limiting step in a reaction.

The appearance of a **primary deuterium kinetic isotope effect for a rate constant of an enzymatic reaction** provides experimental evidence that removal of the hydrogen that has been substituted, as either a hydron, hydrogen atom, or hydride, from the reactant is a step in the enzymatic reaction and that the step is a rate-affecting step.

The **hydron** at carbon 6 in 5-*O*-(1-carboxyvinyl)-3-phosphoshikimate is removed by nitrogen 5 of the prosthetic flavin[298] in the active site of chorismate synthase from *Neurospora crassa* during the elimination catalyzed by the enzyme. When the protium at the *pro-R* position on carbon 6 is replaced synthetically by deuterium, the catalytic constant of the enzyme for deuterated reactant

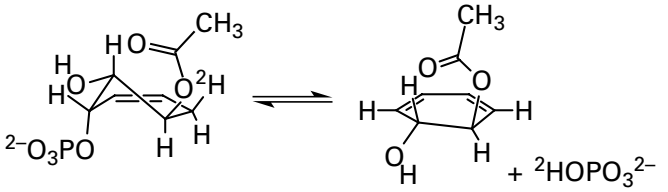

(4–175)

is 2.7 ± 0.2 times smaller than it is for undeuterated reactant, and the specificity constant k_{CPS} for the synthetic (6*R*)-[6-^{2}H]-5-*O*-(1-carboxyvinyl)-3-phosphoshikimate (CPS) is 1.6 ± 0.1 times smaller.[299]

A **hydrogen atom** is removed from the methyl group of toluene by a glycyl radical in the active site of benzylsuccinate synthase from *Thauera aromatica* before addition of the resulting benzyl radical to the double bond of fumarate to produce benzylsuccinate. When perdeuterated toluene is used as a reactant, the catalytic constant of the enzyme is 1.7 ± 0.2 times smaller than when undeuterated toluene (tol) is used as a reactant, and the specificity constant k_{tol} is 2.9 ± 0.1 times smaller.[300]

A **hydride** is transferred from the 4*S* position of reduced thionicotinamide-adenine dinucleotide phosphate to an oxidized flavin adenine dinucleotide in the active site of trypanothione-disulfide reductase from *Trypanosoma congolense*. When reduced (4*S*)-[4-^{2}H]thionicotinamide-adenine dinucleotide phosphate is used as a reactant, the catalytic constant of the enzyme is 4.7 ± 1.0 times smaller than when reduced, undeuterated 3-thionicotinamide-adenine dinucleotide phosphate (tNADPH) is used as a reactant, and the specificity constant k_{tNADPH} is 6.9 ± 0.9 times smaller.[301]

The **deuterium kinetic isotope effect**, ${}^{D}k_i$, on a particular rate constant, k_i, is the ratio between the rate constant for undeuterated reactant, $k_{i\mathrm{H}}$, and the rate constant for the deuterated reactant, $k_{i\mathrm{D}}$

$$ {}^{\mathrm{D}}k_i \equiv \frac{k_{i\mathrm{H}}}{k_{i\mathrm{D}}} \qquad (4\text{–}176) $$

For example, the primary deuterium kinetic isotope effect[299] on the catalytic constant, ${}^{D}k_0$, of chorismate synthase (Equation 4–175) from *N, crassa* for replacement of the *pro-R* hydrogen at carbon 6 in 5-*O*-(1-carboxyvinyl)-3-phosphoshikimate with deuterium is 2.7 ± 0.2.

In the case of the reaction catalyzed by trypanothione-disulfide reductase, the existence of the significant primary deuterium kinetic isotope effects is evidence that the transfer of an actual hydride between the nicotinamide and the flavin is occurring in this enzymatic reaction rather than consecutive transfers of an electron, a hydron, and an electron. In many of the **reactions catalyzed by flavoenzymes** that have NADH or NADPH as substrates, there are significant, often quite large, primary deuterium kinetic isotope effects more consistent with the transfer of a hydride between NADH or NADPH and oxidized flavin than two successive single electron transfers.

If **two hydrogens are removed from the reactant** by the active site, the primary deuterium kinetic isotope effect is usually greater for the reactant in which these two hydrogens are replaced by deuterium than for the two respective reactants in which only one is replaced.[302] For example, in the reduction catalyzed by human dihydroorotate dehydrogenase (quinone)

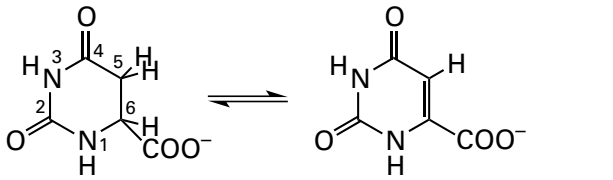

(4–177)

where flavin is a prosthetic flavin mononucleotide in the active site, the primary deuterium kinetic isotope effect on the rate constant for reduction of flavin at saturating dihydroorotate is 4.2 ± 0.1 for [5,5-$^2H_2$]-(*S*)-dihydroorotate, 3.8 ± 0.1 for [6-^{2}H]-(*S*)-dihydroorotate, and 8.0 ± 0.2 for [5,5,6-$^2H_3$]-(*S*)-dihydroorotate.[303] In the reaction catalyzed by histidinol dehydrogenase from *Salmonella typhimurium*

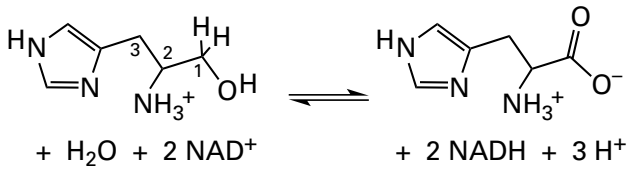

(4–178)

the two hydrides are removed from carbon 1 of the histidinol in two distinct steps that are separated from each other by dissociation of the NADH formed in the first oxidation and association of NAD^+ for the second oxidation. It has been observed that, at pH 6.7, the primary deuterium kinetic isotope effect on the catalytic constant for (1*S*)-[1-^{2}H]histidinol is 1.6 ± 0.1, that for (1*R*)-[1-^{2}H]histidinol is 1.5 ± 0.1, and that for [1,1,-$^2H_2$]histidinol is 2.0 ± 0.2. These observations demonstrate that each of these two steps, in which one of the two hydrides is transferred, is a rate-affecting step in the overall enzymatic reaction.[304]

Kinetic isotope effects can also be used to provide **evidence for removal of a hydrogen** in an enzymatic mechanism even though that hydrogen ends up occupying the same position in the respective product. For example, substitution of a hydrogen with deuterium at carbon 5 on D-glucose 6-phosphate produced a deuterium kinetic isotope effect of 1.5 on the rate of the reaction catalyzed by inositol-3-phosphate synthase

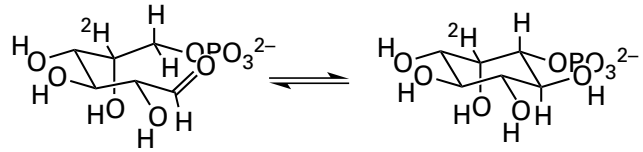

(4–179)

from *R. norvegicus*. This isotope effect was used as evidence that this hydrogen is removed in one rate-affecting step of the enzymatic reaction even though it remains at the same location in the product of the overall reaction.[305]

In the isomerization catalyzed by tRNA pseudouridine[55] synthase

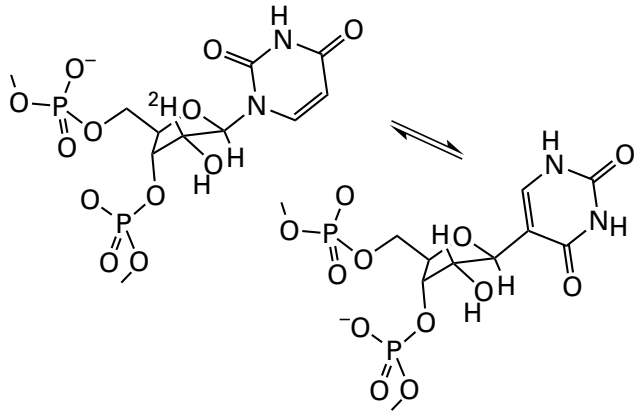

(4–180)

from *E. coli*, the hydrogen on carbon 2′ of uridine seems to be uninvolved. Nevertheless, when it is replaced with a deuterium, the deuterium kinetic isotope effect on the specificity constant, k_U, for a uridine (U) in the proper position in a polyribonucleotide that is a reactant for the enzyme is 3.6. This value is so large that it must be a primary deuterium kinetic isotope effect, and the hydrogen at carbon 2′ must be removed by a base in the active site during the isomerization.[306] The conclusion drawn from this observation is that, following dissociation of the anionic eneimide that is the leaving group and that is the conjugate base at nitrogen 1 of the uracil ($pK_a = 9.5$), the resulting oxocarbenium ion of the ribose, which is quite unstable, is stabilized as the neutral enol ether by removal of the now-acidic hydron from carbon 2′ until the eneimide of the uracil can rotate to the proper orientation so that carbon 5 of the eneimide, which is also nucleophilic, rather than nitrogen 1 can add to carbon 1′ of the ribose. Consequently, addition of carbon 5 as a nucleophile should be a simple addition to the double bond between carbons 1′ and 2′ of the enol ether either before, after, or coincident with readdition of the hydron to carbon 2′.

α-Galactosidase MelA from *Citrobacter freundii* catalyzes the hydrolysis of α-galactosides, which appears to be simply a dissociative nucleophilic substitution with an oxocarbenium ion as an intermediate. When either phenyl α-D-[2-^{2}H]galactopyranoside or phenyl α-D-[3-^{2}H]galactopyranoside is used as a reactant, however, the deuterium kinetic isotope effects on the respective specificity constants for these galactosides were both 1.74.[307,308] These isotope effects are again too large to be secondary or tertiary kinetic isotope effects and must be primary deuterium kinetic isotope effects. These deuterium kinetic isotope effects, and the fact that there is a prosthetic NAD^+ in the active site of the enzyme, led to two conclusions: first, that the NAD^+ removes the hydride from carbon 3 of D-galactose, and second, that the enol formed by removal of a hydron from carbon 2 by a catalytic base permits β-elimination of the phenolate rather than a nucleophilic substitution like the one in the active site of lysozyme.

Another conclusion that can be drawn from a primary deuterium kinetic isotope effect is that **the chemical mechanism of an enzymatic mechanism is the same as the chemical mechanism of the reaction in solution.** For example, strictosidine synthase from *Rauvolfia serpentina* catalyzes intramolecular addition to carbon 2 of the indolyl group of an electrophilic iminium in the adduct between tryptamine and an aldehyde, followed by rearomatization of the indolyl group

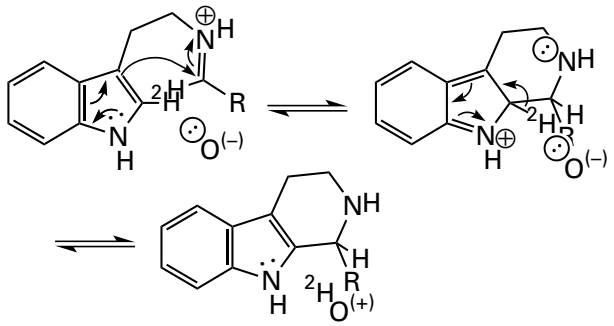

(4–181)

When the protium on carbon 2 of the indolyl group of the tryptamine is replaced by deuterium, the primary deuterium kinetic isotope effect (2.7 ± 0.1) on the catalytic constant of the enzymatic reaction is indistinguishable from the primary deuterium kinetic isotope effect (2.0–2.6) for the same substitution in the nonenzymatic electrophilic aromatic substitution.[309] It was concluded that the chemical mechanism on the active site was the same as that in solution, a Pictet–Spengler electrophilic aromatic substitution, the mechanism for which has been extensively studied.[310] The fact that the deuterium isotope effect results from substitution of the hydrogen on carbon 2 requires that, in both the enzymatic reaction and the reaction in solution, the rearomatization of the adduct between iminium and the indolyl group be at least rate-affecting if not rate-limiting. Consequently, this specific substitution has focused attention on this particular step in the mechanism. In solution, the intramolecular electrophilic aromatic substitution is catalyzed by acetate as a general base, so it was also concluded that there should be a catalytic base in the active site

responsible for accepting the hydron during the rearomatization in the active site.

Tritium kinetic isotope effects are also observed in enzymatic reactions. A **tritium kinetic isotope effect** is a kinetic isotope effect produced by substitution of a tritium (T) for a protium in a reactant. For example, the tritium kinetic isotope effect, ${}^{T}k_{DA}$, for the specificity constant, k_{DA}, for [2-^{3}H]-D-alanine (DA) when it is oxidized to pyruvate by porcine D-amino-acid oxidase is 12.6 ± 0.1.[311]

Deuterium or tritium can be substituted synthetically for a hydrogen on carbon, on hydrogen, or on phosphorus,[312] and it can be expected to remain on that carbon, hydrogen, or phosphorus long enough to perform an experiment. Deuterons or tritons on sulfur, oxygen, or nitrogen, however, exchange rapidly with the hydrons of the water. If deuterium oxide is used in place of water to ensure that deuterium is present on a particular oxygen, nitrogen, or sulfur, then all the oxygens, nitrogens, and sulfurs accessible to the solution will have their hydrogens replaced with deuterium. Because it is not possible to confine deuterium to just one oxygen, nitrogen, or sulfur in either a reactant or the enzyme itself, and because enzymes having molecular hydrogen or phosphites[312,313] as their substrates are rare, almost all hydrogen kinetic isotope effects reported in studies of enzymes are primary deuterium or tritium kinetic isotope effects produced by **synthetic or enzymatic replacement of a hydrogen on a carbon in a reactant by deuterium or tritium**, respectively.

Again, as always, a distinction should be made between observation and explanation. The explanation for an observed primary deuterium isotope effect on one of the steady-state rate constants follows from **the kinetic mechanism chosen for the reaction by the investigator**. If the kinetic mechanism, which is the product of his intuition, is wrong, even though it is consistent with all the observations, the conclusions drawn from the explanation of the observed primary deuterium isotope effect may be mistaken.

An enzymatic reaction always consists of three or more microscopic steps, each, by definition, with its own distinct transition state. To obtain information beyond the fact that dissociation of the bond between a particular carbon and its hydrogen does or does not occur in a rate-affecting step in an enzymatic reaction, the deuterium or tritium kinetic isotope effect on the microscopic rate constant for the step in which that carbon–hydrogen bond dissociates must be measured directly or extracted from the steady-state rate constants. A primary kinetic isotope effect is the kinetic isotope effect on a steady-state rate constant for an enzymatic reaction during which the bond between the atom that has been isotopically substituted and an atom to which it is covalently attached is broken. An **intrinsic kinetic isotope effect** is the kinetic isotope effect on the microscopic rate constant for a specific step in an enzymatically catalyzed reaction, not necessarily a step in which the bond at which the substitution has taken place is broken. An **intrinsic, primary deuterium kinetic isotope effect** is the deuterium kinetic isotope effect on a microscopic rate constant for the specific step in an enzymatic reaction in which the bond is broken between another atom and a hydrogen that has been isotopically substituted with deuterium.

Usually, rate constants for several rate-affecting microscopic steps in the kinetic mechanism of an enzymatic reaction contribute to the observed steady-state rate constants, such as the catalytic constant and the specificity constants. Usually, however, **only one of these microscopic steps can display intrinsic, primary deuterium kinetic isotope effects** on its forward reaction and its reaction in reverse. This microscopic step is the one in which the bond between the carbon and the hydrogen that is isotopically substituted is broken or re-formed, respectively. It necessarily follows that the observed primary deuterium kinetic isotope effect on any one of the steady-state rate constants for the enzymatic reaction is less than the intrinsic, primary deuterium kinetic isotope effects for the step in which hydrogen is actually transferred.

For a particular kinetic mechanism, the observed primary deuterium kinetic isotope effect on one steady-state rate constant is the consequence of the intrinsic, primary deuterium kinetic isotope effect on the microscopic rate constants for the step in the kinetic mechanism in which a bond between the hydrogen that is isotopically substituted and another atom is broken. Because, for hydrogen, such a bond is always broken during the transfer of hydrogen from one atom to another atom and because this transfer is usually reversible in the kinetic mechanism of an enzyme, a bond between the isotopically substituted hydrogen and another atom is **broken in both directions of a particular microscopic step** in which the transfer of that hydrogen occurs. Consequently, each of the two rate constants, forward and reverse, for the step in which hydrogen is transferred exhibits an intrinsic, primary deuterium kinetic isotope effect. These two

intrinsic, primary deuterium kinetic isotope effects, however, do not have to be equal. If they differ, then there must also be a deuterium isotope effect on the equilibrium constant for that microscopic step, which is the ratio of the two rate constants, forward and reverse.

The first step in attempting to formulate an **explanation of the observed primary deuterium kinetic isotope effect** on one steady-state rate constant by dissecting the kinetics of the enzymatic reaction into its components is to examine the ratio between the definition of that steady-state rate constant when the microscopic rate constants, forward and reverse, for the step in which hydrogen is transferred are those for the carbon–hydrogen bond and the definition of that steady-state rate constant when the microscopic rate constants for that same step are for the carbon–deuterium bond. For example, for the kinetic mechanism (previously Equation 3–109)

$$\begin{aligned} E + A + B &\underset{k_{-1}}{\overset{k_1}{\rightleftharpoons}} E{\cdot}A + B \underset{k_{-2}}{\overset{k_2}{\rightleftharpoons}} E{\cdot}A{\cdot}B \underset{k_{-3}}{\overset{k_3}{\rightleftharpoons}} \\ E{\cdot}Z{\cdot}Y &\xrightarrow{k_4} E{\cdot}Z + Y \xrightarrow{k_5} E + Y + Z \end{aligned} \tag{4–182}$$

the steady-state rate constants are (previously Equations 3–117 through 3–120)

$$k_0 = \frac{k_3k_4k_5}{k_3k_4 + k_3k_5 + k_{-3}k_5 + k_4k_5} \tag{4–183}$$

$$k_B = \frac{k_2k_3k_4}{k_{-2}k_{-3} + k_{-2}k_4 + k_3k_4} \tag{4–184}$$

$$k_A = k_1 \tag{4–185}$$

and

$$k_{AB} = \frac{k_1k_2k_3k_4}{k_{-1}(k_{-2}k_{-3} + k_{-2}k_4 + k_3k_4)} \tag{4–186}$$

If the microscopic step governed by k_3 and k_{-3} is the step in which hydrogen that is isotopically substituted is transferred, then

$$^{D}k_0 \equiv \frac{k_{0,H}}{k_{0,D}} = \frac{(k_{3D}k_4 + k_{3D}k_5 + k_{-3D}k_5 + k_4k_5)k_{3H}}{(k_{3H}k_4 + k_{3H}k_5 + k_{-3H}k_5 + k_4k_5)k_{3D}} \tag{4–187}$$

$$^{D}k_B \equiv \frac{k_{B,H}}{k_{B,D}} = \frac{(k_{-2}k_{-3D} + k_{-2}k_4 + k_{3D}k_4)k_{3H}}{(k_{-2}k_{-3H} + k_{-2}k_4 + k_{3H}k_4)k_{3D}} \tag{4–188}$$

and

$$^{D}k_{AB} \equiv \frac{k_{AB,H}}{k_{AB,D}} = {}^{D}k_B \tag{4–189}$$

where k_{3H} and k_{-3H} and k_{3D} and k_{-3D} are the microscopic rate constants for undeuterated substrate and deuterated substrate, respectively.

These **ratios defining the primary deuterium kinetic isotope effect on the steady-state rate constants based on the chosen kinetic mechanism** can be useful in dissecting the relative magnitudes of the microscopic rate constants in a kinetic mechanism. For example, a kinetic mechanism consistent with all the steady-state kinetic observations for peptidylglycine monooxygenase from *R. norvegicus* is

$$\begin{aligned} E + HA + O_2 &\underset{k_{-1}}{\overset{k_1}{\rightleftharpoons}} E{\cdot}HA + O_2 \underset{k_{-2}}{\overset{k_2}{\rightleftharpoons}} \\ E{\cdot}HA{\cdot}O_2 &\xrightarrow{k_3} E{\cdot}HAOH \xrightarrow{k_4} E + HAOH \end{aligned} \tag{4–190}$$

where HA is hippurate (benzoylglycine)

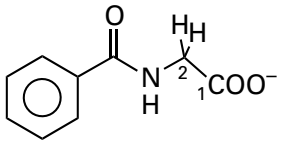

4–44

an analogue of a peptide with a carboxy-terminal glycine, and HAOH is the product of the hydroxylation, (*S*)-2-hydroxyhippurate. For this kinetic mechanism, the primary deuterium kinetic isotope effect on the specificity constant k_{HA} for [2,2-$^2H_2$]hippurate, at any concentration of oxygen, should be

$$^{D}k_{HA} = \frac{^{D}k_3k_{-1}k_{-2} + k_{3H}(k_{-1} + k_2[O_2])}{k_{-1}k_{-2} + k_{3H}(k_{-1} + k_2[O_2])} \tag{4–191}$$

where ${}^{D}k_3$ is the intrinsic, primary deuterium kinetic isotope effect for removal of hydrogen from the glycyl group of hippurate. The fact that the concentration of O_2 had no effect within experimental error on the observed primary deuterium kinetic isotope effect for the specificity constant ${}^{D}k_{HA}$ (4.8) led to the conclusions that $k_{-1} > k_2[O_2]$ and that the first step in the enzymatic reaction, the binding of hippurate, is at equilibrium in the range of concentrations of O_2 examined.[314] If this conclusion is correct, if the kinetic mechanism chosen is correct, and if $k_{-2} > k_{3H}$, which seems likely considering how small a molecule of O_2 is, then ${}^{D}k_3 = 4.8$. Even if all these assumptions are correct, this assignment could still be incorrect if the kinetic mechanism that has been chosen by the investigators is incorrect.

Taking the ratios of the definitions of the observed steady-state rate constants derived from the chosen kinetic mechanism is a simple and unambiguous way to interpret the degree to which an intrinsic, primary isotope effect could manifest itself in the primary deuterium kinetic isotope effect on these rate constants. As with the effects of pH on the kinetics of an enzymatic reaction, however, the interpretation of a primary deuterium kinetic isotope effect is most straightforward if the step in the mechanism in which hydrogen is transferred can be studied directly. For example, when a high molar concentration of bovine primary-amine oxidase, in the oxidized form, was mixed with a high concentration of the reactant dopamine, the transfer of hydride from the dopamine to the prosthetic 2,4,5-trihydroxyphenylalanylquinone (previously **2–156**)

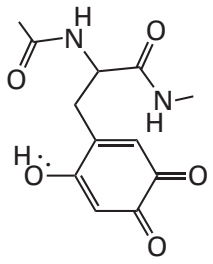

4–45

on the protein[315] could be followed directly by the change in absorbance that occurs during the transfer.[316] The rate of the reaction was extrapolated to saturation with dopamine to eliminate the contributions of the rate of association of dopamine with the active site. The deuterium kinetic isotope effect upon the rate of reduction of 2,4,5-trihydroxyphenylalanylquinone observed when [1,1-$^2H_2$]dopamine was used as reactant was 13. In the mechanism usually written for this reaction, the hydrogen in question is removed as a hydron by a catalytic base within the active site,[315] and the observed kinetic isotope effect is assumed to be the intrinsic, primary deuterium kinetic isotope effect for this step. When the specificity constant k_{DAm} for [1,1-$^2H_2$]dopamine (DAm) was assessed, the primary deuterium kinetic isotope effect was only 6. When the same experiments, however, were performed with another reactant, [1,1-$^2H_2$]benzylamine,[317] the intrinsic, primary deuterium kinetic isotope effect observed directly (13) was the same as the primary deuterium kinetic isotope effect (12) on the specificity constant k_{BAm} for benzylamine (BAm).

The effect of an intrinsic kinetic isotope effect on the steady-state rate constants can also be defined in terms of the commitment forward and the commitment in reverse. Consider an enzymatic reaction that proceeds through a series of steps that occur in a linear, unbranched order, for example

$$\begin{array}{l} E_1 \underset{k_{-1}}{\overset{k_1[A]_0}{\rightleftharpoons}} E_2 \underset{k_{-2}}{\overset{k_2[B]_0}{\rightleftharpoons}} E_3 \underset{k_{-3}}{\overset{k_3}{\rightleftharpoons}} E_4 \underset{k_{-4}}{\overset{k_4}{\rightleftharpoons}} \\ \qquad\qquad E_5 \underset{k_{-5}}{\overset{k_5}{\rightleftharpoons}} E_6 \underset{k_{-6}[Y]_0}{\overset{k_6}{\rightleftharpoons}} E_7 \underset{k_{-7}[Z]_0}{\overset{k_7}{\rightleftharpoons}} E_1 \end{array} \qquad (4\text{–}192)$$

If neither product Y nor product Z is present and the initial rates are being measured, the conversion of E_6 to E_7 is irreversible. If the reactant that is isotopically substituted is reactant B, if the step at which the carbon–hydrogen bond is broken is the step governed by rate constants k_4 and k_{-4}, if reactant A is present at saturation, and if all forms of the enzyme are in steady state, then Equation 4–192 can be rewritten as

$$E_2 \underset{k_{-23}}{\overset{k_{23}[B]_0}{\rightleftharpoons}} E_4 \underset{k_{-4}}{\overset{k_4}{\rightleftharpoons}} E_5 \xrightarrow{k_{56}} E_7 \xrightarrow{k_7} E_2 \qquad (4\text{–}193)$$

where the composite rate constants are defined as

$$k_{23} = \frac{k_2 k_3}{k_{-2} + k_3} \qquad (4\text{–}194)$$

$$k_{-23} = \frac{k_{-2} k_{-3}}{k_{-2} + k_3} \qquad (4\text{–}195)$$

and

$$k_{56} = \frac{k_5 k_6}{k_{-5} + k_6} \tag{4–196}$$

Suppose that the step in a linear unbranched kinetic mechanism in which an isotopically substituted hydrogen is transferred is step i, the step governed by rate constants k_i and k_{-i}. The **commitment forward**, c_f, is the ratio[318] between the forward elementary rate constant ($k_{i\mathrm{H}}$) for step i when the reactant is not deuterated and the composite rate constant k_{ri} for reversal of the reaction from the form of the enzyme immediately preceding this step, E_i, to the point at which the reactant that is isotopically substituted has been released back into the solution. For example, for the mechanism of Equation 4–192

$$c_f \equiv \frac{k_{i\mathrm{H}}}{k_{ri}} = \frac{k_{4\mathrm{H}}}{k_{-23}} = \frac{k_{4\mathrm{H}}(k_{-2} + k_3)}{k_{-2}k_{-3}} \tag{4–197}$$

The **commitment in reverse**, c_r, is defined as the ratio between the reverse elementary rate constant ($k_{-i\mathrm{H}}$) for step i and the composite rate constant k_{fi} for forward flux from the form of the enzyme immediately following this step, E_{i+1}, through the first kinetically irreversible step in the mechanism. For example, for the mechanism of Equation 4–192

$$c_r \equiv \frac{k_{-i\mathrm{H}}}{k_{fi}} = \frac{k_{-4\mathrm{H}}}{k_{56}} = \frac{k_{-4\mathrm{H}}(k_{-5} + k_6)}{k_5 k_6} \tag{4–198}$$

Many kinetic mechanisms for enzymatic reactions, no matter how complex, can be rewritten in the form of the kinetic mechanism in Equation 4–109 by using composite rate constants. Once this conversion has been done, all the mechanisms become formally equivalent, and the definitions of the two commitments become the same as Equations 4–197 and 4–198.

It can be shown[318,319] that, for any linear, unbranched kinetic mechanism, if the reactant that is deuterated is reactant B and if substitution of a hydrogen by a deuterium affects rates of only step i, then the **primary deuterium kinetic isotope effect on the specificity constant** k_B for reactant B

$${}^{D}k_B \equiv \frac{k_{BH}}{k_{BD}} = \frac{{}^{D}k_i + c_f + c_r({}^{D}K_{eqi})}{1 + c_f + c_r} \tag{4–199}$$

where ${}^{D}k_i$ is the intrinsic, primary deuterium kinetic isotope effect ($k_{i\mathrm{H}}\ k_{i\mathrm{D}}^{-1}$) for the forward reaction of step i and ${}^{D}K_{eqi}$ is the primary equilibrium isotope effect for that same step

$${}^{D}K_{eqi} \equiv \frac{K_{eqi\mathrm{H}}}{K_{eqi\mathrm{D}}} = \frac{[E_{i+1,\mathrm{H}}]_{eq}\,[E_{i,\mathrm{D}}]_{eq}}{[E_{i,\mathrm{H}}]_{eq}\,[E_{i+1,\mathrm{D}}]_{eq}} = \frac{k_{i\mathrm{H}}k_{-i\mathrm{D}}}{k_{-i\mathrm{H}}k_{i\mathrm{D}}} \tag{4–200}$$

where $E_{i,\mathrm{H}}$ and $E_{i+1,\mathrm{H}}$ are the respective forms of the enzyme with protiated reactant and protiated catalytic acid, respectively, and $E_{i,\mathrm{D}}$ and $E_{i+1,\mathrm{D}}$ are forms of the enzyme with deuterated reactant and deuterated catalytic acid, respectively. The same equation should hold for any isotopic substitution, either in the reactant or in the enzyme itself, that affects the rate constants, forward and reverse, for only one step in the kinetic mechanism. This equation applies because the derivation deals only with the elementary rate constants for the mechanism, not with the identity of the isotopic substitution that causes the change in the two elementary rate constants and not with whether or not a bond to the substituted element is broken and re-formed, respectively, in the step governed by those rate constants.

A **primary equilibrium isotope effect** is the effect substitution of one isotope for another isotope at a particular atom that is transferred during a reaction has on the equilibrium constant for that reaction. The **primary deuterium equilibrium isotope effect** that results when a protium is substituted by deuterium depends upon the stability of the σ bond between product and deuterium relative to the stability of the σ bond between product and protium and the stability of the σ bond between reactant and deuterium relative to the stability of the σ bond between reactant and protium.

The difference in the stabilities of a carbon–protium bond and a carbon–deuterium bond, or in the stabilities of a bond between another atom and a protium and a bond between that atom and a deuterium, can be estimated from vibrational frequencies in infrared spectra. These estimates are tabulated as fractionation factors.[320,321] **Fractionation factors** are theoretically calculated primary equilibrium isotope effects for transfer of a hydrogen from a particular position in a particular molecule to a reference molecule such as acetylene (carbon to carbon) or water (carbon to oxygen).

An estimate of a particular equilibrium primary isotope effect is made by dividing the fractionation factor for the hydrogen in the reactant by the frac-

tionation factor for the hydrogen in the product. For example, the estimated equilibrium primary isotope effect for transfer of a hydrogen from acetone to hydroxide to form the enolate and water should be 0.93, given the tabulated fractionation factors (relative to acetylene) of 1.432 and 1.539 for acetone and water, respectively. Primary deuterium equilibrium isotope effects vary from 0.8 to 1.2 for transfer of a deuterium from carbon to a carboxylic acid or an amine, from 2.0 to 2.5 for transfer from carbon to a sulfanyl group, and from 0.7 to 1.5 for transfer between two carbons.

For a linear, unbranched mechanism such as that in Equation 4–192, the **primary deuterium kinetic isotope effect on the catalytic constant**, k_0, of the enzyme can be expressed in a form similar to that in Equation 4–199

$$^{D}k_0 \equiv \frac{k_{0,H}}{k_{0,D}} = \frac{^{D}k_i + \alpha_0 + c_r(^{D}K_{eqi})}{1 + \alpha_0 + c_r} \qquad (4–201)$$

where $^{D}k_i$, K_{eqi}, and c_r are the same as they are in Equation 4–199. The ratio α_0, however, is not a commitment but a ratio of rate constants

$$\alpha_0 = \frac{k_{iH}}{\{k_{(i-1)} + k_{-(i-1)}\}\alpha_{i-1}} \qquad (4–202)$$

where k_{iH} is the forward rate constant for step i when the reactant is protiated and the term $\{k_{i-1} + k_{-(i-1)}\}$ is the rate constant for the approach to equilibrium of the step preceding the step in which the intrinsic, primary isotope effect is exerted. The term α_{i-1} is a fraction determined by the mechanism chosen for the reaction. It is the quotient of the steady-state concentration of E_{i-1}, the form of the enzyme preceding E_i, divided by the sum of the concentrations of all forms of the enzyme other than E_i. This quotient is for the situation in which all reactants are at saturation. In estimating the value for α_{i-1}, the step preceding the step in which the isotopically substituted hydrogen is transferred, step $i-1$, is considered to be irreversible with a rate constant of $k_{(i-1)}$. Taken together, the denominator in Equation 4–202 is a measure of the rate at which E_i is regenerated from E_{i+1} in the forward direction.

The accepted kinetic mechanism of D-xylose reductase

$$NADH + H^+ + \text{D-xylose} \rightleftharpoons \text{xylitol} + NAD^+ \qquad (4–203)$$

from *S. cerevisiae* has seven consecutive, unbranched steps. Values for all 14 of the individual rate constants in this kinetic mechanism, forward and reverse, have been determined,[322] and the intrinsic, primary deuterium kinetic isotope effect (6.5) on the step in which hydrogen is transferred from [5-^{2}H]NADH to D-xylose has been determined independently of the steady-state kinetics.[323] The appropriate microscopic rate constants were used to calculate the commitment forward (3.1) and the ratio α_0 (10.6). The value calculated for the commitment in reverse (0.00004), even though it must have a value other than 0, is not significantly different from 0 and, in any case, is too small to affect the observed kinetic isotope effect (see Equation 4–201). All these numerical values and an estimate from fractionation factors of $^{D}K_{eq}$ for the transfer of hydrogen were used to calculate the expected observed primary deuterium kinetic isotope effect (Equation 4–201) on the catalytic constant $^{D}k_0$ (1.5) and the observed primary kinetic isotope effect (Equation 4–199) on the specificity constant $^{D}k_{xyl}$ (2.3) for xylose (xyl). These estimates agreed with observed values (1.55 ± 0.1 and 2.1 ± 0.3, respectively) for these kinetic isotope effects. This agreement between calculated and observed primary deuterium kinetic isotope effects was presented as one piece of evidence that the individual rate constants determined for the kinetic mechanism, the calculated intrinsic, primary deuterium kinetic isotope effect, and the kinetic mechanism itself were correct. In this instance, rather than gaining insight into the step in the mechanism in which hydrogen is transferred, the primary deuterium kinetic isotopic effects were used to validate a particular kinetic mechanism.

Another reason for expressing a kinetic isotope effect in terms of the commitment forward c_f and the commitment in reverse c_r and the ratio α_0, rather than a simple ratio of definitions of the steady-state rate constants, is to understand **what causes the kinetic isotope effect on a steady-state rate constant to be less than the intrinsic kinetic isotope effect** for the microscopic step in which the isotopically substituted bond is broken. The fraction of the intrinsic, primary deuterium isotope effect on step i, $^{D}k_i$, that is seen in the observed kinetic isotope effect on the specificity constant, $^{D}k_B$, for reactant B will depend on the magnitudes of c_f and c_r, respectively (Equation 4–199).

If c_f is large so that E_i is almost always converted to E_{i+1} without significant reversal from E_i to reactant free in solution, then almost every molecule of reactant that associates with the enzyme is converted to product, regardless of whether it is proteated or deuterated. Because those isotope effects on association of substrates with an active site that have been measured are small,[324,325] it is usually assumed that they are negligible. If this assumption is correct, there is no discrimination between substituted and unsubstituted reactant at the step of association, and there are no kinetic isotope effects on the steady-state rate constants for the overall reaction.

If c_r is large so that E_{i+1} often reverses to E_i before the first product is released, and c_f is small so that E_i often reverses to release reactant B, then both reactant and product come to equilibrium on the active site and association of the reactant also comes to equilibrium. Under these conditions, the kinetic isotope effect observed for the specificity constant for isotopically substituted reactant will be the equilibrium isotope effect of only the affected step, and this isotope effect can be less than 1 or greater than 1.

The full intrinsic kinetic isotope effect will be seen on the kinetic isotope effect for the specificity constant only if two conditions apply. First, the commitment forward c_f is small because the form of the enzyme immediately preceding the step in which the intrinsic kinetic isotope effect occurs is in equilibrium with free reactant. Second, the commitment in reverse c_r is small either because the chemical step is kinetically irreversible or because once the product of that step is formed, it immediately dissociates as free product. Under these conditions, the rate-limiting step in the reaction, which is the only significant rate-affecting step, is the step in which the full instrinsic kinetic isotope effect occurs, and the observed isotope effect on the specificity constant, $^{D}k_B$, for reactant B is the intrinsic isotope effect on step i, $^{D}k_i$. This equivalence does happen, as in the case of peptidylglycine monooxygenase, but not so often as one might expect.

Because the equation for the kinetic isotope effect on the catalytic constant k_0 (Equation 4–201) is of the same form as the equation for the specificity constant for isotopically substituted reactant (Equation 4–199), arguments similar to those that were just made can be made again. In this case, however, the ratio α_0 takes the place of c_f, and the reason for a large or a small value for α_0 are quite different from the reasons for a large or small value for c_f.

If, when all the reactants are at saturation, the rate at which E_i is replenished from E_{i+1} in the forward direction, through all the consecutive steps in the reaction other than that governed by k_i and k_{-i}, is slow relative to the forward rate constant k_{iH} for the step in which the intrinsic kinetic isotope effect occurs so that α_0 is large, then there will be little or no kinetic isotope effect on the catalytic constant k_0 because the step with rate constant k_i is not a significant rate-affecting step.

If, however, the rate of the step in which the intrinsic kinetic isotope effect occurs is slow relative to the rate at which E_i is regenerated in the forward direction from E_{i+1} so that as soon as E_{i+1} is formed, it is converted to E_i, and if c_r is small, then step i becomes the only significant rate-affecting step, as well as the rate-limiting step in the enzymatic reaction. Under these conditions, the intrinsic kinetic isotope effect is fully expressed on the catalytic constant. This situation again does not occur so often as one might expect.

It should be noted that formally equivalent circumstances cause values for the observed acid dissociation constants in the pH–rate profiles for the steady-state rate constants of an enzymatic reaction to differ from the intrinsic acid dissociation constants for the active site. The only difference is that a kinetic isotope effect changes an intrinsic rate constant discontinuously while variation of the pH changes it continuously.

An example of the **masking of an intrinsic, primary deuterium kinetic isotope effect** by another step in the reaction occurs with equine alcohol dehydrogenase (Equation 4–158).[326] With the native enzyme, the primary deuterium kinetic isotope effect on the catalytic constant, $^{D}k_0$, is only 1.3 for deuterioethanol as a reactant because dissociation of NADH as a product, which is a step subsequent to hydride transfer, is the rate-limiting step in the reaction. Slow dissociation of NADH causes the commitment in reverse to be large. When the enzyme is modified at several lysines within its active site by amidination with the methyl imidate of 2-pyridinecarboxylic acid, the rate constant for dissociation of NADH is increased more than 30-fold. With the modified enzyme, the primary deuterium kinetic isotope effect on the catalytic constant is 5. The increase observed in the primary deuterium kinetic isotope effect upon amidination arises because c_r has decreased to insignificance and the step in which hydride is transferred has become rate-limiting rather than the subsequent dissociation of NADH.

In the case of L-lactate dehydrogenase (previously Equations 1–90 and 3–27)

$$\text{NADH} + \text{H}^+ + \text{pyruvate} \rightleftharpoons \text{NAD}^+ + \text{L-lactate} \quad (4\text{–}204)$$

from *Oryctolagus cuniculus*, L-lactate usually must dissociate as a product before NAD^+ can dissociate. As the concentration of the product L-lactate in the solution increases, inhibiting dissociation of NAD^+ and causing c_r to increase rather than decrease, the primary deuterium kinetic isotope effects for isotopic substitution at carbon 4 of NADH on the specificity constant k_{pyr} for pyruvate (pyr) and the catalytic constant k_0 decrease from 1.93 ± 0.02 and 1.75 ± 0.03 to 1.16 ± 0.02 and 0.93 ± 0.05, respectively.[327] The fact that the primary deuterium kinetic isotope effect on the catalytic constant is now less than 1 suggests that it is actually registering the equilibrium isotope effect for the step in which the deuterium is transferred from NADH to pyruvate and that, at steady state, the transfer of the hydride is at equilibrium.

A smaller-than-expected kinetic isotope effect on a steady-state rate constant is often cited as evidence that the intrinsic kinetic isotope effect has been masked by other rate-affecting steps. For example, from the fact that the primary tritium kinetic isotope effect on the catalytic constant of methylmalonyl-CoA mutase from *Propionibacterium freudenreichii* was only 4.9, it was concluded that removal of the protium by a catalytic base in the active site was not the only rate-affecting step in the enzymatic reaction.[328]

Because c_f and the ratio α_0 are not determined by the same intrinsic rate constants, it is usually the case that if an intrinsic, primary deuterium kinetic isotope effect is masked by steps other than the step in which hydrogen is transferred, the primary deuterium kinetic isotope effect on the catalytic constant k_0 and the primary deuterium kinetic isotope effect on the specificity constant, ^Dk_B, for isotopically substituted reactant B, will be different. In fact, it is usually the case that they differ, and the difference is assumed to mean that isotopically insensitive steps are rate-affecting at least in the case of the smaller value of the two.[329]

When c_f, c_r, and the ratio α_0, however, are all insignificant (Equations 4–199 and 4–201), then the observed primary deuterium kinetic isotope effect for the specificity constant, ^Dk_B, for reactant B equals the observed primary deuterium kinetic isotope effect, $^Dk_0$, for the catalytic constant k_0 because both are equal to the intrinsic isotope effect on step i, ^Dk_i. The **equivalence of the observed primary deuterium kinetic isotope effects for the catalytic constant and the specificity constant** for isotopically substituted reactant is usually assumed to mean that the intrinsic, primary deuterium kinetic isotope effect is fully manifest in both rate constants. For example, at pH 5, the primary deuterium kinetic isotope effects for both the specificity constant $^Dk_{NE}$ for nitroethane (NE) and the catalytic constant $^Dk_0$ for nitroalkane oxidase from *F. oxysporum* are 7.5 and 7.4, respectively.[330] These values are within the range for the observed primary deuterium kinetic isotope effects for removal of a hydron from a nitroalkane by a general base in solution,[331] which is an intrinsic deuterium kinetic isotope effect. This latter coincidence and the equivalence of the two primary deuterium kinetic isotope effects on the steady-state rate constants led to the conclusion that both rate constants were registering the intrinsic, primary deuterium kinetic isotope effect in the active site of the enzyme.

The Swain–Schaad relation provides another equation that can be used to dissect contributions of the various steps in a kinetic mechanism to the observed kinetic isotope effects on the steady-state rate constants and to obtain values for the intrinsic kinetic isotope effects on the step in which the bond that is isotopically substituted is broken and re-formed. From a semiclassical explanation of primary kinetic isotope effects, which is based on differences in ground-state vibrational energies, it has been proposed that, on the basis of the differences in mass among hydrogen, deuterium, and tritium, the following relation, the Swain–Schaad relation, should hold[332] for intrinsic, primary kinetic isotope effects on the rate constant k_i

$$^Tk_i \equiv \frac{k_{iH}}{k_{iT}} = \left(\frac{k_{iH}}{k_{iD}}\right)^{1.44} = {}^Dk_i{}^{1.44} \quad (4\text{–}205)$$

As an example, if an intrinsic, primary deuterium kinetic isotope effect for a step in a given reaction is 7, then the intrinsic, primary tritium kinetic isotope effect for the same step should be 16. This relation is consistent with observed values for the primary deuterium and tritium kinetic isotope effects for various reactions, and it is used widely as an established fact.[333] It has been pointed out, however, that the exponent on the relation is not precise: it

should fall in a range between 1.33 and 1.58 for a reaction in which an intrinsic, primary deuterium kinetic isotope effect is greater than 3, but it will have a much wider range when an intrinsic, primary deuterium kinetic isotope effect is less than 3.[334,335] Consequently, deviations from the equality of Equation 4–205 within these ranges are not unexpected and cannot be used to make the argument that the values observed require a special explanation. In spite of this uncertainty, the value of 1.44 for the exponent is usually considered to be precise when the relation is used in calculations.[336]

One use of the Swain–Schaad relation is to **validate a conclusion** that the observed primary deuterium kinetic isotope effect on a steady-state rate constant is actually the intrinsic, primary deuterium kinetic isotope effect for the step in which the bond is broken. For example, the observed primary deuterium kinetic isotope effect (4.4) on the specificity constant k_{DS} for [2-^{2}H]-D-serine (DS) in the reaction catalyzed by porcine D-amino-acid oxidase and the observed primary tritium isotope effect (8.6) on the same rate constant satisfy Equation 4–205. Consequently, it was concluded that the observed primary deuterium kinetic isotope effect must be the intrinsic, primary deuterium kinetic isotope effect on the step in the enzymatic reaction in which hydrogen is transferred, and the commitments forward and in reverse, which by definition cannot be affected by isotopic substitution, must be negligible (Equation 4–199).[311]

Another use of this correlation is **to estimate the intrinsic, primary deuterium kinetic isotope effect** when the commitments are not negligible.[333,337] Numerical values for these commitments, c_f and c_r, and the ratio α_0 are almost never available as they were for D-xylose reductase. If the equilibrium constant for the step in the enzymatically catalyzed reaction in which the bond is broken is not affected significantly by substitution of deuterium or tritium for hydrogen, then by combining Equations 4–199 and 4–205

$$\frac{^{D}k_B - 1}{^{T}k_B - 1} = \frac{^{D}k_i - 1}{^{D}k_i^{1.44} - 1} \qquad (4\text{–}206)$$

Very accurate values for the deuterium and tritium kinetic isotope effects on the specificity constants, $^{D}k_B$ and $^{T}k_B$, for reactant B are required for the proper use of this equation.[338] For example, it has been used to estimate the intrinsic, primary deuterium kinetic isotope effect in the reaction catalyzed by bovine dopamine β-monooxygenase[339]

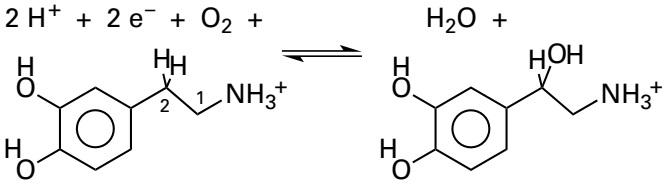

(4–207)

The observed primary deuterium kinetic isotope effect on the specificity constant k_{DAm} for [2,2-^{2}H$_2$]dopamine (DAm) was 2.756 ± 0.054, and the observed primary tritium kinetic isotope effect on k_{DAm} when [2-^{3}H]dopamine was used as a reactant was 6.079 ± 0.220, so the intrinsic, primary deuterium kinetic isotope effect calculated with Equation 4–206 is 9.4 ± 1.3. The magnitude of this value was presented as evidence that the transition state in the step at which hydrogen is removed is symmetric and the equilibrium constant for this step is close to 1.

Malate dehydrogenase (oxaloacetate-decarboxylating) (NADP$^+$) from *Columba livia* catalyzes the reaction

$$NADP^+ + (S)\text{-malate} \rightleftharpoons CO_2 + \text{pyruvate} + NADPH \qquad (4\text{–}208)$$

in which a hydride is removed from malate and carbon dioxide dissociates from the intermediate oxaloacetate, a β-oxo carboxylic acid that would normally be prone to decarboxylation. By measuring deuterium, tritium, and carbon-13 kinetic isotope effects and applying both Equations 4–199 and 4–206 as well as other kinetic measurements, it was possible to calculate[340] an intrinsic, primary deuterium kinetic isotope effect (5.7 ± 0.3) for hydride transfer from malate to NADP$^+$ during formation of the intermediate oxaloacetate. This value is in the range expected for an isoergonic hydride transfer with a symmetric transition state if bending vibrational modes do not contribute significantly to the free energy of activation. The directly observed primary deuterium kinetic isotope effect on the specificity constant k_{mal} for malate (mal), however, is only 1.5 at all values of pH,[318] because hydride transfer is not the only rate-affecting step in the overall reaction.

If a kinetic mechanism is chosen by the investigator for a particular enzymatic reaction, the cata-

lytic constant and the specificity constant for an isotopically substituted reactant can also be expressed in steady-state rate equations that contain only rate constants for the chemical steps in which the isotope participates and c_f, c_r, and the ratio α_0. Observed values for the catalytic constant and the specificity constant for unsubstituted, deuterated, and tritiated reactant each provide two simultaneous equations for these two kinetic parameters, for a total of six simultaneous equations. The Swain–Schaad relations for the forward and reverse rate constants of the step in which the carbon–protium bond, the carbon–deuterium bond, and the carbon–tritium bond are broken provide **four more simultaneous equations**. Although the Swain–Schaad relations are transcendental, these ten simultaneous equations containing ten or fewer unknowns can be solved by successive approximation for values of the intrinsic deuterium kinetic isotope effect, c_f, c_r, and the ratio α_0. For example, values for these four parameters—4.91 ± 0.01, 4.6, 0.1, and 0.2—for the reaction catalyzed by phosphogluconate dehydrogenase (NADP$^+$-dependent, decarboxylating)

$$\text{NADPH} + \text{D-ribulose 5-phosphate} + \text{CO}_2 \rightleftharpoons \text{6-phospho-D-gluconate} + \text{NADP}^+ \quad (4\text{–}209)$$

from *Cyberlindnera jadinii* were estimated from the six equations for the observed catalytic constants and the observed specificity constants for D-[1-^{1}H]ribulose 5-phosphate, D-[1-^{2}H]ribulose 5-phosphate, and D-[1-^{3}H]ribulose 5-phosphate and the four Swain–Schaad relations.[341]

Consequently, in advantageous circumstances, values of the deuterium and tritium kinetic isotope effects on the catalytic constant and the specificity constant for the reactant permit extraction of the primary kinetic isotope effects on the microscopic rate constant for the step in the kinetic mechanism in which a bond involving the atom substituted is broken and, with luck, the numerical value for that rate constant.

Any alteration in the active site that decreases the rate constants for the microscopic step in which hydrogen is transferred will increase the magnitude of the effects of the intrinsic, primary deuterium kinetic isotope effect on the primary deuterium or tritium kinetic isotope effects on the catalytic constant (Equation 4–201) and the specificity constant for isotopically substituted reactant (Equation 4–199). One way to decrease these rate constants is to **mutate an amino acid**, the side chain of which is a catalyst in the step in which hydrogen is transferred. For example, when Glutamate 182 in fructose-bisphosphate aldolase

$$\text{glycerone phosphate} + \text{D-glyceraldehyde 3-phosphate} \rightleftharpoons \text{D-fructose 1,6-bisphosphate} \quad (4\text{–}210)$$

from *E. coli* is mutated to alanine, the primary deuterium kinetic isotope effect on the catalytic constant for the condensation of [3(*S*)-^{2}H]glycerone phosphate increases from 1.04 to 6.0, while the catalytic constant itself decreases 60-fold.[342] The problem with this approach is that the catalytic acid–base has been changed from the one in the native enzyme to probably a molecule of water, and this change should have a significant effect on the intrinsic, primary kinetic isotope effect. One way to get around this problem is to decrease the rate constant for the microscopic step in which hydrogen is transferred by mutating an amino acid peripheral to the site at which the transfer occurs[343,344] rather than one participating directly in the transfer. All that is required is that mutation decreases the microscopic rate constants.

Another way to decrease the microscopic rate constants for the step in which hydrogen is transferred is to **increase or decrease the pH**. As the concentration of the enzymatically active tautomers catalyzing the step in which hydrogen is transferred decreases with the change in pH, rate constants for that step decrease, the commitments and the ratio α_0 decrease, and the primary deuterium kinetic isotope effects on the specificity constant and the catalytic constant increase.[345,346] For example, the specificity constant k_{Met} for L-methionine as an alternative reactant for tryptophan 2-monooxygenase from *Pseudomonas savastanoi* decreases below a pK_a of 5.0 and above a pK_a of 9.8. The primary deuterium kinetic isotope effect on the specificity constant, $^D k_{Met}$, for [β,β,β,α-^{2}H$_4$]-L-methionine increases below a pK_a of 5.1 and above a pK_a of 10.0 from 1.8 ± 0.2 in the midrange. At both low and high pH, these primary deuterium kinetic isotope effects approach a limiting value of 5.2 ± 0.8,[347] which is probably the intrinsic, primary deuterium kinetic isotope effect for the step in which hydrogen is transferred. In each case, as the microscopic rate constants for the step in which hydrogen is trans-

ferred decrease as the pH is decreased or as the pH is increased, this decrease causes that step to become more and more rate-affecting, if not rate-limiting, and the intrinsic, primary deuterium kinetic isotope effect to become more and more manifest.

When the value for a steady-state rate constant decreases as the pH is lowered below an apparent pK_a, the increase in the primary deuterium isotope effect often sets in at a lower pH than that pK_a. Likewise, when the value for a steady-state constant decreases as the pH is raised above an apparent pK_a, the increase in the primary deuterium isotope effect often sets in at a higher pH than that pK_a. In both cases, the rate of the step in which hydrogen is transferred usually has to **decrease a certain amount before the step becomes significantly rate-affecting** or rate-limiting. For example, the specificity constant k_{glyc} for glycerol (glyc) for the reaction catalyzed by glycerol dehydrogenase from *Cellulomonas* decreases as the pH is lowered below a pK_a of 7.8, but the primary deuterium kinetic isotope effect for [2-^{2}H]glycerol[348] increases below an apparent pK_a of 7.3 from a constant value of 1.15 to a limiting value of 2.44. The catalytic constant for the reaction catalyzed by dihydrofolate reductase from *M. tuberculosis* decreases as the pH is raised above a pK_a of 6.8, but the primary deuterium kinetic isotope effect for (4*R*)-[4-^{2}H]NADH[349] increases above an apparent pK_a of 7.4 from a constant value of 1.1 to a limiting value of 2.6.

Decreasing the rate constants of the step in which hydrogen is transferred, however, **does not always completely reveal an intrinsic, primary deuterium kinetic isotope effect**. For example, when the pH is decreased below an apparent pK_a of 6.5 that governs the behavior of both the specificity constant k_{DHO} for dihydroorotate (DHO) and the catalytic constant of orotate reductase (NADH) from *Clostridium oroticum*, the primary deuterium kinetic isotope effect for L-[5*R*,5*S*-$^2H_2$]dihydroorotate on k_{DHO} increases from 1.0 to a limiting value of 1.9, and that on k_0 increases from 1.0 to a limiting value of 1.3.[350] Neither limit, however, is probably the intrinsic, primary deuterium kinetic isotope effect.

Each mutation and each decrease or increase in pH just discussed must have decreased a rate constant for the step in which hydrogen is transferred, rather than other steps governing the commitments, to be able to increase the primary deuterium kinetic isotope effect on a steady-state rate constant (Equations 4–199 and 4–201). Consequently, the fact that each mutation and each decrease or increase in pH increases the respective primary deuterium kinetic isotope effect proves that the amino acid mutated or the side chain titrating participates catalytically in this step but not that it necessarily is the catalytic base that removes the hydron. Contrariwise, if the mutation of an amino acid does not increase a small primary deuterium kinetic isotope effect on one steady-state rate constant, even though it decreases that steady-state rate constant dramatically, then that side chain is probably not a catalytic acid–base in the step in which the hydrogen is transferred.[351]

In the preceding discussion, the difficulties of extracting an intrinsic, primary kinetic isotope effect from steady-state kinetic observations have been presented, as well as ways to extract those kinetic isotope effects. The following discussion will **assume that an intrinsic, primary kinetic isotope effect has been extracted** one way or another and that its value is reliable.

The semiclassical explanation for an intrinsic, primary deuterium kinetic isotope effect is based on an examination of vibrational energy levels.[352] An intrinsic, primary deuterium kinetic isotope effect on the microscopic step in which hydrogen is transferred is for a transition state in which the bond between carbon and hydrogen is breaking and a new bond between the hydrogen and another atom is forming. In the reactant, the carbon–hydrogen bond in the ground state participates in a stretching vibration. In the transition state a portion or all of this stretching vibration is lost. Consider a linear, symmetric transition state in which hydrogen is being transferred as a hydron, hydrogen atom, or hydride from carbon to a lone pair of electrons on a general base, radical, or electrophile such as NAD^+ or $flavin_{ox}$, respectively. Suppose that the carbon–hydrogen bond has been broken completely but the bond to that general base, radical, or electrophile has not yet begun to form. In such a transition state, all the stretching vibration present in the reactant has been converted into translational motion along the reaction coordinate. The vibrational energy that has been converted into translational energy is part of the free energy of activation. The conversion of vibrational energy into translational energy causes the kinetic isotope effect.

In either a molecule or a transition state, the arrangement of nuclei and the accompanying electrons in space creates a surface of potential energy. If one nucleus is moved with respect to the other nuclei, the potential energy varies. If, for example, only the hydrogen in a carbon–hydrogen bond in

the ground state of a molecule is moved along the axis of the bond, the function for the potential energy for stretching that bond is generated (Figure 4–23). Because the nucleus of a deuterium atom has the same charge number as the nucleus of a protium atom, the function for the potential energy of a carbon–deuterium bond is identical to that for a carbon–protium bond.

Stretching vibration along a particular carbon–hydrogen bond in a molecule is controlled by the function for the potential energy of this vibrational mode, but it is quantized. This stretching vibration of a particular carbon–hydrogen bond is only one of many vibrational modes in the molecule. In the semiclassical treatment, the energy for each vibrational energy level in vibrational mode j in a particular molecule

$$E_{n,j} = \frac{h}{2\pi}\left(n + \tfrac{1}{2}\right)\sqrt{\frac{f_j}{\mu_j}} \qquad (4\text{–}211)$$

where h is the Planck constant, f_j is the force constant for vibrational mode j, n is the quantum number for energy level n, and μ_j is the reduced mass

$$\frac{1}{\mu_j} = \sum_{k=1}^{o} \frac{1}{m_k} \qquad (4\text{–}212)$$

of the o atoms participating in vibrational mode j. The force constant, f_j, for vibrational mode j is determined only by the function for the potential energy of vibrational mode j.

For the stretching vibrational mode of a carbon–hydrogen bond, the **force constant** is determined by the function for the potential energy for stretching along that bond. Because potential energy is not a function of mass but only of electric charge, the function is the same for both a carbon–protium bond and a carbon–deuterium bond. If the function for the potential energy, and hence the force constant f_j for vibrational mode j, remains the same when one of the o atoms participating in vibrational mode j is replaced by an isotope of greater mass so that the lighter atom (l) becomes a heavier atom (h), the **change in zero-point energy** ($n = 0$) caused by the isotope effect

$$\Delta E_{0,\mathrm{ie},j} = \frac{h\sqrt{f_j}}{4\pi}\left(\sqrt{\frac{1}{\mu_{j,\mathrm{h}}}} - \sqrt{\frac{1}{\mu_{j,\mathrm{l}}}}\right) < 0 \qquad (4\text{–}213)$$

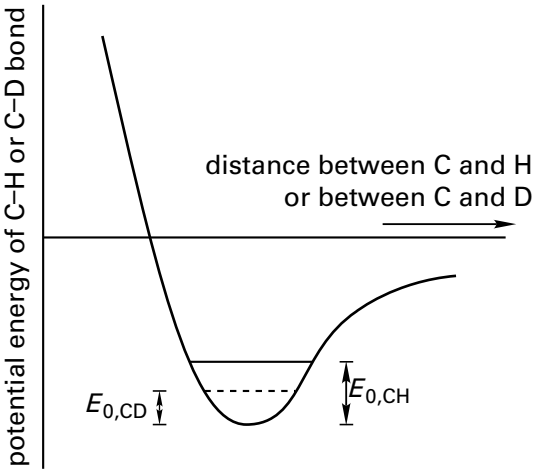

Figure 4–23: Schematic drawing of the potential energy for the stretching of a carbon–hydrogen bond. The potential energy is plotted as a function of the distance between the nuclei of the carbon atom and the respective isotope of the hydrogen atom. When that distance is short, the nuclei repel and the potential energy rises dramatically. When the distance is long, the atoms do not interact and the potential energy is near zero. At intermediate distances, electron overlap creates a covalent bond, which is a favorable interaction with a negative potential energy. The potential energy for a carbon–deuterium bond is the same as that for a carbon–protium bond. Because the stretching vibrations within the bottom of the potential well are quantized, they can only take on certain energies. The zero-point energy for a carbon–protium bond, $E_{0,\mathrm{CH}}$, is higher than that for a carbon–deuterium bond, $E_{0,\mathrm{CD}}$, because of the difference in mass between a hydron (1.67×10^{-24} g) and a deuteron (2.34×10^{-24} g). The drawing is not even close to scale. The ground-state energy of the carbon–hydrogen bond should be about –340 kJ mol^{-1} below the origin, while $E_{0,\mathrm{CH}}$ should be only +17.4 kJ mol^{-1}.

Because, as the equation demonstrates, $\Delta E_{0,\mathrm{ie},j}$ is less than 0, the zero-point energy always decreases when a heavier isotope replaces a lighter isotope.

The frequency, ν_j, of a quantum of light that, during its absorption, excites vibrational mode j from its zero point ($n = 0$) to its first excited state ($n = 1$) is directly proportional to the difference in energy between these two energy levels

$$h\nu_j = \frac{h}{2\pi}\sqrt{\frac{f_j}{\mu_j}} \qquad (4\text{–}214)$$

the constant of proportionality being the Planck constant. It follows from Equations 4–213 and 4–214 that

$$\Delta E_{0,\mathrm{ie},j} = \frac{h\nu_{j,\mathrm{l}}}{2}\left(\sqrt{\frac{\mu_{j,\mathrm{l}}}{\mu_{j,\mathrm{h}}}} - 1\right) \qquad (4\text{–}215)$$

where $\nu_{j,l}$ is the **frequency of the infrared light absorbed by vibrational mode *j*** in the molecule with the lighter element, $\mu_{j,l}$ is the reduced mass of the atoms participating in vibrational mode j for the molecule with the lighter element, and $\mu_{j,h}$ is the reduced mass of the atoms participating in vibrational mode j for the molecule with the heavier element.

The infrared absorptions for the stretching vibrations of carbon–protium bonds in alkanes, alcohols, and ketones fall at frequencies between 2900 and 3000 cm^{-1}. Consequently, the difference in zero-point energies between a carbon–deuterium bond and a carbon–protium bond from Equation 4–215 should be 4.7 ± 0.1 kJ mol^{-1}. If all the zero-point free energy were lost in the transition state, a carbon–protium bond would require **4.7 kJ mol^{-1} less free energy of activation** to reach the transition state than a carbon–deuterium bond because it would start out at a level of energy 4.7 kJ mol^{-1} higher. This situation should lead to an enhancement in rate of the reaction when protium is present rather than deuterium, and

$$\frac{k_{CH}}{k_{CD}} = e^{-\Delta\Delta G^{\circ\ddagger}/RT} = 7 \qquad (4\text{–}216)$$

It should be kept in mind that, in the derivation of this equation, several assumptions have been made along the way.

Extensive tabulations are available of the observed primary deuterium kinetic isotope effects for nonenzymatic removal of hydrogen as a hydron from various carbons by various general bases in solution.[296] If a large number of these values for the simple intrinsic, primary deuterium kinetic isotope effects for nonenzymatic removals of hydrons from carbon by general bases are plotted as a function of the difference in pK_a between the carbon acid and the conjugate acid of the general base, there seems to be a **maximum when the two values of the pK_a are the same**,[296] but it is not a dramatic one. As the pK_a for the conjugate acid of the general base becomes larger or smaller than the pK_a for the carbon acid, the primary deuterium kinetic isotope effect decreases monotonically. When the difference in pK_a is 10, about half of the primary deuterium kinetic isotope effect has been lost. For example, the primary deuterium kinetic isotope effect for removal of a hydron from sulfonatoacetone[353] by hydroxide anion ($\Delta pK_a = -2.0$) is 7.4, but the primary deuterium kinetic isotope effect for removal of the same hydron by acetate anion ($\Delta pK_a = 9.6$) is 3.8. These decreases in the kinetic isotope effect on either side of the maximum are thought to result from increasing asymmetry of the transition state due to changes in the relative attractive forces of the two lone pairs for the hydron that sits between them in that transition state.[352]

When the pK_a for the conjugate acid of the general base is equal to the pK_a for the carbon acid, values of the observed primary deuterium kinetic isotope effects for nonenzymatic removal of hydrogen as a hydron from various carbons by various general bases in solution lie between 6 and 12. Because such **isoergonic transfers of a hydron** should proceed through symmetric transition states, they should represent maximum values that can be obtained.[352] Values in excess of 7 are usually explained by physical organic chemists by assuming that zero-point energy from the bending vibrations of the carbon–hydrogen bond, which also disappear in the transition state, as well as zero-point energy from the stretching vibrations is incorporated into the translational energy along the reaction coordinate.

The stretching frequency of the bond between hydrogen and the carbon of the acid is completely converted into translational motion along the reaction coordinate, and as a result, this vibrational mode disappears. The transition state, however, sits at a col on the potential energy surface. Because the potential energy surface in the vicinity of the transition state has literally the shape of a col, perpendicular to the reaction coordinate at the col is a another potential well with the col at its bottom. This potential well has a symmetrical vibrational mode associated with it. If the carbon and the base that removes the hydron have equal affinity for the hydron, then the hydron remains stationary as vibration occurs in this perpendicular symmetrical vibrational mode of the transition state, and there is no difference in energy between the transition state with protium and the one with deuterium. In this situation, the maximum change in standard free energy of vibration between the transition state and the zero point of the vibration is realized. If, however, the affinities of the carbon and the base differ from each other, then the hydron moves in concert with the atom that has the higher affinity, and the transition state containing deuterium will have a lower energy than that containing protium. This deuterium kinetic isotope effect on standard free energy of the transition state decreases the difference in the primary deuterium kinetic isotope effect on the reaction. As a result, the greater the difference in pK_a, regardless of its sign, between the

carbon and the conjugate acid of the base, the smaller will be the primary deuterium kinetic isotope effect on the rate of the hydron transfer.

Similar arguments have been applied to intrinsic, primary deuterium kinetic isotope effects for **transfer of a hydrogen atom**[354] and **transfer of a hydride**. For example, the reduction potential of the hydride acceptor in the oxidation–reductions of benzyl alcohol catalyzed by alcohol dehydrogenase from *S. cerevisiae* and equine alcohol dehydrogenase (Equation 4–158) was changed monotonically from –0.32 to –0.26 V by using four different analogues of NAD^+, and the intrinsic, primary deuterium kinetic isotope effect observed with [1,1-$^2H_2$]benzyl alcohol increased from 4 to 6.5. This increase was presented as evidence that as the reduction potential became more positive, the transition state for hydride transfer became more symmetric.[355] Because an increase in reduction potential should cause the transition state to occur earlier, the change is proposed to be between a late transition state and a more symmetric transition state.

The maximum magnitudes expected from a semiclassical explanation for intrinsic, primary deuterium kinetic isotope effects and intrinsic, primary tritium kinetic isotope effects for bonds other than carbon–deuterium and carbon–tritium bonds depend on the reduced mass of the two atoms participating in the bond (Equation 4–215). The differences in zero-point energies between protium and deuterium for **nitrogen–hydrogen** (3300 cm^{-1}) and **oxygen–hydrogen** (3300 cm^{-1}) bonds[296] are between 5 and 6 kJ mol^{-1}, so the maximum primary deuterium kinetic isotope effects seen with these bonds are in the same range as those for carbon–hydrogen bonds. Again, however, it should be mentioned that although these estimates are of interest, it is not possible to measure a primary kinetic isotope effect for a specific nitrogen–hydrogen bond or a specific oxygen–hydrogen bond in an enzymatic reaction, which of necessity must occur in aqueous solution.

One purpose for measuring an intrinsic, primary deuterium isotope effect is to use its value to make arguments, such as those made for removal of a hydron from sulfonatoacetone or oxidation–reduction of benzyl alcohol catalyzed by alcohol dehydrogenase, about **the structure of the transition state** using the ratio between the observed intrinsic, primary deuterium isotope effect and a theoretical primary deuterium kinetic isotope effect calculated from semiclassical theory. It is common practice to equate this ratio to the fraction of the bond in question that has been broken in the transition state. Any such argument, however, must make the **assumption that there are no other contributions beyond the differences in zero-point energies** producing that kinetic isotope effect. Even with this assumption, the argument would not be valid if, in addition to differences in zero-point energy, quantum mechanical tunneling of the protium also contributes to the differences between the intrinsic rate constants for protium and deuterium for the transfer of hydrogen. If quantum mechanical tunneling contributes to a significant degree, arguments about the structure of the transition state would be equivocal because the magnitude of the kinetic isotope effect would no longer be related only to vibrational parameters. Consequently, it would not be possible to calculate an upper limit to the intrinsic, primary deuterium kinetic isotope effect with which to compare the observed kinetic isotope effect.

Quantum mechanical tunneling is a result of the uncertainty principle. If the uncertainty principle is valid, it follows that the actual position of a protium is only a distribution of probabilities that it will occupy a precise location. This distribution of probabilities is unaffected by the distribution of the potential energy of that protium as a function of its position relative to the other atoms. A barrier of potential energy along a reaction coordinate (Figure 3–25) lies between the position of a hydrogen atom in the reactant and its position in the product. In the semiclassical treatment, the height of this impenetrable barrier determines the rate constant for transfer of the protium. If, however, the width of this barrier of potential energy at some point below its summit is of the same order of magnitude as the width of the distribution of probabilities for the position of the protium, then there will be a large enough probability that the protium is located on the other side of the barrier and that it will be there in a shorter period of time than would be required for it to pass over the barrier through a semiclassical transition state.* Its existence on the other side of the barrier in this shorter period of time is its ability to **tunnel through the barrier of potential energy**. Because uncertainty in position is inversely proportional to the mass of a particle, protium tunnels more effectively than deuterium because it can tunnel at a lower point below the summit.

*This view of the uncertainty principle assumes that it applies to the actual position of the protium and not just to the uncertainty in ascertaining its position.

There are behaviors that are supposed to be **signatures of quantum mechanical tunneling** and that have been observed for intrinsic, primary deuterium kinetic isotope effects for the transfer of hydrogen in enzymatic reactions.

Intrinsic, primary deuterium kinetic isotope effects greater than around 10 are thought to be an indication that quantum mechanical tunneling is occurring.[356,357] For example, the intrinsic, primary deuterium kinetic isotope effect for removal of a hydron from the carbon between the 9Z double bond and the 12,13-radical cation of (9*Z*,12*Z*)-9,12-octadecadienoate[358-360] at 30 °C by a catalytic base in the active site of lipoxygenase from *Glycine max* is 60. The primary deuterium kinetic isotope effect for removal of a hydrogen atom from (*R*)-methylmalonyl-SCoA by the prosthetic adenosylcobalamin[361] in the active site of methylmalonyl-CoA mutase from *P. freudenreichii* is 30. The primary deuterium kinetic isotope effect for inner-sphere transfer of a hydrogen atom from D-galactose to a tyrosyl radical[362] within the coordination sphere of the copper ion in the active site of galactose oxidase from *Hypomyces rosellus* is 16, and the primary deuterium kinetic isotope effect on the catalytic constant for production of perdeutero-13-hydroperoxy-(9*Z*,11*E*)-9,11-octadecadienoate from perdeutero-(9*Z*,12*Z*)-9,12-octadecadienoate by human prostaglandin-endoperoxide synthase,[363] which also involves the transfer of a hydrogen atom from carbon 11 of (9*Z*,12*Z*)-9,12-octadecadienoate to a tyrosyl radical in the active site, is 22 at 50 °C.*

Primary deuterium kinetic isotope effects that are larger than the maximum expected from a semiclassical description, however, could have **other explanations** than quantum mechanical tunneling. In addition to the loss of bending vibrations of the carbon–hydrogen bond, it could also be the case that the zero-point vibrational energies of other covalent bonds in the vicinity that are coupled to the stretching vibration of the carbon–hydrogen bond change as the carbon–hydrogen bond disappears in the transition state. These changes in zero-point energies of other vibrational levels should contribute to the magnitude of the observed primary deuterium isotope effect. This coupling could be significant in a situation such as the active site of a protein in which there are a significant number of covalent bonds in the vicinity of the carbon–hydrogen bond being broken, the vibrations of which could be coupled to it. When the atoms of carbon-12, nitrogen-14, and nonexchangeable protium in the protein of pentaerythritol tetranitrate reductase from *Enterobacter cloacae* were substituted with carbon-13, nitrogen-15, and deuterium, the intrinsic, primary deuterium kinetic isotope for transfer of the hydride on the reactant NADH to the prosthetic flavin in the active site decreased from 8.2 to 5.4.[365] When the nonexchangeable atoms of protium in the protein of alanine racemase from *Geobacillus stearothermophilus* were substituted with deuterium, the primary deuterium kinetic isotope on the specificity constant for L-alanine increased from 1.6 to 3.8.[366]

The **lack of an effect of temperature** on the value for an enzymatic intrinsic, primary deuterium kinetic isotope effect is inconsistent with the semiclassical explanation and is thought to indicate a significant contribution from tunneling.[367-370] Intrinsic deuterium kinetic isotope effects that are considerably larger than the semiclassical maxima are usually invariant with temperature. For example, the intrinsic deuterium kinetic isotope effect of 60 for lipoxygenase from *G. max* is temperature-independent,[359] as well as the deuterium kinetic isotope effect of 45 for the specificity constant, k_{LA}, for perdeuterated (9Z,12Z)-octadeca-9,12-dienoic acid (linoleic acid; LA) in the reaction catalyzed by human arachidonate 15-lipoxygenase[371] and the deuterium kinetic isotope effect of 22 for the catalytic constant of the reaction catalyzed by human prostaglandin-endoperoxide synthase with perdeuterated linoleic acid.[363] Most investigators who study enzymatic primary deuterium kinetic isotope effects attribute large primary deuterium kinetic isotope effects that are invariant with temperature to quantum mechanical tunneling.

Even in situations in which the observed intrinsic kinetic isotope effect is not outside the semiclassical range, however, invariance of the kinetic isotope effect with changes in temperature is considered to be strong evidence for tunneling. For example, one step in the reaction catalyzed by sarcosine oxidase from *Arthrobacter* is transfer of a hydride from the methyl group of *N*-methylglycine (sarcosine) to the oxidized, prosthetic flavin in the active site. The intrinsic, primary deuterium kinetic isotope effect for this step is 7.3, which is not significantly larger than the semiclassical maximum, but the slope of the plot of the natural logarithm of the intrinsic kinetic isotope effect as a function of inverse temperature (0.07 ± 0.25) is indistinguishable from 0 between

*Although not necessarily the case in these instances, there are kinetic anomalies that can inflate estimates of intrinsic, primary deuterium kinetic isotope effects artifactually, and that should be avoided.[364]

277 and 307 K. This invariance of the intrinsic kinetic isotope effect with temperature was presented as evidence for quantum mechanical tunneling. The lack of a statistically significant effect of temperature on the intrinsic kinetic tritium kinetic isotope effect of 6.1 for hydride transfer from (*R*)-[4-^{3}H]NADPH to 7,8-dihydrofolate[372] in the active site of dihydrofolate reductase (Equation 4–148) from *E. coli* between 278 and 317 K and the lack of a statistically significant effect of temperature on the intrinsic kinetic isotope effect of 2.3 for hydride transfer from phosphite to NAD^+ in the active site of phosphonate dehydrogenase[313] from *Pseudomonas stutzeri* between 278 and 317 K were presented as evidence for the involvement of quantum mechanical tunneling in these enzymatic reactions even though the observed primary kinetic isotope effects are significantly less than the semiclassical maxima.

Secondary deuterium and tritium kinetic isotope effects are also thought to reveal quantum mechanical tunneling. A **secondary kinetic isotope effect** is a kinetic isotope effect in which the isotopic substitution occurs at another atom that is attached to an atom participating in the breaking of a bond, other than the two atoms between which the bond is broken.* Alcohol dehydrogenase from *S. cerevisiae* removes the *pro-R* hydride from benzyl alcohol

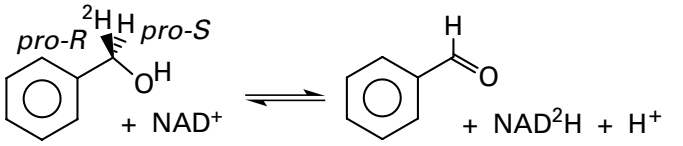

(4–217)

The secondary tritium kinetic isotope effect resulting from substitution of the *pro-S* protium with a tritium when the *pro-R* hydrogen is a protium is 1.30 ± 0.02, but the secondary tritium kinetic isotope effect resulting from substitution of the *pro-S* protium with a tritium when the *pro-R* hydrogen is a deuterium is 1.18 ± 0.03. These results are consistent with the distance between the carbon of benzyl alcohol and carbon 4 of the nicotinamide being greater in the transition state for protide transfer than in the transition state for deuteride transfer.[373] Quantum mechanical tunneling of a protide should occur at longer distances than the distance required by quantum mechanical tunneling of deuteride.

*Because the primary use of secondary kinetic isotope effects is to identify intermediates in enzymatic reactions, they will be discussed in detail in Chapter 5.

Because vibrational frequencies, and hence zero-point energies, are unaffected by increases in hydrostatic pressure,[374] there should be no **effect of hydrostatic pressure** on an enzymatic primary deuterium kinetic isotope effect. There are, however, enzymatic primary deuterium kinetic isotope effects that decrease in magnitude as hydrostatic pressure is applied.[375-377] These results, however, suggest only that something other than the semiclassical explanation is operating, not necessarily tunneling.

Nonenzymatic transfers of hydrogen homologous to those that occur in active sites can also display these signatures of quantum mechanical tunneling. These observations have led to the conclusion that tunneling also occurs in many of these reactions in free solution.[378-380] These observations raise the question of **whether the active site of an enzyme can enhance the amount of tunneling that occurs in the same reaction nonenzymatically** or the amount of tunneling that occurs in the active site is the same as the amount of tunneling that occurs in the same reaction in solution, and hence not indicative of some extraordinary property of an active site. For example, the abstraction of hydrogen atoms from methylmalonyl-SCoA and ethylene glycol by the 5′-deoxyadenosyl radicals formed from the prosthetic adenosylcobalamins in the active sites of methylmalonyl-CoA mutase from *P. freudenreichii*[361] and propanediol dehydratase from *Klebsiella pneumoniae*,[381] respectively, have very similar, elevated primary deuterium kinetic isotope effects that have the signature of quantum mechanical tunneling. Measurements that quantify the contribution of tunneling during the abstraction of a hydrogen from ethylene glycol by adenosylcobalamin in free solution, an analogous nonenzymatic reaction, gave identical results within experimental error to the primary deuterium kinetic isotope effects in the enzymatic reactions. It was concluded that, in this case, these active sites do not enhance the tunneling inherent in the nonenzymatic reaction.[382] The same conclusion was reached for the tunneling that has been proposed to occur in the hydron transfers catalyzed by a lipoxygenase from *G. max*[383] and nitroalkane oxidase from *F. oxysporum*.[384] Observations of secondary kinetic isotope effects, however, suggest that the active site of steroid Δ-isomerase from *C. testosteroni* produces tunneling that does not occur when the hydron transfer proceeds nonenzymatically in solution.[385] Nevertheless, any claim that an active site enhances tunneling requires that the tunneling involved in the nonenzymatic reaction be assessed. In most instance where this claim is made about

enzymatic active sites, this requirement has not been satisfied.

One simple way an active site could increase the contribution of quantum mechanical tunneling, once reactants are properly aligned for in-line transfer of a hydron, hydrogen atom, or hydride, is by **narrowing the distance between the hydrogen in the reactant and the location of its destination in the product** to increase the overlap between the probability densities of the hydrogen in the donor and the hydrogen at the destination.[386] When the distance between an amino nitrogen and a phenolate oxygen was increased from what should be a compressed distance of 0.26 nm to a longer distance of 0.27 nm, the kinetic isotope effect for the intramolecular transfer of a hydron from oxygen to nitrogen, coupled to an oxidative electron transfer, decreased from 2.1 to 1.3, consistent with a decreased contribution of tunneling to the transfer.[387] Steric forces in a protein can compress and shorten a hydrogen bond,[388] and compressed hydrogen bonds between catalytic acids and catalytic bases in active sites and their acceptors and donors on analogues for intermediates of high energy are often observed. It is possible that the distance between a hydrogen on carbon and either a catalytic base, an atom supporting an unpaired electron, or an electrophilic atom such as carbon 4 on NAD^+ could be shortened in a complex between an active site and a reactant by **steric compression** to enhance tunneling and catalyze the transfer of hydrogen. For example, in triose-phosphate isomerase from *S. cerevisiae* (Equations 4–46 and 4–55 and Figure 3–37), an enzyme that has anomalies in kinetic isotope effects considered to be indicative of quantum mechanical tunneling,[389] the oxygen of the carboxylate responsible for removing the hydron from carbon is only 0.30 and 0.308 nm from the two carbons between which it transfers the hydron.[23] Both distances are less than 0.38 nm, which is the sum of the van der Waals radii of oxygen (0.15 nm) and hydrogen (0.115 nm) and the length of a carbon–hydrogen bond (0.11 nm).[390]

From the crystallographic molecular model of a complex between aralkylamine dehydrogenase (azurin) from *Alcaligenes faecalis* and phenylhydrazine, it was concluded that the basic oxygen of the carboxylate of Aspartate 128β would be compressed below the van der Waals limit against the carbon–hydrogen bond of a reactant from which it is required to remove a hydron.[391] The intrinsic, primary deuterium kinetic isotope effect for the dehydrogenation of [1,1-$^2H_2$]tryptamine catalyzed by this enzyme is 55 at 20 °C, well in excess of the semiclassical limit, a fact that suggests tunneling could be occurring in this enzymatic reaction.

In crystallographic molecular models of complexes of NAD^+, trifluoroethanol, an inactive analogue of the reactant ethanol, and two mutants of equine alcohol dehydrogenase (Equation 4–158), changes in the distance between carbon 4 of NAD^+ and carbon 1 of trifluoroethanol, the carbon from which a hydride is removed from the normal reactant ethanol, were observed.[392] In the mutant in which Phenylalanine 93 was mutated to tryptophan, the distance was 0.32 nm—less than the sum (0.4 nm) of the van der Waals radii of carbon (0.175 nm) and hydrogen (0.115 nm) and the length of a carbon–hydrogen bond (0.11 nm)—but in the mutant in which Valine 23 was mutated to alanine, the distance was 0.40 nm. This increase in distance, and presumably an accompanying decrease in compression, led to a decrease in anomalous primary deuterium kinetic isotope effects for hydride transfer, a change that may indicate a decrease in quantum mechanical tunneling as compression is decreased.

In the crystallographic molecular model[393] of the complex between dihydrofolate reductase (Equation 4–148) from *E. coli* and $NADP^+$ and folate, the two oxidized substrates between which there is no hydride to transfer, the distance between carbon 4 of nicotinamide and carbon 6 of folate, between which a hydride is transferred in the normal enzymatic reaction, is 0.33 nm. This distance is already less than van der Waals contact (0.35 nm) between two carbon atoms even without the hydride being there and not counting the radii of hydrogens that are on these carbons in the two substrates. This compression exerted by the active site between the donor and the acceptor of the hydride is a steric effect caused by the shoving of the nicotinamide up against the folate by the side chain of Isoleucine 14. The intrinsic, primary tritium kinetic isotope effect for transfer of the hydride from (*R*)-[4-^{3}H]NADPH to 7,8-dihydrofolate, although only 6 at 25 °C, is invariant with temperature, a fact that is consistent with quantum mechanical tunneling. When Isoleucine 14 is mutated to valine, alanine, or glycine so that the size of the side chain decreases mutant to mutant and the nicotinamide is held more and more loosely until the compression is eliminated, the intrinsic, primary tritium kinetic isotope effect for hydride transfer becomes more and more dependent on temperature until it has become consistent with the semiclassical description in the absence of quantum mechanical tunneling.[372]

If steric compression that enhances tunneling is actually **yet another strategy that can be used by enzymes** to catalyze reactions, it is not surprising that natural selection has discovered it.

Primary kinetic isotope effects also result from isotopic substitutions of the heavier atoms that are within the second row. The fractional difference in mass is much smaller between carbon-13 and carbon-12, between carbon-14 and carbon-12, between nitrogen-15 and nitrogen-14, between oxygen-17 and oxygen-16, and between oxygen-18 and oxygen-16 than between hydrogen-2 and hydrogen-1 and between hydrogen-3 and hydrogen-1. Consequently, primary kinetic isotope effects for carbon-13, carbon-14, nitrogen-15, oxygen-17, and oxygen-18 are much smaller than primary kinetic isotope effects for deuterium or tritium (Equation 4–215). Using the semiclassical treatment, assuming that the bond being broken is between carbon-12 and the respective element from the second row that is being substituted, and assuming that only the respective stretching vibrational modes of the bond between carbon-12 and the respective element in the second row being substituted contribute to the primary kinetic isotope effects, maximum values expected for primary kinetic isotope effects of carbon-13, carbon-14, nitrogen-15, oxygen-17, and oxygen-18 (Equation 4–215) should be 1.05, 1.09, 1.04, 1.03, and 1.07, respectively.

Primary kinetic isotope effects for substitutions of carbons and oxygens have been often measured. When a carbon–carbon bond is broken during a rate-limiting step, if one carbon-12 is replaced with carbon-13, the largest primary kinetic isotope effects, ^{13}k, that have been observed[394,395] are about 1.07. When a carbon–carbon bond is broken during a rate-limiting step, if one carbon-12 is replaced instead with carbon-14, the largest primary kinetic isotope effects, ^{14}k, that have been observed[396] are between 1.09 and 1.15. When a carbon–nitrogen bond is broken during a rate-limiting step, if nitrogen-14 is replaced with nitrogen-15, the largest primary kinetic isotope effects, ^{15}k, that have been observed[397] are about 1.025. When a carbon–oxygen bond is broken during a rate-limiting step, if oxygen-16 is replaced with oxygen-18, the largest primary kinetic isotope effects, ^{18}k, that have been observed[398] are about 1.08. The fact that the largest primary carbon kinetic isotope effects observed are greater than those expected is probably due to changes in the transition state of other vibrational modes in which the carbon that is isotopically substituted participates, because, unlike a hydrogen atom, carbon is usually bonded to two or three other atoms.

Primary kinetic isotope effects produced by these isotopic substitutions of larger atoms are used in similar arguments to those used for primary deuterium kinetic isotope effects. The observation of such a primary kinetic isotope effect is presented as evidence that the bond containing the substituted atom is broken in a rate-limiting[399,400] or rate-affecting[401] step in the kinetic mechanism of the enzymatic reaction. Increases in a primary kinetic isotope effect when a mutation is made in the active site[402] can demonstrate that a change in the rate-limiting step is caused by the mutation. Both a change[403,404] and the lack of a change[405] in the primary kinetic isotope effect when the concentration of a reactant is varied during measurements of initial rates have been cited as evidence for a particular kinetic mechanism.

Because tunneling cannot occur in such reactions, the magnitude of an intrinsic, primary kinetic isotope effect[406] for the isotopic substitution of one of these heavier elements is often **used to define the structure of the transition state** for the step in which the bond containing the substituted atom is broken. For example, the primary carbon-13 kinetic isotope effect for the reactant [1-^{13}C]chorismate is 5-fold smaller than the primary oxygen-18 kinetic isotope effect for the reactant [3-^{18}O]chorismate for the concerted rearrangement catalyzed by chorismate mutases (previously Equation 1–161)

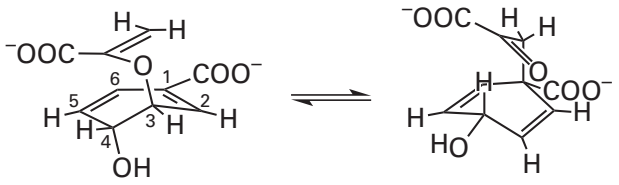

(4–218)

from *Bacillus subtilis* and *E. coli*. This fact was one of the observations used to conclude that, in the transition state, the bond between the oxygen of the migrating *enol*pyruvyl group and carbon 3 of the chorismate is almost completely broken while the bond between the vinyl carbon of the migrating *enol*pyruvyl group and carbon 1 is just beginning to form.[407,408]

The intrinsic, primary carbon-13 kinetic isotope effect for the step in the enzymatic mechanism of orotidine-5′-phosphate decarboxylase from *E. coli*

in which [*carboxy*-^{13}C]orotidine 5′-monophosphate is decarboxylated

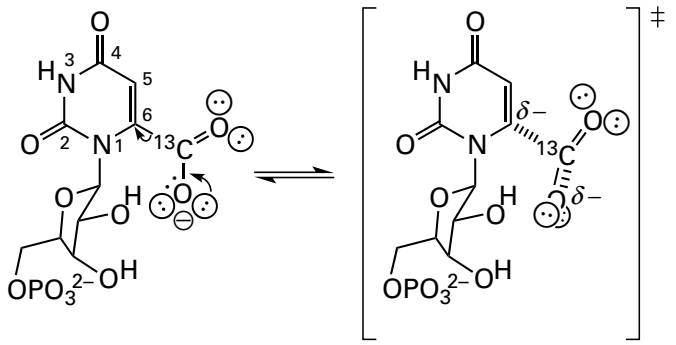

(4–219)

is 1.05–1.07. This fact suggests that the carbon–carbon bond is almost completely broken in the transition state for this step in the enzymatic reaction.[409] The primary carbon-13 kinetic isotope effect on the specificity constant, k_{OMP}, for [*carboxy*-^{13}C]orotidine 5′-monophosphate (OMP) is 1.0255 ± 0.0005 while that on the specificity constant, k_{FOMP}, for [*carboxy*-^{13}C]-5-fluoroorotidine 5′-monophosphate (FOMP) is smaller, 1.0106 ± 0.0001. This fact suggests that the transition state occurs earlier in the latter reaction than in the former,[410] a conclusion consistent with heterolytic dissociation of the carbon–carbon bond that produces a carbanion at carbon 6 of orotidine 5′-monophosphate. Because this carbanion would be destabilized by the 5-fluoro group and significantly more difficult to form, the transition state should occur earlier for the fluoro reactant.

The intrinsic, primary nitrogen-15 kinetic isotope effect on the rate-liming step in hydrolysis of *N*-benzoyl-L-arginine amide by papain from *C. papaya* is 1.024. Because this value is at the upper limit for observed primary nitrogen-15 kinetic isotope effects on nonenzymatic reactions, this result was presented as evidence that the rate-limiting step in the enzymatic reaction is dissociation of the α-amino group of the L-arginine amide from the tetrahedral intermediate formed when the sulfido group of Cysteine 25 in the active site adds nucleophilically to the amide in the reactant.[397]

Secondary isotope effects, although they are quite small, are also observed for isotopic substitutions of carbon, nitrogen, and oxygen at atoms adjacent to an atom at which a bond is broken. For example, the intrinsic secondary nitrogen-15 kinetic isotope effect is 1.0025 ± 0.0002 for the step in the mechanism of aspartate carbamoyltransferase from *E. coli* in which the carbamoyl group in carbamoyl phosphate is transferred in a nucleophilic substitution from the oxygen of phosphate to the α-amino group of L-aspartate. The secondary nitrogen-15 kinetic isotope effect on dissociation of monomeric metaphosphate from the monoanion of carbamoyl phosphate during its decomposition is 1.0028 ± 0.0002. This fact suggests that, in the active site of the enzyme, the nucleophilic substitution is dissociative, with monomeric metaphosphate leaving before the α-amino group adds to the carbonic carbon of the resulting carbamate.[411]

Solvent kinetic isotope effects are the effects on the rate of a reaction that result when another isotopic form of the solvent is substituted for the naturally occurring isotopic form. The only solvent kinetic isotope effects that can be measured for enzymatic reactions, **solvent deuterium kinetic isotope effects**, are those observed when ^2H_2O is used as solvent instead of ^1H_2O.* It is possible to use the existence of a solvent deuterium kinetic isotope effect on the catalytic constant or a specificity constant as evidence for a contribution of hydron transfer to a rate-affecting step in the enzymatic mechanism.[412] The quantitative interpretation of the observed effects is similar to that for a primary deuterium kinetic isotope effect (Equations 4–199 and 4–201). Major drawbacks of these measurements, however, are that the hydron being transferred cannot be identified and that it is possible for the rates of several steps in the mechanism to be affected rather than just one. These drawbacks make the interpretation considerably less informative.

When ^2H_2O is substituted for ^1H_2O, **only hydrons on heteroatoms**—in the case of enzymes and substrates, oxygen, nitrogen, and sulfur—can exchange rapidly enough with the deuterons in solution and subsequently produce the resulting kinetic isotope effects that are observed. Hydrogens that are transferred during the enzymatic reaction as hydrogen atoms or hydrides are almost always uninvolved in such exchanges. Consequently, unlike experiments in which a hydrogen on a carbon in a substrate is synthetically changed to a deuterium, the deuterons that are participating in the enzymatic reaction and producing the solvent deuterium kinetic isotope effect can be on either heteroatoms in the substrate or, more likely, heteroatoms of the catalytic acid–bases in the active site. These catalytic acid–bases often are the same ones responsible for the decreases in steady-state kinetic constants above or below

*It should be obvious that, for practical reasons, solvent tritium kinetic isotopic effects cannot be measured.

particular values of pK_a observed in pH–rate profiles. By examining the solvent deuterium kinetic isotope effects on pH–rate profiles, the solvent deuterium kinetic isotope effects observed at a particular pH can be understood.

When ^2H_2O is substituted for ^1H_2O, apparent values of pK_a governing the pH–rate profiles for enzymatic reactions almost always shift to higher values of pH. These **upward shifts in pK_a** are revealed in pH–rate profiles of the common logarithms of steady-state rate constants (Figure 4–24).[413,414] The shift in pK_a can be only for the acid dissociation of the conjugate acid of the catalytic acid–base, and an acid dissociation constant is an equilibrium constant. Consequently, an acid dissociation constant always decreases when ^2H_2O is substituted for ^1H_2O. Therefore, each shift in pK_a is an upward shift, both when an apparent steady-state rate constant decreases below a particular pK_a, because the catalytic acid–base is acting as a base, and when an apparent steady-state rate constant decreases above a particular pK_a, because the catalytic acid–base is acting as an acid. The increases in pK_a observed for catalytic acid–bases in enzymatic reactions that result from substitution of ^2H_2O for ^1H_2O are usually in the range of 0.4–1.0 unit of pH.[413-416]

These upward shifts of pK_a have a significant effect on the value for a solvent deuterium kinetic isotope effect when it is measured at only one particular pH. In such an instance, the observed value could either be a result of an intrinsic, primary deuterium kinetic isotope effect on the actual transfer of the hydron between the heteroatom on the reactant and the catalytic acid–base that accepts or donates the hydron, an informative value, or simply due to the usual uninformative shift in pK_a. Consequently, a solvent deuterium isotope effect measured in the absence of a pH–rate profile can be misleading.

When an apparent steady-state rate constant decreases below an apparent pK_a but does not decrease above an apparent pK_a (Figure 4–24B), the solvent deuterium kinetic isotope effect at all values of pH will usually be normal. A **normal kinetic isotope effect** is a decrease in a rate constant that results from substitution of a lighter isotope with a heavier isotope. Measurements of a solvent deuterium kinetic isotope effect at values of pH below a pK_a at which the rate constant is decreasing is normal because both the decrease in the solvent deuterium kinetic isotope effect resulting from the shift in pK_a and the intrinsic solvent deuterium kinetic isotope effect on the pH-independent microscopic rate constant for transfer of the hydron are in the same direction.

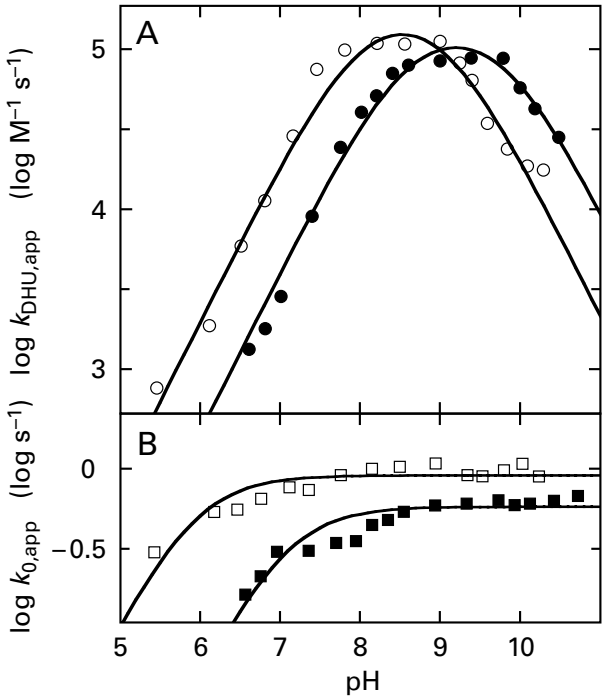

Figure 4–24: Effect of pH on the solvent deuterium kinetic isotope effect for the reaction catalyzed by porcine dihydropyrimidinase.[413] Initial rates for the conversion of 5,6-dihydrouracil into 3-ureidopropanoate that is catalyzed by the enzyme were measured spectrophotometrically at 225 nm in solutions prepared in H_2O and in D_2O with various concentrations of 5,6-dihydrouracil at various values of pH. Values for the specificity constant $k_{DHU,app}$ (○, ●, molar^{-1} second^{-1}) for 5,6-dihydrouracil (DHU) and the catalytic constant $k_{0,app}$ (□, ■, second^{-1}) were determined at each pH in H_2O (○, □) and at each pD in D_2O (●, ■), and their common logarithms are plotted as a function of the pH. The curves fit to the data for the steady-state rate constant $k_{DHU,app}$ are those for Equation 4–97 (replacing AG6 with DHU) with pK_{a3} = 8.05, pK_{a4} = 9.0, and k_{DHU} = 220 mM^{-1} s^{-1} in H_2O and pK_{a3} = 8.6, pK_{a4} = 9.8, and k_{DHU} = 160 mM^{-1} s^{-1} in D_2O. The curves fit to the data for the catalytic constant $k_{0,app}$ are those for Equation 4–80 with pK_a = 5.9 and k_0 = 0.91 s^{-1} in H_2O and pK_{a3} = 7.05 and k_0 = 0.58 s^{-1} in D_2O.

When a apparent steady-state rate constant decreases above an apparent pK_a, however, the solvent deuterium kinetic isotope effect at values of pH greater than the apparent pK_a will usually be inverse (Figure 4–24A). An **inverse kinetic isotope effect** is a counterintuitive increase in an apparent rate constant resulting from substitution of a lighter isotope for a heavier isotope. This inverse solvent deuterium kinetic isotope effect at a particular pH results from the fact that the upward shift in pK_a

produced by substitution of a hydron with a deuteron raises the profile at values of pH greater than the pK_a of the deuterated acid–base. This increase resulting from the shift in pK_a usually has a greater effect on the rate constant at a given pH than the normal kinetic isotope effect on the underlying pH-independent microscopic rate constant for transfer of the hydron from the catalytic acid that is observed at low pH.

Usually, the **pH-independent solvent deuterium kinetic isotope effects on the underlying apparent rate constants are normal**, as they are in Figure 4–24 (notice that, at the respective maxima in Figure 4–24A and at the pH-independent plateaus in Figure 4–24B, the apparent rate constants have normal solvent deuterium kinetic isotope effects). When a hydron is substituted with a deuteron, the transfer of the hydron usually becomes slower. In some instances, however, the solvent deuterium kinetic isotope effects on the pH-independent rate constants are inverse.[416,417] As with inverse primary deuterium kinetic isotope effects, one reason for inverse solvent deuterium kinetic isotope effects is that c_r is large and the equilibrium isotope effect, $^{D}K_{eq}$, is inverse. Another possibility is that the tautomeric equilibrium between an active and an inactive tautomer of the active site is shifted by substitution of deuterons for hydrons in favor of the active tautomer, again by an equilibrium isotope effect.

If the only effect of changing solvent from ^1H_2O to ^2H_2O is on hydron transfer in a single microscopic step in the kinetic mechanism and if c_f, c_r, and the ratio α_0 are small, the solvent deuterium kinetic isotope effects on the steady-state rate constants should be the same and equal to the intrinsic solvent deuterium kinetic isotope effect. If they are not the same, it is, as usual, taken as evidence that other steps in the reaction are rate-affecting and suppress the intrinsic solvent deuterium kinetic isotope effect.[418] As with primary deuterium kinetic isotope effects, if mutation of an amino acid[419,420] or changes in the reactant[421] decrease a steady-state rate constant but increase the solvent deuterium kinetic isotope effect on that rate constant, one can conclude that the amino acid or the reactant is a direct participant in a step in which a hydron that is in rapid exchange with hydrons in the solution is transferred.

In simple situations in which all hydron transfers occur in only one step, it is also possible to use solvent deuterium kinetic isotope effects at a fixed pH, if they exist, to **estimate how many hydrons are being transferred in the transition state** of that step.[422] The equation[423,424] that is used to describe the value of a particular rate constant as a function of the mole fraction of D_2O in a solvent of H_2O, x_{D_2O}, is

$$\frac{k_x}{k_{ref}} = \prod_{i=1}^{n} \left(1 - x_{D_2O} + \phi_i^{\ddagger} x_{D_2O}\right) \qquad (4\text{–}220)$$

where k_x is the rate constant in a solvent of mole fraction x_{D_2O}, k_{ref} is the rate constant in ^1H_2O, $^{\ddagger}\phi_i$ is a fractionation factor for the ith hydron that is transferred in the transition state (‡), and n is the number of hydrons being transferred. In theory, there is a unique fractionation factor for each hydron; in practice, values for the fractionation factors obtained from the fit of the equation to the data are usually the same within the error of measurement.[424-426] This equation applies for both normal and inverse[414] solvent deuterium kinetic isotope effects. It must be the case, however, that the kinetic isotope effect being plotted is an intrinsic solvent deuterium kinetic isotope effect that is not masked by commitments.[427] It is also necessary to distinguish solvent deuterium kinetic isotope effects on the transfer of hydrons in a transition state from the effect of ^2H_2O on the viscosity of the solution[428] or on conformational changes in the enzyme.[429]

If only one hydron is being transferred in the transition state of the step that displays the intrinsic solvent deuterium kinetic isotope effect, there should be a linear relation between the fraction of protium in the solvent that has been replaced by deuterium and the numerical value for that kinetic isotope effect.[415,430] As hydrogen is replaced by deuterium, the microscopic rate constant should change linearly in concert. Such a linear solvent deuterium kinetic isotope effect on the catalytic constant of L-aspartate oxidase from *E. coli* was the basis of the conclusion that only one hydron was being transferred in the transition state of the reaction, a conclusion consistent with the mechanism of the enzyme being the same as other amino acid oxidases even though it is unrelated to them.[431]

If, however, two hydrons are being transferred in the transition state of the step in the reaction producing the deuterium solvent kinetic isotope effect, then the numerical value for the intrinsic deuterium solvent kinetic isotope effect should be a quadratic function (Equation 4–220) of the fraction of hydrogen that has been replaced with deuterium, as was seen with the solvent deuterium kinetic isotope effect on the catalytic constant of nitrile hydratase from *Pseudonocardia thermophila* (Figure 4–25).[424-426]

The result in this instance cannot distinguish between a quadratic fit and a cubic fit, but it definitely indicates that more than one hydron is being transferred in the transition state. This conclusion was used to argue that, in the transition state for the reaction, a hydron is removed from the water that adds nucleophilically to the nitrile by the hydroxy group of Serine 112 in the active site simultaneously with the transfer of the hydron that was on the hydroxy group of the serine to the 4-oxidophenyl group of Tyrosine 68.[432] In this way, the basicity of the oxido group of Tyrosine 68 is relayed through Serine 112 by two coincident hydron transfers.

In addition to identifying steps in a kinetic mechanism in which a hydrogen is transferred, primary deuterium kinetic isotope effects can also be used to determine the regiochemistry or stereochemistry of a transfer of a hydrogen catalyzed by an enzyme.[433,434] For example, the primary deuterium kinetic isotope effect for the desaturation of a [4,4-$^2H_2$]ceramide by sphingolipid 4-desaturase

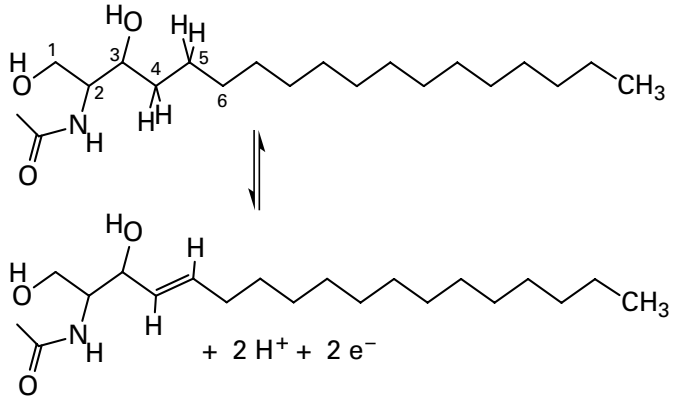

(4–221)

from *R. norvegicus* was 8.3 while that for the [5,5-$^2H_2$]ceramide was 1.02, even though a hydrogen is removed from both carbon 4 and carbon 5 during the enzymatic reaction. These observations demonstrate that the rate-limiting step in the reaction is removal of the hydrogen atom from carbon 4 by the prosthetic oxodiiron(IV) in the active site[435]

The primary deuterium kinetic isotope effect for the specificity constant k_{Ppc} for the oxidation of (2*S*,6*R*)-[6-^{2}H]pipecolate (Ppc) by L-pipecolate oxidase from *Macaca mulatta* is 3.7 while that for (2*S*,6*S*)-[6-^{2}H]pipecolate is 1.0. This fact indicates that the enzyme removes the *pro-R* hydrogen rather than the *pro-S* hydrogen from carbon 6 during the

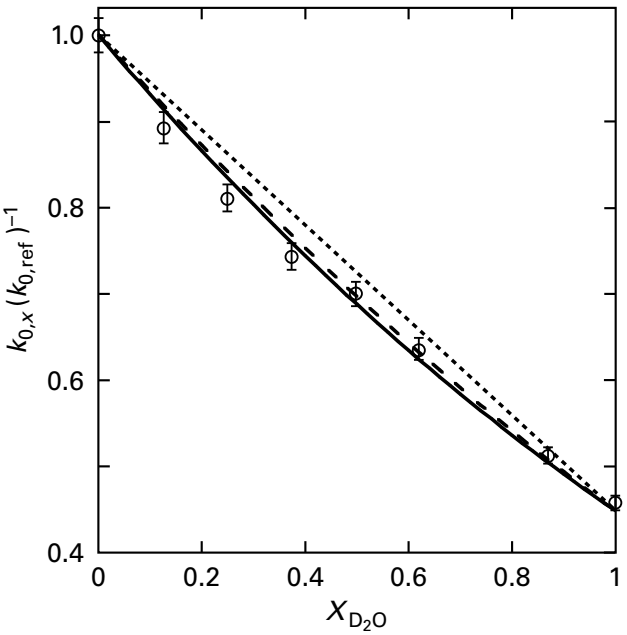

Figure 4–25: Variation in the numerical value of the catalytic constant k_0 for nitrile hydratase from *P. thermophila* with changes in the mole fraction (x_{D_2O}) of D_2O in the solvent.[425] Solutions containing various concentrations of benzonitrile were prepared at pH 7.6 and 25 °C. The solutions were prepared with various mole fractions of D_2O in H_2O. The hydration of benzonitrile was followed by the change in absorbance at 242 nm. For each mole fraction of D_2O, the initial rates at several concentrations of benzonitrile were used to obtain the catalytic constant k_0. The ratio of the catalytic constant, $k_{0,x}$, at each mole fraction (x_{D_2O}) of D_2O to the catalytic constant, $k_{0,ref}$, in pure H_2O is presented as a function of the mole fraction (x_{D_2O}) of D_2O. The solid curve is for the cubic version of Equation 4–220 ($n = 3$) with a common fractionation factor $^{\ddagger}\phi = 0.765$. The curve of long dashes is for the quadratic version of Equation 4–220 ($n = 2$) with fractionation factors of $^{\ddagger}\phi_1 = 0.66$ and $^{\ddagger}\phi_2 = 0.68$. The line of short dashes simply connects the values of the two curves at 0 and 1.

oxidation.[433,436] The **stereochemistry for removal of hydrogen** from a reactant, such as the one in this last example, provides information about the orientation of the acceptor for the hydrogen in an active site.

Suggested Reading

Farnum, M., Palcic, M., and Klinman, J. P. (1986) pH Dependence of deuterium kinetic isotope effects and tritium exchange in the bovine plasma amine oxidase reaction: A role for single-base catalysis in amine oxidation and imine exchange, *Biochemistry 25,* 1898–1904.https://doi.org/10.1021/bi00356a010

Zgiby, S., Plater, A. R., Bates, M. A., Thomson, G. J., and Berry, A. (2002) A functional role for a flexible loop containing Glu182 in the class II fructose-1,6-bisphosphate aldolase from *Escherichia coli*. *J. Mol. Biol. 315*, 131–140. https://doi.org/10.1006/jmbi.2001.5237

Problem 4–12: Phosphopyruvate hydratase catalyzes the reaction

$$\text{2-phospho-D-glycerate} \rightleftharpoons \text{phospho}\textit{enol}\text{pyruvate} + H_2O$$

(A) Write a mechanism for this reaction that has at least two steps, in each of which a hydron transfer occurs. Indicate all removals and additions of hydrons. Incorporate catalytic acids, –$NH^{(+)}$, and catalytic bases, –$B\odot^{(-)}$, on the enzyme into your mechanism.

2-Phospho[2-^{2}H]glycerate was synthesized as a reactant for phosphopyruvate hydratase from *S. cerevisiae*. There are 46,700 g for every mole of active sites. The following data were obtained under the same set of conditions (0.9 μg of phosphopyruvate hydratase mL^{-1} at pH 7.81 and 30 °C) for the two reactants.[437]

2-phospho-[2-^{1}H]glycerate		2-phospho-[2-^{2}H]glycerate	
$[PGA]_0$[a] (mM)	v_0 (ΔA_{230} min^{-1})	$[PGA]_0$[a] (mM)	v_0 (ΔA_{230} min^{-1})
0.25	0.480	0.25	0.228
0.10	0.369	0.10	0.169
0.05	0.274	0.05	0.123
0.025	0.180	0.025	0.086

[a]Concentration of phosphoglycerate (PGA) of noted isotopic composition.

where v_0 is the initial rate of the dehydration.

(B) Determine the limiting rate V (Equation 3–45) and the Michaelis constant K_m (Equation 3–44) for each substrate under these conditions.

(C) How are they related to the catalytic constant and the steady-state rate constant k_{PGA} for phosphogylycerate (PGA)?

(D) What piece of information is missing to prevent the calculation of k_0 and k_{PGA}?

The limiting rate V for the enzymatic reaction was measured in the direction of dehydration, as a function of pH for the reactants containing protium and deuterium, respectively.[437]

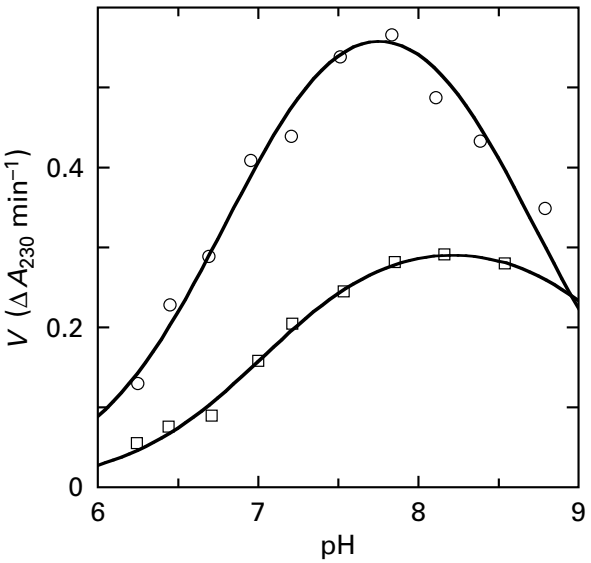

Maximum rates V (ΔA_{230} min^{-1}) for (○) protiated and (□) deuterated reactants as a function of pH.

(E) Why would a plot of the catalytic constant (Equation 3–46) for protiated reactant show a maximum?

When the ratios between the maximum rates for protiated reactant and deuterated reactant, $V_H (V_D)^{-1}$, are plotted as a function of pH, the following results were obtained.[437]

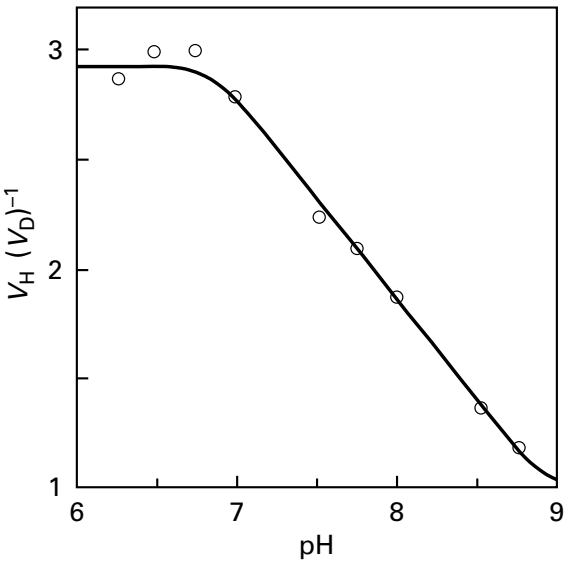

(F) Explain, in terms of the considerations you made in parts A–C, why the magnitude of the

primary deuterium kinetic isotope effect diminishes as the pH is raised.

Problem 4–13: The primary deuterium kinetic isotope effects on the specificity constant k_{NE} (○) for [1,1-$^2H_2$]nitroethane (NE) and the catalytic constant k_0 (□) for the reaction catalyzed by nitroalkane oxidase from *F. oxysporum* are plotted as a function of pH.[330]

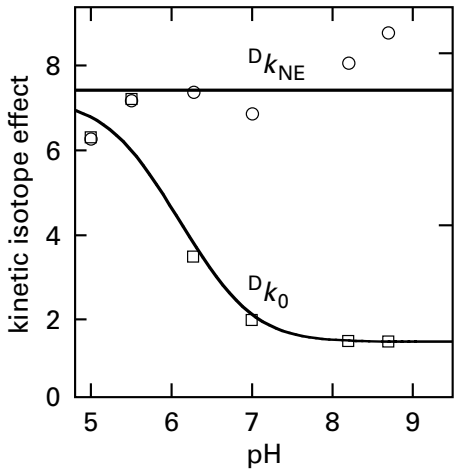

(A) Why does the primary deuterium kinetic isotope effect for k_0 increase as the pH is decreased?
(B) What is probably the intrinsic, primary deuterium kinetic isotope effect for the step in which the hydrogen on nitroethane is transferred?
(C) What can be deduced about the magnitudes of the commitment forward, c_f, the commitment in reverse, c_r, and the ratio α_0 at pH 8?
(D) The change in which of these three parameters is responsible for the increase in $^Dk_0$ at low pH?

Problem 4–14: The enzyme steroid Δ-isomerase catalyzes the following reaction.

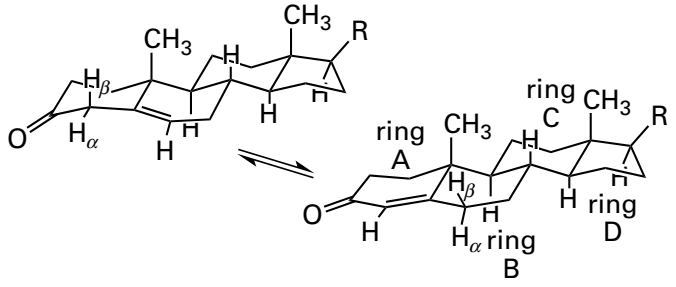

(1)

The enzyme has been purified from *C. testosteroni* and *P. putida*. The enzyme is rather tolerant about R, using many steroids as substrates. Since the chemical transformation occurs in only the A and B rings, the C and D rings will no longer be drawn. The same transformation catalyzed by the enzyme occurs spontaneously, albeit at a much reduced rate, under acidic conditions. The mechanism of this nonenzymatic reaction is

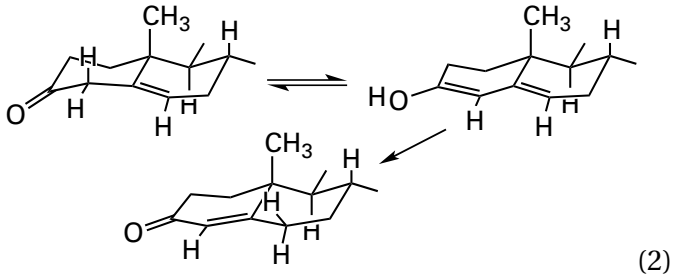

(2)

When the following deuterated reactants were synthesized and mixed with the enzyme in buffered H_2O, the noted products were obtained.[438] The numbers in parentheses below each structure are the moles of deuterium for each mole of the respective compound.

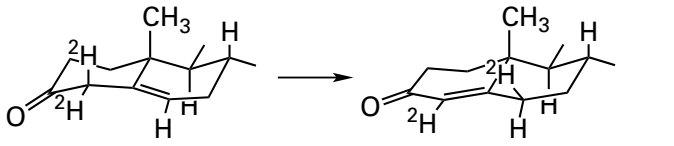

(3)

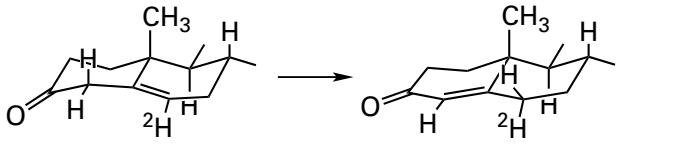

(4)

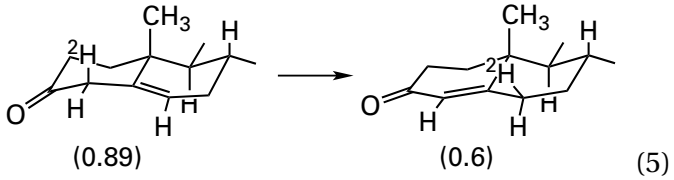

(5)

In each case, the reaction is written as if it were irreversible because the equilibrium strongly favors the conjugated product. The absolute configuration of each deuterated product was verified by infrared spectroscopy; and its deuterium content, by mass spectrometry.

The kinetics of the reaction in Equation 5, in which the 4β-monodeuterated ketosteroid was used as substrate, were compared with those of the reaction in which the undeuterated ketosteroid of

the same structure was used as substrate. It was determined that the deuterium kinetic isotope effect on the catalytic constant was 5.35.

(A) Write out a detailed enzymatic mechanism that explains the observations. Choose specific amino acid side chains to perform various catalytic functions. At the moment, you do not know which amino acid side chains actually perform these roles, but you should pick appropriate ones. Start with reactant bound to the active site and finish with product bound to the active site. Draw the structure of substrate, intermediates, and product in sawhorse configuration, and indicate clearly all stereochemistry. Your mechanism must explain the absolute configuration of the deuterated products and the retention of deuterium in the product.

(B) When the enzymatic reaction was performed in deuterium oxide (^2H_2O) with an undeuterated reactant, 0.12 mole of deuterium was incorporated at the 6β position for every mole of product produced. As the reactions of Equations 3 and 5 proceed, some deuterium is lost to the solvent. Explain all these observations by referring to your mechanism in part A. At which step is the deuterium gained from or lost to the solvent, and how does this happen? Present your answer in a series of acid–base equilibria.

The magnitude of the primary deuterium kinetic isotope effect observed for the catalytic constant suggests that dissociation of the 4β carbon–hydrogen bond is the rate-limiting step in the reaction. If it is, all subsequent steps are very rapid and can be ignored. Convince yourself that, under these circumstances, the simplest kinetic mechanism, the one in Equation 4–149, is appropriate. The specificity constant, k_{KS}, for β-monodeuterated ketosteroid (KS) for the reaction of Equation 5 is ${}^{D}k_{KS} = 380\ \mu M^{-1}\ s^{-1}$, while that for the same reactant when the ketosteroid is undeuterated is ${}^{H}k_{KS} = 910\ \mu M^{-1}\ s^{-1}$. The catalytic constant ${}^{H}k_0$ for the undeuterated substrate is $2.8 \times 10^5\ s^{-1}$.

(C) Make the reasonable assumption that the presence of a deuterium at the 4β position has no effect on the binding of substrate to the enzyme so that ${}^{D}k_1 = {}^{H}k_1$ and ${}^{D}k_{-1} = {}^{H}k_{-1}$. Explain mathematically why ${}^{H}k_{KS} \neq {}^{D}k_{KS}$, and determine definite values for k_1, k_{-1}, and ${}^{D}k_2$.

(D) Copy the drawing of the structure of the A and B rings of a ketosteroid; and, on your drawing, indicate how the enzyme could strain it and cause it to resemble the intermediate in the enzymatic reaction.

Problem 4–15: Human adenine phosphoribosyltransferase catalyzes the following reaction.

magnesium 5-phospho-α-D-ribose 1-diphosphate
+ adenine $\rightleftharpoons$ adenosine 5′-phosphate
+ magnesium diphosphate

(A) Draw a chemical mechanism for the enzymatic reaction as it would occur within the active site. Use specific amino acid side chains as catalytic acids and bases. Draw the reaction with proper stereochemistry at carbon 1 of the ribose throughout.

The kinetics of the enzymatic reaction have been examined as a function of pH (Figure A),[439] and a solvent deuterium kinetic isotope effect was observed when the enzymatic reaction is carried out in ^2H_2O.[439]

Figure: Effect of pH and solvent deuterium isotope effect for the reaction catalyzed by human adenine phosphoribosyltransferase.[439] (**A**) The limiting rate V of the enzymatic reaction at 10 °C and at saturation with both 5-phospho-α-D-ribose 1-diphosphate and adenine is plotted as a function of pH. (B) Reciprocals of the maximum rates V^{-1} at saturation with adenine and different unsaturating concentrations of 5-phospho-α-D-ribose 1-diphosphate (■) in H_2O, maximum rates at saturation with 5-phospho-α-D-ribose 1-diphosphate and different unsaturating concentrations of adenine (●) in H_2O, maximum rates at saturation with adenine and different unsaturating concentrations of 5-phospho-α-D-ribose 1-diphosphate (□) in D_2O, and maximum rates at saturation with 5-phospho-α-D-ribose 1-diphosphate and different unsaturating concentrations of adenine (■) in H_2O are plotted as a function of the reciprocals of the concentration of reactant present below saturation.

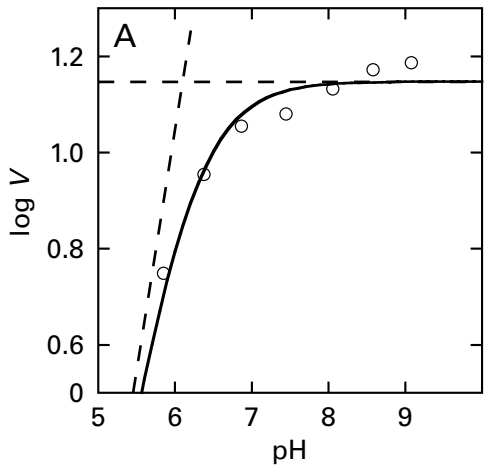

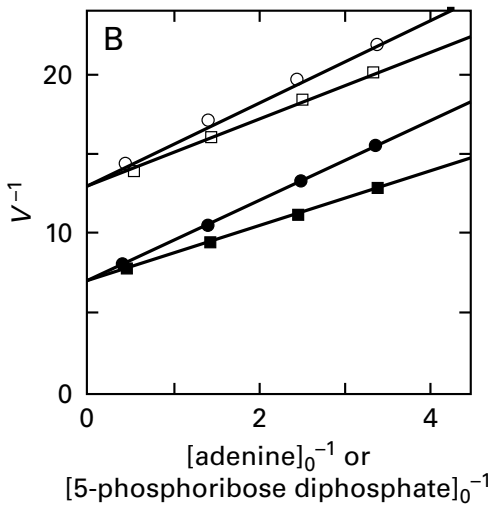

(B) What appears to be the pK_a of the group in the active site the ionization of which causes the behavior observed in Figure A? Is it a catalytic acid or a catalytic base in the mechanism of the enzymatic reaction? What form of the enzyme is titrating? What side chain in your mechanism could be the group that is titrating?

In ^2H_2O, the only form of adenine present is N^6,N^6,N^9-trideuteroadenine. The possibility can now be examined that the deuterium solvent kinetic isotope effect seen in Figure B could arise from removal of a deuterium atom from N^6,N^6,N^9-trideuteroadenine during a rate-limiting step in the enzymatic reaction.

(C) From the value for the equilibrium constant for the following acid–base reaction in solution

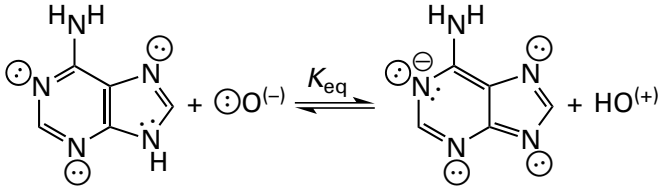

where HO has a pK_a = 6.1 and adenine has a pK_a = 9.8 and with the assumption that hydron transfer in the direction of hydronating the adenine anion is encounter-controlled with a value of 10^{10} M^{-1} s^{-1} (Figure 1–1B), calculate the rate constant for transfer of the hydron from adenine to the base.

(D) Considering the effect of approximation, what would you expect to be the first-order rate constant for hydron removal from adenine on the active site?

(E) The catalytic constant of human adenine phosphoribosyltransferase is 4 s^{-1} at 37 °C.[440] To what is the solvent deuterium kinetic isotope effect not due, and to what else could it be due?

Stereochemistry

Enzymes usually catalyze reactions in which only one enantiomer or diastereomer of each reactant is converted into only one enantiomer or diastereomer of each product. This behavior is so fundamental to biochemistry that different diastereomers of the same compound are given different names. For example, (3*S*,4*R*,5*R*)-1,3,4,5,6-pentahydroxyhexan-2-one is called D-fructose and (3*S*,4*S*,5*R*)-1,3,4,5,6-pentahydroxyhexan-2-one is called D-tagatose.

The **chiral exclusivity of the usual active site** is illustrated in the extreme by the L-methionine *S*-oxide reductases. Two enantiomers of methionine sulfoxide

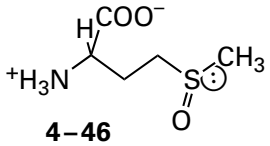

4–46

L-methionine (*R*)-sulfoxide

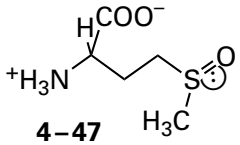

4–47

L-methionine (*S*)-sulfoxide

are produced at random when methionines in proteins are oxidized adventitiously, unavoidably, and nonenzymatically. Even though the structures differ by only the stereochemistry of a lone pair of electrons, the spontaneous inversion of the lone pair of electrons at the sulfur to equilibrate the two diastereomers does not occur at a significant rate at physiological temperatures[441] Consequently, two different, unrelated enzymes, L-methionine (*R*)-*S*-oxide reductase and L-methionine (*S*)-*S*-oxide reductase, are required to reduce the two enantiomers back to L-methionine[442,443] because the catalytic groups

operating on the one enantiomer must be in a different orientation from those operating on the other when the respective substrate is bound within the respective active site.

For enzymes that catalyze bimolecular or trimolecular reactions, the identities of the diastereomers or enantiomers that are substrates for enzymatic reactions **dictate how these substrates must be positioned by the active site** relative to each other to maintain the stereochemistry required of reactants and products. These relative orientations are observed in the crystallographic molecular model of a particular active site for such an enzyme when it is occupied by more than one of its substrates or analogues of its substrates. For example, there are two different enzymes, fructose-bisphosphate aldolase (Equation 4–210) and a class II tagatose-bisphosphate aldolase, in the cytoplasm of *E. coli*. These two enzymes convert the same two substrates, D-glyceraldehyde 3-phosphate and glycerone phosphate, into D-fructose 1,6-bisphosphate and D-tagatose 1,6-bisphosphate, respectively. Two different enzymes are required because the enamine of glycerone phosphate is aligned on the opposite faces of the carbonyl carbon on glyceraldehyde 3-phosphate in the respective active sites to accomplish the proper aldol condensations.[444]

The chiral exclusivity of active sites, however, is not universal. There are a few enzymes that are able to perform the same reaction on several different substrates as long as the differences are not at the positions at which the reaction occurs. The absolute configuration of each of these different substrates at these positions must be the same[445] because each of the different reactants still must be complementary to the one and only configuration of the catalytic groups in the active site.

An even rarer exception to the rule of chiral exclusivity, however, is a class I fructose-bisphosphate aldolase in *S. aureus* that produces D-tagatose 1,6-bisphosphate, D-psicose 1,6-bisphosphate, and D-sorbose 1,6-bisphosphate in addition to D-fructose 1,6-bisphosphate; each product is formed from D-glyceraldehyde 3-phosphate and glycerone phosphate.[446] These four products are the four 2-oxo-D-hexoses that are diastereomeric at carbons 3 and 4, the two carbons that are joined in the aldol condensations catalyzed by the enzyme. This **rare stereochemical promiscuity** results from two departures from the usual requirement that reactants be held in the active site by donors and acceptors for hydrogen bonds and steric effects in only one rigid orientation relative to each other so that only one of the possible diastereomeric products results. In fact, this particular exception to the rule illustrates how the stereochemical requirement is enforced in most cases. First, there are two different sets of donors and acceptors for hydrogen bonds that permit the hydroxy group on the nucleophilic carbon in the enamine that is the intermediate in the reaction catalyzed by the enzyme (Figure 4–26) to assume either the *E* or *Z* configuration,[447] which directs either the *Re* or *Si* face*, respectively, of carbon 3 in the enamine toward the aldehyde and produces the *R* or *S* configuration at carbon 3 in the product. Second, the aldehyde of D-glyceraldehyde 3-phosphate is able to present either its *Si* or *Re* face to the double bond of the enamine (Figure 4–26),† which produces the *R* or *S* configuration, respectively, at carbon 4.

In the case of class II tagatose-bisphosphate aldolase from *E. coli*, the active site provides donors and acceptors for the hydroxy group of the enamine of glycerone phosphate in only one orientation so that only the *Si* face of carbon 3 is directed toward the aldehyde, and the active site holds the carbonyl group of the aldehyde of D-glyceraldehyde 3-phosphate tightly so that only its *Re* face is directed toward the enolate. Consequently, only D-tagatose 1,6-bisphosphate is the product. In the case of fructose-bisphosphate aldolase from *E. coli*, the *Si* face of the enolate is directed to the *Si* face of the aldehyde so that only fructose 1,6-bisphosphate is the product.

Another departure from the almost universal stereochemical rigor of active sites, albeit less dramatic than that of fructose-bisphosphate aldolase from *S. aureus*, occurs in *N*-acetylneuraminate lyase from *E. coli*, in which either the *Si* or the *Re* face of an aldehyde is presented to the enolate of pyruvate.[448] In this instance, however, the face of the aldehyde presented to the enolate depends on the identity of that aldehyde, so for each aldehyde, the reaction is stereospecific.

*If the substituents around a trigonal carbon, when one of its two faces is being viewed, appear in a clockwise sense in order of priority, the face that is being viewed is the *Re* face. The opposite face, in which they appear to the observer in counterclockwise order, is the *Si* face.

†The sawhorse drawings of open-chain molecules used in this book are oriented so that the lower carbon in a carbon–carbon bond that is drawn diagonally is always in front of the upper carbon.

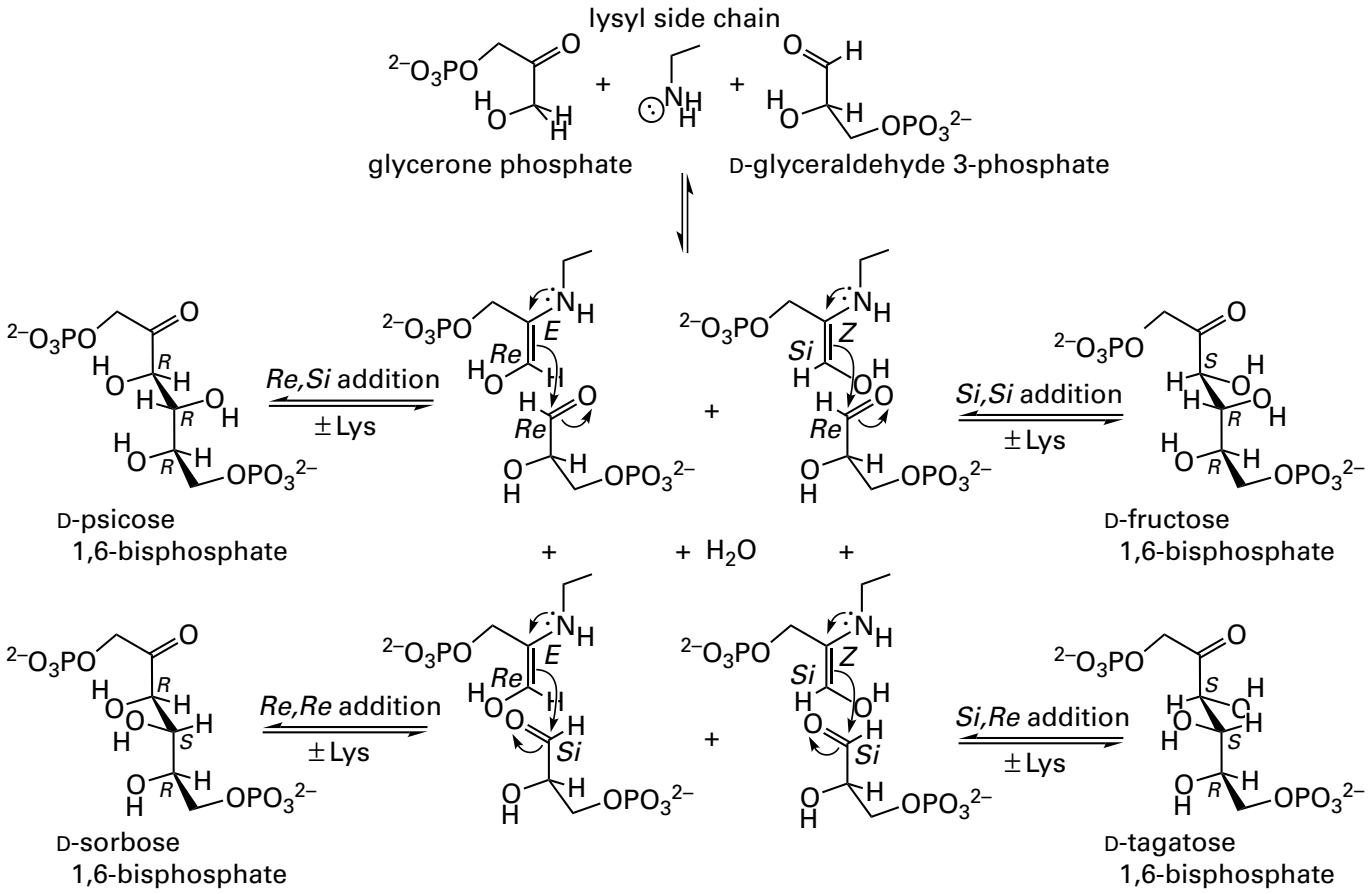

Figure 4–26: Stereochemical explanation for the promiscuity of the products from the reaction catalyzed by class I fructose-bisphosphate aldolase in *S. aureus* that produces D-psicose 1,6-bisphosphate, D-sorbose 1,6-bisphosphate, and D-tagatose 1,6-bisphosphate, in addition to D-fructose 1,6-bisphosphate, from glycerone phosphate and D-glyceraldehyde 3-phosphate. Stereochemical designations are given for the three chiral carbons in each of the four products, the double bond in each of the four enamines, the distal carbon in each of the four enamines, and the front face of each of the four aldehyde carbons. In each of the four additions, the enolate is added to the back face of the aldehyde, so the stereochemical designation for the addition (written above the arrows) is opposite from that for the front face.

There are also examples where the same enzyme in two different species catalyzes the **same chemical reaction but with different stereochemical outcome**s even though each enzyme operates with chiral exclusivity. For example, the TDP-4-oxo-6-deoxy-α-D-glucose-3,4-oxoisomerases

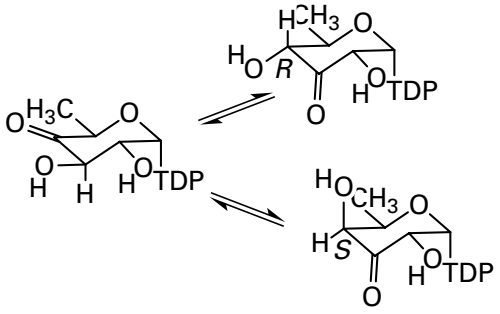

(4–222)

from *Thermoanaerobacterium thermosaccharolyticum* and *Aneurinibacillus thermoaerophilus*, respectively, are closely related enzymes (48% identity; 0 gap percent), but the former produces exclusively the *R* epimer at carbon 4 of the hexose and the latter produces exclusively the *S* epimer (Equation 4–222). Strangely enough, both active sites contain the histidine responsible for transferring the hydron between the two oxygens, the tyrosine responsible for hydronating carbon 4 to produce the *R* epimer in the former instance, and the histidine responsible for removing the hydron from carbon 3 in both instances and hydronating carbon 4 to produce the *S* epimer in the latter instance, and these catalytic acid–bases are in the same locations in both active sites.[449] Presumably, the structures of the two active sites are different enough that the histidine cannot

reach carbon 4 in the former instance and the tyrosine cannot reach carbon 4 in the latter instance.

In spite of the few exceptions that prove the rule, the degree of **stereochemical preference displayed by an active site for the formation of bonds between elements of the second and third rows is usually quite high** because, in most cases, whenever the incorrect diastereomer is produced by the enzyme in either direction, it cannot participate in the next reaction in the metabolic pathway to which the enzyme contributes. An extreme case is that of enoyl-CoA hydratase

trans-2-enoyl-SCoA + H_2O $\rightleftharpoons$ (3*S*)-3-hydroxyacyl-SCoA (4–223)

from *R. norvegicus*, which produces 400,000 times more (3*S*)-3-hydroxybutyryl-SCoA than (3*R*)-3-hydroxybutyryl-SCoA.[450] The chiral exclusivity of a particular enzyme can be decreased or the chirality of the product can even be inverted by mutation of amino acids in the active site,[451-455] but these mutant enzymes are not required to participate in metabolism and be subjected to natural selection. Whether or not cells of *S. aureus* do anything with the D-sorbose 1,6-bisphosphate and D-psicose 1,6-bisphosphate produced by their class I tagatose-bisphosphate aldolase is unclear, but they are able to ferment D-sorbitol.[456] Because it is so fundamental to the coordination of metabolism and so easy to understand, the stereochemical exclusivity of enzymatic catalysis when substrates are participants in metabolism is taken for granted.

There are natural instances, however, in which reactants and products of an enzymatic reaction do not participate in metabolism and are not required to have a particular stereochemistry, but the enzymatic reaction still proceeds with high stereochemical preference. For example, haloacetate dehalogenase from *Rhodopseudomonas palustris* dehalogenates a wide variety of haloacetates, including 2-fluoro-2-phenylacetate. When racemic 2-fluoro-2-phenylacetate is used as a reactant, the enzyme defluoronates only (*S*)-2-fluoro-2-phenylacetate (selectivity for *S* over *R* greater than 500) and produces only (*R*)-2-hydroxy-2-phenylacetate.[457] The observed inversion of configuration is consistent with the established mechanism for the reaction in which the carboxylato group of Aspartate 110 displaces the fluorine in a concerted nucleophilic substitution with inversion of configuration, followed by hydrolysis of the resulting aspartyl ester. Whenever (*R*)-2-fluoro-2-phenylacetate associates with the active site, the fluoro group ends up on the same side of the reactant as the carboxylato group of Aspartate 110, and the nucleophilic substitution cannot occur. Consequently, the strict stereochemistry observed for most enzymatic reactions, even in cases where it is unnecessary, is a consequence of the inescapable orientation of the catalytic groups in the active site relative to the orientation in which the reactant is bound within the active site. These facts are common to almost all active sites, regardless of the purpose of the enzymatic reaction.

The **stereochemistry of the diastereomers and enantiomers that are substrates for the enzymes** and that dictate the structure of active sites were, by and large, determined by organic chemists interested only in the stereochemistry of metabolites and natural products but not in their biosynthesis or catabolism. As a result of these determinations, in most cases the stereochemistry of the substrates for a particular enzymatic reaction had been elucidated before the enzymatic reaction itself was discovered. Consequently, the chemical determination of the absolute* stereochemistry of substrates is usually not a subject for a study of enzymatic mechanisms.

There are exceptions to this generalization. Citrate

4–48

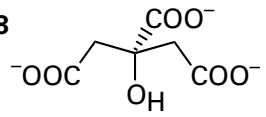

is achiral because the two carboxymethyl groups on the tertiary carbon are identical. To an organic chemist, citrate is simply 3-carboxy-3-hydroxypentanedioate, a molecule of little stereochemical interest. Citrate, however, is prochiral.

A prochiral molecule is a molecule that is achiral but that could become chiral by a single substitution or addition. Citrate is a prochiral molecule because if one, and only one, of the carboxymethyl groups is substituted, say by a carboxydideuteromethyl group, the product of the substitution would be chiral. A **prochiral carbon** is any tetrahedral carbon to which are attached two chemically identical functional groups and two other functional groups, each of which is different from the two

*The absolute stereochemistry of enantiomers and diastereomers that had been previously related to each other was established in 1951 from anomalous scattering of X-rays.[458]

identical ones and different from each other, and that is capable of becoming chiral if one of the identical functional groups were replaced by a functional group different from the other two or a trigonal carbon to which are attached three different functional groups and that is capable of becoming chiral if an additional functional group, different from the other three, were attached. Although chemically identical, the two identical functional groups on a prochiral carbon can be distinguished as unique by a diastereomeric observer. For example, you, as a diastereomeric observer, can readily tell the difference between the two carboxymethyl groups on citrate: one is to the left and the other is to the right when the carboxy group is pointed away from you and the hydroxy group is pointed downward. A substitution of one and only one carboxymethyl group is formally equivalent to distinguishing the left carboxymethyl group from the right carboxymethyl group.

Properly, a prochiral, tetrahedral carbon to which the identical functional groups are attached is distinguished from the functional groups themselves, which should not be described as prochiral. The functional groups are classified as enantiotopic or diastereotopic. If replacement of one of the two identical functional groups on a prochiral, tetrahedral carbon with an achiral functional group different from the other two on the same atom would form one of a pair of enantiomers, then the two identical functional groups are **enantiotopic functional groups**. If replacement of one of the two identical functional groups on a prochiral, tetrahedral carbon with a functional group different from the other two on the same atom would form one of a pair of diastereomers, then the two identical functional groups are **diastereotopic functional groups**. If the two identical functional groups are diastereotopic, there must be a chiral center in one of the nonidentical functional groups. **Stereoheterotopic functional groups** are two identical functional groups that are either enantiotopic or diastereotopic.

The two identical but distinguishable stereoheterotopic functional groups on a prochiral center can be unambiguously designated as *pro-R* or *pro-S*.[459] Choose one of the two identical functional groups and assume that its priority is greater than the other. If this choice makes carbon *R*, the functional group chosen for elevation is the ***pro-R* functional group**; if this choice makes carbon *S*, the functional group chosen for elevation is the ***pro-S* functional group**.

A **trigonal carbon**, such as one carbon in a carbon–carbon double bond or a carbonyl carbon, can also be a prochiral carbon. A trigonal carbon is a **prochiral carbon** if addition of a functional group to that carbon, different from the other three functional groups on that carbon, would cause it to be chiral. In practice, this property usually requires that the three functional groups on the prochiral, trigonal carbon are all different from each other. The two faces of a trigonal, prochiral carbon are **enantiotopic faces** if addition to that carbon of an achiral functional group different from the other three would form one of a pair of enantiomers, and the two faces of a trigonal carbon are **diastereotopic faces** if addition to that carbon of a functional group different from the other three would form one of a pair of diastereomers. A **stereoheterotopic face** is a face that is either enantiotopic or diastereotopic. The stereoheterotopic face of a trigonal carbon is the ***Re* face** if the three functional groups, when viewed from that side of the carbon, appear in a clockwise sense in order of priority. The stereoheterotopic face of a trigonal carbon is the ***Si* face** if the three functional groups, when viewed from that side of the carbon, appear in a counterclockwise sense in order of priority.

Unlike chirality, **prochirality has been of great interest in enzymology**. For example, citrate (*Si*)-synthase (previously Equation 3–226)

$$H^+ + \text{HSCoA} + \text{citrate} \rightleftharpoons H_2O + \text{oxaloacetate} + \text{acetyl-SCoA} \qquad (4\text{–}224)$$

catalyzes the aldol condensation between the enolate of acetyl-SCoA and the carbonyl group on oxaloacetate (2-oxobutanedioate) to produce citrate. In solution, the enolate would add to the carbonyl carbon in oxaloacetate from one or the other of its two surfaces with equal probability because oxaloacetate is achiral. In the active site of citrate synthase, however, it can approach from only one of the two possible directions because both the enolate and the carbonyl group are held in unique orientations. Because this stereochemical question arises only in the context of the enzymatic reaction, it is relevant to the mechanism of the enzyme but not to the stereochemistry of citrate itself.

In a homogenate from *Klebsiella aerogenes* containing ^3H_2O, NADH, and two enzymes, 3-dehydroquinate dehydratase and quinate dehydrogenase, 3-dehydroshikimate is hydrated by the first enzyme

and then reduced by the second to produce (6*R*)-[6-^{3}H]-L-quinate. L-Quinate is a compound the absolute stereochemistry of which had been determined by organic chemists in the past. The (6*R*)-[6-^{3}H]-L-quinic acid produced by the two enzymes was oxidized with periodic acid and then further oxidized with bromine

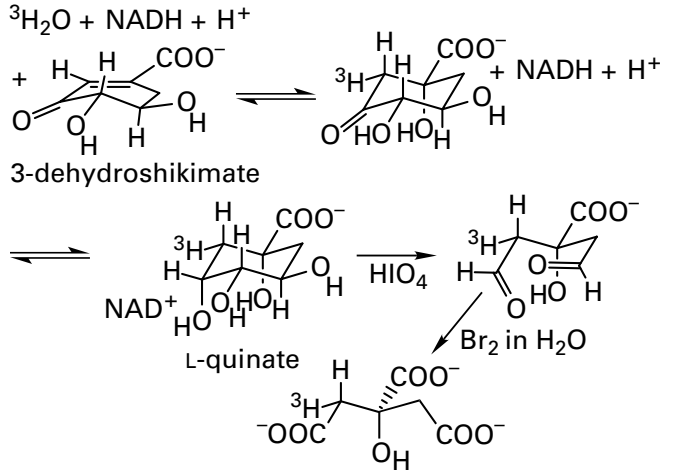

(4–225)

to produce citrate tritiated only in the *pro-R* carboxymethyl group.* This synthetic (2*R*,3*R*)-[2-^{3}H]citrate, when equilibrated with porcine aconitate hydratase, lost all its tritium to water. It had been previously demonstrated that one of the two tritiums in citrate produced from [3,3-$^3H_2$]oxaloacetate is also lost to water on equilibration with aconitate hydratase while neither of the two tritiums on citrate produced from [2,2,2-$^3H_3$]acetyl-SCoA is lost to water on equilibration with aconitate hydratase. Consequently, the *pro-R* carboxymethyl group in citrate produced by animal citrate synthase must come from oxaloacetate, and the *pro-S* carboxymethyl group must come from the enolate of acetyl-SCoA.[460]

It was later found that the citrate synthase from *Clostridium kluyveri* produces citrate in which the *pro-R* carboxymethyl group, rather than the *pro-S* carboxymethyl group, comes from the enolate of acetyl-SCoA.[461] In the two active sites, the enolates of acetyl-SCoA are held on opposite sides of the carbonyl, the *Si* face and the *Re* face, respectively, of oxaloacetate.[462] The animal enzyme is citrate (*Si*)-synthase, and the bacterial enzyme is citrate (*Re*)-synthase. Since it is cryptic, the stereochemistry of citrate synthase is irrelevant to metabolism.

An elucidation of the stereochemistry of an enzymatic reaction that removes a stereoheterotopic hydron from a prochiral methylene carbon or that adds a stereoheterotopic hydron to a trigonal, prochiral carbon to produce a prochiral methylene carbon provides information about the relative positions of catalytic acids and bases within the active site. As with a skeletal model of citrate, when you observe the skeletal model of a substrate such as (*S*)-malate

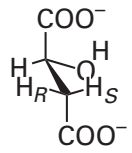

4–49

you can readily distinguish the two hydrogens on carbon 3 because you are diastereomeric. If carbon 2 is placed behind and carbon 4 is placed in front and down, as in the view of **4–49,** one hydrogen on carbon 3 is to the right and the other is to the left. No matter how the skeletal model is rotated in space or about its bonds, you can always identify the right hydrogen and the left hydrogen. In this instance, the two hydrogens are diastereotopic hydrogens. Replacement of either would produce a diastereomer because of the chiral center at carbon 2.

When (*S*)-malate is bound as a reactant to fumarate hydratase

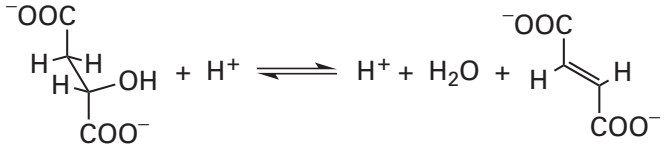

(4–226)

from *M. tuberculosis*, it is bound with the two carboxylato groups in the trans configuration because the product, fumarate, is the *trans*-acid. The two carboxylato groups and the hydroxy group participate in hydrogen bonds with particular amino acids at the proper locations (Figure 4–27),[463,464] and these hydrogen bonds pin the substrate in the trans configuration with the carboxylate adjacent to the hydron to be removed in the proper rotational orientation

*Although it is not relevant to the stereochemical determination because all that was required was to place a tritium anywhere on only the *pro-R* carboxymethyl group, the stereochemistry of the hydration catalyzed by 3-dehydroquinate dehydratase is a syn addition as shown.

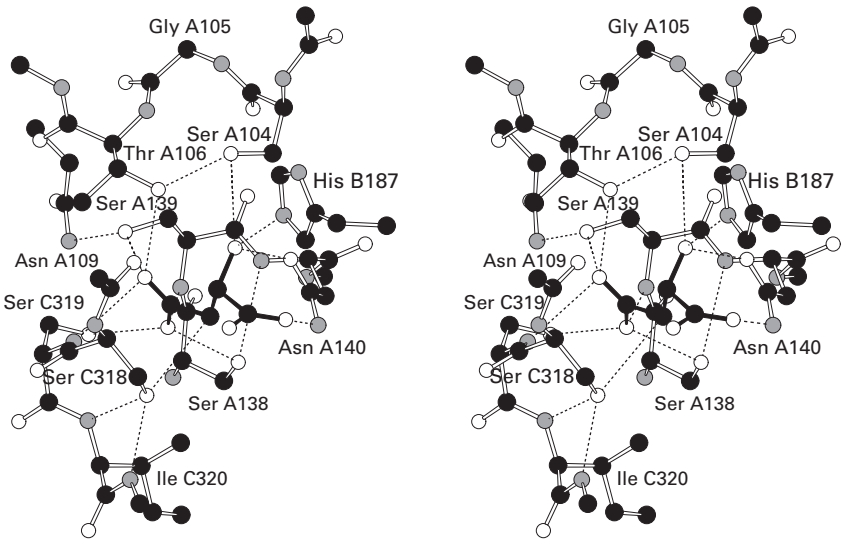

Figure 4–27: Stereodrawing[134] of the crystallographic molecular model of the active site of fumarate hydratase from *M. tuberculosis* occupied by the substrate (*S*)-malate (black bonds).[464] Black atoms are carbons, white atoms are oxygens, and small gray atoms are nitrogens. The enzyme was expressed in *E. coli*, purified, and crystallized in 26.5% (v/v) PEG400, 5% (v/v) glycerol, 200 mM $CaCl_2$, and 100 mM 2-ammonio-2-(hydroxymethyl)-propane-1,3-diol chloride at pH 8.6. Crystals of the enzyme were soaked in the solution from which they were crystallized, supplemented with 20 mM fumarate. A data set to Bragg spacing of 0.22 nm was collected. Electron density consistent only with (*S*)-malate was observed in the active site. Each of the four active sites in the homotetramer is constructed from amino acids from three of the subunits. In the drawing, the amino acids from each subunit are distinguished with the letters A, B, and C. There is only one paradigmatic catalytic acid–base, Histidine B187, which is responsible for hydronating the leaving hydroxy group. The two oxyanions at carbon 1 of the *gem*-enediolate occupy two adjacent oxyanion holes, one formed by the amido nitrogen–hydrogen of Serine A139 and the hydroxy groups of Serine A138 and Serine C319 and the other formed by the amido nitrogen–hydrogen of Serine C319 and the hydroxy groups of Threonine A106 and Serine A139. Notice that the elimination is forced by the active site to be almost precisely anti.

to achieve maximal overlap between its π molecular orbital system and the σ bond between carbon 3 and the hydron that will be removed. There is a catalytic base within the active site responsible for removing the hydron from carbon 3 during the elimination. That **catalytic base is positioned so that it can remove only one of the two stereoheterotopic hydrons on the prochiral carbon**. This positioning results from the fact that the most efficient way to accomplish such a difficult transfer is for the **the hydron to be on the line of centers** between carbon 3 and the heteroatom of the catalytic base. Consequently, during the enzymatic reaction, the hydron removed from almost every molecule of (*S*)-malate will be the same one, either *pro-R* or *pro-S*, in almost every turnover, and the hydron added to carbon 3 of almost every molecule of fumarate will end up being only the *pro-R* or the *pro-S* hydrogen because every active site in the solution is the same diastereomer.

The stereochemistry for the removal of a stereoheterotopic hydron, hydrogen atom, or hydride is usually elucidated by using deuterium or tritium to replace selectively one of the two stereoheterotopic hydrogens, or both of them in turn, in the reactant. Likewise, the stereochemistry for addition of a hydron, hydrogen, or hydride to produce a prochiral carbon is usually elucidated by requiring the enzyme to add deuterium or tritium to produce a chiral carbon in the product rather than a prochiral carbon. For example, when the hydration of fumarate by porcine fumarate hydratase (50% identity and 1.1 gap percent relative to that from *M. tuberculosis*) proceeds in ^2H_2O, the product is (2*S*,3*R*)-[3-^{2}H]malate.[465-467] Consequently, every time a molecule of fumarate is converted by the active site to (*S*)-malate, the hydron almost always is added to the *Re* face of carbon 3 and becomes the *pro-R* hydrogen on carbon 3. Conversely, every time a molecule of (*S*)-malate is converted to fumarate by porcine fumarate hydratase, the *pro-R* hydrogen on carbon 3 is almost always removed, not the *pro-S*, because the *pro-R* side is the side of the reactant on which the catalytic base in the active site just happened to end up as evolution by natural selection proceeded.

If a catalytic base in an active site removes only one of the two stereoheterotopic hydrons from a prochiral carbon, as is the case in fumarate hydratase, it must also be true that the resulting catalytic acid in the active site of an enzyme can create a prochiral carbon by **stereoheterotopic addition of a hydron**, as is also in the case in fumarate hydratase. Any **planar, trigonal, prochiral carbon** has a *Re* face and a *Si* face, which can be distinguished as unique by a diastereomeric observer or active site. If one and only one of the three functional groups around a trigonal, prochiral carbon is a hydrogen, then addition of another hydrogen to that carbon produces a tetrahedral, prochiral carbon. For example, galactarate dehydratase (D-*threo*-forming) from *Agrobacterium tumefaciens* catalyzes the dehydration of *meso*-galactarate* and subsequent tautomerization of the resulting enol

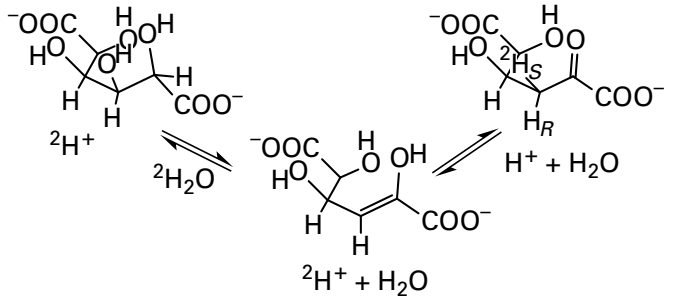

(4–227)

to give (2*S*,3*R*)-2,3-dihydroxy-5-oxohexanedioate. When the reaction is carried out in ^2H_2O, a deuteron ends up in the *pro-S* position on carbon 4 of (2*S*,3*R*)-2,3-dihydroxy-5-oxohexanedioate (Figure 4–28) because the catalytic acid that adds the hydron is on the *Si* face of the carbon–carbon double bond in the enol.[468] The *S*-hydroxy group on the carbon in the reactant is replaced by the *pro-S* deuteron in the product, so the reaction proceeds with **retention of configuration** at carbon 4. Because the deuteron from ^2H_2O ends up on only one of the two diastereotopic positions on carbon 3, it must be the case that a catalytic acid in the active site adds the hydron to carbon 3 rather than the keto–enol tautomerization occurring in solution after the enol is released as a product. This determination is not inconsequential because the keto–enol tautomerization in solution would be facile.

Unlike the active site of fumarate hydratase, however, in which the orientation of the catalytic acid–base was established by happenstance because the two faces of the achiral fumarate are identical to each other in reactivity, it may be the case that, in some instances in which diastereomeric molecules

*A *meso* compound is an achiral member of a set of diastereoisomers which also includes one or more chiral members. A *meso* compound is achiral because it is superposable on its mirror image, but it nevertheless contains two or more chiral centers so that one or more members of the set of diastereomers are chiral.

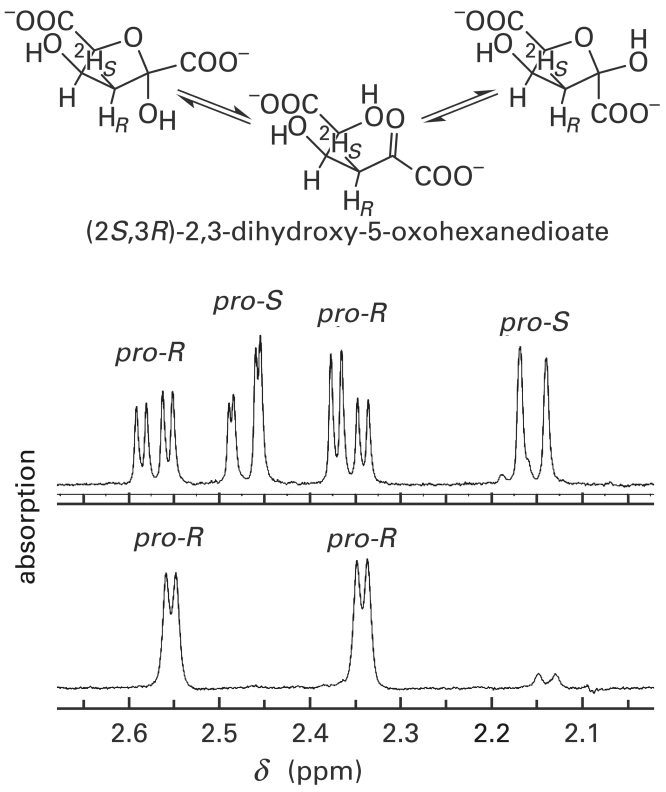

Figure 4–28: Determination of the prochiral stereochemistry of the reaction catalyzed by galactarate dehydratase (D-*threo*-forming) from *A. tumefaciens*.[468] Portions (those between 2.7 and 2.0 ppm) of two proton nuclear magnetic resonance spectra of different samples of (2*S*,3*R*)-2,3-dihydroxy-5-oxohexanedioate, the product of the enzymatic reaction when *meso*-galactarate is the reactant, are shown. These portions of the spectra contain the absorptions from the two protons on carbon 4 in the two furano anomers of (2*S*,3*R*)-2,3-dihydroxy-5-oxohexanedioate present at equilibrium in the solution. The (2*S*,3*R*)-2,3-dihydroxy-5-oxohexanedioate that gave the upper spectrum was obtained when *meso*-galactarate was dehydrated by galactarate dehydratase (D-*threo*-forming) in ^1H_2O. Absorptions from both the 4-*pro*-*S* and the 4-*pro*-*R* hydrons in (2*S*,3*R*)-2,3-dihydroxy-5-oxohexanedioate are observed. These assignments for the spectra of the anomers were made from the respective magnitudes of the vicinal C3–C4 ^1H–^1H coupling constants, ^1H–^{13}C heteronuclear single quantum coherence nuclear Overhauser effects, and ^{13}C nuclear magnetic resonance spectra. The respective absorptions are split by the other hydrogen on carbon 4 and the hydrogen on carbon 3 into doublets of doublets. Dehydration of *meso*-galactarate by the enzyme was then performed in ^2H_2O so that the hydrogen on prochiral carbon 4 that was added by the enzyme in place of the hydroxy group removed during the dehydration (Equation 4–227) would be a deuterium. The absorption from the 4-*pro*-*S* proton was missing from the spectrum (lower two panels) of the deuterated product, and the vicinal splitting of the 4-*pro*-*R* proton by the 4-*pro*-*S* hydrogen was also missing from the absorption of the 3-*pro*-*R* proton. These observations demonstrate that the hydron added by the enzyme to carbon 4 is the 4-*pro*-*S* hydrogen from (2*S*,3*R*)-2,3-dihydroxy-5-oxohexanedioate. Adapted with permission from reference 468. Copyright 2014 American Chemical Society. https://pubs.acs.org/doi/10.1021/bi5005377

are substrates, steric differences or differences in acidity caused by differences in the electronic configurations in the two possible diastereomeric transition states influence which hydron on the substrate is chosen by natural selection for removal. Any **isotropic solution of achiral molecules**—for example, an aqueous solution containing salts and achiral general acids and achiral general bases or achiral oxidants and achiral reductants—can make **no distinction between two enantiotopic hydrogens** on a prochiral carbon and will usually make little distinction between diastereotopic hydrogens.

This conclusion, that a particular reaction, if carried out in free solution, would proceed with little or no distinction between *pro*-*R* and *pro*-*S* hydrogens, however, cannot be drawn unconditionally if the reactant itself, as in the case of (*S*)-malate, has a chiral center in the vicinity of the site of reaction so that the two hydrogens are diastereotopic. For example, (*S*)-5,6-dihydroorotate undergoes hydron exchange in a free solution of ^2H_2O, at pH 7.8 and 37 °C, 10-fold more rapidly at the *pro*-*R* position at carbon 5 than at its *pro*-*S* position[469]

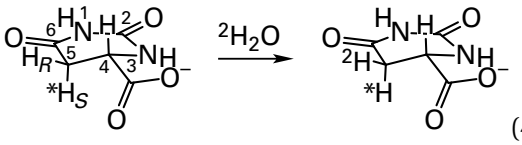

(4–228)

presumably because of the rigidity provided by the ring, the proximity of the chirality at carbon 4, and the steric hindrance produced by the carboxylato group. Regardless, however, of this steric preference in solution, bovine dihydroorotate dehydrogenase (quinone), within the error of measurement, removes only the *pro*-*S* hydrogen from carbon 5. The intermediate enol in the enzymatic reaction is generated by removal of a hydron by a catalytic base in the active site positioned by natural selection, for no apparent reason, to remove the less acidic, more sterically hindered hydron of the reactant.

The example of dihydroorotate dehydrogenase illustrates the point that **the final choice of which stereoheterotopic hydron on a prochiral carbon is removed by a catalytic base or added by a catalytic acid in the reverse reaction proceeding in an active site is arbitrary**. Unless there are overriding chemical advantages, the choice is the random outcome of evolution by natural selection, has no metabolic consequences, and is **inconsequential, cryptic, and not a factor in natural selection**. The choice of which stereoheterotopic hydron is removed or added is a result only of the arbitrary absolute config-

uration of the active site. For the same reason that you are, the active site of an enzyme is also diastereomeric. Just as you are formed from diastereomeric molecules of protein, it is formed from a diastereomeric molecule of protein. A molecule of protein is diastereomeric in large part because it is assembled from only L-amino acids. When 2-hydroxymuconate tautomerase

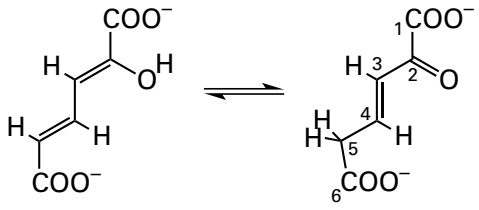

(4–229)

from *P. putida* was synthesized from D-amino acids, the synthetic D-enzyme catalyzed the same reaction because the two substrates are achiral, but its active site produced [5*R*-^{2}H]-(3*E*)-2-oxohex-3-enedioate from (2*Z*,4*E*)-2-hydroxyhexa-2,4-dienedioate when the reaction was run in ^2H_2O by adding the hydron to the *Re* face of the carbon–carbon double bond. In contrast, the natural L-enzyme in ^2H_2O produces [5*S*-^{2}H]-(3*E*)-2-oxohex-3-enedioate by adding the hydron to the *Si* face of the carbon–carbon double bond.[470]

Although most active sites are not nearly so selective as that of enoyl-CoA hydratase (Equation 4–223), the **selectivity of an active site for removal of stereoheterotopic hydrogens is usually quite high**. For example, the diastereotopic hydrogen removed from carbon 6 of methyl α-D-galactopyranoside by galactose oxidase (previously Equation 2–305)

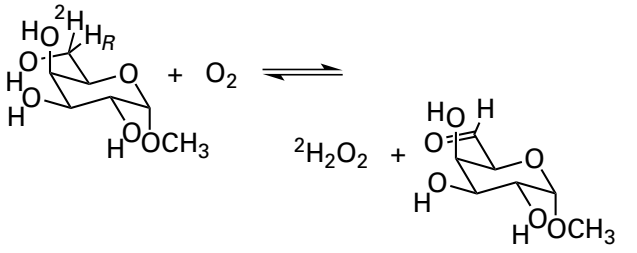

(4–230)

from *Gibberella zeae* is the *pro-S* hydrogen 98% ± 2% of the time,[433] and the enantiotopic hydrogen abstracted from glycine by glycine oxidase from *B. subtilis* is the *pro-S* hydrogen 99% of the time.[471] That **the stereoheterotopic preference at a prochiral carbon is never absolute**, however, is indicated by the fact that when deuterium rather than protium must be removed during the enzymatic reaction, the degree of stereochemical preference is usually measurably less.[433,469,471]

In the cases of hydronation of fumarate in the active site of fumarate hydratase and hydronation of the intermediate enol in the active site of galactarate dehydratase (D-*threo*-forming), the hydron or deuteron is added to one face of a prochiral carbon. If the two other positions around a carbon in a double bond are hydrogens, then the carbon itself is not prochiral. If, however, the carbon at the other end of the double bond has two different functional groups, then the two hydrogens on the first carbon can nevertheless be distinguished as **the *E* and *Z* hydrogens**, respectively, depending on their locations relative to the functional group of higher priority on the adjacent carbon across the double bond. For example, the two protiums on 2-methyleneglutarate can be distinguished as *E* (*entgegen*) or *Z* (*zusammen*) relative to the carboxy group, which has the highest priority

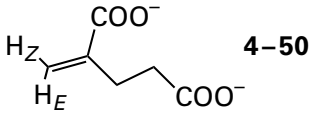

4–50

The absorptions of *E* and *Z* hydrogens in a nuclear magnetic resonance spectrum have different chemical shifts. For example, when the *E* protium is replaced synthetically by deuterium, the equilibration of the deuteron between the *E* and *Z* positions positions in the reactant [*E*-^{2}H]-2-methyleneglutarate by 2-methyleneglutarate mutase (Table 2–3) from *Eubacterium barkeri* can be followed by nuclear magnetic resonance spectroscopy.[472] This equilibration is evidence that there is an intermediate in the enzymatic isomerization such as a radical, carbanion, or carbenium ion in which the double bond has been broken; that the radical, carbanion, or carbenium ion is on the carbon with the hydrogen and the deuterium; and that the intermediate has a lifetime long enough to permit free rotation at the methylene carbon. Free rotation of a planar trigonal carbon with two hydrogens around a single bond to the rest of the molecule is difficult if not impossible to prevent.

Phospho*enol*pyruvate with a carbon–carbon double bond in which one carbon has two hydrogens attached to it is involved in many enzymatic reactions. Both **(*E*)- and (*Z*)-[3-^{2}H]phospho*enol*-pyruvate** have been synthesized[473-475] and have been used in stereochemical studies. Addition of carbon, nitrogen, oxygen, or sulfur to carbon 3 of

phospho*enol*pyruvate causes carbon 3 to become prochiral. For example, in the enzymatic reaction catalyzed by 3-deoxy-8-phosphooctulonate synthase

D-arabinose 5-phosphate + phospho*enol*pyruvate + H_2O ⇌ phosphate + 2-dehydro-3-deoxy-D-octonate 8-phosphate (4–231)

the trigonal carbon 3 of phospho*enol*pyruvate becomes the tetrahedral, prochiral carbon 3 of the 2-dehydro-3-deoxy-D-octonate 8-phosphate, which is (4*R*,5*R*,6*R*,7*R*)-4,5,6,7,8-pentahydroxy-2-oxooctanate 8-phosphate. When the active site of the enzyme from *E. coli* adds the enolate of (*Z*)-[3-^{2}H]phospho-*enol*pyruvate to the aldehydic carbonyl of arabinose 5-phosphate, the product is (3*S*)-[3-^{2}H]-2-dehydro-3-deoxy-D-octonate 8-phosphate. When (*E*)-[3-^{2}H]phospho*enol*pyruvate is used as reactant, the product is (3*R*)-[3-^{2}H]-2-dehydro-3-deoxy-D-octonate 8-phosphate.[476] In each product, when unlabeled phospho*enol*pyruvate is used as reactant, carbon 3 is prochiral. Both of these complementary stereochemical observations, as well as the known stereochemistry of the undeuterated product, demonstrate that the *Si* face of the enolate of pyruvate, resulting from hydrolysis of the phospho group of phospho*enol*pyruvate, adds to the *Re* face of the formyl group of D-arabinose 5-phosphate[477]

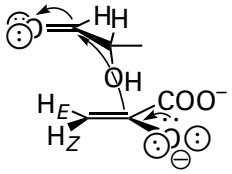

4–51

In this instance, the **stereochemistry of the prochiral product defines the orientation of each reactant relative to the other** rather than the orientation of a catalytic acid–base because neither hydrogen is removed during the enzymatic reaction. Consequently, in this instance, the two hydrogens are reporter groups reporting on the stereochemistry.

Fumarate hydratase catalyzes an anti **addition–elimination** (Equation 4–226). This conclusion was based on the facts that the (*S*)-hydroxy group is the leaving group in the elimination, addition of the hydroxy group always produces (*S*)-malate, the hydron is added to the *Re* face of carbon 3 in fumarate, the *pro-R* hydrogen on carbon 3 of (*S*)-malate is removed during the elimination, and fumarate is the *trans*-diacid. In aqueous solution, such **addition–eliminations that involve general base catalysis usually proceed in an anti sense**, with the general base that removes the hydron from the side of the reactant opposite the side from which the leaving group departs.[478] This preference may be due entirely or only in part to steric effects that would result if the general base and the leaving group were required to sit on the same side of the reactant in a syn elimination.

As in the case of fumarate hydratase, many **enzymatic reactions also show this anti preference**. For example, histidine ammonia-lyase from *Pseudomonas striata* catalyzes the anti elimination of ammonia from L-histidine

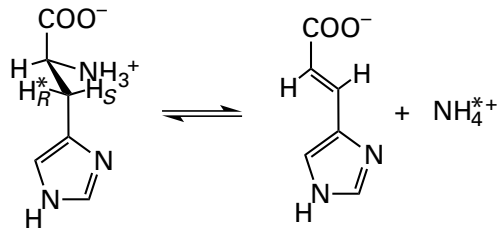

(4–232)

because the *pro-R* hydron is removed[479] and added[480] during the reaction and the product of elimination is the *trans*-acid. Addition of water to the aliphatic double bond in oleic acid, catalyzed by an enzyme from a pseudomonad, also proceeds in an anti sense

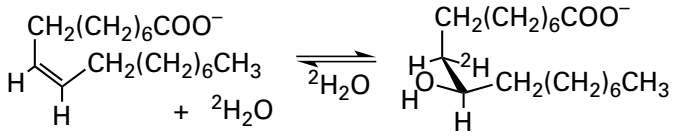

(4–233)

because the reactant acid is cis, carbon 10 in the product is *R*, and deuterium ends up at the *pro-R* position on carbon 9 when the reaction is carried out in ^2H_2O.[481]

It has been found, however, that certain eliminations that occur in solution, in particular, eliminations proceeding through carbanionic intermediates or eliminations involving ion pairing between the leaving group and the general base that removes the hydron, can yield variable percentages of the products of syn elimination.[478] A particularly relevant example for the present purposes is the elimination of acetate from (2*R*,3*R*)-*S*-*tert*-butyl-3-acetoxy-[2-^{2}H]butanethioate with catalysis by hydroxide[482]

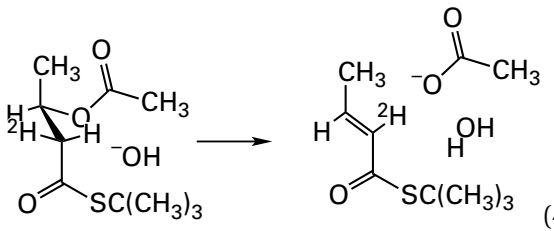

(4–234)

The yield of deuterated product (43% of the total yield of the *E* isomer) was used to calculate that when carbon 2 has two hydrogens and no deuterium kinetic isotope effect is operating, the yield of syn product (Equation 4–234) would be 14%. This elimination probably proceeds through an intermediate enol

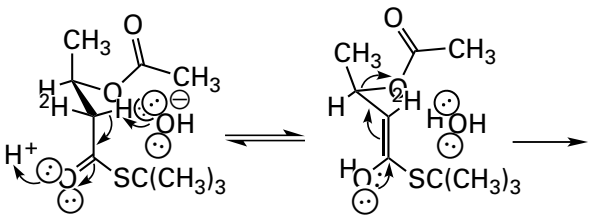

(4–235)

In any event, the product ratios observed suggest that the difference in free energy of activation between syn and anti elimination–addition is probably fairly small and can be influenced considerably by the conditions.

Syn elimination–additions adjacent to a carbonyl group or an acyl group permitting an intermediate enol have also been observed in enzymatically catalyzed reactions. The dehydration of (2*R*,3*S*)-3-hydroxy[2-^{3}H]butyryl-SCoA to produce crotonyl-SCoA, catalyzed by bovine enoyl-CoA hydratase

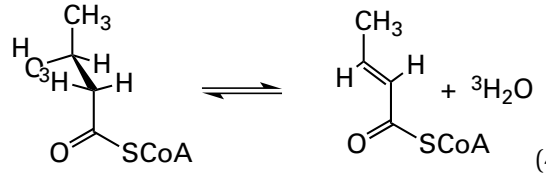

(4–236)

produces trans product that has only 20% the specific radioactivity of the reactant.[483] Therefore, even though the tritium kinetic isotope effect would be against the reaction as it is found to occur, the enzyme nevertheless removes the triton because it is in the *pro-R* position and aligned with a catalytic base in the active site, and the reaction is a syn elimination. Upon correction for the kinetic isotope effect, a hydron in the *pro-S* position is removed by the enzyme from (3*S*)-3-hydroxybutyryl-SCoA at a rate more than 200 times slower than a hydrogen in the *pro-R* position,[289,450] even though the carbon–hydrogen bond should be more sterically accessible, because it is on the opposite side of the reactant from the hydroxy group as it is held in the active site with the methyl and acyl carbons in the necessary trans configuration. The reason that the exclusivity is probably greater than a factor of 200 is that tritium remaining in the product (20%) of elimination from tritiated reactant probably arises in part from nonenzymatic racemization of the reactant during its synthesis or during the incubation

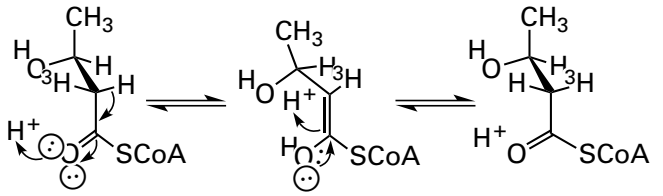

(4–237)

Addition of ^2H_2O to the cis double bond in *Z*-2-oxohept-4-ene-1,7-dioate catalyzed by 2-oxohept-4-ene-1,7-dioate hydratase from *E. coli*

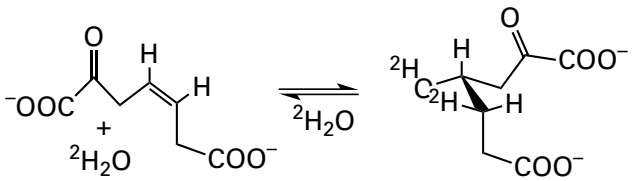

(4–238)

is a syn addition because the reactant is cis and the product has the *S* configuration at both carbon 4 and carbon 5.[484] At first glance, hydration would seem to be an addition to a carbon–carbon double bond unconjugated to a carbonyl, but during the overall addition, a deuteron stereospecifically replaces a hydron on carbon 3 that is α to the carbonyl group at carbon 2, so the mechanism[485] is initiated by removal of this hydrogen as a hydron to produce the conjugated dienolate. Then carbon 5 of the dienolate is hydronated to produce the α,β-unsaturated carbonyl, and the equivalent of a hydroxide adds to carbon 4, the β carbon, in a Michael addition to produce the enolate, which is then rehydronated on carbon 3. The last step places the deuteron from ^2H_2O on carbon 3. Nevertheless, additions of a hydron to carbon 4 and of a hydroxide to carbon 5 are syn, a stereochemical result suggesting that the conjugate base of the catalytic acid that added the hydron

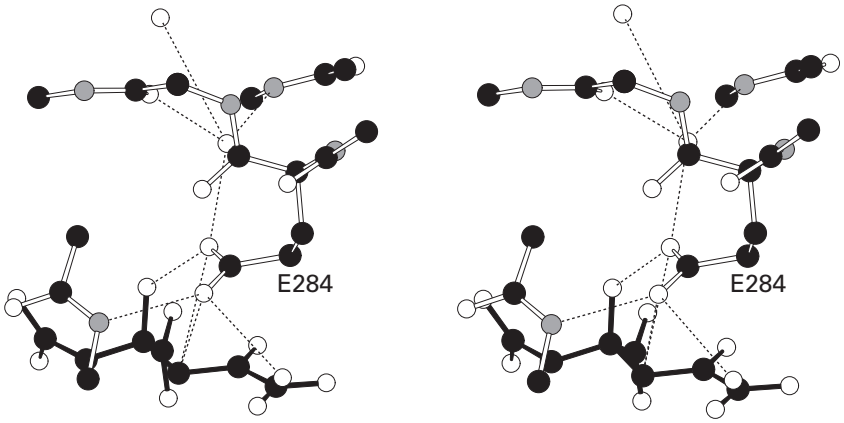

Figure 4–29: Stereodrawing[134] of the active site in the crystallographic molecular model of 2-oxo-4-carboxy-3-hexenedioate hydratase from *Sphingobium* occupied by (4*S*)-2-oxo-4-carboxy-4-hydroxyhexanedioate (black bonds).[487] Black atoms are carbons, white atoms are oxygens, and small gray atoms are nitrogens. Deoxyribonucleic acid encoding the entire gene of the enzyme was chemically synthesized and incorporated into a plasmid that permitted it to be expressed in *E. coli* with six consecutive histidines at its amino terminus. The protein was purified on a solid phase on which nickel ions had been chelated. The purified protein was crystallized from a solution in which (4*S*)-2-oxo-4-carboxy-4-hydroxyhexanedioate and 2-oxo-4-carboxyhex-3-enedioate were first brought to equilibrium by the enzyme in a total concentration of 1.3 mM along with 12% poly(ethylene glycol) and 0.1 M sodium malonate at pH 5. Diffraction data to Bragg spacing of 0.202 nm were collected, and a map of electron density was calculated. Phases were obtained by molecular replacement using the crystallographic molecular model of the enzyme from *R. palustris*. The substrate (4*S*)-2-oxo-4-carboxy-4-hydroxyhexanedioate within the active site is drawn along with the side chain of Glutamate 284. Several molecules of water, which connect the oxygens of the carboxy group of Glutamate 284 with the solution, are also drawn, as well as donors and acceptors for hydrogen bonds to the molecules of water and one of the oxygens of the carboxy group. The two donors and the one acceptor are from amido groups in the polypeptide backbone.

to carbon 5 of the dienolate, possibly the carboxy group of Aspartic Acid 79,[486] then removes a hydron from the molecule of water that adds to carbon 4 from the same side of the resulting α,β-unsaturated carbonyl.

In the active site of 2-oxo-4-carboxy-3-hexenedioate hydratase from *Sphingobium*, which performs a syn addition of water to carbon 3 and carbon 4 of the α,β-unsaturated carbonyl in (3*Z*)-2-oxo-4-carboxyhex-3-enedioate when it is the reactant, one of the oxygens of the carboxylato group of Glutamate 284 removes the hydron from the molecule of water as it adds to the β carbon to produce the enolate. This oxygen also delivers a hydron to the α carbon of the enolate to complete the hydration. Ironically, in this instance, the stereochemistry was assigned as syn from the crystallographic molecular model of the complex between the active site and the substrate (4*S*)-2-oxo-4-carboxy-4-hydroxyhexanedioate (Figure 4–29),[487] which is the product of the hydration and the preferred participant in the equilibrium within the active site. One of the oxygens of the carboxy group of Glutamate 284, which was shown to be the required catalytic acid–base by site-directed mutation, is only 0.28 nm from the *pro-S* hydrogen on carbon 3 that is hydronated in the hydration but distant from the *pro-R* hydrogen. The other oxygen of the carboxy group forms a hydrogen bond (0.22 nm) with the hydroxy group that is added during the hydration, identifying its role as the catalytic base in the hydration. The hydration is a syn addition because the carboxy group can be on only one side of the carbon–carbon double bond.

Enzymatically catalyzed **dehydrogenation–hydrogenations** at positions adjacent to a carbonyl or acyl group, because they can also involve rigid intermediate enolates, proceed with either exclusively syn or exclusively anti stereochemistry. For example, UDP-*N*-acetylmuramate dehydrogenase from *E. coli* reduces the (*E*)-1-carboxy-2-methylvinyl group

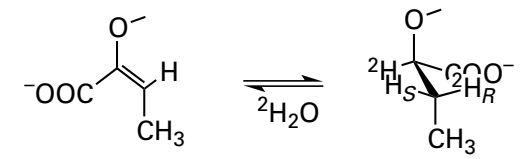

(4–239)

on the reactant, UDP-*N*-acetyl-3-*O*-[(*E*)-1-carboxy-2-methylvinyl]-D-glucosamine, with anti addition of a hydron and a hydride. This conclusion follows from the fact that when hydrogenation is run with NADP^{2}H in ^2H_2O, the (*E*)-1-carboxy-2-methylvinyl group becomes a (1*R*,2*R*)-[1,2-$^2H_2$]-1-carboxypropyl group.[488]

Enoyl thioester reductases reduce the double bond on their substrates with a hydride from NAD or NADPH and a hydron

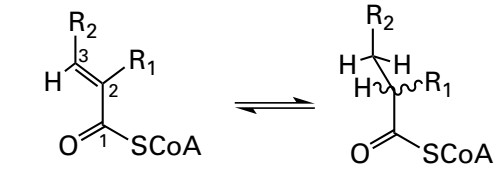

(4–240)

Enzymes catalyzing this reduction, depending on the reactant reduced and the species from which they are isolated, add the hydride to either the *Re* face or the *Si* face of carbon 3 to produce the enolate. The hydron is then added to either the *Re* face or the *Si* face of carbon 2 of the enolate to proceed with either syn or anti hydrogenation.[489] For example, enoyl-[acyl-carrier-protein] reductase (NADPH) in the fatty-acyl-CoA synthase from *S. cerevisiae* performs the anti addition of a hydride from NADPH to the *Si* face of carbon 3 and of a hydron to the *Si* face of carbon 2 of crotonyl-SCoA[490]

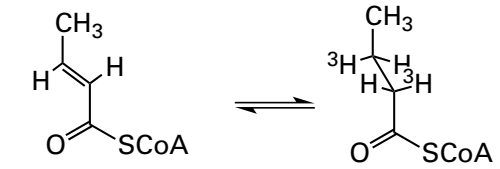

(4–241)

The same enzyme (35% identity; 2.2 gap percent) in the fatty acid synthase from *G. gallus* performs the syn addition of a hydride from NADPH to the *Re* face of carbon 3 and of a hydron to the *Si* face of carbon 2 of crotonyl-SCoA.[491]

Such examples of both stereochemical outcomes in both elimination–additions and dehydrogenation–hydrogenations adjacent to carbonyl and acyl groups again illustrate the fact that the stereochemical outcome of an enzymatic reaction often depends on the adventitious positioning of the catalytic acids and bases and prosthetic groups within the active site relative to the bound reactant or the adventitious positioning of the bound reactant within the active site relative to catalytic acids and bases and prosthetic groups, rather than any innate electronic preference of the reaction.

Enzymatically catalyzed **dehydrogenation–hydrogenations at positions unconjugated to a carbonyl**

or acyl group usually proceed with syn stereochemistry.[492] The dehydrogenation of 5-α-cholestan-3β-ol to Δ^7-5α-cholestan-3β-ol, catalyzed by an enzyme in *Eurycotis floridana*

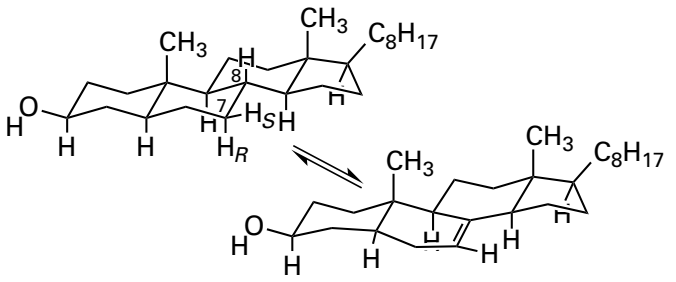

(4–242)

proceeds with removal of the methine hydrogen at carbon 8 and the *pro-S* hydrogen at carbon 7. This conclusion follows from the facts that, when (7*S*)-[7-^{3}H]-5α-cholestan-3β-ol was fed to roaches, the tritium was removed (>90%), but when (7*R*)-[7-^{3}H]-5α-cholestan-3β-ol was fed to roaches, the tritium was retained (>85%) in the product.[493] By use of the four (*Z*)-hexadec-11-enoates stereospecifically monodeuterated at the *pro-R* and *pro-S* positions at carbons 13 and 14, it could be shown that a desaturase from *Thaumetopoea pityocampa* removes the *pro-S* hydrogens from each carbon during the syn dehydrogenation of (*Z*)-hexadec-11-enoate to produce (*Z*,*Z*)-hexadeca-11,13-dienoate.[494] The oxidants in these two reactions are unknown.

The stereochemistry of **enzymatic reactions that involve radical intermediates** provides insight into the orientation in the active site relative to the substrate of a prosthetic group containing a radical or the side chain of an amino acid, such as tyrosine or tryptophan, containing a radical that can abstract a hydrogen atom from a carbon or that, in their respective hydrogenated forms, can add a hydrogen atom to a carbon radical. Such reactions involving the **abstraction of hydrogen atoms from carbon** producing intermediate radicals usually proceed in an active site with stereoheterotopic selectivity during the abstraction and during addition of a functional group to the resulting carbon radical, even though the carbon radical produced by the abstraction must be planar and chemically equivalent on both sides of the plane. For example, as noted above in passing, porcine peptidylglycine monooxygenase (previously Equation 2–309)

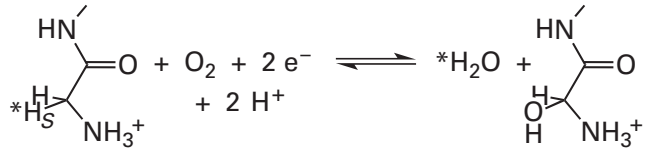

(4–243)

removes the *pro-S* hydrogen from the glycyl group of a reactant[495] and replaces that hydrogen with the equivalent of a hydroxyl radical with retention of configuration.[496] This result is consistent with a mechanism in which the hydroxylating species produced from molecular oxygen bound to one or both of the prosthetic copper ions in the active site (Figure 2–58C) abstracts the hydrogen atom and also hydroxylates the resulting glycyl radical from the same side. Consequently, the stereochemistry is consistent with the favored mechanism for the reaction and adds support to it.

A methyltransferase from *Micromonospora echinospora* uses a 5′-adenosyl radical produced from *S*-adenosyl-L-methionine to remove a hydrogen atom from the methylene of a hydroxymethyl group on a reactant and a methylcobalamin to methylate the resulting radical on the carbon of the former hydroxymethyl group. Sterically, it would make chemical sense to have the 5′-adenosyl radical positioned on one side of the plane of the radical and the methylcobalamin on the other side because both of these participants are quite large and electron density for the radical exists on both sides, but the reaction proceeds with retention of configuration.[497] Several results with alternative reactants for the enzyme and the fact that the *pro-R* hydrogen is abstracted greater than 95% of the time suggest that the hydroxymethyl group is held firmly in one orientation, presumably by hydrogen bonds to its hydroxy group. Therefore, it seems that both the methylcobalamin and the adenosyl radical produced from *S*-adenosyl-L-methionine, which are sizable molecules, somehow have access to the same side of the carbon. There is an unrelated methyltransferase from *Streptomyces fradiae* that also methylates the methylene in a hydroxymethyl group, also using both a 5′-adenosyl radical produced from *S*-adenosyl-L-methionine and methylcobalamin in apparently the same mechanism, but the methylation occurs with inversion of configuration,[498] as one might expect.

A mutant of 2-enoate reductase, a flavoenzyme from *Gluconobacter oxydans*, is able to replace bromine on ethyl 2-bromo-2-methyl-2-phenyl acetate with hydrogen. The reaction proceeds through the widely delocalized ethyl 2-phenylcarboxymethyl radical

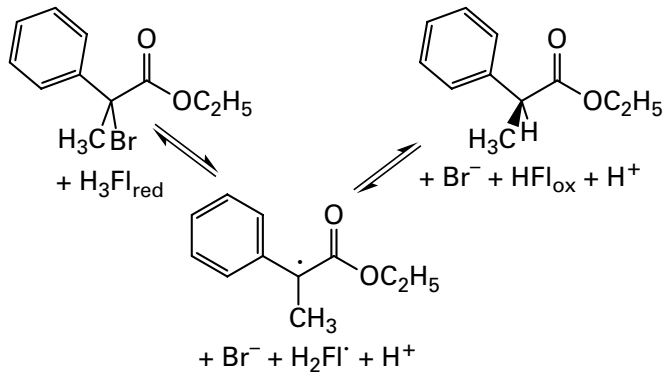

(4–244)

which must be planar and chemically equivalent on each of its faces, *Re* and *Si*. Nevertheless, when racemic 2-bromo-2-methyl-2-phenyl acetate is used as a reactant, the enzyme debrominates both enantiomers at the same rate, but the product is almost exclusively (*S*)-2-methyl-2-phenyl acetate (97%).[499] In this instance, the prosthetic flavin that provides the hydrogen atom that adds to the radical, which is bound in the active site in only one orientation, can only be on one side of its plane, and it just happens to be on the *Re* face.

Racemization is one criterion for a nonenzymatic dissociative nucleophilic substitution at a saturated carbon that proceeds with an intermediate carbenium ion in solution. Human protein farnesyltransferase and human protein geranylgeranyltransferase, which share the same catalytic subunit, catalyze a nucleophilic substitution in which a farnesyl group or a geranylgeranyl group is transferred to the sulfido group of a cysteine in one of a set of particular proteins

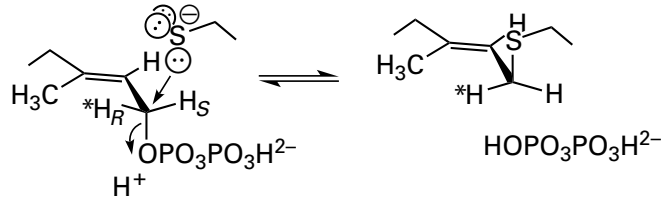

(4–245)

The nucleophilic substitution may[500] proceed through an allyl carbenium ion, which would be a logical intermediate because of its stability.[501] Both the (*S*)-[1-^{2}H] and (*R*)-[1-^{2}H] enantiomers of both farnesyldiphosphate[502] and geranylgeranyldiphosphate[503] were prepared synthetically. The products of their reactions with cysteinyl peptides, when catalyzed by the respective enzyme, had nuclear magnetic resonance spectra demonstrating that inversion of configuration at prochiral carbon 1 of the respective reactant had occurred in each case. This inversion of configuration is consistent with crystallographic molecular models of protein farnesyltransferase from *R. norvegicus* (97% identity relative to human) in complexes with farnesyldiphosphate and a farnesylated peptide, respectively, in which the diphospho group that leaves and the sufido group that adds are found on opposite sides of the active site.[504] They are too far apart, however, for an associative, concerted nucleophilic substitution. This separation is consistent with the evidence suggesting a dissociative nucleophilic substitution and would make perfect sense because, if the diphosphate anion were required to dissociate from the active site to make room for the sulfido group on the same side of the alkyl carbenium ion, water would certainly intervene and react with it to produce the alcohol. Consequently, the sulfido group must be waiting on the other side to react as soon as the dissociation producing the allyl carbenium ion has occurred. In reactions catalyzed by enzymes, inversion of configuration or **the lack of racemization cannot be used as an argument against a dissociative mechanism because the active site necessarily positions reactants in a particular orientation regardless of whether the reaction is dissociative or associative.**

There are instances, however, in which removal or addition of a stereoheterotopic hydrogen from or to a prochiral carbon or stereoheterotopic addition of a functional group to produce a prochiral carbon **does proceed with racemization**. For example, tyrosine 2,3-aminomutase from *Chondromyces crocatus* converts (2*S*)-[3,3-^{2}H$_2$]-L-tyrosine into a mixture of (2*S*,3*R*)- and (2*R*,3*S*)-[2,3-^{2}H$_2$]-3-amino-3-(4-hydroxyphenyl)propanoate even though the catalytic base in the active site always removes the *pro-S* deuteron from carbon 3 of the reactant. From these observations, it was concluded that the resulting deuteronated catalytic base transfers its deuteron to the *S* position on carbon 2 when the product is to be (3*R*)-[2,3-^{2}H$_2$]-3-amino-3-(4-hydroxyphenyl)-propanoate or to the *R* position on carbon 2 when the product is to be (3*S*)-[2,3-^{2}H$_2$]-3-amino-3-(4-hydroxyphenyl)propanoate. The relative proportions of the two products in the mixture vary as the pH of the solution is changed.[505]

If it can be shown that only one of the two stereoheterotopic hydrogens on a prochiral carbon is removed or added as a hydron during an enzymatic reaction, then it is evident that a catalytic base in the active site always removes that hydron or that a catalytic acid in the active site always adds that hydron, respectively. In such instances, the catalytic

base or acid could be a molecule of water, but it must be confined by the active site to act at only one stereoheterotopic position. If, however, the step in the reaction in which the hydron is removed or added had occurred in solution, such an absolute preference would not have been displayed. Consequently, one explanation for the occasional lack of stereoheterotopic discrimination leading to racemization is that the prochiral carbon from which a stereoheterotopic hydron is removed or to which a hydron is stereoheterotopically added is **well exposed to the solution while on the active site**, and molecules of water, hydroniums, or hydroxides free in the solution are relied upon by the enzyme to receive or give that hydron. It is often assumed that this involvement of the solvent is the case,[506] even in the absence of any supporting evidence.

Abstraction of hydrogen from a substrate or abstraction of hydrogen by a radical intermediate in an enzymatic reaction can also proceed with racemization. Isobutyryl-CoA mutase from *Streptomyces cinnamonensis*, which catalyzes its reaction with a prosthetic adenosylcobalamin (Table 2–3), produces [3-^{2}H]butyryl-SCoA from [2-^{2}H]isobutyryl-SCoA that is 60% *pro-R* and 40% *pro-S*.[507] Primary-amine oxidase from *O. cuniculus* produces 74% 1-deuterio-2-(4-hydroxyphenyl)ethanal from (*R*)-[1-^{2}H]tyramine

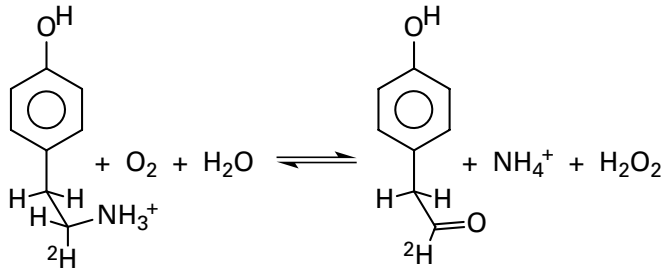

(4–246)

and 81% 1-deuterio-2-(4-hydroxyphenyl)ethanal from (*S*)-[1-^{2}H]tyramine.[508] These results, after correction for the kinetic isotope effect, are consistent with the enzyme removing the *pro-R* hydrogen from tyramine only 1.2 times more often than the *pro-S* hydrogen.

An assessment of the stereochemical outcome of an enzymatic reaction in which stereospecifically deuterated reactants are used or stereospecifically deuterated products are formed is usually made by nuclear magnetic resonance spectroscopy, optical rotation, circular dichroism, or mass spectrometry.

Two enantiotopic protons on a prochiral carbon in an achiral molecule are identical and indistinguishable in a nuclear magnetic resonance spectrum. If, however, there are one or more chiral centers elsewhere in the molecule, then the absorptions of the two diastereotopic protons on the prochiral carbon in the **nuclear magnetic resonance spectrum** have different chemical shifts. If the difference is large enough, then the two protons can be distinguished from each other (Figure 4–28). Because through-bond electron withdrawal is the same for both diastereotopic protons on a prochiral carbon, there is no reliable way to assign the absorptions in the spectrum to the two protons in the absence of other information. It is possible, however, as was done for the spectrum of (2*S*,3*R*)-2,3-dihydroxy-5-oxohexanedioate, to use through-space nuclear Overhauser effects to make the assignments unambiguously.[468] When a deuteron is added stereoheterotopically to a carbon that would be prochiral were a proton added, the absorption for the stereoheterotopic proton at that position in undeuterated product is no longer present in the spectrum of deuterated product (Figure 4–28), and its absence identifies the diastereotopic hydron on the prochiral carbon that is added by the catalytic acid in the active site.

The **optical rotation** of a deuterated product can be measured to determine the outcome of an enzymatic reaction. If a hydrogen is added stereoheterotopically to a reactant to produce a prochiral carbon in the product, the enzymatic reaction is run, on the one hand, with a reactant in which the lone hydrogen on the carbon that will become prochiral has been replaced by deuterium and, on the other hand, with undeuterated reactant but with a deuterated source of the hydrogen that will be added to that carbon, usually the water. The resulting deuterated products from these two reactions will be of opposite stereochemistry at the carbon to which hydrogen or deuterium, respectively, has been added. Because they are enantiomers or diastereomers, their optical rotation can be measured and compared with the optical rotation of synthetic versions of the deuterated product of known stereochemistry.

Diaminopimelate decarboxylase from *Lysinibacillus sphaericus* catalyzes the decarboxylation of *meso*-(2*S*,6*R*)-2,6-diaminopimelate by forming its external pyridoximine in the active site from a prosthetic pyridoxal 5′-diphosphate. Because the biologically relevant (*S*)-lysine is the product, the enzyme must decarboxylate the *R* end of the *meso* reactant. Undeuterated *meso*-(2*S*,6*R*)-2,6-diaminopimelate was converted to (2*S*)-[6-^{2}H]lysine in ^2H_2O

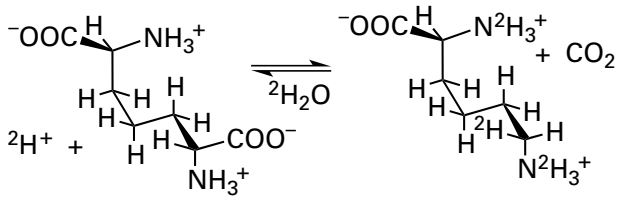

(4–247)

and *meso*-(2*S*,6*R*)-2,6-diamino-[2,6-$^2H_2$]pimelate was converted to (2*S*)-[2,6-$^2H_2$]lysine in H_2O

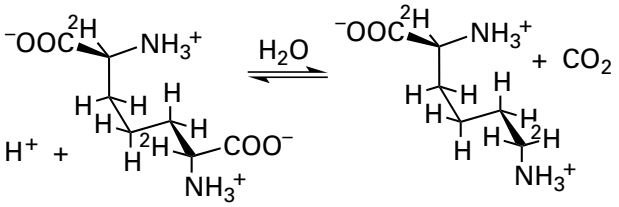

(4–248)

Each product, which should have the opposite stereochemistry from the other at carbon 6, was separately converted to the respective phthalimido valerate **4–52**

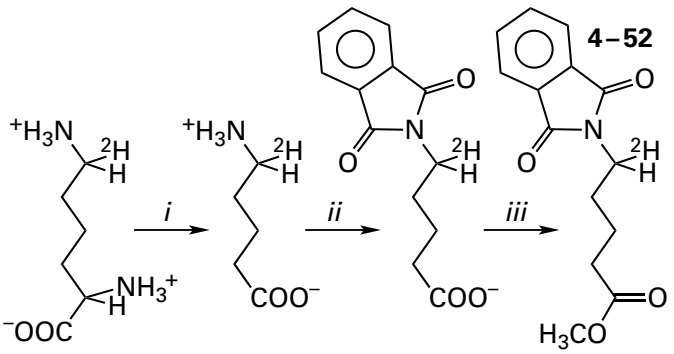

(4–249)

with (*i*) L-lysine oxidase,[509] (*ii*) phthalic anhydride, and (*iii*) diazomethane.[510] The resulting product has only one chiral carbon, the one on which the deuterium is located, so the two products are enantiomers of each other.

The two products had equal but opposite specific rotations at 589 nm. The specific rotation of the product from the decarboxylation of Equation 4–247 was –0.92°, and that of Equation 4–248 was +0.84°. The specific rotation of authentic (*R*)-5-phthalimido-[5-^{2}H]valerate, synthesized from L-glutamate, had a specific rotation of –0.95°. This observation demonstrated that the product from the decarboxylation of Equation 4–247 had *R* stereochemistry and that of Equation 4–248 had *S* stereochemistry. Therefore, in the normal enzymatic reaction carried out in ^1H_2O, the hydron that replaces carbon dioxide becomes the *pro-R* hydrogen at carbon 6 of the product, and the reaction proceeds with inversion of configuration at that carbon.

When a stereoheterotopic hydrogen in a compound is replaced by deuterium, the replacement either creates **circular dichroism,** if the compound was achiral before the replacement, or alters the prexisting circular dichroism, if the compound was chiral before the replacement. For example, (3*E*)-2-oxohex-3-enedioate, the product of the reaction catalyzed by 2-hydroxymuconate tautomerase (Equation 4–229), is an achiral molecule. When the reaction is run in ^2H_2O, a deuterium is added by the active site to carbon 5. The [5-^{2}H]-(3*E*)-2-oxohex-3-enedioate produced by the enzyme was converted, with lead acetate in acetic acid followed by potassium permanganate in sulfuric acid, into [2-^{2}H]glutaric acid, which had a molar ellipticity of +180° at 210 nm. (2*S*)-[2-^{2}H]Glutaric acid and (2*R*)-[2-^{2}H]glutaric acid were synthesized chemically in a route that involved significant racemization at carbon 2. Nevertheless, the synthetic (2*S*)-[2-^{2}H]glutaric acid had a molar ellipticity of +110° at 210 nm, and the synthetic (2*R*)-[2-^{2}H]glutaric acid had a negative molar ellipticity. These results demonstrate that the catalytic acid in the active site of the enzyme adds the hydron that becomes the *pro-S* hydron at carbon 5 in (3*E*)-2-oxohex-3-enedioate.

When a particular stereoheterotopic hydrogen is removed by an active site from a prochiral carbon and the two stereoheterotopic hydrogens on the chiral carbon in the reactant are replaced in turn by deuterium, **mass spectrometry** can determine the outcome of the two reciprocal reactions. The pair of monodeuterated reactants in which the *pro-R* and *pro-S* hydrogens, respectively, have been replaced by deuterium are synthesized, and the mass spectra of products of the enzymatic reaction from each reactant can reveal which hydrogen is removed by the active site. For example, synthetic methyl [6*S*-^{2}H]-*α*-D-galactopyranoside was converted to 1-*O*-methyl-*α*-D-galactose-6-aldehyde by galactose oxidase (Equation 4–230), and the enzymatic product was then converted chemically with *tert*-butyldimethylsilyl trifluoromethanesulfonate to 1-*O*-methyl-2,3,4-tris-(*tert*-butyldimethylsilyl)-*α*-D-*galacto*-pyran-6-aldehyde. The molecular ion of this final silylated product had a mass of 409 unified atomic mass units, but when synthetic methyl [6*R*-^{2}H]-*α*-D-galactopyranoside was used as a reactant and the product of the enzymatic reaction was *tert*-butyldimethylsilylated, the molecular ion of the final product had a mass of 410 unified atomic mass units. Further-

more, the pattern of secondary ions for the final product from the [6*S*-^{2}H] diastereomer was the same as that from undeuterated reactant, and the pattern of secondary ions for the final product from the [6*R*-^{2}H] diastereomer was the same as that from the deuterated [6,6-$^2H_2$] reactant.[433] These results demonstrate that the *pro-S* hydrogen is abstracted from methyl α-D-galactopyranoside by the prosthetic copper–hydroxyphenyl radical in the active site.

To avoid any ambiguity, stereochemical studies of enzymatic reactions should be designed so that **both stereochemical outcomes at a prochiral carbon are examined** by one of these techniques in turn.

If the question to be answered is which of the two stereoheterotopic hydrogens on a particular **prochiral carbon in the reactant** is removed by a catalytic base or prosthetic group in the active site, then deuterium is positioned synthetically at each of the two stereoheterotopic positions on that chiral carbon in turn. For example, both the synthetic 6*S* and the synthetic 6*R* diastereomers of methyl [6-^{2}H]-α-D-galactopyranoside were converted to 1-*O*-methyl-α-D-galactose-6-aldehyde by galactose oxidase (Equation 4–230), and the catalytic base in the active site removed the 6*S* deuterium from the former but removed the 6*S* hydrogen from the latter.[233] Consequently, the prosthetic copper–hydroxyphenyl radical always abstracts the *pro-S* hydrogen from methyl α-D-galactopyranoside during the normal enzymatic reaction.

If the question to be answered is which of the stereoheterotopic hydrogens on a particular chiral carbon has been added to give a **prochiral product** by a catalytic acid or a prosthetic group in the active site, then the stereochemistry of the product of the enzymatic reaction is inverted to give two opposite stereochemical products at that chiral carbon. For example, in the stereochemical study of the reaction catalyzed by diaminopimelate decarboxylase, (2*S*,6*R*)-2,6-diaminopimelate was converted to (6*R*)-[6-^{2}H]-L-lysine in ^2H_2O (Equation 4–247), and (2*S*,6*R*)-2,6-diamino-[2,6-$^2H_2$]pimelate was converted to (6*S*)-[2,6-$^2H_2$]-L-lysine in H_2O (Equation 4–248). It could be concluded from the results that the hydron that replaces carbon dioxide during the normal enzymatic reaction almost always becomes the *pro-R* hydrogen in the product. The occurrence of the reciprocal outcomes in a stereochemical study provides reassurance that the observations resulted from only the stereochemistry of the active site rather than some anomalous kinetic isotope effect.

The ultimate assignment of the absolute stereochemistry of the pair of reactants presented separately to an enzyme or the pair of products produced separately by an enzyme is usually **based on an unambiguous stereochemical synthesis**, either enzymatic or chemical, of one or both members of the labeled pair of reactants or products. For example, the two deuterated stereoisomers of the reactant methyl α-D-galactopyranoside that were converted 1-*O*-methyl-α-D-galactose-6-aldehyde by galactose oxidase (Equation 4–230) were synthesized stereospecifically, and the two stereoisomers of the product, L-lysine, in the case of diaminopimelate decarboxylase (Equations 4–247 and 4–248) were synthesized stereospecifically.

An example of such a stereochemical synthesis would be that for the two diastereomers of D-[6-^{2}H]shikimate with opposite stereochemistry at carbon 6 (Figure 4–30).[511] The stereochemistry of the final product at carbon 6 is dictated by the fact that the Diels–Alder cycloaddition retains the stereochemistry of the dienophile, so H_Z ends up cis to the methoxycarbonyl group and H_E ends up trans.[512] The two D-[6-^{2}H]shikimates of known stereochemistry were synthesized from the two appropriate methyl deuterioacrylates. In the separate syntheses, methyl (*Z*)-[3-^{2}H]acrylate yields (3*R*,4*S*,5*R*,6*R*)-[6-^{2}H]shikimate, and methyl (*E*)-[2,3-$^2H_2$]acrylate yields (3*R*,4*S*,5*R*,6*S*)-[6-^{2}H]shikimate.[511]

When these two diastereomers, each the product of a separate stereochemical synthesis, were separately incubated with the bacterium *E. coli*, (3*R*,4*S*,5*R*,6*S*)-[6-^{2}H]shikimate was the precursor to deuterio-L-phenylalanine and (3*R*,4*S*,5*R*,6*R*)-[6-^{2}H]shikimate was the precursor to undeuterated L-phenylalanine, as determined by mass spectrometry of the products. Between shikimate and L-phenylalanine, the hydrogen at carbon 6 of the shikimate is removed during the elimination catalyzed by chorismate synthase

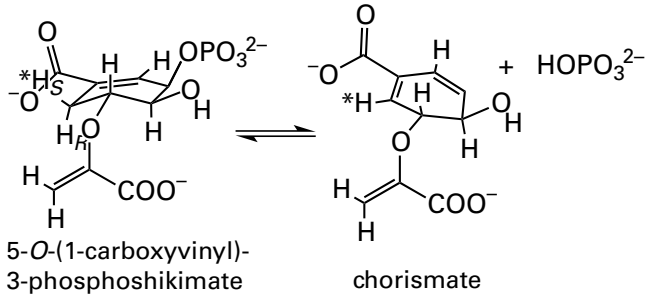

(4–250)

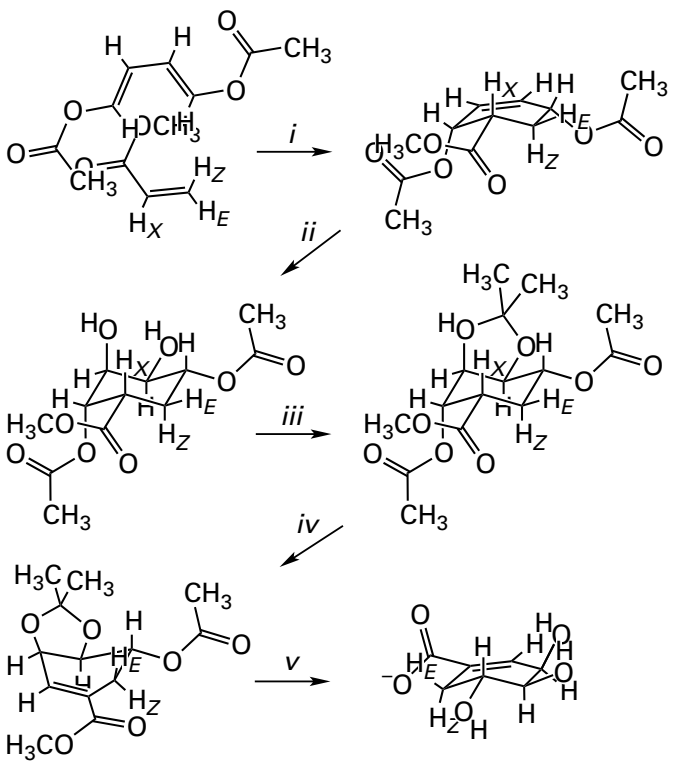

Figure 4–30: Synthesis of D-shikimate from methyl acrylate and *trans,trans*-1,4-diacetoxy-1,3-butadiene.[511,512] (*i*) The diene and dienophile were condensed in anhydrous xylene at reflux in a Diels–Alder cycloaddition that proceeded with the usual stereochemical consequences. In the direction of approach shown, methyl acrylate is below the diene. The two inwardly directed hydrogens on the diene are pushed upward, and the two outwardly directed acetoxy groups respond by rotating downward. The *Z*-hydrogen and the methoxycarbonyl group of the dienophile are pushed downward, and the *E*-hydrogen and the *X*-hydrogen respond by rotating upward to give the enantiomer drawn. The other enantiomer of the endo product is produced when the dienophile approaches from the top of the diene. (*ii*) Osmium tetroxide in tetrahydrofuran/pyridine was used to perform a cis-hydroxylation of the carbon–carbon double bond. The hydroxylation proceeded trans to the two adjacent acetoxy groups because of their bulk and the bulk of the osmium tetroxide. (*iii*) The two vicinal cis-hydroxy groups were incorporated into an acetal with anhydrous acetone under a stream of hydrochloric acid. (*iv*) The elimination of acetic acid by concerted loss of the acidic hydron, H_X^+, and the good leaving group, CH_3COO^-, was accomplished by pyrolysis in a sealed tube at 285 °C. (*v*) The acetal and the two esters were hydrolyzed in 60% acetic acid to yield racemic shikimic acid. The D-enantiomer of shikimate was isolated as the crystalline salt with (–)-1-amino-1-phenylethane.

Therefore, the *pro-R* hydrogen is removed during this anti elimination. Removal of this nonacidic hydrogen at carbon 6 is catalyzed by flavin mononucleotide, which is situated in the active site adjacent to the *pro-R* hydrogen on 5-*O*-(1-carboxyvinyl)-3-phosphoshikimate in the crystallographic molecular model of the complex between chorismate synthase from *Streptococcus pneumoniae* (37% identity; 2.2 gap percent) and oxidized flavin mononucleotide and 5-*O*-(1-carboxyvinyl)-3-phosphoshikimate.[298]

Determination of the stereoheterotopic preference of an active site can be used to identify in a crystallographic molecular model the catalytic acid–base or prosthetic group responsible for removing a stereoheterotopic hydrogen or for adding a hydrogen to a prochiral carbon. For example, every time a molecule of (*S*)-malate is converted to fumarate by the active site of porcine fumarate hydratase, the *pro-R* hydrogen is always removed. This fact identifies Serine C318 in the active site of fumarate hydratase from *M. tuberculosis* (Figure 4–27)[464] as the catalytic base responsible for removal of the hydrogen, even though the hydroxy group of serine ($pK_{a1} = -3$ and $pK_{a2} = 14.2$) seems to be an unlikely catalytic base. The hydroxy group of the serine, however, is located in an oxyanion hole formed by two amido groups of the polypeptide backbone, which should lower its second pK_a significantly by stabilizing the oxido group that is the conjugate base.

In the active site in a crystallographic molecular model of the bimolecular complex between UDP-*N*-acetyl-3-*O*-[(*E*)-1-carboxy-2-methylvinyl]-D-glucosamine and UDP-*N*-acetylmuramate dehydrogenase from *E. coli*, which performs the anti addition of a hydride and a hydron to the carbon–carbon double bond in the (*E*)-1-carboxy-2-methylvinyl group (Equation 4–239), the prosthetic flavin providing the hydride is on one face of the double bond. Consequently, the hydroxy group of Serine 229 on the other face has been assigned as the donor of the hydron during the addition on the basis of the observed anti addition. The more acidic hydron on Tyrosine 125 is relayed to the hydroxy group of this serine through three fixed molecules of water in the active site[513] to increase its acidity.

In the reaction catalyzed by (2*E*,6*E*)-farnesyldiphosphate synthase (previously Equation 3–406)

magnesium isopentenyl diphosphate +
magnesium geranyl diphosphate $\rightleftharpoons$
$MgOPO_3PO_3^{2-}$ + H^+ +
magnesium (2*E*,6*E*)-farnesyl diphosphate
(4–251)

from *E. coli*, the *pro-R* hydron is removed from carbon 2 of isopentenyl diphosphate in the final step of the reaction during formation of the new 2*E* double bond in the product (see Figure 1–26).[514] In the crystallographic molecular model of the active site of the enzyme, occupied by isopentenyl diphosphate and dimethylallyl *S*-thiolodiphosphate, the *pro-R* hydrogen on carbon 2 of isopentenyl diphosphate is directed toward one oxyanion of the diphosphate on dimethylallyl *S*-thiolodiphosphate, and the distance between carbon 2 of isopentenyl diphosphate and that oxygen is 0.42 nm.[515] This distance is close to the sum (0.38 nm) of the van der Waals radii of oxygen (0.15 nm) and hydrogen (0.115 nm) and the length of a carbon–hydrogen bond (0.11 nm), and no other catalytic acid–base is in the immediate vicinity. Knowledge of the prochiral stereochemistry of the reaction identifies this oxygen as the catalytic base that removes the hydron during the reaction.

Several other enzymes that catalyze homologous alkylations of polyisoprenoids proceed with prochiral stereochemistry that is always consistent with the diphosphate that leaves ending up immediately adjacent to the enantiotopic hydrogen on carbon 2 of isopentenyl diphosphate that is removed during the reaction.[516] The conformation of dimethylallyl *S*-thiolodiphosphate, an inactive analogue of the substrate dimethylallyl diphosphate, in the active site of isoprene synthase from *Populus canescens* places one oxygen of the diphospho group immediately adjacent to the hydron removed from carbon during the production of isoprene from dimethylallyl diphosphate by the enzyme.[517]

In the tautomerization of 2-hydroxy-*trans,trans*-muconate catalyzed by 2-hydroxymuconate tautomerase from *P. putida* (Equation 4–229), a hydron is added to a trigonal, prochiral carbon that has a hydrogen as a substituent. When the enzymatic reaction is carried out in ^2H_2O, a hydron is added stereospecifically to carbon 5 to produce only one prochiral product, (5*S*)-5-carboxy-2-oxo-3(*E*)-[5-^{2}H]pentenoate.[518] This stereochemical result confirmed the identification of the amino-terminal proline of the protein in the active site of a crystallographic molecular model of the enzyme from *P. putida*[262] as the catalytic acid that adds the hydron to the *Si* face

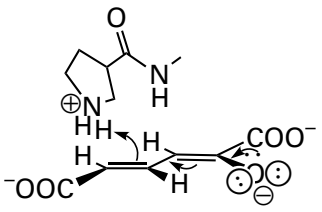

4–53

of carbon 5 of the conjugate base of 2-hydroxy-*trans,trans*-muconate.

The determination of retention of configuration, as in the case of galactarate dehydratase (Equation 4–227) and peptidylglycine monooxygenase (Equation 4–243), determines the orientation of one catalytic group. In instances such as the decarboxylation catalyzed by diaminopimelate decarboxylase (Equations 4–247 and 4–248), however, **the determination of inversion of configuration defines the relative orientation of more than one catalytic group.** This definition can be used to assign the role of particular catalytic groups in the crystallographic molecular model of an active site. The simplest example of such an assignment is that for the active site of mandelate racemase

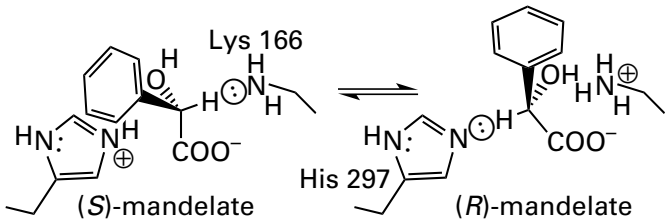

(4–252)

which by definition proceeds with inversion of configuration. As previously noted, in the active site in the crystallographic molecular model of a complex between the enzyme from *P. putida* and 4-iodomandelate, Lysine 166 sits on the same side as the hydrogen on carbon 2 of (*S*)-mandelate, and Histidine 297 sits on the same side as the hydrogen on carbon 2 of (*R*)-mandelate.[100]

Isomerizations catalyzed by a set of related isomerases—glucose-6-phosphate isomerase from *O. cuniculus*, ribose-5-phosphate isomerase from *Spinacia oleracea*, mannose-6-phosphate isomerase from *O. cuniculus*, triose-phosphate isomerase (Equation 4–46) from *O. cuniculus*, xylose isomerase from *Levilactobacillus brevis*, L-arabinose isomerase from *L. brevis*, and L-fucose isomerase from *K. aerogenes*—share a common mechanism, which has been demonstrated by stereochemical studies. In each reaction, an aldose is isomerized to a ketose. The aldose that is the natural substrate in each

reaction has a chiral center at carbon 2 next to the carbonyl carbon of its aldehyde, but both possible enantiomorphs at carbon 3, *S* and *R*, are represented within the set. The ketose that is a substrate in each reaction is a primary alcohol with a prochiral center at carbon 1 where the aldehyde of the corresponding aldose is located.

The stereochemistry for addition of hydrogen to produce prochiral carbon 1 of the ketose has been determined for each isomerase. When the aldose is *R* at carbon 2 (D-glyceraldehyde 3-phosphate, D-glucose 6-phosphate, D-ribose 5-phosphate, and L-arabinose), the ketose produced in the enzymatic reaction has the hydrogen that was added to it at the *pro-R* position on carbon 1

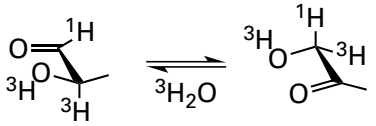

(4–253)

When the aldose is *S* at carbon 2 (D-mannose 6-phosphate and L-fucose), the ketose produced has the hydrogen that was added to it at the *pro-S* position on carbon 1

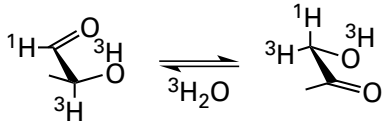

(4–254)

These conclusions were reached by bringing the reactions to equilibrium in ^3H_2O, isolating products, and determining their absolute stereochemistries.[519-522]

This set of enzymes also displays various degrees of **internal hydron transfer** between carbons 2 and 1 during their isomerizations. For example, when the product of the reaction is trapped by glucose-6-phosphate dehydrogenase, it can be shown that the glucose-6-phosphate isomerases from *Homo sapiens*, *O. cuniculus*, and *S. cerevisiae* will transfer a tritium from carbon 1 of [2*R*-^{3}H]-D-fructose 6-phosphate to carbon 2 of D-glucose 6-phosphate

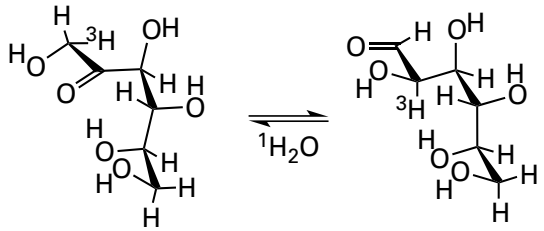

(4–255)

when the reaction is run in ^1H_2O.[523] The ratio between transfer of the tritium intramolecularly and its loss to solvent while it is briefly located on the catalytic base responsible for removing it and then adding it back varies from 5 to 0.3 depending on the species and the conditions. Within the active site of triose-phosphate isomerase (Equation 4–46) from *O. cuniculus*, it can be calculated that 18% of the protium in an unlabeled molecule of glycerone phosphate is transferred from carbon 3 to carbon 2 of D-glyceraldehyde 3-phosphate at pH 7.9 and 25 °C.[524] Similar results have been observed with D-mannose 6-phosphate and mannose-6-phosphate isomerase.[525]

All these facts have led to the conclusion that **a single catalytic base–acid** in the active site of each isomerase removes the hydron from the carbon with the hydroxy group in the substrate to form a *cis*-enediol, moves **across the face of the planar *cis*-enediol**, and adds the hydron back to the intermediate *cis*-enediol from the same face from which it was removed. Later, when crystallographic molecular models of complexes between the active sites of these enzymes and substrates and inhibitors were constructed,[526-531] these stereochemical results identify each catalytic acid–base in the respective active sites that is properly positioned to transfer the hydron between the two carbons, as does Glutamate 164 in the active site of triose-phosphate isomerase (see Equation 4–55 and Figure 3–37).

In this instance, **the stereochemistry was crucial to the identification**. For example, in the active site of triose-phosphate isomerase from *S. cerevisiae*, in the absence of the determination of the stereoheterotopic preference of the active site, Lysine 11 and Glutamate 164 would both be candidates for the role of the catalytic acid–base or catalytic acid–bases that add and remove hydrons from the two carbons. There is no reason that the hydron should be transferred between the two carbons in one of these isomerizations rather than being removed by one base and added by another acid. Furthermore, the prochiral stereochemistries of the primary alcohols in the ketoses are inconsequential to metabolism, so there is no reason for natural selection to pick Glutamic Acid 164 as the sole catalytic acid–base on the basis of this criterion. Consequently, the stereochemical observations of hydron addition and transfer provide the information that allows assignments of the roles of the catalytic acid–bases observed crystallographically.

In contradistinction to the absolute stereochemistry of these isomerases, the catalytic base in human lactoylglutathione lyase can remove the

lone hydron on the chiral carbonyl carbon of either the *S* or the *R* thiohemiacetal formed between glutathione and carbon 1 of a lactaldehyde to produce a *cis*-enediol. Nevertheless, it always delivers the hydron to the *Si* face of the carbon in the *cis*-enediol that was carbon 2 of the lactaldehyde.[532]

A number of stereochemical determinations have been performed for active sites containing **prosthetic pyridoxal 5′-phosphates** that have provided information about the orientations and identities of their catalytic acid–bases. The reaction catalyzed by diaminopimelate decarboxylase (Equations 4–247 and 4–248) introduces the conclusions that can be drawn from stereochemical determinations for active sites with this prosthetic group. The base to which the hydron is added by the catalytic acid within the active site of diaminopimelate decarboxylase is quinonoid intermediate **4–54** formed by the decarboxylation of the external pyridoxamine of the amino group on carbon 6 of *meso*-(2*S*,6*R*)-2,6-diaminopimelate

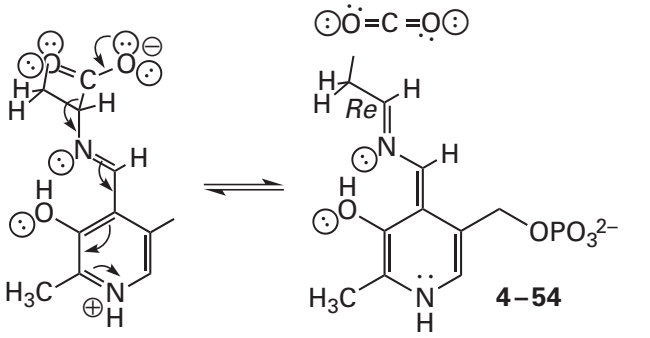

(4–256)

Because the 6*R* carbon in the reactant is decarboxylated and because the *pro-R* hydrogen in the product is added by the active site of the enzyme from *L. sphaericus*, the decarboxylation occurs with inversion of configuration. The catalytic acid must add a hydron to the *Re* face (the face toward the viewer in Equation 4–256) of the carbon that has just been decarboxylated in the quinonoid intermediate. Therefore, determining the stereochemistry of this reaction has revealed the relative orientation of the catalytic acid–base within the active site relative to the planar π molecular orbital system of the quinonoid intermediate.

In the crystallographic molecular model of diaminopimelate decarboxylase from *Arabidopsis thaliana* (28% identity; 2.1 gap percent) in which the 6-amino group of L-lysine has formed an external pyridoximine with the prosthetic pyridoxal 5′-phosphate,[533] the *pro-R* hydrogen on carbon 4 of L-lysine in one of the two active sites in the α_2 dimer is in van der Waals contact (0.41 nm) with the sulfido group of Cysteine 366 from the opposite subunit, and the sulfido group and carbon 4 are in the proper orientation for transfer of a hydron between them. The homologous cysteine is in the same position in both aligned sequences of amino acids of the enzymes from *L. sphaericus* and *A. thaliana*. The *pro-S* hydrogen in the external pyridoximine with L-lysine, however, is pointed toward an open space in the active site occupied by one fixed molecule of water but large enough to accommodate a carboxylato group. The imidazolio group of Histidine 218 is adjacent to the open space, and it could form a hydrogen bond with one oxygen on the carboxylato group of *meso*-2,6-diaminoheptanedioate when it is the reactant to ensure that the carboxylato group bears a negative elementary charge as required by the decarboxylation.

Diaminopimelate decarboxylase catalyzes a decarboxylation of an (*R*)-amino acid that occurs with inversion of configuration. D-Ornithine/D-lysine decarboxylase from *Salmonella enterica*, which is a homologue of diaminopimelate decarboxylase from *L. sphaericus* (27% identity; 1.8 gap percent), also catalyzes a decarboxylation of an (*R*)-amino acid that occurs with inversion of configuration, and the homologous cysteine, Cysteine 387, is also in the same location in the active site adjacent to pyridoxal 5′-phosphate.[534]

There are many enzymes using **pyridoxal 5′-phosphate as a prosthetic group to catalyze decarboxylations of amino acids** that are chemically equivalent to those catalyzed by diaminopimelate decarboxylase and D-ornithine/D-lysine decarboxylase. Each of these other enzymes, however, usually has as its reactant the respective naturally occurring (*S*)-amino acid, but the hydron added nevertheless becomes the *pro-R* hydrogen in the product,[510] as does the hydron added by diaminopimelate decarboxylase. Each of these other decarboxylases must have, as has diaminopimelate decarboxylase, a catalytic acid in its active site on the *Re* face of the respective enamine **4–54** (Equation 4–256). In these decarboxylases, carbon dioxide leaves from the *Re* face of the quinonoid intermediate rather than the *Si* face because the amino acid has the *S* configuration. Therefore, these other enzymes proceed with retention of configuration. The catalytic acid–bases that catalyze the decarboxylation step, if any are required, must reside on the same face (the *Re* face) as the catalytic acid that hydronates the resulting enamine in the next step, and there must

be enough space on the *Re* face to accommodate the carboxylato group of the (*S*)-amino acid.

A **more extensive set of stereochemical conclusions** has been drawn for the nucleophilic substitution catalyzed by the active site of cystathionine γ-synthase (previously Equation 2–31)

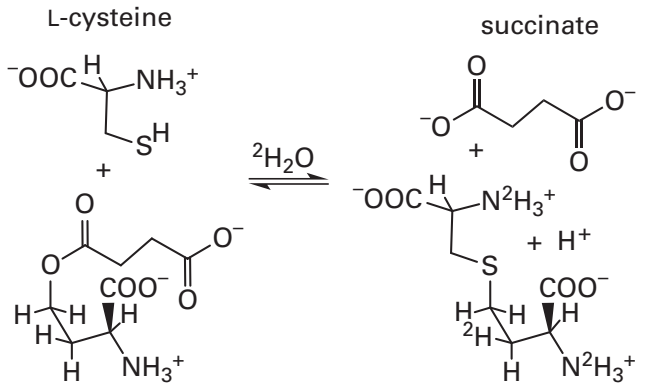

(4–257)

from *S. typhimurium*[535] and its prosthetic pyridoxal 5′-phosphate. In the normal reaction, the stripped intermediate **4–55** is formed from O^4-succinyl-(*S*)-homoserine by tautomerization of its external pyridoximine to form the *N*-pyridoxylimine

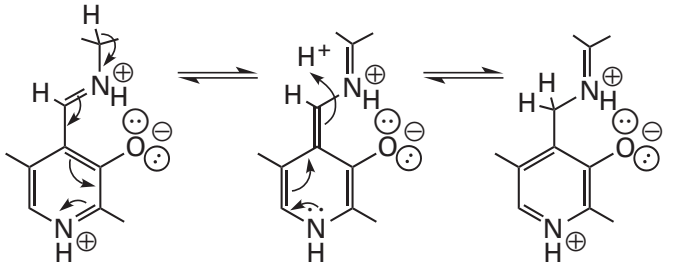

(4–258)

followed by the elimination that proceeds through removal of the β-hydron and expulsion of the leaving group, succinate, from the γ carbon (Equations 2–4, 2–21, 2–32, and 2–34, respectively)

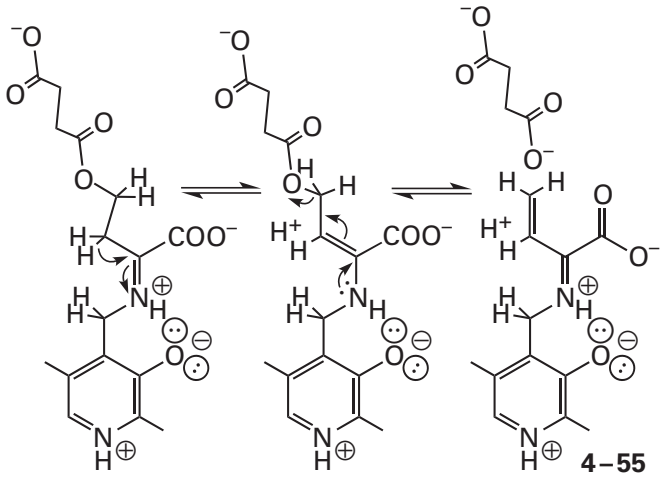

(4–259)

The sulfido group of L-cysteine then replaces the carboxylato group of the succinate, and the sequence of steps proceeds in reverse.

N-Pyridoxylimine **4–55** happens to be the *N*-pyridoxylimine (Equation 4–258) of vinylglycine, and the enzyme will also accept (*S*)-vinylglycine as a reactant

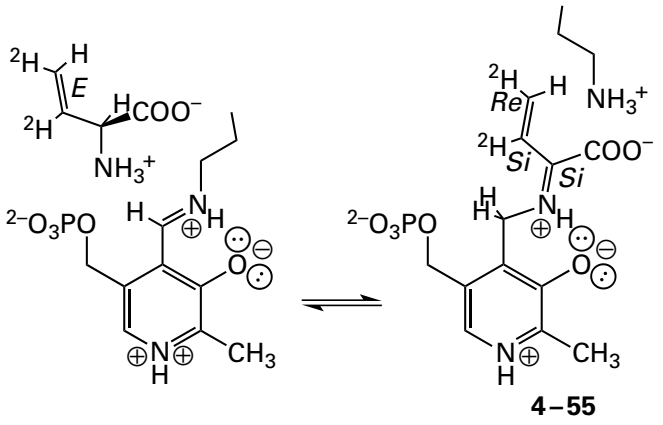

(4–260)

and produce L-cystathionine from it. Both (*E*)-[3,4-$^2H_2$]-(*S*)-vinylglycine and (*Z*)-[4-^{2}H]-(*S*)-vinylglycine were synthesized chemically, and the absolute stereochemistries of the L-cystathionines produced from these two vinylglycines were determined. From these results, it was concluded that the sulfido group of L-cysteine is added to the *Re* face of (*E*)-[3,4-$^2H_2$]vinylglycine (the face toward the viewer in Equation 4–260) and to the stereochemically equivalent *Si* face of (*Z*)-[4-^{2}H]vinylglycine during the respective productions of L-cystathionine. The hydron added to intermediate **4–55** at the β carbon was already known to become the *pro-R* hydrogen of the product (Equation 4–257)[536] so it must be added to the *Si* face of the β carbon in intermediate

4–55.* There are more consequential requirements at the α carbon in proceeding from the reactant and generating the product, both of which must be 2*S*-amino acids. The hydron removed from the α carbon of O^4-succinyl-(*S*)-homoserine to produce the initial quinonoid intermediate (Equation 4–258) must have been removed from what becomes its *Re* face, and the hydron added to the α carbon of the final quinonoid intermediate, which results from addition of the sulfanyl group to intermediate **4–55** and its dehydronation at the 4′ carbon of the pyridoxyl group, must be added to its *Re* face (the face opposite the *Si* face at the α carbon in Equation 4–260).

In the crystallographic molecular model[537] of the complex between cystathionine γ-synthase from *Nicotiana tabacum* (34% identity; 0.8 gap percent relative to *S. typhimurium*) and an inhibitor of the enzyme that forms an intermediate analogous to **4–55**, the 4-hydroxy group of Tyrosine 163 sits on the *Si* face of the β carbon at a distance of 0.30 nm from it and in a location from which its conjugate base could remove a hydron from the incoming sulfido group of L-cysteine and deliver that hydron to the *Si* face of the β carbon (see reverse of Equation 4–259). Because the succinyl group leaves to produce intermediate **4–55** (Equation 4–259) from the same face at which the sulfido group adds to intermediate **4–55**,[535] the hydroxy group of Tyrosine 163 must remove the hydron from the β carbon of the *N*-pyridoxylimine of O^4-succinyl-(*S*)-homoserine and probably hydronates the oxygen of the leaving group in the steps that follow formation of the *N*-pyridoxylimine. All these assignments for the role of Tyrosine 163 based on the crystallographic molecular model **required unambiguous knowledge of the stereochemistry of the enzymatic reaction** because there is also a tyrosine that could act as a catalytic acid–base on the *Si*, *Re*, *Re* face of intermediate **4–55**.

Lysine 261, which forms the internal pyridoximine in the resting enzyme,[538] sits on the *Re* face of the α carbon in the complex with the inhibitor, at a distance of 0.34 nm from it and in a location from which it can remove a hydron from the 4′ carbon of the 5′-phosphopyridoxyl group of the tautomer of the external pyridoximine and deliver it to the *Re* face of the α carbon in the quinonoid intermediate (reverse of the first step in Equation 4–258) to form the external pyridoximine of the product L-cystathionine. Presumably, Lysine 261 removes the hydron from the *Re* face of the α carbon of the initial external pyridoximine of O^4-succinyl-(*S*)-homoserine to form the quinonoid intermediate and then hydronates carbon 4′ of the 5′-phosphopyridoxyl group during the tautomerization (Equation 4–258).

Determination of the stereochemistry of **carboxylases** provides information about the orientations and identities of catalytic acid–bases in the respective active sites. The enzymatic reaction catalyzed by porcine propionyl-CoA carboxylase

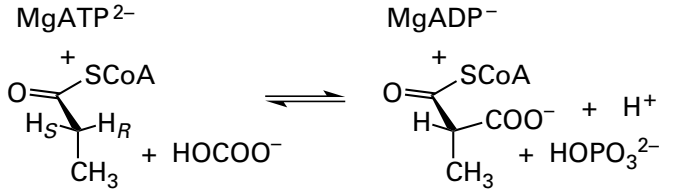

(4–261)

proceeds with retention of configuration at carbon 2. This conclusion is based on two observations. When either deuterium[539] or tritium[540] is substituted for the *pro-S* hydrogen, it is retained in the product. When deuterium is substituted for the *pro-R* hydrogen, it is not retained in the product.[540] Therefore, the catalytic base in the active site that removes the hydron to produce the enolate at carbon 2 must be on the same side of the reactant as the 1-(*N*-carboxy)biotin that delivers the activated carbonic acid to that same carbon in the enolate.

In the crystallographic molecular model of the complex between propionyl-CoA carboxylase from *Streptomyces coelicolor* and biotin and propionyl-SCoA, the *pro-R* hydrogen of carbon 2 of propionyl-SCoA is directed toward nitrogen 1 of biotin, and the distance between carbon and nitrogen is 0.42 nm. It has been proposed that, during the enzymatic carboxylation, biotin dissociates from the carboxy group at nitrogen 1 of 1-(*N*-carboxy)biotin (**1–107**) to give CO_2

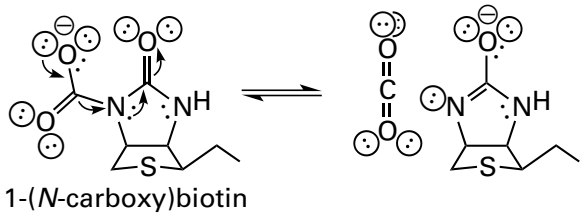

(4–262)

which is held in place by the active site. The resulting conjugate base of the biotin, which, because it is, at the moment of dissociation, the ureido anion, is a

*Note that the priorities for the β carbon and the γ carbon reverse when an oxygen or sulfur is added to the γ carbon.

strong base ($pK_a \cong 27$), then removes the *pro-R* hydron from carbon 2 of propionyl-SCoA, and the adjacent, entrapped CO_2 then adds to the resulting enolate at the same face from which the hydron was removed.[541] These assignments of the several roles are based almost entirely on the stereochemical determinations.

In the carboxylation catalyzed by peptidyl–glutamate 4-carboxylase from *R. norvegicus*, however, in which biotin is not involved, the *pro-S* hydron is removed from carbon 4 of L-glutamate also by a strong base (previously Equation 2–222)

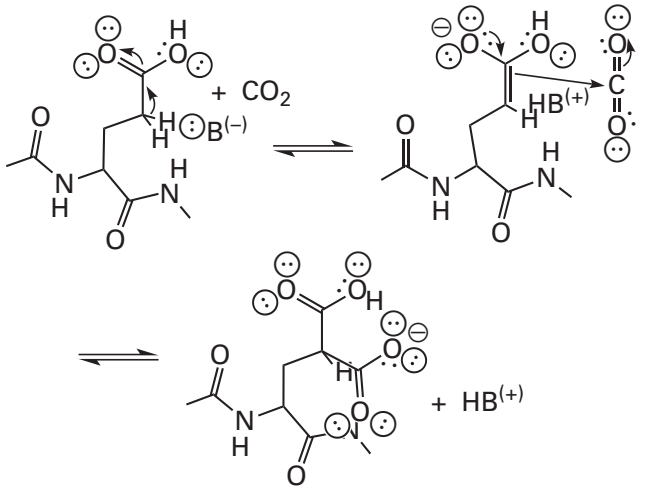

(4–263)

but in this case the strong base is provided by vitamin K (previously in Equation 2–225)

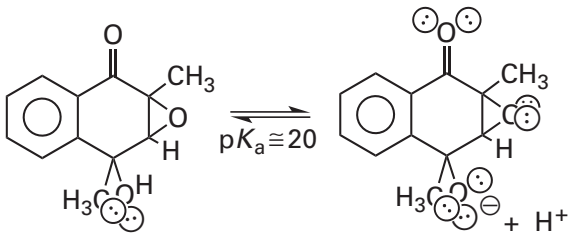

(4–264)

and carbon dioxide adds to the enolate from its other face, so the carboxylation in this case proceeds with inversion of configuration.[542]

Information about the relative orientation of reactants or catalytic functional groups or both of them within the active site can be gained by determining whether an **addition–elimination** catalyzed by an enzyme proceeds in a syn sense or an anti sense. This information is analogous to that gained by determining whether retention or inversion of configuration occurs at a particular chiral or prochiral carbon. For example, in the elimination–addition catalyzed by phosphopyruvate hydratase

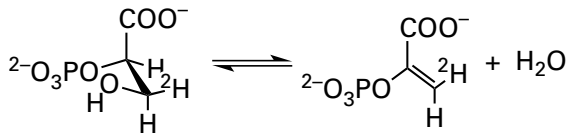

(4–265)

from *O. cuniculus*, the reaction proceeds with anti elimination or addition of water, because the deuterium of (3*R*)-[3-^{2}H]-D-2-phosphoglycerate is found trans to the phosphate in (*E*)-[3-^{2}H]phospho*enol*pyruvate that is the product, with no detectable (*Z*)-[3-^{2}H]phospho*enol*pyruvate.[543] Therefore, in the active site of the enzyme, the catalytic base that removed the hydron from carbon 2 of D-2-phosphoglycerate is on the *Si* face of carbon 2 in the resulting phospho*enol*pyruvate, and the catalytic acid that hydronated the hydroxy group of D-2-phosphoglycerate to convert it to a competent leaving group is on the *Re* face of carbon 3 in the resulting phospho*enol*pyruvate. In the crystallographic molecular model of the complex between phosphopyruvate hydratase from *S. cerevisiae* (62% identity; 0.5 gap percent relative to *O. cuniculus*) and an equilibrium mixture of phospho*enol*pyruvate and 2-phospho-D-glycerate, the 6-ammonio group of Lysine 345 is on the *Si* face of carbon 2 of phospho*enol*pyruvate, its nitrogen atom 0.31 nm from carbon 2. Consequently, this amino group has been assigned as the base that removes the hydron from carbon 2 of 2-phospho-D-glycerate. As expected from the stereochemical observations, the hydroxy group that is added to phospho*enol*pyruvate is found on its *Re* face of carbon 3, accepting hydrogen bonds from the carboxy group of Glutamic Acid 211 and the imidazolyl group of Histidine 373. Consequently, both of these acids have been assigned as catalytic acids that improve the leaving group or, in reverse, the nucleophile.[544]

There are several **related dehydratases that share a common set of acid–bases catalyzing anti eliminations**. Phosphopyruvate hydratase, mandelate racemase, glucarate dehydratase, D(–)-tartrate dehydratase, L-fuconate dehydratase, muconate cycloisomerase, and galactonate dehydratase all share a common ancestor, a conclusion based on alignment of sequences and superposition of crystallographic molecular models.[545-551] Each enzyme uses the 6-amino group of a lysine to remove a hydron α to a carboxy group,[100,101,543,544,549,551-557] as in the active site of phosphopyruvate hydratase (Equation 4–265).

In the active site of mandelate racemase from *P. putida*, Histidine 297, in a homologous position to Histidine 345 in phosphopyruvate hydratase, sits on the opposite side of the substrates from this lysine, Lysine 166, to operate on the other hydron in the racemization catalyzed by the enzyme[558] (Equation 4–252).

In the active site of glucarate dehydratase from *E. coli*,[554] Histidine 339, in the homologous position to Histidine 297 in mandelate racemase, sits on the opposite side of the substrates from Lysine 207, in the homologous position to Lysine 166 in mandelate racemase. Histidine 339 removes the hydron on carbon 5 of D-glucarate and Lysine 207 adds a hydron to carbon 5 during the epimerization between D-glucarate and L-idarate catalyzed by the enzyme[559] (upper equilibrium in Equation 4–266)

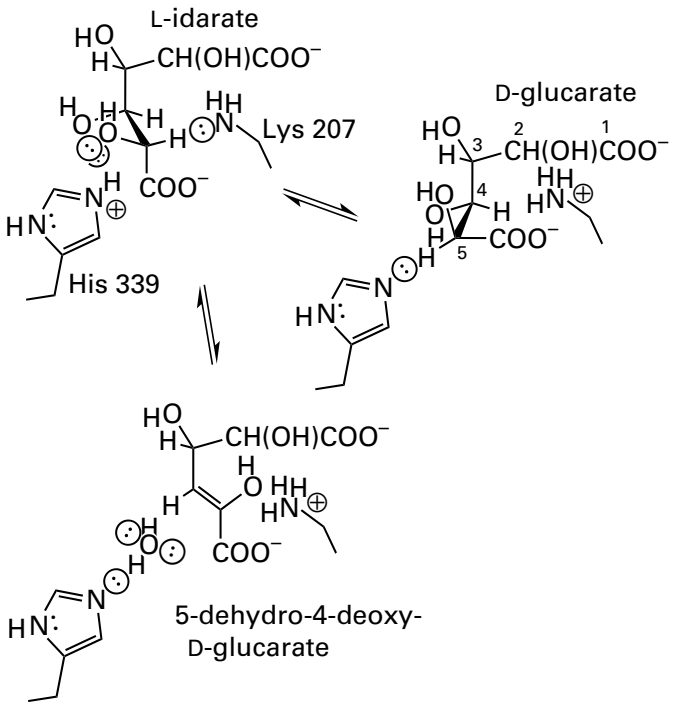

(4–266)

the same roles played by the homologous amino acids in the epimerization of mandelate by mandelate racemase. Histidine 339, however, also hydronates the hydroxy group that leaves from the carbon equivalent to carbon 4 of D-glucarate in the dehydration of L-idarate that is also catalyzed by the active site of glucarate dehydratase,[556] as does the homologous histidine in phosphopyruvate hydratase. In this instance, in contradistinction to the theme of the present discussion, the conclusions that the dehydration of L-idarate must be anti and that the hydron that is removed during the dehydration must be removed by the amino group of Lysine 207 are based so far only on arguments of homology and on the orientation of the product, 4-deoxy-5-dehydro-D-glucarate, when it is bound in the active site in the crystallographic molecular model of its complex with the enzyme,[554] rather than any stereochemical observations.

In the active site of D(–)-tartrate dehydratase from *Bradyrhizobium japonicum*, the homologous Histidine 322 sits on opposite side of the substrates from the homologous Lysine 184, which removes the hydron from (*S,S*)-tartrate during its dehydration to the enol of oxaloacetate. The imidazolyl group of Histidine 322 hydronates the hydroxy group that leaves in the elimination catalyzed by the enzyme.[551]

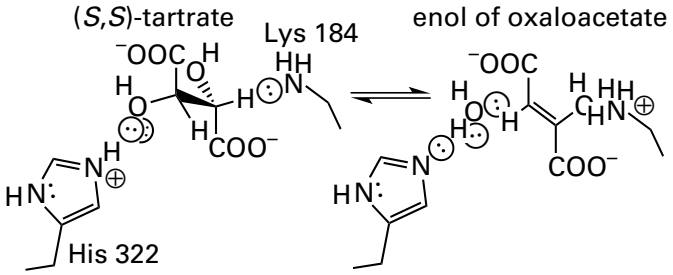

(4–267)

Again, the dehydration is assigned as an anti elimination based only on the conformation assumed by (*S,S*)-tartrate in the crystallographic molecular model of its complex with a mutant of the enzyme in which Lysine 184 has been replaced with alanine.

In the active site of L-fuconate dehydratase from *Xanthomonas campestris*, the homologous Histidine 351, which also hydronates the hydroxy group that leaves in the dehydration catalyzed by the enzyme, sits on the opposite side of the substrates from the homologous Lysine 220, which removes the hydron from carbon 2 of L-fuconate during its dehydration.[549] The fact that the hydron ending up on prochiral carbon 3 of 2-dehydro-3-deoxy-L-fuconate (the ultimate product) is the *pro-S* hydrogen suggests that the 6-ammonio group of Lysine 220, operating on the same face of the intermediate enol **4–56** as it did when it removed the hydron from carbon 2, provides the hydron added to carbon 3.

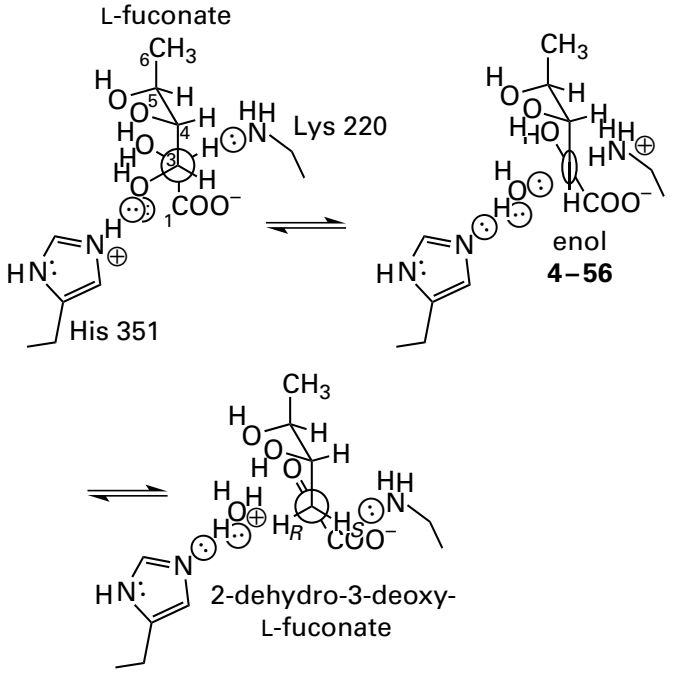

(4–268)

The fact that the *pro-S* hydrogen on carbon 3 of the product is always a deuteron[549] when the reaction is performed in ^2H_2O means that the 6-amino group of Lysine 220, if it does operate on both of these carbons as shown in Equation 4–268, does not transfer the same hydron from carbon 2 to carbon 3 but equilibrates completely with the solution before adding the hydron to carbon 3.

In the active site of muconate cycloisomerase from *Mycolicibacterium smegmatis*, the 6-amino group of the homologous Lysine 162 removes the *pro-S* hydron from the carboxymethyl group of the lactone, (2*S*)-2-(5-oxo-2*H*-furan-2-yl)acetate, in the anti elimination catalyzed by this enzyme.[553,560] In the sequence of amino acids for the protein, however, the homologous histidine is replaced by Glycine 292 and the leaving group in the elimination is instead improved by the 6-ammonio group of Lysine 266, acting as a catalytic acid, and a hydrogen bond from the amido group of Glutamine 294. This glutamine is only two positions in the sequence of amino acids away from that normally occupied by the homologous histidine, and along with the hydroxy group of Threonine 54, it acts as an oxyanion hole

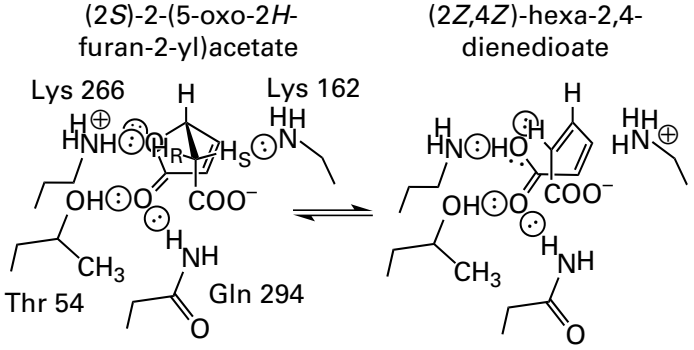

(4–269)

All these observations on homologous enzymes that nevertheless catalyze different reactions **illustrate the versatility of an active site in which there are two catalytic acid–bases**, one on each side of the position in which substrates are bound, to which natural selection can add a third or fourth catalytic acid–base as circumstances require. Such an anti arrangement of catalytic acid–bases can catalyze epimerization or anti elimination. These results also illustrate that a determination that an elimination is anti identifies at least two catalytic acid–bases in the active site of a crystallographic molecular model. This family of enzymes is also an example of the fact that when the reaction catalyzed by an enzyme is changed by evolution through natural selection, the same catalytic groups are often co-opted to play similar roles even though the new reaction may be completely different from the old.[561]

Addition–eliminations discussed so far have all been anti eliminations, but **syn eliminations** also occur in active sites within the same family. In the active site of muconate cycloisomerase from *P. putida*, the *pro-R* hydron is removed by homologous Lysine 171 from the carboxymethyl group of (2*S*)-2-(5-oxo-2*H*-furan-2-yl)acetate, rather than the *pro-S* hydron as in muconate cycloisomerase from *M. smegmatus* (Equation 4–269). In the resulting **syn elimination**, rather than the anti elimination, the leaving group is improved by the imidazolyl group of nonhomologous Histidine 24.[552,553,562] Thus there are muconate cycloisomerases that share a common ancestor (35% identity) and catalyze the same reaction with the same apparent stereochemistry but have a different, albeit cryptic, prochiral stereochemistry enforced by different, nonhomologous catalytic groups in the respective active sites. The related enzyme 3-carboxy-*cis*,*cis*-muconate cycloisomerase also shows both syn[563] and anti[552] stereochemistry in different species. That both syn and anti stereochemistries can occur for the same addition–

elimination reiterates that there are no significant inherent preferences for one over the other.

One of the most sophisticated stereochemical tools to study the orientation of catalytic acid–bases within an active site has been chiral methyl groups. The first compound with a chiral methyl group to be prepared was [^{3}H,^{2}H]acetate in its two enantiomeric forms

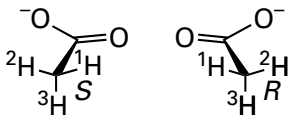

4–57 **4–58**

One of the two original **syntheses of enantiomeric [^{2}H,^{3}H]acetate** proceeds from [^{3}H]glyoxylate* (Figure 4–31)[564] by (*i*) reduction with NAD^{1}H and L-lactate dehydrogenase (Equation 4–204) from mammalian muscle, (*ii*) reduction of the carboxylate to the alcohol with lithium aluminum hydride, (*iii*) activation for nucleophilic substitution of one of the two equivalent hydroxy groups of the ethylene glycol at random with 4-bromobenzenesulfonyl chloride, (*iv*) nucleophilic substitution with a deuteride from lithium aluminum deuteride with inversion of configuration, and (*v*) oxidation of the alcohol to the carboxylic acid with oxygen over platinum. The synthesis provides an equimolar mixture of [^{2}H]acetate and (*R*)-[^{2}H,^{3}H]acetate. The stereochemistry of tritiated product is assigned directly as *R* because L-lactate dehydrogenase (Equation 4–204) is known[565] to produce the *S* isomer of glycolate from [^{3}H]glyoxylate and unlabeled NADH and the nucleophilic substitution with deuteride proceeds with inversion of configuration. The (*S*)-[^{2}H,^{3}H]acetate can be obtained by the same sequence of reactions with the exception that glyoxylate reductase from *S. oleracea* is used in the first step to produce stereochemically pure (*R*)-[^{3}H]glycolate rather than (*S*)-[^{3}H]glycolate. The two enantiomeric acetates can be converted readily to the two acetylcoenzymes A, which are the usual substrates for enzymes operating on acetate, with acetate kinase and phosphate acetyltransferase.[566]

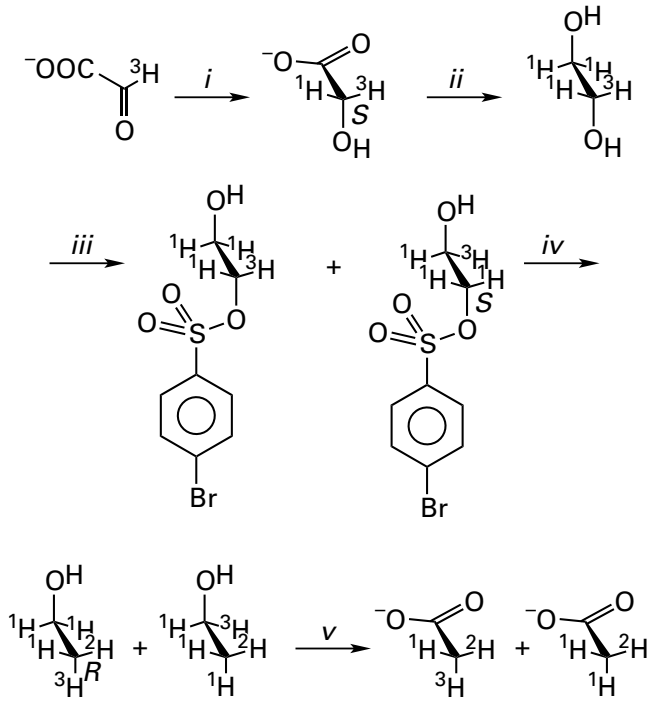

Figure 4–31: Synthesis of chiral acetate from [2-^{3}H]glyoxylate.[564] (*i*) [2-^{3}H]Glyoxylate was reduced with NADH and L-lactate dehydrogenase to produce (2*S*)-[2-^{3}H]glycolate. (*ii*) The methyl ester of (2*S*)-[2-^{3}H]glycolate was reduced chemically with $LiAlH_4$ to produce (1*S*)-[1-^{3}H]ethylene glycol. (*iii*) An equimolar mixture of the two 4-bromobenzenesulfonates (brosylates) of the labeled ethylene glycol was produced by sulfonylation with 4-bromobenzenesulfonyl chloride. (*iv*) The leaving ability of a 4-bromobenzenesulfonyl group was exploited to promote reduction of the two regioisomers with [^{2}H]$LiAlH_4$ by substitution with deuteride with inversion of configuration. (*v*) The resulting equimolar mixture of (2*R*)-[2,2-^{2}H,^{3}H]ethanol and (1*S*)-1-tritio-2-deuterioethanol was oxidized with O_2 over a platinum catalyst, producing a mixture of (*R*)-[^{2}H,^{3}H]acetate and [^{2}H$_1$]acetate. Because only a portion of the original [2-^{3}H]glyoxylate was actually tritiated, the only effect of the equimolar yield of [^{2}H$_1$]acetate was to halve the specific radioactivity of the product relative to that of the initial [2-^{3}H]glyoxylate, not to introduce a species of acetate that was not already unavoidably present.

Other syntheses of enantiomeric [^{2}H,^{3}H]acetate avoid the requirement for enzymatic steps by resolving two enantiomers as diastereomeric salts or adducts[566-568] and then converting the two resolved enantiomers separately to the respective enantiomeric acetates. For example, the carbon–carbon triple bond in [2-^{2}H]-1-phenylethyne was (*i*) reduced stereospecifically with diimide to give (*Z*)-[2-^{2}H]-1-phenylethene, which was then (*ii*) epoxidized with peroxybenzoic acid to give an equimolar mixture of the two diastereomers of (*Z*)-[2-^{2}H]-1-phenyloxirane resulting from epoxidation at the two faces of (*Z*)-[2-^{2}H]-1-phenylethene. This diastereomeric mixture of the two (*Z*)-[2-^{2}H]-1-phenyloxiranes

*Although it is prohibitive to synthesize glyoxylate in which all of the hydrogen is tritium—in other words, the tritium is "carrier free"—the fact that most of the [^{3}H]glyoxylate has a hydrogen at carbon 2, and consequently most of the [^{2}H,^{3}H]acetate has a hydrogen rather than a tritium at carbon 2, is inconsequential to the way in which the final analysis of chirality is performed.

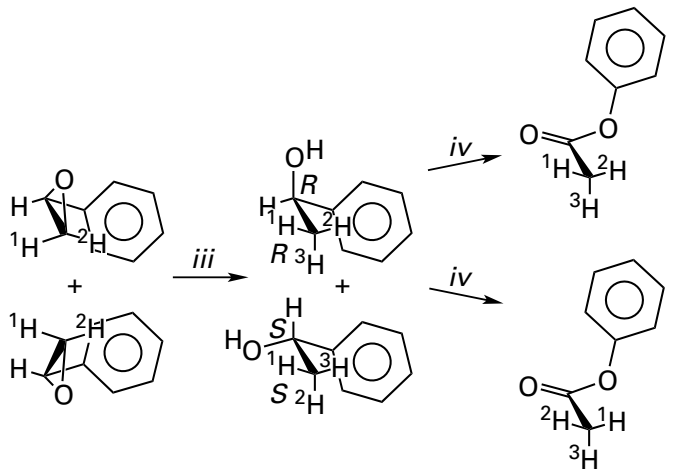

(4–270)

was then (*iii*) reduced with $Li^3HB(C_2H_5)_3$ to produce an equimolar mixture of [2*R*-^{2}H,^{3}H]-(*R*)-1-phenylethanol and [2*S*-^{2}H,^{3}H]-(*S*)-1-phenylethanol. The chirality at carbon 1 was exploited to resolve the two diastereomers of 1-phenylethanol by fractional crystallization of their brucine phthalates. The two diastereomers were then (*iv*) oxidized to the respective [2,2-^{2}H,^{3}H]phenyl ketones with CrO_3 followed by oxidation with peroxytrifluoroacetic acid to produce a Baeyer–Villiger rearrangement (Equation 4–270). The two enantiomeric phenyl [^{2}H,^{3}H]acetates were (*v*) saponified, and the acetates were collected as the respective sodium salts.[566] Another synthesis begins with (*S*)-[1,1-^{2}H,^{3}H]ethanol and (*R*)-[1,1-^{2}H,^{3}H]ethanol prepared by reduction of [1-^{2}H]ethanal with two enantiomeric 9-borabicylo[3.3.1]nonanes,[569] and yet another relies on the ability of rhenium to participate in a planar double bond with carbon and yet remain tetrahedral and enantiomeric.[570]

The **use of enantiomeric [^{2}H,^{3}H]acetyl-SCoA to answer a stereochemical question relies upon the kinetic isotope effect** and the planar, rigid structure of an enolate. Consider (*R*)-[^{2}H,^{3}H]acetyl-SCoA bound to an active site (Figure 4–32). The first step in most enzymatic reactions using acetyl-SCoA as a reactant is removal of a hydron from the acetyl group to create its enolate. The acetyl-SCoA will be bound unavoidably to the active site through its coenzyme A and should form a hydrogen bond at its acyl oxygen with at least the catalytic acid, $–NH^{(+)}$, that hydronates the oxo oxygen to catalyze formation of the enol or the oxyanion hole required to stabilize the oxyanion of the enolate. The chiral methyl group, because it cannot participate in a hydrogen bond or be hindered sterically, will be free to rotate. Assume that the catalytic base required to remove the hydron

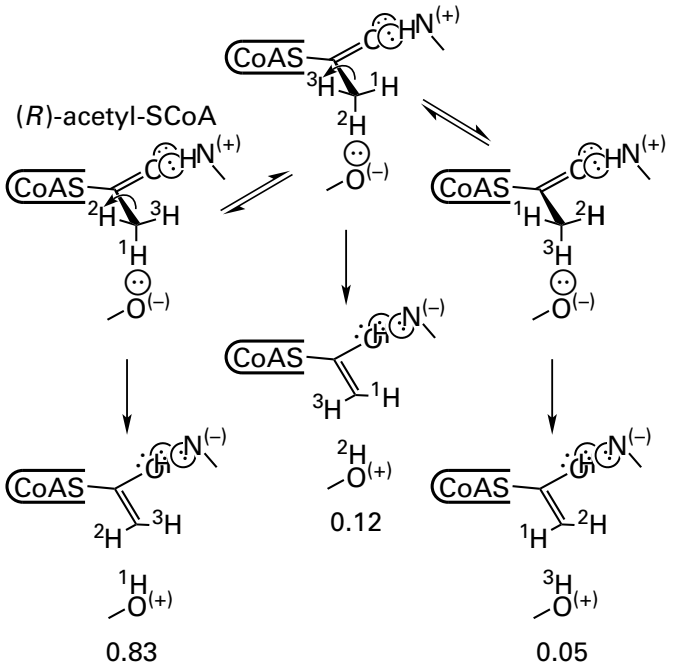

Figure 4–32: Production of three respective enols of (*R*)-[^{2}H,^{3}H]acetyl-SCoA at the active site of an enzyme. In the active site of the enzyme, the coenzyme A thioester of the reactant will be extensively immobilized by noncovalent interactions (symbolized by a cup), and the acyl oxygen will be hydrogen-bonded by at least the catalytic acid, $–NH^{(+)}$ responsible for hydronation of the enolate. As each hydrogen spins by the catalytic base, $–O\odot^{(–)}$, responsible for its removal, the probability that it will be removed should be directly proportional to the appropriate kinetic isotope effect. If the kinetic isotope effects for this hydron removal were ${}^{H}k/{}^{D}k = 7$ and ${}^{H}k/{}^{T}k = 16$, then the probability that the base will remove the protium is 0.83; the deuterium, 0.12; and the tritium, 0.05. The products of each reaction are planar and rigid, and they are pinned to the active site.

from the carbon of the methyl group, $–O\odot^{(–)}$, to form the enolate is on the *Si* face of the acyl carbon and that normal, semiclassical maximum kinetic isotope effects of ${}^{D}k = 7$ and ${}^{T}k = 16$ govern removal of the hydron by the base. If this kinetic isotope effect applies and the base is on the *Si* face, 83% of the enolate formed would be the (*E*)-[^{2}H,^{3}H]enolate and 12% would be the (*Z*)-[^{3}H]enolate. A fraction (5%) of the enolate would be the (*E*)-[^{2}H]enolate and would have lost its tritium altogether and would no longer be radioactive. Rotation about the carbon–carbon bond of the enolate cannot occur because of its double bond. The electrophile added to the nucleophilic enolate in the second step of the reaction will approach either from the respective upper faces in the drawing, in which case inversion of configuration will occur at the α carbon, or from

the respective lower faces in the drawing, in which case retention of configuration will occur at the α carbon.

In the reaction catalyzed by malate synthase

acetyl-SCoA + glyoxylate + H_2O $\rightleftharpoons$ (*S*)-malate + HSCoA (4–271)

the electrophile is the carbonyl group of glyoxylate

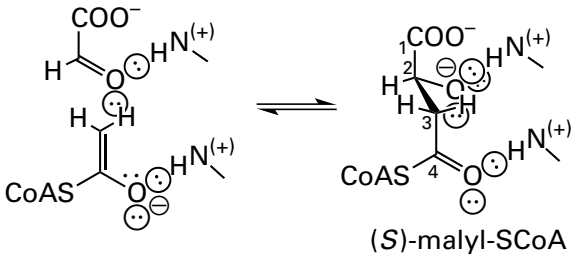

(4–272)

where the numbering is for the malate that is the final product. Because (*S*)-malate is the product of the reaction, the enolate of acetyl-SCoA must add to the *Si* face of the glyoxylate as shown. This stereochemical conclusion follows only from the known stereochemistry of the product. The cryptic stereochemistry at the methylene carbon of the enolate of acetyl-SCoA can be assessed by using the pair of enantiomeric [^{2}H,^{3}H]acetyl-SCoAs.

The strategy for determining the cryptic stereochemistry is most easily understood by making a prediction (Figure 4–33). Consider for the moment only the major product (87%) of acid dissociation, the [^{2}H,^{3}H]enolate of acetyl-SCoA (Figure 4–32). If the reaction proceeds with retention of configuration at carbon 3 of malate, then (*R*)-[^{2}H,^{3}H]acetyl-SCoA should give (2*S*,3*R*)-[3,3-^{2}H,^{3}H]malate as the major product and (*S*)-[^{2}H,^{3}H]acetyl-SCoA should give (2*S*,3*S*)-[3,3-^{2}H,^{3}H]malate as the major product. If the reaction proceeds with inversion of configuration at carbon 3 of malate, then (*R*)-[^{2}H,^{3}H]acetyl-SCoA should give (2*S*,3*S*)-[3,3-^{2}H,^{3}H]malate as the major product and (*S*)-[^{3}H,^{3}H]acetyl-SCoA should give (2*S*,3*R*)-[3,3-^{2}H,^{3}H]malate as the major product. The product of retention from (*R*)-[^{2}H,^{3}H]acetyl-SCoA is identical to the product of inversion from (*S*)-[^{2}H,^{3}H]acetyl-SCoA, and the product of retention from (*S*)-[^{2}H,^{3}H]acetyl-SCoA is identical to the product of inversion from (*R*)-[^{2}H,^{3}H]acetyl-SCoA. The same respective identities are true for the other two products of acid dissociation, the [^{3}H]enolate and the [^{2}H]enolate (Figure 4–32).

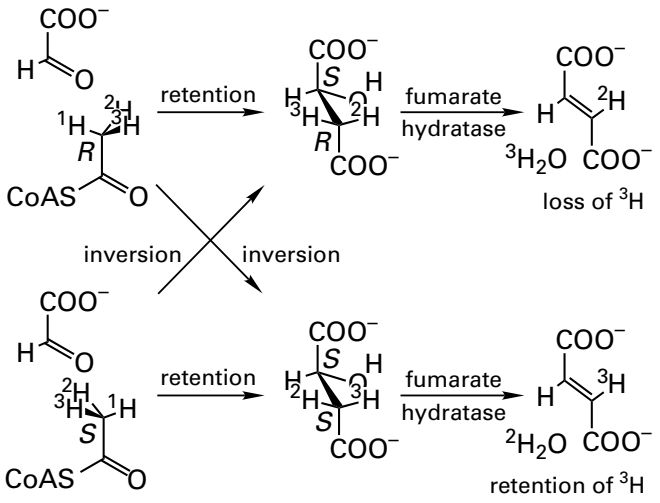

Figure 4–33: Predictions for the stereochemical consequences of the malate synthase reaction if it proceeds either with inversion of configuration or with retention of configuration from either (*R*)-[^{2}H,^{3}H]acetyl-SCoA or (*S*)-[^{2}H,^{3}H]acetyl-SCoA. The actual stereochemistries of the products from each enzymatically catalyzed nucleophilic addition of each enantiomer to glyoxylate are assessed by examining the loss of tritium upon dehydration of the two respective (2*S*)-malates with fumarate hydratase.

Fumarate hydratase is used to distinguish the labeled products from malate synthase. The dehydration catalyzed by fumarate hydratase is always anti regardless of the disposition of isotopes of hydrogen on carbon 3 of the malate (Figure 4–27). Fumarate hydratase removes the tritium from (2*S*,3*R*)-[3,3-^{2}H,^{3}H]malate (as shown in Figure 4–33) but removes the hydrogen from (2*S*,3*S*)-[3-^{3}H]malate and the deuterium from (2*S*,3*R*)-[3-^{2}H]malate. The latter two products always accompany (2*S*,3*R*)-[3,3-^{2}H,^{3}H]malate (Figure 4–32). Fumarate hydratase, however, removes the deuterium from (2*S*,3*S*)-[3,3-^{2}H,^{3}H]malate (as shown in Figure 4–33), but it removes the tritium from (2*S*,3*R*)-[3-^{3}H]malate and the hydrogen from (2*S*,3*S*)-[3-^{2}H]malate. The latter two products, in turn, always accompany (2*S*,3*S*)-[3,3-^{2}H,^{3}H]malate.

If the kinetic isotope effects in the active site of malate synthase had been $^{D}k = 7$ and $^{T}k = 16$ and if the stereochemistry at carbon 3 is disregarded for a short moment, then 83% of the malate produced from either enantiomer of [^{2}H,^{3}H]acetyl-SCoA should have been (2*S*)-[3,3-^{2}H,^{3}H]malate; 12%, (2*S*)-[3-^{3}H]malate; and 5%, (2*S*)-[3-^{2}H]malate (Figure 4–32). Consequently, 95% of the malate produced has a tritium at carbon 3. Now, if the stereochemistry at carbon 3 is considered, then upon incubation with fumarate hydratase, the malate

that is the product of the reaction should lose 87% (83/95) of its tritium if it is a mixture of 83% (2*S*,3*R*)-[3,3-^{2}H,^{3}H]malate, 12% (2*S*,3*S*)-[3-^{3}H]malate, and 5% (2*S*,3*R*)-[3-^{2}H]malate. It should lose 13% (12/95) of its tritium if it is a mixture of 83% (2*S*,3*S*)-[3,3-^{2}H,^{3}H]malate, 12% (2*S*,3*R*)-[3-^{3}H]malate, and 5% (2*S*,3*S*)-[3-^{2}H]malate.

When (*R*)-[^{2}H,^{3}H]acetyl-SCoA was incubated with glyoxylate and malate synthase from *S. cerevisiae*, the [^{3}H]malate produced lost only 31% of its tritium upon conversion to fumarate,[566] so it must have been a mixture of (2*S*,3*S*)-[3,3-^{2}H,^{3}H]malate, (2*S*,3*R*)-[3-^{3}H]malate, and (2*S*,3*S*)-[3-^{2}H]malate. When (*S*)-[^{2}H,^{3}H]acetyl-SCoA was incubated with glyoxylate and malate synthase, the [^{3}H]malate produced lost 69% of its tritium upon conversion to fumarate, so it must have been a mixture of (2*S*,3*R*)-[3,3-^{2}H,^{3}H]malate, (2*S*,3*S*)-[3-^{3}H]malate, and (2*S*,3*R*)-[3-^{2}H]malate. Therefore, malate synthase catalyzes the condensation with inversion of configuration at the methyl carbon of acetyl-SCoA.

The losses of tritium observed (31% and 69%) were closer to 50% than the predicted losses (13% and 87%). In independent experiments,[571] it was determined that the intrinsic kinetic isotope effect ^Dk for malate synthase is 3.7. This observation explains, in part, the percentages of tritium loss that are greater and less than theoretical, respectively. Usually, the actual intrinsic kinetic isotope effects will be less than the theoretical maxima. In addition, exchange of the various isotopes of hydrogen on the acetyl-SCoA, both enzymatic and nonenzymatic, leading to racemization and eventually resulting in a ratio of 50% and 50%, will occur slowly but continuously in the aqueous solutions used for the experimental mixtures. Both the less-than-maximum intrinsic deuterium and tritium kinetic isotope effects and the racemization will tend to cause the two losses of tritium to become closer to 50%.

If the reaction catalyzed by malate synthase proceeds by inversion of configuration, then the catalytic base within the active site that removes the hydron from the methyl group to form the enolate must be on the opposite side of bound acetyl-SCoA from the position at which the carbonyl of glyoxylate is held within the active site, with its *Si* face directed toward the methyl carbon of bound acetyl-SCoA. Because the glyoxylate could be on either side of the enolate, there is no way to learn from the stereochemical result alone whether the catalytic base in the active site is on the *Si* face of the acyl group of bound acetyl-SCoA, as shown in Figure 4–32, or on its *Re* face. **Only the relative stereochemistry of the reaction is assessed**. On the basis of these stereochemical observations, however, it was possible for the crystallographers to assign the role of removing the hydron from the acetyl-SCoA to the carboxy groups of the homologous Aspartate 632 and Aspartate 631, respectively, in the crystallographic molecular models of complexes between the homologous (56% identity; 0.4 gap percent) malate synthases from *E. coli*[572] and *M. tuberculosis*[573] and various substrates and inhibitors. Both homologous aspartates are in locations that would position them on the *Si* face of acyl carbon of the enolate (as in Figure 4–32), the face of the enolate opposite from the glyoxylate when it occupies the active site. Crystallographic determination of the position of the glyoxylate within the active site resolves the ambiguity.

Once it was shown that malate synthase proceeds with inversion of configuration at the methyl carbon of acetyl-SCoA, a criterion for deciding the chirality of any chiral [^{2}H,^{3}H]acetate produced in any enzymatic reaction became available.[574] (*R*)-[^{2}H,^{3}H]Acetate is the enantiomeric [^{2}H,^{3}H]acetate which, when converted to malate by malate synthase, produces [^{3}H]malate that retains most of its tritium upon incubation with fumarate hydratase, and (*S*)-[^{2}H,^{3}H]acetate is the enantiomeric [^{2}H,^{3}H]acetate which, when converted to malate by malate synthase, produces [^{3}H]malate that loses most of its tritium upon incubation with fumarate hydratase. A method for determining by tritium nuclear magnetic resonance spectroscopy the absolute stereochemistry of any [^{3}H,^{3}H]methyl group that can be converted to methylamine has also been devised.[575]

The assay that uses malate synthase and fumarate hydratase can be expanded to assess the absolute stereochemistry of any [^{2}H,^{3}H]methyl group in a molecule if that methyl group can be converted into the methyl group of [^{2}H,^{3}H]acetate without racemization. This conversion is usually done by chemically oxidizing the immediate product of the enzymatic reaction. For example, a culture of *Streptomyces cattleya* incorporates a methyl group derived from L-methionine, through *S*-adenosyl-L-methionine, into thienamycin

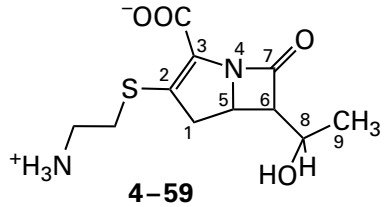

4–59

The methyl group ends up as carbon 9 of the thienamycin. After the 6*S* and 6*R* diastereomers of [6,6-^{2}H,^{3}H]-L-methionine, which were synthesized from (*R*)-[^{2}H,^{3}H]acetate and (*S*)-[^{2}H,^{3}H]acetate, respectively,[576] were fed separately to cultures, the thienamycin produced by the bacteria was oxidized with CrO_3 in H_2SO_4 to give [^{2}H,^{3}H]acetic acid containing the undisturbed methyl group. The [^{2}H,^{3}H]acetates were determined to be *S* and *R*, respectively,[577] by the criterion of tritium loss or tritium retention following treatment with malate synthase and fumarate hydratase. Consequently, the reaction at the methyl groups of the two respective *S*-adenosyl-L-methionines produced from the two diastereomers of L-methionine proceeds with retention of configuration. This conclusion is of interest because almost every other methylation performed by active sites using *S*-adenosyl-L-methionine as the methyl donor proceeds with inversion of configuration in a concerted nucleophilic substitution.

Coenzyme-B sulfoethylthiotransferase (previously Equation 2–358)

$$\text{CoBSH + methyl-SCoM} \rightleftharpoons \text{methane + CoBS–SCoM} \quad (4\text{–}273)$$

where CoBSH is coenzyme B and methyl-SCoM is methylcoenzyme M, in addition to producing methane from methyl-SCoM (previously **2–173**)

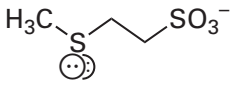

4–60

will produce ethane from ethyl-SCoM. The *R* and *S* enantiomers of [1,1-^{2}H,^{3}H]ethyl-SCoM were produced from [1-^{2}H]acetaldehyde in separate stereospecific syntheses that differed only in the stereoisomer of *B*-(3-pinanyl)-9-borabicyclo[3.3.1]-nonane used as a reductant. These enantiomers were separately incubated with a cell-free extract from the methanogenic bacterium *Methanosarcina barkeri* in ^1H_2O and the resulting ethanes were photochemically chlorinated and oxidized with basic permanganate, the radioactive products were the *R* and *S* enantiomers of [^{2}H,^{3}H]acetate, respectively. Consequently, the overall substitution of the sulfanyl group by a hydride* to produce the ethane proceeds with net inversion of configuration.[569]

*The replacement of a sulfur with a tritium inverts the priority relative to carbon.

Unlike the result for the methylation producing thienamycin (**4–59**), this result is consistent with the expected nucleophilic substitution at that carbon by the nucleophilic nickel(I) in coenzyme F_{430} (previously **2–175**)

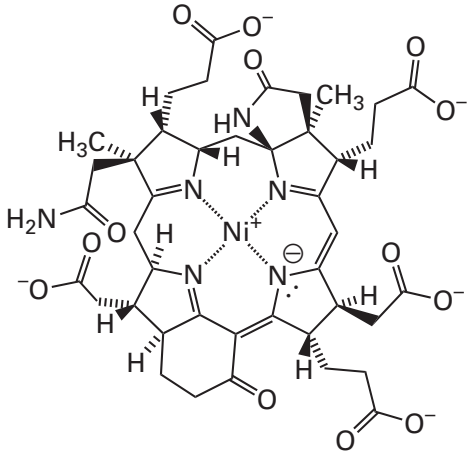

4–61

with $^-$SCoM as the leaving group, which should proceed with inversion of configuration, followed by reduction of the resulting methyl nickel with retention of configuration, presumably the result of the nickel in the methyl coenzyme F_{430} delivering the hydride to its own methyl group from a ligand position immediately adjacent to the carbon–nickel bond. The enantiomers of [1,1-^{2}H,^{3}H]ethane itself have been used to examine the stereochemistry of soluble methane monooxygenase from *Methylococcus capsulatus* (previously Equation 2–295)

$$H^+ + NADH + CH_4 + O_2 \rightleftharpoons CH_3OH + NAD^+ + H_2O \quad (4\text{–}274)$$

which also will accept ethane as a substrate.[578]

Both the ***Z* and *E* stereoisomers of [3,3-^{2}H,^{3}H]phospho*enol*pyruvate** have been synthesized enzymatically (see Problem 4–26)[579,580] and can be used as complementary reactants for one of the many enzymes using phospho*enol*pyruvate. For example, the active site of pyruvate kinase produces a methyl group from a methylene group of phospho*enol*pyruvate during its enzymatic reaction

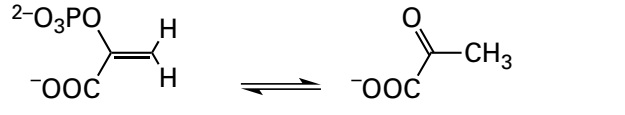

+ $MgADP^-$ + H^+ + $MgATP^{2-}$ (4–275)

by adding a hydron to carbon 3 of the enolate of phospho*enol*pyruvate. The *Z* and *E* stereoisomers of [3,3-^{2}H,^{3}H]phospho*enol*pyruvate were separately incubated with pyruvate kinase from *O. cuniculus* in ^1H_2O to generate the two respective enantiomers of [3,3-^{2}H,^{3}H]pyruvate. These enantiomers were oxidized with H_2O_2 to produce the respective enantiomeric [^{2}H,^{3}H]acetates. The [3,3-^{2}H,^{3}H]pyruvate produced by the enzyme from (*E*)-[3,3-^{2}H,^{3}H]phospho*enol*pyruvate gave (*R*)-[^{2}H,^{3}H]acetate (68% retention of ^{3}H)

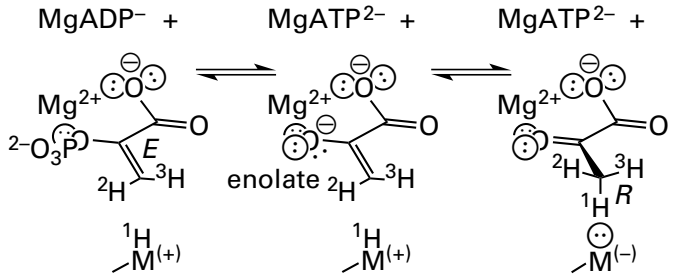

(4–276)

and the [3,3-^{2}H,^{3}H]pyruvate from (*Z*)-[3,3-^{2}H,^{3}H]phospho*enol*pyruvate gave (*S*)-[^{2}H,^{3}H]acetate (84% loss of ^{3}H).[579] Therefore, the catalytic acid that adds the hydron to the enolate of pyruvate during the enzymatic reaction must be on its *Si* face.

In the crystallographic molecular model of a complex between pyruvate kinase from *O. cuniculus* and $MgATP^{2-}$ and glyoxylate, which is an analogue of the enolate of pyruvate (Equation 4–276), a molecule of water, which is a ligand to the Mg^{2+} in $MgATP^{2-}$, is the only catalytic acid that sits on the face of the glyoxylate that would be the *Si* face of the enolate of pyruvate being mimicked by the glyoxylate and that could provide the hydron to the *Si* face.[581] Although this molecule of water is a decent acid in isolation,* a hydron from Glutamic Acid 363 can be relayed through two other molecules of water and the hydroxy group of Serine 361 through this molecule of water on the *Si* face of the enolate to its carbon 3.

The two **enantiomeric [3,3-^{2}H,^{3}H]pyruvates of known absolute stereochemistry** that were produced by pyruvate kinase (Equation 4–276), the stereochemistry of which were determined from the respective chiral acetates, can be used to follow stereochemistry in the many enzymatic reactions involving pyruvate as a reactant. For example, bovine 4-hydroxy-2-oxoglutarate aldolase

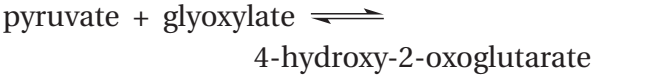

(4–277)

removes an acidic hydron from carbon 3 of pyruvate when it is in the enamine formed by addition of the amino group of Lysine 196 and then condenses this enamine of pyruvate with the carbonyl of glyoxylate. The 4-hydroxy-2-oxoglutarate produced can be converted directly to malate by oxidation with H_2O_2 rather than converting it to acetate and then to malate. The [^{3}H]malate produced from (3*R*)-[3,3-^{2}H,^{3}H]pyruvate lost 81% of its tritium upon incubation with fumarate hydratase, and the [^{3}H]malate produced from (3*S*)-[3,3-^{2}H,^{3}H]pyruvate retained 63% of its tritium upon incubation with fumarate hydratase.[582] Therefore, 4-hydroxy-2-oxoglutarate aldolase proceeds with retention of configuration at carbon 3 of pyruvate

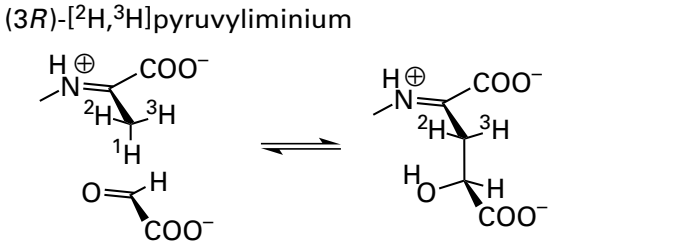

(4–278)

In this case, it seems likely that the same catalytic base that removed the hydron from pyruvate to form its enolate then acts as a catalytic acid to hydronate the carbonyl oxygen of glyoxalate to improve its electrophilicity, or at least transfer the hydron during nucleophilic addition of the enolate, because, as the retention of configuration reveals, the hydron is removed from the same side of the pyruvate to which the aldehyde adds.

In the crystallographic molecular model of human 4-hydroxy-2-oxoglutarate aldolase (90% identity; 0 gap percent) in which the imine between Lysine 196 and pyruvate has been formed in the active site, a fixed molecule of water is located 0.3 nm from the carbon of the methyl group of the imine and 0.26 nm from the 4-hydroxy group of Tyrosine 168 on the same side that, in the enamine, adds to the aldehyde of the glyoxalate.[583] This molecule of water, through which the basicity of the 4-oxido group of Tyrosine 168 can be relayed, seems to be the base that removes the hydron from the imine to

*The pK_a of a molecule of water in the inner coordination sphere of a magnesium ion free in aqueous solution is 11.4.

form the enamine, and then the enamine adds to the carbonyl at the same face from which the hydron was removed.

As with reactions involving enantiomeric [^{2}H,^{3}H]acetyl-SCoA, conclusions drawn from reactions involving enantiomeric [^{2}H,^{3}H]pyruvate depend upon an intrinsic kinetic isotope effect and the inability of an enol, enolate, enaminium, or enamine of pyruvate to undergo rotation between carbons 2 and 3 (Equation 4–276) because of the double bond. The fact that chirality, the result of either inversion or retention of configuration, is actually retained in products of these reactions states that the intermediate, in which the formerly chiral carbon has lost the protium, deuterium, or tritium, cannot, as expected, rotate around the bond because such rotation would lead to racemization.

The stereochemistry of an enzymatic reaction involving a chiral methyl group can also **demonstrate that an intermediate in the reaction is able to rotate** around an adjacent carbon–carbon bond during its lifetime. When either the *R* or the *S* enantiomer of [2,2-^{2}H,^{3}H]ethanolamine is converted to [^{2}H,^{3}H]acetaldehyde

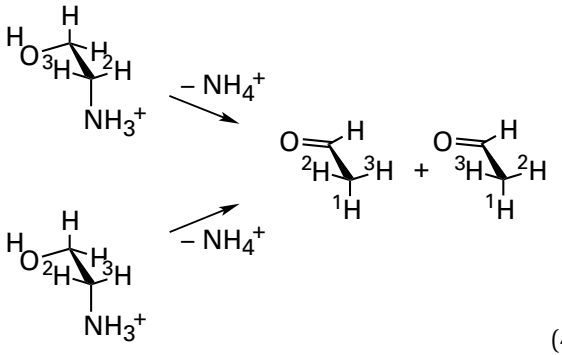

(4–279)

by clostridial ethanolamine ammonia-lyase (Table 2–3), an enzyme with a prosthetic coenzyme B_{12} in its active site, the [^{2}H,^{3}H]methyl group on the resulting [^{2}H,^{3}H]acetaldehyde is racemic.[584] This racemization is not due to the release of an achiral but rigid intermediate that is then rendered racemic by further reaction with the solvent, because when either the *R* or the *S* enantiomer of 2-aminopropanol is used as a reactant with the same enzyme, the products are enantiomeric rather than racemic. When (2*R*)-2-aminopropanol is converted to propionaldehyde with ethanolamine ammonia-lyase containing [5′-^{3}H]adenosylcobalamin, (2*S*)-[2-^{3}H]propionaldehyde is the product, but when (2*S*)-2-aminopropanol is the reactant, (2*S*)-[2-^{3}H]propionaldehyde is again the product[585]

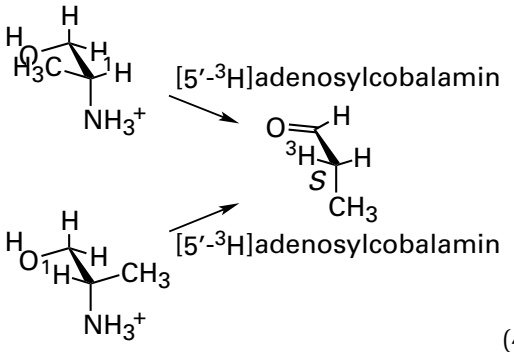

(4–280)

All these results can be explained if an intermediate formed at some step in the reaction catalyzed by ethanolamine ammonia-lyase is free to rotate about its carbon–carbon bond while bound in the active site. For example, if the intermediate is the radical, produced by removal of a hydrogen atom from the *pro-S* position[585] of carbon 1 followed by a 1,2-migration of the amino group across one of its faces, then the resulting radical at carbon 2 produced from (2*S*)-2-aminopropanol

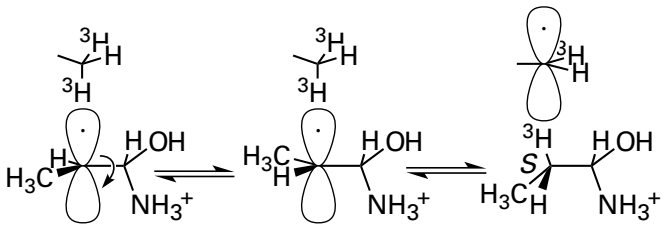

(4–281)

should be able to rotate before it is quenched by the return of the hydrogen atom from [5′-^{3}H]-5′-deoxyadenosine in order to explain the stereochemistry of the product. A similar argument, however, can be made if the intermediate is a carbenium ion or a carbanion rather than the radical. The intermediate produced from (2*R*)-2-aminopropanol would already be the second rotamer in Equation 4–281 rather than the first rotamer. If the second rotamer is the more stable one in the cases of both the 2*S* and 2*R* enantiomers of 2-aminopropanol because of steric interactions in the active site, then both enantiomers would give the same product, (2*S*)-[2-^{3}H]propionaldehyde, as is observed. Rotation of the type described would also explain the racemization observed in the case of [2,2-^{2}H,^{3}H]ethanolamine in which the two substituents on carbon 2 are merely isotopes of hydrogen, which cannot be sterically distinguished,

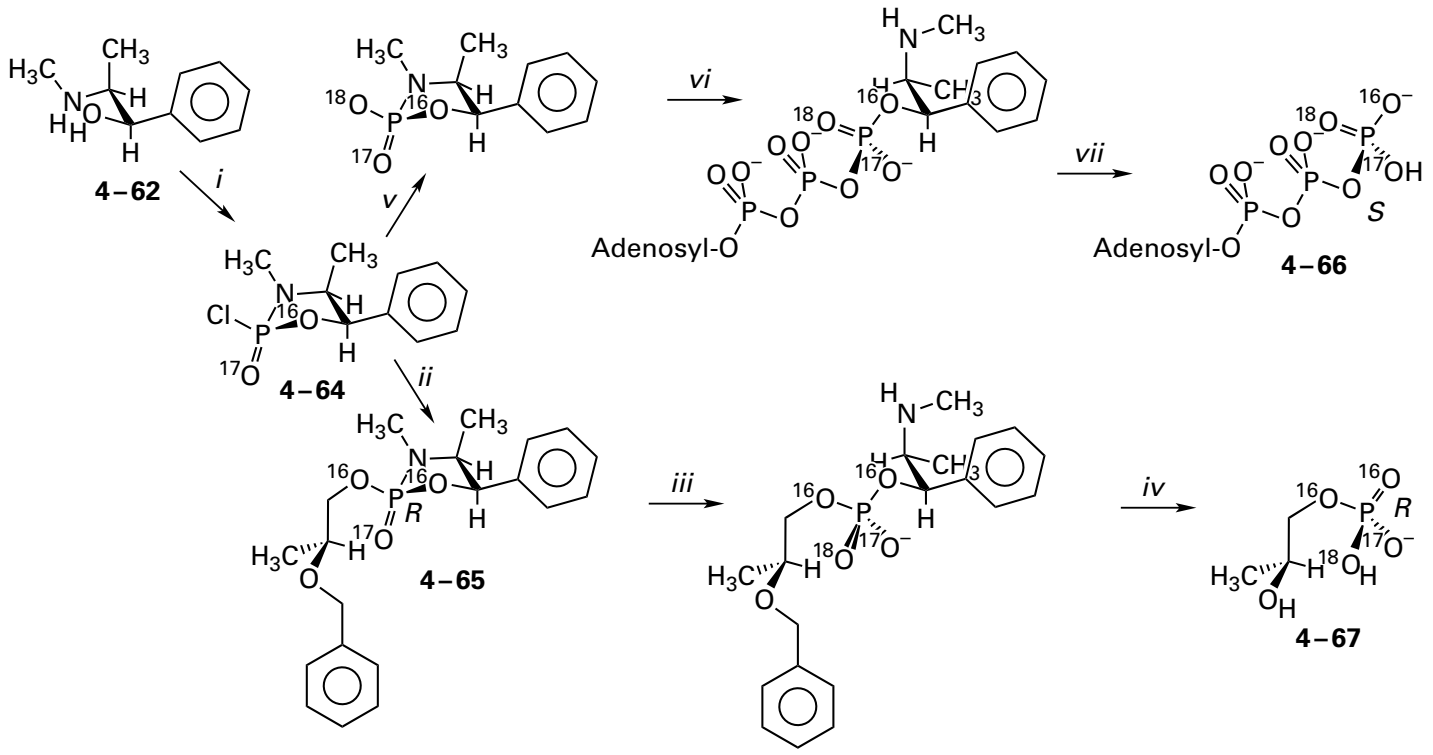

Figure 4–34: Synthesis of either 1-(*R*)-[^{17}O,^{18}O]phospho-(2*S*)-propane-1,2-diol (**4–67**)[586] or adenosine (*S*)-[γ,γ-^{17}O,^{18}O]triphosphate (**4–66**).[588] (1*R*,2*S*)-2-(Methylamino)-1-phenylpropanol (**4–62**) was (*i*) converted to the cyclic phosphoramidochloridic ester **4–64** with [^{17}O]$POCl_3$ in ether with triethylamine as the base. (*ii*) Cyclic phosphoramidochloridic ester **4–64** was submitted to substitution with 2-benzyl-(*S*)-propane-1,2-diol, again with triethylamine as the base, and the two diastereomeric epimers at phosphorus were resolved chromatographically. (*iii*) The major epimer was hydrolyzed in acidic $H_2{}^{18}O$, and (*iv*) the phosphate amido ester was reduced with H_2 over palladium on carbon to produce the monoester **4–67**. The two diastereomeric epimers at phosphorus of cyclic phosphoramidochloridic ester **4–64** were separated chromatographically, and (*v*) the major one was hydrolyzed with Li^{18}OH in $H_2{}^{18}O$ and dioxane. (*vi*) The product of this reaction was submitted to nucleophilic substitution with ADP^{3-} in dimethyl sulfoxide, and (*vii*) adenosine (*S*)-[γ,γ-^{17}O,^{18}O]triphosphate was released by reduction with H_2 over palladium on carbon in ethanol–water.

rather than the methyl group in the intermediate from 2-aminopropanol, which can. In this instance, stereochemistry has provided information about two properties of the reaction: namely, that the intermediate is capable of dihedral rotation about its central carbon–carbon bond within its lifetime and that it is sterically confined by its surroundings.

The wide use of enantiomeric [^{2}H,^{3}H]acetate, in which three otherwise identical hydrogen atoms are distinguished by using the three isotopes protium, deuterium, and tritium, inspired the synthesis and use of chiral phospho groups in which three otherwise identical oxygen atoms are distinguished by using the three isotopes oxygen-16, oxygen-17, and oxygen-18. A chiral phospho group can be **prepared synthetically from specific diastereomers of vicinal bisnucleophiles**, such as 2-(methylamino)-1-phenyl-1-propanol (**4–62**)[586] or 1,2-diphenylethylene glycol (**4–63**)[587]

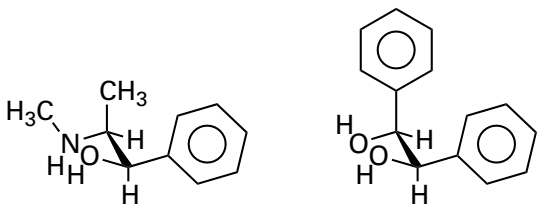

The particular diastereomer chosen to initiate the synthesis determines the stereochemistry of the ultimate phospho group (Figure 4–34).[586,588] For example, 1-[(*R*)-^{17}O,^{18}O]phospho-(2*S*)-propane-1,2-diol (**4–67**) was synthesized from (1*R*,2*S*)-2-(methylamino)-1-phenylpropanol (**4–62**) as follows. (1*R*,2*S*)-2-(Methylamino)-1-phenylpropanol was

(*i*) converted to the cyclic phosphoramidochloridic ester **4–64** with [^{17}O]phosphoryl trichloride. Cyclic phosphoramidochloridic ester **4–64** was then submitted to (*ii*) nucleophilic substitution with 2-benzyl-(*S*)-propane-1,2-diol, and the two epimers at the phosphorus of the resulting diastereomeric cyclic [^{17}O]phosphoramidic diester **4–65** were resolved chromatographically. The major epimer from the chromatography was (*iii*) hydrolyzed in acidic $H_2{}^{18}O$, and the resulting phosphate diester was (*iv*) reduced with H_2 over palladium on carbon to produce a stereochemically pure monoester.

Because the chirality of the major epimer at phosphorus of the phosphoramidate chosen for further reaction after the chromatography was unknown and because the stereochemistry of the nucleophilic substitution at this particular phosphorus had never been determined, the synthesis itself, although stereospecific, did not define the chirality at phosphorus in the final monoester, 1-[^{17}O,^{18}O]phospho-(2*S*)-propane-1,2-diol. Because, however, the final product was a diastereomer, the stereochemistry at phosphorus could be assigned unambiguously as *R* by **metastable ion mass spectrometry** of the cyclic products of intramolecular nucleophilic substitution at phosphorus by the hydroxy group in the (2*S*)-2-hydroxypropyl group.[586] This assignment serves as the basis for stereochemical assignments of the other diastereomeric phosphates in the synthesis. Because reduction with H_2 over palladium on carbon (step *iv*) does not disturb the chirality at phosphorus and hydrolysis in acidic $H_2{}^{18}O$ (step *iii*) proceeds with inversion of configuration, it follows that the major epimer of the cyclic [^{17}O]phosphoramidic diester **4–65** that was purified chromatographically and chosen blindly must have had the *R* configuration at phosphorus as shown.

Once the assignment of the absolute stereochemistry of 1-(*R*)-[^{17}O,^{18}O]phospho-(2*S*)-propane-1,2-diol had been established, a rapid **routine assay for the stereochemistry of a [^{17}O,^{18}O]phospho group** in either the reactant or the product of a chemical synthesis, chemical reaction, or enzymatic reaction by phosphorus nuclear magnetic resonance spectroscopy became available. Usually, the chiral [^{17}O,^{18}O]phospho group in the product of a reaction is transferred enzymatically by reactions of known stereochemistries to a reference diol, either *S*-propane-1,2-diol (dephospho **4–67** in Figure 4–34)[589] or D-glucose.[590] The resulting phosphate monoester is then intramolecularly cyclized to the cyclic diester with inversion of configuration to produce three unique cyclic diesters, which are methylated at random to produce six *O*-methyl diastereomers. Because the presence of oxygen-17 broadens the absorbances of phosphorus in a nuclear magnetic resonance spectrum, signals from only the four cyclic diesters that contain only oxygen-16 and oxygen-18 are observed. The mixture of these four diastereomers from 1-(*R*)-[^{17}O,^{18}O]phospho-(2*S*)-propane-1,2-diol has a phosphorus nuclear magnetic resonance spectrum that can be readily distinguished from the spectrum for the mixture of the four diastereomers from 1-(*S*)-[^{17}O,^{18}O]phospho-(2*S*)-propane-1,2-diol.

Adenosine [γ,γ-^{17}O,^{18}O]triphosphate (**4–66**)[588] can also be synthesized from (1*R*,2*S*)-2-(methylamino)-1-phenylpropanol (Figure 4–34). (*v*) The major epimer of diastereomeric cyclic phosphoramidochloridic ester **4–64** is chromatographically purified and then hydrolyzed with $Li^{18}OH$ in $H_2{}^{18}O$ and dioxane with retention of configuration. (*vi*) The product of this hydrolysis is submitted to nucleophilic substitution at phosphorus with ADP^{3-} with inversion of configuration, and (*vii*) adenosine [γ,γ-^{17}O,^{18}O]triphosphate is released by reduction with H_2 over palladium on carbon. Again, the synthesis does not define the stereochemistry at phosphorus. When, however, the γ-phospho group of adenosine [γ,γ-^{17}O,^{18}O]triphosphate was transferred, with retention of configuration,[591] to 1-phospho-(*S*)-propane-1,2-diol, using alkaline phosphatase from *E. coli*, the nuclear magnetic resonance spectrum identified the product of the synthesis as adenosine (*R*)-[γ,γ-^{17}O,^{18}O]triphosphate.

Another approach to enantiomeric phosphate has been to use two isotopes of oxygen, oxygen-16 and oxygen-18, and replace the third oxygen with sulfur.[592] For example, two syntheses of adenosine (*R*)-[γ-^{18}O]-γ-thiotriphosphate have been developed,[593,594] and the absolute stereochemical preferences of acetate kinase and pyruvate kinase have been exploited to determine the absolute stereochemistry of any [^{18}O]thiophosphate that can be transferred to become the β-phosphate on ADP^{3-}.[595] A chiral triester of thiophosphate, in which a cyclohexyl group, a methyl group, and a 4-nitrophenyl group are substituents on the three oxygens of thiophosphate, has been used as a chiral reactant for aryldialkylphosphatase from *Sphingobium fuliginis* to demonstrate that the enzyme proceeds with inversion of configuration at phosphorus. In this case, no isotopes had to be used because the product of the reaction was the chiral ethylcyclohexylthiophosphodiester.[596]

Chiral phospho groups have been used to examine the stereochemistry of nucleophilic substitutions at phosphorus of the type

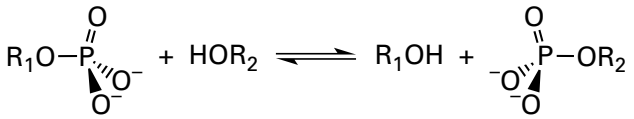

(4–282)

catalyzed by a large collection of enzymes. In all cases, the enzymes catalyze the transfer of a phospho group from an atom of oxygen in one compound to an atom of oxygen in another compound. The significant majority of these enzymatic reactions **proceed with inversion of configuration at phosphorus**. For example, glycerol kinase from *E. coli* proceeds with inversion of configuration at phosphorus[588]

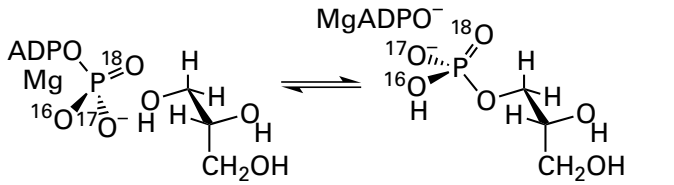

(4–283)

These observations suggest that such enzymatic reactions are simple in-line nucleophilic substitutions at phosphorus. If a **phosphorane** (see **1–56**)

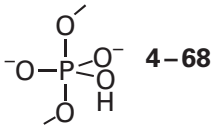

4–68

is formed during this nucleophilic substitution, it necessarily has the oxygen of the acceptor at one axial position and the oxygen of the donor at the other axial position, and these inversions of configuration imply that no pseudorotation takes place. A mechanism in which the oxygen that is the donor resides at an equatorial position in the phosphorane and then assumes an axial position by pseudorotation prior to departure would proceed with retention of configuration. In the active sites of those enzymes that catalyze nucleophilic substitutions at phosphorus that proceed with inversion of configuration, the donor and acceptor must be held in such a way that the oxygen of the acceptor lies upon the opposite side of phosphorus on the line of the phosphorus–oxygen bond of the donor, as in Figures 3–38 and 3–40.

Inversion of configuration, however, **cannot rule out monomeric metaphosphate** as an intermediate in an enzymatically catalyzed nucleophilic substitution at phosphorus because, in the active site of an enzyme, the acceptor and the phospho group of the donor are always held rigidly in place by the noncovalent forces and steric forces of the surroundings. Consequently, inversion of configuration is to be expected of a nucleophilic substitution at phosphorus that involves monomeric metaphosphate as an intermediate (Figure 3–41).

There are several enzymatic nucleophilic substitutions at phosphorus, however, that proceed with **retention of configuration at phosphorus**. In these instances, there is independent evidence that a phosphorylated form of the enzyme acts as a **phosphorylated intermediate** in the enzymatic mechanism. For example, alkaline phosphatase catalyzes nucleophilic substitutions at phosphorus in which the donor and acceptor can be any two alcohols, including water, which is the alcohol where R is H. Because water is usually present at high concentration, it is usually the acceptor when any phosphate monoester is the reactant for alkaline phosphatase. For this reason, the enzymatic reaction is usually hydrolysis of a phosphate monoester (previously Equation 3–380)

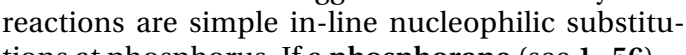

(4–284)

If, however, an alcohol other than water is present in the solution at high concentration, the phosphate will be transferred from the donor to that alcohol as well. Alkaline phosphatase from *E. coli* transfers phosphate from phenylphosphate to (*S*)-propane-1,2-diol with retention of configuration[591]

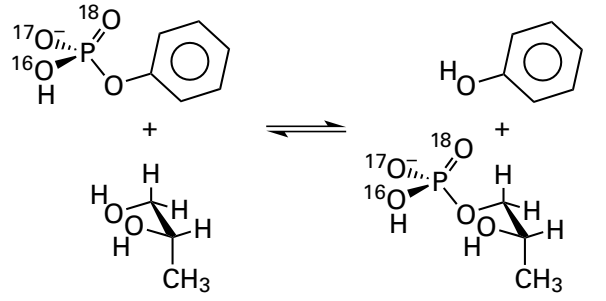

(4–285)

It has been established independently that, in the first step of the enzymatic reaction, the donor transfers the phosphate to Serine 102 within the active site of the enzyme.[597] The donor then leaves the active site and is replaced by the acceptor, and the phosphate is transferred from Serine 102 to the acceptor.

The detailed structure of the active site[597] is consistent with both transfers occurring with inversion of configuration, which would produce net retention of configuration.

Nucleoside-diphosphate kinase catalyzes a nucleophilic substitution at phosphorus

$$MgXTP^{2-} + MgYDP^{-} \rightleftharpoons MgXDP^{-} + MgYTP^{2-} \quad (4\text{–}286)$$

where XTP and YTP are any number of nucleoside 5′-triphosphates and XDP and YDP are the corresponding nucleoside 5′-diphosphates. Its usual purpose is to use $MgATP^{2-}$ to phosphorylate a nucleoside 5′-diphosphate other than $MgADP^{-}$ by transferring the γ-phospho group from $MgATP^{2-}$ to one oxygen in the β-phospho group of the nucleoside 5′-diphosphate and, in this way, to maintain the concentrations of all the nucleoside 5′-triphosphates at high levels relative to their 5′-diphosphates. Bovine nucleoside-diphosphate kinase proceeds with **retention of configuration at phosphorus**,[598] and independent results for the enzyme from *S. cerevisiae* (58% identity; 0 gap percent) are consistent with a mechanism in which the nucleoside triphosphate phosphorylates the imidazolyl group of a histidine within the active site, leaves as the nucleoside diphosphate, and is replaced by the other nucleoside diphosphate, which accepts the phosphate from the resulting *N*-phosphoimidazolyl group.[599-601]

The results with nucleoside diphosphate kinase can be contrasted with those obtained with adenylate kinase

$$MgATP^{2-} + AMP^{2-} \rightleftharpoons ADP^{3-} + MgADP^{-} \quad (4\text{–}287)$$

an enzyme that catalyzes a chemically equivalent reaction. Adenylate kinase from *O. cuniculus* proceeds with **inversion of configuration at phosphorus**.[593] The difference between the reactions catalyzed by nucleoside-diphosphate kinase and adenylate kinase is that the phospho group in the phosphoimidazolyl intermediate in the former reaction (Equation 4–286) always reacts with a nucleoside diphosphate, including the $MgADP^{-}$ that results from phosphorylation of the enzyme by $MgATP^{2-}$. If there were a phosphoimidazolyl intermediate in the active site of adenylate kinase, it would have to transfer its phospho group to both a nucleoside monophosphate, AMP^{2-}, and a nucleoside diphosphate, $MgADP^{-}$. In addition, the active site would have to be able to recognize each as an adenine nucleotide. These two nucleoside phosphates, AMP^{2-} and $MgADP^{-}$, are quite different structurally when viewed back into the respective molecules from the oxygens donating and accepting the phospho group. For both of these reasons, an active site could not be designed so that the same constellation of amino acids is able to recognize in turn the donor and the acceptor. Consequently, the active site of adenylate kinase must form hydrogen bonds over the complete structure of both the donor of the phospho group and the acceptor for the phospho group. As a result, adenylate kinase catalyzes the direct transfer of the phospho group from donor to acceptor while both are bound simultaneously to different regions of the active site.[602] The transfer is accomplished by aligning the nucleophilic oxygen on the α-phospho group of AMP^{2-} with the bridging oxygen–phosphorus bond of the γ-phospho group of $MgATP^{2-}$ and proceeding with an in-line transfer with inversion of configuration with $MgADP^{-}$ as the leaving group.[603,604] Further evidence for this conclusion is that P^1,P^5-bis-(5′-adenosyl)pentaphosphate, a linear pentaphosphate with adenosines at each end that should mimic the transition state in the nucleophilic substitution at phosphorus, is a strong inhibitor ($K_i = 2$ nM) of the enzymatic activity,[605] and a crystallographic molecular model of this complex in the active site has been reported.[606]

The fact that enzymatic nucleophilic substitutions at phosphorus occur with inversion of configuration whenever there is no intermediate phosphoenzyme and the fact that enzymatic nucleophilic substitutions at phosphorus occur with retention of configuration when there a phosphoenzyme intermediate both require that, in these reactions, no pseudorotation can occur. All these results together lead to the conclusion that pseudorotation, which is of accepted chemical interest, is not involved in enzymatic mechanisms.

The three isotopes of oxygen have been used along with sulfur to produce **chiral thiophosphate**[592]

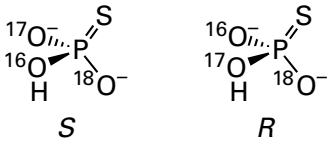

S **4–69** *R* **4–70**

and a method has been developed to distinguish the two enantiomers of [^{17}O,^{18}O]thiophosphate.

Each enantiomer, separately, is converted to adenosine [β,β-^{17}O, ^{18}O]-β-thiotriphosphate by using, in sequence, glyceraldehyde-3-phosphate dehydrogenase (phosphorylating) from *O. cuniculus*, phosphoglycerate kinase from *S. cerevisiae*, adenylate kinase from *O. cuniculus*, and then phosphoglycerate kinase a second time. The diastereomers of adenosine [β,β-^{17}O, ^{18}O]-β-thiotriphosphate produced by this sequence of reactions from (*S*)-[^{17}O,^{18}O]thiophosphate have a phosphorus nuclear magnetic resonance spectrum that is different from those produced from (*R*)-[^{17}O,^{18}O]thiophosphate.[607]

The production of chiral thiophosphate and assays for its chirality have been used to determine the stereochemical consequences of reactions in which $MgATP^{2-}$ is hydrolyzed to phosphate

$$MgATP^{2-} + H_2O \rightleftharpoons H^+ + HOPO_3^{2-} + MgADP^- \quad (4\text{–}288)$$

to provide energy. The consumption of chiral thiophosphate has also been used to determine the stereochemical consequences when $MgATP^{2-}$ is synthesized from phosphate to store energy.[608] When adenosine [(*S*)-γ,γ-^{17}O,^{18}O]-γ-thiotriphosphate is hydrolyzed in $H_2{}^{16}O$ by Ca^{2+}-transporting ATPase from *O. cuniculus*, an enzyme that uses standard free energy from the hydrolysis of $MgATP^{2-}$ for the active transport of calcium across cellular membranes, the [^{17}O,^{18}O]thiophosphate produced has the *S* configuration.[609] The **retention of configuration** observed is due to a phosphorylated intermediate in the mechanism of the enzymatic reaction. The γ-phospho group of $MgATP^{2-}$ is transferred to an aspartate in the active site to produce a mixed anhydride,[610] which is then hydrolyzed by water. The **two successive steps**, each proceeding with inversion of configuration, cause the net result to be retention of configuration. When adenosine (*S*)-[γ^{18}O]-γ-thiotriphosphate, however, is hydrolyzed in $H_2{}^{17}O$ by the ATPase of myosin from *O. cuniculus*, (*S*)-[^{17}O,^{18}O]thiophosphate is produced.[611] The **inversion of configuration** observed in this case has been used as evidence that water directly hydrolyzes the $MgATP^{2-}$ on the active site of myosin in a **single step** through an in-line nucleophilic substitution at phosphorus.

When adenosine (*R*)-[γ,γ-^{17}O,^{18}O]-γ-thiotriphosphate is used as a reactant for glutamine synthetase from *S. typhimurium* (previously Equation 3–405)

$$\text{L-glutamate} + NH_3 + MgATP^{2-} \rightleftharpoons MgADP^- + HOPO_3^{2-} + \text{L-glutamine} \quad (4\text{–}289)$$

in $H_2{}^{16}O$, (*S*)-[^{16}O,^{17}O,^{18}O]thiophosphate was produced.[594] This result is consistent with in-line attack of the oxygen in the carboxy group of the reactant, L-glutamate, bound in the active site, on the immediately adjacent γ-phospho group of the reactant, $MgATP^{2-}$, also bound in the active site, with $MgADP^-$ as the leaving group. This single step in the overall reaction would proceed with inversion of configuration at phosphorus, as is usually the case. The next step in the enzymatic reaction would be the nucleophilic substitution of the phosphate at the carboxyl carbon in the resulting γ-glutamyl phosphate by the third reactant, ammonia, to produce the product, L-glutamine.[612] This step would have no effect on the chirality of the phospho group that is the leaving group during the nucleophilic substitution at the acyl carbon of the acylphosphate. The initial inversion of configuration at phosphorus explains the inversion of configuration observed for the overall reaction.

Suggested Reading

Willadsen, P., and Eggerer, H. (1975) Substrate stereochemistry of the enoyl-CoA hydratase reaction, *Eur. J. Biochem. 54,* 247–252. https://doi.org/10.1111/j.1432-1033.1975.tb04134.x

Willadsen, P., and Eggerer, H. (1975) Substrate stereochemistry of the acetyl-CoA acetyl transferase reaction, *Eur. J. Biochem. 54,* 253–258. https://doi.org/10.1111/j.1432-1033.1975.tb04135.x

Lees, W. J., Benson, T. E., Hogle, J. M., and Walsh, C. T. (1996) (*E*)-Enolbutyryl-UDP-*N*-acetylglucosamine as a mechanistic probe of UDP-*N*-acetylenolpyruvylglucosamine reductase (MurB), *Biochemistry 35,* 1342–1351.https://doi.org/10.1021/bi952287w

Problem 4–16: In the enzymatic reaction catalyzed by arginase

$$\text{L-arginine} + H_2O \rightleftharpoons \text{urea} + \text{L-ornithine}$$

how does a catalytic acid–base in the active site enforce the regiospecificity of the reaction so that ornithine is formed rather than citrulline? Write a mechanism explaining this regiospecificity.

Problem 4–17:

(A) Write the steps in the mechanism of the reaction catalyzed by D-serine ammonia-lyase

$$\text{D-serine} \rightleftharpoons NH_4^+ + \text{pyruvate}$$

The active site uses a prosthetic pyridoxal 5′-phosphate to perform the reaction, so your mechanism should incorporate the pyridoxal 5′-phosphate performing its usual sequence of events as well as one unusual step.

In this enzymatic reaction, the oxygen on carbon 3 of D-serine is replaced by hydrogen. D-Serine ammonia-lyase uses only D-serine [(2*R*)-serine] as a substrate, never L-serine [(2*S*)-serine]. Likewise, the enzyme D-amino-acid oxidase turns only D-serine into 3-hydroxypyruvate, never L-serine. Therefore, in a mixture of the two enantiomers of serine, only the (2*R*)-serine is a substrate for either enzyme and the (2*S*)-serine is untouched.

(*E*)-[3-^{3}H]Propenoic acid was dissolved in methanol, and solid $Ag(CH_3COO)_2$ was added, followed by Br_2. Among other products, a diastereomeric pair of [3-^{3}H]-2-bromo-3-methoxypropanoic acids was formed by anti addition to the double bond. Ammonia (NH_3) was then added to the solution to displace the Br in a concerted nucleophilic substitution with inversion of configuration. After several hours, the whole mixture was treated with HBr to remove the methyl group from the oxygen of the methoxy group by a nucleophilic substitution at the methyl group. After purification, a diastereomeric pair of [^{3}H]serines was obtained from the overall reaction.[613]

(B) Draw, in the sawhorse convention, the absolute structures of the two diastereomeric serines in the diastereomeric mixture obtained from this synthesis, and label each chiral carbon as *R* or *S*.

A portion of this diastereomeric mixture was treated with porcine D-amino-acid oxidase, and [^{3}H]-3-hydroxypyruvate was isolated. This product was treated with H_2O_2 to produce glycolate, which was then turned into glyoxylate by (*S*)-2-hydroxy-acid oxidase from *S. oleracea*. The glyoxylate contained 80% of the tritium originally in the pyruvate; the other 20% was lost as ^3H_2O by slow exchange.

A portion of the original diastereomeric mixture of [^{3}H]serines was also dissolved in ^2H_2O and treated with a mixture of D-serine ammonia-lyase from *E. coli*, pyruvate carboxylase from *G. gallus*, CO_2, $MgATP^{2-}$, malate dehydrogenase, and NADH, all in ^2H_2O. The resulting [3,3-^{2}H,^{3}H]malate was purified from the reaction. Pyruvate carboxylase replaces a hydron on pyruvate with CO_2, which is added with retention of configuration, and the enzyme prefers to remove a hydron by a factor of 3 over a deuteron. Malate dehydrogenase produces only (*S*)-malate from oxaloacetate. When the [3,3-^{2}H,^{3}H]malate was incubated with fumarate hydratase, 41% of the ^{3}H was found in the fumarate, and 58% was recovered as ^3H_2O.

(C) Draw, in the sawhorse convention, the absolute structures of the [3,3-^{2}H,^{3}H]malate, the intermediate [3,3-^{2}H,^{3}H]pyruvate, and the diastereomer of the serine that was the reactant for D-serine ammonia-lyase. Label each chiral carbon as *R* or *S*.

A portion of the original enantiomeric mixture of [^{3}H]serines obtained from the synthesis was acetylated on their amino nitrogens to produce an enantiomeric pair of [3-^{3}H]-*N*-acetylserines. This mixture was treated with porcine aminoacylase, an enzyme that hydrolyzes acetyl groups only from *N*-acetyl-L-amino acids [(2*S*)-*N*-acetyl amino acids]. The optically pure L-[3-^{3}H]serine that was formed by this enzyme was purified, and this optically pure compound was racemized only at carbon 2 to give an equal mixture of the 2*R* and 2*S* enantiomers of [3-^{3}H]serine. This final mixture contained a pair of diastereomers.

(D) Draw, in the sawhorse convention, the absolute structure of the two stereoisomers of [3-^{3}H]serine that were present in this latter diastereomeric mixture, and label each chiral carbon as *R* or *S*.

(E) When this diastereomeric mixture was treated with porcine D-amino-acid oxidase, and the [3-^{3}H]-3-hydroxypyruvate was purified and treated with H_2O_2 followed by (*S*)-2-hydroxy-acid oxidase, how much of the tritium in [3-^{3}H]-3-hydroxypyruvate was retained in the glyoxylate?

When the latter diastereomeric mixture, dissolved in ^2H_2O, was incubated with D-serine ammonia-lyase from *E. coli*, pyruvate carboxylase, CO_2, $MgATP^{2-}$, malate dehydrogenase, and NADH in ^2H_2O, [3,3-^{2}H,^{3}H]malate could be isolated. When this [3,3-^{2}H,^{3}H]malate was incubated with fumarate hydratase, 37% of the ^{3}H was released as ^3H_2O and 63% of the ^{3}H was retained in the fumarate.

(F) Refer to your mechanism for D-serine ammonia-lyase in part A and draw the dissociation of the hydroxy group from the quinonoid intermediate and addition of a hydron to the resulting carbon–carbon double bond with the proper stereochemistry based on all these results. Do these two steps result in retention or inversion of configuration at this carbon?

(G) Does the enzyme release into solution the enamine of pyruvate or pyruvate itself as the product? How can you be sure?

Problem 4–18: Draw in the sawhorse convention the structure of each intermediate product in the following synthesis of the two enantiomers of malonate.[614] In your drawings label each chiral carbon as *R* or *S*. Abbreviate menthyl as $C_{10}H_{19}$.

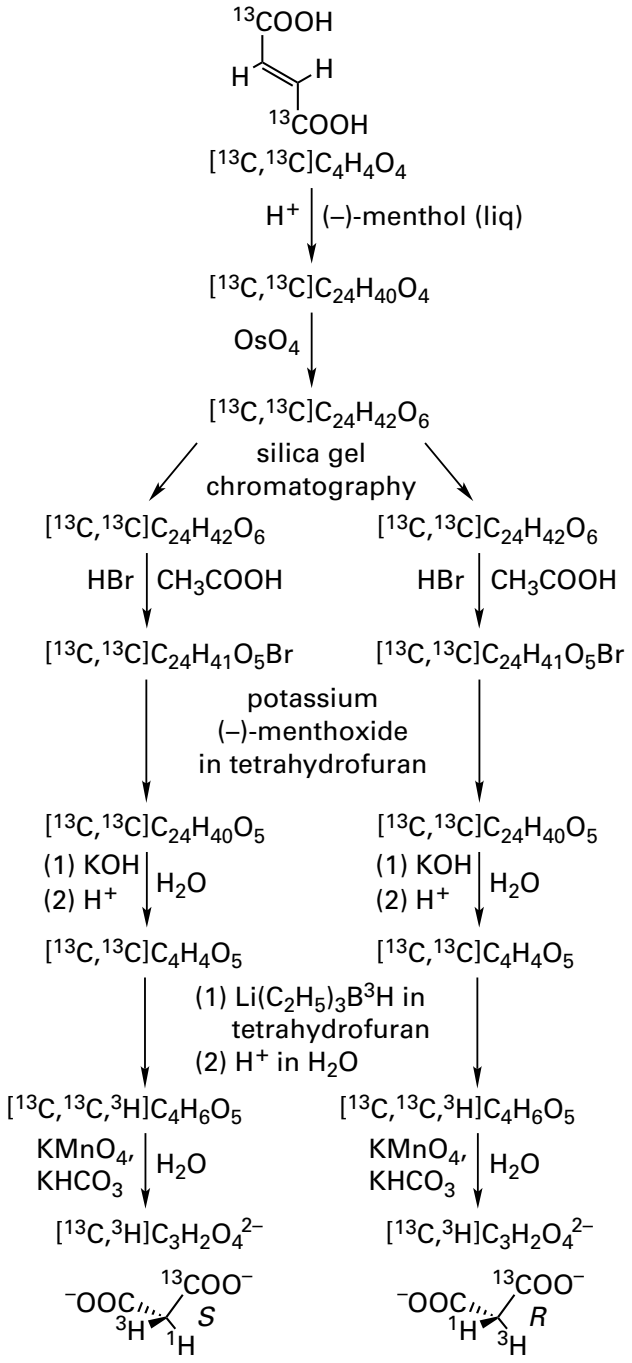

What is (–)-menthol and what purpose does it serve? What is potassium (–)-menthoxide and what purpose does it serve?

Problem 4–19: 2-Methylacyl-CoA dehydrogenase from *R. norvegicus* is a flavoenzyme that catalyzes the following reactions.[615]

(*S*)-2-methylbutanoyl-SCoA $\rightleftharpoons$
(*E*)-2-methylbut-2-enoyl-SCoA + 2 H^+ + 2 e^-

(*R*)-2-methylbutanoyl-SCoA $\rightleftharpoons$
2-ethylpropenoyl-SCoA + 2 H^+ + 2 e^-

2-methylpropanoyl-SCoA $\rightleftharpoons$
2-methylpropenoyl-SCoA + 2 H^+ + 2 e^-

For the moment, assume that the hydron on carbon 2 of each reactant is removed as a hydron to form the enolate and the other hydrogen is removed as a hydride by flavin in the equivalent of a β elimination.

(A) Explain the regiochemistry and stereochemistry of the products by drawing three pictures of the active site of the enzyme. In each case, the disposition of the catalytic base and the flavin in the active site must be the same, but a different one of the three reactants will be bound to it. The drawings must clearly indicate the three-dimensional dispositions of catalytic base, flavin, and reactants that explain the stereochemical results. Abbreviate coenzyme A as SCoA and disregard its detailed structure, and abbreviate flavin as HFl_{ox} and $H_2Fl_{red}^-$, as appropriate, and disregard its detailed structure. Choose a specific side chain to be the catalytic base.

(B) Explain why the enzyme is unable to catalyze the following oxidation because of an absolute stereochemical requirement.

(*R*)-2-methylbutanoyl-SCoA $\rightleftharpoons$
(*Z*)-2-methylbut-2-enoyl-SCoA + 2 H^+ + 2 e^-

The K_m for (*S*)-2-methylbutanoyl-SCoA is 20 μM. Both *n*-butanoyl-SCoA and *n*-pentanoyl-SCoA inhibit the oxidation of (*S*)-2-methylbutanoyl-SCoA. At 100 μM (*S*)-2-methylbutanoyl-SCoA, 100 μM *n*-butanoyl-SCoA inhibits the initial rate for oxidation of (*S*)-2-methylbutanoyl-SCoA by 58%, and 100 μM *n*-pentanoyl-SCoA inhibits the initial rate for oxidation of 2-methylbutanoyl-SCoA by 52%.

(C) Assume that *n*-butanoyl-SCoA and *n*-pentanoyl-SCoA are competitive inhibitors of the enzyme, and calculate the K_i for each.

n-Butanoyl-SCoA is oxidized by the enzyme at a rate only 5% that of the rate for oxidation of (*S*)-2-methylbutanoyl-SCoA when either of these reactants is present at a concentration of 100 μM. *n*-Pentanoyl-SCoA is not oxidized at all by the enzyme.

(D) Provide an explanation, consistent with both your structure of the active site in part A and the dissociation constants calculated in part C, for the fact that *n*-butanoyl-SCoA is a poor substrate and *n*-pentanoyl-SCoA is not a substrate for the enzyme.

Problem 4–20: Fatty-acid synthase system from *G. gallus*, in addition to catalyzing the internal reactions of Equations 3–495 through 3–498, also catalyzes the following homologous external reactions.

acetyl-SCoA + malonyl-SCoA + H^+ $\rightleftharpoons$
HSCoA + CO_2 + acetoacetyl-SCoA (1)

NADPH + acetoacetyl-SCoA + H^+ $\rightleftharpoons$
(*R*)-3-hydroxybutanoyl-SCoA + $NADP^+$ (2)

(*R*)-3-hydroxybutanoyl-SCoA $\rightleftharpoons$
H_2O + (*E*)-but-2-enoyl-SCoA (3)

NADPH + (*E*)-but-2-enoyl-SCoA + H^+ $\rightleftharpoons$
butanoyl-SCoA + $NADP^+$ (4)

(*E*)-But-2-enoyl-SCoA was hydrated by fatty-acid synthase system in ^2H_2O to (3*R*)-[2-^{2}H]-3-hydroxybutyryl-SCoA until equilibrium was reached (Equation 3), and the resulting (3*R*)-[2-^{2}H]-3-hydroxybutyryl-SCoA was purified. The (3*R*)-[2-^{2}H]-3-hydroxybutyryl group was transferred to benzylamine to produce *N*-benzyl-(3*R*)-[2-^{2}H]-3-hydroxybutyramide. The nuclear magnetic resonance spectrum of this product displayed a doublet at 2.4 ppm that was assigned to the proton on carbon 2 of the (3*R*)-[2-^{2}H]-3-hydroxybutyryl group.[491] The doublet integrated with a magnitude of only one proton, which is consistent with the conclusion that carbon 2 had both a hydrogen and a deuterium attached to it.

(A) Which proton on the 3-hydroxybutyryl group is responsible for splitting the absorption of the single proton on carbon 2 into a doublet?

The coupling constant for splitting the absorption of the proton on carbon 2 was 5.5 Hz. When the enzymatic reaction was brought to equilibrium with (3*R*)-[2,2-$^2H_2$]-3-hydroxybutyryl-SCoA in H_2O, the resulting *N*-benzyl-(3*R*)-[2-^{2}H]-3-hydroxybutyramide again displayed a doublet in its nuclear magnetic spectrum at 2.4 ppm, but the coupling constant was 8.4 Hz.

(B) In the spectrum of the first product that has a doublet with a coupling constant of 5.5 Hz, no contribution from a doublet with a coupling constant of 8.4 Hz was detected, and in the spectrum of the second product with a doublet with a coupling constant of 8.4 Hz, no contribution from a doublet with a coupling constant of 5.5 Hz could be detected. What does this observation demonstrate about the stereochemical purity of the two products?

(C) When (*E*)-2,3-epoxybutyric acid was reduced with sodium borodeuteride (NaB^2H_4) in ^2H_2O, the diastereomeric [2-^{2}H]-3-hydroxybutyric acid produced also displayed a doublet in its nuclear magnetic resonance spectrum at 2.5 ppm. The doublet integrated with a magnitude of one proton.[616] This doublet had a coupling constant of 9.0 Hz. What is the absolute stereochemistry at carbon 2 of (3*R*)-[2-^{2}H]-3-hydroxybutyric acid in this racemic synthetic product?

(D) Assume that the (3*R*)-[2-^{2}H]-3-hydroxybutyryl group on *N*-benzyl-(3*R*)-[2-^{2}H]-3-hydroxybutyramide that displayed a doublet with a coupling constant of 8.4 Hz had the same absolute stereochemistry as the (3*R*)-[2-^{2}H]-3-hydroxybutyric acid synthesized in part C, the doublet of which had a coupling constant of 9.0, and assume that the enzymatic product that displayed a doublet with a coupling constant of 5.5 Hz had the opposite stereochemistry at carbon 2. Write a chemical reaction with all reactants and products in the proper stereochemistry that describes the enzymatic hydration of (*E*)-but-2-enoyl-SCoA. Is this a syn addition or an anti addition?

(E) Write the chemical mechanism for the reaction of Equation 1 (the external homologue of Equation 3–495), in which malonyl-SCoA contributes carbons 1 and 2 of the acetoacetyl-SCoA and acetyl-SCoA contributes carbons 3 and 4.

Malonyl-SCoA is produced from acetyl-SCoA in a reaction catalyzed by acetyl-CoA carboxylase

$$\begin{aligned} MgATP^{2-} + HCO_3^- + \\ \text{acetyl-SCoA} \rightleftharpoons MgADP^- + HOPO_3^{2-} \\ + H^+ + \text{malonyl-SCoA} \end{aligned}$$

that uses biotin as a prosthetic group. As is the case with propionyl-CoA carboxylase (Equation 4–261), a hydrogen on acetyl-SCoA is replaced by the carboxy group from 1-(*N*-carboxy)biotin (Equation 4–262) with retention of configuration.

(F) If (*R*)-[^{2}H,^{3}H]acetyl-SCoA were carboxylated by acetyl-CoA carboxylase, what would be the stereochemistry of the [^{2}H,^{3}H]malonyl-SCoA produced?

When (*R*)-[^{2}H,^{3}H]acetyl-SCoA was incubated with acetyl-CoA carboxylase from *G. gallus* and fatty-acid synthase system simultaneously, the butyryl-SCoA produced[617] retained 30.4% of the tritium at carbon 2. When (*S*)-[^{2}H,^{3}H]acetyl-SCoA was incubated with this mixture of enzymes, the butyryl-SCoA retained 34.3% of the tritium at carbon 2. When racemic [2-^{3}H]acetyl-SCoA was incubated with this mixture of enzymes, the butyryl-SCoA retained 32.3% of the tritium at carbon 2.

(G) The first hydrogen is removed from carbon 2 of the original acetyl-SCoA by acetyl-CoA carboxylase. At which step is the second hydrogen removed? What is the absolute stereochemistry of this step?

(H) Draw, with correct stereochemistry, reactants and products for the reaction of Equation 1 if it were performed with (*R*)-[^{3}H]malonyl-SCoA and unlabeled acetyl-SCoA. Does the reaction of Equation 1 proceed with retention of configuration, inversion of configuration, syn addition, or anti addition? Only one answer is correct.

The hydrogen added as a hydron from solution in Equation 4 is added to carbon 2 of (*E*)-but-2-enoyl-SCoA, and the hydrogen added as a hydride, ultimately from NADPH, is added to carbon 3 of (*E*)-but-2-enoyl-SCoA. When the reaction of Equation 4 is carried out in ^2H_2O, with unlabeled (*E*)-but-2-enoyl-SCoA and unlabeled NADPH, the absorption assigned to the two protons on carbon 2 in the nuclear magnetic resonance spectrum of the

N-benzylbutyramide, derived from the butyryl-SCoA produced in the reaction, integrates with a magnitude of only one proton.

Porcine acyl-CoA dehydrogenase (Equation 4–147) converts butyryl-SCoA to (*E*)-but-2-enoyl-SCoA by removing the *pro-R* hydrogen[618] from carbon 3 and the *pro-R* hydrogen[619] from carbon 2. The butyryl-SCoA formed during the enzymatic conversion in ^2H_2O was isolated and then incubated with acyl-CoA dehydrogenase in ^1H_2O. None (<10%) of the deuterium incorporated by fatty-acid synthase system was lost upon this second incubation. The product formed during conversion of (*E*)-but-2-enoyl-SCoA to butyryl-SCoA with [^{3}H]NADPH (Equation 4) was isolated and then incubated with acyl-CoA dehydrogenase. Most of the tritium (83%) incorporated by fatty-acid synthase system (Equation 4) was lost during the second incubation.

(I) Draw a mechanism with proper stereochemistry for Equation 4 if it were carried out in ^2H_2O with [^{3}H]NADPH. The mechanism should proceed through a reasonable enol intermediate.

(J) Does the reaction of Equation 4 proceed with syn addition or anti addition?

Problem 4–21: Imidazoleglycerol-phosphate dehydratase, histidinol-phosphate transaminase, and histidinol-phosphatase from *E. coli* in sequence convert D-*erythro*-1-(imidazol-4-yl)glycerol phosphate in ^2H_2O into [3-^{2}H]-L-histidinol. The peak of absorption from the only proton on carbon 3 of the product in its nuclear magnetic resonance spectrum has the same chemical shift as that for the protons on carbon 3 in an equimolar mixture of (2*S*,3*S*)-[3-^{2}H]histidinol and (2*R*,3*R*)-[3-^{2}H]histidinol prepared synthetically, which was the same chemical shift as the peak of absorption from one of the two protons on carbon 3 of unlabeled L-histidinol. When [3-^{2}H]-D-*erythro*-1-(imidazol-4-yl)glycerol phosphate was used as the initial reactant with the three enzymes in ^1H_2O, the absorption from the only proton on carbon 3 of the resulting [3-^{2}H]-L-histidinol had a chemical shift equal to that of the other proton on carbon 3 of unlabeled L-histidinol.[620] Write a two-step mechanism for imidazoleglycerol-phosphate dehydratase, showing the stereochemistry of each step.

Problem 4–22: At pH 7, tyrosine 2,3-aminomutase from *C. crocatus* converts (2*S*)-[3,3-$^2H_2$]-L-tyrosine into a 3:1 mixture of (2*S*,3*R*)-[2,3-$^2H_2$]-3-amino-3-(4-hydroxyphenyl)propanoate and (2*R*,3*S*)-[2,3-$^2H_2$]-3-amino-3-(4-hydroxyphenyl)propanoate.[505] There is a prosthetic pyridoxal 5′-diphosphate in the active site that forms an external pyridoximine with the amino group of the reactant to convert it to a good leaving group and, once it has left, an adequate nucleophile. The reaction proceeds by an elimination followed by an addition with 3-(4-hydroxyphenyl)propenoic acid as an intermediate. Write a mechanism for the reaction that explains the stereochemical results, in particular why two products are produced from the same reactant. Substrates, intermediates, and catalytic acid–bases in your mechanism should be drawn so that their relative orientation is clearly indicated because the relative orientations determine the stereochemistry.

Problem 4–23: Citrate (*Re*)-synthase adds the enol of acetyl-SCoA to the *Re* face of oxaloacetate to produce citrate in which the *pro*-3*R* carboxymethyl group is derived from acetyl-SCoA.[461] Citrate (*Si*)-synthase (Equation 4–224) adds the enol of acetyl-SCoA to the *Si* face of oxaloacetate to produce citrate in which the *pro*-3*S* carboxymethyl group is derived from acetyl-SCoA.[460] Citrate (*pro*-3*S*)-lyase cleaves citrate to oxaloacetate and acetate by removing the *pro*-3*S* carboxymethyl group.

(A) Copy the structure of citrate

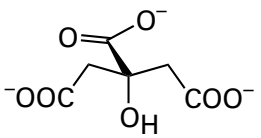

and identify the *pro*-3*S* and *pro*-3*R* carboxymethyl groups.

(B) If [3-^{14}C]oxaloacetate were converted to citrate by citrate (*Re*)-synthase and the [^{14}C]citrate produced were converted to oxaloacetate by citrate (*pro*-3*S*) lyase, which final product would be radioactive?

Two specimens of [^{3}H]malate were synthesized. [^{3}H]Malate, specimen 1, was made by incubating fumarate with fumarate hydratase in ^3H_2O. [^{3}H]Malate, specimen 2, was made by incubating [2,3-$^3H_2$]fumarate with fumarate hydratase in ^1H_2O. [^{3}H]Malate, specimen 1, was incubated with

malate dehydrogenase, NAD^+, acetyl-SCoA, and citrate (*Re*)-synthase from *Clostridium acidurici*. The [^{3}H]citrate produced was incubated with citrate (*pro*-3*S*)-lyase in ^2H_2O, and the [^{3}H,^{2}H]acetate produced was incubated with $MgATP^{2-}$, acetate kinase, phosphate acetyltransferase, HSCoA, glyoxylate, and malate synthase. The [^{3}H,^{2}H]malate produced in this last reaction retained 61% of its tritium upon incubation with fumarate hydratase in ^1H_2O. [^{3}H]Malate, specimen 2, was submitted to the same cycle of reactions, and the [^{3}H,^{2}H]malate produced lost 56% of its tritium upon incubation with fumarate hydratase in ^1H_2O.[574]

(C) Write out each step in this cycle that begins with [^{3}H]malate, specimen 1. Show proper stereochemistry at each step unambiguously.

(D) Draw the mechanism of the reaction of citrate (*pro*-3*S*)-lyase operating in ^2H_2O with the stereochemistry defined by these experiments on [^{3}H]citrate derived from [^{3}H]malate, specimen 1. Indicate stereochemistry unambiguously in your drawings. Use an enol as the leaving group, and hydronate the enol stereochemically on carbon while it is in the active site. Does the reaction proceed with inversion or retention of configuration at carbon 2 of acetate?

(E) Draw the mechanism for the reaction of citrate (*pro*-3*S*)-lyase, with proper stereochemistry, operating in ^2H_2O on [^{3}H]citrate derived from [^{3}H]malate, specimen 2.

(*R*)-[^{2}H,^{3}H]Acetyl-SCoA was incubated with citrate (*Si*)-synthase, and the [^{2}H,^{3}H]citrate produced was cleaved by citrate (*pro*-3*S*)-lyase to [^{2}H,^{3}H]acetate. The [^{2}H,^{3}H]acetate produced was converted to [^{3}H,^{2}H]malate by incubation with $MgATP^{2-}$, acetate kinase, phosphate acetyltransferase, SHCoA, glyoxylate, and malate synthase. The [^{3}H,^{2}H]malate produced retained 65% of its tritium upon incubation with fumarate hydratase. When the complete cycle was repeated with (*S*)-[2,2-^{2}H,^{3}H]acetyl-SCoA, the [^{3}H,^{2}H]malate produced lost 60% of its tritium upon incubation with fumarate hydratase.[574]

(F) Draw, with proper stereochemistry, the mechanism of the reaction catalyzed by citrate (*Si*)-synthase operating on (*R*)-[^{2}H,^{3}H]acetyl-SCoA. Use a stereochemically generated enol as the nucleophile. Does the reaction proceed with retention or inversion of configuration?

Problem 4–24: The unhydrated, carbonyl forms of the substrates are the only ones recognized by triosephosphate isomerase (Equation 4–46) from *O. cuniculus*, although they are the minor forms present in aqueous solution.

(A, B) Draw, with proper stereochemistry where necessary, two possible chemical mechanisms for this reaction and label them A and B. Mechanism A must involve hydron transfers only, while mechanism B must involve a 1,2-hydride migration.

When glycerone phosphate and glyceraldehyde 3-phosphate were incubated with the enzyme in ^3H_2O, tritium was incorporated into the glycerone phosphate.[621]

		specific activity (cpm μatom^{-1})	
compound	isomerase (units)	^3H_2O	compound
experiment 1			
glycerone phosphate	none	699	0
glyceraldehyde 3-phosphate	none	699	0
experiment 2			
glycerone phosphate	1600	278	303
experiment 3			
glycerone phosphate	475	3590	3150

When [^{3}H]glycerone phosphate (777 cpm μmol^{-1}) obtained in a similar experiment was oxidized to 2-phosphoglycolate and formaldehyde with periodate, the formaldehyde was radioactive (835 cpm μmol^{-1}), but the 2-phosphoglycolate was not.

(C) How many hydrogens on which carbon of glycerone phosphate are equilibrated by the enzyme with ^3H_2O during catalysis?

The intention of the next series of experiments[521] was to establish the stereochemistry of this incorporation of tritium into glycerone phosphate. To make this assessment, the absolute stereochemistry of (*S*)-2-hydroxy-acid oxidase from *N. tabacum* was determined. This enzyme catalyzes the reaction

$$O_2 + \underset{\text{glycolate}}{HOCH_2COO^-} \rightleftharpoons H_2O_2 + \underset{\text{glyoxylate}}{OCHCOO^-}$$

(*S*)-2-Hydroxy-acid oxidase readily converts (*S*)-lactate into pyruvate but fails entirely to catalyze the same reaction with (*R*)-lactate. Bovine L-lactate dehydrogenase (Equation 4–204) will convert glyoxylate and NAD^3H into NAD^+ and [^{3}H]glycolate (78,050 cpm μmol^{-1}). When this [^{3}H]glycolate is turned into glyoxylate by (*S*)-2-hydroxy-acid oxidase, all the ^3H ($\leq$100 cpm μmol^{-1} remains) is lost to the solution. Notice that glycolate and lactate differ only by a methyl group.

(D) Indicate, on a stereochemically unambiguous drawing of glycolate, which hydrogen is removed by (*S*)-2-hydroxy-acid oxidase.

A sample of [^{3}H]glycerone phosphate (24,000 cpm μmol^{-1}), prepared as in part C above, was dephosphorylated to glycerone, which was oxidized to glycolate, formaldehyde, and CO_2 by careful treatment with periodate. The [^{3}H]glycolate from this mixture (10,800 cpm $\mu mol^{-1)}$ was isolated and turned into glyoxylate with (*S*)-2-hydroxy-acid oxidase. The specific radioactivity of the resulting glyoxylate was 188 cpm μmol^{-1}.

(E) Why was the specific radioactivity of glycolate half that of glycerone phosphate?

(F) Indicate, on a stereochemically unambiguous drawing of glycerone phosphate, the hydrogen or hydrogens equilibrated with ^3H_2O by triose-phosphate isomerase.

(G) Which mechanism, A or B, is consistent with these observations?

Problem 4–25: The three enzymes 3-carboxy-*cis,cis*-muconate cycloisomerase, 4-carboxymuconolactone decarboxylase, and muconolactone Δ-isomerase from *P. putida* convert *cis,cis*-butadiene-1,2,4-tricarboxylate into (*S*)-5-oxo-2,5-dihydrofuran-2-acetate

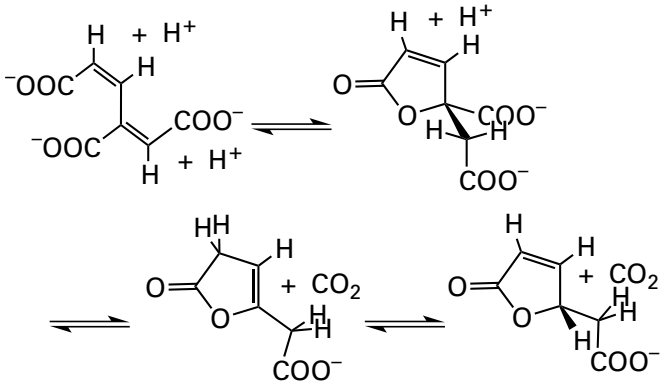

When *cis,cis*-butadiene-1,2,4-tricarboxylate is mixed with all three enzymes in ^2H_2O, the product of the combined sequence of reactions is (2*S*)-[4-^{2}H]-5-oxo-2,5-dihydrofuran-2-[(*R*)-[^{2}H]acetate].[622]

(A) What is the stereochemistry of addition in the first reaction?

(B) What is the stereochemistry of hydron transfers in the third reaction? [Hint: How many protiums are there in the starting material and how many in the final product?]

(C) What is the stereochemistry of the second reaction?

Problem 4–26: [1-^{3}H]-D-Glucose was converted to [1,1-^{3}H,^{2}H]fructose 6-phosphate with hexokinase and glucose-6-phosphate isomerase in ^2H_2O. [1-^{3}H]-D-Mannose was converted to [1,1-^{3}H,^{2}H]fructose 6-phosphate with hexokinase and mannose-6-phosphate isomerase in ^2H_2O. The two respective stereoisomers of [1,1-^{3}H,^{2}H]fructose 6-phosphate produced were of opposite stereochemistry at carbon 1.[520]

(A) Assume that the enzymatic mechanisms for triose-phosphate isomerase, D-glucose-6-phosphate isomerase, and mannose-6-phosphate isomerase are all the same. From your knowledge of the active site of triose-phosphate isomerase, draw two mechanisms, one for glucose-6-phosphate isomerase and one for mannose-6-phosphate isomerase, that explain why the stereochemistries at carbon 1 of the two stereoisomers of [1,1-^{3}H,^{2}H]fructose 6-phosphate are opposite to each other. Use the same amino acids as are found in the active site of triose-phosphate isomerase in the same roles as acid–base catalysts.

(B) Explain how deuterium was introduced at carbon 1 of each fructose 6-phosphate and why, after a sufficient time at equilibrium, the percent deuterium in the proper location on carbon 1 of fructose 6-phosphate should become equivalent to the percent deuterium for each atom of hydrogen in ^2H_2O.

(C) What are the absolute stereochemistries at carbon 1 of the [1,1-^{3}H,^{2}H]fructose 6-phosphates from [1-^{3}H]-D-glucose and [1-^{3}H]-D-mannose, respectively?

The two stereoisomers of [1,1-^{3}H,^{2}H]fructose 6-phosphate were separately incubated with 6-phosphofructokinase and fructose-bisphosphate aldolase (Equation 4–210), and the two stereoisomers of [1,1-^{3}H,^{2}H]glycerone 1-phosphate were isolated. These stereoisomers of [1,1-^{3}H,^{2}H]glycerone 1-phosphate were converted to the *E* and *Z* stereoisomers of [^{3}H,^{2}H]phospho*enol*pyruvate, respectively[543,579]

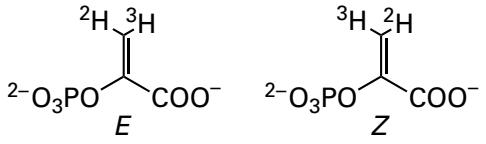

by incubation with triose-phosphate isomerase, glyceraldehyde-3-phosphate dehydrogenase in the presence of arsenate, bisphosphoglycerate mutase, and phosphopyruvate hydratase. Each stereoisomer of [^{3}H,^{2}H]phospho*enol*pyruvate was incubated separately with 3-phosphoshikimate 1-carboxyvinyltransferase from *K. aerogenes* and 3-phosphoshikimate

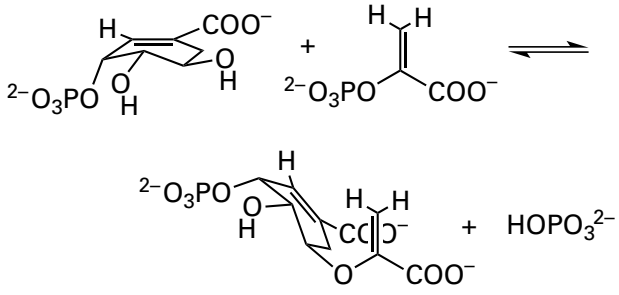

The 5-*O*-(1-carboxyvinyl)-3-phosphoshikimate was converted to chorismate

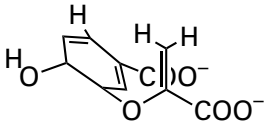

with chorismate synthase, also from *K. aerogenes*. The chorismate was converted to lactate by the following sequence of chemical reactions.

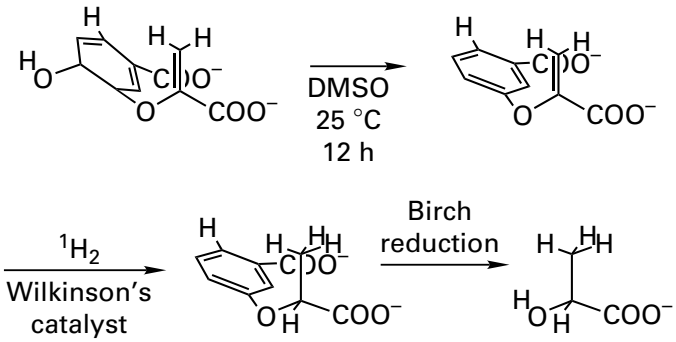

Wilkinson's catalyst performs a syn addition of H_2 to a double bond and ultimately produces both the 2*S* and the 2*R* enantiomers of lactate because it does not distinguish one face of the carbon–carbon double bond from the other. The (2*S*)-lactate was eliminated by incubation with (*S*)-lactate dehydrogenase (Equation 4–204), and the stereochemically pure (2*R*)-lactate was submitted to Kuhn–Roth oxidation to produce chiral [^{3}H,^{2}H]acetate. When 5-*O*-(1-carboxyvinyl)-3-phosphoshikimate derived from (*E*)-[^{3}H,^{2}H]phospho*enol*pyruvate was submitted to this sequence, (*R*)-[^{3}H,^{2}H]acetate was the preferential product. When 5-*O*-(1-carboxyvinyl)-3-phosphoshikimate derived from (*Z*)-[^{3}H,^{2}H]phospho*enol*pyruvate was submitted to this sequence, (*S*)-[^{3}H,^{2}H]acetate was the preferential product.[580]

(D) Show by drawing the proper stereochemistry of every product between phospho*enol*pyruvate and acetate, including both lactates, why these two results demonstrate that (*E*)-[^{3}H,^{2}H]phospho*enol*pyruvate yields (*E*)-[5,5-^{3}H,^{2}H]-5-*O*-(1-carboxyvinyl)-3-phosphoshikimate and (*Z*)-[^{3}H,^{2}H]phospho*enol*pyruvate yields (*Z*)-[5,5-^{3}H,^{2}H]-5-*O*-(1-carboxyvinyl)-3-phosphoshikimate.

(E) Explain why the (*S*)-lactate was eliminated before Kuhn–Roth oxidation was performed.

(F) Draw a mechanism for 3-phosphoshikimate 1-carboxyvinyltransferase with correct stereochemistry for addition of shikimate 3-phosphate to phospho*enol*pyruvate and removal of phosphate to produce 5-*O*-(1-carboxyvinyl)-3-phosphoshikimate. Assume that a hydron is added to and removed from phospho*enol*pyruvate by the same acid–base in the active site and that, as has been demonstrated,

addition of a hydron and removal of that same hydron is in preference to addition and removal of a deuteron or a triton and that this explains why chiral acetate is the final product. Your mechanism must explain the observed retention of configuration in the product. Provide specific amino acids of your own choice as acid–base catalysts of these two steps.

Problem 4–27: When D-glyceraldehyde is used in place of glycerol, glycerol kinase (Equation 4–283)

$$MgATP^{2-} + \text{glycerol} \rightleftharpoons \text{sn-glycerol-3-phosphate} + MgADP^{-}$$

from *E. coli* becomes an ATPase that hydrolyzes $MgATP^{2-}$ (Equation 4–288). When adenosine (*R*)-[γ,γ-^{17}O,^{18}O]-γ-thiotriphosphate is used as a reactant for this adventitious ATPase, (*S*)-[^{17}O,^{18}O]thiophosphate is the product.[623] Write a mechanism for this ATPase that explains the stereochemistry.

Labeling of Active Sites

The acid–bases catalyzing the reactions that occur within the active site of an enzyme are usually the side chains of amino acids within the sequence of the folded polypeptide. The particular amino acid that acts as a catalytic acid–base in a specific step in the mechanism of the enzyme can be identified with an active-site label. An active-site label can be used to locate the active site of an enzyme and identify a catalytic acid–base within that active site in a crystallographic molecular model. And an active-site label can be used to inactivate a particular enzyme within a mixture of different enzymes or, in ideal situations, in cytoplasm.

An active-site label is a reagent that has been designed to associate specifically, noncovalently, and in a defined orientation within the active site of a particular enzyme at the location normally occupied by a substrate and then modify covalently a particular catalytic acid–base or particular side chain that participates in association of a substrate with the active site. Because there are nucleophilic side chains but no electrophilic side chains on the amino acids in a protein, an active-site label is almost always **designed to position an electrophile adjacent to a catalytic acid–base or another nucleophilic side chain**. The electrophilic center on the active-site label, when it is bound in the active site, reacts covalently with the lone pair of electrons on the conjugate base of the side chain of the catalytic acid–base.

The usual sequence of events in the labeling of an active site is a description of the kinetic characteristics of the inactivation and the covalent modification of the enzyme, followed by identification of the amino acid that is modified by isolating and sequencing a peptide containing the modified amino acid. Ultimately, the role of the side chain of that amino acid in the mechanism of the enzyme is defined crystallographically.

Before crystallographic molecular models of triose-phosphate isomerase (Equation 4–46) were available, it was presumed that a catalytic base in the active site of the enzyme was responsible for removing a hydron from carbon 3 of glycerone phosphate during its conversion to D-glyceraldehyde 3-phosphate. To identify the catalytic base, the reagents 3-iodo-, 3-bromo-, and 3-chloro-1-hydroxypropan-2-one phosphate were synthesized. Each reagent, when it is bound in the active site, should place an electrophilic alkyl halide adjacent to that catalytic base, $-O^{(-)}$

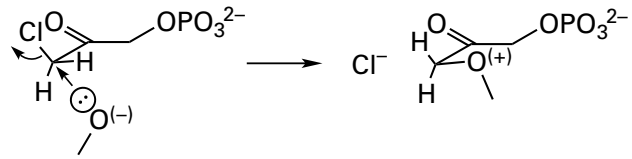

(4–290)

If these reagents are capable of alkylating the actual catalytic base, they should have inactivated the enzyme irreversibly, and it was observed that each did inactivate triose-phosphate isomerase from *O. cuniculus* in a pseudo-first-order reaction (Figure 4–35).[624] 3-Chloro-1-hydroxypropan-2-one [^{32}P]phosphate was prepared, and triose-phosphate isomerase was modified with this reagent. The modified enzyme was then denatured and digested with trypsin. Only one radioactive peptide was observed upon peptide mapping. This tryptic peptide was purified, and its sequence of amino acids was found to be WVLAYEPVWAIGTGK. When the modified peptide was treated with hydroxylamine, the hydroxamate of glutamic acid was identified as the product

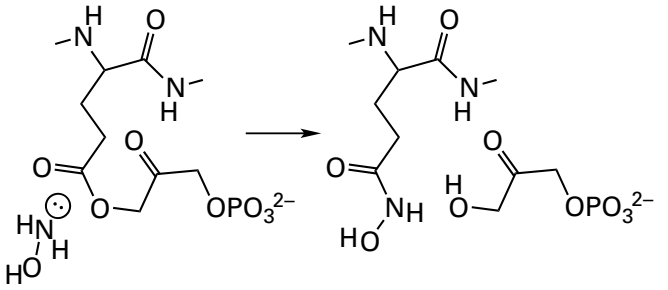

(4–291)

Therefore, the glutamate in this peptide was the nucleophile that had been alkylated by the reagent. The sequence of amino acids for the peptide identifies the glutamate as Glutamate 165[625] in triosephosphate isomerase from *O. cuniculus*. From the results of several such experiments, Glutamate 165 was deduced to be the base responsible for removing the hydron from carbon during the enzymatic reaction. This conclusion about the enzyme from *O. cuniculus* was subsequently confirmed by X-ray crystallography (Figure 3–37)[626] of the enzyme from *S. cerevisiae* (52% identity; 0.4 gap percent)* and site-directed mutation.[627]

There are many **electrophiles that have been incorporated into active-site labels**. In addition to alkyl chlorides,[628] alkyl bromides,[629-640] and alkyl iodides,[641] such as those used to modify triose-phosphate isomerase, alkyl fluorides[628,642,643] *O*-acetylalcohols,[628] sulfate esters,[644] oxiranes,[645-650] aziridines,[651,652] *N,N*-dimethylaziridinium ions,[653,654] aldehydes,[655], vicinal diones,[656-666] α,β-unsaturated imines,[667] and 2-methylenecyclopropyl groups[668] have been used as the electrophiles incorporated into analogues of various substrates. Electrophilic analogues of carboxy groups or acyl groups, or analogues of tetrahedral intermediates in their reactions, such as α-diazoketones,[669,670] fluorophosphono groups,[671] or phenylphosphono groups,[672] have been used as electrophiles in analogues of substrates to modify catalytic bases in an active site that would normally associate with or react with carboxy groups or acyl groups on its substrates. *S*-(4-Bromo-2,3-dioxobutyl)thiophosphate, which positions a vicinal dione in the location that would be occupied by the second phospho group in diphosphate, can be incorporated into nucleotides to position the vicinal dione adjacent to the guanidinio group of an arginine that would be a ligand for that phospho group in the active site.[666] This latter active-site label is a member of a large class of electrophiles designed to modify amino acids in active sites with which nucleotides or coenzymes containing nucleotides associate.[665]

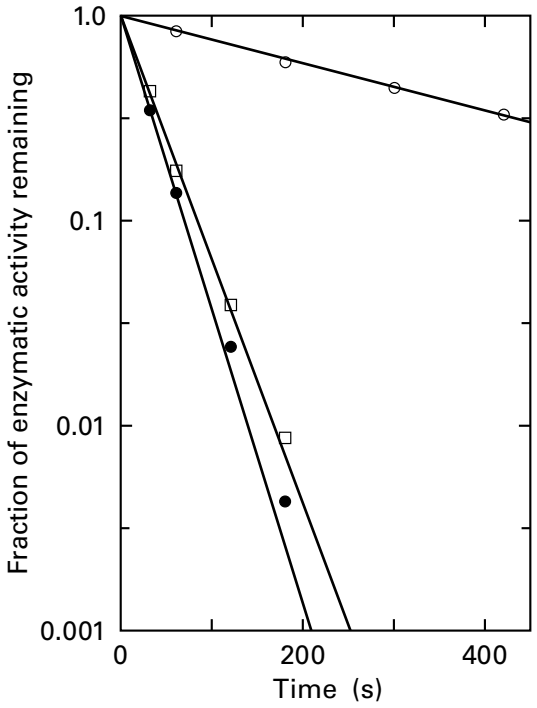

Figure 4–35: Inactivation of triose-phosphate isomerase from *O. cuniculus* by 3-halo-1-hydroxypropan-2-one phosphates.[624] Mixtures containing 0.9 μM active sites of triose-phosphate isomerase in 0.1 M imidazolium chloride, pH 6.5, at 2 °C were prepared with either 10 μM 3-iodo-1-hydroxy-2-propanone phosphate (○), 10 μM 3-chloro-1-hydroxy-2-propanone phosphate (□), or 10 μM 3-bromo-1-hydroxy-2-propanone phosphate (●). At the times indicated, 0.1 mL samples from each mixture were removed and diluted into 4.9 mL of 10 mM 2-sulfanylethanol in 0.02 M triethanolammonium chloride at pH 7.9, to discharge rapidly the respective halopropanone. These quenched samples were then assayed for enzymatic activity. The common logarithm of the fraction of enzymatic activity remaining is plotted as a function of the time (seconds) the enzyme was exposed to the halopropanone before alkylation of the active site was halted by the quenching solution. The data were fit directly with Equation 4–298 to obtain values for $k_{i,app}$ (0.0027 s^{-1}, 0.027 s^{-1}, and 0.033 s^{-1} for iodo, chloro, and bromo reagents, respectively). These values were then used to draw the lines in the figure.

There are also **simple, widely applicable bis-electrophiles**, such as bromoacetyl bromide, that can be incorporated covalently into more complex substrates or analogues of substrates to create active-site labels. For example, bromoacetyl bromide could be used to acylate 5,8-dideazafolate to produce 10-(bromoacetyl)-5,8-dideazafolate (**4–71**)[673]

*The homologue of Glutamate 165 in the enzyme from *O. cuniclus* is Glutamate 164 in the enzyme from *S. cerevisiae*.

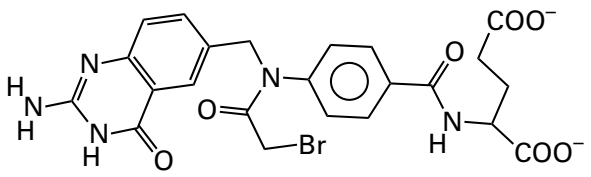

4–71

an analogue of 10-formyltetrahydrofolate

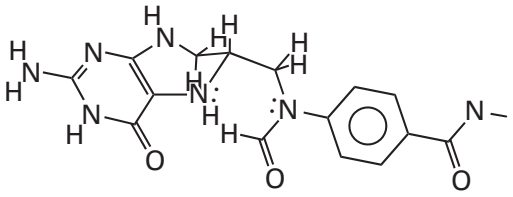

4–72

This analogue modifies the carboxy group of the catalytic acid, Aspartate 144[674] of phosphoribosylglycinamide formyltranferase from *E. coli*, that forms a hydrogen bond to the acyl oxygen of the formyl group in 10-formyltetrahydrofolate to improve the electrophilicity of that acyl group in the formyl transfer catalyzed by the enzyme.[675]

An example of the use of such a biselectrophile to synthesize an active-site label that **modifies an amino acid providing a ligand to a substrate** is the alkylation of 6-sulfanylpurine ribonucleoside 5′-monophosphate by 1,4-dibromobutane-2,3-dione to produce the nucleotide

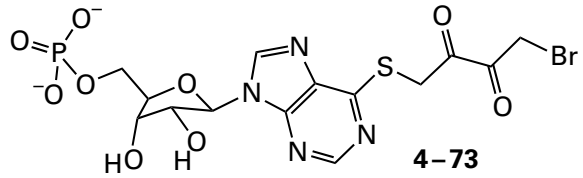

4–73

This active-site label is an analogue of N^6-(1,2-dicarboxyethyl)-AMP,[663,665] one substrate for adenylosuccinate synthase

$$N^6\text{-(}S\text{-1,2-dicarboxyethyl)-AMP}^- + \mathrm{HOPO_3^{2-}} + \mathrm{MgGDP^-} \rightleftharpoons \text{L-aspartate} + \mathrm{MgGTP^{2-}} + \text{inosine monophosphate} \quad (4\text{–}292)$$

from *E. coli*. Nucleotide **4–73** modifies the guanidinio group of Arginine 303 that forms a hydrogen bond to the distal 2-carboxy group of the usual substrate, N^6-(*S*-1,2-dicarboxyethyl)-AMP, in the active site of the enzyme.[676] This carboxy group is not a catalytic acid–base.

It is also possible to **alter an electrophile already present in a substrate** to convert it into an active-site label. As part of its normal mechanism, thymidylate synthase forms a covalent adduct between the sulfido group of a cysteine in its active site and the 5,6-double bond of 2′-deoxyuridine 5′-monophosphate

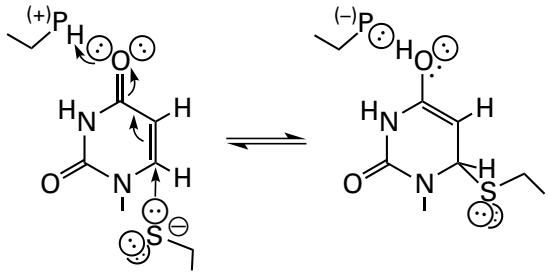

(4–293)

1-(β-D-2′-Deoxyribofuranosyl)-3-azapurin-2-one 5′-monophosphate (**4–74**) is an active-site label that capitalizes on the existence of this nucleophilic addition to an α,β-unsaturated amide[677]

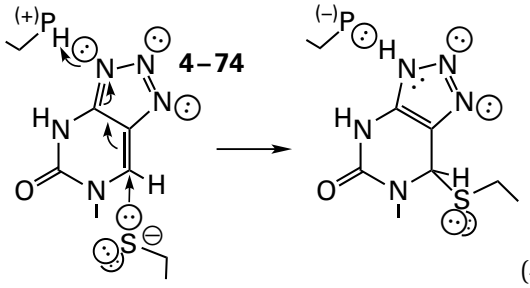

4–74

(4–294)

The aromatization of the triazole causes the nucleophilic addition to be kinetically irreversible and causes the active-site label to inactivate the enzyme from *L. casei*. Other strategies have been used to produce analogues of substrates that become aromatic during their covalent modification of the respective targeted enzymes, and hence modify the enzyme irreversibly.[678,679]

Natural products, the role of which is to inactivate enzymes in organisms other than the one producing that natural product, can contain electrophilic functional groups such as oxiranes[650] that alkylate catalytic bases in the active sites of the enzymes inactivated. They are **natural active-site labels**.

The **exact location that the electrophilic center occupies** when the active-site label is associated specifically with the active site can affect the outcome of the modification and provide additional information.[680] For example, both (2*R*,6*S*) and (2*S*,6*S*) enantiomers of 2-(4-amino-4-carboxybutyl)aziridene-2-carboxylate (**4–76**)

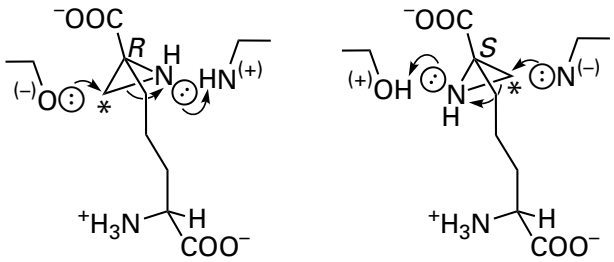

4–75 **4–76**

where the asterisks indicate the electrophilic carbon, were synthesized as active-site labels for diaminopimelate epimerase

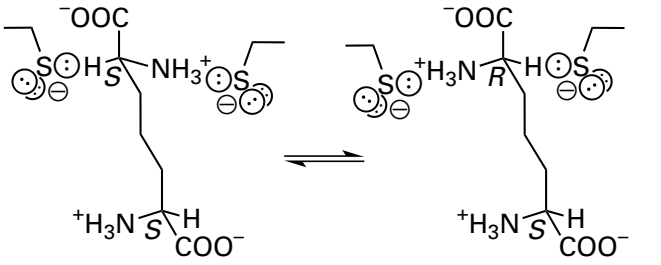

(4–295)

These two diastereomers should place an electrophilic carbon adjacent to the base responsible for removing the hydron from (2*S*,6*S*)-diaminopimelate and adjacent to the base responsible for removing the hydron from (2*R*,6*S*)-diaminopimelate, respectively, in the normal reaction.[681,682] Diaminopimelate epimerase from *Haemophilus influenzae*[652] and diaminopimelate epimerase from *A. thaliana*[654] (39% identity; 1.8 gap percent) were modified by these two active-site labels. In crystallographic molecular models of the modified enzymes, it can be seen that (2*R*)-aziridine **4–75** has alkylated the sulfanyl groups of the homologous cysteines in these two enzymes responsible for removing the hydron from (2*S*,6*S*)-diaminopimelate. Likewise, (2*S*)-aziridine **4–76** has alkylated the sulfanyl groups of the homologous cysteines in these two enzymes responsible for removing the hydron from (2*R*,6*S*)-diaminopimelate in the normal enzymatic reaction.

Glutamate racemase from *Limosilactobacillus fermentum* also uses two cysteines as catalytic acid–bases[683] for its epimerization that are situated on the two sides of the α carbon of D-glutamate.[684] Only one of these cysteines, however, is modified by the analogous racemic aziridine 2-(2-amino-2-carboxyethyl)aziridene-2-carboxylate.[651]

Mandelate racemase also catalyzes an epimerization (Equation 4–252), and (*R*)-2-phenyloxirane-2-carboxylate (**4–77**)* is an active-site label that inactivates the enzyme from *P. putida*[558] by alkylating Lysine 166

4–77

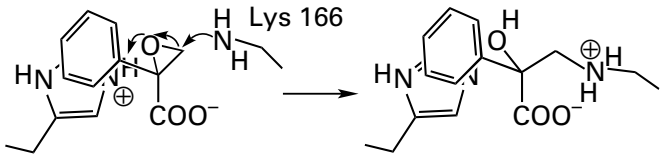

(4–296)

(*S*)-2-Phenyloxirane-2-carboxylate does not inactivate the enzyme or modify the active site because it places the electrophilic carbon 3 of the oxirane on the opposite side of the plane of 2-phenylacetate, distant from the amino group of the lysine, and the imidazolyl group at this location is perhaps not nucleophilic enough or not properly oriented.

Active-site labels can also modify prosthetic groups in the active site rather than catalytic acid–bases. For example, (*R*)-4-amino-4,5-dihydrothiophenecarboxylic acid

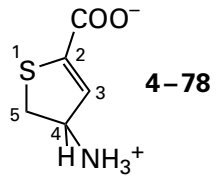

4–78

inactivates D-amino-acid transaminase from *Bacillus* by covalently modifying the prosthetic pyridoxal phosphate. The external pyridoximine is formed between the active-site label and the prosthetic pyridoxal 5′-phosphate. Hydrons are removed from carbons 4 and 5 of 4-amino-4,5-dihydrothiophenecarboxylic acid by the usual steps (see Equations 4–258 and 4–259) to produce the aromatic thiophene, which is so stable that further reaction cannot occur. In this instance the stable, aromatic product of the reaction was identified crystallographically.[678]

2α,3α-Cyclopropano-5α-cholestan-3β-ol

*Note that the priorities for assigning *R* and *S* reverse in going from the amino acid to the aziridine in the case of diaminopimelate epimerase and from the mandelate to the oxirane in the case of mandelate racemase.

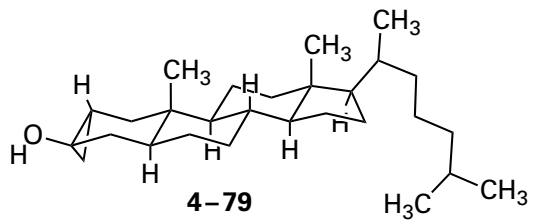

4–79

is an active-site label for the flavoenzyme cholesterol oxidase from *Streptomyces*.[685] It covalently modifies the isoalloxazine ring of the prosthetic flavin (previously **2–42**)

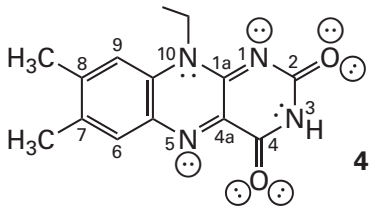

4–80

at carbon 6, and the product of the reaction is consistent with dehydronation of the 3-hydroxy group of 2α,3α-cyclopropano-5α-cholestan-3β-ol by a catalytic base on the enzyme, heterolytic opening of the adjacent cyclopropane to produce a nucleophilic primary carbanion of the secondary carbon of the cyclopropane, and nucleophilic addition of that carbanion to the flavin. *N*-(Cyclopropyl)glycine is a mechanism-based label for sarcosine oxidase from *Bacillus*.[686] In this instance, however, it is thought that the oxidized prosthetic flavin (**4–80**) in the active site removes one electron from the lone pair of electrons on the nitrogen of *N*-(cyclopropyl)glycine, the cyclopropyl ring opens homolytically rather than heterolytically, and the primary radical at carbon 3 of the propanal in the resulting imine with the amino group of glycine colligates with the radical of flavin semiquinone formed upon transfer of the electron. The product of the radical colligation is an adduct that has been alkylated at carbon 4a of the flavin by carbon 3 of propanal.[687]

In one sense, however, the modifications of these prosthetic groups did not identify them as participants in the respective reaction because that fact was already known.

There are several criteria that should be met before a reagent synthesized as an active-site label can be designated as capable of modifying the enzyme while it is bound in place of a substrate within the active site. First, the rate of the reaction between enzyme and active-site label should display saturation as a function of the concentration of the active-site label, just as association of the substrate being mimicked does. Second, a natural substrate or competitive inhibitor of the enzyme should competitively inhibit the inactivation produced by the active-site label. Third, the inhibition constant K_i for a substrate or competitive inhibitor of the inactivation produced by an active-site label should be the same as the Michaelis constant of the substrate or the dissociation constant of the competitive inhibitor from the active site in the absence of the active-site label. Fourth, at short times before covalent modification occurs, the active-site label should be a competitive inhibitor of the normal enzymatic reaction with respect to the reactant that it resembles. Fifth, the inhibition constant K_i for this reversible competitive inhibition of the normal enzymatic reaction by the active-site label should be the same as the dissociation constant from the active site that governs its irreversible inactivation of the enzymatic activity. Sixth, if the behavior of the specificity constant k_A for reactant A that is being mimicked by the active-site label is pH-dependent, decreasing below a pK_a for a catalytic base involved in the reaction (as in Figure 4–10A–D), and the active-site label is thought to modify that same base, then the pH–rate profile for the rate constant of inactivation should be governed by the same pK_a. Seventh, the covalent incorporation of active-site label into the protein should be proportional to the loss of enzymatic activity, and the stoichiometry of incorporation at full inactivation should be 1.0 mol (mol of active sites)$^{-1}$. The first criterion shows that the active-site label binds to the enzyme before it can inactivate the enzyme. The next five criteria connect this binding to the normal binding of substrates or competitive inhibitors to the active site. The last criterion is consistent with the hope that the only significant covalent modification of the protein occurs while the electrophile is occupying the active site in the proper orientation.

The **criterion of saturation** can be explained by an examination of the rate equations for specific labeling. If an active-site label (ASL) first associates with the active site of an enzyme and then modifies a catalytic group within the active site, it follows that

$$\mathrm{E} + \mathrm{ASL} \underset{k_{-1}}{\overset{k_1}{\rightleftharpoons}} \mathrm{E{\cdot}ASL} \xrightarrow{k_i} \mathrm{E{-}ASL} \qquad (4\text{–}297)$$

where k_i is the rate constant for inactivation and E–ASL is the enzyme that has been modified covalently and irreversibly by the active-site label. If the

concentration of active-site label is in large molar excess over the concentration of active sites in the solution and if the active-site label is lost from the solution only by reaction with the active site, then its concentration will remain essentially constant throughout the reaction. In this case, it can be shown[688] that

$$\frac{[E]_0 - [E\text{–}ASL]}{[E]_0} = e^{-k_{i,app}\,t} \tag{4–298}$$

where $[E]_0$ is the initial total concentration of enzyme

$$k_{i,app} = \frac{k_i\,k_{ASL}[ASL]}{k_i + k_{ASL}[ASL]} \tag{4–299}$$

and

$$k_{ASL} = \frac{k_i\,k_1}{k_i + k_{-1}} \tag{4–300}$$

If covalent modification by the active-site label is the only reason that enzymatic activity is disappearing, the term $([E]_0 - [E\text{–}ASL])\,[E]_0^{-1}$ is equal to the fraction of enzymatic activity remaining at a particular time.

The **disappearance of enzymatic activity** is followed in the experiment by removing samples of enzyme from the solution containing the active-site label at various times and immediately diluting each sample or otherwise quenching the inactivation while performing an assay of the remaining enzymatic activity.

The observed fraction of enzymatic activity remaining as a function of time can be fit directly to an exponential equation by usual least-squares analysis to obtain the rate constant $k_{i,app}$. Just as in the case of the effects of pH on the rate of an enzymatic reaction, however, it is easier to evaluate visually how well the data satisfies the exponential equation if the natural logarithm of the fraction of enzymatic activity remaining is plotted as a function of time[640]

$$\ln\left(\frac{[E]_0 - [E\text{–}ASL]}{[E]_0}\right) = -k_{i,app}\,t \tag{4–301}$$

By this criterion, the inactivations of triose-phosphate isomerase by 3-halo-1-hydroxypropan-2-one phosphates are **pseudo-first-order reactions** (Figure 4–35) as predicted by Equation 4–298.

Because the covalent reaction leading to inactivation is usually slow, $k_{-1} >> k_i$ and

$$k_i\,k_{ASL}^{-1} \cong \frac{k_{-1}}{k_1} = K_{dASL} = \frac{[ASL][E]}{[E{\cdot}ASL]} \tag{4–302}$$

where K_{dASL} is the dissociation constant for the complex between the active-site label and the active site, so the apparent first-order rate constant for the inactivation

$$k_{i,app} = \frac{k_i[ASL]}{[ASL] + K_{dASL}} \tag{4–303}$$

The **behavior of the observed pseudo-first-order rate constant of inactivation**, $k_{i,app}$, as a function of the molar concentration of active-site label (Equation 4–299) demonstrates saturation.[640]

One step in the reaction catalyzed by fructose-bisphosphate aldolase (Equation 4–210) is formation of an enamine of glycerone phosphate. The enamine (Figure 4–36) is formed from the imine between glycerone phosphate and a lysine on the enzyme by removal of a hydron from carbon 3

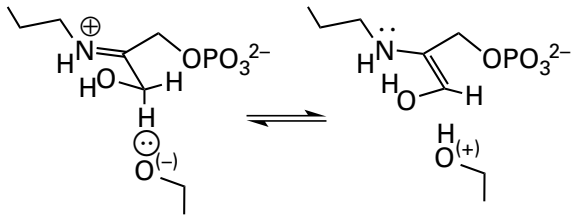

(4–304)

1-Hydroxy-2-oxobut-3-ene phosphate was synthesized as an active-site label for fructose-bisphosphate aldolase.[667] 1-Hydroxy-2-oxobut-3-ene phosphate, when bound to the active site as the analogous adduct of the same lysine (**4–81**), should place an electrophilic α,β-unsaturated imine adjacent to the amino acid responsible for removing the hydron in the normal reaction, and a Michael addition should result

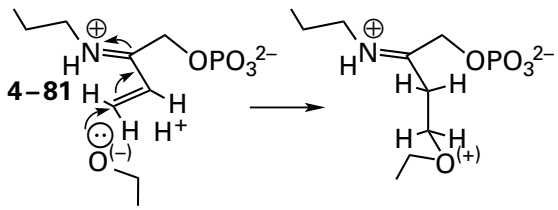

(4–305)

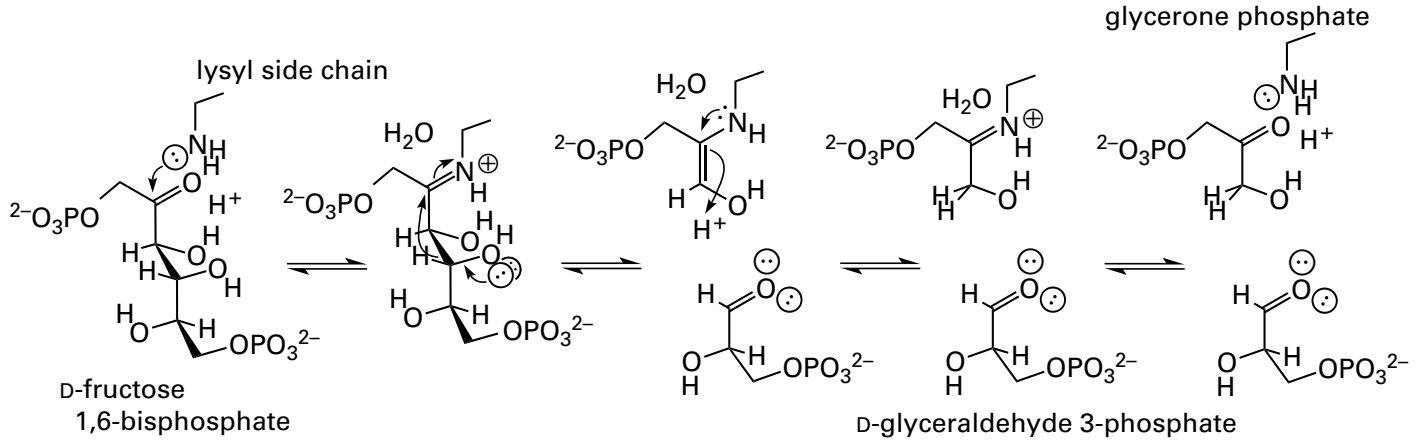

Figure 4–36: Steps in the retroaldol condensation catalyzed by fructose-bisphosphate aldolase. The amino group of a lysine in the active site adds to the carbonyl in D-fructose 1,6-bisphosphate to give the iminium, with the hemiketal as an intermediate. The bond between carbons 3 and 4, weakened by the iminium at carbon 2, breaks to give the enamine and D-glyceraldehyde 3-phosphate, one of the products of the retroaldol condensation. The enamine is hydronated at its basic carbon to give the iminium, and the iminium is hydrolyzed to give glycerone phosphate, the other product.

When 1-hydroxy-2-oxobut-3-ene phosphate was added to a solution of fructose-bisphosphate aldolase from *O. cuniculus* and samples were withdrawn at various intervals and diluted to dissociate the reversibly bound inhibitor, the enzymatic activity was observed to disappear irreversibly in a pseudo-first-order process.[689] From these measurements, observed pseudo-first-order rate constants of inactivation were obtained by fitting Equation 4–298 to the data. When these observed rate constants of inactivation are plotted as a function of the concentration of active-site label, saturation is observed (Figure 4–37).[689] The continuous curve drawn in the figure is defined by Equation 4–303 with $k_i = 0.11\ s^{-1}$ and $K_{dASL} = 100\ \mu M$. Therefore, the observed behavior is consistent with a kinetic mechanism in which the active-site label binds to the active site before covalently modifying it.

Often an active-site label is an active enough electrophile to react with the water or other bases in the solution. In this instance, the **total concentration of active-site label decreases systematically during the reaction**, and the activity of the enzyme does not decrease in a simple first-order reaction.[641] The initial rate of decrease in the enzymatic activity could be used as $k_{i,app}$ in Equation 4–299, but it is often technically difficult to make this measurement accurately at short times. The situation, however, can be viewed as a competition for the reagent between the nucleophile in the active site and nucleophiles in the solution. Under these circumstances, the final yield of modified enzyme after all

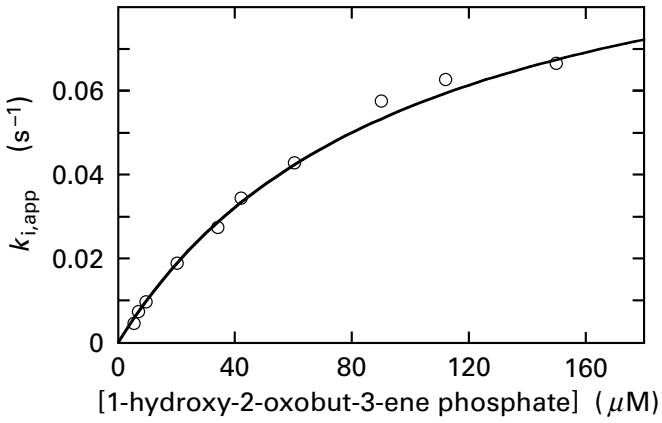

Figure 4–37: Behavior of the observed pseudo-first-order rate constant for inactivation of fructose-bisphosphate aldolase by 1-hydroxy-2-oxobut-3-ene phosphate as a function of the concentration of active-site label.[689] Mixtures were prepared containing various concentrations of 1-hydroxy-2-oxobut-3-ene phosphate at pH 7.0 and 37 °C. The reaction was initiated in each case by adding fructose-bisphosphate aldolase. Samples (50 μL) were removed at various times (at intervals of about 1 min) and were diluted immediately into an assay mixture (750 μL) for measuring enzymatic activity. The initial rate of the enzymatic reaction was measured continuously at 340 nm by coupling the production of triose phosphates to the reduction of NADH with triose-phosphate isomerase and glycerol-3-phosphate dehydrogenase. The initial rate of enzymatic activity was plotted as a function of the time of exposure to 1-hydroxy-2-oxobut-3-ene phosphate, and an observed pseudo-first-order rate constant of inactivation, $k_{i,app}$, was calculated from the time course for each concentration of active-site label. The observed pseudo-first-order rate constants, $k_{i,app}$ (second^{-1}), are plotted as a function of the concentration of 1-hydroxybut-3-en-2-one phosphate (micromolar). The curve drawn in the figure is that defined by Equation 4–303 with $k_i = 0.11\ s^{-1}$ and $K_{dASL} = 99\ \mu M$.

the active-site label has been quenched by reacting with the solution, the yield at infinite time, can be expressed as a fraction of the amount of enzyme originally present. This fractional yield, $\alpha_{E-ASL\infty}$, is simply the enzymatic activity at the end of the reaction divided by the enzymatic activity at the start of the reaction.

If the active site cannot recognize the product of the reaction between the active-site label and the solution, it can be shown[690] that

$$\ln(1 - \alpha_{E-ASL\infty}) = \frac{k_i}{k_D} \ln\left(\frac{K_{dASL}}{[ASL]_0 + K_{dASL}}\right) \quad (4–306)$$

where k_D is the first-order rate constant for the reaction in which the active-site label is destroyed by reaction with the solution, k_i is the first-order rate constant for its reaction with the active site, $[ASL]_0$ is the initial molar concentration of active-site label, and K_{dASL} is its dissociation constant from the active site.

If the active site, however, can bind the product of the reaction between the active-site label and the solution, then as product builds up, it will compete with the active-site label for the active site but be unable to modify it covalently. If the product has the same dissociation constant, K_{dASL}, as the active-site label itself and the initial concentration of the active-site label is always in large excess over the concentration of sites, then it can be shown that

$$\ln(1 - \alpha_{E-ASL\infty}) = -\frac{k_i}{k_D}\left(\frac{[ASL]_0}{[ASL]_0 + K_{dASL}}\right) \quad (4–307)$$

Whether the reaction behaves as described by Equation 4–306 or 4–307, which define significantly different behavior, makes the decision as to whether or not the product of reaction of the active-site label with the solution is able to associate with the active site. From Equation 4–306 or 4–307, it can then be ascertained whether or not the reaction between the active site and the active-site label displays saturation,[690] and a dissociation constant for the active-site label from the enzyme can be determined.

The **criterion of competition by a substrate or competitive inhibitor and the criterion of identity between the respective inhibition constant and either the Michaelis constant of the substrate or the dissociation constant of the competitive inhibitor** are explained by examining an expanded kinetic mechanism for specific labeling. If an active-site label binds in the active site at the same location as the substrate it was designed to resemble before modifying the enzyme, then that substrate should decrease the rate of modification by occupying the active site in its stead. For example, addition of the natural substrate glycerone phosphate at increasing concentrations causes the rate of inactivation of fructose-bisphosphate aldolase by 1-hydroxy-2-oxo-but-3-ene phosphate (Equation 4–305) to decrease accordingly.[689]

If natural reactant A and the active-site label are competing for the same location within the active site and if the concentration of reactant remains relatively constant during the inactivation even though it is being converted to product, then a simple kinetic mechanism for the competition is

$$\begin{array}{c} E{-}ASL + A \xleftarrow{k_i} E{\cdot}ASL + A \overset{K_{dASL}}{\rightleftharpoons} \\ ASL + E + A \underset{k_{-5}}{\overset{k_5}{\rightleftharpoons}} ASL + E{\cdot}A \underset{k_{-6}}{\overset{k_6}{\rightleftharpoons}} \\ ASL + E{\cdot}Z \xrightarrow{k_7} ASL + E + Z \end{array} \quad (4–308)$$

Under these circumstances, or analogous circumstances dictated by the established kinetic mechanism for a particular enzymatic reaction, the derivation of the rate equation from the kinetic mechanism leads to the conclusion[691] that the observed pseudo-first-order rate constant for irreversible inactivation

$$k_{i,app} = \frac{k_i [ASL]}{K_{dASL}\left(\frac{[A] + K_{mA}}{K_{mA}}\right) + [ASL]} \quad (4–309)$$

where K_{mA} is the Michaelis constant for turnover of reactant A in the absence of active-site label. It follows that reactant A, which is being mimicked by the active-site label, is a competitive inhibitor of labeling, with a competitive inhibition constant equal to its Michaelis constant.

Isocitrate lyase performs an aldol condensation between succinate and glyoxylate to produce isocitrate[692]

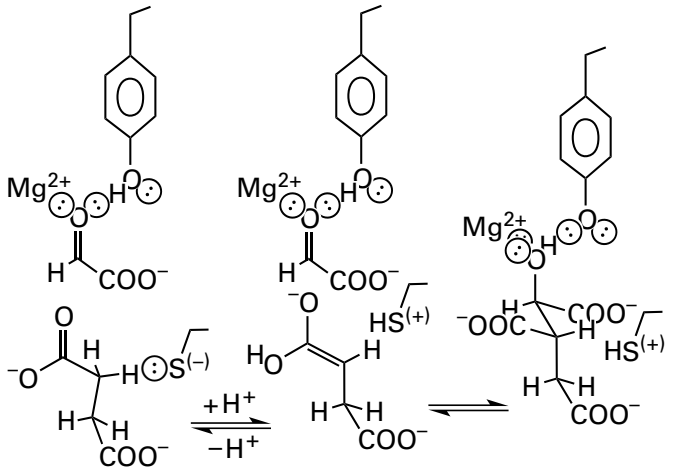

(4–310)

3-Bromopyruvate has a carboxylato group that should occupy one of the three subsites for carboxylato groups on the two substrates and may position an electrophile

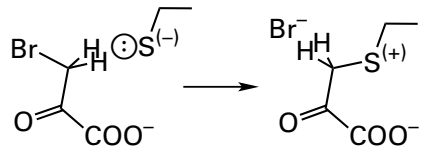

(4–311)

in the vicinity of the catalytic base $^{(-)}$⊙S– responsible for removing the hydron from carbon 2 of succinate. It was selected, for the sake of convenience, as an active-site label for isocitrate lyase.[629] 3-Bromopyruvate inactivates isocitrate lyase from *Vogesella indigofera* in a pseudo-first-order reaction, and the observed pseudo-first-order rate constants of inactivation for various concentrations of the active-site label, 3-bromopyruvate, and the reactant, (2*R*,3*S*)-isocitrate, were determined.

When reciprocals of the observed rate constants for inactivation, $k_{i,app}$, were plotted as a function of reciprocals of the concentrations of 3-bromopyruvate at two fixed concentrations of isocitrate, competitive inhibition of the inactivation was observed (Figure 4–38).[629] The inhibition constant for isocitrate as a competitive inhibitor of the inactivation, calculated from the data directly, was 90 μM, which compares favorably to the Michaelis constant of 110 μM for isocitrate as a reactant for the enzyme. The **coincidence of the inhibition constant and the Michaelis constant** demonstrates that isocitrate binds to the same site on the enzyme when it is a reactant as when it is a competitive inhibitor of the irreversible inactivation caused by 3-bromopyruvate.

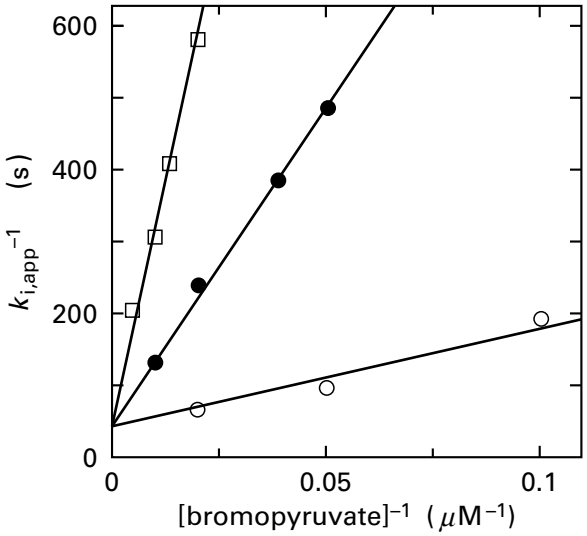

Figure 4–38: Competition between isocitrate and 3-bromopyruvate during the inactivation of isocitrate lyase from *V. indigofera*.[629] Mixtures containing various concentrations of 3-bromopyruvate and 0.5 mM isocitrate (●), 2.0 mM isocitrate (□), or no isocitrate (○) were prepared at pH 7.7 and 30 °C. Enzyme was added to initiate the inactivation. For each mixture, inactivation of the enzyme was followed as a function of time, and pseudo-first-order rate constants of inactivation were calculated from the loss of activity over the first half-time of the reaction. The reciprocals of the observed rate constants for inactivation, $k_{i,app}^{-1}$ (second^{-1}), derived from these time courses are plotted as a function of the reciprocals of the concentrations of 3-bromopyruvate (Brpyr), [bromopyruvate]$^{-1}$ (micromolar^{-1}), in the mixtures after addition of the enzyme. The lines drawn are those defined by the reciprocal of Equation 4–309 for k_i = 0.016 min^{-1}, $K_{m,isc}$ = 90 μM, and $K_{d,Brpyr}$ = 30 μM.

Therefore, 3-bromopyruvate alkylates the enzyme while it is bound at the active site in a portion of the location occupied by isocitrate.

For enzymes with more than one reactant, if the turnover of reactant A is prevented by leaving out reactant B or reactant C or both of them during the inactivation by an active-site label designed to resemble reactant A, then the Michaelis constant in Equation 4–309 is replaced by the dissociation constant of reactant A from the active site, K_{dA}, in the absence of reactant B or reactant C or both of them. For example, glycerone phosphate (reactant A) in the absence of glyceraldehyde 3-phosphate (reactant B) is a competitive inhibitor of the irreversible inactivation of fructose-bisphosphate aldolase caused by 1-hydroxy-2-oxobut-3-ene phosphate (Equation 4–305). Values for the various pseudo-first-order rate constants of inactivation were used to calculate the inhibition constant of glycerone phosphate for inactivation of the enzyme. The value

calculated (1.4 μM) was close enough to the value for the dissociation constant (4.5 μM) for glycerone phosphate from the active site under different circumstances for the authors to conclude that inactivation was occurring within the active site.[689]

A **competitive inhibitor** of the normal enzymatic reaction can also be used to demonstrate the specificity of an active-site label. *N*-Bromoacetyl-*N*-methyl-L-phenylalanine (**4–82**; BramF) was synthesized as an active-site label for carboxypeptidase A.[630] In the normal enzymatic reaction of carboxypeptidase A (Equation 4–172), a catalytic base, $-O\odot^{(-)}$, must remove a hydron from the water that adds to the acyl carbon, and *N*-bromoacetyl-*N*-methyl-L-phenylalanine was designed to modify this catalytic base

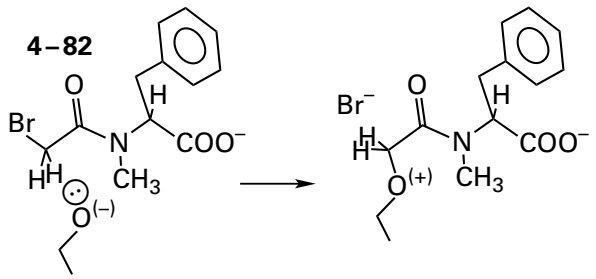

(4–312)

N-Bromoacetyl-*N*-methyl-L-phenylalanine inactivated the enzyme in a pseudo-first-order process, and the observed rate constants displayed saturation (K_{dBramF} = 5 mM). A competitive inhibitor of the enzyme, 2-phenylacetate, competitively inhibited the irreversible inactivation produced by *N*-bromoacetyl-*N*-methyl-L-phenylalanine. The inhibition constant for 2-phenylacetate as a competitive inhibitor of inactivation (1.1 mM) was in reasonable agreement with its inhibition constant as a competitive inhibitor of enzymatic activity (0.4 mM), and this agreement was used as evidence that the inactivation occurred while the active-site label was bound to the active site of the enzyme.

The **criterion that the active-site label should be a competitive inhibitor of the normal enzymatic reaction and the criterion that it should have the same inhibition constant as its dissociation constant** when it is irreversibly inactivating the enzyme are self-evident. The rate at which an active-site label modifies an enzyme is usually slow (Figures 4–35 and 4–37) compared to the rates at which it associates and dissociates from the active site and the rate at which normal reactants are converted to normal products. This difference in rates means that the initial rate of the enzymatic reaction can usually be measured in the presence of the active-site label over an interval short enough that significant inactivation has not yet occurred. In this way, the ultimately irreversible inhibitor can be assessed for its **ability to inhibit the enzymatic reaction reversibly.** If the active-site label does enter the active site before it reacts with the enzyme, then it should be a competitive inhibitor with respect to the reactant that it resembles. If the covalent inactivation is from the same position it occupies as a competitive inhibitor, then its competitive inhibition constant should be the same as its dissociation constant for inactivation.

Amidophosphoribosyltransferase

$$\text{manganese 5-phospho-}\alpha\text{-D-ribose 1-diphosphate} + \text{L-glutamine} + H_2O \rightleftharpoons \text{L-glutamate} + H^+ + MnOPO_3PO_3^{2-} + \text{5-phospho-}\beta\text{-D-ribosylamine} \quad (4\text{–}313)$$

transfers the ammonia produced by hydrolysis of L-glutamine at the active site for glutaminase through a tunnel[693] to 5-phospho-α-D-ribose 1-diphosphate, where the ammonia participates in a nucleophilic substitution at carbon 1 with diphosphate as the leaving group. 6-Diazo-5-oxo-(*S*)-2-aminohexanoic acid (**4–83**) was chosen[669] as an active-site label to modify any base involved in hydrolysis of L-glutamine (**4–84**) at the active site for glutaminase because it should place a diazoketone adjacent to such a base

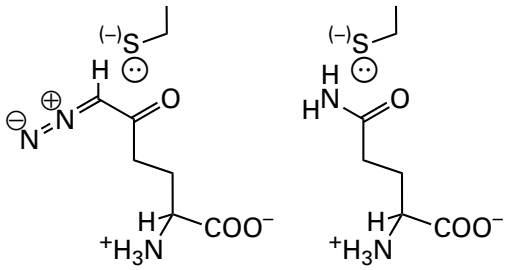

6-Diazo-5-oxo-(*S*)-2-aminohexanoic acid inactivates amidophosphoribosyltransferase from *G. gallus* irreversibly, and at short times it is a reversible competitive inhibitor of the normal enzymatic reaction with respect to L-glutamine. Its inhibition constant as a reversible competitive inhibitor (K_{iDon} = 20 μM) is close to its dissociation constant as an irreversible active-site label (K_{dDon} = 30 μM), and this coincidence is evidence that the irreversible modification occurs while 6-diazo-5-oxo-(*S*)-2-amino-

hexanoic acid is occupying the active site for glutaminase in place of L-glutamine.

When 5-phospho-α-D-ribose 1-diphosphate is present at saturation and occupying the other active site on amidophosphoribosyltransferase that is responsible for the nucleophilic substitution of ammonia by the diphospho group, the rate for inactivation by 6-diazo-5-oxo-(*S*)-2-aminohexanoic acid of the glutaminase increases 15-fold. This fact suggests that there must be a conformational change in the enzyme that causes the active site for deamination of L-glutamine to become more efficient when 5-phospho-α-D-ribose 1-diphosphate has associated with the active site for amination. This communication between the active sites could be a way to prevent molecules of ammonia from piling up in the tunnel and leaking into the solution, leading to the nonproductive, and energetically wasteful, hydrolysis of L-glutamine, and the change in rate of inactivation has revealed this adaptation.

The usual purpose of active-site labeling is to modify the conjugate base of a catalytic acid–base involved in the catalytic mechanism of an enzyme. The **criterion that the same pK_a should govern the steady-state kinetics and the inactivation by an active-site label** connects the pK_a for the catalytic acid–base that is revealed in the pH–rate profile for a steady-state rate constant and the pK_a for the catalytic acid–base that is modified by the active-site label. The kinetic mechanism of Equation 4–297 can be expanded[636] to include acid dissociations of the base being modified, which is nucleophilic only when it is unhydronated

$$\begin{array}{ccccc} EH^{(+)} + ASL & & EH^{(+)}\cdot ASL & & \\ \Big\downarrow\uparrow K_{aE} & & \Big\downarrow\uparrow K_{aE\cdot ASL} & & \\ H^+ & & H^+ & & \\ + & & + & & \\ E^{(-)} + ASL & \underset{k_{-1}}{\overset{k_1}{\rightleftharpoons}} & E^{(-)}\cdot ASL & \xrightarrow{k_i} & E\text{–}ASL \end{array} \qquad (4\text{–}314)$$

from which it follows that

$$k_{ASL,app} = k_{ASL}\left(\frac{K_{aE}}{[H^+] + K_{aE}}\right) \qquad (4\text{–}315)$$

and

$$k_{i,app} = k_i\left(\frac{K_{aE\cdot ASL}}{[H^+] + K_{aE\cdot ASL}}\right) \qquad (4\text{–}316)$$

The rate constants $k_{ASL,app}$ and $k_{i,app}$ are the observed values at a given pH, and k_{ASL} and k_i are asymptotic values for these rate constants (Equation 4–299) at values of pH greater than pK_{aE} and p$K_{aE\cdot ASL}$, respectively, where rate constants become invariant with pH (as in Figure 4–10A–D). Because **the conjugate base of the catalytic acid–base is the nucleophile** that adds to the electrophilic center in the active-site label, the rate of inactivation decreases below a particular value of pK_a as the conjugate base is hydronated. At values of pH greater than that pK_a, all the active sites contain the unhydronated conjugate base.

3-Bromopyruvate (Equation 4–311) inactivates 2-hydroxymuconate tautomerase

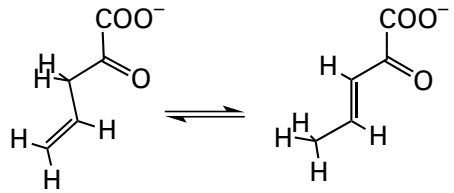

(4–317)

from *P. putida*.[694] Upon entering the active site, 3-bromopyruvate (Brpyr) should place the alkyl bromide immediately adjacent to the base in the active site responsible for removing the hydron from carbon 3 of 2-oxopent-4-enoate during its tautomerization by the enzyme. The inactivation by 3-bromopyruvate was followed as a function of pH (Figure 4–39A).[636,645] The observed rate constant for the inactivation, $k_{Brpyr,app}$ (Equation 4–299), that was produced by 3-bromopyruvate decreased below a pK_a of 6.7 ± 0.3. This pK_a should be the pK_a in the empty active site of the free enzyme (Equation 4–315) for the base that is alkylated by 3-bromopyruvate. It was found that 3-bromopyruvate alkylates the amino-terminal proline of the enzyme,[636] which has been shown, by nuclear magnetic resonance spectroscopy,[116] to have a pK_a of 6.4 ± 0.2 in the unoccupied enzyme. The specificity constant $k_{OPE,app}$ for the enzymatically catalyzed tautomerization of 2-oxopent-4-enoate (OPE) decreases below a pK_a of 6.2 ± 0.3. The fact that all these values of pK_a are identical within the errors of measurement is consistent with two conclusions: first, that 3-bromopyruvate inactivates the enzyme by alkylating the catalytic base that is responsible for the decrease in

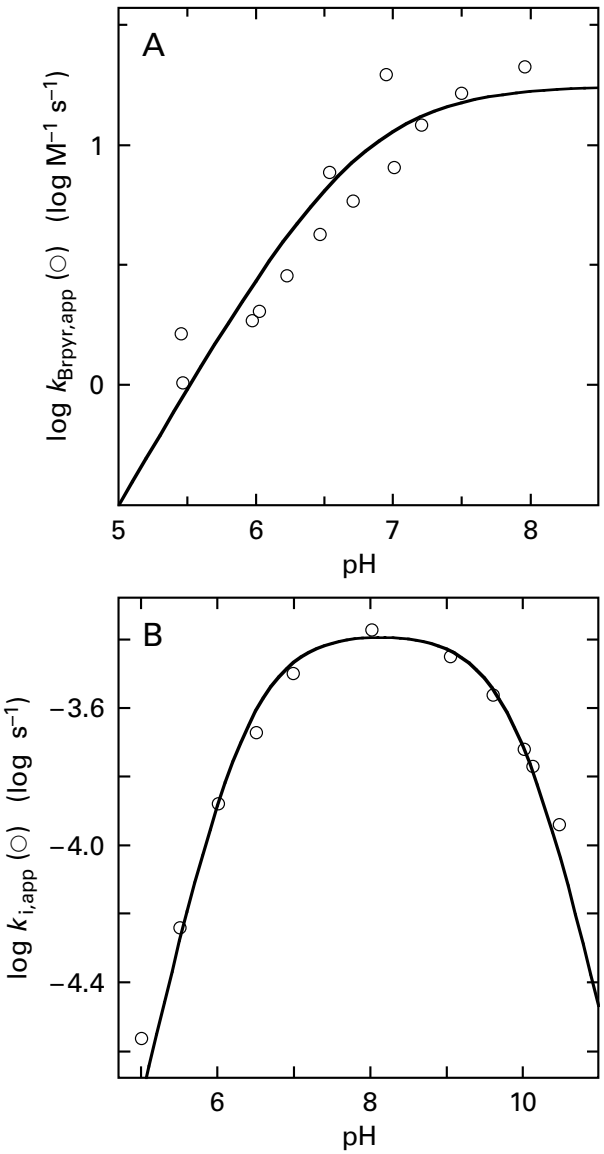

Figure 4–39: Dependence on pH of the common logarithms of the rate constants for inactivation by active-site labels. (**A**) Inactivation of 2-hydroxymuconate tautomerase from *P. putida* by 3-bromopyruvate.[636] Solutions containing 0.45–4.5 mM 3-bromopyruvate were prepared at various values of pH buffered with 0.1 M sodium phosphate at 23 °C . Inactivation of the enzyme was initiated by adding enzyme to 1.7 μM in active sites and was followed by withdrawing samples at appropriate times, diluting the sample 200-fold, and performing an assay for enzymatic activity. The observed pseudo-first-order rate constants of inactivation for each value of pH and each concentration of 3-bromopyruvate were determined from a nonlinear least-squares fit of the data for the loss in enzymatic activity as a function of time to Equation 4–298. These observed rate constants as a function of the concentrations of 3-bromopyruvate (Brpyr) for each pH were then fit to Equation 4–299 to obtain values for $k_{Brpyr,app}$. The common logarithms of these values for $k_{Brpyr,app}$ (molar^{-1} second^{-1}) are plotted as a function of the pH of the solution in which the inactivation occurred. The curve fit to the data is that for Equation 4–89, with $k_{Brpyr,app}$ substituted for $k_{0,app}$ and k_{Brpyr} substituted for k_0. The resulting parameters of the fit are pK_a = 6.74 and k_{Brpyr} = 17.7 M^{-1} s^{-1}. (**B**) Inactivation of glucose-6-phosphate isomerase from *S. cerevisiae* by 1,2-anhydro-D-mannitol 6-phosphate.[645] Solutions containing 2 or 4 mM (2*R*)-1,2-anhydro-D-mannitol 6-phosphate were prepared at various values of pH buffered with sodium acetate, imidazolium chloride, triethanolammonium chloride, or sodium glycinate at 25 °C. The two concentrations of reagent chosen were known to be saturating for the active site, and the fact that the rates of inactivation were the same for each verified this expectation. Inactivation of the enzyme was initiated by adding yeast glucose-6-phosphate isomerase and was followed by withdrawing samples at appropriate times, diluting the sample 100-fold with cold assay buffer, and performing an assay for enzymatic activity. The observed pseudo-first-order rate constants of inactivation, $k_{i,app}$, for each value of pH and each concentration of the epoxide were obtained by plotting the common logarithms of the residual enzymatic activity as a function of time. The common logarithms of these rate constants, log $k_{i,app}$ (second^{-1}), are plotted as a function of pH. The curve fit to the data is that for Equation 4–96, with $k_{i,app}$ substituted for $k_{0,app}$ and k_i substituted for k_0. The resulting parameters of the fit are pK_{a1} = 6.34, pK_{a2} = 9.95, and k_i = 1.5 h^{-1}.

the specificity constant for tautomerization of 2-oxopent-4-enoate below a pK_a of 6.2; and second, that the catalytic base responsible for this decrease in the specificity constant and also responsible for removing the hydron from carbon 3 of 2-oxohex-4-enedioate (Equation 4–317) is the amino-terminal proline of the enzyme.

The reaction catalyzed by glucose-6-phosphate isomerase

D-glucose 6-phosphate ⇌ D-fructose 6-phosphate (4–318)

proceeds through a *cis*-enediol, as does that catalyzed by triose-phosphate isomerase (Equations 4–46 and 4–55 and Figure 3–37). The *cis*-enediol in this case is the conjugate base of both D-glucose 6-phosphate and D-fructose 6-phosphate. To produce this common conjugate base, a catalytic base is necessary to remove a hydron from carbon 1 of D-glucose 6-phosphate or carbon 2 of D-fructose 6-phosphate, and the conjugate acid of this base is necessary to add a hydron to carbon 2 or carbon 1, respectively, of the resulting enediol. Catalytic acid–bases are also necessary to operate on the oxygens on carbons 1 and 2 to stabilize the enolate (see Figure 3–37).

The oxirane 1,2-anhydro-D-mannitol 6-phosphate (**4–85**) was chosen[645] as an active-site label for glucose-6-phosphate isomerase

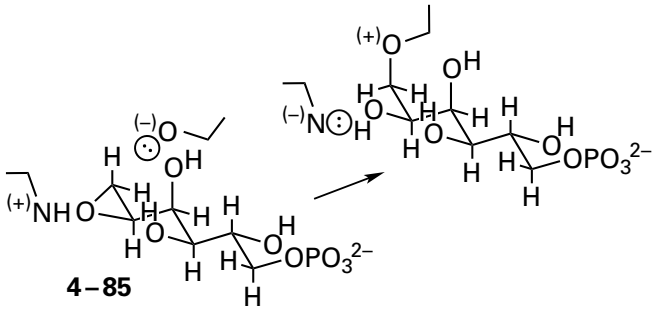

(4–319)

Under catalysis by –NH$^{(+)}$, the catalytic acid responsible for adding the hydron to oxygen in the normal reaction, the epoxide should alkylate –O$\odot^{(-)}$, the catalytic base responsible for removing the hydron from carbon. Rate constants at saturation, $k_{\text{anMP,app}}$ (Equation 4–299), for the irreversible inactivation of glucose-6-phosphate isomerase from *S. cerevisiae* caused by 1,2-anhydro-D-mannitol 6-phosphate (anMP) were determined as a function of pH (Figure 4–39B).[645] The two values of pK_a (6.3 and 10.0) are thought to correspond to the microscopic pK_a of the conjugate acid of the catalytic base responsible for the nucleophilic substitution resulting in inactivation and the microscopic pK_a for the catalytic acid that hydronates the oxygen of the epoxide, respectively. Because values of pK_a measured are for the active site occupied by the epoxide, they should be closest to values of pK_a for the active site occupied by reactant and hence values of pK_a governing the behavior of the catalytic constant. The catalytic constant of the enzymatic reaction has a similar dependence on pH with apparent values for pK_a of 6.6 and 9.8. Acid dissociation constants that govern the inactivation of the enzyme by the epoxide, however, are uncomplicated by rate constants of other steps in the catalytic reaction, and they should be more direct measurements of actual acid dissociation constants for these amino acids within the active site when it is occupied by 1,2-anhydro-D-mannitol 6-phosphate or by either substrate.

The criterion that covalent incorporation of the active-site label into the protein should be **proportional to the loss of enzymatic activity** and that the **stoichiometry of incorporation** at full inactivation should be 1.0 mol (mol of active sites)$^{-1}$ ensures that the major modified peptide that will be derived from digestion of the enzyme will be the peptide containing the amino acid the modification of which led to the inactivation of the enzyme.[640] For example, amidophosphoribosyltransferase from *B. subtilis* (Equation 4–313) is irreversibly inactivated by [6-^{14}C]-6-diazo-5-oxo-(*S*)-2-aminohexanoic acid (**4–86**), an electrophilic analogue of the substrate L-glutamine. [6-^{14}C]-6-Diazo-5-oxo-(*S*)-2-aminohexanoic acid is a diazoketone that covalently modifies an adjacent acid when it is bound in an active site. The covalent incorporation results from a nucleophilic substitution with the conjugate base of the acid after the acid has hydronated carbon 6 of the active-site label. Molecular nitrogen is the leaving group[669,670]

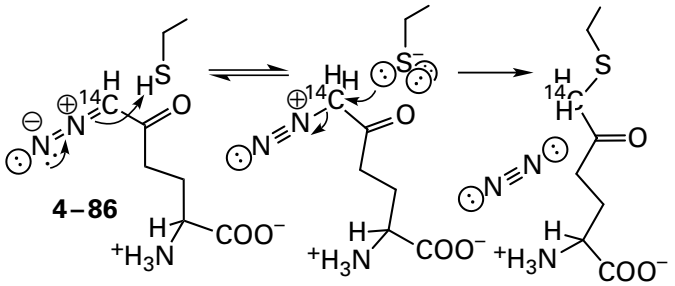

(4–320)

Both the covalent incorporation of the radioactive reagent into amidophosphoribosyltransferase and the irreversible loss of enzymatic activity were followed as a function of time in the same samples. A close correlation between these two properties was observed (Figure 4–40).[695] The incorporation of radioactivity into the protein rises as the enzymatic activity falls (Figure 4–40A). The fraction of enzymatic activity lost is directly proportional to the moles of carbon-14 incorporated into the protein (Figure 4–40B). The **extrapolated value for incorporation at full inactivation** was 0.85 mole of reagent for every mole of protomer, and hence every mole of active sites, estimated to be in the solution.

When intact, fully inactivated amidophosphoribosyltransferase covalently modified by [6-^{14}C]-6-diazo-5-oxo-(*S*)-2-aminohexanoic acid was submitted to Edman degradation, all the carbon-14 that had been incorporated was released in the first cycle. This result identified the sulfido group of the amino-terminal cysteine in the amino-terminal domain of the enzyme as the nucleophile that had been modified. The amino-terminal cysteine in the homologous (36% identity; 3.0 gap percent) amino-terminal glutaminase domain in amidophosphoribosyltransferase from *E. coli* is also alkylated specifically by 6-diazo-5-oxo-(*S*)-2-aminohexanoic acid,[696] and the sulfanyl group of this cysteine has been identified as the nucleophile releasing ammonia from L-glutamine by nucleophilic substitution to form a thioester, which is subsequently hydrolyzed to regenerate the sulfanyl group.[693,697-700]

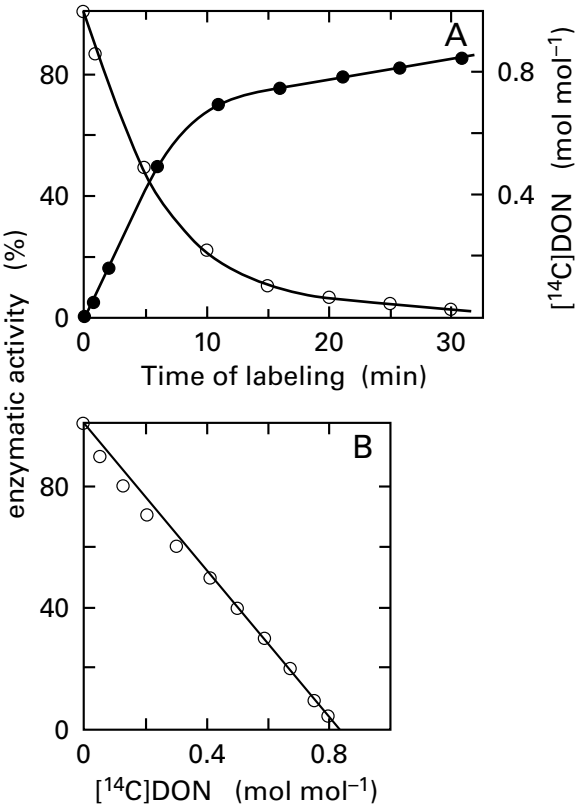

Figure 4–40: Incorporation of [6-^{14}C]-6-diazo-5-oxo-(*S*)-2-aminohexanoic acid into amidophosphoribosyltransferase from *B. subtilis*.[695] A solution containing 10 μM [6-^{14}C]-6-dazo-5-oxo-(*S*)-2-aminohexanoic acid, 7.5 mM $MgCl_2$, and 5 mM 5-phosphoribosyl 1-diphosphate was prepared at pH 7.5 and 37 °C. Amidophosphoribosyltransferase (5 μM final concentration of active sites) was added to initiate the reaction. At the noted times, samples (10 μL) were removed for assay of enzymatic activity, and other samples (75 μL) were removed and quenched with 175 μL of 10% trichloroacetic acid at 0 °C. Serum albumin (0.1 mg) was added to each of these latter samples as a coprecipitant. It was assumed that the precipitated carbon-14 was attached covalently to the amidophosphoribosyltransferase. After 4 h, the precipitates in the latter samples were washed with ethanol, dissolved in 1 M NaOH, neutralized with HCl, and submitted to scintillation counting. (**A**) Enzymatic activity (○), as a percentage of initial activity, and covalent incorporation of carbon-14 into protein (●), as moles of [6-^{14}C]-6-diazo-5-oxo-(*S*)-2-aminohexanoic acid ([^{14}C]DON) incorporated for each mole of active sites in the solution, are presented as a function of time (minutes). (**B**) Enzymatic activity (○), as a percentage of initial activity, is plotted as a function of the covalent incorporation of [6-^{14}C]-6-diazo-5-oxo-(*S*)-2-aminohexanoic acid, in moles of incorporation for each mole of active sites.

Pyridoxal 5′-phosphate (**4–87**) is electrophilic at its aldehyde. It forms unstable pyridoximines with primary amines, just as it forms external pyridoximines during the normal reactions catalyzed by enzymes that use it as a prosthetic group (Equation 4–258). Pyridoximines of primary amines can be reduced with borohydride, BH_4^-, or cyanoborohydride, $N{\equiv}CBH_3^-$, to the corresponding, stable secondary amines. Pyridoxal 5′-phosphate only vaguely resembles 3-phosphoshikimate (**4–88**)

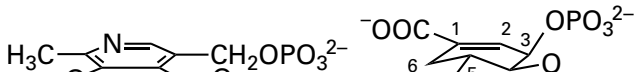

Nevertheless, it is an active-site label for 3-phosphoshikimate 1-carboxyvinyltransferase (previously Equation 3–262)

phospho*enol*pyruvate + 3-phosphoshikimate
$\rightleftharpoons$ phosphate +
5-*O*-(1-carboxyvinyl)-3-phosphoshikimate
(4–321)

from *E. coli* (see Problem 4–26) that satisfies most of the criteria for specific active-site labeling.[655] 3-Phosphoshikimate 1-carboxyvinyltransferase was mixed with a solution of pyridoxal 5′-phosphate, and samples were removed at consecutive intervals and reduced with $[^3H]BH_4^-$. The irreversible, covalent incorporation of [4′-^{3}H]pyridoxamine 5′-phosphate into the protein was directly proportional to the loss of enzymatic activity, and at complete inactivation, 1.0 mole of pyridoxal 5′-phosphate was incorporated for every mole of protomer of the enzyme in the solution. When the fully inactivated enzyme, reduced with $[^3H]BH_4^-$, was digested with trypsin, only one of the resulting tryptic peptides was radioactive. This peptide had the sequence VDGTINLPGSX*XVSNR, where the asterisk denotes the cycle of Edman degradation in which a radioactive amino acid was released. This sequence identifies the labeled amino acid as Lysine 22 in the complete sequence of the enzyme.

In the crystallographic molecular model between 3-phosphoshikimate 1-carboxyvinyltransferase from *E. coli* and 3-phosphoshikimate and 2-(phosphonomethylamino)acetic acid, an enzymatically inactive analogue of phospho*enol*pyruvate, Lysine 22 forms a hydrogen bond (0.28 nm) to the 5-hydroxy group of 3-phosphoshikimate (**4–88**).[701] In crystallographic molecular models of 3-phosphoshikimate

1-carboxyvinyltransferase from both *E. coli* and *Agrobacterium* and several analogues of the tetrahedral intermediate in the enzymatic reaction, Lysine 22 has been identified as the catalytic base that removes the hydron from the 5-hydroxy group of 3-phosphoshikimate to increase the nucleophilicity of the oxygen and initiate transfer of the 1-carboxyvinyl group to this hydroxy group in the first step of the enzymatic reaction.[702] Pyridoxal 5-phosphate, binding in place of 3-phosphoshikimate, serendipitously places its electrophilic aldehyde adjacent to the amino group of this catalytic lysine and modifies it.

As was the case for amidophosphoribosyltransferase (Figure 4–40B), extrapolated values for the moles of reagent incorporated into the protein at complete inactivation are **rarely the hoped-for value of 1.0 mol (mol of active sites)$^{-1}$**. In situations[639] when it is 1.0 mol mol^{-1}, such as that for the incorporation of [4′-^{3}H]pyridoxamino 5′-phosphate into 3-phosphoshikimate 1-carboxyvinyltransferase, the agreement with expectation is probably only by chance. First, an incorporation in excess of 1.0 mol (mol of active sites)$^{-1}$ may only mean that **the electrophile is reactive enough to modify other amino acids** at random on the surface of the protein present in the solution in addition to the targeted catalytic base in the active site of interest. Second, an extrapolated value for incorporation at full inactivation significantly different from 1.0 mol mol^{-1} can also be due to inaccuracies in estimation of the concentration of active sites in the solution because the concentration of active sites is almost always estimated from the concentration of total protein in the preparations, and it is quite **difficult to measure the concentration of protein in any solution** accurately.[703] Third, even if the concentration of protein has been measured accurately, **inactive molecules of enzyme in the solution** and other contaminating proteins will cause the estimate of the concentration of active sites in the solution to be too high. All the foregoing problems probably apply to every measurement of covalent incorporation of an active-site label into an enzyme, so it is remarkable, and perhaps suspicious, that the extrapolated values for incorporation at full inactivation obtained are so often so close to 1.0 mol mol^{-1}.

This last criterion of active-site labeling is confirmatory when it is fulfilled, but it is not a requirement for a modification that occurs specifically in an active site. An extrapolated value for incorporation at full inactivation that is greater than 1.0 or a percent of inactivation that is not directly proportional to incorporation of the active-site label does not rule out the possibility that the reagent did inactivate the enzyme while it was bound in place of a substrate within the active site. The product of the reaction that occurred within the active site can be distinguished from products of other reactions that occurred outside the active site by **changes in the yield of these products in response to ligands for the active site**. The yield of the product of modification from within the active site will decrease significantly when the amino acid involved is protected from modification by adding substrates or competitive inhibitors, but the yield of the products of modification at other amino acids outside the active site should be unaffected by these additions.

When bovine carboxypeptidase A (Equation 4–172) was modified to complete inactivation with *N*-([1-^{14}C]bromoacetyl)-*N*-methyl-L-phenylalanine (Equation 4–312), 2 moles of the reagent were incorporated for every mole of enzyme.[704] Two cyanogen bromide fragments of the protein became radioactive during the modification. When the modification was repeated under the same conditions but in the presence of the competitive inhibitor L-phenylalanine, only 10% of the enzymatic activity was lost, and incorporation of radioactivity into one of the two fragments decreased 10-fold while incorporation into the other was unchanged. This experiment was sufficient to identify the fragment containing the amino acid modified from within the active site. This **ability of substrates or competitive inhibitors to protect a particular peptide against incorporation of the active-site label** is a further necessary criterion to demonstrate that a peptide which has been isolated contains the amino acid from the active site the modification of which was correlated with the inactivation.

A determination of the position of the modified amino acid in the sequence of amino acids for an enzyme connects the results of active-site labeling to the structure of the protein.[641] For example, the modification of triose-phosphate isomerase identified Glutamate 165 as a catalytic acid–base, the modification of amidophosphoribosyltransferase identified the amino-terminal cysteine as a catalytic acid–base, and the modification of 3-phosphoshikimate 1-carboxyvinyltransferase identified Lysine 22 as a catalytic acid–base.

When porcine pepsin, an enzyme that catalyzes the hydrolysis of peptide bonds in peptides and proteins, was completely inactivated with the active-site label *N*-(diazo[^{14}C]acetyl)-L-phenylalanine methyl ester, 1.0 mole of the reagent was incorporated for

every mole of enzyme.[705] The modified protein was digested with pepsin, and a radioactive peptide was partially purified by chromatography. The peptide was then purified to homogeneity by two-dimensional diagonal electrophoresis. The peptides were submitted to electrophoresis in one dimension, treated with triethylamine, and submitted to electrophoresis again in the orthogonal dimension. Only one peptide, which was radioactive after the first separation, changed its mobility and moved off the diagonal. The isolated peptide, which no longer was labeled, was found to be IVDTGTS. It was concluded that the (diazoacetyl)-L-phenylalanine, while it was in the active site, had formed an ester with Aspartate 215 in the sequence of amino acids for the protein

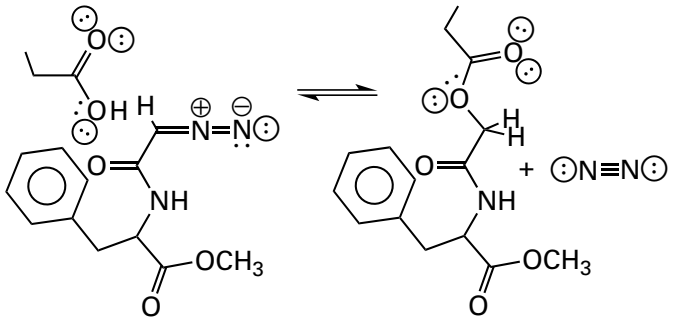

(4–322)

Such an ester is susceptible to aminolysis by ethylamine.

The active-site label 3,4-epoxybutyl β-D-cellobiose

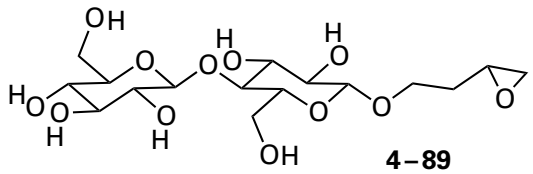

4–89

(molar mass = 412.39 g mol^{-1}) should place an electrophilic epoxy group adjacent to a catalytic acid–base responsible for either stabilizing an intermediate oxocarbenium ion

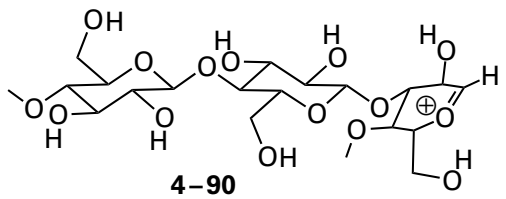

4–90

or adding a hydron to the leaving hydroxy group (previously Equation 1–23)

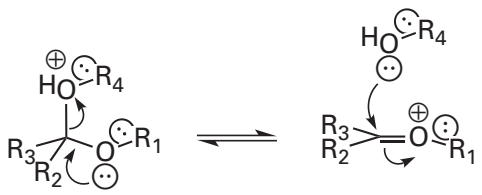

(4–323)

and removing a hydron from water during the hydrolysis of (β1,3)-(β1,4)-glucan

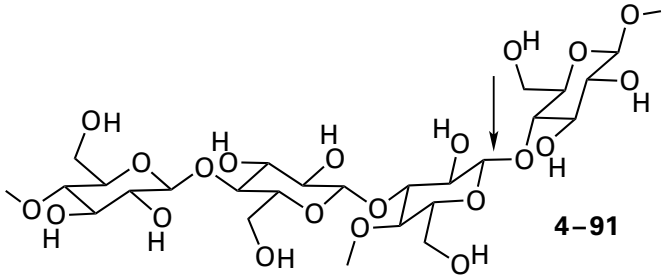

4–91

catalyzed by licheninase, where the arrow marks the site of hydrolysis. When licheninase from *B. amyloliquefaciens* was inactivated with 3,4-epoxybutyl β-[^{14}C]cellobiose, 1.1 mole of the [^{14}C]active-site label was incorporated for each mole of enzyme, and almost all the molecules of enzyme increased in mass by 412 unified atomic mass units (major) or 825 unified atomic mass units (minor), upon mass spectrometry. When the modified protein was digested separately by glutamyl endopeptidase and trypsin, the sequences of amino acids and mass spectrometry of the resulting radioactive peptides obtained from the digests identified Glutamate 105 as the modified amino acid.[648]

Complications can arise when **the product of a modification is too unstable** to survive the digestion, chromatography, and sequencing required to identify the amino acid modified. For example, 2-dehydro-3-deoxy-phosphogluconate aldolase from *Pseudomonas* catalyzes the aldol condensation

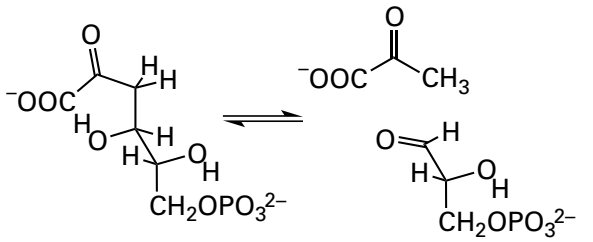

(4–324)

An imine between a lysine in the active site and the 2-oxo group on 2-dehydro-3-deoxyphosphogluconate is formed during the enzymatic reaction to facilitate the retroaldol condensation.[706] Therefore,

an imine between the same lysine and pyruvate forms as a step in the aldol condensation, and this imine can be identified by reducing it with sodium borohydride[707]

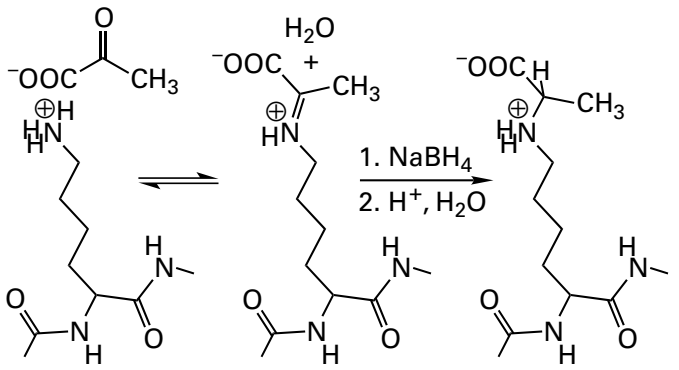

(4–325)

When 3-bromopyruvate is mixed with enzyme, not only does the imine form with the carbonyl of 3-bromopyruvate, but the primary bromide in the resulting imine alkylates another amino acid in the vicinity. When 2-dehydro-3-deoxy-phosphogluconate aldolase that had been inactivated with [^{14}C]-3-bromopyruvate but not reduced with sodium borohydride was digested with trypsin, a radioactive tryptic peptide could be purified to homogeneity.[637] The sequence of this peptide was TLEVTLR, which tentatively identified Glutamate 56 in the complete sequence of the protein[708] as the alkylated nucleophile

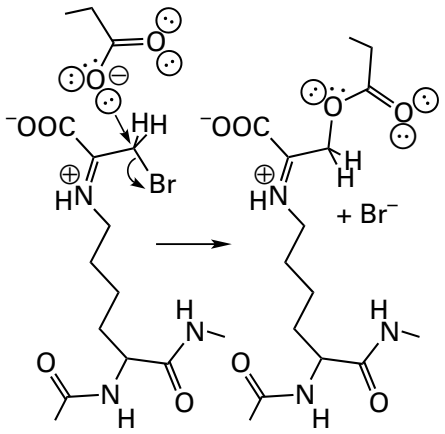

(4–326)

but all the [^{14}C]-3-hydroxypyruvate, presumably esterified to Glutamate 56, was lost at the first step of sequencing due to hydrolysis of the ester.

To confirm that the [^{14}C]-3-hydroxypyruvate actually was esterified to the glutamate as a result of the active-site labeling prior to sequencing, the isolated, radioactive peptide was submitted to a Lossen rearrangement, which requires that an ester be present

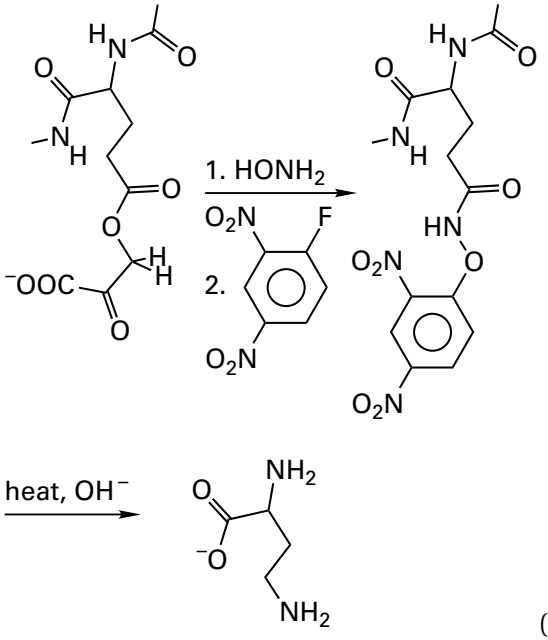

(4–327)

The recovery of 2,4-diaminobutyrate (0.8 mol mol^{-1}) could only be explained if the glutamate in the radioactive peptide was esterified.[637] After the Lossen rearrangement, the peptide was no longer intact, so it could not be sequenced to show that 2,4-diaminobutyrate had replaced glutamate, but there is no other amino acid in the peptide that could have been converted into 2,4-diaminobutyrate. Consequently, it could be concluded that Glutamate 56 had been modified by esterification.

After this discussion of historical examples of identification of labeled amino acids in the sequence of a modified protein, it should be mentioned that advances in mass spectrometry have rendered many of the specific approaches described so far obsolete. Consequently, they are presented not as examples of what would now be done, but as examples of the knowledge gained by identifying a particular amino acid as the site of modification.

Although it is not a frequent occurrence, the group covalently modifying a catalytic acid–base can **move to another amino acid** in the active site that is not a catalytic acid–base. For example, (2-methylenecyclopropyl)formyl-SCoA (**4–92**) inactivates bovine enoyl-CoA hydratase (Equation 4–236) in a reaction that satisfies many of the criteria of active-site labeling.[709] The tryptic peptide modified by the active-site label was ALGGGXEL, where X was the modified amino acid released in that cycle of sequencing.[710] Consequently, the 2-methylenecyclopropyl group had modified Cysteine 114 in the sequence

of amino acids for the enzyme. A mutant of the enzyme, however, in which Cysteine 114 had been changed to alanine, had a catalytic constant and a specificity constant for crotonyl-SCoA that were only 60% and 50%, respectively, of the values for the wild-type enzyme. Furthermore, (2-methylenecyclopropyl)formyl-SCoA inactivated the mutant in a reaction that resulted in modification of Glutamate 115 rather than the missing cysteine.[668] It was concluded that the catalytic acid–base was actually Glutamate 115 and that, after the initial modification of Glutamate 115, the resulting vinyl ester migrated to the sulfido group of Cysteine 114

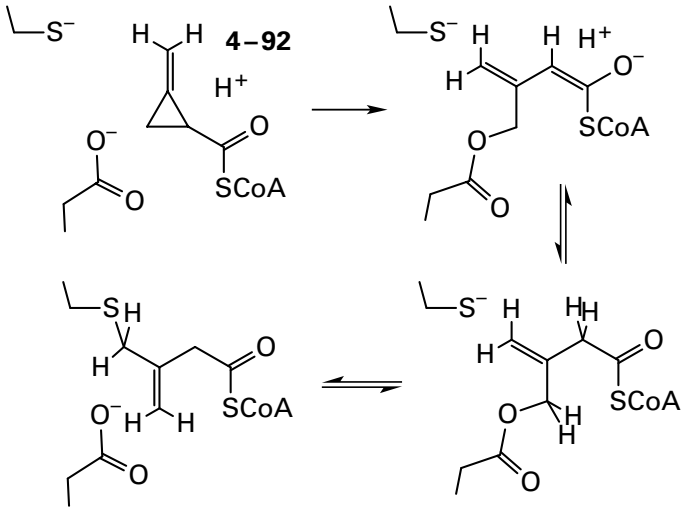

(4–328)

Although the migration should be a pseudosymmetric, reversible reaction, the equilibrium strongly favors the sulfide over the ester. The sulfido group is a strong nucleophile and a poor leaving group while the carboxylate is a weak nucleophile and a good leaving group.

The amino acid in the sequence of the protein that has been modified can also be identified directly in a crystallographic molecular model of the modified enzyme. For example, (1*S*,3*S*)-3-amino-4-(perfluoropropan-2-ylidene)cyclopentane-1-carboxylate inactivates human ornithine aminotransferase. Its 3-amino group forms an external pyridoximine with the prosthetic pyridoxal 5′-phosphate in the active site and positions the perfluoropropan-2-ylidene group, which is turned into an electrophile by the external pyridoximine, adjacent to a catalytic acid–base in the active site and modifies it. A crystallographic molecular model of the modified enzyme identified the structure of the product of modification and identified Lysine 292, a lysine other than the one that forms the internal pyridoximine (Equation 4–129), as the modified amino acid.[711] The product observed crystallographically was consistent with the mass spectrum of the modified enzyme, but the mass spectrum alone would not have identified the product. It is possible that chemical identification of the amino acid modified by an active-site label has been rendered obsolete by advances in the ease with which crystallography can be performed.

As with the active-site labeling of triosephosphate isomerase, diaminopimelate epimerase, 3-phosphoshikimate 1-carboxyvinyltransferase, and ornithine aminotransferase, the success of an active-site label in identifying a catalytic acid–base that participates in the catalysis accomplished by an active site relies on crystallography.

The catalytic roles of the acid–bases of particular amino acids the conjugate bases of which are modified by electrophilic active-site labels are verified crystallographically.[649,670,671,712-714] It is usually the case that the crystallographic molecular model that provides this assignment is for the same enzyme from a different species because crystallization is usually serendipitous and the serendipity depends on the source of the enzyme.

3-Bromopyruvate inactivates isocitrate lyase (Equation 4–310) from *V. indigofera* (Figure 4–38).[629] 3-Bromopyruvate also inactivates[715] the homologous (73% identity; 0.7 gap percent) isocitrate lyase from *E. coli* by alkylating the sulfido group of Cysteine 195 (Equation 4–311), and it inactivates the homologous (63% identity; 0.7 gap percent) isocitrate lyase from *M. tuberculosis* by alkylating the homologous Cysteine 191.[692] There is a mutant of isocitrate lyase from *M. tuberculosis* in which this cysteine has been mutated to serine. In a crystallographic molecular model[692] of a complex between this mutant enzyme and glyoxylate and the *aci*-nitro tautomer of 3-nitropropionate (**4–93**)

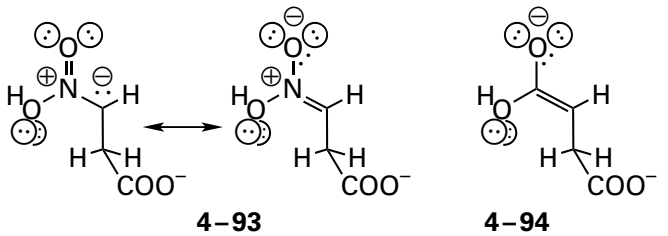

4–93 **4–94**

which is an inactive, isosteric, and isoelectronic analogue of the *gem*-enediolate of succinate (**4–94**), the γ-oxygen of the serine replacing Cysteine 191 is in the location necessary to remove the correct

hydron[716] from succinate and is only 0.29 nm from carbon 3 on the 3-nitropropionate. Presumably, the γ-oxygen forms a hydrogen bond with the anionic carbon of the *aci*-nitro tautomer of nitropropionate. In the normal enzymatic reaction, the sulfido group of the unmutated cysteine would be the catalytic base that removes the correct hydron from succinate (Equation 4–310) with the assistance of the adjacent carboxylato group of Aspartate 108, with which it forms a hydrogen bond, and the acidic molecule of water on a nearby Mg^{2+}, with which the same oxygen on the carboxylato group forms a hydrogen bond.

N-Bromoacetyl-*N*-methyl-L-phenylalanine (Equation 4–312) alkylates Glutamate 270 of bovine carboxypeptidase A.[704] This glutamate has been assigned crystallographically as the catalytic base that removes the hydron from the molecule of water that adds to the acyl carbon to initiate hydrolysis of the peptide bond (Equation 4–172).[234,259]

1,2-Anhydro-D-mannitol 6-phosphate (**4–85** in Equation 4–319) alkylates Glutamate 366 of glucose-6-phosphate isomerase from *S. cerevisiae*.[645] The homologous glutamate, Glutamate 357 in the active site of glucose-6-phosphate isomerase from *O. cuniculus* (59% identity; 0.7 gap percent), has been assigned crystallographically[717] as the catalytic base that transfers the hydron between carbons 1 and 2 of the hexose 6-phosphates in a role analogous to that played by Glutamate 164 in triose-phosphate isomerase from *S. cerevisiae* (Equations 4–46 and 4–55 and Figure 3–37).

(Diazoacetyl)-L-phenylalanine modifies Aspartate 215 in the sequence of amino acids for porcine pepsin (Equation 4–322). In the crystallographic molecular model of a complex between human pepsin (86% identity; 0 gap percent) and a phosphonate analogue of the tetrahedral intermediate in hydrolysis of a peptide that would be a normal reactant for the enzyme,[718] it can be seen that the homologous aspartate, Aspartate 215, is responsible for removing a hydron from the molecule of water that adds nucleophilically to the acyl carbon of the amide that is to be hydrolyzed when it occupies the active site to produce the tetrahedral intermediate in the hydrolysis.

Glutamate 156 in 2-dehydro-3-deoxyphosphogluconate aldolase from *Pseudomonas* is modified by 3-bromopyruvate (Equation 4–326). In a crystallographic molecular model[719] of 2-dehydro-3-deoxyphosphogluconate aldolase from *E. coli* (45% identity; 0 gap percent), in which the active site is occupied by the hemiaminal between pyruvate and the side chain of a lysine, and in a crystallographic molecular model of 2-dehydro-3-deoxy-phosphogluconate aldolase from *Thermotoga maritima* (29% identity; 2.5 gap percent), in which the active site is occupied by the imine between pyruvate and the side chain of a homologous lysine, the homologous glutamates are in a location in which they could easily be alkylated by the imine between 3-bromopyruvate and the lysine (Equation 4–326). In each case, however, in what appears to be the complex competent for catalysis, the carboxy group of the glutamate is too far (0.47 and 0.58 nm, respectively) from the methyl group of pyruvate to be the catalytic base that removes one of the hydrons from the methyl group on the pyruvyl group to form the enolate during the normal aldol condensation, as Glutamate 164 removes the hydron from carbon in the active sites of triosephosphate isomerase (Equation 4–55). Rather, the role that has been assigned to these two glutamates, homologous to Glutamate 156 in 2-dehydro-3-deoxy-phosphogluconate aldolase from *Pseudomonas*, is to hydronate the oxygen of the oxo group of pyruvate to increase its electrophilicity during formation of the hemiaminal and then to hydronate the hydroxy group of the hemiaminal to improve its ability to leave to form the necessary imine (Figure 1–7) between lysine and pyruvate.

The **crystallographic molecular models of actual products of active-site labeling**, in addition to sometimes identifying the product of a particular modification, have been used to provide the first identification of the active site in the molecular model and to identify catalytic bases. For example, the 4-hydroxy-3-(γ-glutamyl)butyl β-D-cellobiose in the crystallographic molecular model of licheninase from *Bacillus macerans* that had been modified by 3,4-epoxybutyl β-D-cellobiose (**4–89**) provided the first identification of the active site of the enzyme and its catalytic functional groups.[720] These assignments were later verified in the crystallographic molecular model of the complex between a β-glucan tetrasaccharide and a mutant of the enzyme in which the two catalytic glutamates had been mutated to glutamines.[721]

Although they are designed to label the active sites of enzymes and they inactivate those enzymes in reactions satisfying the criteria of active-site labeling, there are apparent active-site labels that do not actually modify catalytic amino acids or even amino acids in the active site of an enzyme. For example, 3-bromo-2-oxoglutarate was chosen as an active-site label for isocitrate dehydrogenase ($NADP^+$)

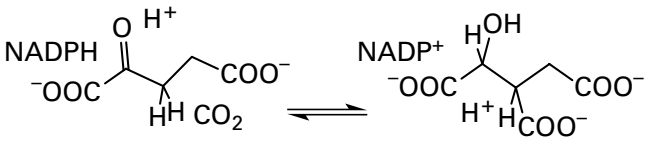

(4–329)

because it is an electrophilic analogue that differs from the natural substrate, 2-oxoglutarate, only by addition of a bromine. The hydroxy group at carbon 2 of isocitrate is converted in the active site to an oxo group by $NADP^+$, and the resulting 3-carboxy-2-oxoglutarate is decarboxylated by the enzyme at carbon 3 to form 2-oxoglutarate. When it is bound in the active site, 3-bromo-2-oxoglutarate should place an electrophile in the location where the catalytic acid–bases that facilitate decarboxylation from carbon 3 of 3-carboxy-2-oxoglutarate are located. Its inactivation of the porcine enzyme is an archetype of active-site labeling, satisfying most of the accepted criteria.[632] Nevertheless, in crystallographic molecular models of the complexes between the porcine α_2 dimer and isocitrate,[722] between the human α_2 dimer and $NADP^+$ and isocitrate,[723] and between the human α_2 dimer and isocitrate (Protein Data Bank 5YFN), the closest sulfanyl group of the two Cysteines 379 in each dimer, which are the nucleophiles alkylated by the reagent,[724] is 2.2 nm away from carbon 3 of isocitrate, the carbon from which modification of the enzyme was supposedly proceeding. Each Cysteine 379 is also 1.1 nm away from the closest atom on the two molecules of $NADP^+$ in the crystallographic molecular model of the complex between the human α_2 dimer and $NADP^+$ and isocitrate. Consequently, it is unclear how modification of these cysteines by 3-bromo-2-oxo-glutarate even leads to inactivation.

A possible explanation of how the modification of an amino acid distant from the active site could nevertheless lead to an inactivation of the enzyme that satisfies the criteria of active-site labeling is **syncatalytic modification**.[725] Cysteine 390 of porcine aspartate transaminase (Equation 4–108) is on the surface of the protein, 1.2 nm from carbon 4a of the prosthetic pyridoxal phosphate in the active site of the enzyme.[187] When an external pyridoximine (Figure 2–2) is formed in the active site between the prosthetic pyridoxal 5′-phosphate and an amino acid that is a reactant for the enzyme, the rate of reaction of the sulfido group of this cysteine with nonspecific electrophiles increases 20–80-fold, and the enzyme alkylated at this cysteine by any electrophile has lost more than 95% of its activity.[726] The reason for this loss of activity is probably that the enzyme can no longer accomplish the conformational change required to pass from an open to a closed conformation[187] upon association of the reactants when this cysteine is modified. Inactivation of the enzyme by 3-bromopyruvate satisfies several criteria of successful active-site labeling.[633] This inactivation, however, results from the fact that 3-bromopyruvate can be mistaken for 2-oxoglutarate and act as a reactant for the pyridoxamine form of the enzyme (previously **2–16**)

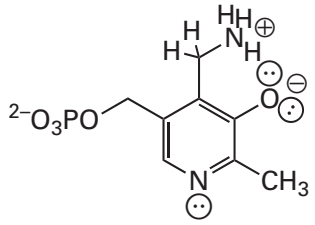

4–95

While one molecule of 3-bromopyruvate is bound in the active site, the active site closes and the rate at which the sulfido group of Cysteine 390 is alkylated by another molecule of 3-bromopyruvate free in the solution increases as usual.[725] The kinetic properties of this increase in the rate of alkylation upon closure of the active site around the 3-bromopyruvate masquerade as several of the criteria of active-site labeling.

Another explanation for modification of an enzyme outside the active site that nevertheless leads to inactivation that displays several of the criteria of active-site labeling is that the **enzyme catalytically transforms the intended active-site label into a more electrophilic reagent** that is released into the solution and then inactivates the enzyme. For example, the active site of phospho*enol*pyruvate carboxylase from *Zea mays* converts electrophilically inactive (*Z*)-3-bromophospho*enol*pyruvate into electrophilic 3-bromopyruvate that then inactivates the enzyme.[727] Because the production of 3-bromopyruvate is enzymatically catalyzed, it and the resulting inactivation display, in retrospect falsely, several of the criteria of successful active-site labeling.[631] Such a conversion of a weakly electrophilic reagent into a strongly electrophilic reagent by the active site of the enzyme is one major drawback of mechanism-based labeling.

A mechanism-based label[728] is an active-site label that must be chemically altered at the active site, in a reaction resembling the one normally catalyzed by the enzyme, before it can modify a catalytic acid–base or side chain in the active site. For example, although its triple bond is not electro-

philic, dec-3-ynoyl-*N*-acetylcysteamine (**4–96**) behaves as an irreversible, covalent inhibitor for 3-hydroxydecanoyl-[acyl-carrier-protein] dehydratase from *E. coli*.[729] One of the reactions normally catalyzed by this enzyme is the tautomerization

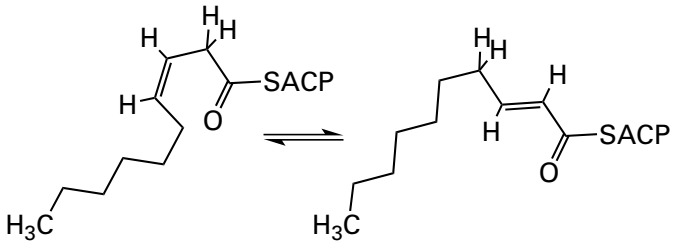

(4–330)

Dec-3-ynoyl-*N*-acetylcysteamine inactivates the enzyme by first being converted in the active site to the electrophilic **allene** deca-2,3-dienoyl-*N*-acetylcysteamine (**4–97**)[729,730]

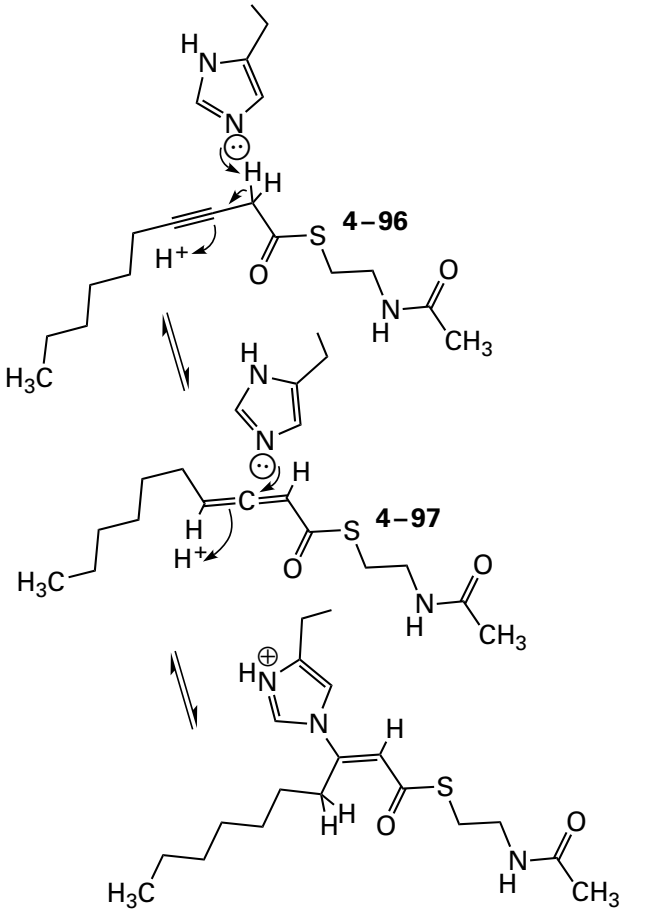

(4–331)

in a reaction that mimics the normal enzymatic reaction. Deca-2,3-dienoyl-*N*-acetylcysteamine then modifies Histidine 70 of the protein.[731] In the crystallographic molecular model of the enzyme modified by dec-3-ynoyl-*N*-acetylcysteamine,[730] the dec-2-enoyl-*N*-acetylcysteamine covalently attached at carbon 3 to Histidine 70 was used to identify and map the active site and to assign Histidine 70 as the catalytic base that removes the hydron from carbon 2 of the substrate (Equation 4–331) before any complexes of the enzyme with substrates or inhibitors were submitted to crystallography. The molecular model of the modified enzyme verified that, in the product of the modification, the double bond was between carbons 2 and 3 as drawn, conjugated to the acyl oxo group, which is the equilibrium product, rather than between carbons 3 and 4 of the decenoyl group, which would have been the kinetic product of the modification.

Acyl-carrier protein, rather than just *N*-acetylcysteamine, acylated with a dec-3-ynoyl group has also been synthesized and used to crosslink acyl-carrier protein from *E. coli* to 3-hydroxyacyl-[acyl-carrier-protein] dehydratase from *E. coli*.[732]

Ethynylene mechanism-based labels have also been used to modify other enzymes that, like 3-hydroxydecanoyl-[acyl-carrier-protein] dehydratase, proceed through intermediate enols or enolates. These enols or enolates are necessarily formed when a catalytic base removes a hydron from the carbon α to a carbonyl or acyl group, and the acidity at that carbon is required to turn the ethyne into the allene. For example, 2-hydroxymuconate tautomerase removes the hydron from carbon 5 of the reactant 2-oxo-(*E*)-pent-3-enoate to form (2*Z*)-2-hydroxy-2,4-pentadienoate (Equation 4–131). The active site of the enzyme mistakes 2-oxopent-3-ynoate (**4–98**) for the reactant, removes a hydron from carbon 5 of 2-oxopent-3-ynoate to form the cumulene, and adds a hydron to carbon 3 to produce 2-oxopenta-3,4-diene (**4–99**)

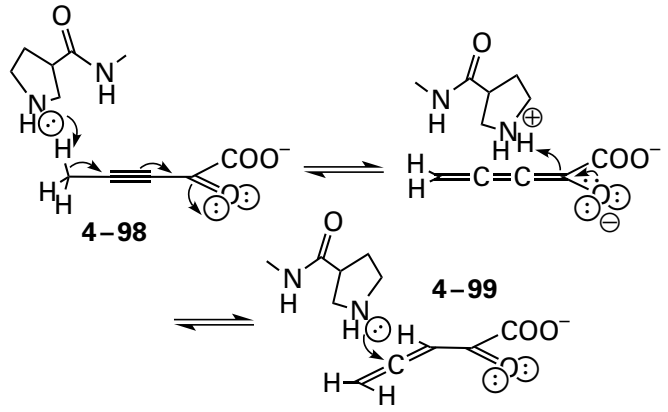

(4–332)

which is the allene that modifies the amino group of amino-terminal proline in the enzyme from

P. putida.[733] In the crystallographic molecular model of the modified enzyme, the position of the resulting 2-oxopent-3-enyl group that is covalently attached at carbon 3 to the amino-terminal proline was used to identify and map the active site.[262]

The inactivation of 2-hydroxymuconate tautomerase by 3-bromopyruvate results from a nucleophilic substitution at a carbon positioned in the active site at the location of carbon 3 in its substrates;[694] the inactivation of 2-hydroxymuconate tautomerase by 2-oxopent-3-ynoate results from a nucleophilic substitution at carbon positioned in the active site at the location of carbon 4 in its substrates (Equation 4–332); and the inactivation of 2-hydroxymuconate tautomerase by 5-bromo-(3*E*)-2-oxohex-3-enedioate results from a nucleophilic substitution at carbon positioned in the active site at the location of carbon 5 in its substrates.[117] In each alkylation, the nucleophile that is modified is the amino group of the amino-terminal proline. These three observations together illustrate the ability of the amino-terminal proline to move among these three carbons in the various substrates for the enzyme and act at a catalytic acid–base at each location at the appropriate times.

The flavoenzyme butyryl-CoA dehydrogenase catalyzes the oxidation of butyryl-SCoA

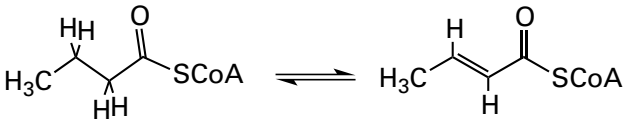

(4–333)

It is believed that this reaction passes through an enolate, formed by removal of the acidic hydron at carbon 2 of butyryl-SCoA, and that two electrons are then transferred from the electron-rich enolate to the prosthetic flavin. If an enolate is the intermediate, then locating an ethynyl group immediately adjacent to carbon 2 of the acyl-SCoA should permit formation of an allene

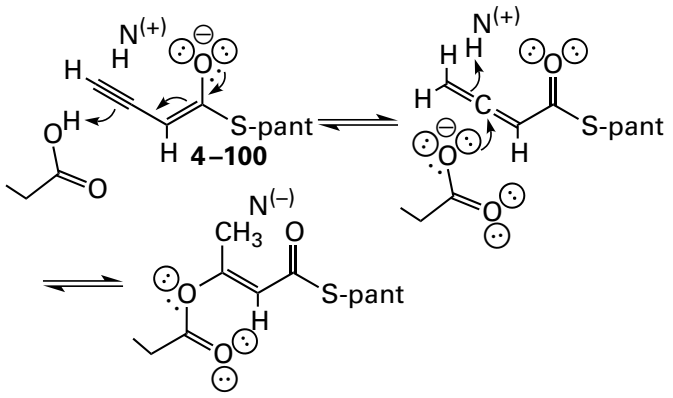

(4–334)

that should be able to react with the catalytic base responsible for removing the hydron from carbon 2.* When (3-pentynoyl)pantetheine (**4–100**) was incubated with butyryl-CoA dehydrogenase from *Megasphaera elsdenii*, the enzyme was irreversibly inactivated coincidently with covalent incorporation of the mechanism-based label into the protein.[734] The catalytic base modified by (3-pentynoyl)pante-theine is Glutamate 367.[735]

In the crystallographic molecular model of the complex between butyryl-CoA dehydrogenase from *M. elsdenii* and acetoacetyl-SCoA,[736] the distance between carbon 2 of acetoacetyl-SCoA and one oxygen in the carboxy group of Glutamate 367 (0.39 nm) is equal to the sum (0.38 nm) of the van der Waals radii of oxygen (0.15 nm) and hydrogen (0.115 nm) and the length of a carbon–hydrogen bond (0.11 nm), the distance of van der Waals contact. Carbon 2 of acetoacetyl-SCoA is the analogue of carbon 2 in butyryl-SCoA from which a hydron is removed during the normal reaction to create the enolate. This same oxygen, however, is within the distance of van der Waals contact with carbon 4 of acetoacetyl-SCoA (0.36 nm), analogous to carbon 4 of the (3-pentynoyl)-pantetheine to which a hydron must be added to create the allene. The distance (0.36 nm) between the same oxygen in the carboxy group of Glutamate 367 and carbon 3 of acetoacetyl-SCoA, analogous to the electrophilic carbon of the allene to which the oxygen of Glutamate 367 adds, is close to the sum of the van der Waals radii of carbon (0.175 nm) and oxygen (0.15 nm). It seems reasonable that, to accomplish the mechanism-based labeling,

*In Equation 4–334, the product of nucleophilic addition to the allene is shown as the conjugated but-2-enoyl adduct, again the equilibrium product. When the carboxylato group adds to the central carbon of the allene, the more stable intermediate would be the enolate, in which the negative charge ends up on the acyl oxygen. Hydronation of this intermediate enolate would give the but-3-enoyl adduct, the kinetic product.

this oxygen in the carboxy group of Glutamate 367 removes the hydron from carbon 2, adds the hydron to carbon 4, and then adds to carbon 3 of the resulting allene.

Usually, an ethynylene active-site label is designed with the ethynylene group a methylene away from an oxo group, so it is converted by the targeted active site into an allene, the electrophile with which a nucleophile in the active site then reacts (Equation 4–331). In at least one case, however, an ethynylene group not a methylene away from an oxo group was used as an active-site label, and the sulfido group of a cysteine in the active site added nucleophilically directly to the ethynylene[737]

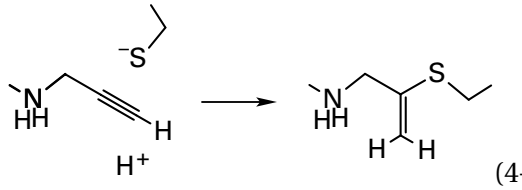

(4–335)

Like an ethynylene group, a 1-fluorovinyl group on a carbon from which an enzyme removes a hydron can be incorporated into a homologue of a substrate to produce a mechanism-based label that, upon removal of that hydron, then eliminates a fluoride ion to produce an allene

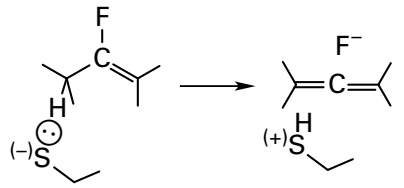

(4–336)

For example, the *N*-pyridoxylimine of vinylglycine (**4–55**, Equation 4–260) is an intermediate in the reaction catalyzed by tryptophan synthase. The enzyme from *S. typhimurium* is inactivated by (1-fluorovinyl)glycine in a reaction that satisfies several of the criteria of active-site labeling.[738] Upon formation of the external pyridoximine of (1-fluorovinyl)glycine, a catalytic base in the active site removes the hydron on the α carbon, the fluoride leaves, and the resulting allene modifies a catalytic acid–base in the active site.

A rather unusual mechanism-based label was synthesized for benzoylformate decarboxylase from *P. putida*. This enzyme decarboxylates 2-oxo-2-phenylacetate (benzoylformate) by forming the usual adduct between its 2-oxo group and the conjugate base of the prosthetic thiamine diphosphate in the active site. In the mechanism-based label 1-phosphonobenzaldehyde, the carboxylato group of 2-oxo-2-phenylacetate is replaced by a phosphono group. Instead of producing carbon dioxide from the carboxylato group, the active site produces monomeric metaphosphate from the phosphono group in an electrophilic elimination that mimics a decarboxylation. The monomeric metaphosphate phosphorylates Serine 26, which is adjacent to the thiamine diphosphate in the active site, and this modification inactivates the enzyme.[739]

The original scenario for mechanism-based labeling was that an unreactive analogue of one of the substrates, the mechanism-based label, would associate with the active site because it was mistaken for the normal reactant in the enzymatic reaction, and it would be converted to an electrophile so reactive that it would modify the enzyme before it could leave the active site.[729] Few electrophiles, however, are so reactive. Furthermore, it is difficult to distinguish the situation in which the electrophile, once it is formed on the active site of one molecule of enzyme, alkylates that molecule of enzyme before it dissociates from the active site from the situation in which one molecule of the enzyme simply produces the electrophile, which dissociates as a free product that then inactivates another molecule of enzyme from solution as a normal active-site label. In the case of 3-hydroxydecanoyl-[acyl-carrier-protein] dehydratase, deca-2,3-dienoyl-*N*-acetylcysteamine, which is the electrophile produced by the active site (Equation 4–331), is itself far superior at inactivating the enzyme than the alkyne when it is added directly to the solution rather than being produced on an active site.[731]

This latter scenario has probably played out in almost every instance of mechanism-based inactivation. The **active site converts the mechanism-based label into a strong electrophile that dissociates from the active site** before there is sufficient time for it to modify a catalytic base in the active site in which it is formed. This is probably what happens during the modifications of 3-hydroxydecanoyl-[acyl-carrier-protein] dehydratase, butyryl-CoA dehydrogenase, and 2-hydroxymuconate tautomerase during their inactivation by the respective alkynes. If so, in each case, the enzyme has simply serendipitously identified the respective allene as as an effective active-site label. In each instance, the crystallographically verified modification of a catalytic base probably results from the fact that the respective allene is an effective and specific active-site label so that even though it is released into the solution from

one active site, it still returns to modify another active site with high specificity.

There is, however, a problem when the electrophile is produced by the enzyme and released into solution, as occurred in the attempt to use (*Z*)-3-bromophospho*enol*pyruvate to label phospho*enol*pyruvate carboxylase. In this instance, the 3-bromopyruvate produced from (*Z*)-3-bromophospho*enol*pyruvate by the active site dissociated into the solution and modified the enzyme nonspecifically. Allyl alcohol inactivates alcohol dehydrogenase (Equation 4–158) because it is converted by the enzyme to acrolein. The acrolein, however, dissociates from the active site and then inactivates the enzyme nonspecifically from solution.[740] 5,6-Dichloro-7,7,7-trifluoro-4-thiahept-5-enoyl-SCoA (**4–101**) inactivates enoyl-CoA hydratase from *R. norvegicus* because the enzyme converts it to 1,2-dichloro-3,3,3-trifluoroprop-1-enethiolate (**4–102**)

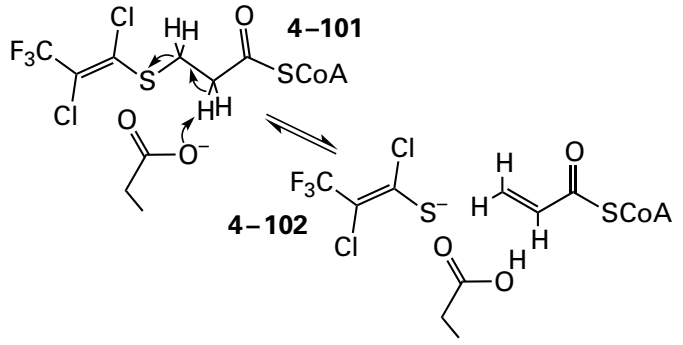

(4–337)

which is an unstable precursor to the electrophilic thioketene or thionoacyl fluoride. This precursor or one of the electrophiles, however, rather than reacting with a catalytic base in the active site, dissociates into the solution. From the solution, it modifies Cysteines 62 and 111 of the enzyme,[741] which are distant from the location in the active site where 1,2-dichloro-3,3,3-trifluoroprop-1-enethiolate is created,[742] and these nonspecific modifications inactivate the enzyme.

As was demonstrated experimentally with 3-hydroxydecanoyl-[acyl-carrier-protein] dehydratase, in such situations, the strong electrophile that has dissociated from the active site into the solution becomes indistinguishable from the same compound if it were added directly to the solution, with the exception that its **specificity is more difficult to verify**. The reason for this difficulty is that it is hard to distinguish effects of competitive inhibitors and substrates on production of the activated inhibitor from their effects on modification of the enzyme by that activated inhibitor that has dissociated into the solution. For example, the inactivation of 4-oxalocrotonate dehydrogenase by 2-oxopent-3-ynoate (Equation 4–332) shows a pseudo-first-order rate that displays saturation ($K_I = 30\ \mu M$, $k_i = 0.31\ s^{-1}$), and its rate decreases when the substrate, (3*E*)-2-oxo-3-pentenedioate, is present.[733] These criteria of specificity, however, may only be features of the kinetics of the enzymatic production and dissociation into the solution of 2-oxopenta-2,3-dienoate, the actual active-site label.

A mechanism-based label is designed to enter the active site and be converted to a strong electrophile. To enable some understanding of the inactivation that it produces, the electrophilic product of the enzymatic conversion of the label can be positively identified and both the **rate of its production and the rate of inactivation** can be measured. For example, ethyl vinyl sulfide inactivates murine thioether *S*-methyltransferase

alkyl alkyl sulfide + *S*-adenosylmethionine ⇌ *S*-adenosylhomocysteine + methyl alkyl alkylsulfonium (4–338)

As expected, the inactive ethyl vinyl sulfide is methylated by the enzyme to form the actual electrophile, methyl ethyl vinylsulfonium ion, that then inactivates the enzyme.[743] For every 100 moles of methyl ethyl vinylsulfonium ion produced by the enzyme, however, only one mole of enzyme is inactivated. From this result, it is clear that the electrophile produced by the active site seldom inactivates the enzyme before it dissociates into the solution.

Aryldialkylphosphatase from *Brevundimonas diminuta* is inactivated by hex-1-ynyl diethyl phosphate. The inactivation levels off at a maximum yield at long times as the presumed electrophile produced by the active site, the ketene hex-1-en-1-one, participates in a rapid nucleophilic addition with water. The maximum yield of inactivation is a linear function of the initial concentration of hex-1-ynyl diethyl phosphate, but to reach complete inactivation requires 500 moles of hex-1-ynyl diethyl phosphate for every mole of enzyme.[744]

Bovine dopamine β-monooxygenase is inactivated by 3-aminomethyl-3-(4-hydroxyphenyl)propyne. The intended reactive intermediate that should be responsible for enzymatic inactivation is 3-aminomethyl-3-(4-hydroxyphenyl)propa-1,2-dien-1-yl radical, formed by abstraction of a hydrogen atom from carbon 3 of the active-site label by the pros-

thetic copper ion in the active site. This radical either inactivates the enzyme or is converted innocuously, in a reaction homologous to the normal enzymatic reaction, into 3-aminomethyl-3-hydroxy-3-(4-hydroxyphenyl)propyne, a product as unreactive as the original 3-aminomethyl-3-(4-hydroxyphenyl)propyne. Only 2.5 moles of 3-aminomethyl-3-hydroxy-3-(4-hydroxyphenyl)propyne are produced by the enzyme for every mole of enzyme inactivated,[680] so it was presumed that at least a fraction of the 3-aminomethyl-3-(4-hydroxyphenyl)propa-1,2-dien-1-yl radical inactivated the enzyme while still associated with the active site at which it was produced.

n-Hexanal phenylhydrazone (**4–103**) is converted by linoleate 13*S*-lipoxygenase from *G. max* into its α-azoperoxide (**4–104**)

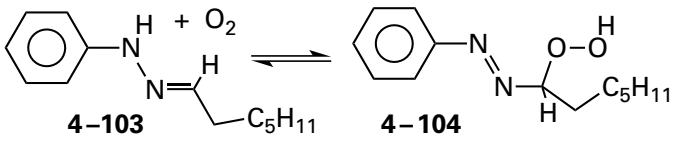

(4–339)

which inactivates the enzyme. From the kinetics of the inactivation, the yield of peroxide **4–104** after full inactivation as a function of the initial concentration of phenylhydrazone **4–103**, and the effect of scavengers on the yield of inactivated enzyme, it could be concluded that 20% of the inactivation observed was due to reaction of peroxide **4–104** before it dissociated from the enzyme and 80% of the inactivation was due to reassociation of peroxide **4–104** from solution.[745] This last investigation shows that it is possible to determine what is actually happening in a mechanism-based labeling.

As in these experiments with linoleate 13*S*-lipoxygenase, one way to prevent the released electrophile from inactivating the enzyme from solution, rather than before it can leave the active site, is to add a **scavenger** to the solution that intercepts the electrophile after it dissociates from the active site. For example, one observation demonstrating that acrolein was inactivating alcohol dehydrogenase after it had been released from the active site was that dithiothreitol prevented the inactivation of the enzyme by allyl alcohol. 2-Aminobut-3-enoic acid inactivates porcine aspartate transaminase (Equation 4–108) irreversibly. The enzyme, in a reaction analogous to its nominal reaction, produces 2-oxobut-3-enoic acid, an electrophilic Michael acceptor that could have been acting as an active-site label from the solution, but 2-sulfanylethanol, which scavenges 2-oxobut-3-enoic acid by Michael addition to its α,β-unsaturated carbonyl, has no effect on inactivation of the enzyme.[746] Consequently, it was assumed that 2-aminobut-3-enoic acid was the species inactivating the enzyme as a true mechanism-based label. Adding a scavenger, however, will preclude the serendipitous, successful identification of a specific and useful active-site label that is produced by an enzyme from a mechanism-based label, as occurred in the case of modification of 3-hydroxydecanoyl-[acyl-carrier-protein] dehydratase by dec-3-ynoyl-*N*-acetylcysteamine.

As with the inactivation of aryldialkylphosphatase by hex-1-ynyl diethyl phosphate, another way to avoid the ambiguity resulting from dissociation of the electrophile and at the same time prevent the dissociated electrophile from modifying the protein from solution is to design a mechanism-based label that **produces an electrophile that reacts with water** rapidly after it is released from the active site. For example, while it is in the active site, 3-thiaoctanoyl-SCoA (**4–105**) is converted by the flavoenzyme porcine medium-chain acyl-CoA dehydrogenase (previously Equation 2–114)

octanoyl-SCoA +
oxidized electron-transfer flavoprotein
⇌ *trans*-oct-2-enoyl-SCoA +
reduced electron-transfer flavoprotein

(4–340)

into an *S*-alkylthiocarbonyl cation

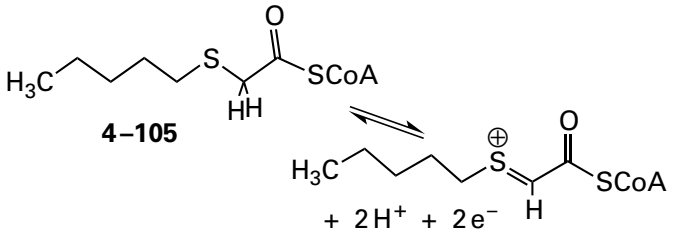

(4–341)

that is electrophilic at its α carbon. The *S*-alkylthiocarbonyl cation is rapidly hydrolyzed when it dissociates from the enzyme. In an exception to the general rule, however, and in spite of the ingenious design of a mechanism-based label electrophilic enough to be scavenged by water, the *S*-alkylthiocarbonyl cation is so electrophilic that only 1 mole of 3-thiaoctanoyl-SCoA for every mole of enzyme is sufficient to produce complete inactivation.[747] Therefore, this reagent is actually a mechanism-based label that does react before dissociating from the active site. The carboxy group of Glutamate 376 is

modified in the labeling, and the carboxy group has been assigned crystallographically to be the catalytic base that removes the hydron from the α carbon of octanoyl-SCoA to produce the enolate in the normal reaction catalyzed by the enzyme.[748]

As was probably the case with inactivation of aspartate transaminase by 2-aminobut-3-enoic acid, another way to avoid the ambiguity between mechanism-based labeling and simple active-site labeling by the product of turnover of the label is to design a **mechanism-based inhibitor that remains bound tightly or even covalently to the active site** after it has been activated.[740] For example, human persulfide dioxygenase uses O_2 to oxidize *S*-sulfanylglutathione, a persulfide between the sulfanyl group of glutathione and hydrogen sulfide, to glutathione and sulfite. The oxidation occurs at a prosthetic iron ion in the active site. During the oxidation, there is an oxidized intermediate in which the sulfino group in *S*-sulfinoglutathione is a tightly bound ligand to the prosthetic Fe^{2+}. This intermediate then undergoes a nucleophilic substitution at the sulfur of the sulfino group, with a molecule of water as the nucleophile and the sulfanyl group of the glutathione as a leaving group. L-γ-Glutamyl-L-homocysteinylglycine, a derivative of glutathione in which L-cysteine is replaced by L-homocysteine, was designed to be a mechanism-based inhibitor. In the inhibitor, the distal sulfur of the reactant *S*-sulfanylglutathione has been replaced with carbon so that hydrolysis at the sulfino group of *S*-sulfinoglutathione cannot occur, and it is locked on the active site inhibiting the enzyme.[749] This inactivation is stoichiometric—one L-γ-glutamyl-L-homocysteinylglycine inactivates one molecule of enzyme—but no catalytic acid–base is modified, only the Fe^{2+}.

Some of the earliest mechanism-based labels were **chloromethyl ketones**, such as 1-chloro-2-oxo-3-(toluenesulfonyl)amino-4-phenylbutane[750]

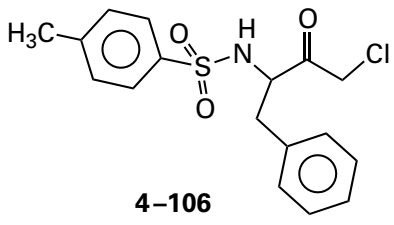

4–106

that vaguely resemble a segment of polypeptide and that inactivate serine endopeptidases, such as chymotrypsin. The serine in the active site of a serine endopeptidase normally forms an intermediate ester from the amido group at the site of cleavage (Figure 3–6) in the first step in hydrolysis of a peptide bond in the polypeptide that is the reactant for the enzyme. The same serine forms the oxyanionic conjugate base of the hemiacetal between the serine in the active site and the 2-carbonyl group of the chloromethyl ketone,[751] locking it onto the active site of the enzyme

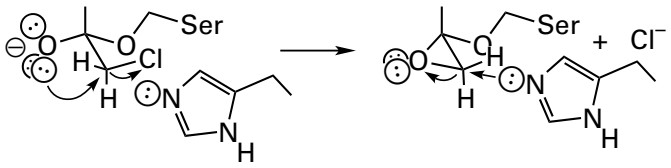

(4–342)

with its anionic oxygen in the oxyanion hole. This oxyanion then displaces the chloro group to form the 2-alkoxyepoxide,[752] and the imidazolyl group of the histidine, which is the catalytic base responsible for removing the hydron from the serine and the hydron from the water hydrolyzing the acyl enzyme, is then alkylated irreversibly by the epoxyether in a concerted nucleophilic substitution.[753,754] These two nucleophilic substitutions proceed with net retention of configuration resulting from two inversions at carbon 1 of the original chloromethyl ketone.[752] The ether between the serine and the epoxide (product in Equation 4–342) locks the electrophile on the active site, so it cannot dissociate.

Another way a mechanism-based label can be locked covalently in the active site is formation of a covalent adduct with a prosthetic pyridoxal 5′-phosphate. A number of **mechanism-based labels for enzymes that use pyridoxal 5′-phosphate** as a prosthetic group have been synthesized. One of these is 2-aminobut-3-enoic acid, which inactivates porcine aspartate transaminase as a true mechanism-based label. Each label is locked onto the active site because it has a primary amino group that forms an external pyridoximine, quinonoid intermediate, or *N*-pyridoxylimine with the prosthetic pyridoxal 5′-phosphate (Figure 2–2 and Equation 4–258). Nonspecific labeling is also avoided because, although the adduct formed between pyridoxal 5′-phosphate and the label is electrophilic, the ultimate product released into the solution, when the electrophilic adduct fails to label a catalytic base, is usually not a strong electrophile.

Ethynylene mechanism-based labels have been used for active sites containing prosthetic pyridoxal 5′-phosphates. For example, 2-amino-4-pentynoic acid[755] is a mechanism-based inhibitor of cystathionine γ-synthase (Equation 4–257) from

S. typhimurium.[756] The inactivation is thought to result from formation of the allene

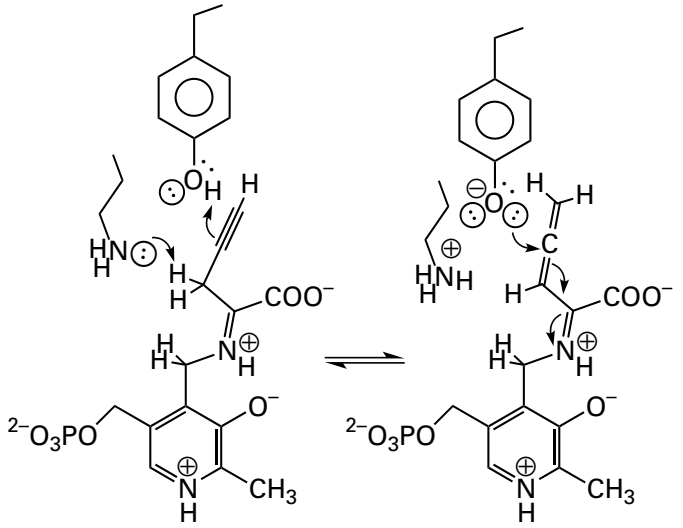

(4–343)

by acid–base reactions analogous to those of the normal mechanism (Equations 4–258 and 4–259). In this case, the allene that is formed, is attached covalently to the pyridoxamine phosphate as the *N*-pyridoxylimine of propadienylglycine. The electrophilic, covalently attached allene can then alkylate one of the catalytic bases within the active site. Even so, 4 moles of 2-aminopent-4-ynoic acid was required to inactivate 1 mole of active sites, and it has been shown that after the mechanism-based inhibitor is converted at the active site, the majority of the reagent (75%) is released as an unidentified product into the solution before it can inactivate the enzyme directly. In the related enzyme human cystathionine γ-lyase (39% identity; 0.5 gap percent)

2-ammoniobut-2-enoate + L-cysteine
$\rightleftharpoons$ L-cystathionine

(4–344)

2-aminopent-4-ynoic acid specifically labels Tyrosine 114 in the active site,[757] which is in the homologous position of Tyrosine 101 in the sequence of amino acids for cystathionine γ-synthase from *S. typhimurium,* and Tyrosine 101 has been assigned crystallographically as the catalytic acid–base that hydronates and dehydronates the γcarbon of the normal substrates in the active site of cystathionine γ-synthase from *N. tabacum* (33% identity; 1.3 gap percent).[537]

(*R*)-2-Amino-3-chlorobut-3-enoate is an irreversible inhibitor of alanine racemase from *E. coli*[758,759]

L-alanine $\rightleftharpoons$ D-alanine (4–345)

It forms an external pyridoximine that is converted in the quinonoid intermediate, following the usual removal of the αhydron catalyzed by the enzyme (Equation 4–258), into an electrophilic allene

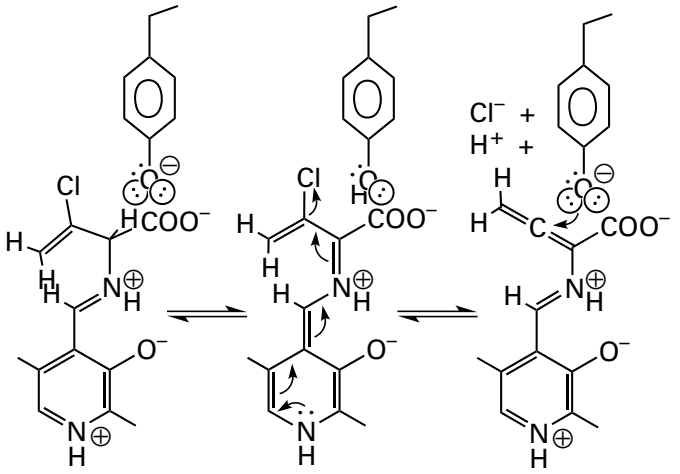

(4–346)

that specifically modifies Tyrosine 253 in the active site of the enzyme.[759] In this instance, the 4-oxidophenyl group of Tyrosine 253 is the catalytic base responsible for removing the αhydron[760] from L-alanine[761] after it has formed an external pyridoximine. The enzyme turns over 2.2 moles of 2-amino-3-chlorobut-3-enoic acid for every mole of enzyme inactivated,[759] but the product of this turnover, 2-aminobuta-2,3-dienoic acid, which would be a strong electrophile, is scavenged by being immediately hydrolyzed to the weak electrophile 2-oxobut-3-enoic acid[746]

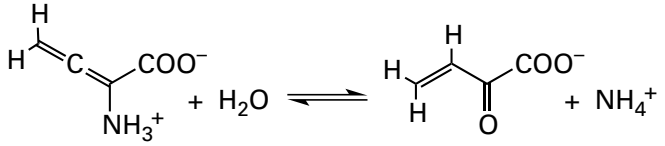

(4–347)

There is an alternate route to the same α,β-allene of an external pyridoximine by using the more paradigmatic α-ethynyl analogue of a substrate for the enzyme.[762]

Two other **electrophilic adducts of pyridoxal phosphate** (**4–107** and **4–108**)

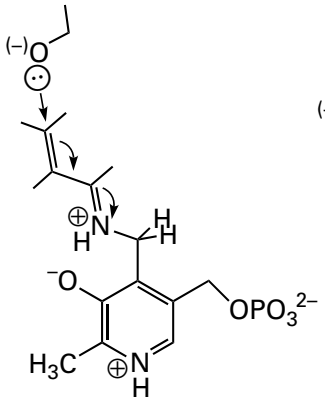

4–107

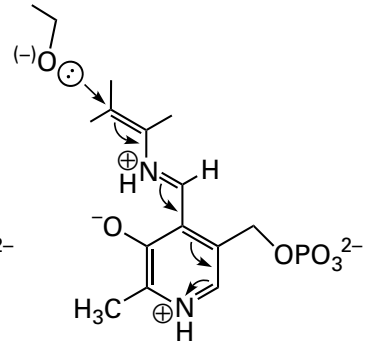

4–108

can be generated by using the mechanism-based label appropriate to the reaction that is performed by a particular enzyme with a prosthetic pyridoxal 5′-phosphate in its active site. The functional groups at the α, β, and γcarbons of these adducts depend upon the mechanism-based inhibitor used, which in turn is determined by the reaction catalyzed by the enzyme.

N-Pyridoxylimine **4–107**, with methyl groups on the α and γcarbons, is the electrophile produced by using 2-aminobut-3-enoic acid as a mechanism-based inhibitor[746] by the usual dehydronation of the αcarbon and the usual hydronation of the aldehydic carbon of the resulting quinonoid intermediate (Equation 4–258). The product released into solution from this adduct is the inert saturated carbonyl compound 2-oxobutanoic acid.[763] 2-Aminobut-3-enoic acid is converted to 2-oxobutanoic acid that dissociates into the solution from the active site of 1-aminocyclopropane-1-carboxylate synthase from *Malus domestica* 500 times more often than the electrophilic adduct **4–107** inactivates the enzyme. The electrophilic adduct specifically alkylates a catalytic base in the active site of the enzyme.[763]

External pyridoximine **4–108**, which places the electrophilic carbon–carbon double bond one atom closer to the pyridoxyl group, is produced by using an analogue of the substrate in which a good leaving group such as a fluorine,[628,642,762,764-766] chlorine,[628,764] acetyl group, or sulfate[644,767] is synthetically placed on a carbon next to the carbon on which the primary amino group is located. For example, α-(difluoromethyl)ornithine (**4–109**)

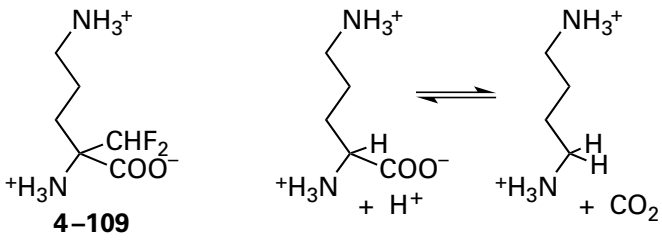

4–109

(4–348)

is a mechanism-based label for ornithine decarboxylase (Equation 4–348) from *R. norvegicus*.[762] Following the decarboxylation of its external pyridoximine to form the quinonoid intermediate (see Equation 4–256), the fluorine on the βcarbon is eliminated in a normal βelimination from a quinonoid intermediate. The result of βelimination is the electrophilic adduct (**4–108** with a 3-aminopropyl group on the αcarbon and fluorine and hydrogen on the βcarbon) of the prosthetic pyridoxal 5′-phosphate in the active site. This particular adduct is the electrophile that modifies Cysteine 360.[643] Cysteine 360 is immediately adjacent (3.5 nm) to what would be the αcarbon in the adduct between the prosthetic pyridoxal 5′-phosphate and 1-aminooxy-3-aminopropane in the crystallographic molecular model of human ornithine decarboxylase (92% identity; 0 gap percent).[768] The product released from the electrophilic adduct **4–108** in this instance is 5-amino-1-fluoro-2-oxopentane, which is only weakly electrophilic.

Unfortunately, however, unlike the example of the successful modification of ornithine decarboxylase with α-(difluoromethyl)ornithine just described, in most instances where the electrophilic external pyridoximine of an enamine, such as **4–108,** is produced by elimination of a good leaving group, it does not react with a catalytic base in the active site. Instead, the respective enamine is released by transimination with the usual lysine (Figure 2–2). The now nucleophilic enamine, before it dissociates from the active site, inserts into the adjacent electrophilic carbon 4′ of the internal lysylpyridoximine to inactivate the enzyme by **labeling the pyridoxal 5′-phosphate**,[628,644,766] which is already known to be a catalytic player. For example, 3-amino-4-fluorocyclopentanecarboxylate is a general active-site label for enzymes that have a prosthetic pyridoxal 5′-phosphate in their active sites. The amino group

forms an external pyridoximine, and the fluorine leaves to produce the external pyridoximine of the enamine, 3-aminocyclopent-3-enylcarboxylate. Upon transimination, carbon 4 of 3-aminocyclopent-3-enylcarboxylate adds irreversibly to carbon 4′ of the internal lysylpyridoximine in an aldol condensation.[769] A covalent modification of carbon 4′ of the internal lysylpyridoximine occurs even when α-(difluoromethyl)ornithine modifies human ornithine aminotransferase[770] rather than ornithine decarboxylase from *R. norvegicus* (91% identity; 0 gap percent).

Even when an enzyme, such as enoyl-CoA hydratase (Equation 4–337), converts a mechanism-based label into a reactive but nonspecific electrophile that dissociates before it can react and is not hydrolyzed, the electrophile, although no longer associated with functional groups mimicking those on a substrate, nevertheless may serendipitously enter another active site and modify a catalytic base because that catalytic base is unusually reactive.

Bases performing catalytic roles in the active sites of enzymes often display exceptional nucleophilicity and react readily with an unexceptional and undirected electrophile that should otherwise react nonspecifically with every nucleophilic amino acid in the protein. Presumably, this results from the fact that these exceptional nucleophiles are found in special environments that are tailored to their assignments in the enzymatic reaction.

When pancreatic ribonuclease (Equation 4–104) was mixed with a molar excess of iodoacetate (8 mol mol^{-1}), the enzymatic activity was lost rapidly. When most of the inactivation had occurred, products were separated chromatographically (Figure 4–41).[771] Aside from some remaining, unalkylated enzyme, only two products were isolated. One was shown to be alkylated only at nitrogen 1 of Histidine 119; the other was shown to be alkylated only at nitrogen 3 of Histidine 12. Neither of the other two histidines in the enzyme, Histidine 48 and Histidine 105, nor any other nucleophilic amino acid, had been alkylated significantly under these circumstances even though iodoacetate is a promiscuous, nonspecific electrophile. These results demonstrate that both Histidine 119 and Histidine 12 in native pancreatic ribonuclease are exceptionally nucleophilic. Furthermore, no bisalkylated product was isolated, and this result suggested that once one of the histidines had reacted, the other became much less nucleophilic. This observation was later explained by the fact that Histidine 12 and Histidine 119 are adjacent to each other in the active site of the enzyme,[151] and

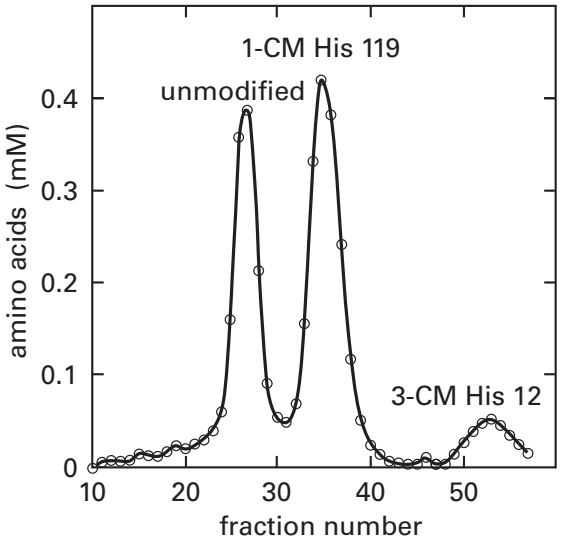

Figure 4–41: Separation of the two monoalkylated derivatives of bovine pancreatic ribonuclease produced by alkylation of the enzyme with iodoacetic acid.[771] A solution containing 16 mM iodoacetic acid and 2 mM pancreatic ribonuclease was prepared at pH 5.5 and 25 °C. After 2 h, the solution was brought to 0.2 M in sodium phosphate at pH 6.5, and it was immediately submitted to cation-exchange chromatography on a column of Amberlite IRC 50 (0.9 × 30 cm) eluted with 0.2 M sodium phosphate, pH 6.5. The several products were located by an alkaline ninhydrin assay that registers the concentration of amino groups in an alkaline hydrolysis of the protein and hence the approximate concentration (millimolar, based on the extinction coefficient for leucine in the assay) of total amino acids in each fraction. The concentration of amino groups (millimolar) is presented as a function of the number of the fraction of eluent collected. Each fraction contained 1 mL. The products were identified as unmodified pancreatic ribonuclease (unmodified), pancreatic ribonuclease carboxymethylated at nitrogen 1 of Histidine 119 (1-CM His 119), and pancreatic ribonuclease carboxymethylated at nitrogen 3 of Histidine 12 (3-CM His 12). The identification was performed by tryptic digestion of each component and subsequent identification of carboxymethylated peptides by chromatography.

steric hindrance prevents alkylation of one of them after the other has become alkylated. The product alkylated at Histidine 119 was completely inactive (<1% activity remaining), but the product alkylated at Histidine 12, although significantly inhibited, retained 7% of the enzymatic activity of native pancreatic ribonuclease. At the time, this result suggested that Histidine 12 might not be involved in the mechanism of the reaction as an essential catalytic acid–base,[771] and this suggestion was later confirmed crystallographically.[152]

The disadvantage of using **reagents for the general modification of particular types of amino acids** to identify amino acids within an active site is that the electrophile has **unbiased access to all the amino acids on the surface of the protein** as well as

those in the active site, rather than being carried into the active site and juxtaposed to a particular amino acid or being created within the active site during turnover. Nevertheless, various reagents for the general modification of particular types of amino acids have been used to identify exceptionally reactive amino acids, the modification of which inactivates the respective enzyme. For example, when bovine phospholipase A_2 was methylated with the reactive electrophile methyl 4-toluenesulfonate, a product could be isolated chromatographically that had been N-methylated exclusively at Histidine 48 and that retained only 1% of the activity of the original enzyme.[772] Histidine 48 is the catalytic base that removes a hydron from the molecule of water that hydrolyzes the ester within the glycerolipid that is a reactant for the enzyme.[773]

When glyceraldehyde-3-phosphate dehydrogenase (phosphorylating) (previously Equation 3–32)

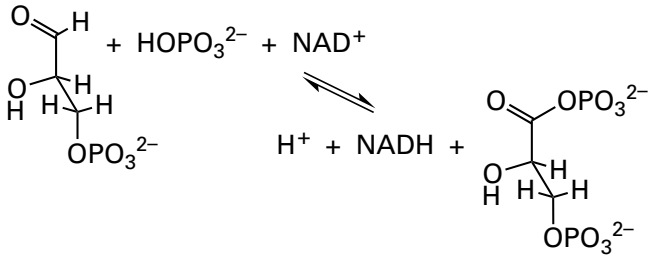

(4–349)

from *O. cuniculus* was mixed with a concentration of [^{14}C]iodoacetic acid equivalent to the total concentration of cysteine in the protein, the enzymatic activity was rapidly lost. After the inactivation was complete and the reaction was terminated, the protein was digested with trypsin. Only one radioactive tryptic peptide was produced in significant yield by the digestion, and it could be shown that the sulfido group of only Cysteine 149, of the four cysteines present in the protein, had been alkylated significantly by iodoacetic acid.[774] Cysteine 149 is the cysteine that forms the hemithioacetal with glyceraldehyde 3-phosphate during the normal enzymatic reaction,[775] and its exceptional nucleophilicity, as demonstrated by its apparently exclusive reaction with iodoacetic acid, may be essential for this role in the mechanism. If so, this essentiality would be the reason for the specificity of the alkylation in this instance.

There are other examples of inactivations caused by the **exclusive modification of particularly nucleophilic amino acids** in active sites. 1,3-Dibromoacetone, a bifunctional alkylating agent, crosslinks Cysteine 25 and Histidine 159 in the active site[776] of papain to inactivate the enzyme.[777,778] Dicyclohexylcarbodiimide exclusively and selectively crosslinks Aspartate 184 and Lysine 72 within the active site of porcine non-specific serine/threonine protein kinase to inactivate the enzyme.[779]

The modification of a single arginine in a subunit of bovine ornithine carbamoyltransferase by butanedione led to inactivation of the enzyme,[780] and the exclusive arylation of one exceptionally reactive lysine, the apparent pK_a of which is 8.0, with trinitrobenzenesulfonate led to inactivation of bovine isocitrate dehydrogenase (NAD^+).[781] Addition of the respective substrates to the solution prevents both of these modifications and the accompanying inactivation of the respective enzyme. Such **protection by a substrate or inhibitor** for the enzyme against the modification of a particular amino acid by a nonspecific electrophile is often the only criterion suggesting that the modification is labeling a nucleophile in the active site.

It is usually unclear why a particular amino acid in a protein is extraordinarily reactive relative to other amino acids of the same type in the same protein. One possibility already mentioned is that the enzymatic reaction requires that the nucleophile be particularly reactive. Even though the nucleophile in the active site is not particularly reactive and the reagent bears no resemblance to a substrate or ligand, it nevertheless may be guided by the high concentration of donors and acceptors for hydrogen bonds within an active site to bind, preferentially but adventitiously, adjacent to the nucleophile with which it reacts. Other acid–bases clustered together in an active site in the vicinity of the nucleophile that is modified may act as catalytic acid–bases to catalyze the modification reaction itself even though the electrophilic reagent does not associate with the active site and modifies the nucleophile in a random encounter complex.

There is also the broader question of **why the nonspecific modification of a particularly reactive nucleophilic amino acid causes the inactivation of an enzyme**. So far, examples of modifications of catalytic acid–bases that produce inactivation have been presented, but there are other reasons for the inactivation caused by a nonspecific reagent.

Cyclohexane-1,2-dione[659] and 2,3-dioxobutane[657,658] have been shown to react with the guanidinio group on L-arginine to produce the bicyclic adduct **4–110**[656]

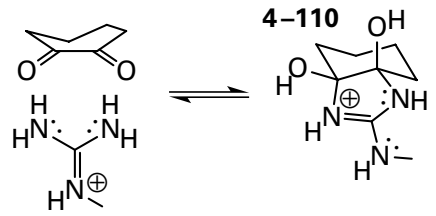

(4–350)

This adduct is formed reversibly but can be stabilized by adding borate,[658] which forms a borocycle with the vicinal hydroxy groups in the adduct. 1-Phenyl-2,3-dioxobutane is another vicinal dione that modifies arginines[660-662] and forms a stable 4-hydroxy-5-phenylimidazol-2-yl group

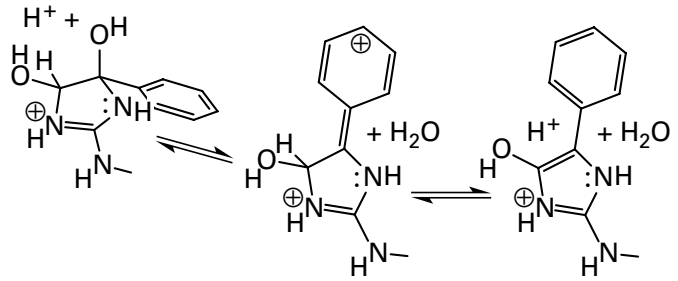

(4–351)

(+116 unified atomic mass units) with the arginine[782] in a dehydration that is not possible with a fully saturated adduct such as **4–110**. 1-Phenyl-2,3-dioxobutane has been widely used to modify arginines in active sites. A 4-bromo-2,3-dioxobutyl group can be attached to nucleophilic atoms in various substrates and ligands by using 1,4-dibromo-2,3-dioxobutane.[665,666] The bromine in the 4-bromo-2,3-dioxobutyl group stabilizes the adduct of the vicinal dione with the guanidinio group enough that the adduct with an arginine in an active site survives digestion and chromatography.[663,664]

When fructose-bisphosphate aldolase (Equation 4–210 and Figure 4–36) from *O. cuniculus* was mixed with cyclohexane-1,2-dione in sodium borate buffer, the enzymatic activity was rapidly lost.[783] When glycerone phosphate or fructose 1,6-bisphosphate was present, however, no activity was lost. During this modification of the enzyme, less than 2 moles of cyclohexane-1,2-dione was incorporated for each mole of the polypeptide comprising the enzyme even though cyclohexane-1,2-dione is not an active-site label. Only one tryptic peptide in a digest of the enzyme modified with [^{14}C]cyclohexane-1,2-dione incorporated radioactivity to a significant level (Figure 4–42A),[783] and the incorporation into this peptide was prevented by addition of fructose 1,6-bisphosphate (Figure 4–42B). The remainder of

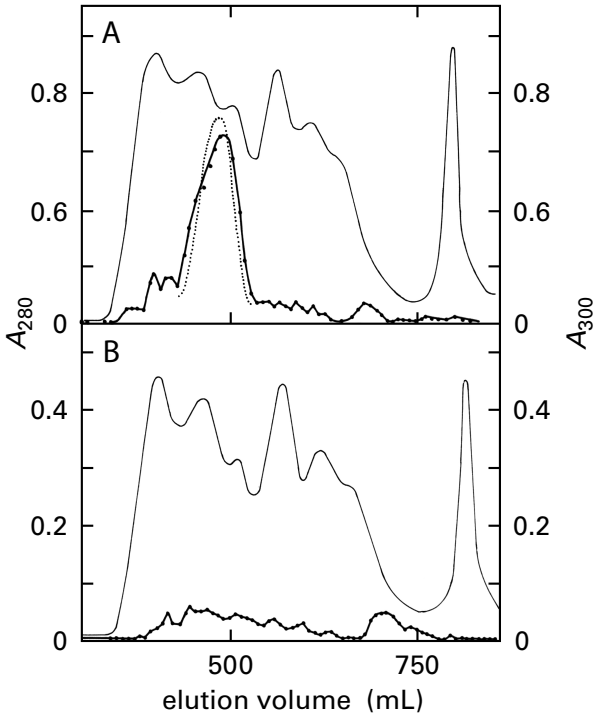

Figure 4–42: Distribution of N^{ω},N^{ω}-(1,2-dihydroxycyclohexyl)-arginine side chains among the tryptic peptides of rabbit muscle fructose-bisphosphate aldolase inactivated with cyclohexane-1,2-dione.[783] Two solutions (60 mL) containing 50 mM cyclohexane-1,2-dione and 0.1 M sodium borate at pH 8.0 and 25 °C were prepared. One of the two solutions contained 5 mM fructose 1,6-bisphosphate to protect the active site. The inactivation was initiated by adding fructose-bisphosphate aldolase (0.2 mM final concentration in protomers) and was allowed to proceed until the residual enzymatic activity in the unprotected sample was 10%, and in the protected sample, 90%. The pH of the two solutions was dropped to 4, and both were dialyzed into deionized water and submitted to performic acid oxidation. The protein was then submitted to digestion by trypsin. The resulting tryptic peptides were submitted to chromatography by size exclusion on Sephadex G-25 in 30% acetic acid. The absorbance of the effluent at 280 nm was monitored continuously. Samples were removed from the various fractions to assay for cyclohexane-1,2-dione released from modified arginines by treatment at alkaline pH. The released cyclohexane-1,2-dione in samples exposed to alkaline pH was assayed by its reaction with (trimethylamino)acetohydrazide, which forms an adduct with vicinal diones that absorbs at 300 nm. The absorbance at 280 nm (thin line) and the absorbance of the adduct at 300 nm (thick line or dashed line) are plotted as a function of the elution volume (milliliters) from the chromatographic column (3 × 140 cm). (**A**) Unprotected product. (**B**) Product from enzyme protected with 5 mM fructose 1,6-bisphosphate.

the incorporation was spread over a number of other peptides indiscriminately. The selectively modified peptide was isolated and sequenced, and from these results it could be concluded that modification of Arginine 148 had inactivated the enzyme. Only Arginine 148, of the 15 arginines present in the enzyme, reacted appreciably with cyclohexane-

1,2-dione under these circumstances even though cyclohexane-1,2-dione is an uncharged, nonspecific reagent for arginines in general.

In the crystallographic molecular model of the complex between fructose-bisphosphate aldolase from *O. cuniculus* and fructose 1,6-bisphosphate, Arginine 148 is near the 6-phospho group of the substrate, well away from the catalytic center of the active site in the immediate vicinity of carbons 3 and 4, and forms a hydrogen bond to a molecule of water that in turn forms a hydrogen bond to the 6-phospho group.[784] Consequently, the arginine is neither a catalytic acid–base nor directly associated with a bound substrate. Nevertheless, modification of Arginine 148 by a bulky cyclohexane-1,2-dione and the accompanying borocycle should **sterically hinder the association of substrates** fructose 1,6-bisphosphate and D-glyceraldehyde 3-phosphate with the active site and prevent catalysis. Conversely, association of either of these substrates should prevent the modification of Arginine 148 by cyclohexane-1,2-dione.

A nonspecific electrophile can also **sterically hinder the access of substrates to an active site** upon its incorporation. For example, at the entrance to the active site of *S*-formylglutathione hydrolase from *A. thaliana*, there is a cysteine the modification of which sterically blocks access to the active site.[785]

There are other instances in which the **steric bulk of a nonspecific electrophile** affects the outcome of inactivation of an enzyme. The sulfido group of Cysteine 565 in native bovine aconitate hydratase is exceptionally nucleophilic and can be modified exclusively with several electrophiles.[786,787] When its sulfanyl group is alkylated with phenacyl bromide, a bulky electrophile, enzymatic activity is completely abolished, but when it is simply methylated, one of the least bulky alterations possible, enzymatic activity is inhibited by only 50%.[788] In the crystallographic molecular model of a complex between a mutant of porcine aconitate hydratase (98% identity; 0 gap percent) and isocitrate,[789] Cysteine 565 is too far away (1.6 nm) from the nearest atom of isocitrate to have a direct steric effect on the enzymatic reaction, as was the case in the modification of fructose-bisphosphate aldolase by cyclohexane-1,2-dione. It is more likely that the bulky phenacyl group **hinders a conformational change**, such as the closing of the active site around one substrate for the enzyme, and that that conformational change is required for catalysis. The small methyl group is not bulky enough to affect the conformational change. A similar difference between complete inactivation upon alkylation with a bulky group and only partial inactivation upon alkylation with a methyl group is observed for modification of the sulfido group of Cysteine 16 in phosphoribulokinase from *S. oleracea*[790]

As the result with aconitate hydratase illustrates, **the question of whether or not an exceptionally nucleophilic amino acid is located within the active site**, even though it inactivates the enzyme, is one that cannot be settled in experiments that only examine the kinetics of inactivation and identify the amino acid modified. Usually, in experiments of this type, only two observations are available. First, the enzymatic activity is irreversibly and completely, or almost completely, inhibited when only 1–2 moles of reagent have become incorporated for every mole of active sites. Second, when a substrate, inhibitor, or ligand is present, the enzyme is protected against inactivation, and incorporation of the reagent is blocked.

Regarding the first observation, there are ways an enzyme can be inactivated other than through modification at the active site. The alkylation of Cysteine 565 in aconitate hydratase probably prevents a conformational change required for enzymatic activity. The modification of Cysteine 45 in porcine glutathione transferase produces an inactive enzyme[791,792] even though its sulfanyl group is 1.9 nm from the active site.[793] In the conformation of the enzyme induced by the association of substrates, Cysteine 45 is buried in a hydrophobic pocket and inaccessible to the solution. If it were modified with a bulky functional group, it would be sterically unable to enter this pocket, and the conformational change required for the active site to close around substrates would be prevented.

Regarding the second observation, the protection of a particular amino acid in an enzyme by a substrate or inhibitor against modification by an electrophile does not prove that the amino acid is located within the active site. For example, modification of the carboxy group of Aspartate 176 in glucan 1,4-α-glucosidase from *Aspergillus awamori* by 1-ethyl-3-(4-azonia-4,4-dimethylpentyl)carbodiimide is prevented by association of the inhibitor acarbose with the active site,[794] even though its carboxy group is 0.9 nm from the nearest atom in this particular inhibitor.[795] The reason that the enzyme is protected from reaction with the carbodiimide is that this carboxy group becomes incorporated into a network of hydrogen bonds created by binding of the inhibitor to the active site. When tryptophan synthase from *E. coli* was irreversibly inactivated with 1-phenyl-2,3-dioxobutane, 1 mole of arginine was modified for each mole of inactive enzyme, and the

modification responsible for the inhibition occurred at Arginine 148 in the β subunit.[796] Because the enzyme could be protected from irreversible inhibition by pyridoxal phosphate and L-serine but not by pyridoxal phosphate alone, and because 1-phenyl-2,3-dioxobutane was a competitive inhibitor with respect to serine in the normal enzymatic reaction, it was concluded that serine binds to Arginine 148 within the active site during catalysis. In the crystallographic molecular model of the β_2 dimer of tryptophan synthase in complex with pyridoxal 5-phosphate, however, the guanidinio group of Arginine 148 is 1.5 nm away from the 4′ carbon of the pyridoxal phosphate[797] Consequently, it cannot be a ligand to the serine.

It is usually difficult to decide whether the residual enzymatic activity present after modification of an enzyme represents the modified enzyme itself or enzyme that is as yet unmodified. This distinction is important because if the actually modified enzyme still possesses significant enzymatic activity, then the amino acid that has been modified must not be essential for catalysis. When human carbonic anhydrase 1 was alkylated with iodoacetate, Histidine 200 was modified to produce an enzyme that, depending on the pH, had 3–15% the catalytic constant of the native enzyme.[798] From these results, it was concluded that Histidine 200 is not essential for enzymatic activity, even though its alkylation does inhibit the enzyme extensively. Histidine 200, however, as in the case of Histidine 12 in pancreatic ribonuclease, is in the active site of the enzyme,[799] and its imidazolyl group is probably catalytic. It is possible that alkylation of its π nitrogen, which is directed away from the site of catalysis, would still permit its τ nitrogen to participate in catalysis, albeit less effectively.

When 2-nitro-5-(thiocyanato)benzoate was used to inactivate 3-oxoacid-CoA transferase, it produced two products, one enzymatically inactive and the other still enzymatically active. It was demonstrated that in each product the sulfido group of the same cysteine had been modified. In the enzymatically active product, however, the cysteine was cyanylated, while in the enzymatically inactive product, it had been oxidized by formation of a mixed disulfide with the 2-nitro-5-thiobenzoate that is a product of cyanylation. In the latter instance, in which the mixed disulfide is far bulkier than the cyanylated sulfanyl group, the inactivation was a steric effect. If only the enzymatically inactive product had been obtained, it might have been concluded, incorrectly, that this cysteine was essential for enzymatic activity.[800]

The strategy of active-site labeling and mechanism-based labeling, in which a reagent is designed to associate specifically with an active site and identify a particular catalytic base–acid responsible for removal or addition of a particular hydron, can be expanded to encompass reagents that are intended simply to identify amino acids in the vicinity of an active site or a site for the binding of a ligand by specifically associating with an active site or binding site and bringing a covalently attached electrophile into its vicinity even though the amino acid or amino acids modified by that electrophile are not catalytic functional groups.

An affinity label is a compound that contains a reactive center and that is designed to resemble the substrate of an enzyme or ligand for a protein so closely that it will bind specifically to the active site or binding site, and while it is bound the reactive center will covalently modify an amino acid in or near the site. If the reagent is designed with the intention of placing the electrophile immediately adjacent to a catalytic acid–base in the normal mechanism of an enzymatic reaction, the affinity label is an active-site label. Often, however, a reagent intended to be an active-site label modifies a nucleophilic side chain that is not involved in the catalytic mechanism and is only near the location at which catalysis occurs, in which case the active-site label is in fact a more general affinity label.[801] In many experiments, however, information about functional groups in the enzymatic mechanism is irrelevant; the actual intention of the labeling is the identification of any amino acid in the vicinity of the active site or the binding site for a particular ligand or, in many cases, simply the identification of the protein to which the ligand binds.

This difference in intent, in part, distinguishes more general affinity labeling from specific active-site labeling. For example, the electrophilic *N,N*-dimethyl-2-phenylaziridium cation

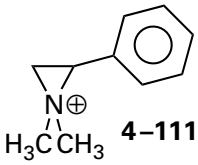

4–111

was used as an affinity label for acetylcholinesterase from *Torpedo californica*. Rather than labeling a catalytic base in the active site that was responsible

for the hydrolysis of acetylcholine, the intention was to modify the amino acids that form the **pocket for the quaternary ammonio group** in acetylcholine (previously Equation 3–341)

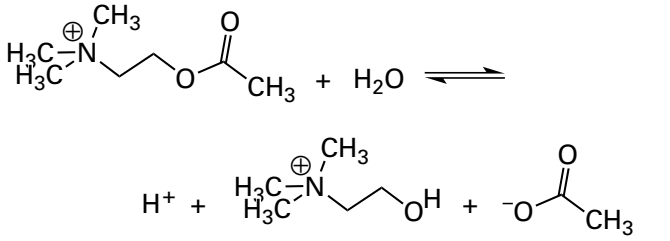

(4–352)

The aziridium participated in an electrophilic aromatic substitution of the indolinyl group of Tryptophan 84,[653] which is one of the three aromatic amino acids that form the pocket for the quaternary ammonium cation,[802] which associates through π–cation interactions.

In many instances, the intended target of the affinity labeling is not an active site at all but the **site for binding a ligand that is not catalytically altered** by the enzyme or the site for binding a ligand on a nonenzymatic protein. For example, adenosine 5′-*O*-[*S*-4-bromo-2,3-dioxobutyl)thiophosphate

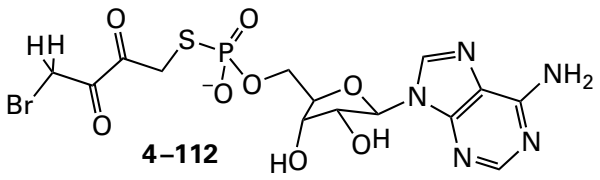

4–112

was used as a label for the modification of one side chain forming the binding site for ADP^{3-}, an activator of bovine glutamate dehydrogenase [$NAD(P)^+$] that is not catalytically involved in the enzymatic oxidation–reduction. It covalently modifies Arginine 459 in the enzyme,[664] which forms a hydrogen bond to the β-phosphate of ADP^{3-} in a crystallographic molecular model[803] of the complex between the enzyme and ADP^{3-}. 8-Azidoadenosine triphosphate

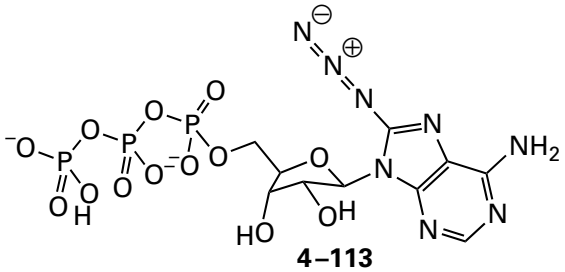

4–113

was used as an affinity label for the noncatalytic binding site for ATP^{4-} on actin from *O. cuniculus*. It was photolytically converted to the nitrene while the label was bound in the site on this nonenzymatic protein, and the electrophilic nitrene modified Lysine 336,[804] which is immediately adjacent to carbon 8 of ATP^{4-} in the crystallographic molecular model[805] of the complex between actin and ATP^{4-}.

Usually, a portion of an affinity label is designed to bind to the site, and a different portion, often quite distinct or even quite distant from the portion that binds, provides the electrophile, diradical, or some other group capable of modifying amino acids in the protein. If the designer is lucky, association of the portion of the affinity label responsible for specificity will position the portion performing the covalent modification close enough to a suitable side chain. For example, ribulose-bisphosphate carboxylase (previously Equation 3–424)

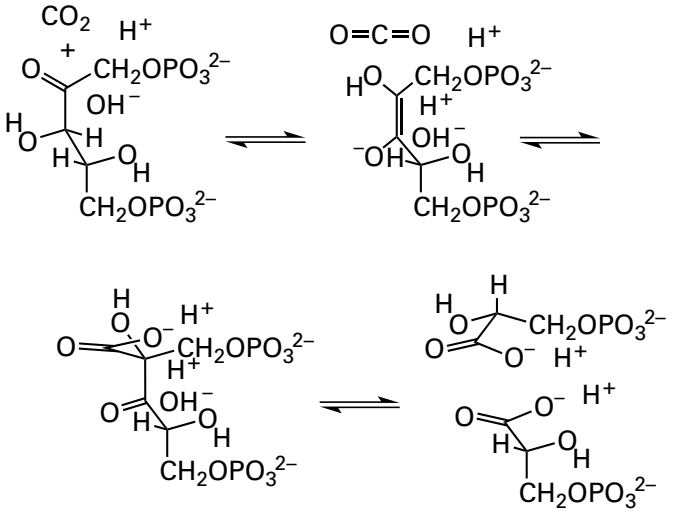

(4–353)

catalyzes the carboxylation of the enediolate of D-ribulose 1,5-bisphosphate.[806,807] Although there should be two or more catalytic base–acids involved in a Claisen condensation, none should be in the vicinity of the electrophilic carbon of *N*-bromoacetyl-2-amino-2-deoxypentitol 1,5-bisphosphate

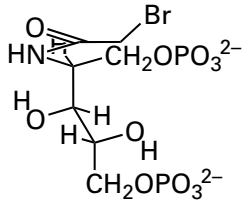

4–114

when it binds to the active site of the enzyme in place of the substrate. Nevertheless, *N*-bromoacetyl-2-amino-2-deoxypentitol 1,5-bisphosphate irreversibly inactivates ribulose-bisphosphate carboxylase from *R. rubrum* in a reaction the properties of which meet all the criteria for specific labeling within the active site.[808] It was shown that the covalently modified amino acid was methionine

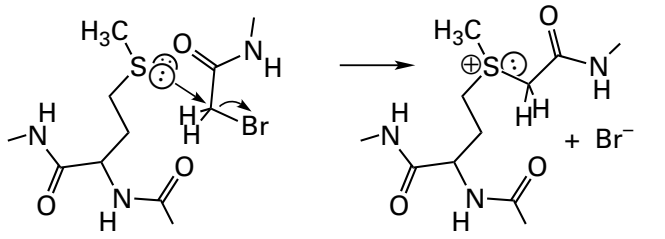

(4–354)

Since methionine cannot act as a catalytic acid or base or as an acceptor or donor for a hydrogen bond, the conclusion reached from these observations is that this methionine is, by chance, **one of the amino acids within or immediately adjacent to the active site**. In the sequence of amino acids for ribulose-bisphosphate carboxylase from *R. rubrum*, Methionine 115 takes the place of Phenylalanine 125 in the enzyme (Figure 3–53) from *S. oleracea* (27% identity; 2.5 gap percent). In the crystallographic molecular model of the enzyme from *R. rubrum* in a complex with D-ribulose 1,5-bisphosphate,[809] Methionine 115 is the closest methionine and in the same location relative to D-ribulose 1,5-bisphosphate as it is in the active site of the enzyme from *S. oleracea*. There are no atoms from the protein between it and D-ribulose 1,5-bisphosphate, but its sulfur is 1.1 nm from carbon 2, which seems a stretch.

An affinity label for creatine kinase, *N*-(2,3-epoxypropyl)-*N*-amidinoglycine (**4–115**)[810]

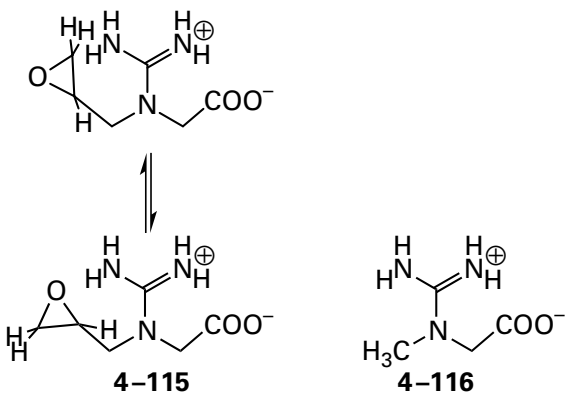

4–115 **4–116**

tacks an epoxide onto the *N*-methyl group in the substrate creatine (**4–116**). This point of attachment places the electrophilic distal carbon of the epoxide at what seems to be a significant remove from the site of phosphorylation, which occurs at one of the distal amidino nitrogens of the creatine. This fact suggested that the reagent was modifying an amino acid only in the vicinity of the active site. Cysteine 282 in creatine kinase from *O. cuniculus* is the site of modification.[811] In the crystallographic molecular model between creatine kinase from *O. cuniculus* and creatine, nitrate, and $MgADP^-$, the sulfur of Cysteine 282 is 0.56 nm from any of the atoms involved in the nucleophilic substitution at phosphorus,[812] which would be consistent with this conclusion that it is not a catalytic acid–base.

In this crystallographic molecular model of the analogue for the transition state (see Figure 3–41), however, the sulfido group of Cysteine 282 is only 0.32 nm from the other distal nitrogen in creatine, the one that is uninvolved directly in the reactions, so it could be increasing the nucleophilicity of the distal nitrogen that is involved. The orientation of the sulfido group of Cysteine 282 with respect to the distal nitrogen is not proper for a hydrogen bond, and the sulfido group participates in three proper hydrogen bonds with an amido nitrogen–hydrogen from the polypeptide, the hydroxy group of a serine, and a molecule of water. Nevertheless, the sulfido group of Cysteine 282, by electron repulsion, could shift electron density in the π molecular orbital system of the guanidinio group from the lobe over the nitrogen adjacent to it to the lobe on the nitrogen that is phosphorylated and make that lobe a more nucleophilic participant in the nucleophilic substitution at phosphorus catalyzed by the enzyme.[813] From the orientation of the participants in the crystallographic molecular model of the complex between creatine kinase from *O. cuniculus* and creatine, nitrate, and $MgADP^-$ and the complex between the related (46% identity; 2 gap percent) arginine kinase from *Limulus polyphemus* and L-arginine, $MgADP^-$, and nitrate (Figure 3–41), it can be seen that this lobe in the π molecular orbital system of the guanidinio group is the nucleophile, not a localized lone pair of electrons in the plane of the conjugate base of the guanidinio group. In the active site of arginine kinase from *L. polyphemus*, the homologous sulfido group on the homologous cysteine is in a similar location.[814]

As was the case with *N*-bromoacetyl-2-amino-2-deoxypentitol 1,5-bisphosphate, the methyl group on creatine to which the epoxide is attached seems too distant (0.61 nm) in the molecular model from the sulfido group of Cysteine 282 that is modified,

and it would be positioned on the opposite side of the guanidinio group, which would lie between it and the sulfido group. There is a rotational isomer (**4–115**) that places the electrophilic carbon immediately adjacent to one of the distal nitrogens, but according to the molecular model, the nitrogen is the nucleophile in the nucleophilic substitution at phosphorus. The labeling was performed in the absence of adenine nucleotide, and the combination of $MgADP^-$ and nitrate, in the absence of creatine, prevents the modification.[810] For both of these reasons, it seems reasonable to assume that the complex between the active site and *N*-(2,3-epoxy-propyl)-*N*-amidinoglycine that is responsible for the modification is the one in which the *N*-methyl-guanidinio group is flipped over relative to its competent orientation in the crystallographic molecular model, in part because this flipped disposition would be precluded when $MgATP^{2-}$ and nitrate are bound, and hence their presence should prevent the modification.

It is possible to perform affinity labeling with **a reagent attached covalently within the active site**. A diazoacetyl group was transesterified onto Serine 195 in chymotrypsin to form a stable acyl intermediate[815] by taking advantage of the first step in the normal enzymatic reaction (Figure 3–6)

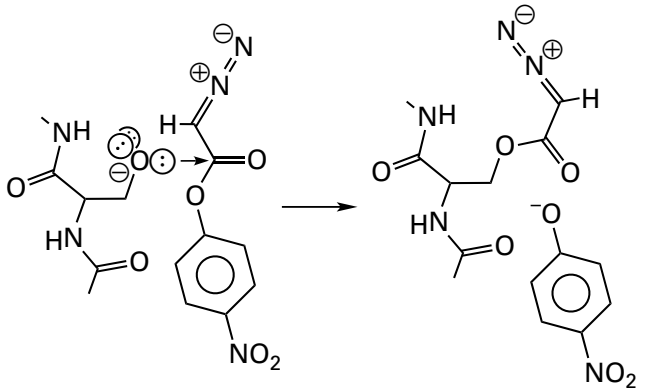

(4–355)

Upon photolysis, a carbene was formed that inserted at random into any one of several oxygen–hydrogen bonds of amino acids surrounding the active site.

8-Azidoadenosine triphosphate (**4–113**) and 4-nitrophenyl diazoacetate (Equation 4–355) are examples of a large class of **photoaffinity labels** that have been widely used to perform affinity labeling. These photoaffinity labels usually contain either a diazoketone or a diazo ester[816] or an azido group.[817] When a diazoketone or diazo ester is photolyzed, a **carbene** is formed

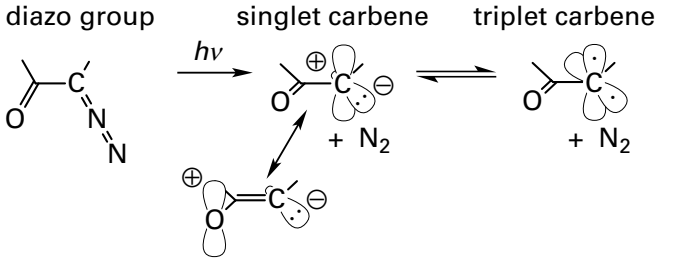

(4–356)

and when an azido group is photolyzed, a **nitrene** is formed

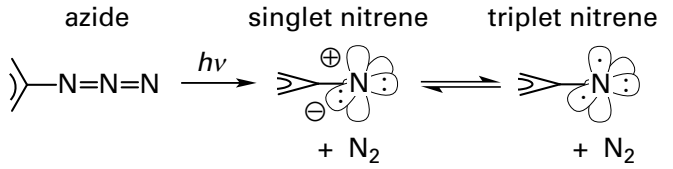

(4–357)

Both carbenes and nitrenes are dramatically electron-deficient. A carbene has only six valence electrons around the single carbon, and a nitrene has only six valence electrons around the single nitrogen.

A carbene or nitrene can react either as a **singlet electrophile**, in which the two nonbonding electrons occupy only one atomic orbital on carbon or nitrogen, or as a **triplet diradical**, in which each of two nonbonding σ atomic orbitals on carbon or nitrogen, respectively, are occupied by one of two unpaired electrons. The singlet state of a carbene or a nitrene has a vacant atomic orbital at carbon or nitrogen, respectively, and consequently it is a strong electrophile that can form a covalent bond with a nucleophilic atom that has a lone pair of electrons in a simple nucleophilic addition, followed by hydronation of the resulting carbanion or azanide. The triplet diradical is capable of abstracting a hydrogen from an atom in its vicinity to produce a radical at that atom and a single radical on the former carbon of the carbene or nitrogen of the nitrene, and then the two adjacent radicals can colligate to form a covalent bond between the carbon or nitrogen of the carbene or nitrene and the atom from which hydrogen was abstracted. Because the reactants in both photochemical dissociations—the diazoketone or diazoacetyl group and the azido group and their respective photochemically excited states—are singlets and molecular nitrogen is a singlet, the initial products of the photolysis are the respective singlets. Each singlet then equilibrates (Equations 4–356 and 4–357) with the triplet state, which is usually the more stable state, by intersystem crossing.

Table 4–1: Affinity Labels

enzyme or protein	substrate or ligand mimicked	affinity label
pyruvate kinase[823]	ADP^{3-}	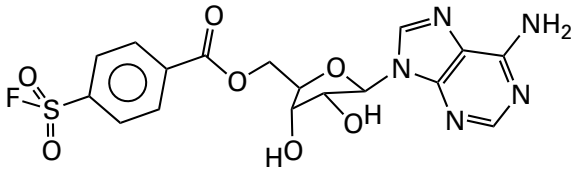
tryptophan synthase[824]	tryptophan	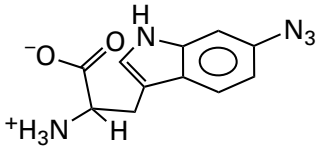
cytochrome bo_3 ubiquinol oxidase[825]	ubiquinone	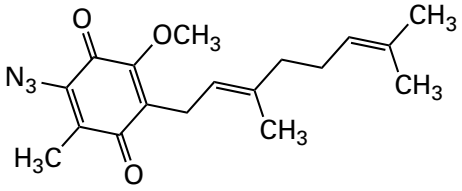
acyl-CoA oxidase[826]	stearoyl-SCoA	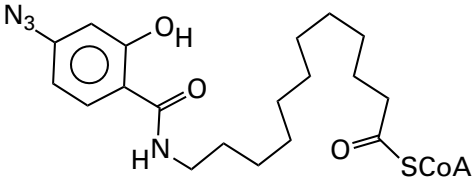
procollagen-proline 3-dioxygenase[827]	procollagen	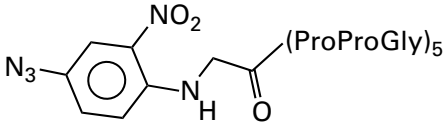
immunoglobulin G anti-estradiol[828]	estradiol	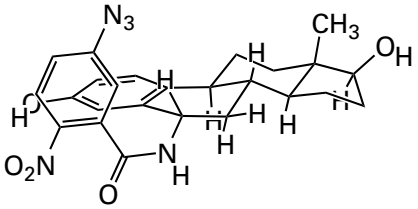
β-adrenergic receptor [829]	benzylpindolol	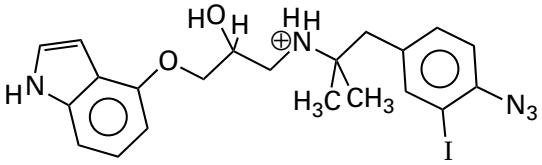

Although there is an example of insertion of a carbene into a carbon–hydrogen bond, albeit at low yield,[818] the majority of the products from modification within active sites or binding sites in proteins by either carbenes[816] or nitrenes[804,817,819,820] are consistent with nucleophilic addition of an oxygen, nitrogen, or sulfur to the respective singlet electrophile. This regioselectivity is observed even when the vast majority of the covalent bonds surrounding a nitrene or carbene are carbon–hydrogen bonds.[821,822]

There are many examples of the use of affinity labels (Table 4–1).[665,823-829] Rather than being used to identify a particular amino acid or set of amino acids in a protein, affinity labels have frequently been **used to identify a particular protein or region within the sequence of amino acids for a protein**[830,831] that contains or comprises the active site or binding site of interest. Although functional groups capable of alkylation, acylation, or sulfonylation are often used as the electrophiles, the most common choice, when the affinity label is not being used as an active-site label, has been an aryl azide (Equation 4–357). This choice increases the chance that a sufficiently reactive nucleophile will be encountered by the electrophile. Nevertheless, it is still necessary that a nucleophile, however unreactive, be accessible to the nitrene resulting from the photolysis. To increase the probability of this juxtaposition, the aryl azide can be attached flexibly to the portion of the reagent conferring specificity so that it can reach several side chains in the vicinity of the active site or binding site, as in the aryl azide

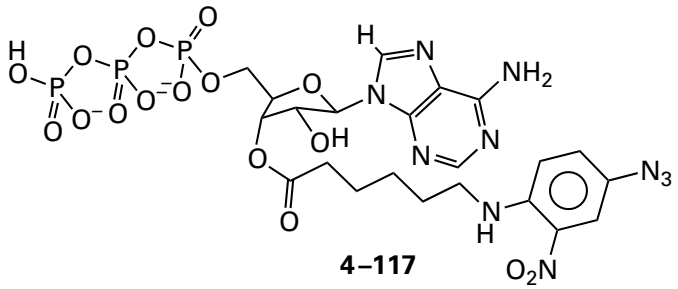

4–117

that was used to modify amino acids surrounding the active site of myosin ATPase (Equation 4–288).[832]

A few of the natural substrates and ligands for enzymes and proteins are themselves photochemically active, and upon photolysis they are converted into products that can covalently modify a site to which they are bound. For example, magnesium thymidine triphosphate modifies Histidine 881 in DNA-directed DNA polymerase I from *E. coli* when it is photolyzed with ultraviolet light while bound at the catalytic site for deoxynucleoside triphosphates on the enzyme.[833]

Derivatives of large nucleic acids that position a group capable of modifying amino acids in a protein with which the nucleic acid associates have been used as affinity labels. For example, the precursor to $tRNA^{Phe}$ into which either 4-thiouridine or 5-bromouridine had been incorporated at each position occupied by uridine was used to modify photolytically RNA ligase (ATP) from *S. cerevisiae* and identify all the uracils in $tRNA^{Phe}$ that come in contact with the enzyme.[834] A 1-pyrrolidinyl ester, which is able to modify the amino group on a lysine, was attached in turn to four different cytosines in $tRNA^{fMet}$. In each instance, the 1-pyrrolidinyl ester was at the end of a long chain of 17 atoms, the bonds between which are free to rotate, permitting the electrophile to survey a wide area on the adjacent surface of the enzyme. Each affinity label modified a different lysine in methionine—tRNA ligase from *E. coli*, and the tryptic peptides containing each modification were isolated and sequenced to identify each site of modification in the sequence of amino acids in the enzyme.[835]

The ribose at the 3′ end of a transfer RNA, which is the only ribosyl group in the nucleic acid with vicinal hydroxy groups, can be oxidized exclusively with periodate, and a dialdehyde is produced from the ribose. This dialdehyde is able to form an imine with the amino group of a lysine in a protein, which can then be reduced with cyanoborohydride.[836] Oxidized $tRNA^{Ala}$ specifically modifies Lysine 73 in alanine—tRNA ligase from *E. coli*.[837] In the crystallographic molecular model of the complex between alanine—tRNA ligase from *Archaeoglobus fulgidus* (24% identity; 2.3 gap percent) and $tRNA^{Ala}$, the leucine that occupies the same position in the aligned sequences as Lysine 73 is immediately adjacent to the 3′ end of the tRNA.[838] It obviously is not a catalytic acid–base, and since Lysine 73 is not conserved, it also is probably not a catalytic acid–base.

Suggested Reading

Holland, P. C., Clark, M. G., and Bloxham, D. P. (1973) Inactivation of pig heart thiolase by 3-butynoyl coenzyme A, 3-pentynoyl coenzyme A, and 4-bromocrotonyl coenzyme A, *Biochemistry 12*, 3309–3315. https://doi.org/10.1021/bi00741a024

Toney, M. D., and Kirsch, J. F. (1993) Lysine 258 in aspartate aminotransferase: Enforcer of the Circe effect for amino acid substrates and general-base catalyst for the 1,3-prototropic shift, *Biochemistry 32*, 1471–1479. https://doi.org/10.1021/bi00057a010

Kreutter, K., Steinmetz, A. C. U., Liang, T.-C., Prorok, M., Abeles, R. H., and Ringe, D. (1994) Three-dimensional structure of chymotrypsin inactivated with (2*S*)-*N*-acetyl-L-alanyl-L-phenylalanyl α-chloroethane: Implications for the mechanism of inactivation of serine proteases by chloroketones, *Biochemistry 33*, 13792–13800. https://doi.org/10.1021/bi00250a033

Problem 4–28: Glycine hydroxymethyltransferase (previously Equation 2–10) uses pyridoxal phosphate as a prosthetic group in its active site to catalyze the reversible interconversion of glycine and L-serine.

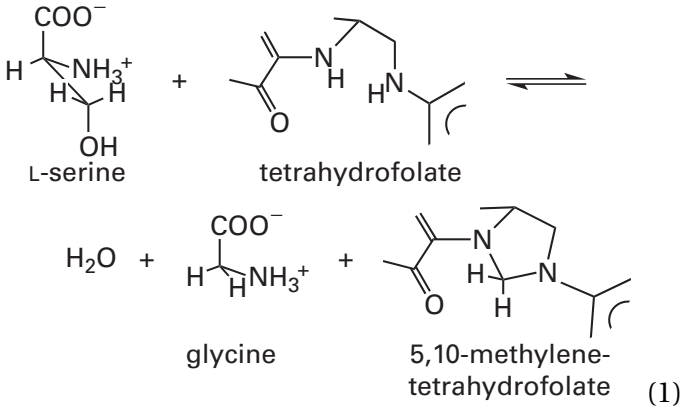

(1)

This reaction is the major source of 5,10-methylene-tetrahydrofolate in mammals. The enzyme also carries out the following transformations.

L-allothreonine $\rightleftharpoons$ acetaldehyde + glycine (2)

L-3-phenylserine $\rightleftharpoons$ benzaldehyde + glycine (3)

aminomalonate + H^+ $\rightleftharpoons$ CO_2 + glycine (4)

L-2-methylserine + tetrahydrofolate $\rightleftharpoons$ H_2O + D-alanine + 5,10-methylenetetrahydrofolate (5)

D-alanine + internal pyridoximine + H_2O $\rightleftharpoons$ lysyl side chain + pyruvate + pyridoxamine (6)

R-2-amino-3-fluoropropionate (D-fluoroalanine) + H_2O $\rightleftharpoons$ F^- + H^+ + pyruvate + NH_4^+ (7)

(A) Write the common mechanism for each of these seven reactions that explains each outcome, both the chemistry and the stereochemistry. Make it clear that each mechanism is just a variation of the common theme. Start with the external pyridoximine of each amine. In every step of each mechanism, write out only the imino carbon and the imino nitrogen of the pyridoximine and the remainder of the respective adduct. Abbreviate the tetrahydrofolate as in Equation 1. Indicate acids and bases as $HN^{(+)}$and $\odot O^{(-)}$ to save time.

(B) Explain the following results from a study[642] of the reaction in Equation 7

reactant	k_{FA} (M^{-1} s^{-1})
D-[2-^{1}H]fluoroalanine	0.37
D-[2-^{2}H]fluoroalanine	0.07

where k_{FA} is the specificity constant for the respective fluoroalanine (FA). When tetrahydrofolate is present, D-fluoroalanine is turned into pyruvate 100 times faster than L-fluoroalanine is turned into pyruvate. The normal substrate for the enzyme, however, is L-serine.

(C) Draw two structures, side by side, of adducts formed at the active sites between pyridoxal phosphate and D-fluoroalanine and between pyridoxal phosphate and L-serine, respectively, that explain why D-fluoroalanine is the preferred substrate over L-fluoroalanine but L-serine is the preferred substrate over D-serine.

(D) Draw a chemical mechanism involving a nucleophilic amino acid side chain, $-S\odot^{(-)}$, in the active site to explain one way the enzyme could become irreversibly inactivated while it is performing the reaction in Equation 7.

Problem 4–29: 2′,3′-Epoxypropyl β-di(*N*-acetyl-D-glucosamine)glycoside

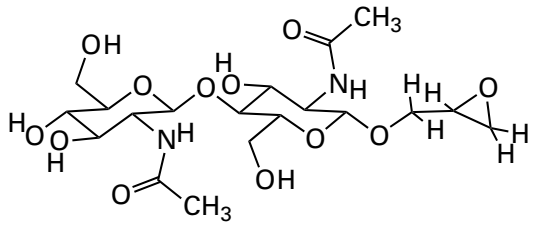

was synthesized as an active-site label for lysozyme (Figure 3–27) from *G. gallus*. After binding to the active site, 2′,3′-epoxypropyl β-di(*N*-acetyl-D-glucosamine)glycoside reacts with the enzyme to form a covalent derivative that is inactive and that contains 1 mole of the label attached to Aspartate 52 for each mole of the enzyme.[646]

(A) Write the chemical mechanism for the reaction between Aspartate 52 and 2′,3′-epoxypropyl β-di(*N*-acetyl-D-glucosamine)glycoside.
(B) Use steric arguments to predict which electrophilic carbon in the epoxide is the most likely electrophile.

Lysozyme, which had been modified by 2′,3′-epoxypropyl β-di(*N*-acetyl-D-glucosamine)glycoside and rendered inactive, was crystallized, and a crystallographic molecular model was constructed.[646]

(C) Which subsites (Figure 3–27) on the inactive lysozyme molecule were occupied by the two *N*-acetyl-D-glucosamino groups of the affinity label?

When the covalently modified enzyme was reduced with $NaBH_4$, the ester was reduced to an alcohol and a derivative of lysozyme with homoserine at position 52 resulted.[839]

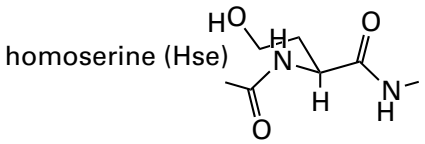

(D) Lysozyme(Hse52) is catalytically inactive but binds hexasaccharide substrates such as $(GlcNAc)_6$ with the same affinity as the native enzyme. Explain this observation.

Problem 4–30: Aldolases are enzymes that catalyze aldol condensations such as those in Equations 4–278 and 4–324 and Figures 4–26 and 4–36. It has been shown that when a ketone that is a substrate is mixed with its aldolase and allowed to equilibrate, and then the mixture is treated with $NaBH_4$ (a mild reducing reagent), a lysine in the protein is irreversibly modified and a secondary amine resulting from reduction of the imine of the ketone with that lysine (Equation 4–325) can be isolated from a hydrolysate of the protein. This result is evidence for the existence of the respective imine of a lysine in the active site.

(A) Write out the steps involved in an aldolase mechanism. Where are hydrons rearranged?

2-Dehydro-3-deoxyphosphogluconate aldolase (Equation 4–324) from *Pseudomonas* was mixed with pyruvate in the presence of ^3H_2O and equilibrated for the times noted in the table.[706] Following the reaction, pyruvate was purified on an ion-exchange column, and fractions were examined for the incorporation of tritium.

enzyme	time (h)	$\frac{\mu mol\ of\ ^3H}{\mu mol\ of\ pyruvate}$
none	1	<0.005
boiled	1	<0.005
active	1	0.585
none	16	0.073
active	16	2.310

(B) To which carbon in pyruvate is tritium added? How does this process fit into the overall mechanism? Draw what you think is occurring at the active site, and explain the super-stoichiometry of the incorporation. Include hydron donors and acceptors.

2-Dehydro-3-deoxyphosphogluconate aldolase was mixed with 1 mM 3-bromopyruvate at pH 6. Samples were removed at various intervals and immediately diluted 200-fold into a solution at pH 8 to hydrolyze the 3-bromopyruvate. The enzyme, following this dilution procedure, was then assayed for aldolase activity.[691]

time of initial incubation with bromopyruvate (min)	enzymatic activity remaining (%)
0	100
1	78
2	65
3	50
4	41
5	28

The 3-bromopyruvate irreversibly inactivates the enzyme.

(C) Why was 3-bromopyruvate chosen? Examine your diagram for the enzyme mechanism. What group is the intended target of 3-bromopyruvate, and what type of chemical reaction should be occurring?

(D) Assume that the kinetic mechanism of Equation 4–297 describes this inactivation and that

$$\frac{d[\text{E–ASL}]}{dt} \equiv v_i = k_i[\text{E}\cdot\text{ASL}]$$

and show that

$$\frac{d[\text{E–ASL}]}{dt} = \frac{k_i([\text{E}]_0 - [\text{E–ASL}])\,k_{ASL}[\text{ASL}]}{k_i + k_{ASL}[\text{ASL}]}$$

where k_{ASL} is defined by Equation 4–300.

(E) Show by integration that Equation 4–298 describes the inactivation.

(F) Show that the reaction corresponds to this expectation by plotting the data from the table in the form of Equation 4–298 or in its common logarithmic form, Equation 4–301. Assume that the concentration of 3-bromopyruvate, [ASL], is 1 mM at all times t, because $[\text{E}]_0 \ll [\text{ASL}]$.

(G) If $t_{½}$ is defined as the time required to inactivate half the enzyme, show that

$$t_{½} = \ln 2\left(\frac{k_{ASL}^{-1} + k_i^{-1}[\text{ASL}]}{[\text{ASL}]}\right)$$

Values of $t_{½}$ for several 3-bromopyruvate concentrations were calculated from curves such as the one you drew earlier.[691]

[bromopyruvate] (mM)	$t_{½}$ (s)
0.21	330
0.30	250
0.46	190
0.89	140
1.5	100
3.5	80

(H) Do these data conform to expectations? Explain.

(I) What are numerical values for k_{ASL} and k_i?

If 3-bromopyruvate is binding to the active site of 2-dehydro-3-deoxyphosphogluconate aldolase at the same position as pyruvate, then pyruvate should protect the enzyme. The following values for $t_{½}$ were measured when 6 mM pyruvate was present in addition to 3-bromopyruvate.[691]

[bromopyruvate] (mM)	$t_{½}$ (s)
5	500
10	280
20	170

(J) What kind of an inhibitor is pyruvate with respect to the inactivation caused by 3-bromopyruvate? Is this observation expected? Why?

Radioactive [^{14}C]-3-bromopyruvate was synthesized by direct bromination of [^{14}C]pyruvate. 2-Dehydro-3-deoxy-D-gluconate 6-phosphate was incubated at pH 6 for 20 min in the presence of 1 mM unradioactive 3-bromopyruvate and 40 mM pyruvate. The enzyme was dialyzed exhaustively and then treated with 1 mM [^{14}C]-3-bromopyruvate at pH 6 in the absence of pyruvate for 20 min. The enzyme was precipitated 3–4 times with $(NH_4)_2SO_4$ until constant counts per minute of ^{14}C (milligram of precipitated protein)$^{-1}$ were obtained. It was found that 90% of the activity had disappeared and 1.1 mol of ^{14}C (mol of enzyme protomer)$^{-1}$ had been covalently incorporated. When the radioactive protein was incubated with 0.5 M NaOH or unfolded in 10 M urea and reacted with hydroxylamine, 90–95% of the radioactivity was removed from the protein. Ethers, phenol ethers, and secondary amines are all stable under these conditions. When the ^{14}C-labeled

protein was hydrolyzed in 6 M HCl at 100 °C for 24 h, 99% of the ^{14}C was released as hydroxypyruvic acid.[634]

(K) What type of amino acid side chain has probably reacted covalently with 3-bromopyruvate to inactivate the enzyme?

[^{14}C]-2-Dehydro-3-deoxy-D-gluconate 6-phosphate aldolase that had been inactivated with [^{14}C]-3-bromopyruvate was prepared and divided into two fractions. One fraction was unfolded with 1% sodium dodecyl sulfate. Both native and unfolded [^{14}C]aldolase were then reacted with $NaBH_4$ for 30 min at 50 °C. When these two fractions were hydrolyzed in 6 M HCl, the unfolded sample yielded only [^{14}C]glyceric acid, but the hydrolysate of the native enzyme contained a new [^{14}C]amino acid (60% yield). When enzyme, purified from bacteria grown on [^{3}H]-L-lysine, was reacted with [^{14}C]-3-bromopyruvate, reduced, and hydrolyzed, the new amino acid contained both ^{14}C and ^{3}H in a 1:1 molar ratio.[634]

(L) What is this novel amino acid, and what occurred during inactivation and then reduction?

(M) Look again at your diagram of hydron movements during the aldolase reaction. Notice that during the retroaldol dissociation a hydron is removed from the hydroxy group on carbon 4 of 2-dehydro-3-deoxy-6-phospho-D-gluconate, but during the reverse reaction a hydron is removed from the methyl group of carbon 3 of pyruvate. Consider the amino acid that performs this function. What is there about its functional group that makes it particularly suitable?

Problem 4–31: 2,3-Epoxypropanol 1-phosphate, glycidol phosphate (GcP), is an irreversible inhibitor of triose-phosphate isomerase (Equations 4–46 and 4–55 and Figure 3–37). When glycidol phosphate is added to a solution of triose-phosphate isomerase from *O. cuniculus*, in large excess over the concentration of enzyme, the enzymatic activity disappears in a pseudo-first-order fashion such that a plot of log([active enzyme]) against time (Equation 4–301) is linear, and a rate constant, $k_{i,app}$, could be obtained from the slope. It was found that $k_{i,app}$ varied with the concentration of glycidol phosphate and was affected by addition of a competitive inhibitor of the enzymatic activity, glycerol 1-phosphate.[647]

[glycidol phosphate] (mM)	$k_{i,app}$ ($s^{-1} \times 10^6$)	
	enzyme alone	enzyme + 0.3 mM glycerol 1-phosphate
0.15	6.4	
0.3	12.0	
0.6	18.4	
1.2	28.7	14.0
1.9	37.5	20.7
3.8		34.0
5.2		49.3

(A) Plot these data in an informative format and determine K_{dGcP}, the dissociation constant of glycidol phosphate from the active site, and K_{dGoP}, the dissociation constant of glycerol 1-phosphate.

(B) What two features of the kinetics of inactivation lead to the conclusion that glycidol phosphate is an active-site label?

(C) What participant in Equation 4–55 is reacting with glycidol phosphate?

When the enzyme was fully inactivated, 0.9 ± 0.1 mol of [^{32}P]glycidol phosphate (mol of active sites)$^{-1}$ was incorporated into the protein.[840] The radioactive protein was digested with pepsin, and a radioactive peptide was isolated. Upon hydrolysis, the amino acid composition of the peptide was

amino acid	mol of amino acids (100 mol of total amino acids)$^{-1}$
Glu	20
Pro	22
Ala	18
Val	21
Tyr	19

The optical density of the peptide at 280 nm was 5800 M^{-1} cm^{-1}.

(D) Find this peptide in the sequence of triose-phosphate isomerase from *O. cuniculus* and write out its sequence.

This peptide was radioactive (^{32}P) and lost its radioactivity upon either alkali treatment, which will not cleave phosphate esters, or phosphatase

treatment, which will. The same peptide was isolated from unmodified enzyme and from enzyme modified with 2,3-epoxypropan-1-ol (glycidol) and $HOPO_3^{2-}$. Upon electrophoresis, the following behavior was observed

peptide	electrophoretic mobility (relative to aspartate) pH 6.5	electrophoretic mobility (relative to serine) pH 1.9
unlabeled	–0.21	+0.43
labeled with glycidol phosphate	–0.27	0
labeled with glycidol + $HOPO_3^{2-}$	0	+0.42

(E) Which amino acid in the peptide had reacted with glycidol phosphate?

Problem 4–32: 3-Hydroxydecanoyl-[acyl-carrier-protein] dehydratase from *E. coli* can catalyze both of the following reactions.[841]

(R)-3-hydroxydecanoyl-SACP $\rightleftharpoons$ H_2O + *trans*-dec-2-enoyl-SACP $\rightleftharpoons$ H_2O + *cis*-dec-3-enoyl-SACP

The abbreviation SACP is for acyl-carrier protein, a small protein in which the sulfanyl group of a prosthetic 4′-phosphopantetheine forms a thioester with the respective fatty acids. Substrates that are thioesters of *N*-acetylcysteamine (SNAC) are as effective as substrates for the enzyme as the thioesters of acyl-carrier protein.

(A) Provide a mechanistic reason to explain why the enzyme cannot convert (*R*)-3-hydroxydecanoyl-SACP directly into *cis*-dec-3-enoyl-SACP.

(B) If any one of the substrates were mixed with a high enough concentration of the enzyme in D_2O, so that the three reactions catalyzed by the enzyme come to equilibrium faster than nonenzymatic hydron exchange could occur, then deuterium would be incorporated by the enzyme into some or all of the three substrates. Assume that the dehydration is trans and that the hydron is moved across the face of the intermediate in the second reaction from carbon 4 to carbon 2. How many deuteriums should incorporated into each of the three substrates, and what are the absolute stereochemistries of each deuterated substrate?

The effect of pH on the catalytic constant of the enzyme, k_0, for isomerization of *cis*-dec-3-enoyl-SNAC to *trans*-dec-2-enoyl-SNAC was measured at various values of pH and at constant temperature (30 °C) and ionic strength (0.05 M).[842]

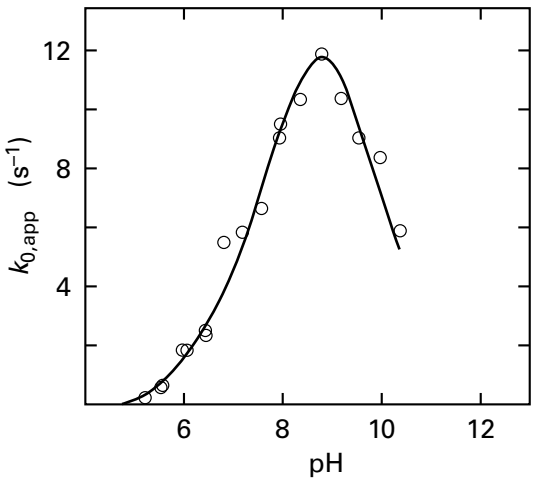

Reactions were initiated by addition of 4 μg of dehydratase to cuvettes containing 1.0 mL of substrate, the concentration of which had been determined by measuring absorbance at 232 nm. Product formation was monitored by measuring A_{263}. Values for k_0 were calculated from double-reciprocal plots of the data at each pH. At least 10 different substrate concentrations were used for each point. The buffer systems were sodium acetate, imidazolium chloride, potassium phosphate, tris(hydroxymethyl)aminomethane hydrochloride, and sodium glycinate.

(C) Write a mechanism for isomerization of *cis*-dec-3-enoyl-SNAC as it occurs within the active site of the enzyme. Your mechanism must contain the explanation for the behavior observed in the figure. Use amino acid side chains of your choice to act as catalytic side chains. Choose a different one for each role to distinguish them in later answers.

(D) Explain the observed effect of pH on k_0 observed in the preceding figure in terms of acid dissociations of the catalytic acids and catalytic bases that you chose in part C. Consider both the free enzyme and the enzyme–

substrate complex. Remember that in this particular experiment *cis*-dec-3-enoyl-SNAC is the substrate.

Both dec-3-ynoyl-SNAC (alkyne) and deca-2,3-dienoyl-SNAC (allene) are irreversible inhibitors of the enzyme.[729]

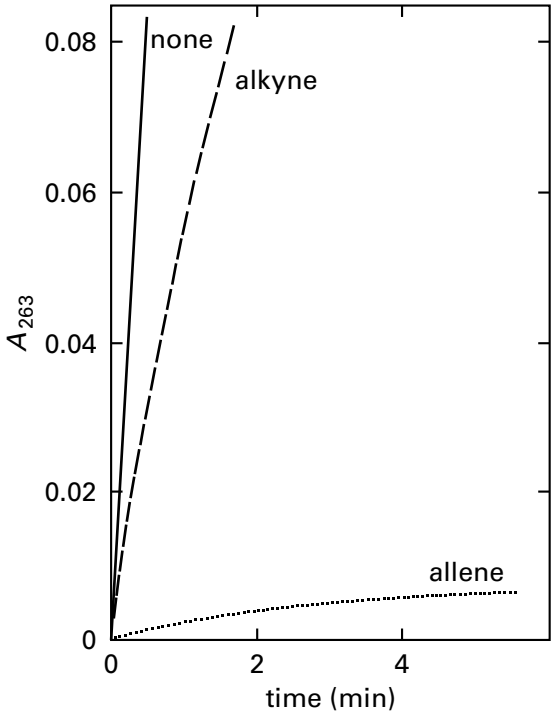

To a cuvette containing 10 μM of the respective inhibitor and 400 μM *cis*-dec-3-enoyl-SNAC in 0.01 M potassium phosphate at pH 7.0 was added 6 μg of purified 3-hydroxydecanoyl-[acyl-carrier-protein] dehydratase at zero time. The rate of *trans*-2-decenoyl-SNAC production was measured spectrophotometrically by absorbance at 263 nm (A_{263}).

(E) Write the nucleophilic addition that explains why one of these compounds is so much more reactive than the other. Use one of the nucleophiles in your active site for the addition.

(F) Draw at least two possible products of the reaction of deca-2,3-dienoyl-SNAC with amino acid side chains in the active site that you constructed in the answer to part B.

2,2-Dideuterodec-3-ynoyl-SNAC was synthesized as well as dec-3-ynoyl-SNAC, and these two compounds were tested together as inactivators of the enzyme.[729] To cuvettes containing 0.5 mL of potassium phosphate at pH 6.0 and an ionic strength of 0.05 M were added, to a final concentration of 8 μM, either dec-3-ynoyl-SNAC (●) or 2,2-dideuterodec-3-ynoyl-SNAC (○) and, at zero time, 33 μg of dehydrase. At various times, 0.5 mL of 3.1×10^{-4} M *cis*-dec-3-enoyl-SNAC in the same buffer was added, and the initial rate of product formation was recorded. The degree of inactivation was based on comparison with a similar reaction to which no ethynylene thioester had been added. Since the amount of ethynylene thioester was present at a 60-fold molar excess over dehydrase, the inactivation data were treated in a first-order manner.

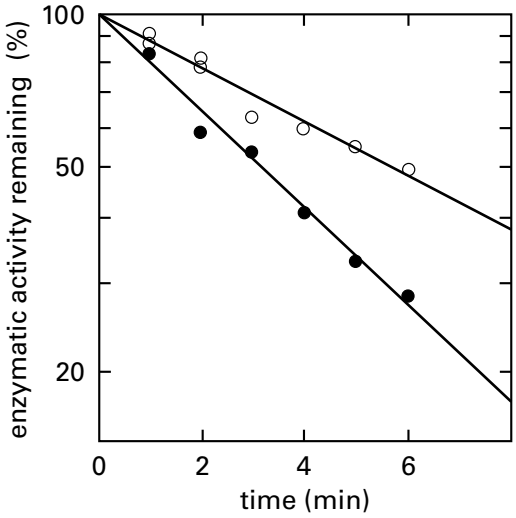

The deuterium kinetic isotope effect observed ($^{H}k/^{D}k = 2.60$) is similar in magnitude to that seen for 2,2-dideutero-3-hydroxydecanoyl-SNAC during its dehydration to *trans*-2-decanoyl-SNAC ($^{H}k/^{D}k = 2.25$). 2-Deuterodeca-2,3-dienoyl-SNAC, however, shows no isotope effect during its inactivation of the enzyme.

(G) What does the deuterium kinetic isotope effect suggest that the enzyme must be doing to dec-3-ynoyl-SNAC before this active-site label can inactivate the enzyme?

(H) What must dec-3-ynoyl-SNAC be turned into before it can inactivate the enzyme?

(I) Incorporate the mechanism for this transformation into your active site from part B.

(J) Write an overall mechanism that incorporates the three reactions naturally catalyzed by the enzyme, inactivation by the allene, and mechanism-based inactivation by the alkyne.

(K) Is the enzyme catalyzing its natural reaction through an enolate, through an intermediate carbenium ion, or by a concerted mechanism?

Problem 4–33: The following mechanism-based labels[679,843-846] were designed to modify the noted enzymes.

enzymatic reaction or enzyme	mechanism-based label
cis-3-chloropropenoate ⇌ 3-oxopropanoate	
4-aminobutyrate transaminase	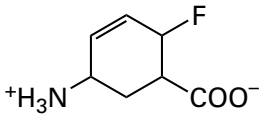
isopentenyl-diphosphate Δ-isomerase	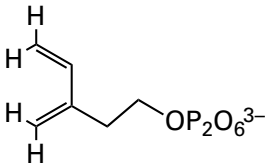
glutaryl-SCoA ⇌ CO_2 + crotonyl-SCoA + 2 e^-	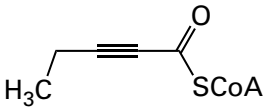
thymidylate synthase	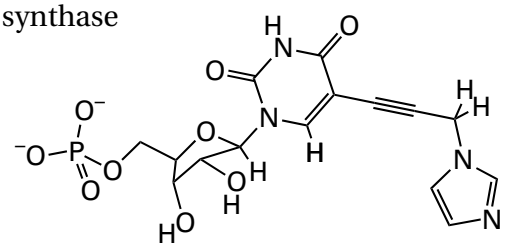

(A) Draw the structure of the substrate for each enzyme that the mechanism-based label is designed to mimic.

(B) Draw the structure of each electrophile that the respective enzyme produces from each mechanism-based label. The electrophile in each case is produced in the same step or sequence of steps through which the enzyme takes the substrate that the mechanism-based label mimics.

Problem 4–34: (1*S*,3*S*)-3-Amino-4-(perfluoropropan-2-ylidene)cyclopentane-1-carboxylate

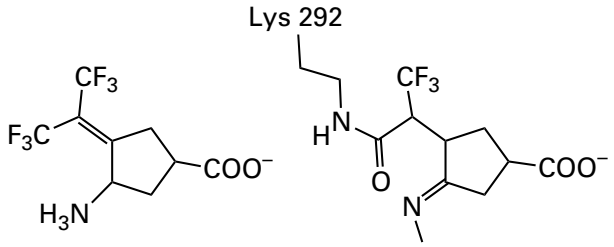

inactivates human ornithine aminotransferase.[711] The product of the reaction has been identified in a crystallographic molecular model of the modified enzyme as the amide between the amino group of Lysine 292 and the N^3-(5′-phosphopyridoxyl)imine of (1*S*)-3-imino-4-(3,3,3-trifluoro-1-carboxypropan-2-yl)cyclopentane-1-carboxylate, and the identification was verified by the mass spectrum of the inactivated enzyme. In the initial step of the reaction, the 3-amino group of the (1*S*,3*S*)-3-amino-4-(perfluoropropan-2-ylidene)cyclopentane-1-carboxylate forms the external pyridoximine with the prosthetic pyridoxal 5′-phosphate in the active site. Write a mechanism for formation of the amide from the perfluoropropan-2-ylidene that involves the 5′-phosphopyridoxyl group in every step except the last one.

Problem 4–35: L-Lactate dehydrogenase catalyzes the reaction of Equation 4–204.

(A) Write a chemical mechanism for the oxidation–reduction as it would occur in the active site, using $HN^{(+)}$ and $\odot O^{(-)}$ to indicate any necessary acid or base. Abbreviate NAD^+ as

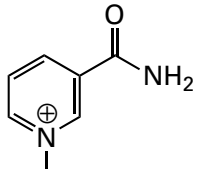

Porcine L-lactate dehydrogenase is inactivated irreversibly by the nonspecific electrophile diethyl dicarbonate.[847]

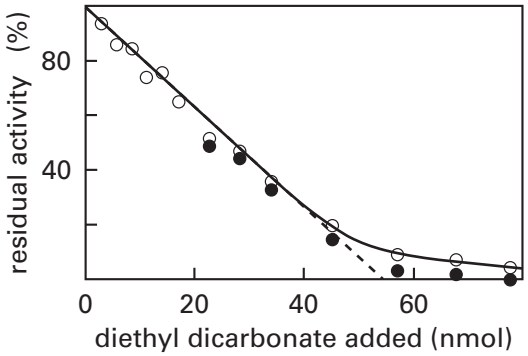

Freshly diluted samples of diethyl dicarbonate were added to solutions of enzyme (56 nmol of subunits) in 0.08 mL of 0.1 M sodium phosphate at pH 6.0 and 20 °C. After 1 min, the enzyme was diluted 200-fold into ice-cold buffer, and a sample was used to measure the enzymatic activity about 5 min after the initial addition of diethyl dicarbonate. The percentage of residual activity is expressed relative to that of an untreated control (○), and the percentage of residual activity, after being corrected for the reactivation (about 5%) that occurs during the 5 min necessary to assay the enzyme, is expressed as a percentage, relative to that of that of an untreated control (●).

(B) Explain why this experiment was done, what the results demonstrate, and why there must be one particularly reactive amino acid in the protein.
(C) Write a kinetic mechanism for the reaction between the nucleophilic form of the enzyme and diethyl dicarbonate. Do not solve the rate equation.
(D) Why is the observed rate of the reaction kinetically first-order when the inactivation of the enzyme is followed as a function of time, and what is the observed rate constant equal to in terms of your kinetic mechanism?

The rate of reaction of diethyl dicarbonate was measured by rapidly mixing a solution of 30 μM L-lactate dehydrogenase in sodium diphosphate at pH 8.4 and an ionic strength of 150 mM with an equal volume of a solution of 11 mM diethyl dicarbonate and following at an absorbance of 251 nm. The product of the reaction between diethyl dicarbonate and the amino acid in the active site absorbs most strongly at 251 nm.

The concentrations of both L-lactate dehydrogenase and diethyl dicarbonate and the ionic strength were kept constant in a series of experiments in which the pH was varied systematically. The apparent first-order rate constant for the change in absorbance at 251 nm was determined for each pH.[847]

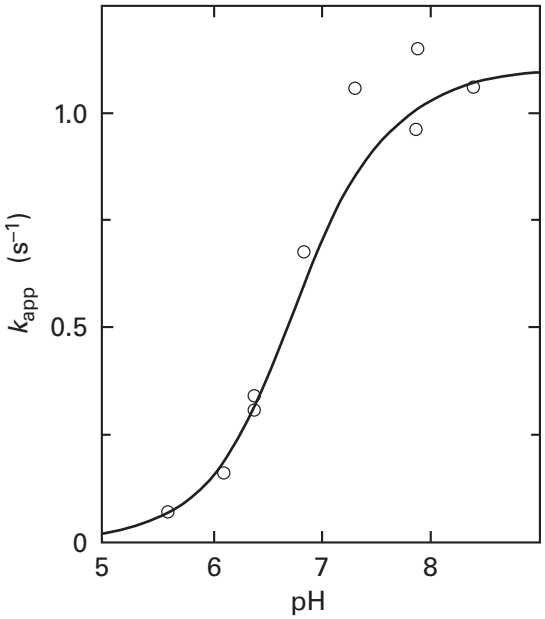

The observed first-order rate constant for the reaction is plotted as a function of the pH. The concentration of enzyme after mixing was 15 μM, and that of diethyl dicarbonate was 5.5 mM. Buffers were sodium diphosphate.

(E) Write a kinetic mechanism for this inactivation describing it as the carbonylation of the conjugate base of an amino acid on the protein. Incorporate acid dissociation of the conjugate acid of that amino acid in your mechanism. Derive an equation for the observed first-order rate constant, k_{app}, in terms of the intrinsic rate constant, k_{DD}, between diethyl dicarbonate and the conjugate base of the amino acid and the acid dissociation constant, K_{aNH}, of the amino acid.
(F) What is the pK_a of the nucleophilic amino acid?

Catalytic Acid–Bases in Crystallographic Molecular Models

It would seem that, when a crystallographic molecular model of the empty active site of a particular enzyme became available, the catalytic acid–bases involved in the enzymatic mechanism could be identified immediately by inspection. Unfortunately, this hope has not been realized. The reasons for the almost universal ambiguity that accompanies crystallographic molecular models of empty active sites are

that there are usually too many acid–bases, that they are too flexible, and that there are many heteroatoms that do not seem to be possible catalytic acid–bases that turn out to be. The reason that there are too many acid–bases in an active site is that substrates, in addition to presenting to the active site the hydrons that must be removed and the lone pairs of electrons that must be hydronated for the reaction to occur, also have significant numbers of donors and acceptors for hydrogen bonds, and these must be occupied by acceptors and donors from the active site. These acceptors and donors within the active site are usually acid–bases in their own right, and they are indistinguishable chemically from the catalytic acid–bases.

Consequently, the active site must be occupied by an informative set of ligands that identifies the catalytic acid–bases responsible for the hydron transfers necessary for the enzymatic reaction.

The most informative ligands are the **complete set of substrates in a complex with the enzyme** in which reactants and products are in rapid equilibrium with each other within the active site. For example, the crystallographic molecular model (Figure 3–36) of the complex between murine cytidine deaminase and a cytidine, a water, a uridine, and an ammonia in equilibrium with each other clearly identifies one oxygen of the carboxylato group of Glutamate 67 as the catalytic base that removes the hydron from hydroxide on the Zn^{2+} (0.28 nm) while it adds as the nucleophile to cytidine in the direction of hydrolysis. Removal of this hydron turns the hydroxide into the oxyanion still coordinated to the Zn^{2+} in the tetrahedral intermediate to provide push. The resulting carboxy group on Glutamate 67 then becomes the catalytic acid that adds the hydron to the amino group in the tetrahedral intermediate at carbon 4, as is required to permit the nitrogen to leave as ammonia. By microscopic reversibility, this same oxygen in the carboxylato group of Glutamate 67 must be the catalytic base that removes the hydron from ammonia (0.29 nm) while it adds as the nucleophile to uridine and then adds that hydron to the oxyanion coordinated to the Zn^{2+} in the resulting tetrahedral intermediate in the direction of aminolysis so that it can leave as a zinc hydroxide. In each case, this catalytic oxygen moves from oxygen to nitrogen and nitrogen to oxygen by pivoting on the hydrogen bond of its other oxygen to nitrogen 3 of cytidine (0.29 nm) or uridine (0.27 nm).[848] While the carboxy group is pivoting, the hydron within this stationary hydrogen bond that acts as the pivot moves from the oxygen to nitrogen 3 as the other oxygen of the carboxy group removes the hydron from the hydroxide group; and in reverse, the hydron within the hydrogen bond moves from nitrogen 3 to the oxygen as the other oxygen of the carboxy group adds the hydron to the oxygen of the oxyanion in the tetrahedral intermediate.

The crystallographic molecular model of phosphopyruvate hydratase (Equation 4–128) from *S. cerevisiae* and an equilibrium mixture (Figure 3–35) of its three substrates—phospho*enol*pyruvate, water, and 2-phospho-D-glycerate—unambiguously identifies the amino group of Lysine 345 (0.32 nm) as the catalytic base responsible for removing the hydron from carbon 2 of 2-phospho-D-glycerate during the anti elimination and the catalytic acid responsible for adding a hydron to carbon 2 during the anti addition (Figure 4–43).[544,849-851] Oxygens from the carboxy groups of Glutamate 168 (0.24 nm) and Glutamate 211 (0.26 nm) form hydrogen bonds to the 3-hydroxy group. One of the glutamates is the catalytic acid responsible for hydronating the leaving hydroxy group during the anti elimination and the catalytic base responsible for removing a hydron from a molecule of water during the anti addition.

In most instances, however, the equilibrium within an **active site favors the set of substrates on one side of the equation** over the set on the other side when together they occupy the active site. For example, in the case of nicotinate-nucleotide—dimethylbenzimidazole phosphoribosyltransferase from *S. typhimurium* (Figure 3–31), in a complex with its substrates at equilibrium within the active site, nicotinate and α-ribazole 5′-phosphate are the favored pair. In this case, Glutamate 317 can be assigned the role of hydronating nitrogen 3 of the benzimidazolyl group (0.26 nm) in α-ribazole 5′-phosphate to improve its ability as a leaving group. The crystallographic molecular model of the complex between triose-phosphate isomerase (Equations 4–46 and 4–55) from *S. cerevisiae* and glycerone phosphate and D-glyceraldehyde 3-phosphate (Figure 3–37) identifies unambiguously one of the two oxygens of the carboxy group of Glutamate 164 as the catalytic base that transfers the hydron between the two carbons. Even though the equilibrium in the active site favors glycerone phosphate,[852] the oxygen is equidistant from the two carbons (0.3 and 0.3 nm) in the complex.

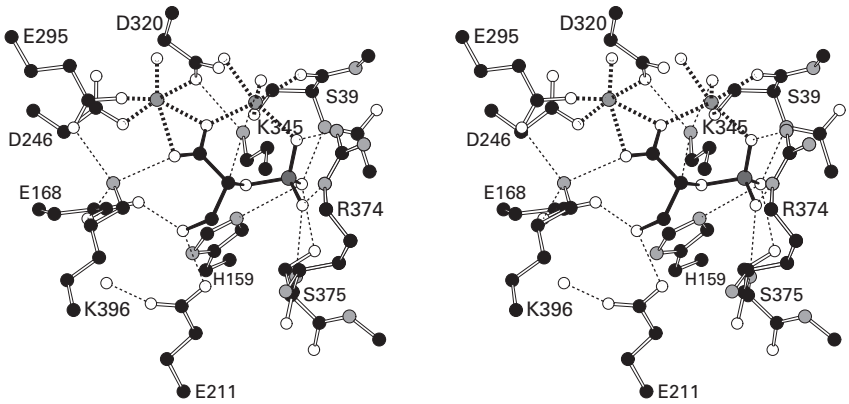

Figure 4–43: Stereodrawing[134] of the crystallographic molecular model of the active site of phosphopyruvate hydratase from *S. cerevisiae* occupied by an equilibrium mixture of 2-phospho-D-glycerate and phospho*enol*pyruvate and H_2O.[544] Black atoms are carbons, white atoms are oxygens, small gray atoms are nitrogens, the large dark gray atom is a phosphorus, and the two small dark gray spheres are magnesium ions surrounded by their ligands. Crystals of the enzyme were grown from solutions of phosphopyruvate hydratase (0.3 mM in active sites), 2 mM phospho*enol*pyruvate, 2 mM $MgCl_2$, 15% PEG 8000, 0.25 M KCl, and 50 mM potassium 3-[4-(2-hydroxyethyl)piperazin-1-yl]propane-1-sulfonate at pH 8.0. The omit maps of electron density from these crystals were consistent with the conclusion that an equilibrium mixture of phospho*enol*pyruvate and H_2O and 2-phospho-D-glycerate occupies the active sites in the crystals (Figure 3–35).[851] For simplicity, however, only a molecule of 2-phospho-D-glycerate is drawn (black bonds). The two catalytic Mg^{2+} in the active site, their eleven ligands, and the catalytic acid–bases participating in the reaction were also chosen for inclusion in the drawing, as well as the donors for hydrogen bonds forming the cup for the phospho group of the substrates. This cup anchors the substrates in the active site by their respective phospho groups as they are interconverted at equilibrium.

Chondroitin AC lyase from *Paenarthrobacter aurescens* catalyzes a syn elimination to cleave the polymer chondroitin sulfate between one of its *N*-acetylgalactosamine 4-sulfates and one of its glucuronic acids

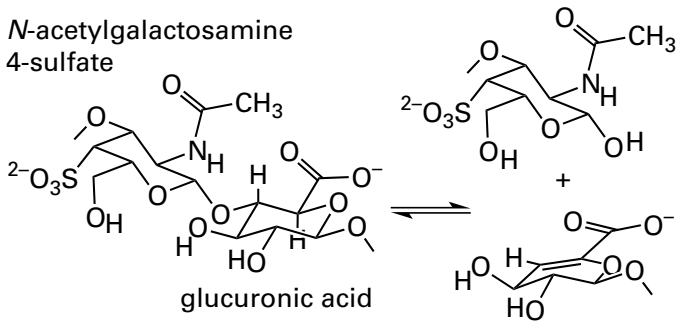

(4–358)

In a crystallographic molecular model of a complex between a tetrasaccharide of chondroitin sulfate and the enzyme (Figure 4–44),[853] the equilibrium in the active site favors uncleaved reactant, and no electron density is observed for the two separate disaccharides that would be products of the elimination occupying the active site simultaneously. The distance (0.29 nm) between the oxygen of the 4-oxidophenyl group of Tyrosine 242 and carbon 5 of the glucuronic acid, from which the hydron is removed during the elimination, is well within the sum (0.38 nm) of the van der Waals radii of oxygen (0.15 nm) and hydrogen (0.115 nm) and the length of a carbon–hydrogen bond (0.11 nm). The plane of its phenyl ring is oriented such that the lone pair of electrons on the oxygen of its 4-oxidophenyl group, which is in the same plane as the ring, points directly at the carbon–hydrogen bond. The oxygen of the 4-oxidophenyl group of Tyrosine 242 is also only 0.31 nm from the oxygen of the leaving group on carbon 1 of *N*-acetylgalactosamine 4-sulfate. Consequently, during the elimination, the hydron is removed from carbon 5 of glucuronic acid by the oxygen of the 4-oxidophenyl group of Tyrosine 242 to produce the *gem*-enediolate at the 6-carboxy group of glucuronic acid, which is hydronated on one of its two enolate oxygens by Histidine 233 during removal of the hydron. The 4-hydroxyphenyl group then rotates around the bond between carbons β and γ of Tyrosine 242 to swing over and hydronate the leaving oxygen on carbon 1 of *N*-acetylgalactosamine 4-sulfate.

Chalcone isomerase from *M. sativa* catalyzes nucleophilic addition of a weakly basic ($pK_a < 8.4$) phenolate oxygen to an α,β-unsaturated carbonyl

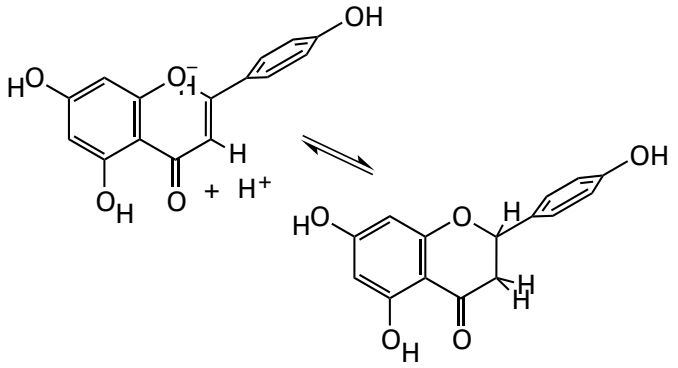

(4–359)

presumably by the usual β addition with an enol as an intermediate. In the crystallographic molecular model of the complex between substrates and the active enzyme, the equilibrium within the active site favors the cyclized adduct.[854] The electron-releasing 4-hydroxyphenyl group on the β carbon of the α,β-unsaturated carbonyl (upper right-hand corner in the respective drawings in Equation 4–359) is rotated by the active site out of conjugation with the α,β-unsaturated carbonyl to prevent the decrease of its electrophilicity by electron donation. The carbonyl oxygen accepts a hydrogen bond from a molecule of water that is a participant in a compound acid formed from a network of hydrogen bonds consisting of that molecule of water, another molecule of water, two oxygens of the 4-oxidophenyl groups from Tyrosines 106 and 152, and the ammonio group of Lysine 97. Together these participants in the compound acid hydronate the carbonyl oxygen, forming the enol during addition of the nucleophilic phenolate oxygen. The hydrogen bond is between the hydron on the immediately adjacent molecule of water in the compound acid and the π system of the carbonyl oxygen, rather than either of its two lone pairs, and the effect of this hydrogen bond is to increase the electrophilicity of the β carbon in the α,β-unsaturated carbonyl to encourage addition of the weak nucleophile.

It is also possible to create an equilibrium between **an intermediate in the reaction** and a substrate that represents one step in a multistep reaction. The nucleophilic addition catalyzed by hydroxymethylglutaryl-CoA synthase

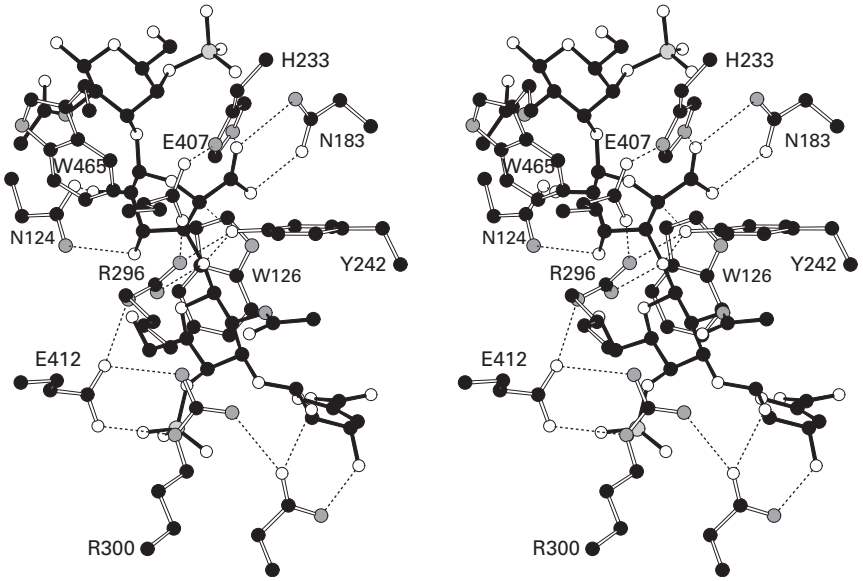

Figure 4–44: Stereodrawing[134] of the crystallographic molecular model of the active site of chondroitin AC lyase from *P. aurescens* occupied by the tetrasaccharide 4-deoxy-α-L-*threo*-hex-4-enuronosyl-(β1,3)-*N*-acetyl-2-deoxy-2-amino-4-sulfato-D-galactosyl-(β1,4)-D-glucuronosyl-(β1,3)-*N*-acetyl-2-deoxy-2-amino-4-sulfato-D-galactose (black bonds).[853] Black atoms are carbons, white atoms are oxygens, small gray atoms are nitrogens, and large light gray atoms are the sulfurs of the two sulfates. Crystals of the enzyme were suspended in a solution containing 5 mM tetrasaccacharide for 30 s and then rapidly frozen to around 100 K. The omit maps of electron density from the resulting crystals were consistent with the presence of intact molecules of tetrasaccharide in the active sites in the crystals. If the soaking was prolonged, only the disaccharide 4-deoxy-α-L-*threo*-hex-4-enuronosyl-(β1,3)-*N*-acetyl-2-deoxy-2-amino-4-sulfato-D-galactose, which is one of the products of hydrolysis, was present in the active site in the same location its glycosyl groups occupy in the complex with the intact reactant. Consequently, it was concluded that the enzyme was active in the crystal and that the tetrasaccharide in the active site was the favored substrate in the equilibrium catalyzed by the enzyme. The catalytic acid–bases participating in the reaction, Tyrosine 242 and Histidine 233, and donors and acceptors for hydrogen bonds to the tetrasaccharide were chosen for inclusion in the drawing, as well as the indolyl groups of two tryptophans the hydrophobic faces of which stack against the hydrophobic faces of two of the glycosyl groups in the tetrasaccharide. The 4-oxidophenyl group of Tyrosine 242 is responsible for removing a hydron from carbon, and it is connected to the carbon that it services by thinner dashed line to indicate that it may or may not participate in a hydrogen bond with this carbon.

acetyl-SCoA + acetoacetyl-SCoA + H_2O $\rightleftharpoons$ H^+ + HSCoA + (*S*)-3-hydroxy-3-methylglutaryl-SCoA (4–360)

displays ping-pong kinetics[855] and proceeds through two separate steps. In the first step, acetyl-SCoA acetylates the sulfanyl group of a cysteine in the active site.[856,857] In the second step, the enolate of the acetylated cysteine adds to the 3-oxo group of acetoacetyl-SCoA, and the resulting thioester of cysteine is hydrolyzed. In the crystal of the complex between acetoacetyl-SCoA and hydroxymethylglutaryl-CoA synthase from *S. aureus* (Equation 4–361) that had been acetylated on Cysteine 111, the equilibrium between acetyl enzyme and acetoacetyl-SCoA and unacetylated enzyme and (*S*)-3-hydroxy-3-methylglutaryl-SCoA is established with about equal concentrations of reactants and products.[858] In the crystallographic molecular model, it can be seen that the carboxylato group of Glutamate 79 (0.30 nm) is the base that removes the hydron from the acetyl group on Cysteine 111, and the imidazolio group of Histidine 233 (0.31 nm) is the acid that hydronates the 3-oxo group of acetoacetyl-SCoA

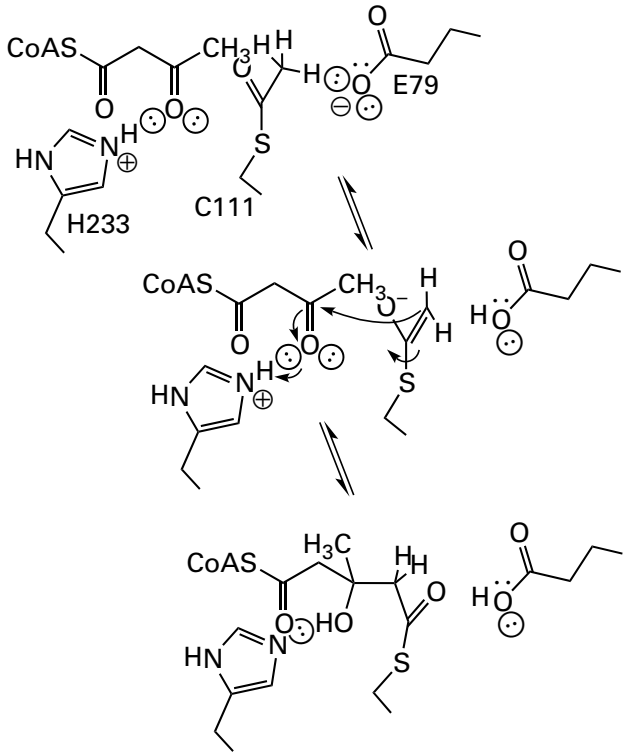

(4–361)

during nucleophilic addition of the enolate to the carbonyl.

The only structures in which the catalytic acid–bases are revealed unambiguously are the transition states themselves, but these, by definition, are inaccessible to crystallography. By the Hammond postulate,[859] however, crystallographic molecular models of **complexes between analogues for intermediates of high energy and active sites** are close representations of transition states. For example, the crystallographic molecular model (Figure 3–42) of the complex between thermolysin from *Bacillus thermoproteolyticus* and phosphonamidate

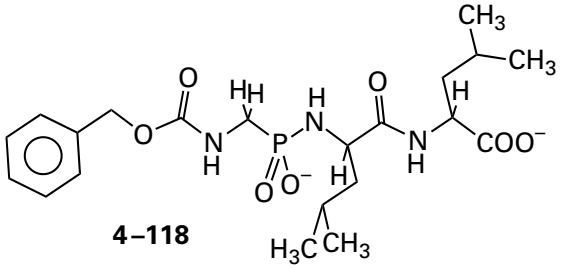

4–118

which mimics the tetrahedral intermediate in the enzymatic reaction, clearly identifies the composite catalytic base formed from the side chains of Histidine 231 and Aspartate 226 as the catalytic base (0.32 nm) that removes the hydron from the molecule of water that is bound to Zn^{2+} and that adds nucleophilically to the acyl carbon of the peptide bond hydrolyzed by the enzyme. The molecular model also identifies the carboxy group of Glutamate 143 as the catalytic acid (0.34 nm) that performs the inescapable hydronation of the amino group that leaves the resulting tetrahedral intermediate in the hydrolysis. The crystallographic molecular model of the complex between the phosphatase encoded by the BT4131 gene of *Bacteroides thetaiotaomicron* and vanadate (Figure 3–43), which mimics the phosphorane that is the intermediate in the hydrolysis catalyzed by this enzyme, clearly identifies the carboxy group of Aspartate 10 as the catalytic base (0.27 nm) that removes the hydron from the nucleophilic molecule of water or the catalytic acid that adds a hydron to the leaving group in reverse.

Fumarylacetoacetase catalyzes a Claisen condensation

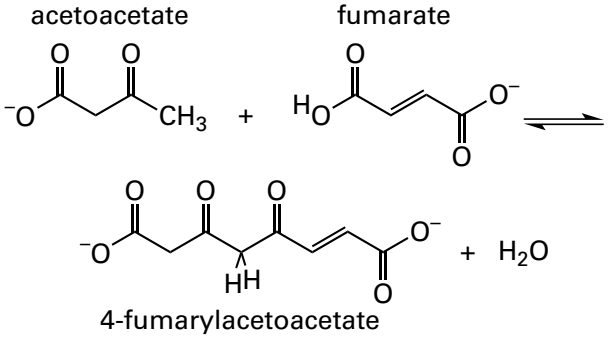

(4–362)

that passes through a tetrahedral intermediate (**4–119**)

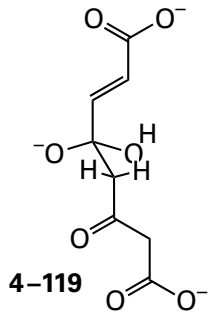

4–119

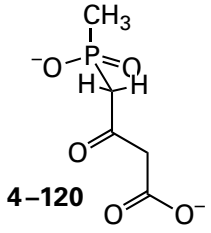

4–120

This tetrahedral intermediate is mimicked by 4-(hydroxymethylphosphinoyl)-3-oxobutanoate (**4–120**). In the crystallographic molecular model of the murine enzyme in a complex with phosphinate **4–120**,[860] the distance (0.42 nm) between the nitrogen of the amino group of Lysine 253 and methylene carbon 4 of the analogue of the intermediate is close to the sum (0.39 nm) of the van der Waals radii of nitrogen (0.16 nm) and hydrogen (0.115 nm) and the length of a carbon–hydrogen bond (0.11 nm). This amino group has been assigned as the catalytic base that removes the hydron from the methyl group of acetoacetate (Equation 4–362)[861] to form its enolate, the oxyanion of which is a ligand to a Ca^{2+}. The hole for the other oxyanion in the enzymatic reaction, that of intermediate **4–119**, is formed by the ammonio group of Lysine 253, the guanidinio group of Arginine 237, and the amido group of Glutamine 240. The hydroxy group that is analogous to the leaving group from intermediate **4–119** during the final step of the Claisen condensation forms a hydrogen bond with the imidazolyl group of Histidine 133 (0.27 nm) in the complex with the analogue of the intermediate and has been assigned as the catalytic acid that is responsible for its hydronation to enhance its ability to leave as a molecule of water

There is a crystallographic molecular model (Figure 4–45)[862] of the complex between (*R*)-1-(2-aminophenoxy)glycerol 3-phosphate (**4–121**)

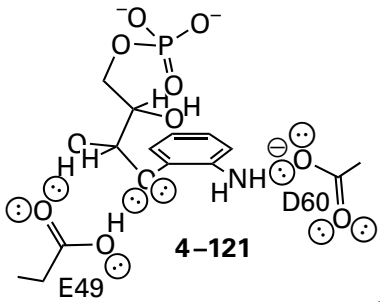

4–121

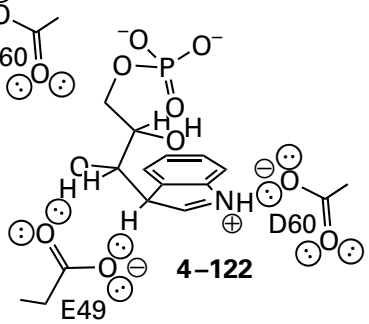

4–122

and the active site for indole-3-glycerol-phosphate lyase within tryptophan synthase from *S. typhimurium*, which condenses indole and D-glyceraldehyde 3-phosphate (previously Equation 3–524)

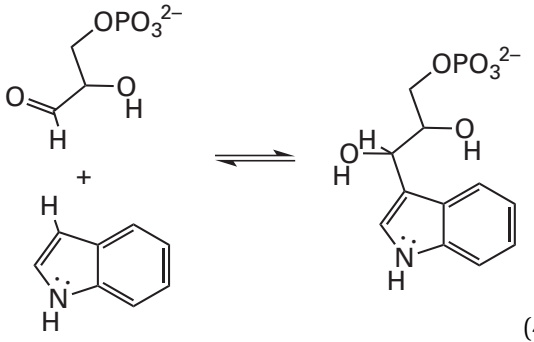

(4–363)

Hemiacetal **4–121** is an analogue of intermediate **4–122** in addition of the enamine in the pyrrolyl group of the indole to the carbonyl group of D-glyceraldehyde 3-phosphate catalyzed by the enzyme. In this molecular model, Glutamic Acid 49 is identified as the catalytic acid that hydronates the carbonyl oxygen of glyceraldehyde 3-phosphate to increase its electrophilicity and also the catalytic base, after the hydronation, that accepts the hydron that is removed from the indolyl group to restore the aromaticity. The molecular model also identifies Aspartate 60 as the catalytic base that stabilizes the cationic iminium nitrogen in the intermediate formed after addition of the enamine, perhaps by fleetingly dehydronating it. In the crystallographic molecular model of the complex between the enzyme

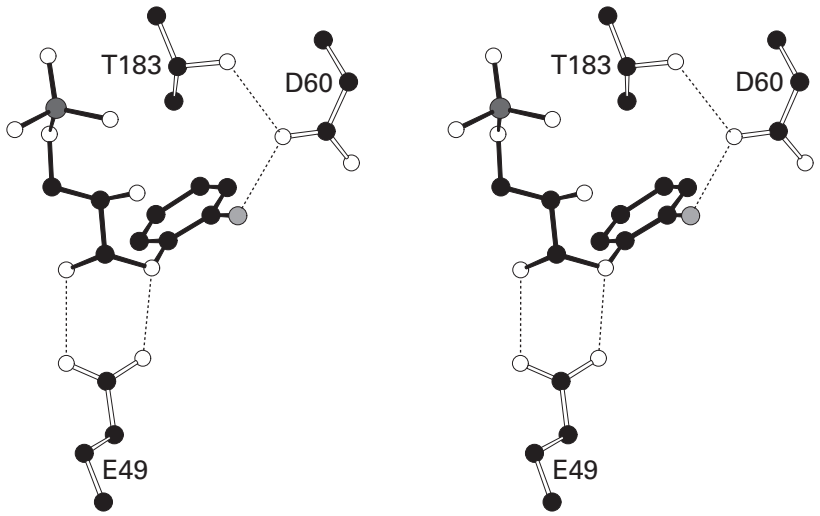

Figure 4–45: Stereodrawing[134] of the crystallographic molecular model of catalytic acid–bases in the active site of tryptophan synthase from *S. typhimurium* occupied by the hemiacetal (*R*)-1-(2-aminophenoxy)glycerol 3-phosphate.[862] Black atoms are carbons, white atoms are oxygens, small gray atoms are nitrogens, and the large dark gray atom is a phosphorus. Crystals of the enzyme and crystals of solid 2-aminophenol to achieve saturation were suspended in a solution containing 70 mM D-glyceraldehyde 3-phosphate, 20% (w/v) PEG 8000, 20% (v/v) glycerol, and 75 mM 2-[bis(2-hydroxyethyl)amino]acetate at pH 7.8 for 20 min and then rapidly frozen. The omit maps of electron density from the resulting crystals were consistent with molecules of (*R*)-1-(2-aminophenoxy)glycerol 3-phosphate (black bonds), the hemiacetal of D-glyceraldehyde 3-phosphate and 2-aminophenol, occupying the active sites of the enzyme in the crystals. Only the catalytic acid–bases participating in the reaction, Glutamate 49 and Aspartate 60, as well as Threonine 183, which positions the carboxy group of Aspartate 60, were chosen for inclusion in the drawing.

and 3-(indol-3-yl)propanol phosphate, an analogue of the substrate 1-*C*-(indol-3-yl)glycerol 3-phosphate (product in Equation 4–363) rather than the intermediate, Aspartate 60 forms a hydrogen bond (0.28 nm) with nitrogen 1 of the indolyl group[863] that is to become the iminium nitrogen during hydronation at carbon 3 of the indolyl group, which is the first step in the reverse reaction.

In aqueous solutions, oxovanadium(IV) usually forms octahedral complexes with its oxo group and five oxygens from its other ligands at the six octahedral positions, but complexes in which only five oxygens surround the vanadium(IV) have also been observed. A complex between uridine and oxovanadium(IV) was found to inhibit bovine ribonuclease competitively (K_i = 10 μM).[864] Ribonuclease, as the second half of its complete mechanism, catalyzes the hydrolysis of nucleoside 2′,3′-cyclic phosphates (Equation 4–104). During that reaction, phosphorane **4–123** should be formed in which the leaving group, the oxygen of the hydroxy group on carbon 2′, should be at an apical position in a trigonal bipyramid

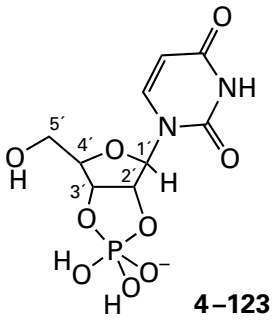

4–123

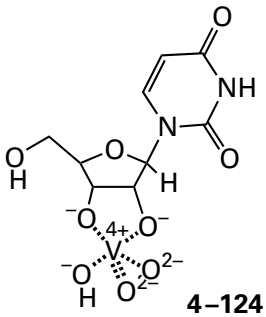

4–124

As originally proposed,[864] it was seen in the subsequent crystallographic molecular model that the strong inhibition observed with the complex between oxovanadium(IV) and uridine results from binding to the active site of the pentacoordinate complex **4–124** between uridine, vanadate, and water (Figure 4–46)[152,865] that mimics the phosphorane.*

This crystallographic molecular model between bovine ribonuclease and uridine 2′,3′-cyclic vanadate identifies Lysine 41 as the catalytic base responsible for that removes the hydron from the 2′-hydroxy group during the first half of the cleavage of a molecule of RNA

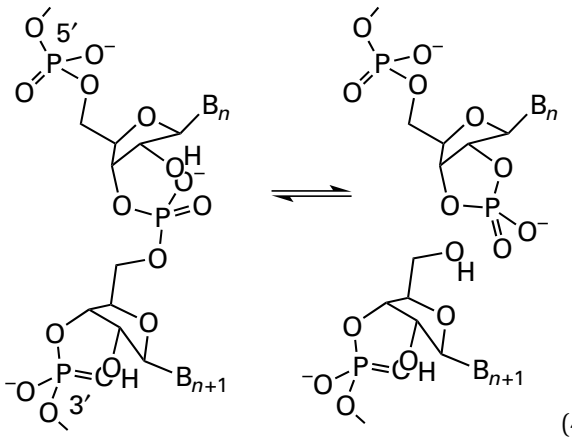

(4–364)

that produces the 2′,3′-cyclic phosphate; and it also identifies Lysine 41 as the catalytic acid that hydronates the leaving 2′-oxygen during the subsequent hydrolysis of the 2′,3′-cyclic phosphate (Equation 4–104) that constitutes the second half of the complete reaction. In addition, this molecular model identifies Histidine 119 as the catalytic acid that hydronates the leaving 5′-hydroxy group during the initial cleavage of a molecule of RNA (Equation 4–364) and also the catalytic base that removes the hydron from a molecule of water during hydrolysis of the resulting 2′,3′-cyclic phosphate. These assignments follow from the fact that these two oxygens at the axial positions in the vanadyl complex are acceptors in hydrogen bonds with the side chains of these two amino acids. The role of Histidine 12 is to stabilize the phosphorane by forming a hydrogen bond with one of the axial oxygens.

Crystallographic molecular models of inert complexes between one reactant and one product, in which **a group normally transferred between two reactants is missing**, also identify acid–bases catalyzing the reaction. For example, in the complex between guanidinoacetate *N*-methyltransferase from *R. norvegicus* and *S*-adenosyl-L-homocysteine and guanidinoacetate (Figure 3–34), which is missing the methyl group that is transferred in the normal reaction between these two substrates, it can be seen that a carboxylato oxygen of Aspartate 134 is the catalytic base (0.30 nm) responsible for removing a hydron from the guanidino nitrogen of guanidinoacetate to turn it into a nucleophile. In the complex between human 2,4-dienoyl-CoA reductase [(3*E*)-enoyl-CoA-producing] and $NADP^+$ and hexa-2,4-dienoyl-SCoA, the hydride transferred between NADPH and hexa-2,4-dienoyl-SCoA in the normal reaction is missing. The crystallographic molecular model[866] identifies Tyrosine 199 as the catalytic acid (0.25 nm) that hydronates the acyl oxygen to increase

*The van der Waals radius of vanadium (0.179 nm) is the same as that of phosphorus (0.180 nm).

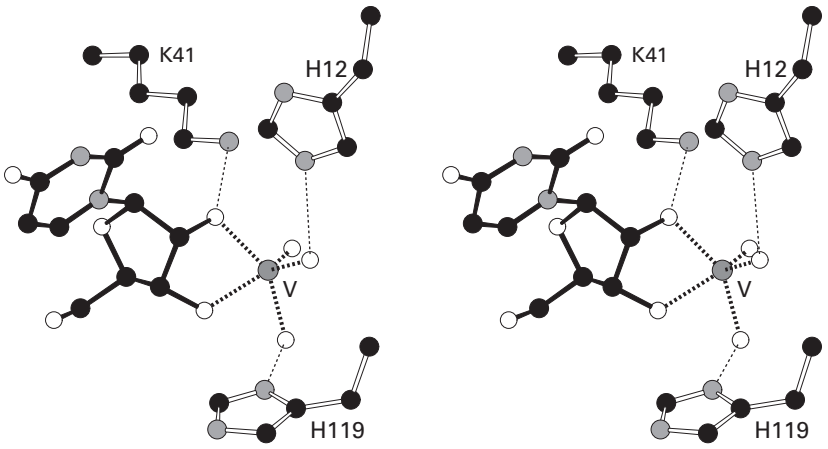

Figure 4–46: Stereodrawing[134] of the crystallographic molecular model of catalytic acid–bases in the active site of bovine pancreatic ribonuclease occupied by uridine 2′,3′-cyclic vanadate, an analogue of the phosphorane that is an intermediate in the reaction.[865] Black atoms are carbons, white atoms are oxygens, small gray atoms are nitrogens, and the dark gray sphere is a vanadium ion surrounded by its ligands. Crystals of bovine pancreatic ribonuclease were produced in 43% (v/v) 2-methyl-2-propanol at pH 5.3; transferred to a solution of 15 mM ammonium uridyl vanadate, 60 mM NH_4VO_3, 50% (v/v) 2-methyl-2-propanol, and 25 mM imidazole at pH 6.2; and soaked for 10 days. Omit maps of electron density from the resulting crystals were consistent with the presence of a molecule of uridine 2′,3′-cyclic vanadate (**4–124**, solid bonds) in each active site in the crystals. Only the key catalytic acid–bases participating in the reaction—Histidine 12, Histidine 119, and Lysine 41—were chosen for inclusion in the drawing.

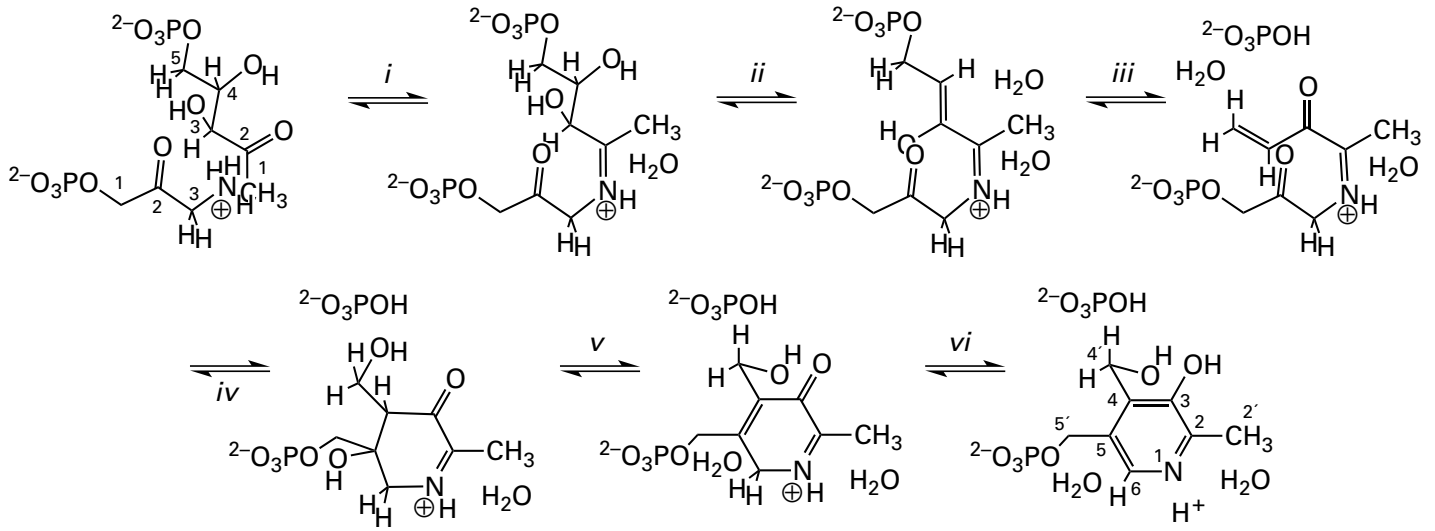

Figure 4–47: Steps in the mechanism for the reaction catalyzed by pyridoxine 5′-phosphate synthase.[867] The reactants for the direction shown are 1-deoxy-D-xylulose 5-phosphate (upper right in first panel) and 3-amino-2-oxopropyl phosphate (lower left in first panel). (*i*) Nucleophilic addition of the amino group to the 2-oxo group of 1-deoxy-D-xylulose 5-phosphate produces the iminium. (*ii*) Dehydration produces the *α,β*-unsaturated iminium, the enol in which then undergoes (*iii*) *β* elimination of phosphate to produce the *α,β*-unsaturated ketone. (*iv*) Addition of hydroxide, which takes the place of the phosphate that left, to the distal carbon of the *α,β*-unsaturated ketone produces the enolate, the anionic carbon of which adds to the ketone across the way to cyclize the intermediate and produce the six-membered ring. (*v*) Dehydration then produces the second unsaturation in the ring, followed by (*vi*) tautomerization of the newly formed *α,β*-unsaturated ketone by removal of its *γ* hydron to aromatize the ring and produce pyridoxine 5′-phosphate.

the electrophilicity of carbon 5 of hexa-2,4-dienoyl-SCoA for the hydride from NADPH

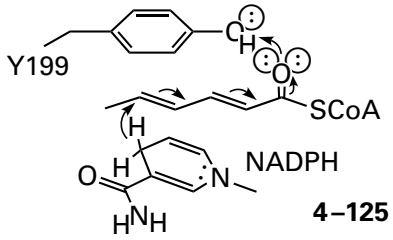

4–125

For enzymes with two reactants, the crystallographic molecular model of an **inert complex between the enzyme and one reactant and an analogue of the other** can identify catalytic acid–bases operating on the actual reactant and can tentatively identify those acting on groups in common between the other reactant that has been substituted by the analogue. For example, pyridoxine 5′-phosphate synthase catalyzes a reaction

1-deoxy-D-xylulose 5-phosphate +
3-amino-2-oxopropyl phosphate $\rightleftharpoons$
pyridoxine 5′-phosphate + phosphate + 2 H_2O (4–365)

that proceeds through five intermediates (Figure 4–47).[867] Each step between one intermediate and the next requires both a catalytic base and a catalytic acid. In the crystallographic molecular model of an inert complex between the enzyme from *E. coli* and 1-deoxy-D-xylulose 5-phosphate and D-glycerol phosphate [(*R*)-2,3-dihydroxypropyl phosphate], which is an analogue of the normal substrate 3-amino-2-oxopropyl phosphate, the catalytic acids and bases for the first steps in the mechanism line up along 1-deoxy-D-xylulose (Figure 4–48A). In the crystallographic molecular model of an enzymatically active complex between the enzyme and pyridoxine 5′-phosphate, phosphate, and water, which are the substrates favored by the equilibrium in the active site, the catalytic acids and bases for the last steps in the mechanism line up around pyridoxine 5′-phosphate and phosphate (Figure 4–48B).[868] These two models together assign the catalytic acids and bases responsible for all six of the individual steps (Figure 4–47).

In the first crystallographic molecular model (Figure 4–48A), it can be seen that Glutamate 72 consecutively removes the two hydrons from the 3-ammonio group of 3-ammonio-2-oxopropyl phosphate, represented by the 3-hydroxy group of

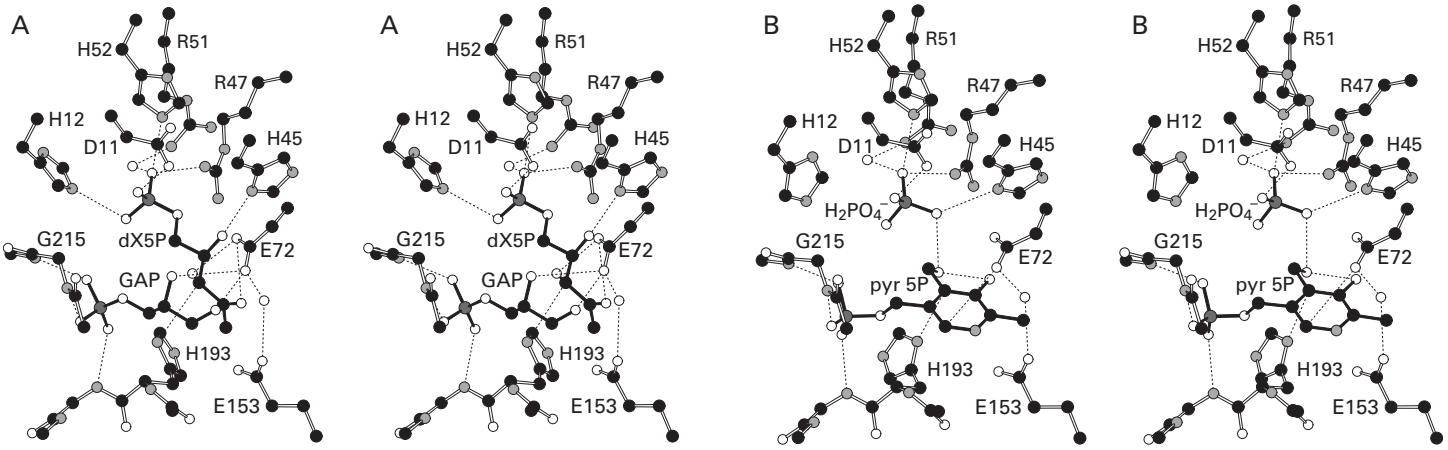

Figure 4–48: Stereodrawings[134] of crystallographic molecular models of the active site of pyridoxine 5′-phosphate synthase from *E. coli* occupied by (**A**) the substrate 1-deoxy-D-xylulose 5-phosphate (dX5P) and glyceraldehyde 3-phosphate (GAP), an analogue of the cosubstrate 3-amino-2-oxopropyl phosphate, or by (**B**) the substrate pyridoxine 5′-phosphate (pyr 5P) and its cosubstrate, phosphate ($H_2PO_4^-$).[868] Black atoms are carbons, white atoms are oxygens, small gray atoms are nitrogens, and the two large dark gray atoms are atoms of phosphorus. The enzyme was overexpressed in *E. coli*, purified, and crystallized from 10% poly(ethylene glycol) and 2 M NaCl at pH 8.0, and the crystals were then isolated and soaked in a solution of (**A**) 2.5 mM 1-deoxy-D-xylulose 5-phosphate and 2.5 mM glyceraldehyde 3-phosphate for 4 h or (**B**) 5 mM pyridoxine 5′-phosphate, 5 mM glyceraldehyde 3-phosphate, and $H_2PO_4^-$ for 1 h. The three substrates and the analogue in the resulting crystallographic molecular models of Panels A and B are anchored firmly in the active sites by the respective phospho groups sitting in their cups of donors for hydrogen bonds. The catalytic acid–bases are shown in the drawing forming hydrogen bonds to the heteroatoms that they service. Acid–bases responsible for removing hydrons from carbon are connected to the carbons that they service by thinner dashed lines (one in Panel A and two in Panel B) to indicate that they may or may not participate in hydrogen bonds with those carbons.

glycerol phosphate (0.24 nm)*, and transfers them consecutively to the 2-carbonyl oxygen of 1-deoxy-D-xylulose 5-phosphate (0.34 nm) that leaves as water in step *i*. Histidine 193 removes the hydron from former carbon 3 of 1-deoxy-D-xylulose 5-phosphate (0.37 nm), and Histidine 45 hydronates the former 4-hydroxy group (0.26 nm) that leaves as water in step *ii*. Glutamate 72 removes the hydron from the former 3-hydroxy group (0.29 nm) of 1-deoxy-D-xylulose 5-phosphate in step *iii*, and Glutamate 72 then hydronates the former carbonyl group of 3-amino-2-oxopropyl phosphate, represented by the 2-hydroxy group (0.34 nm) of the glycerol phosphate, in step *iv*.

In the second crystallographic molecular model (Figure 4–48B), it can be seen that Histidine 45 hydronates the oxygen of the phosphate (0.31 nm) that leaves in step *iii* and that the composite base formed from Histidine 45 and the oxygen of that phosphate removes the hydron from the molecule of water that becomes the eventual 4′-hydroxy group (0.29 nm) of pyridoxine 5′-phosphate in step *iv*. Glutamate 72 then adds a hydron, perhaps shuttled from Glutamate 153, to the hydroxy group that leaves as water, and Histidine 193 removes the hydron from carbon (0.41 nm) in step *v*. A hydron is then relayed from Histidine 45 through the oxygen (0.31 nm) of the phosphate and the 4′-hydroxy group (0.29 nm) of pyridoxine 5′-phosphate to the carbonyl that becomes the 3-hydroxy group (0.25 nm) of pyridoxine 5′-phosphate, and Glutamate 72 removes the hydron from carbon 6 (0.37 nm) of the soon-to-become pyridoxine 5′-phosphate in step *vi*.

Analogue **4–126** of 5-phospho-α-D-ribofuranose 1-diphosphate (**4–127**)[869,870]

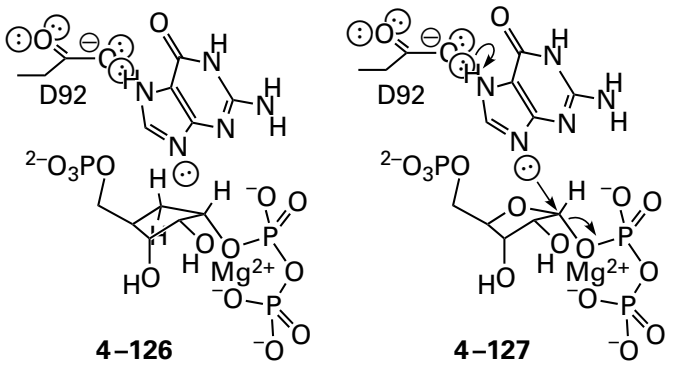

because it lacks the oxygen that stabilizes the transition state resembling an oxocarbenium ion in the enzymatic reaction, is not a substrate for xanthine phosphoribosyltransferase

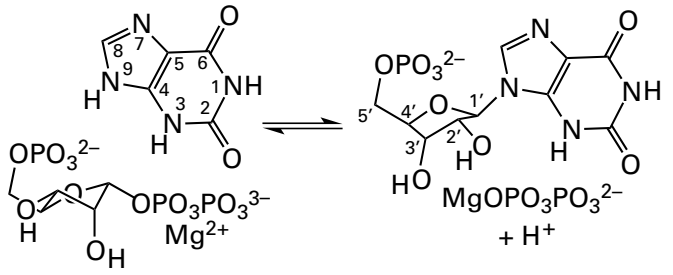

(4–366)

from *E. coli* (see Equations 3–251 and 3–398).

From an examination of the crystallographic molecular model[870] of a complex of the enzyme with analogue **4–126** and guanine, which is also a substrate for the enzyme, one oxygen of the carboxy group of Aspartate 92 can be assigned as the catalytic acid (0.26 nm) that hydronates nitrogen 7 of xanthine or guanine to stabilize the tautomer with a hydron on nitrogen 7 rather than nitrogen 9. The only catalytic base in the vicinity of nitrogen 9 that could remove a hydron from it and in turn stabilize the same tautomer, which lacks a hydron on nitrogen 9 as required by the reaction (**4–127**), is the oxygen (0.39 nm away) on the α-phospho group of the magnesium diphosphate of analogue **4–126**. The hydron or the lone pair of electrons on nitrogen 9 in the molecular model is pointed straight at this oxygen. Neither of the nonbonding oxygens on the α-phospho group is a ligand to the Mg^{2+}. Nevertheless, the α-phospho group on the usual substrate, 5-phospho-α-D-ribofuranose 1-diphosphate, should be a rather weak base ($pK_a \cong 2$), but once nitrogen 7 is hydronated, the hydron on nitrogen 9 should be a fairly strong acid ($pK_a \cong 4$), and when analogue **4–126** is bound in the active site, the α-phospho group is exposed over most of its surface to the aqueous phase, which would serve as a sink to which it could transfer the hydron. As the reaction proceeds, the carboxylato group of Aspartate 92 acts as a catalytic base that removes the hydron from nitrogen 7 and increases the nucleophilicity of the lone pair of electrons on nitrogen 9. Nitrogen 7 of guanine is homologous to nitrogen 3 of 5,6-dimethylbenzimidazole in the reaction catalyzed by nicotinate-nucleotide—dimethylbenzimidazole phosphoribosyltransferase (Figure 3–31) from which a carboxylato

*The numbers in parentheses are the distances in the relevant crystallographic molecular model, either that in Panel A or that in Panel B, between the two atoms between which a hydron is transferred during the steps in the enzymatic reaction.

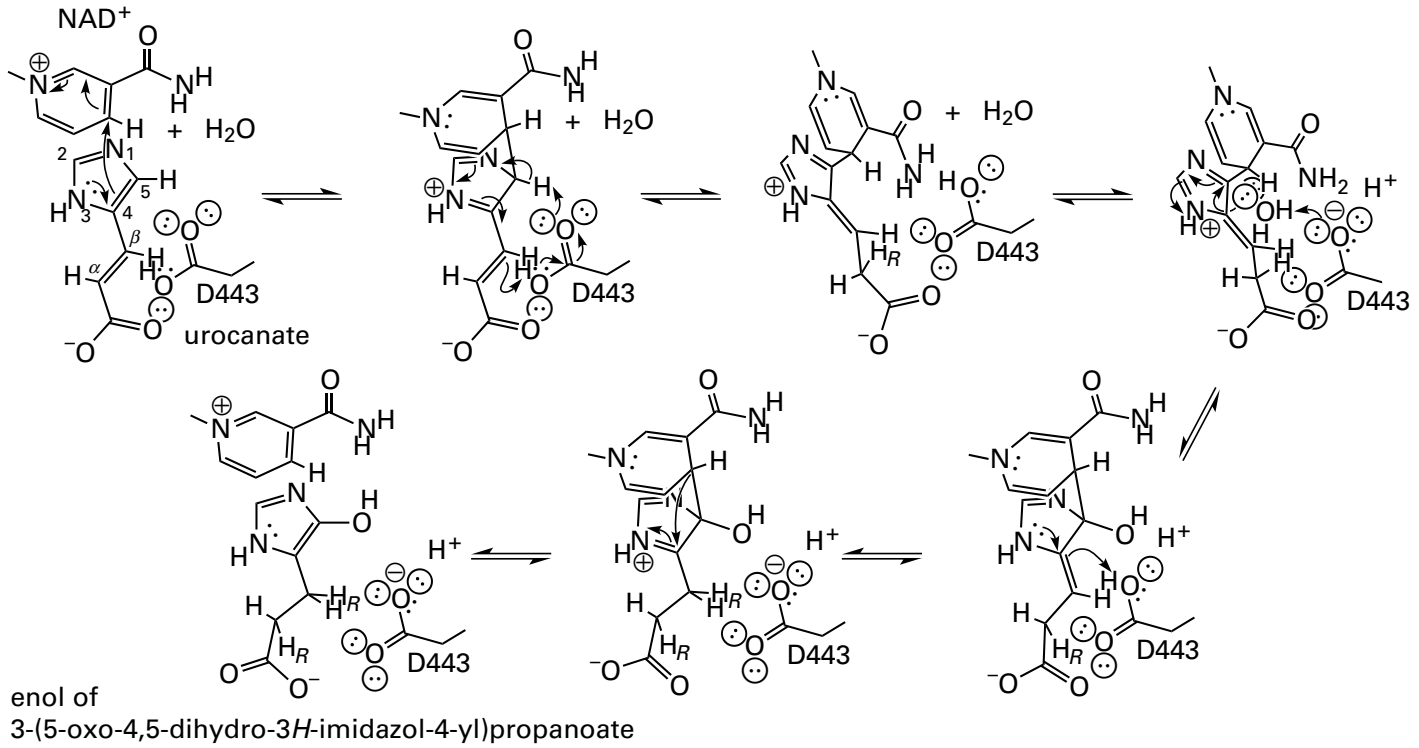

Figure 4–49: Steps in the mechanism for the reaction catalyzed by urocanate hydratase.[871] The reactants for the direction shown are urocanate and water, and the enzyme has a tightly bound NAD^+ as a prosthetic group in its active site. Nucleophilic addition of carbon 4 in the electron-rich imidazolyl group in urocanate to the electrophilic carbon 4 of NAD^+ initiates the reaction. In the resulting adduct, the aromaticity of the imidazolyl group is broken so that it has become two imines linked head to tail. The next step is a tautomerization to produce the exocyclic enamine of one of these imines. A molecule of water then adds nucleophilically to the imino carbon of the other imine to produce a hemiaminal next to a now-neutral enamine. The enamine is hydronated on its carbanionic carbon to produce the corresponding iminium. The parallel π system of this iminium withdraws electrons from the bond to the nicotinamide, and it breaks heterolytically to regenerate NAD^+ and the enol of the product, 3-(5-oxo-4,5-dihydro-3*H*-imidazol-4-yl)propanoate. Every hydron transfer is catalyzed by the carboxy group of Aspartate 443 in the enzyme from *P. putida* (Figure 4–50).

group removes a hydron to increase the nucleophilicity of the other nitrogen in the imidazolyl group.

Crystallographic molecular models of **complexes between inactive mutants and the usual substrates** can identify catalytic acids and bases. The crystallographic molecular model of the complex between an inactive mutant of phosphoserine phosphatase from *Methanocaldococcus jannaschii*, and the usual reactant *O*-phospho-L-serine (Figure 3–56) identifies Aspartate 13 as the catalytic acid that hydronates the β-oxygen of the L-seryl group to ensure its ability to leave from phosphorus. In the normal reaction catalyzed by the enzyme, the phospho group is transferred to the carboxy group of Aspartate 11, which has been changed to asparagine in the mutant, causing it to be inactive.

A less drastic change results from the mutation of Arginine 455 in the active site of urocanate hydratase (previously Equation 1–84)

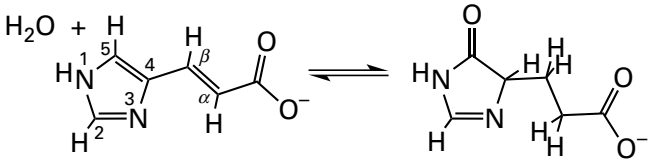

(4–367)

from *P. putida*. The guanidinio group of Arginine 455 is not a catalytic acid–base. Rather, in the unmutated active site of this enzyme, it sterically pushes on carbon 2 of the nicotinamide ring in the prosthetic nicotinamide adenine dinucleotide that is within the active site. When the guanidinio group is removed by mutation, the nicotinamide ring relaxes and tilts away from its proper position for its electrophilic addition to the urocanate (Figure 4–49),[871] and the mutant is catalytically inactive. Crystallographic molecular models of the unliganded native enzyme and of the mutant enzyme with its active site occupied by urocanate were prepared. In a hybrid molecular model (Figure 4–50)[872] of the active site

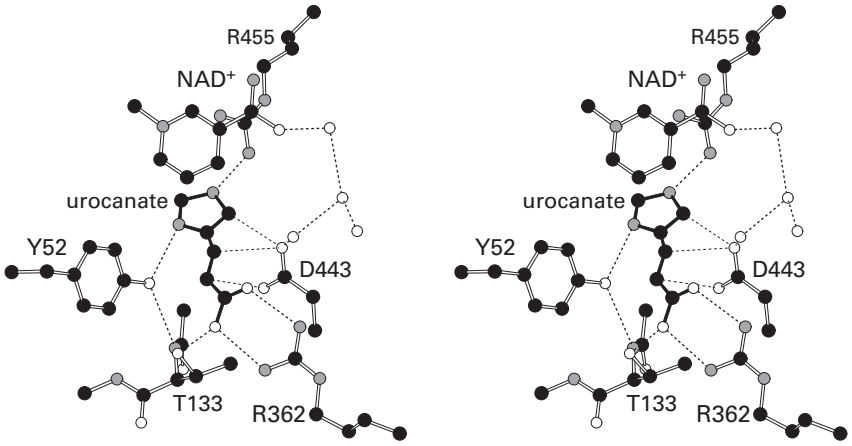

Figure 4–50: Stereodrawing[134] of the crystallographic molecular model of the active site of urocanate hydratase from *P. putida* occupied by the substrate urocanate.[872] Black atoms are carbons, white atoms are oxygens, and small gray atoms are nitrogens. Genes for both the native enzyme and an enzymatically inactive mutant in which Arginine 455 had been changed to alanine were overexpressed in *E. coli*. The two enzymes were purified and crystallized from 12% (w/v) poly(ethylene glycol) 8000, 90 mM sodium acetate, and 50 mM sodium cacodylate at pH 5.8. Crystals of the mutant were soaked in a solution of 10 mM urocanate. In the molecular model of the active site of the native enzyme, Arginine 455 was seen to be sterically tilting the ring of NAD^+, a tightly bound prosthetic group in the active site of the enzyme, into a conformation believed to be required for activity. In the active site of the molecular model of the mutant enzyme soaked in the solution of urocanate, electron density for urocanate could be observed in the active site. The drawing was made by combining urocanate, three molecules of water, and the side chains of Tyrosine 52, Threonine 133, Arginine 362, and Aspartate 443 from the molecular model of the active site of the mutant enzyme with NAD^+, a molecule of water, and the side chain of Arginine 455 from the molecular model of the native unoccupied enzyme. Consequently, the tilt produced by the arginine, which does not occur in the mutant, is depicted in the drawing. The most active acid–base catalyzing the reaction (Figure 4–49) is the carboxy group of Aspartate 443, which adds and removes hydrons from the three carbons connected to it in the drawing by thin dashed lines. The carboxy group swings between the two upper carbon atoms and to the molecule of water that is a substrate in the reaction by rotating around the α,β bond and swings up to the lower carbon by rotating around the β,γ bond. Tyrosine 52 ensures that nitrogen 3 of the imidazolyl group remains hydronated during the reaction, and Arginine 455 ensures that nitrogen 1 remains unhydronated. The four molecules of water clustered at the top right are connected directly to the solution and represent the source of the water that is a substrate in the reaction.

constructed from the model of the mutant protein occupied by urocanate and the model of the native enzyme, it can be seen that the carboxy group of Aspartate 443 is positioned to perform by itself all four of the hydron transfers required by the mechanism of the enzyme (Figure 4–49). It was known from stereochemical experiments that hydrons from the solution assumed the *pro-R* positions on carbons 2 and 3 of the product 3-(5-oxo-4,5-dihydro-3*H*-imidazol-4-yl)propanoate.[873] The stereochemical observations agree with the location of the carboxy group of Aspartate 443 in the model and serve to confirm its identity as the catalytic acid–base.

When Tyrosine 146 in fructose-bisphosphate aldolase from *Thermoproteus tenax* is mutated to phenylalanine, the enzyme is inactivated. In the normal reaction catalyzed by the enzyme (Figure 4–36), Lysine 177 forms an imine with the carbonyl carbon of fructose 1,6-bisphosphate in a nucleophilic substitution. In a crystallographic molecular model of the complex between the inactive enzyme and fructose 1,6-bisphosphate,[874] the enzymatic reaction is stalled at the zwitterion of the hemiaminal between the carbonyl of fructose 1,6-bisphosphate and the amino group of Lysine 177 in the active site (see Figure 1–7). The enzymatic reaction stalls at the zwitterion of the hemiaminal because Tyrosine 146, which has been mutated, is normally responsible for hydronating the oxygen of the hemiaminal and then shuttling a hydron from the ammonio group of Lysine 177 to the same oxygen so that it can leave as water to produce the iminium*

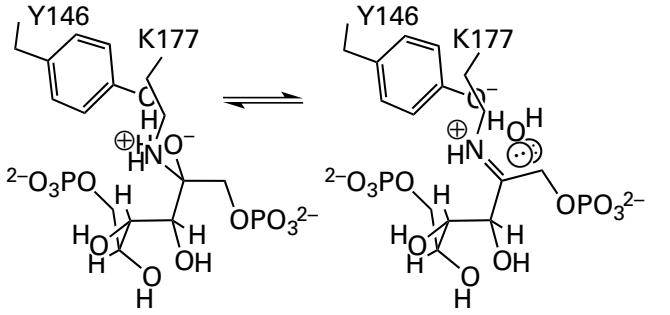

(4–368)

The fact that the enzymatic reaction stalls at this step is another example of the impossibility of transferring a hydron intramolecularly between two heteroatoms that are attached to the same carbon.

For enzymes with only one reactant and one product, other than water, crystallographic molecular models of **complexes between the enzyme and an inactive analogue of the sole reactant or product** can identify catalytic acid–bases. For example, the complex between creatinase from *P. putida* and carbamoyl sarcosine (**4–128**)

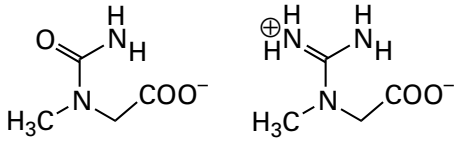

4–128 **4–129**

an inactive analogue of creatine (**4–129**) identifies the imidazolyl group of Histidine 232 as the catalytic base that removes the hydron from a fixed molecule of water in the active site to promote its nucleophilic addition to the guanidinio carbon in the hydrolysis catalyzed by the enzyme

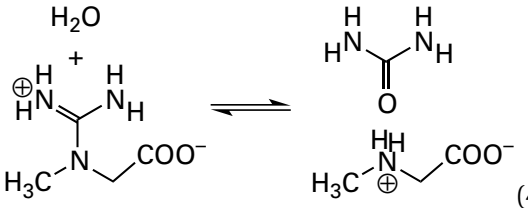

(4–369)

and then as the catalytic acid that hydronates the nitrogen of the *N*-methylglycine that leaves from the tetrahedral intermediate.[875]

R-Mandelate (**4–130**)

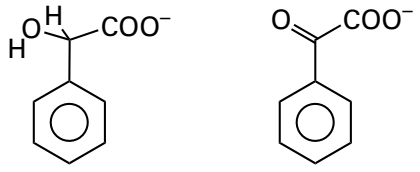

4–130 **4–131**

is an analogue of benzoylformate (**4–131**), which is decarboxylated to benzaldehyde by benzoylformate decarboxylase, an enzyme that uses thiamine diphosphate as a prosthetic group. The crystallographic molecular model of a complex between the enzyme from *P. putida* and *R*-mandelate identifies Histidine 70 as the catalytic acid that hydronates the carbonyl group of benzoylformate (**4–131**) during nucleophilic addition of the ylide of thiamine diphosphate (previously Equation 2–49)

*Carbon 4 of the phenylalanine is equidistant (0.42 nm) from the oxygen and the nitrogen of the hemiaminal and oriented so that, if it had a hydroxy group, as it does in Tyrosine 146, that hydroxy group would sit between the oxygen and the nitrogen of the hemiaminal within the length of a hydrogen bond to each.

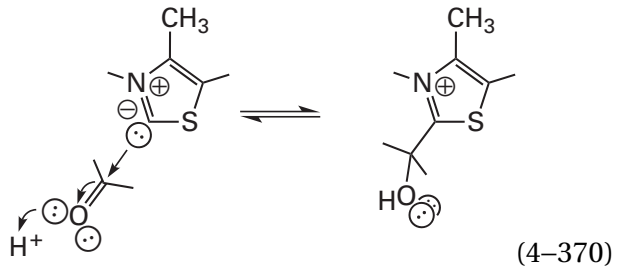

(4–370)

and Histidine 281 as the catalytic acid that hydronates the eventual carbonyl carbon of the incipient benzaldehyde

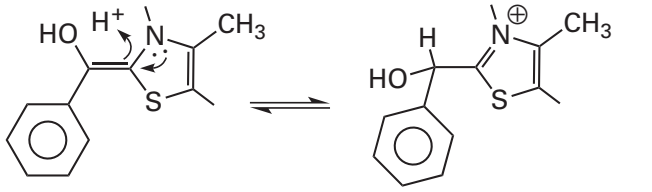

(4–371)

following the decarboxylation[876] (see Equations 2–51 and 2–54)

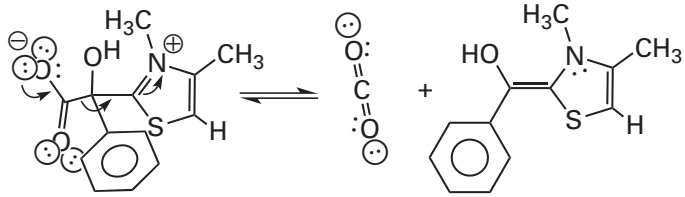

(4–372)

When Histidine 70 is mutated to alanine, the rate constant $k_0\,K_m^{-1}$ decreases by a factor of 18,000, and when Histidine 281 is mutated to alanine, it decreases by a factor of 800.

If an enzyme has two reactants, it is often possible to form a **complex with just one of the two reactants.** The crystallographic molecular model of such a complex, however, **can be misleading** because in many instances the active site is not fully assembled, nor are the catalytic groups properly aligned, until the protein closes around both reactants. For example, when ribulose-bisphosphate carboxylase (Equation 4–353) from *S. oleracea* associates with D-ribulose 1,5-bisphosphate and not with CO_2,[877] the active site fails to close completely around the substrate as it does when it closes around 2-carboxyarabinitol,[878] an analogue of the carboxylated enolate of D-ribulose 1,5-bisphosphate, the central intermediate in the mechanism of the reaction. Consequently, the identification of the N^6-carboxy group of carboxylated Lysine 201, acting alone, as the base that removes the hydron from carbon 3 of D-ribulose 1,5-bisphosphate (0.31 nm) to form the enolate in the first step in the reaction is equivocal. The proximate oxygen of the carboxy group on N^6-carboxylysine, because the other oxygen is a ligand to a Mg^{2+}, would be a weak base indeed ($pK_a < -2$). One possible solution to this problem is that a composite base could form between the proximate oxygen of the carboxy group and the τ nitrogen of Histidine 327 (0.36 nm) upon closure of the active site, and the oxygen of the carboxy group could relay the basicity of the imidazolio group.

In the active site[719] of 2-dehydro-3-deoxyphosphogluconate aldolase from *E. coli* (Equation 4–324), when only pyruvate is present, the equilibrium for formation of the imine of pyruvate (Equation 4–325) lies in favor of the hemiaminal (see Figure 1–7), so the key question of which base removes the hydron from carbon 3 of the imine of pyruvate cannot be answered.

Such observations, however, **need not be equivocal.** In the crystallographic molecular model of the complex between chloramphenicol *O*-acetyltransferase

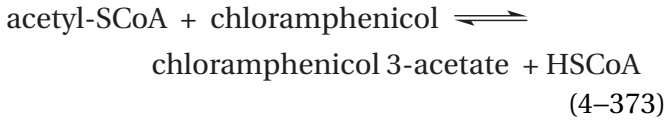

(4–373)

from *E. coli* and chloramphenicol in the absence of acetyl-SCoA, the imidazolyl group of Histidine 195 forms a hydrogen bond with the 3-hydroxy group of chloramphenicol to which the acetyl group is transferred. This hydrogen bond identifies Histidine 195 as the catalytic base that removes the hydron from the hydroxy group to enhance its nucleophilicity during formation of the tetrahedral intermediate in the reaction.[879] In the crystallographic molecular model of a complex between chloramphenicol *O*-acetyltransferase and coenzyme A in the absence of chloramphenicol 3-acetate, the same imidazolyl group forms a hydrogen bond with the sulfanyl group of the coenzyme A.[880] Taken together, these two observations suggest that this imidazolyl group, because it can form a hydrogen bond with each substrate when it is present alone, is responsible for hydronating either the oxygen or the sulfur in the tetrahedral intermediate

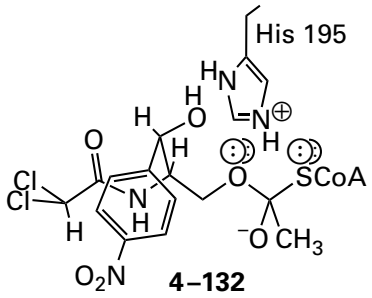

4–132

to make one or the other the leaving group. In addition, the imidazolyl group of Histidine 195 removes either the hydron from the hydroxy group of chloramphenicol or the hydron from the sulfanyl group of coenzyme A to produce the respective nucleophile during the two forward and two reverse routes to formation of the tetrahedral intermediate.

In the crystallographic molecular model of the complex between glucose 1-dehydrogenase [$NAD(P)^+$]

$$\beta\text{-D-glucopyranose} + NADP^+ \rightleftharpoons \text{D-glucono-1,5-lactone} + NADPH + H^+ \quad (4\text{–}374)$$

from *Thermoplasma acidophilum* and an alternate substrate, D-mannose, in the absence of NAD^+, Tyrosine 145 forms a hydrogen bond with the 1-hydroxy group of D-mannose, which probably identifies it as the catalytic base that removes the hydron during the enzymatically catalyzed oxidation by NAD^+ of D-mannose to D-mannono-1,5-lactone.[881]

There are **acid–bases other than the side chains of amino acids** in the polypeptide that accept and donate hydrons. The most common is a molecule of **water**. That molecule of water can be fixed in the active site by several donors and acceptors for hydrogen bonds,[581] or it may be an unfixed molecule of water in an exposed region of the active site, such as a wide opening to the solution[882] or simply due to the fact that the active site is only a depression on the surface of the enzyme, fully exposed on one side, as is the active site of xanthine phosphoribosyltransferase. As also in the case of xanthine phosphoribosyltransferase, a phospho group on a substrate (see Figure 3–44) or a phosphate that is itself a substrate (Figure 4–48B) can act as a catalytic acid–base. The phospho group on the prosthetic pyridoxal 5′-phosphate in glycogen phosphorylase, which is neither a substrate nor a direct participant in any step in the reaction catalyzed by the enzyme, acts as a catalytic acid–base that transfers a hydron to and from an oxygen on the phosphate that is a substrate in the reaction.[883] In this instance, a rather complicated prosthetic group is used by the active site only for its phospho group.

There are many **temporary hydronations at steps in the enzymatic reaction**. In the temporary nucleophilic addition of the sulfanyl group of Cysteine 81 to carbon 6 of cytosine

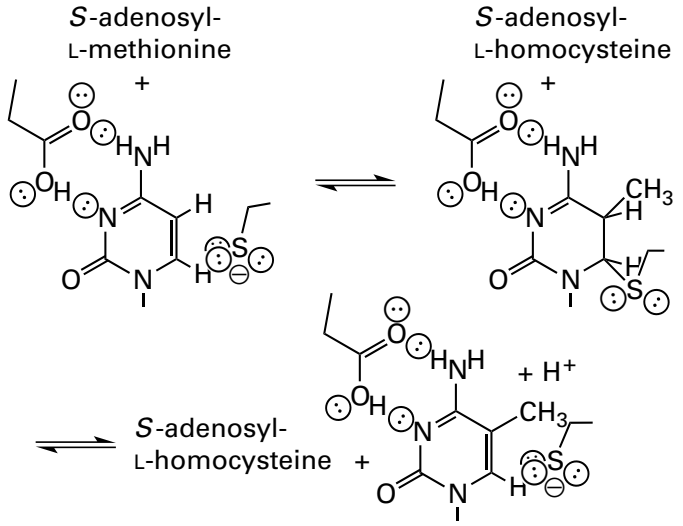

(4–375)

in the methylation of carbon 5 of cytosines in DNA by *S*-adenosyl-L-methionine catalyzed by DNA (cytosine-5-)-methyltransferase from *Haemophilus parahaemolyticus*, Glutamic Acid 119 transiently hydronates nitrogen 3 of the *N*-acylamidine in cytosine during nucleophilic addition of the sulfanyl group to carbon 6 to increase its electrophilicity, dehydronates nitrogen 3 during addition of the electrophilic methyl group from *S*-adenosyl-L-methionine to increase the nucleophilicity of the resulting *gem*-enediamine, and then rehydronates the nitrogen to acidify the hydron on carbon 5 following the methylation, and then dehydronates the nitrogen so that its πlone pair of electrons can push out the sulfanyl group during the final elimination.[884]

In crystallographic molecular models obtained from **neutron diffraction** of deuterated protein[135,885,886] or crystallography from the diffraction of X-rays at **short Bragg spacing**[887,888] or a combination of the two,[889,890] the **deuterons or hydrons on catalytic acid–bases in an active site can be observed directly**. For example, in the imidazolyl-carboxy composite acid–base in bovine trypsin (Equation 4–134), the deuteron in the hydrogen bond between the imidazolyl group and the carboxy group in the molecular model derived from a map of scattering density from neutron diffraction is on the imidazolyl group, even when it is the cationic imidazolium, rather than the carboxy group

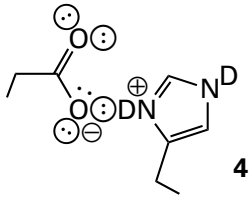

4–133

as expected from the respective values of pK_a.[135] The same is true of the imidazolyl-carboxy composite base in α-lytic endopeptidase from *Lysobacter enzymogenes*[891] and the one in xylose isomerase from *Streptomyces rubiginosus*.[892] In the unoccupied active site of cysteine endopeptidase from severe acute respiratory syndrome coronavirus 2, within the hydrogen bond between the nucleophilic sulfido group of Cysteine 145 and the imidazolio group of Histidine 41, the map of scattering density from neutron diffraction clearly shows the deuteron on the nitrogen of the imidazolyl group.[893] In the X-ray crystallographic molecular model (0.088 nm Bragg spacing) of the complex between β-lactamase CTX-M-9 from *E. coli* and a phosphate anion (Figure 4–51), an analogue of the tetrahedral intermediate in the enzymatic reaction, the hydron relayed by the hydroxy group of Serine 130 from the 6-ammonio group of Lysine 234 to the atom in the analogue representing the leaving nitrogen sits on the serine in the hydrogen bond with that oxygen on the phosphate, again as expected from the respective values of pK_a. All three hydrons on the ammonio group of Lysine 234 and the hydron on the hydroxy group of Serine 130 can be observed.[894]

Aspartic endopeptidases (pepsins) hydrolyze the amide of a peptide bond by catalyzing the nucleophilic substitution of a molecule of water for the amino group in the amide without a covalent intermediate (Figure 1–10). In a crystallographic molecular model from neutron diffraction of a deuterated complex between the aspartic endopeptidase endothiapepsin from *Cryphonectria parasitica* and an analogue of the tetrahedral intermediate, the deuteronation states of the carboxy groups on both catalytic aspartates, Aspartates 35 and 219, can be observed directly.[890] Aspartate 219 is deuteronated in the complex and Aspartate 35 is not deuteronated (but is the carboxylate), and the complex is an analogue of the tetrahedral intermediate, not the Michaelis complex. For these reasons, Aspartate 219 can be assigned as the catalytic base that removes the hydron from the molecule of water that adds to the amido group to form the tetrahedral intermediate. Aspartate 35 must be either the catalytic acid that hydronates the oxyanion of the tetrahedral intermediate

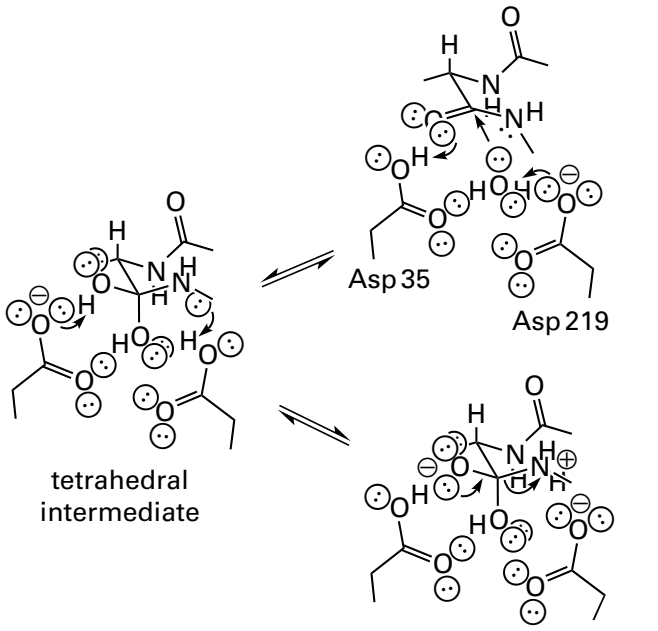

(4–376)

or the catalytic acid that deuteronates the homologous oxygen in the analogue of the tetrahedral intermediate but merely participates in an oxyanion hole for the actual intermediate in the enzymatic reaction.

The assignments of these roles, based on the locations of the deuterons in the crystallographic molecular model of endothiapepsin from neutron diffraction, are consistent with several other crystallographic observations. The molecule of water that is shared by the two carboxy groups in the active site before the reactant associates and that adds nucleophilically to the amido group of the peptide bond can be observed in the crystallographic molecular model[895] of unoccupied porcine pepsin (25% identity; 3.8 gap percent). This model identifies the location of that molecule of water in the Michaelis complex. In a crystallographic molecular model of a complex between HIV-1 retropepsin, encoded in the genome of human immunodeficiency virus, and an inert analogue of a peptide that is hydrolyzed by the enzyme, the carboxy group on the aspartate homologous to Aspartate 219 (Equation 4–376) is positioned to hydronate the leaving nitrogen.[896] In a crystallographic molecular model of a complex between HIV-1 retropepsin[897] and an actual tetrahedral intermediate, the aspartate homologous to Aspartate 219 forms a hydrogen bond with the amino group in the tetrahedral intermediate while retaining

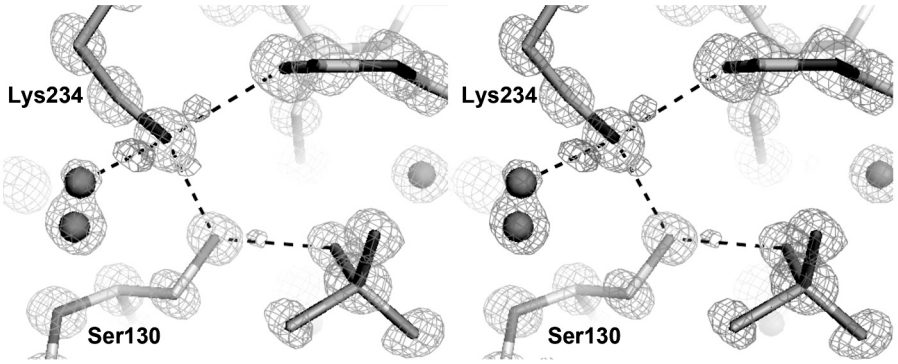

Figure 4–51: Crystallographic molecular model of β-lactamase CTX-M-9 from *E. coli* superposed on the map of electron density.[894] A data set from crystals of the enzyme was collected to Bragg spacing of 0.088 nm and submitted to molecular replacement. The polypeptide was inserted into the initial map of electron density and submitted to refinement. In the end there were three data sets: the observed amplitudes, F_o; the best estimates of the phases following the refinement, α_c; and the amplitudes calculated from the final refined molecular model, F_c. A data set $2F_o - F_c$ was created by subtracting the value for each calculated amplitude from twice the value for the respective observed amplitude, and a map of electron density was calculated from this data set and α_c. The resulting map gave the features of electron density centered on each of the heavy atoms of the molecular model in the drawing and represents the electron density from each of these atoms. A data set $F_o - F_c$ was created by subtracting the value for each calculated amplitude from the value for the respective observed amplitude, and a map of electron density was calculated from this data set and α_c. The resulting map gave three small features of electron density arranged tetrahedrally around the 6-ammonio group of Lysine 234 and a single small feature of electron density at one of the tetrahedral positions next to the oxygen of Serine 130. These four small features of electron density arise from the hydrons at these positions in the active site of β-lactamase CTX-M-9 but not in the refined crystallographic molecular model. They appear because they represent information about electron density within the crystal that is not represented in the molecular model. It can be seen that, within the composite acid–base formed from a molecule of water that is in equilibrium between two fixed positions, the 6-ammonio group of Lysine 234, and the hydroxy group of Serine 130, the hydron in the hydrogen bond between the ammonio group and the hydroxy group is located on the ammonio group. In the hydrogen bond between the 6-ammonio group and an acyl oxygen in the polypeptide backbone (upper right), the hydron, as expected, is on the 6-ammonio group, and in the hydrogen bond to the peripatetic molecule of water, the hydron is also on the 6-ammonio group. There is a phosphate occupying the location (lower right) at which the lactam hydrolyzed by the enzyme would be located in the Michaelis complex, and in the hydrogen bond between one of its oxygens and the hydroxy group of Serine 130, the hydron is, as expected, on the hydroxy group. Reprinted with permission from reference 894. Copyright 2007 American Chemical Society. https://doi.org/10.1021/ja0712064

its hydrogen bond with the oxygen that was the molecule of water, a fact that demonstrates its ability to remove a hydron from the water and then add a hydron to the nitrogen (Equation 4–376). In a crystallographic molecular model of a complex between HIV-1 retropepsin and the two products of the reaction,[897] the aspartate homologous to Aspartate 219 retains its contact with the nitrogen that it has just hydronated as the acceptor in a hydrogen bond with the amino group after it has left the tetrahedral intermediate.

As has already been noted, active sites use composite acid–bases. The simplest of all acids in aqueous solution, the hydronium ion, is itself a composite acid of at least four molecules of water and a hydron, all participating in a complex of hydrogen bonds.[898-907] In the composite acid of four waters and a hydron that may be the smallest hydronium ion, there are six equivalent hydrogens on the periphery, any one of which is acidic. In the simplest composite base of four molecules of water lacking one hydron, there are six lone pairs of basic electrons on the periphery, any one of which is basic. These two composite acid–bases are believed to be responsible for the fact that a hydronium as a catalytic acid in solution is often more acidic than its corrected pK_a would suggest (Figure 4–5B) and the fact that a hydroxide as a catalytic acid is often more basic than its corrected pK_a would suggest. Given the precedent of hydronium and hydroxide, it is not surprising that catalytic acid–bases in an active site are often composites of several side chains and often fixed molecules of water. In a composite acid–base in an active site, one or two heteroatoms on the periphery of the composite acid–base and immediately adjacent to a substrate are catalytic.

The first composite acid–base that was observed crystallographically is the one formed from the imidazolyl group of Histidine 57 and the carboxy group of Aspartate 102 in bovine chymotrypsin (Equation 4–134).[908] The proximal nitrogen on the imidazolyl group in this composite acid–base is responsible for removing the hydron from the hydroxy group on Serine 195 during its nucleophilic addition to a peptide bond (Figure 3–6).

Imidazolyl-carboxy* composite acid–bases have been identified in many active sites. For example, **imidazolyl-carboxy composite acid–bases** remove the hydron from the nucleophilic molecule of water bound to Zn^{2+} in thermolysin (His 231 and Asp 226 in Figure 3–42), and they remove the hydrons from the respective hydroxy groups on the carbons oxidized by L-lactate dehydrogenase (Equation 4–204)[909] and malate dehydrogenase[910]

$$(S)\text{-malate} + NAD^+ \rightleftharpoons NADH + H^+ + \text{oxaloacetate} \qquad (4\text{–}377)$$

As is the case in the active site of chymotrypsin, a number of serine endopeptidases, carboxypeptidases D,[911] lipases,[912-914] esterases,[915] and phospholipases[916] use an imidazolyl-carboxy composite base to remove a hydron from serine, cysteine,[917] or a molecule of water[916] during their nucleophilic additions to the respective acyl derivatives hydrolyzed by these enzymes. The active sites of formamidase from *Helicobacter pylori*[918] and β-lactamase from *S. aureus*,[919] however, use 6-amino-carboxy composite bases, formed from the amino group of lysine and the carboxy group of glutamate or aspartate, to remove a hydron from the sulfanyl group of cysteine and the hydroxy group of serine, respectively, during their nucleophilic additions to the respective acyl derivatives. Composite acid–bases are so common among the hydrolases of acyl compounds that the absence of a composite acid–base in one of these enzymes is considered peculiar.[920,921] Two imidazolyl-carboxy composite acids are used to hydronate one of the equatorial oxygens in an intermediate phosphorane and to hydronate the leaving oxygen from that intermediate phosphorane, respectively, in bovine deoxyribonuclease I.[922] Imidazolyl-carboxy composite acid–bases are also used to add a hydron to a carbonyl oxygen[909,923] and even to remove a hydron from carbon.[924-926]

In some instances, an imidazolyl-carboxy composite acid–base is extended further.[266] For example, in porcine phospholipase A_2, the composite acid–base, the catalytic hydron of which is on the π nitrogen of Histidine 48,[927] has the extended structure[916]

*__Proximal__ refers to positions in the composite acid–base nearer to the point where the catalytic hydron is transferred back and forth between acid–base and substrate, and **distal** refers to positions in the composite acid–base farther from the point at which the catalytic hydron is transferred, respectively. The functional groups in the composite acid–base are written from proximal to distal.

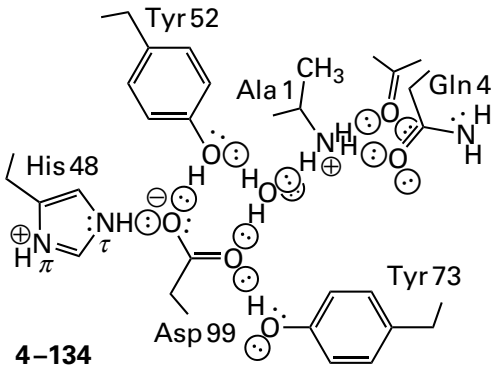

4–134

Mutation of both tyrosines to phenylalanines, however, decreases the rate constant $k_0 K_m^{-1}$ by only a factor of 7 while mutating the aspartate to asparagine decreases it by a factor of 1200.[928] The results of these mutations suggest that in many instances the purpose of the more distal participants in an extended composite acid–base may be structural rather than catalytic, as seems to be the case in the original composite acid–base, the one in the active site of chymotrypsin, in which the carboxy group is responsible only for orienting the imidazolyl group rather than significantly affecting its pK_a or effectiveness as a catalyst.[136,139]

As in the active sites of formamidase and β-lactamase, there are many composite acid–bases other than imidazolyl-carboxy ones. An imidazolyl-carbamoyl composite acid–base between histidine and asparagine removes the hydron from the nucleophilic sulfanyl group of a cysteine in the active site of actinidain from *Actinidia chinensis*,[929] and the two imido hydrogens of the carbamoyl group of the asparagine are buried respectively in the two π electron clouds of two tryptophans.[930] A carboxy-guanidinio composite acid–base removes the hydron from the nucleophilic molecule of water in the active site of the phosphatase encoded by the BT4131 gene of *B. thetaiotaomicron* (Asp10 and Arg45 in Figure 3–43). In the active site of chondroitin AC lyase (Equation 4–358 and Figure 4–44), the 4-hydroxyphenyl group (Tyrosine 242) responsible for the transfer of the hydron is the proximal participant in a composite acid–base. It is connected through a guanidinio group (Arginine 296) to two carboxy groups (Glutamate 412 and Glutamate 407), another guanidinio group (Arginine 300) and an imidazolyl group (Histidine 233). When the proximal guanidinio group on Arginine 296 is removed by mutation, the activity of the enzyme decreases by a factor of 100.[931] In the active site of pyruvate carboxylase from *Rhizobium etli*, the carboxylato group on Glutamate 305, which is responsible for removing a hydron from bicarbonate during the carboxylation of the prosthetic biotin, is the proximal participant in a composite acid–base with a carboxy group on Glutamate 218 and the imidazolyl group of Histidine 216. When any one of these three amino acids is mutated, the catalytic constant of the enzyme decreases by a similar factor (50–100),[932] a result suggesting that their effects on catalysis are concerted.

In the crystallographic molecular model[933] of asparaginase from *E. coli* in a complex with aspartate, one of its substrates, but not the cosubstrate ammonia, there is a continuous network of hydrogen bonds surrounding the substrate that consists of, in order, the side chains of Threonine 89, Lysine 162, Aspartate 90, Asparagine 248, Glutamate 283, Tyrosine 25, and Threonine 12. Calculations suggest that the amino group of Lysine 162, the hydroxy group of Threonine 89, and the hydroxy group of Threonine 12 within this extensive composite catalytic acid–base in turn transfer hydrons to and from substrates and the tetrahedral intermediate in three steps comprising the nucleophilic substitution catalyzed by the enzyme.[934]

Aside from their role in **orienting the heteroatom of the catalytic acid–base** that actually participates in transfer of the hydron to or from a substrate, a role that is usually essential, composite acid–bases, by combining several acid–bases of different intrinsic pK_a, participate in **adjusting the pK_a for that heteroatom**. In the unfolded polypeptide that folds to become the enzyme, the donors and acceptors for hydrogen bonds on the side chain in which the eventually catalytic heteroatom is located, including those on that heteroatom itself, are occupied by molecules of water, and this normal, unheralded network of hydrogen bonds determines in part the pK_a for the heteroatom in the unfolded polypeptide; in fact, this network determines in part the pK_a for any acid–base in solution. When these molecules of water are replaced as donors and acceptors in hydrogen bonds by other acid–bases during folding of the polypeptide and subsequent association of substrates, the pK_a changes for the heteroatom that is the ultimate catalytic acid–base.

When the polypeptide of endo-1,4-β-xylanase from *B. circulans* folds to produce the active site, the pK_a for the catalytic carboxy group of Glutamate 172 shifts from 4.3, the value it has when fully exposed to bulk water,[32] to 6.7.[124] When it is in the native active site, Glutamate 172 forms hydrogen bonds with Tyrosine 80, Asparagine 35, and a molecule of water to connect it to a large composite acid–base

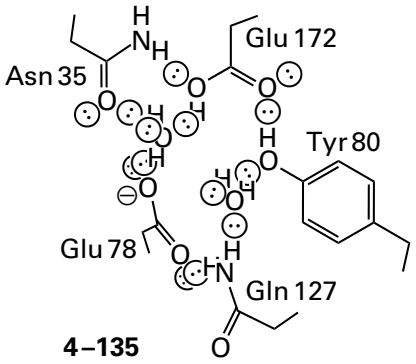

4–135

When Tyrosine 80 is mutated to phenylalanine, the pK_a for the carboxy group of Glutamate 172 increases to 7.9[157] because there is no longer an acidic donor of a hydrogen bond to the distal oxygen of the carboxy group, although an unresolved, less acidic (pK_a = 15.7) molecule of water may take its place. When Asparagine 35, the carboxamido group of which donates a hydrogen bond to the proximal oxygen of the carboxy group of Glutamate 172, is changed to aspartate, the pK_a for the carboxy group rises to 8.4, presumably because the neutral amido group that is the donor of the hydrogen bond (**4–135**) has been replaced by an anionic carboxylato group. The observed increase in the pK_a of Glutamate 172 from 4.3 to 6.7 upon folding, however, is due mainly to the juxtaposition of the anionic, catalytic carboxylato group of Glutamate 78,[124] which is linked to the carboxy group of Glutamate 172 through a molecule of water (**4–135**) at the pH that is optimal for enzymatic activity. This molecule of water is replaced by the oxygen that is the leaving group in the substrate upon its association with the active site so that Glutamic Acid 172 can hydronate that leaving group during hydrolysis of a xylan.[123,935]

When the polypeptide of glyceraldehyde-3-phosphate dehydrogenase (phosphorylating) from *E. coli* folds to produce the active site, the pK_a for the catalytic sulfanyl group of Cysteine 149 should have increased from its value of 8.7 when immersed in bulk water[32] because of a decrease in the relative permittivity from that of liquid water. In this instance, however, a hydrogen bond between the sulfanyl group of Cysteine 149 and the imidazolyl group of Histidine 176[936] maintains the pK_a for the sulfanyl group at 8.6 to facilitate its dehydronation.[937]

The evolution of a composite acid–base by natural selection is a special case, albeit a more obvious example, of the **ability of the active site to adjust the acidity and basicity of a catalytic acid–base**, and a crystallographic molecular model often identifies the reasons for this adjustment. For example, as has already been mentioned, the decrease in pK_a for the 6-amino group of Lysine 115 in acetoacetate decarboxylase from *C. acetobutylicum* from 10.5 to 6.0 (Figure 4–15) is not due to the proximity of Lysine 116, as was originally proposed.[938] Instead, the decrease is the result of Lysine 115 being situated in a hydrophobic region of low relative permittivity in the native enzyme.[165]

When a polypeptide folds and a donor or acceptor for a hydrogen bond on a particular heteroatom within its sequence of amino acids retains a molecule of water* or that fixed molecule of water is replaced by the hydroxy group of serine, threonine, or a substrate, there is no direct effect of that retention or that isoergonic substitution on the pK_a for that heteroatomic donor or acceptor in the native protein, even though other features of the active site, such as its relative permittivity, usually do affect the pK_a. Nevertheless, the **retained molecule of water or the hydroxy group replacing it can relay the acidity or basicity of the heteroatom** to a bound substrate or to another acid–base, much as the molecules of water in a hydronium ion or a hydroxide ion in solution can relay its acidity or basicity, respectively, or a hydron wire can relay a hydron. For example, the hydroxy group on the substrate pyridoxine 5-phosphate (Figure 4–48B) relays the hydron from the phosphate-imidazolyl composite acid in which Histidine 45 is a participant to the carbonyl oxygen on 2-methyl-3-oxo-4-hydroxymethyl-5-phosphomethyl-3,6-dihydropyridine (step *vi*, Figure 4–47) to catalyze its aromatization. A molecule of water relays the acidity of the amino-terminal ammonio group to the carboxy group of Aspartate 99 in the composite acid–base in phospholipase A_2 (**4–134**). A molecule of water relays the basicity of the carboxylato group of Glutamate 78 to the carboxy group of Glutamate 172 (**4–135**) in the empty active site of endo-1,4-β-xylanase from *B. circulans*.

The hydron on Tyrosine 125 in the active site of UDP-*N*-acetylmuramate dehydrogenase (Equation 4–239) is relayed through three molecules of water and the hydroxy group of Serine 229

*It should be reiterated that *the* same molecule of water is not retained, only *a* molecule of water, which is constantly exchanging.

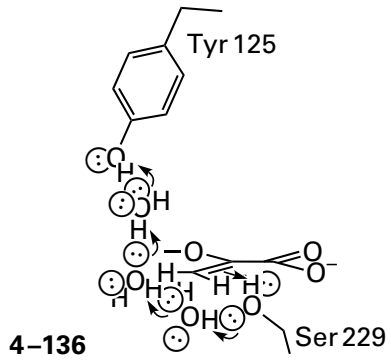

4–136

to hydronate carbon 1 of the enolpyruvyl group on the substrate, UDP-*N*-acetyl-3-*O*-(1-carboxyvinyl)-α-D-glucosamine, as the hydride is added to carbon 2 of the 1-carboxyvinyl group.[513] When that serine is mutated to alanine,[939] interrupting the relay, the rate of the reaction catalyzed by the enzyme decreases by a factor of 10^7.

A single molecule of water relays the basicity of Lysine 518 during removal of a hydron from the 2-hydroxy group of α-D-fructofuranose 6-phosphate

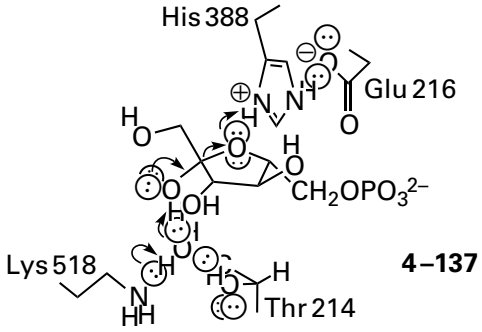

4–137

during the opening of the furanose catalyzed by glucose-6-phosphate isomerase from *O. cuniculus*.[940]

The enzyme 6-aminohexanoate-cyclic-dimer hydrolase from *Arthrobacter* hydrolyzes one of the two identical amides in 1,8-diazacyclotetradecane-2,9-dione, the tetradecacyclic, diamido dimer of two 6-aminohexanoates. In its active site, the hydroxy group of Serine 150 first relays the basicity of the amino group of Lysine 72 to remove the hydron from the hydroxy group of Serine 174

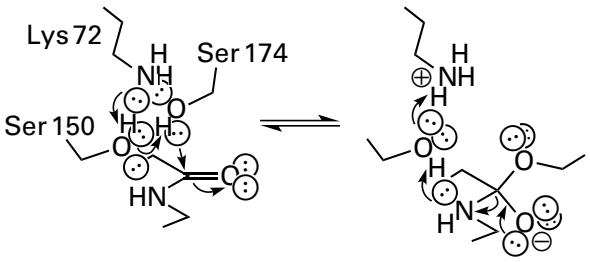

(4–378)

during its nucleophilic addition to the acyl carbon of the amido group. The hydroxy group of Serine 150 then relays the acidity of the resulting ammonio group of Lysine 72 to hydronate the amino nitrogen of the tetrahedral intermediate, permitting it to be the leaving group.[941] When either Serine 150 (the central relay) or Lysine 72 (the catalytic acid–base) is mutated to alanine, enzymatic activity decreases by a factor of greater than 4000.

In the active site of N^4-(β-*N*-acetylglucosaminyl)-L-asparaginase from *Elizabethkingia miricola*, the hydroxy group of Threonine 170 relays the basicity of the amino-terminal amino group of Threonine 152, which is exposed during an endopeptidolytic cleavage that activates the enzyme, to remove a hydron from the hydroxy group of Threonine 152[942]

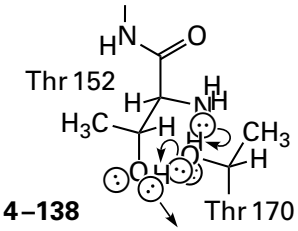

4–138

during its nucleophilic addition to the acyl carbon of the amido group in the reactant N^4-(β-*N*-acetylglucosaminyl)-L-asparagine. The amino-terminal amino group cannot remove the hydron on the hydroxy group effectively on its own because only three atoms separate its nitrogen from the hydron.

When a molecule of water or the hydroxy group on a serine or threonine relays the acidity or basicity of a catalytic acid–base, –NH, in a composite catalytic acid–base to or from a lone pair of electrons on reactant A, a tautomerization occurs

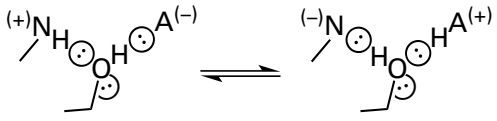

(4–379)

Since there is a hydroxy group in both reactant and product, the standard free energy change for the reaction is about the same as that for the reaction in which the catalytic acid–base would have directly transferred a hydron to and from the substrate. In this sense, the acidity in the forward reaction or the basicity in the reverse reaction is relayed. A hydrogen bond between the conjugate acid of the catalytic acid–base, $-NH^{(+)}$, and a hydroxy group, in the absence of hydron transfer, however, increases the acidity of the hydron on the hydroxy group only

slightly. Likewise, a hydrogen bond between the conjugate base of reactant A, $\odot A^{(-)}$, and the hydroxy group increases the basicity of one lone pair on the hydroxy group only slightly. Consequently, the fraction of the acidity or basicity relayed in the transition state is determined by the extent to which the hydrons are transferred to and from the hydroxy group to the reactant in the transition state. If the hydrons have been transferred almost completely in the transition state, the acidity or basicity has been fully relayed. If they are transferred only partially, then the acidity or basicity is only partially relayed.

The positions of basic lone pairs of electrons and acidic hydrons are revealed by the orientations of catalytic bases and catalytic acids on side chains of the amino acids, respectively, relative to hydrons to be removed from a substrate and lone pairs of electrons to be hydronated on a substrate. In most of the crystallographic molecular models discussed so far and in most others, neither hydrons nor lone pairs of electrons in hydrogen bonds are features in the map of electron density, yet they are there. An acidic hydrogen on a heteroatom in the side chain of an amino acid, although it is engaged in a covalent bond with the heteroatom, can be thought of as a hydron occupying a lone pair of electrons. Consequently, although the location of the hydron in the hydrogen bond cannot be observed in a crystallographic molecular model, the position of the lone pair in a hydrogen bond between a catalytic base and a hydron on a substrate, or the position of a hydron in a hydrogen bond between a catalytic acid and a lone pair on a substrate, are the same. All that remains ambiguous is the location of the hydron.

Leaving aside the question of their orientation in an aprotic solvent or the gas phase, the orientation of the lone pairs on the conjugate bases of the **five most common catalytic acid–bases** among the side chains of the amino acids when they are participating in hydrogen bonding, which they must be to be catalytic acid–bases and which they do when fully exposed to the solution when the polypeptide is unfolded, can be drawn

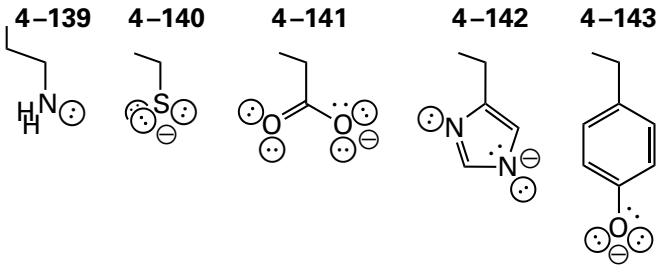

In both the amino group (**4–139**) of lysine and the sulfanyl group (**4–140**) of cysteine, the lone pairs and acidic hydrons are directed tetrahedrally from the heteroatom. This disposition is also true of the amino terminus of the polypeptide, which is sometimes used as a catalytic acid–base. In the carboxylato groups (**4–141**) of glutamate and aspartate, the imidazolyl group (**4–142**) of histidine, and the 4-hydroxyphenyl group (**4–143**) of tyrosine, the lone pairs are in the respective σ planes of these groups sandwiched between the respective π systems, and they are directed trigonally from their heteroatoms. Each side chain has **more than one lone pair of electrons or more than one acidic hydron,** giving it several orientational options and also allowing it to accept one hydron while it is donating another, as when it is a participant in a hydron wire or a composite catalytic acid–base.

The amino group (**4–139**) of lysine, the sulfanyl group (**4–140**) of cysteine, and the 4-hydroxyphenyl group (**4–143**) of tyrosine are particularly adept at removing a hydron from one atom and then pivoting to add a hydron to another atom that is two atoms removed from the first (Figure 4–44, Equation 4–368). This adeptness results from the freedom of nitrogen and sulfur to rotate around the carbon–nitrogen bond and the carbon–sulfur bond, respectively, and also from the collinearity of oxygen in the 4-hydroxyphenyl group with the β-carbon–γ-carbon bond of tyrosine. In a carboxy group, the two oxygens are symmetrically arrayed about the axis of the carbon–carbon bond, but rotation around that bond can have a much wider span. A rotation of 180° around this bond interchanges the two oxygens. Usually, however, one of the oxygens removes a hydron, pivots through a small arc, and then donates a hydron, as in the active site of triose-phosphate isomerase (Equation 4–55), where the carboxy group transfers the hydron between two adjacent carbons. Even though both nitrogens of an imidazolyl group in an enzyme almost always participate in hydrogen bonds, usually only one of the two nitrogens in a catalytic imidazolyl group functions as the acid–base, (Figures 3–37, 3–42, 4–46, and 4–48 and

4–132), and it often pivots on the noncatalytic hydrogen bond to service more than one atom. Lysine has the advantage that its 6-amino group is at the end of a flexible tether that allows it to move around more widely and more freely.

When it is participating in the transfer of a hydron, **each catalytic acid–base** must be oriented such that the atom in the substrate, the heteroatom in the side chain, the hydron being transferred, and the lone pairs of electrons on substrate and side chain between which it is being transferred are as **collinear** as possible. These components are not always precisely collinear because of the extreme steric challenges faced by natural selection in folding a polypeptide to create an active site, but they are usually remarkably close to collinear given these challenges. When you are examining the following stereodrawings from crystallographic molecular models and reexamining the stereodrawings you have already seen, pay particular attention to these orientations. Keep in mind the hybridization of the lone pairs in situations in which hydrogen bonding is occurring and the locations of the hydrons, usually unobserved, on the oxygens, nitrogens, sulfurs, and carbons in the molecular models.

Crystallographic molecular models of informative complexes have delineated the extensive group of catalytic acid–bases that are available to an enzyme for providing or removing a hydron during its catalysis. The set is diverse. In addition to the most common catalytic acid–bases (**4–139** to **4–143**) as well as molecules of water, there is a set of **less common catalytic acid–bases** such as the guanidinio group of arginine[943] and the hydroxy groups of serines[432,464,513] and threonines. Perhaps the most unexpected catalytic base is the indolyl group of tryptophan

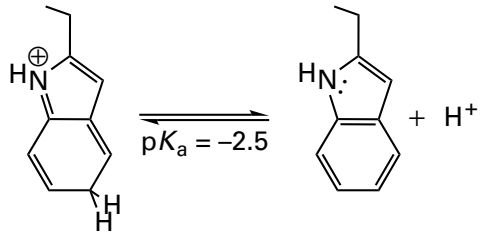

(4–380)

Like pyrrole, the indolyl group hydronates on any one of its carbons with a macroscopic pK_a of –2.5,[944] which is, within experimental error, the same as the pK_a for hydronation of the hydroxy group in serine.[388] The indolyl group of tryptophan has been proposed to be the base that removes a hydron adjacent to a carbenium ion to produce an alkene.[945] Any of the more conventional bases would be alkylated irreversibly by a carbenium ion. The hydron on the nitrogen in the indolyl group of tryptophan is a very weak acid (pK_a = 16), as is the hydron on the nitrogen in pyrrole (pK_a = 17), and it is seldom used as a catalytic acid–base, but when it is, advantage is taken of its weakness.

The present set of crystallographic molecular models of informative complexes has identified the types of catalytic acid–bases used for particular types of hydron transfer. These purposes range in necessity from the apparently unnecessary—acting as the donor of a hydrogen bond to a chloro group to enhance its ability as a leaving group—to the absolutely necessary—removing or adding a hydron from or to carbon. The unexpected result is how broad a spectrum of acid–bases have been called upon for each purpose, from the easiest to the most difficult.

In almost every chemical reaction catalyzed by an enzyme, there are hydron transfers between substrates and catalytic acid–bases in the active site or molecules of water in a region of the active site exposed to the solution or connected to the solution by a hydron wire. In order to understand the acid–base catalysis being performed by a particular active site, **each of its catalytic acid–bases must be identified and their roles defined**. To make this identification and establish this definition, an understanding of what the reaction requires is essential. Although the roles of the side chains in enzymatic reactions have been tabulated in a general sense,[946,947] these tabulations have not been dissected into **specific chemical roles**, such as removing a hydron from a hydroxy group in one direction and adding a hydron to the same oxygen in the other direction or removing a hydron from carbon in one direction and adding a hydron to the same carbon in the other direction. Each bidirectional role is chemically distinct and should be discussed systematically.

In most enzymatic reactions, **hydrons are transferred back and forth between two heteroatoms**: one on a substrate and another on a catalytic acid–base. Heteroatoms on substrates that participate in an enzymatic reaction usually participate as **nucleophiles and leaving groups**. When a heteroatom on a substrate acts in one direction as a nucleophile, it is a leaving group in the other direction, and vice versa. For the same type of heteroatom in a substrate, be it sulfur, oxygen, or nitrogen, the nucleophilicity of one of its lone pairs of electrons increases as the pK_a for its conjugate acid increases, and the ability

of the same heteroatom to leave decreases as the pK_a for its conjugate acid increases. Consequently, as discussed before, the measure of the nucleophilicity of a lone pair of electrons on a heteroatom in a substrate is the pK_a for its conjugate acid, and the measure of the ability of a leaving group to leave is the pK_a for the conjugate acid of the leaving group after it has left. When, however, the difficulty of hydronating a leaving group to improve its ability to leave is considered, that difficulty is measured by the pK_a for the conjugate acid of the leaving group while it is still in the reactant before it leaves. In the following discussion, unless otherwise defined, values of pK_a listed are for the conjugate acid of the nucleophile and the conjugate acid of the leaving group, either before or after it has left depending on the situation. Values of pK_a listed[948] are approximate because they depend significantly on the actual substituents on the particular type of heteroatom.

Strong heteroatomic nucleophiles in substrates, because they are usually hydronated at neutral pH, require a catalytic base to dehydronate them before or while they are adding to an electrophile. A strong nucleophile in the direction of addition is a poor leaving group in the direction of dissociation. Because a catalytic base is required to remove a hydron from a strong nucleophile on the approach to a transition state, by microscopic reversibility, the conjugate acid of that catalytic base will hydronate that same atom as it leaves, which will automatically improve the poor leaving group. These reciprocal requirements explain why, **in most dissociations of weak leaving groups and nucleophilic additions of strong nucleophiles, the active site provides a catalytic acid–base for the heteroatom that is leaving and adding**. It follows that, in a transition state within an active site catalyzing such a reaction, there is usually a catalytic acid–base that forms a hydrogen bond to a heteroatom that is about to leave or has just entered the transition state. This hydrogen bond in the transition state—between the heteroatom of the catalytic acid–base and the heteroatom that was or will be in the substrate and that will be or was the heteroatom of the leaving group or the nucleophile—lowers the standard free energy of formation of the transition state.

Weak heteroatomic nucleophiles, because their conjugate acids are strong, are usually unhydronated at neutral pH. Consequently, they should not require a catalytic base to ensure that they are unhydronated in the ground state. Weak heteroatomic nucleophiles in reverse are good leaving groups. In instances in which the leaving group is a good one and hence the nucleophile is a weak one and a catalytic acid–base should be unnecessary in both directions, one is nevertheless often provided even though it would seem to be counterproductive. If the catalytic acid hydronates the leaving group, then its conjugate acid must donate a hydrogen bond to the weakly basic nucleophile. This hydrogen bond would lower the nucleophilicity of the weak nucleophile from which a hydron does not have to be removed because it is already unhydronated in solution. In such cases, the catalytic acid base is probably used to orient the nucleophile by forming a hydrogen bond with it. For example, **chlorine in an alkyl chloride** is an excellent heteroatomic leaving group (p$K_{aHCl} = -7$) and should not need a catalytic acid, and it is a poor nucleophile in the other direction, the nucleophilicity of which would be decreased by the donor of a hydrogen bond. In haloalkane dehalogenase from *Xanthobacter autotrophicus*, however, the nitrogen–hydrogens in the indolyl groups of two **tryptophans** (p$K_a = 16$) donate their hydrons to the chloride as it leaves from a haloalkane.[949,950] In this instance, the nucleophile displacing the chloride is the carboxy group of an aspartate in the active site, which is a weak nucleophile, so acid catalysis of this nucleophilic substitution at chlorine is appropriate but the two acids in this case are weak ones so that their effect on the nucleophile is minimal.

Sulfur in a sulfanyl group

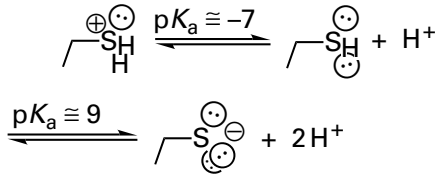

(4–381)

would seem also to need little assistance as a leaving group or a nucleophile. A sulfanyl group has a fairly low pK_a (p$K_a = 9$) and is, consequently, a decent leaving group; the pK_a of the conjugate acid of the sulfur in a sulfide (where one H in Equation 4–381 is a carbon) is quite low (p$K_a = -7$), making it difficult to hydronate before or as it leaves; and the unhydronated sulfido group, because it is in the third row, is a stronger nucleophile than its pK_a would suggest, so removal of a hydron should not be necessary. Yet catalytic acid–bases are almost always supplied. For example, in hydroxymethylglutaryl-CoA synthase (Equation 4–360) from *S. aureus*, the carboxy group of **Glutamate** 79 removes the hydron from the sulfanyl

group of Cysteine 111 (0.34 nm)* during its nucleophilic substitution on acetyl-SCoA. In chloramphenicol *O*-acetyltransferase from *E. coli*, **Histidine** 195 performs a similar role (**4–132**). In formamidase from *H. pylori*, a 6-amino group from lysine and a carboxy group from glutamate form a **lysyl-glutamyl composite base** that removes the hydron from the sulfanyl group of a cysteine during its nucleophilic addition to formamide.[918] In glyceraldehyde-3-phosphate dehydrogenase from *E. coli*, Histidine 176, by providing a catalytic imidazolyl group, ensures that the sulfanyl group of Cysteine 149 is unhydronated and properly oriented during its nucleophilic addition to the aldehyde of glyceraldehyde-3-phosphate.[936] In the human glutathione transferases, the 4-hydroxyphenyl group of **Tyrosine** 7 removes the hydron from the nucleophilic sulfanyl group in glutathione that participates in nucleophilic additions performed by these enzymes.[951,952] These examples indicate how eclectic is the choice of a catalytic acid–base, at least for removing a hydron from a sulfanyl group or adding a hydron to the sulfur in a leaving group.

Nitrogen in an amino group (–NH_2) or a secondary amino group (–NRH)

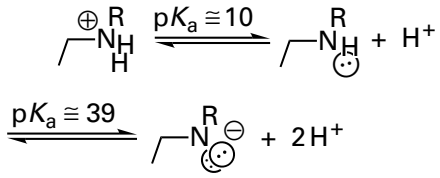

(4–382)

where R can be either a hydrogen or a carbon, rarely leaves a saturated carbon but often leaves carbon in a tetrahedral intermediate or participates in a tetrahedral intermediate by adding nucleophilically to a carbonyl or acyl group. Regardless of the type of carbon from which it leaves, a nitrogen in an amino or alkylamino group must be hydronated and cationic before it can leave (Figure 1–10) because the respective azanide anion, H_2N^- or RHN^-, is an exceptionally strong base ($pK_a = 39$) and hence an exceptionally poor leaving group. Whenever an amino or alkylamino group is **leaving carbon**, the active site must provide a catalytic acid to hydronate the nitrogen before or during the step in which the carbon–nitrogen bond is broken. This requirement is inescapable but also relatively simple to fulfill because an amino or alkylamino group, the conjugate acids of which have values for pK_a of 10, is easily hydronated by any of the catalytic acids available, and the resulting hydronated cationic ammonio or alkylammonio group, in contradistinction to, for example, a hydronated cationic oxygen, is a weak acid and remains hydronated as long as it takes to reach the transition state.

In the other direction (Figure 1–10), when ammonia or an alkylamine **adds to carbon**, it is always as ammonia or the neutral alkylamine (Figure 1–7), which are, respectively, the only accessible species in which the respective nitrogen has a nucleophilic σ lone pair of electrons. Consequently, if the amine enters the active site as the ammonium cation ($pK_a = 10$), there must be a catalytic base ready to remove its hydron before the nucleophilic addition. This participant is often the same catalytic base that removes a second hydron from the amino group as the reaction progresses. Consequently, if the same catalytic base performs both functions, it must either dissociate the hydron it took from the entering ammonium, if the nucleophilic addition is to a saturated carbon, or pass the hydron over to the oxyanion formed during addition of an amino group to a carbonyl or acyl carbon (left path of the tautomerization in Figure 1–7) because it must again be a base to dehydronate the again-ammonio group a second time. In reverse, the conjugate acid of this base would have to hydronate a leaving amino group, which is inescapable, so that it can leave as the amine. Furthermore if dehydronation of the initial ammonio group is required before the nucleophilic addition, then, by microscopic reversibility, it must be hydronated again after it leaves. The catalytic base that just hydronated the leaving group must gain a hydron from somewhere, usually from the atom of the nucleophile that just produced a tetrahedral intermediate, so that it can hydronate the amino group again after it has dissociated as the leaving group.

Formation of the iminium required for the retro-aldol condensation catalyzed by fructose-bisphosphate aldolase from *T. tenax* illustrates these consecutive roles in the two directions. The 4-oxidophenyl group of **Tyrosine** 146 has to remove a hydron from the 6-ammonio group of Lysine 177 before its nitrogen can add nucleophilically to the carbonyl of fructose 1,6-bisphosphate (Equation 4–368), and the resulting 4-hydroxyphenyl group either hydronates the resulting oxyanion of the former carbonyl oxygen in the resulting hemi-

*There is controversy surrounding the question of whether or not sulfanyl groups participate in hydrogen bonds, but this oxygen–sulfur distance is well within the sum (0.40 nm) of a hydrogen–sulfur bond (0.135 nm) and the van der Waals radii of hydrogen (0.115 nm) and oxygen (0.15 nm).

aminal or hydronates the carbonyl oxygen as the amino group is adding to the carbonyl group to form the hemiaminal. The second hydron is then shuttled by the 4-oxidophenyl group from the ammonio group in the hemiaminal to the resulting hydroxy group that is leaving as a molecule of water to give the lysyl imine. In reverse, the 4-oxidophenyl group of Tyrosine 146 removes a hydron from the molecule of water, before or as the water is adding to the lysyl iminium; the resulting 4-hydroxyphenyl group then transfers the hydron to the lone pair of electrons on the nitrogen in the resulting hemiaminal to create a leaving group; and then the resulting 4-oxidophenyl group removes a hydron from the hydroxy group in hemiaminal to give the oxyanion that provides the push to dissociate the amino group. The 4-hydroxyphenyl group then transfers the hydron to the amino group to give the 6-ammonio group of Lysine 177.

A large array of catalytic acid–bases are called upon to be the necessary catalytic acid–bases in reactions in which an amino group is the nucleophile in one direction and the leaving group in the other. **Glutamic Acid** 143 must hydronate the alkylamino group before it can leave as an amine from the tetrahedral intermediate during the reaction catalyzed by thermolysin from *B. thermoproteolyticus* (Figure 3–42). Aspartic Acid 126 must hydronate the alkylamino group before it can leave as an amine from the tetrahedral intermediate in the reaction catalyzed by endothiapepsin from *C. parasitica* (Equation 4–376). The carboxylato group of **Glutamate** 72 has to remove a hydron from the 3-ammonio group of 3-ammonio-2-oxopropyl phosphate before its nitrogen can add nucleophilically to carbonyl carbon 2 of 1-deoxy-D-xylulose during first step in the reaction (Equation 4–365) catalyzed by pyridoxine 5′-phosphate synthase from *E. coli* (Figure 4–48A). **Serine** 150 must relay the acidity of the 6-ammonio group of **Lysine** 72 to hydronate the alkylamino group before it can leave as an amine from the tetrahedral intermediate in the reaction catalyzed by 6-aminohexanoate-cyclic-dimer hydrolase from *Arthrobacter* (Equation 4–378). The **amino-terminal α-ammonio group** of the protein must hydronate the amino group before it can leave as ammonia from the tetrahedral intermediate in the hydrolysis catalyzed by the active site in the glutaminase domain (previously Equation 3–528)

$$\text{L-glutamine} + H_2O \rightleftharpoons \text{L-glutamate} + NH_4^+$$

(4–383)

of asparagine synthase (glutamine-hydrolyzing) from *E. coli*.[953] **Histidine** 232 must hydronate the dialkylamino group before it can leave as the dialkyl secondary amine *N*-methylglycine from the tetrahedral intermediate in the reaction catalyzed by creatinase from *P. putida* (Equation 4–369),[875] and the imidazolyl group of Histidine 141 has to remove the hydron from the 6-ammonio group of GDP-4-amino-4,6-dideoxy-α-D-mannose in the active site of GDP-perosamine *N*-acetyltransferase from *Caulobacter vibrioides* before it can add to the acyl carbon of acetyl-SCoA to initiate the acetyl transfer catalyzed by the enzyme.[954] In the first step of the nucleophilic substitution catalyzed by arginine dihydrolase from *Synechocystis*, Histidine 248 must hydronate one of the two amino groups before it can leave as ammonia from a tetrahedral intermediate in which the four substituents are all heteroatoms: the sulfur of Cysteine 365 and the three nitrogens in the guanidinio group of the substrate L-arginine to which the sulfido group of the cysteine has added nucleophilically.[955] The **phenolate oxygen of a lysylpyridoximine** or some other base has to remove a hydron from the α-ammonio group of the substrate before its nitrogen can add nucleophilically to the iminium carbon of an internal lysylpyridoximine (Figure 2–2), and the resulting conjugate acid of the phenolate oxygen or of the other base hydronates the amino group of the former iminium nitrogen of the internal lysylpyridoximine before it can shuttle the second hydron between the two nitrogens in the tetrahedral intermediate.

Histidine 57 in bovine trypsin is the histidine in the **imidazolyl-carboxy composite acid–base** that is homologous to the one in chymotrypsin (Equation 4–134). After Histidine 57 has removed the hydron from Serine 194 during formation of the tetrahedral intermediate, its imidazolyl group pivots around to the alkylamino group in the tetrahedral intermediate and hydronates the nitrogen before it can leave during the acylation of Serine 194 catalyzed by the enzyme (Figure 3–6).[135,956]

In the nucleophilic substitution catalyzed by ornithine carbamoyltransferase from *E. coli*, the side chain of an amino acid does not act as a catalytic base, but **one oxygen of the phospho group** of the reactant, carbamoyl phosphate[957]

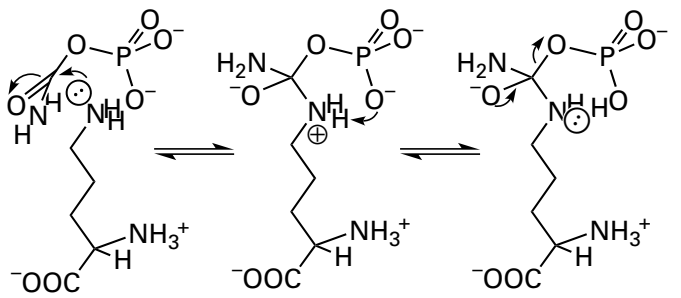

(4–384)

is conveniently positioned 4 atoms away. Ornithine binds to the enzyme as the neutral zwitterion with a nucleophilic 5-amino group that adds directly to the carbonato carbon of carbamoyl phosphate.[109] The phospho group of carbamoyl phosphate then removes the *pro-S* hydron from the now-ammonio nitrogen in the tetrahedral intermediate to make the phosphate the preferred leaving group.[957] The hydrogen bond between phosphoryl oxygen and ammonio group in the tetrahedral intermediate forms a five-membered ring, which is ideal for the transfer of a hydron. Removal of this hydron is unavoidable because only after it is dehydronated can the amino group become the required secondary ureido nitrogen in L-citrulline.

The choices by natural selection of an acid–base for the role of removing a hydron from an ammonio group or adding a hydron to an amine seem arbitrary. In the examples just cited, a carboxy group, an amino terminus, an imidazolyl group, a 4-hydroxyphenyl group, a composite hydroxy-6-amino group, and a phospho group have been chosen as catalytic acid–bases. In GTP cyclohydrolase I from *E. coli*, Histidine 179 hydronates the vinylamine that leaves from the tetrahedral intermediate in the latter of two consecutive hydrolyses catalyzed by the enzyme[958]

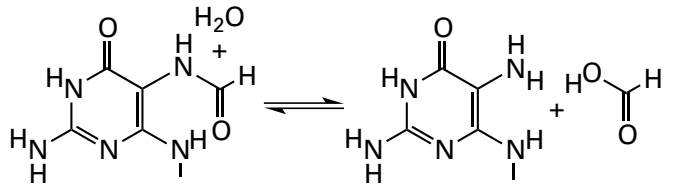

(4–385)

In the unrelated GTP cyclohydrolase II from *E. coli*, however, which catalyzes exactly the same hydrolysis, Tyrosine 105 hydronates the same nitrogen.[959]

Nitrogen in an aniline

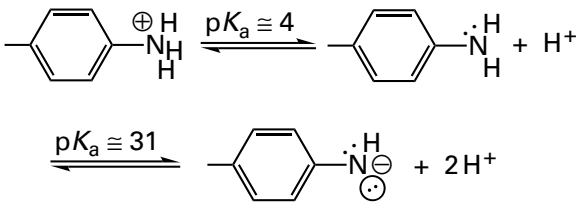

(4–386)

is a poor nucleophile but likely to be unhydronated at neutral pH. In the role of a leaving group, however, the nitrogen in a neutral anilino group inescapably requires a catalytic acid to hydronate it because the anilino anion is an impermissible leaving group ($pK_a = 31$). This hydronation of the leaving nitrogen is not such an inescapable requirement as the one for nitrogen in an amino group, but it is nevertheless imperative.

Both nitrogen 5 and nitrogen 10 of **tetrahydrofolate** (previously **1–81**)

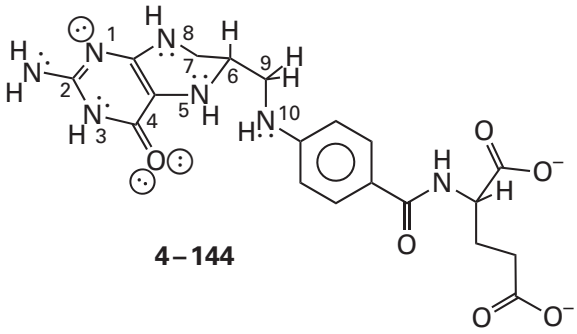

4 – 144

are anilino nitrogens on the basis of acid dissociation constants of their conjugate acids,[960] and they require a catalytic acid to add a hydron to them before they can leave. By microscopic reversibility, in the reverse reaction the resulting catalytic base removes a hydron from the anilino nitrogen as it adds and thus increases its nucleophilicity. For example, when the α carbon of the quininoid intermediate of glycine is adding to the hydroxymethyl group of the hydrate of N^5-methylenetetrahydrofolate, the anilino nitrogen 5 of tetrahydrofolate must be hydronated in order to leave

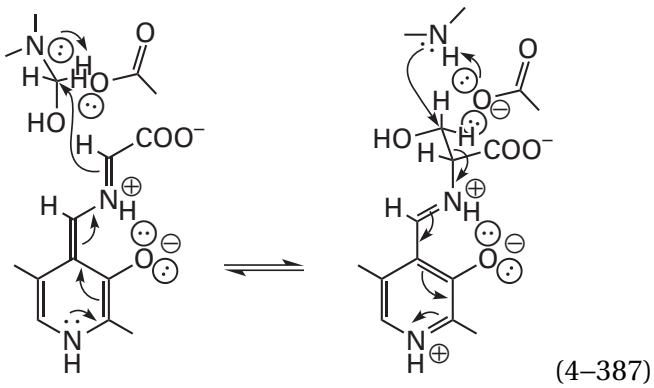

(4–387)

and this role is fulfilled by the carboxy group of **Glutamate** 75 in the active site of murine glycine hydroxymethyltransferase.[961] In the reverse reaction, the carboxylato group of Glutamate 75 removes the hydron from nitrogen 5 to improve its nucleophilicity.

When either anilino nitrogen in tetrahydrofolate enters into or leaves from the successive intermediates in the enzymatic **transfer of a methenyl to or from tetrahydrofolate**

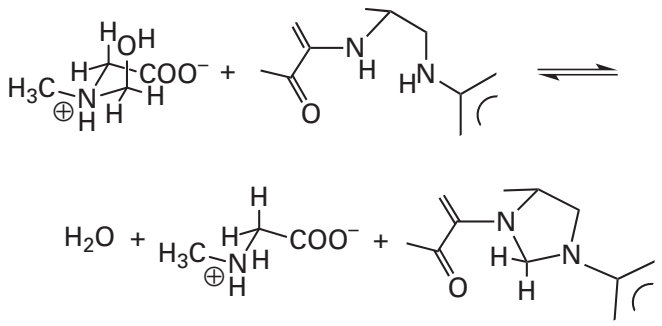

(4–388)

a catalytic acid–base hydronates or dehydronates the respective nitrogens. In the second half of the reaction catalyzed by dimethylglycine dehydrogenase (Equation 4–388) from *A. globiformis*, the carboxy group of **Aspartate** 552 dehydronates nitrogen 10 of tetrahydrofolate, and the 4-oxidophenyl group of the conjugate base of **Tyrosine** 651, through a hydron wire (0.33, 0.26, and 0.28 nm) of two molecules of water, dehydronates nitrogen 5.[962]

Furthermore, when either anilino nitrogen leaves from or enters into the tetrahedral intermediate in the enzymatic **transfer of a formyl group to or from tetrahydrofolate**

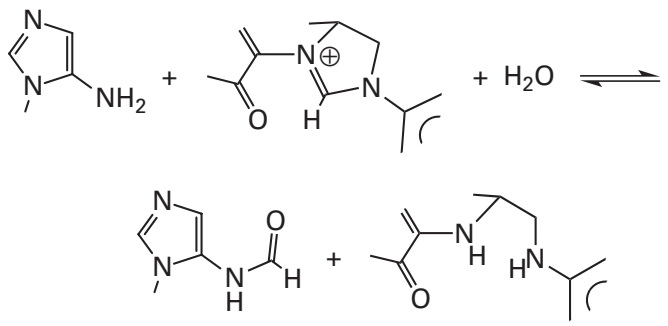

(4–389)

a catalytic acid–base must hydronate or dehydronate the respective nitrogens. In phosphoribosylaminoimidazolecarboxamide formyltransferase from *G. gallus*, the 6-ammonio group of **Lysine** 267 plays at least one of these roles, and perhaps the hydroxy group of **Serine** 451 plays the other.[963]

Nitrogen in the imidazolyl group of an imidazole

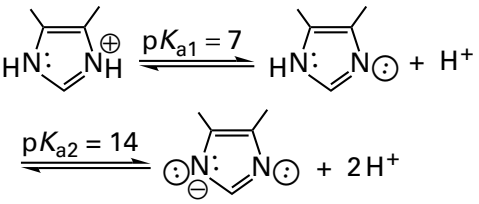

(4–390)

a benzimidazole ($pK_{a1} = 5$, $pK_{a2} = 13$) or the imidazolyl group of a purine such as adenine ($pK_{a1} = 4$, $pK_{a2} = 10$) or guanine ($pK_a = 3$, $pK_a = 9$) is a poor to middling leaving group when it is unhydronated on the distal nitrogen. As has already been noted, the ability of nitrogen in a covalent bond with carbon to leave is usually improved by providing a catalytic acid to hydronate the other, distal nitrogen in the imidazolyl group ($pK_a = 7$), the benzimidazolyl group ($pK_a = 5$), or the adeninyl ($pK_a = 4$) or guaninyl group ($pK_a = 3$), the one that is not leaving.[964,965] For example, **Glutamic Acid** 317 hydronates the other nitrogen in dimethylbenzimidazole as it leaves in the reaction catalyzed by nicotinate-nucleotide—dimethylbenzimidazole phosphoribosyltransferase from *S. typhimurium* (Figure 3–31). Aspartate 92 removes the hydron from the distal nitrogen in the imidazolyl group as guanine adds to 5-phospho-α-D-ribose 1-diphosphate in the active site of xanthine phosphoribosyltransferase from *E. coli* (**4–127**), and **Aspartic Acid** 137 adds a hydron to the distal nitrogen in the imidazolyl group when hypoxanthine or guanine leaves during the reaction catalyzed by human hypoxanthine phosphoribosyltransferase (Figure 3–38). The **carboxy-terminal carboxy group** of Tyrosine 158 in the active site of

nucleoside deoxyribosyltransferase from *Lactobacillus helveticus* hydronates the distal nitrogen in the imidazolyl group of an adenine that is a leaving group from a reactant while the other oxygen of the carboxy group is pinned in a hydrogen bond to the amido group on carbon 6 of the adenine.[966]

Nitrogen in a guanidinio group

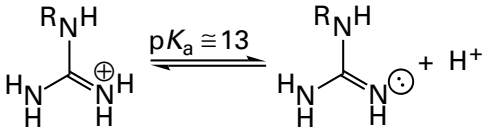

(4–391)

where R can be a carbon or a hydrogen, is a strong nucleophile when it is the neutral, unhydronated conjugate base, but for the same reason it is unlikely to be unhydronated at neutral pH. It follows that even when a guanidinio group is the hydronated, cationic conjugate acid, it is a poor leaving group. In the active site of guanidinoacetate *N*-methyltransferase from *R. norvegicus* (Figure 3–34), Aspartate 134 removes the hydron from the guanidinio nitrogen to unveil its nucleophilic σ lone pair of electrons that can participate in a concerted nucleophilic substitution at the methyl group of *S*-adenosyl-L-methionine. In the reverse reaction, Aspartate 134 must hydronate the same nitrogen as it is leaving to improve its ability as a leaving group. It has already been noted, however, that in the active sites of creatine kinase and arginine kinase (Figure 3–41), the electrons in the π molecular orbital system are the nucleophile, rather than a lone pair of electrons in the plane of the guanidino group of the conjugate base, and Aspartate 134 in guanidinoacetate *N*-methyltransferase is also not situated within the plane of the guanidinio group.

During addition **of a nucleophile to an imine**

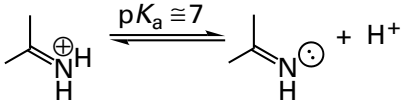

(4–392)

an imidoester

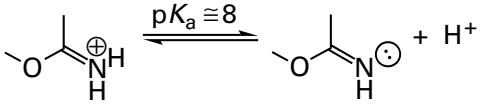

(4–393)

or an amidine

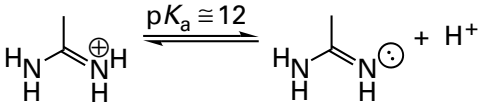

(4–394)

the imino nitrogen in each of these reactants must be hydronated, either before or during the addition to the carbonyl or acyl carbon that forms the respective tetrahedral intermediate. Otherwise an azanide (p$K_a = 39$) or an anilino anion (p$K_a = 31$), which are both more basic than an oxyanion (p$K_a = 15$), would be formed. As with nucleophilic addition to a carbonyl or acyl carbon, one of the simplest examples of such a nucleophilic addition is the addition of a hydride to an imino group catalyzed by a dehydrogenase or reductase.[967,968] For example, a molecule of water (0.26 nm) relays the hydron from Lysine 78 (0.26 nm) in the active site of phenylalanine dehydrogenase from *Rhodococcus* to the imino nitrogen in 2-imino-3-phenylpropionate either before or while a hydride is transferred stereospecifically from NADH to carbon 2 to reduce 2-imino-3-phenylpropionate to L-phenylalanine[969]

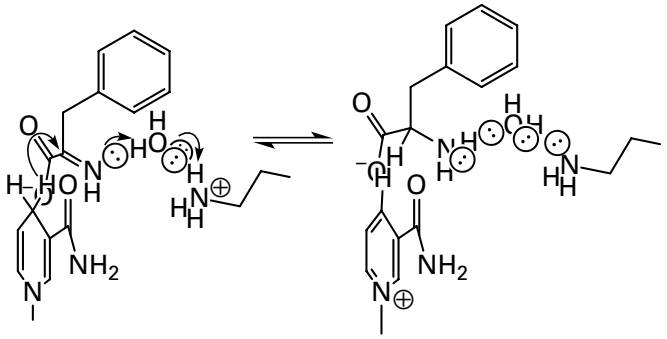

(4–395)

One of the most puzzling instances of this requirement for hydronation upon hydride transfer is the as yet unanswered question of what catalytic acid in the active site of dihydrofolate reductase (Equation 4–148) could hydronate nitrogen 5 during addition of a hydride by NADPH to carbon 6 of dihydrofolate

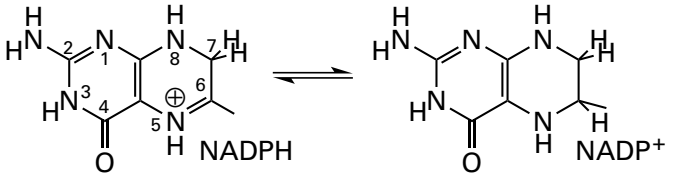

(4–396)

to give tetrahydrofolate.[970,971] Again, the requirement that nitrogen 5 be hydronated must be unavoidable because, if the nitrogen were not hydronated,

the anionic conjugate base of an aniline would be formed. The answer to the question is probably that the dihydrofolate has to enter the active site as the conjugate acid at nitrogen 5 ($pK_a = 4.82$), which is present in solution at reasonable levels, before the reaction can proceed. When dihydrofolate enters the active site as the conjugate base at nitrogen 5, hydride transfer cannot occur, and it simply dissociates.

Tyrosine 146 in fructose-bisphosphate aldolase from *T. tenax* (Equation 4–368) has to ensure that the nitrogen of the lysylimine of glycerone phosphate remains hydronated while a hydron is removed from carbon 3, because an azanide anion would be formed during removal of the hydron from carbon if the imine were not hydronated.

In the nucleophilic substitution catalyzed by murine adenosine deaminase

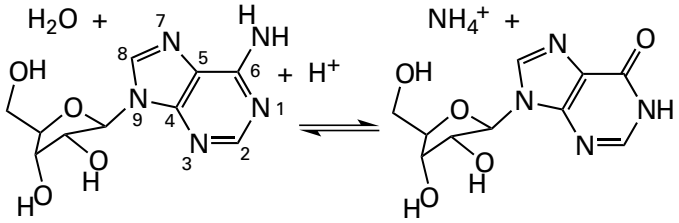

(4–397)

nitrogen 1 is hydronated by Glutamic Acid 217 to make the amidine in the adenine more electrophilic and avoid an anionic nitrogen in the tetrahedral intermediate either before or during nucleophilic addition of the hydroxy group of water to carbon 6.[972]

Oxygen in a hydroxy group

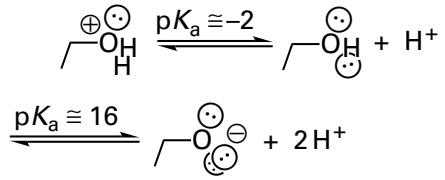

(4–398)

because its pK_a is so large, is a poor leaving group, and although hydroxide and alkoxide anions are strong nucleophiles, water and hydroxy groups are almost completely neutral at neutral pH. Consequently, a catalytic acid is required to hydronate a leaving oxygen in a hydroxy or alkoxy group. In the other direction, the conjugate catalytic base of that catalytic acid is required to remove a hydron from the corresponding water or hydroxy group to make it a nucleophile. Unlike the situation with a chloro group or even a guanidino group, these are inescapable requirements. Furthermore, one would expect that because hydronating an oxygen that is leaving is difficult and removing the hydron from a hydroxy group or a molecule of water that is adding is also difficult, only certain catalytic acid–bases would be capable of these responsibilities. Again, however, the choice of catalytic acid–bases made by natural selection is curiously eclectic.

The imidazolyl group of **Histidine** 322 must hydronate the hydroxy group of (*S*,*S*)-tartrate while that hydroxy group is leaving as water during the elimination catalyzed by D(–)-tartrate dehydratase from *B. japonicum* (Equation 4–267). The imidazolyl group of Histidine 231 must remove the hydron from the molecule of water while it adds nucleophilically to the acyl carbon of the peptide bond during the hydrolysis catalyzed by thermolysin (Figure 3–42). Histidine 195 must remove a hydron from the primary hydroxy group of chloramphenicol while it is adding nucleophilically to the acyl carbon of acetyl-SCoA in the active site of chloramphenicol *O*-acetyltransferase from *E. coli* (**4–132**). The imidazolyl group of Histidine 45 must hydronate the 4-hydroxy group while it leaves as water, and the **phospho-imidazolyl composite** base must remove a hydron from the molecule of water as it adds to carbon 5 during the reaction catalyzed by pyridoxine 5′-phosphate synthase from *E. coli* (Figures 4–47 and 4–48). The **imidazolyl-carboxy composite** acid must hydronate the furanose oxygen of α-D-fructofuranose 6-phosphate during the ring opening catalyzed by glucose-6-phosphate isomerase (**4–137**). The imidazolyl-carboxy composite base (Equation 4–134) must remove the hydron from the hydroxy group of Serine 195 (see **4–39** and the second stereodrawing in Problem 3–30) in bovine chymotrypsin while it adds nucleophilically to the acyl carbon of a peptide bond during the hydrolysis (Figure 3–6) catalyzed by the enzyme.

The carboxy group of **Glutamate** 211 or Glutamate 168 (Figure 4–43)—or possibly the imidazolyl group of Histidine 373 (not shown in Figure 4–43)—must hydronate the 3-hydroxy group of 2-phospho-D-glycerate while it is leaving as water during the elimination catalyzed by phosphopyruvate hydratase (Equation 4–128) from *S. cerevisiae*. Aspartate 215 must remove a hydron from the molecule of water while it adds nucleophilically to the acyl carbon of a peptide bond during the hydrolysis catalyzed by endothiapepsin from *C. parasitica* (Equation 4–376). Aspartate 443 must remove a hydron from the molecule of water while it adds nucleophilically to the imidazolyl group during the reaction catalyzed by

urocanate hydratase from *P. putida* (Figures 4–49 and 4–50).

The 4-hydroxyphenyl group of **Tyrosine** 146 must shuttle two hydrons to the oxyanion in the tetrahedral intermediate so that it can leave as water during formation of the imine in the reaction catalyzed by fructose-bisphosphate aldolase from *T. tenax* (Equation 4–368). The 4-hydroxyphenyl group of Tyrosine 242 must hydronate the oxygen of the glycosidic linkage to *N*-acetylgalactosaminyl 4-sulfate while that oxygen is leaving during the elimination catalyzed by chondroitin AC lyase from *P. aurescens* (Equation 4–358 and Figure 4–44).

An ester between the hydroxy group of Threonine 12 and the β-carboxy group of L-aspartate is a covalent acyl intermediate in hydrolysis of L-asparagine catalyzed by asparaginase from *E. coli*. The basicity of the 4-oxidophenyl group of Tyrosine 25 in the active site is relayed through a molecule of water that removes a hydron from a second molecule of water. This second molecule of water is the nucleophile that adds to the acyl intermediate to form the tetrahedral intermediate, which has been observed in a crystallographic molecular model.[973] The resulting 4-hydroxyphenyl group of Tyrosine 25 then hydronates the oxygen of Threonine 12 as the hydron on the hydroxy group of the tetrahedral intermediate, which was the molecule of water, is transferred through the intervening molecule of water to the 4-hydroxyphenyl group. This transfer of a hydron allows the developing oxido group in the tetrahedral intermediate to provide push while the hydroxy group of Threonine 12 being hydronated leaves. In the transition state, a hydron is leaving the 4-hydroxyphenyl group as another hydron is arriving from the relay, and a hydron is leaving the relay as another hydron is arriving.

The guanidinio group of **Arginine** 241 must hydronate the oxygen of the glycosidic linkage to an α-L-guluronoyl group while that oxygen is leaving during the elimination catalyzed by guluronate-specific alginate lyase from *Paraglaciecola chathamensis*.[974] **Serine** 150 must relay the basicity of **Lysine** 72 to remove a hydron from Serine 174 while it adds to the acyl oxygen of the substrate during the hydrolysis catalyzed by 6-aminohexanoate-cyclic-dimer hydrolase from *Arthrobacter* (Equation 4–378). The 6-ammonio group of Lysine 207 directly hydronates the oxygen on carbon 2 of phosph*enol*pyruvate while it leaves phosphorus during the hydrolytic nucleophilic substitution at phosphorus that forms the enol of pyruvate

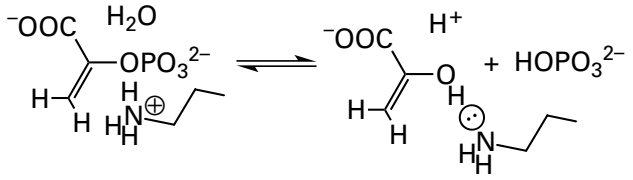

(4–399)

during the aldol condensation catalyzed by 3-deoxy-7-phosphoheptulonate synthase from *T. maritima*.[975]

Glycosidases are enzymes that hydrolyze *O*-glycosyl oligosaccharides and polysaccharides. In most glycosidases, a carboxy group—usually in the side chain of a **glutamic acid**,[795,976-983] such as Glutamate 35 in lysozyme (Figure 3–27) from *G. gallus*, but occasionally[984] in the side chain of an **aspartic acid**—performs the necessary hydronation of oxygen in the alkoxy group in the monosaccharide toward the reducing end of the oligosaccharide while it is leaving from the acetal or ketal that is the glycosidic linkage

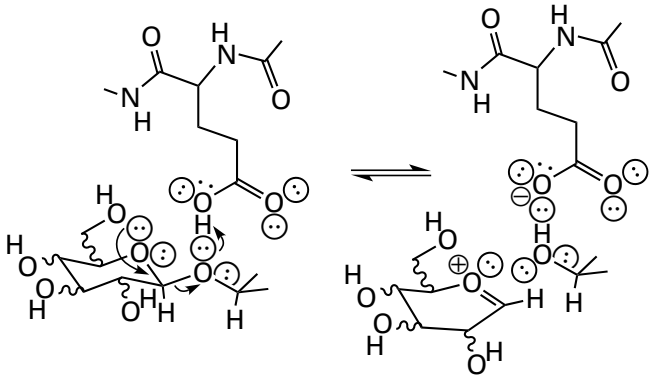

(4–400)

The oxygen of the carboxy group is positioned so that it forms a hydrogen bond with an sp^3-hybridized lone pair on the oxygen of the acetal and an sp^3-hybridized lone pair on the hydroxy group of the alcohol that leaves.[985] In the absence of hydronation, the alkoxide would have to be the leaving group, which would make dissociation difficult. In the unoccupied active site of lysozyme, Glutamate 35 has a pK_a of 6.0, and in the unoccupied active site of endo-1,4-β-xylanase from *B. circulans*, Glutamate 172, which hydronates the leaving group in this glycosidase,[935] has a pK_a of 6.7. These values are too high for the respective acids to hydronate the oxygen of the acetal (pK_a = –2) in the ground state before it leaves, so it must be the case that hydronation occurs as it leaves.

In most glycosidases, the leaving group dissociates from the active site and a molecule of water takes its place. The carboxylato group on the same

glutamate or aspartate then removes a hydron while the molecule of water adds nucleophilically, in the reverse of Equation 4–400, resulting in **retention of configuration** at the glycosidic carbon.

There are also glycosidases, however, that hydrolyze oligosaccharides and polysaccharides with **inversion of configuration** at the glycosidic carbon to produce, for example, an α glycoside from a β oligosaccharide or polysaccharide.[986,987] In these enzymes, a catalytic carboxy group from glutamate or aspartate still hydronates the leaving group (Equation 4–400), but a second carboxylato group acts as a catalytic base, performing the necessary removal of a hydron from a fixed molecule of water or hydroxy group on the opposite side of the glycosidic carbon from the leaving group. That molecule of water or that hydroxy group adds nucleophilically to the glycosidic carbon either during or immediately after dissociation of the leaving group and while this other carboxylato group is removing one of its hydrons.[976,984,988] In at least one inverting glycosidase, the required role of removing this hydron has been assumed by the 4-hydroxyphenyl group of a tyrosine rather than a carboxylato group.[983]

Oxygen in a carboxy group

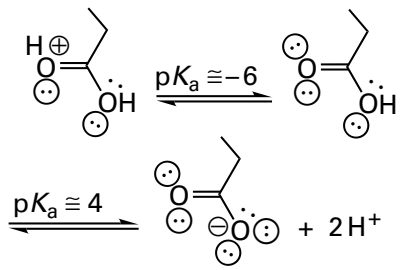

(4–401)

is a weak nucleophile, but it is usually already unhydronated and anionic at neutral pH. Oxygen in a carboxy group is also an excellent leaving group. Nevertheless, as a nucleophile and as a leaving group, it is usually provided with a catalytic acid–base by the active site. For example, in phosphatase from *B. thetaiotaomicron* (Figure 3–43), **Lysine** 188 provides a hydrogen bond (0.29 nm) to enhance the ability of the oxygen in the carboxy group of Aspartate 8 to leave the phosphorane that is the intermediate in the reaction. The 4-hydroxyphenyl group of **Tyrosine** 163 in cystathionine γ-synthase from *N. tabacum* provides a hydrogen bond for the oxygen of the succinyl group that leaves from O^4-succinyl-L-homoserine (Equation 4–259) as well as providing a hydrogen bond for the sulfur of the L-cysteine that leaves from cystathionine in the reverse reaction (Equation 4–257).[537]

The **oxygen in a carbonyl**

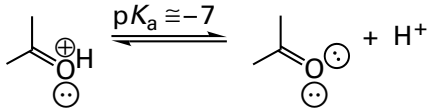

(4–402)

an ester

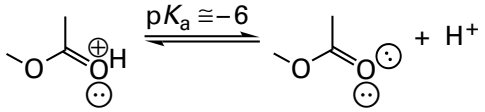

(4–403)

or **an amide**[989]

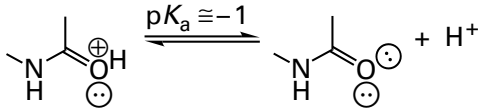

(4–404)

cannot be hydronated by any available catalytic acid in an active site. Nevertheless, when it is to become a hydroxy group in the product, the **oxyanion that results from nucleophilic addition to a carbonyl, ester, or amide** is almost always hydronated by a catalytic acid in an active site as it is being formed. One of the simplest examples is an oxygen that becomes a hydroxy group upon nucleophilic addition of a hydride to a carbonyl or acyl carbon catalyzed by a dehydrogenase or reductase. For example, in the active site of porcine lactate hydrogenase (Equation 4–204), **Histidine** 195 hydronates the developing oxyanion while NADH adds a hydride to the carbonyl of pyruvate.[909] In the active site of sorbose reductase from *Gluconobacter frateurii*, a hydron wire culminating in **Tyrosine** 157 hydronates the developing oxyanion as NADPH adds a hydride to the carbonyl of L-sorbose.[990] In the active site of dTDP-glucose 4,6-dehydratase from *E. coli*, however, Tyrosine 160 by itself dehydronates the developing carbonyl group as the prosthetic NAD^+ in the active site removes a hydride from carbon 4 of dTDP-α-D-glucose.[991] In the active site of human glycerol-3-phosphate dehydrogenase (NAD^+), the ammonio groups from **Lysine**s 120 and 204 form hydrogen bonds with the oxygen of the carbonyl in glycerone phosphate that is reduced.[992]

When the carbanionic carbon of an enolate, enol, or enamine is added to a carbonyl carbon to convert it to an alcohol, a catalytic acid is supplied to hydronate the oxygen. For example, during the aldol condensation between the lysyl enamine of glycerone phosphate and D-glyceraldehyde 3-phosphate, **Aspartic Acid** 24 in the active site of fructose-

bisphosphate aldolase (Equation 4–210) from *T. tenax* hydronates the oxygen of the carbonyl in D-glyceraldehyde 3-phosphate that eventually becomes the 4-hydroxy group in D-fructose 1,6-bisphosphate[874]

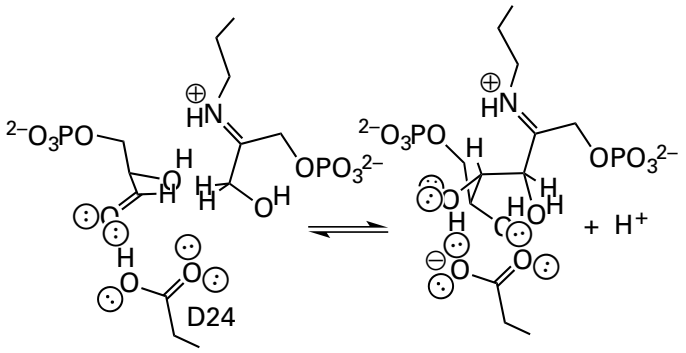

(4–405)

Glutamic Acid 49 in the active site of indole-3-glycerol-phosphate lyase within tryptophan synthase (**4–122**) hydronates the oxygen of the carbonyl of glyceraldehyde 3-phosphate (Figure 4–45) that becomes a hydroxy group during nucleophilic addition of the enamine of indole to that carbonyl carbon (Equation 4–363).

Even when the **oxyanion formed from a nucleophilic addition is transient** and will become an unhydronated carbonyl or acyl group in the product, a catalytic acid is sometimes provided rather than the far more common oxyanion hole. For example, in chalcone isomerase from *M. sativa* (Equation 4–359), the acidity of Tyrosine 106 is relayed through a molecule of water to hydronate the carbonyl oxygen during nucleophilic addition to the α,β-unsaturated carbonyl;[854] in the active site of hydroxymethylglutaryl-CoA synthase from *S. aureus* (Equation 4–360), Histidine 233 transiently hydronates the acyl oxygen of acetoacetyl-SCoA during nucleophilic addition of the enolate of acetyl-SCoA (Equation 4–361);[858] and in endothiapepsin from *C. parasitica* (Equation 4–376), Aspartic Acid 32 hydronates the acyl oxygen of the peptide bond during nucleophilic addition of a molecule of water. In the nucleophilic addition of a hydride catalyzed by human 2,4-dienoyl-CoA reductase (NADPH)

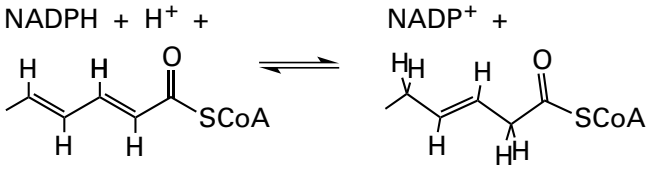

(4–406)

the acyl oxygen of a dienoyl-SCoA, which transiently becomes the oxygen of an enol, is hydronated by Tyrosine 199 (see **4–125**).[866]

Nitrogen 1 of a pyrimidine such as cytosine ($pK_a = 8$), uracil ($pK_a = 10$), or thymine can be turned into a better leaving group by hydronating the carbonylbis(azanediyl) oxygen on carbon 2

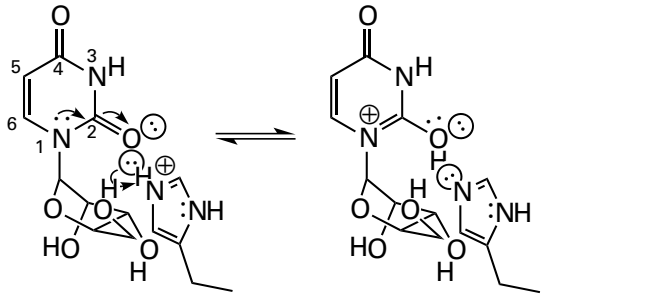

(4–407)

as in the active site of ribosylpyrimidine nucleosidase from *E. coli*.[993] Furthermore, if an acceptor for a hydrogen bond with the hydron on nitrogen 3 and a donor for a hydrogen bond with the oxygen on carbon 4 of uridine (Equation 4–407) are provided by the active site, in addition to hydronating the oxygen on carbon 2, then these three catalytic acid–bases increase the concentration of the unstable tautomer of uridine in which the ring is an aromatic 2,4-dihydroxypyrimidinio group.[994] This tautomer simulates the pyridinio group in an *N*-alkylpyridinium, which is an excellent leaving group. In the case of cytidine, all that is needed is to hydronate the oxygen on carbon 2 to produce the aromatic 4-amino-2-hydroxypyrimidinio group. A similar way in which an active site can make guanine a better leaving group is to hydronate the amido oxygen on carbon 6, as does the hydron on the carboxy group of Glutamate 201, which is relayed through a molecule of water, in the active site of bovine purine-nucleoside phosphorylase.[995]

Oxygen in hydrogen phosphate dianion, $HOPO_3^{2-}$

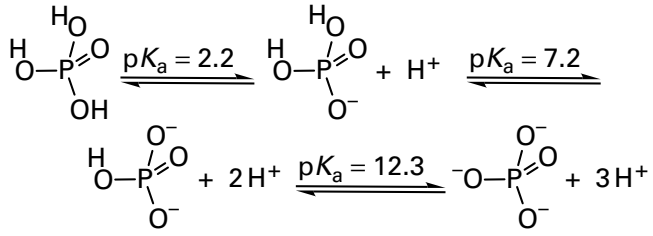

(4–408)

is more nucleophilic than a carboxy group. The pK_a for its conjugate acid, dihydrogen phosphate

monoanion, $HOPO_3H^-$, is 7.2, so at neutral pH there should be a significant fraction of the phosphate in a solution present as the nucleophilic dianion. Because the pK_a for its conjugate acid is 7.2, hydrogen phosphate dianion, without further assistance, is a good leaving group from the carbon in a monoanionic hydrogen phosphomonoester, $ROPO_3H^-$

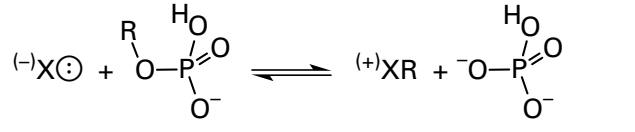

(4–409)

Because its pK_a is around 6.5, at neutral pH a significant fraction of the phospho group in a phosphomonoester should be the monoanionic hydrogen phosphomonoester

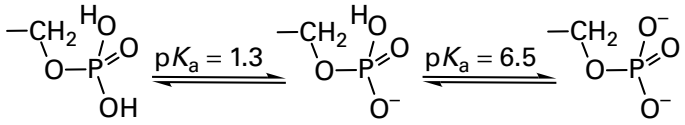

(4–410)

as required. Because a phosphate trianion (pK_a = 12.3) cannot leave from a completely unhydronated dianionic phosphomonoester, $ROPO_3^{2-}$, which should be the major fraction of a phosphomonoester at neutral pH, at least one of the two nonbridging oxygens in a phosphomonoester must be kept hydronated (Equation 4–409) if a phospho group is to function as a leaving group.

Regardless of the fact that hydrogen phosphate dianion by itself is a good nucleophile, a catalytic acid–base is usually supplied to orient that oxygen by a hydrogen bond and to **ensure that the oxygen that is the nucleophile is unhydronated**, and a conjugate base is often supplied to ensure that its other hydron (pK_a = 12.3) is removed as the nucleophilic substitution proceeds. For example, in the active site of glycogen phosphorylase from *O. cuniculus*, phosphate is the nucleophile in a nucleophilic substitution at carbon in which it replaces, at carbon 1 of a D-glucosyl group, the 4-hydroxy group of an adjacent D-glucosyl group in glycogen, poly(α1,4)-D-glucose. Lysine 574, Arginine 569, and an amido nitrogen–hydrogen from the polypeptide, by forming hydrogen bonds, ensure that two oxygens of the phosphate remain unhydronated during the reaction. The remaining, hydronated oxygen of the phosphate dianion (Equation 4–408) hydronates the leaving 4-hydroxy group of the D-glucosyl group (0.29 nm) while one of the other, previously anionic, oxygens of the phosphate is hydronated, to avoid formation of the trianion of phosphate, by the phospho group of a prosthetic pyridoxal 5′-phosphate (0.27 nm) in the active site as the 4-hydroxy group of the D-glucosyl group leaves to form the oxocarbenium ion. The nucleophilic oxygen in the resulting dianion of the phosphate, which just gave its hydron to the leaving group and which remains unhydronated because of hydrogen bonds to Lysine 574 and Arginine 569, then adds to the oxocarbenium ion at carbon 1 of the other D-glucosyl group as the phospho group of pyridoxal 5′-phosphate removes the hydron it just added to the phosphate to increase the nucleophilicity of the dianion.[996]

Regardless of the fact that hydrogen phosphate dianion by itself is a good leaving group (pK_a = 7.2), from carbon, catalytic acids are usually supplied both to **hydronate the bridging oxygen leaving from a monoanionic phosphomonoester** and to ensure that at least one of its nonbridging oxygens remains hydronated to ensure its ability to leave. For example, the imidazolyl groups of Histidine 12 and Histidine 52 and the carboxy group of Aspartate 11, acting in concert, ensure that the phospho group of 1-deoxy-D-xylulose 5-phosphate in the active site of pyridoxine 5′-phosphate synthase from *E. coli* remains at least monoanionic (Figure 4–48A), but the imidazolyl group of **Histidine** 45 hydronates the phospho oxygen that actually leaves (Figure 4–48B). The acidity of a composite acid formed from the carboxy group of the substrate and the imidazolyl group of Histidine 110 is relayed through three molecules of water to the phospho oxygen that leaves carbon 3 during the elimination catalyzed by chorismate synthase (Equation 4–250) from *S. pneumoniae*.[298] In (2*E*,6*E*)-farnesyl diphosphate synthase (Figure 3–44),[515] **Lysine** 202 provides a hydrogen bond to the oxygen of the diphosphate that actually leaves from the carbon of geranyl diphosphate to produce the methylalkylallyl carbenium ion (see Figure 1–26), even though the diphosphate has three Mg^{2+} as ligands.

The many nucleophilic substitutions at phosphorus catalyzed by enzymes almost always involve the transfer of a phospho group from one oxygen to another oxygen. In many of these instances, one or both oxygens are hydroxy groups on carbon or one is a hydroxy group on carbon and the other is a a hydroxy group on a molecule of water. In these cases, **a catalytic acid must be provided to hydronate the weakly acidic oxygen that is leaving, and a catalytic base must be provided to remove a hydron**

from the weakly basic hydroxy group while it is adding as a nucleophile. For example, the carboxy group of **Aspartate** 13 must hydronate the oxygen of serine phosphate while it leaves during the nucleophilic substitution at phosphorus catalyzed by phosphoserine phosphatase from *M. jannaschii* (Figure 3–56). In many instances, however, one or both oxygens are bound to phosphorus. In these cases, the conjugate acid of the leaving group or the nucleophilic oxygen, or both of them, are respectively acidic enough to leave or basic enough to add without assistance. Nevertheless, a catalytic acid is often provided to hydronate the oxygen that is leaving, and a catalytic base is provided to ensure that the nucleophilic oxygen is unhydronated.

Catalytic acid–bases are provided for the oxygens that leave from and add to phosphorus, regardless of whether the nucleophilic substitution is associative with a **phosphorane** as an intermediate

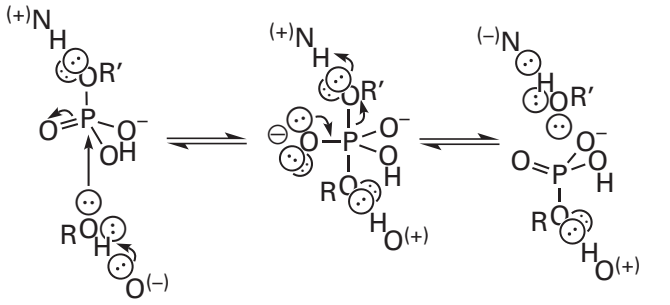

(4–411)

or dissociative with **monomeric metaphosphate** as an intermediate (see Figure 3–41). As with almost all classes of nucleophilic substitution, many if not most of the actual transition states fall between the two extremes of phosphorane and monomeric metaphosphate.

The active site of bovine **pancreatic ribonuclease** (Figure 4–46) is a paradigm of the requirements for catalytic acid–bases in nucleophilic substitutions at phosphorus. In the first step of the reaction, a molecule of RNA is cleaved to produce the 2′,3′-cyclic phosphate

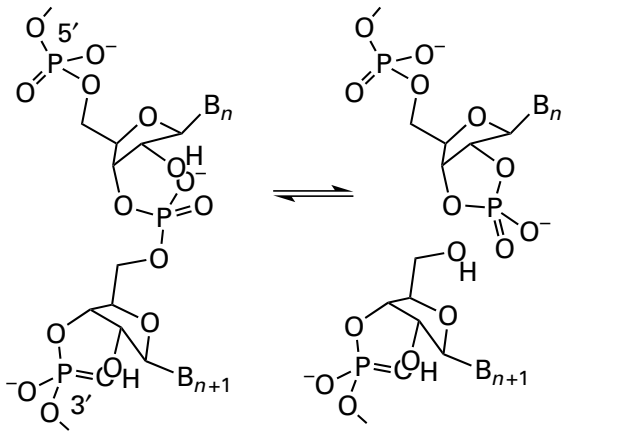

(4–412)

In the second step, the 2′,3′-cyclic phosphate is hydrolyzed

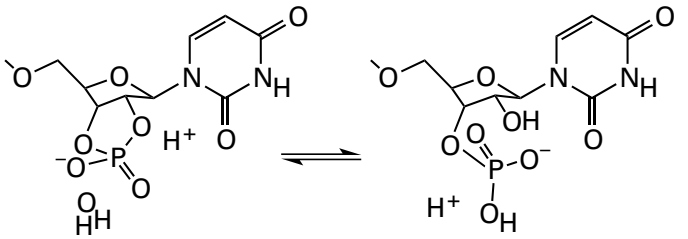

(4–413)

In these two steps, either the intermediates[997] are fully formed phosphoranes (Equation 4–411),[998] as they are in the alkaline hydrolyses of uridine 3′-phosphate esters in solution,[999] or the transition states[1000,1001] are phosphoranes with partial bonds at their axial positions. It is most likely that both of them are intact phosphoranes because, as in nucleophilic substitutions at phosphorus in solution that proceed through intermediate phosphoranes,[1002] all three oxygens involved in the two successive nucleophilic substitutions in the active site of ribonuclease, the two hydroxy groups and the molecule of water, are weak bases.

In the two halves of the full hydrolysis, the roles of the two catalytic acid–bases at the axial positions are switched. During the first half (Equation 4–412), the imidazolyl group of Histidine 119 ($^{(+)}$NH in Equation 4–411) hydronates the leaving 5′-hydroxy group (Figure 4–46), and the 6-ammonio group of Lysine 41 (⊙O$^{(-)}$ in Equation 4–411) removes the hydron from the 2′-hydroxy group that adds nucleophilically to the phosphorus. During the hydrolysis of 2′,3′-cyclic phosphodiester (Equation 4–413), the 6-ammonio group of Lysine 41 ($^{(+)}$NH in Equation 4–411) hydronates the leaving 2′-hydroxy group (Figure 4–46), and the imidazolyl group of Histidine 119 (⊙O$^{(-)}$ in Equation 4–411)

removes the hydron from the molecule of water that adds nucleophilically to phosphorus. When Lysine 41 is replaced by cysteine, the rate constant $k_0 K_m^{-1}$ for hydrolysis of RNA catalyzed by the enzyme decreases by a factor of 100,000;[1003] and when Histidine 119 is replaced by alanine, it decreases by a factor of 8000.[1004]

From the crystallographic molecular model for the complex between bovine pancreatic ribonuclease and the vanadyl analogue of the phosphorane (Figure 4–46), a crystallographic molecular model from neutron diffraction of the same complex,[152] a crystallographic molecular model of the complex between bovine pancreatic ribonuclease and uridine 5′-phosphate,[1005] a crystallographic molecular model of the complex between bovine pancreatic ribonuclease and uridine 3′-phosphate,[1006] and the pH–rate behavior of the enzyme (Figure 4–11), the following description of the two nucleophilic substitutions at phosphorus performed by the active site of pancreatic ribonuclease can be formulated.*

The reactant ribonucleic acid (Equation 4–412) enters the active site with the two nonbridging oxygens on the phosphodiester that will be cleaved sharing, as usual, the equivalent of a charge number of –1, and they remain at that charge number until the reaction commences. Before the first nucleophilic substitution at phosphorus, the imidazolio group on Histidine 119 must be hydronated as the cationic conjugate acid, the imidazolyl group on Histidine 12 must be unhydronated as the neutral conjugate base, and the ammonio group on Lysine 41 must be hydronated as the conjugate acid. Before addition of the nucleophile itself commences, one of the nitrogen–hydrogen bonds of the cationic ammonio group on Lysine 41 forms a hydrogen bond with one of the two lone pairs of electrons on the oxygen of the 2′-hydroxy group from the ribose in the 5′-nucleotide; the unhydronated lone pair of electrons on the proximal nitrogen of the neutral imidazolyl group on Histidine 12 forms a hydrogen bond with the hydrogen of the same 2′-hydroxy group;[1005] and the nitrogen–hydrogen bond of the cationic imidazolio group of Histidine 119 forms a hydrogen bond with the leaving 5′-oxygen from the ribose in the 3′-nucleotide esterified to the phospho group at which the cleavage will occur. The hydron in the hydrogen bond between the neutral imidazolyl group on Histidine 12 and the 2′-hydroxy group moves from oxygen to nitrogen at the same time that the hydron in the hydrogen bond between the ammonio group on Lysine 41 and the 2′-hydroxy group moves from nitrogen to oxygen. The now-cationic imidazolio group on Histidine 12 swings away from the 2′-hydroxy group,* and its nitrogen–hydrogen bond forms a hydrogen bond (Figure 4–46) with one of the lone pairs of electrons on the closest of the two nonbridging oxygens of the phospho group.[1006]

The empty lone pair of electrons on the 2′-hydroxy group from the ribose in the 5′-nucleotide, which was released as the imidazolio group of Histidine 12 swung away, adds nucleophilically to phosphorus. The bond between this oxygen and phosphorus forms at the same time that the hydron in the hydrogen bond between this oxygen and the amino group of Lysine 41 is moving from oxygen to nitrogen (first step in the reverse of Equation 4–411) and the hydron in the hydrogen bond between the imidazolio group of Histidine 12 and the nonbridging oxygen is moving from nitrogen to oxygen. Formation of the covalent bond between the oxygen at the 2′-position on the ribose in the 5′-nucleotide and phosphorus produces the phosphorane (the intermediate in Equation 4–411). The two axial oxygens of the phosphorane are the oxygen at the 2′-position of the ribose in the 5′-nucleotide and the oxygen at the 5′-position of the ribose in the 3′-nucleotide. The three equatorial positions are occupied by the two nonbridging oxygens, one of which has been hydronated by the imidazolio group of Histidine 12, and the oxygen at the 3′-position on the ribose in the 5′-nucleotide (Figure 4–46).

In the phosphorane (Equation 4–411), the neutral imidazolyl group of Histidine 12 is forming a hydrogen bond with the nearest neutral, hydronated equatorial oxygen of the phosphorane; the cationic ammonio group of Lysine 41 is forming a hydrogen bond with the uncharged oxygen at the 2′-position on the ribose in the 5′-nucleotide that is at one axial position in the phosphorane; and the cationic imidazolio group of Histidine 119 is forming a hydrogen bond with the uncharged oxygen that is about to leave the 5′-position of the ribose in the 3′-nucleotide at the other axial position in the phosphorane.

The next step is dissociation of the phosphorane. As the bond between phosphorus in the phosphorane and the 5′-oxygen of the ribose of the leaving nucleo-

*While you proceed through the discussion, view Figure 4–46.

*It has also been proposed that the imidazolyl group of Histidine 12 remains hydrogen-bonded to the 2′-oxygen and is the catalytic base that dehydronates it, rather than Lysine 41.[1007] This proposal, however, disagrees with the disposition of catalytic acid–bases in the vanadyl complex.

tide is breaking, the hydron in the bond between the imidazolio group of Histidine 12 and the equatorial oxygen is moving from oxygen to nitrogen, and the hydron in the hydrogen bond between the imidazolio group of Histidine 119 and the 5′-oxygen is moving from nitrogen to oxygen. Consequently, when the bond between oxygen and phosphorus has broken, there is now a hydrogen bond between the neutral imidazolyl group of Histidine 119 and the 5′-hydroxy group from the ribose in the 3′-nucleotide. The 3′-fragment of RNA departs from the active site as one product of the reaction (Equation 4–412) because it is no longer attached covalently to phosphorus.

At this point, the other product is the nucleoside 2′,3′-cyclic phosphate (Equation 4–412). Its negatively charged nonbridging oxygen forms a hydrogen bond with the cationic imidazolio group of Histidine 12 (Figure 4–11), and the uncharged oxygen from the 2′-position of its ribose forms a hydrogen bond with the cationic ammonio group of Lysine 41. Forget for the moment that this cyclic nucleotide can leave the active site at this point and enter the active site of another molecule of pancreatic ribonuclease.

A molecule of water enters the active site and occupies a location identical to the location that had been occupied by the 5′-hydroxy group from the ribose in the 3′-nucleotide that just left, and one of its two hydrons forms an identical hydrogen bond to the lone pair of electrons on the nitrogen of the neutral imidazolyl group of Histidine 119 (Figure 4–11). At this point the roles of the amino group of Lysine 41 and the imidazolyl group of Histidine 119 reverse. The nucleoside 2′,3′-cyclic phosphate still has one of its negatively charged, nonbridging oxygens forming a hydrogen bond to the cationic imidazolio group of Histidine 12 and the uncharged oxygen from the 2′-position of its ribose forming a hydrogen bond to the cationic ammonio group of Lysine 41. As the bond between phosphorus and the oxygen of water that will become an axial oxygen in the second phosphorane is forming, the hydron in the hydrogen bond between the imidazolio group of Histidine 12 and the nonbridging oxygen is moving from nitrogen to oxygen, and the hydron in the hydrogen bond between that molecule of water and the imidazolyl group of Histidine 119 is moving from oxygen to nitrogen.

When the axial bond has formed and the phosphorane occupies the active site, there is a hydrogen bond between the cationic imidazolio group of Histidine 119 and one of the lone pairs of electrons of the hydroxy group that was in the molecule of water but is now one of the axial oxygens of the resulting phosphorane. The other axial oxygen of the phosphorane is the 2′-oxygen of the ribose. The three equatorial positions are occupied by the two nonbridging oxygens and the oxygen at the 3′-position of the nucleotide (Figure 4–46). In the phosphorane, the neutral imidazolyl group on Histidine 12 forms a hydrogen bond with the nearest hydronated, neutral nonbridging oxygens of the phosphorane; and the cationic ammonio group on Lysine 41 forms a hydrogen bond with the uncharged oxygen at the 2′-position of the ribose in the phosphorane.[152]

The next step is dissociation of the phosphorane. As the bond between the phosphorus and the 2′-oxygen of the ribose is breaking, the hydron in the hydrogen bond between the neutral oxygen at the 2′-position and the nitrogen of the cationic ammonio group of Lysine 41 is moving from nitrogen to oxygen, and the hydron in the hydrogen bond between the imidazolyl group of Histidine 12 and the nonbridging oxygen is moving from oxygen to nitrogen. When the dissociation of the 2′-oxygen is complete, there is a hydrogen bond between the anionic nonbridging oxygen of the phospho group on the 3′-oxygen of the ribose and the cationic imidazolio group of Histidine 12, and there is also a hydrogen bond between the now 2′-hydroxy group of the ribose and the amino group of Lysine 41. The overall reaction is now complete.

Transfer of the hydron in the hydrogen bond from the ammonio group of Lysine 41 to the 2′-oxygen that is leaving during the hydrolysis of uridine 2′,3′-cyclic phosphate occurs at the point on the reaction coordinate at which the pK_a for the conjugate acid of that oxygen equals the pK_a for the ammonio group. In the phosphorane, the pK_a for the conjugate acid of the 2′-oxygen in the hydrogen bond to the ammonio group of Lysine 41 is less than 0. After the 2′-oxygen has become the 2′-hydroxy group in a hydrogen bond to the amino group of Lysine 41 following its dissociation from phosphorus, the pK_a is around 14. Consequently, as the reaction proceeds along the reaction coordinate in the direction of dissociation of the 2′-oxygen from phosphorus, the hydrogen bond between the ammonio group (p$K_a \cong 11$) and 2′-oxygen increases in enthalpy of formation by about -1.3 kJ mol^{-1} for each unit of increase in pK_a for the congugate acid of the 2′-oxygen, until its pK_a equals than of the ammonio group.[1008] There is no additional increase in enthalpy of formation when the pK_a for the ammonio group

is equal to that of the conjugate acid of the oxygen,[1009,1010] especially because the two heteroatoms are different. The increase in enthalpy of formation of this hydrogen bond as the reaction moves along the reaction coordinate lowers the height of the transition state relative to the ground state and promotes catalysis.

This **increase in enthalpy of formation of a hydrogen bond** as the reaction progresses, however, also occurs during general acid catalysis in aqueous solution. Consequently, it cannot be a factor in explaining the increase in the rate of reaction in the active site relative to that same reaction under general acid catalysis in solution because the same effect is operating in each situation. Furthermore, one would expect that this increase in enthalpy of formation due to the increasing strength of the hydrogen bond as the reaction proceeds along the reaction coordinate would be diminished by changing the catalytic acid—in the case of pancreatic ribonuclease, the ammonio group—to an acid of lower pK_a. This expected decrease, however, must be less than the increase in rate that would be caused by the increased acidity of the conjugate acid because rates of reactions in solution always increase as one general acid catalyst is replaced by another that is a stronger acid. The larger the Brønsted coefficient of the reaction is, the larger is this increase in rate. The increase in enthalpy of formation of the hydrogen bond cannot appreciably increase the rate of the reaction in the active site relative to the same reaction under general acid catalysis in water, and this increase in enthalpy is not so consequential as the absolute acidity of the acid catalyst. These two facts apply to any transfer of a hydron within a hydrogen bond during acid or base catalysis that is coincident with formation and dissociation of covalent bonds while passing along a reaction coordinate in an active site or in solution.

The other requirement for catalytic acid–bases in the transition state or transition states of a nucleophilic substitution at phosphorus

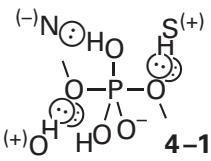

4–145

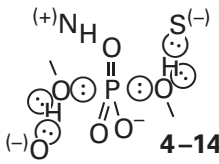

4–146

in addition to the requirements at the nucleophile and the leaving group (the acid–bases OH and SH), is manifest at **the equatorial oxygens on phosphorus** in the intermediate or the transition state. A phosphorane (**4–145**) and a monomeric metaphosphate sandwiched between two hydroxy groups (**4–146**) are the two extremes in a spectrum of transition states or intermediates in a nucleophilic substitution at phosphorus. When a phospho group is transferred between two poor leaving groups, such as two hydroxy groups on alkyl carbons or a hydroxy group on carbon and water (as in pancreatic ribonuclease), a phosphorane will usually be the intermediate, or there will be a transition state closely resembling a phosphorane. When a phospho group is transferred between two good leaving groups, such as two nucleoside diphosphates or a nucleoside diphosphate and a carboxylate, monomeric metaphosphate will usually be the intermediate, or there will be a transition state closely resembling monomeric metaphosphate. In the former instance, the leaving group is too poor an acid to leave before the nucleophile adds; in the latter instance, the leaving group is such a good acid that it leaves before the nucleophile can add.

In the former case, **a phosphomonoester or phosphodiester becomes a monoanionic phosphorane (4–146)** or its equivalent. A phosphorane is required to be at least a monoanion because the pK_a of a fully hydronated phosphorane is around 9 and because the oxyanion must be present to push out one or the other of the leaving groups at its axial positions. When the nucleophile adds to a phosphoester to create a phosphorane, it pushes a negative elementary charge out onto one of the oxygens, which is the automatic origin of the one negative elementary charge in the phosphorane. Consequently, the conjugate acid, $^{(+)}$NH in **4–145**, of at least one acid–base is required to hydronate the inescapable oxyanion on the phosphomonoester (pK_{a1} between 1 and 2) or phosphodiester (pK_a also between 1 and 2). This hydronation also guarantees that the phospho group is electrophilic either before or during the nucleophilic addition of a weak nucleophile. The same acid–base is required to guarantee that the phosphorane is dehydronated either before or while the poor leaving group departs from it to increase the push on phosphorus. In pancreatic ribonuclease, which has both phosphodiesters and phosphomonoesters as substrates, the acid–base that performs this role of hydronating and dehydronating a nonbridging oxygen is Histidine 12. When this histidine is mutated to alanine[1004] rather than simply being carboxymethylated, the rate constant $k_0\,K_m^{-1}$ for the enzymatic reaction decreases by a factor of 17,000. While a phosphodiester must enter the active site as the monoanion, a phosphomonoester can enter

the active site as either a monoanion or dianion. If the phosphomonoester ($pK_{a2} \cong 6$) enters the active site as a monoanion, then only that one acid–base is required at one of the equatorial oxygens, but if it enters as a dianion, a second acid–base is required so that both anionic oxygens can be hydronated during the nucleophilic addition.

In the latter case, **a phosphomonoester becomes a monoanionic monomeric metaphosphate** or its equivalent. Monomeric metaphosphate ($pK_a \cong -11$) must always be monoanionic, and there must be the equivalent of an oxyanionic hole to accommodate the anion. Either a phosphomonoester must enter the active site as the unhydronated dianion or there must be a catalytic acid–base, $^{(-)}$N⊙ in **4–146**, in the active site to remove the hydron from the hydronated monoanion. Because the next step in the nucleophilic substitution at phosphorus is usually equivalent to the first step in reverse, either the product of the nucleophilic substitution must be the unhydronated dianion or there must be a catalytic acid–base responsible for hydronating it to give a monoanionic product. Because it must always be monoanionic, monomeric metaphosphate cannot be an intermediate in a nucleophilic substitution at phosphorus in a phosphodiester.

Acetate kinase from *Methanosarcina thermophila*[1011] is one of the enzymes most likely to have monomeric metaphosphate for an intermediate, and both acetyl phosphate (pK_a for the monoanion is around 1) in one direction and $MgATP^{2-}$ in the other direction enter the active site unhydronated. The crystallographic molecular model for the active site of arginine kinase, however, strongly indicates that the nucleophilic substitution at phosphorus must pass through monomeric metaphosphate (Figure 3–41).[814] In this case, one equatorial oxygen of monomeric metaphosphate participates in hydrogen bonds with the guanidinio group of an arginine and the amido group of an asparagine, each of the other two oxygens participates in a hydrogen bond with one of the guanidinio nitrogens of the same arginine, and one of these two oxygens is also a ligand to the Mg^{2+} that entered the active site on $MgATP^{2-}$. These ligands form an extensive cationic oxyanion hole. The lack of a catalytic acid–base at the equatorial oxygens suggests that one is unneeded. Rather, the arginines surrounding the phospho group that participates in the nucleophilic substitution ensure that both arginine phosphate (pK_a for the monoanionic phosphoramidate is 9.6) and $MgATP^{2-}$ enter the active site as dianions at the phospho group involved in the reaction. In the active site of adenylate kinase from *E. coli*,[603,606] which transfers a phospho group between a monophosphate and a diphosphate and should pass through monomeric metaphosphate, the equatorial oxygens accept hydrogen bonds from two guanidinio groups of two arginines.

In other instances, the catalytic acid–bases that form hydrogen bonds to equatorial oxygens are the 6-ammonio groups of lysine,[1012-1020] which are competent catalytic acid–bases; or the guanidinio groups of arginines,[1021-1024] one or more guanidinio groups and a metallic dication,[1025] or two or more metallic dications,[1026] all of which are unlikely catalytic acid–bases. It has been shown, however, that although catalytic acid–bases provided for the equatorial oxygens increase rates of the respective enzymatic reactions, they do not seem to change the degree to which the nucleophilic substitution at phosphorus is associative or dissociative.[1027]

The slowest and most difficult hydron to remove or add is a hydron on carbon. In the reaction catalyzed by 3-phosphoshikimate 1-carboxyvinyltransferase (Equation 4–321; Problem 4–26) from *E. coli*, the 5-hydroxy group of shikimate 3-phosphate is added to phospho*enol*pyruvate, and hydrogen phosphate is eliminated from the resulting adduct[1028,1029]

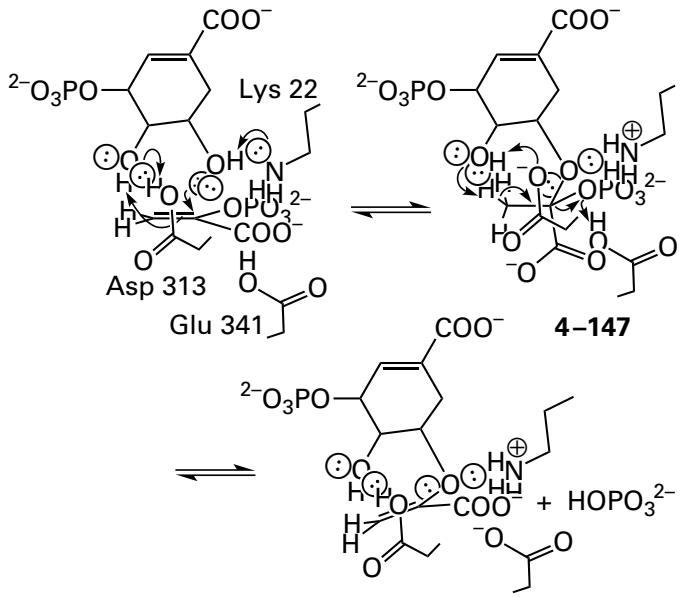

(4–414)

In both the elimination that takes place in the second step in the forward direction of Equation 4–414 and the elimination that takes place in the first step in reverse, a hydron is **removed from a methyl carbon that is not adjacent to a carbonyl or an acyl carbon**, probably the least acidic carbon–hydrogen bond in enzymatically catalyzed reactions. This remarkable

feat in each elimination from tetrahedral intermediate **4–147**, however, is performed by the 4-hydroxy group of shikimate 3-phosphate, the oxygen of which is only 0.31 nm from the methyl carbon of the enol pyruvyl group in tetrahedral intermediate **4–147**.[1029] In each elimination, this hydroxy group relays the basicity of the anionic carboxylato group of Aspartate 313. The same 4-hydroxy group, now relaying the acidity of the neutral carboxy group of Aspartate 313, must also accomplish the difficult hydronation of the methylene carbon of phospho*enol*-pyruvate during the addition that takes place in the first step in the forward direction, and it must hydronate the methylene carbon of the carboxyvinyl group in the addition that takes place in the second step in reverse.[702,1030] Another example of the ability of an active site to remove a hydron from a methyl carbon that is not adjacent to a carbonyl or acyl carbon is the removal of the hydron from the methyl group of *S*-adenosyl-L-methionine by the active site of carboxy-*S*-adenosyl-L-methionine synthase from *E. coli*.[1031]

3-Phosphoshikimate 1-carboxyvinyltransferase and carboxy-*S*-adenosyl-L-methionine synthase are two of the few exceptions, however, to the rule that when a hydron is removed from carbon by a catalytic base in the active site, that hydron is removed from a carbon immediately adjacent to a carbonyl carbon, acyl carbon, imido carbon, or imine or from a carbon conjugated to one of these groups, and addition of a hydron to carbon is to a carbon in an enol or enolate or to an enamine or to the carbon in a carbon–carbon bond conjugated to an enol, enolate, or enamine.

The **hydron on a carbon immediately adjacent to a carbonyl carbon, acyl carbon, imido carbon, or imine** is acidic, and its acid dissociation constant is usually in a reasonable range (Figure 1–23) that widely encompasses the acid dissociation constant for a hydroxy group. Nevertheless, the slowest and most difficult transfer of a hydron in biochemical reactions is the transfer of a hydron from and to carbon, for reasons already discussed in the first chapter. Removal of an acidic hydron from carbon is slow and difficult even for a base as strong as hydroxide, and addition of a hydron to nucleophilic carbon is also slow and difficult even for an acid as strong as hydronium. Hydroxide is a stronger base and hydronium is a stronger acid than any of the catalytic acid–bases available in an active site.

The kinetic difficulty of removing a hydron from carbon, and the fact that the Brønsted coefficient for general bases that remove a hydron from carbon in solution is 0.8,[1032-1034] would suggest that only the strongest bases available are used by an enzyme for this role. This expectation has proven to be mistaken. **Almost every catalytic base available has been chosen** at one time or another for what natural selection seems to find a simple task. For example, to remove a hydron from carbon, a **carboxylato group** is used by triose-phosphate isomerase (Figure 3–37), by tryptophan synthase (**4–122**),[863] by hydroxymethylglutaryl-CoA synthase (Equation 4–361), and by urocanate hydratase (Figure 4–50); a **6-amino group** is used by phosphopyruvate hydratase (Figure 4–43) and the enzymes that are related to it (Equations 4–126 and 4–266 through 4–269); an **imidazolyl group** is used by mandelate racemase (Equation 4–126) and its cousin glucarate dehydratase (Equation 4–266); an imidazolyl group and a carboxylato group are used by pyridoxine 5′-phosphate synthase (Figure 4–48); and a **4-oxidophenyl group** is used by chondroitin AC lyase from *P. aurescens* (Equation 4–358 and Figure 4–44). There are many examples of carboxylato groups of aspartates and glutamates, formally the weakest bases available, that remove hydrons from carbon,[1035-1037] as well as imidazolyl groups of histidines,[226,876,925,1038,1039] **sulfido groups** of cysteines,[652,654,1040-1042] 4-oxidophenyl groups of tyrosines,[761,1043] 6-amino groups of lysines,[1044-1046] **amino-terminal α-amino groups** (**4–53**),[1047-1049] and even **guanidinio groups** of arginines.[943,1050,1051]

In the reverse direction of each removal of a hydron from carbon, a hydron is added to the carbon from which it is removed in the forward direction, so each catalytic acid–base has been chosen by natural selection for both roles. Addition of a hydron to carbon is so difficult that it is also surprising that all these catalytic acids are capable of accomplishing this role effectively, rather than only the most acidic. A choice of the most acidic catalytic acid, however, for addition of a hydron to carbon would mean that the least basic catalytic base had been chosen for removal of a hydron from carbon in the other direction. The solution to this conundrum is to remember that the only relevant ability of a catalytic acid–base is its ability to lower the standard free energy of formation of the transition state for the step in question, and by microscopic reversibility, the same transition state is passed through in either direction.

In the active site of fumarate hydratase (Equation 4–226) from *M. tuberculosis*, the alkoxide of **Serine** 318, conveniently stabilized in a classic oxyanion hole, removes the hydron from carbon 3 of (*S*)-malate (Figure 4–27).[464] In the active site of the

related ethylenediamine-*N,N′*-disuccinate lyase from *Chelativorans*, the alkoxide of Serine 280, within a homologous sequence of amino acids[1052] and also stabilized in a classic oxyanion hole, removes the hydron from carbon 3 of one of the succinyl groups in ethylenediamine-*N,N′*-disuccinate.[1053] An alkoxide is a strong base. Nevertheless, each hydroxy group is forced up against the carbon–hydrogen bond so strongly (0.32 and 0.30 nm, respectively, between carbon and oxygen) by the oxyanion hole that there is no space to accommodate an atom larger than its oxygen. When Serine 318 in fumarate hydratase from *M. tuberculosis* is mutated to cysteine, the enzyme is inactivated. The cysteinate anion would be a satisfactory base, but the sulfur is too large (0.36 nm compared to 0.30 nm for oxygen). This rather unusual use of the alkoxide of serine as the catalytic base that removes a hydron from carbon is found in the large family of enzymes of which fumarate hydratase and ethylenediamine-*N,N′*-disuccinate lyase are members.[1052]

Rather than acting directly as a catalytic base, the basicity of the side chain of an amino acid,[513] a base on a substrate,[1054] or a base on a prosthetic group in the active site[1055] can also be **relayed through the neutral hydroxy group** of threonine or serine or through a molecule[1056] or two molecules of water.[1057] When this occurs, a lone pair of electrons on a neutral hydroxy group or molecule of water, which is even less basic than one on a carboxylato group, can nevertheless formally remove a hydron from carbon. In the active site of 1,4-dihydroxy-2-naphthoyl-CoA synthase from *E. coli*, a bicarbonate, bound in the active site from solution, acts as a catalytic base that removes a hydron from carbon.[275]

During the dehydration catalyzed by 2-oxo-4-carboxy-3-hexenedioate hydratase from *Sphingobium*, the carboxy group of Glutamate 284 in the active site forms a hydrogen bond with the 4-hydroxy group in (4*S*)-2-oxo-4-carboxy-4-hydroxyhexanedioate, the substrate that dominates the equilibrium for this addition–elimination within the active site in the crystallographic molecular model (Figure 4–29),[487] and the carboxy group is responsible for hydronating this hydroxy group in the direction of elimination. It is also the only catalytic acid–base in the vicinity of the hydron on carbon 3, which is removed during the dehydration, so it must also be responsible for this dehydronation. One might think that the reaction could be concerted, with the carboxy group adding a hydron to the hydroxy group while it removes the hydron from carbon 3, but this concerted removal would require that the acyl oxygen in the carboxy group ($pK_a = -7$) act as the base that removes a hydron from carbon because the other oxygen in the carboxy group has to be hydronated to add a hydron to the hydroxy group. The reaction could be stepwise, but the first step must be removal of the hydron from carbon 3 by the basic unhydronated carboxylato group to produce the enolate. For both steric reasons and a consideration of hydrogen bonding, however, it seems that the now-carboxy group could not flip over, carrying the hydron with it, to hydronate the hydroxy group. It is also possible that only one oxygen of the carboxy group is involved in a transfer of the hydron from carbon 3 to the hydroxy group because the oxygen forming the hydrogen bond to the hydroxy group is the same distance (0.34 nm) from carbon 3 as the other oxygen, but the angle between it and carbon 3 is much less appropriate for the transfer of a hydron. Each oxygen of the carboxy group, however, forms hydrogen bonds to a molecule of water, and each fixed molecule of water is in direct contact with the solution. Consequently, it is also possible that hydron on the carboxy group that was just removed from carbon 3 to form the enolate is shuttled into the solution while a hydron is shuttled from the solution onto the other oxygen of the carboxy group so that it can hydronate the hydroxy group. This example illustrates the fact that it is often difficult to be sure of how hydrons move during what seems to be a simple reaction, even when a crystallographic molecular model of high accuracy for the complex between an unmutated active site and the full complement of substrates at equilibrium is available.

It may be the case that the basicities of the various side chains, when they are acting as catalytic bases in active sites that remove a hydron from carbon, are much more similar to each other than the acid dissociation constants of their conjugate acids in solution would suggest. There may well be **shifts in pK_a caused by the lower relative permittivity** of the surroundings after the active site has closed around its substrates, isolating them and one of these catalytic bases from the high relative permittivity of the surrounding water. Anionic carboxylato groups become neutral when they remove a hydron from carbon, and neutral amino and guanidino groups become cationic when they remove a hydron from carbon. Consequently, in an environment of low relative permittivity, carboxylato groups of aspartates and glutamates are more basic, and amino groups of lysines and guanidino groups of arginines are less basic than they are in water. Such shifts in the values of pK_a for the conjugate acids would explain

the low pK_a for the catalytic lysine (pK_a = 6.0) in the active site of acetoacetate decarboxylase from *C. acetobutylicum*[938] and the high pK_a for the catalytic glutamic acid (pK_a = 6.7) in the active site of endo-1,4-β-xylanase. Carboxylato groups, amino groups, and guanidino groups are the outliers in the complete spectrum of basicity, so they would require the most adjustment, but the low relative permittivity of an active site also would make an imidazolyl group less basic (as is does to an amino or guanidino group) and would make a 4-oxidophenyl group more basic (as it does to a carboxylato group).*

When a hydron is removed from carbon adjacent to a carbonyl or acyl carbon, an **enolate or enol** is formed

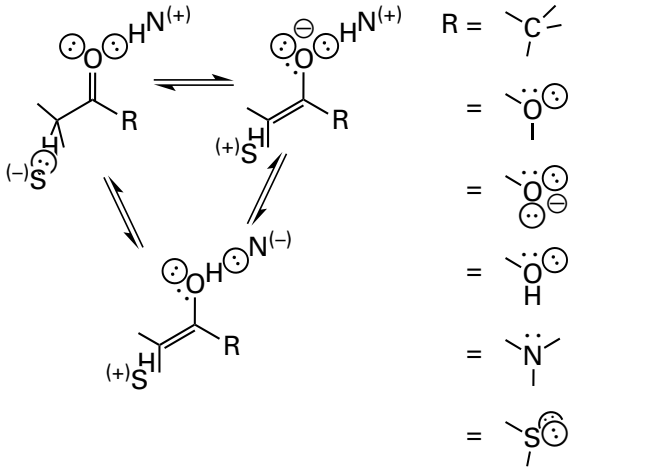

(4–415)

The enzyme always provides a **mechanism to stabilize an enolate**, either by providing hydrogen bonds from within an oxyanion hole for the oxyanion of the enolate or by hydronating the enolate on its oxyanion while it is being formed to produce the enol. It is possible that the enolate can be stabilized sufficiently that the rate for removal of a hydron from the α carbon by a mediocre base can be significantly increased. As has already been mentioned, however, the carbonyl oxygen (pK_a = –7) or acyl oxygen (pK_a = –6) cannot be hydronated to improve the acidity at carbon before the enolization proceeds.

The enolate

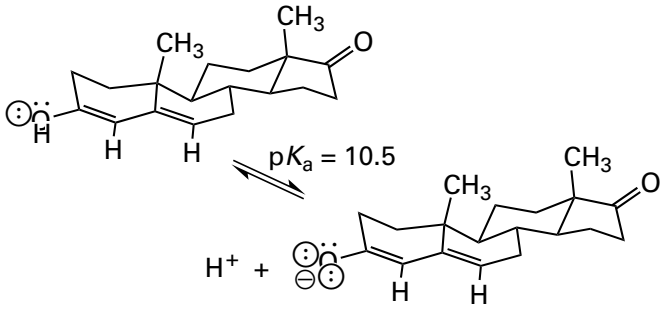

(4–416)

that is the intermediate in the reaction catalyzed by steroid Δ-isomerase

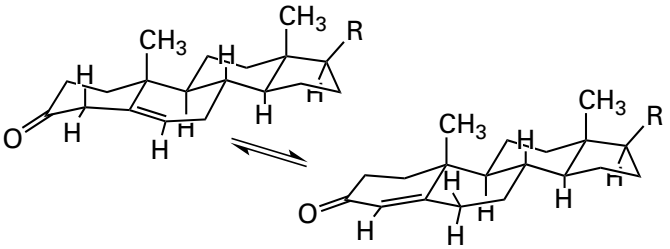

(4–417)

is produced by removal of the hydron from carbon 4 of the 3-oxo-Δ^5-steroid that is the reactant, the carbon adjacent to the carbonyl group. This intermediate illustrates the issues addressed by natural selection when stabilizing an transient enolate. Either the enolate (Equation 4–416) or the enol can be formed when a hydron is removed from carbon 4 of the steroid (pK_a = 12.8) by Aspartate 40 in the active site of the enzyme from *P. putida*.[1058] In the next step of the reaction, the enolate or enol is hydronated on carbon 6. The pK_a for the conjugate acid of the oxyanion in the enolate is 10.5 (Figure 1–23). If a strong acid were used to stabilize this intermediate enolate by hydronating its oxyanion while it was being formed to produce the enol, the weak conjugate base of that acid would not provide much kinetic assistance in dehydronating the hydroxy group of the enol in the second step when the hydron is being added to carbon 6 to form the α,β-unsaturated ketone,* and addition of a hydron to carbon would also be difficult. If a weak acid were used, such as an oxyanion hole, the oxyanion of the enolate would not be hydronated during removal of the hydron from carbon in the first step, but the enolate formed in the first step would be stabilized only by one or more hydrogen bonds from weak acids.

*In the case of a 4-oxidophenyl group, however, the effect of the relative permittivity would be diminished because the negative charge would be delocalized over the ring.

*The conversion of an enol to its keto form is almost always exergonic and therefore requires little thermodynamic assistance, but the issue in catalysis is kinetic assistance.

Consequently, in stabilizing any enolate formed from a reactant, which then returns to a carbonyl in the product, a compromise must be made between creating an enol by hydronation of the carbonyl or acyl oxygen as the hydron is removed from carbon and forming hydrogen bonds to the oxyanion of the enolate that results from dehydronation. If the enolate is hydronated as the hydron is removed from carbon, the act of removing the hydron gets the maximum kinetic assistance. If one or more donors of hydrogen bonds are provided, the return to the oxo group in the second step is less difficult because it does not require dehydronation of the enol. The conjugate acids of most oxyanions of enolates have a pK_a in the range 8–12 (Figure 1–23). Consequently, depending on the requirements of the reaction, it is not difficult for the enzyme either to hydronate the enolate or to provide a hole for its oxyanion. In the case of steroid Δ-isomerase, the hydron that must be removed from carbon is fairly acidic (pK_a = 12.8), and the oxyanion of the enolate is formed from an oxo oxygen that must return to an oxo oxygen in the second step of the reaction.

The active site of steroid Δ-isomerase seems to compromise. In the active site of steroid Δ-isomerase from *P. putida*, the 3-oxo group of the ketosteroid that is the reactant accepts hydrogen bonds from the carboxy group of Aspartate 103 and the 4-hydroxyphenyl group of Tyrosine 16.[1059,1060] The 4-hydroxy group of Tyrosine 16 is the proximal hydroxy group of a composite acid–base formed from 4-hydroxy groups of three tyrosines,[1061] but it is surrounded by three methyl groups from three methionines on one side and a valine and an isoleucine on the other,[1060] which should significantly raise its pK_a. The pK_a for the carboxy group of Aspartate 103 is greater than 9,[1062] probably because it is surrounded by the side chains of the same three methionines, a phenylalanine, a valine, and an alanine. The values of pK_a for both Tyrosine 16 and Aspartate 103, although perhaps higher, are in the vicinity of the pK_a for the enol (10.5). It seems as though, in this instance, natural selection may have matched values of pK_a for the enol, the carboxy group, and the 4-hydroxyphenyl group. Consequently, it is difficult to decide if the 4-hydroxyphenyl group or the carboxy group in the complex with the oxyanion of the dienolate hydronates the enolate to stabilize it while it is being formed or if these two catalytic acids simply create an oxyanion hole that provides two hydrogen bonds to the enolate to stabilize it.

The active site of steroid Δ-isomerase from *P. putida* binds various phenolates, in part by providing an oxyanion hole formed by the carboxy group of Aspartate 103 and the 4-hydroxyphenyl group of Tyrosine 16 into which the respective phenolate oxyanion inserts.[1063] Phenols with values of pK_a up to 9.7 occupy this oxyanion hole as the respective phenolates, and their oxygens are not hydronated by the oxyanion hole. These observations suggest that the intermediate is the enolate (Equation 4–416). If, however, the pK_a of Tyrosine 16 is lowered by replacing it semisynthetically in turn with one of three fluorotyrosines, there is no statistically significant change in either the catalytic constant or the specificity constant for estr-5(10)-ene-3,17-dione.[1064] These observations suggest that the intermediate, even when the tyrosine is unmodified, is the enol.

There is another way to look at this situation. Before Aspartate 40 removes the hydron from carbon 4, which is the difficult step in the reaction, its carboxylato group bears a delocalized negative elementary charge. After the hydron is removed, that negative elementary charge is either delocalized in the enolate, delocalized over the ring of the 4-oxidophenyl group of Tyrosine 16, or delocalized in the carboxylato group of Aspartate 103, depending on which is the more stable tautomer of the active site occupied by the intermediate. It may well be that the choice between these delocalized options is determined by the relative permittivity in the immediate vicinity of each possible anion.

The hydron on carbon 4 of a 3-oxo-Δ^5-steroid (Equation 4–417) is a particularly acidic hydron because its dissociation creates an enolate conjugated to a carbon–carbon double bond (Equation 4–416). Most hydrons on carbons adjacent to a carbonyl or acyl carbon are much less acidic. In such cases, the decision **whether or not the enolate should be hydronated** during removal of the hydron should be influenced by this poor acidity. Consider the dehydronation of the α carbon of ethyl acetate

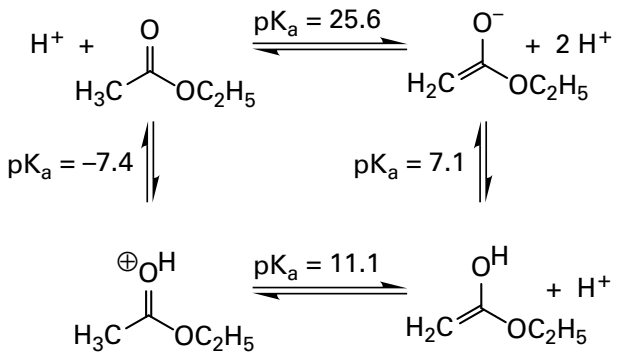

(4–418)

If the acyl oxygen is not hydronated, the pK_a for the adjacent carbon–hydrogen bond is 25.6, but if the oxygen is first hydronated, its pK_a is 11.1. Hydronation leads to a dramatic increase in acidity. In solution, of course, the pH at which the acyl oxygen is hydronated (pH < –7.4) and the pH at which the carbon of the hydronated ester has dissociated a hydron to form the enol (pH > 11.1) are so different from one another that these two steps cannot occur in the order of hydronation followed by dehydronation, even though such a scenario explains in part the specific acid catalysis of aldol condensations involving ethyl acetate.

On an active site, where there is no pH, if a catalytic acid forms a hydrogen bond to the carbonyl or acyl oxygen and a catalytic base is placed adjacent to the carbon–hydrogen bond, and if the active site waits long enough, the oxygen can be hydronated before the hydron is removed. The question is whether or not the wait is longer than the wait necessary for the transition state to be achieved by **hydronating the oxygen while the hydron is being transferred** to the catalytic base. If the wait to hydronate the carbonyl or acyl oxygen is too long, the obvious advantage of hydronating the oxygen *before* the hydron is transferred (Equation 4–418) is nevertheless the reason that hydronating the oxygen *while* the hydron is being transferred is advantageous, just not so advantageous as hydronating it first, if that were even possible.

In triose-phosphate isomerase from *S. cerevisiae* (Equations 4–46 and 4–55 and Figure 3–37), either Lysine 11 or Histidine 94 probably hydronates the 2-oxo group of glycerone phosphate and Histidine 94 probably hydronates the 1-oxo group of glyceraldehyde 3-phosphate during removal of the hydron from either carbon 3 or carbon 2, producing the respective enol as the intermediate. These assignments are reasonable because these two hydrons are difficult to remove (Figure 1–23) and because one of the oxygens is eventually going to leave the active site as a hydroxy group on the product anyway.

In the active site of pyridoxine 5′-phosphate synthase, a hydron is removed from carbon 4 of one of the intermediates (step *v* in Figure 4–47), and as the hydron is removed from carbon, the 4′-hydroxy group of the intermediate (Figure 4–48B) probably relays a hydron from the imidazolyl group of Histidine 45 through an oxygen of the phospho group to hydronate the developing oxyanion while the hydron is removed, because removal of the hydron from carbon is also difficult in this instance. During removal of a hydron from carbon 6 (step *vi* in Figure 4–47), the 4′-hydroxy group of the intermediate (Figure 4–48B) again relays a hydron from the imidazolyl group of Histidine 45 through an oxygen of the phospho group to hydronate the developing oxyanion either while the hydron is being removed from carbon or immediately after it has been removed, because the oxygen becomes a hydroxy group in the product.

In the active site of citrate (*Si*)-synthase (Equation 4–224, Problem 4–23) from *G. gallus*, Aspartate 375 removes a hydron from the methyl group of the substrate, acetyl-SCoA,[462,1065] so that its enol can participate in the aldol condensation with the carbonyl of oxaloacetate that produces citrate. Histidine 274 simultaneously hydronates the acyl oxygen of acetyl-SCoA as the hydron is removed to give the enol of acetyl-SCoA, which is the intermediate in the enzymatic reaction.[1066]

In 2-hydroxymuconate tautomerase (Equation 4–317), however, the guanidinio group of Arginine 39 probably just provides a hydrogen bond to **create an oxyanion hole** for stabilizing the enolate formed during removal of the hydron from carbon 3 of the substrate by the amino-terminal proline of the enzyme (**4–53**). In this instance, again, the hydron is quite acidic (p$K_a \cong 13$) because its dissociation creates an enolate conjugated to a carbon–carbon double bond and the oxyanion in the enolate is not basic enough to remove a hydron from a guanidinio group (Figure 1–23). In the active site of hydroxymethylglutaryl-CoA synthase from *S. aureus* (Equation 4–361), the oxyanion of the enolate of acetylated Cysteine 111, even though the cysteinyl thioester is much less acidic at carbon (p$K_a = 21$), is also stabilized not by hydronation but by a hydrogen bond from an amido nitrogen–hydrogen of the polypeptide backbone and perhaps a hydrogen bond—if formation of such a hydrogen bond is even possible—from the acidic hydron on acetoacetyl-SCoA.[858] The oxyanion of the enolate remains unhydronated (the pK_a of the enol is 8) and becomes an acyl oxygen after nucleophilic addition of the carbanionic carbon to acetoacetyl-SCoA. In the active site of allantoin racemase from *K. pneumoniae*, the oxyanion of the enolate of allantoin is stabilized by a classic oxyanion hole formed from two amido nitrogen–hydrogens pointed directly at the oxygen.[1042]

There are instances in which hydronating an enolate is clearly counterproductive. For example, during the reaction catalyzed by phospho*enol*pyruvate carboxykinase[1067]

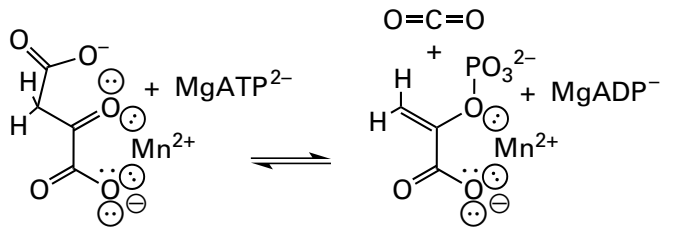

(4–419)

the enolate formed upon decarboxylation of oxaloacetate must remain nucleophilic at its oxygen in order to add to the γ-phospho group of $MgATP^{2-}$, so instead of being hydronated, it is coordinated to a Mn^{2+} so that it retains most of its nucleophilicity.[1068,1069]

Because of its excess negative charge, **one of the most difficult enolates to produce is the *gem*-enediolate** produced by removal of a hydron ($pK_a \cong 33$; Figure 1–23) from a carbon adjacent to a carboxylato group

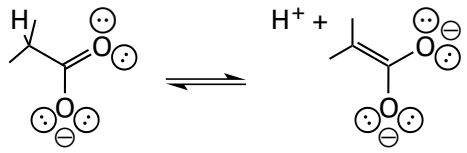

(4–420)

Hydronating one of the two oxygens prior to removal of the hydron is the equivalent of turning a carboxylato group into an ester, so **hydronation of one oxygen** lowers the pK_a for the acidic carbon by more than 7 units (Figure 1–23). It follows that at least one oxygen of an incipient *gem*-enediolate should be hydronated by a catalytic acid in the active site and forced to stay hydronated before removal of the hydron from the α carbon. For example, in the active site of porcine aconitate hydratase (Figure 3–52), the 3-carboxylato group of isocitrate becomes the *gem*-enediolate upon removal of a hydron from carbon 3 of isocitrate during the elimination that turns isocitrate into *cis*-aconitate. The 3-carboxylato group is hydronated by a molecule of water (0.29 nm) that is a ligand to a hexacoordinate[1070] Fe^{2+} in the prosthetic [4Fe–4S] iron–sulfur cluster in the active site of the enzyme.[1054] This molecule of water, although it is itself a competent catalytic acid ($pK_a = 10$), relays a hydron from the imidazolyl group (0.26 nm) of Histidine 167 or the carboxy group of Aspartate 165 (0.26 nm) so that it remains a molecule of water. The fact that the hydron is added to the oxygen in an orientation normal to the plane of the 3-carboxylato group causes the hydrogen bond between the resulting hydronated oxygen of the carboxy group and the molecule of water on Fe^{2+} to be parallel to the π molecular orbital system of the carbon–oxygen double bond to the other oxygen of the carboxy group. This disposition ensures that there is no conjugation between the hydronated oxygen and the carbon–oxygen double bond, so that it becomes the equivalent of a simple carbonyl group or thioester, which also lowers the pK_a for the α carbon significantly (Figure 1–23).

The conjugate acid of the remaining oxyanion in a *gem*-enediolate produced by removing a hydron on the carbon adjacent to a now-neutral carboxy group has a pK_a around 7 (Figure 1–23) so that it can be hydronated or it can be stabilized by a hydrogen bond or an oxyanion hole, depending on the situation. In the case of porcine aconitate hydratase, the other oxygen is in an oxyanion hole formed from two amido nitrogen–hydrogens from two peptide bonds (0.29 and 0.30 nm) and the hydroxy group of Serine 642 (0.29 nm).

In the active site of ulvan lyase from *Alteromonas*, one oxygen of the carboxylato group that is to become a *gem*-enediolate on the oligosaccharide that is the substrate forms a hydrogen bond with the imidazolyl group of Histidine 144, which probably hydronates the carboxylato group before the hydron is removed from the α carbon by the imidazolyl group of Histidine 123 to form the *gem*-enediolate and initiate the elimination catalyzed by the enzyme.[1071] The two oxygens of the carboxylato group also form hydrogen bonds with the two ω-nitrogen–hydrogens of the guanidinio group of Arginine 236. These hydrogen bonds to the cationic guanidinio group should provide even more stabilization to the monoanionic *gem*-enediolate after it forms following hydronation of the carboxylato group by the imidazolyl group.

It most cases, however, it seems that active sites are not so logical. For example, in the active site of chondroitin AC lyase from *P. aurescens* (Equation 4–358 and Figure 4–44), one of the oxygens of the carboxy group that becomes the *gem*-enediolate does accept a hydrogen bond from the imidazolyl group of Histidine 233, which at first glance seems to be a catalytic acid. The two oxygens of the carboxylato group, however, participate in two hydrogen bonds (0.27 and 0.31 nm) with the carbamoyl group of Asparagine 183. In the map of electron density, it cannot be determined which atom in the carbamoyl group is nitrogen and which is oxygen. If the amido group of the carbamoyl group forms the hydrogen bond (0.31 nm) with the oxygen that forms a hydrogen bond with the imidazolyl group, which is the choice made by the authors, then the acyl oxygen

of the carbamoyl group must form the hydrogen bond (0.27 nm) with the other oxygen of the carboxylato group, which must have been hydronated before that hydrogen bond formed because a hydrogen bond must have a hydron. In this instance, the oxygen of the carboxylato group that forms a hydrogen bond with the imidazolyl group could be hydronated by the imidazolyl group either in the ground state or in the transition state to form the enediol. If, however, the acyl oxygen of the carbamoyl group forms the hydrogen bond with the oxygen that forms a hydrogen bond with the imidazolyl group, then that oxygen of the carboxylato group must be hydronated, but the hydron must be directed toward the carbamoyl oxygen rather than the imidazolyl group. In addition, the imidazolyl group must be the imidizolium because a hydrogen bond requires a hydron, and that hydron must be on the nitrogen. In this instance, the amido group of the carbamoyl group must form a hydrogen bond with the other oxygen of the carboxylato group, which is probably not hydronated. In neither case does a catalytic acid hydronate one oxygen of the anionic carboxylato group prior to enolization, even though either disposition does guarantee that it becomes hydronated.

The *gem*-enediolate in the active site of proline racemase from *Trypanosoma cruzi* is stabilized in two **oxyanion holes** that together provide four peptide amido nitrogen–hydrogens and the hydroxy group of threonine as donors for two hydrogen bonds to one oxygen and three hydrogen bonds to the other.[1072] A similar arrangement of two oxyanion holes, in which there are two hydroxy groups and an amido nitrogen–hydrogen for each oxyanion, is found in the active site of fumarate hydratase from *M. tuberculosis* (Figure 4–27) and other members of the family of homologous enzymes to which it belongs.[464,1052] In both cases, it is possible that one oxygen on the *gem*-enediolate is a strong enough base to remove the hydron from one of these donors, which all have values of pK_a between 14 and 15, while the hydron is being removed from carbon, but this remains unlikely (Figure 1–23). If neither oxygen removes a hydron from a donor, then the active site removes a hydron from a carbon α to a carboxylato group without hydronating one of its oxygens prior to removal of the hydron or on the approach to the transition state. It has been suggested that one way the active site of these enzymes could stabilize the *gem*-enediolate instead of hydronating it would be to hold the carbon and the two oxygens of the carboxy group and the two adjacent carbons of the respective substrate in the same plane.

Formation of a hydrogen bond between a reasonably strong catalytic acid and the oxygen in a carbonyl or acyl group should lower the pK_a for the hydron on the α carbon (Equation 4–418). Nevertheless, even for the more acidic α carbons with fairly low values of pK_a, removal of their hydrons, even by a base as strong as hydroxide, is slow and difficult. Likewise, even for the more basic carbons in enols, enolates, and enamines, the conjugate acids of which have fairly high values of pK_a, addition of a hydron, even by an acid as strong as hydronium, is slow and difficult. These observations in solution beg the question of **how an active site is able to remove a hydron rapidly from carbon**, even a poorly acidic carbon, or to add a hydron rapidly to carbon, even a poorly basic carbon, with such ease, even with the relatively weak catalytic bases and acids that it generally uses. One explanation is that **steric effects engendered by the active site compress the catalytic base or the catalytic acid against the carbon–hydrogen bond or the trigonal carbon**, respectively, to bring the complex closer to the transition state for transfer of the hydron.

In crystallographic molecular models of enzymatically active complexes between the active site and a complete complement of substrates at equilibrium within an enzyme that removes a hydron from and adds a hydron to a carbon, the **distance between that carbon and the heteroatom of the base** that removes the hydron or the acid that adds the hydron is usually shorter than the sum (0.38–0.41 nm) of the van der Waals radii of hydrogen (0.115 nm); the heteroatom, oxygen (0.15 nm), nitrogen (0.16 nm), or sulfur (0.18 nm); and the length of a carbon–hydrogen bond (0.11 nm). For example, for the enzymatically active complex of triosephosphate isomerase from *S. cerevisiae* and glycerone phosphate (Equations 4–46 and 4–55 and Figure 3–37), the distance between the oxygen of the carboxylato group and the carbon is 0.31 nm; for the enzymatically active complex of phosphopyruvate hydratase from *S. cerevisiae* (Figure 4–43), the distance between the nitrogen of the amino group and the carbon is 0.32 nm; for the enzymatically active complex of chondroitin AC lyase from *P. aurescens* (Equation 4–358 and Figure 4–44), the distance between the oxygen of the 4-hydroxyphenyl group and the carbon is 0.29 nm; for the enzymatically active complex of hydroxymethylglutaryl-CoA synthase from *S. aureus* (Equation 4–361), the distance between the oxygen of the carboxylato group and the carbon is 0.30 nm;[858] for the enzymatically active complex of fumarate hydratase from *M. tuberculosis*

(Figure 4–27), the distance between the oxyanion of Serine C319 and the carbon is 0.32 nm;[464] and for the enzymatically active complex of pyridoxine 5′-phosphate synthase from *E. coli* (Figure 4–48B), the distance between the oxygen of the carboxylato group and the carbon is 0.37 nm. In the active site of an enzymatically inactive mutant of 3-phosphoshikimate 1-carboxyvinyltransferase (Equation 4–321; Problem 4–26) from *E. coli* and its tetrahedral intermediate, the distance between the hydroxy group of the intermediate and the carbon from which it remove a hydron (Equation 4–414) is 0.31 nm.[1029]

In a crystallographic molecular model of the complex between steroid Δ-isomerase (Equation 4–417) from *C. testosteroni* and androst-4-ene-3,17-dione,[1073] which is one substrate of the enzymatic reaction, the distance between the carboxylato oxygen of Aspartate 38 and carbon 4, the carbon from which this oxygen removes a hydron from the reactant androst-5-ene-3,17-dione or adds a hydron to the product androst-4-ene-3,17-dione to give the intermediate enolate, is 0.27 nm. There are at least 29 crystallographic molecular models of complexes between steroid Δ-isomerase from *P. putida* (32% identity; 1.6 gap percent) and equilenin, an analogue of the intermediate dienol (Equation 4–416) in which the A and B rings are an aromatic 2-hydroxynaphthyl group. In these models, the distances between the oxygen of Aspartate 38, responsible for transferring the hydron between carbons 4 and 6, and the carbon analogous to carbon 4 varied between 0.31 and 0.36 nm, and the distances between the oxygen and carbon 6 varied between 0.30 and 0.38 nm.[1074] All these distances are less than the distance of van der Waals contact (0.39 nm) expected for a hydrogen on an oxygen and the π molecular orbital system of a naphthyl group (0.17 nm).[1075] Consequently, in these complexes that resemble the acceptor of the hydron by the intermediate in the addition, rather than the donor of the hydron by the substrate in the elimination, the catalytic acid is also compressed against the carbon.

One caveat concerning such conclusions about these apparent compressions is that the positions in a particular crystallographic molecular model of the carbon and the heteroatom between which a hydron is transferred may not be defined with sufficient accuracy to support them. In the collection of 29 crystallographic molecular models of complexes between steroid Δ-isomerase from *P. putida* and equilenin, the mean deviation of the position for both the oxygen atom of Aspartate 103 and the oxygen atom of Tyrosine 16, which together form the oxyanion hole for the dienolate, from their mean position in the aligned models is only 0.02 nm.[1074] These two oxygens do not have to move during the enzymatic reaction, and they are remarkably fixed in position by the methionines, the valine, the isoleucine, the phenylalanine, and the alanine that surround them as well as the strands of polypeptide, and this steric confinement is reflected in the crystallographic molecular models. The side chain of Aspartate 40, like the side chain of Glutamate 164 in the active site of triose-phosphate isomerase (Equations 4–46 and 4–55 and Figure 3–37), has to transfer a hydron between carbons 4 and 6 of the substrate, which are even farther apart. Consequently, the mean deviation of the position for the oxygen atom of the carboxy group in Aspartate 103 that transfers the hydron from its mean position in the aligned models is 0.1 nm. Nevertheless, the oxygen is never more than 0.38 nm from both carbons and usually significantly less. The oxygen, in turn, is confined within these boundaries by the side chains of an alanine, a phenylalanine, a valine, and a methionine that surround it. All these considerations suggest that the distances observed in crystallographic molecular models between a catalytic acid–base and the carbon from which it adds or removes a hydron are accurate descriptions of the compression applied by the active site to facilitate the transfer of the hydron to or from the carbon.

The oxygen of the carboxylato group of Aspartate 103 is compressed against carbon 4 in the complex between the active site of steroid Δ-isomerase from *C. testosteroni* and androst-4-ene-3,17-dione in part by a steric interaction (0.36 nm) between its other oxygen and the methyl group of Alanine 114. When Alanine 114 is mutated to glycine, a mutation that eliminates the methyl group (0.15 nm) and relieves the compression, the value of the catalytic constant for the reactant estr-5(10)-ene-3,17-dione decreases by a factor of 225.[1076] For comparison, when Tyrosine 16 in steroid Δ-isomerase from *P. putida* was mutated to phenylalanine or when Aspartate 103 was mutated to leucine, the catalytic constants for the reactant estr-5(10)-ene-3,17-dione decreased by factors of 17,000 and 230. These are the two catalytic acid–bases that stabilize the intermediate enolate by directly providing hydrogen bonds or an oxyanion hole to its oxygen rather than engendering a steric effect.

It is hard to avoid the conclusion that all these observations of distances less than van der Waals contact represent an **intentional compression of the heteroatoms of the catalytic acid–bases against the**

respective carbon–hydrogen bonds accomplished by steric effects within the active site. In solution, there are large differences between rates for the transfer of a hydron between two heteroatoms and rates for the transfer of a hydron between a carbon atom and a heteroatom. It has been argued that a significant portion of this difference results from the fact that in the former instance a preexisting hydrogen bond decreases the distance between the two heteroatoms, and hence the barrier to hydron transfer, while no such decrease can occur in the latter instance in which a hydrogen bond cannot form.[1077] Consequently, compressing the distance between the heteroatom of a base and the carbon atom by an active site should accomplish much the same thing that is accomplished in solution by a hydrogen bond, and it should significantly accelerate the otherwise slow transfer of a hydron from carbon. It has also been proposed, however, that hydrogen bonds can actually form between an acidic carbon–hydrogen bond and a heteroatom.[1078] If such a hydrogen bond can form, then the short distances observed could be the result of their formation, a process that should achieve the same objective.

In **the transition state for transfer of a hydron from carbon to a heteroatom**, the distance between carbon and heteroatom is significantly shorter than the distance between these two atoms upon their van der Waals contact in the ground state. For example, it has been calculated that in the transition state for transfer of a hydron from carbon 2 of D-glyceraldehyde 3-phosphate to the oxygen of the catalytic carboxy group in the active site of triose-phosphate isomerase (Equations 4–46 and 4–55 and Figure 3–37), the distance between carbon and oxygen should be 0.27 nm; and in the transition state for transfer of a hydron from carbon 3 of glycerone phosphate to the oxygen of the carboxy group, the distance between carbon and oxygen should also be 0.27 nm.[1079] These two distances are less than the compressed distance (0.31 nm) observed in the crystallographic molecular model of the enzyme while it is catalyzing its reaction. Nevertheless, the enzyme has compressed the distance from that of van der Waals contact (0.38 nm) in the direction of the transition state, and this compression would be an example of the use of strain to catalyze the reaction.

In crystallographic molecular models of complexes between enzymes and substrates or analogues of intermediates in an enzymatic reaction, there are also many instances of hydrogen bonds between two heteroatoms that are shorter than expected. For example, in the enzymatically active complex of triose-phosphate isomerase (Figure 3–37), the distance between the τ nitrogen of Histidine 94 and the 2-oxo group of the substrate is 0.26 nm; in the complex between steroid Δ-isomerase (Equation 4–417) from *P. putida* and equilenin, a phenolic analogue of the actual dienol intermediate in the enzymatic reaction (Equation 4–416), the distance between the oxygen of the 4-oxidophenyl group of Tyrosine 16 and the phenolic oxygen of the analogue is 0.25 nm, and the distance between the oxygen in the carboxy group of Aspartate 103 and the same phenolic oxygen on the analogue is also 0.25 nm;[712] and in a complex between penicillopepsin from *Penicillium janthinellum* and an analogue of the tetrahedral intermediate in the enzymatic reaction, the distance between an oxygen of Aspartate 33 and an oxygen of the analogue is 0.24 nm.[1080] In the complex between bovine chymotrypsin and an analogue of the tetrahedral intermediate in the enzymatic reaction, the distance (0.26 nm) between the π nitrogen of Histidine 57 and the oxygen in the carboxy group of Aspartate 102 within the imidazolyl-carboxy composite acid–base (Equation 4–134) is thought to be shorter than that of an unconstrained hydrogen bond.[1081-1083] One explanation for the shorter lengths in complexes between active sites and analogues for intermediates in the enzymatic reactions is that these complexes are unnatural and the analogues necessarily contain atoms of a different type in place of one or more of the atoms in the natural intermediate. These differences will produce steric effects not present in the natural intermediate that could cause the observed shortening.

One almost always unexamined question, however, relevant to these observations of short hydrogen bonds is **what would be the unconstrained lengths of these specific hydrogen bonds**. Most tabulated values for the lengths of unconstrained hydrogen bonds are those between two acids or between two bases. For example, the lengths of hydrogen bonds[1084] between two carboxylic acids are 0.26 ± 0.1 nm, those between two phenols are 0.27 ± 0.1 nm, those between the nitrogen–hydrogen of an amide and the acyl oxygen of the same amide are 0.29 ± 0.1 nm, and those between two amines are 0.31 ± 0.1 nm. In all these instances, the difference between the pK_a of the donor and the pK_a of the acceptor is large. For example, in the hydrogen bond between two carboxylic acids, the pK_a of the donor is around 5 while the pK_a of the acceptor is around –6, and in the hydrogen bond between two amines, the pK_a of the

donor is around 40 while the pK_a of the acceptor is around 10.

It is known, however, that hydrogen bonds between an acid as a donor and the conjugate base of that acid as an acceptor, in which the difference in pK_a between donor and acceptor is 0, are about 0.02–0.03 nm shorter[1085] than the hydrogen bonds between two molecules of the same conjugate acid or the same conjugate base. For example, the bond length for the hydrogen bond between an amine and its ammonium is around 0.28 nm. The bond length for the hydrogen bond between a phenol and its phenolate anion is around 0.245 nm. This distance is almost identical to the length of the hydrogen bond between the phenolic oxygen of Tyrosine 103 and the phenolate oxygen of equilenin in the active site of steroid Δ-isomerase, two phenols of almost the same pK_a. The bond length for a carboxylic acid and its conjugate base is also around 0.245 nm. This distance is almost identical to the bond length (0.248 nm) between the carboxy group of Aspartate 103 and the phenolate oxygen of equilenin,[712] two oxygens also with closely matched values of pK_a, and it is also almost identical to the bond length of the hydrogen bond between Aspartate 24 and Aspartate 15 in the crystallographic molecular model of human protein deglycase DJ-1, which was thought to be shorter than expected.[1086] In an extensive compilation of the lengths of hydrogen bonds in small molecules in solution and in crystallographic molecular models,[1087] it was shown that the length of the bonds decreased linearly with the difference in pK_a between donor and acceptor, reaching a minimum when the pK_a of the donor was equal to the pK_a of the conjugate acid of the acceptor. For hydrogen bonds between two oxygens, the length decreased from 0.29 nm to a minimum of 0.245 nm; for hydrogen bonds between nitrogen and oxygen, the length decreased from 0.30 nm to a minimum of 0.255 nm; and for hydrogen bonds between two nitrogens, the length decreased from 0.31 nm to a minimum of 0.27 nm,* in agreement with the earlier, far more limited compilation.[1085]

Although unconstrained bond lengths for even one of the short hydrogen bonds observed in crystallographic molecular models between a native active site and its substrates or an analogue of an intermediate or between two side chains within a protein cannot be ascertained, it is likely that they are almost the same as those observed in the molecular model, and the conclusion that active sites or protein molecules often compress hydrogen bonds between two heteroatoms may be mistaken.

Some of these bond lengths for hydrogen bonds between two heteroatoms, however, may actually be shorter than the unconstrained length. In a compilation[1086] of all the hydrogen bonds in the Protein Data Bank between a carboxylato group and a carboxy group on the side chains of aspartates and glutamates, which are usually hydrogen bonds between an acid and its conjugate base, 85% of these hydrogen bonds were longer than 0.245 nm, but 15% were shorter than 0.245 nm. The most likely explanation for these shorter-than-unconstrained hydrogen bonds in the native structures of these proteins, as well as those observed between substrates and analogues of intermediates and catalytic acid–bases, is **adventitious steric compression**. The almost impossible process of folding a polypeptide to form an active site in which catalytic groups are properly arrayed around the associated substrates cannot always accommodate hydrogen bonds of unconstrained length. Some pushing, pulling and shoving must take place. In fact, there are more hydrogen bonds in these complexes that are longer than the unconstrained length than there are hydrogen bonds that are shorter, but the longer ones go unremarked. To compress a hydrogen bond by 0.02 nm decreases its strength by only around 3 kJ mol^{-1}, which is only about 15% of its energy of formation.[1088] A shortening of another 0.01 nm would result in a further loss of only 4 kJ mol^{-1}.

Adventitiously compressed hydrogen bonds between heteroatomic donors and acceptors should be less stable than if they were uncompressed, but the compression may nevertheless accelerate transfer of the hydron between donor and acceptor, a possibility that has been dwelled upon. In most cases, however, transfer of a hydron between two heteroatoms is extremely rapid (Figure 1–1), and unless the difference in pK_a between donor and acceptor is remarkably large, no acceleration should be required. Consequently, any acceleration arising from the observed compression should be inconsequential to natural selection.

The donors and acceptors for hydrogen bonds on the molecules of water, side chains, and polypeptide backbone within an active site that participate in hydrogen bonds with substrates and with

*In all the instances that were tabulated, there was no obvious discontinuous decrease in the length of hydrogen bonds when the difference in pK_a reached 0, and consequently there is no evidence for shorter, stronger "low-barrier" hydrogen bonds in this situation, just as there was no obvious decrease in the dissociation constant of a hydrogen bond in the same situation.[1009]

transition states for the enzymatic reaction are usually identified by crystallographic molecular models. These functional groups form direct, unambiguous contacts with substrates that can be observed unambiguously in models of appropriate complexes. They unquestionably participate in either the association of substrates with the active site or catalysis itself. Other adjacent functional groups that do not make direct contact with substrates but that may participate in catalysis can also be identified in molecular models. One way in which such action at a distance can be performed is electrostatically. It seems to be the case that, in addition to positioning donors and acceptors for hydrogen bonds, enzymatic active sites also position charged side chains to produce appropriate electrostatic fields that stabilize the transition state and thereby increase the rate of the enzymatic reaction.

Electrostatic catalysis is enhancement of the rate of a reaction that results from the electrostatic field created by the formal elementary charge of one or several nearby functional groups. For example, the transition state of the reaction catalyzed by chorismate mutase (Equation 4–218) involves a separation of charge (Figure 1–30). The separation of charge creates a dipole, and any electrostatic field that stabilizes the dipole will stabilize the transition state and increase the rate of the enzymatic reaction. In an analogue of the transition state in chorismate mutase, the ether oxygen in bicyclic ether

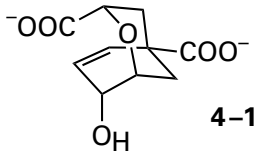

4–148

accepts hydrogen bonds from the ammonio group of a lysine and the carboxy group of a glutamate in the crystallographic molecular models of its complexes with the chorismate mutases from *S. cerevisiae*[1089] and from *E. coli*.[1090] The former hydrogen bond would position the ammonio group of the lysine adjacent to the oxygen

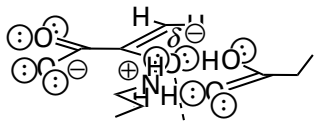

4–149

in each substrate for the enzyme, chorismate and prephenate. In chorismate mutase from *M. tuberculosis*, the ether oxygen in **4–148** accepts hydrogen bonds from the ammonio group of a lysine and the amido group of a glutamine.[1091]

Because the ether oxygen of the analogue is at the location at which the negative charge is concentrated in the transition state, it has been proposed that the positive elementary charges of these lysines stabilize the transition state electrostatically. The hydrogen bonds from these electropositive donors suggest that in the transition state for this reaction, as expected, the bond between the oxygen and the allyl carbon is dissociating heterolytically and that the oxygen, therefore, increases in negative charge as the transition state is approached.

In the chorismate mutase from *B. subtilis*, which is unrelated to the aforementioned chorismate mutases and hence a test of this proposal, Arginine 90 is at the same location in the crystallographic molecular model of the complex between the enzyme and bicyclic ether **4–148** as the lysine in the other enzymes. This arginine is the donor in the only hydrogen bond to the ether oxygen in the analogue of the transition state, and it also forms a hydrogen bond to the carboxy group of the analogue.[1092] Again, these two hydrogen bonds would position the guanidinio group of the arginine adjacent to the oxygen

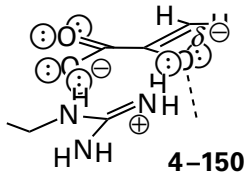

4–150

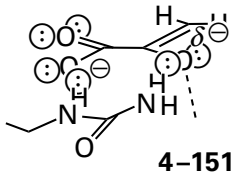

4–151

in each substrate for the enzyme, chorismate and prephenate. When this arginine is replaced by site-directed mutation with a citrulline (**4–151**), which is isosteric to arginine but lacks the positive elementary charge, the value for rate constant $k_0\,K_m^{-1}$ decreases by a factor of 50,000.[1093] In crystallographic molecular models of **4–148** complexed with the mutated enzyme and with the unmutated enzyme, citrulline superposes precisely with arginine[1094] and forms the same two hydrogen bonds (**4–151**) as arginine. These observations are consistent with the conclusion that the catalytic role of arginine in the native enzyme is to stabilize electrostatically the charge developing on the oxygen in the transition state (Figure 1–30) rather than simply to provide hydrogen bonds.

If, during hydrolysis of the acetal in the glycosidic linkage by the active site of lysozyme, the true intermediate is an oxocarbenium ion because the nearby anionic carboxylato group of Aspartate 52 is sterically prevented from adding to the carbon of the oxycarbenium ion despite sitting next to it, then the carboxylato group is stabilizing the oxocarbenium ion electrostatically. It has been proposed that the oxocarbenium ion that is an intermediate in the hydrolysis of poly(ADP-ribose) by poly(ADP-ribose) glycohydrolase from *Thermomonospora curvata* is stabilized electrostatically by the anionic, nonbridging oxygen on the α-phospho group of the ADP-D-ribosyl leaving group. In the crystallographic molecular model of the complex between the enzyme and ADP-D-ribose,[1095] this anionic oxygen is only 0.41 nm away from oxygen 4′ in the ribosyl ring, which is the oxygen onto which formal positive elementary charge in the oxocarbenium ion is delocalized. The anionic oxygen on the α-phospho group is held firmly and is unable to approach any closer than 0.45 nm to carbon 1′ of ADP-D-ribose, so it cannot stabilize the oxocarbenium ion covalently.

Suggested Reading

Kossiakoff, A. A., and Spencer, S. A. (1981) Direct determination of the protonation states of Aspartic Acid-102 and Histidine-57 in the tetrahedral intermediate of the serine proteases: Neutron structure of trypsin, *Biochemistry 20,* 6462–6474. https://doi.org/10.1021/bi00525a027

Larsen, T. M., Wedekind, J. E., Rayment, I., and Reed, G. H. (1996) A carboxylate oxygen of the substrate bridges the magnesium ions at the active site of enolase: Structure of the yeast enzyme complexed with the equilibrium mixture of 2-phosphoglycerate and phosphoenolpyruvate at 1.8 Å resolution, *Biochemistry 35*, 4349–4358. https://doi.org/10.1021/bi952859c

Garrido-Franco, M., Laber, B., Huber, R., and Clausen, T. (2002) Enzyme–ligand complexes of pyridoxine 5′-phosphate synthase: Implications for substrate binding and catalysis, *J. Mol. Biol. 321*, 601–612. https://doi.org/10.1016/S0022-2836(02)00695-2

Ulaganathan, T., Helbert, W., Kopel, M., Banin, E., and Cygler, M. (2018) Structure–function analyses of a PL24 family ulvan lyase reveal key features and suggest its catalytic mechanism, *J. Biol. Chem. 293*, 4026–4036. https://doi.org/10.1074/jbc.RA117.001642RA117.001642

Problem 4–36: 3-Dehydro-L-gulonate-6-phosphate decarboxylase from *E. coli* catalyzes the reaction

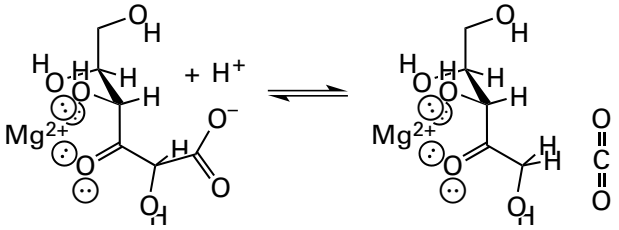

in which a carboxy group is replaced by a hydron.

(A) Write a mechanism for this reaction that proceeds through a *cis*-enediol intermediate.

When the enzymatic reaction is run in ^2H_2O with the wild-type enzyme, both L-(1*S*)-[1-^{2}H]xylulose and L-(1*R*)-[1-^{2}H]xylulose are produced in a 2:1 molar ratio. When the enzymatic reaction is run in ^2H_2O with a mutant in which Glutamate 112 has been changed to glutamine and Histidine 136 has been changed to alanine, L-(1*R*)-[1-^{2}H]xylulose is the exclusive product (>90%). When the enzymatic reaction is run in ^2H_2O with a mutant in which Arginine 139 has been changed to valine, L-(1*S*)-[1-^{2}H]xylulose is the exclusive (>95%) product.[1096]

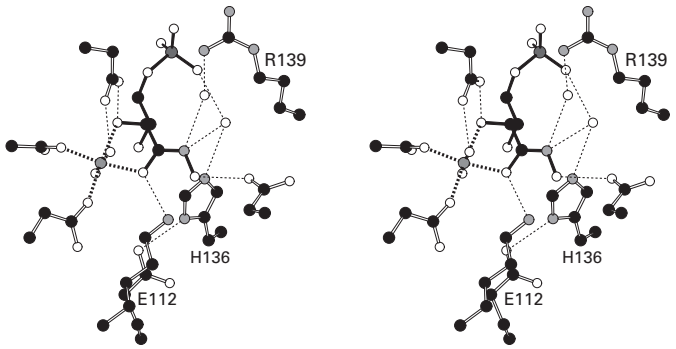

The figure is a stereodrawing of the superposition of two portions of a crystallographic molecular model of a complex between the enzyme and (2*R*,3*S*)-*N*,2,3,4-tetrahydroxybutanamide, a hydroxamate that is an analogue of the *cis*-enediol intermediate.[1097] The asymmetric unit of the crystal is the dimer, and both active sites in the asymmetric unit are occupied by the hydroxamate. Each active site also contains a fixed molecule of water that forms a hydrogen bond to the nitrogen of the hydroxamate, but the the water occupies different locations in the two active sites of the dimer. The drawing includes both molecules of water, positioned in their respective locations in the two active sites in the asymmetric unit. This positioning was achieved

by superposing one of the occupied active sites in the asymmetric unit with its molecule of water with only the molecule of water in the other active site. It seems that both molecules of water cannot be in the same active site at the same time, probably because of steric exclusion.

(B) Draw the structure of the *cis*-enediol intermediate that is formed from 3-dehydro-L-gulonate 6-phosphate and (2*R*,3*S*)-*N*,2,3,4-tetrahydroxybutanamide side by side in the same orientation.
(C) What is the complete description of the acid that hydronates the *cis*-enediol on the *Si* face of carbon 1 in the normal enzymatic reaction?
(D) What is the complete description of the acid that hydronates the *cis*-enediol on the *Re* face of carbon 1 in the normal enzymatic reaction?
(E) Explain the stereochemical observations. In your explanation, discuss the difference in the positions of the molecules of water in the two active sites. This discussion should indicate your understanding of the difference between an enzyme in a crystal and an enzyme in solution.

Problem 4–37: Aspartoacylase catalyzes the nucleophilic substitution

N-acetyl-L-aspartate + H_2O $\rightleftharpoons$ acetate + L-aspartate

(A) Write a step-by-step mechanism for this hydrolysis.

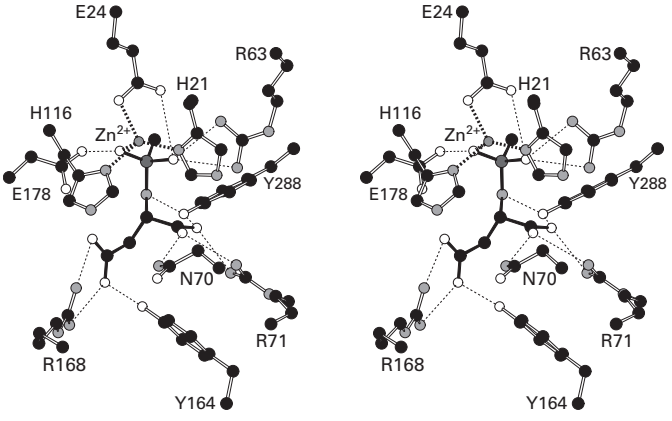

The figure is a stereodrawing of a crystallographic molecular model of the active site of human aspartoacylase occupied by *N*-[hydroxy(methyl)phosphinyl)-L-aspartate.[1098]

(B) Draw the structure of *N*-[hydroxy(methyl)phosphinyl)-L-aspartate.
(C) Why is *N*-[hydroxy(methyl)phosphinyl)-L-aspartate a potent competitive inhibitor of the enzymatic reaction?

What is the role of each of the following in the enzymatic hydrolysis?

(D) The imidazolyl group of Histidine 21
(E) The carboxylato group of Glutamate 24
(F) The carboxamido group of Asparagine 70
(G) The guanidinio group of Arginine 71
(H) The imidazolyl group of Histidine 116
(I) The 4-hydroxyphenyl group of Tyrosine 164
(J) The guanidinio group of Arginine 168
(K) The carboxylate group of Glutamate 178
(L) The 4-hydroxyphenyl group of Tyrosine 288
(M) The Zn^{2+} cation

Metalloenzymes

A limited set of metallic cations is incorporated into proteins as prosthetic groups or transient occupants of their active sites and participate in their function. These are the cations of magnesium, potassium, calcium, vanadium, manganese, iron, cobalt, nickel, copper, zinc, molybdenum, cadmium, and tungsten. Because of their several accessible oxidation states, the transition metals iron and copper, and occasionally manganese, are used as carriers of single electrons (Chapter 2). In this role, they alternate between oxidation states such as Fe^{2+} and Fe^{3+} or Cu^{+} and Cu^{2+}. The metallic cations of cobalt with different formal oxidation states are used enzymatically within the respective cobalamins (Figure 2–67). The cations of the transition metals vanadium, manganese, iron, nickel, copper, molybdenum, and tungsten catalyze reactions involving molecular hydrogen, molecular nitrogen, or molecular oxygen (Chapter 2), and their oxidation states are required to change in these roles. The metallic dications Mn^{2+}, Fe^{2+}, Co^{2+}, and Ni^{2+}, however, are also used by enzymes in situations in which a change in oxidation state is not required and in fact must be avoided; if such a change is encountered adventitiously, it

must be corrected. Cations of the alkaline earth metals magnesium and calcium and the transition metals zinc and cadmium occur naturally only in the dicationic oxidation state as Mg^{2+}, Ca^{2+}, Zn^{2+}, and Cd^{2+}. When they perform enzymatic roles as solely metallic dications, Mg^{2+}, Ca^{2+}, Mn^{2+}, Fe^{2+}, Co^{2+}, Ni^{2+}, Zn^{2+}, and Cd^{2+} usually act as Lewis acids and are, in effect, **surrogate hydrons.** In this role, they fulfill a catalytic requirement in an enzymatic reaction that would otherwise be fulfilled by a hydron from a catalytic Brønsted acid.

Because a metallic dication is larger than a hydron and consequently has a lower density of positive charge, each of them is **less acidic than a hydron**. This difference in acidity can be quantified. It has already been noted that H^+ and H_3O^+ are used as shorthand for the actual cation $[H(OH_2)_n]^+$, where n is variously depicted as having a value between 4 and 21. Values for m in the homologous complexes of water with a metallic dication, $[Me(OH_2)_m]^{2+}$, are between 4 and 9. As a result, $[H(OH_2)_n]^+$ and $[Me(OH_2)_m]^{2+}$ are analogous Brønsted acids, and their **values of pK_a** can be compared. The hydronium cation, $[H(OH_2)_n]^+$, as a Brønsted acid, displays a pK_a for the reaction

$$H^+(OH_2)_n \rightleftharpoons H^+ + HOH(OH_2)_{n-1} \quad (4\text{–}421)$$

of –1.75. Metallic dications, $[Me(OH_2)_m]^{2+}$, in dilute aqueous solution acting as Brønsted acids display analogous values of pK_a for the reaction

$$Me^{2+}(OH_2)_m \rightleftharpoons H^+ + MeOH^+(OH_2)_{m-1} \quad (4\text{–}422)$$

These values of pK_a, as well as those for metallic trications, have been determined in water for metallic cations that act as Lewis acids in metalloenzymes (Table 4–2).[1099-1101] From these values of pK_a, it can be concluded that none of these metallic cations, even the trications, is so effective as a hydron at lowering the acid dissociation constant of the cluster of water that surrounds it and that a hydron is a stronger Lewis acid than any of these metallic cations.

The advantage of a metallic dication, however, is that at neutral pH the molar concentration of hydronium is very small, while the molar concentration of the complex between water and a metallic cation will be equal to the free molar concentration of that metallic cation. There is also another advantage to this weakness of acidity. When a hydron occupies a lone pair of electrons on a nitrogen, oxygen, or sulfur, the other lone pairs on that nitrogen, oxygen, or sulfur become poorer nucleophiles. When, however, a metallic dication occupies one of the lone pairs of electrons, rather than a hydron, the other lone pairs retain much of their nucleophilicity.

Because it is larger than a hydron, a metallic cation is usually **surrounded in its inner sphere of coordination by four or more ligands**. Metallic cations used catalytically as prosthetic Lewis acids within the active sites of enzymes in aqueous solution are at all times surrounded by Lewis bases. The strongest Lewis bases present in biological fluids are the lone pairs of electrons on oxygen, nitrogen, and sulfur. A hydron is also a Lewis acid, and in biological fluids every acidic hydron is always surrounded by lone pairs of electrons on oxygen, nitrogen, or sulfur. A hydron is so small, however, that it can accommodate as ligands only two Lewis bases at a time in one hydrogen bond. Because a metallic cation has core electrons, it is larger than a hydron and can sterically accommodate more Lewis bases simultaneously. The metallic cations incorporated into enzymes are always surrounded by four to nine lone pairs of electrons from oxygen, nitrogen, sulfur, or a halide whether they are in the active site or in the solution before they enter the active site. These four to nine lone pairs of electrons coordinate the metallic dication.

Table 4–2: Acid Dissociation Constants for Aquo Complexes of Metallic Cations[1099-1101]

cation	pK_a	cation	pK_a
K^+	>15[a]	Cd^+	10.1[b]
Ca^{2+}	12.7[a]	Ni^{2+}	9.9[b]
Mg^{2+}	11.4[a]	Co^{2+}	9.6[a,b]
Mn^{2+}	10.6[a,b]	Zn^{2+}	9.0[b]
Fe^{2+}	10.1[a]	Fe^{3+}	2.3[a,b]
		Co^{3+}	0.7[a]

[a]Reference 1101. [b]Reference 1099.

The preference of a metallic cation for a particular type of lone pair of electrons is usually discussed in terms of **hardness** or **softness** of the Lewis acid and the Lewis base.[1102] The rule is that hard acids prefer hard bases and soft acids prefer soft bases. Of the metallic dications acting catalytically in active sites as Lewis acids, K^+, Mg^{2+}, Ca^{2+}, and Mn^{2+} are hard Lewis acids; Fe^{2+}, Co^{2+}, Ni^{2+}, and Zn^{2+} are borderline; and Cd^{2+} is soft. For the commonly encountered bases, lone pairs of electrons on oxygen are harder than lone pairs of electrons on nitrogen, which are harder than lone pairs of electrons on sulfur. These rankings, for example, are consistent with the fact that Ca^{2+} has a strong preference for lone pairs of electrons on oxygen while Zn^{2+} and Co^{2+} have a preference for lone pairs of electrons on sulfur. It also explains why the bases on metallothionein, a protein responsible for chelating soft, toxic cations of heavy metals such as Hg^{2+}, Cd^{2+}, and Pb^{2+}, are entirely the soft sulfanyl groups of cysteine side chains in the protein.

The Lewis bases surrounding a metallic cation in solution are held by interactions the characteristics of which span the spectrum between ionic and covalent. **Ionic interactions** are created by electrostatic forces between the metallic cation and an anion or the dipole on a ligand. If the forces were entirely ionic, the number and orientation of the Lewis bases around the cation would be determined solely by steric considerations. The larger the cation or the smaller the bases, the more bases should be gathered. Usually, the interactions between hard metallic cations and hard bases are close to being purely ionic. The calcium dication is an example of a hard, ionic metallic cation, and it is also large. When it is bound to a protein or when it is in the solution that surrounds the protein, Ca^{2+} is coordinated by six to nine lone pairs of electrons, invariably from oxygen atoms,[1103] which are the hardest of bases. The number and orientation of these lone pairs of electrons from the atoms of oxygen around the calcium depend entirely on the size and shape of the bases that provide the lone pairs, as well as any steric constraint upon those bases.[1104] The Zn^{2+} in the crystallographic molecular model[1105,1106] of aspartate carbamoyltransferase

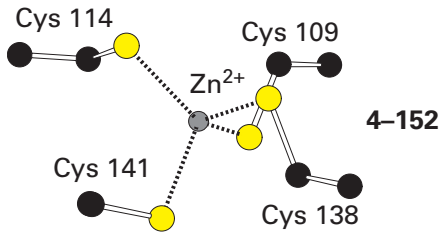

4–152

from *E. coli*, however, is a good example of a metallic cation participating in almost purely **covalent bonds**. In this arrangement, a borderline metallic cation bonds covalently to four soft bases. When the ligands coordinating the dication of a transition metal form covalent bonds in such a tetrahedral geometry, the empty valence 4*s* orbital of the transition metal and its three empty valence 4*p* orbitals form four sp^3 hybrid orbitals, each of which is occupied by a lone pair of electrons from one of the four soft bases that are ligands to the metallic dication to form the four mostly covalent bonds.*

Zinc dication has 10 valence electrons that occupy its five 3*d* orbitals and **completely fill the *d* shell**, and this completion causes the 3*d* electrons to be unavailable for covalent bonding.† In the case of Fe^{2+} in reduced rubredoxin (previously **2–63**)

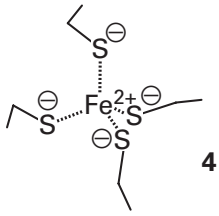

4–153

the metallic dication has only 6 valence electrons, which fill the five 3*d* orbitals. The 3*d* electrons in Fe^{2+}, unlike those in Zn^{2+}, can participate in covalent bonding because, like the valence electrons on a carbon, nitrogen, or oxygen atom, **the *d* shell they occupy is unfilled**. Consequently, in the case of Fe^{2+}, both the partially filled 3*d* orbitals and the unfilled 4*s* and 4*p* orbitals are all available for covalent bonding.

The major structural difference, as opposed to electronic difference, between ionic interactions and

*A comprehensive description of the covalency of the interactions between metallic dications and their ligands is beyond the scope of this discussion and not germane to the participation of metallic dications as Lewis acids in enzymatic reactions. As before, in drawings, all interactions will be considered to be intermediate between ionic and covalent and will be designated by thick dotted lines. The two examples here are close to the extremes of ionic and covalent.

†The electrons occupying all these orbitals cannot be distinguished in terms of their origins, but giving them arbitrary origins makes the counting easier.

covalent bonds is the **directional properties of the arrangements of ligands**. Covalent bonds usually position the participating atoms in strict geometric orientations, such as tetrahedral in the case of Zn^{2+} in **4–152**, while ionic interactions are malleable, resembling pigs at a trough. The fact that covalent bonds involving metals are so reliable is reflected by the practice of geometrically restricting them during crystallographic refinement, as is done for bonds involving carbon, nitrogen, and oxygen. For example, in the initial crystallographic molecular model of aspartate carbamoyltransferase built directly from the unrefined map of electron density, the arrangement of sulfurs around the Zn^{2+} was constrained to tetrahedral geometry, just as all sp^3 carbons were, in all subsequent refinements.[1107] This practice can be dangerous, however, particularly if the metallic cation is harder or if the ligands to the metallic cation are harder, less covalent bases.[1108] In such intermediate cases, various mixtures of ionic and covalent behavior are observed. The main structural indication of such deviations from covalent behavior is the loss of directional ligation.

When a metallic cation leaves the solution and is incorporated into an active site, it exchanges some or all of the lone pairs of electrons from the ligands that coordinated it in solution for lone pairs of electrons provided by the polypeptide backbone or the side chains of the protein. The **coordination observed within the active site** is somewhat characteristic of the type of cation, but similar dications are often accommodated by natural selection with indistinguishable coordinations.

Potassium ion, K^+, is the hard monocation of an alkali metal. It is so hard that it is always surrounded by lone pairs of electrons from oxygens, the hardest bases. Potassium ion is the largest of all the metallic cations that are incorporated naturally into molecules of protein, and it is the only monovalent metallic cation used catalytically as a Lewis acid by enzymes. It has a large enough ionic radius (Table 4–3)* to accommodate as many as eight lone pairs of electrons from oxygens, and because K^+ is so hard, the association is entirely ionic.

A typical arrangement of ligands coordinating K^+ when it is bound in an enzyme occurs in 2,2-dialkylglycine decarboxylase (pyruvate) from *Burkholderia cepacia*[1110]

*Even though an ion is obviously not a hard sphere but a continuous distribution of electron density that decreases with distance from the nucleus, effective ionic radii[1109] are commonly used to quantify the dimensions of this distribution.

Table 4–3: Effective Ionic Radii of Metallic Cations Used by Enzymes as Lewis Acids[1109]

cation	ionic radius (nm)	cation	ionic radius (nm)
K^+	0.14	Fe^{2+} (ls)[a]	0.061
Mg^{2+}	0.072	Fe^{2+} (hs)[b]	0.078
Ca^{2+}	0.11	Ni^{2+}	0.06
Mn^{2+}	0.083	Zn^{2+}	0.07
Co^{2+} (ls)[a]	0.065	Cd^{2+}	0.09
Co^{2+} (hs)[b]	0.075		

[a]Low-spin state. [b]High-spin state.

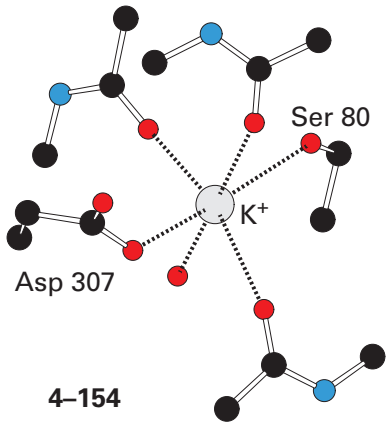

4–154

The six ligands are three acyl oxygens from the peptide backbone, an oxygen in the carboxy group of Aspartate 307, the hydroxy group from Serine 80, and a molecule of water. In the occupied active site of [formate-*C*-acetyltransferase]-activating enzyme from *E. coli* occupied by its substrate L-methionine, the K^+ that activates the enzymatic activity[1111] is coordinated by five ligands—two oxygens, one from each of two carboxy groups from two aspartates, the acyl oxygen of a peptide bond, the hydroxy group of threonine, and the carboxylato group of L-methionine—but no molecules of water.[1112] The number of fixed **molecules of water remaining on K^+** following its incorporation into a protein varies[1113,1114] from none, as in the occupied active sites of [formate-*C*-acetyltransferase]-activating enzyme and carbam-

oyl-phosphate synthase (glutamine-hydrolyzing) from *E. coli*,[1115] to five, as in a mutant of UDP-glucose–hexose-1-phosphate uridylyltransferase from *E. coli*.[1116]

Potassium ion is present in cytoplasm at concentrations of 0.1–0.8 M, making it the **dominant cation in all cells**. Because its presence is as reliable as that of water, it is not surprising that, just as are molecules of water, ions of potassium are incorporated structurally into many proteins. It is also not surprising that many enzymatic reactions are inhibited partially or fully by removal of K^+ from solution,[1117] as they would be if water were removed. In most instances, this inhibition of enzymatic activity results from the fact that, as with 2,2-dialkylglycine decarboxylase (pyruvate) and carbamoyl-phosphate synthase, a K^+ is bound so close to the active site that its removal disrupts the structure of the active site.

There are, however, a few instances in which an oxygen on a substrate that is involved closely in the enzymatic reaction becomes a ligand to K^+ upon association with the active site, and the K^+ performs a **catalytic role**. For example, pyruvate kinase (Equation 4–275) has an absolute requirement for a monovalent cation to catalyze its reaction.[1118] Although ammonium and rubidium cations can fulfill this role as well, in the cytoplasm, where neither of these other ions is present in significant concentration, K^+ is the cation involved in normal catalysis. In steady-state kinetic measurements of the reaction catalyzed by pyruvate kinase, K^+ behaves as if it were one reactant in a multireactant mechanism.[1119] In the crystallographic molecular model of the active site of pyruvate kinase from *O. cuniculus* occupied by K^+, $MgATP^{2-}$, and oxalate (an analogue of the enol of pyruvate),[581] one nonbridging oxygen of the γ-phospho group of $MgATP^{2-}$ is one of the six oxygens that coordinate the K^+ (Figure 4–52). During the nucleophilic substitution at phosphorus catalyzed by the enzyme, this K^+ ensures that the γ-phospho group of $MgATP^{2-}$ remains dianionic and stabilizes the intermediate monomeric metaphosphate or phosphorane.

The enzymatic activity of [formate-*C*-acetyltransferase]-activating enzyme from *E. coli* is activated 10-fold by K^+. It is also activated[1111] by Li^+, Na^+, NH_4^+, and Rb^+. Because, however, K^+ is the most effective and because these other monovalent cations are not present at significant concentrations, in the cytoplasm it must be K^+ that activates the enzyme. When this active site is occupied by the substrate *S*-adenosyl-L-methionine,[1112] the carboxy group of *S*-adenosyl-L-methionine is a monodentate ligand to K^+. Because the carboxy group is distant from *S*-adenosyl-methysulfanyl group of L-methionine, which is the functional group participating in catalysis, the only role for K^+ in this case is to contribute to the recognition of *S*-adenosyl-L-methionine.

With a few exceptions such as pyruvate kinase, where it is involved only peripherally in catalysis, K^+ usually has a structural role in the protein. The K^+ in 2,2-dialkylglycine decarboxylase (**4–154**) and the K^+ in carbamoyl-phosphate synthase (glutamine-hydrolyzing) from *E. coli*[1115] are examples of K^+ in a structural role. Potassium ion is seldom used catalytically because its large size and low density of charge cause it to be the **weakest of the Lewis acids** (Table 4–2). Consequently, the remainder of the discussion will focus on only the metallic dications that are used almost exclusively as Lewis acids in catalytic roles.

The divalent metallic cations used as Lewis acids in the active sites of enzymes each have particular properties.

Magnesium ion, Mg^{2+}, is a hard, small, alkaline earth, metallic dication. Because it is hard, it is almost[1120] always coordinated by lone pairs of electrons from atoms of oxygen. Because it is small (Table 4–3) and therefore has a high density of charge, Mg^{2+} gathers as many oxygen ligands as it can. It almost always ends up with six lone pairs from six oxygens arranged octahedrally. This octahedral arrangement is not, however, the result of covalence. It is a consequence of the fact that the sterically least repulsive way to crowd six oxygens around a cation with such a small ionic radius is octahedrally. In its preferred coordination, with six lone pairs from six atoms of oxygen in an octahedral arrangement, the interatomic distances between Mg^{2+} and the atoms of oxygen (0.20–0.21 nm) are shorter and much less variable than those (0.23–0.26 nm) for Ca^{2+}, its larger sibling. Even these short and less variable distances are probably the result of steric effects. If each atom of oxygen is only 0.205 nm from Mg^{2+}, then the distance between each oxygen and its four neighbors in the octahedral array must be 0.29 nm, which is the distance for van der Waals contact. Consequently, the distance between the cation and its ligands is as short as it can be if six of them are gathered around it. Because of the shorter distance between the metallic cation and the oxygens, the acidity of Mg^{2+} is somewhat stronger than that of Ca^{2+} (Table 4–2).

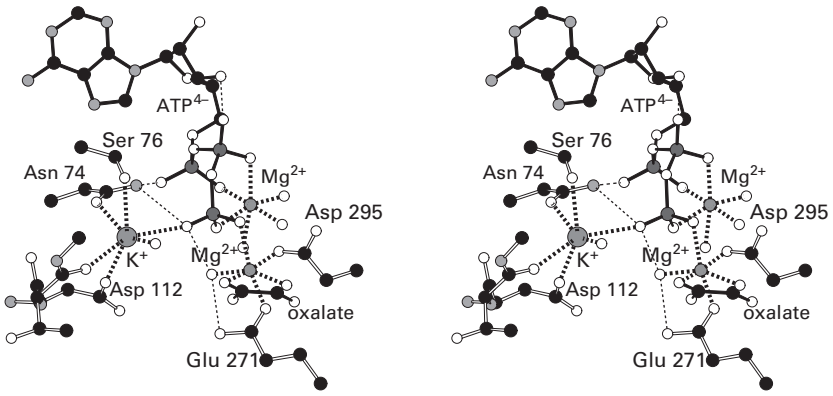

Figure 4–52: Stereodrawing[134] of the crystallographic molecular model of the active site of pyruvate kinase from *O. cuniculus* occupied by K^+, the substrate $MgATP^{2-}$, and oxalate, an analogue of the intermediate enolate of pyruvate that is the nucleophile or leaving group, respectively, in the reaction.[581] Black atoms are carbons, white atoms are oxygens, small gray atoms are nitrogens, and the three large dark gray atoms are three atoms of phosphorus. The smaller dark gray spheres are two magnesium ions surrounded by their ligands, and the larger dark gray sphere is a potassium ion surrounded by its ligands. The enzyme was purified from muscle of *O. cuniculus* and crystallized from 7.8% (w/v) poly(ethylene glycol) 8000, 0.16 M KCl, 5 mM $MgCl_2$, 5 mM ATP^{4-}, 1 mM oxalate, and 50 mM succinate at pH 6.0. Electron density for $MgATP^{2-}$, K^+, oxalate, and an additional Mg^{2+} could be observed in the active site. Molecules of water and side chains of the amino acids that are ligands to K^+ and the other Mg^{2+} are included. The two carboxy groups of the oxalate are monodentate ligands to the other Mg^{2+}.

Magnesium ion is the only metallic dication present at significant free concentration in cytoplasm (Table 4–4). As a result, a prominent role for free Mg^{2+} in the cytoplasm of a cell is to form **complexes with oligophosphates**. The paradigm of such a complex is $MgATP^{2-}$, which is the predominant form[1122] of adenosine triphosphate present in solution in cytoplasm. In $MgATP^{2-}$, three coordination sites on Mg^{2+} are occupied by oxygens of phosphates and the other three by waters.[1123] When the complex associates with the active site of an enzyme, the three sites occupied by water can retain their aquo ligands or become occupied by Lewis bases from the active site. When the waters on Mg^{2+} are not replaced by ligands from the enzyme, donors and acceptors from the protein often form hydrogen bonds to these fixed molecules of water that remain associated with Mg^{2+}.[1124] In the active site of pyruvate kinase (Figure 4–52), the $MgATP^{2-}$ that is bound retains all three of the fixed molecules of water on Mg^{2+} (the upper Mg^{2+} in the drawing) that it had in solution as well as the three oxygens from ATP^{4-}. The structure of this $MgATP^{2-}$ in the active site of pyruvate kinase is almost identical* to the structure of free $MgATP^{2-}$ that has been crystallized from solution.[1123] This fact suggests that the $MgATP^{2-}$ in the active site of pyruvate kinase is little changed upon associating with the enzyme and simply carries Mg^{2+} into the active site as if there were covalent bonds between the three oxygens and Mg^{2+}.

One advantage of using magnesium rather than a hydron as the Lewis acid neutralizing ATP^{4-} is that **more of the oxygens are neutralized**. At pH 7, the predominant forms of free ATP are the unhydronated form (ATP^{4-}) and the monohydronated form ($HATP^{3-}$) in about equal proportions.[1122] In $MgATP^{2-}$, the predominant form of the magnesium complex, however, two oxyanions are fully neutralized by Mg^{2+}.

Another advantage is that the **triphosphate is rigidified by the chelation**, which hinders free rotation around the bonds between the atoms of phosphorus and the bridging oxygens. This rigidification of $MgATP^{2-}$ significantly restricts the conformations that it can assume while still in solution. This decrease in the number of conformations in turn decreases the entropic barrier for association of $MgATP^{2-}$ with an active site, as long as the active site is complementary to the set of these conformations. Because an active site is rigid, the $MgATP^{2-}$ is required to assume a single conformation once it is bound.

Table 4–4: Free Concentrations of Metallic Cations in Cytoplasm[1121]

cation	free concentration[a]	cation	free concentration[a]
K^+	100 mM	Ni^{2+}	<1 nm
Mg^{2+}	1 mM	Zn^{2+}	10 pM
Ca^{2+}	0.1 μM	Co^{2+}	<1 nm
Mn^{2+}	0.1 μM	Cu^{2+}	<10 fM
Fe^{2+}	0.1 μM		

[a]These concentrations are estimates believed to be accurate to within a factor of 10. In most cases, they are not based on direct measurements of free concentration.

Other **nucleoside triphosphates**, such as $MgGTP^{2-}$, $MgCTP^{2-}$, $MgUTP^{2-}$, and $MgdTTP^{2-}$, also enter active sites coordinated[1012] to Mg^{2+}, as do nucleoside diphosphates such as adenosine diphosphate,[1015,1125,1126] thiamine diphosphate,[1127] and diphosphate itself.[1128,1129] In at least one instance, Mg_2ATP seems to have been the substrate that entered the active site.[1024]

The free concentration of Mg^{2+} in the cytoplasm and intracellular compartments is around 1 mM,[1130] Although this free concentration is well below the free concentration of K^+, it is still fairly high, and it does not fluctuate significantly. As a result, natural selection has sometimes incorporated Mg^{2+} into an enzyme in a purely structural role simply because it was an available structural component. An example is the Mg^{2+} in alcohol dehydrogenase ($NADP^+$) from *L. brevis* that is coordinated by the acyl oxygens of two glutamines and four molecules of water.[1131] Even though this bound Mg^{2+} is greater than 1 nm from the active site and not involved in catalysis, its removal completely inactivates the enzyme.

A **typical arrangement of the ligands** coordinating Mg^{2+} that is not coordinated by an oligophosphate occurs in the active site of malate synthase from *E. coli*[1132]

*The complex between the triphosphate of ATP^{4-} and Mg^{2+} in $MgATP^{2-}$ crystallized from solution is, within the triphosphate, the same enantiomer as that in the active site of pyruvate kinase, but the conformations of one of the two six-membered rings around Mg^{2+} are slightly different in the two complexes within the asymmetric unit.

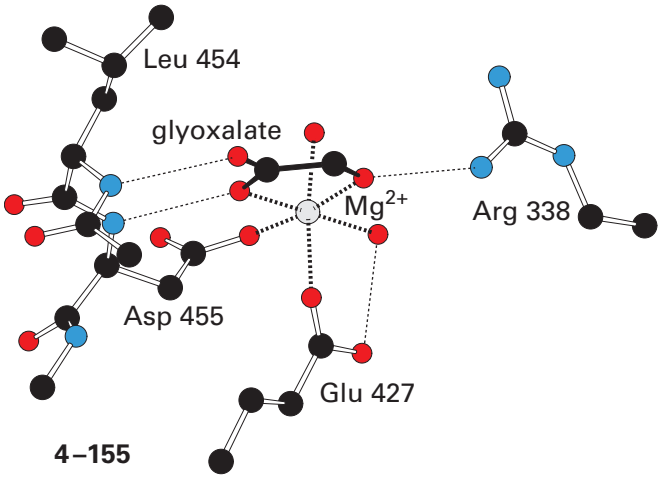

The Mg^{2+} is octahedrally coordinated by two oxygens of carboxy groups, one from Aspartate 455 and one from Glutamate 427; two molecules of water; and two oxygens in glyoxylate, one substrate in the enzymatic reaction (Equation 4–271). This arrangement of ligands is almost identical to that for the Mg^{2+} that did not arrive in the active site of pyruvate kinase on $MgATP^{2-}$ (the lower Mg^{2+} in Figure 4–52), if it is realized that the bridging oxygen between the β-phosphate and the γ-phospho group of $MgATP^{2-}$ in the active site of pyruvate kinase occupies the same position as a molecule of water in the active site of malate synthase.

The two Mg^{2+} in the active site of phosphopyruvate hydratase from *S. cerevisiae* (Figure 4–43) are additional paradigms. The one on the right is coordinated by the hydroxy group and the amido oxygen of Serine 39, two molecules of water, and the oxygen from a carboxy group and an oxygen from a phospho group in the substrate. The one on the left is coordinated by three oxygens from carboxy groups, one from Aspartate 246, one from Glutamate 295, and one from Aspartate 320; a molecule of water; and the two oxygens on the carboxy group of the substrate. These latter two oxygens are an example of the frequent use of a carboxy group as a **bidentate ligand** to a metallic cation, and one of them is in turn a ligand to both Mg^{2+}. Usually there are two, three, or four oxygens from the carboxy groups of aspartates or glutamates, or one or more carboxy groups from substrates and one, two, or three molecules of water or hydroxy groups coordinating Mg^{2+} in an active site.[692,1133-1135] Even though they are usually considered to be carboxylato groups in the absence of evidence, **whether or not the carboxy groups are hydronated on their other oxygens** is generally unknown, but in most instances some or most of them are probably unhydronated and anionic. When Mg^{2+} is acting as a Lewis acid, one or two of the ligands are oxygens from the substrate, one or both of which is a Lewis base acted upon by Mg^{2+} in its catalytic role.

If Mg^{2+} is bound to the active site in the absence of substrate, the positions to be occupied by oxygens from a substrate after it has associated are occupied by fixed molecules of water before it associates. This hydration is commonly the case for the sites on any metallic dication. In the absence of substrate, **the sites to be occupied by the substrate are usually occupied by water**, as are the donors and acceptors for hydrogen bonds that will form with a substrate in any active site.

Calcium ion, Ca^{2+}, is another hard, alkaline earth, metallic dication. Like Mg^{2+}, Ca^{2+} participates in purely ionic interactions. Because it has a significantly larger ionic radius than Mg^{2+} (Table 4–3), the ligands around the cation are not so sterically crowded. Consequently, there are fewer geometric requirements, and Ca^{2+} can be coordinated by as many as nine lone pairs of electrons. Calcium has an even lower affinity for nitrogen[1103] than Mg^{2+}, so the lone pairs of electrons that are its **ligands are**

When Ca^{2+} is bound to proteins, it often **serves in a structural role**[1136-1138] by gathering around itself oxygens from the polypeptide, its side chains, and molecules of water (Figure 4–53).[1139] These associations are highly specific, but the specificity is provided by the distribution of oxygens within the protein and the donors and acceptors for hydrogen bonds between the protein and associated molecules of water, not by the calcium. Although its free concentration in present-day cytoplasm is low (Table 4–4),[1130,1140] the free concentration of Ca^{2+} may have been significantly higher, close to that of its concentration in present-day seawater (10 mM), when it was first being incorporated structurally into the proteins of primitive organisms and before it assumed a role in cellular signaling that required its free concentration in cytoplasm to be maintained at these low levels. The **more flexible steric requirements** for Ca^{2+} may also give it advantages in a purely structural role.

Calcium ion, however, can also play a **catalytic role as a Lewis acid** in enzymatic reactions.[1022,1141]

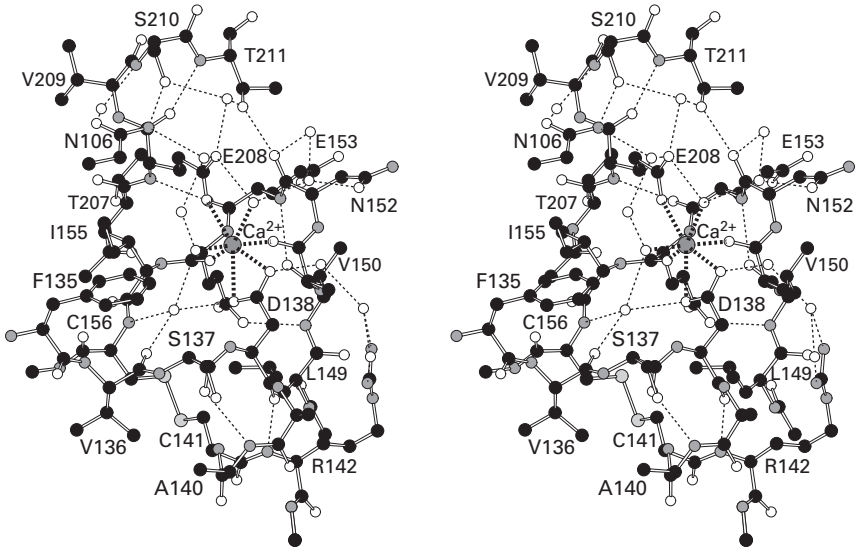

Figure 4–53: Stereodrawing[134] of the crystallographic molecular model of the site in which a Ca^{2+} is coordinated in trypsin from the bacterium *S. griseus*.[1139] Black atoms are carbons, white atoms are oxygens, small gray atoms are nitrogens, large light gray atoms are sulfurs, and the large dark gray sphere is a calcium ion surrounded by its ligands. Crystals were grown in solutions of the purified protein (10–15 mg mL^{-1}) in 10 mM calcium acetate at pH 6.2 by varying the concentration of ammonium sulfate. Reflections from four isomorphous replacements were collected to Bragg spacing of 0.28 nm, and a data set was collected from crystals of the native enzyme to Bragg spacing of 0.17 nm. The phases were estimated from multiple isomorphous replacements and also from molecular replacement using molecular models of bovine trypsin (31% identity; 3.1 gap percent) and bovine chymotrypsin (30% identity; 4.0 gap percent) as guides. The site at which Ca^{2+} is coordinated is distant from the active site in which the nucleophilic serine, Serine 172, as well as Aspartate 82 and Histidine 37 are located, so the Ca^{2+} performs only a structural role. It is located in a pocket on the surface of the protein, and the view in the drawing is into the pocket from the solution.

It performs that role in the active site of murine fumarylacetoacetase (Equation 4–362).[860] In this instance

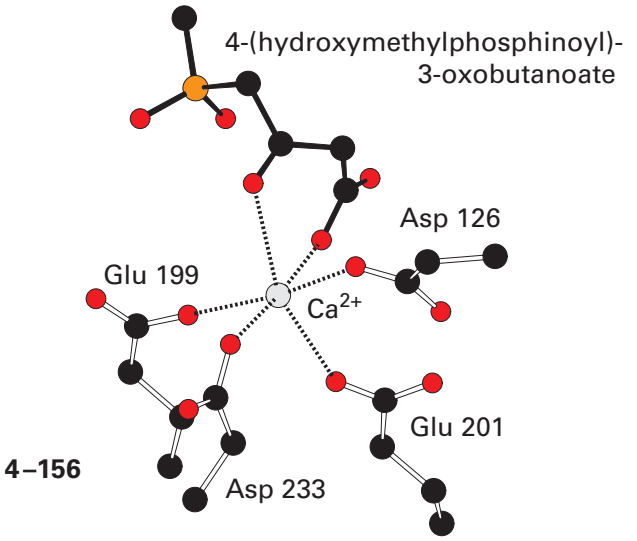

Ca^{2+} is coordinated monodentally by five carboxy oxygens, one from each carboxy group in two aspartates and two glutamates and one oxygen from the carboxy group of 4-(hydroxymethylphosphinoyl)-3-oxobutanoate (**4–120**), an analogue of the tetrahedral intermediate that is formed by nucleophilic addition of the peripheral enolate of acetoacetate to a carboxy group of the fumarate. The carbonyl group of 4-(hydroxymethylphosphinoyl)-3-oxobutanoate represents the oxyanion of the enolate, which is stabilized by Ca^{2+} in the usual reaction. In the active sites of both micrococcal nuclease from *S. aureus*[1021] and diisopropyl fluorophosphatase from *Loligo vulgaris*,[1142] a Ca^{2+} acts catalytically as a Lewis acid. In both active sites, the Lewis base on the substrate that is a ligand to Ca^{2+} is the oxygen of a phospho group. The Ca^{2+} forms only this one contact with the substrate, and its role appears to be the neutralization of negative charge that develops on the oxygen as the phosphorane is formed during the reaction.

Calcium dication is not used often in the role of a Lewis acid because its acidity is weak (Table 4–2). Nevertheless, it is sometimes used as a Lewis acid, and perhaps in these situations weak acidity may actually be advantageous, just as the weak acidity of an oxyanion hole is often advantageous. Its inability to form sterically reliable interactions and thereby provide a firm anchor to distort substrates may also be a drawback. It has already been noted, however, that the Ca^{2+} in the cluster of four manganese ions and a Ca^{2+} (Figure 2–59) in the active site of photosystem II at which water is oxidized to molecular oxygen has exploited this lack of firm coordination to permit molecules of water to rotate across the surface of the Ca^{2+} as they are fed into the cluster of manganese ions to be oxidized,[1143,1144] as if on a conveyer belt.

Manganese dication, Mn^{2+}, is a transition metallic cation rather than an alkaline earth metallic cation. Nevertheless, like Mg^{2+}, Mn^{2+} is also hard and small, although less hard than Mg^{2+}. Its ionic radius (Table 4–3) is only about 10% larger than that of Mg^{2+}, so it has a similar density of charge and size, and for all the same reasons, Mn^{2+} usually gathers six ligands octahedrally around itself. Each of these six ligands, as with all ligands to metallic dications, directs a lone pair of electrons, and hence the dipole associated with that lone pair of electrons, toward Mn^{2+}.

Because it is the **ion of a transition metal**, Mn^{2+}, unlike Mg^{2+}, has **electrons in 3*d* orbitals**. Manganese dication has a half-filled d^5 electronic configuration in which its five valence electrons are distributed one into each of the five 3*d* orbitals (Figure 2–24). In octahedral coordination, the 3*d* orbitals have orientations that cause the two singly occupied orbitals that are aligned with its six ligands ($3d_{z^2}$ and $3d_{x^2-y^2}$) to increase in energy because of electron repulsion and the three singly occupied orbitals that are not aligned with the ligands ($3d_{xy}$, $3d_{xz}$, and $3d_{yz}$) to decrease in energy, relative to a situation in which the sum of the electric fields of the ligands is redistributed mathematically as a uniform spherical field. These increases and decreases in energy result from the fact that the dipoles and elementary charges of the ligands are discretely oriented rather than distributed over a uniform spherical field. Their sum is the **ligand field stabilization** provided by the ligands. Because its five 3*d* electrons are evenly distributed over the five 3*d* orbitals, the increases and decreases in energy nearly cancel, and the ligand field stabilization for octahedrally coordinated Mn^{2+} is negligible. This lack of ligand field stabilization and the fact that the two orbitals aligned with the ligands, $3d_{z^2}$ and $3d_{x^2-y^2}$, are each occupied by an electron makes the bonding between Mn^{2+} and its ligands predominantly ionic, similar to the bonding between Mg^{2+} and its ligands. Consequently, as with Mg^{2+}, the main reason for the octahedral coordination around Mn^{2+} is steric.

While Mg^{2+}, both in solution and when bound to the active site of an enzyme, prefers oxygen ligands, particularly the oxygens of carboxy groups, the softer metallic dication Mn^{2+} in solution forms complexes with both nitrogen bases and oxygen

bases such as ammonia, imidazole, 1,2-diaminoethane, water, alcohols, carboxylates, the carbonyl oxygens of ketones and aldehydes, and the acyl oxygens of amides. Oxygen bases and nitrogen bases are roughly equivalent in their affinities for Mn^{2+}. In aqueous solution, the hexaammonium complex is observed only at concentrations of ammonia greater than 2 M; hexaimidazole salts can be crystallized from anhydrous ethanol. Like those for Mg^{2+}, all these complexes between unhindered bases and Mn^{2+} are hexacoordinate and octahedral. In these complexes, mixtures of various ligands around manganese can occur. For example, each of the species $[Mn(OH_2)_n(NH_3)_{6-n}]^{2+}$ with $0 < n \leq 6$ is observed in mixtures of ammonia and water. When Mn^{2+} is engaged catalytically as a Lewis acid in an enzymatic reaction, it is complexed octahedrally by Lewis bases from amino acids in the active site, molecules of water, and substrates.

As does Mg^{2+}, Mn^{2+} can form a complex in solution with one of the nominal reactants to produce the actual reactant entering the active site from the solution. For example, the requirement for Mn^{2+} in kinetic studies of the reduction catalyzed by isocitrate dehydrogenase (NAD^+)

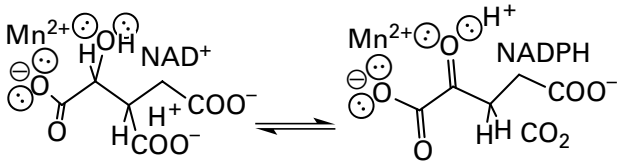

(4–423)

results from the fact that the actual reactant entering the active site is the complex between Mn^{2+} and the isocitrate dianion,[722,1145] and Mn^{2+} enters the active site within this complex just as Mg^{2+} often enters active sites in a complex with an oligophosphate. Because Mg^{2+}, however, was able to substitute for Mn^{2+} in this role, albeit with a lower catalytic constant, it may be the case that in cytoplasm, where the concentration of Mn^{2+} is quite low (Table 4–4), Mg^{2+} is the ligand to the isocitrate that enters the active site.

A typical arrangement of ligands coordinating Mn^{2+} when it is acting as a Lewis acid in an active site occurs in human pyruvate carboxylase[1146,1147]

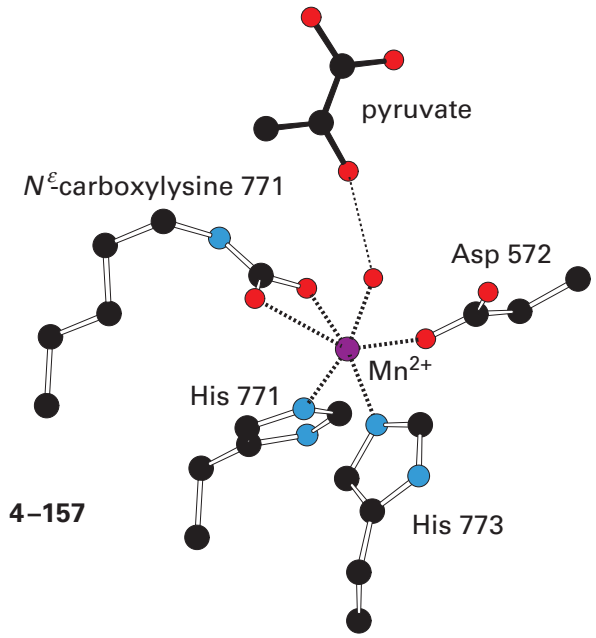

In the crystallographic molecular model, pyruvate, which is one of the six substrates for the enzyme

$$MgATP^{2-} + HOCO_2^- + \text{pyruvate} \rightleftharpoons H^+ + MgADP^- + HOPO_3^{2-} + \text{oxaloacetate}$$

(4–424)

is bound to the active site. The Mn^{2+} is coordinated by imidazolyl groups from Histidines 771 and 773, a carboxylato oxygen from Aspartate 572, the two oxygens of the N^6-carboxy group on Lysine 741, and a molecule of water* that sits between the carbonyl oxygen of pyruvate and Mn^{2+} and connects them.

Iron dication, Fe^{2+}, is a small dication that is borderline in hardness. It is a d^6 transition metallic dication, and its six valence electrons are distributed over five 3*d* orbitals (Figure 2–24). Unlike Mn^{2+}, in which the five 3*d* electrons are all unpaired, causing the ion to have significant unpaired electron spin, Fe^{2+} can exist in both low-spin and high-spin states. Low-spin Fe^{2+} usually adopts octahedral coordination with significant covalent character while high-spin Fe^{2+} exhibits more varied coordination with more ionic character.

Whether Fe^{2+} adopts a high-spin or low-spin state depends on the orientation of its ligands and

*There are no waters in the crystallographic molecular model of the human enzyme, so the molecule of water shown is a ligand to the metal and forms a hydrogen bond to the pyruvate found in the same location in the crystallographic molecular model of the homologous (46% identity; 0.6 gap percent) enzyme from *R. etli*.[1148]

whether they are strong or weak field ligands. These latter designations depend on the magnitude of the effect of a particular ligand on the energy of the ligand field. When octahedrally coordinated Fe^{2+} is in its **high-spin state** (Figure 2–25), two of its six valence electrons as a pair occupy one of the 3*d* orbitals ($3d_{xy}$, $3d_{xz}$, or $3d_{yz}$) that is of low energy because it does not align with any of the ligands. The other four valence electrons are distributed over the other four 3*d* orbitals: the remaining two of the $3d_{xy}$, $3d_{xz}$, and $3d_{yz}$ orbitals of lower energy and the $3d_{z^2}$ and $3d_{x^2-y^2}$ orbitals of higher energy that do align with the ligands. When octahedrally coordinated Fe^{2+} is in its **low-spin state**, its six valence electrons, in three pairs, occupy the three 3*d* orbitals of lower energy ($3d_{xy}$, $3d_{xz}$, or $3d_{yz}$) that are not aligned with the ligands. The 3*d* orbitals that align with the ligands, $3d_{z^2}$ and $3d_{x^2-y^2}$, are empty so that electron repulsion is minimized. The stronger the effect of the ligands is on the ligand field, the stronger will be the electron repulsion exerted by the ligands, and the more favorable will be the low-spin state. When Fe^{2+} is not octahedrally coordinated, the disposition of its 3*d* electrons, and hence its spin state, is determined more subtly, but strong field ligands usually promote octahedral coordination with a low-spin state because in this situation maximum ligand field stabilization is achieved. Because antibonding orbitals on Fe^{2+} are occupied by the lone pairs of electrons of the ligands when Fe^{2+} is in the high-spin state, pentacoordination or tetracoordination is preferred for high-spin Fe^{2+}, but that preference is not absolute. In an active site, steric effects are often more relevant to the distribution of ligands around Fe^{2+} than the electronic effects of the ligand field.

The high-spin state of octahedral Fe^{2+}, like the high-spin state of octahedral Mn^{2+}, does not have much ligand field stabilization. The fact that the two orbitals aligned with the ligands, $3d_{z^2}$ and $3d_{x^2-y^2}$, are each occupied by an electron precludes covalent bonding and makes the bonding of Fe^{2+} with its ligands predominantly ionic. The low-spin state of octahedral Fe^{2+} has maximum ligand field stabilization because the valence electrons are not aligned with the ligands and the lone pairs of the ligands are aligned with empty $3d_{z^2}$ and $3d_{x^2-y^2}$ orbitals. Because of this alignment, when Fe^{2+} is in the low-spin state, its interactions with its ligands have more of a covalent character.

When Fe^{2+} is used as a Lewis acid in an active site, one significant difference between its high-spin and low-spin states is ionic radius (Table 4–3). In the high-spin state of Fe^{2+}, its radius is larger by almost 0.02 nm, so its ligands are coordinated less tightly, as well as more ionically, and they are **more easily substituted**. In the low-spin state of Fe^{2+}, its ligands are coordinated more tightly, as well as more covalently, and they are **more inert to substitution**. These differences are consequential when substrates for the enzyme must become ligands to Fe^{2+} for the reaction catalyzed to proceed.

Iron dication is significantly softer than either Mn^{2+} or Mg^{2+}, so **its ligands are far more eclectic**. For example, in the crystallographic molecular model of peptide deformylase

N-formyl-L-methionyl peptide + H_2O $\rightleftharpoons$ formate + L-methionyl peptide (4–425)

from *E. coli*[121] in a complex with its substrate formate, the Fe^{2+} that acts as a Lewis acid in the reaction catalyzed by the enzyme[1149] is pentacoordinated by five ligands[1150]

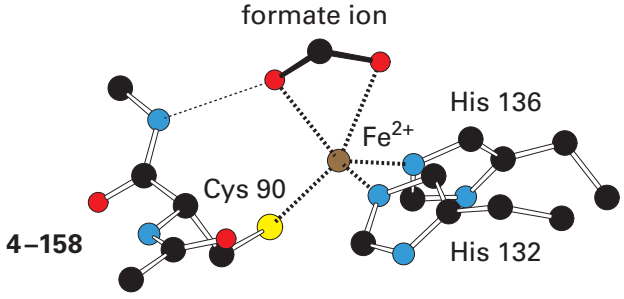

4–158

the imidazolyl groups of Histidines 132 and 136, the sulfanyl group of Cysteine 90, and the two oxygens of formate.

In addition to the covalency of the interactions of its empty 3*d* orbitals with its ligands in the low-spin state, Fe^{2+} can also participate with soft ligands in coordinations that have even more covalency. In these more covalent bonds, the lone pairs of electrons from four ligands fill the four vacant sp^3 orbitals formed from the vacant 4*s* orbital and the three vacant 4*p* orbitals of the dication. Consequently, as is the case with Zn^{2+} in aspartate carbamoyltransferase (**4–152**), this **primarily covalent bonding** always occurs with **tetrahedral coordination**. For example, the four Fe^{2+} in a tetranuclear [4Fe–4S] iron–sulfur cluster (Figure 2–21),* which form covalent bonds with sulfides and sulfanyl groups, are tetrahedrally

*Note the difference in tetrahedrality between the iron ions and the sulfide anions in the distorted cube.

coordinated. In these tetrahedral complexes, ligand field stabilization is negligible.

In the active site of aconitate hydratase (Figure 3–52), one of the four irons in the [4Fe–4S] cluster is missing the usual ligand from the sulfanyl group of a cysteine and is held in the active site only by the three inorganic sulfides. The requirement of aconitate hydratase to be activated with Fe^{2+} to observe enzymatic activity results from the fact that this loosely held Fe^{2+} readily dissociates from the iron–sulfur cluster and must be replaced.[1151] The enzyme is inactive if the cluster has lost this fourth iron. The absence of the sulfanyl group as a ligand to this Fe^{2+} in the cluster, however, although it labilizes the Fe^{2+}, permits the coordination of this Fe^{2+} in the tetranuclear [4Fe–4S] iron–sulfur cluster to expand from tetracoordinate to hexacoordinate when substrates are bound. This hexacoordinate Fe^{2+} provides an example of how important steric effects are in the orientation of ligands coordinating a metallic dication. The three sulfur atoms of the sulfides are significantly larger than the three oxygen atoms in the shell of coordination. As a result, the usual octahedral array around this Fe^{2+} is significantly distorted. The three vertices at which the atoms of sulfur are located move farther apart, increasing the angles between them, and force the three oxygens to move closer together, decreasing the angles between them. When the substrate isocitrate is bound to the hexacoordinate Fe^{2+} in aconitate hydratase (Figure 3–52) and when the substrate citrate is bound to the same Fe^{2+}, each provides a hydroxy group and a carboxylato group as ligands while the third open site is occupied by the molecule of water. When either substrate is bound, the hexacoordinate Fe^{2+} is in the high-spin state.[1070] In this high-spin state, substrates can enter and leave the coordination sphere of Fe^{2+} rapidly enough for catalysis to proceed.

Cobalt dication, Co^{2+}, has ionic radii (Table 4–3) indistinguishable from those of Fe^{2+}, and it is also borderline in hardness. It is a d^7 transition metallic dication, and its seven valence electrons are distributed over five $3d$ orbitals (Figure 2–24). Like Fe^{2+}, Co^{2+} can exist in both low-spin and high-spin states, but unlike Fe^{2+}, in its low-spin state it still has one unpaired electron in one of its $3d$ orbitals (see Figure 2–25). It is as acidic as most of the transition metallic dications (Table 4–2) and exchanges ligands as rapidly as Fe^{2+} (Table 4–5). Metalloenzymes, however, seldom[1152] have Co^{2+} as their naturally occurring prosthetic metallic dication, perhaps because of its extremely low free concentration in cytoplasm (Table 4–4), but it can often substitute effectively in the laboratory for the naturally occurring prosthetic metallic dication in a particular enzyme.

Table 4–5: Rates of Exchange of Water Bound in an Inner-Sphere Complex of a Metallic Cation at 25 °C[1153,1154]

cation	rate constant[a] (μs^{-1})	cation	rate constant[a] (μs^{-1})
K^+	4000	Zn^{2+}	30
Mg^{2+}	0.6	Co^{2+}	1
Ca^{2+}	>10000	Cu^{2+}	5000
Mn^{2+}	20	Fe^{3+}	2×10^{-4}
Fe^{2+}	3	Co^{3+}	1×10^{-7}
Ni^{2+}	0.03	Cr^{3+}	7×10^{-13}

[a]For the reaction
$[Me(OH_2)_m]^{n+} + H_2O^* \rightarrow [Me(OH_2)_{m-1}(O^*H_2)]^{n+} + H_2O$

Nickel dication, Ni^{2+}, is a small transition metallic dication that is also borderline in hardness. Its ionic radius is similar to that of low-spin Fe^{2+} (Table 4–3). Nickel dication has eight electrons in its five $3d$ orbitals (Figure 2–24). In octahedral coordination, the $3d_{xy}$, $3d_{xz}$, and $3d_{yz}$ orbitals are doubly occupied, and the $3d_{z^2}$ and $3d_{x^2-y^2}$ orbitals are each occupied by an unpaired electron. The doubly occupied $3d_{xy}$, $3d_{xz}$, and $3d_{yz}$ orbitals do provide significant ligand field stabilization in favor of octahedral coordination, but the singly occupied $3d_{z^2}$ and $3d_{x^2-y^2}$ orbitals are destabilizing, causing ligand field stabilization in fully octahedral coordination to be weak.

Both the fact that the orbitals oriented toward the ligands are singly occupied and the fact that it has more valence electrons make Ni^{2+} more reluctant to participate in fully occupied octahedral coordination because of electron repulsion. This reluctance and the lack of ligand field stabilization means that Ni^{2+} is **often coordinated by fewer than six ligands**. If one octahedral site is vacant, then **square pyramidal pentacoordination** results. If two octahedral sites are vacant, then **square planar tetracoordination** results. For example, when Ni^{2+} is in an enforced square planar coordination, as in coenzyme F_{430} (**4–61**), the two axial positions can be unoccupied (square planar tetracoordinate), one can be occupied (square pyramidal pentacoordinate), or both can

be occupied (octahedral hexacoordinate), depending on the strength of the ligands available.

In the Ni^{2+} state of the superoxide dismutases from *Streptomyces seoulensis*[1155] and *S. coelicolor*,[1156] the ligands coordinating Ni^{2+} are the sulfido groups of two cysteines and the unhydronated amido nitrogens of two peptide bonds. These ligands produce strong fields that would destabilize an octahedral coordination. In this instance, the four ligands are in a square planar array and both axial positions are unoccupied. In a square planar coordination, strong field ligands, such as dehydronated amido nitrogens of peptide bonds and sulfido groups, promote a **low-spin state** for Ni^{2+} in which the axial $3d_{z^2}$ orbital is doubly occupied and the $3d_{x^2-y^2}$ orbital, oriented toward the ligands, is vacant.[1157] The stability of this configuration is the reason that unconstrained, low-spin Ni^{2+} is nearly always square planar. In this low-spin state, axial ligands, if they are present, are only weakly associated.

Although a square planar coordination, such as those just described, that increases in covalency with softer ligands is common with Ni^{2+}, other dispositions of ligands are possible. For example, in the reduced nickel–iron hydrogenases, Ni^{2+} is coordinated with four sulfanyl groups from four cysteines in a distorted square planar array in which one of the four sulfurs is bent up away from the plane of the other three until it is almost normal to the plane.[1158,1159] This disposition of ligands is neither a tetrahedral nor a square planar arrangement. It must result from **steric effects** exerted by the active site.

There is a binuclear cluster of two Ni^{2+} in the active site of urease

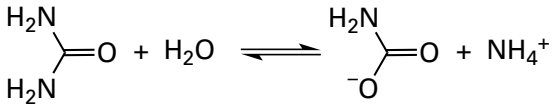

(4–426)

In the crystallographic molecular model of the enzyme from *Sporosarcina pasteurii* in a complex wih phosphorodiamidate, an analogue of the tetrahedral intermediate in the reaction (Figure 4–54),[1160] each Ni^{2+} is coordinated by two imidazolyl groups from two histidines and one of the two oxygens from the carboxy group on N^6-carboxy-Lysine 219. One oxygen of phosphorodiamidate is a μ-oxo ligand between the two Ni^{2+}. The other oxygen is a ligand to one Ni^{2+}, and one nitrogen is a ligand to the other Ni^{2+}. One Ni^{2+} has these five ligands in a sterically distorted square pyramidal coordination; the other Ni^{2+} has an oxygen of the carboxy group of Aspartate 362 as a sixth ligand in a sterically distorted octahedral coordination.

Zinc dication, Zn^{2+}, is a small transition metallic cation that is borderline in hardness. Its ionic radius (Table 4–3) is indistinguishable from those of Mg^{2+}, Fe^{2+}, and Ni^{2+} and somewhat smaller than that of Mn^{2+}. It is a d^{10} metallic cation, so all five of its $3d$ orbitals are occupied by pairs of electrons, a configuration that fills the $3d$ shell. Because the $3d$ shell is fully occupied, there is only a low-spin state. It has already been noted that Zn^{2+} is able to form tetrahedral, mostly covalent complexes (**4–152**) by using the sp^3 hybrids of its vacant $4s$ and $4p$ orbitals.

Zinc dication is the **most versatile metallic cation functioning as a Lewis acid** in the active sites of metalloenzymes. Its versatility in this role arises from its stability to oxidation and reduction because its $3d$ orbitals are fully occupied; its ability to form tetracoordinate, pentacoordinate, and hexacoordinate complexes with Lewis bases; and its ability to be coordinated with lone pairs from oxygen, nitrogen, and sulfur. Often two or three of these rather different bases coordinate the Zn^{2+} in an active site. When Zn^{2+} is coordinated by four sulfurs (**4–152**), which are soft bases, the interaction is usually tetrahedral and almost entirely covalent. The complex between Zn^{2+} and the harder base ammonia, $[Zn(NH_3)_4]^{2+}$, is also tetracoordinate and tetrahedral. This tetrahedral coordination of Zn^{2+} is observed when Zn^{2+} forms complexes with 1,2-diaminoethane, cyclic lactams, and imidazole. As the ligands become harder, however, geometries become more variable as the bonding becomes less covalent and tetrahedral and more ionic and flexible. For example, the complex $[Zn(OH_2)_6]^{2+}$ between Zn^{2+} and water, a hard base, is hexacoordinate and octahedral for the same reasons that ligands around Mg^{2+}, a metallic dication of the same radius, are octahedral. As hydrons are removed, however, and the donor strength of the ligands increases, covalency becomes more favorable because of decreases in ligand field stabilization, and the coordination decreases to four ligands, as $[Zn(OH)_3(OH_2)]^-$.

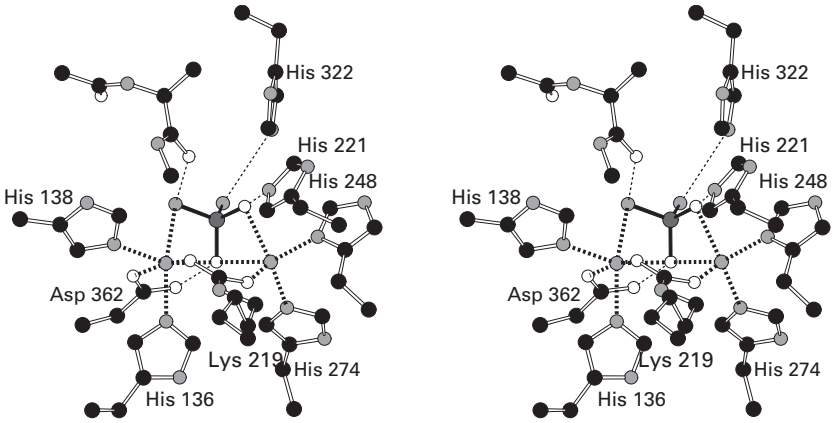

Figure 4–54: Stereodrawing[134] of the crystallographic molecular model of the active site of urease from *S. pasteurii* occupied by two Ni^{2+} and phosphorodiamidate (**4–76**), a analogue of the tetrahedral intermediate in the enzymatic reaction.[1160] Black atoms are carbons, white atoms are oxygens, small gray atoms are nitrogens, and the large dark gray atom is an atom of phosphorus. The small dark gray spheres are the nickel ions surrounded by their ligands. The enzyme was purified from cytoplasm of *S. pasteurii* and crystallized from 1 M $(NH_4)_2SO_4$, 4 mM phosphorodiamidate, 10 mM 2-ammonio-2-hydroxymethylpropane-1,3-diol, and 50 mM citrate at pH 7. Electron density for phosphoramidate and two Ni^{2+} could be observed in the active site. The molecular model of phosphorodiamidate is in the center of the figure. The hexacoordinate Ni^{2+} has as four of its monodentate ligands the imidazolyl groups of Histidines 136 and 138, an oxygen from the carboxylato group of Aspartate 362, and an amido nitrogen of phosphorodiamidate. The pentacoordinate Ni^{2+} has as three of its monodentate ligands the imidazolyl groups of Histidines 248 and 274 and an oxygen from the phosphorodiamidate. One oxygen of phosphorodiamidate is a μ-oxo ligand between the two Ni^{2+}, and each Ni^{2+} is coordinated by one of the two oxygens from the carboxy group on *N*-carboxy-Lysine 219. Histidine 322 forms a hydrogen bond with one of the nitrogens in the phosphorodiamidate, and the acyl oxygen of a peptide bond in the polypeptide forms a hydrogen bond with the other nitrogen.

A distorted octahedral complex (**4–159**) forms with two acetates[1161,1162]

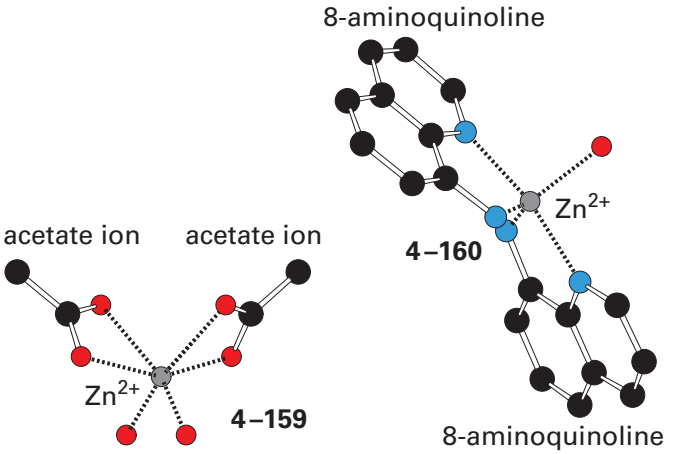

The zinc ion forms a trigonal bipyramidal pentacoordinate complex with, among other ligands, 8-aminoquinoline **4–160**.[1163] In this case, the four nitrogens from two aminoquinolines and a molecule of water are the five Lewis bases that generate the complex $[Zn(N_2C_9H_8)_2(OH_2)]^{2+}$.

The ability of Zn^{2+} to be coordinated effectively by lone pairs on nitrogen, oxygen, and sulfur is also exploited in the association of substrates. For example, the amido nitrogen in cyanamide becomes a ligand to the prosthetic Zn^{2+} in the active site of cyanamide hydratase from *S. cerevisiae* during its hydration;[1164] the acyl oxygen in a peptide bond becomes a ligand to the prosthetic Zn^{2+} in the active site of thermolysin (Figure 3–42) during its hydrolysis by a molecule of water, the oxygen of which is also a ligand to Zn^{2+}; and the sulfanyl group of a cysteine in a substrate becomes a ligand to the prosthetic Zn^{2+} in the active site of protein farnesyltransferase from *S. cerevisiae* during its farnesylation.[1165]

There is no typical arrangement for the ligands coordinating Zn^{2+} when it is bound in an active site (Figure 4–55).[1166-1173] Examples from its eclectic set of **mononuclear coordinations** in the active sites of enzymes are two imidazolyl groups, the oxygen from a monodentate carboxy group, and the oxygen of what was the molecule of water that added nucleophilically to the acyl oxygen of the peptide bond of the substrate in the active site of thermolysin (Figure 3–42); three sulfanyl groups and a molecule of water or the 4-oxo oxygen of uridine in cytidine deaminase (Figure 3–36); two sulfanyl groups, an imidazolyl group, and a molecule of water in GTP cyclohydrolase I from *E. coli*;[1174] three imidazolyl groups and an oxygen from the substrate bicarbonate in human carbonic anhydrase 1 (Figure 4–55A);[1169] three imidazolyl groups and the two oxygens of the *cis*-enediol intermediate in fructose-bisphosphate aldolase from *M. tuberculosis* (Figure 4–55B);[1171] the oxygen from a carboxy group, the acyl oxygen from the γ-carbamoyl group of a glutamine, an imidazolyl group, and the two oxygens from an analogue of the *cis*-enediol intermediate in human lactoylglutathione lyase (Figure 4–55C);[1167] and an imidazolyl group, the two oxygens of a bidentate carboxylato group, an oxygen from another carboxy group, a sulfanyl group, and the carbonyl oxygen from the substrate D-arabinose 5-phosphate in 3-deoxy-8-phosphooctulonate synthase from *A. aeolicus* (Figure 4–55D).[1168] Adjacent to the active site in isopentenyl-diphosphate Δ-isomerase from *E. coli*, there is a structural Zn^{2+} hexacoordinated by three imidazolyl groups, bidentately by the two oxygens of a carboxylato group, and monodentately by one oxygen of another carboxy group.[1175,1176] The tetracoordinate Zn^{2+} in aspartate carbamoyltransferase (**4–152**) is distant from the active site and performs only a structural role.

Many zinc metalloenzymes have **dinuclear clusters of Zn^{2+}, often bridged by a single atom** of one of the ligands. One example is the dinuclear cluster of two Zn^{2+} in the active site of aryldialkylphosphatase from *B. diminuta* (Figure 4–55E).[1166,1177] One pentacoordinated Zn^{2+} is coordinated by two imidazolyl groups and the oxygen of a carboxy group, and the other is coordinated by two imidazolyl groups and the phospho oxygen of diisopropyl methylphosphonate, an analogue of a substrate. In addition, a μ-hydroxide, located between the two Zn^{2+} and bridging them, provides one lone pair to each Zn^{2+}, and the carboxylato group of an N^6-carboxylysine provides one oxygen as a ligand to one Zn^{2+} and the other oxygen as a ligand to the other Zn^{2+}. In the active site of succinyl-diaminopimelate desuccinylase from *H. influenzae* (Figure 4–55F),[1170] each of the two pentacoordinated Zn^{2+} is coordinated by an imidazolyl group and bidentately by the two oxygens of a carboxylato group. In addition, a μ-hydroxide, located between the two Zn^{2+} and bridging them, provides one lone pair to each Zn^{2+}, and the carboxylato group of an aspartate provides one oxygen as a ligand to one Zn^{2+} and the other oxygen as a ligand to the other Zn^{2}.

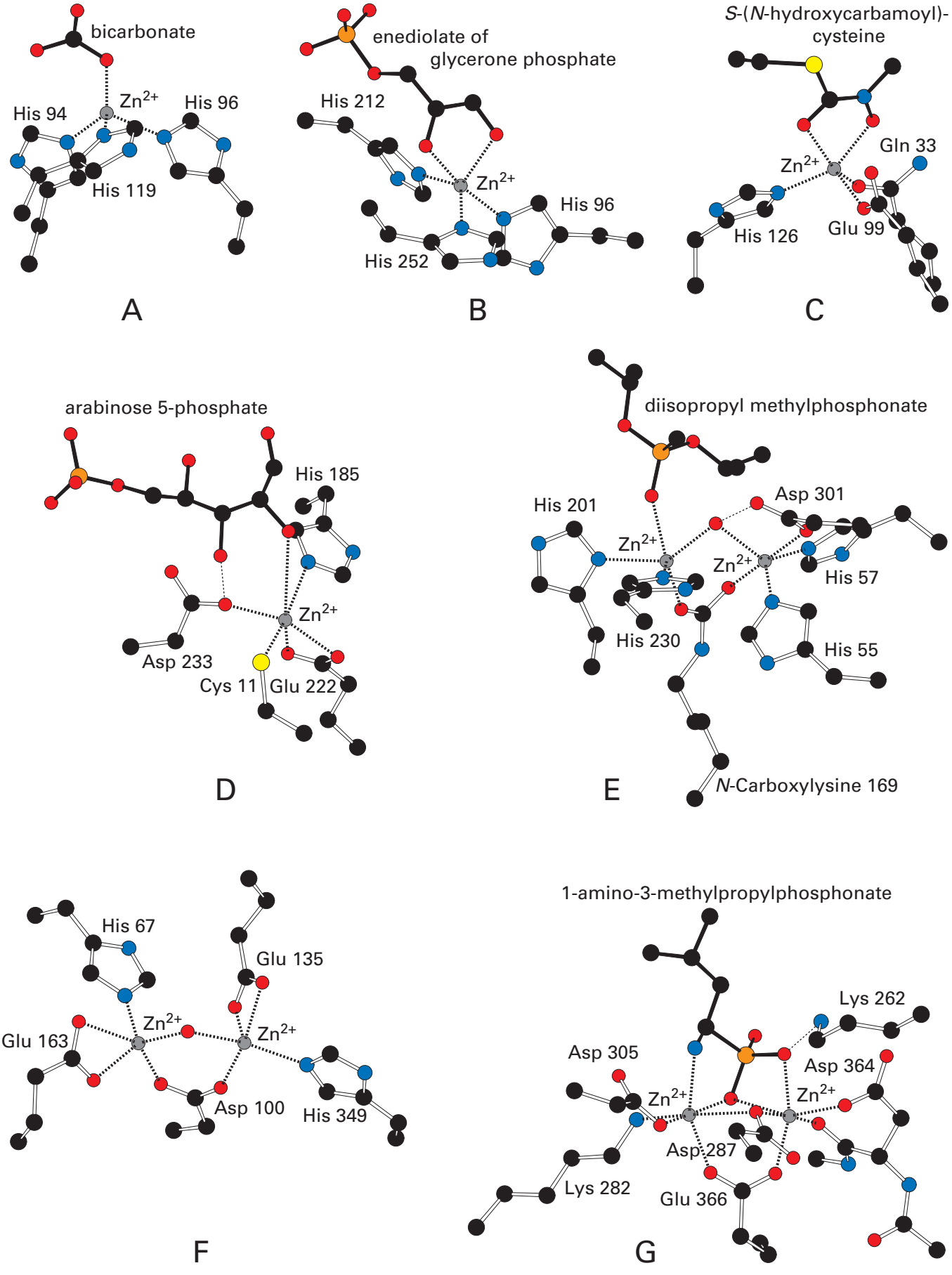
bicarbonate
Zn^{2+}
His 94
His 96
His 119
A
enediolate of
glycerone phosphate
His 212
Zn^{2+}
His 96
His 252
B
S-(*N*-hydroxycarbamoyl)-
cysteine
Gln 33
Zn^{2+}
His 126
Glu 99
C
arabinose 5-phosphate
His 185
Zn^{2+}
Asp 233
Cys 11
Glu 222
D
diisopropyl methylphosphonate
His 201
Asp 301
Zn^{2+}
Zn^{2+}
His 57
His 230
His 55
N-Carboxylysine 169
E
His 67
Glu 135
Zn^{2+}
Zn^{2+}
Glu 163
Asp 100
His 349
F
1-amino-3-methylpropylphosphonate
Lys 262
Asp 305
Asp 364
Zn^{2+}
Zn^{2+}
Asp 287
Lys 282
Glu 366
G

Figure 4–55: Ligands to zinc dications in drawings[134] of the crystallographic molecular models for the active sites of metalloenzymes. Black atoms are carbons, white atoms are oxygens, small darker gray atoms are nitrogens, large lighter gray atoms are sulfurs, and large dark gray atoms are atoms of phosphorus. The small dark gray spheres are zinc ions surrounded by their ligands. (**A**) The Zn^{2+} in the active site of human carbonic anhydrase 1, which is occupied with its substrate bicarbonate, has as its four tetrahedrally arrayed ligands the imidazolyl groups of Histidines 94, 96, and 119 and one of the oxyanions from bicarbonate.[1169] (**B**) The Zn^{2+} in the active site of fructose-bisphosphate aldolase from *M. tuberculosis*, which is occupied with what has been assigned as the *cis*-enediolate of its substrate glycerone phosphate, has as its five ligands the imidazolyl groups of Histidine 96, 212, and 252 and the two oxygens from the *cis*-enediolate.[1171] (**C**) The Zn^{2+} in the active site of human lactoylglutathione lyase, which is occupied with *S*-(*N*-hydroxy-*N*-4-iodophenylcarbamoyl)glutathione, an analogue of the *S*-(*cis*-enediolato) intermediate in the enzymatic reaction, has as its five ligands the oxygens of the amido group of Glutamine 33 and the carboxylato group of Glutamate 99 from one subunit of the enzyme, the imidazolyl group of Histidine 126 from the other subunit, and the two oxygens of the *N*-hydroxycarbamoyl group that are homologues of the two oxygens of the *S*-(*cis*-enediolato) intermediate. Only the side chain of the *S*-(*N*-hydroxycarbamoyl)cysteinyl portion of the analogue without the iodophenyl group is drawn.[1167] (**D**) The Zn^{2+} in the active site of 3-deoxy-8-phosphooctulonate synthase from *A. aeolicus*, which is occupied with the substrates phospho*enol*-pyruvate and D-arabinose 5-phosphate, has as its six ligands the sulfanyl group of Cysteine 11, the imidazolyl group of Histidine 185, the two oxygens of the carboxylato group of Glutamate 222, the carboxylato group of Aspartate 233, and the oxo oxygen of the D-arabinose 5-phosphate.[1168] (**E**) One of the two Zn^{2+} in the active site of aryldialkylphosphatase from *B. diminuta*, which is occupied with diisopropyl methylphosphonate (an analogue of a phosphotriester substrate) has as three of its ligands the imidazolyl groups of Histidines 201 and 230 and the phospho oxygen of the diisopropyl methylphosphonate. The other Zn^{2+} has as three of its ligands the oxyanion of the carboxylato group of Aspartate 301 and the imidazolyl groups of Histidines 55 and 57. A μ-hydroxide is located between the two Zn^{2+} and serves as a ligand to each ion. Each oxygen of the carboxylato group of *N*-carboxy-Lysine 169 provides a ligand[1166,1173] to one of the Zn^{2+}. (**F**) One of the two Zn^{2+} in the active site of succinyl-diaminopimelate desuccinylase from *H. influenzae* has as three of its ligands the two oxygens of the carboxylato group of Glutamate 163 and the imidazolyl group of Histidine 67. The other Zn^{2+} has as three of its ligands the two oxygens of the carboxylato group of Glutamate 135 and the imidazolyl group of Histidine 349. A μ-hydroxide is located between the two Zn^{2+} and serves as a ligand to each ion. Each oxygen of the carboxylato group of Aspartate 100 provides a ligand[1170] to one of the Zn^{2+}. (**G**) One of the two Zn^{2+} in the active site of bovine leucyl aminopeptidase, which is occupied by 1-amino-3-methylpropylphosphonate (an analogue of the tetrahedral intermediate) has as three of its ligands the 6-amino group of Lysine 282, the carboxylato group of Aspartate 305, and the amino group of 1-amino-3-methylpropylphosphonate. The other Zn^{2+} has as three of its ligands the carboxylato group of Aspartate 364, the amido oxygen of the peptide bond following Aspartate 364, and one of the phospho oxygens of 1-amino-3-methylpropylphosphonate. A carboxylato oxygen of Aspartate 287 and a phospho oxygen of 1-amino-3-methylpropylphosphonate are μ-oxo ligands located between the two Zn^{2+}, and each oxygen acts as a ligand to each Zn^{2+}. Each oxygen of the carboxylato group of Glutamate 366 provides a ligand[1172] to one of the Zn^{2+}.

In the active site of bovine leucyl aminopeptidase (Figure 4–55G),[1172] one of the hexacoordinated Zn^{2+} is coordinated by one oxygen from an aspartate and its peptidyl acyl oxygen as well as an oxygen from the phosphonyl group of 1-amino-3-methylpropylphosphonate, an analogue of the tetrahedral intermediate in the enzymatic hydrolysis; and the other hexacoordinated Zn^{2+} is coordinated by the 6-amino group of a lysine, the amino group of 1-amino-3-methylpropylphosphonate, and the oxygen of the carboxylato group of an aspartate. In addition, one carboxylato oxygen of an aspartate and one phospho oxygen of 1-amino-3-methylpropylphosphonate are located between the two Zn^{2+} and provide bridging ligands to both; and the carboxylato group of a glutamate provides one oxygen as a ligand to one Zn^{2+} and the other oxygen as a ligand to the other Zn^{2+}.

In the complete collection of these examples of Zn^{2+} in active sites (Figure 4–55), there are tetracoordinate, pentacoordinate, and hexacoordinate arrangements that are more or less sterically distorted from the paradigmatic tetrahedral, trigonal bipyramidal, tetragonal pyramidal, and octahedral geometries, respectively, and lone pairs of electrons on sp^3 and sp^2 oxygens, sp^3 and sp^2 nitrogens, and sp^3 sulfurs serve as ligands. One conclusion from this promiscuity is that the identities of **ligands to Zn^{2+} in active sites are in part arbitrary**. For example, the homologous (26% identity; 2.7 gap percent) murine cytidine deaminases from *Mus musculus* (Figure 3–36) and *E. coli*[1178] and the unrelated cytosine deaminase from *E. coli*[1179] all use a single Zn^{2+} as a Lewis acid to catalyze the same reaction. The Zn^{2+} is coordinated in the murine enzyme by three sulfanyl groups,[848] in the homologous enzyme from *E. coli* by two sulfanyl groups and an imidazolyl group, and in the nonhomologous enzyme from *E. coli* by three imidazolyl groups. Two of the three sulfanyl groups in the murine enzyme are acceptors for hydrogen bonds from the guanidinio group of an arginine, which may modulate their field strengths.[1180]

It also seems that **the number of ligands to Zn^{2+} is flexible**. For example, the ability of Zn^{2+} to alternate between tetracoordination and pentacoordination while bound as a Lewis acid in the active site of an enzyme has been demonstrated in studies of thermolysin (Figure 3–42). In the crystallographic molecular model of the unoccupied active site in the native enzyme, the Zn^{2+} is **pentacoordinate**. Histidines 142 and 146 each provide a lone pair of electrons, Glutamate 166 provides two lone pairs of electrons as a bidentate ligand, and the fifth position is occupied by a molecule of water.[1181,1182] There are several different complexes in which the active site of thermolysin is occupied by ligands. The first (**4–161**) is a complex with the competitive inhibitor 3-phenylpropionyl-L-phenylalanine

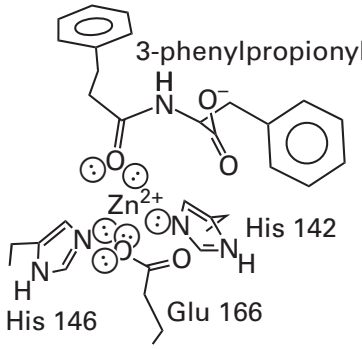

4–161

phosphonamidate **4–163**

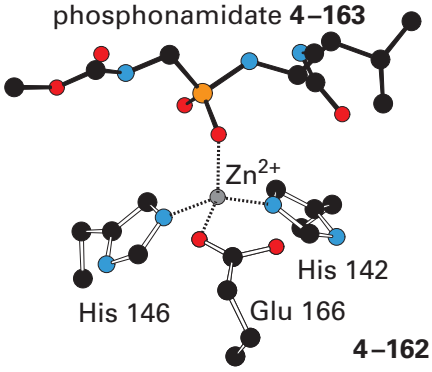

4–162

in which the peptide bond is intact.[1183] Figure 3–42 and **4–162** depict a second complex between the active site of thermolysin and a phosphonamidate (previously **3–83**)

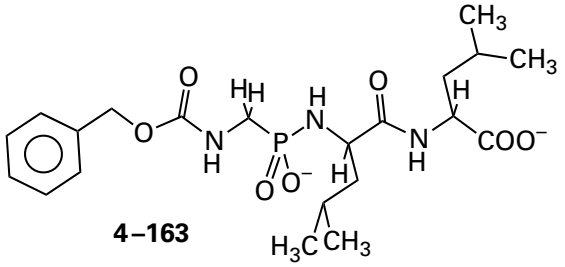

4–163

an analogue of the tetrahedral intermediate.[1184] There is a third complex of the active site of thermolysin with *N*-(1-carboxy-3-phenylpropyl)-L-leucyl-L-tryptophan, an analogue of the carboxy terminus of the amino-terminal product of hydrolysis of a peptide bond.[1185] In crystallographic molecular models of these three complexes, Glutamate 166 has become a monodentate ligand at only one of its oxygens. The molecule of water in the unliganded enzyme has been replaced by a monodentate ligand—the acyl oxygen of 3-phenylpropionyl-L-phenylalanine (**4–161**), the oxyanion of phosphonamidate **4–163** (**4–162**), or the carboxylato group of the carboxy terminus—and the Zn^{2+} has become **tetracoordinate**.

Each complex, representing in turn three major intermediates in the enzymatic reaction, has almost identical tetrahedral tetracoordination (**4–162**). Dissociation of the other oxygen of the carboxy group of Glutamate 166 from the Zn^{2+} is probably the result of a steric effect. Each bulky ligand—attached to the active site in multiple locations, as are the actual substrates and intermediates in the normal enzymatic reaction—draws the zinc toward itself into a location that can no longer accommodate bidentate coordination by the carboxy group of Glutamate 166.

Hydroxamate **4–164**

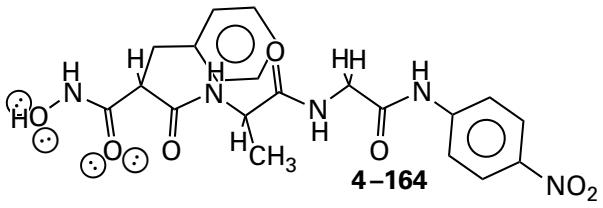

4–164

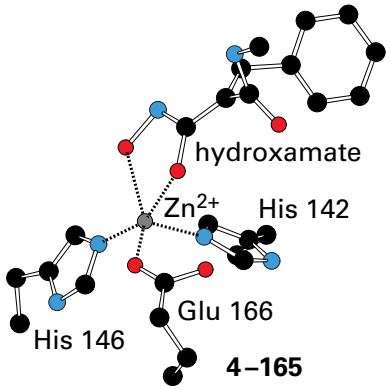

4–165

is also a competitive inhibitor for the enzyme. In the crystallographic molecular model of the complex with the active site,[1108] the hydroxamate provides two ligands to Zn^{2+}—a lone pair of electrons from the acyl oxygen and a lone pair of electrons on the

oxygen in the hydroxy group of the hydroxamate—to accomplish its pentacoordination (**4–165**). This complex probably represents the Michaelis complex between a polypeptide and the active site. The acyl oxygen of the peptide bond in the Michaelis complex is represented by the acyl oxygen of the hydroxamate. The molecule of water that was bound to the Zn^{2+} before association of the polypeptide, which will add nucleophilically to the acyl carbon of the peptide bond in the next step to form the tetrahedral intermediate, is represented by the hydroxy group of the hydroxamate. In this complex, Glutamate 166 is also a monodentate ligand and the pentacoordination is different from the pentacoordination in the unoccupied active site.

In the active site of threonine–tRNA ligase from *E. coli*, the Zn^{2+} that recognizes the L-threonine is tetracoordinate in the unoccupied state with a sulfanyl, two imidazolyl groups, and a molecule of water as ligands

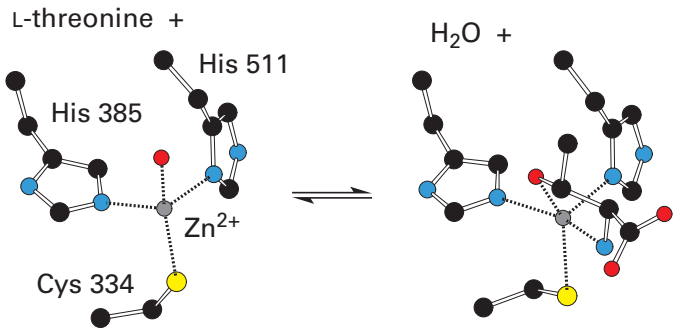

(4–427)

When the L-threonine, however, occupies the active site, both its hydroxy group and its amino group are ligands to the Zn^{2+}, making it pentacoordinate in a distorted tetragonal pyramid.[1186]

Cadmium is in the same group, immediately below zinc in the periodic table, so **cadmium dication**, Cd^{2+}, is a larger and hence softer transition metallic cation than Zn^{2+}. Nevertheless, it is used instead of Zn^{2+} in carbonic anhydrase from *Thalassiosira weissflogii*, which can live in regions of the ocean with very low levels of Zn^{2+}. The Cd^{2+} is coordinated in the resting enzyme in this rare if not exclusive appearance by two sulfanyl groups, an imidazolyl group, and two molecules of water.[1187]

One might imagine that there would be little doubt as to which of the metallic dications just described are incorporated into a particular metalloenzyme to fulfill its particular role when the enzyme is in the cytoplasm, the solution in which it has evolved, but unfortunately, in many instances it is difficult, if not impossible, to ascertain this seemingly simple fact.

There are **enzymes that retain one or more metallic dications** as a part of their structure as they are being purified and also retain their full enzymatic activity throughout. For example, Zn^{2+}, which is the native metallic dication in the active site of *N*-acetylglucosamine-6-phosphate deacetylase from *E. coli*,[1188] is retained during purification. When fructose-bisphosphate aldolase is purified from *S. cerevisiae*, the enzyme is found to contain one tightly bound Zn^{2+} for each active site (Figure 4–55B).[1189] If the Zn^{2+} is removed from the enzyme, its enzymatic activity is lost.[1190] Purified thermolysin (Figure 3–42),[1191] cytidine deaminase (Figure 3–36),[1178] carbonic anhydrase (Figure 4–55A),[1192] lactoylglutathione lyase (Figure 4–55C),[1193] 3-deoxy-8-phosphooctulonate synthase (Figure 4–55D),[1194] aryldialkylphosphatase (Figure 4–55E),[1177] succinyl-diaminopimelate desuccinylase (Figure 4–55F),[1195] and leucyl aminopeptidase (Figure 4–55G)[1196] are other examples of metalloenzymes that retain their Zn^{2+} during purification to homogeneity. Urease (Figure 4–54)[1197,1198] retains its Ni^{2+}, and pyruvate carboxylase from *G. gallus*[1146] retains its Mn^{2+}. Because they seem to be permanent participants in the active site, these metallic dications that purify with the enzyme can be considered to be **prosthetic**.

The Zn^{2+} in the active site of native *N*-acetylglucosamine-6-phosphate deactylase can be removed and replaced with Cd^{2+}, Co^{2+}, Mn^{2+}, Fe^{2+}, or Ni^{2+}, each of which reactivates the enzyme[1199] to catalytic constants about the same as that for Zn^{2+}. Fructose-bisphosphate aldolase in which the native Zn^{2+} has been replaced by Ni^{2+}, Cu^{2+}, or Mg^{2+} is inactive (<0.5% activity).[1190] When, however, the Zn^{2+} is replaced[1189] by Co^{2+}, Fe^{2+}, or Mn^{2+}, the enzyme regains activity, but its catalytic constant has decreased by factors of 2, 2.7, and 7, respectively,[1190] relative to the enzyme in which Zn^{2+} has been reincorporated. Even though a limited number of replacements are permitted, there can be little doubt that the metallic dication normally incorporated into *N*-acetylglucosamine-6-phosphate deactylase and fructose-bisphosphate aldolase is Zn^{2+}, because that dication is still present following purification.

Several of the enzymes that retain their metallic dications during purification because they are so tightly bound in the active site require specific **chaperones that are essential for the incorporation of the metallic dications** during their folding and maturation.[1200] Metallochaperones are able to bind tightly metallic dications that are present at extremely

low free concentrations in the cytoplasm (Table 4–4), such as Ni^{2+}, Zn^{2+}, and Cu^{2+}, and deliver them to the folding metalloenzyme for insertion into their active sites.[1201] For example, a chaperone produced by expression of the *UreE* genes in bacteria is able to bind Ni^{2+} tightly and participate in its incorporation into urease,[1202,1203] the active site of which contains a dinuclear cluster of Ni^{2+}. The fact that such an elaborate system is required to incorporate the metallic dication in the first place suggests that once a metal is incorporated into an active site by a metallochaperone, it will remain incorporated throughout the lifetime of the enzyme.

There is one caveat concerning identification of the metallic cation that is bound so tightly that it copurifies with the enzyme. In the past, when an enzyme retained its cytoplasmic metallic cation, a definitive identification of that prosthetic metallic cation was usually made by standard qualitative and quantitative inorganic analysis. One difficulty with this approach is that significant amounts of protein are needed and are usually lost during the procedure. Methods that require less protein, such as mass spectrometry, X-ray absorption spectroscopy,[1204] X-ray fluorescence,[1205] and particle-induced X-ray emission,[1206] can be used to make identifications when the presence of a metallic cation is suspected. A difficulty arises when a metallic cation that is yet to be identified is observed in a crystallographic molecular model. There are procedures for identifying it provisionally by varying the wavelength of the X-rays used to determine the map of electron density through the absorption edges of the various metals.[1207] It has been noted, however, that when identification of the metallic cation in an active site is made based only on crystallography, that identification is often incorrect.[1206]

There are other **metalloenzymes that require a metallic dication to be added to the solution** after they have been purified as well as during their purification before they display any catalytic activity, but they are themselves, following purification, devoid of any metallic dication. In these situations, either the metallic dication present in the active site when the enzyme is in the cytoplasm is bound weakly and dissociates as the enzyme is purified, or the procedures for purifying the enzyme are so harsh that they promote dissociation of an otherwise tightly bound metallic dication. For **enzymes that lose their metallic dications** during purification, it is unlikely that metallochaperones are involved in incorporating the metal during the folding of their polypeptides because the metallic dications are probably dissociating and associating constantly. In this case, association with the active site is an equilibrium between bound metallic dication and metallic dication free in the cytoplasm. Because, in this instance, the metallic dications are not permanent or even semipermanent participants in the active site, although they are cofactors, they are obviously not prosthetic.

For enzymes in this class, when they are in the cytoplasm under normal circumstances, it is possible that the sites at which the required metallic dications are coordinated are occupied because the concentrations of those metallic dications in the cytoplasm are high enough to saturate those sites, and their association with the preferred metallic dication is specific enough to exclude significant association of other metallic dications. It is also possible, however, that many of these enzymes with loosely bound catalytic metallic dications are able to use more than one particular metallic dication for effective catalysis in the cytoplasm.

When phosphoglucomutase is purified from muscle of *O. cuniculus*, it contains no metallic dications, but its enzymatic activity displays an **absolute requirement** for one (activity in the absence of metallic dication is <0.001% that in the presence of Mg^{2+}).[1208] The requirement for a metallic dication can be fulfilled by Mg^{2+}, Ni^{2+}, Co^{2+}, Mn^{2+}, or Zn^{2+}. Although the relative capacity of each metallic dication to reactivate the enzyme varies with temperature and pH,[1209] Mg^{2+}, Ni^{2+}, and Co^{2+} are almost equally effective at restoring a high catalytic constant, while the catalytic constants of the enzyme reconstituted with Mn^{2+} and Zn^{2+} are much less. Purified 3-dehydroquinate synthase from *Aspergillus nidulans* requires addition of a metallic dication before it will catalyze its enzymatic reaction, and the requirement can be fulfilled[1210] by Zn^{2+} and Co^{2+} and to a lesser extent by Fe^{2+} and Ni^{2+}. In addition, Eu^{3+} and Sm^{3+}, which are definitely nonphysiological metallic dications, work almost as well as Zn^{2+} and Co^{2+}. The requirement for a metallic dication displayed by *N*-formylmethionylaminoacyl-tRNA deformylase from *E. coli*[1211] can be fulfilled only by Mn^{2+} and Ni^{2+}.

Either **the catalytic constant or the specificity constant for a substrate can differ**, depending on the metallic dication that is chosen to occupy the active site and activate the enzymatic reaction. For example, when Co^{2+} is used as the prosthetic metal in the active site of 3-dehydroquinate synthase from *E. coli*,[1212] its catalytic constant is 14 s^{-1}, but when Zn^{2+} is used,[1152] it is 7 s^{-1}; with Ni^{2+}, it is 3.3 s^{-1}; with Cd^{2+}, it is 1.7 s^{-1}; with Mn^{2+}, it is 1.4 s^{-1};

and with Cu^{2+}, it is 1.3 s^{-1}. When Co^{2+} is the prosthetic metal in the active site of xylose isomerase from *Piromyces*,[1213] its specificity constant for xylose is 3300 M^{-1} s^{-1}; with Mn^{2+}, it is 1100 M^{-1} s^{-1}; with Mg^{2+}, it is 270 M^{-1} s^{-1}; and with Ca^{2+}, it is 0.2 M^{-1} s^{-1}. The apparent dissociation constant for the metallic dication can also vary widely. For xylose isomerase from *Piromyces*, the apparent dissociation constants for Mn^{2+}, Co^{2+}, Mg^{2+}, and Ca^{2+} are 1.4, 6.5, 100, and 160 μM, respectively.

In at least one instance, there seems to be a linear correlation between standard free energy of association with the active site for nine metallic dications that activate an enzyme and density of charge for the respective dication.[1214] In most instances, however, there seems to be **little rationale for which metallic dications are effective** at performing the role of a Lewis acid in the active site of an enzyme that loses its native metallic dication during purification. The distinction between dications that are effective and those that are not may arise from subtle differences in the arrangement of ligands that coordinate the metallic dication. For example, mammalian lactoylglutathione lyase (Figure 4–55C) retains its Zn^{2+} during purification.[1193] The homologous enzyme from *E. coli* (38% identity; 2.3 gap percent) loses its metallic dication during purification and can use Ni^{2+}, Co^{2+}, and Mn^{2+} as catalytic Lewis acids but not Zn^{2+}.[1215] The difference in the two enzymes is the identity and arrangement of the ligands coordinating the respective metallic dications.[1216]

When an enzyme loses its metallic dication during purification, the question that arises is **which metallic dication performs the role of a Lewis acid in the active site when the enzyme is in the cytoplasm**. Estimates of free concentrations* of the metallic dications in cytoplasm (Table 4–4)[1130] can provide limits on which metallic dication may be functioning physiologically.† For example, the Michaelis constants for Mg^{2+} and Mn^{2+} for the initial rate of the reaction catalyzed by phosphopyruvate hydratase from *S. cerevisiae* are 0.50 mM and 5 μM, respectively, while the catalytic constants of the enzyme are about the same for the two dications.[1217] Because the free concentration of Mg^{2+} in cytoplasm is about 10,000 times higher than the free concentration of Mn^{2+} (Table 4–4), only about 1% of the total activity of the enzyme in the cytoplasm should result from active sites using Mn^{2+}. Dimethylsulfoniopropionate lyase from *Pelagibacter ubique* requires a metallic dication for enzymatic activity, and that requirement can be filled by Ni^{2+}, Mn^{2+}, Fe^{2+}, Co^{2+}, Zn^{2}, and Cu^{2+}. Because Ni^{2+} gives the highest specific activity of all these metallic dications and is present in seawater at relatively high concentrations, it was concluded that Ni^{2+} is the metallic dication normally present in the active site.[1218] In the case of xylose isomerase from *Piromyces*, it was concluded that, in the cytoplasm, each active site of the enzyme was occupied by one of several different metallic dications.[1213]

There is a group of enzymes that can **use as their required Lewis acid either Mg^{2+} or Mn^{2+}**, two hard metallic dications of small, almost equivalent ionic radius (Table 4–3) and acidity (Table 4–2) but significantly different rates of exchange (Table 4–5). Phosphopyruvate hydratase (Equation 4–128) from *S. cerevisiae*,[1217] pyruvate kinase from *O. cuniculus*,[1219-1221] and mandelate racemase (Equation 4–126) from *P. putida*[1222] are typical members of this group. For xylose isomerase from *Streptomyces violaceoruber*, the Michaelis constant for Mg^{2+}, K_{mMg}, is the same[1223] as that for Mn^{2+}, but the catalytic constant when the enzyme is using Mg^{2+} as its Lewis acid is 5 times greater than when it is using Mn^{2+}. For xylose isomerase from *L. brevis* (23% identity; 2.2 gap percent), however, only Mn^{2+}, not Mg^{2+}, is catalytically effective.[1224]

When Mg^{2+} is able to fulfill the role of a Lewis acid in the active site of a metalloenzyme that has lost its native metallic dication, Mg^{2+} usually performs that role in the cytoplasm as well. For example, in the cytoplasm, Mg^{2+} is probably the metallic dication responsible for all the activity of phosphoglucomutase.[1209] 3-Deoxy-8-phosphooctulonate synthase from *A. aeolicus* requires a metallic dication for its catalysis, and the requirement can be fulfilled by Cd^{2+}, Mn^{2+}, Co^{2+}, or Ni^{2+} and to a lesser extent Cu^{2+}, Zn^{2+}, and Mg^{2+}.[1225] Even though much higher concentrations of Mg^{2+} are required to activate the enzyme than most of the other dications, the concentration of Mg^{2+} in cytoplasm is also much

*These estimates of free concentrations are imprecise because metallic dications are usually bound tightly to proteins, nucleic acids, and carbohydrates in the cytoplasm. Consequently, the free concentration of any one of these dications, the concentration that is relevant to an equilibrium constant for association with an active site, is only a small fraction of its total concentration, which is usually the only precisely known value. The imprecision in these estimates of free concentration for metallic dications other than Mg^{2+} is thought to be plus or minus a factor of 10.[1130]

†Cadmium dication, Cd^{2+}, and the dications and trications of the other soft metals are almost always toxic, and there usually are physiological mechanisms for keeping their free concentrations in cytoplasm at vanishingly low levels.

higher. Consequently, in the cytoplasm, active sites using Mg^{2+} as the Lewis acid are probably responsible for most of the enzymatic activity, with the remainder coming from active sites using Mn^{2+}. Glutamine synthetase from *E. coli* is controlled[1226] by the adenylation of Tyrosine 397. Unadenylated enzyme can use only Mg^{2+} as a Lewis acid[1227] (K_{mMg} = 17 mM)[1228] while adenylated enzyme can use only Mn^{2+} (K_{mMn} = 1.7 mM), and the catalytic constant for unadenylated enzyme using Mg^{2+} is 4 times that for adenylated enzyme using Mn^{2+}. From values for Michaelis constants, catalytic constants, and free concentrations of Mg^{2+} and Mn^{2+} (Table 4–4), it can be concluded that, in the cytoplasm, even though the activity of the adenylated enzyme at saturating concentrations of Mn^{2+} is significant, the adenylated enzyme is essentially inactive relative to the unadenylated enzyme. Phospho*enol*-pyruvate carboxykinase (ATP), however, has been shown to require both Mg^{2+} and Mn^{2+} for effective catalysis:[1229-1231] the Mg^{2+} enters the active site as $MgATP^{2-}$ while the Mn^{2+} acts as a Lewis acid to catalyze the reaction.[1232]

When Mg^{2+} cannot perform the role of a Lewis acid in a metalloenzyme that can use one of several other metallic dications, the metallic dication performing that role in the cytoplasm is harder to identify. Because the free concentration of Ni^{2+} in cytoplasm is vanishingly small (Table 4–4), *N*-formylmethionylaminoacyl-tRNA deformylase[1211] must use Mn^{2+}. *S*-Ribosyl homocysteine lyase can use Fe^{2+}, Zn^{2+}, and Co^{2+} as a required Lewis acid in its active site but must use Fe^{2+} in the cytoplasm because only Fe^{2+} produces enzymatic activity with the same stability to temperature and oxidation and the same K_m for its substrate *S*-(5-deoxy-D-ribos-5-yl)-L-homocysteine as the enzymatic activity in a homogenate of cells.[1233] In addition, Fe^{2+} is at a higher free concentration in cytoplasm than Co^{2+} and Zn^{2+}. Methionyl aminopeptidase from *E. coli* can use Mn^{2+}, Fe^{2+}, Zn^{2+}, and Co^{2+} as a required Lewis acid,[1234,1235] but only the enzyme operating with Fe^{2+} has the same pattern of inhibition for a set of six synthetic inhibitors as the enzyme in a homogenate of cells.[1236] In addition, the total cellular concentration of iron increases about 5 times more than those of the other metals when the enzyme is overexpressed in bacteria.[1235] This latter fact can be explained if the free concentration of Fe^{2+} in the cytoplasm remains constant, as expected, and the excess in the total concentration of Fe^{2+} is that bound to the enzyme. Phosphoprotein phosphatase from bacteriophage λ can use Mn^{2+}, Fe^{2+}, Zn^{2+}, and Co^{2+} as well as nonphysiological Ga^{3+} as a Lewis acid in its active site,[1237,1238] but the total concentration of manganese in cells of *E. coli* overexpressing the enzyme increases 4 times more than those of the other metals.[1239]

When the question of which metallic dication performs the role of Lewis acid in the cytoplasm remains unanswered, metallic dications that eventually turn out **not to be the ones used physiologically** are often used experimentally. For example, *S*-ribosylhomocysteine lyase from *B. subtilis* was crystallized with Co^{2+} coordinated in its active site[1240] to obtain the initial crystallographic molecular model, rather than the Fe^{2+} that was eventually shown to be the cytoplasmic metallic dication. Before it was known that Fe^{2+} was the native Lewis acid, methionyl aminopeptidase from *E. coli* was crystallized with Co^{2+} coordinated in its active site[1241,1242] rather than Fe^{2+}, the cytoplasmic metallic dication, to obtain the initial crystallographic molecular model. Experiments to screen pharmacological inhibitors of methionyl aminopeptidase also used the enzyme with Co^{2+} in its active site, but potent inhibitors of the enzymatic activity elicited by Co^{2+} unfortunately had little effect on the cellular enzymatic activity.[1236]

Although it does lead to uncertainty as to which metallic dication is used by an enzyme in its native cytoplasm, the chemical lesson to be learned from the promiscuity displayed by many purified metalloenzymes, regardless of which dication plays that role in the cytoplasm, is that **it often does not really matter what metallic dication is used as a Lewis acid**. This fact, which is a common observation, seems counterintuitive, given the significant differences in electronic configuration and effects of ligand field among the divalent metallic dications. As has been noted, even metalloenzymes that retain their metallic dication during purification can be promiscuous. Often the tightly bound, physiological metallic dication can be removed and replaced with other metallic dications that can also promote catalytic activity.[1243-1246] One conclusion from this frequent promiscuity of metalloenzymes is that the number of 3*d* electrons and their distribution in the five 3*d* orbitals is of little consequence for effective catalysis in metalloenzymes. All that seems to be of consequence is that the metallic cation be dicationic and be able to occupy the available coordination.

Now that the chemical characteristics of the individual metallic dications and the difficulty of determining the cytoplasmic actor in many instances have been discussed, the roles of the metallic dicat-

ions incorporated into an active site or into the protein surrounding the active site can be described.

There are metallic dications in enzymes that do not perform catalytic roles but that are nevertheless required for their functions. The Mg^{2+} in alcohol dehydrogenase ($NADP^+$) from *L. brevis*, the Ca^{2+} in trypsin from *Streptomyces griseus* (Figure 4–53), and the Zn^{2+} in aspartate carbamoyltransferase (**4–152**) are examples of metallic dications incorporated into enzymes in an **exclusively structural role.** In these instances the metallic dication, by drawing together several ligands from the polypeptide, determines the structure of the protein in its vicinity. Such a structural role should be distinguished from a catalytic role in which the metallic dication is a direct participant in catalysis performed by the active site. In the absence of an informative crystallographic molecular model, it is often difficult to distinguish whether the requirement for a metallic dication for the expression of enzymatic activity results from its participation in a structural role or a catalytic role.

In those instances in which **a metallic cation has a catalytic function**, the catalysis is classified as outer-sphere or inner-sphere. **Outer-sphere catalysis** at a catalytic metallic cation occurs when ligands coordinated to the metallic cation are the catalysts rather than the metallic cation itself. An example of outer-sphere catalysis would be a molecule of water, the pK_a of which has been lowered by the metallic cation (Table 4–2), acting as a catalytic Brønsted acid–base. **Inner-sphere catalysis** at a catalytic metallic cation occurs when one or more reactants become inner-sphere ligands to a catalytic metallic cation and, during their coordination, participate in the reaction. For example, it has been shown[1247] that metallic dications such as Zn^{2+} or Cu^{2+} can increase the rate constants for decarboxylation of β-oxo carboxylic acids by factors of at least 100 if the β-oxo carboxylic acid is designed to promote formation of a complex with the dication and if the complex coordinates the metallic dication directly to the oxygen of the developing enolate

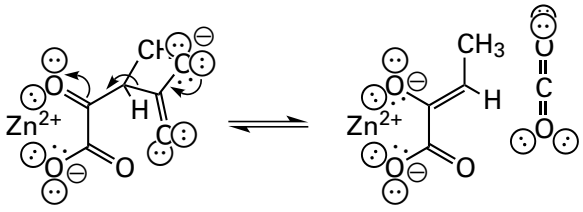

(4–428)

In these examples of inner-sphere catalysis, Zn^{2+} or Cu^{2+} serves the role of a weak hydron by forming a more weakly acidified (Table 4–2) analogue of an enol.

A **molecule of water bound to a metallic dication often acts as an outer-sphere, catalytic Brønsted acid** in an active site to hydronate a substrate, or its conjugate base, a hydroxide bound to the metallic dication, acts as a catalytic Brønsted base that removes a hydron from a substrate. For example, in the active site of 4-hydroxy-2-oxoheptanedioate aldolase from *E. coli*, a molecule of water on the prosthetic metallic dication acts as a catalytic acid that hydronates the carbonyl oxygen of the succinate semialdehyde that is the electrophile in the aldol condensation catalyzed by the enzyme. In addition, a hydroxide on the metallic dication acts as a base that removes a hydron from the 4-hydroxy group in 4-hydroxy-2-oxoheptanedioate in a retroaldol dissociation.[1248] In such a situation, all the ligands to the metallic dication remain as they were, and no exchange of ligands at the metallic dication is required for the reaction to proceed.

Molecules of water on metallic dications have **a variety of values of pK_a** (Table 4–2), a fact that would seem to make them attractive candidates for outer-sphere Brønsted acid–bases in enzymatic active sites. For example, the molecule of water on the Mn^{2+} in the active site of pyruvate carboxylase (**4–157**) is a catalytic Brønsted acid. The anionic 2-oxido oxygen of the enolate of pyruvate that is the intermediate in this reaction is in the outer sphere of the octahedrally coordinated Mn^{2+}, and it participates in a hydrogen bond with the molecule of water that is in the inner sphere.[1148] The pK_a for this molecule of water—were it on $Mn^{2+}(H_2O)_6$ rather than Mn^{2+} coordinated by two imidazolyl groups, a carboxy group, a bidentate carboxylato group, and the molecule of water itself—would be 10.6 (Table 4–2), close to the pK_a for the enol of pyruvate, which is 11.6 (Figure 1–23). Consequently, it is impossible to tell whether or not the molecule of water hydronates the enolate. Were the enolate to remain unhydronated, the carbanionic carbon would more readily add nucleophilically to the electrophilic carbon dioxide or the electrophilic 1-(*N*-carboxy)biotin (Equation 4–262); were the enolate hydronated during its formation, it would be easier for the catalytic base in the active site to remove the hydron from the pyruvate.

In the active site of 3-deoxy-*manno*-octulosonate cytidyltransferase from *E. coli*, $Mg^{2+}{\cdot}OH^-$ acts as a Brønsted base to remove a hydron from the anomeric

2-hydroxy group on the pyranose of 3-deoxy-D-*manno*-octulosonate. The resulting oxyanion then adds nucleophilically to the phosphorus of the α-phospho group of $MgCTP^{2-}$, with magnesium diphosphate as the leaving group, during the formation of CMP-3-deoxy-D-*manno*-octulosonate.[1249] In the active site of isopentenyl-diphosphate Δ-isomerase from *E. coli*, a hexacoordinated Zn^{2+} has one oxygen of the carboxy group of Glutamate 116 as its sixth ligand. The pK_a for the conjugate acid of the other oxygen of the carboxy group of Glutamate 116, which acts as a Brønsted acid in the reaction catalyzed by the enzyme, must be lowered significantly by the Zn^{2+}.[1176]

Such outer-sphere acid–bases, however, regardless of their appeal in the abstract, are seldom used in enzymatic active sites, perhaps because they are more complicated than the simple side chain of an amino acid.

In most cases, **the role of a catalytic metallic dication in an active site is to be a Lewis acid**. If the dication is to act as a Lewis acid, it must directly coordinate a lone pair of electrons on a substrate or an intermediate in the enzymatic reaction. Consequently, when the metallic dication is acting as a Lewis acid, the catalysis it provides must be **inner-sphere**. In nonenzymatic reactions in solution in which a metallic dication participates as a Lewis acid, the base on the reactant that is acidified is almost always bound in direct coordination to the metallic dication.

When a metallic dication acts as an inner-sphere Lewis acid in an enzymatic reaction, the first step is the **exchange of its ligands**. If the metallic dication is to be an inner-sphere, catalytic Lewis acid, the ligand or ligands from the reactant must exchange with the ligand or ligands at the catalytic position or positions that are already on the cation. In addition, the ligand or ligands on the next reactant, or other ligands in solution, must exchange at the dication with the ligand or ligands from the product in order to release product and maintain turnover of molecules of reactant. Therefore, an important feature of the ability of a metallic dication to act directly as a Lewis acid in an enzymatic reaction is the rate at which the ligands surrounding that dication can be exchanged (Table 4–5).*

Rates of exchange for Ca^{2+}, Mn^{2+}, Zn^{2+}, and Co^{2+} are rapid (>1 μs^{-1}) and could be accommodated easily during an enzymatic reaction. The rate of exchange for Mg^{2+}, however, is slow and, given that Mg^{2+} is often used as an inner-sphere Lewis acid, this fact suggests that catalysis of the exchange of ligands or the use of coordinations that promote exchange might be required. The rate of exchange for Fe^{2+} is reasonably fast, but the rate of exchange for Ni^{2+} is slow. In the particular environment of an active site, in which the equilibrium between the low-spin and high-spin state for metallic cations such as Fe^{2+}, Ni^{2+}, and Fe^{3+} shifts in response to the particular coordination that exists, rates of exchange could be hastened by coordination that favors the **high-spin state**. The same could be true for the few active sites that use Fe^{3+} as a Lewis acid because exchange rates for this metallic trication are extremely slow.

The exchange of ligands coordinating a metallic cation can be associative or dissociative. **Associative exchange** is a mechanism in which the entering ligand associates with the metallic cation, expanding its coordination, and then the leaving ligand dissociates. Associative exchange is thought to occur at the Zn^{2+} in thermolysin (Figure 3–42) when the inhibitor 3-phenylpropionyl-L-phenylalanine (**4–161**) binds.[1108] In the resting active site, the Zn^{2+} is pentacoordinate with a molecule of water as one of its ligands. The acyl oxygen of the inhibitor associates with the Zn^{2+}, pushing the molecule of water to one side and causing one oxygen of the carboxy group of Glutamate 166 to dissociate from the Zn^{2+}. This dissociation produces a pentacoordinate arrangement of ligands (**4–165**) from which the molecule of water then dissociates so that the Zn^{2+} becomes tetracoordinate (**4–162**). **Dissociative exchange** is a mechanism in which the leaving ligand dissociates from the metallic cation, contracting its coordination, and then the entering ligand occupies the open site of coordination. Ligands exchange at Mg^{2+} dissociatively because there is no room around the crowded octahedrally hexacoordinated cation for a seventh ligand to occupy.

When $MgATP^{2-}$ and pyruvate enter the active site of pyruvate kinase, one oxygen of the phospho group, the oxygen of the carbonyl group, and one oxygen of the carboxy group enter the inner sphere of the catalytic Mg^{2+}, which is not the Mg^{2+} that entered on the $MgATP^{2-}$ (Equation 4–275 and Figure 4–52). Therefore, as the two substrates associate with the enzyme, these three oxygens must exchange dissociatively with three molecules of water from

*The rates of exchange tabulated are for the exchange of molecules of water from hydrated metallic cations in water. Table 4–5 is only a rough measure of actual rates of exchange in the more complicated coordinations within an active site and with ligands other than water.

the coordination shell of the already bound Mg^{2+}. This ligand exchange must not be a very rapid process (Table 4–5), and this **displacement of the molecules of water may become rate-limiting** under certain circumstances. There is an apparent pK_a of 9.2 above which both the catalytic constant and the specificity constants for pyruvate and $MgATP^{2-}$ in the steady-state kinetics of pyruvate kinase decrease. This pK_a has been assigned to dissociation of a hydron from a molecule of water bound to Mg^{2+} in the free enzyme.[1250,1251] It has been proposed that when this hydron is lost to produce a hydroxide at the magnesium, the exchange required for the oxygens on the substrates to enter the inner sphere of the bound magnesium, which is already slow, becomes too slow to support catalysis.

When a metallic dication acts as a Lewis acid in the active site of an enzyme, it **performs many of the same roles as a hydron**. Unlike a hydron, however, it is not transferred to an oxygen or a nitrogen, and it usually does not leave the active site on that oxygen or nitrogen as the metallic analogue of a hydroxy group or an amine, respectively. A metallic dication is also a weaker acid than is a hydron (Table 4–2), but this weakness is an advantage in circumstances in which a weaker acid is an improvement: for example, in a situation where a strong catalytic acid would be unhydronated. In a sense, the set of metallic dications provides natural selection with a range of surrogate hydrons of unique acidities (Table 4–2) from which to make, in some situations, a choice appropriate to the reaction being catalyzed.

One role of a metallic dication is to **stabilize the oxyanion of an enolate**. The choice between whether to hydronate or provide an oxyanion hole for an enolate can be avoided by using a metallic dication rather than a hydron. For example, the Mg^{2+} that is coordinated by the two oxygens of oxalate in the active site of pyruvate kinase (Figure 4–52) has the homologous two oxygens of pyruvate as ligands when pyruvate occupies the active site.[1252] This Mg^{2+} must be the Lewis acid stabilizing the oxyanion of the enolate of pyruvate (**4–166**)

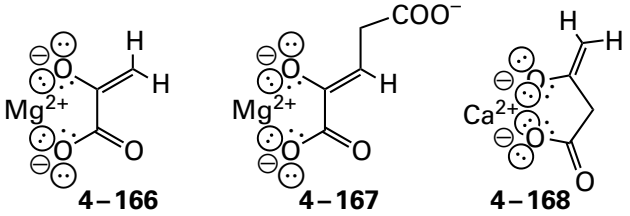

4–166 **4–167** **4–168**

that leaves from the phospho group of phospho*enol*pyruvate during the nucleophilic substitution at phosphorus that transfers the phospho group from phospho*enol*pyruvate to $MgADP^-$. By providing Mg^{2+}, the active site makes hydronation of the carbon of the enolate in the next step easier than if the enolate had been hydronated on its anionic oxygen. In 4-hydroxy-2-oxoheptanedioate aldolase, the enolate of the pyruvate that is a reactant in the aldol condensation catalyzed by the enzyme forms a similar complex (**4–166**) with a Mg^{2+} coordinated in the active site,[1135] but the carbanionic carbon 3 of the enolate of pyruvate in this case adds to the electrophilic carbonyl carbon of succinate semialdehyde, rather than to an electrophilic hydron as in pyruvate kinase. In the active site of isocitrate dehydrogenase ($NADP^+$) from *E. coli* (Equation 4–329), a similar complex is formed between Mg^{2+} and the enolate of 2-oxoglutarate (**4–167**) following the decarboxylation of oxalosuccinate.[1253] In a crystallographic molecular model of the active site of murine fumarylacetoacetase (**4–156**), the oxyanion of the enolate of acetoacetate is a ligand to a Ca^{2+} (**4–168**) acting as a Lewis acid to stabilize the enolate and retain its carbanionic carbon so that it can add nucleophilically to the carboxy group of fumarate in the Claisen condensation catalyzed by the enzyme (Equation 4–362).[860] In these four examples, the enolate stabilized by the metallic dication in the active site is a bidentate ligand, so two exchanges are required to form the respective complexes from reactants.

In the active site of phospho*enol*pyruvate mutase

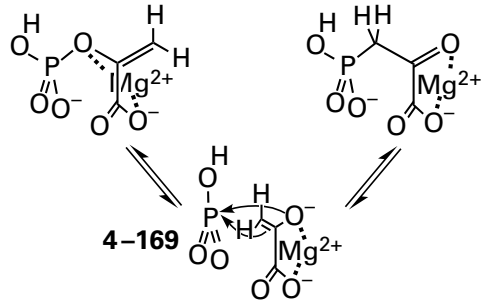

(4–429)

from *Mytilus edulis*,[1254] the enolate of pyruvate that is the intermediate is a bidentate ligand to a coordinated Mg^{2+} (**4–166**). The electrophilic phosphorus atom in the monomeric metaphosphate (**4–169**) that dissociates from phospho*enol*pyruvate to form the enolate is to the left in the orientation of the drawings in Equation 4–429 and above the plane of drawing **4–166**. The plane of the enolate is in the plane of the page in the orientation of drawing **4–166** and perpendicular to the page in the orientation of the drawing of Equation 4–429. The monomeric metaphosphate is perpendicular to the page

in the drawing of Equation 4–429, and its electrophilic phosphorus is approximately equidistant from carbanionic carbon and the anionic 2-oxido group, the two nucleophilic centers in the resulting coordinated enolate. When the carbanionic carbon adds to the monomeric metaphosphate, 3-phosphonopyruvate is formed; when the oxyanion of the enolate adds, phospho*enol*pyruvate is formed. In the former instance, the 2-oxo oxygen of 3-phosphonopyruvate ends up to the right side of the product as drawn in Equation 4–429; in the latter, the same oxygen, now in the phosphoester, ends up to the left side of phospho*enol*pyruvate as drawn in Equation 4–429.

In the complex with the enolate, the 2-oxido oxygen ends up below the plane of the page as drawn in Equation 4–429 as a ligand to the Mg^{2+}, which is also below the plane of the page, and the 2-oxido oxygen is as close as possible to the anionic oxygen of the 1-carboxylato group in the enolate, as in drawing **4–166**. During addition of either carbanionic carbon 3 or the 2-oxido oxygen to the monomeric metaphosphate, the 2-oxido oxygen is forced to move away from the anionic oxygen of the carboxylato group, and the Mg^{2+} attached to it, into the plane of the page in Equation 4–429 because the phosphorus atom is in the plane of the page. These respective pivots to the left and to the right distort the tight octahedral arrangement of ligands around Mg^{2+} (dashed lines in Equation 4–429).[1254] Consequently, the complex with either substrate is strained at Mg^{2+}, and the strain is relieved in the complex with the enolate. This relief decreases the difference in standard free energy between the coordinated substrates and the coordinated enolate intermediate.

***cis*-Enediolates are stabilized** by bidentate ligation to metallic dications. These common intermediates can be separated into two groups. In the first group, an electrophile is removed from one of the two carbons to form the *cis*-enediolate, and an electrophile is added to the other carbon of the *cis*-enediolate to produce an oxo group in the product on a carbon adjacent to the oxo group in the reactant. In the second group, one electrophile is exchanged for another at the same carbon with the *cis*-enediolate as an intermediate, and the oxo group is on the same carbon in reactant and product. In the first group, a hydron must be removed from one oxygen and a hydron added to the other oxygen to form the tautomer of the *cis*-enediolate

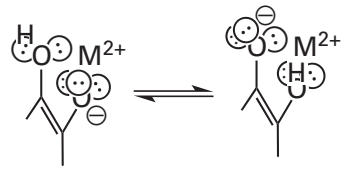

(4–430)

where M^{2+} is a metallic ion. In the second group, no hydron is removed from or added to either oxygen.

The *cis*-enediolate that is coordinated to Zn^{2+} in the active site of human lactoylglutathione lyase (Figure 4–55C) is an example of the first group of *cis*-enediolates. It is an intermediate in an isomerization

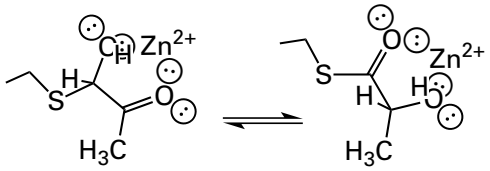

(4–431)

analogous to that catalyzed by triose-phosphate isomerase (Equations 4–46 and 4–55 and Figure 3–37), and lactoylglutathione lyase also uses glutamate to transfer the hydron between the two carbons.[1167] In this isomerization, the 2-oxo group becomes a hydroxy group and the 1-hydroxy group becomes an oxo group—and the other way around in reverse—so a hydron is added to the one oxygen and a hydron is removed from the other. Because Zn^{2+} is stabilizing the *cis*-enediolate, each hydron transfer at oxygen need not be concerted with the one at carbon. In fact, unlike the situation in the active site of triose-phosphate isomerase, in the active site of lactoylglutathione lyase, there are no obvious catalytic acid–bases forming hydrogen bonds to the two oxygens that could hydronate or dehydronate them. Lactoylglutathione lyase from *E. coli*, although clearly related to the human enzyme (34% identity; 1.4 gap percent), uses Ni^{2+} as its Lewis acid[1215] rather than Zn^{2+}.

The *cis*-enediolate that is coordinated to Zn^{2+}

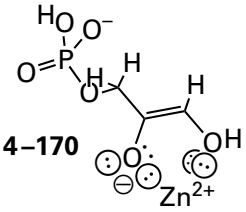

in the active site of fructose-bisphosphate aldolase (Equation 4–210) from *M. tuberculosis* (Figure 4–55B) is an example of the second group of *cis*-enediolates. The *cis*-enediolate of glycerone phosphate is formed

by removal of a hydron from carbon 3, and the carbanionic carbon 3 of the *cis*-enediolate adds nucleophilically to the carbonyl of D-glyceraldehyde 3-phosphate in the aldol condensation catalyzed by the enzyme. In this instance, the 3-hydroxy group provides a second ligand to Zn^{2+} but remains a hydroxy group throughout the reaction. No hydron must be removed from or added to either oxygen because a hydron on carbon 3 of glycerone phosphate is replaced by the carbon of a carbonyl and the oxygen in the carbonyl group of glycerone phosphate ends up as the oxygen in the carbonyl group of D-fructose bisphosphate. In rhamnulose-1-phosphate aldolase from *E. coli*, a Zn^{2+} in the active site also stabilizes the *cis*-enediolate of glycerone phosphate in a similar bidentate complex.[1255]

In the triose-phosphate isomerases, an intermediate *cis*-enediolate is formed by removal of a hydron from either carbon 1 of glycerone phosphate or carbon 2 of D-glyceraldehyde 3-phosphate by the carboxylato group of a glutamate (Figure 3–37) or its respective homologue. In xylose isomerase and L-rhamnose isomerase, however, both of which also interconvert an aldose and a ketose with the analogous stereochemistry (Equation 4–253), there is no glutamate or any other base in the appropriate location. Instead, the hydrogen that is transferred back and forth during the isomerization is, in both the aldose and the ketose, sitting up against the π cloud on one face of the indolyl group of a tryptophan and enclosed by the phenyl groups of two phenylalanines.[1256-1259] In crystallographic molecular models of the active sites of xylose isomerases[892,1120,1256,1260,1261] and rhamnose isomerase[1258,1262] from various species in complexes with substrates or intermediate analogues and catalytic[1224] or noncatalytic metallic dications, the two oxygens that are interconverted between an oxo group and a hydroxy group during the isomerizations catalyzed by these enzymes are ligands to one or both of two catalytic metallic dications, and the oxygen on carbon 1 forms a hydrogen bond with the ammonio group of a lysine. Consequently, the isomerizations must proceed by acid catalysis by these two Lewis acids and this Brønsted acid, since there is no base available.

The role of these acids at the two oxygens is to polarize in turn the carbonyl groups on substrates to promote a 1,2-hydride migration[1261]

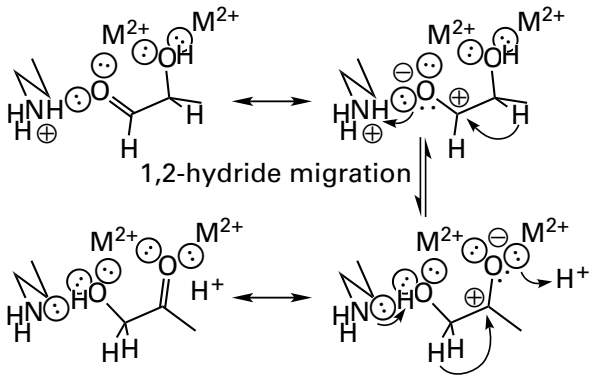

(4–432)

In solution, only about half of the nonenzymatic isomerization between aldose and ketose in strong acid,[1263] in strong base,[1264,1265] or under catalysis by Zn^{2+} at pH 6[1265] proceeds by removal of a hydron from one carbon and addition of a hydron to the other as it does in triose-phosphate isomerase (Equations 4–46 and 4–55 and Figure 3–37). The other half of the isomerizations in solution proceed by 1,2-hydride migration. The 1,2-hydride migration is analogous to the 1,2-hydride migrations and 1,2-alkyl migrations that occur in carbenium ions that are intermediate in terpene cyclizations (Figure 3–50), and the polarization of the respective carbonyl group by the acids makes its carbon resemble a carbenium ion (Equation 4–432).

These isomerizations also require dehydronation of one oxygen and hydronation of the other. The oxygen on carbon 2 in a substrate for one of these two enzymes is dehydronated or hydronated by a fixed molecule of water that, in most cases, forms a hydrogen bond to it. Depending on the crystallographic molecular model, however, the molecule of water either is a ligand to the central metallic dication[1120,1256,1261] or forms a hydrogen bond with the 1-oxygen[1258] to relay the hydron directly. Again, the transfers of the hydrons are not necessarily concerted with the 1,2-hydride migration because the metallic dications coordinate the oxygens.

Certain **epimerases have *cis*-enediolate intermediates that are stabilized** by metallic dications. These epimerases remove either an *R* or *S* hydrogen as a hydron from an acidic carbon adjacent to a carbonyl, and then they add another hydron to the same carbon with the opposite stereochemistry[1266-1269]

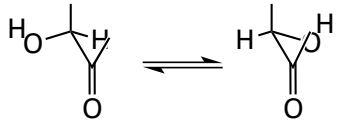

(4–433)

For example, D-psicose 3-epimerase from *A. tumefaciens* equilibrates D-psicose and D-fructose, which are epimers at carbon 3 that is adjacent to the carbonyl group at carbon 2 in the two substrates. The *cis*-enediolate intermediate in this epimerization is a bidentate ligand to the prosthetic Mn^{2+}.[1270] Two carboxylato groups, from Glutamates 244 and 150, are monodentate ligands to Mn^{2+}. Their other, unliganded oxygens are on opposite sides of the *cis*-enediolate, and these unliganded oxygens are the catalytic bases that remove the hydrons from carbon 3 in the respective ketoses and add the hydrons to one of the two faces of carbon 3 in the *cis*-enediolate

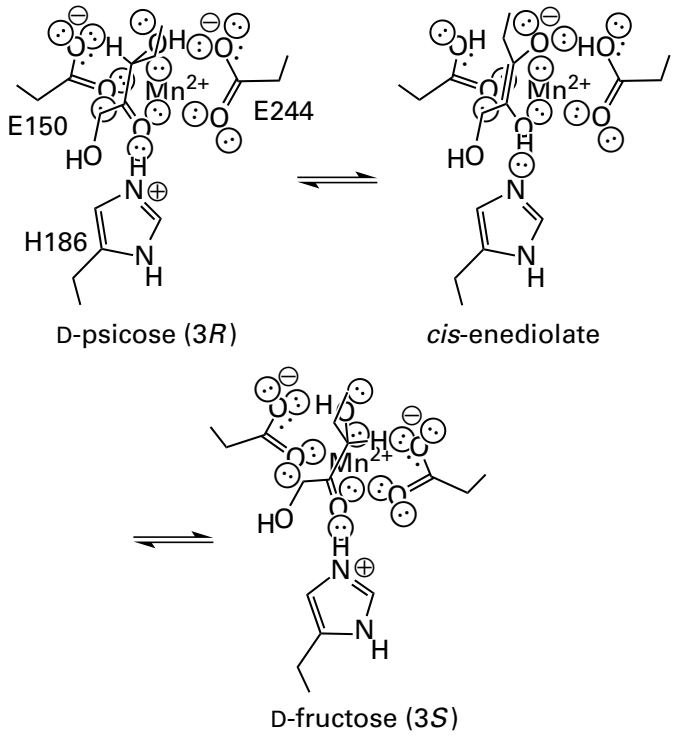

(4–434)

to accomplish the respective epimerization. When Glutamate 240 in the active site of 3-dehydro-D-guloside 4-epimerase from *E. coli*, which is homologous to Glutamate 244, was mutated to glutamine, the enzyme, although unable to perform the epimerization, was still able to exchange a deuterium from ^2H_2O at carbon 4 of the substrate α-methyl 3-dehydro-D-glucoside, presumably because Glutamate 146, the glutamate homologous to Glutamate 150, was unmutated and still able to remove the 4*S*-hydrogen on carbon 4 and replace it with a deuterium. When Glutamate 146 was mutated to glutamine, however, the enzyme was again unable to catalyze the epimerization but also was unable to exchange this hydrogen for a deuterium,[1271] presumably because the carboxy oxygen of the unmutated Glutamate 244 is located on the opposite side of carbon 4 in α-methyl 3-dehydro-D-glucoside from the 4*S*-hydrogen.

In the intermediate *cis*-enediolate resulting from either dehydronation in the active site of D-psicose 3-epimerase, a hydron has been added to the oxygen on carbon 2 that was the carbonyl oxygen by the imidazolium of Histidine 186. Hydronation at the oxygen of the *cis*-enediolate on carbon 2 during removal of the hydron from carbon 3 by the unliganded oxygen of one of the carboxylato groups produces a neutral *cis*-enediol. A hydron is then removed from the 3-hydroxy group of the *cis*-enediol by the unliganded, unhydronated oxygen of the other carboxylato group to form the *cis*-enediolate with a 2-hydroxy group and a 3-oxido group. The resulting hydronated oxygen on this second carboxy group provides the hydron that is then added to carbon 3 of the *cis*-enediolate. The hydron that was originally removed by the other carboxy group from carbon 3 to form the *cis*-enediolate is added to the 3-oxido oxygen of the *cis*-enediolate, either before or while the hydron is being added to carbon 3 on the opposite face of the *cis*-enediolate, to complete the epimerization.[1268,1270]

In the crystallographic molecular model of the complex between D-psicose 3-epimerase from *Ruminiclostridium cellulolyticum* (61% identity; 0 gap percent) and D-psicose, the unliganded oxygen of the carboxy group of Glutamate 150 is 0.28 nm from carbon 3, well within van der Waals contact, and 0.27 nm from the oxygen of the 3-hydroxy group of D-psicose, the length of a hydrogen bond. In the complex of the enzyme with D-fructose, the oxygen of the carboxy group of Glutamate 244 is 0.29 nm from carbon 3 and 0.31 nm from the oxygen of the 3-hydroxy group of D-fructose.[1272] The carboxy group of Glutamate 150 hydronates carbon 3 of the *cis*-enediolate to form D-psicose, and the carboxy group of Glutamate 244 hydronates carbon 3 of the *cis*-enediolate to form D-fructose, so these distances are consistent with, and seem to compel, the conclusion that each glutamate transfers a hydron between oxygen and carbon. D-Tagatose 3-epimerase from *Pseudomonas cichorii* (39% identity; 0.4 gap percent) has the same disposition of Mn^{2+} and the carboxy groups of Glutamates 152 and 246 in the crystallographic molecular models of complexes with D-fructose and D-tagatose, respectively.[1268]

Each of the two carboxy groups in these epimerases is an example of a carboxy group that dedicates one of its oxygens to act as a ligand to a metallic

dication but uses its other oxygen for Brønsted acid–base catalysis. The metallic dication affects the pK_a for each carboxy group but also pins down one oxygen in each carboxy group so that the other oxygen on the respective **carboxy group can pivot back and forth** between carbon 3 and the oxygen on carbon 3 of the *cis*-enediolate.

***Gem*-enediolates can be stabilized** by metallic dications. For example, the *gem*-enediolate that is the intermediate[1273] in the dehydration catalyzed by phosphopyruvate hydratase (Equation 4–128) from *S. cerevisiae* is produced by removal of the hydron from carbon 2 of 2-phospho-D-glycerate by Lysine 345 (Figure 4–43) and is stabilized by two Mg^{2+} and a hydrogen bond with the amino group of Lysine 396 (**4–171**)[544]

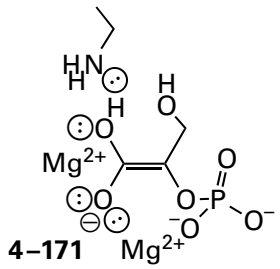

4–171

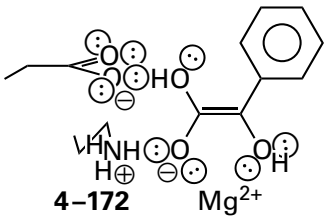

4–172

The *gem*-enediolate that is an intermediate in the racemization catalyzed by the related enzyme, mandelate racemase (Equation 4–126) is stabilized by only one Mg^{2+} but also by a hydrogen bond with the ammonio group of a lysine after being hydronated by a carboxy group (**4–172**).[212] In each instance, the substrates, before removal of the hydron from carbon to produce the *gem*-enediolate, are bidentate ligands to each Mg^{2+}. The *gem*-enediolate formed during the elimination of dimethyl sulfide from 3-dimethylsulfoniopropionate in the active site of dimethylpropiothetin dethiomethylase from *P. ubique* is a also a bidentate ligand at its two carboxy oxygens to the prosthetic Ni^{2+} in the active site.[1218] In pectate lyase 10 from *Cellvibrio japonicus*, however, which catalyzes an elimination analogous to that catalyzed by chondroitin AC lyase (Equation 4–358 and Figure 4–44), the *gem*-enediolate intermediate is a monodentate ligand to a Ca^{2+} through only one of its two carboxylato oxyanions; the other oxyanion is an acceptor for a hydrogen bond from the amido oxygen of the polypeptide, and both carboxylato oxygens form a canonical pair of hydrogen bonds with the *ω*-nitrogens of the guanidinio group of an arginine.[1050] The *gem*-enediolate that is an intermediate in the elimination catalyzed by guluronate-specific alginate lyase from *P. chathamensis* is also a monodentate ligand to a prosthetic Ca^{2+} in the active site.[974]

Metallic dications are also used to **polarize a carbonyl** (Figure 4–55D) to which an enolate[692,975,1168,1274] or a hydride[1275,1276] is to be added, to make the carbonyl more electrophilic. For example, the Mg^{2+} in malate synthase, in addition to the guanidinio group of Arginine 338 (**4–155**), polarizes the carbonyl of oxalate to which the enolate of acetyl-SCoA is added (Equation 4–272). In the active site of 3-deoxy-7-phosphoheptulonate synthase from *S. cerevisiae*, which catalyzes addition of the enolate of pyruvate to D-erythrose 4-phosphate

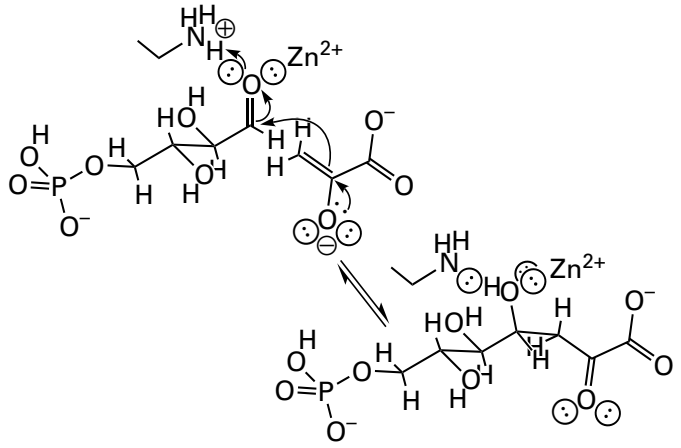

(4–435)

the carbonyl oxygen of D-erythrose 4-phosphate is a ligand to a metallic dication, which is probably Zn^{2+} in the native enzyme,[1277-1279] and the metallic dication polarizes the carbonyl, increasing its electrophilicity.[1274] In the active site of equine alcohol dehydrogenase (Equation 4–158), a Zn^{2+}, which is coordinated by two sulfanyl groups and an imidazolyl group, polarizes the carbonyl in a substrate, increasing its electrophilicity for the hydride transferred from NADH.[1275,1276] In the active site of the unrelated alcohol dehydrogenase from *Zymomonas mobilis*, the same function is performed by an Fe^{2+} that is tetracoordinated by three imidazolyl groups from three histidines and the oxygen of the carboxy group of an aspartate and that becomes pentacoordinated in the complex with substrates.[1280]

Unlike enolates in which an oxyanion stabilized by a metallic dication begins the reaction and ends the reaction as a carbonyl oxygen, in most instances in which a metallic dication **polarizes a carbonyl for nucleophilic addition**, the oxygen of the carbonyl becomes a hydroxy group, and there is usually a catalytic Brønsted acid in a hydrogen bond to the carbonyl oxygen to provide the necessary hydron.

In 3-deoxy-7-phosphoheptulonate synthase (Equation 4–435) from *S. cerevisiae*, it is the ammonio group of a lysine;[1274] in isocitrate lyase (Equation 4–310) from *M. tuberculosis*, it is the 4-hydroxyphenyl group of a tyrosine;[692] and in equine alcohol dehydrogenase, the hydroxy group of a serine relays a hydron ultimately from the imidazolium of a histidine.[1276]

In the **reverse of each of these reactions**, by microscopic reversibility, the substrate with a hydroxy group is the reactant, and the oxygen of the hydroxy group is a ligand to the metallic dication. The Lewis acid lowers the pK_a for the hydroxy group (Table 4–2) so that the hydron can be removed more readily by the now-catalytic Brønsted base to **produce an oxyanion that pushes out the leaving nucleophile**, the enolate or the hydride, far more effectively than a lone pair of electrons on a hydroxy group. For example, pH–rate profiles of enzymatic activity indicate that there is a catalytic acid in the binary complex between NAD^+ and equine alcohol dehydrogenase with an apparent pK_a of 7.6; this acid has been assigned[1281] to the molecule of water bound to the prosthetic Zn^{2+} in the active site. Presumably, after the molecule of water has been replaced by the hydroxy group of the reactant to form the ternary Michaelis complex, the pK_a for that hydroxy group in the alcohol is also shifted into the same range by the Zn^{2+} to which it is a ligand. Upon dissociation of the hydron from this hydroxy group, the resulting oxyanion provides push to the hydride being transferred. There is a synthetic model compound containing a Zn^{2+} that is able to lower the pK_a for a secondary alcohol and accelerate its oxidation to the corresponding ketone by stabilizing the alkoxide so that it can push out the hydride.[1282] In solution, in another nonenzymatic reaction, metallic dications catalyze the decomposition of hemiaminals to aldehydes (reverse of reaction in Figure 1–7) by coordinating to their hydroxy groups, promoting dissociation of a hydron, and increasing the push that pushes out the amine.[1283]

In most cases, a carbonyl participating in an enzymatic reaction is hydronated during a nucleophilic addition to improve the electrophilicity of its carbon rather than becoming a ligand to a metallic dication. An even more common hydronation performed by an active site is one that improves the ability of a leaving group. Consequently, it is not surprising that a metallic dication can act as a Lewis acid to **improve the ability of one of its ligands to act as a leaving group**. For example, Zn^{2+} accelerates the nonenzymatic hydrolysis of *N*-acetylimidazole by coordinating with its peripheral nitrogen

4–173

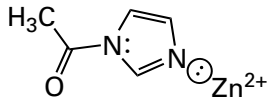

to make the imidazolyl group a better leaving group.[1284] Although Mg^{2+} is a much weaker Lewis acid than the hydron (Table 4–2), the effect of its **complexation of a phospho group** is similar to the enhancement of the ability of a phosphate to act as a leaving group that would result from hydronation.[1285] For example, at high concentration (0.1 M), Mg^{2+} enhances the nonenzymatic solvolysis of geranyl diphosphate, which proceeds through dissociation of the diphospho group that produces the allyl carbenium ion

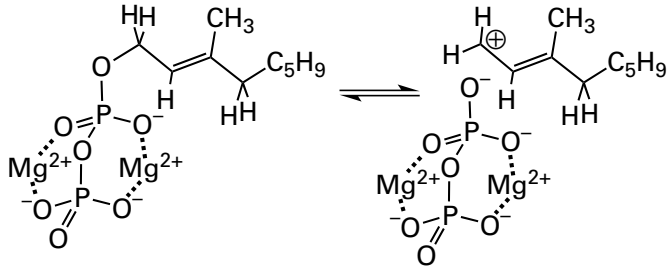

(4–436)

From a consideration of dissociation constants for the complexes between geranyl diphosphate and Mg^{2+}, it could be concluded that the form of geranyl diphosphate showing enhanced reactivity had two Mg^{2+} bound as Lewis acids to the departing diphosphate.

Such catalysis at the leaving group is observed in enzymatic reactions as well. In the nucleophilic substitution catalyzed by xanthine phosphoribosyltransferase from *E. coli*, a Mg^{2+} coordinating the leaving oxygen (**4–127**) improves its ability to leave;[870] in DNA β-glucosyltransferase from T4 bacteriophage, a Mg^{2+} coordinating the leaving oxygen of UDP^{3-} improves its ability to leave;[1286] and in methionine adenosyltransferase from *E. coli*, two Mg^{2+} coordinating the triphosphate of ATP^{4-} improve the ability of triphosphate to leave.[1287]

A hydroxy or alkoxy group on a substrate can become a ligand to a metallic dication, and the metallic dication **enhances the ability of the hydroxy or alkoxy group to leave** without the usual requirement for its oxygen to be hydronated by a Brønsted acid. For example, in the crystallographic molecular model (Figure 3–52)[1054] of the enzymatically active

complex between isocitrate and porcine aconitate hydratase (previously Equation 3–423)

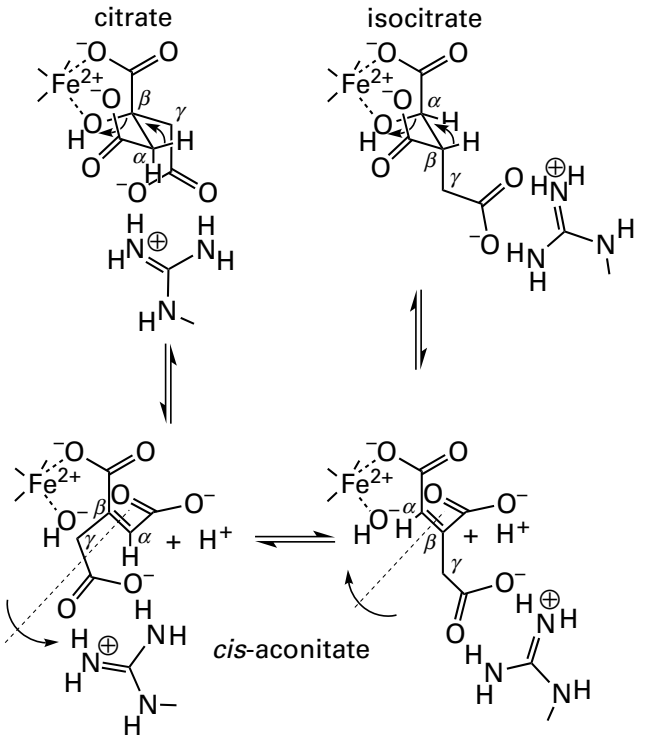

(4–437)

the 2-hydroxy group, which is to leave in the elimination producing *cis*-aconitate, occupies one of the three open coordination sites on the hexacoordinate Fe^{2+} that is situated at the labile site in the tetranuclear [4Fe–4S] iron–sulfur cluster.[789] In the crystallographic molecular model[789] of the complex between citrate and an inactive mutant of bovine aconitate hydratase (98% identity; 0 gap percent), in which Serine 642 has been changed to alanine, the 3-hydroxy group, which is to leave in the elimination also producing *cis*-aconitate, occupies the same open coordination site on the hexacoordinate Fe^{2+}.

Iron dication acts as a Lewis acid in the reactions catalyzed by aconitate hydratase,[1288] maleate hydratase,[1289] fumarate hydratase A,[1290-1292] dihydroxy-acid dehydratase,[1293,1294] and L-serine ammonia-lyase.[1295] These five enzymes catalyze the hydration of 3-carboxymethyl-(*Z*)-butenedioic acid (*cis*-aconitate), (*Z*)-butenedioic acid (maleate), (*E*)-butenedioic acid (fumarate), 2-hydroxy-3-methylbutenoic acid (the enol of 3-methyl-2-oxobutanoate), and 2-amino-propenoic acid (the enamine of pyruvate), respectively. Each enzyme has a tetranuclear [4Fe–4S] iron–sulfur cluster in its active site. Each hydration proceeds by a mechanism that differs from the others only in the identity of the functional groups on the two ends of the carbon–carbon double bond.

The active site of aconitate hydratase (Figure 3–52) is a paradigm of the active site in each hydratase. Because, however, each carbon in the double bond of *cis*-aconitate is adjacent to a carboxy group that can become a *gem*-enediolate, the active site of aconitate hydratase (Equation 4–437) unlike the other enzymes in the family, adds the hydroxy group to *cis*-aconitate at one or the other of the carbons in the double bond, rather than at the only carbon adjacent to a carboxy group, and therefore produces two products, citrate and isocitrate.

During the elimination that converts isocitrate to *cis*-aconitate, a hydron is removed from carbon 3 of isocitrate to form the *gem*-enediolate at the 3-carboxy group; and during the elimination that converts citrate to *cis*-aconitate, a hydron is removed from carbon 2 of citrate to form the *gem*-enediolate at the 1-carboxy group. In each instance, the hydroxy group of the substrate that is a ligand to Fe^{2+} then leaves the *gem*-enediolate to complete the elimination of water from citrate or isocitrate, respectively, that in each case produces *cis*-aconitate. The hydroxide leaves as ferrous hydroxide, $Fe^{2+}{\cdot}OH^-$, instead of the usual situation in which it would leave as water, HOH, after being hydronated by a catalytic acid. The resulting hydroxide on Fe^{2+} participates in the respective reverse directions during the hydrations of *cis*-aconitate producing isocitrate and citrate, respectively (Equation 4–437). The Fe^{2+} lowers the pK_a for the conjugate acid of the hydroxide (Table 4–2) to around 10 so that it can remain unhydronated after it leaves and so that it can add nucleophilically to *cis*-aconitate to produce the *gem*-enediolate during the conversion of citrate to isocitrate and during the conversion of isocitrate to citrate. In order for this lowering of the pK_a for the hydroxy group to occur, the other molecule of water that is also a ligand to the iron (Figure 3–52) cannot also be a hydroxide. In fact, if it were, it could not fulfill its role in the dehydration, which is to relay the acidity of Aspartate 165 or Histidine 167 to hydronate the carboxy group that becomes the *gem*-enediolate in one of the two eliminations catalyzed by the enzyme.

4-Hydroxy-3-methylbut-2-en-1-yl diphosphate reductase from *E. coli*, like aconitate hydratase, has a tetranuclear [4Fe–4S] iron–sulfur cluster in which one iron ion is missing the sulfanyl group of a cysteine that would normally be its ligand. This tetranuclear [4Fe–4S] iron–sulfur cluster is also prone to losing its unliganded Fe^{2+}. In a crystallographic molecular model of the native enzyme with its active site occupied by the substrate (*E*)-4-hydroxy-3-methylbut-

2-en-1-yl diphosphate,[1296] which presumably represents the Michaelis complex, the 4-hydroxy group of (*E*)-4-hydroxy-3-methylbut-2-en-1-yl diphosphate is a ligand to this Fe^{2+} in the intact [4Fe–4S] iron–sulfur cluster. If the reaction then parallels that of aconitate hydratase, the 4-hydroxy group would become the hydroxide in $Fe^{2+}OH^-$, leaving behind an allyl carbenium ion, a logical intermediate in the reaction. In this case, however, unlike in aconitate hydratase, two electrons would then be transferred, one at a time, from two reduced ferredoxins, through the the prosthetic [4Fe–4S] iron–sulfur cluster, to the allyl carbenium ion to produce an intermediate allyl radical and then isopentenyl diphosphate or dimethylallyl diphosphate, the products produced in a 5:1 ratio by the enzyme. An alternative, but more complicated, mechanism has been proposed on the basis of crystallographic molecular models of the substrate (*E*)-4-hydroxy-3-methyl-but-2-en-1-yl diphosphate occupying in turn the active sites of three site-directed mutants, rather than the native enzyme, each the mutant of one of the three side chains that form a composite acid responsible for hydronating the 4-hydroxy group as it is leaving. In these molecular models, the 4-hydroxy group has swung away from the Fe^{2+} and forms hydrogen bonds with the peripheral phospho group of diphosphate and Glutamate 126. In this alternative mechanism, Glutamate 126 hydronates the 4-hydroxy group to catalyze its departure, and the [4Fe–4S] iron–sulfur cluster acts simply as a relay of the two electrons required for the reduction catalyzed by the enzyme.[1297]

The dehydrations and hydrations catalyzed by aconitate hydratase during the conversions of citrate to isocitrate and isocitrate to citrate (Equation 4–437) are particularly apt illustrations of the fact that when a metallic dication improves the ability of a hydroxy group to leave so that it leaves as the metallic hydroxide, the metallic hydroxide is the nucleophile in the reverse of such a dissociation. A metallic dication decreases the pK_a for a molecule of water that is coordinated to it (Table 4–2) and facilitates removal of one of its hydrons by a Brønsted base or simply by dissociation of the hydron into the solution. Dissociation of the hydron from a molecule of water that is a ligand to the metallic dication produces a metallic hydroxide. There are many enzymes in which such metallic hydroxides are used in hydrations and hydrolyses.

Carbonic anhydrase (Equation 4–83) is a metalloenzyme that uses Zn^{2+} in its active site to catalyze the **hydration of carbon dioxide** to produce bicarbonate. In the crystallographic molecular model of the active site of human carbonic anhydrase 1 occupied by bicarbonate (Figure 4–55A), the Zn^{2+} is fixed in position by three imidazolyl groups positioned by the active site in orientations that together promote tetrahedral coordination. A fourth position, one unoccupied sp^3 orbital formed from the 4*s* and 4*p* atomic orbitals of the metallic dication, is occupied by one oxyanion of the bicarbonate. In the unoccupied active site of human carbonic anhydrase 1, the fourth coordinate position is occupied by a molecule of water.[1298] In the active site of the closely related human carbonic anhydrase 2 (60% identity; 0.0 gap percent), the pK_a for this molecule of water[1299-1301] is 6.8, and $Zn^{2+}\cdot OH^-$ rather than $Zn^{2+}\cdot OH_2$ is the catalytically active species.

Because one oxyanion of bicarbonate is a ligand in the inner sphere to the Zn^{2+} in carbonic anhydrase (Figure 4–55A), during the hydration, by microscopic reversibility, the hydroxide anion on Zn^{2+} must add nucleophilically to CO_2 to produce $HOCO_2^-$

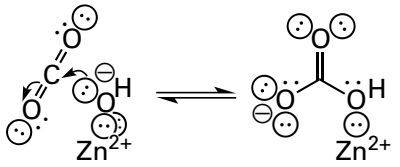

(4–438)

The CO_2 occupies a hydrophobic pocket in the active site of human carbonic anhydrase 2, immediately adjacent to the metallic hydroxide, before the nucleophilic addition occurs.[1299] One of the oxygens in CO_2 is in an oxyanion hole formed from a fixed molecule of water in the active site and the amido nitrogen–hydrogen of a peptide bond.[1302] A molecule of water from solution exchanges at the Zn^{2+} with bicarbonate as it vacates the active site. One hydron on this molecule of water entering form solution then dissociates into a hydron wire[1303] that connects it to the solution to form $Zn^{2+}\cdot OH^-$, prepared for the next turnover.

In most instances, a **metallic hydroxide in an active site is used for hydrolysis**. For example, in the active site of murine cytidine deaminase (Figure 3–36), the hydroxide on Zn^{2+} adds nucleophilically to the carbon of the *N*-carbamoylamidine in cytidine to produce a tetrahedral intermediate from which ammonia is the leaving group in the hydrolysis of cytidine to uridine.[1178,1304] The carboxylato group of Glutamate 67 removes the hydron from the water on Zn^{2+} to produce $Zn^{2+}\cdot OH^-$. The resulting carboxy group shuttles the hydron to the

nitrogen that will leave from the tetrahedral intermediate and then removes the hydron on the hydroxy group of the tetrahedral intermediate, which is acidic because it is still a ligand to the Zn^{2+}, to improve the push of oxygen in ejecting the ammonia. When the homologous[1178] glutamate in cytidine deaminase from *E. coli* was mutated to alanine,[199] the catalytic constant of the enzyme decreased by a factor of 10^8. The enzyme dCTP deaminase from *M. jannaschii*, which is completely unrelated but nevertheless catalyzes the same reaction, has no metallic dication in its active site, but it does use the carboxy group of a glutamate to hydronate the leaving ammonia.[1305] Adenine deaminase from *E. coli*, however, which catalyzes the homologous reaction on the *N*-carbamoylamidine in adenine, has a prosthetic diferric cluster in its active site that uses a dimetallic μ-hydroxide as the nucleophile.[1306]

Histone deacetylase 10 from *D. rerio* hydrolyzes acetyl groups from lysines in histones, which are proteins involved in assembling chromatin. A molecule of water that is a ligand to the prosthetic Zn^{2+} in the active site is the nucleophile in the nucleophilic substitution catalyzed by the enzyme. Upon association with the active site, the acyl oxygen of the acetyl group on a substrate associates with an open site on Zn^{2+}, and the 4-hydroxy group of Tyrosine 307 also forms a hydrogen bond to the acyl oxygen. Together Zn^{2+} and the 4-hydroxy group withdraw electron density from the acyl carbon, making it more electrophilic, and the 4-hydroxyphenyl group hydronates the oxygen as the tetrahedral intermediate forms by addition of the adjacent hydroxide. The imidazolyl group of Histidine 136 removes a hydron from the water either before or during its addition to the acyl carbon of the acetyl group, and the imidazolio group of Histidine 137 adds a hydron to the amino group in the resulting tetrahedral intermediate to permit the nitrogen of the 6-amino group of lysine in the reactant to leave. In the crystallographic molecular model of the active site of a mutant in which Tyrosine 307 was mutated to phenylalanine, an unhydrolyzed N-acetylated substrate occupies the active site because there is no catalytic acid to hydronate the acyl oxygen as the tetrahedral intermediate forms. In this analogue of the Michaelis complex, the τ nitrogen of Histidine 137 is pointed at the amido nitrogen that it would normally hydronate, at a distance of 0.37 nm and in the proper orientation for hydronation. In the crystallographic molecular model of the active site of a mutant in which Histidine 137 was mutated to alanine, the active site is occupied by the tetrahedral intermediate itself because there is no imidazolyl group to hydronate the leaving nitrogen, an inescapable requirement.[137] This molecular model is one of the few instances in which the actual tetrahedral intermediate in the nucleophilic substitution of an acyl derivative has been observed.

Thermolysin (Figure 3–42) is the paradigm of a metalloendopeptidase that uses a metallic hydroxide to **hydrolyze a peptide bond**. In the unoccupied active site of thermolysin, the molecule of water that occupies the fourth position on the tetrahedrally coordinated Zn^{2+} participates in a hydrogen bond with the carboxylato group of Glutamate 143.[1181,1182] The carboxylato group of Glutamate 143 is responsible for removing the acidic hydron from the molecule of water on the prosthetic Zn^{2+} to produce $Zn^{2+}{\cdot}OH^-$, which is the nucleophile in the hydrolysis, and its carboxy group is now responsible for adding the hydron to the departing nitrogen[1307]

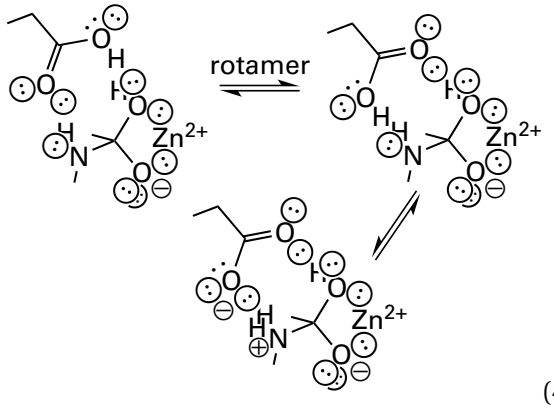

(4–439)

This mechanism allows Zn^{2+} as well as the imidazolium of Histidine 231 (Figure 3–42) to polarize the carbon–oxygen double bond of the amido group to increase the electrophilicity of the acyl carbon. The mechanism has the disadvantage of increasing the occupancy of Zn^{2+}, which should increase the pK_a for the molecule of water and make it more difficult for the carboxylato group to remove the hydron,[1308,1309] but it has the advantage of increasing the nucleophilicity of the resulting zinc hydroxide.

Peptide deformylase from *E. coli* uses $Fe^{2+}{\cdot}OH^-$ instead of $Zn^{2+}{\cdot}OH^-$ in its active site (**4–158**)[1149] to catalyze hydrolysis of an amino-terminal formyl group on a polypeptide (Equation 4–425). The enzyme also uses the carboxylato group of a glutamate to remove a hydron from a molecule of water on Fe^{2+} to produce $Fe^{2+}{\cdot}OH^-$ and to then hydronate the leaving amino group (see Equation 4–439).[121]

The mechanism for hydrolysis of a carboxy-terminal peptide bond in the active site of the zinc metalloenzyme bovine carboxypeptidase A (Equation 4–172) is also almost the same as that used by thermolysin. The hydron is removed from a molecule of water on Zn^{2+} by the carboxylato group of Glutamate 270, the same carboxylato group labeled by *N*-bromoacetyl-*N*-methyl-L-phenylalanine (Equation 4–312), but the carboxylato group does not seem to be properly oriented to hydronate the leaving group.[259] In the active site of GTP cyclohydrolase I from *E. coli*, which hydrolyzes the cyclic amidine in the imidazolyl ring of the guanine in $MgGTP^{2-}$, the hydron is removed from the molecule of water on Zn^{2+} by Histidine 112 while Histidine 179 hydronates the leaving group.[1174]

A metallic dication in an active site can also be used as a Lewis acid to lower the pK_a for an alcohol or thiol to ease its dehydronation, just as it is able to lower the pK_a of a molecule of water. For example, in the active site of catechol *O*-methyltransferase from *R. norvegicus*, the two ortho hydroxy groups of a catechol such as 4-(2-aminoethyl)-benzene-1,2-diol are both ligands to a Mg^{2+} that lowers the pK_a of the hydroxy group that is to be methylated by *S*-adenosyl-L-methionine, so that it is unhydronated and nucleophilic at the start of the reaction.[1310] The Zn^{2+} in the active site of protein farnesyltransferase (Equation 4–245) from *S. cerevisiae* lowers by 3 units the pK_a of the sulfanyl group of cysteine in a protein that is a substrate to which the farnesyl group is transferred during the enzymatic reaction.[1165] When the Zn^{2+} in protein farnesyltransferase from *R. norvegicus* is replaced with Cd^{2+}, a pK_a of 6.0 in the pH–rate profile for the enzyme decreases by 1.0 unit, as expected for replacement of Zn^{2+} by the softer metal.[1311] Consequently, the zinc(II) thiolate is the nucleophile in the enzymatic reaction, and the role of Zn^{2+} is to lower the pK_a for the sulfanyl group in the substrate into the physiological range.

Usually, because of the Brønsted relation, when the pK_a for the conjugate acid of a nucleophile is decreased, its nucleophilicity also decreases. There are indications that this decrease in nucleophilicity can be minimized by coordination with a metallic dication. In dimethyl sulfoxide as a solvent, the rate of nonenzymatic methyl transfer from trimethyl phosphate, $(CH_3O)_3P{=}O$, to the sulfido group of a thiolate in $Zn(SC_6H_5)_4^{2-}$ is equal to the rate for the same methyl transfer to $^-SC_6H_5$, but it is more than 100 times faster than methyl transfer to HSC_6H_5.[1312] Consequently, at least in this instance, Zn^{2+} lowers the pK_a for the sulfanyl group without affecting its nucleophilicity proportionally. When a hydron is added to a sulfido group, however, it has a dramatic effect on the nucleophilicity of sulfur. In solution, $Zn^{2+}{\cdot}OH^-$ in a synthetic, pentacoordinated complex is almost as effective as free OH^- at hydrolyzing a strained lactam and only 100 times less effective at hydrolyzing an ester,[1309] even though the pK_a for $Zn^{2+}{\cdot}OH_2$ in the complex is 8 units lower than that of H_2O the conjugate acid of OH^-. Both observations suggest that use of a metallic dication in the active site of an enzyme could be a general strategy for lowering the pK_a for one of its ligands toward the physiological range of pH without at the same time dramatically decreasing the nucleophilicity of the ligand after it has been dehydronated.[1313]

Upon associating with the active site of 5-methyltetrahydropteroyltriglutamate—homocysteine *S*-methyltransferase from *Candida albicans*,[1314] the sulfanyl group of the substrate L-homocysteine becomes a ligand on the prosthetic Zn^{2+}, and in the complex at neutral pH, the sulfido group is unhydronated.[1313] The concerted nucleophilic substitution at the 5-methyl group in 5-methyltetrahydropteroyltri-L-glutamate by the sulfido group of L-homocysteine is a difficult one because the leaving group, nitrogen 5 of tetrahydropteroyltri-L-glutamate, is an anilino nitrogen. Consequently, the sulfido group has to retain as much of its nucleophilicity as possible even though the Zn^{2+} has lowered its pK_a sufficiently to ensure that the sulfanyl group is the sulfido group, its conjugate base, at neutral pH.

***μ*-Hydroxides bridging two metallic dications** in enzymatic active sites (Figure 4–55E,F), such as the one in the active site of adenine deaminase from *E. coli*, are also used in hydrolyses.[1315-1317] For example, in the active site of creatininase

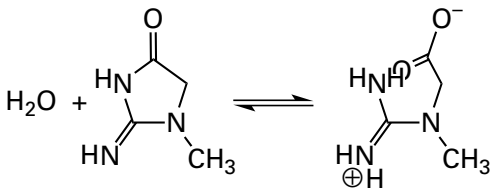

(4–440)

from *P. putida*, a *μ*-hydroxide bridging[1318] two Zn^{2+} adds nucleophilically to the acyl carbon of the (*N*-acyl-*N*′-alkyl)guanidino group in creatinine while the acyl oxygen on that carbon is a ligand to one of the Zn^{2+} to increase the electrophilicity of the carbonyl carbon. Acting as a Brønsted acid, a molecule of water on the same Zn^{2+} that coordinates the acyl oxygen hydronates the leaving nitrogen.[1319] In this

instance, the dinuclear cluster seems to do everything: provide the nucleophile, polarize the carbonyl, and hydronate the leaving group. In the active site of human glutamate carboxypeptidase II, an enzyme that hydrolyzes a peptide bond, the nucleophile in the hydrolysis that adds to the acyl carbon is a μ-hydroxide bridging two Zn^{2+}. The carboxy group of Glutamate 424 that forms a hydrogen bond with this hydroxide at one of its oxygens hydronates the leaving amino nitrogen in the tetrahedral intermediate with the hydron on its other oxygen.[1320]

The main purpose of the two metallic dications in one of these dinuclear clusters is to **lower the pK_a for a molecule of water** bridging the two dications even more than if it were a ligand to only one dication, so that it is a μ-hydroxide sitting between them at physiological pH rather than a μ-molecule of water. For example, a synthetic mononuclear complex of Zn^{2+}, in which one ligand to the metallic dication is the hydroxy group of an aliphatic alcohol, can be induced to dimerize. In the dimer, the same hydroxy group ends up as a ligand to both Zn^{2+}. At pH 6.0, the μ-hydroxy group that sits between the two Zn^{2+} in the dimer is the unhydronated μ-alkoxide; but at pH 9.1, the μ-hydroxy group in the mononuclear complex of Zn^{2+} is still hydronated.[1321] Consequently, the μ-hydroxy group between the two Zn^{2+} must have a pK_a less than 6 while the same hydroxy group on the lone Zn^{2+}, which has the same coordination as each of the two Zn^{2+} in the dimer, must have a pK_a greater than 9. The pK_a for a molecule of the μ-water bridging the two Zn^{2+} in the active site of aryldialkylphosphatase[1322] (Figure 4–55E) is 5.8, so at pH 7, it will be a μ-hydroxide bridging the metals.

In nonenzymatic examples, even though values of pK_a for their conjugate acids, μ-molecules of water, are low, the bridging μ-hydroxides in synthetic dinuclear metallic hydroxides are **competent nucleophiles**. A synthetic dinuclear cluster of two Ni^{2+} bridged by a μ-hydroxide is able to hydrolyze urea,[1323] as does $(Ni^{2+})_2{\cdot}OH^-$ in urease (Figure 4–54). A synthetic dinuclear cluster[1324] of two Ni^{2+} bridged by a μ-hydroxide and a synthetic dinuclear cluster[1325] of two Zn^{2+} bridged by a μ-hydroxide are both able to hydrolyze amides, as does $(Zn^{2+})_2{\cdot}OH^-$ in β-lactamase[1315,1316] or $(Zn^{2+})_2{\cdot}OH^-$ in leucyl aminopeptidase (Figure 4–55G).[1160] A synthetic dinuclear cluster of two Co^{2+} bridged by a μ-hydroxide is able to hydrolyze a guanidino group,[1326] as does $(Mn^{2+})_2{\cdot}OH^-$ in the active site of arginase.[1327]

In the active site of urease (Equation 4–426)[1328] from *S. pasteurii*, which catalyzes a nucleophilic substitution at a carbonato carbon, there is a dinuclear cluster[1329] of two Ni^{2+}. When the active site is occupied by phosphorodiamidate **4–174**

4–174 **4–175**

an analogue of tetrahedral intermediate **4–175** in the enzymatic reaction, one oxygen of the phosphorodiamidate bridges the two Ni^{2+} (Figure 4–54).[1160] In the unoccupied enzyme, there is a μ-hydroxide bridging the two Ni^{2+} at the same location as the bridging oxygen of the phosphorodiamidate. From these observations, it can be concluded that the bridging hydroxide is the nucleophile that adds to the acyl carbon of the urea

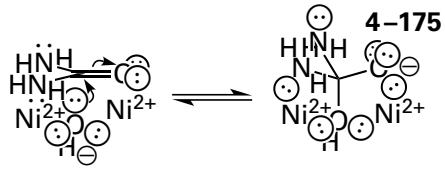

(4–441)

Because two ligand positions, one on each of the two Ni^{2+} in the active site, are occupied by the other oxygen and one nitrogen of phosphorodiamidate **4–174**, respectively (Figure 4–54), it can be concluded that one nitrogen in tetrahedral intermediate **4–175** when it is in the active site is a ligand to one Ni^{2+}, and the oxygen from urea is a ligand to the other Ni^{2+}. Each position for a ligand is occupied by a molecule of water in the unoccupied active site. Upon entering the active site, the urea exchanges with these two molecules of water. The two lone pairs of σ electrons that are ligands to the Ni^{2+} in tetrahedral intermediate **4–175** are π electrons in the urea in the Michaelis complex (Equation 4–441). As these π electrons become σ electrons in the transition state, the **strength of their ligation to the metal increases** dramatically, stabilizing the transition state and promoting catalysis.

The carboxylato group of Aspartate 362 dehydronates the μ-hydroxy group bridging the two Ni^{2+} in tetrahedral intermediate **4–175** (Equation 4–441) to give the resulting μ-oxido group the ability, along with the other oxyanion, to push out the leaving group. The ammonia that is the leaving group from the tetrahedral intermediate in urease can only leave if its nitrogen in tetrahedral intermediate **4–175** is hydronated. If the nitrogen that leaves as ammonia is the one that is a ligand to one of the Ni^{2+} (Figure

4–54), the carboxylato group of Aspartate 362 that has just dehydronated the μ-hydroxy group bridging the two Ni^{2+} in the tetrahedral intermediate (Equation 4–441) would then pivot on the ligation of its other oxygen to that Ni^{2+} and hydronate the nitrogen so that it can leave as ammonia. In this case, the carboxy group would dedicate one of its oxygens to act as a ligand to the nickel and the other oxygen to act as a catalytic acid–base, just as the carboxy groups do in the active site of D-psicose 3-epimerase (Equation 4–434). If, however, the ammonia that is the leaving group from the tetrahedral intermediate is the one that is forming a hydrogen bond with the imidazolyl group of Histidine 322 (Figure 4–54), then the imidazolyl group provides the hydron necessary to make the nitrogen a leaving group.[1330]

In the active site of dihydroorotase

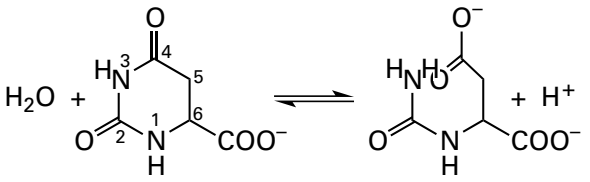

(4–442)

from *E. coli*, which, unlike urease, catalyzes a nucleophilic substitution at an acyl carbon rather than a carbonato carbon, a μ-hydroxide bridging two Zn^{2+} adds nucleophilically to carbon 4, the acyl carbon of the (*N*-acyl-*N*-alkyl)urea in dihydroorotate, just as $(Ni^{2+})_2{\cdot}OH^-$ does to urea in urease (Equation 4–441). The acyl oxygen of carbon 4 is a ligand to one of the two Zn^{2+} in the cluster, which serves to stabilize the oxyanion in the tetrahedral intermediate, just as one of the Ni^{2+} does in urease. The carboxylato group of Aspartate 250 is a ligand to the other Zn^{2+}. It dehydronates the resulting hydroxy group of the tetrahedral intermediate, just as Aspartate 362 in urease does (Figure 4–54), and then the **carboxylato group pivots around its ligation to Zn^{2+}** and hydronates the nitrogen that is a ligand to this same Zn^{2+} in the dinuclear cluster and that leaves as the ureido group,[1331] just as the carboxylato group of Aspartate 362 in the active site of urease might do (Figure 4–54).

Human arginase catalyzes a nucleophilic substitution at a carbonato carbon, as does urease, but in arginase the carbonato carbon is part of a guanidinio group

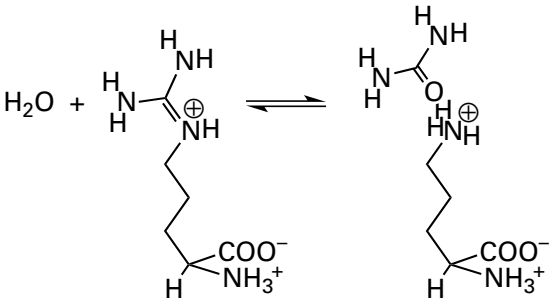

(4–443)

A μ-hydroxide bridging[1332,1333] two Mn^{2+} adds nucleophilically to the guanidinio carbon while one peripheral nitrogen in the guanidinio group is a ligand to one of the Mn^{2+}. The imidazolyl group of Histidine 141 then hydronates the leaving amino group in the tetrahedral intermediate to give L-ornithine,[1334-1336] just as the imidazolyl group of Histidine 322 in the active site of urease might do (Figure 4–54).

The ambiguity in assigning the leaving nitrogen in urease again illustrates the value of stereochemical information, which is necessarily lacking in this case. The uncertainty results from the fact that there are two equivalent nitrogens in tetrahedral intermediate **4–175**, either of which could represent the leaving group in the actual reaction. In the cases of dihydroorotase and arginase, as well as creatinase (**4–128**), the catalytic acids were identified when a substrate or an analogue of an intermediate was bound in the active site and the leaving group or the atom representing the leaving group could be unambiguously identified.

An uncertainty similar to that for urease exists for the complex (Figure 4–55G) between bovine leucyl aminopeptidase and 1-amino-3-methylpropylphosphonic acid (**4–176**)

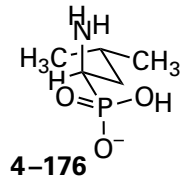

4–176

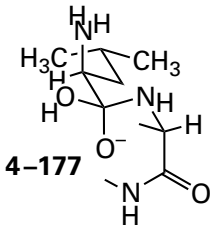

4–177

which is an analogue of tetrahedral intermediate **4–177** in the hydrolysis of a peptide bond to an amino-terminal leucine catalyzed by the enzyme. The phosphono group has two oxygens that are ligands to the two Zn^{2+}, respectively; either the one to the right or the one to the left in drawing **4–176** could represent the leaving amine.[1172] The oxygen on the right, however, is more likely the representative because the ammonio group of Lysine 262 forms a

hydrogen bond to it (Figure 4–55G), perhaps identifying that lysine as the acid that must hydronate the α-amino group before it can leave. In the crystallographic molecular model of the complex between methionyl aminopeptidase from *E. coli*, which has a dinuclear cluster of two Fe^{2+} in its active site, and 1-amino-3-(methylsulfanyl)propylphosphonic acid (the 3-methylsulfanyl analogue of **4–176**), two oxygens of this analogue of the tetrahedral intermediate, either of which may represent the leaving amine, accept hydrogen bonds from the imidazolyl groups of Histidine 79 and 178, respectively, either of which could be the unavoidable catalytic acid that hydronates the actual leaving amino group.[1242]

The enzymatic reaction catalyzed by 3,4-dihydroxy-2-butanone-4-phosphate synthase

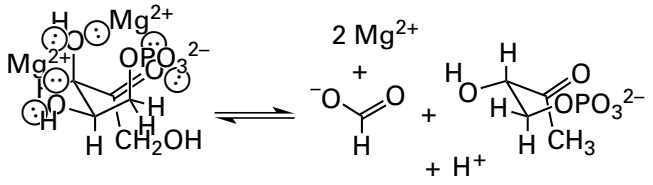

(4–444)

from *M. jannaschii* is centered on the 3-hydroxy group of the D-ribulose 5-phosphate that is its substrate. On one side of the 3-hydroxy group, the reaction involves a 1,2-hydride migration to the carbonyl group of the reactant, analogous to that performed by xylose isomerase (Equation 4–432), or an isomerization analogous to that performed by triose-phosphate isomerase that involves an enolate (Equation 4–55), followed by an elimination that exploits the newly formed carbonyl at carbon 3 or the enolate itself. On the other side of the 3-hydroxy group that has now become a carbonyl, a 1,2-phosphomethide migration then occurs, analogous to a 1,2-methyl migration, followed by a retro-Claisen dissociation during which a metallic hydroxide adds to a carbonyl group.[1337] Consequently, it is one of the most unusual heterolytic reactions catalyzed by an enzyme, and a captivating puzzle to solve (Problem 4–48).

During the steps in the reaction, the oxygen on carbon 3 of D-ribulose 5-phosphate is required to be a hydroxy group, the oxyanion of an enolate, and the oxygen of a carbonyl group at various stages in the mechanism. In order to accommodate these various roles, this oxygen is coordinated by two Mg^{2+}. One Mg^{2+} is additionally coordinated by the 2-carbonyl group of D-ribulose 5-phosphate, and the other Mg^{2+} is additionally coordinated by the 4-hydroxy group of D-ribulose 5-phosphate[882,1338]

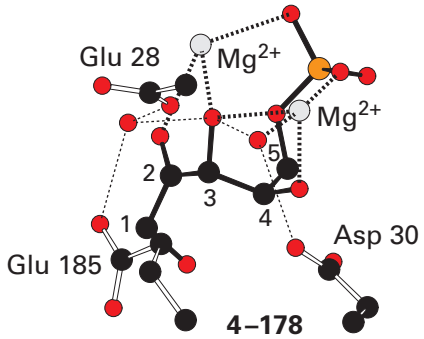

The 3-hydroxy group of D-ribulose 5-phosphate bridges the two Mg^{2+}, so it is formally equivalent to a μ-molecule of water or a μ-hydroxy group bridging the metallic dications in the usual dinuclear cluster and almost, but not quite, as acidic as a typical bridging oxygen (Table 4–2). The purpose of the two Mg^{2+} is to lower the pK_a for the hydroxy group as well as to stabilize the oxyanion of the enolate.

In addition to the two Mg^{2+} that are acting as the usual Lewis acids, two molecules of water form hydrogen bonds to the central 3-hydroxy group. One molecule of water also participates in a hydrogen bond with Aspartate 30, and the other molecule of water also participates in hydrogen bonds with Glutamates 28 and 185. Consequently, the central 3-hydroxy group, in addition to its covalent bond to carbon 3, is surrounded by a crowd of four ligands: two Mg^{2+} and two oxygens from the molecules of water. The molecules of water act as Brønsted acids to give and take hydrons from the oxygen on carbon 3 of D-ribulose 5-phosphate while it assumes its different roles as the reaction proceeds through its several steps. This enzymatic reaction in turn provides, in each of its steps (Problem 4–48), a paradigm of one of several of the roles played by metallic dications as Lewis acids.

In most cases, as in those that have just been discussed, the two metallic dications in a dinuclear cluster in an active site are of the same metal, but several active sites have **two different metallic dications in their dinuclear clusters**. For example, in the active site of enamidase from *E. barkeri*, which hydrolyzes the amido group in 6-oxo-1,4,5,6-tetrahydronicotinate, the dinuclear cluster consists of one Fe^{2+} and one Zn^{2+}, bridged by a μ-hydroxide.[1339]

In addition to acting as Lewis acids, metallic dications or dinuclear clusters can catalyze reactions by approximating a nucleophile and the electrophile to which it is to add in a nucleophilic substitution at carbon. For example, formate, a substrate for peptide deformylase (Equation 4–425), is a

bidendate ligand to Fe^{2+} in the crystallographic molecular model of the active site (**4–158**). This fact implies that Fe^{2+} not only lowers the pK_a for the molecule of water that is one of its ligands but also coordinates the acyl oxygen of the formyl group on an N-formylated polypeptide, the substrate in the hydrolytic direction, and consequently approximates the hydroxide to the formyl carbon to which it adds during the hydrolysis.

The Zn^{2+} in thermolysin can be either tetracoordinate (**4–162**) or pentacoordinate (**4–165**) in crystallographic molecular models of different complexes between inhibitors and the enzyme. This fact suggests that the acyl oxygen of the peptide bond in the normal reactant for the enzyme associates as a monodentate, fifth ligand to Zn^{2+}, pushing to one side that molecule of water, which remains as a ligand to Zn^{2+} while still forming a hydrogen bond with the carboxy group rather than leaving Zn^{2+} as it would in a dissociative exchange. The hydroxide on Zn^{2+} in the tautomer of the pentacoordinate complex would then attack nucleophilically the acyl carbon of the peptide bond that is also coordinated to Zn^{2+} through its acyl oxygen

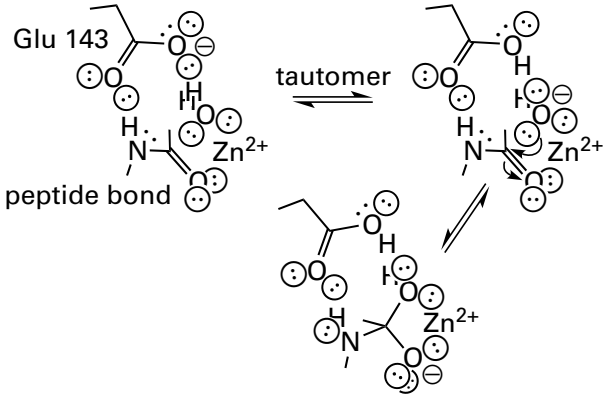

(4–445)

In this way, Zn^{2+} approximates the hydroxide and the acyl carbon of the peptide bond.

Metallic hydroxides are also effective in the nonenzymatic hydrolyses of substrates. The nonenzymatic hydrolysis of *N*-acylbenzimidazole **4–179**, in which the acyl group is designed to chelate Zn^{2+}, proceeds through nucleophilic addition of zinc hydroxide to the acyl group, which is also coordinated by the Zn^{2+}. In this instance, Zn^{2+} approximates the nucleophile and electrophile as well as coordinating the two oxygens of the tetrahedral intermediate[1340]

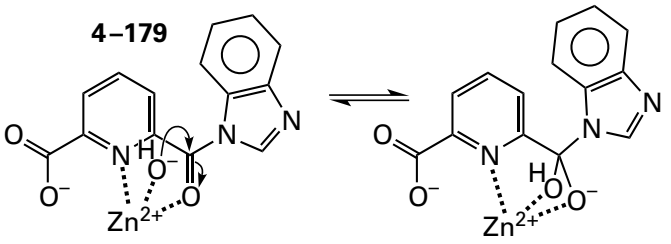

(4–446)

In both enzymatic and nonenzymatic nucleophilic substitutions at an acyl group taking place on a metallic dication, addition of the nucleophile—in the previous three instances a hydroxide on the metallic dication—to the acyl carbon, the oxygen of which is also a ligand to the dication, produces a four-membered metallocycle (zinc, oxygen, carbon, oxygen; see Equation 4–446). In the active site of thermolysin, this metallocycle, unlike the five-membered metallocycle in the complex between the active site and hydroxamate **4–165**, would be strained. In the crystallographic molecular model of the complex between thermolysin and phosphonamidate **4–180**

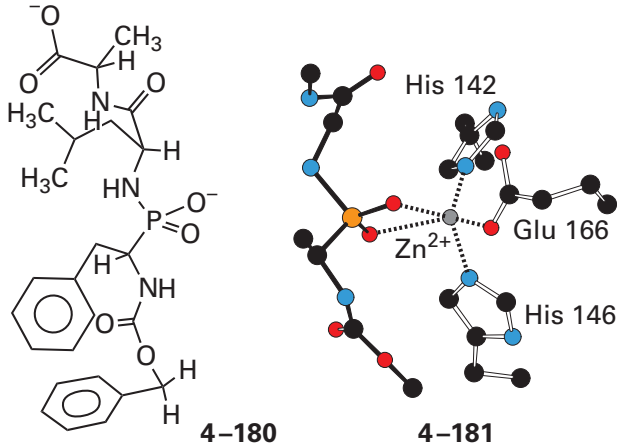

just such a four-membered metallocycle is formed (**4–181**).[1184] In the normal reaction, however, this metallocycle containing a pentacoordinate Zn^{2+} should break at the weakest bond, that between the hydroxy group of the tetrahedral intermediate and Zn^{2+}, to generate the tetracoordinate complex represented in Figure 3–42.

The Zn^{2+} in the active site of bovine carboxypeptidase A (Equation 4–172), just as does the Zn^{2+} in thermolysin, coordinates both the hydroxide that adds to the acyl carbon of the peptide bond and the acyl oxygen; and, in this way, it approximates the nucleophile and the electrophile. The Zn^{2+} in carboxypepidase A forms a metallocycle, analogous to that formed by Zn^{2+} in the active site of thermolysin

(**4–181**), with a phospho analogue of the tetrahedral intermediate in its enzymatic reaction.

The hydrolysis catalyzed by urease (Equation 4–441) illustrates the fact that because **a dinuclear cluster has coordination sites on two metallic dications** instead of just one, it provides more opportunities for catalysis by approximation. In the Michaelis complex between the active site of urease and urea, one Ni^{2+} coordinates the carbonato oxygen and the other Ni^{2+} coordinates one ureido nitrogen. This dinuclear coordination approximates the nucleophilic μ-hydroxide and the electrophilic carbonato carbon in the correct orientation for nucleophilic addition. In tetrahedral intermediate **4–175**, there are two metallocycles—composed of nickel, oxygen, carbon, oxygen and nickel, oxygen, carbon, nitrogen—rather than just one as in the active site of thermolysin, which has only one metallic dication. In the active sites of creatininase[1319] (Equation 4–440), dihydroorotase[1331] (Equation 4–442), arginase[1335] (Equation 4–443), leucyl aminopeptidase[1172] (**4–176**), and methionyl aminopeptidase,[1242] however, although they contain dinuclear clusters of dimetallic dications, only one dimetallic dication (rather than both) approximates the electrophile and the nucleophile by coordinating the respective acyl oxygens and the bridging μ-hydroxide. Creatininase, dihydroorotase, leucyl aminopeptidase, and methionyl aminopeptidase hydrolyze acyl derivatives rather than carbonato derivatives, so there are fewer opportunities for coordination.

Metallic dications are also used as Lewis acids in nucleophilic substitutions at phosphorus. Most nucleophilic substitution at phosphorus, unlike that catalyzed by pancreatic ribonuclease (Figure 4–46), rely on catalysis by metallic dications. For example, pyruvate kinase (Equation 4–275 and Figure 4–52) has two prosthetic Mg^{2+} in its active site when it is occupied by reactants in the productive Michaelis complex. The unliganded enzyme binds one Mg^{2+} from solution at the active site, and the second Mg^{2+} arrives complexed with ATP^{4-} or ADP^{3-}.[1341] This fact was shown by using, in place of $MgATP^{2-}$, a Cr^{3+} complex of ATP, which is a stable covalent complex almost completely inert to exchange (Table 4–5). The enzyme transferred the γ-phospho group from $CrATP^{-}$ to an analogue of *enol*pyruvate but only when Mg^{2+} was also present to occupy the site on the free enzyme for the second, uncomplexed metallic dication.

Both Mg^{2+} involved in the normal reaction catalyzed by pyruvate kinase (Equation 4–275), the one bound to free enzyme and the one brought in by $MgATP^{2-}$, have been located in maps of electron density derived from crystals of the enzyme in which the active site is occupied by substrates and inhibitors.[581,1342,1343] In the complex between the enzyme and Mg^{2+}, oxalate, and $MgATP^{2-}$, one oxygen of the phospho group that is transferred, as well as the oxygen of oxalate that represents the enol oxygen of the enol of pyruvate, are both ligands to the Mg^{2+} that is not brought in on $MgATP^{2-}$ (Figure 4–52). In the complex[1343] between the enzyme and pyruvate and Mg^{2+}, the carbonyl oxygen of pyruvate that was or that becomes the enol oxygen of phospho*enol*-pyruvate is a ligand to this same Mg^{2+} at the same position. Consequently, the role of this prosthetic Mg^{2+} that is not brought in on $MgATP^{2-}$ is to act as a Lewis acid to improve the ability of the enol oxygen to leave phosphorus during transfer of the phospho group from phospho*enol*pyruvate to $MgADP^{-}$. The intermediate in the reaction is probably monomeric metaphosphate, so this Mg^{2+}, by also coordinating one phospho oxygen, ensures that the phospho group on phospho*enol*pyruvate is dianionic, as is required to form monomeric metaphosphate, as well as to provide push to the dissociation

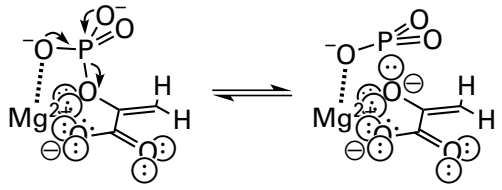

(4–447)

In the active site of phospho*enol*pyruvate carboxykinase, which catalyzes a reaction similar to that catalyzed by pyruvate kinase, one Mg^{2+} enters the active site on $MgATP^{2-}$, but Mn^{2+} rather than Mg^{2+} acts as the Lewis acid for the oxygen of the enolate of pyruvate.[1232]

In the reverse reaction catalyzed by pyruvate kinase (Equation 4–275), the role of the Mg^{2+} that is not brought into the active site on $MgATP^{2-}$ is to **stabilize the enolate and prevent its hydronation** so that its oxyanion can act as a nucleophile on phosphorus, albeit a phosphorus probably in monomeric metaphosphate. A similar role is played by the Mg^{2+} that is not brought into the active site on the nucleoside triphosphate in DNA-directed DNA polymerase β from *R. norvegicus*,[1344] DNA-directed DNA polymerase encoded by the genome of T7 bacteriophage,[1345,1346] and DNA-directed DNA polymerase encoded by the genome of hepatitis C virus.[1347] These Mg^{2+} coordinate the respective

3′-hydroxy groups that add to the α-phospho group of the next deoxynucleoside triphosphate to elongate the DNA. In each instance, this catalytic Mg^{2+} lowers the pK_a for the hydroxy group so that it can be dehydronated and act as a nucleophile at the α phosphorus

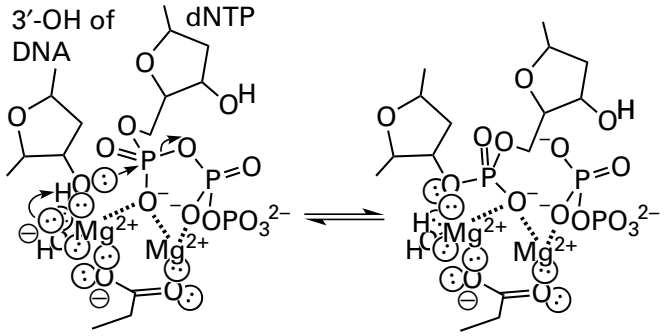

(4–448)

where 3′-OH is the 3′-hydroxy group at the end of the strand of DNA being elongated and dNTP is the deoxynucleoside triphosphate that is being added. In RNA-directed DNA polymerase from human immunodeficiency virus, this catalytic Mg^{2+} is loosely bound to the active site (K_d = 4 mM) and only associates after the magnesium nucleoside triphosphate has associated,[1348] so it is not a prosthetic Mg^{2+}.

In the case of the two Mg^{2+} in the active site of UDP-*N*-acetylglucosamine diphosphorylase

N-acetyl-α-D-glucosamine 1-phosphate^{2-} +
$MgUTP^{2-} \rightleftharpoons MgOPO_3PO_3^{2-}$ +
MgUDP-*N*-acetyl-α-D-glucosamine^{2-}

(4–449)

from *M. tuberculosis*, when it is occupied by magnesium diphosphate^{2-} and MgUDP-*N*-acetyl-α-D-glucosamine, it seems that neither Mg^{2+} fulfills a catalytic function other than entering the active site on the two substrates.[1349] The Mg^{2+} that enters on diphosphate leaves on $MgUTP^{2-}$, in which it is coordinated as the usual enantiomer at the Mg^{2+} on a triphosphate. The Mg^{2+} that enters on MgUDP-*N*-acetyl-α-D-glucosamine ends up on the phospho group of *N*-acetyl-α-D-glucosamine 1-phosphate and probably leaves on its own from the active site. Neither Mg^{2+} is coordinated by the two oxygens between which the phospho group is transferred; rather, each is coordinated by equatorial oxygens in the phosphorane or monomeric metaphosphate that is the intermediate in the nucleophilic substitution at phosphorus.

It is tempting to assign a **role for the Mg^{2+} on nucleoside triphosphates** that enter the active sites of the many enzymes like pyruvate kinase (Figure 4–52), the DNA-directed DNA polymerases, and on both substrates of UDP-*N*-acetylglucosamine diphosphorylase. In solution, addition of Mg^{2+} to an alkyl diphosphate, as opposed to a phosphodiphosphate, significantly enhances the ability of the diphosphate to act as a leaving group in a nonenzymatic nucleophilic substitution at the carbon to which it is attached.[1350] This enhancement results from the decrease in negative charge in the leaving group when it is magnesium diphosphate rather than diphosphate. The same enhancement, however, is not observed for nonenzymatic phosphorylations effected by H_2ATP^{2-}, which is a model for all nucleoside triphosphates. Most of the reactions in which magnesium nucleoside triphosphates engage are phosphorylations, and in these phosphorylations the magnesium nucleoside diphosphate is the leaving group. As has been mentioned, the major form[1122] of nucleoside triphosphates in cytoplasm, is $MgATP^{2-}$, and the Mg^{2+} probably enters the active site of an enzyme for which a nucleoside triphosphate is a substrate automatically rather than purposefully. In most instances of such a Mg^{2+} bound to oligophospho groups in a substrate, the dication ends up coordinated to one or two equatorial oxygens in the phosphorane or monomeric metaphosphate that is the intermediate in the nucleophilic substitution at phosphorus, and this coordination may enhance catalysis, albeit at the periphery. The argument for a mechanistic purpose for these Mg^{2+} could extend, but probably should not, to assigning that purpose as the reason that cellular free concentrations of Mg^{2+} are so high.

Regardless of the role played by a Mg^{2+} brought into the active site on a nucleoside triphosphate or a nucleoside diphosphate, the Mg^{2+} or other metallic dication that is not brought in by $MgATP^{2-}$ can be thought of as acting alone as a catalyst: **stabilizing the phosphorane or monomeric metaphosphate** that is an intermediate in the reaction, stabilizing the nucleophilic oxyanion in one direction, and stabilizing the leaving group in the other direction.

There are, however, a number of instances in which **two metallic dications**, neither of which is brought in by a substrate and both of which are bound as prosthetic groups in the active site in the absence of substrates,[1351-1354] act in concert to catalyze a nucleophilic substitution at phosphorus.

For example, in the active site of aryldialkylphosphatase (Figure 4–55E), which hydrolyzes triesters of phosphoric acid, the μ-hydroxide bridging two Zn^{2+} is the nucleophile that adds to the phosphorus of the triester. In the Michaelis complex, the single, unarylated and unalkylated phospho oxygen on the phosphotriester is a ligand to one of the Zn^{2+}, which withdraws electron density from phosphorus and makes it more electrophilic. The conjugate acid of the unliganded oxygen in the carboxy group of Aspartate 301 that is a monodentate ligand to the other Zn^{2+} is in van der Waals contact (0.39 nm) with the methyl group of diisopropyl methylphosphonate, which is an analogue of a phosphotriester and occupies the active site in the crystallographic molecular model.[1166,1354] This carboxy group hydronates the leaving group that, in a substrate, would sit in the location of the methyl group. This carboxy group also forms a hydrogen bond with the μ-hydroxide in the unoccupied active site,[1354] so it is responsible for removing a hydron from the μ-hydroxide during the nucleophilic addition to phosphorus that forms the phosphorane. The dimetallic cluster and the carboxy group of Glutamate 407 in the active site of aryldialkylphosphatase from *Sphingobium* also seem to be exclusively responsible for the nucleophilic substitution at phosphorus catalyzed by the enzyme. Therefore, the pK_a of 7.9, below which the specificity constant for the aryl dialkyl substrate paraoxon decreases, has been assigned to the hydron in the hydrogen bond between this carboxy group and the μ-hydroxide.[1355]

Two of the four Mg^{2+} in the active site of inorganic diphosphatase

$$Mg_2O_3POPO_3 + H_2O \rightleftharpoons 2\,HOPO_3^{2-} + 2\,Mg^{2+} \qquad (4\text{–}450)$$

from *E. coli* when it is occupied by diphosphate are brought in with the diphosphate, but the other two are metallic dications present in the active site before the substrate binds.[1356] There is a μ-hydroxide bridging these latter two Mg^{2+}. This bridging hydroxide is the nucleophile that adds to the one phosphorus from which the other phospho group leaves during the hydrolysis catalyzed by the enzyme.[1357-1359] Aspartate 117 in inorganic diphosphatase from *S. cerevisiae* removes the hydron from this hydroxide as it adds to the electrophilic phosphorus[1358]

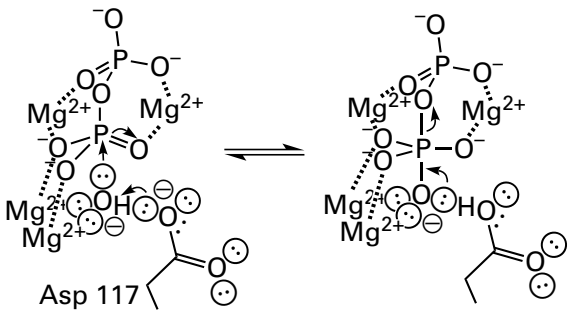

(4–451)

There are other **enzymes that use a μ-hydroxide bridging two metallic dications to hydrolyze phosphoesters**[1360-1362] by a mechanism in which **two oxygens on the phosphoester are ligands**, one to each metallic dication, as in the active site of inorganic diphosphatase (Equation 4–451). There is even an inorganic diphosphatase in which a μ-hydroxide bridging three metallic dications acts as the nucleophile in hydrolysis of diphosphate.[1363] In the active site of histidinol-phosphatase from *Lactococcus lactis*, which hydrolyzes the monoester L-histidinol phosphate, the nucleophile is a μ-hydroxide bridging two Zn^{2+}, and a third Zn^{2+}, not coordinated by the hydroxide, has the leaving oxygen of L-histidinol as a ligand and, as a Lewis acid, enhances its ability to leave from the phosphorane that forms upon nucleophilic addition of the hydroxide to the phospho group.[1364] In the active site of the enzyme from *Vibrio cholerae*, which is responsible for hydrolysis of the phosphodiester at the 3′-hydroxy group of adenylate in 3′,3′-cyclic guanosine monophosphate-adenosine monophosphate, there is a μ-hydroxide bridging two Fe^{2+}.[1365,1366] When either one or both Fe^{2+} are adventitiously oxidized to Fe^{3+}, the enzyme loses its catalytic activity, perhaps because exchange is so much faster at the dication than the trication. A nonenzymatic, synthetic dinuclear $(Co^{2+})_2{\cdot}OH^-$ has been shown to hydrolyze a phosphodiester[1367] by nucleophilic addition of the μ-hydroxide to phosphorus in a complex in which one nonbridging oxygen is the ligand to one Co^{2+} and the other is a ligand to the other Co^{2+}. In most cases, however, the mechanism of nucleophilic substitution at phosphorus catalyzed enzymatically by a dinuclear metallic cluster is the same as that catalyzed by alkaline phosphatase.

Alkaline phosphatase (Equation 4–284) from *E. coli* hydrolyzes a phosphomonoester by transferring the phospho group to Serine 102

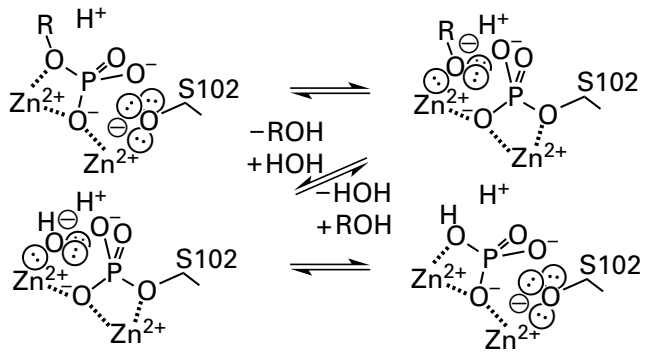

(4–452)

and then transferring it to a molecule of water that enters and replaces the leaving alcohol after it dissociates.[1368] When alkaline phosphatase is hydrolyzing arylphosphomonoesters, in which the leaving groups are acidic ($pK_a \leq 10$), the transition state has considerable dissociative character,[1369] a fact suggesting the intermediate is more like monomeric metaphosphate than a phosphorane. It seems likely, however, that when alkylphosphomonoesters are hydrolyzed by the enzyme, the intermediate is closer to a phosphorane because the leaving groups are poor. In any case, vanadate (Table 3–7) forms an analogue (see **4–124**) for the two phosphoranes of Serine 102 or the two monomeric metaphosphates that are the respective intermediates in the two consecutive nucleophilic substitutions at phosphorus.

The crystallographic molecular model of the vanadyl complex with the active site (Figure 4–56)[1370] demonstrates that one of the equatorial oxygens of each phosphorane or monomeric metaphosphate in the normal reaction (phosphorus in place of vanadium) ends up bridging the two Zn^{2+} in the active site, rather than the oxygen of either the hydroxide or one of the two alkoxides that are substrates for the enzyme. The oxygen of the hydroxy group of Serine 102 is successively a nucleophile and a leaving group, the oxygen of the hydroxy group of the alcohol is successively a leaving group (Equation 4–452) and a nucleophile, and the hydroxy group of the molecule of water replacing the hydroxy group of the alcohol is successively a nucleophile and a leaving group. At one time or another, all three of these oxygens are ligands to one or the other Zn^{2+}, but never both at the same time, as the reaction progresses through the two phosphoranes or the two monomeric metaphosphates, with overall retention of configuration (Equation 4–285).[591]

The **μ-oxygen between the two Zn^{2+}** is one of the equatorial oxygens in each of the two phosphoranes or two monomeric metaphosphates that are intermediates in the overall reaction. The two Zn^{2+} may well **stabilize the negative charge that builds up on the equatorial oxygen** in the phosphorane or monomeric metaphosphate,[1371] but the role of the two Zn^{2+} in the rigid dinuclear cluster may instead be entirely that of both **approximating and orienting reactants** during the respective formations of the two phosphoranes or two monomeric metaphosphates.[107,1370,1372,1373]

One Zn^{2+} (the seryl Zn^{2+}) is also coordinated to the nucleophilic oxygen while the other Zn^{2+} (the aquo Zn^{2+}) is coordinated to the leaving oxygen in the first step of the reaction, and they switch roles in the second step. The seryl Zn^{2+} lowers the pK_a for the hydroxy group of Serine 102, one of its constant ligands, so that the hydroxy group is unhydronated and nucleophilic. The seryl Zn^{2+} then improves the ability of the oxygen of Serine 102 to leave in the next nucleophilic substitution at phosphorus. The aquo Zn^{2+} improves the ability of the hydroxy group of the alcohol, one of its exchangeable ligands, to leave. The aquo Zn^{2+} then lowers the pK_a for the molecule of water that replaces the alcohol so that it dissociates a hydron to become an unhydronated $Zn^{2+}OH^-$. There is also a Mg^{2+} in the active site that is coordinated by a carboxylato group, a hydroxy group, and four molecules of water. One of the molecules of water on this Mg^{2+} acts as the donor of a hydrogen bond to one of the other equatorial oxygens in the two consecutive phosphoranes or monomeric metaphosphates, relaying the Lewis acidity of Mg^{2+}.

The exchanges necessary for association of substrates with the prosthetic Mg^{2+} in the active site of pyruvate kinase are prevented when one water on the prosthetic Mg^{2+} dissociates its hydron and becomes a hydroxide.[1250,1251] Although Zn^{2+} exchanges its ligands more rapidly than Mg^{2+} (Table 4-5), this fact suggests that an **alkoxide anion sitting as an inner-sphere ligand on a Zn^{2+}**, rather than Mg^{2+}, such as the alkoxide that has left the phosphorane or monomeric metaphosphate in the first step of the reaction catalyzed by alkaline phosphatase (Equation 4–452 and Figure 4–56), also **cannot dissociate rapidly** from the aquo Zn^{2+}, and hence leave the active site efficiently as a product, until it is hydronated by a Brønsted acid. The most likely catalytic acid is the molecule of water 0.38 nm from the axial

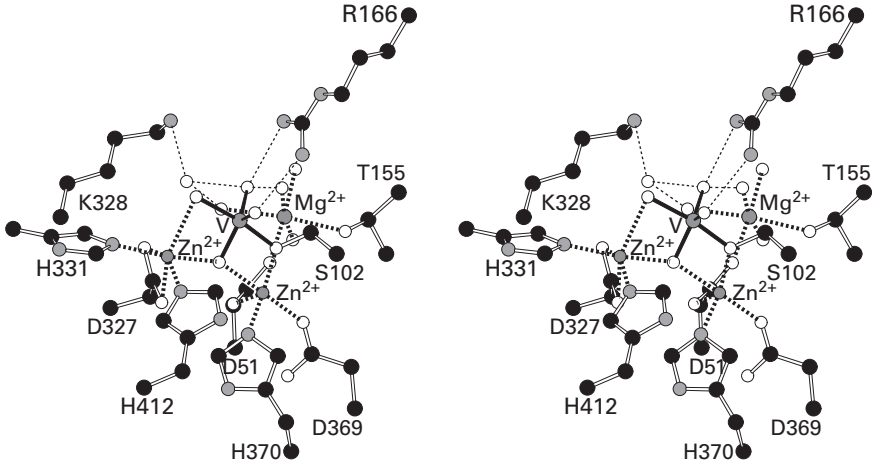

Figure 4–56: Stereodrawing[134] of the crystallographic molecular model of the active site of alkaline phosphatase from *E. coli* occupied by two Zn^{2+}, a Mg^{2+}, and a vanadyl ester (**3–63**) of Serine 102, an analogue of the phosphorane that is an intermediate in the enzymatic reaction.[1370] Black atoms are carbons, white atoms are oxygens, and small gray atoms are nitrogens. The smaller dark gray spheres are two zinc ions surrounded by their ligands, and the larger dark gray sphere is a magnesium ion surrounded by its ligands. The enzyme was purified from cytoplasm of *E. coli* that had been infected with a plasmid encoding the gene for the enzyme that overexpressed the protein and crystallized. The crystals were soaked in a solution containing 1 mM $ZnCl_2$, 10 mM $MgCl_2$, and 100 μM NH_4VO_3 and submitted to X-ray diffraction in that solution. Electron density for two Zn^{2+}, a Mg^{2+}, and a vanadyl ester of Serine 102 could be observed in each active site in the dimer that occupied the asymmetric unit. The molecular model of the vanadyl ester with its five oxygens is in the center of the figure. One of the two Zn^{2+} has as four of its ligands the imidazolyl groups of Histidines 331 and 412, an oxygen from the carboxylato group of Aspartate 327, and one of the oxygens of the vanadyl ester. The other Zn^{2+} has as four of its ligands the imidazolyl group of Histidine 370, the carboxy groups of Aspartates 51 and 369, and the esterified oxygen of Serine 102. One of the oxygens of the vanadyl group is between the two Zn^{2+}, as a ligand to each of them. The Mg^{2+} has retained four molecules of water as ligands and is held in the active site by ligation to one of the oxygens of the carboxy group of Aspartate 51 and the hydroxy group of Threonine 155.

oxygen of the vanadate, which represents the leaving alkoxide in the normal reaction. This molecule of water can form a hydrogen bond (0.26 nm) with the ammonio group of Lysine 238, or it can interact with another molecule of water that bridges the gap but is unresolved in the map of electron density. In either case, a hydron is relayed from Lysine 328 to the alkoxide, converting it to an alcohol that can readily dissociate from the aquo Zn^{2+}.

The alkoxide of Serine 102, however, which is the nucleophile that adds initially to the phosphoester to form the first phosphorane (Equation 4–452) or monomeric metaphosphate, is never required to leave the active site and could remain a metallic alkoxide even after it leaves the second phosphorane or monomeric metaphosphate in the later step of the enzymatic reaction. When it is a ligand to the seryl Zn^{2+}, the oxyanion of Serine 102 is surrounded by an oxygen in the carboxylato group of Aspartate 51 (0.38 nm) and a molecule of water (0.35 nm) that are both ligands on the Mg^{2+} that is also in the active site (Figure 4–56). When the oxyanion of Serine 102 swings away from the seryl Zn^{2+}, it forms a hydrogen bond (0.32 nm) to the hydroxy group of Threonine 155 that is also a ligand to Mg^{2+}.[1374] Because a hydroxy group or a molecule of water on Mg^{2+} is a weaker acid than a hydroxy group on Zn^{2+} (Table 4–2) neither the molecule of water nor the hydroxy group of Threonine 155, which are both permanent ligands to Mg^{2+}, can hydronate the hydroxy group of Serine 102 as long as it is a ligand to the seryl Zn^{2+}. These neighbors, which form a cup surrounding the oxyanion of Serine 102, ensure that the hydroxy group on Serine 102 remains the unhydronated, nucleophilic oxyanion when it is bound to the seryl Zn^{2+}. It is possible that this constellation is responsible for the values for pK_a of 7.4 and 7.3 in the pH–rate profiles for the enzyme below which its catalytic constant and specificity constant k_{phs} for a phospho substrate (phs), respectively, decrease.[1375] If so, these two values for pK_a, identical within the error of measurement, both represent hydronation of the oxyanion of Serine 102 as the pH is lowered and both would be the pK_a for its conjugate acid.

There are also enzymes[1376-1382] that use two Mg^{2+} or two Mn^{2+} in the same way that alkaline phosphatase uses its two Zn^{2+} to coordinate dinuclearly an equatorial oxygen in the phosphorane or monomeric metaphosphate (Figure 4–56) and to increase the electrophilicity of phosphorus in the respective phosphoesters, as well as to anchor the oxygens of the nucleophiles and leaving groups to Zn^{2+} to lower the values of pK_a for the nucleophilic oxygens and to improve, in turn, the leaving groups (Equation 4–452). In a nonenzymatic instance of catalysis by a dinuclear complex of two Zn^{2+}, the hydron dissociates from a hydroxy group on one Zn^{2+} and the resulting zinc alkoxide adds to the phosphorus of a phosphodiester that is tightly bound to the two Zn^{2+} by the two nonbridging oxygens as the first step in a nucleophilic substitution.[1383]

In most reactions in which a metallic dication is used by an active site to catalyze a nucleophilic substitution at phosphorus, the metallic dication also **catalyzes the nucleophilic addition by approximating the two reactants**. This approximation is achieved by coordination of the reactants to the metallic dication or dications. Examples are approximation of the enolate oxygen and the γ-phospho group of $MgATP^{2-}$ by the prosthetic Mg^{2+} in the active site of pyruvate kinase (Equation 4–447 and Figure 4–52); approximation of the 3′-hydroxy group and the α-phospho group of $MgdNTP^{2-}$ by the prosthetic Mg^{2+} in the active site of DNA-directed DNA polymerase (Equation 4–448); approximation of the bridging μ-hydroxide and the phosphorus in diphosphate by coordination of two phospho oxygens by the dinuclear cluster of Mg^{2+} in the active site of inorganic diphosphatase (Equation 4–451); and both approximation of the oxido group of Serine 102 and the phospho group and approximation of the nucleophilic molecule of water or an alcohol and the phospho group in the active site of alkaline phosphatase (Equation 4–452). The ability of the Mg^{2+} in $Mg^{2+}(H_2O)_5OH^-$ to approximate the respective phospho group and hydroxide by coordinating one oxygen of the phospho group has been proposed in part as an explanation for the effective catalysis exhibited by Mg^{2+} for the hydrolyses of phosphopyridiniums[1384] and phosphodiesters.[1385]

In the active site of glutamine synthetase (previously Equation 3–405)

$$\text{L-glutamate} + NH_3 + MgATP^{2-} \rightleftharpoons MgADP^- + HOPO_3^{2-} + \text{L-glutamine} \qquad (4\text{–}453)$$

from *S. typhimurium*, a prosthetic Mg^{2+} coordinates both the γ-carboxy oxygen of L-glutamate, which is the nucleophile, and one nonbridging oxygen of the γ-phospho group of $MgATP^{2-}$, which is the electro-

phile,[1386] during transfer of the phospho group from $MgATP^{2-}$ to the γ-carboxy group. Since the carboxylato group of L-glutamate in the Michaelis complex with the active site requires no assistance to remain unhydronated and its nucleophilicity can be decreased only by being a ligand to Mg^{2+}, the role of Mg^{2+} in this case must be mainly that of approximating the nucleophilic oxygen and the phosphorus of the phospho group by having both the carboxylato group and the phospho group as inner-sphere ligands.

In all these complexes, the **metallocycle** or each of the two metallocycles that approximates the nucleophilic oxygen and phosphorus of the phospho group has four atoms: the metallic dication, the nucleophilic oxygen, the phosphorus, and its oxyanion that is a ligand to the metallic dication (Equations 4–447, 4–448, 4–451, and 4–452). In the nucleophilic substitution at phosphorus catalyzed by dTMP kinase

$$MgATP^{2-} + \text{deoxythymidine 5′-phosphate} \rightleftharpoons MgADP^{-} + \text{deoxythymidine 5′-diphosphate} \quad (4\text{–}454)$$

from *M. tuberculosis*, however, the metallocycle that brings the two phospho groups together has six atoms in its ring[1387,1388]

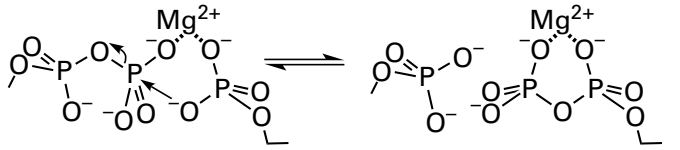

(4–455)

In nucleophilic additions both to an electrophilic carbon and to an electrophilic phosphorus in which metallic dications approximate nucleophile and electrophile, the electrophilic carbon and the electrophilic phosphorus are not themselves direct ligands to the respective metallic dications. The nucleophilic addition occurs at an electrophilic position one atom removed from the metallic dication, and an oxygen attached to either the electrophilic carbon or the electrophilic phosphorus is the inner-sphere ligand. There are, however, many nonenzymatic examples of **inner-sphere additions** in organometallic compounds. A Ni^{2+} in the active site of CO-methylating acetyl-CoA synthase catalyzes such an inner-sphere addition between an electrophilic carbon and the carbon of a nucleophilic methyl group and between an electrophilic carbon and the sulfur of a nucleophilic sulfido group. In each case, both the nucleophile and the electrophile are direct ligands to the metallic dication.

CO-Methylating acetyl-CoA synthase is a metalloenzyme responsible for fixing carbon monoxide in the form of acetyl-SCoA

$$\text{methyl-Co(III) corrinoid} + CO + e^{-} + {}^{-}SCoA \rightleftharpoons \text{Co(I) corrinoid} + \text{acetyl-SCoA} \quad (4\text{–}456)$$

The cobalt corrinoids are located within large (1520 aa) homodimeric $\alpha_2\beta_2$ heterotetramers.[1389,1390] Each heterotetrameric protein contains two identical sites, each of which is occupied by one cobalt corrinoid. As such, they are rather elaborate methyl-carrier proteins that supply the methyl group to CO-methylating acetyl-CoA synthase. Because the carbon and the oxygen of the acyl group in the acetyl group of acetyl-SCoA are derived from carbon monoxide itself,[1391] the enzyme simply stitches together a formal carbanide ion, a molecule of carbon monoxide, and a sulfido group, without changing them in the process other than forming bonds between them. Although there would be a two-electron oxidation were this actually what is occurring, there is no net oxidation–reduction in the complete reaction because the methyl-Co(III) corrinoid becomes a Co(I) corrinoid. Nevertheless, the cobalt corrinoid is acting neither as an oxidant nor as a reductant; rather, it is a leaving group in the forward reaction and a nucleophile in the reverse reaction, while the sulfido group is a nucleophile in the forward reaction and a leaving group in the reverse reaction. All these roles balance in the overall reaction.

In the active site of CO-methylating acetyl-CoA synthase, there is a **dinuclear cluster of nickel ions**.[1207,1392] One of these clusters is found in the crystallographic molecular model of the active site of monomeric (732 aa) CO-methylating acetyl-CoA synthase from *Carboxydothermus hydrogenoformans*

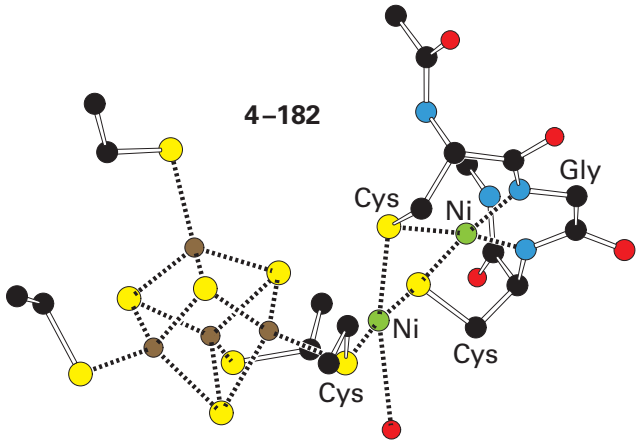

One nickel ion in this cluster is electronically coupled to a normal [4Fe–4S] iron–sulfur cluster[1393,1394] by the sulfanyl group of a cysteine, which is a ligand in the inner spheres of both this nickel ion and one iron ion in the cluster. This **central nickel ion** is also electronically coupled to the **peripheral nickel** ion in the cluster by the sulfanyl groups of two other cysteines, each of which is a ligand in the inner spheres of both nickel ions in the dinuclear cluster.[1207,1392] The peripheral nickel ion is also gripped tightly by two amido groups, one from the carboxy-terminal cysteine and one from the glycine between the two cysteines. Because they are obviously ligands to a nickel ion (bond lengths of 0.190 and 0.188 nm), because both amido groups and the nickel are in the same plane, and because the nitrogen–hydrogen of the amido group carboxy-terminal to the carboxy-terminal cysteine is pointed at the nitrogen of the amido group of glycine, each of the two nitrogens must be the unhydronated, anionic conjugate base of the respective amido group. Consequently, the peripheral nickel ion is coordinated by two strongly basic ligands and **enfolded by the polypeptide** in a five-membered metallocycle.

The central nickel ion that is electronically coupled to both the [4Fe–4S] iron–sulfur cluster and the other nickel ion is coordinated much less tightly by the sulfanyl groups of the three cysteines performing the electronic coupling. During the purification of CO-methylating acetyl-CoA synthase, this latter, unenfolded nickel ion can dissociate, much as the Fe^{2+} in aconitate hydratase can, and be replaced adventitiously by Zn^{2+} or Cu^{2+}.[1207,1395,1396] These substitutions decrease significantly or eliminate the catalytic activity of the enzyme because the trisulfido-dinickel cluster is the active species.[1207,1392,1397]

The first step in the enzymatic reaction of CO-methylating acetyl-CoA synthase[1398] is thought[1399] to be either **association of carbon monoxide** with Ni^{+}, to give a complex in which carbon monoxide is an inner-sphere ligand,[1400-1402] or **concerted nucleophilic substitution of a nucleophilic Ni^{+}** in the cluster for the cobalt cation in methyl-Co(III) corrinoid, in which the leaving group is the nucleophilic Co(I) corrinoid[1403-1405]

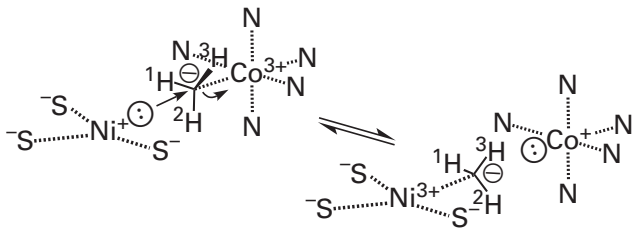

(4–457)

If the carbonylation is the first step in the reaction, the methylation is the second, and vice versa. If the carbonylation is the first step, then the Ni^{+} that participates in the nucleophilic substitution (Equation 4–457) has carbon monoxide as its fourth ligand in addition to the three sulfido groups.

The Ni^{+} that is carbonylated and then methylated or methylated and then carbonylated is the central nickel ion, which shares the sulfanyl group of cysteine with the [4Fe–4S] iron–sulfur cluster (**4–182**) and is prone to dissociation and replacement with other metallic dications.[1405] In the resting enzyme, this nickel ion is Ni^{2+}. Transfer of an electron from the [4Fe–4S] iron–sulfur cluster in the entire complex **4–182,** preceding or concurrently with association of carbon monoxide, or association of the protein containing the methyl-Co(III) corrinoid, which also has a [4Fe–4S] iron–sulfur cluster that can provide the necessary electron,[1406] promotes reduction **of the central Ni^{2+} in the trisulfido-dinickel cluster to Ni^{+}**, which is the participant in either the coordination of carbon monoxide or the nucleophilic substitution. This Ni^{+} can also be produced in the active site of the enzyme from *Moorella thermoacetica* by reduction with titanium(III) citrate.[1394]

Whether association of carbon monoxide with Ni^{+} is the first or second step in the reaction of CO-methylating acetyl-CoA synthetase, carbon monoxide arrives at the active site either directly from the solution—in those enzymes that are independent proteins such as the one in *R. rubrum*—or by passing through a tunnel from the active site of anaerobic carbon monoxide dehydrogenase—in those enzymes (Figure 3–69) that are found in multienzymatic

complexes, such as those in *M. thermoacetica* and *M. barkeri*. CO-Methylating acetyl-CoA synthase from *C. hydrogenoformans* can function either as an independent protein or in complex with carbon monoxide dehydrogenase.[1392] At the end of the tunnel in CO-methylating acetyl-CoA synthase from *M. thermoacetica*, immediately adjacent to the two nickel ions in the cluster, there is a cavity that can be occupied by one xenon atom and that is the proper size for a carbon monoxide.[1407] When the cavity is expanded by mutating a phenylalanine in its wall to alanine, the activity of the enzyme decreases by a factor of 10 and the cluster becomes more flexible.[1408] These facts suggest a steric requirement for the active site to hold carbon monoxide firmly during its association with the cluster.

Before CO-methylating acetyl-CoA synthase from *M. thermoacetica* has been methylated by methyl-Co(III) corrinoid, it is possible to form a complex in which one iron ion in the [4Fe–4S] iron–sulfur cluster (see **4–182**), presumably the one closest to the labile nickel ion, has been coordinated by carbon monoxide.[1409,1410] Some kinetic studies are consistent with this carbonmonoxy iron intermediate being a precursor to the acyl carbon and acyl oxygen in the product acetyl-SCoA[1411] while also being consistent with either methylation of the nickel ion or carbonylation of the iron ion being the first step in the normal enzymatic reaction.[1412] The proposal is that before it can add to the methylnickel(II), carbon monoxide must first become a ligand to the iron ion and then be transferred. The situation is complicated by the fact that carbon monoxide inhibits the enzymatic reaction,[1413] and there are other kinetic results consistent with a requirement that the methylation precedes productive association of the carbon monoxide destined to become the carbon and oxygen of the acyl group of acetyl-SCoA.[1398]

Nucleophilic substitution of Ni^+ for the Co(I) corrinoid (Equation 4–457), regardless of whether or not a carbon monoxide is associated with the Ni^+ as a fourth ligand, is a concerted in-line transfer of the methyl group[1414] between cobalt and nickel with inversion of configuration at the methyl group. Although the methyl group in methyl-Co(III) corrinoid bears a formal negative elementary charge because carbon is more electronegative than cobalt, this designation is a formal one and the methyl group on cobalt is actually electrophilic. The nucleophilic substitution requires that the nickel ion be at least as reduced as Ni^+, which is nucleophilic. The leaving group is the Co^+ in Co(I) corrinoid, which is itself (as is the case with all leaving groups) a nucleophile, but less of a nucleophile than Ni^+. Methyl transfer from Co^+ to Ni^+ (Equation 4–457) in the active site of the enzyme from *M. thermoacetica* is rapidly reversible[1415] and has an equilibrium constant of 2.3.

During the nucleophilic substitution, preceding it, or immediately following it, an electron is transferred to nickel, so the final adduct is methylnickel(II), which is diamagnetic.[1405,1415,1416] The order in which the two steps, methylation and transfer of this other electron to Ni^+, occur is not clear. The single nickel atom in a model compound, in which the nickel is Ni^0, readily reacts nucleophilically with a methyl-Co(III) corrinoid, and the product is directly methylnickel(II).[1417] This result suggests that the second electron could be transferred to Ni^+ before the nucleophilic substitution occurs to make it Ni^0, which would be even more nucleophilic. This proposal would explain the fact that paramagnetic methylnickel(III), which would be the product of the nucleophilic substitution in which Ni^+ is the nucleophile (Equation 4–457), has never been observed during the enzymatic reaction.[1399] The Ni^+, however, in the reduced state of a mutant of azurin in which the native copper cation has been replaced with a nickel ion does react with CH_3I to form an adduct, but again methylnickel(III) was not observed. It was believed that the reductant present in the solution to maintain the reduced state of Ni^+-azurin immediately reduced methylnickel(III) as it was formed to diamagnetic methylnickel(II). In this instance, the reductant present was not able to reduce Ni^+-azurin to Ni^0-azurin before the CH_3I was added to the solution, so the nickel in Ni^+-azurin must have been the nucleophile.

Regardless of whether carbonylation of nickel or methylation of nickel is the first step, after both have occurred, the product is a pentacoordinate Ni^{2+} with three sulfido groups, a formal methide ion, and carbon monoxide as the five ligands.[1418] This complex then undergoes formally a nucleophilic addition of the methide ion as the nucleophile to carbon monoxide as the electrophile

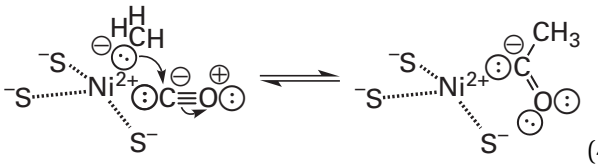

(4–458)

Both the nucleophilic carbon and the electrophilic carbon are ligands to Ni^{2+}, so this addition is a **nucleo-**

philic addition that takes place in the inner sphere of the metallic dication. This inner-sphere nucleophilic addition produces an acetylnickel(II).[1405]

There is a synthetic model reaction that replicates this methylation of carbon monoxide. A Ni^{2+}, coordinated with a ligand that provides three sulfides and a tertiary amine, was methylated with Grignard reagent

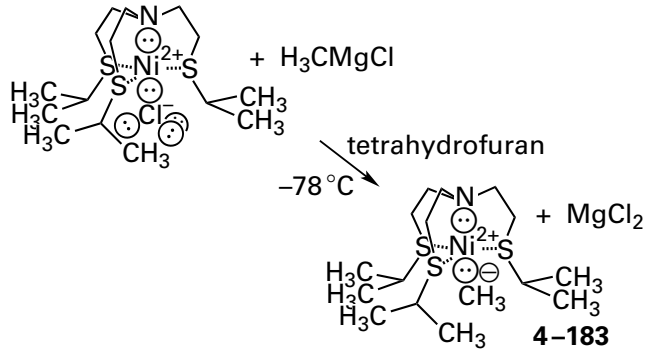

(4–459)

This methylation involves the transfer of the formal equivalent of a methide ion from a hard metal, Mg^{2+}, to a soft metal, Ni^{2+}, and as such it is not a model for the first step in the enzymatic reaction. The methylated Ni^{2+} that is the product, however, is equivalent to the methylnickel(II) produced in the enzymatic reaction. When the synthetic methylnickel(II) is mixed with carbon monoxide, an acetylnickel(II) is produced[1419]

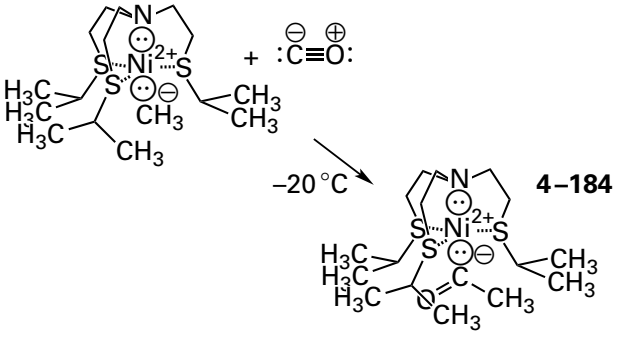

(4–460)

Methylnickel(II) **4–183** and acetylnickel(II) **4–184** have both been crystallized, and the crystallographic molecular models verify their structures.[1420] A similar CO insertion produces an acylnickel(II) from a synthetic alkylnickel(II) in a model compound in which the nickel ion is coordinated by the two sulfido groups of a bisthiolate and a phosphine and in which the alkyl group is larger than a methyl group.[1421]

In the final chemical step in the mechanism, the acetylnickel(II) intermediate in the enzymatic reaction is subjected to a nucleophilic substitution that forms acetyl-SCoA.[1405] In this final nucleophilic substitution, the sulfido group of coenzyme A is the nucleophile and Ni^0 is the leaving group. Because Ni^0, a strong nucleophile, can be considered equivalent to an alkoxide, the acetylnickel(II) intermediate is analogous to an acetyl ester, so it could be the case that there is a tetrahedral intermediate in the reaction, with the oxyanion of the tetrahedral intermediate expelling Ni^0. When synthetic acetylnickel(II) **4–184** is mixed with phenylmethanethiol, a high yield (75%) of the corresponding acetyl thioester is obtained.[1419,1420] Because there seems to be little room for the phenylmethanethiolate to coordinate with the nickel before the acetyl group is transferred to it, it may be the case that, in this particular model system, the sulfido group of the thiolate adds directly to the acyl carbon that is a ligand to Ni^{2+}, forming a tetrahedral intermediate.

In another synthetic model system, however, in which the nickel ion is coordinated at only two sites by a bispyridine, an acetylnickel(II) can be formed by adding an equivalent of carbon monoxide to a square planar complex in which the other two sites are occupied by a methide and a thiolate. A crystallographic molecular model verifies the direct coordination of both the acetyl group and the thiolate in this product. Upon addition of excess carbon monoxide, a strong ligand for Ni^{2+}, the immediately adjacent sulfanyl group on the nickel ion adds in the inner sphere to the acetyl group to produce the acetyl thioester, which is released from the Ni^{2+} as two carbon monoxides associate with it.[1422]

This model reaction suggests that **the $^-$SCoA may first coordinate to Ni^{2+}** in the acetylnickel(II) intermediate in the enzymatic reaction, which has open sites for ligands, before adding to the acetyl group to produce acetyl-SCoA, the product of the overall enzymatic reaction (Equation 4–456). If the sulfur of the sulfido group does become a ligand to Ni^{2+}, this does not happen until the acetylnickel(II) intermediate has formed because HSCoA is the last reactant to associate with the enzyme and does so only after the acetylnickel(II) intermediate is present.[1412] If this intramolecular addition is the mechanism of the enzymatic reaction, rather than a normal nucleophilic substitution in which the nucleophile adds directly to the acyl carbon of the acyl derivative, then there are two steps in the overall mechanism in which a nucleophilic substitution between a nucleophile and an electrophile that are both ligands to Ni^{2+} occurs in the inner sphere. The difficulty with this proposal is that if the sulfido group of

coenzyme A adds to the acetyl group while both are ligands to the Ni^{2+}, then what is to prevent a sulfido group from one of the cysteines that also coordinate the Ni^{2+} from adding to the acetyl group, which would be counterproductive? In fact, in another synthetic model system, where the Ni^{2+} has a bisthiolate and a phosphine as ligands, one sulfido group of the bisthiolate also becomes acetylated upon addition of carbon monoxide,[1421] just as the sulfido group that is a substrate in the other model compound does. Somehow the active site has to prevent this unfortunate side reaction.

The steps in the reaction catalyzed by CO-methylating acetyl-CoA synthase from *M. thermoacetica* between the methylated intermediate and the final product, acetyl-SCoA, are rapidly reversible. When the enzyme is mixed with [1-^{14}C]acetyl-SCoA and [^{12}C]carbon monoxide, [^{14}C]carbon monoxide is formed continuously[1423] at a maximum rate of 440 min^{-1} at pH 6.0 and 55 °C.[1424]

In the model reaction in which acetylnickel(II) **4–184** is mixed with phenylmethanethiol to produce the acetyl thioester, the nickel ends up as Ni^0 and precipitates from the solution as nickel metal, which would certainly be counterproductive in the enzymatic reaction. In order to precipitate as nickel metal, however, the atoms of nickel must be able to collide with each other in solution, which is precluded by the fact that the nickel atoms in the enzymatic reaction are individually buried in active sites in proteins. This protection is similar to the long-term protection that an active site can provide to the sulfenic acid of a cysteine. Sulfenic acids do not exist in free solution because they immediately disproportionate to a thiol and a sulfinic acid, a disproportionation that is precluded when they are located in an active site. Because Ni^0 would be protected by the surroundings of the active site, it could be the case that Ni^0 is stable and able to participate as the nucleophile in the next round of the reaction with the next molecule of methyl-Co(III) corrinoid (see Equation 4–457) and produce methylnickel(II) directly. In this case, no source of electrons would be needed to sustain successive turnovers.

Another possibility, however, is that the [4Fe–4S] iron–sulfur cluster in cluster **4–182**, perhaps in concert with the peripheral nickel ion, instantaneously removes an electron from Ni^0 to return it to Ni^+, which then participates in the next round of the reaction. This electron would then be returned to the Ni^{3+} in methylnickel(III) during its formation or immediately after it is formed by the nucleophilic substitution (Equation 4–457). If these transfers of an electron are the actual sequence of events, the purpose of the other participants in the complete cluster would be to poise the central nickel ion by transferring an electron back and forth so that it is either Ni^+ or methylnickel(II) or acetylnickel(II) while the enzyme is turning over.

A few enzymes have metallic trications as Lewis acid catalysts in their active sites. For example, in the dinuclear[1425] cluster in the active site of purple acid phosphatase, one position is occupied by Zn^{2+}, Fe^{2+}, or Mn^{2+} depending on the species from which the enzyme is purified,[1426-1430] but the other position is always occupied by Fe^{3+}.[1431,1432] Even though all these enzymes have Fe^{3+} in their active sites, all that is required for catalysis is a metallic trication that can occupy the available coordination because Ga^{3+} can substitute effectively for Fe^{3+}.[1238]

There are at least two problems with using a metallic trication as a Lewis acid. First, the conjugate acid of an alkoxide or hydroxide that is a ligand to a metallic trication has such a low pK_a (Table 4–2) that it is a weak Brønsted base and a weak nucleophile. It is also difficult to hydronate so that it can be used as a Brønsted acid or so that it can leave the metallic trication as an alcohol or a molecule of water. Second, the exchange rates of even a neutral molecule of water at a metallic trication are so slow (Table 4–5) that association of a reactant with or dissociation of a product from the inner sphere of the trication would limit rates of catalysis. These difficulties illustrate the advantages of metallic dications for catalysis.

In the active site of alkaline phosphatase PhoX from *Pseudomonas fluorescens*, an oxide bridges two Fe^{3+} and a Ca^{2+}. In a crystallographic molecular model[1433] of a complex between the enzyme and β,γ-methylene ATP^{4-}, which is a nonhydrolyzable analogue of the substrate ATP^{4-}, two nonbridging oxygens of the γ-phosphono group are ligands to the two Fe^{3+}, and the third nonbridging oxygen is a ligand to the Ca^{2+}. The hydroxide is directed toward phosphorus and oriented for an in-line addition directly opposite the methylene group that represents the leaving group. The two Fe^{3+} are high-spin, but it is not clear how the two nonbridging oxygens are able to exchange into their inner spheres rapidly enough and how the phosphate that is the product of the hydrolysis, which would have three of its oxygens as ligands to the two Fe^{3+}, is able to dissociate rapidly enough to sustain catalysis. That the iron ions must be Fe^{3+} for catalysis to occur is demonstrated by

the fact that reduction of both to Fe^{2+} inactivates the enzyme.[1433]

Nitrile hydratase

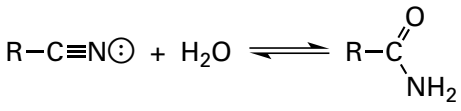

(4–461)

has either Co^{3+} or Fe^{3+} in its active site depending on the species from which the enzyme is purified.[1434] The enzymes with the different metallic trications, however, are very similar (40% identity; 1.0 gap percent), so they must have the same catalytic mechanism. The metallic trications in each unoccupied active site have the same ligands

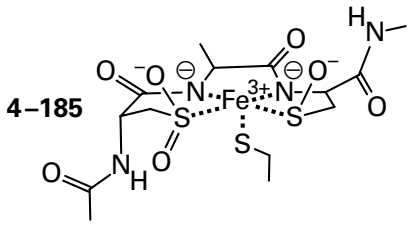

4–185

which are the sulfanyl group of a cysteine; two unhydronated, negative amido nitrogens from the peptide backbone; a cysteinyl sulfinate ($-SO_2^-$); and a cysteinyl sulfenate ($-SO^-$).[1435-1439] The last ligand is an example of a sulfenate that is protected from disproportionation by being in the active site of an enzyme. The pK_a for a sulfinic acid is around 3 while that of a sulfenic acid is around 12, but the cysteinyl sulfenate has a hydrogen bond to the guanidinio group of an arginine, which should lower its pK_a.

The following mechanism has been proposed[1440] for the hydration catalyzed by the enzymes with Fe^{3+} in their active sites

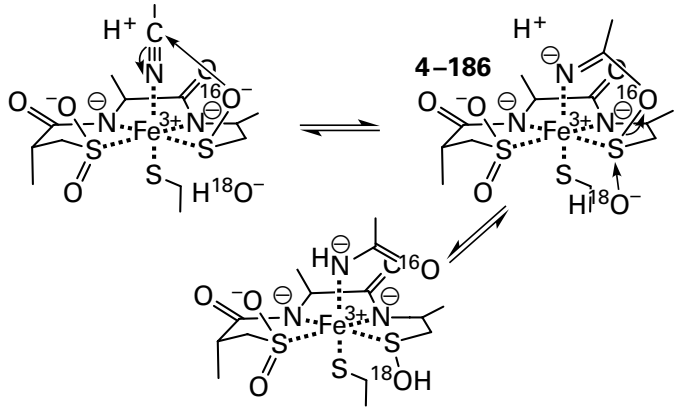

(4–462)

4–186

and by extension those with Co^{3+} in their active sites. The nitrogen of the nitrile would associate with the metallic trication, and the oxyanion of the sulfenate would add nucleophilically to the carbon of the nitrile. A hydroxide would then perform a nucleophilic substitution at sulfur with the amido oxygen as the leaving group while the amido nitrogen is hydronated by a catalytic acid. The nucleophilic substitution at sulfur is analogous to the nucleophilic substitution of one sulfido group for another in a disulfide.

There are a number of observations consistent with this mechanism. Intermediate **4–186** has been observed in a crystallographic molecular model[1440] of the complex between 2,2-dimethylpropanenitrile, a hindered analogue of the substrate, and the active site of a mutant of the ferric nitrile hydratase from *Rhodococcus erythropolis* in which the arginine that forms the hydrogen bond to sulfenate has been mutated to lysine, decreasing the turnover of the enzyme by a factor of 500. Both 1-butaneboronic acid and phenylboronic acid form adducts[1441] with the oxygen of sulfenate in the active site of cobaltic nitrile hydratase from *P. thermophila.* In these adducts, the boronate is trigonal and isosteric with the amido group in intermediate **4–186**, and the only oxygen from boronic acid that remains is a ligand to the Co^{3+}, as is the nitrogen in the proposed intermediate. When cobaltic nitrile hydratase from *Streptomyces rimosus*, which has been preequilibrated in $H_2{}^{16}O$, is mixed with the nitrile toyocamycin (a natural substrate) in $H_2{}^{18}O$, the hydrated product from the first turnover contains oxygen-16 in the amide, but products from the next turnovers contain oxygen-18. During the first turnover, the enzyme itself covalently incorporates one oxygen-18, but it incorporates no further oxygen-18 in later turnovers.[1442] When iron nitrile hydratase from *Rhodococcus hoagii* was mixed rapidly with 2-methylprop-2-enenitrile, an intermediate appears with a rate constant of 60 $mM^{-1}\,s^{-1}$ and a visible absorption spectrum that has been assigned as that of a complex between nitrile and Fe^{3+} in the active site.[1443]

The problem with the proposed mechanism is rate constants and equilibrium constants. The Fe^{3+} in ferric nitrile hydratase is in the low-spin state.[1444] Ferric iron in its low-spin state and Co^{3+} are usually almost inert to ligand exchange, and since there is only one open site on the prosthetic metallic complexes in the several active sites, that exchange would have to be dissociative. The crystallographic molecular model in which intermediate **4–186** occupied the open position on Fe^{3+} was from a crystal in which each lone open site on Fe^{3+}

was occupied by a molecule of nitric oxide, and a molecule of 2,2-dimethylpropanenitrile occupied a nearby site in the outer sphere.[1440] Nitric oxide then dissociated photolytically and vacated the active site almost immediately. Nevertheless, it took the nitrile more than 25 min ($0.001\ s^{-1}$) at 20 °C to move 1 nm from the site in the outer sphere to the open site on Fe^{3+}. A synthetic complex of Fe^{3+} coordinated by three amino nitrogens and two sulfanyl groups, which is similar to the coordination in the active site of ferric nitrile hydratase, is able to associate with nitriles such as acetonitrile ($K_d = 33$ M at 2 °C; $k_{ex} = 10^5\ s^{-1}$ at 2 °C) and forms an octahedral complex with thiocyanate that could be crystallized.[1445] Most synthetic model compounds, however, with either Fe^{3+} or Co^{3+} that have similar ligands, do not associate with nitriles.[1446-1449] There is a synthetic complex of Co^{3+} that is coordinated by three amino nitrogens, an imino nitrogen, and the sulfido group of a thiolate and that was synthesized with a nitrile at the sixth position.[1450] When the complex is mixed with hydroxide, the nitrile is hydrated with a rate constant of $3\ M^{-1}\ s^{-1}$. The rate, however, for exchange of the nitrile at Co^{3+} is $0.01\ s^{-1}$ at 7 °C. The amide on Co^{3+} that is the product of nucleophilic addition of hydroxide to the nitrile is inert to exchange.

It is unclear how nitrile hydratase can accelerate the exchanges at the single open site on either Fe^{3+} or Co^{3+}, which are required for the mechanism of Equation 4–462, to accommodate rate constants for the turnover of the various enzymes. Such considerations have led to the proposition that the metallic trication, if it is involved in catalysis, must provide a Brønsted acid–base in a reaction at its outer sphere.[1437,1447]

Suggested Reading

Holden, H. M., Tronrud, D. E., Monzingo, A. F., Weaver, L. H., and Matthews, B. W. (1987) Slow- and fast-binding inhibitors of thermolysin display different modes of binding: Crystallographic analysis of extended phosphonamidate transition-state analogues, *Biochemistry 26*, 8542–8553. https://doi.org/10.1021/bi00400a008

Stavropoulos, P., Muetterties, M. C., Carrie, M., and Holm, R. H. (1991) Structural and reaction chemistry of nickel complexes in relation to carbon monoxide dehydrogenase: A reaction system simulating acetyl-coenzyme A synthase activity, *J. Am. Chem. Soc. 113*, 8485–8492. https://doi.org/10.1021/ja00022a041

Lauble, H., Kennedy, M. C., Beinert, H., and Stout, C. D. (1992) Crystal structures of aconitase with isocitrate and nitroisocitrate bound, *Biochemistry 31*, 2735–2748. https://doi.org/10.1021/bi00125a014

Benini, S., Rypniewski, W. R., Wilson, K. S., Miletti, S., Ciurli, S., and Mangani, S. (1999) A new proposal for urease mechanism based on the crystal structures of the native and inhibited enzyme from *Bacillus pasteurii*: Why urea hydrolysis costs two nickels, *Structure 7*, 205–216. https://doi.org/10.1016/S0969-2126(99)80026-4

Problem 4–38: Write a mechanism for the complete reaction catalyzed by 4-hydroxy-2-oxoheptanedioate aldolase that uses Mg^{2+} (**4–166**) as a Lewis acid in the active site.

Problem 4–39: Write a mechanism for the complete reaction catalyzed by isocitrate dehydrogenase ($NADP^+$) that uses Mg^{2+} (**4–167**) as a Lewis acid in the active site.

Problem 4–40: Write a mechanism for the complete reaction catalyzed by fumarylacetoacetase (Equation 4–362) that uses Ca^{2+} (**4–168**) as a Lewis acid in the active site.

Problem 4–41: Write a mechanism for the complete reaction catalyzed by fructose-bisphosphate aldolase (Equation 4–210) that uses Zn^{2+} (**4–170**) as a Lewis acid in the active site.

Problem 4–42: Write a mechanism for the complete reaction catalyzed by lactoylglutathione lyase (Equation 4–431) that uses Zn^{2+} (Figure 4–55C) as a Lewis acid in the active site.

Problem 4–43: Write a mechanism for the complete reaction catalyzed by malate synthase (Equation 4–271) that uses Mg^{2+} (**4–155**) as a Lewis acid in the active site.

Problem 4–44: Write a mechanism for the complete reaction catalyzed by peptide deformylase (Equation 4–425) that uses Fe^{2+} (**4–158**) as a Lewis acid in the active site.

Problem 4–45: Write a mechanism for the complete reaction catalyzed by alkaline phosphatase (Equation 4–452) that incorporates the two respective phosphoranes. Include the two Zn^{2+} in each successive structure.

Problem 4–46: The following is a direct quotation from reference 1022.

> Staphylococcal nuclease [micrococcal nuclease] catalyzes the hydrolysis of both DNA and RNA at the 5′ position of the phosphodiester bond yielding a free 5′-hydroxyl group and a 3′-phosphate monoester. The pH optimum is between 8.6 and 10.3 and varies inversely with the Ca^{2+} concentration, but at any pH rather high levels of Ca^{2+}, typically 0.01 M, are required for optimal activity. With minor exceptions, which will be discussed later, Ca^{2+} is required for activity with all substrates and cannot be replaced with other ions, although Ca^{2+} and a number of other ions do promote the binding of various inhibitors. The 5′-*p*-nitrophenyl esters of pdT and pdTp are the simplest known good substrates for the nuclease. Both these esters are hydrolized [sic] at essentially the same rate via P–O bond cleavage of the 5′–C–O–P bond, but the pdTp-based ester has a K_m showing almost two orders of magnitude tighter binding to enzyme. Both the 5′-methyl ester of pdT and thymidine 5′-fluorophosphate are poor substrates. With these simple substrates, the products of enzyme-catalyzed reaction are exclusively *p*-nitrophenyl phosphate and dT or dTp for the first two and methylphosphate or fluorophosphate plus dT for the second two …, a striking and significant contrast to the products of a nonenzymatic hydrolysis of these compounds where *p*-nitrophenol, fluoride ion, or at least some methanol along with pdT or pdTp would result. Simple diesters of phosphate are not substrates, so this enzyme is indeed a nuclease and not a general phosphodiesterase. For a series of dinucleotides, $dN^{\alpha}pdN^{\beta}$, as substrates, there is a distinct order of preference (dT > dA >> dC >> dG) for the base in the β-nucleotide position, but little base specificity in the α-position. The presence of a terminal 3′-phosphate results in a better substrate than the plain dinucleotide; a terminal 5′ phosphate results in a poorer substrate. In the presence of Ca^{2+}, or a wide variety of other metallic dications, pA, pdA, and pdT are good inhibitors ($K_i \cong 10^{-5}$); pdTp is the best known inhibitor ($K_i \cong 10^{-7}$). The binding of the nucleoside 5′-monophosphates involves a single Ca^{2+} ion; the binding of pdTp and of DNA and RNA appears to involve two. Nucleosides themselves and nucleoside 2′- or 3′-monophosphates are not inhibitory. Mapping studies of the active site region with oligonucleotides having a terminal 5′ phosphate $(pdT)_n$, show maximum binding when $n = 3$, suggesting the presence of a third, probably ionic, binding site in addition to those for the 5′- and 3′-phosphates of pdTp. Studies of the interactions among the inhibitors, the simple substrates, DNA, and RNA strongly imply a single, common binding and hydrolytic site on the nuclease, although, as noted elsewhere, there are differences between DNA and RNA as substrates that may indicate different hydrolytic mechanisms.

In the abbreviation used for mononucleotides, a p before the capital letter, such as pdT, stands for a phosphate attached to the 5′-hydroxy group of the ribose; a p after, such as dTp, stands for a phosphate attached to the 3′-hydroxy group. The d stands for 2′-deoxyribose in a 2′-deoxyribonucleotide. The capital letters stand for the various nucleosides.

The point of the preceding brief, but fairly comprehensive, review of the enzymological properties of micrococcal nuclease is to establish that the crystal structure of the nuclease–pdTp–Ca^{2+} complex should resemble fairly closely that of the actual enzymatically active complex of micrococcal nuclease, a substrate for the enzyme, and Ca^{2+}. Because a diester will have a single negative elementary charge on the phosphate when it is associated with the hydrolytic site and pdTp has two negative elementary charges on its 5′ phosphate, some difference is, of course, to be expected.

(A) Write the mechanism for hydrolysis of the 5′-(4-nitrophenyl) ester of pdTp, as it would occur during a nonenzymatic reaction that produces 4-nitrophenol and pdTp. Draw your intermediates, for example a phosphorane, with proper stereochemistry.

(B) Why is 4-nitrophenol rather than 4-nitrophenyl phosphate the product of the nonenzymatic reaction?

(C) Write the mechanism for hydrolysis of the 5′-(4-nitrophenyl) ester of pdTp as it would occur under catalysis by micrococcal nuclease, which produces 4-nitrophenyl phosphate and dTp. Draw your intermediates with proper stereochemistry, and include catalytic acids, $HA^{(+)}$, or catalytic bases, $\odot B^{(-)}$, where appropriate.

Crystals of the complex between micrococcal nuclease, Ca^{2+}, and pdTp were submitted to diffraction, and a map of electron density from a data set with minimum Bragg spacing of 0.17 nm was obtained. A molecular model built from the sequence of the protein, the Ca^{2+}, and the known structure of the inhibitor were placed into the map. The stereodrawing of the active site

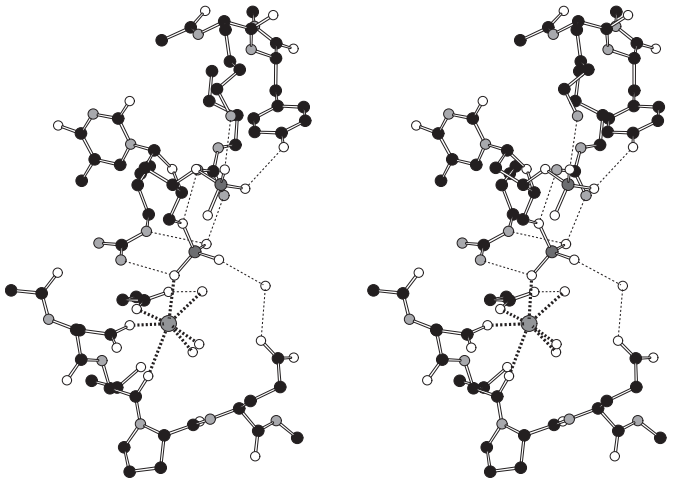

has been derived from the final refined molecular model.[1021]

(D) The various side chains, inhibitor, and prosthetic groups in the stereodrawing are not identified. Make a copy of one side of the drawing. Expand the scale so that you have plenty of room, and clearly identify with labels each side chain, the inhibitor, and the prosthetic groups. On each hydrogen bond indicated in the figure, draw a hydron next to the donor for that hydrogen bond. Attach a 4-nitrophenyl group to the appropriate oxygen.

(E) What are the smaller detached, open spheres in the crystallographic molecular model?

(F) Which is the most likely molecule of water for the role of the nucleophile in hydrolysis of 5′-(4-nitrophenyl)pdTp? Write a mechanism for the hydrolysis that uses this molecule of water. What are the catalytic acid–bases activating the molecule of water?

(G) Why is 4-nitrophenyl phosphate rather than 4-nitrophenol the product of the enzymatic reaction? Invoke two rules of phosphate chemistry in your explanation. What must the active site be preventing the phosphorane from undergoing that would enable the best leaving group? Decide which would be the best leaving group by looking up values for pK_a.

(H) What is the identity of the catalytic acid that hydronates the leaving group in the mechanism that you presented in part C? Why is this choice peculiar?

Problem 4–47: 3,4-Dihydroxy-2-butanone-4-phosphate synthase is a metalloenzyme that catalyzes the conversion of D-ribulose 5-phosphate to 3,4-dihydroxybutan-2-one-4-phosphate and formate.

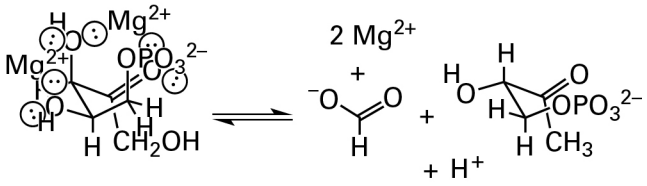

(A) Write a mechanism for the multistep transformation catalyzed by the unmutated enzyme that involves an isomerization proceeding by a 1,2-hydride migration as occurs in xylose isomerase (Equation 4–432), followed by removal of a hydron α to a carbonyl to produce an enolate, a β elimination, a hydronation, a 1,2-phosphomethide migration analogous to a 1,2-methyl migration, and a retro-Claisen condensation.[1337] (Hint: Write the mechanism in reverse first.)

(B) Write an alternative mechanism that lacks the isomerization and 1,2-hydride migration steps but includes the remaining five steps in part A. (Hint: As in part A, write the mechanism in reverse first.)

There is a crystallographic molecular model of a complex of D-ribulose 5-phosphate with a mutant of the enzyme from *M. jannaschii* in which Histidine 147 has been replaced by serine and in which one of the two Mg^{2+} normally in the active site has been replaced with Zn^{2+} and the other Mg^{2+} has been replaced by Ca^{2+} to produce an inactive enzyme. D-Ribulose 5-phosphate coordinates Ca^{2+} with its 2-oxo and 3-hydroxy groups, and it coordinates Zn^{2+} with its 3-hydroxy and 4-hydroxy groups.[882] Recall that, in the unmutated active enzyme, Ca^{2+} and Zn^{2+} are replaced by two Mg^{2+} (**4–178**).

In the following drawing

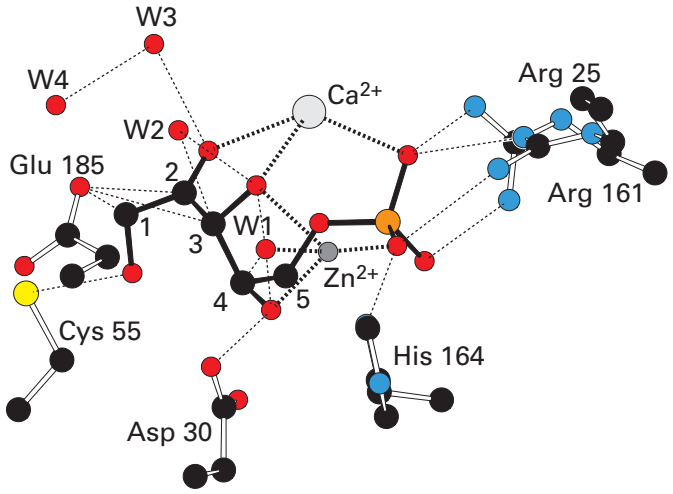

of a portion of the active site in this crystallographic molecular model, the carbons of D-ribulose 5-phosphate are numbered. The 1-hydroxy group of D-ribulose 5-phosphate forms a hydrogen bond (0.31 nm) with the sulfanyl group of Cysteine 55. The distance (0.34 nm) between carbon 1 and an oxygen in the carboxy group of Glutamate 185 is within van der Waals contact (0.38 nm). The oxygen of the 2-carbonyl group of D-ribulose 5-phosphate is coordinated to Ca^{2+} (see **4–178**) and participates in a hydrogen bond (0.27 nm) with water W3 that in turn forms a hydrogen bond (0.29 nm) with water W4 that in turn is in contact with the bulk solution. The distance (0.35 nm) between carbon 2 and the same oxygen in the carboxy group of Glutamate 185 is within van der Waals contact (0.38 nm). The 3-hydroxy group of D-ribulose 5-phosphate is coordinated to Ca^{2+} and Zn^{2+} (see **4–178**) and forms hydrogen bonds (0.31 and 0.27 nm) with both waters W1 and W2, which in turn form hydrogen bonds with carboxy groups of two glutamates and an aspartate (see **4–178**). The distance (0.32 nm) between carbon 3 and water W2 is within van der Waals contact (0.38 nm). The distance (0.35 nm) between carbon 3 and the same oxygen in the carboxy group of Glutamate 185 is within van der Waals contact (0.38 nm). The 4-hydroxy group of D-ribulose 5-phosphate is coordinated to the Zn^{2+} and forms a hydrogen bond (0.24 nm) with the carboxy group of Aspartate 30 and a hydrogen bond (0.30 nm) with water W1 that is also coordinated to that Zn^{2+}. The distance (0.39 nm) between carbon 4 and water W1 is at van der Waals contact (0.38 nm). Nitrogen τ of Histidine 147 (missing in the drawing because it is the mutated amino acid) forms a hydrogen bond (≥0.29 nm) in a crystallographic molecular model of the unmutated enzyme with the oxygen of the carboxy group of Glutamate 185 that is in contact with carbons 1, 2, and 3 of D-ribulose 5-phosphate.

(C) Referring to the drawing from the crystallographic molecular model of the occupied active site in the mutant enzyme, the numbered side chains it contains, and the contacts just described between them and the D-ribulose 5-phosphate, identify the catalytic acid–base that performs the removal or addition of a hydron in each step of your two mechanisms whenever a hydron must be removed or added to an oxygen or a carbon.

(D) Which metallic hydroxide is the nucleophile in the retro-Claisen condensation?

(E) Why does the active site enforce the rotational isomer between carbons 3 and 4 observed in the drawing?

(F) Why does the active site enforce the rotational isomer between carbons 4 and 5 observed in the drawing?

In a 1,2-phosphomethide migration, the carbon migrating carries with it the two electrons in the bond, so formally it bears a negative elementary charge that is stabilized by conjugation to phosphorus. It migrates across the plane of a vicinal dicarbonyl. The carbon from which the phosphomethide leaves becomes a carbonyl, and the oxygen on the carbon to which it adds becomes a hydroxy group.

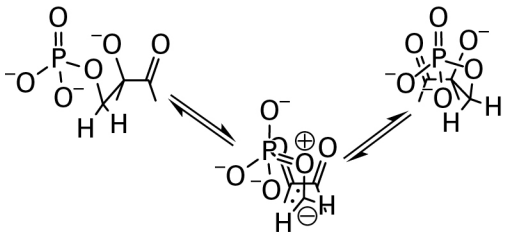

(G) Discuss the several ways in which the active site encourages the 1,2-phosphomethide migration both sterically and electronically.

References

1. Loudon, G. M., and Ryono, D. E. (1976) Electrostatic facilitation of general acid catalyzed α-oxonium ion formation in a lysozyme-like environment: Kinetic investigations, *J. Am. Chem. Soc. 98*, 1900–1907.
2. Dookhun, V., and Bennet, A. J. (2005) Unexpected stability of aryl β-*N*-acetylneuraminides in neutral solution: Biological implications for sialyl transfer reactions, *J. Am. Chem. Soc. 127*, 7458–7465.
3. Cordes, E. H. (1967) Mechanism and catalysis for the hydrolysis of acetals, ketals, and ortho esters, *Prog. Phys. Org. Chem. 4*, 144.
4. Fife, T. H., and Natarajan, R. (1986) General acid-catalyzed acetal hydrolysis; The hydrolysis of acetals and ketals of *cis*-1,2-cyclohexanediol and *trans*-1,2-cyclohexanediol: Changes in rate-determining step and mechanism as a function of pH, *J. Am. Chem. Soc. 108*, 8050–8056.
5. Jencks, W. P., and Carriuolo, J. (1959) Imidazole catalysis. II. Acyl transfer and the reactions of acetyl imidazole with water and oxygen anions, *J. Biol. Chem. 234*, 1272–1279.
6. Bearne, S. L., and Wolfenden, R. (1997) Mandelate racemase in pieces: Effective concentrations of enzyme functional groups in the transition state, *Biochemistry 36*, 1646–1656.
7. Kresge, A. J., Leibovitch, M., and Sikorski, J. A. (1992) Acid-catalyzed hydrolysis of 5-enolpyruvylshikimate 3–phosphate (EPSP) and some simple-models of its vinyl ether functional-group, *J. Am. Chem. Soc. 114*, 2618–2622.
8. Funderburk, L. H., Aldwin, L., and Jencks, W. P. (1978) Mechanisms of general acid and base catalysis of the reactions of water and alcohols with formaldehyde, *J. Am. Chem. Soc. 100*, 5444–5459.
9. Sorensen, P. E., and Jencks, W. P. (1987) Acid-catalyzed and base-catalyzed decomposition of acetaldehyde hydrate and hemiacetals in aqueous-solution, *J. Am. Chem. Soc. 109*, 4675–4690.
10. Jencks, W. P., and Carriuolo, J. (1959) Imidazole catalysis. III. General base catalysis and the reactions of acetyl imidazole with thiols and amines, *J. Biol. Chem. 234*, 1280–1285.
11. Hegarty, A. F., Dowling, J. P., Eustace, S. J., and McGarraghy, M. (1998) Enolization of aldehydes and ketones: Structural effects on concerted acid-base catalysis, *J. Am. Chem. Soc. 120*, 2290–2296.
12. Dunn, B. M., and Bruice, T. C. (1970) Steric and electronic effects on the neighboring general acid catalyzed hydrolysis of methyl phenyl acetals of formaldehyde, *J. Am. Chem. Soc. 92*, 2410–2416.
13. Capon, B., and Zucco, C. (1982) Simple enols: 2. Kinetics and mechanism of the ketonization of vinyl alcohol, *J. Am. Chem. Soc. 104*, 7567–7572.
14. Jencks, W. P., and Carriuolo, J. (1961) General base catalysis of ester hydrolysis, *J. Am. Chem. Soc. 83*, 1743–1750.
15. Chiang, Y., Chwang, W. K., Kresge, A. J., and Yin, Y. (1989) Acid-catalyzed hydrolysis of vinyl acetals: Reaction through the acetal rather than the vinyl ether functional-group, *J. Am. Chem. Soc. 111*, 7185–7190.
16. Jencks, W. P. (1969) *Catalysis in chemistry and enzymology*, McGraw-Hill, New York.
17. Ewing, S. P., Lockshon, D., and Jencks, W. P. (1980) Mechanism of cleavage of carbamate anions, *J. Am. Chem. Soc. 102*, 3072–3084.
18. Young, P. R., and Jencks, W. P. (1977) Nonenforced catalysis of the bisulfite carbonyl addition reaction by hydrogen bonding, *J. Am. Chem. Soc. 99*, 1206–1214.
19. Banait, N. S., and Jencks, W. P. (1991) General-acid and general-base catalysis of the cleavage of α-D-glucopyranosyl fluoride, *J. Am. Chem. Soc. 113*, 7958–7963.
20. Murray, C. J., and Jencks, W. P. (1988) Proton transfer reactions of sulfonium ylides: Unit Brønsted slopes do not require diffusion-controlled proton transfer, *J. Am. Chem. Soc. 110*, 7561–7563.
21. Coleman, C. A., and Murray, C. J. (1991) Characterization of transition states by isotopic mapping and structure-reactivity coefficients: Solvent and secondary deuterium isotope effects for the base-catalyzed breakdown of acetaldehyde hemiacetals, *J. Am. Chem. Soc. 113*, 1677–1684.
22. Nissen, P., Hansen, J., Ban, N., Moore, P. B., and Steitz, T. A. (2000) The structural basis of ribosome activity in peptide bond synthesis, *Science (Washington, DC, U. S.) 289*, 920–930.
23. Jogl, G., Rozovsky, S., McDermott, A. E., and Tong, L. (2003) Optimal alignment for enzymatic proton transfer: Structure of the Michaelis complex of triosephosphate isomerase

at 1.2-Å resolution, *Proc. Natl. Acad. Sci. U. S. A. 100*, 50–55.
24. Zhang, Z., Sugio, S., Komives, E. A., Liu, K. D., Knowles, J. R., Petsko, G. A., and Ringe, D. (1994) Crystal structure of recombinant chicken triosephosphate isomerase-phosphoglycolohydroxamate complex at 1.8-Å resolution, *Biochemistry 33*, 2830–2837.
25. Lodi, P. J., and Knowles, J. R. (1991) Neutral imidazole is the electrophile in the reaction catalyzed by triosephosphate isomerase: Structural origins and catalytic implications, *Biochemistry 30*, 6948–6956.
26. Lodi, P. J., Chang, L. C., Knowles, J. R., and Komives, E. A. (1994) Triosephosphate isomerase requires a positively charged active site: The role of Lysine-12, *Biochemistry 33*, 2809–2814.
27. Go, M. K., Koudelka, A., Amyes, T. L., and Richard, J. P. (2010) Role of Lys-12 in catalysis by triosephosphate isomerase: A two-part substrate approach, *Biochemistry 49*, 5377–5389.
28. Nickbarg, E. B., Davenport, R. C., Petsko, G. A., and Knowles, J. R. (1988) Triosephosphate isomerase: Removal of a putatively electrophilic histidine residue results in a subtle change in catalytic mechanism, *Biochemistry 27*, 5948–5960.
29. Swain, C. G., and Brown, J. F., Jr. (1952) Concerted displacement reactions. VII. The mechanism of acid-base catalysis in nonaqueous solvents, *J. Am. Chem. Soc. 74*, 2534–2537.
30. Rony, P. R., McCormack, W. E., and Wunderly, S. W. (1969) Polyfunctional catalysis. II. General base catalysis of the mutarotation of tetramethyl-D-glucose in benzene and methanol-benzene, *J. Am. Chem. Soc. 91*, 4244–4251.
31. Swain, C. G., and Brown, J. F., Jr. (1952) Concerted displacement reactions. VIII. Polyfunctional catalysis, *J. Am. Chem. Soc. 74*, 2538–2543.
32. Kyte, J. (2007) *Structure in Protein Chemistry: Second Edition*, p 75, Garland Science, New York.
33. Roux, B., Yu, H. A., and Karplus, M. (1990) Molecular-basis for the Born model of ion solvation, *J. Phys. Chem. 94*, 4683–4688.
34. Born, M. (1920) Volumes and hydration warmth of ions, *Z. Phys. 1*, 45–48.
35. Rashin, A. A., and Honig, B. (1985) Reevaluation of the Born model of ion hydration, *J. Phys. Chem. 89*, 5588–5593.
36. Czerwinski, R. M., Harris, T. K., Massiah, M. A., Mildvan, A. S., and Whitman, C. P. (2001) The structural basis for the perturbed pK_a of the catalytic base in 4–oxalocrotonate tautomerase: Kinetic and structural effects of mutations of Phe-50, *Biochemistry 40*, 1984–1995.
37. Yasuda, M. (1959) Dissociation constants of some carboxylic acids in mixed aqueous solvents, *Bull. Chem. Soc. Jpn. 32*, 429–432.
38. Lee, C. K., Jeoung, E. H., and Lee, I.-S. H. (2000) Effect of mixtures of water and organic solvents on the acidities of 5–membered heteroaromatic carboxylic acids, *J. Heterocycl. Chem. 37*, 159–166.
39. Rahman, M. A., Ghosh, A. K., and Bose, R. N. (1979) Dissociation constants of long chain fatty acids in methanol-water and ethanol-water mixtures, *J. Chem. Technol. Biotechnol. 29*, 158–162.
40. Zielinska, J., Makowski, M., Maj, K., Liwo, A., and Chmurzynski, L. (1999) Acid-base and hydrogen-bonding equilibria in aliphatic amine and carboxylic acid systems in nonaqueous solutions, *Anal. Chim. Acta 401*, 317–321.
41. Clare, B. W., Cook, D., Ko, E. C. F., Mac, Y. C., and Parker, A. J. (1966) Solvation of ions: 9. Effect of anion solvation on acid dissociation constants in methanol, water, dimethylformamide, and dimethyl sulfoxide, *J. Am. Chem. Soc. 88*, 1911–1916.
42. Koeppe, B., Guo, J., Tolstoy, P. M., Denisov, G. S., and Limbach, H. H. (2013) Solvent and H/D isotope effects on the proton transfer pathways in heteroconjugated hydrogen-bonded phenol-carboxylic acid anions observed by combined UV-vis and NMR spectroscopy, *J. Am. Chem. Soc. 135*, 7553–7566.
43. Isom, D. G., Castaneda, C. A., Cannon, B. R., and Garcia-Moreno, B. (2011) Large shifts in pK_a values of lysine residues buried inside a protein, *Proc. Natl. Acad. Sci. U. S. A. 108*, 5260–5265.
44. Deno, N. C., and Wisotsky, M. J. (1963) Quantitative Raman spectroscopy for the determination of base strengths of weak organic bases, *J. Am. Chem. Soc. 85*, 1735–1738.
45. Deno, N. C., Gaugler, R. W., and Wisotsky, M. J. (1966) Base strengths and chemical behav-

ior of nitriles in sulfuric acid and oleum systems, *J. Org. Chem. 31*, 1967–1968.
46. Zheng, Y.-J., and Ornstein, R. L. (1996) What happens to salt-bridges in nonaqueous environments: Insights from quantum mechanics calculations, *J. Am. Chem. Soc. 118*, 11237–11243.
47. Simonson, T., and Brooks, C. L., III. (1996) Charge screening and the dielectric constant of proteins: Insights from molecular dynamics, *J. Am. Chem. Soc. 118*, 8452–8458.
48. Hartwell, E., Hodgson, D. R. W., and Kirby, A. J. (2000) Exploring the limits of efficiency of proton-transfer catalysis in models and enzymes, *J. Am. Chem. Soc. 122*, 9326–9327.
49. Bender, M. L., and Lawlor, J. M. (1963) Isotopic and kinetic studies of the mechanism of hydrolysis of salicyl phosphate. Intramolecular general acid catalysis, *J. Am. Chem. Soc. 85*, 3010–3017.
50. Kirby, A. J., Dutta-Roy, N., da Silva, D., Goodman, J. M., Lima, M. F., Roussev, C. D., and Nome, F. (2005) Intramolecular general acid catalysis of phosphate transfer. Nucleophilic attack by oxyanions on the PO_3^{2-} group, *J. Am. Chem. Soc. 127*, 7033–7040.
51. Orth, E. S., Brandao, T. A., Milagre, H. M., Eberlin, M. N., and Nome, F. (2008) Intramolecular acid-base catalysis of a phosphate diester: Modeling the ribonuclease mechanism, *J. Am. Chem. Soc. 130*, 2436–2437.
52. Orth, E. S., Brandao, T. A., Souza, B. S., Pliego, J. R., Vaz, B. G., Eberlin, M. N., Kirby, A. J., and Nome, F. (2010) Intramolecular catalysis of phosphodiester hydrolysis by two imidazoles, *J. Am. Chem. Soc. 132*, 8513–8523.
53. Kirby, A. J., and Younas, M. (1970) Reactivity of phosphate esters. Diester hydrolysis, *J. Chem. Soc. B*, 510–513.
54. Keillor, J. W., and Brown, R. S. (1992) Attack of zwitterionic ammonium thiolates on a distorted anilide as a model for the acylation of papain by amides. A simple demonstration of a bell-shaped pH/rate profile, *J. Am. Chem. Soc. 114*, 7983–7989.
55. Kellogg, B. A., Neverov, A. A., Aman, A. M., and Brown, R. S. (1996) Catalysis of acyl transfer from amides to thiolate nucleophiles: The reaction of a distorted anilide with thioglycolic acid and ethyl 2-mercaptoacetate, *J. Am. Chem. Soc. 118*, 10829–10837.
56. Ora, M., Linjalahti, H., and Lonnberg, H. (2005) Phosphodiester cleavage of guanylyl-(3′,3′)-(2′-amino-2′-deoxyuridine): Rate acceleration by the 2′-amino function, *J. Am. Chem. Soc. 127*, 1826–1832.
57. Komiyama, M., Roesel, T. R., and Bender, M. L. (1977) Intramolecular general base-catalyzed ester hydrolyses by the imidazolyl group, *Proc. Natl. Acad. Sci. U. S. A. 74*, 23–25.
58. Page, M. I., and Jencks, W. P. (1972) Intramolecular general base catalysis in the aminolysis of acetylimidazole and methyl formate by diamines, *J. Am. Chem. Soc. 94*, 8818–8827.
59. Dietze, P. E., and Jencks, W. P. (1989) General-base catalysis of nucleophilic substitution at carbon, *J. Am. Chem. Soc. 111*, 340–344.
60. Smith, R. M., and Hansen, D. E. (1998) The pH–rate profile for the hydrolysis of a peptide bond, *J. Am. Chem. Soc. 120*, 8910–8913.
61. Richard, J. P., and Nagorski, R. W. (1999) Mechanistic imperatives for catalysis of aldol addition reactions: Partitioning of the enolate intermediate between reaction with Brønsted acids and the carbonyl group, *J. Am. Chem. Soc. 121*, 4763–4770.
62. Lienhard, G. E., and Wang, T.-C. (1969) Mechanism of acid-catalyzed enolization of ketones, *J. Am. Chem. Soc. 91*, 1146–1153.
63. Bruice, T. C., and Benkovic, S. J. (1966) *Bioorganic mechanisms*, Vol. II, Benjamin, New York.
64. Hine, J., Cholod, M. S., and Chess, W. K., Jr. (1973) Kinetics of the formation of imines from acetone and primary amines. Evidence for internal acid-catalyzed dehydration of certain intermediate carbinolamines, *J. Am. Chem. Soc. 95*, 4270–4276.
65. Coward, J. K., and Bruice, T. C. (1969) Intramolecular amine-catalyzed ketone enolization. A search for concerted intramolecular general-base, general-acid catalysis, *J. Am. Chem. Soc. 91*, 5339–5345.
66. Knowles, J. R. (1976) The intrinsic pK_a values of functional groups in enzymes: Improper deductions from the pH-dependence of steady-state parameters, *CRC Crit. Rev. Biochem. 4*, 165–173.
67. Gloss, L. M., and Kirsch, J. F. (1995) Use of site-directed mutagenesis and alternative substrates to assign the prototropic groups important to catalysis by *Escherichia coli* as-

partate aminotransferase, *Biochemistry 34*, 3999–4007.
68. Hicks, K. A., Yuen, M. E., Zhen, W. F., Gerwig, T. J., Story, R. W., Kopp, M. C., and Snider, M. J. (2016) Structural and biochemical characterization of 6-hydroxynicotinic acid 3-monooxygenase: A novel decarboxylative hydroxylase involved in aerobic nicotinate degradation, *Biochemistry 55*, 3432–3446.
69. Tobin, A. J. (1970) Carbonic anhydrase from parsley leaves, *J. Biol. Chem. 245*, 2656–2666.
70. Plaut, B., and Knowles, J. R. (1972) pH-Dependence of the triose phosphate isomerase reaction, *Biochem. J. 129*, 311–320.
71. Dixon, M. (1953) The effect of pH on the affinities of enzymes for substrates and inhibitors, *Biochem. J. 55*, 161–170.
72. Waley, S. G. (1953) Some aspects of the kinetics of enzymic reactions, *Biochim. Biophys. Acta 10*, 27–34.
73. Alberty, R. A., and Massey, V. (1954) On the interpretation of the pH variation of the maximum initial velocity of an enzyme-catalyzed reaction, *Biochim. Biophys. Acta 13*, 347–353.
74. Ghanem, M., Fan, F., Francis, K., and Gadda, G. (2003) Spectroscopic and kinetic properties of recombinant choline oxidase from *Arthrobacter globiformis*, *Biochemistry 42*, 15179–15188.
75. Zheng, J., Avvaru, B. S., Tu, C., McKenna, R., and Silverman, D. N. (2008) Role of hydrophilic residues in proton transfer during catalysis by human carbonic anhydrase II, *Biochemistry 47*, 12028–12036.
76. Xu, H., Alguindigue, S. S., West, A. H., and Cook, P. F. (2007) A proposed proton shuttle mechanism for saccharopine dehydrogenase from *Saccharomyces cerevisiae*, *Biochemistry 46*, 871–882.
77. Xu, Y., and Grubmeyer, C. (1998) Catalysis in human hypoxanthine-guanine phosphoribosyltransferase: Asp 137 acts as a general acid/base, *Biochemistry 37*, 4114–4124.
78. Valley, M. P., and Fitzpatrick, P. F. (2003) Inactivation of nitroalkane oxidase upon mutation of the active site base and rescue with a deprotonated substrate, *J. Am. Chem. Soc. 125*, 8738–8739.
79. Cornish-Bowden, A. J., and Knowles, J. R. (1969) The pH-dependence of pepsin-catalysed reactions, *Biochem. J. 113*, 353–362.
80. Banerjee, S. K., Kregar, I., Turk, V., and Rupley, J. A. (1973) Lysozyme-catalyzed reaction of the *N*-acetylglucosamine hexasaccharide. Dependence of rate on pH, *J. Biol. Chem. 248*, 4786–4792.
81. Eftink, M. R., and Biltonen, R. L. (1983) Energetics of ribonuclease A catalysis. 1. pH, ionic strength, and solvent isotope dependence of the hydrolysis of cytidine cyclic 2′,3′-phosphate, *Biochemistry 22*, 5123–5134.
82. del Rosario, E. J., and Hammes, G. G. (1969) Kinetic and equilibrium studies of the ribonuclease-catalyzed hydrolysis of uridine 2′,3′-cyclic phosphate, *Biochemistry 8*, 1884–1889.
83. Machuga, E., and Klapper, M. H. (1977) Catalytic activity of N^{τ}-carboxymethylhistidine-12 ribonuclease: pH Dependence, *Biochim. Biophys. Acta 481*, 526–541.
84. Herries, D. G., Mathias, A. P., and Rabin, B. R. (1962) The active site and mechanism of action of bovine pancreatic ribonuclease. 3. The pH-dependence of the kinetic parameters for the hydrolysis of cytidine 2′,3′-phosphate, *Biochem. J. 85*, 127–134.
85. Kiick, D. M., and Cook, P. F. (1983) pH Studies toward the elucidation of the auxiliary catalyst for pig heart aspartate aminotransferase, *Biochemistry 22*, 375–382.
86. Lu, Z., Feng, X., Song, L., Han, Y., Kim, A., Herzberg, O., Woodson, W. R., Martin, B. M., Mariano, P. S., and Dunaway-Mariano, D. (2005) Diversity of function in the isocitrate lyase enzyme superfamily: The *Dianthus caryophyllus* petal death protein cleaves α-keto and α-hydroxycarboxylic acids, *Biochemistry 44*, 16365–16376.
87. Kiick, D. M., and Phillips, R. S. (1988) Mechanistic deductions from kinetic isotope effects and pH studies of pyridoxal phosphate dependent carbon-carbon lyases: *Erwinia herbicola* and *Citrobacter freundii* tyrosine phenol-lyase, *Biochemistry 27*, 7333–7338.
88. Cho, Y. K., and Cook, P. F. (1989) pH Dependence of the kinetic parameters for the pyrophosphate-dependent phosphofructokinase reaction supports a proton-shuttle mechanism, *Biochemistry 28*, 4155–4160.
89. Qian, J., West, A. H., and Cook, P. F. (2006) Acid–base chemical mechanism of homocitrate synthase from *Saccharomyces cerevisiae*, *Biochemistry 45*, 12136–12143.
90. Magalhaes, M. L., and Blanchard, J. S. (2005) The kinetic mechanism of AAC(3)-IV amino-

glycoside acetyltransferase from *Escherichia coli*, *Biochemistry 44*, 16275–16283.
91. Arabshahi, A., Flentke, G. R., and Frey, P. A. (1988) Uridine diphosphate galactose 4-epimerase. pH Dependence of the reduction of NAD^+ by a substrate analog, *J. Biol. Chem. 263*, 2638–2643.
92. Holyoak, T., and Nowak, T. (2004) pH Dependence of the reaction catalyzed by avian mitochondrial phosphoenolpyruvate carboxykinase, *Biochemistry 43*, 7054–7065.
93. Rao, S., and Holz, R. C. (2008) Analyzing the catalytic mechanism of the Fe-type nitrile hydratase from *Comamonas testosteroni* Ni1, *Biochemistry 47*, 12057–12064.
94. Case, A., and Stein, R. L. (2003) Mechanistic origins of the substrate selectivity of serine proteases, *Biochemistry 42*, 3335–3348.
95. Cleland, W. W. (1977) Determining the chemical mechanisms of enzyme-catalyzed reactions by kinetic studies, *Adv. Enzymol. Relat. Areas Mol. Biol. 45*, 273–387.
96. Frankel, B. A., Kruger, R. G., Robinson, D. E., Kelleher, N. L., and McCafferty, D. G. (2005) *Staphylococcus aureus* sortase transpeptidase SrtA: Insight into the kinetic mechanism and evidence for a reverse protonation catalytic mechanism, *Biochemistry 44*, 11188–11200.
97. LoGrasso, P. V., Tu, C., Chen, X., Taoka, S., Laipis, P. J., and Silverman, D. N. (1993) Influence of amino acid replacement at position 198 on catalytic properties of zinc-bound water in human carbonic anhydrase III, *Biochemistry 32*, 5786–5791.
98. St Maurice, M., and Bearne, S. L. (2002) Kinetics and thermodynamics of mandelate racemase catalysis, *Biochemistry 41*, 4048–4058.
99. Haldane, J. B. S. (1930) *Enzymes*, p 20, Longmans, Green, London.
100. Neidhart, D. J., Howell, P. L., Petsko, G. A., Powers, V. M., Li, R. S., Kenyon, G. L., and Gerlt, J. A. (1991) Mechanism of the reaction catalyzed by mandelate racemase. 2. Crystal structure of mandelate racemase at 2.5-Å resolution: Identification of the active site and possible catalytic residues, *Biochemistry 30*, 9264–9273.
101. Landro, J. A., Kallarakal, A. T., Ransom, S. C., Gerlt, J. A., Kozarich, J. W., Neidhart, D. J., and Kenyon, G. L. (1991) Mechanism of the reaction catalyzed by mandelate racemase. 3. Asymmetry in reactions catalyzed by the H297N mutant, *Biochemistry 30*, 9274–9281.
102. Roberts, D. D., Lewis, S. D., Ballou, D. P., Olson, S. T., and Shafer, J. A. (1986) Reactivity of small thiolate anions and Cysteine-25 in papain toward methyl methanethiosulfonate, *Biochemistry 25*, 5595–5601.
103. Mortensen, U. H., Remington, S. J., and Breddam, K. (1994) Site-directed mutagenesis on (serine) carboxypeptidase Y. A hydrogen bond network stabilizes the transition state by interaction with the C-terminal carboxylate group of the substrate, *Biochemistry 33*, 508–517.
104. Cohn, E. J., Edsall, J. T., Kirkwood, J. G., Mueller, H., Oncley, J. L., and Schatchard, G. (1943) *Proteins,amino acids and peptides as ions and dipolar ions*, Reinhold, New York.
105. Belasco, J. G., Herlihy, J. M., and Knowles, J. R. (1978) Critical ionization states in the reaction catalyzed by triosephosphate isomerase, *Biochemistry 17*, 2971–2978.
106. Kim, K., and Cole, P. A. (1998) Kinetic analysis of a protein tyrosine kinase reaction transition state in the forward and reverse directions, *J. Am. Chem. Soc. 120*, 6851–6858.
107. O'Brien, P. J., and Herschlag, D. (2002) Alkaline phosphatase revisited: Hydrolysis of alkyl phosphates, *Biochemistry 41*, 3207–3225.
108. Jez, J. M., and Noel, J. P. (2002) Reaction mechanism of chalcone isomerase. pH Dependence, diffusion control, and product binding differences, *J. Biol. Chem. 277*, 1361–1369.
109. Kuo, L. C., Herzberg, W., and Lipscomb, W. N. (1985) Substrate specificity and protonation state of ornithine transcarbamoylase as determined by pH studies, *Biochemistry 24*, 4754–4761.
110. Pitsawong, W., Chenprakhon, P., Dhammaraj, T., Medhanavyn, D., Sucharitakul, J., Tongsook, C., van Berkel, W. J. H., Chaiyen, P., and Miller, A. F. (2020) Tuning of pK_a values activates substrates in flavin-dependent aromatic hydroxylases, *J. Biol. Chem. 295*, 3965–3981.
111. Vinarov, D. A., and Nowak, T. (1998) pH Dependence of the reaction catalyzed by yeast Mg-enolase, *Biochemistry 37*, 15238–15246.
112. Brauenstein, A. E. (1973) Amino group transfer, In *The enzymes, third edition, volume IX, group transfer, part B* (Boyer, P. D., Ed.), pp 379–481, Academic Press, New York.

113. Liu, Y., Thoden, J. B., Kim, J., Berger, E., Gulick, A. M., Ruzicka, F. J., Holden, H. M., and Frey, P. A. (1997) Mechanistic roles of Tyrosine 149 and Serine 124 in UDP-galactose 4-epimerase from *Escherichia coli*, *Biochemistry 36*, 10675–10684.
114. Berger, E., Arabshahi, A., Wei, Y., Schilling, J. F., and Frey, P. A. (2001) Acid-base catalysis by UDP-galactose 4-epimerase: Correlations of kinetically measured acid dissociation constants with thermodynamic values for Tyrosine 149, *Biochemistry 40*, 6699–6705.
115. Subramanya, H. S., Roper, D. I., Dauter, Z., Dodson, E. J., Davies, G. J., Wilson, K. S., and Wigley, D. B. (1996) Enzymatic ketonization of 2-hydroxymuconate: Specificity and mechanism investigated by the crystal structures of two isomerases, *Biochemistry 35*, 792–802.
116. Stivers, J. T., Abeygunawardana, C., Mildvan, A. S., Hajipour, G., and Whitman, C. P. (1996) 4-Oxalocrotonate tautomerase: pH Dependence of catalysis and pK_a values of active site residues, *Biochemistry 35*, 814–823.
117. Stack, T. M. M., Li, W., Johnson, W. H., Jr., Zhang, Y. J., and Whitman, C. P. (2018) Inactivation of 4-oxalocrotonate tautomerase by 5-halo-2-hydroxy-2,4-pentadienoates, *Biochemistry 57*, 1012–1021.
118. Cosgrove, M. S., Gover, S., Naylor, C. E., Vandeputte-Rutten, L., Adams, M. J., and Levy, H. R. (2000) An examination of the role of Asp-177 in the His-Asp catalytic dyad of *Leuconostoc mesenteroides* glucose 6–phosphate dehydrogenase: X-ray structure and pH dependence of kinetic parameters of the D177N mutant enzyme, *Biochemistry 39*, 15002–15011.
119. Cosgrove, M. S., Loh, S. N., Ha, J. H., and Levy, H. R. (2002) The catalytic mechanism of glucose 6-phosphate dehydrogenases: Assignment and ^{1}H NMR spectroscopy pH titration of the catalytic histidine residue in the 109 kDa *Leuconostoc mesenteroides* enzyme, *Biochemistry 41*, 6939–6945.
120. Clements, J. M., Beckett, R. P., Brown, A., Catlin, G., Lobell, M., Palan, S., Thomas, W., Whittaker, M., Wood, S., Salama, S., Baker, P. J., Rodgers, H. F., Barynin, V., Rice, D. W., and Hunter, M. G. (2001) Antibiotic activity and characterization of BB-3497, a novel peptide deformylase inhibitor, *Antimicrob. Agents Chemother. 45*, 563–570.
121. Becker, A., Schlichting, I., Kabsch, W., Groche, D., Schultz, S., and Wagner, A. F. (1998) Iron center, substrate recognition and mechanism of peptide deformylase, *Nat. Struct. Biol. 5*, 1053–1058.
122. Deng, H., Callender, R., Zhu, J., Nguyen, K. T., and Pei, D. (2002) Determination of the ionization state and catalytic function of Glu-133 in peptide deformylase by difference FTIR spectroscopy, *Biochemistry 41*, 10563–10569.
123. Wakarchuk, W. W., Campbell, R. L., Sung, W. L., Davoodi, J., and Yaguchi, M. (1994) Mutational and crystallographic analyses of the active site residues of the *Bacillus circulans* xylanase, *Protein Sci. 3*, 467–475.
124. McIntosh, L. P., Hand, G., Johnson, P. E., Joshi, M. D., Korner, M., Plesniak, L. A., Ziser, L., Wakarchuk, W. W., and Withers, S. G. (1996) The pK_a of the general acid/base carboxyl group of a glycosidase cycles during catalysis: A ^{13}C-NMR study of *Bacillus circulans* xylanase, *Biochemistry 35*, 9958–9966.
125. Ludwiczek, M. L., D'Angelo, I., Yalloway, G. N., Brockerman, J. A., Okon, M., Nielsen, J. E., Strynadka, N. C., Withers, S. G., and McIntosh, L. P. (2013) Strategies for modulating the pH-dependent activity of a family 11 glycoside hydrolase, *Biochemistry 52*, 3138–3156.
126. Krekel, F., Samland, A. K., Macheroux, P., Amrhein, N., and Evans, J. N. (2000) Determination of the pK_a value of C115 in MurA (UDP-*N*-acetylglucosamine enolpyruvyltransferase) from *Enterobacter cloacae*, *Biochemistry 39*, 12671–12677.
127. Schmidt, D. E., Jr., and Westheimer, F. H. (1971) pK of the lysine amino group at the active site of acetoacetate decarboxylase, *Biochemistry 10*, 1249–1253.
128. Cheng, K. C., and Nowak, T. (1989) A histidine residue at the active site of avian liver phosphoenolpyruvate carboxykinase, *J. Biol. Chem. 264*, 19666–19676.
129. Knuckley, B., Bhatia, M., and Thompson, P. R. (2007) Protein arginine deiminase 4: Evidence for a reverse protonation mechanism, *Biochemistry 46*, 6578–6587.
130. Tsukada, H., and Blow, D. M. (1985) Structure of α-chymotrypsin refined at 1.68 Å resolution, *J. Mol. Biol. 184*, 703–711.
131. Blow, D. M., Birktoft, J. J., and Hartley, B. S. (1969) Role of a buried acid group in the

mechanism of action of chymotrypsin, *Nature (London, U. K.) 221*, 337–340.
132. Cruickshank, W. H., and Kaplan, H. (1972) Competitive labeling method for determining the ionization constants and reactivity of individual histidine residues in proteins. Histidines of α-chymotrypsin, *Biochem. J. 130*, 1125–1131.
133. Ryan, M., Liu, T., Dahlquist, F. W., and Griffith, O. H. (2001) A catalytic diad involved in substrate-assisted catalysis: NMR study of hydrogen bonding and dynamics at the active site of phosphatidylinositol-specific phospholipase C, *Biochemistry 40*, 9743–9750.
134. Kraulis, P. J. (1991) Molscript: A program to produce both detailed and schematic plots of protein structures, *J. Appl. Crystallogr. 24*, 946–950.
135. Kossiakoff, A. A., and Spencer, S. A. (1981) Direct determination of the protonation states of Aspartic Acid-102 and Histidine-57 in the tetrahedral intermediate of the serine proteases: Neutron structure of trypsin, *Biochemistry 20*, 6462–6474.
136. Everill, P., Sudmeier, J. L., and Bachovchin, W. W. (2012) Direct NMR observation and pK_a determination of the Asp102 side chain in a serine protease, *J. Am. Chem. Soc. 134*, 2348–2354.
137. Herbst-Gervasoni, C. J., and Christianson, D. W. (2021) X-ray crystallographic snapshots of substrate binding in the active site of histone deacetylase 10, *Biochemistry 60*, 303–313.
138. Hardman, M. J., Valenzuela, P., and Bender, M. L. (1971) Acylation of α- and δ-chymotrypsins by *p*-nitrophenyl acetate. Enzyme-substrate complex formation and pH dependence, *J. Biol. Chem. 246*, 5907–5913.
139. Stratton, J. R., Pelton, J. G., and Kirsch, J. F. (2001) A novel engineered subtilisin BPN′ lacking a low-barrier hydrogen bond in the catalytic triad, *Biochemistry 40*, 10411–10416.
140. Tremblay, L. W., Xu, H., and Blanchard, J. S. (2010) Structures of the Michaelis complex (1.2 Å) and the covalent acyl intermediate (2.0 Å) of cefamandole bound in the active sites of the *Mycobacterium tuberculosis* β-lactamase K73A and E166A mutants, *Biochemistry 49*, 9685–9687.
141. Charlier, H. A., Jr., Runquist, J. A., and Miziorko, H. M. (1994) Evidence supporting catalytic roles for aspartate residues in phosphoribulokinase, *Biochemistry 33*, 9343–9350.
142. Runquist, J. A., Harrison, D. H., and Miziorko, H. M. (1999) *Rhodobacter sphaeroides* phosphoribulokinase: Identification of lysine-165 as a catalytic residue and evaluation of the contributions of invariant basic amino acids to ribulose 5–phosphate binding, *Biochemistry 38*, 13999–14005.
143. Damblon, C., Raquet, X., Lian, L. Y., Lamotte-Brasseur, J., Fonze, E., Charlier, P., Roberts, G. C., and Frere, J. M. (1996) The catalytic mechanism of β-lactamases: NMR titration of an active-site lysine residue of the TEM-1 enzyme, *Proc. Natl. Acad. Sci. U. S. A. 93*, 1747–1752.
144. Knap, A. K., and Pratt, R. F. (1991) Inactivation of the RTEM-1 cysteine β-lactamase by iodoacetate. The nature of active-site functional groups and comparisons with the native enzyme, *Biochem. J. 273(Pt 1)*, 85–91.
145. Edsall, J. T., and Wyman, J. (1958) *Biophysical chemistry: Volume I*, Academic Press, New York.
146. Blake, C. C., Johnson, L. N., Mair, G. A., North, A. C., Phillips, D. C., and Sarma, V. R. (1967) Crystallographic studies of the activity of hen egg-white lysozyme, *Proc. R. Soc. London, B 167*, 378–388.
147. Parsons, S. M., and Raftery, M. A. (1972) Ionization behavior of the catalytic carboxyls of lysozyme. Effects of temperature, *Biochemistry 11*, 1630–1633.
148. Sims, P. A., Larsen, T. M., Poyner, R. R., Cleland, W. W., and Reed, G. H. (2003) Reverse protonation is the key to general acid-base catalysis in enolase, *Biochemistry 42*, 8298–8306.
149. Larson, S. B., Day, J. S., Nguyen, C., Cudney, R., and McPherson, A. (2010) Structure of bovine pancreatic ribonuclease complexed with uridine 5′-monophosphate at 1.60 Å resolution, *Acta Crystallogr., Sect. F: Struct. Biol. Commun. 66*, 113–120.
150. Crestfield, A. M., Stein, W. H., and Moore, S. (1963) Properties and conformation of the histidine residues at the active site of ribonuclease, *J. Biol. Chem. 238*, 2421–2428.
151. Wyckoff, H. W., Tsernoglou, D., Hanson, A. W., Knox, J. R., Lee, B., and Richards, F. M. (1970) The three-dimensional structure of ribonuclease-S. Interpretation of an electron

density map at a nominal resolution of 2 Å, *J. Biol. Chem. 245*, 305–328.
152. Wlodawer, A., Miller, M., and Sjolin, L. (1983) Active site of RNase: Neutron diffraction study of a complex with uridine vanadate, a transition-state analog, *Proc. Natl. Acad. Sci. U. S. A. 80*, 3628–3631.
153. Meadows, D. H., Roberts, G. C., and Jardetzky, O. (1969) Nuclear magnetic resonance studies of the structure and binding sites of enzymes. 8. Inhibitor binding to ribonuclease, *J. Mol. Biol. 45*, 491–511.
154. Markley, J. L. (1975) Correlation proton magnetic resonance studies at 250 MHz of bovine pancreatic ribonuclease. I. Reinvestigation of the histidine peak assignments, *Biochemistry 14*, 3546–3554.
155. Patel, D. J., Canuel, L. L., and Bovey, F. A. (1975) Reassignment of the active site histidines in ribonuclease A by selective deuteration studies, *Biopolymers 14*, 987–997.
156. Markley, J. L., and Finkenstadt, W. R. (1975) Correlation proton magnetic resonance studies at 250 MHz of bovine pancreatic ribonuclease. III. Mutual electrostatic interaction between histidine residues 12 and 119, *Biochemistry 14*, 3562–3566.
157. Joshi, M. D., Sidhu, G., Nielsen, J. E., Brayer, G. D., Withers, S. G., and McIntosh, L. P. (2001) Dissecting the electrostatic interactions and pH-dependent activity of a family 11 glycosidase, *Biochemistry 40*, 10115–10139.
158. Kotzler, M. P., Robinson, K., Chen, H. M., Okon, M., McIntosh, L. P., and Withers, S. G. (2018) Modulating the nucleophile of a glycoside hydrolase through site-specific incorporation of fluoroglutamic acids, *J. Am. Chem. Soc. 140*, 8268–8276.
159. Goldberg, R. N., Kishore, N., and Lennen, R. M. (2002) Themodynamic quantities for the ionization reactions of buffers, *J. Phys. Chem. Ref. Data 31*, 231–370.
160. Jackson, D. Y., Burnier, J., Quan, C., Stanley, M., Tom, J., and Wells, J. A. (1994) A designed peptide ligase for total synthesis of ribonuclease A with unnatural catalytic residues, *Science (Washington, DC, U. S.) 266*, 243–247.
161. Oda, Y., Yamazaki, T., Nagayama, K., Kanaya, S., Kuroda, Y., and Nakamura, H. (1994) Individual ionization constants of all the carboxyl groups in ribonuclease HI from *Escherichia coli* determined by NMR, *Biochemistry 33*, 5275–5284.
162. Guillen Schlippe, Y. V., and Hedstrom, L. (2005) Guanidine derivatives rescue the Arg418Ala mutation of *Tritrichomonas foetus* IMP dehydrogenase, *Biochemistry 44*, 16695–16700.
163. Guillen Schlippe, Y. V., and Hedstrom, L. (2005) Is Arg418 the catalytic base required for the hydrolysis step of the IMP dehydrogenase reaction?, *Biochemistry 44*, 11700–11707.
164. Rudik, I., Ghisla, S., and Thorpe, C. (1998) Protonic equilibria in the reductive half-reaction of the medium-chain acyl-CoA dehydrogenase, *Biochemistry 37*, 8437–8445.
165. Ho, M. C., Menetret, J. F., Tsuruta, H., and Allen, K. N. (2009) The origin of the electrostatic perturbation in acetoacetate decarboxylase, *Nature (London, U. K.) 459*, 393–397.
166. Schwans, J. P., Sunden, F., Gonzalez, A., Tsai, Y., and Herschlag, D. (2013) Uncovering the determinants of a highly perturbed tyrosine pK_a in the active site of ketosteroid isomerase, *Biochemistry 52*, 7840–7855.
167. Hoskins, A. A., Morar, M., Kappock, T. J., Mathews, II, Zaugg, J. B., Barder, T. E., Peng, P., Okamoto, A., Ealick, S. E., and Stubbe, J. (2007) N^5–CAIR mutase: Role of a CO_2 binding site and substrate movement in catalysis, *Biochemistry 46*, 2842–2855.
168. Nandy, A., Kieweg, V., Krautle, F. G., Vock, P., Kuchler, B., Bross, P., Kim, J. J., Rasched, I., and Ghisla, S. (1996) Medium-long-chain chimeric human acyl-CoA dehydrogenase: Medium-chain enzyme with the active center base arrangement of long-chain acyl-CoA dehydrogenase, *Biochemistry 35*, 12402–12411.
169. Drohat, A. C., and Stivers, J. T. (2000) *Escherichia coli* uracil DNA glycosylase: NMR characterization of the short hydrogen bond from His187 to uracil O2, *Biochemistry 39*, 11865–11875.
170. Parikh, S. S., Mol, C. D., Slupphaug, G., Bharati, S., Krokan, H. E., and Tainer, J. A. (1998) Base excision repair initiation revealed by crystal structures and binding kinetics of human uracil-DNA glycosylase with DNA, *EMBO J. 17*, 5214–5226.
171. Viola, R. E., and Cleland, W. W. (1978) Use of pH studies to elucidate the chemical mecha-

nism of yeast hexokinase, *Biochemistry 17*, 4111–4117.
172. Grace, S., and Dunaway-Mariano, D. (1983) Examination of the solvent perturbation technique as a method to identify enzyme catalytic groups, *Biochemistry 22*, 4238–4247.
173. Di Nardo, G., Breitner, M., Bandino, A., Ghosh, D., Jennings, G. K., Hackett, J. C., and Gilardi, G. (2015) Evidence for an elevated aspartate pK_a in the active site of human aromatase, *J. Biol. Chem. 290*, 1186–1196.
174. Malabanan, M. M., Nitsch-Velasquez, L., Amyes, T. L., and Richard, J. P. (2013) Magnitude and origin of the enhanced basicity of the catalytic glutamate of triosephosphate isomerase, *J. Am. Chem. Soc. 135*, 5978–5981.
175. Jencks, W. P. (1959) Mechanism of oxime and semicarbazone formation, *J. Am. Chem. Soc. 81*, 475–481.
176. Coggins, B. E., McClerren, A. L., Jiang, L., Li, X., Rudolph, J., Hindsgaul, O., Raetz, C. R., and Zhou, P. (2005) Refined solution structure of the LpxC-TU-514 complex and pK_a analysis of an active site histidine: Insights into the mechanism and inhibitor design, *Biochemistry 44*, 1114–1126.
177. Fierke, C. A., Johnson, K. A., and Benkovic, S. J. (1987) Construction and evaluation of the kinetic scheme associated with dihydrofolate reductase from *Escherichia coli*, *Biochemistry 26*, 4085–4092.
178. Stone, S. R., and Morrison, J. F. (1984) Catalytic mechanism of the dihydrofolate reductase reaction as determined by pH studies, *Biochemistry 23*, 2753–2758.
179. Jeong, S. S., and Gready, J. E. (1995) pH Dependence of enzyme reaction rates and deuterium isotope effects on the reduction of a new mechanism-based substrate by dihydrofolate reductase (DHFR), *Biochemistry 34*, 3734–3741.
180. Murphy, D. J., and Benkovic, S. J. (1989) Hydrophobic interactions via mutants of *Escherichia coli* dihydrofolate reductase: Separation of binding and catalysis, *Biochemistry 28*, 3025–3031.
181. Hale, S. P., Poole, L. B., and Gerlt, J. A. (1993) Mechanism of the reaction catalyzed by staphylococcal nuclease: Identification of the rate-determining step, *Biochemistry 32*, 7479–7487.
182. Adams, J. A., and Taylor, S. S. (1993) Phosphorylation of peptide substrates for the catalytic subunit of cAMP-dependent protein kinase, *J. Biol. Chem. 268*, 7747–7752.
183. Lin, Y., Volkman, J., Nicholas, K. M., Yamamoto, T., Eguchi, T., Nimmo, S. L., West, A. H., and Cook, P. F. (2008) Chemical mechanism of homoisocitrate dehydrogenase from *Saccharomyces cerevisiae*, *Biochemistry 47*, 4169–4180.
184. LeBrun, L. A., Park, D. H., Ramaswamy, S., and Plapp, B. V. (2004) Participation of Histidine-51 in catalysis by horse liver alcohol dehydrogenase, *Biochemistry 43*, 3014–3026.
185. Brooks, R. L., and Shore, J. D. (1972) The effects of pH and temperature on hydrogen transfer in the liver alcohol dehydrogenase mechanism, *J. Biol. Chem. 247*, 2382–2383.
186. Colby, T. D., Bahnson, B. J., Chin, J. K., Klinman, J. P., and Goldstein, B. M. (1998) Active site modifications in a double mutant of liver alcohol dehydrogenase: Structural studies of two enzyme-ligand complexes, *Biochemistry 37*, 9295–9304.
187. Rhee, S., Silva, M. M., Hyde, C. C., Rogers, P. H., Metzler, C. M., Metzler, D. E., and Arnone, A. (1997) Refinement and comparisons of the crystal structures of pig cytosolic aspartate aminotransferase and its complex with 2-methylaspartate, *J. Biol. Chem. 272*, 17293–17302.
188. Zhai, X., Reinhardt, C. J., Malabanan, M. M., Amyes, T. L., and Richard, J. P. (2018) Enzyme architecture: Amino acid side-chains that function to optimize the basicity of the active site glutamate of triosephosphate isomerase, *J. Am. Chem. Soc. 140*, 8277–8286.
189. Smith, R., Brereton, I. M., Chai, R. Y., and Kent, S. B. (1996) Ionization states of the catalytic residues in HIV-1 protease, *Nat. Struct. Biol. 3*, 946–950.
190. Blanchard, J. S., and Cleland, W. W. (1980) Kinetic and chemical mechanisms of yeast formate dehydrogenase, *Biochemistry 19*, 3543–3550.
191. Guo, Q., Gakhar, L., Wickersham, K., Francis, K., Vardi-Kilshtain, A., Major, D. T., Cheatum, C. M., and Kohen, A. (2016) Structural and kinetic studies of formate dehydrogenase from *Candida boidinii*, *Biochemistry 55*, 2760–2771.
192. Bouhss, A., Dementin, S., Parquet, C., Mengin-Lecreulx, D., Bertrand, J. A., Le Beller, D., Dideberg, O., van Heijenoort, J., and Blanot, D. (1999) Role of the ortholog and

paralog amino acid invariants in the active site of the UDP-murNAc-L-alanine:D-glutamate ligase (MurD), *Biochemistry 38*, 12240–12247.
193. Cantwell, J. S., Novak, W. R., Wang, P. F., McLeish, M. J., Kenyon, G. L., and Babbitt, P. C. (2001) Mutagenesis of two acidic active site residues in human muscle creatine kinase: Implications for the catalytic mechanism, *Biochemistry 40*, 3056–3061.
194. Henn-Sax, M., Thoma, R., Schmidt, S., Hennig, M., Kirschner, K., and Sterner, R. (2002) Two $(\beta\alpha)_8$-barrel enzymes of histidine and tryptophan biosynthesis have similar reaction mechanisms and common strategies for protecting their labile substrates, *Biochemistry 41*, 12032–12042.
195. Kumar, V. P., Thomas, L. M., Bobyk, K. D., Andi, B., Cook, P. F., and West, A. H. (2012) Evidence in support of Lysine 77 and Histidine 96 as acid–base catalytic residues in saccharopine dehydrogenase from *Saccharomyces cerevisiae*, *Biochemistry 51*, 857–866.
196. Stapleton, M. A., Javid-Majd, F., Harmon, M. F., Hanks, B. A., Grahmann, J. L., Mullins, L. S., and Raushel, F. M. (1996) Role of conserved residues within the carboxy phosphate domain of carbamoyl phosphate synthetase, *Biochemistry 35*, 14352–14361.
197. Yang, G., Sandalova, T., Lohman, K., Lindqvist, Y., and Rendina, A. R. (1997) Active site mutants of *Escherichia coli* dethiobiotin synthetase: Effects of mutations on enzyme catalytic and structural properties, *Biochemistry 36*, 4751–4760.
198. Basarab, G. S., Steffens, J. J., Wawrzak, Z., Schwartz, R. S., Lundqvist, T., and Jordan, D. B. (1999) Catalytic mechanism of scytalone dehydratase: Site-directed mutagenesis, kinetic isotope effects, and alternate substrates, *Biochemistry 38*, 6012–6024.
199. Carlow, D. C., Smith, A. A., Yang, C. C., Short, S. A., and Wolfenden, R. (1995) Major contribution of a carboxymethyl group to transition-state stabilization by cytidine deaminase: Mutation and rescue, *Biochemistry 34*, 4220–4224.
200. Carter, P., and Wells, J. A. (1988) Dissecting the catalytic triad of a serine protease, *Nature (London, U. K.) 332*, 564–568.
201. Chiu, Y. C., Okajima, T., Murakawa, T., Uchida, M., Taki, M., Hirota, S., Kim, M., Yamaguchi, H., Kawano, Y., Kamiya, N., Kuroda, S., Hayashi, H., Yamamoto, Y., and Tanizawa, K. (2006) Kinetic and structural studies on the catalytic role of the aspartic acid residue conserved in copper amine oxidase, *Biochemistry 45*, 4105–4120.
202. Cosgrove, M. S., Naylor, C., Paludan, S., Adams, M. J., and Levy, H. R. (1998) On the mechanism of the reaction catalyzed by glucose 6–phosphate dehydrogenase, *Biochemistry 37*, 2759–2767.
203. Gibbs, C. S., and Zoller, M. J. (1991) Rational scanning mutagenesis of a protein kinase identifies functional regions involved in catalysis and substrate interactions, *J. Biol. Chem. 266*, 8923–8931.
204. Gopalan, K. V., and Srivastava, D. K. (2002) Beyond the proton abstracting role of Glu-376 in medium-chain acyl-CoA dehydrogenase: Influence of Glu-376→Gln substitution on ligand binding and catalysis, *Biochemistry 41*, 4638–4648.
205. Gross, J. W., Hegeman, A. D., Gerratana, B., and Frey, P. A. (2001) Dehydration is catalyzed by Glutamate-136 and Aspartic Acid-135 active site residues in *Escherichia coli* dTDP-glucose 4,6-dehydratase, *Biochemistry 40*, 12497–12504.
206. Hibler, D. W., Stolowich, N. J., Reynolds, M. A., Gerlt, J. A., Wilde, J. A., and Bolton, P. H. (1987) Site-directed mutants of staphylococcal nuclease. Detection and localization by ^{1}H NMR spectroscopy of conformational changes accompanying substitutions for Glutamic Acid-43, *Biochemistry 26*, 6278–6286.
207. Kallarakal, A. T., Mitra, B., Kozarich, J. W., Gerlt, J. A., Clifton, J. G., Petsko, G. A., and Kenyon, G. L. (1995) Mechanism of the reaction catalyzed by mandelate racemase: Structure and mechanistic properties of the K166R mutant, *Biochemistry 34*, 2788–2797.
208. Kuliopulos, A., Talalay, P., and Mildvan, A. S. (1990) Combined effects of two mutations of catalytic residues on the ketosteroid isomerase reaction, *Biochemistry 29*, 10271–10280.
209. Lewendon, A., Murray, I. A., Shaw, W. V., Gibbs, M. R., and Leslie, A. G. (1994) Replacement of catalytic Histidine-195 of chloramphenicol acetyltransferase: Evidence for a general base role for glutamate, *Biochemistry 33*, 1944–1950.
210. Li, C., Montgomery, M. G., Mohammed, F., Li, J. J., Wood, S. P., and Bugg, T. D. (2005)

Catalytic mechanism of C-C hydrolase MhpC from *Escherichia coli*: Kinetic analysis of His263 and Ser110 site-directed mutants, *J. Mol. Biol. 346*, 241–251.
211. Meng, M., and Chuang, D. T. (1994) Site-directed mutagenesis and functional analysis of the active-site residues of the E2 component of bovine branched-chain α-keto acid dehydrogenase complex, *Biochemistry 33*, 12879–12885.
212. Mitra, B., Kallarakal, A. T., Kozarich, J. W., Gerlt, J. A., Clifton, J. G., Petsko, G. A., and Kenyon, G. L. (1995) Mechanism of the reaction catalyzed by mandelate racemase: Importance of electrophilic catalysis by Glutamic Acid 317, *Biochemistry 34*, 2777–2787.
213. Poyner, R. R., Laughlin, L. T., Sowa, G. A., and Reed, G. H. (1996) Toward identification of acid/base catalysts in the active site of enolase: Comparison of the properties of K345A, E168Q, and E211Q variants, *Biochemistry 35*, 1692–1699.
214. Rydberg, E. H., Li, C., Maurus, R., Overall, C. M., Brayer, G. D., and Withers, S. G. (2002) Mechanistic analyses of catalysis in human pancreatic α-amylase: Detailed kinetic and structural studies of mutants of three conserved carboxylic acids, *Biochemistry 41*, 4492–4502.
215. Sakurai, M., Cook, P. F., Haseman, C. A., and Uyeda, K. (2000) Glutamate 325 is a general acid–base catalyst in the reaction catalyzed by fructose-2,6-bisphosphatase, *Biochemistry 39*, 16238–16243.
216. Samuel, J., Luo, Y., Morgan, P. M., Strynadka, N. C., and Tanner, M. E. (2001) Catalysis and binding in L-ribulose-5–phosphate 4-epimerase: A comparison with L-fuculose-1-phosphate aldolase, *Biochemistry 40*, 14772–14780.
217. Serpersu, E. H., Hibler, D. W., Gerlt, J. A., and Mildvan, A. S. (1989) Kinetic and magnetic resonance studies of the Glutamate-43 to serine mutant of staphylococcal nuclease, *Biochemistry 28*, 1539–1548.
218. Shim, J. H., and Benkovic, S. J. (1999) Catalytic mechanism of *Escherichia coli* glycinamide ribonucleotide transformylase probed by site-directed mutagenesis and pH-dependent studies, *Biochemistry 38*, 10024–10031.
219. Steyaert, J., Hallenga, K., Wyns, L., and Stanssens, P. (1990) Histidine-40 of ribonuclease T1 acts as base catalyst when the true catalytic base, Glutamic Acid-58, is replaced by alanine, *Biochemistry 29*, 9064–9072.
220. Strater, N., Sun, L., Kantrowitz, E. R., and Lipscomb, W. N. (1999) A bicarbonate ion as a general base in the mechanism of peptide hydrolysis by dizinc leucine aminopeptidase, *Proc. Natl. Acad. Sci. U. S. A. 96*, 11151–11155.
221. Wang, Y., Li, Y., and Yan, H. (2006) Mechanism of dihydroneopterin aldolase: Functional roles of the conserved active site glutamate and lysine residues, *Biochemistry 45*, 15232–15239.
222. Wikner, C., Nilsson, U., Meshalkina, L., Udekwu, C., Lindqvist, Y., and Schneider, G. (1997) Identification of catalytically important residues in yeast transketolase, *Biochemistry 36*, 15643–15649.
223. Zhang, L., Chooback, L., and Cook, P. F. (1999) Lysine 183 is the general base in the 6-phosphogluconate dehydrogenase-catalyzed reaction, *Biochemistry 38*, 11231–11238.
224. Zhuang, Z., Song, F., Zhang, W., Taylor, K., Archambault, A., Dunaway-Mariano, D., Dong, J., and Carey, P. R. (2002) Kinetic, Raman, NMR, and site-directed mutagenesis studies of the *Pseudomonas* sp. strain CBS3 4–hydroxybenzoyl-CoA thioesterase active site, *Biochemistry 41*, 11152–11160.
225. Appleby, T. C., Kinsland, C., Begley, T. P., and Ealick, S. E. (2000) The crystal structure and mechanism of orotidine 5′-monophosphate decarboxylase, *Proc. Natl. Acad. Sci. U. S. A. 97*, 2005–2010.
226. Dunn, G., Montgomery, M. G., Mohammed, F., Coker, A., Cooper, J. B., Robertson, T., Garcia, J. L., Bugg, T. D., and Wood, S. P. (2005) The structure of the C-C bond hydrolase MhpC provides insights into its catalytic mechanism, *J. Mol. Biol. 346*, 253–265.
227. Harris, P., Navarro Poulsen, J. C., Jensen, K. F., and Larsen, S. (2000) Structural basis for the catalytic mechanism of a proficient enzyme: Orotidine 5′-monophosphate decarboxylase, *Biochemistry 39*, 4217–4224.
228. Hellinga, H. W., and Evans, P. R. (1987) Mutations in the active site of *Escherichia coli* phosphofructokinase, *Nature (London, U. K.) 327*, 437–439.
229. Kiema, T. R., Engel, C. K., Schmitz, W., Filppula, S. A., Wierenga, R. K., and Hiltunen, J. K. (1999) Mutagenic and enzymological

studies of the hydratase and isomerase activities of 2–enoyl-CoA hydratase-1, *Biochemistry 38*, 2991–2999.
230. Liu, D., Karsten, W. E., and Cook, P. F. (2000) Lysine 199 is the general acid in the NAD-malic enzyme reaction, *Biochemistry 39*, 11955–11960.
231. Miller, B. G., Snider, M. J., Wolfenden, R., and Short, S. A. (2001) Dissecting a charged network at the active site of orotidine-5′-phosphate decarboxylase, *J. Biol. Chem. 276*, 15174–15176.
232. Phillips, M. A., Fletterick, R., and Rutter, W. J. (1990) Arginine 127 stabilizes the transition state in carboxypeptidase, *J. Biol. Chem. 265*, 20692–20698.
233. Tao, X., Yang, Z., and Tong, L. (2003) Crystal structures of substrate complexes of malic enzyme and insights into the catalytic mechanism, *Structure (Cambridge, MA, U. S.) 11*, 1141–1150.
234. Kim, H., and Lipscomb, W. N. (1990) Crystal structure of the complex of carboxypeptidase A with a strongly bound phosphonate in a new crystalline form: Comparison with structures of other complexes, *Biochemistry 29*, 5546–5555.
235. Liu, D. R., Cload, S. T., Pastor, R. M., and Schultz, P. G. (1996) Analysis of active site residues in *Escherichia coli* chorismate mutase by site-directed mutagenesis, *J. Am. Chem. Soc. 118*, 1789–1790.
236. Vinarov, D. A., and Nowak, T. (1999) Role of His159 in yeast enolase catalysis, *Biochemistry 38*, 12138–12149.
237. Berger, S. A., and Evans, P. R. (1992) Site-directed mutagenesis identifies catalytic residues in the active site of *Escherichia coli* phosphofructokinase, *Biochemistry 31*, 9237–9242.
238. Tsai, C. L., Gokulan, K., Sobrado, P., Sacchettini, J. C., and Fitzpatrick, P. F. (2007) Mechanistic and structural studies of H373Q flavocytochrome b_2: Effects of mutating the active site base, *Biochemistry 46*, 7844–7851.
239. Ciulli, A., Chirgadze, D. Y., Smith, A. G., Blundell, T. L., and Abell, C. (2007) Crystal structure of *Escherichia coli* ketopantoate reductase in a ternary complex with $NADP^+$ and pantoate bound: Substrate recognition, conformational change, and cooperativity, *J. Biol. Chem. 282*, 8487–8497.
240. Sunden, F., Peck, A., Salzman, J., Ressl, S., and Herschlag, D. (2015) Extensive site-directed mutagenesis reveals interconnected functional units in the alkaline phosphatase active site, *eLife 4*, e06181.
241. Joerger, A. C., Gosse, C., Fessner, W. D., and Schulz, G. E. (2000) Catalytic action of fuculose 1-phosphate aldolase (class II) as derived from structure-directed mutagenesis, *Biochemistry 39*, 6033–6041.
242. Street, I. P., Coffman, H. R., Baker, J. A., and Poulter, C. D. (1994) Identification of Cys139 and Glu207 as catalytically important groups in the active site of isopentenyl diphosphate:Dimethylallyl diphosphate isomerase, *Biochemistry 33*, 4212–4217.
243. Hondal, R. J., Zhao, Z., Kravchuk, A. V., Liao, H., Riddle, S. R., Yue, X., Bruzik, K. S., and Tsai, M. D. (1998) Mechanism of phosphatidylinositol-specific phospholipase C: A unified view of the mechanism of catalysis, *Biochemistry 37*, 4568–4580.
244. Cobucci-Ponzano, B., Trincone, A., Giordano, A., Rossi, M., and Moracci, M. (2003) Identification of the catalytic nucleophile of the family 29 α-L-fucosidase from *Sulfolobus solfataricus* via chemical rescue of an inactive mutant, *Biochemistry 42*, 9525–9531.
245. Liu, Y., Barrett, J. E., Schultz, P. G., and Santi, D. V. (1999) Tyrosine 146 of thymidylate synthase assists proton abstraction from the 5-position of 2′-deoxyuridine 5′-monophosphate, *Biochemistry 38*, 848–852.
246. Gardell, S. J., Hilvert, D., Barnett, J., Kaiser, E. T., and Rutter, W. J. (1987) Use of directed mutagenesis to probe the role of Tyrosine 198 in the catalytic mechanism of carboxypeptidase A, *J. Biol. Chem. 262*, 576–582.
247. Krautwurst, H., Encinas, M. V., Marcus, F., Latshaw, S. P., Kemp, R. G., Frey, P. A., and Cardemil, E. (1995) *Saccharomyces cerevisiae* phosphoenolpyruvate carboxykinase: Revised amino acid sequence, site-directed mutagenesis, and microenvironment characteristics of Cysteines 365 and 458, *Biochemistry 34*, 6382–6388.
248. Cho, J. H., Kim, D. H., Lee, K. J., Kim, D. H., and Choi, K. Y. (2001) The role of Tyr248 probed by mutant bovine carboxypeptidase A: Insight into the catalytic mechanism of carboxypeptidase A, *Biochemistry 40*, 10197–10203.

249. Fischer, M., Haase, I., Kis, K., Meining, W., Ladenstein, R., Cushman, M., Schramek, N., Huber, R., and Bacher, A. (2003) Enzyme catalysis via control of activation entropy: Site-directed mutagenesis of 6,7-dimethyl-8-ribityllumazine synthase, *J. Mol. Biol. 326*, 783–793.
250. Naught, L. E., Regni, C., Beamer, L. J., and Tipton, P. A. (2003) Roles of active site residues in *Pseudomonas aeruginosa* phosphomannomutase/phosphoglucomutase, *Biochemistry 42*, 9946–9951.
251. Susan-Resiga, D., and Nowak, T. (2003) The proton transfer step catalyzed by yeast pyruvate kinase, *J. Biol. Chem. 278*, 12660–12671.
252. Toke, D. A., McClintick, M. L., and Carman, G. M. (1999) Mutagenesis of the phosphatase sequence motif in diacylglycerol pyrophosphate phosphatase from *Saccharomyces cerevisiae*, *Biochemistry 38*, 14606–14613.
253. Seemann, M., Zhai, G. Z., Umezawa, K., and Cane, D. (1999) Pentalenene synthase. Histidine-309 is not required for catalytic activity, *J. Am. Chem. Soc. 121*, 591–592.
254. Dolence, J. M., Rozema, D. B., and Poulter, C. D. (1997) Yeast protein farnesyltransferase. Site-directed mutagenesis of conserved residues in the β-subunit, *Biochemistry 36*, 9246–9252.
255. Huang, H.-H., Arscott, L. D., Ballou, D. P., and Williams, C. H. (2008) Acid-base catalysis in the mechanism of thioredoxin reductase from *Drosophila melanogaster*, *Biochemistry 47*, 1721–1731.
256. Wang, Y., Darnay, B. G., and Rodwell, V. W. (1990) Identification of the principal catalytically important acidic residue of 3–hydroxy-3–methylglutaryl coenzyme A reductase, *J. Biol. Chem. 265*, 21634–21641.
257. Steussy, C. N., Robison, A. D., Tetrick, A. M., Knight, J. T., Rodwell, V. W., Stauffacher, C. V., and Sutherlin, A. L. (2006) A structural limitation on enzyme activity: The case of HMG-CoA synthase, *Biochemistry 45*, 14407–14414.
258. Savenkova, M. I., Kuo, J. M., and Ortiz de Montellano, P. R. (1998) Improvement of peroxygenase activity by relocation of a catalytic histidine within the active site of horseradish peroxidase, *Biochemistry 37*, 10828–10836.
259. Kim, H., and Lipscomb, W. N. (1991) Comparison of the structures of three carboxypeptidase A-phosphonate complexes determined by X-ray crystallography, *Biochemistry 30*, 8171–8180.
260. Rees, D. C., and Lipscomb, W. N. (1981) Binding of ligands to the active site of carboxypeptidase A, *Proc. Natl. Acad. Sci. U. S. A. 78*, 5455–5459.
261. Gardell, S. J., Craik, C. S., Hilvert, D., Urdea, M. S., and Rutter, W. J. (1985) Site-directed mutagenesis shows that Tyrosine 248 of carboxypeptidase A does not play a crucial role in catalysis, *Nature (London, U. K.) 317*, 551–555.
262. Taylor, A. B., Czerwinski, R. M., Johnson, W. H., Jr., Whitman, C. P., and Hackert, M. L. (1998) Crystal structure of 4–oxalocrotonate tautomerase inactivated by 2–oxo-3–pentynoate at 2.4 Å resolution: Analysis and implications for the mechanism of inactivation and catalysis, *Biochemistry 37*, 14692–14700.
263. Czerwinski, R. M., Johnson, W. H., Jr., and Whitman, C. P. (1997) Kinetic and structural effects of mutations of the catalytic amino-terminal proline in 4–oxalocrotonate tautomerase, *Biochemistry 36*, 14551–14560.
264. Leveque, V. J., Stroupe, M. E., Lepock, J. R., Cabelli, D. E., Tainer, J. A., Nick, H. S., and Silverman, D. N. (2000) Multiple replacements of Glutamine 143 in human manganese superoxide dismutase: Effects on structure, stability, and catalysis, *Biochemistry 39*, 7131–7137.
265. Mowat, C. G., Pankhurst, K. L., Miles, C. S., Leys, D., Walkinshaw, M. D., Reid, G. A., and Chapman, S. K. (2002) Engineering water to act as an active site acid catalyst in a soluble fumarate reductase, *Biochemistry 41*, 11990–11996.
266. Dajnowicz, S., Parks, J. M., Hu, X., Gesler, K., Kovalevsky, A. Y., and Mueser, T. C. (2017) Direct evidence that an extended hydrogen-bonding network influences activation of pyridoxal 5′-phosphate in aspartate aminotransferase, *J. Biol. Chem. 292*, 5970–5980.
267. Toney, M. D., and Kirsch, J. F. (1989) Direct Brønsted analysis of the restoration of activity to a mutant enzyme by exogenous amines, *Science (Washington, DC, U. S.) 243*, 1485–1488.

268. Harpel, M. R., and Hartman, F. C. (1994) Chemical rescue by exogenous amines of a site-directed mutant of ribulose 1,5–bisphosphate carboxylase/oxygenase that lacks a key lysyl residue, *Biochemistry 33*, 5553–5561.
269. Admiraal, S. J., Schneider, B., Meyer, P., Janin, J., Veron, M., Deville-Bonne, D., and Herschlag, D. (1999) Nucleophilic activation by positioning in phosphoryl transfer catalyzed by nucleoside diphosphate kinase, *Biochemistry 38*, 4701–4711.
270. Lehoux, I. E., and Mitra, B. (1999) (*S*)-Mandelate dehydrogenase from *Pseudomonas putida*: Mutations of the catalytic base Histidine-274 and chemical rescue of activity, *Biochemistry 38*, 9948–9955.
271. Rynkiewicz, M. J., and Seaton, B. A. (1996) Chemical rescue by guanidine derivatives of an arginine-substituted site-directed mutant of *Escherichia coli* ornithine transcarbamylase, *Biochemistry 35*, 16174–16179.
272. Lamba, V., Yabukarski, F., Pinney, M., and Herschlag, D. (2016) Evaluation of the catalytic contribution from a positioned general base in ketosteroid isomerase, *J. Am. Chem. Soc. 138*, 9902–9909.
273. Perona, J. J., Hedstrom, L., Wagner, R. L., Rutter, W. J., Craik, C. S., and Fletterick, R. J. (1994) Exogenous acetate reconstitutes the enzymatic activity of trypsin Asp189Ser, *Biochemistry 33*, 3252–3259.
274. MacLeod, A. M., Lindhorst, T., Withers, S. G., and Warren, R. A. (1994) The acid/base catalyst in the exoglucanase/xylanase from *Cellulomonas fimi* is Glutamic Acid 127: Evidence from detailed kinetic studies of mutants, *Biochemistry 33*, 6371–6376.
275. Sun, Y. R., Song, H. G., Li, J., Jiang, M., Li, Y., Zhou, J. H., and Guo, Z. H. (2012) Active site binding and catalytic role of bicarbonate in 1,4–dihydroxy-2–naphthoyl coenzyme A synthases from vitamin K biosynthetic pathways, *Biochemistry 51*, 4580–4589.
276. Rishavy, M. A., Hallgren, K. W., Yakubenko, A. V., Shtofman, R. L., Runge, K. W., and Berkner, K. L. (2006) Brønsted analysis reveals Lys218 as the carboxylase active site base that deprotonates vitamin K hydroquinone to initiate vitamin K-dependent protein carboxylation, *Biochemistry 45*, 13239–13248.
277. Gloss, L. M., and Kirsch, J. F. (1995) Examining the structural and chemical flexibility of the active site base, Lys-258, of *Escherichia coli* aspartate aminotransferase by replacement with unnatural amino acids, *Biochemistry 34*, 12323–12332.
278. Harpel, M. R., Larimer, F. W., and Hartman, F. C. (2002) Multifaceted roles of Lys166 of ribulose-bisphosphate carboxylase/oxygenase as discerned by product analysis and chemical rescue of site-directed mutants, *Biochemistry 41*, 1390–1397.
279. Smiley, J. A., and Jones, M. E. (1992) A unique catalytic and inhibitor-binding role for Lys93 of yeast orotidylate decarboxylase, *Biochemistry 31*, 12162–12168.
280. Zhang, Z. Y., Wang, Y., and Dixon, J. E. (1994) Dissecting the catalytic mechanism of protein-tyrosine phosphatases, *Proc. Natl. Acad. Sci. U. S. A. 91*, 1624–1627.
281. Oyugi, M. A., Bashiri, G., Baker, E. N., and Johnson-Winters, K. (2016) Investigating the reaction mechanism of F_{420}-dependent glucose-6-phosphate dehydrogenase from *Mycobacterium tuberculosis*: Kinetic analysis of the wild-type and mutant enzymes, *Biochemistry 55*, 5566–5577.
282. McClerren, A. L., Zhou, P., Guan, Z., Raetz, C. R., and Rudolph, J. (2005) Kinetic analysis of the zinc-dependent deacetylase in the lipid A biosynthetic pathway, *Biochemistry 44*, 1106–1113.
283. Beebe, J. A., Arabshahi, A., Clifton, J. G., Ringe, D., Petsko, G. A., and Frey, P. A. (2003) Galactose mutarotase: pH Dependence of enzymatic mutarotation, *Biochemistry 42*, 4414–4420.
284. Erman, J. E., Vitello, L. B., Miller, M. A., Shaw, A., Brown, K. A., and Kraut, J. (1993) Histidine 52 is a critical residue for rapid formation of cytochrome *c* peroxidase compound I, *Biochemistry 32*, 9798–9806.
285. Wang, Q., Trimbur, D., Graham, R., Warren, R. A., and Withers, S. G. (1995) Identification of the acid/base catalyst in *Agrobacterium faecalis* β-glucosidase by kinetic analysis of mutants, *Biochemistry 34*, 14554–14562.
286. Hiller, D. A., Dunican, B. F., Nallur, S., Li, N. S., Piccirilli, J. A., and Strobel, S. A. (2020) The positively charged active site of the bacterial toxin RelE causes a large shift in the general base pK_a, *Biochemistry 59*, 1665–1671.
287. Klein, C., Chen, P., Arevalo, J. H., Stura, E. A., Marolewski, A., Warren, M. S., Benkovic, S. J., and Wilson, I. A. (1995) Towards structure-based drug design: Crystal structure of a

multisubstrate adduct complex of glycinamide ribonucleotide transformylase at 1.96 Å resolution, *J. Mol. Biol. 249*, 153–175.
288. Sugio, S., Amisaki, T., Ohishi, H., and Tomita, K. (1988) Refined X-ray structure of the low pH form of ribonuclease T1–2′-guanylic acid complex at 1.9 Å resolution, *J. Biochem. 103*, 354–366.
289. Hofstein, H. A., Feng, Y., Anderson, V. E., and Tonge, P. J. (1999) Role of Glutamate 144 and Glutamate 164 in the catalytic mechanism of enoyl-CoA hydratase, *Biochemistry 38*, 9508–9516.
290. Sideraki, V., Wilson, D. K., Kurz, L. C., Quiocho, F. A., and Rudolph, F. B. (1996) Site-directed mutagenesis of Histidine 238 in mouse adenosine deaminase: Substitution of Histidine 238 does not impede hydroxylate formation, *Biochemistry 35*, 15019–15028.
291. Bong, S. M., Moon, J. H., Nam, K. H., Lee, K. S., Chi, Y. M., and Hwang, K. Y. (2008) Structural studies of human brain-type creatine kinase complexed with the ADP-Mg^{2+}-NO^{3-}-creatine transition-state analogue complex, *FEBS Lett. 582*, 3959–3965.
292. Yep, A., Kenyon, G. L., and McLeish, M. J. (2008) Saturation mutagenesis of putative catalytic residues of benzoylformate decarboxylase provides a challenge to the accepted mechanism, *Proc. Natl. Acad. Sci. U. S. A. 105*, 5733–5738.
293. Holman, C. M., and Benisek, W. F. (1994) Extent of proton transfer in the transition states of the reaction catalyzed by the Δ^5-3-ketosteroid isomerase of *Comamonas (Pseudomonas) testosteroni*: Site-specific replacement of the active site base, Aspartate 38, by the weaker base alanine-3–sulfinate, *Biochemistry 33*, 2672–2681.
294. O'Brien, P. J., and Ellenberger, T. (2003) Human alkyladenine DNA glycosylase uses acid–base catalysis for selective excision of damaged purines, *Biochemistry 42*, 12418–12429.
295. Denu, J. M., Zhou, G., Guo, Y., and Dixon, J. E. (1995) The catalytic role of Aspartic acid-92 in a human dual-specific protein-tyrosine-phosphatase, *Biochemistry 34*, 3396–3403.
296. Hupe, D. J., and Pohl, E. R. (1984) On the magnitude of primary isotope effects for proton abstraction from carbon, *J. Am. Chem. Soc. 106*, 5634–5640.
297. Rocek, J., Westheimer, F. H., Eschenmoser, A., Moldovanyi, L., and Schreiber, J. (1962) Chromic acid esters as intermediates in the oxidation of alcohols. Rate-limiting esterification of a sterically hindered alcohol, *Helv. Chim. Acta 45*, 2554–2567.
298. Maclean, J., and Ali, S. (2003) The structure of chorismate synthase reveals a novel flavin binding site fundamental to a unique chemical reaction, *Structure (Cambridge, MA, U. S.) 11*, 1499–1511.
299. Balasubramanian, S., Abell, C., and Coggins, J. R. (1990) Observation of an isotope effect in the chorismate synthase reaction, *J. Am. Chem. Soc. 112*, 8581–8583.
300. Li, L., and Marsh, E. N. (2006) Deuterium isotope effects in the unusual addition of toluene to fumarate catalyzed by benzylsuccinate synthase, *Biochemistry 45*, 13932–13938.
301. Leichus, B. N., Bradley, M., Nadeau, K., Walsh, C. T., and Blanchard, J. S. (1992) Kinetic isotope effect analysis of the reaction catalyzed by *Trypanosoma congolense* trypanothione reductase, *Biochemistry 31*, 6414–6420.
302. Pohl, B., Raichle, T., and Ghisla, S. (1986) Studies on the reaction mechanism of general acyl-CoA dehydrogenase. Determination of selective isotope effects in the dehydrogenation of butyryl-CoA, *Eur. J. Biochem. 160*, 109–115.
303. Fagan, R. L., Nelson, M. N., Pagano, P. M., and Palfey, B. A. (2006) Mechanism of flavin reduction in class 2 dihydroorotate dehydrogenases, *Biochemistry 45*, 14926–14932.
304. Grubmeyer, C., and Teng, H. (1999) Mechanism of *Salmonella typhimurium* histidinol dehydrogenase: Kinetic isotope effects and pH profiles, *Biochemistry 38*, 7355–7362.
305. Loewus, M. W. (1977) Hydrogen isotope effects in the cyclization of D-glucose 6-phosphate by *myo*-inositol-1–phosphate synthase, *J. Biol. Chem. 252*, 7221–7223.
306. Veerareddygari, G. R., Singh, S. K., and Mueller, E. G. (2016) The pseudouridine synthases proceed through a glycal intermediate, *J. Am. Chem. Soc. 138*, 7852–7855.
307. Sannikova, N., Gerak, C. A. N., Shidmoossavee, F. S., King, D. T., Shamsi Kazem Abadi, S., Lewis, A. R., and Bennet, A. J. (2018) Both chemical and non-chemical steps limit the catalytic efficiency of family 4 glycoside hydrolases, *Biochemistry 57*, 3378–3386.

308. Chakladar, S., Cheng, L., Choi, M., Liu, J., and Bennet, A. J. (2011) Mechanistic evaluation of *MelA* α-galactosidase from *Citrobacter freundii*: A family 4 glycosyl hydrolase in which oxidation is rate-limiting, *Biochemistry 50*, 4298–4308.
309. Maresh, J. J., Giddings, L. A., Friedrich, A., Loris, E. A., Panjikar, S., Trout, B. L., Stockigt, J., Peters, B., and O'Connor, S. E. (2008) Strictosidine synthase: Mechanism of a Pictet–Spengler catalyzing enzyme, *J. Am. Chem. Soc. 130*, 710–723.
310. Cox, E. D., and Cook, J. M. (1995) The Pictet–Spengler condensation: A new direction for an old reaction, *Chem. Rev. 95*, 1797–1842.
311. Denu, J. M., and Fitzpatrick, P. F. (1994) Intrinsic primary, secondary, and solvent kinetic isotope effects on the reductive half-reaction of D-amino acid oxidase: Evidence against a concerted mechanism, *Biochemistry 33*, 4001–4007.
312. Vrtis, J. M., White, A. K., Metcalf, W. W., and van der Donk, W. A. (2001) Phosphite dehydrogenase: An unusual phosphoryl transfer reaction, *J. Am. Chem. Soc. 123*, 2672–2673.
313. Howe, G. W., and van der Donk, W. A. (2019) Temperature-independent kinetic isotope effects as evidence for a Marcus-like model of hydride tunneling in phosphite dehydrogenase, *Biochemistry 58*, 4260–4268.
314. Francisco, W. A., Merkler, D. J., Blackburn, N. J., and Klinman, J. P. (1998) Kinetic mechanism and intrinsic isotope effects for the peptidylglycine α-amidating enzyme reaction, *Biochemistry 37*, 8244–8252.
315. Janes, S. M., and Klinman, J. P. (1991) An investigation of bovine serum amine oxidase active site stoichiometry: Evidence for an aminotransferase mechanism involving two carbonyl cofactors per enzyme dimer, *Biochemistry 30*, 4599–4605.
316. Palcic, M. M., and Klinman, J. P. (1983) Isotopic probes yield microscopic constants: Separation of binding energy from catalytic efficiency in the bovine plasma amine oxidase reaction, *Biochemistry 22*, 5957–5966.
317. Farnum, M., Palcic, M., and Klinman, J. P. (1986) pH dependence of deuterium isotope effects and tritium exchange in the bovine plasma amine oxidase reaction: A role for single-base catalysis in amine oxidation and imine exchange, *Biochemistry 25*, 1898–1904.
318. Schimerlik, M. I., Grimshaw, C. E., and Cleland, W. W. (1977) Determination of the rate-limiting steps for malic enzyme by the use of isotope effects and other kinetic studies, *Biochemistry 16*, 571–576.
319. Cook, P. F., and Cleland, W. W. (1981) Mechanistic deductions from isotope effects in multireactant enzyme mechanisms, *Biochemistry 20*, 1790–1796.
320. Shiner, V. J., and Neumann, T. E. (1989) Protium-deuterium fractionation factors for organic molecules calculated from vibrational force fields, *Z. Naturforsch., A: Phys. Sci. 44*, 337–354.
321. Cook, P. F., and Cleland, W. W. (2007) *Enzyme kinetics and mechanism*, Garland Science, New York.
322. Nidetzky, B., Klimacek, M., and Mayr, P. (2001) Transient-state and steady-state kinetic studies of the mechanism of NADH-dependent aldehyde reduction catalyzed by xylose reductase from the yeast *Candida tenuis*, *Biochemistry 40*, 10371–10381.
323. Grimshaw, C. E., Bohren, K. M., Lai, C. J., and Gabbay, K. H. (1995) Human aldose reductase: Rate constants for a mechanism including interconversion of ternary complexes by recombinant wild-type enzyme, *Biochemistry 34*, 14356–14365.
324. Lewis, B. E., and Schramm, V. L. (2003) Glucose binding isotope effects in the ternary complex of brain hexokinase demonstrate partial relief of ground-state destabilization, *J. Am. Chem. Soc. 125*, 4672–4673.
325. LaReau, R. D., Wan, W., and Anderson, V. E. (1989) Isotope effects on binding of NAD^+ to lactate dehydrogenase, *Biochemistry 28*, 3619–3624.
326. Plapp, B. V., Brooks, R. L., and Shore, J. D. (1973) Horse liver alcohol dehydrogenase. Amino groups and rate-limiting steps in catalysis, *J. Biol. Chem. 248*, 3470–3475.
327. Cook, P. F., Yoon, M. Y., Hara, S., and McClure, G. D., Jr. (1993) Product dependence of deuterium isotope effects in enzyme-catalyzed reactions, *Biochemistry 32*, 1795–1802.
328. Meier, T. W., Thoma, N. H., and Leadlay, P. F. (1996) Tritium isotope effects in adenosylcobalamin-dependent methylmalonyl-CoA mutase, *Biochemistry 35*, 11791–11796.
329. Cheng, M. C., and Marsh, E. N. (2005) Isotope effects for deuterium transfer between

substrate and coenzyme in adenosylcobalamin-dependent glutamate mutase, *Biochemistry 44*, 2686–2691.
330. Gadda, G., and Fitzpatrick, P. F. (2000) Mechanism of nitroalkane oxidase: 2. pH and kinetic isotope effects, *Biochemistry 39*, 1406–1410.
331. Bell, R. P., and Goodall, D. M. (1966) Kinetic hydrogen isotope effects in the ionization of some nitroparaffins, *Proc. R. Soc. London, A 294*, 273–297.
332. Swain, C. G., Stivers, E. C., Reuwer, J. F., Jr., and Schaad, L. J. (1958) Use of hydrogen isotope effects to identify the attacking nucleophile in the enolization of ketones catalyzed by acetic acid, *J. Am. Chem. Soc. 80*, 5885–5893.
333. Northrop, D. B. (1975) Steady-state analysis of kinetic isotope effects in enzymic reactions, *Biochemistry 14*, 2644–2651.
334. Stern, M. J., and Vogel, P. C. (1971) Relative tritium-deuterium isotope effects in the absence of large tunneling factors, *J. Am. Chem. Soc. 93*, 4664–4675.
335. Hirschi, J., and Singleton, D. A. (2005) The normal range for secondary Swain–Schaad exponents without tunneling or kinetic complexity, *J. Am. Chem. Soc. 127*, 3294–3295.
336. Tipton, P. A. (1993) Intermediate partitioning in the tartrate dehydrogenase-catalyzed oxidative decarboxylation of D-malate, *Biochemistry 32*, 2822–2827.
337. Sen, A., Yahashiri, A., and Kohen, A. (2011) Triple isotopic labeling and kinetic isotope effects: Exposing H-transfer steps in enzymatic systems, *Biochemistry 50*, 6462–6468.
338. Albery, W. J., and Knowles, J. R. (1977) The determination of the rate-limiting step in a proton transfer reaction from the breakdown of the Swain-Schaad relation, *J. Am. Chem. Soc. 99*, 637–638.
339. Miller, S. M., and Klinman, J. P. (1983) Magnitude of intrinsic isotope effects in the dopamine β-monooxygenase reaction, *Biochemistry 22*, 3091–3096.
340. Grissom, C. B., and Cleland, W. W. (1985) Use of intermediate partitioning to calculate intrinsic isotope effects for the reaction catalyzed by malic enzyme, *Biochemistry 24*, 944–948.
341. Hanau, S., Montin, K., Cervellati, C., Magnani, M., and Dallocchio, F. (2010) 6–Phosphogluconate dehydrogenase mechanism: Evidence for allosteric modulation by substrate, *J. Biol. Chem. 285*, 21366–21371.
342. Zgiby, S., Plater, A. R., Bates, M. A., Thomson, G. J., and Berry, A. (2002) A functional role for a flexible loop containing Glu182 in the class II fructose-1,6–bisphosphate aldolase from *Escherichia coli*, *J. Mol. Biol. 315*, 131–140.
343. Xu, Y., Dewanti, A. R., and Mitra, B. (2002) Arginine 165/Arginine 277 pair in (*S*)-mandelate dehydrogenase from *Pseudomonas putida*: Role in catalysis and substrate binding, *Biochemistry 41*, 12313–12319.
344. Gong, J., Hunter, G. A., and Ferreira, G. C. (1998) Aspartate-279 in aminolevulinate synthase affects enzyme catalysis through enhancing the function of the pyridoxal 5′-phosphate cofactor, *Biochemistry 37*, 3509–3517.
345. Hines, V., and Johnston, M. (1989) Mechanistic studies on the bovine liver mitochondrial dihydroorotate dehydrogenase using kinetic deuterium isotope effects, *Biochemistry 28*, 1227–1234.
346. Wagner, W., Breksa, A. P., 3rd, Monzingo, A. F., Appling, D. R., and Robertus, J. D. (2005) Kinetic and structural analysis of active site mutants of monofunctional NAD-dependent 5,10-methylenetetrahydrofolate dehydrogenase from *Saccharomyces cerevisiae*, *Biochemistry 44*, 13163–13171.
347. Emanuele, J. J., and Fitzpatrick, P. F. (1995) Mechanistic studies of the flavoprotein tryptophan 2-monooxygenase. 2. pH and kinetic isotope effects, *Biochemistry 34*, 3716–3723.
348. Leichus, B. N., and Blanchard, J. S. (1994) Isotopic analysis of the reaction catalyzed by glycerol dehydrogenase, *Biochemistry 33*, 14642–14649.
349. Czekster, C. M., Vandemeulebroucke, A., and Blanchard, J. S. (2011) Kinetic and chemical mechanism of the dihydrofolate reductase from *Mycobacterium tuberculosis*, *Biochemistry 50*, 367–375.
350. Argyrou, A., Washabaugh, M. W., and Pickart, C. M. (2000) Dihydroorotate dehydrogenase from *Clostridium oroticum* is a class 1B enzyme and utilizes a concerted mechanism of catalysis, *Biochemistry 39*, 10373–10384.
351. Hong, B., Maley, F., and Kohen, A. (2007) Role of Y94 in proton and hydride transfers

catalyzed by thymidylate synthase, *Biochemistry 46*, 14188–14197.
352. Westheimer, F. H. (1961) The magnitude of the primary kinetic isotope effect for compounds of hydrogen and deuterium, *Chem. Rev. 61*, 265–273.
353. Barnes, D. J., and Bell, R. P. (1970) Kinetic hydrogen isotope effects in the ionization of some carbon acids, *Proc. R. Soc. London, A 318*, 421–440.
354. Atkinson, J. K., Hollenberg, P. F., Ingold, K. U., Johnson, C. C., Le Tadic, M. H., Newcomb, M., and Putt, D. A. (1994) Cytochrome P450–catalyzed hydroxylation of hydrocarbons: Kinetic deuterium isotope effects for the hydroxylation of an ultrafast radical clock, *Biochemistry 33*, 10630–10637.
355. Scharschmidt, M., Fisher, M. A., and Cleland, W. W. (1984) Variation of transition-state structure as a function of the nucleotide in reactions catalyzed by dehydrogenases. 1. Liver alcohol dehydrogenase with benzyl alcohol and yeast aldehyde dehydrogenase with benzaldehyde, *Biochemistry 23*, 5471–5478.
356. Nesheim, J. C., and Lipscomb, J. D. (1996) Large kinetic isotope effects in methane oxidation catalyzed by methane monooxygenase: Evidence for C-H bond cleavage in a reaction cycle intermediate, *Biochemistry 35*, 10240–10247.
357. Ambundo, E. A., Friesner, R. A., and Lippard, S. J. (2002) Reactions of methane monooxygenase intermediate Q with derivatized methanes, *J. Am. Chem. Soc. 124*, 8770–8771.
358. Glickman, M. H., and Klinman, J. P. (1995) Nature of rate-limiting steps in the soybean lipoxygenase-1 reaction, *Biochemistry 34*, 14077–14092.
359. Jonsson, T., Glickman, M. H., Sun, S. J., and Klinman, J. P. (1996) Experimental evidence for extensive tunneling of hydrogen in the lipoxygenase reaction: Implications for enzyme catalysis, *J. Am. Chem. Soc. 118*, 10319–10320.
360. Hatcher, E., Soudackov, A. V., and Hammes-Schiffer, S. (2007) Proton-coupled electron transfer in soybean lipoxygenase: Dynamical behavior and temperature dependence of kinetic isotope effects, *J. Am. Chem. Soc. 129*, 187–196.
361. Chowdhury, S., and Banerjee, R. (2000) Evidence for quantum mechanical tunneling in the coupled cobalt-carbon bond homolysis-substrate radical generation reaction catalyzed by methylmalonyl-CoA mutase, *J. Am. Chem. Soc. 122*, 5417–5418.
362. Whittaker, M. M., Ballou, D. P., and Whittaker, J. W. (1998) Kinetic isotope effects as probes of the mechanism of galactose oxidase, *Biochemistry 37*, 8426–8436.
363. Danish, H. H., Doncheva, I. S., and Roth, J. P. (2011) Hydrogen tunneling steps in cyclooxygenase-2 catalysis, *J. Am. Chem. Soc. 133*, 15846–15849.
364. Francis, K., and Gadda, G. (2009) Inflated kinetic isotope effects in the branched mechanism of *Neurospora crassa* 2-nitropropane dioxygenase, *Biochemistry 48*, 2403–2410.
365. Pudney, C. R., Guerriero, A., Baxter, N. J., Johannissen, L. O., Waltho, J. P., Hay, S., and Scrutton, N. S. (2013) Fast protein motions are coupled to enzyme H-transfer reactions, *J. Am. Chem. Soc. 135*, 2512–2517.
366. Toney, M. D., Castro, J. N., and Addington, T. A. (2013) Heavy-enzyme kinetic isotope effects on proton transfer in alanine racemase, *J. Am. Chem. Soc. 135*, 2509–2511.
367. Kohen, A., Cannio, R., Bartolucci, S., and Klinman, J. P. (1999) Enzyme dynamics and hydrogen tunnelling in a thermophilic alcohol dehydrogenase, *Nature (London, U. K.) 399*, 496–499.
368. Harris, R. J., Meskys, R., Sutcliffe, M. J., and Scrutton, N. S. (2000) Kinetic studies of the mechanism of carbon–hydrogen bond breakage by the heterotetrameric sarcosine oxidase of *Arthrobacter* sp. 1–in, *Biochemistry 39*, 1189–1198.
369. Knapp, M. J., Rickert, K., and Klinman, J. P. (2002) Temperature-dependent isotope effects in soybean lipoxygenase-1: Correlating hydrogen tunneling with protein dynamics, *J. Am. Chem. Soc. 124*, 3865–3874.
370. Francisco, W. A., Knapp, M. J., Blackburn, N. J., and Klinman, J. P. (2002) Hydrogen tunneling in peptidylglycine α-hydroxylating monooxygenase, *J. Am. Chem. Soc. 124*, 8194–8195.
371. Wecksler, A. T., Kenyon, V., Garcia, N. K., Deschamps, J. D., van der Donk, W. A., and Holman, T. R. (2009) Kinetic and structural investigations of the allosteric site in human epithelial 15-lipoxygenase-2, *Biochemistry 48*, 8721–8730.

372. Stojkovic, V., Perissinotti, L. L., Willmer, D., Benkovic, S. J., and Kohen, A. (2012) Effects of the donor-acceptor distance and dynamics on hydride tunneling in the dihydrofolate reductase catalyzed reaction, *J. Am. Chem. Soc. 134*, 1738–1745.
373. Roston, D., and Kohen, A. (2013) A critical test of the "tunneling and coupled motion" concept in enzymatic alcohol oxidation, *J. Am. Chem. Soc. 135*, 13624–13627.
374. Isaacs, N. S. (1984) The effect of pressure on kinetic isotope effects, In *Isotope effects in organic chemistry, Vol. 6* (Buncel, E., and Lee, C. C., Eds.), pp 67–105, Elsevier, New York.
375. Northrop, D. B., and Cho, Y. K. (2000) Effect of pressure on deuterium isotope effects of yeast alcohol dehydrogenase: Evidence for mechanical models of catalysis, *Biochemistry 39*, 2406–2412.
376. Park, H., Girdaukas, G. G., and Northrop, D. B. (2006) Effect of pressure on a heavy-atom isotope effect of yeast alcohol dehydrogenase, *J. Am. Chem. Soc. 128*, 1868–1872.
377. Pudney, C. R., Hay, S., Levy, C., Pang, J., Sutcliffe, M. J., Leys, D., and Scrutton, N. S. (2009) Evidence to support the hypothesis that promoting vibrations enhance the rate of an enzyme catalyzed H-tunneling reaction, *J. Am. Chem. Soc. 131*, 17072–17073.
378. Northrop, D. B. (1999) Effects of high pressure on isotope effects and hydrogen tunneling, *J. Am. Chem. Soc. 121*, 3521–3524.
379. Shelton, G. R., Hrovat, D. A., and Borden, W. T. (2007) Tunneling in the 1,5-hydrogen shift reactions of 1,3-cyclopentadiene and 5-methyl-1,3-cyclopentadiene, *J. Am. Chem. Soc. 129*, 164–168.
380. Amin, M., Price, R. C., and Saunders, W. H., Jr. (1988) Isotope effects on isotope effects. Failure of the rule of the geometric mean as evidence for tunneling, *J. Am. Chem. Soc. 110*, 4085–4086.
381. Moore, K. W., Bachovchin, W. W., Gunter, J. B., and Richards, J. H. (1979) Hydrogen transfer in catalysis by adenosylcobalamin-dependent diol dehydratase, *Biochemistry 18*, 2776–2782.
382. Doll, K. M., Bender, B. R., and Finke, R. G. (2003) The first experimental test of the hypothesis that enzymes have evolved to enhance hydrogen tunneling, *J. Am. Chem. Soc. 125*, 10877–10884.
383. Pan, Z., Horner, J. H., and Newcomb, M. (2008) Tunneling in C–H oxidation reactions by an oxoiron(IV) porphyrin radical cation: Direct measurements of very large H/D kinetic isotope effects, *J. Am. Chem. Soc. 130*, 7776–7777.
384. Valley, M. P., and Fitzpatrick, P. F. (2004) Comparison of enzymatic and nonenzymatic nitroethane anion formation: Thermodynamics and contribution of tunneling, *J. Am. Chem. Soc. 126*, 6244–6245.
385. Wilde, T. C., Blotny, G., and Pollack, R. M. (2008) Experimental evidence for enzyme-enhanced coupled motion/quantum mechanical hydrogen tunneling by ketosteroid isomerase, *J. Am. Chem. Soc. 130*, 6577–6585.
386. Cheatum, C. M., and Kohen, A. (2013) Relationship of femtosecond-picosecond dynamics to enzyme-catalyzed H-transfer, *Top. Curr. Chem. 337*, 1–39.
387. Markle, T. F., Rhile, I. J., and Mayer, J. M. (2011) Kinetic effects of increased proton transfer distance on proton-coupled oxidations of phenol-amines, *J. Am. Chem. Soc. 133*, 17341–17352.
388. Kyte, J. (2007) *Structure in protein chemistry: Second edition*, pp 213–215, Garland Science, New York.
389. Alston, W. C., 2nd, Kanska, M., and Murray, C. J. (1996) Secondary H/T and D/T isotope effects in enzymatic enolization reactions. Coupled motion and tunneling in the triosephosphate isomerase reaction, *Biochemistry 35*, 12873–12881.
390. Kyte, J. (2007) *Structure in protein chemistry: Second edition*, p 277, Garland Science, New York.
391. Masgrau, L., Roujeinikova, A., Johannissen, L. O., Hothi, P., Basran, J., Ranaghan, K. E., Mulholland, A. J., Sutcliffe, M. J., Scrutton, N. S., and Leys, D. (2006) Atomic description of an enzyme reaction dominated by proton tunneling, *Science (Washington, DC, U. S.) 312*, 237–241.
392. Bahnson, B. J., Colby, T. D., Chin, J. K., Goldstein, B. M., and Klinman, J. P. (1997) A link between protein structure and enzyme catalyzed hydrogen tunneling, *Proc. Natl. Acad. Sci. U. S. A. 94*, 12797–12802.
393. Sawaya, M. R., and Kraut, J. (1997) Loop and subdomain movements in the mechanism of *Escherichia coli* dihydrofolate reductase:

Crystallographic evidence, *Biochemistry 36*, 586–603.
394. O'Leary, M. H., and Limburg, J. A. (1977) Isotope effect studies of the role of metal ions in isocitrate dehydrogenase, *Biochemistry 16*, 1129–1135.
395. Silva, R. G., and Schramm, V. L. (2011) Uridine phosphorylase from *Trypanosoma cruzi*: Kinetic and chemical mechanisms, *Biochemistry 50*, 9158–9166.
396. Goitein, R. K., Chelsky, D., and Parsons, S. M. (1978) Primary ^{14}C and α secondary ^{3}H substrate kinetic isotope effects for some phosphoribosyltransferases, *J. Biol. Chem. 253*, 2963–2971.
397. O'Leary, M. H., Urberg, M., and Young, A. P. (1974) Nitrogen isotope effects on the papain-catalyzed hydrolysis of *N*-benzoyl-L-argininamide, *Biochemistry 13*, 2077–2081.
398. Rosenberg, S., and Kirsch, J. F. (1981) Oxygen-18 leaving group kinetic isotope effects on the hydrolysis of nitrophenyl glycosides. 2. Lysozyme and β-glucosidase: Acid and alkaline hydrolysis, *Biochemistry 20*, 3196–3204.
399. Stanley, T. M., Johnson, W. H., Jr., Burks, E. A., Whitman, C. P., Hwang, C. C., and Cook, P. F. (2000) Expression and stereochemical and isotope effect studies of active 4-oxalocrotonate decarboxylase, *Biochemistry 39*, 718–726.
400. Rishavy, M. A., Cleland, W. W., and Lusty, C. J. (2000) ^{15}N Isotope effects in glutamine hydrolysis catalyzed by carbamyl phosphate synthetase: Evidence for a tetrahedral intermediate in the mechanism, *Biochemistry 39*, 7309–7315.
401. Axelsson, B. S., Bjurling, P., Matsson, O., and Laengstroem, B. (1992) Carbon-11/carbon-14 kinetic isotope effects in enzyme mechanism studies. $^{11}C/^{14}C$ Kinetic isotope effect of the tyrosine phenol-lyase catalyzed α,β-elimination of L-tyrosine, *J. Am. Chem. Soc. 114*, 1502–1503.
402. Swanson, T., Brooks, H. B., Osterman, A. L., O'Leary, M. H., and Phillips, M. A. (1998) Carbon-13 isotope effect studies of *Trypanosoma brucei* ornithine decarboxylase, *Biochemistry 37*, 14943–14947.
403. Parmentier, L. E., O'Leary, M. H., Schachman, H. K., and Cleland, W. W. (1992) ^{13}C Isotope effects as a probe of the kinetic mechanism and allosteric properties of *Escherichia coli* aspartate transcarbamylase, *Biochemistry 31*, 6570–6576.
404. Mundle, S. O., Rathgeber, S., Lacrampe-Couloume, G., Sherwood Lollar, B., and Kluger, R. (2009) Internal return of carbon dioxide in decarboxylation: Catalysis of separation and $^{12}C/^{13}C$ kinetic isotope effects, *J. Am. Chem. Soc. 131*, 11638–11639.
405. Paneth, P., and O'Leary, M. H. (1987) Isotope effect evidence for the zinc hydroxide mechanism of carbonic anhydrase catalysis, *Biochemistry 26*, 1728–1731.
406. Snider, M. J., Reinhardt, L., Wolfenden, R., and Cleland, W. W. (2002) ^{15}N Kinetic isotope effects on uncatalyzed and enzymatic deamination of cytidine, *Biochemistry 41*, 415–421.
407. Gustin, D. J., Mattei, P., Kast, P., Wiest, O., Lee, L., Cleland, W. W., and Hilvert, D. (1999) Heavy atom isotope effects reveal a highly polarized transition state for chorismate mutase, *J. Am. Chem. Soc. 121*, 1756–1757.
408. Wright, S. K., DeClue, M. S., Mandal, A., Lee, L., Wiest, O., Cleland, W. W., and Hilvert, D. (2005) Isotope effects on the enzymatic and nonenzymatic reactions of chorismate, *J. Am. Chem. Soc. 127*, 12957–12964.
409. Ehrlich, J. I., Hwang, C.-C., Cook, P. F., and Blanchard, J. S. (1999) Evidence for a stepwise mechanism of OMP decarboxylase, *J. Am. Chem. Soc. 121*, 6966–6967.
410. Van Vleet, J. L., Reinhardt, L. A., Miller, B. G., Sievers, A., and Cleland, W. W. (2008) Carbon isotope effect study on orotidine 5′-monophosphate decarboxylase: Support for an anionic intermediate, *Biochemistry 47*, 798–803.
411. Waldrop, G. L., Urbauer, J. L., and Cleland, W. W. (1992) ^{15}N Isotope effects on nonenzymatic and aspartate transcarbamylase catalyzed-reactions of carbamyl phosphate, *J. Am. Chem. Soc. 114*, 5941–5945.
412. Horenstein, B. A., Parkin, D. W., Estupinan, B., and Schramm, V. L. (1991) Transition-state analysis of nucleoside hydrolase from *Crithidia fasciculata*, *Biochemistry 30*, 10788–10795.
413. Jahnke, K., Podschun, B., Schnackerz, K. D., Kautz, J., and Cook, P. F. (1993) Acid-base catalytic mechanism of dihydropyrimidinase from pH studies, *Biochemistry 32*, 5160–5166.
414. Merkler, D. J., and Schramm, V. L. (1993) Catalytic mechanism of yeast adenosine 5′-monophosphate deaminase. Zinc content,

substrate specificity, pH studies, and solvent isotope effects, *Biochemistry 32*, 5792–5799.
415. Klimacek, M., and Nidetzky, B. (2002) Examining the relative timing of hydrogen abstraction steps during NAD^+-dependent oxidation of secondary alcohols catalyzed by long-chain D-mannitol dehydrogenase from *Pseudomonas fluorescens* using pH and kinetic isotope effects, *Biochemistry 41*, 10158–10165.
416. Podschun, B., Jahnke, K., Schnackerz, K. D., and Cook, P. F. (1993) Acid–base catalytic mechanism of the dihydropyrimidine dehydrogenase from pH studies, *J. Biol. Chem. 268*, 3407–3413.
417. Weiss, P. M., Cook, P. F., Hermes, J. D., and Cleland, W. W. (1987) Evidence from nitrogen-15 and solvent deuterium isotope effects on the chemical mechanism of adenosine deaminase, *Biochemistry 26*, 7378–7384.
418. Wolthers, K. R., and Schimerlik, M. I. (2002) Neuronal nitric oxide synthase: Substrate and solvent kinetic isotope effects on the steady-state kinetic parameters for the reduction of 2,6-dichloroindophenol and cytochrome c^{3+}, *Biochemistry 41*, 196–204.
419. Vidakovic, M., Sligar, S. G., Li, H., and Poulos, T. L. (1998) Understanding the role of the essential Asp251 in cytochrome P450cam using site-directed mutagenesis, crystallography, and kinetic solvent isotope effect, *Biochemistry 37*, 9211–9219.
420. Vergis, J. M., and Beardsley, G. P. (2004) Catalytic mechanism of the cyclohydrolase activity of human aminoimidazole carboxamide ribonucleotide formyltransferase/inosine monophosphate cyclohydrolase, *Biochemistry 43*, 1184–1192.
421. Bosma, T., Pikkemaat, M. G., Kingma, J., Dijk, J., and Janssen, D. B. (2003) Steady-state and pre-steady-state kinetic analysis of halopropane conversion by a *Rhodococcus* haloalkane dehalogenase, *Biochemistry 42*, 8047–8053.
422. Venkatasubban, K. S., and Schowen, R. L. (1984) The proton inventory technique, *CRC Crit. Rev. Biochem. 17*, 1–44.
423. Schowen, K. B. J. (1978) Solvent hydrogen isotope effects, In *Transition states of biochemical processes* (Gandour, R. D., and Schowen, R. L., Eds.), pp 225–279, Plenum Press Springer-Verlag, Boston, MA.
424. Hyland, L. J., Tomaszek, T. A., Jr., and Meek, T. D. (1991) Human immunodeficiency virus-1 protease. 2. Use of pH rate studies and solvent kinetic isotope effects to elucidate details of chemical mechanism, *Biochemistry 30*, 8454–8463.
425. Mitra, S., and Holz, R. C. (2007) Unraveling the catalytic mechanism of nitrile hydratases, *J. Biol. Chem. 282*, 7397–7404.
426. Matta, M. S., and Diep Thi, V. (1986) Proton inventory of the second step of ribonuclease catalysis, *J. Am. Chem. Soc. 108*, 5316–5318.
427. Kiick, D. M. (1991) Effect of commitments to catalysis on the degree of curvature in proton inventories of the kinetic parameters for enzyme-catalyzed reactions: Application to tryptophan indole-lyase, *J. Am. Chem. Soc. 113*, 8499–8504.
428. Karsten, W. E., Lai, C.-J., and Cook, P. F. (1995) Inverse solvent isotope effects in the NAD-malic enzyme reaction are the result of the viscosity difference between D_2O and H_2O: Implications for solvent isotope effect studies, *J. Am. Chem. Soc. 117*, 5914–5918.
429. Karsten, W. E., Chooback, L., and Cook, P. F. (1998) Glutamate 190 is a general acid catalyst in the 6-phosphogluconate-dehydrogenase-catalyzed reaction, *Biochemistry 37*, 15691–15697.
430. Acheson, S. A., Dedopoulou, D., and Quinn, D. M. (1987) Simple general acid-base catalysis and virtual transition states for acetylcholinesterase-catalyzed hydrolysis of phenyl esters, *J. Am. Chem. Soc. 109*, 239–245.
431. Chow, C., Hegde, S., and Blanchard, J. S. (2017) Mechanistic characterization of *Escherichia coli* L-aspartate oxidase from kinetic isotope effects, *Biochemistry 56*, 4044–4052.
432. Miyanaga, A., Fushinobu, S., Ito, K., Shoun, H., and Wakagi, T. (2004) Mutational and structural analysis of cobalt-containing nitrile hydratase on substrate and metal binding, *Eur. J. Biochem. 271*, 429–438.
433. Minasian, S. G., Whittaker, M. M., and Whittaker, J. W. (2004) Stereoselective hydrogen abstraction by galactose oxidase, *Biochemistry 43*, 13683–13693.
434. Jordan, D. B., Zheng, Y. J., Lockett, B. A., and Basarab, G. S. (2000) Stereochemistry of the enolization of scytalone by scytalone dehydratase, *Biochemistry 39*, 2276–2282.
435. Savile, C. K., Fabrias, G., and Buist, P. H. (2001) Dihydroceramide Δ^4 desaturase initiates substrate oxidation at C-4, *J. Am. Chem. Soc. 123*, 4382–4385.

436. Zabriskie, T. M., Kelly, W. L., and Liang, X. (1997) Stereochemical course of the oxidation of L-pipecolic acid by the flavoenzyme L-pipecolate oxidase, *J. Am. Chem. Soc. 119*, 6446–6447.
437. Shen, T. Y., and Westhead, E. W. (1973) Divalent cation and pH dependent primary isotope effects in the enolase reaction, *Biochemistry 12*, 3333–3337.
438. Malhotra, S. K., and Ringold, H. J. (1965) Chemistry of conjugate anions and enols. V. Stereochemistry, kinetics, and mechanism of the acid- and enzymatic-catalyzed isomerization of Δ^5-3-keto steroids, *J. Am. Chem. Soc. 87*, 3228–3236.
439. Gadd, R. E., and Henderson, J. F. (1970) The rate-limiting step in the adenine phosphoribosyltransferase reaction, *Biochem. Biophys. Res. Commun. 38*, 363–368.
440. Thomas, C. B., Arnold, W. J., and Kelley, W. N. (1973) Human adenine phosphoribosyltransferase. Purification, subunit structure, and substrate specificity, *J. Biol. Chem. 248*, 2529–2535.
441. Rayner, D. R., Gordon, A. J., and Mislow, K. (1968) Thermal racemization of diaryl, alkyl aryl, and dialkyl sulfoxides by pyramidal inversion, *J. Am. Chem. Soc. 90*, 4854–4860.
442. Kryukov, G. V., Kumar, R. A., Koc, A., Sun, Z., and Gladyshev, V. N. (2002) Selenoprotein R is a zinc-containing stereo-specific methionine sulfoxide reductase, *Proc. Natl. Acad. Sci. U. S. A. 99*, 4245–4250.
443. Lowther, W. T., Weissbach, H., Etienne, F., Brot, N., and Matthews, B. W. (2002) The mirrored methionine sulfoxide reductases of *Neisseria gonorrhoeae* pilB, *Nat. Struct. Biol. 9*, 348–352.
444. Hall, D. R., Bond, C. S., Leonard, G. A., Watt, C. I., Berry, A., and Hunter, W. N. (2002) Structure of tagatose-1,6–bisphosphate aldolase. Insight into chiral discrimination, mechanism, and specificity of class II aldolases, *J. Biol. Chem. 277*, 22018–22024.
445. Liu, D., Hwang, C. C., and Cook, P. F. (2002) Alternative substrates for malic enzyme: Oxidative decarboxylation of L-aspartate, *Biochemistry 41*, 12200–12203.
446. Bissett, D. L., and Anderson, R. L. (1980) Lactose and d-galactose metabolism in *Staphylococcus aureus*. IV. Isolation and properties of a class I D-ketohexose-1,6–diphosphate aldolase that catalyzes the cleavage of D-tagatose 1,6-diphosphate, *J. Biol. Chem. 255*, 8750–8755.
447. LowKam, C., Liotard, B., and Sygusch, J. (2010) Structure of a class I tagatose-1,6-bisphosphate aldolase: Investigation into an apparent loss of stereospecificity, *J. Biol. Chem. 285*, 21143–21152.
448. Lin, C. H., Sugai, T., Halcomb, R. L., Ichikawa, Y., and Wong, C. H. (1992) Unusual stereoselectivity in sialic acid aldolase-catalyzed aldol condensations: Synthesis of both enantiomers of high-carbon monosaccharides, *J. Am. Chem. Soc. 114*, 10138–10145.
449. Thoden, J. B., Vinogradov, E., Gilbert, M., Salinger, A. J., and Holden, H. M. (2015) Bacterial sugar 3,4–ketoisomerases: Structural insight into product stereochemistry, *Biochemistry 54*, 4495–4506.
450. Wu, W.-J., Feng, Y., He, X., Hofstein, H. A., Raleigh, D. P., and Tonge, P. J. (2000) Stereospecificity of the reaction catalyzed by enoyl-CoA hydratase, *J. Am. Chem. Soc. 122*, 3987–3994.
451. Feng, Y., Hofstein, H. A., Zwahlen, J., and Tonge, P. J. (2002) Effect of mutagenesis on the stereochemistry of enoyl-CoA hydratase, *Biochemistry 41*, 12883–12890.
452. Harris, T. K., Czerwinski, R. M., Johnson, W. H., Jr., Legler, P. M., Abeygunawardana, C., Massiah, M. A., Stivers, J. T., Whitman, C. P., and Mildvan, A. S. (1999) Kinetic, stereochemical, and structural effects of mutations of the active site arginine residues in 4-oxalocrotonate tautomerase, *Biochemistry 38*, 12343–12357.
453. van Den Heuvel, R. H., Fraaije, M. W., Ferrer, M., Mattevi, A., and van Berkel, W. J. (2000) Inversion of stereospecificity of vanillyl-alcohol oxidase, *Proc. Natl. Acad. Sci. U. S. A. 97*, 9455–9460.
454. Obata, R., and Nakasako, M. (2010) Structural basis for inverting the enantioselectivity of arylmalonate decarboxylase revealed by the structural analysis of the Gly74Cys/Cys188Ser mutant in the liganded form, *Biochemistry 49*, 1963–1969.
455. Watson, J. N., Dookhun, V., Borgford, T. J., and Bennet, A. J. (2003) Mutagenesis of the conserved active-site tyrosine changes a retaining sialidase into an inverting sialidase, *Biochemistry 42*, 12682–12690.

456. Adegoke, G. O., and Ojo, M. O. (1982) Biochemical characterization of Staphylococci isolated from goats, *Vet Microbiol 7*, 463–470.
457. Wang, J. B., Ilie, A., Yuan, S., and Reetz, M. T. (2017) Investigating substrate scope and enantioselectivity of a defluorinase by a stereochemical probe, *J. Am. Chem. Soc. 139*, 11241–11247.
458. Bijvoet, J. M., Peerdeman, A. F., and Vanbommel, A. J. (1951) Determination of the absolute configuration of optically active compounds by means of X-rays, *Nature (London, U. K.) 168*, 271–272.
459. Hanson, K. R. (1966) Applications of the sequence rule. I. Naming the paired ligands g,g at a tetrahedral atom Xggij. II. Naming the two faces of a trigonal atom Yghi, *J. Am. Chem. Soc. 88*, 2731–2742.
460. Hanson, K. R., and Rose, I. A. (1963) The absolute stereochemical course of citric acid biosynthesis, *Proc. Natl. Acad. Sci. U. S. A. 50*, 981–988.
461. Gottschalk, G., and Barker, H. A. (1966) Synthesis of glutamate and citrate by *Clostridium kluyveri*. A new type of citrate synthase, *Biochemistry 5*, 1125–1133.
462. Karpusas, M., Branchaud, B., and Remington, S. J. (1990) Proposed mechanism for the condensation reaction of citrate synthase: 1.9-Å Structure of the ternary complex with oxaloacetate and carboxymethyl coenzyme A, *Biochemistry 29*, 2213–2219.
463. Estevez, M., Skarda, J., Spencer, J., Banaszak, L., and Weaver, T. M. (2002) X-ray crystallographic and kinetic correlation of a clinically observed human fumarase mutation, *Protein Sci. 11*, 1552–1557.
464. Mechaly, A. E., Haouz, A., Miras, I., Barilone, N., Weber, P., Shepard, W., Alzari, P. M., and Bellinzoni, M. (2012) Conformational changes upon ligand binding in the essential class II fumarase Rv1098c from *Mycobacterium tuberculosis*, *FEBS Lett. 586*, 1606–1611.
465. Fisher, H. F., Frieden, C., Mckee, J. S. M., and Alberty, R. A. (1955) Concerning the stereospecificity of the fumarase reaction and the demonstration of a new intermediate, *J. Am. Chem. Soc. 77*, 4436–4436.
466. Gawron, O., and Fondy, T. P. (1959) Stereochemistry of the fumarase- and aspartase-catalyzed reactions and of the Krebs cycle from fumaric acid to D-isocitric acid, *J. Am. Chem. Soc. 81*, 6333–6334.
467. Anet, F. A. L. (1960) Configuration of deuterio-L-malic acid produced enzymically. Synthesis of *threo*-3-deuterio-DL-malic acid, *J. Am. Chem. Soc. 82*, 994–995.
468. Groninger-Poe, F. P., Bouvier, J. T., Vetting, M. W., Kalyanaraman, C., Kumar, R., Almo, S. C., Jacobson, M. P., and Gerlt, J. A. (2014) Evolution of enzymatic activities in the enolase superfamily: Galactarate dehydratase III from *Agrobacterium tumefaciens* C58, *Biochemistry 53*, 4192–4203.
469. Keys, L. D., III, and Johnston, M. (1985) Stereoselectivity in the enzymatic oxidation and nonenzymatic hydrogen-exchange reactions of dihydroorotate, *J. Am. Chem. Soc. 107*, 486–492.
470. Fitzgerald, M. C., Chernushevich, I., Standing, K. G., Kent, S. B. H., and Whitman, C. P. (1995) Total chemical synthesis and catalytic properties of the enzyme enantiomers L- and D-4-oxalocrotonate tautomerase, *J. Am. Chem. Soc. 117*, 11075–11080.
471. Jamil, F., Gardner, Q.-t.-A. A., Bashir, Q., Rashid, N., and Akhtar, M. (2010) Mechanistic and stereochemical studies of glycine oxidase from *Bacillus subtilis* strain R5, *Biochemistry 49*, 7377–7383.
472. Edwards, C. H., Golding, B. T., Kroll, F., Beatrix, B., Broker, G., and Buckel, W. (1996) Rotation of the exo-methylene group of 2-methyleneglutarate catalyzed by coenzyme B_{12}-dependent 2-methyleneglutarate mutase from *Clostridium barkeri*, *J. Am. Chem. Soc. 118*, 4192–4193.
473. Gore, M. P., Nanjappan, P., Hoops, G. C., and Woodard, R. W. (1990) Synthesis of (*E*)-3-deuteriophosphoenolpyruvate and (*Z*)-3-deuteriophosphoenolpyruvate, *J. Org. Chem. 55*, 758–760.
474. Onderka, D. K., and Floss, H. G. (1969) Steric course of chorismate synthetase reaction and 3-deoxy-D-arabino-heptulosonate 7-phosphate (DAHP) synthetase reaction, *J. Am. Chem. Soc. 91*, 5894–5896.
475. Rose, I. A., O'Connell, E. L., Noce, P., Utter, M. F., Wood, H. G., Willard, J. M., Cooper, T. G., and Benziman, M. (1969) Stereochemistry of the enzymatic carboxylation of phosphoenolpyruvate, *J. Biol. Chem. 244*, 6130–6133.
476. Dotson, G. D., Nanjappan, P., Reily, M. D., and Woodard, R. W. (1993) Stereochemistry

of 3-deoxyoctulosonate 8-phosphate synthase, *Biochemistry 32*, 12392–12397.
477. Vainer, R., Belakhov, V., Rabkin, E., Baasov, T., and Adir, N. (2005) Crystal structures of *Escherichia coli* KDO8P synthase complexes reveal the source of catalytic irreversibility, *J. Mol. Biol. 351*, 641–652.
478. Bartsch, R. A., and Zavada, J. (1980) Stereochemical and base species dichotomies in olefin-forming E2 eliminations, *Chem. Rev. 80*, 453–494.
479. Sawada, S., Tanaka, A., Yuzoinouye, Hirasawa, T., and Soda, K. (1974) Biostereochemistry of histidine metabolism. II. The steric course of ammonia elimination from L-histidine, *Biochim. Biophys. Acta 350*, 354–357.
480. Retey, J., Fierz, H., and Zeylemaker, W. P. (1970) Steric course of the histidase reaction, *FEBS Lett. 6*, 203–205.
481. Schroepfer, G. J., Jr. (1966) Stereospecific conversion of oleic acid to 10-hydroxystearic acid, *J. Biol. Chem. 241*, 5441–5447.
482. Mohrig, J. R., Schultz, S. C., and Morin, G. (1983) Syn and anti stereochemistry in elimination reactions producing acyclic conjugated thioesters, *J. Am. Chem. Soc. 105*, 5150–5151.
483. Willadsen, P., and Eggerer, H. (1975) Substrate stereochemistry of the enoyl-CoA hydratase reaction, *Eur. J. Biochem. 54*, 247–252.
484. Burks, E. A., Johnson, W. H., Jr., and Whitman, C. P. (1998) Stereochemical and isotopic labeling studies of 2-oxo-hept-4-ene-1,7-dioate hydratase: Evidence for an enzyme-catalyzed ketonization step in the hydration reaction, *J. Am. Chem. Soc. 120*, 7665–7675.
485. Johnson, W. H., Jr., Stack, T. M., Taylor, S. M., Burks, E. A., and Whitman, C. P. (2016) Stereochemical consequences of vinylpyruvate hydratase-catalyzed reactions, *Biochemistry 55*, 4055–4064.
486. Izumi, A., Rea, D., Adachi, T., Unzai, S., Park, S. Y., Roper, D. I., and Tame, J. R. (2007) Structure and mechanism of HpcG, a hydratase in the homoprotocatechuate degradation pathway of *Escherichia coli*, *J. Mol. Biol. 370*, 899–911.
487. Hogancamp, T. N., Mabanglo, M. F., and Raushel, F. M. (2018) Structure and reaction mechanism of the LigJ hydratase: An enzyme critical for the bacterial degradation of lignin in the protocatechuate 4,5-cleavage pathway, *Biochemistry 57*, 5841–5850.
488. Lees, W. J., Benson, T. E., Hogle, J. M., and Walsh, C. T. (1996) (*E*)-Enolbutyryl-UDP-*N*-acetylglucosamine as a mechanistic probe of UDP-*N*-acetylenolpyruvylglucosamine reductase (MurB), *Biochemistry 35*, 1342–1351.
489. Liu, H., Wallace, K. K., and Reynolds, K. A. (1997) Linking diversity in evolutionary origin and stereospecificity for enoyl thioester reductases: Determination and interpretation of the novel stereochemical course of reaction catalyzed by crotonyl CoA reductase from *Streptomyces collinus*, *J. Am. Chem. Soc. 119*, 2973–2979.
490. Sedgwick, B., and Morris, C. (1980) Stereochemical course of hydrogen transfer catalyzed by the enoyl reductase of the yeast fatty acid synthetase, *J. Chem. Soc., Chem. Commun.*, 96–97.
491. Anderson, V. E., and Hammes, G. G. (1984) Stereochemistry of the reactions catalyzed by chicken liver fatty acid synthase, *Biochemistry 23*, 2088–2094.
492. Wilton, D. C., and Akhtar, M. (1970) The stereochemistry of hydrogen elimination during 7,8-double bond formation by *Tetrahymena pyriformis*, *Biochem. J. 116*, 337–339.
493. Clayton, R. B., and Edwards, A. M. (1963) Conversion of 5-α-cholestan-3-β-ol to Δ^7-5-α-cholesten-3-β-ol in cockroaches, *J. Biol. Chem. 238*, 1966–1972.
494. Abad, J. L., Camps, F., and Fabrias, G. (2007) Substrate-dependent stereochemical course of the (*Z*)-13-desaturation catalyzed by the processionary moth multifunctional desaturase, *J. Am. Chem. Soc. 129*, 15007–15012.
495. Ramer, S. E., Cheng, H., Palcic, M. M., and Vederas, J. C. (1988) Formation of peptide amides by peptidylglycine α-amidating monooxygenase: A new assay and stereochemistry of hydrogen loss, *J. Am. Chem. Soc. 110*, 8526–8532.
496. Ping, D., Katopodis, A. G., and May, S. W. (1992) Tandem stereochemistry of peptidylglycine α-monooxygenase and peptidylamidoglycolate lyase, the two enzymes involved in peptide amidation, *J. Am. Chem. Soc. 114*, 3998–4000.
497. Kim, H. J., Liu, Y. N., McCarty, R. M., and Liu, H. W. (2017) Reaction catalyzed by GenK, a cobalamin-dependent radical *S*-adenosyl-L-methionine methyltransferase in the bio-

synthetic pathway of gentamicin, proceeds with retention of configuration, *J. Am. Chem. Soc. 139*, 16084–16087.
498. Schweifer, A., and Hammerschmidt, F. (2018) Stereochemical course of methyl transfer by cobalamin-dependent radical SAM methyltransferase in fosfomycin biosynthesis, *Biochemistry 57*, 2069–2073.
499. Sandoval, B. A., Meichan, A. J., and Hyster, T. K. (2017) Enantioselective hydrogen atom transfer: Discovery of catalytic promiscuity in flavin-dependent 'ene'-reductases, *J. Am. Chem. Soc. 139*, 11313–11316.
500. Weller, V. A., and Distefano, M. D. (1998) Measurement of the α-secondary kinetic isotope effect for a prenyltransferase by MALDI mass spectrometry, *J. Am. Chem. Soc. 120*, 7975–7976.
501. Poulter, C. D., Wiggins, P. L., and Le, A. T. (1981) Farnesylpyrophosphate synthetase. A stepwise mechanism for the 1′-4 condensation reaction, *J. Am. Chem. Soc. 103*, 3926–3927.
502. Mu, Y., Omer, C. A., and Gibbs, R. A. (1996) On the stereochemical course of human protein-farnesyl transferase, *J. Am. Chem. Soc. 118*, 1817–1823.
503. Clausen, V. A., Edelstein, R. L., and Distefano, M. D. (2001) Stereochemical analysis of the reaction catalyzed by human protein geranylgeranyl transferase, *Biochemistry 40*, 3920–3930.
504. Long, S. B., Casey, P. J., and Beese, L. S. (2002) Reaction path of protein farnesyltransferase at atomic resolution, *Nature (London, U. K.) 419*, 645–650.
505. Wanninayake, U., and Walker, K. D. (2013) A bacterial tyrosine aminomutase proceeds through retention or inversion of stereochemistry to catalyze its isomerization reaction, *J. Am. Chem. Soc. 135*, 11193–11204.
506. Woo, E. R., Fujii, I., Ebizuka, Y., Sankawa, U., Kawaguchi, A., Huang, S., Beale, J. M., Shibuya, M., Mocek, U., and Floss, H. G. (1989) Nonstereospecific proton removal in the enzymatic formation of orsellinic acid from chiral malonate, *J. Am. Chem. Soc. 111*, 5498–5500.
507. Moore, B. S., Eisenberg, R., Weber, C., Bridges, A., Nanz, D., and Robinson, J. A. (1995) On the stereospecificity of the coenzyme B_{12}-dependent isobutyryl-CoA mutase reaction, *J. Am. Chem. Soc. 117*, 11285–11291.
508. Coleman, A. A., Scaman, C. H., Kang, Y. J., and Palcic, M. M. (1991) Stereochemical trends in copper amine oxidase reactions, *J. Biol. Chem. 266*, 6795–6800.
509. Kusakabe, H., Kodama, K., Kuninaka, A., Yoshino, H., Misono, H., and Soda, K. (1980) A new antitumor enzyme, L-lysine α-oxidase from *Trichoderma viride*. Purification and enzymological properties, *J. Biol. Chem. 255*, 976–981.
510. Asada, Y., Tanizawa, K., Sawada, S., Suzuki, T., Misono, H., and Soda, K. (1981) Stereochemistry of *meso*-α,ε-diaminopimelate decarboxylase reaction: The first evidence for pyridoxal 5′-phosphate dependent decarboxylation with inversion of configuration, *Biochemistry 20*, 6881–6886.
511. Hill, R. K., and Newkome, G. R. (1969) Stereochemistry of chorismic acid biosynthesis, *J. Am. Chem. Soc. 91*, 5893–5894.
512. Smissman, E. E., Suh, J. T., Oxman, M., and Daniels, R. (1962) A stereospecific synthesis of D(−)-skikimic acid, *J. Am. Chem. Soc. 84*, 1040–1041.
513. Benson, T. E., Walsh, C. T., and Hogle, J. M. (1997) X-ray crystal structures of the S229A mutant and wild-type MurB in the presence of the substrate enolpyruvyl-UDP-N-acetylglucosamine at 1.8-Å resolution, *Biochemistry 36*, 806–811.
514. Thulasiram, H. V., and Poulter, C. D. (2006) Farnesyl diphosphate synthase: The art of compromise between substrate selectivity and stereoselectivity, *J. Am. Chem. Soc. 128*, 15819–15823.
515. Hosfield, D. J., Zhang, Y., Dougan, D. R., Broun, A., Tari, L. W., Swanson, R. V., and Finn, J. (2004) Structural basis for bisphosphonate-mediated inhibition of isoprenoid biosynthesis, *J. Biol. Chem. 279*, 8526–8529.
516. Ito, M., Kobayashi, M., Koyama, T., and Ogura, K. (1987) Stereochemical analysis of prenyltransferase reactions leading to (*Z*)- and (*E*)-polyprenyl chains, *Biochemistry 26*, 4745–4750.
517. Koksal, M., Zimmer, I., Schnitzler, J. P., and Christianson, D. W. (2010) Structure of isoprene synthase illuminates the chemical mechanism of teragram atmospheric carbon emission, *J. Mol. Biol. 402*, 363–373.
518. Whitman, C. P., Hajipour, G., Watson, R. J., Johnson, W. H., Jr., Bembenek, M. E., and Stolowich, N. J. (1992) Stereospecific keton-

ization of 2-hydroxymuconate by 4-oxalocrotonate tautomerase and 5-(carboxymethyl)-2-hydroxymuconate isomerase, *J. Am. Chem. Soc. 114*, 10104–10110.
519. Rose, I. A., O'Connell, E. L., and Mortlock, R. P. (1969) Stereochemical evidence for a *cis*-enediol intermediate in Mn-dependent aldose isomerases, *Biochim. Biophys. Acta 178*, 376–379.
520. Topper, Y. J. (1957) On the mechanism of action of phosphoglucose isomerase and phosphomannose isomerase, *J. Biol. Chem. 225*, 419–425.
521. Rose, I. A. (1958) Absolute configuration of dihydroxyacetone phosphate tritiated by aldolase reaction, *J. Am. Chem. Soc. 80*, 5835–5836.
522. Rose, I. A., and O'Connell, E. L. (1960) Stereospecificity of the sugarphosphate isomerase reactions: A uniformity, *Biochim. Biophys. Acta 42*, 159–160.
523. Rose, I. A., and O'Connell, E. L. (1961) Intramolecular hydrogen transfer in the phosphoglucose isomerase reaction, *J. Biol. Chem. 236*, 3086–3092.
524. O'Donoghue, A. C., Amyes, T. L., and Richard, J. P. (2005) Hydron transfer catalyzed by triosephosphate isomerase. Products of isomerization of dihydroxyacetone phosphate in D_2O, *Biochemistry 44*, 2622–2631.
525. Simon, H., and Medina, R. (1966) Mannose-6–phosphate isomerase reaction with mannose-2-^{3}H, *Z. Naturforsch., B: J. Chem. Sci. 21*, 496–497.
526. Seemann, J. E., and Schulz, G. E. (1997) Structure and mechanism of L-fucose isomerase from *Escherichia coli*, *J. Mol. Biol. 273*, 256–268.
527. Davies, C., Muirhead, H., and Chirgwin, J. (2003) The structure of human phosphoglucose isomerase complexed with a transition-state analogue, *Acta Crystallogr., Sect. D: Biol. Crystallogr. 59*, 1111–1113.
528. Roos, A. K., Burgos, E., Ericsson, D. J., Salmon, L., and Mowbray, S. L. (2005) Competitive inhibitors of *Mycobacterium tuberculosis* ribose-5–phosphate isomerase B reveal new information about the reaction mechanism, *J. Biol. Chem. 280*, 6416–6422.
529. Sagurthi, S. R., Gowda, G., Savithri, H. S., and Murthy, M. R. (2009) Structures of mannose-6-phosphate isomerase from *Salmonella typhimurium* bound to metal atoms and substrate: Implications for catalytic mechanism, *Acta Crystallogr., Sect. D: Biol. Crystallogr. 65*, 724–732.
530. Takeda, K., Yoshida, H., Izumori, K., and Kamitori, S. (2010) X-ray structures of *Bacillus pallidus* D-arabinose isomerase and its complex with L-fucitol, *Biochim. Biophys. Acta 1804*, 1359–1368.
531. Arsenieva, D., Hardre, R., Salmon, L., and Jeffery, C. J. (2002) The crystal structure of rabbit phosphoglucose isomerase complexed with 5-phospho-D-arabinonohydroxamic acid, *Proc. Natl. Acad. Sci. U. S. A. 99*, 5872–5877.
532. Landro, J. A., Brush, E. J., and Kozarich, J. W. (1992) Isomerization of (*R*)- and (*S*)-glutathiolactaldehydes by glyoxalase I: The case for dichotomous stereochemical behavior in a single active site, *Biochemistry 31*, 6069–6077.
533. Crowther, J. M., Cross, P. J., Oliver, M. R., Leeman, M. M., Bartl, A. J., Weatherhead, A. W., North, R. A., Donovan, K. A., Griffin, M. D. W., Suzuki, H., Hudson, A. O., Kasanmascheff, M., and Dobson, R. C. J. (2019) Structure-function analyses of two plant *meso*-diaminopimelate decarboxylase isoforms reveal that active-site gating provides stereochemical control, *J. Biol. Chem. 294*, 8505–8515.
534. Phillips, R. S., Poteh, P., Krajcovic, D., Miller, K. A., and Hoover, T. R. (2019) Crystal structure of D-ornithine/D-lysine decarboxylase, a stereoinverting decarboxylase: Implications for substrate specificity and stereospecificity of fold III decarboxylases, *Biochemistry 58*, 1038–1042.
535. Chang, M. N. T., and Walsh, C. T. (1981) Stereochemical analysis of γ-replacement and γ-elimination processes catalyzed by a pyridoxal phosphate dependent enzyme, *J. Am. Chem. Soc. 103*, 4921–4927.
536. Fuganti, C., and Coggiola, D. (1977) Further information on the mechanism of the cystathionine-λ-synthase catalyzed reactions from the assignment of the proton NMR spectrum of homoserine, *Experientia 33*, 847.
537. Steegborn, C., Laber, B., Messerschmidt, A., Huber, R., and Clausen, T. (2001) Crystal structures of cystathionine gamma-synthase inhibitor complexes rationalize the increased affinity of a novel inhibitor, *J. Mol. Biol. 311*, 789–801.

538. Steegborn, C., Messerschmidt, A., Laber, B., Streber, W., Huber, R., and Clausen, T. (1999) The crystal structure of cystathionine gamma-synthase from *Nicotiana tabacum* reveals its substrate and reaction specificity, *J. Mol. Biol. 290*, 983–996.
539. Prescott, D. J., and Rabinowitz, J. L. (1968) The enzymatic carboxylation of propionyl coenzyme A. Studies involving deuterated and tritiated substrates, *J. Biol. Chem. 243*, 1551–1557.
540. Retey, J., and Lynen, F. (1965)[On the biochemical function of biotin. IX. The steric course in the carboxylation of propionyl-CoA], *Biochem. Z. 342*, 256–271.
541. Diacovich, L., Mitchell, D. L., Pham, H., Gago, G., Melgar, M. M., Khosla, C., Gramajo, H., and Tsai, S.-C. (2004) Crystal structure of the β-subunit of acyl-CoA carboxylase: Structure-based engineering of substrate specificity, *Biochemistry 43*, 14027–14036.
542. Dubois, J., Dugave, C., Foures, C., Kaminsky, M., Tabet, J. C., Bory, S., Gaudry, M., and Marquet, A. (1991) Vitamin K dependent carboxylation: Determination of the stereochemical course using a 4-fluoroglutamyl-containing substrate, *Biochemistry 30*, 10506–10512.
543. Cohn, M., Pearson, J. E., O'Connell, E. L., and Rose, I. A. (1970) Nuclear magnetic resonance assignment of the vinyl hydrogens of phospho*enol*pyruvate. Stereochemistry of the enolase reaction, *J. Am. Chem. Soc. 92*, 4095–4098.
544. Larsen, T. M., Wedekind, J. E., Rayment, I., and Reed, G. H. (1996) A carboxylate oxygen of the substrate bridges the magnesium ions at the active site of enolase: Structure of the yeast enzyme complexed with the equilibrium mixture of 2–phosphoglycerate and phospho*enol*pyruvate at 1.8 Å resolution, *Biochemistry 35*, 4349–4358.
545. Duquerroy, S., Camus, C., and Janin, J. (1995) X-ray structure and catalytic mechanism of lobster enolase, *Biochemistry 34*, 12513–12523.
546. Babbitt, P. C., Mrachko, G. T., Hasson, M. S., Huisman, G. W., Kolter, R., Ringe, D., Petsko, G. A., Kenyon, G. L., and Gerlt, J. A. (1995) A functionally diverse enzyme superfamily that abstracts the α protons of carboxylic acids, *Science (Washington, DC, U. S.) 267*, 1159–1161.
547. Babbitt, P. C., Hasson, M. S., Wedekind, J. E., Palmer, D. R., Barrett, W. C., Reed, G. H., Rayment, I., Ringe, D., Kenyon, G. L., and Gerlt, J. A. (1996) The enolase superfamily: A general strategy for enzyme-catalyzed abstraction of the α-protons of carboxylic acids, *Biochemistry 35*, 16489–16501.
548. Wedekind, J. E., Reed, G. H., and Rayment, I. (1995) Octahedral coordination at the high-affinity metal site in enolase: Crystallographic analysis of the Mg^{II}–enzyme complex from yeast at 1.9 Å resolution, *Biochemistry 34*, 4325–4330.
549. Yew, W. S., Fedorov, A. A., Fedorov, E. V., Rakus, J. F., Pierce, R. W., Almo, S. C., and Gerlt, J. A. (2006) Evolution of enzymatic activities in the enolase superfamily: L-Fuconate dehydratase from *Xanthomonas campestris*, *Biochemistry 45*, 14582–14597.
550. Petsko, G. A., Kenyon, G. L., Gerlt, J. A., Ringe, D., and Kozarich, J. W. (1993) On the origin of enzymatic species, *Trends Biochem. Sci. 18*, 372–376.
551. Yew, W. S., Fedorov, A. A., Fedorov, E. V., Wood, B. M., Almo, S. C., and Gerlt, J. A. (2006) Evolution of enzymatic activities in the enolase superfamily: D-Tartrate dehydratase from *Bradyrhizobium japonicum*, *Biochemistry 45*, 14598–14608.
552. Chari, R. V. J., Whitman, C. P., Kozarich, J. W., Ngai, K. L., and Ornston, L. N. (1987) Absolute stereochemical course of the 3-carboxymuconate cycloisomerases from *Pseudomonas putida* and *Acinetobacter calcoaceticus*: Analysis and implications, *J. Am. Chem. Soc. 109*, 5514–5519.
553. Sakai, A., Fedorov, A. A., Fedorov, E. V., Schnoes, A. M., Glasner, M. E., Brown, S., Rutter, M. E., Bain, K., Chang, S., Gheyi, T., Sauder, J. M., Burley, S. K., Babbitt, P. C., Almo, S. C., and Gerlt, J. A. (2009) Evolution of enzymatic activities in the enolase superfamily: Stereochemically distinct mechanisms in two families of *cis,cis*-muconate lactonizing enzymes, *Biochemistry 48*, 1445–1453.
554. Gulick, A. M., Hubbard, B. K., Gerlt, J. A., and Rayment, I. (2000) Evolution of enzymatic activities in the enolase superfamily: Crystallographic and mutagenesis studies of the reaction catalyzed by D–glucarate dehydratase from *Escherichia coli*, *Biochemistry 39*, 4590–4602.

555. Gulick, A. M., Palmer, D. R., Babbitt, P. C., Gerlt, J. A., and Rayment, I. (1998) Evolution of enzymatic activities in the enolase superfamily: Crystal structure of D-glucarate dehydratase from *Pseudomonas putida*, *Biochemistry 37*, 14358–14368.
556. Gulick, A. M., Hubbard, B. K., Gerlt, J. A., and Rayment, I. (2001) Evolution of enzymatic activities in the enolase superfamily: Identification of the general acid catalyst in the active site of D-glucarate dehydratase from *Escherichia coli*, *Biochemistry 40*, 10054–10062.
557. Wieczorek, S. J., Kalivoda, K. A., Clifton, J. G., Ringe, D., Petsko, G. A., and Gerlt, J. A. (1999) Evolution of enzymatic activities in the enolase superfamily: Identification of a "new" general acid catalyst in the active site of D-galactonate dehydratase from *Escherichia coli*, *J. Am. Chem. Soc. 121*, 4540–4541.
558. Landro, J. A., Gerlt, J. A., Kozarich, J. W., Koo, C. W., Shah, V. J., Kenyon, G. L., Neidhart, D. J., Fujita, S., and Petsko, G. A. (1994) The role of Lysine 166 in the mechanism of mandelate racemase from *Pseudomonas putida*: Mechanistic and crystallographic evidence for stereospecific alkylation by (*R*)-α-phenylglycidate, *Biochemistry 33*, 635–643.
559. Palmer, D. R. J., and Gerlt, J. A. (1996) Evolution of enzymatic activities: Multiple pathways for generating and partitioning a common enolic intermediate by glucarate dehydratase from *Pseudomonas putida*, *J. Am. Chem. Soc. 118*, 10323–10324.
560. Sakai, A., Fedorov, A. A., Fedorov, E. V., Schnoes, A. M., Glasner, M. E., Brown, S., Rutter, M. E., Bain, K., Chang, S., Gheyi, T., Sauder, J. M., Burley, S. K., Babbitt, P. C., Almo, S. C., and Gerlt, J. A. (2009) Evolution of enzymatic activities in the enolase superfamily: Stereochemically distinct mechanisms in two families of *cis,cis*-muconate lactonizing enzymes. [Correction], *Biochemistry 48*, 2569–2570.
561. Bartlett, G. J., Borkakoti, N., and Thornton, J. M. (2003) Catalysing new reactions during evolution: Economy of residues and mechanism, *J. Mol. Biol. 331*, 829–860.
562. Avigad, G., and Englard, S. (1969) Stereochemistry of the enzymic reactions involved in *cis,cis* muconic acid utilization, *Fed. Proc. 28*, 345.
563. Kirby, G. W., O'Loughlin, G. J., and Robins, D. J. (1975) Stereochemistry of the enzymic cyclization of 3-carboxymuconic acid to 3-carboxymuconolactone, *J. Chem. Soc., Chem. Commun.*, 402–403.
564. Luthy, J., Retey, J., and Arigoni, D. (1969) Preparation and detection of chiral methyl groups, *Nature (London, U. K.) 221*, 1213–1215.
565. Johnson, C. K., Gabe, E. J., Taylor, M. R., and Rose, I. A. (1965) Determination by neutron and X-ray diffraction of absolute configuration of an enzymatically formed α-monodeuterioglycolate, *J. Am. Chem. Soc. 87*, 1802–1804.
566. Cornforth, J. W., Redmond, J. W., Eggerer, H., Buckel, W., and Gutschow, C. (1969) Asymmetric methyl groups, and the mechanism of malate synthase, *Nature (London, U. K.) 221*, 1212–1213.
567. Townsend, C. A., Scholl, T., and Arigoni, D. (1975) New synthesis of chiral acetic acid, *J. Chem. Soc., Chem. Commun.*, 921–922.
568. Coates, R. M., Koch, S. C., and Hegde, S. (1986) Stereochemistry of the terminating methyl→methylene elimination in kaurene biosynthesis, *J. Am. Chem. Soc. 108*, 2762–2764.
569. Ahn, Y., Krzycki, J. A., and Floss, H. G. (1991) Steric course of the reduction of ethyl coenzyme M to ethane catalyzed by methyl coenzyme M reductase from *Methanosarcina barkeri*, *J. Am. Chem. Soc. 113*, 4700–4701.
570. O'Connor, E. J., Kobayashi, M., Floss, H. G., and Gladysz, J. A. (1987) A versatile new synthesis of organic compounds with chiral methyl groups: Stereochemistry of protolytic rhenium-carbon bond cleavage in chiral alkyl complexes (η^5-C_5H_5)Re(NO)(PPh_3)(R), *J. Am. Chem. Soc. 109*, 4837–4844.
571. Lenz, H., and Eggerer, H. (1976) Enzymic generation of chiral acetates. A quantitative evaluation of their configurational assay, *Eur. J. Biochem. 65*, 237–246.
572. Anstrom, D. M., and Remington, S. J. (2006) The product complex of *M. tuberculosis* malate synthase revisited, *Protein Sci. 15*, 2002–2007.
573. Smith, C. V., Huang, C. C., Miczak, A., Russell, D. G., Sacchettini, J. C., and Honer zu Bentrup, K. (2003) Biochemical and structural studies of malate synthase from *Mycobac-*

terium tuberculosis, *J. Biol. Chem. 278*, 1735–1743.
574. Eggerer, H., Buckel, W., Lenz, H., Wunderwald, P., Gottschalk, G., Cornforth, J. W., Donninger, C., Mallaby, R., and Redmond, J. W. (1970) Stereochemistry of enzymic citrate synthesis and cleavage, *Nature (London, U. K.) 226*, 517–519.
575. Anet, F. A. L., O'Leary, D. J., Beale, J. M., and Floss, H. G. (1989) Stereogenic (chiral) methyl groups: Determination of configuration by direct tritium NMR spectroscopy, *J. Am. Chem. Soc. 111*, 8935–8936.
576. Woodard, R. W., Mascaro, L., Horhammer, R., Eisenstein, S., and Floss, H. G. (1980) Stereochemistry of indolmycin biosynthesis: Steric course of C-methylation and N-methylation reactions, *J. Am. Chem. Soc. 102*, 6314–6318.
577. Houck, D. R., Kobayashi, K., Williamson, J. M., and Floss, H. G. (1986) Stereochemistry of methylation in thienamycin biosynthesis: Example of a methyl transfer from methionine with retention of configuration, *J. Am. Chem. Soc. 108*, 5365–5366.
578. Valentine, A. M., Wilkinson, B., Liu, K. E., Komar-Panicucci, S., Priestley, N. D., Williams, P. G., Morimoto, H., Floss, H. G., and Lippard, S. J. (1997) Tritiated chiral alkanes as substrates for soluble methane monooxygenase from *Methylococcus capsulatus* (bath): Probes for the mechanism of hydroxylation, *J. Am. Chem. Soc. 119*, 1818–1827.
579. Rose, I. A. (1970) Stereochemistry of pyruvate kinase, pyruvate carboxylase, and malate enzyme reactions, *J. Biol. Chem. 245*, 6052–6056.
580. Grimshaw, C. E., Sogo, S. G., Copley, S. D., and Knowles, J. R. (1984) Synthesis of stereoselectively labeled [9-^{2}H,^{3}H]chorismate and the stereochemical course of 5-enolpyruvoylshikimate-3-phosphate synthetase, *J. Am. Chem. Soc. 106*, 2699–2700.
581. Larsen, T. M., Benning, M. M., Rayment, I., and Reed, G. H. (1998) Structure of the bis(Mg^{2+})-ATP-oxalate complex of the rabbit muscle pyruvate kinase at 2.1 Å resolution: ATP binding over a barrel, *Biochemistry 37*, 6247–6255.
582. Meloche, H. P., and Mehler, L. (1973) The stereochemistry at carbon 3 of pyruvate lyase condensation products. Aldolases forming condensation products racemic at carbon 4, *J. Biol. Chem. 248*, 6333–6338.
583. Riedel, T. J., Johnson, L. C., Knight, J., Hantgan, R. R., Holmes, R. P., and Lowther, W. T. (2011) Structural and biochemical studies of human 4-hydroxy-2-oxoglutarate aldolase: Implications for hydroxyproline metabolism in primary hyperoxaluria, *PLoS One 6*, e26021.
584. Retey, J., Suckling, C. J., Arigoni, D., and Babior, B. M. (1974) Stereochemistry of the reaction catalyzed by ethanolamine ammonia-lyase, an adenosylcobalamin-dependent enzyme. Example of racemization accompanying substitution, *J. Biol. Chem. 249*, 6359–6360.
585. Diziol, P., Haas, H., Retey, J., Graves, S. W., and Babior, B. M. (1980) The substrate-dependent steric course of the ethanolamine ammonia-lyase reaction, *Eur. J. Biochem. 106*, 211–224.
586. Abbott, S. J., Jones, S. R., Weinman, S. A., Bockhoff, F. M., McLafferty, F. W., and Knowles, J. R. (1979) Chiral [^{16}O,^{17}O,^{18}O]phosphate monoesters. Asymmetric synthesis and stereochemical analysis of [1(*R*)-^{16}O,^{17}O,^{18}O]-phospho-(*S*)-propane-1,2–diol, *J. Am. Chem. Soc. 101*, 4323–4332.
587. Cullis, P. M., and Lowe, G. (1981) Synthesis of chiral [^{16}O,^{17}O,^{18}O]phosphate esters, *J. Chem. Soc., Perkin Trans. 1 (1972–1999)*, 2317–2321.
588. Blattler, W. A., and Knowles, J. R. (1979) Stereochemical course of phosphokinases. The use of adenosine [γ-(*S*)-^{16}O,^{17}O,^{18}O]triphosphate and the mechanistic consequences for the reactions catalyzed by glycerol kinase, hexokinase, pyruvate kinase, and acetate kinase, *Biochemistry 18*, 3927–3933.
589. Buchwald, S. L., and Knowles, J. R. (1980) Determination of the absolute configuration of [^{16}O,^{17}O,^{18}O]phosphate monoesters by using phosphorus-31 NMR, *J. Am. Chem. Soc. 102*, 6601–6602.
590. Jarvest, R. L., Lowe, G., and Potter, B. V. L. (1981) Analysis of the chirality of oxygen-16, -17, and -18 phosphate esters by phosphorus-31 nuclear magnetic resonance spectroscopy, *J. Chem. Soc., Perkin Trans. 1 (1972–1999)*, 3186–3195.
591. Jones, S. R., Kindman, L. A., and Knowles, J. R. (1978) Stereochemistry of phosphoryl group transfer using a chiral [^{16}O,^{17}O,^{18}O]

stereochemical course of alkaline phosphatase, *Nature (London, U. K.) 275*, 564–565.
592. Eckstein, F., Romaniuk, P. J., and Connolly, B. A. (1982) Stereochemistry of enzymic phosphoryl and nucleotidyl transfer, *Methods Enzymol. 87*, 197–212.
593. Richard, J. P., and Frey, P. A. (1978) Stereochemical course of thiophosphoryl group transfer catalyzed by adenylate kinase, *J. Am. Chem. Soc. 100*, 7757–7758.
594. Bethell, R. C., and Lowe, G. (1988) A new synthesis of adenosine 5′-([$\gamma(R)$-^{17}O,^{18}O]-γ-thiotriphosphate) and its use to determine the stereochemical course of the activation of glutamate by glutamine synthetase, *Biochemistry 27*, 1125–1131.
595. Richard, J. P., Ho, H.-T., and Frey, P. A. (1978) Synthesis of nucleoside [^{18}O]pyrophosphorothioates with chiral [^{18}O]phosphorothioate groups of known configuration. Stereochemical orientations of enzymatic phosphorylations of chiral [^{18}O]phosphorothioates, *J. Am. Chem. Soc. 100*, 7756–7757.
596. Bigley, A. N., Xiang, D. F., Ren, Z., Xue, H., Hull, K. G., Romo, D., and Raushel, F. M. (2016) Chemical mechanism of the phosphotriesterase from *Sphingobium* sp. Strain TCM1, an enzyme capable of hydrolyzing organophosphate flame retardants, *J. Am. Chem. Soc. 138*, 2921–2924.
597. Sowadski, J. M., Handschumacher, M. D., Murthy, H. M., Foster, B. A., and Wyckoff, H. W. (1985) Refined structure of alkaline phosphatase from *Escherichia coli* at 2.8 Å resolution, *J. Mol. Biol. 186*, 417–433.
598. Sheu, K. F., Richard, J. P., and Frey, P. A. (1979) Stereochemical courses of nucleotidyltransferase and phosphotransferase action. Uridine diphosphate glucose pyrophosphorylase, galactose-1-phosphate uridylyltransferase, adenylate kinase, and nucleoside diphosphate kinase, *Biochemistry 18*, 5548–5556.
599. Garces, E., and Cleland, W. W. (1969) Kinetic studies of yeast nucleoside diphosphate kinase, *Biochemistry 8*, 633–640.
600. Edlund, B., Rask, L., Olsson, P., Walinder, O., Zetterqvist, O., and Engstrom, L. (1969) Preparation of crystalline nucleoside diphosphate kinase from baker's yeast and identification of 1-[^{32}P]phosphohistidine as the main phosphorylated product of an alkaline hydrolysate of enzyme incubated with adenosine [^{32}P]triphosphate, *Eur. J. Biochem. 9*, 451–455.
601. Chen, Y., Gallois-Montbrun, S., Schneider, B., Veron, M., Morera, S., Deville-Bonne, D., and Janin, J. (2003) Nucleotide binding to nucleoside diphosphate kinases: X-Ray structure of human NDPK-A in complex with ADP and comparison to protein kinases, *J. Mol. Biol. 332*, 915–926.
602. Pai, E. F., Sachsenheimer, W., Schirmer, R. H., and Schulz, G. E. (1977) Substrate positions and induced-fit in crystalline adenylate kinase, *J. Mol. Biol. 114*, 37–45.
603. Berry, M. B., Meador, B., Bilderback, T., Liang, P., Glaser, M., and Phillips, G. N., Jr. (1994) The closed conformation of a highly flexible protein: The structure of *E. coli* adenylate kinase with bound AMP and AMPPNP, *Proteins 19*, 183–198.
604. Abele, U., and Schulz, G. E. (1995) High-resolution structures of adenylate kinase from yeast ligated with inhibitor AP5A, showing the pathway of phosphoryl transfer, *Protein Sci. 4*, 1262–1271.
605. Lienhard, G. E., and Secemski, I. I. (1973) P^1,P^5-Di(adenosine-5′)pentaphosphate, a potent multisubstrate inhibitor of adenylate kinase, *J. Biol. Chem. 248*, 1121–1123.
606. Muller, C. W., and Schulz, G. E. (1992) Structure of the complex between adenylate kinase from *Escherichia coli* and the inhibitor AP5A refined at 1.9 Å resolution. A model for a catalytic transition state, *J. Mol. Biol. 224*, 159–177.
607. Webb, M. R., and Trentham, D. R. (1980) Analysis of chiral inorganic [^{16}O,^{17}O,^{18}O]thiophosphate and the stereochemistry of the 3-phosphoglycerate kinase reaction, *J. Biol. Chem. 255*, 1775–1778.
608. Webb, M. R., Grubmeyer, C., Penefsky, H. S., and Trentham, D. R. (1980) The stereochemical course of phosphoric residue transfer catalyzed by beef heart mitochondrial ATPase, *J. Biol. Chem. 255*, 11637–11639.
609. Webb, M. R., and Trentham, D. R. (1981) The stereochemical course of phosphoric residue transfer catalyzed by sarcoplasmic reticulum ATPase, *J. Biol. Chem. 256*, 4884–4887.
610. Bastide, F., Meissner, G., Fleischer, S., and Post, R. L. (1973) Similarity of the active site of phosphorylation of the adenosine triphosphatase from transport of sodium and potassium ions in kidney to that for transport of

calcium ions in the sarcoplasmic reticulum of muscle, *J. Biol. Chem. 248*, 8385–8391.
611. Webb, M. R., and Trentham, D. R. (1980) The stereochemical course of phosphoric residue transfer during the myosin ATPase reaction, *J. Biol. Chem. 255*, 8629–8632.
612. Krajewski, W. W., Collins, R., Holmberg-Schiavone, L., Jones, T. A., Karlberg, T., and Mowbray, S. L. (2008) Crystal structures of mammalian glutamine synthetases illustrate substrate-induced conformational changes and provide opportunities for drug and herbicide design, *J. Mol. Biol. 375*, 217–228.
613. Cheung, Y. F., and Walsh, C. (1976) Letter: Stereospecific synthesis of isotopically labeled serine at carbon 3 and stereochemical analysis of D-serine dehydrase reaction, *J. Am. Chem. Soc. 98*, 3397–3398.
614. Micklefield, J., Harris, K. J., Groeger, S., Mocek, U., Hilbi, H., Dimroth, P., and Floss, H. G. (1995) Stereochemical course of malonate decarboxylation in *Malonomonas rubra*, *J. Am. Chem. Soc. 117*, 1153–1154.
615. Ikeda, Y., and Tanaka, K. (1983) Purification and characterization of 2–methyl-branched chain acyl coenzyme A dehydrogenase, an enzyme involved in the isoleucine and valine metabolism, from rat liver mitochondria, *J. Biol. Chem. 258*, 9477–9487.
616. Mohrig, J. R., Vreede, P. J., Schultz, S. C., and Fierke, C. A. (1981) Stereospecific reduction of 2,3-epoxybutanoic acid. Synthesis of (*R*,*R*)- and (*S*,*S*)-3–hydroxybutanoic-*2-d* acid and *S*-tert-butyl 3-acetoxythiobutanoate-*2-d*, *J. Org. Chem. 46*, 4655–4658.
617. Sedgwick, B., and Cornforth, J. W. (1977) The biosynthesis of long-chain fatty acids. Stereochemical differentiation in the enzymic incorporation of chiral acetates, *Eur. J. Biochem. 75*, 465–479.
618. Biellmann, J. F., and Hirth, C. G. (1970) Stereochemistry of the oxidation at the β-carbon of butyryl-SCoA, *FEBS Lett. 8*, 55–56.
619. Biellmann, J. F., and Hirth, C. G. (1970) Stereochemistry of the oxidation at the α carbon of butyryl-CoA and of the enzymic hydrogen exchange, *FEBS Lett. 9*, 335–336.
620. Parker, A. R., Moore, J. A., Schwab, J. M., and Davisson, V. J. (1995) *Escherichia coli* imidazoleglycerol phosphate dehydratase: Spectroscopic characterization of the enzymic product and the steric course of the reaction, *J. Am. Chem. Soc. 117*, 10605–10613.
621. Rieder, S. V., and Rose, I. A. (1959) The mechanism of the triosephosphate isomerase reaction, *J. Biol. Chem. 234*, 1007–1010.
622. Chari, R. V. J., Whitman, C. P., Kozarich, J. W., Ngai, K. L., and Ornston, L. N. (1987) Absolute stereochemical course of muconolactone Δ-isomerase and of 4–carboxymuconolactone decarboxylase: Proton NMR "ricochet" analysis, *J. Am. Chem. Soc. 109*, 5520–5521.
623. Bethell, R. C., and Lowe, G. (1988) The stereochemical course of D-glyceraldehyde-induced ATPase activity of glycerokinase from *Escherichia coli*, *Eur. J. Biochem. 174*, 387–389.
624. Hartman, F. C. (1971) Haloacetol phosphates. Characterization of the active site of rabbit muscle triose phosphate isomerase, *Biochemistry 10*, 146–154.
625. Corran, P. H., and Waley, S. G. (1975) The amino acid sequence of rabbit muscle triose phosphate isomerase, *Biochem. J. 145*, 335–344.
626. Lolis, E., and Petsko, G. A. (1990) Crystallographic analysis of the complex between triosephosphate isomerase and 2-phosphoglycolate at 2.5-Å resolution: Implications for catalysis, *Biochemistry 29*, 6619–6625.
627. Straus, D., Raines, R., Kawashima, E., Knowles, J. R., and Gilbert, W. (1985) Active site of triosephosphate isomerase: *In vitro* mutagenesis and characterization of an altered enzyme, *Proc. Natl. Acad. Sci. U. S. A. 82*, 2272–2276.
628. Roise, D., Soda, K., Yagi, T., and Walsh, C. T. (1984) Inactivation of the *Pseudomonas striata* broad specificity amino acid racemase by D and L isomers of β-substituted alanines: Kinetics, stoichiometry, active site peptide, and mechanistic studies, *Biochemistry 23*, 5195–5201.
629. Roche, T. E., and McFadden, B. A. (1969) Active site modification of isocitrate lyase, *Biochem. Biophys. Res. Commun. 37*, 239–246.
630. Hass, G. M., and Neurath, H. (1971) Affinity labeling of bovine carboxypeptidase Aγ^{Leu} by *N*-bromoacetyl-*N*-methyl-L-phenylalanine. I. Kinetics of inactivation, *Biochemistry 10*, 3535–3540.
631. O'Leary, M. H., and Diaz, E. (1982) Phosphoenol-3-bromopyruvate. A mechanism-based inhibitor of phosphoenolpyruvate

carboxylase from maize, *J. Biol. Chem. 257*, 14603–14605.
632. Hartman, F. C. (1981) Interaction of isocitrate dehydrogenase with (*RS*)-3-bromo-2-ketoglutarate. A potential affinity label for α-ketoglutarate binding sites, *Biochemistry 20*, 894–898.
633. Okamoto, M., and Morino, Y. (1973) Affinity labeling of aspartate aminotransferase isozymes by bromopyruvate, *J. Biol. Chem. 248*, 82–90.
634. Meloche, H. P. (1973) The substrate analog, bromopyruvate, as a bridging agent for the active site of 2-keto-3-deoxy-6-phosphogluconic aldolase. Chemical evidence for a carboxylate adjacent to the Schiff's base-forming lysine, *J. Biol. Chem. 248*, 6945–6951.
635. Bednar, R. A., Hartman, F. C., and Colman, R. F. (1982) 3-Bromo-2-ketoglutarate: A substrate and affinity label for diphosphopyridine nucleotide dependent isocitrate dehydrogenase, *Biochemistry 21*, 3681–3689.
636. Stivers, J. T., Abeygunawardana, C., Mildvan, A. S., Hajipour, G., Whitman, C. P., and Chen, L. H. (1996) Catalytic role of the amino-terminal proline in 4-oxalocrotonate tautomerase: Affinity labeling and heteronuclear NMR studies, *Biochemistry 35*, 803–813.
637. Meloche, H. P., Monti, C. T., and Hogue-Angeletti, R. A. (1978) Identification of the bromopyruvate-sensitive glutamate within the active site of 2-keto-3-deoxygluconate-6-P aldolase, *Biochem. Biophys. Res. Commun. 84*, 589–594.
638. Moe, O. A., Baker-Malcolm, J. F., Wang, W., Kang, C., Fromm, H. J., and Colman, R. F. (1996) Involvement of Arginine 143 in nucleotide substrate binding at the active site of adenylosuccinate synthetase from *Escherichia coli*, *Biochemistry 35*, 9024–9033.
639. Lee, T. T., Worby, C., Dixon, J. E., and Colman, R. F. (1997) Identification of His141 in the active site of *Bacillus subtilis* adenylosuccinate lyase by affinity labeling with 6-(4-bromo-2,3-dioxobutyl)thioadenosine 5′-monophosphate, *J. Biol. Chem. 272*, 458–465.
640. Park, I., Ozturk, D. H., Soundar, S., and Colman, R. F. (1993) Nicotinamide ribose 5′-*O*-[*S*-(3-bromo-2-oxopropyl)]thiophosphate: A new affinity label for NMN sites in enzymes, *Arch. Biochem. Biophys. 303*, 483–488.
641. Vargo, M. A., and Colman, R. F. (2001) Affinity labeling of rat glutathione *S*-transferase isozyme 1-1 by 17β-iodoacetoxy-estradiol-3-sulfate, *J. Biol. Chem. 276*, 2031–2036.
642. Wang, E. A., Kallen, R., and Walsh, C. (1981) Mechanism-based inactivation of serine transhydroxymethylases by D-fluoroalanine and related amino acids, *J. Biol. Chem. 256*, 6917–6926.
643. Grishin, N. V., Osterman, A. L., Brooks, H. B., Phillips, M. A., and Goldsmith, E. J. (1999) X-Ray structure of ornithine decarboxylase from *Trypanosoma brucei*: The native structure and the structure in complex with α-difluoromethylornithine, *Biochemistry 38*, 15174–15184.
644. Ueno, H., Likos, J. J., and Metzler, D. E. (1982) Chemistry of the inactivation of cytosolic aspartate aminotransferase by serine *O*-sulfate, *Biochemistry 21*, 4387–4393.
645. O'Connell, E. L., and Rose, I. A. (1973) Affinity labeling of phosphoglucose isomerase by 1,2-anhydrohexitol-6-phosphates, *J. Biol. Chem. 248*, 2225–2231.
646. Moult, J., Eshdat, Y., and Sharon, N. (1973) The identification by X-ray crystallography of the site of attachment of an affinity label to hen egg-white lysozyme, *J. Mol. Biol. 75*, 1–4.
647. Rose, I. A., and O'Connell, E. L. (1969) Inactivation and labeling of triose phosphate isomerase and enolase by glycidol phosphate, *J. Biol. Chem. 244*, 6548–6550.
648. Hoj, P. B., Condron, R., Traeger, J. C., McAuliffe, J. C., and Stone, B. A. (1992) Identification of glutamic acid 105 at the active site of *Bacillus amyloliquefaciens* 1,3-1,4-β-D-glucan 4-glucanohydrolase using epoxide-based inhibitors, *J. Biol. Chem. 267*, 25059–25066.
649. Bounds, P. L., and Pollack, R. M. (1987) Affinity alkylation of 3-oxo-Δ^5-steroid isomerase by steroidal 3 β-oxiranes: Identification of the modified amino acid by reduction with hydroxyborohydride, *Biochemistry 26*, 2263–2269.
650. Liu, S., Widom, J., Kemp, C. W., Crews, C. M., and Clardy, J. (1998) Structure of human methionine aminopeptidase-2 complexed with fumagillin, *Science (Washington, DC, U. S.) 282*, 1324–1327.
651. Tanner, M. E., and Miao, S. C. (1994) The synthesis and stability of aziridino-glutamate, an irreversible inhibitor of glutamate racemase, *Tetrahedron Lett. 35*, 4073–4076.

652. Pillai, B., Cherney, M. M., Diaper, C. M., Sutherland, A., Blanchard, J. S., Vederas, J. C., and James, M. N. (2006) Structural insights into stereochemical inversion by diaminopimelate epimerase: An antibacterial drug target, *Proc. Natl. Acad. Sci. U. S. A. 103*, 8668–8673.
653. Kreienkamp, H. J., Weise, C., Raba, R., Aaviksaar, A., and Hucho, F. (1991) Anionic subsites of the catalytic center of acetylcholinesterase from torpedo and from cobra venom, *Proc. Natl. Acad. Sci. U. S. A. 88*, 6117–6121.
654. Pillai, B., Moorthie, V. A., van Belkum, M. J., Marcus, S. L., Cherney, M. M., Diaper, C. M., Vederas, J. C., and James, M. N. (2009) Crystal structure of diaminopimelate epimerase from *Arabidopsis thaliana*, an amino acid racemase critical for L-lysine biosynthesis, *J. Mol. Biol. 385*, 580–594.
655. Huynh, Q. K., Kishore, G. M., and Bild, G. S. (1988) 5-Enolpyruvyl shikimate 3-phosphate synthase from *Escherichia coli*. Identification of Lys-22 as a potential active site residue, *J. Biol. Chem. 263*, 735–739.
656. Patthy, L., and Smith, E. L. (1975) Reversible modification of arginine residues. Application to sequence studies by restriction of tryptic hydrolysis to lysine residues, *J. Biol. Chem. 250*, 557–564.
657. Yankeelov, J. A., Jr., Mitchell, C. D., and Crawford, T. H. (1968) A simple trimerization of 2,3-butanedione yielding a selective reagent for the modification of arginine in proteins, *J. Am. Chem. Soc. 90*, 1664–1666.
658. Riordan, J. F. (1973) Functional arginyl residues in carboxypeptidase A. Modification with butanedione, *Biochemistry 12*, 3915–3923.
659. Toi, K., Bynum, E., Norris, E., and Itano, H. A. (1967) Studies on the chemical modification of arginine. I. The reaction of 1,2–cyclohexanedione with arginine and arginyl residues of proteins, *J. Biol. Chem. 242*, 1036–1043.
660. Takahashi, K. (1968) The reaction of phenylglyoxal with arginine residues in proteins, *J. Biol. Chem. 243*, 6171–6179.
661. Takahashi, K. (1977) The reactions of phenylglyoxal and related reagents with amino acids, *J. Biochem. 81*, 395–402.
662. Riordan, J. F. (1979) Arginyl residues and anion binding sites in proteins, *Mol. Cell Biochem. 26*, 71–92.
663. Lee, P., Gorrell, A., Fromm, H. J., and Colman, R. F. (1999) Implication of Arginine-131 and Arginine-303 in the substrate site of adenylosuccinate synthetase of *Escherichia coli* by affinity labeling with 6-(4-bromo-2,3-dioxobutyl)thioadenosine 5′-monophosphate, *Biochemistry 38*, 5754–5763.
664. Wrzeszczynski, K. O., and Colman, R. F. (1994) Activation of bovine liver glutamate dehydrogenase by covalent reaction of adenosine 5′-*O*-[*S*-(4-bromo-2,3-dioxobutyl)thiophos-phate]with Arginine-459 at an ADP regulatory site, *Biochemistry 33*, 11544–11553.
665. Colman, R. F. (2006) Insights from affinity labeling into nucleotide and coenzyme-dependent enzyme catalysis and regulation, *Letters in Drug Design and Discovery 3*, 462–480.
666. Vollmer, S. H., Walner, M. B., Tarbell, K. V., and Colman, R. F. (1994) Guanosine 5′-*O*-[*S*-(4-bromo-2,3-dioxobutyl)thiophosphate] and adenosine 5′-*O*-[*S*-(4-bromo-2,3-dioxobutyl)thiophosphate]. New nucleotide affinity labels which react with rabbit muscle pyruvate kinase, *J. Biol. Chem. 269*, 8082–8090.
667. Wilde, J., Hunt, W., and Hupe, D. J. (1977) An inhibitor for aldolase, *J. Am. Chem. Soc. 99*, 8319–8321.
668. Agnihotri, G., He, S., Hong, L., Dakoji, S., Withers, S. G., and Liu, H. W. (2002) A revised mechanism for the inactivation of bovine liver enoyl-CoA hydratase by (methylenecyclopropyl)formyl-CoA based on unexpected results with the C114A mutant, *Biochemistry 41*, 1843–1852.
669. Hartman, S. C. (1963) The interaction of 6-diazo-5-oxo-L-norleucine with phosphoribosyl pyrophosphate amidotransferase, *J. Biol. Chem. 238*, 3036–3047.
670. Kaartinen, V., Williams, J. C., Tomich, J., Yates, J. R., 3rd, Hood, L. E., and Mononen, I. (1991) Glycoasparaginase from human leukocytes. Inactivation and covalent modification with diazo-oxonorvaline, *J. Biol. Chem. 266*, 5860–5869.
671. Inoue, M., Hiratake, J., Suzuki, H., Kumagai, H., and Sakata, K. (2000) Identification of catalytic nucleophile of *Escherichia coli* γ-glutamyltranspeptidase by γ-monofluoro-

phosphono derivative of glutamic acid: *N*-Terminal Thr-391 in small subunit is the nucleophile, *Biochemistry 39*, 7764–7771.
672. Bone, R., Sampson, N. S., Bartlett, P. A., and Agard, D. A. (1991) Crystal structures of α-lytic protease complexes with irreversibly bound phosphonate esters, *Biochemistry 30*, 2263–2272.
673. Daubner, S. C., Young, M., Sammons, R. D., Courtney, L. F., and Benkovic, S. J. (1986) Structural and mechanistic studies on the HeLa and chicken liver proteins that catalyze glycinamide ribonucleotide synthesis and formylation and aminoimidazole ribonucleotide synthesis, *Biochemistry 25*, 2951–2957.
674. Inglese, J., Smith, J. M., and Benkovic, S. J. (1990) Active-site mapping and site-specific mutagenesis of glycinamide ribonucleotide transformylase from *Escherichia coli*, *Biochemistry 29*, 6678–6687.
675. Greasley, S. E., Yamashita, M. M., Cai, H., Benkovic, S. J., Boger, D. L., and Wilson, I. A. (1999) New insights into inhibitor design from the crystal structure and NMR studies of *Escherichia coli* GAR transformylase in complex with β-GAR and 10-formyl-5,8,10-trideazafolic acid, *Biochemistry 38*, 16783–16793.
676. Iancu, C. V., Zhou, Y., Borza, T., Fromm, H. J., and Honzatko, R. B. (2006) Cavitation as a mechanism of substrate discrimination by adenylosuccinate synthetases, *Biochemistry 45*, 11703–11711.
677. Kalman, T. I., and Goldman, D. (1981) Inactivation of thymidylate synthetase by a novel mechanism-based enzyme inhibitor: 1–(β-D-2′-deoxyribofuranosyl) 8-azapurin-2-one 5′-monophosphate, *Biochem. Biophys. Res. Commun. 102*, 682–689.
678. Lepore, B. W., Liu, D., Peng, Y., Fu, M., Yasuda, C., Manning, J. M., Silverman, R. B., and Ringe, D. (2010) Chiral discrimination among aminotransferases: Inactivation by 4-amino-4,5-dihydrothiophenecarboxylic acid, *Biochemistry 49*, 3138–3147.
679. Wang, Z., Yuan, H., Nikolic, D., Van Breemen, R. B., and Silverman, R. B. (2006) (+/−)-(1*S*,2*R*,5*S*)-5-amino-2-fluorocyclohex-3-enecarboxylic acid. A potent GABA aminotransferase inactivator that irreversibly inhibits via an elimination-aromatization pathway, *Biochemistry 45*, 14513–14522.
680. DeWolf, W. E., Jr., Chambers, P. A., Southan, C., Saunders, D., and Kruse, L. I. (1989) Inactivation of dopamine β-hydroxylase by β-ethynyltyramine: Kinetic characterization and covalent modification of an active site peptide, *Biochemistry 28*, 3833–3842.
681. Higgins, W., Tardif, C., Richaud, C., Krivanek, M. A., and Cardin, A. (1989) Expression of recombinant diaminopimelate epimerase in *Escherichia coli*. Isolation and inhibition with an irreversible inhibitor, *Eur. J. Biochem. 186*, 137–143.
682. Diaper, C. M., Sutherland, A., Pillai, B., James, M. N., Semchuk, P., Blanchard, J. S., and Vederas, J. C. (2005) The stereoselective synthesis of aziridine analogues of diaminopimelic acid (DAP) and their interaction with DAP epimerase, *Org. Biomol. Chem. 3*, 4402–4411.
683. Glavas, S., and Tanner, M. E. (2001) Active site residues of glutamate racemase, *Biochemistry 40*, 6199–6204.
684. Ruzheinikov, S. N., Taal, M. A., Sedelnikova, S. E., Baker, P. J., and Rice, D. W. (2005) Substrate-induced conformational changes in *Bacillus subtilis* glutamate racemase and their implications for drug discovery, *Structure 13*, 1707–1713.
685. McCann, A. E., and Sampson, N. S. (2000) A C6–flavin adduct is the major product of irreversible inactivation of cholesterol oxidase by 2α,3α-cyclopropano-5α-cholestan-3β-ol, *J. Am. Chem. Soc. 122*, 35–39.
686. Zhao, G., Qu, J., Davis, F. A., and Jorns, M. S. (2000) Inactivation of monomeric sarcosine oxidase by reaction with *N*-(cyclopropyl)-glycine, *Biochemistry 39*, 14341–14347.
687. Chen, Z. W., Zhao, G., Martinovic, S., Jorns, M. S., and Mathews, F. S. (2005) Structure of the sodium borohydride-reduced *N*-(cyclopropyl)glycine adduct of the flavoenzyme monomeric sarcosine oxidase, *Biochemistry 44*, 15444–15450.
688. Gold, A. M., and Fahrney, D. (1964) Sulfonyl fluorides as inhibitors of esterases. II. Formation and reactions of phenylmethanesulfonyl α-chymotrypsin, *Biochemistry 3*, 783–791.
689. Motiu-DeGrood, R., Hunt, W., Wilde, J., and Hupe, D. J. (1979) Rates and equilibria for the inactivation of muscle aldolase by an active site directed Michael reaction, *J. Am. Chem. Soc. 101*, 2182–2190.

690. Kyte, J. (1981) The utilization of inactivation kinetics to demonstrate specificity of photoaffinity labeling, *J. Biol. Chem. 256*, 3231–3232.
691. Meloche, H. P. (1967) Bromopyruvate inactivation of 2-keto-3-deoxy-6-phosphogluconic aldolase. I. Kinetic evidence for active site specificity, *Biochemistry 6*, 2273–2280.
692. Sharma, V., Sharma, S., Hoener zu Bentrup, K., McKinney, J. D., Russell, D. G., Jacobs, W. R., Jr., and Sacchettini, J. C. (2000) Structure of isocitrate lyase, a persistence factor of *Mycobacterium tuberculosis*, *Nat. Struct. Biol. 7*, 663–668.
693. Krahn, J. M., Kim, J. H., Burns, M. R., Parry, R. J., Zalkin, H., and Smith, J. L. (1997) Coupled formation of an amidotransferase interdomain ammonia channel and a phosphoribosyltransferase active site, *Biochemistry 36*, 11061–11068.
694. Chen, L. H., Kenyon, G. L., Curtin, F., Harayama, S., Bembenek, M. E., Hajipour, G., and Whitman, C. P. (1992) 4-Oxalocrotonate tautomerase, an enzyme composed of 62 amino acid residues per monomer, *J. Biol. Chem. 267*, 17716–17721.
695. Vollmer, S. J., Switzer, R. L., Hermodson, M. A., Bower, S. G., and Zalkin, H. (1983) The glutamine-utilizing site of *Bacillus subtilis* glutamine phosphoribosylpyrophosphate amidotransferase, *J. Biol. Chem. 258*, 10582–10585.
696. Tso, J. Y., Hermodson, M. A., and Zalkin, H. (1982) Glutamine phosphoribosylpyrophosphate amidotransferase from cloned *Escherichia coli* purF. NH_2-Terminal amino acid sequence, identification of the glutamine site, and trace metal analysis, *J. Biol. Chem. 257*, 3532–3536.
697. Raushel, F. M., Thoden, J. B., and Holden, H. M. (1999) The amidotransferase family of enzymes: Molecular machines for the production and delivery of ammonia, *Biochemistry 38*, 7891–7899.
698. Kim, J. H., Krahn, J. M., Tomchick, D. R., Smith, J. L., and Zalkin, H. (1996) Structure and function of the glutamine phosphoribosylpyrophosphate amidotransferase glutamine site and communication with the phosphoribosylpyrophosphate site, *J. Biol. Chem. 271*, 15549–15557.
699. van den Heuvel, R. H., Svergun, D. I., Petoukhov, M. V., Coda, A., Curti, B., Ravasio, S., Vanoni, M. A., and Mattevi, A. (2003) The active conformation of glutamate synthase and its binding to ferredoxin, *J. Mol. Biol. 330*, 113–128.
700. Dossena, L., Curti, B., and Vanoni, M. A. (2007) Activation and coupling of the glutaminase and synthase reaction of glutamate synthase is mediated by E1013 of the ferredoxin-dependent enzyme, belonging to loop 4 of the synthase domain, *Biochemistry 46*, 4473–4485.
701. Schonbrunn, E., Eschenburg, S., Shuttleworth, W. A., Schloss, J. V., Amrhein, N., Evans, J. N., and Kabsch, W. (2001) Interaction of the herbicide glyphosate with its target enzyme 5-enolpyruvylshikimate 3-phosphate synthase in atomic detail, *Proc. Natl. Acad. Sci. U. S. A. 98*, 1376–1380.
702. Funke, T., Healy-Fried, M. L., Han, H., Alberg, D. G., Bartlett, P. A., and Schonbrunn, E. (2007) Differential inhibition of class I and class II 5-enolpyruvylshikimate-3-phosphate synthases by tetrahedral reaction intermediate analogues, *Biochemistry 46*, 13344–13351.
703. Moczydlowski, E. G., and Fortes, P. A. (1981) Characterization of 2′,3′-*O*-(2,4,6–trinitrocyclohexadienylidine)adenosine 5′-triphosphate as a fluorescent probe of the ATP site of sodium and potassium transport adenosine triphosphatase. Determination of nucleotide binding stoichiometry and ion-induced changes in affinity for ATP, *J. Biol. Chem. 256*, 2346–2356.
704. Hass, G. M., and Neurath, H. (1971) Affinity labeling of bovine carboxypeptidase $A\gamma^{Leu}$ by *N*-bromoacetyl-*N*-methyl-L-phenylalanine. II. Sites of modification, *Biochemistry 10*, 3541–3546.
705. Bayliss, R. S., Knowles, J. R., and Wybrandt, G. B. (1969) An aspartic acid residue at the active site of pepsin. The isolation and sequence of the heptapeptide, *Biochem. J. 113*, 377–386.
706. Meloche, H. P., and Wood, W. A. (1964) The mechanism of 2-keto-3-deoxy-6-phosphogluconic aldolase, *J. Biol. Chem. 239*, 3511–3514.
707. Grazi, E., Meloche, H., Martinez, G., Wood, W. A., and Horecker, B. L. (1963) Evidence for Schiff base formation in enzymatic aldol condensations, *Biochem. Biophys. Res. Commun. 10*, 4–10.

708. Suzuki, N., and Wood, W. A. (1980) Complete primary structure of 2-keto-3-deoxy-6-phosphogluconate aldolase, *J. Biol. Chem. 255*, 3427–3435.
709. Li, D., Agnihotri, G., Dakoji, S., Oh, E., Lantz, M., and Liu, H. W. (1999) The toxicity of methylenecyclopropylglycine: Studies of the inhibitory effects of (methylenecyclopropyl)formyl-CoA on enzymes involved in fatty acid metabolism and the molecular basis of its inactivation of enoyl-CoA hydratases, *J. Am. Chem. Soc. 121*, 9034–9042.
710. Dakoji, S., Li, D., Agnihotri, G., Zhou, H. Q., and Liu, H. W. (2001) Studies on the inactivation of bovine liver enoyl-CoA hydratase by (methylenecyclopropyl)formyl-CoA: Elucidation of the inactivation mechanism and identification of Cysteine-114 as the entrapped nucleophile, *J. Am. Chem. Soc. 123*, 9749–9759.
711. Moschitto, M. J., Doubleday, P. F., Catlin, D. S., Kelleher, N. L., Liu, D., and Silverman, R. B. (2019) Mechanism of inactivation of ornithine aminotransferase by (1*S*,3*S*)-3-amino-4-(hexafluoropropan-2-ylidenyl)cyclopentane-1-carboxylic acid, *J. Am. Chem. Soc. 141*, 10711–10721.
712. Kim, S. W., Cha, S. S., Cho, H. S., Kim, J. S., Ha, N. C., Cho, M. J., Joo, S., Kim, K. K., Choi, K. Y., and Oh, B. H. (1997) High-resolution crystal structures of Δ^5-3-ketosteroid isomerase with and without a reaction intermediate analogue, *Biochemistry 36*, 14030–14036.
713. Okada, T., Suzuki, H., Wada, K., Kumagai, H., and Fukuyama, K. (2006) Crystal structures of γ-glutamyltranspeptidase from *Escherichia coli*, a key enzyme in glutathione metabolism, and its reaction intermediate, *Proc. Natl. Acad. Sci. U. S. A. 103*, 6471–6476.
714. Oinonen, C., Tikkanen, R., Rouvinen, J., and Peltonen, L. (1995) Three-dimensional structure of human lysosomal aspartylglucosaminidase, *Nat. Struct. Biol. 2*, 1102–1108.
715. Ko, Y. H., and McFadden, B. A. (1990) Alkylation of isocitrate lyase from *Escherichia coli* by 3-bromopyruvate, *Arch. Biochem. Biophys. 278*, 373–380.
716. Sprecher, M., Berger, R., and Sprinson, D. B. (1964) Stereochemistry of the isocitrate lyase reaction, *Biochem. Biophys. Res. Commun. 16*, 254–257.
717. Jeffery, C. J., Hardre, R., and Salmon, L. (2001) Crystal structure of rabbit phosphoglucose isomerase complexed with 5-phospho-D-arabinonate identifies the role of Glu357 in catalysis, *Biochemistry 40*, 1560–1566.
718. Fujinaga, M., Cherney, M. M., Tarasova, N. I., Bartlett, P. A., Hanson, J. E., and James, M. N. (2000) Structural study of the complex between human pepsin and a phosphorus-containing peptidic-transition-state analog, *Acta Crystallogr., Sect. D: Biol. Crystallogr. 56*, 272–279.
719. Allard, J., Grochulski, P., and Sygusch, J. (2001) Covalent intermediate trapped in 2-keto-3-deoxy-6-phosphogluconate (KDPG) aldolase structure at 1.95-Å resolution, *Proc. Natl. Acad. Sci. U. S. A. 98*, 3679–3684.
720. Keitel, T., Simon, O., Borriss, R., and Heinemann, U. (1993) Molecular and active-site structure of a *Bacillus* 1,3-1,4-β-glucanase, *Proc. Natl. Acad. Sci. U. S. A. 90*, 5287–5291.
721. Gaiser, O. J., Piotukh, K., Ponnuswamy, M. N., Planas, A., Borriss, R., and Heinemann, U. (2006) Structural basis for the substrate specificity of a *Bacillus* 1,3-1,4-β-glucanase, *J. Mol. Biol. 357*, 1211–1225.
722. Ceccarelli, C., Grodsky, N. B., Ariyaratne, N., Colman, R. F., and Bahnson, B. J. (2002) Crystal structure of porcine mitochondrial $NADP^+$-dependent isocitrate dehydrogenase complexed with Mn^{2+} and isocitrate. Insights into the enzyme mechanism, *J. Biol. Chem. 277*, 43454–43462.
723. Xu, X., Zhao, J., Xu, Z., Peng, B., Huang, Q., Arnold, E., and Ding, J. (2004) Structures of human cytosolic NADP-dependent isocitrate dehydrogenase reveal a novel self-regulatory mechanism of activity, *J. Biol. Chem. 279*, 33946–33957.
724. Smyth, G. E., and Colman, R. F. (1992) Inactivation of pig heart NADP-specific isocitrate dehydrogenase by two affinity reagents is due to reaction with a cysteine not essential for function, *Arch. Biochem. Biophys. 293*, 356–361.
725. Birchmeier, W., and Christen, P. (1974) The reaction of cytoplasmic aspartate aminotransferase with bromopyruvate. Syncatalytic modification simulates affinity labeling, *J. Biol. Chem. 249*, 6311–6315.
726. Birchmeier, W., Wilson, K. J., and Christen, P. (1973) Cytoplasmic aspartate aminotransferase: Syncatalytic sulfhydryl group modification, *J. Biol. Chem. 248*, 1751–1759.

727. Diaz, E., O'Laughlin, J. T., and O'Leary, M. H. (1988) Reaction of phosphoenolpyruvate carboxylase with (*Z*)-3-bromophosphoenolpyruvate and (*Z*)-3-fluorophosphoenolpyruvate, *Biochemistry 27*, 1336–1341.
728. Bloch, K. (1987) Summing up, *Annu. Rev. Biochem. 56*, 1–19.
729. Endo, K., Helmkamp, G. M., Jr., and Bloch, K. (1970) Mode of inhibition of β-hydroxydecanoyl thioester dehydrase by 3-decynoyl-*N*-acetylcysteamine, *J. Biol. Chem. 245*, 4293–4296.
730. Leesong, M., Henderson, B. S., Gillig, J. R., Schwab, J. M., and Smith, J. L. (1996) Structure of a dehydratase-isomerase from the bacterial pathway for biosynthesis of unsaturated fatty acids: Two catalytic activities in one active site, *Structure (Cambridge, MA, U. S.) 4*, 253–264.
731. Cronan, J. E., Jr., Li, W. B., Coleman, R., Narasimhan, M., de Mendoza, D., and Schwab, J. M. (1988) Derived amino acid sequence and identification of active site residues of *Escherichia coli* β-hydroxydecanoyl thioester dehydrase, *J. Biol. Chem. 263*, 4641–4646.
732. Ishikawa, F., Haushalter, R. W., Lee, D. J., Finzel, K., and Burkart, M. D. (2013) Sulfonyl 3-alkynyl pantetheinamides as mechanism-based cross-linkers of acyl carrier protein dehydratase, *J. Am. Chem. Soc. 135*, 8846–8849.
733. Johnson, W. H., Jr., Czerwinski, R. M., Fitzgerald, M. C., and Whitman, C. P. (1997) Inactivation of 4-oxalocrotonate tautomerase by 2-oxo-3-pentynoate, *Biochemistry 36*, 15724–15732.
734. Fendrich, G., and Abeles, R. H. (1982) Mechanism of action of butyryl-CoA dehydrogenase: Reactions with acetylenic, olefinic, and fluorinated substrate analogues, *Biochemistry 21*, 6685–6695.
735. Lundberg, N. N., and Thorpe, C. (1993) Inactivation of short-chain acyl-coenzyme A dehydrogenase from pig liver by 2-pentynoyl-coenzyme A, *Arch. Biochem. Biophys. 305*, 454–459.
736. Djordjevic, S., Pace, C. P., Stankovich, M. T., and Kim, J.-J. P. (1995) Three-dimensional structure of butyryl-CoA dehydrogenase from *Megasphaera elsdenii*, *Biochemistry 34*, 2163–2171.
737. Ekkebus, R., van Kasteren, S. I., Kulathu, Y., Scholten, A., Berlin, I., Geurink, P. P., de Jong, A., Goerdayal, S., Neefjes, J., Heck, A. J., Komander, D., and Ovaa, H. (2013) On terminal alkynes that can react with active-site cysteine nucleophiles in proteases, *J. Am. Chem. Soc. 135*, 2867–2870.
738. Xu, Y., and Abeles, R. H. (1993) Inhibition of tryptophan synthase by (1-fluorovinyl)glycine, *Biochemistry 32*, 806–811.
739. Bera, A. K., Polovnikova, L. S., Roestamadji, J., Widlanski, T. S., Kenyon, G. L., McLeish, M. J., and Hasson, M. S. (2007) Mechanism-based inactivation of benzoylformate decarboxylase, a thiamin diphosphate-dependent enzyme, *J. Am. Chem. Soc. 129*, 4120–4121.
740. Rando, R. R. (1974) Allyl alcohol-induced irreversible inhibition of yeast alcohol dehydrogenase, *Biochem. Pharmacol. (Amsterdam, Neth.) 23*, 2328–2331.
741. Baker-Malcolm, J. F., Lantz, M., Anderson, V. E., and Thorpe, C. (2000) Novel inactivation of enoyl-CoA hydratase via β-elimination of 5,6-dichloro-7,7,7-trifluoro-4-thia-5-heptenoyl-CoA, *Biochemistry 39*, 12007–12018.
742. Engel, C. K., Kiema, T. R., Hiltunen, J. K., and Wierenga, R. K. (1998) The crystal structure of enoyl-CoA hydratase complexed with octanoyl-CoA reveals the structural adaptations required for binding of a long chain fatty acid-CoA molecule, *J. Mol. Biol. 275*, 847–859.
743. Warner, D. R., and Hoffman, J. L. (1996) Suicide inactivation of thioether *S*-methyltransferase by ethyl sulfide, *Biochemistry 35*, 4480–4484.
744. Banzon, J. A., Kuo, J. M., Miles, B. W., Fischer, D. R., Stang, P. J., and Raushel, F. M. (1995) Mechanism-based inactivation of phosphotriesterase by reaction of a critical histidine with a ketene intermediate, *Biochemistry 34*, 743–749.
745. Galey, J. B., Bombard, S., Chopard, C., Girerd, J. J., Lederer, F., Thang, D. C., Nam, N. H., Mansuy, D., and Chottard, J. C. (1988) Hexanal phenylhydrazone is a mechanism-based inactivator of soybean lipoxygenase 1, *Biochemistry 27*, 1058–1066.
746. Rando, R. R. (1974) Irreversible inhibition of aspartate aminotransferase by 2-amino-3-butenoic acid, *Biochemistry 13*, 3859–3863.
747. Schaller, R. A., and Thorpe, C. (1995) Oxidative inactivation of a charge transfer complex

in the medium-chain acyl-CoA dehydrogenase, *Biochemistry 34*, 16424–16432.
748. Kim, J. J., Wang, M., and Paschke, R. (1993) Crystal structures of medium-chain acyl-CoA dehydrogenase from pig liver mitochondria with and without substrate, *Proc. Natl. Acad. Sci. U. S. A. 90*, 7523–7527.
749. Kabil, O., Motl, N., Strack, M., Seravalli, J., Metzler-Nolte, N., and Banerjee, R. (2018) Mechanism-based inhibition of human persulfide dioxygenase by γ-glutamyl-homocysteinyl-glycine, *J. Biol. Chem. 293*, 12429–12439.
750. Schoellmann, G., and Shaw, E. (1963) Direct evidence for the presence of histidine in the active center of chymotrypsin, *Biochemistry 2*, 252–255.
751. Weiner, H., White, W. N., Hoare, D. G., and Koshland, D. E., Jr. (1966) The formation of anhydrochymotrypsin by removing the elements of water from the serine at the active site, *J. Am. Chem. Soc. 88*, 3851–3859.
752. Kreutter, K., Steinmetz, A. C., Liang, T. C., Prorok, M., Abeles, R. H., and Ringe, D. (1994) Three-dimensional structure of chymotrypsin inactivated with (2*S*)-*N*-acetyl-L-alanyl-L-phenylalanyl α-chloroethane: Implications for the mechanism of inactivation of serine proteases by chloroketones, *Biochemistry 33*, 13792–13800.
753. Stevenson, K. J., and Smillie, L. B. (1965) The reaction of phenoxymethyl chloromethyl ketone with nitrogen 3 of Histidine-57 of chymotrypsin, *J. Mol. Biol. 12*, 937–941.
754. Navia, M. A., McKeever, B. M., Springer, J. P., Lin, T. Y., Williams, H. R., Fluder, E. M., Dorn, C. P., and Hoogsteen, K. (1989) Structure of human neutrophil elastase in complex with a peptide chloromethyl ketone inhibitor at 1.84-Å resolution, *Proc. Natl. Acad. Sci. U. S. A. 86*, 7–11.
755. Abeles, R. H., and Walsh, C. T. (1973) Acetylenic enzyme inactivators. Inactivation of γ-cystathionase, *in vitro* and *in vivo* by propargylglycine, *J. Am. Chem. Soc. 95*, 6124–6125.
756. Johnston, M., Jankowski, D., Marcotte, P., Tanaka, H., Esaki, N., Soda, K., and Walsh, C. (1979) Suicide inactivation of bacterial cystathionine γ-synthase and methionine γ-lyase during processing of L–propargylglycine, *Biochemistry 18*, 4690–4701.
757. Sun, Q., Collins, R., Huang, S., Holmberg-Schiavone, L., Anand, G. S., Tan, C. H., van-den-Berg, S., Deng, L. W., Moore, P. K., Karlberg, T., and Sivaraman, J. (2009) Structural basis for the inhibition mechanism of human cystathionine γ-lyase, an enzyme responsible for the production of H_2S, *J. Biol. Chem. 284*, 3076–3085.
758. Thornberry, N. A., Bull, H. G., Taub, D., Greenlee, W. J., Patchett, A. A., and Cordes, E. H. (1987) 3-Halovinylglycines. Efficient irreversible inhibitors of *Escherichia coli* alanine racemase, *J. Am. Chem. Soc. 109*, 7543–7544.
759. Thornberry, N. A., Bull, H. G., Taub, D., Wilson, K. E., Gimenez-Gallego, G., Rosegay, A., Soderman, D. D., and Patchett, A. A. (1991) Mechanism-based inactivation of alanine racemase by 3-halovinylglycines, *J. Biol. Chem. 266*, 21657–21665.
760. Fenn, T. D., Stamper, G. F., Morollo, A. A., and Ringe, D. (2003) A side reaction of alanine racemase: Transamination of cycloserine, *Biochemistry 42*, 5775–5783.
761. Watanabe, A., Yoshimura, T., Mikami, B., Hayashi, H., Kagamiyama, H., and Esaki, N. (2002) Reaction mechanism of alanine racemase from *Bacillus stearothermophilus*: X-Ray crystallographic studies of the enzyme bound with *N*-(5′-phosphopyridoxyl)alanine, *J. Biol. Chem. 277*, 19166–19172.
762. Metcalf, B. W., Bey, P., Danzin, C., Jung, M. J., Casara, P., and Vevert, J. P. (1978) Catalytic irreversible inhibition of mammalian ornithine decarboxylase (E.C.4.1.1.17) by substrate and product analogs, *J. Am. Chem. Soc. 100*, 2551–2553.
763. Feng, L., and Kirsch, J. F. (2000) L-Vinylglycine is an alternative substrate as well as a mechanism-based inhibitor of 1-aminocyclopropane-1-carboxylate synthase, *Biochemistry 39*, 2436–2444.
764. Badet, B., Roise, D., and Walsh, C. T. (1984) Inactivation of the *dadB Salmonella typhimurium* alanine racemase by D and L isomers of β-substituted alanines: Kinetics, stoichiometry, active site peptide sequencing, and reaction mechanism, *Biochemistry 23*, 5188–5194.
765. Bhattacharjee, M. K., and Snell, E. E. (1990) Pyridoxal 5′-phosphate-dependent histidine decarboxylase. Mechanism of inactivation by α-fluoromethylhistidine, *J. Biol. Chem. 265*, 6664–6668.

766. Storici, P., Qiu, J., Schirmer, T., and Silverman, R. B. (2004) Mechanistic crystallography. Mechanism of inactivation of γ-aminobutyric acid aminotransferase by (1*R*,3*S*,4*S*)-3-amino-4-fluorocyclopentane-1-carboxylic acid as elucidated by crystallography, *Biochemistry 43*, 14057–14063.
767. Contestabile, R., Jenn, T., Akhtar, M., Gani, D., and John, R. A. (2000) Reactions of glutamate 1-semialdehyde aminomutase with *R*- and *S*-enantiomers of a novel, mechanism-based inhibitor, 2,3-diaminopropyl sulfate, *Biochemistry 39*, 3091–3096.
768. Zhou, X. E., Suino-Powell, K., Schultz, C. R., Aleiwi, B., Brunzelle, J. S., Lamp, J., Vega, I. E., Ellsworth, E., Bachmann, A. S., and Melcher, K. (2021) Structural basis of binding and inhibition of ornithine decarboxylase by 1-amino-oxy-3-aminopropane, *Biochem. J. 478*, 4137–4149.
769. Mascarenhas, R., Le, H. V., Clevenger, K. D., Lehrer, H. J., Ringe, D., Kelleher, N. L., Silverman, R. B., and Liu, D. (2017) Selective targeting by a mechanism-based inactivator against pyridoxal 5′-phosphate-dependent enzymes: Mechanisms of inactivation and alternative turnover, *Biochemistry 56*, 4951–4961.
770. Storici, P., Capitani, G., Muller, R., Schirmer, T., and Jansonius, J. N. (1999) Crystal structure of human ornithine aminotransferase complexed with the highly specific and potent inhibitor 5-fluoromethylornithine, *J. Mol. Biol. 285*, 297–309.
771. Crestfield, A. M., Stein, W. H., and Moore, S. (1963) Alkylation and identification of the histidine residues at the active site of ribonuclease, *J. Biol. Chem. 238*, 2413–2419.
772. Verheij, H. M., Volwerk, J. J., Jansen, E. H., Puyk, W. C., Dijkstra, B. W., Drenth, J., and de Haas, G. H. (1980) Methylation of Histidine-48 in pancreatic phospholipase A2. Role of histidine and calcium ion in the catalytic mechanism, *Biochemistry 19*, 743–750.
773. Sekar, K., Kumar, A., Liu, X., Tsai, M. D., Gelb, M. H., and Sundaralingam, M. (1998) Structure of the complex of bovine pancreatic phospholipase A2 with a transition-state analogue, *Acta Crystallogr., Sect. D: Biol. Crystallogr. 54*, 334–341.
774. Harris, I., Meriwether, B. P., and Park, J. H. (1963) Chemical nature of the catalytic sites in glyceraldehyde-3-phosphate dehydrogenase, *Nature (London, U. K.) 198*, 154–157.
775. Buehner, M., Ford, G. C., Olsen, K. W., Moras, D., and Rossman, M. G. (1974) Three-dimensional structure of D-glyceraldehyde-3-phosphate dehydrogenase, *J. Mol. Biol. 90*, 25–49.
776. Drenth, J., Kalk, K. H., and Swen, H. M. (1976) Binding of chloromethyl ketone substrate analogues to crystalline papain, *Biochemistry 15*, 3731–3738.
777. Husain, S. S., and Lowe, G. (1968) The location of the active-site histidine residue in the primary sequence of papain, *Biochem. J. 108*, 861–866.
778. Husain, S. S., and Lowe, G. (1970) The amino acid sequence around the active-site cysteine and histidine residues of stem bromelain, *Biochem. J. 117*, 341–346.
779. Buechler, J. A., and Taylor, S. S. (1989) Dicyclohexylcarbodiimide cross-links two conserved residues, Asp-184 and Lys-72, at the active site of the catalytic subunit of cAMP-dependent protein kinase, *Biochemistry 28*, 2065–2070.
780. Marshall, M., and Cohen, P. P. (1980) Evidence for an exceptionally reactive arginyl residue at the binding site for carbamyl phosphate in bovine ornithine transcarbamylase, *J. Biol. Chem. 255*, 7301–7305.
781. Fan, C. C., and Plaut, G. W. (1974) Functional groups of diphosphopyridine nucleotide linked isocitrate dehydrogenase from bovine heart. I. Studies of an active amino group by amidination, arylation, acetylation, and carbamylation, *Biochemistry 13*, 45–51.
782. Wood, T. D., Guan, Z., Borders, C. L., Jr., Chen, L. H., Kenyon, G. L., and McLafferty, F. W. (1998) Creatine kinase: Essential arginine residues at the nucleotide binding site identified by chemical modification and high-resolution tandem mass spectrometry, *Proc. Natl. Acad. Sci. U. S. A. 95*, 3362–3365.
783. Patthy, L., Varadi, A., Thesz, J., and Kovacs, K. (1979) Identification of the C-1-phosphate-binding arginine residue of rabbit-muscle aldolase. Isolation of 1,2-cyclohexanedione-labeled peptide by chemisorption chromatography, *Eur. J. Biochem. 99*, 309–313.
784. St-Jean, M., and Sygusch, J. (2007) Stereospecific proton transfer by a mobile catalyst in mammalian fructose-1,6-bisphosphate aldolase, *J. Biol. Chem. 282*, 31028–31037.

785. Cummins, I., McAuley, K., Fordham-Skelton, A., Schwoerer, R., Steel, P. G., Davis, B. G., and Edwards, R. (2006) Unique regulation of the active site of the serine esterase *S*-formylglutathione hydrolase, *J. Mol. Biol. 359*, 422–432.
786. Johnson, P. G., Waheed, A., Jones, L., Glaid, A. J., and Gawron, O. (1977) Identification of an essential residue of pig heart aconitase, *Biochem. Biophys. Res. Commun. 74*, 384–389.
787. Plank, D. W., and Howard, J. B. (1988) Identification of the reactive sulfhydryl and sequences of cysteinyl-tryptic peptides from beef heart aconitase, *J. Biol. Chem. 263*, 8184–8189.
788. Kennedy, M. C., Spoto, G., Emptage, M. H., and Beinert, H. (1988) The active site sulfhydryl of aconitase is not required for catalytic activity, *J. Biol. Chem. 263*, 8190–8193.
789. Lloyd, S. J., Lauble, H., Prasad, G. S., and Stout, C. D. (1999) The mechanism of aconitase: 1.8 Å Resolution crystal structure of the S642A:citrate complex, *Protein Sci. 8*, 2655–2662.
790. Porter, M. A., and Hartman, F. C. (1988) Catalytic nonessentiality of an active-site cysteinyl residue of phosphoribulokinase, *J. Biol. Chem. 263*, 14846–14849.
791. Schaffer, J., Gallay, O., and Ladenstein, R. (1988) Glutathione transferase from bovine placenta. Preparation, biochemical characterization, crystallization, and preliminary crystallographic analysis of a neutral class pi enzyme, *J. Biol. Chem. 263*, 17405–17411.
792. Tamai, K., Satoh, K., Tsuchida, S., Hatayama, I., Maki, T., and Sato, K. (1990) Specific inactivation of glutathione S-transferases in class pi by SH-modifiers, *Biochem. Biophys. Res. Commun. 167*, 331–338.
793. Dirr, H., Reinemer, P., and Huber, R. (1994) Refined crystal structure of porcine class Pi glutathione *S*-transferase (pGST P1-1) at 2.1 Å resolution, *J. Mol. Biol. 243*, 72–92.
794. Svensson, B., Clarke, A. J., Svendsen, I., and Moller, H. (1990) Identification of carboxylic acid residues in glucoamylase G2 from *Aspergillus niger* that participate in catalysis and substrate binding, *Eur. J. Biochem. 188*, 29–38.
795. Harris, E. M., Aleshin, A. E., Firsov, L. M., and Honzatko, R. B. (1993) Refined structure for the complex of 1-deoxynojirimycin with glucoamylase from *Aspergillus awamor*i var. X100 to 2.4-Å resolution, *Biochemistry 32*, 1618–1626.
796. Tanizawa, K., and Miles, E. W. (1983) L-Serine binds to Arginine-148 of the β_2 subunit of *Escherichia coli* tryptophan synthase, *Biochemistry 22*, 3594–3603.
797. Nishio, K., Ogasahara, K., Morimoto, Y., Tsukihara, T., Lee, S. J., and Yutani, K. (2010) Large conformational changes in the *Escherichia coli* tryptophan synthase β_2 subunit upon pyridoxal 5′-phosphate binding, *FEBS J. 277*, 2157–2170.
798. Khalifah, R. G., and Edsall, J. T. (1972) Carbon dioxide hydration activity of carbonic anhydrase: Kinetics of alkylated anhydrases B and C from humans, *Proc. Natl. Acad. Sci. U. S. A. 69*, 172–176.
799. Srivastava, D. K., Jude, K. M., Banerjee, A. L., Haldar, M., Manokaran, S., Kooren, J., Mallik, S., and Christianson, D. W. (2007) Structural analysis of charge discrimination in the binding of inhibitors to human carbonic anhydrases I and II, *J. Am. Chem. Soc. 129*, 5528–5537.
800. Kindman, L. A., and Jencks, W. P. (1981) Modification and inactivation of CoA transferase by 2-nitro-5-(thiocyanato)benzoate, *Biochemistry 20*, 5183–5187.
801. Mueller, M. J., Andberg, M., and Haeggstrom, J. Z. (1998) Analysis of the molecular mechanism of substrate-mediated inactivation of leukotriene A4 hydrolase, *J. Biol. Chem. 273*, 11570–11575.
802. Dvir, H., Jiang, H. L., Wong, D. M., Harel, M., Chetrit, M., He, X. C., Jin, G. Y., Yu, G. L., Tang, X. C., Silman, I., Bai, D. L., and Sussman, J. L. (2002) X-ray structures of *Torpedo californica* acetylcholinesterase complexed with (+)-huperzine A and (–)-huperzine B: Structural evidence for an active site rearrangement, *Biochemistry 41*, 10810–10818.
803. Banerjee, S., Schmidt, T., Fang, J., Stanley, C. A., and Smith, T. J. (2003) Structural studies on ADP activation of mammalian glutamate dehydrogenase and the evolution of regulation, *Biochemistry 42*, 3446–3456.
804. Hegyi, G., Szilagyi, L., and Elzinga, M. (1986) Photoaffinity labeling of the nucleotide binding site of actin, *Biochemistry 25*, 5793–5798.
805. Kabsch, W., Mannherz, H. G., Suck, D., Pai, E. F., and Holmes, K. C. (1990) Atomic struc-

ture of the actin:DNAse I complex, *Nature (London, U. K.) 347*, 37–44.
806. Lorimer, G. H. (1978) Retention of the oxygen atoms at carbon-2 and carbon-3 during the carboxylation of ribulose 1,5-bisphosphate, *Eur. J. Biochem. 89*, 43–50.
807. Pierce, J., Tolbert, N. E., and Barker, R. (1980) Mass spectrometric analysis of the reactions of ribulosebisphosphate carboxylase/ oxygenase, *J. Biol. Chem. 255*, 509–511.
808. Fraij, B., and Hartman, F. C. (1982) 2–Bromoacetylaminopentitol 1,5-bisphosphate as an affinity label for ribulose bisphosphate carboxylase/oxygenase from *Rhodospirillum rubrum*, *J. Biol. Chem. 257*, 3501–3505.
809. Lundqvist, T., and Schneider, G. (1991) Crystal structure of activated ribulose-1,5-bisphosphate carboxylase complexed with its substrate, ribulose-1,5-bisphosphate, *J. Biol. Chem. 266*, 12604–12611.
810. Marletta, M. A., and Kenyon, G. L. (1979) Affinity labeling of creatine kinase by *N*-(2,3-epoxypropyl)-*N*-amidinoglycine, *J. Biol. Chem. 254*, 1879–1886.
811. Buechter, D. D., Medzihradszky, K. F., Burlingame, A. L., and Kenyon, G. L. (1992) The active site of creatine kinase. Affinity labeling of Cysteine 282 with *N*-(2,3-epoxypropyl)-*N*-amidinoglycine, *J. Biol. Chem. 267*, 2173–2178.
812. Ohren, J. F., Kundracik, M. L., Borders, C. L., Jr., Edmiston, P., and Viola, R. E. (2007) Structural asymmetry and intersubunit communication in muscle creatine kinase, *Acta Crystallogr., Sect. D: Biol. Crystallogr. 63*, 381–389.
813. Gattis, J. L., Ruben, E., Fenley, M. O., Ellington, W. R., and Chapman, M. S. (2004) The active site cysteine of arginine kinase: Structural and functional analysis of partially active mutants, *Biochemistry 43*, 8680–8689.
814. Zhou, G., Somasundaram, T., Blanc, E., Parthasarathy, G., Ellington, W. R., and Chapman, M. S. (1998) Transition state structure of arginine kinase: Implications for catalysis of bimolecular reactions, *Proc. Natl. Acad. Sci. U. S. A. 95*, 8449–8454.
815. Hexter, C. S., and Westheimer, F. H. (1971) Intermolecular reaction during photolysis of diazoacetyl -chymotrypsin, *J. Biol. Chem. 246*, 3928–3933.
816. Shafer, J., Baronowsky, P., Laursen, R., Finn, F., and Westheimer, F. H. (1966) Products from the photolysis of diazoacetyl chymotrypsin, *J. Biol. Chem. 241*, 421–427.
817. Fleet, G. W., Knowles, J. R., and Porter, R. R. (1972) The antibody binding site. Labelling of a specific antibody against the photoprecursor of an aryl nitrene, *Biochem. J. 128*, 499–508.
818. Vaughan, R. J., and Westheimer, F. H. (1969) A method for marking hydrophobic binding sites of enzymes. An insertion into methyl group of an alanine residue of trypsin, *J. Am. Chem. Soc. 91*, 217–218.
819. Lifter, J., Hew, C. L., Yoshioka, M., Richards, F. F., and Konigsberg, W. H. (1974) Affinity-labeled peptides obtained from the combining region of myeloma protein 460. I. Heavy-chain-labeling patterns using dinitrophenyl azide photoaffinity label, *Biochemistry 13*, 3567–3571.
820. Quirk, S., and Seley, K. L. (2005) Identification of catalytic amino acids in the human GTP fucose pyrophosphorylase active site, *Biochemistry 44*, 13172–13178.
821. Brunner, J., and Richards, F. M. (1980) Analysis of membranes photolabeled with lipid analogues. Reaction of phospholipids containing a disulfide group and a nitrene or carbene precursor with lipids and with gramicidin A, *J. Biol. Chem. 255*, 3319–3329.
822. Takagaki, Y., Radhakrishnan, R., Gupta, C. M., and Khorana, H. G. (1983) The membrane-embedded segment of cytochrome b_5 as studied by cross-linking with photoactivatable phospholipids, *J. Biol. Chem. 258*, 9128–9135.
823. Wyatt, J. L., and Colman, R. F. (1977) Affinity labeling of rabbit muscle pyruvate kinase by 5′-p-fluorosulfonylbenzoyladenosine, *Biochemistry 16*, 1333–1342.
824. Miles, E. W., and Phillips, R. S. (1985) Photoinactivation and photoaffinity labeling of tryptophan synthase $\alpha_2\beta_2$ complex by the product analogue 6-azido-L-tryptophan, *Biochemistry 24*, 4694–4703.
825. Tsatsos, P. H., Reynolds, K., Nickels, E. F., He, D. Y., Yu, C. A., and Gennis, R. B. (1998) Using matrix-assisted laser desorption ionization mass spectrometry to map the quinol binding site of cytochrome bo_3 from *Escherichia coli*, *Biochemistry 37*, 9884–9888.
826. Rajasekharan, R., Marians, R. C., Shockey, J. M., and Kemp, J. D. (1993) Photoaffinity labeling of acyl-CoA oxidase with 12-azido-

oleoyl-CoA and 12-[(4-azidosalicyl)amino]-dodecanoyl-CoA, *Biochemistry 32*, 12386–12391.
827. de Waal, A., de Jong, L., Hartog, A. F., and Kemp, A. (1985) Photoaffinity labeling of peptide binding sites of prolyl 4-hydroxylase with *N*-(4-azido-2-nitrophenyl)glycyl-(Pro-Pro-Gly)$_5$, *Biochemistry 24*, 6493–6499.
828. Rousselot, P., Mappus, E., Blachere, T., de Ravel, M. R., Grenot, C., Tonnelle, C., and Cuilleron, C. Y. (1997) Specific photoaffinity labeling of Tyr-49 on the light chain in the steroid-combining site of a mouse monoclonal anti-estradiol antibody using two epimeric 6α- and 6β-(5-azido-2-nitrobenzoyl)-amidoestradiol photoreagents, *Biochemistry 36*, 7860–7868.
829. Rashidbaigi, A., and Ruoho, A. E. (1981) Iodoazidobenzylpindolol, a photoaffinity probe for the β-adrenergic receptor, *Proc. Natl. Acad. Sci. U. S. A. 78*, 1609–1613.
830. DiPaola, M., Kao, P. N., and Karlin, A. (1990) Mapping the α-subunit site photolabeled by the noncompetitive inhibitor [^{3}H]quinacrine azide in the active state of the nicotinic acetylcholine receptor, *J. Biol. Chem. 265*, 11017–11029.
831. Corey, E. J., Cheng, H., Baker, C. H., Matsuda, S. P. T., Li, D., and Song, X. (1997) Studies on the substrate binding segments and catalytic action of lanosterol synthase. Affinity labeling with carbocations derived from mechanism-based analogs of 2,3-oxidosqualene and site-directed mutagenesis probes, *J. Am. Chem. Soc. 119*, 1289–1296.
832. Jeng, S. J., and Guillory, R. J. (1975) The use of aryl azido ATP analogs as photoaffinity labels for myosin ATPase, *J. Supramol. Struct. 3*, 448–468.
833. Pandey, V. N., Williams, K. R., Stone, K. L., and Modak, M. J. (1987) Photoaffinity labeling of the thymidine triphosphate binding domain in *Escherichia coli* DNA polymerase I: Identification of Histidine-881 as the site of cross-linking, *Biochemistry 26*, 7744–7748.
834. Tanner, N. K., Hanna, M. M., and Abelson, J. (1988) Binding interactions between yeast tRNA ligase and a precursor transfer ribonucleic acid containing two photoreactive uridine analogues, *Biochemistry 27*, 8852–8861.
835. Leon, O., and Schulman, L. H. (1987) tRNA Recognition site of *Escherichia coli* methionyl-tRNA synthetase, *Biochemistry 26*, 5416–5422.
836. Buonocore, V., and Schlesinger, S. (1972) Interactions of tyrosyl transfer ribonucleic acid synthetase from *Escherichia coli* with its substrates. Inhibition by transfer ribonucleic acid, *J. Biol. Chem. 247*, 1343–1348.
837. Hill, K., and Schimmel, P. (1989) Evidence that the 3′ end of a tRNA binds to a site in the adenylate synthesis domain of an aminoacyl-tRNA synthetase, *Biochemistry 28*, 2577–2586.
838. Naganuma, M., Sekine, S., Chong, Y. E., Guo, M., Yang, X. L., Gamper, H., Hou, Y. M., Schimmel, P., and Yokoyama, S. (2014) The selective tRNA aminoacylation mechanism based on a single G•U pair, *Nature (London, U. K.) 510*, 507–511.
839. Eshdat, Y., Dunn, A., and Sharon, N. (1974) Chemical conversion of Aspartic Acid 52, a catalytic residue in hen egg-white lysozyme, to homoserine, *Proc. Natl. Acad. Sci. U. S. A. 71*, 1658–1662.
840. Miller, J. C., and Waley, S. G. (1971) The active centre of rabbit muscle triose phosphate isomerase. The site that is labelled by glycidol phosphate, *Biochem. J. 123*, 163–170.
841. Rando, R. R., and Bloch, K. (1968) Mechanism of action of β-hydroxydecanoyl thioester dehydrase, *J. Biol. Chem. 243*, 5627–5634.
842. Helmkamp, G. M., Jr., and Bloch, K. (1969) β-Hydroxydecanoyl thioester dehydrase. Studies on molecular structure and active site, *J. Biol. Chem. 244*, 6014–6022.
843. Poelarends, G. J., Serrano, H., Person, M. D., Johnson, W. H., Jr., Murzin, A. G., and Whitman, C. P. (2004) Cloning, expression, and characterization of a *cis*-3-chloroacrylic acid dehalogenase: Insights into the mechanistic, structural, and evolutionary relationship between isomer-specific 3-chloroacrylic acid dehalogenases, *Biochemistry 43*, 759–772.
844. Wu, Z., Wouters, J., and Poulter, C. D. (2005) Isopentenyl diphosphate isomerase. Mechanism-based inhibition by diene analogues of isopentenyl diphosphate and dimethylallyl diphosphate, *J. Am. Chem. Soc. 127*, 17433–17438.
845. Rao, K. S., Albro, M., Vockley, J., and Frerman, F. E. (2003) Mechanism-based inactivation of human glutaryl-CoA dehydrogenase

by 2-pentynoyl-CoA: Rationale for enhanced reactivity, *J. Biol. Chem. 278*, 26342–26350.
846. Saxl, R. L., Reston, J., Nie, Z., Kalman, T. I., and Maley, F. (2003) Modification of *Escherichia coli* thymidylate synthase at Tyrosine-94 by 5-imidazolylpropynyl-2′-deoxyuridine 5′-monophosphate, *Biochemistry 42*, 4544–4551.
847. Holbrook, J. J., and Ingram, V. A. (1973) Ionic properties of an essential histidine residue in pig heart lactate dehydrogenase, *Biochem. J. 131*, 729–738.
848. Teh, A.-H., Kimura, M., Yamamoto, M., Tanaka, N., Yamaguchi, I., and Kumasaka, T. (2006) The 1.48 Å resolution crystal structure of the homotetrameric cytidine deaminase from mouse, *Biochemistry 45*, 7825–7833.
849. Sims, P. A., Menefee, A. L., Larsen, T. M., Mansoorabadi, S. O., and Reed, G. H. (2006) Structure and catalytic properties of an engineered heterodimer of enolase composed of one active and one inactive subunit, *J. Mol. Biol. 355*, 422–431.
850. Zhang, E., Brewer, J. M., Minor, W., Carreira, L. A., and Lebioda, L. (1997) Mechanism of enolase: The crystal structure of asymmetric dimer enolase-2-phospho-D-glycerate/enolase-phosphoenolpyruvate at 2.0 Å resolution, *Biochemistry 36*, 12526–12534.
851. Burbaum, J. J., and Knowles, J. R. (1989) Internal thermodynamics of enzymes determined by equilibrium quench: Values of k_{int} for enolase and creatine kinase, *Biochemistry 28*, 9306–9317.
852. Rozovsky, S., and McDermott, A. E. (2007) Substrate product equilibrium on a reversible enzyme, triosephosphate isomerase, *Proc. Natl. Acad. Sci. U. S. A. 104*, 2080–2085.
853. Lunin, V. V., Li, Y., Linhardt, R. J., Miyazono, H., Kyogashima, M., Kaneko, T., Bell, A. W., and Cygler, M. (2004) High-resolution crystal structure of *Arthrobacter aurescens* chondroitin AC lyase: An enzyme-substrate complex defines the catalytic mechanism, *J. Mol. Biol. 337*, 367–386.
854. Jez, J. M., Bowman, M. E., Dixon, R. A., and Noel, J. P. (2000) Structure and mechanism of the evolutionarily unique plant enzyme chalcone isomerase, *Nat. Struct. Biol. 7*, 786–791.
855. Middleton, B. (1972) The kinetic mechanism of 3-hydroxy-3-methylglutaryl-coenzyme A synthase from baker's yeast, *Biochem. J. 126*, 35–47.
856. Middleton, B., and Tubbs, P. K. (1974) An enzyme-bound intermediate in the biosynthesis of 3-hydroxy-3-methylglutaryl-coenzyme A, *Biochem. J. 137*, 15–23.
857. Misra, I., Narasimhan, C., and Miziorko, H. M. (1993) Avian 3-hydroxy-3-methylglutaryl-CoA synthase. Characterization of a recombinant cholesterogenic isozyme and demonstration of the requirement for a sulfhydryl functionality in formation of the acetyl-enzyme reaction intermediate, *J. Biol. Chem. 268*, 12129–12135.
858. Theisen, M. J., Misra, I., Saadat, D., Campobasso, N., Miziorko, H. M., and Harrison, D. H. (2004) 3–hydroxy-3-methylglutaryl-CoA synthase intermediate complex observed in "real-time", *Proc. Natl. Acad. Sci. U. S. A. 101*, 16442–16447.
859. Hammond, G. S. (1955) A correlation of reaction rates, *J. Am. Chem. Soc. 77*, 334–338.
860. Bateman, R. L., Bhanumoorthy, P., Witte, J. F., McClard, R. W., Grompe, M., and Timm, D. E. (2001) Mechanistic inferences from the crystal structure of fumarylacetoacetate hydrolase with a bound phosphorus-based inhibitor, *J. Biol. Chem. 276*, 15284–15291.
861. Timm, D. E., Mueller, H. A., Bhanumoorthy, P., Harp, J. M., and Bunick, G. J. (1999) Crystal structure and mechanism of a carbon–carbon bond hydrolase, *Structure (Cambridge, MA, U. S.) 7*, 1023–1033.
862. Kulik, V., Hartmann, E., Weyand, M., Frey, M., Gierl, A., Niks, D., Dunn, M. F., and Schlichting, I. (2005) On the structural basis of the catalytic mechanism and the regulation of the α subunit of tryptophan synthase from *Salmonella typhimurium* and BX1 from maize, two evolutionarily related enzymes, *J. Mol. Biol. 352*, 608–620.
863. Rhee, S., Parris, K. D., Hyde, C. C., Ahmed, S. A., Miles, E. W., and Davies, D. R. (1997) Crystal structures of a mutant (βK87T) tryptophan synthase $\alpha_2\beta_2$ complex with ligands bound to the active sites of the α- and β-subunits reveal ligand-induced conformational changes, *Biochemistry 36*, 7664–7680.
864. Lindquist, R. N., Lynn, J. L., Jr., and Lienhard, G. E. (1973) Possible transition-state analogs for ribonuclease. Complexes of uridine with oxovanadium(IV) ion and vanadium(V) ion, *J. Am. Chem. Soc. 95*, 8762.

865. Ladner, J. E., Wladkowski, B. D., Svensson, L. A., Sjolin, L., and Gilliland, G. L. (1997) X-Ray structure of a ribonuclease A-uridine vanadate complex at 1.3 Å resolution, *Acta Crystallogr., Sect. D: Biol. Crystallogr. D53*, 290–301.
866. Alphey, M. S., Yu, W., Byres, E., Li, D., and Hunter, W. N. (2005) Structure and reactivity of human mitochondrial 2,4-dienoyl-CoA reductase: Enzyme-ligand interactions in a distinctive short-chain reductase active site, *J. Biol. Chem. 280*, 3068–3077.
867. Laber, B., Maurer, W., Scharf, S., Stepusin, K., and Schmidt, F. S. (1999) Vitamin B_6 biosynthesis: Formation of pyridoxine 5′-phosphate from 4-(phosphohydroxy)-L-threonine and 1-deoxy-D-xylulose-5-phosphate by PdxA and PdxJ protein, *FEBS Lett. 449*, 45–48.
868. Garrido-Franco, M., Laber, B., Huber, R., and Clausen, T. (2002) Enzyme-ligand complexes of pyridoxine 5′-phosphate synthase: Implications for substrate binding and catalysis, *J. Mol. Biol. 321*, 601–612.
869. Parry, R. J., Burns, M. R., Jiralerspong, S., and Alemany, L. (1997) Synthesis of (+)-(1*S*)-1-pyrophosphoryl-(2*R*,3*R*)-2,3-dihydroxy-(4*S*)-4-(phosphoryloxymethyl)cyclopentane: A stable, optically-active carbocyclic analog of 5-phosphoribosyl-1-pyrophosphate (PRPP), *Tetrahedron 53*, 7077–7088.
870. Vos, S., Parry, R. J., Burns, M. R., de Jersey, J., and Martin, J. L. (1998) Structures of free and complexed forms of *Escherichia coli* xanthine-guanine phosphoribosyltransferase, *J. Mol. Biol. 282*, 875–889.
871. Klepp, J., Fallert-Muller, A., Grimm, K., Hull, W. E., and Retey, J. (1990) Mechanism of action of urocanase. Specific ^{13}C-labelling of the prosthetic NAD^+ and revision of the structure of its adduct with imidazolylpropionate, *Eur. J. Biochem. 192*, 669–676.
872. Kessler, D., Retey, J., and Schulz, G. E. (2004) Structure and action of urocanase, *J. Mol. Biol. 342*, 183–194.
873. Kaeppeli, F., and Retey, J. (1971) Studies on the mechanism and stereospecificity of the urocanase reaction, *Eur. J. Biochem. 23*, 198–202.
874. Lorentzen, E., Siebers, B., Hensel, R., and Pohl, E. (2005) Mechanism of the Schiff base forming fructose-1,6-bisphosphate aldolase: Structural analysis of reaction intermediates, *Biochemistry 44*, 4222–4229.
875. Hoeffken, H. W., Knof, S. H., Bartlett, P. A., Huber, R., Moellering, H., and Schumacher, G. (1988) Crystal structure determination, refinement and molecular model of creatine amidinohydrolase from *Pseudomonas putida*, *J. Mol. Biol. 204*, 417–433.
876. Polovnikova, E. S., McLeish, M. J., Sergienko, E. A., Burgner, J. T., Anderson, N. L., Bera, A. K., Jordan, F., Kenyon, G. L., and Hasson, M. S. (2003) Structural and kinetic analysis of catalysis by a thiamin diphosphate-dependent enzyme, benzoylformate decarboxylase, *Biochemistry 42*, 1820–1830.
877. Taylor, T. C., and Andersson, I. (1997) The structure of the complex between rubisco and its natural substrate ribulose 1,5-bisphosphate, *J. Mol. Biol. 265*, 432–444.
878. Andersson, I. (1996) Large structures at high resolution: The 1.6 Å crystal structure of spinach ribulose-1,5-bisphosphate carboxylase/oxygenase complexed with 2-carboxyarabinitol bisphosphate, *J. Mol. Biol. 259*, 160–174.
879. Leslie, A. G. (1990) Refined crystal structure of type III chloramphenicol acetyltransferase at 1.75 Å resolution, *J. Mol. Biol. 213*, 167–186.
880. Leslie, A. G., Moody, P. C., and Shaw, W. V. (1988) Structure of chloramphenicol acetyltransferase at 1.75-Å resolution, *Proc. Natl. Acad. Sci. U. S. A. 85*, 4133–4137.
881. Yasutake, Y., Nishiya, Y., Tamura, N., and Tamura, T. (2007) Structural insights into unique substrate selectivity of *Thermoplasma acidophilum* D-aldohexose dehydrogenase, *J. Mol. Biol. 367*, 1034–1046.
882. Steinbacher, S., Schiffmann, S., Richter, G., Huber, R., Bacher, A., and Fischer, M. (2003) Structure of 3,4-dihydroxy-2-butanone 4-phosphate synthase from *Methanococcus jannaschii* in complex with divalent metal ions and the substrate ribulose 5-phosphate: Implications for the catalytic mechanism, *J. Biol. Chem. 278*, 42256–42265.
883. Johnson, L. N., Acharya, K. R., Jordan, M. D., and McLaughlin, P. J. (1990) Refined crystal structure of the phosphorylase-heptulose 2-phosphate-oligosaccharide-AMP complex, *J. Mol. Biol. 211*, 645–661.
884. O'Gara, M., Klimasauskas, S., Roberts, R. J., and Cheng, X. (1996) Enzymatic C5-cytosine methylation of DNA: Mechanistic implications of new crystal structures for HhaI me-

thyltransferase-DNA-AdoHcy complexes, *J. Mol. Biol. 261*, 634–645.
885. Schoenborn, B. P. (1972) A neutron diffraction analysis of myoglobin. 3. Hydrogen-deuterium bonding in side chains, *Cold Spring Harbor Symp. Quant. Biol. 36*, 569–575.
886. Shu, F., Ramakrishnan, V., and Schoenborn, B. P. (2000) Enhanced visibility of hydrogen atoms by neutron crystallography on fully deuterated myoglobin, *Proc. Natl. Acad. Sci. U. S. A. 97*, 3872–3877.
887. Lario, P. I., Sampson, N., and Vrielink, A. (2003) Sub-atomic resolution crystal structure of cholesterol oxidase: What atomic resolution crystallography reveals about enzyme mechanism and the role of the FAD cofactor in redox activity, *J. Mol. Biol. 326*, 1635–1650.
888. Minasov, G., Wang, X., and Shoichet, B. K. (2002) An ultrahigh resolution structure of TEM-1 β-lactamase suggests a role for Glu166 as the general base in acylation, *J. Am. Chem. Soc. 124*, 5333–5340.
889. Blakeley, M. P., Ruiz, F., Cachau, R., Hazemann, I., Meilleur, F., Mitschler, A., Ginell, S., Afonine, P., Ventura, O. N., Cousido-Siah, A., Haertlein, M., Joachimiak, A., Myles, D., and Podjarny, A. (2008) Quantum model of catalysis based on a mobile proton revealed by subatomic X-ray and neutron diffraction studies of h-aldose reductase, *Proc. Natl. Acad. Sci. U. S. A. 105*, 1844–1848.
890. Coates, L., Tuan, H. F., Tomanicek, S., Kovalevsky, A., Mustyakimov, M., Erskine, P., and Cooper, J. (2008) The catalytic mechanism of an aspartic proteinase explored with neutron and X-ray diffraction, *J. Am. Chem. Soc. 130*, 7235–7237.
891. Fuhrmann, C. N., Daugherty, M. D., and Agard, D. A. (2006) Subångstrom crystallography reveals that short ionic hydrogen bonds, and not a His-Asp low-barrier hydrogen bond, stabilize the transition state in serine protease catalysis, *J. Am. Chem. Soc. 128*, 9086–9102.
892. Kovalevsky, A. Y., Katz, A. K., Carrell, H. L., Hanson, L., Mustyakimov, M., Fisher, S. Z., Coates, L., Schoenborn, B. P., Bunick, G. J., Glusker, J. P., and Langan, P. (2008) Hydrogen location in stages of an enzyme-catalyzed reaction: Time-of-flight neutron structure of D-xylose isomerase with bound D-xylulose, *Biochemistry 47*, 7595–7597.
893. Kneller, D. W., Phillips, G., Weiss, K. L., Pant, S., Zhang, Q., O'Neill, H. M., Coates, L., and Kovalevsky, A. (2020) Unusual zwitterionic catalytic site of SARS–CoV-2 main protease revealed by neutron crystallography, *J. Biol. Chem. 295*, 17365–17373.
894. Chen, Y., Bonnet, R., and Shoichet, B. K. (2007) The acylation mechanism of CTX-M β-lactamase at 0.88 Å resolution, *J. Am. Chem. Soc. 129*, 5378–5380.
895. Sielecki, A. R., Fedorov, A. A., Boodhoo, A., Andreeva, N. S., and James, M. N. (1990) Molecular and crystal structures of monoclinic porcine pepsin refined at 1.8 Å resolution, *J. Mol. Biol. 214*, 143–170.
896. Miller, M., Schneider, J., Sathyanarayana, B. K., Toth, M. V., Marshall, G. R., Clawson, L., Selk, L., Kent, S. B., and Wlodawer, A. (1989) Structure of complex of synthetic HIV-1 protease with a substrate-based inhibitor at 2.3 Å resolution, *Science (Washington, DC, U. S.) 246*, 1149–1152.
897. Shen, C. H., Tie, Y., Yu, X., Wang, Y. F., Kovalevsky, A. Y., Harrison, R. W., and Weber, I. T. (2012) Capturing the reaction pathway in near-atomic-resolution crystal structures of HIV-1 protease, *Biochemistry 51*, 7726–7732.
898. Jiang, J.-C., Wang, Y.-S., Chang, H.-C., Lin, S. H., Lee, Y. T., Niedner-Schatteburg, G., and Chang, H.-C. (2000) Infrared spectra of $H^+(H_2O)_{5\text{-}8}$ clusters: Evidence for symmetric proton hydration, *J. Am. Chem. Soc. 122*, 1398–1410.
899. Miyazaki, M., Fujii, A., Ebata, T., and Mikami, N. (2004) Infrared spectroscopic evidence for protonated water clusters forming nanoscale cages, *Science (Washington, DC, U. S.) 304*, 1134–1137.
900. Shin, J. W., Hammer, N. I., Diken, E. G., Johnson, M. A., Walters, R. S., Jaeger, T. D., Duncan, M. A., Christie, R. A., and Jordan, K. D. (2004) Infrared signature of structures associated with the $H^+(H_2O)_n$ ($n = 6$ to 27) clusters, *Science (Washington, DC, U. S.) 304*, 1137–1140.
901. Okumura, M., Yeh, L. I., Myers, J. D., and Lee, Y. T. (1990) Infrared-spectra of the solvated hydronium ion-vibrational predissociation spectroscopy of mass-selected $H_3O^+ \cdot (H_2O)_n \cdot (H_2)_m$, *J. Phys. Chem. 94*, 3416–3427.
902. Yang, X. L., and Castleman, A. W. (1989) Large protonated water clusters $H^+(H_2O)_n$ ($1 \leq n > 60$): The production and reactivity of

clathrate-like structures under thermal conditions, *J. Am. Chem. Soc. 111*, 6845–6846.
903. Wei, S., Shi, Z., and Castleman, A. W., Jr. (1991) Mixed cluster ions as a structure probe: Experimental evidence for clathrate structure of water-hydrogen ion clusters $(H_2O)_{20}H^+$ and $(H_2O)_{21}H^+$, *J. Chem. Phys. 94*, 3268–3270.
904. Zundel, G., and Metzger, H. (1968) IR Spectroscopic study of the hydration of polystyrenesulfonic acid, *Z. Phys. Chem. (Muenchen, Ger.) 59*, 225–241.
905. Schwarz, H. A. (1977) Gas phase infrared spectra of oxonium hydrate ions from 2 to 5 μ, *J. Chem. Phys. 67*, 5525–5534.
906. Marx, D., Tuckerman, M. E., Hutter, J., and Parrinello, M. (1999) The nature of the hydrated excess proton in water, *Nature (London, U. K.) 397*, 601–604.
907. Eigen, M. (1964) Proton transfer, acid-base catalysis, and enzymatic hydrolysis. Part I: Elementary processes, *Angew. Chem., Int. Ed. Engl. 3*, 1–19.
908. Steitz, T. A., Henderson, R., and Blow, D. M. (1969) Structure of crystalline α-chymotrypsin. 3. Crystallographic studies of substrates and inhibitors bound to the active site of α-chymotrypsin, *J. Mol. Biol. 46*, 337–348.
909. Grau, U. M., Trommer, W. E., and Rossmann, M. G. (1981) Structure of the active ternary complex of pig heart lactate dehydrogenase with *S*-lac-NAD at 2.7 Å resolution, *J. Mol. Biol. 151*, 289–307.
910. Birktoft, J. J., and Banaszak, L. J. (1983) The presence of a histidine-aspartic acid pair in the active site of 2-hydroxyacid dehydrogenases. X-Ray refinement of cytoplasmic malate dehydrogenase, *J. Biol. Chem. 258*, 472–482.
911. Liao, D. I., Breddam, K., Sweet, R. M., Bullock, T., and Remington, S. J. (1992) Refined atomic model of wheat serine carboxypeptidase II at 2.2-Å resolution, *Biochemistry 31*, 9796–9812.
912. Brady, L., Brzozowski, A. M., Derewenda, Z. S., Dodson, E., Dodson, G., Tolley, S., Turkenburg, J. P., Christiansen, L., Huge-Jensen, B., Norskov, L., Thim, L., and Menge, U. (1990) A serine protease triad forms the catalytic centre of a triacylglycerol lipase, *Nature (London, U. K.) 343*, 767–770.
913. Winkler, F. K., D'Arcy, A., and Hunziker, W. (1990) Structure of human pancreatic lipase, *Nature (London, U. K.) 343*, 771–774.
914. Mancheno, J. M., Pernas, M. A., Martinez, M. J., Ochoa, B., Rua, M. L., and Hermoso, J. A. (2003) Structural insights into the lipase/esterase behavior in the *Candida rugosa* lipases family: Crystal structure of the lipase 2 isoenzyme at 1.97 Å resolution, *J. Mol. Biol. 332*, 1059–1069.
915. Weadge, J. T., and Clarke, A. J. (2007) *Neisseria gonorrheae O*-acetylpeptidoglycan esterase, a serine esterase with a Ser-His-Asp catalytic triad, *Biochemistry 46*, 4932–4941.
916. Dijkstra, B. W., Renetseder, R., Kalk, K. H., Hol, W. G., and Drenth, J. (1983) Structure of porcine pancreatic phospholipase A_2 at 2.6 Å resolution and comparison with bovine phospholipase A_2, *J. Mol. Biol. 168*, 163–179.
917. Pathak, D., and Ollis, D. (1990) Refined structure of dienelactone hydrolase at 1.8 Å, *J. Mol. Biol. 214*, 497–525.
918. Hung, C. L., Liu, J. H., Chiu, W. C., Huang, S. W., Hwang, J. K., and Wang, W. C. (2007) Crystal structure of *Helicobacter pylori* formamidase AmiF reveals a cysteine-glutamate-lysine catalytic triad, *J. Biol. Chem. 282*, 12220–12229.
919. Herzberg, O. (1991) Refined crystal structure of β-lactamase from *Staphylococcus aureus* PC1 at 2.0 Å resolution, *J. Mol. Biol. 217*, 701–719.
920. Duggleby, H. J., Tolley, S. P., Hill, C. P., Dodson, E. J., Dodson, G., and Moody, P. C. (1995) Penicillin acylase has a single-amino-acid catalytic centre, *Nature (London, U. K.) 373*, 264–268.
921. Wei, Y., Schottel, J. L., Derewenda, U., Swenson, L., Patkar, S., and Derewenda, Z. S. (1995) A novel variant of the catalytic triad in the *Streptomyces scabies* esterase, *Nat. Struct. Biol. 2*, 218–223.
922. Weston, S. A., Lahm, A., and Suck, D. (1992) X-Ray structure of the DNase I-d$(GGTATACC)_2$ complex at 2.3 Å resolution, *J. Mol. Biol. 226*, 1237–1256.
923. Clarke, A. R., Wilks, H. M., Barstow, D. A., Atkinson, T., Chia, W. N., and Holbrook, J. J. (1988) An investigation of the contribution made by the carboxylate group of an active site histidine-aspartate couple to binding and catalysis in lactate dehydrogenase, *Biochemistry 27*, 1617–1622.

924. Xia, Z. X., and Mathews, F. S. (1990) Molecular structure of flavocytochrome b_2 at 2.4 Å resolution, *J. Mol. Biol. 212*, 837–863.
925. Gondry, M., and Lederer, F. (1996) Functional properties of the histidine-aspartate ion pair of flavocytochrome b_2 (L-lactate dehydrogenase): Substitution of Asp282 with asparagine, *Biochemistry 35*, 8587–8594.
926. Bhaumik, P., Schmitz, W., Hassinen, A., Hiltunen, J. K., Conzelmann, E., and Wierenga, R. K. (2007) The catalysis of the 1,1-proton transfer by α-methyl-acyl-CoA racemase is coupled to a movement of the fatty acyl moiety over a hydrophobic, methionine-rich surface, *J. Mol. Biol. 367*, 1145–1161.
927. Thunnissen, M. M., Ab, E., Kalk, K. H., Drenth, J., Dijkstra, B. W., Kuipers, O. P., Dijkman, R., de Haas, G. H., and Verheij, H. M. (1990) X-ray structure of phospholipase A_2 complexed with a substrate-derived inhibitor, *Nature (London, U. K.) 347*, 689–691.
928. Dupureur, C. M., Deng, T., Kwak, J. G., Noel, J. P., and Tsai, M. D. (1990) Phospholipase A_2 engineering. 4. Can the active-site Aspartate-99 function alone?, *J. Am. Chem. Soc. 112*, 7074–7076.
929. Baker, E. N. (1980) Structure of actinidin, after refinement at 1.7 Å resolution, *J. Mol. Biol. 141*, 441–484.
930. Bromme, D., Bonneau, P. R., Purisima, E., Lachance, P., Hajnik, S., Thomas, D. Y., and Storer, A. C. (1996) Contribution to activity of histidine–aromatic, amide–aromatic, and aromatic–aromatic interactions in the extended catalytic site of cysteine proteinases, *Biochemistry 35*, 3970–3979.
931. Huang, W., Boju, L., Tkalec, L., Su, H., Yang, H. O., Gunay, N. S., Linhardt, R. J., Kim, Y. S., Matte, A., and Cygler, M. (2001) Active site of chondroitin AC lyase revealed by the structure of enzyme-oligosaccharide complexes and mutagenesis, *Biochemistry 40*, 2359–2372.
932. Adina-Zada, A., Jitrapakdee, S., Wallace, J. C., and Attwood, P. V. (2014) Coordinating role of His216 in MgATP binding and cleavage in pyruvate carboxylase, *Biochemistry 53*, 1051–1058.
933. Swain, A. L., Jaskolski, M., Housset, D., Rao, J. K., and Wlodawer, A. (1993) Crystal structure of *Escherichia coli* L-asparaginase, an enzyme used in cancer therapy, *Proc. Natl. Acad. Sci. U. S. A. 90*, 1474–1478.
934. Gesto, D. S., Cerqueira, N. M., Fernandes, P. A., and Ramos, M. J. (2013) Unraveling the enigmatic mechanism of L-asparaginase II with QM/QM calculations, *J. Am. Chem. Soc. 135*, 7146–7158.
935. Sidhu, G., Withers, S. G., Nguyen, N. T., McIntosh, L. P., Ziser, L., and Brayer, G. D. (1999) Sugar ring distortion in the glycosyl-enzyme intermediate of a family G/11 xylanase, *Biochemistry 38*, 5346–5354.
936. Yun, M., Park, C. G., Kim, J. Y., and Park, H. W. (2000) Structural analysis of glyceraldehyde 3-phosphate dehydrogenase from *Escherichia coli*: Direct evidence of substrate binding and cofactor-induced conformational changes, *Biochemistry 39*, 10702–10710.
937. Soukri, A., Mougin, A., Corbier, C., Wonacott, A., Branlant, C., and Branlant, G. (1989) Role of the Histidine 176 residue in glyceraldehyde-3-phosphate dehydrogenase as probed by site-directed mutagenesis, *Biochemistry 28*, 2586–2592.
938. Highbarger, L. A., Gerlt, J. A., and Kenyon, G. L. (1996) Mechanism of the reaction catalyzed by acetoacetate decarboxylase. Importance of Lysine 116 in determining the pK_a of active-site Lysine 115, *Biochemistry 35*, 41–46.
939. Benson, T. E., Walsh, C. T., and Massey, V. (1997) Kinetic characterization of wild-type and S229A mutant MurB: Evidence for the role of Ser 229 as a general acid, *Biochemistry 36*, 796–805.
940. Lee, J. H., Chang, K. Z., Patel, V., and Jeffery, C. J. (2001) Crystal structure of rabbit phosphoglucose isomerase complexed with its substrate D-fructose 6-phosphate, *Biochemistry 40*, 7799–7805.
941. Yasuhira, K., Shibata, N., Mongami, G., Uedo, Y., Atsumi, Y., Kawashima, Y., Hibino, A., Tanaka, Y., Lee, Y. H., Kato, D., Takeo, M., Higuchi, Y., and Negoro, S. (2010) X-Ray crystallographic analysis of the 6-aminohexanoate cyclic dimer hydrolase: Catalytic mechanism and evolution of an enzyme responsible for nylon-6 byproduct degradation, *J. Biol. Chem. 285*, 1239–1248.
942. Wang, Y., and Guo, H. C. (2007) Crystallographic snapshot of a productive glycosylasparaginase-substrate complex, *J. Mol. Biol. 366*, 82–92.

943. Doherty, M. K., Pealing, S. L., Miles, C. S., Moysey, R., Taylor, P., Walkinshaw, M. D., Reid, G. A., and Chapman, S. K. (2000) Identification of the active site acid/base catalyst in a bacterial fumarate reductase: A kinetic and crystallographic study, *Biochemistry 39*, 10695–10701.
944. Balon, M., Carmona, M. C., Munoz, M. A., and Hidalgo, J. (1989) The acid-base properties of pyrrole and its benzologs indole and carbazole. A reexamination from the excess acidity method, *Tetrahedron 45*, 7501–7504.
945. Starks, C. M., Back, K., Chappell, J., and Noel, J. P. (1997) Structural basis for cyclic terpene biosynthesis by tobacco 5-epi-aristolochene synthase, *Science (Washington, DC, U. S.) 277*, 1815–1820.
946. Holliday, G. L., Almonacid, D. E., Mitchell, J. B., and Thornton, J. M. (2007) The chemistry of protein catalysis, *J. Mol. Biol. 372*, 1261–1277.
947. Torrance, J. W., Holliday, G. L., Mitchell, J. B., and Thornton, J. M. (2007) The geometry of interactions between catalytic residues and their substrates, *J. Mol. Biol. 369*, 1140–1152.
948. March, J. (1992) *Advanced organic chemistry: Reactions, mechanisms, and structure: Fourth edition*, pp 250–252, Wiley, New York.
949. Verschueren, K. H., Seljee, F., Rozeboom, H. J., Kalk, K. H., and Dijkstra, B. W. (1993) Crystallographic analysis of the catalytic mechanism of haloalkane dehalogenase, *Nature (London, U. K.) 363*, 693–698.
950. Verschueren, K. H. G., Kingma, J., Rozeboom, H. J., Kalk, K. H., Janssen, D. B., and Dijkstra, B. W. (1993) Crystallographic and fluorescence studies of the interaction of haloalkane dehalogenase with halide ions. Studies with halide compounds reveal a halide binding site in the active site, *Biochemistry 32*, 9031–9037.
951. Oakley, A. J., Lo Bello, M., Battistoni, A., Ricci, G., Rossjohn, J., Villar, H. O., and Parker, M. W. (1997) The structures of human glutathione transferase P1-1 in complex with glutathione and various inhibitors at high resolution, *J. Mol. Biol. 274*, 84–100.
952. Ji, X., Zhang, P., Armstrong, R. N., and Gilliland, G. L. (1992) The three-dimensional structure of a glutathione *S*-transferase from the Mu gene class. Structural analysis of the binary complex of isoenzyme 3–3 and glutathione at 2.2-Å resolution, *Biochemistry 31*, 10169–10184.
953. Larsen, T. M., Boehlein, S. K., Schuster, S. M., Richards, N. G., Thoden, J. B., Holden, H. M., and Rayment, I. (1999) Three-dimensional structure of *Escherichia coli* asparagine synthetase B: A short journey from substrate to product, *Biochemistry 38*, 16146–16157.
954. Thoden, J. B., Reinhardt, L. A., Cook, P. D., Menden, P., Cleland, W. W., and Holden, H. M. (2012) Catalytic mechanism of perosamine *N*-acetyltransferase revealed by high-resolution X-ray crystallographic studies and kinetic analyses, *Biochemistry 51*, 3433–3444.
955. Zhuang, N., Zhang, H., Li, L., Wu, X., Yang, C., and Zhang, Y. (2020) Crystal structures and biochemical analyses of the bacterial arginine dihydrolase ArgZ suggests a "bond rotation" catalytic mechanism, *J. Biol. Chem. 295*, 2113–2124.
956. Stroud, R. M., Kay, L. M., and Dickerson, R. E. (1974) The structure of bovine trypsin: Electron density maps of the inhibited enzyme at 5 Å and at 2.7 Å resolution, *J. Mol. Biol. 83*, 185–208.
957. Langley, D. B., Templeton, M. D., Fields, B. A., Mitchell, R. E., and Collyer, C. A. (2000) Mechanism of inactivation of ornithine transcarbamoylase by N^{δ}-(*N'*-sulfodiaminophosphinyl)-L-ornithine, a true transition state analogue? Crystal structure and implications for catalytic mechanism, *J. Biol. Chem. 275*, 20012–20019.
958. Nar, H., Huber, R., Auerbach, G., Fischer, M., Hosl, C., Ritz, H., Bracher, A., Meining, W., Eberhardt, S., and Bacher, A. (1995) Active site topology and reaction mechanism of GTP cyclohydrolase I, *Proc. Natl. Acad. Sci. U. S. A. 92*, 12120–12125.
959. Ren, J., Kotaka, M., Lockyer, M., Lamb, H. K., Hawkins, A. R., and Stammers, D. K. (2005) GTP Cyclohydrolase II structure and mechanism, *J. Biol. Chem. 280*, 36912–36919.
960. Kallen, R. G., and Jencks, W. P. (1966) Dissociation constants of tetrahydrofolic acid, *J. Biol. Chem. 241*, 5845–5850.
961. Szebenyi, D. M., Liu, X., Kriksunov, I. A., Stover, P. J., and Thiel, D. J. (2000) Structure of a murine cytoplasmic serine hydroxymethyltransferase quinonoid ternary complex: Evidence for asymmetric obligate dimers, *Biochemistry 39*, 13313–13323.

962. Tralau, T., Lafite, P., Levy, C., Combe, J. P., Scrutton, N. S., and Leys, D. (2009) An internal reaction chamber in dimethylglycine oxidase provides efficient protection from exposure to toxic formaldehyde, *J. Biol. Chem. 284*, 17826–17834.
963. Wolan, D. W., Greasley, S. E., Wall, M. J., Benkovic, S. J., and Wilson, I. A. (2003) Structure of avian AICAR transformylase with a multisubstrate adduct inhibitor β-DADF identifies the folate binding site, *Biochemistry 42*, 10904–10914.
964. Versees, W., Barlow, J., and Steyaert, J. (2006) Transition-state complex of the purine-specific nucleoside hydrolase of *T. vivax*: Enzyme conformational changes and implications for catalysis, *J. Mol. Biol. 359*, 331–346.
965. Focia, P. J., Craig, S. P., 3rd, and Eakin, A. E. (1998) Approaching the transition state in the crystal structure of a phosphoribosyltransferase, *Biochemistry 37*, 17120–17127.
966. Anand, R., Kaminski, P. A., and Ealick, S. E. (2004) Structures of purine 2′-deoxyribosyltransferase, substrate complexes, and the ribosylated enzyme intermediate at 2.0 Å resolution, *Biochemistry 43*, 2384–2393.
967. Gourley, D. G., Schuttelkopf, A. W., Leonard, G. A., Luba, J., Hardy, L. W., Beverley, S. M., and Hunter, W. N. (2001) Pteridine reductase mechanism correlates pterin metabolism with drug resistance in trypanosomatid parasites, *Nat. Struct. Biol. 8*, 521–525.
968. Stenmark, P., Moche, M., Gurmu, D., and Nordlund, P. (2007) The crystal structure of the bifunctional deaminase/reductase RibD of the riboflavin biosynthetic pathway in *Escherichia coli*: Implications for the reductive mechanism, *J. Mol. Biol. 373*, 48–64.
969. Brunhuber, N. M., Thoden, J. B., Blanchard, J. S., and Vanhooke, J. L. (2000) *Rhodococcus* L-phenylalanine dehydrogenase: Kinetics, mechanism, and structural basis for catalytic specificity, *Biochemistry 39*, 9174–9187.
970. Wan, Q., Bennett, B. C., Wilson, M. A., Kovalevsky, A., Langan, P., Howell, E. E., and Dealwis, C. (2014) Toward resolving the catalytic mechanism of dihydrofolate reductase using neutron and ultrahigh-resolution X-ray crystallography, *Proc. Natl. Acad. Sci. U. S. A. 111*, 18225–18230.
971. Liu, C. T., Francis, K., Layfield, J. P., Huang, X., Hammes-Schiffer, S., Kohen, A., and Benkovic, S. J. (2014) *Escherichia coli* dihydrofolate reductase catalyzed proton and hydride transfers: Temporal order and the roles of Asp27 and Tyr100, *Proc. Natl. Acad. Sci. U. S. A. 111*, 18231–18236.
972. Mohamedali, K. A., Kurz, L. C., and Rudolph, F. B. (1996) Site-directed mutagenesis of active site Glutamate-217 in mouse adenosine deaminase, *Biochemistry 35*, 1672–1680.
973. Lubkowski, J., Vanegas, J., Chan, W. K., Lorenzi, P. L., Weinstein, J. N., Sukharev, S., Fushman, D., Rempe, S., Anishkin, A., and Wlodawer, A. (2020) Mechanism of catalysis by L-asparaginase, *Biochemistry 59*, 1927–1945.
974. Xu, F., Dong, F., Wang, P., Cao, H. Y., Li, C. Y., Li, P. Y., Pang, X. H., Zhang, Y. Z., and Chen, X. L. (2017) Novel molecular insights into the catalytic mechanism of marine bacterial alginate lyase AlyGC from polysaccharide lyase family 6, *J. Biol. Chem. 292*, 4457–4468.
975. Shumilin, I. A., Bauerle, R., Wu, J., Woodard, R. W., and Kretsinger, R. H. (2004) Crystal structure of the reaction complex of 3-deoxy-D-arabino-heptulosonate-7-phosphate synthase from *Thermotoga maritima* refines the catalytic mechanism and indicates a new mechanism of allosteric regulation, *J. Mol. Biol. 341*, 455–466.
976. Brux, C., Ben-David, A., Shallom-Shezifi, D., Leon, M., Niefind, K., Shoham, G., Shoham, Y., and Schomburg, D. (2006) The structure of an inverting GH43 β-xylosidase from *Geobacillus stearothermophilus* with its substrate reveals the role of the three catalytic residues, *J. Mol. Biol. 359*, 97–109.
977. Qian, M., Haser, R., Buisson, G., Duee, E., and Payan, F. (1994) The active center of a mammalian α-amylase. Structure of the complex of a pancreatic α-amylase with a carbohydrate inhibitor refined to 2.2-Å resolution, *Biochemistry 33*, 6284–6294.
978. Varrot, A., Tarling, C. A., Macdonald, J. M., Stick, R. V., Zechel, D. L., Withers, S. G., and Davies, G. J. (2003) Direct observation of the protonation state of an imino sugar glycosidase inhibitor upon binding, *J. Am. Chem. Soc. 125*, 7496–7497.
979. Weaver, L. H., Grutter, M. G., and Matthews, B. W. (1995) The refined structures of goose lysozyme and its complex with a bound trisaccharide show that the "goose-type" lysozymes lack a catalytic aspartate residue, *J. Mol. Biol. 245*, 54–68.

980. Shaw, A., Bott, R., Vonrhein, C., Bricogne, G., Power, S., and Day, A. G. (2002) A novel combination of two classic catalytic schemes, *J. Mol. Biol. 320*, 303–309.
981. Miyake, H., Kurisu, G., Kusunoki, M., Nishimura, S., Kitamura, S., and Nitta, Y. (2003) Crystal structure of a catalytic site mutant of β-amylase from *Bacillus cereus* var. mycoides cocrystallized with maltopentaose, *Biochemistry 42*, 5574–5581.
982. Fujimoto, Z., Takase, K., Doui, N., Momma, M., Matsumoto, T., and Mizuno, H. (1998) Crystal structure of a catalytic-site mutant α-amylase from *Bacillus subtilis* complexed with maltopentaose, *J. Mol. Biol. 277*, 393–407.
983. Guimaraes, B. G., Souchon, H., Lytle, B. L., Wu, J. H. D., and Alzari, P. M. (2002) The crystal structure and catalytic mechanism of cellobiohydrolase CelS, the major enzymatic component of the *Clostridium thermocellum* cellulosome, *J. Mol. Biol. 320*, 587–596.
984. Davies, G. J., Tolley, S. P., Henrissat, B., Hjort, C., and Schulein, M. (1995) Structures of oligosaccharide-bound forms of the endoglucanase V from *Humicola insolens* at 1.9 Å resolution, *Biochemistry 34*, 16210–16220.
985. Sakon, J., Adney, W. S., Himmel, M. E., Thomas, S. R., and Karplus, P. A. (1996) Crystal structure of thermostable family 5 endocellulase E1 from *Acidothermus cellulolyticus* in complex with cellotetraose, *Biochemistry 35*, 10648–10660.
986. Kuhn, R. (1924) The constitution of starch and the different modes of action of amylases, *Ber. Dtsch. Chem. Ges. B 57*, 1965–1968.
987. Parrish, F. W., and Reese, E. T. (1967) Anomeric form of D-glucose produced during enzymolysis, *Carbohydr. Res. 3*, 424–429.
988. Guerin, D. M., Lascombe, M. B., Costabel, M., Souchon, H., Lamzin, V., Beguin, P., and Alzari, P. M. (2002) Atomic (0.94 Å) resolution structure of an inverting glycosidase in complex with substrate, *J. Mol. Biol. 316*, 1061–1069.
989. Cox, R. A., Druet, L. M., Klausner, A. E., Modro, T. A., Wan, P., and Yates, K. (1981) Protonation acidity constants for some benzamides, acetamides, and lactams, *Can. J. Chem. 59*, 1568–1573.
990. Kubota, K., Nagata, K., Okai, M., Miyazono, K., Soemphol, W., Ohtsuka, J., Yamamura, A., Saichana, N., Toyama, H., Matsushita, K., and Tanokura, M. (2011) The crystal structure of L-sorbose reductase from *Gluconobacter frateurii* complexed with NADPH and L-sorbose, *J. Mol. Biol. 407*, 543–555.
991. Gerratana, B., Cleland, W. W., and Frey, P. A. (2001) Mechanistic roles of Thr134, Tyr160, and Lys164 in the reaction catalyzed by dTDP-glucose 4,6-dehydratase, *Biochemistry 40*, 9187–9195.
992. Mydy, L. S., Cristobal, J. R., Katigbak, R. D., Bauer, P., Reyes, A. C., Kamerlin, S. C. L., Richard, J. P., and Gulick, A. M. (2019) Human glycerol 3-phosphate dehydrogenase: X-Ray crystal structures that guide the interpretation of mutagenesis studies, *Biochemistry 58*, 1061–1073.
993. Iovane, E., Giabbai, B., Muzzolini, L., Matafora, V., Fornili, A., Minici, C., Giannese, F., and Degano, M. (2008) Structural basis for substrate specificity in group I nucleoside hydrolases, *Biochemistry 47*, 4418–4426.
994. Das, R., Vazquez-Montelongo, E. A., Cisneros, G. A., and Wu, J. I. (2019) Ground state destabilization in uracil DNA glycosylase: Let's not forget "tautomeric strain" in substrates, *J. Am. Chem. Soc. 141*, 13739–13743.
995. Mao, C., Cook, W. J., Zhou, M., Federov, A. A., Almo, S. C., and Ealick, S. E. (1998) Calf spleen purine nucleoside phosphorylase complexed with substrates and substrate analogues, *Biochemistry 37*, 7135–7146.
996. Watson, K. A., McCleverty, C., Geremia, S., Cottaz, S., Driguez, H., and Johnson, L. N. (1999) Phosphorylase recognition and phosphorolysis of its oligosaccharide substrate: Answers to a long outstanding question, *EMBO J. 18*, 4619–4632.
997. Breslow, R. (1993) Kinetics and mechanism in RNA cleavage, *Proc. Natl. Acad. Sci. U. S. A. 90*, 1208–1211.
998. Elsasser, B., Valiev, M., and Weare, J. H. (2009) A dianionic phosphorane intermediate and transition states in an associative A_N+D_N mechanism for the ribonuclease A hydrolysis reaction, *J. Am. Chem. Soc. 131*, 3869–3871.
999. Lonnberg, H., Stromberg, R., and Williams, A. (2004) Compelling evidence for a stepwise mechanism of the alkaline cyclisation of uridine 3′-phosphate esters, *Org. Biomol. Chem. 2*, 2165–2167.
1000. Sowa, G. A., Hengge, A. C., and Cleland, W. W. (1997) ^{18}O Isotope effects support a con-

certed mechanism for ribonuclease A, *J. Am. Chem. Soc. 119*, 2319–2320.
1001. Deng, H., Burgner, J. W., and Callender, R. H. (1998) Structure of the ribonuclease·uridine–vanadate transition state analogue complex by Raman difference spectroscopy: Mechanistic implications, *J. Am. Chem. Soc. 120*, 4717–4722.
1002. Westheimer, F. H. (1968) Pseudo-rotation in the hydrolysis of phosphate esters, *Acc. Chem. Res. 1*, 70–78.
1003. Messmore, J. M., Fuchs, D. N., and Raines, R. T. (1995) Ribonuclease A: Revealing structure-function relationships with semisynthesis, *J. Am. Chem. Soc. 117*, 8057–8060.
1004. Thompson, J. E., and Raines, R. T. (1994) Value of general acid-base catalysis to ribonuclease A, *J. Am. Chem. Soc. 116*, 5467–5468.
1005. Tsirkone, V. G., Dossi, K., Drakou, C., Zographos, S. E., Kontou, M., and Leonidas, D. D. (2009) Inhibitor design for ribonuclease A: The binding of two 5′-phosphate uridine analogues, *Acta Crystallogr., Sect. F: Struct. Biol. Commun. 65*, 671–677.
1006. Fisher, B. M., Schultz, L. W., and Raines, R. T. (1998) Coulombic effects of remote subsites on the active site of ribonuclease A, *Biochemistry 37*, 17386–17401.
1007. Gu, H., Zhang, S., Wong, K. Y., Radak, B. K., Dissanayake, T., Kellerman, D. L., Dai, Q., Miyagi, M., Anderson, V. E., York, D. M., Piccirilli, J. A., and Harris, M. E. (2013) Experimental and computational analysis of the transition state for ribonuclease A-catalyzed RNA 2′-O-transphosphorylation, *Proc. Natl. Acad. Sci. U. S. A. 110*, 13002–13007.
1008. Arnett, E. M., Mitchell, E. J., and Murty, T. S. S. R. (1974) Basicity. Comparison of hydrogen bonding and proton transfer to some Lewis bases, *J. Am. Chem. Soc. 96*, 3875–3891.
1009. Shan, S. O., Loh, S., and Herschlag, D. (1996) The energetics of hydrogen bonds in model systems: Implications for enzymatic catalysis, *Science (Washington, DC, U. S.) 272*, 97–101.
1010. Perrin, C. L., and Nielson, J. B. (1997) "Strong" hydrogen bonds in chemistry and biology, *Annu. Rev. Phys. Chem. 48*, 511–544.
1011. Gorrell, A., Lawrence, S. H., and Ferry, J. G. (2005) Structural and kinetic analyses of arginine residues in the active site of the acetate kinase from *Methanosarcina thermophila*, *J. Biol. Chem. 280*, 10731–10742.
1012. Richard, S. B., Bowman, M. E., Kwiatkowski, W., Kang, I., Chow, C., Lillo, A. M., Cane, D. E., and Noel, J. P. (2001) Structure of 4-diphosphocytidyl-2-C-methylerythritol synthetase involved in mevalonate- independent isoprenoid biosynthesis, *Nat. Struct. Biol. 8*, 641–648.
1013. Madhusudan, Akamine, P., Xuong, N. H., and Taylor, S. S. (2002) Crystal structure of a transition state mimic of the catalytic subunit of cAMP-dependent protein kinase, *Nat. Struct. Biol. 9*, 273–277.
1014. Zheng, J., Knighton, D. R., ten Eyck, L. F., Karlsson, R., Xuong, N., Taylor, S. S., and Sowadski, J. M. (1993) Crystal structure of the catalytic subunit of cAMP-dependent protein kinase complexed with MgATP and peptide inhibitor, *Biochemistry 32*, 2154–2161.
1015. Gil-Ortiz, F., Ramon-Maiques, S., Fita, I., and Rubio, V. (2003) The course of phosphorus in the reaction of *N*-acetyl-L-glutamate kinase, determined from the structures of crystalline complexes, including a complex with an AlF_4^- transition state mimic, *J. Mol. Biol. 331*, 231–244.
1016. Huang, W., Jia, J., Gibson, K. J., Taylor, W. S., Rendina, A. R., Schneider, G., and Lindqvist, Y. (1995) Mechanism of an ATP-dependent carboxylase, dethiobiotin synthetase, based on crystallographic studies of complexes with substrates and a reaction intermediate, *Biochemistry 34*, 10985–10995.
1017. Richard, S. B., Lillo, A. M., Tetzlaff, C. N., Bowman, M. E., Noel, J. P., and Cane, D. E. (2004) Kinetic analysis of *Escherichia coli* 2-C-methyl-D-erythritol-4-phosphate cytidyltransferase, wild type and mutants, reveals roles of active site amino acids, *Biochemistry 43*, 12189–12197.
1018. Krautwurst, H., Bazaes, S., Gonzalez, F. D., Jabalquinto, A. M., Frey, P. A., and Cardemil, E. (1998) The strongly conserved Lysine 256 of *Saccharomyces cerevisiae* phosphoenolpyruvate carboxykinase is essential for phosphoryl transfer, *Biochemistry 37*, 6295–6302.
1019. Smith, C. A., and Rayment, I. (1996) X-Ray structure of the magnesium(II)·ADP·vanadate complex of the *Dictyostelium discoideum* myosin motor domain to 1.9 Å resolution, *Biochemistry 35*, 5404–5417.
1020. Lahiri, S. D., Zhang, G., Dunaway-Mariano, D., and Allen, K. N. (2003) The pentacovalent phosphorus intermediate of a phosphoryl

transfer reaction, *Science (Washington, DC, U. S.) 299*, 2067–2071.
1021. Loll, P. J., and Lattman, E. E. (1989) The crystal structure of the ternary complex of staphylococcal nuclease, Ca^{2+}, and the inhibitor pdTp, refined at 1.65 Å, *Proteins 5*, 183–201.
1022. Cotton, F. A., Hazen, E. E., Jr., and Legg, M. J. (1979) Staphylococcal nuclease: Proposed mechanism of action based on structure of enzyme-thymidine 3′,5′-bisphosphate-calcium ion complex at 1.5-Å resolution, *Proc. Natl. Acad. Sci. U. S. A. 76*, 2551–2555.
1023. Gassler, C. S., Ryan, M., Liu, T., Griffith, O. H., and Heinz, D. W. (1997) Probing the roles of active site residues in phosphatidylinositol-specific phospholipase C from *Bacillus cereus* by site-directed mutagenesis, *Biochemistry 36*, 12802–12813.
1024. Arnez, J. G., Augustine, J. G., Moras, D., and Francklyn, C. S. (1997) The first step of aminoacylation at the atomic level in histidyl-tRNA synthetase, *Proc. Natl. Acad. Sci. U. S. A. 94*, 7144–7149.
1025. Shirakihara, Y., and Evans, P. R. (1988) Crystal structure of the complex of phosphofructokinase from *Escherichia coli* with its reaction products, *J. Mol. Biol. 204*, 973–994.
1026. Hibi, T., Nii, H., Nakatsu, T., Kimura, A., Kato, H., Hiratake, J., and Oda, J. i. (2004) Crystal structure of γ-glutamylcysteine synthetase: Insights into the mechanism of catalysis by a key enzyme for glutathione homeostasis, *Proc. Natl. Acad. Sci. U. S. A. 101*, 15052–15057.
1027. O'Brien, P. J., and Herschlag, D. (1999) Does the active site arginine change the nature of the transition state for alkaline phosphatase-catalyzed phosphoryl transfer?, *J. Am. Chem. Soc. 121*, 11022–11023.
1028. Anderson, K. S., and Johnson, K. A. (1990) "Kinetic competence" of the 5-enolpyruvoylshikimate-3-phosphate synthase tetrahedral intermediate, *J. Biol. Chem. 265*, 5567–5572.
1029. Eschenburg, S., Kabsch, W., Healy, M. L., and Schonbrunn, E. (2003) A new view of the mechanisms of UDP-*N*-acetylglucosamine enolpyruvyl transferase (MurA) and 5-enolpyruvylshikimate-3-phosphate synthase (AroA) derived from X-ray structures of their tetrahedral reaction intermediate states, *J. Biol. Chem. 278*, 49215–49222.
1030. Priestman, M. A., Healy, M. L., Becker, A., Alberg, D. G., Bartlett, P. A., Lushington, G. H., and Schonbrunn, E. (2005) Interaction of phosphonate analogues of the tetrahedral reaction intermediate with 5-enolpyruvylshikimate-3-phosphate synthase in atomic detail, *Biochemistry 44*, 3241–3248.
1031. Kim, J., Xiao, H., Bonanno, J. B., Kalyanaraman, C., Brown, S., Tang, X. Y., Al-Obaidi, N. F., Patskovsky, Y., Babbitt, P. C., Jacobson, M. P., Lee, Y. S., and Almo, S. C. (2013) Structure-guided discovery of the metabolite carboxy-SAM that modulates tRNA function, *Nature (London, U. K.) 498*, 123–126.
1032. Bender, M. L., and Williams, A. (1966) Ketimine intermediates in amine-catalyzed enolization of acetone, *J. Am. Chem. Soc. 88*, 2502–2508.
1033. Feather, J. A., and Gold, V. (1965) Catalytic power of pyridine and related Brønsted bases in iodination of ketones and nitromethane, *J. Chem. Soc.*, 1752–1761.
1034. Bell, R. P., and Lidwell, O. M. (1940) The base catalysed prototropy of substituted acetones, *Proc. R. Soc. London, A 176*, 0088–0113.
1035. Partanen, S. T., Novikov, D. K., Popov, A. N., Mursula, A. M., Hiltunen, J. K., and Wierenga, R. K. (2004) The 1.3 Å crystal structure of human mitochondrial Δ^3-Δ^2-enoyl-CoA isomerase shows a novel mode of binding for the fatty acyl group, *J. Mol. Biol. 342*, 1197–1208.
1036. Vincent, F., Davies, G. J., and Brannigan, J. A. (2005) Structure and kinetics of a monomeric glucosamine 6-phosphate deaminase: Missing link of the NagB superfamily?, *J. Biol. Chem. 280*, 19649–19655.
1037. Parsons, J. F., Calabrese, K., Eisenstein, E., and Ladner, J. E. (2003) Structure and mechanism of *Pseudomonas aeruginosa* PhzD, an isochorismatase from the phenazine biosynthetic pathway, *Biochemistry 42*, 5684–5693.
1038. Benning, M. M., Haller, T., Gerlt, J. A., and Holden, H. M. (2000) New reactions in the crotonase superfamily: Structure of methylmalonyl CoA decarboxylase from *Escherichia coli*, *Biochemistry 39*, 4630–4639.
1039. Moynie, L., Leckie, S. M., McMahon, S. A., Duthie, F. G., Koehnke, A., Taylor, J. W., Alphey, M. S., Brenk, R., Smith, A. D., and Naismith, J. H. (2013) Structural insights into the mechanism and inhibition of the β-hydroxydecanoyl-acyl carrier protein dehydratase from *Pseudomonas aeruginosa*, *J. Mol. Biol. 425*, 365–377.

1040. May, M., Mehboob, S., Mulhearn, D. C., Wang, Z., Yu, H., Thatcher, G. R., Santarsiero, B. D., Johnson, M. E., and Mesecar, A. D. (2007) Structural and functional analysis of two glutamate racemase isozymes from *Bacillus anthracis* and implications for inhibitor design, *J. Mol. Biol. 371*, 1219–1237.
1041. Ploom, T., Thony, B., Yim, J., Lee, S., Nar, H., Leimbacher, W., Richardson, J., Huber, R., and Auerbach, G. (1999) Crystallographic and kinetic investigations on the mechanism of 6-pyruvoyl tetrahydropterin synthase, *J. Mol. Biol. 286*, 851–860.
1042. French, J. B., Neau, D. B., and Ealick, S. E. (2011) Characterization of the structure and function of *Klebsiella pneumoniae* allantoin racemase, *J. Mol. Biol. 410*, 447–460.
1043. Maruyama, Y., Hashimoto, W., Mikami, B., and Murata, K. (2005) Crystal structure of *Bacillus* sp. GL1 xanthan lyase complexed with a substrate: Insights into the enzyme reaction mechanism, *J. Mol. Biol. 350*, 974–986.
1044. Vogan, E. M., Bellamacina, C., He, X., Liu, H. W., Ringe, D., and Petsko, G. A. (2004) Crystal structure at 1.8 Å resolution of CDP-D-glucose 4,6-dehydratase from *Yersinia pseudotuberculosis*, *Biochemistry 43*, 3057–3067.
1045. Klenchin, V. A., Schmidt, D. M., Gerlt, J. A., and Rayment, I. (2004) Evolution of enzymatic activities in the enolase superfamily: Structure of a substrate-liganded complex of the L-Ala-D/L-Glu epimerase from *Bacillus subtilis*, *Biochemistry 43*, 10370–10378.
1046. Jensen, M. H., Otten, H., Christensen, U., Borchert, T. V., Christensen, L. L. H., Larsen, S., and Lo Leggio, L. (2010) Structural and biochemical studies elucidate the mechanism of rhamnogalacturonan lyase from *Aspergillus aculeatus*, *J. Mol. Biol. 404*, 100–111.
1047. de Jong, R. M., Bazzacco, P., Poelarends, G. J., Johnson, W. H., Jr., Kim, Y. J., Burks, E. A., Serrano, H., Thunnissen, A. M., Whitman, C. P., and Dijkstra, B. W. (2007) Crystal structures of native and inactivated *cis*-3-chloroacrylic acid dehalogenase. Structural basis for substrate specificity and inactivation by (*R*)-oxirane-2–carboxylate, *J. Biol. Chem. 282*, 2440–2449.
1048. Lubetsky, J. B., Swope, M., Dealwis, C., Blake, P., and Lolis, E. (1999) Pro-1 of macrophage migration inhibitory factor functions as a catalytic base in the phenylpyruvate tautomerase activity, *Biochemistry 38*, 7346–7354.
1049. Almrud, J. J., Kern, A. D., Wang, S. C., Czerwinski, R. M., Johnson, W. H., Jr., Murzin, A. G., Hackert, M. L., and Whitman, C. P. (2002) The crystal structure of YdcE, a 4-oxalocrotonate tautomerase homologue from *Escherichia coli*, confirms the structural basis for oligomer diversity, *Biochemistry 41*, 12010–12024.
1050. Charnock, S. J., Brown, I. E., Turkenburg, J. P., Black, G. W., and Davies, G. J. (2002) Convergent evolution sheds light on the anti-β-elimination mechanism common to family 1 and 10 polysaccharide lyases, *Proc. Natl. Acad. Sci. U. S. A. 99*, 12067–12072.
1051. Taylor, P., Pealing, S. L., Reid, G. A., Chapman, S. K., and Walkinshaw, M. D. (1999) Structural and mechanistic mapping of a unique fumarate reductase, *Nat. Struct. Biol. 6*, 1108–1112.
1052. Puthan Veetil, V., Fibriansah, G., Raj, H., Thunnissen, A. M., and Poelarends, G. J. (2012) Aspartase/fumarase superfamily: A common catalytic strategy involving general base-catalyzed formation of a highly stabilized *aci*-carboxylate intermediate, *Biochemistry 51*, 4237–4243.
1053. Poddar, H., de Villiers, J., Zhang, J., Puthan Veetil, V., Raj, H., Thunnissen, A. W. H., and Poelarends, G. J. (2018) Structural basis for the catalytic mechanism of ethylenediamine-*N*,*N*′-disuccinic acid lyase, a carbon-nitrogen bond-forming enzyme with a broad substrate scope, *Biochemistry 57*, 3752–3763.
1054. Lauble, H., Kennedy, M. C., Beinert, H., and Stout, C. D. (1992) Crystal structures of aconitase with isocitrate and nitroisocitrate bound, *Biochemistry 31*, 2735–2748.
1055. Sheng, X., and Liu, Y. (2014) QM/MM study of the reaction mechanism of the carboxyl transferase domain of pyruvate carboxylase from *Staphylococcus aureus*, *Biochemistry 53*, 4455–4466.
1056. Karthikeyan, S., Zhou, Q., Zhao, Z., Kao, C. L., Tao, Z., Robinson, H., Liu, H. W., and Zhang, H. (2004) Structural analysis of *Pseudomonas* 1-aminocyclopropane-1-carboxylate deaminase complexes: Insight into the mechanism of a unique pyridoxal-5′-phosphate dependent cyclopropane ring-opening reaction, *Biochemistry 43*, 13328–13339.

1057. LeVieux, J. A., Medellin, B., Johnson, W. H., Jr., Erwin, K., Li, W., Johnson, I. A., Zhang, Y. J., and Whitman, C. P. (2018) Structural characterization of the hydratase-aldolases, NahE and PhdJ: Implications for the specificity, catalysis, and *N*-acetylneuraminate lyase subgroup of the aldolase superfamily, *Biochemistry 57*, 3524–3536.
1058. Cho, H. S., Ha, N. C., Choi, G., Kim, H. J., Lee, D., Oh, K. S., Kim, K. S., Lee, W., Choi, K. Y., and Oh, B. H. (1999) Crystal structure of Δ^5-3-ketosteroid isomerase from *Pseudomonas testosteroni* in complex with equilenin settles the correct hydrogen bonding scheme for transition state stabilization, *J. Biol. Chem. 274*, 32863–32868.
1059. Choi, G., Ha, N. C., Kim, S. W., Kim, D. H., Park, S., Oh, B. H., and Choi, K. Y. (2000) Asp-99 donates a hydrogen bond not to Tyr-14 but to the steroid directly in the catalytic mechanism of Δ^5-3-ketosteroid isomerase from *Pseudomonas putida* biotype B, *Biochemistry 39*, 903–909.
1060. Ha, N. C., Kim, M. S., Lee, W., Choi, K. Y., and Oh, B. H. (2000) Detection of large pK_a perturbations of an inhibitor and a catalytic group at an enzyme active site, a mechanistic basis for catalytic power of many enzymes, *J. Biol. Chem. 275*, 41100–41106.
1061. Sigala, P. A., Fafarman, A. T., Schwans, J. P., Fried, S. D., Fenn, T. D., Caaveiro, J. M., Pybus, B., Ringe, D., Petsko, G. A., Boxer, S. G., and Herschlag, D. (2013) Quantitative dissection of hydrogen bond-mediated proton transfer in the ketosteroid isomerase active site, *Proc. Natl. Acad. Sci. U. S. A. 110*, E2552–2561.
1062. Thornburg, L. D., Henot, F., Bash, D. P., Hawkinson, D. C., Bartel, S. D., and Pollack, R. M. (1998) Electrophilic assistance by Asp-99 of 3-oxo-Δ^5-steroid isomerase, *Biochemistry 37*, 10499–10506.
1063. Kraut, D. A., Sigala, P. A., Pybus, B., Liu, C. W., Ringe, D., Petsko, G. A., and Herschlag, D. (2006) Testing electrostatic complementarity in enzyme catalysis: Hydrogen bonding in the ketosteroid isomerase oxyanion hole, *PLoS Biol. 4*, e99.
1064. Natarajan, A., Schwans, J. P., and Herschlag, D. (2014) Using unnatural amino acids to probe the energetics of oxyanion hole hydrogen bonds in the ketosteroid isomerase active site, *J. Am. Chem. Soc. 136*, 7643–7654.
1065. van der Kamp, M. W., Perruccio, F., and Mulholland, A. J. (2007) Substrate polarization in enzyme catalysis: QM/MM analysis of the effect of oxaloacetate polarization on acetyl-CoA enolization in citrate synthase, *Proteins 69*, 521–535.
1066. Kurz, L. C., Shah, S., Crane, B. R., Donald, L. J., Duckworth, H. W., and Drysdale, G. R. (1992) Proton uptake accompanies formation of the ternary complex of citrate synthase, oxaloacetate, and the transition-state analog inhibitor, carboxymethyl-CoA. Evidence that a neutral enol is the activated form of acetyl-CoA in the citrate synthase reaction, *Biochemistry 31*, 7899–7907.
1067. Sullivan, S. M., and Holyoak, T. (2007) Structures of rat cytosolic PEPCK: Insight into the mechanism of phosphorylation and decarboxylation of oxaloacetic acid, *Biochemistry 46*, 10078–10088.
1068. Sudom, A. M., Prasad, L., Goldie, H., and Delbaere, L. T. (2001) The phosphoryl-transfer mechanism of *Escherichia coli* phospho*enol*pyruvate carboxykinase from the use of AlF_3, *J. Mol. Biol. 314*, 83–92.
1069. Holyoak, T., Sullivan, S. M., and Nowak, T. (2006) Structural insights into the mechanism of PEPCK catalysis, *Biochemistry 45*, 8254–8263.
1070. Kent, T. A., Emptage, M. H., Merkle, H., Kennedy, M. C., Beinert, H., and Munck, E. (1985) Mössbauer studies of aconitase. Substrate and inhibitor binding, reaction intermediates, and hyperfine interactions of reduced 3Fe and 4Fe clusters, *J. Biol. Chem. 260*, 6871–6881.
1071. Ulaganathan, T., Helbert, W., Kopel, M., Banin, E., and Cygler, M. (2018) Structure-function analyses of a PL24 family ulvan lyase reveal key features and suggest its catalytic mechanism, *J. Biol. Chem. 293*, 4026–4036.
1072. Buschiazzo, A., Goytia, M., Schaeffer, F., Degrave, W., Shepard, W., Gregoire, C., Chamond, N., Cosson, A., Berneman, A., Coatnoan, N., Alzari, P. M., and Minoprio, P. (2006) Crystal structure, catalytic mechanism, and mitogenic properties of *Trypanosoma cruzi* proline racemase, *Proc. Natl. Acad. Sci. U. S. A. 103*, 1705–1710.
1073. Ruben, E. A., Schwans, J. P., Sonnett, M., Natarajan, A., Gonzalez, A., Tsai, Y., and Herschlag, D. (2013) Ground state destabili-

zation from a positioned general base in the ketosteroid isomerase active site, *Biochemistry 52*, 1074–1081.
1074. Yabukarski, F., Biel, J. T., Pinney, M. M., Doukov, T., Powers, A. S., Fraser, J. S., and Herschlag, D. (2020) Assessment of enzyme active site positioning and tests of catalytic mechanisms through X-ray-derived conformational ensembles, *Proc. Natl. Acad. Sci. U. S. A. 117*, 33204–33215.
1075. Piacenza, M., and Grimme, S. (2005) Van der Waals complexes of polar aromatic molecules: Unexpected structures for dimers of azulene, *J. Am. Chem. Soc. 127*, 14841–14848.
1076. Schwans, J. P., Hanoian, P., Lengerich, B. J., Sunden, F., Gonzalez, A., Tsai, Y., Hammes-Schiffer, S., and Herschlag, D. (2014) Experimental and computational mutagenesis to investigate the positioning of a general base within an enzyme active site, *Biochemistry 53*, 2541–2555.
1077. Costentin, C., and Saveant, J.-M. (2004) Why are proton transfers at carbon slow? Self-exchange reactions, *J. Am. Chem. Soc. 126*, 14787–14795.
1078. Horowitz, S., and Trievel, R. C. (2012) Carbon–oxygen hydrogen bonding in biological structure and function, *J. Biol. Chem. 287*, 41576–41582.
1079. Cui, Q., and Karplus, M. (2002) Quantum mechanical/molecular mechanical studies of the triosephosphate isomerase-catalyzed reaction: Verification of methodology and analysis of reaction mechanisms, *J. Phys. Chem. B 106*, 1768–1798.
1080. Fraser, M. E., Strynadka, N. C., Bartlett, P. A., Hanson, J. E., and James, M. N. (1992) Crystallographic analysis of transition-state mimics bound to penicillopepsin: Phosphorus-containing peptide analogues, *Biochemistry 31*, 5201–5214.
1081. Neidhart, D., Wei, Y., Cassidy, C., Lin, J., Cleland, W. W., and Frey, P. A. (2001) Correlation of low-barrier hydrogen bonding and oxyanion binding in transition state analogue complexes of chymotrypsin, *Biochemistry 40*, 2439–2447.
1082. Kuhn, P., Knapp, M., Soltis, S. M., Ganshaw, G., Thoene, M., and Bott, R. (1998) The 0.78 Å structure of a serine protease: *Bacillus lentus* subtilisin, *Biochemistry 37*, 13446–13452.
1083. Takeuchi, Y., Satow, Y., Nakamura, K. T., and Mitsui, Y. (1991) Refined crystal structure of the complex of subtilisin BPN′ and *Streptomyces* subtilisin inhibitor at 1.8 Å resolution, *J. Mol. Biol. 221*, 309–325.
1084. Kyte, J. (2007) *Structure in protein chemistry: Second edition*, p 205, Garland Science, New York.
1085. Kyte, J. (2007) *Structure in protein chemistry: Second edition*, p 214, Garland Science, New York.
1086. Lin, J., Pozharski, E., and Wilson, M. A. (2017) Short carboxylic acid-carboxylate hydrogen bonds can have fully localized protons, *Biochemistry 56*, 391–402.
1087. Herschlag, D., and Pinney, M. M. (2018) Hydrogen bonds: Simple after all?, *Biochemistry 57*, 3338–3352.
1088. Singh, U. C., and Kollman, P. A. (1985) A water dimer potential based on *ab initio* calculations using Morokuma component analyses, *J. Chem. Phys. 83*, 4033–4040.
1089. Strater, N., Schnappauf, G., Braus, G., and Lipscomb, W. N. (1997) Mechanisms of catalysis and allosteric regulation of yeast chorismate mutase from crystal structures, *Structure (Cambridge, MA, U. S.) 5*, 1437–1452.
1090. Lee, A. Y., Karplus, P. A., Ganem, B., and Clardy, J. (1995) Atomic structure of the buried catalytic pocket of *Escherichia coli* chorismate mutase, *J. Am. Chem. Soc. 117*, 3627–3628.
1091. Okvist, M., Dey, R., Sasso, S., Grahn, E., Kast, P., and Krengel, U. (2006) 1.6 Å Crystal structure of the secreted chorismate mutase from *Mycobacterium tuberculosis*: Novel fold topology revealed, *J. Mol. Biol. 357*, 1483–1499.
1092. Chook, Y. M., Gray, J. V., Ke, H., and Lipscomb, W. N. (1994) The monofunctional chorismate mutase from *Bacillus subtilis*. Structure determination of chorismate mutase and its complexes with a transition state analog and prephenate, and implications for the mechanism of the enzymatic reaction, *J. Mol. Biol. 240*, 476–500.
1093. Kienhofer, A., Kast, P., and Hilvert, D. (2003) Selective stabilization of the chorismate mutase transition state by a positively charged hydrogen bond donor, *J. Am. Chem. Soc. 125*, 3206–3207.
1094. Burschowsky, D., van Eerde, A., Okvist, M., Kienhofer, A., Kast, P., Hilvert, D., and Krengel, U. (2014) Electrostatic transition state stabilization rather than reactant destabiliza-

tion provides the chemical basis for efficient chorismate mutase catalysis, *Proc. Natl. Acad. Sci. U. S. A. 111*, 17516–17521.
1095. Slade, D., Dunstan, M. S., Barkauskaite, E., Weston, R., Lafite, P., Dixon, N., Ahel, M., Leys, D., and Ahel, I. (2011) The structure and catalytic mechanism of a poly(ADP-ribose) glycohydrolase, *Nature (London, U. K.) 477*, 616–620.
1096. Yew, W. S., Wise, E. L., Rayment, I., and Gerlt, J. A. (2004) Evolution of enzymatic activities in the orotidine 5′-monophosphate decarboxylase suprafamily: Mechanistic evidence for a proton relay system in the active site of 3-keto-L-gulonate 6-phosphate decarboxylase, *Biochemistry 43*, 6427–6437.
1097. Wise, E. L., Yew, W. S., Gerlt, J. A., and Rayment, I. (2003) Structural evidence for a 1,2-enediolate intermediate in the reaction catalyzed by 3-keto-L-gulonate 6-phosphate decarboxylase, a member of the orotidine 5′-monophosphate decarboxylase suprafamily, *Biochemistry 42*, 12133–12142.
1098. Le Coq, J., Pavlovsky, A., Malik, R., Sanishvili, R., Xu, C., and Viola, R. E. (2008) Examination of the mechanism of human brain aspartoacylase through the binding of an intermediate analogue, *Biochemistry 47*, 3484–3492.
1099. Barnum, D. W. (1983) Hydrolysis of cations. Formation constants and standard free energies of formation of hydroxy complexes, *Inorg. Chem. 22*, 2297–2305.
1100. Yatsimirsky, K. B., and Vasil'ev, V. P. (1960) *Instability constants of complex compounds*, Pergamon Press, Oxford.
1101. Huheey, J. E. (1972) *Inorganic chemistry; principles of structure and reactivity*, Harper and Row, New York.
1102. Pearson, R. G. (1966) Acids and bases, *Science (Washington, DC, U. S.) 151*, 172–177.
1103. Martin, R. B. (1984) Bioinorganic chemistry of calcium, In *Calcium and its role in biology* (Sigel, H., and Sigel, A., Eds.), pp 1–50, Marcel Dekker, New York.
1104. Einspahr, H., and Bugg, C. E. (1984) Crystal structure studies of calcium complexes and implications for biological systems, In *Calcium and its role in biology* (Sigel, H., and Sigel, A., Eds.), pp 51–97, Marcel Dekker, New York.
1105. Honzatko, R. B., Crawford, J. L., Monaco, H. L., Ladner, J. E., Ewards, B. F., Evans, D. R., Warren, S. G., Wiley, D. C., Ladner, R. C., and Lipscomb, W. N. (1982) Crystal and molecular structures of native and CTP-liganded aspartate carbamoyltransferase from *Escherichia coli*, *J. Mol. Biol. 160*, 219–263.
1106. Huang, J., and Lipscomb, W. N. (2006) T-State active site of aspartate transcarbamylase: Crystal structure of the carbamyl phosphate and L-alanosine ligated enzyme, *Biochemistry 45*, 346–352.
1107. Kim, K. H., Pan, Z., Honzatko, R. B., Ke, H. M., and Lipscomb, W. N. (1987) Structural asymmetry in the CTP-liganded form of aspartate carbamoyltransferase from *Escherichia coli*, *J. Mol. Biol. 196*, 853–875.
1108. Holmes, M. A., and Matthews, B. W. (1981) Binding of hydroxamic acid inhibitors to crystalline thermolysin suggests a pentacoordinate zinc intermediate in catalysis, *Biochemistry 20*, 6912–6920.
1109. Shannon, R. D. (1976) Revised effective ionic-radii and systematic studies of interatomic distances in halides and chalcogenides, *Acta Crystallogr., Sect. A: Found. Adv. 32*, 751–767.
1110. Toney, M. D., Hohenester, E., Keller, J. W., and Jansonius, J. N. (1995) Structural and mechanistic analysis of two refined crystal structures of the pyridoxal phosphate-dependent enzyme dialkylglycine decarboxylase, *J. Mol. Biol. 245*, 151–179.
1111. Shisler, K. A., Hutcheson, R. U., Horitani, M., Duschene, K. S., Crain, A. V., Byer, A. S., Shepard, E. M., Rasmussen, A., Yang, J., Broderick, W. E., Vey, J. L., Drennan, C. L., Hoffman, B. M., and Broderick, J. B. (2017) Monovalent cation activation of the radical SAM enzyme pyruvate formate-lyase activating enzyme, *J. Am. Chem. Soc. 139*, 11803–11813.
1112. Vey, J. L., Yang, J., Li, M., Broderick, W. E., Broderick, J. B., and Drennan, C. L. (2008) Structural basis for glycyl radical formation by pyruvate formate-lyase activating enzyme, *Proc. Natl. Acad. Sci. U. S. A. 105*, 16137–16141.
1113. Morrison, S. D., Roberts, S. A., Zegeer, A. M., Montfort, W. R., and Bandarian, V. (2008) A new use for a familiar fold: The X-ray crystal structure of GTP-bound GTP cyclohydrolase III from *Methanocaldococcus jannaschii* reveals a two metal ion catalytic mechanism, *Biochemistry 47*, 230–242.

1114. Isupov, M. N., Antson, A. A., Dodson, E. J., Dodson, G. G., Dementieva, I. S., Zakomirdina, L. N., Wilson, K. S., Dauter, Z., Lebedev, A. A., and Harutyunyan, E. H. (1998) Crystal structure of tryptophanase, *J. Mol. Biol. 276*, 603–623.
1115. Thoden, J. B., Holden, H. M., Wesenberg, G., Raushel, F. M., and Rayment, I. (1997) Structure of carbamoyl phosphate synthetase: A journey of 96 Å from substrate to product, *Biochemistry 36*, 6305–6316.
1116. Thoden, J. B., Ruzicka, F. J., Frey, P. A., Rayment, I., and Holden, H. M. (1997) Structural analysis of the H166G site-directed mutant of galactose-1-phosphate uridylyltransferase complexed with either UDP-glucose or UDP-galactose: Detailed description of the nucleotide sugar binding site, *Biochemistry 36*, 1212–1222.
1117. Suelter, C. H. (1970) Enzymes activated by monovalent cations, *Science (Washington, DC, U. S.) 168*, 789–795.
1118. Kachmar, J. F., and Boyer, P. D. (1953) Kinetic analysis of enzyme reactions. II. The potassium activation and calcium inhibition of pyruvic phosphoferase, *J. Biol. Chem. 200*, 669–682.
1119. Suelter, C. H., Singleton, R., Jr., Kayne, F. J., Arrington, S., Glass, J., and Mildvan, A. S. (1966) The interaction of substrate and univalent and bivalent cations with pyruvic kinase, *Biochemistry 5*, 131–139.
1120. Allen, K. N., Lavie, A., Glasfeld, A., Tanada, T. N., Gerrity, D. P., Carlson, S. C., Farber, G. K., Petsko, G. A., and Ringe, D. (1994) Role of the divalent metal ion in sugar binding, ring opening, and isomerization by D-xylose isomerase: Replacement of a catalytic metal by an amino acid, *Biochemistry 33*, 1488–1494.
1121. Frausto da Silva, J. J. R., and Williams, R. J. P. (1991) *The biological chemistry of the elements: The inorganic chemistry of life*, Clarendon Press, Oxford, England.
1122. Alberty, R. A. (1969) Standard Gibbs free energy, enthalpy, and entropy changes as a function of pH and pMg for several reactions involving adenosine phosphates, *J. Biol. Chem. 244*, 3290–3302.
1123. Cini, R., Burla, M. C., Nunzi, A., Polidori, G. P., and Zanazzi, P. F. (1984) Preparation and physicochemical properties of the ternary complexes formed between adenosine 5′-triphosphoric acid, bis(2-pyridyl)amine, and divalent metal ions. Crystal and molecular structures of the compounds containing magnesium(II) and calcium(II), *J. Chem. Soc., Dalton Trans.*, 2467–2476.
1124. Tari, L. W., Matte, A., Pugazhenthi, U., Goldie, H., and Delbaere, L. T. (1996) Snapshot of an enzyme reaction intermediate in the structure of the ATP-Mg^{2+}-oxalate ternary complex of *Escherichia coli* PEP carboxykinase, *Nat. Struct. Biol. 3*, 355–363.
1125. Hartley, A., Glynn, S. E., Barynin, V., Baker, P. J., Sedelnikova, S. E., Verhees, C., de Geus, D., van der Oost, J., Timson, D. J., Reece, R. J., and Rice, D. W. (2004) Substrate specificity and mechanism from the structure of *Pyrococcus furiosus* galactokinase, *J. Mol. Biol. 337*, 387–398.
1126. Joyce, M. A., Fraser, M. E., James, M. N., Bridger, W. A., and Wolodko, W. T. (2000) ADP-Binding site of *Escherichia coli* succinyl-CoA synthetase revealed by X-ray crystallography, *Biochemistry 39*, 17–25.
1127. Arjunan, P., Umland, T., Dyda, F., Swaminathan, S., Furey, W., Sax, M., Farrenkopf, B., Gao, Y., Zhang, D., and Jordan, F. (1996) Crystal structure of the thiamin diphosphate-dependent enzyme pyruvate decarboxylase from the yeast *Saccharomyces cerevisiae* at 2.3 Å resolution, *J. Mol. Biol. 256*, 590–600.
1128. Heroux, A., White, E. L., Ross, L. J., Davis, R. L., and Borhani, D. W. (1999) Crystal structure of *Toxoplasma gondii* hypoxanthine-guanine phosphoribosyltransferase with XMP, pyrophosphate, and two Mg^{2+} ions bound: Insights into the catalytic mechanism, *Biochemistry 38*, 14495–14506.
1129. Shi, W., Munagala, N. R., Wang, C. C., Li, C. M., Tyler, P. C., Furneaux, R. H., Grubmeyer, C., Schramm, V. L., and Almo, S. C. (2000) Crystal structures of *Giardia lamblia* guanine phosphoribosyltransferase at 1.75 Å, *Biochemistry 39*, 6781–6790.
1130. Frausto da Silva, J. J. R., and Williams, R. J. P (2001) *The biological chemistry of the elements: The inorganic chemistry of life*, Second Edition, Oxford University Press, Oxford.
1131. Niefind, K., Muller, J., Riebel, B., Hummel, W., and Schomburg, D. (2003) The crystal structure of *R*-specific alcohol dehydrogenase from *Lactobacillus brevis* suggests the structural basis of its metal dependency, *J. Mol. Biol. 327*, 317–328.

1132. Howard, B. R., Endrizzi, J. A., and Remington, S. J. (2000) Crystal structure of *Escherichia coli* malate synthase G complexed with magnesium and glyoxylate at 2.0 Å resolution: Mechanistic implications, *Biochemistry 39*, 3156–3168.
1133. Thompson, T. B., Garrett, J. B., Taylor, E. A., Meganathan, R., Gerlt, J. A., and Rayment, I. (2000) Evolution of enzymatic activity in the enolase superfamily: Structure of *o*-succinylbenzoate synthase from *Escherichia coli* in complex with Mg^{2+} and *o*-succinylbenzoate, *Biochemistry 39*, 10662–10676.
1134. Jia, Y., Lu, Z., Huang, K., Herzberg, O., and Dunaway-Mariano, D. (1999) Insight into the mechanism of phospho*enol*pyruvate mutase catalysis derived from site-directed mutagenesis studies of active site residues, *Biochemistry 38*, 14165–14173.
1135. Rea, D., Fulop, V., Bugg, T. D., and Roper, D. I. (2007) Structure and mechanism of HpcH: A metal ion dependent class II aldolase from the homoprotocatechuate degradation pathway of *Escherichia coli*, *J. Mol. Biol. 373*, 866–876.
1136. Bode, W., and Schwager, P. (1975) Refined crystal structure of bovine β-trypsin at 1.8 Å resolution. II. Crystallographic refinement, calcium binding site, benzamidine binding site, and active site at pH 7.0, *J. Mol. Biol. 98*, 693–717.
1137. Feinberg, H., Mitchell, D. A., Drickamer, K., and Weis, W. I. (2001) Structural basis for selective recognition of oligosaccharides by DC-SIGN and DC-SIGNR, *Science (Washington, DC, U. S.) 294*, 2163–2166.
1138. McPhalen, C. A., and James, M. N. (1988) Structural comparison of two serine proteinase-protein inhibitor complexes: Eglin-C-subtilisin carlsberg and CI-2-subtilisin novo, *Biochemistry 27*, 6582–6598.
1139. Read, R. J., and James, M. N. (1988) Refined crystal structure of *Streptomyces griseus* trypsin at 1.7 Å resolution, *J. Mol. Biol. 200*, 523–551.
1140. Torrecilla, I., Leganes, F., Bonilla, I., and Fernandez-Pinas, F. (2000) Use of recombinant aequorin to study calcium homeostasis and monitor calcium transients in response to heat and cold shock in cyanobacteria, *Plant Physiol. 123*, 161–176.
1141. Suck, D., and Oefner, C. (1986) Structure of DNAse I at 2.0 Å resolution suggests a mechanism for binding to and cutting DNA, *Nature (London, U. K.) 321*, 620–625.
1142. Blum, M. M., Lohr, F., Richardt, A., Ruterjans, H., and Chen, J. C. (2006) Binding of a designed substrate analogue to diisopropyl fluorophosphatase: Implications for the phosphotriesterase mechanism, *J. Am. Chem. Soc. 128*, 12750–12757.
1143. Young, I. D., Ibrahim, M., Chatterjee, R., Gul, S., Fuller, F., Koroidov, S., Brewster, A. S., Tran, R., Alonso-Mori, R., Kroll, T., Michels-Clark, T., Laksmono, H., Sierra, R. G., Stan, C. A., Hussein, R., Zhang, M., Douthit, L., Kubin, M., de Lichtenberg, C., Long Vo, P., Nilsson, H., Cheah, M. H., Shevela, D., Saracini, C., Bean, M. A., Seuffert, I., Sokaras, D., Weng, T. C., Pastor, E., Weninger, C., Fransson, T., Lassalle, L., Brauer, P., Aller, P., Docker, P. T., Andi, B., Orville, A. M., Glownia, J. M., Nelson, S., Sikorski, M., Zhu, D., Hunter, M. S., Lane, T. J., Aquila, A., Koglin, J. E., Robinson, J., Liang, M., Boutet, S., Lyubimov, A. Y., Uervirojnangkoorn, M., Moriarty, N. W., Liebschner, D., Afonine, P. V., Waterman, D. G., Evans, G., Wernet, P., Dobbek, H., Weis, W. I., Brunger, A. T., Zwart, P. H., Adams, P. D., Zouni, A., Messinger, J., Bergmann, U., Sauter, N. K., Kern, J., Yachandra, V. K., and Yano, J. (2016) Structure of photosystem II and substrate binding at room temperature, *Nature (London, U. K.) 540*, 453–457.
1144. Kim, C. J., and Debus, R. J. (2020) Roles of D1-Glu189 and D1-Glu329 in O_2 formation by the water-splitting Mn_4Ca cluster in photosystem II, *Biochemistry 59*, 3902–3917.
1145. Cohen, P. F., and Colman, R. F. (1974) Role of manganous ion in the kinetics of pig heart NAD-specific isocitrate dehydrogenase, *Eur. J. Biochem. 47*, 35–45.
1146. Scrutton, M. C., Utter, M. F., and Mildvan, A. S. (1966) Pyruvate carboxylase. VI. The presence of tightly bound manganese, *J. Biol. Chem. 241*, 3480–3487.
1147. Xiang, S., and Tong, L. (2008) Crystal structures of human and *Staphylococcus aureus* pyruvate carboxylase and molecular insights into the carboxyltransfer reaction, *Nat. Struct. Mol. Biol. 15*, 295–302.
1148. Lietzan, A. D., and St Maurice, M. (2013) A substrate-induced biotin binding pocket in the carboxyltransferase domain of pyruvate carboxylase, *J. Biol. Chem. 288*, 19915–19925.

1149. Rajagopalan, P. T. R., Yu, X. C., and Pei, D. (1997) Peptide deformylase: A new type of mononuclear iron protein, *J. Am. Chem. Soc. 119*, 12418–12419.
1150. Jain, R., Hao, B., Liu, R. P., and Chan, M. K. (2005) Structures of *E. coli* peptide deformylase bound to formate: Insight into the preference for Fe^{2+} over Zn^{2+} as the active site metal, *J. Am. Chem. Soc. 127*, 4558–4559.
1151. Kennedy, M. C., Emptage, M. H., Dreyer, J. L., and Beinert, H. (1983) The role of iron in the activation-inactivation of aconitase, *J. Biol. Chem. 258*, 11098–11105.
1152. Bender, S. L., Mehdi, S., and Knowles, J. R. (1989) Dehydroquinate synthase: The role of divalent metal cations and of nicotinamide adenine dinucleotide in catalysis, *Biochemistry 28*, 7555–7560.
1153. Margerum, D. W., Cayley, G. R., Weatherburn, D. C., and Pagenkopf, G. K. (1978) Kinetics and mechanism of complex formation and ligand exchange, In *Coordination chemistry: Volume 2* (Martell, A. E., Ed.), pp 1–220, American Chemical Society, Washington, D. C.
1154. Lee, Y., Thirumalai, D., and Hyeon, C. (2017) Ultrasensitivity of water exchange kinetics to the size of metal ion, *J. Am. Chem. Soc. 139*, 12334–12337.
1155. Wuerges, J., Lee, J. W., Yim, Y. I., Yim, H. S., Kang, S. O., and Djinovic Carugo, K. (2004) Crystal structure of nickel-containing superoxide dismutase reveals another type of active site, *Proc. Natl. Acad. Sci. U. S. A. 101*, 8569–8574.
1156. Barondeau, D. P., Kassmann, C. J., Bruns, C. K., Tainer, J. A., and Getzoff, E. D. (2004) Nickel superoxide dismutase structure and mechanism, *Biochemistry 43*, 8038–8047.
1157. Huang, H. T., Dillon, S., Ryan, K. C., Campecino, J. O., Watkins, O. E., Cabelli, D. E., Brunold, T. C., and Maroney, M. J. (2018) The role of mixed amine/amide ligation in nickel superoxide dismutase, *Inorg. Chem. 57*, 12521–12535.
1158. Higuchi, Y., Ogata, H., Miki, K., Yasuoka, N., and Yagi, T. (1999) Removal of the bridging ligand atom at the Ni-Fe active site of [NiFe] hydrogenase upon reduction with H_2, as revealed by X-ray structure analysis at 1.4 Å resolution, *Structure (Cambridge, MA, U. S.) 7*, 549–556.
1159. Volbeda, A., Amara, P., Darnault, C., Mouesca, J. M., Parkin, A., Roessler, M. M., Armstrong, F. A., and Fontecilla-Camps, J. C. (2012) X-Ray crystallographic and computational studies of the O_2-tolerant [NiFe]-hydrogenase 1 from *Escherichia coli*, *Proc. Natl. Acad. Sci. U. S. A. 109*, 5305–5310.
1160. Benini, S., Rypniewski, W. R., Wilson, K. S., Miletti, S., Ciurli, S., and Mangani, S. (1999) A new proposal for urease mechanism based on the crystal structures of the native and inhibited enzyme from *Bacillus pasteurii*: Why urea hydrolysis costs two nickels, *Structure (Cambridge, MA, U. S.) 7*, 205–216.
1161. Ishioka, T., Murata, A., Kitagawa, Y., and Nakamura, K. T. (1997) Zinc(II) acetate dihydrate, *Acta Crystallogr., Sect. C Cryst. Struct. Commun. C53*, 1029–1031.
1162. Van Niekerk, J. N., Schoening, F. R. L., and Talbot, J. H. (1953) The crystal structure of zinc acetate dihydrate, $Zn(CH_3COO)_2{\cdot}2H_2O$, *Acta Crystallogr. 6*, 720–723.
1163. Kerr, M. C., Preston, H. S., Ammon, H. L., Huheey, J. E., and Stewart, J. M. (1981) The crystal structure of *trans*-bis(8-aminoquinoline)aquazinc(II) tetrachlorozincate(II), *J. Coord. Chem. 11*, 111–115.
1164. Li, J., Jia, Y., Lin, A., Hanna, M., Chelico, L., Xiao, W., and Moore, S. A. (2019) Structure of Ddi2, a highly inducible detoxifying metalloenzyme from *Saccharomyces cerevisiae*, *J. Biol. Chem. 294*, 10674–10685.
1165. Rozema, D. B., and Poulter, C. D. (1999) Yeast protein farnesyltransferase. pK_as of peptide substrates bound as zinc thiolates, *Biochemistry 38*, 13138–13146.
1166. Benning, M. M., Hong, S. B., Raushel, F. M., and Holden, H. M. (2000) The binding of substrate analogs to phosphotriesterase, *J. Biol. Chem. 275*, 30556–30560.
1167. Cameron, A. D., Ridderstrom, M., Olin, B., Kavarana, M. J., Creighton, D. J., and Mannervik, B. (1999) Reaction mechanism of glyoxalase I explored by an X-ray crystallographic analysis of the human enzyme in complex with a transition state analogue, *Biochemistry 38*, 13480–13490.
1168. Kona, F., Tao, P., Martin, P., Xu, X., and Gatti, D. L. (2009) Electronic structure of the metal center in the Cd^{2+}, Zn^{2+}, and Cu^{2+} substituted forms of KDO8P synthase: Implications for catalysis, *Biochemistry 48*, 3610–3630.

1169. Kumar, V., and Kannan, K. K. (1994) Enzyme-substrate interactions. Structure of human carbonic anhydrase I complexed with bicarbonate, *J. Mol. Biol. 241*, 226–232.
1170. Nocek, B. P., Gillner, D. M., Fan, Y., Holz, R. C., and Joachimiak, A. (2010) Structural basis for catalysis by the mono- and dimetalated forms of the dapE-encoded *N*-succinyl-L,L-diaminopimelic acid desuccinylase, *J. Mol. Biol. 397*, 617–626.
1171. Pegan, S, D., Rukseree, K., Franzblau, S. G., and Mesecar, A. D. (2009) Structural basis for catalysis of a tetrameric class IIa fructose 1,6-bisphosphate aldolase from *Mycobacterium tuberculosis*, *J. Mol. Biol. 386*, 1038–1053.
1172. Strater, N., and Lipscomb, W. N. (1995) Transition state analogue L-leucinephosphonic acid bound to bovine lens leucine aminopeptidase: X-ray structure at 1.65 Å resolution in a new crystal form, *Biochemistry 34*, 9200–9210.
1173. Vanhooke, J. L., Benning, M. M., Raushel, F. M., and Holden, H. M. (1996) Three-dimensional structure of the zinc-containing phosphotriesterase with the bound substrate analog diethyl 4-methylbenzylphosphonate, *Biochemistry 35*, 6020–6025.
1174. Rebelo, J., Auerbach, G., Bader, G., Bracher, A., Nar, H., Hosl, C., Schramek, N., Kaiser, J., Bacher, A., Huber, R., and Fischer, M. (2003) Biosynthesis of pteridines. Reaction mechanism of GTP cyclohydrolase I, *J. Mol. Biol. 326*, 503–516.
1175. Wouters, J., Oudjama, Y., Barkley, S. J., Tricot, C., Stalon, V., Droogmans, L., and Poulter, C. D. (2003) Catalytic mechanism of *Escherichia coli* isopentenyl diphosphate isomerase involves Cys-67, Glu-116, and Tyr-104 as suggested by crystal structures of complexes with transition state analogues and irreversible inhibitors, *J. Biol. Chem. 278*, 11903–11908.
1176. Lee, S., and Poulter, C. D. (2006) *Escherichia coli* type I isopentenyl diphosphate isomerase: Structural and catalytic roles for divalent metals, *J. Am. Chem. Soc. 128*, 11545–11550.
1177. Dumas, D. P., Caldwell, S. R., Wild, J. R., and Raushel, F. M. (1989) Purification and properties of the phosphotriesterase from *Pseudomonas diminuta*, *J. Biol. Chem. 264*, 19659–19665.
1178. Betts, L., Xiang, S., Short, S. A., Wolfenden, R., and Carter, C. W., Jr. (1994) Cytidine deaminase. The 2.3 Å crystal structure of an enzyme: transition-state analog complex, *J. Mol. Biol. 235*, 635–656.
1179. Ireton, G. C., McDermott, G., Black, M. E., and Stoddard, B. L. (2002) The structure of *Escherichia coli* cytosine deaminase, *J. Mol. Biol. 315*, 687–697.
1180. Johansson, E., Mejlhede, N., Neuhard, J., and Larsen, S. (2002) Crystal structure of the tetrameric cytidine deaminase from *Bacillus subtilis* at 2.0 Å resolution, *Biochemistry 41*, 2563–2570.
1181. Holland, D. R., Hausrath, A. C., Juers, D., and Matthews, B. W. (1995) Structural analysis of zinc substitutions in the active site of thermolysin, *Protein Sci. 4*, 1955–1965.
1182. English, A. C., Done, S. H., Caves, L. S., Groom, C. R., and Hubbard, R. E. (1999) Locating interaction sites on proteins: The crystal structure of thermolysin soaked in 2% to 100% isopropanol, *Proteins 37*, 628–640.
1183. Kester, W. R., and Matthews, B. W. (1977) Crystallographic study of the binding of dipeptide inhibitors to thermolysin: Implications for the mechanism of catalysis, *Biochemistry 16*, 2506–2516.
1184. Holden, H. M., Tronrud, D. E., Monzingo, A. F., Weaver, L. H., and Matthews, B. W. (1987) Slow- and fast-binding inhibitors of thermolysin display different modes of binding: Crystallographic analysis of extended phosphonamidate transition-state analogues, *Biochemistry 26*, 8542–8553.
1185. Monzingo, A. F., and Matthews, B. W. (1984) Binding of *N*-carboxymethyl dipeptide inhibitors to thermolysin determined by X-ray crystallography: A novel class of transition-state analogues for zinc peptidases, *Biochemistry 23*, 5724–5729.
1186. Sankaranarayanan, R., Dock-Bregeon, A.-C., Rees, B., Bovee, M., Caillet, J., Romby, P., Francklyn, C. S., and Moras, D. (2000) Zinc ion mediated amino acid discrimination by threonyl-tRNA synthetase, *Nat. Struct. Biol. 7*, 461–465.
1187. Xu, Y., Feng, L., Jeffrey, P. D., Shi, Y., and Morel, F. M. M. (2008) Structure and metal exchange in the cadmium carbonic anhydrase of marine diatoms, *Nature (London, U. K.) 452*, 56–61.
1188. Ferreira, F. M., Mendoza-Hernandez, G., Castaneda-Bueno, M., Aparicio, R., Fischer, H., Calcagno, M. L., and Oliva, G. (2006)

Structural analysis of *N*-acetylglucosamine-6-phosphate deacetylase apoenzyme from *Escherichia coli*, *J. Mol. Biol. 359*, 308–321.
1189. Kobes, R. D., Simpson, R. T., Vallee, R. L., and Rutter, W. J. (1969) A functional role of metal ions in a class II aldolase, *Biochemistry 8*, 585–588.
1190. Kadonaga, J. T., and Knowles, J. R. (1983) Role of mono- and divalent metal cations in the catalysis by yeast aldolase, *Biochemistry 22*, 130–136.
1191. Latt, S. A., Holmquist, B., and Vallee, B. L. (1969) Thermolysin: A zinc metalloenzyme, *Biochem. Biophys. Res. Commun. 37*, 333–339.
1192. Keilin, D., and Mann, T. (1939) Carbonic anhydrase, *Nature (London, U. K.) 144*, 442–443.
1193. Aronsson, A. C., Marmstal, E., and Mannervik, B. (1978) Glyoxalase I, a zinc metalloenzyme of mammals and yeast, *Biochem. Biophys. Res. Commun. 81*, 1235–1240.
1194. Krosky, D. J., Alm, R., Berg, M., Carmel, G., Tummino, P. J., Xu, B., and Yang, W. (2002) *Helicobacter pylori* 3-deoxy-D-manno-octulosonate-8-phosphate (KDO-8-P) synthase is a zinc-metalloenzyme, *Biochim. Biophys. Acta 1594*, 297–306.
1195. Born, T. L., Zheng, R., and Blanchard, J. S. (1998) Hydrolysis of *N*-succinyl-L,L-diaminopimelic acid by the *Haemophilus influenzae* dapE-encoded desuccinylase: Metal activation, solvent isotope effects, and kinetic mechanism, *Biochemistry 37*, 10478–10487.
1196. Himmelhoch, S. (1969) Leucine aminopeptidase: A zinc metalloenzyme, *Arch. Biochem. Biophys. 134*, 597–602.
1197. Christians, S., and Kaltwasser, H. (1986) Nickel-content of urease from *Bacillus pasteurii*, *Arch. Microbiol. 145*, 51–55.
1198. Dixon, N. E., Gazzola, C., Asher, C. J., Lee, D. S., Blakeley, R. L., and Zerner, B. (1980) Jack bean urease (EC 3.5.1.5). II. The relationship between nickel, enzymatic activity, and the "abnormal" ultraviolet spectrum. The nickel content of jack beans, *Can. J. Biochem. 58*, 474–480.
1199. Hall, R. S., Xiang, D. F., Xu, C., and Raushel, F. M. (2007) *N*-Acetyl-D-glucosamine-6-phosphate deacetylase: Substrate activation via a single divalent metal ion, *Biochemistry 46*, 7942–7952.
1200. Capdevila, D. A., Edmonds, K. A., and Giedroc, D. P. (2017) Metallochaperones and metalloregulation in bacteria, *Essays Biochem 61*, 177–200.
1201. Ranieri-Raggi, M., Moir, A. J., and Raggi, A. (2014) The role of histidine-proline-rich glycoprotein as zinc chaperone for skeletal muscle AMP deaminase, *Biomolecules 4*, 474–497.
1202. Song, H. K., Mulrooney, S. B., Huber, R., and Hausinger, R. P. (2001) Crystal structure of *Klebsiella aerogenes* UreE, a nickel-binding metallochaperone for urease activation, *J. Biol. Chem. 276*, 49359–49364.
1203. Zambelli, B., Musiani, F., Benini, S., and Ciurli, S. (2011) Chemistry of Ni^{2+} in urease: Sensing, trafficking, and catalysis, *Acc. Chem. Res. 44*, 520–530.
1204. Ascone, I., and Strange, R. (2009) Biological X-ray absorption spectroscopy and metalloproteomics, *J. Synchrotron Radiat. 16*, 413–421.
1205. Fruncillo, S., Trande, M., Blanford, C. F., Astegno, A., and Wong, L. S. (2019) A method for metal/protein stoichiometry determination using thin-film energy dispersive X-ray fluorescence spectroscopy, *Anal. Chem. 91*, 11502–11506.
1206. Grime, G. W., Zeldin, O. B., Snell, M. E., Lowe, E. D., Hunt, J. F., Montelione, G. T., Tong, L., Snell, E. H., and Garman, E. F. (2020) High-throughput PIXE as an essential quantitative assay for accurate metalloprotein structural analysis: Development and application, *J. Am. Chem. Soc. 142*, 185–197.
1207. Darnault, C., Volbeda, A., Kim, E. J., Legrand, P., Vernede, X., Lindahl, P. A., and Fontecilla-Camps, J. C. (2003) Ni-Zn-[Fe_4–S_4] and Ni-Ni-[Fe_4–S_4] clusters in closed and open α-subunits of acetyl-CoA synthase/carbon monoxide dehydrogenase, *Nat. Struct. Biol. 10*, 271–279.
1208. Ray, W. J., Jr. (1969) Role of bivalent cations in the phosphoglucomutase system. I. Characterization of enzyme-metal complexes, *J. Biol. Chem. 244*, 3740–3747.
1209. Ray, W. J., Jr., Goodin, D. S., and Ng, L. (1972) Cobalt(II) and nickel(II) complexes of phosphoglucomutase, *Biochemistry 11*, 2800–2804.
1210. Moore, J. D., Skinner, M. A., Swatman, D. R., Hawkins, A. R., and Brown, K. A. (1998) Reactivation of 3-dehydroquinate synthase by lanthanide cations, *J. Am. Chem. Soc. 120*, 7105–7106.

1211. Ragusa, S., Blanquet, S., and Meinnel, T. (1998) Control of peptide deformylase activity by metal cations, *J. Mol. Biol. 280*, 515–523.
1212. Frost, J. W., Bender, J. L., Kadonaga, J. T., and Knowles, J. R. (1984) Dehydroquinate synthase from *Escherichia coli*: Purification, cloning, and construction of overproducers of the enzyme, *Biochemistry 23*, 4470–4475.
1213. Lee, M., Rozeboom, H. J., de Waal, P. P., de Jong, R. M., Dudek, H. M., and Janssen, D. B. (2017) Metal dependence of the xylose isomerase from *Piromyces* sp. E2 explored by activity profiling and protein crystallography, *Biochemistry 56*, 5991–6005.
1214. Lu, Z. J., and Markham, G. D. (2007) Metal ion activation of *S*-adenosylmethionine decarboxylase reflects cation charge density, *Biochemistry 46*, 8172–8180.
1215. Clugston, S. L., Barnard, J. F., Kinach, R., Miedema, D., Ruman, R., Daub, E., and Honek, J. F. (1998) Overproduction and characterization of a dimeric non-zinc glyoxalase I from *Escherichia coli*: Evidence for optimal activation by nickel ions, *Biochemistry 37*, 8754–8763.
1216. He, M. M., Clugston, S. L., Honek, J. F., and Matthews, B. W. (2000) Determination of the structure of *Escherichia coli* glyoxalase I suggests a structural basis for differential metal activation, *Biochemistry 39*, 8719–8727.
1217. Hanlon, D. P., and Westhead, E. W. (1969) Kinetic studies on the activation of yeast enolase by divalent cations, *Biochemistry 8*, 4255–4260.
1218. Schnicker, N. J., De Silva, S. M., Todd, J. D., and Dey, M. (2017) Structural and biochemical insights into dimethylsulfoniopropionate cleavage by cofactor-bound DddK from the prolific marine bacterium *Pelagibacter*, *Biochemistry 56*, 2873–2885.
1219. Tietz, A., and Ochoa, S. (1958) Fluorokinase and pyruvic kinase, *Arch. Biochem. Biophys. 78*, 477–493.
1220. Melchior, J. B. (1965) The role of metal ions in the pyruvic kinase reaction, *Biochemistry 4*, 1518–1525.
1221. Mildvan, A. S., and Cohn, M. (1965) Kinetic and magnetic resonance studies of the pyruvate kinase reaction. I. Divalent metal complexes of pyruvate kinase, *J. Biol. Chem. 240*, 238–246.
1222. Fee, J. A., Hegeman, G. D., and Kenyon, G. L. (1974) Mandelate racemase from *Pseudomonas putida*. Subunit composition and absolute divalent metal ion requirement, *Biochemistry 13*, 2528–2532.
1223. Callens, M., Kersters-Hilderson, H., Van Opstal, O., and De Bruyne, C. K. (1986) Catalytic properties of D-xylose isomerase from *Streptomyces violaceoruber*, *Enzyme Microb. Technol. 8*, 696–700.
1224. Yamanaka, K. (1968) Purification, crystallization and properties of the D-xylose isomerase from *Lactobacillus brevis*, *Biochim. Biophys. Acta 151*, 670–680.
1225. Duewel, H. S., and Woodard, R. W. (2000) A metal bridge between two enzyme families. 3-Deoxy-D-manno-octulosonate-8-phosphate synthase from *Aquifex aeolicus* requires a divalent metal for activity, *J. Biol. Chem. 275*, 22824–22831.
1226. Shapiro, B. M., and Stadtman, E. R. (1968) 5′-Adenylyl-*O*-tyrosine. The novel phosphodiester residue of adenylylated glutamine synthetase from *Escherichia coli*, *J. Biol. Chem. 243*, 3769–3771.
1227. Ginsburg, A., Yeh, J., Hennig, S. B., and Denton, M. D. (1970) Some effects of adenylylation on the biosynthetic properties of the glutamine synthetase from *Escherichia coli*, *Biochemistry 9*, 633–649.
1228. Woolfolk, C. A., Shapiro, B., and Stadtman, E. R. (1966) Regulation of glutamine synthetase. I. Purification and properties of glutamine synthetase from *Escherichia coli*, *Arch. Biochem. Biophys. 116*, 177–192.
1229. Rohrer, S. P., Saz, H. J., and Nowak, T. (1986) Purification and characterization of phospho*enol*pyruvate carboxykinase from the parasitic helminth *Ascaris suum*, *J. Biol. Chem. 261*, 13049–13055.
1230. Goldie, A. H., and Sanwal, B. D. (1980) Allosteric control by calcium and mechanism of desensitization of phospho*enol*pyruvate carboxykinase of *Escherichia coli*, *J. Biol. Chem. 255*, 1399–1405.
1231. Lee, M. H., Hebda, C. A., and Nowak, T. (1981) The role of cations in avian liver phospho*enol*pyruvate carboxykinase catalysis. Activation and regulation, *J. Biol. Chem. 256*, 12793–12801.
1232. Tari, L. W., Matte, A., Goldie, H., and Delbaere, L. T. (1997) Mg^{2+}-Mn^{2+} Clusters in enzyme-catalyzed phosphoryl-transfer reactions, *Nat. Struct. Biol. 4*, 990–994.

1233. Zhu, J., Dizin, E., Hu, X., Wavreille, A. S., Park, J., and Pei, D. (2003) *S*-Ribosylhomocysteinase (LuxS) is a mononuclear iron protein, *Biochemistry 42*, 4717–4726.
1234. Hu, X. V., Chen, X., Han, K. C., Mildvan, A. S., and Liu, J. O. (2007) Kinetic and mutational studies of the number of interacting divalent cations required by bacterial and human methionine aminopeptidases, *Biochemistry 46*, 12833–12843.
1235. D'Souza V, M., and Holz, R. C. (1999) The methionyl aminopeptidase from *Escherichia coli* can function as an iron(II) enzyme, *Biochemistry 38*, 11079–11085.
1236. Chai, S. C., Wang, W. L., and Ye, Q. Z. (2008) Fe(II) is the native cofactor for *Escherichia coli* methionine aminopeptidase, *J. Biol. Chem. 283*, 26879–26885.
1237. Chu, Y., Lee, E. Y., and Schlender, K. K. (1996) Activation of protein phosphatase 1. Formation of a metalloenzyme, *J. Biol. Chem. 271*, 2574–2577.
1238. Merkx, M., and Averill, B. A. (1998) Ga^{3+} as a functional substitute for Fe^{3+}: Preparation and characterization of the $Ga^{3+}Fe^{2+}$ and $Ga^{3+}Zn^{2+}$ forms of bovine spleen purple acid phosphatase, *Biochemistry 37*, 8490–8497.
1239. Reiter, T. A., Reiter, N. J., and Rusnak, F. (2002) Mn^{2+} is a native metal ion activator for bacteriophage lambda protein phosphatase, *Biochemistry 41*, 15404–15409.
1240. Rajan, R., Zhu, J., Hu, X., Pei, D., and Bell, C. E. (2005) Crystal structure of *S*-ribosylhomocysteinase (LuxS) in complex with a catalytic 2-ketone intermediate, *Biochemistry 44*, 3745–3753.
1241. Roderick, S. L., and Matthews, B. W. (1993) Structure of the cobalt-dependent methionine aminopeptidase from *Escherichia coli*: A new type of proteolytic enzyme, *Biochemistry 32*, 3907–3912.
1242. Lowther, W. T., Zhang, Y., Sampson, P. B., Honek, J. F., and Matthews, B. W. (1999) Insights into the mechanism of *Escherichia coli* methionine aminopeptidase from the structural analysis of reaction products and phosphorus-based transition-state analogues, *Biochemistry 38*, 14810–14819.
1243. Tse, P., Scopes, R. K., and Wedd, A. G. (1989) Iron-activated alcohol dehydrogenase from *Zymomonas mobilis*: Isolation of apoenzyme and metal dissociation constants, *J. Am. Chem. Soc. 111*, 8703–8706.
1244. Marti-Arbona, R., and Raushel, F. M. (2006) Mechanistic characterization of *N*-formimino-L-glutamate iminohydrolase from *Pseudomonas aeruginosa*, *Biochemistry 45*, 14256–14262.
1245. Shim, H., and Raushel, F. M. (2000) Self-assembly of the binuclear metal center of phosphotriesterase, *Biochemistry 39*, 7357–7364.
1246. Huang, D. T., Thomas, M. A., and Christopherson, R. I. (1999) Divalent metal derivatives of the hamster dihydroorotase domain, *Biochemistry 38*, 9964–9970.
1247. Kubala, G., and Martell, A. E. (1982) Zinc(II)-, aluminum(III)-, and copper(II)-catalyzed decarboxylation of 2-oxalopropionic acid, *J. Am. Chem. Soc. 104*, 6602–6609.
1248. Coincon, M., Wang, W., Sygusch, J., and Seah, S. Y. (2012) Crystal structure of reaction intermediates in pyruvate class II aldolase: Substrate cleavage, enolate stabilization, and substrate specificity, *J. Biol. Chem. 287*, 36208–36221.
1249. Jelakovic, S., and Schulz, G. E. (2002) Catalytic mechanism of CMP:2-keto-3-deoxy-manno-octonic acid synthetase as derived from complexes with reaction educt and product, *Biochemistry 41*, 1174–1181.
1250. Dougherty, T. M., and Cleland, W. W. (1985) pH Studies on the chemical mechanism of rabbit muscle pyruvate kinase. 2. Physiological substrates and phosphoenol-α-ketobutyrate, *Biochemistry 24*, 5875–5880.
1251. Dougherty, T. M., and Cleland, W. W. (1985) pH Studies on the chemical mechanism of rabbit muscle pyruvate kinase. 1. Alternate substrates oxalacetate, glycolate, hydroxylamine, and fluoride, *Biochemistry 24*, 5870–5875.
1252. Fenton, A. W., Johnson, T. A., and Holyoak, T. (2010) The pyruvate kinase model system, a cautionary tale for the use of osmolyte perturbations to support conformational equilibria in allostery, *Protein Sci. 19*, 1796–1800.
1253. Hurley, J. H., Dean, A. M., Koshland, D. E., Jr., and Stroud, R. M. (1991) Catalytic mechanism of $NADP^+$-dependent isocitrate dehydrogenase: Implications from the structures of magnesium-isocitrate and $NADP^+$ complexes, *Biochemistry 30*, 8671–8678.
1254. Liu, S., Lu, Z., Jia, Y., Dunaway-Mariano, D., and Herzberg, O. (2002) Dissociative phosphoryl transfer in PEP mutase catalysis:

Structure of the enzyme/sulfopyruvate complex and kinetic properties of mutants, *Biochemistry 41*, 10270–10276.
1255. Kroemer, M., Merkel, I., and Schulz, G. E. (2003) Structure and catalytic mechanism of L-rhamnulose-1-phosphate aldolase, *Biochemistry 42*, 10560–10568.
1256. Collyer, C. A., Henrick, K., and Blow, D. M. (1990) Mechanism for aldose-ketose interconversion by D-xylose isomerase involving ring opening followed by a 1,2-hydride shift, *J. Mol. Biol. 212*, 211–235.
1257. Meng, M., Bagdasarian, M., and Zeikus, J. G. (1993) The role of active-site aromatic and polar residues in catalysis and substrate discrimination by xylose isomerase, *Proc. Natl. Acad. Sci. U. S. A. 90*, 8459–8463.
1258. Yoshida, H., Yamada, M., Ohyama, Y., Takada, G., Izumori, K., and Kamitori, S. (2007) The structures of L-rhamnose isomerase from *Pseudomonas stutzeri* in complexes with L-rhamnose and D-allose provide insights into broad substrate specificity, *J. Mol. Biol. 365*, 1505–1516.
1259. Lambeir, A. M., Lauwereys, M., Stanssens, P., Mrabet, N. T., Snauwaert, J., van Tilbeurgh, H., Matthyssens, G., Lasters, I., De Maeyer, M., Wodak, S. J., Jenkins, J., Chiadmi, M., and Janin, J. (1992) Protein engineering of xylose (glucose) isomerase from *Actinoplanes missouriensis*. 2. Site-directed mutagenesis of the xylose binding site, *Biochemistry 31*, 5459–5466.
1260. Lavie, A., Allen, K. N., Petsko, G. A., and Ringe, D. (1994) X-Ray crystallographic structures of D-xylose isomerase-substrate complexes position the substrate and provide evidence for metal movement during catalysis, *Biochemistry 33*, 5469–5480.
1261. Allen, K. N., Lavie, A., Petsko, G. A., and Ringe, D. (1995) Design, synthesis, and characterization of a potent xylose isomerase inhibitor, D-threonohydroxamic acid, and high-resolution X-ray crystallographic structure of the enzyme-inhibitor complex, *Biochemistry 34*, 3742–3749.
1262. Korndorfer, I. P., Fessner, W. D., and Matthews, B. W. (2000) The structure of rhamnose isomerase from *Escherichia coli* and its relation with xylose isomerase illustrates a change between inter and intra-subunit complementation during evolution, *J. Mol. Biol. 300*, 917–933.
1263. Harris, D. W., and Feather, M. S. (1975) Mechanism of the interconversion of D-glucose, D-mannose, and D-fructose in acid solution, *J. Am. Chem. Soc. 97*, 178–181.
1264. Nagorski, R. W., and Richard, J. P. (1996) Mechanistic imperatives for enzymic catalysis of aldose-ketose isomerization: Isomerization of glyceraldehyde in weakly alkaline aqueous solution occurs with intramolecular transfer of a hydride ion, *J. Am. Chem. Soc. 118*, 7432–7433.
1265. Nagorski, R. W., and Richard, J. P. (2001) Mechanistic imperatives for aldose-ketose isomerization in water: Specific, general base- and metal ion-catalyzed isomerization of glyceraldehyde with proton and hydride transfer, *J. Am. Chem. Soc. 123*, 794–802.
1266. Jelakovic, S., Kopriva, S., Suss, K. H., and Schulz, G. E. (2003) Structure and catalytic mechanism of the cytosolic D-ribulose-5-phosphate 3-epimerase from rice, *J. Mol. Biol. 326*, 127–135.
1267. Kim, K., Kim, H. J., Oh, D. K., Cha, S. S., and Rhee, S. (2006) Crystal structure of D-psicose 3-epimerase from *Agrobacterium tumefaciens* and its complex with true substrate D-fructose: A pivotal role of metal in catalysis, an active site for the non-phosphorylated substrate, and its conformational changes, *J. Mol. Biol. 361*, 920–931.
1268. Yoshida, H., Yamada, M., Nishitani, T., Takada, G., Izumori, K., and Kamitori, S. (2007) Crystal structures of D-tagatose 3–epimerase from *Pseudomonas cichorii* and its complexes with D-tagatose and D-fructose, *J. Mol. Biol. 374*, 443–453.
1269. Liang, W., Ouyang, S., Shaw, N., Joachimiak, A., Zhang, R., and Liu, Z. J. (2011) Conversion of D-ribulose 5-phosphate to D-xylulose 5-phosphate: New insights from structural and biochemical studies on human RPE, *FASEB J. 25*, 497–504.
1270. Kim, H. J., Hyun, E. K., Kim, Y. S., Lee, Y. J., and Oh, D. K. (2006) Characterization of an *Agrobacterium tumefaciens* D-psicose 3-epimerase that converts D-fructose to D-psicose, *Appl. Environ. Microbiol. 72*, 981–985.
1271. Mabanglo, M. F., Huddleston, J. P., Mukherjee, K., Taylor, Z. W., and Raushel, F. M. (2020) Structure and reaction mechanism of YcjR, an epimerase that facilitates the interconversion of D-gulosides to D-glucosides in *Escherichia coli*, *Biochemistry 59*, 2069–2077.

1272. Chan, H. C., Zhu, Y., Hu, Y., Ko, T. P., Huang, C. H., Ren, F., Chen, C. C., Ma, Y., Guo, R. T., and Sun, Y. (2012) Crystal structures of D-psicose 3-epimerase from *Clostridium cellulolyticum* H10 and its complex with ketohexose sugars, *Protein Cell 3*, 123–131.
1273. Dinovo, E. C., and Boyer, P. D. (1971) Isotopic probes of the enolase reaction mechanism. Initial and equilibrium isotope exchange rates. Primary and secondary isotope effects, *J. Biol. Chem. 246*, 4586–4593.
1274. Konig, V., Pfeil, A., Braus, G. H., and Schneider, T. R. (2004) Substrate and metal complexes of 3-deoxy-D-arabino-heptulosonate-7-phosphate synthase from *Saccharomyces cerevisiae* provide new insights into the catalytic mechanism, *J. Mol. Biol. 337*, 675–690.
1275. Eklund, H., Plapp, B. V., Samama, J. P., and Branden, C. I. (1982) Binding of substrate in a ternary complex of horse liver alcohol dehydrogenase, *J. Biol. Chem. 257*, 14349–14358.
1276. Ramaswamy, S., Eklund, H., and Plapp, B. V. (1994) Structures of horse liver alcohol dehydrogenase complexed with NAD^+ and substituted benzyl alcohols, *Biochemistry 33*, 5230–5237.
1277. Zhou, L., Wu, J., Janakiraman, V., Shumilin, I. A., Bauerle, R., Kretsinger, R. H., and Woodard, R. W. (2012) Structure and characterization of the 3-deoxy-D-arabino-heptulosonate 7-phosphate synthase from *Aeropyrum pernix*, *Bioorg. Chem. 40*, 79–86.
1278. Wu, J., Sheflyan, G. Y., and Woodard, R. W. (2005) *Bacillus subtilis* 3-deoxy-D-arabino-heptulosonate 7-phosphate synthase revisited: Resolution of two long-standing enigmas, *Biochem. J. 390*, 583–590.
1279. Schnappauf, G., Hartmann, M., Kunzler, M., and Braus, G. H. (1998) The two 3-deoxy-D-arabino-heptulosonate-7-phosphate synthase isoenzymes from *Saccharomyces cerevisiae* show different kinetic modes of inhibition, *Arch. Microbiol. 169*, 517–524.
1280. Moon, J. H., Lee, H. J., Park, S. Y., Song, J. M., Park, M. Y., Park, H. M., Sun, J., Park, J. H., Kim, B. Y., and Kim, J. S. (2011) Structures of iron-dependent alcohol dehydrogenase 2 from *Zymomonas mobilis* ZM4 with and without NAD^+ cofactor, *J. Mol. Biol. 407*, 413–424.
1281. Evans, S. A., and Shore, J. D. (1980) The role of zinc-bound water in liver alcohol dehydrogenase catalysis, *J. Biol. Chem. 255*, 1509–1514.
1282. Kimura, E., Shionoya, M., Hoshino, A., Ikeda, T., and Yamada, Y. (1992) A model for catalytically active zinc(II) ion in liver alcohol dehydrogenase: A novel "hydride transfer" reaction catalyzed by zinc(II)-macrocyclic polyamine complexes, *J. Am. Chem. Soc. 114*, 10134–10137.
1283. Takahashi, K., Harada, S., Higashimoto, Y., Shimokawa, C., Sato, H., Sugishima, M., Kaida, Y., and Noguchi, M. (2009) Involvement of metals in enzymatic and nonenzymatic decomposition of C-terminal α-hydroxyglycine to amide: An implication for the catalytic role of enzyme-bound zinc in the peptidylamidoglycolate lyase reaction, *Biochemistry 48*, 1654–1662.
1284. Neverov, A. A., Montoya-Pelaez, P. J., and Brown, R. S. (2001) Catalysis of the methanolysis of activated amides by divalent and trivalent metal ions. The effect of Zn^{2+}, Co^{2+}, and La^{3+} on the methanolysis of acetylimidazole and its $(NH_3)_5Co(III)$ complex, *J. Am. Chem. Soc. 123*, 210–217.
1285. Brems, D. N., and Rilling, H. C. (1977) The mechanism of the prenyltransferase reaction. Metal ion dependent solvolysis of an allylic pyrophosphate, *J. Am. Chem. Soc. 99*, 8351–8352.
1286. Morera, S., Lariviere, L., Kurzeck, J., Aschke-Sonnenborn, U., Freemont, P. S., Janin, J., and Ruger, W. (2001) High resolution crystal structures of T4 phage β-glucosyltransferase: Induced fit and effect of substrate and metal binding, *J. Mol. Biol. 311*, 569–577.
1287. Komoto, J., Yamada, T., Takata, Y., Markham, G. D., and Takusagawa, F. (2004) Crystal structure of the *S*-adenosylmethionine synthetase ternary complex: A novel catalytic mechanism of *S*-adenosylmethionine synthesis from ATP and Met, *Biochemistry 43*, 1821–1831.
1288. Kennedy, S. C., Rauner, R., and Gawron, O. (1972) On pig heart aconitase, *Biochem. Biophys. Res. Commun. 47*, 740–745.
1289. Dreyer, J. L. (1985) Isolation and biochemical characterization of maleic-acid hydratase, an iron-requiring hydro-lyase, *Eur. J. Biochem. 150*, 145–154.
1290. Flint, D. H., Emptage, M. H., and Guest, J. R. (1992) Fumarase A from *Escherichia coli*: Purification and characterization as an iron–sulfur

cluster containing enzyme, *Biochemistry 31*, 10331–10337.
1291. Feliciano, P. R., Drennan, C. L., and Nonato, M. C. (2016) Crystal structure of an Fe-S cluster-containing fumarate hydratase enzyme from *Leishmania major* reveals a unique protein fold, *Proc. Natl. Acad. Sci. U. S. A. 113*, 9804–9809.
1292. Feliciano, P. R., and Drennan, C. L. (2019) Structural and biochemical investigations of the [4Fe-4S] cluster-containing fumarate hydratase from *Leishmania major*, *Biochemistry 58*, 5011–5021.
1293. Flint, D. H., Tuminello, J. F., and Emptage, M. H. (1993) The inactivation of Fe-S cluster containing hydro-lyases by superoxide, *J. Biol. Chem. 268*, 22369–22376.
1294. Flint, D. H., and Emptage, M. H. (1988) Dihydroxy acid dehydratase from spinach contains a [2Fe-2S] cluster, *J. Biol. Chem. 263*, 3558–3564.
1295. Hofmeister, A. E., Berger, S., and Buckel, W. (1992) The iron–sulfur-cluster-containing L-serine dehydratase from *Peptostreptococcus asaccharolyticus*. Stereochemistry of the deamination of L-threonine, *Eur. J. Biochem. 205*, 743–749.
1296. Grawert, T., Span, I., Eisenreich, W., Rohdich, F., Eppinger, J., Bacher, A., and Groll, M. (2010) Probing the reaction mechanism of IspH protein by X-ray structure analysis, *Proc. Natl. Acad. Sci. U. S. A. 107*, 1077–1081.
1297. Span, I., Grawert, T., Bacher, A., Eisenreich, W., and Groll, M. (2012) Crystal structures of mutant IspH proteins reveal a rotation of the substrate's hydroxymethyl group during catalysis, *J. Mol. Biol. 416*, 1–9.
1298. Kannan, K. K., Ramanadham, M., and Jones, T. A. (1984) Structure, refinement, and function of carbonic anhydrase isozymes: Refinement of human carbonic anhydrase I, *Ann. N. Y. Acad. Sci. 429*, 49–60.
1299. Domsic, J. F., Avvaru, B. S., Kim, C. U., Gruner, S. M., Agbandje-McKenna, M., Silverman, D. N., and McKenna, R. (2008) Entrapment of carbon dioxide in the active site of carbonic anhydrase II, *J. Biol. Chem. 283*, 30766–30771.
1300. Silverman, D. N., Tu, C. K., Lindskog, S., and Wynns, G. C. (1979) Rate of exchange of water from the active site of human carbonic anhydrase C, *J. Am. Chem. Soc. 101*, 6734–6740.
1301. Lindskog, S. (1997) Structure and mechanism of carbonic anhydrase, *Pharmacol. Ther. 74*, 1–20.
1302. Sjoblom, B., Polentarutti, M., and Djinovic-Carugo, K. (2009) Structural study of X-ray induced activation of carbonic anhydrase, *Proc. Natl. Acad. Sci. U. S. A. 106*, 10609–10613.
1303. Fisher, Z., Kovalevsky, A. Y., Mustyakimov, M., Silverman, D. N., McKenna, R., and Langan, P. (2011) Neutron structure of human carbonic anhydrase II: A hydrogen-bonded water network "switch" is observed between pH 7.8 and 10.0, *Biochemistry 50*, 9421–9423.
1304. Xiang, S., Short, S. A., Wolfenden, R., and Carter, C. W., Jr. (1995) Transition-state selectivity for a single hydroxyl group during catalysis by cytidine deaminase, *Biochemistry 34*, 4516–4523.
1305. Huffman, J. L., Li, H., White, R. H., and Tainer, J. A. (2003) Structural basis for recognition and catalysis by the bifunctional dCTP deaminase and dUTPase from *Methanococcus jannaschii*, *J. Mol. Biol. 331*, 885–896.
1306. Kamat, S. S., Bagaria, A., Kumaran, D., Holmes-Hampton, G. P., Fan, H., Sali, A., Sauder, J. M., Burley, S. K., Lindahl, P. A., Swaminathan, S., and Raushel, F. M. (2011) Catalytic mechanism and three-dimensional structure of adenine deaminase, *Biochemistry 50*, 1917–1927.
1307. Matthews, B. W. (1988) Structural basis of the action of thermolysin and related zinc peptidases, *Acc. Chem. Res. 21*, 333–340.
1308. Silver, G. C., Gantzel, P., and Trogler, W. C. (1995) Characterization of (trimethyltriazacyclononane)triaquozinc(II) nitrate. A nonbridged isomer, *Inorg. Chem. 34*, 2487–2489.
1309. Koike, T., Takamura, M., and Kimura, E. (1994) Role of zinc(II) in β-lactamase II: A model study with a zinc(II)-macrocyclic tetraamine (1,4,7,10–tetraazacyclododecane, cyclen) complex, *J. Am. Chem. Soc. 116*, 8443–8449.
1310. Vidgren, J., Svensson, L. A., and Liljas, A. (1994) Crystal structure of catechol *O*-methyltransferase, *Nature (London, U. K.) 368*, 354–358.
1311. Saderholm, M. J., Hightower, K. E., and Fierke, C. A. (2000) Role of metals in the reaction catalyzed by protein farnesyltransferase, *Biochemistry 39*, 12398–12405.
1312. Wilker, J. J., and Lippard, S. J. (1995) Modeling the DNA methylphosphotriester repair

site in *Escherichia coli* Ada. Why zinc and four cysteines?, *J. Am. Chem. Soc. 117*, 8682–8683.
1313. Matthews, R. G., Smith, A. E., Zhou, Z. H. S., Taurog, R. E., Bandarian, V., Evans, J. C., and Ludwig, M. (2003) Cobalamin-dependent and cobalamin-independent methionine synthases: Are there two solutions to the same chemical problem?, *Helv. Chim. Acta 86*, 3939–3954.
1314. Ubhi, D. K., and Robertus, J. D. (2015) The cobalamin-independent methionine synthase enzyme captured in a substrate-induced closed conformation, *J. Mol. Biol. 427*, 901–909.
1315. Fabiane, S. M., Sohi, M. K., Wan, T., Payne, D. J., Bateson, J. H., Mitchell, T., and Sutton, B. J. (1998) Crystal structure of the zinc-dependent β-lactamase from *Bacillus cereus* at 1.9 Å resolution: Binuclear active site with features of a mononuclear enzyme, *Biochemistry 37*, 12404–12411.
1316. Ullah, J. H., Walsh, T. R., Taylor, I. A., Emery, D. C., Verma, C. S., Gamblin, S. J., and Spencer, J. (1998) The crystal structure of the L1 metallo-β-lactamase from *Stenotrophomonas maltophilia* at 1.7 Å resolution, *J. Mol. Biol. 284*, 125–136.
1317. Abendroth, J., Niefind, K., and Schomburg, D. (2002) X-Ray structure of a dihydropyrimidinase from *Thermus* sp. at 1.3 Å resolution, *J. Mol. Biol. 320*, 143–156.
1318. Beuth, B., Niefind, K., and Schomburg, D. (2003) Crystal structure of creatininase from *Pseudomonas putida*: A novel fold and a case of convergent evolution, *J. Mol. Biol. 332*, 287–301.
1319. Yoshimoto, T., Tanaka, N., Kanada, N., Inoue, T., Nakajima, Y., Haratake, M., Nakamura, K. T., Xu, Y., and Ito, K. (2004) Crystal structures of creatininase reveal the substrate binding site and provide an insight into the catalytic mechanism, *J. Mol. Biol. 337*, 399–416.
1320. Klusak, V., Barinka, C., Plechanovova, A., Mlcochova, P., Konvalinka, J., Rulisek, L., and Lubkowski, J. (2009) Reaction mechanism of glutamate carboxypeptidase II revealed by mutagenesis, X-ray crystallography, and computational methods, *Biochemistry 48*, 4126–4138.
1321. Iranzo, O., Kovalevsky, A. Y., Morrow, J. R., and Richard, J. P. (2003) Physical and kinetic analysis of the cooperative role of metal ions in catalysis of phosphodiester cleavage by a dinuclear Zn(II) complex, *J. Am. Chem. Soc. 125*, 1988–1993.
1322. Aubert, S. D., Li, Y., and Raushel, F. M. (2004) Mechanism for the hydrolysis of organophosphates by the bacterial phosphotriesterase, *Biochemistry 43*, 5707–5715.
1323. Barrios, A. M., and Lippard, S. J. (2000) Interaction of urea with a hydroxide-bridged dinuclear nickel center: An alternative model for the mechanism of urease, *J. Am. Chem. Soc. 122*, 9172–9177.
1324. Barrios, A. M., and Lippard, S. J. (1999) Amide hydrolysis effected by a hydroxo-bridged dinickel(II) complex: Insights into the mechanism of urease, *J. Am. Chem. Soc. 121*, 11751–11757.
1325. Kaminskaia, N. V., Spingler, B., and Lippard, S. J. (2000) Hydrolysis of β-lactam antibiotics catalyzed by dinuclear zinc(II) complexes: Functional mimics of metallo-β-lactamases, *J. Am. Chem. Soc. 122*, 6411–6422.
1326. He, C., and Lippard, S. J. (1998) Aminoguanidinium hydrolysis effected by a hydroxo-bridged dicobalt(II) complex as a functional model for arginase and catalyzed by mononuclear cobalt(II) complexes, *J. Am. Chem. Soc. 120*, 105–113.
1327. Kim, N. N., Cox, J. D., Baggio, R. F., Emig, F. A., Mistry, S. K., Harper, S. L., Speicher, D. W., Morris, S. M., Jr., Ash, D. E., Traish, A., and Christianson, D. W. (2001) Probing erectile function: *S*-(2–Boronoethyl)-L-cysteine binds to arginase as a transition state analogue and enhances smooth muscle relaxation in human penile corpus cavernosum, *Biochemistry 40*, 2678–2688.
1328. Jencks, W. P. (1963) Infrared measurements in aqueous media, *Methods Enzymol. 6*, 914–928.
1329. Dixon, N. E., Gazzola, T. C., Blakeley, R. L., and Zermer, B. (1975) Letter: Jack bean urease (EC 3.5.1.5). A metalloenzyme. A simple biological role for nickel?, *J. Am. Chem. Soc. 97*, 4131–4133.
1330. Pearson, M. A., Park, I. S., Schaller, R. A., Michel, L. O., Karplus, P. A., and Hausinger, R. P. (2000) Kinetic and structural characterization of urease active site variants, *Biochemistry 39*, 8575–8584.
1331. Thoden, J. B., Phillips, G. N., Jr., Neal, T. M., Raushel, F. M., and Holden, H. M. (2001) Molecular structure of dihydroorotase: A paradigm

for catalysis through the use of a binuclear metal center, *Biochemistry 40*, 6989–6997.
1332. Kanyo, Z. F., Scolnick, L. R., Ash, D. E., and Christianson, D. W. (1996) Structure of a unique binuclear manganese cluster in arginase, *Nature (London, U. K.) 383*, 554–557.
1333. Reczkowski, R. S., and Ash, D. E. (1992) EPR Evidence for binuclear manganese(II) centers in rat liver arginase, *J. Am. Chem. Soc. 114*, 10992–10994.
1334. Cox, J. D., Kim, N. N., Traish, A. M., and Christianson, D. W. (1999) Arginase-boronic acid complex highlights a physiological role in erectile function, *Nat. Struct. Biol. 6*, 1043–1047.
1335. Di Costanzo, L., Sabio, G., Mora, A., Rodriguez, P. C., Ochoa, A. C., Centeno, F., and Christianson, D. W. (2005) Crystal structure of human arginase I at 1.29-Å resolution and exploration of inhibition in the immune response, *Proc. Natl. Acad. Sci. U. S. A. 102*, 13058–13063.
1336. Hai, Y., Edwards, J. E., Van Zandt, M. C., Hoffmann, K. F., and Christianson, D. W. (2014) Crystal structure of *Schistosoma mansoni* arginase, a potential drug target for the treatment of schistosomiasis, *Biochemistry 53*, 4671–4684.
1337. Volk, R., and Bacher, A. (1991) Biosynthesis of riboflavin. Studies on the mechanism of L-3,4-dihydroxy-2-butanone 4-phosphate synthase, *J. Biol. Chem. 266*, 20610–20618.
1338. Kumar, P., Singh, M., Gautam, R., and Karthikeyan, S. (2010) Potential antibacterial drug target: Structural characterization of 3,4-dihydroxy-2-butanone-4-phosphate synthase from *Salmonella typhimurium* LT2, *Proteins 78*, 3292–3303.
1339. Kress, D., Alhapel, A., Pierik, A. J., and Essen, L. O. (2008) The crystal structure of enamidase: A bifunctional enzyme of the nicotinate catabolism, *J. Mol. Biol. 384*, 837–847.
1340. Fife, T. H., and Przystas, T. J. (1986) Divalent metal ion catalysis in amide hydrolysis. The hydrolysis of *N*-acylimidazoles, *J. Am. Chem. Soc. 108*, 4631–4636.
1341. Dunaway-Mariano, D., Benovic, J. L., Cleland, W. W., Gupta, R. K., and Mildvan, A. S. (1979) Stereospecificity of the metal-adenosine 5′-triphosphate complex in reactions of muscle pyruvate kinase, *Biochemistry 18*, 4347–4354.
1342. Muirhead, H., Clayden, D. A., Cuffe, S. P., and Davies, C. (1987) Crystallographic studies on the structure and catalytic activity of pyruvate kinase from skeletal muscle, *Biochem. Soc. Trans. 15*, 996–999.
1343. Larsen, T. M., Laughlin, L. T., Holden, H. M., Rayment, I., and Reed, G. H. (1994) Structure of rabbit muscle pyruvate kinase complexed with Mn^{2+}, K^+, and pyruvate, *Biochemistry 33*, 6301–6309.
1344. Pelletier, H., Sawaya, M. R., Kumar, A., Wilson, S. H., and Kraut, J. (1994) Structures of ternary complexes of rat DNA polymerase β, a DNA template-primer, and ddCTP, *Science (Washington, DC, U. S.) 264*, 1891–1903.
1345. Doublie, S., Tabor, S., Long, A. M., Richardson, C. C., and Ellenberger, T. (1998) Crystal structure of a bacteriophage T7 DNA replication complex at 2.2 Å resolution, *Nature (London, U. K.) 391*, 251–258.
1346. Brautigam, C. A., and Steitz, T. A. (1998) Structural and functional insights provided by crystal structures of DNA polymerases and their substrate complexes, *Curr. Opin. Struct. Biol. 8*, 54–63.
1347. Appleby, T. C., Perry, J. K., Murakami, E., Barauskas, O., Feng, J., Cho, A., Fox, D., 3rd, Wetmore, D. R., McGrath, M. E., Ray, A. S., Sofia, M. J., Swaminathan, S., and Edwards, T. E. (2015) Viral replication. Structural basis for RNA replication by the hepatitis C virus polymerase, *Science (Washington, DC, U. S.) 347*, 771–775.
1348. Gong, S., Kirmizialtin, S., Chang, A., Mayfield, J. E., Zhang, Y. J., and Johnson, K. A. (2021) Kinetic and thermodynamic analysis defines roles for two metal ions in DNA polymerase specificity and catalysis, *J. Biol. Chem. 296*, 100184.
1349. Jagtap, P. K., Verma, S. K., Vithani, N., Bais, V. S., and Prakash, B. (2013) Crystal structures identify an atypical two-metal-ion mechanism for uridyltransfer in GlmU: Its significance to sugar nucleotidyl transferases, *J. Mol. Biol. 425*, 1745–1759.
1350. Gopinath, P., Ramalingam, V., and Breslow, R. (2015) Magnesium pyrophosphates in enzyme mimics of nucleotide synthases and kinases and in their prebiotic chemistry, *Proc. Natl. Acad. Sci. U. S. A. 112*, 12011–12014.
1351. Xu, R. X., Hassell, A. M., Vanderwall, D., Lambert, M. H., Holmes, W. D., Luther, M.

A., Rocque, W. J., Milburn, M. V., Zhao, Y., Ke, H., and Nolte, R. T. (2000) Atomic structure of PDE4: Insights into phosphodiesterase mechanism and specificity, *Science (Washington, DC, U. S.) 288*, 1822–1825.
1352. Davies, J. F., 2nd, Hostomska, Z., Hostomsky, Z., Jordan, S. R., and Matthews, D. A. (1991) Crystal structure of the ribonuclease H domain of HIV-1 reverse transcriptase, *Science (Washington, DC, U. S.) 252*, 88–95.
1353. Beernink, P. T., Segelke, B. W., Hadi, M. Z., Erzberger, J. P., Wilson, D. M., 3rd, and Rupp, B. (2001) Two divalent metal ions in the active site of a new crystal form of human apurinic/apyrimidinic endonuclease, Ape1: Implications for the catalytic mechanism, *J. Mol. Biol. 307*, 1023–1034.
1354. Benning, M. M., Kuo, J. M., Raushel, F. M., and Holden, H. M. (1995) Three-dimensional structure of the binuclear metal center of phosphotriesterase, *Biochemistry 34*, 7973–7978.
1355. Bigley, A. N., Xiang, D. F., Narindoshvili, T., Burgert, C. W., Hengge, A. C., and Raushel, F. M. (2019) Transition state analysis of the reaction catalyzed by the phosphotriesterase from *Sphingobium* sp. TCM1, *Biochemistry 58*, 1246–1259.
1356. Harutyunyan, E. H., Oganessyan, V. Y., Oganessyan, N. N., Avaeva, S. M., Nazarova, T. I., Vorobyeva, N. N., Kurilova, S. A., Huber, R., and Mather, T. (1997) Crystal structure of holo inorganic pyrophosphatase from *Escherichia coli* at 1.9 Å resolution. Mechanism of hydrolysis, *Biochemistry 36*, 7754–7760.
1357. Tuominen, V., Heikinheimo, P., Kajander, T., Torkkel, T., Hyytia, T., Kapyla, J., Lahti, R., Cooperman, B. S., and Goldman, A. (1998) The R78K and D117E active-site variants of *Saccharomyces cerevisiae* soluble inorganic pyrophosphatase: Structural studies and mechanistic implications, *J. Mol. Biol. 284*, 1565–1580.
1358. Heikinheimo, P., Tuominen, V., Ahonen, A. K., Teplyakov, A., Cooperman, B. S., Baykov, A. A., Lahti, R., and Goldman, A. (2001) Toward a quantum-mechanical description of metal-assisted phosphoryl transfer in pyrophosphatase, *Proc. Natl. Acad. Sci. U. S. A. 98*, 3121–3126.
1359. Samygina, V. R., Moiseev, V. M., Rodina, E. V., Vorobyeva, N. N., Popov, A. N., Kurilova, S. A., Nazarova, T. I., Avaeva, S. M., and Bartunik, H. D. (2007) Reversible inhibition of *Escherichia coli* inorganic pyrophosphatase by fluoride: Trapped catalytic intermediates in cryo-crystallographic studies, *J. Mol. Biol. 366*, 1305–1317.
1360. Omi, R., Goto, M., Miyahara, I., Manzoku, M., Ebihara, A., and Hirotsu, K. (2007) Crystal structure of monofunctional histidinol phosphate phosphatase from *Thermus thermophilus* HB8, *Biochemistry 46*, 12618–12627.
1361. Gabelli, S. B., Bianchet, M. A., Ohnishi, Y., Ichikawa, Y., Bessman, M. J., and Amzel, L. M. (2002) Mechanism of the *Escherichia coli* ADP-ribose pyrophosphatase, a Nudix hydrolase, *Biochemistry 41*, 9279–9285.
1362. Bellinzoni, M., Wehenkel, A., Shepard, W., and Alzari, P. M. (2007) Insights into the catalytic mechanism of PPM Ser/Thr phosphatases from the atomic resolution structures of a mycobacterial enzyme, *Structure 15*, 863–872.
1363. Fabrichniy, I. P., Lehtio, L., Tammenkoski, M., Zyryanov, A. B., Oksanen, E., Baykov, A. A., Lahti, R., and Goldman, A. (2007) A trimetal site and substrate distortion in a family II inorganic pyrophosphatase, *J. Biol. Chem. 282*, 1422–1431.
1364. Ghodge, S. V., Fedorov, A. A., Fedorov, E. V., Hillerich, B., Seidel, R., Almo, S. C., and Raushel, F. M. (2013) Structural and mechanistic characterization of L-histidinol phosphate phosphatase from the polymerase and histidinol phosphatase family of proteins, *Biochemistry 52*, 1101–1112.
1365. Lovering, A. L., Capeness, M. J., Lambert, C., Hobley, L., and Sockett, R. E. (2011) The structure of an unconventional HD-GYP protein from *Bdellovibrio* reveals the roles of conserved residues in this class of cyclic-di-GMP phosphodiesterases, *mBio 2*, 10.1128/mbio.00163-11.
1366. Miner, K. D., Klose, K. E., and Kurtz, D. M., Jr. (2013) An HD-GYP cyclic di-guanosine monophosphate phosphodiesterase with a non-heme diiron-carboxylate active site, *Biochemistry 52*, 5329–5331.
1367. Humphry, T., Forconi, M., Williams, N. H., and Hengge, A. C. (2002) An altered mechanism of hydrolysis for a metal-complexed phosphate diester, *J. Am. Chem. Soc. 124*, 14860–14861.
1368. Bobyr, E., Lassila, J. K., Wiersma-Koch, H. I., Fenn, T. D., Lee, J. J., Nikolic-Hughes, I.,

Hodgson, K. O., Rees, D. C., Hedman, B., and Herschlag, D. (2012) High-resolution analysis of Zn^{2+} coordination in the alkaline phosphatase superfamily by EXAFS and X-ray crystallography, *J. Mol. Biol. 415*, 102–117.
1369. Hollfelder, F., and Herschlag, D. (1995) The nature of the transition state for enzyme-catalyzed phosphoryl transfer. Hydrolysis of *O*-aryl phosphorothioates by alkaline phosphatase, *Biochemistry 34*, 12255–12264.
1370. Holtz, K. M., Stec, B., and Kantrowitz, E. R. (1999) A model of the transition state in the alkaline phosphatase reaction, *J. Biol. Chem. 274*, 8351–8354.
1371. Nikolic-Hughes, I., O'Brien P, J., and Herschlag, D. (2005) Alkaline phosphatase catalysis is ultrasensitive to charge sequestered between the active site zinc ions, *J. Am. Chem. Soc. 127*, 9314–9315.
1372. Kim, E. E., and Wyckoff, H. W. (1991) Reaction mechanism of alkaline phosphatase based on crystal structures. Two-metal ion catalysis, *J. Mol. Biol. 218*, 449–464.
1373. Zalatan, J. G., Fenn, T. D., Brunger, A. T., and Herschlag, D. (2006) Structural and functional comparisons of nucleotide pyrophosphatase/phosphodiesterase and alkaline phosphatase: Implications for mechanism and evolution, *Biochemistry 45*, 9788–9803.
1374. Stec, B., Holtz, K. M., and Kantrowitz, E. R. (2000) A revised mechanism for the alkaline phosphatase reaction involving three metal ions, *J. Mol. Biol. 299*, 1303–1311.
1375. Krishnaswamy, M., and Kenkare, U. W. (1970) The effect of pH, temperature, and organic solvents on the kinetic parameters of *Escherichia coli* alkaline phosphatase, *J. Biol. Chem. 245*, 3956–3963.
1376. Patel, S., Yenush, L., Rodriguez, P. L., Serrano, R., and Blundell, T. L. (2002) Crystal structure of an enzyme displaying both inositol-polyphosphate-1-phosphatase and 3′-phosphoadenosine-5′-phosphate phosphatase activities: A novel target of lithium therapy, *J. Mol. Biol. 315*, 677–685.
1377. Beese, L. S., and Steitz, T. A. (1991) Structural basis for the 3′-5′ exonuclease activity of *Escherichia coli* DNA polymerase I: A two metal ion mechanism, *EMBO J. 10*, 25–33.
1378. Curley, J. F., Joyce, C. M., and Piccirilli, J. A. (1997) Functional evidence that the 3′-5′ exonuclease domain of *Escherichia coli* DNA polymerase I employs a divalent metal ion in leaving group stabilization, *J. Am. Chem. Soc. 119*, 12691–12692.
1379. Horton, N. C., Connolly, B. A., and Perona, J. J. (2000) Inhibition of *Eco*RV endonuclease by deoxyribo-3′-*S*-phosphorothiolates: A high-resolution X-ray crystallographic study, *J. Am. Chem. Soc. 122*, 3314–3324.
1380. Kostrewa, D., and Winkler, F. K. (1995) Mg^{2+} Binding to the active site of *Eco*RV endonuclease: A crystallographic study of complexes with substrate and product DNA at 2 Å resolution, *Biochemistry 34*, 683–696.
1381. Baldwin, G. S., Vipond, I. B., and Halford, S. E. (1995) Rapid reaction analysis of the catalytic cycle of the *Eco*RV restriction endonuclease, *Biochemistry 34*, 705–714.
1382. Viadiu, H., and Aggarwal, A. K. (1998) The role of metals in catalysis by the restriction endonuclease BamHI, *Nat. Struct. Biol. 5*, 910–916.
1383. Gao, H., Ke, Z., DeYonker, N. J., Wang, J., Xu, H., Mao, Z. W., Phillips, D. L., and Zhao, C. (2011) Dinuclear Zn(II) complex catalyzed phosphodiester cleavage proceeds via a concerted mechanism: A density functional theory study, *J. Am. Chem. Soc. 133*, 2904–2915.
1384. Herschlag, D., and Jencks, W. P. (1990) Catalysis of the hydrolysis of phosphorylated pyridines by $Mg(OH)^+$: A possible model for enzymatic phosphoryl transfer, *Biochemistry 29*, 5172–5179.
1385. Cassano, A. G., Anderson, V. E., and Harris, M. E. (2004) Analysis of solvent nucleophile isotope effects: Evidence for concerted mechanisms and nucleophilic activation by metal coordination in nonenzymatic and ribozyme-catalyzed phosphodiester hydrolysis, *Biochemistry 43*, 10547–10559.
1386. Liaw, S. H., and Eisenberg, D. (1994) Structural model for the reaction mechanism of glutamine synthetase, based on five crystal structures of enzyme-substrate complexes, *Biochemistry 33*, 675–681.
1387. Fioravanti, E., Haouz, A., Ursby, T., Munier-Lehmann, H., Delarue, M., and Bourgeois, D. (2003) *Mycobacterium tuberculosis* thymidylate kinase: Structural studies of intermediates along the reaction pathway, *J. Mol. Biol. 327*, 1077–1092.
1388. Ursby, T., Weik, M., Fioravanti, E., Delarue, M., Goeldner, M., and Bourgeois, D. (2002) Cryophotolysis of caged compounds: A technique for trapping intermediate states in

protein crystals, *Acta Crystallogr., Sect. D: Biol. Crystallogr. D58*, 607–614.
1389. Seravalli, J., Brown, K. L., and Ragsdale, S. W. (2001) Acetyl coenzyme A synthesis from unnatural methylated corrinoids: Requirement for "base-off" coordination at cobalt, *J. Am. Chem. Soc. 123*, 1786–1787.
1390. Hu, S. I., Pezacka, E., and Wood, H. G. (1984) Acetate synthesis from carbon monoxide by *Clostridium thermoaceticum*. Purification of the corrinoid protein, *J. Biol. Chem. 259*, 8892–8897.
1391. Menon, S., and Ragsdale, S. W. (1996) Evidence that carbon monoxide is an obligatory intermediate in anaerobic acetyl-CoA synthesis, *Biochemistry 35*, 12119–12125.
1392. Svetlitchnyi, V., Dobbek, H., Meyer-Klaucke, W., Meins, T., Thiele, B., Romer, P., Huber, R., and Meyer, O. (2004) A functional Ni-Ni-[4Fe-4S] cluster in the monomeric acetyl-CoA synthase from *Carboxydothermus hydrogenoformans*, *Proc. Natl. Acad. Sci. U. S. A. 101*, 446–451.
1393. Kumar, M., Lu, W. P., Liu, L. F., and Ragsdale, S. W. (1993) Kinetic evidence that carbon-monoxide dehydrogenase catalyzes the oxidation of carbon-monoxide and the synthesis of acetyl-CoA at separate metal centers, *J. Am. Chem. Soc. 115*, 11646–11647.
1394. Tan, X., Martinho, M., Stubna, A., Lindahl, P. A., and Munck, E. (2008) Mossbauer evidence for an exchange-coupled $\{[Fe_4S_4]^{1+}Ni_p^{1+}\}$ A-cluster in isolated α subunits of acetyl-coenzyme A synthase/carbon monoxide dehydrogenase, *J. Am. Chem. Soc. 130*, 6712–6713.
1395. Russell, W. K., Stalhandske, C. M. V., Xia, J. Q., Scott, R. A., and Lindahl, P. A. (1998) Spectroscopic, redox, and structural characterization of the Ni-labile and nonlabile forms of the acetyl-CoA synthase active. Site of carbon monoxide dehydrogenase, *J. Am. Chem. Soc. 120*, 7502–7510.
1396. Doukov, T. I., Iverson, T. M., Seravalli, J., Ragsdale, S. W., and Drennan, C. L. (2002) A Ni-Fe-Cu center in a bifunctional carbon monoxide dehydrogenase/acetyl-CoA synthase, *Science (Washington, DC, U. S.) 298*, 567–572.
1397. Seravalli, J., Xiao, Y., Gu, W., Cramer, S. P., Antholine, W. E., Krymov, V., Gerfen, G. J., and Ragsdale, S. W. (2004) Evidence that Ni-Ni acetyl-CoA synthase is active and that the CuNi enzyme is not, *Biochemistry 43*, 3944–3955.
1398. Gencic, S., Kelly, K., Ghebreamlak, S., Duin, E. C., and Grahame, D. A. (2013) Different modes of carbon monoxide binding to acetyl-CoA synthase and the role of a conserved phenylalanine in the coordination environment of nickel, *Biochemistry 52*, 1705–1716.
1399. Manesis, A. C., O'Connor, M. J., Schneider, C. R., and Shafaat, H. S. (2017) Multielectron chemistry within a model nickel metalloprotein: Mechanistic implications for acetyl-CoA synthase, *J. Am. Chem. Soc. 139*, 10328–10338.
1400. Ragsdale, S. W., Wood, H. G., and Antholine, W. E. (1985) Evidence that an iron-nickel-carbon complex is formed by reaction of Co with the Co dehydrogenase from *Clostridium thermoaceticum*, *Proc. Natl. Acad. Sci. U. S. A. 82*, 6811–6814.
1401. Kumar, M., and Ragsdale, S. W. (1992) Characterization of the CO binding site of carbon monoxide dehydrogenase from *Clostridium thermoaceticum* by infrared spectroscopy, *J. Am. Chem. Soc. 114*, 8713–8715.
1402. Chen, J., Huang, S., Seravalli, J., Gutzman, H., Jr., Swartz, D. J., Ragsdale, S. W., and Bagley, K. A. (2003) Infrared studies of carbon monoxide binding to carbon monoxide dehydrogenase/acetyl-CoA synthase from *Moorella thermoacetica*, *Biochemistry 42*, 14822–14830.
1403. Harder, S. R., Lu, W. P., Feinberg, B. A., and Ragsdale, S. W. (1989) Spectroelectrochemical studies of the corrinoid/iron–sulfur protein involved in acetyl coenzyme A synthesis by *Clostridium thermoaceticum*, *Biochemistry 28*, 9080–9087.
1404. Kumar, M., Qiu, D., Spiro, T. G., and Ragsdale, S. W. (1995) A methylnickel intermediate in a bimetallic mechanism of acetyl-coenzyme A synthesis by anaerobic bacteria, *Science (Washington, DC, U. S.) 270*, 628–630.
1405. Barondeau, D. P., and Lindahl, P. A. (1997) Methylation of carbon monoxide dehydrogenase from *Clostridium thermoaceticum* and mechanism of acetyl coenzyme A synthesis, *J. Am. Chem. Soc. 119*, 3959–3970.
1406. Grahame, D. A. (1993) Substrate and cofactor reactivity of a carbon monoxide dehydrogenase-corrinoid enzyme complex: Stepwise reduction of iron–sulfur and corrinoid centers, the corrinoid $Co^{2+/1+}$ redox midpoint

potential, and overall synthesis of acetyl-CoA, *Biochemistry 32*, 10786–10793.
1407. Doukov, T. I., Blasiak, L. C., Seravalli, J., Ragsdale, S. W., and Drennan, C. L. (2008) Xenon in and at the end of the tunnel of bifunctional carbon monoxide dehydrogenase/acetyl-CoA synthase, *Biochemistry 47*, 3474–3483.
1408. James, C. D., Wiley, S., Ragsdale, S. W., and Hoffman, B. M. (2020) ^{13}C Electron nuclear double resonance spectroscopy shows acetyl-CoA synthase binds two substrate CO in multiple binding modes and reveals the importance of a CO-binding "alcove", *J. Am. Chem. Soc. 142*, 15362–15370.
1409. Qiu, D., Kumar, M., Ragsdale, S. W., and Spiro, T. G. (1994) Nature's carbonylation catalyst: Raman-spectroscopic evidence that carbon monoxide binds to iron, not nickel, in CO dehydrogenase, *Science (Washington, DC, U. S.) 264*, 817–819.
1410. Qiu, D., Kumar, M., Ragsdale, S. W., and Spiro, T. G. (1995) Freeze–quench resonance Raman spectroscopic evidence for an Fe–CO adduct during acetyl-CoA synthesis and Ni involvement in CO oxidation by carbon monoxide dehydrogenase from *Clostridium thermoaceticum*, *J. Am. Chem. Soc. 117*, 2653–2654.
1411. George, S. J., Seravalli, J., and Ragsdale, S. W. (2005) EPR and infrared spectroscopic evidence that a kinetically competent paramagnetic intermediate is formed when acetyl-coenzyme A synthase reacts with CO, *J. Am. Chem. Soc. 127*, 13500–13501.
1412. Seravalli, J., and Ragsdale, S. W. (2008) Pulse-chase studies of the synthesis of acetyl-CoA by carbon monoxide dehydrogenase/acetyl-CoA synthase: Evidence for a random mechanism of methyl and carbonyl addition, *J. Biol. Chem. 283*, 8384–8394.
1413. Maynard, E. L., Sewell, C., and Lindahl, P. A. (2001) Kinetic mechanism of acetyl-CoA synthase: Steady-state synthesis at variable CO/CO_2 pressures, *J. Am. Chem. Soc. 123*, 4697–4703.
1414. Lebertz, H., Simon, H., Courtney, L. F., Benkovic, S. J., Zydowsky, L. D., Lee, K., and Floss, H. G. (1987) Stereochemistry of acetic-acid formation from 5-methyltetrahydrofolate by *Clostridium thermoaceticum*, *J. Am. Chem. Soc. 109*, 3173–3174.
1415. Tan, X. S., Sewell, C., and Lindahl, P. A. (2002) Stopped-flow kinetics of methyl group transfer between the corrinoid-iron–sulfur protein and acetyl-coenzyme A synthase form *Clostridium thermoaceticum*, *J. Am. Chem. Soc. 124*, 6277–6284.
1416. Tan, X. S., Sewell, C., Yang, Q. W., and Lindahl, P. A. (2003) Reduction and methyl transfer kinetics of the α subunit from acetyl coenzyme A synthase, *J. Am. Chem. Soc. 125*, 318–319.
1417. Eckert, N. A., Dougherty, W. G., Yap, G. P. A., and Riordan, C. G. (2007) Methyl transfer from methylcobaloxime to (triphos)Ni(PPh_3): Relevance to the mechanism of acetyl coenzyme A synthase, *J. Am. Chem. Soc. 129*, 9286–9287.
1418. Ragsdale, S. W. (2004) Life with carbon monoxide, *Crit. Rev. Biochem. Mol. Biol. 39*, 165–195.
1419. Stavropoulos, P., Carrie, M., Muetterties, M. C., and Holm, R. H. (1990) Reaction sequence related to that of carbon-monoxide dehydrogenase (acetyl coenzyme A synthase): Thioester formation mediated at structurally defined nickel centers, *J. Am. Chem. Soc. 112*, 5385–5387.
1420. Stavropoulos, P., Muetterties, M. C., Carrie, M., and Holm, R. H. (1991) Structural and reaction chemistry of nickel-complexes in relation to carbon monoxide dehydrogenase: A reaction system simulating acetyl-coenzyme A synthase activity, *J. Am. Chem. Soc. 113*, 8485–8492.
1421. Sellmann, D., Haussinger, D., Knoch, F., and Moll, M. (1996) Transition metal complexes with sulfur ligands. 117. A reaction cycle for nickel mediated thioester formation from alkyl, CO, and thiolate groups modeling the acetyl-coenzyme A synthase function of CO dehydrogenase, *J. Am. Chem. Soc. 118*, 5368–5374.
1422. Tucci, G. C., and Holm, R. H. (1995) Nickel-mediated formation of thioesters from bound methyl, thiols, and carbon-monoxide: A possible reaction pathway of acetyl-coenzyme A synthase activity in nickel-containing carbon monoxide dehydrogenases, *J. Am. Chem. Soc. 117*, 6489–6496.
1423. Ragsdale, S. W., and Wood, H. G. (1985) Acetate biosynthesis by acetogenic bacteria. Evidence that carbon monoxide dehydrogenase is the condensing enzyme that catalyzes the final

steps of the synthesis, *J. Biol. Chem. 260*, 3970–3977.
1424. Raybuck, S. A., Bastian, N. R., Orme-Johnson, W. H., and Walsh, C. T. (1988) Kinetic characterization of the carbon monoxide-acetyl-CoA (carbonyl group) exchange activity of the acetyl-CoA synthesizing CO dehydrogenase from *Clostridium thermoaceticum*, *Biochemistry 27*, 7698–7702.
1425. Campbell, H. D., Dionysius, D. A., Keough, D. T., Wilson, B. E., de Jersey, J., and Zerner, B. (1978) Iron-containing acid phosphatases: Comparison of the enzymes from beef spleen and pig allantoic fluid, *Biochem. Biophys. Res. Commun. 82*, 615–620.
1426. Debrunner, P. G., Hendrich, M. P., De Jersey, J., Keough, D. T., Sage, J. T., and Zerner, B. (1983) Mossbauer and EPR study of the binuclear iron centre in purple acid phosphatase, *Biochim. Biophys. Acta 745*, 103–106.
1427. Merkx, M., and Averill, B. A. (1998) The activity of oxidized bovine spleen purple acid phosphatase is due to an Fe(III)Zn(II) 'impurity', *Biochemistry 37*, 11223–11231.
1428. Davis, J. C., and Averill, B. A. (1982) Evidence for a spin-coupled binuclear iron unit at the active site of the purple acid phosphatase from beef spleen, *Proc. Natl. Acad. Sci. U. S. A. 79*, 4623–4627.
1429. Beck, J. L., De Jersey, J., Zerner, B., Hendrich, M. P., and Debrunner, P. G. (1988) Properties of the Fe(II)-Fe(III) derivative of red kidney bean purple phosphatase. Evidence for a binuclear zinc-iron center in the native enzyme, *J. Am. Chem. Soc. 110*, 3317–3318.
1430. Schenk, G., Gahan, L. R., Carrington, L. E., Mitic, N., Valizadeh, M., Hamilton, S. E., de Jersey, J., and Guddat, L. W. (2005) Phosphate forms an unusual tripodal complex with the Fe-Mn center of sweet potato purple acid phosphatase, *Proc. Natl. Acad. Sci. U. S. A. 102*, 273–278.
1431. Strater, N., Klabunde, T., Tucker, P., Witzel, H., and Krebs, B. (1995) Crystal structure of a purple acid phosphatase containing a dinuclear Fe(III)-Zn(II) active site, *Science (Washington, DC, U. S.) 268*, 1489–1492.
1432. Uppenberg, J., Lindqvist, F., Svensson, C., Ek-Rylander, B., and Andersson, G. (1999) Crystal structure of a mammalian purple acid phosphatase, *J. Mol. Biol. 290*, 201–211.
1433. Yong, S. C., Roversi, P., Lillington, J., Rodriguez, F., Krehenbrink, M., Zeldin, O. B., Garman, E. F., Lea, S. M., and Berks, B. C. (2014) A complex iron-calcium cofactor catalyzing phosphotransfer chemistry, *Science (Washington, DC, U. S.) 345*, 1170–1173.
1434. Nagasawa, T., Takeuchi, K., and Yamada, H. (1991) Characterization of a new cobalt-containing nitrile hydratase purified from urea-induced cells of *Rhodococcus rhodochrous* J1, *Eur. J. Biochem. 196*, 581–589.
1435. Huang, W., Jia, J., Cummings, J., Nelson, M., Schneider, G., and Lindqvist, Y. (1997) Crystal structure of nitrile hydratase reveals a novel iron centre in a novel fold, *Structure (Cambridge, MA, U. S.) 5*, 691–699.
1436. Brodkin, H. R., Novak, W. R., Milne, A. C., D'Aquino, J. A., Karabacak, N. M., Goldberg, I. G., Agar, J. N., Payne, M. S., Petsko, G. A., Ondrechen, M. J., and Ringe, D. (2011) Evidence of the participation of remote residues in the catalytic activity of Co-type nitrile hydratase from *Pseudomonas putida*, *Biochemistry 50*, 4923–4935.
1437. Yamanaka, Y., Hashimoto, K., Ohtaki, A., Noguchi, K., Yohda, M., and Odaka, M. (2010) Kinetic and structural studies on roles of the serine ligand and a strictly conserved tyrosine residue in nitrile hydratase, *J. Biol. Inorg. Chem. 15*, 655–665.
1438. Tsujimura, M., Odaka, M., Nakayama, H., Dohmae, N., Koshino, H., Asami, T., Hoshino, M., Takio, K., Yoshida, S., Maeda, M., and Endo, I. (2003) A novel inhibitor for Fe-type nitrile hydratase: 2-Cyano-2-propyl hydroperoxide, *J. Am. Chem. Soc. 125*, 11532–11538.
1439. Miyanaga, A., Fushinobu, S., Ito, K., and Wakagi, T. (2001) Crystal structure of cobalt-containing nitrile hydratase, *Biochem. Biophys. Res. Commun. 288*, 1169–1174.
1440. Yamanaka, Y., Kato, Y., Hashimoto, K., Iida, K., Nagasawa, K., Nakayama, H., Dohmae, N., Noguchi, K., Noguchi, T., Yohda, M., and Odaka, M. (2015) Time-resolved crystallography of the reaction intermediate of nitrile hydratase: Revealing a role for the cysteine-sulfenic acid ligand as a catalytic nucleophile, *Angew. Chem. Int. Ed. Engl. 54*, 10763–10767.
1441. Martinez, S., Wu, R., Sanishvili, R., Liu, D., and Holz, R. (2014) The active site sulfenic acid ligand in nitrile hydratases can function as a nucleophile, *J. Am. Chem. Soc. 136*, 1186–1189.

1442. Nelp, M. T., Song, Y., Wysocki, V. H., and Bandarian, V. (2016) A protein-derived oxygen is the source of the amide oxygen of nitrile hydratases, *J. Biol. Chem. 291*, 7822–7829.
1443. Gumataotao, N., Kuhn, M. L., Hajnas, N., and Holz, R. C. (2013) Identification of an active site-bound nitrile hydratase intermediate through single turnover stopped-flow spectroscopy, *J. Biol. Chem. 288*, 15532–15536.
1444. Sugiura, Y., Kuwahara, J., Nagasawa, T., and Yamada, H. (1987) Nitrile hydratase: The first nonheme iron enzyme with a typical low-spin Fe(III)-active center, *J. Am. Chem. Soc. 109*, 5848–5850.
1445. Shearer, J., Jackson, H. L., Schweitzer, D., Rittenberg, D. K., Leavy, T. M., Kaminsky, W., Scarrow, R. C., and Kovacs, J. A. (2002) The first example of a nitrile hydratase model complex that reversibly binds nitriles, *J. Am. Chem. Soc. 124*, 11417–11428.
1446. Shearer, J., Kung, I. Y., Lovell, S., Kaminsky, W., and Kovacs, J. A. (2001) Why is there an "inert" metal center in the active site of nitrile hydratase? Reactivity and ligand dissociation from a five-coordinate Co(III) nitrile hydratase model, *J. Am. Chem. Soc. 123*, 463–468.
1447. Noveron, J. C., Olmstead, M. M., and Mascharak, P. K. (2001) A synthetic analogue of the active site of Fe-containing nitrile hydratase with carboxamido N and thiolato S as donors: Synthesis, structure, and reactivities, *J. Am. Chem. Soc. 123*, 3247–3259.
1448. Kung, I., Schweitzer, D., Shearer, J., Taylor, W. D., Jackson, H. L., Lovell, S., and Kovacs, J. A. (2000) How do oxidized thiolate ligands affect the electronic and reactivity properties of a nitrile hydratase model compound? *J. Am. Chem. Soc. 122*, 8299–8300.
1449. Ellison, J. J., Nienstedt, A., Shoner, S. C., Barnhart, D., Cowen, J. A., and Kovacs, J. A. (1998) Reactivity of five-coordinate models for the thiolate-ligated Fe site of nitrile hydratase, *J. Am. Chem. Soc. 120*, 5691–5700.
1450. Swartz, R. D., Coggins, M. K., Kaminsky, W., and Kovacs, J. A. (2011) Nitrile hydration by thiolate- and alkoxide-ligated Co-NHase analogues. Isolation of Co(III)-amidate and Co(III)-iminol intermediates, *J. Am. Chem. Soc. 133*, 3954–3963.

Chapter 5
Intermediates in Enzymatic Reactions

Almost all chemical reactions catalyzed by enzymes pass through two or more transition states and one or more intermediates after the complete set of substrates has been assembled in the active site. An intermediate in the mechanism of any chemical reaction can be distinguished from a transition state in that mechanism by the length of time it exists. A **transition state** lasts only as long as is necessary to pass over a maximum in the reaction coordinate (Figure 3–25). Because the movement over such a maximum resembles only half the stroke of an intramolecular vibration, the time required to pass over the top is less than the time required for a complete intramolecular vibration ($<10^{-12}$ s). Because the movement through the transition state is over a maximum of potential energy, a transition state does not have a finite lifetime. An **intermediate** in a reaction is an arrangement of atoms in the mechanism of a chemical reaction that has a lifetime longer than the time required for the intramolecular and intermolecular vibrations among those atoms to become established and that is formed from the reactants and reacts further to give the products. For any arrangement of atoms to persist for this length of time, the connections holding them together must be full covalent bonds or fully established noncovalent interactions, not partial bonds in the process of forming and unforming as is the case in a transition state. In this sense, an intermediate in any reaction must itself be either **one molecule or the noncovalent complex of two or more molecules**, even though the one molecule or these several noncovalently associated molecules together may be of higher energy than either reactants or products of the overall reaction.

Because intermediates have finite lifetimes, an intermediate in any reaction must have a potential energy that is less than the potential energy of the transition state immediately preceding it on the reaction coordinate leading from reactants and less than the potential energy of the transition state immediately following it on the reaction coordinate proceeding toward products. In other words, the constellation of atoms defining an intermediate is always an arrangement that occupies a potential well on the reaction coordinate (Figure 5–1). If the potential energy of an intermediate were not such a local minimum on the reaction coordinate, the intermediate would not have a finite lifetime.

Two examples of specific reactions will serve to illustrate the **distinction between transition states and intermediates**. An example of a reaction that proceeds without an intermediate is the transfer of the methyl group from the sulfur of *S*-adenosyl-L-methionine to the nitrogen of glycine in the concerted nucleophilic substitution catalyzed by glycine *N*-methyltransferase (Equation 1–19) after reactants have been gathered in the active site (see Figure 3–34). This reaction passes through a single transition state in which the past bond to the methyl carbon is being broken as the future bond to the methyl carbon is being formed. An example of a reaction in which there are intermediates is hydrolysis of an amide (Figure 1–10). In this reaction, the tetrahedral intermediate formed must exist for a period of time sufficient for hydronation of the nitrogen that is on the leaving group to occur. Otherwise, the leaving group would be an amide anion, which is 17 orders of magnitude more basic than the hydroxide anion that attacked the acyl carbon or 35 orders of magnitude more basic than the molecule of water that attacked the acyl carbon. The nitrogen of the amide cannot be hydronated before the nucleophilic addition occurs because it is not basic. Furthermore, if water was the initial nucleophile rather than hydroxide anion, as in the acid-catalyzed hydrolysis of an amide, the tetrahedral intermediate must also exist long enough for the hydron to be removed from the cationic oxygen that was derived from the oxygen in water. Each hydronation and dehydronation produces a new tetrahedral intermediate of unique structure, each a molecule in its own right, and each hydronation or dehydronation itself passes through a transition state, even though the respective free energies of activation for each transition state may be only slightly greater than the chemical potentials of the respective tetrahedral intermediates.

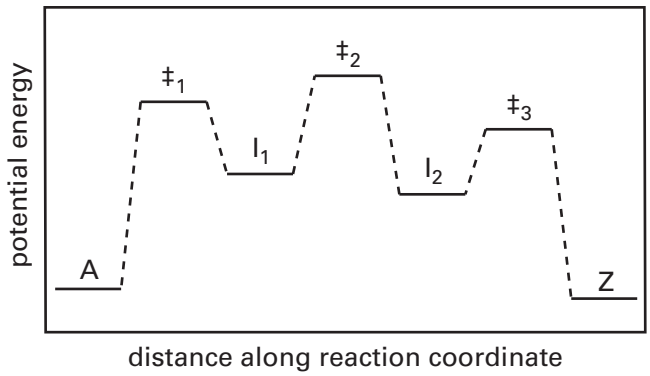

Figure 5–1: Diagrammatic representation of a reaction coordinate between reactant (A) and product (Z) that passes through three transition states ($\ddagger_1$, $\ddagger_2$, and $\ddagger_3$) and two intermediates (I_1 and I_2). Potential energies are presented as a function of distance along the reaction coordinate.

An alternative to the existence of the tetrahedral intermediate in hydrolysis of an amide, in which an intermediate would not be involved, would be a concerted nucleophilic substitution at the acyl carbon of the amide

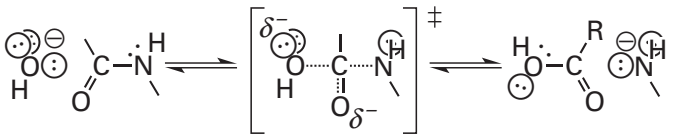

(5–1)

For various reasons, such a reaction, although it does not immediately seem unreasonable, would have a significantly higher standard free energy of activation than the standard free energies of activation for formation of a tetrahedral intermediate, its tautomerizations, and its decomposition. Consequently, the chemical reaction in solution proceeds through the tetrahedral intermediates and their accompanying transition states rather than through only the one transition state.

An enzymatic reaction involves intermediates for the same reason that a nonenzymatic reaction does. The reaction coordinate, passing through a series of successive intermediates, encounters a series of standard free energies of activation that are all smaller than the standard free energy of activation for even the least endergonic of the alternative reaction coordinates that have only one transition state. It should not be thought that in this way the enzyme divides up the larger free energy of activation associated with the one step. Rather, it happens that there is an alternative, but independent, reaction coordinate passing through the intermediates, and this reaction coordinate has **transition states that are all lower in free energy of activation** than that for any of the reaction coordinates with only a single transition state. This conclusion follows from the fact that the mechanism with intermediates is the one actually observed.

In reactions that occur in solution, an intermediate is usually described as if it were a single molecule—for example, a tetrahedral intermediate in hydrolysis of an amide. This description may be reasonable in other solvents; but in water, an intermediate in the mechanism for the usual reaction, in addition to a layer of hydration, has molecules of water or general acid–bases or both noncovalently bound to it through hydrogen bonds. These bound molecules are usually essential participants in the intermediate both structurally and energetically. For this reason, an intermediate in an enzymatic reaction can be viewed as a simpler structure than the analogous intermediate in a nonenzymatic, aqueous reaction because much or all of the layer of hydration, some or all of the necessary molecules of water, and all the molecules of general acid–bases have been replaced by the surrounding, well-structured protein, well-oriented donors and acceptors of hydrogen bonds, and catalytic acid–bases, respectively, from within the folded polypeptide and its associated prosthetic groups. An intermediate in an enzymatic reaction is the **complex between the catalytic functional groups in the active site and a particular covalent arrangement of the atoms** that had composed together the reactants that precede the intermediate and that will compose together the products that follow the intermediate in the enzymatic reaction. As is the case for the fully hydrated complex in aqueous solution, an intermediate in an enzymatic reaction is the entire complex between the rearranged atoms of the reactants and the protein surrounding the active site, as well as any adjacent fixed or unfixed molecules of water. To simplify matters, however, the intermediate in an enzymatic reaction is often discussed as if it were only the molecule or molecules formed from the atoms of reactants or products, and the active site itself is often not explicitly mentioned even though it is inescapably a participant.

The intermediates encountered in enzymatic reactions can be divided into two classes. On the one hand, an enzymatic reaction can pass through the **same series of intermediates** that the same chemical reaction would pass through in the same aqueous solution in the absence of enzyme. This situation is the basis for the paradigm of the enzyme associating with a transition state or an intermediate

of high energy in the reaction more tightly than the reactants. An example of such a reaction is hydrolysis of a peptide bond catalyzed by an aspartic endopeptidase, in which the carboxylato group of an aspartate removes a hydron from a molecule of water either before or as it attacks the acyl carbon of the amide to form the tetrahedral intermediate, and the carboxy group of the same aspartic acid hydronates the nitrogen of the tetrahedral intermediate to produce the leaving group (Equation 4–376). These two steps in hydrolysis of an amide would occur in solution under catalysis by acetate and acetic acid. On the other hand, because the active site of an enzyme resembles an aqueous solution only remotely, **unique intermediates**, which do not participate in the uncatalyzed reaction, may participate in the enzymatically catalyzed reaction. For example, although the serine endopeptidases in the family represented by trypsin and chymotrypsin catalyze a reaction identical to that catalyzed by an aspartic endopeptidase, these enzymes use a serine in the active site as the initial nucleophile to produce an ester between the enzyme and the acyl carbon of the original amide, and then the internal ester is hydrolyzed by water (Figure 3–6).[1,2] Both formation of the acyl enzyme and its hydrolysis must pass through the respective tetrahedral intermediates. It is not immediately obvious, however, that the reaction catalyzed by a serine endopeptidase can be described by the rule that an enzyme associates with a transition state that would normally exist in solution more tightly than it associates with the reactants. Why the seryl intermediate was chosen by natural selection to catalyze a reaction that other enzymes perform without one is, for obvious reasons, unknown.

The serine endopeptidases use an amino acid in the active site to form an intermediate unique to their enzymatic reactions relative to the mechanism of the reaction in solution, but adenosylhomocysteinase

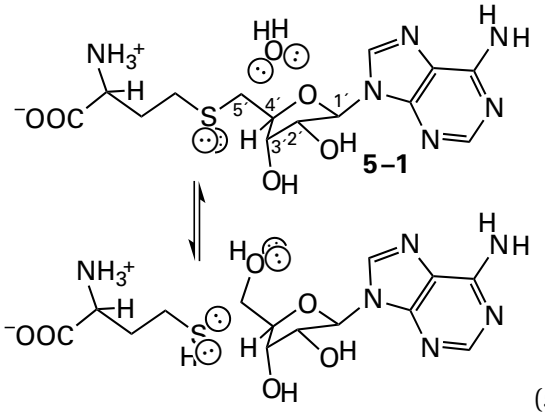

(5–2)

uses a prosthetic group in the active site to form an intermediate unique to its enzymatic reaction. The reaction catalyzed by the enzyme is formally a nucleophilic substitution at a primary carbon. In solution, it would probably be concerted, but it would be a difficult reaction because the sulfido anion is a poor leaving group and hydronating the sulfide to cause the sulfanyl group to be the leaving group is difficult.

The following results, however, are consistent with a mechanism for the enzymatic reaction (Figure 5–2) in which 3′-oxo-4′,5′-dehydroadenosine is the central intermediate.[3,4] The enzyme contains NAD^+ bound tightly as a prosthetic group to its active site. When *S*-adenosyl-L-homocysteine (**5–1**) is added to bovine adenosylhomocysteinase, NADH is transiently formed. When the reaction is run in ^2H_2O, deuterium appears at carbon 4′ in the unreacted *S*-adenosyl-L-homocysteine. The hydrolysis of [4′-^{2}H]-*S*-adenosyl-L-homocysteine by the enzyme displays a deuterium kinetic isotope effect of 1.5. 4′,5′-Dehydroadenosine is oxidized by the enzyme and converted into adenosine. A crystallographic molecular model of the intermediate 3′-deoxy-3′-oxoadenosine occupying the active site of adenosylhomocysteinase from *Mycobacterium tuberculosis* (56% identity; 0.8 gap percent) with the prosthetic NAD^+—oxidant next to oxidant to prevent any reaction from occurring—places carbon 3′ of 3′-deoxy-3′-oxoadenosine immediately adjacent (0.39 nm) to carbon 4 of the nicotinamide and in the proper orientation to be reduced were the NAD^+ an NADH.[4]

If a mechanism in which 3′-oxo-4′,5′-dehydroadenosine is the central intermediate applies to adenosylhomocysteinase, the nucleophilic substitution occurs indirectly rather than directly, by an elimination–addition β to a carbonyl, a reaction in which thiols readily participate. This mechanism is reminiscent of the mechanism of cystathionine γ-synthase, in which a substitution of a succinyl group by the sulfanyl group of L-cysteine was accomplished by an even more complicated elimination–addition involving formation of the 1-carboxyprop-2-enimine of pyridoxal 5′-phosphate. In the case of adenosylhomocysteinase, the fact that the enzyme can catalyze hydrogen exchange at carbon 4′ of 5′-deoxyadenosine is consistent with the enzymatic reaction proceeding through the two respective enolates as intermediates in the elimination and addition, respectively, as shown, and this enzymatic reaction has at least five unique intermediates. Both

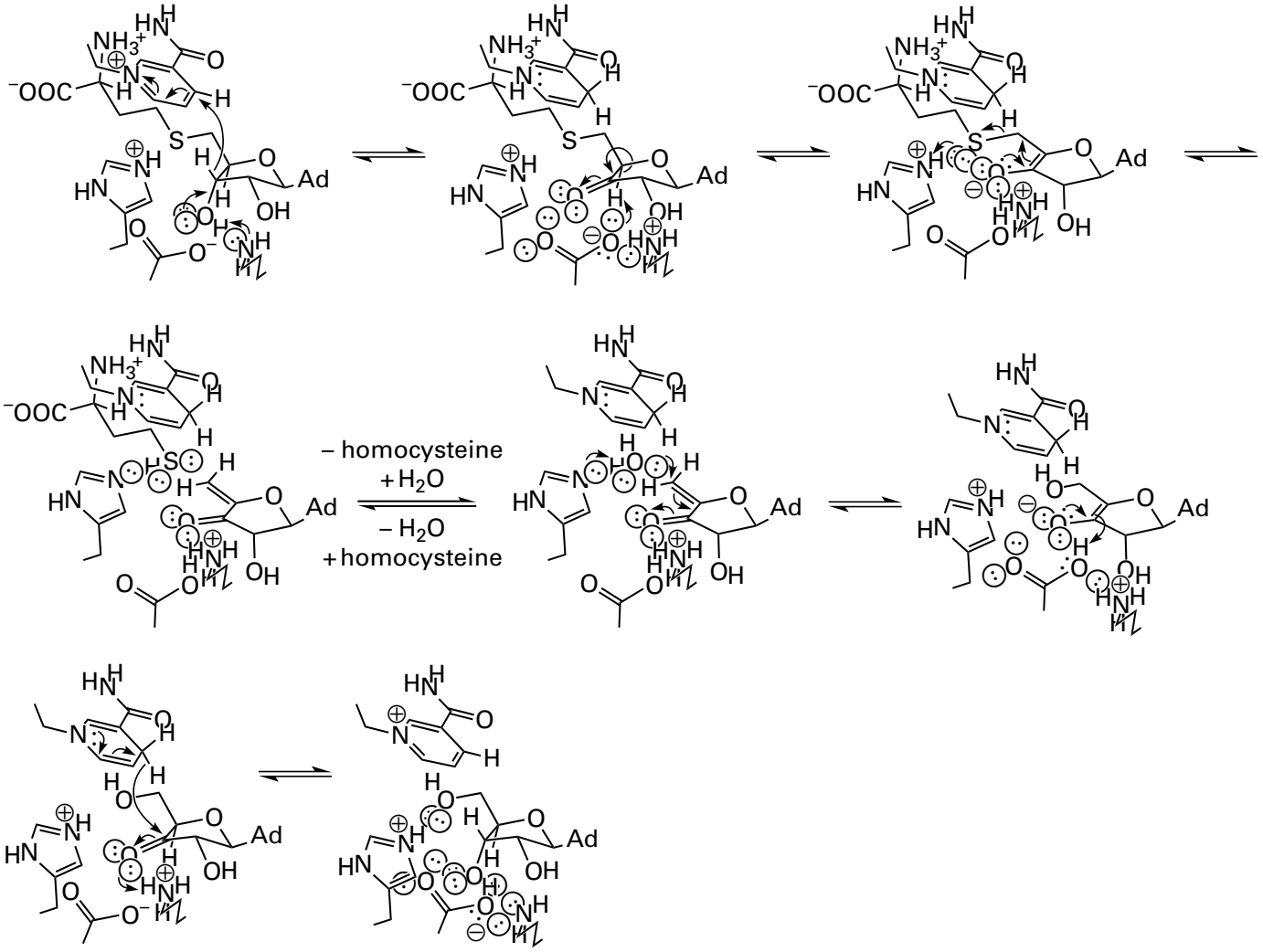

Figure 5–2: Mechanism proposed for adenosylhomocysteinase.[3,4] While a lysine removes a hydron from the 3′-hydroxy group, the prosthetic NAD^+ removes a hydride from carbon 3′ of adenosyl-L-homocysteine (Ad = adenosyl) to produce a 3′-deoxy-3′-oxoribosyl group that now has an acidic hydron at carbon 4′, which is then removed by an aspartate. Elimination from the resulting enolate of the sulfur of the homocysteinyl group, which is hydronated by a histidine, breaks the carbon–sulfur bond and produces 4′,5′-didehydro-3′,5′-dideoxy-3′-oxoadenosine as the central intermediate in the enzymatic reaction. After a molecule of water replaces the L-homocysteine, this α,β-unsaturated carbonyl compound is hydrated across the double bond, and the resulting ketone is reduced by hydride transfer from the NADH to produce adenosine as the other product of the enzymatic reaction.

the enzymatic reaction catalyzed by pyridoxine 5′-phosphate synthase (Figure 4–47) and that catalyzed by urocanate hydratase (Figure 4–49) also pass through at least five intermediates.

In the discussion so far, as it has proceeded in the earlier chapters, a number of intermediates in enzymatic reactions have been encountered. Together they have represented in turn different **classes of intermediates**. These classes can be distinguished by what is added or what is subtracted from the reactant or reactants to produce the intermediate.

A **covalent intermediate** is an intermediate in an enzymatic reaction in which the enzyme itself and the other atoms participating in the intermediate are covalently attached to each other. A covalent intermediate results when a functional group on the side chain of an amino acid in the active site or a functional group on a prosthetic group covalently attached to the active site is added to one reactant or to the product of the covalent association of two or more reactants. Often a portion of one of the original reactants departs as a leaving group as the covalent intermediate is formed. Examples of covalent intermediates are the acylseryl intermediates in serine endopeptidases (Figure 3–6) and acetyl-

cholinesterase (Equation 3–385), the acylcysteinyl intermediate in hydroxymethylglutaryl-CoA synthase (Equation 4–361), the phosphoaspartyl intermediate in the phosphatase encoded by the BT3141 gene of *Bacteroides thetaiotaomicron* (Figure 3–43), the phosphoseryl intermediates in phosphoglycerate mutase (Equation 3–421) and alkaline phosphatase (Equation 4–452), the phosphohistidinyl intermediates in pyruvate, phosphate dikinase (Equations 3–501 and 3–502), the adenylyl intermediate in sulfate adenylyltransferase (ADP) (Equation 3–161), and the lysylimines in fructose-bisphosphate aldolase (Figure 4–36 and Equations 4–304, 4–368, and 4–405) and 2-dehydro-3-deoxyphosphogluconate aldolase (Equation 4–325).

A **covalent prosthetic intermediate** is an intermediate in an enzymatic reaction in which the other atoms participating in the intermediate that are derived from the reactants are covalently attached to a prosthetic group that is itself covalently or noncovalently attached to the active site. In this class of intermediates, there is no covalent linkage formed between the substrate and the protein itself, only with the prosthetic group, which may or may not be covalently attached to the enzyme. Covalent prosthetic intermediates have already been discussed in detail in Chapters 1 and 2.

A **diamagnetic, noncovalent intermediate** is any intermediate in an enzymatic reaction that forms within the active site, that is noncovalently associated with the active site, and in which all electrons are paired in atomic and molecular orbitals. Examples of diamagnetic, noncovalent intermediates are the ketones produced by the prosthetic NAD^+ in UDP-glucose-4-epimerase (Equation 4–130) and adenosylhomocysteinase (Figure 5–2); the tetrahedral intermediates in aspartate—ammonia ligase (**3–75**), thermolysin (Figure 3–42 and Equation 4–445), glutamine synthetase (**3–98**), chloramphenicol *O*-acetyltransferase (**4–132**), endothiapepsin (Equation 4–376), urease (**4–175**), and leucyl aminopeptidase (**4–177**); the tetrahedral carbonyl adduct in the active site of fumarylacetoacetase (Equation 4–362); the tetrahedral adduct in the active site of 3-phosphoshikimate 1-carboxyvinyltransferase (**3–81** and Equation 4–414); the phosphorane in the active site of ribonuclease (**4–123**); and the carboxylated enolate in the active site of ribulose-bisphosphate carboxylase (Equation 3–424 and Figure 3–53).

Diamagnetic, noncovalent intermediates are independent molecules,* but because they are often unstable, they are usually bound tightly in the active site. For example, 3′-oxo-4′,5′-dehydroadenosine (Figure 5–2) is held so tightly in the active site of adenosylhomocysteinase by noncovalent forces that it cannot escape into the solution. If 3′-oxo-4′,5′-dehydroadenosine were to escape from the active site, the enzyme would be left in its reduced inactive form, incapable of reaction with the next homocysteinyladenosine, and 3′-oxo-4′,5′-dehydroadenosine would readily form Michael adducts with proteins in the cytoplasm. Both of these consequences would be unfortunate.

In the case of phosphoglucomutase (α-D-glucose-1,6-bisphosphate-dependent)

$$\alpha\text{-D-glucose 1-phosphate} \rightleftharpoons \text{D-glucose 6-phosphate} \qquad (5\text{–}3)$$

however, dissociation of the diamagnetic, noncovalent intermediate, α-D-glucose 1,6-bisphosphate, which does occur slowly, inactivates the enzyme but is not otherwise harmful. Nevertheless, a sufficient concentration of α-D-glucose 1,6-bisphosphate must always be present in the cytoplasm so that it can reassociate with the enzyme and continuously reactivate it. Consequently, another enzyme, glucose-1,6-bisphosphate synthase, is required to maintain proper levels of this **escaped intermediate**. Its only purpose is to service phosphoglucomutase.

In spite of the fact that it has provided the name for the enzyme and in spite of the fact that it is often included in the equation for the reaction (Equation 4–437), *cis*-aconitate, which is released into solution from the active site of aconitate hydratase, is not a product of the reaction but a diamagnetic, noncovalent intermediate that has escaped. Little if anything in the metabolism of a cell is produced from *cis*-aconitate, so its release from the active site is fortuitous rather than purposeful. Because *cis*-aconitate is unreactive and because the enzyme is not inactivated by its dissociation, its escape is harmless, and it is readily re-bound by the active site and converted into citrate or isocitrate. It is possible that some metabolites for which purposes have been found were once escaped intermediates.

*Diamagnetic, noncovalent intermediates are often ionic at the site of reaction, but since most biochemical molecules are ions, it would be meaningless to separate them into the categories of nonionic, diamagnetic, noncovalent intermediates and ionic, diamagnetic, noncovalent intermediates.

There are several classes of diamagnetic, noncovalent intermediates that are usually distinguished because of the special properties of their members.

A **carbanionic intermediate** is a diamagnetic, noncovalent intermediate that forms in an active site when a hydron or another electrophile dissociates heterolytically from a carbon in a reactant—usually a carbon adjacent to a carbonyl, imino, or acyl group—and that dissociation produces a carbanion or that forms when a nucleophile associates hetereolytically with a carbon in a reactant—usually a carbon conjugated to a carbonyl, imino, or acyl carbon—and that association produces a carbanion. Examples are the enolates and their conjugate acids in the active sites of 3-deoxy-8-phosphooctulonate synthase (**4–51**), L-fuconate dehydratase (Equation 4–268), malate synthase (Equation 4–272), pyruvate kinase (Equation 4–276), phospho*enol*pyruvate carboxykinase (Equation 4–419), 4-hydroxy-2-oxoheptanedioate aldolase (**4–166**), isocitrate dehydrogenase (**4–167**), and fumarylacetoacetase (**4–168**); the *cis*-enediolates in the active sites of triose-phosphate isomerase (Equations 4–46 and 4–55), fructose-bisphosphate aldolase (**4–170**), and D-psicose 3-epimerase (Equation 4–434); the *gem*-enediolates in the active sites of isocitrate lyase (Equation 4–310), chondroitin AC lyase (Figure 4–44), phosphopyruvate hydratase (**4–171**), and mandelate racemase (**4–172**); and the α,β-unsaturated enolates in the active sites of 4-chlorobenzoyl-CoA dehalogenase (**3–110**), steroid Δ-isomerase (Equation 4–416), and 2-hydroxymuconate tautomerase (**4–53**). It has already been noted that an enzyme may or may not stabilize an enolate by hydronating its oxyanion during or after its formation.

A **carbocationic intermediate** is a diamagnetic, noncovalent intermediate that forms in an active site when a leaving group dissociates heterolytically from a carbon in a reactant and that dissociation produces a carbocation or that forms when a hydron or another electrophile associates heterolytically with carbon in a reactant and that addition produces a carbocation. Examples are the carbenium ion in the active site of 3-deoxy-8-phosphooctulosonate synthase (**3–96**); the carbocationic intermediate in the electrophilic aromatic substitution catalyzed by tryptophan synthase (**4–122**); the oxocarbenium ions in the active sites of lysozyme (**3–26**), hypoxanthine phosphoribosyltransferase (**3–91**), and other glycosidases (Equation 4–400); and the carbenium ions that are intermediates in terpenoid synthesis (Figures 3–48 and 3–50 and Equation 3–368).

A **radical intermediate** is a paramagnetic noncovalent intermediate that possesses an unpaired electron and that forms in an active site when a hydrogen atom is abstracted from a reactant, when an electron is added or subtracted from a reactant, or when a reactant dissociates homolytically. Because they are so different from diamagnetic, noncovalent intermediates, radical intermediates can be treated separately. They are tightly held in an active site, unable to escape during their usually short lifetimes. Far fewer enzymes have radical intermediates than diamagnetic, noncovalent intermediates, but because of their unique peculiarities, these enzymes have received much attention. Examples that have been previously discussed are the radical intermediates in the active sites of enzymes that use cobalamin as a prosthetic group (**2–182** and Equations 2–369 through 2–373) and the radical intermediates in certain monooxygenases (**2–95**).

Chemical and Crystallographic Identification of Covalent Intermediates

If a covalent intermediate between an amino acid in the active site and a portion of a reactant or portions of two reactants is formed during the overall enzymatic reaction, the enzyme itself is transiently and covalently modified during its normal reaction. Chemical identification of this modification often involves the isolation of a peptide from the enzyme bearing the modification, as was the case for identification of an amino acid modified by an active-site label. **Chemical identification** of the modification can be used as evidence for involvement of the covalent intermediate in the enzymatic reaction. For example, when chymotrypsin catalyzes hydrolysis of 4-nitrophenyl acetate, the fast step in the overall reaction is formation of an intermediate *O*-acetylserine, which is the esterolytic homologue of the intermediate *O*-peptidylserine in the endopeptidolytic hydrolysis of a peptide bond normally catalyzed by the enzyme (Figure 3–6). The intermediate *O*-acetylserine accumulates because its hydrolysis, which is the second step in the esterolysis, is slow. When 4-nitrophenyl [^{14}C]acetate was used as a substrate, [^{14}C]acetyl-enzyme was formed, and the acetyl group was shown to be incorporated as an ester of Serine 195 by isolation of the acetylated peptide, GDS(acetyl)-GGPL,[1] where (acetyl) indicates modification of the serine. 4-Methylbenzenesulfonyl chloride inactivates chymotrypsin[5] by tosylating the same serine, and a crystallographic molecular model of the modified

enzyme could be obtained.[6] **Crystallographic molecular models** for the normal intermediate *O*-acylserine of other serine endopeptidases, such as those of trypsin[7,8] and pancreatic elastase,[9] have been reported.

Covalent acyl intermediates in enzymatic nucleophilic substitutions are common. For example, in β-lactamase, an enzyme that catalyzes the hydrolysis of a strained cyclic amide rather than a linear amide, the intermediate ***O*-acylserine** in the enzymatic reaction was **identified spectrophotometrically** by its characteristic stretching frequency in the infrared at 1753 cm^{-1} for the carbon–oxygen double bond of the seryl ester. The intermediate was trapped by using a reactant that produces an intermediate *O*-acylserine that, like the intermediate *O*-acetylserine in chymotrypsin, is hydrolyzed much more slowly than it is formed.[10] The existence of this particular intermediate *O*-acylserine was also verified crystallographically.[11]

Crystallographic molecular models of serine endopeptidases complexed with inhibitors that are designed to react with the respective nucleophilic serines and form analogues of the **covalent tetrahedral intermediates** leading to and from the covalent intermediate *O*-acylserine have also been reported,[8,12-14] as well as a crystallographic molecular model of the actual tetrahedral intermediate produced during hydrolysis of a reactant for pancreatic elastase.[15] These latter results verify the complete mechanism of hydrolysis for serine endopeptidases (Figure 3–6). They also identify, in each case, the imidazolyl group of the homologous histidine that removes a hydron from the hydroxy group of serine, swings over to hydronate the leaving amino group, unhydronates the water that replaces that leaving amino group and that will hydrolyze the intermediate *O*-acylserine, and then swings back to hydronate the leaving hydroxy group of the serine. When the nucleophilic serine in the active site of subtilisin, another serine endopeptidase, is mutated to alanine, the value for $k_0\,K_m^{-1}$ decreases 3×10^6-fold.[16] All these results confirm the existence and importance of a covalent *O*-acylseryl intermediate in the reaction catalyzed by the various serine endopeptidases.

There are esterases that also proceed through intermediate *O*-acylserines during the hydrolyses of the particular esters that they catalyze. In the case of carboxylesterase from *Geobacillus stearothermophilus*, a covalent tetrahedral intermediate on the serine, again implicating a single imidazolyl group as the only catalytic acid–base, has been observed crystallographically.[17]

Intermediate *O*-acylserines, however, are often so transient that they cannot be identified either chemically or crystallographically. A method has been developed to incorporate 2,3-diaminopropionate in place of serine in an active site, in this way replacing a hydroxy group at a particular position with an amino group. The acyl intermediate that is formed in the resulting enzymatic reaction is an amide rather than an ester and is much more stable.[18]

2,6-Dioxo-6-phenylhexa-3-enoate hydrolase from *Paraburkholderia xenovorans* performs a retro-Claisen condensation on 2,6-dioxo-6-phenylhexa-3-enoate

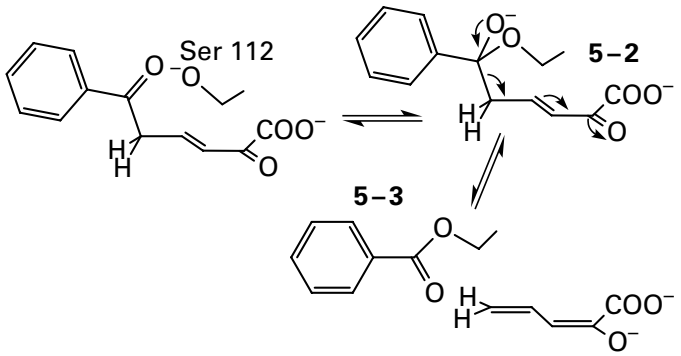

(5–4)

with benzoic acid and 2-oxopent-4-enoate, the more stable tautomer of the conjugate acid of the 2-oxidopenta-2,4-dienoate shown in the equation, as the two products. The thiohemiketal, homologous to the proposed hemiketal **5–2** between Serine 112 and 2,6-dioxo-6-phenylhexa-3-enoate in the normal enzymatic mechanism (Equation 5–4), has been observed in a crystallographic molecular model of a mutant in which Serine 112 was replaced by cysteine.[19] In this model, the bond between carbons 5 and 6 is parallel to the π molecular orbital system of the α,β-unsaturated carbonyl group from carbon 2 to carbon 4, as expected if the π molecular orbital system withdraws electron density from this carbon–carbon bond during the retro-Claisen condensation. Intermediate **benzoylserine 5–3** could be isolated in a peptic peptide purified from a digest of 2,6-dioxo-6-phenylhexa-3-enoate hydrolase mixed with 2,6-dioxo-6-phenylhexa-3-enoate. The modified Serine 112 was identified by mass spectrometry of the modified peptide. The same benzoylserine could be observed in the active site in a crystallographic molecular model of a mutant of the enzyme in which Histidine 265 had been mutated to glutamine to decrease the rate of hydrolysis of benzoylserine.[20]

2,6-Dioxo-6-phenylhexa-3-enoate hydrolase also catalyzes hydrolysis and methanolysis of 4-nitrophenyl benzoate with a catalytic constant identical, within experimental error, to the rate at which it catalyzes the retro-Claisen condensation, and the ratios of the products methyl benzoate and benzoic acid in mixtures of methanol in water for both reactions are the same. These latter results suggest that benzoylserine **5–3** is a common intermediate in both reactions and that hydrolysis of benzoylserine is the rate-limiting step, not the retro-Claisen condensation.[21] Using benzoylserine **5–3** as an intermediate in the reaction avoids the necessity for the less stable *gem*-dienolate as an intermediate. Esters are also the most common reactants chosen in nonenzymatic Claisen condensations for the same reason.

***S*-Acylcysteines** are also intermediates in hydrolyses catalyzed by enzymes. The intermediate *S*-acylcysteine in the endopeptidolytic hydrolysis catalyzed by papain was trapped by using the reactant methyl benzoylcarbamothioate, a methyl ester that produces an intermediate cysteinyl benzoylcarbamothioate

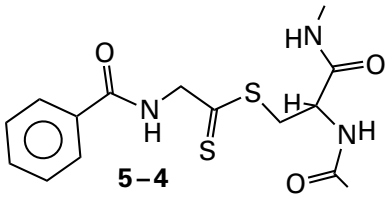

5–4

Again, intermediate **5–4** is formed on the active site more rapidly than it is hydrolyzed. Formation of this dithioester was demonstrated by its characteristic absorbance at 313 nm.[22] The cysteine that was thioacylated was later identified by modifying it with several chloromethyl ketones and identifying the products crystallographically.[23]

The homologous glutaminase domains[24] attached to various carbon–nitrogen ligases hydrolyze L-glutamine to provide the ammonia for the subsequent ligation. During hydrolysis, an *S*-(γ-L-glutamyl)-cysteine is formed as a covalent intermediate

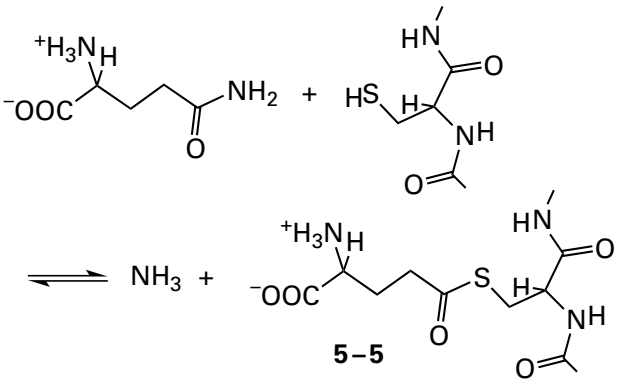

5–5

(5–5)

which is then hydrolyzed. A significant amount of this intermediate is present at steady state during catalysis by asparagine synthase (glutamine-hydrolysing) from *Escherichia coli*,[25] and the cysteine that is acylated is the same one modified by 6-diazo-5-oxo-L-2-aminohexanoic acid, which produced a covalent modification that could be identified crystallographically.[26] Intermediate *S*-(γ-L-glutamyl)cysteines (**5–5**) have been observed crystallographically in the active sites of some of these enzymes.[27,28]

There are a number of **acyltransferases** that transfer an acyl group from one reactant to another. Usually a covalent acylenzyme holds the acyl group. For example, glutamate *N*-acetyltransferase transfers an acetyl group from N^{α}-acetyl-L-ornithine to L-glutamate to produce N^{α}-acetyl-L-glutamate. When the enzyme from *Streptomyces clavuligerus* is mixed with only N^{α}-acetyl-L-glutamate, it becomes acetylated,[29] and the acetylated peptide TLLTFFATDAR is identified in a tryptic digest of the acetylated enzyme. A crystallographic molecular model of the acetylated enzyme identified Threonine 181, which is the amino-terminal threonine in this peptide, as the site of the acetylation (**5–6**)[30]

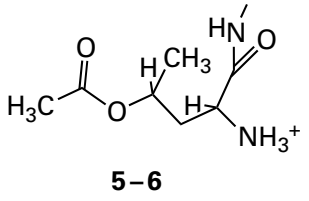

5–6

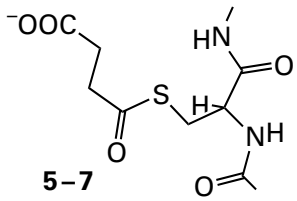

5–7

Consequently, it is inferred that during the overall acetyl transfer catalyzed by the enzyme, either N^{α}-acetyl-L-ornithine or N^{α}-acetyl-L-glutamate associates with the enzyme, the acetyl group is transferred to the threonine, and L-ornithine or L-glutamate dissociates. When L-glutamate or L-ornithine, respectively, associates and the acetyl group is transferred from ***O*-acetylthreonine** to its

α-amino group, the net reaction is accomplished. The fact that glutamate *N*-acetyltransferase from *G. stearothermophilus* (38% identity; 1.5 gap percent) displays steady-state kinetics in which

$$v_0 = \frac{k_0 k_A k_B [E]_t [A]_0 [B]_0}{k_0 k_A [A]_0 + k_0 k_B [B]_0 + k_A k_B [A]_0 [B]_0} \quad (5\text{–}6)$$

when N^{α}-acetyl-L-ornithine and L-glutamate are reactants is consistent with a ping-pong mechanism (compare Equation 3–148) in which L-ornithine dissociates as a product before L-glutamate can associate as a reactant.[31] In a crystallographic molecular model of glutamate *N*-acetyltransferase from *M. tuberculosis* (31% identity; 1.7 gap percent), the active site seems to be designed to associate with either L-ornithine or L-glutamate in turn.[32]

There are acyltransferases that transfer an acetyl group between coenzyme A and the hydroxy group of L-homoserine, parking the acetyl group on the hydroxy group of a serine.[33-36] There are also acyltransferases that transfer a succinyl group between coenzyme A and the hydroxy group of L-homoserine, parking the succinyl group on the sulfanyl group of a cysteine as an ***S*-succinylcysteine** (**5–7**).[37-39] In addition, there are acyltranferases that transfer a γ-glutamyl group between the amino group of L-cysteinylglycine and the α-amino groups of other amino acids or peptides, parking the γ-glutamyl group on the hydroxy group of a threonine.[40,41]

Covalent intermediates of derivatives of carbonic acid are also formed during enzymatic reactions. For example, addition of the sulfanyl group of a cysteine to the hypoxanthinyl group in inosine 5′-phosphate when it is bound in the active site of IMP dehydrogenase[42-45]

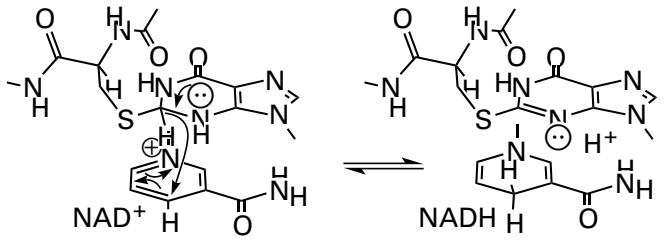

(5–7)

produces a tetrahedral covalent intermediate in the *N*-acyl-*N*′-alkylformamidine portion of the hypoxanthinyl group, a derivative of formic acid. Instead of one of the two nitrogens being expelled from the tetrahedral intermediate to form an acyl derivative, a hydride is expelled as a leaving group while being transferred to NAD^+. This expulsion of the hydride oxidizes the tetrahedral intermediate, which was an acyl derivative of formic acid, to an ***S*-alanyl-*N*-acyl-*N*′-alkylthiourea** (Equation 5–7), a derivative of carbonic acid that is the covalent intermediate in the reaction catalyzed by the enzyme. A peptide containing the covalent intermediate formed from [8-^{14}C]inosine 5′-phosphate was isolated from a digest of the enzyme from *Tritrichomonas foetus* that had been mixed with [8-^{14}C]inosine 5′-phosphate and NAD^+. Sequencing of the peptide showed that Cysteine 319 was the participant in the covalent intermediate.[43] The *S*-alanyl-*N*-acyl-*N*′-alkylthiourea (Equation 5–7) has also been observed crystallographically in the active site of IMP dehydrogenase from *Cricetulus griseus*.[45] In the enzymatic reaction, the *S*-alanyl-*N*-acyl-*N*′-alkylthiourea is then hydrolyzed to the *N*-acyl-*N*′-alkylurea in xanthosine 5′-phosphate, which is the final product in the direction written, and this hydrolysis also regenerates the cysteine.

Arginine deiminase from *Pseudomonas aeruginosa*

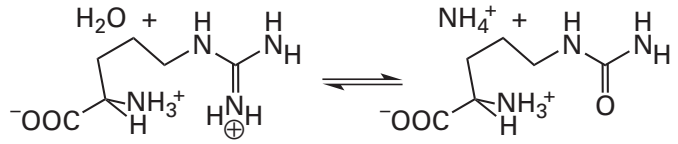

(5–8)

incorporates L-[1-^{14}C]-L-arginine covalently during its hydrolysis of L-arginine to L-citrulline; and when Cysteine 405 is mutated to serine, the enzyme no longer catalyzes the hydrolysis and no longer incorporates [1-^{14}C]-L-arginine.[46] A crystallographic molecular model has defined this intermediate as[47]

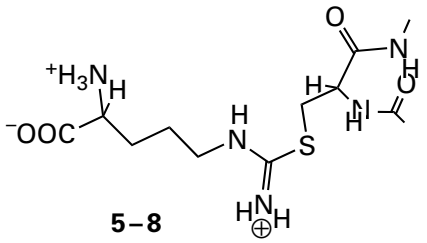

5–8

In the case of porcine glycine amidinotransferase

L-arginine + glycine $\rightleftharpoons$ L-ornithine + guanidinoacetate

(5–9)

mixing the enzyme with the amidino donor, [guanidinio-^{14}C]-L-arginine, in the absence of the acceptor, glycine, produces a covalent intermediate in which Cysteine 370[48] is amidinated (**5–9**)

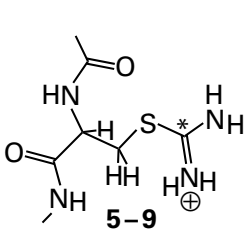

5–9

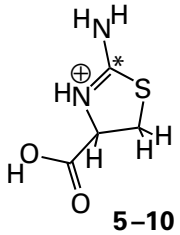

5–10

The ***S*-[^{14}C]amidinocysteine** (**5–9**; asterisk indicates carbon-14) in the [^{14}C]amidino enzyme cyclizes during acid hydrolysis of the protein to 2-amino-4-carboxy-[2-^{14}C]-4,5-dihydro-1,3-thiazole (**5–10**), a product that provided the initial identification of the intermediate.[49]

Esters of the carboxy groups on aspartates and glutamates in active sites are used as covalent intermediates in enzymatic nucleophilic substitutions. For example, in each active site of the related enzymes[50,51] epoxide hydrolase, haloalkane dehalogenase, and haloacid dehalogenase, there is an aspartate the carboxylato group of which performs a nucleophilic substitution on the electrophilic epoxide, haloalkane, or haloacid, respectively[52-54]

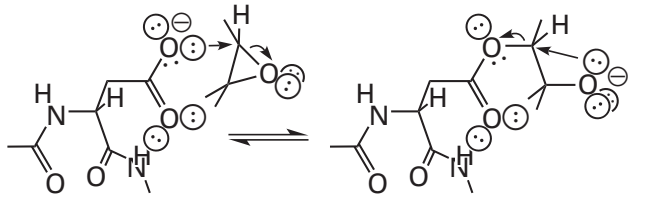

(5–10)

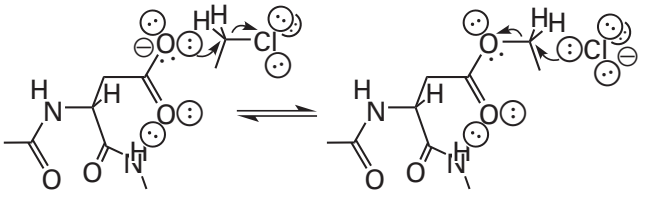

(5–11)

and the resulting covalent ***β*-aspartyl ester** is then hydrolyzed at its acyl carbon

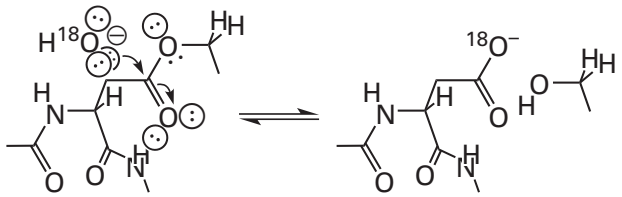

(5–12)

There is chemical evidence for this mechanism. Oxygen-18 from [^{18}O]H_2O is incorporated during the reaction into the aspartate in the active site of haloalkane dehalogenase from *Xanthobacter autotrophicus*. The [*β*-^{18}O]aspartate was isolated in a chymotryptic peptide to identify the particular aspartate that was labeled.[55] During the first turnover of epoxide hydrolase from *Rattus norvegicus* in [^{18}O]H_2O, no oxygen is incorporated into the product alcohol, but once the aspartate becomes isotopically labeled, it is incorporated into the product during later turnovers.[50] The crystallographic evidence for this mechanism is observation of the respective *β*-aspartyl esters (Equations 5–12) formed from the usual substrates in the active sites of haloalkane dehalogenase from *X. autotrophicus*[52] and haloacid dehalogenase from *Burkholderia cepacia*.[56]

Many, if not most, of the **glycosyltransferases** that retain the configuration of the glycosidic linkage in their product glycosides, as well as glycosidases that retain the configuration of the glycosidic linkage they hydrolyze, are thought to use mechanisms that pass through **covalent glycosyl intermediates**, which are *β*-aspartyl esters or *γ*-glutamyl esters formed between the respective glycosidic carbons and the carboxy groups of aspartates or glutamates in the active sites. For the overall nucleophilic substitution, a decision must be made: either a covalent glycosyl intermediate between two consecutive nucleophilic substitutions or an intermediate oxocarbenium ion and a single dissociative nucleophilic substitution.

An example of an active site that performs two successive nucleophilic substitutions with a covalent glycosyl intermediate is 4-*α*-glucanotransferase. The role of this enzyme is to transfer a maltotriose from the 4-hydroxy group of a D-glucose in a polysaccharide to the 4-hydroxy group of another D-glucose at the nonreducing end of another polysaccharide. The covalent glycosyl intermediate in the active site of 4-*α*-glucanotransferase from *Oryctolagus cuniculus* can be trapped, in the absence of an acceptor, with the covalent maltotriosyl intermediate[57]

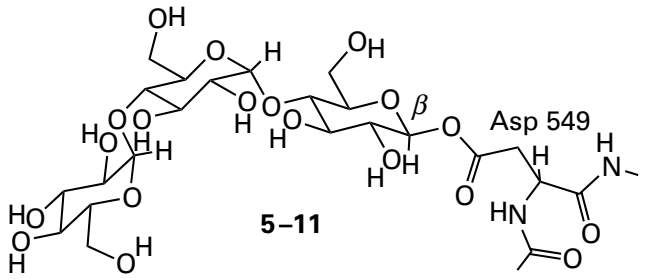

in its active site. When an acceptor is added, the enzyme transfers the maltotriosyl group to that acceptor in its normal reaction, but in the absence of acceptor, the maltotriosyl enzyme is stable. The glycosylated enzyme was digested with pepsin, and a peptide glycosylated on Aspartate 549 of the intact protein was isolated to identify the site of the modification.[58] Likewise, in the absence of an acceptor, cyclomaltodextrin glucanotransferase from *Niallia circulans* can be glycosylated with a 4-deoxymaltotriosyl group, and the resulting covalent glycosyl intermediate on Aspartate 229 can be observed crystallographically.[59]

Both 4-α-glucanotransferase and cyclomaltodextrin glucanotransferase are examples of glycosyltransferases in which the monosaccharide or oligosaccharide is transferred between a donor and an acceptor that are similar in structure—in these two examples, the nonreducing ends of polysaccharides. In such cases, the acceptor can associate with the same subsite as the donor, and the donor and acceptor can change places while the covalent intermediate holds on to the monosaccharide or oligosaccharide being transferred. There are, however, glycosyltransferases for which the donor and acceptor are structurally unrelated, so this strategy cannot be applied.

Just such an enzyme provides an example of an active site that performs a glycosyl transfer with an **oxocarbenium ion as an intermediate**. Lipopolysaccharide 4-α-galactosyltransferase from *Neisseria meningitidis* transfers the α anomer of D-galactose from UDP-α-D-galactose to the 4-hydroxy group of a D-galactosyl group in an elongating lipopolysaccharide with retention of configuration at D-galactose. The UDP in the UDP-α-D-galactose from which the α-D-galactosyl group is transferred and the lipopolysaccharide to which it is transferred are so dissimilar that there is no way they could occupy the same subsite in turn. Consequently, the active site of the enzyme binds both substrates simultaneously. In a crystallographic molecular model of the active site occupied by UDP-α-D-2-deoxy-2-fluoro-D-galactose and 4-deoxylactose, in which the 4-hydroxy group of the D-galactose, which would normally be the acceptor, is missing, carbon 4 of the D-galactosyl group in 4-deoxylactose is only 0.32 nm from carbon 1 of the α-D-galactosyl group in UDP-α-D-2-deoxy-2-fluoro-D-galactose,[60] not enough room to accommodate the missing 4-hydroxy group to which carbon 1 would normally be transferred. Even though the oxygen of the carbamoyl group of Glutamine 189, which is only 0.35 nm from carbon 1, has been proposed as a nucleophile that could form a covalent intermediate, in this glycosyltransferase, neither the carbamoyl nitrogen nor the carbamoyl oxygen is nucleophilic. Consequently, the α-D-galactosyl group is transferred directly to the 4-hydroxy group, with retention of configuration and probably without the intermediacy of a covalent intermediate. The intermediate in the **dissociative nucleophilic substitution** is probably an **oxocarbenium ion**.[61]

The issue in situations in which donor and acceptor are not simultaneously associated with an active site is whether or not an oxocarbenium ion can be an intermediate that lives long enough for the donor to leave and the acceptor to associate. An oxocarbenium ion in solution has a short half life (10^{-12} s).[62] Unless it is stabilized significantly by the enzyme both electronically, by providing a significant negative electric field such as that created by an adjacent carboxylato or carbamoyl group, and sterically, by preventing any nucleophile other than the intended one to approach it, including an adjacent carboxylato group, it would not exist long enough for the nonreducing monosaccharide to leave and be replaced by the intended nucleophile.[63] Both means of stabilization, however, are within the abilities of an active site, and it would not be unreasonable for the lifetime of the oxocarbenium ion to be extended long enough for the leaving hydroxy group of the donor to be replaced by the hydroxy group of the acceptor.

In contradistinction, for many if not all of the glycosidases that proceed by retention of configuration, including lysozyme,[64] it has been proposed that the usually present carboxylato group from an aspartate or glutamate, located on the opposite face of the glycosidic linkage from which the leaving group departs, adds to the oxocarbenium ion as the leaving group is departing to form an ester[65-67]

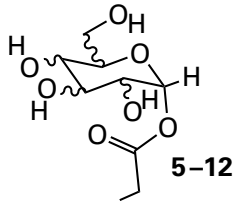

5–12

An ester is so stable that it can exist for as long as is necessary for the nucleophile intended to be the acceptor to arrive. After the nucleophile associates, the ester would then participate in a nucleophilic substitution as the glycosidic carbon during or immediately after the departure of the carboxylato group, which is a competent leaving group, from the glycosidic carbon. This proposal, however, would seem to require that, as is usually the case, a catalytic acid form a hydrogen bond with the ester oxygen of the carboxy group in the acyl intermediate to improve the ability of the carboxy group to leave during its dissociation from the intermediate. The presence of such a catalytic acid has not been mentioned, and in the active sites of many glycosidases that proceed with retention of configuration it seems not to be present. In the active site of lysozyme, there is none. Another drawback of this proposal is that the ester it requires has been observed only with unnatural substrates.

In the case of retaining **glycosidases**, as opposed to retaining glycosyltransferases, the nucleophile is water. In most of these enzymatic reactions, formation of the glycosyl intermediate, if it exists, is slower than its hydrolysis,[68] so even at equilibrium, little of the covalent intermediate should be present. One way to trap an intermediate is to discover a mutant in which hydrolysis of that intermediate is slow.[69] When Histidine 205 in cellulose 1,4-β-cellobiosidase from *Cellulomonas fimi*, a glycosidase that hydrolyzes cellobiose units from the nonreducing end of cellulose, is mutated to asparagine and Glutamate 127 to alanine, a covalent cellobiosyl intermediate at the carboxy group of Glutamate 233 can be trapped and observed crystallographically.[70]

Another way to stabilize a covalent glycosyl intermediate might be to use a reactant in which a fluoro group has been synthetically introduced at the carbon next to the glycosidic carbon that participates in hydrolysis. For example, cellulase from *Acetivibrio thermocellus*[71] releases consecutively the cellobioses 4-(β-D-glucosido)-D-glucose from cellulose. When this enzyme is mixed with dinitrophenyl [^{3}H]fluorocellobioside **5–13**

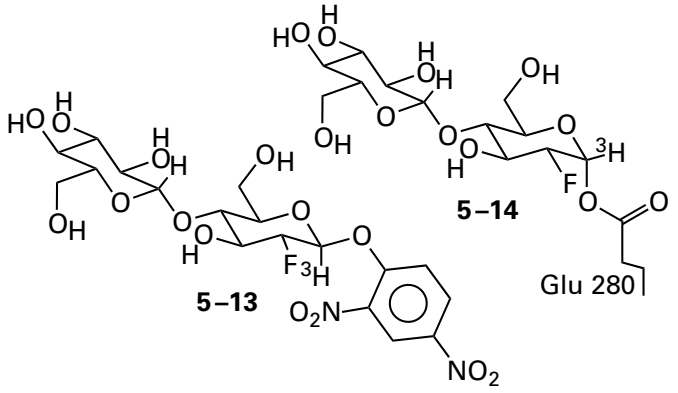

a [^{3}H]fluorocellobiosyl derivative **5–14** of Glutamate 280 forms. This covalent intermediate can be isolated in a peptic peptide, which identifies the site of modification.[72] Fluorocellobioside **5–13** has also been used to form the homologous derivative (see **5–14**) with Glutamate 233 in the active site of cellulose 1,4-β-cellobiosidase from *C. fimi*, and a crystallographic molecular model of the modified active site has been reported.[73]

Covalent fluoroglycosyl derivatives of this type have been prepared from many glycosidases and characterized kinetically,[74,75] chemically,[76-80] and crystallographically.[75,81-86] The problem with these results is that the fluoroglycosides used to modify the carboxy groups in the active sites of these glycosidases are so different chemically from their usual substrates that they may simply be labeling the active site rather than producing an adduct homologous to an actual intermediate in the normal enzymatic reaction. For example, if the actual intermediate in one of these reactions were a glycosyloxocarbenium ion, a noncovalent intermediate, rather than a glycosylcarboxy group, a covalent intermediate, the fluoro substitution would destabilize that intermediate so drastically as to prevent its formation, and the increase in electrophilicity of a carbonyl carbon in the reagent would turn it into an active-site label. For example, when 2-acetamido-2-deoxy-D-glucopyranosyl-(β1,4)-2-deoxy-2-fluoro-β-D-glucopyranosyl fluoride was used to modify lysozyme, Aspartate 52 was modified by the glycoside,[64] but formation of a covalent glycosyl intermediate in the normal enzymatic reaction appears to be sterically precluded,[87] and the carboxylato group of Aspartate 52 probably serves as an anion to stabilize an oxocarbenium ion.

Carboxylic anhydrides of the carboxy groups of glutamates and aspartates are covalent intermediates for the common mechanism of the various CoA-transferases[88]

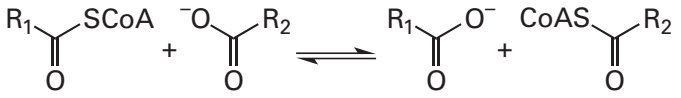

(5–13)

In the case of porcine 3-oxoacid CoA-transferase, chemical evidence for the existence of a **γ-glutamyl-SCoA thioester** at a glutamate in the protein, which participates in the mechanism of the enzymatic reaction as a covalent intermediate, has been presented.[89] A covalent γ-glutamyl-SCoA thioester in the active site of this enzyme[90] and the one in the active site of acetate CoA-transferase from *E. coli* have been observed crystallographically.[91] In the case of formyl CoA-transferase from *Oxalobacter formigenes*, both a covalent β-aspartyl-SCoA intermediate and a covalent β-aspartyl formyl anhydride have been observed crystallographically.[92] All these results are consistent with a general mechanism for coenzyme A transfer that includes a γ-glutamyl-SCoA

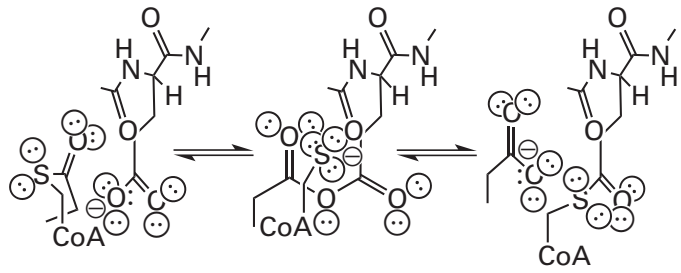

(5–14)

or a β-aspartyl-SCoA as a covalent intermediate, formation of either of which proceeds through the respective γ-glutamyl anhydride or β-aspartyl anhydride, also a covalent intermediate.

Because a hydron α to a thioester is significantly more acidic than a hydron α to an ester (Figure 1–23), covalent *S*-acylcysteinyl intermediates are often used as precursors to the respective α-enolates. An example is the intermediate in the reaction catalyzed by hydroxymethylglutaryl-CoA synthase, which catalyzes an aldol condensation (previously Equation 4–361)

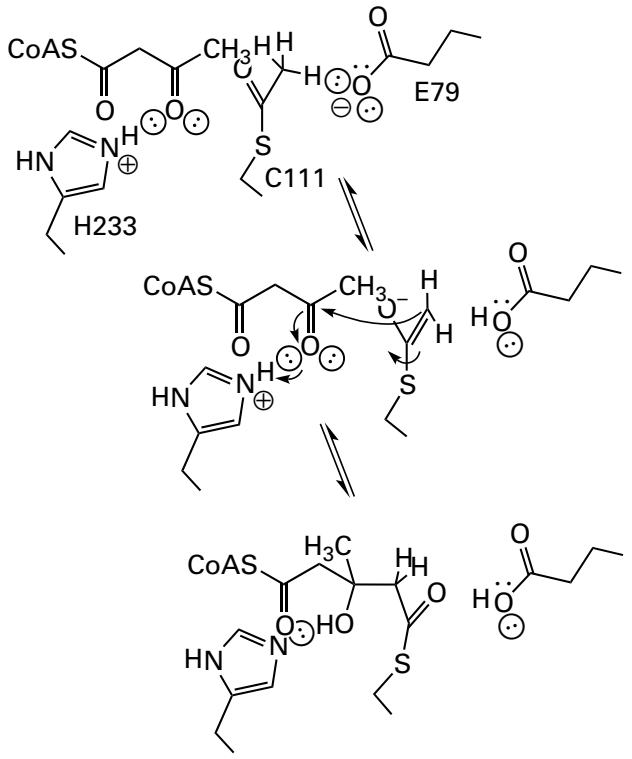

(5–15)

In the case of this enzyme, the covalent [1-^{13}C]acetylcysteinyl intermediate was first detected in a nuclear magnetic resonance spectrum of the enzyme from *Gallus gallus* that had been mixed with [1-^{13}C]acetyl-SCoA in the absence of the cosubstrate acetoacetyl-SCoA,[93] before it was observed crystallographically in the enzyme from *Staphylococcus aureus* (28 % identity; 3.1 gap percent).[94] Acetoacetyl-SCoA itself is produced by acetyl-CoA *C*-acetyltransferase, an enzyme that transfers an acetyl group from acetyl-SCoA to the sulfanyl of a cysteine and then adds the enolate of this acetyl group to a second acetyl-SCoA to produce acetoacetyl-SCoA in a Claisen condensation. A crystallographic molecular model of acetylated acetyl-CoA *C*-acetyltransferase from *Zoogloea ramigera* in a complex with acetyl-SCoA identifies acetylated Cysteine 89. In this complex, the α-carbon of the acetyl-SCoA, which becomes the enolate during the reaction, is immediately adjacent to the acyl carbon of the acetylcysteine, which is the electrophilic carbon in this Claisen condensation.[95]

Citrate (*pro*-3*S*)-lyase (see Problem 4–23) also catalyzes an aldol condensation

(5–16)

Following purification, the enzyme from *Klebsiella aerogenes* slowly loses activity in a process hastened by addition of citrate and Mg^{2+} or addition of hydroxylamine.[96] The inactive enzyme can be reactivated by exposure to acetic anhydride[96] or acetyl-SCoA.[97] During reactivation, the enzyme becomes acetylated on the sulfanyl group of the **4′-phosphopantetheinyl group**

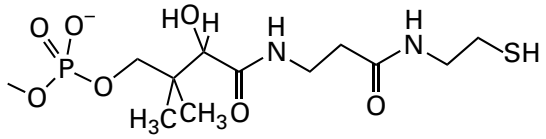

5–15

in a molecule of coenzyme A covalently bound to a serine as a prosthetic group to the protein. This prosthetic coenzyme A is attached through a (β1,2)-glycosidic linkage between the 2′-hydroxy group on its ribosyl group and carbon 1 of a 5-phosphoribosyl group, which in turn is bound through its 5-phospho group in a phosphodiester to a serine of the polypeptide.[98] Only the enzyme acetylated on the sulfanyl group of this prosthetic coenzyme A is active as citrate lyase.

The enzyme lacking the covalently bound acetyl group, however, will carry out reactions in which it uses either extraneously added acetyl-SCoA or citryl-SCoA as if they were covalently bound to the protein.[99] Presumably this occurs because the extraneous acetyl-SCoA or citryl-SCoA displaces the covalently bound coenzyme A, which is only distantly tethered to the enzyme, from the active site. From products of these reactions of the unattached acyl-coenzymes A, it could be inferred that the normal enzymatic reaction proceeds through a covalent citryl intermediate in the sequence

$$\text{E·CoAS-acetyl} + \text{citrate} \rightleftharpoons \text{E·CoAS-citryl} + \text{acetate} \qquad (5\text{–}17)$$

$$\text{E·CoAS-citryl} \rightleftharpoons \text{E·CoAS-acetyl} + \text{oxaloacetate} \qquad (5\text{–}18)$$

where E-CoASH is the prosthetic coenzyme A covalently attached to the enzyme. The advantage of forming the citryl thioester in Equation 5–17 is obvious because the carbon–carbon bond cleaved or formed during the retro-Claisen or Claisen condensation, respectively (Equation 5–18 in the respective direction), is weakened considerably (Figure 1–23).

In both the fatty-acid synthase system and citrate (*pro*-3*S*)-lyase, active sites that have covalently bound 4′-phosphopantetheinyl groups (**5–15**), the respective sulfanyl groups are used to provide the intermediate thioesters for the respective Claisen condensations. That this might be only marginally advantageous is suggested by the fact that isocitrate lyase, which also catalyzes a similar aldol condensation

$$\text{glyoxylate} + \text{succinate} \rightleftharpoons \text{isocitrate} \qquad (5\text{–}19)$$

proceeds without forming any thioesters.[100] In this instance, a *gem*-enediolate must be formed from the unesterified carboxy group of the isocitrate that is adjacent to the carbon–carbon bond to be cleaved. In the active site of isocitrate lyase from *M. tuberculosis* occupied by isocitrate, the incipient *gem*-enediolate is firmly hydronated by the carboxy group of a glutamate during the cleavage of that carbon–carbon bond. The two peripheral nitrogen–hydrogen bonds of the guanidinio group of an arginine and an amido nitrogen–hydrogen from the polypeptide form an oxyanion hole for the other oxygen. These groups, as well as the carbamoyl group of an asparagine, stabilize the *gem*-enediol, 4,4-dihydroxy-3-butenoate, that is the noncovalent intermediate in the reaction as its monoanionic *gem*-enediolate[101]

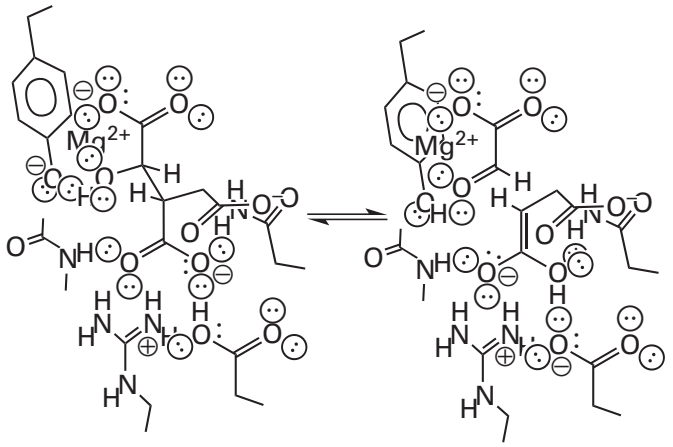

(5–20)

The hydroxy group of the isocitrate, which is a ligand to a Mg^{2+}, is dehydronated by a tyrosinate as the bond cleaves. Carbon 2 of the *gem*-enediolate is then hydronated by the hydroxy group of a serine (0.29 nm) that relays, through a molecule of water, a hydron from a histidine.[102] As with the endopeptidases, these two different examples of aldol condensations illustrate the fact that **different strategies**

involving different intermediates are often used by enzymes to catalyze the same reaction.

The fatty-acid synthase system (see Equations 3–492 through 3–499)

$$\text{acetyl-SCoA} + n\,\text{malonyl-SCoA} + 2n\,\text{NADPH} + (3n-1)\text{H}^+ \rightleftharpoons 2n\,\text{NADP}^+ + n\,\text{CO}_2 + (n+1)\text{HSCoA} + \text{CH}_3(\text{CH}_2\text{CH}_2)_n\text{COO}^- \quad (5\text{–}21)$$

is a multienzymatic complex, within which the active site of 3-oxoacyl-[acyl-carrier-protein] synthase catalyzes the Claisen condensation (see Equation 3–495)

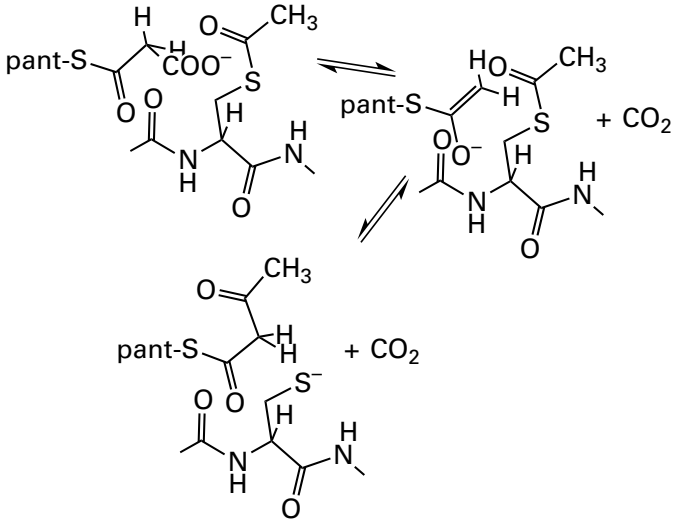

(5–22)

that initiates the synthesis of a fatty acid. The malonyl group is a thioester of a 4′-phosphopantetheinyl group (HS-pant; **5–15**) covalently attached directly (rather than indirectly) through its 4′-phospho group in a phosphodiester to a serine located in the acyl-carrier domain of the multienzymatic complex, which is a homologue of the independent acyl-carrier proteins found in the cytoplasm of prokaryotes and plants.[103] The serine to which the 4′-phosphopantetheinyl group is attached was identified by isolating a [^{14}C]palmitoyl-4′-phosphopantetheinyl peptide from the fatty-acid synthase system from *Saccharomyces cerevisiae* that had been mixed with [^{14}C]palmitoyl-SCoA.[104] The acetyl group with which the enol is condensed during the first round in the synthesis of a fatty acid is also bound as a thioester, but it is bound to the sulfanyl group of a cysteine in the active site of 3-oxoacyl-[acyl-carrier-protein] synthase.

Both the acetyl group and the malonyl group, the enolate of which is the eventual nucleophile, arrive initially at the respective active sites of [acyl-carrier-protein] *S*-acetyltransferase (see Equation 3–492)

$$\text{CH}_3\text{CSCoA} + \text{HS-pant} \rightleftharpoons \text{HSCoA} + \text{CH}_3\text{CS-pant} \quad (5\text{–}23)$$

and [acyl-carrier-protein] *S*-malonyltransferase (see Equation 3–493)

$$^-\text{OOCCH}_2\text{CSCoA} + \text{HS-pant} \rightleftharpoons \text{HSCoA} + {}^-\text{OOCCH}_2\text{CS-pant} \quad (5\text{–}24)$$

in the fatty-acid synthase system as thioesters of coenzyme A. Again, HS-pant indicates a 4′-phosphopantetheinyl group in the same acyl-carrier domain.

The transfer of the two groups to their respective locations for subsequent condensation within the active site of 3-oxoacyl-[acyl-carrier-protein] synthase (Equation 5–22) is not direct; the two groups pass through a sequence of other covalent intermediates, each formed by a nucleophilic substitution of one heteroatom for another heteroatom at an acyl group. In the fatty-acid synthase system from *S. cerevisiae*, the acetyl group of acetyl-SCoA is transferred first to a serine to form an *O*-acetylserine[105] in the active site of [acyl-carrier-protein] *S*-acetyltransferase (Equation 5–23), then to the sulfanyl group of the 4′-phosphopantetheinyl group in the acyl-carrier-protein domain to form a thioester again, and then from that sulfanyl group to the sulfanyl group of the cysteine in the active site of 3-oxoacyl-[acyl-carrier-protein] synthase to situate it for the Claisen condensation. The malonyl group of malonyl-SCoA is transferred first to a serine to form an ***O*-malonylserine**[106] in the active site of [acyl-carrier-protein] *S*-malonyltransferase (Equation 5–24) and then to the sulfanyl group of the 4′-phosphopantetheinyl group in the same acyl-carrier domain to form the necessary thioester that becomes the enolate within the active site of 3-oxoacyl-[acyl-carrier-protein] synthase that is the nucleophile in the Claisen condensation.

The two respective serines that pass on the acetyl group and the malonyl group to the sulfanyl group of the 4′-phosphopantetheinyl group in [acyl-

carrier-protein] *S*-acetyltransferase and [acyl-carrier-protein] *S*-malonyltransferase were identified by alkylating all accessible sulfanyl groups in the fatty-acid synthase system to prevent subsequent transfers, forming the esters with [^{14}C]acetyl-SCoA or [^{14}C]malonyl-SCoA, and isolating and sequencing the two unique peptides containing the respective esters.[105,106] The cysteine that holds the acetyl group during the condensation in the active site of 3-oxoacyl-[acyl-carrier-protein] synthase (Equation 5–22) was identified by its high reactivity to iodoacetamide and by subsequent isolation of the peptide modified by [^{14}C]iodoacetamide.[107]

The sequence of events just described, however, has one drawback. If a malonyl group arrives first, its occupation of the sulfanyl group of the 4′-phosphopantetheinyl group on the sole acyl-carrier domain would block the transfer of the acetyl group to the sulfanyl group of the cysteine in the active site of 3-oxoacyl-[acyl-carrier-protein] synthase. For this reason, the presence of free coenzyme A is an absolute requirement for synthesis of a fatty acid by the fatty-acid synthase system. In its absence, the multienzymatic complex rapidly becomes occupied by malonyl groups, which cannot be removed because the reverse reaction is blocked, and the acetyl groups cannot be transferred onto the active site.[108] Consequently, the reversibility of the malonyl transfer and the presence of coenzyme A, the malonyl acceptor, permits the proper order of transfer to occur.

Thiohemiacetals are covalent intermediates in enzymatic oxidation–reductions. In such oxidation–reductions, thiohemiacetals are precursors to thioesters. For example, during the oxidation of aldehydes, *S*-(1-hydroxyalkyl)cysteines (**5–16**) are formed in an active site

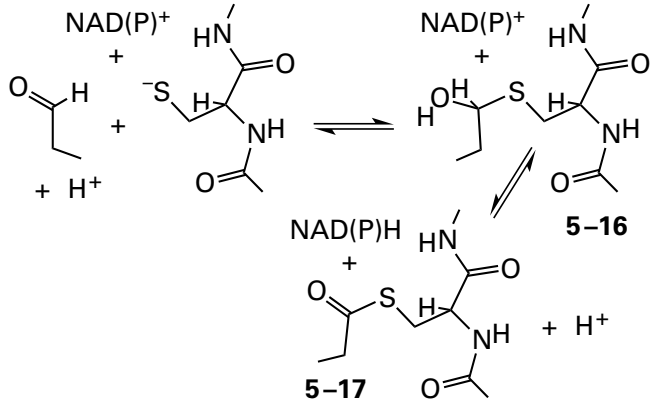

(5–25)

and their existence is inferred from the chemical or crystallographic identification of the more stable *S*-acylcysteine (**5–17**). In the oxidation–reduction (previously Equation 4–349)

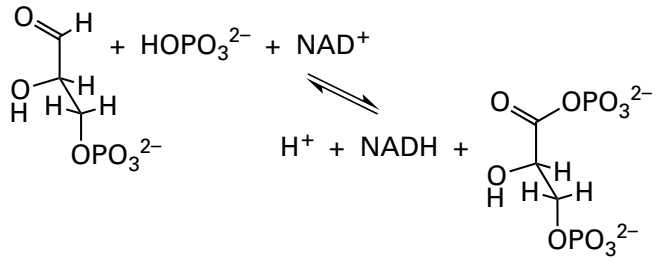

(5–26)

catalyzed by glyceraldehyde-3-phosphate dehydrogenase (phosphorylating), a 3-phospho-D-glyceroyl thioester[109] is phosphorylyzed to produce 3-phospho-D-glyceroyl phosphate

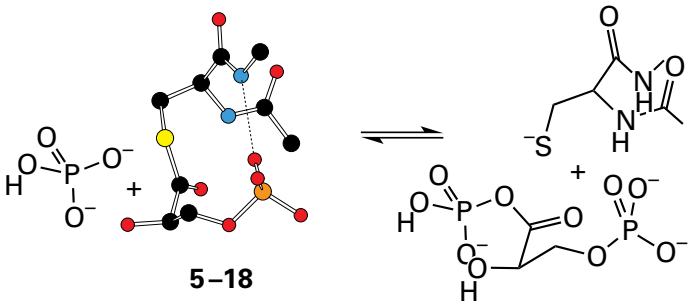

(5–27)

Acetylphosphate acetylates Cysteine 149 of the enzyme from *O. cuniculus* and is reduced by the enzyme to acetaldehyde, a reaction homologous to the normal reduction of 3-phospho-D-glyceroyl phosphate (reverse of Equation 5–26).[110,111] The peptide acetylated with [1-^{14}C]acetylphosphate was purified and sequenced to identify Cysteine 149 as the site of the modification. A crystallographic molecular model of the authentic 3-phospho-D-glyceroyl thioester intermediate (**5–18**) for glyceraldehyde-3-phosphate dehydrogenase (phosphorylating) from *G. stearothermophilus* (54 % identity; 1.2 gap percent) demonstrated the existence of the thioacylation and identified the cysteine homologous to Cysteine 149 in the enzyme from *O. cuniculus* as the site of acylation.[109] In the case of aspartate-semialdehyde dehydrogenase from *E. coli*, an enzyme homologous to glyceraldehyde-3-phosphate dehydrogenase (phosphorylating),[112] the β-aspartyl thioester of the homologous cysteine has also been observed crystallographically.[113]

In reduction of the cyano group of 7-cyano-7-deazaguanine by preQ$_1$ synthase from *Bacillus subtilis*, a thioimidate is formed as a covalent intermediate by nucleophilic addition of the sulfido group of Cysteine 55 to the cyano group

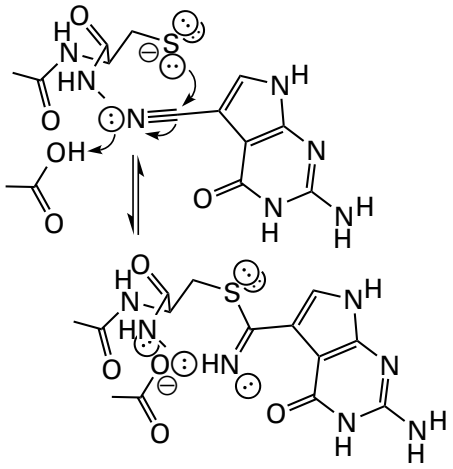

(5–28)

The **thioimidate** is then reduced by NADPH to the thiohemiaminal in the usual addition of a hydride to its imino group. The resulting **thiohemiaminal** then dissociates from the sulfur of Cysteine 55 to give the imine, which is reduced to the amine by a second NADPH. The intermediate thioimidate (Equation 5–28) has been observed in a crystallographic molecular model of the enzyme that was crystallized in the presence of 7-cyano-7-deazaguanine but in the absence of NADPH.[114] The hydron required for the nucleophilic addition to avoid an anionic nitrogen is provided by Aspartate 62, which forms a hydrogen bond (0.31 nm) with the nitrogen of the thioimidate in the crystallographic molecular model. When reduction of 7-cyano-7-deazaguanine is being catalyzed by a mutant of preQ$_1$ synthase from *E. coli* (26% identity; 1.9 gap percent), the intermediate imine that results from reduction of the thioimidate and dissociation of the sulfido group from the thiohemiaminal and that is a noncovalent intermediate in the normal reaction is released into the solution, and the aldehyde that is the product of its hydrolysis could be identified by nuclear magnetic resonance spectroscopy.[115]

The active site of UDP-glucose dehydrogenase

$$2\,NAD^+ + \text{UDP-}\alpha\text{-D-glucose} + H_2O \rightleftharpoons \text{UDP-}\alpha\text{-D-glucuronate} + 2\,NADH + 3\,H^+ \quad (5\text{–}29)$$

catalyzes two successive oxidations of carbon 6 of the glucosyl group in UDP-α-D-glucose. The first oxidation turns UDP-α-D-glucose into the aldehyde UDP-α-6-oxo-6-deoxy-D-glucose. The sulfanyl group of a cysteine in the active site then forms a thiohemiacetal with the carbonyl at carbon 6, which is oxidized to the thioester at carbon 6 of the glucuronyl group by the second NAD$^+$. The thioester is then hydrolyzed to give UDP-α-D-glucuronate. The nucleophilic cysteine that forms the thiohemiacetal and the subsequent thioester in the active site of UDP-glucose dehydrogenase from *Streptococcus pyogenes* was mutated to serine so that the seryl ester of UDP-α-D-glucuronic acid—rather than the cysteinyl ester, which was unstable—could be isolated in a peptic peptide from the UDP-α-D-glucuronyl enzyme.[116] The actual thiohemiacetal has also been observed crystallographically in a mutant of human UDP-glucose dehydrogenase, lacking its carboxy-terminal 27 amino acids, in which Glutamate 161 was mutated to glutamine to decrease the rate at which the thiohemiacetal of UDP-α-6-oxo-6-deoxy-D-glucose was oxidized to the thioester.[117] The intermediate thiohemiacetal of this mutant was also identified by mass spectrometry. The intact mutant enzymes—both unoccupied and containing the covalent intermediate thiohemiacetal in the active site—were in turn submitted to electrospray ionization mass spectrometry. The molecular mass of the unoccupied mutant was 52,019.3 Da, and the molecular mass of the covalent intermediate of the mutant enzyme was 52,581.6 Da. The molecular mass of UDP-α-6-oxo-6-deoxy-D-glucose, the intermediate aldehyde, is 564.3 Da, which should be equal to the increase in molecular mass upon formation of the hemiacetal.

What happens to the structure of a protein such as UDP-glucose dehydrogenase upon atomization in the gas phase of the mass spectrometer is unknown. The fact that the molecular mass of the unmodified protein observed in the mass spectrometer was 52,019.3 Da, together with the fact that the molecular mass of the protein calculated from its sequence of amino acids is 52,019.6 Da, confirms that all the water associated with the native protein definitely does dissociate in the vacuum. It has always been assumed that other noncovalently associated ligands, including inorganic ions, dissociate in the vacuum as well, which also seems to be confirmed in this case. That UDP-glucose dehydrogenase in the gas phase is dehydrated and unliganded also suggests that it no longer assumes its native tertiary structure because if it did, buried molecules of water and

buried adventitious ions would probably remain. The fact that the molecular mass observed for the covalent thiohemiacetal is within the molecular mass of two hydrons of that expected seems to confirm that the covalent intermediate is the actual vaporized molecule being detected by the spectrometer. It also demonstrates that the thiohemiacetal, which would rapidly hydrolyze were the molecule of protein to unfold while still in an aqueous solution, nevertheless does not hydrolyze upon atomization in the electrospray.

Phosphate esters, phosphoanhydrides, or phosphoramidates of amino acids are covalent intermediates in the active sites of enzymes that perform nucleophilic substitutions at phosphorus. These are usually formed by a nucleophilic substitution of the bridging oxygen in a phosphoric ester

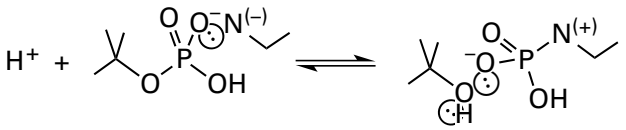

(5–30)

or the bridging oxygen in a phosphoanhydride

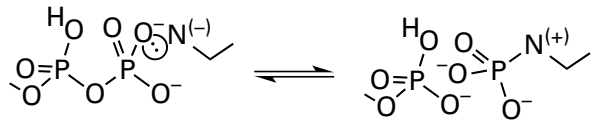

(5–31)

by a nucleophile, ⊙N$^{(-)}$–, in the active site to form a **phosphorylated intermediate**. Examples of such phosphorylated intermediates are ***O*$^{\beta}$-phosphoserine (5–19), *O*$^{\beta}$-phosphoaspartate (5–20), *O*$^{\gamma}$-phosphoglutamate, *S*-phosphocysteine (5–21) *N*$^{\tau}$-phosphohistidine, or *N*$^{\pi}$-phosphohistidine (5–22)**

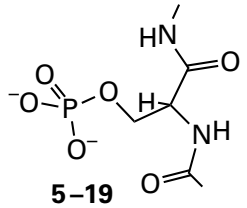

5–19

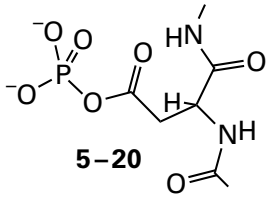

5–20

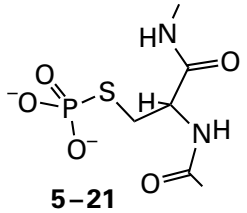

5–21

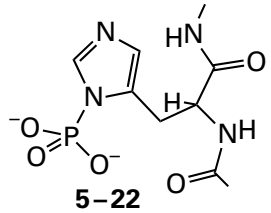

5–22

One advantage of such a phosphorylated intermediate is that the same catalytic groups in the active site that are used to activate the phospho donor by acid–base catalysis can serve to activate the phospho acceptor in an identical, but reciprocal, manner. For example, in the reaction catalyzed by nucleoside-diphosphate kinase (previously Equation 4–286)

$$MgXTP^{2-} + MgYDP^{-} \rightleftharpoons MgXDP^{-} + MgYTP^{2-} \qquad (5–32)$$

in which X and Y represent different nitrogenous bases, the oxygens acting as phosphate donor and phosphate acceptor are chemically identical because both are the most distal oxygens in a nucleoside diphosphate. As a result, the enzymatic reaction can proceed through a phosphorylated intermediate,[118] formed by transfer of a phosphate from a nucleoside triphosphate to an amino acid in the active site to produce its nucleoside diphosphate and unformed by transfer of the phosphate to the other nucleoside diphosphate to produce the other nucleoside triphosphate. By remaining in the active site as the phosphorylated intermediate, the free energy of hydrolysis of the phosphoanhydride of the nucleoside triphosphate can be retained to facilitate transfer to the acceptor.

Because nucleoside-diphosphate kinase is only marginally selective as to the nucleotide, it must recognize mainly the complex between magnesium and the triphosphate (see Figure 4–52) and carbons 3′ through 5′ of the ribose or deoxyribose. This intuition is validated in crystallographic molecular models[119,120] of the enzyme from *Dictyostelium discoideum* in complexes with MgADP^{-} and MgTDP^{-}. The ribose rings and the $Mg(H_2O)_4$ diphospho groups in the two complexes are caught firmly in a web of hydrogen bonds deep in the active site. The web is formed from the same donors and acceptors, which donate and accept at the same locations in the substrates. The adenine and thymine bases, however, are near the opening of the active site with their π systems stacked against the π system of the same phenylalanine, but they participate in no hydrogen bonds with the enzyme that might distinguish between them.

If the mechanism for nucleoside-diphosphate kinase is the one just described, then the donor of the phospho group must dissociate from the active site as MgXDP^{-}, an irreversible step during measurement of the initial rate for the enzymatic reaction, before the acceptor is bound as MgYDP^{-}. This

sequence of events is consistent with the fact that steady-state kinetics of the enzymatic reaction display the behavior of Equation 5–6, which is that expected for a ping-pong mechanism.[121] The steady-state kinetics are chemical evidence consistent with a phosphorylated intermediate.

In the reaction catalyzed by alkaline phosphatase (previously Equation 4–452)

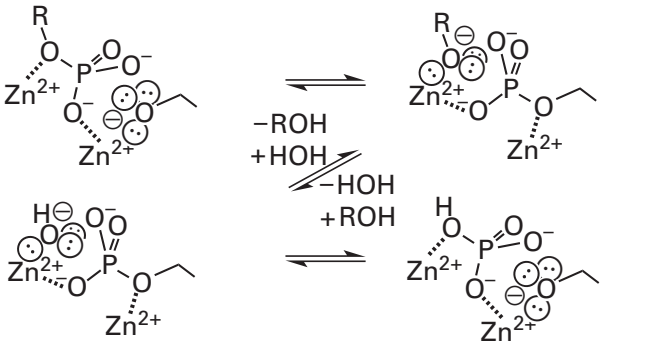

(5–33)

the various donors of the phospho group that can be substrates for the enzyme and the water that is the usual acceptor may not resemble each other at first glance, but they are all alcohols. The crystallographic molecular model suggests that only the phospho ester itself forms contacts with the active site to be activated by catalytic acids and bases.[122] For this reason, the enzyme has a broad specificity for phosphate monoesters, and it is not surprising that there is a phosphorylated intermediate in this enzymatic reaction. The fact that the reaction proceeds with retention of configuration at phosphorus is consistent with the existence of a phosphorylated intermediate.[123]

Demonstration of the existence of phosphorylated intermediates in enzymatic reactions usually begins with the observation that [^{32}P]phosphate is transferred from the substrate that is a phospho donor in the reaction to the enzyme itself to form a **covalently [^{32}P]phosphorylated protein**. The phosphoamino acid formed in this transfer can sometimes be identified directly by hydrolyzing the modified protein and isolating the covalently modified amino acid. For example, succinate-CoA ligase (ADP-forming) from *E. coli* proceeds through a phosphorylated intermediate,[124] and the [^{32}P]phosphate incorporated during this reaction into the bovine enzyme was isolated as N^{τ}-phospho-L-histidine after alkaline hydrolysis or enzymatic digestion of the protein.[125] The phosphorylated intermediate in the reaction catalyzed by nucleoside-diphosphate kinases (Equation 5–32) from both *Bos taurus* and *S. cerevisiae* has been identified in the same way as N^{π}-phospho-L-histidine (**5–22**).[118,126] In these two instances, the phosphorylation occurred exclusively at the τ nitrogen and the π nitrogen, respectively, as would be expected from the regioselectivity usually displayed by active sites.

The phosphorylated protein formed as an intermediate in the reaction catalyzed by alkaline phosphatase from *E. coli* has been digested with pepsin at low pH, to prevent alkaline hydrolysis, and an analysis of the resulting peptides showed that the phosphate is covalently attached to Serine 102, the first serine in the sequence TGKPDYVTDSAASA.[127] When Serine 102 is mutated to alanine, the enzymatic activity decreases by a factor of 100,000.[128]

The phosphorylated intermediate in the enzymatic reaction catalyzed by P-type Ca^{2+} transporter [129] from *O. cuniculus* has been identified indirectly as O^{γ}-phosphoaspartate (**5–20**) by reducing it to [^{3}H]homoserine with sodium [^{3}H]borohydride

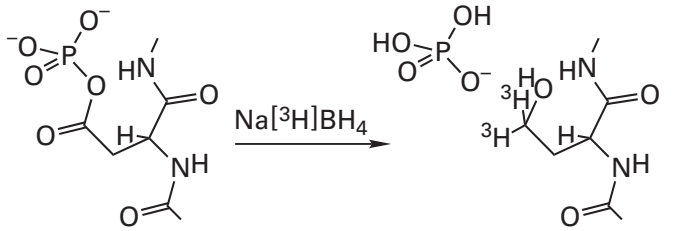

(5–34)

and isolating the [^{3}H]homoserine produced upon hydrolysis of the polypeptide in acid.[130]

The phosphorylated intermediate in the enzymatic reaction catalyzed by enzyme II of the phosphotransferase system from *E. coli* has been identified as an *S*-phosphocysteine (**5–21**) both by isolation of the phosphopeptide and by analysis with nuclear magnetic resonance spectroscopy.[131]

Phosphorylated intermediates have also been **observed crystallographically**. For example, N^{τ}-phosphohistidine in the active site of succinate-CoA ligase (ADP-forming) from *E. coli*,[132] N^{π}-phosphohistidine (**5–22**) in the active sites of the nucleoside-diphosphate kinases from *D. discoideum* and *Drosophila melanogaster*,[133] N^{τ}-phosphohistidine in phospholipase D from *Streptomyces*,[134] N^{τ}-phosphohistidine in fructose-2,6-bisphosphate 2-phosphatase from *R. norvegicus*,[135] and N^{τ}-phosphohistidine in human bisphosphoglycerate mutase[136] have all been captured crystallographically. The O^{β}-phosphoseryl intermediate (**5–19**) in alkaline phosphatase from *E. coli* has been observed in the active site of a crystallographic molecular model of a mutant in

which Histidine 331 has been mutated to glutamine to decrease the rate of its dephosphorylation.[137] The O^{γ}-phosphoaspartyl intermediate in histidinol-phosphatase from *E. coli* has been observed crystallographically in the active site of the enzyme in which Ca^{2+} replaces the required Mg^{2+} to decrease its rate of dephosphorylation.[138] The *S*-phospho-cysteinyl intermediate[139] in human protein-tyrosine-phosphatase has been observed crystallographically in a mutant in which Glutamine 262 has been mutated to alanine to decrease the rate of its dephosphorylation.[140]

Bisphosphoglycerate mutase catalyzes the transfer of the 1-phospho group of 3-phospho-D-glyceroyl phosphate to its 2-hydroxy group

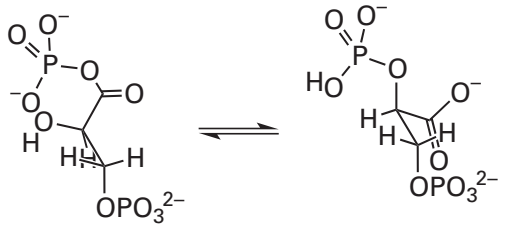

(5–35)

The phosphorylated intermediate in the reaction is an N^{τ}-phosphohistidine. Either substrate, 3-phospho-D-glyceroyl phosphate or 2,3-diphospho-D-glycerate, can phosphorylate the imidazolyl group.[141] Within the active site, the 3-phospho group of the intermediate 3-phospho-D-glycerate that results from either nucleophilic substitution is anchored firmly in a cup of seven donors of hydrogen bonds.[136] The carboxyhydroxymethyl group of the 3-phospho-D-glycerate can pivot around this anchor along the bond between carbons 2 and 3 (as in Equation 5–35) so that the phospho group can be transferred from the N^{τ}-phosphohistidine to the carboxy group or the hydroxy group to complete the reaction.

Phosphoglucomutase (α-D-glucose-1,6-bisphosphate-dependent) catalyzes the transfer of the 1-phospho group of α-D-glucose 1-phosphate to its 6-hydroxy group[142]

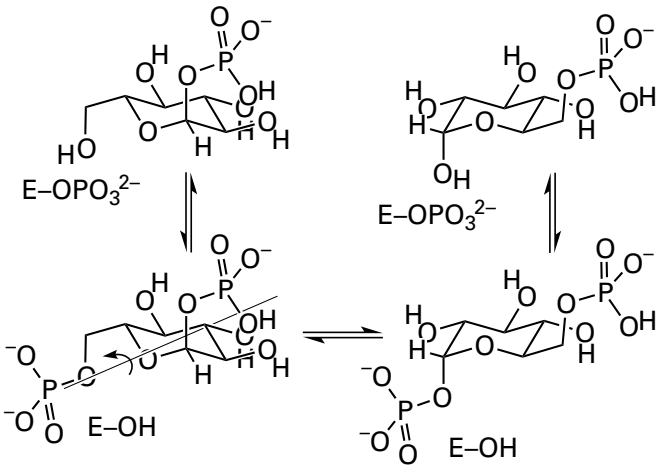

(5–36)

The phosphorylated intermediate ($E–OPO_3^{2-}$) is an O^{β}-phosphoserine (**5–19**) in the active site, which is roughly isoergonic with the phospho groups on carbons 1 and 6. The same phosphorylated enzyme[143] acts on the two monophospho substrates, turning each into the intermediate, α-D-glucose 1,6-bisphosphate, by transferring its phospho group to either the unphosphorylated 6-hydroxy group of α-D-glucose 1-phosphate or the unphosphorylated 1-hydroxy group of D-glucose 6-phosphate, respectively.[144] The intermediate α-D-glucose 1,6-bisphosphate, although occasionally dissociating, usually flips over (around the axis indicated in Equation 5–36) while enclosed tightly within the active site, and then it transfers the other phospho group back to the enzyme, after which the respective monophospho product dissociates.[145]

β-Phosphoglucomutase catalyzes the transfer of the 1-phospho group of β-D-glucose-1-phosphate to its 6-hydroxy group, rather than the 1-phospho group of α-D-glucose 1-phosphate, as was the case with phosphoglucomutase (α-D-glucose-1,6-bisphosphate-dependent). The phosphorylated intermediate in this instance is an O^{γ}-phosphoaspartate even though there seems to be little difference in the enzymatic reaction catalyzed by it and the one catalyzed by phosphoglucomutase (α-D-glucose-1,6-bisphosphate-dependent). β-D-Glucose 1,6-bisphosphate is produced from either β-D-glucose 1-phosphate or D-glucose 6-bisphosphate by the phosphorylated enzyme, but because the active site is open to the solution,[146] the β-D-glucose 1,6-bisphosphate usually dissociates completely and rebinds in the opposite orientation rather than flipping over in the active site to transfer the other phosphate back to the enzyme to complete the reaction.[147]

In the case of phosphoglucomutase (α-D-glucose-1,6-bisphosphate-dependent), the intermediate α-D-glucose 1,6-bisphosphate slowly dissociates from the active site as the reaction progresses, inactivating the enzyme, so a reliable concentration of α-D-glucose 1,6-bisphosphate in the solution is maintained by glucose-1,6-bisphosphate synthase. Because β-D-glucose 1,6-bisphosphate normally dissociates from the active site of β-phosphoglucomutase, the enzyme itself maintains an equilibrium concentration of the intermediate in the solution.

The N^{τ}-phosphohistidinyl intermediate in equine bisphosphoglycerate mutase was identified by isolating a tryptic [^{32}P]phosphorylated peptide.[148] The O^{β}-phosphoseryl intermediate[149] in phosphoglucomutase from *O. cuniculus* was identified by isolating a [^{32}P]phosphorylated peptide from a partial acid hydrolysis of the enzyme.[150] The O^{γ}-phosphoaspartyl intermediate in β-phosphoglucomutase from *Lactococcus lactis* was observed in a crystallographic molecular model of the enzyme.[146]

As was noted earlier, the **stereochemistry** of an enzymatic reaction can also be consistent with the existence of a covalent phosphorylated intermediate.[151] If the overall enzymatic reaction is observed to proceed with inversion of configuration at the phosphorus that is transferred, this observation is consistent with direct in-line transfer between donor and acceptor without the involvement of a phosphorylated intermediate. If the overall reaction is observed to proceed with **retention of configuration at phosphorus**, this is consistent with two successive phosphotransfers both taking place with inversion, one from donor to enzyme and the other from enzyme to acceptor.

There are also phosphorylated intermediates formed from substituted phospho groups. A phosphorylated intermediate[152] in the reaction catalyzed by pyruvate, phosphate dikinase from *Clostridium symbiosum* (previously Equation 3–500)

$$\text{phospho}\textit{enol}\text{pyruvate} + MgOPO_3PO_3^{2-} + 2\,H^+ + AMP^{2-} \rightleftharpoons MgATP^{2-} + HOPO_3^{2-} + \text{pyruvate} \quad (5\text{–}37)$$

is an ***N*$^{\tau}$-diphosphohistidine** (**5–23**)[153,154]

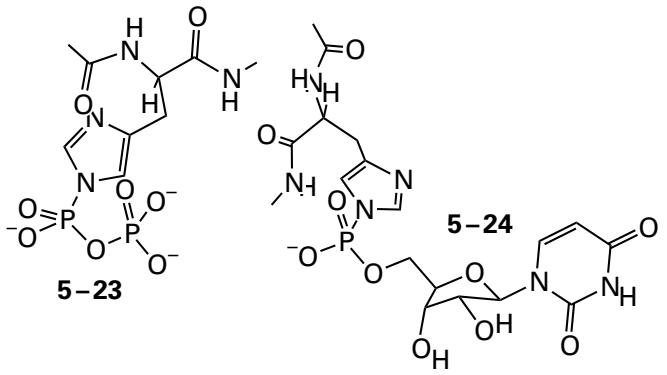

The phosphorylated intermediate in UDP-glucose—hexose-1-phosphate uridylyltransferase

$$\text{UDP-}\alpha\text{-D-glucose} + \alpha\text{-D-galactose 1-phosphate} \rightleftharpoons \alpha\text{-D-glucose 1-phosphate} + \text{UDP-}\alpha\text{-D-galactose} \quad (5\text{–}38)$$

from *E. coli* is an ***N*$^{\tau}$-uridylylhistidine** (**5–24**), the existence of which was confirmed crystallographically[155] after the modified histidine had been identified chemically.[156,157] There is an ***N*$^{\tau}$-adenylylhistidinyl intermediate**, which was identified crystallographically, in the reaction catalyzed by ADP-glucose phosphorylase from *Arabidopsis thaliana*.[158] The existence of the **guanylylhistidinyl intermediate** in the reaction catalyzed by GDP-L-galactose phosphorylase from *A. thaliana*[159] was inferred from electrospray ionization mass spectrometry. In this case, the observed molecular mass of the enzyme increased from 53,107 Da to 53,451 Da upon formation of the intermediate, a difference (345 Da) that is within a hydron of the molecular mass of guanosine monophosphate minus the molecular mass of a molecule of water.

When a type I topoisomerase cleaves one of the two strands of double-helical DNA to permit supercoiling to be relieved, the 3′-phospho group on the 5′ end produced by the cleavage remains as a covalent ***O*^{4}-(3′-phosphopolynucleotidyl)tyrosinyl intermediate**[160]

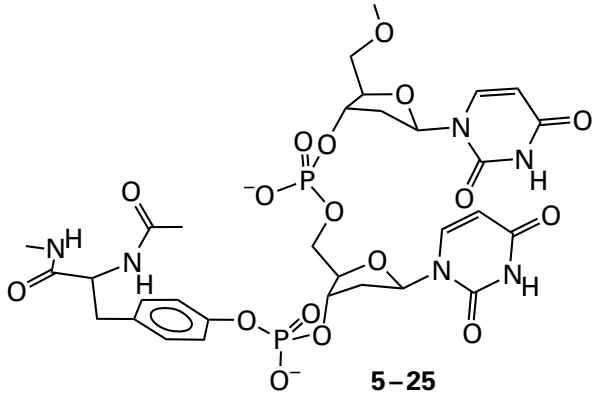

5–25

which has been isolated in a peptide containing the modified tyrosine from topoisomerase I from *S. cerevisiae*[161] and observed crystallographically in a complex between DNA and the active site of human topoisomerase I.[162] This covalent intermediate preserves the free energy of the phospho ester that was in the DNA so that the 3′-phospho group can be rejoined to the 5′-hydroxy group on the 3′ fragment to reconstruct the intact DNA after the supercoiling has been relaxed.

Type II topoisomerase relieves or promotes supercoiling by breaking the two strands of the DNA simultaneously, leaving the two broken strands as O^4-(3′-phosphopolynucleotidyl)tyrosinyl intermediates. The enzyme from *S. cerevisiae* is an α_2 homodimer, so each strand that has been broken ends up with its 5′ end covalently attached to one of the two Tyrosines 782 from the two subunits. The O^4-(3′-phosphopolynucleotidyl)tyrosinyl intermediate has been isolated on a peptide derived from trypsin digestion of topoisomerase II from *S. cerevisiae*,[163] and it has also been observed in a crystallographic molecular model of a complex of topoisomerase II from *S. cerevisiae* and DNA.[164] The two sites of single-strand cleavages on opposite strands of the DNA are immediately adjacent to the crystallographic twofold rotational axis of symmetry in the α_2 homodimer so that there are only four base pairs in the DNA between them.[165] After both covalent intermediates are formed to create the two nearby breaks, there is a conformational change in the protein that dissociates the interface in the α_2 homodimer at which the cleavage has occurred, separating the two ends of the broken DNA and creating a space between them large enough for a portion of the intact, double-helical DNA distant from the site of cleavage to pass through the vacancy.[166-168] The two strands are then rejoined, again taking advantage of the fact that the covalent intermediate has preserved the free energy of the phospho ester.

In the recombinases, there are also covalent phosphotyrosyl intermediates that conserve the free energy of the cleaved phosphodiester after each strand of DNA is severed, but they are formed with phospho groups on the 3′ ends of the strands rather than the 5′ ends.[169]

Lysyliminiums are covalent intermediates in enzymatic aldol condensations, Claisen condensations, dehydrations,[170] and decarboxylations. Covalent ester, thioester, and phosphorylated intermediates are usually stable enough to be identified directly, but lysyliminiums are covalent intermediates that must be **trapped by chemical conversion to a stable species**. Lysyliminiums are usually trapped by reduction. For example, tritium is incorporated into 2-dehydro-3-deoxyphosphogluconate aldolase from *Pseudomonas fluorescens* upon reduction of the intermediate lysyliminium of pyruvate[171] with $Na[^3H]BH_4$ (previously Equation 4–325)

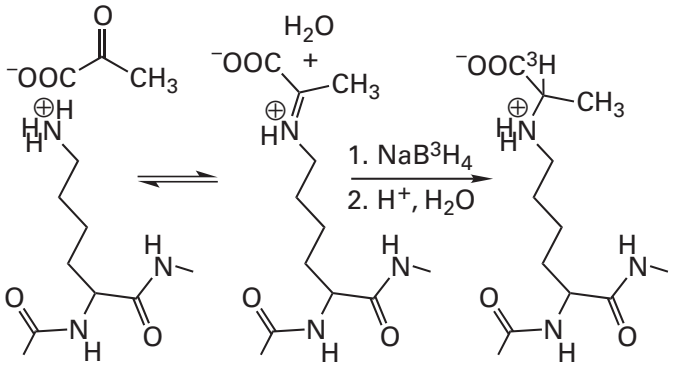

(5–39)

Acetoacetate decarboxylase catalyzes the exchange of one electrophile for another, carbon dioxide for a hydron, at an acidic carbon[172]

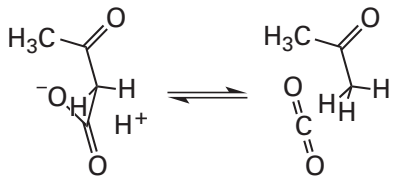

(5–40)

When [3-^{14}C]acetoacetate was mixed with the enzyme from *Clostridium acetobutylicum* in the presence of $NaBH_4$, radioactivity was incorporated into the protein in a reduction analogous to that of the intermediate in 2-dehydro-3-deoxyphosphogluconate aldolase (Equation 5–39). The radioactively modified acetoacetate decarboxylase was digested with trypsin, and the radioactive peptide ELSAYPK([^{14}C]isopropyl)K, in which the radioactive modification was

N^6-[^{14}C]isopropyllysine, was isolated and sequenced.[173] From this observation, it was concluded that the covalent intermediate trapped by **reduction with sodium borohydride** was the lysyliminium between Lysine 115 and acetone

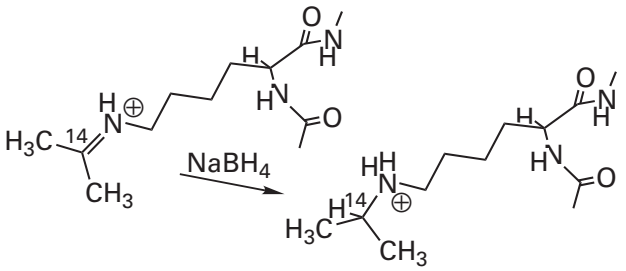

(5–41)

This conclusion is consistent with a mechanism in which the lysyliminium of acetoacetate is formed in the active site to expedite the decarboxylation

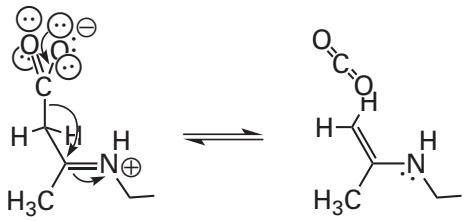

(5–42)

In a crystallographic molecular model of the complex between the enzyme and pentane-2,4-dione, a homologue of acetoacetate in which the carboxy group that would be decarboxylated is replaced by a methyl group, the carbon–carbon bond homologous to the one broken in the normal reaction is positioned by the active site parallel to the π molecular orbital system of the lysyliminium.[172] The enzyme uses the π system of the iminium cation to withdraw electron density from the carbon–carbon σ bond (Equation 5–42).

Mutants of (5-formylfuran-3-yl)methyl phosphate synthase from *Methanocaldococcus jannaschii* that decrease its overall activity, so that intermediates accumulate, were mixed with its substrate, D-glyceraldehyde 3-phosphate. The mixture was reduced with $NaBH_4$ and digested with trypsin, and the resulting **peptides** were submitted to mass spectrometry. In the mass spectrum, there was a peptide that had the mass expected of the tryptic peptide containing Lysine 27 of the enzyme that had been covalently modified at its 6-amino group so that the trypsin was unable to hydrolyze the peptide bond at that location. The modification increased the mass of this peptide and fragments of the peptide containing Lysine 27 by 58 Da, which is the mass of an additional C_3OH_6. This increase is the additional mass expected for the product of reduction by borohydride of the lysyliminium resulting from the α,β-elimination of a phosphate from the lysyliminium of glyceraldehyde 3-phosphate

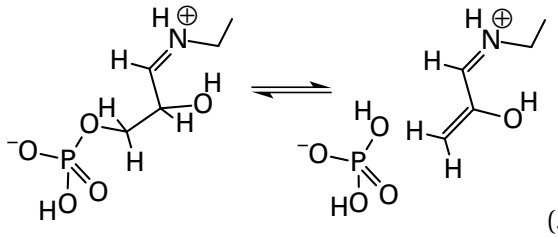

(5–43)

These results from **mass spectrometry** are evidence for the lysyliminium being the initial covalent intermediate in the enzymatic reaction.[174] The lysyliminium accelerates elimination of phosphate to form the enol, which then adds to the carbonyl of the glycerone phosphate that is the second substrate in the reaction that eventually produces (5-formylfuran-3-yl)methyl phosphate.

Both reduction of the lysyliminium in 2-dehydro-3-deoxyphosphogluconate aldolase (Equation 5–39) and reduction of the lysyliminium in acetoacetate decarboxylase (Equation 5–41) were based on earlier observations with fructose-bisphosphate aldolase in which a very similar lysyliminium between a lysine in the active site and glycerone phosphate (Figure 4–36) had been trapped with sodium borohydride.[175,176] When fructose-bisphosphate aldolase from *O. cuniculus* is mixed with glycerone phosphate, a tautomeric equilibrium is established on the active site between the lysyliminium and the lysylenamine that are both covalent intermediates in the enzymatic reaction[176]

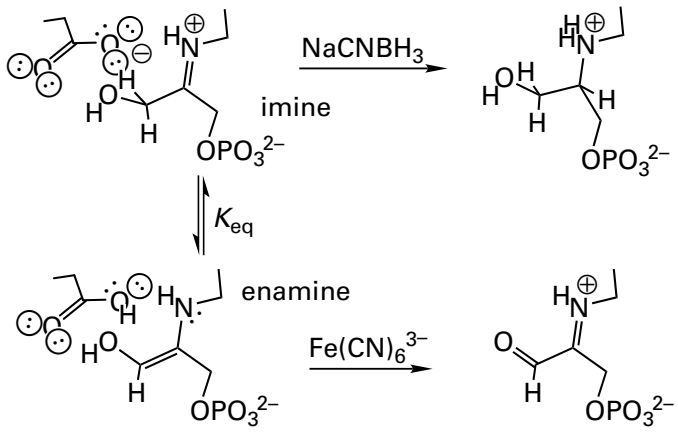

(5–44)

The enzyme could be denatured rapidly in acid, and the **lysylenamine could be trapped by oxidation**,

either with tetranitromethane[177] or with ferricyanide, or the lysyliminium could be trapped with sodium cyanoborohydride.[178] In this way, the equilibrium constant for the tautomerization within the active site ($K_{eq} = 3$) could be ascertained.

Crystallographic molecular models of the lysyliminium intermediates in fructose-bisphosphate aldolase have been presented. When crystals of the enzyme from *O. cuniculus* were suspended in 10 mM D-fructose 1,6-bisphosphate for 3 min and then rapidly frozen, the iminium intermediate of D-fructose 1,6-bisphosphate was captured at equilibrium in the active site (Figure 5–3).[179-182] The carbon–carbon bond weakened by the iminium is held by the active site so that it is parallel to its π system. When Lysine 146, which shuttles a hydron from the 4-hydroxy group of D-fructose 1,6-bisphosphate to carbon 3 of the enamine of glycerone phosphate, was mutated to alanine, the turnover number of the enzyme decreased 30,000-fold.[183] When crystals of the enzyme were suspended for 2 min in 1 mM glycerone phosphate and then rapidly frozen, the lysylenamine of glycerone phosphate (Equation 5–44) was observed in the active site of the crystallographic molecular model.[179] When a similar experiment, however, was performed with crystals of 2-dehydro-3-deoxyphosphogluconate aldolase from *E. coli*, an equilibrium mixture of the lysylhemiaminal and the lysyliminium and water was observed in the active site.[184]

Porphobilinogen synthase catalyzes the condensation of two α-amino ketones to form a pyrrole

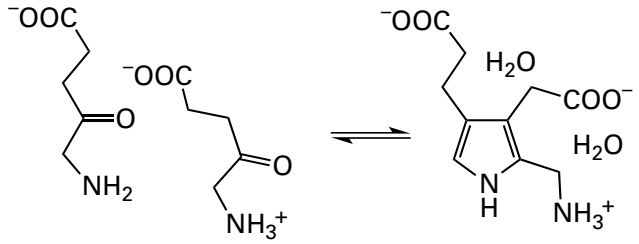

(5–45)

In the active site of the enzyme from *P. aeruginosa*, Lysines 205 and 260 are adjacent to each other,[185] and in a crystallographic molecular model of a mutant in which Aspartate 139 has been changed to asparagine to decrease the catalytic constant of the enzyme, the two reactants, both 5-aminolevulinates, occupy these two lysines as the respective lysyliminiums.[186] The enamine of the lysyliminium of Lysine 205 condenses with the iminium carbon of the lysyliminium of Lysine 260, followed by addition of the amino group of the lysyliminium of Lysine 260 to the lysyliminium of Lysine 205

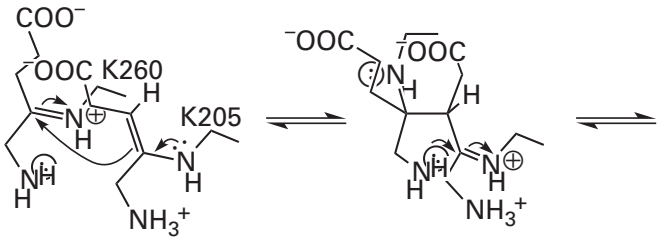

(5–46)

to form the 2,4-diaminopyrrolidine in which the amino groups at carbons 2 and 4 are the amino groups of the two lysines. Two successive eliminations of the amino groups of these two lysines end up aromatizing the pyrrolidine to the pyrrole and simultaneously releasing the ring from the two lysines.

As was the case with (5-formylfuran-3-yl)methyl phosphate synthase, lysyliminium **5–26** that weakens the carbon–phosphorus bond

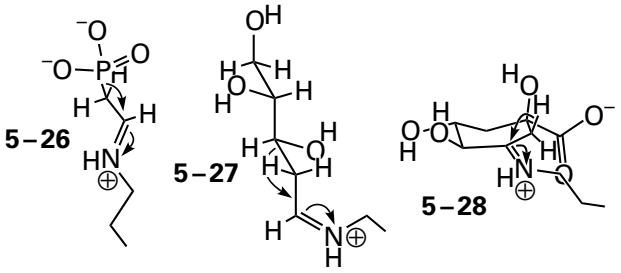

in the active site of phosphonoacetaldehyde hydrolase from *Bacillus cereus* has been trapped by reduction with [^{3}H]$NaBH_4$, and a tryptic peptide has been isolated that contains the resulting N^6-[^{3}H]ethyllysine, which is the product of reduction by [^{3}H]BH_4^- of the N^6-vinyllysine formed by dissociation of the monomeric metaphosphate.[187] This same *N*-ethyllysine has also been observed crystallographically.[188] Both lysyliminium **5–27,** which weakens the carbon–carbon bond in 2-deoxy-D-ribose 5-phosphate in the active site of deoxyribose-phosphate aldolase from *E. coli*, and the hemiaminal that precedes lysyliminium **5–27** in the mechanism of the reaction have been observed crystallographically.[189]

Lysyliminium **5–28**,[190] which results from the nucleophilic substitution of the amino group of a lysine in the active site of 3-dehydroquinate dehydratase for the carbonyl oxygen at carbon 3 of the substrate 3-dehydroquinate, weakens the adjacent carbon–hydrogen bond so that it can be removed as a

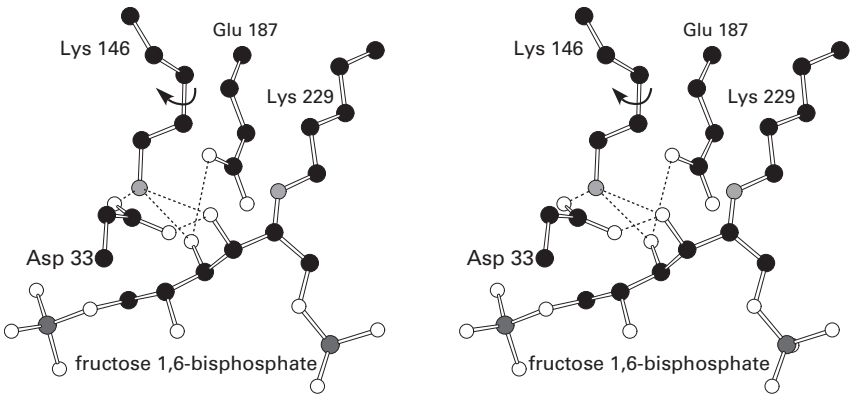

Figure 5–3: Stereodrawing[181] of a crystallographic molecular model of the active site of fructose-bisphosphate aldolase from *O. cuniculus* occupied by D-fructose 1,6-bisphosphate.[179] Black atoms are carbons, white atoms are oxygens, small gray atoms are nitrogens, and large dark gray atoms are atoms of phosphorus. Crystals of fructose-bisphosphate aldolase from *O. cuniculus*, which had been expressed in *E. coli*, were soaked for 3 min in a solution containing 10 mM D-fructose 1,6-bisphosphate and then quickly frozen. In the map of electron density, there was a feature that could unambiguously be accounted for as the iminium adduct between a molecule of D-fructose 1,6-bisphosphate and the 6-amino group of Lysine 229. The bond between carbons 3 and 4 of D-fructose 1,6-bisphosphate in this adduct is held by the active site so that it is parallel to the π system of the iminium cation that is withdrawing its electron density. The 3-hydroxy and 4-hydroxy groups of D-fructose 1,6-bisphosphate form a network of hydrogen bonds with the side chains of Aspartate 33, Lysine 146, and Glutamate 187. During the reaction, the 6-amino group of Lysine 146 removes the hydron from the 4-hydroxy group as it becomes the carbonyl of glyceraldehyde 3-phosphate while the bond between carbons 3 and 4 is broken. Lysine 146 then pivots about the bond between its γ and δ carbons to align its now 6-ammonio group to hydronate carbon 3 of the enamine that eventually becomes glycerone phosphate. The enzymatic reaction proceeds with retention of configuration at carbon 3 of D-fructose 1,6-bisphosphate.[182]

hydron to initiate the dehydration of 3-dehydroquinate. Evidence for the existence of lysyliminium **5–28** was provided by mass spectrometry. 3-Dehydroquinate dehydratase from *E. coli* was mixed with the reactant 3-dehydroquinate and then immediately injected into an electrospray mass spectrometer. A component with a mass of 27,618 mass units, which is 151 mass units greater than the observed mass of the unliganded enzyme (27,467 mass units), was detected in the mass spectrum.[191] This increase is within two hydrons of the mass expected for the lysyliminium of the product of dehydration, 3-dehydroshikimate (molar mass 171 g mol^{-1}). When the lysyliminium forms, the other product is a molecule of water (molar mass 18 g mol^{-1}) containing the oxygen of the original carbonyl group of 3-dehydroshikimate. The lysyliminium with the lysine before the dehydration has been observed in the active site of a crystallographic molecular model of 3-dehydroquinate dehydratase from *Salmonella enterica* in a complex with the substrate 3-dehydroquinate, and the lysyliminium with the lysine in the active site following the dehydration has been observed in the crystallographic molecular model of 3-dehydroquinate dehydratase from *Clostridioides difficile* in a complex with 3-dehydroshikimate.[192] In the crystallographic molecular models of the complexes between the active site of 3-dehydroquinate dehydratase from *E. coli* and either quinate or shikimate,[193] the analogues of the respective substrates that have hydroxy groups at carbon 3, rather than carbonyl groups at which addition of the amino group of the lysine would occur, the distances between the respective carbons 3 and the amino groups of the same lysines in each model are each only 0.36 nm.

Mass spectrometry was also used to identify a covalent intermediate in the nucleophilic substitution catalyzed by aminodeoxychorismate synthase from *E. coli* (52,984 mass units) When the enzyme was mixed with the substrate chorismate (225 g mol^{-1}) in the absence of L-glutamine, the source of the ammonia in the nucleophilic substitution of an amino group for a hydroxy group catalyzed by the enzyme, a new peak of 53,192 mass units was observed in the mass spectrum of the enzyme,[194] consistent with the existence of the covalent intermediate formed between chorismate and Lysine 274 in the active site

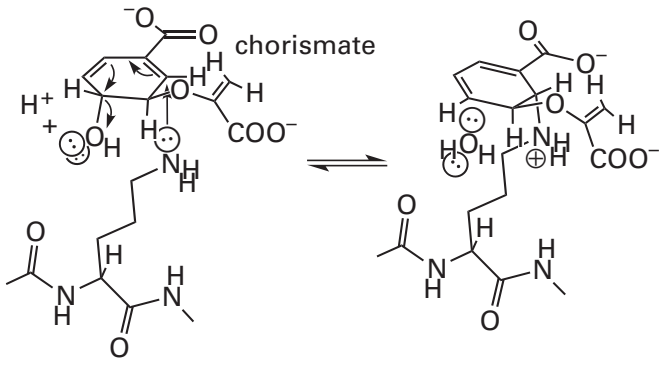

(5–47)

Nucleophilic addition of ammonia to carbon 4 of this adduct from which a molecule of water has just left would give, in reverse, 4-amino-4-deoxychorismate, the normal product in this enzymatic reaction.

The central covalent intermediate in the enzymatic reaction catalyzed by DNA-formamidopyrimidine glycosylase, which has been observed crystallographically within the active site of the enzyme from *Thermus thermophilus*,[195] is a **prolyliminium** formed with the amino-terminal proline of the protein

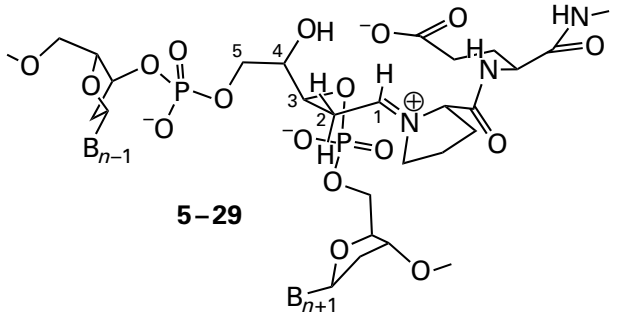

5–29

where B_{n+1} and B_{n-1} are the bases in the DNA on the deoxyriboses that precede and follow the deoxyribose at which the enzyme cleaves the strand of DNA, and the carbons in that deoxyribose are numbered.* The advantage of a prolyliminium is that it does not need to retain a hydron to be cationic and hence more electrophilic. This intermediate then participates in a β-elimination of the 5′-phospho group at carbon 3, followed by a δ-elimination of the 3′-phospho group at carbon 5. The two eliminations cleave the strand of DNA, and they leave clean 5′ and 3′ phosphorylated ends. The other product is the prolylimine of 2,4-hydroxypenta-2,4-dienal.

*The central deoxyribose ring has been opened at the glycosidic carbon during the formation of the imine.

Addition of the sulfido group of a cysteine to the β carbon in an α,β-unsaturated carbonyl or acyl derivative produces in one step a covalently bound enolate. A covalent intermediate, **2-(cysteinyl)-butanedioate** (**5–30**), is formed between Cysteine 76 and maleate

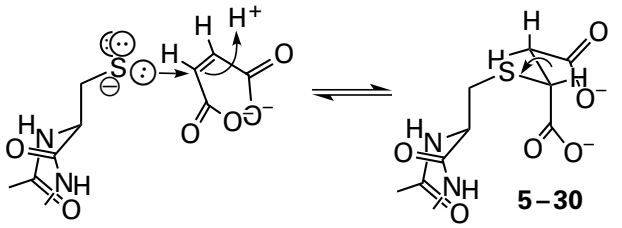

(5–48)

in the active site of maleate isomerase

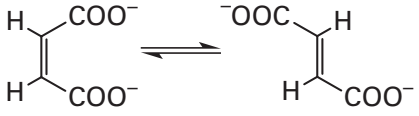

(5–49)

from *Nocardia farcinica*. The initial step in formation of adduct **5–30** is the direct formation of the *gem*-enediolate at the carbon adjacent to the one to which the sulfido group adds. The *gem*-enediolate would then be hydronated on the α carbon either during or after its formation. The resulting 2-(cysteinyl)-butanedioate (**5–30**), an unprecedented intermediate, was discovered in the crystallographic map of electron density (Figure 5–4)[196] for a mutant of the enzyme in which Cysteine 194, a catalytic acid in the enzymatic reaction, was converted to an alanine and that had been crystallized in a solution of 50 mM maleate. It is formed in a Michael addition of the sulfanyl group of Cysteine 76 to one or the other of the α,β-unsaturated carboxylic acids that are substrates for the enzyme. The purpose of the adduct is to break the double bond in either maleate or fumarate and permit a rotation about the now single bond (indicated by the arrow in covalent intermediate **5–30**). Consequently, when the sulfanyl group of the cysteine leaves in a retro-Michael addition, either maleate [(*Z*)-but-2-enedioate] or fumarate [(*E*)-but-2-enedioate] is produced on the active site. In the Michael adduct observed in the crystallographic molecular model (Figure 5–4), the dihedral angle along the central carbon–carbon bond is almost exactly halfway between the dihedral angle for the *Z*-configuration and the one for the *E*-configuration of the respective substrates.

Thymidylate synthase is responsible for providing the methyl group on thymidine (previously Equation 3–535)

5,10-methylenetetrahydrofolate + dUMP $\rightleftharpoons$ dTMP + 7,8-dihydrofolate

(5–50)

where dUMP is 2′-deoxyuridine 5′-monophosphate and dTMP is thymidine 5′-monophosphate. During this reaction, the methylene carbon of 5,10-methylenetetrahydrofolate, an electrophile, becomes the methyl group of dTMP, in a substitution for the hydron at carbon 5 of the uracil in dUMP, which is also an electrophile. Thymidylate synthase is an excellent example of the array of chemical transformations that an active site can apply consecutively to the same covalent intermediate and the **evidence that can be assembled to validate such a multistep mechanism**. Support for the existence of each of the several covalent intermediates in the reaction has been provided either chemically or crystallographically or by both procedures.

Thymidylate synthase is covalently inactivated[197,198] by 2′-deoxy-5-fluorouridine 5′-monophosphate in a reaction involving nucleophilic addition of the sulfido group of a cysteine in the active site of the enzyme to carbon 6 in the α,β-unsaturated *N*-carbamoylcarbamoyl group of 2′-deoxy-5-fluorouridine 5′-monophosphate[199]

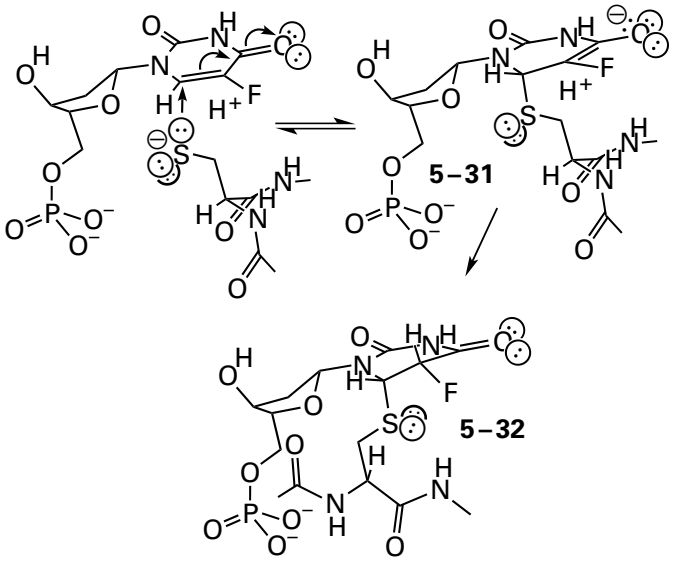

(5–51)

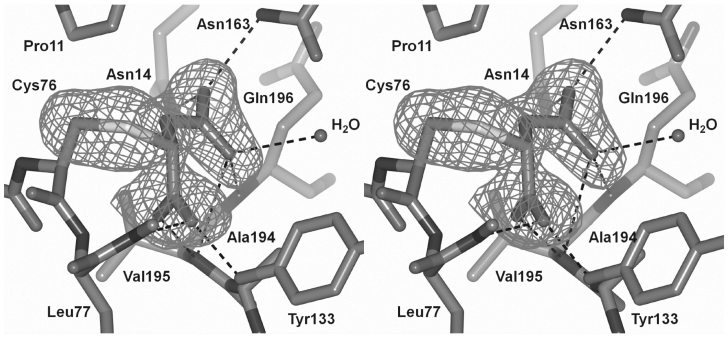

Figure 5–4: Crystallographic molecular model of the active site of maleate isomerase from *N. farcinica* occupied by the covalent intermediate that results from nucleophilic addition of the sulfanyl group of Cysteine 76.[196] An almost completely inactive mutant of the enzyme, in which Cysteine 194 had been mutated to alanine, was crystallized from a solution containing 50 mM maleate. In the resulting map of electron density, there was a feature immediately adjacent to the sulfanyl group of Cysteine 76 that was consistent with the nucleophilic adduct of that sulfanyl group with the carbon–carbon double bond of maleate. Because the 4-carboxy group of the adduct was held in the active site in the same plane as the bond between carbons 2 and 3, the adduct could have been the *gem*-enediolate or the hydronated *gem*-enediolate. A model of *S*-[(2*R*)-succinyl]cysteine was inserted into the map of electron density in place of Cysteine 76, and the resulting crystallographic molecular model was submitted to refinement. As the refinement converged, the succinyl group and the side chain of Cysteine 76 were removed from the model, and the final rounds of refinement were performed to produce the omit map of electron density drawn in the figure. The omit map of electron density is superposed on the refined structure from which the succinate and the side chain were not removed. Reprinted with permission from reference 196. Copyright 2010 American Chemical Society. https://doi.org/10.1021/ja1053576

The cysteine that forms covalently bound enolate **5–31**, Cysteine 198 in the enzyme from *Lactobacillus casei*, was identified by isolating and sequencing a cyanogen bromide fragment from a sample of the enzyme that had been covalently modified by 2′-deoxy-[2-^{14}C]-5-fluorouridine 5′-monophosphate.[200] In the process of digestion and isolation of the peptide, enolate **5–31** is hydronated and stabilized as adduct **5–32**, which is the product of a Michael addition of the sulfanyl group of the cysteine to the α,β-unsaturated acyl group in the substrate. It is assumed that, during the normal reaction, the same cysteine also adds in the same manner to carbon 6 of the natural reactant, dUMP, to produce the homologous enolate (**5–31** with H in place of F) of the homologous *N*-carbamoylamide. The normal reaction, however, immediately proceeds to completion for two reasons: first, there is not a fluorine at carbon 5 in dUMP strongly withdrawing electron density, as there is in enolate **5–31**, and second, in the 2′-deoxyuridine 5′-monophosphate there is not a fluorine taking the place of the hydrogen on carbon 5, which is removed as a hydron in the later steps of the reaction.

The advantage of this nucleophilic addition in the normal reaction is to turn carbon 5 in the uracil in one step into the carbanionic carbon of an enolate. This enolate is the conjugate base of an *N*-carbamoylamide (see Equation 5–51). That formation of the covalent intermediate leads to a dramatic increase in the basicity of carbon 5 has been demonstrated in a model system by noting the appearance of hydrogen exchange at carbon 5 of uridine upon addition of thiols[201]

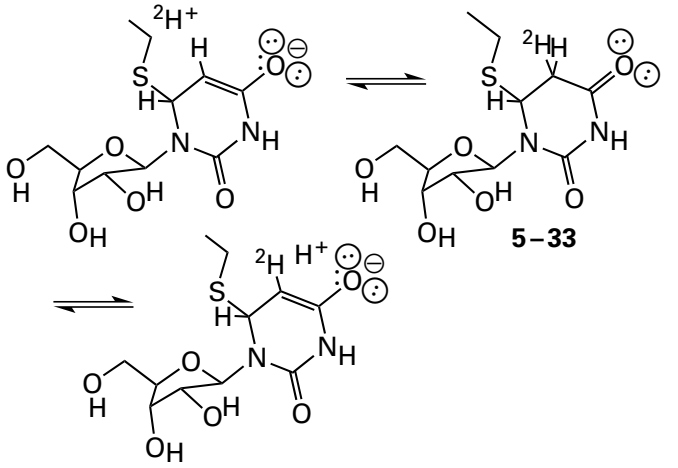

(5–52)

as would be expected for the α-position of saturated *N*-carbamoylamide **5–33**.

The enolate of the normal substrate, dUMP, has been observed in several crystallographic molecular models of the active site of thymidylate synthase from *E. coli* (60% identity; 0.4 gap percent) in which either inactive analogues of 5,10-methylenetetrahydrofolate are also occupying the active site or the enzyme had been mutated to decrease its catalytic constant.[202-204]

On the basis of all these observations, it can be concluded that addition of the cysteine to carbon 6 of dUMP produces the respective enolate (**5–31** with H in place of F or Equation 5–52 with deoxyribose in place of ribose) in the active site as the **first covalent intermediate** in the normal mechanism.

In crystallographic molecular models, this enolate, formed by addition of the sulfanyl group of the homologous Cysteine 146 to dUMP in the active site of the enzyme from *E. coli*, is stabilized in an oxyanion hole formed by an amido nitrogen–hydrogen of the side chain of Asparagine 177 and a molecule of water relaying the acidity of Glutamic Acid 58.[202-208] When the homologous asparagine in the enzyme from *L. casei* is mutated to serine,[199] the rate constant $k_0\,(K_{m,dUMP})^{-1}\,(K_{m,mTHF})^{-1}$ for the enzyme, where mTHF is 5,10-methylenetetrahydrofolate, decreases by a factor of 4000, and when the homologous glutamate in the enzyme from *L . casei* is mutated to alanine, the rate constant $k_0\,(K_{m,dUMP})^{-1}\,(K_{m,mTHF})^{-1}$ decreases by a factor of 10^6. The exchange of tritium at carbon 5 of dUMP, however, relative to the rate of thymidylate synthesis increases by a factor of 20.[209] This last observation suggests that the enzymatic reaction has been blocked because the enolate is not properly stabilized so that it cannot rapidly participate in the next step of the reaction and so that the resulting *N*-carbamoylamide (**5–32** with H replacing F or **5–33** with deoxyribose in place of ribose) can participate only in hydrogen exchange (Equation 5–52). Consistent with this explanation is the fact that one of the main effects of mutation of the glutamate is a decrease in the rate of the nucleophilic addition of this enolate that occurs in the next step of the enzymatic reaction.[210]

In the crystallographic map of electron density[208,211] for the complex formed between thymidylate synthase of *E. coli* and 2′-deoxy-5-fluorouridine 5′-monophosphate and 5,10-methylenetetrahydrofolate, both the covalent bond formed between Cysteine 146 from the active site and carbon 6 of 5-fluorouracil (**5–31**) and a new covalent bond between the methylene carbon of N^5-methylenetetrahydrofolate (previously **1–82**)

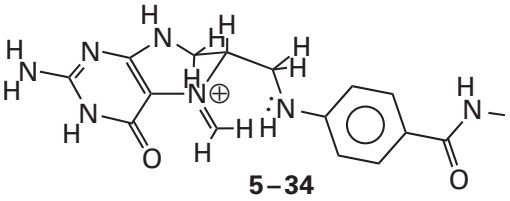

5–34

and carbon 5 of 5-fluorouracil are observed

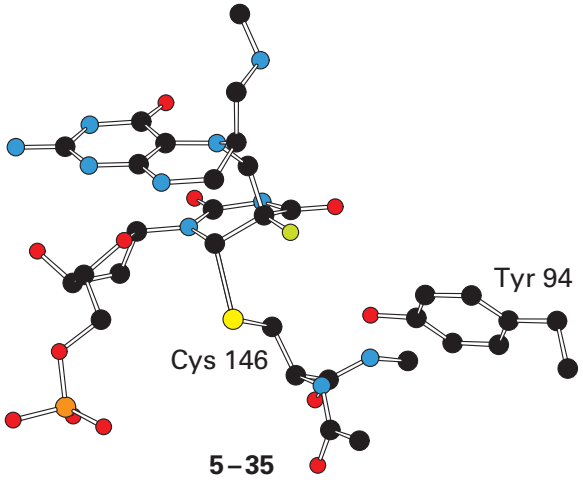

5–35

This **second covalent intermediate** is formed by nucleophilic addition of enolate **5–31** to the electrophilic methylene carbon in N^5-methylenetetrahydrofolate

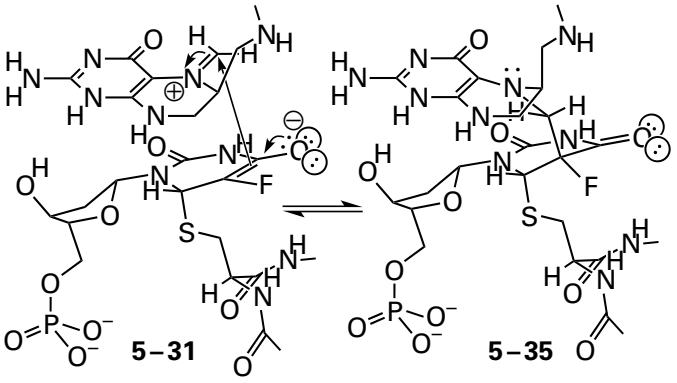

5–31 **5–35**

(5–53)

which is formed from 5,10-methylenetetrahydrofolate by the usual dissociation of nitrogen 10. This crystallographic molecular model of the unnatural intermediate **5–35** verifies the capacity of the normal covalent, intermediate enolate (**5–31** with H in place of F) formed from the cysteine and 2′-deoxyuridine 5′-monophosphate to function as an enolate, as well as the ability of that enolate in the active site to add to the 5-methyleneiminium in N^5-methylenetetrahydrofolate to form adduct **5–36** (Figure 5–5) during the normal enzymatic reaction. If anything, the substitution of that hydrogen with a fluorine should hinder this nucleophilic addition because of the electron withdrawal from the enolate caused by fluorine, yet it does not.

A covalent, intermediate enolate, analogous to enolate **5–31**, the first covalent intermediate of the reaction catalyzed by thymidylate synthase, forms between a cytosine in DNA and a cysteine in the active site of DNA (cytosine-5-)-methyltransferase from *Haemophilus parahaemolyticus*.[212] In this case, however, the covalent, intermediate enolate is methylated in a concerted nucleophilic substitution at carbanionic carbon 5 of this adduct of cytosine by *S*-adenosyl-L-methionine

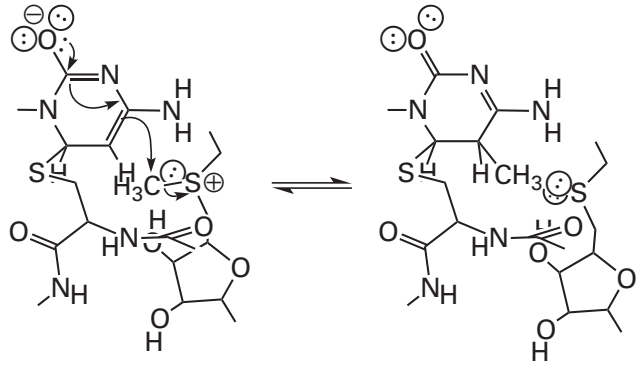

(5–54)

rather than indirectly by 5,10-methylenetetrahydrofolate. This reaction illustrates the nucleophilicity of the intermediate enolate.

An analogous enolate is also formed between carbon 6 in a uracil in tRNA and a cysteine in the active site of methylenetetrahydrofolate—tRNA-(uracil^{54}-C^5)-methyltransferase [NAD(P)H-oxidizing] from *B. subtilis*. The ultimate source of the methyl group in this case is N^5-methylenetetrahydrofolate, but the methylene at carbon 5 of N^5-methylenetetrahydrofolate is first transferred to nitrogen 5 of the prosthetic flavin in the active site of the enzyme, a transfer of a methylene group from one anilino nitrogen to another, where it ends up as a methylene group between nitrogen 5 of the flavin and the sulfanyl group of a cysteine in the active site, before being transferred to carbon 5 of the uracil in the tRNA.[213]

The **fourth covalent intermediate*** in the normal reaction of thymidylate synthase is the exocyclic methylene at carbon 5 of the original uracil in dUMP (**5–38**), which is formed by an elimination (Figure 5–5) in the first step of which the hydrogen on

*This intermediate, the fourth, is presented before the third because its existence, which has been proven, is evidence for the existence of **5–37**, the third intermediate.

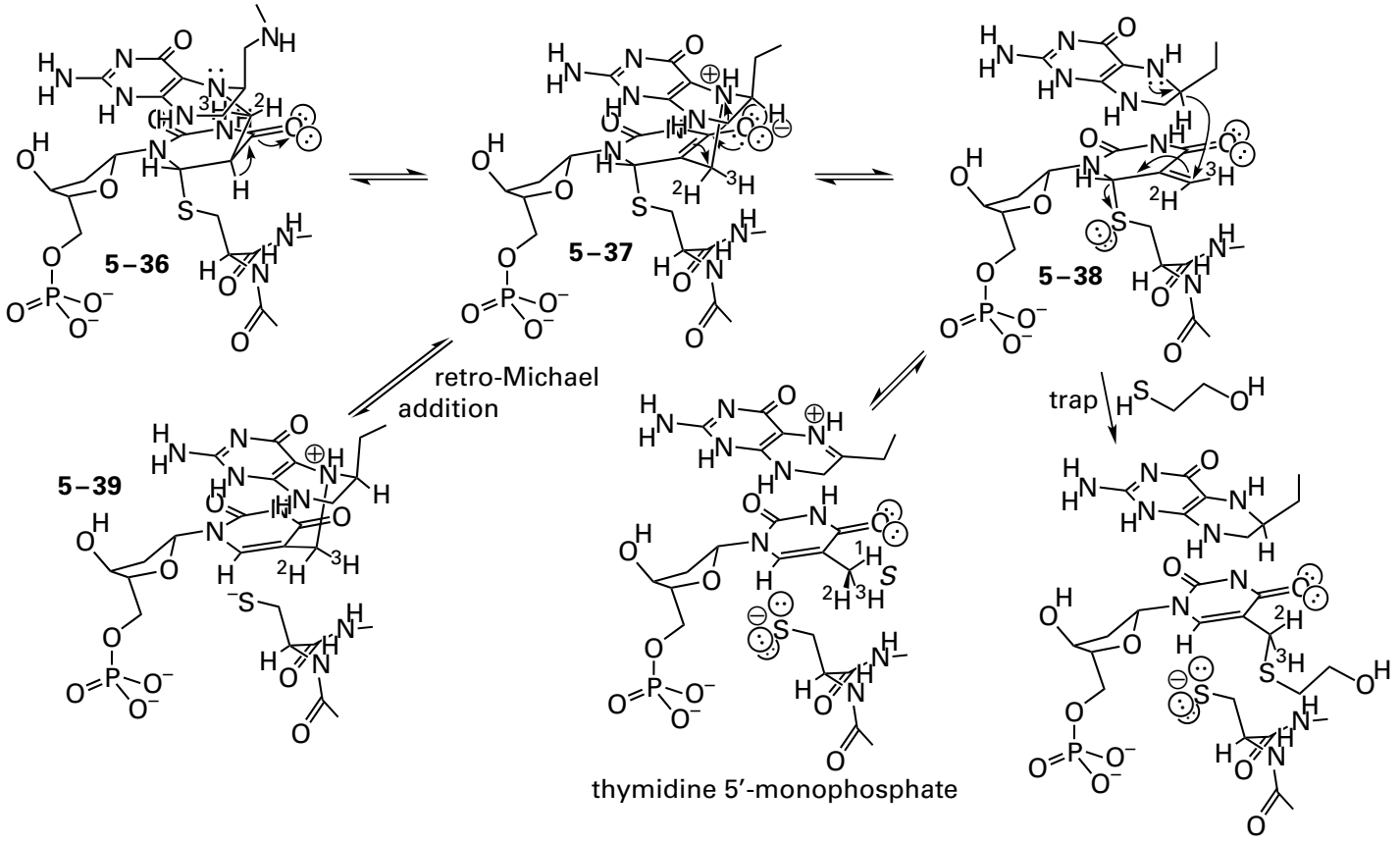

Figure 5–5: Final steps in the mechanism of the reaction catalyzed by thymidylate synthase. The ternary complex **5–36** formed from Cysteine 146, 2′-deoxyuridine 5′-phosphate, and 5,10-methylenetetrahydrofolate is dehydronated at carbon 5 of the former uracil, which is adjacent to the carbamoyl group at carbon 4, and nitrogen 5 of the tetrahydrofolate is hydronated to produce enolate **5–37**. This tautomerization producing enolate **5–37** sets up the elimination that produces exocyclic olefin **5–38** of the uracil. A hydride is transferred from tetrahydrofolate to this exocyclic olefin to produce the enolate, which then undergoes a elimination of cysteine in a step producing the 5-methyluracil (thymine) in the product, thymidine 5′-phosphate. There are two side reactions along the main path. First, thioether **5–37** may dissociate in a retro-Michael addition into the thiolate and adduct **5–39**, but that would decrease dramatically the elimination of the tetrahydrofolate from adduct **5–39** because the enolate would be lost. Second, α,β-unsaturated ketone **5–38** can be trapped with 2-sulfanylethanol.

carbon 5 is removed as a hydron by the 4-hydroxyphenyl group of Tyrosine 94 (see **5–35**). In the crystallographic molecular models[208,211] of the ternary complex **5–35** formed between Cysteine 146 in the active site of thymidylate synthase from *E. coli* and 2′-deoxy-5-fluorouridine 5′-phosphate and N^5-methylenetetrahydrofolate, the complex has the stereochemistry expected for the immediate product of addition of the enolate (Equation 5–53).* The bond just formed between the methylene carbon and carbon 5 of the uracil in dUMP is parallel to the π system of the acyl group at carbon 4 of the uracil, and the new carbon–carbon bond is antiperiplanar to the lone pair of electrons on nitrogen 5 of tetrahydrofolate. For removal of the hydron, however, from carbon 5 by the 4-hydroxyphenyl group of Tyrosine 94 that initiates the elimination leading to the exocyclic methylene (Figure 5–5), the bond to the hydrogen on carbon 5 of the original uracil (the bond to the fluorine in **5–35**) must be parallel to the π system of the acyl group at carbon 4 of the intermediate.[211] This orientation can be achieved in the boat conformation of the ring of the original uracil (compare the conformation of the ring of the original uracil at carbon 5 in **5–35** with its conformation in **5–36**). Following removal of the hydron

*The carbon–sulfur bond (0.216 nm rather than 0.19 nm) is stretched in the crystallographic molecular model of adduct **5–35,** perhaps because of a steric effect resulting from the fact that the hydroxy group of Tyrosine 94 is pushing up on the fluorine (van der Waals radius of 0.15 nm) of **5–35** (0.32 nm). This steric effect is probably much less in the actual intermediate in which there is a hydron (van der Waals radius of 0.115 nm) rather than a fluorine on carbon 5, so in the actual intermediate in the active site, the carbon–sulfur bond could well be unstretched.

on carbon 5 by Tyrosine 194, the bond to nitrogen 5 of tetrahydrofolate, which is now parallel to the π system of enolate **5–37**, which is the **third covalent intermediate** in the reaction, is broken in the elimination* to give the exocyclic methylene in **5–38**.

Aside from these electronic considerations, the intermediacy of enolate **5–37**, which has not been observed crystallographically, is also consistent with the known stereochemistry of the reaction. (6*R*,11*S*)-[11-^{3}H,11-^{2}H]-5,10-Methylenetetrahydrofolate produces (5*S*)-[5-^{3}H,5-^{2}H]thymidine monophosphate.[214,215] Because (6*R*,11*S*)-[11-^{3}H,11-^{2}H]-5,10-methylenetetrahydrofolate has the 11*S* conformation, when the 5-methyleneiminium cation is formed from (6*R*,11*S*)-[11-^{3}H,11-^{2}H]-5,10-methylenetetrahydrofolate, it will be the *Z* isomer[215]

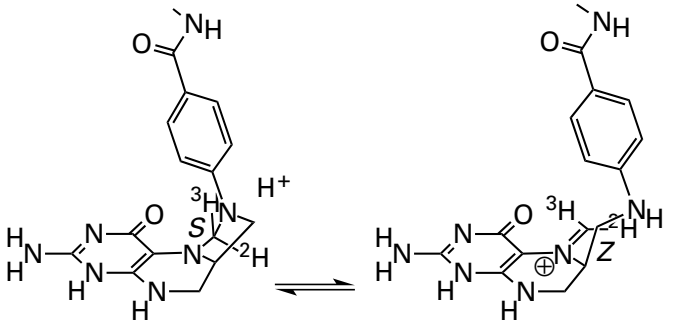

(5–55)

This isomer would produce (Equation 5–53) adduct **5–36** with the noted stereochemistry (Figure 5–5).[211] Upon isomerization, elimination, and direct intramolecular hydride transfer[216,217] from carbon 6 of tetrahydrofolate, which must occur from above in orientation **5–38**, the (*S*)-[^{3}H,^{2}H]methyl group would be generated.

Further evidence for existence of covalent intermediate **5–37** has been provided by chemical synthesis. In intermediate enolate **5–37**, the sulfur of the sulfanyl group of the cysteine in the active site is situated in an electronically equivalent location to nitrogen 5 of tetrahydrofolate because the bond between the original carbon 6 of the uracil in dUMP and this sulfur is parallel to the π molecular orbital system of the enolate, as is the bond between the exocyclic methylene and nitrogen 5 of tetrahydrofolate. Consequently, it would be surprising if the sulfur were not also prone to elimination, just as is nitrogen 5 of tetrahydrofolate, to give intermediate **5–39**. Intermediate **5–39** is no longer a covalent intermediate, and it should be able to leave and enter the active site from the solution. In fact, intermediate **5–39** has been synthesized and shown to be a kinetically competent precursor to 5,10-methylenetetrahydrofolate and dUMP and to tetrahydrofolate and dTMP.[218] Intermediate **5–39** has a catalytic constant that is twice that for the reactants 5,10-methylenetetrahydrofolate and dUMP.

When thymidylate synthase from *E. coli* is in the process of catalyzing the methylation of dUMP, the reaction is quenched with hydrochloric acid, and the quenched solution is submitted to chromatography, intermediate **5–39** is one product of the quench.[219] It has been proposed that intermediate **5–39** is an actual intermediate in the overall reaction, formed by elimination of the sulfido group and a hydron from intermediate **5–36,** and that the readdition of the sulfido group to carbon 6 in intermediate **5–39,** coincident with dissociation of the anilino nitrogen of tetrahydrofolate, then gives intermediate **5–38**. Elimination of the sulfido group of the cysteine, however, from covalent intermediate **5–36**, which is a retro-Michael addition, would require that intermediate **5–37** be formed in any case, so the advantage of forming noncovalent intermediate intermediate **5–39** is far from obvious. In addition, the fact that synthetic intermediate **5–39** is able to enter and presumably escape from the active site with ease, while covalent intermediate **5–37** cannot, seems to mitigate against this proposal.

During the elimination from intermediate **5–36** that produces covalent intermediate **5–38** (Figure 5–5), an elimination which has the enolate **5–37** as an intermediate, the hydron on carbon 5 of what was the uracil in dUMP, because it is acidic as a result of addition of the sulfido group to the uracil, can be removed by Tyrosine 94 of the enzyme from *E. coli*.[205,207,208] When the homologous tyrosine, Tyrosine 146, in the enzyme from *L. casei* is mutated to phenylalanine, the rate constant $k_0\,(K_{m,dUMP})^{-1}$ $(K_{m,mTHF})^{-1}$ decreases by a factor of 10,000. When it is replaced by 2-fluorotyrosine, 3-fluorotyrosine, or 3,5-difluorotyrosine, the pK_a observed in the pH–rate profile for the steady-state Michaelis constant $K_{m,mTHF}$ for 5,10-methylenetetrahydrofolate decreased proportionally to the decrease in pK_a for the respective fluorotyrosine.[220]

The product of the elimination in the mechanism of thymidylate synthase described in the first two steps of Figure 5–5 is the covalent intermediate

*Nitrogen 5 of tetrahydrofolate must be hydronated in the usual inescapable requirement before the elimination can occur. The closest acid (0.41 nm) in the crystallographic molecular model[208] of adduct **5–35** is another molecule of water forming a hydrogen bond to the carboxy group of Glutamate 58 of the enzyme from *E. coli*, and this water could relay the acidity of Glutamate 58 to nitrogen 5.

2′-deoxy-6-cysteinyl-5-methyleneuridine 5′-monophosphate (**5–38**). The exocyclic methylene in the 2′-deoxy-6-cysteinyl-5-methyleneuridine is in a carbon–carbon double bond α,β to an acyl carbon and should be susceptible to nucleophilic additions. In fact, intermediate **5–38** has been trapped in a Michael addition with 2-sulfanylethanol (Figure 5–5) in a mutant of the enzyme from *E. coli* in which Tryptophan 82 has been mutated to tyrosine to decrease the rate of steps that follow its formation in the mechanism of the enzyme. The resulting product of this nucleophilic addition was isolated and identified by nuclear magnetic resonance spectroscopy and mass spectrometry.[221]

The final step in the reaction catalyzed by thymidylate synthase is the transfer of a hydride from carbon 6 of the coenzyme tetrahydrofolate to the 5-methylene group of intermediate **5–38** (Figure 5–5). This transfer is concerted with the leaving of sulfur in the sulfanyl group of cysteine in the active site[222] to give thymidine 5′-monophosphate, the **final product** of the methylation. This reduction is required because the original carbon in 5,10-methylenetetrahydrofolate is at the carbonyl oxidation state and the methyl group in thymidine 5′-monophosphate is the vinylogous *N*-methylurea. In the active site of methylenetetrahydrofolate—tRNA-(uracil^{54}-C^5)-methyltransferase [NAD(P)H-oxidizing] from *B. subtilis*, the reduced flavin that transferred the methylene group to carbon 5 of the uracil provides the hydride.[213] There is a significant kinetic isotope effect for transfer of the hydride in the active site of thymidylate synthase.[223,224] This kinetic isotope effect is independent of temperature,[222] which distinguishes it from the kinetic isotope effect for removal of the hydron by Tyrosine 94 in the elimination that produces intermediate **5–38**.[225] The fact that the decrease in Michaelis constant $K_{m,mTHF}$ for 5,10-methylenetetrahydrofolate as the pH is lowered has been assigned to the pK_a of Tyrosine 94, the fact that there is a kinetic isotope effect for removal of the hydron from carbon 5 by Tyrosine 94, and the fact that there is a kinetic isotope effect for transfer of the hydride all suggest that the rate-limiting step in the enzymatic reaction is transfer of the hydride but that removal of the hydron from carbon 5 is significantly rate-affecting.

Addition of a hydride, formally a nucleophile, to intermediate **5–38** is analogous to addition of a hydroxide ion, actually a nucleophile, to 2′-deoxy-6-cysteinyl-2-methylenecytosine, the homologous covalent intermediate in the reaction catalyzed by deoxycytidylate 5-hydroxymethyltransferase[226]

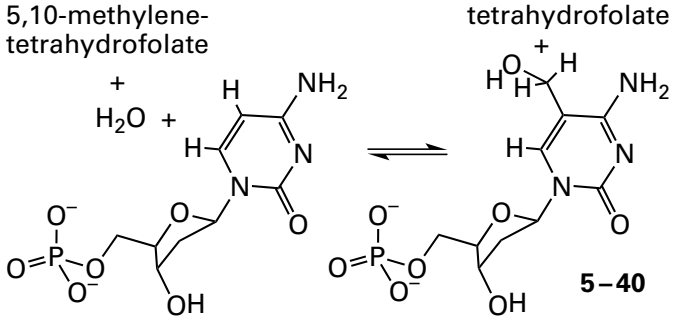

(5–56)

encoded by the genome of Enterobacteria phage T4. In this latter instance, addition of the hydroxide instead of a hydride, which is also analogous to the nucleophilic addition of 2-sulfanylethanol to intermediate **5–38** (Figure 5–5), produces the hydroxymethyl group in the product 5-hydroxymethyldeoxycytidylate (**5–40**) rather than a methyl group.

In the latter steps of the reaction catalyzed by thymidylate synthase (Figure 5–5), following nucleophilic addition of carbon 5 of the enolate that is the first covalent intermediate to the methyleneiminium cation of N^5-methylenetetrahydrofolate, the continued necessity for the covalent intermediate between the uracil in dUMP and the cysteine is evident. This adduct continues to permit carbons 4 and 5 to act as an acyl carbon and a carbon α to an acyl carbon, respectively, so that the necessary enolates and α,β-unsaturated acyl compounds can be formed. Such chemistry at the position α to an acyl carbon would not be possible if the double bond between carbons 5 and 6 of the uracil were intact because the hydron on that carbon is orthogonal to the π molecular orbital system of the acyl group at carbon 4 and hence, unreactive.

There is no cysteine in the active site of the unrelated thymidylate synthase (FAD) from Enterobacteria phage T4 that can participate in a nucleophilic addition to carbon 5 of the uracil in dUMP,[227] even though it catalyzes the same reaction. Thymidylate synthase (FAD), as its name implies, is a flavoenzyme with a prosthetic flavin adenine dinucleotide in its active site, which must be in its reduced form before the methylation can proceed.[228] Even though there is no cysteine in the active site, there are several results that are consistent with formation of an enolate at oxygen 4, carbon 4, and carbon 5, as occurs in the active site of thymidylate synthase. The reduced enzyme catalyzes exchange of the hydron at carbon 5 of dUMP with deuterons in ^2H_2O in the absence of 5,10-methylenetetrahydrofolate, as would be expected if the active site is able to create the enolate.[229] If the enzymatic reaction is quenched

while it is proceeding, 2′-deoxy-5-hydroxymethyluridine 5′-monophosphate can be isolated,[230] which is the product expected from addition of water to the α,β-unsaturated acyl intermediate homologous to intermediate **5-38** (Figure 5–5), as occurs in the active site of deoxycytidylate 5-hydroxymethyltransferase (Equation 5–56). These observations have led to the proposal that the reduced flavin reversibly adds a hydride to carbon 6 of dUMP to produce directly the enolate as the first step in the reaction, which would accomplish the same function as the nucleophilic addition of the sulfanyl group of the cysteine in the active site of thymidylate synthase.[229] Consistent with this explanation is the fact that, in the crystallographic molecular model of the complex between the oxidized enzyme and dUMP, the dUMP stacks upon the isoalloxazine of the flavin, and carbon 6 of the dUMP sits directly on top of nitrogen 5 of the flavin,[227] which would be poised to transfer a hydride if it were reduced flavin. The stacking of the two rings against each other is reminiscent of the complexes between NAD^+ and reduced flavin in active sites in which the NAD^+ is reduced by flavin.

There are several enzymes that have mixed disulfides between cysteines in their active sites and sulfanyl groups in their respective substrates as covalent intermediates in their reactions. For example, in the active site of human glutathione-disulfide reductase, reduced flavin reduces a disulfide between Cysteines 58 and 63 (Figure 2–11). The sulfido group of Cysteine 58 then engages in thiol–disulfide exchange with the disulfide in glutathione disulfide (see Equation 2–136)

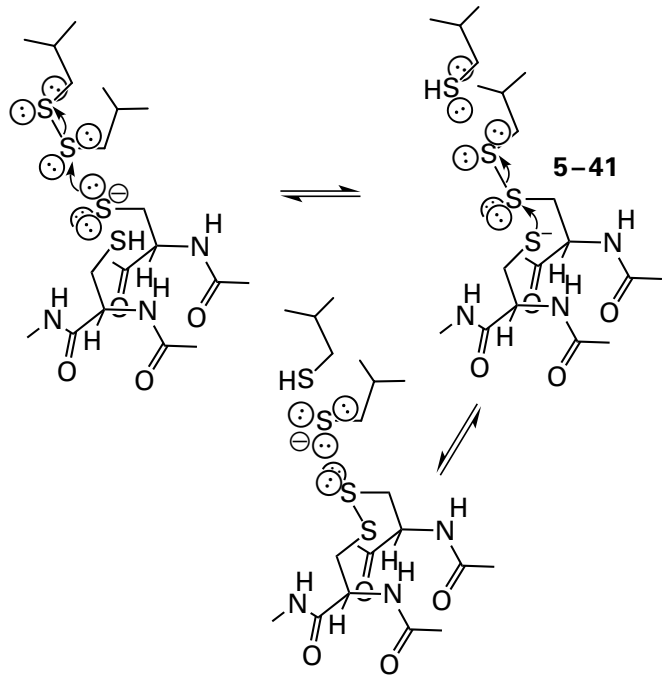

(5–57)

to produce one reduced glutathione and a mixed disulfide (**5–41**) between Cysteine 58 and the other molecule of glutathione. This mixed disulfide has been observed crystallographically.[231] A second thiol–disulfide exchange with the sulfido group of Cysteine 63 then produces the second molecule of reduced glutathione and regenerates the disulfide between Cysteines 58 and 63 awaiting reduction in the next round.

A thiol–disulfide exchange is a **nucleophilic substitution at sulfur**. Nucleophilic substitutions at sulfur also occur in active sites with leaving groups other than a sulfanyl group. For example, in the reaction catalyzed by 2-oxopropyl-CoM reductase (carboxylating), an enolate is the leaving group in a nucleophilic substitution

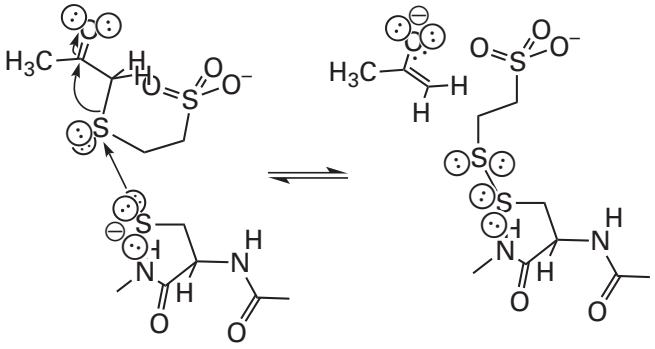

(5–58)

that produces a mixed disulfide between a cysteine in the active site and 2-sulfanylethanesulfonate

(coenzyme M), which is one product of the reaction in the direction written. This covalent intermediate has also been observed crystallographically in the active site of 2-oxopropyl-CoM reductase (carboxylating) from *X. autotrophicus*.[232] The sulfido group of a second cysteine in the active site then releases the 2-sulfanylethanesulfonate in a thiol–disulfide exchange (see Equation 5–57). The enolate of acetone that is the leaving group in the nucleophilic substitution is carboxylated with carbon dioxide within the active site to produce acetoacetate, the other product of the enzymatic reaction in the direction written.

Mixed disulfides between hydrogen sulfide and cysteines form in the active sites of sulfurtransferases. For example, in 3-mercaptopyruvate sulfurtransferase from *E. coli*, a hydrogen sulfide is transferred from 3-sulfanylpyruvate to Cysteine 237 in the active site of the enzyme

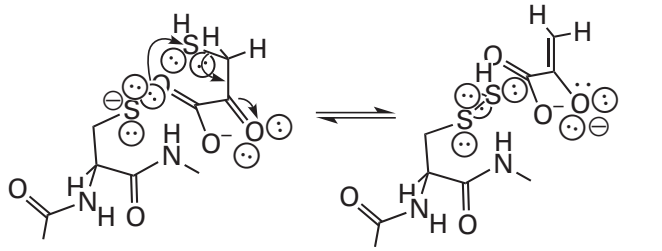

(5–59)

with the enolate of pyruvate as the leaving group. The resulting cysteine persulfide has been observed crystallographically.[233,234] The first persulfide of this type was observed in the crystallographic molecular model of thiosulfate sulfurtransferase (rhodanese).[235,236] Sulfenic acids (RS–OH) are oxygen analogues of these persulfides, and they are covalent intermediates in the active sites of peroxidases.[237,238]

Suggested Reading

Buckel, W., and Bobi, A. (1976) The enzyme complex citramalate lyase from *Clostridium tetanomorphum, Eur. J. Biochem. 64*, 255–262. https://doi.org/10.1111/j.1432-1033.1976.tb10295.x

Buckel, W. (1976) Acetic anhydride: An intermediate analogue in the acyl-exchange reaction of citramalate lyase, *Eur. J. Biochem. 64*, 263–267. https://doi.org/10.1111/j.1432-1033.1976.tb10296.x

Matthews, D. A., Villafranca, J. E., Janson, C. A., Smith, W. W., Welsh, K., and Freer, S. (1990) Stereochemical mechanism of action for thymidylate synthase based on the X-ray structure of the covalent inhibitory ternary complex with 5-fluoro-2′-deoxyuridylate and 5,10-methylenetetrahydrofolate, *J. Mol. Biol. 214*, 937–948. https://doi.org/10.1016/0022-2836(90)90347-O

Hyatt, D. C., Maley, F., and Montfort, W. R. (1997) Use of strain in a stereospecific catalytic mechanism: Crystal structures of *Escherichia coli* thymidylate synthase bound to FdUMP and methylenetetrahydrofolate, *Biochemistry 36*, 4585–4594. https://doi.org/10.1021/bi962936j

Problem 5–1: Homoserine *O*-acetyltransferase from *Haemophilus influenzae*

$$\text{acetyl-SCoA} + \text{L-homoserine} \rightleftharpoons \text{HSCoA} + \textit{O}\text{-acetyl-L-homoserine}$$

displays the following steady-state kinetics.[33]

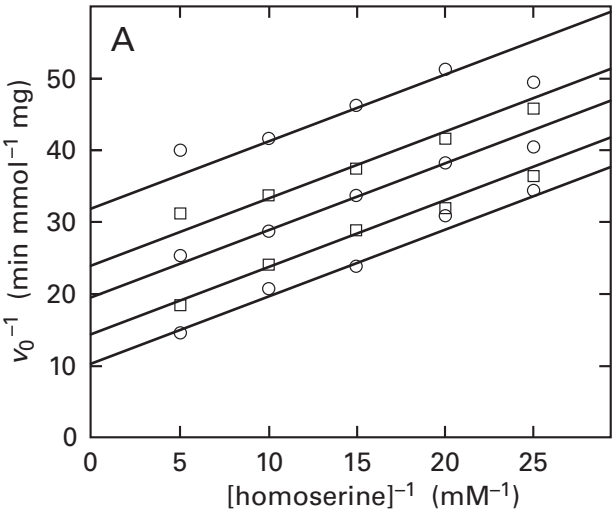

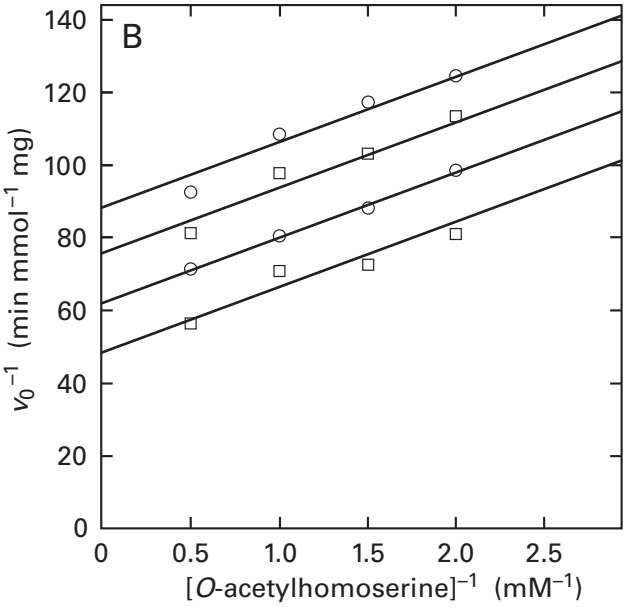

Reciprocals (minutes millimole^{-1} milligram) of the initial rates plotted against the reciprocals (millimolar^{-1}) of the initial concentrations of reactants for the enzymatic reaction catalyzed by homoserine *O*-acetyltransferase from *H. influenzae*. (A) Varying concentrations of L-homoserine at constant concentrations of acetyl-SCoA, in descending order, of 0.042, 0.056, 0.083, 0.143, and 0.33 mM. (B) Varying concentrations of *O*-acetyl-L-homoserine at constant concentrations of coenzyme A, in descending order, of 0.20, 0.25, 0.33, and 0.50 mM.

When the enzyme (0.28 mM) was mixed with [^{3}H]acetyl-SCoA (0.40 mM) for various times and then mixed with 25% trichloroacetic acid to denature and precipitate the protein, and the precipitate was then collected, washed, and submitted to scintillation counting, the following results were observed.

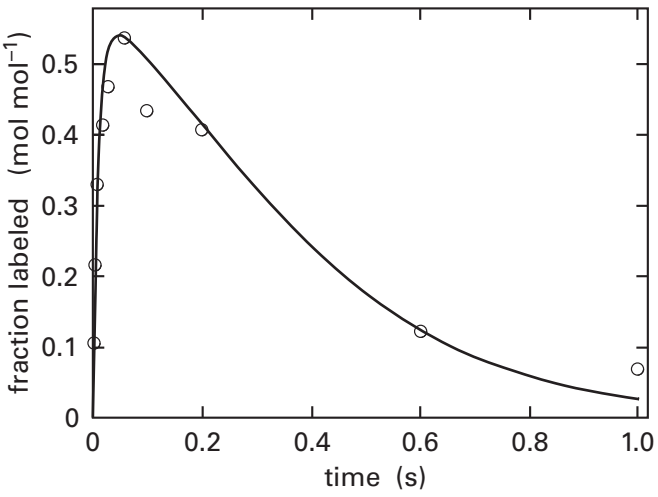

Covalent incorporation of tritium into homoserine *O*-acetyltransferase. The incorporation of radioactivity into the precipitated protein is expressed in terms of moles (mole of active sites)$^{-1}$.

When Serine 163 in the enzyme from *Schizosaccharomyces pombe* was mutated to alanine, no acetylation of the protein occurred.[34]

(A) Write a mechanism for the transacetylation. Include arbitrary but suitable side chains from amino acids in the active site in your mechanism.
(B) What feature of your mechanism is consistent with the steady-state kinetics?
(C) What feature of your mechanism is consistent with the acetylation of the enzyme?
(D) What feature of your mechanism is consistent with the results of the mutation?

Problem 5–2: Aspartate-semialdehyde dehydrogenase catalyzes the reaction

$$\text{NADPH} + \text{L-4-aspartylphosphate} + \text{H}^+ \rightleftharpoons \text{L-aspartate 4-semialdehyde} + \text{HOPO}_3^{2-} + \text{NADP}^+$$

Write a mechanism for the reaction involving a covalent intermediate at a cysteine.

Problem 5–3: Methanol in water reacts about 100-fold more rapidly with the acyl intermediate in the reaction catalyzed by chymotrypsin (Figure 3–6) than does water itself.

(A) If this is the case, explain why the catalytic constant k_0 for the combined hydrolysis and methanolysis of 4-nitrophenyl acetate by chymotrypsin is markedly increased in methanol–water solutions, but that for *N*-acetyl-L-tryptophan amide is unchanged from the value in water alone.
(B) Estimate the value of the catalytic constant k_0 for the combined hydrolysis and methanolysis of 4-nitrophenyl acetate in 1 M methanol in water relative to k_0 in water alone and the fraction of the product that would be methyl acetate.

Problem 5–4: When pseudouridylate synthase

$$\text{pseudouridine 5′-phosphate} + \text{H}_2\text{O} \rightleftharpoons \text{uracil} + \text{D-ribose 5-phosphate}$$

from *E. coli* was crystallized from a solution of D-ribose 5′-phosphate and uracil, the covalent intermediate

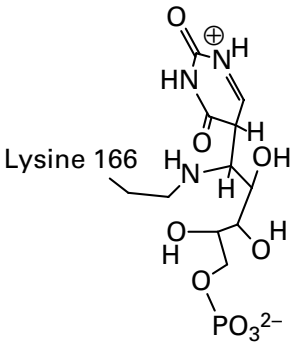

was observed in the map of electron density in its active site.[239] Write a mechanism for the reaction catalyzed by the enzyme that involves this covalent intermediate. Hint: Find the correct enolate in uracil.

Problem 5–5: UDP-Glucose—hexose-1-phosphate uridylyltransferase catalyzes the reaction

$$\text{UDP-}\alpha\text{-D-glucose} + \alpha\text{-D-galactose 1-phosphate} \rightleftharpoons \alpha\text{-D-glucose 1-phosphate} + \text{UDP-}\alpha\text{-D-galactose}$$

(A) Suppose that the reaction proceeded through the two ternary complexes

$$\text{E·UDP-glucose·galactose 1-phosphate} \rightleftharpoons \text{E·glucose 1-phosphate·UDP-galactose}$$

and draw the structure of the pentavalent intermediate at phosphorus that would have to be bound tightly by the active site. Indicate the entering oxygen and the leaving oxygen.

The following results have been observed.[240]

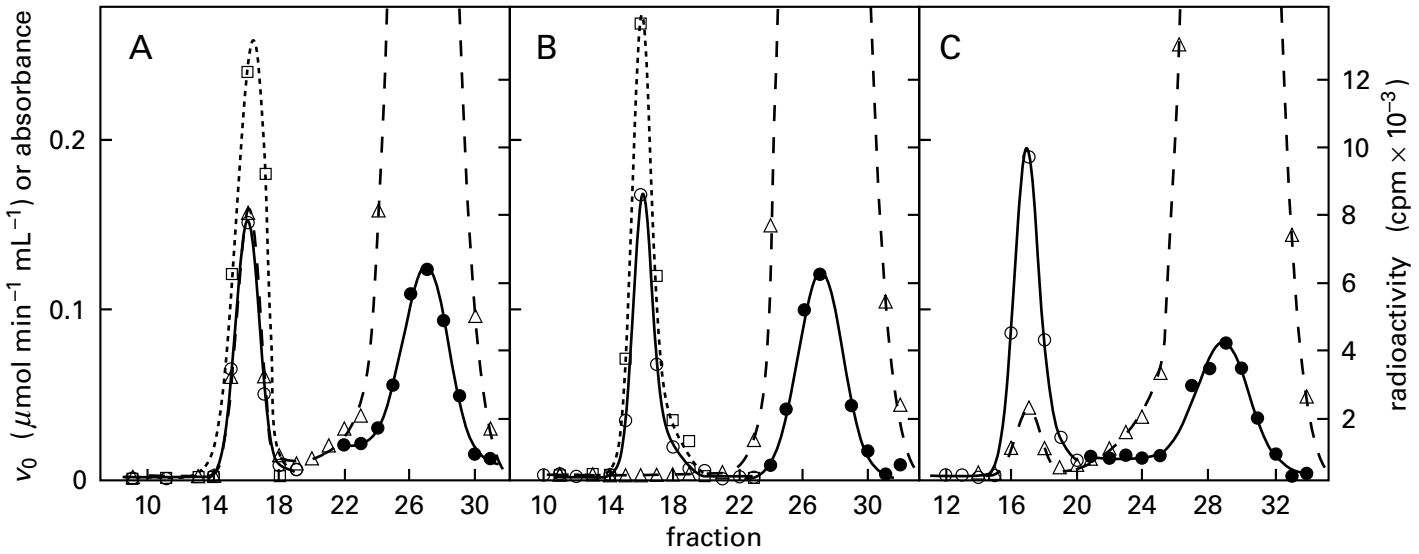

Distribution of (○) A_{280} (protein), (●) A_{260} (nucleotides), (△) radioactivity (counts per minute milliliter^{-1}), and (□) catalytic activity (micromoles minute^{-1} milliliter^{-1}) following chromatography of several mixtures. (A) The mixture of reactants contained initially 8 nmol of active sites for UDP-glucose—hexose-1-phosphate uridylyltransferase from *E. coli* and 32 nmol of [*uracil*-5,6-$^3H_2$] UDP-D-glucose (specific radioactivity 2.0×10^7 cpm μmol^{-1}) in 0.2 mL of 50 μM L-cysteine and 5 mM potassium phosphate, pH 7.5. After 5 min at room temperature, the solution was passed thorough a column (1 × 41 cm) of Sephadex G-25 equilibrated and eluted with the same buffer at 4 °C. Fractions of approximately 1 mL were collected at intervals of 5 min. (B) The mixture of reactants was identical with that of Panel A except that the tritiated UDP-D-glucose was replaced with 34 nmol of UDP-[U-^{14}C]-D-glucose (specific radioactivity 5.8×10^6 cpm μmol^{-1}). (C) The mixture of reactants was identical with that of Panel A except that it also contained 32 nmol of D-glucose 1-phosphate. [240]

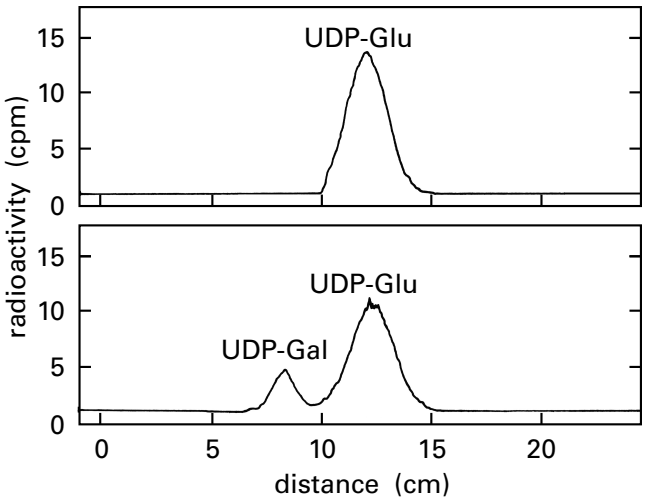

Distribution of radioactivity upon chromatography of two mixtures of reactants. The complete mixture of reactants contained initially 32 nmol of [*uracil*-5,6-$^3H_2$]UDP-D-glucose (6.3×10^5 cpm), 36 nmol of UDP-D-galactose, and UDP-glucose—hexose-1-phosphate uridylyltransferase (0.56 micromolar minute^{-1}) in 25 μL of buffer consisting of 0.5 mM L-cysteine and 5 mM potassium phosphate, pH 7.5. After 25 min at 25 °C, half of the solution was subjected to descending paper chromatography for 92 h with ethanol–methyl ethyl ketone–0.5 M morpholinium tetraborate, pH 8.6 (7:2:3), as the mobile phase. The upper panel is the control without enzyme, and the lower is the complete mixture of reactants.[240]

(B) On the basis of these results, write a mechanism for the enzymatic reaction involving a covalent uridylyl-enzyme intermediate.

(C) On the basis of the mechanism you wrote in part B, explain the uridylyl exchange observed in Figure B.

(D) Draw the complete structure of the covalent uridylyl intermediate formed between a portion of the substrate and a histidine in the active site of the enzyme.[156]

(E) The overall enzymatic reaction proceeds with retention of configuration of phosphorus.[151] To which of the two phosphorus atoms in a uridylyl substrate must this statement refer?

(F) Draw a structure of UDP-D-glucose and indicate the phosphorus with an arrow. Show how this observation rules out a mechanism in which this phosphorus is transferred directly in a ternary complex as in part A and is consistent with formation of the covalent intermediate you drew in part C. Show this by drawing structures of the intermediates in the key steps.

(G) Explain why the mechanism of part B that passes through a covalent intermediate is more economical than the mechanism of part A that passes through a ternary complex.

(H) Consider the amino acids in the active site that must form hydrogen bonds to the UDP monosaccharides and those that activate the phosphate for transfer. Which can be called upon to perform twice the work?

Problem 5–6: Nucleoside-diphosphate kinase catalyzes Equation 5–32. When MgATP^{2-} is used as the phosphate donor (MgXTP^{2-}) and MgdGDP$^-$ as the phosphate acceptor (MgYDP$^-$) in the enzymatic reaction, the following kinetic behavior is observed.

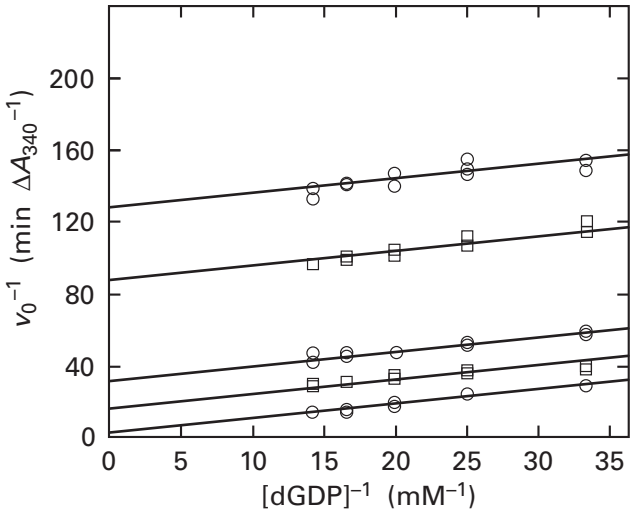

Plot of the reciprocal [minutes (change in A_{340})$^{-1}$] of the initial rate for the enzymatic assay, which is coupled to oxidation of NADH, against the reciprocal (millimolar^{-1}) of the concentration of MgdGDP$^-$ for human nucleoside-diphosphate kinase at concentrations, from top to bottom, of MgATP^{2-} of 15, 25, 50, 100, and 800 μM.[241]

(A) Write a kinetic mechanism that is consistent with these observations. In your mechanism, explicitly name substrates and products as MgATP^{2-}, MgdGDP$^-$, MgADP$^-$, and MgdGTP^{2-}. Abbreviate the enzyme as E.

When human nucleoside-diphosphate kinase was mixed with Mg[^{32}P]ATP^{2-} for 1 min at 30 °C and then the mixture was added to a column of Sephadex G-100, the following elution profile was obtained.

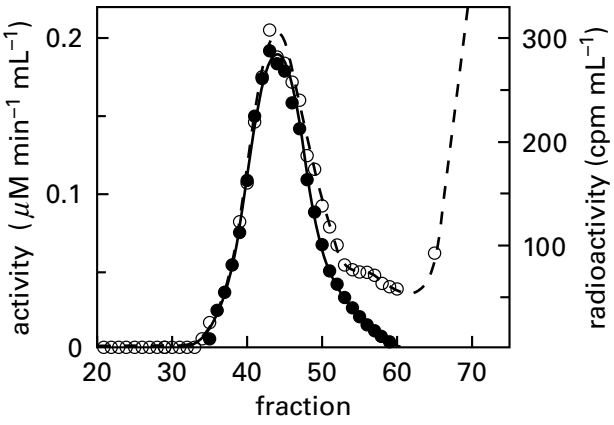

Separation of [^{32}P]nucleoside-diphosphate kinase from Mg[^{32}P]ATP^{2-} on a column of Sephadex G-100.[242] Enzymatic activity (micromolar minute^{-1} milliliter^{-1}) and radioactivity (counts per minute milliliter^{-1}) are plotted as a function of the number of the fraction.

The authors point out in the publication that nucleoside-diphosphate kinase elutes from Sephadex G-100 at a position where the stationary phase for the molecular exclusion is separating proteins on the basis of their size.

(B) How do these results rule out the possibility that ^{32}P is associated with proteins other than nucleoside-diphosphate kinase?
(C) Which phosphate of Mg[^{32}P]ATP^{2-} was certainly radioactive?
(D) Write a chemical mechanism for the reaction of nucleoside-diphosphate kinase that incorporates both your kinetic mechanism and an explicit explanation of the results in Figure B.
(E) When enzyme from fractions 40–45 from the Sephadex G-100 column was mixed with MgGDP^{-}, what radioactive nucleotide was subsequently isolated from the mixture? Indicate precisely where the radioactive phosphorus resides on that nucleotide.

Problem 5–7: Thiazole synthase converts 1-deoxy-D-xylulose 5-phosphate and 2-iminoacetate into 2-[(2*R*,5*Z*)-2-carboxy-4-methylthiazol-5(2*H*)-ylidene]-ethyl phosphate. It has been proposed that the enzymatic mechanism proceeds through the following sequence of covalent intermediates

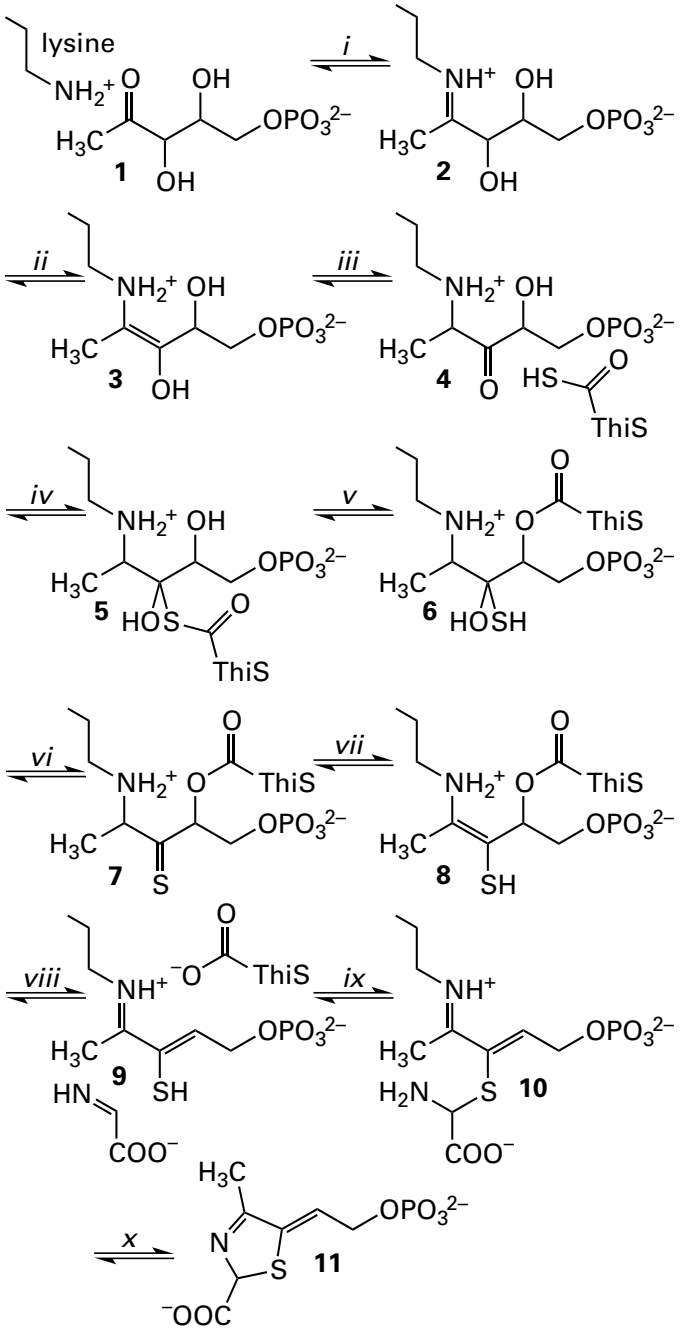

where the primary alkylamino group is the 6-amino group of a lysine in the active site of the enzyme and ThiS is a small protein that carries a sulfide as a monothiocarboxy group at its carboxy terminus. Intermediate **5** has been observed in a crystallographic molecular model.[243]

(A) Using the lowercase Roman numbers for each step, identify the type of chemical reaction and describe what is occurring in each step.
(B) Using the boldface numbers for particular intermediates, identify any reactants or products that do not appear at that point in the chemical equations as written.

(C) Write out the mechanism of each step in detail. Show all removals and additions of hydrons and any reactants or products not shown in the diagram.

Problem 5–8: Write a mechanism for the reaction

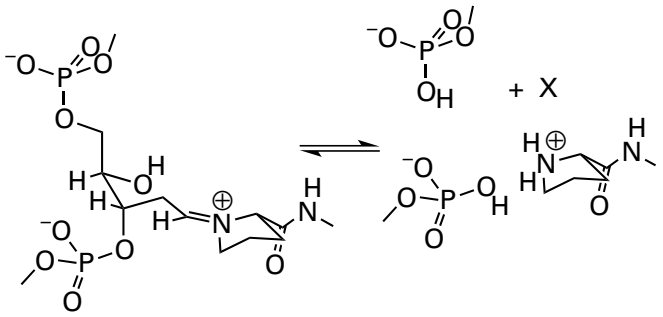

catalyzed by DNA-formamidopyrimidine glycosylase.[195] What is X?

Chemical and Crystallographic Identification of Diamagnetic, Noncovalent Intermediates

There are instances in which a stable noncovalent intermediate is present in an active site at a high enough concentration to be isolated directly and identified chemically or crystallographically. In such cases, there is no need to perform chemical analysis of the protein. For example, poly(*β*-D-mannuronate) C5 epimerase from *P. aeruginosa* catalyzes the epimerization

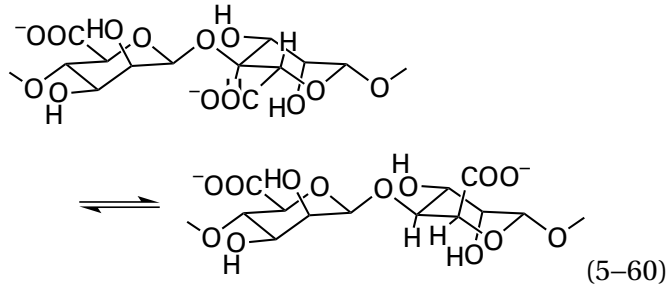

(5–60)

When the enzymatic reaction was quenched 5 s after the enzyme was mixed with a polymer of 34 D-mannurates, fragments of the polymer of various lengths could be isolated from the enzyme in 25% yield based on the concentration of active sites, and each fragment was shown by a colorimetric assay to end in a glycal of mannurate[244]

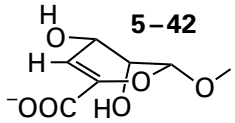

5–42

Consequently, it was concluded that these glycals were noncovalent intermediates in the enzymatic reaction. Each is formed by an elimination at the respective glycosidic linkage (see Equation 4–358)

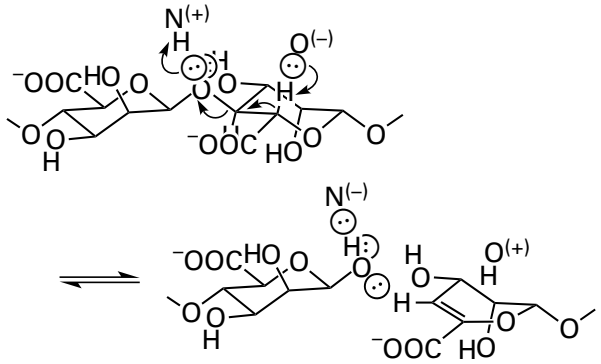

(5–61)

To accomplish the overall epimerization for which the enzyme is responsible, during the readdition of the 1-hydroxy group of the adjacent mannuronate (reverse of Equation 5–61), the hydron is added to carbon 5 of the glycal from the opposite face of the double bond from which it was removed during the initial elimination. In a crystallographic molecular model of the active site of the enzyme from *Azotobacter vinelandii*, Tyrosine 149 is in the proper position to remove the hydron on carbon 5 on the *β*-D-mannuronyl group being epimerized and add the hydron to oxygen 1 of the leaving *β*-D-mannuronate, just as Tyrosine 242 does in the active site of chondroitin AC lyase (Figure 4–44), and Histidine 154 is in the proper position to add a hydron to the other side of the double bond in the glycal to produce the *α*-L-guluronyl group during the readdition of the hydroxy group.[245] The identification of the intermediate led to the rather unexpected conclusion that the polymer is cleaved and then reformed to perform the epimerization, presumably as a way to stabilize the *gem*-dienolate.

In the case of RNA polymerase (see Figure 3–73B) from *E. coli*, samples were removed and quenched at various intervals from 0.5 to 150 s from reaction mixtures in which the synthesis of RNA under the control of the double-stranded DNA of the λP_R promoter had been initiated. Each intermediate

segment of single-stranded RNA 3–16 bases long that was a noncovalent intermediate in the enzymatic reaction could be separated electrophoretically and quantified. The rates of the individual, consecutive steps in which an additional base was added to the elongating strand of RNA could be derived from these observations.[246]

One way to improve the chances of having measurable concentrations of a noncovalent intermediate in the active site is to have all substrates for the enzyme present in the solution at their equilibrium ratios and at concentrations high enough to saturate the active sites. Under these conditions, an **equilibrium between reactants, intermediates, and products** is established in all active sites in the solution. When such an equilibrium was established in the active site[247] of bovine glutamate dehydrogenase [NAD(P)$^+$] (previously Equation 3–319)

$$\text{L-glutamate} + H_2O + NAD(P)^+ \rightleftharpoons 2\text{-oxoglutarate} + NH_4^+ + NAD(P)H \quad (5\text{–}62)$$

imine **5–43** (10%) and hemiaminal **5–44** (60%)

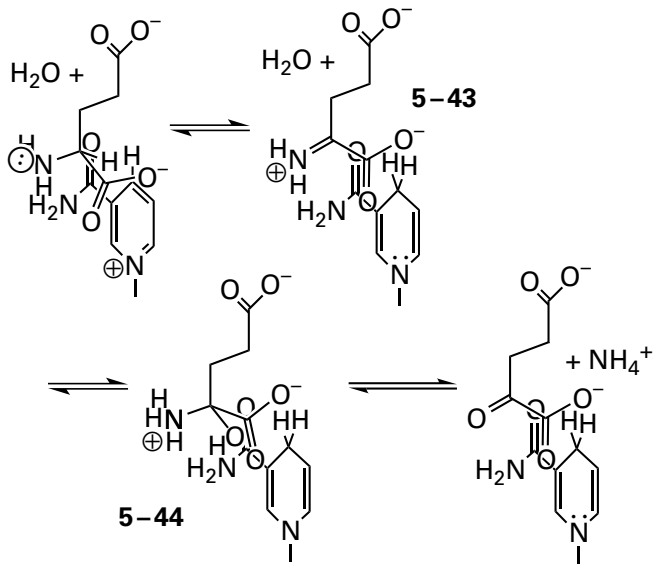

(5–63)

identified spectrophotometrically in the ultraviolet range, were present in the active site at equilibrium.[248]

Noncovalent intermediates sometimes accumulate in an active site when **one reactant is omitted from the solution**. For example, when an electron acceptor, which normally would be oxidized electron-transfer flavoprotein, is omitted from an anaerobic solution of the oxidized flavoenzyme human glutaryl-CoA dehydrogenase (ETF), glutaconyl-SCoA (**5–45**) accumulated (25%) in the active site[249] as a noncovalent intermediate[250]

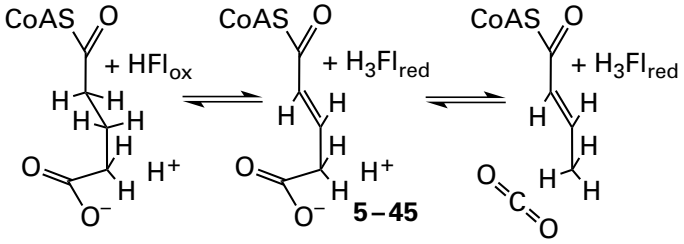

(5–64)

where HFl_{ox} is the oxidized prosthetic flavin and H_3Fl_{red} is the reduced prosthetic flavin. The glutaconyl-SCoA present in the active site as a noncovalent intermediate was identified by high-pressure liquid chromatography and mass spectrometry after inactivation and precipitation of the protein.

The mixed anhydride **5–46**

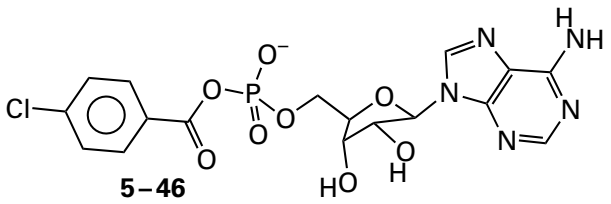

could be isolated from the active site of 4-chlorobenzoate—CoA ligase from *Pseudomonas* when the enzyme was mixed with 4-chlorobenzoate and $MgATP^{2-}$ in the absence of its third reactant, coenzyme A. It was identified by nuclear magnetic resonance spectroscopy.[251] This observation is consistent with the transfer of an adenylyl group from $MgATP^{2-}$ to the carboxy group of 4-chlorobenzoate to form mixed anhydride **5–46** with diphosphate as the leaving group. This nucleophilic substitution at phosphorus activates the carboxy group for a nucleophilic substitution of the sulfanyl group of coenzyme A for the adenylyl group in the intermediate to form the product 4-chlorobenzoate-SCoA.

In the case of squalene synthase from *S. cerevisiae*, the noncovalent intermediate, (+)-presqualene diphosphate (**5–47**),[252-255] is formed in an initial step from two molecules of (2*E*,6*E*)-farnesyl diphosphate

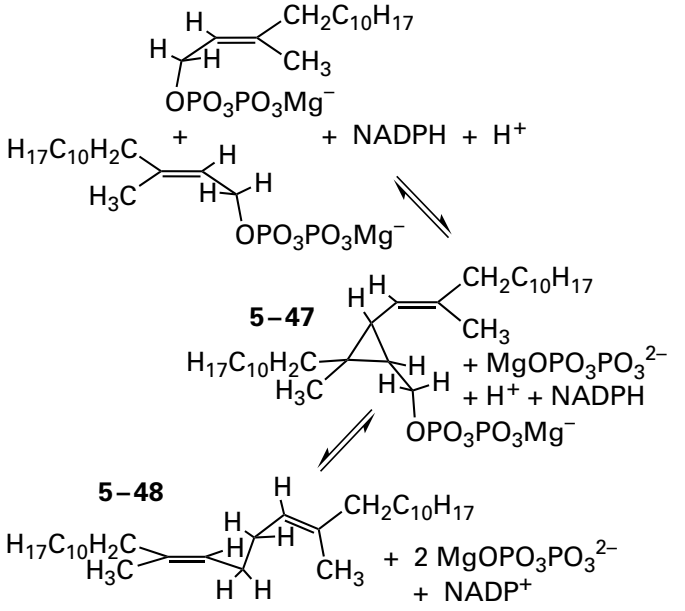

(5–65)

upon dissociation of diphosphate from one of them to form the allyl carbenium ion, which adds to the carbon–carbon double bond of the other to form the cyclopropane. Then, following dissociation of the second diphosphate and a sequence of carbocationic rearrangements (previously Equation 3–368)

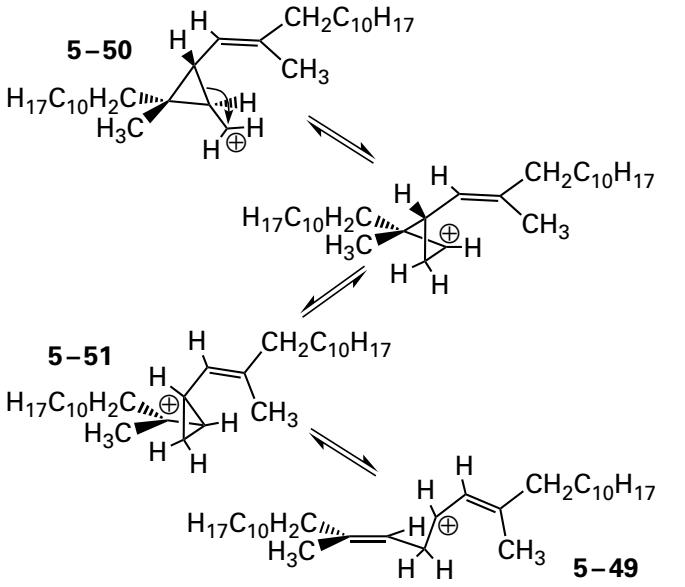

(5–66)

the final carbenium ion (**5–49**) is reduced by a hydride from NADPH to the final product squalene (**5–48**). In the absence of NADPH, the steps in the enzymatic mechanism beyond (+)-presqualene diphosphate (**5–47**) are blocked, and (+)-presqualene diphosphate slowly dissociates as a stable compound from the active site.[256] Under normal circumstances, sufficient NADPH is available to prevent the release of the intermediate. In this instance, the intermediate in the enzymatic reaction was sufficiently complex that total organic synthesis was required to define its structure unambiguously.[253,254]

If a noncovalent intermediate in an enzymatic reaction is **too unstable to isolate**, other approaches are applied. For example, **mixed anhydrides of two carboxylic acids** that are substrates for the enzyme are noncovalent intermediates in acyl exchanges, and these mixed anhydrides are too unstable to isolate. During each turnover, citrate (*pro*-3*S*)-lyase accomplishes the exchange of a citryl group for the initial acetyl group in the thioester of the prosthetic coenzyme A in the active site (Equation 5–17).[257] The most likely noncovalent intermediate in this partial reaction is a mixed anhydride formed between citrate and acetate[258]

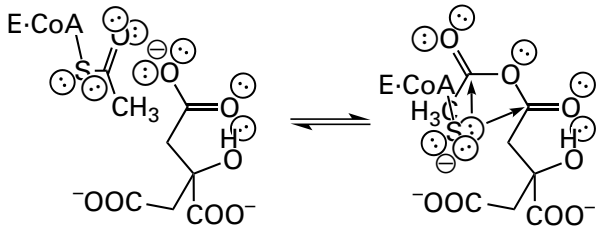

(5–67)

The sulfido group of the prosthetic coenzyme A (as shown), or the sulfido group of a cysteine known to be located nearby in the active site,[259] then adds to the acyl carbon of the citryl group in the mixed anhydride intermediate to complete the substitution of the citryl group for the acetyl group and give the acetate that is one product of the enzymatic retro-Claisen condensation. In reverse, the sulfido group would add to the acyl carbon of the acetyl group in the mixed anhydride to re-form the acetyl intermediate. The existence of this mixed anhydride as an intermediate was demonstrated by the fact that oxygen-18 in the carboxy group of citrate is transferred to the acetate that is the product during a single turnover of the enzyme.

Another approach to identification is to **trap an unstable noncovalent intermediate** by a chemical reaction that produces a stable derivative of it. Carbamoyl-phosphate synthase (glutamine-hydro-lysing) catalyzes three separate reactions (previously Equations 3–531 to 3–533)

$$H_2O + \text{L-glutamine} \rightleftharpoons \text{L-glutamate} + NH_3 + H^+$$

(5–68)

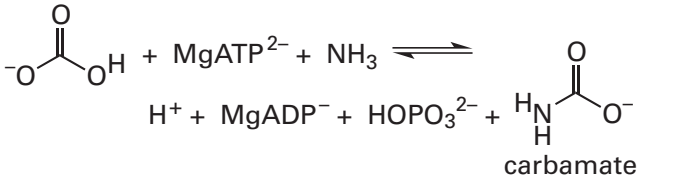

(5–69)

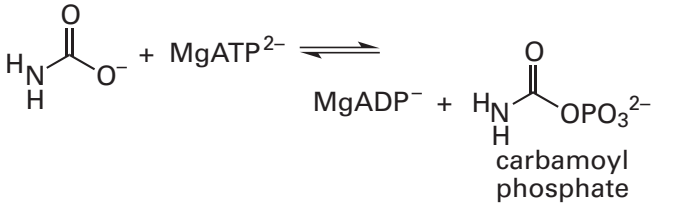

(5–70)

in three separate active sites connected by two tunnels. The phosphocarbonate **5–52**, formed as a noncovalent intermediate at the active site in the enzyme from *E. coli* that is responsible for producing carbamate (Equation 5–69)

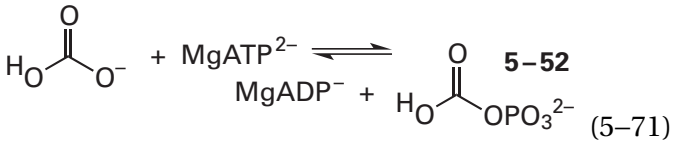

(5–71)

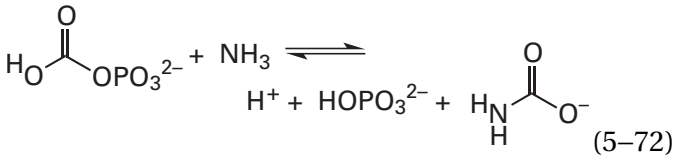

(5–72)

can be trapped by mixing a solution of the enzyme, $MgATP^{2-}$, and bicarbonate with diazomethane[260]

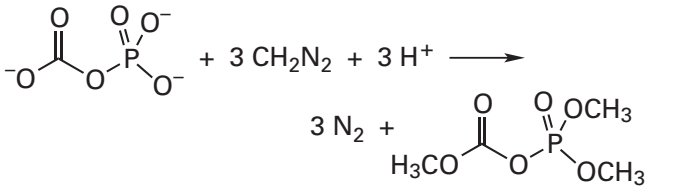

(5–73)

The resulting trimethyl phosphocarbonate is a stable compound, unlike the phosphocarbonate itself, because it has no oxyanions to provide push.

Noncovalent intermediates in enzymatic reactions are often **identified crystallographically**.[261] For example, when a crystal of dethiobiotin synthase from *E. coli*

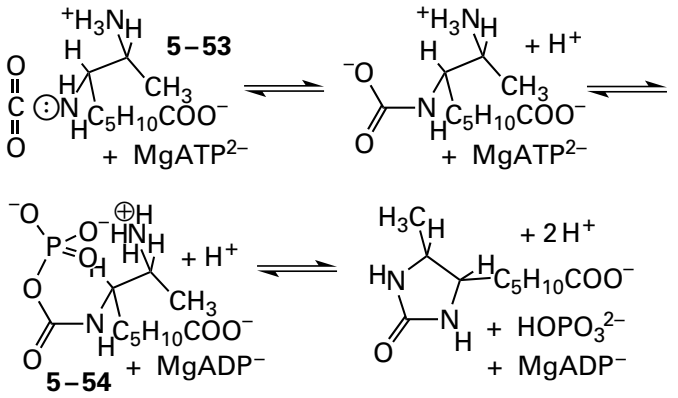

(5–74)

was soaked with $MgATP^{2-}$ and 7,8-diaminononanoate (**5–53**) for 1 h and then $NaHCO_3^{2-}$ was added to the solution for 80 s before the crystal was frozen, carbamic phosphoanhydride **5–54**, an analogue of carbamoyl phosphate, was observed occupying the active site of the enzyme in the map of electron density for this crystal.[262] This noncovalent intermediate had already been isolated from enzyme dissolved in solution that was mixed with these same reactants for 100 s at pH 7.5 and then acidified to pH 4.[263]

The observation of a potential intermediate in a map of electron density **can be deceptive**. The active site of quinolinate synthase[264]

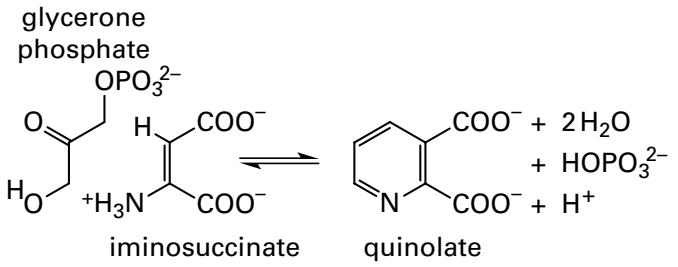

(5–75)

contains a tetranuclear [4Fe–4S] iron–sulfur cluster with an open site[265] on one of the Fe^{2+}, as does aconitate hydratase. Two distinct crystallographic maps of electron density for crystals of quinolinate synthase from *Thermotoga maritima* and *Pyrococcus horikoshii*, respectively, have been reported, each of which is consistent with a different noncovalent intermediate

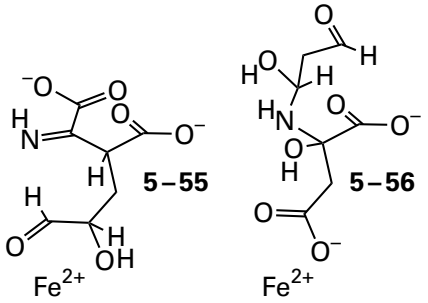

Because of the two carboxylato groups, the two maps of electron density of the potential intermediates are distinct enough that they cannot both be of the same noncovalent intermediate. In the condensation catalyzed by the enzyme, a carbon–carbon bond and a nitrogen–carbon bond are formed between the two reactants. In intermediate **5–55**, the carbon–carbon bond has formed[266,267] and in intermediate **5–56** the nitrogen–carbon bond has formed,[268] so at least one of them cannot be a normal intermediate in the enzymatic reaction. There are two different chemically defensible mechanisms that can include the respective intermediate and convert glycerone phosphate and iminosuccinate into quinolinate, so a decision cannot be made by appeal to mechanism. The active site forms a complex with glycerone phosphate[266,269] in which the hydroxy group and the carbonyl oxygen are ligands to the Fe^{2+}, which would lead to **5–55** in which this ligation is retained. The active site, however, also forms a complex with iminosuccinate in which the 4-carboxy group is a ligand to the Fe^{2+}, which is more similar to the ligation in **5–56**, and it also forms a complex with the nitrogen and the 3-carboxy group of quinolinate.[266,269,270] In its favor, dicarboxylic acid **5–55** associates with the active site with the two oxygens that will eventually leave during the production of quinolinate as ligands to the Fe^{2+}, which would be consistent with the role of such tetranuclear [4Fe–4S] iron–sulfur clusters in other dehydrations.

If the equilibrium in the active site is such that insignificant concentrations of a noncovalent intermediate accumulate or can be caused to accumulate, other strategies must be applied. One of these strategies is to **use an analogue of one substrate as an alternative reactant** that is mistaken by the enzyme for the actual substrate and from which the usual intermediate is formed; but the intermediate formed from the analogue is stable. For example, germacrene A is a noncovalent intermediate in the reaction catalyzed by aristolochene synthase (Figure 3–48) from (2*E*,6*E*)-farnesyl diphosphate. It is never present, however, in sufficient quantities to be isolated. When the enzyme from *Aspergillus terreus* was mixed with (7*R*)-6,7-dihydrofarnesyl diphosphate, which is (2*E*,6*E*)-farnesyl diphosphate reduced at the 6,7 carbon–carbon double bond, the resulting analogue, 1,2-dihydrogermacrene

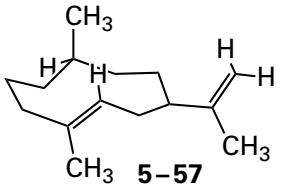

accumulated in the active site at 1.3% of the rate of the normal reaction and was identified by gas chromatography and mass spectrometry.[271] 1,2-Dihydrogermacrene **5–57** lacks the 1,2-double bond present in germacrene that is needed to complete the enzymatic reaction.

In the enzymatic reaction catalyzed by phosphogluconate dehydrogenase ($NADP^+$-dependent, decarboxylating), 6-phospho-D-*ribo*-3-hexulosonate (**5–58**) is the central, noncovalent intermediate formed in the active site[272] from the substrate, 6-phospho-D-gluconate, during the oxidative decarboxylation

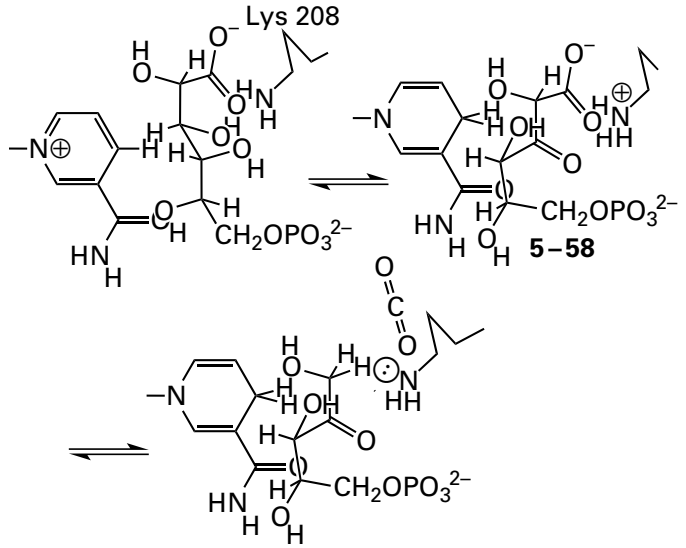

(5–76)

producing D-ribulose 5-phosphate. It had not been trapped chemically, in part because the rate of the initial dehydrogenation that produces it is slower than the rate of the subsequent decarboxylation of the 3-oxo carboxylic acid that eliminates it, so little of the intermediate can accumulate on the active site during the normal reaction.[273] Fortuitously, it was discovered that an analogue of the substrate, 2-deoxy-6-phospho-D-gluconate, is converted by

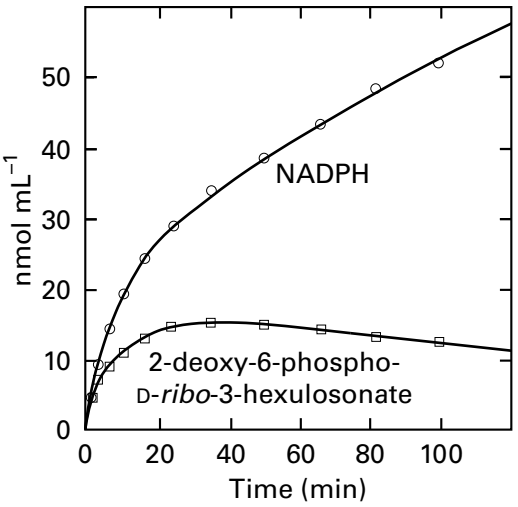

Figure 5–6: Kinetics of formation of 2-deoxy-6-phospho-D-*ribo*-3-hexulosonate and NADPH in the unnatural reaction catalyzed by phosphogluconate dehydrogenase (NADP$^+$-dependent, decarboxylating).[273] To the reaction mixture at 20 °C (final volume of 1 mL buffered at pH 8.0) were added 1.0 μmol of 2-deoxy-6-phospho-D-gluconate, 1.2 μmol of NADP$^+$, and 0.68 unit of phosphogluconate dehydrogenase. (○) The increases in the concentration of NADPH (nanomoles milliliter^{-1}) were followed as a function of the respective intervals (minutes) by the absorbance of the solution at 340 nm. (□) The concentrations of 2-deoxy-6-phospho-D-*ribo*-3-hexulosonate (nanomoles milliliter^{-1}) were assessed at intervals (minutes) by withdrawing samples and forming a formazan derivative from the β-oxo carboxylic acid by reaction with diazotized 4-nitroaniline.

phosphogluconate dehydrogenase (NADP$^+$-dependent, decarboxylating) from *Cyberlindnera jadinii* into 2-deoxy-6-phospho-D-*ribo*-3-hexulosonate

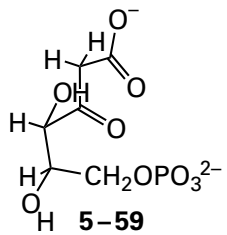

5–59

Unlike the natural intermediate, which remains tightly bound in the active site, the rate at which 2-deoxy-6-phospho-D-*ribo*-3-hexulosonate dissociates from the active site is almost the same as the rate at which it is decarboxylated while on the active site. Consequently, 2-deoxy-6-phospho-D-*ribo*-3-hexulosonate appears in the solution as the reaction progresses (Figure 5–6).[273] This 2-deoxy-6-phospho-D-*ribo*-3-hexulosonate is eventually re-bound at the active site and decarboxylated to 2-deoxy-D-ribulose 5-phosphate, another observation consistent with 6-phospho-D-*ribo*-3-hexulosonic acid (**5–58**) being the normal intermediate. Simply by replacing the hydroxy group at carbon 2 with a hydrogen, an analogue of an otherwise undetectable intermediate was produced and even released into the solution in significant yield by the enzyme.

As with phosphogluconate dehydrogenase (NADP$^+$-dependent, decarboxylating), an alternative reactant has been used with glutamine synthetase (previously Equation 4–453)

$$\text{L-glutamate} + NH_3 + MgATP^{2-} \rightleftharpoons MgADP^- + HOPO_3^{2-} + \text{L-glutamine} \quad (5\text{–}77)$$

to identify an intermediate in the enzymatic reaction. When the enzyme from *E. coli* is mixed with L-glutamate and MgATP^{2-} in the absence of ammonia, a large change in fluorescence of the protein occurs that is consistent with formation of an intermediate.[274] If this intermediate sits in the active site for any length of time in the absence of ammonia, 5-carboxy-2-pyrrolidone is formed by cyclization of an activated L-glutamate

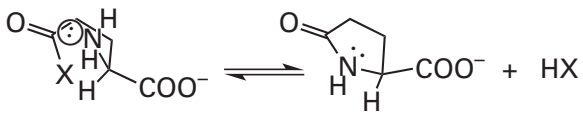

(5–78)

where X is a good leaving group, presumably phosphate. Attempts to isolate directly the expected intermediate, 5-phospho-L-glutamate, usually have been unsuccessful, owing to the spontaneous formation of 5-carboxy-2-pyrrolidone in solution after denaturation of the enzyme. *cis*-1-Amino-1,3-dicarboxycyclohexane, however, is a reactant for glutamine synthetase that resembles L-glutamate[275] but cannot cyclize as L-glutamate can. When *cis*-1-amino-1,3-dicarboxycyclohexane is incubated with ovine glutamine synthetase, in the absence of ammonia, the analogous acyl phosphate is formed, and it can be isolated and identified chemically[276]

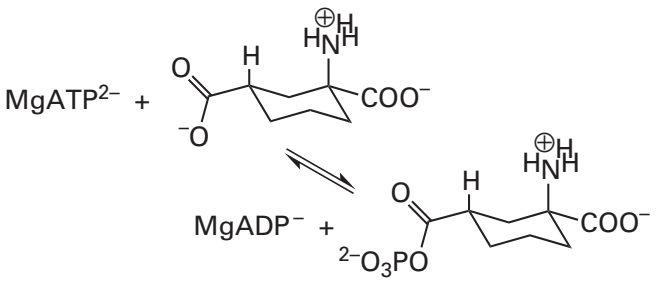

(5–79)

These results demonstrate the ability of the enzyme to form an acyl phosphate at the proper position in a reactant.

If an alternative reactant is used, the intermediate formed by the enzyme can also be unstable but nevertheless **disintegrate in such a way as to implicate the existence of a particular intermediate.** For example, bovine adenosylhomocysteinase, in addition to catalyzing its normal reaction (Equation 5–2), also catalyzes the unnatural oxidative elimination of adenine from 2′-deoxyadenosine

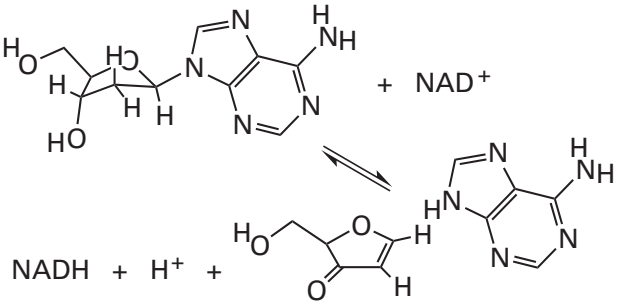

(5–80)

concomitant with reduction of the prosthetic NAD^+ to NADH.[277] This elimination is consistent with the initial formation of 2′-deoxy-3′-oxoadenosine during a reaction analogous to the first step in the normal enzymatic reaction (Figure 5–2).

Another strategy is to **mutate the enzyme** to block the enzymatic reaction in such a way that a noncovalent intermediate will accumulate. For example, when Phenylalanine 337 in 4-hydroxyphenylpyruvate dioxygenase

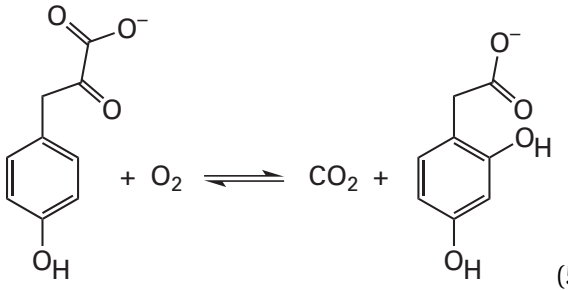

(5–81)

from *Streptomyces avermitilis* was mutated to isoleucine, the enzyme still converted 4-hydroxyphenylpyruvate into homogentisate but also produced oxepinone **5–60**[278]

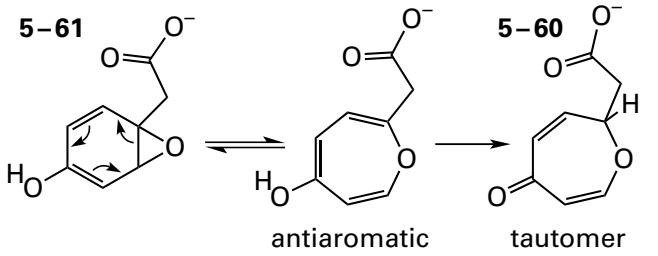

(5–82)

which is the product expected from the rapid, nonenzymatic rearrangement of benzene oxide **5–61** believed to be the noncovalent intermediate in the normal enzymatic reaction.

A noncovalent intermediate can also be accumulated in an active site for crystallographic observation by decreasing the rate of the enzymatic reaction in such a way that the **steps following formation of the intermediate are inhibited**. When crystals of the aspartic endopeptidase HIV-1 retropepsin from human immunodeficiency virus type 1 were soaked in a solution of the peptide AETFYVDGAA at pH 2.5, a pH at which the enzyme has little enzymatic activity, the tetrahedral intermediate in the enzymatic reaction (previously Equation 4–376)

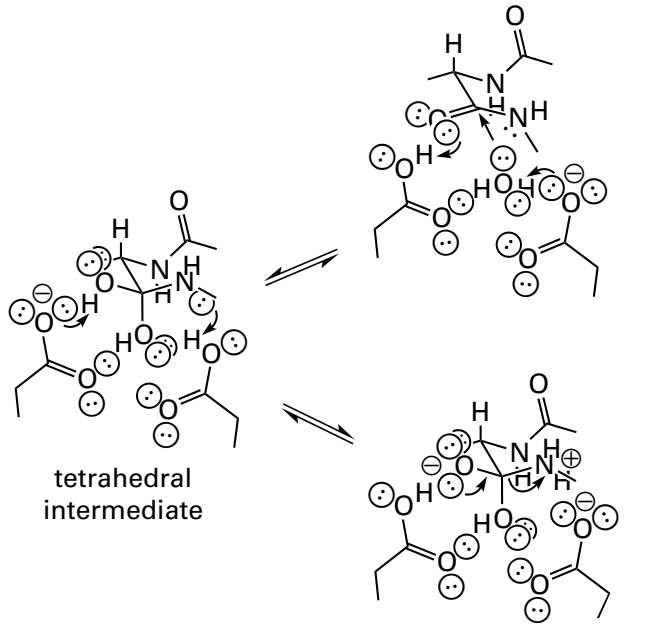

(5–83)

could be observed occupying the active site in the resulting map of electron density.[279] The tetrahedral intermediate for hydrolysis of the peptide NLLTQI was observed crystallographically in the active site of the same enzyme in which Isoleucine 54 had been mutated to valine to decrease enzymatic activity.[280]

Isocitrate dehydrogenase ($NADP^+$) catalyzes the oxidative decarboxylation of isocitrate

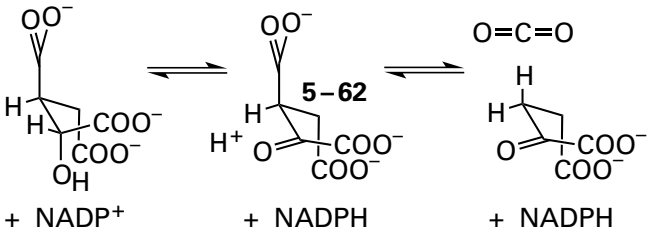

(5–84)

by passing through the noncovalent intermediate oxalosuccinate (**5–62**), an α-oxo acid. A mutant of the enzyme from *E. coli* in which Lysine 230 was changed to methionine was shown to be inhibited in the decarboxylation step of the mechanism.[281] When crystals of the mutant enzyme were soaked in 0.5 M isocitrate, 0.5 M Mg^{2+}, and 0.5 M $NADP^+$ for 60 s and then submitted to diffraction, electron density corresponding to oxalosuccinate was observed in the active site of the resulting crystallographic molecular model.[282] In the map of electron density, the carbon–carbon bond to the carboxylato group that dissociates as CO_2 is held parallel to the π molecular orbital system of the carbonyl by the active site, as one might expect.

Another approach to its chemical identification is to synthesize a noncovalent intermediate, if it is stable enough to be synthesized, and show that the synthetic compound is converted by the enzyme into its usual substrates. For example, enol ether **5–63** is an intermediate in the addition–elimination catalyzed by anthranilate synthase

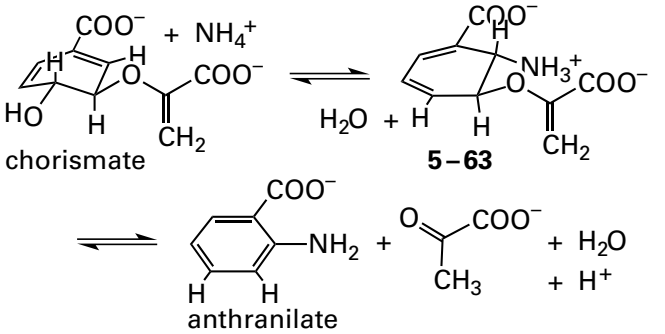

(5–85)

It is stable enough to be synthesized chemically,[283] and when it was mixed with NH_4^+ and anthranilate synthase from *Serratia marcescens*, the enzyme could convert the synthetic compound to anthranilate in an elimination that displayed a limiting rate of 600 nmol min^{-1} mg^{-1} and a Michaelis constant for chorismate of 0.1 mM. The corresponding rate constants for chorismate at saturating NH_4^+ were 500 nmol min^{-1} mg^{-1} and 0.1 mM. These observations demonstrated that the **synthetic intermediate is kinetically competent**. Furthermore, when a mutant of the enzyme from *S. enterica*, in which Histidine 398 had been changed to methionine to decrease the rate of the elimination in the second step of the enzymatic reaction (Equation 5–85), was mixed with chorismate for 3 h, enol ether **5–63** could be isolated from the solution,[284] and at 0 °C, the wild-type enzyme produces enol ether **5–63** and releases a portion of it into the solution.[285]

Unsaturated enol **5–64** (see Equations 4–416 and 4–417)

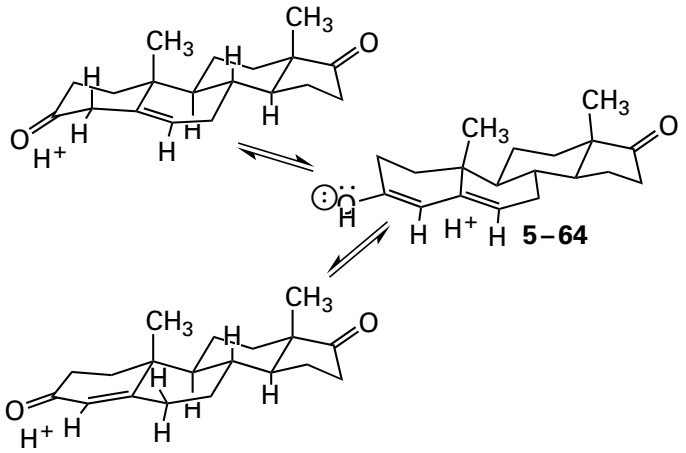

(5–86)

that is the intermediate in the reaction catalyzed by steroid Δ-isomerase has been synthesized.[286] The enzyme from *Comamonas testosteroni* converts the synthetic intermediate (Int) to a mixture of the two steroids that are substrates for the enzyme with a specificity constant, k_{Int}, of 230 μM^{-1} s^{-1} which is indistinguishable from the specificity constant, $k_{\Delta 5}$, of 210 μM^{-1} s^{-1} for the conversion of androst-5-ene-3,17-dione (Δ5) to androst-4-ene-3,17-dione. Again, the synthetic intermediate is kinetically competent.

In many instances, however, a synthetic compound that is identical to an actual **noncovalent intermediate is not kinetically competent** when added to the enzyme and the remainder of the substrates required for enzymatic activity. One reason for this failure is that, to protect the normally formed intermediate from hydrolysis, dissociation, or another alteration that would occur in a partially aqueous environment, the active site of the enzyme closes around the substrates to shield them almost

completely from the solution before the intermediate is formed. Another reason is that, to prevent its undesired rearrangement or decomposition, the intermediate, after it is formed, is tightly circumscribed by the active site. In such instances, it can be difficult for the intermediate, when it is present in the solution, necessarily without a complete set of reactants, to effect the same rearrangements of the active site that occur in the normal sequence of events when a complete set of reactants binds to the active site.

Formate—tetrahydrofolate ligase

$$MgATP^{2-} + \text{formate} + \text{tetrahydrofolate} \rightleftharpoons MgADP^{-} + HOPO_3^{2-} + \text{10-formyltetrahydrofolate} \quad (5\text{–}87)$$

has formyl phosphate as an intermediate in its reaction

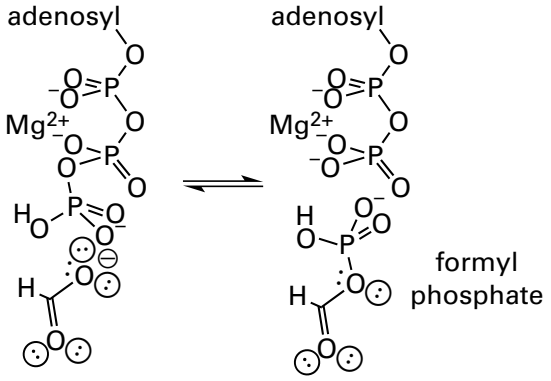

(5–88)

Formyl phosphate is unstable and is rapidly hydrolyzed in solution at neutral pH. Presumably this unstable intermediate is protected from counterproductive hydrolysis by the active site. Electron density for formyl phosphate and $MgADP^-$ has been observed in the active site of the enzyme from *Moorella thermoacetica* crystallized in the presence of $MgATP^{2-}$ and formate but in the absence of tetrahydrofolate.[287] In the absence of tetrahydrofolate, the enzyme from *Clostridium cylindrosporum* slowly releases formyl phosphate, formed at its active site, into the solution.[288] These observations are evidence that formyl phosphate is a genuine noncovalent intermediate.

When synthetic formyl phosphate, however, is mixed with the enzyme in the presence of $MgADP^-$ and tetrahydrofolate, both 10-formyltetrahydrofolate (Equation 5–87 in the forward direction) and $MgATP^{2-}$ (Equation 5–87 in the reverse direction) are produced, but the catalytic constants k_0 for the respective rates of their production from formyl phosphate were only 3% and 1% of the catalytic constants for their rates of production from the usual substrates for the enzyme.[289] Carbamoyl phosphate

5–65

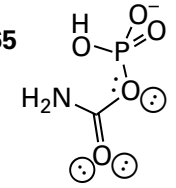

resembles formyl phosphate and is mistaken by the enzyme for formyl phosphate. The enzyme catalyzes phosphotransfer from carbamoyl phosphate to $MgADP^-$ to form $MgATP^{2-}$ (the reverse of Equation 5–88), consistent with the role of formyl phosphate as an intermediate in the enzymatic reaction,[290] but again the rate of the unnatural reaction is only about 1% that of the reaction of $HOPO_3^{2-}$ and 10-formyltetrahydrofolate with $MgADP^-$ to form $MgATP^{2-}$.

The purpose for producing formyl phosphate as an intermediate is to activate the carboxy group by providing an excellent leaving group. This activation permits formate to form the anilide in a nucleophilic substitution with a poor nucleophile

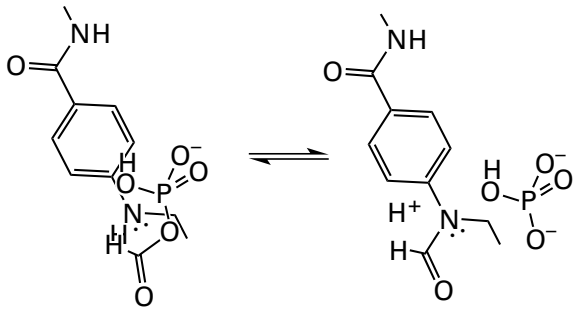

(5–89)

The nucleophile is a poor one ($pK_a = -1.25$) because the pair of electrons on the exocyclic nitrogen of the anilino group is withdrawn into the π system of the phenyl group. This delocalization positions the pair of electrons in a molecular orbital perpendicular to the plane of the phenyl ring rather than residing in an sp^3 atomic orbital on the nitrogen as it would in an amino group.

Analogues for intermediates of high energy can be used as evidence for the existence of that intermediate in an enzymatic reaction. It has already been noted that analogues for intermediates of high energy (Table 3–7) are often competitive inhibitors with high affinity for the active sites of enzymes, and several examples of such analogues have already been presented and discussed at length. The earlier discussion focused on these inhibitors as evidence for the proposal that the active sites of enzymes are constructed to bind intermediates of high energy tightly and thereby lower the free energy required to produce these intermediates at the active site. Another view of such observations is that if a particular compound has been designed to mimic a postulated intermediate in a proposed mechanism for the enzymatic reaction, the fact that it binds tightly to the active site is evidence for the existence of that intermediate. For example, the inhibition of bovine adenosine deaminase by (6*S*)-6-hydroxy-1,6-dihydropurine ribonucleoside (**5–66**)

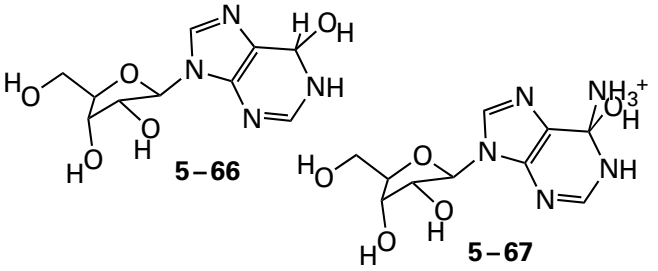

with competitive inhibition constant of 0.2 pM, is strong evidence that the noncovalent intermediate in the enzymatic reaction (see Figure 3–36) is tetrahedral intermediate **5–67**.[291-293]

2-Carboxy-D-arabinitol 1,5-bisphosphate (**5–68**)

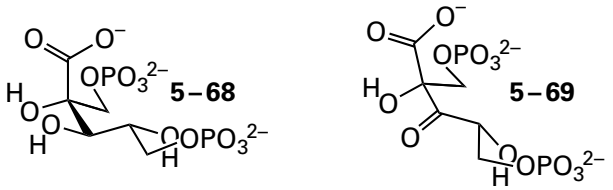

is an inhibitor of ribulose-bisphosphate carboxylase from *Spinacia oleracea* with a dissociation constant around 0.2 pM.[294,295] This observation is one fact providing evidence for the existence of 2-carboxy-3-oxo-D-arabinitol 1,5-bisphosphate (**5–69**) as the noncovalent intermediate[296] preceding the retro-Claisen condensation catalyzed by ribulose-bisphosphate carboxylase (previously Equation 4–173)

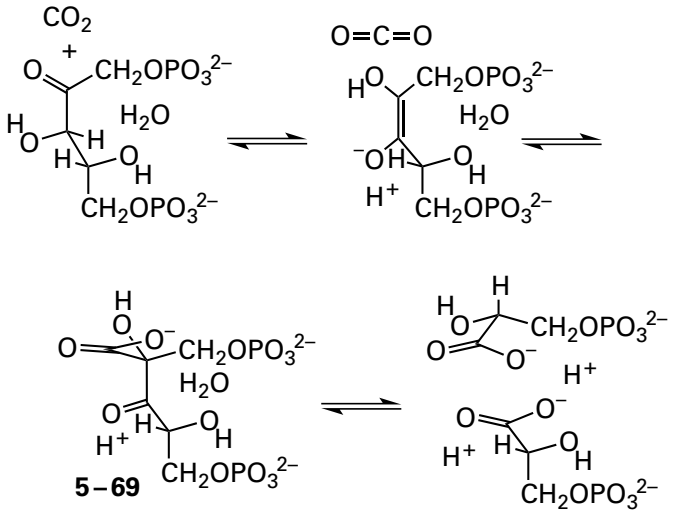

(5–90)

that produces two molecules of 3-phospho-D-glycerate. Intermediate **5–69** is formed from D-ribulose 1,5-bisphosphate at the active site by an isomerization analogous to the one catalyzed by triose-phosphate isomerase, followed by a nucleophilic addition of the resulting *cis*-enediolate to carbon dioxide. When the enzyme from *S. oleracea* was mixed with CO_2 and D-ribulose 1,5-bisphosphate and then denatured with acid after 0.3 s and the resulting solution was reduced immediately with $NaBH_4$, both 2-carboxy-D-arabinitol 1,5-bisphosphate (**5–68**) and 4-carboxy-D-arabinitol 1,5-bisphosphate, the two products expected from nonstereospecific reduction of intermediate **5–69** at the central carbonyl group, were identified as products in 7% yield relative to the concentration of active sites.[297] The reduction produces the diastereomeric mixture because it occurs nonstereospecifically after intermediate **5–69** has been ejected from the active site by acidic denaturation, so the fact that both diastereomers are present is evidence for the existence of the noncovalent intermediate. There are crystallographic molecular models of analogue **5–68** of the noncovalent intermediate, in the active sites of ribulose-bisphosphate carboxylases from *S. oleracea* (Figure 3–53),[298,299] *Rhodospirillum rubrum*,[300] and *Synechococcus*.[301]

Analogue **5–68** is a far more potent inhibitor (K_d = 0.2 pM) of the enzyme than its epimer 2-carboxy-D-ribitol 1,5-bisphosphate (K_d = 1 μM).[294,302] Both inhibitors have the same stereochemistry at carbons 3 and 4 as D-ribulose 1,5-bisphosphate. The only difference between them is the stereochemistry at carbon 2, and the large difference in their dissociation constants, as well as the stereochemistry of the products of reduction of the ejected intermediate,

identifies the stereochemistry of the nucleophilic addition of the *cis*-enediolate to CO_2 (Equation 5–90) during the enzymatic reaction.

The fact that (*R*)-difluoromethylketal phosphate **5–70**

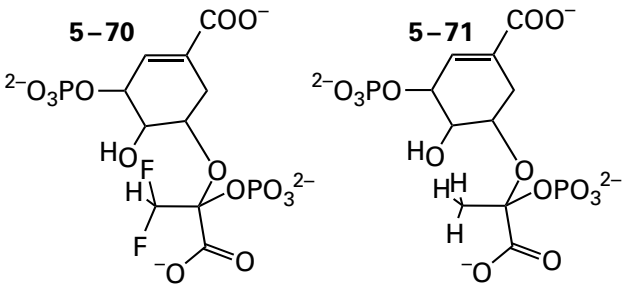

is a competitive inhibitor with a high affinity (K_i = 4 nM)[303] for the active site of 3-phosphoshikimate 1-carboxyvinyltransferase (see Equation 4–321; previously Problem 4–26)

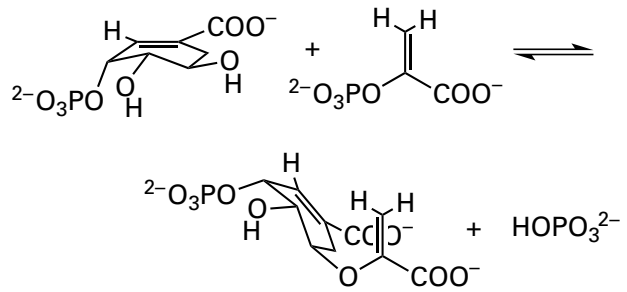

(5–91)

from *Petunia hybrida* has been presented as evidence that (*S*)-methylketal phosphate **5–71*** is an intermediate in the reaction catalyzed by the enzyme (previously Equation 4–414)

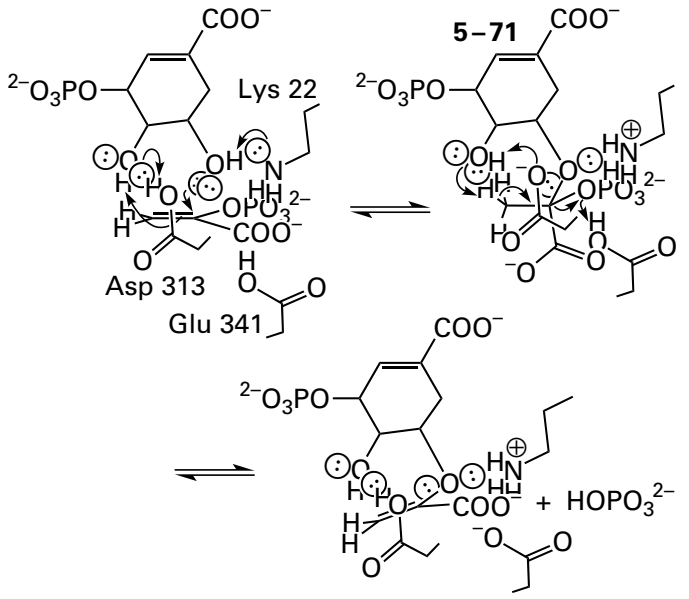

(5–92)

(*S*)-Methylketal phosphate **5–71** has been synthesized; and when it was mixed with the enzyme, it was converted to a 3:1:1 mixture of the substrates 5-*O*-(1-carboxyvinyl)-3-phosphoshikimate (product of Equation 5–91) and phospho*enol*pyruvate and 3-phosphoshikimate (reactants in Equation 5–91), as expected for a noncovalent intermediate in the reaction.[304]

The facts that (*S*)-difluoromethylketal phosphate is a weaker competitive inhibitor (K_i = 75 nm)[303] and that (*R*)-methylketal phosphate is not converted to substrates by the enzyme[304] verify the stereochemistry of the actual intermediate in the enzymatic reaction.

There is a crystallographic molecular model of (*R*)-difluoromethylketal phosphate **5–70** occupying the active site of 3-phosphoshikimate 1-carboxyvinyltransferase from *E. coli*,[305] and noncovalent intermediate **5–71** has been observed crystallographically in the active site of an inactive mutant of the enzyme from *E. coli*—in which the catalytic acid, Aspartate 313, had been changed to alanine—when it was crystallized in the presence of 3-phosphoshikimate and phospho*enol*pyruvate,[306] When the enzyme from *Streptococcus pneumoniae* was crystallized from a solution containing 3-phosphoshikimate and (*Z*)-3-fluorophospho*enol*pyruvate, electron density for the monofluoromethylketal phosphate analogue of **5–70** was found in the active site of the enzyme.[307]

When 3-phosphoshikimate 1-carboxyvinyltransferase from *E. coli* was mixed at high concentration with an equimolar amount of shikimate 3-phosphate and 2 mM phospho*enol*pyruvate and 5 mM phos-

*The two fluorines invert the stereochemical designation.

phate, an equilibrium was established on the active site in which intermediate **5–71** comprised 30% of the several bound reactants[308] and from which, upon alkaline denaturation of the protein, ketal phosphate **5–71** could be isolated and identified by nuclear magnetic resonance spectroscopy.[309] When a solution (450 μL) containing 12 mM shikimate 3-phosphate and a 3.4 mM concentration of active sites for 3-phosphoshikimate 1-carboxyvinyltransferase from *E. coli* was mixed with a solution (21 μL) containing 267 mM [2-^{13}C]phospho*enol*pyruvate (final concentration 12.5 mM) or a solution (450 μL) containing 4 mM shikimate 3-phosphate and a 1.1 mM concentration of active sites was mixed with a solution (8 μL) containing 244 mM [3-^{13}C]phospho*enol*pyruvate (final concentration 4.3 mM), additional absorptions appeared in the nuclear magnetic resonance spectra that were assigned to the respective carbons-13 in intermediate **5–71**, bound at equilibrium in the respective active sites.[310]

When ketal phosphate **5–71,** isolated from the active site of 3-phosphoshikimate 1-carboxyvinyltransferase from *E. coli* by alkaline denaturation, was mixed with fresh enzyme, it was converted to substrates at a rate (120 s^{-1})[311] close to the rate (420 s^{-1}) at which the intermediate was calculated to decompose to substrates of the enzymatic reaction.[308]

From all these observations, it has been concluded that the first step of the reaction catalyzed by 3-phosphoshikimate 1-carboxyvinyltransferase (Equation 5–91) is nucleophilic addition of the 5-hydroxy group of 3-phosphoshikimate to carbon 2 of phospho*enol*pyruvate to produce ketal phosphate **5–71**. This rather unusual nucleophilic addition, which is not stabilized in any usual manner, appears to be an inescapable conclusion. The concerted addition of a hydron to carbon 3 of phospho*enol*pyruvate during nucleophilic addition of the 5-hydroxy group or the initial hydronation of carbon 3 to produce a carbenium ion at carbon 2 must be required to avoid formation of a primary carbanion at carbon 3, which would result from unassisted addition of the 5-oxido group of the conjugate base of 3-phosphoshikimate.

The fact that a minor side product of the enzymatic reaction is ketal **5–72**

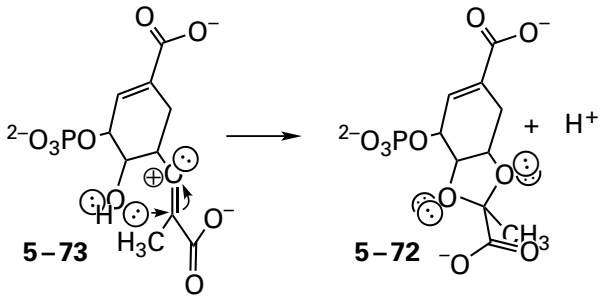

(5–93)

suggests that phosphate leaves from intermediate **5–71** to produce oxocarbenium ion **5–73** as an intermediate before a hydron is removed from the methyl group to form the desired product.[312,313] It is possible, however, that ketal **5–72** is the result of an intramolecular concerted nucleophilic substitution at the tertiary carbon of intermediate **5–71**.

The related enzyme[314] UDP-*N*-acetylglucosamine 1-carboxyvinyltransferase (20% identity; 2.6 gap percent) catalyzes addition of the 3-hydroxy group of UDP-*N*-acetylglucosamine to phospho*enol*pyruvate and the subsequent elimination of phosphate. Chemical and crystallographic evidence has been presented for an intermediate in this enzymatic reaction that is analogous to methylketal phosphate **5–71**.[315-317]

Noncovalent intermediates are also formed by substrate-assisted catalysis. Enzymes such as chymotrypsin (Figure 3–6), 4-α-glucanotransferase (**5–11**), cellulase (**5–14**), and alkaline phosphatase (Equation 5–33) have covalent intermediates in their enzymatic reactions. Each of these covalent intermediates is formed by a nucleophilic substitution in which the electrophile is an atom in a substrate and the nucleophile is a heteroatom in the side chain of an amino acid in the active site. In other instances, however, the nucleophile used in analogous enzymatic reactions is a functional group in the substrate itself rather than in the enzyme, such as the 2′-hydroxy group on the substrate for ribonuclease (Figure 4–46). A noncovalent intermediate, such as 2′,3′-cyclic phosphate in the cleavage of RNA by ribonuclease, results from this intramolecular substrate-assisted catalysis.

β-*N*-Acetylhexosaminidase catalyzes hydrolysis of an *N*-acetylgalactosamine or *N*-acetylglucosamine from the nonreducing end of an oligosaccharide. The fact that thiazoline **5–74**[318]

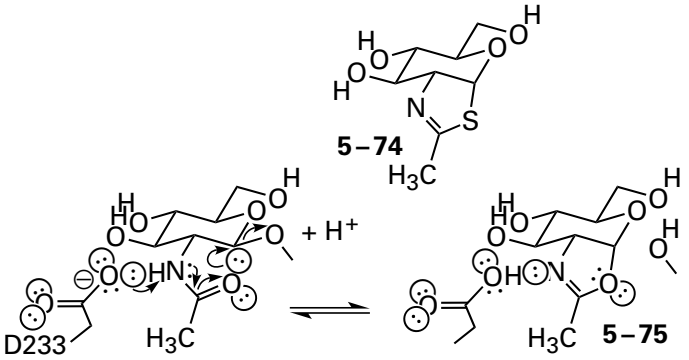

(5–94)

is a competitive inhibitor (K_i = 70 nM) of the human enzyme[319] is evidence that *β*-*N*-acetylhexosaminidase catalyzes its reaction by intramolecular concerted nucleophilic substitution of the hydroxy group of the adjacent saccharide at the reducing end of *N*-acetylgalactosamine or *N*-acetylglucosamine by the acyl oxygen of its *N*-acetyl group (Equation 5–94) with oxazoline **5–75** as a noncovalent intermediate.

In crystallographic molecular models of thiazoline **5–74** in the active sites of isoenzymes of human *β*-*N*-acetylhexosaminidase and a bacterial homologue, the carboxy groups homologous to that of Aspartate 233 in the human A isoenzyme form hydrogen bonds to the respective imino nitrogens of the inhibitor.[320-322] These facts identify that carboxy group as the one performing two roles. First, it acts as the catalytic base required to remove the hydron from the 2-imino nitrogen of the substrate (pK_a = 17) to increase sufficiently the nucleophilicity of the acyl oxygen in the nucleophilic substitution. Second, it acts as a catalytic acid (right side of Equation 5–94) to hydronate the imino nitrogen to make the oxygen a better leaving group in the second concerted nucleophilic substitution of the hydroxy group of a molecule of water for the acyl oxygen of the acetyl group to complete the hydrolysis.

Protein O-GlcNAcase from *B. thetaiotaomicron* is an enzyme that hydrolyzes an *N*-acetylglucosamine from a serine in a glycoprotein by substrate-assisted catalysis through the same oxazoline (**5–75**) as the one formed in the active site of *β*-*N*-acetylhexosaminidase.[319] When Aspartate 242, the aspartate that acts as a catalytic base and then a catalytic acid at the imino group of *N*-acetylglucosamine in the active site of this enzyme, is mutated to asparagine, oxazoline **5–75** can be seen in the map of electron density for the active site computed from the diffraction of a crystal of the enzyme that had been mixed with an *N*-acetylglucoside with a good leaving group.[323] The fact that oxazoline **5–75** is observed in the active site in the mutant but not in the wild type implies that the importance of hydronation of its nitrogen to create a leaving group capable enough to participate in a nucleophilic substitution that breaks the oxazoline, which should be quite stable, is significantly greater than the need to dehydronate the imino group during formation of the oxazoline.

Phosphoinositide phospholipase C hydrolyzes the phosphodiester in 1-phosphatidyl-1D-*myo*-inositol.[324] The enzyme from *B. cereus* converts 1-phosphatidyl-1D-*myo*-inositol (**5–76**) to 1,2-diacyl-*sn*-glycerol and 1D-*myo*-inositol 1,2-cyclic phosphate (**5–77**), which are both released from the active site, and then the enzyme slowly hydrolyzes the 1D-*myo*-inositol 1,2-cyclic phosphate to 1D-*myo*-inositol 1-phosphate

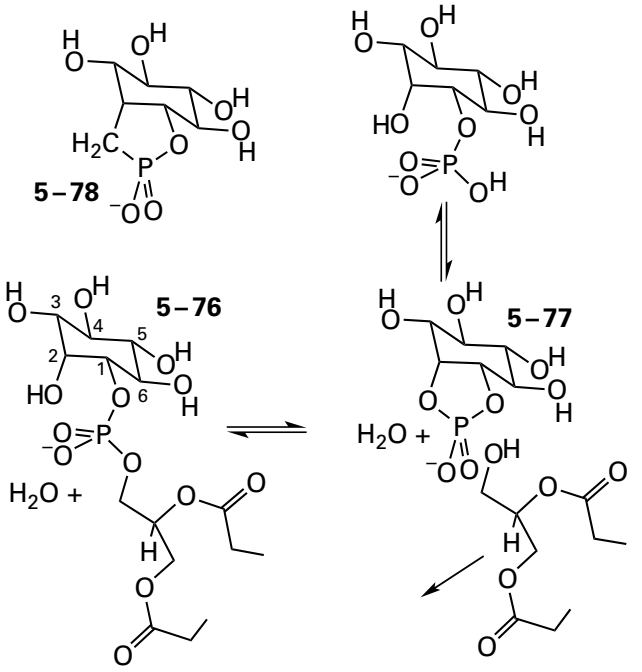

(5–95)

This behavior is analogous to the reaction catalyzed by ribonuclease (previously Equation 4–364)

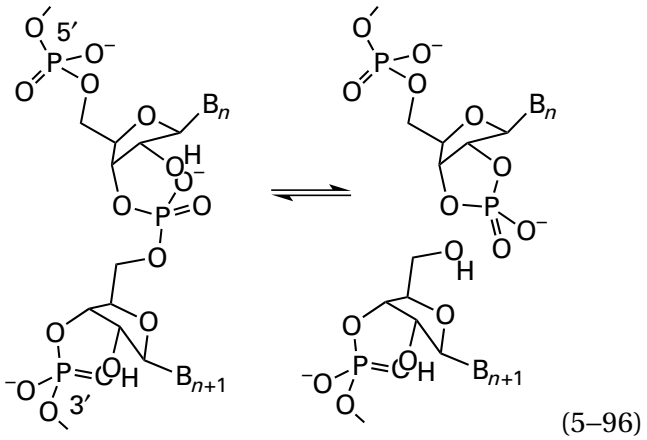

(5–96)

Bovine phosphoinositide phospholipase C, however, produces 90% 1D-*myo*-inositol 1-phosphate and 10% 1D-*myo*-inositol 1,2-cyclic phosphate, and it does not hydrolyze the 1D-*myo*-inositol 1,2-cyclic phosphate once it has been released into the solution.[325] Electron density for the inhibitor 1D-*myo*-inositol-2-methylene-1,2-cyclic phosphonate (**5–78**), a stable analogue of 1D-*myo*-inositol 1,2-cyclic phosphate, has been located in the active site of a crystallographic molecular model of phosphoinositide phospholipase C from *R. norvegicus*.[324] All these results suggest that, in the active site of the enzyme from mammals such as *B. taurus* and *R. norvegicus*, 1D-*myo*-inositol 1,2-cyclic phosphate (**5–77**) is a noncovalent intermediate in the enzymatic reaction that remains bound in the active site and that is converted, almost exclusively, into 1D-*myo*-inositol 1-phosphate, the major product of the enzymatic reaction (Equation 5–95).

Ketones or ketimines transiently formed from alcohols or amines, respectively, are noncovalent intermediates in a number of enzymatic reactions. In most of these instances, a prosthetic NAD^+, tightly bound at the active site, oxidizes a secondary alcohol or internal primary amine that is the reactant to produce the respective ketone or ketimine as an intermediate. This intermediate then undergoes a transformation, and the resulting, transformed ketone or ketimine is then reduced by NADH to a secondary alcohol or primary amine on the same carbon on which it was in the reactant. In the process, the prosthetic NAD^+ is regenerated. For example, in the active site of ADP-*glyceromanno*-heptose 6-epimerase

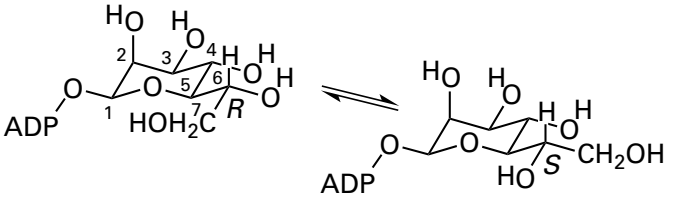

(5–97)

the prosthetic NAD^+ removes the hydride from the secondary alcohol at carbon 6 of the *β*-L-*glycero*-*manno*-heptosyl group, oxidizing it to the ketone, and then the prosthetic NADH reduces the ketone by adding a hydride to the face opposite from the one from which the hydride was removed.[326] The ketone formed by the oxidation leaks slowly from the active site, while ADP-*glyceromanno*-heptose 6-epimerase from *E. coli* is turning over, and the ketone can be trapped with phenylhydrazine.[327] In the active site of the enzyme, however, there seems to be enough room for the ketone at carbon 6 to flip over as a result of rotation about the bond between carbons 5 and 6, dragging along the hydroxymethyl group, and the ketone then can be reduced from the other face to complete the epimerization most of the time before the intermediate ketone can escape from the active site.[328,329]

In the active site of UDP-glucose 4-epimerase (previously Equation 3–422)[330]

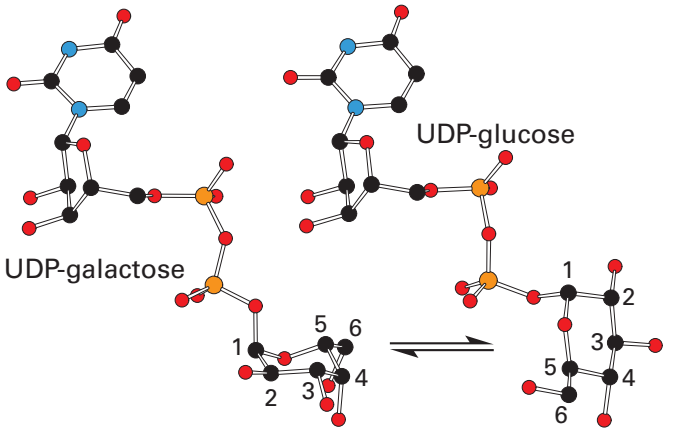

(5–98)

the tightly bound NAD^+ oxidizes UDP-D-galactose to UDP-4-oxo-D-glucopyranoside

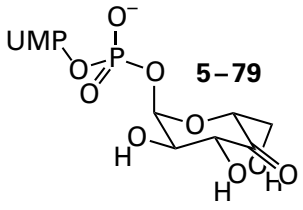

UDP-4-Oxoglucopyranoside **5–79** pivots in the active site,[331] and then the NADH reduces it to UDP-D-glucose.

There are several observations consistent with the existence of UDP-4-oxoglucopyranoside **5–79** as a noncovalent intermediate in the enzymatic reaction. When either UDP-D-glucose or UDP-D-galactose is mixed with the enzyme from *E. coli*, a portion of the bound NAD^+ is reduced to NADH.[332] When TDP-4-oxo-6-deoxy-D-glucose is mixed with enzyme, the prosthetic group of which has been reduced to NADH, TDP-4-oxo-6-deoxy-D-glucose is reduced to a mixture of TDP-6-deoxy-D-glucose and TDP-6-deoxy-D-galactose.[333] When high concentrations of the enzyme are mixed with UDP-D-galactose and $Na[^3H]BH_4$ is subsequently added, the intermediate UDP-4-oxo-D-hexose **5–79** can be trapped as a mixture of UDP-[4-^{3}H]-D-glucose and UDP-[4-^{3}H]-D-galactose.[334,335] Crystallographic molecular models of the NADH form of the enzyme from *E. coli* in a mismatched, inactive complex with UDP-D-glucose[336] and in a mismatched, inactive complex with UDP-D-galactose[331] define the flip that the intermediate UDP-4-oxo-D-hexose **5–79** performs (Equation 5–98). This conformational change is the only transformation the intermediate undergoes between the oxidation and the subsequent reduction, as is the conformational change on a much smaller scale in the epimerization catalyzed by ADP-*glyceromanno*-heptose 6-epimerase (Equation 5–97).

A related enzyme (25% identify, 2.7 gap per cent), CDP-paratose 2-epimerase from *Yersinia pseudotuberculosis*, catalyzes the epimerization of CDP-D-paratose (CDP-3,6-dideoxy-D-glucose) at carbon 2 instead of carbon 4. It does so, however, by oxidizing carbon 4 to the ketone, as might be expected from its similarity, but then performing a retroaldol condensation between carbons 2 and 3 followed by an aldol condensation, after the aldehyde at carbon 2 has flipped over, to produce the other epimer at carbon 2.[337] Oxidation to the ketone permits the retroaldol and aldol condensations to occur.

The reaction catalyzed by CDP-paratose 2-epimerase illustrates the fact that the production of a ketone as an intermediate by a prosthetic NAD^+ **opens up all the chemistry available to a carbonyl group**, such as the acidity of its α carbon, elimination from its β carbon, nucleophilic addition, aldol and retroaldol condensations, and Claisen and retro-Claisen condensations. For example, adenosylhomocysteinase exploits the acidity of the α carbon of the ketone produced as an intermediate in its enzymatic mechanism to set up elimination of a poor leaving group (Figure 5–2).

6-Phospho-β-glucosidase from *T. maritima*[338] uses a similar β-elimination

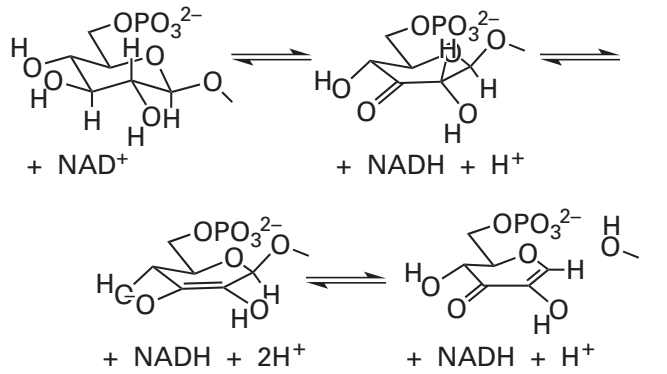

(5–99)

in which a molecule of water substitutes in reverse for the hydroxy group on the alcohol that is the leaving group. This mechanism is an alternative to the usual mechanisms for hydrolysis of a glycoside. The chemical evidence for this alternative mechanism includes a requirement for catalytic amounts of NAD^+ (1 μM) for catalysis; the appearance of deuterium at carbon 2 of the product when the reaction is run in D_2O; the ability of the enzyme to exchange a deuterium for a hydrogen at carbon 2 of 1,5-anhydroglucitol 6-phosphate, an analogue of the product D-glucose 6-phosphate; and a kinetic isotope effect for the substrate 4-nitrophenyl 6-phospho-β-D-[3-^{2}H]glucoside.[339] None of these observations would result from the usual mechanisms for hydrolyzing glycosides in which the leaving group is hydronated, and a covalent intermediate with a carboxylato group from the active site at carbon 1 may or may not form.

Ornithine cyclodeaminase, which catalyzes a formal nucleophilic substitution of an amino group for ammonia at the α carbon of L-ornithine, proceeds through **nucleophilic substitution at an iminium ion**

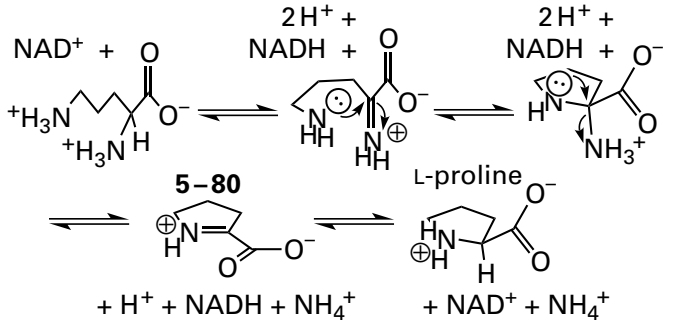

(5–100)

The enzyme contains a tightly bound, prosthetic NAD^+. Upon addition of L-ornithine to ornithine cyclodeaminase from *Clostridium sporogenes*, a portion of the NAD^+ is reduced to NADH.[340] In the crystallographic molecular model of the mismatched complex between the enzyme from *Pseudomonas putida* and NADH and L-ornithine, carbon 2 of L-ornithine and carbon 4 of nicotinamide are in the proper orientation for transfer of a hydride, and they are only 0.38 nm apart.[341] In the reaction catalyzed by the enzyme, the δ nitrogen of L-ornithine is retained in L-proline.[340] All these results are consistent with formation of 3,4-dihydro-2*H*-pyrrole-5-carboxylic acid (**5–80**) as a noncovalent intermediate in the enzymatic reaction (Equation 5–100) by nucleophilic addition to the intermediate imine. In this reaction, a hydride is removed from and returned to the same carbon with the same stereochemistry, so the only role of the oxidation is to produce the imine and exploit its capabilities.

The 2-dehydro-1D-*myo*-inositol 3-phosphate (**5–81**), produced as a noncovalent intermediate in the conversion of D-glucose 6-phosphate to 1D-*myo*-inositol 3-phosphate catalyzed by inositol-3-phosphate synthase (see Equation 4–179)

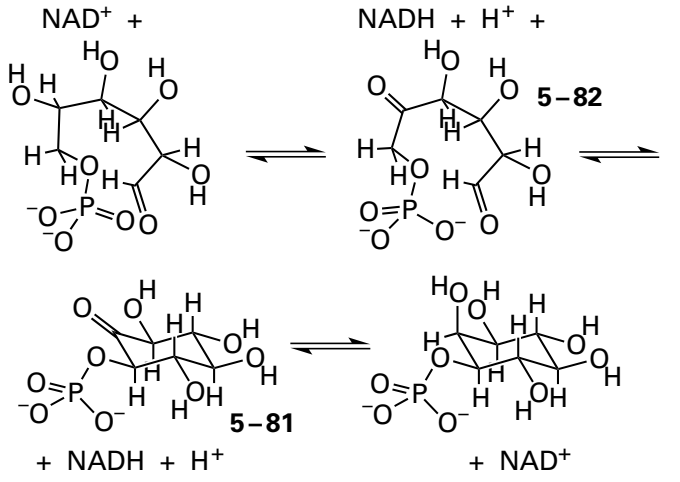

(5–101)

is the product of carbon–carbon bond formation by an **aldol condensation** enabled by the initial oxidation of D-glucose 6-phosphate at carbon 5 by the prosthetic NAD^+. Noncovalent intermediate **5–81** can be trapped nonstereospecifically[342] from the active site of the enzyme from *R. norvegicus* with NaB^3H_4 before it can be reduced stereospecifically in the normal reaction to 1D-*myo*-inositol 3-phosphate by the prosthetic NADH

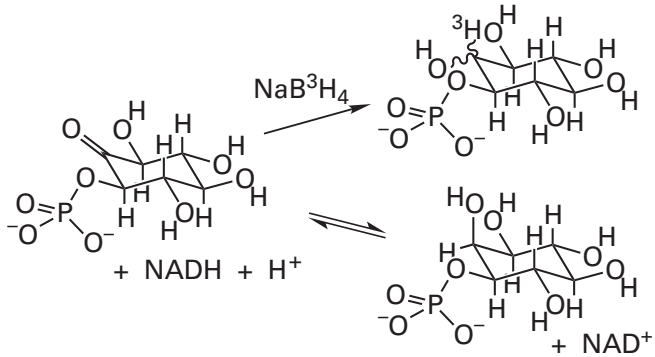

(5–102)

that is the product of the initial oxidation of D-glucose 6-phosphate (Equation 5–101). The lack of stereospecificity in the reaction with NaB^3H_4 demonstrates that it was noncovalent intermediate **5–81** that was reduced because, as usual, the product of the enzymatic reduction is stereospecific.

2-Dehydro-1D-*myo*-inositol 3-phosphate (**5–81**) has been synthesized. It is a competitive inhibitor ($K_i = 4\ \mu M$) of the enzyme from *S. cerevisiae* when the prosthetic group is NAD^+, but it is converted to the product of the enzymatic reaction, 1D-*myo*-inositol 3-phosphate, when the prosthetic group in the active site is NADH.[343] When crystals of the enzyme from *Archaeoglobus fulgidus* are mixed with the substrate D-glucose 6-phosphate and NAD^+ and heated at 80 °C for 15 min in the absence of Mg^{2+}, electron density corresponding to NADH and the ketone 5-dehydro-D-glucose 6-phosphate (**5–82**) could be observed in the active site of the enzyme.[344] In this instance, the absence of Mg^{2+}, a cofactor for the enzyme, prevents the aldol condensation from occurring. In the crystallographic molecular model, carbon 4 of nicotinamide and carbonyl carbon 5 of 5-dehydro-D-glucose 6-phosphate are in the proper orientation for hydride transfer, and they are only 0.35 nm apart, so the ketone and NADH must represent the more favored participants in that particular equilibrium.

Instead of using NAD^+ to oxidize an alcohol or amine to a ketone or ketimine, respectively, phosphopantothenoylcysteine decarboxylase uses a prosthetic

flavin mononucleotide[345] to oxidize a thiol to a thioaldehyde[346]

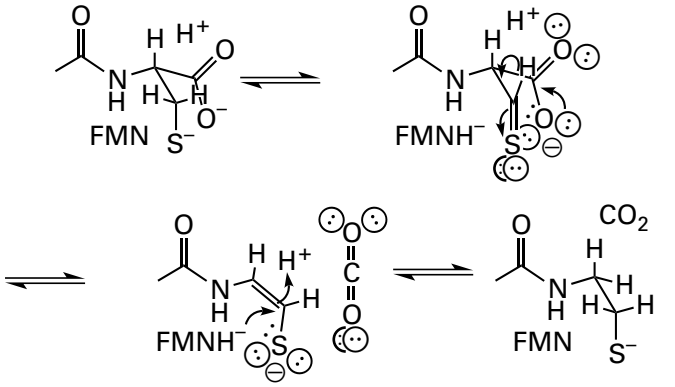

(5–103)

The 1-carboxythioaldehyde is easily decarboxylated, in contrast to the thiol. A hydron then replaces the carboxy group, and the decarboxylated thioaldehyde is reduced back to the thiol to produce pantotheine 4′-phosphate. One piece of evidence for this mechanism is that the analogue of the substrate with a cyclopropyl group at carbon 2 of the cysteinyl group is an active-site label for human phosphopantothenoylcysteine decarboxylase. This ability requires that the thiol be oxidized to the thioaldehyde to make the cyclopropyl group an effective electrophile.[347]

Lactate racemase from *Lactiplantibacillus plantarum* equilibrates (*S*)-lactate and (*R*)-lactate. The active site contains a prosthetic Ni^{2+} that is coordinated by a derivative of nicotinamide mononucleotide. One ligand to the Ni^{2+} is carbon 4 of the nicotinamide ring.[348] The nicotinamide is still reduced by a hydride, and it seems as though the nickel is simply a rather complex substitute for the usual hydrogen atom at carbon 4 of nicotinamide

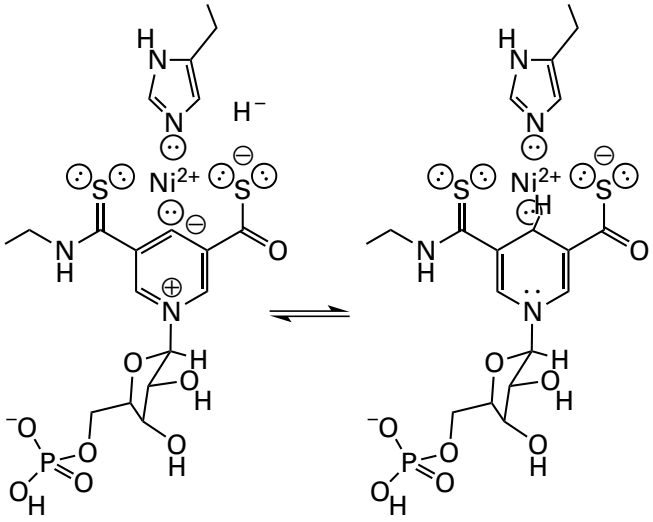

(5–104)

The active site racemizes lactate by using the derivative of nicotinamide mononucleotide to remove a hydride to form pyruvate as an intermediate and then add the hydride to the opposite side of the carbonyl carbon in the pyruvate. Pyruvate (in a constant ratio of greater than 0.30 mole fraction relative to competent active sites) has been isolated upon quenching a solution in which (*S*)-lactate and (*R*)-lactate were being equilibrated.[348] As might be expected, regardless of the mechanism of racemization, a deuterium kinetic isotope effect (2.2) was observed for the racemization of either (*S*)-[2-^{2}H]lactate or (*R*)-[2-^{2}H]lactate.

Enamines, enols, and enolates, the conjugate bases of enols, are common noncovalent heterolytic intermediates in enzymatic reactions.

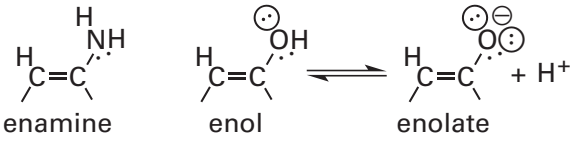

(5–105)

This widespread behavior has already been discussed from a mechanistic standpoint. Several strategies have been used to provide **chemical evidence for their existence**.

In some instances, the enol that is the intermediate can be **synthesized**. For example, *enol*pyruvate, the enol of pyruvate, is unstable in solution relative to the ketone (Figure 1–23)

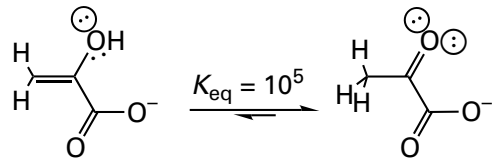

(5–106)

but the enol can be generated rapidly by treatment of phospho*enol*pyruvate with alkaline phosphatase[349] or by fluorolysis of 2-[(trimethylsilyl)oxy]propenoic acid trimethylsilyl ester[350]

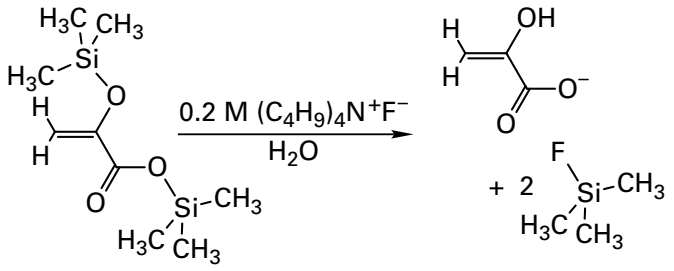

(5–107)

The lifetime of *enol*pyruvate (4 min at pH 6.4 and 20 °C) is long enough that it can be examined as an intermediate in an enzymatic reaction.

The biotinyl enzyme methylmalonyl-CoA carboxytransferase

(*S*)-methylmalonyl-SCoA + pyruvate ⇌ propanoyl-SCoA + oxaloacetate

(5–108)

transfers a carboxy group from (*S*)-methylmalonyl-SCoA to pyruvate by using a prosthetic biotinyl group as the carrier between the active site responsible for decarboxylating (*S*)-methylmalonyl-SCoA and the active site responsible for carboxylating pyruvate, and vice versa. When methylmalonyl-CoA carboxytransferase from *Propionibacterium freudenreichii* is present in a solution made from ^2H_2O, in which either (*Z*)-[3-^{3}H]*enol*pyruvate or (*E*)-[3-^{3}H]*enol*pyruvate is then generated rapidly, the enzyme catalyzes the stereospecific conversion of the respective *enol*pyruvate to [3-^{3}H,3-^{2}H]pyruvate by deuteronating its 2-*Si* face in a reaction requiring the presence of (*S*)-methylmalonyl-SCoA, which itself does not participate in the deuteronation.[351] This ability of the enzyme to accept *enol*pyruvate as a reactant and stereospecifically add a deuteron is consistent with the participation of *enol*pyruvate as an intermediate in the enzymatic reaction occurring at the active site in the enzyme responsible for carboxylating the pyruvate*

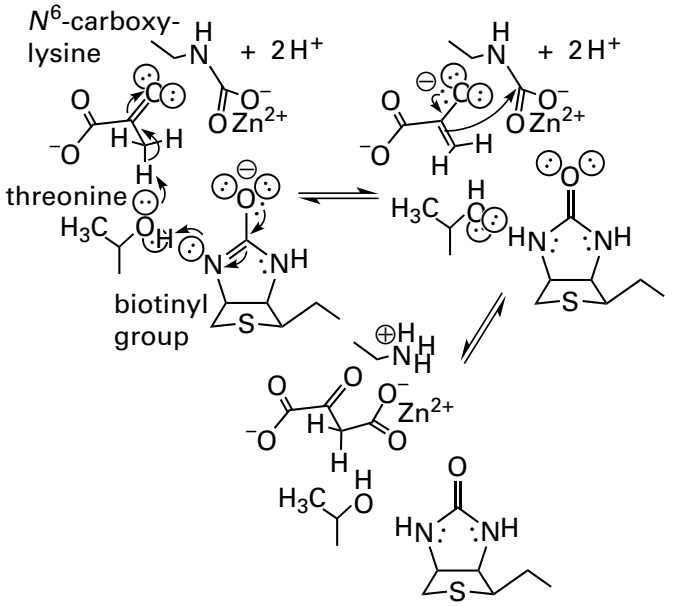

(5–109)

Crystallographic molecular models of the same active site, occupied in turn by pyruvate and oxaloacetate, suggest that the carboxy group is transferred from the biotinyl group to the amino group of Lysine 184 to produce an N^6-carboxylysine, which becomes a ligand to a prosthetic Zn^{2+}, before the carboxy group is transferred to the *enol*pyruvate.[352]

A related (31% identity; 1.5 gap percent) enzyme, pyruvate carboxylase from *Rhizobium etli*, performs the same carboxylation in an almost identical active site. Crystallographic molecular models of two active sites, one occupied by pyruvate and the other by biotin, suggest that the anionic conjugate base of the nitrogen in the ureylene of the biotin, the same one from which the carboxy group was just transferred to Lysine 184, provides the base that removes the hydron from pyruvate to form the enolate of *enol*pyruvate.[353] Its basicity is relayed through a threonine that is at the same location in the active sites of both pyruvate carboxylase and methylmalonyl-CoA carboxytransferase. There is also an N^6-carboxylysine at the same location in the active site of pyruvate carboxylase from *R. etli* as that occupied by the one in methylmalonyl-CoA carboxytransferase.

*The mechanism, as written, does not involve a deuterium, but if it were proceeding in ^2H_2O with phospho*enol*pyruvate as the reactant, deuterium would be added stereospecifically to phospho*enol*pyruvate by reversal of the first step because there would be a deuterium in the active site on threonine.

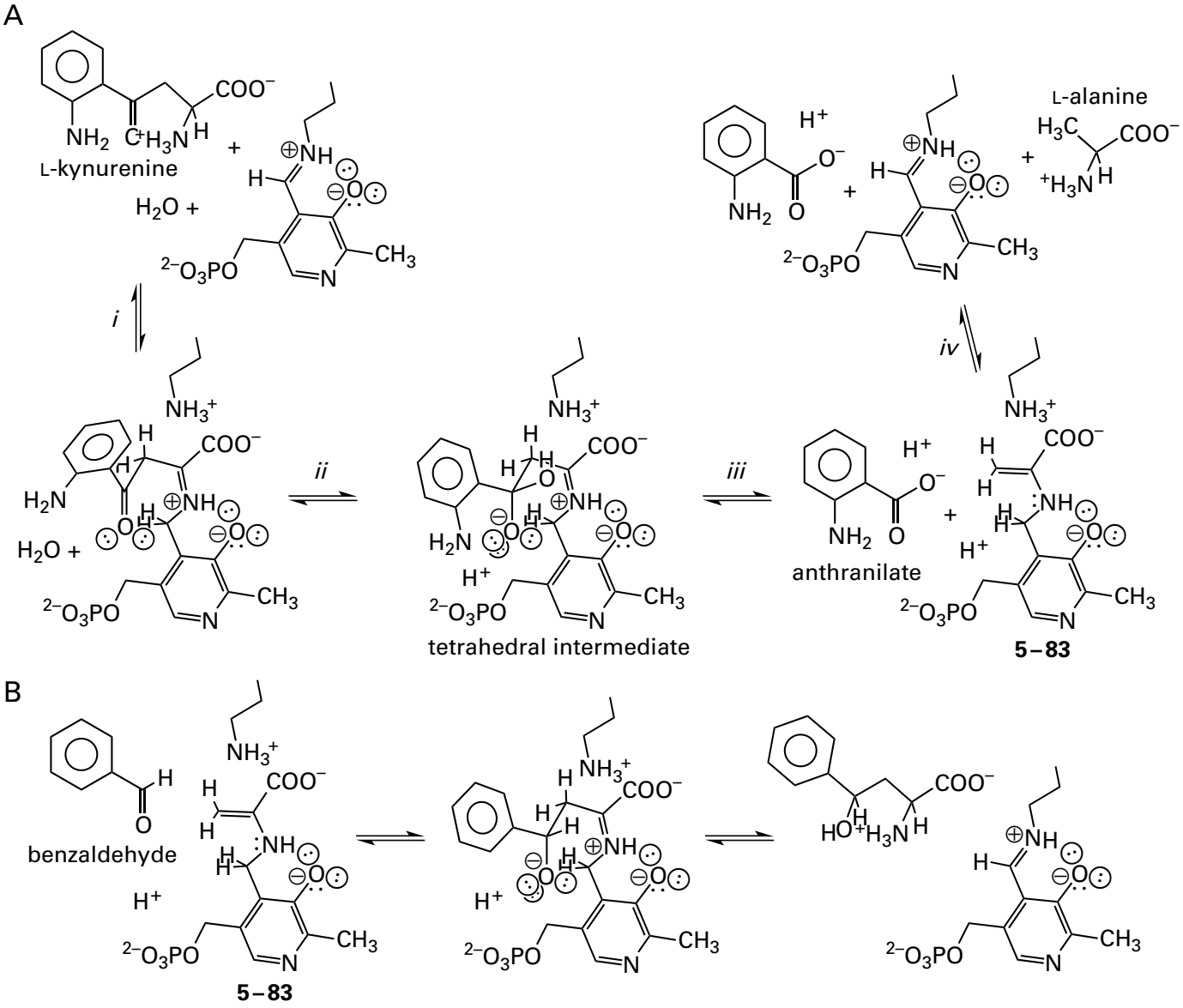

Figure 5–7: Intermediates in the reaction catalyzed by kynureninase. (**A**) Steps in the mechanism. (*i*) The external pyridoximine of L-kynurenine is formed from an internal pyridoximine of the prosthetic pyridoxal 5′-phosphate by transimination (Figure 2–2), and the imine of pyridoxamine 5′-phosphate and 2,4-dioxo-4-(*o*-aminophenyl)butanoic acid is then produced by tautomerization (Equations 2–4 and 2–21). (*ii*) A molecule of water then adds nucleophilically to the former carbonyl of L-kynurenine, and a hydron is removed from the resulting hydronated hydroxy group to yield the tetrahedral intermediate. (*iii*) *N*-Pyridoxylenamine **5–83** then leaves from the tetrahedral intermediate to produce anthranilate. (*iv*) Upon hydronation of the methylene carbon of *N*-pyridoxylenamine **5–83** (not shown), the imine of pyridoxamine 5′-phosphate and pyruvate is produced; the external imine of pyridoxal 5′-phosphate and L-alanine is then formed by the usual tautomerization; and L-alanine is released by transimination. (**B**) *N*-Pyridoxylenamine **5–83** can be trapped by its addition to the carbonyl of benzaldehyde added to the solution to produce the secondary alcohol. 2-Amino-4-hydroxy-4-phenylbutanate is released from the adduct by transimination. The production of 2-amino-4-hydroxy-4-phenylbutanate is a signature of the intermediacy of *N*-pyridoxylenamine **5–83** in the enzymatic reaction.

When phospho*enol*pyruvate carboxylase from *Zea mays*, which is neither a biotinyl enzyme nor related to biotinyl carboxylases, is reconstituted with unphysiological, prosthetic metallic cations such as Ni^{2+} and Co^{2+} that stabilize the intermediate *enol*pyruvate and decrease the rate of carboxylation, *enol*pyruvate leaks out of the active site and can be trapped as pyruvate.[354]

Enamines and enolates are electron-rich nucleophiles, and when one is an intermediate in an enzymatic reaction, it can be **trapped by an electrophile**. For example, *N*-pyridoxylenamine **5–83**, formed from L-kynurenine following the dissociation of anthranilate during the retro-Claisen condensation catalyzed by kynureninase (Figure 5–7) from *Pseudomonas marginalis*, can be trapped with benzalde-

hyde[355] before it is converted to L-alanine, the other usual product of the enzymatic reaction, and the prosthetic pyridoxal 5′-phosphate. The *enol*pyruvate that is an intermediate in the reaction catalyzed by pyruvate kinase (Figure 4–52) could be trapped as bromopyruvate in 2–30% yield, based on the concentration of active sites, when the enzyme from *O. cuniculus* is rapidly mixed with 2 M $HClO_4$ saturated with Br_2, a strong electrophile.[356] Pyruvate itself is not brominated under the same conditions.

Because they are electron-rich, intermediate enolates and enamines in enzymatic reactions have also been identified by their susceptibility to **oxidation**. It has already been noted that the electron-rich 1,2-enaminol produced between fructose-bisphosphate aldolase and glycerone phosphate (Figure 4–36) can be oxidized to the imino aldehyde (Equation 5–44) with $Fe^{III}(CN)_6^{3-}$ as well as other oxidants.[357] Reduction of tetranitromethane in the presence of phosphogluconate dehydrogenase ($NADP^+$-dependent, decarboxylating) from *S. cerevisiae*, ribulose 5-phosphate, and NADPH is thought to represent oxidation of the electron-rich *cis*-enediolate that is an intermediate in the reaction catalyzed by the enzyme (Equation 5–76)[357,358]

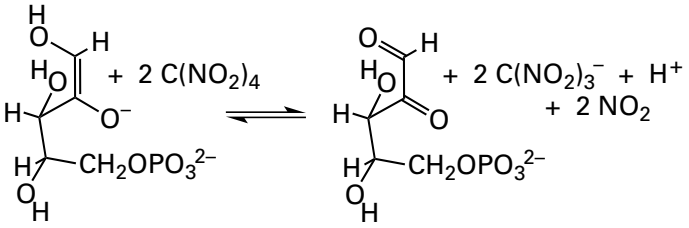

(5–110)

In these oxidations, the reagents used are one-electron oxidants that must remove electrons one at a time from the electron-rich enols or enamines.

If an **analogue of a reactant** is synthesized to incorporate a **good leaving group**, such as a halogen on the β carbon in the enolate formed as an intermediate in the reaction, and if the active site will recognize the analogue as a reactant, then when the enolate forms, the leaving group next to the carbanionic α carbon will leave in a β-elimination

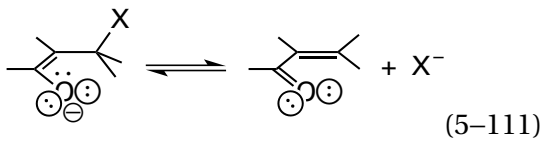

(5–111)

The product of this elimination will identify the carbanionic carbon of the enol. Porcine propionyl-CoA carboxylase* converts 3-fluoropropionyl-SCoA to acrylyl-SCoA[359]

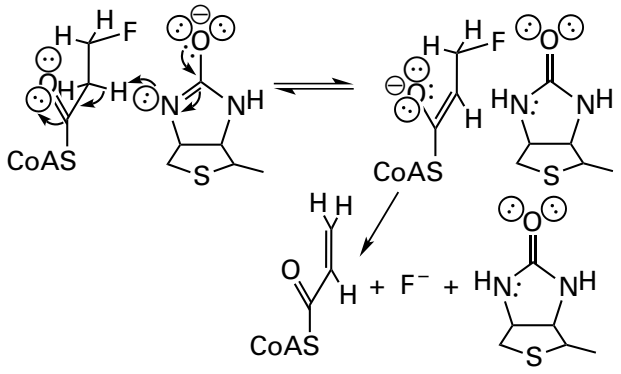

(5–112)

a product that arises from elimination of fluoride from an intermediate enolate.[360] In the absence of a good leaving group, the conjugate base of the substrate propionyl-SCoA, which is the intermediate enolate in the normal reaction catalyzed by the enzyme, is carboxylated by carbon dioxide that has been released from the *N*-carboxybiotin bound at the active site as a prosthetic group

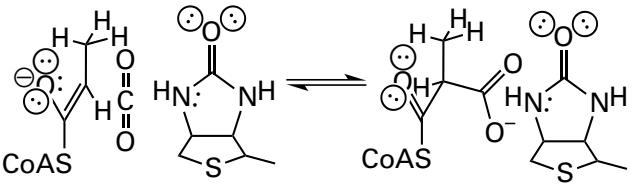

(5–113)

As was the case with the active site responsible for carboxylating pyruvate in methylmalonyl-CoA carboxytransferase (Equation 5–109), following dissociation of carbon dioxide, the anionic nitrogen from which carbon dioxide has just dissociated in the conjugate base of the biotinyl group performs the role of the catalytic base that removes the hydron

*Three different enzymes, methylmalonyl-CoA carboxytransferase, propionyl-CoA carboxylase, and pyruvate carboxylase, contain domains that are related to each other. The domains responsible for the same reaction—carboxylating propionyl-SCoA and decarboxylating methylmalonyl-SCoA—within methylmalonyl-CoA carboxytransferase from *P. freudenreichii* and porcine propionyl-CoA carboxylase are closely related (52% identity; 1.0 gap percent); less so are the domains in porcine pyruvate carboxylase and methylmalonyl-CoA carboxytransferase from *P. freudenreichii* responsible for carboxylating and decarboxylating pyruvate (31% identity; 1.4 gap percent). Both propionyl-CoA carboxylase and pyruvate carboxylase contain a domain responsible for carboxylating biotin (44% identity; 0.9 gap percent), a domain that does not exist in methylmalonyl-CoA carboxytransferase because it is not required to. These three enzymes are examples of subunit swapping and domain swapping.

from carbon during formation of the enolate (Equation 5–112), but in this instance it seems to remove the hydron directly rather than indirectly.[360]

In some instances, placing a group capable of electron withdrawal on its carbanionic α carbon, rather than the β carbon, stabilizes an enolate, and this **stabilization of the enolate** is evidence for its existence as a noncovalent intermediate. For example, 1-deoxy-D-xylulose-5-phosphate reductoisomerase from *E. coli* catalyzes an isomerization[361]

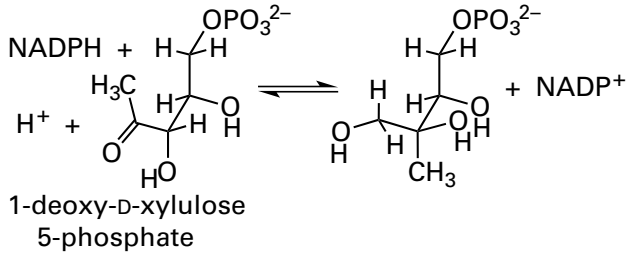

(5–114)

that requires the enolate of 2-hydroxypropanal as an intermediate in an aldol condensation that produces 2-*C*-methyl-D-erythritol 4-phosphate. The enolate of 2-hydroxypropanal in turn is derived from carbons 1 through 3 of 1-deoxy-D-xylulose 5-phosphate in a retroaldol condensation. When 1-fluoro-1-deoxy-D-xylulose 5-phosphate is used as a reactant, which places a fluoromethyl group on the α carbon of the enolate of 2-hydroxypropanal in place of its methyl group, the rate of this isomerization increases. This increase in rate was presented as evidence that the enolate of 2-hydroxypropanal, which would be stabilized by the fluoromethyl group on its carbanionic α carbon, is an intermediate in the reaction.[362]

The **inhibition of an enzyme by an analogue of an enolate** thought to be an intermediate in the reaction (**3–53**, **3–55**, **3–57**, **3–59**, and **3–61** in Table 3–7) is often cited as evidence of its existence. For example, enzymatic addition–eliminations that occur adjacent to carboxylato groups, as in the case of phosphopyruvate hydratase (previously Equation 4–128 and see Figures 3–35 and 4–43)

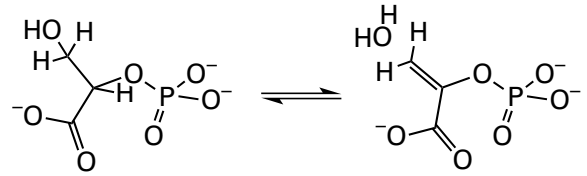

(5–115)

have been observed uniformly to proceed through the intermediate *gem*-enediolates[363]

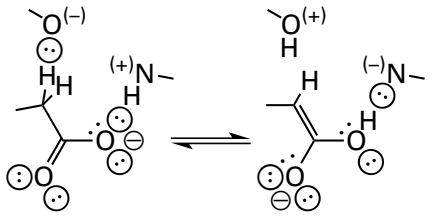

(5–116)

that are the tautomers of the carboxylates rather than through intermediate carbocations. A simple demonstration of this generalization is that these enzymes are strongly and competitively inhibited by the conjugate bases of nitro analogues of the respective enolates

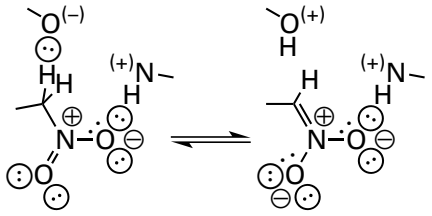

(5–117)

For example, the intermediate *gem*-enediolate

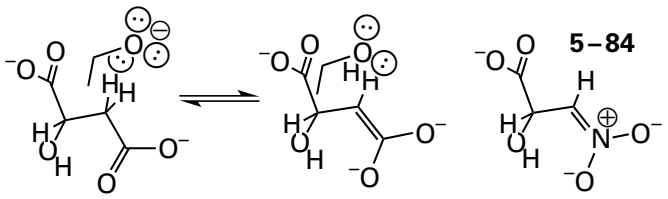

(5–118)

formed during the dehydration of (*S*)-malate and the hydration of fumarate catalyzed by fumarate hydratase (previously Equation 4–226 and see Figure 4–27)[364]

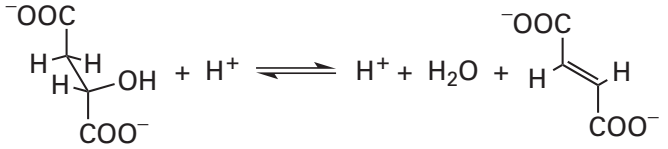

(5–119)

can be mimicked by the conjugate base of 3-nitro-2-hydroxypropionate (**5–84**).[365] The conjugate base of 3-nitro-2-hydroxypropionate is a competitive inhibitor of porcine fumarate hydratase with a dissociation constant (K_i) 10,000 times smaller than the dissociation constant ($K_{d,succ}$) for succinate (succ), also a simple competitive inhibitor of the enzyme, and 1000 times smaller than the Michaelis constant ($K_{m,mal}$) for (*S*)-malate (mal) as a reactant.

Table 5–1: Ratio of Products for the Solvolysis of β-Galactosides by β-Galactosidase[368]

β-galactoside	limiting rate[a] (μmol min^{-1} mg^{-1})	ratio of products[b]
2-nitrophenyl	360	1.97 ± 0.05
3-nitrophenyl	327	1.96 ± 0.13
3-chlorophenyl	180	2.08 ± 0.24
4-nitrophenyl	69	1.99 ± 0.05
phenyl	40	1.94 ± 0.20
4-methoxyphenyl	33	2.14 ± 0.13
4-chlorophenyl	7.5	2.02 ± 0.16
4-bromophenyl	7.0	2.03 ± 0.08

[a]Limiting rate in the absence of methanol. All reactions were run at 25 °C at pH 7.5. [b]Ratio of methyl β-D-galactoside to D-galactose for reactions run in 0.25 M methanol.

Similarly, the conjugate base of 2-amino-3-nitropropionate is a potent competitive inhibitor ($K_{mAsp}\,K_i^{-1} = 200$) of aspartate ammonia-lyase from *Clostridium budayi*;[365] the conjugate base of (3-hydroxy-2-nitropropyl)phosphonate is a potent competitive inhibitor ($K_{m,PGA}\,K_i^{-1} = 1000$) of phosphopyruvate hydratase from *S. cerevisiae*;[363] and the conjugate base of 2-hydroxy-3-nitro-1,2-propanedicarboxylate is a potent competitive inhibitor ($K_{m,cit}\,K_i^{-1} = 3000$) with respect to citrate (cit) for bovine aconitate hydratase.[366]

Although carbocationic intermediates are common in organic reactions under acidic conditions, they are usually encountered in enzymatic reactions only in glycosyl transfer and the biosynthesis of polyisoprenoids.[367] In a glycosyl transfer reaction, carbocationic intermediates are stabilized as oxocarbenium ions

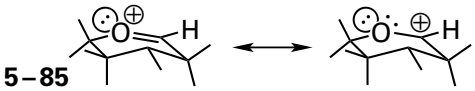

Carbocationic intermediates involved in polyisoprenoid biosynthesis usually begin as allylic carbenium ions

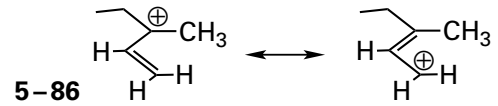

β-Galactosidase is a retaining **glycosyltransferase** that displays little specificity for the alcohols between which the galactosyl group is transferred

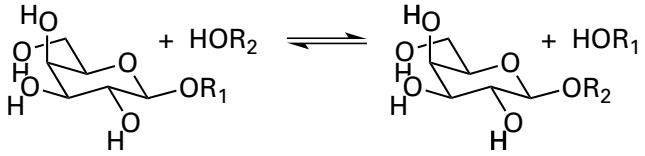

(5–120)

When the enzyme processed any one of a series of β-galactosides in a solution of 0.25 M methanol in water, the products were methyl β-galactoside, arising from transfer to methanol ($R_2 = CH_3$), and D-galactose, arising from transfer to water ($R_2 = H$), in a molar ratio of 2:1, even though the ratio of methanol to water in the solution was 1:220.[368] The molar ratio between the two products remained 2:1 within the experimental error of the measurements when the catalytic constant k_0 of the enzyme was varied over a 50-fold range by choosing a set of reactants that differed in the properties of the leaving group, HOR_1 (Table 5–1).[368] The most reasonable explanation for this observation is that either acceptor, water or methanol, reacts with the galactosyl group only after the leaving group has departed from the active site. The production of an oxocarbenium ion as an intermediate in the reaction

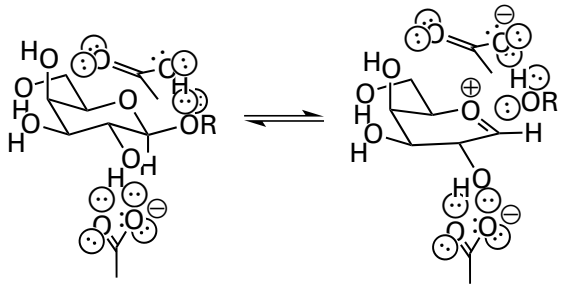

(5–121)

would explain these observations, as would a covalent galactosyl-enzyme intermediate.[81] In either case, the acceptor, methanol or water, would be reacting with the same intermediate left behind by the departing alcohol, regardless of the particular galactoside used to produce that intermediate.

This observation with β-galactosidase again raises the question of whether retaining glycosyl-

transferases such as β-galactosidase have **an oxocarbenium ion or an ester as an intermediate**

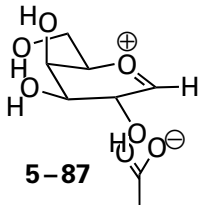

5–87

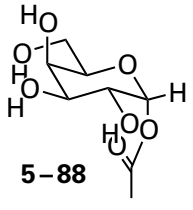

5–88

It has already been mentioned, for example, that there is significant controversy over whether there is an oxocarbenium ion as a stabilized noncovalent intermediate or a ester as a covalent intermediate in the nucleophilic substitutions catalyzed by lysozyme (Figure 3–27).[64] The extreme instability of an oxocarbenium ion in aqueous solution[369] is a point often mentioned in favor of the ester as a covalent intermediate. It is, however, also a point in favor of a stabilized oxocarbenium ion. The advantage of such a oxocarbenium ion as an intermediate is the fact that it would be far more reactive than ester **5–88**. Most glycosyltransferases display behavior consistent with an almost fully dissociative nucleophilic substitution.[367] Formation of a covalent intermediate can have only a small advantageous effect on the departure of the alcohol that is the leaving group while forming the covalent intermediate from a dramatically reactive intermediate that is formed anyway in the enzymatic reaction would be significantly disadvantageous for catalysis. In almost every glycosyltransferase, the rate of dissociation of the alcohol from the reactant is much slower than formation of the glycoside from the intermediate that is left behind during that dissociation. This almost universal observation would be consistent with an intermediate that is far more reactive than an ester.

In the active sites of retaining glycosyltransferases, there is almost always the carboxylato group of a glutamate or aspartate adjacent to the carbonyl carbon that becomes the oxocarbenium ion (bottom carboxylato group in Equation 5–121). Consequently, the question becomes whether the carboxylato group stabilizes an oxocarbenium ion by the effect of its electric field or captures it by forming a covalent bond with the carbonyl carbon in a dissociative nucleophilic substitution. These alternatives differ sterically. Unless the active site is constructed in such a way that the carboxylato oxygen is sterically prevented from forming a covalent bond with the oxocarbenium ion, it will almost certainly do so.

During intramolecular catalysis of the hydrolysis of an enol ether or 4-nitrophenyl riboside by carboxylato groups, oxocarbenium ions are intermediates in the absence of an adjacent carboxylato group. Results from observations of such reactions have reached different conclusions about the possibility of electrostatic stabilization of an oxocarbenium ion. In both cases, a rigid superstructure was designed that held the carboxylato group near the carbon on which the oxocarbenium ion develops but not close enough to form an unstrained ester with the carbon. In both instances, there was no evidence indicating that the adjacent carboxylato group was catalyzing the reaction nucleophilically by adding to the carbon to form an ester as a covalent intermediate in the reaction. In the case of intramolecular catalysis of the 4-nitrophenyl riboside, the carboxylato group was held rigidly by the superstructure at a distance and orientation that stringently precluded formation of an ester. The acceleration of hydrolysis of the enol ether by the nearby carboxylato group was 20-fold, but it was attributed to intramolecular acid catalysis in which the carboxy group added a hydron to the α carbon of the enol ether rather than to electrostatic catalysis.[370] The acceleration of hydrolysis of the 4-nitrophenyl riboside was 900-fold relative to the same superstructure in which the carboxylato group was replaced by a hydrogen, and it was proposed that at least a portion of this acceleration could be attributed to electrostatic catalysis.[371] A problem with these observations is that both hydrolyses were followed in aqueous solution, a situation in which electrostatic interactions are minimized by the high relative permittivity of the solvent. In the active site of an enzyme, however, the relative permittivity is much less, a fact that would increase the effectiveness of electrostatic catalysis.

Chemical evidence to support the existence of oxocarbenium ions in the mechanisms of glycosyltransferases has been presented. For example, in the reaction catalyzed by glycogen phosphorylase, a retaining glycosyltransferase

$$[(1\rightarrow4)\text{-}\alpha\text{-D-glucosyl}]_n + HOPO_3^{2-} \rightleftharpoons [(1\rightarrow4)\text{-}\alpha\text{-D-glucosyl}]_{n-1} + \alpha\text{-D-glucose 1-phosphate} \quad (5\text{–}122)$$

the phosphate could act as the enforced acceptor for an oxocarbenium ion

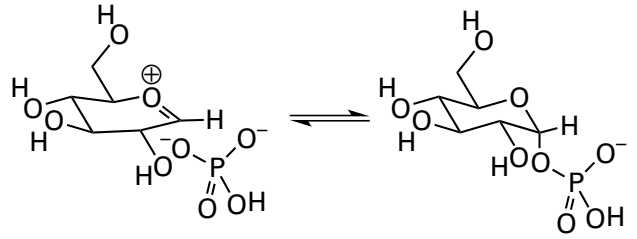

(5–123)

from the same side to which the leaving group in the reaction dissociates. 2,6-Anhydro-1-deoxy-D-*gluco*-hept-1-enitol (**5–89**) and phosphate are converted to 1-deoxy-α-D-*gluco*-heptulose 2-phosphate by phosphorylase from *O. cuniculus* in an addition in which the planar carbon–carbon double bond seems to be mistaken for the planar oxocarbenium ion[372,373]

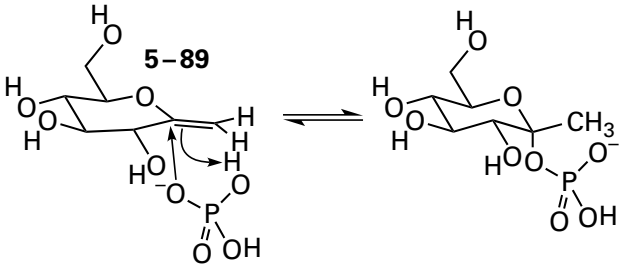

(5–124)

The existence of this reaction is consistent with the existence of oxocarbenium ion in the normal reaction.

5-Deoxy-5-amino-D-glucose (**5–90**, nojirimycin)

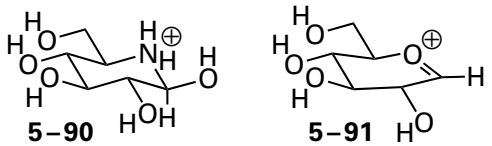

is an antibiotic produced by *Streptomyces* that is a potent competitive inhibitor of glucosidases[374,375] at concentrations of 1–10 μM. It is thought that the ability of nojirimycin to inhibit glucosidases results from its resemblance to the oxocarbenium ion **5–91** that is the common intermediate in these reactions. 1,5-Dideoxy-5-aminoglucopyranose, a stable cyclic amine, also inhibits glucosidases[376] at concentrations of 1–10 μM, and it has been used as an analogue of an oxocarbenium ion in crystallographic studies of the active sites of glucosidases.[377]

Cyclic amines that mimic the oxocarbenium ions that would be intermediates in other glycosidases have also been synthesized and shown to be potent inhibitors.[378]

Fluoro derivatives of substrates for glycosidases have also been synthesized. If a fluoro group occupies a position adjacent to the carbon of an oxocarbenium ion that is an intermediate in an enzymatic reaction, its ability to withdraw electron density strongly should destabilize that intermediate. For example, the fact that GDP-2-deoxy-2-fluoro-β-L-fucose is a reversible, competitive inhibitor of the substrate GDP-β-L-fucose for human glycoprotein 3-α-L-fucosyltransferase, with an inhibition constant of 4 μM, rather than being a substrate itself, suggests that an oxocarbenium ion, which should be destabilized by the adjacent fluorine, is an intermediate in this inverting glycosyltransferase[379]

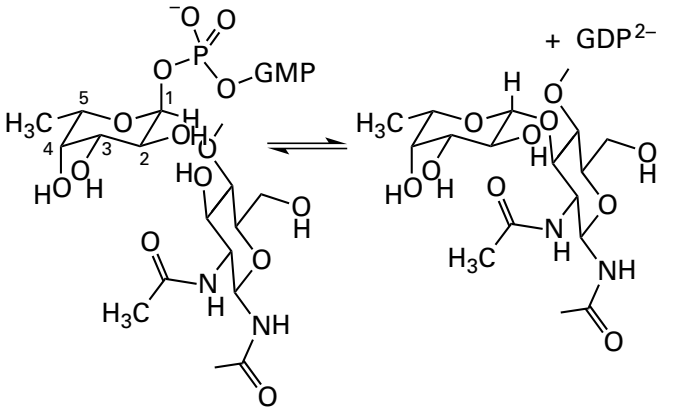

(5–125)

Values of the steady-state rate constants $k_0\,(K_{\mathrm{mUDPX}})^{-1}$ for UDP-α-D-galactofuranose, UDP-α-D-3-deoxy-3-fluorogalactofuranose, and UDP-α-D-2-deoxy-2-fluorogalactofuranose (where UDPX is the respective UDP monosaccharide) in the reaction catalyzed by UDP-galactopyranose mutase from *E. coli* are 1200, 6.6, and 0.51 $\mathrm{nM^{-1}\,s^{-1}}$, respectively. As the 3-hydroxy group is replaced by a fluorine and then the substitution is made closer to the glycosidic carbon of the galactofuranose, the rate of the enzymatic reaction decreases. This trend is consistent with the existence of an oxocarbenium ion as a carbocationic intermediate in the enzymatic reaction.[380]

Although all these results have been interpreted as evidence for the existence of oxocarbenium ions as noncovalent carbocationic intermediates in these glycosyltransferases and the mutase, they are also consistent with the existence of an expanded transition state with oxocarbenium character in which the acceptor, in inverting glycosyltransferases, or the carboxylato group of an aspartate or glutamate, in retaining glycosyltransferases, is adding as the leaving group is departing.

Carbocationic intermediates are definitely produced in the active sites of enzymes catalyzing the biosynthesis of polyisoprenoids. For example, an initial enzyme in all these biosynthetic pathways is (2*E*,6*E*)-farnesyl diphosphate synthase[381-383]

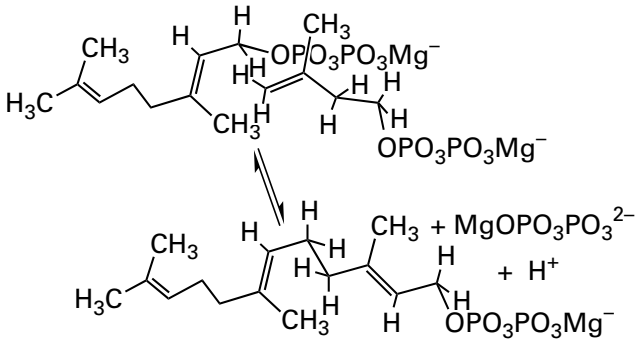

(5–126)

The reaction can be formulated as a dissociative nucleophilic substitution (see Figure 1–26) resembling that for the nonenzymatic cationic polymerization of alkenes at low pH. In this mechanism, a tertiary allylic carbenium ion is formed in the first step by dissociation of diphosphate, a good leaving group, from geranyl diphosphate

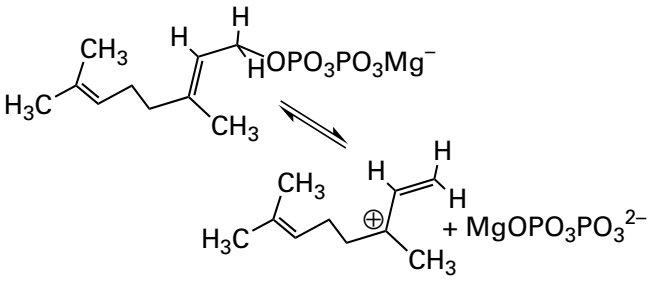

(5–127)

which is an allylic diphosphate. Because the diphosphate in geranyl diphosphate is on a primary carbon and because addition of the alkene proceeds with inversion of configuration at the allylic carbon bearing the diphosphate, it was also possible that a concerted nucleophilic substitution with inversion of configuration could occur at the allylic carbon rather than a dissociative nucleophilic substitution with an allylic carbenium ion as an intermediate.[384]

A decision has been made between these two possibilities by replacing one methyl group of dimethylallyl diphosphate, which is also a substrate for the enzyme in place of geranyl diphosphate, with a trifluoromethyl group.[385] In model studies, it was shown that such a replacement would increase the rate of a concerted nucleophilic substitution by a factor of 10 but would decrease the rate of a dissociative nucleophilic substitution with an allylic carbenium ion as an intermediate by a factor of 10^6 because of the difficulty of forming the carbenium ion next to an electron-withdrawing substituent

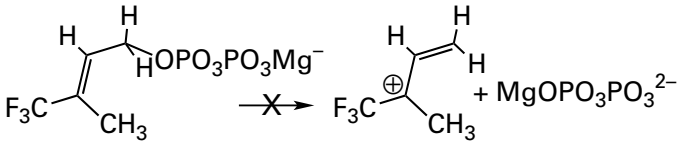

(5–128)

In the reaction catalyzed by porcine (2*E*,6*E*)-farnesyl diphosphate synthase, (trifluoromethyl)methylallyl diphosphate, although it is a competitive inhibitor, shows no reaction ($k_{0,CF3} < 10^{-6} k_{0,CH3}$). These results rule out a concerted nucleophilic substitution and are consistent with the existence of an allylic carbenium ion in the normal reaction.

A series of other **fluorinated derivatives** of geranyl diphosphate were also synthesized, and it was shown that the rate constants for their nonenzymatic solvolysis at low pH, a reaction definitely proceeding by dissociative nucleophilic substitution with an allyl carbenium ion as an intermediate, correlated closely with the catalytic constants, k_0, of the same compounds as reactants in the reaction catalyzed by (2*E*,6*E*)-farnesyl diphosphate synthase from *G. gallus*. These results also support the existence of an allyl carbenium ion as a carbocationic intermediate in this enzymatic reaction.[386]

The other carbocationic intermediate in the reaction catalyzed by (2*E*,6*E*)-farnesyl diphosphate synthase is the tertiary carbenium ion formed upon addition of the initial allylic carbenium ion to the carbon–carbon double bond (see Figure 1–26). A hydron is removed from this other carbenium ion to yield the other double bond in the product. Evidence for the existence of this other carbocationic intermediate was obtained similarly by showing that 2,2-difluoroisopentenyl diphosphate was not utilized as an acceptor in the enzymatic reaction, even when it was incubated for a period of 3 days with the enzyme and geranyl diphosphate serving as the donor of the initially formed carbenium ion.[387] Again, fluorination prevented the reaction from occurring by hindering formation of the tertiary carbenium ion on the acceptor.

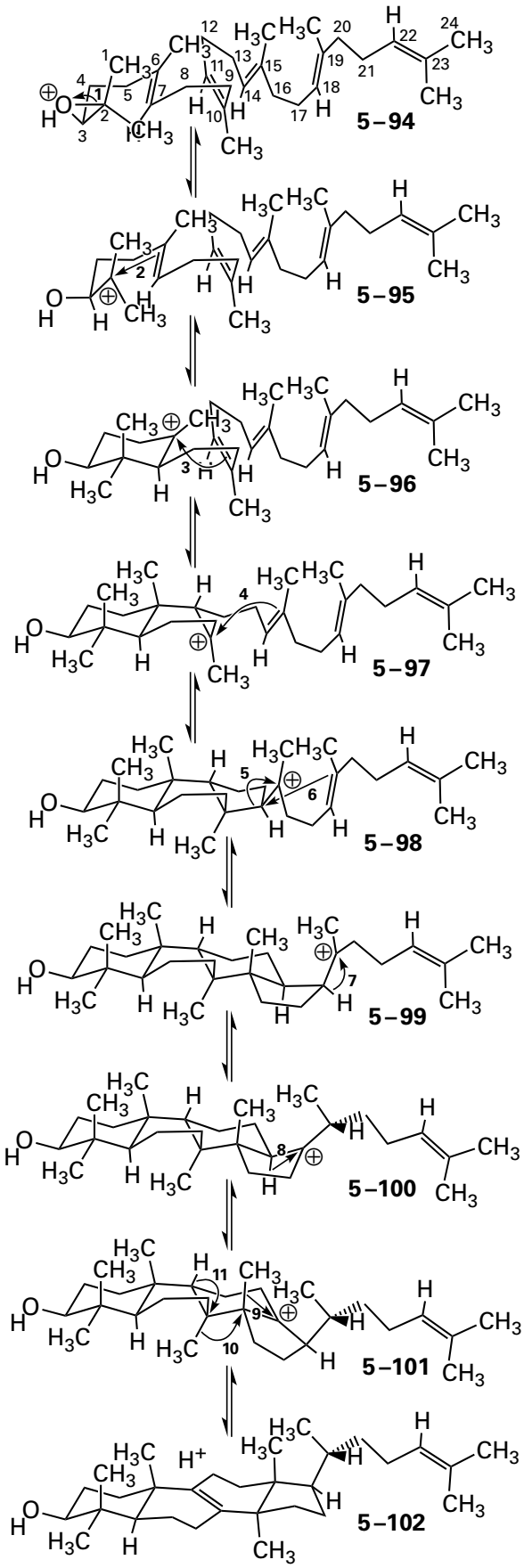

Figure 5–8: Intermediates in the reaction converting (3*S*)-2,3-epoxy-2,3-dihydrosqualene (**5–94**) into lanosterol (**5–102**) catalyzed by lanosterol synthase.[392,393] Each dissociation, ring closure, and 1,2-migration of σ bonds, hydrogens, and methyl groups that consecutively form the ten intermediate carbenium ions is numbered in bold. Seven of the intermediate carbenium ions (**5–95** through **5–101**) are drawn. The undrawn carbenium ions are those produced by 1,2-migrations numbered **5**, **9**, and **10**.

(+)-Presqualene diphosphate (**5–47**) is converted by squalene synthase to squalene (**5–48** in Equation 5–65) through two cyclopropyl carbenium ions **5–50** and **5–51** (Equation 5–66). One set of observations consistent with their existence as carbocationic intermediates is the fact that analogues **5–92** and **5–93**

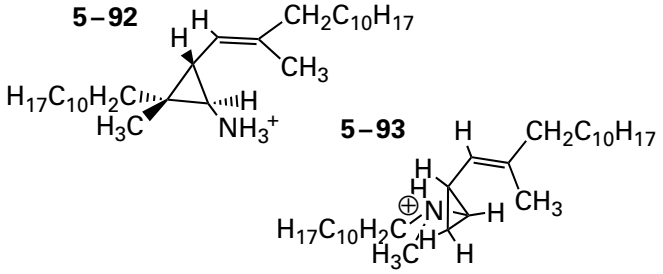

in which a primary ammonio group and a tertiary **ammonio group respectively replaces the carbocationic carbon**, are effective inhibitors of squalene synthase from *S. cerevisiae*.[388] Another observation consistent with the role of carbenium ion **5–51** as an intermediate is that when an inert analogue of NADPH is added to a solution containing the enzyme from *S. cerevisiae* and farnesyl diphosphate, so that the final carbenium ion **5–49** cannot be reduced to squalene, the tertiary alcohol arising from addition of water to carbenium ion **5–51** was produced by the enzyme in 17% yield.[389,390] In the absence of NADPH, the enzyme converts (+)-presqualene diphosphate into a mixture of alcohols, which are products of addition of water to carbenium ion **5–49**, and a carbenium ion, which is the product of the immediate rearrangement of carbenium ion **5–50**.[390,391]

Lanosterol synthase produces lanosterol (**5–102**), the precursor to cholesterol, by cyclizing (3*S*)-2,3-epoxy-2,3-dihydrosqualene (**5–94**). The cyclization and rearrangement passes through ten carbenium ions (Figure 5–8).[392-394] Chemical evidence supports the existence of most of these carbocationic intermediates in the enzymatic reaction. When Histidine 234 in lanosterol synthase from

S. cerevisiae is mutated to each of the other 19 amino acids, one at a time, the various **mutants of the enzyme** produce, from (*S*)-2,3-epoxy-2,3-dihydrosqualene, in addition to lanosterol, steroids that result from the loss of a hydron adjacent to each of the carbenium ions **5–96**, **5–98**, **5–99**, and **5–101**.[395,396] When the electrophilicity of carbenium ion **5–99** is decreased dramatically by **mutating the substrate synthetically** to (20*E*)-20,21-dehydro-2,3-epoxy-2,3-dihydrosqualene, which places a double bond allylic to the carbocation, further rearrangement ceases at this point because of the stability of the allylic carbenium ion, and the alcohol resulting from addition of water to this allylic carbenium ion is produced by lanosterol synthase from *S. cerevisiae* rather than lanosterol.[397] When carbon 20 of (*S*)-2,3-epoxy-2,3-dihydrosqualene is replaced with an oxygen, the resulting oxocarbenium ion, homologous to carbenium ion **5–99**, loses an allyl carbenium ion in the active site[398]

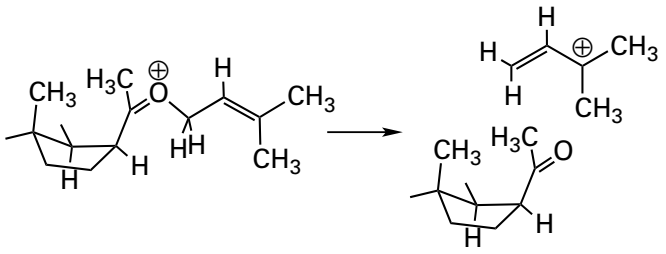

(5–129)

and the production of the ketone by the enzyme from *S. cerevisiae* is evidence for the existence of carbenium ion **5–99**.[399] In the same enzymatic reaction, a minor product that results from a direct rearrangement of the carbenium ion arising from the (*S*)-2,3-epoxy-2,3-dihydro-20-oxasqualene that is analogous to carbenium ion **5–98** is also isolated.[400] This minor product has a cyclopentyl ring at the same location as the unexpanded cyclopentyl ring in carbenium ion **5–98**. The rearrangement of the carbenium ions in the active site probably pauses at carbenium ion **5–98** and its analogues because the next step turns a tertiary carbenium ion into a secondary carbenium ion.

Analogues of (3*S*)-2,3-epoxy-2,3-dihydrosqualene (**5–94**) in which a sulfur replaces either a carbon or a carbon and its attached methyl group have also been synthesized. Analogues, in which carbons 6, 10, 18, and 19 (see Figure 5–8) are replaced by sulfur and the double bonds in which they participate are not present, are potent inhibitors of lanosterol synthase from *Candida albicans* and *R. norvegicus*.[401-403] During the rearrangements of these analogues, following the normal sequence (Figure 5–8), these inhibitors place **sulfur in a sulfide** immediately adjacent to and four atoms away from the carbocationic carbon in carbenium ions **5–95**, **5–96**, ring expanded **5–98**, and **5–98** itself, respectively. The sulfur can add to the respective carbenium ion nucleophilically to produce a five-membered ring containing a sulfonium cation

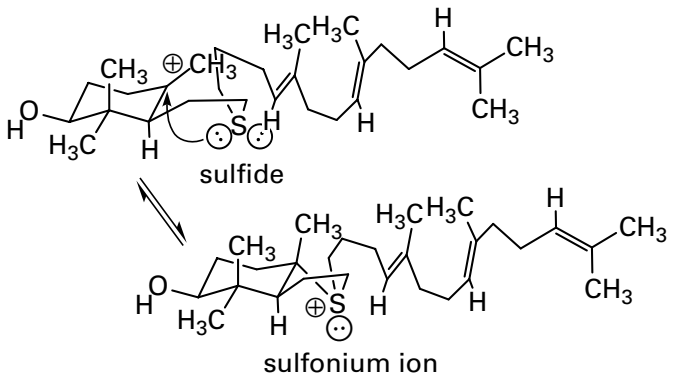

(5–130)

which is far more stable than a carbenium ion[404] and prevents any further rearrangement. The cationic sulfonium observed in each case also ends up at the same location as a carbenium ion in the normal sequence of rearrangements, so in this case, the active site itself produces the positive charge at a location in which it normally would stabilize a positively charged carbenium ion, just as the ammonio inhibitors of squalene synthase (**5–92** and **5–93**) do without the assistance of the active site. Because the active site of the enzyme creates the cation, these sulfides are **mechanism-based inhibitors**. Substitutions at carbons 5, 8, and 13 of (3*S*)-2,3-epoxy-2,3-dihydrosqualene, positions that are sterically prevented from adding nucleophilically (Equation 5–130) to any of the carbocationic carbons in the sequence (see Figure 5–8), produced weak inhibitors of the enzyme.[401,405] Analogues of carbenium ions **5–95**, **5–96**, and **5–97**, in which a nitrogen has been replaced by the carbocationic carbon to produce the ammonium cation, are also strong inhibitors of lanosterol cyclase from *R. norvegicus*.[406]

As has already been discussed, linear head-to-tail polyisoprenoids with an allylic diphosphate at one end, such as geranyl diphosphate, (2*E*,6*E*)-farnesyl diphosphate (Equation 5–126), and geranylgeranyl diphosphate, are susceptible to a vast array of cyclizations that produce monoterpenes, sesquiterpenes, and diterpenes, respectively. For example, (+)-α-pinene synthase from *Salvia officinalis*[407] produces (+)-α-pinene, (+)-limonene, and (+)-camphene from geranyl

diphosphate. The same active site produces all these products[408,409] and all three can be explained as arising from the same carbocationic intermediate **5–103**

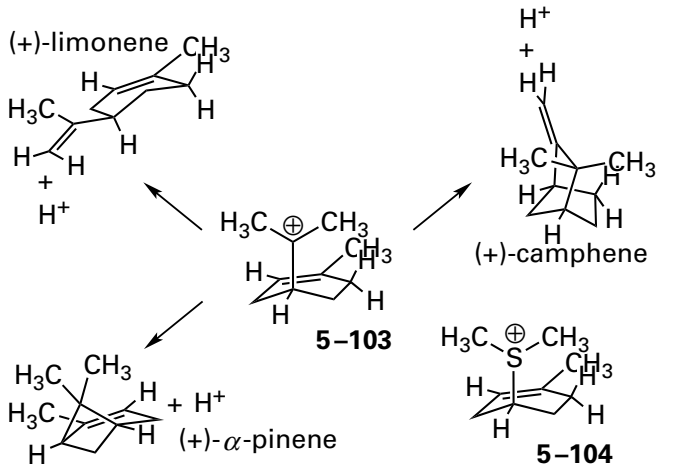

(5–131)

which in turn can be derived from the carbocationic intermediate produced during dissociation of geranyl diphosphate

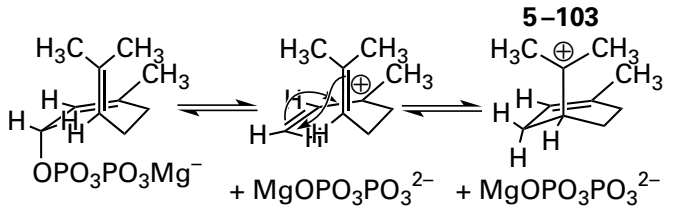

(5–132)

Therefore, the identity of the products is consistent with a particular sequence of carbocationic intermediates in the enzymatic reaction. A **sulfonium cation in an analogue of the intermediate** was chemically synthesized[409] as a mimic of the common carbocationic intermediate (Equation 5–131). Sulfonium cation **5–104** in the presence of diphosphate is a good inhibitor ($K_i = 1\ \mu M$) of (+)-α-pinene synthase, consistent with the involvement of carbocationic intermediate **5–103** in the enzymatic reaction.

Each of the thousands of monoterpenoids, sesquiterpenoids, and diterpenoids that are produced naturally arise from enzymatic cyclizations such as the ones catalyzed by (+)-α-pinene synthase (Equations 5–131 and 5–132) and 5-epiaristolochene synthase (Figure 3–50). The same strategies for identifying the carbocationic intermediates that were used for dimethylallyl*trans*transferase, squalene synthase, lanosterol synthase, and (+)-α-pinene synthase have been used to validate the existence of particular carbocationic intermediates in these enzymatic reactions. A fluorine atom can be placed on a carbon or immediately adjacent to a carbon that should be a carbocation in the proposed intermediate, and the fluoro analogue is shown to be an inhibitor rather than a substrate for the enzyme.[410] Mutants of the enzyme are discovered that produce from the natural reactant unnatural products that arise directly from one or the other of the postulated carbocationic intermediates in the enzymatic mechanism.[411-414] The natural reactant for the enzyme can be mutated synthetically to produce an unnatural reactant that causes the rearrangement to be blocked at one of its steps so that the enzyme produces unnatural products arising from one or the other of the postulated carbocationic intermediates.[415-417] Analogues of the postulated carbocationic intermediates in which an ammonio nitrogen replaces the cationic carbon can be synthesized and shown to inhibit the enzymatic reaction.[407,418]

Similar strategies are used to provide evidence for carbocationic intermediates in the few enzymes other than glycosyltransferases and polyisoprenoid synthases that have them. For example, diphosphomevalonate decarboxylase[419]

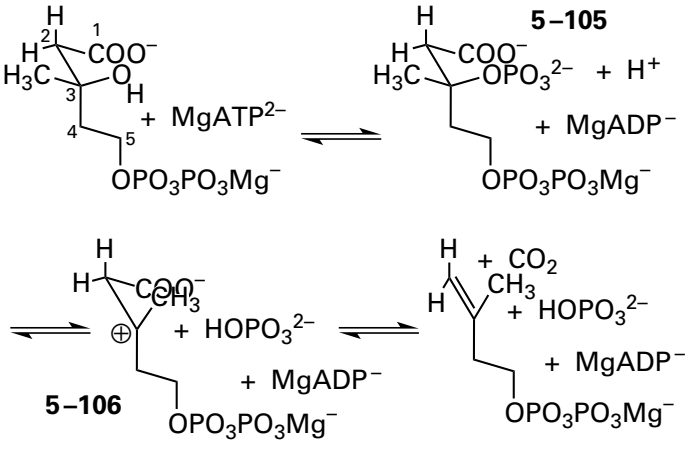

(5–133)

from *S. cerevisiae* catalyzes elimination of the nucleophile, phosphate, and the electrophile, CO_2, from (3*R*)-3-hydroxy-3-(fluoromethyl)-5-diphosphopentanoate, a fluorinated derivative of the normal reactant, that has been phosphorylated at its 3-hydroxy group within the active site by $MgATP^{2-}$ to form the noncovalent intermediate, (3*R*)-3-phospho-3-(fluoromethyl)-5-diphosphopentanoate, at a rate 2500-fold slower than the rate for elimination from the usual noncovalent intermediate, (3*R*)-3-phospho-3-methyl-

5-diphosphopentanoate (**5–105**). This observation is consistent with the existence of tertiary carbocationic intermediate **5–106** in the enzymatic elimination, formed by dissociation from the (3*R*)-3-phospho-3-methyl-5-diphosphopentanoate of phosphate, which is a good leaving group from a tertiary carbon. The resulting carbocationic intermediate at carbon 3 would precede the step in which CO_2 dissociates from carbon 2.[420] The elimination catalyzed by diphosphomevalonate decarboxylase is peculiar because it cannot involve removal of an electrophile such as carbon dioxide or a hydron α to a carbonyl group or acyl group, as almost all biochemical eliminations do. An initial departure of carbon dioxide during the elimination, rather than the phosphate, would produce a primary carbanion with no obvious means of stabilization.

It has already been noted that (*S*)-methylketal phosphate **5–71** is a noncovalent intermediate in the enzymatic reaction catalyzed by 3-phosphoshikimate 1-carboxyvinyltransferase (Equation 5–91) and that oxocarbenium ion **5–73** is probably an intermediate in the elimination that forms the 1-carboxyvinyl group. UDP-*N*-Acetylglucosamine 1-carboxyvinyltransferase also adds phospho*enol*pyruvate to a hydroxy group, the 3-hydroxy group of UDP-*N*-acetyl-α-D-glucosamine. The fact that (*Z*)-3-fluorophospho*enol*pyruvate is a substrate for the enzyme from *E. coli* with a catalytic constant, k_0, 10,000 times slower than that for phospho*enol*pyruvate,[421] is consistent with the existence of an oxocarbenium ion as an intermediate either preceding or following the (*S*)-methylketal phosphate in this enzymatic reaction, or both.

Thiamine phosphate synthase[422]

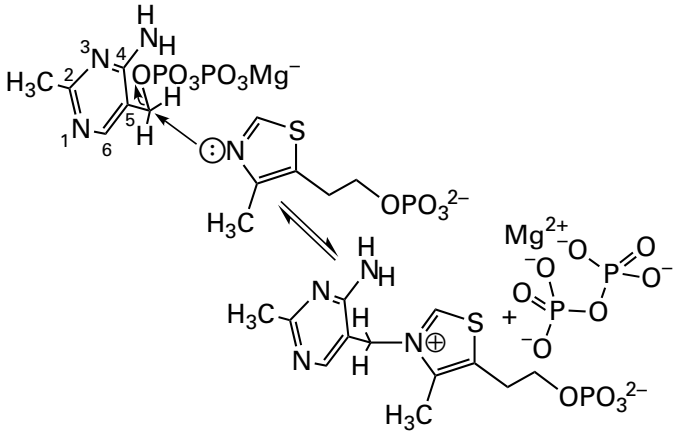

(5–134)

catalyzes the nucleophilic substitution at the 5-diphosphooxymethyl group of 4-amino-2-methyl-5-(diphosphooxymethyl)pyrimidine of the nitrogen in 4-methyl-5-(2-phosphooxyethyl)thiazole for diphosphate. Thiamine phosphate synthase from *B. subtilis* catalyzes its nucleophilic substitution 16 times faster when the 2-methyl group on 4-amino-2-methyl-5-(diphosphooxymethyl)pyrimidine is replaced by a methoxy group and 1300 times more slowly when it is replaced by a trifluoromethyl group.[423] These differences in rate are almost the same as the differences in rate for hydrolysis of 2-chloro-2-(4-methylphenyl)propane when the 4-methyl group in this alkyl chloride undergoes the same substitutions, and this latter reaction is definitely a dissociative nucleophilic substitution with a carbenium ion as an intermediate. These observations are consistent with an enzymatic mechanism in which 4-amino-2-methyl-5-(diphosphooxymethyl)-pyrimidine dissociates to give diphosphate and the carbenium ion **5–107**

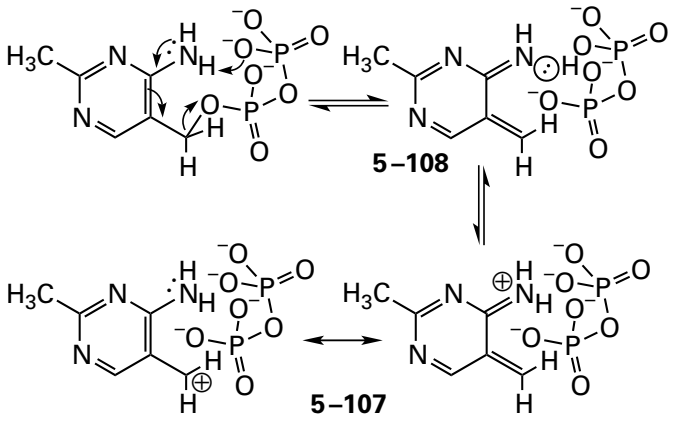

(5–135)

which is stabilized by resonance and to which the nitrogen of the thiazole then adds. In this instance, the reaction is a dissociative nucleophilic substitution.

Crystals of thiamine-phosphate diphosphorylase from *B. subtilis*, in which Serine 130 had been mutated to alanine, were soaked in solutions of the alternative substrate 2-[(2*R*,5*Z*)-2-carboxy-4-methylthiazol-5(2*H*)-ylidene]ethyl phosphate and either the cosubstrate 4-amino-2-methyl-5-(diphosphooxymethyl)pyrimidine or the much slower cosubstrate 4-amino-2-(trifluoromethyl)-5-(diphosphooxymethyl)pyrimidine. In the crystallographic molecular models from these crystals, electron density for separate molecules of diphosphate and the respective intermediate carbenium ion was observed in addition to that for 2-[(2*R*,5*Z*)-2-carboxy-4-methylthiazol-5(2H)-ylidene]ethyl phosphate.[424] In both of these complexes and in complexes with only the intact, unaccompanied substrate 4-amino-2-methyl-

5-(diphosphooxymethyl)pyrimidine, there is a hydrogen bond between a peripheral oxygen of the diphosphate and the 4-imino or 4-amino group of the carbenium ion or the substrate, respectively (Equation 5–135). It is probably the case that the carbenium ion is stabilized in the complexes in which it appears, either during its formation or after its formation, by hydron transfer within this hydrogen bond to produce the neutral noncovalent intermediate **5–108**, which may also be a transient intermediate in the normal reaction.

(*S*)-2-Hydroxypropylphosphonic acid epoxidase catalyzes a 1,2-phosphonomigration when the unnatural substrate (*R*)-2-hydroxypropylphosphonic acid is a reactant. That the migration occurs to an adjacent carbenium ion is consistent with the facts that when the secondary carbon to which the phosphono group migrates is adjacent to a methoxy group or an additional methyl group, groups that stabilize a carbenium ion, the migration occurs, but when the secondary carbon to which the migration would occur is adjacent to a trifluoro methyl group, it does not.[425]

Suggested Reading

Poulter, C. D., Capson, T. L., Thompson, M. D., and Bard, R. S. (1989) Squalene synthetase: Inhibition by ammonium analogues of carbocationic intermediates in the conversion of presqualene diphosphate to squalene, *J. Am. Chem. Soc. 111*, 3734–3739. https://doi.org/10.1021/ja00192a036

An, M., Maitra, U., Neidlein, U., and Bartlett, P. A. (2003) 5-Enolpyruvylshikimate 3-phosphate synthase: Chemical synthesis of the tetrahedral intermediate and assignment of the stereochemical course of the enzymatic reaction, *J. Am. Chem. Soc. 125*, 12759–12767. https://doi.org/10.1021/ja036627+

Problem 5–9: The following reaction is catalyzed by ATP citrate synthase:

$$\text{HSCoA} + \text{citrate} + \text{MgATP}^{2-} \rightleftharpoons \text{MgADP}^{-} + \text{HOPO}_3^{2-} + \text{oxaloacetate} + \text{acetyl-SCoA}$$

On the basis of the following data,[426-428] write a detailed mechanism for the reaction. Give explanations for all the observations. Identify each of your explanations with the letter of its observation.

(A) When Mg[8-^{14}C]ATP^{2-} is incubated with the enzyme in the presence of $MgCl_2$, no radioactivity is associated with the protein that is chromatographically isolated by molecular exclusion.

(B) When Mg[γ-^{32}P]ATP^{2-} is incubated with the enzyme in the presence of $MgCl_2$, radioactivity is associated with the isolated protein. When this radioactive protein is incubated with [1,5-$^{14}C_2$]citrate in the presence of HSCoA but in the absence of $MgCl_2$, [^{14}C]oxaloacetate is formed and all the radioactivity is released from the enzyme.

(C) When the enzyme is incubated with MgATP^{2-} and $HO^{32}PO_3^{2-}$, in the presence of $MgCl_2$, no radioactivity is found in the enzyme or in MgATP^{2-}. When the enzyme is incubated with MgATP^{2-} and Mg[8-^{14}C]ADP^{-} in the presence of $MgCl_2$, no radioactivity is found in the enzyme, but MgATP^{2-} becomes radioactive.

(D) When citryl 1-phosphate is incubated with the enzyme in the presence of HSCoA, oxaloacetate and acetyl-SCoA are formed.

(E) When citryl 1-phosphate and HSCoA are incubated without the enzyme, nothing happens.

Problem 5–10: β-Galactosidase catalyzes the reaction of Equation 5–120. The enzyme acts only on the β-anomer of a galactoside and releases only the β-anomer of the product. It cares little, however, what R_1 and R_2 are.

(A) Write a mechanism for this reaction, as it would occur in the active site, that is consistent with these observations. Position catalytic side chains to explain both the stringency in the stereochemistry of the reaction at carbon 1 and the carelessness in recognizing R. Use

specific amino acid side chains of your choice for catalysis.

(B) The chemical mechanism you have written in part A has the following kinetic mechanism.

$$E + A \underset{k_{-1}}{\overset{k_1}{\rightleftharpoons}} E{\cdot}A \xrightarrow{k_2} E{\cdot}C + Y$$

$$E{\cdot}C + B \underset{k_{-3}}{\overset{k_3}{\rightleftharpoons}} E{\cdot}C{\cdot}B \xrightarrow{k_4} E + Z$$

Write out the complete equation for initial rate for the enzymatic reaction for this kinetic mechanism.

(C) Take the limit

$$\lim_{[A]_0,[B]_0 \to \infty} v_0 ([E]_t)^{-1} = k_0$$

and write an expression for the catalytic constant, k_0, that contains only rate constants (k_i) in the kinetic mechanism of part B.

(D) Refer to your molecular mechanism for β-galactosidase, and determine which rate constant in the kinetic mechanism would be most affected by changes in R.

(E) Consider the following table of relative catalytic constants, where $k_{0,R}$ is the catalytic constant for the β-galactoside with the tabulated functional group and $k_{0,2\text{-nitro}}$ is the catalytic constant for 2-nitrophenyl β-galactoside. The various R groups are listed in order of increasing ability to leave.[368,429,430]

R	$k_{0,R}\ (k_{0,2\text{-nitro}})^{-1}$
methyl	0.06
4-bromophenyl	0.02
4-chlorophenyl	0.02
4-methoxyphenyl	0.1
phenyl	0.1
4-nitrophenyl	0.2
3-chlorophenyl	0.5
3-nitrophenyl	0.9
2-nitrophenyl	1.0
2,5-dinitrophenyl	1.1
3,5-dinitrophenyl	1.1
2,4-dinitrophenyl	1.3

(F) Explain, in terms of the expression you derived in part C, why $k_{0,R}\ (k_{0,2\text{-nitro}})^{-1}$ increases as R becomes a better leaving group and then levels off, showing no further increase.

Problem 5–11: Deoxyhypusine synthase catalyzes the reaction

lysyl side chain + spermidine $\rightleftharpoons$
N^6-(4-aminobutyl)lysyl side chain
+ propane-1,3-diamine

where lysyl side chain is a lysyl side chain in the protein translation initiation factor 4D. The enzyme has a prosthetic NAD^+ in its active site. When the enzyme from *R. norvegicus* was mixed with spermidine in the absence of translation initiation factor 4D, and hence the lysyl side chain, 1-pyrroline and propane-1,3-diamine were isolated from the active site.[431]

(A) What intermediate is formed during the enzymatic reaction?

(B) Write a complete mechanism for the reaction.

Problem 5–12: Riboflavin synthase catalyzes the reaction

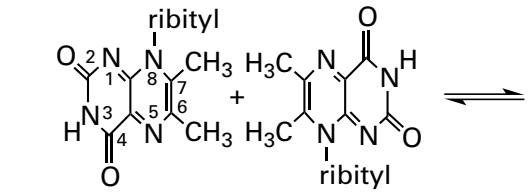

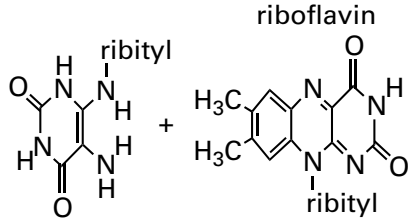

Note that the two reactants are both the same molecule, 6,7-dimethyl-8-(1-D-ribityl)lumazine. The reaction, formally, is the transfer of a 2-butenyl group from two nitrogens to two carbons. That the two molecules of 6,7-dimethyl-8-(1-D-ribityl)lumazine are joined in the noted opposite orientations, one up and the other down, has been demonstrated by

determining the stereochemistry of the product formed from 6-deuteriomethyl-7-methyl-8-(1-D-ribityl)lumazine.[432]

It has been shown that the hydrogens on the 7-methyl group of the lumazine are acidic ($pK_a = 9.8$)[433] and susceptible to exchange with deuterium under basic conditions in the absence of the enzyme.

(A) Write a mechanism for this exchange of protium for deuterium with an enolate as an intermediate.

When one of the two 6,7-dimethyl-9-(1-ribityl)-lumazines associates with riboflavin synthase from *E. coli*, this enolate is formed in its subsite in the active site.[433] The following are two portions of a crystallographic molecular model of the enzyme from *S. pombe* in complex with 6-carboxyethyl-7-oxo-8-(1-D-ribityl)lumazine, an unreactive analogue of 6,7-dimethyl-8-(1-D-ribityl)lumazine.[434]

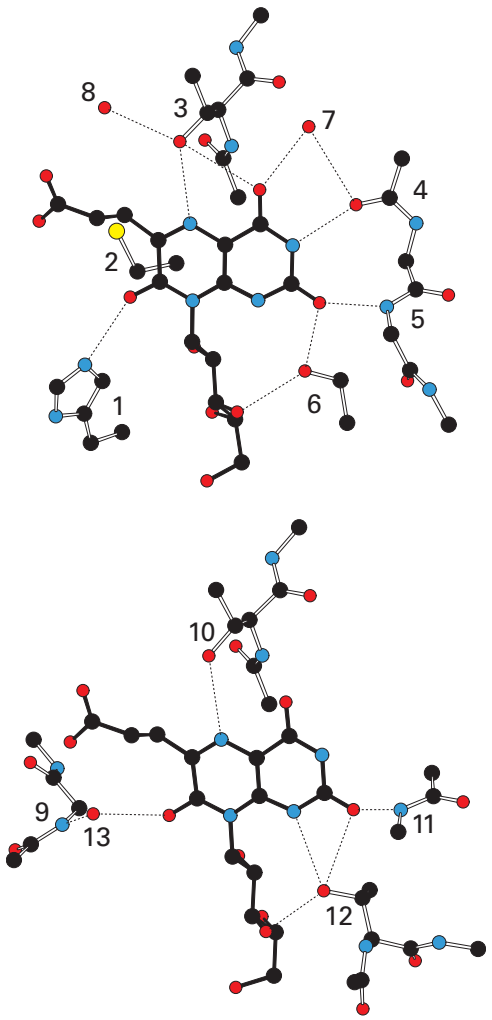

The two drawings are of the two subsites that comprise the active site, one for each of the two 6,7-dimethyl-8-(1-ribityl)lumazines that are substrates for the enzyme and each of which is occupied by a molecule of 6-carboxyethyl-7-oxo-8-(1-D-ribityl)-lumazine.

(B) Make a list numbered 1 to 13 that identifies each donor and acceptor of a hydrogen bond and the side chains of amino acids numbered in the two drawings.

(C) Write a mechanism for the binding of the molecule of 6,7-dimethyl-8-(1-D-ribityl)lumazine that becomes the enolate in the active site. Draw explicitly the functional groups in the crystallographic molecular model of the active site responsible for creating and stabilizing the enolate.

This enolate is the first intermediate in the enzymatic reaction.

Pentacyclic intermediate **1** is produced by a mutant of riboflavin synthase from *E. coli*.

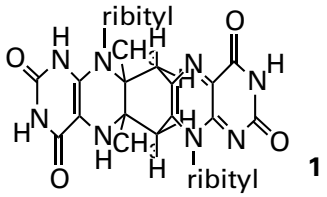

1

When it is mixed with the native, unmutated enzyme, it is converted to riboflavin at a rate that is much greater than the rate at which two molecules of 6,7-dimethyl-8-(1-D-ribityl)lumazine are converted to riboflavin,[435] a fact consistent with it also being an intermediate in the enzymatic reaction. There is a tautomer of the enolate, dienamine **2**, that is nucleophilic at the two requisite carbons.

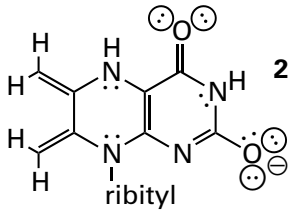

2

(D) Write a mechanism for formation of dienamine **2** from the enolate in the active site of the enzyme using the functional groups observed in the crystallographic molecular model.

(E) Write a mechanism[436] in which dienamine **2** reacts twice, as two different nucleophiles, with 6,7-dimethyl-8-(1-D-ribityl)lumazine to form pentacyclic intermediate **1**. Which nucleophilic addition has to precede the other?

(F) Write a mechanism in which dienamine **2** participates in a cycloaddition with 6,7-dimethyl-8-(1-D-ribityl)lumazine to form pentacyclic intermediate **1** in a single step.

(G) Explain why one of these two mechanisms seems more likely given the functional groups available in the active site.

(H) Write a mechanism to convert pentacyclic intermediate **1** into the products observed in the enzymatic reaction using the catalytic groups found in the active site, labeling each with its name and number.

(I) What essential catalytic group for one of these latter steps seems to be missing?

Chemical and Crystallographic Identification of Radical Intermediates

There are instances in which an intermediate or a sequence of intermediates in an enzymatic reaction are radicals. The chemistry of almost all enzymatic reactions is heterolytic because it is based on hydron transfers performed by acid–bases in the active site, which are themselves heterolytic. Far fewer and far less fundamental instances of enyzmatic reactions with radical intermediates have been described. There are a few prosthetic groups, in particular flavins, hemes, and coenzyme B_{12}, and a few enzymes lacking such prosthetic groups that engage in homolytic chemistry.[437] The reason for the relative rarity of homolytic mechanisms is the **difficulty of catalyzing formation of radical intermediates*** and their ability to participate in random hydrogen abstraction.[438]

Any **organic radical** can be formally **defined as the product of a hydrogen abstraction.** Consequently, a radical is energetically defined by the **bond dissociation energy** (BDE; kilojoules mole^{-1}),† which is the enthalpy required to break the bond homolytically between a hydrogen and the rest of the particular molecule to form a radical, regardless of whether or not that radical was formed by the abstraction of a hydrogen.[439,440] The more energy that is required to break a bond between the radical and a hydrogen, the more energetic is the radical. A radical with a larger bond dissociation energy will abstract a hydrogen from another molecule in a favorable reaction that produces a radical of lower bond dissociation energy.

An example of a radical involved in several enzymatic reactions is the **tyrosyl radical**. A tyrosyl radical can be formed nonenzymatically upon X-irradiation of a crystal of tyrosine hydrochloride. This radical has the resonance hybrids

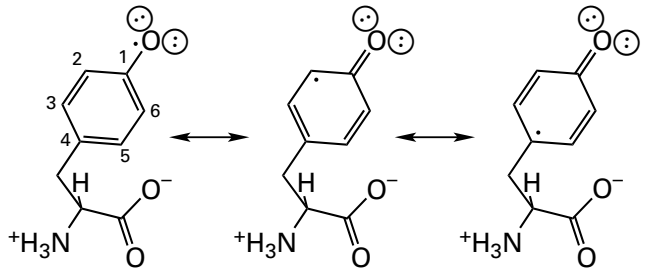

5–109

with spin densities in the solid state of 0.2–0.3 on the oxygen and carbons 1, 3, and 5, respectively,[441] as predicted by the resonance structures. It can be thought of as the product of dissociation of an electron (E^0 = 850 mV) from the π system of the 4-oxidophenyl anion [442]

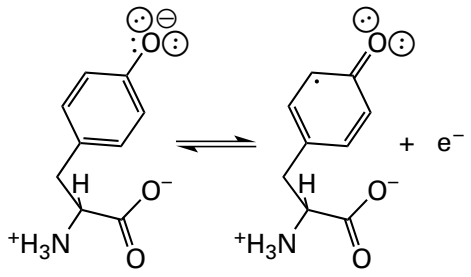

(5–136)

or the product of hydrogen abstraction (BDE = 380 kJ mol^{-1}) from the oxygen of the 4-hydroxyphenyl group[439]

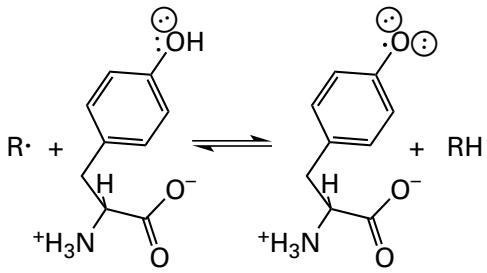

(5–137)

*As the majority of this discussion has emphasized, it is acid–base chemistry that provides the ability to catalyze heterolytic reactions. Nothing equivalent to such catalysis is available for homolytic reactions, except for the prosthetic groups.

†http://aquila.tversu.ru/LIB/Book/ComprehensiveHClBE.pdf

Regardless of the mechanism of its formation, a tyrosyl radical is capable of hydrogen abstraction at its oxygen (reverse of Equation 5–137) from a donor (RH in Equation 5–137) with the same or a smaller bond dissociation energy.

In marked contrast to acid–base chemistry, any hydrogen in a protein or in a substrate is susceptible to **hydrogen abstraction** to form a radical of the protein or substrate itself. The hydrogenated form of any radical is the functional group produced when that radical abstracts a hydrogen from another location. The products of this hydrogen abstraction are a new radical on the atom from which the hydrogen has been abstracted and a new σ covalent bond between the hydrogen and the atom on which the unpaired electron was previously located. If the hydrogenated form of a particular radical formed as an intermediate in an enzymatic reaction has a bond dissociation energy greater than those of hydrogens that necessarily surround it in the active site, the radical will uncontrollably abstract one of these hydrogens—for example, the tertiary hydrogen in a leucine or isoleucine (BDE = 390 kJ mol^{-1})—and produce a radical that would spread over the structure of the protein by successive hydrogen abstractions or electron transfers.

Enzymatic active sites, however, can be constructed so as to surround radicals with hydrogens that are difficult to abstract, such as a hydrogen of water (BDE = 497 kJ mol^{-1}), phenyl hydrogens (BDE = 470 kJ mol^{-1}), or hydrogens in hydroxy groups (BDE = 440 kJ mol^{-1}). The almost unavoidable nature of hydrogen abstraction may explain why most radical intermediates that participate in enzymatic reactions, such as the tyrosine radical (BDE = 380 kJ mol^{-1}), have low values for the bond dissociation energies of their hydrogenated forms, with the notable exceptions of the primary 5′-deoxy-5′-adenosyl radical (BDE = 420 kJ mol^{-1}) and the alkyl radicals thought to be involved in the reactions catalyzed by hemes P-450, which are quite reactive.[443] In these latter two instances, the reactive radicals generated during the enzymatic reaction are either surrounded by molecules of water or are generated immediately adjacent to the hydrogen that is to be abstracted.[438]

The eclectic collection of radicals generated in the mechanisms of enzymes that use a prosthetic adenosylcobalamin; a metallic prosthetic group and molecular oxygen; a prosthetic flavin and molecular oxygen; or a metallic prosthetic group, a prosthetic flavin, and molecular oxygen in concert have already been discussed in detail. There are **three main strategies** that enzymes use to generate radical intermediates without the assistance of any of these previously described prosthetic groups. These three strategies differ in the source of the initial radical that initiates a sequence of radical intermediates in the respective mechanism.

First, there are enzymes that generate a 5′-deoxy-5′-adenosyl radical by catalyzing, with a reduced prosthetic [4Fe–4S] iron–sulfur cluster, the homolytic dissociation* of the appropriate carbon–sulfur bond in *S*-adenosyl-L-methionine[444-448]

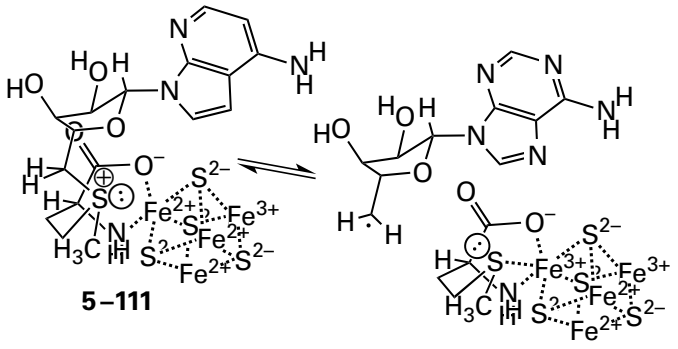

(5–138)

The [4Fe–4S] iron–sulfur cluster and the L-methionine operate as the integrated complex **5–110** in which three lone pairs of electrons from the sulfur, the carboxy oxyanion, and the amino group of the L-methionine are ligands to an iron ion in the cluster. This complex either dissociates homolytically from the 5′-deoxyadenosyl group during association of the sulfur with the iron ion or, in reverse, associates homolytically with the 5′-deoxy-5′-adenosyl radical. Meanwhile, the iron ion adds the other electron to the sulfur or removes the other electron from the sulfur of the sulfide in the L-methioninyl group, respectively. The 5′-deoxy-5′-adenosyl radical produced by this dissociation is identical to the 5′-deoxy-5′-adenosyl radical produced by homolytic dissociation of the carbon–cobalt bond in adenosylcobalamin, but it is surrounded by a different environment.

Second, there are enzymes that contain, at particular locations within their folded polypeptides, a stable glycyl radical (**5–112**)[449,450]

*In the absence of assistance from the [4Fe–4S] iron–sulfur cluster, the bond dissociation energy of the carbon–sulfur bond in *S*-adenosyl-L-methionine is around 300 kJ mol^{-1}.

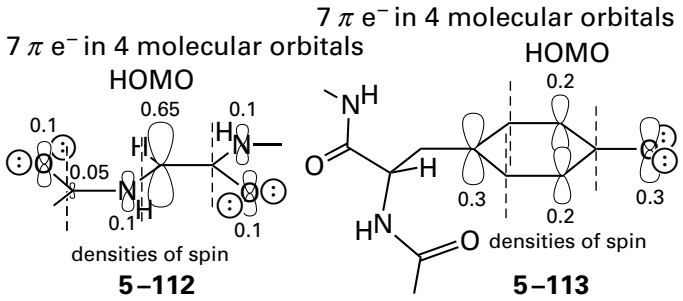

formally the product of abstraction of a hydrogen from a particular glycine within the sequence of the protein located in the active site. This glycyl radical has the noted distribution of unpaired spin in the highest occupied molecular orbital (HOMO).

Third, there are enzymes that contain,[451] within their folded polypeptides, a stable tyrosyl radical (**5–109** and **5–113**).

The homologous enzymes ribonucleoside-diphosphate reductase and ribonucleoside-triphosphate reductase, in their various guises, use all three of these strategies as well as adenosylcobalamin to produce the radical initiating the common reaction. Hence, the respective individuals in this family of enzymes are excellent paradigms for all these strategies. Ribonucleoside-diphosphate reductase (R = $-PO_3^{2-}$) and ribonucleoside-triphosphate reductase (R = $-PO_3PO_3^{3-}$) are two enzymes that catalyze the same oxidation–reduction

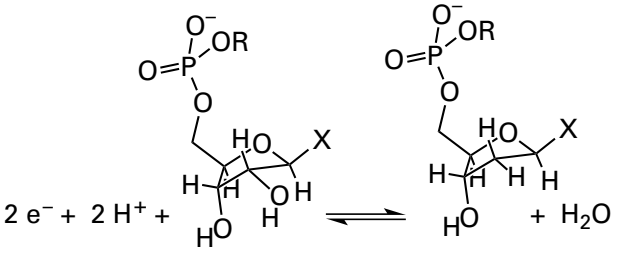

(5–139)

where X can be uracil, cytosine, adenine, or guanine, and R is either a phosphate or a diphosphate, respectively, none of which participate. In almost all cases, the two electrons are supplied stoichiometrically by two adjacent cysteines in the small electron carrier thioredoxin[452,453]

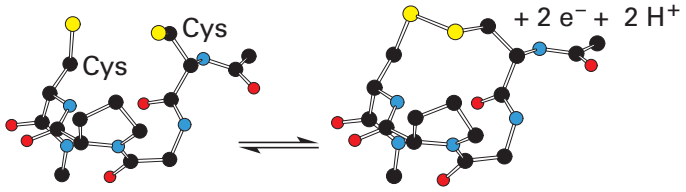

(5–140)

that end up as a cystine at the end of the reaction. Because these two enzymes, ribonucleoside-diphosphate reductase and ribonucleoside-triphosphate reductase, share a common ancestor[454,455] and a common mechanism, they are each usually given the common unofficial name **ribonucleotide reductase**.

Reduction of carbon 2′ in the ribose would be difficult to perform heterolytically because neither the hydron on carbon 1′ nor the hydron on carbon 3′ is acidic, which would permit a β elimination followed by reduction of the resulting carbon–carbon bond, nor is the hydroxy group on carbon 2′ a reasonable leaving group, so natural selection has discovered a homolytic solution. There are several types of ribonucleotide reductases, all of which use the same homolytic mechanism. These types differ depending on the strategy they use to generate the initial radical intermediate in their respective mechanisms.

In one class of ribonucleotide reductases—some members of which are ribonucleoside-triphosphate reductases and some ribonucleoside-diphosphate reductases and which are found in bacteria and a few eukaryotic microorganisms—each active site uses **adenosylcobalamin** in the usual manner to generate the initial radical intermediate in the sequence of intermediates. The adenosylcobalamin, however, is not a firmly attached prosthetic group and must be present in solution at saturating concentrations for maximum enzymatic activity.[456] That the active sites in this class are able to dissociate the carbon–cobalt bond to form a 5′-deoxy-5′-adenosyl radical follows from the fact that stereochemically labeled (5′-*R*)-[5′-^{2}H]adenosylcobalamin is racemized by an inactive mutant of ribonucleoside-triphosphate reductase from *Lactobacillus leichmannii* in which an adjacent catalytic cysteine in the active site has been converted to serine.[457] The equilibrium constant for dissociation of the carbon–cobalt bond in the active site of the same enzyme has been measured spectroscopically[458] to be 0.2.

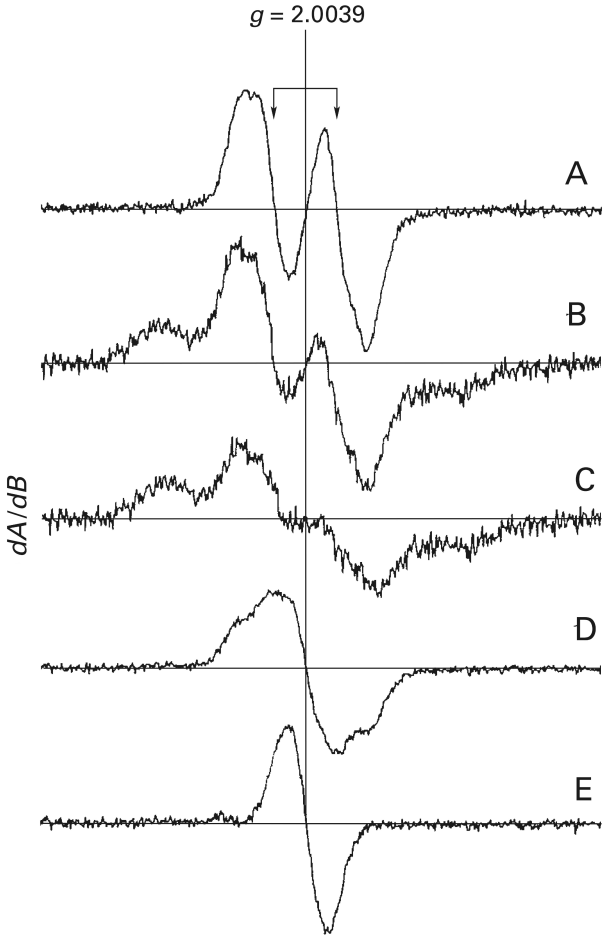

Figure 5–9: Electron paramagnetic resonance spectra of the glycyl radical in anaerobic ribonucleoside-triphosphate reductase encoded by Enterobacteria phage T4.[460] A plasmid encoding the gene from Enterobacteria phage T4 for anaerobic ribonucleoside-triphosphate reductase was replicated anaerobically in *E. coli*. The plasmid permitted significant overexpression so that the final concentration of glycyl radicals in a cytoplasmic extract of the bacteria was 7 μM. Frozen cytoplasmic extracts from the bacteria were used for measurement of electron paramagnetic resonance spectra at 77 K. (**A**) Spectrum of an extract from overexpressing bacterial cells grown on normal medium supplemented with 50 mM unlabeled glycine. (**B**) Spectrum of an extract from overexpressing bacterial cells grown on normal medium supplemented with 50 mM [2-^{13}C]glycine. (**C**) Spectrum B after subtraction of 20% spectrum A to correct for the fact that, in the end, only 80% of the glycine in the enzyme had carbon-13 at its α carbon. (**D**) Spectrum of an extract from overexpressing bacterial cells grown on normal medium supplemented with 50 mM [2,2-$^{2}H_2$]glycine. (**E**) Spectrum D after subtraction of 50% spectrum A to correct for the fact that, in the end, only 50% of the hydrogens on the α carbons of the glycines in the enzyme were deuterium. When Glycine 580 in the enzyme was mutated to alanine, or when the plasmid responsible for overproduction of ribonucleoside-diphosphate reductase was omitted, none of these absorptions were observed in the respective extracts. Vertical lines indicate the center of each absorption at its *g* value.

In the next class—the ribonucleoside-triphosphate reductases found in obligate anaerobic bacteria and facultative anaerobic bacteria under anaerobic conditions—each active site uses an oxygen-sensitive* **glycyl radical** located stably on a particular glycine[459] in the enzyme. The glycyl radical is identified by an absorption in an electron paramagnetic resonance spectrum of the enzyme (Figure 5–9).[460] In the spectrum of a cytoplasmic extract containing the anaerobic ribonucleoside-triphosphate reductase encoded by Enterobacteria phage T4, the absorption of the glycyl radical is a doublet (arrows in Figure 5–9A) because it is split by the nucleus of the single protium on the α carbon of the glycine on which the radical is concentrated (**5–112**). When the bacteria are grown on medium supplemented with [2-^{13}C]glycine, the absorption becomes a complex multiplet (Figure 5–9C) because it is split by the nuclei of both the hydrogen and the carbon-13 on which it is concentrated. When the bacteria are grown on medium supplemented with [2,2-$^{2}H_2$]glycine, the absorption becomes a singlet (Figure 5–9E) because it is not split by either the nucleus of the deuterium on the carbon on which it is concentrated or the nucleus of the carbon-12 on which it is concentrated.† The particular glycine, Glycine 580, that is the radical in the ribonucleoside-triphosphate reductase encoded by Enterobacteria phage T4 has been identified by site-directed mutation.[460] When Glycine 580 is replaced by alanine, electron paramagnetic resonance spectra of the cytoplasmic extracts from bacteria carrying the plasmid with the mutant do not have the absorption due to the radical. The glycyl radical in the enzyme is produced by a 5′-deoxy-5′-adenosyl radical that in turn is formed by the homolytic dissociation of *S*-adenosyl-L-methionine catalyzed by a [4Fe–4S] iron–sulfur cluster (Equation 5–138).[461,462] This 5′-deoxy-5′-adenosyl radical is produced in another protein, anaerobic ribonucleoside-triphosphate reductase-activating protein, that binds tightly to the cognate anaerobic ribonucleoside-triphosphate reductase to effect formation of the glycyl radical.[463]

*The glycyl radical, as is the case with most aliphatic radicals is susceptible to the addition of triplet molecular oxygen.

† Recall that electron paramagnetic resonance spectra are presented as the first derivative of the actual absorption, so the trace in Figure 5–9E is the first derivative of the peak of a singlet and the trace in Figure 5–9A is the first derivative of the peak of a doublet.

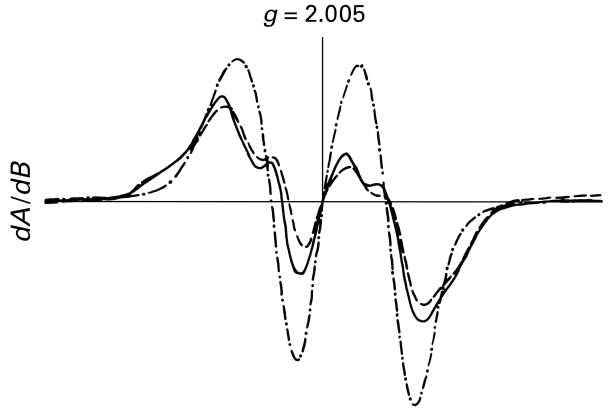

Figure 5–10: Electron paramagnetic resonance spectra of the tyrosyl radical in ribonucleoside-diphosphate reductase.[465] A strain of the bacterium *E. coli* that overproduces its own ribonucleoside-diphosphate reductase was used for these experiments. In this overproducing strain, about 3% of the cytoplasmic protein is the enzyme. Frozen suspensions of intact bacteria were used for measurement of electron paramagnetic resonance spectra at 77 K. Spectra are shown for cells grown on undeuterated L-tyrosine (– – –), for cells grown on [3,5-$^2H_2$]-L-tyrosine (– · – · –), and for cells grown on [2,6-$^2H_2$]-L-tyrosine (——). Vertical lines indicate the center of each absorption at its *g* value. When Tyrosine 122 in the enzyme being overexpressed was mutated to phenylalanine, or when the plasmid responsible for overproduction of ribonucleoside-diphosphate reductase was omitted, none of these absorptions were observed.[464]

The most widely distributed class of ribonucleotide reductases is that of the ribonucleoside-diphosphate reductases found in eukaryotes and most aerobic bacteria. Each member of this class uses a **stable tyrosyl radical** (**5–109** and **5–113**) to generate the initial radical intermediate in the enzymatic mechanism. These enzymes require two proteins for enzymatic activity. One protein, R1, contains the active site for the reduction; the other, R2, contains the tyrosyl radical.

Protein R2 can thought of as a **radical-carrier protein**, serving a role homologous to biotin carboxyl-carrier protein, acyl-carrier protein, or a small protein serving as an electron-transferring coenzyme, but it seems to fulfill this role only with protein R1, rather than being more promiscuous. The polypeptide that comprises protein R2 from *Homo sapiens* is 351 amino acids long, that from *A. thaliana* (60% identity; 0.8 gap percent) is 341 amino acids long, that from *S. cerevisiae* (43% identity; 0.8 gap percent) is 345 amino acids long, and that from *E. coli* (21% identity; 1.8 gap percent) is 375 amino acids long. Tyrosine 122 of protein R2 from *E. coli* has been identified by site-directed mutation as the stable tyrosyl radical.[464] Its unpaired spin can be detected by electron paramagnetic resonance spectroscopy (Figure 5–10).[464,465] That the unpaired spin is on a tyrosine can be demonstrated by replacing specific hydrogens on the tyrosines in protein R2 with deuteriums and observing changes in the spectra. From electron–nuclear double resonance spectra of this radical in protein R2 from *E. coli*, it has been calculated[466,467] that carbons 3 and 5 of the 4-hydroxyphenyl group each bear a spin density of 0.25; carbon 1, a tertiary carbon, bears a spin density of 0.4; and the oxygen bears a spin density of 0.3 while carbons 2, 4, and 6 bear negligible spin density (**5–113**). When cells of *E. coli* are grown on [2,6-$^2H_2$]-L-tyrosine, there is negligible alteration of the absorption of the radical, but when the cells are grown on [3,5-$^2H_2$]-L-tyrosine, the absorption of the radical becomes a doublet (Figure 5–10). These facts are consistent with a radical producing the absorption being located on a tyrosine and its resonance structures. When Tyrosine 122 in the enzyme is mutated to phenylalanine, the absorption is no longer observed.[464]

Immediately adjacent to this tyrosyl radical in the crystallographic molecular model of protein R2 from *E. coli*[468] is a **diferric cluster with a μ-oxo bridge** and ligation similar to that of the dinuclear cluster in diferric methane monooxygenase (soluble) (Figure 2–57I). The distance between the 4-oxidophenyl oxygen and the nearest iron is 0.35 nm, and the tyrosyl radical is magnetically coupled to the dinuclear iron center.[469] In terms of electron exchange, the equilibrium, heavily in favor of the tyrosyl radical, would be

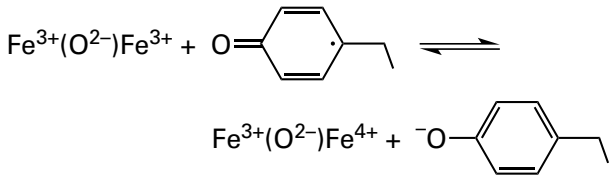

(5–141)

The high-valent species $Fe^{3+}(O^{2-})Fe^{4+}$ is responsible for formation of the tyrosyl radical by establishing this equilibrium.[470,471] There are versions of ribonucleoside-diphosphate reductases in this class that contain a homologous dimanganic, μ-oxo cluster[472-475] rather than a diferric, μ-oxo cluster, and there are versions in which the tyrosine has been replaced by natural selection with phenylalanine, and the unpaired electron responsible for initiating catalysis remains located in a dinuclear $Fe^{3+}(O^{2-})Mn^{4+}$ cluster.[476-478]

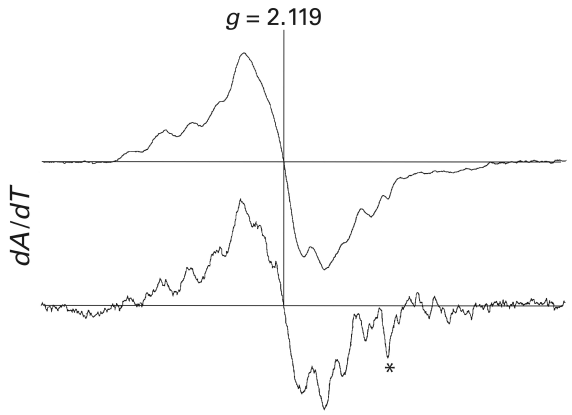

Figure 5–11: Electron paramagnetic resonance spectra of the sulfenyl radical in adenosylcobalamin-dependent ribonucleoside-triphosphate reductase.[479] A solution of 520 μM purified adenosylcobalamin-dependent ribonucleoside-triphosphate reductase from *L. leichmannii*, 50 μM thioredoxin, 3 μM thoredoxin reductase, and 1.7 mM NADPH was mixed with a solution of 400 μM adenosylcobalamin. Each solution also contained 1 μM $dGTP^{4-}$ and 0.1 M sodium dimethylglutarate, pH 7.3. After 175 ms, the mixture was injected into isopentane at −140 °C and then submitted to electron paramagnetic resonance spectroscopy at 100 K. (Upper trace) Unlabeled adenosylcobalamin-dependent ribonucleoside-triphosphate reductase. (Lower trace) Adenosylcobalamin-dependent ribonucleoside-triphosphate in which the cysteines were replaced with [β,β-$^2H_2$]cysteine. The asterisk indicates an absorption arising from a contaminant in the preparation. Reprinted with permission from reference 479. Copyright 1996 American Association for the Advancement of Science. https://doi.org/10.1126/science.271.5248.477

The reaction that initiates the homolytic reduction catalyzed by a ribonucleotide reductase is the production of the **sulfenyl radical** of a particular cysteine in the active site of the enzyme. An intermediate in the reaction catalyzed by the adenosylcobalamin-dependent ribonucleoside-triphosphate reductase from *L. leichmannii*, trapped 175 ms after mixing of the enzyme with adenosylcobalamin and $dGTP^{4-}$, has the electron paramagnetic resonance spectrum (Figure 5–11) of a sulfenyl radical.[479] When the cysteines in the enzyme are replaced with [β,β-$^2H_2$]cysteines, the spectrum of this radical is altered, consistent with it being located on sulfur of a cysteine. This sulfenyl radical is electronically coupled to the cob(II)alamin that results from homolysis of the carbon–cobalt bond.[480] At the same time that the radical is formed, cob(II)alamin and 5′-deoxyadenosine are also formed[481,482]

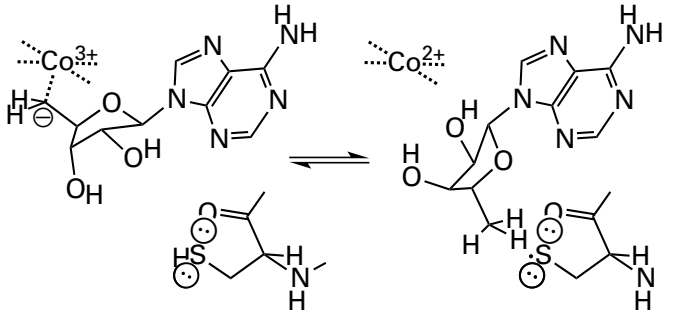

(5–142)

The former is followed by its absorbance at 525 nm; the latter, by chromatographic identification. The sulfanyl group (BDE = 370) of the cysteine that becomes the sulfenyl radical has been identified as Cysteine 408 in the enzyme from *L. leichmannii* by site-directed mutation.[481] Electron paramagnetic absorptions from a transient sulfenyl radical[483] and a stable sulfenyl radical[484] in mutants of protein R1 of ribonucleoside-diphosphate reductase from *E. coli* and *Mus musculus* have also been observed.

The 5′-deoxy-5′-adenosyl radical that is transiently formed during the reaction of Equation 5–142 must **abstract a hydrogen from an acidic position** because tritium is washed out of [5′-^{3}H]adenosylcobalamin, ending up as ^3H_2O, at a rate about as fast as the turnover of the enzyme.[456] This fact is consistent with the conclusion that a 5′-deoxy-5′-adenosyl radical, produced by homolytic dissociation of the carbon–cobalt bond of adenosylcobalamin in the active site of the ribonucleoside-triphosphate reductase of *L. leichmannii*, abstracts a hydrogen directly from the sulfanyl group of Cysteine 408. If this abstraction (Equation 5–142) reverses several times, eventually the tritium will end up on the sulfanyl group and then exchange into the solution.

In the crystallographic molecular model of the complex between ribonucleoside-diphosphate reductase from *T. maritima* and adenosylcobalamin, thymidine triphosphate, and guanosine diphosphate, the ribosyl group of adenosylcobalamin immediately flanks the sulfanyl group of Cysteine 322, which becomes the sulfenyl radical in this structurally homologous enzyme. The 5′-carbon of the adenosyl group in adenosylcobalamin is only 0.65 nm from the sulfur of the sulfanyl group,[482] and there is nothing in the active site to prevent it from reaching the sulfanyl group so that it can **abstract the hydrogen atom directly** once the carbon–cobalt bond dissociates. Nor are there any other nearby hydrogens that the 5′-deoxy-5′-adenosyl radical can abstract on its way to the sulfanyl group, except those on the molecules of water in the vacancy.

There is a crystallographic molecular model of a mutant of the anaerobic ribonucleoside-triphosphate reductase from Enterobacteria phage T4 in which Glycine 580, which harbors the stable radical in this enzyme, has been changed to alanine. The distance between the α carbon of that alanine, on which the glycyl radical resides in the native enzyme, and the sulfanyl group of Cysteine 290, from which a hydrogen is abstracted by the glycyl radical, is 0.55 nm.[485,486] In this instance, unlike that of ribonucleoside-diphosphate reductase from *T. maritima*, in the active site of which the 5′-carbon of the 5′-deoxy-5′-adenosyl radical is free to swing from the cobalt to the sulfanyl group, both the sulfanyl group and the glycine, which is in the polypeptide backbone itself, are rigidly fixed. Consequently, there seems to be no way they can come any closer to each other, and the distance between them is too great for direct hydrogen abstraction. The oxygen of the 4-hydroxy group of Tyrosine 581, however, is only 0.35 nm from the sulfur of the sulfanyl group of Cysteine 290, well within van der Waals contact (0.44 nm). The plane of the 4-hydroxyphenyl group is almost perpendicular to the line between its oxygen and the sulfur, the proper orientation for hydrogen abstraction by a 4-oxyphenyl radical (**5–113**). The stable glycyl radical on Glycine 580, which already has significant spin density (0.05–0.10) on the α-amino group of Tyrosine 581,[449,450] can receive an electron from the 4-oxido group on the anionic conjugate base of Tyrosine 581 by **short-range, through-bond electron transfer**, and the 4-hydroxyphenyl radical that results can then abstract the hydrogen atom directly from the sulfanyl group of Cysteine 290

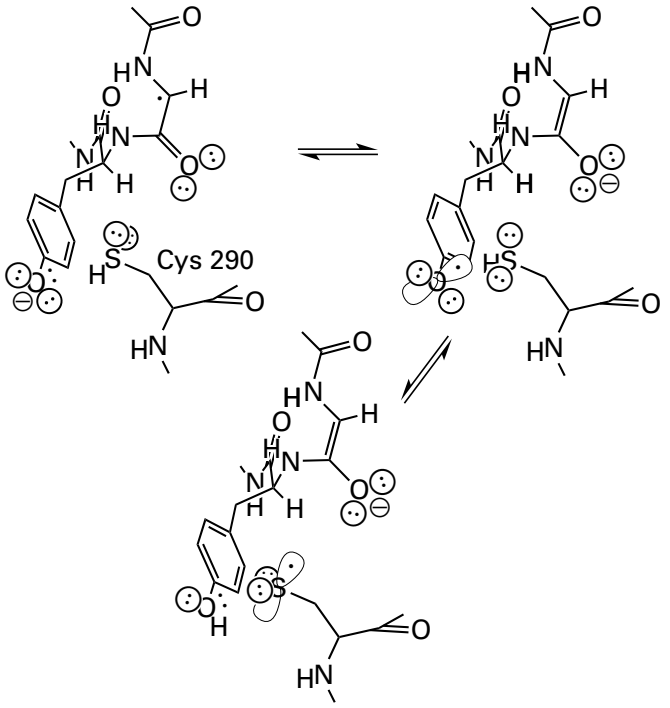

(5–143)

Both the 4-hydroxyphenyl group of a different tyrosine, Tyrosine 507, and the guanidinio group of Arginine 577 are close enough to form an oxyanion hole for the **1,2-diaminoenolate** that forms on Glycine 580 when the electron is transferred from Tyrosine 581.

Neither direct hydrogen abstraction nor direct, short-range electron transfer between their stable tyrosyl radicals and the sulfanyl groups of the catalytic cysteines in their active sites, however, can occur in the ribonucleoside-diphosphate reductases of aerobic bacteria and eukaryotes. In these enzymes, there is a stable tyrosyl radical that provides the hole for an electron, but the tyrosyl radical and the cysteine in the active site are on separate proteins, R1 and R2. Because both the sulfanyl group in the active site and the tyrosyl radical are buried in their respective proteins, the closest approach that they could ever make to each other is 2.5 nm.[487] In fact, there are measurements by electron paramagnetic resonance spectroscopy which suggest that the distance in the productive complex of ribonucleoside-diphosphate reductase from *E. coli* is actually around 3.5 nm.[488,489] It follows that the tyrosyl radical in protein R2 cannot directly abstract the hydrogen from the sulfanyl group in the active site on protein R1. Consequently, the sulfenyl radical (BDE = 370 kJ mol^{-1}) formed in the active site is the result of **long-range electron transfer** over a significant distance from the sulfanyl group to the tyrosyl radical (BDE = 380 kJ mol^{-1})

to produce the required sulfenyl radical and the 4-oxidophenyl group.

This electron transfer occurs by **hopping between identified relay stations**. There are two tyrosines, Tyrosines 730 and 731, in the catalytic R1 protein from *E. coli*. These two tyrosines, which are homologous to Tyrosines 741 and 742 in the active site of R1 protein from *S. cerevisiae* (Figure 5–12),[490,491] are adjacent to the sulfido group of Cysteine 439, which is homologous to Cysteine 443 in the active site of *S. cerevisiae* and which is the sulfido group that becomes the sulfenyl radical in the active site at which the reduction occurs.[483] Tyrosines 730 and 731 are on the path of the electron transfer. When they are replaced, in turn, by 3-aminotyrosines, and the respective mutant R1 proteins are mixed with R2 protein, an unpaired electron, on its way to the hole in the tyrosyl radical in protein R2, appears on the respective 3-aminotyrosine.[492] In a system in which an artificial one-electron oxidant, rhenium bipyridine, replaces protein R2 in the ribonucleoside-diphosphate reductase from *E. coli*, electron transfer from the sulfanyl group of the cysteine in the active site to the photochemical oxidant cannot occur when either Tyrosine 741 or Tyrosine 742 in protein R1 is mutated to phenylalanine.[493]

When Tyrosine 356 in protein R2 of *E. coli* is replaced by tyrosines that have been variously substituted at their 4-hydroxyphenyl groups, the ribonucleoside-diphosphate reductase activity decreases abruptly when the reduction potential of the substituted 4-hydroxyphenyl group becomes 0.1 V (10 kJ mol^{-1}) more positive than that for the unsubstituted tyrosine. When that 4-hydroxyphenyl group is replaced by a 3,4-dihydroxy group, an unpaired electron builds up on it.[494] When rhenium bipyridine is attached covalently to Cysteine 355 in protein R2, an electron can be removed directly from Tyrosine 356 photochemically. Reduction of CDP^{3-} by a complex of this modified R2 protein and native R1 protein can be driven by light.[495] These observations are evidence that Tyrosine 356 in protein R2 is also one of the relay stations between which the electron hops on the path for electron transfer.[496]

No stable complex between the native R1 α_2 dimer and the native R2 β_2 dimer of any ribonucleotide reductase that requires these two proteins for activity has ever been directly observed or crystallized. Attempts to reveal, by quantitative crosslinking, a complex between proteins R1 and R2 from *E. coli* while that complex is catalyzing the reaction failed to observe any crosslinked product.* This failure suggests that the complex, which must form at some point in the catalytic cycle, is transient—lasting only long enough for the electron to be transferred, catalysis to occur, and the electron to be returned—so that most of the time the two proteins are independent of each other. Measurements of the formation of a complex at short times, immediately after R2 β_2 dimer and reduced R1 α_2 dimer from *E. coli* are mixed together at varying ratios, are consistent with a rate of association between the two proteins of 160 $\mu M\ s^{-1}$ and a rate of dissociation of 75 s^{-1} at these initial times. These results require that the dissociation constant for the complex when protein R1 is reduced should be 0.4 μM. It was also concluded, however, that during steady-state turnover, the rate-limiting step of the enzymatic reaction is reduction of the cystine in the active site (2 s^{-1}), which follows dissociation of the complex between R2 β_2 dimer and R1 α_2 dimer. This reduction, which is the last step in the mechanism, must be completed before the two proteins can again form a complex,[497] so most of the time, the two are not associated with each other, in agreement with the results of quantitative crosslinking.

A stable complex, however, can be formed between native R2 β_2 dimer and an R1 α_2 dimer from *E. coli* in which Tyrosine 730 has been mutated to 3-aminotyrosine.[498] What seems to be the same complex can also be formed from a native R1 α_2 dimer and a mutant of R2 β_2 dimer in which Glutamate 52 has been mutated to glutamine and Tyrosine 122 has been mutated to 2,3,5-trifluorotyrosine.[499] The existence of these two complexes suggests that when the electron being transferred is trapped on one of the relay stations, so that it cannot complete its passage in either direction, the complex between the two proteins cannot dissociate as it does at the end of each complete turnover.

Electron micrographic images (80,386) of the complex between the native R1 α_2 dimer and the mutant of R2 β_2 dimer from *E. coli* embedded in amorphous ice were submitted to image reconstruction to obtain a map of scattering density into which the previously reported crystallographic molecular models of the R1 α_2 dimer and the R2 β_2 dimer could be inserted. Following refinement, a complete molecular model of the complex was produced.[499]

*Smith, S. and Kyte, J., personal communication.

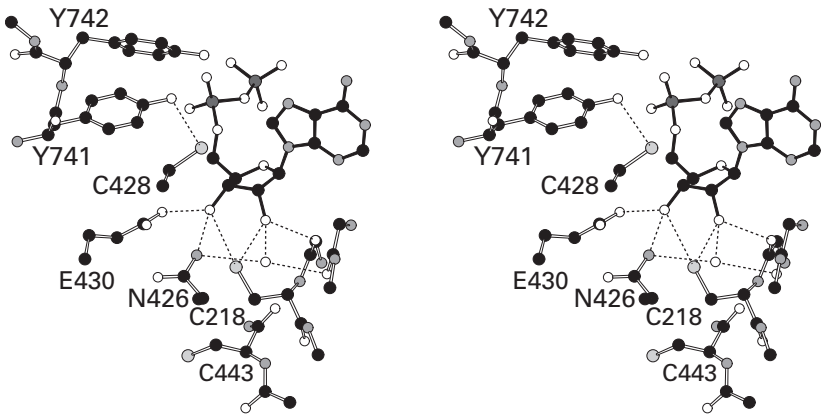

Figure 5–12: Stereodrawing[181] of the crystallographic molecular model[490] of the active site of ribonucleoside-diphosphate reductase from *S. cerevisiae* occupied by the substrate ADP^{3-}. Black atoms are carbons, white atoms are oxygens, small gray atoms are nitrogens, large light gray atoms are sulfurs, and large dark gray atoms are atoms of phosphorus. The small white sphere is a water. The protein was overexpressed in *E. coli* and purified by passing the cellular extract over a solid phase to which a heptapeptide with the carboxy-terminal sequence of the R2 protein from *S. cerevisiae* had been covalently attached.[491] The purified catalytic R1 protein was crystallized, and the crystals were soaked in a solution containing 20 mM ADP^{3-}, 20 mM 2′-deoxyguanosine 5′-triphosphate, and 10 mM $MgCl_2$. Reflections to Bragg spacing of 0.26 nm were then collected. In the resulting map of electron density, there was a feature in the active site into which a molecule of ADP^{3-} (black bonds) could be inserted unambiguously. The ribose of ADP^{3-} is held firmly in the active site by hydrogen bonds to Asparagine 246, Glutamate 430, Cysteine 218, a fixed molecule of water, and the amido oxygen of a peptide bond. The sulfanyl group of Cysteine 428 is 0.33 nm from the 3′ carbon of the ribose, and the 3′ hydrogen is almost on a line of centers between sulfur and carbon. In the active site, there are two tyrosines adjacent to each other in the sequence of amino acids, Tyrosines 741 and 742 (upper left-hand corner). The oxygen of Tyrosine 741 is 0.34 nm from the sulfur of Cysteine 428 and almost perfectly aligned to remove the hydrogen from that sulfur.

This complex between the native R1 α_2 dimer and the mutant R2 β_2 dimer is asymmetric. The main reason for the **asymmetry of the complex** is that the twofold rotational axes of symmetry for the R1 α_2 dimer and the R2 β_2 dimer are far from collinear. Collinearity is a requirement of rotational symmetry in a complex between two dimers.[487] Furthermore, association of the face on the surface of an R2 β_2 dimer with the face on the surface of one of the two R1 α subunits to form the specific interface holding the complex together sterically blocks the symmetrically situated face on the other R1 α subunit; therefore, only one of the two symmetricaly identical faces on the R1 α_2 dimer can be occupied by an R2 β_2 dimer at the same time. Consequently, in the complex between an R1 α_2 dimer and an R2 β_2 dimer, only one of the two active sites on the R1 α_2 dimer can be coupled to a path for electron transfer. The asymmetry of this complex and the consequent steric exclusion of a second R2 β_2 dimer, if the molecular model represents the catalytically competent complex between an R1 α_2 dimer and an R2 β_2 dimer, may explain the fact that only half the active sites and half the tyrosyl radicals in a given solution of the enzyme can be involved in catalysis at the same time.[500-502]

In the molecular model from the reconstruction,[499] there is an extensive interface between one R1 α subunit and faces on both R2 β subunits in the R2 β_2 dimer, but the interface between the other α subunit and a β subunit is almost nonexistent (there is a loop in the other R1 α subunit at the tip of which four amino acids make contact with an R2 β subunit). Consequently, only one active site for the reduction on the R1 α_2 dimer is linked to one of the two tyrosyl radicals on the R2 β_2 dimer. Within the molecular model from the reconstruction, this tyrosine and the sulfido group of Cysteine 439 in the active site for the reduction are linked by a chain of relay stations among which the electron can hop during its transfer. **Side chains of Tryptophan β48, Tyrosine β356, Tyrosine α731, and Tyrosine α730 comprise this chain**. The path on these relay stations from the sulfido group in the active site on the associated R1 α subunit and the radical at the nearest Tyrosine β122 is 3.5 nm long, in agreement with the electron paramagnetic resonance spectra.[488] The distance in the molecular model between Tryptophan β48 and Tyrosine β356 is 1.2 nm, and the distance between Tyrosine β356 and Tyrosine α731 is 0.8 nm. The sum of these two distances in the catalytically competent complex has been estimated to be 2.5 nm by pulsed electron–electron double resonance spectroscopy.[489] Tyrosine β356, through which the electron is transferred, is within the extensive interface between its β subunit and the competent α subunit, and the 20 amino acids between it and the carboxy terminus of its polypeptide are also in the interface. A synthetic heptapeptide with the sequence (FTLDADF) of the carboxy-terminal segment of murine protein R2 inhibits enzymatic activity, an observation from which it was concluded that this sequence is involved in association of the two proteins,[491] and this conclusion agrees with the molecular model. All these observations suggest that the complex observed in the electron micrographs is the catalytically competent complex between the R1 α_2 dimer and the R2 β_2 dimer, in which the electron is transferred from the sulfanyl group of Cysteine α439 to the 4-oxidophenyl radical on Tyrosine β122 over a distance of 3.5 nm.

As was discussed earlier in Chapter 2, the **net transfer of the electron by hopping** among these side chains that comprise the relay is accomplished in a sequence of steps. An electron is transferred from the indolyl group of Tryptophan β48 to the hole in the 4-oxyphenyl radical in Tyrosine β122 to produce an indolyl radical in Tryptophan β48; an electron is transferred from the 4-hydroxyphenyl group of Tyrosine β356 to the hole in the indolyl radical in Tryptophan β48 to produce a 4-oxyphenyl radical in Tyrosine β356; an electron is transferred from the 4-hydroxyphenyl group of Tyrosine α731 to the hole in the 4-oxyphenyl radical in Tyrosine β356 to produce a 4-oxyphenyl radical in Tyrosine α731; and an electron is transferred from the 4-hydroxyphenyl group of Tyrosine α730 to the hole in the 4-oxyphenyl radical in Tyrosine α731 to produce a 4-oxyphenyl radical in Tyrosine α730. The 4-oxyphenyl radical in Tyrosine α730 then abstracts a hydrogen from the sulfanyl group of Cysteine α439 or an electron from the sulfido group of Cysteine α439 to produce the sulfenyl radical. As before, it is obvious that although long-range electron transfer seems to imply that the same electron is transferred from one location to the other, this is never the case in any situation, even when hopping does not occur. In fact, in the net transfer of an electron between each relay station in ribonucleoside-diphosphate reductase on a path of covalent bonds or through space, the same electron that leaves one station is not the same electron that arrives at the next.

When an electron is transferred from an indolyl group, that group becomes an indolyl radical cation. It follows that **dehydronation** of the indolyl nitrogen during the transfer, so that the product is a neutral indolyl radical, should assist in the transfer. When an electron is transferred to a neutral, dehydronated indolyl radical, it becomes the anionic conjugate base of an indolyl group ($pK_a = 17$), so **hydronation** of the nitrogen during the transfer will definitely assist in the transfer. In protein R2 from *E. coli*, the nitrogen of the indolyl group of Tryptophan β48 participates in a hydrogen bond (0.30 nm) with the carboxylato group of Aspartate β237, which can remove and then add back a hydron as required, as the indolyl group gives up and takes up an electron.[468]

When an electron is transferred from a neutral 4-hydroxyphenyl group, that group becomes a 4-hydroxyphenyl radical cation, so dehydronation of its oxygen during the transfer should assist in the transfer. When, however, an electron is transferred from an anionic 4-oxidophenyl group, it becomes a neutral 4-oxyphenyl radical, so hydronation of its oxygen during the transfer could be undesirable. When an electron is transferred to a 4-oxyphenyl radical, it becomes a 4-oxidophenyl group ($pK_a = 9.8$), so hydronation of its oxygen during the transfer might assist in the transfer. When the electron arrives at the 4-oxyphenyl radical on Tyrosine β122 in the active site of ribonucleoside-diphosphate reductase from *E. coli*, the resulting 4-oxido group can be hydronated by a hydron on one oxygen of the carboxy group of Aspartic Acid β84,[468,503] which is nearby (0.34 nm) and in the proper orientation to transfer a hydron to a σ lone pair of electrons on the oxido group. The 4-hydroxy group on Tyrosine β356 in the R2 protein is exposed to the solution and could take up a hydron from and give away a hydron to the solution. The planes of the two adjacent tyrosines in the active site in an R1 α subunit, Tyrosines α731 and α730, are roughly parallel to each other in most crystallographic molecular models, and in the image reconstruction of the complex between protein R1 and protein R2, they are stacked upon each other,[499] probably to facilitate electron transfer. In all cases, their respective oxygens are too far apart (0.35 nm) to form a hydrogen bond, and their disposition, especially when they are stacked upon each other, prevents them from attaining the proper orientation for a hydrogen bond,[504] which is usually if not always a requirement of hydron transfer.* The 4-hydroxy group of Tyrosine α731 in the active site, however, does participate in a hydrogen bond with the carboxy group of Glutamate α623.[499]

The 4-oxido group of Tyrosine α730 and the sulfanyl group of Cysteine α439 in protein R1 of ribonucleoside-diphosphate reductase from *E. coli* are in van der Waals contact (0.35 nm) in the resting state of the enzyme. Consequently, they cannot both be the negatively charged conjugate bases, and there must be a hydron on one of them. When the electron is removed from Tyrosine α730 by the hole in the 4-oxyphenyl radical of Tyrosine α731, the product of the one-electron oxidation must be a neutral, hydronated 4-hydroxy group and a neutral cysteinyl radical. The plane of the 4-hydroxyphenyl group of Tyrosine α741 in the enzyme from *S. cerevisiae* (Figure 5–12), homologous to Tyrosine α730 in the enzyme from *E. coli*, is **normal to the line connecting its 4-hydroxy group to the sulfanyl group** of Cysteine α428, homologous to Cysteine α439 in *E. coli*, and the oxygen and sulfur are in van der Waals contact (0.34 nm). This orientation and this intimate contact are as they should be if the 4-oxyphenyl radical (**5–113**) of Tyrosine α741 abstracts the hydrogen from the sulfanyl group of Cysteine α428, or if an electron from the sulfido group of Cysteine α428 is transferred in concert with the transfer of an electron from the 4-hydroxyphenyl group of Tyrosine α741 to the 4-oxyphenyl radical of Tyrosine α742. Both situations produce the sulfenyl radical and the 4-hydroxyphenyl group.

Ribonucleoside-diphosphate reductase from *Chlamydia trachomatis* is a homologue (22% identity; 1.7 gap percent) of ribonucleoside-diphosphate reductase from *E. coli* in which the tyrosine bearing the radical in protein R2 has mutated over time to a phenylalanine and the unpaired electron resides in a dinuclear $Fe^{3+}(O^{2-})Mn^{4+}$ cluster. In this ribonucleoside-diphosphate reductase, a **tryptophan in the vicinity of the dinuclear $Fe^{3+}(O^{2-})Mn^{4+}$ cluster** assumes the role of the missing tyrosine in the chain of relay stations between which the electron hops,[505] even though the electron does not reside in its indolyl group at rest as it does in the 4-hydroxyphenyl group of Tyrosine 122 in protein R2 from *E. coli*. Other than the substitution of this tryptophan, the relay stations in the electron transfer in proteins R1 and R2 in this enzyme are on tyrosines and a tryptophan in homologous positions in the two polypeptides. Significant differences are observed in the absorptions in the electron paramagnetic resonance spectra of mutants of the enzyme from *C. trachomatis* in which each tyrosine is mutated in

*It is sterically difficult if not impossible for a hydron to be transferred between two tyrosines that are immediately adjacent to each other in a polypeptide.

turn when each mutant is in the normal reaction mixture for enzymatic activity. These differences indicate that each mutation in turn obstructs the transfer of the electron, causing it to assume different distributions over the chain of relay stations.[506]

In protein R2 from *Flavobacterium johnsoniae*, the tyrosine homologous to Tyrosine 122 in protein R2 from *E. coli* is present, but it is not a radical. The unpaired electron **remains in the $Mn^{3+}(O^{2-})Mn^{4+}$ cluster adjacent to the tyrosine**, presumably because the equilibrium analogous to Equation 5–141, with manganese ions replacing the two iron ions, favors the dinuclear cluster.[475]

Transfer of an electron from the sulfido or sulfanyl group on the cysteine in the catalytic site on protein R1 to the tyrosyl radical in protein R2 to create the sulfenyl radical initiates reduction of the nucleoside triphosphate. At the end of the catalytic reaction in the active site, the sulfenyl radical is regenerated. It was possible that it could then remain there and participate in subsequent turnovers. By using a mutant of ribonucleoside-diphosphate reductase from *E. coli*, however, in which Tyrosine 122 in protein R2 has been replaced with 2,3,5-trifluorotyrosine to decrease the rate of electron transfer so that its kinetics could be examined, it has been shown that, **at the end of each turnover, the electron is transferred from Tyrosine 122 back to the sulfenyl radical** in the active site of protein R1.[507] These observations are consistent with the conclusion that the complex between proteins R1 and R2 that is required for enzymatic activity exists only from the time the electron is transferred from the catalytic site until the time that it has returned.

Crystallographic molecular models of the active sites of R1 proteins, in the absence of the respective R2 proteins and their tyrosyl radicals and occupied by ribonucleoside diphosphates (Figure 5–12) have been reported,[490,504] as have crystallographic molecular models of an adenosylcobalamin-dependent ribonucleotide reductase in the absence of thioredoxin and occupied by ribonucleotides and, in one case, a ribonucleotide and adenosylcobalamin.[482,508] In each case, the catalytic groups are homologous and similarly aligned.

There is a common mechanism for the ribonucleotide reductases that is consistent with this arrangement of the catalytic groups around the ribonucleotides in these molecular models and with the available chemical evidence. This common mechanism (Figure 5–13)[509] can be described for the ribonucleoside-diphosphate reductase from *S. cerevisiae* operating on ADP^{3-} (Figure 5–12). The sulfenyl radical (BDE = 370 kJ mol^{-1}) at Cysteine 428, homologous to each sulfenyl radical formed in the various ways, abstracts the hydrogen (BDE = 380 kJ mol^{-1}) from carbon 3′ of ADP^{3-} (0.33 nm). The resulting **α-hydroxyalkyl radical** (**5–114**) at carbon 3′ is stabilized by the captodative effect engendered by electron donation from a lone pair of electrons on the adjacent 3′-hydroxy group. This lone pair of electrons is held parallel to the developing radical on carbon 3′ by hydrogen bonds between the hydroxy group and Asparagine 426 and Glutamate 430. Abstraction of the hydrogen from carbon 3′ permits the conjugation of that same lone pair of electrons with the two electrons in the carbon–oxygen bond of the 2′-hydroxy group, a conjugation that was prevented by the hydrogen on carbon 3′. As a result of the creation of this conjugation, the lone pair of electrons on the 3′-hydroxy group can push. The ribosyl group then undergoes a precedented, acid-catalyzed[510,511] elimination of water from carbon 2′. During this elimination, the sulfanyl group of Cysteine 218, as the required acid catalyst, hydronates the leaving oxygen (0.34 nm) while the 3′-hydroxy group, which is becoming a carbonyl oxygen, hydronates the sulfido group of Cysteine 218 (0.33 nm). The elimination produces an **oxallylic radical** with three electrons in two π molecular orbitals (**5–115**) and a sulfanyl group at Cysteine 218. In the highest occupied molecular orbital (drawn in Figure 5–13), the spin density is concentrated almost exclusively on carbon 2′ and the oxygen on carbon 3′. Carbon 2′ of the oxallylic radical (BDE = 400 kJ mol^{-1}) abstracts the hydrogen (BDE = 370 kJ mol^{-1}) from the sulfanyl group of Cysteine 218 to produce ketone **5–116**.* The resulting sulfenyl radical then adds to the sulfanyl group of Cysteine 443 to form the **disulfide radical anion**.[512,513] The α carbons of Cysteines 218 and 443 are 0.51 nm apart, on the shorter end but within the range of 0.45–0.7 nm for that distance in typical disulfides in proteins.[514] The carboxy group of Glutamate 430 then hydronates the carbonyl oxygen of ketone **5–116** while the electron in the disulfide radical anion (electron affinity = 9 kJ mol^{-1})[515] is transferred to the carbonyl group (electron affinity = 95 kJ mol^{-1})[516] at carbon 3′. The resulting α-hydroxyalkyl radical (**5–117**) at carbon 3′ (BDE = 380 kJ mol^{-1}),

*Cysteine 218 illustrates the unique properties of a sulfanyl group in such a reaction. The hydron that its thiolate removes from the 3′-hydroxy group is the hydrogen atom abstracted by carbon 2′ of the oxallylic radical. Thus a hydron on a sulfanyl group becomes a hydrogen atom.

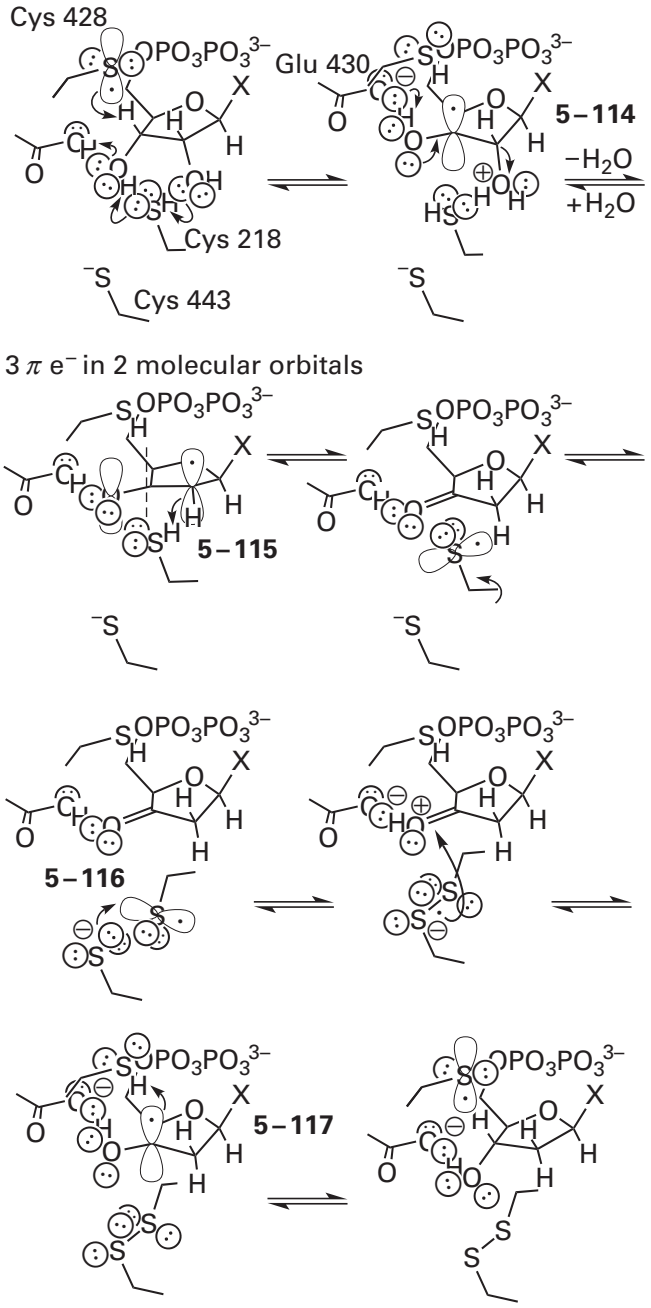

Figure 5–13: A mechanism for ribonucleoside-diphosphate reductase or ribonucleotide-triphosphate reductase involving radical intermediates. The mechanism is drawn as if it were occurring in the active site of ribonucleoside-diphosphate reductase from *S. cerevisiae*. A hydrogen is abstracted from the 3′-carbon of the ribosyl group by the sulfenyl radical of Cysteine 428 to produce the radical **5–114**, and the 2′-hydroxy group of the ribose is hydronated by a composite acid consisting of Cysteine 218, the 3′-hydroxy group of the ribose, and Glutamate 430 to initiate the production of the neutral oxallylic radical **5–115**. The highest occupied molecular orbital (HOMO) of oxallylic radical **5–115** is drawn. It is occupied by the unpaired electron. The complete π molecular orbital system of the oxallylic radical contains three electrons. Formation of this oxallylic radical proceeds by elimination of water and dehydronation of the 3′-hydroxy group so that two electrons can enter the π molecular orbital system of the oxallylic radical. The oxallylic radical abstracts hydrogen from the sulfanyl group of Cysteine 218 to form ketone **5–116**, and the resulting sulfenyl radical of Cysteine 218 forms a cystinyl radical anion with the sulfanylate anion of Cysteine 443. An electron is transferred from the cystinyl radical anion to carbon 3′ of ketone **5–116** to produce the radical at carbon 3′ of the ribose (**5–117**). This radical abstracts the hydrogen from the sulfanyl group of Cysteine 428 to regenerate the original radical at the active site and the 2′-deoxyribosyl group.

which differs from α-hydroxyalkyl radical **5–114** only by the hydrogen that has replaced the hydroxy group at carbon 2′, abstracts the hydrogen (BDE = 370 kJ mol^{-1}) from the sulfanyl group of Cysteine 428, the reverse of the first step in the mechanism, to complete reduction of the substrate. The resulting sulfenyl radical is then converted into a sulfanyl group or a sulfido group by the electron transfer that formed it in the first place. At the end of the reaction, ADP^{3-} has been reduced to deoxyADP^{3-}, and the two cysteines, Cysteines 218 and 443, have been oxidized to a cystine, and everything else is as it was.

This mechanism and the orientation of the catalytic groups in the active site are consistent with the retention of configuration for replacement of the hydroxy group by a tritium observed at carbon 2′.[517] There are also a number of other observations that support this mechanism.*

When Cysteine 225 in ribonucleotide diphosphate reductase from *E. coli* (homologous to Cysteine 218 in the enzyme from *S. cerevisiae*) is mutated to serine and the mutant is mixed with protein R2 and [3′-^{3}H]UDP^{3-}, the ribosyl of UDP^{3-} slowly decomposes, releasing its uracil, and tritium is released as ^3H_2O at the same rate as the tyrosyl radical in protein R2 is lost.[518] Presumably, the abstraction of the hydrogen from carbon 3′ by the sulfenyl radical of Cysteine 439 (homologous to Cysteine 428 in the enzyme from *S. cerevisiae*) and the electron transfer to Tyrosine 122 in protein R2 from *E. coli* from Cysteine 439 reaches equilibrium because the reaction cannot proceed further in the absence of Cysteine 225. As the oxallylic radical **5–115** slowly decomposes, the 4-oxidophenyl ion of Tyrosine 122 in protein R2 cannot be reoxidized to the tyrosyl radical, and the triton stalled on Cysteine 439 exchanges with water.

*While reading the following observations, you should be referring to your copy of the stereodrawing of Figure 5–12, as well as Figure 5–13.

When [3′-^{3}H]UDP^{3-} is used as a reactant in the reaction catalyzed by ribonucleoside-diphosphate reductase from *E. coli*, a **primary kinetic isotope effect** ($^Tk = 3$)[509] is observed, consistent with breaking of the bond between carbon 3′ and its hydrogen. While most of the tritium remains on carbon 3′ in the product [3′-^{3}H]-2′-deoxyuridine diphosphate, about 1% is lost to solvent,[519] a result consistent with a slow loss resulting from isotopic exchange at the sulfanyl group of Cysteine 439 (homologous to Cysteine 428 in the enzyme from *S. cerevisiae*). If the accepted mechanism is correct, the latter observation suggests that either the [^{3}H]sulfanyl group resulting from hydrogen abstraction from carbon 3′ is shielded by the active site from exchange or the lifetime of the [^{3}H]sulfanyl group is so short that very little exchange can occur or both of these possibilities combined.

2′-Chloro-2′-deoxycytidine diphosphate[520] and 2′-chloro-2′-deoxyuridine diphosphate[520,521] are converted by ribonucleoside-diphosphate reductase from *E. coli* to the respective ketones, 2′,3′-dideoxy-3′-oxocytidine diphosphate and 2′,3′-dideoxy-3′-oxouridine diphosphate

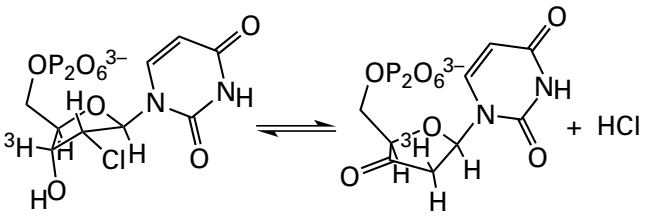

(5–144)

These ketones are the respective noncovalent intermediate ketones **5–116** in the proposed mechanism (Figure 5–13). If [3′-^{3}H]-2′-chloro-2′-deoxyuridine diphosphate is used as a reactant, the tritium is transferred[522] intramolecularly to carbon 2′. Both observations are consistent with **radical-assisted dehydrohalogenation***

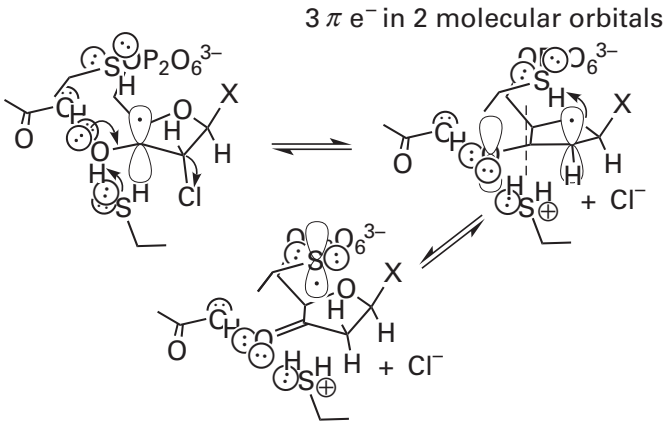

(5–145)

In this explanation for the observations, the same oxallylic radical **5–115** is formed as during the normal reaction (Figure 5–13), and there is no unequivocal explanation for why it must be quenched by abstracting a hydrogen from Cysteine 439 (homologous to Cysteine 428 from *S. cerevisiae*) to form ketone **5–116** rather than abstracting a hydrogen from Cysteine 225 (homologous to Cysteine 218 from *S. cerevisiae*) as usual and continuing on the normal path. For the dehydrohalogenation of these 2′-chloro-2′-deoxynucleotides to occur, the enzyme must be in its reduced, dithiol form even though the reaction is formally a dehydrohalogenation and not a reduction, so it is not that Cysteine 225 is sequestered in the disulfide with Cysteine 462 (homologous to Cysteine 443 from *S. cerevisiae*) and unreactive. The only difference between the normal reactants and the homologous chlorides is the leaving group. Unlike a hydroxy group, a chloro group does not require hydronation before it leaves, and it is also far more difficult to hydronate the chlorine atom in an alkyl chloride than it is to hydronate the hydroxy group in an alcohol.[523] If the active site is occluded so that hydrons cannot leave or enter over the lifetime of the intermediates, which would be consistent with the lack of tritium exchange when [3′-^{3}H]UDP^{3-} is used as a reactant, then the sulfanyl group ($pK_a = -7$ for RSH_2^+) on Cysteine 225 (homologous to Cysteine 218 from *S. cerevisiae*) would be sharing a hydron with the oxo group ($pK_a = -7$ for R_2COH^+) at carbon 3′ that was the 3′-hydroxy group. The sulfanyl group, however, would be unable to lose simultaneously the hydron it already had at the beginning of the reaction by hydronating the chloride ion, and this double hydronation of sulfur, producing the conjugate acid of the sulfanyl group, would prevent it from donating a hydrogen atom to carbon 2′ (Figure 5–13). In this case, Cysteine 439 (homologous to Cysteine 428 from *S. cerevisiae*) would step

*From here on, when a radical intermediate is drawn in orbital notation, only the highest occupied molecular orbital (HOMO) of that intermediate will be represented, with the appropriate nodes, to indicate the locations of the unpaired spin. Because spin densities in the highest occupied molecular orbital of the respective intermediates are almost always unknown, a single dot, representing an unpaired electron will be placed in one of the lobes of the orbital either over a carbon, which is the atom that probably has the highest spin density (see **5–112** and **5–113**), or over a heteroatom, if spin density over that heteroatom is the focus of the reaction.

in to do so. If this is the case, the dehydrohalogenation of the chlorides catalyzed by the enzyme is consistent with the sulfanyl group of Cysteine 225 (homologous to Cysteine 218 from *S. cerevisiae*) being required to remove the hydron from the 3′-hydroxy group as well as adding a hydron to the 2′-hydroxy group during the elimination that produces the oxallylic radical, which its location in the occupied active site suggests that it must do (Figure 5–12).

The same dehydrohalogenation as that catalyzed by ribonucleoside-diphosphate reductase from *E. coli* (Equation 5–144) is also catalyzed by adenosylcobalamin-dependent ribonucleoside-triphosphate reductase from *L. leichmannii*.[524] This additional, unusual observation demonstrates that the fundamental mechanisms of the reactions catalyzed by ribonucleoside-diphosphate reductases and by ribonucleoside-triphosphate reductases are the same.

A result similar to the dehydrohalogenation is observed when **2′-*C*-methyladenosine diphosphate** is used as a reactant with adenosylcobalamin-dependent ribonucleoside-diphosphate reductase from *Corynebacterium nephridii*. In this case, the methyl group on carbon 2′ seems to hinder the abstraction of a hydrogen from carbon 2′ by the sulfanyl group on the *Si* face of the oxallylic radical (the one homologous to Cysteine 218 in the enzyme from *S. cerevisiae*). As a result, about 35% of the time, carbon 2′ in the oxallylic radical abstracts the hydrogen from the cysteine (the one homologous to Cysteine 428 in the enzyme from *S. cerevisiae*) on the *Re* face rather than the *Si* face. This steric hindrance aborts the reaction and leads to production of the 2′-*C*-methyl version of ketone **5–116**.[525]

When proteins R1 and R2 from *E. coli* are mixed with 2′-azido-2′-deoxyuridine 5′-phosphate, the tyrosyl radical on protein R2 is reduced to the tyrosinate, and **sulfenamido radical 5-118**

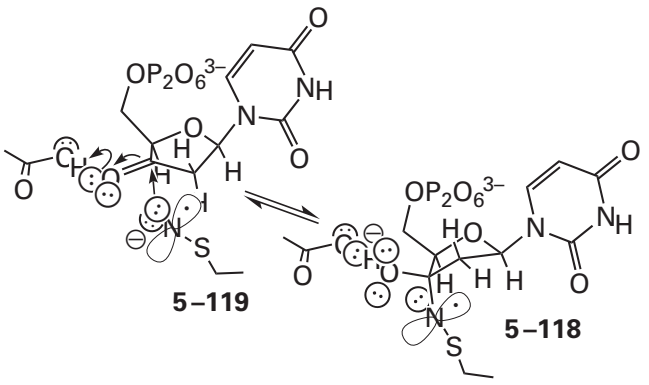

(5–146)

is formed at the active site.[526-528] It has been proposed that the nucleophilic sulfenamido radical anion **5–119** of Cysteine 225 (homologous to Cysteine 218 from *S. cerevisiae*) adds to ketone **5-116** formed by the normal mechanism (Figure 5–13) to form the identified product. The sulfenamido radical anion **5–119** would be formed from the azide anion that leaves rather than water from carbon 2′ as the oxallylic radical **5–115** is formed.

When Glutamate 441 in protein R1 of ribonucleoside-diphosphate reductase from *E. coli* (homologous to Glutamate 430 in the enzyme from *S. cerevisiae*) is mutated to glutamine and the mutant is mixed with protein R2 and cytidine 5′-diphosphate, a portion of the tyrosyl radical is lost and a new radical appears with the **electron paramagnetic resonance spectrum of a disulfide radical anion**.[529] Because the carboxy group of Glutamate 441 is unavailable to hydronate the carbonyl oxygen of ketone **5–116** (Figure 5–13), carbon 3′ is not electropositive enough to accept the electron from the disulfide radical anion, and the reaction is arrested at this step.

Finally, the disulfide between Cysteines 225 and 462 in protein R1 from *E. coli* (homologous to Cysteines 218 and 443 in the enzyme from *S. cerevisiae*) has been shown to be **kinetically competent** because it forms at a rate faster than the normal turnover of the enzyme when fully reduced R1 protein, R2 protein, and cytidine diphosphate are mixed in the absence of thioredoxin.[500]

This disulfide in the active site of ribonucleoside-diphosphate reductase from *E. coli*, at the end of the reduction, is reduced by thiol–disulfide exchange (see Equation 5–57) with Cysteines 754 and 759 in protein R1 (homologous to Cysteines 731 and 736 in the enzyme from *S. cerevisiae*). The homologous cysteines, Cysteines 731 and 736, in the adenosylcobalamin-dependent ribonucleoside-triphosphate reductase of *L. leichmannii* are also responsible for reducing the homologous disulfide in its active site.[518,530-532] The resulting, respective cystine of these two distal cysteines is reduced by thiol–disulfide exchange with the two cysteines in reduced thioredoxin.[533]

Model studies of these reductions of ribonucleotides are also consistent with the proposed mechanism (Figure 5–13).[534,535] For example, when a radical is generated at carbon 3′ of 2′-acetyl-6-(*N*-benzoyl)adenosine by replacing its 3′-hydrogen synthetically with a phenylselenol ester and the phenylselenol ester is submitted to photolysis, the homologue of oxallylic radical **5–115** is formed, but

this conversion occurs only when a base, playing the role of Cysteine 218 (Figure 5–12), is present. This oxallylic radical subsequently participates in hydrogen abstraction to form ketone **5–116**.[536] The analogous radical at carbon 3 of 3-methoxytetrahydrofuran can be produced by intramolecular abstraction of hydrogen 3 by a sulfenyl radical.[537]

Although several ribonucleoside-triphosphate reductases that initiate their catalytic reactions with a stable glycyl radical (Equation 5–143) can use thioredoxin[453] or other reductants[538] as the ultimate source of reducing equivalents, the anaerobic ribonucleoside-triphosphate reductases (formate), which also use a glycyl radical to initiate their reactions, use **formate**

$$HCOOH \rightleftharpoons 2\,e^- + 2\,H^+ + CO_2 \qquad (5\text{–}147)$$

as the ultimate reductant.[539] Anaerobic ribonucleoside-triphosphate reductases (formate) lack the peripheral cysteines to oxidize the thioredoxin that serves as the reductant in the other ribonucleotide reductases, and they also may lack a sulfanyl group that plays the role of Cysteine 443 in the active site of protein R1 from *S. cerevisiae* (Figure 5–12). In the crystallographic molecular model of the unoccupied active site of anaerobic ribonucleoside-triphosphate reductase (formate) from Enterobacteria phage T4, there is a cysteine near the cysteine that becomes the sulfenyl radical, but its sulfur is 0.94 nm away from the sulfur of the sulfenyl radical,[486] which seems too far away to form a cystine. If this is the case, the formate may enter the reaction at an earlier stage than formation of an unavailable disulfide radical anion between two cysteines.[540] In the absence of formate and the presence of CTP^{4-}, however, an absorbance in an electron paramagnetic resonance spectrum of the closely related (68% identity; 2 gap per cent) anaerobic ribonucleoside-triphosphate reductase (formate) from *E. coli* is observed that has been identified as a thiosulfuranyl radical, which in this instance would be a **disulfide radical between the sulfur of a cysteine and the sulfur of a methionine**. In the enzyme from *E. coli*, a methionine does replace the nearby cysteine in the active site of the enzyme from Enterobacteria phage T4, so observation of the thiosulfuranyl radical suggests that a disulfide radical anion, either between the two cysteines or between the cysteine and the methionine, is also an intermediate in the reaction catalyzed by the anaerobic ribonucleoside-triphosphate reductases (formate). Formation of this radical in the active site of the enzyme from *E. coli* has been shown to be kinetically competent to be an intermediate in the reaction.[541] If it is an intermediate, the formate may not become involved at an earlier stage in the reaction.

The bond dissociation energy for the hydrogen of formic acid is 404 kJ mol^{-1}, which seems too large for its abstraction by a sulfenyl radical (BDE = 370 kJ mol^{-1}) but perhaps not too large for its abstraction by a disulfide radical anion or thiosulfuranyl radical, which would regenerate the two cysteines or a cysteine and a methionine. The **carbon dioxide radical anion** that results from abstraction of the hydrogen from formate is a strong one-electron reductant (electron affinity = -60 kJ mol^{-1}),[542] so it could as easily reduce ketone **5–116** to α-hydroxyalkyl radical **5–117**.[540] If a disulfide radical anion is not an intermediate in the reaction, carbon 2′ of oxallylic radical **5–115** (BDE = 400 kJ mol^{-1}) could abstract the hydrogen from formate, and then the carbon dioxide radical anion could reduce ketone **5–116** to α-hydroxyalkyl radical **5–117**. In this case, the only role for the cysteine in these active sites that is homologous to Cysteine 218 in the active site of the enzyme from *S. cerevisiae* would be as a catalytic acid–base.

In the few other instances in which a tyrosyl or glycyl radical is an intermediate in an enzymatic mechanism, the radical is usually transient rather than permanent, and it usually abstracts a hydrogen from the substrate directly. For example, in the active site of prostaglandin-endoperoxide synthase[543]

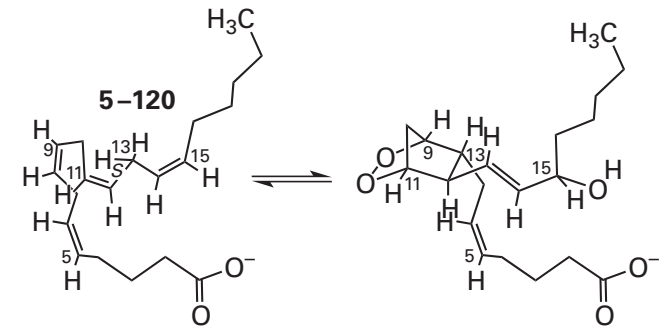

(5–148)

a tyrosine is oxidized to a tyrosyl radical during each turnover of the enzyme. This tyrosyl radical has been identified in ovine prostaglandin-endoperoxide synthase by its characteristic electron paramagnetic resonance spectrum.[544,545] It is a transient intermediate in the enzymatic reaction, and it is followed in the sequence of steps by a **pentadienyl radical**, also

identified by its electron paramagnetic resonance spectrum, that results from abstraction of the *pro-S* hydrogen from carbon 13 (Equation 5–148) of (5*Z*,8*Z*,11*Z*,14*Z*)-icosa-5,8,11,14-tetraenoate (arachidonate, **5–120**).[546] Carbon 13 sits between two carbon–carbon double bonds. In crystallographic molecular models of the complexes of the ovine enzyme[547] or the murine enzyme[543,548] with arachidonate, the 4-hydroxyphenyl group of Tyrosine 385, which becomes the transient radical,[549] is immediately adjacent (0.30 nm) to carbon 13 of arachidonate, well within van der Waals contact (0.44 nm) and in the proper orientation to remove the *pro-S* hydrogen. Consequently, it must be the case that the tyrosyl radical (BDE = 380 kJ mol^{-1}) abstracts a hydrogen directly from carbon 13 (BDE = 320 kJ mol^{-1}) to produce the pentadienyl radical encompassing carbons 11–15 of arachidonate.[437]

The oxidant that produces the tyrosyl radical in prostaglandin-endoperoxide synthase is a ferric heme. This heme is converted first to an oxoiron(IV) porphyrin$^{\bullet+}$ that has an electron paramagnetic resonance spectrum closely resembling that of the oxoiron(IV) porphyrin$^{\bullet+}$ of peroxidase from *Armoracia rusticana*.[550] The porphyrin$^{\bullet+}$ immediately removes an electron from Tyrosine 385 to produce a **hydroxyiron(IV) tyrosyl$^{\bullet+}$** that has an electron paramagnetic resonance spectrum closely resembling that of the hydroxyiron(IV) tryptophanyl$^{\bullet+}$ from cytochrome-*c* peroxidase. One edge of the heme in the murine enzyme is cradled in the segment of polypeptide that Tyrosine 385 and Histidine 386 comprise. One of the pyrroles in this edge of the heme is in van der Waals contact with the imidazolyl group of Histidine 386 (0.37 nm), and one of its vinyl groups is in van der Waals contact with the 4-hydroxyphenyl group of Tyrosine 385 (0.37 nm).[543] These two contacts provide two possible paths for the electron between the tyrosine and the porphyrin$^{\bullet+}$.

In the mechanism of galactose oxidase, a transient tyrosyl radical abstracts a hydrogen directly from the carbon of a primary alcohol (BDE = 390 kJ mol^{-1}) in a substrate [551,552] to form a radical at that location that is stabilized captodatively. In the decarboxylation catalyzed by hydrogen peroxide-dependent heme synthase from *G. stearothermophilus*, a tyrosyl radical, formed by electron transfer to the oxoiron(IV) porphyrin$^{\bullet+}$ of the reactant Fe-coproporphyrin III, abstracts a hydrogen from carbon 1 on a 2-carboxyethyl group on the porphyrin to produce what should be a stable radical because it is **conjugated to the oxoiron(IV)** in the coproheme.[553] The electron in the radical is immediately withdrawn into oxoiron(IV), leaving a carbenium ion that becomes a carbon–carbon double bond by decarboxylation at the adjacent former carbon 2 of the 2-carboxyethyl group on Fe-coproporphyrin III.

There is a group of enzymes,[554-557] all distantly related to anaerobic ribonucleoside-triphosphate reductase (formate) and consequently to each other,[565-567] in each of which a **stable glycyl radical** is formed by a [4Fe–4S] iron–sulfur cluster and *S*-adenosyl-L-methionine.[558-564] In each of these enzymes, other than anaerobic ribonucleoside-triphosphate reductase of Enterobacteria phage T4, a sulfenyl radical produced directly by the glycyl radical is the first intermediate in the reaction. For example, in the active site of formate *C*-acetyltransferase

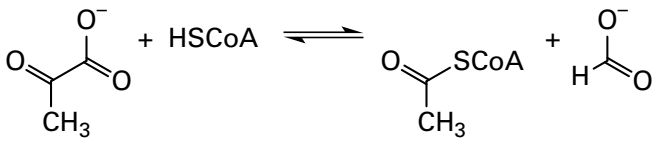

(5–149)

from *E. coli*, the sulfanyl group of Cysteine 419 (the structural homologue of Cysteine 290 in anaerobic ribonucleoside-triphosphate reductase of Enterobacteria phage T4)[566] is only 0.31 nm from the amido oxygen of Glycine 734,[568] the glycine on which the stable radical (**5–112**) is located.[556] This amido oxygen is in the proper orientation[566] to abstract directly the hydrogen atom from the sulfanyl group

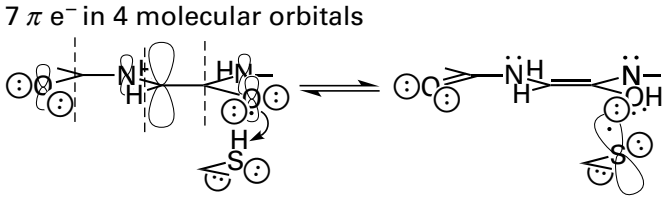

(5–150)

to form the 1,2-diaminoenol and the sulfenyl radical. The radical at Cysteine 419 is then transferred to Cysteine 418, probably by hydrogen abstraction. An absorption from one or the other of these cysteinyl radicals can be observed in an electron paramagnetic resonance spectrum of the enzyme inactivated by 3-sulfanylpyruvate.[569,570] From a crystallographic molecular model of the active site of the enzyme occupied by oxamate,[566] it has been proposed that the radical of Cysteine 418 adds nucleophilically to the carbonyl of pyruvate (0.33 nm away) to create the **radical of a thiohemiacetal** that decomposes to

S-acetylcysteine and a formate radical. The formate radical then abstracts the hydrogen from the sulfanyl group of Cysteine 418. Transfer of the acetyl group on Cysteine 418 to coenzyme A completes the reaction.

In the reaction catalyzed by benzylsuccinate synthase from *Thauera aromatica*, however, the cysteinyl radical itself, formed by abstraction of the hydrogen by the stable glycyl radical from Cysteine 493, abstracts a hydrogen from the methyl group in the reactant toluene to form the delocalized **phenylmethylenyl radical**, which has a benzylic π molecular orbital system. This intermediate radical participates in a radical addition at its methylene group to the carbon–carbon double bond of fumarate, the other reactant. The resulting benzylsuccinyl radical then abstracts the hydrogen from the sulfanyl group of Cysteine 493 to complete the reaction.[555] In a crystallographic molecular model of the active site occupied by toluene and fumarate, the methyl carbon of toluene is 0.39 nm from the sulfanyl group, and the carbon of fumarate to which the phenylmethyl radical adds is 0.34 nm from the methyl carbon of toluene,[571] both distances at or within the respective van der Waals contact.

In a crystallographic molecular model of the active site of 4-hydroxyphenylacetate decarboxylase from *Clostridium scatologenes* occupied by the reactant (4-hydroxyphenyl)acetate, the sulfanyl group of Cysteine 503, the cysteine from which a hydrogen is abstracted by the stable glycyl radical, forms a hydrogen bond with the carboxy group of (4-hydroxyphenyl)acetate.[572] A sulfenyl radical at Cysteine 503 (BDE = 370 kJ mol^{-1}), however, should be unable to abstract a hydrogen from a carboxy group (BDE = 470 kJ mol^{-1}). It has been proposed instead[572,573] that the cysteinyl radical removes an electron from the carboxylato group of (4-hydroxyphenyl)acetate, rather than abstracting a hydrogen. This abstraction forms the **acyloxy radical**. Acyloxy radicals are unstable species that **immediately decarboxylate,** regardless of the carbon radical that results. In this instance, however, the decarboxylation leaves behind a stable, delocalized (4-hydroxyphenyl)methyl radical (BDE = 375 kJ mol^{-1}). The (4-hydroxyphenyl)methyl radical then abstracts the hydrogen from the sulfanyl group of Cysteine 503 (BDE = 370 kJ mol^{-1}), the sulfido group of which was hydronated by Glutamate 505, to regenerate the cysteinyl radical and in the process form 4-methylphenol, the other product of the enzymatic reaction.

A significant number[574] of enzymes use 5′-deoxy-5′-adenosyl radicals directly as intermediates. The 5′-deoxy-5′-adenosyl radicals in the active sites of this superfamily of enzymes are produced by homolytic dissociation of complex **5–111***

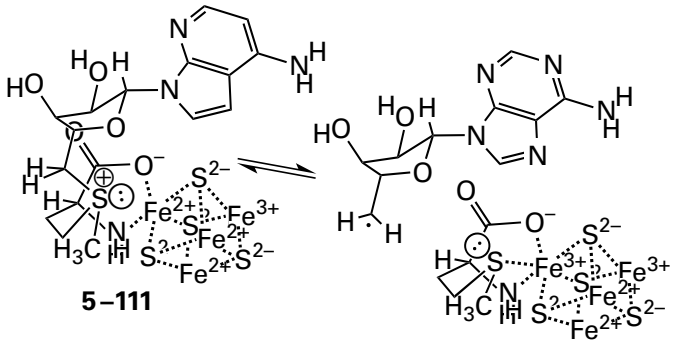

(5–138)

which is formed from *S*-adenosyl-L-methionine and a [4Fe–4S] iron–sulfur cluster, rather than the homolytic dissociation of the carbon–cobalt bond in a prosthetic adenosylcobalamin. In almost all[575,576] enzymatic reactions in which a 5′-deoxy-5′-adenosyl radical is produced by the homolytic dissociation of complex **5–111**, ***S*-adenosyl-L-methionine is a reactant, and L-methionine and 5′-deoxyadenosine are products**, as in the oxidation catalyzed by 2-deoxy-*scyllo*-inosamine dehydrogenase (AdoMet-dependent)[577]

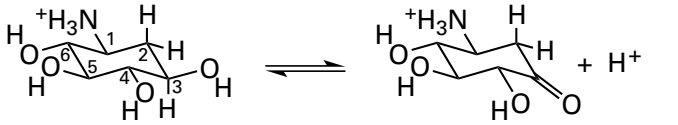

(5–151)

In these enzymatic reactions, the first step is **association of *S*-adenosyl-L-methionine with the prosthetic, catalytic [4Fe–4S] iron–sulfur cluster** in the active site.[578] During this association, both the α-amino group and the α-carboxy group of *S*-adenosyl-L-methionine become ligands to the one iron ion in the [4Fe–4S] iron–sulfur cluster that is not coordinated by a cysteine from the protein and that consequently has open sites for coordination. The conclusion that these two functional groups become ligands to this iron ion was reached by electron–nuclear double resonance spectroscopy[579]

*The enzymes that use a 5′-deoxyadenosyl radical produced by the homolytic dissociation of complex **5–111** are often referred to as *S*-adenosyl-L-methionine-dependent radical enzymes or radical AdoMet enzymes.

and crystallography.[447,561,580-582] In this initial complex, exemplified by the initial complex in the active site of lysine 2,3-aminomutase from *Clostridium subterminale*[447]

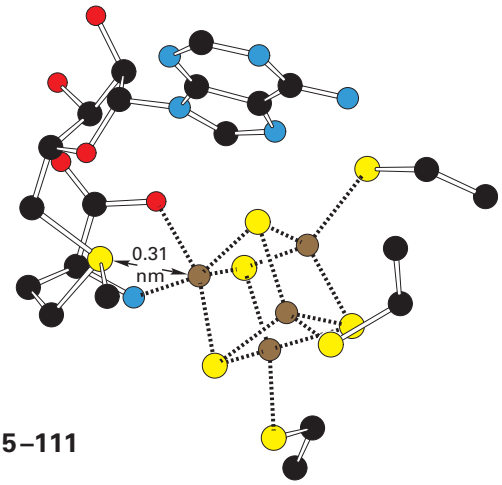

5–111

the sulfur of *S*-adenosyl-L-methionine ends up only 0.29–0.35 nm from the same iron ion to which the α-amino and α-carboxy groups are ligands, and spectroscopic measurements identify the sulfur as a ligand to that iron ion following homolytic dissociation of the sulfur–carbon bond (Equation 5–138; **5–110**)[583] During each turnover of one of these enzymes, the resulting L-methionine dissociates from complex **5–110** and leaves the active site as a product, as does 5′-deoxyadenosine, while the catalytic [4Fe–4S] iron–sulfur cluster, which is a prosthetic group covalently bound through the three cysteines, as is the case for all [4Fe–4S] iron–sulfur clusters, remains.

Because it must provide an electron to the sulfur that dissociates from the deoxyadenosyl group to give the sulfide as the product, the **catalytic [4Fe–4S] iron–sulfur cluster must be in the reduced state**, $[(Fe^{2+})_3(Fe^{3+})(^{2-}S)_4(^{-}S-)_3]^{2-}$, for the reductive homolytic dissociation of complex **5–111** to occur.[584] In solution under cyclic voltammetry, *S*-adenosyl-L-methionine displays an irreversible biochemical reduction potential of –1.4 V during successive sweeps of electrode potential between –0.6 and –1.7 V. When the voltage of the electrode is maintained at –1.5 V, 5′-deoxyadenosine (the product of abstraction of a hydrogen from a solute by a 5′-deoxy-5′-adenosyl radical) and 8,5′-cycloadenosine (the product of the intramolecular cyclization of a 5′-deoxy-5′-adenosyl radical) accumulate at a linear rate in the solution.[585] The accumulation of these products occurs only if the electrode is poised at a voltage less than –1.4 V, and the rate of accumulation increases linearly as the voltage of the poise is lowered to –2.8 V. These observations are consistent with a reductive homolytic dissociation of *S*-adenosyl-L-methionine producing 5′-deoxy-5′-adenosyl radical, as normally occurs in the active sites of the enzymes of this family.

Standard biochemical reduction potentials, however, of the catalytic [4Fe–4S] iron–sulfur clusters in the enzymes that use complex **5–111** to produce a 5′-deoxy-5′-adenosyl radical are all in the range[585] from –0.45 to –0.55 V. Formation of complex **5–111**, however, may shift the required reduction potential significantly. Instantaneous abstraction of the immediately adjacent hydrogen[438] on the reactant bound in the active site could also shift a significantly unfavorable equilibrium for dissociation of complex **5–111** to form the 5′-deoxy-5′-adenosyl radical at these greater reduction potentials into the favorable range by mass action.

The intermediate 5′-deoxy-5′-adenosyl radical assumed to exist in these enzymatic reactions has been produced in the active site of [formate-*C*-acetyltransferase]-activating enzyme from *E. coli* at 12 K by photolytically driven electron transfer from the catalytic [4Fe–4S] iron–sulfur cluster to force dissociation of the carbon–sulfur bond. The resulting 5′-deoxy-5′-adenosyl radical has been characterized by electron paramagnetic resonance and electron–nuclear double resonance spectroscopy using isotopic substitution in its ribosyl group. The radical is in a *p* orbital on carbon 5′ and is rotated out of the plane of the ribose ring by 40° to take advantage of the captodative effect provided by an unconjugated lone pair of electrons on the oxygen of the ribosyl ring.

In all other instances in which it is an intermediate, however, the **existence of intermediate 5′-deoxy-5′-adenosyl radical has only been inferred** from the fact that the product of these enzymatic reactions is 5′-deoxyadenosine, the fact that the deuterium on the reactant that does not remain in the product ends up on the methyl group of 5′-deoxyadenosine, the fact that the hydrogen removed from the reactant is usually not acidic, the fact that the bond dissociation energies of carbon–sulfur bonds are fairly small, and the fact that a [4Fe–4S] iron–sulfur cluster usually provides electrons one at a time, which is what is needed to further weaken the carbon–sulfur bond in *S*-adenosyl-L-methionine.

The sulfur of the sulfonium in *S*-adenosyl-L-methionine in complex **5–111** has two secondary aliphatic carbons and a primary aliphatic carbon

attached to it. In the enzymes that use a 5′-deoxy-5′-adenosyl radical as an intermediate, the bond between the adenosyl group and the sulfur dissociates homolytically, but the **other two carbon–sulfur bonds are also susceptible to homolytic dissociation**. In the active site of 2-(3-amino-3-carboxypropyl)histidine synthase from *P. horikoshii*, in which the ligation of the iron ion in the catalytic [4Fe–4S] iron–sulfur cluster[586] in complex **5–111** is almost identical to that in the active site of lysine 2,3-aminomutase from *C. subterminale*, the carbon–sulfur bond to the **(*S*)-3-amino-3-carboxypropyl group** of *S*-adenosyl-L-methionine (8 o'clock position of the sulfur atom in **5–111**), rather than the carbon–sulfur bond to the 5′-deoxyadenosyl group (10 o'clock position of the sulfur atom in **5–111**), dissociates homolytically to produce the (*S*)-3-amino-3-carboxy-1-propyl radical, which then adds to carbon 2 of the imidazolyl group of a histidine in translation elongation factor 2. An absorption in the electron paramagnetic resonance spectrum of the enzyme when it is mixed with *S*-adenosyl-L-methionine has been assigned to this radical on the basis of changes in the spectrum upon isotopic substitutions.[587]

Complex **5–111** can also dissociate homolytically at the sulfur–carbon bond to the **methyl group**, even though a primary methyl radical is significantly less stable. The methyl radical has been observed in the active site of (FeFe) hydrogenase maturation factor HydG, the enzyme responsible for producing, from L-tyrosine, the carbon monoxide and cyanide found in the [FeFe] hydrogenase of *C. acetobutylicum*. It was produced at 12 K by photolytically driven electron transfer from the catalytic [4Fe–4S] iron–sulfur cluster to force dissociation of the carbon–sulfur bond.[588] The methyl radical was identified by its electron paramagnetic resonance spectrum, which was consistent with the conclusion that it was rapidly rotating within the active site, as one might expect. When the decarboxylated analogue of *S*-adenosyl-L-methionine, *S*-adenosyl-*S*-methyl-3-sulfanyl-1-propylamine, is used as a reactant for 2-(3-amino-3-carboxypropyl)histidine synthase from *P. horikoshii* rather than *S*-adenosyl-L-methionine, the carbon–sulfur bond to the *S*-methyl group dissociates homolytically, and that methyl group ends up on a sulfide adjacent to the catalytic iron ion in the [4Fe–4S] iron–sulfur cluster.[586] In the active site of the carbide synthase NifB from *Methanothrix thermoacetophila*, the methyl group that eventually becomes the mononuclear carbide in the center of the [Mo–7Fe–9S–C] cluster in dinitrogenase during its normal reaction is the methyl group of *S*-adenosyl-L-methionine in complex **5–111**. Rather than to a sulfide in the catalytic [4Fe–4S] iron–sulfur cluster, this methyl group is transferred to a sulfide in another [4Fe–4S] iron–sulfur cluster, which is one of the two [4Fe–4S] iron–sulfur clusters that are reactants for the enzyme and that eventually become the [Mo–7Fe–9S–C] cluster.[589]

In most reactions in which a 5′-deoxy-5′-adenosyl radical is produced by homolytic dissociation of complex **5–111**, **the 5′-deoxy-5′-adenosyl radical abstracts a hydrogen** directly from a reactant. For example, in the **dehydrogenation** catalyzed by 2-deoxy-*scyllo*-inosamine dehydrogenase (AdoMet-dependent), the 5′-deoxy-5′-adenosyl radical produced by homolytic dissociation of complex **5–111** abstracts the hydrogen on carbon 3 in the reactant 2-deoxy-*scyllo*-inosamine[577]

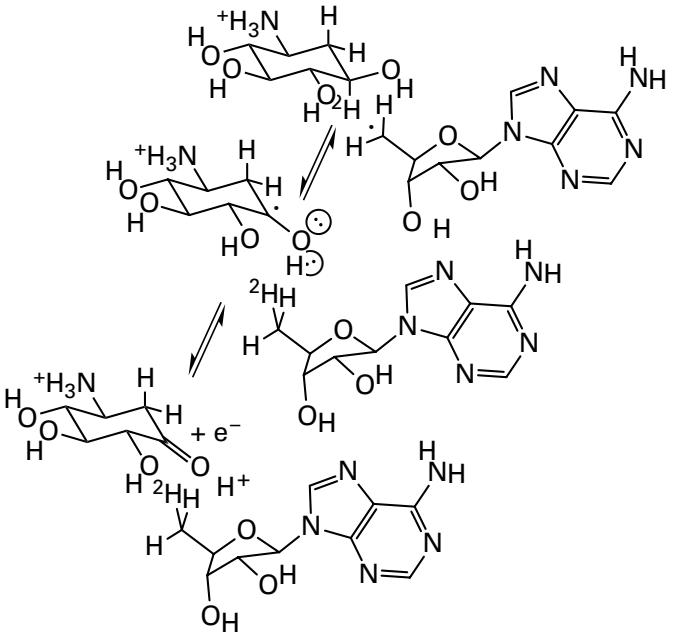

(5–152)

The intermediate radical of 2-deoxy-*scyllo*-inosamine is then **oxidized by the transfer of one electron** to give the ketone, 2,3-dideoxy-3-oxo-*scyllo*-inosamine, which is the product of the reaction. As was observed in this instance,[577] in most cases, the fact that the 5′-deoxy-5′-adenosyl radical has abstracted a hydrogen from one reactant for an enzyme in this superfamily and the identity of the hydrogen abstracted is established by synthetically or biosynthetically deuterating that hydrogen and showing that the deuterium ends up on the 5′-deoxyadenosine that is the product of the reaction.[590-599] Because the deuterium ends up on a methyl group in 5′-deoxyadenosine, it is not susceptible to exchange.

The radical produced by **abstracting a hydrogen adjacent to any hydroxy group**, as occurs in the reaction of ribonucleotide reductase or 2-deoxy-*scyllo*-inosamine dehydrogenase (AdoMet-dependent), is 30 kJ mol^{-1} more stable than the one produced by abstracting a hydrogen from the analogue in which the hydroxy group is replaced by a hydrogen.[440] This stability arises from a **captodative effect**.[600] In both ribonucleotide reductase and 2-deoxy-*scyllo*-inosamine dehydrogenase (AdoMet-dependent), the captodative effect that stabilizes the radical results from electron exchange between the unpaired electron and electrons in a lone pair on a hydroxy group. For this captodative effect to occur, the lone pair must be parallel to the π molecular orbital system of the radical, as it is in the active site of ribonucleotide reductase (Figure 5–12). The radical produced by abstracting a hydrogen adjacent to an amino group is 40 kJ mol^{-1} more stable than the one produced by abstracting a hydrogen from the analogue in which the amino group is replaced by a hydrogen, and the stabilization provided by a sulfanyl group is of the same order of magnitude.

In enzymatic dehydrogenations analogous to that catalyzed by 2-deoxy-*scyllo*-inosamine dehydrogenase (AdoMet-dependent), a 5′-deoxy-5′-adenosyl radical, produced from the adenosyl group by homolytic dissociation of complex **5–111**, abstracts a hydrogen from a carbon bearing a primary hydroxy group,[601] a secondary amino group,[602] or a primary sulfanyl group,[603] each of which can stabilize the resulting radical captodatively. When the reactant is a secondary amine or primary thiol, the product resulting from subsequent removal of the unpaired electron is an imine or thioaldehyde, usually hydrolyzed to a ketone or aldehyde, respectively, to complete the oxidation. In these instances the products are the same as when the hydrogen is abstracted next to a hydroxy group.

Mycofactocin radical SAM maturase from *Mycolicibacterium smegmatis*.[604,605] uses a 5′-deoxy-5′-adenosyl radical produced by homolytic dissociation of complex **5–111** to abstract a hydrogen from the β-carbon of a tyrosine at the carboxyterminus of a short peptide (31aa). In this instance, the unpaired electron in the intermediate radical (**5–121**) is delocalized in a **benzylic π molecular orbital system**

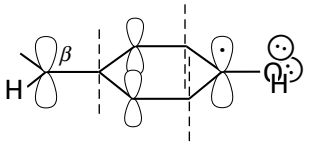

5–122

over its 4-hydroxyphenyl group and stabilized further by a captodative effect of a lone pair of electrons on the 4-hydroxy group.

There is a corollary to the captodative effect in situations in which there is an extended π molecular orbital system, as in the case of mycofactocin radical SAM maturase. When an unpaired electron is delocalized in such a way that there is a **lobe in the highest occupied molecular orbital** of the π molecular orbital system, as identified by resonance structures, on a carbon **next to a heteroatom** with a lone pair of electrons that can exchange with that unpaired electron, the spin density at that carbon will be increased by the interaction, as indicated by placing the unpaired electron at that carbon. This electron exchange increases the stability of the delocalized radical and lowers its potential to abstract a hydrogen from its surroundings, a fact that would be advantagous in a crowded active site. When, however, there is a node in the highest occupied molecular orbital next to a heteroatom, there is no possibility of electron exchange with the unpaired electron.

In the tyrosyl radical

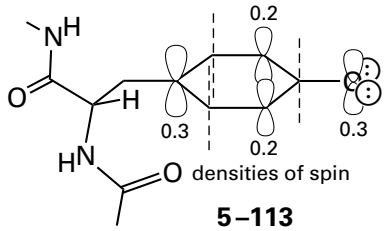

5–113

there is a different type of stabilization. The π molecular orbital system in this radical is also benzylic, and there is a node on the carbon adjacent to the exocyclic oxygen, but there is a lobe on oxygen in the highest occupied molecular orbital system because a hydrogen has been formally abstracted from this oxygen. The increase in spin density in this lobe is not due to the lone pairs of electrons on the oxygen because they are orthogonal to the π molecular orbital system; it is due to the fact that the oxygen, as is the case with a nitrogen, is more electronegative than carbon. The **electronegativity of oxygen increases the spin density** on oxygen.

As has already been discussed, the significant reactivity of the primary radical on carbon 5′ of the 5′-deoxy-5′-adenosyl radical presents a challenge. The active site in an enzyme in the superfamily guards against unfortunate, **unintentional abstractions of hydrogens** in the vicinity that could result from such a reactive primary radical in at least two ways.

First, the 5′-deoxy-5′-adenosyl radical is usually **generated immediately adjacent to the hydrogen that is to be abstracted**. When *S*-3′,4′-anhydroadenosyl-L-methionine is used as a reactant for lysine 2,3-aminomutase from *C. subterminale*, the complex between this analogue of *S*-adenosyl-L-methionine and the catalytic [4Fe–4S] iron–sulfur cluster dissociates in the active site to produce an **allylic analogue** of the 5′-deoxy-5′-adenosyl radical

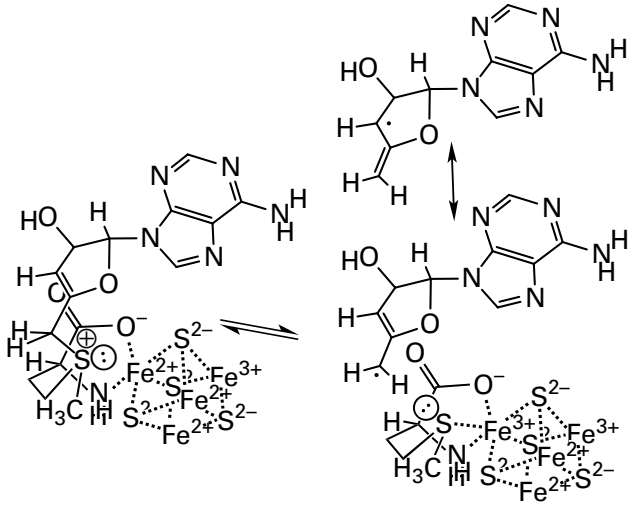

(5–153)

in which the unpaired electron is delocalized over carbons 3′, 4′, and 5′. This allylic 5′-deoxy-3′,4′-anhydroadenosyl radical is much less reactive (BDE = 370 kJ mol^{-1}) than the primary radical in the 5′-deoxy-5′-adenosyl radical and is unable to abstract a hydrogen efficiently from carbon 3 of L-lysine, the reactant in this enzymatic reaction, when it is formed from *S*-3′,4′-anhydroadenosyl-L-methionine. As a result, the allylic radical accumulates in the active site when the enzyme is in a reaction mixture for the enzymatic reaction, and its absorption in an electron paramagnetic resonance spectrum can be observed and definitively identified.[606]

Electron–nuclear double resonance spectra of L-lysines in which various atoms have been isotopically substituted provide estimates of the distances between a radical on carbon 5′ and both carbons 2 and 3 of L-lysine within the complex between the active site of lysine 2,3-aminomutase from *C. subterminale* and a 5′-deoxy-3′,4′-anhydroadenosyl radical and L-lysine.[438] The measured distance between carbon 5′ of the allylic radical and the hydrogen on carbon 3 of the L-lysines in the respective complexes, the hydrogen that ends up on the product 5′-deoxyadenosine, is 0.2 nm, well within van der Waals contact (0.29 nm). The measured distance between carbon 5′ of the allylic radical and carbon 2 of L-lysine in the complex, the carbon to which the hydrogen is transferred, is 0.3 nm, also within van der Waals contact (0.40 nm). From these measurements, it could be concluded that in the case of the active site of lysine 2,3-aminomutase—and presumably in many, if not most, of the other active sites of enzymes that share this mechanism—the 5′-deoxy-5′-adenosyl radical is generated during turnover of the enzyme at a location so close to the hydrogen it is supposed to abstract that there is no opportunity for it to abstract a hydrogen from any other location in the active site, which it could easily do. This intimacy guarantees the proper outcome for the enzymatic reaction.

Second, if the reactant is not present in the active site of the enzyme when the 5′-deoxy-5′-adenosyl radical is generated, it can add to the catalytic iron ion in the catalytic [4Fe–4S] iron–sulfur cluster to produce a organometallic product with an iron–carbon bond between this iron ion and carbon 5′. This adduct has been observed in electron–nuclear double resonance spectra of intermediates in several of the enzymes in this family.[607] This organometallic complex is analogous to an adenosylcobalamin. It is a way to store the 5′-deoxy-5′-adenosyl radical safely while retaining its reactivity. [4Fe–4S] Iron–sulfur clusters in which one of the iron ions is alkylated with a benzyl group or an *n*-octyl group have been synthesized.[608] The iron–carbon bond in each synthetic complex dissociates readily to give the benzyl radical or the *n*-octyl radical, results that demonstrate the ability of such a complex to preserve the reactivity of the radical. It is also possible that this adenosyliron could be an obligate intermediate in the creation of the 5′-deoxy-5′-adenosyl radical,[607] but this possibility seems unrealistic considering the distance between carbon 5′ and the iron in complex **5–111**.

Most of the intermediate radicals that are formed in the active sites of enzymes that share this mechanism to initiate their reactions are either localized on a carbon adjacent to a heteroatom with a lone pair of electrons that can participate in a captodative effect or are in the highest occupied molecular orbital of a π molecular orbital system that has a lobe or lobes adjacent to one or more heteroatoms with lone pairs of electrons that can participate in a captodative effect. Consequently, it may be the case that these are the intermediate radicals that are produced in the active site simply because they are the **most stable alternatives**. In other words, the 5′-deoxy-5′-adenosyl radical and the subsequent radicals

may be sterically able to abstract more than one hydrogen atom on the reactant in their immediate vicinity, as in the case of lysine 2,3-aminomutase, but the hydrogen each of them abstracts is the one that produces the more stable subsequent radical. If so, this discrimination follows the rule governing the regiochemistry of a nonenzymatic radical chain reaction. It is possible that the particular products of these various enzymatic reactions first appeared adventitiously solely because the intermediates were the most stable before a use was found for those products.

Abstraction of a hydrogen by the 5′-deoxy-5′-adenosyl radical from a substrate usually produces a **radical intermediate of significant lifetime** at the carbon from which it is removed. This longevity was demonstrated by synthesizing an analogue of the substrate for sporulation killing factor maturation protein SkfB from *B. subtilis* in which a cyclopropyl group was added to the carbon from which hydrogen is abstracted. The product of the reaction was not the usual crosslink produced by the enzyme but an ethylmethylene group at that carbon, resulting from the opening of the cyclopropyl ring.[609] This result is consistent with abstraction of a hydrogen from that carbon, producing a radical that has a lifetime long enough (>10 ns) to permit the cyclopropyl ring to open.

Following dissociation of the 5′-deoxy-5′-adenosyl radical from complex **5–111,** the catalytic [4Fe–4S] iron–sulfur cluster in complex **5–110** ends up in the oxidized state, $[(Fe^{2+})_2(Fe^{3+})_2(^{2-}S)_4(^{-}S^{-})_3]^{-}$. Consequently, it is **available to accept an electron** from an intermediate radical in a one-electron oxidation. Most, but not all,[610-612] of the enzymes that share this mechanism, however, also have at least one **auxiliary iron–sulfur cluster** in addition to the catalytic [4Fe–4S] iron–sulfur cluster, so the oxidant in these reactions is often ambiguous. In some instances, an auxiliary cluster may accept the electron from the intermediate radical and transfer it to the oxidized catalytic [4Fe–4S] iron–sulfur cluster of complex **5–110**.

In 2-deoxy-*scyllo*-inosamine dehydrogenase (AdoMet-dependent) (Equation 5–152), there is an auxiliary [4Fe–4S] iron–sulfur cluster in addition to the catalytic [4Fe–4S] iron–sulfur cluster.[613] In a crystallographic molecular model of the enzyme occupied by 2,3-dideoxy-3-oxo-*scyllo*-inosamine, carbon 3, at which the hydrogenation–dehydrogenation occurs (Equation 5–152), is almost equidistant from the two [4Fe–4S] iron–sulfur clusters.[580] The phenyl ring of Phenylalanine 188, however, is almost normal to a line between one of the sulfides in the auxiliary [4Fe–4S] iron–sulfur cluster and carbon 3. A carbon in the phenyl ring is 0.4 nm from carbon 1 of 2,3-dideoxy-3-oxo-*scyllo*-inosamine, and another is 0.5 nm from the sulfide. The phenyl ring could serve as an intermediate relay station for electron transfer from the radical at carbon 1 to the oxidized auxiliary [4Fe–4S] iron–sulfur cluster. The low biochemical reduction potential (–765 mV) of the auxiliary [4Fe–4S] iron–sulfur cluster, however, suggests that it is not a competent oxidant.

In a crystallographic molecular model of a dehydrogenase from *Streptoalloteichus tenebrarius*, which performs an identical dehydrogenation at carbon 4 of a terminal 2-deoxy-2-amino-D-glucosyl group in an oligosaccharide and which contains only the catalytic [4Fe–4S] iron–sulfur cluster, the 4-hydroxyphenyl group of Tyrosine 216 sits between the catalytic [4Fe–4S] iron–sulfur cluster and carbon 4 of a 2-deoxy-2-amino-D-glucosyl group that occupies the active site and forms a hydrogen bond to the hydroxy group on carbon 3. It has been proposed that this tyrosine transfers the electron from the intermediate radical at carbon 3 of 2-deoxy-*scyllo*-inosamine (see Equation 5–152) to the oxidized catalytic [4Fe–4S] iron–sulfur cluster.[614]

There is also a subfamily of enzymes each of which uses a 5′-deoxy-5′-adenosyl radical generated by the homolytic dissociation of complex **5–111** and each of which contains a **cobalamin**. In the crystallographic molecular model of the complex between *S*-adenosyl-L-methionine and OxsB protein from *Priestia megaterium*,[581] a member of this subfamily, the prosthetic cobalamin in the active site is in contact with the catalytic [4Fe–4S] iron–sulfur cluster, which is the only iron–sulfur cluster in the enzyme, but the cobalt in the cobalamin is too far away (0.75 nm) from carbon 5′ of *S*-adenosyl-L-methionine in complex **5–111** for carbon 5′ to ever become a ligand to the cobalt. In this case, the cobalamin serves the same role as an auxiliary iron–sulfur cluster acting as the acceptor of an electron and then being rereduced.

There are also reactions catalyzed by active sites that share this mechanism in which an **intermediate radical is reduced by accepting an electron** rather than being oxidized by losing an electron. Because the catalytic [4Fe–4S] iron–sulfur cluster is oxidized during the generation of the 5′-deoxy-5′-adenosyl radical, it cannot provide the necessary electron. Consequently, in these cases an auxiliary iron–sulfur cluster in the active site or nearby is usually able to donate the necessary electron and in

turn is rereduced by one of the usual small electron carriers present in the cytoplasm. This auxiliary iron–sulfur cluster can also be involved in reduction of the oxidized catalytic [4Fe–4S] iron–sulfur cluster in complex **5–110**.

In the **epimerization** catalyzed by neomycin C epimerase from *Streptomyces fradiae*

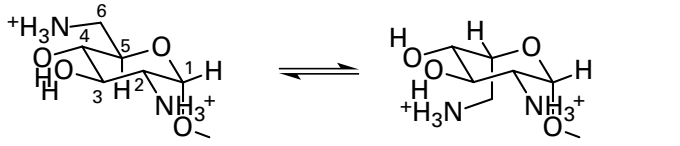

+ *S*-adenosyl-L-methionine + H^+ + 2 e^- ⇌ + 5′-deoxyadenosine + L-methionine

(5–154)

the 5′-deoxy-5′-adenosyl radical abstracts the hydrogen from carbon 5 of the 2,6-diamino-2,6-dideoxy-D-glucosyl group to produce a planar tertiary radical, stabilized by a lone pair on the adjacent oxygen. The tertiary radical, on its opposite face, then abstracts a hydrogen from the sulfanyl group of Cysteine 249 to achieve the epimerization. A signal from the intermediate tertiary radical has been observed in the electron paramagnetic resonance spectrum of the enzyme in which Cysteine 249 has been mutated to alanine when the mutant is mixed with reactant. This result is consistent with this cysteine being the source of the hydrogen abstracted by the initial radical. The resulting sulfenyl radical at Cysteine 249 and the oxidized catalytic [4Fe–4S] iron–sulfur cluster in complex **5–110** are then reduced back to the sulfanyl group and the reduced catalytic [4Fe–4S] iron–sulfur cluster by respective one-electron transfers from an auxiliary [4Fe–4S] iron–sulfur cluster within the active site.[597] These transfers provide in turn the two electrons needed for the overall reaction. The auxiliary [4Fe–4S] iron–sulfur cluster is reduced in two one-electron steps by small electron carriers in the cytoplasm. The two electrons are required because the S-adenosyl-L-methionine becomes 5′-deoxyadenosine and L-methionine. An epimerase in an uncharacterized bacterial symbiont in the sponge *Theonella swinhoei* uses the same mechanism to epimerize L-valine to D-valine in a peptide that is a precursor to polytheonamide A.[615]

The rather remarkable diversity (Figure 5–14) of the reactions catalyzed within the family of enzymes that initiate their respective reactions by homolytic dissociation of complex 5–111 illustrates the variety of homolytic transformations that active sites are able to perform and the control over regiochemistry they are able to exert. This regiospecificity, in particular, is a further demonstration of the steric control possible in an active site, reminiscent of the stereochemical control in the terpene cyclases.

Mycofactocin radical SAM maturase (Figure 5–14A) abstracts a hydrogen from a tyrosine at the carboxy terminus of mycofactocin precursor peptide during the synthesis of mycofactocin.[604,605] The resulting intermediate 4-hydroxybenzylic radical (**5–122**) is then oxidized by the transfer of an electron to one of the three [4Fe–4S] iron–sulfur clusters in the enzyme to produce the intermediate 1-carboxymethylene-2,5-cyclohexadien-4-one, which is a ketone at carbon 4 of the former 4-hydroxyphenyl group. This intermediate, which is a vinylogous β-oxo acid, then decarboxylates.

In biotin synthase

sulfur–(sulfur carrier) + 2 reduced [2Fe–2S] ferredoxin + dethiobiotin + 2 *S*-adenosyl-L-methionine ⇌ biotin + 2 L-methionine + 2 5′-deoxyadenosine + 2 oxidized [2Fe–2S] ferredoxin + (sulfur carrier)

(5–155)

which is a **sulfurtransferase**, two *S*-adenosyl-L-methionines are reactants, and they are converted in succession to two 5′-deoxyadenosines and two L-methionines that leave the active site as products during each turnover.[590] In the active site of biotin synthase, there is a single catalytic [4Fe–4S] iron–sulfur cluster that generates these two 5′-deoxy-5′-adenosyl radicals in succession by consecutive homolytic dissociations of complex **5–111**. The two reduced [2Fe–2S] ferredoxins that are reactants for the enzyme each provide an electron that is needed to rereduce complex **5–110** after each of the two rounds of hydrogen abstraction. An auxiliary [2Fe–2S] iron–sulfur cluster, which does not act as a donor or acceptor of an electron from an intermediate radical, is the source of the necessary sulfide ion.

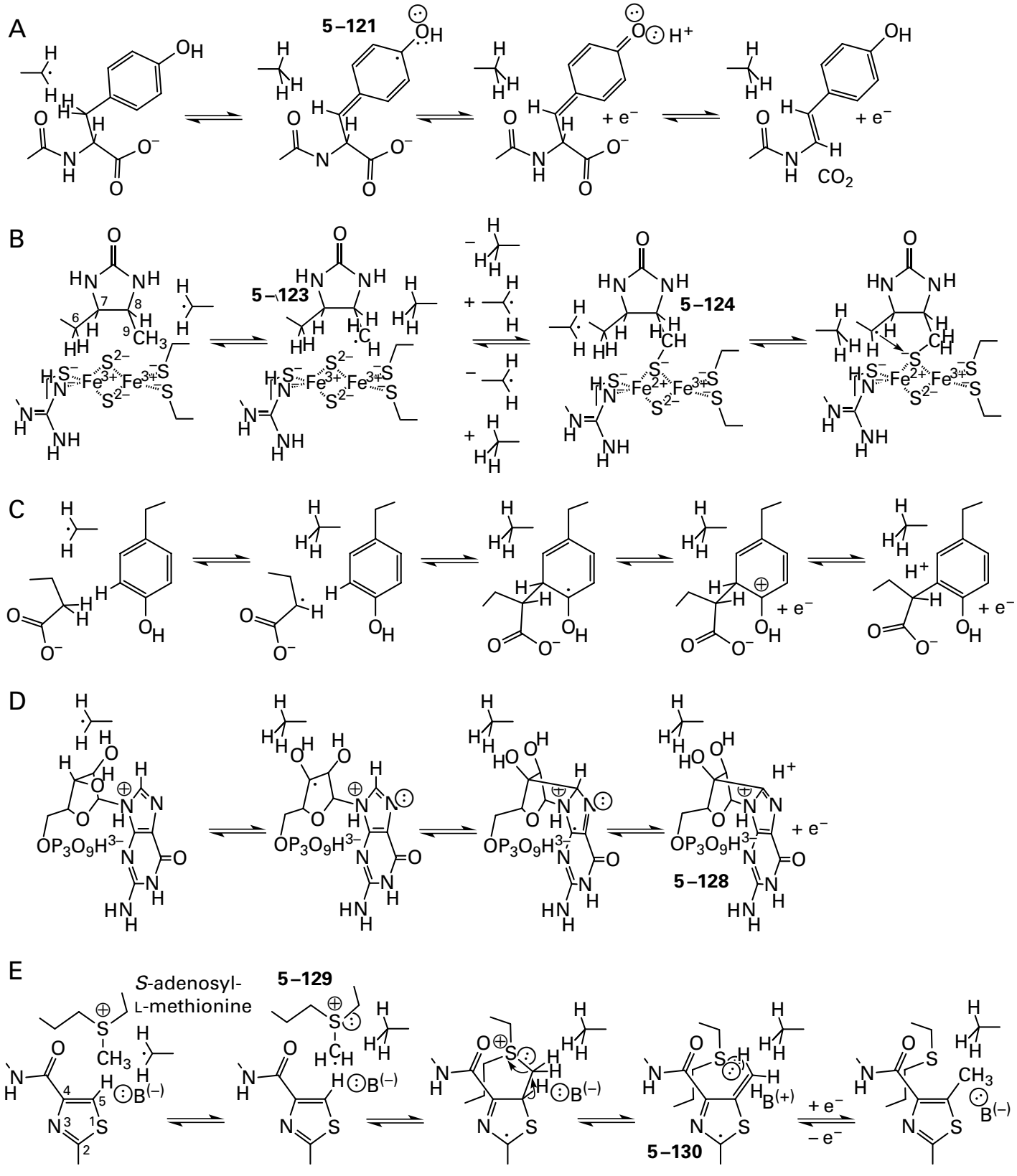
A
5–121
+ e⁻
+ e⁻
CO2
B
5–123
5–124
C
+ e⁻
+ e⁻
D
5–128
+ e⁻
E
S-adenosyl-
L-methionine
5–129
5–130
+ e⁻
– e⁻

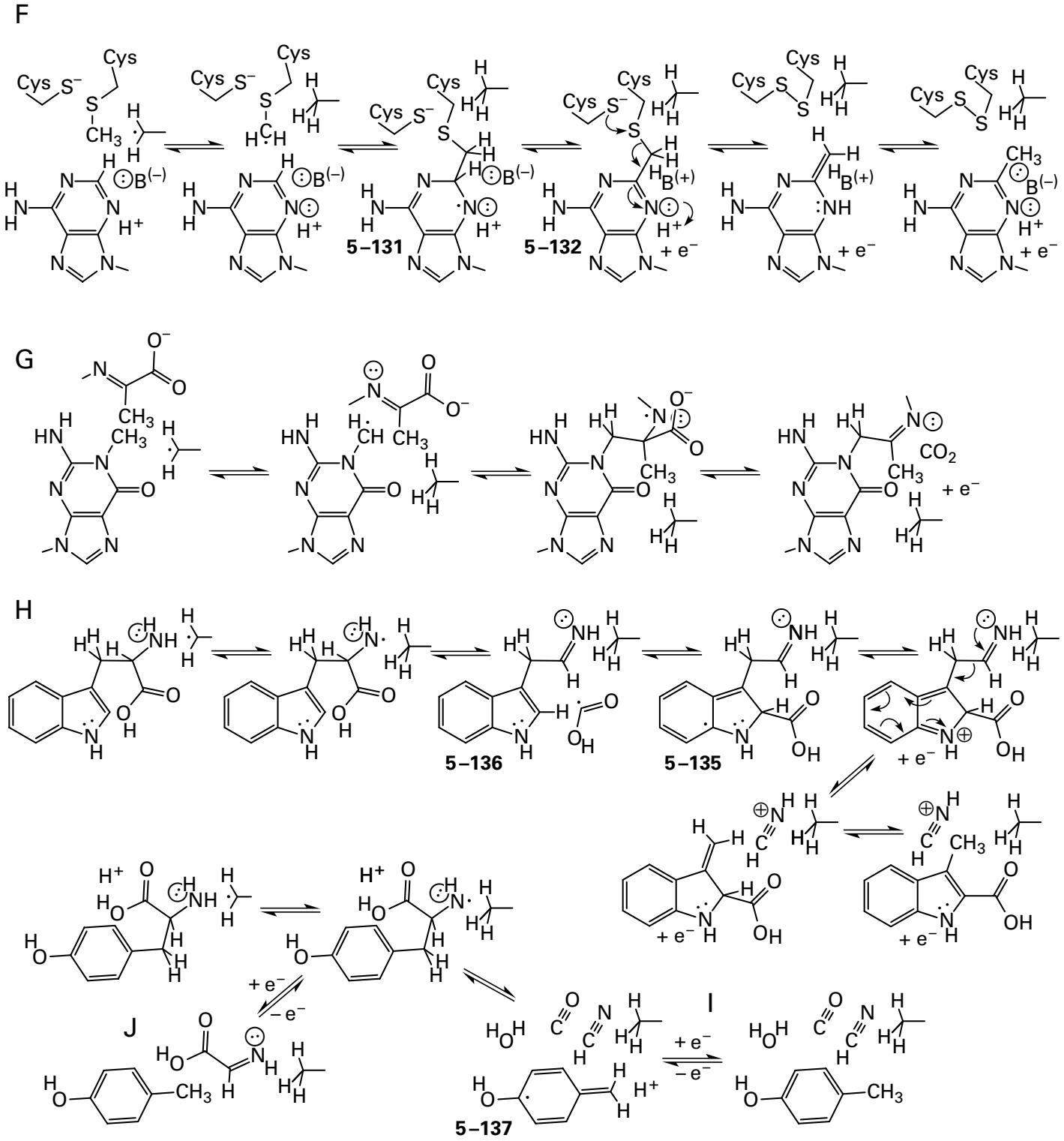

Figure 5–14: Reactions catalyzed by enzymes that use as an intermediate a 5′-deoxy-5′-adenosyl radical produced by the homolytic dissociation of complex **5–111**. (**A**) Mycofactocin radical SAM maturase. (**B**) Biotin synthase. (**C**) PqqA Peptide cyclase. (**D**) GTP 3′,8-Cyclase. (**E**) Thiazole methyltransferase. (**F**) 23S rRNA (Adenine^{2503}-C^2)-methyltransferase. (**G**) tRNA 4-Demethylwyosine synthase (AdoMet-dependent). (**H**) 3-Methyl-2-indolic acid synthase. (**I**) (FeFe) Hydrogenase maturation factor HydG. (J) 2-Iminoacetate synthase.

The first 5′-deoxy-5′-adenosyl radical generated in the active site of biotin synthase by homolytic dissociation of complex **5–111**[616] abstracts a hydrogen from carbon 9 of dethiobiotin (Figure 5–14B),[590,617] and the resulting dethiobiotin radical **5–123** then **inserts into a sulfide** in the auxiliary [2Fe–2S] iron–sulfur cluster[616,618,619] that is immediately adjacent to it.[612] The conjugate base of the 9-sulfanyldethiobiotin (**5–124**) that is formed as an intermediate in this first half of the overall reaction remains as a ligand through its sulfur to one or both of the iron ions in the auxiliary [2Fe–2S] iron–sulfur cluster, and an absorption in an electron paramagnetic resonance spectrum has been assigned to this complex on the basis of changes that occur on isotopic substitutions.[620] 9-Sulfanyldethiobiotin has been isolated from a reaction mixture containing biotin synthase from *E. coli* and identified chemically.[621] In the second half of the overall reaction, a second 5′-deoxy-5′-adenosyl radical, produced in the same way at the same catalytic [4Fe–4S] iron–sulfur cluster, abstracts a hydrogen from carbon 6 of the intermediate 9-sulfanyldethiobiotin, and the resulting radical inserts into the same sulfur, in a sequence of steps similar to the first, to produce biotin

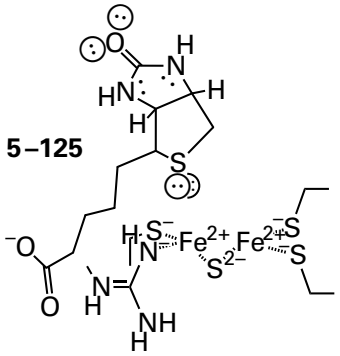

That each hydrogen is abstracted by the respective 5′-deoxy-5′-adenosyl radical follows from the fact that deuterium on carbon 9 and tritium on carbon 6 of dethiobiotin end up in 5′-deoxyadenosine produced in the reaction catalyzed by biotin synthase from *E. coli*.[590] The auxiliary [2Fe–2S] iron–sulfur cluster is reassembled after each turnover by an assembly system that uses a sulfur atom on a sulfur-carrier protein, which becomes a sulfide in the reassembled auxiliary cluster.

Lipoyl synthase also catalyzes two successive radical additions to sulfides. The first 5′-deoxy-5′-adenosyl radical generated in the active site of lipoyl synthase by homolytic dissociation of complex **5–111** abstracts a hydrogen from carbon 6 of an octanoyl group in an amide with the 6-amino group of a lysine in a protein that is a substrate for the enzyme. The resulting secondary alkyl radical at carbon 6 then inserts into a sulfide in an auxiliary [4Fe–4S] iron–sulfur cluster that is immediately adjacent to it. The sulfide becomes a sulfido group on carbon 6 of the octanoyl group. In a crystallographic molecular model between a peptide containing this 6-sulfidooctanoyl group and lipoyl synthase from *E. coli*,[622] the **sulfido group remains a ligand to three iron ions** in the auxiliary [4Fe–4S] iron–sulfur cluster.[623] In a second round, a second 5′-deoxy-5′-adenosyl radical generated in the active site by homolytic dissociation of a subsequent complex **5–111** at the same catalytic [4Fe–4S] iron–sulfur cluster abstracts a hydrogen from carbon 8 of the 6-sulfanyloctanoyl group. The resulting primary radical inserts into a sulfide across the face of the auxiliary [4Fe–4S] iron–sulfur cluster in which the first sulfide was located to form a sulfido group on carbon 8. The N^6-(dihydrolipoyl)lysine

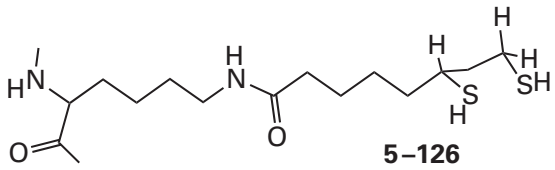

in the peptide or protein that is a substrate for the enzyme then dissociates from the auxiliary [4Fe–4S] iron–sulfur cluster as the nominal product of the reaction, leaving two vacancies where the two sulfides once were. The auxiliary [4Fe–4S] iron–sulfur cluster has to be regenerated before the next turnover can occur.

In addition to the dehydrogenases, the epimerases, and sulfurtransferases that have already been discussed, there are enzymes that use 5′-deoxy-5′-adenosyl radicals generated by homolytic dissociation of complexes **5–111** to initiate numerous posttranslational crosslinkings within peptides; alkylations and methylations of purines; alkylations and methylations by radical additions; and oxidative decarboxylations. There are also lyases that use L-tyrosine and L-tryptophan as substrates. These disparate outcomes result from an initial abstraction of a hydrogen by a 5′-deoxy-5′-adenosyl radical. Nevertheless, it seems again as if the various outcomes may well have been adventitious because the products of many of these enzymatic reactions are of only isolated utility, unlike the product of lipoyl synthase, which is present in all organisms,

and the product of biotin synthase, which is present in bacteria and plants.

There are a number of **posttranslational crosslinks** that enzymes from prokaryotes perform on short peptides to produce natural products by using a 5′-deoxy-5′-adenosyl radical generated by homolytic dissociation of complex **5–111**.[604,624-631] For example, PqqA peptide cyclase from *Methylorubrum extorquens* catalyzes formation of a crosslink between Glutamate 16 and Tyrosine 20 (Figure 5–14C) in PqqA, a peptide 29 amino acids long, as the first step in the biosynthesis of pyrroloquinoline quinone (**5–127**)[632]

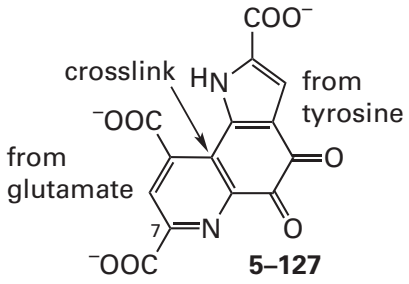

5–127

In the mechanism of this enzyme, an intermediate radical is formed by **radical aromatic addition** of the initial intermediate radical at the γcarbon of Glutamate 16 to carbon 3 of the 4-hydroxyphenyl group of Tyrosine 20. The unpaired electron in the resulting intermediate radical in the radical aromatic addition is delocalized over five carbons of the former 4-hydroxyphenyl group in the highest occupied molecular orbital of a pentadienyl πmolecular orbital system that has a lobe adjacent to the original 4-hydroxy group. This delocalized intermediate radical is oxidized by one electron, which is removed either by the oxidized catalytic [4Fe–4S] iron–sulfur cluster or one of the two auxiliary iron–sulfur clusters, a [4Fe–4S] iron–sulfur cluster and a [2Fe–2S] iron–sulfur cluster,[632] also in the enzyme. Following removal of a hydron from the resulting cyclopentadienyl carbenium ion or removal of a hydron during the transfer of the electron, the crosslinked product is formed.

A homologous (20% identity; 1.4 gap percent)[632] enzyme from streptococci, KxxxW cyclic peptide radical SAM maturase, forms a similar crosslink between Lysine 15 and Tryptophan 19 in a peptide 29 amino acids long by an analogous mechanism as the first step in the biosynthesis of streptide, a cyclic peptide secreted by the bacteria. Addition of the initial intermediate radical, located on the β-carbon of Lysine 15, to carbon 7 of Tryptophan 19 also produces an intermediate radical with an unpaired electron delocalized in the highest occupied molecular orbital of a pentadienyl πmolecular orbital system that has a lobe adjacent to the nitrogen of the indolyl group. The fact that enzymatic activity is lost when one of the two auxiliary [4Fe-4S] iron–sulfur clusters in this enzyme,[633] the one homologous to the lone auxiliary [4Fe–4S] iron–sulfur cluster in PqqA peptide cyclase, is removed by site-directed mutation suggests that this auxiliary [4Fe–4S] iron–sulfur cluster is the one-electron oxidant of this delocalized radical[627] rather than the catalytic [4Fe–4S] iron–sulfur cluster.

GTP 3′,8-Cyclase from *S. aureus* catalyzes the intramolecular **radical addition** of carbon 3′ in the ribosyl group of GTP^{4-} to carbon 8 of GTP^{4-} (Figure 5–14D). The 5′-deoxy-5′-adenosyl radical generated in the active site abstracts the hydrogen from carbon 3′ and the resulting initial radical, adjacent to the 3′-hydroxy group, adds to carbon 8 to produce an intermediate radical with an unpaired electron delocalized in the highest occupied molecular orbital of an allyl πmolecular orbital system that has a lobe adjacent to nitrogen 3 of the former guanine. Oxidation of this intermediate radical by one-electron transfer and the loss of a hydron produces tetracyclic product **5–128**. There is an auxiliary [4Fe–4S] iron–sulfur cluster in the active site, and it has been shown by electron paramagnetic resonance spectroscopy[634] and crystallography[635] that the *N*-acylguanidino group of the guanine associates with this cluster in a coordination with nitrogen 1 and its 2-amino group as ligands to an iron ion. Because the electron to be transferred in the one-electron oxidation is in the guanine, this auxiliary [4Fe–4S] iron–sulfur cluster may be the acceptor in this oxidation. The tetracyclic product **5–128** of these steps in the enzymatic reaction is actually an intermediate in the overall reaction, which produces pyranopterin monophosphate, a precusor to molybdopterin, so this enzyme is found in all organisms. Tetracyclic intermediate **5–128** has been isolated and identified by mass spectrometry from reaction mixtures of enzyme and substrates.[636]

So far, in the various reactions in which 5′-deoxy-5′-adenosyl radicals produced by homolytic dissociation of complex **5–111**, 5′-deoxy-adenosine and L-methionine are products of the overall reaction. In the condensation catalyzed by viperin, an enzyme in animals that has antiviral activity, 5′-deoxy-adenosine is incorporated into one of the products. The 5′-deoxy-5′-adenosyl radical produced in the active site, instead of abstracting a hydrogen to give a radical of one of the reactants which then adds to

an unsaturated carbon, adds directly to the peripheral carbon in the carbon–carbon bond of isopentenyl diphosphate to give a tertiary radical at the distal carbon. The tertiary radical is then reduced by an electron and a hydron to give the unsaturated alkane. The product of the condensation is 5′-deoxy-5′-(4-diphospho-2-methylbutyl)adenosine.[637]

A number of enzymes that share this common mechanism catalyze **methylations**. The methyl group is usually derived from a second molecule of *S*-adenosyl-L-methionine, either directly or indirectly. For example, thiazole methyltransferase (Figure 5–14E) **uses the second *S*-adenosyl-L-methionine directly** as the source of the methyl group. The 5′-deoxy-5′-adenosyl radical initially abstracts a hydrogen from the methyl group of the second *S*-adenosyl-L-methionine, and the resulting *S*-methylene radical **5–129**, captodatively stabilized by a lone pair of electrons on the sulfonium sulfur, participates in a radical aromatic addition at carbon 5 of a thiazolyl group. This radical aromatic addition produces an intermediate radical with an unpaired electron delocalized over the highest occupied molecular orbital of an allyl π molecular orbital system that has a lobe adjacent to the sulfur of the thiazolyl group and a node on the nitrogen of the thiazolyl group. Elimination of an acidic hydron and L-methionine, which is an excellent leaving group, from the sulfonium ion, leads to an even more stable intermediate, radical **5–130**, in which the unpaired electron is in the highest occupied molecular orbital of a pentadienyl π molecular orbital system. Radical **5–130** is reduced by one electron, concerted with the transfer of a hydron to the distal carbon of its exocyclic carbon–carbon bond. The product of this reduction and hydronation is the methylated thiazolyl group. It has been shown, by using deuterated reactants and the enzyme from *Thermobispora bispora*, that the hydrogen abstracted from the methyl group of the second *S*-adenosyl-L-methionine ends up on 5′-deoxyadenosine and the hydrogen on carbon 5 of the thiazolyl group ends up on the final methyl group (Figure 5–14E).[592]

An enzyme in *Streptomyces actuosus* transfers a methylene radical from the same initial *S*-methylene radical **5–129** of *S*-adenosyl-L-methionine[595] to carbon 4 of an indolyl group by radical aromatic addition to produce an intermediate radical with an exocyclic double bond, analogous to intermediate radical **5–130**. Transfer of the methylene occurs through an intermediate formed by addition of *S*-methylene radical **5–129** to carbon 4 of the indolyl group to form a chemically identified adduct in which the methylene group bridges the indolyl and *S*-adenosylhomocysteinyl groups.[638] The adduct then undergoes heterolytic elimination of the hydrogen that was on carbon 4 as a hydron and *S*-adenosyl-L-homocysteine, again an excellent leaving group from the sulfonium that is the adduct, to produce the 4-methyleneindolyl radical. This intermediate radical is oxidized by the transfer of one electron, and the resulting **electrophilic exocyclic carbon on the 4-methylene group,** on the antiaromatic 4-methyleneindole, then reacts with a nucleophilic carboxylato group to give the aromatic adduct

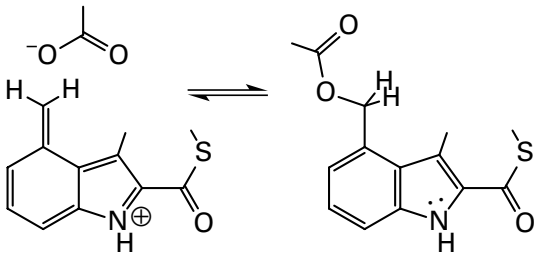

(5–156)

23S rRNA (Adenine^{2503}-C^2)-methyltransferase (Figure 5–14F) from *E. coli* uses the other *S*-adenosyl-L-methionine **indirectly as the source of the methyl group** in the methylation that it catalyzes. Cysteine 355 in the active site is methylated[611] by an *S*-adenosyl-L-methionine in complex **5–111** with the catalytic [4Fe–4S] iron–sulfur cluster. This initial methylation of the cysteine is an example of complex **5–111** dissociating at the methyl group rather than at the 5′-deoxyadenosyl group. The resulting *S*-adenosyl-L-homocysteine dissociates from complex with the catalytic [4Fe–4S] iron–sulfur cluster and is replaced by a second *S*-adenosyl-L-methionine. The resulting second complex **5–111**,[639] dissociates homolytically at the 5′-deoxy-5′-adenosyl group to give the 5′-deoxy-5′-adenosyl radical necessary to abstract a hydrogen from the methyl group on Cysteine 355. The enzyme contains only this one iron–sulfur cluster,[640] so it is required to do double duty.

The intermediate *S*-methylene radical on Cysteine 355 then participates in a radical addition to carbon 2 of Adenine 2503 in 23S rRNA to form intermediate radical **5–131** with an unpaired electron delocalized in the highest occupied molecular orbital of a 3-vinylpentadienyl π molecular orbital system that has lobes over nitrogens 1 and 3 of adenine that stabilize the radical by their electronegativity. Intermediate radical **5–131** within the active site of the native enzyme has been observed by electron

paramagnetic resonance spectroscopy.[641] This radical has also been observed crystallographically[640] and by electron paramagnetic resonance spectroscopy[642] in the active site of a mutant of the enzyme in which Cysteine 118, the base that removes the hydron from carbon 2 during its oxidation, has been mutated to alanine. These latter observations suggest that removal **of the hydron must be concerted with the one-electron oxidation**. Intermediate radical **5–131** is then oxidized by the transfer of one electron—concerted with removal of a hydron—to the oxidized catalytic [4Fe–4S] iron–sulfur cluster in complex **5–110**, which is the only iron–sulfur cluster in the enzyme,[611] to produce covalent intermediate **5–132**. A peptide containing covalent intermediate **5–132** was isolated from a tryptic digest of the same mutant, and its structure was defined by collision-induced dissociation in a mass spectrometer.[643]

The sulfido group of Cysteine 105 then participates[641] in a nucleophilic substitution at the sulfur of Cysteine 355 that produces a cystine and a non-covalent intermediate in which the adenine has gained an exocyclic methylene group. The carbon of this methylene group is in an enamine and can be easily hydronated. Results from reactions with deuterated substrates are consistent with the conclusion that the exocyclic methylene group is deuteronated by the same deuteron that was removed from carbon 2 of intermediate radical **5–131**. The product of the reaction[591] is 2-methyladenine[2503].

In the active site of an enzyme in *Cystobacter* that methylates the methyl group in a 3-methoxy group on a 4-aminobenzoyl thioester, the methyl group is transferred from the other *S*-adenosyl-L-methionine to a cob(I)alamin rather than the sulfido group of a cysteine.[644] Cob(I)alamin is the nucleophile in the usual concerted nucleophilic substitution that forms methylcob(III)alamin rather than adenosylcob(III)alamin. Methylcob(III)alamin then provides the equivalent of a methyl radical that colligates with a methylene radical on the methoxy group formed by abstraction of a hydrogen from the methyl group by the 5′-deoxy-5′-adenosyl radical to produce a carboxyethyl group. The resulting cob(II)alamin is eventually reduced by one electron to regenerate cob(I)alamin.

The 5′-deoxy-5′-adenosyl radical generated by homolytic dissociation of complex **5–111** in the active site of tRNA 4-demethylwyosine synthase (AdoMet-dependent) from *M. jannaschii* (Figure 5–14G) abstracts a hydrogen atom from the methyl group of 1-methylguanine[594] at position 37 in transfer RNA^{Phe}. This intermediate radical adjacent to nitrogen 1 of guanine then adds to carbon 2 of an imine of pyruvate, which spectroscopic studies indicate is a bidentate ligand to a open iron ion on an auxiliary [4Fe–4S] iron–sulfur cluster,[645,646] to give the intermediate radical on the iminium nitrogen. One-electron oxidation of this intermediate radical, coupled to its decarboxylation, produces the imine of 1-(acetylmethyl)guanine, a precusor to 4-demethylwyosine. Consistent with this mechanism, it has been shown that all the hydrogens on the methyl group of pyruvate remain on the methyl group in the product.[594] The extreme exclusivity of 23S rRNA (adenine^{2503}-C^2)-methyltransferase and tRNA 4-demethylwyosine synthase (AdoMet-dependent) are examples of the boutique character of many of the reactions catalyzed by enzymes in this family.

Several **lyases of L-tryptophan and L-tyrosine** use a 5′-deoxy-5′-adenosyl radical generated by homolytic dissociation of complex **5–111** to rearrange or decompose these amino acids and in the process provide unusual products for particular purposes. For example, 3-methyl-2-indolic acid synthase (Figure 5–14H) **decomposes the entire aminocarboxymethyl group** of L-tryptophan while transferring the carboxy group to carbon 2 of the indolyl group to produce 3-methyl-2-indolic acid, which is incorporated into the antibiotic nosiheptide. (FeFe) hydrogenase maturation factor HydG (Figure 5–14I) decomposes the entire aminocarboxymethyl group of L-tyrosine, turning it into carbon monoxide[647] and hydrogen cyanide,[648] which are then incorporated into the prosthetic iron cluster (previously **2–137**)

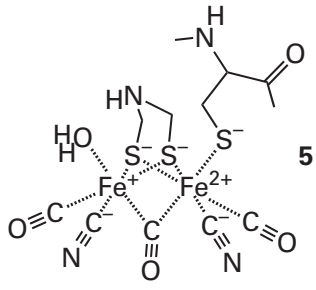

5–133

of ferredoxin hydrogenase.[649] These decompositions are reminiscent of the decomposition of the aminocarboxymethyl group of the serine that replaces Cysteine 225 (homologous to Cysteine 218 in the enzyme from *S. cerevisiae*; Figure 5–13) in a mutant of ribonucleoside-diphosphate reductase from *E. coli* when it is mixed with a nucleoside diphosphate.[650] In this instance, it is assumed that a radical is formed on the serine that then decomposes.

2-Iminoacetate synthase (Figure 5–14J), however, simply dissociates the aminocarboxymethyl group of L-tyrosine and converts it into 2-iminoacetate,[651] the useful product of the reaction, which becomes carbon 2 and nitrogen 3 of thiamine diphosphate

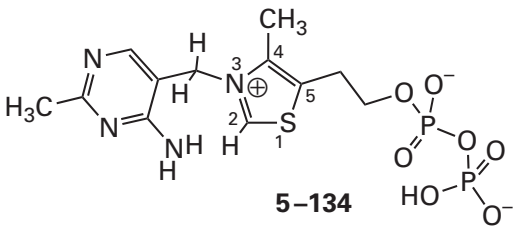

5–134

The 5′-deoxy-5′-adenosyl radical generated in the active site of 3-methyl-2-indolic acid synthase from *S. actuosus* initiates the reaction (Figure 5–14H) by abstracting a hydrogen from the α-amino group of L-tryptophan. This conclusion follows from several facts. First, a hydrogen abstracted and ending up in the 5′-deoxyadenosine that is the product of the enzymatic oxidation is on a heteroatom in L-tryptophan that exchanges with deuterons when ^2H_2O is used as the solvent.[652] Second, when analogues of L-tryptophan in which the only exchangeable hydrogens are on the α-amino nitrogen are used in the enzymatic oxidation, deuterons from solvent are again incorporated into 5′-deoxyadenosine.[653-655] Third, a hydrogen on the amino group of L-tryptophan is only 0.33 nm from carbon 5′ of 5′-deoxyadenosine in a crystallographic molecular model of the active site occupied by this reactant and this product of the enzymatic oxidation.[610]

In the next step, a **carboxy radical** dissociates from the α carbon and adds to carbon 2 of the indolyl group.[656] This conclusion follows in part from the fact that the carbon of the α-carboxy group of L-tryptophan in the crystallographic molecular model is only 0.34 nm from carbon 2 of the indolyl group. The result of this radical aromatic addition is radical **5–135**, an intermediate radical with an unpaired electron delocalized in the highest occupied molecular orbital of a heptatrienyl π molecular orbital system that has a lobe adjacent to the nitrogen of the former indolyl group. An absorption in the electron paramagnetic resonance spectrum taken while the enzyme was catalyzing its reaction has been identified as radical **5–135** on the basis of both its pattern of splitting and changes in its shape when various atoms in the L-tryptophan used as a reactant were replaced with deuterium, nitrogen 15, and carbon 13, respectively.[657] In radical **5–135**, the aminocarboxymethyl group of L-tryptophan has become an imine, a conclusion consistent with the fact that when L-tryptophan thiocarboxylate is used as a reactant, the product of the enzymatic reaction is (1*H*-indol-3-yl)-3-propanal. This aldehyde is the product expected if the thiocarboxy radical that dissociates from the initial intermediate radical, which results from the abstraction of a hydrogen from the α-amino group of the L-tryptophan thiocarboxylate, is too weak or decomposes too rapidly to participate in intramolecular radical aromatic addition to carbon 2. In this case, the reaction goes no further than the production of 3-(2-iminoethyl)-indole (**5–136**), which dissociates from the active site and hydrolyzes to (1*H*-indol-3-yl)-3-propanal.[655]

In the normal reaction, radical **5–135** is then oxidized by one electron. Since the enzyme contains only the catalytic iron–sulfur cluster complex **5–110**,[610] it must be the one-electron oxidant in this step. The penultimate step is dissociation of an electrophile, dihydrogen cyanide, from the vinylogous iminium ion. In the crystallographic molecular model of the active site occupied by L-tryptophan, the carbon–carbon bond between the α and β carbons, which will be the bond broken in this penultimate step, is parallel to the π molecular orbital system of the indolyl group in the active site,[610] as it should be. The final step is a tautomerization initiated by removal of a hydron from an acidic carbon α to a carboxy group.

Both (FeFe) hydrogenase maturation factor HydG (Figure 5–14I) from *C. acetobutylicum* (21% identity; 3 gap percent) and 2-iminoacetate synthase (Figure 5–14J) from *E. coli* (22% identity; 3.4 gap percent) are homologues of 3-methyl-2-indolic acid synthase from *S. actuosus*, and both are even closer homologues (27% identity; 1.9 gap percent) of each other. One product of the reaction catalyzed by (FeFe) hydrogenase maturation factor HydG is hydrogen cyanide, which is also a product of 3-methyl-2-indolic acid synthase.[658] The 5′-deoxy-5′-adenosyl radical generated by homolytic dissociation of complex **5–111** in the active site of this latter enzyme initiates its reaction by abstracting a hydrogen atom from the amino group of L-tyrosine.[659] These facts imply that the mechanisms of these three enzymes should be similar and that each amino acid that is a reactant is positioned in the respective active site in the same orientation.

Because the product in each case[651] is 4-methylphenol—unlike the reaction catalyzed by 3-methyl-2-indolic acid synthase, which is electron neutral (Figure 5–14H)—the reactions catalyzed by (FeFe) hydrogenase maturation factor HydG and 2-iminoacetate synthase each require two electrons from

small electron carriers. An absorption in the electron paramagnetic resonance spectrum taken while (FeFe) hydrogenase maturation factor HydG was catalyzing its reaction[660] has been identified as the **radical of 4-methylphenol** (**5–137**; Figure 5–14I) on the basis of both its pattern of splitting and changes in its shape when 3-hydroxy-L-phenylalanine replaces L-tyrosine. This radical of 4-methylphenol is an intermediate radical with an unpaired electron delocalized in the highest occupied molecular orbital of a benzyl π molecular orbital system that has a lobe adjacent to the oxygen of the hydroxy group (**5–122**). Consequently, one of the two electrons required by the reaction catalyzed by this enzyme reduces the radical of 4-methylphenol and the other rereduces the catalytic [4Fe–4S] iron–sulfur cluster. (FeFe) Hydrogenase maturation factor HydG from *C. acetobutylicum* has an auxiliary [4Fe–4S] iron–sulfur cluster that may be able to shuttle these two electrons to these intermediates.[661] 2-Iminoacetate synthase from *E. coli*, however, does not have the same auxiliary [4Fe–4S] iron–sulfur cluster. Nevertheless, two reduced flavodoxins are able to provide the required two electrons, one at a time, to this latter enzyme,[662] presumably through the catalytic [4Fe–4S] iron–sulfur cluster.

There seems to be no reasonable heterolytic way to break the bond between the α and β carbons of the L-tyrosine that is a substrate in these two tyrosine lyases as there was in the reaction catalyzed by the tryptophan lyase, 3-methyl-2-indolic acid synthase. There are, however, homolytic possibilities. For (FeFe) hydrogenase maturation factor HydG, the homolytic dissociation

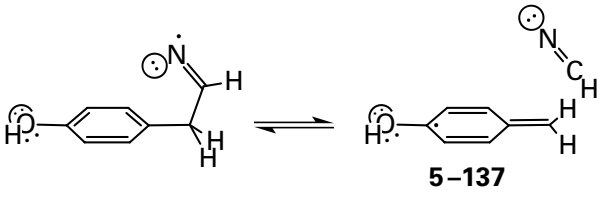

(5–157)

would break the carbon–carbon bond and give both the observed radical of 4-methylphenol and hydrogen cyanide, one product of the reaction. The initial radical in this enzymatic reaction is formed by abstraction of a hydrogen from a heteroatom, presumably—by analogy with the reaction catalyzed by 3-methyl-2-indolic acid synthase—a hydrogen on the α-amino group of the L-tyrosine that is a reactant, because a deuterium is abstracted by the 5′-deoxy-5′-adenosyl radical when the reaction is run in ^2H_2O.[659] Following formation of this initial radical, nothing is known about the later steps, but an intermediate radical formed in the reaction could easily abstract a hydrogen from the nitrogen (BDE = 360 kJ mol^{-1}) of 4-(2-iminoethyl)phenol, the homologue of 3-(2-iminoethyl)indole (**5–136**), to give its radical. For 2-iminoacetate synthase, the homolytic dissociation

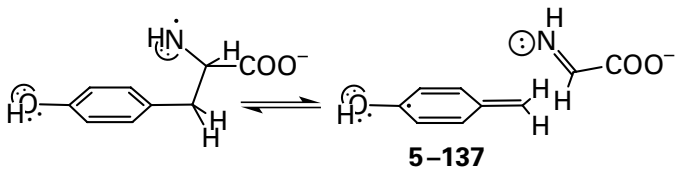

(5–158)

would break the carbon–carbon bond and give both the radical of 4-methylphenol and 2-iminoacetate, one product of the reaction.

Lysine 2,3-aminomutase uses a 5′-deoxy-5′-adenosyl radical produced by homolytic dissociation of complex **5–111** to initiate a **migration**[663]

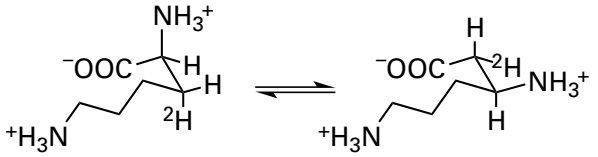

(5–159)

homologous to those performed by mutases

(5–160)

that use a 5′-deoxy-5′-adenosyl radical produced by homolytic dissociation of a prosthetic adenosylcobalamin. In the reaction catalyzed by lysine 2,3-aminomutase, X is the external pyridoximine of the L-lysine, the reactant, and the external pyridoximine of the (3*S*)-3,6-diaminohexanoate, the product, just as in the reaction catalyzed by the active site of β-lysine 5,6-aminomutase (Table 2–3), in which there is a prosthetic adenosylcobalamin.

The difference between lysine 2,3-aminomutase and the other enzymes that use a 5′-deoxy-5′-adenosyl radical produced by homolytic dissociation of complex **5–111** and that have been discussed so far is that ***S*-adenosyl-L-methionine is not a reactant** in the overall reaction, nor are L-methionine and 5′-deoxyadenosine products. Undissociated complex **5–111** is a prosthetic group covalently

bound to the active site through three cysteines, and it is re-formed by reassociation of the 5′-deoxy-5′-adenosyl radical that is regenerated during every turnover by the reverse of Equation 5–138 with the methionyl [4Fe–4S] iron–sulfur cluster, just as adenosylcobalamin is re-formed after each turnover by reassociation of the 5′-deoxy-5′-adenosyl radical that is regenerated during every turnover with cob(II)alamin. Nevertheless, *S*-adenosyl-L-methionine must be present in the solution for efficient enzymatic turnover to occur,[664] presumably because it is not bound to the active site tightly enough and slowly dissociates from complex **5–111**.

The 5′-deoxy-5′-adenosyl radical produced in the active site of lysine 2,3-aminomutase abstracts a hydrogen from carbon 2 of the reactant (3*S*)-3,6-diaminohexanoate to produce the radical at that location. The external pyridoximine of the amino group at carbon 3 of the radical[665] migrates to the site of the radical at carbon 2, leaving behind a radical at carbon 3, which then abstracts a hydrogen from 5′-deoxyadenosine to regenerate the 5′-deoxy-5′-adenosyl radical, which reassociates with complex **5–110** to re-form complex **5–111**. The absorption of the former intermediate, the radical of (3*S*)-3,6-diaminohexanoate at carbon 2, has been observed in an electron paramagnetic resonance spectrum of a reaction mixture,[666] and isotopic substitutions identify it as the source of the absorption.[667] This radical was shown to be kinetically competent to be an intermediate in the enzymatic reaction.[668] The absorption of the latter radical, the one at carbon 3, has been observed in an electron paramagnetic resonance spectrum of a reaction mixture of the enzyme and either the alternative reactant 4-thialysine, the sulfur of which stabilizes the radical at carbon 3,[669] or the alternative reactant *trans*-4,5-dehydro-L-lysine,[670] which gives an allylic radical at carbons 3, 4, and 5. There is a nonenzymatic radical reaction, initiated by forming a radical on a carbon immediately adjacent to a carbon the amino group of which is in a benzylimine, that mimics the migration of the external pyridoximine of the amino group of either L-lysine or (3*S*)-3,6-diaminohexanoate between the two adjacent carbons.[671]

Propanediol dehydratase from *Klebsiella oxytoca*, unlike a propanediol dehydratase that requires adenosylcobalamin as a prosthetic group (Table 2–3), uses a 5′-deoxy-5′-adenosyl radical produced by homolytic dissociation of complex **5–111**. As in the case of lysine 2,3-aminomutase, *S*-adenosyl-L-methionine is not a reactant in the overall reaction, nor are L-methionine and 5′-deoxyadenosine products. Unlike the reaction catalyzed by lysine 2,3-aminomutase, however, the reaction catalyzed by propanediol dehydratase from *K. oxytoca* does not involve a migration because when the hydroxy group on carbon 2 is labeled with oxygen-18, none of the oxygen-18 ends up in the product.[672]

Spore photoproduct lyase, as does lysine 2,3-aminomutase, uses a 5′-deoxy-5′-adenosyl radical produced by homolytic dissociation of complex **5–111**; but when the enzyme is turning over at limiting rate, the 5′-deoxy-5′-adenosyl radical is regenerated at the end of each turnover[673] rather than complex **5–111**. Complex **5–110**, however, is present in the active site, presumably to capture the 5′-deoxy-5′-adenosyl radical when turnover is not proceeding at a rapid enough pace. As with lysine 2,3-aminomutase, even though *S*-adenosyl-L-methionine is not a reactant in the overall reaction, it must be present in the solution.

There are several enzymes that use a [4Fe–4S] iron–sulfur cluster alone to produce a radical or a carbanion on a substrate. For example, there is a [4Fe–4S] iron–sulfur cluster in the active site of (*R*)-2-hydroxyisocaproyl-CoA dehydratase

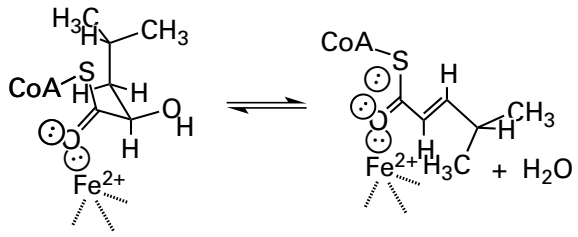

(5–161)

from *C. difficile*.[674] In this elimination, the hydrogen involved is not on a carbon α to either a carbonyl or an acyl group, so it cannot be removed as a hydron before the hydroxy group leaves; and the hydroxy group cannot leave first because it is α to the electropositive carbon of a thioacyl group. Natural selection has solved these problems by performing the reaction homolytically. The only iron ion in the [4Fe–4S] iron–sulfur cluster that lacks a cysteine as a ligand associates with the acyl oxygen of the substrate.[674] The reduced [4Fe–4S] iron–sulfur cluster then donates an electron to the acyl group while the acyl oxygen is hydronated by Glutamic Acid 55 to produce a radical on carbon 1 (**5–138**)

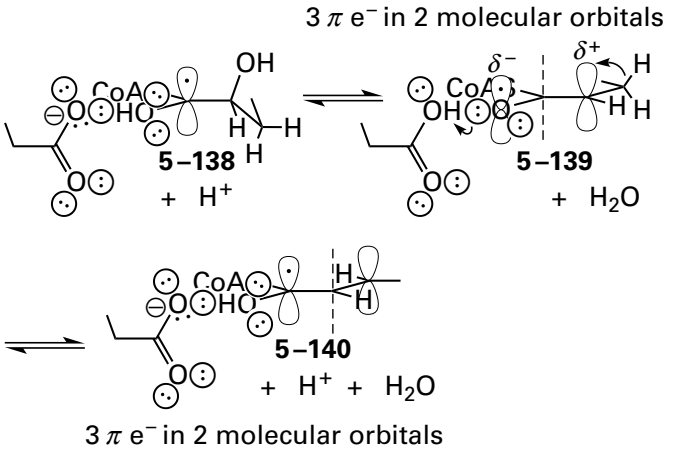

(5–162)

The electron that is donated to produce radical **5–138** has to be one of quite low biochemical reduction potential (<–600 mV), and there is another protein, (*R*)-2-hydroxyisocaproyl-CoA dehydratase activator, that provides this **electron of low potential** to the catalytic [4Fe–4S] iron–sulfur cluster. Remarkably, it is structurally unrelated but functionally related to dinitrogenase reductase.[675] As with dinitrogenase reductase, (*R*)-2-hydroxyisocaproyl-CoA dehydratase activator is a homodimer with only one [4Fe–4S] iron–sulfur cluster, and it lowers dramatically the reduction potential of this [4Fe–4S] iron–sulfur cluster[676] by hydrolyzing $MgATP^{2-}$.

Radical **5–138** conjugates the lone pair of electrons on the oxygen of the former acyl group with the carbon–oxygen bond of the hydroxy group on carbon 2, just as such a conjugation is established in the active site of ribonucleotide reductase (Figure 5–13). While Glutamate 55 dehydronates the former acyl oxygen of radical **5–138**, the hydroxy group, following its hydronation, leaves as a molecule of water to form the oxallylic radical **5–139** (see second step in Figure 5–13). While the acyl oxygen is again hydronated, oxallylic radical **5–139** dissociates a hydron to become the allylic radical **5–140**, the electron paramagnetic resonance spectrum of which has been observed in the active site of the enzyme.[677] While the acyl oxygen is again dehydronated, the unpaired electron in the highest occupied molecular orbital of the allylic radical is then transferred back to the oxidized [4Fe–4S] iron–sulfur cluster, still attached to the acyl oxygen, to produce the product.

There are several enzymes that can use a [4Fe–4S] iron–sulfur cluster to produce **carbanionic intermediates that are neither enolates or enamines** in reactants that have neither a carbonyl, nor an imine, nor a derivative of a carboxylic acid. As do the catalytic [4Fe–4S] iron–sulfur clusters discussed so far, the [4Fe–4S] iron–sulfur clusters in the active sites of these enzymes have an iron ion that is not coordinated by a sulfido group from a cysteine and is open to coordination by substrates.

In the active site of 4-hydroxy-3-methylbut-2-en-1-yl diphosphate reductase from *E. coli*, the open site on the reduced [4Fe–4S] iron–sulfur cluster forms a π adduct with a carbon–carbon double bond in the reactant (*E*)-4-hydroxy-3-methylbut-2-en-1-yl diphosphate adjacent to carbon 4 that has the hydroxy group. After the [4Fe–4S] iron–sulfur cluster is further reduced by one electron, the hydroxy group is hydronated by Glutamic Acid 126 in the active site and dissociates heterolytically from carbon 4 as a molecule of water while two electrons flow from the overreduced [4Fe–4S] iron–sulfur cluster onto the 4-hydroxy-3-methylbut-2-en-1-yl diphosphate to produce an **intermediate allylic carbanion**, coordinated to the iron ion in the now-oxidized [4Fe–4S] iron–sulfur cluster. The allylic carbanion is hydronated at one end or the other to produce either isopentenyl diphosphate or dimethylallyl diphosphate, the two products of the reaction.[678,679] An absorption in electron paramagnetic resonance spectra has been assigned to an unpaired electron within the [4Fe–4S] iron–sulfur cluster in the π adduct of the overreduced [4Fe–4S] iron–sulfur cluster in the active site of a mutant in which Glutamate 126 was converted to alanine or glutamine to prevent hydronation of the hydroxy group.[680,681] Another absorption in electron paramagnetic resonance spectra has been assigned to the unpaired electron in the [4Fe–4S] iron–sulfur in the complex between the allyl carbanion and the oxidized [4Fe–4S] iron–sulfur in the active site of the unmutated enzyme.[681] Finally, there is a crystallographic molecular model of the π adduct between 4-fluoro-3-methylbut-2-en-1-yl diphosphate and the [4Fe–4S] iron–sulfur cluster in the active site of the enzyme.[679]

In the active site of (*E*)-4-hydroxy-3-methylbut-2-enyl-diphosphate synthase (flavodoxin), which produces the reactant for 4-hydroxy-3-methylbut-2-en-1-yl diphosphate reductase, the conjugate base of the 3-hydroxy group on the reactant 2-*C*-methyl-D-erythritol 2,4-cyclodiphosphate becomes a ligand to the open site on the reduced [4Fe–4S] iron–sulfur cluster. The diphosphate dissociates from carbon 2 of 2-*C*-methyl-D-erythritol 2,4-cyclodiphosphate to form a tertiary carbenium ion stabilized by intramolecular electron transfer from the reduced [4Fe–4S] iron–sulfur cluster. An electron is then

transferred from a flavodoxin in the solution while **two electrons are transferred to the carbenium ion to produce the tertiary carbanion** stabilized by intramolecular electron transfer and perhaps direct coordination to the iron ion in the now-oxidized [4Fe–4S] iron–sulfur cluster group. This intermediate has an unpaired electron, which resides mainly on the oxidized [4Fe–4S] iron–sulfur cluster, and has an absorption in an electron paramagnetic resonance spectrum.[682,683] Following reduction of the oxidized [4Fe–4S] iron–sulfur cluster by one electron, the oxygen of the former 3-hydroxy group dissociates from the carbanionic intermediate while the two electrons in the carbanion push in to produce the carbon–carbon double bond in the product, (*E*)-4-hydroxy-3-methylbut-2-enyl-diphosphate. The 2-*C*-methyl-D-erythritol 2,4-cyclodiphosphate coordinated to the iron ion,[684] the carbenium ion stabilized by the reduced [4Fe–4S] iron–sulfur cluster, the carbanion stabilized by the oxidized [4Fe–4S] iron–sulfur cluster, and the hydroxide that leaves coordinated to the iron ion adjacent to the product (*E*)-4-hydroxy-3-methylbut-2-enyl-diphosphate have all been observed in crystallographic molecular models of the active site of (*E*)-4-hydroxy-3-methylbut-2-enyl-diphosphate synthase (flavodoxin) from *T. thermophilus*.[683]

Suggested Reading

Licht, S., Gerfen, G. J., and Stubbe, J. (1996) Thiyl radicals in ribonucleotide reductases, *Science 271*, 477–481. https://doi.org/10.1126/science.271.5248.477

Zhang, Z., Mahanta, N., Hudson, G. A., Mitchell, D. A., and van der Donk, W. A. (2017) Mechanism of a class C radical *S*-adenosyl-L-methionine thiazole methyl transferase, *J. Am. Chem. Soc. 139*, 18623–18631. https://doi.org/10.1021/jacs.7b10203

Quitterer, F., Frank, A., Wang, K., Rao, G., O'Dowd, B., Li, J., Guerra, F., Abdel-Azeim, S., Bacher, A., Eppinger, J., Oldfield, E., and Groll, M. (2015). Atomic-resolution structures of discrete stages on the reaction coordinate of the $[Fe_4S_4]$ enzyme IspG (GcpE), *J. Mol. Biol. 427*, 2220–2228. https://doi.org/10.1016/j.jmb.2015.04.002

Problem 5–13: Write a complete mechanism for the reaction catalyzed by prostaglandin-endoperoxide synthase (Equation 5–148). The mechanism should include reductions and oxidations of both the heme and the complex between the heme and molecular oxygen, formation of the tyrosyl radical, abstraction of a hydrogen by the tyrosyl radical, and formation of the two rings with an allylic carbocation as an intermediate. Abbreviate the heme as a parallelogram as usual (see Chapter 2).

Problem 5–14: An enzyme from *Streptomyces venezuelae* catalyzes the reaction[602]

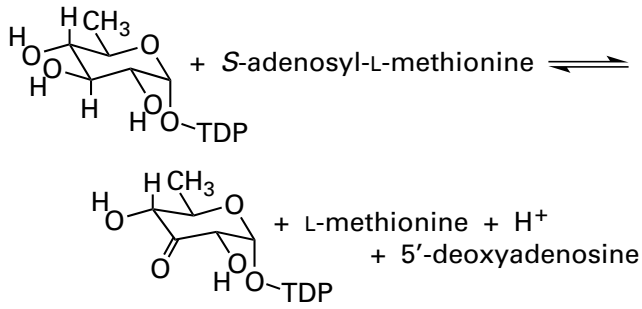

where TDP^{3-} is a thymidine diphospho group. The enzyme contains a [4Fe–4S] iron–sulfur cluster as a prosthetic group.

(A) Write a complete mechanism for the reaction. Note the oxidation state of the [4Fe–4S] iron–sulfur cluster at each step.

(B) Write a complete mechanism for the following reaction

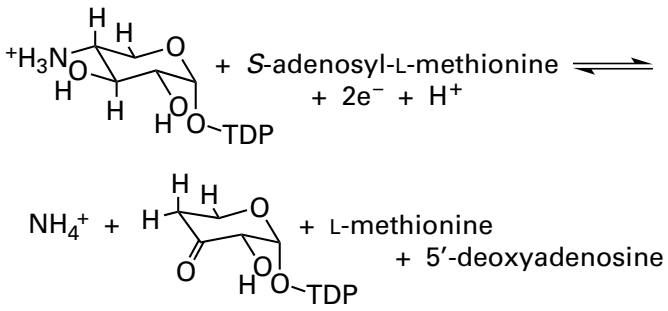

catalyzed by the same enzyme.

(C) If the second reaction were carried out in ^2H_2O, what should be the products? Why is this question ambiguous?

Problem 5–15: Based on the description given in the text, draw a detailed mechanism for the reaction catalyzed by 4-hydroxy-3-methylbut-2-en-1-yl diphosphate reductase[681] and a detailed mechanism for the reaction catalyzed by (*E*)-4-hydroxy-3-methylbut-2-enyl-diphosphate synthase (flavodoxin).[683]

Secondary Kinetic Isotope Effects

The kinetic isotope effects discussed in Chapter 4 were for isotopic substitutions in which an atom in a bond that is broken during an enzymatic reaction is replaced with a heavier isotope of the same element. The resulting decrease in the rate of the enzymatic reaction is used to give either an indication of the extent to which that bond is broken in the transition state for the step in which it is broken or, in a less sophisticated sense, simply to provide evidence that the bond in question is broken in a rate-affecting step in the enzymatic mechanism. These are **primary kinetic isotope effects**. Kinetic isotope effects also can be observed when the isotopic substitution occurs at another atom that is attached covalently to an atom participating in the breaking of a bond, other than the two atoms between which the bond is broken. For example, when the hydrogen on the anomeric carbon in α-D-glucopyranosyl 4′-bromoisoquinolinium (**5–141**)

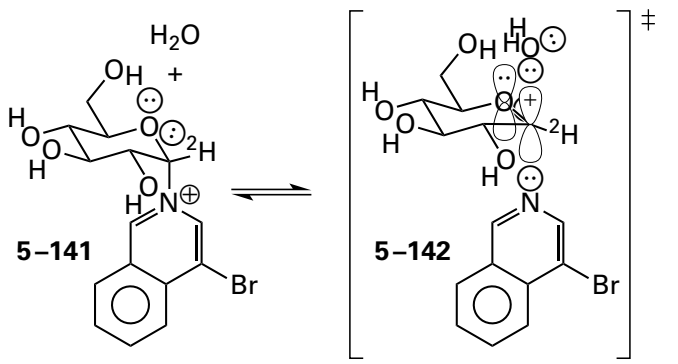

(5–163)

is replaced with a deuterium, the rate constant for the uncatalyzed hydrolysis of the glucopyranoside at 80 °C decreases, and the deuterium kinetic isotope effect, ${}^{D}k_{hyd}$,* is 1.19 ± 0.01.[685] Such changes in rate constant are secondary kinetic isotope effects, and they provide information about **how the neighboring bond is being broken** in the transition state.

A secondary kinetic isotope effect is a kinetic isotope effect in which the isotopic substitution occurs at another atom that is attached covalently to an atom participating in the breaking of a bond, other than the two atoms between which the bond is broken. A secondary kinetic isotope is a **reporter of a change in the zero-point energies** of vibrational modes in which the atom to be substituted participates between ground state and transition state as the ground state of the molecule is turned into the transition state during the reaction involving dissociation of the neighboring bond. A change in zero-point energy, $E_{0,j}$, of vibrational mode j in which the atom that will be substituted participates will change the frequency of the absorption of infrared light by that vibrational mode j, ν_j, as the transition state is approached, even though that change in absorption cannot be measured as the reaction coordinate is traversed. As before (Equations 4–211, 4–212, and 4–214)

$$E_{0,j} = \frac{h}{4\pi}\sqrt{\frac{f_j}{\mu_j}} \tag{5–164}$$

and

$$h\nu_j = \frac{h}{2\pi}\sqrt{\frac{f_j}{\mu_j}} \tag{5–165}$$

where h is Planck's constant, f_j is the force constant for vibrational mode j, and μ_j is the reduced mass

$$\frac{1}{\mu_j} = \sum_{k=1}^{o}\frac{1}{m_k} \tag{5–166}$$

of the o atoms participating in vibrational mode j.

If the force constant, f_j, for vibrational mode j is determined only by the function for the potential energy of vibrational mode j and unaffected by the change in isotope and if, during a reaction in which a molecule participates, the frequency of the quantum of light absorbed by vibrational mode j in the molecule containing the unsubstituted, lighter atom changes when the ground state is transformed into the transition state, then it follows that the change in frequency

$$\Delta\nu^{\ddagger}_{j,l} = \frac{1}{2\pi\sqrt{\mu_{j,l}}}\left(\sqrt{f^{\ddagger}_{j}} - \sqrt{f_{j,gs}}\right) \tag{5–167}$$

where ${}^{\ddagger}f_j$ is the force constant for vibrational mode j in the transition state and $f_{j,gs}$ is the force constant for vibrational mode j in the ground state. In either the ground state or the transition state, the difference between the zero-point energy for vibrational mode j for the heavy isotope and the zero-point energy for vibrational mode j for the light isotope (previously Equation 4–213)

*As before (Equation 4–176), ${}^{D}k_i = k_{iH}\,k_{iD}^{-1}$.

$$\Delta E_{0,\mathrm{ie},j} = \frac{h\sqrt{f_j}}{4\pi}\left(\sqrt{\frac{1}{\mu_{j,\mathrm{h}}}} - \sqrt{\frac{1}{\mu_{j,\mathrm{l}}}}\right) < 0 \qquad (5\text{–}168)$$

It follows from all these considerations that the difference in the differences in zero-point energy between ground state and transition state when the lighter isotope is replaced by the heavier

$$\Delta\Delta E^{\ddagger}_{0,\mathrm{ie},j} = \sqrt{\frac{1}{\mu_{j,\mathrm{h}}}}\left(\frac{h\sqrt{f^{\ddagger}_j}}{4\pi} - \frac{h\sqrt{f_{j,\mathrm{gs}}}}{4\pi}\right) - \sqrt{\frac{1}{\mu_{j,\mathrm{l}}}}\left(\frac{h\sqrt{f^{\ddagger}_j}}{4\pi} - \frac{h\sqrt{f_{j,\mathrm{gs}}}}{4\pi}\right) = \frac{h}{2}\left(\sqrt{\frac{\mu_{j,\mathrm{l}}}{\mu_{j,\mathrm{h}}}} - 1\right)\Delta\nu^{\ddagger}_{j,\mathrm{l}} \qquad (5\text{–}169)$$

Because $\mu_{j,\mathrm{h}}$ is greater than $\mu_{j,\mathrm{l}}$, it follows that the change in the difference in zero-point energy between ground state and transition state, $\Delta\Delta^{\ddagger}E_{0,\mathrm{ie},j}$, for a particular vibrational mode j in which the atom to be substituted participates will have a sign opposite to the difference in zero-point energies between transition state and ground state for vibrational mode j in the unsubstituted molecule containing the lighter isotope (Equation 5–169).

Consider the sums of the zero-point energies for those vibrational modes in which the atom to be substituted participates. If the sum in the transition state for the unsubstituted molecule is *less* than the sum in the ground state, so that the difference in the two sums between the two states is a negative number, then $\Delta\Delta^{\ddagger}E_{0,\mathrm{ie},j}$ will be a positive number; it will take more energy for the molecule substituted with the heavier isotope to reach the transition state than it does for the unsubstituted molecule; and a kinetic isotope effect greater than 1, a **normal kinetic isotope effect**, will be observed. Contrariwise, if the sum in the transition state for the unsubstituted molecule is *greater* than the sum in the ground state, so that the difference in the two sums between the two states is a positive number, then $\Delta\Delta^{\ddagger}E_{0,\mathrm{ie},j}$ will be a negative number; it will take less energy for the molecule substituted with the heavier isotope to reach the transition state than for the unsubstituted molecule; and a kinetic isotope effect less than 1, an **inverse kinetic isotope effect**, will be observed. For example, the secondary deuterium kinetic isotope effect on the rate of hydrolysis of α-D-glucopyranosyl 4′-bromoisoquinolinium ion is a normal kinetic isotope effect of 1.19. This fact means that the sum of the zero-point energies for the vibrational modes in which the hydrogen that is to be substituted participates decreases as the transition state is approached, and $\Delta\Delta^{\ddagger}E_{0,\mathrm{ie},j}$ has a positive value. If this is so, then $\Delta^{\ddagger}\nu_{j,\mathrm{l}}$ must have a negative value since $\mu_{j,\mathrm{h}}$ is greater than $\mu_{j,\mathrm{l}}$. Consequently, at least one of the infrared vibrational absorptions must decrease significantly in frequency in the transition state relative to the ground state (Equation 5–169).

An α-secondary kinetic isotope effect is a secondary kinetic isotope effect in which the isotopic substitution occurs at an atom bonded directly to one atom in a bond being broken during the reaction. The secondary kinetic isotope effect on hydrolysis of α-D-glucopyranosyl 4′-bromoisoquinolinium is an example of an α-secondary kinetic isotope effect. In the case of an α-secondary kinetic isotope effect from a carbon–hydrogen bond, the difference in zero-point energies, $\Delta E_{0,\mathrm{ie},j}$, on arrival at the transition state (Equation 5–168) is usually believed to result from a change in the hybridization of the carbon atom to which the hydrogen is attached.[686] In the case of hydrolysis of α-D-glucopyranosyl 4′-bromoisoquinolinium ion, the uninvolved carbon–hydrogen bond has become a **reporter of the change in hybridization**.

The absorptions of infrared light by stretching vibrations of carbon–hydrogen bonds on sp^3 carbons in hydrocarbons (2850–3000 cm^{-1}) are not significantly different from the absorptions of those on sp^2 carbons (2950–3100 cm^{-1}),[687] and the absorptions of infrared light by in-plane bending vibrations for carbon–hydrogen bonds on sp^2 carbons (1250–1450 cm^{-1}) are not significantly different from the absorptions of those on sp^3 carbons (1350–1500 cm^{-1}). The absorptions of infrared light by the **out-of-plane bending vibrations**, however, for carbon–hydrogen bonds on sp^2 carbons in hydrocarbons occur at considerably lower frequencies (650–1000 cm^{-1}), and these out-of-plane vibrational modes are unique to sp^2 carbons. This lower frequency of absorption results from the lack of steric hindrance and a decrease in electron repulsion above and below the plane of an sp^2 carbon relative to an sp^3 carbon.

The frequency at which an out-of-plane bending mode for a carbon–hydrogen bond on an sp^2 carbon absorbs infrared light is less than the frequency at which the bending modes on an sp^3 carbon absorb infrared light. Consequently, when an sp^3 carbon is becoming an sp^2 carbon in a transition state, the

zero-point energy is decreasing as the transition state is approached. In addition, the zero-point energy for that particular bending vibration is smaller in the transition state than in the ground state. As a result, the difference in energy between the transition state and the ground state is more positive for the deuterated molecule than the protiated molecule (Equations 5–168 and 5–169), and the rate of the reaction should decrease when a hydrogen is replaced by a deuterium. **When a carbon to which a hydrogen is bound changes from sp^3 hybridization in the ground state in the direction of sp^2 hybridization in the transition state, the α-secondary kinetic deuterium isotope effect will be normal**. A normal α-secondary kinetic deuterium isotope effect is usually taken to mean that the sp^3 carbon on which the hydrogen is located has become more like an sp^2 carbon in the transition state.

In theory, if it is assumed that the change in absorption frequency for the bending vibrational mode that becomes the out-of-plane vibration when an sp^3 carbon is converted to an sp^2 carbon is 500–600 cm^{-1}, then the change in the difference in zero-point energy producing the α-secondary deuterium kinetic isotope effect should be between 800 and 960 J mol^{-1} (Equation 5–169). When this difference is inserted into the Arrhenius equation (previously Equation 4–216)

$$\frac{k_{CH}}{k_{CD}} = e^{-\Delta\Delta G^{\circ\ddagger}/RT} = 7 \qquad (5\text{–}170)$$

The result is an α-secondary deuterium kinetic isotope effect of 1.4–1.5. The usual α-secondary deuterium kinetic isotope effect on the rate constant for reaction i, ${}^{\alpha D}k_i$, when reaction i is thought to involve, or proven to involve, a change from an sp^3 carbon in the direction of an sp^2 carbon in its transition state[686] is normal, but the observed values are usually between 1.0 and 1.2. An sp^3 carbon seldom if ever becomes a fully hybridized sp^2 carbon in the transition state, and even if it were to become fully rehybridized, a transition state is quite different from a simple ground state in which a carbon has sp^2 hybridization. Changes in the zero-point energies of other vibrational modes—in particular the small increases in the frequencies of stretching vibration and in-plane bending vibrations of the carbon–hydrogen bond—also contribute to the magnitude of the maximum value to be expected for an α-secondary deuterium kinetic isotope effect as an sp^3 carbon is becoming an sp^2 carbon. When an sp^2 carbon in the ground state is becoming an sp^3 carbon in the transition state of a reaction, the α-secondary deuterium kinetic isotope effect is inverse, with observed values between 0.83 and 1.0.

Because the reaction has a normal α-secondary deuterium kinetic isotope of 1.19 ± 0.01, it was proposed that the transition state for the uncatalyzed hydrolysis of α-D-glucopyranosyl 4′-bromoisoquinolinium (Equation 5–163) resembles an oxocarbenium ion, in which the carbon has vibrational energy levels resembling those on an sp^2 carbon, and that the 4′-bromoisoquinoline has almost completely left the carbon, while the molecule of water has not yet significantly added (**5–142**). If the leaving group is still associated with the oxocarbenium ion, the reaction would be a concerted nucleophilic substitution with a single **expanded transition state** proceeding with inversion of configuration at the anomeric carbon. If the leaving group has completely departed from the oxocarbenium ion, the oxocarbenium ion would be an intermediate in a dissociative nucleophilic substitution, and the reaction would proceed with racemization at the anomeric carbon.[688]

The distinction between concerted and dissociative nucleophilic substitution in the mechanism of such a reaction in solution is significant. In the active site of an enzyme, however, it is usually insignificant. For example, uracil-DNA glycosylase from *E. coli*[689] catalyzes the nucleophilic substitution of the uridinyl group in the trinucleotide 5′-phosphodeoxyuridyl-deoxyadenosyl-3′,5′-dideoxyguanosine (UAG) by a molecule of water after the uracil has been hydronated on oxygen 2

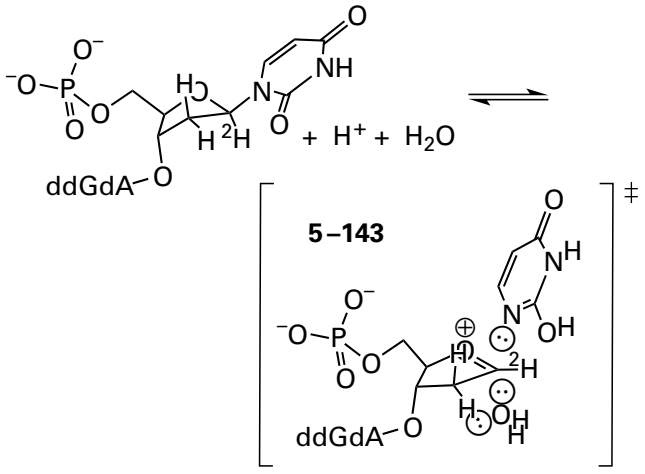

(5–171)

The reaction proceeds with inversion of configuration at the glycosidic carbon. The α-secondary deuterium kinetic isotope effect, however, on the specificity

constant, ${}^{\alpha D}k_{UAG}$, for the enzymatic reaction when the protium on the glycosidic carbon is replaced with deuterium is 1.20 ± 0.02.[690] This result is consistent with a transition state that contains almost an oxocarbenium ion from which the leaving group has almost completely departed and to which the molecule of water may or may not already be adding. Consequently, this kinetic isotope effect is consistent with a concerted nucleophilic substitution with a single, expanded transition state (**5–143**) in which the carbon is planar, with vibrational energy levels resembling those of an sp^2 carbon, or a dissociative nucleophilic substitution with an oxocarbenium ion as an intermediate. On the active site of the enzyme, however, where the molecule of water is held in position adjacent to the glycosidic carbon directly opposite the leaving group,[690] the difference between these two possibilities is inconsequential. For most glycosidases and glycosyltransferases that have been examined, the α-secondary kinetic isotope effects are normal and fall between 1.07 and 1.20.[690,691] This fact suggestis that most if not all glycosidases and glycosyltransferases have mechanisms that pass through **transition states resembling oxocarbenium ions** or that actual oxocarbenium ions are intermediates in the nucleophilic substitutions.

The catalytic constant for the elimination catalyzed by exo-(1→4)-α-D-glucan lyase

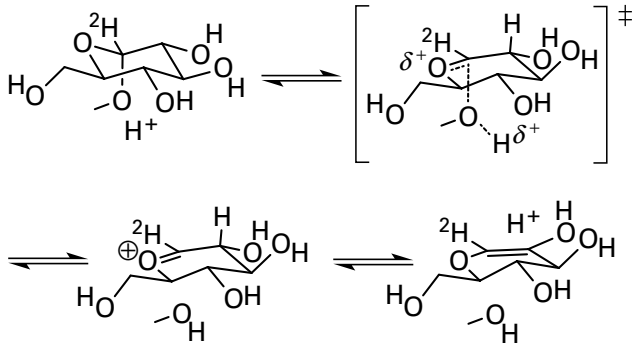

(5–172)

from *Gracilariopsis lemaneiformis* has a large normal α-secondary deuterium kinetic isotope effect of 1.19 ± 0.02 and a Brønsted coefficient for the leaving group of 0.32. From these values, it was concluded that the transition state for the first step in the reaction resembles an oxocarbenium ion and involves considerable hydron donation to the leaving group.[692]

In the case of soluble epoxide hydrolase from *Glycine max*

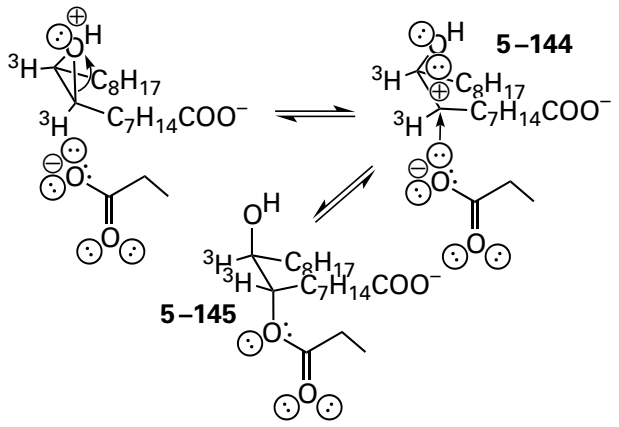

(5–173)

which has a covalent acyl intermediate at Aspartate 126 in the active site,[693,694] the specificity constant for 9,10-epoxystearic acid (eps) for the enzymatic reaction has an ***α*-secondary tritium kinetic isotope effect**, ${}^{\alpha T}k_{eps}$, of 1.30 ± 0.06 when the enzyme is hydrolyzing (*R*,*S*)-[9,10-$^3H_2$]-9,10-epoxystearic acid.[694] This result suggests two possibilities. First, a secondary **carbocationic intermediate** (**5–144**) may precede the covalent acyl intermediate (**5–145**). Second, there may be a single transition state for the nucleophilic substitution, in which the bond to the leaving hydroxy group is mostly broken and the bond to the carboxy group of Aspartate 126 has only begun to form, and the carbon is planar, with vibrational energy levels resembling those of an sp^2 carbon. In this situation, in which a carbenium ion and the nucleophile would be held in place, the difference between these two possibilities is again inconsequential.

The primary deuterium and tritium kinetic isotope effect for the catalytic and specificity constants for thymidylate synthase (Equation 5–50) from *E. coli* for [6-^{2}H]-5,10-methylenetetrahydrofolate and [6-^{3}H]- 5,10-methylenetetrahydrofolate, respectively, where the isotopic substitution is at the hydride on carbon 6 of the tetrahydrofolate that is transferred to the methylene at carbon 5 of the thiolyl adduct of deoxyuridine 5′-monophosphate in the last step of the proposed mechanism (Figure 5–5), demonstrate that hydride transfer is the rate-limiting step in the reaction and that hydride transfer is kinetically irreversible when 5,10-methylenetetrahydrofolate and deoxyuridine 5′-monophosphate are reactants.[223,224] There is, however, an α-secondary tritium kinetic isotope effect of 1.104 ± 0.004 on the specificity constant, ${}^{\alpha T}k_{dUMP}$, for deoxyuridine 5′-monophosphate (dUMP) when the hydrogen on carbon 6 of deoxyuridine 5′-monophosphate is replaced with tritium.[222] This hydrogen is on the

carbon from which the sulfanyl sulfur of the cysteine that forms the covalent adduct leaves in the last step of the mechanism. If this sulfur were to leave in a separate step, which would have to be after the transfer of the hydride from carbon 6 of tetrahydrofolate, there could not be an α-secondary kinetic isotope effect because the transfer of the hydride between carbon 6 of tetrahydrofolate and the methylene at carbon 5 of the thiolyl adduct of deoxyuridine 5′-monophosphate is the rate-limiting step in the reaction, and by definition, no step following the rate-limiting step can affect the kinetics of the reaction. Consequently, hydride transfer and the leaving of the sulfanyl group of cysteine from carbon 6 of the thiolyl adduct must be concerted (as shown in Figure 5–5).[222] The fact that the α-secondary kinetic isotope effect is greater than 1 is consistent with a change in hybridization at the carbon that becomes carbon 6 of thymidine 5′-monophosphate from sp^3 to sp^2, as expected.

An **inverse α-secondary deuterium or tritium kinetic isotope effect** is consistent with the **conversion of an sp^2 carbon into an sp^3 carbon** in the transition state for the reaction. For example, dihydropyrimidine dehydrogenase (NADP$^+$) is a flavoenzyme that reduces the carbon–carbon double bond in uracil through transfer of the hydride on nitrogen 5 of flavin to carbon 6 of the uracil[695]

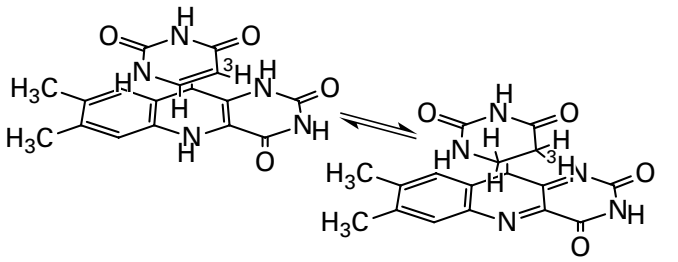

(5–174)

When the hydrogen at carbon 5 on uracil is replaced with tritium, the α-secondary tritium kinetic isotope effect on the specificity constant for uracil of porcine dihydropyrimidine dehydrogenase (NADP$^+$)[696] is inverse, with a value of 0.90 ± 0.03. This result indicates that carbon 5 is converted from the sp^2 carbon in the ground state in the direction of an sp^3 carbon in the transition state and is consistent with hydronation of carbon 5 occurring in the rate-limiting step in the reaction, which may or may not be concerted with transfer of the hydride. If transfer of the hydride precedes hydronation of the carbon, the enolate of the *N*-carbamoylcarbamoyl group in uracil, in which carbon 5 remains hybridized sp^2, would be an intermediate in the reduction.

An inverse α-secondary deuterium kinetic isotope effect is also observed for a fully **concerted nucleophilic substitution** that has a transition state in which the bond to the leaving group is mostly intact while the bond to the nucleophile has been mostly established so that there is a pentavalent transition state. In the confines of the pentavalent carbon, what were ground-state energies for vibrational modes become more positive because steric effects and electron repulsion increase in the transition state relative to the ground state. For example, in the concerted nucleophilic substitution at a primary methyl carbon catalyzed by cyclopropane-fatty-acyl-phospholipid synthase from *E. coli*

phospholipid olefinic fatty acid +
S-adenosyl-L-methionine $\rightleftharpoons$
S-adenosyl-L-homocysteine + H^+ +
phospholipid cyclopropane fatty acid
(5–175)

in which a carbon–carbon double bond, as a nucleophile, attacks the electrophilic methyl group on *S*-adenosyl-L-methionine. The fact that the α-secondary deuterium kinetic isotope effect on the catalytic constant, ${}^{\alpha D}k_0$, for [*methyl*-$^2H_3$]-*S*-adenosyl-L-methionine is 0.87 ± 0.08 is consistent with a concerted nucleophilic substitution,[697] as one might expect for a nucleophilic substitution at a methyl group. Even though the nucleophile is a poor one and the leaving group is a good one, a dissociative nucleophilic substitution would require a methyl carbenium ion.

Because the α-secondary deuterium or tritium kinetic isotope effect on a concerted nucleophilic substitution is always inverse, the significant normal α-secondary deuterium and tritium kinetic isotope effects observed for the glycosidases and epoxide hydrolase, and any other enzymatic reaction, must result from either a dissociative nucleophilic substitution or a nucleophilic substitution with a transition state that is so expanded that the usual constraints on the out-of-plane vibrational energies in the transition state for a concerted nucleophilic substitution do not occur. Consequently, the normal α-secondary deuterium and tritium kinetic isotope effects observed in these situations are definitive.

Another example of an inverse α-secondary tritium kinetic isotope effect is encountered in the reaction catalyzed by methylaspartate mutase (previously Equation 2–360)

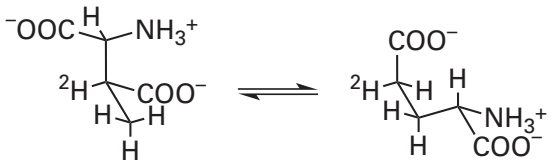

(5–176)

from *Clostridium* sp. When [5′-^{3}H]-5′-adenosylcobalamin, in which the tritium is upon the carbon that dissociates from cobalt (previously Equation 2–362)

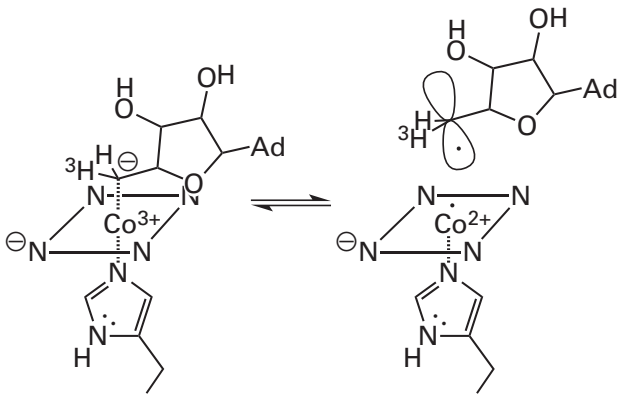

(5–177)

was incorporated into the enzyme as a prosthetic group, an α-secondary tritium kinetic isotope effect on the catalytic constant, $^{\alpha T}k_0$, of 0.76 ± 0.02 was observed.[698] This inverse effect, however, cannot be the result of a transition state in which there is concerted formation of a radical on the *threo*-3-methyl-L-aspartate proceeding through a pentavalent transition state in which the cobalt is leaving and the hydrogen being abstracted from *threo*-3-methyl-L-aspartate is entering carbon 5′. Such a transition state cannot occur because in the crystallographic molecular model of a complex between methylaspartate mutase from *Clostridium cochlearium* and cobalamin, 5′-deoxyadenosine, and L-glutamate, the cobalt from which the 5′-deoxy-5′-adenosyl radical leaves is 0.7 nm from the γcarbon of the glutamate from which a hydrogen is abstracted.[699] It follows that, as might be expected, the rate-limiting step in the reaction is abstraction of hydrogen from *threo*-3-methyl-L-aspartate (Equation 5–176), a step in which an sp^2 radical at carbon 5′ becomes an sp^3 carbon.

α-Secondary kinetic isotope effects are also observed when an atom of carbon, nitrogen, or oxygen adjacent to one atom in the bond that is being broken is replaced with another of its isotopes. For example, the normal **α-secondary carbon-13 kinetic isotope effect** on the specificity constant, $^{\alpha 13}k_{mgp}$, for hydrolysis of methyl [2-^{13}C]-α-D-glucopyranoside (mgp) by α-glucosidase from *S. cerevisiae* of 1.01 ± 0.004. This value is consistent with a transition state resembling an oxocarbenium ion.[700]

An **α-secondary oxygen-18 kinetic isotope effect indicates a change in bond order to oxygen** in the transition state. If a double bond between oxygen and the adjacent atom is partially or entirely broken in the transition state, the α-secondary oxygen-18 kinetic isotope effect will be normal; if a double bond between oxygen and the adjacent atom is partially or entirely formed, the effect will be inverse. For example, the first step in the nucleophilic substitution of an alcohol, 3-phosphoshikimate, by phosphate catalyzed by 3-phosphoshikimate 1-carboxyvinyltransferase (Equations 5–91 and 5–92)

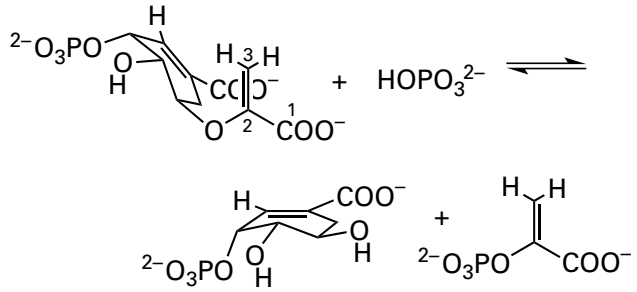

(5–178)

from *E. coli* is thought to be hydronation of carbon 3 of the carboxyvinyl group to form an oxocarbenium ion at carbon 2. Because this hydronation is a rather difficult one, this first step should be rate-limiting for the nucleophilic substitution. The enzyme also catalyzes the hydrolysis of 5-*O*-(1-carboxyvinyl)-3-phosphoshikimate, in a nucleophilic substitution in which a molecule of water is the nucleophile instead of phosphate, a nucleophilic substitution with a much more favorable equilibrium constant than that for the phosphorolysis. The inverse α-secondary oxygen-18 kinetic isotope effect for the oxygen on carbon 2 of the carboxyvinyl group is 0.986 ± 0.008. This value is consistent with a transition state that resembles an oxocarbenium ion, with a carbon–oxygen double bond at carbon 2 resulting from hydronation of carbon 3, where there was a carbon–oxygen single bond in the ground state. The inverse secondary oxygen-18 kinetic isotope effect for the two oxygens of the carboxy group at carbon 1 is 0.979 ± 0.006. This value is also consistent with such a carbocationic transition state, in which the positive charge on carbon 2 draws electron density from the oxygens onto carbon 1, increasing the bond order of those oxygens. There is also an inverse α-secondary deuterium kinetic isotope effect of 0.990 ± 0.001 for the two hydrogens on carbon 3.

This value is consistent with a conversion of this carbon from sp^2 to sp^3 in the transition state[701] as a result of its hydronation.

An α-secondary oxygen-18 kinetic isotope effect can be observed when one or both of the nonbridging oxygen-16 atoms on phosphorus in the reactant for a **nucleophilic substitution at phosphorus** are replaced by oxygen-18. It is usually assumed that such an α-secondary oxygen-18 kinetic isotope effect arises when the bonds between these oxygens and phosphorus change from double to single bonds or vice versa.[702] The theoretically calculated, normal α-secondary oxygen-18 kinetic isotope effect when a P=O double bond becomes a P–O single bond should be 1.04. The α-secondary oxygen-18 kinetic isotope effect for the uncatalyzed alkaline hydrolysis of *O,O*-diethyl-*O*-(4-carbamoylphenyl)phosphate is 1.025 ± 0.002.[703] This normal α-secondary oxygen-18 kinetic isotope effect is evidence for the conclusion that, in this nucleophilic substitution at phosphorus, the transition state is associative and resembles a phosphorane

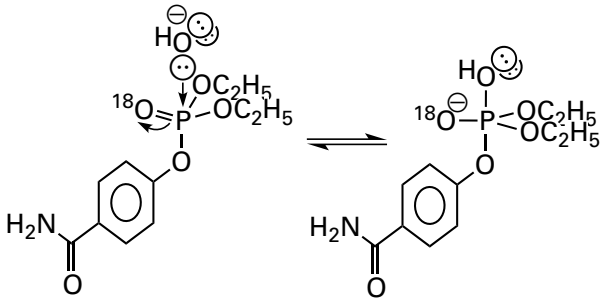

(5–179)

This phosphorane, in which the bonds are fully formed, is probably an intermediate in the reaction because the nucleophile is a strong one and the leaving group ($pK_a \cong 8.6$) is a poor one. If the transition state resembles this intermediate phosphorane, the phosphorus–oxygen double bond in the phospho group has been almost completely converted to a phosphorus–oxygen single bond, and a normal kinetic isotope of this magnitude is to be expected. In contrast, the normal α-secondary oxygen-18 kinetic isotope effect on the specificity constant, ${}^{\alpha 18}k_{\mathrm{nbp}}$, for the transfer of a 3-nitrobenzyl phosphate from 3-nitrobenzyl triphosphate (nbp) to kanamycin by gentamicin 2″-nucleotidyltransferase from *S. aureus* is 1.0033 ± 0.0004. This much smaller value has been interpreted to indicate that the bond order of phosphorus decreases partially in a slightly associative transition state resembling an expanded phosphorane.[704]

A dissociative nucleophilic substitution at phosphorus with a transition state that resembles monomeric metaphosphate should have an inverse α-secondary oxygen-18 kinetic isotope effect because monomeric metaphosphate has two phosphorus–oxygen double bonds while a phospho group has only one. The α-secondary oxygen-18 kinetic isotope effect for the specificity constant for $MgATP^{2-}$ in the nucleophilic substitution catalyzed by hexokinase from *S. cerevisiae* is 0.996 ± 0.002. This value has been presented as evidence for a partially dissociative transition state in the enzymatic reaction.[705]

Conclusions from α-secondary oxygen-18 kinetic isotope effects for nucleophilic substitutions at phosphorus involving phosphomonoesters, however, are complicated by questions of whether the monoanion or the dianion is the reactant and whether or not a nonbridging oxygen is being hydronated or dehydronated in the transition state.[702] As a result, they are often uninformative.

A β-secondary kinetic isotope effect is a secondary kinetic isotope effect in which the isotopic substitution occurs at an atom bonded to an atom that, in turn, is bonded to an atom in the bond being broken during a reaction. For example, when the two hydrogens on carbon 3 of UMP-*N*-acetylneuraminate (Uran, **5–146**)

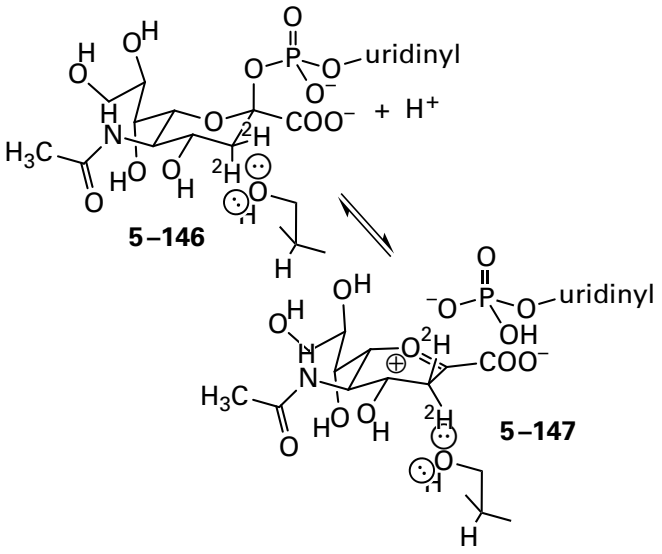

(5–180)

are replaced with deuteriums, the specificity constant k_{Uran} for transfer of the sialyl group to the 6-hydroxy group of *N*-acetyllactosamine catalyzed by β-galactoside α-2,6-sialyltransferase from *R. norvegicus* decreases. This normal, double **β-secondary deuterium kinetic isotope** effect, ${}^{\beta D}k_{\mathrm{Can}}$, is 1.22 ± 0.01,[706]

close to the value (1.28 ± 0.01) for the uncatalyzed hydrolysis of [3,3-$^2H_2$]-CMP-*N*-acetylneuraminidate, in which the alcohol to which the sialyl group is transferred is water. A normal β-secondary deuterium isotope effect of this magnitude suggests that, in the transition state, the carbon–hydrogen bond that is to be isotopically substituted has become hyperconjugated to an adjacent carbenium ion, such as the oxocarbenium ion **5–147**, that is developing in the transition state. This **hyperconjugation in the transition state** weakens the carbon–hydrogen bond that is to be isotopically substituted. This weakening of the bond decreases the zero-point energy of the carbon–hydrogen stretching vibration in the transition state, which produces a normal β-secondary deuterium kinetic isotope effect (Equation 5-169). Again, the kinetic isotope effect is reporting this decrease in the zero-point energy of the stretching vibration as ground state becomes transition state.

The product following the transition state in the active site of this inverting glycosyltransferase could be oxocarbenium ion **5–147** as a carbocationic intermediate (Equation 5–180), or the bond to the 6-hydroxy group of the *N*-acetyllactosamine could be starting to form as the bond to the phospho leaving group is almost completely broken. Again, however, the difference between these alternatives, in the case of the enzymatic reaction, is slight.

That the establishment of hyperconjugation can be the explanation for a normal β-secondary deuterium kinetic isotope effect is consistent with the kinetic isotope effects observed[707] with exo-α-sialidase from *Vibrio cholerae*, which hydrolyzes a peripheral α-sialyl group from an oligosaccharide

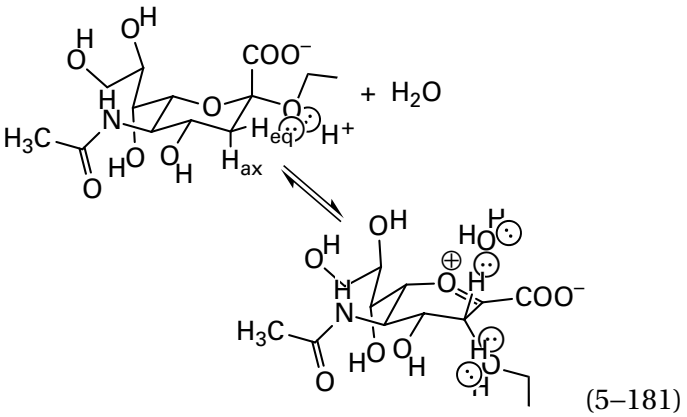

(5–181)

The β-secondary deuterium kinetic isotope effect for the axial hydrogen on carbon 3, the σ bond of which is parallel to the developing oxocarbenium ion and properly positioned for hyperconjugation, is 1.043 ± 0.002. The β-secondary deuterium kinetic isotope effect for the equatorial hydrogen on carbon 3, however, which is not parallel in the ground state but is approaching an orientation equivalent to that of the axial hydrogen in the transition state but not quite there, is only 1.034 ± 0.002.

The β-secondary deuterium kinetic isotope effect, $^{\beta D}k_{hyd}$, for the uncatalyzed hydrolysis of α-D-glucopyranosyl 4′-bromoisoquinolinium (**5–141**), produced by replacement of the protium on carbon 2 of the glucosyl group by a deuterium, is 1.09 ± 0.01.[685] This value is also consistent with a dissociative transition state that resembles an oxocarbenium ion (Equation 5–163). The β-secondary deuterium kinetic isotope effect for the same replacement on the catalytic constant, $^{\beta D}k_0$, for hydrolysis of α-D-glucopyranosyl isoquinolinium by α-glucosidase from *S. cerevisiae* is 1.11 ± 0.01. This value suggests that the transition state for the enzymatic reaction closely resembles that for the uncatalyzed reaction.

Inverse β-secondary kinetic isotope effects are also observed. For example, there is an inverse β-secondary deuterium kinetic isotope effect on the catalytic constant, $^{\beta D}k_0$, of 0.81 ± 0.02 for hydrolysis by β-lactamase from *S. aureus* at pH 6.0 of a 3-carboxyphenyl ester in which the two protiums on the α carbon of the carboxylic acid in the ester are replaced with deuteriums. This value suggests that, at least in this instance, the rate-limiting step in the mechanism is nucleophilic addition of the hydroxy group of Serine 70 in the active site[708] to the acyl carbon of the 3-carboxyphenyl ester or addition of water to the acyl carbon of the seryl ester. In either instance, the sp^2 carbon that is hyperconjugated in the ground state to these two α-hydrogens is converted in the transition state to a carbon resembling the sp^3 carbon of the tetrahedral intermediate that cannot hyperconjugate.[709]

Peptidylprolyl isomerase catalyzes isomerization of a *cis*-prolyl peptide bond to a *trans*-prolyl peptide bond

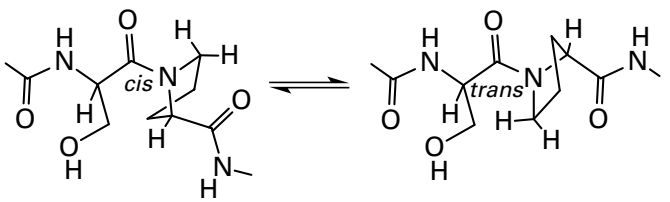

(5–182)

Because an amide is planar,[710] the hybridization of the nitrogen in a peptide bond in which proline

participates is sp^2. The lowest unoccupied σ^* antibonding orbital of the carbon–hydrogen bond on the α carbon adjacent to that nitrogen, which is parallel to the π molecular orbital system of the amide, can engage in hyperconjugation with the lobe on nitrogen in the highest occupied π molecular orbital of the amide. The inverse β-secondary deuterium kinetic isotope on the catalytic constant of human peptidylprolyl isomerase is 0.86 ± 0.08 when all seven hydrogens in the proline in a peptide substrate are changed to deuteriums. This value is consistent with a decrease in this hyperconjugation in the transition state.[711] It was concluded that, in the transition state, the nitrogen rehybridizes from sp^2 toward sp^3 in such a way that the now developing σ lone pair of electrons on the nitrogen can no longer participate in this hyperconjugation.

The more interesting kinetic isotope effect, however, is the normal α-secondary deuterium kinetic isotope of 1.6 ± 0.2 observed on the catalytic constant when the three hydrogens in the serine on the amino-terminal side of the proline (Equation 5–182) are changed to deuterium. In an amide, the π molecular orbital system has a node over the acyl carbon in its lowest unoccupied molecular orbital so that carbon cannot participate in hyperconjugation with the carbon–hydrogen bond of the α carbon of the serine. If in the transition state, however, the nitrogen in the amide can no longer conjugate with the carbon–oxygen double bond, then the amide becomes a carbonyl group that has a lobe of its lowest unoccupied molecular orbital over a partially positive carbon and that can participate in hyperconjugation with the carbon–hydrogen bond on the α carbon if the serine. The loss of the π molecular orbital system of the amide in the transition state that is reported by both of these secondary kinetic isotope effects could result from its hydronation ($pK_a = -6$). A more likely explanation, however, is a steric effect that twists the two carbons of the proline to which the nitrogen in the amide is attached, turning the nitrogen and forcing it to lose its conjugation with the carbon–oxygen double bond even though it is not hydronated. If it is, however, twisted out of conjugation by a steric effect, then the nitrogen becomes equivalent to an amino nitrogen, which is far more basic, so twisting and hydronation could function in concert.

The intrinsic primary and secondary kinetic isotope effects arising from several single isotopic substitutions in the same reactant can be **combined to obtain a fuller definition of the transition state** for a particular step in an enzymatic reaction. Orotate phosphoribosyltransferase (previously Equation 3–227)

$$\begin{gathered}\text{orotidine 5′-phosphate} + H^+ + \\ MgOPO_3PO_3^{2-} \rightleftharpoons \text{orotate} + \\ \text{magnesium 5-phospho-}\alpha\text{-D-ribose 1-diphosphate}\end{gathered} \qquad (5\text{–}183)$$

transfers a 5-phospho-D-ribosyl group between orotate and magnesium diphosphate. The rate-limiting step of the reaction becomes this nucleophilic substitution at carbon 1 of the ribosyl group if a slow substrate such as phosphonoacetic acid (an analogue of diphosphate) or orotidine (which is dephosphorylated orotidine 5′-phosphate) is used in kinetic studies. In this way, intrinsic isotopic effects can be measured directly. When various isotopic substitutes of orotidine 5′-phosphate were used as reactants in transfer of the 5-phospho-D-ribosyl group from orotate to phosphonoacetic acid catalyzed by human orotate phosphoribosyltransferase, the intrinsic kinetic isotope effects for the step in the enzymatic mechanism in which the carbon–nitrogen bond is broken were[712]

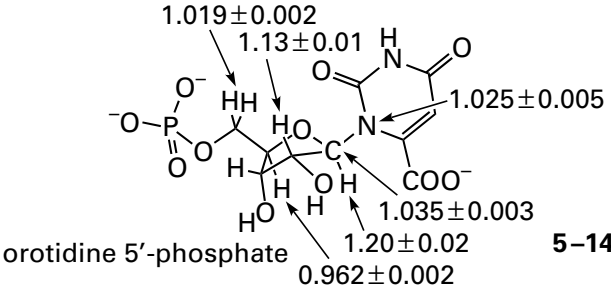

5–148

where the observed kinetic isotope effects are the numbers connected with the atom that was substituted with a heavier isotope. Each kinetic isotope effect is for a single isotopic substitution of tritium for protium, carbon-14 for carbon-12, or nitrogen-15 for nitrogen-14. Values for kinetic isotope effects that are identical or almost identical within experimental error to these values had been observed earlier for orotate phosphoribosyltransferase from *S. enterica*[713] and subsequently for human orotate phosphoribosyltransferase with orotidine and magnesium diphosphate as substrates.[714]

Nitrogen-15 and carbon-14 primary kinetic isotope effects for the reaction catalyzed by orotate phosphoribosyltransferase are consistent with significant dissociation of the carbon–nitrogen bond in the transition state. The sizable normal α-secondary tritium kinetic isotope effect for the hydrogen at

carbon 1′ is consistent with a rehybridization of carbon 1 from sp^3 to sp^2. The normal β-secondary tritium kinetic isotope effect for the hydrogen at carbon 2′ is consistent with the establishment of hyperconjugation with a developing oxocarbenium ion. The inverse γ-secondary tritium kinetic isotope effect for the hydrogen at carbon 4′ is consistent with a decrease of hyperconjugation between the σ^* antibonding orbital of the 4′ carbon–hydrogen bond and a lone pair of electrons on the 4′-oxygen in the furanosyl ring, as an incipient carbenium ion at carbon 1′ draws electron density away from the 4′-oxygen into an oxocarbenium ion. This inverse γ-secondary kinetic isotope effect at the hydrogen on a carbon adjacent to the oxygen in a furanosyl or pyranosyl ring has been observed for another ribosyltransferase[715] and has also been observed for the uncatalyzed hydrolysis of both methyl α-glucopyranoside and methyl β-glucopyranoside in strong acid.[716] The normal δ-secondary tritium kinetic isotope effect at carbon 5′ is consistent with a change in the conformation of this exocyclic carbon as a transition state resembling an oxocarbenium ion is achieved.

All kinetic isotope effects for human orotate phosphoribosyltransferase (**5–148**) are those expected from **calculations for a transition state** in which the bond between the nitrogen and the anomeric carbon (0.15 nm in the ground state) is almost completely broken (0.28 nm); the bond to the phospho oxygen (0.14 nm in the ground state) is beginning to form (0.22 nm); and the 5′-phosphoribosyl group is similar if not identical to an oxocarbenium ion.[712,714] In the case of orotate phosphoribosyltransferase from *S. enterica* (25% identity; 2.2 gap percent), rather than the human enzyme, the kinetic isotope effects observed for the reaction of orotidine 5′-phosphate and diphosphate were consistent with a calculated transition state in which the distance between the leaving nitrogen and the anomeric carbon is only 0.19 nm while that between the phospho oxygen and the anomeric carbon is 0.38 nm, even though the respective kinetic isotope effects were either identical or almost identical within experimental error to those for the human enzyme (**5–148**).[713] For human nicotinamide phosphoribosyltransferase, however, in which nicotinamide replaces orotate and nicotinamide D-ribonucleotide replaces orotidine 5′-phosphate, these two calculated distances are 0.23 and 0.26 nm, which are much closer to those for human orotate phosphoribosyltransferase even though four of the six kinetic isotope effects, although in the same direction, are different in magnitude.[717] In the case of purine nucleosidase

$$\text{a purine nucleoside} + H_2O \rightleftharpoons \text{a purine base} + \text{D-ribose} \qquad (5\text{–}184)$$

from *Crithidia fasciculata*, the observed kinetic isotope effects were consistent with a calculated transition state in which the distance between the leaving nitrogen and the anomeric carbon is 0.20 nm while that between the entering oxygen of the water is 0.30 nm, even though, again, the respective kinetic isotope effects were similar in direction and magnitude to those (**5–148**) for human orotate phosphoribosyltransferase.[715] All these results suggest that calculations of dimensions in a transition state are quite sensitive to the exact values for the individual kinetic isotope effects. Nevertheless, in these instances, in which the nucleophilic substitutions all occur at carbon 1 of a ribosyl group, the kinetic isotope effects are consistent with the respective transition states resembling an oxocarbenium ion with nucleophile approaching but only weakly bonded and a leaving group well dissociated and only weakly bonded.

Alcohol dehydrogenase removes the *pro-R* hydrogen from benzyl alcohol (bna) during its oxidation to benzaldehyde. When the *pro-S* hydrogen is replaced with tritium, the α-secondary tritium kinetic isotope effect for the specificity constant of alcohol dehydrogenase from *S. cerevisiae*, which is the ratio between the specificity constants, k_{bna}, for oxidation of benzyl alcohol and [1(*S*)-^{3}H]benzyl alcohol,[718-720] is 1.30 ± 0.02. This tritium kinetic isotope effect is normal, as would be expected for a transition state in which a carbon is changing from sp^3 to sp^2 hybridization. When the enzyme removes a deuterium rather than a hydrogen, however, from [1(*S*)-^{3}H,1(*R*)-^{2}H]benzyl alcohol, the α-secondary tritium kinetic isotope effect[718] decreases to 1.18 ± 0.03. The numerical values for these two α-secondary tritium kinetic isotope effects have been cited as evidence for a particular theoretical explanation of hydrogen tunneling in this particular reaction. In this instance, the rate-limiting step in the enzymatic reaction is transfer of the hydride, so these two kinetic isotope effects are thought to be intrinsic. Formally, however, the latter measurement is that for a double kinetic isotope effect, in which a

kinetic isotope effect decreases when a second heavy isotope is incorporated into a substrate. Double kinetic isotope effects are usually evidence for the existence of two rate-affecting steps in the kinetic mechanism of an enzymatic reaction.

Suggested Reading

Huang, X., Tanaka, K. S. E., and Bennet, A. J. (1997) Glucosidase-catalyzed hydrolysis of α-D-glucopyranosyl pyridinium salts: Kinetic evidence for nucleophilic involvement at the glucosidation transition state, *J. Am. Chem. Soc. 119*, 11147–11154. https://doi.org/10.1021/ja963733l

Lou, M., Burger, S. K., Gilpin, M. E., Gawuga, V., Capretta, A., and Berti, P. J. (2012) Transition state analysis of enolpyruvylshikimate 3-phosphate (EPSP) synthase (AroA)-catalyzed EPSP hydrolysis, *J. Am. Chem. Soc. 134*, 12958–12969. https://doi.org/10.1021/ja304339h

Problem 5–16: When the hydrogen on carbon 3 of 1-deoxy-D-xylulose 5-phosphate is replaced by deuterium, the deuterium kinetic isotope effect on the catalytic constant, ${}^{D}k_0$, for 1-deoxy-D-xylulose-5-phosphate reductoisomerase (Equation 5–114) from *E. coli* is 1.04 ± 0.02. When the hydrogen on carbon 4 is replaced by deuterium, it is 1.11 ± 0.02.[721]

(A) Write a mechanism for the reaction catalyzed by 1-deoxy-D-xylulose-5-phosphate reductioisomerase consistent with these kinetic isotope effects.

L-Ribulose-5-phosphate 4-epimerase from *E. coli*, which does not contain a nicotinamide-adenine dinucleotide as a prosthetic group, catalyzes the reaction

L-ribulose 5-phosphate $\rightleftharpoons$ D-xylulose 5-phosphate

When carbon 3 of L-ribulose-5-phosphate (r5p) is replaced with carbon-13, the kinetic isotope effect on the specificity constant, ${}^{13}k_{r5p}$, is 1.025 ± 0.001, and when carbon 4 is replaced by carbon-13, it is 1.021 ± 0.001. When the protium on carbon 3 is replaced by deuterium, the kinetic isotope effect, ${}^{D}k_{r5p}$, is 1.03 ± 0.01, and when the protium on carbon 4 is replaced by deuterium, it is 1.14 ± 0.01 at pH 5.5.[722]

(B) Write a mechanism for L-ribulose-5-phosphate 4-epimerase consistent with these kinetic isotope effects.

Problem 5–17: When [β,β-${}^{2}H_2$]-L-tryptophan is used as a reactant for tryptophanase (Equation 2–14), there is a kinetic isotope effect of 1.17 ± 0.03.[723] With what intermediate in the enzymatic reaction is this consistent?

Double Kinetic Isotope Effects

If one remembers that association of a hydron is formation of a bond and dissociation of a hydron is breaking of a bond, it follows that in almost every enzymatically catalyzed reaction more than one bond is formed or broken. If each of these bonds is formed or broken in a different kinetic step, then intermediates are necessarily produced during the reaction. If two or more bonds are formed or broken in the same step through a single transition state, then these formations or breakings are concerted, and fewer or perhaps no intermediates are involved in the mechanism. Therefore, the order in which or simultaneity with which specific bonds are made or broken can **define the chemical structures and the number of intermediates in a particular enzymatic reaction**.

To review, if a particular bond in reactant A is broken during a particular step *i* in the kinetic mechanism of an enzymatic reaction and an atom participating in that bond is changed to a heavier isotope, step *i* will experience an **intrinsic primary kinetic isotope effect**, and the microscopic rate constants for that step, both forward and reverse, will decrease. The **influence of the intrinsic primary kinetic isotope effect for step *i* on a steady-state rate constant** for the overall enzymatic reaction is determined by the extent to which that step is a rate-affecting step in the overall kinetic mechanism. For example, for a primary deuterium kinetic isotope effect resulting from the substitution of a hydrogen in reactant A with a deuterium on the specificity constant for reactant A (previously Equation 4–199)

$$ {}^{D}k_A \equiv \frac{k_{AH}}{k_{AD}} = \frac{{}^{D}k_i + c_f + c_r({}^{D}K_{eqi})}{1 + c_f + c_r} \qquad (5–185) $$

where ${}^{D}k_i$ is the intrinsic primary deuterium isotope effect on step *i*, c_f is the commitment forward, c_r is the commitment in reverse, and ${}^{D}K_{eqi}$ is the equilibrium isotope effect for step *i*. This equation determines whether or not the step in which the intrinsic primary kinetic isotope effect is exerted has an effect on the specificity constant significant enough to be measured.

Malate dehydrogenase (oxaloacetate-decarboxylating) ($NADP^+$)[724] catalyzes an oxidative decarboxylation (previously Equation 4–208)

$$NADP^+ + (S)\text{-malate} \rightleftharpoons CO_2 + \text{pyruvate} + NADPH \qquad (5\text{–}186)$$

In the direction written, the bond between carbon 2 of malate and its hydrogen is necessarily broken when it is removed as a hydride, and the bond between carbons 4 and 3 of malate is necessarily broken as carbon dioxide dissociates. Both a primary deuterium kinetic isotope effect and a primary carbon-13 kinetic isotope effect are observed on the steady-state kinetics[725] of the overall reaction catalyzed by the enzyme from *G. gallus*, resulting from substitutions of the hydrogen on carbon 2 and carbon 4 itself, respectively.

A double kinetic isotope effect is the change in a primary kinetic isotope effect associated with the overall enzymatic reaction brought about by substituting a heavier isotope at another position in the molecule at which another bond is formed or broken. For example, in the case of malate dehydrogenase (oxaloacetate-decarboxylating) ($NADP^+$), a double kinetic isotope effect would be either a change in the overall primary carbon-13 kinetic isotope effect at carbon 4 of malate on a steady-state rate constant brought about by substituting a deuterium at carbon 2 or a change in the overall primary deuterium kinetic isotope effect at carbon 2 of malate on a steady-state rate constant brought about by substituting a carbon-13 at carbon 4. Because, however, heavy atom kinetic isotope effects are so small, it is technically difficult or impossible to detect the small change in a deuterium kinetic isotope effect produced by the substitution of a heavy atom with a heavier isotope, such as carbon-13 for carbon-12. Only the **effect of substituting a deuterium** for a hydrogen on a deuterium, tritium, carbon-13, nitrogen-15, or oxygen-18 primary kinetic isotope effect, or even a secondary tritium kinetic isotope effect,[696,718] usually can be measured with sufficient precision.

A double kinetic isotope effect can be used to determine whether, in a particular enzymatic reaction, **breakings of two different bonds occur in two separate steps or take place in one step** and are concerted.[725] For example, based on the fact that 2-oxo carboxylic acids readily decarboxylate under catalysis by a metallic cation and the fact that there is a Mn^{2+} cation at the appropriate location in the active site,[726] a possible mechanism for the oxidative decarboxylation catalyzed by malate dehydrogenase (oxaloacetate-decarboxylating) ($NADP^+$) involves two steps

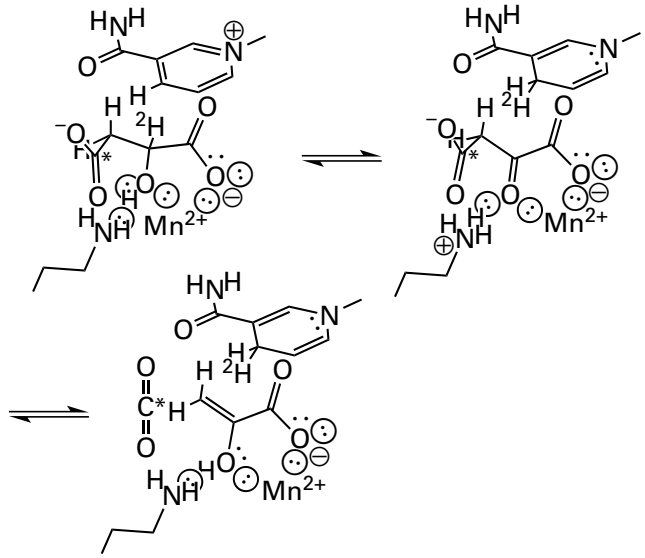

(5–187)

with oxaloacetate as an intermediate. If each of the two bonds is broken in a separate step, the substitution of hydrogen with deuterium at carbon 2 will decrease the rate only of the step involving hydride transfer, causing it to become more rate-affecting at the expense of the other steps in the reaction. Consequently, the primary carbon-13 kinetic isotope effect on the overall reaction would have to decrease in magnitude because the step in which this bond is broken has **become less rate-affecting**. It is also possible, however, that the two bond breakings, carbon–hydrogen and carbon–carbon, are concerted and occur in the same step. If the reaction were concerted and both bonds were broken in the same step, the substitution of hydrogen with deuterium at carbon 2 would decrease the rate of this single step, **causing it to become more rate-affecting** in the overall reaction, and the primary carbon-13 kinetic isotope effect on the overall reaction would have to increase in magnitude. Such an argument can apply to any two bond breakings or bond formations in any enzymatic reaction.

This intuition can be verified mathematically.[725,727] The primary carbon-13 kinetic isotope effect on the specificity constant for [4-^{13}C]-(*S*)-malate (mal), when it is a reactant in the oxidative decarboxylation catalyzed by malate dehydrogenase (oxaloacetate-decarboxylating)(NADP$^+$) (Equation 5–185)

$$^{13}k_{\text{mal}} \equiv \frac{k_{\text{mal},12}}{k_{\text{mal},13}} = \frac{^{13}k_i + c_\text{f} + c_\text{r}(^{13}K_{\text{eq}i})}{1 + c_\text{f} + c_\text{r}} \tag{5–188}$$

where the rate constants $k_{\text{mal},12}$ and $k_{\text{mal},13}$ are the specificity constants for malate for the reaction run with unsubstituted [4-^{12}C]-(*S*)-malate and with [4-^{13}C]-(*S*)-malate, respectively; $^{13}k_i$ is the intrinsic primary carbon-13 kinetic isotope effect on the forward rate constant for step *i*, the step in which the bond to carbon 4 is broken; c_f and c_r are the commitments forward and in reverse, respectively; and $^{13}K_{\text{eq}i}$ is the carbon-13 equilibrium isotope effect on step *i*. Suppose that the kinetic mechanism for the reaction is (previously Equation 4–192)

$$\begin{aligned} \text{E}_1 \underset{k_{-1}}{\overset{k_1[\text{A}]_0}{\rightleftharpoons}} \text{E}_2 \underset{k_{-2}}{\overset{k_2[\text{B}]_0}{\rightleftharpoons}} \text{E}_3 \underset{k_{-3}}{\overset{k_3}{\rightleftharpoons}} \text{E}_4 \underset{k_{-4}}{\overset{k_4}{\rightleftharpoons}} \\ \text{E}_5 \underset{k_{-5}[\text{X}]_0}{\overset{k_5}{\rightleftharpoons}} \text{E}_6 \underset{k_{-6}[\text{Y}]_0}{\overset{k_6}{\rightleftharpoons}} \text{E}_7 \underset{k_{-7}[\text{Z}]_0}{\overset{k_7}{\rightleftharpoons}} \text{E}_1 \end{aligned} \tag{5–189}$$

where reactants A and B are NADP$^+$ and (*S*)-malate, respectively; products X and Y are either carbon dioxide and pyruvate or pyruvate and carbon dioxide, respectively; and product Z is NADPH.[728] If the step in which the hydride is transferred between carbon 2 and NADP$^+$ (step 3) precedes the step in which the bond between carbons 3 and 4 is broken (step 4), the more chemically reasonable order, then when $[\text{B}]_0 > 0$, the commitment forward (see Equation 4–197)

$$c_\text{f} \equiv \frac{k_{4,12}}{k_{\text{r}i}} = \frac{k_{4,12}(k_2k_3[\text{B}]_0 + k_3k_{-1} + k_{-1}k_{-2})}{k_{-1}k_{-2}k_{-3}} \tag{5–190}$$

where $k_{4,12}$ is the forward rate constant for step 4 when the carbon is carbon-12. The **commitment forward will increase** because k_{-3} decreases when deuterium replaces protium. If the step in which the hydrogen is transferred between carbon 2 and NADP$^+$ (step 4) follows the step in which the carbon–carbon bond is broken during the decarboxylation (step 3), then the commitment in reverse (see Equation 4–198)

$$c_\text{r} \equiv \frac{k_{4,12}}{k_{\text{f}i}} = \frac{k_{4,12}(k_{-3}k_{-4} + k_{-3}k_5 + k_4k_5)}{k_3k_4k_5} \tag{5–191}$$

The **commitment in reverse will increase** because k_4 decreases when deuterium replaces protium. Neither $^{13}k_i$ nor $^{13}K_{\text{eq}i}$ will be affected significantly in either case when a hydrogen on carbon is changed to a deuterium because the β-secondary kinetic isotope effect should be insignificant. Therefore, because $^{13}k_i > 1$, the observed kinetic isotope effect on the specificity constant, $^{13}k_{\text{mal}}$, will be less when deuterium is on carbon 2 than when protium is on carbon 2, regardless of whether the step in which the hydrogen is removed precedes or follows the step in which the carbon–carbon bond breaks.

If the step in which the hydrogen is transferred between carbon 2 and NADP$^+$ is the same step in which the carbon–carbon bond is broken, then c_f (Equation 5–190) decreases because k_i, the rate constant for step *i* in which the carbon–carbon bond is broken, decreases when the hydrogen is replaced by deuterium. Therefore, because $^{13}k_i > 1$, the observed kinetic isotope effect increases when transfer of the hydrogen between carbon 2 and NADP$^+$ occurs in the same transition state in which the carbon–carbon bond is breaking.

Whether the actual change in a carbon-13 kinetic isotope effect is large enough to be observed will depend on the respective magnitudes of the commitments themselves as well as the changes that occur in them. For example, if both c_f and c_r are small so that the carbon-13 kinetic isotope effect on the specificity constant is the intrinsic kinetic isotope effect, there will be a negligible effect of substituting the deuterium for the protium; and if either commitment is large, there will also be a negligible effect. In the former case, however, there will be only a small primary deuterium kinetic isotope effect on the specificity constant, and in the latter case, there will not be a significant primary carbon-13 kinetic isotope effect on the specificity constant. If both deuterium and carbon-13 kinetic isotope effects are observed, then there is a good chance that they will interact with each other.

What this explanation emphasizes is that the double kinetic isotope effect arising from substituting the second atom with a heavier isotope is not exerted on the intrinsic kinetic isotope effect itself

for breaking the bond in which the first atom participates. Rather, the effect of substituting the second atom with a heavier isotope results from the effect that the intrinsic kinetic isotope effect for the second atom has on the primary kinetic isotopic effect for the substitution of the first atom on the specificity constants or the catalytic constant, or both of them, for the overall reaction. In other words, it is an **effect on the steady-state rate constants**. A double kinetic isotope effect is observed because specificity constants and catalytic constants are usually composite macroscopic rate constants, often quite complicated ones, determined by several or many microscopic rate constants, and an intrinsic kinetic isotope effect is exerted on only two microscopic rate constants.

The foregoing mathematical development is not unique to carbon-13–deuterium double kinetic isotope effects and can be applied to the double kinetic isotope effect between deuterium and any other isotopic substitution.

For malate dehydrogenase (oxaloacetate-decarboxylating) ($NADP^+$) from *G. gallus* at pH 8.0 and 25 °C, the carbon-13 kinetic isotope effect, $^{13}k_{mal}$, on the specificity constant for malate (mal) is 1.0302 ± 0.0005.[725] If the hydrogen at carbon 2 is changed to a deuterium, this carbon-13 kinetic isotope effect decreases to 1.0250 ± 0.0007. Therefore, the bond between carbon 2 and hydrogen is broken in a different step in the kinetic mechanism than that in which the bond between carbons 4 and 3 is broken. There must be **two steps and an intermediate**. When 3-acetylpyridine adenine dinucleotide phosphate, however, is used as a reactant in place of nicotinamide adenine dinucleotide phosphate, the catalytic constant increases twofold and the specificity constant for 3-acetylpyridine adenine dinucleotide phosphate increases threefold. The fact that the primary carbon-13 kinetic isotope effect on the specificity constant for substituting carbon 4 now increases from 1.0056 ± 0.0005 to 1.0087 ± 0.0007 when a deuterium replaces a hydrogen at carbon 2 indicates that the reaction has become concerted, with removal of the hydride coinciding with breaking of the carbon–carbon bond, and that oxaloacetate can no longer be an intermediate.[729]

Only when the microscopic rate constants for each of the two steps altered by the respective isotopic substitutions are by themselves rate-affecting will a double kinetic isotope effect be observed. Unless the single concerted step or each of the two steps involving breaking and formation of the two bonds is rate-affecting, a **shift in the relative importance of the rate-affecting steps** cannot occur. Consequently, each isotopic substitution alone must produce a primary kinetic isotope effect on a steady-state rate constant, and to be reassured of the interpretations of the results of these experiments, both single kinetic isotope effects must be observed. In the case of malate dehydrogenase (oxaloacetate-decarboxylating) ($NADP^+$), the primary deuterium kinetic isotope effect, $^{D}k_{mal}$, on the specificity constant for malate is 1.47, and as already mentioned, the primary carbon-13 kinetic isotope effect, $^{13}k_{mal}$, is 1.302.[725] In this case, the primary deuterium kinetic isotope effect is not that much different from 1, which suggests, as required by all the foregoing development, that while it is rate-affecting, transfer of the hydride from (*S*)-malate to $NADP^+$ is not rate-limiting.

If breakings or formings of the two bonds, respectively, are not concerted and if the equilibrium isotope effects for the two steps in a mechanism in which their intrinsic kinetic isotope effects are exerted are sufficiently different from each other, then it is also **possible to determine which step precedes the other.** In this situation, because c_r is multiplied by the equilibrium isotope effect in Equation 5–188 and c_f is not, different relations will exist among the various observed kinetic isotope effects, depending on which step comes first.[725] For example, malate dehydrogenase (oxaloacetate-decarboxylating) ($NADP^+$) has a deuterium equilibrium isotope effect[730] of 1.18. In other words, the equilibrium constant for the reaction when hydride is transferred between oxaloacetate and $NADP^+$ is 1.18 times greater, in favor of oxaloacetate and NADPH, than the equilibrium constant when deuteride is transferred between oxaloacetate and $NADP^+$ (Equation 5–187). Taken together, this value for the deuterium equilibrium isotope effect and values for the carbon-13 equilibrium isotope effect, deuterium kinetic isotope effect, carbon-13 kinetic isotope effect, and carbon-13 kinetic isotope effect after substitution of deuterium at carbon 2 are consistent only with a kinetic mechanism in which hydride transfer precedes decarboxylation.[725] Therefore, oxaloacetate must be an intermediate in the enzymatic reaction, the conclusion which always made the most chemical sense.

Phosphogluconate dehydrogenase ($NADP^+$-dependent, decarboxylating) catalyzes formally the same reaction (compare Equations 5–76 and 5–187) as does malate dehydrogenase (oxaloacetate-decarboxylating) ($NADP^+$). The carbon-13 kinetic isotope effect for carbon-13 substitution at carbon 1 of 6-phospho-D-gluconate on the specificity con-

stant, k_{6pg}, for 6-phospho-D-gluconate (6pg) for the enzyme from *S. cerevisiae* is 1.0096 ± 0.0006. When the hydrogen on carbon 3 of 6-phospho-D-gluconate is replaced with deuterium, the carbon-13 kinetic isotope effect on the specificity constant decreases to 1.0081 ± 0.0002. Therefore, hydride transfer from carbon 3 and decarboxylation of carbon 1 are not concerted.[731] Similar results were obtained with the ovine enzyme and the enzyme from *C. jadinii*.[732] In the enzyme from *S. cerevisiae*, the magnitudes of the various kinetic isotope effects are together consistent with a kinetic mechanism in which hydride transfer precedes decarboxylation and in which 3-oxo-6-phospho-D-gluconate is the β-oxo acid that is the intermediate in the enzymatic reaction (Equation 5–76).

Prephenate dehydrogenase also catalyzes a reaction in which a hydride transfer and a decarboxylation occur. The reaction can be written with a reasonable divinylketone (**5–149**), a vinylogous β-oxo acid, as an intermediate

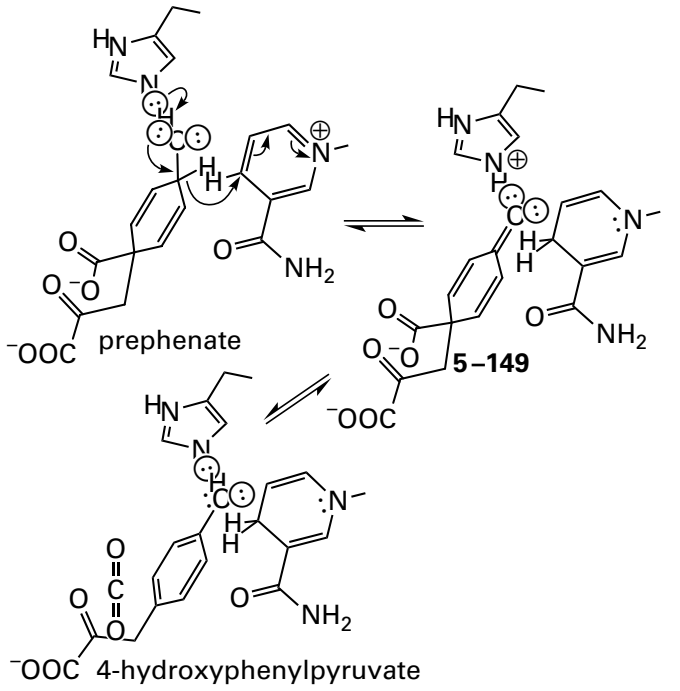

(5–192)

The divinyl ketone resembles the intermediate in the electrophilic aromatic substitution of a phenol at its carbon 4

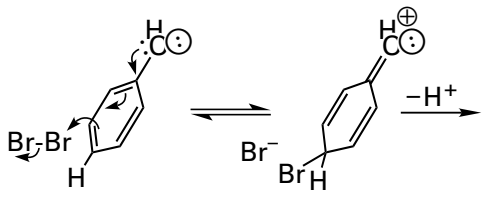

(5–193)

and explains the role of the imidazolyl group of a histidine that forms a hydrogen bond to the hydroxy group of the substrate 4-hydroxyphenylpyruvate in the active site.[733] It has also been shown[734] that the related nonenzymatic, acid-catalyzed 1,4-elimination of water and carbon dioxide from prephenate passes through a carbocationic intermediate

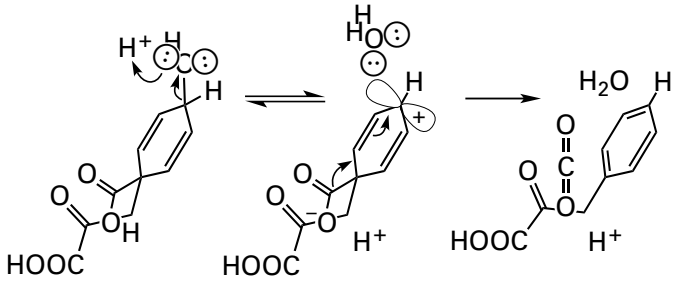

(5–194)

even though that intermediate is even less stable than divinyl ketone **5–149**.

Nevertheless, when the hydrogen on carbon 4 of the alternative reactant for prephenate dehydrogenase, 3-(*cis*-1-carboxy-4-hydroxy-2,5-cyclohexadien-1-yl)propanoic acid (chp)

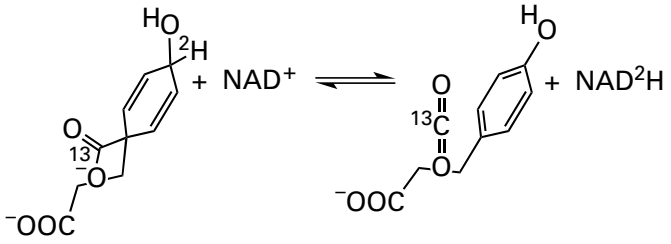

(5–195)

is replaced with a deuterium, the carbon-13 kinetic isotope effect on the specificity constant, k_{chp}, for [^{13}C]carboxy substitution at carbon 1 increases from 1.0033 ± 0.0008 to 1.0103 ± 0.0013.[734] This unmistakable, statistically significant increase is consistent only with a concerted mechanism for prephenate dehydrogenase in which hydride transfer and decarboxylation occur in the same transition state. This mechanism is different from the one expected (Equation 5–192), and intermediate **5–149** must not be formed. Therefore, the σ bond between carbon 1 and the carboxylato group that is forming

carbon dioxide must provide antarafacial push to the hydride leaving the 3-(*cis*-1-carboxy-4-hydroxy-2,5-cyclohexadien-1-yl)propanoic acid from carbon 4, in addition to the push provided by the 4-hydroxy group, in a **concerted reaction with no intermediate**

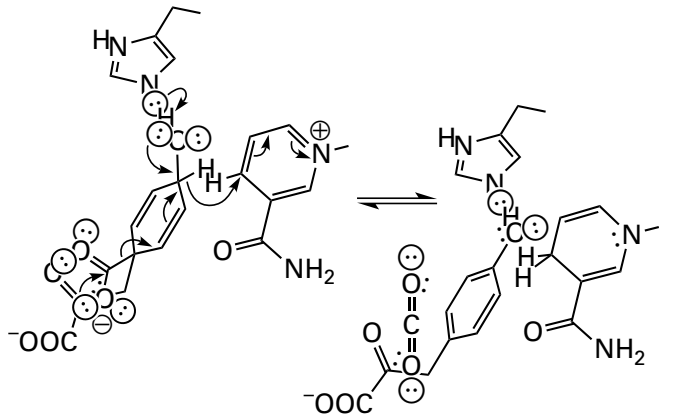

(5–196)

The double kinetic isotope effects discussed so far have been for situations in which a primary kinetic isotope effect increases or decreases when another atom is changed to a heavier isotope. It is also possible that **no change occurs in the kinetic isotope effect** upon isotopic substitution at the other position even though individual kinetic isotope effects are observed for isotopic substitution at each position independently. Formate dehydrogenase (previously Equation 4–171)

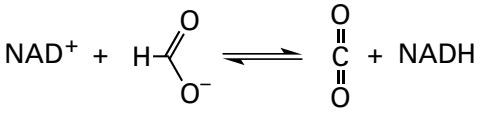

(5–197)

from *S. cerevisiae* displays both a primary carbon-13 kinetic isotope effect (1.0413 ± 0.0006) for [^{13}C]formate and a primary deuterium kinetic isotope effect (2.85 ± 0.04) for [^{2}H]formate on the specificity constant, k_{fm}, for formate (fm) when the pyridine aldehyde derivative of NAD$^+$, 3-formylpyridine adenine dinucleotide, is used as the other reactant.[735] When the two deuterated formates, [^{12}C,^{2}H]formate and [^{13}C,^{2}H]formate, are used as reactants, the carbon-13 kinetic isotope effect is identical (1.414 ± 0.0001) to that for the hydronated formates. In this instance, the bond involving the deuterium is the same bond as that involving carbon-13—namely, the carbon–hydrogen bond of formate—so these results can say nothing about intermediates in the reaction. They do, however, speak to the issue of the rate-limiting step in the enzymatic reaction. If any steps other than hydride transfer contributed to the rate constant k_{fm}—in other words, if the commitments c_f and c_r in the equivalent of Equation 5–188 were other than nearly zero—then the carbon-13 kinetic isotope effect would have to increase when deuterium replaces hydrogen. Only if hydride transfer is the rate-limiting step in the enzymatic reaction and if all steps preceding it are so much faster that they do not contribute to the value for k_{fm} will the slowing of this step by substituting deuterium for hydrogen have no effect on the observed carbon-13 kinetic isotope effect. Because no effect was seen, it could be concluded[736] that both the deuterium and carbon-13 kinetic isotope effects were the intrinsic isotope effects for the step in which the carbon–hydrogen bond was broken heterolytically. From these intrinsic kinetic isotope effects, arguments could be made concerning the structure of the transition state for the step in which hydride transfer occurs at the active site.[735]

Even though they rely only on kinetic isotope effects on steady-state rate constants, double kinetic isotope effects, again because they provide additional independent equations, can be used in concert with other results to **estimate intrinsic kinetic isotope effects**. For example, intrinsic kinetic isotope effects for malate dehydrogenase (oxaloacetate-decarboxylating) (NADP$^+$) could be calculated from carbon-13–deuterium double kinetic isotope effects and tritium, deuterium, and carbon-13 primary kinetic isotope effects on the steady-state rate constants.[725] For carbon–hydrogen bond cleavage during hydride transfer, the intrinsic primary deuterium kinetic isotope effect, ^{D}k, was estimated to be 5.6 ± 0.5. For carbon–carbon bond cleavage during decarboxylation, the intrinsic primary carbon-13 kinetic isotope effect, ^{13}k, was estimated to be 1.05 ± 0.01. These values were confirmed by later intermediate partitioning experiments.[737] They define, in the absence of tunneling, a transition state for hydride transfer in which the bond to malate is almost entirely broken and a transition state in which the bond to the carbon that becomes carbon dioxide is also almost entirely broken.

So far, only double kinetic isotope effects for the substitution of hydrogen with deuterium on a primary carbon-13 kinetic isotope effect have been described. If two bonds broken or formed during an enzymatic reaction involve hydrogen, but the hydrogens are on different atoms, a **deuterium–deuterium double kinetic isotope effect** for substitution of the other protium with deuterium on a primary deuterium kinetic isotope effect may be observed.[738] For example, in the reaction catalyzed

by the flavoenzyme dihydroorotate dehydrogenase (fumarate), the prosthetic flavin mononucleotide is oxidized by fumarate, and the oxidized flavin mononucleotide then oxidizes dihydroorotate by removing two hydrogens (previously Equation 4–177)

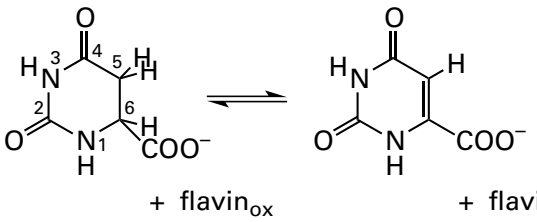

(5–198)

The latter reaction, in isolation, can be followed spectrophotometrically by monitoring the decrease in A_{475} of the flavin after oxidized enzyme is rapidly mixed with a saturating concentration of dihydroorotate in the absence of fumarate. The primary deuterium kinetic isotope effect on the catalytic constant for this reduction of the oxidized enzyme from *L. lactis* for substitution of the two hydrogens at carbon 5 with deuterium is 1.83 ± 0.04. When this same substitution is made when there is deuterium rather than hydrogen at carbon 6, the primary deuterium kinetic isotope effect is 1.95 ± 0.12. The primary deuterium kinetic isotope effect on this same rate constant for substitution of the hydrogen on carbon 6 with deuterium is 2.21 ± 0.04. If this same substitution is made when there are two deuteriums in place of protiums on carbon 5, the primary kinetic isotope effect is 2.35 ± 0.16.[739] The facts that, within the margin of error, neither primary kinetic isotope effect was affected by the other substitution, but that in both cases the primary kinetic isotope effects increase, are consistent with three conclusions: both hydrogens are removed in the same transition state; the commitments forward and reverse from this step are negligible within the error of the measurements; and concerted removal of the hydrogens is the rate-limiting step in the reaction.

It is also possible to measure the double kinetic isotope effect of a solvent deuterium kinetic isotope effect on a primary deuterium kinetic isotope effect and vice versa. For example, isocitrate dehydrogenase (NADP$^+$)

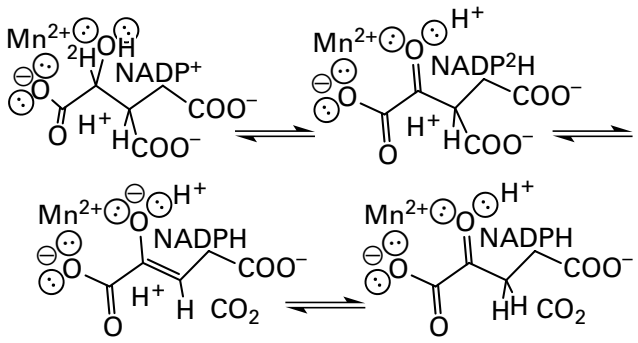

(5–199)

from *M. tuberculosis* catalyzes a reaction analogous to that catalyzed by malate dehydrogenase (oxaloacetate-decarboxylating) (NADP$^+$) (Equations 5–186 and 5–187), in which a reduction by nicotinamide and a decarboxylation occur. When isocitrate and [2-^{2}H]isocitrate are used as reactants in H_2O, the primary deuterium kinetic isotope effect on the catalytic constant is 1.3 ± 0.1, and the primary deuterium kinetic isotope effect on the specificity constant for isocitrate is 1.5 ± 0.2. In ^2H_2O, these primary kinetic isotope effects decrease to 1.2 ± 0.1 and 1.0 ± 0.3, respectively. When unsubstituted isocitrate is used as a reactant, the solvent deuterium kinetic isotope effect on the catalytic constant is 3.0 ± 0.2, and the solvent deuterium kinetic isotope effect on the specificity constant for isocitrate is 1.5 ± 0.3. When [2-^{2}H]isocitrate is used as a reactant, these solvent deuterium kinetic isotope effects decrease to 1.7 ± 0.2 and 1.0 ± 0.2, respectively.

The fact that both primary deuterium kinetic isotope effects decrease when H_2O is changed to ^2H_2O and the fact that both solvent deuterium kinetic isotope effects decrease when isocitrate is changed to [2-^{2}H]isocitrate[740] are consistent with transfer of the hydride from carbon 2 of isocitrate to NADP$^+$ occurring in a step separate from hydron transfer from or to a catalytic acid–base. The manganese complex of isocitrate is the reactant, and as a result, removal of the hydron from the hydroxy group should be so rapid as to not be rate-affecting and probably concerted with transfer of the hydride. Consequently, the only reasonable transfer of a hydron that could produce the solvent deuterium kinetic isotope effects is transfer from a catalytic acid in the active site, which has been identified crystallographically[741] as Tyrosine 142, to carbon 3 of the enolate (Equation 5–199). Hydronation of carbon is always a slow reaction.

The deuterium kinetic isotope effect for hydride transfer from [4(*R*)-^{2}H]NADH to pyruvate by human L-lactate dehydrogenase, however, increases from

2.64 ± 0.02 to 2.74 ± 0.04 when the solvent is changed from H_2O to ^2H_2O. The solvent deuterium kinetic isotope effect increases from 2.51 ± 0.02 to 2.61 ± 0.04 when NADH is changed to [4(*R*)-^{2}H]NADH. These increases in the two kinetic isotope effects are consistent with concerted transfer of the hydride and a hydron in the same step in the kinetic mechanism of the enzyme.[742]

The pyridoximine of 2-aminoacrylate (see Equation 2–13)

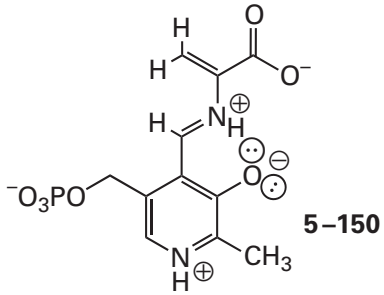

5–150

absorbs strongly at 340 nm. It is possible to follow formation of the pyridoximine of 2-aminoacrylate on the active site of tryptophanase (see Equation 2–14)

$$\text{L-tryptophan} + H_2O \rightleftharpoons \text{indole} + \text{pyruvate} + NH_4^+ \qquad (5\text{–}200)$$

from *E. coli* by following the increase in A_{345} after rapid mixing of the enzyme and a saturating concentration of L-tryptophan. The solvent deuterium kinetic isotope effect on the rate constant for formation of this intermediate is 1.8 ± 0.1. The primary kinetic isotope kinetic effect on the same rate constant when [α-^{3}H]-L-tryptophan is used as a reactant increases from 3.0 ± 0.3 to 4.3 ± 0.2 when the water used as the solvent for the reaction is replaced with deuterium oxide.[723] This result suggests that, in the same transition state in which the hydron is removed from the α carbon of the external pyridoximine of L-tryptophan, another exchangeable hydron on a catalytic acid in the active site is being transferred to this same intermediate in the enzymatic reaction. The most likely candidate for this acid is the carboxy group of Aspartic Acid 227, which forms a hydrogen bond to the pyrimidino nitrogen of pyridoxal phosphate in the active site.[743] This carboxy group would be hydronating the pyrimidino nitrogen as the α-hydron is being removed from the external pyridoximine to give the quinonoid intermediate derived from L-tryptophan (see Equation 2–4)

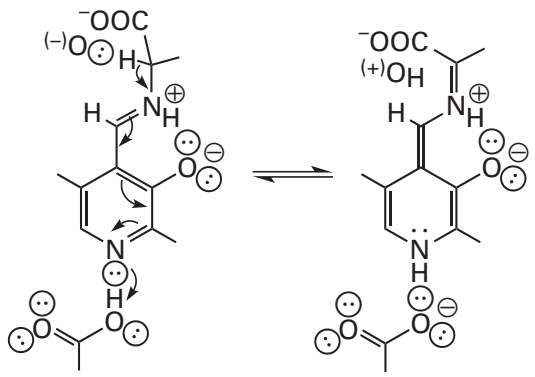

(5–201)

Unfortunately, the rates of most of the steps in an enzymatic reaction, even steps involving conformational changes of the protein, are decreased when water is replaced by deuterium oxide, so no unambiguous conclusions, even the conclusion that a dissociable hydron on a catalytic base is not transferred in the step exhibiting the primary kinetic isotope effect, can be reached from the observation that a primary kinetic isotope effect decreases when water is replaced by deuterium oxide.[744,745]

Suggested Reading

Hermes, J. D., Roeske, C. A., O'Leary, M. H., and Cleland, W. W. (1982) Use of multiple isotope effects to determine enzyme mechanisms and intrinsic isotope effects: Malic enzyme and glucose-6-phosphate dehydrogenase, *Biochemistry 21*, 5106–5114. https://doi.org/10.1021/bi00263a040

Quartararo, C. E., Hazra, S., Hadi, T., and Blanchard, J. S. (2013) Structural, kinetic and chemical mechanism of isocitrate dehydrogenase-1 from *Mycobacterium tuberculosis*, *Biochemistry 52*, 1765–1775. https://doi.org/10.1021/bi400037w

Problem 5–18: The catalytic constant k_0 for mandelate racemase from *P. putida* for [α-^{1}H]-(*R*)-mandelate in H_2O is 370 ± 20 s^{-1}; for [α-^{2}H]-(*R*)-mandelate in H_2O, it is 120 ± 10 s^{-1}; for [α-^{1}H]-(*R*)-mandelate in D_2O, it is 170 ± 10 s^{-1}; and for [α-^{2}H]-(*R*)-mandelate in D_2O, it is 80 ± 10 s^{-1}.[746]

(A) Calculate the primary deuterium kinetic isotope effect on the catalytic constant, $^Dk_0$, for the enzymatic reaction in H_2O.

(B) Calculate the primary deuterium kinetic isotope effect on the catalytic constant, $^{D}k_0$, for the enzymatic reaction in D_2O.
(C) What do these results suggest about the enzymatic reaction? Why is this suggestion ambiguous?

Isotopic Exchange

Isotopic exchange is the exchange of one isotope of an atom in a reactant for a different isotope of that atom catalyzed by the active site of an enzyme. The exchanged isotope then appears in the solution in the reactant or a product of the enzymatic reaction. A simple example of isotopic exchange is that observed when glycerone phosphate, in the absence of D-glyceraldehyde 3-phosphate, is mixed with fructose-bisphosphate aldolase (Figure 4–36) from *O. cuniculus* in tritiated water (^3H_2O).[747] When the specific radioactivity of the water was 9800 cpm (μmol of hydrogen)$^{-1}$, the specific radioactivity of glycerone phosphate in the solution monotonically increased from 0 to 9800 cpm (μmol of glycerone phosphate)$^{-1}$, after which only a slow nonenzymatic increase in its specific radioactivity was seen. Because no glyceraldehyde 3-phosphate was added, no fructose 1,6-bisphosphate was produced. The enzyme, however, was able to transform one reactant in the absence of the other by exchanging a tritium for a protium. This situation is an example of **hydrogen isotopic exchange**, which is the exchange of one isotope of hydrogen—protium, deuterium, or tritium—for a different isotope of hydrogen, catalyzed by the active site of an enzyme. Usually, the protium, deuterium, or tritium in the reactant or an intermediate produced from the reactant is at an acidic position and is removed as a **hydron**—a proton, deuteron, or triton—by a catalytic base in the active site from the reactant or intermediate, replaced on the resulting catalytic conjugate acid by a hydron of the other isotope in a series of acid–base reactions, and then returned as the other isotope—a triton, deuteron, or proton—to the reactant or intermediate.

A simple example of oxygen isotopic exchange is encountered in the reaction catalyzed by deoxycytidylate 5-hydroxymethyltransferase (Equation 5–56) from Enterobacteria phage T4

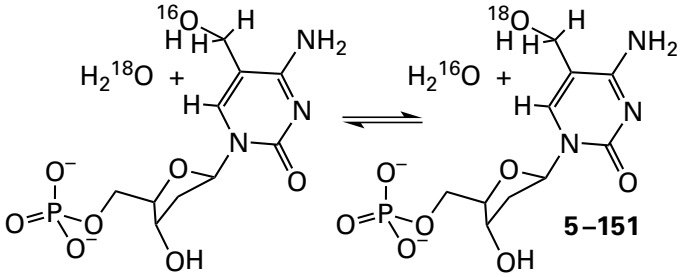

(5–202)

In the penultimate step of the reaction, a hydroxide anion, or a molecule of water from which a hydron is being removed in concert by a catalytic base, adds as a nucleophile to the methylene of the intermediate homologous to intermediate **5–38** for the reaction catalyzed by thymidylate synthase (Figure 5–5)

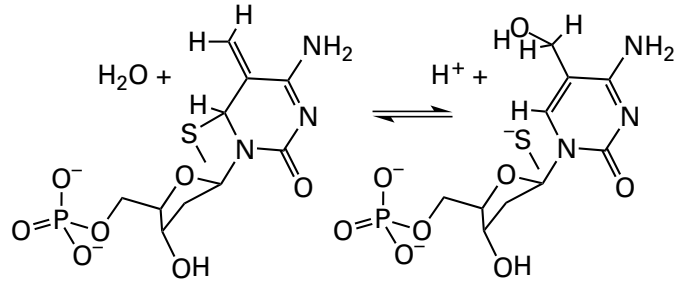

(5–203)

rather than a hydride from 5,6,7,8-tetrahydrofolate. In the absence of 5,6,7,8-tetrahydrofolate, deoxycytidylate 5-hydroxymethyltransferase catalyzes the isotopic exchange of oxygen-16 in the hydroxy group of the substrate 5-hydroxymethylcytidine 5′-monophosphate (**5–151**) for oxygen-18 in $H_2{}^{18}O$ (Equation 5–202), which was followed in mass spectra by the transformation of [5-^{16}O]-5-hydroxymethylcytidine 5′-monophosphate into [5-^{18}O]-5-hydroxymethylcytidine 5′-monophosphate.[748]

Oxygen isotopic exchange is the exchange of one isotope of oxygen—oxygen-16, oxygen-17, or oxygen-18—for a different isotope of oxygen catalyzed by the active site of an enzyme. Usually, oxygen isotopic exchange **involves molecules of water**. The oxygen-16, oxygen-17, or oxygen-18 in the reactant or an intermediate produced from the reactant leaves as a hydroxide that is being hydronated as it leaves by a catalytic acid in the active site. The resulting molecule of water is replaced by a molecule of water containing an oxygen of the other isotope, and then that exchanged molecule of water returns as a nucleophile to the reactant or intermediate in the reverse of the original elimination.

With both hydrogen isotopic exchange and oxygen isotopic exchange, there is significant ambiguity about the origin of the hydron or the molecule of water with the different isotope that ultimately registers the respective isotopic exchange. Originally, it was thought that active sites would be accessible enough to the solution that any hydron removed from the substrate by a catalytic base or any molecule of water that was a leaving group in the active site would exchange almost immediately with a hydron or a molecule of water in solution.[749] How this might occur at the molecular level seemed to draw little attention. As more and more crystallographic molecular models of enzymatic active sites became available, it became apparent that the catalytic acid–bases and molecules of water in the active site were often, if not usually, occluded from contact with the solvent, especially in active sites that closed around their substrates. There were also situations where a substrate or the intermediates themselves sat between the catalytic acid–base or the molecule of water and the solvent, preventing exchange with the solvent.

For a hydrogen isotopic exchange at an acidic position in a reactant, there is a catalytic acid–base in the active site that removes a proton, deuteron, or triton from—or adds a proton, deuteron, or triton to—the reactant or an intermediate produced from that reactant. For example, a catalytic acid–base removes a hydron from the lysyl imine of glycerone phosphate in the active site of fructose-bisphosphate aldolase, and the glycerone phosphate, into which a tritium from ^3H_2O is exchanged,[747] is the reactant that ultimately registers this isotopic exchange. The **catalytic acid–bases** performing these hydrogen isotopic exchanges have almost always been identified in crystallographic molecular models, so the actual molecular events leading to the particular hydrogen isotopic exchange being followed can be surmised. For example, there is a crystallographic molecular model[179] of the active site of fructose-bisphosphate aldolase from *O. cuniculus* occupied by the imine between Lysine 229 and the carbonyl of glycerone phosphate from which a hydron is removed or to which a hydron is added. In this model, the catalytic base that removes the *pro-S* hydrogen from carbon 3 of glycerone phosphate to produce the enamine during the normal enzymatic reaction has been identified as either a molecule of water relaying the basicity of the carboxylato group of Glutamate 187

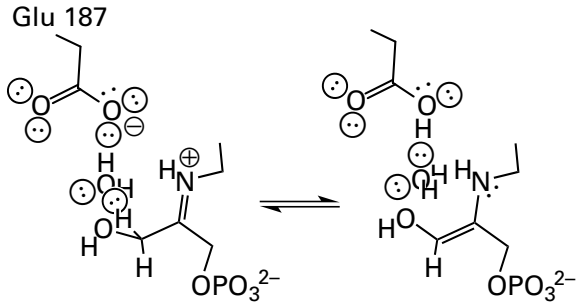

(5–204)

or the compound base formed by the carboxylato group of Glutamate 187 and the 4-hydroxyphenyl group of Tyrosine 363. The hydroxy group on the 4-hydroxyphenyl group displaces the molecule of water as Tyrosine 363 swings into the active site, in a conformational change reminiscent of the swoop of Tyrosine 248 into the active site of bovine carboxypeptidase A.

The molecule of water that may relay the basicity of Glutamate 187 is part of an extensive cluster of hydrogen bonds in which both oxygens in the carboxylato group of Glutamate 187, another molecule of water, both oxygens in the carboxy group of Glutamate 189, the 6-amino group of Lysine 146, the 3-hydroxy group of glycerone phosphate, both oxygens of the carboxy group of Aspartate 33, yet another molecule of water, an oxygen on the phospho group of glycerone phosphate, and a guanidinio nitrogen of Arginine 303 are participants. Within this cluster there are 11 hydrogen bonds and, therefore, at least 11 tritons when the enzyme is dissolved in ^3H_2O. These tritons comprise a **reservoir of tritons available for isotopic exchange**. Once the hydron is removed from carbon 3 of glycerone phosphate, if the molecule of water removes it, there is a high probability that the hydron will be rapidly replaced by a triton in the reservoir. When Tyrosine 363 swings into the active site, its hydroxy group is surrounded by two molecules of water with four tritons and its hydroxy group brings in a triton. If its hydroxy group removes the hydron by relaying the basicity of Glutamate 187, there will be at least five tritons available to rapidly exchange with the hydron. In fact, if Tyrosine 363 actually does swing in and out of the active site, isotopic exchange of the hydron with a triton in the solution would be inescapable. Consequently, whether the molecule of water or the 4-hydroxyphenyl group relays the basicity of Glutamate 187, the hydron that was removed will usually exchange with a triton in the active site, which in the back reaction will be

added to glycerone phosphate to accomplish the hydrogen isotopic exchange.

These considerations illustrate the fact that, in many if not most cases of hydrogen isotopic exchange at an acidic position, there are **more than enough hydrons, deuterons, or tritons**, depending on the design of the experiment, within the active site itself. There is no need for the proton, deuteron, or triton exchanging to enter and leave the active site from the solution, although such an isotopic exchange with hydrons in the solvent may indeed be involved. This consideration simply is a corollary to the fact that active sites occupied by substrates are usually rich in hydrogen bonds, in each of which there must be a hydron.

When an **active site is occluded from the solution** by a conformational change that occurs after all reactants have associated and when the occlusion persists for the entire duration of the chemical steps in its mechanism, hydrogen isotopic exchange can still occur while the reactants are occluded. For example, when either glycerone phosphate or D-glyceraldehyde 3-phosphate associates with the active site of triose-phosphate isomerase (previously Equation 3–384)

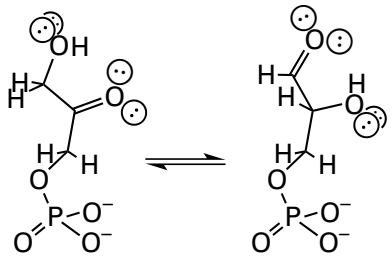

(5–205)

a lid closes over the active site, occluding it from the solution (Figure 3–58). Even so, the enzyme from *G. gallus* in ^3H_2O catalyzes the isotopic exchange of the hydron at carbon 3 of glycerone phosphate for a triton at early times during the approach to equilibrium before the back reaction becomes established.[750] When triose-phosphate isomerase from *O. cuniculus* or *S. cerevisiae* is equilibrated in ^3H_2O in the absence of glycerone phosphate and then diluted rapidly into a large volume of ^1H_2O containing a saturating concentration of glycerone phosphate, the observed amount of tritium incorporated into glycerone phosphate by hydrogen isotopic exchange can be explained only if the equivalent of one triton (in the case of the enzyme from *O. cuniculus*) or 2–3 tritons (in the case of the enzyme from *S. cerevisiae*) trapped in the respective occluded active site are able to exchange with the hydron removed by the catalytic base.[751] These tritons, in the active site before the dilution, must be trapped in the active site during association of glycerone phosphate and the subsequent closing of the lid because the solution is mainly ^1H_2O. If isotopic exchange of the hydron on glutamate were occurring only with the hydrons in this solution of ^1H_2O, then no hydrogen isotopic exchange would be observed. The difference between the enzymes from the different species in the number of tritons trapped in the active site that are able to exchange with the hydron is not due to a difference in the catalytic groups in the respective active sites because they are all the same (52% identity; 0.4 gap percent); it is due to a difference in how many tritons exchange for hydrons before the respective active site closes around glycerone phosphate. It follows that, in the situation in which the solvent is continuously ^3H_2O, more tritons capable of exchanging with a hydron on carbon 3 of glycerone phosphate are occluded within the active site upon closing of the lid than when the solvent has been rapidly changed from ^3H_2O to ^1H_2O before the occlusion begins.

Crystallographic observations (Figure 3–37) and active-site labeling[752] have shown that the catalytic base that removes the hydron from carbon 3 of glycerone phosphate in the active site of triose-phosphate isomerase is the carboxylato group of a glutamate. The tritons trapped in an occluded active site and available internally for isotopic exchange with the hydron removed from carbon 3 of glycerone phosphate by the carboxylato group are probably located on the fixed molecule of water that forms a hydrogen bond to the other oxygen of the carboxy group (0.27 nm), on the π nitrogen of the imidazolyl group in van der Waals contact (0.38 nm) with that molecule of water, and on the oxygen on carbon 2 of glycerone phosphate. This last oxygen is in van der Waals contact (0.35 nm) with the oxygen on the carboxy group that removed the hydron and which becomes a tritoxy group during the reaction by being tritonated on the 6-amino group of the lysine that is in a hydrogen bond (0.27 nm) with it (Figure 3–37).[753,754]

In an oxygen isotopic exchange, a molecule of water is the leaving group from the reactant in one direction and the nucleophile in the other direction. This molecule of water can also be identified in a crystallographic molecular model. For example, the molecule of water that leaves and returns in the elimination–addition catalyzed by deoxycytidylate 5-hydroxymethyltransferase from Enterobacteria phage T4 (Equation 5–203) has been identified in the crystallographic model of a complex between 5,6,7,8-tetrahydrofolate and 2′-deoxycytidine

5′-monophosphate, in which the methylene that is normally transferred in the enzymatic reaction is missing.[755] This molecule of water is found on the periphery of a **hydrogen-bonded cluster of six molecules of water** fixed in the active site. The five molecules of $H_2{}^{18}O$ that are not the leaving group are available to rapidly change places with it and then be incorporated into 5-hydroxymethylcytidine 5′-monophosphate. There are always fewer fixed molecules of water occupying an active site in which substrates are undergoing their transformation than there are hydrons in hydrogen bonds; nevertheless, because water is the solvent in which a protein has evolved, there are usually some. There may, however, be situations in which the active site is so dehydrated that there are no molecules of water within it that can exchange with the molecule of water that is a leaving group. It is even less likely that an active site would be so bereft of hydrons that there would be no hydrons within it that were derived from the solvent and that are available to exchange with a hydron removed from a substrate.

There are several ways in which isotopic exchanges are observed. They differ in how the solution in which they are observed is prepared, which reactants are used, and how the isotopic exchange is monitored.

Isotopic exchange in the absence of one or more reactants is exemplified by the hydrogen isotopic exchange observed for glycerone phosphate catalyzed by fructose-bisphosphate aldolase and the oxygen isotopic exchange observed for 5-hydroxymethylcytidine 5′-monophosphate catalyzed by deoxycytidylate 5-hydroxymethyltransferase (Equation 5–202). If an intermediate in the enzymatic reaction can be formed in the absence of the missing reactant or reactants and if the intermediate has lost one or more of the atoms present in the added reactant, then isotopic exchange of those atoms in that reactant may be observed.

All observed properties for hydrogen isotopic exchange in glycerone phosphate catalyzed by fructose-bisphosphate aldolase are **consistent with the existence of an intermediate in the enzymatic reaction** and consistent with the mechanism (Figure 4–36) in which an intermediate enamine is formed stereospecifically at the active site and the reaction can proceed no further because the electrophile to which the enamine would normally add, glyceraldehyde 3-phosphate, has been omitted. Even though there are four acidic hydrogens on the iminium adduct, two on carbon 3 and two on carbon 1 (Equation 5–204), the final specific radioactivity of glycerone phosphate at equilibrium was not 39,000 cpm μmol^{-1} when the specific activity of the water was 9800 cpm (μmol of hydrogen)$^{-1}$ because only one of the four acidic hydrons, the *pro-S* hydrogen on carbon 3, is removed and replaced with a triton by the molecule of water or the 4-hydroxyphenyl group in the active site. When the enzymatic reaction comes to equilibrium, the specific radioactivity of that one hydrogen, and hence that of glycerone phosphate itself, must be equivalent to the specific radioactivity of a hydrogen in the water. The slow increase in specific radioactivity of glycerone phosphate results from nonenzymatic isotopic exchange of the other three acidic hydrons.

The fact that, in the absence of 5,6,7,8-tetrahydrofolate, deoxycytidylate 5-hydroxymethyltransferase catalyzes oxygen isotopic exchange at the hydroxy group of the reactant 5-hydroxymethylcytidine 5′-monophosphate (Equation 5–202)[748] is evidence for the reversible addition of hydroxide anion or a molecule of water to the methylene group in the intermediate in the enzymatic mechanism (Equation 5–203), as well as the existence of the intermediate itself. The oxygen isotopic exchange arises from association of [5-^{16}O]-5-hydroxymethylcytidine 5′-monophosphate with the active site, dehydration to produce the intermediate, isotopic exchange of the molecule of $H_2{}^{16}O$ that was the leaving group for a molecule of $H_2{}^{18}O$, conversion of the intermediate to [5-^{18}O]-5-hydroxymethylcytidine 5′-monophosphate, and dissociation of [5-^{18}O]-5-hydroxymethylcytidine 5′-monophosphate into the solution. In this oxygen isotopic exchange, the reactant added is 5-hydroxymethylcytidine 5′-monophosphate, and the reactant omitted is 5,6,7,8-tetrahydrofolate. When 5-deazatetrahydrofolate, an inactive analogue of 5,6,7,8-tetrahydrofolate, is added to the reaction, oxygen isotopic exchange increases 26-fold, a fact that can be explained if 5-deazatetrahydrofolate produces an induced fit of the active site that aligns the catalytic groups more effectively.

Isotopic exchange into an analogue of a reactant that is incapable of participating in the complete enzymatic reaction resembles the strategy for isotopic exchange in the absence of one or more reactants because the use of the analogue prevents the reaction from proceeding beyond a particular step in the kinetic mechanism, as does the omission of one reactant. For example, 3-dehydroquinate synthase catalyzes a reaction in which a ketone is formed so that an elimination can occur[756]

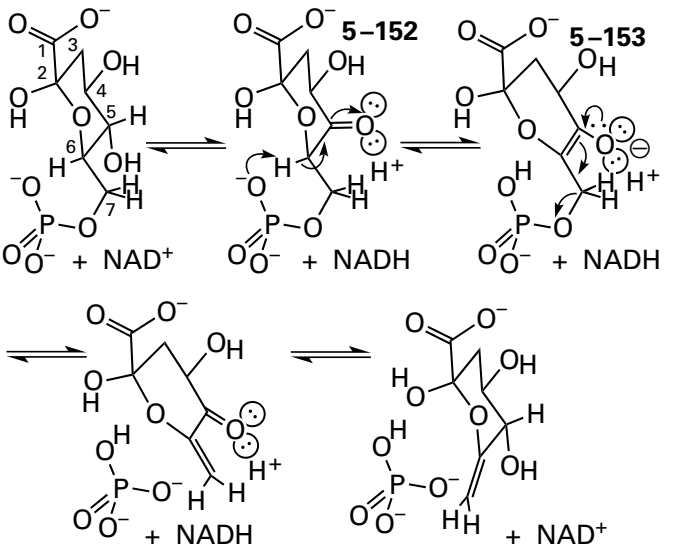

(5–206)

The enzyme requires only catalytic amounts of NAD^+ ($K_{mNAD} = 1\ \mu M$)[757] since NAD^+ is not a stoichiometric participant in the overall reaction and is regenerated in the last step of the mechanism. Chemical evidence for the requirement for intermediate ketone **5–152** is that the carbacyclic phosphonate **5–154**

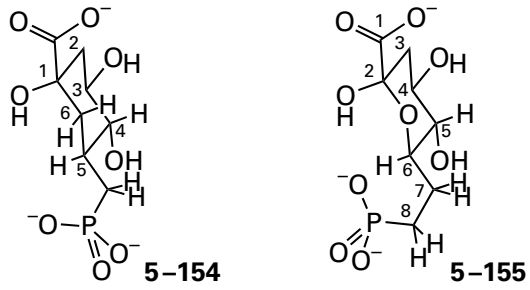

which is an analogue of the substrate 3-deoxy-D-*arabino*-hept-2-ulosonate 7-phosphate, is oxidized to the corresponding ketone by the enzyme from *E. coli* at its carbon 4, which is in the analogous position to carbon 5 of the normal substrate. Isotopic evidence for removal of the hydron from carbon 6 of ketone **5–152** prior to the elimination is that that the enzyme in ^2H_2O catalyzes hydrogen isotopic exchange at carbon 6 of phosphonate **5–155**, which is also an analogue of 3-deoxy-D-*arabino*-hept-2-ulosonate 7-phosphate.[758] Analogue **5–155** is the phosphonate rather than the phosphate, so the forward reaction is blocked at the step in which elimination of phosphate would normally occur because the phospho oxygen has been replaced with a carbon, and there is no competition in the forward direction with the reversal of the reaction following removal of the hydron. Consequently, hydrogen isotopic exchange supports the conclusion that elimination of phosphate must take place in a step following removal of the hydron from carbon 6.

In the crystallographic molecular model of the active site of dehydroquinate synthase from *Aspergillus nidulans* (Equation 5–206) occupied by carbacyclic phosphonate **5–154**, the hydron on its carbon 5 is immediately adjacent (0.32 nm) to an oxygen on the phosphono group.[759] The other two oxygens of the phosphono group have the 6-ammonio groups of Lysine 152 and Lysine 356, respectively, as ligands. Most likely the hydrogen isotopic exchange in analogue **5–155** occurs by exchange of the hydron on the phosphono group in the analogue of intermediate enolate **5–153**, which has just been removed from intermediate **5–152**, for one of the six deuterons on these two lysines.

Isotopic exchange at initial rate is the isotopic exchange observed at an atom in one reactant when all the reactants and none of the products are present and the reaction is proceeding only in one direction. For example, urocanate hydratase (Figures 4–49 and 4–50) has a tightly bound, prosthetic NAD^+ at its active site, and the ultimate product of the reaction has been formally oxidized to an oxo group at carbon 5 of its imidazolyl group

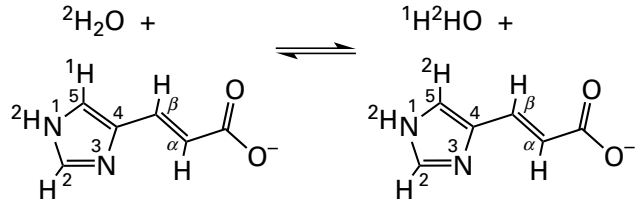

(5–207)

while being formally reduced at other carbons in the reactant. These facts raised the possibility that the hydrogen at carbon 5 was removed by this prosthetic NAD^+ as a hydride during the reaction. [5-^{1}H]Urocanate was mixed with the enzyme from *P. putida* in ^2H_2O. At various times, the reaction was stopped, and the concentrations of [5-^{1}H]urocanate and [5-^{2}H]urocanate were determined (Figure 5–15).[760] Although urocanate was continuously disappearing, [5-^{2}H]urocanate was being produced by hydrogen isotopic exchange of the hydron for a deuteron at a rate significantly in excess of the rate of the overall reaction, and it accumulated before it was in turn converted to product.

Because the hydrogens at carbon 4 of the nicotinamide in NADH are not acidic, the existence of this rapid hydrogen isotopic exchange is consistent with the proposed mechanism for the reaction (first two steps in Figure 4–49) in which the hydrogen at carbon 5 of urocanate becomes acidic during the reaction and is removed as a hydron by the carboxylato group of Aspartate 443 (Figure 4–50). The oxygen in this carboxylato group that removes the hydron is also in a hydrogen bond within a chain of molecules of water leading out of the active site, and the deuteron leaves the active site and enters this chain, to be replaced by a hydron already in the chain.[761] In this instance, the hydron removed is formally exchanging with a deuteron in the solution, but the isotopic exchange at Aspartic Acid 443 probably involves a deuteron already in the active site on a fixed molecule of water.

Positional isotopic exchange is the intramolecular exchange of one atom in a substrate with another atom, of the same element but a different isotope, in such a way that the product of the isotopic exchange is chemically identical to the reactant except that the two isotopes within the molecule have been interchanged. The interchange of the isotopically different atoms within the same molecule registers the fact that a reaction has occurred even though no otherwise apparent chemical change has taken place. For example, when $MgATP^{2-}$ containing **oxygen-18 in the bridging position** between the β and γ phosphorus atoms, as well as the other three positions on the γ phosphorus, was mixed with L-glutamate and ovine glutamine synthetase (previously Equation 3–405)

$$\text{L-glutamate} + NH_3 + MgATP^{2-} \rightleftharpoons MgADP^{-} + HOPO_3^{2-} + \text{L-glutamine} \qquad (5\text{–}208)$$

or glutamine synthetase from *E. coli*, in the absence of ammonia, the ^{18}O was found[762] to exchange to a nonbridging position on the β-phosphate of the $MgATP^{2-}$

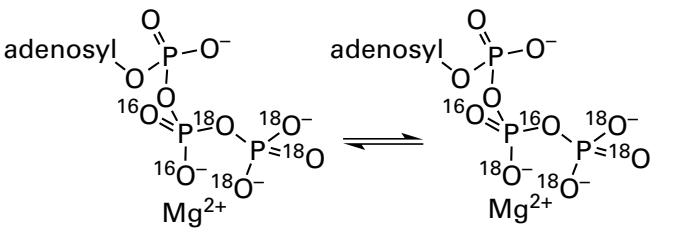

(5–209)

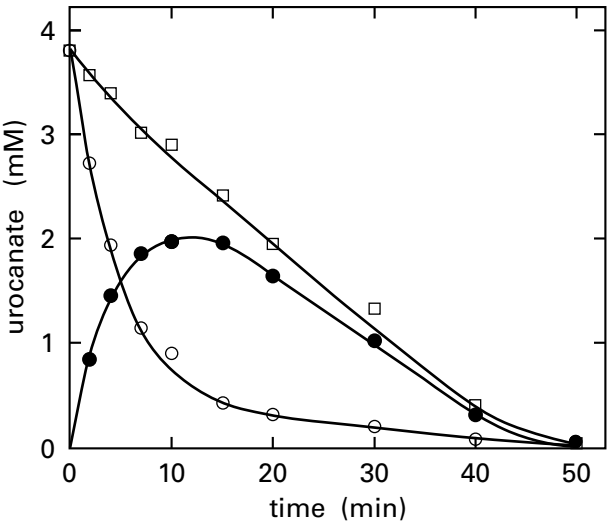

Figure 5–15: Isotopic exchange of hydrogen at carbon 5 of urocanate during the reaction catalyzed by urocanate hydratase from *P. putida*.[760] The reaction mixture (3 mL) contained 4 mM urocanate in ^2H_2O (99.9% deuterium) at p^{2}H 7.5 and 25 °C. The reaction was initiated with 0.4 mg of urocanate hydratase. The total concentration of urocanate (millimolar) was followed by its absorbance at 317 nm (□). Samples were removed at various intervals, quickly frozen, and lyophilized. The fraction of the remaining urocanate that had incorporated one deuterium at carbon 5 was assessed by gas chromatography followed by mass spectrometry. That the deuterium substitution was at carbon 5 was confirmed by nuclear magnetic resonance spectroscopy. From the fraction of urocanate that was deuterated and the total concentration of urocanate, the millimolar concentrations of [5-^{2}H]urocanate (●) and [5-^{1}H]urocanate (○) could be calculated. These concentrations are plotted as a function of the respective intervals (minutes).

even though no other isotopic exchanges could be observed.

Three steps provide the explanation for this positional oxygen isotopic exchange. First, in the active site,[763] the γ-phosphate is transferred to the oxygen of L-glutamate to form L-γ-glutamyl phosphate. Second, the β-phosphate of $MgADP^-$, tightly held in the active site at other positions in its structure, rotates about the oxygen–phosphorus bond to interchange the oxygen-18 and an oxygen-16

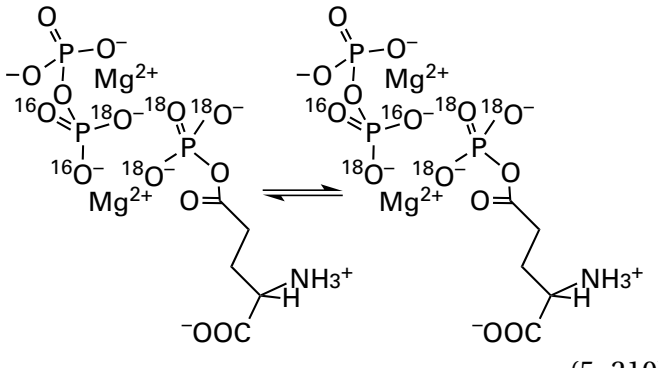

(5–210)

Third, the phospho group is transferred back from the L-glutamate to this oxygen-16 of the rotationally isomerized MgADP$^-$. This positional oxygen isotopic exchange can occur because the reaction cannot proceed beyond the complex of the active site with MgADP$^-$ and L-γ-glutamyl phosphate because no ammonia was added to the solution. When ammonia was added to permit the reaction to proceed forward, the rate of the positional oxygen isotopic exchange was diminished. In the absence of ammonia, the initial rate for the positional oxygen isotopic exchange was equal to the initial rate for the complete enzymatic reaction in the presence of ammonia, and this equality demonstrated the kinetic competence of the positional exchange. All these results are consistent with the existence of L-γ-glutamyl phosphate as an intermediate in the enzymatic reaction.

Intermediate isotopic exchange is hydrogen isotopic exchange or oxygen isotopic exchange observed at a position in one product as the reaction is proceeding in one direction, but the exchanged isotope is not an atom that would have been incorporated into the product from a stoichiometric hydron or a stoichiometric molecule of water during the normal course of the reaction.[764,765] Intermediate isotopic exchange can detect the **reversibility of intermediate steps** that occur after association of the reactant with the active site. During intermediate isotopic exchange, one reactant enters the active site. Isotopic exchange occurs while that reactant is reversibly converted to an intermediate, while an intermediate in the reaction is reversibly converted into another intermediate, or while the last intermediate is converted reversibly into product; and the product leaves the active site bearing the exchanged isotope. For example, intermediate hydrogen isotopic exchange could be observed in the reaction catalyzed by porcine citrate (*Si*)-synthase (see Equation 4–224)

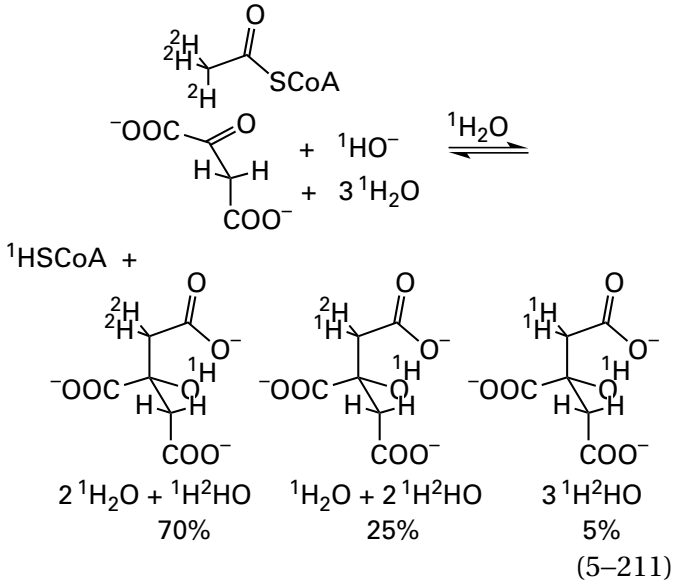

(5–211)

When [$^2H_3$]acetyl-SCoA was used as a reactant in ^1H_2O, 0.35 atom of protium was incorporated at carbon 2 of the [2-^{2}H]citrate produced.[766] This **superstoichiometric incorporation** of protium was the result of hydrogen isotopic exchange at that carbon in an intermediate in the reaction. Furthermore, when [^{18}O]acetyl-SCoA was used as a reactant in $H_2{}^{16}O$, 0.26 atom of oxygen-16 beyond the one oxygen-16 stoichiometrically incorporated was found in the carboxylato group of citrate derived from the thioester of the citryl-SCoA that is the intermediate in this reaction

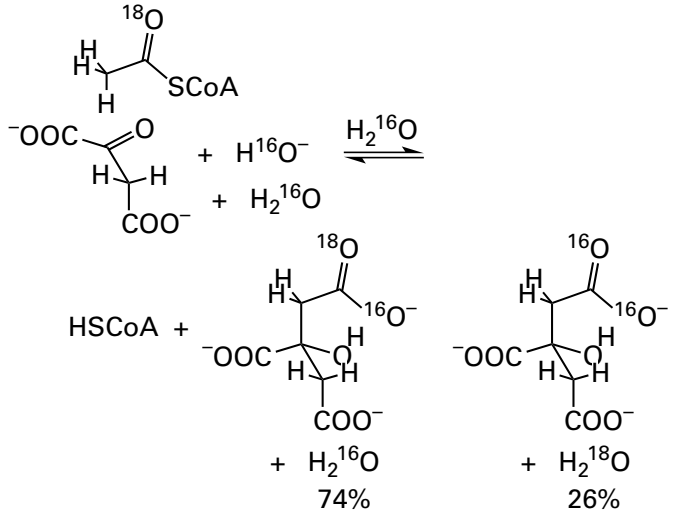

(5–212)

In the active site of citrate (*Si*)-synthase, the enolate of acetyl-SCoA is formed, and it adds in an aldol condensation to the carbonyl of oxaloacetate. The resulting citryl-SCoA is then hydrolyzed in the next step in the reaction. The intermediate hydrogen

isotopic exchange (Equation 5–211) during the reaction catalyzed by porcine citrate (*Si*)-synthase occurs because the step in which the enolate of acetyl-SCoA is formed, before formation of the carbon–carbon bond in its nucleophilic addition to the carbonyl, is reversible. This step reverses after the deuteron on the carboxy group of Aspartic Acid 375 in the active site,[767] which removed the deuteron from [$^2H_3$]acetyl-SCoA, is exchanged for a proton, probably a proton on a nearby (0.27 nm)[768-770] molecule of water fixed in the active site. The enolate is protonated, once and sometimes twice, before citryl-SCoA is formed from that molecule of [$^2H_3$]acetyl-SCoA and then is turned into citrate and released as a product. The isotopic exchange of two or even three deuterons does not have to occur in consecutive steps while a molecule of acetyl-SCoA is bound in an active site. The singly labeled acetyl-SCoA can dissociate and then reassociate with a different active site between each exchange.

The intermediate oxygen isotopic exchange (Equation 5–212) occurs because the step during which [1-^{18}O]citryl-SCoA is hydrolyzed by $H_2{}^{16}O$ to [1-^{18}O,1-^{16}O]citrate, the major product, reverses after the carboxylato group of [1-^{18}O,1-^{16}O]citrate flips over in the active site. This reversal of the hydrolysis forms [1-^{16}O]citryl-SCoA, which is then hydrolyzed by another molecule of $H_2{}^{16}O$, but it must occur before citrate and HSCoA can be released as products. The molecule of $H_2{}^{16}O$ that is responsible for the both the first and the second hydrolysis of citryl-SCoA forms a hydrogen bond (0.32 nm) with a second molecule of $H_2{}^{16}O$ within the active site.[770] This second molecule of water, after exchanging with the molecule of $H_2{}^{18}O$ that dissociates during the reversal of the hydrolysis that forms [1-^{16}O]citryl-SCoA, could easily be responsible for all 26% of intermediate oxygen isotopic exchange that is observed. The fact that intermediate oxygen isotopic exchange is observed requires that hydrolysis of a thioester, which is exergonic in solution (–18 kJ mol^{-1}, Table 1–3) is nevertheless reversible in the active site.

For intermediate isotopic exchange to be observed, the atom in either the reactant or product on which the atom is being exchanged must be bound to **more than one of the type of atom** that is being substituted. In most cases, at least one of those equivalent atoms being substituted is a stoichiometric participant in the reaction. For example, the carbon atom on which the deuteriums were exchanged for protiums in the case of citrate (*Si*)-synthase has three equivalent hydrons on the methyl group in the reactant, and one of them is a silent stoichiometric product of the reaction. The carboxy carbon of the product, citrate, has two equivalent oxygens, one of which comes from the water that is a designated stoichiometric reactant and is therefore also silent. The distinction between isotopic exchange at initial rate and intermediate isotopic exchange is that the isotopic exchange that occurs into the intermediate is **registered in the product rather than in the reactant**. The intermediate isotopic exchanges of hydrogen and oxygen that occur with citrate (*Si*)-synthase, however, could also have been registered in the reactant acetyl-SCoA at initial rate if acetyl-SCoA is produced in the back reaction from the respective isotopically exchanged intermediate and dissociates from the enzyme at a great enough rate.

Isotopic exchange at equilibrium is the isotopic exchange within one reactant that is observed when all reactants and products of the enzymatic reaction are present in the solution at concentrations that satisfy the equation for the equilibrium constant. If the absolute molar concentrations of reactants and products present in solution are such that their ratio is equal to the equilibrium constant, the reaction does not cease; rather, the rate at which reactants are converted to products will simply be equal to the rate at which products are converted to reactants. This balance of rapid conversions is an important feature of the state of equilibrium that is often not stressed sufficiently, so the mistaken impression is often left that a reaction at equilibrium is quiescent. Actually, it is often at equilibrium that the most is happening. When appropriate isotopes are used, the rates of these otherwise hidden reactions contributing to this active interconversion of reactants and products can be determined.

For the reaction catalyzed by phosphopyruvate hydratase

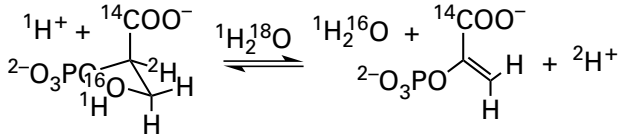

(5–213)

the equilibrium constant between pH 6 and 8 is

$$\frac{[\text{phospho}\textit{enol}\text{pyruvate}]_{eq}}{[\text{2-phospho-D-glycerate}]_{eq}} = K_{eq} = 6.3 \qquad (5\text{–}214)$$

Equilibrium concentrations of phospho*enol*pyruvate (0.11 M) and 2-phospho-D-[2-^{2}H]glycerate (0.018 M), as well as a trace amount of 2-phospho-D-[1-^{14}C]glycerate, dissolved in $H_2{}^{18}O$ (isotopic labels in Equation 5–213), were mixed with phosphopyruvate hydratase from *O. cuniculus*. The trace amount of 2-phospho-D-[1-^{14}C]glycerate provided a radioactive label for 2-phospho-D-glycerate without diluting the 2-phospho-D-[2-^{2}H]glycerate. A trace amount of 2-phospho-D-[2-^{3}H]glycerate was also added to the first solution so that the exchange of protium for tritium in D-glycerate could be followed simultaneously. In this mixture, several isotopic exchanges could be monitored as a function of time.[749]

Because the concentrations of phospho*enol*pyruvate and 2-phospho-D-glycerate remained constant, appearance of phospho[1-^{14}C]*enol*pyruvate in the solution is the result of a **carbon isotopic exchange** at equilibrium

$$\begin{aligned}&\text{phospho[1-}^{12}\text{C]}\textit{enol}\text{pyruvate} + \\ &\quad \text{2-phospho-D-[1-}^{14}\text{C]glycerate} \rightleftharpoons \\ &\qquad \text{2-phospho-D-[1-}^{12}\text{C]glycerate} + \\ &\qquad\quad \text{phospho[1-}^{14}\text{C]}\textit{enol}\text{pyruvate}\end{aligned} \qquad (5\text{–}215)$$

This carbon isotopic exchange at equilibrium is accomplished in six steps: association of phospho[1-^{12}C]*enol*pyruvate with the active site; its conversion to 2-phospho-D-[1-^{12}C]glycerate; dissociation of this product; association of 2-phospho-D-[1-^{14}C]glycerate with the active site; its conversion to phospho-[1-^{14}C]*enol*pyruvate; and dissociation of this product. The same exchange can be accomplished by association of 2-phospho-D-[1-^{14}C]glycerate with the active site; its conversion to phospho[1-^{14}C]*enol*-pyruvate; dissociation of this product; association of phospho[1-^{12}C]*enol*pyruvate with the active site; its conversion to 2-phospho-D-[1-^{12}C]glycerate; and dissociation of this product.

In contrast to hydrogen isotopic exchange involving hydrons or oxygen isotopic exchange involving molecules of water, in the case of the carbon isotopic exchange observed with phosphopyruvate hydratase, there is **no ambiguity about the source of the exchanged isotope**—it must be a molecule of 2-phospho-D-[1-^{14}C]glycerate or a molecule of phospho[1-^{12}C]*enol*pyruvate from the solution. This certainty results from the fact that the carbon is an integral part of the substrates and remains in the intermediates as other transformations—removal of a hydron and dissociation of the leaving hydroxy group—occur at other locations. The carbon in this instance has to associate with the active site as a part of the reactant, remain in the body of the molecule as it is transformed into product, and then dissociate from the active site in the product. In other words, this isotopic exchange monitors the complete reaction. This sequence of events is a consequence of the fact that carbon-14 is neither in a hydron nor in a molecule of water, both of which are ubiquitous.

The appearance of oxygen-18 in 2-phospho-D-[3-^{18}O]glycerate is a direct measure of the **oxygen isotopic exchange**

$$\begin{aligned}&\text{2-phospho-D-[3-}^{16}\text{O]glycerate} + H_2{}^{18}O \rightleftharpoons \\ &\qquad H_2{}^{16}O + \text{2-phospho-D-[3-}^{18}\text{O]glycerate}\end{aligned} \qquad (5\text{–}216)$$

This oxygen isotopic exchange at equilibrium is accomplished in five steps: association of 2-phospho-D-[3-^{16}O]glycerate with the active site; breaking of the carbon–oxygen bond in 2-phospho-D-[3-^{16}O]glycerate on the active site to produce a molecule of $H_2{}^{16}O$ and an intermediate bound in the active site; isotopic exchange of that molecule of $H_2{}^{16}O$ for a molecule of $H_2{}^{18}O$; insertion of that molecule of $H_2{}^{18}O$ back into the intermediate still bound in the active site; and dissociation of 2-phospho-D-[3-^{18}O]glycerate from the active site.

There is a molecule of water, which must be $H_2{}^{18}O$ in the case where oxygen isotopic exchange is observed, in van der Waals contact (0.36 nm) with the 3-hydroxy group of 2-phospho-D-glycerate in the complex between this substrate and the active site and in a hydrogen bond (0.26 nm) with the other oxygen of the carboxy group of Glutamic Acid 211 that hydronates the leaving group (Figure 4–43).[155] This $H_2{}^{18}O$ could change places with the $H_2{}^{16}O$ that is the leaving group in the elimination catalyzed by the enzyme and could be responsible for some of the oxygen isotopic exchange that is observed, but there is probably some isotopic exchange of $H_2{}^{16}O$ with $H_2{}^{18}O$ in the solvent as well.

The appearance of $^{3}H_2{}^{18}O$ is a direct measure of the **hydrogen isotopic exchange**

$$\begin{aligned}&\text{2-phospho-D-[2-}^{3}\text{H]glycerate} + {}^{1}H_2{}^{18}O \rightleftharpoons \\ &\qquad {}^{3}H_2{}^{18}O + \text{2-phospho-D-[2-}^{1}\text{H]glycerate}\end{aligned} \qquad (5\text{–}217)$$

This hydrogen isotopic exchange at equilibrium is accomplished in five steps: association of 2-phospho-D-[2-^{3}H]glycerate with the active site; removal of the triton from carbon 2 of 2-phospho-D-[2-^{3}H]glycerate by the amino group of Lysine 345 (Figure 4–43); rotation of the ammonio group; addition of one of its two protons, or one of the two protons on the molecule of water on the Mg^{2+} to which the ammonio group is hydrogen-bonded, to carbon 2; and dissociation of 2-phospho-D-[2-^{1}H]glycerate.

The appearance of $^2H_2{}^{18}O$ is a direct measure of the hydrogen isotopic exchange

2-phospho-D-[2-^{2}H]glycerate + $^1H_2{}^{18}O$ $\rightleftharpoons$
$^2H_2{}^{18}O$ + 2-phospho-D-[2-^{1}H]glycerate

(5–218)

Site-directed mutation of the enzyme can reveal or accentuate an isotopic exchange. The enzyme dTDP-glucose 4,6-dehydratase catalyzes a reaction

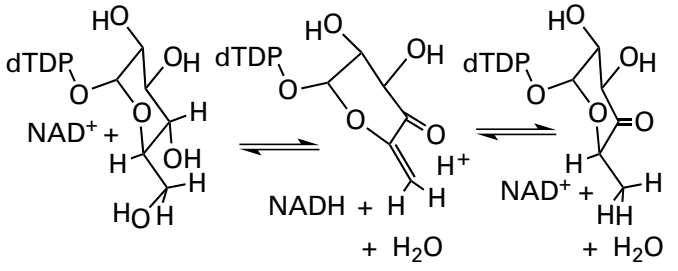

(5–219)

similar to the one catalyzed by 3-dehydroquinate synthase (Equation 5–206), with the exception that NADH reduces the methylene group in the intermediate α,β-unsaturated ketone by adding a hydride to carbon 6 rather than adding a hydride to the carbonyl at carbon 4 to complete the reaction. The carboxy group of Aspartic Acid 135 in the active site of the enzyme from *E. coli* is responsible for hydronating the leaving hydroxy group at carbon 6.[771] In a mutant of the enzyme, in which Aspartate 135 is replaced by alanine, the catalytic constant is decreased by a factor of 220. Unlike the wild-type enzyme, the mutant catalyzes hydrogen isotopic exchange of a deuteron at carbon 5 of dTDP-D-glucose for a hydron.[772] The mutation has decreased elimination of the hydroxy group significantly so that removal of the hydron is able to reverse.

Just as in the case of site-directed mutation, using an **alternative reactant**, equivalent to mutating the normal reactant, can reveal an isotopic exchange catalyzed by an enzyme. For example, when 4-fluoro-L-tryptophan ($k_0\,K_{m,FTrp}{}^{-1}$ = 5 $mM^{-1}\,s^{-1}$) is used as a reactant in the reaction catalyzed by N^1-(1,1-dimethylallyl)tryptophan synthase

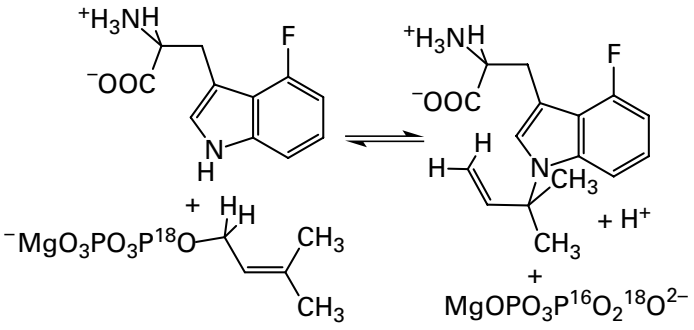

(5–220)

from *Salinispora arenicola*, a positional oxygen isotopic exchange at initial rate for the bridging oxygen-18 between the diphospho group and carbon 1 of the dimethylallyl diphosphate into a nonbridging position is observed even though this exchange is not observed when the natural reactant, L-tryptophan ($k_0\,K_{m,Trp}{}^{-1}$ = 26 $mM^{-1}\,s^{-1}$), is used.[773] This observation is evidence for the existence of a dimethylallyl carbenium ion as an intermediate in the enzymatic reaction (see Figure 1–26). Fluorination increases the pK_a of the indolyl nitrogen and slows its dehydronation sufficiently that dissociation of the diphosphate from the dimethylallyl diphosphate to form dimethylallyl carbenium ion is able to reverse.

Crystallographic molecular models provide explanations for situations in which hydrogen isotopic exchange is not observed when it is expected. Whenever an example of hydrogen isotopic exchange was discussed in the foregoing definitions of the various types of isotopic exchange, the reservoir of hydrons in the respective crystallographic molecular model of the enzyme being discussed that is connected directly to the catalytic acid–base performing hydrogen isotopic exchange was described. The hydrons in these reservoirs are able to provide the hydrons that exchange with the one that the catalytic acid–base has removed from the reactant or intermediate, whether or not the active site is completely sequestered from the solution. Since such reservoirs should be common, it is actually situations in which hydrogen isotopic exchange is not observed that are unexpected, not situations in which it is. For example, fumarate hydratase (Equation 5–119) catalyzes a hydration homologous to that catalyzed by phosphopyruvate hydratase (Equation 5–213). There is ample, convincing evidence that dehydra-

tion of (*S*)-malate in the active site of this enzyme proceeds with initial removal of the hydron from carbon 3 to produce a *gem*-enediolate (Equation 5–118).[365] Hydrogen isotopic exchange, however, of tritium at carbon 3 of (2*S*,3*R*)-[3-^{3}H]malate with a hydron, catalyzed by porcine fumarate hydratase in ^1H_2O, is slower than isotopic exchange of carbon-14 in [1-^{14}C]fumarate into (*S*)-malate at equilibrium, even though isotopic exchange of the hydroxy group in unlabeled (*S*)-malate with oxygen-18 in $H_2{}^{18}O$ at equilibrium is more rapid than isotopic exchange of the carbon-14 in [1-^{14}C]fumarate into (*S*)-malate.[774]

These observations require that the triton removed from carbon 3 of (2*S*,3*R*)-[3-^{3}H]malate cannot exchange with any of the hydrons in the active site and also must dissociate from and reassociate with the active site more slowly than the product fumarate. That this counterintuitive conclusion is correct follows from the fact that porcine fumarate hydratase is able to transfer tritium from (2*S*,3*R*)-[1,4-$^{14}C_2$,3-^{3}H]malate to unlabeled [1,4-$^{12}C_2$]fumarate.[775] This capability requires that the product [1,4-$^{14}C_2$]fumarate must be able to dissociate from the enzyme and be replaced by unlabeled fumarate before the triton that was removed from (2*S*,3*R*)-[1,4-$^{14}C_2$,3-^{3}H]malate can dissociate from the active site. That this conclusion is correct also follows from the fact that the enzyme is able to transfer deuterium from (2*S*,3*R*)-[3-^{2}H]malate to 1,2-dicarboxyethyne, an analogue of fumarate, to produce [3-^{2}H]-2-hydroxyfumarate.[776] Nevertheless, the fact that the rate of dissociation of the tritium removed from (2*S*,3*R*)-[3-^{3}H]malate from the active site is accelerated by certain general bases added to the solution demonstrates that it is located on a catalytic acid–base.[775]

In the active site of porcine fumarate hydratase, tritium is removed from (2*S*,3*R*)-[3-^{3}H]malate by the oxido group of Serine C318 (Figure 4–27). This **oxido group is in an oxyanion hole** formed by two hydronated amido groups from the polypeptide backbone. The role of this oxyanion hole is to lower the pK_a of the hydroxy group so that its conjugate base, an oxido group, is present upon association of substrate and can remove the triton. Presumably, the protons on the amido groups do not participate in hydrogen isotopic exchange with the now-hydroxy group of Serine C318 because, to do so, one of them (pK_a = 17) would have to protonate the hydroxy group (pK_a = –3), which would be difficult, if not impossible, in the time available. Why the hydroxy group on the serine does not exchange with hydrons in the solution while fumarate dissociates and reassociates nevertheless remains puzzling.

Mandelate racemase (previously Equation 4–126)

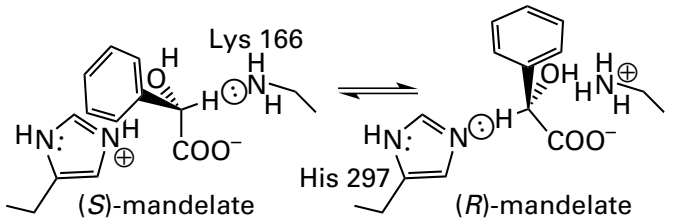

(5–221)

provides the clearest example of the effect that the identity of the catalytic acid–base and hydrogen bonds in which it participates has on an observed hydrogen isotopic exchange. In this instance, because the enzyme has only one reactant and one product, one reactant cannot be omitted to observe hydrogen isotopic exchange. Consequently, it was followed at initial rate before significant concentrations of product accumulated. When mandelate racemase from *P. putida* is catalyzing the epimerization of (*S*)-mandelate in ^2H_2O*

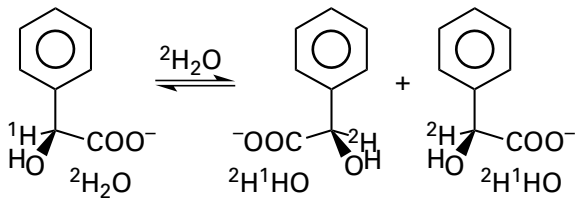

(5–222)

deuterium appears on the α carbon of the reactant, (*S*)-mandelate, as well as in the product, (*R*)-mandelate.[777] This observation has been presented as evidence that the enzyme proceeds through an intermediate *gem*-enediolate formed by direct removal of a hydron from the α carbon by a catalytic base in the active site. The observation that the enzyme catalyzes elimination of HBr from racemic 4-(bromomethyl)mandelate[778]

*Equal quantities of both (*S*)-mandelate and (*R*)-mandelate are produced, regardless of which enantiomer is the reactant, because the equilibrium constant for the epimerization must be 1.

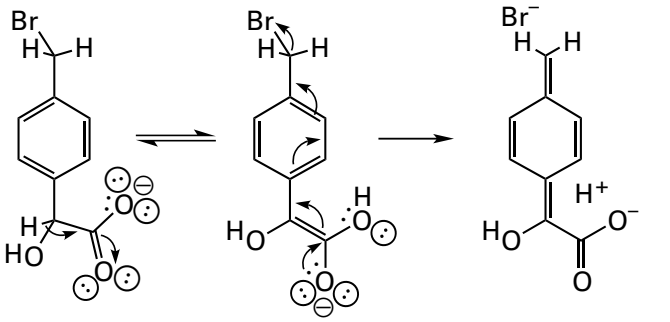

(5–223)

is also consistent with the participation of the *gem*-enediolate in the normal reaction.

While mandelate racemase catalyzes the hydrogen isotopic exchange (4%) of protium at the α carbon of (*S*)-mandelate for deuterium in ^2H_2O (Equation 5–222) during early stages (<5%) of the approach to equilibrium, no measurable hydrogen isotopic exchange (≤0.4%) is observed at the α carbon of (*R*)-mandelate when it is the reactant over the same extent of the approach to equilibrium.[779] One explanation for this difference between the two enantiomers is that there are two bases involved in the mechanism, one that removes the hydron from (*S*)-mandelate and another that removes the hydron from (*R*)-mandelate. If there were only one base, after it had removed a hydron from either enantiomer of mandelate, there would be the same *gem*-enediolate and the same conjugate acid. That acid should then participate in hydrogen isotopic exchange at the same initial rate in both cases, not just in the case of (*S*)-mandelate.

The bases in the active site of mandelate racemase from *P. putida* that remove the hydrons from (*S*)-mandelate and (*R*)-mandelate have been unambiguously assigned crystallographically as Lysine 166 and Histidine 297, respectively (Equation 5–221).[780,781] The 6-amino group of Lysine 166 has only two deuteriums on it whenever the active site associates with (*S*)-mandelate because it is the catalytic base. In addition, however, Lysine 166 is a participant in a cluster of hydrogen bonds in which the two oxygens of the carboxy group of Glutamate 221, a molecule of water, the hydroxy group of Serine 139, the 6-amino group of Lysine 164, and the 4-hydroxy group of Tyrosine 137 are participants. There are six hydrogen bonds in this cluster and, consequently, at least six deuterons. In any reversal of formation of the intermediate *gem*-dienolate from (*S*)-mandelate at the active site, deuterium would almost always be incorporated into the resulting (*S*)-mandelate, as is observed.

The τ nitrogen of the imidazolyl group of Histidine 297 removes the hydron from (*R*)-mandelate, and the π nitrogen–hydrogen of its imidazolyl group forms a hydrogen bond (0.28 nm) with an oxygen of the carboxy group of Aspartate 270. This hydrogen bond is responsible for holding the imidazolyl group in the proper orientation. In this distal hydrogen bond, there must be a deuteron, but the imidazolyl group of Histidine 297 would have to flip over to bring that deuteron into the vicinity of carbon 2 of the enolate. If it were to flip over, however, the nitrogen–deuterium bond of the π nitrogen would be in a completely different orientation and location, relative to the carbanionic carbon of the enolate, than the nitrogen–hydrogen bond of the τ nitrogen

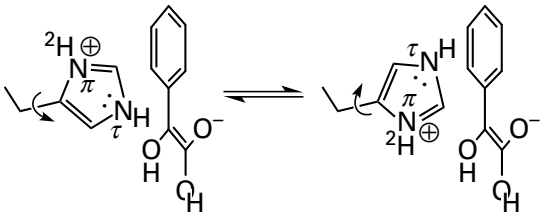

(5–224)

and it would be difficult, if not impossible, for the deuteron on the π nitrogen to deuteronate that carbon. Consequently, hydrogen isotopic exchange into (*R*)-mandelate should be significantly slower than that into (*S*)-mandelate, as is observed. This instance is an educational example of the fact that **the two nitrogens in the imidazolyl group of a histidine are not symmetrically arrayed**, as well as an illustration of the fact that hydrogens exchanged in most hydrogen isotopic exchanges are already within the active site.

Hydrogen isotopic exchange is usually taken as evidence that a hydrogen is removed from the substrate as a hydron. For example, GDP-mannose 3,5-epimerase, which contains a prosthetic NAD^+ in its active site,[782] is able to interconvert GDP-L-galactose and GDP-D-mannose, a reaction requiring a double epimerization*

*Upon double epimerization, the more stable configuration of the ring changes due to the shift of the two substituents from equatorial to axial in the initial configuration.

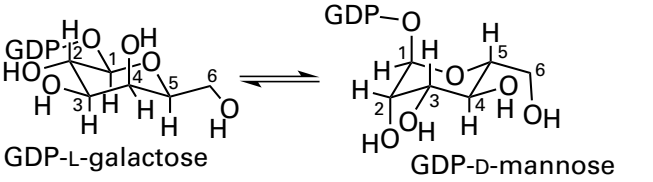

(5–225)

one at carbon 3 and one at carbon 5. Neither position in either substrate is acidic. When the reaction, however, is carried out with the enzyme from *Auxenochlorella pyrenoidosa* in ^3H_2O, tritium is incorporated into both GDP-L-galactose and GDP-D-mannose at both carbons 3 and 5.[783] The existence of these hydrogen isotopic exchanges suggests a mechanism in which GDP-4-oxo-4-dehydro-L-galactose (**5–156**) is formed from GDP-L-galactose and GDP-4-oxo-4-dehydro-D-mannose (**5–157**) is formed from GDP-D-mannose. The two adjacent epimerizations occur through the two respective enolates at carbon 3 and the two respective enolates at carbon 5

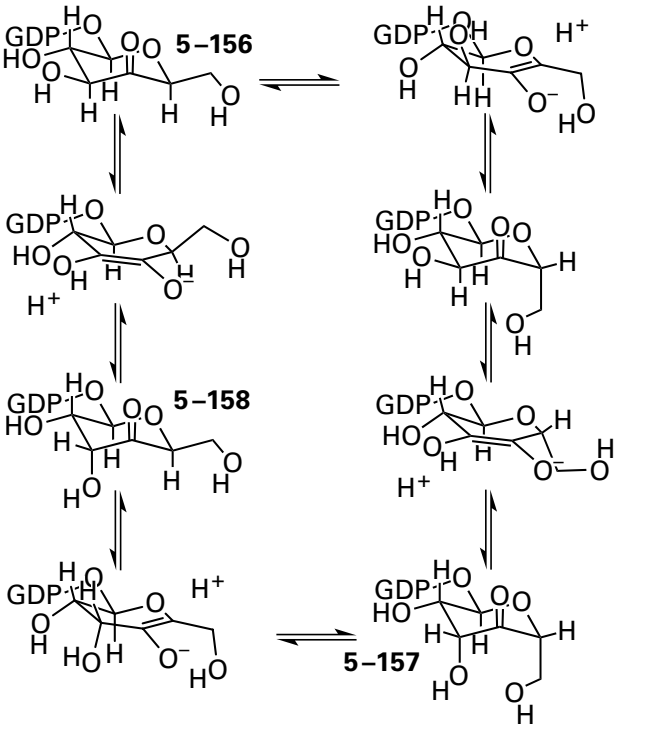

(5–226)

formed by removals of hydrons from the respective carbons α to the respective oxo group. Because the percentage of tritium incorporated into the two substrates at carbon 3 was the same as that incorporated into carbon 5, the hydrogen isotopic exchange provides no indication of a preferential order for the double epimerizations, forward and reverse. On the path to the left, the hydron on carbon 3 of **5–156** is removed first and the hydron on carbon 5 of **5–157** is removed first. On the path to the right, the hydron on carbon 5 of **5–156** is removed first and the hydron on carbon 3 of **5–157** is removed first. One product at equilibrium, however, when the reaction is catalyzed by GDP-mannose 3,5-epimerase from *A. thaliana* (72% identity; 0.5 gap percent), is GDP-L-gulose, the monosaccharide that is the product of reduction of GDP-4-oxo-4-dehydro-L-gulose (**5–158**).[784] This observation suggests that, at least in the case of this species, the left path in Equation 5–226 predominates.

The existence of hydrogen isotopic exchange, however, does not necessarily demonstrate that a hydrogen was initially removed as a hydron. During the reaction catalyzed by the flavoenzyme glutaryl-CoA dehydrogenase (ETF) (Equation 5–64) from *P. fluorescens* with glutarylpantetheine as the reactant in ^2H_2O, hydrogen isotopic exchange of protium for deuterium at carbon 3 of glutarylpantetheine is observed.[785] The first step in this reaction is removal of a hydron from carbon 2 of the reactant to produce the enolate with its oxyanion sitting in an oxyanion hole.[249] The enolate is then oxidized to the olefin by flavin

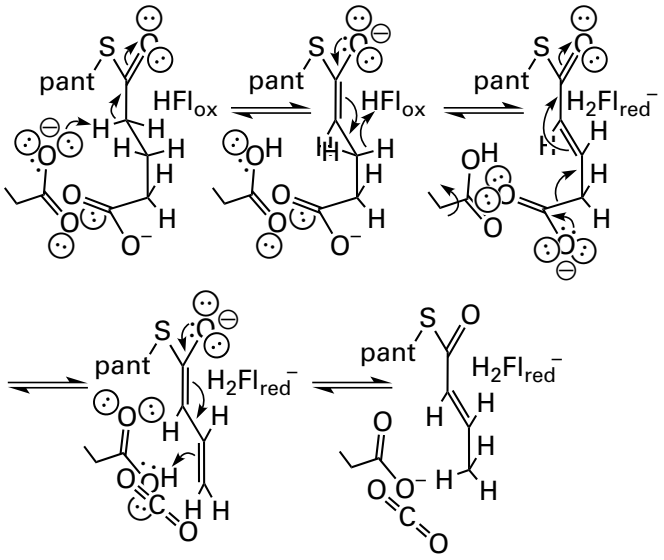

(5–227)

During this second step, the hydrogen on carbon 3 is probably transferred to nitrogen 5 of the oxidized flavin (HFl_{ox}) as a hydride. On nitrogen 5 of the flavin, the hydride becomes acidic and susceptible to isotopic exchange, probably with the deuterons on the deuteroxy group of Threonine 172 that forms a hydrogen bond with nitrogen 5 (0.28 nm) or the molecule of ^2H_2O that is in a hydrogen bond

(0.24 nm) with that deuteroxy group.[249] This example illustrates a feature peculiar to flavin, which is the ability to convert a hydride into a hydron.

Isotopic exchange in the absence of one or more reactants, isotopic exchange into an analogue of a reactant, isotopic exchange at initial rate, positional isotopic exchange, and intermediate isotopic exchange usually provide information about the existence of intermediates in the enzymatic reaction. The isotopic exchanges observed with fructose-bisphosphate aldolase, deoxycytidylate 5-hydroxymethyltransferase, 3-dehydroquinate synthase, urocanate hydratase, glutamine synthetase, and citrate (*Si*)-synthase are examples of this ability.

In the absence of the appropriate transfer RNA but the presence of the appropriate amino acid, amino acid—tRNA ligases catalyze **phosphorus isotopic exchange**[786]

$$Mg[^{32}P]OPO_3PO_3^{2-} + Mg[^{31}P]ATP^{2-} \rightleftharpoons Mg[^{32}P]ATP^{2-} + Mg[^{31}P]OPO_3PO_3^{2-} \quad (5\text{–}228)$$

It was the existence of this phosphorus isotopic exchange in the absence of a reactant in leucine—tRNA ligase from *E. coli* that led to the identification of the **amino acid adenylates**[787] that are the central intermediates in these fundamental enzymatic nucleophilic substitutions.

Pyruvate carboxylase catalyzes the carboxylation of pyruvate (previously Equation 1–144)

$$\text{pyruvate} + HOCO_2^- + MgATP^{2-} \rightleftharpoons HOPO_3^{2-} + MgADP^- + H^+ + \text{oxaloacetate} \quad (5\text{–}229)$$

Consistent with the existence of ***N*-carboxybiotin** as the central intermediate in this carboxylation (Figure 1–29), both the enzyme from *G. gallus*[788] and the enzyme from *R. norvegicus*[789] catalyze the carbon isotopic exchange

$$Mg[^{12}C]ATP^{2-} + Mg[^{14}C]ADP^- \rightleftharpoons Mg[^{12}C]ADP^- + Mg[^{14}C]ATP^{2-} \quad (5\text{–}230)$$

that requires addition of bicarbonate[788,789] but proceeds in the absence of pyruvate. Unfortunately, this carbon isotopic exchange in the absence of pyruvate is eliminated by removal of biotin from the active site,[790] so it could not be determined if the exchange results from reversal of the first step in the phosphorylation of bicarbonate by $MgATP^{2-}$

$$E{\cdot}MgATP^{2-}{\cdot}HCO_3^-{\cdot}\text{biotin} \rightleftharpoons E{\cdot}MgADP^-{\cdot}HOPO_3CO_2^{2-}{\cdot}\text{biotin} \rightleftharpoons E{\cdot}MgADP^-{\cdot}HOPO_3^{2-}{\cdot}\textit{N}\text{-carboxybiotin} + H^+ \quad (5\text{–}231)$$

a result that would provide evidence for carboxyphosphate as an intermediate. In the absence of HCO_3^-, $MgATP^{2-}$, $MgADP^-$, and $HOPO_3^{2-}$, the enzyme catalyzes the carbon isotopic exchange

$$[3\text{-}^{14}C]\text{pyruvate} + [3\text{-}^{12}C]\text{oxaloacetate} \rightleftharpoons [3\text{-}^{14}C]\text{oxaloacetate} + [3\text{-}^{12}C]\text{pyruvate} \quad (5\text{–}232)$$

that results from reversible formation of the intermediate, *N*-carboxybiotin

$$E{\cdot}\text{oxaloacetate}{\cdot}\text{biotin} \rightleftharpoons E{\cdot}\text{pyruvate}{\cdot}\textit{N}\text{-carboxybiotin} \quad (5\text{–}233)$$

The design of these experiments was based on similar isotopic exchanges that had been observed with porcine propionyl-CoA carboxylase[791] and methylcrotonyl-CoA carboxylase from *Mycobacterium* and *Achromobacter*.[792]

Pyruvate, phosphate dikinase from *P. freudenreichii* catalyzes the phosphorylation of phosphate by the γ-phospho group of $MgATP^{2-}$ and then the phosphorylation of pyruvate by the β-phospho group of $MgATP^{2-}$ (previously Equation 3–500)

$$MgATP^{2-} + HOPO_3^{2-} + \text{pyruvate} \rightleftharpoons 2\,H^+ + AMP^{2-} + MgOPO_3PO_3^{2-} + \text{phospho}\textit{enol}\text{pyruvate} \quad (5\text{–}234)$$

The enzyme catalyzes the carbon isotopic exchange[793]

$$Mg[^{12}C]ATP^{2-} + [^{14}C]AMP^{2-} \rightleftharpoons [^{12}C]AMP^{2-} + Mg[^{14}C]ATP^{2-} \quad (5\text{–}235)$$

in the absence of all four of the other substrates. It catalyzes the phosphorus isotopic exchange

$$[^{32}P]HOPO_3^{2-} + Mg[^{31}P]OPO_3PO_3^{2-} \rightleftharpoons Mg[^{32}P]OPO_3PO_3^{2-} + [^{31}P]HOPO_3^{2-} \quad (5\text{–}236)$$

in the presence of $MgATP^{2-}$ but the absence of the three other substrates. It catalyzes the carbon isotopic exchange

$$[^{14}C]\text{pyruvate} + \text{phospho}[^{12}C]\textit{enol}\text{pyruvate} \rightleftharpoons \text{phospho}[^{14}C]\textit{enol}\text{pyruvate} + [^{12}C]\text{pyruvate} \quad (5\text{–}237)$$

in the absence of all four of the other substrates.

A kinetic mechanism[794,795] that is consistent with all these isotopic exchanges in the absence of one or more substrates has been proposed that involves a diphosphorylated intermediate[796]

$$EH + MgATP^{2-} \rightleftharpoons E\text{-}PO_3PO_3^{3-}\cdot Mg^{2+} + H^+ + AMP^{2-} \quad (5\text{–}238)$$

as the first chemical step in the direction written (Equation 5-234). This first step by itself explains the carbon isotopic exchange of Equation 5–235. The covalent intermediate $E\text{-}PO_3PO_3Mg^-$ is a **diphosphoimidazolyl group**[154,797] on Histidine 453 (previously Equation 3–503)

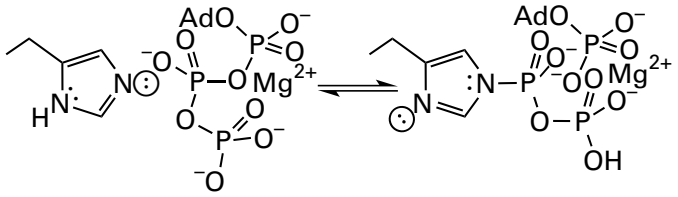

(5–239)

The diphosphorylated covalent intermediate first phosphorylates phosphate (see Equation 3–502)

$$E\text{-}PO_3PO_3^{3-}\cdot Mg^{2+} + HOPO_3^{2-} \rightleftharpoons E\text{-}PO_3^{2-} + MgOPO_3PO_3^{2-} + H^+ \quad (5\text{–}240)$$

to produce magnesium diphosphate. This second step explains the phosphorus isotopic exchange of Equation 5–236 and its requirement for $MgATP^{2-}$, which is necessary to produce the diphosphoimidazolyl group. The resulting phosphoimidazolyl intermediate, $E\text{-}PO_3^{2-}$, then phosphorylates the enolate of pyruvate (see Equation 3–501)

$$E\text{-}PO_3^{2-} + \text{pyruvate} \rightleftharpoons EH + \text{phospho}\textit{enol}\text{pyruvate} \quad (5\text{–}241)$$

This third step by itself explains the carbon isotopic exchange of Equation 5–237, and the fact that it occurs in the absence of any other substrates.

Pyruvate, phosphate dikinase from *Clostridium symbiosum* (Equation 5–234) also catalyzes the positional oxygen isotopic exchange of oxygen-18 from the $\alpha\beta$-bridging position in $Mg[\alpha\beta\text{-}^{18}O,\beta,\beta\text{-}^{18}O_2]ATP^{2-}$ to a nonbridging position on the α-phospho group. This positional oxygen isotopic exchange[794] produces $Mg[\alpha\text{-}^{18}O,\ \beta,\beta\text{-}^{18}O_2]ATP^{2-}$. Its existence is also consistent with the involvement of a covalent diphospho intermediate. The fact that this positional oxygen isotopic exchange is almost completely dependent on the presence of $HOPO_3^{2-}$ suggests that the active site in this species must close around both $MgATP^{2-}$ and $HOPO_3^{2-}$ before the covalent diphospho intermediate can form (Equation 5–238). The same positional isotopic exchange within $MgATP^{2-}$ is observed during the reaction catalyzed by glutamine kinase

$$MgATP^{2-} + \text{L-glutamine} + H_2O \rightleftharpoons N^5\text{-phospho-L-glutamine} + Mg^{2+} + HOPO_3^{2-} + AMP^{2-} + 2\,H^+ \quad (5\text{–}242)$$

from *Campylobacter jejuni*, which also has a diphosphoimidazolyl group as a covalent intermediate.[798] The diphosphoimidazolyl intermediate phosphorylates a molecule of water to produce phosphate, and the resulting phosphoimidazolyl group phosphorylates the nitrogen of the carbamoyl group of L-glutamine rather than the oxygen of *enol*pyruvate.

Orotidine-5′-phosphate decarboxylase catalyzes the exchange of carbon dioxide, a Lewis acid, for a hydron, a Brønsted acid[799]

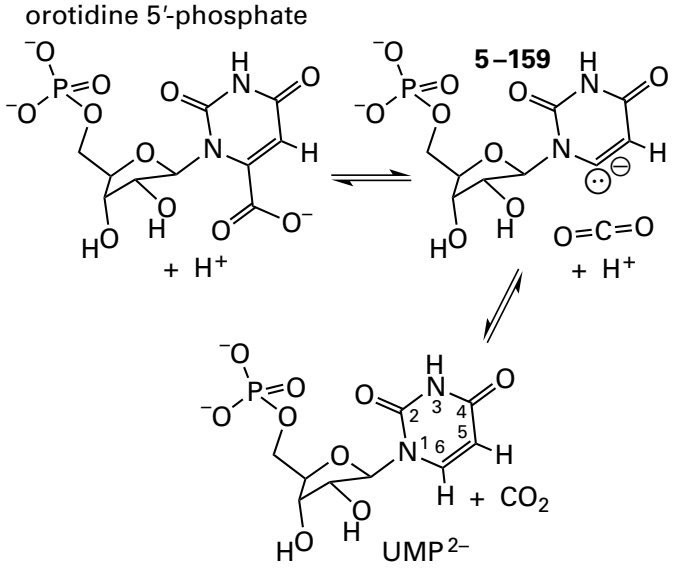

(5–243)

The strongest evidence for the existence of **carbanionic intermediate 5–159** is that, in ^2H_2O and in the absence of CO_2, the enzyme from *S. cerevisiae* catalyzes hydrogen isotopic exchange[800] of a deuteron for the hydron on carbon 6 of UMP^{2-}. The catalytic base in the active site of the enzyme from *Methanothermobacter thermoautotrophicus* that is responsible for removing the hydron from carbon 6 of UMP during this hydrogen isotopic exchange is Lysine 72.[801,802] The 6-amino group of Lysine 72 is in a hydrogen-bonded cluster in which the two oxygens of the carboxy group of Aspartate 70, the two oxygens of the carboxy group of Aspartate 75, the amino group of Lysine 42, and the two hydroxy groups on the ribosyl group of orotidine 5′-phosphate are participants. There are five hydrogen bonds in this cluster and, consequently at least five deuterons. The 6-amino group of Lysine 72 removes the hydron on carbon 6 of [6-^{1}H]UMP^{2-}, the hydron on the ammonio group can exchange for a deuteron in the cluster, and the deuteron on the ammonio group deuteronates carbanionic intermediate **5–159** to form [6-^{2}H]UMP^{2-}.

Additional evidence for the existence of carbanionic intermediate **5–159** comes from experiments with orotidine-5′-phosphate decarboxylase from *S. cerevisiae*. When the complete enzymatic reaction is run in a 1:1 mixture of H_2O to D_2O, the rate at which a deuteron is incorporated at carbon 6 of the product UMP^{2-} is equal to the rate for incorporation of protium, as would be expected if a base considerably more basic than hydroxide were an intermediate in the reaction.[803] A strongly basic carbanion, such as carbanionic intermediate **5–159**, would not discriminate between removing a hydron from the catalytic ammonio group of the lysine and removing a deuteron. When the hydrogen on carbon 5 of UMP^{2-} is replaced with a fluorine to give 5-fluoro-UMP^{2-}, the initial rate constant for hydrogen isotopic exchange[800,804] increases from 1.2×10^{-5} s^{-1} (0.04 h^{-1}) to 0.04 s^{-1}. This increase is consistent with the conclusion that the normal mechanism includes carbanionic intermediate **5–159**, which would be stabilized by the electron withdrawal of the adjacent fluorine. Finally, when the hydrogen on carbon 5 of the orotyl group in 1-(*β*-D-erythrofuranosyl)orotic acid (EO), a poor alternative reactant (k_{EO} = 0.026 M^{-1} s^{-1}), is replaced with a fluorine to give 1-(*β*-D-erythrofuranosyl)-5-fluoroorotic acid (FEO), the specificity constant (k_{FEO} = 10 M^{-1} s^{-1}) for the decarboxylation increases significantly.[805] This result is also consistent with the electron withdrawal of fluorine stabilizing a carbanionic intermediate in the orotyl group. There is, however, still the difficulty that the hydrogen isotopic exchange is far slower than the catalytic constant (20 s^{-1} at 25 °C) for the decarboxylation.[806] The equilibrium constant for the decarboxylation might provide an explanation of this disparity by providing estimates of the intrinsic rate constant for removal of the hydrogen from UMP^{2-} during the carboxylation catalyzed by the enzyme.

The intermediate carbanion **5–159**, if it exists, is one of the few carbanionic intermediates in an enzymatic reaction that is **not an enolate**, a fact that has contributed to the reluctance to accept its existence. The pK_a of UMP at carbon 6 while it is in the active site of the enzyme has been estimated from the rate of hydrogen isotopic exchange at carbon 6 to be less than or equal to 22.[800] The pK_a of the hydrogen on carbon 6 of UMP in solution is 34,[807] which is consistent with lack of conjugation of the lone pair of electrons in carbanion **5–159** with anything that can withdraw its electron density in the unsubstituted orotyl group. Its inability to conjugate with anything results from the fact that the lone pair of electrons is orthogonal to the π molecular orbital system of the orotyl group. Consequently, the enzyme would be able to stabilize the carbanion by a factor of 10^{12} or 68 kJ mol^{-1}, if the estimate is accurate.

Although intermediate carbanion **5–159** is a strong base and consequently difficult to form, it has been pointed out that it may be the case that decarboxylation produces the carbene

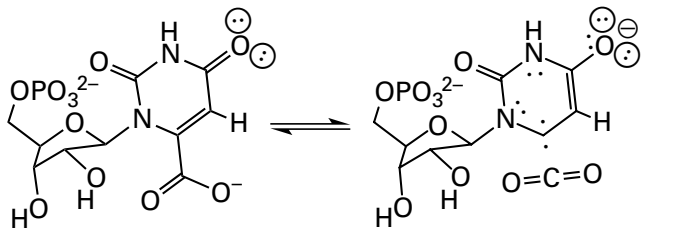

(5–244)

rather than the carbanion. The carbene should be more stable than the carbanion,[808] but its formation would require an intersystem crossing, which may not be kinetically competent. Intersystem crossing would be required both during formation of the carbene and in the transformation of the carbene into the carbanion, either before or during the hydronation. If this **intermediate carbene** can be formed in the active site, it should be an oxyanion. The nitrogen–hydrogen bond of the amido group of Serine 154 in the polypeptide backbone of orotidine-5′-phosphate decarboxylase from *S. cerevisiae* forms a hydrogen bond (0.29 nm) with the oxygen of the carbonyl group in the crystallographic molecular model of the active site occupied by 6-hydroxyuridine 5′-phosphate.[799] When the homologous amido group in orotidine-5′-phosphate decarboxylase from *Methanothermobacter thermautotrophicus* (24% identity; 4.4 gap percent) is chemically mutated to an ester oxygen,[809] the value for $k_0\,K_{m,OMP}{}^{-1}$ decreases by a factor of 75.

Hydronation of the acyl oxygen at carbon 2 in orotidine 5′-phosphate should increase[810,811] its rate of decarboxylation by a factor of 10^8. In a crystallographic molecular model of the active site of the enzyme from *M. thermautotrophicus* occupied by 6-aza-UMP, an analogue[812] of carbanionic intermediate **5–159**, the amido nitrogen in the carbamoyl group of Glutamine 185 forms a hydrogen bond (0.27 nm) with the acyl oxygen on carbon 2 of 6-aza-UMP.[802] This hydrogen bond could explain in part, but only in small part, the stabilization of intermediate carbanionic intermediate **5–159** by the active site.

Another contributor to the stabilization of carbanionic intermediate **5–159,** relative to the substrate orotidine 5′-phosphate, is the carboxylato group of Aspartate 70 in orotidine-5′-phosphate decarboxylase from *M. thermautotrophicus*, which is immediately adjacent to the carboxylato group of orotidine 5′-phosphate when it is bound to the active site. The carboxylato group of the aspartate should destabilize orotidine 5′-monophosphate by electrostatic repulsion relative to carbanionic intermediate **5–159,** in which the anion is farther away.[801,813] When the homologous aspartate, Aspartate 91, in the enzyme from *S. cerevisiae* is mutated to alanine,[814] the catalytic constant decreases by a factor of greater than 10^5, When the homologous aspartate, Aspartate 70, in the enzyme from *M. thermautotrophicus* is mutated to glycine, the rate constant $k_0\,(K_{mOMP})^{-1}$ for decarboxylation of orotidine 5′-phosphate (OMP)[802] decreases by a factor of 10^4 while the rate constant for isotopic exchange of the hydrogen on carbon 6 of 5-fluoro-UMP catalyzed by unmutated Lysine 72, which does not involve the carboxy group, is unchanged.

Finally, in the crystallographic molecular model[815] of a complex between orotidine-5′-phosphate decarboxylase from *E. coli* and 6-hydroxy-UMP$^-$ and the crystallographic molecular model[802] of a complex between orotidine-5′-phosphate decarboxylase from *M. thermautotrophicus* and 5,6-dihydro-UMP, the respective uracilyl groups are surrounded by hydrophobic amino acids, which form a hydrophobic pocket similar to that found in the active sites of other decarboxylases.[816] When these side chains are mutated in turn, decreases in the rate constant $k_0\,(K_{mOMP})^{-1}$ of 10–400 are observed.[817] These decreases recall the observation that decarboxylation of 2-(1′-carboxy-1′-hydroxyethyl)-3,4-dimethylthiazolium (previously Equation 2–54)

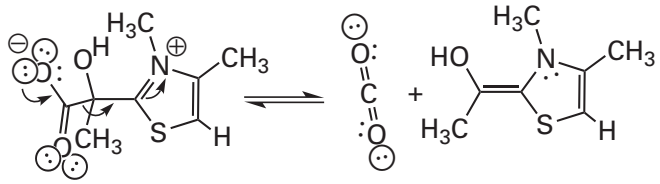

(5–245)

occurs about 10^5 times more rapidly in ethanol than in water.[818] The role of these hydrophobic amino acids in catalysis is supported by the fact that the rate of decarboxylation of 1-methylorotate, a model compound for orotidine 5′-monophosphate, increases 6000-fold when the decarboxylation occurs in tetrahydrofuran or dioxane rather than in water.[819]

Methionine γ-lyase uses pyridoxal 5′-phosphate as a prosthetic group to catalyze the elimination

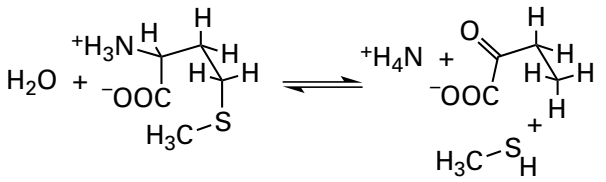

(5–246)

The reaction is based on the ability of the pyridoxal phosphate to project a π molecular orbital system over the carbon skeleton of L-methionine until it is adjacent to the methylsulfanyl group and to provide push to the leaving group, methanethiol (see Equation 4–259)[820]

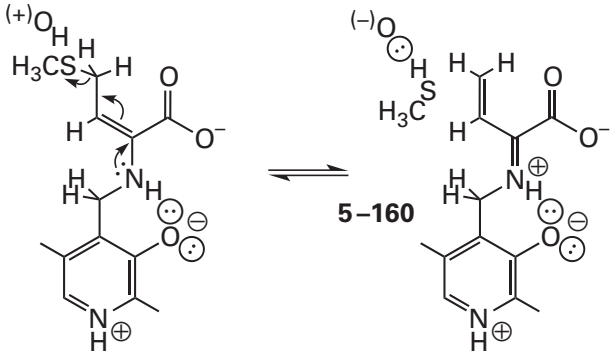

(5–247)

The ultimate intermediate in elimination of the methanethiol is ***N*-(5′-phosphopyridoxyl)-1-carboxyprop-2-enimine (5–160).**

The **individual steps in the expansion of this π molecular orbital system** and the sequence of intermediates could be followed by hydrogen isotopic exchange at initial rate. L-Methionine (100 mM) was mixed with methionine γ-lyase (2.4 μM) from *P. putida* in ^2H_2O, and the α-hydrogen and β-hydrogens on the L-methionine in the solution were monitored by nuclear magnetic resonance spectroscopy. The initial rate at which the α-hydrogen of L-methionine was replaced by deuterium was more rapid than the initial rate at which one of the two β-hydrogens was replaced by deuterium, and formation of the products, 2-oxobutanoate and methanethiol, was much slower than both hydrogen isotopic exchanges (Figure 5–16).[821] This hierarchy provides evidence for sequential formation of the three intermediates—the quinonoid, *N*-(5′-phosphopyridoxyl)imine, and *N*-(5′-phosphopyridoxyl)enamine

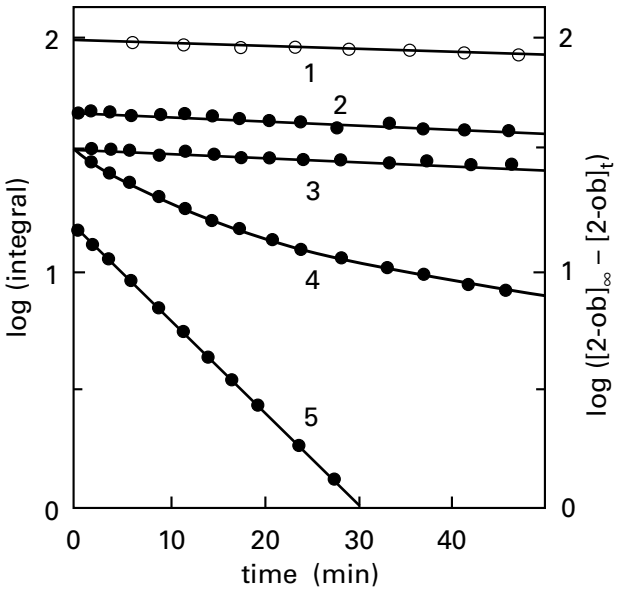

Figure 5–16: Isotopic exchange of hydrogens on the α and β carbons of L-methionine, as well as loss of methanethiol during the overall reaction, for the enzymatic reaction catalyzed by methionine γ-lyase from *P. putida*.[821] A solution (0.5 mL) was prepared at p^{2}H 8.6 and 28 °C that contained 100 mM L-methionine in ^2H_2O (99.8% isotopic enrichment). The reaction was initiated by adding 0.8 nmol of active sites of methionine γ-lyase, and the solution was placed in a nuclear magnetic resonance spectrometer. At various intervals, spectra were recorded. Amplitudes of the absorptions in spectra from the α-hydrogen (curve 5), the β-hydrogens (curve 4), the γ-hydrogens (curve 3), and the *S*-methyl hydrogens (curve 2) were determined by integration of the respective peaks on each spectrum. The common logarithms of these integrals are plotted (●) as a function of the intervals (minutes) that had elapsed from initiation of the reaction to the time at which each peak was recorded. The two β-hydrogens exchange at different rates, and this heterogeneity accounts for the nonlinear behavior of their absorption. At various intervals, samples were withdrawn and quenched, and the appearance of 2-oxobutanoate was followed by reacting the ketone with 3-methyl-2-benzothiozolone. The disappearance of L-methionine as a result of the enzymatic reaction was assumed to be equal to the difference between the concentration (millimolar) of 2-oxobutanoate (2-ob) at infinite time ($[2\text{-ob}]_\infty$) and its concentration at any particular time ($[2\text{-ob}]_t$). The common logarithms of these differences (○) are plotted as a function of time (minutes). Because the equilibrium for the enzymatic reaction favors the products (methanethiol, NH_4^+, and 2-oxobutanoate), the yield of 2-oxobutanoate at the completion of the reaction was close to 100 mM. The fact that absorptions from the γ-hydrogens and the *S*-methyl hydrogens decrease at the same rate as the concentration of reactant indicates that no isotopic exchange takes place at these positions.

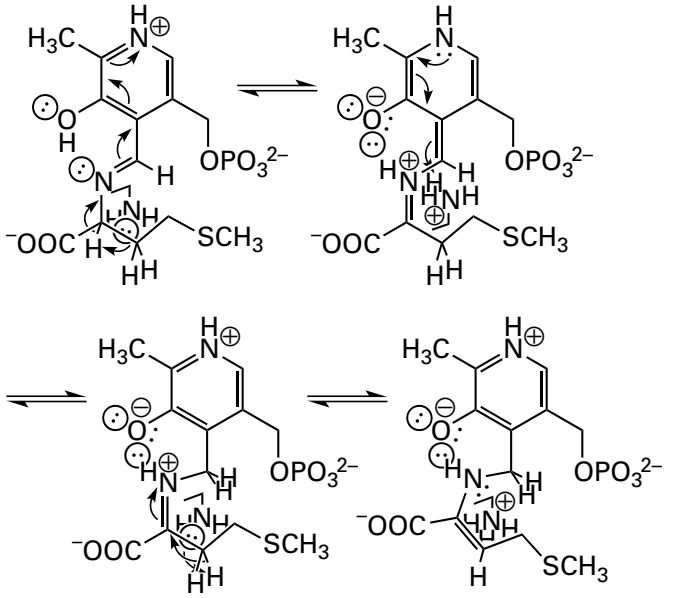

(5–248)

in the enzymatic reaction before elimination of methanethiol (Equation 5–247). The catalytic base that removes the hydrons from the α carbon, hydronating carbon 4′ of the 5′-phosphopyridoxyl group, and the β carbon and that is responsible for the hydrogen isotopic exchanges is the 6-amino group of Lysine 211, which also forms the internal pyridoximine.[820,822] Between removal of each hydron and the addition of each deuteron to the intermediates, the amino group of Lysine 211 is in a cluster of hydrogen bonds in which the 4-hydroxy group of Tyrosine 59, an oxygen from the phosphate of the pyridoxal 5′-phosphate, and the hydroxy group of Serine 340 are participants. This cluster has three hydrogen bonds and, consequently, contains at least three deuterons, and it is probably the immediate source of the deuterons incorporated by hydrogen isotopic exchange at initial rate into the L-methionine.

Bovine glutamate dehydrogenase [NAD(P)$^+$] catalyzes a reaction with three reactants and three products (previously Equation 3–319)[247,823]

$$\text{NAD(P)H} + \text{2-oxoglutarate} + \text{NH}_4^+ + \text{H}^+ \rightleftharpoons \text{H}_2\text{O} + \text{L-glutamate} + \text{NAD(P)}^+$$

(5–249)

The intermediate after the first two chemical steps should be the iminium of 2-oxoglutarate

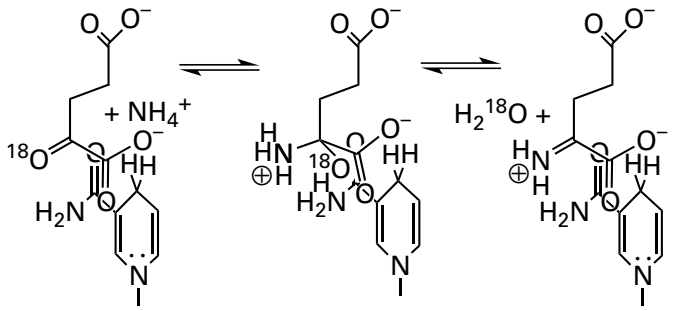

(5–250)

along with a molecule of water that should be able to participate in oxygen isotopic exchange. The molecule of water of the other isotope with which it exchanges should be able to hydrolyze the imine back to ammonia and 2-oxoglutarate. Enzymatically catalyzed oxygen isotopic exchange, however

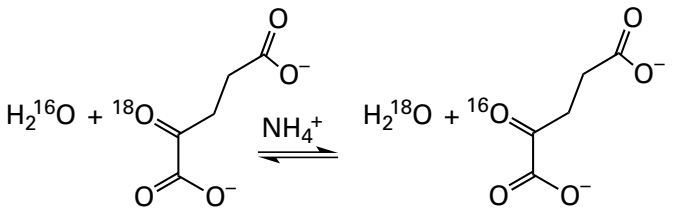

(5–251)

could not be observed in the absence of NADPH, which should be unnecessary for oxygen isotopic exchange.[824]

The following strategy was designed to reveal oxygen isotopic exchange at initial rate during a period in which the forward reaction dominates. The enzyme (250 μM in active sites) was mixed with [2-^{18}O]-2-oxoglutarate (0.3 mM, 58% isotopic enrichment), NADPH (1.1 mM), and amounts of ammonium less than the concentration of active sites (<200 μM), so that when the reaction had reached equilibrium, most of the 2-oxoglutarate would still remain in solution. Under these conditions, a rapid decrease is observed in [2-^{18}O]-2-oxoglutarate over a period of less than 10 s (Figure 5–17) as a result of oxygen isotopic exchange occuring in the first two chemical steps on the active site (Equation 5–250) and their subsequent reversal.[824] This rapid depletion of [2-^{18}O]-2-oxoglutarate was followed by the normal uncatalyzed oxygen isotopic exchange that takes place in solution and that results from nonenzymatic hydration of the ketone

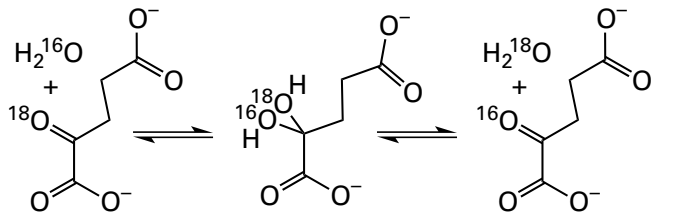

(5–252)

The slow decrease in the isotopic enrichment of [2-^{18}O]-2-oxoglutarate over the next 150 s is a consequence of this uncatalyzed oxygen isotopic exchange ($t_{1/2}$ = 5 min), the rate of which is defined by the course of oxygen isotopic exchange in the absence of enzyme (●). For each course in the presence of enzyme, the rapid decrease in [2-^{18}O]-2-oxoglutarate occurs during the rapid, unresolved approach to equilibrium. In each course, this rapid decrease is revealed by extrapolation (dashed lines) of the uncatalyzed course to zero time. The oxygen isotopic exchange revealed in these measurements is consistent with nucleophilic substitution at the carbonyl groups of 2-oxoglutarate producing the **iminium of 2-oxoglutarate as an intermediate** (Equation 5–250) prior to the reduction.

The enzymatically catalyzed oxygen isotopic exchange occurs only during the rapid approach to equilibrium of the enzymatic reaction. After equilibrium has been established, almost all the ammonium has been converted to glutamate, and the rates of the enzymatic reaction in both directions are much less than the rate of the forward reaction when ammonium was still present. Because the rate of oxygen isotopic exchange decreases dramatically as the ammonia is depleted, it could be concluded that the oxygen isotopic exchange observed in less than 10 s is isotopic exchange during the approach to equilibrium and is not due to reversal of the complete reaction. If it were due to reversal, the oxygen isotopic exchange would have proceeded at the same rapid rate after equilibrium had been reached, but only the uncatalyzed oxygen isotopic exchange (Equation 5–252) is observed at longer times. It was concluded that, to observe the isotopic exchange, NADPH had to be present to close the active site around the reactants, but its reduction of the imine was not required for the isotopic exchange to proceed. Because the uncatalyzed oxygen isotopic exchange by itself was appreciable ($t_{1/2}$ = 5 min), large concentrations of the enzyme (250 μM) were used to complete the approach to equilibrium immediately (<1 s) so that the rapid enzymatically

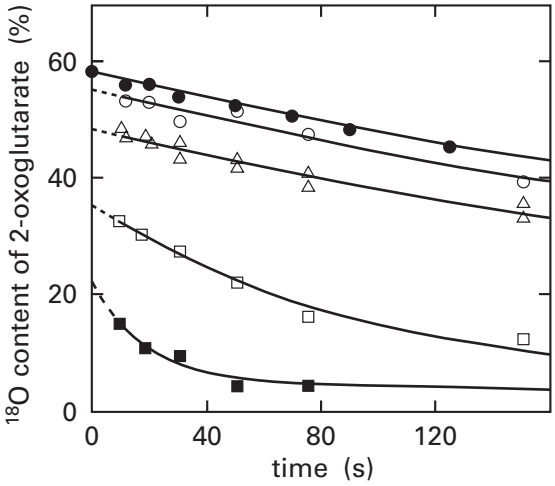

Figure 5–17: Rate of oxygen isotopic exchange from the carbonyl group of 2-oxoglutarate catalyzed by bovine glutamate dehydrogenase (NADP$^+$).[824] Solutions at pH 7.6 and 25 °C contained 250 μM glutamate dehydrogenase (NADP$^+$) and 1.1 mM NADPH and 6 μM (○), 55 μM (△), 118 μM (□), or 180 μM (■) ammonium ion. As ammonium ion was always present at concentrations less than that of the enzyme, each molecule of enzyme on average could complete less than one turnover before equilibrium was reached. The reaction was initiated by adding [2-^{18}O]-2-oxoglutarate (58% isotopic enrichment) to a final concentration of 310 μM. Samples of the reaction mixture were withdrawn at intervals and quenched with an equal volume of 50% H_2O_2, which converted [2-^{18}O]-2-oxoglutarate to [^{18}O]succinate by oxidative decarboxylation, and the oxygen-18 contents of the succinate were determined by mass spectrometry. These values were used to calculate the percentages of isotopic enrichment in the carbonyl oxygen of [2-^{18}O]-2-oxoglutarate (percent ^{18}O content) as a function of each interval (seconds). For each set of data, the solid line extending from 10 to 160 s represents a single first-order curve fit to the loss of ^{18}O due to uncatalyzed isotopic exchange. These solid lines are extrapolated to zero time by dashed lines to indicate the level of oxygen-18 that would be in 2-oxoglutarate if the enzymatically catalyzed reaction had reached equilibrium instantaneously following addition of reactant. The difference between these extrapolated values and the initial value of 58% isotopic enrichment is the amount of oxygen-18 isotopic exchange that occurred before the ammonia had been depleted by the enzymatic reaction. The uncatalyzed oxygen isotopic exchange from [2-^{18}O]-2-oxoglutarate in the absence of enzyme, ammonia, and NADPH is also plotted (●).

catalyzed isotopic exchange could be clearly distinguished from the slower uncatalyzed isotopic exchange.

The enzyme GMP synthase (glutamine-hydrolysing) catalyzes the conversion of xanthosine monophosphate to guanosine monophosphate

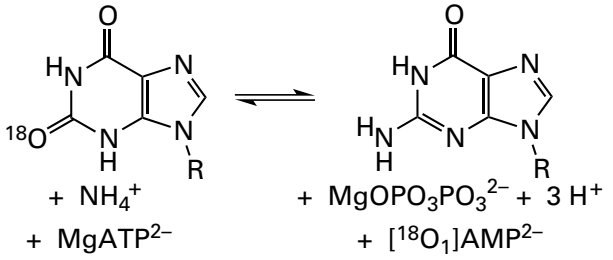

(5–253)

where R is D-ribos-1-yl 5′-monophosphate. The enzyme uses L-glutamine and a glutaminase at a distant active site as the source of the ammonia, hence the notation in parenthesis within the name of the enzyme. Formally, the reaction is a simple nucleophilic substitution at a carbonate carbon in which the nitrogen of ammonia as a nucleophile replaces the oxygen on the ureido carbon 2 of xanthosine 5′-monophosphate with water as the leaving group. That substitution, however, has quite a small equilibrium constant, so the enzyme couples it to hydrolysis of $MgATP^{2-}$. When [2-^{18}O]xanthosine 5′-monophosphate was used as a reactant for GMP synthase (glutamine-hydrolysing) from *Columba livia*, oxygen-18 was found in the phosphate of the AMP^{-} formed during the reaction.[825] This incorporation of isotope led to the suggestion that xanthosine adenylate[826] is formed as an intermediate

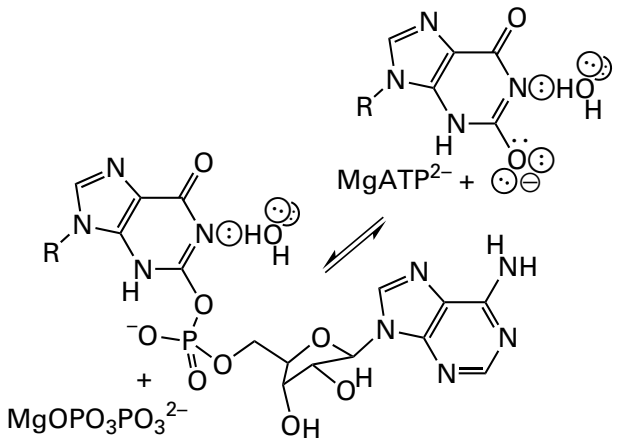

(5–254)

by the nucleophilic substitution at phosphorus of the conjugate base of xanthosine ($pK_a = 13.0$) for magnesium diphosphate. This nucleophilic substitution would create an activated O-adenylated ureido group and, in the process, couple directly and chemically the hydrolysis of $MgATP^{2-}$ to the nucleophilic substitution. This direct chemical coupling ensures that every time the nucleophilic substitution occurs, a molecule of $MgATP^{2-}$ is hydrolyzed. This enforcement necessarily adds the free energy of hydrolysis of $MgATP^{2-}$ to the change of free energy for the overall reaction.

The direct MgATP–diphosphate phosphorus isotopic exchange

$$Mg[\gamma\text{-}^{31}P]ATP^{2-} + Mg[^{32}P]OPO_3PO_3^{2-} \rightleftharpoons Mg[^{31}P]OPO_3PO_3^{2-} + Mg[\gamma\text{-}^{32}P]ATP^{2-}$$

(5–255)

that might have accompanied this mechanism could not be detected in the absence of ammonia. It was possible, however, to detect a positional oxygen isotopic exchange of a nonbridging oxygen into a bridging position

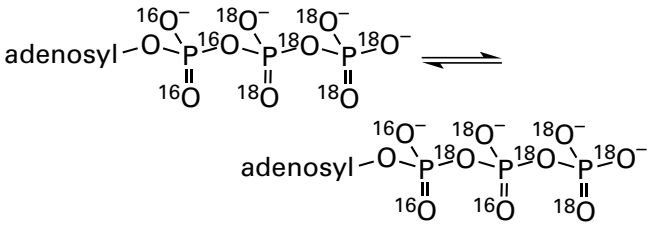

(5–256)

that required the presence of xanthosine but not ammonia.[827] This positional oxygen isotopic exchange is consistent with the existence of **xanthosine adenylate** as an intermediate. The explanation for why positional oxygen isotopic exchange (Equation 5–256) is observed but not phosphorus isotopic exchange (Equation 5–255) is that the active site seems to remain closed to protect the xanthosine adenylate, prohibiting the diphosphate from leaving, a requirement for phosphorus isotopic exchange, until the guanosine monophosphate is formed after the ammonia has been delivered.

Positional oxygen isotopic exchange of a bridging oxygen into a nonbridging position was observed for the diphosphate in 4-amino-2-methyl-5-(diphosphooxymethyl)pyrimidine

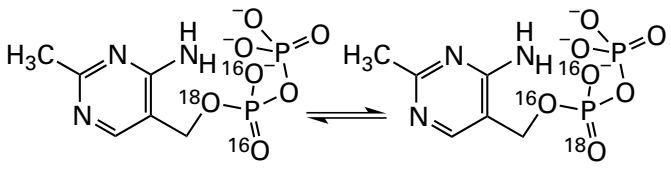

(5–257)

when thiamine phosphate synthase (Equation 5–134) from *B. subtilis* was mixed with 4-amino-2-methyl-5-(diphospho[^{18}O]oxymethyl)pyrimidine in the absence of the other substrate in the enzymatic

reaction, 4-methyl-5-(2-phosphooxyethyl)thiazole.[828] The reaction catalyzed by the enzyme is the nucleophilic substitution of diphosphate by the nitrogen of the thiazolyl group in 4-methyl-5-(2-phosphooxyethyl)thiazole at a primary carbon. This positional oxygen isotopic exchange in the absence of the thiazolyl group requires that the diphosphate dissociate reversibly from the carbon, which is consistent with it being the leaving group in a **dissociative nucleophilic substitution** (Equation 5–135) with 2-methyl-4-imino-5-methylenepyrimidine (**5–108**) or its conjugate acid (**5–107**), a formal carbenium ion, as an intermediate.

Positional isotopic exchange at initial rate within the reactant UDP-α-D-galactopyranose of a bridging oxygen-18 between the diphospho group of UDP and carbon 1 of galactopyranose into a nonbridging position during the ring contraction catalyzed by UDP-galactopyranose mutase

$$\text{UDP-}\alpha\text{-D-galactopyranose} \rightleftharpoons \text{UDP-}\alpha\text{-D-galactofuranose} \qquad (5\text{–}258)$$

from *E. coli* was also consistent with a dissociative nucleophilic substitution of the diphospho group for nitrogen 5 of the prosthetic flavin in the active site with an oxocarbenium ion as an intermediate. In the case of thiamine phosphate synthase, positional oxygen isotopic exchange was observed in the absence of 4-methyl-5-(2-phosphonooxyethyl)-thiazole. In contrast, when nitrogen 5 of the prosthetic flavin, which is the nucleophile in the reaction, was replaced by a carbon by using 5-deazaflavin as the prosthetic group, the positional oxygen isotopic exchange no longer occurred.[829] This result **ruled out an intermediate oxocarbenium ion** and a dissociative nucleophilic substitution, and it is consistent with a concerted nucleophilic substitution in which a covalent bond to nitrogen 5 must be forming as the covalent bond to the phospho oxygen is breaking.

Myosin ATPase hydrolyzes $MgATP^{2-}$ to $MgADP^{-}$ and $HOPO_3^{2-}$ to obtain the free energy necessary for contraction of muscle. On the active site of myosin ATPase, hydrolysis occurs without any intermediates by a direct in-line attack of water

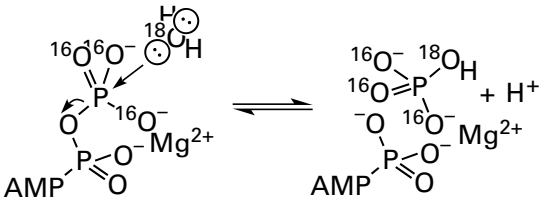

(5–259)

with inversion of configuration at phosphorus.[830] When myosin ATPase from *O. cuniculus*, in the absence of actin, hydrolyzes $MgATP^{2-}$ to $MgADP^{-}$ and $HOPO_3^{2-}$ in $[^{18}O]H_2O$, instead of containing only one atom of oxygen-18, as expected (Equation 5–259), $HOPO_3^{2-}$ contains almost four atoms of oxygen-18.[765,831] The reasons for this intermediate oxygen isotopic exchange at initial rate are that, on the active site, the equilibrium constant for hydrolysis of $MgATP^{2-}$ has been shifted dramatically in the direction of 1 and that the **release of products from the active site** of myosin ATPase is very slow in the absence of actin.[832] For both reasons, hydrolysis of $MgATP^{2-}$ (Equation 5–259) reverses many times, as the phosphate tumbles in the active site, before the products depart. In this instance, because there are no fixed molecules of water in its vicinity[833] aside from two molecules of water on the nearby Mg^{2+}, the molecule of H_2O that is a reactant probably has enough time to enter and leave the active site during these reversals while the $MgATP^{2-}$ remains tightly bound. The $H_2{}^{16}O$ leaving the active site carries away, one at a time and at random,[834] oxygens-16 on phosphorus; and the $H_2{}^{18}O$ entering the active site replaces them with oxygens-18. The existence of this rapid reversal of a reaction that is significantly exergonic in solution is one demonstration that the standard free energy of a particular reaction catalyzed by an enzyme can be dramatically altered by the environment of the active site.

As actin is added to the solution, the rate of the overall hydrolysis increases and the magnitude of the intermediate oxygen isotopic exchange decreases[831] by a relation predicted for random isotopic exchange of all three oxygens on the γ-phosphate of $MgATP^{2-}$ until high concentrations of actin are reached. At this point, only one atom of oxygen-18, from the stoichiometric $H_2{}^{18}O$, is incorporated into the phosphate during the hydrolysis, and no intermediate oxygen isotopic exchange is observed (Figure 5–18).[835,836] This result is one illustration of the fact that the main effect of actin on the rate at which myosin ATPase hydrolyzes $MgATP^{2-}$ in the solution to $MgADP^{-}$ and $HOPO_3^{2-}$ in the solution, as opposed to on its active site, is to accelerate the rate at

which the two products dissociate from the active site, not an acceleration of the hydrolysis of $MgATP^{2-}$ itself on the active site. At high enough concentrations of actin, products are released from the active site so rapidly that no reversal of hydrolysis of $MgATP^{2-}$ can occur before their dissociation.

Such measurements of intermediate oxygen isotopic exchange can also **rule out the existence of two paths** as an explanation for the decrease in incorporation of oxygen-18 into phosphate upon acceleration of a reaction in which $MgATP^{2-}$ is hydrolyzed. Bovine H^+-transporting two-sector ATPase also catalyzes hydrolysis of $MgATP^{2-}$ as well as its synthesis from $MgADP^-$ and $HOPO_3^{2-}$, the reverse reaction. As the rate for hydrolysis of $MgATP^{2-}$ decreases when the concentration of $MgATP^{2-}$ is lowered, the number of oxygens-18 incorporated into the product $HOPO_3^{2-}$ increases, just as when the concentration of actin is decreased with myosin ATPase. One explanation for such an observation is that at high concentrations of $MgATP^{2-}$ the reaction proceeds on a path in which reversal of hydrolysis cannot occur, while at low concentrations of $MgATP^{2-}$ the reaction proceeds on a different path on which complete reversal and consequently complete isotopic exchange occurs at the hydrolytic step. By determining the relative concentrations of the isomeric forms of $HOPO_3^{2-}$ with one, two, three, and four oxygens-18 at several different concentrations of $MgATP^{2-}$, the possibility that two paths were operating could be ruled out.[837]

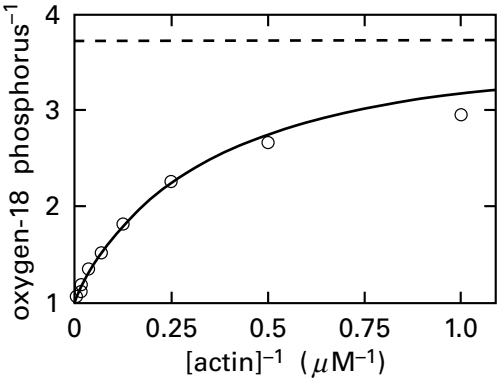

Figure 5–18: Effect of the concentration of actin on intermediate isotopic exchange of oxygen-18 for oxygen-16 into the phosphate produced from $Mg[^{16}O]ATP^{2-}$ in $[^{18}O]H_2O$ by subfragment 1 of myosin.[835] Myosin was digested with chymotrypsin, and the large globular fragment (subfragment 1), missing the coiled coil of the intact protein[836] but still containing the active site at which $MgATP^{2-}$ is hydrolyzed, was purified by anion-exchange chromatography. Solutions (3 mL) containing 1 mM $MgCl_2$, 0.5 mM $MgATP^{2-}$, 1.75 mM phospho*enol*pyruvate, and 200 μg of pyruvate kinase (to regenerate the $Mg[^{16}O]ATP^{2-}$ as it was hydrolyzed) were prepared at pH 7 and 23 °C. Various amounts of actin were added, and hydrolysis of $MgATP^{2-}$ was initiated in each case by adding enough subfragment 1 to produce 80% hydrolysis of $MgATP^{2-}$ and phospho*enol*pyruvate over 2 h. Reaction mixtures were quenched at 2 h with perchloric acid, and the remaining nucleotide and protein were removed by adding activated charcoal and submitting the samples to centrifugation. The phosphate was isolated, and oxygens in the phosphate were converted to gaseous carbon dioxide by reaction with guanidinium chloride. The isotopic composition of $[^{18}O]CO_2$ was determined by mass spectrometry. From these measurements, the ratios of oxygen-18 to phosphorus (oxygen-18 phosphorus^{-1}) in the phosphate could be calculated. These ratios are plotted as a function of the inverse of the concentrations of actin (micromolar^{-1}). The horizontal dashed line is placed at the value for oxygen-18 phosphorus^{-1} for the phosphate produced by subfragment 1 in the absence of actin.

The observed rate of a particular isotopic exchange is determined by a sequence of rates. If a reactant is registering the isotopic exchange, as in the case of fructose-bisphosphate aldolase, then the sequence of rates is the rate of association of the reactant in which the isotope is to be exchanged; the rate at which the bound reactant is transformed into the species responsible for the actual exchange of the isotope; the rate at which this species with the original isotope is exchanged for the same species but with the other isotope; the rate at which the species with the other isotope is modified to re-form the isotopically substituted reactant on the active site; and the rate at which that now isotopically exchanged reactant dissociates from the active site. If a product is registering the isotopic exchange, as in the case of citrate (*Si*)-synthase, then the sequence of rates is the rate of association of the reactant in which the isotope is to be exchanged; the rate at which the bound reactant is transformed into the species responsible for the actual exchange of the isotope; the rate at which this species with the original isotope is exchanged for the same species but with the other isotope; the rate at which the species with the other isotope is converted into the product associated with the active site; and the rate at which that product with the other isotope dissociates from the active site. These considerations emphasize that, because the isotopic exchange is registered in isotopically exchanged reactant or isotopically exchanged product, both accumulating in the solution, associations and dissociations of substrates with the active site are essential steps in the isotopic exchange.

Isotopic exchange can be described by a **universal kinetic mechanism**[838,839]

$$\begin{array}{ccccc} E_1 + A & \underset{k_{-1i}}{\overset{k_{1i}}{\rightleftharpoons}} & E_i(I)(X) & \underset{k_{-i1}}{\overset{k_{i1}}{\rightleftharpoons}} & E_1 + Z \\ & & k_{ex} \Big\downarrow \Big\uparrow k_{-ex} & & \\ E_1 + A' & \underset{k'_{-1i}}{\overset{k'_{1i}}{\rightleftharpoons}} & E_i(I)(X') & \underset{k'_{-i1}}{\overset{k'_{i1}}{\rightleftharpoons}} & E_1 + Z' \end{array} \qquad (5\text{–}260)$$

If **isotopic exchange into a reactant** is being observed, reactant A carries the original isotope and reactant A′ carries the exchanged isotope. The species that accomplishes the switch of the isotopes is indicated as X with the original isotope or X′ with the other isotope. Species X′ may already be in the active site—for example, a hydron or a molecule of water—and simply switch places with species X, in which case the rate constants k_{ex} and k_{-ex} are simple first-order rate constants. Species X may have to dissociate from the active site and species X′ may have to associate with the active site, in which case the rate constants k_{ex} and k_{-ex} are composite rate constants involving concentrations of species X and X′ in solution. Species X can be a nonstoichiometric molecule from the solution entering and leaving the active site—for example, a molecule of water carrying hydrons or an oxygen of the other isotope in and out of the active site—even though a hydron or a molecule of water does not appear in the stoichiometric reaction for the enzymatic reaction. Species E_i can be a complex between the enzyme and an intermediate in the reaction from which species X has just dissociated and with which species X′ associates to accomplish the isotopic exchange. Species X, however, could itself be a substrate for the enzyme, substrate X, and its dissociation from the active site and subsequent association of species X′, a molecule of substrate X bearing the other isotope, accomplishes the isotopic exchange. In this case, the rate constants k_{ex} and k_{-ex} are again composite rate constants involving concentrations of species X and X′ in solution.

If **isotopic exchange into a product** is being observed, product Z is the product of the reaction that carries the original isotope. This product may or may not be present in the solution, and it may or may not be required to associate with the active site for isotopic exchange to be observed. Product Z′ is the product of the reaction that carries the other isotope. When species X itself is a stoichiometric product of the reaction, it carries the original isotope and species X′ is the same stoichiometric product of the reaction that carries the other isotope. In this case, there is no product Z or Z′, and product X or X′ simply dissociates from the active site. Most if not all types of isotopic exchange can be described by Equation 5–260.

Oxygen isotopic exchange in the absence of 5,6,7,8-tetrahydrofolate catalyzed by deoxycytidylate 5-hydroxymethyltransferase (Equation 5–202) is an isotopic exchange in the absence of one or more reactants. In this example, reactant A is 5-hydroxymethylcytidine 5′-monophosphate; species X is a molecule of $H_2{}^{16}O$; and species X′ is a molecule of $H_2{}^{18}O$. A molecule of water is formally a product of the reaction in the direction written, but the molecule of $H_2{}^{18}O$ that switches with the molecule of $H_2{}^{16}O$ is probably already in the active site. After 5-hydroxymethylcytidine 5′-monophosphate has associated with the active site, a molecule of $H_2{}^{16}O$ leaves the 5-hydroxymethylcytidine 5′-monophosphate to produce species E_i, which is a complex between the active site and the methylene intermediate. The molecule of $H_2{}^{16}O$ is then replaced by the molecule of $H_2{}^{18}O$, and isotopically substituted 5-hydroxymethylcytidine 5′-monophosphate dissociates from the active site. Because the other reactant, 5,6,7,8-tetrahydrofolate, has been omitted, no stoichiometric products of the reaction, 5,10-methylenetetrahydrofolate and deoxycytidylate, can be produced; the reaction cannot proceed beyond the methylene intermediate; and the reaction is confined to the left half and central vertical step of Equation 5–260.

The hydrogen isotopic exchange catalyzed by 3-dehydroquinate synthase (Equation 5–206) is an example of an isotopic exchange into an analogue of a reactant. In this instance, reactant A is phosphonate **5–155**; species X is a hydron removed from carbon 6 of the ketone formed from phosphonate **5–155**; species E_i is a complex between the active site and the enolate resulting from removal of the hydron from the ketone; and species X′ is a deuteron probably already in the active site. Again, because phosphonate **5–155** cannot be turned into the product of the reaction, 3-dehydroquinate, the reaction is confined to the left half and central vertical step of Equation 5–260.

The hydrogen isotopic exchange catalyzed by urocanate hydratase (Equation 5–207) is an example of an isotopic exchange at initial rate. Reactant A is urocanate; species X is the hydron that has been removed from carbon 5 of the intermediate formed from urocanate; species E_i is a complex between the active site and the second intermediate result-

ing from removal of the hydron from the first; and species X′ is a deuteron, probably on a molecule of water already in the active site. In this instance, the product of the reaction, 3-(5-oxo-4,5-dihydro-3*H*-imidazol-4-yl)propanoate, species Z, is accumulating as the isotopic exchange into urocanate is proceeding. Although carbon 5 of the product 3-(5-oxo-4,5-dihydro-3*H*-imidazol-4-yl)propanoate no longer has a hydrogen, there must be exchange of a deuteron into the intermediate that is then removed in later steps. Product Z′ is the product that arises from the deuterated intermediate and product Z is the product that arises from the hydronated intermediate, but products Z′ and Z are indistinguishable because neither bears a deuterium. The kinetic mechanism is the complete form of Equation 5–260.

The oxygen isotopic exchange catalyzed by glutamine synthetase (Equation 5–209) is an example of positional isotopic exchange. Reactant A is $MgATP^{2-}$; species X is oxygen-18 on the β-phospho group of $MgADP^-$ with that oxygen-18 having just left and still directed at the phosphorus of L-glutamyl phosphate; species E_i is the complex between the active site and $MgADP^-$ and L-glutamyl phosphate; and species X′ is the rotated [^{18}O]-β-phospho group with one of its two oxygens-16 now directed at the phosphorus of L-glutamyl phosphate and about to add as a nucleophile. Because ammonia is not present, no products of the reaction—$MgADP^-$, phosphate, and L-glutamine—can be produced, and the reaction is confined to the left half and central vertical step of Equation 5–260.

The oxygen isotopic exchange catalyzed by citrate (*Si*)-synthase (Equation 5–212) is an example of intermediate isotopic exchange. Reactant A is [^{18}O]acetyl-SCoA; reactant A′ is [^{16}O]acetyl-SCoA; product Z is [1-^{18}O]citrate; product Z′ is [$^{16}O_7$]citrate; species X is a molecule of $H_2{}^{18}O$ formed during reversal of the hydrolysis of [1-^{18}O]citryl-SCoA; species X′ is a molecule of $H_2{}^{16}O$ that switches with the molecule of $H_2{}^{18}O$ and then hydrolyzes the [1-^{16}O]citryl-SCoA formed by reversal of the hydrolysis of [1-^{18}O]citryl-SCoA; and species E_i is the complex between the active site and that molecule of [1-^{16}O]citryl-SCoA. In this instance, both products Z and Z′ are produced, so the kinetic mechanism is Equation 5–260 in its entirety. There is, however, another reactant, oxaloacetate, and another product, coenzyme A, in the enzymatic reaction. Consequently, regeneration of the form of the enzyme E_1, with which acetyl-SCoA associates, from the form of the enzyme from which citrate dissociates may involve dissociation of coenzyme A and association of oxaloacetate.

The carbon isotopic exchange catalyzed by phosphopyruvate hydratase (Equation 5–215) is an example of isotopic exchange at equilibrium. Reactant A is phospho[1-^{12}C]*enol*pyruvate; species X is 2-phospho-D-[1-^{12}C]glycerate; species X′ is 2-phospho-D-[1-^{14}C]glycerate; and reactant A′ is phospho-[1-^{14}C]*enol*pyruvate. In reverse, reactant A is 2-phospho-D-[1-^{14}C]glycerate; species X is phospho[1-^{14}C]-*enol*pyruvate; species X′ is phospho[1-^{12}C]*enol*pyruvate; and reactant A′ is 2-phospho-D-[1-^{12}C]glycerate. Species E_i is simply the empty active site from which the respective substrates have dissociated. Because species X is product Z and species X′ is product Z′, there is neither product Z nor product Z′, and the reaction is confined to the left half and central vertical step of Equation 5–260. Species X must dissociate from the active site and be replaced by species X′ associating with the active site from solution.

In the forward direction, E_1 is the form of the enzyme that associates with reactant A, the reactant in which the isotopic exchange occurs or the reactant that is transformed into the intermediate in which the isotopic exchange occurs. In the reverse direction after the switching of the isotopes has occurred, E_1 is also the form of the enzyme from which the isotopically exchanged reactant A′ has just dissociated. The form of the enzyme E_i(X) is the one in which species X has just been formed. The form of the enzyme E_i(X′) is the one with which species X′ either has just associated after species X has dissociated or in which species X′ has just switched places with species X′ if species X′ is already in the active site. The rate constant k_{1i} in Equation 5–260 is the forward composite rate constant for all steps between the two forms of the enzyme, E_1 and E_i(X). The rate constant k_{-1i} is the backward composite rate constant for all steps between the two forms of the enzyme, E_i(X) and E_1, from which reactant A dissociates. The rate constants k'_{1i} and k'_{-1i} are similar to the rate constants just described, but they occur between the form of the enzyme E_1 and the complex E_i(X′). The primes indicate that these two rate constants may be different from the rate constants k_{1i} and k_{-1i}, respectively, because of the isotopic substitution.

The rate constant k_{i1} in Equation 5–260 is the forward composite rate constant for all steps between the two forms of the enzyme, E_i(X) and E_1, with which reactant A associates in the next round of catalysis. This composite rate constant includes the steps between E_i(X) and the form of the enzyme from

which product Z dissociates and the steps between the form of the enzyme from which product Z dissociates and E_1. The steps in the latter sequence of steps may include dissociation of another product to clear the active site, a conformational change in the unoccupied enzyme to prepare it for association of reactant A, or association of another reactant that must precede association of reactant A, or two or all three of these transformations. The term k_{-i1} is the backward composite rate constant for all steps in the mechanism between the two forms of the enzyme, E_1 and E_i(X). This composite rate constant includes the steps between E_1 and the form of the enzyme with which product Z associates and the steps between the form of the enzyme with which product Z associates and E_i(X). The steps in the former sequence may include dissociation of another reactant that clears the active site, a conformational change in the enzyme to prepare it for association of product Z, or association of another product that must precede association of product Z, or two or all three of these transformations. Again, the rate constants k'_{i1} and k'_{-i1} are similar to the rate constants just described, but they occur between the complex of the enzyme with species X′ and the form of the enzyme with which reactant A associates.

The rate constant k_{ex} is the rate constant for replacement of species X by species X′. It is usually a composite rate constant as well. Even in cases where species X′ is already in the active site and simply switches places with species X so that k_{ex} is a first-order rate constant, there are probably several steps in this switching of places, each with its own intrinsic forward and reverse rate constants. In situations in which species X must dissociate into the solution from the active site and species X′ must then associate with the active site, the rate constant k_{ex} is a composite rate constant that includes the intrinsic rate constants for dissociations and associations of both species X and X′. The rate constant k_{-ex} is the composite rate constant for the reverse reaction.

The **initial rate for any particular isotopic exchange** ($v_{0,ie}$) can be defined by the equation

$$v_{0,ie} = \frac{d[Q']}{dt} \qquad (5\text{–}261)$$

where $d[Q']/dt$ is the initial rate at which the other isotope, replacing the initial isotope, appears in the molecule Q into which it is being exchanged and which is registering the isotopic exchange. Molecule Q can be either a reactant, reactant A, or a product, species X or product Z. For example, the initial rate for isotopic exchange could be the initial rate at which [5-^{2}H]urocanate, reactant A′, is produced in the hydrogen isotopic exchange at initial rate catalyzed by urocanate hydratase (Figure 5–15) before the rate at which this [5-^{2}H]urocanate is converted into 3-(5-oxo-4,5-dihydro-3*H*-imidazol-4-yl)propanoate, product Z, is sufficient to decrease the rate at which [5-^{2}H]urocanate is formed. The initial rate for isotopic exchange could also be the initial rate at which carbon-14 appears in phospho*enol*pyruvate in the isotopic exchange catalyzed by phosphopyruvate hydratase before enough of this phospho-[1-^{14}C]*enol*pyruvate, reactant A′, has accumulated that it is converted back to 2-phospho-D-[1-^{14}C]glycerate, species X, at a rate sufficient to begin to decrease the rate at which 2-phospho-D-[1-^{14}C]glycerate is converted to phospho-[1-^{14}C]*enol*pyruvate. The initial rate for isotopic exchange could also be the initial rate at which [$^{16}O_7$]citrate, product Z′, appears before [$^{16}O_7$]citrate produced by the reassociation of [1-^{18}O]citrate, product Z, with the active site of citrate (*Si*)-synthase and the reversal of its hydrolysis begins to increase the rate of production of [$^{16}O_7$]citrate.

By defining the rate of isotopic exchange as an initial rate, the intention is to determine the **rate of isotopic exchange in the absence of isotopic exchange resulting from any back reaction**. The conversion of reactant to final product through the steps that accomplish the complete, stoichiometric reaction catalyzed by the enzyme and the subsequent conversion of that product back to reactant almost always produces isotopic exchange, which is uninformative and complicates measurement of the informative isotopic exchange. In situations in which the complete, stoichiometric reaction is not permitted to occur, at isotopic equilibrium for whatever transformation is occurring, the rate of isotopic exchange, by definition, becomes zero. It follows that the initial rate constant for a particular isotopic exchange provides the most uncomplicated information.

The difficulty with measuring the initial rates for isotopic exchange, which is seldom encountered with measurements of the initial rates for enzymatic reactions because there is no product in the solution to begin with, is that accurately measuring the amount of isotope incorporated into a molecule already present at significant concentration in the solution requires that a significant percentage of that molecule be converted to the form containing the exchanged isotope. If the system, however, is **at chemical**

equilibrium, even though it is not at isotopic equilibrium, the incorporation of the other isotope into the substrate registering the isotopic exchange can be treated as a simple **approach to isotopic equilibrium**. The integrated equation for the initial rate of isotopic exchange at chemical equilibrium from the observed concentrations of the products of isotopic exchange measured over the entire course of the reaction is[838,840]

$$v_{0,ie} = \frac{[A]_t[X]_t}{[A]_t + [X]_t}\left[\frac{\ln(1-f)}{t}\right] \qquad (5\text{–}262)$$

where $[A]_t$ and $[X]_t$ are the total molar concentrations of reactant A and species X, and f is the fraction of isotopic exchange achieved at time t relative to the level of isotopic exchange achieved at isotopic equilibrium. It should be emphasized that Equation 5–262 is used to determine the numerical value for the initial rate from a set of experimental observations in the absence of any assignment of kinetic mechanism.

The four isotopic exchanges at equilibrium catalyzed by phosphopyruvate hydratase—the appearance of phospho[1-^{14}C]*enol*pyruvate (Equation 5–215), the appearance of oxygen-18 in 2-phospho-D-[3-^{18}O]glycerate (Equation 5–216), the appearance of ^3H_2O (Equation 5–217), and the appearance of ^2H_2O (Equation 5–218)—behaved as approaches to equilibrium (Figure 5–19)[749] that could be fit by Equation 5–262 to obtain the initial rate for each isotopic exchange (Table 5–2).[749] In both of the two latter isotopic exchanges, reactant A is 2-phospho-D-glycerate and species X is a hydron. Because the concentration of hydrons was 110 M in the solution

$$\frac{[A]_t[X]_t}{[A]_t + [X]_t} = [A]_t \qquad (5\text{–}263)$$

In the case of the oxygen isotopic exchange at equilibrium, the concentration of $H_2{}^{18}O$ was 0.7 M, so Equation 5–263 is approximately correct.

It is obvious that for observations of isotopic exchange at equilibrium, such as the isotopic exchanges observed with phosphopyruvate hydratase, the **system is at chemical equilibrium** because that is the design of the experiment. It is also the case, however, that in measurements of isotopic exchange in the absence of one or more reactants, isotopic exchange into an analogue of a substrate, positional

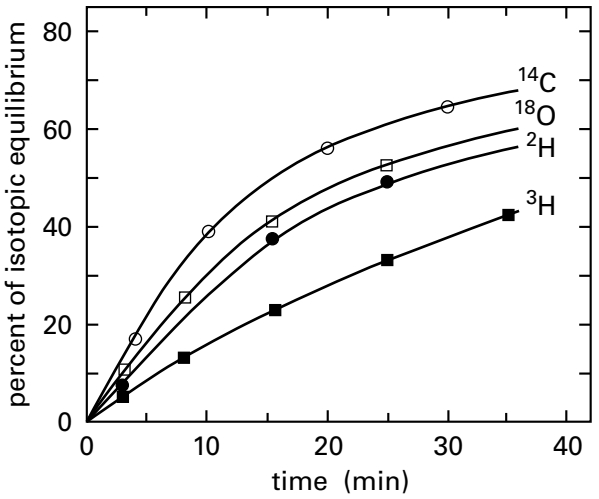

Figure 5–19: Time courses for isotopic exchange at equilibrium of carbon-14, oxygen-18, deuterium, and tritium into and out of 2-phospho-D-glycerate catalyzed by phosphopyruvate hydratase from *O. cuniculus*.[749] The reaction mixture contained 18 mM 2-phospho-D-[2-^{2}H]glycerate (97% ^{2}H), 25 mM $MgCl_2$, traces of 2-phospho-D-[1-^{14}C]glycerate and 2-phospho-D-[2-^{3}H]glycerate, and 110 mM phospho*enol*pyruvate, pH 6.5, in a total volume of 1.5 mL of 1.33 atom % $H_2{}^{18}O$. The reaction was initiated by adding 50 μg of phosphopyruvate hydratase. At various intervals, samples (50 μL) were removed and quenched at 115 °C for 40 s. Values for the isotopic distributions at equilibrium were measured at 18 h. The ^{2}H and ^{3}H exchanged into the H_2O in each sample were determined by distilling the water. The ^{18}O exchanged into 2-phospho-D-glycerate was determined from the residue following distillation of the water. Carbon-14 exchanged into phospho*enol*pyruvate was determined by separating the two substrates chromatographically. For each isotope, the values at each interval (minutes) are plotted as a percentage of their values at equilibrium (18 h). The data were fit to the general equation for isotopic exchange at equilibrium,[840] rate = $\{[A][X]/([A] + [X])\}\{[\ln(1-f)]/t\}$, where "rate" is the rate of the isotopic exchange, [A] and [X] are total molar concentrations of each of the two species exchanging the isotope, and f is the fraction of isotopic exchange achieved at time t. From these fits, the rates (millimolar minute^{-1}) can be calculated for each isotopic exchange (Table 5–2). When one of the species that is exchanging is H_2O, the factor to the left of the expression becomes unity.

isotopic exchange in the absence of a reactant, and intermediate isotopic exchange in the absence of a reactant, the various steps in the truncated reaction come to equilibrium on the active site almost immediately because in each instance, by design, the enzymatic reaction is not progressing to products and the time required to reach equilibrium is less than the time required to complete one round of catalysis. Consequently, in these situations, the system is at chemical equilibrium during the entire course of its approach to isotopic equilibrium, and Equation 5–262 can be fit to the incorporation of the other isotope as a function of time to determine the initial rate of the isotopic exchange.

Table 5–2: Rates of Equilibrium Isotopic Exchange for Phosphopyruvate Hydratase[749]

isotopic equilibrium[a]	observed initial rate[b] (mM min^{-1})	relative rate
[^{14}C]PGA ⇌ [^{14}C]PEP	0.68	1.0
[^{18}O]H_2O ⇌ [^{18}O]PGA	0.71	1.1
[^{3}H]PGA ⇌ [^{3}H]H_2O	0.34	0.5
[^{2}H]PGA ⇌ [^{2}H]H_2O	0.62	0.8
[^{1}H]PGA ⇌ [^{1}H]H_2O		6.2[c]

[a]2-Phospho-D-glycerate is abbreviated as PGA, and phospho-*enol*pyruvate is abbreviated as PEP. [b]Reaction conditions and measurements are given in the legend for Figure 5–19. [c]Estimated from exchange rates for ^{2}H and ^{3}H.

The isotopic exchanges at equilibrium catalyzed by phosphopyruvate hydratase illustrate the use of numerical values of the initial rates for isotopic exchange, rather than the simple fact that the isotopic exchanges occur, to draw a mechanistic conclusion. The initial rates for the observed tritium and deuterium isotopic exchanges at equilibrium catalyzed by phosphopyruvate hydratase were each slower than the initial rate for protium isotopic exchange would have been because of the respective primary **kinetic isotope effects**, but from the initial rates of tritium and deuterium isotopic exchanges, the initial rate for protium isotopic exchange

$$\text{2-phospho-D-[2-}^{1}\text{H]glycerate} + {}^{1}H_2O \rightleftharpoons {}^{1}H_2O + \text{2-phospho-D-[2-}^{1}\text{H]glycerate} \quad (5\text{–}264)$$

could be calculated (previously Equations 4–205 and 4–199)

$${}^{T}k_i \equiv \frac{k_{i\mathrm{H}}}{k_{i\mathrm{T}}} = \left(\frac{k_{i\mathrm{H}}}{k_{i\mathrm{D}}}\right)^{1.44} = {}^{D}k_i{}^{1.44} \quad (5\text{–}265)$$

$${}^{D}k_{\mathrm{B}} \equiv \frac{k_{\mathrm{BH}}}{k_{\mathrm{BD}}} = \frac{{}^{D}k_i + c_{\mathrm{f}} + c_{\mathrm{r}}({}^{D}K_{\mathrm{eq}i})}{1 + c_{\mathrm{f}} + c_{\mathrm{r}}} \quad (5\text{–}266)$$

The initial rate for **hydrogen isotopic exchange of a proton for a proton** at carbon 2 of 2-phospho-D-glycerate was faster than the initial rate for oxygen isotopic exchange at carbon 3 of 2-phospho-D-glycerate (Table 5–2), which was the same as the initial rate for carbon isotopic exchange accomplished by the forward and then the backward operation of the entire reaction. The hydrogen isotopic exchange of a proton for a proton (Equation 5–218) at carbon 2 of 2-phospho-D-glycerate does not require that a proton enter the active site because there are two protons already present on the ammonio group of Lysine 345 and two protons on the molecule of water on the Mg^{2+} that is in a hydrogen bond with the ammonio group. The oxygen isotopic exchange (Equation 5–216) may also involve a molecule of $H_2{}^{18}O$ already in the active site, but there seems to be only one other molecule of water nearby (Figure 4–43), so this isotopic exchange should be slower than a hydrogen isotopic exchange that has four protons on which to draw. The carbon isotopic exchange must incorporate all steps in the hydrogen and oxygen isotopic exchanges as well as dissociation of phospho[^{14}C]*enol*pyruvate, so it is strange that it should have the same initial rate as the oxygen isotopic exchange. The fact that the initial rate for oxygen isotopic exchange is the same as that for carbon isotopic exchange, however, would be consistent with steps in these two isotopic exchanges following a common rate-limiting step that obscures any difference in their respective isotopic exchanges. This rate-limiting step should be removal of the hydron from carbon, which is the most difficult chemical step in the reaction.

Both hydrogen and oxygen isotopic exchanges at equilibrium in the reaction catalyzed by phosphopyruvate hydratase start with association of 2-phosphoglycerate. Consequently, the fact that the initial rate for hydrogen isotopic exchange on carbon 2 of 2-phospho-D-glycerate at equilibrium was greater than the initial rate for oxygen isotopic exchange on carbon 3 at equilibrium was originally presented as evidence that the hydron is removed by a catalytic base in the active site from 2-phospho-D-glycerate before the hydroxy group dissociates as a molecule of water and that there is a *gem*-enediolate as an intermediate in the reaction.[749] This conclusion, drawn from the relative initial rates for the isotopic exchanges, although chemically reasonable, was based on the assumption that the isotopic exchanges at each step in the enzymatic reaction would be so rapid that they would be complete before the next step commenced.

This assumption seems to be too wishful. The rate of exchange (governed by the rate constant k_{ex} in Equation 5–260) of one isotope of a hydron for another isotope of a hydron should be greater than the initial rate for one isotope of oxygen for another isotope of oxygen if there are four hydrons to draw upon but only one molecule of water. Consequently, it seems reasonable that if the water were to leave before the hydron in the enzymatic reaction, oxygen isotopic exchange of $H_2{}^{16}O$ for $H_2{}^{18}O$ could still be slower than hydrogen isotopic exchange of a proton for the proton that is removed from the substrate or an intermediate in the reaction and exchanged for another hydron. Furthermore, the exchange of a fixed molecule of water, almost always pinned down by four hydrogen bonds, should be slower intrinsically than the exchange of a hydron. In this instance, however, hydrogen isotopic exchange is considerably more rapid than oxygen isotopic exchange, a fact in favor of removal of the hydron preceding dissociation of the hydroxy group.

Nevertheless, this particular ambiguity is an example of the fact that, unlike simple observation of the existence of isotopic exchange in the absence of one or more reactants or into an analogue of a reactant, both of which are not based on any reference to initial rates, the relative initial rates for isotopic exchange do not provide unambiguous information for the identification of intermediates in an enzymatic reaction. The ambiguity arises from the details of the exchange of species X′ for species X. If species X′ is a hydron or molecule of water within the active site, its exchange for species X may be slower than the rates of the steps that convert intermediates into subsequent intermediates or into the product within the active site. If species X is a product in the stoichiometric reaction other than a hydron or molecule of water, so that it must dissociate from the active site and a molecule of species X′ must associate with the active site before isotopic exchange can occur, and if species X remains in the active site and only dissociates from the active site after product Z, then an isotopic exchange in which species X is a participant will be less rapid than an isotopic exchange in which product Z participates, even though species X is formed in a chemical step in the active site before the chemical step forming product Z occurs.

So far the kinetics of situations in which the system is at chemical equilibrium while measurements of the initial rate for the isotopic exchange are made have been examined. In contrast, for measurements of isotopic exchange at initial rate, positional isotopic exchange at initial rate, and intermediate isotopic exchange at initial rate, the system is not at chemical equilibrium, and the chemical **concentrations of substrates and intermediates are constantly changing**. This constant change makes determination of the initial rate for isotopic exchange more difficult. In such situations, the percentage of isotopic exchange at a particular time relative to the percentage at complete equilibration of isotope can be plotted as a function of the percentage of conversion of reactant into product relative to the concentration of product at complete chemical equilibration. The data on such a plot can then be fit to equations derived from the universal kinetic mechanism.[839,841] These equations are complex and their form depends on the particular situation, so there is no common equation for all situations. Fitting the data to the appropriate equation for the particular set of measurements, however, can provide the initial rate for isotopic exchange. When the system is in neither isotopic equilibrium nor chemical equilibrium, the fit to the data also provides **information about the partition of an intermediate back into reactant and forward into product.**

Hydrogen isotopic exchange at initial rate for tritons from ^3H_2O onto carbon 2 of D-[2-^{1}H]alanine is observed during the conversion of D-[2-^{1}H]alanine to L-[2-^{3}H]alanine catalyzed by alanine racemase (previously Equation 4–345)

$$\text{D-alanine} \rightleftharpoons \text{L-alanine} \qquad (5\text{–}267)$$

of *G. stearothermophilus*. The intermediate in the reaction is quinonoid **5–161** (see Equation 2–4)

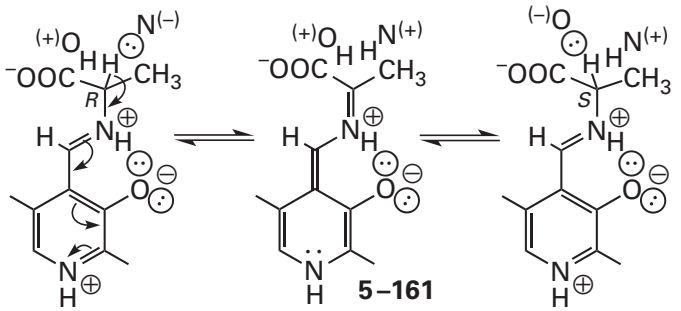

(5–268)

The catalytic acid, $^{(+)}$OH, that normally hydronates quinonoid intermediate **5–161** to give the product L-alanine is the 4-hydroxyphenyl group of Tyrosine 265, which should be completely tritonated throughout the reaction, so the product of the reaction is exclusively L-[2-^{3}H]alanine. The catalytic base, $\odot N^{(-)}$, that normally removes the hydron from D-alanine

to give quinonoid intermediate **5–161** is the 6-amino group of Lysine 39,[842] which is also ditritonated. Consequently, the reactant at early intervals, before the back reaction is significant, is a mixture of the original D-[2-^{1}H]alanine and the exchanged D-[2-^{3}H]alanine. The 6-amino group of Lysine 39 that is responsible for the hydrogen isotopic exchange participates in a cluster of hydrogen bonds involving an oxygen from the carboxy group of an aspartate, a molecule of water, an oxygen in the carboxy group and the imino nitrogen in quinonoid intermediate **5–161**, and a nitrogen in the guanidinio group of an arginine. This cluster contains five hydrogen bonds and therefore at least five tritons, more than enough to exchange with the proton removed from D-[2-^{1}H]alanine by the 6-amino group of Lysine 39 without having to go outside the active site. The 4-hydroxyphenyl group of Tyrosine 265 that removes the hydron from the α carbon of the external pyridoximine of L-alanine is the donor to a cluster of three molecules of water,[842] which provide ample hydrons for hydrogen isotopic exchange into L-alanine that was observed when L-[2-^{1}H]alanine rather than D-[2-^{1}H]alanine was chosen as the reactant.

The percentages of hydrogen isotopic exchange relative to complete isotopic equilibration were plotted as a function of the percentage of conversion of reactant into product relative to the concentration of product at complete chemical equilibration to determine the initial rates for the hydrogen isotopic exchanges. The initial rate for hydrogen isotopic exchange of tritium into the initial D-[2-^{1}H]alanine derived from fitting the data is 0.5 times the initial rate for its conversion to L-[2-^{3}H]alanine. For the reaction in reverse (Equations 5–267 and 5–268), the extrapolated initial rate for hydrogen isotopic exchange of tritium into the initial L-[2-^{1}H]alanine is 0.33 times the initial rate for its conversion to D-[2-^{3}H]alanine.[841] These results, along with steady-state rate constants and kinetic isotope effects, could be used to calculate that under normal circumstances, when no tritium is present in the solvent, the initial rate at which quinonoid intermediate **5–161** is converted to D-alanine free in solution is twice the initial rate at which quinonoid intermediate **5–161** is converted to L-alanine free in solution.*

As was the case with alanine racemase, the initial rate for an isotopic exchange, when combined with other kinetic observations, can provide **rate constants for the steps in the kinetic mechanism** of an enzymatic reaction. For example, the initial rate for positional oxygen isotopic exchange of the bridging oxygen in $MgATP^{2-}$ (Equation 5–209) in the absence and presence of the other two reactants, coenzyme A and citrate; the rate at which the covalent phosphorylated intermediate of the enzyme is formed as a function of the concentration of $MgATP^{2-}$; the catalytic constant; and the two specificity constants from steady-state kinetics could be used to provide experimentally observed parameters within the necessary simultaneous equations. From these equations, the rate constants, both forward and reverse, and hence the equilibrium constants for each step in the kinetic mechanism proposed for the reaction catalyzed by human ATP citrate synthase

$$MgATP^{2-} + \text{citrate} + HSCoA \rightleftharpoons MgADP^{-} + HOPO_3^{2-} + \text{acetyl-SCoA} + \text{oxaloacetate} \quad (5\text{–}269)$$

could be calculated.[843] Such calculations, however, are valid only if the kinetic mechanism proposed for the reaction is correct. Usually, however, if the proposed mechanism is not correct but only incomplete, then the calculated rate constants are composite rate constants that combine steps that occur but do not appear in the proposed kinetic mechanism.

If measurements are confined to the relative initial rates for individual isotopic exchanges into stoichiometric substrates in the enzymatic reaction that are neither hydrogen nor oxygen isotopic exchanges, then isotopic exchange at equilibrium can provide information about the sequence in which reactants associate and products dissociate rather than information about the order of the chemical transformations that occur within the active site and the existence of particular intermediates. Such determinations provide information about a kinetic mechanism rather than a chemical mechanism. Isotopic exchanges in which neither a molecule of water nor a hydron carries the isotope exchanged always require that a stoichiometric reactant participating in the isotopic exchange must associate with the active site and be chemically converted to a stoichiometric product, and this product must dissociate into the solution before the same product with a different isotope, participating in the isotopic exchange in the other direction,

*These rates do not violate the requirement that the equilibrium constant for the reaction must be 1. The rates of formation of the quinonoid intermediate from the two enantiomers differ by the correct amount to satisfy the Haldane relation.

takes the place of the just-dissociated product in the active site. Following its association, this isotopically different product must be chemically transformed into the original reactant, albeit with a different isotopic signature, and that reactant must dissociate from the active site for the isotopic exchange to be accomplished.

Glutamine synthetase (previously Equation 4–453)

$$\text{L-glutamate} + NH_4^+ + MgATP^{2-} \rightleftharpoons MgADP^- + H_2OPO_3^- + \text{L-glutamine} \quad (5\text{–}270)$$

catalyzes a reaction with three reactants and three products. On the basis of other evidence,[763,844,845] including positional isotopic exchange (Equation 5–209),[762] it has been concluded that the central intermediate in the reaction is L-γ-glutamyl phosphate (Equation 5–210). Formation of L-γ-glutamyl phosphate should require only L-glutamate and $MgATP^{2-}$. In the simplest situation, $MgATP^{2-}$, should reversibly phosphorylate an oxygen in the γ-carboxy group of L-glutamate in the absence of ammonium ion; yet, in the presence of L-glutamate but in the absence of ammonium ion, no carbon isotopic exchange (<0.01% that seen in the presence of ammonium ion) between $MgATP^{2-}$ and $MgADP^-$

$$Mg[^{12}C]ATP^{2-} + Mg[^{14}C]ADP^- \rightleftharpoons Mg[^{12}C]ADP^- + Mg[^{14}C]ATP^{2-} \quad (5\text{–}271)$$

was observed with the enzyme from *E. coli*.[846] This isotopic exchange would result from formation of a ternary complex of L-γ-glutamyl phosphate ($GluOPO_3^{2-}$), $Mg[^{12}C]ADP^-$, and enzyme from $Mg[^{12}C]ATP^{2-}$ and L-glutamate (Glu^-)

$$E + Glu^- + Mg[^{12}C]ATP^{2-} \rightleftharpoons E{\cdot}GluOPO_3^{2-}{\cdot}Mg[^{12}C]ADP^- \quad (5\text{–}272)$$

dissociation of the $Mg[^{12}C]ADP^-$ formed

$$E{\cdot}GluOPO_3^{2-}{\cdot}Mg[^{12}C]ADP^- \rightleftharpoons E{\cdot}GluOPO_3^{2-} + Mg[^{12}C]ADP^- \quad (5\text{–}273)$$

association of $Mg[^{14}C]ADP^-$ with the complex of enzyme and glutamyl phosphate, formation of $Mg[^{14}C]ATP^{2-}$ and L-glutamate in the active site, and dissociation of $Mg[^{14}C]ATP^{2-}$ from the active site

$$E{\cdot}GluOPO_3^{2-} + Mg[^{14}C]ADP^- \rightleftharpoons E + Glu^- + Mg[^{14}C]ATP^{2-} \quad (5\text{–}274)$$

The explanation for why no carbon isotopic exchange (Equation 5–271) occurs in the absence of ammonium while positional oxygen isotopic exchange (Equation 5–209) is observed is that, in the absence of ammonium ion, $Mg[^{12}C]ADP^-$ cannot dissociate from the active site, which is a requirement for the carbon isotopic exchange to occur (Equation 5–273). The reason $Mg[^{12}C]ADP^-$ cannot dissociate is that the active site closes around $MgATP^{2-}$, L-glutamate, $MgADP^-$, and L-γ-glutamyl phosphate, preventing $MgADP^-$ from dissociating and exposing L-γ-glutamyl phosphate to hydrolysis.[763,845] When equilibrium concentrations of all six substrates are present, however, MgATP–MgADP carbon isotopic exchange at equilibrium (Equation 5–271) is observed. Because this isotopic exchange does not occur in the absence of ammonium ion, it must result from reversal of the complete reaction at equilibrium.

The initial rates for several of the isotopic exchanges at equilibrium observed with glutamine synthetase from *E. coli* are contrary to expectation. They present an even clearer example of the danger of attempting to correlate relative initial rates for isotopic exchange with the sequence in which covalent bonds are formed or broken within the active site. The initial rate for the carbon isotopic exchange between L-glutamate and L-glutamine

$$\text{L-}[^{14}C]\text{glutamate} + \text{L-}[^{12}C]\text{glutamine} \rightleftharpoons \text{L-}[^{14}C]\text{glutamine} + \text{L-}[^{12}C]\text{glutamate} \quad (5\text{–}275)$$

at equilibrium is 3.6-fold greater than the initial rate for the carbon isotopic exchange between $MgATP^{2-}$ and $MgADP^-$ at equilibrium (Equation 5–271).[846] The carbon isotopic exchange between L-glutamate and L-glutamine must represent the sum of all chemical steps in the reaction in which bonds are formed and broken because, once L-glutamate has been converted to L-glutamine, all chemical steps have been accomplished. Because L-γ-glutamyl phosphate is the intermediate in the enzymatic reaction, $MgADP^-$ must be formed in a step in the overall

enzymatic reaction that precedes the step in which L-glutamine is formed, yet the magnitudes of the initial rates for the isotopic exchanges were in the opposite relation. Even the initial rate for the **nitrogen isotopic exchange**

$$\text{L-}[^{14}\text{N}]\text{glutamine} + [^{15}\text{N}]\text{NH}_4^+ \rightleftharpoons [^{14}\text{N}]\text{NH}_4^+ + \text{L-}[^{15}\text{N}]\text{glutamine} \quad (5\text{–}276)$$

at equilibrium, which requires that phosphate ion, a poor nucleophile, engage in a nucleophilic substitution for ammonia, a poor leaving group, at the γ-carboxy group of the L-glutamyl group was 2.1-fold greater than the initial rate for the MgATP–MgADP isotopic exchange at equilibrium, which only requires that $MgATP^{2-}$ be able to phosphorylate a carboxylato group and then $MgADP^-$ be rephosphorylated by the resulting acyl phosphate in an almost isoergonic nucleophilic substitution at phosphorus. Clearly the relative initial rates for the various isotopic exchanges provide no information about the intermediate in the enzymatic reaction.

The ultimate product $MgADP^-$ must be formed within the active site of glutamine synthetase before L-glutamine is formed in the direction written (Equation 5–270). Nonetheless, at equilibrium, the initial rates for glutamate–glutamine carbon isotopic exchange (Equation 5–275) and ammonium–glutamine nitrogen isotopic exchange (Equation 5–276) are more rapid than the initial rate for MgATP–MgADP carbon isotopic exchange (Equation 5–271). This fact means that either $MgATP^{2-}$ is slower to dissociate from the enzyme than L-glutamate and ammonia in the reverse direction or $MgADP^-$ is slower to dissociate than L-glutamine in the forward direction or both of these requirements apply or $MgATP^{2-}$ is required to associate with the active site before L-glutamate and ammonium can associate or L-glutamine must dissociate from the active site before $MgADP^-$ can dissociate or both of these requirements apply. In other words, associations and dissociations have a preferential order or they have a required order.

Consequently, these relative initial rates, although they fail to provide reliable information about the intermediate in the enzymatic reaction, provide supporting evidence for the conclusion, drawn from steady-state kinetic measurements in the forward direction of the enzymatic reaction (Equation 5–270), that association of reactants is ordered, and $MgATP^{2-}$ is the first reactant to add, L-glutamate the second, and ammonia the third.[845,847] It follows that $MgADP^-$ should be the last product to dissociate and L-glutamine the penultimate product to dissociate. If all these orders of association and dissociation are those followed by the enzymatic reaction, the MgATP–MgADP isotopic exchange at equilibrium would have to be the isotopic exchange accomplished by the entire enzymatic reaction in one direction and then the entire enzymatic reaction in the other while the glutamate–glutamine and nitrogen isotopic exchanges would be accomplished by shorter sequences of interior steps of associations and dissociations of L-glutamate, L-glutamine, and ammonia. Consequently, at the very least, isotopic exchanges at equilibrium provide **evidence consistent with a preferential order for association of reactants and a preferential order for dissociation of products in the enzymatic reaction.**

As already discussed, however, there is a distinction between a situation in which reactants associate with, and products dissociate from, an active site in a preferential order because the rate of association of one reactant is simply greater than that of the other at all concentrations of reactants examined or the rate of dissociation of one product is greater than the rate of dissociation of another, and a situation in which reactants are required to add to, or products are required to dissociate from, the active site in an obligatory order. For example, a second reactant may not be able to associate with the active site until the first reactant does because the first reactant forms a portion of the site with which the second associates or induces a conformational change in the active site required to create the site with which the second reactant associates. In either case, the site for the second reactant does not exist until the first reactant associates. Another example would be a situation in which a second product cannot dissociate from the active site until the first product dissociates because the first product is bound in the active site between the second product and the solution and sterically prevents the second from dissociating or dissociation of the first induces a conformational change required to occur before the second product can dissociate.

Isotopic exchange at equilibrium can be used to draw a distinction between a preferential order, resulting from a simple difference in the rates of association with and dissociation from the active site, and an obligatory order in which one substrate must associate before its cosubstrate can and that same substrate must dissociate only after its cosubstrate has dissociated.[838,848] The following distinctions

are one of the few ways to **assess the difference between obligation and preference**.

Suppose that substrates A and Z must associate with the active site before the active site is capable of associating with their respective cosubstrates, B and Y, and that substrates B and Y must dissociate from the active site before their respective cosubstrates, A and Z, can gain access to the solution and dissociate

$$\mathrm{E + A + B} \underset{k_{-1}}{\overset{k_1}{\rightleftharpoons}} \mathrm{E{\cdot}A + B} \underset{k_{-2}}{\overset{k_2}{\rightleftharpoons}} \mathrm{E{\cdot}A{\cdot}B} \underset{k_{-3}}{\overset{k_3}{\rightleftharpoons}} \mathrm{E{\cdot}Z{\cdot}Y} \underset{k_{-4}}{\overset{k_4}{\rightleftharpoons}} \mathrm{E{\cdot}Z + Y} \underset{k_{-5}}{\overset{k_5}{\rightleftharpoons}} \mathrm{E + Y + Z} \qquad (5\text{–}277)$$

Suppose also that one isotopic exchange at equilibrium can be measured between substrates B and Y, the proximal pair, and another isotopic exchange at equilibrium can be measured between substrates A and Z, the distal pair. When the absolute equilibrium concentrations of all substrates are raised in concert, the distal isotopic exchange between A and Z will increase, reach a maximum, and decrease to zero because the concentrations of E·A and E·Z, from which the respective substrates must dissociate for the distal isotopic exchange to occur, will begin to decrease and approach zero as the concentrations of B and Y are increased and the complexes E·A·B and E·Z·Y come to account for almost all the enzyme in the solution. The proximal isotopic exchange at equilibrium between B and Y, however, will increase and approach a maximum asymptotically because substrate B will always be able to dissociate from the complex E·A·B and substrate Y will always be able to dissociate from the complex E·Z·Y. The rates of these two dissociations are not influenced by the concentrations of substrates. In addition, reformation of complex E·A·B following dissociation of substrate B and re-formation of complex E·Z·Y following dissociation of substrate Y will be almost immediate because there are high concentrations of substrates B and Y to capture the complexes E·A and E·Z immediately after the respective dissociations and before substrates A and Z, respectively, are able to dissociate.

If there is no obligate order and substrates can associate at random

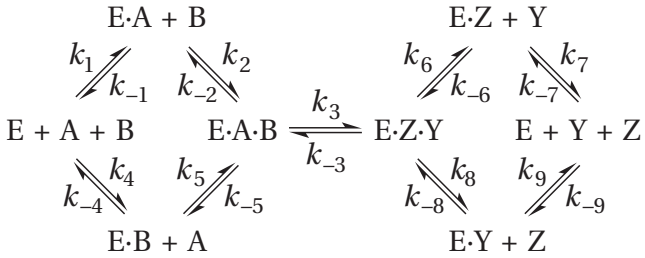

(5–278)

All isotopic exchanges will increase and approach a maximum asymptotically, even though the rates of association and dissociation for one substrate are such that it almost always associates with the active site before its cosubstrate can and, because it binds more tightly, dissociates less readily than its cosubstrate. In this instance, there will be a preferential order in which substrates associate with and dissociate from the enzyme. Complexes E·A and E·B are not distinguished from each other by the order in which substrates A and B are required to associate with and dissociate from complex E·A·B. In addition, complexes E·Z and E·Y are also not distinguished from each other by the order in which substrates Z and Y are required to associate with and dissociate from complex E·Z·Y.

Because glutamate–glutamine carbon isotopic exchange (Equation 5–275) is catalyzed by glutamine synthetase (Equation 5–270) more rapidly than MgATP–MgADP carbon isotopic exchange (Equation 5–271), it was possible that there might be an obligatory order in which substrates must associate with and dissociate from the active site. Other kinetic observations[847] and crystallographic observations[845] were also consistent with an obligate order of addition for substrates $MgATP^{2-}$ and L-glutamate, the former preceding the latter, and an obligate order for association of substrates $MgADP^{-}$ and L-glutamine, the former preceding the latter. Both isotopic exchanges at equilibrium, however, increased and approached their respective maxima asymptotically when the concentrations of substrates were increased in concert for both glutamine synthetase from *E. coli*[846] and ovine glutamine synthetase.[849] It follows that either substrate, $MgATP^{2-}$ or L-glutamate, or either substrate, $MgADP^{-}$ or L-glutamine, may associate with and dissociate from the active site first. The microscopic rate constants for associations and dissociations of the nucleotides, however, are such that they usually associate first with the empty active site and usually dissociate last from a fully occupied active site, but they are not required to do so.

Similar results were observed with isotopic exchanges at equilibrium catalyzed by bovine ketohexokinase[850]

$$MgATP^{2-} + \text{D-fructose} \rightleftharpoons \text{D-fructose 1-phosphate} + MgADP^{-} + H^{+} \quad (5\text{–}279)$$

Although the initial rate for MgATP–MgADP carbon isotopic exchange

$$Mg[^{14}C]ATP^{2-} + Mg[^{12}C]ADP^{-} \rightleftharpoons Mg[^{14}C]ADP^{-} + Mg[^{12}C]ATP^{2-} \quad (5\text{–}280)$$

at equilibrium is 4 times greater at saturation than the initial rate for fructose–fructose phosphate carbon isotopic exchange

$$\text{D-}[^{12}C]\text{fructose 1-phosphate} + \text{D-}[^{14}C]\text{fructose} \rightleftharpoons \text{D-}[^{12}C]\text{fructose} + \text{D-}[^{14}C]\text{fructose 1-phosphate} \quad (5\text{–}281)$$

at equilibrium, the initial rates for both carbon isotopic exchanges at equilibrium approach their respective maxima asymptotically as concentrations of reactants and products are increased. Therefore, any of the four reactants can associate first and any of the four products can dissociate first, but the microscopic rate constants for associations or dissociations of the nucleotides are such that they usually associate after instead of before, and dissociate before instead of after, the monosaccharides.

In the case of diphosphate—fructose-6-phosphate 1-phosphotransferase from *P. freudenreichii*

$$\text{D-fructose 6-phosphate} + MgOPO_3PO_3^{2-} \rightleftharpoons Mg^{2+} + HOPO_3^{2-} + \text{D-fructose 1,6-bisphosphate} \quad (5\text{–}282)$$

the initial rates for three isotopic exchanges at equilibrium—carbon isotopic exchange for D-[U-^{14}C]fructose 1,6-bisphosphate with D-[U-^{12}C]fructose 1-phosphate, phosphorus isotopic exchange for [^{32}P]phosphate with magnesium [^{31}P]diphosphate, and phosphorus isotopic exchange for magnesium [^{32}P]diphosphate with D-fructose [1,6-$^{31}P_2$]bisphosphate—increased in concert when each concentration of the four possible substrate pairs—diphosphate and phosphate, magnesium diphosphate and D-fructose 1,6-bisphosphate, D-fructose 6-phosphate and phosphate, and D-fructose 6-phosphate and D-fructose 1,6-bisphosphate—were increased.* The initial rates for each of the three isotopic exchanges reached the **same limiting rate at saturation** with all substrates.[851] These results are **evidence consistent with a kinetic mechanism in which substrates associate with and dissociate from the active site at random**.

Intramolecular isotopic transfer is sometimes observed in enzymatic reactions. For example, in the reaction catalyzed by steroid Δ-isomerase

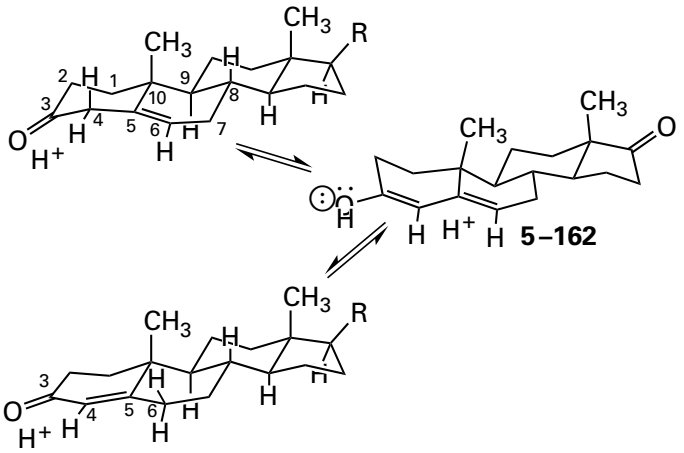

(5–283)

from *C. testosteroni* in ^2H_2O with the reactant androst-5-ene-3,17-dione, only a small amount of deuterium (6–9%) is incorporated into the product androst-4-ene-3,17-dione.[852] Because the enzyme was initially dissolved in ^2H_2O and all the hydrons on any possible catalytic acid were immediately exchanged for deuterons before the reaction was initiated, the only source of protons in this instance is androst-5-ene-3,17-dione itself. Because only the hydron on carbon 4 is removed from androst-5-ene-3,17-dione, this observation requires that the hydron be intramolecularly transferred between carbons 4 and 6 during the enzymatic reaction. When the reaction is catalyzed by the enzyme in ^1H_2O with the reactant [4,4-$^2H_2$]androst-5-ene-3,17-dione, a deuterium on carbon 4 is transferred intramolecularly to carbon 6 of the steroid that is a reactant with little isotopic exchange.[853] Aspartate 38 in the active site of the enzyme performs this intramolecular transfer of a deuteron or hydron, respectively.[854] The carboxy

*Recall that in the equilibrium constant for the reaction, these four pairs appear as quotients, so increasing them in concert does not affect the equilibrium.

group of an aspartate can carry only one hydron at a time, and all that is needed to perform the intramolecular transfer from one carbon to the other is for the carboxy group of Aspartate 38 to rotate around the β carbon–γ carbon bond since removal of the hydron from carbon 4 of androst-5-ene-3,17-dione and its addition to carbon 6 occurs on the same face of the steroid.[853] The carboxy group must, however, also be isolated from hydrons on other acid–bases in the active site that could participate in exchange of its hydron before it has a chance to hydronate carbon 6 of the steroid, which must be relatively slow because it is a hydronation of carbon.

In the reaction catalyzed by glutaryl-CoA dehydrogenase (ETF) from *P. fluorescens*

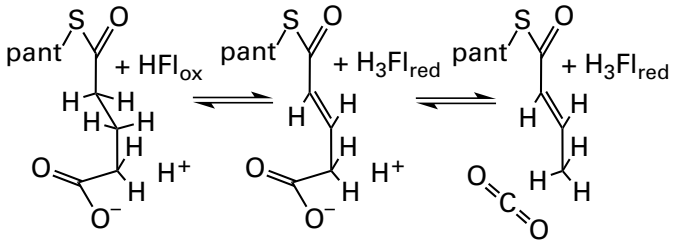

(5–284)

where pant is a pantetheinyl group, there is no incorporation (≤0.5%) of tritium into (*E*)-but-2-enoyl-pantetheine when glutarylpantetheine is oxidized and decarboxylated by the enzyme in ^3H_2O and no hydrogen isotopic exchange of protium with tritium at carbon 2 of the unreacted glutarylpantetheine.[785] The former result requires that the hydron removed from carbon 2 of glutarylpantetheine by a catalytic base be transferred without hydrogen isotopic exchange to carbon 4 because the formal protide ion removed by the prosthetic flavin from carbon 3 does undergo hydrogen isotopic exchange with tritons and therefore cannot be the source of the protium at carbon 4 in the product. The hydron is transferred between carbons 2 and 4 by the catalytic carboxy group of a glutamate that is located in the active site immediately adjacent to carbons 2 and 4 of glutarylpantetheine (Equation 5–227).[249] Again, all that is required for intramolecular isotopic transfer is for the carboxy group of the glutamate to be isolated from other hydrons and to rotate around its γ carbon–δ carbon bond.

The fact that there is no incorporation of tritium from ^3H_2O is consistent with a requirement that no hydrogen isotopic exchange of a proton on the carboxy group of glutamate occur with a triton. Human glutaryl-CoA dehydrogenase (decarboxylating), however, which is closely related (57% identity; 0.5 gap percent), does catalyze hydrogen isotopic exchange of protium for deuterium at both carbon 4 of (*E*)-but-2-enoyl-SCoA ($k_{ex} = 10\ s^{-1}$) and carbon 2 of glutaryl-SCoA in ^2H_2O.[855] In this enzyme with these substrates, the hydron on the carboxy group of the homologous glutamate must be able to exchange ($k_{ex} \geq 10\ s^{-1}$) with deuterons, either on other acid–bases in the active site or in the solvent. The side chains of the amino acids surrounding the carboxy group of the glutamate responsible for dehydronation and hydronation of carbons 2 and 4 in the human enzyme are all hydrophobic,[249] two leucines and a valine, but the same side chains are present at the homologous positions in the enzyme from *P. fluorescens*, so there is no obvious molecular explanation for the difference in isotopic exchange between these two species of the enzyme.

The addition–elimination catalyzed by aconitate Δ-isomerase could have proceeded either of two ways[856]

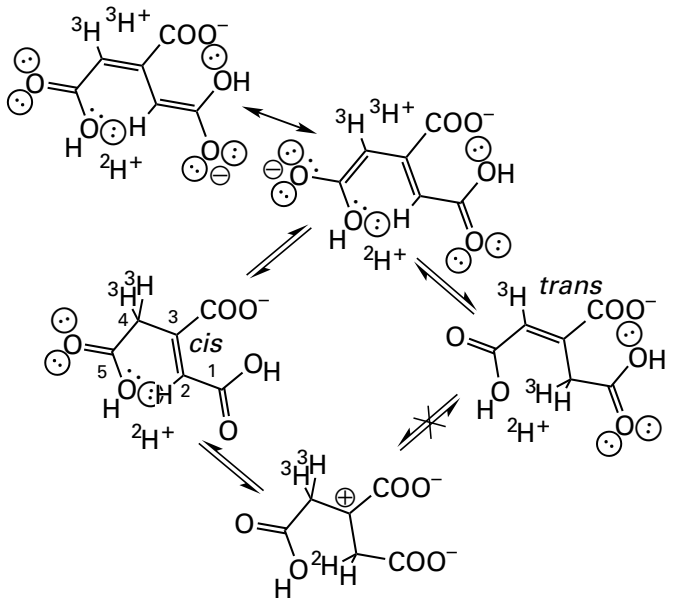

(5–285)

where the reactant is *cis*-aconitate and the product is *trans*-aconitate. The lower path would be through a carbenium ion as an intermediate and the upper through an enolate. The carbocation is not so appealing because the hydron would have to add to a carbon next to the electropositive carbon of a carboxy group and the resulting carbenium ion would also be forced to reside next to a carboxy group. The enolate is the more appealing possibility because it spreads the negative charge over seven atoms in its highest occupied π molecular orbital with lobes over the two electropositive oxygens at its two ends.

Because, in the complete reaction, a hydron is added to carbon 2 and a hydron is removed from carbon 4, the issue again is the timing. It was observed[856] that during the enzymatic isomerization of *cis*-[4*S*-$^3H_2$]aconitate in ^2H_2O, the *pro*-*S* tritium was removed from carbon 4 of the reactant and a fraction of that tritium (44%) was transferred to carbon 2. The tritium or deuterium added to carbon 2 occupied the *S* position in the product. All these observations are consistent with removal of a hydron from carbon 4 of the reactant by a base, its transfer across that same face of the intermediate by the base, and its subsequent addition to carbon 2 from that same face. Consequently, the intermediate should be the more appealing enolate (Equation 5–285).

Aspartate 4-decarboxylase uses a prosthetic pyridoxal 5′-phosphate to catalyze the reaction

$$\text{L-aspartate} + H^+ \rightleftharpoons CO_2 + \text{L-alanine} \qquad (5\text{–}286)$$

the replacement of carbon dioxide by a hydron. Occasionally (0.05% of the time) the enzyme from *Alcaligenes faecalis* fails to complete the normal reaction and the following side reaction occurs

$$\text{L-aspartate} + H^+ + \text{pyridoxal 5′-phosphate} \rightleftharpoons CO_2 + \text{pyruvate} + \text{pyridoxamine 5′-phosphate} \qquad (5\text{–}287)$$

In the abortive reaction, the prosthetic group has become a substrate. When L-[2-^{3}H]aspartate is used as a reactant, a significant amount of tritium (equivalent to 17% intramolecular transfer)[857] is found at carbon 4′ of the pyridoxamine phosphate formed as a result of abortive Equation 5–287. The existence of this intramolecular isotopic transfer suggests that the same base that removes the α-hydron from the external succinyl pyridoximine hydronates the 4′-carbon of pyridoxal phosphate to form *N*-pyridoxylimine **5–164**, which would be necessary to promote the decarboxylation (see Equation 2–5)[858]

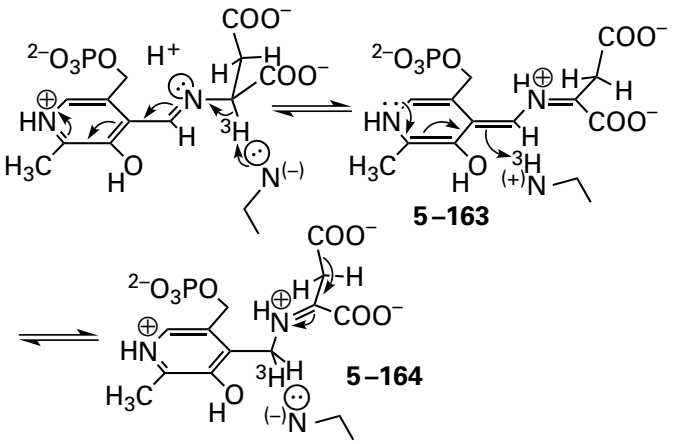

(5–288)

Following decarboxylation and hydronation, the resulting *N*-pyridoxylimine hydrolyzes occasionally before the hydron can be transferred back to the carbon of the imino group

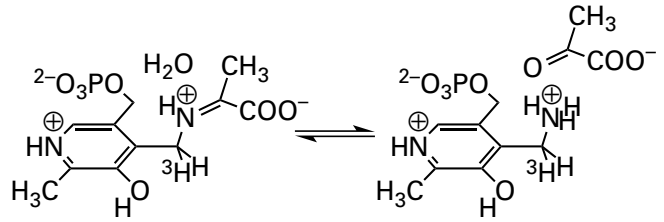

(5–289)

This hydrolysis could occur either on the active site or after the decarboxylated *N*-pyridoxylimine has dissociated intact from the active site. The existence of the intramolecular isotopic transfer, as well as the existence of the abortive reaction itself, provides evidence that *N*-pyridoxylimine **5–164** is an obligatory intermediate in the enzymatic reaction. This conclusion is reasonable because quinonoid **5–163** should be too electron-rich to promote decarboxylation, a reaction that requires π electron withdrawal. In other words, the carbanion that would be formed if quinonoid **5–163** decarboxylated directly would have 10 π molecular orbitals—5 bonding and 5 antibonding—and 12 π electrons, a circumstance that would require two π electrons to occupy an antibonding molecular orbital or two degenerate molecular orbitals.

Methylphosphonate synthase is an oxygenase that converts 2-hydroxyethylphosphonate to methylphosphonate by oxidizing the hydroxymethyl group in 2-hydroxyethylphosphonate to carbon dioxide. The two hydrogens on carbon 1 of 2-hydroxyethylphosphonate remain in the final methyl group in methylphosphonate, but the active site transfers the *pro*-*R* hydrogen on the hydroxymethyl group in

2-hydroxyethylphosphonate to carbon 1 during the oxidation so that it ends up on the methyl group of methylphosphonate.[859] In this instance, however, a catalytic base does not perform the transfer because there is none in the vicinity.[860] It has been proposed that, in the process of oxidizing carbon 2, a formate on a prosthetic iron ion is produced and its **hydrogen is directly transferred** either as a hydrogen atom to a phosphonomethyl radical or, less likely, as a hydride to a primary phosphonomethylene carbenium ion.

Isotopic transfer between a substrate of the enzymatic reaction and the enzyme itself has also been observed. The mechanism of 3-oxoacid CoA-transferase involves formation of an anhydride between a glutamate at the active site[90] and the carboxylic acids that are substrates for the enzyme (Equation 5–14). When [^{18}O]succinate and acetoacetyl-SCoA were used as reactants for the porcine enzyme, the isotopic transfer

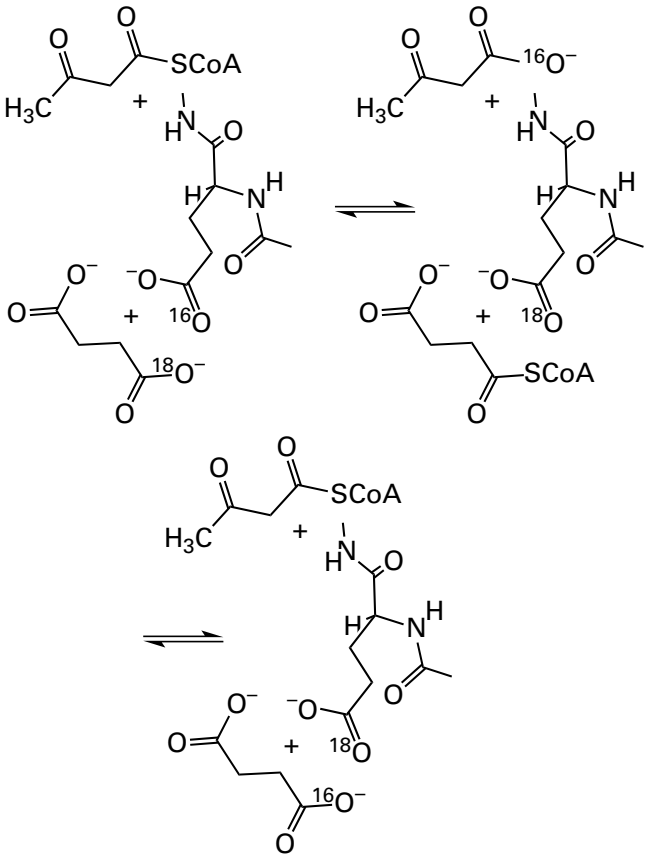

(5–290)

into the protein itself could be detected.[861] This isotopic transfer into the protein is consistent with the existence of the anhydride as an intermediate in the enzymatic reaction. The incorporation of one atom of oxygen-18 into 3-hydroxyisobutyryl-CoA hydrolase from *P. aeruginosa* during the hydrolysis catalyzed by the enzyme

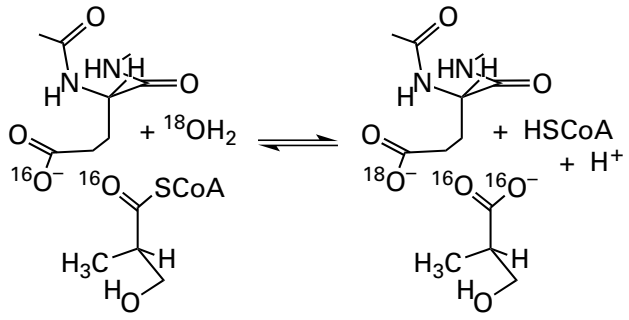

(5–291)

was also presented as evidence for an intermediate anhydride.[862]

Suggested Reading

Fisher, H. F., and Viswanathan, T. S. (1984) Carbonyl oxygen exchange evidence of imine formation in the glutamate dehydrogenase reaction and identification of the "occult role" of NADPH, *Proc. Natl. Acad. Sci. U.S.A. 81*, 2747–2751. https://doi.org/10.1073/pnas.81.9.2747

Furuta, T., Takahashi, H., and Kasuya, Y. (1990) Evidence for a carbanion intermediate in the elimination of ammonia from L-histidine catalyzed by histidine ammonia-lyase, *J. Am. Chem. Soc. 112*, 3633–3636. https://doi.org/10.1021/ja00165a058

Schwede, T. F., Retey, J., and Schulz, G. E. (1999) Crystal structure of histidine ammonia-lyase revealing a novel polypeptide modification as the catalytic electrophile, *Biochemistry 38*, 5355–5361. https:// doi.org/10.1021/bi982929q

Qian, Q., Schultz, A. W., Moore, B. S., and Tanner, M. E. (2012) Mechanistic studies on CymD: A tryptophan reverse *N*-prenyltransferase, *Biochemistry 51*, 7733–7739. https://doi.org/10.1021/bi3009054

Problem 5–19: 2-Aminohexano-6-lactam racemase is an enzyme that uses pyridoxal phosphate as a prosthetic group to catalyze the racemization of the lactam of lysine.

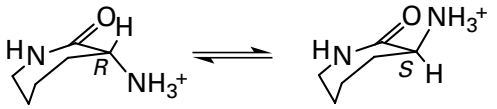

When (*R*)-[2-^{1}H]-2-aminohexano-6-lactam was mixed with the enzyme from *Achromobacter obae* in ^2H_2O, (*R*)-[2-^{2}H]-2-aminohexano-6-lactam was formed at an initial rate that was 80% the initial rate at which (*S*)-2-aminohexano-6-lactam was formed.[863]

(A) Write a mechanism for the enzymatic reaction, incorporating the pyridoxal phosphate and catalytic acids and bases, that explains this hydrogen isotopic exchange at initial rate.

(*R*)-[2-^{1}H]-2-Aminohexano-6-lactam was converted with 2-aminohexano-6-lactam racemase to (*S*)-2-aminohexano-6-lactam in ^2H_2O in the presence of excess L-lysine-lactamase so that the product of the first reaction was immediately hydrolyzed. A significant fraction (17%) of the resulting L-lysine had protium at carbon 2.

(B) What does this observation suggest about the catalytic acid and catalytic base catalyzing the racemization?

(C) There are two reasons to suspect that one particular amino acid is used as a catalytic acid–base in this reaction.[864] What is the amino acid and what are the two reasons? Use this amino acid as the catalytic base in your answer to part A.

Problem 5–20: The reaction catalyzed by ribulose-bisphosphate carboxylase (Equations 3–424 and 5–90) was initiated by mixing enzyme from *R. rubrum* with D-ribulose 1,5-bisphosphate and CO_2 in ^3H_2O. As the reaction progressed at initial rate, tritium appeared at carbon 3 of the ribulose 1,5-bisphosphate remaining in the solution.[865]

extent of reaction (%)	specific radioactivity of remaining ribulose bisphosphate (cpm μmol$^{-1} \times 10^{-5}$)
21	0.9
38	1.9
56	3.3
70	5.2
82	7.4
86	8.4
98	17

(A) Write a mechanism demonstrating why this hydrogen isotopic exchange at initial rate is evidence for an enediol intermediate in the enzymatic reaction.

(B) The specific radioactivity of the water was 7.0×10^5 cpm (μmol of hydrogen)$^{-1}$. Why does the specific radioactivity of the remaining ribulose bisphosphate exceed this value when the reaction has reached equilibrium (98% completion)?

Problem 5–21: Na^+/K^+-Exchanging ATPase catalyzes the following reaction

$$2\,K_o^+ + H_2O + MgATP^{2-} + 3\,Na_i^+ \rightleftharpoons H^+ + HOPO_3^{2-} + 2\,K_i^+ + MgADP^- + 3\,Na_o^+$$

in which the subscripts i and o refer to the inside and the outside of a cell, respectively. This reaction will be referred to as overall turnover. Overall turnover is always measured in, and requires, the presence of all substrates: $MgATP^{2-}$, Na^+, and K^+. In the cell, the cations are moved against their concentration gradients at the expense of hydrolysis of $MgATP^{2-}$. When the cell is fragmented, the enzyme continues to move the cations across itself but accomplishes nothing even though it still hydrolyzes $MgATP^{2-}$. Thus, it is named an adenosinetriphosphatase (ATPase).

The enzyme catalyzes several isotopic exchanges in the absence of certain reactants. In the presence of K^+ and Mg^{2+} but the absence of Na^+ and $MgATP^{2-}$, porcine Na^+/K^+-exchanging ATPase catalyzes the following oxygen isotopic exchange.[866]

$$[^{16}O]HOPO_3^{2-} + [^{18}O]H_2O \rightleftharpoons [^{16}O]H_2O + [^{18}O]HOPO_3^{2-}$$

This oxygen isotopic exchange occurs at an initial rate greater than that of the overall turnover seen when Na^+ and $MgATP^{2-}$ are added. In the presence of Na^+ but the absence of K^+, the enzyme very slowly catalyzes the following carbon isotopic exchange.[867]

$$Mg[^{12}C]ATP^{2-} + Mg[^{14}C]ADP^- \rightleftharpoons Mg[^{12}C]ADP^- + Mg[^{14}C]ATP^{2-}$$

When the enzyme is treated with *N*-ethylmaleimide, the initial rate for this ATP–ADP carbon isotopic exchange increases greater than 100-fold and becomes 3 times faster than the overall turnover was before the treatment. The overall turnover is eliminated by treatment with *N*-ethylmaleimide. *N*-Ethylmaleimide, however, has no effect on the $HOPO_3^{2-} \rightleftharpoons H_2O$ oxygen isotopic exchange observed in the absence of Na^+ and $MgATP^{2-}$. When both Na^+ and K^+ are omitted, none of the isotopic exchanges occur.

(A) Write a kinetic mechanism for the overall reaction, involving a covalent intermediate, that explains both the $HOPO_3^{2-} \rightleftharpoons H_2O$ oxygen isotopic exchange and the ATP–ADP carbon isotopic exchange.
(B) Write the steps in the overall mechanism that produce the Na^+-dependent ATP–ADP carbon isotopic exchange.
(C) Write the steps in the overall mechanism that produce the K^+-dependent $HOPO_3^{2-} \rightleftharpoons H_2O$ oxygen isotopic exchange.
(D) Considering the initial rates for the isotopic exchanges when the enzyme is not treated with *N*-ethylmaleimide, decide whether the intermediate is a high-energy or a low-energy intermediate in this situation.
(E) Show that the effects of *N*-ethylmaleimide can be explained by adding to your mechanism a step that involves a conformational change between two forms of the covalent intermediate, a high-energy form and a low-energy form, and that is blocked by reaction with *N*-ethylmaleimide.
(F) Considering your mechanism and assuming that all biochemical phosphostransfers are in-line, draw the two products, with proper stereochemistry, that result when the following substrate is hydrolyzed by the enzyme in $[^{17}O]H_2O$.

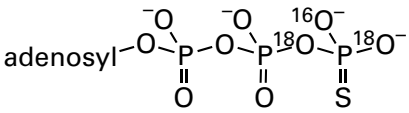

Oxygen-17 ends up in one product.

Problem 5–22: When the reaction catalyzed by 2-hydroxy-6-oxonona-2,4-dienedioate hydrolase

(2*Z*,4*E*)-2-hydroxy-6-oxonona-2,4-diene-1,9-dioate + $H_2O \rightleftharpoons$ succinate + H^+ + (2*Z*)-2-hydroxypenta-2,4-dienoate

from *E. coli* is performed in $H_2{}^{18}O$ with the reactant [6-^{16}O]-(2*Z*,4*E*)-2-hydroxy-6-oxonona-2,4-diene-1,9-dioate, [^{18}O]succinate (95%) and doubly labeled [1,1-$^{18}O_2$]succinate (5%) are produced as products and oxygen isotopic exchange of oxygen-16 for oxygen-18 at the carbonyl group on carbon 6 of 2-hydroxy-6-oxonona-2,4-diene-1,9-dioate is observed as well.[868]

(A) Write a mechanism for the enzymatic reaction consistent with both the intermediate oxygen isotopic exchange and the oxygen isotopic exchange into the reactant at initial rate.
(B) Write out separately the sequence of individual steps in the mechanism of part A that explains the respective oxygen isotopic exchanges.

Problem 5–23: Carbamoyl-phosphate synthase (ammonia) catalyzes the reaction comprising just Equations 3–532 and 3–533

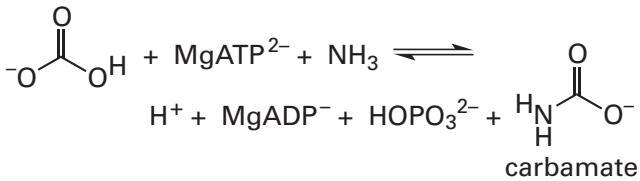

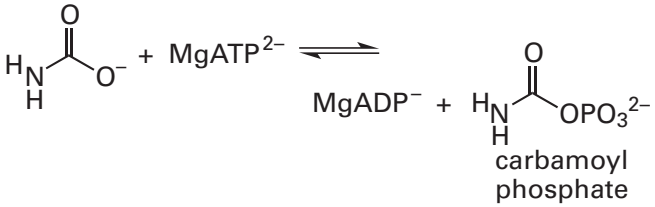

using stoichiometric ammonia rather than ammonia derived from hydrolysis of L-glutamine. In the presence of HCO_3^- but the absence of NH_4^+, the

enzyme from *R. norvegicus* catalyzes the positional oxygen isotopic exchange[869]

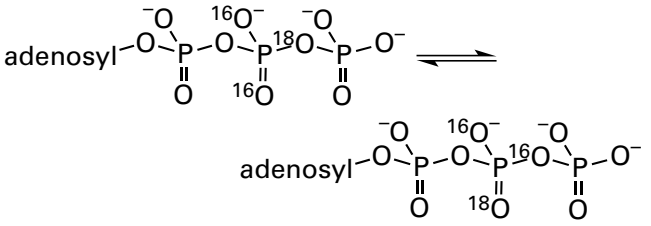

When the enzyme is mixed with $MgATP^{2-}$ and $[^{18}O]HOCO_2^-$ in the absence of NH_4^+, it catalyzes a slow ATPase activity in which 1 mol of oxygen-18 appears in $HOPO_3^{2-}$ for every $MgATP^{2-}$ hydrolyzed. There is a related enzyme (39% identity; 0.7 gap percent) in *E. coli*, carbamoyl-phosphate synthase (glutamine-hydrolysing), that catalyzes the same sequence of reactions and that produces the necessary NH_4^+ by hydrolyzing L-glutamine in a distant glutaminase domain. It also catalyzes a slow bicarbonate-dependent ATPase reaction and the same positional oxygen isotopic exchange.[870] When carbamoyl-phosphate synthase (glutamine-hydrolysing) is mixed with $MgATP^{2-}$ and $HOCO_3^-$ in $H_2{}^{18}O$ in the absence of L-glutamine and NH_4^+, it catalyzes the oxygen isotopic exchange

$$H^{16}OC^{16}O_2^- + {}^{18}OH_2 \rightleftharpoons {}^{16}OH_2 + H^{18}OC^{16}O_2^-$$

at an initial rate equal to the initial rate for the bicarbonate-dependent ATPase reaction.[871]

(A) Write a mechanism for the overall enzymatic reaction that is catalyzed by both enzymes from NH_4^+, $MgATP^{2-}$, and $HOCO_2^-$ and that contains an intermediate that can explain these observations.
(B) Why is the positional oxygen isotopic exchange in the enzyme from *R. norvegicus* inhibited by NH_4^+?
(C) Why is oxygen isotopic exchange of oxygen-18 into $HC^{16}O_3^-$ catalyzed by the enzyme from *E. coli* eliminated in the presence of saturating L-glutamine?
(D) If necessary, add side reactions involving nonstoichiometric species from your main linear mechanism for formation of carbamoyl phosphate from $HOCO_2^-$, $MgATP^{2-}$, and NH_4^+ that explain the positional oxygen isotopic exchange, ATPase reaction, incorporation of oxygen-18 into $HOPO_3^{2-}$, and oxygen isotopic exchange of oxygen-18 into $HOCO_2^-$.

Problem 5–24: UDP-*N*-Acetylglucosamine 2-epimerase (non-hydrolysing)

UDP-*N*-acetyl-α-D-glucosamine $\rightleftharpoons$ UDP-*N*-acetyl-α-D-mannosamine

catalyzes the following positional oxygen isotopic exchange[872]

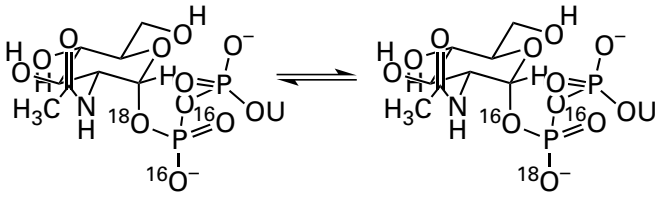

where U is uridinyl.

(A) Write a mechanism that explains both the epimerization and the positional oxygen isotopic exchange catalyzed by the enzyme.
(B) Write just the sequence of steps from the overall mechanism that explains the positional oxygen isotopic exchange.
(C) In a crystallographic molecular model of the active site occupied by UDP-*N*-acetyl-α-D-glucosamine,[873] one of the two nonbridging oxygens on the phospho group attached directly to carbon 1 of *N*-acetyl-α-D-glucosamine forms a hydrogen bond to the τ-nitrogen of the imidazolyl group of a histidine. What is the role of this histidine in catalysis?
(D) What should be the most important acid–base catalyst in the active site?

Problem 5–25: 3-Phosphoshikimate 1-carboxyvinyltransferase (Equation 5–178; Problem 4–26) is present in plants and bacteria and has been purified from *Klebsiella pneumoniae*. From here on, you should abbreviate 3-phosphoshikimate as ROH because the only participant in the reaction is its hydroxy group. When 3-phosphoshikimate and phospho*enol*pyruvate labeled with ^{18}O in the oxygen between phosphorus and carbon 2 are converted by the enzyme, the products are $[^{18}O]HOPO_3^{2-}$ and unlabeled 5-*O*-(1-carboxyvinyl)-3-phosphoshikimate. When [3,3-$^2H_2$]phospho*enol*pyruvate was used as a substrate in the enzymatic reaction and the reaction was allowed to proceed in $[^1H]H_2O$ only a short way (7–18%) toward equilibrium, the isotopic composition of the product 5-*O*-(1-carboxyvinyl)-3-phospho-

shikimate and of the remaining phospho*enol*pyruvate were as follows.[874]

pH	extent of reaction (%)		initial PEP (%)	5-*enol*pyruvylshikimate 3-phosphate (%)	final PEP (%)
6.25	14	d_0	<1	9	<1
		d_1	8	47	7
		d_2	92	44	93
6.25	13	d_0	<1	6	<1
		d_1	5	47	6
		d_2	95	46	93
9.35	18	d_0	<1	6	<1
		d_1	8	42	10
		d_2	92	52	89
10.4	7	d_0	<1	6	<1
		d_1	5	40	7
		d_2	95	54	93

In this table, d_0, d_1, and d_2 signify the percent of molecules of 5-*O*-(1-carboxyvinyl)-3-phosphoshikimate or percent of molecules of phospho*enol*pyruvate, either as initially present or after the reaction was quenched, that were produced during the reaction and that contain no deuterium, one deuterium, or two deuteriums, respectively, as determined by mass spectrometry. By nuclear magnetic resonance spectroscopy, it was shown that the ^{1}H introduced into the product was uniformly distributed between the *E* and *Z* positions.

(A) Write a mechanism to explain the appearance of ^{1}H in the product. Your mechanism should contain a step in which a hydrogen or deuterium is removed from carbon.

(B) For the sake of argument, assume every step in your mechanism is irreversible, and from the percentages of deuterium in the products when the reaction is run at pH 10.4, calculate the deuterium isotope effect for the step in the reaction during which hydrogen or deuterium is removed from carbon. Do not forget that intermediates with two deuteriums and one hydrogen are twice as likely to lose a deuterium as a hydrogen and that intermediates with two hydrogens and one deuterium are twice as likely to lose a hydrogen as a deuterium even when no isotope effect is operating.

3-Phosphoshikimate 1-carboxyvinyltransferase was mixed with phospho*enol*pyruvate in $[^3H]H_2O$ in the absence of 3-phosphoshikimate and incubated under the noted conditions. Phospho*enol*pyruvate was isolated, and its radioactivity was determined.[875]

additions[a]	reaction time (h)	total cpm of ^{3}H in PEP ($\times 10^{-3}$)
1 mM PEP	3	<1
5 mM PEP	3	<1.5
1 mM PEP, 20 mM dd3PS	3	76.4
5 mM PEP, 20 mM dd3PS	3	185
1 mM PEP, 20 mM dd3PS	1	28.7
1 mM PEP, 20 mM dd3PS, 5 mM glyphosate	3	54.5

[a]Phospho*enol*pyruvate is abbreviated as PEP, and 4,5-dideoxy-3-phosphoshikimate is abbreviated as dd3PS. The reaction at 37 °C contained, in addition to the noted ingredients, 10 mM NaF and 100 mM 2-ammonio-2-hydroxymethylpropane-1,3-diol chloride, pH 7.6, in a total volume of 0.25 mL of $[^3H]H_2O$ (3×10^{11} cpm mL^{-1}) and 0.29 unit [0.29 μmol of 5-*O*-(1-carboxyvinyl)-3-phosphoshikimate min^{-1}]of enzyme.

(C) Write a mechanism to explain tritium incorporation into phospho*enol*pyruvate in the presence of 4,5-dideoxy-3-phosphoshikimate.

(D) The 4,5-dideoxy-3-phosphoshikimate is acting by an induced-fit mechanism. Explain what this means in this situation.

(E) What damaging side reaction is the induced-fit mechanism of this enzyme designed to prevent?

Glyphosate, *N*-phosphonomethylglycine (previously **3–51**)

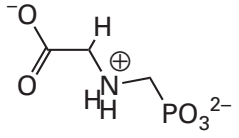

inhibits 3-phosphoshikimate 1-carboxyvinyltransferase. When the kinetics of its inhibition were examined, the following results were obtained.[876]

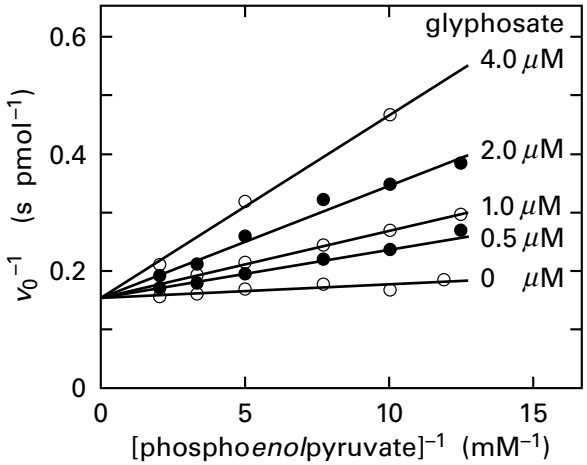

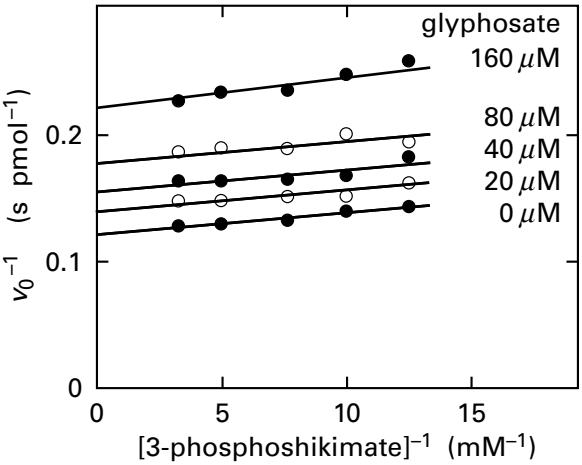

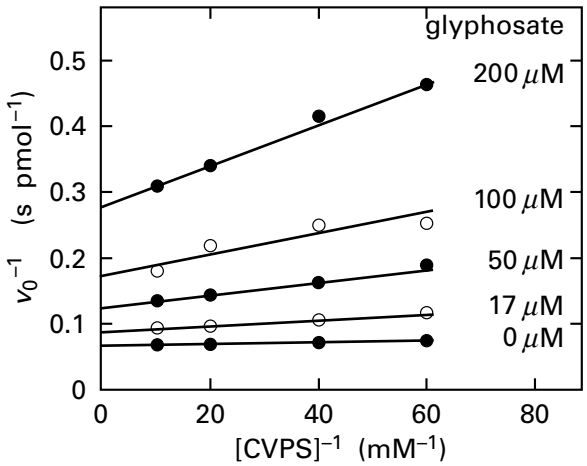

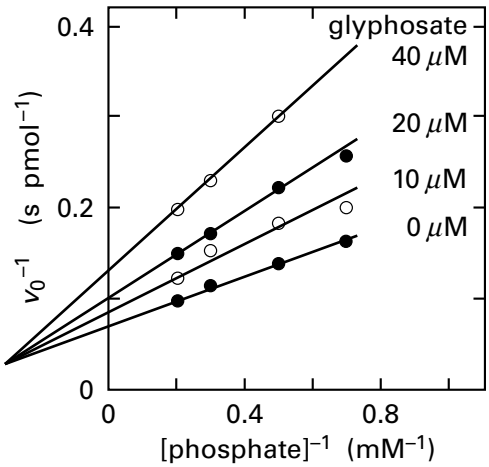

Kinetic analysis of inhibition of 3-phosphoshikimate 1-carboxyvinyltransferase by glyphosate.[876] Enzymatic assays were run in 20 mM sodium 2-[4-(2-hydroxyethyl)piperazin-1-yl]ethanesulfonate, pH 7 and 30 °C. One reactant was varied while the other remained at a constant concentration. The reactants varied and the identities and concentrations of the unvaried reactants are (A) phospho*enol*pyruvate ([3-phosphoshikimate] = 5 mM); (B) 3-phosphoshikimate ([phospho*enol*pyruvate] = 5 mM); (C) 5-*O*-(1-carboxyvinyl)-3-phosphoshikimate ([phosphate] = 20 mM); (D) phosphate ([5-*O*-(1-carboxyvinyl)-3-phosphoshikimate] = 0.2 mM). 5-*O*-(1-Carboxyvinyl)-3-phosphoshikimate is abbreviated as CVPS. In each panel, the reciprocals of the observed initial rates (picomoles second^{-1}) are plotted as a function of the reciprocals of the concentrations of the varied reactant (millimolar). To the right of each line is listed the concentration of glyphosate in the set of assays defining that line.

(F) Against which substrate is glyphosate a competitive inhibitor?

The inhibition caused by glyphosate was also examined as a function of pH.[876]

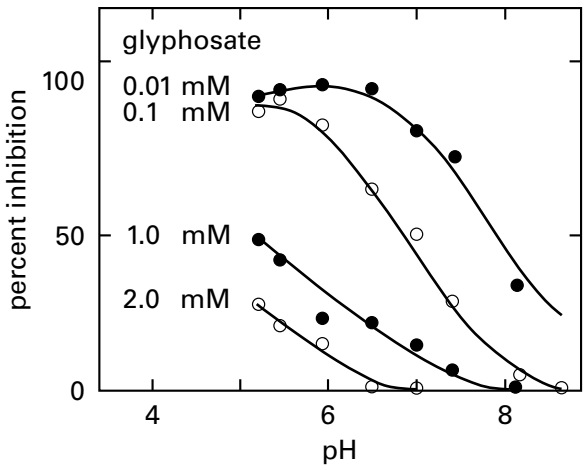

Dependence of inhibition of 3-phosphoshikimate 1-carboxyvinyltransferase by glyphosate on pH.[876] Initial rates for the reaction in the direction from phospho*enol*pyruvate (5 mM) and 3-phosphoshikimate (5 mM) to phosphate and 5-*O*-(1-carboxyvinyl)-3-phosphoshikimate were measured in 100 mM tris(hydroxymethyl)methylammonium maleate at different values of pH in the absence and presence of glyphosate at the four indicated concentrations. The results are presented as the percent of activity at the same pH in the absence of glyphosate as a function of pH.

(G) Complete this table for the experiments described in the second figure. Parameter I_{50} is defined as the concentration of inhibitor necessary to inhibit an enzyme by 50% under a set of fixed conditions.

pH	I_{50} (mM)
	2
	1
	0.1
	0.01

(H) To explain this behavior, assume the following kinetic mechanism.

$$\mathrm{I{\cdot}E + H^+ + A \overset{K_I}{\rightleftharpoons} I + E + H^+ + A \overset{K_a}{\rightleftharpoons}}$$

$$\mathrm{I + EH + A \underset{k_{-1}}{\overset{k_1}{\rightleftharpoons}} I + EH{\cdot}A \xrightarrow{k_2} I + E + Z}$$

Assume that A is the reactant with which the glyphosate, I, competes, and assume that the other reactant is saturating and does not enter the mechanism, and determine the rate equation for the initial rate of the enzymatic reaction, v_0, from this mechanism.

(I) When [I] = 0, $v_0 = v_{\text{uninhibited}}$, and when [I] = I_{50}, $v_0 = 0.5 v_{\text{uninhibited}}$. Using the equation you derived in part H, solve for I_{50} as a function of $[H^+]$ and [A].

(J) Show that the behavior of I_{50} with pH seen in part G can be explained by the equation you derived in part I.

(K) What intermediate in your mechanism for part C is glyphosate supposed to resemble?

(L) Why would glyphosate bind to a form of the enzyme with one less hydron than the form to which phospho*enol*pyruvate binds? Answer this question by drawing two structures of the active site, one occupied by the intermediate and one by glyphosate, and include a catalytic acid–base from the enzyme in your drawing.

(M) What other kinetic mechanism would also explain the observations?

(N) What would you need to know to decide between the two possible mechanisms?

Problem 5–26: Phospho*enol*pyruvate carboxylase from *E. coli* catalyzes the following reaction.

$$\text{phospho}\textit{enol}\text{pyruvate} + HOCO_2^- \rightleftharpoons HOPO_3^{2-} + \text{oxaloacetate}$$

When the reaction is carried out with $[^{18}O_3]HOCO_2^-$, one atom of oxygen-18 is incorporated into the $HOPO_3^{2-}$ formed. When the reaction is carried out with $[^{18}O_3]HOCO_2^-$ and chiral $[^{16}O,^{17}O]$thiophospho*enol*pyruvate, inversion of configuration at phosphorus is observed. 3-Methylphospho*enol*pyruvate does not substitute for phospho*enol*pyruvate in the normal reaction but is slowly hydrolyzed to 3-methylpyruvate and $HOPO_3^{2-}$ in a reaction catalyzed by the enzyme and requiring the presence of $HOCO_2^-$. When this bicarbonate-dependent hydrolysis is performed in the presence of $[^{18}O_3]HOCO_2^-$, oxygen-18 is incorporated into the $HOPO_3^{2-}$ produced during the hydrolysis. The molar proportions of this labeled phosphate having one, two, or three atoms of oxygen-18 were 70%, 25%, and 5%.[877] Write a mechanism for the bicarbonate-dependent hydrolysis of 3-methylphospho*enol*pyruvate that explains the observed intermediate oxygen isotopic exchange and incorporates the inversion of configuration at phosphorus observed in the normal reaction.

Problem 5–27: Write a mechanism for 3-oxoacid CoA-transferase that can explain the oxygen isotopic exchange observed between succinate and the enzyme (Equation 5–290) by proceeding through an anhydride as an intermediate.

Stopped Flow and Quenched Flow

If sufficiently high molar concentrations of the active site of an enzyme are used in an experiment, then measurable quantities of the intermediates in the enzymatic reaction can be generated. The catalytic constants, however, of most enzymes between 20 and 37 °C lie in the range between 1 and 10^6 s^{-1}. This range of rate constants means that once reactants are assembled on the active site of an enzyme, each individual step between the successive intermediates in the enzymatic reaction usually has rate constants in excess of 1 s^{-1}, and **each step in the chemical mechanism of the enzymatic reaction takes less than a second to occur**.

The device used to observe formation, interconversion, or decay of these intermediates must be able to initiate a particular step in an enzymatic reaction rapidly and immediately (<10 ms) monitor its progress. For most kinetic studies, reactions are usually **initiated by mixing two solutions**. If the two solutions to be mixed are introduced through separate ports of a specially designed mixing chamber at rapid, continuous, and uniform flows, then the fluid emerging immediately adjacent to the mixing chamber will have been mixed for only a short time.[878] If the flow through the mixing chamber is stopped abruptly, then the reaction occurring in the fluid immediately adjacent to the mixing chamber will have progressed during the short time it was passing through the mixing chamber but will continue to proceed in the fluid now at rest.[879] If an observation chamber is located as close to the mixing chamber as possible and the flow is stopped as abruptly as possible,[880,881] the fluid within the observation chamber will have been mixed only a short time before, and the progress of the reaction can then be followed within the still fluid. The interval between the time at which the fluid in the observation chamber was mixed and the time at which the flow has ceased completely is referred to as the **dead time** because no observation can be made of changes occurring during this interval. An important focus in advancing the design of such an apparatus has been to decrease its dead time so that measurements can be made at shorter times after the mixing occurs.

A device that accomplishes this strategy is an **apparatus for stopped flow** (Figure 5–20).[881,882] The two solutions are delivered to the mixer by two syringes that are driven by a plunger. The window to the observation chamber is immediately adjacent to the mixer. During the flowing phase, the continuously emerging fluid fills and expands a stop syringe until its distending plunger strikes a solid barrier. This collision stops the flow abruptly within the completely sealed system. The progress of the reaction in the observation chamber is usually followed spectroscopically by passing light through the chamber. Apparatuses for stopped flow of this type can have dead times of less than 1 ms.[883]

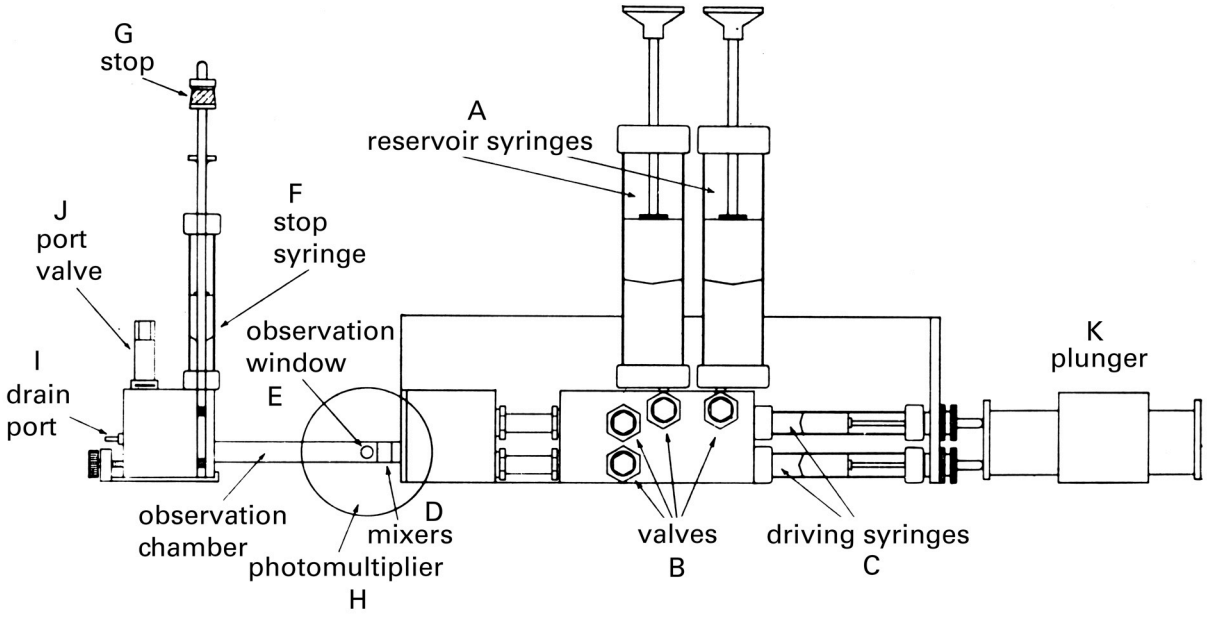

Figure 5–20: Apparatus for stopped flow.[882] The two reservoir syringes (A) store large quantities of the two solutions to be mixed. Small amounts of these two solutions are introduced through valves (B) into the two respective driving syringes (C). After the driving syringes are filled, the valves are turned so that the two drive syringes become connected directly to the two ports of the mixing chamber (D), which efficiently mixes the two fluids passing through it at high velocity. Just to the downstream side of the mixing chamber is a window (E) through which observations can be made. The observation chamber that contains this window is connected directly to a syringe (F) that fills as the fluid flows through the chamber until the end of its shaft hits a solid barrier or stop (G). After the stop has been struck by the shaft, all flow through the apparatus ceases. A photomultiplier (H) monitors the change in absorbance in the still fluid inside the observation window. Light of the desired wavelength passing through the observation window is produced by a monochromator. The stop syringe is drained through a port (I) by turning a valve (J). The hydraulic plunger (K), because it travels so rapidly in order to promote flow of high velocity, develops significant hydrostatic pressure in the fluids, so all valves and tubes must be designed to withstand this high pressure. Reprinted with permission from reference 882. Copyright 1963 Wiley-Interscience. https://archive.org/details/techniqueoforgan0008slfr

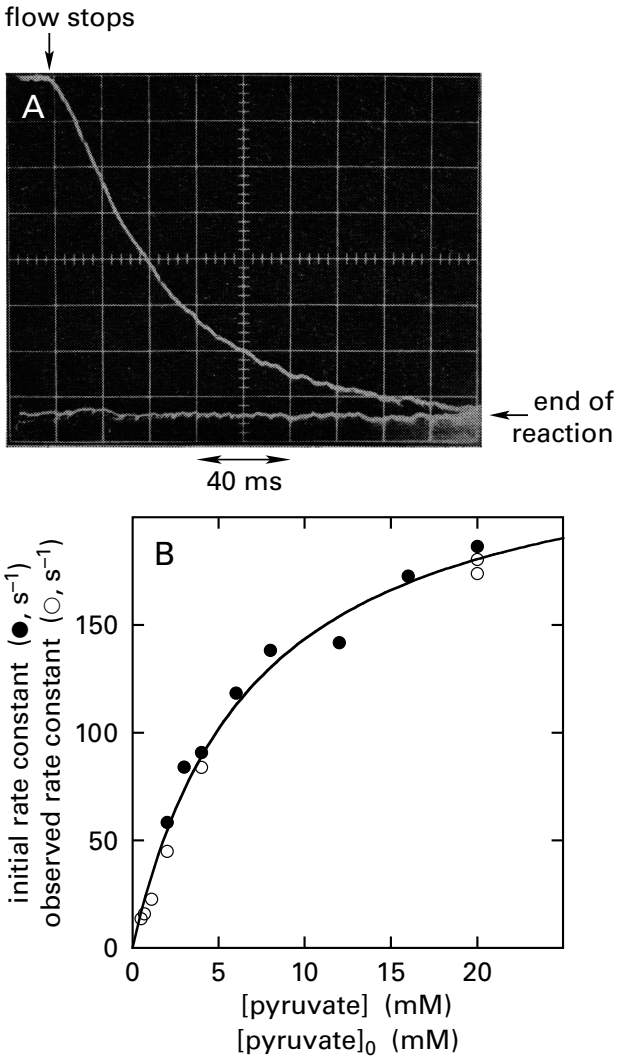

Figure 5–21: Monitoring the transfer of a hydride from NADH to pyruvate at the active site of L-lactate dehydrogenase by stopped flow.[884] A solution of porcine L-lactate dehydrogenase (28 μM in active sites) and NADH (20 μM) in one syringe of the apparatus for stopped flow was mixed with an equal volume of a solution of pyruvate (2.0 mM) in the other syringe. Both solutions were at pH 9.0 and 22 °C. The dead time of the apparatus was 1.3 ms. (**A**) Kinetic course of the reaction. The flow of fluid through the apparatus ceased at the point indicated by the arrow (labeled "flow stops"), and the absorbance of the solution in the observation chamber was monitored at 340 nm, the wavelength at which NADH absorbs. The upper trace on the oscilloscope displays the voltage from the photomultiplier tube as a function of time (milliseconds) immediately following cessation of flow. The lower, flat trace is a second sweep after all change in voltage had ceased (labeled "end of reaction"). (**B**) Observed first-order rate constants from stopped flow and steady-state kinetics. Values for the first-order rate constants from stopped flow were obtained by fitting an exponential function to the observed decrease in absorbance (Panel A) as a function of time at each concentration of pyruvate (pyr). First-order rate constants for hydride transfer (second^{-1}) measured by stopped flow are plotted (○) as a function of the concentrations of pyruvate (millimolar). The initial rates of the enzymatic reaction, v_0, were also measured at several different initial concentrations of pyruvate at saturating concentrations of NADH, also at pH 9.0 and 22 °C. Each initial rate (micromolar second^{-1}) was divided by the respective molar concentration of active sites (micromolar) in the solution to obtain an initial rate constant (v_0 $[E]_t^{-1}$) for the active site in catalyzing the overall reaction at that initial concentration of pyruvate. These initial rate constants (second^{-1}) are also plotted (●) as a function of the initial concentrations of pyruvate (millimolar). The curve is a fit of Equation 5–328 to the data with $k_2 = 243 \pm 9$ s^{-1} and $K_{pyr} = 7 \pm 0.5$ mM. Adapted with permission from ref 884. Copyright 1971 Biochemical Society. https://doi.org/10.1042/bj1210235

From an examination of this apparatus for stopped flow, it is clear that **the contents of the two syringes define the reaction observed.** For example, one of the two syringes in an apparatus for stopped flow was filled with a solution 20 μM in NADH and 30 μM in active sites of porcine L-lactate dehydrogenase (previously Equation 3–27)

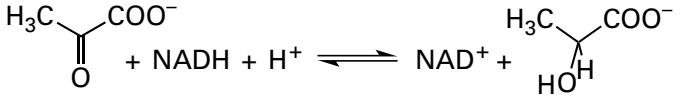

(5–292)

At these concentrations, almost all (85%) of the NADH present was already bound to active sites of the enzyme before mixing occurred, and the solution in this syringe contained almost entirely the complex, E·NADH, and free enzyme. The other syringe was filled with 2.0 mM pyruvate. After cessation of flow, the fluid in the observation chamber was monitored by its absorbance at 340 nm, a wavelength at which NADH absorbs light strongly but NAD^+ does not. Therefore, the decrease in absorbance at 340 nm (Figure 5–21A)[884] directly monitors the transfer of a hydride from NADH to pyruvate

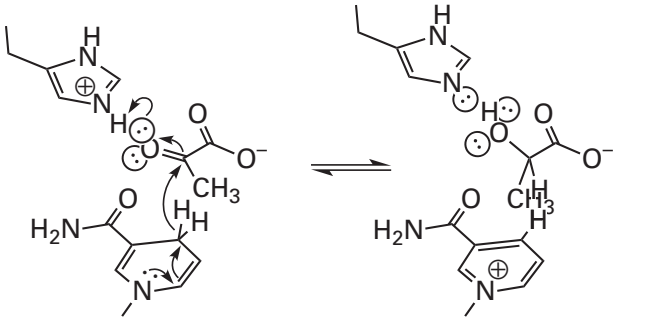

(5–293)

as it occurs on the active site.[885] Because the dead time of the apparatus was 1.3 ms, this reaction could be monitored from 1.3 ms after mixing to its completion. One advantage of the ability to monitor the transfer of a hydride from NADH or NADPH to a reactant by stopped flow is that by using [4′(*R*)-^{2}H]NADH or [4′(*R*)-^{2}H]NADPH, the intrinsic kinetic isotope effect for the transfer can often be obtained directly.[886]

Changes that have occurred within the dead time of the apparatus can be documented even though their kinetic courses cannot be recorded. For example, protocatechuate 3,4-dioxygenase (previously Equation 2–274)

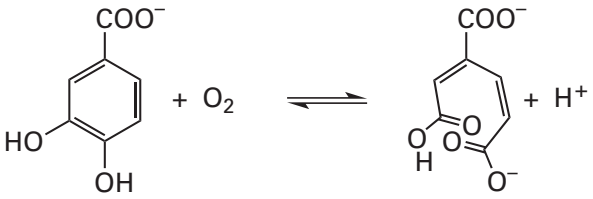

(5–294)

contains tightly bound prosthetic iron (Figure 2–57B), and in the absence of oxygen, its active site forms a complex with protocatechuate that absorbs visible light in a broad range from 400 to 600 nm. Changes in the composition of this complex could be followed by monitoring absorbance in this range. When a solution of the complex between the enzyme from *P. putida* and protocatechuate in one syringe of a stopped-flow spectrophotometer was mixed with a solution of oxygen in the other, a three-step process was observed (Figure 5–22).[887] The steps of this process could be dissected by performing measurements at two different wavelengths (403 and 460 nm). The initial absorbance at either wavelength at the dead time following mixing (1.3 ms) was substantially different from the absorbance of the complex of enzyme and protocatechuate that would have been observed in the absence of oxygen (arrows).

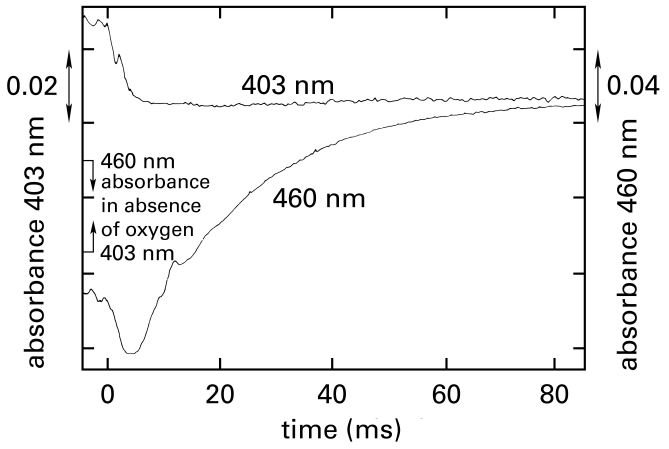

Figure 5–22: Three successive relaxations that occur when the complex between protocatechuate and protocatechuate 3,4-dioxygenase from *P. putida* is mixed with oxygen.[887] A solution containing 0.24 mM protocatechuate and 0.24 mM active sites of protocatechuate 3,4-dioxygenase was mixed with an equal volume of a solution containing 12 mM O_2. The solutions were at pH 8.3 and 10 °C . The absorbance of the mixture was followed at either 403 nm (top trace) or 460 nm (bottom trace). The absorbance (0.02 absorbance unit division^{-1} at 403 nm and 0.04 unit division^{-1} at 460 nm) was monitored as a function of time (milliseconds) in the still fluid just beyond the mixing chamber after flow stopped (at 0 ms). The absorbances at 460 and 403 nm that would have been observed had an oxygen-free solution been mixed are indicated on the respective axes of the ordinate. That these levels differ from those observed at cessation of flow shows that a relaxation faster than the dead time of the apparatus (1.3 ms) had occurred immediately upon mixing. The second relaxation is observed at both 403 and 460 nm and is complete after 5 ms. The third relaxation is observed only at 460 nm and is complete at 100 ms.

Because the absorbance at 403 nm increased within the dead time and was observed to be decreasing following the dead time, an initial intermediate, the absorbance of which at 403 nm is greater than that of the complex between enzyme and protocatechuate in the absence of oxygen as well as being greater than that of the second intermediate that is being formed following the dead time, must have formed during the dead time. The conversion of the first intermediate into this second intermediate is registered by the observed decrease in absorbance at 403 nm. An increase in absorbance at 460 nm then occurs while the absorbance at 403 nm remains constant. This increase in absorbance at 460 nm is due to formation of a third intermediate in the reaction. The absorbance at 403 nm remains constant because it is at an isosbestic point in the transition from the second to the third intermediate.

In an apparatus for stopped flow, the fluid emerging from the mixing chamber usually enters an optical

cuvette and must be **monitored by either absorbance**, as for NADH in the active site of porcine L-lactate dehydrogenase or prosthetic iron in protocatechuate 3,4-dioxygenase, **or fluorescence**, which is often a more sensitive, albeit more complicated, property and which can permit lower concentrations of enzyme to be used.

Complete spectra of absorbance can be followed at successive short intervals. For example, when β-lactamase encoded by the bacterial plasmid NDM-1, which has two prosthetic Zn^{2+} in its active site, was mixed with the chromogenic reactant nitrocefin (**5–165**) and spectra of absorbance were recorded every 2 ms (Figure 5–23A),[888] it could be observed that the absorbance of nitrocefin (λ_{max} = 390 nm) was rapidly lost as a new peak of absorbance (λ_{max} = 665 nm) appeared in a transition that displayed an isosbestic point at 425 nm (dashed vertical line). The majority of this first transition was complete in the dead time (2 ms) of the instrument. The intermediate responsible for the peak of absorbance at 665 nm was then more slowly (15 s^{-1}) converted into hydrolyzed nitrocefin (λ_{max} = 485 nm) in a transition with isosbestic points at 382 and 550 nm (dashed vertical lines). The existence of the initial isosbestic point and the subsequent pair of isosbestic points establish that there are only three species interconverting: nitrocefin, the intermediate that absorbs at 665 nm, and hydrolyzed nitrocefin. The intermediate has been assigned as the trianion of hydrolyzed nitrocefin (**5–166**)

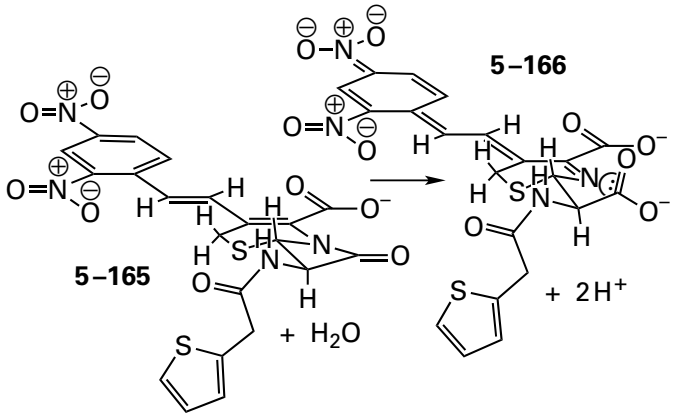

(5–295)

In this trianion, the negative elementary charge, other than the two negative elementary charges on the carboxylato groups, is delocalized from the nitrogen that has just left the tetrahedral intermediate formed by addition of a hydroxide on one catalytic Zn^{2+} in the active site to the acyl carbon of the lactam in nitrocefin (the four-membered ring in **5–165**).

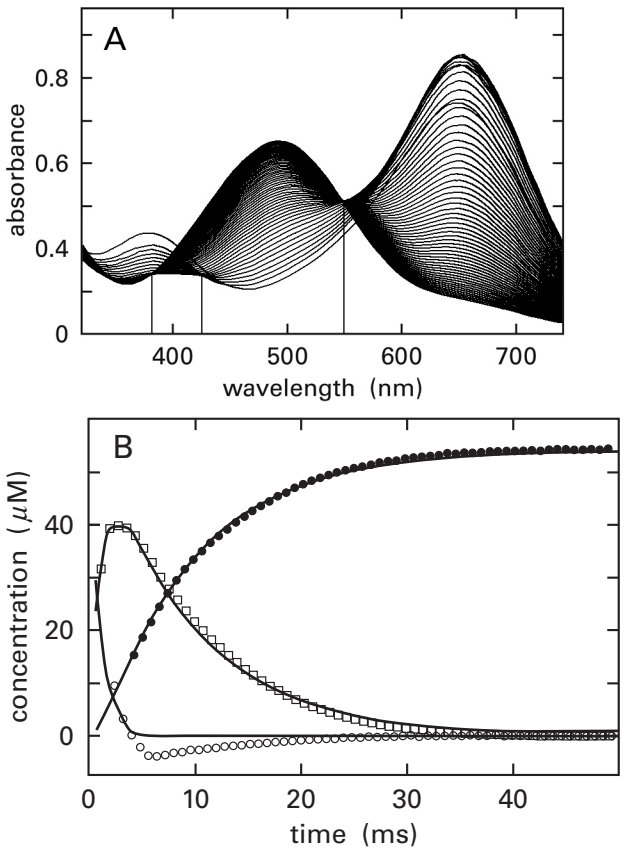

Figure 5–23: Monitoring hydrolysis of nitrocefin (**5–165**) at the active site of the metallo-β-lactamase encoded by the bacterial plasmid NDM-1 by stopped flow.[888] A solution of β-lactamase (100 μM) in one syringe of the apparatus for stopped flow (dead time of 2 ms) was mixed with an equal volume of a solution of nitrocefin (100 μM) in the other syringe. Both solutions also contained 0.2 M NaCl and 30 mM 2-ammonio-2-hydroxymethylpropane-1,3-diol chloride, at pH 7.6 and 22 °C. (**A**) Kinetic course of the reaction. After the flow of fluid through the apparatus ceased, the absorbance of the solution in the observation chamber was monitored at wavelengths between 320 and 740 nm every 2 ms. The resulting spectra are superposed in the drawing. After 50 ms, no further changes were observed. Isosbestic points are indicated with vertical lines. (**B**) Concentrations of the three species observed in a kinetic course of the reaction as a function of time. The peaks of absorbance at 390, 485, and 665 nm were identified as nitrocefin (**5–165**), hydrolyzed nitrocefin, and the trianion of hydrolyzed nitrocephin (**5–166**), respectively (see Equation 5–295). With extinction coefficients for each of these three species, the absorbances at the various intervals were converted to molar concentrations. These molar concentrations of nitrocefin (○), hydrolyzed nitrocefin (●), and the trianion of hydrolyzed nitrocephin (□) are plotted as a function of the intervals between mixing and observation (milliseconds). The curves are fits of the data by numerical integration to a kinetic mechanism in which the complex between enzyme and nitrocephin is formed reversibly, and hydrolysis of nitrocephin to the anion in the active site is also reversible, but hydronation of the anion on the active site and its release from the active site are both kinetically irreversible. Adapted with permission from reference 888. Copyright 2012 American Chemical Society. https://doi.org/10.1021/bi300056y

This accumulating negative charge is delocalized from the nitrogen as it is leaving the tetrahedral intermediate through the extensive π molecular orbital system of ten carbons, two nitrogens, and four oxygens that is conjugated with it, and it ends up concentrated on the four oxygens of the two nitro groups (Equation 5–295). This extensive delocalization allows the nitrogen to leave the tetrahedral intermediate without the hydronation that is required during hydrolysis of a normal lactam by the enzyme. A molecule of water on the other catalytic Zn^{2+} normally hydronates the nitrogen as it is leaving from the tetrahedral intermediate formed from a normal lactam.[889] During hydrolysis of nitrocefin, however, this molecule of water hydronates the anionic nitrogen in intermediate **5–166** after it has left the tetrahedral intermediate, rather than while it leaves. This hydronation gives the secondary amine that is the product of hydrolysis and that is the third spectral component in Figure 5–23A, and the second transition is a simple hydronation.

The progress of the reaction within the cuvette of an apparatus for stopped flow can be monitored in a number of different ways. The experiment is often designed to follow the chemical transformation of the molecule that is absorbing or fluorescing, as was the case with β-lactamase. It is also possible, however, to obtain information even when that molecule remains intact. For example, the absorbance of NADH, bound to an active site as a coenzyme, can **respond to nearby changes in the active site** prior to the transfer of its hydride. In the active site of bovine glutamate dehydrogenase [$NAD(P)^+$], the absorbance of NADPH bound in the active site shifts to longer wavelengths as 2-oxoglutarate becomes hemiaminal **5–167** and then to shorter wavelengths when the hemiaminal becomes 2-iminoglutarate (**5–168**)

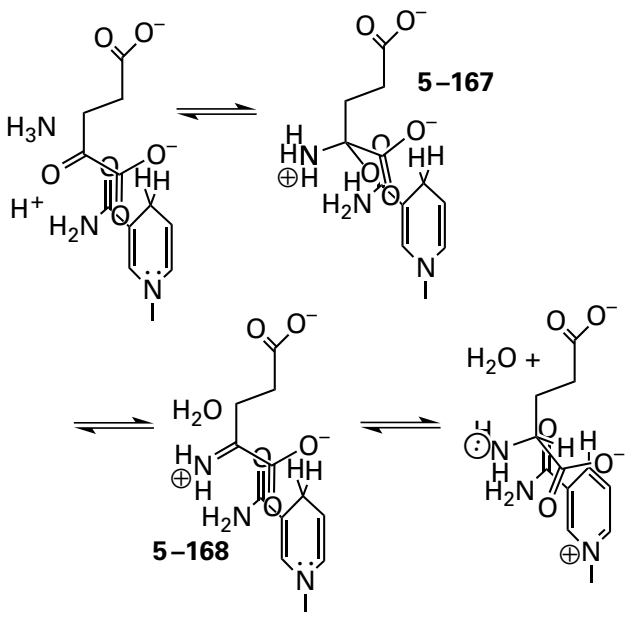

(5–296)

These two steps occur before the hydride is transferred (last step in Equation 5–296).[890] The fluorescence of NADPH in an active site can also be used to monitor events occurring in its vicinity before the transfer of the hydride.[891] For example, the fluorescence of prosthetic NADPH in glucose-fructose oxidoreductase from *Zymomonas mobilis* is quenched as the reactant gluconolactone associates with the active site before its absorbance decreases as the hydride is transferred to gluconolactone.[892]

The **absorbance or fluorescence of a normal reactant** for a particular enzyme other than NADH can also be followed. For example, the absorbance between 340 and 400 nm of the normal reactant, 2-amino-3-(3-oxoprop-1-en-1-yl)but-2-enedioate, in the active site of aminocarboxymuconate-semialdehyde decarboxylase from *P. fluorescens*[893] and the fluorescence of the normal reactant, *N*-(5-phospho-β-D-ribosyl)anthranilate, in the active site of phosphoribosylanthranilate isomerase from *E. coli*[894] have been used to monitor the respective enzymatic reactions by stopped flow. The **absorbance of a normal product**, such as the absorbance of AMP^{2-} as it is produced in the active site of adenine phosphoribosoyltransferase from *Leishmania donovani*,[895] or the fluorescence of a normal product can also be used.

In most instances, a distinction cannot be made between a reactant that is bound in the active site and a reactant that is still in solution before it associates with the active site or between a product that is bound in the active site and a product that has dissociated from the active site and is now free in

solution. If, however, an assay can couple rapidly enough, through one or two other enzymatic reactions, the release of product into the solution to the production of the chromophore or the fluorophore being monitored spectroscopically, then only **product that is free in solution** is observed. For example, $MgGDP^-$ that dissociates from the active site of the GTPase associated with sulfate adenyltransferase from *E. coli* can be monitored over milliseconds by coupling its appearance in solution to a decrease in the concentration of NADH by using pyruvate kinase and phospho*enol*pyruvate to rephosphorylate $MgGDP^-$ to $MgGTP^{2-}$ and reduce the resulting pyruvate to lactate while NADH is oxidized to NAD^+ by L-lactate dehydrogenase.[896] At high enough concentrations of these other two enzymes and their substrates, the rates for conversion of $MgGDP^-$ and disappearance of NADH are rapid enough to be essentially instantaneous relative to the rate at which $MgGDP^-$ dissociates from the active site of the GTPase into the solution. The decrease in the concentration of NADH was monitored by its fluorescence.

A **chromophoric or fluorophoric analogue of the natural reactant**, such as nitrocefin (Figure 5–23; Equation 5–295), can also be used to monitor rapid enzymatic reactions occurring in the cuvette. For example, 2-hydroxy-4-nitrophenol (**5–169**) is an enzymatically active analogue of the natural reactant 3,4-dihydroxyphenylacetate (**5–170**)

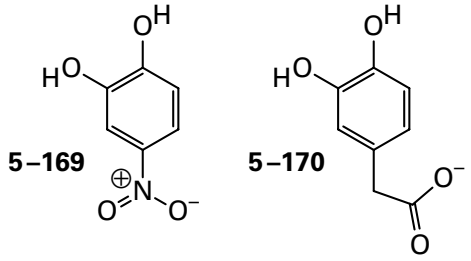

for 3,4-dihydroxyphenylacetate 2,3-dioxygenase (see Equation 2–278)

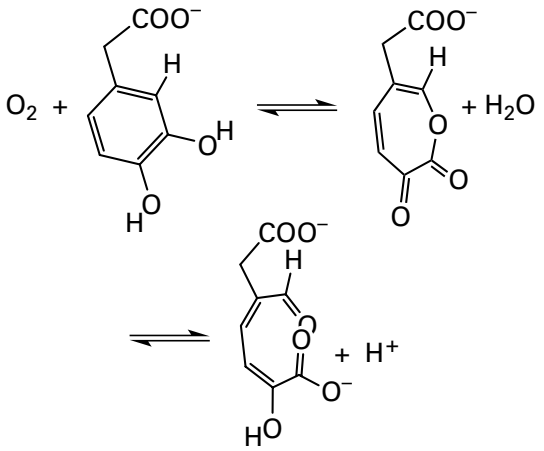

(5–297)

from *Brevibacterium fuscum*. The changes in absorbance of 2-hydroxy-4-nitrophenol can be followed as it associates with the active site and is then converted successively into two intermediates in the enzymatic reaction.[897]

In another example, the chromophoric reactant (*E*,2*S*)-2-amino-5-phenylpent-4-enoic acid, which is the styryl analogue of the normal reactant L-phenylalanine, is also a reactant for phenylalanine aminomutase (L-β-phenylalanine forming) from *Taxus canadensis*. The first step in the chemical mechanism of the aminomutase when L-phenylalanine is the reactant is an elimination of the *pro-S* hydron on its β carbon as well as the α-amino group to form 3-phenylpropenoic acid as an intermediate in the enzymatic reaction. When (*E*,2*S*)-2-amino-5-phenylpent-4-enoic acid is the reactant, the analogous intermediate in the enzymatic reaction is (2*E*,4*E*)-5-phenylpenta-2,4-dienoic acid, the appearance of which can be monitored by the strong absorbance at 310 nm of the π molecular orbital system that includes the entire molecule.[898]

In a third example, the fluorescence of magnesium 2′(3′)-*O*-(*N*-methylanthraniloyl)adenosine 5′-triphosphate, which is $MgATP^{2-}$ with an attached fluorescent *N*-methylanthraniloyl group, could be monitored as it associated with the active site of human kinesin ATPase and was then hydrolyzed.[899]

If an enzyme contains a **prosthetic group that absorbs or that absorbs and then fluoresces**, it can be used to monitor changes in the active site as the enzyme steps through its reaction. **Pyridoxal 5′-phosphate** is particularly useful in this regard because the absorption spectra of many of the intermediates in the reactions that it catalyzes are well characterized (Figure 2–1). For example, cysteine synthase

O-acetyl-L-serine + H_2S $\rightleftharpoons$ H^+ + acetate + L-cysteine (5–298)

from *S. enterica* was mixed with only one reactant, *O*-acetyl-L-serine, and spectra of absorbance were collected over 1.7 s (Figure 5–24).[900] It was observed that absorbance of the internal pyridoximine (λ_{max} = 412 nm) rapidly shifts to higher wavelength in a transition with an isosbestic point at 340 nm (thin vertical line) as the external pyridoximine forms (Figure 2–1; λ_{max} = 416 nm). The external pyridoximine is then converted (see Equation 2–13) into the pyridoximine of 2-aminoacrylate (λ_{max} = 330 and 469 nm)

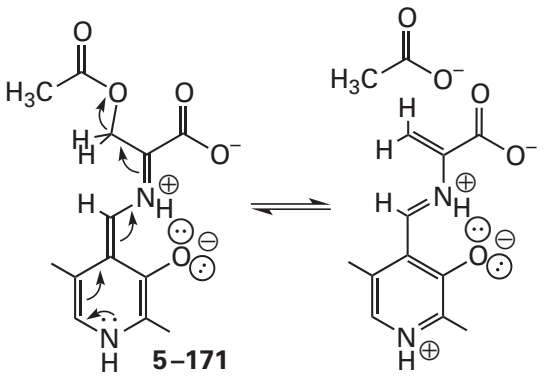

(5–299)

in a transition with isosbestic points at 363 and 430 nm (thin vertical lines). In this case, quinonoid intermediate **5–171** was not observed, probably because the elimination (Equation 5–299) is almost immediate after removal of the hydron from the α carbon.

The same intermediate pyridoximine of 2-aminoacrylate is the central intermediate in cysteine lyase from *Fusobacterium nucleatum*. This active site can form the intermediate by β-elimination of acetate from the quinonoid of *O*-acetyl-L-serine (**5–171** in Equation 5–299) but also by β-elimination of hydrogen sulfide from the quinonoid of L-cysteine or β-elimination of L-cysteine from the quinonoid of L-lanthionine. Changes in the absorbance between 300 and 500 nm could be followed by stopped flow from 0.75 ms to monitor conversion of the respective internal pyridoximines to *gem*-diamines, to external pyridoximines (Figure 2–1), and then to the pyridoximine of 2-aminoacrylate, but again, in each case, the quinonoid intermediate between the external pyridoximine and the pyridoximine of 2-aminoacrylate was not observed.[901]

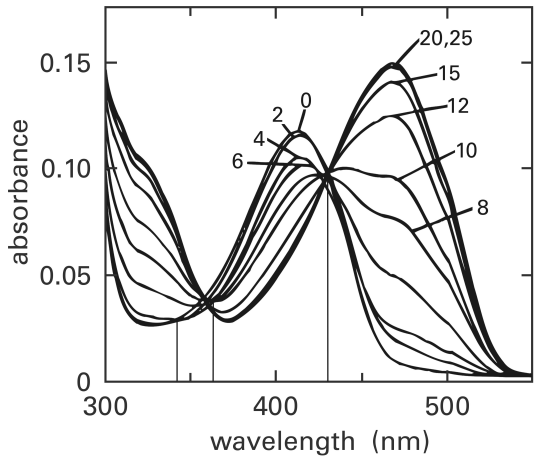

Figure 5–24: Monitoring the intermediates formed on the prosthetic pyridoxal 5′-phosphate in the active site of cysteine synthase from *S. enterica* by stopped flow.[900] A solution of cysteine synthase (20 μM) in one syringe of the apparatus for stopped flow was mixed with an equal volume of a solution of *O*-acetyl-L-serine (2 mM) in the other syringe. Both solutions also contained 0.1 M KCl and 100 mM sodium 2-(*N*-morpholino)-ethanesulfonate, pH 6.5. After the flow of fluid through the apparatus ceased, the absorbance of the solution in the observation chamber was monitored at wavelengths between 300 and 550 nm at the noted intervals (numbers designating each trace in milliseconds). The resulting spectra are superposed in the drawing. After 25 ms, no further changes were observed. Isosbestic points are indicated with thin vertical lines. Adapted with permission from reference 900. Copyright 1996 American Chemical Society. https://doi.org/10.1021/bi952938o

In the case of ornithine decarboxylase

L-ornithine + H^+ $\rightleftharpoons$ 1,4-diaminobutane + CO_2 (5–300)

from *Trypanosoma brucei brucei*, which also has pyridoxal phosphate as a prosthetic group, full spectra taken at intervals of 1.3 ms, following the mixing of the enzyme with L-ornithine, could be resolved into four distinct components. The spectrum for the first species detected was assigned to the external pyridoximine of the reactant L-ornithine, which formed within the dead time of the apparatus. The spectrum of the second intermediate was assigned to the quinonoid (previously Equation 2–5)

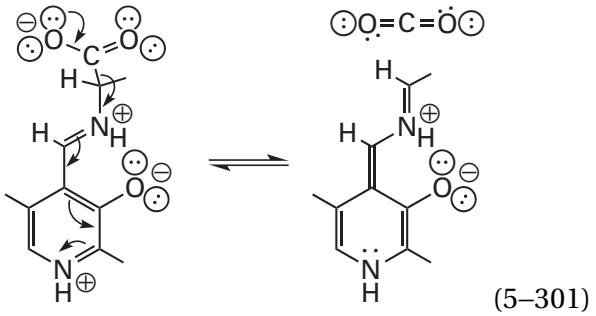

(5–301)

that follows the decarboxylation of L-ornithine, and the spectrum of the fourth species was assigned to the external pyridoximine of the product 1,4-diaminobutane. Consequently, three consecutive chemical intermediates in the enzymatic reaction—the external pyridoximine of the reactant L-ornithine, the quinonoid that follows the decarboxylation of L-ornithine, and the external pyridoximine of the product 1,4-diaminobutane—could be followed (Figure 5–25).[902]

Histidine 123 is the catalytic base that removes a hydron from Cysteine 364, the nucleophile in the active site of cysteine desulfurase from *E. coli* that participates in nucleophilic substitution at the sulfanyl group in *N*-(5′-phosphopyridoxyl)-1-carboxy-2-sulfanylethylimine produced by hydronation of carbon 4′ of the 5′-phosphopyridoxyl group in the quinonoid of L-cysteine (see Equation 5–288). This nucleophilic substitution transfers that sulfanyl group from the 1-carboxy-2-sulfanylethylimine to Cysteine 364 during the desulfurization of L-cysteine. When Histidine 123 is mutated to alanine, the rate at which *N*-(5′-phosphopyridoxyl)-1-carboxy-2-sulfanylethylimine is formed can be followed by stopped flow[903] by its absorbance at 350 nm. In the native enzyme this intermediate is converted to the *N*-(5′-phosphopyridoxyl)-1-carboxyenamine, under catalysis by Histidine 123, too rapidly to be observed.

Flavins, however, are the prosthetic groups most often used to monitor steps in an enzymatic reaction by stopped flow. For example, the steps in the addition of molecular oxygen to flavin (Equation 2–217) to create an oxidant able to perform several oxygenations

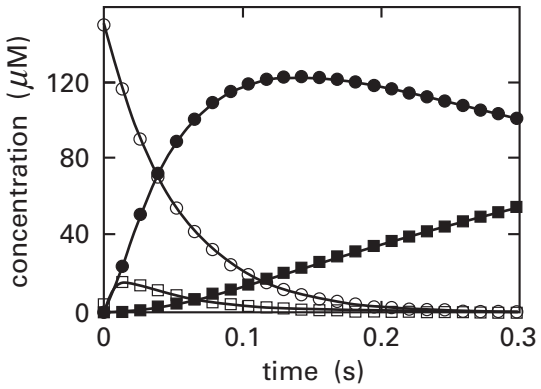

Figure 5–25: Kinetic courses for the concentrations of four intermediates in the reaction catalyzed by ornithine decarboxylase.[902] Full spectra between 310 and 500 nm were gathered at intervals of 3 ms after a solution of ornithine decarboxylase from *T. brucei brucei* (0.32 mM) was mixed with an equal volume of a solution of L-ornithine (20 mM) in 10 mM sodium phosphate, pH 7.3. All solutions were at 4 °C. The resulting spectra could be resolved by numerical analysis into spectra for four different intermediates, the contributions of which to the complete spectrum changed with time. Three intermediates were assigned, by their spectra (see Figure 2–1), to be the external pyridoximine of the reactant L-ornithine (○; λ_{max} = 337 and 424 nm), the quinonoid that follows the decarboxylation of L-ornithine (□; λ_{max} = 349 and 447 nm), and the external pyridoximine of the product, putrescine (■; λ_{max} = 335 and 420 nm). The other intermediate (●; λ_{max} = 338 and 422 nm) could not be assigned definitively. From the complete spectrum at each point, the magnitudes of the constituent spectra for the four intermediates at each point, and the fact that the molar concentrations of the four intermediates at each point had to sum to give the molar concentration of active sites in the solution, the concentrations of each of the intermediates at each of intervals could be calculated. The concentrations of each intermediate (micromolar) are plotted as a function of the intevals between mixing and observation (seconds). The curves are a fit of the kinetic mechanism of Equation 5–359 to the data by numerical analysis with rate constants of $k_1 = 21.1 \pm 0.4\ s^{-1}$, $k_2 = 145 \pm 5\ s^{-1}$, and $k_3 = 1.03 \pm 0.01\ s^{-1}$.

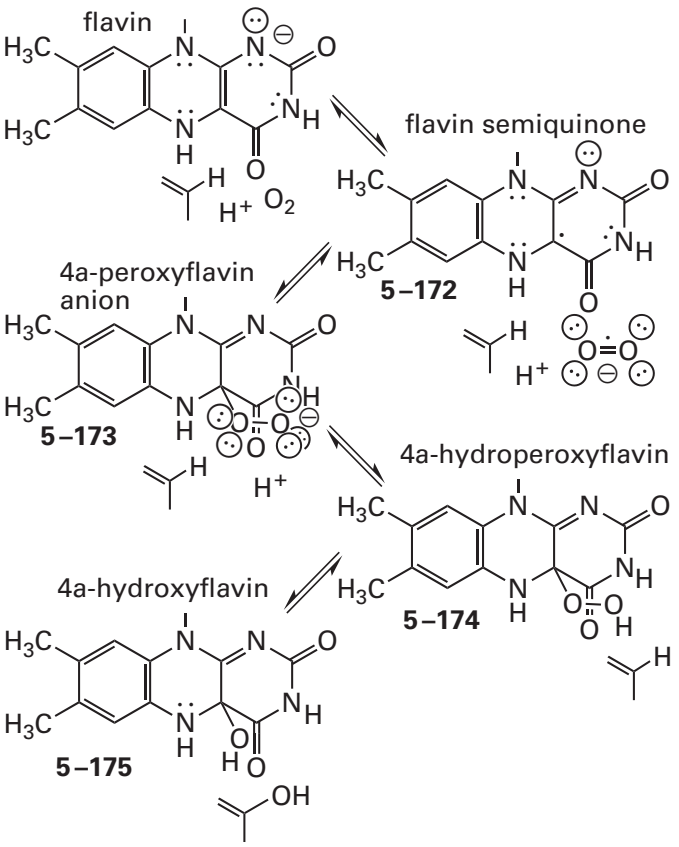

(5–302)

can be followed. Upon mixing human (*S*)-2-hydroxy-acid oxidase containing reduced prosthetic flavin with high concentrations of O_2 dissolved in the second solution, the rapid (2 ms), transient appearance of absorbance that could be assigned to flavin semiquinone (**5–172**) could be observed during the formation of 4a-peroxyflavin anion (**5–173**) from O_2 and the prosthetic flavin.[904] The semiquinone is formed by the transfer of an electron from the reduced flavin to the O_2. Formation of 4a-peroxyflavin anion (**5–173**) in the active site of cyclohexanone mono-oxygenase (previously Equation 2–213)

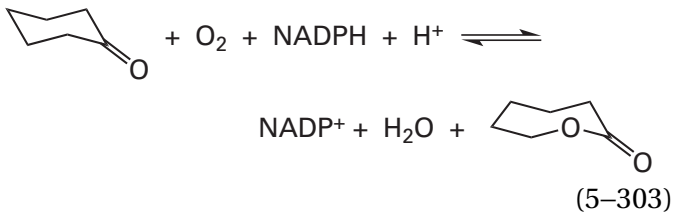

(5–303)

from *Acinetobacter* could be monitored by changes in the spectrum of the reduced prosthetic flavin as oxygen was adding to it. After formation of the 4a-peroxyflavin anion, the subsequent oxidation of cyclohexanone to produce hexano-6-lactone and oxidized flavin (Figure 2–47) could also be monitored.[905] In the case of 3-hydroxybenzoate 6-mono-oxygenase

$$\text{3-hydroxybenzoate} + \text{NADPH} + \text{H}^+ + \text{O}_2 \rightleftharpoons \text{3,6-dihydroxybenzoate} + \text{NADP}^+ + \text{H}_2\text{O} \quad (5\text{–}304)$$

association of oxygen, formation of 4a-peroxyflavin anion (**5–173**), hydronation of the 4a-peroxyflavin anion to form 4a-hydroperoxyflavin (**5–174**), and hydroxylation of the 3-hydroxybenzoate at carbon 6 by the 4a-hydroperoxyflavin (see Figure 2–48) could all be followed by monitoring changes in absorbance at wavelengths characteristic for these intermediates.[906] The subsequent hydrolysis of the 4a-hydroxyflavin (**5–175**) produced during the hydroxylation of the 3-hydroxybenzoate was too rapid, which precluded its observation, but the case of the flavoenzyme 4-hydroxybenzoate 3-monooxygenase [NAD(P)H] from *P. aeruginosa*, formation of the 4a-hydroxyflavin produced on its active site during the hydroxylation of 4-hydroxybenzoate by 4a-hydroperoxyflavin (**5–174**) could be followed by its strong fluorescence.[907]

Changes in the absorbance spectra of prosthetic **hemes**,[908] **iron–sulfur clusters**,[909,910] and prosthetic **nonheme iron clusters** (Figure 2–57)[911] are further examples of prosthetic groups the spectroscopy of which can be used to follow steps in an enzymatic reaction by stopped flow.

It is often the case, however, that neither substrates for the enzyme nor enzymatically active analogues of those substrates absorb or fluoresce, and the enzyme has no prosthetic groups that do either. In such cases, there may be a **tryptophan in the protein**, in the vicinity of the active site or affected by conformational changes, the absorbance or fluorescence of which changes as the enzyme steps through its reaction. For example, association of each of the two reactants, $MgATP^{2-}$ and L-threonine, with the active site of threonine—tRNA ligase from *E. coli,* as well as conversion of the complex of both reactants to the threonyladenylate that is an intermediate in the reaction, could be monitored by following changes in fluorescence of one or more of the 11 tryptophans in the enzyme.[912]

Crystallographic molecular models suggest that when NADH and pyruvate bind to L-lactate dehydrogenase (Equation 5–292) from *G. stearothermophilus*, a lid composed of a loop of polypeptide closes over the active site. When the three tryptophans in the enzyme were replaced with tyrosines and a **trypto-**

phan was inserted by site-directed mutation into this loop, the closure of the lid could be followed by the quenching of fluorescence of this tryptophan when it is transferred from the solution to the surface of the protein. The fact that the rate constant ($125\ s^{-1}$) for the closing of the lid upon NADH and oxamate, an analogue of pyruvate, is equal to the rate constant ($140\ s^{-1}$) for production of a molecule of L-lactate when the complex between NADH and the enzyme is mixed with pyruvate (see Figure 5–21A) suggests that closing of this lid is the rate-limiting step in reduction of pyruvate by the enzyme.[913]

It is also possible to **modify a protein with a fluorescent functional group** other than an indolyl group of a tryptophan to produce an even more fluorescent protein. If the modification occurs near enough to the active site, the **fluorescent reporter** incorporated into the enzyme can register, by changes in its fluorescence, changes occuring in the active site as reactants associate and are converted into intermediates. For example, a fluorescent 3,6-diamino-9-(2,4-dicarboxyphenyl)-4,5-disulfoxanthylium was covalently attached to a loop of polypeptide that closes down over the active site of dihydrofolate reductase (previously Equation 4–148)

$$\text{NADPH} + \text{7,8-dihydrofolate} + \text{H}^+ \rightleftharpoons \text{5,6,7,8-tetrahydrofolate} + \text{NADP}^+ \qquad (5\text{–}305)$$

from *E. coli* after the reactants 7,8-dihydrofolate and NADPH associate with the enzyme, and its fluorescence could be used to monitor rates of association of each reactant, closing of the lid, and hydride transfer in the active site.[914]

The rates of **hydron uptake into or hydron release** from the active site of an enzyme can also be observed by stopped flow by adding an **pH indicator** to the solution. For example, release of a hydron from the active site of equine alcohol dehydrogenase at pH 5.9 during the oxidation of 1-propanol by NAD^+ could be monitored by following the absorbance of chlorophenol red in the solution.[915]

The progress of a reaction can also be followed by the technique of quenched flow. If the outlet from a mixing chamber fed by two coupled syringes that are compressed at a constant rate by a plunger is attached to a length of tubing that is connected to a second mixing chamber or that simply ends in a quench solution, the time that the fluid spends between the first mixing chamber and the second mixing chamber or the quench solution is determined only by the flow rate through the first mixing chamber and the length and cross-sectional area of the tubing. Suppose the reaction is initiated in the first mixing chamber, by analogy with the apparatus for stopped flow, and abruptly halted at the second mixing chamber or in the solution into which it flows at the end of the tubing, for example, by quenching with strong acid. The final solution produced by the device will provide a measure of the progress of the reaction over the time spent within the tubing between the two mixing chambers or between the first mixing chamber and the quench solution. The advantage of this technique of quenched flow is that products of the reaction are collected and can be assayed chemically rather than only spectroscopically. Its disadvantage is that only one time point in the progress of the reaction is provided by each measurement. To obtain the whole course of the reaction, a sequence of tubings that vary in length or a coupled pair of syringes driven by a plunger the speed of which can be varied[916] is used to provide a sequence of reaction times.

One syringe of an apparatus for quenched flow was filled with a solution of 3-phosphoshikimate 1-carboxyvinyltransferase ($20\ \mu M$ in active sites) from *E. coli* (Equation 5–178) and $200\ \mu M$ 3-phosphoshikimate, and the other syringe was filled with $7\ \mu M$ phospho[^{14}C]*enol*pyruvate. After these solutions were mixed in a mixing chamber at a constant rate of flow, the mixture passed through a tube of a particular length and was then quenched with 0.6 M HCl. This sequence of events was repeated 18 times with tubing of varying lengths (Figure 5–26). Each quenched sample, each of which spent a different interval of time between mixing and quenching, or in the case of reproduction, the same amount of time, was then submitted to chromatography to separate the reactant phospho[^{14}C]*enol*pyruvate (○) and the product 5-*O*-(1-[^{14}C]carboxyvinyl)-3-phosphoshikimate (□).[308] Because the concentration of active sites ($20\ \mu M$) was greater than the concentration of phospho[^{14}C]*enol*pyruvate ($7\ \mu M$), only one turnover or no turnovers occurred at each active site. Because all the reactant was converted into product over a period of 100 ms, the decrease in the concentration of phospho*enol*pyruvate and the increase in the concentration of 5-*O*-(1-carboxyvinyl)-3-phosphoshikimate could both be accurately followed at intervals of 5 ms.

Often, especially when the concentrations of reactants are required to be much greater than the concentration of enzyme so that the decrease in

the concentration of reactants is insignificant, only the **accumulation of a product of the enzymatic reaction** is followed by quenched flow. For example, formation of orotidine 5′-phosphate from orotate and 5-phospho-α-D-ribose and, in the opposite direction, formation of orotate from orotidine 5′-phosphate and diphosphate catalyzed by orotate phosphoribosyltransferase (Equation 5–183) from *S. enterica* could be followed by quenched flow. The respective products from each quenched solution were separated from the much larger amounts of reactants by thin-layer chromatography.[917]

Usually, as in the preceding examples, the reactants or products or both of them in the quenched solutions are separated and identified chromatographically, but other **types of analysis** can be used. Differences in the partition of reactants and products between water and an organic solvent[918,919] or differences in their adsorption to a solid phase[920] can be used as rapid assays for a large number of samples. When the various products and reactants are identified chromatographically or separated by solvent extraction or adsorption, radioactive reactants are often used to increase the sensitivity of the assay and decrease the needed concentration of enzyme, which determines the concentration of intermediates accumulated or product produced during a single turnover and which determines the amount of enzyme irretrievably lost in each quenched sample. Other methods that have been used to quantify products from quenched flow are mass spectrometry,[921] electron paramagnetic resonance spectroscopy,[922,923] and Mössbauer spectroscopy.[924] It is also possible to assay the concentration of a particular reactant or product in a quenched sample by using a sensitive coupled enzymatic assay.[925] In all these instances, because the samples must always be quenched, a step that must inactivate and usually denature the enzyme, reactants and products that were free in solution at the time the sample was quenched cannot be distinguished from reactants and products that were bound in the active site.

If the identity of an intermediate is known, it is also possible to follow the **appearance of an intermediate** in an enzymatic reaction by quenched flow as the reaction progresses by identifying it chromatographically[926] or by mass spectrometry.[921] For example, solutions of acyl-homoserine-lactone-synthase[927]

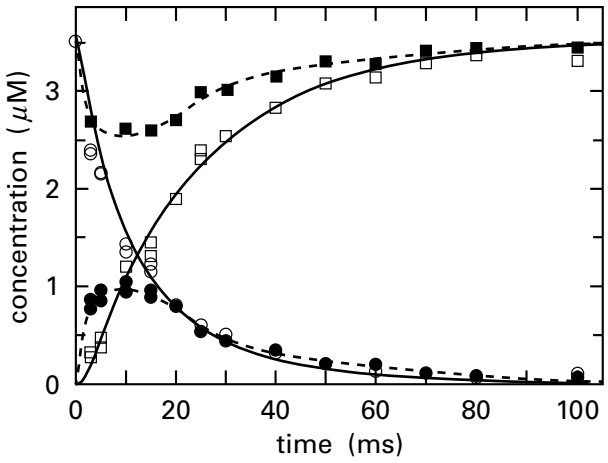

Figure 5–26: Kinetic courses for the concentrations of the reactant phospho*enol*pyruvate, the product 5-*O*-(1-carboxyvinyl)-3-phosphoshikimate, and an intermediate in the reaction catalyzed by 3-phosphoshikimate 1-carboxyvinyltransferase from *E. coli*.[308] A solution of 3-phosphoshikimate 1-carboxyvinyltransferase (20 μM in active sites) and 200 μM 3-phosphoshikimate was mixed with an equal volume of a solution of 7 μM phospho[^{14}C]*enol*pyruvate (32 mCi mmol^{-1}). Both solutions contained 50 mM KCl and 50 mM potassium 2-[4-(2-hydroxyethyl)piperazin-1-yl]ethanesulfonate, pH 7.0 and 20 °C. The two solutions were mixed in a mixing chamber, the mixture flowed through a tube of a particular length, and the mixture was then quenched with 0.6 M HCl. This procedure was repeated with the same two solutions, varying the time each mixture spent between the mixing chamber and the quench solution by choosing different lengths of tubing. Each quenched solution was then extracted with chloroform and neutralized with KOH. Phospho[^{14}C]*enol*pyruvate (○, solid line), 5-*O*-(1-[^{14}C]carboxyvinyl)-3-phosphoshikimate (□, solid line), and [^{14}C]pyruvate (●, dashed line) were separated by high-pressure liquid chromatography and quantified by their counts per minute. The concentrations of each compound in the unquenched mixture (micromolar) are plotted as a function of the intervals between mixing and quenching (milliseconds). The sums of the concentrations of phospho[^{14}C]*enol*pyruvate and 5-*O*-(1-[^{14}C]carboxyvinyl)-3-phosphoshikimate are also plotted (■, dashed line). The concentrations of [^{14}C]pyruvate observed were equal to the missing differences between sums of the concentrations of the other two substrates and the initial concentration of phospho*enol*pyruvate, and the [^{14}C]pyruvate observed was assumed to represent an intermediate in the unquenched mixture that decomposed to pyruvate during the quench. The curves for the concentrations of phospho[^{14}C]*enol*pyruvate and 5-*O*-(1-[^{14}C]carboxyvinyl)-3-phosphoshikimate are fits of the kinetic mechanism of Equation 5–360 to the data by numerical integration.

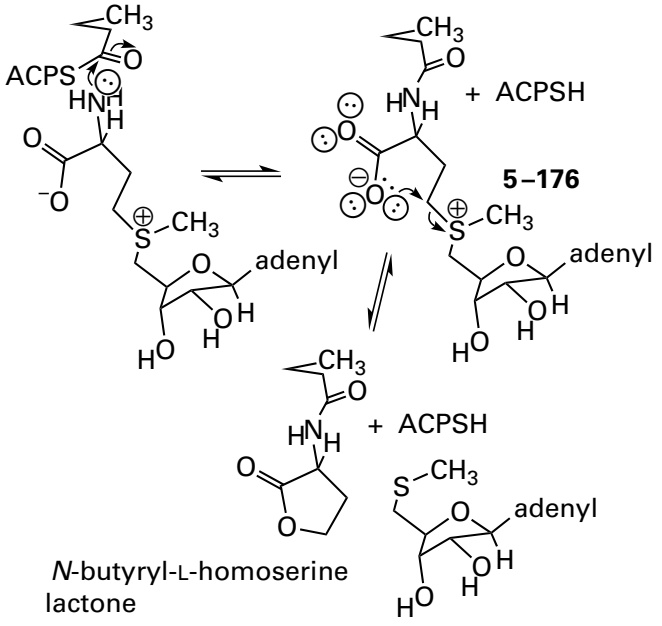

(5–306)

from *P. aeruginosa* and *S*-adenosyl-[*carboxy*-^{14}C]-L-methionine were mixed with solutions of butyryl-SACP, where ACP is acyl-carrier protein, and the reactions were quenched after various intervals. The decrease in *S*-adenosyl-[*carboxy*-^{14}C]-L-methionine and the increase in the intermediate *N*-butyryl-2-adenosyl-[*carboxy*-^{14}C]-L-methionione (**5–176)** could be followed chromatographically. The decrease in the intermediate could then be followed as *N*-butyryl-[*carboxy*-^{14}C]-L-homoserine lactone, the ultimate product of the enzymatic reaction, was formed at the active site by intramolecular nucleophilic substitution.[926]

It is also possible to follow formation of the **covalent intermediate of an enzyme** by quenched flow. For example, one syringe in an apparatus for quenched flow was filled with a solution of active, ^{31}P-phosphorylated phosphoglucomutase (α-D-glucose-1,6-bisphosphate-dependent) (Equation 5–36) from *O. cuniculus*, and the other was filled with D-glucose 1-[^{32}P]phosphate. After these solutions were mixed in a rapid mixing chamber at a constant flow rate, the mixture passed through a tube of a particular length and was then mixed with trichloroacetic acid to precipitate the protein. Using a series of tubes of different lengths, the amount of [^{32}P]phosphate attached covalently to the protein resulting from its phosphorylation of the 6-hydroxy group of D-glucose 1-[^{32}P]phosphate and the subsequent phosphorylation of the enzyme by the 1-[^{32}P]phospho group (Equation 5–36). This exchange of phospho groups on the enzyme could be followed as a function of the time spent between the mixing chamber and the quench solution (Figure 5–27).[928]

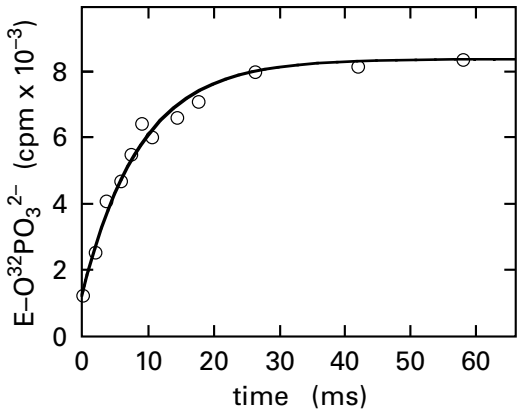

Figure 5–27: Increase in [^{32}P]phosphoenzyme after active, fully phosphorylated phosphoglucomutase from *O. cuniculus* was mixed with D-glucose 1-[^{32}P]phosphate.[928] A solution containing ^{32}P-phosphorylated phosphoglucomutase [8.1×10^3 cpm (nmol of active sites)$^{-1}$] at a concentration of 0.15 μM was mixed with an equal volume of a solution of 2 μM D-glucose 1-[^{32}P]phosphate (75×10^3 cpm nmol^{-1}). Both solutions contained 1 mM $MgCl_2$ and were buffered at pH 7.5 and room temperature. The two solutions were mixed in a mixing chamber, the mixture flowed through a tube of a particular length, and the mixture was then introduced through the end of the tube into a rapidly swirling quench solution of 5% trichloroacetic acid. The protein that precipitated was collected by filtration, and the radioactivity (counts per minute) attached to the protein was determined by liquid scintillation counting. This procedure was repeated with the same two solutions, varying the interval each mixture spent between the mixing chamber and the quench solution by choosing different lengths of tubing. The individual measurements of the amount of phosphorus-32 attached to protein (E–O^{32}PO$_3^{2-}$ in counts per minute $\times 10^{-3}$) are plotted as a function of intervals the mixtures spent in the tubing between the mixing chamber and the quench solution (milliseconds). Because the enzyme had some phosphorus-32 attached at the beginning of the reaction, the amount at time zero does not equal 0. The curve is a fit of the data to Equation 5–321 with a rate constant, k_{obs}, of 112 s^{-1}.

Pyruvate, phosphate dikinase from *C. symbiosum* (Equation 5–234) was rapidly mixed with Co[β-^{32}P]ATP^{2-} to follow the sum of the concentrations of [^{32}P]diphosphoenzyme (Equation 5–238) and [^{32}P]phosphoenzyme (Equation 5–240) or with Co[γ-^{32}P]ATP^{2-} to follow only the concentration of [^{32}P]diphosphoenzyme. These mixtures were then quenched with 0.6 M HCl after various intervals (Figure 5–28).[929] When the protein from these two time courses was precipitated with CCl_4, it could be shown, by difference, that formation of [^{32}P]diphosphoenzyme (●) preceded formation of [^{32}P]phosphoenzyme (■), a result consistent with the proposed

mechanism of the enzyme.[929] It could also be shown that formation of [^{32}P]diphosphate (□) followed formation of [^{32}P]diphosphoenzyme (●) and that formation of [^{32}P]phospho*enol*pyruvate (△) followed formation of [^{32}P]phosphoenzyme (■). This entire sequence is that expected from the proposed mechanism (Equations 5–238 to 5–241).

It is also possible to **inject the effluent** emerging from the mixing chamber, after it passes for a certain amount of time through a segment of tubing, directly **into a mass spectrometer** and thereby monitor the mass of the enzyme. For example, endo-1,4-β-xylanase from *N. circulans* was mixed with the unnatural reactant 2,5-dinitrophenyl-β-xylobioside and, after passing for a defined interval through a length of tubing, the mixture was injected as an electrospray into a mass spectrometer. The appearance of a peak of molecular mass 20,649 Da could be followed as a function of time.[930] This peak represents a xylobiosyl group (molecular mass = 265 Da) esterified to a glutamyl group

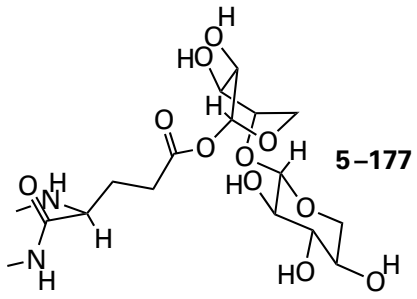

that is a covalent intermediate[931,932] in the reaction catalyzed by the enzyme (molecular mass = 20,384 Da). Again, only atoms covalently attached to the protein, not those noncovalently attached such as molecules of water, remain associated with the polypeptide in the vacuum of the instrument.

More chemically explicit information about the identity of a covalent intermediate of an enzyme can be obtained as its formation is being followed. For example, the two cysteines that form a cystine during the mechanism of ribonucleoside-diphosphate reductase from *E. coli* (Figure 5–13) are found in the sequences –RQFSSCVLIECGD– and –ENGEIALCTLSAFNLG–. When the enzyme is digested with glutamyl endopeptidase and chymotrypsin, these two cysteines end up in the peptides SSCVLIE and IALCTLSAF. Ribonucleoside-diphosphate reductase was mixed with the reactant CDP^{3-}, and the effluent from the mixing chamber was quenched with acetic acid after various intervals. The protein was then

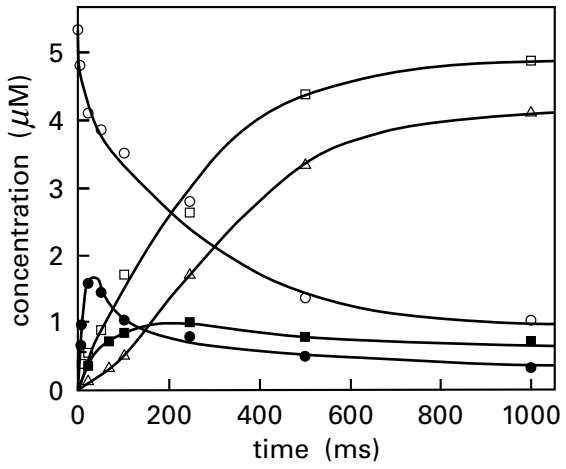

Figure 5–28: Kinetic courses for the concentrations of the reactant MgATP^{2-}, the diphosphorylated enzymatic intermediate, the product diphosphate, the phosphorylated intermediate, and the product phospho*enol*pyruvate in the reaction catalyzed by pyruvate, phosphate dikinase from *C. symbiosum*.[929] A solution containing pyruvate, phosphate dikinase (40 μM in active sites) was mixed with an equal volume of a solution of 12 μM AT[γ-^{32}P]P^{2-} or 12 μM AT[β-^{32}P]P^{2-} and 2 mM pyruvate. Both solutions contained 2.5 mM $CoCl_2$, 10 mM NH_4Cl, 2 mM $HOPO_3^{2-}$, and 50 mM potassium 2-[4-(2-hydroxyethyl)piperazin-1-yl]ethanesulfonate, pH 7.0 and 25 °C. The two solutions were mixed in a mixing chamber, the mixture flowed through a tube of a particular length, and the mixture was then quenched with 0.6 M HCl. The protein in the quenched solution was precipitated with CCl_4, and the radioactivity in the precipitate was measured. This procedure was repeated with the same two solutions, varying the time each mixture spent between the mixing chamber and the quench solution by choosing different lengths of tubing. Radioactivity in the precipitates from AT[γ-^{32}P]P^{2-} was assumed to represent only the diphosphorylated intermediate while that from AT[β-^{32}P]P^{2-} was assumed to represent both the diphosphorylated and phosphorylated intermediates. The supernate that remained after collecting the precipitated protein was submitted to high-pressure liquid chromatography to separate unreacted MgAT[^{32}P]P^{2-}, magnesium [^{32}P]diphosphate, and [^{32}P]phospho*enol*pyruvate, which were quantified by their radioactivity. The concentrations (micromolar) of MgAT[^{32}P]P^{2-} (○), ^{32}P-diphosphorylated intermediate (●), magnesium [^{32}P]diphosphate (□), ^{32}P-phosphorylated intermediate (■), and [^{32}P]phospho*enol*pyruvate (△) in the reaction mixtures are plotted as a function of the intervals between mixing and quenching (milliseconds).

digested with glutamyl endopeptidase and chymotrypsin, the digest was passed over an immunoadsorbent specific for the carboxy-terminal sequence –VLIE, and the peptides eluted from the immunoadsorbent were submitted to chromatography. By this procedure, transformation of the peptide SSCVLIE into the peptide in which SSCVLIE is connected by a cystine with the peptide IALCTLSAF could be followed.[500]

Enzymatic reactions can also be initiated rapidly by using a caged reactant without the need for the methods of either stopped flow or quenched flow. A caged reactant is a photolabile derivative of the reactant for an enzyme that is catalytically inactive but that decomposes upon photolysis to produce the catalytically active reactant. The photolysis that releases the actual reactant takes place in an optical cuvette, and the subsequent reaction, following release from the cage, can be followed spectroscopically. For example, caged ATP^{3-}

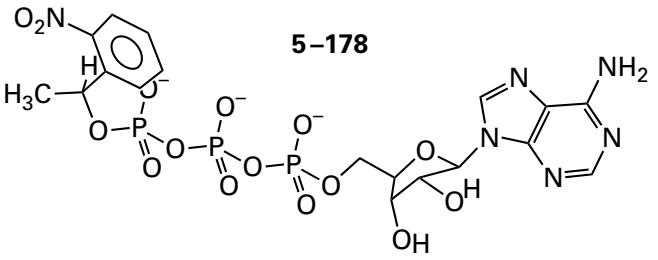

5–178

when photolyzed at 347 nm, decomposes to produce ATP^{4-} at a rate of 2.2×10^6 $[H^+]$ M^{-1} ms^{-1}, which at pH 6 is 2.2 ms^{-1}. The released ATP^{4-} then combines with Mg^{2+} in the solution to give $MgATP^{2-}$. Depending on the structure of the active site, a caged reactant can either associate to form a catalytically inactive complex or fail to associate with the active site at all until photolysis is performed.[933]

A solution of cytochrome-*c* oxidase and the binuclear complex

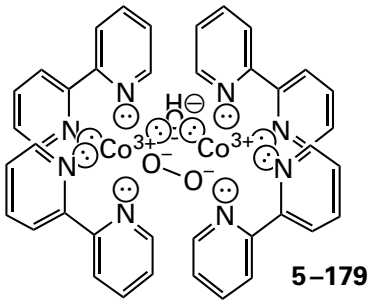

5–179

which upon photolysis at 355 nm decomposes in less than 40 ns to produce O_2 from the peroxide coordinated to the two Co^{3+},[934] was submitted to photolysis. Reduction of the O_2 released from the cage by the two reduced hemes and the two Cu^+ in the active site of cytochrome-*c* oxidase could be followed spectroscopically in the range between 450 and 750 nm.[935] The enzymatic reaction passed through three distinct intermediates over an interval of 1 μs–10 ms. At least two of these intermediates would have formed and decayed within the dead time for stopped flow and would have been inaccessible by that method.

There is a similar strategy to observe intermediates that form in microseconds and that has long been employed in the study of hemoproteins. The tight complex between the iron of a hemoprotein and carbon monoxide is dissociated by light.[936] Such a complex is mixed in an apparatus for stopped flow with a solution of another ligand for the iron in the hemoprotein at a concentration high enough to outcompete carbon monoxide for reassociation with the iron. Upon cessation of the flow, the solution is exposed to an intense flash that causes the carbon monoxide to dissociate immediately, and association of the other ligand with the vacant iron and subsequent events can be monitored. For example, a complex between carbon monoxide and ferrous ubiquinol oxidase (H^+-transporting)

$$2\ \text{ubiquinol} + O_2 + n\,H^+_{\text{cyt}} \rightleftharpoons 2\ \text{ubiquinone} + 2\,H_2O + n\,H^+_{\text{extra}} \qquad (5\text{–}307)$$

from *E. coli*, where cyt refers to the cytoplasmic face of the enzyme and extra to the extracellular face, was mixed rapidly, in the absence of ubiquinol to prevent rereduction of the hemes, with a saturated solution of O_2. The mixture was immediately exposed to a short (7 ns) flash of light (532 nm) from a neodymium:yttrium–aluminum–garnet laser. Carbon monoxide dissociated, and from the first microsecond, association of oxygen and the sequence of five subsequent intermediates formed during reduction of the O_2 to two molecules of water could be observed by following the absorbance spectrum of the heme between 350 and 500 nm.[937]

There are two regimes under which an observation can be made by stopped flow or quenched flow. First, if the enzyme is mixed with concentrations of reactants that are all significantly greater than the concentrations of enzyme, then the enzyme will turn over many times until the equilibrium it catalyzes is reached. Rapid changes, however, occur as the steady state is being established during the pre-steady state. After this initial period, the appearance of products or the disappearance of reactants then proceeds at the normal, steady-state rate, and the concentrations of intermediates remain constant at their steady-state levels. Second, if the kinetic experiment is purposely designed so that the enzyme

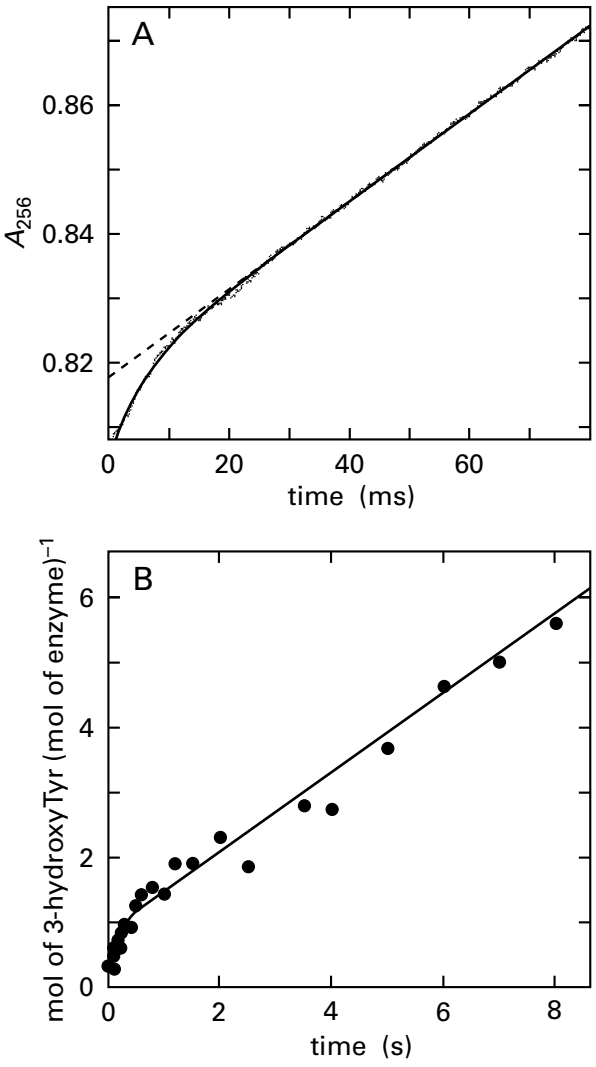

Figure 5–29: Bursts monitored by stopped flow and quenched flow. (**A**) Burst in formation of AMP^{2-} observed by stopped flow after the complex between adenine phosphoribosyltransferase and magnesium 5-phospho-α-D-ribose 1-diphosphate was mixed with a solution of adenine.[895] A solution containing 250 μM magnesium 5-phospho-α-D-ribose 1-diphosphate and 11 μM active sites of adenine phosphoribosyltransferase from *L. donovani* was mixed with an equal volume of a solution of 70 μM adenine in an apparatus for stopped flow. The solutions contained 10 mM MgCl and 100 mM tris(hydroxymethyl)methylammonium chloride at pH 7.5 and 27 °C. The absorbance of the solution was monitored at 256 nm, the wavelength at which there is the largest difference in absorbance between AMP^{2-} and adenine, and the absorbance (A_{256}) is plotted as a function of time (milliseconds). The curve is a fit of Equation 5–309 to the data (irregular dotted line), and the dashed line is an extrapolation of the later, linear portion of the curve (k_0t). (**B**) Burst in formation of 3-hydroxy-L-tyrosine observed by quenched flow after solutions of tyrosine 3-monooxygenase saturated with 6-methyltetrahydropterin were mixed with solutions of L-tyrosine and O_2.[938] A solution of tyrosine 3-monooxygenase (40 μM in active sites) from *R. norvegicus* and 2 mM 6-methyltetrahydropterin was mixed with an equal volume of a solution containing 500 μM L-tyrosine and 1.9 mM O_2. Both solutions contained 10% glycerol, 0.1 M KCl, and 200 mM potassium 2-[4-(2-hydroxyethyl)piperazin-1-yl]ethanesulfonate, pH 7.5 and 5 °C. The two solutions were mixed in a mixing chamber, the mixture flowed through a tube of a particular length, and the mixture was then quenched with 5 M HCl. The quenched solution was submitted to high-pressure liquid chromatography to isolate 3-hydroxy-L-tyrosine, which was quantified by its fluorescence. This procedure was repeated with the same two solutions, varying the time each mixture spent between the mixing chamber and the quench solution by choosing different lengths of tubing. The moles of 3-hydroxy-L-tyrosine (mole of active sites of tyrosine 3-monooxygenase)$^{-1}$ in the reaction mixtures are plotted as a function of the intervals (seconds) between mixing and quenching. Adapted with permission from reference 895. Copyright 2002 American Chemical Society. https://doi.org/10.1021/bi0158730

is prevented from completing more than one turnover, then the enzymatic reaction will proceed until a single turnover or a portion of a single turnover has been completed and will proceed no further. The rapid changes observed are uncomplicated by the establishment of a steady state when molecules of enzyme individually and stochastically complete their first turnover. These molecules of enzyme proceed with the second or even third turnover while other molecules are still finishing their first or have finished their first earlier.

In a measurement of the **pre-steady state**, when the appearance of a certain product or intermediate in an enzymatic reaction is being monitored by stopped flow or quenched flow, if that product or intermediate is formed in a step followed by significantly slower steps, then a burst of that product or intermediate will be observed before the steady state is established.

A **burst of product** is the rapid appearance of an amount of product that is equal in molar concentration to the molar concentration of active sites in the solution and that can be distinguished kinetically from the much slower accumulation of product that follows the burst and proceeds at the normal steady-state rate. For example, when a solution of adenine phosphoribosyltransferase (Problem 3–15)

$$\text{magnesium 5-phospho-}\alpha\text{-D-ribose 1-diphosphate} + \text{adenine} \rightleftharpoons AMP^{2-} + MgOPO_3PO_3^{2-} + H^+ \quad (5\text{–}308)$$

from *L. donovani*, the active site of which had been saturated with magnesium 5-phospho-α-D-ribose 1-diphosphate, was mixed with a solution of adenine, an increase in the molar concentration of AMP^{2-} proceeded rapidly in a burst (Figure 5–29A).[895] The data could be fit to the equation

$$A_{256} = \Delta A e^{-k_{obs}t} + k_0 t \qquad (5\text{–}309)$$

The size of the burst (ΔA), determined by extrapolation to zero time, was directly proportional to the molar concentration of active sites in a series of measurements at different concentrations of enzyme. Following the burst, AMP^{2-} was produced at a linear rate equal to the steady-state initial rate (v_0) separately measured under these conditions. The explanation for this behavior is that there is a step in the enzymatic reaction following formation of AMP^{2-} on the active site that is slower than all steps preceding formation of AMP^{2-}. For that reason, the initial formation of AMP^{2-} at each active site is more rapid than the steady-state rate for subsequent formation of AMP^{2-}, which is limited by the slower steps following the production of AMP^{2-}.

A solution of tyrosine 3-monooxygenase

$$\text{tetrahydrobiopterin} + \text{L-tyrosine} + O_2 \rightleftharpoons \text{3-hydroxy-L-tyrosine} + \text{4a-hydroxytetrahydrobiopterin} \qquad (5\text{–}310)$$

from *R. norvegicus*, the active site of which had been saturated with 6-methyltetrahydropterin, was mixed with a solution of L-tyrosine and O_2, and then the reaction was quenched after various intervals with 5 M HCl. An increase in the concentration of the product 3-hydroxy-L-tyrosine in the quenched solutions proceeded rapidly in a burst (Figure 5–29B),[938] the size of which was equivalent to the molar concentration of active sites, and then 3-hydroxy-L-tyrosine was produced at the steady-state rate for the concentrations present.

In observations made by stopped flow or quenched flow, it is also possible to observe a **lag** in the accumulation of product. If the actual formation of the product being monitored is preceded by one or several slow steps, the increase in its concentration will proceed slowly at first and then accelerate until the steady-state rate is established. For example, when sulfate adenylyltransferase from *E. coli*, saturated with AMP^{2-} and magnesium diphosphate, is mixed with $MgGTP^{2-}$, the GTPase that is an inherent activity of the enzyme, even though it is unrelated to catalysis, is initiated. The $MgGDP^-$ released from the active site of this GTPase into the solution was monitored in an apparatus for stopped flow by a coupled enzymatic assay that registered $MgGDP^-$ in the solution by a decrease in the absorbance of NADH. Since its dissociation from the active site is the last step in the enzymatic reaction, it is not surprising that a lag in its appearance in the solution was observed (Figure 5–30, lower trace).[896] When the production of $MgGDP^-$ was followed by quenched flow, however, where $MgGDP^-$ in solution and $MgGDP^-$ within the

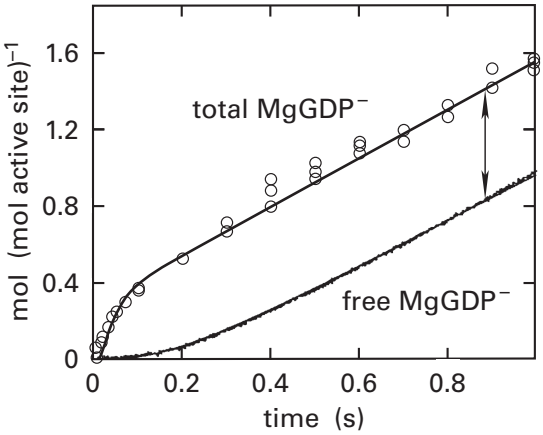

Figure 5–30: Lag in formation of $MgGDP^-$ free in solution, observed by stopped flow, and burst in formation of $MgGDP^-$ within the site for hydrolysis of $MgGTP^{2-}$ on sulfate adenylyltransferase, observed by quenched flow.[896] A solution of sulfate adenylyltransferase from *E. coli* (40 μM in active sites) was mixed with an equal volume of a solution of 1.0 mM $MgGTP^{2-}$ at 25 °C. Both solutions also contained 1.0 mM AMP, 0.1 mM diphosphate, 2.2 mM $MgCl_2$, and 50 mM potassium 2-[4-(2-hydroxyethyl)-piperazin-1-yl]ethanesulfonate, pH 8.0. For the stopped-flow observations, the second solution also contained a coupled assay for $MgGDP^-$ free in solution consisting of 200 μM pyruvate kinase, 2.0 mM phospho*enol*pyruvate, 72 mM lactate dehydrogenase, and 0.28 mM NADH. For the quenched-flow observations, the second solution contained 80 mCi mL^{-1} of [γ-^{32}P]$MgGTP^{2-}$. In the stopped-flow experiments, the $MgGDP^-$ free in solution was converted to $MgGTP^{2-}$ by pyruvate kinase; the pyruvate produced was converted to lactate by lactate dehydrogenase; and the NADH, monitored by its fluorescence, decreased in concentration as it was converted to NAD^+. The increase in $MgGDP^-$ free in solution (data points in lower trace) was calculated from the decrease in fluorescence. In the quenched-flow experiments, the two solutions were mixed in a mixing chamber, the mixture flowed through a tube of a particular length, and the mixture was then quenched with 0.1 M sodium hydroxide and 0.1 M sodium ethylenediaminetetraacetate. This procedure was repeated with the same two solutions, varying the time each mixture spent between the mixing chamber and the quench solution by choosing different lengths of tubing. Each quenched solution was submitted to thin-layer chromatography to isolate GDP^{3-}, which was quantified by its radioactivity. The moles of $MgGDP^-$ free in solution (mole of active sites of GTPase)$^{-1}$ (data points in lower trace) and the moles of total $MgGDP^-$ (mole of active sites of GTPase)$^{-1}$ (○) in the reaction mixtures are plotted as a function of the intervals between mixing and observation or between mixing and quenching (seconds). The curves through the data are fits of a kinetic mechanism proposed by the authors. Adapted with permission from reference 896. Copyright 2001 American Chemical Society. https://doi.org/10.1021/bi015735a

active site cannot be distinguished because the quench denatured the enzyme and released $MgGDP^-$ bound in the active site, it was observed that $MgGDP^-$ appeared rapidly in a burst rather than a lag (Figure 5–30; ○). These results together demonstrate that the rate-limiting step of the reaction is not hydrolysis of $MgGTP^{2-}$ on the active site but dissociation of $MgGDP^-$ from the active site into the solution. In this sense, the reaction resembles that of myosin ATPase in the absence of actin. After the burst and after the lag, once the steady state had been established, both the appearance of $MgGDP^-$ in the solution and the appearance of $MgGDP^-$ within the active site proceeded at the same rate because that is a fundamental property of a steady state. By definition, once an active site has achieved steady state, all the rates for formation of intermediates and products are identical. The size of the burst (extrapolation of the rate at steady state) was equivalent to 0.32 active site. After the steady state was established, however, the lag between the two lines, which registers the amount of $MgGDP^-$ bound in the active site in the steady state, is equivalent to 0.57 active site (vertical double arrow). This increase in the amount of $MgGDP^-$ associated with the active site occurs as the steady state is established.

A paradigm of an experiment in which an **active site is confined to a single turnover** is the one in which a solution of chorismate synthase (previously Equation 4–175)

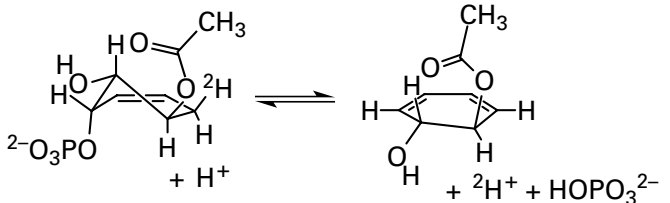

(5–311)

from *E. coli* was mixed with a solution of its single reactant 5-*O*-(1-carboxyvinyl)-3-phosphoshikimate so that the final concentrations were 105 μM in active sites and 70 μM in reactant. The dissociation constant for enzyme and reactant is less than 0.2 μM, so as soon as the reactant had associated with the enzyme (> 50 ms^{-1}), every molecule of the reactant (>99.4%) was associated with an active site of the enzyme and was then converted to product in a single turnover.[939]

In the experiment in which pyruvate is reduced by the complex between L-lactate dehydrogenase and NADH (Figure 5–21), almost all (85%) of the molecules of NADH (20 μM) in the initial solution with the enzyme (28 μM) are associated with active sites (K_d = 2 μM) and are oxidized to NAD^+ in a single turnover. In the experiment (Figure 5–26) in which 3-phosphoshikimate 1-carboxyvinyl transferase (20 μM), the active sites of which were fully saturated (96%) with 3-phosphoshikimate (200 μM; K_d = 7 μM), was mixed with a solution of phospho[^{14}C]*enol*pyruvate, so that the final concentration of the complex of enzyme and 3-phosphoshikimate was 9.3 μM and that of phospho[^{14}C]*enol*pyruvate was 3.5 μM, the active sites initially were only partially occupied by phospho*enol*pyruvate. In this instance, however, the almost 3-fold excess of enzyme over phospho*enol*-pyruvate ensured that the reaction was confined to a single turnover. An extreme example of enzyme in excess is a kinetic experiment with orotidine-5′-phosphate decarboxylase (Equation 5–243) from *S. cerevisiae*, in which enzyme (7 μM) was mixed at 14-fold molar excess over orotidine 5′-phosphate (0.5 μM) so that almost all (86%) of the molecules of orotidine 5′-phosphate would occupy an active site initially. As these molecules of orotidine 5′-phosphate were decarboxylated, their decarboxylation would draw the rest into other active sites by mass action. In this way, a minority of the active sites ended up catalyzing only a single turnover while the majority catalyzed no turnover at all.

Enzymatic reactions that convert more than one reactant to products, which represent the majority of enzymes, can be **confined to only a portion of their reaction by leaving out one reactant**. For example, when cysteine synthase (Equation 5–298) is mixed only with *O*-acetyl-L-serine, the enzymatic reaction ceases after the pyridoximine of 2-aminoacrylate (Equation 5–299) is formed (Figure 5–24) because no hydrogen sulfide is present. The steps preceding production of the pyridoximine of 2-aminoacrylate could be spectroscopically defined. The pyridoximine of 2-aminoacrylate was pre-formed in the active site of the enzyme under the same conditions and then mixed with hydrogen sulfide, and its conversion to L-cysteine (k_{obs} > 1 ms^{-1}) could be followed separately.[900]

When 3-hydroxy-2-methylquinolin-4-one 2,4-dioxygenase

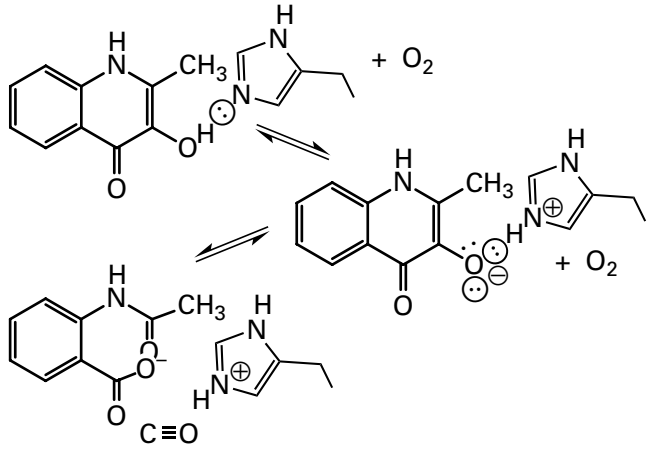

(5–312)

from *Paenarthrobacter nitroguajacolicus* is mixed with the reactant 3-hydroxy-2-methyl-1*H*-quinolin-4-one in the absence of oxygen, the active site is unable to complete the reaction (second step in Equation 5–312). Upon mixing the reactant and the enzyme anaerobically at pH 6.5 in an apparatus for stopped flow, there is a rapid (430 s^{-1}) change in the absorbance spectrum of the solution as an intermediate in the enzymatic reaction is formed. The absorbance spectrum of the intermediate is that of the anionic conjugate base of 3-hydroxy-2-methyl-1*H*-quinolin-4-one, which is not present at pH 6.5 ($pK_a = 10.4$). It was concluded that the first step in the reaction is removal of a hydron from the 3-hydroxy group of 3-hydroxy-2-methyl-1*H*-quinolin-4-one by a catalytic base in the active site.[940] In the crystallographic molecular model of the active site of a mutant of the enzyme occupied by 3-hydroxy-2-methyl-1*H*-quinolin-4-one, the side chain adjacent to the 3-hydroxy group is the imidazolyl group of Histidine 251. When Histidine 251 is mutated to alanine, the rate constant $k_0\,K_m^{-1}$ at pH 6.5 decreases by a factor of 5×10^5, and there was no longer a change in absorbance indicative of dehydronation of 3-hydroxy-2-methyl-1*H*-quinolin-4-one even at long times after it was mixed anaerobically with the enzyme. The rate constant for dehydronation of 3-hydroxy-2-methyl-1*H*-quinolin-4-one in the unmutated active site increases through an apparent pK_a of 7.2 to a maximum rate of 1.3 ms^{-1}. This pK_a has been assigned to the imidazolyl group of Histidine 251 when it is in a hydrogen bond with the 3-hydroxy group of 3-hydroxy-2-methyl-1*H*-quinolin-4-one in the Michaelis complex. At low pH, the imidazolyl group is hydronated and unable to participate in the hydrogen bond. **Direct observation of the transfer of the hydron** simplifies the assignment of this pK_a.

A variation on this strategy of leaving out one reactant is applied when the enzyme of interest catalyzes an oxidation–reduction and **oscillates between a reduced and an oxidized form**. Usually, a prosthetic group on the enzyme is either oxidized or reduced. For example, fructosyl amine oxidase (glucosone-forming)

N-(1-deoxy-D-fructos-1-yl)glycine + O_2 + H_2O
$\rightleftharpoons$ D-*arabino*-hexos-2-ulose + glycine + H_2O_2

(5–313)

from *Aspergillus fumigatus* is a flavoenzyme. When enzyme in which the flavin is oxidized is mixed with only *N*-(1-deoxy-D-fructos-1-yl)glycine, the flavin is reduced, and the reaction ceases in the middle of the first turnover because no O_2 is present to reoxidize the flavin. When enzyme in which the flavin is reduced is mixed with O_2, the flavin is oxidized, and the reaction ceases in the middle of the first turnover because no *N*-(1-deoxy-D-fructos-1-yl)glycine is present.[941] Consequently, both reduction and oxidation of the flavin, each of which are half of a single turnover, can be monitored separately.

When the active site of 4-hydroxybenzoate 3-monooxygenase [NAD(P)H] (see Equation 5–304) was occupied by 4-hydroxybenzoate at saturation and its prosthetic flavin was then reduced with dithionite, a solution of the complex of 4-hydroxybenzoate and reduced enzyme was produced. This complex was then mixed with a solution containing O_2. Following addition of O_2 to the flavin (Equation 5–302) to produce 4a-hydroperoxyflavin (**5–174**), hydroxylation of 4-hydroxybenzoate by 4a-hydroperoxyflavin (Figure 2–48) proceeds, but the reaction ceases in the middle of the first turnover because there is no NADPH to reduce the oxidized flavin. By monitoring changes in absorbance of the flavin at 385 and 470 nm as well as the fluorescence of 4a-hydroxyflavin (**5–175**), three individual steps—formation of 4a-hydroperoxyflavin from oxygen and a hydron, hydroxylation of 4-hydroxybenzoate by 4a-hydroperoxyflavin, and dissociation of the resulting 4a-hydroxyflavin (**5–175**) to produce oxidized flavin and a molecule of water—could each be followed.[907]

A major reason for examining an enzymatic reaction by stopped flow or quenched flow is to discover intermediates. As the last example and several earlier ones demonstrate, stopped flow and quenched flow can be used to observe the enzyme **stepping through its intermediates**. So far, examples

have been presented in which the accumulation of an intermediate and its conversion to the next intermediate or to product are followed directly. In the case of hydrolysis of nitrocefin by β-lactamase (Figure 5–23), the accumulation and subsequent conversion of the single intermediate in the reaction was monitored by its absorbance (λ_{max} = 655 nm). In this case of acyl-homoserine-lactone synthase (Equation 5–306), the accumulation and subsequent conversion of the single kinetic intermediate (**5–176**) in the enzymatic reaction was followed chromatographically. The single covalent xylobiosyl covalent intermediate (**5–177**) in the reaction catalyzed by endo-1,4-β-xylanase was observed by mass spectrometry. In the cases of cysteine synthase (Figure 5–24) and ornithine decarboxylase (Figure 5–25), the two intermediates and the three intermediates, respectively, were distinguished by the unique spectra of their adducts with pyridoxal phosphate. The prosthetic flavins in the three consecutive intermediates in reduction of the oxidized prosthetic flavin in the active site of dihydrolipoyl dehydrogenase from *M. tuberculosis* have unique absorption spectra and could be monitored spectrally as they successively increased and then decreased in concentration,[942] just as consecutive spectra of the prosthetic flavin and its fluorescence could be used to monitor the consecutive intermediates in oxidation of reduced 4-hydroxybenzoate 3-monooxygenase and in oxidation of reduced 3-hydroxybenzoate 6-monooxygenase.

A deoxygenation is catalyzed by CDP-4-dehydro-6-deoxyglucose reductase (previously Equation 2–41)

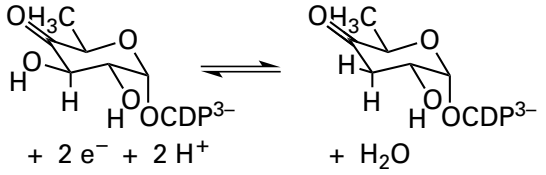

(5–314)

The overall reaction is a reduction requiring two electrons. These two electrons are provided in two consecutive electron transfers from a single prosthetic [4Fe–4S] iron–sulfur cluster within the active site. The prosthetic [4Fe–4S] iron–sulfur cluster in the active site is reduced in turn by a unique electron-carrier protein, which is a flavoprotein containing its own single prosthetic [4Fe–4S] iron–sulfur cluster, and, upon transferring two electrons, with flavin semiquinone as an intermediate, its oxidized prosthetic flavin is reduced by NADH. CDP-4-Dehydro-6-deoxyglucose reductase from *Y. pseudotuberculosis*, in which the prosthetic [4Fe–4S] iron–sulfur cluster is oxidized and in the absence of the electron-carrier protein, was mixed with CDP-4-dehydro-6-deoxyglucose. Four consecutive intermediates (previously Equation 2–42)

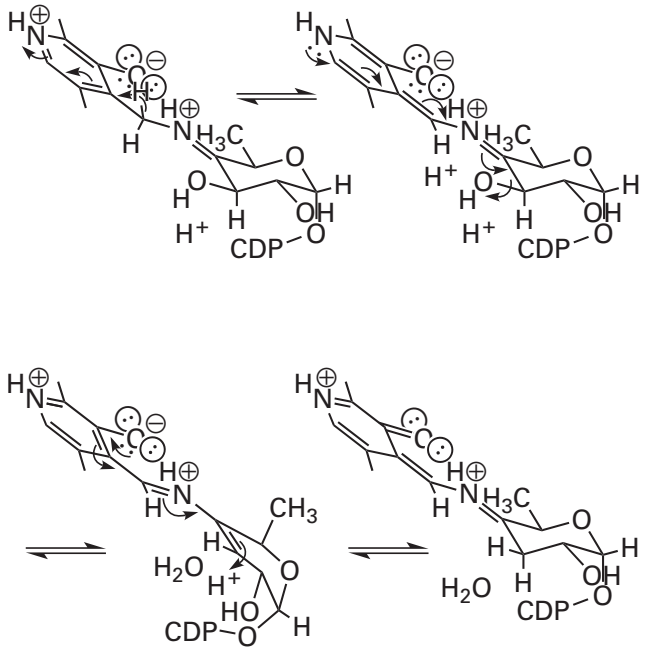

(5–315)

each of which accumulates and is then turned into the next, could be identified in an apparatus for stopped flow by following the absorbance of the prosthetic pyridoxamine 5′-phosphate at eight different wavelengths. The reaction ceases when the fourth intermediate has formed because no reductant is available. CDP-4-Dehydro-6-deoxyglucose reductase on which the fourth intermediate had accumulated was then mixed with NADH and reduced flavoprotein in an apparatus for quenched flow in which the solution emerging after passage through tubes of different lengths was rapidly frozen. A fifth intermediate, which was a radical that could be identified by electron paramagnetic resonance spectroscopy of the frozen samples, was formed from the fourth intermediate by transfer of one electron from the now-reduced prosthetic [4Fe–4S] iron–sulfur cluster in the active site. A sixth, fully reduced intermediate, the *N*-(5′-phosphopyridoxyl)-imine of the final product CDP-4-dehydro-3,6-dideoxy-D-glucose, was then produced by a second electron transfer. These results from quenched flow revealed the intermediate radical in the final reduction, which is widely delocalized over the π molecular orbital system of the *N*-(5′-phosphopyridoxyl)imine.[943]

There are also several ways in which formation and conversion of intermediates can be **observed indirectly**.

When the concentrations of both reactants and products of the stoichiometric reaction catalyzed by an enzyme are followed, a **failure of the sum of the molar concentrations of reactants and products to remain constant** with time and to equal the initial concentration of reactant is evidence that an intermediate which accounts for the missing moles is accumulating. For example, the sum of the molar concentrations (Figure 5–26) of phospho[^{14}C]*enol*-pyruvate (○), a stoichiometric reactant in the reaction catalyzed by 3-phosphoshikimate 1-carboxyvinyltransferase from *E. coli* (Equation 5–178), and 5-*O*-(1-[^{14}C]carboxyvinyl)-3-phosphoshikimate (□), a stoichiometric product, could be calculated for each interval of quenched flow.[308] This sum of the concentrations (■) decreases and then increases as the single turnover of the enzyme proceeds. In this instance, the missing moles could be accounted for by an increase and then a decrease in the concentration of [^{14}C]pyruvate (●), which also appeared on the chromatograms of the quenched samples. The accepted intermediate in this enzymatic reaction (previously **3–81**)

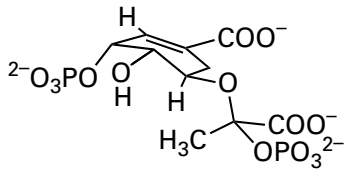

5–180

because it is the phosphorylated hemiketal of pyruvate, should be hydrolyzed in the strong acid used to quench the reaction to give pyruvate, so the increase and then the decrease in the amounts of [^{14}C]pyruvate in the quenched solutions represent the accumulation of this intermediate on the active site and then its conversion to product, respectively.

In the case of the single turnover of chorismate synthase from *E. coli*, the sum of the molar concentrations of the reactant, 5-*O*-(1-carboxyvinyl)-3-phosphoshikimate, and the product, chorismate, in measurements quenched flow decreases as the reaction begins and then increases again as it ends, just as was observed for 3-phosphoshikimate 1-carboxyvinyltransferase (Figure 5–26). The missing moles increase to a maximum at 20 ms and then decrease. This increase and decrease in the missing moles coincides with the increase and decrease in the amount of an intermediate detected spectrally by following the changes in the complete absorption spectrum of the prosthetic flavin in the active site of the enzyme.[939] In this instance, because no extinction coefficient for the intermediate observed spectroscopically was available, its molar concentration could not be estimated from the spectra alone. Nevertheless, because of the coincidence over the course of the reaction, it was concluded that this spectrally identified species accounted entirely for the missing moles, and hence its molar concentration and consequently its extinction coefficient could be estimated.

Another indication of the accumulation of an intermediate in an active site is a **lag between the appearance of one product of the reaction and the appearance of another product**. For example, haloalkane dehalogenase (750 μM) from *Rhodococcus rhodochrous*, which catalyzes the reaction

$$\text{1,3-dibromopropane} + H_2O \rightleftharpoons \text{3-bromopropan-1-ol} + Br^- + H^+ \qquad (5\text{–}316)$$

was mixed with 1,3-dibromopropane (400 μM; K_d = 200 μM), and the concentrations of reactants and products were followed by quenching the reaction at different times and submitting the quenched samples to chromatography (Figure 5–31).[944] The increase in the concentration of Br^- (□) over the first 20 ms (0.3 ms^{-1}) was stoichiometric with the decrease in the concentration of 1,3-dibromopropane (○), but the appearance of the other product, 3-bromopropan-1-ol (●), was much slower (0.015 ms^{-1}) and lagged significantly behind the production of Br^-. It was concluded that this behavior was a consequence of rapid accumulation of the β-aspartyl ester of 3-bromopropan-1-ol as a covalent intermediate (see Equations 5–10 and 5–11), which was stable in the 0.6 M HCl used to quench the reaction, and its subsequent slow hydrolysis (Equation 5–12).

In the case of argininosuccinate synthase, the lag between the appearance of two products is not the result of formation of a covalent intermediate but formation of a noncovalent intermediate. Argininosuccinate synthase catalyzes the nucleophilic substitution

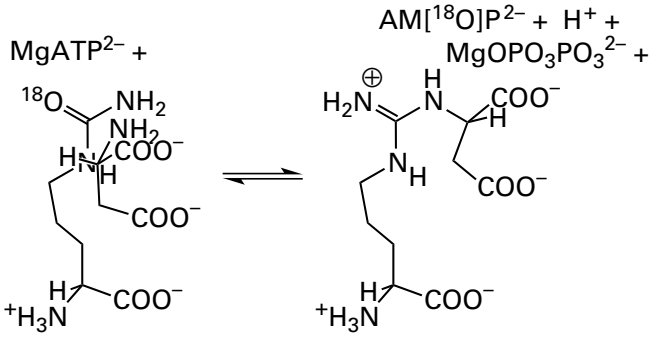

(5–317)

at a carbonate carbon. During the reaction catalyzed by the bovine enzyme, oxygen-18 in [*ureido*-^{18}O]-L-citrulline is transferred to the phosphate of the product AMP^{2-}.[945] This observation suggests that L-citrulline adenylate is formed as a noncovalent intermediate in the enzymatic reaction in the active site[946]

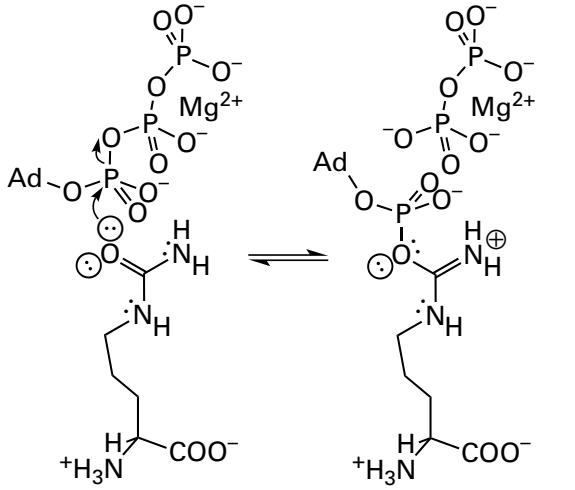

(5–318)

This adenylation would activate the L-citrulline for nucleophilic substitution and explain in molecular terms how the free energy of hydrolysis of $MgATP^{2-}$ is firmly and chemically coupled to the nucleophilic substitution. No isotopic exchanges in the absence of L-aspartate, however, which would be expected from Equation 5–318, have been observed.[947]

Solutions of bovine argininosuccinate synthase were mixed in an apparatus for quenched flow with solutions containing L-citrulline, $MgATP^{2-}$, and L-aspartate, the stoichiometric reactants in the equation. After each individual reaction had proceeded for a specific interval, the mixtures were quenched with 0.25 M H_2SO_4. The molar concentrations of AMP^{2-} (○) and 2-(N^{ω}-L-arginino)succinate (●), the

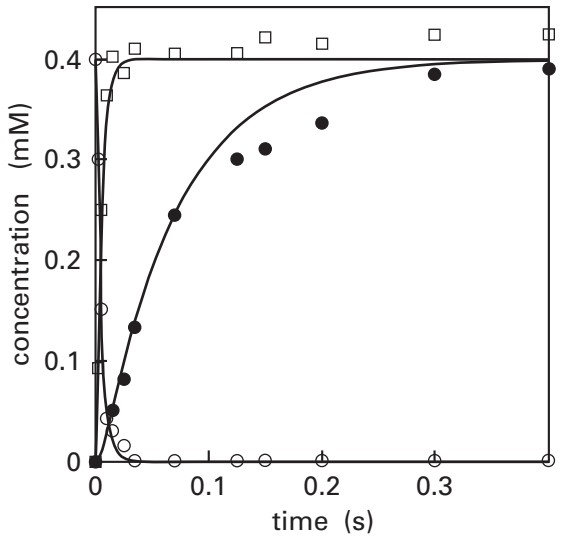

Figure 5–31: Kinetic courses for the concentrations of the reactant 1,3-dibromopropane and the products Br^- and 3-bromopropan-1-ol in the reaction catalyzed by haloalkane dehalogenase from *R. rhodochrous*.[944] A solution of haloalkane dehalogenase (1.5 mM in active sites) was mixed with an equal volume of a solution of 0.8 mM 1,3-dibromopropane. Both solutions contained 1 mM dithiothreitol and 50 mM $NaHCO_3$, pH 9.4 and 30 °C. The two solutions were mixed in a mixing chamber, the mixture flowed through a tube of a particular length, and the mixture was then quenched with 0.8 M H_2SO_4. This procedure was repeated with the same two solutions, varying the time each mixture spent between the mixing chamber and the quench solution by choosing different lengths of tubing. Each quenched solution was then extracted with diethyl ether and neutralized with $NaHCO_3$. 1,3-Dibromopropane (○) and 3-bromopropan-1-ol (●) in the diethyl ether were separated and quantified by gas chromatography, and Br^- (□) in the aqueous phase was isolated by ion-exchange chromatography and quantified. The concentrations of each compound in the unquenched mixture (millimolar) are plotted as a function of the intervals between mixing and quenching (seconds). The curves are the fit to the data by numerical integration of the kinetic mechanism of Equation 5–368.

stoichiometric products, in the acid solutions emerging from the second mixing chamber increased as the time spent between the two mixing chambers was increased (Figure 5–32).[948] The concentration of 2-(N^{ω}-L-arginino)succinate increased at a rate equal to the steady-state rate of the enzymatic reaction from the first instant, but a burst in the concentration of AMP^{2-} occurred before the rate of its production became equal to that of 2-(N^{ω}-L-arginino)succinate. An explanation for these observations is that the burst of AMP^{2-} in the acid solution resulted from a burst of L-citrulline adenylate in the active site that decomposed rapidly to AMP^{2-} and L-citrulline after

being released from the active site by denaturation of the protein. If this is so, then L-citrulline adenylate is formed rapidly (k_{obs} = 9.7 s^{-1}), early in the enzymatic reaction, and 2-(N^{ω}-L-arginino)succinate is formed subsequently in a slow step (k_{obs} = 0.6 s^{-1}) that is rate-limiting for turnover of the enzyme.

Another purpose of stopped flow and quenched flow is to determine numerical values for the rate constants governing the steps in the enzymatic reaction in which intermediates participate. Because these measurements, both for pre-steady-state observations and for observations of single turnovers, are made before a steady state is established, the kinetics are not steady-state kinetics, such as those applied to initial rates for enzymatic reactions, but those for normal chemical reactions. Consequently, standard derivations of integrated rate equations for first-order, pseudo-first-order, second-order, and consecutive first-order reactions and numerical integration of the differential equations for more complex circumstances are the relevant treatments. Again, as with all kinetic measurements, **the observations must be distinguished from the explanation** in the form of a kinetic mechanism provided by the investigators for those observations and the observed rate constants.

Most of the kinetic courses in observations made by stopped flow or quenched flow are, by design, for first-order reactions or consecutive first-order reactions. The kinetic course of such a reaction or series of reactions is referred to as a first-order relaxation or a sequence of first-order relaxations. The reciprocal of the first-order rate constant observed for a given first-order relaxation is referred to as a **relaxation time**, τ. It is the time during which the overall change in concentration falls to e^{-1} of its initial value. If a first-order relaxation or a series of first-order relaxations is not observed, the system is often altered by varying the initial conditions until one is.

The general equation for **a single first-order relaxation*** is

$$\frac{\xi - \xi_{\infty}}{\xi_0 - \xi_{\infty}} = e^{-k_{obs}t} \qquad (5\text{–}319)$$

where ξ is either the molar concentration of a reactant, intermediate, or product in the reaction or any physical property—such as absorbance, fluorescence, or counts per minute—that is directly proportional to the concentration of a reactant, intermediate, or product; ξ_0 is the value for that quantity at time zero; ξ is the value for that quantity at any time during the kinetic course; and ξ_{∞} is the value for that quantity when the reaction reaches equilibrium and changes in physical properties cease.

Because the extinction coefficients or any other constants proportional to concentration are the same for all ξ, these constants of proportionality, as well as the units of concentration, cancel in the quotient. The rate constant obtained by the fit of

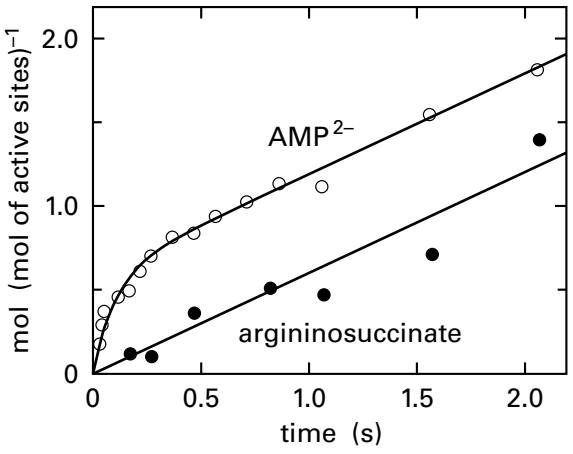

Figure 5–32: Burst in formation of AMP^{2-} observed by quenched flow during the reaction of argininosuccinate synthase.[948] A solution of bovine argininosuccinate synthase (34 μM in active sites) was mixed with an equal volume of a solution containing 5.0 mM L-citrulline, 2.0 mM $MgATP^{2-}$, and 5.0 mM L-aspartate. Both solutions contained 9 mM $MgCl_2$ and 100 mM 2-amino-2-(hydroxymethyl)propane-1,3-diol chloride, pH 8.0 and 22 °C. The two solutions were mixed in a mixing chamber, the mixture flowed through a tube of a particular length, and the mixture was then quenched with 0.25 M H_2SO_4. This procedure was repeated with the same two solutions, varying the time each mixture spent between the mixing chamber and the quench solution by choosing different lengths of tubing. A portion of each quenched solution was submitted to high-pressure liquid chromatography to isolate AMP^{2-}, which was quantified by its absorbance. Another portion of each quenched solution was brought to pH 7 and mixed with a solution of bovine argininosuccinate lyase to hydrolyze 2-(N^{ω}-L-arginino)succinate (argininosuccinate) to fumarate and L-arginine. Each sample was then submitted to high-pressure liquid chromatography to isolate fumarate, which was quantified by its absorbance. The moles of AMP^{2-} (mole of active sites of argininosuccinate synthase)$^{-1}$ and the moles of 2-(N^{ω}-L-arginino)succinate (mole of active sites of argininosuccinate synthase)$^{-1}$ in the reaction mixtures are plotted as a function of the intervals between mixing and quenching (seconds).

*The relaxation time is formally defined as the time, τ, during which the overall change in concentration falls to e^{-1} of its initial value. Consequently, at the relaxation time, the quotient in Equation 5–319 is equal to e^{-1} and $k_{obs}\tau$ must equal 1.

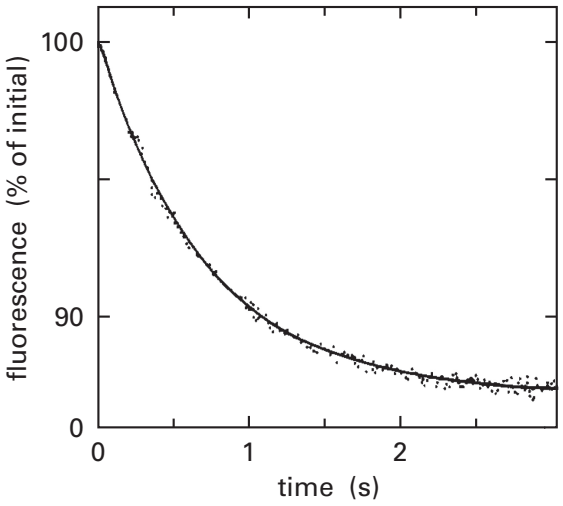

Figure 5–33: Monitoring the dissociation of 5,6,7,8-tetrahydrofolate from the active site of dihydrofolate reductase by stopped flow.[950] A solution containing dihydrofolate reductase from *E. coli* (1.0 μM in active sites) and 4.4 μM 5,6,7,8-tetrahydrofolate was mixed with an equal volume of a solution of 106 μM methotrexate in an apparatus for stopped flow. Both solutions also contained 50 mM sodium 2-(*N*-morpholino)-ethanesulfonate, 25 mM 2-amino-2-(hydroxymethyl)propane-1,3-diol chloride, and 25 mM ethanolammonium chloride, pH 6.0 and 25 °C. The solution in the observation chamber was monitored by fluorescence at 340 nm with excitation at 290 nm. The intrinsic fluorescence of the enzyme was monitored in this way. The decrease in intrinsic fluorescence of the enzyme as a percentage of the initial reading (data points) is presented as a function of time (seconds). The solid curve is the fit of Equation 5–319 to the data with a rate constant of $1.4 \pm 0.2\ s^{-1}$. Adapted with permission from reference 950. Copyright 1987 American Chemical Society. https://doi.org/10.1021/bi00387a052

Equation 5–319 to the data is an **observed rate constant**. For example, the kinetic course for the absorbance at 340 nm (A_{340}), recording the loss of NADH in the active site of L-lactate dehydrogenase (Figure 5–21), could be fit with the equation

$$\frac{A_{340} - A_{340,\infty}}{A_{340,0} - A_{340,\infty}} = e^{-k_{obs}t} \qquad (5–320)$$

The observed rate constant (k_{obs}) governing the first-order decrease in absorbance[884] is 22 s^{-1}. The increase in counts per minute of phosphorus-32 bound to phosphoglucomutase (E–$O^{32}PO_3^{2-}$ in Figure 5–27) could be fit (solid line) with the equation

$$\frac{E{-}^{32}P - E{-}^{32}P_\infty}{E{-}^{32}P_0 - E{-}^{32}P_\infty} = e^{-k_{obs}t} \qquad (5–321)$$

where E–^{32}P is E–$O^{32}PO_3^{2-}$. The observed rate constant governing the first-order increase in counts per minute is 110 s^{-1}.

An observed first-order rate constant provides no insight into the events that are occurring in the active site. As usual, an explanation for the observed rate constant requires that the investigator propose a kinetic mechanism. The simplest case of a first-order relaxation is a situation in which **a reaction, by design, is confined to one step**. For example, dihydrofolate reductase (1.0 μM) from *E. coli* (Equation 5–305) that was saturated with 5,6,7,8-tetrahydrofolate (4.4 μM; $K_d = 0.1\ \mu$M) was mixed with a solution of methotrexate (106 μM), which rapidly associates, with high affinity ($K_d = 9$ nM),[949] with an empty active site of the enzyme in place of 5,6,7,8-tetrahydrofolate. As 5,6,7,8-tetrahydrofolate dissociates from an active site, that active site is immediately and stoichiometrically occupied with methotrexate. As methotrexate associates with vacated active sites, its fluorescence is quenched. The decrease in fluorescence of methotrexate measures the rate at which 5,6,7,8-tetrahydrofolate vacates the active site (Figure 5–33).[950] The first-order decrease in fluorescence can be fit with Equation 5–319 (solid line).

To explain this observed behavior, it was assumed by the investigators that the dissociation of 5,6,7,8-tetrahydrofolate being monitored is a **simple uncomplicated dissociation** that proceeds in a single step, for which the kinetic mechanism is

$$E{\cdot}A \xrightarrow{k_{-1}} E + A \qquad (5–322)$$

where, in this instance, E is an active site of dihydrofolate reductase that does not have 5,6,7,8-tetrahydrofolate associated with it and A is 5,6,7,8-tetrahydrofolate. Because methotrexate immediately occupies any empty active sites, at the outset of the observation all active sites that will be monitored as time passes are occupied with 5,6,7,8-tetrahydrofolate so that at any time t

$$[E] + [E{\cdot}A] = [E{\cdot}A]_0 \qquad (5–323)$$

where [E] is the concentration of active sites from which 5,6,7,8-tetrahydrofolate has dissociated since the reaction was initiated and that have been filled immediately with methotrexate, [E·A] is the concentration of active sites still occupied by 5,6,7,8-tetrahydrofolate, and $[E{\cdot}A]_0$ is the concentration of occupied active sites at the beginning of the

reaction. From **the kinetic mechanism proposed** in Equation 5–322, it follows that

$$\frac{d[\mathrm{E}]}{dt} = k_{-1}[\mathrm{E{\cdot}A}] \tag{5–324}$$

The rate equation upon integration is

$$[\mathrm{E}] = [\mathrm{E{\cdot}A}]_0\left(1 - \mathrm{e}^{-k_{-1}t}\right) \tag{5–325}$$

which, because $[\mathrm{E}]_\infty = [\mathrm{E{\cdot}A}]_0$ and $[\mathrm{E}]_0 = 0$, upon rearrangement becomes

$$\frac{[\mathrm{E}] - [\mathrm{E}]_\infty}{[\mathrm{E}]_0 - [\mathrm{E}]_\infty} = \frac{F - F_\infty}{F_0 - F_\infty} = \mathrm{e}^{-k_{-1}t} \tag{5–326}$$

where F is fluorescence, the quenching of which is directly proportional to [E]. From an examination of this integrated rate equation, it can be seen that $k_{obs} = k_{-1}$. A rate constant k_{-1} of 1.4 s^{-1} was obtained from a fit of Equation 5–326 to the data.

In the case of L-lactate dehydrogenase (Figure 5–21), the observed first-order rate constants (k_{obs}) measured at various concentrations of pyruvate displayed saturation (Figure 5–21B), an observation that can be explained with the kinetic mechanism

$$\mathrm{E{\cdot}NADH} + \text{pyruvate} \underset{k_{-1}}{\overset{k_1}{\rightleftharpoons}} \mathrm{E{\cdot}NADH{\cdot}pyruvate} \xrightarrow{k_2} \mathrm{E} + \mathrm{NAD^+} + \text{lactate} \tag{5–327}$$

but only if k_1 and k_{-1} are so large that the complex E·NADH·pyruvate is in equilibrium at all times with E·NADH and free pyruvate (pyr). If this is the case, then the observed first-order rate constant, k_{obs}, will be

$$k_{obs} = \frac{k_2[\mathrm{pyr}]}{K_{pyr} + [\mathrm{pyr}]} \tag{5–328}$$

where the dissociation constant for pyruvate $K_{pyr} = k^{-1}\,(k_{-1})^{-1}$. Therefore, at saturation with pyruvate, the observed first-order rate constant for the reaction should be k_2, the rate constant for transfer of the hydride from NADH to pyruvate after both NADH and pyruvate are bound to the active site. This process was measured directly by stopped flow. At pH 9.0 and 22 °C, k_2 had a value of 243 ± 9 s^{-1} and K_{pyr} had a value of 7 ± 0.5 mM. The rate constants for transfer of the hydride measured directly in these experiments made with stopped flow (○) at several concentrations of pyruvate equaled the rate constant for the steady-state initial rates (●) for the overall reaction at the same concentration of pyruvate (Figure 5–21B). All these observations suggest that, for the reaction catalyzed by porcine lactate dehydrogenase under these conditions, the rate-limiting step in the reaction is transfer of the hydride.

As with most kinetic explanations, however, there are alternatives. For example, the observations are also consistent with the mechanism

$$\mathrm{E{\cdot}NADH} + \text{pyruvate} \underset{k_{-1}}{\overset{k_1}{\rightleftharpoons}} \mathrm{E{\cdot}NADH{\cdot}pyruvate} \underset{k_{-2}}{\overset{k_2}{\rightleftharpoons}} \mathrm{E{\cdot}NAD^+{\cdot}}\text{lactate} \xrightarrow{k_3} \mathrm{E} + \mathrm{NAD^+} + \text{lactate} \tag{5–329}$$

where $k_{-1} >> k_2$, $k_{-2} >> k_3$, and $k_{-2} > k_2$ and dissociation of the lactate is the rate-limiting step.

The first-order relaxations observed with dihydrofolate reductase and lactate dehydrogenase were explained with kinetic mechanisms (Equations 5–322 and 5–327, respectively) in which the governing steps were irreversible first-order steps. All chemical reactions, however, are approaches to equilibrium. If the equilibrium constant for a first-order reaction is heavily in favor of the reactant, no reaction will be observed even though a small, perhaps immeasurable, concentration of the product must be formed to reach equilibrium. If the equilibrium constant is heavily in favor of product, the reaction will proceed to apparent completion, even though a small, perhaps immeasurable, equilibrium concentration of reactant remains. If the equilibrium constant for a first-order reaction is neither too large nor too small, a measurable quantity of reactant will remain when the reaction ceases and a measurable quantity of product will be formed. In this case, the **approach to equilibrium is a first-order relaxation**.

Suppose that, by designing the experiment properly, the kinetic mechanism for the reaction being followed is

$$\mathrm{E_2} \underset{k_{-2}}{\overset{k_2}{\rightleftharpoons}} \mathrm{E_3} \tag{5–330}$$

where E_2 and E_3 are two forms of the enzyme, for example, E·NADH·pyruvate and E·NAD^+·lactate at saturation with pyruvate or E–^{31}P·Glc-1-^{32}P and E–^{32}P·Glc-6-^{31}P at saturation with D-glucose 1-[^{32}P]phosphate. Suppose that, again by design, the sum

$$[E_2] + [E_3] = [E]_t \tag{5–331}$$

at all time points, where $[E]_t$ is the total concentration of enzyme. As a result, the sum must remain constant over the duration of the reaction. Suppose also, for the sake of argument, that the physical property being monitored is absorbance, A, but any other property, such as counts per minute incorporated into protein, that is proportional to the molar concentration of either form of the enzyme would be equivalent. The absorbance due to the two forms of the enzyme at any time is then

$$A = \varepsilon_2[E_2] + \varepsilon_3[E_3] \tag{5–332}$$

where ε_2 and ε_3 are the respective extinction coefficients. From Equations 5–330 and 5–331

$$-\frac{d[E_2]}{dt} = k_2[E_2] - k_{-2}[E_3] \tag{5–333}$$

$$-\frac{d[E_2]}{(k_2 + k_{-2})[E_2] - k_{-2}[E]_t} = dt \tag{5–334}$$

which upon integration gives

$$-\ln\left\{\frac{(k_2 + k_{-2})[E_2] - k_{-2}[E]_t}{(k_2 + k_{-2})[E_2]_0 - k_{-2}[E]_t}\right\} = (k_2 + k_{-2})t \tag{5–335}$$

where $[E_2]_0$ is the concentration of form E_2 at the beginning of the reaction and $[E_2]$ is its concentration at any instant. If $[E_2]_{eq}$ and $[E_3]_{eq}$ are the concentrations of the two forms at the end of the reaction

$$k_2[E_2]_{eq} = k_{-2}[E_3]_{eq} \tag{5–336}$$

$$k_{-2}[E]_t = (k_2 + k_{-2})[E_2]_{eq} \tag{5–337}$$

$$-\ln\left\{\frac{[E_2] - [E_2]_{eq}}{[E_2]_0 - [E_2]_{eq}}\right\} = (k_2 + k_{-2})t \tag{5–338}$$

$$\frac{(\varepsilon_2 - \varepsilon_3)[E_2] - (\varepsilon_2 - \varepsilon_3)[E_2]_{eq}}{(\varepsilon_2 - \varepsilon_3)[E_2]_0 - (\varepsilon_2 - \varepsilon_3)[E_2]_{eq}} = e^{-(k_2 + k_{-2})t} \tag{5–339}$$

$$\frac{\varepsilon_2[E_2] + \varepsilon_3[E_3] - \varepsilon_3[E]_t - \varepsilon_2[E_2]_{eq} - \varepsilon_3[E_3]_{eq} + \varepsilon_3[E]_t}{\varepsilon_2[E_2]_0 + \varepsilon_3[E_3]_0 - \varepsilon_3[E]_t - \varepsilon_2[E_2]_{eq} - \varepsilon_3[E_3]_{eq} + \varepsilon_3[E]_t} = e^{-(k_2 + k_{-2})t} \tag{5–340}$$

$$\frac{A - A_{eq}}{A_0 - A_{eq}} = e^{-(k_2 + k_{-2})t} \tag{5–341}$$

Equation 5–341 states that if the reaction observed is described by the kinetic mechanism of Equation 5–330, then the behavior of any physical property the magnitude of which is proportional to the concentrations of both product and reactant will display first-order behavior. First-order behavior will be seen regardless of whether measurements were initiated when all the enzyme was E_2 or in midreaction ($[E_3]_0 > 0$); regardless of whether the reaction goes to completion ($k_{-2} = 0$) or reaches an equilibrium; regardless of whether both product and reactant display the physical property ($\varepsilon_2 > 0$ and $\varepsilon_3 > 0$) or only one displays the physical property; and regardless of whether the rate constants k_{-2} and k_2 are unimolecular rate constants or pseudo-first-order rate constants ($k_2 = k_2'[A]$ or $k_{-2} = k_{-2}'[Z]$). The only requirement for observing the reaction is that the two extinction coefficients (constants of proportionality) for the two forms of the enzyme must be different enough that a significant change occurs in the magnitude of the physical property during the measurement. Because of this generality, such first-order relaxations are commonly observed in kinetic measurements. It can also be seen that a reaction consisting of a single irreversible first-order step is simply a special case of an approach to equilibrium.

Because it does not matter whether or not one of the concentrations of the participants in an approach to equilibrium is initially zero, it follows that when a system at equilibrium is perturbed in some way that changes the value for the equilibrium constant, the

system will then approach the new, perturbed equilibrium. Each microscopic step in the overall equilibrium will approach its own new equilibrium, with a rate constant governed by Equation 5–341. This fact is the basis for temperature jump. **Temperature jump** is a relaxation technique in which the temperature of a chemical system is suddenly raised, and the system then relaxes to a new state of equilibrium. Analysis of the relaxation process provides rate constants for the step or steps through which the system proceeds to reach the new equilibrium. The advantage of temperature jump is that the dead time during which the temperature is raised can be much shorter than the dead times for stopped flow and quenched flow, so measurements can be made at much shorter times. The disadvantage is that, when the system is at equilibrium before the temperature is raised, there should be measurable concentrations of reactants, products, and intermediates to follow as the new equilibrium is achieved. Consequently, temperature jump has seldom been applied to enzymatic reactions, but there are situations in which it has. For example, temperature jump monitoring the absorbance of proflavin has been applied to a solution of this competitive inhibitor in equilibrium with its complex with the active site of bovine chymotrypsin. Upon a jump of temperature, the system relaxes to the new equilibrium in a process that involves the rate constants for association and dissociation of the inhibitor and rate constants for a transition assigned to a conformational change in the enzyme.[951] Temperature jump has also been applied to the complex of lactate dehydrogenase from *G. stearothermophilus* and the coenzyme NADH at saturation. In this instance, both fluorescence of NADH and fluorescence of four tryptophans placed in turn by site-directed mutation at different locations in the protein were monitored in order to measure rate constants for rapid conformational changes of the protein within the complex as equilibrium is reestablished.[952]

Because it does not matter whether the rate constants governing the relaxation for the approach to an equilibrium are unimolecular or pseudo-first-order rate constants, the first-order rate constant observed for association of reactant A with an active site E

$$\mathrm{E} + \mathrm{A} \underset{k_{-1}}{\overset{k_1}{\rightleftharpoons}} \mathrm{E{\cdot}A} \qquad (5\text{–}342)$$

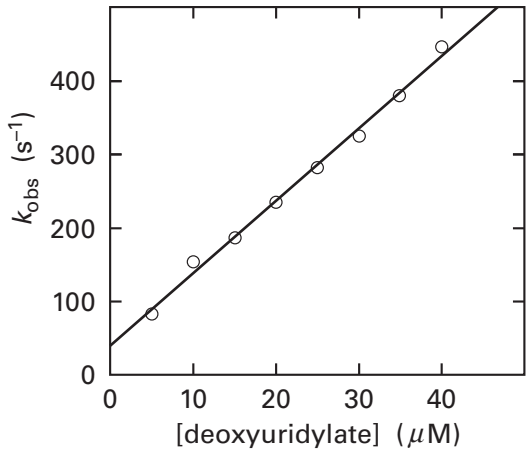

Figure 5–34: Effect of the concentration of deoxyuridylate on the observed rate constant for its association with the active site of thymidylate synthase.[224] A solution of thymidylate synthase from *E. coli* (2.1 μM in active sites) in one syringe of an apparatus for stopped flow was mixed with an equal volume of a solution of deoxyuridylate in the other syringe, and the mixture was immediately introduced into a cuvette. Both solutions contained 50 mM 2-sulfanylethanol, 1 mM ethylenediaminetetraacetate, and 100 mM 2-ammonio-2-hydroxymethylpropane-1,3-diol chloride, pH 7.4 and 20 °C. This procedure was repeated several times with different concentrations of deoxyuridylate. The kinetic courses for association of deoxyuridylate with the active site of the enzyme were followed by monitoring the fluorescence of one or more of the seven tryptophans in a subunit of the enzyme, which decreases as the deoxyuridylate binds. The decreases in fluorescence with time could all be fit with Equation 5–319 to obtain observed first-order rate constants, k_{obs}. The rate constants (second^{-1}) are plotted as a function of the final concentrations (micromolar) of deoxyuridylate in the reaction mixture. The line is a fit of Equation 5–343 to the data.

when the concentration of reactant is in great excess over the concentration of active sites, is

$$k_{obs} = k_1[\mathrm{A}] + k_{-1} \qquad (5\text{–}343)$$

Consequently, if the **observed rate constant for association of reactant A is plotted as a function of the concentration of reactant A,** a straight line with a slope of k_1(molar^{-1} second^{-1}) and an intercept of k_{-1} (second^{-1}) will be observed if this is the applicable mechanism. For example, when the individually observed rate constants for the purely first-order relaxations produced by association of deoxyuridine monophosphate with the active site of thymidylate synthase (Equation 5–50) from *E. coli*, in the absence of 5,10-methylenetetrahydrofolate, are plotted as a function of the concentration of deoxyuridine monophosphate (Figure 5–34), they define a line with a slope of 10 μM^{-1} s^{-1} and an intercept of 40 s^{-1}. Because (previously Equation 3–338)

$$K_{dL} = \frac{k_{-1}}{k_1} \tag{5–344}$$

together these rate constants give a dissociation constant of 4 μM, which is the same as the dissociation constant measured directly.[224]

Association of a reactant can also be an essentially irreversible reaction. When the observed rate constant for association of oxygen with the complex between protocatechuate 3,4-dioxygenase and protocatechuate (see Figure 5–22) was plotted against the molar concentration of O_2 in the solution, it was a linear relation, but the intercept at the axis of the ordinate, which would be the rate of dissociation of O_2 from the complex, was <5 s^{-1} and indistinguishable from zero.[887]

A behavior of **first-order relaxations at different concentrations of a reactant** is also observed that is a hybrid of the behavior of first-order relaxations observed at different concentrations of pyruvate with L-lactate dehydrogenase (Figure 5–21B) and the behavior of first-order relaxations observed at different concentrations of deoxyuridine monophosphate with thymidylate synthase (Figure 5–34). For example, when fluorescence from tryptophans in glutamine synthetase (Equation 5–270) from *E. coli* was followed after the enzyme was mixed with the substrate MnADP$^-$ in the absence of phosphate and L-glutamine, the change in fluorescence was a first-order relaxation at all concentrations of MnADP$^-$. A plot of the observed first-order rate constants as a function of the concentration of MnADP$^-$ (Figure 5–35)[953] could be fit (solid line) with the equation

$$k_{obs} = \frac{k_a[\text{MnADP}^-]}{k_b + [\text{MnADP}^-]} + k_c \tag{5–345}$$

This observed behavior can be explained with the kinetic mechanism

$$\text{E} + \text{MnADP}^- \underset{K_{dADP}}{\rightleftharpoons} \text{E}\cdot\text{MnADP}^- \underset{k_{-2}}{\overset{k_2}{\rightleftharpoons}} \text{E}^*\cdot\text{MnADP}^- \tag{5–346}$$

where E* is a different conformation of the enzyme. The observed first-order rate constant for the analytically integrated rate equation for this kinetic mechanism

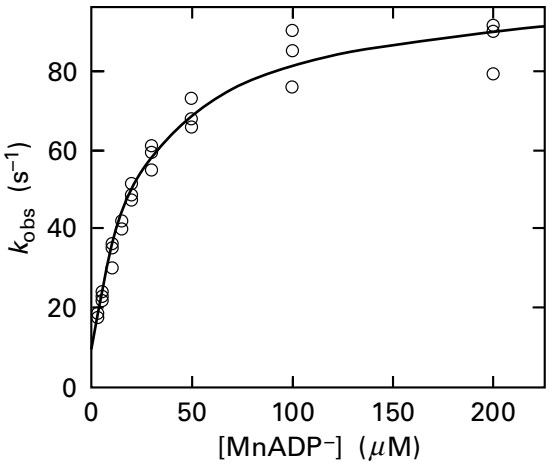

Figure 5–35: Effect of the concentration of MnADP$^-$ on the observed rate constant for its association with the active site of glutamine synthetase.[953] A solution containing glutamine synthetase from *E. coli* (2 μM in active sites) in one syringe of an apparatus for stopped flow was mixed with an equal volume of a solution of MnADP$^-$ in the other syringe, and the mixture was immediately introduced into a cuvette. Both solutions contained 0.1 M KCl, 1 mM $MnCl_2$, and 50 mM potassium 2-[4-(2-hydroxyethyl)piperazin-1-yl]ethanesulfonate, pH 7.0 and 15 °C. This procedure was repeated several times with different concentrations of MnADP$^-$. The kinetic courses for association of MnADP$^-$ with the active site of the enzyme were followed by monitoring the fluorescence of one or both of the two tryptophans in a subunit of the enzyme, which increases as the MnADP$^-$ binds. The increases in fluorescence with time could all be fit with Equation 5–319 to obtain observed first-order rate constants, k_{obs}. The rate constants ($second^{-1}$) are plotted as a function of the final concentrations (micromolar) of MnADP$^-$ in the reaction mixtures. The curve is a fit of Equation 5–347 to the data.

$$k_{obs} = \frac{k_2[\text{MnADP}^-]}{K_{dADP} + [\text{MnADP}^-]} + k_{-2} \tag{5–347}$$

In this case, at low [MnADP$^-$] the initial line for k_{obs} is defined by

$$k_{obs} = \frac{k_2}{K_{dADP}}[\text{MnADP}^-] + k_{-2} \tag{5–348}$$

and at high [MnADP$^-$] the observed rate constant is equal to $k_2 + k_{-2}$. The two rate constants (k_2 = 90 s^{-1} and k_{-2} = 9 s^{-1}) and the dissociation constant (K_{dADP} = 25 μM) can be calculated from parameters of the fit of Equation 5–347 to the data. In this situation, there is a change in rate-limiting step from the rate of association of MnADP$^-$ to the rate of approach to equilibrium between E·MnADP$^-$ and E*·MnADP$^-$. The fact that the directly measured, apparent disso-

ciation constant ($K_{d,app}$) for $MnADP^-$ ($4.6 \pm 1.5\ \mu M$) is within statistical error of the dissociation constant ($2.7 \pm 0.6\ \mu M$) calculated from these values ($K_{d,app} = k_{-2}\ K_{dADP}\ k_2^{-1}$) is evidence in favor of the mechanism proposed as the explanation of the observed behavior.

As the examples of L-lactate dehydrogenase (Figure 5–21B) and glutamine synthetase (Figure 5–35) illustrate, the dependence or lack of dependence of an observed rate constant on the concentration of a reactant is often used to incorporate association of the reactant into the kinetic mechanism and obtain values for the dissociation constant of the reactant or the rate constants for its dissociation and association.[897,899,954,955]

When there are **two consecutive first-order relaxations** connecting three distinct species, the equation fit to observations has the general form

$$\frac{\xi - \xi_\infty}{\xi_0 - \xi_\infty} = a + b e^{-k_{obs1} t} + c e^{-k_{obs2} t} \qquad (5\text{–}349)$$

where, as before, ξ is either the molar concentration of one reactant, intermediate, or product in the reaction or any physical property—such as absorbance, fluorescence, or counts per minute—that is directly proportional to the concentration of a reactant, intermediate, or product in the reaction. In this instance, the magnitudes of the parameters in the equation, *a*, *b*, and *c*, depend on the species being observed. For example, the three species the concentrations of which are being followed in the kinetic course of hydrolysis of nitrocefin by β-lactamase (Figure 5–23) were assigned to be the Michaelis complex with nitrocefin, [E·nit], formed during the dead time for the apparatus; the complex between the active site and the intermediate anion, [E·an] (Equation 5–295); and the neutral hydrolyzed nitrocefin, [hyd], that is the product of the enzymatic reaction. These three kinetic courses (Figure 5–23B) can be fit with the equations

$$[E{\cdot}nit] = [E{\cdot}nit]_0\, e^{-k_{obs1} t} \qquad (5\text{–}350)$$

which is Equation 5–349 with $a = 0$, $b = 0$, and $c = [E{\cdot}nit]_0$

$$[E{\cdot}an] = [E{\cdot}nit]_0 \left(b_2 e^{-k_{obs1} t} + c_2 e^{-k_{obs2} t}\right) \qquad (5\text{–}351)$$

which is Equation 5–349 with $a = 0$, and

$$[hyd] = [E{\cdot}nit]_0 \left(1 + b_3 e^{-k_{obs1} t} + c_3 e^{-k_{obs2} t}\right) \qquad (5\text{–}352)$$

which is Equation 5–349 with all three of its terms. In these equations, $[E{\cdot}nit]_0$ is the initial concentration of the Michaelis complex between enzyme and nitrocefin. Fitting the equations to the data gives the following parameters: $k_{obs1} = 150 \pm 30\ s^{-1}$, $k_{obs2} = 13 \pm 1\ s^{-1}$, $b_2 = -1.09$, $c_2 = 1.09$, $b_3 = 0.095$, and $c_3 = -1.09$.

The simplest and most obvious explanation for such behavior is that the reaction passes through three species, A, B, and C, that are connected by **two consecutive irreversible steps** governed by rate constants k_1 and k_2

$$A \xrightarrow{k_1} B \xrightarrow{k_2} C \qquad (5\text{–}353)$$

for which the integrated rate equations are[956]

$$[A] = [A]_0\, e^{-k_1 t} \qquad (5\text{–}354)$$

$$[B] = [A]_0 \left(\frac{k_1}{k_2 - k_1}\right)\left(e^{-k_1 t} - e^{-k_2 t}\right) \qquad (5\text{–}355)$$

$$[C] = [A]_0 \left(1 + \frac{k_2}{k_1 - k_2} e^{-k_1 t} - \frac{k_1}{k_1 - k_2} e^{-k_2 t}\right) \qquad (5\text{–}356)$$

It was concluded that hydrolysis of nitrocefin by β-lactamase in the apparatus for stopped flow proceded with this kinetic mechanism[888] with rate constants of $k_1 = 150\ s^{-1}$ and $k_2 = 13\ s^{-1}$. The kinetic courses of the absorbances at 403 and 460 nm for the reaction of the complex between protocatechuate 3,4-dioxygenase and protocatechuate with O_2 (Figure 5–22) in an apparatus for stopped flow following the abrupt changes in absorbance during the dead time could be fit[887] by the integrated rate equations for a simple two-step mechanism with $k_2 = 450\ s^{-1}$ and $k_3 = 36\ s^{-1}$. The respective kinetic courses for the concentrations of *S*-adenosyl-L-methionine, intermediate **5–176**, and *N*-butyryl-L-homoserine lactone for the reaction catalyzed by acylhomoserine-lactone synthase (Equation 5–306) could also be fit satisfactorily with Equations 5–354 through 5–356, respectively, when enzyme saturated with *S*-adenosyl-[*carboxy*-^{14}C]-L-methionine (91%) was mixed in an

apparatus for quenched flow in 2.5-fold molar excess with butyryl-SACP.[926]

As is the case with a single first-order relaxation, it is also possible to fit such data with more complicated kinetic mechanisms. For example, the inclusion of rapid, kinetically silent steps or rapid intermediate equilibria do not affect the form of the derived equations.

The kinetic mechanism with **two consecutive reversible steps**

$$\mathrm{A} \underset{k_{-1}}{\overset{k_1}{\rightleftharpoons}} \mathrm{B} \underset{k_{-2}}{\overset{k_2}{\rightleftharpoons}} \mathrm{C} \qquad (5\text{–}357)$$

also produces observed behavior that can be fit by Equations 5–354 through 5–356 even though the reverse rate constants, k_{-1} and k_{-2}, do not appear in these equations. If it cannot be demonstrated that addition of two reverse rate constants improves the fit significantly in comparison with the irreversible mechanism of Equation 5–353,[957] there is no justification for adding them.[926] If they do exist, however, and are of significant magnitude, then the rate constants obtained by fitting the data to the irreversible kinetic mechanism of Equation 5–353 will not be accurate.

The general form of the equation for **multiple first-order relaxations** is

$$\frac{\xi - \xi_\infty}{\xi_0 - \xi_\infty} = a_0 + \sum_{i=1}^{n} a_i e^{-k_{\mathrm{obs}i}t} \qquad (5\text{–}358)$$

and again the explicit form of this equation in a given circumstance depends on which species, reactant, Michaelis complex, intermediate, or product, is being monitored, which, in turn, determines the physical property that is being monitored. In many instances, the different species connected consecutively by the relaxations can be independently followed. For example, four spectrally distinct intermediates in the reaction catalyzed by ornithine decarboxylase (Figure 5–25),[902] the first of which is formed in the dead time of the apparatus, can be distinguished one from the other by their unique absorbance spectra. The increases and decreases in the concentrations of intermediate A (○), intermediate B (□), intermediate C (●), and intermediate D (■), over the course of the observations can each be fit with Equation 5–358. The observed behavior can be satisfactorily explained with the proposal that the kinetic mechanism is the simplest one possible

$$\mathrm{A} \xrightarrow{k_1} \mathrm{B} \xrightarrow{k_2} \mathrm{C} \xrightarrow{k_3} \mathrm{D} \qquad (5\text{–}359)$$

with rate constants $k_1 = 21\ \mathrm{s}^{-1}$, $k_2 = 145\ \mathrm{s}^{-1}$, and $k_3 = 1.03\ \mathrm{s}^{-1}$. The fact that $k_1 < k_2$ explains why so little of the second intermediate accumulates during the reaction.

Often, however, only one species can be distinguished, for example, the product of the reaction. In such instances, Equation 5–358 is fit to the data, using the smallest number of relaxations necessary to fit the data satisfactorily. Since the inclusion of more terms always improves the fit of any equation to any set of data, the question of how many terms to include is, to a certain extent, a subjective decision, but usually it is obvious how many are required.[909,958]

Once it has been decided how many first-order relaxations are required to fit the data satisfactorily and observed pre-exponential parameters and observed rate constants have been estimated from the fits of the data to Equation 5–358, it is then incumbent upon the investigators to provide a kinetic mechanism with its accompanying rate constants to explain the observations. Because of the significant difficulties in directly deriving an analytical solution, integrated rate equations for a proposed kinetic mechanism involving a sequence of three or more irreversible steps or a sequence of two or more reversible steps can be derived by **linear algebra**.[959]

The observed pre-exponential parameters and first-order rate constants governing a sequence of first-order relaxations are functions of the microscopic rate constants in the actual kinetic mechanism of the enzyme being studied. As always, there is no way to determine the actual kinetic mechanism of a particular enzyme at the level of its microscopic rate constants. As was the case in the simpler examples of kinetic mechanisms—for dihydrofolate reductase (Equation 5–322), L-lactate dehydrogenase (Equation 5–327), glutamine synthetase (Equation 5–346), β-lactamase (Equation 5–353), and ornithine decarboxylase (Equation 5–359)—the investigator, usually relying on an intuitive understanding of the chemical mechanism of the events occurring in the active site as well as knowledge of the relaxations that have been observed, proposes a kinetic mechanism and then demonstrates that the **proposed kinetic mechanism** is consistent with all available observations. The examples presented so far of this process have been simple enough that algebraic derivations of integrated rate equations can be readily derived from a proposed kinetic mechanism

and its rate constants and fit to the experimental data.

In complicated situations, however, that involve two or more reversible rate-affecting steps and branching within the kinetic mechanism, rather than performing the derivation of a set of analytical, integrated rate equations by linear algebra, **the differential equations describing the steps in the proposed kinetic mechanism are usually submitted to numerical integration.**[960] For example, 3-phosphoshikimate 1-carboxyvinyltransferase (E) from *E. coli* saturated with 3-phosphoshikimate (3PS) was mixed with phospho*enol*pyruvate (PEP) (Figure 5–26)[308] so that the final concentrations of enzyme and phospho*enol*pyruvate were only 10 μM and 3.5 μM, respectively. At these concentrations, even if association of phospho*enol*pyruvate were rapid, only 30% of the phospho*enol*pyruvate (K_d = 20 μM) in the solution would occupy an active site at the beginning of the reaction. It was proposed that the kinetic mechanism for the reaction being observed was

$$\begin{aligned} \text{E}\cdot\text{3PS} + \text{PEP} &\underset{k_{-2}}{\overset{k_2}{\rightleftharpoons}} \text{E}\cdot\text{3PS}\cdot\text{PEP} \underset{k_{-3}}{\overset{k_3}{\rightleftharpoons}} \\ \text{E}\cdot\text{I} &\underset{k_{-4}}{\overset{k_4}{\rightleftharpoons}} \text{E}\cdot\text{CVPS} \xrightarrow{k_5} \text{E} + \text{CVPS} \end{aligned} \qquad (5\text{–}360)$$

where I (●) is intermediate **5–180** and CVPS (□) is the product 5-*O*-(1-carboxyvinyl)-3-phosphoshikimate (Equation 5–178). The differential equations that describe this kinetic mechanism were submitted to numerical integration. The curves drawn in Figure 5–26 are fits produced by this numerical integration for rate constants k_2 = 15 μM^{-1} s^{-1}, k_{-2} = 280 s^{-1}, k_3 = 1200 s^{-1}, k_{-3} = 100 s^{-1}, k_4 = 320 s^{-1}, k_{-4} = 240 s^{-1}, and k_5 = 100 s^{-1}.

When D-amino-acid oxidase from *Trigonopsis variabilis* with its prosthetic flavin in the oxidized state ($E\cdot Fl_{ox}$) was mixed anaerobically in an apparatus for stopped flow with the reactant D-phenylglycine (DPG)

$$\begin{aligned} \text{E}\cdot\text{HFl}_{ox} + \text{D-phenylglycine} + \text{H}_2\text{O} &\rightleftharpoons \\ \text{E}\cdot\text{H}_3\text{Fl}_{red} + \text{phenylglyoxylate} + \text{NH}_4^+ & \end{aligned} \qquad (5\text{–}361)$$

so that there was no O_2 to reoxidize the reduced flavin, each active site could complete only one turnover regardless of the concentration of D-phenylglycine. Reduction of the prosthetic flavin during a single turnover could be followed as the absorbance at 454 nm decreased. The decreases in absorbance for a series of concentrations of D-phenylglycine could be fit satisfactorily with the equation

$$\frac{A_{454} - A_{454,\infty}}{A_{454,0} - A_{454,\infty}} = a_0 - a_1 e^{-k_{obs1}t} - a_2 e^{-k_{obs2}t} \qquad (5\text{–}362)$$

The kinetic mechanism

$$\begin{aligned} \text{E}\cdot\text{Fl}_{ox} + \text{DPG} &\underset{k_{-1}}{\overset{k_1}{\rightleftharpoons}} \text{E}\cdot\text{Fl}_{ox}\cdot\text{DPG} \\ &\underset{k_{-2}}{\overset{k_2}{\rightleftharpoons}} \text{E}\cdot\text{Fl}_{red}\cdot\text{PGO} \xrightarrow{k_3} \text{E}\cdot\text{Fl}_{red} + \text{PGO} \end{aligned} \qquad (5\text{–}363)$$

where PGO is phenylglyoxylate, the product of oxidation of D-phenylglycine, can explain the observed behavior of the two observed first-order rate constants, k_{obs1} and k_{obs2}, as a function of the concentration of reactant.[961] This kinetic mechanism was fit by numerical integration of its differential equations to the changes in absorbance for the series of single turnovers at different concentrations of D-phenylglycine with k_1 = 60 mM^{-1} s^{-1}, k_{-1} = 40 s^{-1}, k_2 = 30 s^{-1}, k_{-2} = 4 s^{-1}, and k_3 = 6 s^{-1}.

These observations of the behavior of D-amino-acid oxidase by stopped flow probably give values of the microscopic rate constants for the transfer of a hydride between D-phenylglycine and the prosthetic flavin. Consequently by the use of [2-^{2}H]-D-phenylglycine as a reactant, it was possible to obtain values for the intrinsic kinetic deuterium isotope effects (6.3 and 4.7, respectively) on the rate constants k_2 and k_{-2}, as well as a value for the intrinsic deuterium isotope effect on the equilibrium constant (1.35) for the transfer. Because the deuterated reactant decreases the rate constant k_2 by a factor of 6.3, association of [2-^{2}H]-D-phenylglycine reaches equilibrium before the hydride is transferred, and this association becomes a pre-equilibrium in the kinetic mechanism with the deuterated reactant.

When halohydrin dehalogenase

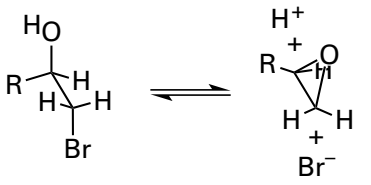

(5–364)

from *Rhizobium radiobacter* is mixed with the reactant (1*R*)-2-bromo-1-(4-nitrophenyl)ethanol (Equation 5–364 with R = 4-nitrophenyl)) under conditions permitting the enzyme to complete only one turnover, the production of Br^- in the active site of the enzyme during that single turnover can be followed as fluorescence of one or more of the four tryptophans in the protein increases. The fluorescence of those tryptophans then returns to the value for the unoccupied active site as the Br^- dissociates (trace a in Figure 5–36A).[962] This change in fluorescence (F) for the production and dissociation of Br^- at this one concentration of reactant can be fit satisfactorily with the equation

$$\frac{F_t - F_\infty}{F_0 - F_\infty} = ae^{-k_{obs2}t} - ae^{-k_{obs1}t} \quad (5–365)$$

which is consistent for an intermediate in a kinetic mechanism with two consecutive first-order reactions (Equation 5–355). The enzyme can also be mixed with concentrations of (1*R*)-2-bromo-1-(4-nitrophenyl)ethanol over a broad range. At these higher concentrations of reactant, multiple turnovers of the enzyme have to occur. Each burst of fluorescence that is observed preceding the multiple turnovers can be fit with a first-order relaxation to provide a first-order rate constant k_{obs}.

The kinetic mechanism

$$E + BNE \underset{K_{dBNE}}{\rightleftharpoons} E{\cdot}BNE \underset{k_{-2}}{\overset{k_2}{\rightleftharpoons}} E{\cdot}epox{\cdot}Br^- \xrightarrow{k_3} E + epox + Br^- \quad (5–366)$$

where BNE is the reactant (1*R*)-2-bromo-1-(4-nitrophenyl)ethanol and epox is the product (*S*)-(4-nitrophenyl)oxirane, can explain the observed behavior of these observed first-order rate constants, k_{obsi}, as a function of the concentration of reactant (Figure 5–36B). In this instance, as was the case with the deuterated reactant for D-amino-acid oxidase, association of the reactant is a pre-equilibrium. This kinetic mechanism (Equation 5–366) can be fit

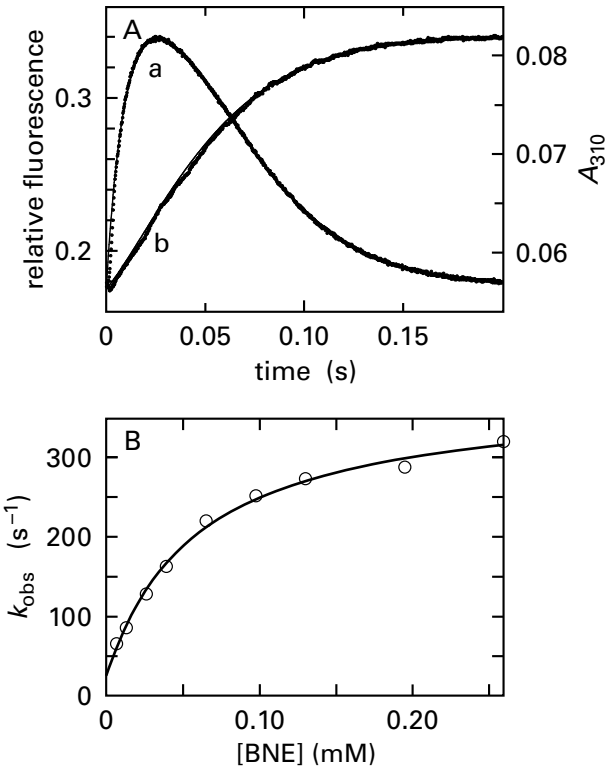

Figure 5–36: Stopped-flow measurements of the kinetics of the reaction catalyzed by halohydrin dehalogenase from *R. radiobacter*.[962] (**A**) Observation of a single turnover of the enzyme. Halohydrin dehalogenase (26.5 μM in active sites) in one syringe was rapidly mixed with (1-*R*)-2-bromo-1-(4-nitrophenyl)-ethanol (23.5 μM) in the other syringe. Fluorescence (curve a; $\lambda_{excitation}$ = 290 nm, $\lambda_{emission}$ = >320 nm), arising from an enhancement of the fluorescence of tryptophans by Br^- bound in the active site, and absorbance at 310 nm (curve b, A_{310}), arising from the change in absorbance as (*S*)-(4-nitrophenyl)oxirane dissociates, were monitored as a function of time (seconds). The solid curves are fits by numerical integration of the differential equations for the mechanism in Equation 5–366. (**B**) Rate constants for bursts of fluorescence. Halohydrin dehalogenase (0.8 μM in active sites) in one syringe was mixed with increasing concentrations of (1*R*)-2-bromo-1-(4-nitrophenyl)ethanol in the other syringe. The observed rate constants for the bursts ($second^{-1}$) are plotted as a function of the final concentrations of (1*R*)-2-bromo-1-(4-nitrophenyl)ethanol (millimolar). The solid curve is a fit of Equation 5–367 to the data. Adapted with permission from reference 962. Copyright 2003 American Chemical Society. https://doi.org/10.1021/bi0273361

by numerical integration of its differential equations to the change in fluorescence during the single turnover with $K_{dBNE} = 100 \pm 9$ μM, $k_2 = 380 \pm 20$ s^{-1}, $k_{-2} = 3$ s^{-1}, and $k_3 = 21 \pm 1$ s^{-1} (solid curve a in Figure 5–36A). The change in absorbance at 310 nm rather than fluorescence that occurs during the single turnover (trace b in Figure 5–36A) could also be fit with the equilibrium constant and the rate constants (solid curve b in Figure 5–36A) derived from measurements of fluorescence. To obtain a satisfactory fit with the same rate and equilibrium constants, however,

it had to be assumed that the absorbance of the 4-nitrophenyl group increases significantly only when (*S*)-(4-nitrophenyl)oxirane dissociates from the active site. From the kinetic mechanism (Equation 5–366), an integrated equation for the behavior of k_{obs} for the bursts

$$k_{obs} = k_{-2} + k_3 + \frac{k_2\,[BNE]}{[BNE] + K_{dBNE}} \quad (5–367)$$

can be derived analytically, and the same values for the dissociation constant and the three rate constants that fit the data for the single turnover provide a satisfactory fit, within experimental error, of the behavior of k_{obs} for the bursts as a function of the concentration of (1*R*)-2-bromo-1-(4-nitrophenyl)-ethanol (solid curve in Figure 5–36B).

The kinetic mechanism

$$E + DBP \underset{k_{-1}}{\overset{k_1}{\rightleftharpoons}} E{\cdot}DBP \xrightarrow{k_2} E{-}I + Br^- \xrightarrow{k_3} E{\cdot}BrPOH \quad (5–368)$$

was proposed to explain the data for hydrolysis of 1,3-dibromopropane (DBP) by haloalkane dehalogenase (E) (Figure 5–31),[944] which passes through the covalent acyl intermediate E–I before the product 3-bromopropan-1-ol (BrPOH) is produced. Numerical integration was used to obtain rate constants $k_1 = 1\ \mu M\ s^{-1}$, $k_{-1} = 200\ s^{-1}$, $k_2 = 300\ s^{-1}$, and $k_3 = 15\ s^{-1}$ that could fit (solid curves) simultaneously the kinetic mechanism to the data for the decrease in concentration of 1,3-dibromopropane (○) and the production of Br^- (□), as well as the production of 3-bromopropan-1-ol (●).

The animal fatty-acid synthase system is known to catalyze five consecutive reactions (see Equations 3–492 to 3–496, Problem 4–20)

$$\text{acetyl-SCoA} + \text{HSACD} \rightleftharpoons \text{HSCoA} + \text{acetyl-SACD} \quad (5–369)$$

$$\text{acetyl-SACD} + \text{HSE} \rightleftharpoons \text{HSACD} + \text{acetyl-SE} \quad (5–370)$$

$$\text{malonyl-SCoA} + \text{HSACD} \rightleftharpoons \text{HSCoA} + \text{malonyl-SACD} \quad (5–371)$$

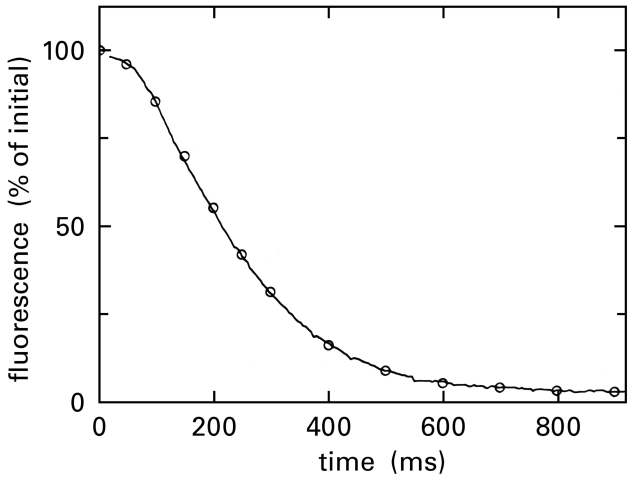

Figure 5–37: Lag in oxidation of NADPH when the complex between NADPH and the fatty-acid synthase system is mixed with acetyl-SCoA and malonyl-SCoA.[963] A solution containing the fatty-acid synthase system from *G. gallus* (4.3 μM in active sites) and 1.5 μM NADPH was mixed with a solution of 110 μM acetyl-SCoA and 200 μM malonyl-SCoA in an apparatus for stopped flow (dead time 2 ms). The two solutions were buffered at pH 7.0 with 0.1 M potassium phosphate at 25 °C. Fluorescence of the solution in the observation chamber at wavelengths greater than 420 nm ($\lambda_{excitation} = 367$ nm), which was due to NADPH, was monitored as a function of time (milliseconds). The solid trace is the direct observation of fluorescence as a percentage of the initial reading, and the open circles are values calculated by Equation 5–376 with $k_1 = 4.3\ s^{-1}$, $k_2 = 9.5\ s^{-1}$, and $[NADPH]_0 = 100\%$. It was necessary to add a background of 18% to all calculated values to obtain a satisfactory fit. Adapted with permission from reference 963. Copyright 1983 American Chemical Society. https://doi.org/10.1021/bi00295a037

$$\text{acetyl-SE} + \text{malonyl-SACD} + H^+ \rightleftharpoons \text{HSE} + CO_2 + \text{acetoacetyl-SACD} \quad (5–372)$$

$$\text{NADPH} + \text{acetoacetyl-SACD} + H^+ \rightleftharpoons (R)\text{-3-hydroxybutanoyl-SACD} + NADP^+ \quad (5–373)$$

where HSACD is a sulfanyl group on the phosphopantotheinyl group attached as a phosphodiester to a serine in the acyl-carrier domain and HSE is a sulfanyl group of a cysteine in the active site of β-ketoacyl-[acyl-carrier-protein] synthase I. When a solution of the fatty-acid synthase system from *G. gallus* and NADPH in one syringe was mixed with a solution of acetyl-SCoA and malonyl-SCoA in the other syringe so that the final concentrations of enzyme (2.1 μM) and NADPH (0.8 μM) were less than their dissociation constant (6.0 μM), a lag was observed in oxidation of NADPH (Figure 5–37).[963]

In part to avoid numerical integration, the situation was considerably simplified. The first four reactions were considered to be only one composite reaction

$$\text{acetyl-SCoA} + \text{malonyl-SCoA} + \text{H}^+ + \text{HSACD} \rightleftharpoons 2\,\text{HSCoA} + \text{CO}_2 + \text{acetoacetyl-SACD} \quad (5\text{–}374)$$

Furthermore, the 15% of NADPH that was already associated with the active site for 3-oxoacyl-[acyl-carrier-protein]reductase (Equation 5–373) before mixing was ignored, and it was assumed that, within the dead time of the apparatus, the various active sites were saturated with acetyl-SCoA and malonyl-SCoA. The significantly simplified kinetic mechanism that was proposed to explain the observations was

$$\text{E·acSCoA·malSCoA} + \text{HSACD} \xrightarrow{k_1} 2\,\text{HSCoA} + \text{CO}_2 + \text{E·acacSACD} + \text{NADPH} \xrightarrow{k_2} \text{E·hbSACD·NADP}^+ \quad (5\text{–}375)$$

where E·acSCoA·malSCoA is the complex between the enzyme and acetyl-SCoA and malonyl-SCoA, E·acacSACD is the acetoacetyl thioester of the acyl-carrier domain, and E·hbSACD is the (3*R*)-3-hydroxybutyryl thioester of the acyl-carrier domain. The analytically integrated rate equation for this simplified kinetic mechanism for the concentration of NADPH is

$$[\text{NADPH}] = [\text{NADPH}]_0 \exp\left\{-k_2\left(t + \frac{e^{-k_1 t} - 1}{k_1}\right)\right\} \quad (5\text{–}376)$$

which fits the data satisfactorily (open circles in Figure 5–37). This exercise again illustrates the fact that kinetic measurements often cannot reveal steps in the mechanism of an enzymatic reaction that are known to exist if Occam's razor that the simplest kinetic mechanism consistent with the observations is accepted.

Monitoring association of reactants with an active site by stopped flow or quenched flow or both methods can provide an answer to the vexing question of whether reactants associate with the active site in an obligate order or a preferential order. For example, coenzyme-B sulfoethylthiotransferase (previously Equation 4–273)

$$\text{CoBSH} + \text{methyl-SCoM} \rightleftharpoons \text{methane} + \text{CoBS–SCoM} \quad (5\text{–}377)$$

from *Methanothermobacter marburgensis* catalyzes a reaction with two reactants, coenzyme B (CoBSH) and methylcoenzyme M (methyl-SCoM). Association of each reactant alone with the active site could be followed in an apparatus for stopped flow by changes in fluorescence of the prosthetic nickel tetrapyrrole, coenzyme F_{430}, in the active site, and rate constants for these respective associations and dissociations could be obtained. The complexes between each reactant and the active site at saturation could then be mixed in turn with the other reactant in the apparatus for stopped flow, and association of the other reactant to the complex of the coreactant could be monitored again by changes in the absorbance of coenzyme F_{430}. Finally, the disappearance of [^{14}C]methyl-SCoM and the coincident appearance of [^{14}C]methane could be monitored by quenched flow. From the observed rate constants for the relaxations observed in these separate experiments, numerical values for all rate constants for association and dissociation of each reactant, both in the absence and in the presence of the other, and the rate constant for the production of methane in the active site occupied by both reactants could be calculated. It was found that either reactant can associate first with the active site, but if coenzyme B associates before methyl-SCoM, a nonproductive complex is formed that cannot produce methane. For methane production, methyl-SCoM must associate before coenzyme B.[964] Consequently, in this instance, which probably represents the minority, there is an obligate order to addition of reactants for the enzyme to catalyze its reaction.

Similar measurements were performed for the reaction catalyzed by phenylalanine 4-monooxygenase

$$\text{5,6,7,8-tetrahydrobiopterin} + \text{L-phenylalanine} + \text{O}_2 \rightleftharpoons \text{L-tyrosine} + \text{4a-hydroxy-5,6,7,8-tetrahydrobiopterin} \quad (5\text{–}378)$$

from *Chromobacterium violaceum*. Association of the reactant 5,6,7,8-tetrahydrobiopterin alone with the active site could be followed in an apparatus for

stopped flow by monitoring changes in the absorbance of the prosthetic mononuclear nonheme iron ion in the active site. Unfortunately, no absorbance changes were observed when the enzyme was mixed with L-phenylalanine, so the rates of its association and dissociation from the active site could not be monitored directly. When the enzyme, however, was premixed with various concentrations of L-phenylalanine and then mixed with 5,6,7,8-tetrahydrobiopterin and when the enzyme was premixed with various concentrations of 5,6,7,8-tetrahydrobiopterin and then mixed with L-phenylalanine, distinct relaxations in absorbance of the prosthetic mononuclear nonheme iron ion were observed that were unique to each order of addition. These relaxations could only be explained if both L-phenylalanine and 5,6,7,8-tetrahydrobiopterin are able to associate with the active site in the absence of the other before the other reactant then associates. Finally, when the complex between the enzyme and L-phenylalanine and 5,6,7,8-tetrahydrobiopterin was first formed and then mixed with O_2, the relaxations in absorbance that were observed were consistent with the conclusions that the ternary complex formed when L-phenylalanine associates first is the same as the ternary complex when 5,6,7,8-tetrahydrobiopterin associates first and that a single ternary complex is catalytically competent.

When a kinetic mechanism incorporating all these conclusions was fit to all changes in absorbance with time, although the kinetic mechanism must be one with random association of reactants, three additional determinations were made. First, the bimolecular rate constant for association of 5,6,7,8-tetrahydrobiopterin with the empty active site is 170 times greater than that for L-phenylalanine. Second, the bimolecular rate constant for association of L-phenylalanine with the active site occupied by 5,6,7,8-tetrahydrobiopterin is 80 times greater than that for its association with the empty active site. Third, the bimolecular rate constant for association of 5,6,7,8-tetrahydrobiopterin with the active site occupied by L-phenylalanine is 0.5 times that for its association with the empty active site.[965] Consequently, association of these two reactants is preferential, with initial association of 5,6,7,8-tetrahydrobiopterin highly favored over initial association of L-phenylalanine because of the values for these rate constants and equilibrium constants, but the order of association is not obligate.

Yet another purpose for stopped flow and quenched flow is to demonstrate the kinetic competence of an intermediate. The kinetic competence of any intermediate in an enzymatic reaction is its capacity to be formed and unformed, or unformed and formed, at rates equal to or greater than the overall rate of the normally occurring enzymatic reaction. All actual intermediates in the actual mechanism for an enzyme must be kinetically competent, even though this has not been demonstrated that they are. It is, however, important to know that they are. If a particular molecule, either a noncovalently bound molecule or a covalent adduct of the enzyme, is not kinetically competent, then that molecule cannot be an intermediate on the main path of the enzymatic mechanism. For example, both the peptide SSCVLIE and the peptide in which SSCVLIE is covalently attached to the peptide IALCTLSAF by a disulfide between the respective cysteines can be isolated from a digest of ribonucleoside-diphosphate reductase from *E. coli* by immunoadsorption. When ribonucleoside-diphosphate reductase was mixed in an apparatus for quenched flow with its reactant CDP in the absence of its reactant thioredoxin, it could be shown that this disulfide, which had been proposed to be an intermediate in the enzymatic reaction (Figure 5–13), was formed with an observed rate constant of 8 s^{-1}.[500] The catalytic constant for turnover of the enzyme at steady state under the same conditions is 4 s^{-1}. Because the rate constant for formation of the disulfide is larger than the rate constant for a complete turnover, the disulfide that is formed in the active site is kinetically competent.

In the enzymatic reaction catalyzed by phosphoglucomutase (Equation 5–3), only enzyme already covalently phosphorylated at its active site is enzymatically active. If phosphoglucomutase from *O. cuniculus* that has [^{32}P]phosphate covalently attached at its active site is mixed in an apparatus for quenched flow with D-glucose 1-[^{31}P]phosphate, the [^{32}P]phosphate is replaced by [^{31}P]phosphate with a rate constant[928] of 98 s^{-1}. If enzyme phosphorylated with [^{31}P]phosphate is mixed with D-glucose 1-[^{32}P]phosphate, the enzyme becomes phosphorylated with [^{32}P]phosphate with a rate constant of 110 s^{-1} (solid curve in Figure 5–27). Under the same conditions, the catalytic constant for the enzyme with D-glucose 1-phosphate as reactant is 103 s^{-1}. Because these three numbers are identical within experimental error, the intermediate phosphoenzyme is kinetically competent. When Mg^{2+}, an obligatory cofactor that was present in both solutions that were mixed together, is replaced with Zn^{2+}, the rate constant for loss of the [^{32}P]phosphoenzyme inter-

mediate upon addition of D-glucose 1-[^{31}P]phosphate decreases to 25 s^{-1}, but the catalytic constant for the enzyme decreases to 10 s^{-1}. Again, the phosphoenzyme intermediate is kinetically competent. In the mechanism proposed for this enzymatic reaction (Equation 5–36),[966,967] the phosphate on the enzyme is replaced by a phosphate from one substrate during each turnover. The active form of the enzyme that binds the reactant is phosphorylated, and the enzyme from which the product dissociates is also phosphorylated.

A remarkable result of studying enzymatic reactions by stopped flow and quenched flow has been the discovery that steps other than those in which the actual chemical transformations occur are often kinetically rate-affecting or rate-limiting. When experiments are performed at saturating concentrations of reactants, associations of reactants cannot be rate-limiting, but dissociations of products often are. Myosin ATPase from *O. cuniculus* (Equation 5–259) is an extreme case of this situation, in which hydrolysis of the reactant is 1000 times more rapid than dissociation of products in the absence of actin. The rate-limiting step in the reaction catalyzed by hexokinase from *S. cerevisiae* is the release of $MgADP^-$ as a product from the active site.[968]

In many instances, however, relaxations have been observed that cannot be assigned either to the chemical transformation of substrates bound at the active site or to dissociation of products from the active site. Such unexplained relaxations have been **observed when substrates or intermediates are being monitored.** Relaxations in the reductive dephosphorylation catalyzed by glyceraldehyde-3-phosphate dehydrogenase (phosphorylating) from *Homarus gammarus* (Equation 5–26), which were observed while monitoring the change in absorbance of NADH, were assigned to a conformational change in the enzyme.[969] A comparison of the steady-state rate constants with rate constants for relaxations observed in the transfer of a hydride from NADH to 2-amino-4-hydroxy-6,7-dimethyldihydropteridine during its reduction by bovine 6,7-dihydropteridine reductase led to the conclusion that a step preceding hydrogen transfer was a conformational change in the enzyme.[970] Relaxations in the hydrolysis of 2,4-dinitrophenyl phosphate catalyzed by alkaline phosphatase (Equation 5–33) from *E. coli*, which were observed while monitoring the absorbance of 2,4-dinitrophenol formed during the hydrolysis, were assigned to a conformational change in the enzyme.[971]

Other similar intramolecular relaxations occur following association of competitive inhibitors. Relaxations in the absorbance of proflavin, which is a competitive inhibitor of bovine chymotrypsin (Figure 3–6), as it associates with the active site were assigned to a conformational change in the enzyme.[951] Relaxations in the absorbance of 2-hydroxy-5-nitrobenzylphosphonate, which is a competitive inhibitor of alkaline phosphatase from *E. coli*, as it associates with the active site were assigned to a conformational change in the enzyme.[972] Relaxations for which there are no other conceivable explanations are usually assigned by exclusion, and often in the absence of any other information, to conformational changes in the protein. It should be pointed out that argument by exclusion is invalid in chemistry.

Assignments of relaxations to conformational changes in the enzyme are far more defensible when the chromophore or fluorophore monitoring the progress of the reaction is located in the protein at a position well removed from the active site so that association of reactants and their chemical conversion cannot be responsible for those relaxations. Five relaxations[883] observed in the fluorescence of 2-aza-1,N^6-etheno-AMP, covalently attached through its phospho group to the 4-hydroxyphenyl group of Tyrosine 398, upon mixing glutamine synthetase from *E. coli* (Equation 5–270) with its several reactants—L-glutamate, $MgATP^{2-}$, and NH_4^+—can be assigned more confidently as conformational changes in the protein that occur in five steps during the progress of the two nucleophilic substitutions because the 4-hydroxyphenyl group of Tyrosine 398 is at least 2 nm from the active site.[973] Five relaxations[974] observed in the absorbance and fluorescence of tryptophans in the protein upon mixing GMP synthase (glutamine-hydrolysing) from *E. coli* with its several reactants—L-glutamine, $MgATP^{2-}$, and xanthosine 5′-phosphate—either by themselves or in various combinations can be assigned more confidently as conformational changes in the protein that occur in five steps during the progress of the two nucleophilic substitutions catalyzed by the enzyme because each of the eight tryptophans is 2–3 nm from the active site.[975] Three relaxations[976] observed in the fluorescence of Tryptophan 8 in the protein, as well as fluorophores attached covalently to a cysteine inserted in place of Aspartate 61, upon mixing indole-3-glycerol-phosphate synthase from *Saccharolobus solfataricus* with its single reactant, 1-(2-carboxyphenylamino)-1-deoxy-D-ribulose 5-phosphate, can be assigned more confidently as conformational

changes in the protein that occur in three steps during the progress of the electrophilic aromatic substitution catalyzed by the enzyme because Tryptophan 8 is 1 nm from the active site, with a loop of polypeptide in between, and the carboxy group of Aspartate 61 is 1.7 nm from the active site.[977] The initial conformational change monitored by the fluorophores attached to position 61 probably resulted from the closing of the loop in which it is located over the active site once it has been occupied by the reactant.

Even though conformational changes are being monitored by these reporter groups, the effects of changing the concentrations of reactants on these various relaxations indicate that many of them are accompanying associations and dissociations of reactants and chemical steps in the mechanism of the enzyme. These observations suggest that many, if not most, associations and dissociations of substrates with an active site and chemical transformations that subsequently occur within an active site may require coincident conformational changes in the protein to proceed. If so, it is possible that these conformational changes are necessary for catalysis to occur and that controlling them could be a way to control association of reactants and the overall rate of the enzymatic reaction.

Suggested Reading

Rhee, S. G., Ubom, G. A., Hunt, J. B., and Chock, P. B. (1982) Catalytic cycle of the biosynthetic reaction catalyzed by adenylylated glutamine synthetase from *Escherichia coli, J. Biol. Chem. 257*, 289–297. https://doi.org/10.1016/S0021-9258(19)68360-2

Brooks, H. B., and Phillips, M. A. (1997) Characterization of the reaction mechanism for *Trypanosoma brucei* ornithine decarboxylase by multiwavelength stopped-flow spectroscopy, *Biochemistry 36*, 15147–15155. https://doi.org/10.1021/bi971652b

Roberts, K. M., Pavon, J. A., and Fitzpatrick, P. F. (2013) Kinetic mechanism of phenylalanine hydroxylase: Intrinsic binding and rate constants from single-turnover experiments, *Biochemistry 52*, 1062–1073. https://doi.org/10.1021/bi301675e

Wongnate, T., and Ragsdale, S. W. (2015) The reaction mechanism of methyl-coenzyme M reductase: How an enzyme enforces strict binding order, *J. Biol. Chem. 290*, 9322–9334. https://doi.org/10.1074/jbc.M115.636761

Problem 5–28: In the reaction catalyzed by L-lactate dehydrogenase (Equation 5–327), the substrate NADH absorbs light with $\lambda_{max} = 339$ nm, while the substrate NAD^+ has negligible absorbance (<1% of that for NADH) at this wavelength.

(A) Write the simplest kinetic mechanism that could describe this enzymatic reaction. Do not derive an equation for v_0. Include in your kinetic mechanism only steps involving binding of substrates and the interconversion of substrates and products once they are bound.

This enzymatic reaction has been studied by stopped-flow spectrophotometry. A solution containing a higher concentration of active sites (28 μM) than NADH (20 μM) was added to one syringe of an apparatus for stopped flow, and a solution of pyruvate at a saturating concentration (2 mM) was added to the other. The decrease in A_{340} was followed (Figure 5–21A). At the original concentrations of enzyme (28 μM) and NADH (20 μM) in the experiment described in Figure 5–21, almost all (>85%) of the NADH was bound to active sites of the enzyme.

(B) Write the step or steps in your kinetic mechanism from part A that are being directly monitored in Figure 5–21.

This stopped-flow experiment was repeated at several different concentrations of pyruvate (pyr), and an observed first-order rate constant (k_{obs}) was calculated for each of them. Measurements of initial rate were also made at saturating NADH, and initial rate constants ($v_0\,[E]_t^{-1}$) at various pyruvate concentrations were calculated from these measurements. Both the first-order rate constants (k_{obs}) from measurements by stopped flow and the rate constants from measurements of initial rate for the enzymatic reaction were plotted on the same graph against the initial concentration of pyruvate ($[pyruvate]_0$) (Figure 5–21B). The rate constants from the steady-state experiments are equal, within experimental error, to the observed rate constants from stopped flow as a function of the concentration of pyruvate. The value for the catalytic constant determined from Figure 5–21B is 260 s^{-1}.

(C) The bimolecular rate constant for association of pyruvate with the enzyme under the conditions of Figure 5–21 is greater than 10^3 mM^{-1} s^{-1}. Calculate the lower limit of the pseudo-first-order rate constant for association

of pyruvate with the enzyme at the smallest concentration (1 mM) used in these experiments.

(D) According to the results in Figure 5–21 and the calculation of part C, which step in the mechanism that you wrote in part A is rate-limiting for L-lactate dehydrogenase in the direction of pyruvate reduction?

(E) When the experiment shown in Figure 5–21 was repeated with NAD^{2}H, both the catalytic constant and the observed rate constant from stopped flow at a saturating concentration of pyruvate were found to be 200 s^{-1}. Why does this result suggest that the actual kinetic mechanism is more complicated than what you wrote in part A?

Enzyme and a saturating concentration of NAD^+ were added to one syringe of an apparatus for stopped flow, and a saturating concentration of lactate was added to the other. The solutions were rapidly mixed in an apparatus for stopped flow that had a dead time of 1.3 ms. A burst in A_{340}, the rate of which was so fast that it was complete within the dead time ($k_{obs} > 1\ ms^{-1}$), occurred upon mixing. The size of this burst of NADH production could be calculated from the extinction coefficient of enzyme-bound NADH. At pH 9, the nanomoles of NADH formed in the burst were equal to the nanomoles of active sites present.[884]

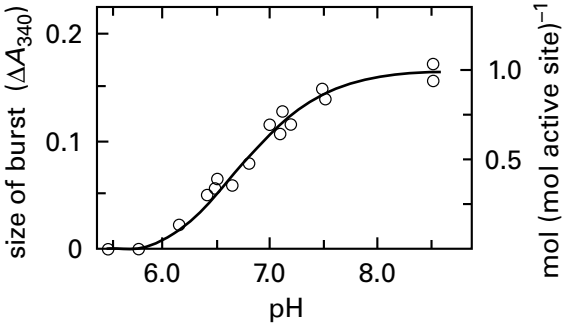

Effect of pH on the magnitude of the initial burst of NADH production. A solution of 40 mM NAD^+ and 55 μM lactate dehydrogenase was mixed with an equal volume of 0.50 M lithium DL-lactate. The buffer was 67 mM potassium phosphate and the temperature was 22 °C. Each pH was recorded after completion of the reaction.

(F) Write the step or steps in the kinetic mechanism in part A that are being monitored in this last experiment.

The catalytic constant k_0 of porcine L-lactate dehydrogenase for oxidation of lactate by NAD^+ was determined to be 150 s^{-1} at pH 9 when measurements of initial rate were performed under the conditions of those for measurements from stopped flow, but the rate of the burst described in the figure is greater than the dead time of the instrument ($k > 1\ ms^{-1}$). It was calculated that pyruvate release from the enzyme is greater than 10,000 s^{-1} under the conditions of these experiments. The rate constant of the reaction E·NADH → E + NADH was measured at pH 8 and found to be 460 s^{-1}.

(G) The results just described and those presented in part E are inconsistent with the mechanism of part A but can be explained if a required conformational change of the enzyme is added as a step of the kinetic mechanism. Write a kinetic mechanism that incorporates the conformational change in the proper place and makes the mechanism consistent with the results.

Problem 5–29: Dihydrolipoyl dehydrogenase is a flavoenzyme that reduces or oxidizes N^6-(lipoyl)-lysines (**2–31**) by using NADH to reduce the oxidized prosthetic flavin and NAD^+ to oxidize the reduced prosthetic flavin (Equations 2–71 and 2–112)

$$N^6\text{-(dihydrolipoyl)lysine} + NAD^+ \rightleftharpoons N^6\text{-(lipoyl)lysine} + NADH + H^+$$

The enzyme is responsible for reducing or oxidizing lipoyl groups on a separate enzyme, dihydrolipoyllysine-residue acetyltransferase, using the same mechanism that the related enzyme (23% identity; 1.4 gap percent) glutathione-disulfide reductase (Equation 2–134, Figure 2–11) uses to reduce or oxidize glutathiones.

When a 20 μM solution of dihydrolipoyl dehydrogenase from *M. tuberculosis*, the prosthetic flavin and catalytic cysteines of which were fully oxidized, was mixed with a solution of 2 mM NADH and the mixture was monitored at 435, 458, 530, and 670 nm, the following kinetic courses were observed.[942]

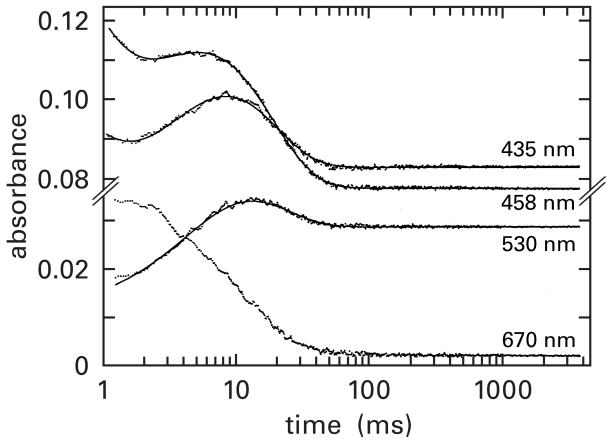

Kinetic courses of absorbance in stopped flow. In addition to oxidized dihydrolipoyl dehydrogenase and NADH, each solution contained 0.1 M sodium phosphate, pH 7.5 and 4 °C. The time elapsed following mixing (milliseconds) is shown on a logarithmic scale. The dots are the experimental data, and the solid lines are fits of a proposed kinetic mechanism to the data.

The dissociation constant for NADH from the enzyme is 180 μM.

(A) What chromophore is being monitored?
(B) Why does the reaction cease after 100 ms even though a large excess of reactant over enzyme was added?
(C) Write complete chemical equations for the three consecutive reductions that are occurring during reduction of the fully oxidized dihydrolipoyl dehydrogenase.
(D) How many relaxations are observed in the four kinetic traces? The same relaxation observed in two or more traces is considered to be only one relaxation.
(E) Over what range of times (milliseconds) does each relaxation occur?
(F) A charge-transfer band can be observed in partially reduced dihydrolipoyl dehydrogenase that arises from electron transfer between oxidized flavin and the closest of the two catalytic cysteines in the active site of the enzyme. Over which range of times is this charge-transfer band lost? In which of the relaxations you identified in part D is the charge-transfer band lost?

The first phase of the kinetic course shows a kinetic isotope effect of 4.2 when [4,4-$^2H_2$]NADH is used as reactant.

(G) Propose assignments for each relaxation to a specific step in your mechanism for the reduction of dihydrolipoyl dehydrogenase being observed.

Problem 5–30: Succinate—CoA ligase (ADP-forming) from *E. coli* catalyzes the following reaction.

$$\text{succinate} + \text{MgATP}^{2-} + \text{CoASH} \rightleftharpoons \text{MgADP}^{-} + \text{HOPO}_3^{2-} + \text{succinyl-SCoA}$$

The purified enzyme contains a stable N^{τ}-phosphohistidinyl group in its active site.[132] The following three steps have been proposed for the overall reaction

$$\text{E}\sim\text{PO}_3^{2-} + \text{succinate} \rightleftharpoons \text{E}\cdot\text{succinyl phosphate}$$

$$\text{E}\cdot\text{succinyl phosphate} + \text{CoASH} \rightleftharpoons \text{E} + \text{succinyl-SCoA} + \text{HOPO}_3^{2-}$$

$$\text{E} + \text{MgATP}^{2-} \rightleftharpoons \text{E}\sim\text{PO}_3^{2-} + \text{MgADP}^{-}$$

where succinyl phosphate is 1-phosphobutanedioic acid.

Two experiments were performed on the dephosphorylated form (E) of succinate—CoA ligase (ADP-forming) by quenched flow. In both experiments, the two syringes of the apparatus were connected to a mixing chamber, the outlet of which was attached to a tube that terminated in a solution of 8% phenol, which inactivated the enzyme instantaneously. The time between mixing of the two solutions and entry into the quench solution was varied between 20 and 100 ms by changing the flow rates of the fluids that entered the mixing chamber. The results are displayed in the following two figures.

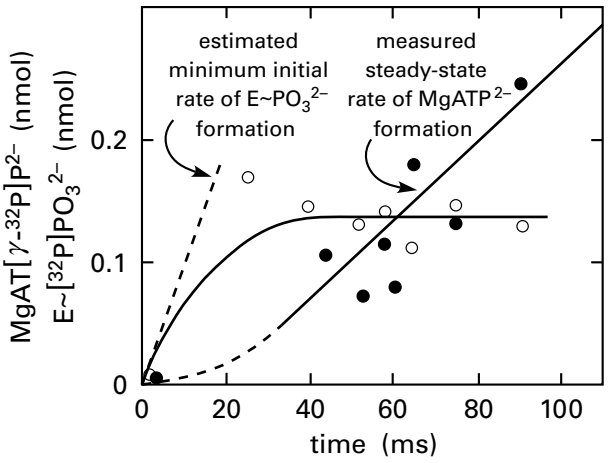

Rates of E~$[^{32}P]PO_3^{2-}$ and MgAT[γ-$^{32}P]P^{2-}$ formation from $HO[^{32}P]PO_3^{2-}$.[978] Measurements were made at 24 °C. One syringe contained 0.05 mM $HO[^{32}P]PO_3^{2-}$ (1.2×10^7 cpm μmol^{-1}), 0.1 mM ADP^{3-}, and 0.2 mM succinyl-SCoA at pH 6.6. The other syringe contained 17 μM dephosphoenzyme in 0.1 M KCl, 8 mM $MgCl_2$, and 0.1 mM EDTA at pH 7.4. The observed MgAT[γ-$^{32}P]P^{2-}$ (nanomoles; ●) and the observed E~$[^{32}P]PO_3^{2-}$(nanomoles; ○) are plotted as a function of time (milliseconds). The slope of the solid line that was chosen to fit the points for the observed nanomoles of MgAT[γ-$^{32}P]P^{2-}$ as a function of time is that of the initial steady-state rate for formation of $MgATP^{2-}$ that was measured separately in reactions of 2–15 s duration under the same conditions. The horizontal placement of that solid line was determined by the points for the observed nanomoles of MgAT[γ-$^{32}P]P^{2-}$.

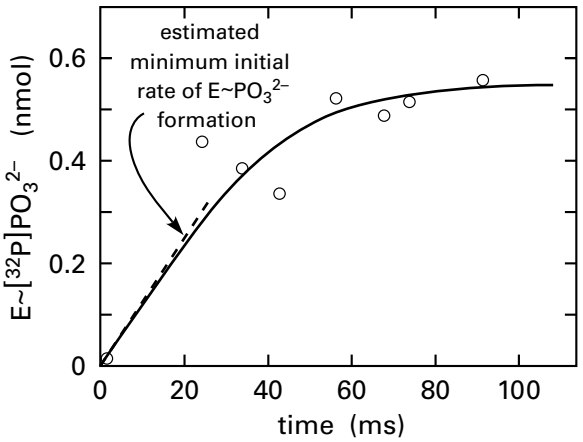

Rate of E~$[^{32}P]PO_3^{2-}$ formation from MgAT[γ-$^{32}P]P^{2-}$.[978] One syringe contained 8 μM dephosphoenzyme in 0.1 M KCl, 8 mM $MgCl_2$, and 0.1 mM EDTA at pH 7.4. The other syringe contained 0.02 mM HSCoA, 0.08 mM AT[γ-$^{32}P]P^{4-}$(900 cpm nmol^{-1}), and 0.05 M sodium succinate at pH 7.4. The observed values for E~$[^{32}P]PO_3^{2-}$ (nanomoles) are plotted as a function of time (milliseconds).

(A) Write the step-by-step mechanism for the enzymatic reaction that produces the E~$[^{32}P]PO_3^{2-}$ and MgAT[γ-$^{32}P]P^{2-}$ observed in the first figure. Draw the structures of all substrates explicitly, abbreviating coenzyme A as $CoAS^-$, $MgATP^{2-}$ as $MgADPOPO_3^{2-}$, and $MgADP^-$ as $MgADPO^-$. Use the explicit structure of the imidazolyl group and the β carbon of the histidine.

(B) Write the step-by-step mechanism for the enzymatic reaction that produces the E~$[^{32}P]PO_3^{2-}$ observed in the second figure as well as the $HO[^{32}P]PO_3^{2-}$ at completion of the overall reaction.

The two mechanisms you write in parts A and B must be identical to each other, except for the isotopes and the direction of each, because of the principle of microscopic reversibility.

In the reaction displayed in the first figure, the rate of E~$[^{32}P]PO_3^{2-}$ formation was ≥10 nmol s^{-1} because equilibrium had been reached at the earliest times that could be measured. The steady-state rate for production of MgAT[γ-$^{32}P]P^{2-}$ under the same conditions was measured in a separate experiment and found to be 3 nmol s^{-1}. The solid line in the first figure has this slope but has been shifted to coincide with the actual measurements of MgAT[γ-$^{32}P]P^{2-}$ in the apparatus for quenched flow.

For the experiment displayed in the second figure, the rate of E~$[^{32}P]PO_3^{2-}$ formation was ≥13 nmol s^{-1} and the steady-state rate of $HOPO_3^{2-}$ formation, determined with the same preparations under the same conditions in a separate experiment, was 10 nmol s^{-1}.

(C) What important fact concerning formation of E~$[^{32}P]PO_3^{2-}$ do these two experiments establish? Why was quenched flow needed to establish this fact?

Succinate—CoA ligase (ADP-forming) from *E. coli* was mixed with several substrates, the phosphate bearing the noted isotopic labels, as described in the following paragraph and table, which are quoted with slight adaptation from the original report.[979]

> The incubation of the purified enzyme with O^{18}-labeled phosphate in the presence of succinate, ATP, and CoA led to a rapid exchange of oxygen between succinate and phosphate (table). The phosphate was additionally labeled with phosphorus^{32} [sic] to indicate the extent of over-all reversal of the reaction. The use of relatively large amounts of enzyme in this

experiment to achieve 50% equilibration between inorganic phosphate and ATP revealed a slow phosphate–ATP exchange in the absence of succinate (line 5, table). This probably is due to the presence of an unknown contaminating enzyme since succinate—CoA ligase (ADP-forming) isolated from other sources has an absolute succinate requirement for the phosphate–ATP exchange. Within experimental error, the O^{18} exchange reaction between inorganic phosphate and succinate is completely dependent upon ATP, CoA, and enzyme. A comparison of the rate of O^{18} exchange into succinate and the P^{32} exchange into ATP indicates that oxygen exchange can occur independently of the over-all reaction. Assuming that the one succinate oxygen would be replaced during complete reversal of the reaction, the theoretical per cent O^{18} exchange into succinate would be ¼ the value for the ^{32}P exchange into ATP (100% exchange representing replacement of all four succinate oxygen atoms). In contrast to this prediction, the O^{18} exchange into succinate is some 5-fold greater than the theoretical value (table). This finding implies the reversible formation and cleavage of an intermediate compound, independent of the over-all reversal of the reaction.

additions[a]	$[^{32}P]HOPO_3^{2-}$–$MgATP^{2-}$ exchange		$[^{18}O]HOPO_3^{2-}$–succinate exchange		
	cpm μmol^{-1} in $MgATP^{2-}$	% exchange	mass ratio of CO_2 (46/44)	oxygen-18 (% excess)	% exchange[b]
complete system	20,650	56	0.00762 0.00744	0.338	66.9
complete system – enzyme	<100	<1	0.00422 0.00421	<0.001	<0.1
complete system – CoASH	2000	5	0.00439 0.00441	0.024	4.7
complete system – $MgATP^{2-}$	<100	<1	0.00441 0.00447	0.024	4.7
complete system – succinate	5900	16	0.00433 0.00425[c]	0.010	2.0

[a]The complete system contained 10 mM $MgCl_2$, 10 mM L-cysteine, 5 mM $MgATP^{2-}$, 50 mM succinate, 1 mM CoASH, 1.6 mg mL^{-1} enzyme, and either 5 mM $K_2[^{32}P]HOPO_3$ (73,400 cpm μmol^{-1}) or 5 mM $K_2[^{18}O]HOPO_3$ (5.05% excess ^{18}O). The reaction was run at 30 °C for 1 h. [b]Calculated on the basis of 100% exchange being equal to replacement of four oxygens-18 on succinate by oxygens-18 from phosphate and corrected for the 10-fold excess of succinate over phosphate. [c]Succinate added after acidification and extraction.

(D) Write a step-by-step mechanism to explain the transfer of oxygen-18 from $[^{18}O]HOPO_3^{2-}$ to succinate.

(E) Expand your mechanism to show why this exchange is 5 times faster than the overall reaction.

(F) What is the "intermediate compound" required for this exchange of oxygen for phosphate into succinate?

A solution containing succinate—CoA ligase (ADP-forming) from *E. coli* and $MgADP^-$ was mixed with other substrates, as described in the following figure, and the synthesis of $MgATP^{2-}$ was followed.[980]

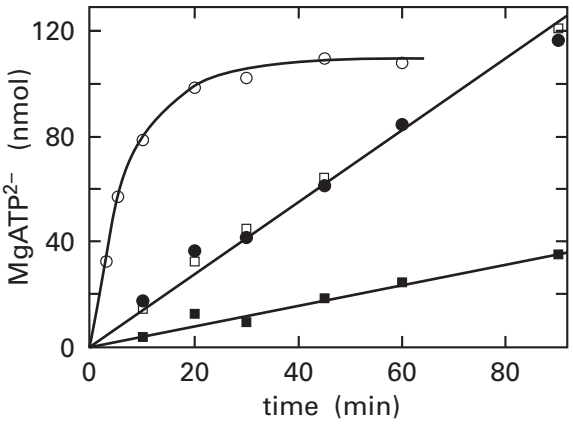

Synthesis of $MgATP^{2-}$ from succinyl phosphate and from succinyl-SCoA plus phosphate.[980] To a solution of 5 mM $MgADP^{-}$, 5 mM $MgSO_4$, 0.08 mM dithiothreitol, 1 mM ethylenediaminetetraacetate, and 50 mM 2-ammonio-2-(hydroxymethyl)-propane-1,3-diol, pH 7.8 and 17 °C, were added the following: (○) 0.20 mM succinyl-SCoA and 0.20 mM potassium phosphate; (●) 1.0 mM succinyl phosphate and 0.025 mM HSCoA; (□) 1.0 mM succinyl phosphate and 0.025 mM desulfoCoA; (■) 1.0 mM succinyl phosphate.

(G) Write a step-by-step mechanism to explain the synthesis of $MgATP^{2-}$ from succinyl phosphate (■). Expand your mechanism to explain synthesis of $MgATP^{2-}$ from succinyl-SCoA and $HOPO_3^{2-}$ (○). How could a reaction with fewer steps (■) be slower than one with more steps (○)?

(H) Desulfocoenzyme A is coenzyme A lacking the sulfanyl group. How can it activate formation of $MgATP^{2-}$ from succinyl phosphate? Why does coenzyme A have the same effect?

(I) What other isotopic exchanges, such as the $[^{18}O]HOPO_3^{2-} \rightleftharpoons$ succinate reaction described above, should succinate—CoA ligase (ADP-forming) catalyze if the three-step mechanism presented in the first paragraph of this problem is correct?

References

1. Oosterbaan, R. A., and van Adrichem, M. E. (1958) Isolation of acetyl peptides from acetylchymotrypsin, *Biochim. Biophys. Acta 27*, 423–425.
2. Bender, M. L., and Kezdy, F. J. (1964) The mechanism of action of proteolytic enzymes. XXXII. The current status of the α-chymotrypsin mechanism, *J. Am. Chem. Soc. 86*, 3704–3714.
3. Palmer, J. L., and Abeles, R. H. (1979) The mechanism of action of *S*-adenosylhomocysteinase, *J. Biol. Chem. 254*, 1217–1226.
4. Reddy, M. C., Kuppan, G., Shetty, N. D., Owen, J. L., Ioerger, T. R., and Sacchettini, J. C. (2008) Crystal structures of *Mycobacterium tuberculosis S*-adenosyl-L-homocysteine hydrolase in ternary complex with substrate and inhibitors, *Protein Sci. 17*, 2134–2144.
5. Fahrney, D. E., and Gold, A. M. (1963) Sulfonyl fluorides as inhibitors of esterases. I. Rates of reaction with acetylcholinesterase, α-chymotrypsin, and trypsin, *J. Am. Chem. Soc. 85*, 997–1000.
6. Sigler, P. B., Blow, D. M., Matthews, B. W., and Henderson, R. (1968) Structure of crystalline α-chymotrypsin. II. A preliminary report including a hypothesis for the activation mechanism, *J. Mol. Biol. 35*, 143–164.
7. Mangel, W. F., Singer, P. T., Cyr, D. M., Umland, T. C., Toledo, D. L., Stroud, R. M., Pflugrath, J. W., and Sweet, R. M. (1990) Structure of an acyl-enzyme intermediate during catalysis: (Guanidinobenzoyl)trypsin, *Biochemistry 29*, 8351–8357.
8. Radisky, E. S., Lee, J. M., Lu, C. J., and Koshland, D. E., Jr. (2006) Insights into the serine protease mechanism from atomic resolution structures of trypsin reaction intermediates, *Proc. Natl. Acad. Sci. U.S.A. 103*, 6835–6840.
9. Ding, X., Rasmussen, B. F., Petsko, G. A., and Ringe, D. (1994) Direct structural observation of an acyl-enzyme intermediate in the hydrolysis of an ester substrate by elastase, *Biochemistry 33*, 9285–9293.
10. Fisher, J., Belasco, J. G., Khosla, S., and Knowles, J. R. (1980) β-Lactamase proceeds via an acyl-enzyme intermediate. Interaction of the *Escherichia coli* RTEM enzyme with cefoxitin, *Biochemistry 19*, 2895–2901.
11. Strynadka, N. C., Adachi, H., Jensen, S. E., Johns, K., Sielecki, A., Betzel, C., Sutoh, K., and James, M. N. (1992) Molecular structure of the acyl-enzyme intermediate in β-lactam hydrolysis at 1.7 Å resolution, *Nature (London, U. K.) 359*, 700–705.
12. Bone, R., Sampson, N. S., Bartlett, P. A., and Agard, D. A. (1991) Crystal structures of α-lytic protease complexes with irreversibly bound phosphonate esters, *Biochemistry 30*, 2263–2272.

13. Takahashi, L. H., Radhakrishnan, R., Rosenfield, R. E., Jr., Meyer, E. F., Jr., and Trainor, D. A. (1989) Crystal structure of the covalent complex formed by a peptidyl α,α-difluoro-β-keto amide with porcine pancreatic elastase at 1.78 Å resolution, *J. Am. Chem. Soc. 111*, 3368–3374.
14. Nicola, G., Peddi, S., Stefanova, M., Nicholas, R. A., Gutheil, W. G., and Davies, C. (2005) Crystal structure of *Escherichia coli* penicillin-binding protein 5 bound to a tripeptide boronic acid inhibitor: A role for Ser-110 in deacylation, *Biochemistry 44*, 8207–8217.
15. Wilmouth, R. C., Edman, K., Neutze, R., Wright, P. A., Clifton, I. J., Schneider, T. R., Schofield, C. J., and Hajdu, J. (2001) X-Ray snapshots of serine protease catalysis reveal a tetrahedral intermediate, *Nat. Struct. Biol. 8*, 689–694.
16. Carter, P., and Wells, J. A. (1988) Dissecting the catalytic triad of a serine protease, *Nature (London, U. K.) 332*, 564–568.
17. Liu, P., Wang, Y. F., Ewis, H. E., Abdelal, A. T., Lu, C. D., Harrison, R. W., and Weber, I. T. (2004) Covalent reaction intermediate revealed in crystal structure of the *Geobacillus stearothermophilus* carboxylesterase Est30, *J. Mol. Biol. 342*, 551–561.
18. Huguenin-Dezot, N., Alonzo, D. A., Heberlig, G. W., Mahesh, M., Nguyen, D. P., Dornan, M. H., Boddy, C. N., Schmeing, T. M., and Chin, J. W. (2019) Trapping biosynthetic acyl-enzyme intermediates with encoded 2,3-diaminopropionic acid, *Nature (London, U. K.) 565*, 112–117.
19. Horsman, G. P., Ke, J., Dai, S., Seah, S. Y., Bolin, J. T., and Eltis, L. D. (2006) Kinetic and structural insight into the mechanism of BphD, a C–C bond hydrolase from the biphenyl degradation pathway, *Biochemistry 45*, 11071–11086.
20. Ruzzini, A. C., Ghosh, S., Horsman, G. P., Foster, L. J., Bolin, J. T., and Eltis, L. D. (2012) Identification of an acyl-enzyme intermediate in a *meta*-cleavage product hydrolase reveals the versatility of the catalytic triad, *J. Am. Chem. Soc. 134*, 4615–4624.
21. Ruzzini, A. C., Horsman, G. P., and Eltis, L. D. (2012) The catalytic serine of *meta*-cleavage product hydrolases is activated differently for C–O bond cleavage than for C–C bond cleavage, *Biochemistry 51*, 5831–5840.
22. Lowe, G., and Williams, A. (1965) Direct evidence for an acylated thiol as an intermediate in papain- and ficin-catalysed hydrolyses, *Biochem. J. 96*, 189–193.
23. Drenth, J., Kalk, K. H., and Swen, H. M. (1976) Binding of chloromethyl ketone substrate analogues to crystalline papain, *Biochemistry 15*, 3731–3738.
24. Schendel, F. J., Mueller, E., Stubbe, J., Shiau, A., and Smith, J. M. (1989) Formylglycinamide ribonucleotide synthetase from *Escherichia coli*: Cloning, sequencing, overproduction, isolation, and characterization, *Biochemistry 28*, 2459–2471.
25. Schnizer, H. G., Boehlein, S. K., Stewart, J. D., Richards, N. G. J., and Schuster, S. M. (1999) Formation and isolation of a covalent intermediate during the glutaminase reaction of a class II amidotransferase, *Biochemistry 38*, 3677–3682.
26. Kim, J. H., Krahn, J. M., Tomchick, D. R., Smith, J. L., and Zalkin, H. (1996) Structure and function of the glutamine phosphoribosylpyrophosphate amidotransferase glutamine site and communication with the phosphoribosylpyrophosphate site, *J. Biol. Chem. 271*, 15549–15557.
27. Thoden, J. B., Miran, S. G., Phillips, J. C., Howard, A. J., Raushel, F. M., and Holden, H. M. (1998) Carbamoyl phosphate synthetase: Caught in the act of glutamine hydrolysis, *Biochemistry 37*, 8825–8831.
28. Anand, R., Hoskins, A. A., Stubbe, J., and Ealick, S. E. (2004) Domain organization of *Salmonella typhimurium* formylglycinamide ribonucleotide amidotransferase revealed by X-ray crystallography, *Biochemistry 43*, 10328–10342.
29. Kershaw, N. J., McNaughton, H. J., Hewitson, K. S., Hernandez, H., Griffin, J., Hughes, C., Greaves, P., Barton, B., Robinson, C. V., and Schofield, C. J. (2002) ORF6 from the clavulanic acid gene cluster of *Streptomyces clavuligerus* has ornithine acetyltransferase activity, *Eur. J. Biochem. 269*, 2052–2059.
30. Iqbal, A., Clifton, I. J., Bagonis, M., Kershaw, N. J., Domene, C., Claridge, T. D., Wharton, C. W., and Schofield, C. J. (2009) Anatomy of a simple acyl intermediate in enzyme catalysis: combined biophysical and modeling studies on ornithine acetyl transferase, *J. Am. Chem. Soc. 131*, 749–757.

31. Marc, F., Weigel, P., Legrain, C., Almeras, Y., Santrot, M., Glansdorff, N., and Sakanyan, V. (2000) Characterization and kinetic mechanism of mono- and bifunctional ornithine acetyltransferases from thermophilic microorganisms, *Eur. J. Biochem. 267*, 5217–5226.
32. Sankaranarayanan, R., Cherney, M. M., Garen, C., Garen, G., Niu, C., Yuan, M., and James, M. N. (2010) The molecular structure of ornithine acetyltransferase from *Mycobacterium tuberculosis* bound to ornithine, a competitive inhibitor, *J. Mol. Biol. 397*, 979–990.
33. Born, T. L., Franklin, M., and Blanchard, J. S. (2000) Enzyme-catalyzed acylation of homoserine: Mechanistic characterization of the *Haemophilus influenzae met2*-encoded homoserine transacetylase, *Biochemistry 39*, 8556–8564.
34. Nazi, I., and Wright, G. D. (2005) Catalytic mechanism of fungal homoserine transacetylase, *Biochemistry 44*, 13560–13566.
35. Mirza, I. A., Nazi, I., Korczynska, M., Wright, G. D., and Berghuis, A. M. (2005) Crystal structure of homoserine transacetylase from *Haemophilus influenzae* reveals a new family of α/β-hydrolases, *Biochemistry 44*, 15768–15773.
36. Zubieta, C., Arkus, K. A., Cahoon, R. E., and Jez, J. M. (2008) A single amino acid change is responsible for evolution of acyltransferase specificity in bacterial methionine biosynthesis, *J. Biol. Chem. 283*, 7561–7567.
37. Born, T. L., and Blanchard, J. S. (1999) Enzyme-catalyzed acylation of homoserine: Mechanistic characterization of the *Escherichia coli metA*-encoded homoserine transsuccinylase, *Biochemistry 38*, 14416–14423.
38. Ziegler, K., Noble, S. M., Mutumanje, E., Bishop, B., Huddler, D. P., and Born, T. L. (2007) Identification of catalytic cysteine, histidine, and lysine residues in *Escherichia coli* homoserine transsuccinylase, *Biochemistry 46*, 2674–2683.
39. Zubieta, C., Krishna, S. S., McMullan, D., Miller, M. D., Abdubek, P., Agarwalla, S., Ambing, E., Astakhova, T., Axelrod, H. L., Carlton, D., Chiu, H. J., Clayton, T., Deller, M., DiDonato, M., Duan, L., Elsliger, M. A., Grzechnik, S. K., Hale, J., Hampton, E., Han, G. W., Haugen, J., Jaroszewski, L., Jin, K. K., Klock, H. E., Knuth, M. W., Koesema, E., Kumar, A., Marciano, D., Morse, A. T., Nigoghossian, E., Oommachen, S., Reyes, R., Rife, C. L., van den Bedem, H., Weekes, D., White, A., Xu, Q., Hodgson, K. O., Wooley, J., Deacon, A. M., Godzik, A., Lesley, S. A., and Wilson, I. A. (2007) Crystal structure of homoserine *O*-succinyltransferase from *Bacillus cereus* at 2.4 Å resolution, *Proteins: Struct., Funct., Bioinf. 68*, 999–1005.
40. Inoue, M., Hiratake, J., Suzuki, H., Kumagai, H., and Sakata, K. (2000) Identification of catalytic nucleophile of *Escherichia coli* γ-glutamyltranspeptidase by γ-monofluorophosphono derivative of glutamic acid: *N*-terminal Thr-391 in small subunit is the nucleophile, *Biochemistry 39*, 7764–7771.
41. Okada, T., Suzuki, H., Wada, K., Kumagai, H., and Fukuyama, K. (2006) Crystal structures of γ-glutamyltranspeptidase from *Escherichia coli*, a key enzyme in glutathione metabolism, and its reaction intermediate, *Proc. Natl. Acad. Sci. U.S.A. 103*, 6471–6476.
42. Link, J. O., and Straub, K. (1996) Trapping of an IMP dehydrogenase-substrate covalent intermediate by mycophenolic acid, *J. Am. Chem. Soc. 118*, 2091–2092.
43. Huete-Perez, J. A., Wu, J. C., Whitby, F. G., and Wang, C. C. (1995) Identification of the IMP binding site in the IMP dehydrogenase from *Tritrichomonas foetus*, *Biochemistry 34*, 13889–13894.
44. Zhang, R., Evans, G., Rotella, F. J., Westbrook, E. M., Beno, D., Huberman, E., Joachimiak, A., and Collart, F. R. (1999) Characteristics and crystal structure of bacterial inosine-5′-monophosphate dehydrogenase, *Biochemistry 38*, 4691–4700.
45. Sintchak, M. D., Fleming, M. A., Futer, O., Raybuck, S. A., Chambers, S. P., Caron, P. R., Murcko, M. A., and Wilson, K. P. (1996) Structure and mechanism of inosine monophosphate dehydrogenase in complex with the immunosuppressant mycophenolic acid, *Cell (Cambridge, MA, U. S.) 85*, 921–930.
46. Lu, X., Galkin, A., Herzberg, O., and Dunaway-Mariano, D. (2004) Arginine deiminase uses an active-site cysteine in nucleophilic catalysis of L-arginine hydrolysis, *J. Am. Chem. Soc. 126*, 5374–5375.
47. Galkin, A., Lu, X., Dunaway-Mariano, D., and Herzberg, O. (2005) Crystal structures representing the Michaelis complex and the thiouronium reaction intermediate of *Pseudo-*

monas aeruginosa arginine deiminase, *J. Biol. Chem. 280*, 34080–34087.
48. Humm, A., Fritsche, E., Steinbacher, S., and Huber, R. (1997) Crystal structure and mechanism of human L-arginine:glycine amidinotransferase: A mitochondrial enzyme involved in creatine biosynthesis, *EMBO J. 16*, 3373–3385.
49. Grazi, E., and Rossi, N. (1968) Transamidinase of hog kidney. VII. Cysteine at the amidine-binding site, *J. Biol. Chem. 243*, 538–542.
50. Lacourciere, G. M., and Armstrong, R. N. (1993) The catalytic mechanism of microsomal epoxide hydrolase involves an ester intermediate, *J. Am. Chem. Soc. 115*, 10466–10467.
51. Argiriadi, M. A., Morisseau, C., Hammock, B. D., and Christianson, D. W. (1999) Detoxification of environmental mutagens and carcinogens: Structure, mechanism, and evolution of liver epoxide hydrolase, *Proc. Natl. Acad. Sci. U.S.A. 96*, 10637–10642.
52. Verschueren, K. H. G., Seljee, F., Rozeboom, H. J., Kalk, K. H., and Dijkstra, B. W. (1993) Crystallographic analysis of the catalytic mechanism of haloalkane dehalogenase, *Nature (London, U. K.) 363*, 693–698.
53. Eldrup, A. B., Soleymanzadeh, F., Taylor, S. J., Muegge, I., Farrow, N. A., Joseph, D., McKellop, K., Man, C. C., Kukulka, A., and De Lombaert, S. (2009) Structure-based optimization of arylamides as inhibitors of soluble epoxide hydrolase, *J. Med. Chem. 52*, 5880–5895.
54. Gomez, G. A., Morisseau, C., Hammock, B. D., and Christianson, D. W. (2004) Structure of human epoxide hydrolase reveals mechanistic inferences on bifunctional catalysis in epoxide and phosphate ester hydrolysis, *Biochemistry 43*, 4716–4723.
55. Pries, F., Kingma, J., Pentenga, M., van Pouderoyen, G., Jeronimus-Stratingh, C. M., Bruins, A. P., and Janssen, D. B. (1994) Site-directed mutagenesis and oxygen isotope incorporation studies of the nucleophilic aspartate of haloalkane dehalogenase, *Biochemistry 33*, 1242–1247.
56. Schmidberger, J. W., Wilce, J. A., Tsang, J. S. H., and Wilce, M. C. J. (2007) Crystal structures of the substrate free-enzyme, and reaction intermediate of the HAD superfamily member, haloacid dehalogenase DehIVa from *Burkholderia cepacia* MBA4, *J. Mol. Biol. 368*, 706–717.
57. Barends, T. R., Bultema, J. B., Kaper, T., van der Maarel, M. J., Dijkhuizen, L., and Dijkstra, B. W. (2007) Three-way stabilization of the covalent intermediate in amylomaltase: An α-amylase-like transglycosylase, *J. Biol. Chem. 282*, 17242–17249.
58. Braun, C., Lindhorst, T., Madsen, N. B., and Withers, S. G. (1996) Identification of Asp 549 as the catalytic nucleophile of glycogen-debranching enzyme via trapping of the glycosyl-enzyme intermediate, *Biochemistry 35*, 5458–5463.
59. Uitdehaag, J. C., Mosi, R., Kalk, K. H., van der Veen, B. A., Dijkhuizen, L., Withers, S. G., and Dijkstra, B. W. (1999) X-Ray structures along the reaction pathway of cyclodextrin glycosyltransferase elucidate catalysis in the α-amylase family, *Nat. Struct. Biol. 6*, 432–436.
60. Persson, K., Ly, H. D., Dieckelmann, M., Wakarchuk, W. W., Withers, S. G., and Strynadka, N. C. (2001) Crystal structure of the retaining galactosyltransferase LgtC from *Neisseria meningitidis* in complex with donor and acceptor sugar analogs, *Nat. Struct. Biol. 8*, 166–175.
61. Gomez, H., Polyak, I., Thiel, W., Lluch, J. M., and Masgrau, L. (2012) Retaining glycosyltransferase mechanism studied by QM/MM methods: Lipopolysaccharyl-α-1,4–galactosyltransferase c transfers α-galactose via an oxocarbenium ion-like transition state, *J. Am. Chem. Soc. 134*, 4743–4752.
62. Banait, N. S., and Jencks, W. P. (1991) General-acid and general-base catalysis of the cleavage of α-D-glucopyranosyl fluoride, *J. Am. Chem. Soc. 113*, 7958–7963.
63. Kirby, A. J. (2001) The lysozyme mechanism sorted -- after 50 years, *Nat. Struct. Biol. 8*, 737–739.
64. Vocadlo, D. J., Davies, G. J., Laine, R., and Withers, S. G. (2001) Catalysis by hen egg-white lysozyme proceeds via a covalent intermediate, *Nature (London, U. K.) 412*, 835–838.
65. Withers, S. G., Street, I. P., Bird, P., and Dolphin, D. H. (1987) 2-Deoxy-2-fluoroglucosides: a novel class of mechanism-based glucosidase inhibitors, *J. Am. Chem. Soc. 109*, 7530–7531.

66. Davies, G. J., Mackenzie, L., Varrot, A., Dauter, M., Brzozowski, A. M., Schulein, M., and Withers, S. G. (1998) Snapshots along an enzymatic reaction coordinate: Analysis of a retaining β-glycoside hydrolase, *Biochemistry 37*, 11707–11713.
67. Tao, B. Y., Reilly, P. J., and Robyt, J. F. (1989) Detection of a covalent intermediate in the mechanism of action of porcine pancreatic α-amylase by using ^{13}C nuclear magnetic resonance, *Biochim. Biophys. Acta 995*, 214–220.
68. Tull, D., and Withers, S. G. (1994) Mechanisms of cellulases and xylanases: A detailed kinetic study of the exo-β-1,4-glycanase from *Cellulomonas fimi, Biochemistry 33*, 6363–6370.
69. Czjzek, M., Ben David, A., Bravman, T., Shoham, G., Henrissat, B., and Shoham, Y. (2005) Enzyme-substrate complex structures of a GH39 β-xylosidase from *Geobacillus stearothermophilus*, *J. Mol. Biol. 353*, 838–846.
70. Notenboom, V., Birsan, C., Nitz, M., Rose, D. R., Warren, R. A. J., and Withers, S. G. (1998) Insights into transition state stabilization of the β-1,4-glycosidase Cex by covalent intermediate accumulation in active site mutants, *Nat. Struct. Biol. 5*, 812–818.
71. Money, V. A., Smith, N. L., Scaffidi, A., Stick, R. V., Gilbert, H. J., and Davies, G. J. (2006) Substrate distortion by a lichenase highlights the different conformational itineraries harnessed by related glycoside hydrolases, *Angew. Chem., Int. Ed. Engl. 45*, 5136–5140.
72. Wang, Q., Tull, D., Meinke, A., Gilkes, N. R., Warren, R. A., Aebersold, R., and Withers, S. G. (1993) Glu280 is the nucleophile in the active site of *Clostridium thermocellum* CelC, a family A endo-β-1,4-glucanase, *J. Biol. Chem. 268*, 14096–14102.
73. White, A., Tull, D., Johns, K., Withers, S. G., and Rose, D. R. (1996) Crystallographic observation of a covalent catalytic intermediate in a β-glycosidase, *Nat. Struct. Biol. 3*, 149–154.
74. Street, I. P., Kempton, J. B., and Withers, S. G. (1992) Inactivation of a β-glucosidase through the accumulation of a stable 2-deoxy-2-fluoro-α-D-glucopyranosyl-enzyme intermediate: A detailed investigation, *Biochemistry 31*, 9970–9978.
75. Goddard-Borger, E. D., Sakaguchi, K., Reitinger, S., Watanabe, N., Ito, M., and Withers, S. G. (2012) Mechanistic insights into the 1,3-xylanases: useful enzymes for manipulation of algal biomass, *J. Am. Chem. Soc. 134*, 3895–3902.
76. Gebler, J. C., Aebersold, R., and Withers, S. G. (1992) Glu-537, not Glu-461, is the nucleophile in the active site of (lac Z) β-galactosidase from *Escherichia coli*, *J. Biol. Chem. 267*, 11126–11130.
77. Vocadlo, D. J., Mayer, C., He, S., and Withers, S. G. (2000) Mechanism of action and identification of Asp242 as the catalytic nucleophile of *Vibrio furnisii N*-acetyl-β-D-glucosaminidase using 2-acetamido-2-deoxy-5-fluoro-α-L-idopyranosyl fluoride, *Biochemistry 39*, 117–126.
78. Watts, A. G., Damager, I., Amaya, M. L., Buschiazzo, A., Alzari, P., Frasch, A. C., and Withers, S. G. (2003) *Trypanosoma cruzi trans*-sialidase operates through a covalent sialyl-enzyme intermediate: Tyrosine is the catalytic nucleophile, *J. Am. Chem. Soc. 125*, 7532–7533.
79. Lee, S. S., Yu, S., and Withers, S. G. (2002) α-1,4-Glucan lyase performs a trans-elimination via a nucleophilic displacement followed by a *syn*-elimination, *J. Am. Chem. Soc. 124*, 4948–4949.
80. Nieman, C. E., Wong, A. W., He, S., Clarke, L., Hopwood, J. J., and Withers, S. G. (2003) Family 39 α-L-Iduronidases and β-D-xylosidases react through similar glycosyl-enzyme intermediates: Identification of the human iduronidase nucleophile, *Biochemistry 42*, 8054–8065.
81. Juers, D. H., Heightman, T. D., Vasella, A., McCarter, J. D., Mackenzie, L., Withers, S. G., and Matthews, B. W. (2001) A structural view of the action of *Escherichia coli* (lacZ) β-galactosidase, *Biochemistry 40*, 14781–14794.
82. Hidaka, M., Fushinobu, S., Ohtsu, N., Motoshima, H., Matsuzawa, H., Shoun, H., and Wakagi, T. (2002) Trimeric crystal structure of the glycoside hydrolase family 42 β-galactosidase from *Thermus thermophilus* A4 and the structure of its complex with galactose, *J. Mol. Biol. 322*, 79–91.
83. Yang, J. K., Yoon, H. J., Ahn, H. J., Lee, B. I., Pedelacq, J. D., Liong, E. C., Berendzen, J., Laivenieks, M., Vieille, C., Zeikus, G. J., Vocadlo, D. J., Withers, S. G., and Suh, S. W. (2004) Crystal structure of β-D-xylosidase

from *Thermoanaerobacterium saccharolyticum*, a family 39 glycoside hydrolase, *J. Mol. Biol. 335*, 155–165.
84. Watts, A. G., Oppezzo, P., Withers, S. G., Alzari, P. M., and Buschiazzo, A. (2006) Structural and kinetic analysis of two covalent sialosyl-enzyme intermediates on *Trypanosoma rangeli* sialidase, *J. Biol. Chem. 281*, 4149–4155.
85. Newstead, S. L., Potter, J. A., Wilson, J. C., Xu, G., Chien, C. H., Watts, A. G., Withers, S. G., and Taylor, G. L. (2008) The structure of *Clostridium perfringens* NanI sialidase and its catalytic intermediates, *J. Biol. Chem. 283*, 9080–9088.
86. Knott, B. C., Haddad Momeni, M., Crowley, M. F., Mackenzie, L. F., Gotz, A. W., Sandgren, M., Withers, S. G., Stahlberg, J., and Beckham, G. T. (2014) The mechanism of cellulose hydrolysis by a two-step, retaining cellobiohydrolase elucidated by structural and transition path sampling studies, *J. Am. Chem. Soc. 136*, 321–329.
87. Strynadka, N. C., and James, M. N. (1991) Lysozyme revisited: Crystallographic evidence for distortion of an *N*-acetylmuramic acid residue bound in site D, *J. Mol. Biol. 220*, 401–424.
88. White, H., and Jencks, W. P. (1976) Mechanism and specificity of succinyl-CoA:3-ketoacid coenzyme A transferase, *J. Biol. Chem. 251*, 1688–1699.
89. Solomon, F., and Jencks, W. P. (1969) Identification of an enzyme-γ-glutamyl coenzyme A intermediate from coenzyme A transferase, *J. Biol. Chem. 244*, 1079–1081.
90. Fraser, M. E., Hayakawa, K., and Brown, W. D. (2010) Catalytic role of the conformational change in succinyl-CoA:3-oxoacid CoA transferase on binding CoA, *Biochemistry 49*, 10319–10328.
91. Rangarajan, E. S., Li, Y., Ajamian, E., Iannuzzi, P., Kernaghan, S. D., Fraser, M. E., Cygler, M., and Matte, A. (2005) Crystallographic trapping of the glutamyl-CoA thioester intermediate of family I CoA transferases, *J. Biol. Chem. 280*, 42919–42928.
92. Berthold, C. L., Toyota, C. G., Richards, N. G., and Lindqvist, Y. (2008) Reinvestigation of the catalytic mechanism of formyl-CoA transferase, a class III CoA-transferase, *J. Biol. Chem. 283*, 6519–6529.
93. Vinarov, D., Narasimhan, C., and Miziorko, H. M. (1999) Detection of acetyl-*S*-enzyme reaction intermediates of hydroxymethylglutaryl-CoA synthase and β-ketothiolase by ^{13}C NMR, *J. Am. Chem. Soc. 121*, 270–271.
94. Theisen, M. J., Misra, I., Saadat, D., Campobasso, N., Miziorko, H. M., and Harrison, D. H. (2004) 3-Hydroxy-3-methylglutaryl-CoA synthase intermediate complex observed in "real-time", *Proc. Natl. Acad. Sci. U.S.A. 101*, 16442–16447.
95. Modis, Y., and Wierenga, R. K. (2000) Crystallographic analysis of the reaction pathway of *Zoogloea ramigera* biosynthetic thiolase, *J. Mol. Biol. 297*, 1171–1182.
96. Buckel, W., Buschmeier, V., and Eggerer, H. (1971) The action mechanism of citrate lyase from *Klebsiella aerogenes*, *Hoppe-Seyler's Z. Physiol. Chem. 352*, 1195–1205.
97. Schmellenkamp, H., and Eggerer, H. (1972) Enzyme catalyzed reactivation of inactive citrate lyase, *Hoppe-Seyler's Z. Physiol. Chem. 353*, 1563–1564.
98. Oppenheimer, N. J., Singh, M., Sweeley, C. C., Sung, S. J., and Srere, P. A. (1979) The configuration and location of the ribosidic linkage in the prosthetic group of citrate lyase (*Klebsiella aerogenes*), *J. Biol. Chem. 254*, 1000–1002.
99. Buckel, W., Ziegert, K., and Eggerer, H. (1973) Acetyl-CoA-dependent cleavage of citrate on inactivated citrate lyase, *Eur. J. Biochem. 37*, 295–304.
100. Dimroth, P., Mayer, K., and Eggerer, H. (1975) On the mechanism of action of isocitrate lyase, *Eur. J. Biochem. 51*, 267–273.
101. Sharma, V., Sharma, S., Hoener zu Bentrup, K., McKinney, J. D., Russell, D. G., Jacobs, W. R., Jr., and Sacchettini, J. C. (2000) Structure of isocitrate lyase, a persistence factor of *Mycobacterium tuberculosis*, *Nat. Struct. Biol. 7*, 663–668.
102. Sprecher, M., Berger, R., and Sprinson, D. B. (1964) Stereochemistry of the isocitrate lyase reaction, *Biochem. Biophys. Res. Commun. 16*, 254–257.
103. Mohamed, A. H., Chirala, S. S., Mody, N. H., Huang, W. Y., and Wakil, S. J. (1988) Primary structure of the multifunctional α subunit protein of yeast fatty acid synthase derived from FAS2 gene sequence, *J. Biol. Chem. 263*, 12315–12325.

104. Schreckenbach, T., Wobser, H., and Lynen, F. (1977) The palmityl binding sites of fatty acid synthetase from yeast, *Eur. J. Biochem. 80*, 13–23.
105. Ziegenhorn, J., Niedermeier, R., Nussler, C., and Lynen, F. (1972) Study of the acetyltransferase component of fatty acid synthetase of yeast, *Eur. J. Biochem. 30*, 285–300.
106. Schweizer, E., Piccinini, F., Duba, C., Gunther, S., Ritter, E., and Lynen, F. (1970) Malonyl binding site of yeast fatty acid synthetase complex, *Eur. J. Biochem. 15*, 483–499.
107. Kresze, G. B., Steber, L., Oesterhelt, D., and Lynen, F. (1977) Reaction of yeast fatty acid synthetase with iodoacetamide. 2. Identification of the amino acid residues reacting with iodoacetamide and primary structure of a peptide containing the peripheral sulfhydryl group, *Eur. J. Biochem. 79*, 181–190.
108. Stern, A., Sedgwick, B., and Smith, S. (1982) The free coenzyme A requirement of animal fatty acid synthetase. Participation in the continuous exchange of acetyl and malonyl moieties between coenzyme A thioester and enzyme, *J. Biol. Chem. 257*, 799–803.
109. Moniot, S., Bruno, S., Vonrhein, C., Didierjean, C., Boschi-Muller, S., Vas, M., Bricogne, G., Branlant, G., Mozzarelli, A., and Corbier, C. (2008) Trapping of the thioacylglyceraldehyde-3-phosphate dehydrogenase intermediate from *Bacillus stearothermophilus*. Direct evidence for a flip-flop mechanism, *J. Biol. Chem. 283*, 21693–21702.
110. Krimsky, I., and Racker, E. (1955) Acyl derivatives of glyceraldehyde-3-phosphate dehydrogenase, *Science (Washington, DC, U. S.) 122*, 319–321.
111. Harris, I., Meriwether, B. P., and Park, J. H. (1963) Chemical nature of the catalytic sites in glyceraldehyde-3-phosphate dehydrogenase, *Nature (London, U. K.) 198*, 154–157.
112. Hadfield, A., Kryger, G., Ouyang, J., Petsko, G. A., Ringe, D., and Viola, R. (1999) Structure of aspartate-β-semialdehyde dehydrogenase from *Escherichia coli*, a key enzyme in the aspartate family of amino acid biosynthesis, *J. Mol. Biol. 289*, 991–1002.
113. Faehnle, C. R., Le Coq, J., Liu, X., and Viola, R. E. (2006) Examination of key intermediates in the catalytic cycle of aspartate-β-semialdehyde dehydrogenase from a gram-positive infectious bacteria, *J. Biol. Chem. 281*, 31031–31040.
114. Chikwana, V. M., Stec, B., Lee, B. W., de Crecy-Lagard, V., Iwata-Reuyl, D., and Swairjo, M. A. (2012) Structural basis of biological nitrile reduction, *J. Biol. Chem. 287*, 30560–30570.
115. Jung, J., and Nidetzky, B. (2018) Evidence of a sequestered imine intermediate during reduction of nitrile to amine by the nitrile reductase QueF from *Escherichia coli*, *J. Biol. Chem. 293*, 3720–3733.
116. Ge, X., Campbell, R. E., van de Rijn, I., and Tanner, M. E. (1998) Covalent adduct formation with a mutated enzyme: Evidence for a thioester intermediate in the reaction catalyzed by UDP-glucose dehydrogenase, *J. Am. Chem. Soc. 120*, 6613–6614.
117. Egger, S., Chaikuad, A., Klimacek, M., Kavanagh, K. L., Oppermann, U., and Nidetzky, B. (2012) Structural and kinetic evidence that catalytic reaction of human UDP-glucose 6-dehydrogenase involves covalent thiohemiacetal and thioester enzyme intermediates, *J. Biol. Chem. 287*, 2119–2129.
118. Colomb, M. G., Cheruy, A., and Vignais, P. V. (1972) Nucleoside diphosphokinase from beef heart cytosol. II. Characterization of the phosphorylated intermediate, *Biochemistry 11*, 3378–3386.
119. Morera, S., Lascu, I., Dumas, C., LeBras, G., Briozzo, P., Veron, M., and Janin, J. (1994) Adenosine 5′-diphosphate binding and the active site of nucleoside diphosphate kinase, *Biochemistry 33*, 459–467.
120. Cherfils, J., Morera, S., Lascu, I., Veron, M., and Janin, J. (1994) X-Ray structure of nucleoside diphosphate kinase complexed with thymidine diphosphate and Mg^{2+} at 2 Å resolution, *Biochemistry 33*, 9062–9069.
121. Colomb, M. G., Cheruy, A., and Vignais, P. V. (1972) Nucleoside diphosphokinase from beef heart cytosol. I. Physical and kinetic properties, *Biochemistry 11*, 3370–3378.
122. Sowadski, J. M., Handschumacher, M. D., Murthy, H. M., Foster, B. A., and Wyckoff, H. W. (1985) Refined structure of alkaline phosphatase from *Escherichia coli* at 2.8 Å resolution, *J. Mol. Biol. 186*, 417–433.
123. Jones, S. R., Kindman, L. A., and Knowles, J. R. (1978) Stereochemistry of phosphoryl group transfer using a chiral [^{16}O, ^{17}O, ^{18}O]stereochemical course of alkaline phosphatase, *Nature (London, U. K.) 275*, 564–565.

124. Ramaley, R. F., Bridger, W. A., Moyer, R. W., and Boyer, P. D. (1967) The preparation, properties, and reactions of succinyl coenzyme A synthetase and its phosphorylated form, *J. Biol. Chem. 242*, 4287–4298.
125. Deluca, M., Ebner, K. E., Hultquist, D. E., Kreil, G., Peter, J. B., Moyer, R. W., and Boyer, P. D. (1963) The isolation and identification of phosphohistidine from mitochondrial protein, *Biochem. Z. 338*, 512–525.
126. Edlund, B., Rask, L., Olsson, P., Walinder, O., Zetterqvist, O., and Engstrom, L. (1969) Preparation of crystalline nucleoside diphosphate kinase from baker's yeast and identification of [^{32}P]phosphohistidine as the main phosphorylated product of an alkaline hydrolysate of enzyme incubated with adenosine [^{32}P]triphosphate, *Eur. J. Biochem. 9*, 451–455.
127. Schwartz, J. H., Crestfield, A. M., and Lipmann, F. (1963) The amino acid sequence of a tetradecapeptide containing the reactive serine in *E. coli* alkaline phosphatase, *Proc. Natl. Acad. Sci. U.S.A. 49*, 722–729.
128. Stec, B., Hehir, M. J., Brennan, C., Nolte, M., and Kantrowitz, E. R. (1998) Kinetic and X-ray structural studies of three mutant *E. coli* alkaline phosphatases: Insights into the catalytic mechanism without the nucleophile Ser102, *J. Mol. Biol. 277*, 647–662.
129. Yamamoto, T., and Tonomura, Y. (1967) Reaction mechanism of the Ca^{++}-dependent ATPase of sarcoplasmic reticulum from skeletal muscle. I. Kinetic studies, *J. Biochem. (Tokyo) 62*, 558–575.
130. Degani, C., and Boyer, P. D. (1973) A borohydride reduction method for characterization of the acyl phosphate linkage in proteins and its application to sarcoplasmic reticulum adenosine triphosphatase, *J. Biol. Chem. 248*, 8222–8226.
131. Pas, H. H., Meyer, G. H., Kruizinga, W. H., Tamminga, K. S., van Weeghel, R. P., and Robillard, G. T. (1991) ^{31}Phospho-NMR demonstration of phosphocysteine as a catalytic intermediate on the *Escherichia coli* phosphotransferase system EII^{Mtl}, *J. Biol. Chem. 266*, 6690–6692.
132. Fraser, M. E., James, M. N., Bridger, W. A., and Wolodko, W. T. (1999) A detailed structural description of *Escherichia coli* succinyl-CoA synthetase, *J. Mol. Biol. 285*, 1633–1653.
133. Morera, S., Chiadmi, M., LeBras, G., Lascu, I., and Janin, J. (1995) Mechanism of phosphate transfer by nucleoside diphosphate kinase: X-Ray structures of the phosphohistidine intermediate of the enzymes from *Drosophila* and *Dictyostelium*, *Biochemistry 34*, 11062–11070.
134. Leiros, I., McSweeney, S., and Hough, E. (2004) The reaction mechanism of phospholipase D from *Streptomyces* sp. strain PMF. Snapshots along the reaction pathway reveal a pentacoordinate reaction intermediate and an unexpected final product, *J. Mol. Biol. 339*, 805–820.
135. Lee, Y. H., Olson, T. W., Ogata, C. M., Levitt, D. G., Banaszak, L. J., and Lange, A. J. (1997) Crystal structure of a trapped phosphoenzyme during a catalytic reaction, *Nat. Struct. Biol. 4*, 615–618.
136. Wang, Y., Liu, L., Wei, Z., Cheng, Z., Lin, Y., and Gong, W. (2006) Seeing the process of histidine phosphorylation in human bisphosphoglycerate mutase, *J. Biol. Chem. 281*, 39642–39648.
137. Murphy, J. E., Stec, B., Ma, L., and Kantrowitz, E. R. (1997) Trapping and visualization of a covalent enzyme-phosphate intermediate, *Nat. Struct. Biol. 4*, 618–622.
138. Rangarajan, E. S., Proteau, A., Wagner, J., Hung, M. N., Matte, A., and Cygler, M. (2006) Structural snapshots of *Escherichia coli* histidinol phosphate phosphatase along the reaction pathway, *J. Biol. Chem. 281*, 37930–37941.
139. Guan, K. L., and Dixon, J. E. (1991) Evidence for protein-tyrosine-phosphatase catalysis proceeding via a cysteine-phosphate intermediate, *J. Biol. Chem. 266*, 17026–17030.
140. Pannifer, A. D., Flint, A. J., Tonks, N. K., and Barford, D. (1998) Visualization of the cysteinyl-phosphate intermediate of a protein-tyrosine phosphatase by X-ray crystallography, *J. Biol. Chem. 273*, 10454–10462.
141. Rose, Z. B., and Dube, S. (1976) Rates of phosphorylation and dephosphorylation of phosphoglycerate mutase and bisphosphoglycerate synthase, *J. Biol. Chem. 251*, 4817–4822.
142. Schramm, A. M., Mehra-Chaudhary, R., Furdui, C. M., and Beamer, L. J. (2008) Backbone flexibility, conformational change, and catalysis in a phosphohexomutase from *Pseudo-*

monas aeruginosa, *Biochemistry 47*, 9154–9162.
143. Ray, W. J., Jr., and Roscelli, G. A. (1964) The phosphoglucomutase pathway. An investigation of phospho-enzyme isomerization, *J. Biol. Chem. 239*, 3935–3941.
144. Najjar, V. A., and Pullman, M. E. (1954) The occurrence of a group transfer involving enzyme (phosphoglucomutase) and substrate, *Science (Washington, DC, U. S.) 119*, 631–634.
145. Naught, L. E., and Tipton, P. A. (2005) Formation and reorientation of glucose 1,6-bisphosphate in the PMM/PGM reaction: transient-state kinetic studies, *Biochemistry 44*, 6831–6836.
146. Lahiri, S. D., Zhang, G., Dunaway-Mariano, D., and Allen, K. N. (2002) Caught in the act: The structure of phosphorylated β-phosphoglucomutase from *Lactococcus lactis*, *Biochemistry 41*, 8351–8359.
147. Dai, J., Wang, L., Allen, K. N., Radstrom, P., and Dunaway-Mariano, D. (2006) Conformational cycling in β-phosphoglucomutase catalysis: Reorientation of the β-D-glucose 1,6-(bis)phosphate intermediate, *Biochemistry 45*, 7818–7824.
148. Han, C. H., and Rose, Z. B. (1979) Active site phosphohistidine peptides from red cell bisphosphoglycerate synthase and yeast phosphoglycerate mutase, *J. Biol. Chem. 254*, 8836–8840.
149. Anderson, L., and Jolles, G. R. (1957) A study of the linkage of phosphorus to protein in phosphoglucomutase, *Arch. Biochem. Biophys. 70*, 121–128.
150. Milstein, C., and Sanger, F. (1961) An amino acid sequence in the active centre of phosphoglucomutase, *Biochem. J. 79*, 456–469.
151. Sheu, K. F., Richard, J. P., and Frey, P. A. (1979) Stereochemical courses of nucleotidyltransferase and phosphotransferase action. Uridine diphosphate glucose pyrophosphorylase, galactose-1-phosphate uridylyltransferase, adenylate kinase, and nucleoside diphosphate kinase, *Biochemistry 18*, 5548–5556.
152. Thrall, S. H., Mehl, A. F., Carroll, L. J., and Dunaway-Mariano, D. (1993) Characterization of the covalent enzyme intermediates formed during pyruvate phosphate dikinase catalysis, *Biochemistry 32*, 1803–1809.
153. Spronk, A. M., Yoshida, H., and Wood, H. G. (1976) Isolation of 3-phosphohistidine from phosphorylated pyruvate, phosphate dikinase, *Proc. Natl. Acad. Sci. U.S.A. 73*, 4415–4419.
154. Goss, N. H., Evans, C. T., and Wood, H. G. (1980) Pyruvate phosphate dikinase: Sequence of the histidyl peptide, the pyrophosphoryl and phosphoryl carrier, *Biochemistry 19*, 5805–5809.
155. Wedekind, J. E., Frey, P. A., and Rayment, I. (1996) The structure of nucleotidylated Histidine-166 of galactose-1-phosphate uridylyltransferase provides insight into phosphoryl group transfer, *Biochemistry 35*, 11560–11569.
156. Yang, S. L., and Frey, P. A. (1979) Nucleophile in the active site of *Escherichia coli* galactose-1-phosphate uridylyltransferase: Degradation of the uridylyl-enzyme intermediate to N^3-phosphohistidine, *Biochemistry 18*, 2980–2984.
157. Kim, J., Ruzicka, F., and Frey, P. A. (1990) Remodeling hexose-1-phosphate uridylyltransferase: Mechanism-inspired mutation into a new enzyme, UDP-hexose synthase, *Biochemistry 29*, 10590–10593.
158. McCoy, J. G., Arabshahi, A., Bitto, E., Bingman, C. A., Ruzicka, F. J., Frey, P. A., and Phillips, G. N., Jr. (2006) Structure and mechanism of an ADP-glucose phosphorylase from *Arabidopsis thaliana*, *Biochemistry 45*, 3154–3162.
159. Linster, C. L., Adler, L. N., Webb, K., Christensen, K. C., Brenner, C., and Clarke, S. G. (2008) A second GDP-L-galactose phosphorylase in *Arabidopsis* en route to vitamin C. Covalent intermediate and substrate requirements for the conserved reaction, *J. Biol. Chem. 283*, 18483–18492.
160. Tse, Y. C., Kirkegaard, K., and Wang, J. C. (1980) Covalent bonds between protein and DNA. Formation of phosphotyrosine linkage between certain DNA topoisomerases and DNA, *J. Biol. Chem. 255*, 5560–5565.
161. Lynn, R. M., Bjornsti, M. A., Caron, P. R., and Wang, J. C. (1989) Peptide sequencing and site-directed mutagenesis identify Tyrosine-727 as the active site tyrosine of *Saccharomyces cerevisiae* DNA topoisomerase I, *Proc. Natl. Acad. Sci. U. S. A. 86*, 3559–3563.
162. Redinbo, M. R., Stewart, L., Kuhn, P., Champoux, J. J., and Hol, W. G. (1998) Crystal structures of human topoisomerase I in covalent and noncovalent complexes with

DNA, *Science (Washington, DC, U. S.) 279*, 1504–1513.
163. Worland, S. T., and Wang, J. C. (1989) Inducible overexpression, purification, and active site mapping of DNA topoisomerase II from the yeast *Saccharomyces cerevisiae*, *J. Biol. Chem. 264*, 4412–4416.
164. Schmidt, B. H., Burgin, A. B., Deweese, J. E., Osheroff, N., and Berger, J. M. (2010) A novel and unified two-metal mechanism for DNA cleavage by type II and IA topoisomerases, *Nature (London, U. K.) 465*, 641–644.
165. Morrison, A., and Cozzarelli, N. R. (1979) Site-specific cleavage of DNA by *E. coli* DNA gyrase, *Cell (Cambridge, MA, U. S.) 17*, 175–184.
166. Williams, N. L., and Maxwell, A. (1999) Locking the DNA gate of DNA gyrase: Investigating the effects on DNA cleavage and ATP hydrolysis, *Biochemistry 38*, 14157–14164.
167. Morais Cabral, J. H., Jackson, A. P., Smith, C. V., Shikotra, N., Maxwell, A., and Liddington, R. C. (1997) Crystal structure of the breakage-reunion domain of DNA gyrase, *Nature (London, U. K.) 388*, 903–906.
168. Fass, D., Bogden, C. E., and Berger, J. M. (1999) Quaternary changes in topoisomerase II may direct orthogonal movement of two DNA strands, *Nat. Struct. Biol. 6*, 322–326.
169. Guo, F., Gopaul, D. N., and van Duyne, G. D. (1997) Structure of Cre recombinase complexed with DNA in a site-specific recombination synapse, *Nature (London, U. K.) 389*, 40–46.
170. Watanabe, S., Watanabe, Y., Nobuchi, R., and Ono, A. (2020) Biochemical and structural characterization of L-2-keto-3–deoxyarabinonate dehydratase: A unique catalytic mechanism in the class I aldolase protein superfamily, *Biochemistry 59*, 2962–2973.
171. Grazi, E., Meloche, H., Martinez, G., Wood, W. A., and Horecker, B. L. (1963) Evidence for Schiff base formation in enzymatic aldol condensations, *Biochem. Biophys. Res. Commun. 10*, 4–10.
172. Ho, M. C., Menetret, J. F., Tsuruta, H., and Allen, K. N. (2009) The origin of the electrostatic perturbation in acetoacetate decarboxylase, *Nature (London, U. K.) 459*, 393–397.
173. Laursen, R. A., and Westheimer, F. H. (1966) The active site of acetoacetate decarboxylase, *J. Am. Chem. Soc. 88*, 3426–3430.
174. Wang, Y., Jones, M. K., Xu, H., Ray, W. K., and White, R. H. (2015) Mechanism of the enzymatic synthesis of 4-(hydroxymethyl)-2-furancarboxaldehyde-phosphate (4-HFC-P) from glyceraldehyde-3-phosphate catalyzed by 4-HFC-P synthase, *Biochemistry 54*, 2997–3008.
175. Grazi, E., Rowley, P. T., Cheng, T., Tchola, O., and Horecker, B. L. (1962) The mechanism of action of aldolases. III. Schiff base formation with lysine, *Biochem. Biophys. Res. Commun. 9*, 38–43.
176. Choi, K. H., Shi, J., Hopkins, C. E., Tolan, D. R., and Allen, K. N. (2001) Snapshots of catalysis: the structure of fructose-1,6-(bis)phosphate aldolase covalently bound to the substrate dihydroxyacetone phosphate, *Biochemistry 40*, 13868–13875.
177. Healy, M. J., and Christen, P. (1972) Reaction of the carbanionic aldolase-substrate intermediate with tetranitromethane. Identification of the products, hydroxypyruvaldehyde phosphate and D-5-ketofructose 1,6–diphosphate, *J. Am. Chem. Soc. 94*, 7911–7916.
178. Kuo, D. J., and Rose, I. A. (1985) Chemical trapping of complexes of dihydroxyacetone phosphate with muscle fructose-1,6-bisphosphate aldolase, *Biochemistry 24*, 3947–3952.
179. St-Jean, M., and Sygusch, J. (2007) Stereospecific proton transfer by a mobile catalyst in mammalian fructose-1,6-bisphosphate aldolase, *J. Biol. Chem. 282*, 31028–31037.
180. St-Jean, M., Lafrance-Vanasse, J., Liotard, B., and Sygusch, J. (2005) High resolution reaction intermediates of rabbit muscle fructose-1,6-bisphosphate aldolase: substrate cleavage and induced fit, *J. Biol. Chem. 280*, 27262–27270.
181. Kraulis, P. J. (1991) MOLSCRIPT: A program to produce both detailed and schematic plots of protein structures, *J. Appl. Crystallogr. 24*, 946–950.
182. Rose, I. A. (1958) Absolute configuration of dihydroxyacetone phosphate tritiated by aldolase reaction, *J. Am. Chem. Soc. 80*, 5835–5836.
183. Morris, A. J., and Tolan, D. R. (1994) Lysine-146 of rabbit muscle aldolase is essential for cleavage and condensation of the C3–C4 bond of fructose 1,6-bis(phosphate), *Biochemistry 33*, 12291–12297.

184. Allard, J., Grochulski, P., and Sygusch, J. (2001) Covalent intermediate trapped in 2-keto-3-deoxy-6-phosphogluconate (KDPG) aldolase structure at 1.95 Å resolution, *Proc. Natl. Acad. Sci. U.S.A. 98*, 3679–3684.
185. Erskine, P. T., Senior, N., Awan, S., Lambert, R., Lewis, G., Tickle, I. J., Sarwar, M., Spencer, P., Thomas, P., Warren, M. J., Shoolingin-Jordan, P. M., Wood, S. P., and Cooper, J. B. (1997) X-ray structure of 5-aminolaevulinate dehydratase, a hybrid aldolase, *Nat. Struct. Biol. 4*, 1025–1031.
186. Frere, F., Schubert, W. D., Stauffer, F., Frankenberg, N., Neier, R., Jahn, D., and Heinz, D. W. (2002) Structure of porphobilinogen synthase from *Pseudomonas aeruginosa* in complex with 5-fluorolevulinic acid suggests a double Schiff base mechanism, *J. Mol. Biol. 320*, 237–247.
187. Olsen, D. B., Hepburn, T. W., Moos, M., Mariano, P. S., and Dunaway-Mariano, D. (1988) Investigation of the *Bacillus cereus* phosphonoacetaldehyde hydrolase. Evidence for a Schiff base mechanism and sequence analysis of an active-site peptide containing the catalytic lysine residue, *Biochemistry 27*, 2229–2234.
188. Lahiri, S. D., Zhang, G., Dunaway-Mariano, D., and Allen, K. N. (2006) Diversification of function in the haloacid dehalogenase enzyme superfamily: The role of the cap domain in hydrolytic phosphorus–carbon bond cleavage, *Bioorg. Chem. 34*, 394–409.
189. Heine, A., DeSantis, G., Luz, J. G., Mitchell, M., Wong, C. H., and Wilson, I. A. (2001) Observation of covalent intermediates in an enzyme mechanism at atomic resolution, *Science (Washington, DC, U. S.) 294*, 369–374.
190. Light, S. H., Anderson, W. F., and Lavie, A. (2013) Reassessing the type I dehydroquinate dehydratase catalytic triad: Kinetic and structural studies of Glu86 mutants, *Protein Sci. 22*, 418–424.
191. Shneier, A., Kleanthous, C., Deka, R., Coggins, J. R., and Abell, C. (1991) Observation of an imine intermediate on dehydroquinase by electrospray mass spectrometry, *J. Am. Chem. Soc. 113*, 9416–9418.
192. Light, S. H., Minasov, G., Shuvalova, L., Duban, M. E., Caffrey, M., Anderson, W. F., and Lavie, A. (2011) Insights into the mechanism of type I dehydroquinate dehydratases from structures of reaction intermediates, *J. Biol. Chem. 286*, 3531–3539.
193. Light, S. H., Antanasijevic, A., Krishna, S. N., Caffrey, M., Anderson, W. F., and Lavie, A. (2014) Crystal structures of type I dehydroquinate dehydratase in complex with quinate and shikimate suggest a novel mechanism of Schiff base formation, *Biochemistry 53*, 872–880.
194. He, Z., and Toney, M. D. (2006) Direct detection and kinetic analysis of covalent intermediate formation in the 4-amino-4-deoxychorismate synthase catalyzed reaction, *Biochemistry 45*, 5019–5028.
195. Fromme, J. C., and Verdine, G. L. (2002) Structural insights into lesion recognition and repair by the bacterial 8-oxoguanine DNA glycosylase MutM, *Nat. Struct. Biol. 9*, 544–552.
196. Fisch, F., Fleites, C. M., Delenne, M., Baudendistel, N., Hauer, B., Turkenburg, J. P., Hart, S., Bruce, N. C., and Grogan, G. (2010) A covalent succinylcysteine-like intermediate in the enzyme-catalyzed transformation of maleate to fumarate by maleate isomerase, *J. Am. Chem. Soc. 132*, 11455–11457.
197. Langenbach, R. J., Danenberg, P. V., and Heidelberger, C. (1972) Thymidylate synthetase: Mechanism of inhibition by 5-fluoro-2′-deoxyuridylate, *Biochem. Biophys. Res. Commun. 48*, 1565–1571.
198. Santi, D. V., and McHenry, C. S. (1972) 5-Fluoro-2′-deoxyuridylate: Covalent complex with thymidylate synthetase, *Proc. Natl. Acad. Sci. U.S.A. 69*, 1855–1857.
199. Costi, P. M., Liu, L., Finer-Moore, J. S., Stroud, R. M., and Santi, D. V. (1996) Asparagine 229 mutants of thymidylate synthase catalyze the methylation of 3-methyl-2′-deoxyuridine 5′-monophosphate, *Biochemistry 35*, 3944–3949.
200. Bellisario, R. L., Maley, G. F., Galivan, J. H., and Maley, F. (1976) Amino acid sequence at the FdUMP binding site of thymidylate synthetase, *Proc. Natl. Acad. Sci. U.S.A. 73*, 1848–1852.
201. Kalman, T. I. (1971) Glutathione-catalyzed hydrogen isotope exchange at position 5 of uridine. A model for enzymic carbon alkylation reactions of pyrimidines, *Biochemistry 10*, 2567–2573.
202. Sage, C. R., Rutenber, E. E., Stout, T. J., and Stroud, R. M. (1996) An essential role for wa-

ter in an enzyme reaction mechanism: The crystal structure of the thymidylate synthase mutant E58Q, *Biochemistry 35*, 16270–16281.
203. Stroud, R. M., and Finer-Moore, J. S. (2003) Conformational dynamics along an enzymatic reaction pathway: Thymidylate synthase, "the movie", *Biochemistry 42*, 239–247.
204. Montfort, W. R., Perry, K. M., Fauman, E. B., Finer-Moore, J. S., Maley, G. F., Hardy, L., Maley, F., and Stroud, R. M. (1990) Structure, multiple site binding, and segmental accommodation in thymidylate synthase on binding dUMP and an anti-folate, *Biochemistry 29*, 6964–6977.
205. Matthews, D. A., Appelt, K., Oatley, S. J., and Xuong, N. H. (1990) Crystal structure of *Escherichia coli* thymidylate synthase containing bound 5-fluoro-2′-deoxyuridylate and 10-propargyl-5,8-dideazafolate, *J. Mol. Biol. 214*, 923–936.
206. Huang, W., and Santi, D. V. (1997) Active site general catalysts are not necessary for some proton transfer reactions of thymidylate synthase, *Biochemistry 36*, 1869–1873.
207. Finer-Moore, J. S., Santi, D. V., and Stroud, R. M. (2003) Lessons and conclusions from dissecting the mechanism of a bisubstrate enzyme: Thymidylate synthase mutagenesis, function, and structure, *Biochemistry 42*, 248–256.
208. Hyatt, D. C., Maley, F., and Montfort, W. R. (1997) Use of strain in a stereospecific catalytic mechanism: Crystal structures of *Escherichia coli* thymidylate synthase bound to FdUMP and methylenetetrahydrofolate, *Biochemistry 36*, 4585–4594.
209. Huang, W., and Santi, D. V. (1994) Isolation of a covalent steady-state intermediate in Glutamate 60 mutants of thymidylate synthase, *J. Biol. Chem. 269*, 31327–31329.
210. Hardy, L. W., Graves, K. L., and Nalivaika, E. (1995) Electrostatic guidance of catalysis by a conserved glutamic acid in *Escherichia coli* dTMP synthase and bacteriophage T4 dCMP hydroxymethylase, *Biochemistry 34*, 8422–8432.
211. Matthews, D. A., Villafranca, J. E., Janson, C. A., Smith, W. W., Welsh, K., and Freer, S. (1990) Stereochemical mechanism of action for thymidylate synthase based on the X-ray structure of the covalent inhibitory ternary complex with 5-fluoro-2′-deoxyuridylate and 5,10-methylenetetrahydrofolate, *J. Mol. Biol. 214*, 937–948.
212. Klimasauskas, S., Kumar, S., Roberts, R. J., and Cheng, X. (1994) HhaI methyltransferase flips its target base out of the DNA helix, *Cell (Cambridge, MA, U. S.) 76*, 357–369.
213. Hamdane, D., Argentin, M., Cornu, D., Golinelli-Pimpaneau, B., and Fontecavet, M. (2012) FAD/Folate-dependent tRNA methyltransferase: Flavin as a new methyl-transfer agent, *J. Am. Chem. Soc. 134*, 19739–19745.
214. Tatum, C., Vederas, J., Schleicher, E., Benkovic, S. J., and Floss, H. (1977) Stereospecificity of thymidylate synthetase, *J. Chem. Soc., Chem. Commun.*, 218–220.
215. Slieker, L. J., and Benkovic, S. J. (1984) Synthesis of (6*R*,11*S*)- and (6*R*,11*R*)-5,10-methylene[11-^{1}H,^{2}H]tetrahydrofolate. Stereochemical paths of serine hydroxymethyltransferase, 5,10-methylenetetrahydrofolate dehydrogenase, and thymidylate synthetase catalysis, *J. Am. Chem. Soc. 106*, 1833–1838.
216. Pastore, E. J., and Friedkin, M. (1962) The enzymatic synthesis of thymidylate. II. Transfer of tritium from tetrahydrofolate to the methyl group of thymidylate, *J. Biol. Chem. 237*, 3802–3810.
217. Lorenson, M. Y., Maley, G. F., and Maley, F. (1967) The purification and properties of thymidylate synthetase from chick embryo extracts, *J. Biol. Chem. 242*, 3332–3344.
218. Kholodar, S. A., and Kohen, A. (2016) Noncovalent intermediate of thymidylate synthase: Fact or fiction?, *J. Am. Chem. Soc. 138*, 8056–8059.
219. Kholodar, S. A., Ghosh, A. K., Swiderek, K., Moliner, V., and Kohen, A. (2018) Parallel reaction pathways and noncovalent intermediates in thymidylate synthase revealed by experimental and computational tools, *Proc. Natl. Acad. Sci. U. S. A. 115*, 10311–10314.
220. Liu, Y., Barrett, J. E., Schultz, P. G., and Santi, D. V. (1999) Tyrosine 146 of thymidylate synthase assists proton abstraction from the 5-position of 2′-deoxyuridine 5′-monophosphate, *Biochemistry 38*, 848–852.
221. Barrett, J. E., Maltby, D. A., Santi, D. V., and Schultz, P. G. (1998) Trapping of the C5 methylene intermediate in thymidylate synthase, *J. Am. Chem. Soc. 120*, 449–450.
222. Islam, Z., Strutzenberg, T. S., Gurevic, I., and Kohen, A. (2014) Concerted versus stepwise

mechanism in thymidylate synthase, *J. Am. Chem. Soc. 136*, 9850–9853.
223. Agrawal, N., Hong, B. Y., Mihai, C., and Kohen, A. (2004) Vibrationally enhanced hydrogen tunneling in the *Escherichia coli* thymidylate synthase catalyzed reaction, *Biochemistry 43*, 1998–2006.
224. Spencer, H. T., Villafranca, J. E., and Appleman, J. R. (1997) Kinetic scheme for thymidylate synthase from *Escherichia coli*: Determination from measurements of ligand binding, primary and secondary isotope effects, and pre-steady-state catalysis, *Biochemistry 36*, 4212–4222.
225. Wang, Z., and Kohen, A. (2010) Thymidylate synthase catalyzed H-transfers: Two chapters in one tale, *J. Am. Chem. Soc. 132*, 9820–9825.
226. Graves, K. L., Butler, M. M., and Hardy, L. W. (1992) Roles of Cys148 and Asp179 in catalysis by deoxycytidylate hydroxymethylase from bacteriophage T4 examined by site-directed mutagenesis, *Biochemistry 31*, 10315–10321.
227. Mathews, I. I,, Deacon, A. M., Canaves, J. M., McMullan, D., Lesley, S. A., Agarwalla, S., and Kuhn, P. (2003) Functional analysis of substrate and cofactor complex structures of a thymidylate synthase-complementing protein, *Structure 11*, 677–690.
228. Conrad, J. A., Ortiz-Maldonado, M., Hoppe, S. W., and Palfey, B. A. (2014) Detection of intermediates in the oxidative half-reaction of the FAD-dependent thymidylate synthase from *Thermotoga maritima*: Carbon transfer without covalent pyrimidine activation, *Biochemistry 53*, 5199–5207.
229. Mishanina, T. V., Corcoran, J. M., and Kohen, A. (2014) Substrate activation in flavin-dependent thymidylate synthase, *J. Am. Chem. Soc. 136*, 10597–10600.
230. Mishanina, T. V., Koehn, E. M., Conrad, J. A., Palfey, B. A., Lesley, S. A., and Kohen, A. (2012) Trapping of an intermediate in the reaction catalyzed by flavin-dependent thymidylate synthase, *J. Am. Chem. Soc. 134*, 4442–4448.
231. Karplus, P. A., Pai, E. F., and Schulz, G. E. (1989) A crystallographic study of the glutathione binding site of glutathione reductase at 0.3-nm resolution, *Eur. J. Biochem. 178*, 693–703.
232. Pandey, A. S., Nocek, B., Clark, D. D., Ensign, S. A., and Peters, J. W. (2006) Mechanistic implications of the structure of the mixed-disulfide intermediate of the disulfide oxidoreductase, 2–ketopropyl-coenzyme M oxidoreductase/carboxylase, *Biochemistry 45*, 113–120.
233. Spallarossa, A., Forlani, F., Carpen, A., Armirotti, A., Pagani, S., Bolognesi, M., and Bordo, D. (2004) The "rhodanese" fold and catalytic mechanism of 3–mercaptopyruvate sulfurtransferases: Crystal structure of SseA from *Escherichia coli*, *J. Mol. Biol. 335*, 583–593.
234. Yadav, P. K., Yamada, K., Chiku, T., Koutmos, M., and Banerjee, R. (2013) Structure and kinetic analysis of H_2S production by human mercaptopyruvate sulfurtransferase, *J. Biol. Chem. 288*, 20002–20013.
235. Ploegman, J. H., Drent, G., Kalk, K. H., and Hol, W. G. (1979) The structure of bovine liver rhodanese. II. The active site in the sulfur-substituted and the sulfur-free enzyme, *J. Mol. Biol. 127*, 149–162.
236. Bordo, D., Deriu, D., Colnaghi, R., Carpen, A., Pagani, S., and Bolognesi, M. (2000) The crystal structure of a sulfurtransferase from *Azotobacter vinelandii* highlights the evolutionary relationship between the rhodanese and phosphatase enzyme families, *J. Mol. Biol. 298*, 691–704.
237. Choi, H. J., Kang, S. W., Yang, C. H., Rhee, S. G., and Ryu, S. E. (1998) Crystal structure of a novel human peroxidase enzyme at 2.0 Å resolution, *Nat. Struct. Biol. 5*, 400–406.
238. Yeh, J. I., Claiborne, A., and Hol, W. G. (1996) Structure of the native cysteine-sulfenic acid redox center of enterococcal NADH peroxidase refined at 2.8 Å resolution, *Biochemistry 35*, 9951–9957.
239. Huang, S., Mahanta, N., Begley, T. P., and Ealick, S. E. (2012) Pseudouridine monophosphate glycosidase: A new glycosidase mechanism, *Biochemistry 51*, 9245–9255.
240. Wong, L. J., and Frey, P. A. (1974) Galactose 1-phosphate uridylyltransferase. Isolation of a uridylyl-enzyme intermediate, *J. Biol. Chem. 249*, 2322–2324.
241. Mourad, N., and Parks, R. E., Jr. (1965) NDP Kinase: Demonstration of phosphorylated enzyme as the reactive intermediate, *Biochem. Biophys. Res. Commun. 19*, 312–316.

242. Mourad, N., and Parks, R. E., Jr. (1966) Erythrocytic nucleoside diphosphokinase. 3. Studies with free and phosphorylated enzyme and evidence for an essential thiol group, *J. Biol. Chem. 241*, 3838–3844.
243. Settembre, E. C., Dorrestein, P. C., Zhai, H., Chatterjee, A., McLafferty, F. W., Begley, T. P., and Ealick, S. E. (2004) Thiamin biosynthesis in *Bacillus subtilis*: structure of the thiazole synthase/sulfur carrier protein complex, *Biochemistry 43*, 11647–11657.
244. Jerga, A., Stanley, M. D., and Tipton, P. A. (2006) Chemical mechanism and specificity of the C5–mannuronan epimerase reaction, *Biochemistry 45*, 9138–9144.
245. Rozeboom, H. J., Bjerkan, T. M., Kalk, K. H., Ertesvag, H., Holtan, S., Aachmann, F. L., Valla, S., and Dijkstra, B. W. (2008) Structural and mutational characterization of the catalytic A-module of the mannuronan C-5-epimerase AlgE4 from *Azotobacter vinelandii*, *J. Biol. Chem. 283*, 23819–23828.
246. Henderson, K. L., Evensen, C. E., Molzahn, C. M., Felth, L. C., Dyke, S., Liao, G., Shkel, I. A., and Record, M. T., Jr. (2019) RNA Polymerase: Step-by-step kinetics and mechanism of transcription initiation, *Biochemistry 58*, 2339–2352.
247. Peterson, P. E., and Smith, T. J. (1999) The structure of bovine glutamate dehydrogenase provides insights into the mechanism of allostery, *Structure 7*, 769–782.
248. Maniscalco, S. J., Tally, J. F., Harris, S. W., and Fisher, H. F. (2003) The direct measurement of thermodynamic parameters of reactive transient intermediates of the L-glutamate dehydrogenase reaction, *J. Biol. Chem. 278*, 16129–16134.
249. Rao, K. S., Fu, Z., Albro, M., Narayanan, B., Baddam, S., Lee, H. J., Kim, J. J., and Frerman, F. E. (2007) The effect of a Glu370Asp mutation in glutaryl-CoA dehydrogenase on proton transfer to the dienolate intermediate, *Biochemistry 46*, 14468–14477.
250. Westover, J. B., Goodman, S. I., and Frerman, F. E. (2001) Binding, hydration, and decarboxylation of the reaction intermediate glutaconyl-coenzyme A by human glutaryl-CoA dehydrogenase, *Biochemistry 40*, 14106–14114.
251. Chang, K. H., and Dunaway-Mariano, D. (1996) Determination of the chemical pathway for 4-chlorobenzoate:coenzyme A ligase catalysis, *Biochemistry 35*, 13478–13484.
252. Sasiak, K., and Rilling, H. C. (1988) Purification to homogeneity and some properties of squalene synthetase, *Arch. Biochem. Biophys. 260*, 622–627.
253. Altman, L. J., Kowerski, R. C., and Rilling, H. C. (1971) Synthesis and conversion of presqualene alcohol to squalene, *J. Am. Chem. Soc. 93*, 1782–1783.
254. Coates, R. M., and Robinson, W. H. (1971) Stereoselective total synthesis of (±)-presqualene alcohol, *J. Am. Chem. Soc. 93*, 1785–1786.
255. Popjak, G., Edmond, J., and Wong, S.-M. (1973) Absolute configuration of presqualene alcohol, *J. Am. Chem. Soc. 95*, 2713–2714.
256. Rilling, H. C. (1966) A new intermediate in the biosynthesis of squalene, *J. Biol. Chem. 241*, 3233–3236.
257. Wood, T. G., Weisz, O. A., and Kozarich, J. W. (1984) Acyl-enzyme exchange detection by intermolecular oxygen scrambling: An application of the oxygen-18 isotope effect in carbon-13 NMR, *J. Am. Chem. Soc. 106*, 2222–2223.
258. Buckel, W. (1976) Acetic anhydride: An intermediate analogue in the acyl-exchange reaction of citramalate lyase, *Eur. J. Biochem. 64*, 263–267.
259. Basu, A., Subramanian, S., Hiremath, L. S., and SivaRaman, C. (1983) *S*-Acylated residues of the acyl-carrier protein subunit of *Klebsiella aerogenes* citrate lyase, *Biochem. Biophys. Res. Commun. 114*, 310–317.
260. Powers, S. G., and Meister, A. (1976) Identification of enzyme-bound activated CO_2 as carbonic-phosphoric anhydride: Isolation of the corresponding trimethyl derivative from the active site of glutamine-dependent carbamyl phosphate synthetase, *Proc. Natl. Acad. Sci. U.S.A. 73*, 3020–3024.
261. Wang, S., and Eisenberg, D. (2003) Crystal structures of a pantothenate synthetase from *M. tuberculosis* and its complexes with substrates and a reaction intermediate, *Protein Sci. 12*, 1097–1108.
262. Kack, H., Gibson, K. J., Lindqvist, Y., and Schneider, G. (1998) Snapshot of a phosphorylated substrate intermediate by kinetic crystallography, *Proc. Natl. Acad. Sci. U.S.A. 95*, 5495–5500.
263. Gibson, K. J. (1997) Isolation and chemistry of the mixed anhydride intermediate in the

reaction catalyzed by dethiobiotin synthetase, *Biochemistry 36*, 8474–8478.
264. Reichmann, D., Coute, Y., and Ollagnier de Choudens, S. (2015) Dual activity of quinolinate synthase: Triose phosphate isomerase and dehydration activities play together to form quinolinate, *Biochemistry 54*, 6443–6446.
265. Cherrier, M. V., Chan, A., Darnault, C., Reichmann, D., Amara, P., Ollagnier de Choudens, S., and Fontecilla-Camps, J. C. (2014) The crystal structure of Fe_4S_4 quinolinate synthase unravels an enzymatic dehydration mechanism that uses tyrosine and a hydrolase-type triad, *J. Am. Chem. Soc. 136*, 5253–5256.
266. Volbeda, A., Darnault, C., Renoux, O., Reichmann, D., Amara, P., Ollagnier de Choudens, S., and Fontecilla-Camps, J. C. (2016) Crystal structures of quinolinate synthase in complex with a substrate analogue, the condensation intermediate, and substrate-derived product, *J. Am. Chem. Soc. 138*, 11802–11809.
267. Volbeda, A., Saez Cabodevilla, J., Darnault, C., Gigarel, O., Han, T. H., Renoux, O., Hamelin, O., Ollagnier-de-Choudens, S., Amara, P., and Fontecilla-Camps, J. C. (2018) Crystallographic trapping of reaction intermediates in quinolinic acid synthesis by NadA, *ACS Chem. Biol. 13*, 1209–1217.
268. Esakova, O. A., Silakov, A., Grove, T. L., Warui, D. M., Yennawar, N. H., and Booker, S. J. (2019) An unexpected species determined by X-ray crystallography that may represent an intermediate in the reaction catalyzed by quinolinate synthase, *J. Am. Chem. Soc. 141*, 14142–14151.
269. Fenwick, M. K., and Ealick, S. E. (2016) Crystal structures of the iron-sulfur cluster-dependent quinolinate synthase in complex with dihydroxyacetone phosphate, iminoaspartate analogues, and quinolinate, *Biochemistry 55*, 4135–4139.
270. Esakova, O. A., Silakov, A., Grove, T. L., Saunders, A. H., McLaughlin, M. I., Yennawar, N. H., and Booker, S. J. (2016) Structure of quinolinate synthase from *Pyrococcus horikoshii* in the presence of its product, quinolinic acid, *J. Am. Chem. Soc. 138*, 7224–7227.
271. Cane, D. E., and Tsantrizos, Y. S. (1996) Aristolochene synthase. Elucidation of the cryptic germacrene A synthase activity using the anomalous substrate dihydrofarnesyl diphosphate, *J. Am. Chem. Soc. 118*, 10037–10040.
272. Adams, M. J., Ellis, G. H., Gover, S., Naylor, C. E., and Phillips, C. (1994) Crystallographic study of coenzyme, coenzyme analogue and substrate binding in 6-phosphogluconate dehydrogenase: Implications for NADP specificity and the enzyme mechanism, *Structure 2*, 651–668.
273. Rippa, M., Signorini, M., and Dallocchio, F. (1973) A multiple role for the coenzyme in the mechanism of action of 6-phosphogluconate dehydrogenase. The oxidative decarboxylation of 2-deoxy-6-phosphogluconate, *J. Biol. Chem. 248*, 4920–4925.
274. Timmons, R. B., Rhee, S. G., Luterman, D. L., and Chock, P. B. (1974) Mechanistic studies of glutamine synthetase from *Escherichia coli*. Fluorometric identification of a reactive intermediate in the biosynthetic reaction, *Biochemistry 13*, 4479–4485.
275. Gass, J. D., and Meister, A. (1970) 1-Amino-1,3-dicarboxycyclohexane (cycloglutamic acid), a new glutamic acid analog and a substrate of glutamine synthetase, *Biochemistry 9*, 842–846.
276. Tsuda, Y., Stephani, R. A., and Meister, A. (1971) Direct evidence for the formation of an acyl phosphate by glutamine synthetase, *Biochemistry 10*, 3186–3189.
277. Abeles, R. H., Fish, S., and Lapinskas, B. (1982) *S*-Adenosylhomocysteinase: Mechanism of inactivation by 2′-deoxyadenosine and interaction with other nucleosides, *Biochemistry 21*, 5557–5562.
278. Gunsior, M., Ravel, J., Challis, G. L., and Townsend, C. A. (2004) Engineering *p*-hydroxyphenylpyruvate dioxygenase to a *p*-hydroxymandelate synthase and evidence for the proposed benzene oxide intermediate in homogentisate formation, *Biochemistry 43*, 663–674.
279. Das, A., Mahale, S., Prashar, V., Bihani, S., Ferrer, J. L., and Hosur, M. V. (2010) X-ray snapshot of HIV-1 protease in action: observation of tetrahedral intermediate and short ionic hydrogen bond SIHB with catalytic aspartate, *J. Am. Chem. Soc. 132*, 6366–6373.
280. Kovalevsky, A. Y., Chumanevich, A. A., Liu, F., Louis, J. M., and Weber, I. T. (2007) Caught in the Act: the 1.5 Å resolution crystal structures of the HIV-1 protease and the I54V

mutant reveal a tetrahedral reaction intermediate, *Biochemistry 46*, 14854–14864.
281. Lee, M. E., Dyer, D. H., Klein, O. D., Bolduc, J. M., Stoddard, B. L., and Koshland, D. E., Jr. (1995) Mutational analysis of the catalytic residues Lysine 230 and Tyrosine 160 in the $NADP^+$-dependent isocitrate dehydrogenase from *Escherichia coli*, *Biochemistry 34*, 378–384.
282. Bolduc, J. M., Dyer, D. H., Scott, W. G., Singer, P., Sweet, R. M., Koshland, D. E., Jr., and Stoddard, B. L. (1995) Mutagenesis and Laue structures of enzyme intermediates: Isocitrate dehydrogenase, *Science (Washington, DC, U. S.) 268*, 1312–1318.
283. Teng, C. Y. P., and Ganem, B. (1984) Shikimate-derived metabolites. 13. A key intermediate in the biosynthesis of anthranilate from chorismate, *J. Am. Chem. Soc. 106*, 2463–2464.
284. Morollo, A. A., Finn, M. G., and Bauerle, R. (1993) Isolation and structure determination of 2-amino-2-deoxyisochorismate: An intermediate in the biosynthesis of anthranilate, *J. Am. Chem. Soc. 115*, 816–817.
285. Morollo, A. A., and Bauerle, R. (1993) Characterization of composite aminodeoxyisochorismate synthase and aminodeoxyisochorismate lyase activities of anthranilate synthase, *Proc. Natl. Acad. Sci. U.S.A. 90*, 9983–9987.
286. Hawkinson, D. C., Eames, T. C., and Pollack, R. M. (1991) Kinetic competence of an externally generated dienol intermediate with steroid isomerase, *Biochemistry 30*, 6956–6964.
287. Celeste, L. R., Chai, G., Bielak, M., Minor, W., Lovelace, L. L., and Lebioda, L. (2012) Mechanism of N^{10}–formyltetrahydrofolate synthetase derived from complexes with intermediates and inhibitors, *Protein Sci. 21*, 219–228.
288. Mejillano, M. R., Jahansouz, H., Matsunaga, T. O., Kenyon, G. L., and Himes, R. H. (1989) Formation and utilization of formyl phosphate by N^{10}–formyltetrahydrofolate synthetase: Evidence for formyl phosphate as an intermediate in the reaction, *Biochemistry 28*, 5136–5145.
289. Smithers, G. W., Jahansouz, H., Kofron, J. L., Himes, R. H., and Reed, G. H. (1987) Substrate activity of synthetic formyl phosphate in the reaction catalyzed by formyltetrahydrofolate synthetase, *Biochemistry 26*, 3943–3948.
290. Buttlaire, D. H., Himes, R. H., and Reed, G. H. (1976) Formyltetrahydrofolate synthetase-catalyzed formation of ATP from carbamyl phosphate and ADP. Evidence for a formyl phosphate intermediate in the enzyme's catalytic mechanism, *J. Biol. Chem. 251*, 4159–4161.
291. Wolfenden, R., Kaufman, J., and Macon, J. B. (1969) Ring-modified substrates of adenosine deaminases, *Biochemistry 8*, 2412–2415.
292. Jones, W., Kurz, L. C., and Wolfenden, R. (1989) Transition-state stabilization by adenosine deaminase: 1,6-Addition of water to purine ribonucleoside, the enzyme's affinity for 6-hydroxy-1,6-dihydropurine ribonucleoside, and the effective concentration of substrate water at the active site, *Biochemistry 28*, 1242–1247.
293. Wang, Z., and Quiocho, F. A. (1998) Complexes of adenosine deaminase with two potent inhibitors: X-Ray structures in four independent molecules at pH of maximum activity, *Biochemistry 37*, 8314–8324.
294. Pierce, J., Tolbert, N. E., and Barker, R. (1980) Interaction of ribulosebisphosphate carboxylase/oxygenase with transition-state analogues, *Biochemistry 19*, 934–942.
295. Schloss, J. V. (1988) Comparative affinities of the epimeric reaction-intermediate analogs 2- and 4-carboxy-D-arabinitol 1,5-bisphosphate for spinach ribulose 1,5-bisphosphate carboxylase, *J. Biol. Chem. 263*, 4145–4150.
296. Siegel, M. I., and Lane, M. D. (1973) Chemical and enzymatic evidence for the participation of a 2-carboxy-3-ketoribitol-1,5-diphosphate intermediate in the carboxylation of ribulose 1,5-diphosphate, *J. Biol. Chem. 248*, 5486–5498.
297. Schloss, J. V., and Lorimer, G. H. (1982) The stereochemical course of ribulosebisphosphate carboxylase. Reductive trapping of the 6-carbon reaction-intermediate, *J. Biol. Chem. 257*, 4691–4694.
298. Andersson, I. (1996) Large structures at high resolution: the 1.6 Å crystal structure of spinach ribulose-1,5–bisphosphate carboxylase/oxygenase complexed with 2-carboxyarabinitol bisphosphate, *J. Mol. Biol. 259*, 160–174.
299. Knight, S., Andersson, I., and Branden, C. I. (1990) Crystallographic analysis of ribulose 1,5-bisphosphate carboxylase from spinach

at 2.4 Å resolution. Subunit interactions and active site, *J. Mol. Biol. 215*, 113–160.
300. Andersson, I., Knight, S., Schneider, G., Lindqvist, Y., Lundqvist, T., Braenden, C. I., and Lorimer, G. H. (1989) Crystal structure of the active site of ribulose-bisphosphate carboxylase, *Nature (London, U. K.) 337*, 229–234.
301. Newman, J., and Gutteridge, S. (1993) The X-ray structure of *Synechococcus* ribulose-bisphosphate carboxylase/oxygenase-activated quaternary complex at 2.2-Å resolution, *J. Biol. Chem. 268*, 25876–25886.
302. Wishnick, M., Lane, M. D., and Scrutton, M. C. (1970) The interaction of metal ions with ribulose 1,5-diphosphate carboxylase from spinach, *J. Biol. Chem. 245*, 4939–4947.
303. Alberg, D. G., Lauhon, C. T., Nyfeler, R., Faessler, A., and Bartlett, P. A. (1992) Inhibition of 5-enolpyruvoylshikimate 3–phosphate (EPSP) synthase by analogs of the tetrahedral intermediate and of EPSP, *J. Am. Chem. Soc. 114*, 3535–3546.
304. An, M., Maitra, U., Neidlein, U., and Bartlett, P. A. (2003) 5-Enolpyruvylshikimate 3-phosphate synthase: Chemical synthesis of the tetrahedral intermediate and assignment of the stereochemical course of the enzymatic reaction, *J. Am. Chem. Soc. 125*, 12759–12767.
305. Funke, T., Healy-Fried, M. L., Han, H., Alberg, D. G., Bartlett, P. A., and Schonbrunn, E. (2007) Differential inhibition of class I and class II 5-enolpyruvylshikimate-3-phosphate synthases by tetrahedral reaction intermediate analogues, *Biochemistry 46*, 13344–13351.
306. Eschenburg, S., Kabsch, W., Healy, M. L., and Schonbrunn, E. (2003) A new view of the mechanisms of UDP-*N*-acetylglucosamine enolpyruvyl transferase (MurA) and 5-enolpyruvylshikimate-3-phosphate synthase (AroA) derived from X-ray structures of their tetrahedral reaction intermediate states, *J. Biol. Chem. 278*, 49215–49222.
307. Park, H., Hilsenbeck, J. L., Kim, H. J., Shuttleworth, W. A., Park, Y. H., Evans, J. N., and Kang, C. (2004) Structural studies of *Streptococcus pneumoniae* EPSP synthase in unliganded state, tetrahedral intermediate-bound state and S3P-GLP-bound state, *Mol. Microbiol. 51*, 963–971.
308. Anderson, K. S., Sikorski, J. A., and Johnson, K. A. (1988) A tetrahedral intermediate in the EPSP synthase reaction observed by rapid quench kinetics, *Biochemistry 27*, 7395–7406.
309. Anderson, K. S., Sikorski, J. A., Benesi, A. J., and Johnson, K. A. (1988) Isolation and structural elucidation of the tetrahedral intermediate in the EPSP synthase enzymic pathway, *J. Am. Chem. Soc. 110*, 6577–6579.
310. Barlow, P. N., Appleyard, R. J., Wilson, J. O., and Evans, J. N. (1989) Direct observation of the enzyme-intermediate complex of 5-enolpyruvylshikimate-3-phosphate synthase by ^{13}C NMR spectroscopy, *Biochemistry 28*, 7985–7991.
311. Anderson, K. S., and Johnson, K. A. (1990) "Kinetic competence" of the 5-enolpyruvoylshikimate-3-phosphate synthase tetrahedral intermediate, *J. Biol. Chem. 265*, 5567–5572.
312. Byczynski, B., Mizyed, S., and Berti, P. J. (2003) Nonenzymatic breakdown of the tetrahedral (α-carboxyketal phosphate) intermediates of MurA and AroA, two carboxyvinyl transferases. Protonation of different functional groups controls the rate and fate of breakdown, *J. Am. Chem. Soc. 125*, 12541–12550.
313. Clark, M. E., and Berti, P. J. (2007) Enolpyruvyl activation by enolpyruvylshikimate-3-phosphate synthase, *Biochemistry 46*, 1933–1940.
314. Schonbrunn, E., Eschenburg, S., Shuttleworth, W. A., Schloss, J. V., Amrhein, N., Evans, J. N., and Kabsch, W. (2001) Interaction of the herbicide glyphosate with its target enzyme 5-enolpyruvylshikimate 3-phosphate synthase in atomic detail, *Proc. Natl. Acad. Sci. U. S. A. 98*, 1376–1380.
315. Kim, D. H., Lees, W. J., and Walsh, C. T. (1995) Stereochemical analysis of the tetrahedral adduct formed at the active site of UDP-GlcNAc enolpyruvyl transferase from the pseudosubstrates, (*E*)- and (*Z*)-3-fluorophosphoenolpyruvate, in D_2O, *J. Am. Chem. Soc. 117*, 6380–6381.
316. Ramilo, C., Appleyard, R. J., Wanke, C., Krekel, F., Amrhein, N., and Evans, J. N. (1994) Detection of the covalent intermediate of UDP-*N*-acetylglucosamine enolpyruvyl transferase by solution-state and time-resolved solid-state NMR spectroscopy, *Biochemistry 33*, 15071–15079.
317. Skarzynski, T., Kim, D. H., Lees, W. J., Walsh, C. T., and Duncan, K. (1998) Stereochemical course of enzymatic enolpyruvyl transfer and

catalytic conformation of the active site revealed by the crystal structure of the fluorinated analogue of the reaction tetrahedral intermediate bound to the active site of the C115A mutant of MurA, *Biochemistry 37*, 2572–2577.
318. Knapp, S., Vocadlo, D., Gao, Z., Kirk, B., Lou, J., and Withers, S. G. (1996) NAG-Thiazoline, an *N*-acetyl-β-hexosaminidase inhibitor that implicates acetamido participation, *J. Am. Chem. Soc. 118*, 6804–6805.
319. Macauley, M. S., Whitworth, G. E., Debowski, A. W., Chin, D., and Vocadlo, D. J. (2005) *O*-GlcNAcase uses substrate-assisted catalysis: Kinetic analysis and development of highly selective mechanism-inspired inhibitors, *J. Biol. Chem. 280*, 25313–25322.
320. Mark, B. L., Vocadlo, D. J., Knapp, S., Triggs-Raine, B. L., Withers, S. G., and James, M. N. (2001) Crystallographic evidence for substrate-assisted catalysis in a bacterial β-hexosaminidase, *J. Biol. Chem. 276*, 10330–10337.
321. Mark, B. L., Mahuran, D. J., Cherney, M. M., Zhao, D., Knapp, S., and James, M. N. (2003) Crystal structure of human β-hexosaminidase B: Understanding the molecular basis of Sandhoff and Tay-Sachs disease, *J. Mol. Biol. 327*, 1093–1109.
322. Lemieux, M. J., Mark, B. L., Cherney, M. M., Withers, S. G., Mahuran, D. J., and James, M. N. (2006) Crystallographic structure of human β-hexosaminidase A: Interpretation of Tay-Sachs mutations and loss of GM2 ganglioside hydrolysis, *J. Mol. Biol. 359*, 913–929.
323. He, Y., Macauley, M. S., Stubbs, K. A., Vocadlo, D. J., and Davies, G. J. (2010) Visualizing the reaction coordinate of an *O*-GlcNAc hydrolase, *J. Am. Chem. Soc. 132*, 1807–1809.
324. Essen, L. O., Perisic, O., Katan, M., Wu, Y., Roberts, M. F., and Williams, R. L. (1997) Structural mapping of the catalytic mechanism for a mammalian phosphoinositide-specific phospholipase C, *Biochemistry 36*, 1704–1718.
325. Bruzik, K. S., Morocho, A. M., Jhon, D. Y., Rhee, S. G., and Tsai, M. D. (1992) Phospholipids chiral at phosphorus. Stereochemical mechanism for the formation of inositol 1-phosphate catalyzed by phosphatidylinositol-specific phospholipase C, *Biochemistry 31*, 5183–5193.
326. Read, J. A., Ahmed, R. A., Morrison, J. P., Coleman, W. G., Jr., and Tanner, M. E. (2004) The mechanism of the reaction catalyzed by ADP-β-L-glycero-D-manno-heptose 6-epimerase, *J. Am. Chem. Soc. 126*, 8878–8879.
327. Mayer, A., and Tanner, M. E. (2007) Intermediate release by ADP-L-glycero-D-manno-heptose 6-epimerase, *Biochemistry 46*, 6149–6155.
328. Deacon, A. M., Ni, Y. S., Coleman, W. G., Jr., and Ealick, S. E. (2000) The crystal structure of ADP-L-glycero-D-mannoheptose 6-epimerase: Catalysis with a twist, *Structure 8*, 453–462.
329. Kowatz, T., Morrison, J. P., Tanner, M. E., and Naismith, J. H. (2010) The crystal structure of the Y140F mutant of ADP-L-glycero-D-manno-heptose 6-epimerase bound to ADP-β-D-mannose suggests a one base mechanism, *Protein Sci. 19*, 1337–1343.
330. Maxwell, E. S. (1957) The enzymic interconversion of uridine diphosphogalactose and uridine diphosphoglucose, *J. Biol. Chem. 229*, 139–151.
331. Thoden, J. B., and Holden, H. M. (1998) Dramatic differences in the binding of UDP-galactose and UDP-glucose to UDP-galactose 4-epimerase from *Escherichia coli*, *Biochemistry 37*, 11469–11477.
332. Wilson, D. B., and Hogness, D. S. (1964) The enzymes of the galactose operon in *Escherichia coli*. I. Purification and characterization of uridine diphosphogalactose 4-epimerase, *J. Biol. Chem. 239*, 2469–2481.
333. Nelsestuen, G., and Kirkwood, S. (1970) Mechanism of action of uridine diphosphoglucose 4-epimerase, *Fed. Proc. 29*, 337.
334. Maitra, U. S., and Ankel, H. (1971) Uridine diphosphate-4-keto-glucose, an intermediate in the uridine diphosphate-galactose-4-epimerase reaction, *Proc. Natl. Acad. Sci. U.S.A. 68*, 2660–2663.
335. Maitra, U. S., and Ankel, H. (1973) The intermediate in the uridine diphosphate galactose 4-epimerase reaction. Resolution of an apparent ambiguity, *J. Biol. Chem. 248*, 1477–1479.
336. Thoden, J. B., Frey, P. A., and Holden, H. M. (1996) Molecular structure of the NADH/UDP-glucose abortive complex of UDP-galactose 4-epimerase from *Escherichia coli*: implications for the catalytic mechanism, *Biochemistry 35*, 5137–5144.

337. Hallis, T. M., and Liu, H.-W. (1999) Mechanistic studies of the biosynthesis of tyvelose: Purification and characterization of CDP-D-tyvelose 2-epimerase, *J. Am. Chem. Soc. 121*, 6765–6766.
338. Varrot, A., Yip, V. L., Li, Y., Rajan, S. S., Yang, X., Anderson, W. F., Thompson, J., Withers, S. G., and Davies, G. J. (2005) NAD^+ and metal-ion dependent hydrolysis by family 4 glycosidases: Structural insight into specificity for phospho-β-D-glucosides, *J. Mol. Biol. 346*, 423–435.
339. Yip, V. L., Varrot, A., Davies, G. J., Rajan, S. S., Yang, X., Thompson, J., Anderson, W. F., and Withers, S. G. (2004) An unusual mechanism of glycoside hydrolysis involving redox and elimination steps by a family 4 β-glycosidase from *Thermotoga maritima*, *J. Am. Chem. Soc. 126*, 8354–8355.
340. Muth, W. L., and Costilow, R. N. (1974) Ornithine cyclase (deaminating). III. Mechanism of the conversion of ornithine to proline, *J. Biol. Chem. 249*, 7463–7467.
341. Goodman, J. L., Wang, S., Alam, S., Ruzicka, F. J., Frey, P. A., and Wedekind, J. E. (2004) Ornithine cyclodeaminase: Structure, mechanism of action, and implications for the μ-crystallin family, *Biochemistry 43*, 13883–13891.
342. Chen, C. H., and Eisenberg, F., Jr. (1975) Myoinososse-2 1-phosphate: An intermediate in the myoinositol 1-phosphate synthase reaction, *J. Biol. Chem. 250*, 2963–2967.
343. Migaud, M. E., and Frost, J. W. (1995) Inhibition of *myo*-inositol-1-phosphate synthase by a reaction coordinate intermediate, *J. Am. Chem. Soc. 117*, 5154–5155.
344. Neelon, K., Roberts, M. F., and Stec, B. (2011) Crystal structure of a trapped catalytic intermediate suggests that forced atomic proximity drives the catalysis of mIPS, *Biophys. J. 101*, 2816–2824.
345. Kupke, T., Hernandez-Acosta, P., Steinbacher, S., and Culianez-Macia, F. A. (2001) *Arabidopsis thaliana* flavoprotein AtHAL3a catalyzes the decarboxylation of 4′-phosphopantothenoylcysteine to 4′-phosphopantetheine, a key step in coenzyme A biosynthesis, *J. Biol. Chem. 276*, 19190–19196.
346. Strauss, E., and Begley, T. P. (2001) Mechanistic studies on phosphopantothenoylcysteine decarboxylase, *J. Am. Chem. Soc. 123*, 6449–6450.
347. Strauss, E., Zhai, H., Brand, L. A., McLafferty, F. W., and Begley, T. P. (2004) Mechanistic studies on phosphopantothenoylcysteine decarboxylase: Trapping of an enethiolate intermediate with a mechanism-based inactivating agent, *Biochemistry 43*, 15520–15533.
348. Rankin, J. A., Mauban, R. C., Fellner, M., Desguin, B., McCracken, J., Hu, J., Varganov, S. A., and Hausinger, R. P. (2018) Lactate racemase nickel-pincer cofactor operates by a proton-coupled hydride transfer mechanism, *Biochemistry 57*, 3244–3251.
349. Kuo, D. J., O'Connell, E. L., and Rose, I. A. (1979) Physical, chemical, and enzymological characterization of enolpyruvate, *J. Am. Chem. Soc. 101*, 5025–5030.
350. Peliska, J. A., and O'Leary, M. H. (1991) Preparation and properties of enolpyruvate, *J. Am. Chem. Soc. 113*, 1841–1842.
351. Kuo, D. J., and Rose, I. A. (1982) Utilization of enolpyruvate by the carboxybiotin form of transcarboxylase: Evidence for a nonconcerted mechanism, *J. Am. Chem. Soc. 104*, 3235–3236.
352. Hall, P. R., Zheng, R., Antony, L., Pusztai-Carey, M., Carey, P. R., and Yee, V. C. (2004) Transcarboxylase 5*S* structures: Assembly and catalytic mechanism of a multienzyme complex subunit, *EMBO J. 23*, 3621–3631.
353. Lietzan, A. D., and St Maurice, M. (2013) A substrate-induced biotin binding pocket in the carboxyltransferase domain of pyruvate carboxylase, *J. Biol. Chem. 288*, 19915–19925.
354. Ausenhus, S. L., and O'Leary, M. H. (1992) Hydrolysis of phospho*enol*pyruvate catalyzed by phospho*enol*pyruvate carboxylase from *Zea mays*, *Biochemistry 31*, 6427–6431.
355. Bild, G. S., and Morris, J. C. (1984) Detection of β-carbanion formation during kynurenine hydrolysis catalyzed by *Pseudomonas marginalis* kynureninase, *Arch. Biochem. Biophys. 235*, 41–47.
356. Seeholzer, S. H., Jaworowski, A., and Rose, I. A. (1991) Enolpyruvate: Chemical determination as a pyruvate kinase intermediate, *Biochemistry 30*, 727–732.
357. Healy, M. J., and Christen, P. (1973) Mechanistic probes for enzymatic reactions. Oxidation-reduction indicators as oxidants of intermediary carbanions (studies with aldolase, aspartate aminotransferase, pyruvate decarboxylase, and 6–phosphogluconate dehydrogenase), *Biochemistry 12*, 35–41.

358. Sundaramoorthy, R., Iulek, J., Barrett, M. P., Bidet, O., Ruda, G. F., Gilbert, I. H., and Hunter, W. N. (2007) Crystal structures of a bacterial 6–phosphogluconate dehydrogenase reveal aspects of specificity, mechanism and mode of inhibition by analogues of high-energy reaction intermediates, *FEBS J. 274*, 275–286.
359. Stubbe, J., Fish, S., and Abeles, R. H. (1980) Are carboxylations involving biotin concerted or nonconcerted?, *J. Biol. Chem. 255*, 236–242.
360. Diacovich, L., Mitchell, D. L., Pham, H., Gago, G., Melgar, M. M., Khosla, C., Gramajo, H., and Tsai, S. C. (2004) Crystal structure of the β-subunit of acyl-CoA carboxylase: Structure-based engineering of substrate specificity, *Biochemistry 43*, 14027–14036.
361. Mac Sweeney, A., Lange, R., Fernandes, R. P., Schulz, H., Dale, G. E., Douangamath, A., Proteau, P. J., and Oefner, C. (2005) The crystal structure of *E.coli* 1-deoxy-D-xylulose-5-phosphate reductoisomerase in a ternary complex with the antimalarial compound fosmidomycin and NADPH reveals a tight-binding closed enzyme conformation, *J. Mol. Biol. 345*, 115–127.
362. Fox, D. T., and Poulter, C. D. (2005) Mechanistic studies with 2-C-methyl-D-erythritol 4-phosphate synthase from *Escherichia coli*, *Biochemistry 44*, 8360–8368.
363. Anderson, V. E., Weiss, P. M., and Cleland, W. W. (1984) Reaction intermediate analogues for enolase, *Biochemistry 23*, 2779–2786.
364. Mechaly, A. E., Haouz, A., Miras, I., Barilone, N., Weber, P., Shepard, W., Alzari, P. M., and Bellinzoni, M. (2012) Conformational changes upon ligand binding in the essential class II fumarase Rv1098c from *Mycobacterium tuberculosis*, *FEBS Lett. 586*, 1606–1611.
365. Porter, D. J., and Bright, H. J. (1980) 3–Carbanionic substrate analogues bind very tightly to fumarase and aspartase, *J. Biol. Chem. 255*, 4772–4780.
366. Schloss, J. V., Porter, D. J., Bright, H. J., and Cleland, W. W. (1980) Nitro analogues of citrate and isocitrate as transition-state analogues for aconitase, *Biochemistry 19*, 2358–2362.
367. Danby, P. M., and Withers, S. G. (2017) Glycosyl cations versus allylic cations in spontaneous and enzymatic hydrolysis, *J. Am. Chem. Soc. 139*, 10629–10632.
368. Stokes, T. M., and Wilson, I. B. (1972) A common intermediate in the hydrolysis of β-galactosides by β-galactosidase from *Escherichia coli*, *Biochemistry 11*, 1061–1064.
369. Amyes, T. L., and Jencks, W. P. (1988) Absence of a common ion effect on the hydrolysis of an α-azido ether of an aliphatic aldehyde, *J. Am. Chem. Soc. 110*, 3677–3679.
370. Ryono, D. E., and Loudon, G. M. (1976) Electrostatic facilitation of general acid-catalyzed α-oxonium ion formation in a lysozyme-like environment: Synthesis of models, *J. Am. Chem. Soc. 98*, 1889–1899.
371. Cherian, X. M., Vanarman, S. A., and Czarnik, A. W. (1990) Models for nucleoside glycosylase enzymes. Evidence that the hydrolysis of β-D-ribofuranosides requires a backside preassociation nucleophile, *J. Am. Chem. Soc. 112*, 4490–4498.
372. Klein, H. W., Im, M. J., and Palm, D. (1986) Mechanism of the phosphorylase reaction. Utilization of D-*gluco*-hept-1-enitol in the absence of primer, *Eur. J. Biochem. 157*, 107–114.
373. Johnson, L. N., Acharya, K. R., Jordan, M. D., and McLaughlin, P. J. (1990) Refined crystal structure of the phosphorylase-heptulose 2-phosphate-oligosaccharide-AMP complex, *J. Mol. Biol. 211*, 645–661.
374. Niwa, T., Inouye, S., Tsuruoka, T., Koaze, Y., and Niida, T. (1970) "Nojirimycin" as a potent inhibitor of glucosidase, *Agric. Biol. Chem. 34*, 966–968.
375. Grover, A. K., and Cushley, R. J. (1977) Studies on almond emulsin β-D-glucosidase. II. Kinetic evidence for independent glucosidase and galactosidase sites, *Biochim. Biophys. Acta, Enzymol. 482*, 109–124.
376. Saunier, B., Kilker, R. D., Jr., Tkacz, J. S., Quaroni, A., and Herscovics, A. (1982) Inhibition of *N*-linked complex oligosaccharide formation by 1-deoxynojirimycin, an inhibitor of processing glucosidases, *J. Biol. Chem. 257*, 14155–14161.
377. Zechel, D. L., Boraston, A. B., Gloster, T., Boraston, C. M., Macdonald, J. M., Tilbrook, D. M., Stick, R. V., and Davies, G. J. (2003) Iminosugar glycosidase inhibitors: Structural and thermodynamic dissection of the binding of isofagomine and 1-deoxynojirimycin to β-glucosidases, *J. Am. Chem. Soc. 125*, 14313–14323.

378. Jiang, Y. L., Ichikawa, Y., and Stivers, J. T. (2002) Inhibition of uracil DNA glycosylase by an oxacarbenium ion mimic, *Biochemistry 41*, 7116–7124.
379. Murray, B. W., Wittmann, V., Burkart, M. D., Hung, S. C., and Wong, C. H. (1997) Mechanism of human α-1,3-fucosyltransferase V: Glycosidic cleavage occurs prior to nucleophilic attack, *Biochemistry 36*, 823–831.
380. Zhang, Q., and Liu, H. (2001) Mechanistic investigation of UDP-galactopyranose mutase from *Escherichia coli* using 2- and 3-fluorinated UDP-galactofuranose as probes, *J. Am. Chem. Soc. 123*, 6756–6766.
381. Reed, B. C., and Rilling, H. C. (1975) Crystallization and partial characterization of prenyltransferase from avian liver, *Biochemistry 14*, 50–54.
382. Hosfield, D. J., Zhang, Y., Dougan, D. R., Broun, A., Tari, L. W., Swanson, R. V., and Finn, J. (2004) Structural basis for bisphosphonate-mediated inhibition of isoprenoid biosynthesis, *J. Biol. Chem. 279*, 8526–8529.
383. Tarshis, L. C., Proteau, P. J., Kellogg, B. A., Sacchettini, J. C., and Poulter, C. D. (1996) Regulation of product chain length by isoprenyl diphosphate synthases, *Proc. Natl. Acad. Sci. U. S. A. 93*, 15018–15023.
384. Cornforth, J. W., Cornforth, R. H., Popjak, G., and Yengoyan, L. (1966) Studies on the biosynthesis of cholesterol. XX. Steric course of decarboxylation of 5-pyrophosphomevalonate and of the carbon to carbon bond formation in the biosynthesis of farnesyl pyrophosphate, *J. Biol. Chem. 241*, 3970–3987.
385. Poulter, C. D., Satterwhite, D. M., and Rilling, H. C. (1976) Prenyltransferase. The mechanism of the reaction, *J. Am. Chem. Soc. 98*, 3376–3377.
386. Poulter, C. D., Wiggins, P. L., and Le, A. T. (1981) Farnesylpyrophosphate synthetase. A stepwise mechanism for the 1′–4 condensation reaction, *J. Am. Chem. Soc. 103*, 3926–3927.
387. Poulter, C. D., Mash, E. A., Argyle, J. C., Muscio, O. J., and Rilling, H. C. (1979) Farnesyl pyrophosphate synthetase. Mechanistic studies of the 1′–4 coupling reaction in the terpene biosynthetic pathway, *J. Am. Chem. Soc. 101*, 6761–6763.
388. Poulter, C. D., Capson, T. L., Thompson, M. D., and Bard, R. S. (1989) Squalene synthetase. Inhibition by ammonium analogs of carbocationic intermediates in the conversion of presqualene diphosphate to squalene, *J. Am. Chem. Soc. 111*, 3734–3739.
389. Blagg, B. S., Jarstfer, M. B., Rogers, D. H., and Poulter, C. D. (2002) Recombinant squalene synthase. A mechanism for the rearrangement of presqualene diphosphate to squalene, *J. Am. Chem. Soc. 124*, 8846–8853.
390. Jarstfer, M. B., Blagg, B. S. J., Rogers, D. H., and Poulter, C. D. (1996) Biosynthesis of squalene. Evidence for a tertiary cyclopropylcarbinyl cationic intermediate in the rearrangement of presqualene diphosphate to squalene, *J. Am. Chem. Soc. 118*, 13089–13090.
391. Jarstfer, M. B., Zhang, D. L., and Poulter, C. D. (2002) Recombinant squalene synthase. Synthesis of non-head-to-tail isoprenoids in the absence of NADPH, *J. Am. Chem. Soc. 124*, 8834–8845.
392. Jenson, C., and Jorgensen, W. L. (1997) Computational investigations of carbenium ion reactions relevant to sterol biosynthesis, *J. Am. Chem. Soc. 119*, 10846–10854.
393. Hoshino, T., and Sato, T. (2002) Squalene-hopene cyclase: Catalytic mechanism and substrate recognition, *Chem. Commun. (Cambridge, U. K.)*, 291–301.
394. Bloch, K. (1965) The biological synthesis of cholesterol, *Science (Washington, DC, U. S.) 150*, 19–28.
395. Wu, T. K., Liu, Y. T., Chang, C. H., Yu, M. T., and Wang, H. J. (2006) Site-saturated mutagenesis of Histidine 234 of *Saccharomyces cerevisiae* oxidosqualene-lanosterol cyclase demonstrates dual functions in cyclization and rearrangement reactions, *J. Am. Chem. Soc. 128*, 6414–6419.
396. Wu, T.-K., and Griffin, J. H. (2002) Conversion of a plant oxidosqualene-cycloartenol synthase to an oxidosqualene-lanosterol cyclase by random mutagenesis, *Biochemistry 41*, 8238–8244.
397. Corey, E. J., Virgil, S. C., and Sarshar, S. (1991) New mechanistic and stereochemical insights on the biosynthesis of sterols from 2,3-oxidosqualene, *J. Am. Chem. Soc. 113*, 8171–8172.
398. Corey, E. J., Cheng, H., Baker, C. H., Matsuda, S. P. T., Li, D., and Song, X. (1997) Studies on the substrate binding segments and catalytic action of lanosterol synthase. Affinity labeling with carbocations derived from mecha-

nism-based analogs of 2,3-oxidosqualene and site-directed mutagenesis probes, *J. Am. Chem. Soc. 119*, 1289–1296.
399. Corey, E. J., and Virgil, S. C. (1991) An experimental demonstration of the stereochemistry of enzymic cyclization of 2,3-oxidosqualene to the protosterol system, forerunner of lanosterol and cholesterol, *J. Am. Chem. Soc. 113*, 4025–4026.
400. Corey, E. J., Virgil, S. C., Cheng, H., Baker, C. H., Matsuda, S. P. T., Singh, V., and Sarshar, S. (1995) New insights regarding the cyclization pathway for sterol biosynthesis from (*S*)-2,3-oxidosqualene, *J. Am. Chem. Soc. 117*, 11819–11820.
401. Zheng, Y. F., Oehlschlager, A. C., Georgopapadakou, N. H., Hartman, P. G., and Scheliga, P. (1995) Synthesis of sulfur- and sulfoxide-substituted 2,3-oxidosqualenes and their evaluation as inhibitors of 2,3-oxidosqualene-lanosterol cyclase, *J. Am. Chem. Soc. 117*, 670–680.
402. Stach, D., Zheng, Y. F., Perez, A. L., Oehlschlager, A. C., Abe, I., Prestwich, G. D., and Hartman, P. G. (1997) Synthesis and inhibition studies of sulfur-substituted squalene oxide analogues as mechanism-based inhibitors of 2,3-oxidosqualene-lanosterol cyclase, *J. Med. Chem. 40*, 201–209.
403. Zheng, Y. F., Abe, I., and Prestwich, G. D. (1998) Inhibition kinetics and affinity labeling of bacterial squalene:hopene cyclase by thia-substituted analogues of 2,3-oxidosqualene, *Biochemistry 37*, 5981–5987.
404. Abe, I., Liu, W., Oehlschlager, A. C., and Prestwich, G. D. (1996) Mechanism-based active site modification of oxidosqualene cyclase by tritium-labeled 18-thia-2,3-oxidosqualene, *J. Am. Chem. Soc. 118*, 9180–9181.
405. Zheng, Y. F., Dodd, D. S., Oehlschlager, A. C., and Hartman, P. G. (1995) Synthesis of vinyl sulfide analogs of 2,3-oxidosqualene and their inhibition of 2,3-oxidosqualene lanosterol-cyclases, *Tetrahedron 51*, 5255–5276.
406. Taton, M., Benveniste, P., Rahier, A., Johnson, W. S., Liu, H. T., and Sudhakar, A. R. (1992) Inhibition of 2,3-oxidosqualene cyclases, *Biochemistry 31*, 7892–7898.
407. Whittington, D. A., Wise, M. L., Urbansky, M., Coates, R. M., Croteau, R. B., and Christianson, D. W. (2002) Bornyl diphosphate synthase: Structure and strategy for carbocation manipulation by a terpenoid cyclase, *Proc. Natl. Acad. Sci. U.S.A. 99*, 15375–15380.
408. Gambliel, H., and Croteau, R. (1984) Pinene cyclases I and II. Two enzymes from sage (*Salvia officinalis*) which catalyze stereospecific cyclizations of geranyl pyrophosphate to monoterpene olefins of opposite configuration, *J. Biol. Chem. 259*, 740–748.
409. Croteau, R., Wheeler, C. J., Aksela, R., and Oehlschlager, A. C. (1986) Inhibition of monoterpene cyclases by sulfonium analogs of presumptive carbocationic intermediates of the cyclization reaction, *J. Biol. Chem. 261*, 7257–7263.
410. Cane, D. E., Yang, G., Xue, Q., and Shim, J. H. (1995) Trichodiene synthase. Substrate specificity and inhibition, *Biochemistry 34*, 2471–2479.
411. Xu, M., Wilderman, P. R., and Peters, R. J. (2007) Following evolution's lead to a single residue switch for diterpene synthase product outcome, *Proc. Natl. Acad. Sci. U.S.A. 104*, 7397–7401.
412. Wilderman, P. R., and Peters, R. J. (2007) A single residue switch converts abietadiene synthase into a pimaradiene specific cyclase, *J. Am. Chem. Soc. 129*, 15736–15737.
413. Cane, D. E., and Xue, Q. (1996) Trichodiene synthase. Enzymic formation of multiple sesquiterpenes by alteration of the cyclase active site, *J. Am. Chem. Soc. 118*, 1563–1564.
414. Rynkiewicz, M. J., Cane, D. E., and Christianson, D. W. (2002) X-Ray crystal structures of D100E trichodiene synthase and its pyrophosphate complex reveal the basis for terpene product diversity, *Biochemistry 41*, 1732–1741.
415. Jin, Y., Williams, D. C., Croteau, R., and Coates, R. M. (2005) Taxadiene synthase-catalyzed cyclization of 6-fluorogeranylgeranyl diphosphate to 7-fluoroverticillenes, *J. Am. Chem. Soc. 127*, 7834–7842.
416. Croteau, R. B., Wheeler, C. J., Cane, D. E., Ebert, R., and Ha, H. J. (1987) Isotopically sensitive branching in the formation of cyclic monoterpenes: Proof that (–)-α-pinene and (–)-β-pinene are synthesized by the same monoterpene cyclase via deprotonation of a common intermediate, *Biochemistry 26*, 5383–5389.
417. Cane, D. E., Pawlak, J. L., and Horak, R. M. (1990) Studies of the cryptic allylic pyrophosphate isomerase activity of trichodiene

synthase using the anomalous substrate 6,7-dihydrofarnesyl pyrophosphate, *Biochemistry 29*, 5476–5490.
418. Roy, A., Roberts, F. G., Wilderman, P. R., Zhou, K., Peters, R. J., and Coates, R. M. (2007) 16-Aza-*ent*-beyerane and 16-Aza-*ent*-trachylobane: Potent mechanism-based inhibitors of recombinant *ent*-kaurene synthase from *Arabidopsis thaliana*, *J. Am. Chem. Soc. 129*, 12453–12460.
419. Barta, M. L., McWhorter, W. J., Miziorko, H. M., and Geisbrecht, B. V. (2012) Structural basis for nucleotide binding and reaction catalysis in mevalonate diphosphate decarboxylase, *Biochemistry 51*, 5611–5621.
420. Dhe-Paganon, S., Magrath, J., and Abeles, R. H. (1994) Mechanism of mevalonate pyrophosphate decarboxylase: Evidence for a carbocationic transition state, *Biochemistry 33*, 13355–13362.
421. Kim, D. H., Lees, W. J., Haley, T. M., and Walsh, C. T. (1995) Kinetic characterization of the inactivation of UDP-GlcNAC enolpyruvyl transferase by (*Z*)-3-fluorophosphoenolpyruvate: Evidence for two oxocarbenium ion intermediates in enolpyruvyl transfer catalysis, *J. Am. Chem. Soc. 117*, 1494–1502.
422. Chiu, H. J., Reddick, J. J., Begley, T. P., and Ealick, S. E. (1999) Crystal structure of thiamin phosphate synthase from *Bacillus subtilis* at 1.25 Å resolution, *Biochemistry 38*, 6460–6470.
423. Hanes, J. W., Ealick, S. E., and Begley, T. P. (2007) Thiamin phosphate synthase: The rate of pyrimidine carbocation formation, *J. Am. Chem. Soc. 129*, 4860–4861.
424. Peapus, D. H., Chiu, H. J., Campobasso, N., Reddick, J. J., Begley, T. P., and Ealick, S. E. (2001) Structural characterization of the enzyme-substrate, enzyme-intermediate, and enzyme-product complexes of thiamin phosphate synthase, *Biochemistry 40*, 10103–10114.
425. Chang, W. C., Mansoorabadi, S. O., and Liu, H. W. (2013) Reaction of HppE with substrate analogues: Evidence for carbon–phosphorus bond cleavage by a carbocation rearrangement, *J. Am. Chem. Soc. 135*, 8153–8156.
426. Inoue, H., Suzuki, F., Tanioka, H., and Takeda, Y. (1968) Studies on ATP citrate lyase of rat liver. 3. The reaction mechanism, *J. Biochem. (Tokyo) 63*, 89–100.
427. Walsh, C. T., Jr., and Spector, L. B. (1969) Citryl phosphate and the mode of action of the citrate cleavage enzyme, *J. Biol. Chem. 244*, 4366–4374.
428. Wells, T. N. (1991) ATP-Citrate lyase from rat liver. Characterisation of the citryl-enzyme complexes, *Eur. J. Biochem. 199*, 163–168.
429. Viratelle, O. M., and Yon, J. M. (1973) Nucleophilic competition in some β-galactosidase-catalyzed reactions, *Eur. J. Biochem. 33*, 110–116.
430. Sinnott, M. L., and Viratelle, O. M. (1973) The effect of methanol and dioxan on the rates of the β-galactosidase-catalysed hydrolyses of some β-D-galactopyranosides: Rate-limiting degalactosylation. The pH-dependence of galactosylation and degalactosylation, *Biochem. J. 133*, 81–87.
431. Wolff, E. C., Park, M. H., and Folk, J. E. (1990) Cleavage of spermidine as the first step in deoxyhypusine synthesis. The role of NAD, *J. Biol. Chem. 265*, 4793–4799.
432. Beach, R., and Plaut, G. W. E. (1970) Stereospecificity of the enzymic synthesis of the *o*-xylene ring of riboflavin, *J. Am. Chem. Soc. 92*, 2913–2916.
433. Kim, R. R., Illarionov, B., Joshi, M., Cushman, M., Lee, C. Y., Eisenreich, W., Fischer, M., and Bacher, A. (2010) Mechanistic insights on riboflavin synthase inspired by selective binding of the 6,7-dimethyl-8-ribityllumazine exomethylene anion, *J. Am. Chem. Soc. 132*, 2983–2990.
434. Gerhardt, S., Schott, A. K., Kairies, N., Cushman, M., Illarionov, B., Eisenreich, W., Bacher, A., Huber, R., Steinbacher, S., and Fischer, M. (2002) Studies on the reaction mechanism of riboflavin synthase: X-Ray crystal structure of a complex with 6-carboxyethyl-7-oxo-8-ribityllumazine, *Structure 10*, 1371–1381.
435. Illarionov, B., Eisenreich, W., and Bacher, A. (2001) A pentacyclic reaction intermediate of riboflavin synthase, *Proc. Natl. Acad. Sci. U.S.A. 98*, 7224–7229.
436. Breugst, M., Eschenmoser, A., and Houk, K. N. (2013) Theoretical exploration of the mechanism of riboflavin formation from 6,7-dimethyl-8-ribityllumazine: Nucleophilic catalysis, hydride transfer, hydrogen atom transfer, or nucleophilic addition?, *J. Am. Chem. Soc. 135*, 6658–6668.

437. Stubbe, J., and van der Donk, W. A. (1998) Protein radicals in enzyme catalysis, *Chem. Rev. (Washington, DC, U. S.) 98*, 705–762.
438. Horitani, M., Byer, A. S., Shisler, K. A., Chandra, T., Broderick, J. B., and Hoffman, B. M. (2015) Why nature uses radical SAM enzymes so widely: Electron nuclear double resonance studies of lysine 2,3-aminomutase show the 5′-dAdo· "free radical" is never free, *J. Am. Chem. Soc. 137*, 7111–7121.
439. Blanksby, S. J., and Ellison, G. B. (2003) Bond dissociation energies of organic molecules, *Acc. Chem. Res. 36*, 255–263.
440. Luo, Y.-R. (2007) *Comprehensive Handbook of Chemical Bond Energies*, Taylor and Francis, Boca Raton, FL.
441. Fasanella, E. L., and Gordy, W. (1969) Electron spin resonance of an irradiated single crystal of L-tyrosine-HCl, *Proc. Natl. Acad. Sci. U.S.A. 62*, 299–304.
442. Ghosh, D., Roy, A., Seidel, R., Winter, B., Bradforth, S., and Krylov, A. I. (2012) First-principle protocol for calculating ionization energies and redox potentials of solvated molecules and ions: Theory and application to aqueous phenol and phenolate, *J. Phys. Chem. B 116*, 7269–7280.
443. Groves, J. T., and McClusky, G. A. (1978) Aliphatic hydroxylation by highly purified liver microsomal cytochrome P-450. Evidence for a carbon radical intermediate, *Biochem. Biophys. Res. Commun. 81*, 154–160.
444. Frey, M., Rothe, M., Wagner, A. F., and Knappe, J. (1994) Adenosylmethionine-dependent synthesis of the glycyl radical in pyruvate formate-lyase by abstraction of the glycine C-2 *pro-S* hydrogen atom. Studies of [^{2}H]glycine-substituted enzyme and peptides homologous to the Glycine 734 site, *J. Biol. Chem. 269*, 12432–12437.
445. Knappe, J., and Schmitt, T. (1976) A novel reaction of *S*-adenosyl-L-methionine correlated with the activation of pyruvate formate-lyase, *Biochem. Biophys. Res. Commun. 71*, 1110–1117.
446. Baraniak, J., Moss, M. L., and Frey, P. A. (1989) Lysine 2,3-aminomutase. Support for a mechanism of hydrogen transfer involving *S*-adenosylmethionine, *J. Biol. Chem. 264*, 1357–1360.
447. Lepore, B. W., Ruzicka, F. J., Frey, P. A., and Ringe, D. (2005) The X-ray crystal structure of lysine-2,3-aminomutase from *Clostridium subterminale*, *Proc. Natl. Acad. Sci. U.S.A. 102*, 13819–13824.
448. Lees, N. S., Chen, D., Walsby, C. J., Behshad, E., Frey, P. A., and Hoffman, B. M. (2006) How an enzyme tames reactive intermediates: Positioning of the active-site components of lysine 2,3-aminomutase during enzymatic turnover as determined by ENDOR spectroscopy, *J. Am. Chem. Soc. 128*, 10145–10154.
449. Himo, F., and Eriksson, L. A. (1998) Catalytic mechanism of pyruvate formate-lyase (PFL). A theoretical study, *J. Am. Chem. Soc. 120*, 11449–11455.
450. Kacprzak, S., Reviakine, R., and Kaupp, M. (2007) Understanding the electron paramagnetic resonance parameters of protein-bound glycyl radicals, *J. Phys. Chem. B 111*, 820–831.
451. Allard, P., Barra, A. L., Andersson, K. K., Schmidt, P. P., Atta, M., and Graeslund, A. (1996) Characterization of a new tyrosyl free radical in *Salmonella typhimurium* ribonucleotide reductase with EPR at 9.45 and 245 GHz, *J. Am. Chem. Soc. 118*, 895–896.
452. Weichsel, A., Gasdaska, J. R., Powis, G., and Montfort, W. R. (1996) Crystal structures of reduced, oxidized, and mutated human thioredoxins: Evidence for a regulatory homodimer, *Structure 4*, 735–751.
453. Wei, Y., Funk, M. A., Rosado, L. A., Baek, J., Drennan, C. L., and Stubbe, J. (2014) The class III ribonucleotide reductase from *Neisseria bacilliformis* can utilize thioredoxin as a reductant, *Proc. Natl. Acad. Sci. U. S. A. 111*, E3756–3765.
454. Sintchak, M. D., Arjara, G., Kellogg, B. A., Stubbe, J., and Drennan, C. L. (2002) The crystal structure of class II ribonucleotide reductase reveals how an allosterically regulated monomer mimics a dimer, *Nat. Struct. Biol. 9*, 293–300.
455. Stubbe, J., Ge, J., and Yee, C. S. (2001) The evolution of ribonucleotide reduction revisited, *Trends Biochem. Sci. 26*, 93–99.
456. Licht, S. S., Lawrence, C. C., and Stubbe, J. (1999) Class II ribonucleotide reductases catalyze carbon–cobalt bond reformation on every turnover, *J. Am. Chem. Soc. 121*, 7463–7468.
457. Chen, D., Abend, A., Stubbe, J., and Frey, P. A. (2003) Epimerization at carbon-5′ of (5′*R*)-[5′-^{2}H]adenosylcobalamin by ribonu-

cleoside triphosphate reductase: Cysteine 408-independent cleavage of the Co–C5′ bond, *Biochemistry 42*, 4578–4584.
458. Brown, K. L., and Li, J. (1998) Activation parameters for the carbon–cobalt bond homolysis of coenzyme B_{12} induced by the B_{12}–dependent ribonucleotide reductase from *Lactobacillus leichmannii*, *J. Am. Chem. Soc. 120*, 9466–9474.
459. Sun, X., Ollagnier, S., Schmidt, P. P., Atta, M., Mulliez, E., Lepape, L., Eliasson, R., Graslund, A., Fontecave, M., Reichard, P., and Sjoberg, B. M. (1996) The free radical of the anaerobic ribonucleotide reductase from *Escherichia coli* is at Glycine 681, *J. Biol. Chem. 271*, 6827–6831.
460. Young, P., Andersson, J., Sahlin, M., and Sjoberg, B. M. (1996) Bacteriophage T4 anaerobic ribonucleotide reductase contains a stable glycyl radical at position 580, *J. Biol. Chem. 271*, 20770–20775.
461. Ollagnier, S., Mulliez, E., Schmidt, P. P., Eliasson, R., Gaillard, J., Deronzier, C., Bergman, T., Graslund, A., Reichard, P., and Fontecave, M. (1997) Activation of the anaerobic ribonucleotide reductase from *Escherichia coli*. The essential role of the iron-sulfur center for *S*-adenosylmethionine reduction, *J. Biol. Chem. 272*, 24216–24223.
462. Tamarit, J., Gerez, C., Meier, C., Mulliez, E., Trautwein, A., and Fontecave, M. (2000) The activating component of the anaerobic ribonucleotide reductase from *Escherichia coli*. An iron-sulfur center with only three cysteines, *J. Biol. Chem. 275*, 15669–15675.
463. Sun, X., Eliasson, R., Pontis, E., Andersson, J., Buist, G., Sjoberg, B. M., and Reichard, P. (1995) Generation of the glycyl radical of the anaerobic *Escherichia coli* ribonucleotide reductase requires a specific activating enzyme, *J. Biol. Chem. 270*, 2443–2446.
464. Larsson, A., and Sjoberg, B. M. (1986) Identification of the stable free radical tyrosine residue in ribonucleotide reductase, *EMBO J. 5*, 2037–2040.
465. Sjoberg, B. M., Reichard, P., Graslund, A., and Ehrenberg, A. (1978) The tyrosine free radical in ribonucleotide reductase from *Escherichia coli*, *J. Biol. Chem. 253*, 6863–6865.
466. Bender, C. J., Sahlin, M., Babcock, G. T., Barry, B. A., Chandrashekar, T. K., Salowe, S. P., Stubbe, J., Lindström, B., Petersson, L., Ehrenberg, A., and Sjöberg, B. M. (1989) An ENDOR study of the tyrosyl free radical in ribonucleotide reductase from *Escherichia coli*, *J. Am. Chem. Soc. 111*, 8076–8083.
467. Hoganson, C. W., Sahlin, M., Sjoberg, B. M., and Babcock, G. T. (1996) Electron magnetic resonance of the tyrosyl radical in ribonucleotide reductase from *Escherichia coli*, *J. Am. Chem. Soc. 118*, 4672–4679.
468. Nordlund, P., and Eklund, H. (1993) Structure and function of the *Escherichia coli* ribonucleotide reductase protein R2, *J. Mol. Biol. 232*, 123–164.
469. Sahlin, M., Petersson, L., Graslund, A., Ehrenberg, A., Sjoberg, B. M., and Thelander, L. (1987) Magnetic interaction between the tyrosyl free radical and the antiferromagnetically coupled iron center in ribonucleotide reductase, *Biochemistry 26*, 5541–5548.
470. Atkin, C. L., Thelander, L., and Reichard, P. (1973) Iron and free radical in ribonucleotide reductase. Exchange of iron and Moessbauer spectroscopy of the protein B2 subunit of the *Escherichia coli* enzyme, *J. Biol. Chem. 248*, 7464–7472.
471. Sturgeon, B. E., Burdi, D., Chen, S., Huynh, B.-H., Edmondson, D. E., Stubbe, J., and Hoffman, B. M. (1996) Reconsideration of X, the diiron intermediate formed during cofactor assembly in *E. coli* ribonucleotide reductase, *J. Am. Chem. Soc. 118*, 7551–7557.
472. Zhang, Y., and Stubbe, J. (2011) *Bacillus subtilis* class Ib ribonucleotide reductase is a dimanganese(III)-tyrosyl radical enzyme, *Biochemistry 50*, 5615–5623.
473. Cotruvo, J. A., and Stubbe, J. (2011) *Escherichia coli* class Ib ribonucleotide reductase contains a dimanganese(III)-tyrosyl radical cofactor *in vivo*, *Biochemistry 50*, 1672–1681.
474. Boal, A. K., Cotruvo, J. A., Jr., Stubbe, J., and Rosenzweig, A. C. (2012) The dimanganese(II) site of *Bacillus subtilis* class Ib ribonucleotide reductase, *Biochemistry 51*, 3861–3871.
475. Rose, H. R., Ghosh, M. K., Maggiolo, A. O., Pollock, C. J., Blaesi, E. J., Hajj, V., Wei, Y., Rajakovich, L. J., Chang, W. C., Han, Y., Hajj, M., Krebs, C., Silakov, A., Pandelia, M. E., Bollinger, J. M., Jr., and Boal, A. K. (2018) Structural basis for superoxide activation of *Flavobacterium johnsoniae* class I ribonucleotide reductase and for radical initiation by its dimanganese cofactor, *Biochemistry 57*, 2679–2693.

476. Hogbom, M., Stenmark, P., Voevodskaya, N., McClarty, G., Graslund, A., and Nordlund, P. (2004) The radical site in chlamydial ribonucleotide reductase defines a new R2 subclass, *Science (Washington, DC, U. S.) 305*, 245–248.
477. Jiang, W., Yun, D., Saleh, L., Barr, E. W., Xing, G., Hoffart, L. M., Maslak, M. A., Krebs, C., and Bollinger, J. M., Jr. (2007) A manganese(IV)/iron(III) cofactor in *Chlamydia trachomatis* ribonucleotide reductase, *Science (Washington, DC, U. S.) 316*, 1188–1191.
478. Voevodskaya, N., Narvaez, A. J., Domkin, V., Torrents, E., Thelander, L., and Graslund, A. (2006) Chlamydial ribonucleotide reductase: Tyrosyl radical function in catalysis replaced by the FeIII-FeIV cluster, *Proc. Natl. Acad. Sci. U.S.A. 103*, 9850–9854.
479. Licht, S., Gerfen, G. J., and Stubbe, J. (1996) Thiyl radicals in ribonucleotide reductases, *Science (Washington, DC, U. S.) 271*, 477–481.
480. Gerfen, G. J., Licht, S., Willems, J. P., Hoffman, B. M., and Stubbe, J. (1996) Electron paramagnetic resonance investigations of a kinetically competent intermediate formed in ribonucleotide reduction: Evidence for a thiyl radical-cob(II)alamin interaction, *J. Am. Chem. Soc. 118*, 8192–8197.
481. Licht, S. S., Booker, S., and Stubbe, J. (1999) Studies on the catalysis of carbon–cobalt bond homolysis by ribonucleoside triphosphate reductase: Evidence for concerted carbon–cobalt bond homolysis and thiyl radical formation, *Biochemistry 38*, 1221–1233.
482. Larsson, K. M., Logan, D. T., and Nordlund, P. (2010) Structural basis for adenosylcobalamin activation in AdoCbl-dependent ribonucleotide reductases, *ACS Chem. Biol. 5*, 933–942.
483. Persson, A. L., Sahlin, M., and Sjoberg, B. M. (1998) Cysteinyl and substrate radical formation in active site mutant E441Q of *Escherichia coli* class I ribonucleotide reductase, *J. Biol. Chem. 273*, 31016–31020.
484. Adrait, A., Ohrstrom, M., Barra, A. L., Thelander, L., and Graslund, A. (2002) EPR studies on a stable sulfinyl radical observed in the iron-oxygen-reconstituted Y177F/I263C protein R2 double mutant of ribonucleotide reductase from mouse, *Biochemistry 41*, 6510–6516.
485. Logan, D. T., Andersson, J., Sjoberg, B. M., and Nordlund, P. (1999) A glycyl radical site in the crystal structure of a class III ribonucleotide reductase, *Science (Washington, DC, U. S.) 283*, 1499–1504.
486. Larsson, K. M., Andersson, J., Sjoberg, B. M., Nordlund, P., and Logan, D. T. (2001) Structural basis for allosteric substrate specificity regulation in anaerobic ribonucleotide reductases, *Structure 9*, 739–750.
487. Uhlin, U., and Eklund, H. (1994) Structure of ribonucleotide reductase protein R1, *Nature (London, U. K.) 370*, 533–539.
488. Bennati, M., Robblee, J. H., Mugnaini, V., Stubbe, J., Freed, J. H., and Borbat, P. (2005) EPR distance measurements support a model for long-range radical initiation in *E. coli* ribonucleotide reductase, *J. Am. Chem. Soc. 127*, 15014–15015.
489. Seyedsayamdost, M. R., Chan, C. T., Mugnaini, V., Stubbe, J., and Bennati, M. (2007) PELDOR spectroscopy with DOPA-β2 and NH_2Y-α2s: distance measurements between residues involved in the radical propagation pathway of *E. coli* ribonucleotide reductase, *J. Am. Chem. Soc. 129*, 15748–15749.
490. Xu, H., Faber, C., Uchiki, T., Fairman, J. W., Racca, J., and Dealwis, C. (2006) Structures of eukaryotic ribonucleotide reductase I provide insights into dNTP regulation, *Proc. Natl. Acad. Sci. U.S.A. 103*, 4022–4027.
491. Yang, F. D., Spanevello, R. A., Celiker, I., Hirschmann, R., Rubin, H., and Cooperman, B. S. (1990) The carboxyl terminus heptapeptide of the R2 subunit of mammalian ribonucleotide reductase inhibits enzyme activity and can be used to purify the R1 subunit, *FEBS Lett. 272*, 61–64.
492. Seyedsayamdost, M. R., Xie, J., Chan, C. T., Schultz, P. G., and Stubbe, J. (2007) Site-specific insertion of 3-aminotyrosine into subunit α_2 of *E. coli* ribonucleotide reductase: Direct evidence for involvement of Y730 and Y731 in radical propagation, *J. Am. Chem. Soc. 129*, 15060–15071.
493. Holder, P. G., Pizano, A. A., Anderson, B. L., Stubbe, J., and Nocera, D. G. (2012) Deciphering radical transport in the large subunit of class I ribonucleotide reductase, *J. Am. Chem. Soc. 134*, 1172–1180.
494. Seyedsayamdost, M. R., and Stubbe, J. (2007) Forward and reverse electron transfer with the Y356DOPA-β_2 heterodimer of *E. coli* ribonucleotide reductase, *J. Am. Chem. Soc. 129*, 2226–2227.

495. Pizano, A. A., Olshansky, L., Holder, P. G., Stubbe, J., and Nocera, D. G. (2013) Modulation of Y356 photooxidation in *E. coli* class Ia ribonucleotide reductase by Y731 across the α_2:β_2 interface, *J. Am. Chem. Soc. 135*, 13250–13253.
496. Seyedsayamdost, M. R., Yee, C. S., Reece, S. Y., Nocera, D. G., and Stubbe, J. (2006) pH Rate profiles of F_nY_{356}–R2s (n = 2, 3, 4) in *Escherichia coli* ribonucleotide reductase: Evidence that Y_{356} is a redox-active amino acid along the radical propagation pathway, *J. Am. Chem. Soc. 128*, 1562–1568.
497. Ravichandran, K., Olshansky, L., Nocera, D. G., and Stubbe, J. (2020) Subunit interaction dynamics of class Ia ribonucleotide reductases: In search of a robust assay, *Biochemistry 59*, 1442–1453.
498. Minnihan, E. C., Ando, N., Brignole, E. J., Olshansky, L., Chittuluru, J., Asturias, F. J., Drennan, C. L., Nocera, D. G., and Stubbe, J. (2013) Generation of a stable, aminotyrosyl radical-induced $\alpha_2\beta_2$ complex of *Escherichia coli* class Ia ribonucleotide reductase, *Proc. Natl. Acad. Sci. U. S. A. 110*, 3835–3840.
499. Kang, G., Taguchi, A. T., Stubbe, J., and Drennan, C. L. (2020) Structure of a trapped radical transfer pathway within a ribonucleotide reductase holocomplex, *Science (Washington, DC, U. S.) 368*, 424–427.
500. Erickson, H. K. (2000) Formation of the cystine between Cysteine 225 and Cysteine 462 from ribonucleoside diphosphate reductase is kinetically competent, *Biochemistry 39*, 9241–9250.
501. Ge, J., Yu, G., Ator, M. A., and Stubbe, J. (2003) Pre-steady-state and steady-state kinetic analysis of *E. coli* class I ribonucleotide reductase, *Biochemistry 42*, 10071–10083.
502. Seyedsayamdost, M. R., and Stubbe, J. (2006) Site-specific replacement of Y_{356} with 3,4-dihydroxyphenylalanine in the β_2 subunit of *E. coli* ribonucleotide reductase, *J. Am. Chem. Soc. 128*, 2522–2523.
503. Hogbom, M., Galander, M., Andersson, M., Kolberg, M., Hofbauer, W., Lassmann, G., Nordlund, P., and Lendzian, F. (2003) Displacement of the tyrosyl radical cofactor in ribonucleotide reductase obtained by single-crystal high-field EPR and 1.4-Å X-ray data, *Proc. Natl. Acad. Sci. U. S. A. 100*, 3209–3214.
504. Eriksson, M., Uhlin, U., Ramaswamy, S., Ekberg, M., Regnstrom, K., Sjoberg, B. M., and Eklund, H. (1997) Binding of allosteric effectors to ribonucleotide reductase protein R1: Reduction of active-site cysteines promotes substrate binding, *Structure 5*, 1077–1092.
505. Jiang, W., Saleh, L., Barr, E. W., Xie, J., Gardner, M. M., Krebs, C., and Bollinger, J. M., Jr. (2008) Branched activation- and catalysis-specific pathways for electron relay to the manganese/iron cofactor in ribonucleotide reductase from *Chlamydia trachomatis*, *Biochemistry 47*, 8477–8484.
506. Dassama, L. M., Jiang, W., Varano, P. T., Pandelia, M. E., Conner, D. A., Xie, J., Bollinger, J. M., Jr., and Krebs, C. (2012) Radical-translocation intermediates and hurdling of pathway defects in "super-oxidized" (Mn(IV)/Fe(IV)) *Chlamydia trachomatis* ribonucleotide reductase, *J. Am. Chem. Soc. 134*, 20498–20506.
507. Ravichandran, K. R., Minnihan, E. C., Wei, Y., Nocera, D. G., and Stubbe, J. (2015) Reverse electron transfer completes the catalytic cycle in a 2,3,5-trifluorotyrosine-substituted ribonucleotide reductase, *J. Am. Chem. Soc. 137*, 14387–14395.
508. Larsson, K. M., Jordan, A., Eliasson, R., Reichard, P., Logan, D. T., and Nordlund, P. (2004) Structural mechanism of allosteric substrate specificity regulation in a ribonucleotide reductase, *Nat. Struct. Mol. Biol. 11*, 1142–1149.
509. Stubbe, J., Ator, M., and Krenitsky, T. (1983) Mechanism of ribonucleoside diphosphate reductase from *Escherichia coli*. Evidence for 3′-C–H bond cleavage, *J. Biol. Chem. 258*, 1625–1631.
510. Walling, C., and Johnson, R. A. (1975) Fenton's reagent. VI. Rearrangements during glycol oxidations, *J. Am. Chem. Soc. 97*, 2405–2407.
511. Gilbert, B. C., Larkin, J. P., and Norman, R. O. C. (1972) Electron spin resonance studies. XXXIII. Evidence for heterolytic and homolytic transformations of radicals from 1,2-diols and related compounds, *J. Chem. Soc., Perkin Trans. 2*, 794–802.
512. Kyte, J. (1995) *Mechanism in Protein Chemistry*, p 400, Garland Publishing, New York.
513. Asmus, K. D. (1983) Sulfur-centered free radicals, In *Radioprotectors and Anticarcinogens* (Nygaard, O. E., and Simic, M. D., Eds.), pp 23–42, Academic Press, New York.

514. Richardson, J. S. (1981) The anatomy and taxonomy of protein structure, *Adv. Protein Chem. 34*, 167–339.
515. Braida, B., and Hiberty, P. C. (2003) A simplified Gaussian-2 scheme for determining electron affinities of covalent bonds. Application to the disulfide bond RS–SR′ (R, R′ = H, CH_3, C_2H_5), *J. Phys. Chem. A 107*, 4741–4747.
516. Modelli, A., Jones, D., Rossini, S., and Distefano, G. (1984) Electron-affinities of double-bond π^* orbitals determined by means of electron transmission spectroscopy, *Tetrahedron 40*, 3257–3262.
517. Batterham, T. J., Ghambeer, R. K., Blakley, R. L., and Brownson, C. (1967) Cobamides and ribonucleotide reduction. IV. Sterochemistry of hydrogen transfer to the deoxyribonucleotide, *Biochemistry 6*, 1203–1208.
518. Mao, S. S., Holler, T. P., Bollinger, J. M., Jr., Yu, G. X., Johnston, M. I., and Stubbe, J. (1992) Interaction of C225SR1 mutant subunit of ribonucleotide reductase with R2 and nucleoside diphosphates: Tales of a suicidal enzyme, *Biochemistry 31*, 9744–9751.
519. Stubbe, J. (1990) Ribonucleotide reductases: Amazing and confusing, *J. Biol. Chem. 265*, 5329–5332.
520. Thelander, L., and Larsson, B. (1976) Active site of ribonucleoside diphosphate reductase from *Escherichia coli*. Inactivation of the enzyme by 2′-substituted ribonucleoside diphosphates, *J. Biol. Chem. 251*, 1398–1405.
521. Stubbe, J., and Kozarich, J. W. (1980) Inorganic pyrophosphate is released from 2′-chloro-2′-deoxyuridine 5′-diphosphate by ribonucleoside diphosphate reductase, *J. Am. Chem. Soc. 102*, 2505–2507.
522. Ator, M. A., and Stubbe, J. (1985) Mechanism of inactivation of *Escherichia coli* ribonucleotide reductase by 2′-chloro-2′-deoxyuridine 5′-diphosphate: Evidence for generation of a 2′-deoxy-3′-ketonucleotide via a net 1,2 hydrogen shift, *Biochemistry 24*, 7214–7221.
523. Drago, R. S., Ferris, D. C., and Wong, N. (1990) A method for the analysis and prediction of gas-phase ion molecule enthalpies, *J. Am. Chem. Soc. 112*, 8953–8961.
524. Ashley, G. W., Harris, G., and Stubbe, J. A. (1988) Inactivation of the ribonucleoside triphosphate reductase from *Lactobacillus leichmannii* by 2′-chloro-2′-deoxyuridine 5′-triphosphate: A 3′-2′ hydrogen transfer during the formation of 3′-keto-2′-deoxyuridine 5′-triphosphate, *Biochemistry 27*, 7841–7845.
525. McFarlan, S. C., Ong, S. P., and Hogenkamp, H. P. (1996) Mechanism-based inhibition of ribonucleoside diphosphate reductase from *Corynebacterium nephridii* by 2′-C-methyladenosine diphosphate, *Biochemistry 35*, 4485–4491.
526. Salowe, S. P., Ator, M. A., and Stubbe, J. (1987) Products of the inactivation of ribonucleoside diphosphate reductase from *Escherichia coli* with 2′-azido-2′-deoxyuridine 5′-diphosphate, *Biochemistry 26*, 3408–3416.
527. van der Donk, W. A., Stubbe, J., Gerfen, G. J., Bellew, B. F., and Griffin, R. G. (1995) EPR Investigations of the inactivation of *E. coli* ribonucleotide reductase with 2′-azido-2′-deoxyuridine 5′-diphosphate: Evidence for the involvement of the thiyl radical of C225-R1, *J. Am. Chem. Soc. 117*, 8908–8916.
528. Fritscher, J., Artin, E., Wnuk, S., Bar, G., Robblee, J. H., Kacprzak, S., Kaupp, M., Griffin, R. G., Bennati, M., and Stubbe, J. (2005) Structure of the nitrogen-centered radical formed during inactivation of *E. coli* ribonucleotide reductase by 2′-azido-2′-deoxyuridine-5′-diphosphate: Trapping of the 3′-ketonucleotide, *J. Am. Chem. Soc. 127*, 7729–7738.
529. Lawrence, C. C., Bennati, M., Obias, H. V., Bar, G., Griffin, R. G., and Stubbe, J. (1999) High-field EPR detection of a disulfide radical anion in the reduction of cytidine 5′-diphosphate by the E441Q R1 mutant of *Escherichia coli* ribonucleotide reductase, *Proc. Natl. Acad. Sci. U.S.A. 96*, 8979–8984.
530. Thelander, L. (1974) Reaction mechanism of ribonucleoside diphosphate reductase from *Escherichia coli*. Oxidation-reduction-active disulfides in the B1 subunit, *J. Biol. Chem. 249*, 4858–4862.
531. Lin, A. N., Ashley, G. W., and Stubbe, J. (1987) Location of the redox-active thiols of ribonucleotide reductase: Sequence similarity between the *Escherichia coli* and *Lactobacillus leichmannii* enzymes, *Biochemistry 26*, 6905–6909.
532. Booker, S., Licht, S., Broderick, J., and Stubbe, J. (1994) Coenzyme B_{12}-dependent ribonucleotide reductase: Evidence for the participation of five cysteine residues in ribo-

nucleotide reduction, *Biochemistry 33*, 12676–12685.
533. Berardi, M. J., Pendred, C. L., and Bushweller, J. H. (1998) Preparation, characterization, and complete heteronuclear NMR resonance assignments of the glutaredoxin (C14S)-ribonucleotide reductase B1 737–761 (C754S) mixed disulfide, *Biochemistry 37*, 5849–5857.
534. Robins, M. J., Guo, Z., Samano, M. C., and Wnuk, S. F. (1999) Biomimetic simulation of free radical-initiated cascade reactions postulated to occur at the active site of ribonucleotide reductases, *J. Am. Chem. Soc. 121*, 1425–1433.
535. Robins, M. J., Guo, Z., and Wnuk, S. F. (1997) Elimination of chlorine (radical) or tosylate (anion) from C2′ of nucleoside C3′ *J. Am. Chem. Soc. 119*, 3637–3638.
536. Lenz, R., and Giese, B. (1997) Studies on the mechanism of ribonucleotide reductases, *J. Am. Chem. Soc. 119*, 2784–2794.
537. Robins, M. J., and Ewing, G. J. (1999) Biomimetic modeling of the first substrate reaction at the active site of ribonucleotide reductases. Abstraction of H3′ by a thiyl free radical, *J. Am. Chem. Soc. 121*, 5823–5824.
538. Wei, Y., Li, B., Prakash, D., Ferry, J. G., Elliott, S. J., and Stubbe, J. (2015) A ferredoxin disulfide reductase delivers electrons to the *Methanosarcina barkeri* class III ribonucleotide reductase, *Biochemistry 54*, 7019–7028.
539. Mulliez, E., Ollagnier, S., Fontecave, M., Eliasson, R., and Reichard, P. (1995) Formate is the hydrogen donor for the anaerobic ribonucleotide reductase from *Escherichia coli*, *Proc. Natl. Acad. Sci. U.S.A. 92*, 8759–8762.
540. Fontecave, M., Mulliez, E., and Logan, D. T. (2002) Deoxyribonucleotide synthesis in anaerobic microorganisms: The class III ribonucleotide reductase, *Prog. Nucleic Acid Res. Mol. Biol. 72*, 95–127.
541. Wei, Y., Mathies, G., Yokoyama, K., Chen, J., Griffin, R. G., and Stubbe, J. (2014) A chemically competent thiosulfuranyl radical on the *Escherichia coli* class III ribonucleotide reductase, *J. Am. Chem. Soc. 136*, 9001–9013.
542. Compton, R. N., Reinhardt, P. W., and Cooper, C. D. (1975) Collisional ionization of Na, K, and Cs by CO_2, COS, and CS_2: Molecular electron affinities, *J. Chem. Phys. 63*, 3821–3827.
543. Vecchio, A. J., Simmons, D. M., and Malkowski, M. G. (2010) Structural basis of fatty acid substrate binding to cyclooxygenase-2, *J. Biol. Chem. 285*, 22152–22163.
544. Karthein, R., Dietz, R., Nastainczyk, W., and Ruf, H. H. (1988) Higher oxidation states of prostaglandin H synthase. EPR Study of a transient tyrosyl radical in the enzyme during the peroxidase reaction, *Eur. J. Biochem. 171*, 313–320.
545. Tsai, A., Palmer, G., Xiao, G., Swinney, D. C., and Kulmacz, R. J. (1998) Structural characterization of arachidonyl radicals formed by prostaglandin H synthase-2 and prostaglandin H synthase-1 reconstituted with mangano protoporphyrin IX, *J. Biol. Chem. 273*, 3888–3894.
546. Hamberg, M. (1998) Stereochemistry of oxygenation of linoleic acid catalyzed by prostaglandin-endoperoxide H synthase-2, *Arch. Biochem. Biophys. 349*, 376–380.
547. Malkowski, M. G., Ginell, S. L., Smith, W. L., and Garavito, R. M. (2000) The productive conformation of arachidonic acid bound to prostaglandin synthase, *Science (Washington, DC, U. S.) 289*, 1933–1937.
548. Kiefer, J. R., Pawlitz, J. L., Moreland, K. T., Stegeman, R. A., Hood, W. F., Gierse, J. K., Stevens, A. M., Goodwin, D. C., Rowlinson, S. W., Marnett, L. J., Stallings, W. C., and Kurumbail, R. G. (2000) Structural insights into the stereochemistry of the cyclooxygenase reaction, *Nature (London, U. K.) 405*, 97–101.
549. Shimokawa, T., Kulmacz, R. J., DeWitt, D. L., and Smith, W. L. (1990) Tyrosine 385 of prostaglandin endoperoxide synthase is required for cyclooxygenase catalysis, *J. Biol. Chem. 265*, 20073–20076.
550. Dietz, R., Nastainczyk, W., and Ruf, H. H. (1988) Higher oxidation states of prostaglandin H synthase. Rapid electronic spectroscopy detected two spectral intermediates during the peroxidase reaction with prostaglandin G_2, *Eur. J. Biochem. 171*, 321–328.
551. Branchaud, B. P., Montague-Smith, M. P., Kosman, D. J., and McLaren, F. R. (1993) Mechanism-based inactivation of galactose oxidase: Evidence for a radical mechanism, *J. Am. Chem. Soc. 115*, 798–800.
552. Wachter, R. M., Montague-Smith, M. P., and Branchaud, B. P. (1997) β-Haloethanol substrates as probes for radical mechanisms for

galactose oxidase, *J. Am. Chem. Soc. 119*, 7743–7749.
553. Streit, B. R., Celis, A. I., Moraski, G. C., Shisler, K. A., Shepard, E. M., Rodgers, K. R., Lukat-Rodgers, G. S., and DuBois, J. L. (2018) Decarboxylation involving a ferryl, propionate, and a tyrosyl group in a radical relay yields heme *b*, *J. Biol. Chem. 293*, 3989–3999.
554. Duboc-Toia, C., Hassan, A. K., Mulliez, E., Ollagnier-de Choudens, S., Fontecave, M., Leutwein, C., and Heider, J. (2003) Very high-field EPR study of glycyl radical enzymes, *J. Am. Chem. Soc. 125*, 38–39.
555. Krieger, C. J., Roseboom, W., Albracht, S. P., and Spormann, A. M. (2001) A stable organic free radical in anaerobic benzylsuccinate synthase of *Azoarcus* sp. strain T, *J. Biol. Chem. 276*, 12924–12927.
556. Wagner, A. F., Frey, M., Neugebauer, F. A., Schafer, W., and Knappe, J. (1992) The free radical in pyruvate formate-lyase is located on Glycine-734, *Proc. Natl. Acad. Sci. U.S.A. 89*, 996–1000.
557. Shisler, K. A., and Broderick, J. B. (2014) Glycyl radical activating enzymes: Structure, mechanism, and substrate interactions, *Arch. Biochem. Biophys. 546*, 64–71.
558. Walsby, C. J., Hong, W., Broderick, W. E., Cheek, J., Ortillo, D., Broderick, J. B., and Hoffman, B. M. (2002) Electron–nuclear double resonance spectroscopic evidence that *S*-adenosylmethionine binds in contact with the catalytically active $[4Fe–4S]^{+}$ cluster of pyruvate formate-lyase activating enzyme, *J. Am. Chem. Soc. 124*, 3143–3151.
559. Henshaw, T. F., Cheek, J., and Broderick, J. B. (2000) The $[4Fe–4S]^{1+}$ Cluster of pyruvate formate-lyase activating enzyme generates the glycyl radical on pyruvate formate-lyase: EPR-Detected single turnover, *J. Am. Chem. Soc. 122*, 8331–8332.
560. Walsby, C. J., Ortillo, D., Broderick, W. E., Broderick, J. B., and Hoffman, B. M. (2002) An anchoring role for FeS clusters: Chelation of the amino acid moiety of *S*-adenosylmethionine to the unique iron site of the [4Fe–4S] cluster of pyruvate formate-lyase activating enzyme, *J. Am. Chem. Soc. 124*, 11270–11271.
561. Vey, J. L., Yang, J., Li, M., Broderick, W. E., Broderick, J. B., and Drennan, C. L. (2008) Structural basis for glycyl radical formation by pyruvate formate-lyase activating enzyme, *Proc. Natl. Acad. Sci. U.S.A. 105*, 16137–16141.
562. O'Brien, J. R., Raynaud, C., Croux, C., Girbal, L., Soucaille, P., and Lanzilotta, W. N. (2004) Insight into the mechanism of the B_{12}-independent glycerol dehydratase from *Clostridium butyricum*: preliminary biochemical and structural characterization, *Biochemistry 43*, 4635–4645.
563. Demick, J. M., and Lanzilotta, W. N. (2011) Radical SAM activation of the B_{12}-independent glycerol dehydratase results in formation of 5′-deoxy-5′-(methylthio)adenosine and not 5′-deoxyadenosine, *Biochemistry 50*, 440–442.
564. Craciun, S., and Balskus, E. P. (2012) Microbial conversion of choline to trimethylamine requires a glycyl radical enzyme, *Proc. Natl. Acad. Sci. U. S. A. 109*, 21307–21312.
565. Selmer, T., and Andrei, P. I. (2001) *p*-Hydroxyphenylacetate decarboxylase from *Clostridium difficile*. A novel glycyl radical enzyme catalysing the formation of *p*-cresol, *Eur. J. Biochem. 268*, 1363–1372.
566. Becker, A., Fritz-Wolf, K., Kabsch, W., Knappe, J., Schultz, S., and Volker Wagner, A. F. (1999) Structure and mechanism of the glycyl radical enzyme pyruvate formate-lyase, *Nat. Struct. Biol. 6*, 969–975.
567. Leuthner, B., Leutwein, C., Schulz, H., Horth, P., Haehnel, W., Schiltz, E., Schagger, H., and Heider, J. (1998) Biochemical and genetic characterization of benzylsuccinate synthase from *Thauera aromatica*: A new glycyl radical enzyme catalyzing the first step in anaerobic toluene metabolism, *Mol. Microbiol. 28*, 615–628.
568. Becker, A., and Kabsch, W. (2002) X-Ray structure of pyruvate formate-lyase in complex with pyruvate and CoA. How the enzyme uses the Cys-418 thiyl radical for pyruvate cleavage, *J. Biol. Chem. 277*, 40036–40042.
569. Parast, C. V., Wong, K. K., Lewisch, S. A., Kozarich, J. W., Peisach, J., and Magliozzo, R. S. (1995) Hydrogen exchange of the glycyl radical of pyruvate formate-lyase is catalyzed by Cysteine 419, *Biochemistry 34*, 2393–2399.
570. Parast, C. V., Wong, K. K., Kozarich, J. W., Peisach, J., and Magliozzo, R. S. (1995) Electron paramagnetic resonance evidence for a cysteine-based radical in pyruvate formate-

lyase inactivated with mercaptopyruvate, *Biochemistry 34*, 5712–5717.
571. Funk, M. A., Marsh, E. N., and Drennan, C. L. (2015) Substrate-bound structures of benzylsuccinate synthase reveal how toluene is activated in anaerobic hydrocarbon degradation, *J. Biol. Chem. 290*, 22398–22408.
572. Martins, B. M., Blaser, M., Feliks, M., Ullmann, G. M., Buckel, W., and Selmer, T. (2011) Structural basis for a Kolbe-type decarboxylation catalyzed by a glycyl radical enzyme, *J. Am. Chem. Soc. 133*, 14666–14674.
573. Feliks, M., Martins, B. M., and Ullmann, G. M. (2013) Catalytic mechanism of the glycyl radical enzyme 4-hydroxyphenylacetate decarboxylase from continuum electrostatic and QC/MM calculations, *J. Am. Chem. Soc. 135*, 14574–14585.
574. Sofia, H. J., Chen, G., Hetzler, B. G., Reyes-Spindola, J. F., and Miller, N. E. (2001) Radical SAM, a novel protein superfamily linking unresolved steps in familiar biosynthetic pathways with radical mechanisms: Functional characterization using new analysis and information visualization methods, *Nucleic Acids Res. 29*, 1097–1106.
575. Cheek, J., and Broderick, J. B. (2002) Direct H Atom abstraction from spore photoproduct C-6 initiates DNA repair in the reaction catalyzed by spore photoproduct lyase: Evidence for a reversibly generated adenosyl radical intermediate, *J. Am. Chem. Soc. 124*, 2860–2861.
576. Yang, L., Lin, G., Liu, D., Dria, K. J., Telser, J., and Li, L. (2011) Probing the reaction mechanism of spore photoproduct lyase (SPL) via diastereoselectively labeled dinucleotide SP TpT substrates, *J. Am. Chem. Soc. 133*, 10434–10447.
577. Yokoyama, K., Numakura, M., Kudo, F., Ohmori, D., and Eguchi, T. (2007) Characterization and mechanistic study of a radical SAM dehydrogenase in the biosynthesis of butirosin, *J. Am. Chem. Soc. 129*, 15147–15155.
578. Cosper, M. M., Jameson, G. N., Davydov, R., Eidsness, M. K., Hoffman, B. M., Huynh, B. H., and Johnson, M. K. (2002) The $[4Fe–4S]^{2+}$ cluster in reconstituted biotin synthase binds *S*-adenosyl-L-methionine, *J. Am. Chem. Soc. 124*, 14006–14007.
579. Chen, D., Walsby, C., Hoffman, B. M., and Frey, P. A. (2003) Coordination and mechanism of reversible cleavage of *S*-adenosylmethionine by the [4Fe–4S] center in lysine 2,3-aminomutase, *J. Am. Chem. Soc. 125*, 11788–11789.
580. Goldman, P. J., Grove, T. L., Booker, S. J., and Drennan, C. L. (2013) X-Ray analysis of butirosin biosynthetic enzyme BtrN redefines structural motifs for AdoMet radical chemistry, *Proc. Natl. Acad. Sci. U. S. A. 110*, 15949–15954.
581. Bridwell-Rabb, J., Zhong, A., Sun, H. G., Drennan, C. L., and Liu, H. W. (2017) A B_{12}-dependent radical SAM enzyme involved in oxetanocin A biosynthesis, *Nature (London, U. K.) 544*, 322–326.
582. Grell, T. A. J., Kincannon, W. M., Bruender, N. A., Blaesi, E. J., Krebs, C., Bandarian, V., and Drennan, C. L. (2018) Structural and spectroscopic analyses of the sporulation killing factor biosynthetic enzyme SkfB, a bacterial AdoMet radical sactisynthase, *J. Biol. Chem. 293*, 17349–17361.
583. Cosper, N. J., Booker, S. J., Ruzicka, F., Frey, P. A., and Scott, R. A. (2000) Direct FeS cluster involvement in generation of a radical in lysine 2,3-aminomutase, *Biochemistry 39*, 15668–15673.
584. Lieder, K. W., Booker, S., Ruzicka, F. J., Beinert, H., Reed, G. H., and Frey, P. A. (1998) *S*-Adenosylmethionine-dependent reduction of lysine 2,3-aminomutase and observation of the catalytically functional iron-sulfur centers by electron paramagnetic resonance, *Biochemistry 37*, 2578–2585.
585. Miller, S. A., and Bandarian, V. (2019) Analysis of electrochemical properties of *S*-adenosyl-L-methionine and implications for its role in radical SAM enzymes, *J. Am. Chem. Soc. 141*, 11019–11026.
586. Dong, M., Horitani, M., Dzikovski, B., Freed, J. H., Ealick, S. E., Hoffman, B. M., and Lin, H. (2017) Substrate-dependent cleavage site selection by unconventional radical *S*-adenosylmethionine enzymes in diphthamide biosynthesis, *J. Am. Chem. Soc. 139*, 5680–5683.
587. Dong, M., Kathiresan, V., Fenwick, M. K., Torelli, A. T., Zhang, Y., Caranto, J. D., Dzikovski, B., Sharma, A., Lancaster, K. M., Freed, J. H., Ealick, S. E., Hoffman, B. M., and Lin, H. (2018) Organometallic and radical intermediates reveal mechanism of diphthamide biosynthesis, *Science (Washington, DC, U. S.) 359*, 1247–1250.

588. Yang, H., Impano, S., Shepard, E. M., James, C. D., Broderick, W. E., Broderick, J. B., and Hoffman, B. M. (2019) Photoinduced electron transfer in a radical SAM enzyme generates an *S*-adenosylmethionine derived methyl radical, *J. Am. Chem. Soc. 141*, 16117–16124.
589. Fajardo, A. S., Legrand, P., Paya-Tormo, L. A., Martin, L., Pellicer Martínez, M. T., Echavarri-Erasun, C., Vernede, X., Rubio, L. M., and Nicolet, Y. (2020) Structural insights into the mechanism of the radical SAM carbide synthase NifB, a key nitrogenase cofactor maturating enzyme, *J. Am. Chem. Soc. 142*, 11006–11012.
590. Escalettes, F., Florentin, D., Bui, B. T. S., Lesage, D., and Marquet, A. (1999) Biotin synthase mechanism: Evidence for hydrogen transfer from the substrate into deoxyadenosine, *J. Am. Chem. Soc. 121*, 3571–3578.
591. Yan, F., and Fujimori, D. G. (2011) RNA Methylation by radical SAM enzymes RlmN and Cfr proceeds via methylene transfer and hydride shift, *Proc. Natl. Acad. Sci. U.S.A. 108*, 3930–3934.
592. Zhang, Z., Mahanta, N., Hudson, G. A., Mitchell, D. A., and van der Donk, W. A. (2017) Mechanism of a class C radical *S*-adenosyl-L-methionine thiazole methyl transferase, *J. Am. Chem. Soc. 139*, 18623–18631.
593. Mehta, A. P., Hanes, J. W., Abdelwahed, S. H., Hilmey, D. G., Hanzelmann, P., and Begley, T. P. (2013) Catalysis of a new ribose carbon-insertion reaction by the molybdenum cofactor biosynthetic enzyme MoaA, *Biochemistry 52*, 1134–1136.
594. Young, A. P., and Bandarian, V. (2015) Mechanistic studies of the radical *S*-adenosyl-L-methionine enzyme 4-demethylwyosine synthase reveal the site of hydrogen atom abstraction, *Biochemistry 54*, 3569–3572.
595. LaMattina, J. W., Wang, B., Badding, E. D., Gadsby, L. K., Grove, T. L., and Booker, S. J. (2017) NosN, a Radical *S*-adenosylmethionine methylase, catalyzes both C1 transfer and formation of the ester linkage of the side-ring system during the biosynthesis of nosiheptide, *J. Am. Chem. Soc. 139*, 17438–17445.
596. Grove, T. L., Benner, J. S., Radle, M. I., Ahlum, J. H., Landgraf, B. J., Krebs, C., and Booker, S. J. (2011) A radically different mechanism for *S*-adenosylmethionine-dependent methyltransferases, *Science (Washington, DC, U. S.) 332*, 604–607.
597. Kudo, F., Hoshi, S., Kawashima, T., Kamachi, T., and Eguchi, T. (2014) Characterization of a radical *S*-adenosyl-L-methionine epimerase, NeoN, in the last step of neomycin B biosynthesis, *J. Am. Chem. Soc. 136*, 13909–13915.
598. Philmus, B., Decamps, L., Berteau, O., and Begley, T. P. (2015) Biosynthetic versatility and coordinated action of 5′-deoxyadenosyl radicals in deazaflavin biosynthesis, *J. Am. Chem. Soc. 137*, 5406–5413.
599. McCarty, R. M., Krebs, C., and Bandarian, V. (2013) Spectroscopic, steady-state kinetic, and mechanistic characterization of the radical SAM enzyme QueE, which catalyzes a complex cyclization reaction in the biosynthesis of 7-deazapurines, *Biochemistry 52*, 188–198.
600. Viehe, H. G., Janousek, Z., Merenyi, R., and Stella, L. (1985) The captodative effect, *Acc. Chem. Res. 18*, 148–154.
601. McLaughlin, M. I., and van der Donk, W. A. (2018) Stereospecific radical-mediated B_{12}-dependent methyl transfer by the fosfomycin biosynthesis enzyme Fom3, *Biochemistry 57*, 4967–4971.
602. Ruszczycky, M. W., Choi, S. H., Mansoorabadi, S. O., and Liu, H. W. (2011) Mechanistic studies of the radical *S*-adenosyl-L-methionine enzyme DesII: EPR Characterization of a radical intermediate generated during its catalyzed dehydrogenation of TDP-D-quinovose, *J. Am. Chem. Soc. 133*, 7292–7295.
603. Benjdia, A., Leprince, J., Sandstrom, C., Vaudry, H., and Berteau, O. (2009) Mechanistic investigations of anaerobic sulfatase-maturating enzyme: Direct CβH-atom abstraction catalyzed by a radical AdoMet enzyme, *J. Am. Chem. Soc. 131*, 8348–8349.
604. Bruender, N. A., and Bandarian, V. (2016) The radical *S*-adenosyl-L-methionine enzyme MftC catalyzes an oxidative decarboxylation of the C-terminus of the MftA peptide, *Biochemistry 55*, 2813–2816.
605. Khaliullin, B., Ayikpoe, R., Tuttle, M., and Latham, J. A. (2017) Mechanistic elucidation of the mycofactocin-biosynthetic radical *S*-adenosylmethionine protein, MftC, *J. Biol. Chem. 292*, 13022–13033.

606. Magnusson, O. T., Reed, G. H., and Frey, P. A. (2001) Characterization of an allylic analogue of the 5′-deoxyadenosyl radical: An intermediate in the reaction of lysine 2,3-aminomutase, *Biochemistry 40*, 7773–7782.
607. Byer, A. S., Yang, H., McDaniel, E. C., Kathiresan, V., Impano, S., Pagnier, A., Watts, H., Denler, C., Vagstad, A. L., Piel, J., Duschene, K. S., Shepard, E. M., Shields, T. P., Scott, L. G., Lilla, E. A., Yokoyama, K., Broderick, W. E., Hoffman, B. M., and Broderick, J. B. (2018) Paradigm shift for radical *S*-adenosyl-L-methionine reactions: The organometallic intermediate Ω is central to catalysis, *J. Am. Chem. Soc. 140*, 8634–8638.
608. Brown, A. C., and Suess, D. L. M. (2020) Reversible formation of alkyl radicals at $[Fe_4S_4]$ clusters and its implications for selectivity in radical SAM enzymes, *J. Am. Chem. Soc. 142*, 14240–14248.
609. Kincannon, W. M., Bruender, N. A., and Bandarian, V. (2018) A radical clock probe uncouples H atom abstraction from thioether cross-link formation by the radical *S*-adenosyl-L-methionine enzyme SkfB, *Biochemistry 57*, 4816–4823.
610. Nicolet, Y., Zeppieri, L., Amara, P., and Fontecilla-Camps, J. C. (2014) Crystal structure of tryptophan lyase (NosL): Evidence for radical formation at the amino group of tryptophan, *Angew. Chem., Int. Ed. Engl. 53*, 11840–11844.
611. Boal, A. K., Grove, T. L., McLaughlin, M. I., Yennawar, N. H., Booker, S. J., and Rosenzweig, A. C. (2011) Structural basis for methyl transfer by a radical SAM enzyme, *Science (Washington, DC, U. S.) 332*, 1089–1092.
612. Berkovitch, F., Nicolet, Y., Wan, J. T., Jarrett, J. T., and Drennan, C. L. (2004) Crystal structure of biotin synthase, an *S*-adenosylmethionine-dependent radical enzyme, *Science (Washington, DC, U. S.) 303*, 76–79.
613. Maiocco, S. J., Grove, T. L., Booker, S. J., and Elliott, S. J. (2015) Electrochemical resolution of the [4Fe–4S] centers of the AdoMet radical enzyme BtrN: Evidence of proton coupling and an unusual, low-potential auxiliary cluster, *J. Am. Chem. Soc. 137*, 8664–8667.
614. Liu, W. Q., Amara, P., Mouesca, J. M., Ji, X., Renoux, O., Martin, L., Zhang, C., Zhang, Q., and Nicolet, Y. (2018) 1,2-Diol dehydration by the radical SAM enzyme AprD4: A matter of proton circulation and substrate flexibility, *J. Am. Chem. Soc. 140*, 1365–1371.
615. Parent, A., Benjdia, A., Guillot, A., Kubiak, X., Balty, C., Lefranc, B., Leprince, J., and Berteau, O. (2018) Mechanistic investigations of PoyD, a radical *S*-adenosyl-L-methionine enzyme catalyzing iterative and directional epimerizations in polytheonamide A biosynthesis, *J. Am. Chem. Soc. 140*, 2469–2477.
616. Cosper, M. M., Jameson, G. N., Hernandez, H. L., Krebs, C., Huynh, B. H., and Johnson, M. K. (2004) Characterization of the cofactor composition of *Escherichia coli* biotin synthase, *Biochemistry 43*, 2007–2021.
617. Nicolet, Y., Rohac, R., Martin, L., and Fontecilla-Camps, J. C. (2013) X-Ray snapshots of possible intermediates in the time course of synthesis and degradation of protein-bound Fe_4S_4 clusters, *Proc. Natl. Acad. Sci. U. S. A. 110*, 7188–7192.
618. Ugulava, N. B., Sacanell, C. J., and Jarrett, J. T. (2001) Spectroscopic changes during a single turnover of biotin synthase: Destruction of a [2Fe–2S] cluster accompanies sulfur insertion, *Biochemistry 40*, 8352–8358.
619. Jameson, G. N., Cosper, M. M., Hernandez, H. L., Johnson, M. K., and Huynh, B. H. (2004) Role of the [2Fe–2S] cluster in recombinant *Escherichia coli* biotin synthase, *Biochemistry 43*, 2022–2031.
620. Fugate, C. J., Stich, T. A., Kim, E. G., Myers, W. K., Britt, R. D., and Jarrett, J. T. (2012) 9–Mercaptodethiobiotin is generated as a ligand to the $[Fe–2S]^+$ cluster during the reaction catalyzed by biotin synthase from *Escherichia coli*, *J. Am. Chem. Soc. 134*, 9042–9045.
621. Taylor, A. M., Farrar, C. E., and Jarrett, J. T. (2008) 9–Mercaptodethiobiotin is formed as a competent catalytic intermediate by *Escherichia coli* biotin synthase, *Biochemistry 47*, 9309–9317.
622. Lanz, N. D., Pandelia, M. E., Kakar, E. S., Lee, K. H., Krebs, C., and Booker, S. J. (2014) Evidence for a catalytically and kinetically competent enzyme-substrate cross-linked intermediate in catalysis by lipoyl synthase, *Biochemistry 53*, 4557–4572.
623. McLaughlin, M. I., Lanz, N. D., Goldman, P. J., Lee, K. H., Booker, S. J., and Drennan, C. L. (2016) Crystallographic snapshots of sulfur insertion by lipoyl synthase, *Proc. Natl. Acad. Sci. U. S. A. 113*, 9446–9450.

624. Bruender, N. A., Wilcoxen, J., Britt, R. D., and Bandarian, V. (2016) Biochemical and spectroscopic characterization of a radical *S*-adenosyl-L-methionine enzyme involved in the formation of a peptide thioether cross-link, *Biochemistry 55*, 2122–2134.
625. Fluhe, L., Knappe, T. A., Gattner, M. J., Schafer, A., Burghaus, O., Linne, U., and Marahiel, M. A. (2012) The radical SAM enzyme AlbA catalyzes thioether bond formation in subtilosin A, *Nat. Chem. Biol. 8*, 350–357.
626. Benjdia, A., Decamps, L., Guillot, A., Kubiak, X., Ruffie, P., Sandstrom, C., and Berteau, O. (2017) Insights into the catalysis of a lysine-tryptophan bond in bacterial peptides by a SPASM domain radical *S*-adenosylmethionine (SAM) peptide cyclase, *J. Biol. Chem. 292*, 10835–10844.
627. Schramma, K. R., Forneris, C. C., Caruso, A., and Seyedsayamdost, M. R. (2018) Mechanistic investigations of lysine-tryptophan cross-link formation catalyzed by *Streptococcal* radical *S*-adenosylmethionine enzymes, *Biochemistry 57*, 461–468.
628. Fluhe, L., Burghaus, O., Wieckowski, B. M., Giessen, T. W., Linne, U., and Marahiel, M. A. (2013) Two [4Fe–4S] clusters containing radical SAM enzyme SkfB catalyze thioether bond formation during the maturation of the sporulation killing factor, *J. Am. Chem. Soc. 135*, 959–962.
629. Schramma, K. R., Bushin, L. B., and Seyedsayamdost, M. R. (2015) Structure and biosynthesis of a macrocyclic peptide containing an unprecedented lysine-to-tryptophan cross-link, *Nat. Chem. 7*, 431–437.
630. Clark, K. A., Bushin, L. B., and Seyedsayamdost, M. R. (2019) Aliphatic ether bond formation expands the scope of radical SAM enzymes in natural product biosynthesis, *J. Am. Chem. Soc. 141*, 10610–10615.
631. Caruso, A., Martinie, R. J., Bushin, L. B., and Seyedsayamdost, M. R. (2019) Macrocyclization via an arginine-tyrosine crosslink broadens the reaction scope of radical *S*-adenosylmethionine enzymes, *J. Am. Chem. Soc. 141*, 16610–16614.
632. Barr, I., Stich, T. A., Gizzi, A. S., Grove, T. L., Bonanno, J. B., Latham, J. A., Chung, T., Wilmot, C. M., Britt, R. D., Almo, S. C., and Klinman, J. P. (2018) X-Ray and EPR characterization of the auxiliary Fe–S clusters in the radical SAM enzyme PqqE, *Biochemistry 57*, 1306–1315.
633. Davis, K. M., Schramma, K. R., Hansen, W. A., Bacik, J. P., Khare, S. D., Seyedsayamdost, M. R., and Ando, N. (2017) Structures of the peptide-modifying radical SAM enzyme SuiB elucidate the basis of substrate recognition, *Proc. Natl. Acad. Sci. U. S. A. 114*, 10420–10425.
634. Lees, N. S., Hanzelmann, P., Hernandez, H. L., Subramanian, S., Schindelin, H., Johnson, M. K., and Hoffman, B. M. (2009) ENDOR Spectroscopy shows that guanine N1 binds to [4Fe–4S] cluster II of the *S*-adenosylmethionine-dependent enzyme MoaA: Mechanistic implications, *J. Am. Chem. Soc. 131*, 9184–9185.
635. Hanzelmann, P., and Schindelin, H. (2006) Binding of 5′-GTP to the C-terminal FeS cluster of the radical *S*-adenosylmethionine enzyme MoaA provides insights into its mechanism, *Proc. Natl. Acad. Sci. U. S. A. 103*, 6829–6834.
636. Mehta, A. P., Abdelwahed, S. H., and Begley, T. P. (2013) Molybdopterin biosynthesis: Trapping an unusual purine ribose adduct in the MoaA-catalyzed reaction, *J. Am. Chem. Soc. 135*, 10883–10885.
637. Chakravarti, A., Selvadurai, K., Shahoei, R., Lee, H., Fatma, S., Tajkhorshid, E., and Huang, R. H. (2018) Reconstitution and substrate specificity for isopentenyl pyrophosphate of the antiviral radical SAM enzyme viperin, *J. Biol. Chem. 293*, 14122–14133.
638. Wang, B., LaMattina, J. W., Marshall, S. L., and Booker, S. J. (2019) Capturing intermediates in the reaction catalyzed by NosN, a class C radical *S*-adenosylmethionine methylase involved in the biosynthesis of the nosiheptide side-ring system, *J. Am. Chem. Soc. 141*, 5788–5797.
639. Grove, T. L., Radle, M. I., Krebs, C., and Booker, S. J. (2011) Cfr and RlmN contain a single [4Fe–4S]cluster, which directs two distinct reactivities for *S*-adenosylmethionine: Methyl transfer by S_N2 displacement and radical generation, *J. Am. Chem. Soc. 133*, 19586–19589.
640. Schwalm, E. L., Grove, T. L., Booker, S. J., and Boal, A. K. (2016) Crystallographic capture of a radical *S*-adenosylmethionine enzyme in the act of modifying tRNA, *Science (Washington, DC, U. S.) 352*, 309–312.

641. Grove, T. L., Livada, J., Schwalm, E. L., Green, M. T., Booker, S. J., and Silakov, A. (2013) A substrate radical intermediate in catalysis by the antibiotic resistance protein Cfr, *Nat. Chem. Biol. 9*, 422–427.
642. Silakov, A., Grove, T. L., Radle, M. I., Bauerle, M. R., Green, M. T., Rosenzweig, A. C., Boal, A. K., and Booker, S. J. (2014) Characterization of a cross-linked protein-nucleic acid substrate radical in the reaction catalyzed by RlmN, *J. Am. Chem. Soc. 136*, 8221–8228.
643. McCusker, K. P., Medzihradszky, K. F., Shiver, A. L., Nichols, R. J., Yan, F., Maltby, D. A., Gross, C. A., and Fujimori, D. G. (2012) Covalent intermediate in the catalytic mechanism of the radical *S*-adenosyl-L-methionine methyl synthase RlmN trapped by mutagenesis, *J. Am. Chem. Soc. 134*, 18074–18081.
644. Wang, Y., and Begley, T. P. (2020) Mechanistic studies on CysS – a vitamin B_{12}-dependent radical SAM methyltransferase involved in the biosynthesis of the *tert*-butyl group of cystobactamid, *J. Am. Chem. Soc. 142*, 9944–9954.
645. Perche-Letuvee, P., Kathirvelu, V., Berggren, G., Clemancey, M., Latour, J. M., Maurel, V., Douki, T., Armengaud, J., Mulliez, E., Fontecave, M., Garcia-Serres, R., Gambarelli, S., and Atta, M. (2012) 4–Demethylwyosine synthase from *Pyrococcus abyssi* is a radical-*S*-adenosyl-L-methionine enzyme with an additional $[4Fe–4S]^{+2}$ cluster that interacts with the pyruvate co-substrate, *J. Biol. Chem. 287*, 41174–41185.
646. Kathirvelu, V., Perche-Letuvee, P., Latour, J. M., Atta, M., Forouhar, F., Gambarelli, S., and Garcia-Serres, R. (2017) Spectroscopic evidence for cofactor-substrate interaction in the radical-SAM enzyme TYW1, *Dalton Trans. 46*, 13211–13219.
647. Shepard, E. M., Duffus, B. R., George, S. J., McGlynn, S. E., Challand, M. R., Swanson, K. D., Roach, P. L., Cramer, S. P., Peters, J. W., and Broderick, J. B. (2010) [FeFe]-Hydrogenase maturation: HydG-Catalyzed synthesis of carbon monoxide, *J. Am. Chem. Soc. 132*, 9247–9249.
648. Driesener, R. C., Challand, M. R., McGlynn, S. E., Shepard, E. M., Boyd, E. S., Broderick, J. B., Peters, J. W., and Roach, P. L. (2010) [FeFe]-Hydrogenase cyanide ligands derived from *S*-adenosylmethionine-dependent cleavage of tyrosine, *Angew. Chem., Int. Ed. Engl. 49*, 1687–1690.
649. Kuchenreuther, J. M., George, S. J., Grady-Smith, C. S., Cramer, S. P., and Swartz, J. R. (2011) Cell-free H-cluster synthesis and [FeFe] hydrogenase activation: All five CO and CN^- ligands derive from tyrosine, *PLoS One 6*, e20346.
650. van der Donk, W. A., Zeng, C., Biemann, K., Stubbe, J., Hanlon, A., and Kyte, J. (1996) Identification of an active site residue of the R1 subunit of ribonucleotide reductase from *Escherichia coli*: Characterization of substrate-induced polypeptide cleavage by C225SR1, *Biochemistry 35*, 10058–10067.
651. Kriek, M., Martins, F., Challand, M. R., Croft, A., and Roach, P. L. (2007) Thiamine biosynthesis in *Escherichia coli*: Identification of the intermediate and by-product derived from tyrosine, *Angew. Chem., Int. Ed. Engl. 46*, 9223–9226.
652. Zhang, Q., Li, Y., Chen, D., Yu, Y., Duan, L., Shen, B., and Liu, W. (2011) Radical-mediated enzymatic carbon chain fragmentation–recombination, *Nat. Chem. Biol. 7*, 154–160.
653. Bhandari, D. M., Xu, H., Nicolet, Y., Fontecilla-Camps, J. C., and Begley, T. P. (2015) Tryptophan lyase (NosL): Mechanistic insights from substrate analogues and mutagenesis, *Biochemistry 54*, 4767–4769.
654. Ji, X., Li, Y., Ding, W., and Zhang, Q. (2015) Substrate-tuned catalysis of the radical *S*-adenosyl-L-methionine enzyme NosL involved in nosiheptide biosynthesis, *Angew. Chem., Int. Ed. Engl. 54*, 9021–9024.
655. Bhandari, D. M., Fedoseyenko, D., and Begley, T. P. (2018) Mechanistic studies on the radical SAM enzyme tryptophan lyase (NosL), *Methods Enzymol. 606*, 155–178.
656. Amara, P., Mouesca, J. M., Bella, M., Martin, L., Saragaglia, C., Gambarelli, S., and Nicolet, Y. (2018) Radical *S*-adenosyl-L-methionine tryptophan lyase (NosL): How the protein controls the carboxyl radical $\cdot CO_2^-$ migration, *J. Am. Chem. Soc. 140*, 16661–16668.
657. Sicoli, G., Mouesca, J. M., Zeppieri, L., Amara, P., Martin, L., Barra, A. L., Fontecilla-Camps, J. C., Gambarelli, S., and Nicolet, Y. (2016) Fine-tuning of a radical-based reaction by radical *S*-adenosyl-L-methionine tryptophan lyase, *Science (Washington, DC, U. S.) 351*, 1320–1323.

658. Bhandari, D. M., Fedoseyenko, D., and Begley, T. P. (2018) Mechanistic studies on tryptophan lyase (NosL): Identification of cyanide as a reaction product, *J. Am. Chem. Soc. 140*, 542–545.
659. Duffus, B. R., Ghose, S., Peters, J. W., and Broderick, J. B. (2014) Reversible H atom abstraction catalyzed by the radical *S*-adenosylmethionine enzyme HydG, *J. Am. Chem. Soc. 136*, 13086–13089.
660. Kuchenreuther, J. M., Myers, W. K., Stich, T. A., George, S. J., Nejatyjahromy, Y., Swartz, J. R., and Britt, R. D. (2013) A radical intermediate in tyrosine scission to the CO and CN^- ligands of FeFe hydrogenase, *Science (Washington, DC, U. S.) 342*, 472–475.
661. Driesener, R. C., Duffus, B. R., Shepard, E. M., Bruzas, I. R., Duschene, K. S., Coleman, N. J., Marrison, A. P., Salvadori, E., Kay, C. W., Peters, J. W., Broderick, J. B., and Roach, P. L. (2013) Biochemical and kinetic characterization of radical *S*-adenosyl-L-methionine enzyme HydG, *Biochemistry 52*, 8696–8707.
662. Challand, M. R., Martins, F. T., and Roach, P. L. (2010) Catalytic activity of the anaerobic tyrosine lyase required for thiamine biosynthesis in *Escherichia coli*, *J. Biol. Chem. 285*, 5240–5248.
663. Aberhart, D. J., Lin, H. J., and Weiller, B. H. (1981) Stereochemistry of lysine 2,3-aminomutase, *J. Am. Chem. Soc. 103*, 6750–6752.
664. Chirpich, T. P., Zappia, V., Costilow, R. N., and Barker, H. A. (1970) Lysine 2,3-aminomutase. Purification and properties of a pyridoxal phosphate and *S*-adenosylmethionine-activated enzyme, *J. Biol. Chem. 245*, 1778–1789.
665. Ballinger, M. D., Frey, P. A., Reed, G. H., and LoBrutto, R. (1995) Pulsed electron paramagnetic resonance studies of the lysine 2,3-aminomutase substrate radical: Evidence for participation of pyridoxal 5′-phosphate in a radical rearrangement, *Biochemistry 34*, 10086–10093.
666. Ballinger, M. D., Reed, G. H., and Frey, P. A. (1992) An organic radical in the lysine 2,3-aminomutase reaction, *Biochemistry 31*, 949–953.
667. Ballinger, M. D., Frey, P. A., and Reed, G. H. (1992) Structure of a substrate radical intermediate in the reaction of lysine 2,3-aminomutase, *Biochemistry 31*, 10782–10789.
668. Chang, C. H., Ballinger, M. D., Reed, G. H., and Frey, P. A. (1996) Lysine 2,3-aminomutase: rapid mix-freeze-quench electron paramagnetic resonance studies establishing the kinetic competence of a substrate-based radical intermediate, *Biochemistry 35*, 11081–11084.
669. Wu, W., Lieder, K. W., Reed, G. H., and Frey, P. A. (1995) Observation of a second substrate radical intermediate in the reaction of lysine 2,3-aminomutase: A radical centered on the β-carbon of the alternative substrate, 4-thia-L-lysine, *Biochemistry 34*, 10532–10537.
670. Wu, W., Booker, S., Lieder, K. W., Bandarian, V., Reed, G. H., and Frey, P. A. (2000) Lysine 2,3-aminomutase and *trans*-4,5-dehydrolysine: Characterization of an allylic analogue of a substrate-based radical in the catalytic mechanism, *Biochemistry 39*, 9561–9570.
671. Han, O., and Frey, P. A. (1990) Chemical model for the pyridoxal 5′-phosphate dependent lysine aminomutases, *J. Am. Chem. Soc. 112*, 8982–8983.
672. Levin, B. J., and Balskus, E. P. (2018) Characterization of 1,2-propanediol dehydratases reveals distinct mechanisms for B_{12}-dependent and glycyl radical enzymes, *Biochemistry 57*, 3222–3226.
673. Yang, L., Nelson, R. S., Benjdia, A., Lin, G., Telser, J., Stoll, S., Schlichting, I., and Li, L. (2013) A radical transfer pathway in spore photoproduct lyase, *Biochemistry 52*, 3041–3050.
674. Knauer, S. H., Buckel, W., and Dobbek, H. (2011) Structural basis for reductive radical formation and electron recycling in (*R*)-2-hydroxyisocaproyl-CoA dehydratase, *J. Am. Chem. Soc. 133*, 4342–4347.
675. Locher, K. P., Hans, M., Yeh, A. P., Schmid, B., Buckel, W., and Rees, D. C. (2001) Crystal structure of the *Acidaminococcus fermentans* 2-hydroxyglutaryl-CoA dehydratase component A, *J. Mol. Biol. 307*, 297–308.
676. Knauer, S. H., Buckel, W., and Dobbek, H. (2012) On the ATP-dependent activation of the radical enzyme (*R*)-2-hydroxyisocaproyl-CoA dehydratase, *Biochemistry 51*, 6609–6622.
677. Kim, J., Darley, D. J., Buckel, W., and Pierik, A. J. (2008) An allylic ketyl radical intermedi-

ate in clostridial amino-acid fermentation, *Nature (London, U. K.) 452*, 239–242.
678. Span, I., Grawert, T., Bacher, A., Eisenreich, W., and Groll, M. (2012) Crystal structures of mutant IspH proteins reveal a rotation of the substrate's hydroxymethyl group during catalysis, *J. Mol. Biol. 416*, 1–9.
679. Span, I., Wang, K., Wang, W., Jauch, J., Eisenreich, W., Bacher, A., Oldfield, E., and Groll, M. (2013) Structures of fluoro, amino, and thiol inhibitors bound to the $[Fe_4S_4]$ protein IspH, *Angew. Chem., Int. Ed. Engl. 52*, 2118–2121.
680. Xu, W., Lees, N. S., Hall, D., Welideniya, D., Hoffman, B. M., and Duin, E. C. (2012) A closer look at the spectroscopic properties of possible reaction intermediates in wild-type and mutant (*E*)-4-hydroxy-3-methylbut-2-enyl diphosphate reductase, *Biochemistry 51*, 4835–4849.
681. Wang, W., Wang, K., Span, I., Jauch, J., Bacher, A., Groll, M., and Oldfield, E. (2012) Are free radicals involved in IspH catalysis? An EPR and crystallographic investigation, *J. Am. Chem. Soc. 134*, 11225–11234.
682. Xiao, Y., Zahariou, G., Sanakis, Y., and Liu, P. (2009) IspG Enzyme activity in the deoxyxylulose phosphate pathway: Roles of the iron-sulfur cluster, *Biochemistry 48*, 10483–10485.
683. Quitterer, F., Frank, A., Wang, K., Rao, G., O'Dowd, B., Li, J., Guerra, F., Abdel-Azeim, S., Bacher, A., Eppinger, J., Oldfield, E., and Groll, M. (2015) Atomic-resolution structures of discrete stages on the reaction coordinate of the $[Fe_4S_4]$ enzyme IspG (GcpE), *J. Mol. Biol. 427*, 2220–2228.
684. Rekittke, I., Jomaa, H., and Ermler, U. (2012) Structure of the GcpE (IspG)-MEcPP complex from *Thermus thermophilus*, *FEBS Lett. 586*, 3452–3457.
685. Huang, X., Tanaka, K. S. E., and Bennet, A. J. (1997) Glucosidase-catalyzed hydrolysis of α-D-glucopyranosyl pyridinium salts: Kinetic evidence for nucleophilic involvement at the glucosidation transition state, *J. Am. Chem. Soc. 119*, 11147–11154.
686. Anslyn, E. V., and Dougherty, D. A. (2006) *Modern Physical Organic Chemistry*, University Science, Sausalito, CA.
687. Daimay, L.-V., Colthup, N. V., Fateley, W. G., and Grasselli, J. G. (1991) *The Handbook of Infrared and Raman Characteristic Frequencies of Organic Molecules*, Academic Press, Boston.
688. Huang, X. C., Surry, C., Hiebert, T., and Bennet, A. J. (1995) Hydrolysis of (2-deoxy-β-D-glucopyranosyl)pyridinium salts, *J. Am. Chem. Soc. 117*, 10614–10621.
689. Parikh, S. S., Walcher, G., Jones, G. D., Slupphaug, G., Krokan, H. E., Blackburn, G. M., and Tainer, J. A. (2000) Uracil-DNA glycosylase-DNA substrate and product structures: Conformational strain promotes catalytic efficiency by coupled stereoelectronic effects, *Proc. Natl. Acad. Sci. U. S. A. 97*, 5083–5088.
690. Werner, R. M., and Stivers, J. T. (2000) Kinetic isotope effect studies of the reaction catalyzed by uracil DNA glycosylase: Evidence for an oxocarbenium ion-uracil anion intermediate, *Biochemistry 39*, 14054–14064.
691. Vocadlo, D. J., Wicki, J., Rupitz, K., and Withers, S. G. (2002) Mechanism of *Thermoanaerobacterium saccharolyticum* β-xylosidase: Kinetic studies, *Biochemistry 41*, 9727–9735.
692. Lee, S. S., Yu, S., and Withers, S. G. (2003) Detailed dissection of a new mechanism for glycoside cleavage: α-1,4-Glucan lyase, *Biochemistry 42*, 13081–13090.
693. Rink, R., Fennema, M., Smids, M., Dehmel, U., and Janssen, D. B. (1997) Primary structure and catalytic mechanism of the epoxide hydrolase from *Agrobacterium radiobacter* AD1, *J. Biol. Chem. 272*, 14650–14657.
694. Blee, E., Summerer, S., Flenet, M., Rogniaux, H., Van Dorsselaer, A., and Schuber, F. (2005) Soybean epoxide hydrolase: Identification of the catalytic residues and probing of the reaction mechanism with secondary kinetic isotope effects, *J. Biol. Chem. 280*, 6479–6487.
695. Dobritzsch, D., Ricagno, S., Schneider, G., Schnackerz, K. D., and Lindqvist, Y. (2002) Crystal structure of the productive ternary complex of dihydropyrimidine dehydrogenase with NADPH and 5-iodouracil. Implications for mechanism of inhibition and electron transfer, *J. Biol. Chem. 277*, 13155–13166.
696. Rosenbaum, K., Jahnke, K., Schnackerz, K. D., and Cook, P. F. (1998) Secondary tritium and solvent deuterium isotope effects as a probe of the reaction catalyzed by porcine recombinant dihydropyrimidine dehydrogenase, *Biochemistry 37*, 9156–9159.
697. Iwig, D. F., Grippe, A. T., McIntyre, T. A., and Booker, S. J. (2004) Isotope and elemental ef-

fects indicate a rate-limiting methyl transfer as the initial step in the reaction catalyzed by *Escherichia coli* cyclopropane fatty acid synthase, *Biochemistry 43*, 13510–13524.
698. Cheng, M.-C., and Marsh, E. N. G. (2004) Pre-steady-state measurement of intrinsic secondary tritium isotope effects associated with the homolysis of adenosylcobalamin and the formation of 5′-deoxyadensosine in glutamate mutase, *Biochemistry 43*, 2155–2158.
699. Gruber, K., Reitzer, R., and Kratky, C. (2001) Radical shuttling in a protein: Ribose pseudorotation controls alkyl-radical transfer in the coenzyme B_{12} dependent enzyme glutamate mutase, *Angew. Chem. 40*, 3377–3380.
700. Lee, J. K., Bain, A. D., and Berti, P. J. (2004) Probing the transition states of four glucoside hydrolyses with ^{13}C kinetic isotope effects measured at natural abundance by NMR spectroscopy, *J. Am. Chem. Soc. 126*, 3769–3776.
701. Lou, M., Burger, S. K., Gilpin, M. E., Gawuga, V., Capretta, A., and Berti, P. J. (2012) Transition state analysis of *enol*pyruvylshikimate 3-phosphate (EPSP) synthase (AroA)-catalyzed EPSP hydrolysis, *J. Am. Chem. Soc. 134*, 12958–12969.
702. Sowa, G. A., Hengge, A. C., and Cleland, W. W. (1997) ^{18}O Isotope effects support a concerted mechanism for ribonuclease A, *J. Am. Chem. Soc. 119*, 2319–2320.
703. Caldwell, S. R., Raushel, F. M., Weiss, P. M., and Cleland, W. W. (1991) Transition-state structures for enzymatic and alkaline phosphotriester hydrolysis, *Biochemistry 30*, 7444–7450.
704. Gerratana, B., Frey, P. A., and Cleland, W. W. (2001) Characterization of the transition-state structure of the reaction of kanamycin nucleotidyltransferase by heavy-atom kinetic isotope effects, *Biochemistry 40*, 2972–2977.
705. Jones, J. P., Weiss, P. M., and Cleland, W. W. (1991) Secondary ^{18}O isotope effects for hexokinase-catalyzed phosphoryl transfer from ATP, *Biochemistry 30*, 3634–3639.
706. Bruner, M., and Horenstein, B. A. (2000) Use of an altered sugar-nucleotide to unmask the transition state for $\alpha(2\rightarrow6)$ sialyltransferase, *Biochemistry 39*, 2261–2268.
707. Chan, J., Lewis, A. R., Indurugalla, D., Schur, M., Wakarchuk, W., and Bennet, A. J. (2012) Transition state analysis of *Vibrio cholerae* sialidase-catalyzed hydrolyses of natural substrate analogues, *J. Am. Chem. Soc. 134*, 3748–3757.
708. Chen, C. C., Rahil, J., Pratt, R. F., and Herzberg, O. (1993) Structure of a phosphonate-inhibited β-lactamase. An analog of the tetrahedral transition state/intermediate of β-lactam hydrolysis, *J. Mol. Biol. 234*, 165–178.
709. Adediran, S. A., Deraniyagala, S. A., Xu, Y., and Pratt, R. F. (1996) β-Secondary and solvent deuterium kinetic isotope effects on β-lactamase catalysis, *Biochemistry 35*, 3604–3613.
710. Carpenter, G. B., and Donohue, J. (1950) The crystal structure of *N*-acetylglycine, *J. Am. Chem. Soc. 72*, 2315–2328.
711. Mercedes-Camacho, A. Y., Mullins, A. B., Mason, M. D., Xu, G. G., Mahoney, B. J., Wang, X., Peng, J. W., and Etzkorn, F. A. (2013) Kinetic isotope effects support the twisted amide mechanism of Pin1 peptidyl-prolyl isomerase, *Biochemistry 52*, 7707–7713.
712. Zhang, Y., Luo, M., and Schramm, V. L. (2009) Transition states of *Plasmodium falciparum* and human orotate phosphoribosyltransferases, *J. Am. Chem. Soc. 131*, 4685–4694.
713. Tao, W., Grubmeyer, C., and Blanchard, J. S. (1996) Transition state structure of *Salmonella typhimurium* orotate phosphoribosyltransferase, *Biochemistry 35*, 14–21.
714. Zhang, Y., and Schramm, V. L. (2010) Pyrophosphate interactions at the transition states of *Plasmodium falciparum* and human orotate phosphoribosyltransferases, *J. Am. Chem. Soc. 132*, 8787–8794.
715. Horenstein, B. A., Parkin, D. W., Estupinan, B., and Schramm, V. L. (1991) Transition-state analysis of nucleoside hydrolase from *Crithidia fasciculata*, *Biochemistry 30*, 10788–10795.
716. Bennet, A. J., and Sinnott, M. L. (1986) Complete kinetic isotope effect description of transition states for acid-catalyzed hydrolyses of methyl α- and β-glucopyranosides, *J. Am. Chem. Soc. 108*, 7287–7294.
717. Burgos, E. S., Vetticatt, M. J., and Schramm, V. L. (2013) Recycling nicotinamide. The transition-state structure of human nicotinamide phosphoribosyltransferase, *J. Am. Chem. Soc. 135*, 3485–3493.

718. Roston, D., and Kohen, A. (2013) A critical test of the "tunneling and coupled motion" concept in enzymatic alcohol oxidation, *J. Am. Chem. Soc. 135*, 13624–13627.
719. Cha, Y., Murray, C. J., and Klinman, J. P. (1989) Hydrogen tunneling in enzyme reactions, *Science (Washington, DC, U. S.) 243*, 1325–1330.
720. Welsh, K. M., Creighton, D. J., and Klinman, J. P. (1980) Transition-state structure in the yeast alcohol dehydrogenase reaction: The magnitude of solvent and α-secondary hydrogen isotope effects, *Biochemistry 19*, 2005–2016.
721. Munos, J. W., Pu, X., Mansoorabadi, S. O., Kim, H. J., and Liu, H. W. (2009) A secondary kinetic isotope effect study of the 1-deoxy-D-xylulose-5-phosphate reductoisomerase-catalyzed reaction: Evidence for a retroaldol-aldol rearrangement, *J. Am. Chem. Soc. 131*, 2048–2049.
722. Lee, L. V., Vu, M. V., and Cleland, W. W. (2000) ^{13}C and deuterium isotope effects suggest an aldol cleavage mechanism for L-ribulose-5-phosphate 4-epimerase, *Biochemistry 39*, 4808–4820.
723. Phillips, R. S., Sundararaju, B., and Faleev, N. G. (2000) Proton transfer and carbon–carbon bond cleavage in the elimination of indole catalyzed by *Escherichia coli* tryptophan indole-lyase, *J. Am. Chem. Soc. 122*, 1008–1014.
724. Tao, X., Yang, Z., and Tong, L. (2003) Crystal structures of substrate complexes of malic enzyme and insights into the catalytic mechanism, *Structure 11*, 1141–1150.
725. Hermes, J. D., Roeske, C. A., O'Leary, M. H., and Cleland, W. W. (1982) Use of multiple isotope effects to determine enzyme mechanisms and intrinsic isotope effects. Malic enzyme and glucose-6-phosphate dehydrogenase, *Biochemistry 21*, 5106–5114.
726. Yang, Z., Zhang, H., Hung, H. C., Kuo, C. C., Tsai, L. C., Yuan, H. S., Chou, W. Y., Chang, G. G., and Tong, L. (2002) Structural studies of the pigeon cytosolic NADP$^+$-dependent malic enzyme, *Protein Sci. 11*, 332–341.
727. Schimerlik, M. I., Grimshaw, C. E., and Cleland, W. W. (1977) Determination of the rate-limiting steps for malic enzyme by the use of isotope effects and other kinetic studies, *Biochemistry 16*, 571–576.
728. Davisson, V. J., and Schulz, A. R. (1985) The purification and steady-state kinetic behaviour of rabbit heart mitochondrial NADP$^+$ malic enzyme, *Biochem. J. 225*, 335–342.
729. Edens, W. A., Urbauer, J. L., and Cleland, W. W. (1997) Determination of the chemical mechanism of malic enzyme by isotope effects, *Biochemistry 36*, 1141–1147.
730. Cook, P. F., Blanchard, J. S., and Cleland, W. W. (1980) Primary and secondary deuterium isotope effects on equilibrium constants for enzyme-catalyzed reactions, *Biochemistry 19*, 4853–4858.
731. Rendina, A. R., Hermes, J. D., and Cleland, W. W. (1984) Use of multiple isotope effects to study the mechanism of 6-phosphogluconate dehydrogenase, *Biochemistry 23*, 6257–6262.
732. Hwang, C. C., Berdis, A. J., Karsten, W. E., Cleland, W. W., and Cook, P. F. (1998) Oxidative decarboxylation of 6-phosphogluconate by 6-phosphogluconate dehydrogenase proceeds by a stepwise mechanism with NADP and APADP as oxidants, *Biochemistry 37*, 12596–12602.
733. Chiu, H. J., Abdubek, P., Astakhova, T., Axelrod, H. L., Carlton, D., Clayton, T., Das, D., Deller, M. C., Duan, L., Feuerhelm, J., Grant, J. C., Grzechnik, A., Han, G. W., Jaroszewski, L., Jin, K. K., Klock, H. E., Knuth, M. W., Kozbial, P., Krishna, S. S., Kumar, A., Marciano, D., McMullan, D., Miller, M. D., Morse, A. T., Nigoghossian, E., Okach, L., Reyes, R., Tien, H. J., Trame, C. B., van den Bedem, H., Weekes, D., Xu, Q., Hodgson, K. O., Wooley, J., Elsliger, M. A., Deacon, A. M., Godzik, A., Lesley, S. A., and Wilson, I. A. (2010) The structure of *Haemophilus influenzae* prephenate dehydrogenase suggests unique features of bifunctional TyrA enzymes, *Acta Crystallogr., Sect. F: Struct. Biol. Commun. 66*, 1317–1325.
734. Hermes, J. D., Tipton, P. A., Fisher, M. A., O'Leary, M. H., Morrison, J. F., and Cleland, W. W. (1984) Mechanisms of enzymatic and acid-catalyzed decarboxylations of prephenate, *Biochemistry 23*, 6263–6275.
735. Hermes, J. D., Morrical, S. W., O'Leary, M. H., and Cleland, W. W. (1984) Variation of transition-state structure as a function of the nucleotide in reactions catalyzed by dehydrogenases. 2. Formate dehydrogenase, *Biochemistry 23*, 5479–5488.
736. Blanchard, J. S., and Cleland, W. W. (1980) Kinetic and chemical mechanisms of yeast

formate dehydrogenase, *Biochemistry 19*, 3543–3550.
737. Grissom, C. B., and Cleland, W. W. (1985) Use of intermediate partitioning to calculate intrinsic isotope effects for the reaction catalyzed by malic enzyme, *Biochemistry 24*, 944–948.
738. Belasco, J. G., Albery, W. J., and Knowles, J. R. (1983) Double isotope fractionation: Test for concertedness and for transition-state dominance, *J. Am. Chem. Soc. 105*, 2475–2477.
739. Fagan, R. L., Jensen, K. F., Bjornberg, O., and Palfey, B. A. (2007) Mechanism of flavin reduction in the class 1A dihydroorotate dehydrogenase from *Lactococcus lactis*, *Biochemistry 46*, 4028–4036.
740. Quartararo, C. E., Hazra, S., Hadi, T., and Blanchard, J. S. (2013) Structural, kinetic and chemical mechanism of isocitrate dehydrogenase-1 from *Mycobacterium tuberculosis*, *Biochemistry 52*, 1765–1775.
741. Ceccarelli, C., Grodsky, N. B., Ariyaratne, N., Colman, R. F., and Bahnson, B. J. (2002) Crystal structure of porcine mitochondrial $NADP^+$-dependent isocitrate dehydrogenase complexed with Mn^{2+} and isocitrate. Insights into the enzyme mechanism, *J. Biol. Chem. 277*, 43454–43462.
742. Wang, Z., Chang, E. P., and Schramm, V. L. (2016) Triple isotope effects support concerted hydride and proton transfer and promoting vibrations in human heart lactate dehydrogenase, *J. Am. Chem. Soc. 138*, 15004–15010.
743. Isupov, M. N., Antson, A. A., Dodson, E. J., Dodson, G. G., Dementieva, I. S., Zakomirdina, L. N., Wilson, K. S., Dauter, Z., Lebedev, A. A., and Harutyunyan, E. H. (1998) Crystal structure of tryptophanase, *J. Mol. Biol. 276*, 603–623.
744. Spies, M. A., and Toney, M. D. (2003) Multiple hydrogen kinetic isotope effects for enzymes catalyzing exchange with solvent: Application to alanine racemase, *Biochemistry 42*, 5099–5107.
745. Ehrlich, J. I., Hwang, C.-C., Cook, P. F., and Blanchard, J. S. (1999) Evidence for a stepwise mechanism of OMP decarboxylase, *J. Am. Chem. Soc. 121*, 6966–6967.
746. Mitra, B., Kallarakal, A. T., Kozarich, J. W., Gerlt, J. A., Clifton, J. G., Petsko, G. A., and Kenyon, G. L. (1995) Mechanism of the reaction catalyzed by mandelate racemase: Importance of electrophilic catalysis by Glutamic Acid 317, *Biochemistry 34*, 2777–2787.
747. Rose, I. A., and Rieder, S. V. (1958) Studies on the mechanism on the aldolase reaction; Isotope exchange reactions of muscle and yeast aldolase, *J. Biol. Chem. 231*, 315–329.
748. Butler, M. M., Graves, K. L., and Hardy, L. W. (1994) Evidence from ^{18}O exchange studies for an exocyclic methylene intermediate in the reaction catalyzed by T4 deoxycytidylate hydroxymethylase, *Biochemistry 33*, 10521–10526.
749. Dinovo, E. C., and Boyer, P. D. (1971) Isotopic probes of the enolase reaction mechanism. Initial and equilibrium isotope exchange rates. Primary and secondary isotope effects, *J. Biol. Chem. 246*, 4586–4593.
750. Maister, S. G., Pett, C. P., Albery, W. J., and Knowles, J. R. (1976) Energetics of triosephosphate isomerase: The appearance of solvent tritium in substrate dihydroxyacetone phosphate and in product, *Biochemistry 15*, 5607–5612.
751. Rose, I. A., Fung, W. J., and Warms, J. V. (1990) Proton diffusion in the active site of triosephosphate isomerase, *Biochemistry 29*, 4312–4317.
752. Hartman, F. C. (1971) Haloacetol phosphates. Characterization of the active site of rabbit muscle triose phosphate isomerase, *Biochemistry 10*, 146–154.
753. Jogl, G., Rozovsky, S., McDermott, A. E., and Tong, L. (2003) Optimal alignment for enzymatic proton transfer: Structure of the Michaelis complex of triosephosphate isomerase at 1.2-Å resolution, *Proc. Natl. Acad. Sci. U. S. A. 100*, 50–55.
754. Nickbarg, E. B., Davenport, R. C., Petsko, G. A., and Knowles, J. R. (1988) Triosephosphate isomerase: Removal of a putatively electrophilic histidine residue results in a subtle change in catalytic mechanism, *Biochemistry 27*, 5948–5960.
755. Park, S. H., Suh, S. W., and Song, H. K. (2019) A cytosine modification mechanism revealed by the structure of a ternary complex of deoxycytidylate hydroxymethylase from bacteriophage T4 with its cofactor and substrate, *IUCrJ 6*, 206–217.
756. Bartlett, P. A., and Satake, K. (1988) Does dehydroquinate synthase synthesize dehydroquinate? *J. Am. Chem. Soc. 110*, 1628–1630.

757. Srinivasan, P. R., Rothschild, J., and Sprinson, D. B. (1963) The enzymic conversion of 3-deoxy-D-arabino-heptulosonic acid 7-phosphate to 5-dehydroquinate, *J. Biol. Chem. 238*, 3176–3182.
758. Widlanski, T., Bender, S. L., and Knowles, J. R. (1989) Dehydroquinate synthase: a sheep in wolf's clothing? *J. Am. Chem. Soc. 111*, 2299–2300.
759. Carpenter, E. P., Hawkins, A. R., Frost, J. W., and Brown, K. A. (1998) Structure of dehydroquinate synthase reveals an active site capable of multistep catalysis, *Nature (London, U. K.) 394*, 299–302.
760. Egan, R. M., Matherly, L. H., and Phillips, A. T. (1981) Mechanism of urocanase as studied by deuterium isotope effects and labeling patterns, *Biochemistry 20*, 132–137.
761. Kessler, D., Retey, J., and Schulz, G. E. (2004) Structure and action of urocanase, *J. Mol. Biol. 342*, 183–194.
762. Midelfort, C. F., and Rose, I. A. (1976) A stereochemical method for detection of ATP terminal phosphate transfer in enzymatic reactions. Glutamine synthetase, *J. Biol. Chem. 251*, 5881–5887.
763. Krajewski, W. W., Jones, T. A., and Mowbray, S. L. (2005) Structure of *Mycobacterium tuberculosis* glutamine synthetase in complex with a transition-state mimic provides functional insights, *Proc. Natl. Acad. Sci. U. S. A. 102*, 10499–10504.
764. Rosing, J., Kayalar, C., and Boyer, P. D. (1977) Evidence for energy-dependent change in phosphate binding for mitochondrial oxidative phosphorylation based on measurements of medium and intermediate phosphate-water exchanges, *J. Biol. Chem. 252*, 2478–2485.
765. Levy, H. M., and Koshland, D. E., Jr. (1959) Mechanism of hydrolysis of adenosinetriphosphate by muscle proteins and its relation to muscular contraction, *J. Biol. Chem. 234*, 1102–1107.
766. Myers, J. A., and Boyer, P. D. (1984) Oxygen and deuterium exchanges show reversal of catalytic steps of citrate synthase: Catalytic cooperativity is not observed, *Biochemistry 23*, 1264–1269.
767. Karpusas, M., Branchaud, B., and Remington, S. J. (1990) Proposed mechanism for the condensation reaction of citrate synthase: 1.9-Å Structure of the ternary complex with oxaloacetate and carboxymethyl coenzyme A, *Biochemistry 29*, 2213–2219.
768. Schwartz, B., Drueckhammer, D. G., Usher, K. C., and Remington, S. J. (1995) α-Fluoro acid and α-fluoro amide analogs of acetyl-CoA as inhibitors of citrate synthase: Effect of pK_a matching on binding affinity and hydrogen bond length, *Biochemistry 34*, 15459–15466.
769. Remington, S., Wiegand, G., and Huber, R. (1982) Crystallographic refinement and atomic models of two different forms of citrate synthase at 2.7 and 1.7 Å resolution, *J. Mol. Biol. 158*, 111–152.
770. Usher, K. C., Remington, S. J., Martin, D. P., and Drueckhammer, D. G. (1994) A very short hydrogen bond provides only moderate stabilization of an enzyme-inhibitor complex of citrate synthase, *Biochemistry 33*, 7753–7759.
771. Allard, S. T., Beis, K., Giraud, M. F., Hegeman, A. D., Gross, J. W., Wilmouth, R. C., Whitfield, C., Graninger, M., Messner, P., Allen, A. G., Maskell, D. J., and Naismith, J. H. (2002) Toward a structural understanding of the dehydratase mechanism, *Structure 10*, 81–92.
772. Hegeman, A. D., Gross, J. W., and Frey, P. A. (2002) Concerted and stepwise dehydration mechanisms observed in wild-type and mutated *Escherichia coli* dTDP-glucose 4,6-dehydratase, *Biochemistry 41*, 2797–2804.
773. Qian, Q., Schultz, A. W., Moore, B. S., and Tanner, M. E. (2012) Mechanistic studies on CymD: a tryptophan reverse *N*-prenyltransferase, *Biochemistry 51*, 7733–7739.
774. Hansen, J. N., Dinovo, E. C., and Boyer, P. D. (1969) Initial and equilibrium ^{18}O, ^{14}C, ^{3}H, and ^{2}H exchange rates as probes of the fumarase reaction mechanism, *J. Biol. Chem. 244*, 6270–6279.
775. Rose, I. A., Warms, J. V., and Kuo, D. J. (1992) Proton transfer in catalysis by fumarase, *Biochemistry 31*, 9993–9999.
776. Flint, D. H., and McKay, R. G. (1994) *Escherichia coli* fumarase A catalyzed transfer of ^{18}O from C-2 and ^{2}H from C-3 of malate to acetylene dicarboxylate to form ^{18}O and ^{2}H labeled oxalacetate, *J. Am. Chem. Soc. 116*, 5534–5539.
777. Kenyon, G. L., and Hegeman, G. D. (1970) Mandelic acid racemase from *Pseudomonas putida*. Evidence favoring a carbanion in-

termediate in the mechanism of action, *Biochemistry 9*, 4036–4043.
778. Lin, D. T., Powers, V. M., Reynolds, L. J., Whitman, C. P., Kozarich, J. W., and Kenyon, G. L. (1988) Evidence for the generation of α-carboxy-α-hydroxy-*p*-xylylene from *p*-(bromomethyl)mandelate by mandelate racemase, *J. Am. Chem. Soc. 110*, 323–324.
779. Powers, V. M., Koo, C. W., Kenyon, G. L., Gerlt, J. A., and Kozarich, J. W. (1991) Mechanism of the reaction catalyzed by mandelate racemase. 1. Chemical and kinetic evidence for a two-base mechanism, *Biochemistry 30*, 9255–9263.
780. Neidhart, D. J., Howell, P. L., Petsko, G. A., Powers, V. M., Li, R. S., Kenyon, G. L., and Gerlt, J. A. (1991) Mechanism of the reaction catalyzed by mandelate racemase. 2. Crystal structure of mandelate racemase at 2.5-Å resolution: Identification of the active site and possible catalytic residues, *Biochemistry 30*, 9264–9273.
781. Lietzan, A. D., Nagar, M., Pellmann, E. A., Bourque, J. R., Bearne, S. L., and St Maurice, M. (2012) Structure of mandelate racemase with bound intermediate analogues benzohydroxamate and cupferron, *Biochemistry 51*, 1160–1170.
782. Major, L. L., Wolucka, B. A., and Naismith, J. H. (2005) Structure and function of GDP-mannose-3',5′-epimerase: An enzyme which performs three chemical reactions at the same active site, *J. Am. Chem. Soc. 127*, 18309–18320.
783. Barber, G. A. (1979) Observations on the mechanism of the reversible epimerization of GDP-D-mannose to GDP-L-galactose by an enzyme from *Chlorella pyrenoidosa*, *J. Biol. Chem. 254*, 7600–7603.
784. Wolucka, B. A., and Van Montagu, M. (2003) GDP-mannose 3′,5′-epimerase forms GDP-L-gulose, a putative intermediate for the *de novo* biosynthesis of vitamin C in plants, *J. Biol. Chem. 278*, 47483–47490.
785. Gomes, B., Fendrich, G., and Abeles, R. H. (1981) Mechanism of action of glutaryl-CoA and butyryl-CoA dehydrogenases. Purification of glutaryl-CoA dehydrogenase, *Biochemistry 20*, 1481–1490.
786. Hoagland, M. B. (1955) An enzymic mechanism for amino acid activation in animal tissues, *Biochim. Biophys. Acta 16*, 288–289.
787. Demoss, J. A., Genuth, S. M., and Novelli, G. D. (1956) The enzymatic activation of amino acids via their acyl-adenylate derivatives, *Proc. Natl. Acad. Sci. U.S.A. 42*, 325–332.
788. Scrutton, M. C., Keech, D. B., and Utter, M. F. (1965) Pyruvate carboxylase. IV. Partial reactions and the locus of activation by acetyl coenzyme A, *J. Biol. Chem. 240*, 574–581.
789. McClure, W. R., Lardy, H. A., and Cleland, W. W. (1971) Rat liver pyruvate carboxylase. 3. Isotopic exchange studies of the first partial reaction, *J. Biol. Chem. 246*, 3584–3590.
790. Scrutton, M. C., and Utter, M. F. (1965) Pyruvate carboxylase. V. Interaction of the enzyme with adenosine triphosphate, *J. Biol. Chem. 240*, 3714–3723.
791. Kaziro, Y., Hass, L. F., Boyer, P. D., and Ochoa, S. (1962) Mechanism of the propionyl carboxylase reaction. II. Isotopic exchange and tracer experiments, *J. Biol. Chem. 237*, 1460–1468.
792. Lynen, F., Knappe, J., Lorch, E., Juetting, G., Ringelmann, E., and Lachance, J. P. (1961) On the biochemical function of biotin. II. Purification and mode of action of β-methylcrotonyl-carboxylase, *Biochem. Z. 335*, 123–167.
793. Evans, H. J., and Wood, H. G. (1968) The mechanism of the pyruvate, phosphate dikinase reaction, *Proc. Natl. Acad. Sci. U.S.A. 61*, 1448–1453.
794. Wang, H. C., Ciskanik, L., Dunaway-Mariano, D., von der Saal, W., and Villafranca, J. J. (1988) Investigations of the partial reactions catalyzed by pyruvate phosphate dikinase, *Biochemistry 27*, 625–633.
795. Milner, Y., and Wood, H. G. (1976) Steady state and exchange kinetics of pyruvate, phosphate dikinase from *Propionibacterium shermanii*, *J. Biol. Chem. 251*, 7920–7928.
796. Milner, Y., and Wood, H. G. (1972) Isolation of a pyrophosphoryl form of pyruvate, phosphate dikinase from *Propionibacteria*, *Proc. Natl. Acad. Sci. U.S.A. 69*, 2463–2468.
797. Phillips, N. F., and Wood, H. G. (1986) Isolation of pyrophosphohistidine from pyrophosphorylated pyruvate, phosphate dikinase, *Biochemistry 25*, 1644–1649.
798. Taylor, Z. W., Chamberlain, A. R., and Raushel, F. M. (2018) Substrate specificity and chemical mechanism for the reaction catalyzed by glutamine kinase, *Biochemistry 57*, 5447–5455.

799. Miller, B. G., Hassell, A. M., Wolfenden, R., Milburn, M. V., and Short, S. A. (2000) Anatomy of a proficient enzyme: The structure of orotidine 5′-monophosphate decarboxylase in the presence and absence of a potential transition state analog, *Proc. Natl. Acad. Sci. U. S. A. 97*, 2011–2016.
800. Amyes, T. L., Wood, B. M., Chan, K., Gerlt, J. A., and Richard, J. P. (2008) Formation and stability of a vinyl carbanion at the active site of orotidine 5′-monophosphate decarboxylase: pK_a of the C-6 proton of enzyme-bound UMP, *J. Am. Chem. Soc. 130*, 1574–1575.
801. Wu, N., Mo, Y., Gao, J., and Pai, E. F. (2000) Electrostatic stress in catalysis: Structure and mechanism of the enzyme orotidine monophosphate decarboxylase, *Proc. Natl. Acad. Sci. U. S. A. 97*, 2017–2022.
802. Chan, K. K., Wood, B. M., Fedorov, A. A., Fedorov, E. V., Imker, H. J., Amyes, T. L., Richard, J. P., Almo, S. C., and Gerlt, J. A. (2009) Mechanism of the orotidine 5′-monophosphate decarboxylase-catalyzed reaction: Evidence for substrate destabilization, *Biochemistry 48*, 5518–5531.
803. Toth, K., Amyes, T. L., Wood, B. M., Chan, K., Gerlt, J. A., and Richard, J. P. (2007) Product deuterium isotope effect for orotidine 5′-monophosphate decarboxylase: Evidence for the existence of a short-lived carbanion intermediate, *J. Am. Chem. Soc. 129*, 12946–12947.
804. Tsang, W. Y., Wood, B. M., Wong, F. M., Wu, W., Gerlt, J. A., Amyes, T. L., and Richard, J. P. (2012) Proton transfer from C-6 of uridine 5′-monophosphate catalyzed by orotidine 5′-monophosphate decarboxylase: Formation and stability of a vinyl carbanion intermediate and the effect of a 5-fluoro substituent, *J. Am. Chem. Soc. 134*, 14580–14594.
805. Goryanova, B., Spong, K., Amyes, T. L., and Richard, J. P. (2013) Catalysis by orotidine 5′-monophosphate decarboxylase: effect of 5-fluoro and 4′-substituents on the decarboxylation of two-part substrates, *Biochemistry 52*, 537–546.
806. Porter, D. J., and Short, S. A. (2000) Yeast orotidine-5′-phosphate decarboxylase: Steady-state and pre-steady-state analysis of the kinetic mechanism of substrate decarboxylation, *Biochemistry 39*, 11788–11800.
807. Sievers, A., and Wolfenden, R. (2002) Equilibrium of formation of the 6-carbanion of UMP, a potential intermediate in the action of OMP decarboxylase, *J. Am. Chem. Soc. 124*, 13986–13987.
808. Lee, J. K., and Houk, K. N. (1997) A proficient enzyme revisited: The predicted mechanism for orotidine monophosphate decarboxylase, *Science (Washington, DC, U. S.) 276*, 942–945.
809. Desai, B. J., Goto, Y., Cembran, A., Fedorov, A. A., Almo, S. C., Gao, J., Suga, H., and Gerlt, J. A. (2014) Investigating the role of a backbone to substrate hydrogen bond in OMP decarboxylase using a site-specific amide to ester substitution, *Proc. Natl. Acad. Sci. U. S. A. 111*, 15066–15071.
810. Feng, W. Y., Austin, T. J., Chew, F., Gronert, S., and Wu, W. (2000) The mechanism of orotidine 5′-monophosphate decarboxylase: Catalysis by destabilization of the substrate, *Biochemistry 39*, 1778–1783.
811. Beak, P., and Siegel, B. (1976) Mechanism of decarboxylation of 1,3-dimethylorotic acid. A model for orotidine 5′-phosphate decarboxylase, *J. Am. Chem. Soc. 98*, 3601–3606.
812. Levine, H. L., Brody, R. S., and Westheimer, F. H. (1980) Inhibition of orotidine-5′-phosphate decarboxylase by 1-(5′-phospho-β-D-ribo-furanosyl)barbituric acid, 6-azauridine 5′-phosphate, and uridine 5′-phosphate, *Biochemistry 19*, 4993–4999.
813. Wu, N., Gillon, W., and Pai, E. F. (2002) Mapping the active site–ligand interactions of orotidine 5′-monophosphate decarboxylase by crystallography, *Biochemistry 41*, 4002–4011.
814. Miller, B. G., Snider, M. J., Wolfenden, R., and Short, S. A. (2001) Dissecting a charged network at the active site of orotidine-5′-phosphate decarboxylase, *J. Biol. Chem. 276*, 15174–15176.
815. Harris, P., Navarro Poulsen, J. C., Jensen, K. F., and Larsen, S. (2000) Structural basis for the catalytic mechanism of a proficient enzyme: Orotidine 5′-monophosphate decarboxylase, *Biochemistry 39*, 4217–4224.
816. Stunkard, L. M., Dixon, A. D., Huth, T. J., and Lohman, J. R. (2019) Sulfonate/nitro bearing methylmalonyl-thioester isosteres applied to methylmalonyl-CoA decarboxylase structure-function studies, *J. Am. Chem. Soc. 141*, 5121–5124.

817. Iiams, V., Desai, B. J., Fedorov, A. A., Fedorov, E. V., Almo, S. C., and Gerlt, J. A. (2011) Mechanism of the orotidine 5′-monophosphate decarboxylase-catalyzed reaction: Importance of residues in the orotate binding site, *Biochemistry 50*, 8497–8507.
818. Crosby, J., Stone, R., and Lienhard, G. E. (1970) Mechanisms of thiamine-catalyzed reactions. Decarboxylation of 2-(1-carboxy-1-hydroxyethyl)-3,4-dimethylthiazolium chloride, *J. Am. Chem. Soc. 92*, 2891–2900.
819. Lewis, C. A., Jr., and Wolfenden, R. (2009) Orotic acid decarboxylation in water and nonpolar solvents: A potential role for desolvation in the action of OMP decarboxylase, *Biochemistry 48*, 8738–8745.
820. Sato, D., Shiba, T., Karaki, T., Yamagata, W., Nozaki, T., Nakazawa, T., and Harada, S. (2017) X-Ray snapshots of a pyridoxal enzyme: A catalytic mechanism involving concerted [1,5]-hydrogen sigmatropy in methionine γ-lyase, *Sci Rep 7*, 4874.
821. Esaki, N., Nakayama, T., Sawada, S., Tanaka, H., and Soda, K. (1985) ^{1}H NMR Studies of substrate hydrogen exchange reactions catalyzed by L-methionine γ-lyase, *Biochemistry 24*, 3857–3862.
822. Fukumoto, M., Kudou, D., Murano, S., Shiba, T., Sato, D., Tamura, T., Harada, S., and Inagaki, K. (2012) The role of amino acid residues in the active site of L-methionine γ-lyase from *Pseudomonas putida*, *Biosci. Biotechnol. Biochem. 76*, 1275–1284.
823. Smith, T. J., Peterson, P. E., Schmidt, T., Fang, J., and Stanley, C. A. (2001) Structures of bovine glutamate dehydrogenase complexes elucidate the mechanism of purine regulation, *J. Mol. Biol. 307*, 707–720.
824. Fisher, H. F., and Viswanathan, T. S. (1984) Carbonyl oxygen exchange evidence of imine formation in the glutamate dehydrogenase reaction and identification of the "occult role" of NADPH, *Proc. Natl. Acad. Sci. U.S.A. 81*, 2747–2751.
825. Lagerkvist, U. (1958) Biosynthesis of guanosine 5′-phosphate. II. Amination of xanthosine 5′-phosphate by purified enzyme from pigeon liver, *J. Biol. Chem. 233*, 143–149.
826. Fukuyama, T. T. (1966) Formation of an adenyl xanthosine monophosphate intermediate by xanthosine 5′-phosphate aminase and its inhibition by psicofuranine, *J. Biol. Chem. 241*, 4745–4749.
827. von der Saal, W., Crysler, C. S., and Villafranca, J. J. (1985) Positional isotope exchange and kinetic experiments with *Escherichia coli* guanosine-5′-monophosphate synthetase, *Biochemistry 24*, 5343–5350.
828. Reddick, J. J., Nicewonger, R., and Begley, T. P. (2001) Mechanistic studies on thiamin phosphate synthase: Evidence for a dissociative mechanism, *Biochemistry 40*, 10095–10102.
829. Sun, H. G., Ruszczycky, M. W., Chang, W. C., Thibodeaux, C. J., and Liu, H. W. (2012) Nucleophilic participation of reduced flavin coenzyme in mechanism of UDP-galactopyranose mutase, *J. Biol. Chem. 287*, 4602–4608.
830. Webb, M. R., and Trentham, D. R. (1980) The stereochemical course of phosphoric residue transfer during the myosin ATPase reaction, *J. Biol. Chem. 255*, 8629–8632.
831. Shukla, K. K., and Levy, H. M. (1977) Mechanism of oxygen exchange in actin-activated hydrolysis of adenosine triphosphate by myosin subfragment 1, *Biochemistry 16*, 132–136.
832. Lymn, R. W., and Taylor, E. W. (1971) Mechanism of adenosine triphosphate hydrolysis by actomyosin, *Biochemistry 10*, 4617–4624.
833. Fisher, A. J., Smith, C. A., Thoden, J. B., Smith, R., Sutoh, K., Holden, H. M., and Rayment, I. (1995) X-Ray structures of the myosin motor domain of *Dictyostelium discoideum* complexed with MgADP·BeF_x and MgADP·AlF_4^-, *Biochemistry 34*, 8960–8972.
834. Sleep, J. A., Hackney, D. D., and Boyer, P. D. (1980) The equivalence of phosphate oxygens for exchange and the hydrolysis characteristics revealed by the distribution of [^{18}O]P_i species formed by myosin and actomyosin ATPase, *J. Biol. Chem. 255*, 4094–4099.
835. Sleep, J. A., and Boyer, P. D. (1978) Effect of actin concentration on the intermediate oxygen exchange of myosin; Relation to the refractory state and the mechanism of exchange, *Biochemistry 17*, 5417–5422.
836. Kyte, J. (2007) In *Structure in Protein Chemistry: Second Edition*, p 731, Garland Science, New York.
837. Hutton, R. L., and Boyer, P. D. (1979) Subunit interaction during catalysis. Alternating site cooperativity of mitochondrial adenosine

triphosphatase, *J. Biol. Chem. 254*, 9990–9993.
838. Boyer, P. D. (1959) Uses and limitations of measurements of rates of isotopic exchange and incorporation in catalyzed reactions, *Arch. Biochem. Biophys. 82*, 387–410.
839. Albery, W. J., and Knowles, J. R. (1976) Deuterium and tritium exchange in enzyme kinetics, *Biochemistry 15*, 5588–5600.
840. Myers, O. E., and Prestwood, R. J. (1951) Isotopic exchange reactions, In *Radioactivity Applied to Chemistry* (Wahl, A. C., and Bonner, N. A., Eds.), pp 6–43, John Wiley, New York.
841. Faraci, W. S., and Walsh, C. T. (1988) Racemization of alanine by the alanine racemases from *Salmonella typhimurium* and *Bacillus stearothermophilus*: Energetic reaction profiles, *Biochemistry 27*, 3267–3276.
842. Watanabe, A., Yoshimura, T., Mikami, B., Hayashi, H., Kagamiyama, H., and Esaki, N. (2002) Reaction mechanism of alanine racemase from *Bacillus stearothermophilus*: X-ray crystallographic studies of the enzyme bound with *N*-(5′-phosphopyridoxyl)alanine, *J. Biol. Chem. 277*, 19166–19172.
843. Fan, F., Williams, H. J., Boyer, J. G., Graham, T. L., Zhao, H., Lehr, R., Qi, H., Schwartz, B., Raushel, F. M., and Meek, T. D. (2012) On the catalytic mechanism of human ATP citrate lyase, *Biochemistry 51*, 5198–5211.
844. Todhunter, J. A., and Purich, D. L. (1975) Use of the sodium borohydride reduction technique to identify a γ-glutamyl phosphate intermediary in the *Escherichia coli* glutamine synthetase reaction, *J. Biol. Chem. 250*, 3505–3509.
845. Liaw, S. H., Kuo, I., and Eisenberg, D. (1995) Discovery of the ammonium substrate site on glutamine synthetase, a third cation binding site, *Protein Sci. 4*, 2358–2365.
846. Wedler, F. C., and Boyer, P. D. (1972) Substrate binding and reaction intermediates of glutamine synthetase (*Escherichia coli* W) as studied by isotope exchanges, *J. Biol. Chem. 247*, 984–992.
847. Abell, L. M., and Villafranca, J. J. (1991) Effect of metal ions and adenylylation state on the internal thermodynamics of phosphoryl transfer in the *Escherichia coli* glutamine synthetase reaction, *Biochemistry 30*, 1413–1418.
848. Purich, D. L., and Allison, R. D. (1980) Isotope exchange methods for elucidating enzymic catalysis, *Methods Enzymol. 64*, 1–46.
849. Allison, R. D., Todhunter, J. A., and Purich, D. L. (1977) Steady state and equilibrium exchange kinetic studies of the sheep brain glutamine synthetase reaction, *J. Biol. Chem. 252*, 6046–6051.
850. Raushel, F. M., and Cleland, W. W. (1977) Determination of the rate-limiting steps and chemical mechanism of fructokinase by isotope exchange, isotope partitioning, and pH studies, *Biochemistry 16*, 2176–2181.
851. Cho, Y. K., Matsunaga, T. O., Kenyon, G. L., Bertagnolli, B. L., and Cook, P. F. (1988) Isotope exchange as a probe of the kinetic mechanism of pyrophosphate-dependent phosphofructokinase, *Biochemistry 27*, 3320–3325.
852. Wang, S. F., Kawahara, F. S., and Talalay, P. (1963) The mechanism of the Δ^5-3-ketosteroid isomerase reaction: Absorption and fluorescence spectra of enzyme-steroid complexes, *J. Biol. Chem. 238*, 576–585.
853. Malhotra, S. K., and Ringold, H. J. (1965) Chemistry of conjugate anions and enols. V. Stereochemistry, kinetics, and mechanism of the acid- and enzymatic-catalyzed isomerization of Δ^5-3-keto steroids, *J. Am. Chem. Soc. 87*, 3228–3236.
854. Cho, H. S., Ha, N. C., Choi, G., Kim, H. J., Lee, D., Oh, K. S., Kim, K. S., Lee, W., Choi, K. Y., and Oh, B. H. (1999) Crystal structure of Δ^5-3-ketosteroid isomerase from *Pseudomonas testosteroni* in complex with equilenin settles the correct hydrogen bonding scheme for transition state stabilization, *J. Biol. Chem. 274*, 32863–32868.
855. Rao, K. S., Albro, M., Zirrolli, J. A., Vander Velde, D., Jones, D. N., and Frerman, F. E. (2005) Protonation of crotonyl-CoA dienolate by human glutary-CoA dehydrogenase occurs by solvent-derived protons, *Biochemistry 44*, 13932–13940.
856. Klinman, J. P., and Rose, I. A. (1971) Mechanism of the aconitate isomerase reaction, *Biochemistry 10*, 2259–2266.
857. Chang, C. C., Laghai, A., O'Leary, M. H., and Floss, H. G. (1982) Some stereochemical features of aspartate β-decarboxylase, *J. Biol. Chem. 257*, 3564–3569.
858. Chen, H. J., Ko, T. P., Lee, C. Y., Wang, N. C., and Wang, A. H. (2009) Structure, assembly,

and mechanism of a PLP-dependent dodecameric L-aspartate β-decarboxylase, *Structure 17*, 517–529.
859. Cooke, H. A., Peck, S. C., Evans, B. S., and van der Donk, W. A. (2012) Mechanistic investigation of methylphosphonate synthase, a non-heme iron-dependent oxygenase, *J. Am. Chem. Soc. 134*, 15660–15663.
860. Born, D. A., Ulrich, E. C., Ju, K. S., Peck, S. C., van der Donk, W. A., and Drennan, C. L. (2017) Structural basis for methylphosphonate biosynthesis, *Science (Washington, DC, U. S.) 358*, 1336–1339.
861. Benson, R. W., and Boyer, P. D. (1969) The participation of an enzyme-bound oxygen group in a coenzyme A transferase reaction, *J. Biol. Chem. 244*, 2366–2371.
862. Wong, B. J., and Gerlt, J. A. (2003) Divergent function in the crotonase superfamily: An anhydride intermediate in the reaction catalyzed by 3-hydroxyisobutyryl-CoA hydrolase, *J. Am. Chem. Soc. 125*, 12076–12077.
863. Ahmed, S. A., Esaki, N., Tanaka, H., and Soda, K. (1986) Mechanism of α-amino-ε-caprolactam racemase reaction, *Biochemistry 25*, 385–388.
864. Frese, A., Sutton, P. W., Turkenburg, J. P., and Grogan, G. (2017) Snapshots of the catalytic cycle of the industrial enzyme α-amino-ε-caprolactam racemase (ACLR) observed using X-ray crystallography, *ACS Catal. 7*, 1045–1048.
865. Saver, B. G., and Knowles, J. R. (1982) Ribulose-1,5-bisphosphate carboxylase: Enzyme-catalyzed appearance of solvent tritium at carbon 3 of ribulose 1,5-bisphosphate reisolated after partial reaction, *Biochemistry 21*, 5398–5403.
866. Dahms, A. S., and Boyer, P. D. (1973) Occurrence and characteristics of ^{18}O exchange reactions catalyzed by sodium- and potassium-dependent adenosine triphosphatases, *J. Biol. Chem. 248*, 3155–3162.
867. Beauge, L. A., and Glynn, I. M. (1979) Sodium ions, acting at high-affinity extracellular sites, inhibit sodium-ATPase activity of the sodium pump by slowing dephosphorylation, *J. Physiol. (Oxford, U. K.) 289*, 17–31.
868. Fleming, S. M., Robertson, T. A., Langley, G. J., and Bugg, T. D. (2000) Catalytic mechanism of a C–C hydrolase enzyme: Evidence for a *gem*-diol intermediate, not an acyl enzyme, *Biochemistry 39*, 1522–1531.
869. Rubio, V., Britton, H. G., Grisolia, S., Sproat, B. S., and Lowe, G. (1981) Mechanism of activation of bicarbonate ion by mitochondrial carbamoyl-phosphate synthetase: Formation of enzyme-bound adenosine diphosphate from the adenosine triphosphate that yields inorganic phosphate, *Biochemistry 20*, 1969–1974.
870. Meek, T. D., Karsten, W. E., and DeBrosse, C. W. (1987) Carbamoyl-phosphate synthetase II of the mammalian CAD protein: Kinetic mechanism and elucidation of reaction intermediates by positional isotope exchange, *Biochemistry 26*, 2584–2593.
871. Raushel, F. M., Mullins, L. S., and Gibson, G. E. (1998) A stringent test for the nucleotide switch mechanism of carbamoyl phosphate synthetase, *Biochemistry 37*, 10272–10278.
872. Sala, R. F., Morgan, P. M., and Tanner, M. E. (1996) Enzymic formation and release of a stable glycal intermediate: The mechanism of the reaction catalyzed by UDP-*N*-acetylglucosamine 2-epimerase, *J. Am. Chem. Soc. 118*, 3033–3034.
873. Chen, S. C., Huang, C. H., Yang, C. S., Liu, J. S., Kuan, S. M., and Chen, Y. (2014) Crystal structures of the archaeal UDP-GlcNAc 2-epimerase from *Methanocaldococcus jannaschii* reveal a conformational change induced by UDP-GlcNAc, *Proteins: Struct., Funct., Bioinf. 82*, 1519–1526.
874. Grimshaw, C. E., Sogo, S. G., and Knowles, J. R. (1982) The fate of the hydrogens of phospho*enol*pyruvate in the reaction catalyzed by 5-*enol*pyruvylshikimate-3–phosphate synthase. Isotope effects and isotope exchange, *J. Biol. Chem. 257*, 596–598.
875. Anton, D. L., Hedstrom, L., Fish, S. M., and Abeles, R. H. (1983) Mechanism of *enol*pyruvylshikimate-3-phosphate synthase exchange of phosphoenolpyruvate with solvent protons, *Biochemistry 22*, 5903–5908.
876. Steinrucken, H. C., and Amrhein, N. (1984) 5–*Enol*pyruvylshikimate-3-phosphate synthase of *Klebsiella pneumoniae*. 2. Inhibition by glyphosate [*N*-(phosphonomethyl)glycine], *Eur. J. Biochem. 143*, 351–357.
877. Fujita, N., Izui, K., Nishino, T., and Katsuki, H. (1984) Reaction mechanism of phospho*enol*-pyruvate carboxylase. Bicarbonate-dependent dephosphorylation of phospho*enol*-α-ketobutyrate, *Biochemistry 23*, 1774–1779.

878. Hartridge, H., and Roughton, F. J. W. (1923) Method of measuring the velocity of very rapid chemical reactions, *Proc. R. Soc. London, Ser. A 104*, 376–394.
879. Roughton, F. J. W. (1934) Kinetics of hemoglobin. VII. Notes on the reactivity of freshly reduced hemoglobin, *Proc. R. Soc. London, Ser. B 115*, 495–503.
880. Chance, B. (1940) The accelerated-flow method for rapid reactions. I. Analysis, *J. Franklin Inst. 229*, 455–476,613–440.
881. Gibson, Q. H., and Roughton, F. J. (1955) The kinetics of dissociation of the first oxygen molecule from fully saturated oxyhaemoglobin in sheep blood solutions, *Proc. R. Soc. London, Ser. B 143*, 310–334.
882. Roughton, F. J. W., and Chance, B. (1963) Rapid Reactions, In *Technique of Organic Chemistry: Volume VIII, Part II, Investigation of Rates and Mechanisms of Reactions* (Friess, S. L., Lewis, E. S., and Weissberger, A., Eds.), pp 703–792, Wiley-Interscience, New York.
883. Rhee, S. G., Ubom, G. A., Hunt, J. B., and Chock, P. B. (1982) Catalytic cycle of the biosynthetic reaction catalyzed by adenylylated glutamine synthetase from *Escherichia coli*, *J. Biol. Chem. 257*, 289–297.
884. Stinson, R. A., and Gutfreund, H. (1971) Transient-kinetic studies of pig muscle lactate dehydrogenase, *Biochem. J. 121*, 235–240.
885. Swiderek, K., Panczakiewicz, A., Bujacz, A., Bujacz, G., and Paneth, P. (2009) Modeling of isotope effects on binding oxamate to lactic dehydrogenase, *J. Phys. Chem. B 113*, 12782–12789.
886. Fierke, C. A., and Benkovic, S. J. (1989) Probing the functional role of Threonine-113 of *Escherichia coli* dihydrofolate reductase for its effect on turnover efficiency, catalysis, and binding, *Biochemistry 28*, 478–486.
887. Bull, C., Ballou, D. P., and Otsuka, S. (1981) The reaction of oxygen with protocatechuate 3,4-dioxygenase from *Pseudomonas putida*. Characterization of a new oxygenated intermediate, *J. Biol. Chem. 256*, 12681–12686.
888. Yang, H., Aitha, M., Hetrick, A. M., Richmond, T. K., Tierney, D. L., and Crowder, M. W. (2012) Mechanistic and spectroscopic studies of metallo-β-lactamase NDM-1, *Biochemistry 51*, 3839–3847.
889. Kim, Y., Cunningham, M. A., Mire, J., Tesar, C., Sacchettini, J., and Joachimiak, A. (2013) NDM-1, the ultimate promiscuous enzyme: Substrate recognition and catalytic mechanism, *FASEB J. 27*, 1917–1927.
890. Maniscalco, S. J., Saha, S. K., and Fisher, H. F. (1998) Identification and characterization of kinetically competent carbinolamine and α-iminoglutarate complexes in the glutamate dehydrogenase-catalyzed oxidation of L-glutamate using a multiwavelength transient state approach, *Biochemistry 37*, 14585–14590.
891. Cooper, W. C., Jin, Y., and Penning, T. M. (2007) Elucidation of a complete kinetic mechanism for a mammalian hydroxysteroid dehydrogenase (HSD) and identification of all enzyme forms on the reaction coordinate: The example of rat liver 3α-HSD (AKR1C9), *J. Biol. Chem. 282*, 33484–33493.
892. Hardman, M. J., Tsao, M., and Scopes, R. K. (1992) Changes in the fluorescence of bound nucleotide during the reaction catalysed by glucose-fructose oxidoreductase from *Zymomonas mobilis*, *Eur. J. Biochem. 205*, 715–720.
893. Li, T., Ma, J. K., Hosler, J. P., Davidson, V. L., and Liu, A. (2007) Detection of transient intermediates in the metal-dependent nonoxidative decarboxylation catalyzed by α-amino-β-carboxymuconate-ε-semialdehyde decarboxylase, *J. Am. Chem. Soc. 129*, 9278–9279.
894. Hommel, U., Eberhard, M., and Kirschner, K. (1995) Phosphoribosyl anthranilate isomerase catalyzes a reversible Amadori reaction, *Biochemistry 34*, 5429–5439.
895. Bashor, C., Denu, J. M., Brennan, R. G., and Ullman, B. (2002) Kinetic mechanism of adenine phosphoribosyltransferase from *Leishmania donovani*, *Biochemistry 41*, 4020–4031.
896. Sukal, S., and Leyh, T. S. (2001) Product release during the first turnover of the ATP sulfurylase-GTPase, *Biochemistry 40*, 15009–15016.
897. Groce, S. L., Miller-Rodeberg, M. A., and Lipscomb, J. D. (2004) Single-turnover kinetics of homoprotocatechuate 2,3-dioxygenase, *Biochemistry 43*, 15141–15153.
898. Wanninayake, U., and Walker, K. D. (2012) Assessing the deamination rate of a covalent aminomutase adduct by burst phase analysis, *Biochemistry 51*, 5226–5228.

899. Ma, Y. Z., and Taylor, E. W. (1995) Kinetic mechanism of kinesin motor domain, *Biochemistry 34*, 13233–13241.
900. Woehl, E. U., Tai, C. H., Dunn, M. F., and Cook, P. F. (1996) Formation of the α-aminoacrylate intermediate limits the overall reaction catalyzed by *O*-acetylserine sulfhydrylase, *Biochemistry 35*, 4776–4783.
901. Mothersole, R. G., and Wolthers, K. R. (2019) Structural and kinetic insight into the biosynthesis of H_2S and L-lanthionine from L-cysteine by a pyridoxal L-phosphate-dependent enzyme from *Fusobacterium nucleatum*, *Biochemistry 58*, 3592–3603.
902. Brooks, H. B., and Phillips, M. A. (1997) Characterization of the reaction mechanism for *Trypanosoma brucei* ornithine decarboxylase by multiwavelength stopped-flow spectroscopy, *Biochemistry 36*, 15147–15155.
903. Blahut, M., Wise, C. E., Bruno, M. R., Dong, G., Makris, T. M., Frantom, P. A., Dunkle, J. A., and Outten, F. W. (2019) Direct observation of intermediates in the SufS cysteine desulfurase reaction reveals functional roles of conserved active-site residues, *J. Biol. Chem. 294*, 12444–12458.
904. Pennati, A., and Gadda, G. (2011) Stabilization of an intermediate in the oxidative half-reaction of human liver glycolate oxidase, *Biochemistry 50*, 1–3.
905. Sheng, D., Ballou, D. P., and Massey, V. (2001) Mechanistic studies of cyclohexanone monooxygenase: Chemical properties of intermediates involved in catalysis, *Biochemistry 40*, 11156–11167.
906. Sucharitakul, J., Tongsook, C., Pakotiprapha, D., van Berkel, W. J., and Chaiyen, P. (2013) The reaction kinetics of 3-hydroxybenzoate 6-hydroxylase from *Rhodococcus jostii* RHA1 provide an understanding of the *para*-hydroxylation enzyme catalytic cycle, *J. Biol. Chem. 288*, 35210–35221.
907. Ortiz-Maldonado, M., Entsch, B., and Ballou, D. P. (2004) Oxygen reactions in *p*-hydroxybenzoate hydroxylase utilize the H-bond network during catalysis, *Biochemistry 43*, 15246–15257.
908. Koppenhofer, A., Little, R. H., Lowe, D. J., Ferguson, S. J., and Watmough, N. J. (2000) Oxidase reaction of cytochrome cd_1 from *Paracoccus pantotrophus*, *Biochemistry 39*, 4028–4036.
909. Wolfe, M. D., Altier, D. J., Stubna, A., Popescu, C. V., Muenck, E., and Lipscomb, J. D. (2002) Benzoate 1,2-dioxygenase from *Pseudomonas putida*: Single turnover kinetics and regulation of a two-component Rieske dioxygenase, *Biochemistry 41*, 9611–9626.
910. Robinson, W. E., Bassegoda, A., Blaza, J. N., Reisner, E., and Hirst, J. (2020) Understanding how the rate of C–H bond cleavage affects formate oxidation catalysis by a Mo-dependent formate dehydrogenase, *J. Am. Chem. Soc. 142*, 12226–12236.
911. Valentine, A. M., Stahl, S. S., and Lippard, S. J. (1999) Mechanistic studies of the reaction of reduced methane monooxygenase hydroxylase with dioxygen and substrates, *J. Am. Chem. Soc. 121*, 3876–3887.
912. Bovee, M. L., Pierce, M. A., and Francklyn, C. S. (2003) Induced fit and kinetic mechanism of adenylation catalyzed by *Escherichia coli* threonyl-tRNA synthetase, *Biochemistry 42*, 15102–15113.
913. Waldman, A. D., Hart, K. W., Clarke, A. R., Wigley, D. B., Barstow, D. A., Atkinson, T., Chia, W. N., and Holbrook, J. J. (1988) The use of genetically engineered tryptophan to identify the movement of a domain of *B. stearothermophilus* lactate dehydrogenase with the process which limits the steady-state turnover of the enzyme, *Biochem. Biophys. Res. Commun. 150*, 752–759.
914. Zhang, Z., Rajagopalan, P. T. R., Selzer, T., Benkovic, S. J., and Hammes, G. G. (2004) Single-molecule and transient kinetics investigation of the interaction of dihydrofolate reductase with NADPH and dihydrofolate, *Proc. Natl. Acad. Sci. U. S. A. 101*, 2764–2769.
915. Sekhar, V. C., and Plapp, B. V. (1990) Rate constants for a mechanism including intermediates in the interconversion of ternary complexes by horse liver alcohol dehydrogenase, *Biochemistry 29*, 4289–4295.
916. Johnson, K. A. (1986) Rapid kinetic analysis of mechanochemical adenosinetriphosphatases, *Methods Enzymol. 134*, 677–705.
917. Wang, G. P., Lundegaard, C., Jensen, K. F., and Grubmeyer, C. (1999) Kinetic mechanism of OMP synthase: A slow physical step following group transfer limits catalytic rate, *Biochemistry 38*, 275–283.
918. Mathis, J. R., Back, K., Starks, C., Noel, J., Poulter, C. D., and Chappell, J. (1997) Pre-

steady-state study of recombinant sesquiterpene cyclases, *Biochemistry 36*, 8340–8348.
919. Cane, D. E., Chiu, H. T., Liang, P. H., and Anderson, K. S. (1997) Pre-steady-state kinetic analysis of the trichodiene synthase reaction pathway, *Biochemistry 36*, 8332–8339.
920. Grant, B. D., and Adams, J. A. (1996) Pre-steady-state kinetic analysis of cAMP-dependent protein kinase using rapid quench flow techniques, *Biochemistry 35*, 2022–2029.
921. Gross, J. W., Hegeman, A. D., Vestling, M. M., and Frey, P. A. (2000) Characterization of enzymatic processes by rapid mix-quench mass spectrometry: The case of dTDP-glucose 4,6-dehydratase, *Biochemistry 39*, 13633–13640.
922. Brenner, M. C., and Klinman, J. P. (1989) Correlation of copper valency with product formation in single turnovers of dopamine β-monooxygenase, *Biochemistry 28*, 4664–4670.
923. Zhu, J., Egawa, T., Yeh, S. R., Yu, L., and Yu, C. A. (2007) Simultaneous reduction of iron-sulfur protein and cytochrome b_L during ubiquinol oxidation in cytochrome bc_1 complex, *Proc. Natl. Acad. Sci. U. S. A. 104*, 4864–4869.
924. Panay, A. J., Lee, M., Krebs, C., Bollinger, J. M., and Fitzpatrick, P. F. (2011) Evidence for a high-spin Fe(IV) species in the catalytic cycle of a bacterial phenylalanine hydroxylase, *Biochemistry 50*, 1928–1933.
925. Farazi, T. A., Manchester, J. K., and Gordon, J. I. (2000) Transient-state kinetic analysis of *Saccharomyces cerevisiae* myristoylCoA:protein *N*-myristoyltransferase reveals that a step after chemical transformation is rate limiting, *Biochemistry 39*, 15807–15816.
926. Raychaudhuri, A., Tullock, A., and Tipton, P. A. (2008) Reactivity and reaction order in acylhomoserine lactone formation by *Pseudomonas aeruginosa* RhlI, *Biochemistry 47*, 2893–2898.
927. Chung, J., Goo, E., Yu, S., Choi, O., Lee, J., Kim, J., Kim, H., Igarashi, J., Suga, H., Moon, J. S., Hwang, I., and Rhee, S. (2011) Small-molecule inhibitor binding to an *N*-acyl-homoserine lactone synthase, *Proc. Natl. Acad. Sci. U. S. A. 108*, 12089–12094.
928. Walinder, O., and Joshi, J. G. (1974) Mechanism of action of rabbit muscle phosphoglucomutase. Rate of enzyme phosphate turnover studied with a rapid mixing technique, *J. Biol. Chem. 249*, 3166–3169.
929. Carroll, L. J., Mehl, A. F., and Dunaway-Mariano, D. (1989) The mode of triple phosphoryl group transfer in pyruvate phosphate dikinase catalysis. Demonstration of the intermediacy of pyrophosphorylated and phosphorylated enzyme species, *J. Am. Chem. Soc. 111*, 5965–5967.
930. Zechel, D. L., Konermann, L., Withers, S. G., and Douglas, D. J. (1998) Pre-steady state kinetic analysis of an enzymatic reaction monitored by time-resolved electrospray ionization mass spectrometry, *Biochemistry 37*, 7664–7669.
931. Sidhu, G., Withers, S. G., Nguyen, N. T., McIntosh, L. P., Ziser, L., and Brayer, G. D. (1999) Sugar ring distortion in the glycosyl-enzyme intermediate of a family G/11 xylanase, *Biochemistry 38*, 5346–5354.
932. Sabini, E., Sulzenbacher, G., Dauter, M., Dauter, Z., Jorgensen, P. L., Schulein, M., Dupont, C., Davies, G. J., and Wilson, K. S. (1999) Catalysis and specificity in enzymatic glycoside hydrolysis: A $^{2,5}B$ conformation for the glycosyl-enzyme intermediate revealed by the structure of the *Bacillus agaradhaerens* family 11 xylanase, *Chem. Biol. 6*, 483–492.
933. Cohen, B. E., Stoddard, B. L., and Koshland, D. E., Jr. (1997) Caged NADP and NAD. Synthesis and characterization of functionally distinct caged compounds, *Biochemistry 36*, 9035–9044.
934. MacArthur, R., Sucheta, A., Chong, F. F., and Einarsdottir, O. (1995) Photodissociation of a (μ-peroxo)(μ-hydroxo)bis[bis(bipyridyl)-cobalt(III)] complex: A tool to study fast biological reactions involving O_2, *Proc. Natl. Acad. Sci. U. S. A. 92*, 8105–8109.
935. Van Eps, N., Szundi, I., and Einarsdottir, O. (2000) A new approach for studying fast biological reactions involving dioxygen: The reaction of fully reduced cytochrome *c* oxidase with O_2, *Biochemistry 39*, 14576–14582.
936. Haldane, J., and Smith, J. L. (1896) The oxygen tension of arterial blood, *J. Physiol. (Oxford, U. K.) 20*, 497–520.
937. Szundi, I., Kittredge, C., Choi, S. K., McDonald, W., Ray, J., Gennis, R. B., and Einarsdottir, O. (2014) Kinetics and intermediates of the reaction of fully reduced *Escherichia coli*

bo$_3$ ubiquinol oxidase with O_2, *Biochemistry 53*, 5393–5404.
938. Eser, B. E., and Fitzpatrick, P. F. (2010) Measurement of intrinsic rate constants in the tyrosine hydroxylase reaction, *Biochemistry 49*, 645–652.
939. Bornemann, S., Lowe, D. J., and Thorneley, R. N. (1996) The transient kinetics of *Escherichia coli* chorismate synthase: Substrate consumption, product formation, phosphate dissociation, and characterization of a flavin intermediate, *Biochemistry 35*, 9907–9916.
940. Hernandez-Ortega, A., Quesne, M. G., Bui, S., Heuts, D. P., Steiner, R. A., Heyes, D. J., de Visser, S. P., and Scrutton, N. S. (2014) Origin of the proton-transfer step in the cofactor-free (1*H*)-3-hydroxy-4-oxoquinaldine 2,4-dioxygenase: Effect of the basicity of an active site His residue, *J. Biol. Chem. 289*, 8620–8632.
941. Collard, F., Fagan, R. L., Zhang, J., Nemet, I., Palfey, B. A., and Monnier, V. M. (2011) The cation-π interaction between Lys53 and the flavin of fructosamine oxidase (FAOX-II) is critical for activity, *Biochemistry 50*, 7977–7986.
942. Argyrou, A., Blanchard, J. S., and Palfey, B. A. (2002) The lipoamide dehydrogenase from *Mycobacterium tuberculosis* permits the direct observation of flavin intermediates in catalysis, *Biochemistry 41*, 14580–14590.
943. Johnson, D. A., Gassner, G. T., Bandarian, V., Ruzicka, F. J., Ballou, D. P., Reed, G. H., and Liu, H. W. (1996) Kinetic characterization of an organic radical in the ascarylose biosynthetic pathway, *Biochemistry 35*, 15846–15856.
944. Bosma, T., Pikkemaat, M. G., Kingma, J., Dijk, J., and Janssen, D. B. (2003) Steady-state and pre-steady-state kinetic analysis of halopropane conversion by a *Rhodococcus* haloalkane dehalogenase, *Biochemistry 42*, 8047–8053.
945. Rochovansky, O., and Ratner, S. (1961) Biosynthesis of ureas. IX. Further studies on mechanism of argininosuccinate synthetase reaction, *J. Biol. Chem. 236*, 2254–2260.
946. Goto, M., Omi, R., Miyahara, I., Sugahara, M., and Hirotsu, K. (2003) Structures of argininosuccinate synthetase in enzyme-ATP substrates and enzyme-AMP product forms: Stereochemistry of the catalytic reaction, *J. Biol. Chem. 278*, 22964–22971.
947. Hilscher, L. W., Hanson, C. D., Russell, D. H., and Raushel, F. M. (1985) Measurement of positional isotope exchange rates in enzyme-catalyzed reactions by fast atom bombardment mass spectrometry: Application to argininosuccinate synthetase, *Biochemistry 24*, 5888–5893.
948. Ghose, C., and Raushel, F. M. (1985) Determination of the mechanism of the argininosuccinate synthetase reaction by static and dynamic quench experiments, *Biochemistry 24*, 5894–5898.
949. Rajagopalan, P. T., Zhang, Z., McCourt, L., Dwyer, M., Benkovic, S. J., and Hammes, G. G. (2002) Interaction of dihydrofolate reductase with methotrexate: Ensemble and single-molecule kinetics, *Proc. Natl. Acad. Sci. U. S. A. 99*, 13481–13486.
950. Fierke, C. A., Johnson, K. A., and Benkovic, S. J. (1987) Construction and evaluation of the kinetic scheme associated with dihydrofolate reductase from *Escherichia coli*, *Biochemistry 26*, 4085–4092.
951. Havsteen, B. H. (1967) The kinetics of the two-step interaction of chymotrypsin with proflavin, *J. Biol. Chem. 242*, 769–771.
952. Nie, B., Deng, H., Desamero, R., and Callender, R. (2013) Large scale dynamics of the Michaelis complex in *Bacillus stearothermophilus* lactate dehydrogenase revealed by a single-tryptophan mutant study, *Biochemistry 52*, 1886–1892.
953. Rhee, S. G., and Chock, P. B. (1976) Mechanistic studies of glutamine synthetase from *Escherichia coli*: Kinetics of ADP and orthophosphate binding to the unadenylylated enzyme, *Biochemistry 15*, 1755–1760.
954. Phillips, R. S. (1989) Mechanism of tryptophan indole-lyase: Insights from pre-steady-state kinetics and substrate and solvent isotope effects, *J. Am. Chem. Soc. 111*, 727–730.
955. Galletto, R., and Bujalowski, W. (2002) The *E. coli* replication factor DnaC protein exists in two conformations with different nucleotide binding capabilities. I. Determination of the binding mechanism using ATP and ADP fluorescent analogues, *Biochemistry 41*, 8907–8920.
956. Frost, A. A., and Pearson, R. G. (1961) *Kinetics and Mechanism: A Study of Homogeneous Chemical Reactions, Second Edition*, Wiley, New York.

957. Mannervik, B. (1982) Regression analysis, experimental error, and statistical criteria in the design and analysis of experiments for discrimination between rival kinetic models, *Methods Enzymol. 87*, 370–390.
958. Bloom, L. B., Otto, M. R., Eritja, R., Reha-Krantz, L. J., Goodman, M. F., and Beechem, J. M. (1994) Pre-steady-state kinetic analysis of sequence-dependent nucleotide excision by the 3′-exonuclease activity of bacteriophage T4 DNA polymerase, *Biochemistry 33*, 7576–7586.
959. Bujalowski, W., and Jezewska, M. J. (2000) Kinetic mechanism of the single-stranded DNA recognition by *Escherichia coli* replicative helicase DnaB protein. Application of the matrix projection operator technique to analyze stopped-flow kinetics, *J. Mol. Biol. 295*, 831–852.
960. Kuzmic, P. (2009) DynaFit—a software package for enzymology, *Methods Enzymol. 467*, 247–280.
961. Pollegioni, L., Blodig, W., and Ghisla, S. (1997) On the mechanism of D-amino acid oxidase. Structure/linear free energy correlations and deuterium kinetic isotope effects using substituted phenylglycines, *J. Biol. Chem. 272*, 4924–4934.
962. Tang, L., Lutje Spelberg, J. H., Fraaije, M. W., and Janssen, D. B. (2003) Kinetic mechanism and enantioselectivity of halohydrin dehalogenase from *Agrobacterium radiobacter*, *Biochemistry 42*, 5378–5386.
963. Cognet, J. A., Cox, B. G., and Hammes, G. G. (1983) Elementary steps in the reaction mechanism of chicken liver fatty acid synthase: Reduced nicotinamide adenine dinucleotide phosphate binding and formation and reduction of acetoacetyl-enzyme, *Biochemistry 22*, 6281–6287.
964. Wongnate, T., and Ragsdale, S. W. (2015) The reaction mechanism of methyl-coenzyme M reductase: How an enzyme enforces strict binding order, *J. Biol. Chem. 290*, 9322–9334.
965. Subedi, B. P., and Fitzpatrick, P. F. (2016) Kinetic mechanism and intrinsic rate constants for the reaction of a bacterial phenylalanine hydroxylase, *Biochemistry 55*, 6848–6857.
966. Britton, H. G., and Clarke, J. B. (1968) The mechanism of the phosphoglucomutase reaction. Studies on rabbit muscle phosphoglucomutase with flux techniques, *Biochem. J. 110*, 161–180.
967. Ray, W. J., Jr., Hermodson, M. A., Puvathingal, J. M., and Mahoney, W. C. (1983) The complete amino acid sequence of rabbit muscle phosphoglucomutase, *J. Biol. Chem. 258*, 9166–9174.
968. Wilkinson, K. D., and Rose, I. A. (1979) Isotope trapping studies of yeast hexokinase during steady state catalysis. A combined rapid quench and isotope trapping technique, *J. Biol. Chem. 254*, 12567–12572.
969. Trentham, D. R. (1971) Rate-determining processes and the number of simultaneously active sites of D-glyceraldehyde 3-phosphate dehydrogenase, *Biochem. J. 122*, 71–77.
970. Poddar, S., and Henkin, J. (1984) Isotope, pulse-chase, stopped-flow, and rapid quench studies on the kinetic mechanism of bovine dihydropteridine reductase, *Biochemistry 23*, 3143–3148.
971. Halford, S. E. (1971) *Escherichia coli* alkaline phosphatase. An analysis of transient kinetics, *Biochem. J. 125*, 319–327.
972. Halford, S. E., Bennett, N. G., Trentham, D. R., and Gutfeund, H. (1969) A substate-induced conformation change in the reaction of alkaline phosphatase from *Escherichia coli*, *Biochem. J. 114*, 243–251.
973. Gill, H. S., and Eisenberg, D. (2001) The crystal structure of phosphinothricin in the active site of glutamine synthetase illuminates the mechanism of enzymatic inhibition, *Biochemistry 40*, 1903–1912.
974. Oliver, J. C., Linger, R. S., Chittur, S. V., and Davisson, V. J. (2013) Substrate activation and conformational dynamics of guanosine 5′-monophosphate synthetase, *Biochemistry 52*, 5225–5235.
975. Tesmer, J. J., Klem, T. J., Deras, M. L., Davisson, V. J., and Smith, J. L. (1996) The crystal structure of GMP synthetase reveals a novel catalytic triad and is a structural paradigm for two enzyme families, *Nat. Struct. Biol. 3*, 74–86.
976. Schlee, S., Dietrich, S., Kurcon, T., Delaney, P., Goodey, N. M., and Sterner, R. (2013) Kinetic mechanism of indole-3-glycerol phosphate synthase, *Biochemistry 52*, 132–142.
977. Hennig, M., Darimont, B. D., Jansonius, J. N., and Kirschner, K. (2002) The catalytic mechanism of indole-3-glycerol phosphate synthase: Crystal structures of complexes of the enzyme from *Sulfolobus solfataricus* with

substrate analogue, substrate, and product, *J. Mol. Biol. 319*, 757–766.
978. Bridger, W. A., Millen, W. A., and Boyer, P. D. (1968) Substrate synergism and phosphoenzyme formation in catalysis by succinyl coenzyme A synthetase, *Biochemistry 7*, 3608–3616.
979. Hager, L. P. (1957) Oxygen exchange reaction catalyzed by succinic-thiokinase, *J. Am. Chem. Soc. 79*, 4864–4867.
980. Hildebrand, J. G., and Spector, L. B. (1969) Succinyl phosphate and the succinyl coenzyme A synthetase reaction, *J. Biol. Chem. 244*, 2606–2613.

Chapter 6
Global Conformational Change

Because many instances have been documented crystallographically, there is no doubt that most molecules of protein can exist in more than one conformation. In retrospect, this observation is not surprising. If all the information necessary to produce one native structure of lowest free energy is encoded in the sequence of amino acids for the polypeptide or polypeptides comprising the protein, it must also be the case that the **information necessary to produce two or more different native structures** can be encoded in the same sequence of amino acids. If a polypeptide can fold and the folded polypeptides can assemble to produce one particular conformation, there is no reason that the same polypeptide cannot fold and assemble to produce a different conformation or several different conformations as well. The surprising fact is that these different conformations are usually in rapid equilibrium with each other without the necessity of passing through the unfolded random coil during their interconversion. The frequency with which these rapid equilibria between conformations are encountered among the proteins probably reflects the fact that they have been naturally selected during evolution for their significant functional utility.

Although there is a continuous spectrum for the extent of differences between two conformations of the same protein, there are several **classes of conformational changes** that can be distinguished. The conformational changes of least extent—such as local rearrangements of the side chains of amino acids in an active site upon association of reactants (Figures 3–56 and 3–57), closing of a lid over the active site upon assembly of all the reactants (Figure 3–58), and closing of the two domains of a subunit around the reactants to occlude them from the solution and in the process produce the active site (Figure 3–55)—have already been discussed. These are all local conformational changes. A **local conformational change** is a conformational change that occurs within the tertiary structure of a single folded polypeptide, that is confined to that folded polypeptide, and that has an insignificant effect on neighboring subunits when, as is almost always the case, that folded polypeptide is one of several folded polypeptides within a larger oligomer.

Most molecules of protein are **oligomers of subunits** that are folded polypeptides, each of which has the same sequence of amino acids. A conformational change can alter the spatial relations among the subunits in such an oligomer. A **quaternary conformational change** is a conformational change in an oligomer that includes two or more of its subunits (but usually all of them), that usually occurs with retention of the symmetry of the oligomer, and that usually involves a change in the orientation of its constituent folded polypeptides with respect to each other. For example, the conformational change between deoxyhemoglobin, in which all the hemes are unoccupied, and oxyhemoglobin, in which all four hemes have molecular oxygen bound, involves the rotation of one $\alpha\beta$ dimer with respect to the other $\alpha\beta$ dimer by 15° and an increase in the distance between the two dimers of 0.1 nm along a screw axis (Figure 6–1).[1-3]

The conformational change between unliganded aspartate carbamoyltransferase and aspartate carbamoyltransferase in which the bisubstrate analogue *N*-(phosphonacetyl)-L-aspartate (previously **3–6**)

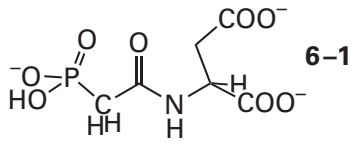

6–1

is bound in all six active sites of the $(\alpha\beta)_6$ oligomer involves a rotation of one catalytic α_3 trimer with respect to the other by 10° and a widening of the distance between the two by 1.2 nm (Figure 6–2)[4-7] and also a reorientation along a screw axis that coincides with the threefold rotational axes of symmetry in each of the two conformations. During this change, the three regulatory β_2 dimers rotate about their respective twofold rotational axes of symmetry by 15°. The interfaces between the regulatory β_2 dimers and the catalytic α_3 trimers act as pivots during this conformational change.

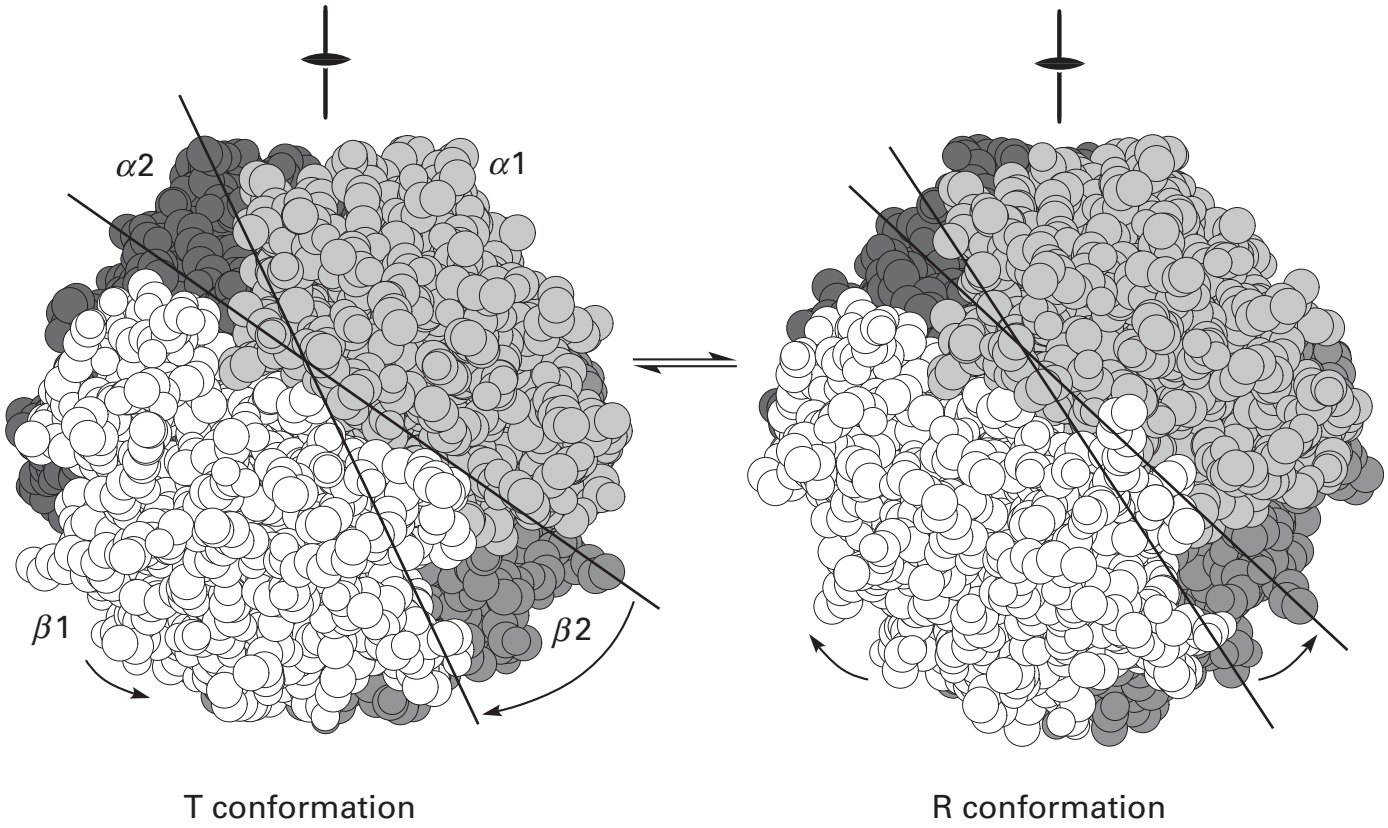

Figure 6–1: Drawings[485] of crystallographic molecular models of human hemoglobin in its two quaternary conformations, the R conformation (oxy) and the T conformation (deoxy).[1] Crystals of hemoglobin in the R conformation, the hemes of which were occupied by carbon monoxide, were grown in 2.5 M sodium/potassium phosphate at pH 6.7. Crystals of the space group $P4_12_12$ were obtained with an $\alpha\beta$ dimer in each asymmetric unit. Reflections were collected from these crystals to Bragg spacing of 0.22 nm.[3] Crystals of hemoglobin in the T conformation, the hemes of which were unoccupied, were grown in solutions of 1 mM ferrous citrate, ammonium sulfate (2–2.5 M), and ammonium phosphate (2–2.5 M) at pH 6.5. Crystals of the space group $P12_11$ were obtained with the entire $(\alpha\beta)_2$ heterotetramer in the asymmetric unit. Reflections were collected from these crystals to Bragg spacing of 0.174 nm.[2] The space-filling drawings are of the two refined, complete crystallographic molecular models, that for the R conformation (left) and that for the T conformation (right). The two $\alpha\beta$ dimers of the $(\alpha\beta)_2$ heterotetramer, $\alpha1\beta1$ to the front and $\alpha2\beta2$ to the back, are drawn in light gray and white and in dark gray and gray, respectively. The two $\alpha\beta$ dimers are arrayed around the exact, crystallographic twofold rotational axis of symmetry of the R conformation or the noncrystallographic twofold rotational axis of symmetry of the T conformation, each running vertically in the plane of the page. There is a twofold rotational axis of pseudosymmetry relating $\alpha1$ and $\beta1$ and $\alpha2$ and $\beta2$, normal to the plane of the page in the middle of the $\alpha1\beta1$ dimer in front, and there is a horizontal twofold rotational axis of pseudosymmetry relating $\alpha1$ and $\beta2$ and $\alpha2$ and $\beta1$ in the plane of the page. The two lines in each drawing are drawn through two side chains on the opposite sides of the $\alpha1\beta1$ dimer and through two side chains on the opposite sides of the $\alpha2\beta2$ dimer, respectively. In each drawing, the lines are drawn through the same side chains to illustrate the 15° rotation between the two dimers that occurs upon the change in conformation.

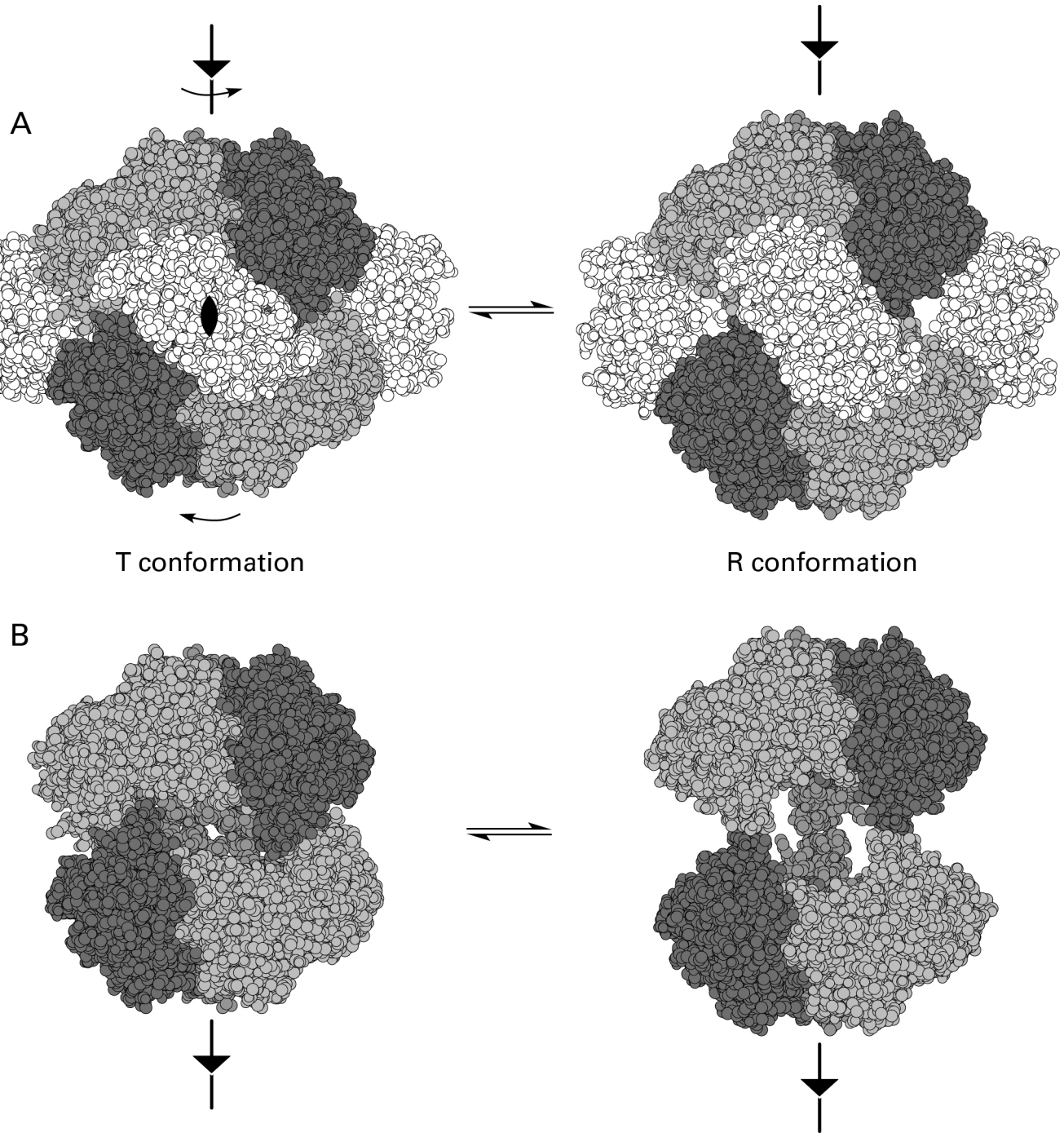

Figure 6–2: Drawings[485] of crystallographic molecular models of aspartate carbamoyltransferase from *E. coli* in its two quaternary conformations.[5] Crystals of the enzyme in the R conformation, the active sites of which were occupied by *N*-(phosphonacetyl)-L-aspartate (**6–1**), were produced by dialyzing the enzyme at high concentration into 50 mM *N*-ethylmorpholinium maleate at pH 6.9 and 21 °C in the presence of 1 mM *N*-(phosphonacetyl)-L-aspartate. Crystals of the space group *P*321 were obtained. Reflections were collected from these crystals to Bragg spacing of 0.25 nm.[6] Crystals of the enzyme in the T conformation, the regulatory sites of which were occupied by CTP^{4-}, were formed by dialysis against 1 mM 2-sulfanylethanol, 0.2 mM ethylenediaminetetraacetic acid, 10 mM 2-ammonio-2-hydroxymethylpropane-1,3-diol chloride, and 100 mM sodium maleate at pH 6.35. Crystals of space group *P*321 were obtained. These were soaked in the aforementioned buffer with 2.5 mM CTP^{4-}. Reflections one at the top in each drawing and one at the bottom, are drawn in three shades of gray, and the three folded α polypeptides in each catalytic α_3 trimer are arrayed around an exact crystallographic threefold rotational axis of symmetry running vertically in the plane of the page. The three regulatory β_2 dimers, drawn in white, connect the two catalytic α_3 trimers, and a twofold rotational axis of symmetry runs through the center of each of the three regulatory β_2 dimers. One of those twofold rotational axes of symmetry is normal to the plane of the page in the middle of the regulatory β_2 dimer in front. Both views are down this twofold rotational axis of symmetry. (**B**) Rearrangement of catalytic α_3 trimers during the conformational change. The drawings of the R conformation (left) and the T conformation (right) are the same drawings as in Panel A except that the three regulatory β_2 dimers have been removed so that the central cavity in the molecule of the enzyme

from the soaked crystals were collected to Bragg spacing of 0.26 nm.[7] (**A**) Equilibrium between the R and T conformations. The space-filling drawings are of the two refined, complete crystallographic molecular models, that for the R conformation (left) and that for the T conformation (right). The two catalytic α_3 trimers, can be seen. As the conformation changes, the two catalytic α_3 trimers rotate in opposite directions. As they slide past each other, they fit together more snugly and the central cavity becomes narrower.

The rotation of the pivoting regulatory β_2 dimers spreads apart and rotates the two catalytic α_3 trimers with respect to each other. In such quaternary conformational changes, the subunits can, to a first approximation, be treated as **rigid bodies that reorient with respect to each other** by mechanical movements of defined geometry.

Within the tertiary conformation of each constituent folded polypeptide of an oligomeric protein, **local conformational changes always accompany a quaternary conformational change** that involves the entire molecule of protein. For example, local conformational changes on the distal side of the heme in hemoglobin (Figure 2–53) occur during the quaternary conformational change promoted by the binding of molecular oxygen. Such local conformational changes within the subunits must occur during a quaternary conformational change. Every inter*face* in a homooligomeric protein, by definition, is formed from two *faces*. These two words must be clearly distinguished because they refer to different things. If the tertiary conformations of the folded polypeptides constituting the subunits were to remain the same, the structures of the faces within the interfaces that create the oligomer would also have to remain the same. Because the structures of these two faces are all that determine the structure of the interface, the quaternary conformational change could not occur. If the faces that form the interface do not change, the interface cannot change. Local conformational changes, however, do not always affect or effect quaternary conformational changes. A local conformational change confined to a region of the subunit well isolated from the interfaces, for example, the closing of a loop of polypeptide over an active site upon association of reactants, **can occur independently of a quaternary conformational change**.

Aspartate carbamoyltransferase (previously Equation 3–220)

$$\text{carbamoyl phosphate} + \text{L-aspartate} \rightleftharpoons \text{H}^+ + \textit{N}\text{-carbamoyl-L-aspartate} + \text{HOPO}_3^{2-} \quad (6\text{–}1)$$

catalyzes the first committed reaction in the metabolic pathway leading to the pyrimidine nucleotides: orotidine 5′-phosphate, uridine 5′-triphosphate, cytidine 5′-triphosphate, thymidine 5′-triphosphate, and deoxycytidine 5′-triphosphate. The **first committed reaction** in any metabolic pathway is the earliest step in the pathway in which a metabolite is produced that can be used only in that pathway. For example, *N*-carbamoyl-L-aspartate, a product of the reaction catalyzed by aspartate carbamoyltransferase (Equation 6–1), is used only to synthesize pyrimidine nucleotides.

The simplest form of metabolic regulation is **end-product inhibition**, a situation where one or several end products of a metabolic pathway inhibit the first committed reaction in that pathway. When the cytoplasmic concentrations of pyrimidine nucleotides are too high, the flux through the pathway for their biosynthesis is diminished by decreasing the rate of the reaction catalyzed by aspartate carbamoyltransferase. This decrease occurs because several of the pyrimidine nucleotides, in particular $MgCTP^{2-}$ and $MgUTP^{2-}$ acting together, are inhibitors of the catalysis performed by the enzyme (Figure 6–3).[8,9] If, however, the concentrations of purine nucleotides, in particular $MgATP^{2-}$ and $MgGTP^{2-}$, are in significant excess over those of pyrimidine nucleotides, the biosynthesis of pyrimidine nucleotides is increased by accelerating the rate of the reaction catalyzed by aspartate carbamoyltransferase. This increase occurs because $MgATP^{2-}$ and $MgGTP^{2-}$ are activators of the catalysis performed by the enzyme. Metabolic regulation can also be exerted at the branch points of major metabolic pathways; for example, citrate activates acetyl-CoA carboxylase to divert acetyl-SCoA from the citric acid cycle to the biosynthesis of fatty acids, from the immediate production of energy to the storage of energy.

It is known, from studies in which the catalytic α_3 trimers were separated from the regulatory β_2 dimers,[10] that the active sites for aspartate carbamoyltransferase from *Escherichia coli* are on its catalytic α subunits[10] and the binding sites for nucleotides are on its regulatory β subunits.[9,11,12] In the intact native enzyme, the six active sites are symmetrically

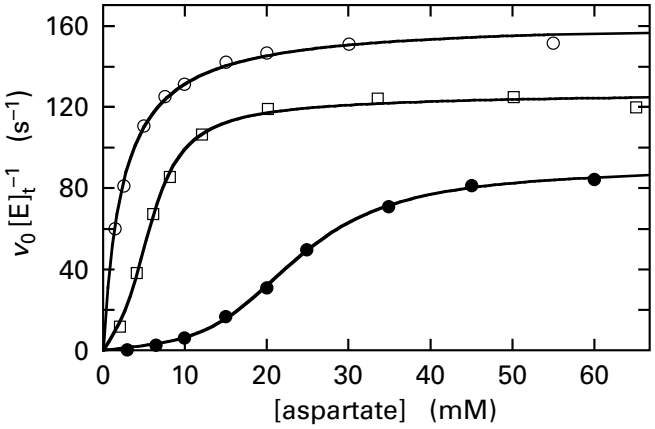

Figure 6–3: Behavior of the initial rates of the reaction catalyzed by aspartate carbamoyltransferase from *E. coli* as a function of the initial concentrations of its reactant L-aspartate.[9] The initial rates of the enzymatic reaction were determined colorimetrically at various concentrations of L-aspartate in 2.0 mM carbamoyl phosphate, 2.0 mM MgCl, 20 mM 2-[bis(2-hydroxyethyl)amino]-2-(hydroxymethyl)propane-1,3-diol, 20 mM 2-amino-2-hydroxymethylpropane-1,3-diol, and 20 mM 3-(cyclohexylamino)-1-propanesulfonic acid at pH 7 and 28 °C with either no other additions (□), 2 mM $MgCTP^{2-}$ and 2 mM $MgUTP^{2-}$ (●), or 2 mM $MgATP^{2-}$ and 2 mM $MgGTP^{2-}$ (○). From the concentration of purified enzyme and its molar mass, the measured activity was converted to moles of *N*-carbamoyl-L-aspartate (mole active sites)$^{-1}$ second^{-1} (s^{-1}). Each initial rate (v_0 in second^{-1}) is plotted as a function of the respective initial concentration of L-aspartate. The curves drawn for the lower two sets of data are fits of Equation 6–36 to the points, and the curve drawn to the upper set of data is a fit of Equation 3–40 to the points.

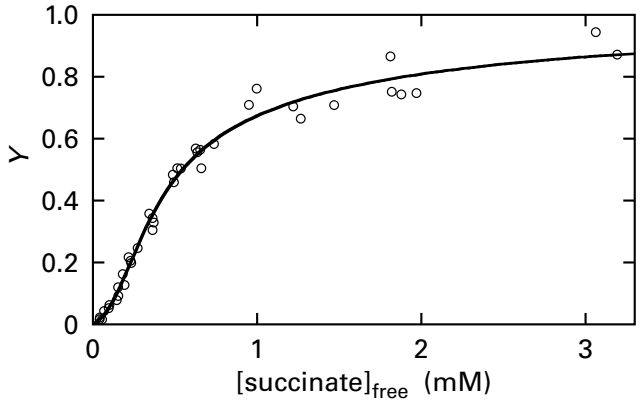

Figure 6–4: Measurement of the binding of [U-^{14}C]succinate to aspartate carbamoyltransferase from *E. coli* by equilibrium dialysis.[11] For measurements by equilibrium dialysis, a series of apparatuses, each separating two chambers by a dialysis membrane, was used. In one chamber of each apparatus, aspartate carbamoyltransferase (5–20 mg mL^{-1}) in buffer containing 4 mM carbamoyl phosphate (CAP) was present; in the other chamber, only buffer and 4 mM carbamoyl phosphate were present. A different initial concentration of [U-^{14}C]succinate (succ) was added to the side of each chamber without enzyme, and the chambers were allowed to reach equilibrium across the membrane. The final concentration of [U-^{14}C]succinate, as determined by scintillation counting, in the chamber lacking enzyme in each apparatus is the free concentration of the succinate at equilibrium in both chambers of that apparatus; the final concentration of [U-^{14}C]succinate in the chamber containing the protein is the sum of free and bound concentrations of ligand. The value for the concentration of bound [U-^{14}C]succinate at saturation was obtained with the version of Equation 6–35 in which the concentration of total sites is a known parameter rather than an unknown variable. With this value for the concentration of bound [U-^{14}C]succinate at saturation, a value for the fraction of sites occupied, Y, was calculated for each point. Each value for Y is plotted as a function of the respective free concentration of succinate at equilibrium. When the data were fit to Equation 6–35 without inserting a value for the concentration of sites, the value for $K'_{d,succ}$ from the fit was a large but negative number. Because negative dissociation constants are meaningless, it was assumed that $K'_{d,succ}$ must be too large to be defined by the observations. Values for $K'_{d,succ}$ larger than 1 M all produced the same fit to the data that was obtained when the value for $K'_{d,succ}$ was not constrained. The curve in the figure[76] is for $K'_{d,succ} = 1$ M, $L_{CAP} = 6.8 \pm 2.4$, and $K_{d,succ} = 0.48 \pm 0.04$ mM.

displayed on the two catalytic α_3 trimers,[5] and the six binding sites for nucleotides are symmetrically displayed on the three regulatory β_2 dimers (Figure 6–2). In the crystallographic molecular model for the intact enzyme,[13] each site on a folded regulatory polypeptide at which nucleotides, either $MgCTP^{2-}$ and $MgUTP^{2-}$ or $MgATP^{2-}$ and $MgGTP^{2-}$, are bound[6,9,14] is 6.0 nm distant from and makes no direct contacts with the closest active site.[5] As a result, the **active sites are distinct and separate from the regulatory sites**, and the inhibition or activation of catalysis is an allosteric effect.[15]

An allosteric effect is an indirect interaction between distinct, spatially separated sites on a protein during which the conformation of the protein is altered by association of a ligand at one or more of the sites, causing a change at one or more of the other sites. The ligands the association of which causes the alteration of the conformation can be inhibitors, activators, antagonists, agonists, or substrates for an active site, and the sites that change as a result of the change in conformation can be active sites or sites for agonists, activators, inhibitors, or antagonists.

A **heterotropic allosteric effect** is the allosteric effect that occurs when the interacting sites bind different ligands. An example of a heterotropic allosteric effect would be an interaction between a regulatory site on aspartate carbamoyltransferase that associates with $MgCTP^{2-}$ and $MgUTP^{2-}$ or $MgATP^{2-}$ and $MgGTP^{2-}$ on the one hand and an active site on aspartate carbamoyltransferase that associates with L-aspartate and carbamoyl phosphate on the other. Two examples of heterotropic

allosteric effects are the inhibition of aspartate carbamoyltransferase from *E. coli* by $MgCTP^{2-}$ and $MgUTP^{2-}$ and the activation of the same enzyme by $MgATP^{2-}$ and $MgGTP^{2-}$ (Figure 6–3).

A **homotropic allosteric effect** is the allosteric effect that occurs when two or more interacting sites are composed of the same respective amino acids within two or more constituent subunits, each formed from a folded polypeptide of the same sequence, and consequently associating with the same ligand or set of ligands. An example of a homotropic allosteric effect would be the interactions among the active sites on aspartate carbamoyltransferase, one on each catalytic α subunit, that, by definition, associate with L-aspartate and carbamoyl phosphate.

There are two consequences of homotropic allosteric effects among the active sites of aspartate carbamoyltransferase from *E. coli*. First, at saturating concentrations of succinate, association of carbamoyl phosphate at one or two of the six active sites in aspartate carbamoyltransferase increases the affinity of the remaining active sites for carbamoyl phosphate.[16] Second, at saturating concentrations of carbamoyl phosphate, association of succinate, an analogue of L-aspartate, at one or two of the six active sites increases the affinity of the remaining active sites for succinate (Figure 6–4).[11] The effect of the concentrations of L-aspartate on the initial rate of the reaction catalyzed by aspartate carbamoyltransferase (Figure 6–3) mimics the dependence of the binding of succinate on its concentration (Figure 6–4). This behavior suggests that when one or two of the active sites become occupied with L-aspartate, the affinity of the remaining active sites for L-aspartate increases.

Homotropic allosteric behavior is also of **regulatory significance**. Because association of the first few molecules of a reactant with active sites on an oligomer that displays homotropic allosteric behavior increases the affinity of the yet-to-be-occupied sites on the same oligomer, the range of concentration for that reactant between an occupancy of 10% and an occupancy of 90% is much narrower than it would have been if a homotropic allosteric effect did not exist. Consequently, increases and decreases in enzymatic activity are more pronounced when changes in the concentration of that reactant occur in the cytoplasm, and such changes in the concentration of reactant exert greater control over the enzymatic activity. In the specific case of aspartate carbamoyltransferase, the activity of the enzyme is shut down more effectively when L-aspartate, which is used widely in other metabolic reactions, is present at a low concentration in the cytoplasm.

Both heterotropic and homotropic allosteric effects are consequences of the ability of the protein to exist in two or more conformations that are in rapid equilibrium with each other. In addition to their role in heterotropic and homotropic allosteric control of enzymatic activity, conformational changes are also used by proteins to convert the potential energy in a covalent bond, usually the potential energy in the γ-phosphoanhydride of $MgATP^{2-}$, into kinetic energy or the electrochemical potential of a gradient of ions across a membrane and vice versa. For example, the movements of muscle, the movements of individual cells, the synthesis of $MgATP^{2-}$ from an electrochemical gradient of hydrons during oxidative phosphorylation, and the maintenance of the concentration gradients of ions and metabolites across the plasma membranes of cells are all a consequence of conformational changes in the enzymes responsible for these processes.

Cooperativity

In the usual, ideal case, when measurements are made of the occupancy for a ligand with a set of independent sites, regardless of whether they are each on a monomer of the protein or they are independent, identical sites on an oligomer, the data follow a rectangular hyperbola. The slope of the curve describing the occupancy decreases continuously from its initial value as it approaches its rectangularly hyperbolic asymptote at saturation (Figure 3–17). Association of succinate, however, with the active sites on aspartate carbamoyltransferase from *E. coli* that are saturated with carbamoyl phosphate (Figure 6–4) displays a **positive deviation from ideal behavior**. Such positive deviation is often referred to as **sigmoid behavior**. Instead of decreasing from its initial value at the lowest concentrations of succinate, the slope of the curve describing occupancy of the sites actually increases as the concentration of succinate is increased before it then decreases. The resulting curve is S-shaped (sigmoid). **Cooperativity** is an allosteric interaction between two or more identical sites, usually but not always active sites, on an oligomeric protein in which the association of a ligand or substrate at one or more of the sites induces conformational changes in the remaining

unoccupied sites, leading to an increase in the affinity of those sites for their ligand or substrate—or an increase in the limiting rate of the remaining active sites—and typically producing sigmoid behavior. Cooperativity is observed in the binding of ligands to many proteins (Figures 6–4 and 6–5). Association of the first ligands with the protein increases its affinity for the last ligands to associate. The ligands cooperate with each other to fill the sites. Because hemoglobin is a protein that displays this type of behavior and because it has been studied longer than any of the others, it serves as a useful example. When the fraction of the hemes in human hemoglobin that are occupied by molecular oxygen is measured as a function of the concentration of molecular oxygen, positive deviation from ideal behavior is observed (Figure 6–5).[17]

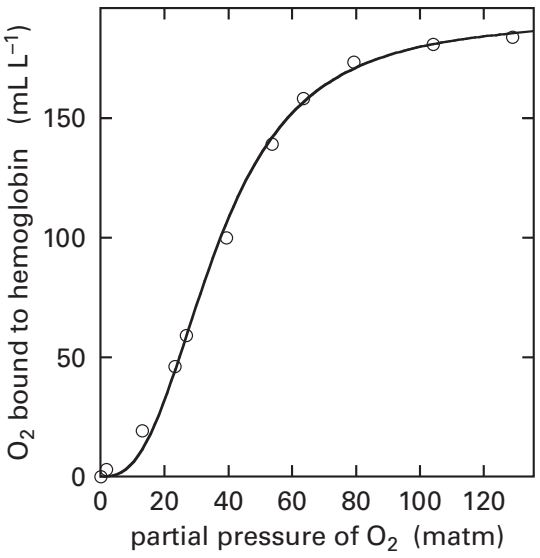

Figure 6–5: Dissociation curve for molecular oxygen from human hemoglobin.[17] Samples of whole blood from C. G. Douglas were equilibrated with various mixtures of N_2 gas and O_2 gas and 53 matm of CO_2 at 38 °C. After equilibrium was reached, the molecular oxygen bound to hemoglobin was driven off the hemes by adding potassium ferricyanide. The volume of O_2 gas liberated into the vapor phase above the blood (milliliters) was then measured manometrically. This volume represents the amount of O_2 bound to hemoglobin in the blood before ferricyanide was added. The volume of O_2 bound [milliliters of O_2 released by ferricyanide (liter of blood)$^{-1}$] is plotted as a function of the respective partial pressure of O_2 over the blood (oxygen tension in milliatmospheres). The curve is a fit of Equation 6–6 to the data with $[ST]_t = 192 \pm 4$ mL of O_2 L^{-1}, $n = 2.7 \pm 0.2$, and $K_d = (16{,}000 \pm 700 \text{ matm})^{2.7}$.

Two equations, the Hill equation and the Adair equation, which involve no explanation for cooperativity, are used to fit sigmoid behavior. They are simply mathematical equations that happen to describe the observations.

Consider a protein, P, with n sites, ST, for ligand L. Suppose that each molecule of protein, for some unknown reason, were required to bind simultaneously all n molecules of ligand L to those n sites and that, as a result, each molecule of that protein were always either fully occupied or completely unoccupied

$$\mathrm{P} + n\mathrm{L} \underset{K_{dL}}{\rightleftharpoons} \mathrm{P}\cdot n\mathrm{L} \tag{6–2}$$

The dissociation constant for this reaction would be

$$K_{dL} = \frac{[\mathrm{P}][\mathrm{L}]^n}{[\mathrm{P}\cdot n\mathrm{L}]} \tag{6–3}$$

and if Y is defined as the fraction of sites occupied (previously Equation 3–293)

$$Y \equiv \frac{[\mathrm{ST}\cdot\mathrm{L}]_{eq}}{[\mathrm{ST}]_t} \tag{6–4}$$

then

$$\frac{[\mathrm{ST}\cdot\mathrm{L}]}{[\mathrm{ST}]_t} \equiv Y = \frac{n[\mathrm{P}\cdot n\mathrm{L}]}{n[\mathrm{P}]_t} = \frac{[\mathrm{L}]^n}{K_{dL} + [\mathrm{L}]^n} \tag{6–5}$$

Equation 6–5 displays sigmoid behavior. It can be rearranged to give the equation

$$[\mathrm{ST}\cdot\mathrm{L}] = \frac{[\mathrm{ST}]_t [\mathrm{L}]^n}{K_{dL} + [\mathrm{L}]^n} \tag{6–6}$$

which is analogous to (previously Equation 3–298)

$$\Delta A = \frac{\Delta A_t [\mathrm{L}]_{eq}}{K_{dL} + [\mathrm{L}]_{eq}} \tag{6–7}$$

Equation 6–6 can be fit directly to the data for the binding of molecular oxygen to hemoglobin (Figure 6–5). Nevertheless, the otherwise rearranged version

$$\frac{Y}{1 - Y} = \frac{[\mathrm{L}]^n}{K_{dL}} \tag{6–8}$$

$$\log\left(\frac{Y}{1-Y}\right) = n\log[\mathrm{L}] + \mathrm{p}K_{\mathrm{dL}} \qquad (6\text{–}9)$$

has historically been used to fit the data and obtain a value for n. Once $[\mathrm{ST}]_t$ is estimated from a fit of Equation 6–6 to the data directly, values for log $[Y(1-Y)^{-1}]$ are plotted as a function of log [L]. The common logarithmic form of the equation (Equation 6–9) is the **Hill equation**.[18] Parameter n, the **Hill coefficient**, is the slope of a plot of log $[Y(1-Y)^{-1}]$ against log [L].

Although the preceding derivation is based on a particular mechanism, the mechanism in which **each molecule of protein is required to bind all its ligands simultaneously** (Equation 6–2), the uselessness of this stipulation as an explanation for the sigmoid behavior of the binding of a ligand to a protein as a function of free concentration of the ligand is apparent. Only a very peculiar protein, unlike any that currently exists, would bind all its ligands simultaneously. Nevertheless, experimental data are often fit with the Hill equation even though it usually fails to fit the data if they are gathered over a large enough range. Observed values for the occupancy of a site by a ligand L or the initial rate of an enzymatic reaction that shows sigmoid behavior as a function of the concentration of a reactant A are plotted in the format log $[Y(1-Y)^{-1}]$ against log [L], or log $[v_0\,(V-v_0)^{-1}]$ against log [A]; and, over a limited range, the plot is usually linear as demanded by the equation.

Even though the Hill coefficient obtained from such a plot provides no insight into the reason for the sigmoid behavior, it serves as a semiquantitative **measure of the degree of cooperativity**. If the number of sites for the ligand on a molecule of the protein is known, the closer the value of the Hill coefficient is to that number, the greater is the cooperativity among the sites. If the Hill coefficient were to equal the number of sites, the cooperativity would be complete; the remaining ligands would associate immediately upon association of the first.

There are several reasons that plotting experimental data by the Hill equation (Equation 6–9) is unsatisfactory. While there are a few instances in which it comes close, such as the α_4 tetramer of 6-phosphofructokinase from *E. coli* ($n = 3.8$),[19] the value of the Hill coefficient rarely equals the known number of sites that are cooperating with each other. In addition, the value of the Hill coefficient is almost never an integer. For example, for human hemoglobin (Figure 6–5) the Hill coefficient is 2.7, which

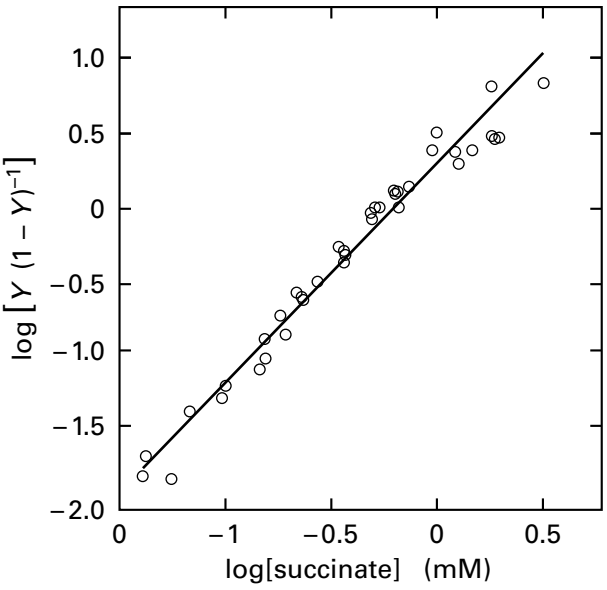

Figure 6–6: Hill plot of the binding of [U-^{14}C]succinate to aspartate carbamoyltransferase from *E. coli*. Values for the total concentration of sites and the fractional saturation Y as a function of the free concentration of ligand are those plotted in Figure 6–4. The quotient $Y(1-Y)^{-1}$ was calculated for each concentration of succinate, and each common logarithm of $Y(1-Y)^{-1}$ is plotted as a function of the respective common logarithm of the concentration of succinate (millimolar). A line was fit to the data. The slope of the line, the Hill coefficient, is 1.45 ± 0.04.

is neither equal to the number of sites for binding molecular oxygen on the protein nor an integer. In theory, the Hill coefficient can never exceed the number of cooperating sites because Equation 6–2 describes, by definition, a completely cooperative situation. In practice, however, there are instances in which the Hill coefficient exceeds the number of protomers in the protein.[20] Finally, the value of the Hill coefficient varies depending on the position on the curve at which the slope is determined. According to the Hill equation (Equation 6–9), a plot of log $[Y(1-Y)^{-1}]$ against log [L] should be a straight line at all values of [L]. Most observations are made around the mid-region (Figure 6–5) of the curve for binding ($0.10 < Y < 0.90$), and within this range the data in a Hill plot, within the errors of the experiment, usually define a line, as is the case for binding of succinate to aspartate carbamoyltransferase (Figure 6–6). When, however, measurements are taken over a broad enough range, log $[Y(1-Y)^{-1}]$ is not a linear function of log [L] (Figure 6–7).[21]

The complete set of observations, however, for association of molecular oxygen with human hemoglobin (Figure 6–7), and almost always, if not always,

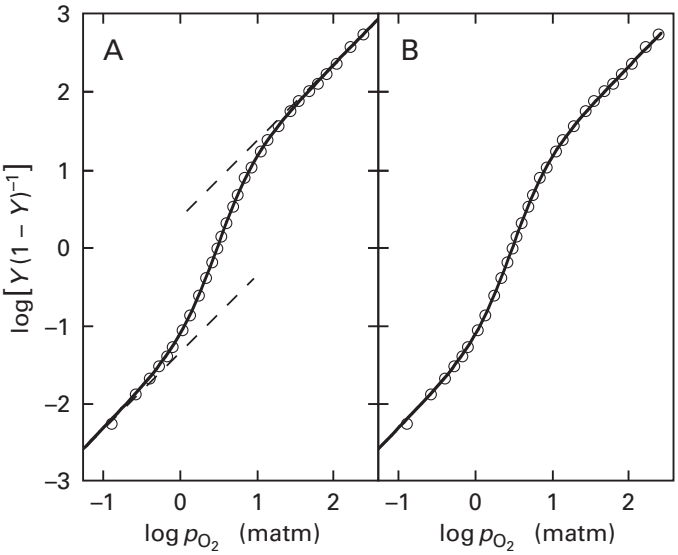

Figure 6–7: Dissociation of molecular oxygen from human hemoglobin,[21] measured over a range of greater than 3 orders of magnitude in the concentration of O_2. Hemoglobin A was prepared from human blood and was stripped of all organic phosphates. Solutions of this hemoglobin at a concentration of 0.6 mM in heme were prepared in 0.1 M NaCl at pH 9.1 and 25 °C. The fractional saturation of hemoglobin, *Y*, was determined as a function of the partial pressure of molecular oxygen (pO_2) in the gas phase above the solution. For each measurement, the concentration of molecular oxygen in the solution of hemoglobin was measured directly with an oxygen electrode that had been calibrated with standard gas mixtures at the same time that transmittance of the solution was measured at a wavelength of 620 nm. Absorbance of the solution purged with N_2 was assumed to be the absorbance of hemoglobin unoccupied with molecular oxygen, and absorbance extrapolated to infinite concentration of molecular oxygen was assumed to be that of hemoglobin fully saturated with molecular oxygen. The fractional saturation, *Y*, was assumed to be directly proportional to the observed absorbance relative to these limits (Equation 3–297). After a measurement was taken at one concentration, the mixture of molecular nitrogen and molecular oxygen was changed. All consecutive readings were taken on the same solution at a particular temperature. The reversibility of the process was demonstrated by returning frequently to concentrations of earlier measurements. From individual measurements of *Y*, the function $\log [Y(1-Y)^{-1}]$ was calculated, and each calculated value is plotted as a function of the respective common logarithm of the partial pressure (milliatmospheres) of molecular oxygen. (**A**) Fit of the data with the Adair equation (Equation 6–11). The dashed lines are the two limits of Equations 6–18 and 6–19. Values for K_{d1} and K_{d4} obtained from these limits were used as starting values for these parameters in a complete fit of the equation to the data. The final values for the dissociation constants from the full fit were $K_{d1} = 5.6 \pm 0.7$ matm, $K_{d2} = 5.8 \pm 2.4$ matm, $K_{d3} = 1.6 \pm 0.7$ matm, and $K_{d4} = 1.9 \pm 0.2$ matm. The solid curve is the fit to the data. (**B**) Fit of the same data with Equation 6–35. Values for parameters of the fit are $L_0 = 1700 \pm 300$, $K'_{dO_2} = 22 \pm 1$ matm, and $K_{dO_2} = 0.49 \pm 0.02$ matm. Again, the solid curve is the fit to the data.

associations of other ligands with other proteins and enzymes that display sigmoid behavior, can be fit with an equation that does not require the unrealistic assumption that the molecule of protein binds all its ligands simultaneously.[22] For example, hemoglobin contains four hemes and binds four molecular oxygens at saturation. If this process, as one might reasonably assume, occurs in four simple steps

$$\begin{aligned} \mathrm{Hb} + 4\,\mathrm{O_2} &\underset{K_{d1}}{\rightleftharpoons} \mathrm{Hb{\cdot}O_2} + 3\,\mathrm{O_2} \\ &\underset{K_{d2}}{\rightleftharpoons} \mathrm{Hb{\cdot}(O_2)_2} + 2\,\mathrm{O_2} \underset{K_{d3}}{\rightleftharpoons} \\ &\mathrm{Hb{\cdot}(O_2)_3} + \mathrm{O_2} \underset{K_{d4}}{\rightleftharpoons} \mathrm{Hb{\cdot}(O_2)_4} \end{aligned} \tag{6–10}$$

where the K_{di} are all macroscopic dissociation constants for molecular oxygen, then

$$Y = \frac{K_{d2}K_{d3}K_{d4}[\mathrm{O_2}] + 2K_{d3}K_{d4}[\mathrm{O_2}]^2 + 3K_{d4}[\mathrm{O_2}]^3 + 4[\mathrm{O_2}]^4}{4(K_{d1}K_{d2}K_{d3}K_{d4} + K_{d2}K_{d3}K_{d4}[\mathrm{O_2}] + K_{d3}K_{d4}[\mathrm{O_2}]^2 + K_{d4}[\mathrm{O_2}]^3 + [\mathrm{O_2}]^4)} \tag{6–11}$$

This relation is an Adair equation.

The **Adair equation** is not exclusive to association of molecular oxygen with hemoglobin. Nor is it only applicable to a molecule of protein with four sites; the number of sites on the molecule of protein can be any integer. As already mentioned, it can be applied to association of any ligand or substrate to any protein, whether or not the association displays sigmoid behavior. In fact, in situations in which there are several different, independent sites on a protein for the same ligand, each of which is composed of a different set of amino acids and each of which associates with a ligand with its own distinct dissociation constant, the Adair equation can be used to obtain values for those several dissociation constants. In such a situation, association of the ligand with the

protein must show **negative deviation from ideal behavior** as the ligand associates successively with sites of lower and lower affinity.

The **general form for the Adair equation** is

$$Y = \frac{\left\{\sum_{i=1}^{n-1} i\left(\prod_{i+1}^{n} K_{\mathrm{d}i}\right)[\mathrm{L}]^i\right\} + n[\mathrm{L}]^n}{\left\{\sum_{i=0}^{n-1} n\left(\prod_{i+1}^{n} K_{\mathrm{d}i}\right)[\mathrm{L}]^i\right\} + n[\mathrm{L}]^n} \qquad (6\text{–}12)$$

where n is the number of sites for ligand L on the protein and $K_{\mathrm{d}i}$ are formally dissociation constants with units of molarity. The Adair equation is also not confined to association of a ligand with a molecule of protein. Association of a ligand with any molecule or ion, for example, association of imidazole with Zn^{2+} and Cu^{2+}, can be described with an Adair equation.[23] From these considerations, it should be clear that the intent of the equation is to be **as independent of any explanation as possible** and to provide a **broadly applicable equation to fit any set of observations**.

Because each coefficient in the Adair equation is simply the previous coefficient multiplied by a number that can have any positive value, each coefficient is actually independent of the others. Consequently, the general form of the Adair equation can be restated as

$$Y = \frac{\left\{\sum_{i=1}^{n-1} i a_i[\mathrm{L}]^i\right\} + n[\mathrm{L}]^n}{\left\{\sum_{i=0}^{n-1} n a_i[\mathrm{L}]^i\right\} + n[\mathrm{L}]^n} \qquad (6\text{–}13)$$

where the n coefficients, a_0 to a_{n-1}, with units of M^{n-i}, can have any value greater than 0. In this formulation, the Adair equation is independent of any proposed mechanism and independent of any explanation for the behavior that is observed. It is simply an equation that has been found to describe accurately observations of association of a ligand with a protein whether cooperative or not.

In the case of hemoglobin, an Adair equation is being applied to a situation where a great deal is known about the protein. It should be noted, however, that in deriving the equation for hemoblobin, no assumptions were made as to the properties of the sites to which molecular oxygen is binding. The only assumption made was that there are four sites on each molecule of protein, a fact which can be ascertained by quantifying the moles of molecular oxygen that associate with each mole of hemoglobin at saturation. In situations in which almost nothing is known about a protein binding a particular ligand other than a fairly accurate approximation of its molar mass,* the first property that is ascertained is the ratio between the moles of bound ligand at saturation and the moles of protein. It is then assumed that each molecule of protein in the solution† can associate with that number of ligands, and the value for n in the Adair equation is chosen to be that molar ratio.

For the general Adair equation (Equation 6–12)[23]

$$\lim_{[\mathrm{L}] \to 0} \log\left(\frac{Y}{1-Y}\right) = \log\left(\frac{1}{nK_{\mathrm{d}1}}\right) \qquad (6\text{–}14)$$

and

$$\lim_{[\mathrm{L}] \to \infty} \log\left(\frac{Y}{1-Y}\right) = \log\left(\frac{n}{K_{\mathrm{d}n}}\right) \qquad (6\text{–}15)$$

and for the algebraic form (Equation 6–13)

$$\lim_{[\mathrm{L}] \to 0} \log\left(\frac{Y}{1-Y}\right) = \log\left(\frac{a_1[\mathrm{L}]}{na_0}\right) \qquad (6\text{–}16)$$

and

$$\lim_{[\mathrm{L}] \to \infty} \log\left(\frac{Y}{1-Y}\right) = \log\left(\frac{n[\mathrm{L}]}{a_{n-1}}\right) \qquad (6\text{–}17)$$

It follows from these limits that the **asymptotes** at either end of plots of $\log [Y(1-Y)^{-1}]$ against $\log [\mathrm{L}]$, which should have slopes of 1 as required by Equations 6–14 and 6–15, fix values for K_1 and K_n. These constraints then allow values for the other parameters to be determined more precisely. For example, for

*Today, the molar mass of a subunit of an enzyme is usually known before it is purified because its sequence of amino acids is usually known before it is purified.

†Some problems with this assumption are that it is quite difficult to determine precisely the concentration of protein in a solution, to estimate the purity of the protein being studied, and to know what percentage of the molecules of that particular protein, although present, are defunct.

*From here on a unidirectional arrow, rather than two opposing arrows, will be used to designate an equilibrium as

dissociation of molecular oxygen from hemoglobin at 30 °C (Figure 6–7), the limits for Equation 6–11 are

$$\lim_{[O_2] \to 0} \log\left(\frac{Y}{1-Y}\right) = \log\left(\frac{[O_2]}{4K_{d1}}\right) \quad (6–18)$$

and

$$\lim_{[O_2] \to \infty} \log\left(\frac{Y}{1-Y}\right) = \log\left(\frac{4[O_2]}{K_{d4}}\right) \quad (6–19)$$

Values for K_{d1} and K_{d4} were determined from the asymptotes (dashed lines in Figure 6–7A), and values for K_{d2} and K_{d3} could then be obtained[23] by fitting the data to Equation 6–11, with the result that $K_{d1} = 5.6 \pm 0.7$ matm, $K_{d2} = 5.8 \pm 2.4$ matm, $K_{d3} = 1.6 \pm 0.7$ matm, and $K_{d4} = 1.9 \pm 0.2$ matm. Because the data are of such high accuracy, extend over almost 4 orders of magnitude in the concentration of molecular oxygen (Figure 6–7), and include both asymptotes, the errors of estimate are small even though the data are fit with four parameters. Much of this precision is due to the fact that the asymptotes, at each end of the curve, were used to determine K_{d1} alone and K_{d4} alone, a fact that explains the greater precision of these two parameters relative to the other two.

If data are available for only the midrange, as is usually the case, then the **errors of estimate** are usually much greater. For example, when the Adair equation is fit to the data for binding of succinate to the active sites on aspartate carbamoyltransferase from *E. coli* that are saturated with carbamoyl phosphate (Figure 6–4), which is an unusually extensive set of observations, a satisfactory coincidence between the resulting curve and the points is obtained ($R = 0.99$), but standard deviations on the six parameters governing the fit are all larger than the numbers for the parameters themselves, and the values for dissociation constants are strange. In this case, the data span only two orders of magnitude, asymptotes of slope 1 with which to fix values for K_1 and K_6 independently are not reached (Figure 6–6), and there are six parameters in the Adair equation rather than four. Nevertheless, the behavior can be fit with the equation.

One of the more important points, however, that can be established by examining an Adair equation is that the sigmoid behavior observed for association of ligands with certain homooligomeric proteins is **not simply a consequence of the fact that a homooligomer has more than one site** for a particular ligand. Unoccupied homooligomers are, with few exceptions, rotationally symmetric. If the asymmetric unit of a symmetric homooligomer has one site with which a ligand associates, then each of the other asymmetric units will have an identical site for that ligand. If they are identical and independent of each other, each site should have the same microscopic dissociation constant, K_{dL}, for the ligand. The macroscopic dissociation constant, however, for the ith step, K_{di}, in the association is the product of a **statistical correction** and that microscopic dissociation constant

$$K_{di} = \frac{i}{n-i+1} K_{dL} \quad (6–20)$$

Before the ith ligand associates with the protein, there are $n-i+1$ identical unoccupied sites at which association can occur, a fact that decreases its macroscopic dissociation constant, while the product of its association has i identical sites occupied by ligand from which dissociation can occur, a fact that increases its macroscopic dissociation constant. For example, in the case of a homotetramer in which every site binds the ligand with the same microscopic dissociation constant, K_{dL}, and every site is independent and unlinked to any other site, when the statistical correction is applied

$$K_{dL} = 4K_{d1} = {}^3/_2 K_{d2} = {}^2/_3 K_{d3} = {}^1/_4 K_{d4} \quad (6–21)$$

The macroscopic dissociation constant for the first step always has one-fourth the value of the microscopic dissociation constant for the sites because the reactant has four sites at which association can occur while the product has only one site from which dissociation can occur. The macroscopic dissociation constant for the second step always has two-thirds the value for the microscopic dissociation constant because the reactant has three sites for association but the product has only two sites for dissociation, and so forth.

When **statistically corrected values of the macroscopic dissociation constants** (Equation 6–20) are entered into the general Adair equation (Equation 6–12)

$$Y = \frac{[L]}{K_{dL} + [L]} \quad (6–22)$$

In this instance, all sites are binding the ligand independently, and no sigmoid behavior is observed, only the usual rectangularly hyperbolic behavior of

binding to unlinked sites. Notice that the number of sites in the oligomer is not involved in Equation 6–22. Only if the macroscopic dissociation constants in the Adair equation (Equation 6–12) differ from the statistically corrected values (Equation 6–20)—in other words, the sites are not independent—does the Adair equation, when plotted, produce deviations from ideal behavior, either positive or negative.

When the statistical corrections are applied to values for the individual macroscopic dissociation constants obtained from the fit of the Adair equation to dissociation of molecular oxygen from hemoglobin (Figure 6–7A), values for the four intrinsic dissociation constants are $K_{d0,1}$ = 22 matm, $K_{d0,2}$ = 8.8 matm, $K_{d0,3}$ = 1.1 matm, and $K_{d0,4}$ = 0.48 matm. On the basis of this analysis, the microscopic dissociation constants, as expected, decrease with occupancy, and the largest increase in intrinsic affinity occurs between association of the second and third oxygens.

Although both the Hill equation within the mid-range (Figures 6–5 and 6–6) and the Adair equation (Figure 6–7) can usually produce curves that fit observed cooperative behavior quite precisely, neither provides an explanation for that observed behavior. An explanation of cooperativity, however, has been provided by Monod, Wyman, and Changeux.[15] This explanation is based on the established ability of many proteins to exist in two conformations, on thermodynamic linkage relations that establish the ability of association of a ligand with such a protein to shift the equilibrium between the two conformations, and, most especially, on the almost universal observation that the quaternary conformations of homooligomeric proteins are rotationally symmetric.

Proteins that display cooperative behavior can be shown by crystallography to exist in at least two different quaternary conformations. It has already been noted that hemoglobin (Figure 6–1) and aspartate carbamoyltransferase (Figure 6–2) do exist in two quaternary conformations. In the simplest situation, one could assume that there are only two quaternary conformations of a protein. For irrelevant historical reasons,[15] these two quaternary conformations are called the T and R conformations. By definition, the **T conformation** is the one that predominates when a ligand or substrate, the behavior of which is being examined and which displays cooperativity in its association with the protein, is absent and often only when an allosteric inhibitor or cosubstrate is present. The **R conformation** is the one that predominates when a ligand or substrate, the behavior of which is being examined and which displays cooperativity in its association with the protein, is present at saturating concentrations and often only when an allosteric activator or cosubstrate is present. In the case of aspartate carbamoyltransferase, the T conformation predominates in the absence of substrates and heterotropic allosteric effectors, and the R conformation predominates in the presence of saturating concentrations of substrates and the absence of heterotropic allosteric effectors. To simplify the following explanation, it can be assumed for the moment that, as is the case with aspartate carbamoyltransferase, the T conformation predominates in the absence of all ligands, even though this assumption will later be shown neither to describe the usual case nor to be a necessary one for the explanation of cooperative behavior to be valid.

The cooperativity displayed by aspartate carbamoyltransferase is **observed only when the R and T conformations can be interconverted**. Alanine 241 in aspartate carbamoyltransferase is in a loop of polypeptide distant from the active site of the enzyme and also distant from the interfaces between catalytic α subunits and regulatory β subunits. It is, however, located in the space between the two catalytic α_3 trimers. Each Alanine 241 from a catalytic α subunit in one catalytic α_3 trimer is immediately adjacent to an Alanine 241 from a catalytic α subunit in the other catalytic α_3 trimer in the R conformation (opposed loops between catalytic α_3 trimers in Figure 6–2B) but not in the T conformation. When the Alanines 241 were replaced with cysteines and cystines were formed between pairs of these cysteines when the enzyme was in the R conformation, the resulting disulfides locked the enzyme in the R conformation (Figure 6–8), and this crosslink prevents the conversion between the T and R conformations. The enzyme locked in the R conformation shows a smaller Michaelis constant for L-aspartate than the concentration of L-aspartate at which the initial rate of the enzymatic reaction is half its limiting rate in the unmodified enzyme, and the initial rate of the enzymatic reaction as a function of the concentration of L-aspartate, unlike the reaction catalyzed by the unmutated enzyme, displays no cooperativity. When the cystines are reduced to cysteines, cooperativity reappears and the concentration of L-aspartate at which the initial rate is half the limiting rate returns to the value for the unmutated enzyme.[24]

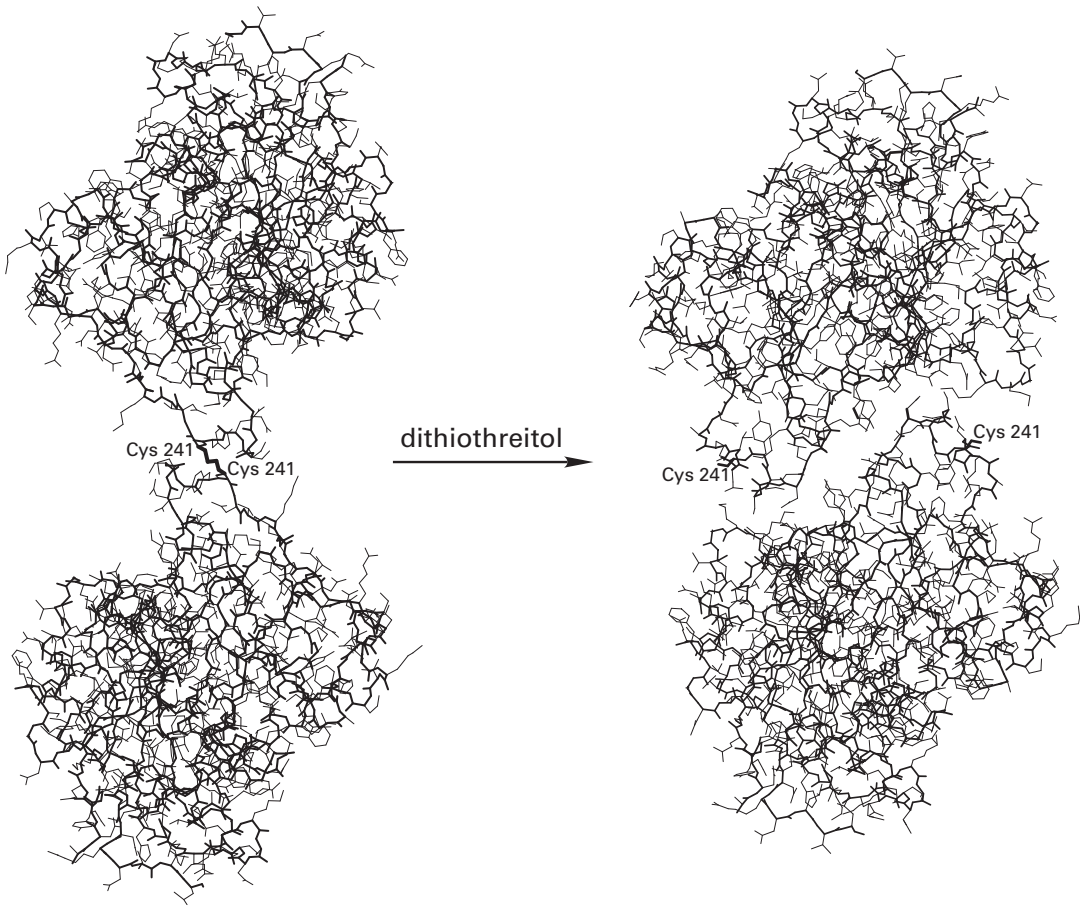

Figure 6–8: Drawings[485] of the locking of aspartate carbamoyltransferase in the R conformation. The codon in the chromosome of *Escherichia coli* for Alanine 241 in the α catalytic subunit of aspartate carbamoyltransferase was changed to a codon for cysteine, and the codon for the only cysteine in the α catalytic subunit was changed to one coding for alanine. The mutant aspartate carbamoyltransferase was overproduced in the resulting cells of *E. coli* and purified to homogeneity. It was discovered that in the purified enzyme, in the absence of reducing agents, there was a cystine connecting each α catalytic subunit in one α_3 trimer to a catalytic α subunit in the opposite α_3 trimer. Only in the R conformation is the single cysteine in a mutated catalytic α subunit, Cysteine 241, close enough to one of the other Cysteines 241 in the intact holoenzyme to form a cystine. The cysteines that are close together in the R conformation are each in a flexible loop of polypeptide. One of these flexible loops in an α catalytic subunit in an α_3 trimer is immediately adjacent to the flexible loop in an α catalytic subunit in the other α_3 trimer (Figure 6–2B). The loops are related to each other by a twofold rotational axis of symmetry, which should pass through the disulfide in the cysteine. It was assumed that the cystines in the purified enzyme formed while it was in the R conformation. It was also assumed that the cystine was between the respective cysteines in the flexible loops in these adjacent catalytic subunits. The crystallographic molecular model of the R conformation used for the drawing in Figure 6–2 was used here to represent two α catalytic subunits in an R conformation covalently connected to each other by a cystine. The crystallographic molecular models of two adjacent α catalytic subunits in the R conformation are presented to the left as skeletal drawings. The polypeptide backbone is drawn with a thicker line than the lines for the side chains of the amino acids. The loops of polypeptide containing Alanine 241 in this crystallographic molecular model of the R conformation were arbitrarily stretched out by rotating bonds in the polypeptide until the β carbons of the Alanines 241 were close enough together, and a cystine (even thicker lines) was then drawn in place of the two alanines. The drawing to the left is therefore not a drawing of an actual crystallographic molecular model. The drawing to the right, however, is of two α catalytic subunits from the crystallographic molecular model of the T conformation used in Figure 6–2 that are related by the same twofold rotational axis of symmetry. The cystine locks the enzyme in the R conformation, but when the cystine is reduced by dithiothreitol, in the absence of any ligands, the enzyme reverts to the T conformation because the two catalytic α_3 trimers can now rotate relative to each other. As the catalytic α_3 trimers rotate, they slide past each other, and this sliding displaces the cysteines.

The explanation of how **association of a ligand is able to shift the equilibrium between two quaternary conformations** of a protein relies upon casting the situation as a linkage relation. If the two conformations, R and T, are accessible to each other, the difference in free energy between them in the absence of ligands defines an equilibrium constant*

$$\mathrm{R} \xrightarrow{L_0} \mathrm{T} \tag{6–23}$$

$$L_0 = \frac{[\mathrm{T}]_{eq}}{[\mathrm{R}]_{eq}} \tag{6–24}$$

For historical reasons again, the equilibrium is written with the T conformation as product and the R conformation as reactant, and the equilibrium constant between the two conformations in the absence of any ligands is designated as L_0, the equilibrium constant between the R and T conformations.[15] This equilibrium constant is an allosteric constant.

An **allosteric constant** is the constant for the equilibrium between two conformations of an enzyme or protein that displays allosteric behavior. A **fundamental allosteric constant**, L_0, is the allosteric constant for an enzyme in the absence of any of its ligands. A **conditional allosteric constant** is the allosteric constant for an enzyme in the presence of saturating concentrations of one or more of its ligands. The following argument is for the general case of association of any ligand capable of shifting any conformational equilibrium of a protein. The special case in which association of a substrate causes an active site to close around that substrate has already been discussed (Equations 3–437 to 3–440). For the moment, it will be assumed that the protein is a monomer and that the sole subunit of the monomer has only one site with which the ligand can associate, even though association of a ligand to a single site on a monomer does not display cooperativity.

If the two conformations of the protein, the T and R conformations, exist as definable states in equilibrium with each other so that each is accessible from the other and both are populated in either the presence or absence of a particular ligand L for the protein, then the following **linkage relation** can be written

$$\begin{array}{ccc} \mathrm{R} + \mathrm{L} & \xleftarrow[K_{dL}]{\Delta G^\circ_L} & \mathrm{R{\cdot}L} \\ L_0 \downarrow \Delta G^\circ_E & & L_L \downarrow \Delta G^\circ_{E\cdot L} \\ \mathrm{T} + \mathrm{L} & \xleftarrow[K'_{dL}]{\Delta G^{\circ\prime}_L} & \mathrm{T{\cdot}L} \end{array} \tag{6–25}$$

where K_{dL} is the dissociation constant for ligand L from the R conformation, K'_{dL} is the dissociation constant for ligand L from the T conformation, and L_L is the equilibrium constant between the two conformations when both are occupied by ligand L. Both conformations have a site for the binding of ligand L, but it is unlikely, given the changes in structure that occur in the protein when one conformation becomes the other, that the dissociation constants for that ligand from that site will be the same in the two conformations. If the ligand L binds more tightly to the R conformation than it does to the T conformation ($K_{dL} < K'_{dL}$), it necessarily follows that **association of the ligand with the protein will shift the equilibrium between T and R** in favor of the R conformation ($L_A < L_0$) because, by linkage

$$\Delta G^\circ_L + \Delta G^\circ_E = \Delta G^\circ_{E\cdot L} + \Delta G^{\circ\prime}_L \tag{6–26}$$

and

$$K_{dL} L_0 = L_L K'_{dL} \tag{6–27}$$

Equation 6–26 is a corollary of the definition of a state function, and Equation 6–27 can be validated by inserting the definitions of the four equilibrium constants. If the **T conformation predominates in the absence of the ligand** ($L_0 < 1$) and the difference in dissociation constants for the ligand between the T and R conformations is large enough $[L_0 K_{dA} (K'_{dA})^{-1} > 1]$, then association of the ligand will shift the equilibrium constant so much that the **R conformation predominates in its presence**, just as association of *N*-(phosphoacetyl)-L-aspartate does to aspartate carbamoyltransferase (Figure 6–2). The difference in standard free energy of dissociation of the ligand from the two conformations provides the standard free energy necessary to shift the equilibrium between the two conformations.

As is the case with quaternary structures observed in crystallographic molecular models of almost all homooligomers in their fully liganded or fully unoccupied states, it is assumed that, when they are in solution, the T and R conformations of

*From here on a unidirectional arrow, rather than two opposing arrows, will be used to designate an equilibrium so that products and reactants are clearly defined.

a homooligomer displaying cooperativity in association of a ligand are rotationally symmetric. Although reasons can be given as to why this rotational symmetry should be so,[15,25] the fact remains that, crystallographically at least, it is so.

The initial rate for the reaction catalyzed by 6-phosphofructokinase (previously Equation 3–300)

$$\text{D-fructose 6-phosphate} + \text{MgATP}^{2-} \rightleftharpoons \text{H}^+ + \text{MgADP}^- + \text{D-fructose 1,6-bisphosphate} \quad (6\text{–}28)$$

from *Geobacillus stearothermophilus* is a sigmoid function of the concentration of the reactant fructose 6-phosphate when the allosteric sites on the enzyme are occupied by the heterotropic allosteric inhibitor phospho*enol*pyruvate,[19,26] as well as when they are not.[27] When the allosteric sites of the enzyme are fully occupied by phosphoglycolate, an analogue of phospho*enol*pyruvate, it crystallizes in the T conformation in the space group $P2_12_12_1$. The α_4 tetramer is necessarily the asymmetric unit in this space group that lacks crystallographic rotational axes of symmetry. Nevertheless, the four subunits in the asymmetric unit of the crystallographic molecular model are arrayed in molecular 222 (D_2) symmetry, and superpositions of α carbons, following rotations around the three molecular axes of symmetry, have root mean square deviations of 0.03 nm,[28] well within the positional errors of the coordinates of the crystallographic molecular model. When the enzyme is in the R conformation, fully occupied by the substrate fructose 6-phosphate in the absence of any heterotropic allosteric inhibitor, it crystallizes in the space group $I222$ with a single subunit of the homotetramer in the asymmetric unit, and all molecular axes of symmetry coincide with crystallographic axes of symmetry and are therefore precise.[29] Even though the R and T conformations crystallized under these different conditions differ significantly in both tertiary structure and the quaternary disposition of the subunits around the molecular axes of symmetry,[28] each tetramer is itself fully symmetric.

When the heterotropic allosteric inhibitor L-phenylalanine occupies its sites on the homotetramer, the initial rate for the reaction catalyzed by pyruvate kinase (previously Equation 3–222)

$$\text{phospho}\textit{enol}\text{pyruvate} + \text{H}^+ + \text{MgADP}^- \rightleftharpoons \text{MgATP}^{2-} + \text{pyruvate} \quad (6\text{–}29)$$

from *Oryctolagus cuniculus* is a sigmoid function of the concentration of the reactant phospho*enol*-pyruvate.[30] The unoccupied T conformation of the mammalian enzyme fails to crystallize, but when the T conformation of the human enzyme is stabilized by the heterotropic allosteric inhibitor L-phenylalanine, it crystallizes in the space group $P2_1$. The R conformation of the enzyme with its active sites occupied by $MgATP^{2-}$ and oxalate, an analogue of the *cis*-enediolate intermediate in the enzymatic reaction (Figure 4–52), also crystallizes in the space group $P2_1$. Although, in each case, the homotetramer is necessarily the asymmetric unit of the space group, the homotetramers in the respective crystallographic molecular models of the T and R conformations both have 222 symmetry (D_2).[31] The homologous homotetramer (47% identity; 0.6 gap percent) of pyruvate kinase from *Leishmania mexicana* does crystallize in its unoccupied conformation, which closely resembles the T conformation of the human enzyme and also has 222 symmetry,[32,33] from which it can be concluded that the unoccupied human enzyme is also a rotationally symmetric homotetramer.

The R conformation of the α_4 homotetramer of porcine fructose-bisphosphatase, with its active sites occupied by the substrates D-fructose 6-phosphate and phosphate, crystallizes in both the space groups $P2_12_12$ and $P3_221$ with the α_2 dimer as the asymmetric unit in each case and one of the three molecular rotational axes of symmetry of the tetramer coinciding with a crystallographic rotational axis of symmetry and consequently precise. Rotational superpositions of the α carbons of the α_2 dimer in the asymmetric unit around its molecular rotational axis of symmetry, however, have root mean square deviations of only 0.02 nm[34] and 0.03 nm.[35] Consequently, the R conformation is rotationally symmetric around all its molecular rotational axes of symmetry within the errors of the coordinates of the two crystallographic molecular models. The T conformation of the enzyme, with its heterotropic allosteric sites occupied by AMP^{2-} and its active sites occupied by fructose 6-phosphate and phosphate, crystallizes in the $P2_12_12$ space group.[36] Although its tertiary structure and arrangement of its subunits around the molecular axes of symmetry are significantly different from those of the R conformation,[37] it is also rotationally symmetric around all three of its molecular rotational axes of symmetry (root mean square deviation within the dimer again equals 0.02 nm).[38] Two other quaternary conformations of this enzyme have been identified, and they also are

rotationally symmetric within the error of the coordinates of their respective crystallographic molecular models.[39,40]

L-Lactate dehydrogenase from *Bifidobacterium longum* is activated by D-fructose 1,6-bisphosphate. The enzyme was crystallized from a solution containing the coenzymatic substrate NADH; oxamate, an analogue of the substrate pyruvate; and D-fructose 1,6-bisphosphate, an activator of the enzyme. Under these conditions, the major conformation present in solution should be the conformation of high enzymatic activity. The space group of the crystal was *F*222. When the map of electron density was examined, it was found that the unit cell contained two subunits of the enzyme and that they were in different conformations. Examination of the arrangement of the unit cells in relation to the three orthogonal arrays of twofold rotational axes of symmetry, however, demonstrated that the crystal was actually an array of two different types of tetramers in equal numbers. All the tetramers were occupied by NADH and D-fructose 1,6-bisphosphate, but one type was unoccupied by oxamate and in the other all four of its active sites were occupied by oxamate.

Within each of the two different quaternary conformations, all four subunits had the same conformation because in each type of tetramer, the three orthogonal, molecular twofold rotational axes of symmetry coincided with crystallographic twofold rotational axes of symmetry. From this fact, it could be concluded that the molecular twofold rotational axes of symmetry were exact; that every subunit in both quaternary conformations of the tetramer had the same local conformations; and that within each conformation of the homotetramer, the subunits were symmetrically arranged.[41] The quaternary conformation of the one type of tetramer in the crystallographic molecular model was identical to that of the tetramer in an earlier crystallographic molecular model of the enzyme crystallized from a solution lacking D-fructose 1,6-bisphosphate.[42] In this conformation, in both the earlier model and the more recent one, an α helix is sterically blocking the site at which oxamate, the analogue of the substrate pyruvate, binds, so it is assumed to be the conformation with low or no activity. In the other type of tetramer, an oxamate is bound in each of the four active sites as well as an NADH, and it is assumed that this tetramer is the active conformation. The fact that molecules of enzyme in the two different fully symmetric quaternary conformations cocrystallized permitted the two quaternary conformations in the crystal to be compared under identical conditions.

The preceding examples are crystallographic observations of the retention of complete rotational symmetry by the conformations of oligomeric proteins that display homotropic cooperativity even though the two conformations differ significantly in both tertiary and quaternary structure. In each instance, however, the conformations crystallized were either unoccupied or fully occupied with their respective ligands. **No crystallographic molecular models of proteins displaying homotropic cooperativity in which the oligomer can be shown to be only partially liganded** rather than fully liganded are available, so intermediate states of ligation have not been directly observed. Even in the case of L-lactate dehydrogenase from *B. longum*, in which both conformations of the enzyme were fully occupied by NADH at the active sites and D-fructose 1,6-bisphosphate at sites for this heterotropic allosteric effector, the active sites, both those occupied by oxamate and those not occupied by oxamate, are fully occupied or fully unoccupied, and each of the two quaternary conformations found in the same crystal are fully symmetric. No molecules of enzyme in intermediate partially occupied, asymmetric conformations are present in these crystals.

As is the case with hemoglobin (Figure 6–1) and aspartate carbamoyltransferase (Figure 6–2), the quaternary conformational changes accompanying allosteric conformational changes that are observed crystallographically can usually be described as the **reorientation of somewhat rigid bodies around rotational axes or around screw axes of symmetry**. The quaternary conformational change in porcine fructose-bisphosphatase is accomplished by a 17° rotation of one of the dimers in the homotetramer around one of the twofold rotational axes of symmetry in the rotationally symmetric homotetramer.[37] The quaternary conformational change in 6-phosphofructokinase from *G. stearothermophilus*[28] can be described as a 7° rotation of one of the dimers in the homotetramer relative to the other about one of the rotational axes of symmetry in the molecule (Figure 6–9).[43] The quaternary conformational change in L-lactate dehydrogenase from *G. stearothermophilus*, however, can be described as rotation of one dimer in the homotetramer relative to the other around three rotational axes, each parallel to a respective molecular rotational axis of symmetry but only one of which coincides with one of these molecular rotational axes of symmetry.[42] Glycogen phosphor-

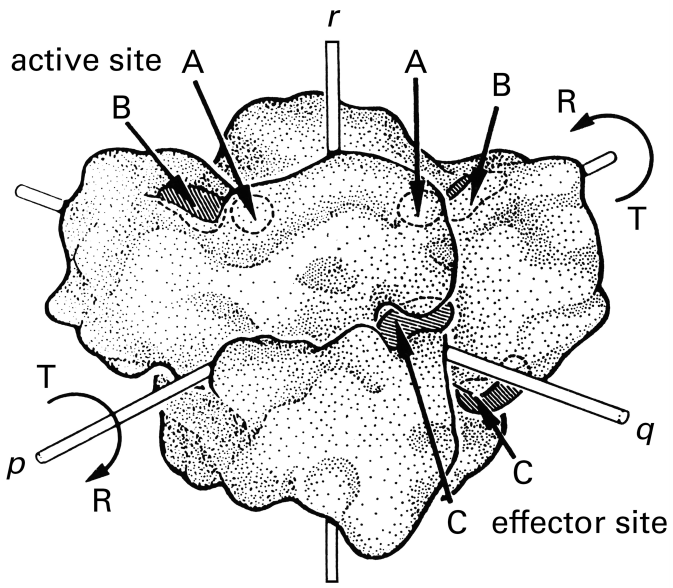

Figure 6–9: Schematic view of the crystallographic molecular model of the tetramer of 6-phosphofructokinase from *E. coli* in the unliganded T conformation.[43] 6-Phosphofructokinase, in the absence of ligands and substrates, was crystallized from 14% poly(ethylene glycol) and 1.0 M NaCl at pH 7.9. The crystals belonged to space group *C*2. Reflections were gathered to Bragg spacing of 0.24 nm. An available refined crystallographic molecular model of the liganded enzyme was used to phase the reflections by molecular replacement, and the initial molecular model of the unliganded enzyme was refined against the data set. A drawing was made of the van der Waals surface of the final molecular model. The four elongated subunits are arranged around the three orthogonal molecular axes of symmetry, *p*, *q*, and *r*. From other maps of electron density of the enzyme complexed with substrates, sites A that bind fructose 6-phosphate and sites B that bind $MgATP^{2-}$ and that together form the active sites could be identified. In the same way, sites C, with which the heterotropic allosteric activators ADP^{3-} and GDP^{3-} or the heterotropic allosteric inhibitor phospho*enol*pyruvate associate, were identified. Both heterotropic allosteric activators and heterotropic allosteric inhibitors in turn occupy the same allosteric site. In comparisons of this crystallographic molecular model of the T conformation with crystallographic molecular models of the enzyme in the R conformation, it could be seen that the conformational change between these two conformations involves a clockwise rotation of one of the dimers through which the *p* molecular axis of symmetry passes relative to the other dimer in the tetramer. Reprinted with permission from reference 43. Copyright 1989 Elsevier. https://doi.org/10.1016/0022-2836(89)90246-5

ylase *b* from *O. cuniculus* is a homodimer, and the allosteric, quaternary conformational change it undergoes cannot be described as a rotation about its only rotational axis of symmetry but can be described as a rotation of 10° of one monomer with respect to the other about a rotational axis, which cannot be a rotational axis of symmetry but is normal to the rotational axis of symmetry.[44] In the case of human pyruvate kinase, the allosteric, quaternary conformational change can be described as the rotation of two of the monomers in the homotetramer in a clockwise direction and two of the monomers in a counterclockwise direction, around identically located rotational axes in each monomer parallel to one of the molecular rotational axes of symmetry.[31] Regardless of the complexity of the rotations describing the quaternary conformational changes, both conformations of each protein are themselves rotationally symmetric.

It was pointed out by Monod, Wyman, and Changeux that if ligand-linked quaternary conformational changes in oligomeric proteins actually do occur with conservation of molecular symmetry, then the homotropic cooperativity often observed in association of ligands to homooligomeric proteins can be readily explained.[15] Consider the simplest case, that of an α_2 dimer that has one site for ligand L on each subunit and that displays a ligand-linked quaternary conformational change that occurs with conservation of symmetry. The dominant quaternary conformation in the population of unoccupied, fully symmetric dimers is designated as T·T, where T stands for the T conformation, and the dominant quaternary conformation in the population of fully occupied, fully symmetric dimers is designated as R·R, where R stands for the R conformation.[15] These are the two quaternary conformations that would usually be examined crystallographically. Because the quaternary conformational change occurs with conservation of symmetry, only two quaternary conformations of the protein itself are present, T·T and R·R. The accessible states are

$$\begin{array}{ccccc} \mathrm{R{\cdot}R} + 2\mathrm{L} & \xleftarrow[1/2\,K_{\mathrm{dL}}]{} & \mathrm{L{\cdot}R{\cdot}R} + \mathrm{L} & \xleftarrow[2\,K_{\mathrm{dL}}]{} & \mathrm{L{\cdot}R{\cdot}R{\cdot}L} \\ \Big\downarrow L_0 & & \Big\downarrow L_0 \dfrac{K_{\mathrm{dL}}}{K'_{\mathrm{dL}}} & & \Big\downarrow L_{\mathrm{L}} \\ \mathrm{T{\cdot}T} + 2\mathrm{L} & \xleftarrow[1/2\,K'_{\mathrm{dL}}]{} & \mathrm{L{\cdot}T{\cdot}T} + \mathrm{L} & \xleftarrow[2\,K'_{\mathrm{dL}}]{} & \mathrm{L{\cdot}T{\cdot}T{\cdot}L} \end{array} \qquad (6\text{–}30)$$

where K_{dL} and K'_{dL} are the intrinsic dissociation constants for ligand L from a site in the T and the R conformations, respectively. Sites in the two quaternary conformations associate with ligand L independently, so the usual statistical corrections (Equation 6–20) for multiple independent sites apply to the microscopic dissociation constants. The equilibrium constant for conversion of the R·R conformation to the T·T conformation when no site is occupied with ligand L

$$L_0 = \frac{[\mathrm{T{\cdot}T}]_{eq}}{[\mathrm{R{\cdot}R}]_{eq}} \qquad (6\text{–}31)$$

and the equilibrium constant for conversion of the L·R·R·T conformation to the L·T·T·T conformation, in both of which sites are fully occupied with ligand L

$$L_L = \frac{[\mathrm{L{\cdot}T{\cdot}T{\cdot}T}]_{eq}}{[\mathrm{L{\cdot}R{\cdot}R{\cdot}T}]_{eq}} \qquad (6\text{–}32)$$

If the mechanism of Equation 6–30 is to explain cooperativity, the observed fact that association with the ligand L is cooperative requires that a molecule of the unoccupied protein in the T·T conformation, on average, has a lower affinity for ligand L than the affinity of a molecule of the protein with one site occupied and the other unoccupied, when that affinity is averaged over the population of L·R·R and L·T·T. The equilibrium between **the quaternary conformations of the enzyme must shift significantly in the direction of the R conformation** after the first ligand has been bound but before the second is bound. For this change in quaternary conformation to be caused by association of the first ligand, K_{dL} must be less than K'_{dL} by a sufficient amount. If it is, then equilibrium will shift from favoring the T conformation in the absence of ligand L to favoring the R conformation when it is occupied by one ligand L, and the second ligand L, on average, will bind more tightly than the first. Consequently, as long as symmetry is conserved during the quaternary conformational change, this difference in the affinity of the two quaternary conformations for ligand L is all that is necessary for the shift in the quaternary conformational equilibrium to produce homotropic cooperativity.

The appeal of this hypothesis is that the same property that tips the conformational equilibrium—the fact that $K_{dL} < K'_{dL}$—also causes the second ligand to bind more tightly than the first once the equilibrium between the quaternary conformations has shifted. The requirement that symmetry be conserved during the quaternary conformational change is responsible for homotropic cooperativity because it necessitates that, during the quaternary conformational change, the dissociation constant of the unoccupied active site decreases in concert with the dissociation constant for the occupied active site.

The simple model of a homodimer can be **expanded to a homooligomer of any number of subunits**. Suppose that a homooligomeric protein has only two symmetric quaternary conformations, T and R, and that each conformation has as many sites for association of a ligand as there are subunits. Suppose also that, in each quaternary conformation, the respective binding sites are formed by the same respective constellations of side chains but in orientations altered by the quaternary conformational change. It is unlikely that the dissociation constants for the ligand from the binding sites will be the same in these two quaternary conformations. Suppose also, for the moment, that the equilibrium constant, L_0, between the R and T conformations is greater than 1 so that the concentration of the latter is greater than the concentration of the former in the absence of the ligand and that the dissociation constant for the ligand from a binding site in the R conformation is smaller than it is for the ligand from a binding site in the T conformation. Because the dissociation constant for the ligand from the R conformation is smaller that that from the T conformation, as the concentration of ligand is increased, association of the ligand with each binding site in turn will shift the equilibrium between the T and R conformations by the same amount of standard free energy in favor of the latter. As the ligand occupies one or more binding sites on each molecule of protein and the level of occupancy reaches **the point at which the quaternary conformation of the majority of the molecules of protein changes** from the T to the R conformation, the dissociation constant for binding of the final few ligands to the protein decreases, and cooperativity will be observed in the binding of the ligand.

A general equation, based on the proposal that the homooligomer undergoes a quaternary conformational change in which symmetry is conserved, has been derived.[15] If the system has the structure

$$\begin{array}{ccccccccccc}
R_n + nL & \xleftarrow{{}^{1}/_{n}K_{dL}} & R_n{\cdot}L + (n-1)L & \xleftarrow{{}^{2}/_{(n-1)}K_{dL}} & R_n{\cdot}L_2 + (n-2)L & \cdots\cdots & R_n{\cdot}L_{(n-1)} + L & \xleftarrow{nK_{dL}} & R_n{\cdot}L_n \\
\Big\downarrow L_0 & & \Big\downarrow L_0\dfrac{K_{dL}}{K'_{dL}} & & \Big\downarrow L_0\left(\dfrac{K_{dL}}{K'_{dL}}\right)^2 & & \Big\downarrow L_0\left(\dfrac{K_{dL}}{K'_{dL}}\right)^{n-1} & & \Big\downarrow L_0\left(\dfrac{K_{dL}}{K'_{dL}}\right)^{n} \\
T_n + nL & \xleftarrow{{}^{1}/_{n}K'_{dL}} & T_n{\cdot}L + (n-1)L & \xleftarrow{{}^{2}/_{(n-1)}K'_{dL}} & T_n{\cdot}L_2 + (n-2)L & \cdots\cdots & T_n{\cdot}L_{(n-1)} + L & \xleftarrow{nK'_{dL}} & T_n{\cdot}L_n
\end{array} \tag{6–33}$$

where n is the number of protomers in the homooligomer, and only quaternary conformational changes that conserve symmetry [$T_n{\cdot}L_i \rightleftharpoons R_n{\cdot}L_i$] are permitted, and if the fraction of sites occupied (see Equation 3–293)

$$Y \equiv \frac{[ST{\cdot}L]}{[ST]_t} = \frac{\left([R_n{\cdot}L] + 2[R_n{\cdot}L_2] + \ldots + n[R_n{\cdot}L_n]\right) + \left([T_n{\cdot}L] + 2[T_n{\cdot}L_2] + \ldots + n[T_n{\cdot}L_n]\right)}{n\left([R_n] + [R_n{\cdot}L] + [R_n{\cdot}L_2] + \ldots + [R_n{\cdot}L_n]\right) + n\left([T_n] + [T_n{\cdot}L] + [T_n{\cdot}L_2] + \ldots + [T_n{\cdot}L_n]\right)} \tag{6–34}$$

then

$$Y = \frac{[ST]_t\left\{L_0\dfrac{[L]}{K'_{dL}}\left(1+\dfrac{[L]}{K'_{dL}}\right)^{n-1} + \dfrac{[L]}{K_{dL}}\left(1+\dfrac{[L]}{K_{dL}}\right)^{n-1}\right\}}{L_0\left(1+\dfrac{[L]}{K'_{dL}}\right)^{n} + \left(1+\dfrac{[L]}{K_{dL}}\right)^{n}} =$$

$$\frac{[ST]_t\left\{L_0[L]K_{dL}{}^n\left(K'_{dL}+[L]\right)^{n-1} + [L]K'_{dL}{}^n\left(K_{dL}+[L]\right)^{n-1}\right\}}{L_0K_{dL}{}^n\left(K'_{dL}+[L]\right)^n + K'_{dL}{}^n\left(K_{dL}+[L]\right)^n} \tag{6–35}$$

This equation is the **Monod–Wyman–Changeux equation** (MWC equation), in keeping with the biochemical habit of naming equations, methods, and ways to present data, even if trivial, after their originators.

If the **initial rate of an enzymatic reaction** as a function of reactant A is being followed and if it can be assumed with reason that the reactant associates with and dissociates from the active site much more rapidly than it is turned over—in other words, its dissociation constant at equilibrium is the same as its Michaelis constant for each quaternary conformation of the enzyme—then

$$\frac{v_0}{[E]_t} = \frac{k_{0,T}L_0\dfrac{[A]}{K'_{dA}}\left(1+\dfrac{[A]}{K'_{dA}}\right)^{n-1} + k_{0,R}\dfrac{[A]}{K_{dA}}\left(1+\dfrac{[A]}{K_{dA}}\right)^{n-1}}{L_0\left(1+\dfrac{[A]}{K'_{dA}}\right)^{n} + \left(1+\dfrac{[A]}{K_{dA}}\right)^{n}} =$$

$$\frac{k_{0,T}L_0[A]K_{dA}{}^n\left(K'_{dA}+[A]\right)^{n-1} + k_{0,R}[A]K'_{dA}{}^n\left(K_{dA}+[A]\right)^{n-1}}{L_0K_{dA}{}^n\left(K'_{dA}+[A]\right)^n + K'_{dA}{}^n\left(K_{dA}+[A]\right)^n} \tag{6–36}$$

where $k_{0,T}$ is the catalytic constant of the T conformation and $k_{0,R}$ is that of the R conformation.

Most, if not all, instances of homotropic cooperativity examined so far can be quantitatively described by the MWC equation, either for binding (Equation 6–35) or for steady-state kinetics (Equation 6–36).

This ability perhaps is not surprising because these equations have three or five adjustable parameters, respectively. For example, curves generated with the MWC equation fit the data for the binding of O_2 to hemoglobin (Figure 6–7B) as well as do curves generated with the Adair equation, even though the MWC equation has only three adjustable parameters while the Adair equation has four adjustable parameters or coefficients. This instance is perhaps the most stringent test of the ability of this equation to fit sigmoid behavior because the data span a wider range of concentrations of ligand than any other extant set of observations of sigmoid behavior. For the binding of O_2, values for the parameters are $L_0 = 1700 \pm 300$, $K'_{dO_2} = 22 \pm 1$ matm, and $K_{dO_2} = 0.49 \pm 0.02$ matm. As expected, the dissociation constant for O_2 from the R conformation is significantly smaller than that from the T conformation, and L_0 is greater than 1 so that, in the absence of O_2, the T conformation predominates.*

There are **informative limits to the MWC equation**.

First, suppose that $L_0 < 1$ so that the R conformation predominates in the absence of ligand but that it is still the case that the R conformation has a greater affinity for the ligand than the T conformation so that $K_{dL} < K'_{dL}$. In this instance, as the concentration of the ligand increases, the equilibrium shifts even more in favor of the R conformation. For all values K_{dL} and K'_{dL}

$$Y \cong \frac{[L]}{K_{dL} + [L]} \tag{6–37}$$

Association of the ligand behaves as if all sites are the same and independent of each other, which is a result of the fact that the T conformation is never present in solution in significant concentration, and association is only with the R conformation, in which all sites are the same.

Second, suppose that $L_0 > 1$ so that the T conformation predominates in the absence of ligand and that $K'_{dL} > K_{dL}$ so that the ligand shifts the equilibrium in favor of the R conformation but that $L_0 > K'_{dL}{}^2 (K_{dL}{}^2)^{-1} > 1$. In this instance, the ligand will be unable to shift the equilibrium sufficiently (Equation 6–33), and the homooligomer will remain in the T conformation at all concentrations of ligand and

$$Y \cong \frac{[L]}{K'_{dL} + [L]} \tag{6–38}$$

Association of the ligand behaves as if all sites are the same and independent of each other, which is a result of the fact that the R conformation is never present in solution in significant concentration, and association is only with the T conformation.

Third, suppose that $L_0 > 1$ so that the T conformation predominates in the absence of ligand but that $K_{dL} (K'_{dL})^{-1}$ is so small that $L_0 K_{dL} (K'_{dL})^{-1} < 1$. In this instance, because $L_0 (K'_{dL})^{-1} < K_{dL}{}^{-1}$, when $K_{dL} < [L] < K'_{dL}$

$$Y \cong \frac{[L]^n}{L_0 K_{dL}{}^n + [L]^n} \tag{6–39}$$

As long as the concentration of ligand is in the stipulated range, association will be defined by the Hill equation, and the Hill coefficient, n, will be equal to the number of symmetric sites on the homooligomer. Since the stipulated range is quite large because $K_{dL} (K'_{dL})^{-1}$ is so small, this behavior should be expected if the other criteria are met. In this situation, as one molecule of ligand associates with an empty site on an unoccupied molecule of the protein, the quaternary conformation of that molecule of protein shifts from the T to the R conformation and the remaining sites are immediately occupied. In other words, it is as if all the ligands were required to associate with each molecule of protein simultaneously, the requirement that produces the Hill equation. As noted earlier, however, the Hill coefficient is almost never equal to the number of sites. The exercise simply demonstrates that the MWC equation can produce the Hill equation. It can also produce the Adair equation.

The MWC equation rests on a specific assumption about the behavior of the protein under consideration: namely, that this behavior the result of the ability of the protein to undergo, within the range of measurements, a quaternary conformational change that proceeds with conservation of symmetry. Consequently, **the MWC equation is an explanation of**

*There is no correspondence between the structural characteristics of the quaternary conformational change and whether it has high affinity for a ligand or low affinity. For example, the quaternary conformation of hemoglobin with the higher affinity for oxygen, the conformation observed in the crystallographic molecular models of the fully liganded conformation, involves an expansion of the molecule from its dimensions in the conformation of lower affinity observed in crystallographic molecular models of the unliganded protein (Figure 6–1). The opposite is true of aspartate carbamoyltransferase (Figure 6–2).

the observations. The intention is to explain observations of sigmoid behavior in molecular terms. Because sigmoid behavior can almost always be fit with an Adair equation even at the extremes, it follows that the general MWC equation and the general Adair equation must be the same if the explanation is to be consistent with observations.* The general form of the Adair equation (Equation 6–13) can be trivially rearranged to give

$$Y = \frac{\left\{\sum_{i=1}^{n-1} \frac{i}{n}\left(\prod_{i+1}^{n} K_{di}\right)[\mathrm{L}]^i\right\} + [\mathrm{L}]^n}{\left\{\sum_{i=0}^{n-1}\left(\prod_{i+1}^{n} K_{di}\right)[\mathrm{L}]^i\right\} + [\mathrm{L}]^n} \tag{6–40}$$

and the four binomials of the general MWC equation, two in the numerator and two in the denominator, can be expanded by the binomial theorem and the terms with the concentration of ligand to the same power can be combined to obtain

$$Y = \frac{\left\{\sum_{i=1}^{n-1}\binom{n-1}{i-1}\frac{L_0 K_{\mathrm{dL}}{}^i + K'_{\mathrm{dL}}{}^i}{(K'_{\mathrm{dL}}K_{\mathrm{dL}})^i}[\mathrm{L}]^i\right\} + \frac{L_0 K_{\mathrm{dL}}{}^n + K'_{\mathrm{dL}}{}^n}{(K'_{\mathrm{dL}}K_{\mathrm{dL}})^n}[\mathrm{L}]^n}{\left\{\sum_{i=0}^{n-1}\binom{n}{i}\frac{L_0 K_{\mathrm{dL}}{}^i + K'_{\mathrm{dL}}{}^i}{(K'_{\mathrm{dL}}K_{\mathrm{dL}})^i}[\mathrm{L}]^i\right\} + \frac{L_0 K_{\mathrm{dL}}{}^n + K'_{\mathrm{dL}}{}^n}{(K'_{\mathrm{dL}}K_{\mathrm{dL}})^n}[\mathrm{L}]^n} \tag{6–41}$$

where the integers within the parentheses are the usual binomial coefficients. Equation 6–41 can be rearranged to give

$$Y = \frac{\frac{(K'_{\mathrm{dL}}K_{\mathrm{dL}})^n}{L_0 K_{\mathrm{dL}}{}^n + K'_{\mathrm{dL}}{}^n}\left\{\sum_{i=1}^{n-1}\binom{n-1}{i-1}\frac{L_0 K_{\mathrm{dL}}{}^i + K'_{\mathrm{dL}}{}^i}{(K'_{\mathrm{dL}}K_{\mathrm{dL}})^i}[\mathrm{L}]^i\right\} + [\mathrm{L}]^n}{\frac{(K'_{\mathrm{dL}}K_{\mathrm{dL}})^n}{L_0 K_{\mathrm{dL}}{}^n + K'_{\mathrm{dL}}{}^n}\left\{\sum_{i=0}^{n-1}\binom{n}{i}\frac{L_0 K_{\mathrm{dL}}{}^i + K'_{\mathrm{dL}}{}^i}{(K'_{\mathrm{dL}}K_{\mathrm{dL}})^i}[\mathrm{L}]^i\right\} + [\mathrm{L}]^n} \tag{6–42}$$

It can be seen that both the general Adair equation and the general MWC equation have the same form. If each coefficient in the general Adair equation is set equal to each coefficient in the binomial expansion of the general MWC equation for the same power of the concentration of ligand, both those in the numerator and those in the denominator, then it can be seen that for all the coefficients

$$(K'_{\mathrm{dL}}K_{\mathrm{dL}})^{n-i}\binom{n}{i}\frac{L_0 K_{\mathrm{dL}}{}^i + K'_{\mathrm{dL}}{}^i}{L_0 K_{\mathrm{dL}}{}^n + K'_{\mathrm{dL}}{}^n} = \prod_{i+1}^{n} K_{di} \tag{6–43}$$

because

$$\frac{n}{i}\binom{n-1}{i-1} = \binom{n}{i} \tag{6–44}$$

Consequently, for every unique coefficient in an Adair equation, there is a unique coefficient in the corresponding MWC equation; and any behavior that can be described by an Adair equation can also be described by an MWC equation. Unlike an Adair equation, however, an MWC equation provides an explanation for the observations.

There are two important mathematical distinctions between an Adair equation and the corresponding MWC equation. First, because the series of coefficients in an MWC equation is a power series of a number that is always greater than 1, the coefficients that precede each power of the concentration of ligand must increase monotonically while the coefficients in the corresponding Adair equation that precede each power of the concentration, although they are always required to be greater than 0, are not required to increase monotonically but can take on any value. Second, an Adair equation has the same number of coefficients, K_{di}, as n, in addition to the value for n chosen.* In other words the number of coefficients increases as n increases. In an MWC equation there are only three parameters, L_0, K_{dL}, and K'_{dL}, in addition to the value for n, which is independently determined by the number of asymmetric units in the protein and consequently not a parameter. It follows that, for both reasons, an MWC equation is more constrained than the corresponding Adair equation if n is greater than 3, and it does not follow from the equality of Equation 6–43 that any behavior that can be described by an Adair equation can also be described by an MWC

*The following development was provided to the author by Stuart Edelstein.

*Recall that the value chosen for n can be arbitrary if nothing is known about the quaternary structure of the protein or if it is not known whether or not each subunit in a protein of known quaternary structure has a functional site for binding the ligand. For example, L-lactate dehydrogenase from *B. longum* is a tetramer of identical subunits, but each tetramer has only two binding sites for D-fructose 1,6-bisphosphate.[41]

equation. Consequently, there could be situations in which the data could be satisfactorily fit by an Adair equation but not by an MWC equation. The fact that this failure seldom if ever occurs might be an argument in favor of the validity of the general MWC equation and its assumptions, were the data always of high precision and over a large range of concentration for the ligand, which they almost always are not.

The major quaternary conformational change of an oligomeric protein that involves reorientation of the protomers in a homooligomer and that permits it in this way to display homotropic cooperative behavior among its widely separated sites should be distinguished from the local conformational changes that occur in the vicinity of the sites themselves as they are occupied by the ligand. These local conformational changes are those described earlier when changes around the active site upon association of a substrate were discussed. They include shifts in the positions of side chains of amino acids (Figures 3–56 and 3–57), the closing of a lid over the active site (Figure 3–58), and even the closing of structural domains around reactants (Figure 3–55), if this closing of structural domains does not always, by itself, precipitate the quaternary conformational change.

When aspartate carbamoyltransferase from *E. coli* is dissociated into its regulatory β_2 dimers and catalytic α_3 trimers, the resulting catalytic trimers are enzymatically active but display no cooperativity. Modification of these isolated, enzymatically active catalytic α_3 trimers with tetranitromethane converts tyrosines in the protein to *o*-nitrotyrosines. The maximum of absorbance for *o*-nitrotyrosine[45] is 430 nm for the anionic phenolate and 355 nm for the neutral phenol, and the pK_a of nitrotyrosine is 7.5. Consequently, any shift in pK_a owing to a change in the environment surrounding a nitrotyrosine will cause a change in its absorbance when the pH of the solution is well-buffered and in the neutral range. When the active site in such a modified catalytic α_3 trimer is first occupied with carbamoyl phosphate, the binding of succinate, a competitive inhibitor of the enzymatic activity, causes a significant decrease in the absorbance at 430 nm, a change expected from an increase in values of pK_a for some of the nitrotyrosines. This decrease in absorbance can be used to monitor directly the proportion of active sites occupied by the succinate,[46] from which it follows that the decrease is monitoring a local change in conformation.

When these nitrated catalytic α subunits are reconstituted with dimers of regulatory β subunits to produce the intact $(\alpha\beta)_6$ hexamer of aspartate carbamoyltransferase, to which succinate binds cooperatively (Figure 6–3), the same change in absorbance upon occupation of the active site persists.[47] It still monitors directly the binding of the succinate rather than the quaternary conformational change involved in homotropic cooperativity. For this reason, it can be assumed that whatever local conformational change leads to the change of absorbance of the nitrotyrosines in these α subunits is not propagated globally.

Comparisons of the crystallographic molecular model of the isolated, unoccupied catalytic α_3 trimer and the catalytic α_3 trimer of intact $(\alpha_3)_2(\beta_2)_3$ aspartate carbamoyltransferase in the R conformation occupied by *N*-(phosphonacetyl)-L-aspartate (Figure 6–2) demonstrate that an induced fit, in which the amino-terminal structural domain of a catalytic protomer closes upon its carboxy-terminal structural domain by a 10° pivot upon a hinge, closes the active site following the assembly of reactants,[48,49] much as the active site of hexokinase closes around its reactants (Figure 3–55).* It may well be that this conformational change is the local conformational change detected by the nitrotyrosines. The local conformational change that closes off the active site could be a significant contributor to the change in free energy shifting the equilibrium between the T and R conformations even though its progress does not coincide with the progress of the quaternary conformational change.

In addition, in aspartate carbamoyltransferase, a short loop of polypeptide, comprising amino acids 80–87 of an adjacent catalytic α subunit in an α_3 trimer, lies over the closed, occupied active site in the crystallographic molecular model of the R conformation fully occupied with substrates or analogues of substrates, but this loop is shifted away to open the active site in the model of the unoccupied, T conformation (Figure 6–10).[6,50-52] Because the active site is shut off from the solution when this loop covers it, it must be the case that the loop closes over the active site after substrates or analogues of substrates have been bound. Therefore, each rearrangement in each catalytic α subunit must be a local conformational change that occurs

*It should be recalled that, just as is the case with quaternary conformational changes, induced fit relies upon the existence of an equilibrium between two local conformations—in the case of hexokinase, open and closed—that is shifted upon the association of a ligand—in the case of hexokinase, D-glucose.

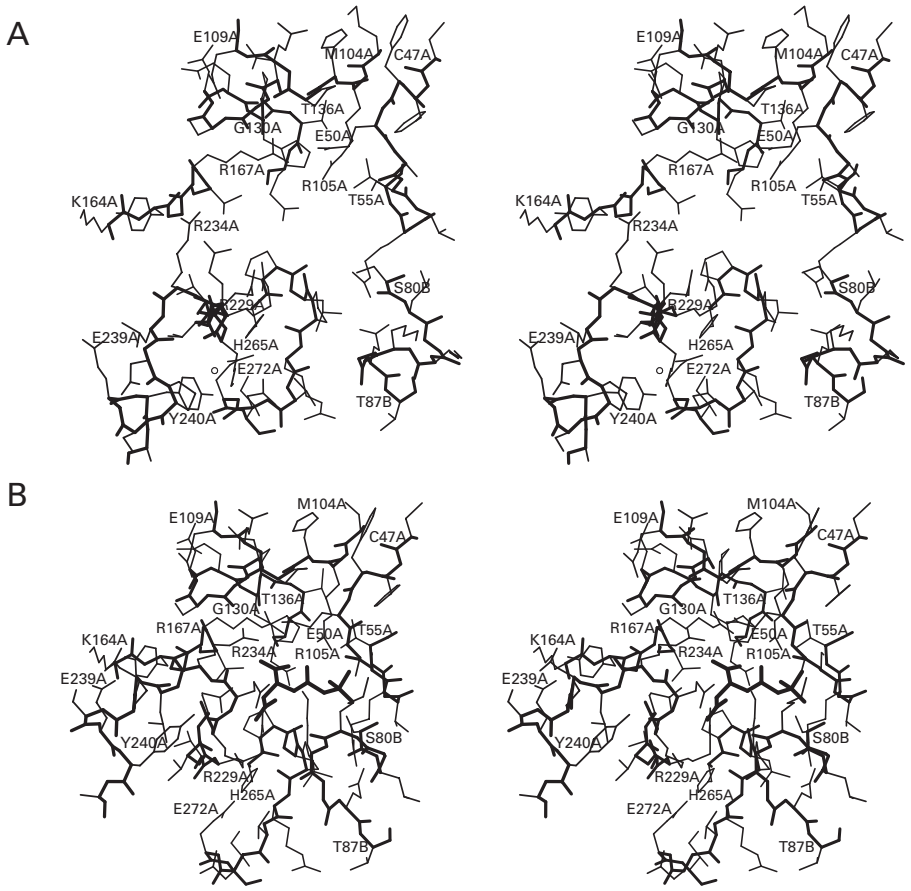

Figure 6–10: Stereodrawings[485] of crystallographic molecular models of the closing of the active site around the bisubstrate analogue *N*-(phosphonacetyl)-L-aspartate during its association with aspartate carbamoyltransferase from *E. coli*. (**A**) Crystals of the enzyme in the T conformation, the regulatory sites of which were occupied by CTP^{4-}, were formed by dialysis of a solution of the enzyme at 18 mg mL^{-1} against a solution of 1 mM cytidine 5′-triphosphate, 3 mM sodium azide, 1 mM 2-sulfanylethanol, 0.2 mM ethylenediamine tetraacetate, and 40 mM sodium citrate at pH 5.7. Crystals of space group *P*321 were obtained. Reflections from the crystals were collected to Bragg spacing of 0.22 nm.[52] (**B**) Crystals of the enzyme in the R conformation, the active sites of which were occupied by *N*-(phosphonacetyl)-L-aspartate (**6–1**), were produced by dialyzing the enzyme at high concentration into 1 mM *N*-(phosphonacetyl)-L-aspartate and 50 mM *N*-ethylmorpholinium maleate at pH 6.9 and 21 °C.[51] Isomorphous crystals of the space group *P*321 were obtained. Reflections were collected from these crystals to Bragg spacing of 0.21 nm.[50] The segments of polypeptide surrounding the active site in each drawing are from Threonine 228A to Alanine 241A, Lysine 164A to Threonine 168A, Cysteine 47A to Threonine 55A, Methionine 104A to Glutamate 109A, Aspartate 129A to Glutamine 137A, and Histidine 265A to Isoleucine 273A from one of the α catalytic polypeptides and a segment from Serine 80B to Threonine 87B from the other. In Panel B, *N*-(phosphonacetyl)-L-aspartate (thickest lines) is seen within the active site surrounded by the catalytic side chains. It has been trapped within the active site by the closing of a lid formed from a loop of polypeptide from Serine 80B to Threonine 87B. In Panel A, the active site in the unliganded crystallographic molecular model is open to the solvent because this lid has swung away, and the active site is much wider (compare the distances between the side chains of Glutamate 50 and Arginine 234) because the two hinged domains forming its top and bottom have swung open.

coincident with association of substrates with the active site and not during the quaternary conformational change because the quaternary conformational change occurs at concentrations of ligands well below saturation. If the closing of the lid were strongly coupled to the quaternary conformational change, then the last ligands, rather than binding with high affinity as a result of the quaternary conformational change, could not bind at all because the lids would be closed. There are also dramatic local changes in conformation of the regulatory β subunits in aspartate carbamoyltransferase upon association of the various nucleotides that act as heterotropic allosteric effectors, but these are local conformational changes that occur within the otherwise unaffected quaternary T and R conformations.[9,53]

Local changes in conformation can be distinguished from quaternary conformational changes by nuclear magnetic resonance spectroscopy.

Cells of *E. coli* were grown in a medium prepared in ^2H_2O with fully deuterated D-glucose as the main source of carbon. Also present in the medium was 2-oxo-[3,3-$^2H_2$,4-^{13}C]butyrate, which during the growth of the bacteria was converted by its metabolic pathways into [2,3,3′,3′,3′,4,4-$^2H_7$,5-$^{13}C^1H_3$]-L-isoleucine. This cellularly created [2,3,3′,3′,3′,4,4-$^2H_7$, 5-$^{13}C^1H_3$]-L-isoleucine was incorporated by the bacteria into the otherwise fully deuterated aspartate carbamoyltransferase. In two-dimensional transverse relaxation-optimized spectroscopy (TROSY) nuclear magnetic resonance spectra, cross peaks arise from through-bond dipolar coupling between carbon-13 and protium atoms in the 5-[$^{13}C^1H_3$]methyl groups of the labeled isoleucines in purified aspartate carbamoyltransferase. From changes in the amplitudes of many of these cross peaks in response to various ligands, it was concluded that these cross peaks come in pairs, each pair arising from one of the isoleucines in the enzyme. One cross peak in each pair arises from this one isoleucine in the T conformation of the enzyme, and the other cross peak from the same isoleucine arises from that isoleucine in the R conformation. It was also concluded that these two conformations were those previously described crystallographically (Figure 6–2).

In the two-dimensional TROSY nuclear magnetic resonance spectra of intact, fully deuterated $(\alpha_3)_2(\beta_2)_3$ aspartate carbamoyltransferase containing [2,3,3′,3′,3′,4,4-$^2H_7$, 5-$^{13}C^1H_3$]isoleucyl groups when it is in the unliganded T conformation, there are several cross peaks the positions of which shift monotonically as phosphonoacetamide, an analogue of the substrate carbamoyl phosphate, occupies the active site as its concentration is increased (Figure 6–11A).[54] Each shifting cross peak has a partner when the enzyme is in the R conformation. The two cross peaks in the respective pair, one from a particular isoleucine in the T conformation (Figure 6–11B) and one from the same isoleucine in the R conformation (Figure 6–11C), both shift as the concentration of phosphonoacetamide increases. These shifts are independent of the reciprocal decrease in amplitude of the former cross peak and the increase in amplitude of the latter that are registering the change from the quaternary T to the quaternary R conformation. The monotonic shifts in position of the peaks on the two-dimensional field are registering local conformational changes that occur upon occupation of each active site in turn, while the reciprocal changes in amplitudes of the two members of each pair of cross peaks are registering the quaternary conformational change from the T to the R conformation.

In two-dimensional TROSY nuclear magnetic resonance spectra of 6-phosphofructokinase from *G. stearothermophilus* labeled in the same way, there are cross peaks from methyl groups of isoleucines in the protein that shift from one position in the T conformation to an adjacent position in the R conformation as the concentration of the substrate D-fructose 6-phosphate, which displays cooperativity in steady-state kinetics,[27] is increased.[55] At intermediate concentrations of D-fructose 6-phosphate, the cross peaks display contributions from each quaternary conformation and monitor the transition from the T to the R conformation, but the positions of the cross peaks for each conformation shift continuously as do those of aspartate carbamoyltransferase (Figure 6–11) as the concentration of D-fructose 6-phosphate is increased. These continuous shifts are monitoring local conformational changes resulting from occupation of the active sites by the D-fructose 6-phosphate.

The closely related enzyme 6-phosphofructokinase (Equation 6–28) from *E. coli* (55% identity; 0.3 gap percent) has been crystallized in two active symmetric conformations, each with the same quaternary R conformation but differing in occupation of the site for the heterotropic allosteric activator, $MgADP^-$. Extensive local changes in conformation around the site for a heterotropic allosteric effector to which $MgADP^-$ binds (Figure 6–9) are observed when the two molecular models are compared, but these conformational changes are not widespread enough to produce any change in the quaternary conformation.[43] Presumably these are local changes

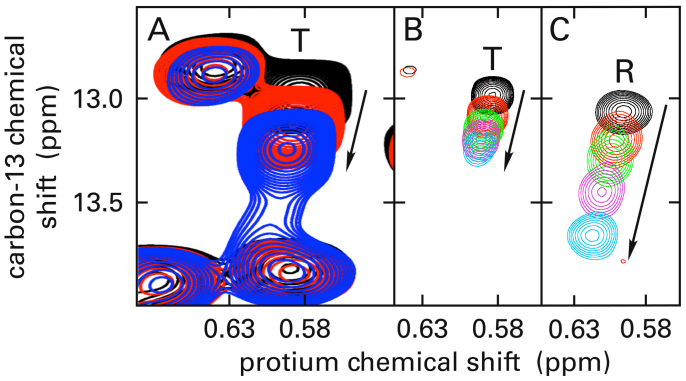

Figure 6–11: Changes in chemical shift caused by local conformational changes resulting from association of phosphonoacetamide with aspartate carbamoyltransferase from *E. coli*.[54] The enzyme was labeled as described in the text. The resulting, fully deuterated enzyme containing one carbon-13 and three protiums in the methyl group at position 5 in each isoleucine was dissolved at concentrations of asparate carbamoyltransferase from 0.3 to 0.9 mM in active sites in deuterium oxide with 50 mM KCl, 20 mM 2-sulfanylethanol, and 20 mM 2-[4-(2-hydroxyethyl)piperazin-1-yl]ethanesulfonic acid at pH 7.5. The coupling that gives rise to the observed cross peaks is that between carbon-13 and protiums in each methyl group. The cross peak for each methyl group in each isoleucine at a particular position in the two sequences of amino acids for the enzyme occupies a unique position on the field of the two-dimensional spectrum that is determined by the chemical shifts of its carbon-13 and protiums. Because each cross peak arises from a methyl group, all 27 cross peaks from the 27 isoleucines in the protein are confined to a range of carbon-13 chemical shift between 9 and 17 ppm and a range of protium chemical shift between 0.2 and 1.2 ppm. As the concentration of phosphonoacetamide was increased, it was observed that several of the cross peaks in the individual complete spectra shifted monotonically. (**A**) Complete spectra. Portions of three complete spectra obtained at different concentrations of phosphonoacetamide are drawn. The ranges of the chemical shifts are noted on the axes. One of the peaks in the three spectra (labeled T) shifted down and to the left as phosphonoacetamide was added. The spectrum of the unliganded enzyme is in black, the spectrum for a saturating concentration of phosphonoacetamide is in blue, and the spectrum for an intermediate concentration of phosphonoacetamide is in red. (**B**) Peak that registers association of phosphonoacetamide with the T conformation. The peak that shifts significantly in the complete spectrum of Panel A could be emphasized because it was the most intense peak in its vicinity. When the contour levels were given a high setting, the titrating peak dominated the field. This presentation made it easier to quantify the distance over which each shift occurs. Five separate peaks from five complete spectra, each from this same isoleucine, are shown: one for the unliganded enzyme (black), one for the enzyme saturated with phosphonoacetamide (cyan), and three for intermediate concentrations of phosphonoacetamide (red, green, and lavender). (**C**) Peak that registers association of phosphonoacetamide with the R conformation. The mutant in which Lysine 164 and Glutamate 239 in the α catalytic subunit have been changed to glutamate and lysine, respectively, is entirely in the R conformation. The peak corresponding to absorbance of the same methyl group on the same isoleucine as that producing the peak in Panel B could be identified in the complete spectra. The peak for that isoleucine was again emphasized. This peak also shifted when phosphonoacetamide was added to the solutions. Five separate peaks are shown: one for the unliganded enzyme (black), one for the enzyme saturated with phosphonoacetamide (cyan), and three for intermediate concentrations of phosphonoacetamide (red, green, and lavender). Adapted with permission from reference 54. Copyright 2007 National Academy of Sciences. https://doi.org/10.1073/pnas.0703347104

in conformation that again may or may not affect the free energy of the equilibrium between the quaternary conformations of the enzyme.

There are many disparate observations that can be explained by the proposal that enzymes displaying cooperativity exist in two rotationally symmetric conformations, the equilibrium between which is linked to association of substrates or heterotropic allosteric effectors. For example, when the initial rate of the reaction catalyzed by aspartate carbamoyltransferase was measured in the direction from *N*-carbamoyl-L-aspartate and phosphate[56] to carbamoyl phosphate and L-aspartate,* ***N*-(phosphonacetyl)-L-aspartate was a potent activator** (Figure 6–12).[57] One explanation for this observation is that the T conformation has low enzymatic activity and neither reactant, unlike the reactants for the reaction in the opposite direction, can shift the conformational equilibrium in favor of the more active R conformation. *N*-(Phosphonacetyl)-L-aspartate, however, can shift the equilibrium in favor of the R conformation. When *N*-(phosphonacetyl)-L-aspartate occupies one or more active sites on a molecule of the enzyme, the distribution of conformations shifts in favor of the R conformation, and the enzymatic activity at the other empty active sites increases dramatically.

Site-directed mutations of amino acids, the side chains of which appear in a crystallographic molecular model to be involved in interactions that change as the quaternary conformations change, can be consistent with the conclusion that shifts in the equilibrium between T and R conformations are responsible for observed allosteric effects. For example, Tyrosine 240 in a catalytic α subunit of aspartate carbamoyltransferase participates in a

*This is the direction of the approach to equilibrium catalyzed by the enzyme that is not usually chosen.

hydrogen bond with a fixed molecule of water that also participates in a hydrogen bond with Glutamate 272 in the crystallographic molecular model of the T conformation but not in the R conformation. The breaking of this cluster of hydrogen bonds, among many other changes, permits contacts to occur between loops in the space between the trimers of catalytic α subunits in the R conformation (Figures 6–2 and 6–8). When Tyrosine 240 is mutated to phenylalanine, so the cluster of hydrogen bonds can no longer form, the apparent affinity of the enzyme for L-aspartate increases.[58] This change is consistent with a destabilization of the T conformation relative to the R conformation, in which each of these two side chains have hydrogen bonds with water in the solvent. Glutamate 50 in a catalytic α subunit of aspartate carbamoyltransferase forms a hydrogen bond with Arginine 105 in the T conformation[6] but forms hydrogen bonds with both Arginines 167 and 234 in the R conformation, one at each of its oxygens (Figure 6–10). When Arginine 105 is mutated to glutamine, so that one of these latter arginines necessarily lacks an acceptor, the apparent affinity of the enzyme for L-aspartate decreases, as well as the cooperativity ($n_H = 1.0$); and these decreases are consistent with a destabilization of the R conformation relative to the T conformation.[59] When both Tyrosine 240 and Glutamate 50 are mutated, the enzyme displays a higher affinity for L-aspartate than when only Glutamate 50 is mutated,[58] consistent with a destabilization of both the R and T conformations. These results suggest that the changes in hydrogen bonds involving these amino acids observed crystallographically are indeed involved in the quaternary conformational change responsible for cooperativity.

When the R and T conformations of hemoglobin were immobilized in silica gel so that the quaternary conformational change was prevented, association of carbon monoxide with the hemes showed two kinetic phases. Various ligands shifted reciprocally the amplitudes of these phases in molecules of hemoglobin trapped in each quaternary conformation. These shifts in amplitude could be explained by assuming that the ligands shifted the equilibrium constants between two or more local conformations that can be achieved by the individual subunits regardless of the quaternary conformation in which they are located.[60]

Following the publication of the explanation of Monod, Wyman, and Changeux, it was pointed out that if a simple model involving only two quaternary conformations of the protein satisfactorily explains homotropic cooperativity, then a model involving more than two quaternary conformations must also be as satisfactory.[61] It has already been pointed out in the discussion of steady-state kinetics that if an explanation based on a particular number of intermediates is consistent with observations, then it necessarily follows that an explanation involving additional intermediates must also be consistent. Therefore, to establish the central hypothesis that, because of the conservation of symmetry, there are only two quaternary conformations, results other than measurements of the binding of a ligand or the behavior of the initial rate of the enzymatic reaction as a function of the concentrations of reactants must be obtained. Experiments addressing this point seek to

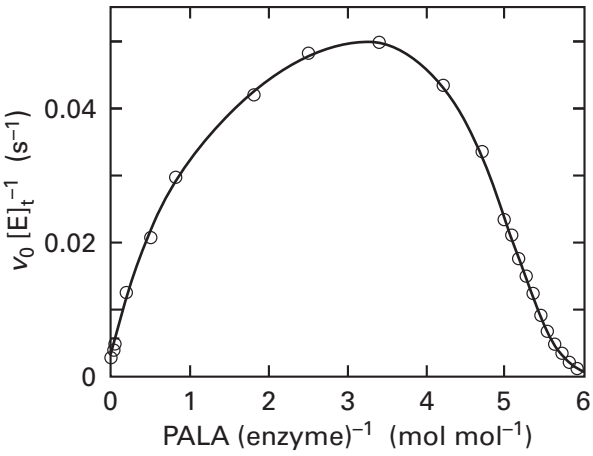

Figure 6–12: Activation of the arsenolysis of *N*-carbamoyl-L-aspartate catalyzed by aspartate carbamoyltransferase from *E. coli* by the binding of *N*-(phosphonacetyl)-L-aspartate stoichiometrically to active sites on the enzyme.[57] The enzymatic reaction was assayed in the direction from *N*-carbamoyl-L-aspartate to L-aspartate by using arsenate in place of phosphate so that the carbamoyl arsenate formed in the reaction would hydrolyze immediately upon formation and drive the reaction in its usually unfavorable direction. The enzyme (70 μM final concentration of active sites) was added to final concentrations of 3 mM arsenate and 5 mM *N*-carbamoyl-L-aspartate at pH 7.0 and 30 °C to initiate the reaction. Production of L-aspartate was monitored continuously by coupling it to oxidation of NADH with aspartate transaminase and malate dehydrogenase. As a result, the reaction mixture contained these two enzymes as well as 0.5 mM 2-oxoglutarate and 0.16 mM NADH. The rate of decrease in the absorbance at 340 nm was used to calculate directly the initial rate of the enzymatic reaction (micromolar second^{-1}). After division by the concentration of active sites, each initial rate (second^{-1}) is plotted as a function of the respective molar ratio of *N*-(phosphonacetyl)-L-aspartate (PALA) to aspartate carbamoyltransferase [moles of PALA (mole of enzyme)$^{-1}$]. At these concentrations of enzyme and *N*-(phosphonacetyl)-L-aspartate, all (>99%) of the *N*-(phosphonacetyl)-L-aspartate is bound by the enzyme ($K_d^{PALA} = 25$ nM) until the concentration of *N*-(phosphonacetyl)-L-aspartate becomes greater than 98% of the concentration of active sites.

demonstrate that only two quaternary conformations of the protein exist over the complete range of concentrations of a ligand that displays cooperativity. Then, because two quaternary conformations have been observed crystallographically, those conformations must be the only two.

In this search for more than two quaternary conformations, it becomes even more important to distinguish local conformational changes from quaternary conformational changes. For example, the closing of the two hinged domains of the α subunits of aspartate carbamoyltransferase upon its assembled reactants is a significant local conformational change. Whether the enzyme is in the T or R conformation, active sites with which reactants have associated will be closed and active sites with which reactants have not associated will be open. Consequently, partially occupied T and R conformations will not actually be rotationally symmetric. On the quaternary level, however, these two partially occupied conformations will be rotationally pseudosymmetric about all four rotational axes of pseudosymmetry. The partially occupied T conformations can still be distinguished from partially occupied R conformations by expansion of the space between the α_3 trimers, rotation of one α_3 trimer relative to the other, and the change in the tilt of the regulatory β_2 dimers (Figure 6–2). Effectively, the partially occupied T or R conformations are formally equivalent to the partially occupied, pseudosymmetric conformations of any rotationally symmetric homooligomer, such as L-lactate dehydrogenase or fumarate hydratase, that does not have different quaternary conformations but, when partially occupied, must be pseudosymmetric rather than symmetric, if only because some of the active sites are occupied.

The most extensive examination of whether or not more than two quaternary conformations exist during the cooperative association of a ligand to a protein has been performed with aspartate carbamoyltransferase from *E. coli*. It should be recalled that association of both carbamoyl phosphate[16] and succinate (Figure 6–4) with aspartate carbamoyltransferase and the behavior of the initial rate of the enzymatic reaction as a function of the concentration of L-aspartate (Figure 6–3) are all cooperative.

Crystals of aspartate carbamoyltransferase of the space group *R*32 form in solutions of the enzyme in the T conformation in the absence of ligands, and the crystallographic asymmetric unit is one folded catalytic polypeptide and one folded regulatory polypeptide. All molecular axes of symmetry coincide with crystallographic axes of symmetry, and the protein in the crystals is necessarily precisely symmetric.[13] Crystals of the protein in which all six catalytic sites are occupied by the bisubstrate analogue *N*-(phosphonacetyl)-L-aspartate (**6–1**) have the space group *P*321, and the crystallographic asymmetric unit is two folded catalytic polypeptides and two folded regulatory polypeptides.[5] The threefold molecular rotational axis of symmetry coincides with the threefold crystallographic rotational axis of symmetry and is precise. Although the twofold molecular axes of symmetry do not coincide with crystallographic axes of symmetry, only small, insignificant deviations from exact symmetry are observed.[6] When a heterotropic allosteric site on the T conformation is occupied with CTP^{4-}, the enzyme also crystallizes in the space group *P*321, with two folded catalytic polypeptides and two folded regulatory polypeptides in the asymmetric unit. Superposition of the folded polypeptides around the twofold noncrystallographic rotational axis of symmetry detects a number of violations of exact symmetry, but almost entirely they are alternative conformations of the side chains of amino acids,[62] rather than significant asymmetry of the polypeptide backbones or orientation of the subunits. There is a crystalline form of the R conformation occupied with *N*-(phosphonacetyl)-L-aspartate in the space group $P2_12_12_1$ in which the entire $(\alpha\beta)_6$ hexamer is the asymmetric unit. Although the folded catalytic α polypeptides superpose closely around the molecular threefold rotational axis of symmetry, the unoccupied, β regulatory polypeptides, which usually display much greater disorder than the folded catalytic polypeptides,[50] superpose poorly around the molecular twofold rotational axis of symmetry (0.15–0.31 nm root mean square deviation).[63] Nevertheless, the conclusion that can be drawn from all these observations taken together is that **both quaternary conformations, the T and R conformations, of aspartate carbamoyltransferase observed crystallographically are rotationally symmetric oligomers** even though they differ dramatically from each other in conformation (Figure 6–2).

Association of *N*-(phosphonacetyl)-L-aspartate with the active sites of aspartate carbamoyltransferase shifts the equilibrium between these two quaternary conformations in favor of the R conformation. In two-dimensional TROSY nuclear magnetic resonance spectra of purified aspartate carbamoyltransferase labeled in the manner described above, several well-resolved cross peaks that monitored conformational

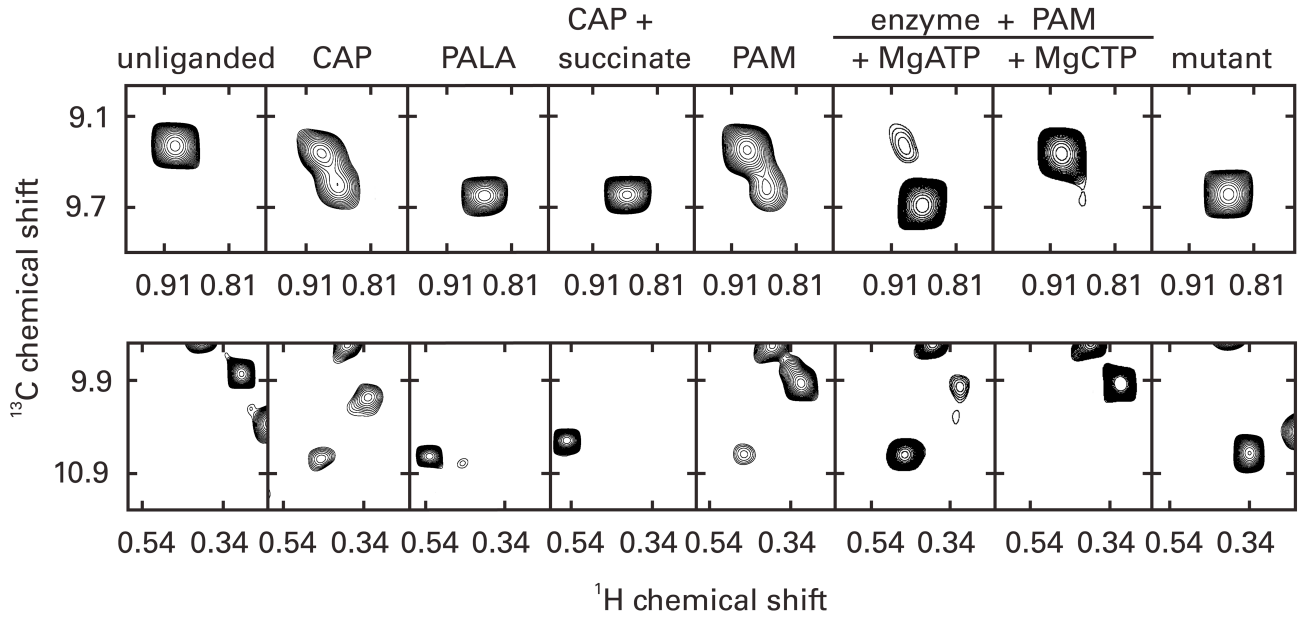

Figure 6–13: Two-dimensional methyl-TROSY (^{1}H–^{13}C) nuclear magnetic resonance spectra of aspartate carbamoyltransferase from *E. coli*.[54] The enzyme was labeled as described in the text and dissolved as described in the legend for Figure 6–11. Only two portions (top row and bottom row) of each complete spectrum are presented in the ranges noted on the respective axes. Further additions to solutions for the respective spectra (from left to right) were as follows: none (unliganded); carbamoyl phosphate (CAP) at a molar ratio of 30 relative to the concentration of active sites; *N*-(phosphonacetyl)-L-aspartate (PALA) at a molar ratio of 1.5; carbamoyl phosphate and succinate (CAP + succinate) at molar ratios of 30 and 75, respectively; phosphonoacetamide (PAM) at a molar ratio of 58; phosphonoacetamide and $MgATP^{2-}$ (enzyme + PAM + MgATP) at molar ratios of 58 and 46, respectively; and phosphonoacetamide and $MgCTP^{2-}$ (enzyme + PAM + MgCTP) at molar ratios of 58 and 32, respectively. Shown in the last column (mutant) are the same regions from a spectrum for a mutant of aspartate carbamoyltransferase in which Lysine 164 and Glutamate 239 in the α catalytic subunit have been changed to glutamate and lysine, respectively. Peaks arising from isoleucines in the R conformation are labeled, and those arising from the same isoleucines in the T conformation are also labeled. Adapted with permission from reference 54. Copyright 2007 National Academy of Sciences. https://doi.org/10.1073/pnas.0703347104

changes could be observed.[54] Many of the isoleucyl 5-methyl groups produced two cross peaks in the spectra, the amplitudes of which were inversely related to each other and changed as the conformation of the enzyme was changed by adding ligands (Figure 6–13). From changes in the amplitudes of each cross peak in response to various ligands, it was concluded that one cross peak from one of these isoleucines arises from the T conformation and the other cross peak from the same isoleucine arises from the R conformation. It was also concluded that these two conformations were those previously described crystallographically. In the presence of *N*-(phosphonacetyl)-L-aspartate, the bisubstrate analogue, only one of these two cross peaks from each isoleucine is observed; and in the absence of ligands, only the other cross peak is observed (Figure 6–13). These observations led to the conclusion that, in each of these two situations, the equilibrium between the R and T conformations was shifted completely to one or the other, as suggested by the crystallographic molecular models (Figure 6–2). In the presence of carbamoyl phosphate, however, about equal amounts of T and R conformations are in equilibrium with each other, but when succinate, an analogue of L-aspartate, is then added, all the molecules of enzyme assume the R conformation. In the presence of 2-phosphonoacetamide, an analogue of carbamoyl phosphate that is stable to hydrolysis, amounts of R and T conformations in a ratio of about 1:3 are present.

The cross peaks of a significant percentage of the isoleucyl 5-methyl groups in the enzyme could be resolved in the spectra. In many of these cases, the cross peaks from a particular methyl group came in pairs that were assumed to represent the T and R conformations. In most of these instances, the ratios of the amplitudes of the cross peaks in each pair were affected in the same way by the association of one or more of the ligands just mentioned. These observations are consistent with the conclusion that under all these circumstances there were **only**

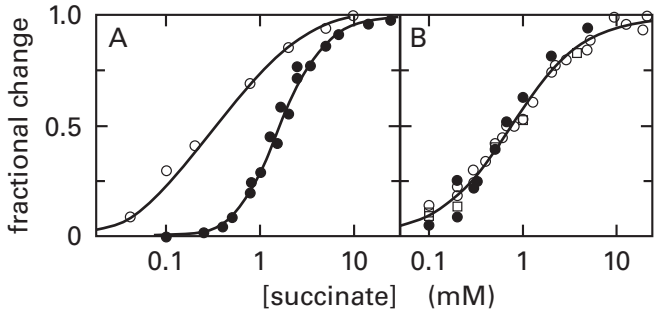

Figure 6–14: Relation between the change in quaternary conformation of *E. coli* aspartate carbamoyltransferase—as monitored by sedimentation velocity, changes in absorbance of nitrotyrosines, or rate of mercuration of cysteines—and the change in occupation of the active sites by succinate—as monitored spectrophotometrically. (**A**) Comparison of the binding of succinate to aspartate carbamoyltransferase and the resulting change in conformation.[47] Catalytic α_3 trimers, made from purified $(\alpha\beta)_6$ hexamers of aspartate carbamoyltransferase, were nitrated with tetranitromethane in the presence of carbamoyl phosphate and succinate so that 0.7 nitrotyrosine was formed for every catalytic α polypeptide and 85% of the enzymatic activity remained. These nitrated (ntr) catalytic α_3 trimers were reconstituted with unmodified regulatory β_2 dimers to form $(\alpha^{ntr}\beta)_6$ hexamers that were enzymatically active and displayed homotropic cooperativity. A change in the spectrum of nitrotyrosines at 430 nm was shown to be directly proportional to the concentration of succinate bound to active sites of the enzyme when carbamoyl phosphate was present at saturating concentration. The fraction of active sites occupied by succinate (●), where 0 is unoccupied and 1.0 is fully occupied with six succinates for each $(\alpha^{ntr}\beta)_6$ hexamer, is plotted as a function of the common logarithm of the succinate concentration (millimolar). The fractional change in sedimentation coefficient ($\Delta s_{max} = -2.9\%$) of these reconstituted $(\alpha^{ntr}\beta)_6$ hexamers (○) was also followed as a function of the molar concentrations of succinate at saturating carbamoyl phosphate under the same conditions. (**B**) Coincidence of three measures of the change in conformation.[67] Nitrated catalytic α_3 trimers, $\alpha_{3,ntr}$, were covalently inactivated by modifying their active sites with pyridoxal phosphate (PLP) and $NaBH_4$. These inactive, nitrated catalytic α_3 trimers, $\alpha_{3,ntr,PLP}$, were then modified with 3,4,5,6-tetrahydrophthalic anhydride to increase their negative charge number. The resulting triply modified catalytic α_3 trimers were reconstituted with native, unmodified catalytic α_3 trimers and regulatory β_2 dimers. The $(\alpha_{3,ntr,PLP}\alpha_{3,native}\beta_6)$ heterohexamers resulting from this reconstitution were isolated by anion-exchange chromatography followed by removal of the phthalyl groups. A nitrated catalytic α_3 trimer in this hybrid could not bind succinate but nevertheless registered the quaternary conformational change of the hexamer through a difference spectrum with a maximum at 450 nm. The quaternary conformation change was monitored by this change in absorbance at 450 nm (○), by the change in sedimentation coefficient (●), and by the change in the rate at which the enzyme was modified by 4-hydroxymercuribenzoate (□). All assays were performed at saturating carbamoyl phosphate (CAP) and at 20 °C. The fractional change in each of these three properties is plotted as a function of the concentration of succinate (molar). The smooth curve is that for Equation 6–48 with $n = 3$, $K_{d,succ} = 0.5$ mM, $K'_{d,succ} = 1.3$ mM, and $L_{CAP} = 3.4$.

two quaternary conformations of aspartate carbamoyltransferase present in the solution and that it is only the ratio between these two conformations that changed. These shifts in the equilibrium between the two conformatations caused the shifts in the ratios of the amplitudes.

The **change in the distribution of quaternary conformations** that occurs in a solution of aspartate carbamoyltransferase upon addition of a ligand can be **monitored by sedimentation velocity**.[64] The sedimentation coefficient of native aspartate carbamoyltransferase decreases by 3.5% as the unliganded enzyme becomes fully occupied either with carbamoyl phosphate and succinate[64,65] or with *N*-(phosphonacetyl)-L-aspartate.[66] This decrease in the sedimentation coefficient is consistent with a change in the frictional coefficient resulting from expansion of the molecule observed crystallographically (Figure 6–2), and it monitors directly the shift in the equilibrium between quaternary conformational states of the enzyme. The cooperative binding of succinate to aspartate carbamoyltransferase (Figure 6–4) can be monitored directly by the change in absorbance at 430 nm in intact aspartate carbamoyltransferase that has been reconstituted from nitrated catalytic α subunits. The absorbance of this modified enzyme changes in direct proportion to the fraction of active sites occupied by succinate.[47] When the change in sedimentation coefficient as a function of the concentration of succinate is compared to the occupation of the active sites as a function of the concentration of succinate, both at saturating carbamoyl phosphate (Figure 6–14A),[47,67] it can be seen that the majority of the shift in the distribution of conformations has occurred significantly before most of the active sites are occupied.[64] This sequence of events is as expected because the last succinates must associate with high affinity in order to explain homotropic cooperativity. Therefore, if the change from the T to R conformation is to explain the cooperativity, then the quaternary conformation must change before the last succinates are bound.

This observation, that completion of the **quaternary conformational change in the protein precedes full occupation of the active sites**, is a commonly observed property of proteins that display homotropic cooperativity. For example, the heterotropic allosteric activator AMP^{2-} binds to tetrameric glycogen phosphorylase *a* with homotropic cooperativity. Its occupation of the binding sites can be followed directly by equilibrium dialysis, and the change in the distribution of quaternary conformations it promotes can be followed separately by monitoring

changes in the electron paramagnetic resonance spectrum of a covalently bound, stable radical, 1-oxyl-2,2,6,6-tetramethylpiperidine. When the distribution of quaternary conformations is displayed as a function of the fraction of sites occupied (Figure 6–15),[68] the quaternary conformational change is also seen to precede occupation of the sites.

This observation, however, is the expected result regardless of the theory used to explain homotropic cooperativity. The last ligands to bind must bind to the quaternary conformations of high affinity stabilized by the binding of the first ligands to the conformations of low affinity. For this requirement to be fulfilled, the population of the quaternary conformations of high affinity must become dominant before all the ligands have been bound by the protein. The more important issue is whether there are only two quaternary conformations populated to any significant degree in these ligand-promoted transitions or more than two quaternary conformations.

Catalytic α_3 subunits of aspartate carbamoyltransferase, nitrated with tetranitromethane to give them a visible absorption spectrum, were then fully and permanently inactivated by modification of a lysine in their active sites with pyridoxal 5′-phosphate and sodium borohydride

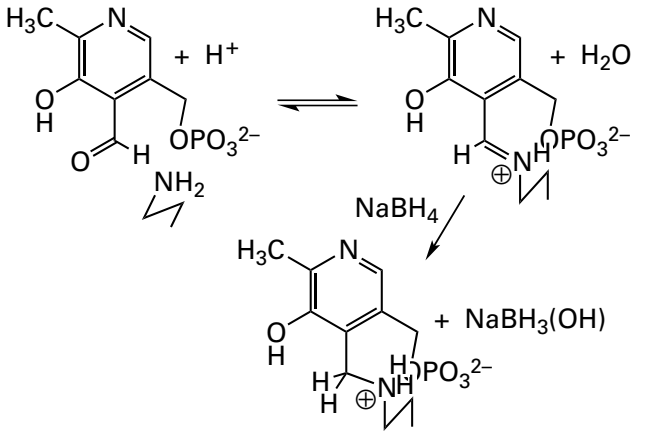

(6–45)

The inactive, modified α_3 subunits were then made more negatively charged by reversible modification of their remaining lysines, which are mostly on the surface of the enzyme, with 3,4,5,6-tetrahydrophthalic anhydride[67,69]

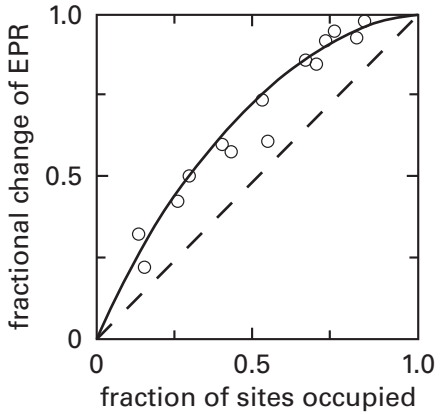

Figure 6–15: Plot of the extent of conformational change[68] of spin-labeled glycogen phosphorylase *a* from *O. cuniculus* as a function of the fraction of sites occupied by the heterotropic allosteric effector AMP^{2-}. Phosphorylase *a* was modified with *N*-(1-oxyl-2,2,6,6-tetramethyl-4-piperidinyl)iodoacetamide to introduce one stable nitroxyl radical into each subunit of the protein. Binding of AMP^{2-} was followed by equilibrium dialysis by measuring at equilibrium the molar concentrations of [U-^{14}C]adenosine 5′-monophosphate in the two chambers, one containing 4 μM phosphorylase *a* and one lacking phosphorylase *a*, for a series of concentrations of the ligand. The binding displayed positive deviation from ideal behavior and could be fit with Equation 6–35 with $L_0 = 3$, $K_{dAMP} = 2$ μM, $K'_{dAMP} = 10$ μM, and $n = 4$. As the occupation of the enzyme by AMP^{2-} was increased by increasing the free concentration of the ligand, the electron paramagnetic resonance (EPR) spectrum changed as the result of broadening of the outer two absorbances of the triplet. The binding of AMP^{2-} was measured and the electron paramagnetic resonance spectra were recorded for a series of samples with the same free concentrations of AMP^{2-}. For each free concentration of AMP^{2-}, the broadening of the spectra observed at that concentration, as a fraction of the broadening observed at saturation with AMP^{2-} [○; fractional change of EPR], is plotted as a function of the respective fraction of sites for AMP^{2-} that were occupied at the same free concentrations of AMP^{2-}. The solid curve is not a fit to the data. It is instead the curve for the function of Equation 6–49 using values for the fraction of the enzyme in the R conformation calculated with Equation 6–48 with $L_0 = 3$, $K_{dAMP} = 2$ μM, $K'_{dAMP} = 10$ μM, and $n = 4$ that were established from the binding of [U-^{14}C]adenosine 5′-monophosphate to the enzyme.

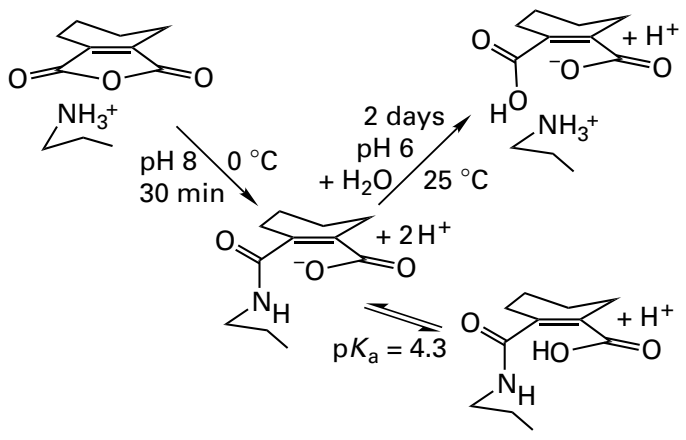

(6–46)

These yellow, inactive, negatively charged subunits were mixed with an equal amount of native unmodified catalytic α_3 subunits, and regulatory β_2 subunits were added to reconstitute $(\alpha\beta)_6$ hexamers. $(\alpha\beta)_6$ Hexamers with **one native catalytic α_3 subunit and one yellow, inactive catalytic α_3 subunit** could be purified by ion-exchange chromatography on a solid phase to which diethylaminoethyl groups are attached, and the tetrahydrophthalyl groups necessary for this separation could then be removed by hydrolysis at pH 6 under intramolecular general base catalysis. When succinate was added to these hybrid molecules saturated with carbamoyl phosphate, an increase in their absorbance at 450 nm was observed. Because neither succinate nor carbamoyl phosphate could bind to the active sites of the yellow, nitrated, inactivated catalytic α_3 subunit in a hexamer, the change in absorbance must have been monitoring a shift in the distribution of quaternary conformations of the nitrated catalytic α_3 subunit brought about by the binding of succinate to the other, unnitrated catalytic α_3 subunit across the twofold rotational axes of pseudosymmetry in the hybrid $(\alpha\beta)_6$ hexamer. The change in absorbance of this hybrid hexamer at 450 nm coincided precisely with the change in sedimentation coefficient. It was also found that the change in **rate constant for the reaction of cysteines in the protein with 4-hydroxymercuribenzoate** coincided with the other two changes (Figure 6–14B) when each of these **three independent monitors of the distribution of quaternary conformations** of the protein was followed as a function of the concentration of succinate.[64,67]

At sufficiently low concentrations of aspartate carbamoyltransferase, the bisubstrate analogue *N*-(phosphonacetyl)-L-aspartate (**6–1**) binds with homotropic cooperativity to the enzyme. The analogue, however, binds so tightly to the active site that it can be used as a stoichiometric ligand at high concentrations of enzyme. For example, when occupation of the active site is followed by ultraviolet difference spectroscopy as a function of moles of *N*-(phosphonacetyl)-L-aspartate added for every mole of hexameric enzyme, a clean titration that inflects at 6 mol mol^{-1} is observed (Figure 6–16A).[66,70,71] When the sedimentation coefficient was followed over the same range of stoichiometries, it was again observed that the change in the distribution of quaternary conformations monitored by sedimentation preceded occupation of the active sites, as expected for a quaternary conformational change producing homotropic cooperativity.

When catalytic α subunits of aspartate carbamoyltransferase were reconstituted with **nitrated regulatory β subunits**, an increase in absorbance at 445 nm and a corresponding decrease in absorbance at 380 nm, arising from a decrease in values of pK_a for some of the *o*-nitrotyrosyl groups in the regulatory β subunits, was observed when *N*-(phosphonacetyl)-L-aspartate was bound to the active sites in the catalytic α subunits of the reconstituted enzyme.[70] As the nitrotyrosines were on the regulatory β subunits, well removed from the active sites,[5] they must have been responding to a quaternary conformational change in the intact enzyme. The changes in absorbance of the *o*-nitrotyrosyl groups at either 380 or 445 nm coincided with the change in sedimentation coefficient when presented as a function of the stoichiometry between *N*-(phosphonacetyl)-L-aspartate and enzyme (Figure 6–16B).[70]

A Zn^{2+} coordinated by four cysteines from a regulatory β subunit is located at the interface between each folded regulatory and catalytic polypeptide in crystallographic molecular models of aspartate carbamoyltransferase.[13] The **zinc can be replaced by nickel**. Bound nickel displays absorption maxima[72] at 360, 440, 660, and 720 nm as well as maxima and minima in the difference circular dichroic spectrum[71] at 360, 405, and 460 nm. Both the absorption spectrum[72] and the difference circular dichroic spectrum[71] of a solution of aspartate carbamoyltransferase display significant changes as the active sites of the modified enzyme are occupied by *N*-(phosphonacetyl)-L-aspartate. The progress of these changes as a function of the stoichiometry of binding of the bisubstrate analogue coincides with the progress of the change in the distribution of quaternary conformations detected by sedimentation (Figure 6–16C).[71]

It follows from all the results just described (Figures 6–14 and 6–16) that the changes in the distribution of quaternary conformations detected by sedimentation, by nitrotyrosines in the inactive catalytic α subunits, by the rate at which the enzyme was modified by 4-hydroxymercuribenzoate, by nitrotyrosines in the regulatory β subunits, and at metallic ions distant from the active sites **all occur in concert** as the active sites of the enzyme become occupied. One explanation for these coincidences is that all these physical measurements are monitoring the same single quaternary conformational change between only two quaternary conformations. In other words, **no combination of these observations was able to detect more than one quaternary conformational change involving only two quaternary conformations**

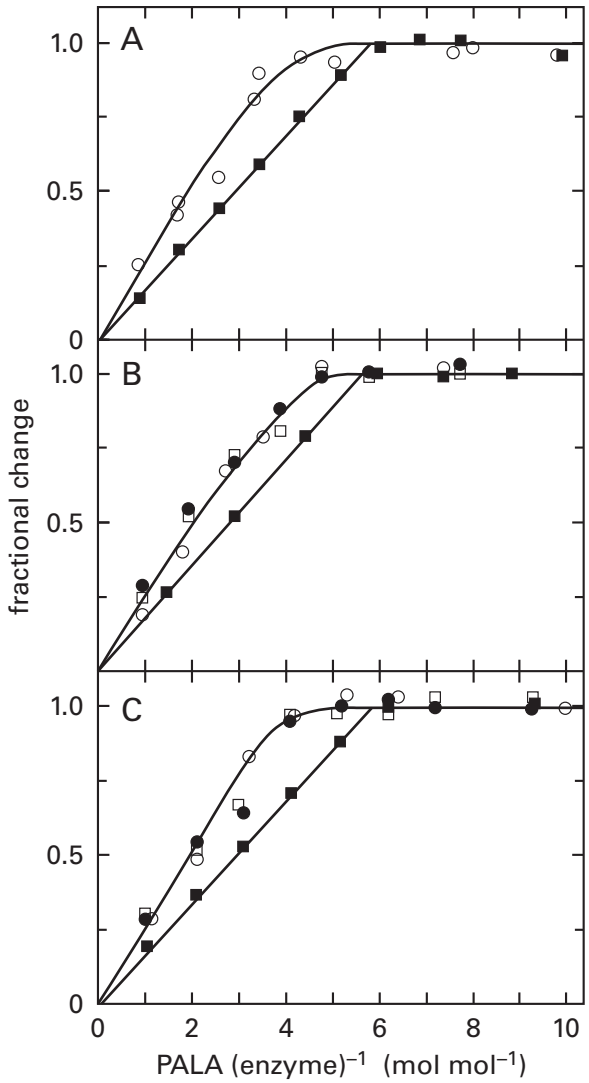

Figure 6–16: Coincidence of several physical measurements monitoring the quaternary conformational change in aspartate carbamoyltransferase from *E. coli* produced by *N*-(phosphonacetyl)-L-aspartate. In all panels, *N*-(phosphonacetyl)-L-aspartate was used to occupy the active sites on the enzyme to varying degrees. This bisubstrate analogue displays homotropic cooperative behavior. In all panels, the change in sedimentation coefficient (○) at various levels of occupation of the active site, measured at 3–4 mg of protein mL^{-1}, was used as the common monitor of the change in quaternary conformation of the enzyme. Association of *N*-(phosphonacetyl)-L-aspartate with aspartate carbamoyltransferase (2.4 mg mL^{-1} in Panel A, 2.1 mg mL^{-1} in Panel B, and 5 mg mL^{-1} in Panel C) was measured directly by following either the difference spectrum of the enzyme at 290 and 286 nm (Panels A and B, ■) or the circular dichroism at 360 nm (Panel C, ■), each of which registers only occupation of the active site with ligand. Each measurement is plotted as the fraction of the respective change (fractional change), relative to the total change between unliganded and fully saturated enzyme, as a function of the respective molar ratio of added *N*-(phosphonacetyl)-L-aspartate (PALA) to aspartate transcarbamoylase [moles of PALA (mole of enzyme)$^{-1}$]. (**A**) Solutions of native protein were monitored at pH 7.0 and 20 °C.[66] (**B**) The protein used for these experiments was reconstituted from native catalytic α_3 subunits and regulatory β_2 subunits modified with tetranitromethane [0.9 nitro group (polypeptide)$^{-1}$]. The change in absorbance (at 17 mg of protein mL^{-1}) at 380 nm (□) or 445 nm (●), both of which are due to absorbance of nitrotyrosines in the regulatory β_2 subunits, as a fraction of the total change between unliganded and fully saturated enzyme, is plotted. The changes were monitored at pH 7.0 and 25 °C.[70] (**C**) The protein used for these experiments was reconstituted from native catalytic and regulatory subunits. stripped of their Zn^{2+}, in the presence of $Ni(NO_3)_2$ (10-fold molar excess over sites) to replace the Zn^{2+} of the native enzyme with Ni^{2+}. The change in circular dichroism (at 5 mg of protein mL^{-1}) at 405 nm (□) or 460 nm (●), arising from absorption bands of complexed Ni^{2+}, as a fraction of the change between unoccupied enzyme and enzyme saturated with *N*-(phosphonacetyl)-L-aspartate, is plotted as a function of the respective molar ratio of *N*-(phosphonacetyl)-L-aspartate to enzyme. Measurements were made at pH 7.0.[71]

of the enzyme. If there were a third quaternary conformation present at significant concentration, the only way that all observations could coincide is if the changes in each observed quantity in the third quaternary conformation were in the same proportion relative to the respective changes in these observed quantities between the T and R conformations, which seems unlikely.

Formally, the coincidence of all these physical measurements is equivalent to observing an isosbestic point in a series of spectra, an observation that has always been accepted as evidence for only two states. If there is only one quaternary conformational change between unoccupied and fully occupied aspartate carbamoyltransferase, then the quaternary conformational change must occur with conservation of symmetry because both unoccupied and fully occupied aspartate carbamoyltransferase are symmetric oligomers.

When the concentration of aspartate carbamoyltransferase is in sufficient excess over the concentration of *N*-(phosphonacetyl)-L-aspartate, each molecule of enzyme to which the inhibitor is bound will have only one molecule of inhibitor bound. The increase in activity in this range of low concentrations of *N*-(phosphonacetyl)-L-aspartate (<0.05 mol mol^{-1}) will then be a function only of the number of active sites converted to the R conformation by one molecule of *N*-(phosphonacetyl)-L-aspartate.[57] Several conditions were chosen in which the equilibrium constant between the T and R conformations was shifted by other ligands sufficiently toward the R conformation that the binding of only one molecule of *N*-(phosphonacetyl)-L-aspartate would convert the T to the R conformation almost quantitatively. Under these conditions, the experimental value for the number of active sites converted to high enzymatic activity was between 4 and 5. Therefore, under these conditions,

association of one, or perhaps two, molecules of *N*-(phosphonacetyl)-L-aspartate at one, or perhaps two. active sites on the enzyme is able to convert the remaining five, or perhaps four, active sites to the R conformation. This result suggests that the conformational change is highly concerted and that only two conformations can exist in significant concentrations.

The curve for the scattering of X-rays at small angles by the R conformation of aspartate carbamoyltransferase, measured with saturating *N*-(phosphonacetyl)-L-aspartate, and the curve for the scattering of X-rays at small angles by the T conformation, measured in the absence of ligands, are significantly different. A molecule of aspartate carbamoyltransferase was constructed with **five mutated, inactive active sites and one normal active site,** and the quaternary conformation of the enzyme was monitored by the scattering of X-rays at small angles. Association of *N*-(phosphonacetyl)-L-aspartate with that one unmutated active site converted this enzyme from the T to the R conformation, and no other conformations could by detected by the measurement.[73]

Crystals of aspartate carbamoyltransferase of the space group *P*321, in the T conformation with its active sites occupied with phosphonoacetamide, were transferred to a solution of 8 mM malonate, which is an analogue of L-aspartate. The T conformation was converted, in the crystals, to the R conformation as the malonate occupied the active sites.[74] The crystals remained in the space group *P*321 with the usual asymmetric unit of two catalytic α subunits and two catalytic β subunits arrayed around the crystallographic threefold rotational axis of symmetry.

The same values for the equilibrium constants between R and T conformations can fit both independently measured changes in the distribution of quaternary conformations of an enzyme and observed cooperativities. From the mechanism of Equation 6–33, the fraction of the enzyme in the R conformation[15]

$$\bar{R} = \frac{[R_n] + [R_n{\cdot}L] + [R_n{\cdot}L_2] + \ldots + [R_n{\cdot}L_n]}{\left([R_n] + [R_n{\cdot}L] + [R_n{\cdot}L_2] + \ldots + [R_n{\cdot}L_n]\right) + \left([T_n] + [T_n{\cdot}L] + [T_n{\cdot}L_2] + \ldots + [T_n{\cdot}L_n]\right)} \quad (6\text{–}47)$$

and

$$\bar{R} = \frac{\left(1 + \frac{[L]}{K_{dL}}\right)^n}{L_0\left(1 + \frac{[L]}{K'_{dL}}\right)^n + \left(1 + \frac{[L]}{K_{dL}}\right)^n} \quad (6\text{–}48)$$

The fractional change (f_ξ) in any property (ξ), such as absorbance, fluorescence, rate of reaction of sulfanyl groups, scattering of X-rays, or sedimentation coefficient, that changes in direct proportion to the fraction of the enzyme in the R conformation is

$$f_\xi = \frac{\bar{R} - \bar{R}_0}{\bar{R}_\infty - \bar{R}_0} \quad (6\text{–}49)$$

where

$$\bar{R}_0 = \lim_{[L] \to 0} \bar{R} = \frac{1}{L_0 + 1} \quad (6\text{–}50)$$

and

$$\bar{R}_\infty = \lim_{[L] \to \infty} \bar{R} = \frac{{K'_{dL}}^n}{L_0 {K_{dL}}^n + {K'_{dL}}^n} \quad (6\text{–}51)$$

The observed behavior of the distribution of conformations of spin-labeled glycogen phosphorylase *a* from *O. cuniculus* as a function of the occupation of the heterotropic allosteric sites in the enzyme by AMP^{2-} could also be described by Equations 6–48 and 6–49 (smooth curve in Figure 6–15),[68] with a value for L_0 of 3. When the MWC equation (Equation 6–35) was constrained by setting the value for L_0 at 3, this constrained equation could fit the data for cooperative binding of AMP^{2-} to the enzyme.

As the concentration of *N*-(phosphonacetyl)-L-aspartate is increased, the fractional changes in sedimentation coefficient of aspartate carbamoyltransferase coincide with those in the rate at which the enzyme is modified at its sulfanyl groups by 4-hydroxymercuribenzoate. It has already been noted that these fractional changes coincide with those in the absorbance of nitrotyrosines in the inactive catalytic α subunits or in the regulatory β subunits and those in the distribution of quaternary conformations detected at metallic ions distant from the active sites (Figures 6–14 and 6–16). The fractional changes in sedimentation coefficient and those in the rate at which the enzyme is modified by 4-hydroxymercuribenzoate can be fit with Equations 6–48 and 6–49.[75] All these observations taken together are consistent with the conclusion that each fractional change is equal to f_ξ, the fraction of the enzyme that has changed from the T conformation into the R conformation, The value for L_0 from this fit is 250, and this value can be inserted into the MWC equation for two reactants that each have a higher affinity for the R conformation than the T conformation. The resulting equation, constrained by fixing L_0, is able to fit both the cooperativity for the initial rate of the enzymatic reaction as a function of the concentration of L-aspartate at saturating concentrations of carbamoyl phosphate and the cooperativity for the initial rate of the enzymatic reaction as a function of the concentration of carbamoyl phosphate at saturating concentrations of L-aspartate. The equation also fits stimulation of the enzymatic activity by succinate (see Problem 6–5 for stimulation by maleate, an analogue of succinate), an effect that is a result of the cooperativity displayed by the enzyme.

As the active sites of fully deuterated aspartate carbamoyltransferase containing [2,3,3′,3′,3′,4,4-$^2H_7$, 5-$^{13}C^1H_3$]isoleucyl groups are filled with phosphonoacetamide, an analogue of carbamoyl phosphate, each pair of cross peaks in the two-dimensional **methyl-TROSY nuclear magnetic resonance spectra** either records only the transition from the T to the R conformation (Figure 6–13) or records both the transition from the T to the R conformation (a reciprocal change in amplitude) and the local conformational changes that accompany the occupation of the active sites (a change in chemical shift).[54] The changes in chemical shift (δ) of nine pairs of cross peaks in the nuclear magnetic resonance spectra that record the local conformational changes accompanying the occupation of the active site by phosphonoacetamide in the R and T conformations, respectively (Figure 6–11B,C), were measured. From the magnitudes of these changes in chemical shift, dissociation constants for phosphonoacetamide from the active sites of the R conformation (K_{dPAM} = 1.8 + 0.1 mM) and the T conformation (K'_{dPAM} = 3.8 + 0.3 mM) could be calculated (see Equations 3–297 and 3–303)

$$Y_{lig} = \frac{\delta_{obs} - \delta_{uo}}{\delta_{sat} - \delta_{uo}} = \frac{\Delta\delta}{\Delta\delta_t} = \frac{[ST]_{eq}}{K_{dL} + [ST]_{eq}} \tag{6–52}$$

These measurements are direct determinations of the dissociation constants that are independent of each other and do not rely on the MWC equation in any way. None of the titration curves for occupation of the active sites by phosphonoacetamide in the R conformation by itself or the T conformation by itself displays cooperativity, which is one of the assumptions in the derivation of the MWC equation. The value for L_{PAM}, the equilibrium constant for the conformational equilibrium when the active site of aspartate carbamoyltransferase occupied by phosphonoacetamide (PAM), estimated from the two-dimensional TROSY nuclear magnetic resonance spectra (Figure 6–13) is 3.4 ± 1.2. From K_{dPAM}, K'_{dPAM}, and L_{PAM} (see Equation 6–33), the equilibrium constant

$$L_0 = L_{PAM}\left(\frac{K'_{d,PAM}}{K_{d,PAM}}\right)^6 \tag{6–53}$$

can be estimated to be 300 ± 190, which is consistent with estimates of L_0 by sedimentation velocity (250).[75] The value for L_{PAM} (3.4 ± 1.2) also agrees, within the errors of measurement, with the value for L_{CAP} (6.8 ± 2.4)[76] derived from a titration of the enzyme saturated with carbamoyl phosphate (CAP) with succinate (Figure 6–4).

The conformations of aspartate carbamoyltransferase were followed by scattering of X-rays at small angles as the active enzyme consumed several different saturating concentrations of L-aspartate and carbamoyl phosphate until equilibrium was reached. Each individual time-resolved scattering curve could be fit by a linear combination of only the scattering curve of the R conformation and the scattering curve of the T conformation, which shift in their relative concentrations as the reaction progresses and the reactants decrease in concentration. There was **no indication of any other conformations**

throughout the course of the reaction.[77] This result is an actual observation of isosbestic behavior. A value for L_0 of 70 was determined by fitting measurements of the scattering of X-rays at small angles as a function of the concentration of *N*-(phosphonacetyl)-L-aspartate to Equations 6–48 and 6–49.[78]

All the foregoing observations demonstrate that, at least in the case of aspartate carbamoyltransferase from *E. coli*, the **cooperativity observed in its association with substrates and analogues of its substrates arises from the existence of two and only two quaternary conformations** that are in equilibrium with each other. They also demonstrate that the equilibrium between these conformations is shifted by thermodynamic linkage because the dissociation constants for both carbamoyl phosphate and L-aspartate from the R conformation are smaller than those from the T conformation. Aside from hemoglobin—where observations are complicated by the fact that it is an asymmetric $(\alpha\beta)_2$ tetramer—in no other protein that displays cooperativity have the correlations between quaternary conformations and cooperativity in its associations with ligands been examined so extensively as in aspartate carbamoyltransferase. It is still possible that there will be one, several, or many proteins that assume several asymmetric quaternary conformations and that the equilibrium among those several conformations will explain the cooperative behavior. At the moment, however, no other protein has been examined extensively enough to draw this conclusion.

Cooperativity observed in measurements of the initial rate of a particular enzymatic reaction also can be explained by the existence of two rotationally symmetric quaternary conformations of the enzyme that differ in their affinity for substrate. The most unambiguous cases in which the explanation of cooperativity provided by the MWC equation can be applied are those in which cooperativity in the binding of ligands, such as molecular oxygen to hemoglobin (Figures 6–5 and 6–7) or succinate to aspartate carbamoyltransferase (Figures 6–4 and 6–14), rather than cooperativity in steady-state kinetics, is observed. This unambiguity results from the fact that differences in the dissociation constants for the binding of ligands to the T and R conformations produce the shift in the equilibrium constant between them. Consequently, cooperativity in these cases is not complicated by the effect of conformational changes on both rate constants and equilibrium constants. There are, however, far fewer measurements of cooperative association of a ligand than there are of cooperativity in the effects of the concentration of a reactant on the initial rates of enzymatic reactions, so some attention must be paid to these measurements of steady-state kinetics.

Suppose that a homooligomeric enzyme has two quaternary conformations and that each conformation has as many active sites as there are subunits. In each conformation, the respective active sites are formed by the same respective constellations of side chains, albeit in orientations altered by the conformational change. It is unlikely that the dissociation constants, the catalytic constants, and the specificity constants for reactants at the active sites will be the same in the two quaternary conformations of the enzyme. Suppose also, for the moment, that the equilibrium constant, L_0, between the R and T conformations is greater than 1 so that the concentration of the latter is greater than the concentration of the former in the absence of reactants; that the dissociation constant for one reactant is smaller in the R conformation than in the T conformation; and that the concentration of only that one reactant is varied. Because the dissociation constant from an active site in the R conformation for the one reactant that is being varied is smaller than that from an active site in the T conformation, as the concentration of that reactant is increased, its association with active sites on the enzyme will shift the equilibrium between the T and R conformations in favor of the latter. As that reactant occupies one or more active sites on each molecule of enzyme and the level of occupancy reaches the point at which most molecules have changed from the T to the R conformation, the catalytic constants and the specificity constants of the remaining active sites will be those of the R conformation.

The problem with assessing the behavior of the initial rate of the enzymatic reaction as a function of the concentration of that reactant is that even though the dissociation constant of the reactant must decrease upon the change in conformation, **the catalytic constants and the specificity constants for that reactant in the two conformations of the active site determine the initial rate for the enzymatic reaction at steady state, not its dissociation constant.** If association and dissociation of that reactant with the active site in both conformations are so rapid that the dissociation constant for that reactant from each conformation is its Michaelis constant, K_m, for that conformation and if the catalytic constant for both active sites is the same, then the initial rate of the enzymatic reaction as a function of the concentration of reactant will be directly proportional to

the occupation of the active site at equilibrium and will simply reflect the cooperative association of reactant. It has already been mentioned that, even with enzymes that do not have two different quaternary conformations, the Michaelis constant for a reactant is rarely its dissociation constant from an active site. Consequently, even though the cooperativity observed in the initial rate of the enzymatic reaction as a function of the concentration of reactant can be fit with Equation 6–36, this fact alone does not permit values to be assigned to the intrinsic dissociation constants and the catalytic constants for that reactant to two conformations of the enzyme from this fit, just as the value for a Michaelis constant in a situation in which cooperativity is not displayed cannot be assigned to the dissociation constant for reactant[79] even though it usually seems to the observer that it should be so and regardless of the units on the Michaelis constant. Nevertheless, cooperative behavior in the initial rate as a function of the concentrations of reactants requires that association of reactants be cooperative and that the cooperative association of reactant be manifest, even if indirectly, as the cooperative effect of its concentration on the enzymatic reaction. It is possible that cooperativity in enzymatic kinetics is so advantageous that natural selection promotes such a manifestation.

In a few instances, the cooperative **binding of a reactant to the otherwise unoccupied active site correlates satisfactorily with the cooperative effect** that its concentration has on the initial rate of the enzymatic reaction. For example, cooperative binding (Hill coefficient = 2.3) of *S*-adenosyl-L-methionine as a function of its concentration to the unoccupied active site of glycine *N*-methyltransferase (previously Equation 1–19)

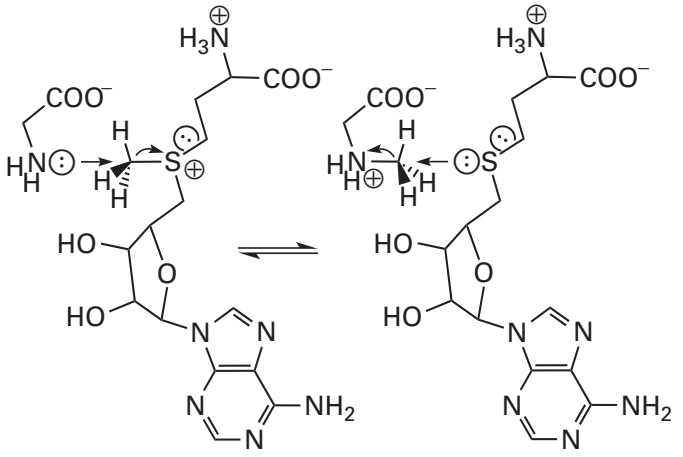

(6–54)

from *Rattus norvegicus* corresponds within the error of measurement with the cooperative effect ($n_H = 2.3$) of its concentration on the initial rate of the enzymatic reaction at 2.0 mM glycine. The concentration of *S*-adenosylmethionine at which half the sites are occupied (50 μM) in the measurement of binding is also indistinguishable from the concentration (43 μM) at which the initial rate is half the limiting rate.[80] In this instance, the initial rate does seem to be registering only association of reactant with the active site.

Fructose 6-phosphate, in the absence of $MgATP^{2-}$, binds cooperatively to the active site of 6-phosphofructokinase (Equation 6–28) from *Saccharomyces cerevisiae*,[81] and the effect of the concentration of fructose 6-phosphate on the initial rate of the enzymatic reaction[82] also displays cooperativity (Figure 6–17C). The value for L_0 (12 ± 3) from a fit of the data for the binding of fructose 6-phosphate in the absence of $MgATP^{2-}$ (○) with the MWC equation and the value for L_{ATP} (20 ± 10) from a fit of the data for the initial rate of the enzymatic reaction (□) as a function of the concentration of fructose 6-phosphate in the presence of a subsaturating concentration of $MgATP^{2-}$ (0.15 mM) with the kinetic version of the MWC equation (Equation 6–36) are indistinguishable, within the margin of error, which may be due to the fact that $MgATP^{2-}$ does not bind cooperatively.[82] The value for the dissociation constant (0.1 ± 0.01 mM) of fructose 6-phosphate from the otherwise unoccupied R conformation of the enzyme obtained by the fit of the MWC equation to the data is somewhat smaller than the dissociation constant (0.25 ± 0.05 mM) for fructose 6-phosphate from the active site of the R conformation occupied by $MgATP^{2-}$ obtained from the fit of Equation 6–36 to the data, as might be expected from steric effects when the two reactants together occupy the active site.

In most instances, however, **the correlation between the cooperative binding of a reactant and the cooperative effect of its concentration on the enzymatic reaction is poor**. For example, the initial rate of 2-dehydropantoate 2-reductase

$$\text{NADPH} + \text{2-dehydropantoate} + \text{H}^+ \rightleftharpoons (R)\text{-pantoate} + \text{NADP}^+ \qquad (6\text{–}55)$$

from *Staphylococcus aureus* as a function of the concentration of NADPH displays cooperativity with a Hill coefficient of 2.5 ± 0.2, even though the enzyme

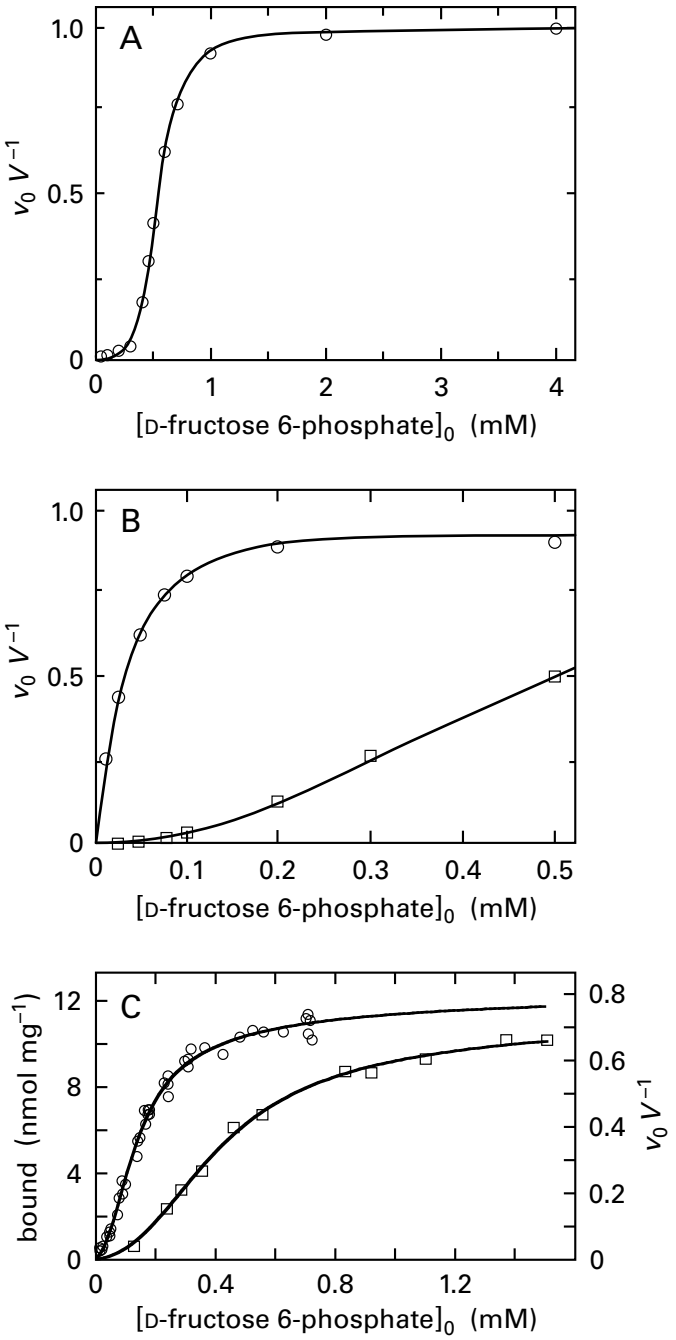

Figure 6–17: Cooperativity in the initial rates as a function of the concentration of D-fructose 6-phosphate and cooperativity in the binding of D-fructose 6-phosphate for 6-phosphofructokinase. (**A**) Cooperativity in the kinetics of 6-phosphofructokinase from *E. coli*.[84] The purified enzyme was assayed in 1 mM $MgATP^{2-}$, 10 mM $MgCl_2$, and 0.1 M 2-amino-2-hydroxymethylpropane-1,3-diol at pH 8.2 and 25 °C and at the noted concentrations of D-fructose 6-phosphate. Each initial rate of the reaction as a fraction of the limiting rate ($v_0\ V^{-1}$) is plotted as a function of the respective initial concentration of D-fructose 6-phosphate (millimolar). (**B**) Lack of cooperativity and induction of cooperativity by a heterotropic allosteric inhibitor in the kinetics of 6-phosphofructokinase from *G. stearothermophilus*.[26] The purified enzyme was assayed in 1 mM $MgATP^{2-}$, 10 mM $MgCl_2$, 5 mM NH_4Cl, 0.2 mM NADH, 10 μg mL^{-1} fructose-bisphosphate aldolase, 18 μg mL^{-1} triose-phosphate isomerase, 2.4 μg mL^{-1} glycerol-3-phosphate dehydrogenase, and 0.1 M 2-amino-2-hydroxymethylpropane-1,3-diol at pH 8.2 and at the noted concentrations of D-fructose 6-phosphate by coupling production of D-fructose 1,6-bisphosphate to the enzymatic reactions catalyzed by fructose-bisphosphate aldolase, triose-phosphate isomerase, and glycerol-3-phosphate dehydrogenase. The initial rates (v_0) of the reaction as a fraction of the limiting rate ($v_0\ V^{-1}$) are plotted as a function of the initial concentrations of D-fructose 6-phosphate (millimolar). Each initial rate was measured in either the absence (○) or presence (□) of 0.5 mM phospho*enol*-pyruvate, a heterotropic allosteric inhibitor of the enzyme. (**C**) Binding of D-fructose 6-phosphate to 6-phosphofructokinase from *S. cerevisiae* (left axis)[81] and the initial rate of the enzymatic reaction as a function of the initial concentration of D-fructose 6-phosphate (right axis).[82] The binding of D-fructose 6-[^{32}P]phosphate to the enzyme (○) was determined by equilibrating enzyme and substrate in 5 mM $MgSO_4$ and 50 mM imidazolium chloride at pH 7.2 and 20 °C and then forcing a portion of the solution through a membrane impermeant to the enzyme. The free concentration of D-fructose 6-[^{32}P]phosphate (F6P) was determined in the fluid passing through the membrane, and the total concentration was determined in the fluid that did not pass through. Each determination of bound D-fructose 6-[^{32}P]phosphate [nanomoles bound (milligram of protein)$^{-1}$] is plotted as a function of the respective free concentration of D-fructose 6-[^{32}P]phosphate, and the curve is a fit of Equation 6–35 to the data with $L_0 = 12 \pm 3$; $K_{dF6P} = 0.1 \pm 0.01$ mM; and $K'_{dF6P} > 10$ mM. The initial rates of the enzymatic reaction (□) were determined in 5 mM $MgCl_2$ at pH 7.1 with the concentration of $MgATP^{2-}$ fixed at 0.15 mM and the concentration of D-fructose 6-phosphate (F6P) varied. "Activity was normalized with respect to the calculated maximum activity." Each normalized activity is plotted as a function of the respective concentration of D-fructose 6-phosphate. The curve is a fit of Equation 6–36 to the data with $L_0 = 20 \pm 10$; $K_{dF6P} = 0.25 \pm 0.05$ mM; and $K'_{dF6P} > 100$ mM.

is an α_2 dimer in which each subunit has only one active site. Association of NADPH with the enzyme at equilibrium, in the absence of 2-dehydropantoate, is cooperative, but it has a Hill coefficient of only 1.3 ± 0.05. This discrepancy could be explained by a kinetic mechanism for the steady-state random bimolecular association of the two reactants (previously Equation 3–136)

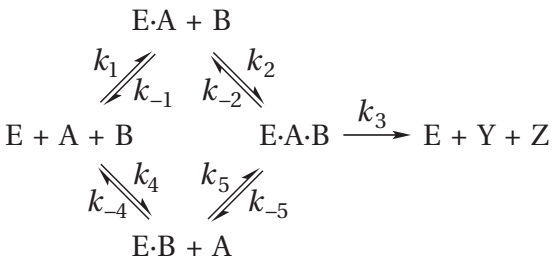

(6–56)

in which the individual associations are not rapid enough to reach equilibrium as the reaction progresses. The rate equation for this mechanism (previously Equation 3–137)

$$v_0 = \frac{a[\mathrm{A}]_0[\mathrm{B}]_0 + b[\mathrm{A}]_0[\mathrm{B}]_0^2 + c[\mathrm{A}]_0^2[\mathrm{B}]_0}{d + e[\mathrm{B}]_0 + f[\mathrm{B}]_0^2 + g[\mathrm{A}]_0 + h[\mathrm{A}]_0^2 + i[\mathrm{A}]_0[\mathrm{B}]_0 + j[\mathrm{A}]_0[\mathrm{B}]_0^2 + l[\mathrm{A}]_0^2[\mathrm{B}]_0} \quad (6\text{–}57)$$

has terms in which the concentrations of reactants are squared, which can explain the greater cooperativity that is observed in the steady-state kinetics.[83]

At pH 8.2, 6-phosphofructokinase (Equation 6–28) from *E. coli* displays cooperativity in the effect of the concentration of the reactant fructose 6-phosphate on the initial rate of the enzymatic reaction at a fixed, saturating concentration of its other reactant, $MgATP^{2-}$ (Figure 6–17A).[19,84] This cooperativity, however, decreases to a Hill coefficient of 1 as the concentration of $MgATP^{2-}$ is decreased, a trend that is consistent with the fact that, in the absence of $MgATP^{2-}$, the binding of fructose 6-phosphate to the active site of the enzyme is not cooperative,[85] unlike the binding of fructose 6-phosphate to the active site of 6-phosphofructokinase from *S. cerevisiae* (Figure 6–17C). At pH 8.2, however, 6-phosphofructokinase from *G. stearothermophilus*, although it is quite similar to that of *E. coli* (55% identity; 0.3 gap percent), displays cooperativity in the effects of the concentration of fructose 6-phosphate on the initial rate of the enzymatic reaction only when phospho*enol*pyruvate, a heterotropic allosteric inhibitor of the enzyme,[28,86] is present as well as saturating concentration of $MgATP^{2-}$ (Figure 6–17B).[26] At pH 7.5, however, the enzyme displays cooperativity in the effects of fructose 6-phosphate on the initial rate in the absence of phospho*enol*pyruvate.[27]

Most enzymes have two or more reactants, and usually, as in the case of aspartate carbamoyltransferase or 6-phosphofructokinase from *E. coli,* **each reactant exerts an effect on the equilibrium** between the T and R conformations (Figure 6–13). As a result, it is difficult to correlate cooperativity in the binding of one reactant to the active site, in the absence of the other reactant or reactants, to the cooperativity observed in the kinetics.

In cases in which the Hill coefficient for the effect of the concentration of reactant on the initial rate of an enzymatic reaction is greater than the number of subunits in a homooligomer,[87] a reasonable explanation would be that rate-limiting steps for the reaction as it occurs on the T conformation are different from those for the reaction on the R conformation.

In the absence of a demonstration that the kinetics are governed only by dissociation constants of the reactants, the function describing the binding of reactant is the same as the function describing the effect of the concentration of that reactant on the initial rate of the enzymatic reaction. Dissociation constants derived from fitting Equation 6–36 to the data are probably illusory because the equation was derived on the assumption that the associations of reactants at steady state are always rapid enough to be at equilibrium. Nevertheless, **any cooperativity observed in kinetic measurements almost always arises, albeit indirectly, from differences in dissociation constants** of reactant from two or more quaternary conformations of the enzyme. Otherwise, reactants would have no effect on the conformation of the enzyme, and noncooperative, rectangularly hyperbolic kinetics would be observed.

In a few exceptional cases, cooperativity or apparent cooperativity in the effect of the concentration of reactant on the initial rate of an enzymatic reaction **arises from causes other than a homotropic allosteric mechanism resulting from changes in quaternary conformations.** For example, L-tryptophan is both a substrate and a heterotropic allosteric activator of tryptophan 2,3-dioxygenase from *Delftia acidovorans* because the reaction is the first step in the catabolism of this amino acid. The two roles of L-tryptophan were distinguished by using analogues. The competitive inhibitor 5-fluorotryptophan binds only at the active site,[88] while 2-methyltryptophan cannot bind at the active site but acts as a heterotropic allosteric activator at a separate site.[89] When a heterotropic allosteric site is saturated with 2-methyltryptophan, the initial rate of the enzymatic reaction is a rectangularly hyperbolic function of the concentration of L-tryptophan; and in the absence of 2-methyltryptophan, the binding of 5-fluorotryptophan to the active site is a rectangularly hyperbolic function of its concentration. In the absence of either 5-fluorotryptophan or 2-methyltryptophan,

however, the initial rate of the enzymatic reaction as a function of the concentration of L-tryptophan displays positive deviation from hyperbolic behavior. An explanation for this behavior consistent with all the facts is that the positive deviation arises because, as the active sites become occupied, heterotropic allosteric sites also become occupied. As a result, the initial rate at higher concentrations of L-tryptophan is greater than those predicted from the initial slope of the curve at concentrations of L-tryptophan where the site for the activator is vacant. This explanation does not invoke homotropic cooperativity among active sites, only a heterotropic allosteric effect between the active site and the site for binding the effector.

In the case of glucokinase from *R. norvegicus*, which is a monomeric enzyme, the apparent cooperativity in the effect of the concentration of D-glucose on the enzymatic reaction arises from the fact that there is a transition from an inactive to an active form of the enzyme that is slower (2–10 min) than the period of time over which the initial rates were measured. Because this transition is accelerated by high concentrations of D-glucose, the initial rate of the enzymatic reaction increases more than it should have if it were only association of D-glucose with one form of the singular active site that was governing the initial rate. When the enzyme is preincubated with high concentrations of D-glucose or with the simple competitive inhibitor *N*-acetylglucosamine, the cooperativity is eliminated.[90] When association of D-glucose with the enzyme is measured under conditions in which each measurement at each concentration of D-glucose is made only after equilibrium is achieved, the association shows no cooperativity.[91] The slow conformational change responsible for the aberrant behavior has been assigned to a loop of 30 amino acids that closes over the active site. In the unoccupied enzyme, the loop is disordered, and the transition between the disordered and ordered states is slow as D-glucose associates with the active site and the loop closes over it. A mutant of the enzyme in which four amino acids in this loop have been switched no longer displays cooperativity in its initial rate as a function of the concentration of D-glucose.[91]

An actual artifact is observed with glycine hydroxymethyltransferase (see Equation 2–10)

$$\text{tetrahydrofolate} + \text{L-serine} \rightleftharpoons H_2O + \text{glycine} + \text{5,10-methylenetetrahydrofolate} \quad (6\text{–}58)$$

from *O. cuniculus*. Originally, it was observed that the initial rate of the enzymatic reaction, as a function of the concentration of the reactant tetrahydrofolate, appeared to display cooperativity. It was later demonstrated that this observation was artifactual and arose from instability of the tetrahydrofolate at low concentrations.[92] As a result, the actual concentrations of reactant in the lower range were less than the nominal concentrations, causing the initial rates measured in this range to be lower than they should have been. At higher concentrations, the tetrahydrofolate was stable, and the initial rates measured in this range were accurate but higher relative to those at the lower concentrations.

Most instances of positive deviations from ideal behavior in association of reactants during measurements of initial rate of an enzymatic reaction, however, probably do involve homotropic allosteric processes.

As the kinetics of the enzymatic reaction catalyzed by phosphofructokinase (Equation 6–28) from *G. stearothermophilus* (Figure 6–17B) illustrate, heterotropic allosteric effectors often cause cooperativity in the effects of the concentration of a reaction to appear, and heterotropic allosteric effectors can also cause cooperativity to disappear (Figure 6–3). As might be expected, these materializations and dematerializations result from the ability of heterotropic allosteric effectors to shift the equilibrium between two or more conformations of the protein. This behavior begs the question of how homotropic and heterotropic allosteric effects are related to each other and whether or not the same conformational changes are responsible for both effects. As might be expected, the answer to these questions depends on the enzyme being examined.

Suggested Reading

Wang, C., Yang, Y. R., Hu, C. Y., & Schachman, H. K. (1981) Communication between subunits in aspartate transcarbamoylase. Effect of active site ligands on the tertiary structure of regulatory chains, *J. Biol. Chem. 256*, 7028–7034. https://doi.org/10.1016/S0021-9258(19)69094-0

Velyvis, A., Yang, Y. R., Schachman, H. K., and Kay, L. E. (2007) A solution NMR study showing that active site ligands and nucleotides directly perturb the allosteric equilibrium in aspartate transcarbamoylase, *Proc. Natl. Acad. Sci. U.S.A. 104*, 8815–8820. https://doi.org/10.1073/pnas.0703347104

Problem 6–1: Derive Equation 6–5 from Equation 6–3 and the conservation of protein.

$$[P] + [P{\cdot}L_n] = [P]_t$$

Problem 6–2: Derive Equation 6–11 from Equation 6–10 and the conservation of protein.

Problem 6–3: Derive Equation 6–42 from Equation 6–35 and the binomial theorem.

Problem 6–4: The mean hemoglobin concentration in the blood of adult human males is 157 g L^{-1}.

(A) Find the molar masses of human α polypeptide, human β polypeptide, and heme B, and calculate the molar concentration of sites for binding of molecular oxygen in the blood of an average adult male.
(B) The capacity of the blood used in the measurements of Figure 6–5 for binding O_2 at saturation, by extrapolation, is 191 mL of O_2 (liter of blood)$^{-1}$. Calculate the capacity of this blood from C. G. Douglas in units of moles of O_2 (mole of heme)$^{-1}$.
(C) What percent of the hemes are binding O_2 if the hemoglobin concentration of the blood of C. G. Douglas were that of the average male?
(D) What might cause this number to be different from 100%?

Problem 6–5: The enzymatic rate of the reaction catalyzed by aspartate carbamoyltransferase is a sigmoid function of the L-aspartate concentration at saturating carbamoyl phosphate (Figure 6–3).

(A) Write a series of linkage boxes to describe the binding of each of the six aspartates to the enzyme and to explain the observed cooperativity. Remember to indicate the statistical corrections.

Maleate is an inhibitor of aspartate carbamoyltransferase that is competitive with L-aspartate. The following behavior was observed when maleate was added to the enzyme along with L-aspartate.

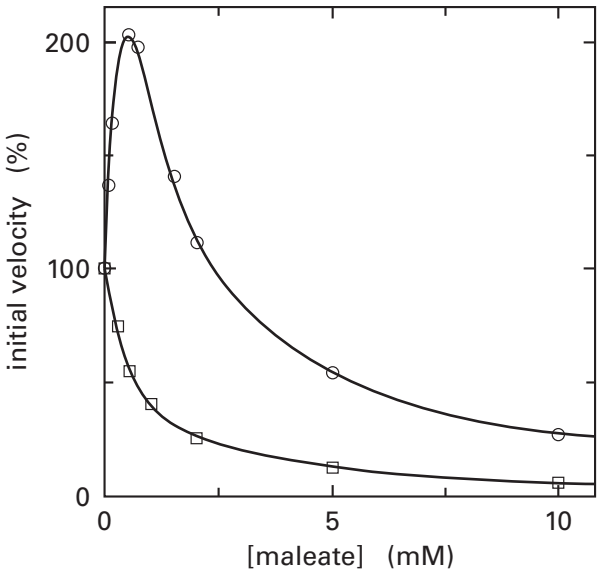

Activation and inhibition of aspartate carbamoyltransferase from *E. coli* by maleate, an analogue of L-aspartate.[93] The reaction mixtures contained 3.6 mM carbamoyl phosphate, 1.0 mM L-aspartate, 0.04 M potassium phosphate at pH 7.0, maleate at the concentrations indicated, and 0.4 μg mL^{-1} native aspartate carbamoyltransferase (○) or 0.2 μg mL^{-1} heated aspartate carbamoyltransferase (□). Heated aspartate carbamoyltransferase was prepared by heating native aspartate carbamoyltransferase at a concentration of 20 μg mL^{-1} in 4 mM potassium phosphate buffer at pH 7.0 and 60 °C for 4 min, followed by rapid cooling in an ice–water bath. The initial rates of enzymatic assays (percent of control) are presented as a function of the concentrations of maleate (millimolar). Note the concentration of L-aspartate and where this concentration falls on the curve in Figure 6–3.

(B) Where approximately is the enzyme in the linkage boxes before maleate is added?
(C) Why does the maleate first stimulate enzymatic activity?
(D) Why does it eventually inhibit enzymatic activity?
(E) What has happened during the heat treatment described in the legend to the figure?

Heterotropic Allosteric Control

A heterotropic allosteric effector is a ligand that acts by associating with a protein or enzyme at a site different from a site for binding another ligand or an active site and altering association of ligands or substrates with this other site or its steady-state kinetics. Consequently, the ultimate decision on whether or not a ligand is a heterotropic allosteric effector is **made crystallographically**. For example, 6-phosphofructokinase (Equation 6–28) from *E. coli* is activated by $MgADP^-$ and $MgGDP^-$ so that, as levels of nucleoside diphosphates rise, glycolysis will accelerate to replenish the levels of nucleoside triphosphates. The enzyme is inhibited by phospho-

*enol*pyruvate[19] so that as levels of this indicator of glycolytic flux rise, the flow of D-fructose 6-phosphate into glycolysis will decrease. The enzyme is an α_4 homotetramer that has been examined extensively by crystallography. The four symmetrically arrayed active sites with which the reactants $MgATP^{2-}$ and D-fructose 6-phosphate associate are distinct and well-separated from the four symmetrically arrayed sites with which heterotropic allosteric effectors associate (Figure 6–9). There is little doubt that both the activation and the inhibition of the enzyme are allosteric.

The enzymatic activity of aspartate carbamoyltransferase (Equation 6–1) from *E. coli* is modulated by nucleoside triphosphates (Figure 6–3). When both $MgCTP^{2-}$ and $MgUTP^{2-}$ are present in solution, the enzyme is inhibited,[94-96] and when both $MgATP^{2-}$ and $MgGTP^{2-}$ are present in solution, the enzyme is activated. That $MgATP^{2-}$ and $MgGTP^{2-}$ are heterotropic allosteric effectors of aspartate carbamoyltransferase follows from the fact that the allosteric site to which they bind is on a different subunit from the one on which the active site resides. Because $MgCTP^{2-}$ and $MgUTP^{2-}$ bind to the same allosteric site at which $MgATP^{2-}$ and $MgGTP^{2-}$ bind,[9] they are also heterotropic allosteric effectors of the enzyme.

When an inhibitor of an enzymatic reaction competes with one of its reactants, a crystallographic decision on whether or not it is a heterotropic allosteric inhibitor is even more important. In particular, in situations where the end product of a metabolic pathway is a competitive inhibitor that does not seem to resemble the reactant with which it competes, the usual impulse is to assume that heterotropic allosteric inhibition is occurring. The dissimilarity of the inhibitor from the substrates, however, cannot be used as an argument that it is a heterotropic allosteric inhibitor. Nor can a decision that the inhibitor is acting at the active site be made from steady-state kinetic measurements demonstrating that the inhibitor is a competitive inhibitor, which would normally be taken as evidence that the inhibitor is competing with the reactant for occupation of the active site. The **definitive decision whether the observed competitive inhibition results from association of the inhibitor with the active site or from heterotropic allosteric inhibition** is also ultimately made by crystallography. Such decisions have been made for a number of inhibitors. For example, mevalonate kinase

$$MgATP^{2-} + (R)\text{-mevalonate} \rightleftharpoons H^+ + (R)\text{-5-phosphomevalonate} + MgADP^- \quad (6\text{–}59)$$

catalyzes an early step in the metabolic pathway for biosynthesis of (2*Z*,6*Z*)-farnesyl diphosphate. In crystallographic molecular models of the enzyme from *R. norvegicus*, it has been observed that farnesyl diphosphate, which is a competitive inhibitor of the human enzyme[97] with respect to $MgATP^{2-}$, which it does not resemble very closely, nevertheless associates with the active site of the enzyme. The diphosphate of (2*Z*,6*Z*)-farnesyl diphosphate overlaps the subsite with which the triphosphate of $MgATP^{2-}$ associates, and the triisoprenoid portion of (2*Z*,6*Z*)-farnesyl diphosphate overlaps the subsite with which the adenosyl group of $MgATP^{2-}$ associates.[98] Consequently, farnesyl diphosphate is not a heterotropic allosteric inhibitor.

L-Lysine is a competitive inhibitor of homocitrate synthase from *S. cerevisiae* with respect to 2-oxoglutarate[99]

$$\text{acetyl-SCoA} + H_2O + \text{2-oxoglutarate} \rightleftharpoons H^+ + \text{HSCoA} + (R)\text{-2-hydroxybutane-1,2,4-tricarboxylate} \quad (6\text{–}60)$$

which it does not resemble very closely. The enzyme catalyzes the first committed step in biosynthesis of L-lysine. L-Lysine associates with the active site of the enzyme from *Schizosaccharomyces pombe* (72% identity; 0 gap percent) at a location that almost completely overlaps that occupied by 2-oxoglutarate.[100] L-Tyrosine (**6–2**) inhibits prephenate dehydrogenase from *Aquifex aeolicus*, the first committed step in its biosynthesis, by occupying the same location in the active site occupied by the reactant prephenate (**6–3**)

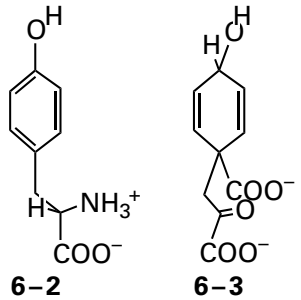

6–2 **6–3**

which it does resemble.[101]

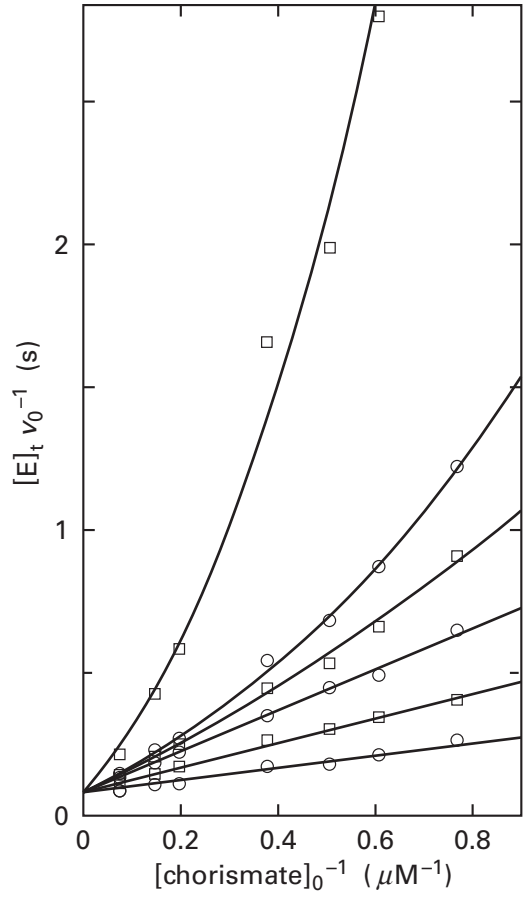

Figure 6–18: Competitive heterotropic allosteric inhibition of anthranilate synthase from *S. typhimurium* by L-tryptophan.[104,105] Solutions contained 20 mM L-glutamine, 10 mM MgCl, various concentrations of chorismate, various concentrations of L-tryptophan, and 0.1 M potassium phosphate at pH 7.0 and 25 °C. The reaction was initiated by adding anthranilate synthase, and the rate of production of anthranilate was followed fluorometrically (λ_{ex} = 308 nm; λ_{em} = 388 nm) over the first few minutes to obtain initial rates. The initial rates were converted to unit of second^{-1}. The reciprocal of each initial rate (v_0^{-1} in seconds) is plotted as a function of the respective reciprocal of the initial concentration of chorismate (micromolar^{-1}) at six fixed concentrations of L-tryptophan: in ascending order of the curves, 0, 2.5, 5.0, 7.5, 10, and 20 μM. The lines and curves are drawn by hand.

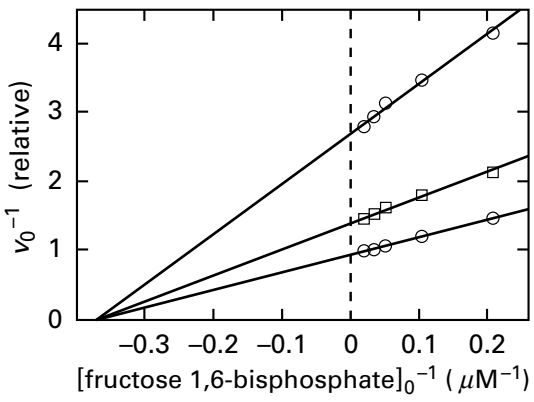

Contrariwise, **a heterotropic allosteric inhibitor is often a competitive inhibitor** even though the site with which it associates is well-removed from the active site. For example, the inhibition of anthranilate synthase (previously Equation 5–85)

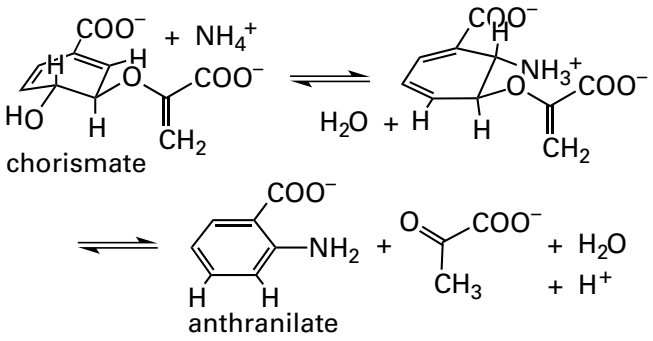

(6–61)

from *Salmonella typhimurium* by L-tryptophan, which is known from crystallographic observations to be a heterotropic allosteric inhibitor,[102,103] is competitive with respect to chorismate (Figure 6–18).[104,105]

When acting to control metabolism, **direct competitive inhibition at an active site and heterotropic allosteric inhibition are not mutually exclusive.** For example, fructose 2,6-bisphosphate inhibits fructose-bisphosphatase

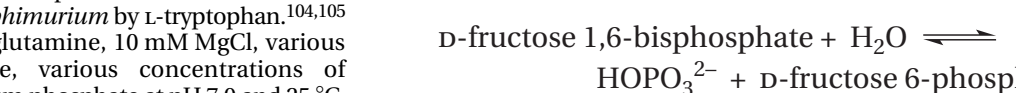

(6–62)

Figure 6–19: Noncompetitive heterotropic allosteric inhibition of fructose-bisphosphatase from *R. norvegicus* by AMP^{2-} with respect to the reactant D-fructose 1,6-bisphosphate.[108] Solutions contained 0.15 mM $NADP^+$, 20 mM 2-sulfanylethanol, 10 mM $MgSO_4$, 2 μmol min^{-1} mL^{-1} D-glucose-6-phosphate isomerase, 0.3 μmol min^{-1} mL^{-1} D-glucose-6-phosphate dehydrogenase ($NADP^+$), fructose-bisphosphatase, and 50 mM 2-ammonio-2-hydroxymethylpropane-1,3-diol chloride at pH 7.5 and 30 °C. Each reaction was initiated by adding one of several concentrations of D-fructose 1,6-bisphosphate, and the rate of production of D-fructose 6-phosphate was followed by coupling it to production of NADPH (λ_{max} = 339 nm) by the use of D-glucose-6-phosphate isomerase and D-glucose-6-phosphate dehydrogenase ($NADP^+$). The reciprocal of each initial rate (v_0^{-1} relative to the limiting rate of the enzymatic reaction in the absence of inhibitor) is plotted as a function of the respective reciprocal of the initial concentration of D-fructose 1,6-bisphosphate (micromolar^{-1}) at three fixed concentrations of the heterotropic allosteric inhibitor AMP^{2-}: in ascending order of the curves, 0, 80, and 160 μM. The lines are drawn by hand, so as to converge at a point on the axis of the abscissa.

from *R. norvegicus*[106] by associating with the active site in place of the reactant D-fructose 1,6-bisphosphate[107] while AMP^{2-}, a noncompetitive inhibitor of the enzyme (Figure 6–19),[108,109] associates at a heterotropic allosteric site.

Crystallographic observations have shown that heterotropic allosteric sites can be located almost anywhere in an enzyme relative to its active site. They can be well within the same subunit in which the active site is located, as is the case for glycogen phosphorylase *b* from *O. cuniculus* (Figure 6–20)[110,111] and anthranilate synthase (Equation 6–61) from *Serratia marcescens*.[103] They can be adjacent to or within the symmetrically arrayed interfaces between the subunits of a homooligomer, as is the case for

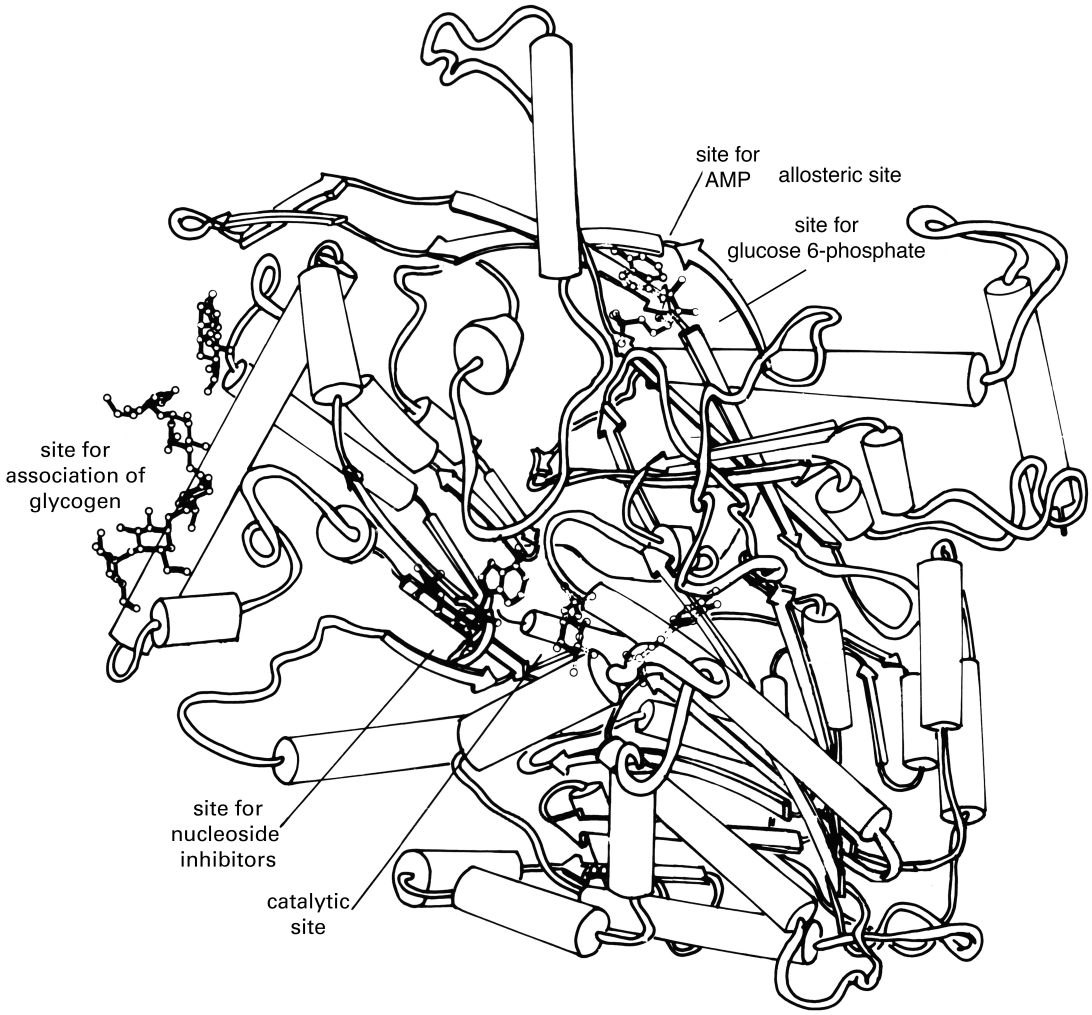

Figure 6–20: Schematic drawing of the crystallographic molecular model of one subunit of glycogen phosphorylase *b* from *O. cuniculus*, indicating all sites for the various heterotropic allosteric effectors.[110] The drawing summarizes a large number of crystallographic studies in which data sets from various liganded forms of the crystalline enzyme were used to provide maps of electron density or difference electron density. In these studies, the crystals were often stabilized by crosslinking to prevent them from shattering as a result of the conformational changes promoted by the binding of certain ligands. Although this shortcut placed in question whether the observed changes in conformation were indicative, it did allow the various binding sites for ligands to be identified. In the drawing, AMP^{2-} is shown bound at the site for heterotropic allosteric effectors. D-Glucose 6-phosphate (not drawn), an allosteric inhibitor, binds next to AMP^{2-} in the site for allosteric effectors. Maltoheptaose, portions of which were not resolved in the respective map of electron density, is shown bound at the site for association of glycogen. D-Glucose 1-phosphate and pyridoxal phosphate are shown bound at the catalytic site. The site for nucleoside inhibitors is occupied by AMP^{2-}. Reprinted with permission from reference 110. Copyright 1984 Portland Press, Ltd. https://doi.org/10.1042/bj2180045

glycogen synthase from *S. cerevisiae*,[112] acetylglutamate kinase from *Thermotoga maritima*,[113] and 6-phosphofructokinase (Figure 6–9). They can reside upon a twofold rotational axis of symmetry within a homooligomer* as do the sites for the pseudosymmetric molecule fructose 1,6-bisphosphate in both L-lactate dehydrogenase from *B. longum*[42] and glycerol kinase (previously Equation 4–283)

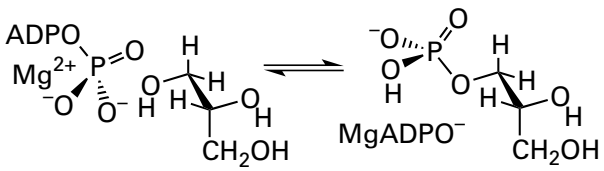

(6–63)

from *E. coli*.[114]

Heterotropic allosteric sites can be located on a regulatory domain within the subunit comprising a homooligomer, distinct from the catalytic domain in which the active site is located, but in the same folded polypeptide, as is the case for sulfate adenylyltransferase from *Penicillium chrysogenum*,[115] porcine fructose-1,6-bisphosphatase,[36] and phosphoglycerate dehydrogenase from *E. coli*.[116,117] In fructose-1,6-bisphosphatase, the regulatory domain (201 aa) is larger than the catalytic domain (137 aa); but in phosphoglycerate dehydrogenase, the regulatory domain (92 aa) is smaller than the catalytic domain (300 aa). Heterotropic allosteric sites can be located on regulatory β subunits in an $(\alpha\beta)_n$ heterooligomer in which the active sites are on the catalytic α subunits, as is the case for aspartate carbamoyltransferase (Figure 6–2) and ATP phosphoribosyltransferase from *Psychrobacter arcticus*.[118] In the former instance, the regulatory subunit (153 aa) is smaller than the catalytic subunit (311 aa); in the latter, the regulatory subunit (387 aa) is larger than the catalytic subunit (231 aa).

Finally, catalytic α subunits and regulatory β subunits can be loosely associated rather than tightly associated. Each can comprise a separate homooligomeric protein, and these two distinct homooligomers can be unassociated with each other in some circumstances but form an allosterically regulated heterooligomer in other circumstances, as is the case for acetolactate synthase[119-121] and bovine cyclic-AMP-dependent non-specific serine/threonine protein kinase.[122,123] In the case of acetolactate synthase from *S. cerevisiae*, the regulatory protein is a β_8 homooctamer with 422(D_4) rotational symmetry with which four catalytic α_2 homodimers can associate to form the regulated $(\alpha_2)_4\beta_8$ heterohexadecamer. Each twofold rotational axis of symmetry in the four catalytic homodimers coincides with a pair of perpendicular twofold rotational axes of symmetry in the homooctamer.[124]

In heterooligomers containing equal numbers of two different subunits, in which one type of subunit contains the active site for an enzymatic activity and the other contains the active site for a different enzymatic activity rather than a site with which a heterotropic allosteric effector can associate, the progress of catalysis in one active site can be coordinated with that in the other by a heterotropic allosteric effect. For example, in tryptophan synthase (previously Equation 3–523)

1-*C*-(indol-3-yl)glycerol 3-phosphate + L-serine $\rightleftharpoons$ L-tryptophan + D-glyceraldehyde 3-phosphate + H_2O

(6–64)

the indole-3-glycerol-phosphate lyase activity, catalyzed by the active site on an α subunit, must be coordinated with the tryptophan synthase (indole-salvaging) activity, catalyzed by the active site on the β subunit to which it is connected, because the former produces the indole that passes through the tunnel between them before it can used by the latter. One way in which this coordination is accomplished is that formation of the pyridoximines of 2-aminoacrylate from serine (see Equation 2–13)

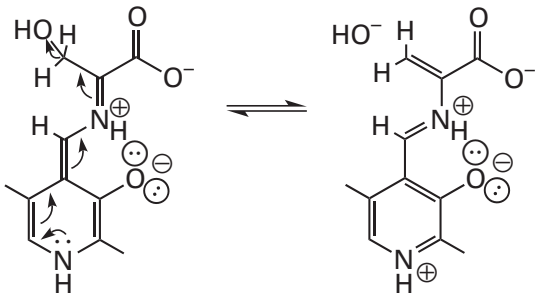

(6–65)

at the active site for tryptophan synthase (indole-scavenging) on a β subunit increases the rate for production of indole at the active site for indole 3-glycerol-phosphate lyase on the α subunit to which it is connected 150-fold.[125] It has been demonstrated crystallographically[126] and by nuclear magnetic resonance spectroscopy of fluorinated analogues of substrates for indole-3-glycerol-phosphate lyase[127] that formation of the pyridoxime of 2-aminoacrylate

*In such instances, there are half as many sites for binding the allosteric ligand as there are subunits in the oligomer.

promotes a quaternary conformational change of the heterooligomer, closing both the active site for tryptophan synthase (indole-scavenging) and the active site for indole-3-glycerol-phosphate lyase around their respective reactants, which leads to an increase in overall enzymatic activity. Another way the coordination is accomplished is that association of substrates and analogues of substrates with an active site for indole-3-glycerol-phosphate lyase on an α subunit increases the affinity for L-serine for the active site for tryptophan synthase (indole-scavenging) on the β subunit to which it is connected and shifts the equilibria among the intermediates at this active site in favor of the pyridoximine of 2-aminoacrylate.[128-130] The quaternary conformational change that accomplishes this heterotropic allosteric effect has also been described crystallographically.[131]

One of the more surprising crystallographic observations is that **the same allosteric site can associate in turn with both a heterotropic allosteric activator and a heterotropic allosteric inhibitor of the enzyme.** In such instances, both heterotropic allosteric inhibition and heterotropic allosteric activation originate from the same site. For example, in the case of aspartate carbamoyltransferase, the same site on a regulatory β subunit associates at the same location with a complex of one CTP^{4-}, one UTP^{4-}, and one Mg^{2+} ($CTP{\cdot}Mg{\cdot}UTP^{6-}$), which leads to heterotropic allosteric inhibition, and with a complex of two ATP^{4-} and one Mg^{2+}($ATP{\cdot}Mg{\cdot}ATP^{6-}$), which leads to heterotropic allosteric activation (Figure 6–3). In both instances, the Mg(ribosyl 5′-triphosphate)$_2^{6-}$ portion of the respective complex occupies exactly the same location in the allosteric site while the bases occupy slightly different locations that nevertheless overlap.[9] In chorismate mutase from *S. cerevisiae*, the heterotropic allosteric inhibitor L-tyrosine and the heterotropic allosteric activator L-tryptophan associate with the same allosteric site. Their carboxy groups, their amino groups, and their α and β carbons occupy identical locations, but the locations occupied by the 4-hydroxyphenyl group and the indolyl group, respectively, only partially overlap (Figure 6–21).[132,133]

A heterotropic allosteric inhibitor and a heterotropic allosteric activator can occupy the same allosteric site even when the inhibitor and activator are much **less similar to each other**. For example, the allosteric site in glycogen phosphorylase (previously Equation 5–122)

$$[(1\rightarrow4)\text{-}\alpha\text{-D-glucosyl}]_n + HOPO_3^{2-} \rightleftharpoons [(1\rightarrow4)\text{-}\alpha\text{-D-glucosyl}]_{n-1} + \alpha\text{-D-glucose 1-phosphate} \quad (6\text{–}66)$$

from *O. cuniculus* binds both AMP^{2-}, a heterotropic allosteric activator of the enzyme, and D-glucose 6-phosphate, a heterotropic allosteric inhibitor. Phospho groups of the effectors occupy the same location in the site, so their association is mutually exclusive, but the glucosyl and adenosyl groups occupy different locations in the respective complexes.[110] In the case of 6-phosphofructokinase from *G. stearothermophilus* (see Figure 6–9),[28,86] the heterotropic allosteric inhibitor phospho*enol*pyruvate associates with the same site as the heterotropic allosteric activator $MgADP^-$. The phospho group of phospho*enol*pyruvate occupies the same location as the β-phospho group of $MgADP^-$, and the carboxylato group of phospho*enol*pyruvate, occupies the same location as the α-phospho group of $MgADP^-$.

In ribonucleoside-diphosphate reductase, $dATP^{4-}$, ATP^{4-}, $dGTP^{4-}$, and $dTTP^{4-}$, as heterotropic allosteric inhibitors and heterotropic allosteric activators, bind to two distinct allosteric sites on the protein.[134] Depending upon what nucleotides are in which sites, the catalytic constant for the enzyme is increased or decreased and the relative values of the specificity constants for the reactants, ADP^{3-}, GDP^{3-}, UDP^{3-}, and CDP^{3-} are determined.[135] In this way, the concentrations in the cytoplasm of the four deoxyribonucleotides, which are the precursors of DNA, are balanced.

So far, the only explanation of heterotropic allosteric effects that can reproduce the observed behavior and explain how association of an effector at a distant site is able to affect catalysis at the active site is that there are two or more conformations of the enzyme, each of which has different steady-state rate constants for the enzymatic reaction and each of which has different dissociation constants for heterotropic allosteric effectors. The fact that each heterotropic allosteric effector for a particular enzyme can shift the equilibrium between the two or more conformations by thermodynamic linkage is the reason that the steady-state kinetics of the enzyme change in the presence of that effector.

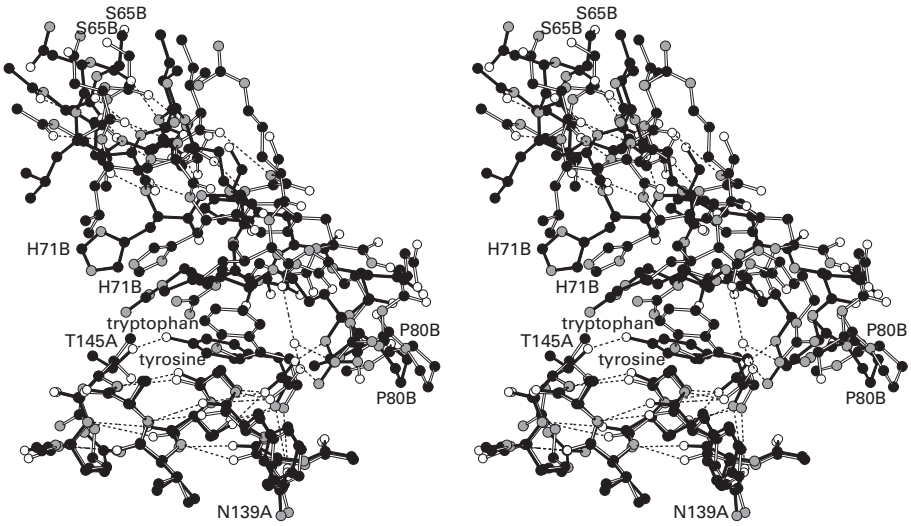

Figure 6–21: Stereodrawings[485] of crystallographic molecular models of the allosteric site on chorismate mutase from *S. cerevisiae* that associates with both the heterotropic allosteric inhibitor L-tyrosine and the heterotropic allosteric activator L-tryptophan.[132,133] Black atoms are carbons, white atoms are oxygens, and gray atoms are nitrogens. The portion of the molecular model with L-tryptophan bound in the site is designated by white bonds, and the portion of the molecular model of the enzyme with L-tyrosine bound in the site is designated by black bonds. The two sites in each dimer of the enzyme both lie in the interface between its two subunits, and they are related to each other by a twofold rotational axis of symmetry running through the interface. Amino acids from Asparagine 139 to Arginine 146 comprise the portion of the lower subunit in the drawing and are labeled with the letter A. Amino acids from Leucine 64 to Proline 80 comprise the portion of the upper subunit in the drawing and are labeled with the letter B. Because the heterotropic allosteric activator L-tryptophan associates preferentially with the R conformation and the heterotropic allosteric inhibitor L-tyrosine associates preferentially with the T conformation, the enzyme crystallized in the R conformation when L-tryptophan was present in the solution but in the T conformation when L-tyrosine was present in the solution. The two different crystallographic molecular models, those of the R and T conformations, were aligned by superposing the α helices formed by Asparagine 139A to Arginine 146A from the two models. When these α helices are superposed, it can be seen that the upper subunit, both its α helix and the loop following the α helix, shifts back and to the left when the conformation changes from the R to the T conformation. Only hydrogen bonds that lie within the α helices are drawn in order to highlight those α helices. The many hydrogen bonds cementing the α-amino group and the carboxy group of each bound amino acid in the site are also drawn. It can be seen that the same amino acids supply those hydrogen bonds in each conformation, with the exception of the intercession of a molecule of water between the side chain of Arginine 75B and the carboxy group of L-tryptophan in the R conformation.

Each of the two or more distinct conformations of an enzyme, the equilibrium among which is being controlled by the differences in dissociation constants for association of a heterotropic allosteric effector, usually is a **rotationally symmetric quaternary conformation**. The control exerted by a heterotropic allosteric effector arises from its association in turn with as many identical heterotropic allosteric sites as there are asymmetric units in the symmetric homo-oligomer of a particular quaternary conformation. Both the control of conformational changes by the thermodynamic linkage between the conformational equilibrium and association of heterotropic allosteric effectors and the multimolecularity of the various associations of both effectors and reactants for the enzyme often cause the binding of several molecules of effector or reactant to be cooperative and display sigmoid behavior. This cooperativity, however, that usually accompanies heterotropic allosteric inhibition and activation complicates the explanation of the observed heterotropic allosteric effects in isolation.

For the moment, it will be assumed that there are only two conformations of the enzyme controlled by heterotropic allosteric effectors. Historically, the conformation from which a heterotropic allosteric inhibitor has the smaller dissociation constant has been designated T and the conformation from which a heterotropic allosteric activator has the smaller dissociation constant has been designated R.[133] These designations, perhaps by design and often in the absence of any experimental validation, conflate the symmetric quaternary conformational changes responsible for cooperativity in the behavior of association of substrates and cooperativity of the initial rate of the enzymatic reaction as a function of the concentration of a reactant with the two conformations responsible for heterotropic allosteric effects. There is, however, no necessary connection between heterotropic allosteric effects and cooperative effects. To avoid this conflation, for the moment, even though it may seem strange to those used to it, the inhibited conformation from which a heterotropic allosteric inhibitor has the smaller dissociation constant will designated the **H conformation**, the in**H**ibited conformation, and the activated conformation from which a heterotropic allosteric activator has the smaller dissociation constant will be designated the **V conformation**, the acti**V**ated conformation.

The fact that, in many cases, a heterotropic allosteric inhibitor and a heterotropic allosteric activator associate with the same site is inconsequential to their ultimate effects on the equilibrium between the H and V conformations. The consequential facts are that the inhibitor has a higher affinity for that site when the enzyme is in the H conformation than when it is in the V conformation and that the activator has a higher affinity for that site when the enzyme is in the V conformation than when it is in the H conformation. All that is necessary is for the activator and inhibitor to be different enough from each other that the affinity of the site for activator increases and the affinity of the site for inhibitor decreases when the H changes to the V conformation. The structure of the allosteric site in chorismate mutase from *S. cerevisiae* in the H conformation when the heterotropic allosteric inhibitor L-tyrosine is associated with it and the structure of the same site in the V conformation when the heterotropic allosteric activator L-tryptophan is associated with it (Figure 6–21) comprise an example of this principle. The conformational change in the structure of the allosteric site when the H becomes the V conformation is able to increase significantly the dissociation constant of L-tyrosine, the heterotropic allosteric inhibitor, and decrease significantly the dissociation constant of L-tryptophan, the heterotropic allosteric activator, and vice versa. In this instance, the only ligands associated with the conformations in the respective crystals were L-tyrosine and L-tryptophan, so the situation is not complicated by the presence of any substrates for the enzyme.

One explanation is that heterotropic allosteric inhibition is based on the ability of a heterotropic allosteric inhibitor to shift the equilibrium from a V to an H conformation and that heterotropic allosteric activation is based on the ability of a heterotropic allosteric activator to shift the equilibrium from an H to a V conformation. If this explanation is to apply to the general case of heterotropic allosteric inhibition and activation,[136] then it must be assumed that the **V conformation of the enzyme has either a larger specificity constant for the reactant affected by the allosteric modulation, or a larger catalytic constant** relative to the H conformation, or both properties. If a heterotropic allosteric inhibitor has a smaller dissociation constant for the H than the V conformation, its association with the enzyme will shift the equilibrium in favor of the H conformation and either decrease the catalytic constant, decrease the specificity constant, or have both effects. For example, both effects are observed when $MgCTP^{2-}$ and $MgUTP^{2-}$ are present and aspartate carbamoyltransferase is catalyzing its reaction (Figure 6–3). If a heterotropic allosteric activator has a smaller dissociation constant for the V than for the H conformation, its association with the enzyme should shift the equilibrium

in favor of the V conformation and increase the catalytic constant, increase the specificity constant, or have both effects. For example, both effects are observed when $MgATP^{2-}$ and $MgGTP^{2-}$ are present and aspartate carbamoyltransferase is catalyzing its reaction. In this way, by controlling the equilibria between the two conformations of the enzyme, heterotropic allosteric effectors are able to control enzymatic reactions.

There are situations in which the V conformation has a larger catalytic constant for reactant than the H conformation, a larger specificity constant for reactant than the H conformation, or both properties. In such situations, when a heterotropic allosteric activator is present in solution, the initial rate of the enzymatic reaction at all concentrations of the varied reactant below saturation is usually greater than or equal to the initial rate in the absence of the activator. In such situations, when a heterotropic allosteric inhibitor is present in solution, the initial rate of the enzymatic reaction at concentrations of the varied reactant below saturation is usually less than or equal to the initial rate in the absence of inhibitor. In other words, the curves for the initial rate as a function of the concentration of reactant in the presence of a heterotropic allosteric activator, in the absence of activators and inhibitors, and in the presence of a heterotropic allosteric inhibitor do not cross each other, as is the case in Figure 6–3.

There is no reason, however, other than perhaps the effects of natural selection, that the catalytic constant of the H conformation cannot be larger than that of the V conformation while the specificity constant for reactant is smaller for the H conformation. Similarly, there is no reason that the specificity constant for reactant of the H conformation cannot be larger than that of the V conformation while the catalytic constant is smaller for the H conformation. In such an instance, at a particular set of concentrations of reactants—usually those in the normal cytoplasmic ranges—a heterotropic allosteric activator can still activate the enzymatic reaction and a heterotropic allosteric inhibitor can still inhibit the enzymatic reaction. Suppose that a heterotropic allosteric effector has a higher affinity for the H conformation than the V conformation. Suppose also that the catalytic constant is larger and the specificity constant is smaller for the H conformation than those for the V conformation. In the presence of a high enough concentration of heterotropic allosteric effector, the limiting rate of the enzymatic reaction will be greater in the presence of the effector than in its absence while the specificity constant will be smaller in its presence than in its absence. The curve for the initial rate for the enzymatic reaction in the presence of effector will cross that for the initial rate in its absence. At low concentrations of heterotropic allosteric effector, it will be an inhibitor; and at high concentrations, it will be an activator.

It is possible that behavior resulting from this rarely observed possibility applies when a combination of L-phenylalanine and L-tyrosine act as heterotropic allosteric inhibitors of 3-deoxy-7-phosphoheptulonate synthase[137] from *Mycobacterium tuberculosis* when the reactant, D-erythrose 4-phosphate, is varied (Figure 6–26B).* In this instance, the curves do cross. Even in this case, however, the difference in maximal rates is small and perhaps not statistically significant. In the case of 6-phosphofructokinase (Equation 6–28) from *E. coli*, the heterotropic allosteric effector $MgADP^-$ increases the specificity constant and decreases the concentration at which the initial rate of the enzymatic reaction as a function of the concentration of D-fructose 6-phosphate is half its limiting rate, but $MgADP^-$ also decreases the limiting rate of the reaction itself as its concentration is increased. Consequently, $MgADP^-$ is both an activator and an inhibitor at the same time, and the curves cross. It could be shown, however, that $MgADP^-$ acts at the active site as a competitive inhibitor of the other reactant $MgATP^{2-}$. When $MgGDP^-$ is used as a heterotropic allosteric activator rather than $MgADP^-$, the limiting rate of the reaction does not decrease as the concentration of $MgGDP^-$ is increased, and the curves do not cross.[19] In almost all cases, the **curve of the initial rate of an enzymatic reaction in the presence of a heterotropic allosteric inhibitor does not cross the curve of the initial rate in the presence of a heterotropic allosteric activator**, and neither curve crosses the curve for the initial rate in the absence of inhibitors or activators.

Rather than controlling the rate of its catalytic reaction, **a heterotropic allosteric conformational change can change the reaction** itself. For example, [glutamate—ammonia-ligase] adenylyltransferase from *E. coli* is responsible for both adenylation and deadenylation of glutamate–ammonia ligase (previously Equation 3–405)

$$\text{L-glutamate} + NH_3 + MgATP^{2-} \rightleftharpoons MgADP^- + HOPO_3^{2-} + \text{L-glutamine} \qquad (6\text{–}67)$$

*This figure is on page 1734.

from *E. coli*. The active site of [glutamate—ammonia-ligase] adenylyltransferase uses $MgATP^{2-}$ as a reactant to adenylate glutamate–ammonia ligase at Tyrosine 397 in a covalent modification that alters its enzymatic activity.[138] [Glutamate—ammonia-ligase] adenylyltransferase can exist in six different conformations, two of which are inactive, three of which catalyze adenylation, and one of which catalyzes deadenylation of glutamate—ammonia ligase. L-Glutamine, acting as a heterotropic allosteric effector of the adenylyltransferase, shifts the equilibrium among the conformations of adenylyltransferase in favor of the three conformations that catalyze adenylation. As a result, L-glutamine is a heterotropic allosteric effector of adenylyltransferase that converts it from an enzyme that deadenylates the ligase to one that adenylates the ligase.[139] The latter reaction is the transfer of an adenylyl group from diphosphate to the 4-hydroxy group of a tyrosine in the ligase, and the former reaction is hydrolysis of that adenylated tyrosine. Both are nucleophilic substitutions at phosphorus, but the leaving group in the adenylation and the nucleophile in the deadenylation are quite different.

The result of a shift in the equilibrium between the conformations of an enzyme accomplished by associations of heterotropic allosteric effectors at its heterotropic allosteric sites is manifested in the steady-state kinetics. Because an enzyme operates within its organism at steady state, these manifestations observed in the experimental steady-state kinetics define the abilities of heterotropic allosteric inhibitors and activators to control the enzymatic activity in the native environment of the enzyme.

As is the case with all kinetic discussions, a distinction must be made between **observations** and explanations for the observed behavior. Heterotropic allosteric inhibitors display properties reminiscent of classical enzymatic inhibitors. In a few instances, **noncompetitive heterotropic allosteric inhibition** is observed. For example, heterotropic allosteric inhibition[36] of fructose-bisphosphatase (Equation 6–62) from *R. norvegicus* at its active sites by AMP^{2-} associating with its allosteric sites is noncompetitive with respect to the reactant D-fructose 1,6-bisphosphate (Figure 6–19). This noncompetitive heterotropic allosteric inhibition is distinguished, as is classical nonallosteric noncompetitive inhibition (previously Equation 3–178)

$$v_0 = \frac{k_{0,A,app}\left(\frac{K_{inI}}{[I] + K_{inI}}\right)[E]_t\,[A]_0}{K_{mA,app} + [A]_0} \tag{6–68}$$

by the fact that the Michaelis constant is unaffected by the inhibitor as the limiting rate of the enzymatic reaction is decreased.

A far more common observation, however, is **competitive heterotropic allosteric inhibition**. For example, heterotropic allosteric inhibition[102,103] of anthranilate synthase (Equation 6–61) from *S. typhimurium* by L-tryptophan is competitive with respect to the reactant chorismate (Figure 6–18). As with classical nonallosteric competitive inhibition (previously Equation 3–170)

$$v_0 = \frac{k_{0,A,app}[E]_t[A]_0}{K_{mA,app}\left(\frac{[I] + K_{icI}}{K_{icI}}\right) + [A]_0} \tag{6–69}$$

competitive heterotropic allosteric inhibition is distinguished by two facts. First, the limiting rate of the enzymatic reaction, at least within the range of concentrations of inhibitor that are chosen, is invariant. Second, the concentration of reactant at which half the limiting rate is attained increases and the specificity constant for reactant decreases.

Finally, there are instances of **mixed heterotropic allosteric inhibition** in which both the limiting rate decreases and the concentration of reactant at which half the limiting rate is attained increases as in the case of the inhibition of aspartate carbamoyltransferase by $MgCTP^{2-}$ and $MgUTP^{2-}$ (Figure 6–3).

One feature of heterotropic allosteric inhibition that distinguishes it from classical inhibition is that there are often **certain limits beyond which the inhibition fails to conform to classical expectations**. For example, heterotropic allosteric inhibition[140] of 4-hydroxy-tetrahydrodipicolinate synthase

$$\text{L-aspartate-4-semialdehyde} + \text{pyruvate} \rightleftharpoons H^+ + H_2O + (2S,4S)\text{-4-hydroxy-2,3,4,5-tetrahydropicolinate} \tag{6–70}$$

from *Campylobacter jejuni* by L-lysine is competitive with respect to the reactant L-aspartate-4-semialdehyde at concentrations less than 0.06 mM, but

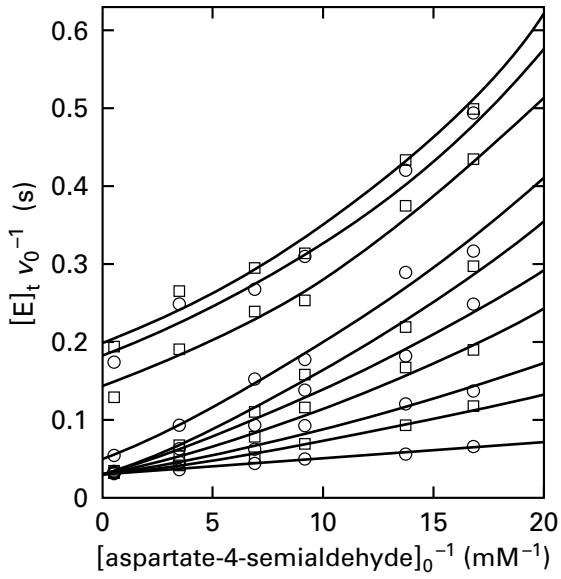

Figure 6–22: Heterotropic allosteric inhibition of 4-hydroxy-tetrahydrodipicolinate synthase from *C. jejuni* by L-lysine.[141] Solutions contained 0.35 mM pyruvate, 0.16 mM NADH, 0.25 μM active sites for 4-hydroxy-tetrahydrodipicolinate reductase, various concentrations of L-aspartate-4-semialdehyde, various concentrations of L-lysine, and 0.1 M 2-[4-(2-hydroxyethyl)-piperazin-1-yl]ethanesulfonic acid at pH 8.0 and 25 °C. The reaction was initiated by adding active sites for 4-hydroxy-tetrahydrodipicolinate synthase to a final concentration of 11 nM, and the rate of production of (2*S*,4*S*)-4-hydroxy-2,3,4,5-tetrahydrodipicolinate was followed by coupling it to the consumption of NADH (λ_{max} = 339 nm) during reduction of (2*S*,4*S*)-4-hydroxy-2,3,4,5-tetrahydrodipicolinate by 4-hydroxy-tetrahydrodipicolinate reductase. The observed initial rates were converted to units of second^{-1}. The reciprocal of each initial rate (v_0^{-1} in seconds) is plotted as a function of the respective reciprocal of the initial concentration of L-aspartate-4-semialdehyde (millimolar^{-1}) at 10 fixed concentrations of L-lysine: in ascending order of the curves, 0, 40, 50, 60, 70, 80, 100, 200, 500, and 1000 μM. The line and the curves are drawn by hand through the data.

the inhibition is no longer competitive at higher concentrations (Figure 6–22).[141] In heterotropic allosteric inhibition of amino-acid *N*-acetyltransferase from *Neisseria gonorrhoeae* by L-arginine, the inhibitor displays mixed inhibition with respect to L-glutamate. L-Arginine decreases the limiting rate of the enzymatic reaction and increases the concentration of L-glutamate at which the initial rate of the enzymatic reaction is half the limiting rate (Figure 6–23A).[142] In this instance, however, at saturating concentrations of the two reactants, L-glutamate and acetyl-SCoA, increasing the concentration of the heterotropic allosteric inhibitor L-arginine decreases the rate of the enzymatic reaction until a plateau is reached at which the enzyme retains 14% of the activity it has in the absence of L-arginine (Figure 6–23B).

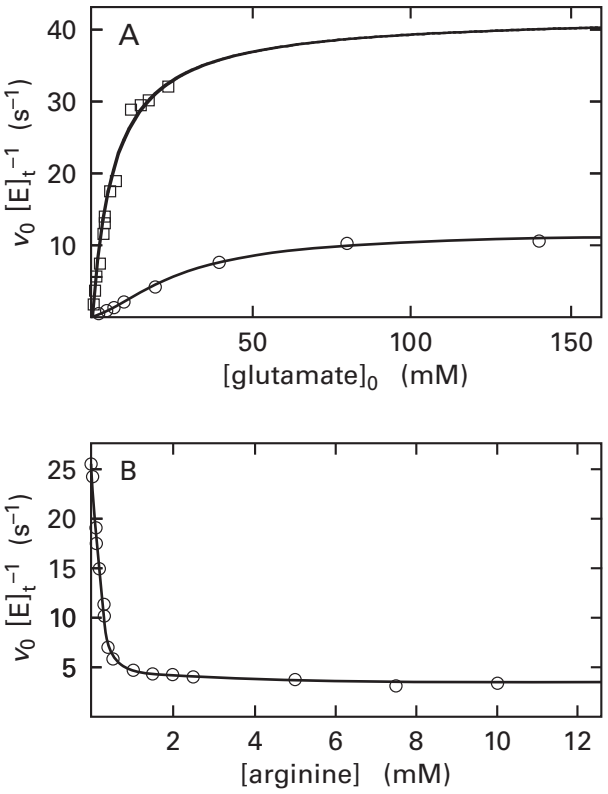

Figure 6–23: Heterotropic allosteric inhibition of amino-acid *N*-acetyltransferase from *N. gonorrhoeae* by L-arginine.[142] The reaction was carried out in 100 μL of 100 mM NaCl, 4 mM acetyl-SCoA, various concentrations of L-glutamate, various concentrations of L-arginine, and 50 mM 2-ammonio-2-hydroxymethylpropane-1,3-diol chloride at pH 8.5 and 30 °C. The reaction was initiated by adding 4 nmol of active sites, and the mixtures were quenched after 1 or 5 min with 100 μL of 30% trichloroacetic acid. The product, *N*-acetyl L-glutamate, was quantified by using liquid chromatography and mass spectrometry. The observed initial rates were converted to units of second^{-1} by dividing by the molar mass of protein for each mole of active sites. (**A**) Each initial rate ($v_0\ [E]_t^{-1}$ in second^{-1}) is plotted as a function of the respective initial concentration of L-glutamate (millimolar) in the presence of (□) 0.1 mM or (○) 1.0 mM L-arginine. (**B**) Each initial rate ($v_0\ [E]_t^{-1}$ in second^{-1}) at 15 mM L-glutamate is plotted as a function of the respective concentration of L-arginine (millimolar^{-1}). The curves are drawn by hand through the data.

A heterotropic allosteric activator almost always decreases the concentration of reactant A required to produce an enzymatic rate that is half the limiting rate and increases the specificity constant for reactant. This is the behavior observed for the activation of aspartate carbamoyltransferase in the presence of the heterotropic allosteric activators $MgATP^{2-}$ and $MgGTP^{2-}$ (Figure 6–3) and for the activation of dCMP deaminase

$$dCMP + H_2O + H^+ \rightleftharpoons NH_4^+ + dUMP \qquad (6\text{–}71)$$

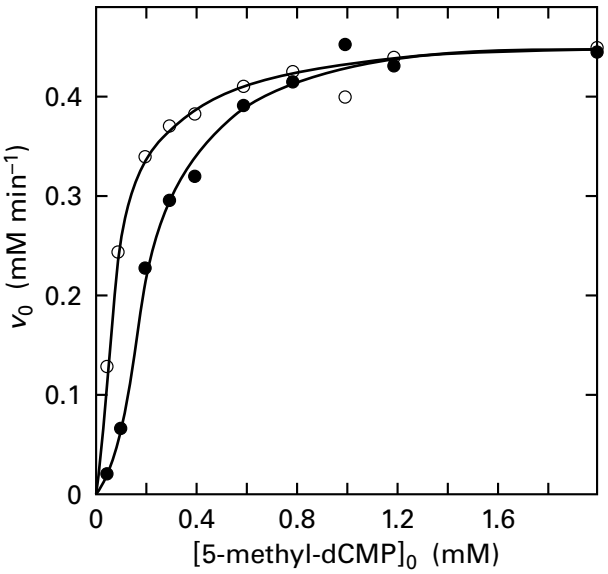

Figure 6–24: Heterotropic allosteric activation of dCMP deaminase from *E. asinus* by MgdCTP^{2-}.[143] The reaction was carried out in 5 mM 2-sulfanylethanol, 1 mM $MgCl_2$, various concentrations of 5-methyldeoxycytidine monophosphate, and 50 mM imidazolium chloride at pH 7.5 and 38 °C. The reaction was initiated by adding dCMP deaminase. The rate of decrease in the concentration of 5-methyldeoxycytidine monophosphate was followed by monitoring its absorbance at 295 nm. Each observed initial rate (micromolar minute^{-1}) is plotted as a function of the respective initial concentration of 5-methyldeoxycytidine monophosphate ([5-methyl-dCMP]$_0$ in millimolar) in the absence of heterotropic allosteric activator (●) and in the presence of 0.3 μM MgdCTP^{2-} (○).

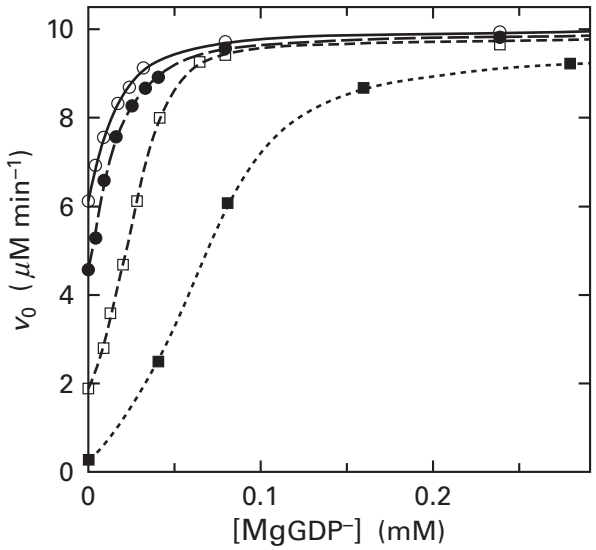

Figure 6–25: Heterotropic allosteric activation of 6-phosphofructokinase from *E. coli* by MgGDP$^-$.[19] The reaction was carried out in 0.1 mM MgATP^{2-}, 0.9 mM $MgCl_2$, various concentrations of D-fructose 6-phosphate, various concentrations of MgGDP$^-$, 0.2 mM NADH, 120 μg mL^{-1} fructose-bisphosphate aldolase, 30 μg mL^{-1} triose-phosphate isomerase, 30 μg mL^{-1} glycerol-3-phosphate dehydrogenase (NAD$^+$), 1 M creatine phosphate, 10 μg mL^{-1} creatine kinase, and 35 mM 2-ammonio-2-hydroxymethylpropane-1,3-diol chloride at pH 8.5 and 28 °C. The reaction was initiated by adding 6-phosphofructokinase. The rate of production of D-fructose 1,6-bisphosphate was followed by coupling it to oxidation of NADH (λ_{max} = 339 nm) by glycerol-3-phosphate dehydrogenase (NAD$^+$) and the glycerone phosphate produced from D-fructose 1,6-bisphosphate by fructose-bisphosphate aldolase and triose-phosphate isomerase. Creatine kinase and phosphocreatine were present to regenerate MgATP^{2-} from the MgADP$^-$ produced during the reaction so that the initial rates remained linear. Each observed initial rate (micromolar minute^{-1}) is plotted as a function of the respective concentration of MgGDP$^-$ (millimolar) at concentrations of D-fructose 6-phosphate of 0.22 mM (■), 0.44 mM (□), 0.7 mM (●), and 1 mM (○).

from *Equus asinus* in the presence of the heterotropic allosteric activator MgCTP^{2-} (Figure 6–24).[143] Were these enzymatic reactions noncooperative in initial rate as a function of the concentration of reactant, this effect would be described as a decrease in the Michaelis constant. In the case of an enzymatic reaction that shows sigmoid behavior, however, there is no longer a Michaelis constant because, by definition, a Michaelis constant is only a parameter of a rectangular hyperbola defining noncooperative kinetics.

The decrease in the concentration of reactant required to produce an enzymatic rate that is half the limiting rate can be far more dramatic that those observed with dCMP deaminase and aspartate carbamoyltransferase. For example, D-fructose 1,6-bisphosphate, a heterotropic allosteric activator of L-lactate dehydrogenase from *Thermus caldophilus*, decreases the concentration of pyruvate required to produce half the limiting rate[144] by a factor of 1000 ± 200.

A heterotropic allosteric activator can either have no **effect on the limiting rate** (Figure 6–24) or increase the limiting rate (Figure 6–3). If, however, a heterotropic allosteric activator does increase the limiting rate of the reaction, there will usually be a concentration of reactant above which the activator, when present at a saturating concentration, will no longer increase the limiting rate. For example, when 6-phosphofructokinase (Equation 6–28) from *E. coli* is catalyzing its reaction at pH 8.5 and at concentrations of D-fructose 6-phosphate of 0.22 mM and greater, addition of increasing concentrations of the heterotropic allosteric activator MgGDP$^-$ increases the steady-state rate to the same level regardless of the concentration of D-fructose-6-phosphate (Figure 6–25).[19]

To avoid the complication of sigmoid behavior while still providing an explanation of heterotropic allosteric inhibition and activation, at least qualitatively, it is useful to derive a kinetic equation for an allosteric monomer. Allosteric enzymes are not homooligomers because they are allosteric but because almost all molecules of protein, allosteric or not, are homooligomers. In fact, it is not necessary for an enzyme to be a homooligomer to display allosteric behavior. For example, the enzymatic activity of ribonucleoside-triphosphate reductase (previously Equation 5–139)

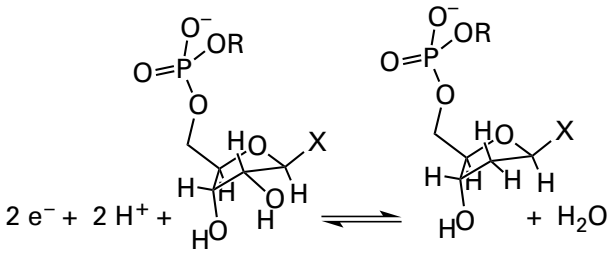

(6–72)

from *Lactobacillus leichmannii* is allosterically[145] activated by deoxyribonucleoside triphosphates,[146-148] even though the enzyme is a monomer of only one folded polypeptide.[145,149] When glycogen phosphorylase *b* (Equation 6–66), which is allosterically activated by AMP^{2-}, is treated with sodium borohydride and then transferred to 7% formamide, it dissociates into monomers. Although the cooperativity of the effect of the concentration of AMP^{2-} on enzymatic activity is lost, AMP^{2-} remains a heterotropic allosteric activator of the enzyme.[150]

If an enzyme were monomeric, were allosterically inhibited or allosterically activated, and association of its reactant and association of a heterotropic allosteric inhibitor or activator were both to reach equilibrium rapidly before the subsequent catalytic steps commence, then the **linkage cube**

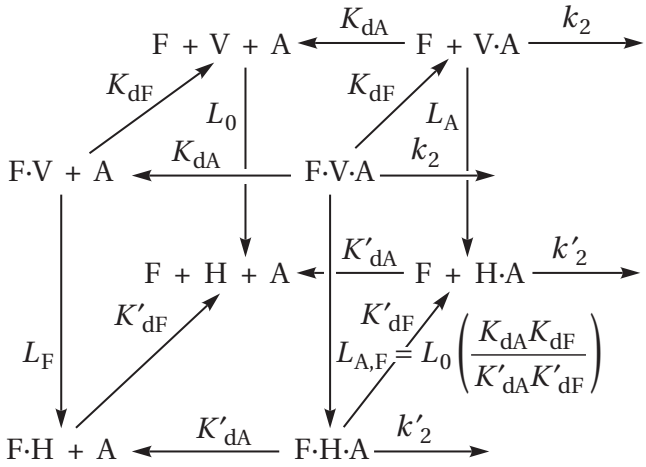

(6–73)

would explain its behavior. The two conformations of the enzyme are designated as the V and H conformations because $K_{dA} < K'_{dA}$, or $k_2 > k'_2$, or both inequalities hold. In this kinetic mechanism the arrows indicate the direction of each equilibrium. Ligand A is the reactant being varied in the measurement, usually while all the other reactants are maintained at saturating concentrations; and ligand F is a heterotropic allosteric effector, either an inhibitor or an activator. The allosteric constants L_0, L_A, L_F, and $L_{A,F}$ are equilibrium constants for the respective equilibria between the V and H conformations when the enzyme is unoccupied, fully occupied by reactant A, fully occupied by heterotropic allosteric effector F, and fully occupied by both A and F, respectively. The latter three are conditional allosteric constants for enzyme occupied by ligands. For the sake of simplicity, dissociation constants for reactant A, K_{dA} and K'_{dA}, and effector F, K_{dF} and K'_{dF}, from the same conformation, H or V, are assumed to be independent of the occupancy of the other site

$$K_{dA} = \frac{[V][A]}{[V{\cdot}A]} = \frac{[F{\cdot}V][A]}{[F{\cdot}V{\cdot}A]} \tag{6–74}$$

$$K'_{dA} = \frac{[H][A]}{[H{\cdot}A]} = \frac{[F{\cdot}H][A]}{[F{\cdot}H{\cdot}A]} \tag{6–75}$$

$$K_{dF} = \frac{[F][V]}{[F{\cdot}V]} = \frac{[F][V{\cdot}A]}{[F{\cdot}V{\cdot}A]} \tag{6–76}$$

$$K'_{dF} = \frac{[F][H]}{[F{\cdot}H]} = \frac{[F][H{\cdot}A]}{[F{\cdot}H{\cdot}A]} \tag{6–77}$$

These assumptions are reasonable because a heterotropic allosteric effector associates at a site separated from the active site and because only the conformational change between the V and H conformations alters the affinity of each site for its ligands and communicates the fact that the other site is occupied by its ligand. By linkage

$$K_{dA} L_0 = L_A K'_{dA} \tag{6–78}$$

$$K_{dF} L_0 = L_F K'_{dF} \tag{6–79}$$

$$K_{dA} L_F = L_{A,F} K'_{dA} \tag{6–80}$$

$$K_{dF} L_A = L_{A,F} K'_{dF} \tag{6–81}$$

The steady-state rate equation derived from this kinetic mechanism has the usual rectangularly hyperbolic form

$$\frac{v_0}{[E]_t} = \frac{k_0[A]_0}{K_{mA} + [A]_0} = \frac{k_0 k_A [A]_0}{k_0 + k_A [A]_0} \tag{6–82}$$

where

$$k_0 = \frac{k_2 K'_{dA} K'_{dF} (K_{dF} + [F]) + k'_2 L_0 K_{dA} K_{dF} (K'_{dF} + [F])}{K'_{dA} K'_{dF} (K_{dF} + [F]) + L_0 K_{dA} K_{dF} (K'_{dF} + [F])} \tag{6–83}$$

$$K_{mA} = K_{dA}\left\{\frac{K'_{dA} K'_{dF} (K_{dF} + [F]) + L_0 K'_{dA} K_{dF} (K'_{dF} + [F])}{K'_{dA} K'_{dF} (K_{dF} + [F]) + L_0 K_{dA} K_{dF} (K'_{dF} + [F])}\right\} \tag{6–84}$$

and

$$k_A = \frac{k_2 K'_{dA} K'_{dF} (K_{dF} + [F]) + k'_2 L_0 K_{dA} K_{dF} (K'_{dF} + [F])}{K_{dA} K'_{dA} K'_{dF} (K_{dF} + [F]) + L_0 K_{dA} K'_{dA} K_{dF} (K'_{dF} + [F])} \tag{6–85}$$

At any fixed concentration of heterotropic allosteric effector, the initial rate for the enzymatic reaction is a rectangularly hyperbolic function of the concentration of reactant A because the enzyme is monomeric. These equations are **in qualitative agreement with the behavior** of heterotropic allosteric effectors.

Given the definitions of the two conformations, it must follow that a heterotropic allosteric inhibitor shifts the equilibrium constant between the two conformations in the direction of the less enzymatically active H conformation. Consequently, for that inhibitor, $K'_{dF} < K_{dF}$. By the same definitions, it must follow that a heterotropic allosteric activator shifts the equilibrium constant between the two conformations in the direction of the more enzymatically active V conformation. Consequently, for that activator, $K'_{dF} > K_{dF}$.

As was the case with cooperativity, there are **limits that apply to the ability of a heterotropic allosteric effector to affect the steady-state kinetics.** If $L_0 < 1$, so that the V conformation predominates in the absence of any ligands, and if $K'_{dF} < K_{dF}$, so that ligand F is a heterotropic allosteric inhibitor that shifts the equilibrium in favor of the H conformation, but $L_0 < K'_{dF} K'_{dA} (K_{dF} K_{dA})^{-1} < 1$, then the inhibitor will be unable to shift the equilibrium (Equation 6–73) sufficiently in favor of the H conformation. The enzyme will remain in the V conformation at all concentrations of inhibitor and reactant, and no inhibition will occur. Because the enzyme is always in the V conformation, it cannot be activated by a heterotropic allosteric activator either. If $L_0 > 1$, so that the H conformation predominates in the absence of any ligands, and if $K'_{dF} > K_{dF}$, so that ligand F is a heterotropic allosteric activator that shifts the equilibrium in favor of the V conformation, but $L_0 > K'_{dF} K'_{dA} (K_{dF} K_{dA})^{-1} > 1$, then the activator will be unable to shift the equilibrium (Equation 6–73) sufficiently in favor of the V conformation. The enzyme will remain in the H conformation at all concentrations of activator and reactant, and no activation will occur. Because the enzyme is always in the H conformation, it cannot be inhibited by a heterotropic allosteric inhibitor either. Such situations have no selective advantage.

To explain noncompetitive heterotropic allosteric inhibition, such as that displayed by the inhibition of fructose-bisphosphatase from *R. norvegicus* by AMP^{2-} (Figure 6–19), $L_0 < 1$, $K_{dA} = K'_{dA}$, $K'_{dF} < K_{dF}$, and $k'_2 < k_2$. With these designations, it can be seen (Equation 6–84) that $K_{mA} = K_{dA}$ for all values of [A] and [F], and it can also be seen (Equation 6–83) that k_0 decreases as [F] increases. Because $K_{dA} = K'_{dA}$,

reactant A cannot affect the equilibrium between the H and V conformations, and the dissociation constant of reactant from the enzyme is always the same regardless of the ratio between the two conformations established by a heterotropic allosteric inhibitor. The decrease in k_0 as [F] increases, however, is significant only if

$$\frac{K'_{dF}}{K_{dF}} < L_0 < \frac{k_2}{k'_2} \tag{6–86}$$

Because $K_{dA} = K'_{dA}$, if L_0 is less than $K'_{dF}\,(K_{dF})^{-1}$, then the ligand will be unable to shift the equilibrium sufficiently and the enzyme will remain in the V conformation. If L_0 is greater than $k_2\,(k'_2)^{-1}$, then the amount of H conformation in the absence of F would be so great that its enzymatic activity would be greater than that of the smaller amount of V conformation present, and no significant decrease in enzymatic activity would be observed as the heterotropic allosteric inhibitor F was added.

Because, as one might expect, the dissociation constant for a reactant is rarely unaffected by the change from the V to the H conformation, noncompetitive heterotropic allosteric inhibition is rarely observed. Competitive heterotropic allosteric inhibition, such as that observed with anthranilate synthase (Figure 6–18), is more common.

There are two **simple explanations for competitive heterotropic allosteric inhibition**. First, from the equation for the catalytic constant k_0 (Equation 6–83), it can be seen that if heterotropic allosteric inhibitor F cannot associate with the V conformation of the enzyme ($K_{dF} = \infty$) and reactant A cannot associate with the H conformation ($K_{dA}' = \infty$), then heterotropic allosteric inhibition will be competitive at all finite concentrations of inhibitor F and k_0 will be equal to k_2 because reactant, when it is at saturation, will always be able to shift the equilibrium entirely to the V conformation because the concentration of inhibitor must always be finite. Second, if the catalytic constant for the V conformation, k_2, is equal to the catalytic constant for the H conformation, k'_2, then heterotropic allosteric inhibition will be competitive because $k_0 = k_2 = k'_2$ at all concentrations of heterotropic allosteric inhibitor (Equation 6–83). The behavior of the initial rate of the enzymatic reaction in each situation mimics classical competitive inhibition, so neither of these simplifications can explain the unique properties of allosteric competitive inhibition, and neither seems likely anyway.

It has already been demonstrated that competitive heterotropic allosteric inhibition has several unique properties that distinguish it from classical competitive inhibition. If the preceding simple conditions do not hold and the kinetic mechanism of Equation 6–73 is the proper explanation, then competitive heterotropic allosteric inhibition can still occur, and the peculiarities that distinguish it from classical competitive inhibition can be explained.

In **classical competitive inhibition**, no matter how high the concentration of inhibitor, increasing the concentration of reactant can always completely overcome the inhibition. The simplest way to understand this fact is to suppose that two ligands, A and B, occupy the same site (ST) on a protein and sterically exclude each other

$$\text{ST·B} + \text{A} \xrightarrow{K_{dB}} \text{B} + \text{ST} + \text{A} \xleftarrow[K_{dA}]{} \text{B} + \text{ST·A} \tag{6–87}$$

The concentration of the complex between the site and ligand A

$$[\text{ST·A}] = \frac{K_{dB}[\text{ST}]_t[\text{A}]}{K_{dA}K_{dB} + K_{dB}[\text{A}] + K_{dA}[\text{B}]} \tag{6–88}$$

The equation states that no matter what the concentration is for ligand B—for example, when B is an inhibitor of the enzymatic activity—if the concentration of ligand A—for example, when A is a reactant for the enzyme—is made large enough, the site will be completely occupied by ligand A. In classical competitive inhibition, at saturating concentrations of reactant, the active sites are fully occupied by molecules of reactant sterically excluding molecules of inhibitor, and thereby the enzyme achieves the same limiting rate as is achieved in the absence of inhibitor. The defining property of classical competitive inhibition is the fact that the same limiting rate is reached at saturating concentrations of reactant regardless of the concentration of inhibitor.

Another signature of classical competitive inhibition with respect to reactant A is that when the concentration of inhibitor is increased, **the Michaelis constant** for reactant A, K_{mA}, increases. The specificity constant for reactant decreases by the same factor because the catalytic constant k_0 does not change (Equation 6–69). If the observed Michaelis constant for the hypothetical heterotropic allosteric monomer is to increase as the concentration of a competitive

heterotropic allosteric inhibitor F increases, then the derivative of Equation 6–84 with respect to the concentration of inhibitor must be greater than 0. By taking the derivative, it can be determined that if that derivative is to be greater than 0*

$$(K'_{dF} - K_{dF})(K_{dA} - K'_{dA}) > 0 \qquad (6–89)$$

If it is stipulated, by definition, that the dissociation constant for a heterotropic allosteric inhibitor is smaller for the H conformation than it is for the V conformation ($K'_{dF} < K_{dF}$), then the Michaelis constant for reactant A will increase upon addition of a competitive heterotropic allosteric inhibitor F only when $K_{dA} < K'_{dA}$. For the increase in K_{mA} to be significant, however, $L_0 K_{dA} < K'_{dA}$. If $L_0 K_{dA}$ were greater than K'_{dA}, the enzyme would always be almost entirely in the H conformation regardless of how much reactant A was present, even in the absence of a heterotropic allosteric inhibitor, because the difference in dissociation constants for reactant A from the two conformations would not be great enough to shift the equilibrium significantly from the H to the V conformation. Consequently, even if $K'_{dF} < K_{dF}$, no inhibition of the reaction would be observed and this discussion would not be occurring.

If the following two limits on the expression for **the catalytic constant** k_0 for heterotropic allosteric inhibition (Equation 6–83) are taken

$$\lim_{[F] \to 0} k_0 = \frac{k_2 K'_{dA} + k'_2 L_0 K_{dA}}{K'_{dA} + L_0 K_{dA}} \qquad (6–90)$$

$$\lim_{[F] \to \infty} k_0 = \frac{k_2 K'_{dA} K'_{dF} + k'_2 L_0 K_{dA} K_{dF}}{K'_{dA} K'_{dF} + L_0 K_{dA} K_{dF}} \qquad (6–91)$$

it can be seen that if $K'_{dF} < K_{dF}$, $K_{dA} < K'_{dA}$, $k'_2 < k_2$, and $L_0 K_{dA} K_{dF} > K'_{dA} K'_{dF}$, then the catalytic constant k_0 will decrease as [F] approaches saturation, regardless of the concentration of reactant. It can also be seen, however, that if Equation 6–83 is factored into terms that depend on [F], then the catalytic constant is always invariant when

$$[F] < K'_{dF} \left\{ \frac{K'_{dA} K_{dF} + L_0 K_{dA} K_{dF}}{K'_{dA} K'_{dF} + L_0 K_{dA} K_{dF}} \right\} \qquad (6–92)$$

This inequality states that in certain situations there is a concentration of heterotropic allosteric inhibitor below which it will appear to be competitive, but that the inhibition observed will no longer be competitive but mixed when the concentration of inhibitor becomes greater than the concentration defined by the inequality.

In other words, unlike classical competitive inhibition, **competitive heterotropic allosteric inhibition can be conditional**. Usually all concentrations of inhibitor chosen for the measurements, by chance, are greater than this limit so that the inhibition appears to be mixed (Figures 6–3 and 6–24) or all concentrations chosen, by chance, are less than this limit so that the inhibition appears to be competitive (Figure 6–18). Occasionally, however, there are situations in which the range of concentrations chosen spans this limit, as is probably the case for heterotropic allosteric inhibition of 4-hydroxy-tetrahydrodipicolinate synthase by L-lysine (Figure 6–22), and **the inhibition can be both mixed and competitive** in different ranges of concentration for a heterotropic allosteric inhibitor.

The various limits on the properties of heterotropic allosteric inhibition of the steady-state kinetics of an enzymatic reaction, which are not observed with classical inhibition and which distinguish heterotropic behavior from classical behavior, are more easily understood by examining the state of the allosteric enzyme when the active site is saturated with reactant and the allosteric site is saturated with a heterotropic allosteric inhibitor (Equation 6–73). **At saturation with both heterotropic allosteric inhibitor and reactant, an allosteric enzyme attains a particular limiting rate that can either be that of the V conformation, that of the H conformation, or a value between** these two limiting rates. Which of these three possiblities will pertain depends on the value of the allosteric equilibrium constant $L_{A,F}$ between the fully occupied V conformation and the fully occupied H conformation.

*This inequality illustrates the fact that the kinetic mechanism of Equation 6–73 and the steady-state kinetic mechanism derived from it do not stipulate anything about the properties of the two conformations of the enzyme. It is only when the properties of the two conformations are defined in terms of their dissociation constants for one of their ligands that the inequality requires a particular inequality between the dissociation constants for another ligand.

Suppose that when the concentrations of both the heterotropic allosteric inhibitor and the reactant are at saturation, and both sites are fully occupied, the V conformation dominates ($L_{A,F} << 1$). In this instance, inhibition by a heterotropic allosteric inhibitor will be competitive at all concentrations of inhibitor because at saturation with reactant, regardless of the concentration of inhibitor, the limiting rate will always be that of the V conformation, which accounts for all of the enzyme when it is fully occupied by reactant and inhibitor.

Suppose, however, that when the concentrations of both the heterotropic allosteric inhibitor and the reactant are at saturation, and both sites are fully occupied, the H conformation predominates either partially ($L_{A,F} > 1$) or fully ($L_{A,F} >> 1$). If the H conformation has a lower catalytic constant, then competitive inhibition can be observed at low concentrations of inhibitor if the saturation by the reactant shifts the equilibrium from the H conformation promoted by the inhibitor in the absence of reactant completely to the V conformation. These low concentrations of inhibitor are unable to shift the equilibrium away from the V conformation when reactant is at saturation. At higher concentrations of the heterotropic allosteric inhibitor, however, the limiting rate must begin to decrease, as it does in the case of inhibition of 4-hydroxy-tetrahydrodipicolinate synthase by L-lysine (Figure 6–22), because saturation by the reactant is no longer able to shift the equilibrium completely to the V conformation. At high enough concentrations of inhibitor to saturate its binding site, the catalytic constant will come closer to or equal that of the H conformation (k'_2 in Equation 6–73) than that of the V conformation. How close depends on the value of $L_{A,F}$.

The inhibition of amino-acid *N*-acetyltransferase by L-arginine (Figure 6–23B) is a clearer example of this behavior. At saturating concentrations of L-arginine, the catalytic constant reaches a constant value, which is probably that of either the H conformation itself (right lower front corner of Equation 6–73) or the weighted average established by the equilibrium ratio of the V and H conformations when the concentration of L-arginine is sufficient to saturate the allosteric sites on the V conformation and the concentration of L-glutamate is sufficient to saturate the active sites on the H conformation (right lower front and right upper front corners in Equation 6–73). The inability of L-arginine to completely inhibit the reaction at any concentration is in contrast to the behavior of classical enzymatic inhibitors.

The inability of a reactant at all concentrations of inhibitor to reach the same limiting rate as its concentration is increased to infinity (Figure 6–22) and the inability of a heterotropic allosteric inhibitor at all concentrations of reactant to decrease the limiting rate of an enzymatic reaction to 0 as its concentration is increased to infinity (Figure 6–23B)—both properties of classical competitive inhibition—are consequences of the same property of heterotropic allosteric inhibition: the fact that the equilibrium constant between the fully saturated V conformation and the fully saturated H conformation, $L_{A,F}$, alone determines the limiting rate.

If, however, the H conformation has the same catalytic constant as the V conformation and only differs by having a larger dissociation constant for reactant, which is one of the simple, but unlikely, explanations for competitive heterotropic allosteric inhibition, then even if the V conformation predominates at saturation with both heterotropic allosteric inhibitor and reactant, competitive inhibition will be observed (Figure 6–18). This explanation may describe the behavior of 6-phosphofructokinase from *E. coli* for which phospho*enol*pyruvate is a competitive heterotropic allosteric inhibitor at concentrations even in the range of its dissociation constant for the V conformation.[19,151]

There are instances in which **two heterotropic allosteric inhibitors reinforce their effects** on a steady-state rate of the reaction. In the case of aspartate carbamoyltransferase, the inhibition caused by $MgUTP^{2-}$ and $MgCTP^{2-}$ together (Figure 6–3) is more effective than that of either alone.[9,94] In has already been noted that one CTP^{4-}, one UTP^{4-}, and one Mg^{2+} are accommodated by the site on each regulatory subunit of the enzyme, an unusual property that explains this behavior. The enzymatic activity of 3-deoxy-7-phosphoheptulonate synthase (see Equation 3–17)

D-erythrose 4-phosphate + phospho*enol*pyruvate + $H_2O \rightleftharpoons HOPO_3^{2-}$ + 3-deoxy-D-*arabino*-hept-2-ulosonate 7-phosphate (6–93)

from *M. tuberculosis* is inhibited allosterically[152] by the aromatic amino acids, L-tryptophan, L-phenylalanine, and L-tyrosine,[137] which are products of the respective metabolic pathways that all begin with this enzymatic reaction. Each aromatic amino acid has its own site on the enzyme so that all three can

bind simultaneously.[152] Combinations of these amino acids are more effective inhibitors than each is alone (Figure 6–26). Although the combination of L-phenylalanine and L-tyrosine (Figure 6–26B) is no more effective than either alone (Figure 6–26A), the combinations of L-tryptophan and L-tyrosine and of L-tryptophan and L-phenylalanine are more effective than either alone, and the combination of all three is more effective than any combination of two.[152] An explanation for this behavior is that each inhibitor has a dissociation constant from the H conformation that is smaller than its dissociation constant from the V conformation. The consequence of these differences is that the equilibrium constant $L_{F1,F2}$ between the V and H conformations in the absence of reactant but at saturation with two inhibitors, F1 and F2, is now $L_0K_{dF1}K_{dF2}\,(K'_{dF1}K'_{dF2})^{-1}$ instead of $L_0K_{dF}\,(K'_{dF})^{-1}$ as it is for a single heterotropic allosteric inhibitor (Equation 6–79), and the equilibrium constant at saturation with reactant and both inhibitors is $L_0K_{dF1}K_{dF2}K_{dA}\,(K'_{dF1}K'_{dF2}K'_{dA})^{-1}$ instead of $L_0K_{df}K_{dA}\,(K_{dF}'K_{dA}')^{-1}$. The differences in dissociation constants multiply together because the differences in standard free energy add together.

Heterotropic allosteric activators almost always decrease the concentration of reactant A required to produce an initial rate for an enzymatic reaction that is half the limiting rate, and they often increase the catalytic constant for the enzymatic reaction (Figure 6–3). Almost all heterotropic allosteric activation are complicated by sigmoid saturation curves resulting from the fact that each enzyme is a symmetric homooligomer that has several identical sites for binding reactants and several identical sites for binding heterotropic allosteric activators. Equations 6–82 to 6–85, however, based on the assumption that the enzyme is a monomer, can provide **qualitative explanations of the increase in the concentration of reactant required to achieve half the limiting rate and any increase in the catalytic constant**. Again, the fact that the enzyme is assumed to be a monomer eliminates the cooperativity that almost always accompanies the steady-state kinetics of an allosteric enzyme. Consequently, there is a Michaelis constant in this hypothetical case because the initial rate is always a rectangularly hyperbolic function of the concentration of reactant.

If the observed Michaelis constant is to decrease as the concentration of a heterotropic allosteric activator F increases, as is almost always observed, then the derivative of Equation 6–84 with respect to

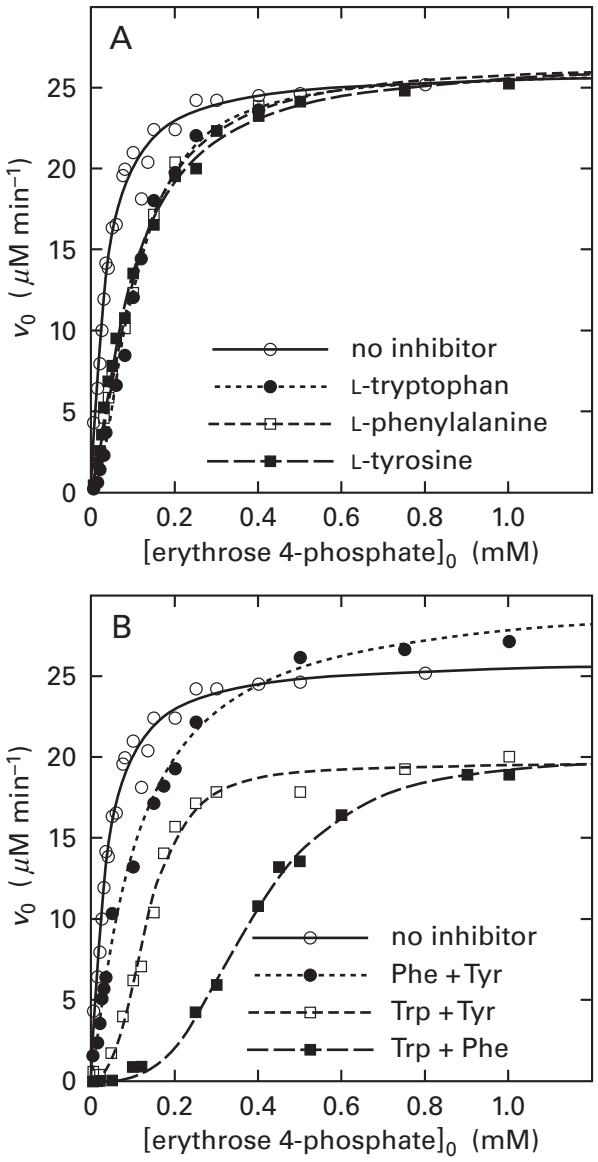

Figure 6–26: Additive heterotropic allosteric inhibition of 3-deoxy-7-phosphoheptulonate synthase from *M, tuberculosis* by L-tryptophan, L-phenylalanine, and L-tyrosine.[137] The reaction was carried out in 0.3 mM phospho*enol*pyruvate, 0.1 mM $MnSO_4$, 3,3′,3″-phosphanetriyltripropanoic acid, various concentrations of D-erythrose 4-phosphate, and 50 mM 2-[bis(2-hydroxyethyl)-amino]-2-(hydroxymethyl)propane-1,3-diol chloride at pH 7.5 and 30 °C. The reaction was initiated by adding 0.09 nmol of active sites. The decrease in the concentration of phospho*enol*-pyruvate was followed by the loss of absorbance at 232 nm. Each observed initial rate (micromolar minute^{-1}) is plotted as a function of the respective initial concentration of D-erythrose 4-phosphate (millimolar). (**A**) Initial rates in the absence of inhibitor (○) and in the presence of 200 μM L-tryptophan (●), 200 μM L-phenylalanine (□), or 200 μM L-tyrosine (■). (**B**) Initial rates in the absence of inhibitor (○) and in the presence of 100 μM L-phenylalanine and 100 μM L-tyrosine (●), 100 μM L-tryptophan and 100 μM L-tyrosine (□), or 100 μM L-tryptophan and 100 μM L-phenylalanine (■). The curves are fits of Equation 3–44 or 6–36, as appropriate, to the data.

the concentration of the activator must be less than 0. For the derivative to be negative, it must be the case that

$$(K'_{dF} - K_{dF})(K_{dA} - K'_{dA}) < 0 \qquad (6\text{–}94)$$

If $K_{dA} < K'_{dA}$, it follows that if the Michaelis constant is to decrease in the presence of a heterotropic allosteric activator, which requires the derivative to be less than 0, then $K_{dF} < K'_{dF}$. As expected, **a heterotropic allosteric activator must have a greater affinity for the V conformation than for the H conformation**.

Because the curves for heterotropic allosteric activation rarely if ever cross, the **limiting rate of the enzymatic reaction** in the presence of a heterotropic allosteric activator must be greater than or equal to the limiting rate in its absence. If the observed catalytic constant is to increase or stay the same as the concentration of a heterotropic allosteric activator F increases, as is almost always observed, then the derivative of Equation 6–83 with respect to the concentration of effector must be equal to or greater than 0. For this to be so, it must be the case that

$$0 \le (k'_2 - k_2)(K_{dF} - K'_{dF}) \qquad (6\text{–}95)$$

Because $K_{dF} < K'_{dF}$, it follows that if the catalytic constant is to stay the same or increase in the presence of a heterotropic allosteric activator, which requires the derivative to be equal to or greater than 0, then it must be the case that $k'_2 \le k_2$.

By examining Equation 6–83, however, it can be seen that if $k'_2 < k_2$, $K_{dA} < K'_{dA}$, and $K_{dF} < K'_{dF}$, so that a heterotropic allosteric activator increases the catalytic constant, then the increase will be significant only if $L_0K_{dA} < K'_{dA}$. If $L_0K_{dA} < K'_{dA}$, then the enzyme will be almost completely in the V conformation at saturation with reactant A in the absence of heterotropic allosteric activator, and addition of the activator can have little effect on k_0 and hence the limiting rate of the enzymatic reaction (Figure 6–24).* If, however, $L_0K_{dA} > K'_{dA}$, then **saturating concentrations of reactant A alone will be unable to shift the equilibrium completely in favor of the V conformation** (Equation 6–73), and addition of a heterotropic allosteric activator will increase the catalytic constant. For example, the fact that $MgATP^{2-}$ and $MgGTP^{2-}$ increase the initial rate of the reaction catalyzed by aspartate carbamoyltransferase even at saturation with L-aspartate (Figure 6–3) indicates that, under these conditions, saturating concentrations of L-aspartate are insufficient to draw the enzyme completely into the V conformation. Another explanation for such an observation would be that there was a third conformation into which the activator could draw the enzyme with an even greater limiting rate than that of the V conformation.

Finally, by taking the limit of Equation 6–83 at which the concentration of heterotropic allosteric activator goes to infinity, it can be seen that if $L_0K_{dA}K_{dF} < K'_{dA}K'_{dF}$ and

$$[A] > K_{dA}\left(\frac{K'_{dF} + L_0K_{dF}}{K'_{dF}}\right) \qquad (6\text{–}96)$$

then the catalytic constant will be equal to k_2. Above this concentration of reactant A, a saturating concentration of reactant is able to shift the equilibrium completely in favor of the V conformation, which has a catalytic constant of k_2 (Figure 6–25) regardless of the concentration of heterotropic allosteric activator. In this case, a heterotropic allosteric activator will be unable to increase the catalytic constant.

In enzymes that do not display heterotropic allosteric behavior, reactants often inhibit the enzymatic activity at higher concentrations (previously Equation 3–256)

$$v_0 = \frac{k_0[E]_t k_A[E]_t[A]_0}{k_0[E]_t + k_A[E]_t[A]_0\left(\frac{K_{iA} + [A]_0}{K_{iA}}\right)} \qquad (6\text{–}97)$$

but are rarely, if ever, able to activate an enzymatic reaction by associating at the active site. **Reactants, however, can activate the enzymatic reaction in which they participate by associating with a heterotropic allosteric site**. For example, L-phenylalanine activates phenylalanine 4-monooxygenase by associating with an allosteric site distinct from the active site in which L-phenylalanine is hydroxylated,[153,154] and pyruvate heterotropically activates pyruvate decarboxylase from *S. cerevisiae*[155] by associating with an allosteric site[156] distinct from the active site in which pyruvate is decarboxylated.

*Again, a trivial, but unlikely, explanation for the invariance of k_0 as the concentration of allosteric activator is increased is that $k_2 = k'_2$.

So far, only the effects of heterotropic allosteric inhibitors or activators on the steady-state kinetics of the overall enzymatic reaction have been examined, again with the caveat that association of reactant must be at equilibrium during its turnover and the enzymatic reaction be occurring at steady state. This latter requirement is met in the cytoplasm where the control of metabolism occurs, but a more comprehensive understanding of the actual mechanism of inhibition or activation can be gained by identifying the **steps in the kinetic mechanism controlled by a heterotropic allosteric effector**. For example, by following the pre-steady-state kinetics of 2-isopropylmalate synthase from *M. tuberculosis* by quenched flow, it could be shown that the heterotropic allosteric inhibitor L-leucine[157] decreases the rates of chemical steps transforming the reactants, acetyl-SCoA and 3-methyl-2-oxobutanoate, into the products, (2*S*)-2-isopropylmalate and coenzyme A. Consequently, the rate-limiting step of the enzymatic reaction, which is the release of products in the absence of inhibitor, becomes the production of the undissociated products on the active site in the presence of inhibitor, and the inhibitor acts by changing the rate-limiting step in the enzymatic reaction.[158] In the case of pyruvate carboxylase (previously Equation 5–229)

$$\text{pyruvate} + HOCO_2^- + MgATP^{2-} \rightleftharpoons HOPO_3^{2-} + MgADP^- + H^+ + \text{oxaloacetate} \quad (6\text{–}98)$$

from *Gallus gallus*, it could be shown by quenched flow that the heterotropic allosteric activator acetyl-SCoA[159] increases the rate of formation of 1-(*N*-carboxy)biotin on the active site by a factor of 200.[160]

To this point, qualitative explanations of heterotropic allosteric inhibition have been provided by examining the behavior of an allosteric monomer. It is possible, however, to derive a kinetic equation that describes heterotropic allosteric behavior of an allosteric oligomer as well as cooperativity of association of heterotropic allosteric effectors and substrates or reactants.

The kinetic mechanism for allosteric effects (Equation 6–73) can be combined with the equilibrium mechanism for cooperativity (Equation 6–33) to obtain an expanded rate equation that can be fit to experimental results in which both heterotropic allosteric effects and cooperativity are observed. This expansion, however, assumes that the **same symmetric quaternary conformational change** between only two conformations that is responsible for cooperativity is the same one that causes heterotropic allosteric inhibition. Consequently, by the usual convention, these two conformations will now be designated the R and T conformations. It should be kept in mind, however, that if this particular explanation of the observed behavior is consistent with a set of observations of the steady-state kinetics of an enzymatic reaction, then explanations involving more than two quaternary conformations must also be consistent.

Pyruvate kinase (Equation 6–29) from *O. cuniculus* is allosterically inhibited by L-phenylalanine (Figure 6–27A).[30] This inhibition regulates the concentration of phospho*enol*pyruvate, a precursor of the aromatic amino acids. Its carbon skeleton eventually becomes the carboxy carbon, the α carbon, and the β carbon of L-phenylalanine and L-tyrosine. Formally, in the range of concentrations examined, L-phenylalanine (Phe) is a competitive inhibitor with respect to phospho*enol*pyruvate (PEP) because it changes only the apparent specificity constant k_{PEP} for phospho*enol*pyruvate and the concentration of phospho*enol*pyruvate at which the enzymatic rate is half the limiting rate, but it does not change the limiting rate of the enzymatic reaction.[161]

Pyruvate kinase is a homotetramer, rather than a monomer; and in the presence of sufficient concentrations of the heterotropic allosteric inhibitor L-phenylalanine, the initial rate of the enzymatic reaction is a cooperative function of the concentration of the reactant phospho*enol*pyruvate (Figure 6–27A). It has been demonstrated, by direct measurement of the binding of phospho*enol*pyruvate to pyruvate kinase (Figure 6–27B), that the observed Michaelis constant for this reactant is equal to its observed dissociation constant in the absence of L-phenylalanine.* In the presence of L-phenylalanine, the concentration of phospho*enol*pyruvate at which the initial rate of the enzymatic reaction is half the limiting rate is also the same as the concentration at which half the active sites are occupied.[161] Consequently, the initial rate of the enzymatic reaction was assumed to be directly proportional to the occupation of the active sites by phospho*enol*pyruvate and determined only by its dissociation constant and its concentration, as required by the kinetic mechanism of Equation 6–73.

*In the absence of L-phenylalanine, the initial rate as a function of phospho*enol*pyruvate is rectangularly hyperbolic and has a Michaelis constant.

Because pyruvate kinase is a symmetric homotetramer of four identical subunits, each of which can bind a molecule of L-phenylalanine and each of which has an active site, the kinetic mechanism of Equation 6–73 must be expanded to account for association of four molecules of L-phenylalanine to four identical heterotropic allosteric sites and four molecules of phospho*enol*pyruvate to four identical active sites on each molecule of pyruvate kinase in both the T and R conformations. Equation 6–73 has been **expanded to include all 25 states of occupation for the tetramer in the R conformation and all 25 states of occupation for the tetramer in the T conformation**, and the states of occupation were connected by 25 allosteric constants and 32 dissociation constants to produce a $2\times5\times5$ linkage network, which is too large to reproduce here. In effect, the kinetic mechanism of Equation 6–73 was multiplied by the linkage relation for association of both reactant and inhibitor of Equation 6–33 to produce the expanded kinetic mechanism.[30]

It has been shown that such a multiplication produces, as the equation for dependence of the initial rate for an enzymatic reaction as a function of the concentration of reactant A

$$\frac{v_0}{[\mathrm{E}]_t} = \frac{k_{0,\mathrm{T}}\,L\,\dfrac{[\mathrm{A}]}{K'_{\mathrm{dA}}}\left(1+\dfrac{[\mathrm{A}]}{K'_{\mathrm{dA}}}\right)^{n-1} + k_{0,\mathrm{R}}\,\dfrac{[\mathrm{A}]}{K_{\mathrm{dA}}}\left(1+\dfrac{[\mathrm{A}]}{K_{\mathrm{dA}}}\right)^{n-1}}{L\left(1+\dfrac{[\mathrm{A}]}{K'_{\mathrm{dA}}}\right)^{n} + \left(1+\dfrac{[\mathrm{A}]}{K_{\mathrm{dA}}}\right)^{n}} \qquad (6\text{–}99)$$

where

$$L = L_0\,\frac{\left(1+\dfrac{[\mathrm{F_{inh}}]}{K'_{\mathrm{d,inh}}}\right)^{n}\left(1+\dfrac{[\mathrm{F_{act}}]}{K'_{\mathrm{d,act}}}\right)^{n}}{\left(1+\dfrac{[\mathrm{F_{inh}}]}{K_{\mathrm{d,inh}}}\right)^{n}\left(1+\dfrac{[\mathrm{F_{act}}]}{K_{\mathrm{d,act}}}\right)^{n}} \qquad (6\text{–}100)$$

where $\mathrm{F_{inh}}$ is a heterotropic allosteric inhibitor, $\mathrm{F_{act}}$ is a heterotropic allosteric activator, and the dissociation constants are as follows: $K_{\mathrm{d,inh}}$ is for inhibitor $\mathrm{F_{inh}}$ from the R conformation, $K'_{\mathrm{d,inh}}$ is for inhibitor $\mathrm{F_{inh}}$ from the T conformation, $K_{\mathrm{d,act}}$ is for activator $\mathrm{F_{act}}$ from the R conformation, and $K'_{\mathrm{d,act}}$ is for activator $\mathrm{F_{act}}$ from the T conformation.[19] Notice that, mathematically, no distinction is made between a heterotropic allosteric inhibitor and a heterotropic allosteric activator. Only when the dissociation constant of the effector is smaller for the T conformation than for the R conformation will the effector be a heterotropic allosteric inhibitor. and only when its dissociation constant is smaller for the R conformation than the T conformation will the effector be a heterotropic allosteric activator. In effect, because their concentrations are constant, because none is chemically altered by the reaction, and because their association with the allosteric sites is always at equilibrium, the presence of heterotropic allosteric effectors simply shifts the value for the equilibrium constant between the R and T conformations. This shifted equilibrium constant then governs the cooperative association of reactant A. Again the assumption behind all these equations is that associations of reactants are always at equilibrium, irrespective of the progress of the enzymatic reaction.

Table 6–1: Equilibrium Constants and Rate Constants for Pyruvate Kinase[30]

equilibrium constant or rate constant[a]	numerical value
L_0	0.094 ± 0.03
K_{dPEP}	$44 \pm 2\ \mu$M
K'_{dPEP}	$440 \pm 40\ \mu$M
$K_{\mathrm{d,Phe}}$	14 ± 3 mM
$K'_{\mathrm{d,Phe}}$	0.6 ± 0.07 mM
k_2	$920 \pm 110\ \mathrm{s^{-1}}$
k'_2	$90 \pm 70\ \mathrm{s^{-1}}$

[a]The numerical values listed are from fits of the expanded MWC equation to the values of the observed initial rates in steady-state kinetics. The dissociation constants are for phospho*enol*pyruvate (PEP) from the active site and L-phenylalanine (Phe) from the heterotropic allosteric site.

The rate equation derived from this expanded kinetic mechanism, where there is only the heterotropic allosteric inhibitor L-phenylalanine ($[\mathrm{F_{act}}] = 0$), could be fit satisfactorily to the observations (Figure 6–27A). From these fits, values for the equilibrium constant L_0 and the various dissociation constants in the proposed kinetic mechanism (Equation 6–73) were obtained (Table 6–1).[30] The fit of the equations to the data was satisfactory even though it was assumed that association of phospho*enol*pyruvate

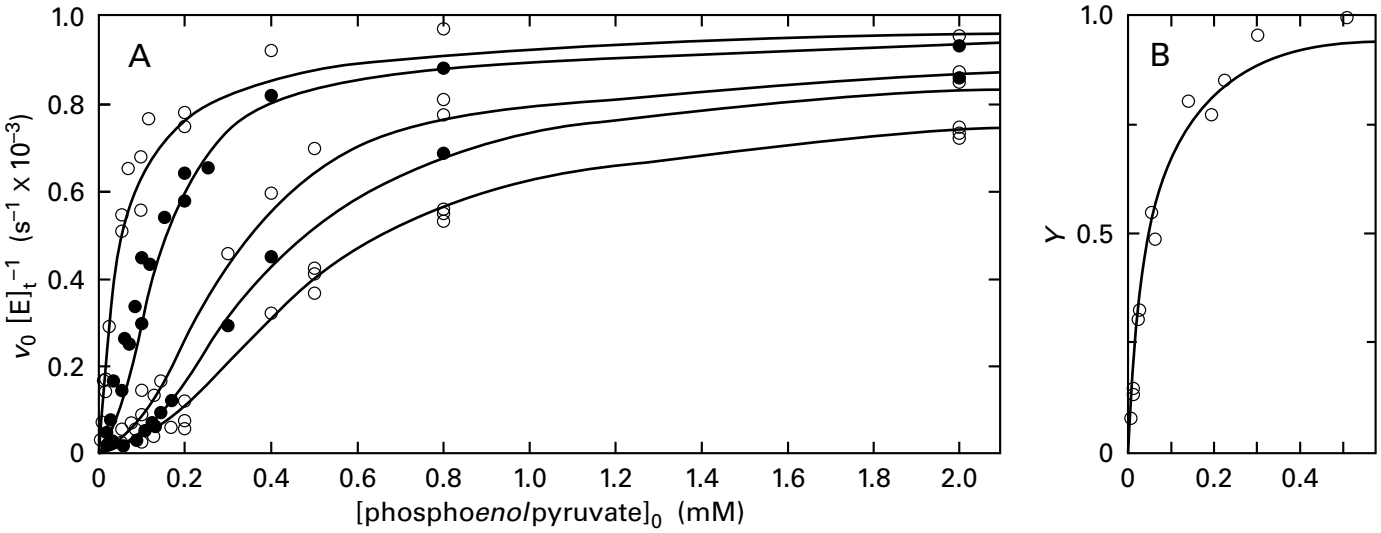

Figure 6–27: Heterotropic allosteric inhibition of pyruvate kinase from *O. cuniculus* by L-phenylalanine and a demonstration that the Michaelis constant and the dissociation constant of phospho*enol*pyruvate from the enzyme are the same.[30] (**A**) Heterotropic allosteric inhibition. Solutions contained 72 mM KCl, 7.2 mM $MgSO_4$, 2.0 mM ADP^{3-}, 0.3 mM NADH, 0.3 μM in active sites of L-lactate dehydrogenase, variable amounts of phospho*enol*pyruvate, variable amounts of L-phenylalanine, and 50 mM 2-ammonio-2-hydroxymethylpropane-1,3-diol chloride, pH 7.5 and 23 °C. Each reaction was initiated by adding pyruvate kinase, and the rate of production of pyruvate was followed by coupling its consumption to the consumption of NADH (λ_{max} = 339 nm) by L-lactate dehydrogenase. Initial rates were calculated from the decrease in absorbance at 340 nm. Each initial rate was divided by the concentration of active sites of pyruvate kinase in the assay ($v_0\,[E]_t^{-1}$ in second^{-1}), and each of these initial rate constants is plotted as a function of the respective initial concentration of phospho*enol*pyruvate (millimolar). Each set of assays had, in descending order 0, 3, 7, 9, or 12 mM L-phenylalanine. The curves are fits of a rate equation for the kinetic mechanism of Equation 6–73 that has been expanded to account for association of four molecules of L-phenylalanine and four molecules of phospho*enol*pyruvate to four identical heterotropic allosteric sites and four identical active sites, respectively, on each molecule of pyruvate kinase in both the T and R conformations. (**B**) Binding of phospho*enol*pyruvate to pyruvate kinase. Binding was measured by molecular exclusion at pH 7.5 and 23 °C. Solutions (0.55 mL) containing pyruvate kinase (150–350 μM in active sites) and various concentrations of [^{14}C]phospho*enol*pyruvate were mixed with 50 mg of dehydrated beads of Sephadex G-50. The Sephadex imbibed a certain amount of the fluid. It was assumed that the free phospho*enol*pyruvate equilibrated between the fluid in the interior of the beads and solution surrounding the beads while the protein remained entirely outside the beads. From the volume of fluid added, the total amount of protein added, the total amount of phospho*enol*pyruvate added, the molar concentration of phospho*enol*pyruvate in the fluid outside the beads (as determined by scintillation counting) and the molar concentration of protein in the fluid outside the beads (as determined by the absorbance at 280 nm), the moles of phospho*enol*pyruvate bound to each mole of active sites could be calculated as a function of the free concentration of phospho*enol*pyruvate (millimolar). The points are the experimental determinations. The line is drawn on the basis of the assumption that the dissociation constant for phospho*enol*pyruvate is the same as the numerical value (0.44 mM) for the Michaelis constant observed kinetically in Panel A. The scale of the axis of the abscissa is the same as the scale in Panel A to facilitate comparison.

to either the R or the T conformation is unaffected by association of L-phenylalanine and that association of L-phenylalanine to either the R or the T conformation is unaffected by association of phospho*enol*pyruvate, as should be the case for this explanation of heterotropic allosteric inhibition (see Equations 6–74 to 6–77).

Both homotropic cooperativity of the initial rate of the reaction catalyzed by pyruvate kinase as a function of the concentration of phospho*enol*pyruvate (PEP) in the presence of sufficient concentrations of L-phenylalanine (Phe) and heterotropic inhibition of the activity of the enzyme by L-phenylalanine (Figure 6–27A) can be **explained simultaneously by the expanded kinetic mechanism based on the existence of only two symmetric quaternary conformations of the enzyme**, R and T, the equilibrium between which is shifted in one direction by phospho*enol*pyruvate and in the other direction by L-phenylalanine. L-Phenylalanine inhibits pyruvate kinase by shifting the conformational equilibrium in favor of the T conformation, which has a lower affinity for phospho*enol*pyruvate (K'_{dPEP} = 440 μM and K_{dPEP} = 44 μM) and a lower catalytic constant (k'_2 = 90 s^{-1} and k_2 = 920 s^{-1}). This shift is accomplished because L-phenylalanine has a greater affinity for the T conformation ($K'_{d,Phe}$ = 0.6 mM and $K_{d,Phe}$ = 14 mM) than it does for the R conformation.

The fundamental allosteric constant is less than 1($L_0 = 0.094$), so pyruvate kinase, unlike aspartate carbamoyltransferase (Figure 6–13), is already mostly in the R conformation in the absence of L-phenylalanine and phospho*enol*pyruvate. Consequently, the initial rate of the enzymatic reaction, in the absence of L-phenylalanine, is a rectangularly hyperbolic function of the concentration of phospho*enol*pyruvate (Figure 6–27A) because association of phospho*enol*-pyruvate can only increase the predominance of the R conformation. At concentrations of L-phenylalanine sufficient to shift the conformational equilibrium in favor of the T conformation, **association of phospho*enol*pyruvate becomes cooperative** because its dissociation constant from the R conformation is smaller than its dissociation constant from the T conformation. Because the binding of L-phenylalanine shifts the conformational equilibrium from one in favor of the R conformation in the absence of ligands to one in favor of the T conformation, its association with the otherwise unoccupied enzyme is cooperative (Figure 6–28).

If only a manageable portion of the expanded $2 \times 5 \times 5$ linkage network[30] is examined

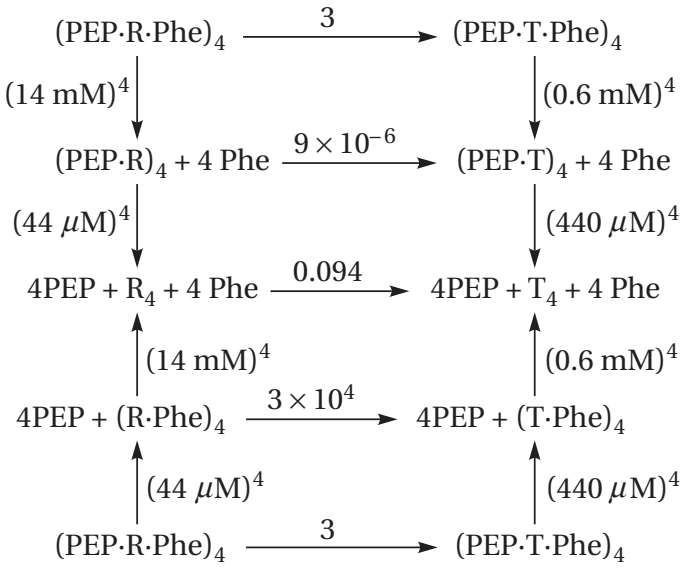

(6–101)

it can be seen that as L-phenylalanine is added to the solution, the equilibrium between the two conformations shifts in favor of the T conformation; and as phospho*enol*pyruvate is added to the solution, it shifts in favor of the R conformation. When the concentration of L-phenylalanine is high enough to saturate the R conformation, pyruvate kinase exists primarily ($L_{\text{Phe,PEP}} = 3$) in the T conformation regardless of how high the concentration of phospho*enol*-pyruvate is. Unlike the case of classical steric competition, saturating concentrations of phospho*enol*pyruvate cannot drive L-phenylalanine off the enzyme because the active site is distant from the heterotropic allosteric site. If $L_{\text{Phe,PEP}} = 3$, competitive inhibition should be observed at low concentrations of inhibitor, as is observed (Figure 6–27A); but as the concentration of heterotropic allosteric inhibitor increases, the limiting rate should begin to decrease; and at high enough concentrations of inhibitor, the limiting rate should be closer to that of the T conformation (K'_2 in Equation 6–73) than that of the R conformation. Unfortunately, in the case of pyruvate kinase, high enough concentrations of L-phenylalanine to observe the decrease in limiting rate ([Phe] > 14 mM), which would have been a further justification of the procedure, simply were not used in the measurements (Figure 6–27A), although an examination of the graph at the highest concentrations of L-phenylalanine used (12 mM) suggests that the inhibition is not competitive.

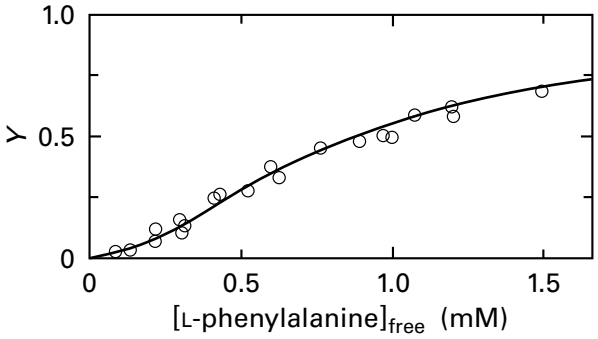

Figure 6–28: Binding of L-phenylalanine to pyruvate kinase from *O. cuniculus*.[30] The binding of [^{3}H]-L-phenylalanine to the enzyme was measured by equilibrium dialysis at pH 7.5 and 23 °C. A solution containing 210 μM pyruvate kinase was placed in one compartment, and a solution of [^{3}H]-L-phenylalanine of an appropriate molar concentration was placed in the other compartment. After equilibrium had been reached (20 h), the final concentration of the protein in its compartment (as determined by absorbance at 280 nm) and the final concentrations of L-phenylalanine in each compartment (as determined by scintillation counting) in each compartment were assessed. From these concentrations, the free concentration of L-phenylalanine as well as the moles of L-phenylalanine bound for each mole of the tetrameric enzyme could be calculated for each measurement. The fractional saturation (Y) is plotted as a function of the free concentration of L-phenylalanine (millimolar). The smooth curve was a fit of Equation 6–35 to the data using the conformational equilibrium constant and the dissociation constants for L-phenylalanine from the R conformation, $K_{\text{d,Phe}}$, and the T conformation, $K'_{\text{d,Phe}}$, of the enzyme that were obtained from the curves in Figure 6–27A (Table 6–1).

The sum of all the conformational changes that produce both cooperativity and heterotropic allosteric effects is observed crystallographically. It should now be clear from the foregoing discussion that there are **several levels of conformational changes** that usually occur in such an enzyme that displays both heterotropic allosteric behavior and cooperativity. First, there are the **local conformational changes** that occur upon association of a heterotropic allosteric effector or association of one or more substrates for the enzyme and are confined to the immediate vicinity of the respective site. Second, there are conformational **changes that occur within the individual subunits** that could be responsible for the observed heterotropic allosteric behavior but may not elicit a quaternary conformational change. Third, there are the **quaternary conformational changes** that are responsible for cooperativity. These quaternary conformational changes could also be responsible for heterotropic allosteric behavior because, as these changes occur, the affinities of the symmetrically displayed heterotropic allosteric sites as well as the active sites change.

One might believe, and many do, that molecular details of the conformational changes that enable heterotropic allosteric behavior to occur should be able to be gathered from examination of crystallographic molecular models of the two or more conformations involved. For example, significant changes occur around the allosteric site in the two conformations of chorismate mutase from *S. cerevisiae*: the V conformation, crystallized with the heterotropic allosteric activator L-tryptophan bound in the allosteric site, and the H conformation, crystallized with the heterotropic allosteric inhibitor L-tyrosine in the allosteric site (Figure 6–21). In addition to a number of reorientations of the side chains in the vicinity of the site, two α helices surrounding the site have shifted in their relative orientation. The enzyme, however, also undergoes a quaternary conformational change between the H and V conformations that involves the entire α_2 dimer.[133] The conformation of an enzyme with high affinity for a particular ligand that is studied crystallographically is usually produced by fully occupying sites on the protein with that ligand, as was the case with chorismate mutase, and it is usually also rotationally symmetric. In such a situation, the local conformational changes, the conformational changes that might be confined to an individual subunit, and the quaternary conformational change have all occurred together and have all been completed. In such a situation, local conformational changes that occur around sites for ligands and substrates and that result only from the binding of the ligand itself are **difficult, if not impossible, to distinguish** from conformational changes confined to an individual subunit and from quaternary conformational changes.

Although crystallographic observations are necessary to define the sum of all the various conformational changes in atomic detail, **other methods are often used to detect particular conformational changes while an enzyme is in solution.** Many examples of these chemical and physical methods normally used to study the structure of native proteins were presented when the cooperativity of aspartate carbamoyltransferase was discussed earlier, but the same physical methods can be used to monitor the conformational changes that mediate heterotropic allosteric effects. For example, isopropyl β-D-thiogalactoside, an analogue of a natural heterotropic allosteric activator, is bound by *lac* repressor from *E. coli* (an α_4 homotetramer) in the absence of DNA. Upon binding, a change in the optical spectrum of *lac* repressor is observed, which indicates alterations in the environments around its tyrosines. Changes in the circular dichroic spectrum and sedimentation coefficient of the protein are also observed.[65,162] In another example, changes in the conformation of hemoglobin documented crystallographically can be followed by observing changes in nuclear magnetic resonance spectra.[163]

The rate of deuteration of the amido nitrogens in segments of the folded polypeptide comprising 4-hydroxy-tetrahydrodipicolinate synthase from *C. jejuni* could be followed by mixing the enzyme with deuterium oxide, removing samples at various times, quenching the deuterium exchange with acid, digesting the unfolded polypeptide with pepsin at low pH, separating the resulting peptic peptides chromatographically, and determining their mass by mass spectrometry. It was found that segments of polypeptide surrounding the active site became less susceptible to deuterium exchange in the presence of L-lysine, a heterotropic allosteric inhibitor (Figure 6–22) of the enzyme. These results suggested that the inhibitor was decreasing the conformational dynamics around the active site because the T conformation was more rigid in this region than the R conformation.[164] Because the active site in the crystallographic molecular model of the enzyme, an α_4 homotetramer, is buried and access to it appears limited,[165] it was proposed that the increase in rigidity observed for the T conformation decreases the rate for association of the reactant L-aspartate-4-semialdehyde with the active site when the enzyme is in

this conformation. At high enough concentrations of L-lysine to cause the T conformation to predominate even in the presence of saturating concentrations of L-aspartate-4-semialdehyde, the limiting rate of the enzymatic reaction decreases (Figure 6–22) because of this rigidification.

In 6-phosphofructokinase (Equation 6–28) from *O. cuniculus*, an α_4 homotetramer, there is a side chain of cysteine in each subunit that reacts preferentially with fluorodinitrobenzene. When a heterotropic allosteric activator of the enzymatic reaction, such as AMP^{2-}, is bound to the enzyme, the rate of this arylation increases. When a heterotropic allosteric inhibitor, such as citrate, is bound, however, the rate decreases.[166] It was assumed that the rate of this reaction responds to shifts in the orientation of amino acids surrounding the cysteine that result from a conformational change in the protein the equilibrium for which is shifted by association of the effectors.

Glycogen phosphorylase *a* (Equation 6–66) from *O. cuniculus*, an α_4 homotetramer, can be modified at a cysteine in each of its subunits by *N*-(1-oxyl-2,2,6,6-tetramethyl-4-piperidinyl)iodoacetamide to introduce a stable radical into the protein. The electron paramagnetic resonance spectrum of this radical shifts, presumably in response to a conformational change in the protein, when AMP^{2-}, a heterotropic allosteric activator of the enzymatic activity, is bound by the enzyme.[68]

If the shifts in equilibria between particular quaternary conformations of an enzyme, brought about by association of ligands and accomplished by thermodynamic linkage, produce a heterotropic allosteric effect and also cooperativity, then it must be the case that these equilibria exist in both the presence and the absence of ligands. For example, in the case of chorismate mutase from *S. cerevisiae*, it seems reasonable to assume that in the absence of ligands there are two conformations of the enzyme: one in which the allosteric site fits L-tryptophan and one in which the allosteric site fits L-tyrosine. From the atomic details of the two respective conformations of the allosteric site when they are occupied in turn by these heterotropic allosteric ligands (Figure 6–21), it can be seen that each conformation would almost exclude the other ligand and that the equilibrium between them would surely be shifted by thermodynamic linkage in one direction by L-tryptophan and in the other direction by L-tyrosine.

That such an equilibrium exists between two conformations in the presence of ligands is clear from results such as those displayed in Figures 6–13 and 6–21.[167,168] It has been far more **difficult to prove** that equilibria between allosteric conformations of a protein exist in the absence of ligands. The reason for this difficulty is that the equilibrium constants are usually significantly different from 1. For example, it can be estimated that, in the absence of ligands, the equilibrium constant L_0 (Equation 6–24) for conversion of the R conformation into the T conformation for aspartate carbamoyltransferase from *E. coli*[54] is around 200 and that for 6-phosphofructokinase from *E. coli*[19] is around 4×10^6. In such situations, it is impossible to measure the small amount of R conformation that should be present in solution in the absence of ligands. In many instances, the equilibrium favors the R conformation in the absence of ligands,[37,142,169,170] but the equilibrium constant in these cases is usually much less than 1.

Serendipitously, in at least one of these latter cases, that of pyruvate kinase (Equation 6–29) from *O. cuniculus*, the equilibrium constant L_0 has been estimated to be 0.1 (Equations 6–100 and 6–101). If this is so, in the absence of ligands, even though the R conformation predominates, about 9% of the enzyme should be in the T conformation. L-Phenylalanine is a heterotropic allosteric inhibitor of pyruvate kinase. Therefore, L-phenylalanine alone should be able to shift the equilibrium distribution between the two conformations in one direction while phospho*enol*pyruvate alone, a reactant that displays cooperativity,[30] should be able to shift it in the other. L-Phenylalanine decreases the sedimentation velocity of pyruvate kinase relative to that when the enzyme is unoccupied ($\Delta s_{20,w} = -0.24$ S), and phospho*enol*pyruvate increases the sedimentation velocity relative to that when the enzyme is unoccupied ($\Delta s_{20,w} = +0.11$ S).[161] From scattering of neutrons at low angles, it can be calculated that association of L-phenylalanine with unliganded pyruvate kinase increases its radius of gyration by 0.08 ± 0.02 nm, and association of phospho*enol*pyruvate with the unliganded enzyme decreases its radius of gyration by 0.06 ± 0.02 nm.[171] L-Phenylalanine increases by 10-fold the rate of reaction of cysteines in the protein with dithiobis(2-nitrobenzoate), and phospho*enol*pyruvate decreases this rate by 5-fold.[161] Each physical and chemical property should be monitoring the average of the two conformations at equilibrium in the absence of either ligand. These observations are consistent with the two respective ligands pulling by linkage in opposite

directions on **a conformational equilibrium that exists in the absence of any ligand**, but they cannot exclude the possibility that the conformations present in the absence of the ligands are only the two that are assumed by the enzyme in the presence of heterotropic allosteric inhibitors and activators.[172]

In another serendipitous instance, the R conformation of 6-phosphofructokinase (Equation 6–28) from *E. coli* crystallized from a solution of the enzyme that did not contain any of its substrates or heterotropic allosteric effectors even though, as has been noted, the equilibrium constant L_0 between the T and R conformations has been estimated to be heavily in favor (4×10^6) of the T conformation in this situation.[43] This outcome certainly suggests that, in this case, the R conformation is present in solution and in equilibrium with the T conformation and that the crystallization itself pulled this equilibrium in the direction of the R conformation by mass action. In every other case with other proteins, however, the T conformation is expected to predominate in a solution that crystallizes in the absence of substrate and heterotropic allosteric effectors.

One approach to this problem of demonstrating that the equilibrium exists in the absence of ligands is to discover a **mutant of the enzyme in which the equilibrium in the absence of ligands has been altered** so that it is in a measurable range. For example, mutation of Lysine 143 in the regulatory β subunits of aspartate carbamoyltransferase to alanine shifts the equilibrium constant between the R and T conformation to a value of 2.7 ± 0.8, a range in which the equilibrium can be monitored by sedimentation velocity.[173] Addition of $MgCTP^{2-}$ shifts the equilibrium constant to 30 ± 20, and addition of $MgATP^{2-}$ shifts the equilibrium constant to 0.2 ± 0.1. When Aspartate 236 in the catalytic α subunit of aspartate carbamoyltransferase from *E. coli* is mutated to alanine, an equilibrium between at least two conformations of the mutant enzyme with an equilibrium constant or constants in the range 0.5–2 can be observed by scattering of X-rays at small angles.[174] This equilibrium shifts to a scattering profile resembling that of the R conformation of the wild-type enzyme upon addition of *N*-(phosphonacetyl)-L-aspartate, and it shifts to a scattering profile closely resembling that of the T conformation of the wild-type enzyme upon addition of $MgCTP^{2-}$.

In spite of the few instances in which the equilibrium between two unoccupied conformations of a heterotropic allosteric enzyme have been directly observed, the possibility must be considered that the conformation or conformations that predominate when the allosteric sites or active sites are occupied cannot exist when these sites are unoccupied.

Crystallographers often succumb to the temptation to identify a "path of conformational changes [that] transmit the inhibitory signal"[175] from an allosteric site to the active site of the enzyme.[118,133] For example, in the case of ATP phosphoribosyltransferase from *P. arcticus*, a detailed, linear mechanical explanation was provided for the allosteric inhibition of the enzyme by histidine.[118] The idea is that there is a concerted set of shifts in the positions and orientations of side chains, polypeptide backbone, and portions of interfaces between subunits, usually chosen by the crystallographer to lie directly between the allosteric site and the active site, that mechanically conveys the information that an effector resides in the allosteric site to the active site without relying on preexisting conformational changes of the protein.[176] One difficulty with such an explanation is that there is no way to validate it. For example, if amino acids participating in such a path are mutated to interfere with the changes observed, the fact that such mutations interfere with a heterotropic allosteric effect is not a validation because such mutations must affect the equilibrium between the two quaternary conformations one way or the other, if that equilibrium actually exists, to the same extent that they disrupt the particular region around the mutation itself, and this effect on the equilibrium would explain the interference of the allosteric effect.

When aspartate carbamoyltransferase from *E. coli* is locked in the R conformation by disulfides between cysteines inserted in place of its Alanines 241 (Figure 6–8), the enzyme, although it is fully active, no longer displays heterotropic allosteric inhibition by $MgCTP^{2-}$ or heterotropic allosteric activation by $MgATP^{2-}$, even though any mechanical path for communication between the allosteric site and active site should not be affected by the alteration. When these disulfides are eliminated by thiol–disulfide exchange with an added thiol, heterotropic allosteric inhibition and activation are restored to the normal levels.[24] Locking of the enzyme in the R conformation prevented the allosteric communication, not some interference in a path between the sites.* The fact that association of either $MgCTP^{2-}$

*In a related example, malate dehydrogenase ($NADP^+$) from *Sorghum bicolor* is allosterically activated by light. In the dark, a disulfide between two cysteines in the enzyme locks it in an inactive T conformation. Illumination activates photosynthesis, producing reduced ferredoxin that ultimately leads to reduction of the disulfide and enables the equilibrium between the inactive T and active R conformations to be established.[178]

or $MgATP^{2-}$ with the allosteric sites on the regulatory β subunits of aspartate carbamoyltransferase in the R conformation has no effect on the chemical shifts of protons on the methyl groups of isoleucines, valines, and leucines in the catalytic α subunits is also consistent with the conclusion that there is no path of conformational changes mechanically altering the active site upon association of the effectors.[179]

Nevertheless, in this view, the ligands themselves mechanically induce the protein to assume the respective conformation or conformations. Large quaternary conformational changes are observed upon association of molecular oxygen with hemoglobin (Figure 6–1), association of *N*-(phosphonacetyl)-L-aspartate with aspartate carbamoyltransferase (Figure 6–2), association of magnesium 5′-adenylic imidodiphosphonic anhydride ($MgAMPPNP^{2-}$) with aspartate kinase (Figure 6–29),[177] and association of AMP^{2-} with fructose-bisphosphatase.[37] It is difficult to believe that association of such small ligands, which upon association are only minor players in the structures of each complex, can somehow physically induce such significant changes in the structures of such large proteins when those changes in structure do not already preexist in a conformation in equilibrium with the unoccupied conformation. Furthermore, if the ligand were able to perform this feat, there would have to be no significant steric or electronic interaction preventing this purportedly sterically enforced rearrangement of the structure. Consequently, there would be no reason that this conformation of the protein could not be achieved in the absence of the ligand.

All these considerations suggest that an equilibrium between the quaternary conformations observed crystallographically exists in the absence of the ligands. If so, the entire quaternary conformational change between the two conformations defined crystallographically or by a set of physical measurements produces the communication. It is counterproductive to focus attention on only one small portion of that overall conformational change, in particular changes that occur in a line between the two sites.

The question that now arises is whether a conformational change between only two quaternary conformations is responsible for both heterotropic allosteric effects and homotropic cooperativity displayed by many enzymes or whether there must be more than two conformations to explain all heterotropic allosteric effects observed. This question is more complicated in situations where there are heterotropic allosteric effectors in addition to cooperatively associating substrates. Most of the peculiar effects of heterotropic allosteric inhibitors and activators can be explained qualitatively by the kinetic mechanism of Equation 6–73, but that explanation is irrelevant to this question because a monomer, which is unable to display cooperative behavior was chosen for the quaternary structure to avoid the complication of cooperativity.

Monod, Wyman, and Changeux pointed out that most enzymes displaying heterotropic allosteric effects also display homotropic cooperativity in association of substrates and in the initial rates as a function of the concentrations of reactants.[15] They proposed that the two properties are usually present together because both require the enzyme to be able to adopt at least two conformations the relative stabilities of which are linked to the binding of ligands. Most proteins are oligomeric for reasons unrelated to cooperativity, but the fact that they are oligomeric is required for homotropic cooperativity to be manifested. When a particular oligomeric enzyme is able to adopt two symmetric quaternary conformations, both heterotropic allosteric behavior and homotropic cooperativity can exploit this quaternary conformational change. The argument is that heterotropic allosteric inhibition and activation and homotropic cooperativity occur simultaneously because the conformational change used for communicating heterotropic allosteric effects is the same one used for communicating homotropic cooperativity. In such a case, the conformational equilibrium is shifted in favor of the less active T conformation by a heterotropic allosteric inhibitor and in favor of the more active R conformation by substrates, reactants, and heterotropic allosteric activators. In effect, this argument is an application of Occam's razor to the question.

Nevertheless, even though they often occur together, there is **no necessary connection between heterotropic allosteric effects and cooperative effects**. For example, α_2 homodimeric phosphoserine phosphatase from *M. tuberculosis*, which hydrolyzes *O*-phospho-L-serine, is allosterically inhibited by L-serine from an allosteric site distinct from the active site. None of the measurements, however, of initial rate of the enzymatic reaction as a function of the reactant *O*-phospho-L-serine in the presence or absence of L-serine display cooperativity, as one might expect were there only two symmetric quaternary conformations responsible for heterotropic allosteric

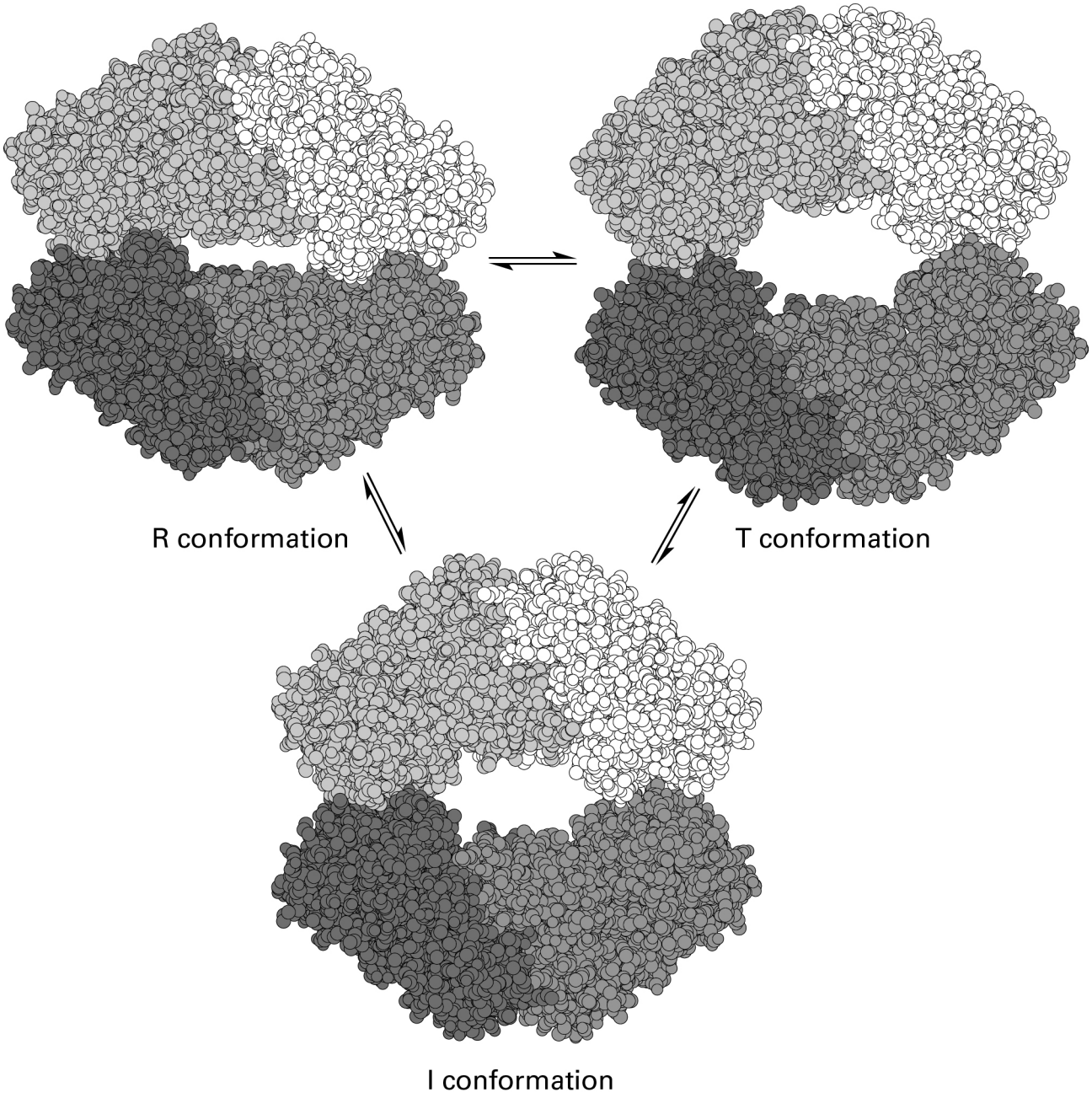

Figure 6–29: Stereodrawings[485] of crystallographic molecular models of aspartate kinase from *M. jannaschii* in its three conformations.[177] Each subunit of the α_4 tetramer is drawn in a different shade of gray. Aspartate kinase was poised in the R conformation, the active sites of which were occupied by L-aspartate and $MgAMPPNP^{2-}$, by dissolving the enzyme (12 mg mL^{-1}) in 5 mM $MgAMPPNP^{2-}$ and 30 mM L-aspartate. Crystals were then grown in 800 mM ammonium formate, 100 mM 2-[bis(2-hydroxyethyl)amino]-2-(hydroxymethyl)propane-1,3-diol at pH 8.0 with 13–15% poly(ethylene glycol) 4000 as the precipitant. Crystals of the space group $P2_12_12_1$ were obtained. Reflections were collected from these crystals to Bragg spacing of 0.23 nm. Aspartate kinase was poised in the T conformation, the active sites of which were occupied by L-threonine, by dissolving the enzyme (12 mg mL^{-1}) in 6 mM L-threonine and 30 mM L-aspartate. Crystals were then grown in 0.2 M KI with 1.4–1.6 M ammonium sulfate as the precipitant. Crystals of the space group $P2_12_12_1$ were obtained. Reflections were collected from these crystals to Bragg spacing of 0.27 nm. After a week at 4 °C, crystals of the enzyme in a third conformation, the active sites of which were occupied only by L-aspartate, appeared in the batches of crystals of the enzyme in the R conformation. These new crystals had the space group $C222_1$. Reflections were collected from these crystals to Bragg spacing of 0.27 nm. It was found that the enzyme in these crystals had a distinct conformation, which can be designated the I conformation. The equilibrium between the R conformation (left), the I conformation (below), and the T conformation (right) is represented with space-filling drawings of the three refined, complete crystallographic molecular models. Noncrystallographic rotational axes of symmetry are vertical and horizontal in the plane of the page and normal to the plane of the page.

inhibition.[180] Consequently, the proposal that an enzyme can exist in a symmetric quaternary T conformation with which, by definition, a heterotropic allosteric inhibitor preferentially associates and a symmetric quaternary R conformation with which, by definition, a substrate or a heterotropic allosteric activator preferentially associates is able to explain heterotropic allosteric effects. This fact, however, does not mean that these are the same T and R conformations that explain homotropic cooperativity in the absence of heterotropic allosteric effectors or that the existence of these two conformations requires the enzyme to display cooperative behavior.

In the case of aspartate carbamoyltransferase, however, most, if not all, experimental observations suggest that the conformations responsible for heterotropic allosteric effects and homotropic cooperativity are the same two symmetric quaternary conformations. Aspartate carbamoyltransferase can exist in R and T conformations. Because $MgATP^{2-}$ shifts the equilibrium between the R and T conformations in favor of the R conformation (Figure 6–13), $MgATP^{2-}$ must have a smaller dissociation constant from the R than it does from the T conformation. Presumably, $MgGTP^{2-}$ does also. Because $MgCTP^{2-}$ shifts the equilibrium between the R and T conformations in favor of the T conformation (Figure 6–13), $MgCTP^{2-}$ must have a smaller dissociation constant from the T than it does from the R conformation. Presumably, $MgUTP^{2-}$ does also. L-Aspartate has a smaller dissociation constant from the R conformation occupied by carbamoyl phosphate than it does from the T conformation occupied by carbamoyl phosphate. As is observed (Figure 6–3), $MgATP^{2-}$ and $MgGTP^{2-}$ should decrease the concentration of L-aspartate required for the initial rate of the enzymatic reaction to reach half its limiting value, and $MgCTP^{2-}$ and $MgUTP^{2-}$ should increase that concentration. If the R conformation of aspartate carbamoyltransferase has a larger catalytic constant than the T conformation, then $MgATP^{2-}$ and $MgGTP^{2-}$ should increase the apparent catalytic constant for the enzymatic reaction, and $MgCTP^{2-}$ and $MgUTP^{2-}$ should decrease the apparent catalytic constant of the enzymatic reaction, as is also observed (Figure 6–3).

A feature of noncompetitive heterotropic allosteric inhibition, albeit a rare one, can support the conclusion that the same two symmetric quaternary conformations responsible for heterotropic allosteric effects are the same two that are responsible for homotropic cooperativity. Association of substrates with the active sites of enzymes, the steady-state kinetics of which display noncompetitive heterotropic allosteric inhibition, is usually not cooperative. One explanation for the fact that **noncompetitive heterotropic allosteric inhibition**, by definition, does not alter the Michaelis constant for reactant is that $K_{dA} = K'_{dA}$. If this equality holds, then the concentration of reactant A cannot affect the equilibrium between the R and T conformations. Consequently, even when the enzyme is homooligomeric, association of reactant cannot be cooperative, nor can the initial rate of the enzymatic reaction as a function of its concentration display cooperativity. For example, fructose-bisphosphatase from *R. norvegicus* is a homotetramer, yet the initial rate of the enzymatic reaction as a function of the concentration of D-fructose 1,6-bisphosphate (Figure 6–19) does not display cooperativity at any of the concentrations of AMP^{2-}, a noncompetitive heterotropic allosteric inhibitor, as expected. In the absence of ligands, fructose-bisphosphatase is in the R conformation,[36,38] and AMP^{2-} shifts the equilibrium in favor of the T conformation, which has a lower catalytic constant for the enzymatic reaction. This shift in the equilibrium constant between the R conformation, with high activity, and the T conformation, with low activity ($k'_2 < k_2$) produced by the inhibitor, which is unaffected by the concentration of D-fructose 1,6-bisphosphate, is the reason for the decrease in the catalytic constant k_0.

In many cases, **only two quaternary conformations have been observed crystallographically**, a fact reinforcing the almost universal convention of the T and R conformations. For example, aspartate carbamoyltransferase from *E. coli* has been examined crystallographically with many different heterotropic allosteric effectors. Although there are significant local conformational changes within the constituent folded polypeptides around the binding sites being occupied when different ligands associate with the same quaternary conformation,[9,48,49,53] all the complexes between ligands and enzyme assume either the T or R conformation when crystallized from solution. The results from nuclear magnetic resonance spectroscopy are also unable to detect any quaternary conformations other than the T and R conformations the equilibrium between which is shifted both by heterotropic allosteric effectors and by homotropic allosteric ligands and substrates (Figure 6–13). The crystallographic molecular models of glycogen phosphorylase *b* (Equation 6–66 and Figure 6–20) from *O. cuniculus*, activated either by association of AMP^{2-} or by covalent phosphorylation at distinct sites, are both in the same quaternary R conformation,[181,182] which is distinct from the

quaternary T conformation observed when the heterotropic allosteric inhibitor D-glucose 6-phosphate is bound in the allosteric site or in the absence of ligands.[183]

In instances in which an enzyme is simply inhibited allosterically by the final product of a metabolic pathway and there are no as-yet-recognized heterotropic allosteric activators, it is less surprising that only T and R conformations are observed crystallographically. Examples of such situations are phosphoglycerate dehydrogenase from *E. coli*, which is allosterically inhibited by L-serine, the final product of the pathway;[117] anthranilate synthase (Equation 6–61) from *S. marcescens*, which is allosterically inhibited by L-tryptophan, the final product of the pathway;[103] 4-hydroxy-tetrahydrodipicolinate synthase from *Nicotiana sylvestris*, which is allosterically inhibited by L-lysine, the final product of the pathway;[184] sulfate adenylyltransferase

$$MgATP^{2-} + \text{sulfate} + Mg^{2+} \rightleftharpoons MgOPO_3PO_3^{2-} + \text{magnesium adenosine 5′-phosphosulfate} \quad (6\text{–}102)$$

from *P. chrysogenum*, which is allosterically inhibited by 3′-phosphoadenylyl sulfate, the final product of the pathway;[115] and 3-deoxy-7-phosphoheptulonate synthase (Equation 6–93) from *E. coli*, which is allosterically inhibited by L-phenylalanine, the final product of the pathway.[175]

There are, however, examples of allosterically controlled enzymes that can assume **at least three distinct quaternary conformations**, the equilibria among which are shifted by association of substrates and heterotropic allosteric effectors. For example, aspartate kinase

$$MgATP^{2-} + \text{L-aspartate} \rightleftharpoons \text{4-phospho-L-aspartate} + MgADP^{-} \quad (6\text{–}103)$$

from *Methanocaldococcus jannaschii* crystallizes in three distinct quaternary conformations (Figure 6–29): one that crystallizes from a solution of the substrate L-aspartate; one that crystallizes from a solution of L-aspartate and $MgAMPPNP^{2-}$; and one that crystallizes from a solution of L-threonine, a heterotropic allosteric inhibitor of the enzyme. Each conformation differs significantly from the others in the disposition of its subunits, and each has the noted ligands bound in all the active sites or allosteric sites on the enzyme. Each of the three quaternary conformations is symmetric, but in the conformation stabilized by association of L-threonine, the symmetrically distributed sites for association of L-threonine are not symmetrically occupied, a fact that suggests there may be subtle asymmetries in the structure of this conformation.

It may also be the case that in some instances in which only two conformations of an allosteric enzyme have been defined crystallographically, **a third may yet be discovered**. The quaternary conformations of porcine fructose-bisphosphatase (Equation 6–62) in crystallographic molecular models of a number of different complexes with heterotropic allosteric inhibitors, substrates, analogues of substrates, and a physiological competitive inhibitor could all be clearly identified as one of two quaternary conformations designated the T and R conformations.[36,37,176,185] It was then later reported that a third, distinct quaternary conformation of the same enzyme crystallized from solution under different conditions.[186] As has already been noted, there is no reason that a molecule of protein should exist in only one conformation or only two conformations in equilibrium with each other. Heterotropic allosteric inhibition and activation would still be a consequence of the existence of three globally symmetric conformations if, for example, there is a quaternary T conformation of low enzymatic activity that is most stable in the presence of saturating concentrations of heterotropic allosteric inhibitor, another quaternary conformation that is most stable in the absence of ligands or in the presence of only one substrate, and a quaternary R conformation of high enzymatic activity stabilized by association of both reactants and heterotropic allosteric activators. Certainly, in the case of aspartate kinase from *M. jannaschii* (Figure 6–29), one could imagine that the equilibrium between the conformation observed at saturating concentrations of L-threonine, a heterotropic allosteric inhibitor of the enzyme,[187] and the conformation observed in the presence of saturating L-aspartate could be responsible for heterotropic allosteric inhibition while the equilibrium between the conformation in the presence of saturating L-aspartate and $MgAMPPNP^{2-}$ could be responsible for homotropic cooperativity.

Contrariwise, at one time, several observations suggested that the heterotropic allosteric effects and the cooperativity observed for aspartate carbamoyltransferase from *E. coli* (Figure 6–3) could be the result of separate conformational changes.[188,189]

The nuclear magnetic resonance spectra (Figure 6–13), however, demonstrate that heterotropic allosteric effectors and reactants and analogues of reactants shift the equilibrium between only two conformations, the R and T conformations. Aspartate carbamoyltransferase was reconstituted from regulatory subunits and nitrated catalytic subunits, and the active sites were saturated with carbamoyl phosphate. Both the homotropic cooperativity observed with L-aspartate as a reactant and the change in sedimentation coefficient upon adding *N*-(phosphonacetyl)-L-aspartate were those expected if the modified protein saturated with carbamoyl phosphate (CAP) was 60% in the T conformation and 40% in the R conformation ($L_{CAP} = 1.5$).[190] This significant shift in the equilibrium constant in favor of the R conformation resulted from nitration as well as from saturation with carbamoyl phosphate. When the heterotropic allosteric inhibitor $MgCTP^{2-}$ was added to the solution, the absorbance of the nitrated enzyme at 450 nm decreased; and when the heterotropic allosteric activator $MgATP^{2-}$ was added, the absorbance increased. These changes were in the directions expected for an increase in the concentration of the less active T conformation or the more active R conformation, respectively. In the presence of $MgCTP^{2-}$, the percentage of T conformation, calculated from both the homotropic cooperativity displayed by L-aspartate and the change in sedimentation coefficient produced by *N*-(phosphonacetyl)-L-aspartate, increased to 80% ($L_{CTP,CAP} = 4$); and in the presence of $MgATP^{2-}$, it decreased to 40% ($L_{ATP,CAP} = 0.7$). These are the changes expected if the heterotropic allosteric effects are coupled to the same quaternary conformational change as homotropic cooperativity.

It has already been noted that the simplest solution to implementing both heterotropic allosteric effects and homotropic cooperativity is to tie them to the same quaternary conformational change and that this solution seems to have been hit upon by natural selection in many instances. There are, however, observations of physical properties of allosteric enzymes for which no more than two quaternary conformations have been observed crystallographically that are presented as **evidence for the existence of more than two quaternary conformations involved in their heterotropic and homotropic allosteric effects**. For example, changes in fluorescence of the single tryptophan in pyruvate kinase from *G. stearothermophilus*, which is distant from both the active sites and the site at which the heterotropic allosteric activator D-ribose 5-phosphate binds, indicate that association of the reactant phospho*enol*pyruvate, the concentration of which affects the initial rate of the enzymatic reaction cooperatively, produces an R conformation that is distinct from the conformation produced by association of D-ribose 5-phosphate.[191]

Ten of the cross peaks that shifted the most in two-dimensional TROSY nuclear magnetic resonance spectra of the methyl groups of isoleucines in 6-phosphofructokinase from *G. stearothermophilus* were observed in solutions containing no ligands, saturating concentrations of the substrate D-fructose-6-phosphate, saturating concentrations of the heterotropic allosteric inhibitor phospho*enol*pyruvate, and saturating concentrations of both D-fructose-6-phosphate and phospho*enol*pyruvate. The shifts observed in these 10 cross peaks indicated that there were more than just two quaternary conformations of the enzyme under all these conditions.[55]

Such observations, however, could be consistent with the existence of only two quaternary conformations of the enzyme if local conformational changes were clearly distinguished from quaternary conformational changes, as was done with aspartate carbamoyltransferase.

At first glance, **mutations of an allosteric enzyme that eliminate cooperativity without eliminating heterotropic allosteric inhibition**[192-194] would seem to suggest that different conformational equilibria are responsible for cooperativity and heterotropic allosteric inhibition. For example, when Arginine 234 in the catalytic subunit of aspartate carbamoyltransferase is mutated to serine, the Hill coefficient describing the effect of the concentration of L-aspartate on the enzymatic activity decreases from 2.3 to a value indistinguishable from 1.0. Another explanation of such an observation, however, is that the mutation has changed the rate-limiting step in the enzymatic reaction so that the initial rate of the enzymatic reaction is no longer directly proportional to the occupation of the active site by reactant. Consequently, the underlying cooperativity in association of reactant with the active site is no longer manifest in the effect of the concentration of reactant on the initial rate. In fact, mutation of Arginine 234 decreases the value for the catalytic proficiency of the enzyme, $k_0\,K_{m,asp}^{-1}$, by a factor of 2000, and it would not be surprising if such a large change were due to a change in rate-limiting step for the enzymatic reaction. The concentration of L-serine, a heterotropic allosteric inhibitor of phosphoglycerate dehydrogenase from *E. coli*, affects the initial rate of the enzymatic reaction

cooperatively (Hill coefficient = 2.0 ± 0.07), but mutation of Glycine 294 to valine eliminates this cooperativity (Hill coefficient = 1.08 ± 0.04) on its effect on the initial rate, even though L-serine binds to its allosteric site on the mutant enzyme with the same degree of cooperativity (Hill coefficient = 2.0) with which it binds to the wild-type enzyme.[195,196]

Unfortunately, in instances in which a mutation eliminates cooperativity in the steady-state kinetics as a function of the concentration of a reactant but does not eliminate heterotropic allosteric effects, a threefold demonstration that the mutation eliminates the cooperativity of the actual association of reactant with the active site, that the mutation does not alter the ability of a heterotropic allosteric inhibitor to inhibit the binding of reactant to the active site, and that, for the mutant, the binding of reactant remains noncooperative even in the presence of inhibitor has not been presented. These three observations would be necessary to conclude that the conformational equilibrium responsible for cooperativity of a reactant is different from the conformational equilibrium responsible for heterotropic allosteric inhibition.

When Glutamate 23 in chorismate mutase (previously Equation 1–161)

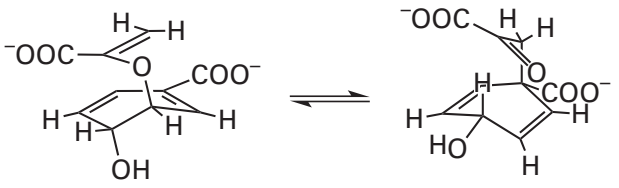

(6–104)

from *S. cerevisiae*, which is a homodimer, is mutated to aspartate, the Hill coefficient describing the effect of the concentration of chorismate on enzymatic activity decreases from 1.5 to a value indistinguishable from 1.0 in the absence of L-tyrosine, its heterotropic allosteric inhibitor, and from 1.7 to a value indistinguishable from 1.0 in the presence of 100 μM L-tyrosine. The concentration of chorismate at which the initial rate of the enzymatic reaction is half the limiting rate, however, is still increased by L-tyrosine from 4.5 to 9.5 mM, a change similar to the increase observed in the wild type (from 4.0 to 6.7 mM).[197] Furthermore, association of L-tyrosine with one heterotropic allosteric site in the homodimer increases the microscopic dissociation constant of L-tryptophan from the other site by a factor of 3, and association of L-tryptophan with one heterotropic allosteric site increases the microscopic dissociation constant of L-tyrosine from the other site by a factor of 3. These two facts would be consistent with their competition for the two quaternary conformations observed crystallographically, but neither L-tyrosine nor L-tryptophan binds to the enzyme cooperatively,* which is inconsistent with the existence of only those two quaternary rotationally symmetric quaternary conformations.[198] If there were only those two conformations, either the heterotropic allosteric inhibitor L-tyrosine or the heterotropic allosteric activator L-tryptophan would have to associate cooperatively with the unoccupied enzyme. These results suggest that heterotropic allosteric effects are confined to the individual subunits, even though the cooperativity in the effect of the concentration of chorismate on the enzymatic activity would seem to require that its association with the active site be linked to the quaternary conformational change between the two rotationally symmetric conformations. These considerations suggest that homotropic cooperativity and heterotropic allosteric behavior in the case of chorismate mutase are not linked to the same conformational change and that there exists at least a third quaternary conformation in which one subunit has assumed an H conformation and the other a V conformation.

Although the simplest strategy for a protein that displays both homotropic cooperativity and heterotropic allosteric behavior is to link these two processes to the same conformational change between two quaternary conformations at equilibrium with each other, it appears that natural selection has produced at least some proteins if not many that have **the ability to assume more than two quaternary conformations**, the conformational changes among which are linked arbitrarily to the binding of the various ligands. The stable radical 1-oxyl-2,2,6,6-tetramethylpiperidine, when it is covalently bound to glycogen phosphorylase from *O. cuniculus* (Figure 6–20), detects changes in the distribution of conformations in solutions of the protein (Figure 6–15). The changes detected by the radical when the heterotropic allosteric activator AMP^{2-} is bound by glycogen phosphorylase *b* differ significantly from those caused by the substrate D-glucose 1-phosphate. The complete set of results suggests that the enzyme can assume four distinct conformations variously linked to the binding of ligands.[199] A distinction between quaternary conformations and local conformations was

*In fact, association of the first L-tyrosine (K_{dY} = 70 μM) seems to increase the microscopic dissociation constant for association of the second (K_{dY} = 180 μM).

not made. The existence, however, of enzymes in which the conformational change responsible for heterotropic allosteric effects is different from that responsible for homotropic cooperativity is irrelevant to the issue of whether or not homotropic cooperativity arises from the ability of an oligomeric protein to exist in only quaternary conformations in which symmetry is conserved that was discussed earlier.

The argument to this point has emphasized, albeit not exclusively, an explanation of heterotropic allosteric effects as a result of the ability of the effector to shift an equilibrium between two or more symmetric quaternary conformations. This argument follows from the principle that symmetry is conserved in the conformational changes of a homooligomeric protein. This view seems to be held by a majority of investigators, given the wide use of the terms T conformation and R conformation. As has been already mentioned, however, there are heterotropic allosteric effects that cannot be explained satisfactorily in this way. The failure of such an explanation often results in cases in which there are a large number of heterotropic allosteric effects on association of a ligand or the kinetics of an enzymatic reaction. For example, there are heterotropic allosteric effects on association of molecular oxygen with hemoglobin caused by changes in pH, as well as heterotropic allosteric effects on the kinetics of association of oxygen, that do not seem to be linked to the quaternary conformational equilibria that conserve symmetry.* In this instance, it has been shown that local conformational changes within the subunits of hemoglobin that do not exert significant influence on the well-established quaternary conformational changes of the protein (Figure 6–1) can explain these effects that cannot be explained solely by a shift in the equilibrium between these quaternary conformations.[200] In a sense, the fact that these allosteric conformational changes that take place entirely within the individual subunits is a corollary to the conclusion that heterotropic allosteric effects can be linked to a conformational change in a monomeric protein. It is still a conformational explanation of heterotropic allosteric effects that relies on the linkage of association of a ligand on a conformational equilibrium, only it is a local conformational equilibrium between two or more conformations confined within each subunit.

*It should be noted that hemoglobin is a weak example of the principle of conservation of symmetry because it is an $(\alpha\beta)_2$ heterodimer. Nevertheless, the issue is the existence of local conformational equilibria unlinked to quaternary conformational equilibria.

Heterotropic allosteric effectors usually alter the cooperativity of association of substrates and reactants with an active site. Such changes are to be expected. Assume for the moment that there are only two symmetric quaternary conformations of the enzyme, the T conformation that predominates in the presence of saturating concentrations of a heterotropic allosteric inhibitor and the R conformation that predominates in the presence of saturating concentrations of reactants for the enzyme or heterotropic allosteric activators. Assume also that cooperativity of the steady-state kinetics mirrors the cooperativity of association of reactants with the active site. If the effects manifested by a heterotropic allosteric effector are exerted through the same quaternary conformational change as that controlled by homotropically cooperative reactant or reactants, then the change in cooperativity of the initial rate as a function of the concentration of a reactant will **depend on which conformation of the enzyme is favored in the absence of heterotropic allosteric ligands.**

If the effect of the concentration of a reactant on the initial rate of the enzymatic reaction or the binding of a substrate to the otherwise unoccupied enzyme is homotropically cooperative, then the T conformation dominates in the absence of all ligands. Because a heterotropic allosteric inhibitor increases the stability of the T conformation and increases the value for the allosteric constant L (Equation 6–100), it should increase the degree of homotropic cooperativity and increase the sigmoidicity, up to the point at which the reactant can no longer significantly shift the equilibrium from the T to the R conformation. For example, the heterotropic allosteric inhibitor L-isoleucine increases the Hill coefficient, n_H, for the initial rate of threonine ammonia-lyase from *Mycolicibacterium smegmatis* as a function of L-threonine[201] from 2.4 to 3.1; the heterotropic allosteric inhibitor phospho*enol*pyruvate increases the Hill coefficient for the initial rate of 6-phosphofructokinase from *Thermus thermophilus* as a function of D-fructose 6-phosphate[202] from 1.5 to 2.5; and the sigmoidicity of the initial rate of aspartate carbamoyltransferase as a function of the concentration of L-aspartate (Figure 6–3) is greater in the presence of $MgCTP^{2-}$ and $MgUTP^{2-}$ ($n_H = 2.7$) than in their absence ($n_H = 2.0$). In the case of aspartate transcarbamoylase, the allosteric constant in the absence of heterotropic allosteric inhibitors, L_0, is greater than 1, but heterotropic allosteric inhibitors increase this conformational equilibrium constant.

Suppose that either the initial rate of the enzymatic reaction as a function of the concentration of a reactant or the association of a reactant for an otherwise unoccupied enzyme that can exist in both T and R conformations is not cooperative but rectangularly hyperbolic. There are two possible explanations for this observation. First, in the absence of substrate or reactant and the absence of heterotropic allosteric effectors, the R conformation is dominant ($L_0 < 1$). Second, the T conformation is so dominant ($L_0 K_{dA} > K'_{dA}$) that neither substrate nor reactant at saturation can shift the equilibrium between the R and T conformations significantly. If the former explanation applies, because the reactant associates only with the dominant R conformation and the allosteric constant L becomes even smaller upon its association, then both binding and transformation of the reactant are noncooperative, rectangularly hyperbolic functions of its concentration. When a heterotropic allosteric inhibitor is added, however, it shifts the conformational equilibrium in favor of the T conformation by increasing the allosteric constant L. If its presence shifts the equilibrium so that the allosteric constant is greater than 1, then homotropic cooperativity of association of reactant or the initial rate as a function of the concentration of reactant will be observed where none was in the absence of inhibitor.

It is frequently observed that **a heterotropic allosteric inhibitor can cause a rectangularly hyperbolic effect of the concentration of a reactant on the initial rate of an enzymatic reaction to become cooperative**.[203,204] For example, the presence of the heterotropic allosteric inhibitor L-lysine causes the effect of L-aspartate-4-semialdehyde on the initial rate of the reaction catalyzed by 4-hydroxy-tetrahydrodipicolinate synthase from from *C. jejuni*, which is rectangularly hyperbolic in the absence of inhibitor, to become cooperative (Figure 6–22). The fact that, in the absence of L-lysine, the enzyme is predominantly in the R conformation, which would explain the absence of cooperativity in this situation, is consistent with the fact that inhibition of the enzyme is a significantly cooperative function ($n_H = 2.0$) of the concentration of L-lysine.[205] L-Arginine, a heterotropic allosteric inhibitor, also converts the effect of the concentration of L-glutamate on the initial rate of amino-acid *N*-acetyltransferase from *N. gonorrhoeae* from rectangularly hyperbolic to cooperative (Figure 6–23).[142] Combinations of the three heterotropic allosteric inhibitors L-tryptophan, L-tyrosine, and L-phenylalanine convert the effect of the concentration of D-erythrose 4-phosphate on the initial rate of 3-deoxy-7-phosphoheptulonate synthase from *M.tuberculosis* from rectangularly hyperbolic to cooperative (Figure 6–26). Phospho*enol*pyruvate, a heterotropic allosteric inhibitor, converts the effect of the concentration of D-fructose 6-phosphate on the initial rate of 6-phosphofructokinase from *G. stearothermophilus* from rectangularly hyperbolic to cooperative (Figure 6–17B).

The most obvious explanation for such behavior is that, in the absence of heterotropic allosteric inhibitor, the allosteric constant L_0 is less than 1, so **the enzyme is almost completely in the R conformation at all concentrations of reactant**. As has already been noted, L-phenylalanine causes the effect of phospho*enol*pyruvate on the initial rate of the reaction catalyzed by pyruvate kinase from *O. cuniculus*, which is rectangularly hyperbolic in the absence of heterotropic allosteric inhibitor, to become cooperative (Figure 6–27A). The fact that the binding of the heterotropic allosteric inhibitor L-phenylalanine with unoccupied pyruvate kinase is cooperative (Figure 6–28)[30] is consistent with the proposal that L_0 is less than 1 for this enzyme, that the R conformation predominates in the absence of ligands, and that L-phenylalanine has a smaller dissociation constant from the T conformation than it does from the R conformation so that association of L-phenylalanine with the otherwise unoccupied enzyme is cooperative. In a situation where L_0 is less than 1, association of reactant with the R conformation would be the same as association of any ligand to a homooligomer with only one quaternary conformation, which is always rectangularly hyperbolic, while association of a heterotropic allosteric inhibitor, by shifting the equilibrium in favor of the T conformation, will be cooperative. Only when a heterotropic allosteric inhibitor shifts the equilibrium between the T and the R conformations so that the T conformation is present in high enough concentration in the absence of reactant will the reactant associate with the enzyme cooperatively. This explanation, however, requires that both heterotropic allosteric inhibitor and reactant shift the same equilibrium between the same two conformations.

Mutations of an allosterically regulated enzyme can also convert the effect of the concentration of a reactant on the initial rate of the enzymatic reaction from rectangularly hyperbolic to cooperative.[206] Again, the explanation is that before the mutation the allosteric equilibrium constant favors the R conformation and after the mutation it favors the T conformation.

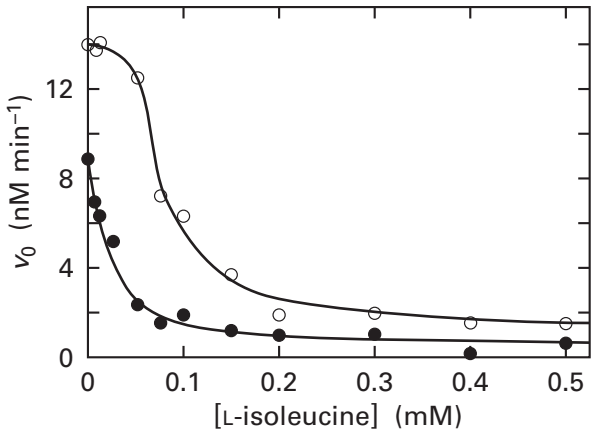

Figure 6–30: Heterotropic allosteric inhibition of threonine ammonia-lyase from *E. coli* by L-isoleucine.[15] Solutions contained 0.4 μM pyridoxal phosphate, 0.1 mM $MgCl_2$, various concentrations of L-isoleucine, various concentrations of L-threonine, and 0.1 M potassium phosphate at pH 8.05 and 27 °C. The reaction was initiated by adding a sample from a partially purified preparation of threonine ammonia-lyase. After suitable intervals, the samples were quenched by adding acid. The concentration of 2-oxobutanoate in each sample was determined by adding 2,4-dinitrophenylhydrazine, extracting the 2,4-dinitrophenylhydrazone of 2-oxobutanoate with ethyl acetate, and measuring the absorbance of the extract at 360 nm. Each initial rate (v_0 in nanomolar minute^{-1}) is plotted as a function of the respective concentration of L-isoleucine (millimolar) at two initial concentrations of L-threonine: 5 mM (●) and 20 mM (○).

Reciprocally, it has also been observed that **a reactant that displays cooperativity in its association with the active site can cause a rectangularly hyperbolic effect of the concentration of a heterotropic allosteric inhibitor on the initial rate of an enzymatic reaction to become cooperative.** For example, the inhibition of threonine ammonia-lyase from *E. coli* by the heterotropic allosteric inhibitor L-isoleucine is rectangularly hyperbolic at low concentrations of the reactant L-threonine but becomes cooperative at higher concentrations (Figure 6–30).[15] An explanation for this behavior is that, at low concentrations of L-threonine, L_0 is greater than 1 and the T conformation predominates. Consequently, L-isoleucine associates noncooperatively with this dominant T conformation, from which it has a smaller dissociation constant than it does from the R conformation, and it simply shifts the equilibrium constant more in favor of the T conformation. The reactant L-threonine, however, has a smaller dissociation constant from the R conformation than from the T conformation, and at high enough concentrations, it shifts the equilibrium in favor of the R conformation. When it does, association of L-isoleucine then becomes cooperative. Again, this explanation requires the same equilibrium between the same two conformations to produce both heterotropic allosteric inhibition and cooperativity; in this case, cooperativity in association of inhibitor rather than in association of reactant.

Because it must increase the stability of the R conformation and decrease the value for the allosteric constant L, a **heterotropic allosteric activator should decrease the degree of homotropic cooperativity** displayed by a reactant. For example, L-valine, a heterotropic allosteric activator of threonine ammonia-lyase from *M. smegmatis*, decreases the Hill coefficient, n_H, of the initial rate of the enzymatic reaction as a function of the concentration of the reactant L-threonine[201] from 2.4 to 1.1. In the extreme, where the difference in affinity of the two conformations for heterotropic allosteric activator is sufficient to invert the value for the equilibrium constant for conformational change in the absence of reactant, the protein will be mostly in the R conformation in the presence of saturating concentrations of the activator even in the absence of other ligands. This latter limit is reached in the activation of aspartate carbamoyltransferase in the presence of $MgATP^{2-}$ and $MgGTP^{2-}$, which activate aspartate carbamoyltransferase from *E. coli* by decreasing both k_0 and k_{asp} and also eliminate cooperativity in the dependence of the initial rate of the enzyme on L-aspartate (Figure 6–3).

Reactants that normally display homotropic cooperativity often no longer display this behavior in the presence of a heterotropic allosteric activator.[15,191,207-209] Acetyl-SCoA is a heterotropic allosteric activator of phospho*enol*pyruvate carboxylase. In this way, flow through the Krebs cycle is increased when levels of acetyl-SCoA are high. Acetyl-SCoA, in its role as heterotropic allosteric activator, eliminates the cooperativity of the initial rate of phospho*enol*pyruvate carboxylase from *S. typhimurium* as a function of the concentration of phospho*enol*pyruvate.[210]

Magnesium ADP^-, a heterotropic allosteric activator of 6-phosphofructokinase from *E. coli*, increases the specificity constant, k_{F6P}, for D-fructose 6-phosphate (F6P) while phospho*enol*pyruvate, a heterotropic allosteric inhibitor, decreases it, yet both $MgADP^-$ and phospho*enol*pyruvate decrease cooperativity in the dependence of the initial rate of the enzyme on the initial concentration of D-fructose 6-phosphate.[19] An explanation for this observation is that the activator shifts the equilibrium between the conformations so that the R conformation dominates in the absence of reactant while the inhibitor shifts the equilibrium so heavily

in the direction of the T conformation that even saturating concentrations of reactant cannot shift it sufficiently in the direction of the R conformation to overcome the shift caused by the inhibitor.

Such situations, however, in which either an activator or an inhibitor decreases cooperativity or both do, **cannot provide evidence for the existence of only one equilibrium between two conformations** of the enzyme. Although this behavior can be explained by the existence of only two conformations, it can also be explained as readily by the existence of separate conformational equilibria, one for heterotropic allosteric effects and another for cooperativity. In this case, a heterotropic allosteric effector would shift the enzyme into the third quaternary conformation, which would simply associate with reactant as would a normal homooligomer in which there is no quaternary conformational change linked to the association. Consequently, such behavior provides no evidence in favor of the effectors and reactants controlling the equilibrium between the same two conformations. Likewise, the observation that a heterotropic allosteric inhibitor causes the effects of a heterotropic allosteric activator to become cooperative[15] can be just as consistent with separate equilibria responsible for heterotropic allosteric effects and for cooperativity. Again this ambiguity is a consequence of the fact that any explanation for observed behavior of equilibria or observed kinetics can always be expanded by adding additional participants and remain consistent with the observations. Nevertheless, these effects of ligands on the observed cooperativity are those expected from the existence of only two quaternary conformations that are responsible for them.

There are many examples of simple heterotropic allosteric inhibition by a single inhibitor, simple heterotropic allosteric activation by a single activator, and even simple heterotropic allosteric inhibition and activation by a single inhibitor and a single activator. Many enzymes, however, are controlled by complicated combinations of classical competitive inhibition, heterotropic allosteric inhibition, and heterotropic allosteric activation exerted by several inhibitors and activators associating both with the active site and with more than one allosteric site.

Glycogen phosphorylase (Equation 6–66) releases D-glucose, the primary source of immediate metabolic energy in an animal, from glycogen. Glycogen phosphorylase *b* from *O. cuniculus* is controlled, as might be expected, by a large collection of different heterotropic allosteric effectors (Table 6–2) that associate with one or more of five distinct sites (Figure 6–20) and affect the equilibrium or equilibria between two or more conformations of the enzyme. The site for heterotropic allosteric effectors (AE) binds AMP^{2-}, a heterotropic allosteric activator of the enzyme that signals a need for metabolic energy,[211,212] but the enzyme is inhibited when this site is occupied by $MgATP^{2-}$.[213] It was proposed that opposite effects from the same site can occur because AMP^{2-} binds more tightly to only one conformation while $MgATP^{2-}$ prevents the binding of AMP^{2-} but has no effect on the conformational equilibria. A similar situation occurs in the catalytic (C) site. D-Glucose 1-phosphate, acting as a reactant, shifts the conformational equilibrium in favor of a more active conformation,[213] while D-glucose, also binding at the active site as a simple competitive inhibitor,[214] shifts it in favor of a less active or inactive conformation to shut down glycogen utilization when levels of D-glucose are high.[215]

Table 6–2: Effects of Various Ligands on the Conformational Equilibria between Enzymatically Active and Inactive Conformations of Glycogen Phosphorylase from *O. cuniculus*

ligand	site[a]	conformer
AMP^{-}	AE	active
$MgATP^{2-}$	AE	neither[b]
D-glucose 6-phosphate	G6P	neither
D-glucose 1-phosphate	C	active
D-glucose	C	inactive
adenosine	I	inactive
caffeine	I	inactive[c]
glycogen	G	active

[a]Named as in Figure 6–20. [b]Competes with AMP for nucleotide site. [c]Synergistic with D-glucose. [d]Binds at a site adjacent to the nucleotide site and competes with AMP.

Sandwiched between Phenylalanine 285 and Tyrosine 613 in the enzyme from *O. cuniculus* is another site, the site for nucleoside inhibitors (I), at which planar heterocycles such as those in caffeine, adenine, inosine, adenosine, AMP^{2-}, $MgATP^{2-}$, or flavin mononucleotide can bind.[216] These ligands are all heterotropic allosteric inhibitors of the enzyme. Because either D-glucose, binding to the active site, or any one of these inhibitors, binding to the site for nucleoside inhibitors, shifts the conformational equilibrium in favor of a less active or inactive conformation or conformations of the enzyme, when both D-glucose and one of these other inhibitors are present, they inhibit the enzyme in concert.[216,217] D-Glucose increases the apparent dissociation constant for any one of these inhibitory heterocyclic compounds by independently shifting the conformational equilibrium constant in favor of the R conformation, with which they associate less avidly.

D-Glucose 6-phosphate binds at a site (G6P) that is immediately adjacent to the site for heterotropic allosteric effectors. When it is bound at this site, one of its phosphate oxygens overlaps the location at which one of the phosphate oxygens of AMP^{2-} is bound.[110] Consequently, AMP^{2-} cannot bind to the site and activate the enzyme because of steric exclusion, which explains the inhibition of activation by AMP^{2-} manifested by D-glucose 6-phosphate. This makes sense because glycogenolysis should not be activated when the concentration of a glycolytic intermediate such as D-glucose 6-phosphate is high.

Finally, there is a site at which the enzyme normally binds to glycogen, the glycogen storage site (G). When a polysaccharide occupies this site, in the absence of AMP^{2-}, the conformational equilibrium or equilibria is shifted in favor of the active conformation and the enzymatic reaction is accelerated.[218]

The first-order rate constants for the conformational changes that accompany changes in the affinity of a homooligomer in either the binding of its ligands or its enzymatic activity have a wide range of values. These conformational changes are unimolecular isomerizations of the folded polypeptides within the oligomer that can lead to alterations in the orientations of its subunits.

The kinetics of isomerizations that occur when carbon monoxide is photodissociated from the four hemes in fully occupied human **hemoglobin** have been studied extensively. Upon complete and almost instantaneous dissociation of bound carbon monoxides, the molecules of hemoglobin are almost all in the R conformation, which then converts to the T conformation (Figure 6–1). A **rapid change** in the scattering of X-rays at small angles, which monitors directly the quaternary conformational change,[219] occurs with a rate constant of approximately 0.5 μs^{-1} at 20° C. This rate constant is indistinguishable from the rate constant of approximately 2 μs^{-1} for a change in circular dichroic absorption at 340 nm, arising from tryptophan and tyrosines in the interfaces between the subunits,[220] and from the rate constant of 1.3 μs^{-1} for a change in absorption between 400 and 480 nm, the region in which the heme absorbs.[221] These coincidences are consistent with the conclusion that these changes all monitor the **rapid global quaternary conformational change** from the R to the T conformation. Less rapid changes in infrared signals in Raman spectra are thought also to arise from the interfaces between the subunits.[222] Less rapid changes in the circular dichroic spectrum at 340 nm[220] occur with rate constants between 0.05 and 0.1 μs^{-1} and may be monitoring final readjustments in the R conformation. There are also more rapid changes in absorption of the heme and in the resonance Raman infrared spectrum that have been assigned to local conformational changes around the heme in response to its unoccupation. The rate constant for the conformational relaxation[223] that occurs after aspartate carbamoyltransferase in the R conformation associates with $MgCTP^{2-}$ is 0.01 μs^{-1} at pH 7.0 and 25 °C. All these processes are quite rapid when compared to catalytic constants of enzymes. The opening and closing of the active sites of enzymes such as hexokinase (Figure 3–55) and citrate synthase must also proceed at rates greater than or equal to the turnover numbers for these enzymes.

There are, however, many **conformational changes that have slow rates**. When 6-phosphofructokinase (Equation 6–28) from *O. cuniculus* is preincubated with heterotropic allosteric activators and then diluted for enzymatic assay, its enzymatic activity is quite high at first but then decreases slowly to the steady-state rate.[224] When the enzyme is preincubated with heterotropic allosteric inhibitors and then diluted for assay, its enzymatic activity is low at first but then increases slowly to the steady-state rate. These decreases and increases in enzymatic activity reflect the slow rate constant for the conformational changes responsible for heterotropic allosteric effects. The first-order rate constants for these relaxations are between 0.003 and 0.03 s^{-1}

at pH 7.5 and 25 °C. Very similar behavior is also observed[225] with human amidophosphoribosyltransferase (previously Equation 4–313)

$$\text{manganese 5-phospho-}\alpha\text{-D-ribose 1-diphosphate} + \text{L-glutamine} + H_2O \rightleftharpoons \text{L-glutamate} + H^+ + MnOPO_3PO_3^{2-} + \text{5-phospho-}\beta\text{-D-ribosylamine} \quad (6\text{–}105)$$

The slow conformational change in this instance has a rate constant of about 0.005 s^{-1} at 25 °C. Formally, there is no distinction except in magnitude between a rapid and a slow conformational relaxation. It may, however, be the case that the rate of conformational change has evolved to match the rates of the particular fluctuations in concentration of effectors to which the enzyme is adapted to respond.

Suggested Reading

Oberfelder, R. W., Lee, L-Y. L., & Lee, J. C. (1984) Thermodynamic linkages in rabbit muscle pyruvate kinase: Kinetic, equilibrium, and structural studies, *Biochemistry 23*, 3813–3821. https://doi.org/10.1021/bi00312a004

Oberfelder, R. W., Barisas, B. G., & Lee, J. C. (1984) Thermodynamic linkages in rabbit muscle pyruvate kinase: Analysis of experimental data by a two-state model, *Biochemistry 23*, 3822–3826. https://doi.org/10.1021/bi00312a005

Cockrell, G. M., Zheng, Y., Guo, W., Peterson, A. W., Truong, J. K., and Kantrowitz, E. R. (2013) New paradigm for allosteric regulation of *Escherichia coli* aspartate transcarbamoylase, *Biochemistry 52*, 8036–8047. https://doi.org/10.1021/bi401205n

Problem 6–6: The reaction catalyzed by 3-deoxy-7-phosphoheptulonate synthase (see Equation 3–17)

$$\text{phospho}\textit{enol}\text{pyruvate} + H_2O + \text{D-erythrose 4-phosphate} \rightleftharpoons HOPO_3^{2-} + \text{3-deoxy-D-}\textit{arabino}\text{-hept-2-ulosonate 7-phosphate}$$

is the first committed reaction in the biosynthesis of L-phenylalanine and L-tyrosine. The reaction of the enzyme from *E. coli* is allosterically inhibited[175] by both L-phenylalanine and L-tyrosine. Below are some of the kinetic results that describe this heterotropic allosteric inhibition.

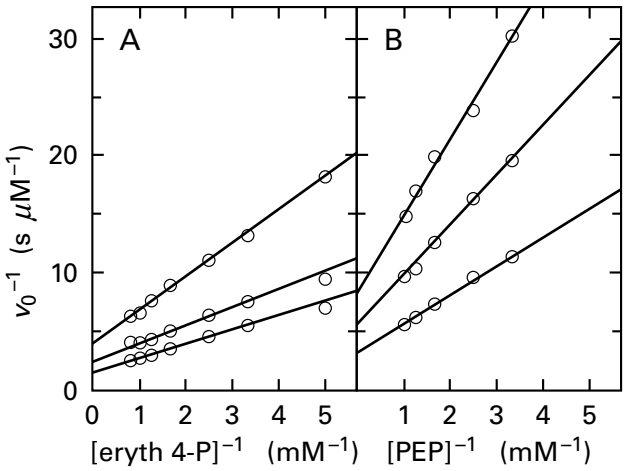

Inhibition of 3-deoxy-7-phosphoheptulonate synthase by L-tyrosine.[226] The reaction mixtures for the observations in Panel A contained 2 mM phospho*enol*pyruvate, D-erythrose 4-phosphate as indicated, 0.13 mg of protein mL^{-1}, and 0.1 M potassium phosphate at pH 6.4. The reaction mixtures for the observations in Panel B contained 2 mM D-erythrose 4-phosphate, phospho*enol*pyruvate as indicated, 0.1 mg of protein mL^{-1}, and 0.1 M potassium phosphate at pH 6.4. All reaction mixtures were incubated for 10 min at 37 °C, and the amount of 3-deoxy-D-*arabino*-hept-2-ulosonate 7-phosphate formed was determined. Each reciprocal of the initial rate of the enzymatic reaction (v_0 in micromolar of 3-deoxy-D-*arabino*-hept-2-ulosonate 7-phosphate produced second^{-1}) is plotted as a function of the reciprocal of the concentrations of reactant, either (A) erythrose 4-phosphate (eryth 4-P; millimolar) or (B) phospho*enol*pyruvate (PEP; millimolar). The concentrations of L-tyrosine in the reaction mixtures for each line were, in each panel in ascending order, 0, 20, and 40 μM.

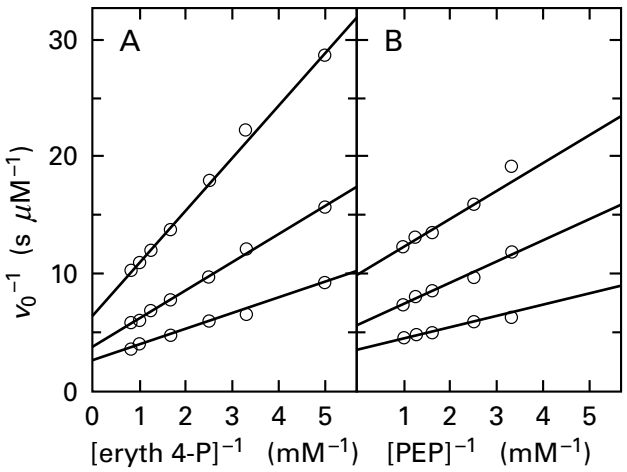

Inhibition of 3-deoxy-7-phosphoheptulonate synthase by L-phenylalanine.[226] The procedure was the same as described above, with the exceptions that L-phenylalanine was used to inhibit the enzyme rather than L-tyrosine and that the reaction mixtures contained 0.13 mg of protein mL^{-1} (Panel A) or 0.09 mg of protein mL^{-1} (Panel B). The concentrations of L-phenylalanine in the reaction mixtures for each line were, in each panel in ascending order, 0, 20, and, 40 μM.

(A) Do the heterotropic allosteric inhibitors L-phenylalanine and L-tyrosine compete with any reactant?
(B) Extend the lines in each figure and decide whether the heterotropic allosteric inhibitors might affect dissociation constants for D-erythrose 4-phosphate (eryth 4-P) from the enzyme.
(C) What kinetic parameter of the enzymatic reaction is affected by association of inhibitors with the enzyme?
(D) Assume that there are two conformations of the enzyme, R and T, in equilibrium with each other and that L-phenylalanine affects this equilibrium. Draw the linkage relation between binding of L-phenylalanine and the conformational equilibrium of the enzyme.
(E) If

$$L_0 = [\mathrm{T}]\,[\mathrm{R}]^{-1}$$
$$K_{\mathrm{dPhe}} = [\mathrm{R}][\mathrm{Phe}]\,[\mathrm{R{\cdot}Phe}]^{-1}$$
$$K'_{\mathrm{dPhe}} = [\mathrm{T}][\mathrm{Phe}]\,[\mathrm{T{\cdot}Phe}]^{-1}$$
$$L_{\mathrm{Phe}} = [\mathrm{T{\cdot}Phe}]\,[\mathrm{R{\cdot}Phe}]^{-1}$$

what is the relation between these four equilibrium constants?
(F) To explain the effect of L-phenylalanine on the properties of the enzyme, what probably are values for L_0 and L_{Phe} with respect to 1 if $K'_{\mathrm{dPhe}} << K_{\mathrm{dPhe}}$?

Problem 6–7: The Bohr effect of hemoglobin is the change in the affinity of hemoglobin (Hb) for molecular oxygen with a change in pH. It is due to a heterotropic allosteric interaction between hydrons (H^+) and molecular oxygen (O_2). The main experimental facts can be approximated in the following way. An approximation is made to simplify the situation and elucidate underlying principles. The main simplification is to ignore homotropic cooperativity.

(a) The reaction between Hb and O_2 can be described by the following equilibrium.

$$\mathrm{HbO_2} \rightleftharpoons \mathrm{Hb} + \mathrm{O_2}$$

(b) At pH 7, the apparent dissociation constant $K_{\mathrm{dO_2,app}}$ for this reaction is 18 μM.

(c) The apparent dissociation constant changes with pH, reaching a constant minimum value of 2.5 μM above pH 9.5 and a constant maximum value of 50 μM below pH 6.0.

(d) If a 0.1 mM solution of oxygenated hemoglobin ($Hb{\cdot}O_2$) in unbuffered 0.2 M NaCl at pH 7 is deoxygenated by bubbling with N_2, the pH of the resulting solution increases by 0.26 pH unit.

(e) Assume that the reaction of interest between hemoglobin and hydronium can be considered a consequence of the ionization of a single amino acid side chain in each $\alpha\beta$ dimer.

(f) The curves for the binding of molecular oxygen by Hb have been determined at several different values of pH. The reaction measured experimentally is

$$\mathrm{HbO_{2,t}} \overset{K_{\mathrm{d,O_2,app}}}{\rightleftharpoons} \mathrm{Hb_t} + \mathrm{O_2}$$

where $[\mathrm{HbO_{2,t}}] = [\mathrm{Hb{\cdot}O_2}] + [\mathrm{Hb{\cdot}H^+{\cdot}O_2}]$, $[\mathrm{Hb_t}] = [\mathrm{Hb}] + [\mathrm{Hb{\cdot}H^+}]$, and $K_{\mathrm{dO_2,app}} = [\mathrm{Hb_t}][\mathrm{O_2}]\,[\mathrm{Hb{\cdot}O_{2,t}}]^{-1}$.

Values of the apparent dissociation constants for molecular oxygen from hemoglobin are as follows.

pH	$K_{\mathrm{dO_2,app}}$ (μM)	pH	$K_{\mathrm{dO_2,app}}$ (μM)
10.0	2.5	7.0	25
9.0	3.0	6.5	37
8.25	4.8	6.0	45
7.6	13	5.0	50

(A) Define the four microscopic equilibrium constants: $K_{\mathrm{dO_2}}$, $K_{\mathrm{dO_2,H^+}}$, K_{aHb}, and $K_{\mathrm{aHb{\cdot}O_2}}$. Write the reactions to which they refer.
(B) Show that $K_{\mathrm{dO_2}}K_{\mathrm{aHbO_2}} = K_{\mathrm{dO_2,H^+}}K_{\mathrm{aHb}}$.
(C) How many equilibrium constants are independent ones?
(D) By using the relations between the equilibrium constants derived above, show that $K_{\mathrm{dO_2,app}}$ is a function of only $[H^+]$ and give the mathematical relation.
(E) Plot log $K_{\mathrm{dO_2,app}}$ against pH. Explain the shape of the curve in terms of the equation in part D.
(F) If the pK_a for the oxygen-linked group in deoxyhemoglobin (pK_{aHb}) were 8.5, what would be the pK_a of this group in oxyhemoglobin, p$K_{\mathrm{aHbO_2}}$?
(G) Explain observation d.

Problem 6–8: The enzyme AMP deaminase from *O. cuniculus* catalyzes the following reaction:

$$AMP^{2-} + H^+ + H_2O \rightleftharpoons IMP^{2-} + NH_4^+$$

The enzyme is a tetramer and is activated by K^+. The kinetics of this activation, with respect to the concentration of AMP^{2-}, are displayed in Panel A of the following figure. Open circles are the data gathered in the presence of a nonactivating cation (tetramethylammonium); filled circles are the data gathered in the presence of K^+. Panel B of the figure is simply a replot of the data by the Hill equation.

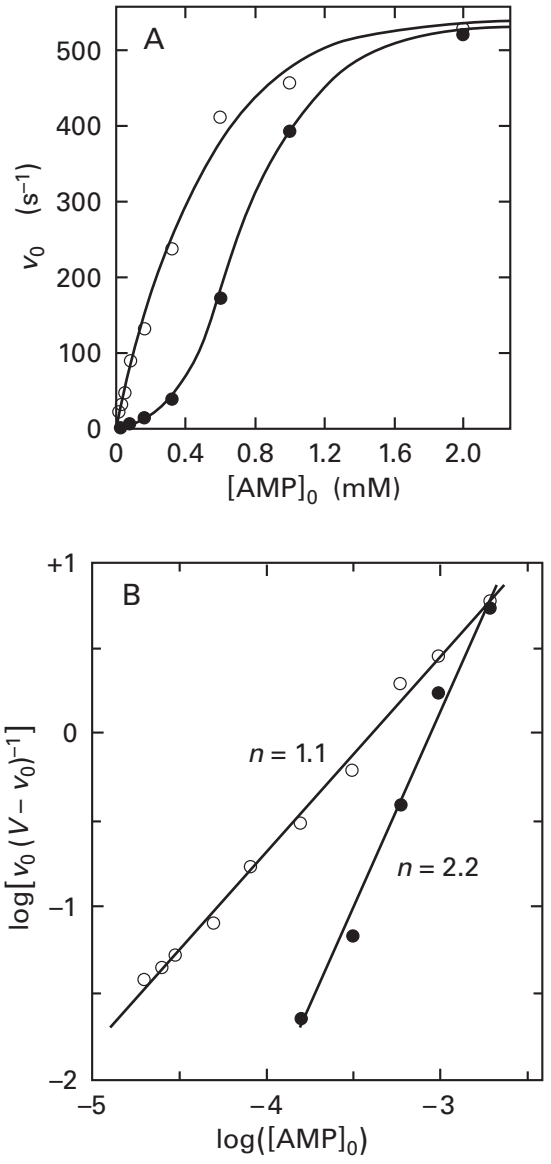

Effect of the concentration of AMP^{2-} on the initial rate of AMP deaminase[227] in the presence and absence of K^+. Assays were run at various concentrations of AMP, 0.15 M tetramethylammonium chloride (●) or 0.15 M KCl (○), and 50 mM imidazolium chloride at pH 6.5 and 30 °C. (A) Initial rate (v_0, in second^{-1}) with respect to the initial concentration of AMP^{2-} ($[AMP]_0$; millimolar). (B) Plots of data from Panel A in the format of the Hill equation (Equation 6–9).

Potassium ion activates the enzyme by increasing its apparent affinity for AMP^{2-} without altering its limiting rate and by eliminating the cooperativity for the effect of AMP^{2-} on enzymatic rate.

(A) Assume that there are two forms of the enzyme, R and T, in equilibrium with each other and that both K^+ and AMP^{2-} can shift that equilibrium. Draw the two linkage relations that connect the binding of either K^+ or the first AMP^{2-} to the conformational equilibrium of the enzyme. Abbreviate K^+ as K and AMP^{2-} as AMP.

(B) By definition

$$L_0 = [T]\,[R]^{-1}$$
$$L_K = [K{\cdot}T]\,[K{\cdot}R]^{-1}$$
$$L_{AMP} = [T{\cdot}AMP]\,[R{\cdot}AMP]^{-1}$$
$$K_{dAMP} = [R][AMP]\,[R{\cdot}AMP]^{-1}$$
$$K'_{dAMP} = [T][AMP]\,[T{\cdot}AMP]^{-1}$$
$$K_{dK} = [K][R]\,[K{\cdot}R]^{-1}$$
$$K'_{dK} = [K][T]\,[K{\cdot}T]^{-1}$$

Write two fundamental equalities relating some of these equilibrium constants with others.

(C) Assume that the R conformation has a higher affinity for AMP^{2-} than the T conformation; in other words, $K_{dAMP} < K'_{dAMP}$. What must be true for the value of L_0 to explain the cooperativity of the enzyme in the absence of K^+?

(D) What must be true for values of L_0 and L_K to explain K^+ activation?

(E) Why does activation by K^+ result in the loss of cooperativity?

(F) Why does K^+ affect only the Michaelis constant for AMP^{2-} rather than the limiting rate, V?

Interfaces and Oligomeric Associations

The quaternary conformational changes controlled by ligands, substrates, and heterotropic allosteric effectors involve reorientations of the folded polypeptides that constitute the oligomer with respect to each other. These reorientations occur at the interfaces between the subunits. Within each interface there are two faces, and it is these faces that reorient relative to each other. For these reorientations to proceed, changes in the molecular **contacts within the interfaces** that hold the oligomer together must occur. These contacts within the interface are between amino acid side chains and portions of the polypeptide backbones that are in the two faces. These changes in orientation can be seen at the interfaces in hemoglobin as their faces shift during the quaternary conformational change.

Crystallographic molecular models are available for human hemoglobin both in its unliganded, deoxy (T) conformation[228] and in its liganded, oxy (R) conformation. The latter hemoglobin is either in a complex with molecular oxygen,[229] its physiological ligand, or in a complex with carbon monoxide,[230] a congener of molecular oxygen. The more extensive[231] identical interfaces between subunits $\alpha 1$ and $\beta 1$ and between subunits $\alpha 2$ and $\beta 2$ (Figure 6–1) remain the same in each quaternary conformation. The two interfaces that change—namely, the less extensive interfaces between subunits $\alpha 1$ and $\beta 2$ (Figure 6–31)[1] and between subunits $\alpha 2$ and $\beta 1$—are also identical to each other both before and after the conformational change because of the twofold rotational axis of symmetry relating the two $\alpha\beta$ dimers. Passing through the center of each identical interface, $\alpha 1\beta 2$ and $\alpha 2\beta 1$, is a twofold rotational axis of pseudosymmetry (normal to the page in Figure 6–31), so each interface has two similar pairs of contacts related by this axis. These two pseudosymmetric pairs of contacts are formed by the third α helix (helix C) of one subunit interdigitating with a loop of polypeptide (the FG corner) between the sixth and seventh α helices of the other subunit and the third α helix (helix C) of the other subunit interdigitating with the loop of polypeptide (the FG corner) between the sixth and seventh α helices of the first subunit.

Because the axis, however, is a rotational axis of pseudosymmetry, these two sets of contacts related by it adjust differently to the conformational change. Within the juxtaposition of the FG corner of subunit $\alpha 1$ and helix C of subunit $\beta 2$ (Figure 6–31), the arrangement of the interlocking contacts among the three amino acids from subunit $\alpha 1$ and the two amino acids from subunit $\beta 2$ remain the same during the conformational change, and the shift in the orientations of the subunits is accommodated by plastically shifting the conformations and atomic contacts among these five amino acids.[1] Within the juxtaposition of the FG corner of subunit $\beta 2$ and helix C of subunit $\alpha 1$ (Figure 6–31), however, which are in the same interface between subunits $\alpha 1$ and $\beta 2$, the order of the amino acids in the interdigitations shifts to accommodate the new orientation as the two faces of this interface slide across each other.

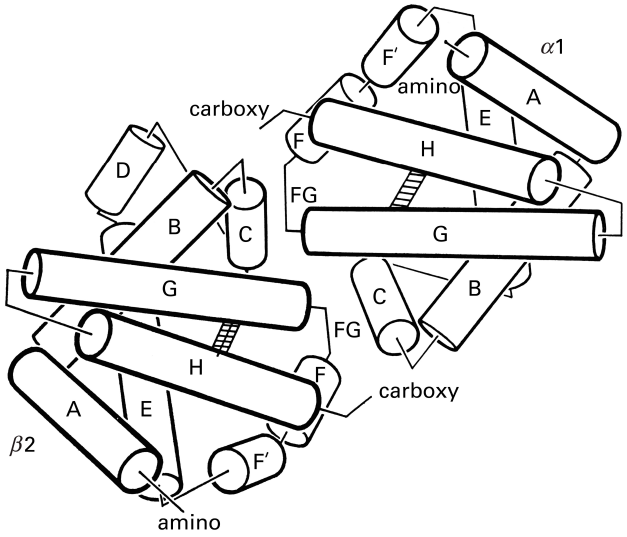

Figure 6–31: Schematic diagram of the arrangement of an $\alpha 1$ subunit and a $\beta 2$ subunit that forms the $\alpha 1\beta 2$ interface in the crystallographic molecular model of hemoglobin.[1] The crystallographic molecular models of deoxyhemoglobin and carbonmonoxyhemoglobin described in Figure 6–1 were used to draw the diagram and provide the disposition of an $\alpha 1$ subunit and a $\beta 2$ subunit. Because the $\alpha 1\beta 2$ interface shown here rearranges significantly during the conformational change, the diagram represents neither model but is an average structure that is intended simply to display the disposition of secondary structures at the interface in both molecular models. The hemes are seen side-on in this view as hatched trapezoids. The α helices that form the majority of the protein are labeled consecutively A–H from the amino terminus (labeled "amino") to the carboxy terminus (labeled "carboxy") of each subunit. The $\alpha 1\beta 2$ interface is formed from the FG corners and the C α helices. The twofold rotational axis of pseudosymmetry is normal to the page and passes through the center of the structure. Reprinted with permission from reference 1. Copyright 1979 Elsevier. https://doi.org/10.1016/0022-2836(79)90277-8

For example, Histidine 97 from the FG corner of the β2 subunit packs between Threonine 41 and Proline 44 from the C helix of subunit α1 in the deoxy conformation, but it shifts over to pack between Threonines 38 and 41 in the oxy conformation. It has been proposed that this alternation between only **two discrete accessible and stable interdigitations** within this second juxtaposition is the reason that there are only two conformations of the oligomer.[1]

At the hemes, the difference in affinity for oxygen between the deoxy and oxy conformations arises from a shift in the position of the sixth helix (helix F) that causes the iron to be pulled out of the plane of the heme in the deoxy conformation but to reside within the plane of the heme in the oxy conformation (Figure 2–53). The connection between this shift and the quaternary conformational change can be thought of in two equivalent ways. On the one hand, it could be concluded that a change in quaternary conformation causes the interfaces involving the FG corners to change their structure, pushing or pulling the covalently connected helix F across the heme and changing the affinity for oxygen. On the other hand, it could be concluded that the binding of oxygen pulls the iron into the plane of the heme, which in turn pulls on helix F and lowers the stability of the deoxy conformation because the shifted helix can be accommodated most effectively in the oxy conformation. These two views of the conformational change are not mutually exclusive; in fact, they are probably two sides of the same coin. The most important point is that the change in conformation be coupled indivisibly to the change in affinity of the hemes for oxygen. This coupling of a conformational change to a functional change is the reason that conformational changes permit cooperativity and heterotropic allosteric control, as well as the conformational conversion of chemical and mechanical energy.

Crystallographic molecular models are available for aspartate carbamoyltransferase in the T conformation, to which $MgCTP^{2-}$ is bound,[62] and in the R conformation, to which *N*-(phosphonacetyl)-L-aspartate is bound.[6,51] During the quaternary conformational change (Figure 6–2)—which involves rotation of the catalytic α subunits relative to each other, opening up of the space between them, and tilting of the regulatory β subunits—several **changes occur in the interfaces** among the subunits.[6] An extensive interface between each catalytic α subunit and the regulatory β subunit immediately adjacent to it but in the other half of the oligomer is present in the T conformation but not in the R conformation because the expansion of the space between the two catalytic trimers sunders it. An interface between each catalytic α subunit and the catalytic α subunit adjacent to it in the other half of the oligomer that is present in the T conformation (Figure 6–8) is also drastically altered and almost eliminated during the conformational change as the α_3 trimers move apart. These two interfaces presumably would act to stabilize the T conformation relative to the R conformation. The interface between adjacent subunits in each trimer of catalytic α subunits, however, becomes more extensive in the R conformation than in the T conformation, which would operate in the opposite direction. The main interface between a catalytic α subunit and a regulatory β subunit, which acts as one of the six identical, symmetrically displayed pivots during the quaternary conformational change, sustains a significant number of changes in atomic contacts, as might be expected during such a rotation of β subunits relative to α subunits. Overall, however, the number of contacts in that interface also increases upon the change from the T to the R conformation.

When **atomic contacts across the various interfaces** are examined in detail, 31 are lost and 25 different ones are gained for each of the six asymmetric units, comprising one catalytic α subunit and one regulatory β subunit, upon the transition from the T to the R conformation. This accounting, however, is a deceptive tally because large changes in the number of contacts (34 lost and 48 gained for each asymmetric unit) also occur within the folded polypeptides themselves, and there is no reason to focus on only one category of changes to explain the overall differences in stability between the two quaternary conformations. In addition, there was no distinction made between the contacts lost and gained within each subunit as a result of local conformational changes and those lost or gained as a result of the quaternary conformational change.

One of the more remarkable aspects of the structure of many of **the interfaces the faces of which shift during the conformational changes** producing allosteric behavior, such as the two in human hemoglobin, is their **relatively small extent**. For example, the homotetramer of porcine fructose-bisphosphatase (Equation 6–62) is held together by four interfaces between the four subunits. Because of the 222(D_2) symmetry of the molecule, the four interfaces consist of two identical pairs. The quaternary conformational change between the T and R conformations includes a reorientation of the subunits that involves only one pair of interfaces. Within each of these two symmetrically identical

interfaces that are involved in the quaternary conformational change, there are two faces, one from each subunit across the interface. It is these faces that reorient, and it is changes in the structures of these faces that cause the reorientation. As a result of these changes, the two faces shift relative to each other, causing the two dimers to rotate by 17° around the twofold rotational axis of symmetry relative to each other.[37] The symmetrically identical interfaces in the other pair are more extensive, and they do not experience a shift in the orientation of their two constituent faces during the quaternary conformational change. In the pair in which the faces reorient, each symmetrically identical interface is formed by contacts among only 20 amino acids from one face and 24 amino acids from the other. In the pair in which the faces do not reorient, each interface is formed by contacts among 48 amino acids from one face and 52 amino acids from the other.[232] In this instance, the interfaces within which the faces shift during the allosteric quaternary conformational change are less extensive by a significant margin.

Each pair of symmetrically related interfaces within which the faces reorient when the deoxy conformation of hemoglobin turns into the oxy conformation (Figure 6–31) involves only 11 amino acids from each subunit.[231] The interface between two subunits in glycogen phosphorylase from *O. cuniculus* is at a neck connecting the two much wider globular subunits (Figure 6–32).[214,486] The twofold rotational axis of symmetry passes through the center of the neck, which is formed from several loops of polypeptide that interdigitate symmetrically around the axis (Figure 6–32). The narrow cross section of the neck relative to the centers of the two subunits causes this interface to be less extensive than those usually encountered in oligomers that do not display allostery.

It is within such **interfaces in which the faces shift** that the changes in orientation among the folded polypeptides occur. Most enzymes (85%) are either dimers or tetramers with 222(D_2) symmetry formed from identical folded polypeptides.[233] **Twofold rotational axes of symmetry** run through the centers of the interfaces holding together such homooligomers, and **an overall change in structure within one of these rotationally symmetric interfaces includes a pair of identical reorientations of its faces**. These interfaces are related to each other by the twofold rotational axis of symmetry. That these pairs of structural changes, because they are identical to each other, are required to occur simultaneously is the reason the symmetry is maintained. The binding of ligand to one subunit causes local conformational changes that destabilize the quaternary conformation. The interfaces, however, remain symmetric and in the unliganded conformation until the number of ligands bound is sufficient to shift the equilibrium constant for the quaternary conformational change of the oligomer to the other side of unity. Then, as the quaternary conformational change of the oligomer commences, it cannot stop at some intermediate asymmetric state because the interfaces among the subunits do not mesh properly until a symmetrical oligomer of the other conformation is formed.[15] The difference of a few kilojoules mole^{-1} of standard free energy between the imprecise fit at the interfaces in an asymmetrical oligomer and the precise fit in a symmetrical oligomer dictates that the ligand-linked quaternary conformational changes built into the sequence of amino acids for each subunit occur in concert during the quaternary conformational change of the oligomer.

When the faces within less extensive interfaces shift relative to each other during a quaternary conformational change, the dissociation constant between the two folded polypeptides on the two sides of the interface necessarily changes. Because these interfaces are often puny, the larger homooligomer in which these puny interfaces are located sometimes dissociates into smaller homooligomers when it associates with or dissociates from its ligands, substrates, or heterotropic allosteric effectors. Dissociation occurs because the dissociation constant for the symmetric interfaces increases as the result of reorientation of its faces that occurs during the quaternary conformational change. In a dimer, there is only one interface with identical halves holding the oligomer together, as with the dimer of glycogen phosphorylase (Figure 6–32). When the dissociation constant for this interface increases, the dimer can split into two monomers. In a tetramer, there are four or six interfaces holding the oligomer together—two or three symmetrically arrayed pairs of identical interfaces—through each of which passes a molecular twofold rotational axis of symmetry. Usually one pair of identical interfaces in a homotetramer is stronger than the other pair or pairs and is much less affected by the quaternary conformational change, as is the case in fructose-bisphosphatase. When dissociation constants for the weaker pair or pairs of interfaces increase during the change in quaternary conformation, whether the change occurs by association or dissociation of ligands, the tetramer

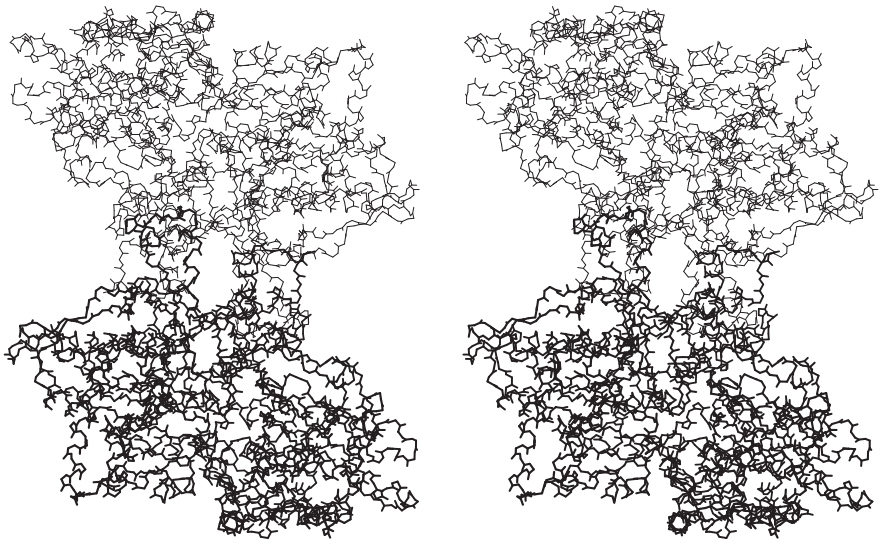

Figure 6–32: Stereodrawing[485] of the two polypeptide backbones in the crystallographic molecular model[486] of the α_2 dimer of glycogen phosphorylase *b* from *O. cuniculus*. The crystals were of space group $P4_32_12$, and a single subunit (841 aa) occupied the asymmetric unit. The only ligand observed in the map of electron density was the prosthetic pyridoxal phosphate. In the figure, the two subunits (thick and thin lines) of the α_2 dimer are displayed around the crystallographic twofold rotational axes of symmetry, which in this view is normal to the page. The interface between the subunits is peculiar in that it is formed by interdigitating strands that create a neck between the two globular structures.

can split into two dimers, each of which retains the strong interface unaffected by the conformational change

A **reactant, heterotropic allosteric activator, or heterotropic allosteric inhibitor can change one or the other of these dissociation constants** and either effect such a dissociation or, in reverse, promote association of the halves that are products of such a dissociation.* The isoenzyme of aspartate kinase (Equation 6–103) in *E. coli* that is inhibited allosterically by L-lysine is a homodimer.[234] Two of these homodimers exist in equilibrium with a tetrameric dimer of dimers within a particular range of concentration of protein. Addition of L-lysine shifts the equilibrium in favor of the tetramer.[235] Human amidophosphoribosyltransferase (Equation 6–105) is a homotetramer that exists in equilibrium with its two dimers. Addition of AMP^{2-}, a heterotropic allosteric inhibitor,[236] also shifts the equilibrium in favor of the tetramer.[237]

In the two previous examples, the binding of a heterotropic allosteric inhibitor promoted association of dimers to a tetramer, but association of **a substrate, heterotropic allosteric inhibitor, or heterotropic activator can promote either association or dissociation of an oligomer**. The heterotropic allosteric inhibitor phospho*enol*pyruvate shifts the equilibrium between dimers and tetramers in favor of dimers of 6-phosphofructokinase from *G. stearothermophilus*, promoting dissociation of the tetramer (Figure 6–9) into dimers, which occurs at the pair of identical symmetrically displayed interfaces in which the faces shift in their relative orientation during the quaternary conformational change.[27,238] In the case of threonine ammonia-lyase from *Arabidopsis thaliana*, the heterotropic allosteric inhibitor L-isoleucine[239] also shifts the equilibrium between dimers and tetramers in favor of dimers.[240] The binding of either molecular oxygen or carbon monoxide, each a homologue of a substrate for an enzyme, promotes dissociation of the stable $(\alpha\beta)_2$ tetramer of human deoxyhemoglobin (Figure 6–1) into $\alpha\beta$ dimers.[241] The heterotropic allosteric activator[242] $MgGTP^{2-}$ shifts the equilibrium between dimers and tetramers in favor of tetramers of uracil phosphoribosyltransferase from *Toxoplasma gondii*.[243] And D-ribulose 5-phosphate, a cooperative substrate, promotes association of two monomers of human ribulose-phosphate 3-epimerase to form a dimer, which is the more enzymatically active quaternary form of the enzyme.[244,245]

In a few instances, dimers of a particular enzyme are in equilibrium with an oligomer larger than a tetramer, and the equilibrium is affected by a substrate or heterotropic allosteric effector.[246] For example, rotationally symmetric dimers of a rare allele of human porphobilinogen synthase are in equilibrium with octamers and also in equilibrium with hexamers.[247] Each octamer is a tetramer of the dimers arrayed around a fourfold rotational axis of symmetry. There are eight identical interfaces among the four dimers, not counting those that hold the dimers together, and these interfaces are symmetrically related by the fourfold rotational axis of symmetry. Each hexamer of dimers is arrayed around a threefold rotational axis of symmetry, and there are six identical interfaces among the dimers, distinct from the eight that produce the octamer, arrayed around the threefold axis of symmetry. In both the octamer and the hexamer, however, none of these interfaces connecting the homodimers—eight in the octamer and six in the hexamer—has a twofold rotational axis running through it because the individual subunits participating in these interfaces are arranged about the threefold and fourfold axes of symmetry, respectively, as are the catalytic subunits in aspartate carbamoyltranferase (Figure 6–2), head to tail. The interface within a dimer is the strong one while the eight and the six interfaces holding together each octamer and hexamer, respectively, are weak. Association of the substrate, 5-aminolevulinate, shifts the equilibrium from one in favor of hexamers to one in favor of octamers.[248] Association of substrate alters the conformation of the surface of each subunit in a dimer in such a way that the two faces on the surface of each subunit that participates in formation of the hexamer no longer can do so and the two faces on each subunit that participates in formation of the octamer can now do so.

So far, all but one of the examples of oligomeric enzymes in which an equilibrium between monomer and dimer or between dimer and tetramer, hexamer, or octamer is shifted by heterotropic allosteric effectors and substrates are cases in which the **active site is removed from or distant from the interface** or interfaces that dissociate or the faces that associate.[234,245,247,249-252] In these instances, a direct effect of dissociation of the interface or association of the faces in the oligomer on the enzymatic activity cannot occur, even though there could well be indirect effects,

*By microscopic reversibility, the removal of any ligand that causes dissociation of a homooligomer must cause its reassociation, and the removal of any ligand that promotes the association of the halves of a homooligomer must cause its dissociation.

which would be difficult to dissect from the global conformational change itself.

In the case of 6-phosphofructokinase from *G. stearothermophilus*, however, **a portion of the active site is in the interface** the faces of which shift upon the quaternary conformational change (Figure 6–9). In the crystallographic molecular model of the homotetramer, the active site of which is occupied by fructose 6-phosphate and $MgADP^-$, it can be seen that fructose 6-phosphate occupies a subsite in which two of the eight side chains forming the subsite are from the subunit opposite the one that provides the other six.[27,253] Both 6-phosphofructokinase from *G. stearothermophilus*[238] and 6-phosphofructokinase from *S. aureus* (59% identity; 0.6 gap percent) are homotetramers that exist in equilibrium with the respective two homodimers. Each tetramer is enzymatically active, and the dimer is inactive. Addition of phospho*enol*pyruvate, a heterotropic allosteric inhibitor, shifts the equilibrium between tetramer and dimers of 6-phosphofructokinase from *G. stearothermophilus* in favor of the enzymatically inactive dimer. Addition of $MgATP^{2-}$, an inhibitor as well as being a substrate, shifts the equilibrium between tetramer and dimers of 6-phosphofructokinase from *S. aureus*[27] in favor of the enzymatically inactive dimer. Because the subsite for fructose 6-phosphate is in the interface, there is no complete active site in the dimer, and it is only formed when the tetramer forms. Consequently, the tetramerization has **a direct effect on the enzymatic activity**, and it seems reasonable to assume that dissociation of the tetramer, at least in part, explains the inhibition. In most cases, however, there cannot be a direct effect because of the usual remove of the active site from the interface.

The observed effect of a substrate or heterotropic allosteric effector on the molar concentrations of monomers and dimers, or of dimers and tetramers, in equilibrium with each other in a particular solution depends on both the dissociation constant for the oligomer and the concentration of the protein in solution. For the moment, define dimer D as either a homodimer of monomers or a homodimer of homodimers, which is by definition a homotetramer of $222(D_2)$ symmetry, and define monomer M as the monomer forming that homodimer or the homodimer forming that homotetramer with $222(D_2)$ symmetry. Also assume, as has been noted, that a homotetramer of $222(D_2)$ symmetry almost always or always dissociates into two homodimers. The equation for the equilibrium between dimer D and monomer M is

$$2\,\mathrm{M} \xleftarrow[K_{d2}]{} \mathrm{D} \tag{6–106}$$

and the dissociation constant for dimer D is

$$K_{d2} = \frac{[\mathrm{M}]^2}{[\mathrm{D}]} \tag{6–107}$$

Because the dissociation constant is the quotient of the square of the concentration of monomer M and the unsquared concentration of dimer D, the observed concentrations of monomers and dimers, respectively, depends on the total concentration of the protein. If

$$[\mathrm{M}]_t = [\mathrm{M}] + 2[\mathrm{D}] \tag{6–108}$$

is the equation for conservation of mass, where $[M]_t$ is the total concentration of monomers in solution, both those present as free monomers M and those present as dimers D, then the fraction of total monomers that are free monomers*

$$f_M = \frac{[\mathrm{M}]}{[\mathrm{M}]_t} = \frac{\left(K_{d2}^2 + 8K_{d2}[\mathrm{M}]_t\right)^{1/2} - K_{d2}}{4[\mathrm{M}]_t} \tag{6–109}$$

and the fraction of total monomers that comprise dimers

$$f_D = \frac{2[\mathrm{D}]}{[\mathrm{M}]_t} = \frac{4[\mathrm{M}]_t + K_{d2} - \left(K_{d2}^2 + 8K_{d2}[\mathrm{M}]_t\right)^{1/2}}{4[\mathrm{M}]_t} \tag{6–110}$$

From these two equations, it can be seen that, when the concentrations of all other components remain the same, as the total concentration of monomers—and hence the concentration of the protein—is increased, the concentration of monomers decreases and the concentration of dimers increases. The equations apply to dissociation of any oligomer, not just homodimers and homotetramers, into two equal parts—for example, dissociation of the hetero-tetramer of hemoglobin.

*This equation differs from that in Yu and Pettigrew[254] only in the definition of what constitutes a subunit.

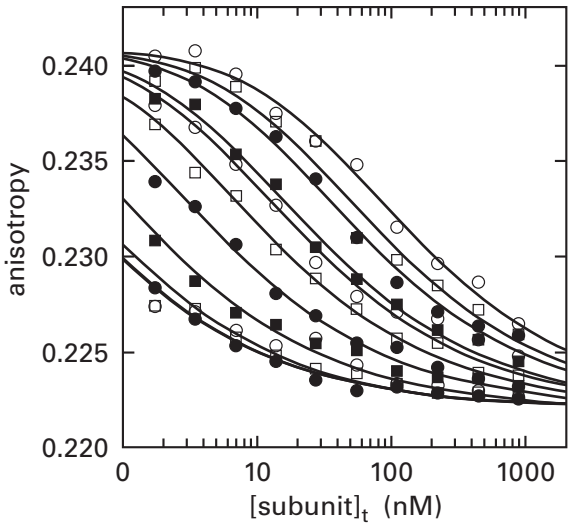

Figure 6–33: Dissociation of glycerol kinase from *E. coli* that occurs when the protein is diluted.[254] Glutamate 478, which is on the surface of glycerol kinase, was mutated to cysteine. Although there are five cysteines in the native protein, none is accessible for reaction when the protein is in a solution containing 2 mM glycerol and 2 mM $MgATP^{2-}$. The mutant protein was modified with 5-(iodoacetamido)-2′,7′-difluorofluorescein in 2 mM glycerol, 2 mM ATP^{4-}, and 0.1 M triethanolammonium chloride at pH 8.0. At the completion of the reaction, 0.35 mole of 2′,7′-difluorofluorescein was incorporated for every mole of subunit. The anisotropy of fluorescence ($\lambda_{excitation}$ = 485 nm; $\lambda_{emission}$ = 515 nm) was assessed in a solution of 2 mM glycerol, 0.1 mM ethylenediaminetetraacetate, 0.1 mM 2-sulfanylethanol, various concentrations of the heterotropic allosteric inhibitor D-fructose 1,6-bisphosphate, and 0.1 M triethylammonium chloride at pH 7.0. The anisotropy is plotted as a function of the total concentration of subunits of glycerol kinase in the solution (nanomolar). The axis of the abscissa is in a common logarithmic scale. The concentrations of D-fructose 1,6-bisphosphate, in descending order, were 0, 0.05, 0.1, 0.2, 0.3, 0.5, 1, 5, 10, 20, and 50 mM. Each curve is a fit of Equations 6–109, 6–110, and 6–112 to the data.

Glycerol kinase (previously Equation 4–283)

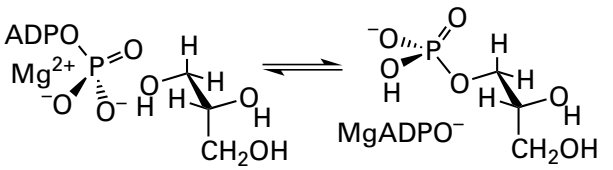

(6–111)

from *E. coli* can be a homodimer or a homotetramer of 222(D_2) symmetry, and these two oligomers are in rapid equilibrium with each other. The active sites are distant from the interfaces involved in dissociation and association.[255] The enzyme was modified with 5-(iodoacetamido)-2′,7′-difluorofluorescein at a cysteine in each of its polypeptides. The steady-state fluorescent anisotropy of the fluorophore, which is a function of rotational diffusion of the oligomer to which it is attached, depends on whether it is attached to a subunit in a dimer or a subunit in a tetramer. The tetramer has lower anisotropy than the dimer because its rotational diffusion is less. Consequently, it is possible to follow, by fluorescent anisotropy, the equilibrium concentrations of dimers and tetramers of glycerol kinase in equilibrium with each other as a function of the total concentration of dimers in solution (Figure 6–33).[254] If the monomer in this dissociation is defined as the homodimer and the dimer in this dissociation is defined as the homotetramer, then the observed steady-state anisotropy

$$\bar{r} = \bar{r}_M f_M + \bar{r}_D f_D \qquad (6–112)$$

where $\bar{r}_M$ is the steady-state anisotropy of the monomer and $\bar{r}_D$ is the steady-state anisotropy of the dimer, and the fractions of monomer and dimer are defined by Equations 6–109 and 6–110. As the total concentration of monomers is increased, the ratio between the concentration of monomers and the concentration of dimers decreases, as expected.

D-Fructose 1,6-bisphosphate is a heterotropic allosteric inhibitor of glycerol kinase from *E. coli*. Its two sites for binding are in two of the interfaces between the subunits in the tetramer of glycerol kinase, and both sites sit upon the same twofold rotational axis of symmetry passing through these two interfaces. Consequently, the site for binding of D-fructose 1,6-bisphosphate is formed from the same side chains on each subunit, which are related by the local twofold rotational axis of symmetry, and there are only two sites on each tetramer.[114] As might be predicted, D-fructose 1,6-bisphosphate binds more tightly to the tetramer, so as the concentration of D-fructose 1,6-bisphosphate is increased, the tetramer becomes more stable (Figure 6–33), and its apparent dissociation constant becomes smaller. The curves in the figure are all fits of Equations 6–109, 6–110, and 6–112 to the data, and the apparent dissociation constant, $K_{d4,app}$, obtained from these fits decreases as the concentration of fructose 1,6-bisphosphate increases.

An equation for the dissociation constant of the tetramer was derived from a simple set of linked equilibria

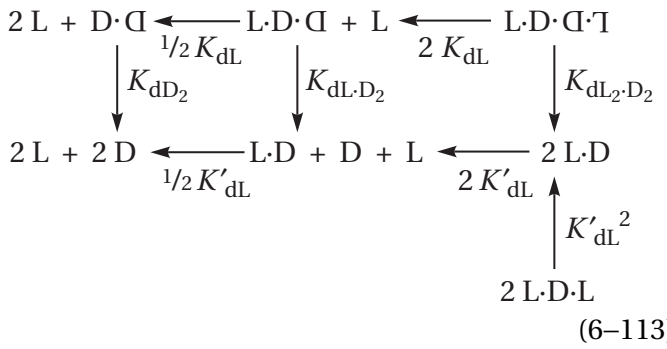

(6–113)

In this equation, the intrinsic dissociation constants of fructose 1,6-bisphosphate from the dimer, K'_{dL}, and from the tetramer, K_{dL}, differ. Consequently, the linked dissociation constants of the unoccupied tetramer, K'_{dD_2}, the tetramer occupied by one fructose 1,6-bisphosphate, $K'_{dL\cdot D_2}$ and the tetramer occupied by two fructose 1,6-bisphosphates, $K'_{dL_2\cdot D_2}$, also must differ from each other. Association of a second fructose 1,6-bisphosphate with the dimer prevents that doubly occupied dimer from associating with another occupied dimer. The decrease in the apparent dissociation constant for the tetramer as the concentration of fructose 1,6-bisphosphate is increased (Figure 6–33) could be fit with the equation derived from these linked equilibria and the intrinsic dissociation constants of $K_{dL} = 0.1$ mM and $K'_{dL} = 20$ mM. As expected, the dissociation constant for fructose 1,6-bisphosphate is smaller for the tetramer than for the dimer.

It is clear, from a consideration of the horizontal asymptotes for the lines in Figure 6–33, that if the dissociation constant for the tetramer of glycerol kinase were large enough, then only dimers of the enzyme would be observed at all concentrations of enzyme and all concentrations of D-fructose 1,6-bisphosphate. It is also clear that if the dissociation constant were small enough, then only tetramers would be observed. Consequently, if concentrations of enzyme that were too small had been chosen, no association of dimers would have been observed, or if concentrations of enzyme that were too large had been chosen, no dissociation of tetramers would have been observed, yet the binding of heterotropic allosteric inhibitor would still be changing the dissociation constant of the tetramer.

In the case of association of fructose 1,6-bisphosphate with glycerol kinase, there was no consideration of the fact that it is a heterotropic allosteric inhibitor of the enzyme, only that it is a ligand that happens to associate within the interface between the dimers in the tetramer, and hence its association is linked to dissociation of the tetramer. The **ability of substrates, heterotropic allosteric effectors, and other ligands to change the dissociation constant for a dimer into two monomers**, or for a dimer of dimers into two dimers, when sites with which they associate are distant from the interfaces that dissociate is also a consequence of linkage. In addition, because the faces in the interface in a dimer or the faces in the two weak interfaces in a dimer of dimers shift during the quaternary conformational changes that are responsible for cooperativity, the same linkage that produces cooperativity is also responsible for changing the dissociation constants for those interfaces.

Assume that the protein is a dimer but remember that the same derivation applies to a tetramer of 222(D_2) symmetry that dissociates into homodimers at the weakest pair or pairs of interfaces. Assume that sites for association of a particular ligand, L, are not within the interface that dissociates so that their effect on dissociation of the dimer is solely the result of their effect on the equilibrium between two quaternary conformations, T and R. Since the allosteric interface between the two monomers in the dimer must differ between the two quaternary conformations and this difference must result in a change in the dissociation constant of the interface, the effect of the ligand on the equilibrium constant between the two conformations results in a linked effect on the dissociation constant for the dimer. Remember also that the allosteric interfaces in an allosteric tetramer of 222(D_2) symmetry change both their structure and the orientation of their two faces upon association of ligand and that they are almost always the weak interfaces that dissociate.

Consider the following **linkage relation** for an allosteric dimer associating with ligand L

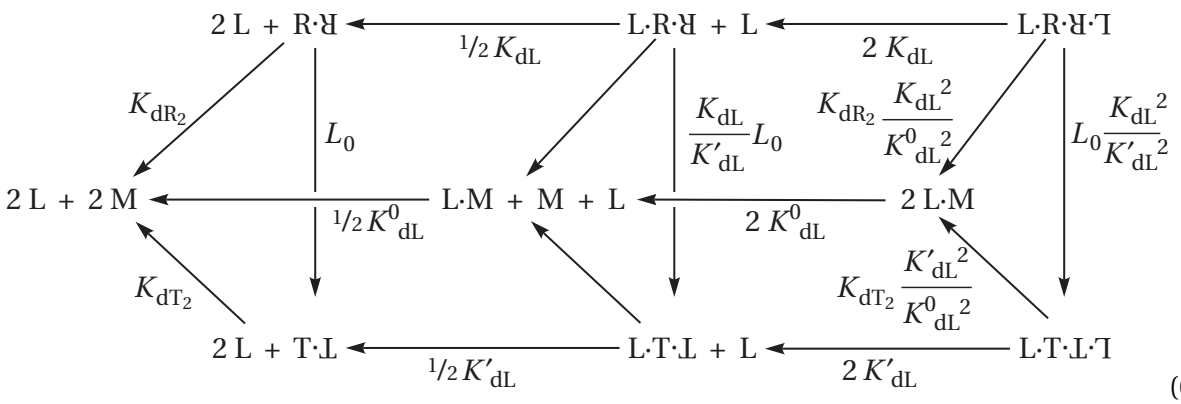

(6–114)

where

$$K_{dT_2} = \frac{[M]^2}{[T{\cdot}T]} \tag{6–115}$$

and

$$K_{dR_2} = \frac{[M]^2}{[R{\cdot}R]} \tag{6–116}$$

The dissociation constant for ligand L from the monomer

$$K^0_{dL} = \frac{[L][M]}{[L{\cdot}M]} \tag{6–117}$$

The rest of the equilibrium constants have their usual definition. The **apparent dissociation constant for the dimer**

$$K_{dD,app} = \frac{([M] + [L{\cdot}M])^2}{[T{\cdot}T] + [L{\cdot}T{\cdot}T] + [L{\cdot}T{\cdot}T{\cdot}L] + [R{\cdot}R] + [L{\cdot}R{\cdot}R] + [L{\cdot}R{\cdot}R{\cdot}L]} \tag{6–118}$$

With the above definitions

$$K_{dD,app} = K_{dR_2} \frac{\left(1 + \frac{[L]}{K^0_{dL}}\right)^2}{\left(1 + \frac{[L]}{K_{dL}}\right)^2 + L_0 \left(1 + \frac{[L]}{K'_{dL}}\right)^2}$$

$$= K_{dR_2} \frac{K_{dL}^2 K'^2_{dL} \left(K^0_{dL} + [L]\right)^2}{K^0_{dL}{}^2 K'^2_{dL} (K_{dL} + [L])^2 + L_0 K^0_{dL}{}^2 K_{dL}^2 (K'_{dL} + [L])^2} \tag{6–119}$$

with the following limits

$$\lim_{[L] \to 0} K_{dD,app} = K_{dR_2} \frac{1}{1 + L_0} \tag{6–120}$$

$$\lim_{[L] \to \infty} K_{dD,app} = K_{dR_2} \frac{K_{dL}^2 K'^2_{dL}}{K^0_{dL}{}^2 (K'^2_{dL} + L_0 K_{dL}^2)} \tag{6–121}$$

When $L_0 > 1$, the T conformation predominates in the absence of ligand. If $K'_{dL} > K_{dL}$, then the ligand shifts the equilibrium in favor of the R conformation. In this situation, in the absence of ligand, the apparent dissociation constant of the dimer into two monomers is $K_{dR_2} L_0^{-1}$, which is simply K_{dT_2}, the dissociation constant for the dimer in the T conformation. In the presence of saturating concentrations of ligand, however, the apparent dissociation constant for the dimer is $K_{dT} K'^2_{dL} (K^0_{dL}{}^2)^{-1}$, which is the dissociation

constant of the dimer in the T conformation shifted by the difference in dissociation constants for the ligand from the T conformation and from the monomer, respectively, just as any dissociation of a dimer is shifted by a difference in the dissociation constant for the ligand between dimer and monomer. If $K'_{dL}{}^2\ (K^0_{dL}{}^2)^{-1} < 1$, then the apparent dissociation constant for the dimer will decrease at all concentrations of ligand L until saturation because the dissociation constant of ligand from the monomer is larger than that from the dimer. If $K'_{dL}{}^2\ (K^0_{dL}{}^2)^{-1} > 1$, then the dissociation constant for the dimer will increase at all concentrations of ligand L until saturation.

When $L_0 < 1$, the R conformation predominates in the absence of ligand. If $K'_{dL} < K_{dL}$, then the ligand shifts the equilibrium in favor of the T conformation. In the absence of ligand, the apparent dissociation constant is K_{dR_2}, the dissociation constant for the R conformation. In the presence of saturating concentrations of ligand, however, the apparent dissociation constant is $K_{dR}K_{dL}{}^2\ (K^0_{dL}{}^2)^{-1}$, which is the dissociation constant of the dimer in the R conformation shifted by the difference in dissociation constants for the ligand from the R conformation and from the monomer. If $K_{dL}{}^2\ (K^0_{dL}{}^2)^{-1} < 1$, then the dissociation constant for the dimer will decrease at all concentrations of ligand L until saturation. If $K_{dL}{}^2\ (K^0_{dL}{}^2)^{-1} > 1$, then the dissociation constant for the dimer will increase at all concentrations of ligand L until saturation.

The **usual limits to cooperative and heterotropic allosteric behavior** apply. If $L_0 > K'_{dL}{}^2\ (K_{dL}{}^2)^{-1} > 1$, then the ligand will be unable to shift the equilibrium sufficiently (Equation 6–114), and almost all the dimer will remain in the T conformation at all concentrations of ligand, and no change in its dissociation constant will be observed. If $L_0 < K'_{dL}{}^2\ (K_{dL}{}^2)^{-1} < 1$, then the ligand will be unable to shift the equilibrium sufficiently to produce significant concentrations of the T conformation, almost all of the dimer will remain in the R conformation at all concentrations of ligand, and no change in its dissociation constant will be observed.

D-Fructose 1,6-bisphosphate is a heterotropic allosteric inhibitor of glycerol kinase, and its inhibition of enzymatic activity shows a degree of cooperativity ($n_H = 1.5$). In the absence of substrates, however, the enzyme is probably in the T conformation and remains in the T conformation as D-fructose 1,6-bisphosphate associates because it is a heterotropic allosteric inhibitor. Consequently, the decrease in dissociation constant observed with increasing concentration of D-fructose 1,6-bisphosphate (Figure 6–33) most likely represents only the fact that the dissociation constant for D-fructose 1,6-bisphosphate from the dimer (the monomer in Equation 6–114) is significantly larger than its dissociation constant from the tetramer in the T conformation (the dimer in the T conformation in Equation 6–114) without the complication of the allosteric conformational change.*

If the ligand is a heterotropic allosteric inhibitor and the inhibitor alone shifts the allosteric equilibrium from the R conformation in its absence to the T conformation at saturating concentrations, then $K'_{dL} < K_{dL}$ and $K'_{dL}{}^2\ (K_{dL}{}^2)^{-1} < L_0 < 1$. In the absence of inhibitor, the apparent dissociation constant of the dimer is

$$\lim_{[L] \to 0} K_{dD,app} \cong K_{dR_2} \tag{6–122}$$

and at saturating concentrations of inhibitor, it is

$$\lim_{[L] \to \infty} K_{dD,app} \cong \frac{K_{dR_2}K'_{dL}{}^2}{L_0 K^0_{dL}{}^2} = K_{dT_2}\frac{K'_{dL}{}^2}{K^0_{dL}{}^2} \tag{6–123}$$

In the absence of inhibitor, the apparent dissociation constant is that of the R conformation; and at saturating concentrations of inhibitor, the apparent dissociation constant is that of the dimer in the T conformation **shifted by the difference in dissociation constants for the ligand** from the T conformation and from the monomer (Equation 6–114).

If $K'_{dL}{}^2\ (L_0 K^0_{dL}{}^2)^{-1} < 1$, then the dissociation constant for the dimer at saturating concentrations of heterotropic allosteric inhibitor will be less than that in the absence of inhibitor. In the case of aspartate kinase from *E. coli*, dimers of the enzyme associate to form dimers of dimers upon binding of the heterotropic allosteric inhibitor L-lysine.[234]

If $K'_{dL}{}^2\ (L_0 K^0_{dL}{}^2)^{-1} > 1$, then the dissociation constant for the dimer at saturating concentrations of heterotropic allosteric inhibitor will be greater than that in the absence of ligand. In the case of 6-phosphofructokinase from *G. stearothermophilus*, the dimer of dimers dissociates into two dimers upon binding of the heterotropic allosteric inhibitor phospho*enol*pyruvate.[238]

*With, however, the already noted complication of the inhibition of association of the dimers caused by the association of two D-fructose 1,6-bisphosphates with the dimer.

If the ligand is a heterotropic allosteric activator or substrate and the ligand alone shifts the allosteric equilibrium from the T conformation in its absence to the R conformation at saturating concentrations, then $K'_{dL} > K_{dL}$ and $K'_{dL}{}^2\ (K_{dL}{}^2)^{-1} > L_0 > 1$. In the absence of activator or substrate, the apparent dissociation constant of the dimer is

$$\lim_{[L] \to 0} K_{dD,app} \cong \frac{K_{dR_2}}{L_0} = K_{dT_2} \qquad (6\text{–}124)$$

and at saturating concentrations of activator or substrate, it is

$$\lim_{[L] \to \infty} K_{dD,app} \cong K_{dR_2} \frac{K_{dL}{}^2}{K^0_{dL}{}^2} = K_{dT_2} L_0 \frac{K_{dL}{}^2}{K^0_{dL}{}^2} \qquad (6\text{–}125)$$

In the absence of ligand, the apparent dissociation constant is that for the T conformation; and at saturating concentrations of ligand, the apparent dissociation constant is that for the dimer in the R conformation shifted by the difference in dissociation constants for the ligand from the R conformation and from the monomer (Equation 6–114).

If $L_0 K_{dL}{}^2\ (K^0_{dL}{}^2)^{-1} < 1$, then the dissociation constant for the dimer at saturating concentrations of activator or substrate will be less than that in the absence of activator or substrate. For example, association of the substrate D-ribulose 5-phosphate with human ribulose-phosphate 3-epimerase causes monomers of the enzyme to dimerize.[244,245]

If $L_0 K_{dL}{}^2\ (K^0_{dL}{}^2)^{-1} > 1$, then the dissociation constant for the dimer at saturating concentrations of activator or substrate will be greater than that in the absence of activator or substrate. For example, $(\alpha\beta)_2$ tetramers of human hemoglobin dissociate to $\alpha\beta$ dimers upon association with molecular oxygen,[241] its substrate.

There is one peculiarity of Equation 6–119. If one examines its behavior as a function of the concentration of ligand when there is no ligand present and when there is a saturating concentration of ligand, the decrease to a smaller value for the apparent dissociation constant at saturation or the increase to a larger value at saturation is not necessarily monotonic. There can be inflections and inversions in the value before saturation is reached. These inflections can be disconcerting.

For the moment, consider the two following, perhaps unlikely, situations. For one particular protein, if a ligand is observed to be a heterotropic allosteric inhibitor and the dissociation constant for that ligand from the dimer in the T conformation is the same as its dissociation constant from the monomer, then the dissociation constant for the dimer at saturation with inhibitor (Equation 6–123) would have to be greater than its dissociation constant in the absence of inhibitor (Equation 6–122) because $L_0 < 1$ or heterotropic allosteric inhibition would not be observed. For a different protein, if a ligand is observed to be a heterotropic allosteric activator and the dissociation constant for that ligand from the dimer in the R conformation is the same as its dissociation constant from the monomer, then the dissociation constant for the dimer at saturation with inhibitor (Equation 6–125) would have to be greater than its dissociation constant in the absence of inhibitor (Equation 6–124) because $L_0 > 1$ or heterotropic allosteric activation would not be observed. These considerations suggest, counterintuitively, that if these equalities and inequalities describe these two different situations, then association of an observed heterotropic allosteric inhibitor to the first protein and association of an observed heterotropic allosteric activator to the second protein **biases each equilibrium between dimer and monomer in favor of the monomer**.

Suppose that the apparent dissociation constant of the dimer is larger when either a heterotropic allosteric inhibitor or activator is present at saturation than in their absence. In this case, addition of the inhibitor or activator could cause dissociation of the dimer, which would diminish and eventually eliminate cooperativity and any further heterotropic allosteric effects because the monomer can display neither of these properties. To avoid this possibility, the quotient of the dissociation constant for the inhibitor from the T conformation and its dissociation constant from the monomer or the quotient of the dissociation constant for the activator from the R conformation and its dissociation constant from the monomer must be small enough to prevent this dissociation of the dimer from occurring.

Nevertheless, it follows from all the foregoing considerations that **the effect of a substrate, heterotropic allosteric inhibitor, or heterotropic allosteric activator on the equilibrium between dimers and**

monomers or between dimers of dimers and dimers bears no relation to its effect on the equilibrium between or among the allosteric quaternary conformations of the dimers or the dimers of dimers that are responsible for the cooperativity and heterotropic allosteric effects that these ligands display. Consequently, any outcome is possible with any ligand that affects the equilibrium between two quaternary conformations. Addition of a heterotropic allosteric inhibitor or activator or a substrate can lead to dissociation of the dimer or the dimer of dimers. Addition of a heterotropic allosteric inhibitor or activator or a substrate can lead to association of monomers into a dimer or to association of dimers into a dimer of dimers.*

All the arguments leading to this conclusion are equally valid for dissociation of any oligomeric protein or enzyme for which an allosteric ligand alters its quaternary conformation and hence the dissociation constants of some or all of its interfaces, even heterooligomers or oligomers with greater than twofold rotational axes of symmetry. An example of both these latter peculiarities would be aspartate carbamoyltransferase, an $(\alpha_3)_2(\beta_2)_3$ heterohexamer with a threefold rotational axis of symmetry. In this instance, however, the $(\alpha_3)_2(\beta_2)_3$ heterohexamer has not yet been observed to dissociate into its parts when any ligand is added, and its dissociation requires either heating or addition of agents that chemically modify the protein. Ligands, however, are able to interconvert dimers, hexamers, and octamers of human porphobilinogen synthase.

It is unlikely that the dissociation constant between dimer and monomer, between tetramer and dimer, or between any other types of oligomers will be unaffected by a change in the quaternary conformation of the protein such as occurs in aspartate carbamoyltransferase because changes in the interfaces that accompany a change in quaternary conformation almost always occur in the weakest interfaces in the oligomer. If, however, the concentration of enzyme is high enough or low enough, these changes in dissociation constant, even though they must occur upon a particular conformational change, **will not cause any measurable change in the state of aggregation of the oligomer**. The question that is far more difficult to answer with any certainty is whether or not changes in the aggregation state of the oligomer at the cytoplasmic concentration of a particular enzyme have any advantageous or disadvantageous effect that might influence natural selection.* These changes in the state of aggregation, if and when they occur, may simply be unavoidable and inconsequential results of the fact that the dissociation constants must change as an allosterically linked quaternary conformational change rearranges the interfaces holding together the dimers, the dimers of dimers, or any other oligomer. This conclusion is valid whether there are only two quaternary conformations of the protein or there are many.

Suggested Reading

Funkhouser, J. D., Abraham, A., Smith, V. A., & Smith, W. G. (1974) Kinetic and molecular properties of lysine-sensitive aspartokinase. Factors influencing the lysine-mediated association reaction and their relationship to the cooperativity of lysine inhibition, *J. Biol. Chem. 249*, 5478–5484. https://doi.org/10.1016/S0021-9258(20)79753-X

Yu, P., and Pettigrew, D. W. (2003) Linkage between fructose 1,6-bisphosphate binding and the dimer–tetramer equilibrium of *Escherichia coli* glycerol kinase: Critical behavior arising from change of ligand stoichiometry, *Biochemistry 42*, 4243–4252. https://doi.org/10.1021/bi027142l

Problem 6–9: Because 2,3-bisphosphoglycerate binds to a site created by the two β subunits in tetrameric hemoglobin, its dissociation constant from the dissociated $\alpha\beta$ dimers must be much larger than that from the intact $(\alpha\beta)_2$ tetramer.

(A) Draw a relation between the binding of 2,3-bisphosphoglycerate and dissociation of deoxyhemoglobin into dimers.

(B) How would the presence of 2,3-bisphosphoglycerate affect the apparent dissociation constant between dimers and tetramers of deoxyhemoglobin?

(C) Derive formulas that relate the dissociation constant of the oligomer to the molar concentration of 2,3-bisphosphoglycerate.

*This consideration causes the historical origins of the names "tight" (T) and "relaxed" (R) to be even more ambiguous.

*There is a slight increase in the osmotic pressure of the cytoplasm when a dimer of protein or a dimer of dimers dissociates.

Conformational Conversion of Energy

A significant portion of the $MgATP^{2-}$ that is consumed in an animal by hydrolysis to $MgADP^{-}$ and $HOPO_3^{2-}$ is consumed by Na^+/K^+-exchanging ATPase, and the majority of the $MgATP^{2-}$ produced in an animal from $MgADP^{-}$ and $HOPO_3^{2-}$ is produced by H^+-transporting two-sector ATPase. Both enzymes convert the chemical standard free energy available from hydrolysis of $MgATP^{2-}$ into **conformational changes that perform work**; or, in reverse, work is performed upon the protein to drive conformational changes that reverse hydrolysis and create $MgATP^{2-}$. As with all enzymes, these two enzymes catalyze approaches to equilibrium, and in each case the outcome, whether it is the net hydrolysis of $MgATP^{2-}$ or the net formation of $MgATP^{2-}$, depends entirely on the activity of the substrates. Both enzymes either hydrolyze $MgATP^{2-}$ or create $MgATP^{2-}$ when the proper concentrations of substrates are imposed. Although these two enzymes are dramatically different in structure and do not share a common ancestor, the strategy that they employ to couple free energy of hydrolysis of $MgATP^{2-}$ to work that they perform or work that is performed upon them is based on their ability to proceed through several conformational changes that are forced by the protein to occur in a particular order.

The work performed by these enzymes or that is performed upon them is the **movement of ions across membranes**. A **gradient** is the change in a quantity—such as temperature, electric potential, or the concentration or chemical activity of a substance—with distance, expressed as a ratio or differential ratio of the quantity. A **chemical gradient** is a gradient in chemical potential established when the molar concentration of uncharged substance A, such as D-glucose, is greater on one side of a biological membrane than on the other side An **electric gradient** is a gradient in electric potential established when the molar concentration of ionically charged substance A, such as sodium ion, is greater on one side of a biological membrane than on the other side. An **electrochemical gradient** is a gradient in chemical activity of a substance, caused by the combination of its chemical and electric gradients. When these enzymes transport ions across membranes, the ions move across an electrochemical gradient in their concentration. Because of microscopic reversibility, if one of these enzymes is able to move its ions against their concentration gradients, it must also be able to move the ions in the other direction with their concentration gradients.

When the concentrations of an neutral molecule, such as D-glucose, are the same on the two sides of membrane, which is the situation at equilibrium, the change in standard free energy, ΔG°, for moving a molecule of that uncharged substance from one side of the membrane (side a) to the other (side b) is 0 by definition. When the concentrations are different on the two sides, however, the usual equation for situational free energy applies

$$\Delta G = \Delta G^\circ + RT \ln \frac{[A]_b}{[A]_a} = RT \ln \frac{[A]_b}{[A]_a} \quad (6\text{–}126)$$

where $[A]_a$ and $[A]_b$ are the molar concentrations of substance A on side a of the membrane, the side from which it is removed, and on side b of the membrane, the side to which it is added. If substance A is charged—for the sake of argument, it has a positive charge of charge number n, A^{n+}—then the difference in electric potential, ΔV_{ab}, between the two sides must be considered

$$\begin{aligned} \Delta G &= RT \ln \frac{[A^{n+}]_b}{[A^{n+}]_a} + zF\Delta V_{ab} \\ &= RT \ln \frac{[A^{n+}]_b}{[A^{n+}]_a} + nF\Delta V_{ab} \end{aligned} \quad (6\text{–}127)$$

where ΔV_{ab} is the electric potential on side b minus the electric potential on side a, z is the charge number of substance A—which in this case is equal to n—and F is the Faraday constant (96.5 kJ V^{-1} mol^{-1}). This equation defines an **electrochemical gradient of the ions**. The first term is the chemical gradient and the second term is the **electric gradient**, the electric potential across the membrane caused by the imbalance of ionic charge.

To move a positively charged ion from a solution with an electrochemical potential that is negative relative to that of the solution to which it is moved requires work and results in an increase in free energy. To accomplish its intended purpose, Na^+/K^+-exchanging ATPase uses the free energy from hydrolysis of $MgATP^{2-}$ to move Na^+ and K^+ across the plasma membrane of animal cells against electrochemical gradients of Na^+ and K^+. The situational free energy, ΔG, for the movement of the ions in these circumstances is positive.

To move a positively charged ion from a solution with an electrochemical potential that is positive relative to that of the solution to which it is moved results in a decrease in free energy that can be used to perform work. To accomplish its intended purpose, H^+-transporting two-sector ATPase moves hydrons down an electrochemical gradient of hydrons across a membrane in mitochondria, chloroplasts, or a bacterium to provide the free energy necessary to reverse hydrolysis and synthesize $MgATP^{2-}$ instead. The situational free energy, ΔG, for the movement of the ions in these circumstances is negative.

The strategy that each enzyme uses is its own particular form of **conformational coupling**. Hydrolysis or, in reverse, creation of $MgATP^{2-}$ is divided by each enzyme into a sequence of steps. The work ultimately accomplished or used by each enzyme is also divided into the same number of steps, which are forced to occur in concert with steps for the hydrolysis.[256] At the same time that each step in the hydrolysis and synthesis of $MgATP^{2-}$ occurs, the corresponding step in the physical transformation performing work or using work is forced to occur. The site at which the $MgATP^{2-}$ is hydrolyzed and, in reverse, created in each case is in a different location in the enzyme from the location at which the physical transformation performing work and, in reverse, having work performed on it is effected. Consequently, the obligation that particular steps for hydrolysis or creation coincide with particular steps for the physical transformation is enforced by accompanying global conformational changes in the enzyme. Each step involves a global conformational change that includes particular local conformational changes both at the hydrolytic site and at the location where the physical transformation is being accomplished. Each global conformational change proceeds only when both the closely circumscribed step in hydrolysis and creation of $MgATP^{2-}$ and the closely circumscribed step in the physical transformation proceed together. As in heterotropic allostery, global conformational changes dependably couple what occurs in one location on the enzyme with what occurs at another, usually distant location on the enzyme. Whenever the two processes are not forced by the conformational changes to occur simultaneously, energy is wasted. Natural selection has naturally minimized such failures. A paradigm of this strategy of conformational coupling is the reaction catalyzed by Na^+/K^+-exchanging ATPase and its close relatives.

Na^+/K^+-Exchanging ATPase[257] catalyzes the reaction

$$2\,K^+_e + MgATP^{2-}_c + 3\,Na^+_c + H_2O \rightleftharpoons 2\,K^+_c + MgADP^-_c + H^+ + 3\,Na^+_e + HOPO_3{}^{2-}_c \quad (6\text{–}128)$$

where the subscripts c and e refer to the cytoplasm and the extracytoplasmic space, respectively.[258,259] It is a protein spanning the plasma membranes[260-262] of all animal cells and catalyzing the active transport of the alkali metallic cations Na^+ and K^+ across itself.

Na^+/K^+-Exchanging ATPase is a member of **a family of enzymes**, the P-type ATPases, each of which spans a bilayer of phospholipids and catalyzes the primary active transport of particular inorganic cations across the plasma membrane or the endoplasmic reticular membranes of a cell between the cytoplasm and an extracytoplasmic space. The particular reactions catalyzed by these enzymes serve to introduce the members of the family (Table 6–3).[257-279] Each couples hydrolysis of $MgATP^{2-}$ to the movement of cations across a membrane up their electrochemical gradients, but the identity and stoichiometry of the cations moving out of and into the cytoplasm differs. A compelling verification that all the enzymes in this family are closely related is that most of the portions of Na^+/K^+-exchanging ATPase in the globular regions outside the membrane, as well as the four of its membrane-spanning α helices peripheral to the central six that create the compartment for cations, can be replaced by homologous segments from H^+/K^+-exchanging ATPase without affecting its ability to transport Na^+ and K^+ across the membrane.[280]

Mammalian Na^+/K^+-exchanging ATPase is composed of two subunits,[281] α (1020 aa)[282,283] and β (300 aa),[284] each present in the active complex in one copy.[285,286] The β subunit is a cell surface glycoprotein uninvolved in catalysis, and the α catalytic subunit performs the active transport. The α subunit is a protein that spans the plasma membrane, and it is so large that it dwarfs the bilayer of the membrane.[287] Each enzyme in the family contains a polypeptide homologous (Table 6–3) to the catalytic α polypeptide of Na^+/K^+-exchanging ATPase[277,288,289] but no glycoprotein homologous to the β subunit of Na^+/K^+-exchanging ATPase. The large **catalytic polypeptide** is fixed in the bilayer, as are all membrane-spanning proteins, and it catalyzes transport not by moving back and forth across the membrane but by **passing the cations back and forth through itself**.[290] In this regard, active transport is not transport through a membrane but transport through a protein.

Table 6–3: Family of P-type ATPases[a]

name[b]	homology	where found	function
Na^+/K^+-exchanging ATPase[257-262]		plasma membranes of animal cells	transports three Na^+ out of the cytoplasm in exchange for two K^+
H^+/K^+-exchanging ATPase[264-266]	62% identity 0 gap percent	plasma membranes of gastric mucosa	transports one or two[c] H^+ out of the cytoplasm in exchange for two K^+
P-type Ca^{2+} transporter[267-269]	27% identity 1.7 gap percent	sarcoplasmic reticulum	transports two Ca^{2+} out of the cytoplasm in exchange for two or three H^+
calmodulin-dependent[270-273] P-type Ca^{2+} transporter	27% identity 2.7 gap percent	plasma membranes of animal cells	transports one Ca^{2+} out of the cytoplasm in exchange for two H^+
P-type H^+ exporting[274-277] transporter	23% identity 2.2 gap percent	plasma membranes of fungi and plants	transports H^+ out of the cytoplasm
P-type Ca^{2+} transporter[278]	29% identity 1.4 gap percent	plasma membranes of fungi	transports Ca^{2+} out of the cytoplasm
P-type Zn^{2+} transporter[279]	23% identity 2.1 gap percent	plasma membranes of bacteria and plants	transports excess[d] Zn^{2+}, as well as Cd^{2+} and Pb^{2+}, out of the cytoplasm

[a]Relative to Na^+/K^+-exchanging ATPase. [b]The names of the enzymes in this family differ significantly from each other because the name of an enzyme is based on the participants in the equilibrium that it catalyzes rather than any ancestral relationships, which usually makes sense. [c]Stoichiometry depends on the gradient of pH. [d]Zn^{2+} is an essential trace metallic ion but is toxic at high concentrations.

The fact that all the sequences of amino acids for all these catalytic polypeptides are homologous to each other (Table 6–3) requires that they have descended from a common ancestor, that they all fold respectively to produce superposable structures, and that they all catalyze active transport by the same stepwise mechanism.

During catalysis of the active transport of the respective cations, each member of this family passes through a homologous sequence of steps coupling hydrolysis of $MgATP^{2-}$ to the movement of the cations. A fundamental aspect of this scheme is the existence of at least four distinct global conformations of the enzyme. These four conformations differ in structure from each other both at the site where the $MgATP^{2-}$ is hydrolyzed and at a compartment that has access alternately to each side of the membrane and through which the transported cations pass. The hydrolytic site in each enzyme is 5 nm away from the compartment through which the respective cations pass (Figure 6–34).[291,292] Consequently, the conformational changes that are responsible for active transport are typical heterotropic allosteric conformational changes that link changes in the structure of the hydrolytic site to distant changes in the structure of the compartment for the cations. Each hydrolytic site is located in a large globular portion of the respective enzyme that comprises more than half its mass and is located on the cytoplasmic side of the membrane. Only on the cytoplasmic side of each membrane in which these enzymes are located is a significant concentration of $MgATP^{2-}$ available. The compartment for the cations is in the middle of a bundle of ten α helices that span the bilayer of the membrane in which the enzyme is found (Figure 6–35).[282,287,291,293-295]

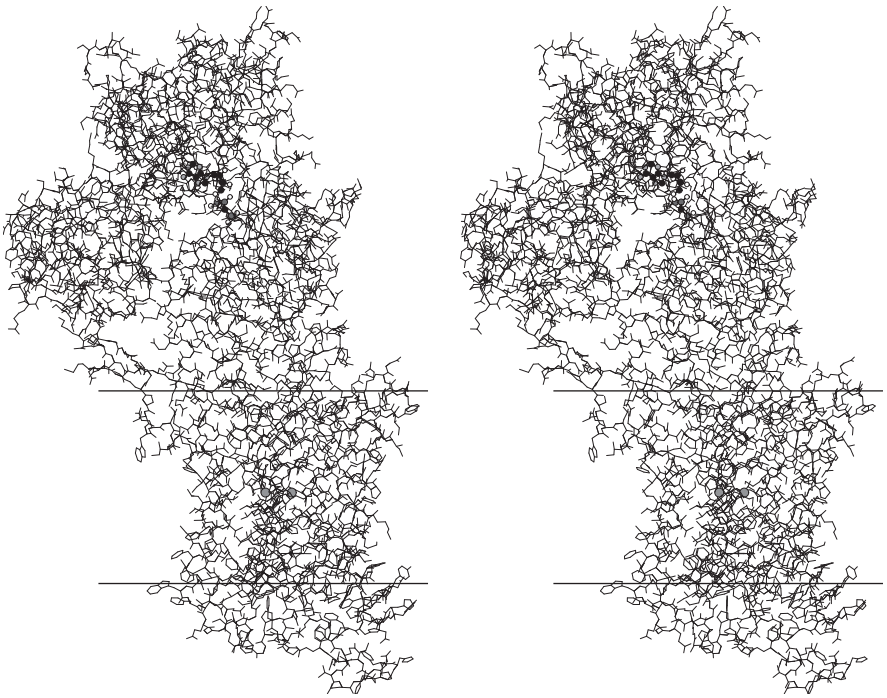

Figure 6–34: Stereodrawing[485] of a crystallographic molecular model of P-type Ca^{2+} transporter from *O. cuniculus* in which the hydrolytic site of the enzyme is occupied by magnesium 5′-adenylic methylenediphosphonic anhydride ($MgAMPPCP^{2-}$) and the compartment for the transported cations is occupied by two Ca^{2+}.[291] Membranes of sarcoplasmic reticulum enriched in P-type Ca^{2+} transporter, isolated from the white muscle of the hind legs of *O. cuniculus,* were dissolved in a 2% solution of the detergent 3,6,9,12,15,18,21,24,27-nonaoxanonatriacontan-1-ol, and P-type Ca^{2+} transporter was purified by nonspecific adsorption to a solid phase of agarose to which the dye reactive red 120 had been covalently attached and then by selective elution of the enzyme from the solid phase by a solution containing 0.4 mM $MgAMPPCP^{2-}$. The purified enzyme was then crystallized from a 2% solution of the detergent 3,6,9,12,15,18,21,24-octaoxahexatriacontan-1-ol containing an undisclosed amount of phosphatidylcholine, 0.5 mM $MgAMPPCP^{2-}$, 5 mM $MgCl_2$, and 10 mM $CaCl_2$. The entire structure of the enzyme is drawn in skeletal format. The polypeptide backbone is shown in thick line segments and the side chains in thin line segments. The $MgAMPPCP^{2-}$ occupying the hydrolytic site is drawn in ball-and-stick format. Black atoms are carbons, white atoms are oxygens, small gray atoms are nitrogens, and large dark gray atoms are the three atoms of phosphorus. The two Ca^{2+} occupying the compartment for cations are the two large gray spheres in the center of the portion of the enzyme that spans the membrane. Although there is no phospholipid bilayer in the map of electron density, presumably because the enzyme is in an unresolved micelle of detergent and phospholipid, the location of the bilayer in the structure (parallel horizontal lines) was assigned by the authors. The cytoplasmic portion of the enzyme is above the membrane, and the extracytoplasmic portion is below the membrane.[287] The enzyme seems to have crystallized in an intermediate conformation between the $E1{\cdot}MgATP^{2-}$ and $[Ca^{2+}]_2{\cdot}E1{\sim}P$ conformations in which the two Ca^{2+} are occluded from both the cytoplasmic and extracytoplasmic solutions in the compartment in the middle of the membrane.[291] Presumably the full conformational change to the $[Ca^{2+}]_2{\cdot}E1{\sim}P$ conformation has been arrested because the $MgAMPPCP^{2-}$ is unable to phosphorylate the aspartate in the hydrolytic site.

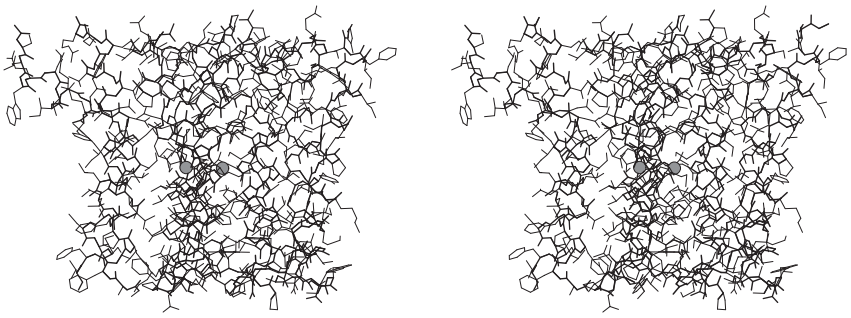

Figure 6–35: Stereodrawing[485] of the ten α helices that span the membrane in P-type Ca^{2+} transporter and form the compartment through which the two Ca^{2+} pass. The two Ca^{2+} occupying the compartment for the cations are the two large gray spheres in the center of the drawing. The portion of the drawing in Figure 6–34 within the volume designated by the authors as spanning the sarcoplasmic reticulum has been magnified to make it easier to observe the individual α helices surrounding the two Ca^{2+}. The ten α helices include amino acids 44–74, 85–115, 249–278, 291–318, 753–782, 783–813, 824–856, 893–922, 926–954, and 960–990, respectively, from the complete sequence of amino acids. Only the α helices that include amino acids 291–318, 753–782, 783–813, and 893–922 provide ligands to the Ca^{2+}. In addition, the two α helices that include amino acids 44–74 and 85–115, which do not provide ligands, form the wall of the compartment for the cations on the left-hand side of the drawing. The two α helices including amino acids 753–782 and 893–922, in addition to providing ligands for the cations, form the wall of the compartment on the right-hand side of the drawing. The α helix including amino acids 783–813 is in the center of the wall in front of the compartment, and the α helix including amino acids 291–318 is in the center of the wall in back of the compartment.

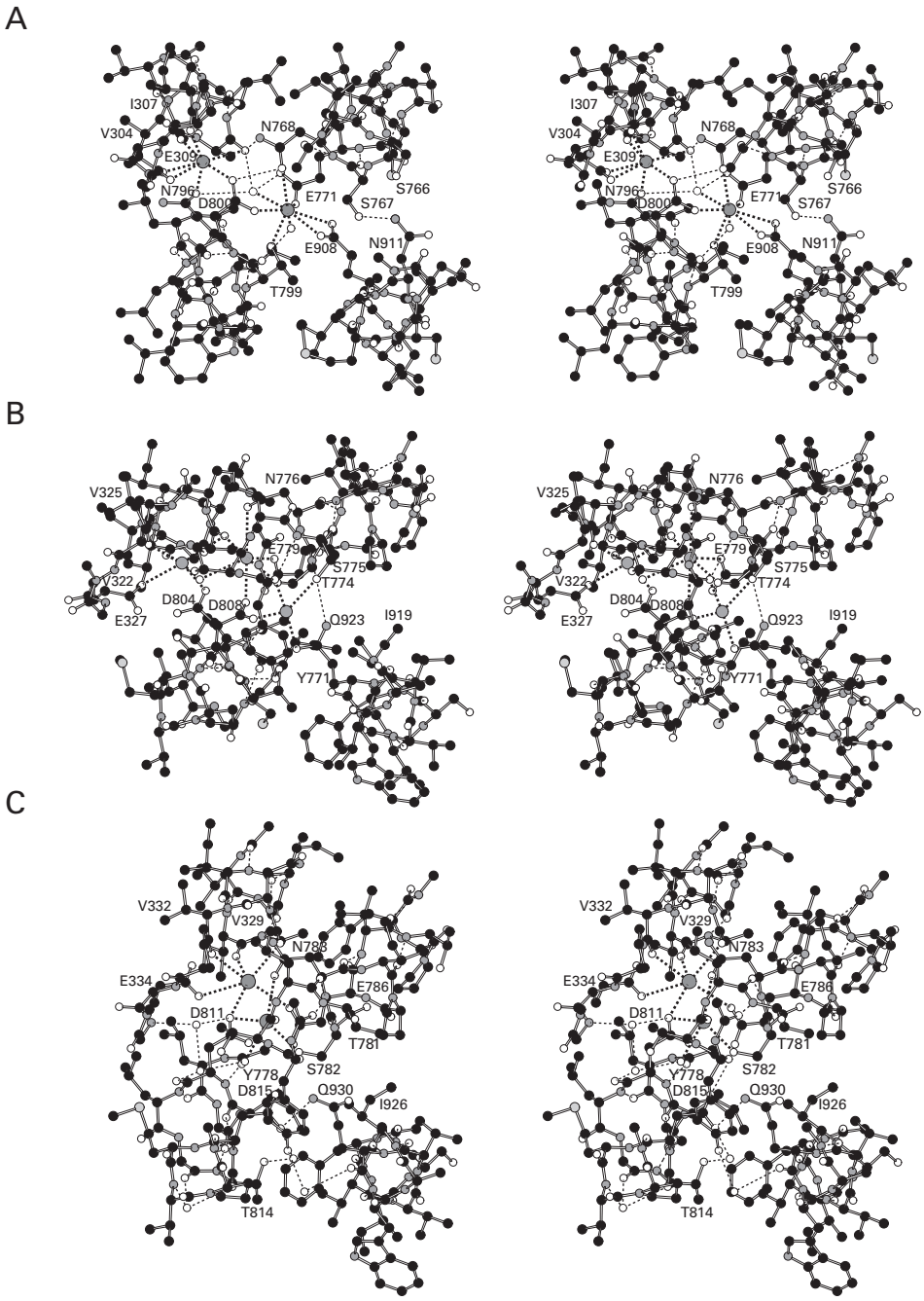
A
I307
V304
N768
E309
N796
D800
E771
S767
S766
E908
N911
T799
B
V325
N776
E779
S775
V322
T774
D804
D808
E327
Q923
I919
Y771
C
V332
V329
N783
E334
E786
D811
T781
Y778
S782
D815
Q930
I926
T814

Figure 6–36: Stereodrawings[485] of crystallographic molecular models of the ligands chelating the hard cations Ca^{2+}, Na^+, and K^+ when they are occluded in the compartments through which they pass in the respective enzymes. Black atoms are carbons, white atoms are oxygens, small gray atoms are nitrogens, and large light gray atoms are sulfurs. The large coordinated gray spheres are the respective metallic cations. (**A**) Two Ca^{2+} occluded within the compartment in P-type Ca^{2+} transporter from *O. cuniculus*.[291] The portion of the crystallographic molecular model of P-type Ca^{2+} transporter drawn in Figure 6–35 was rotated 90° about a horizontal axis in the plane of the page to obtain a view down into the compartment from the cytoplasmic side of the membrane. Only segments from the four α helices that include amino acids 291–318, 753–782, 783–813, and 893–922 and that provide ligands to the two Ca^{2+} are included in the drawing. Each side chain that provides a ligand to a cation is labeled with its identity and its number in the overall sequence of amino acids. (**B**) Three Na^+ occluded within the compartment through which they pass in Na^+/K^+-exchanging ATPase.[292] Membranes from the outer medullae of porcine kidneys enriched in Na^+/K^+-exchanging ATPase[487] were dissolved in a solution of the detergent 3,6,9,12,15,18,21,24-octaoxahexatriacontan-1-ol at a ratio of 1.3 g of detergent (g of protein)$^{-1}$ to obtain a monodisperse solution of the enzyme.[285] The enzyme was then crystallized from a solution containing 150 mM NaCl, 3 mM $MgADP^-$, 1 mM $AlCl_3$, and 0.25 mM oligomycin A. The $MgADP^-$ and $AlCl_3$ formed a complex in the hydrolytic site of the enzyme that promotes formation of the conformation in which three Na^+ are occluded in the compartment for the cations. The drawing was prepared in the same orientation as that in Panel A by superposing only those segments of the crystallographic molecular model of Na^+/K^+-exchanging ATPase that included sequences of amino acids homologous (Figure 6–37) to those comprising the segments from P-type Ca^{2+} transporter represented in Panel A. (**C**) Two K^+ occluded within the compartment through which they pass in Na^+/K^+-exchanging ATPase.[299] Membranes from the rectal glands of *S. acanthias* enriched in Na^+/K^+-exchanging ATPase[302] were dissolved in a solution of the detergent 3,6,9,12,15,18,21,24-octaoxahexatriacontan-1-ol at a ratio of 4 g of detergent (g of protein)$^{-1}$. The enzyme (2.1 mg mL^{-1}) was then crystallized from a 1.5% solution of 3,6,9,12,15,18,21,24-octaoxahexatriacontan-1-ol containing 100 mM KCl, 4 mM MgF_2, and 2.5 mg mL^{-1} phosphatidylcholine. In the presence of K^+ and the absence of nucleotide, the enzyme assumes the E2·$[K^+]_2$ conformation with the two K^+ occluded within the compartment for the cations. The drawing was prepared in the same orientation as that in Panel B by superposing only those segments of the molecular model of Na^+/K^+-exchanging ATPase from *S. acanthias* that included sequences of amino acids homologous (Figure 6–37) to those comprising the segments from porcine Na^+/K^+-exchanging ATPase represented in Panel B. In all three drawings, the ligands are connected to the cations by thick dotted lines, and the thinner dotted lines designate hydrogen bonds. There are two molecules of water (small white solitary spheres) in the drawing in Panel A, one molecule of water in the drawing in Panel B, and six molecules of water in the drawing in Panel C. These molecules of water are fixed by hydrogen bonds to the protein and by coordination to the cations. All of them are within the membrane. There are more in the drawing in Panel C only because there are almost no molecules of water anywhere in the maps of electron density for the other two molecular models. There are empty spaces scattered throughout the membrane-spanning portions of all these molecular models, probably occupied by molecules of water that are simply unobserved.

The compartment through which the cations pass is formed by six of the ten membrane-spanning α helices, but only four of these six α helices provide direct ligands to the cations. The compartment is located in the middle of the bundle at a position that is close to or within the plane defined by the center of the bilayer of phospholipids surrounding the enzyme (Figure 6–35). In each enzyme, this compartment is a **site for binding hard cations, Ca^{2+}, Na^+, or K^+**. Consequently, the ligands are exclusively oxygens: amido oxygens from the polypeptide backbone and oxygens from the side chains of amino acids. Each side chain provides one or two **oxygens as inner-sphere ligands** to the respective cation. Six of the side chains in P-type Ca^{2+} transporter from *O. cuniculus* that provide ligands to the two Ca^{2+} when they occupy the compartment were identified by site-directed mutation,[296] and their assignment was later verified by crystallography.[294] It was then demonstrated by site-directed mutation that the homologous side chains in Na^+/K^+-exchanging ATPase from *S. cerevisiae*[297] as well as three others in the porcine enzyme[298] were involved as ligands to the two K^+ and three Na^+, respectively. These latter assignments were also verified crystallographically.[292,295,299]

When the compartment in the middle of P-type Ca^{2+} transporter from *O. cuniculus* is **occupied by two Ca^{2+}** on their way across the protein, the ligands to the cations can be identified in crystallographic molecular models (Figure 6–36A).[300] The site in the compartment chelating the first Ca^{2+} (to the left in the figure) consists of both oxygens from the carboxylato group of Glutamate 309, the acyl oxygen from the carbamoyl group of Asparagine 796, three amido oxygens from the backbone of the same α helix in the polypeptide, and one oxygen from the carboxylato group of Aspartate 800. The other oxygen from the carboxylato group of Aspartate 800 is a ligand to the second Ca^{2+} (to the right in the figure). The other ligands chelating this second Ca^{2+} are the acyl oxygen from the carbamoyl group of Asparagine 768, the hydroxy oxygen of Threonine 799, two buried molecules of water, one of the carboxylato oxygens of Glutamate 771, and both oxygens from the carboxylato group of Glutamate 908. These are all paradigmatic ligands for Ca^{2+} bound to sites in enzymes (Figure 4–53, **4–156**, and Problem 4–46).

	304 307 309	
O. cuniculus	V A L A **V A** A **I** P **E** G L P	
	322 325 327	
S. scrofa	I G I I **V A** N **V** P **E** G L L	
	329 332 334	
S. acanthias	I G I I **V A** N **V** P **E** G L L	
	763 766 768 771	
O. cuniculus	**Y** L I S S **N** V G **E** V V C I	
	771 774 776 779	
S. scrofa	**Y** T L **T S N** I P **E** I T P F	
	778 781 783 786	
S. acanthias	Y **T** L T **S N** I P **E** I T P F	
	796 799	
O. cuniculus	L W V **N** L V **T D** G L P A T	
	804 807	
S. scrofa	L C I **D** L G T **D** M V P A I	
	811 814	
S. acanthias	L C I **D** L G T D M V P A I	
	908 911	
O. cuniculus	V T I **E** M C N A L N S L S	
	923 926	
S. scrofa	V V V **Q** W A D L V I C K T	
	930 933	
S. acanthias	V V V **Q** W A D L I I C K T	

Figure 6–37: Alignment of the sequences of amino acids for the segments of P-type Ca^{2+} transporter from *O. cuniculus*, porcine (*Sus scrofa*) Na^+/K^+-exchanging ATPase, and Na^+/K^+-exchanging ATPase from *S. acanthias* in the drawings of Figure 6–36. The alignments of the first three segments are obvious by inspection, but the alignment of the last segments of the two Na^+/K^+-exchanging ATPases with the segment from P-type Ca^{2+} transporter was made by structural superposition. The amino acids providing ligands to the respective cations are shown in boldface.

When the compartment in the middle of porcine Na^+/K^+-exchanging ATPase is **occupied by three*** **Na^+** on their way across the protein, the ligands to these three Na^+ can again be identified in crystallographic molecular models (Figure 6–36B).[285,292] The site chelating the first Na^+ (to the left in the figure) consists of one oxygen from each carboxylato group of Aspartate 804 and Glutamate 327, a buried molecule of water, and three amido oxygens from the backbone of an α helix in the polypeptide. Both the α helix and the amido oxygens themselves are homologous to the α helix and the three amido oxygens from the polypeptide, respectively, that chelate the homologously situated Ca^{2+} in P-type Ca^{2+} transporter (Figure 6–37), and the two carboxylato groups providing two of the other ligands to the Na^+ are also on side chains of amino acids in homologous positions in the sequence of amino acids to two of the carboxylato groups chelating the same Ca^{2+}. The second Na^+ (in the middle in the figure) shares one of the amido oxygens from the polypeptide with the first Na^+. Ir is also chelated by two carboxylato oxygens, one from Glutamate 779 and one from Aspartate 808, the acyl oxygen of the carbamoyl group of Asparagine 776, the hydroxy oxygen of Serine 775, and a buried molecule of water. The two carboxylato groups and the carbamoyl group are on side chains in homologous positions in the sequence of amino acids, respectively, to the two carboxylato groups and the carbamoyl group that chelates the homologously situated Ca^{2+} in P-type Ca^{2+} transporter (Figure 6–37). Finally, the site chelating the third Na^+ (to the right in the figure) consists of the other oxygen from the carboxylato group of Aspartate 808 that also coordinates the second Na^+, an amido oxygen from the polypeptide, the acyl oxygen of the carbamoyl group of Glutamine 923, the hydroxy group of Threonine 774, and the π system of Tyrosine 771, in an example of a π–cation interaction.[301]

When the compartment in the middle of Na^+/K^+-exchanging ATPase from *Squalus acanthias* is **occupied by two K^+** on their way across the protein (Figure 6–36C),[299,302] the site chelating the first K^+ (to the left in the figure) consists of an oxygen from each of the carboxylato groups of Aspartate 811 and Glutamate 334, which are homologous to Aspartate 804 and Glutamate 327 in the porcine enzyme, and the same three amido oxygens from the same α helix in the polypeptide as are used for the similarly coordinated Na^+ when Na^+ ions are occupying the compartment (Figure 6–37), as well as an oxygen from the carboxylato group of Glutamate 786, homologous to Glutamate 779 in the porcine enzyme. The second K^+ (to the right in the figure) shares the same oxygen of Aspartate 811 coordinating the first K^+ as well as the hydroxy group of Serine 782 and the carbamoyl oxygen of Asparagine 783, which are homologous to the oxygens of Serine 775 and Asparagine 776 used for the similarly coordinated Na^+ when Na^+ ions are occupying the compartment in the porcine enzyme. In addition, this second K^+ is coordinated by an amido oxygen from the backbone of the polypeptide and a molecule of water. All these oxygens that are ligands are typical of those coor-

*Oligomycin A is bound to the enzyme in the crystals used to produce this crystallographic molecular model to stabilize the complex between the protein and the three Na^+.

dinating K^+ in sites in other enzymes (**4–154** and Figure 4–52).

It is clear from the drawings of the crystallographic molecular models and the foregoing description detailing the homology in the ligands used to coordinate the ions that P-type Ca^{2+} transporter (Figure 6–37) and Na^+/K^+-exchanging ATPase are closely related enzymes.

In the site to the left in the drawings of Na^+/K^+-exchanging ATPase, the same five homologous ligands coordinate Na^+ (Figure 6–36B) or K^+ (Figure 6–36C) while only the sixth ligand differs. The only chemical difference between these two alkali metallic ions that the site can recognize is the **difference in their respective ionic radii**, and the consequent difference in density of charge. The ionic radius of Na^+ with six ligands is 0.102 nm, and the ionic radius of K^+ with six ligands is 0.138 nm, a difference in diameters of only 0.072 nm. It is clear, however, from the role of the enzyme in metabolism, that natural selection was able to exert significant influence on making this discrimination as exclusive as possible because any mistakes would uselessly waste $MgATP^{2-}$.

That almost the same set of ligands make this distinction unerringly is another demonstration of the fundamental rigidity of the positions assumed by the functional groups in an active site. If the protein surrounding this site for one or the other of the two cations were actually soft and able to flex significantly, even though the two global conformations to which the respective cation are bound are different from each other, the ligands would not be able to distinguish between Na^+ and K^+. The rigidity with which the ligands assume their positions is essential to this distinction. The site must be rigid enough to enforce a contraction of the ligands by the necessary 0.07 nm when its specificity for K^+ is changed to its specificity for Na^+.

Each enzyme in the family other than Na^+/K^+-exchanging ATPase transports **hydrons** in one direction in exchange for the K^+ or Ca^{2+} that are transported in the other direction. In some instances, hydrons are actively transported out of the cytoplasm, while in other instances, they are actively transported into the cytoplasm as if they were simply convenient replacements on carboxylato groups for the hard cations. Further complicating the situation is the observation that the stoichiometry for the hydrons that are transported appears to vary with the pH of the solution into which they depart or from which they enter. Such a variation in stoichiometry would be expected if, during the passage of these hydrons through the compartment, they reside, as they must, on one, two, or three of the carboxylato groups that form the sites for the Ca^{2+} or K^+ when those cations are travelling in the opposite direction from the hydrons. Differences in values of pK_a for these carboxy groups dictate the relation between the pH of the solution and the stoichiometry of the occupation.

Hydrons are ubiquitous, so it is difficult to distinguish those hydrons being transported from all the other hydrons both in the enzyme and in the solution. Na^+/K^+-exchanging ATPase, however, transports Na^+ in one direction and K^+ in the other direction, and these cations are easily identified. Consequently, the earliest and most informative observations defining the mechanism of active transport were obtained in studies of Na^+/K^+-exchanging ATPase because the strokes of the pump in the two directions could be distinguished and followed independently by varying the concentrations of the alkali metallic ions.

The global conformational changes responsible for active transport of Na^+, Ca^{2+}, or H^+ in one direction and K^+ or H^+ in the other direction across a membrane couple changes in the accessibility of the compartment for cations to changes at the site for hydrolysis of $MgATP^{2-}$. For Na^+/K^+-exchanging ATPase, the **four major global conformations** that the enzyme assumes during catalysis can be designated as $E2{\cdot}[K^+]_2$, $E1{\cdot}MgATP^{2-}$, $[Na^+]_3{\cdot}E1{\sim}P$, and E2–P (Figure 6–38).[303,304] The mechanism for actively transporting three Na^+ and two K^+ is the same as the respective mechanisms used by other members of the family. Consequently, to maintain consistency, the four conformations can be designated $E2{\cdot}[H^+]_2$, $E1{\cdot}MgATP^{2-}$, $[Ca^{2+}]_2{\cdot}E1{\sim}P$, and E2–P for P-type Ca^{2+} transporter; $E2{\cdot}[K^+]_2$, $E1{\cdot}MgATP^{2-}$, $[H^+]_2{\cdot}E1{\sim}P$, and E2–P for H^+/K^+-exchanging ATPase; and so forth, with the reminder that the stoichiometry for H^+ is usually variable because they are carried by carboxy groups as simple acidic hydrons.

Detailed measurements of the **steady-state kinetics** of purified porcine Na^+/K^+-exchanging ATPase are consistent with this mechanism for the enzymatic reaction.[305] The initial rate as a function of the concentration of Na^+ displays positive deviation

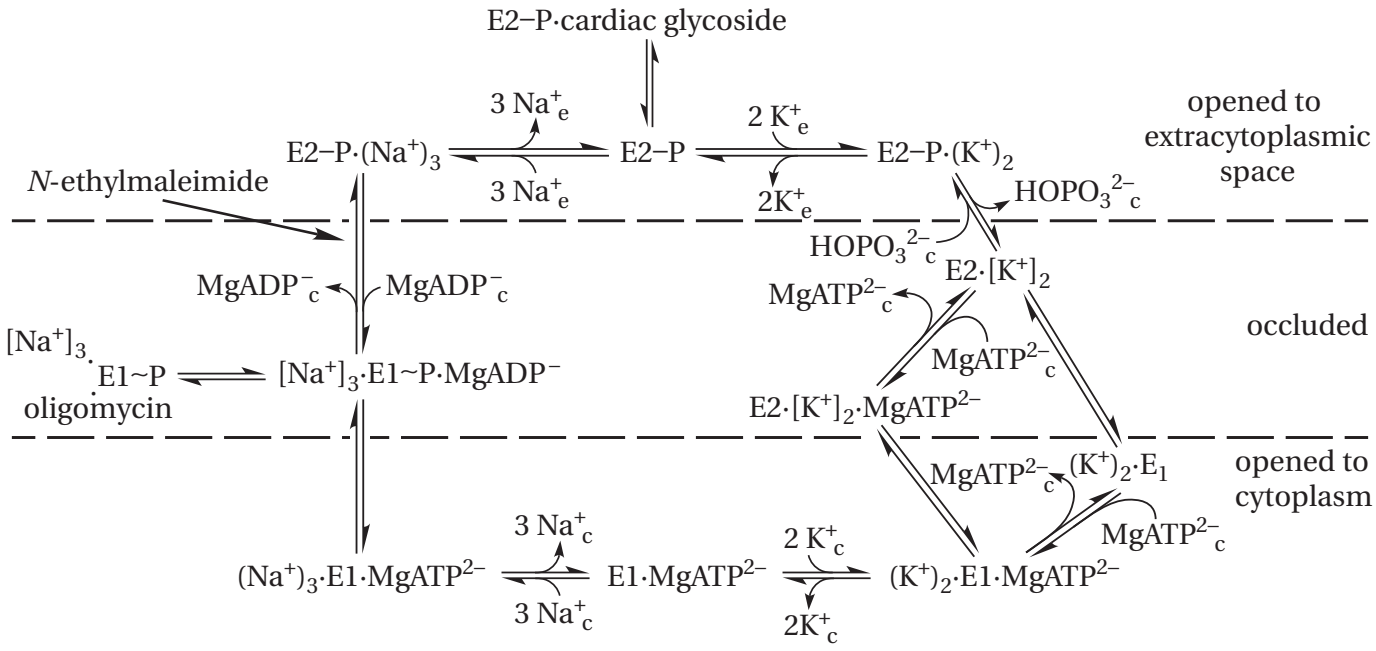

Figure 6–38: Kinetic mechanism for active transport of Na^+ and K^+ catalyzed by Na^+/K^+-exchanging ATPase. The four major conformations of the enzyme are E2·[K+], E1·$MgATP^{2-}$, $[Na^+]_3$·E1~P, and E2–P. Changes at the active site for hydrolysis of $MgATP^{2-}$ are indicated by association of $MgATP^{2-}$, release of $MgADP^-$, formation of the phosphorylated form E1~P and its transformation to the phosphorylated form E2–P, and dephosphorylation of E2–P. Changes in occupation and accessibility of the compartment for cations are indicated by association and dissociation of K^+ and Na^+. The major shifts between the conformation opened to the cytoplasm (E1·$MgATP^{2-}$), the two occluded conformations ($[Na^+]_3$·E1~P and E2·[K+]), and the conformation opened outward (E2–P) are designated by their locations with respect to the dashed lines representing the bilayer. The inhibitor oligomycin is noncovalently bound by a specific conformation, $[Na^+]_3$·E1~P, and modification of the enzyme with *N*-ethylmaleimide prevents the conformational change from E1~P to E2–P. The cardiac glycosides, such as ouabain, and cardiac aglycons, such as strophanthidin, are a set of natural products that inhibit Na^+/K^+-exchanging ATPase by binding from the extracytoplasmic solution[488] and fill the wide channel opening into the empty compartment for cations in the E2–P conformation.[303,304]

from rectangularly hyperbolic behavior. This positive deviation is not due to cooperativity but due to the molecularity of the reaction: three Na^+ together are reactants. In fact, the Michaelis constant for the third Na^+ to associate with the enzyme is greater than the Michaelis constant for the first two rather than smaller, as would be the case if Na^+ were associating cooperatively.

The easiest and least complicated place to start (Figure 6–38) is with Na^+/K^+-exchanging ATPase in the **E2·$[K^+]_2$ conformation** in which two K^+ are enclosed in the compartment for cations and the compartment is occluded, or inaccessible, to the solutions on either side of the membrane. In this conformation, porcine Na^+/K^+-exchanging ATPase encloses two tightly bound $^{86}Rb^+$—which are congeners of two K^+, are transported as efficiently as two K^+, and are also radioactive*—when no other substrates are bound to the enzyme.[306-308] This ability to occlude these Rb^+ is the defining feature of this conformation. In the usual situation, the occluded cations are the two K^+ that have entered the compartment from the extracytoplasmic solution during the normal sequence of events and are in transit to the cytoplasmic solution. In crystallographic molecular models of the E2·$[K^+]_2$ conformation of porcine Na^+/K^+-exchanging ATPase, the two K^+ are occupying their ligands in the compartment for cations

*There are several radioactive isotopes of the alkali metal ions and alkaline earth metal ions, such as $^{86}Rb^+$, $^{42}K^+$, $^{22}Na^+$, $^{45}Ca^{2+}$, and $^{89}Sr^{2+}$ that are used to examine the association of the ions with these enzymes. Their radioactivity allows them to be detected at the low stoichiometric concentrations at which these large, membrane-bound, often impure enzymes must be studied. They are a sensitive method for ascertaining whether or not cations are in the compartment when the enzyme is in one of its conformations.

(Figure 6–36C), and there are no obvious paths on which they can leave the compartment, a fact consistent with their occlusion.[295,299] In the corresponding crystallographic molecular model of P-type Ca^{2+} transporter from *O. cuniculus*, the compartment for cations is vacant but presumably the H^+ passing through it, which are homologues of the K^+ passing through Na^+/K^+-exchanging ATPase, are invisible occupants of several of the carboxy groups that will chelate the Ca^{2+} as carboxylato groups on the return trip,[300,309,310] and the compartment is also occluded. The behavior of the steady-state concentration of occluded $^{86}Rb^+$ as a function of the concentration of Na^+ while porcine Na^+/K^+-exchanging ATPase is hydrolyzing $MgATP^{2-}$ is consistent with its participation in the normal enzymatic reaction and with the kinetic mechanism of Figure 6–38.[305]

During a conformational change, which can be detected in mammalian Na^+/K^+-exchanging ATPase by following either the intrinsic fluorescence of its tryptophans[311] or the response of fluorescent, covalently attached groups that do not otherwise affect the enzyme,[312] the compartment then opens to the cytoplasmic surface. This **E1·MgATP^{2-} conformation** is open to the cytoplasmic solution. Two previously occluded $^{42}K^+$ have been shown to depart from this conformation in canine Na^+/K^+-exchanging ATPase,[313] and three Na^+ bind to it during the normal cycle. In crystallographic molecular models of P-type Ca^{2+} transporter from *O. cuniculus* in this E1·$MgATP^{2-}$ conformation, in which the compartment for cations is vacant (Figure 6–39A),[309,314,315] there are two hydrophilic channels that connect the cytoplasmic solution to the compartment. One of these channels is formed by a dramatic sinking into the bilayer of one of the α helices that span the membrane (arrow in Figure 6–39B).[316] The shift in the position of this α helix opens a wide funnel into one side of the compartment. Passing out from the opposite side of the compartment for the cations in this conformation is a channel, again into the cytoplasm, filled with molecules of water, that meanders among four of the other α helices that span the membrane. This latter channel is neither wide nor obvious, and its opening does not involve any dramatic rearrangement of the α helices,[315] so it may not be an alternative exit from or entrance to the compartment.

In the reaction catalyzed by P-type Ca^{2+} transporter, the two hydrons leaving the compartment, which are homologues of the two K^+ leaving the compartment from Na^+/K^+-exchanging ATPase, and the two Ca^{2+} entering the compartment, which are homologues of the three Na^+, pass through one or the other or both of these hydrophilic channels.[315] The departure of two K^+ and the arrival of three Na^+ through the homologous hydrophilic channels in the E1·$MgATP^{2-}$ conformation of Na^+/K^+-exchanging ATPase produces the competition between these cations both at the cytoplasmic surface of the human enzyme[317] and in the steady-state kinetics of human Na^+/K^+-exchanging ATPase[318] and Na^+/K^+-exchanging ATPase from *Carcinus maenas*.[257] Potassium ion is a competitive product inhibitor of Na^+ in its role as a reactant. In P-type Ca^{2+} transporter from *O. cuniculus*, the two Ca^{2+} that associate with the compartment for cations when it is open to the cytoplasm in the E1·$MgATP^{2-}$ conformation bind sequentially and can be distinguished kinetically.[319] This distinction results from the fact that one of them is deeper in the compartment than the other (Figure 6–39B).

When two K^+ have left and three Na^+ have entered the compartment through one or both of the openings to the cytoplasm, the compartment again closes, and three radioactive $^{22}Na^+$ become locked within the compartment of porcine Na^+/K^+-exchanging ATPase in a different occluded state[320] that defines in part the **[Na^+]$_3$·E1~P conformation**.* In crystallographic molecular models of porcine Na^+/K^+-exchanging ATPase[292,321] occupied by three Na^+ (Figure 6–36B) and P-type Ca^{2+} transporter from *O. cuniculus*[291,315,316] occupied by two Ca^{2+} (Figure 6–36A), which are homologues of the three Na^+, the cytoplasmic entrances to the compartment for cations have closed and the cations are now occluded (Figure 6–39B).

The conformational change in Na^+/K^+-exchanging ATPase that then occurs between the [Na^+]$_3$·E1~P conformation and the **E2–P conformation** can also be followed by covalently attaching fluorescent reporters of the structure of the protein to the canine enzyme.[312] This conformational change opens the compartment for cations to the extracytoplasmic side (Figure 6–40).[291,294] In the crystallographic molecular model of P-type Ca^{2+} transporter from *O. cuniculus* in this conformation, there is a wide hydrophilic channel, open to the extracytoplasmic side of the bilayer and ending in the compartment for cations (Figure 6–40B).[322,323] The opening of this channel, which provides an unobstructed path connecting the compartment with the extracytoplasmic solution, is accomplished by movement of the extracytoplasmic portions of four of the membrane-spanning α helices away from the other six.[315]

*In this instance, the enzyme was modified by *N*-ethylmaleimide (Figure 6–38) to stabilize the occluded state.

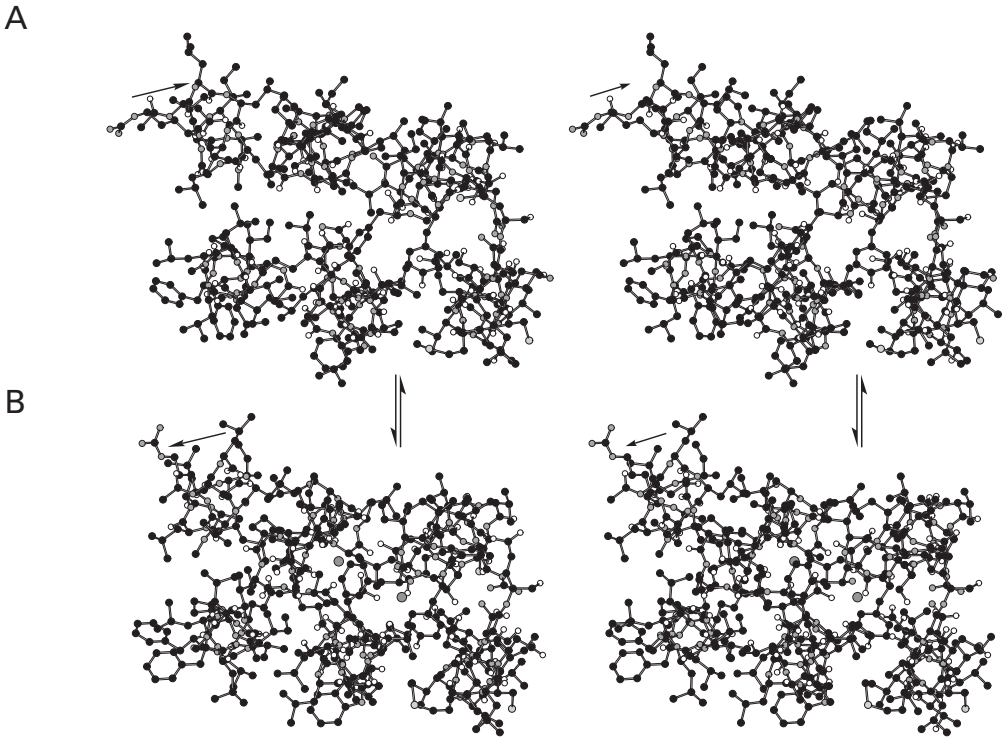

Figure 6–39: Stereodrawings[485] of crystallographic molecular models representing the closing of the cytoplasmic entrance to the compartment for Ca^{2+} in P-type Ca^{2+} transporter from *O. cuniculus* around the two Ca^{2+}. Black atoms are carbons, white atoms are oxygens, small gray atoms are nitrogens, and large light gray atoms are sulfurs. (**A**) Crystallographic molecular model of the compartment when the door is open to the cytoplasmic solution in the E1·MgATP^{2-} conformation and the compartment is ready to associate with Ca^{2+} that have entered the compartment from the cytoplasmic solution.[314] Membranes of sarcoplasmic reticulum enriched in P-type Ca^{2+} transporter were isolated from white muscle of the hind legs of *O. cuniculus*. The membranes (12 mg mL^{-1}) were dissolved in a solution (18 mg mL^{-1}) of the detergent 3,6,9,12,15,18,21,24,27-nonaoxanonatriacontan-1-ol. The dissolved enzyme was then crystallized in the presence of 80 mM KCl, 3 mM $MgCl_2$, and 3.9 mM ethylene glycol bis(2-aminoethyl ether)-*N,N,N′,N′*-tetraacetate to sequester any calcium in solution and prevent it from associating with sites in the compartment. Reflections were collected to Bragg spacing of 0.31 nm. The peptide sarcolipin was also added to stabilize the E1·MgATP^{2-} conformation. The enzyme adopts an α-helical conformation that spans the membrane and lies below the two α helices at the lower left and center left of the drawing. (**B**) Crystallographic molecular model[316] of the closed, occluded compartment in the $[Ca^{2+}]_2$·E1~P conformation occupied by two Ca^{2+}, drawn as large gray spheres. Membranes of sarcoplasmic reticulum enriched in P-type Ca^{2+} transporter were isolated from white muscle of the hind legs of *O. cuniculus*. The membranes were suspended in 0.5 mg mL^{-1} deoxycholate, 0.3 M sucrose, 0.5 M KCI, 1 mM ethylenediaminetetraacetate, 1.25 mM $MgCl_2$, and 10 μM $CaCl_2$ at pH 7.9 to remove any loosely attached protein. The washed membranes at 3.0 mg mL^{-1} were then dissolved in 2.0 mg mL^{-1} deoxycholate, 0.3 M sucrose, 0.5 M KCI, 1 mM ethylenediaminetetraacetate, 1.5 mM $MgCl_2$, and 20 μM $CaCl_2$ at pH 8.0. The supernatant was dialyzed against 0.3 M sucrose, 0.5 M KCI, 1 mM ethylenediaminetetraacetate, 1.5 mM $MgCl_2$, and 20 μM $CaCl_2$ at pH 8.0. The re-formed membranes, which contained only P-type Ca^{2+} transporter, were then dissolved in 30 mM 3,6,9,12,15,18,21,24-octaoxatetratriacontan-1-ol, 20% glycerol, 80 mM KCl, 10 mM $CaCl_2$, 2 mM $MgCl_2$, and 1 mM magnesium 5′-adenylic methylenediphosphonic anhydride (MgAMPPCP^{2-}) at 12 mg mL^{-1} final protein concentration. The solution was mixed with an equal volume of 8% poly(ethylene glycol), 4% *tert*-butanol, 15% glycerol, 5 mM 2-sulfanylethanol, and 200 mM sodium acetate to form crystals. Reflections were collected to Bragg spacing of 0.26 nm. The view in both drawings is from the cytoplasmic side of the membrane into the interior down several of the membrane-spanning α helices. The view is also in the same orientation as in Figure 6–36A. In the present instance, however, the two α helices that form the wall of the compartment on the left in the drawing are included. They were not included in the drawing of Figure 6–36A because they do not provide ligands to the Ca^{2+}. All six of the α helices that form the walls of the compartment were extended up to the cytoplasmic surface of the membrane, to include the door to the compartment from that side. Each stereodrawing includes the same segments of polypeptide from each of these six α helices. In the drawing of the occluded compartment in Panel B, the two Ca^{2+} can be seen at the bottom of the drawing in the same orientation as in Figure 6–36A. This equivalence can be verified by looking for Asparagine 768 and Aspartate 800. The door to the compartment is the α helix in the upper left-hand corner of the two drawings. In the open conformation (Panel A), a large entrance to the compartment can be seen. In the occluded conformation (Panel B), the door has been closed. Opening of the compartment involves a sinking of the upper left-hand α helix into the membrane away from the viewer and movement away from the other five α helices (arrow in Panel B). Closing of the compartment around the two Ca^{2+} involves movement of the α helix in the opposite direction (arrow in Panel A).

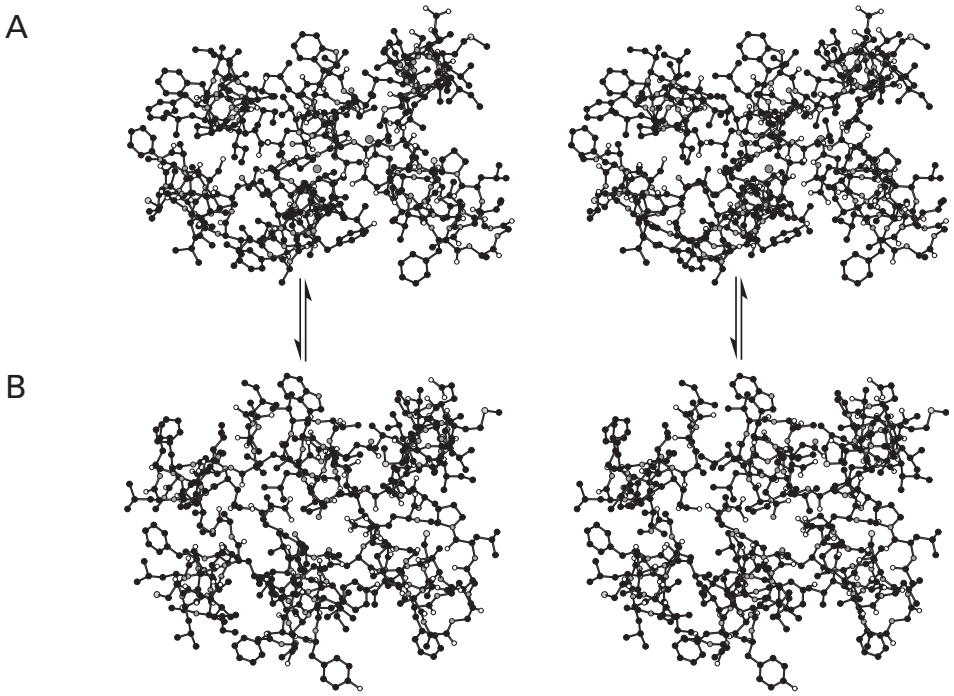

Figure 6–40: Stereodrawings[485] of crystallographic molecular models representing the opening of the extracytoplasmic entrance to the compartment for Ca^{2+} in P-type Ca^{2+} transporter from *O. cuniculus*. Black atoms are carbons, white atoms are oxygens, small gray atoms are nitrogens, and large light gray atoms are sulfurs. (**A**) Crystallographic molecular model of the closed, occluded compartment in the $[Ca^{2+}]_2$·E1~P conformation occupied by two Ca^{2+} (Figure 6–36A), drawn as large gray spheres. The view is from the extracytoplasmic surface of the membrane rather than the cytoplasmic surface. To obtain this view, the molecular model drawn in Figure 6–35 was rotated 90° about a horizontal axis in the plane of the page in the opposite direction from the rotation used to obtain the view in Figure 6–36A. (**B**) Crystallographic molecular model of the compartment when the door is open to the extracytoplasmic solution in the E2–P conformation and the Ca^{2+} have dissociated into the extracytoplasmic solution. To obtain this molecular model of the open compartment,[323] the same preparation of P-type Ca^{2+} transporter described in the legend of Figure 6–34 was used. The enzyme, however, was crystallized from a solution of 2 mM BeF_2, 4 mM NaF, 10 mM $MgCl_2$, and 3 mM ethylene glycol bis(2-aminoethyl ether)-*N,N,N′,N′*-tetraacetate to sequester any calcium in solution and prevent it from associating with sites in the compartment. The beryllium atom in BeF_2 forms a covalent bond (0.16 nm) with one oxygen of the carboxylato group of Aspartate 351 in the hydrolytic site to produce an acyloxy beryllium trifluoride that mimics the phosphorylated intermediate in the E2–P conformation, and there is no free Ca^{2+} in solution to associate with the ligands in the compartment. These two strategies ensure formation of the E2–P conformation. The view in both drawings is from the extracytoplasmic side of the membrane. All six α helices that form the wall of the compartment are included and were extended from the ligands to the Ca^{2+} up to the extracytoplasmic surface of the membrane, to include the door to the compartment from that side. Each drawing includes the same segments of polypeptide from these six α helices. The fact that the drawing is in an orientation that results from a 180° rotation about a horizontal axis in the plane of the page in Figure 6–36A can be verified by finding the two Ca^{2+} in Panel A and looking for Asparagine 768 and Aspartate 800. Although there are significant changes in the orientation and alignments of four or five of the six α helices between the drawings in Panels A and B, the α helix in the middle of the bottom row swings open most dramatically (arrow in Panel A) to produce an open path out of the compartment that allows the Ca^{2+} to dissociate into the extracytoplasmic solution.

This wide funnel opened to the extracytoplasmic side of the enzyme is occupied in its entirety and completely blocked by a molecule of cardiac glycoside in crystallographic molecular models of complexes between cardiac glycoside and Na^+/K^+-exchanging ATPase[303,304,324-326] in this conformation. This fact explains why cardiac glycosides, which are strong inhibitors of the enzyme, associate with only this conformation (Figure 6–38). In P-type Ca^{2+} transporter, two Ca^{2+} depart from this E2–P conformation to be replaced by two or three H^+. In Na^+/K^+-exchanging ATPase, three Na^+ depart from this E2–P conformation to be replaced by two K^+. During this exchange, Na^+ acts as a competitive product inhibitor of K^+ in its role as a reactant in the steady-state kinetics of the enzyme.[257,318]

When the conformational change between the occluded $[Na^+]_3$·E1~P conformation and the open $(Na^+)_3$·E2–P conformation in Na^+/K^+-exchanging ATPase is initiated by a large and rapid voltage change across the plasma membrane of axons from *Doryteuthis pealeii*, there are three movements of positive charge[327] that have been assigned to the individual dissociations of three Na^+ at rates of 1, 10, and >1000 ms^{-1}. In the case of P-type Ca^{2+} transporter from *O. cuniculus*, the conformational change between $[Ca^{2+}]_2$·E1~P and $(Ca^{2+})_2$·E2–P is slow (0.03 ms^{-1} at 25° C) and the subsequent dissociation of the two Ca^{2+} into the extracytoplasmic solution is rapid (>10^2 ms^{-1}) so that the two Ca^{2+} that dissociate cannot be kinetically distinguished.[319,328] These rapid rates for dissociation of the cations from both Na^+/K^+-exchanging ATPase and P-type Ca^{2+} transporter are consistent with the large size of the opening to the compartment for cations from the extracytoplasmic solution in crystallographic molecular models of the E2–P conformation (Figure 6–40B).[322,323]

In the final step in the mechanism, the protein closes around the two K^+ to regenerate the E2·$[K^+]_2$ conformation.[308] During this final step in P-type Ca^{2+} transporter, the protein closes around two or three hydrons to regenerate the occluded E2·$[H^+]_n$ conformation. A mutant of P-type Ca^{2+} transporter from *O. cuniculus*, in which Glutamate 309, one of the glutamates in the compartment, has been mutated to glutamine to simulate its hydronation, crystallizes in a conformation that was proposed to be an intermediate between the E2–P and E2·$[H^+]_n$ conformations as the compartment is closing around the hydrons.[329]

The Michaelis constants for Na^+ and K^+ in the steady-state kinetics of Na^+/K^+-exchanging ATPase are assumed to be the dissociation constants for the respective ions when they are reactants because they are such small, uncomplicated ions that they probably associate and dissociate from their sites in the compartment rapidly. The inhibition constants in steady-state kinetics for Na^+ and K^+ are assumed to be for Na^+ as a product competing with K^+ as reactant for occupation of the compartment when it is open to the extracellular surface of the enzyme and for K^+ as a product competing with Na^+ as reactant for occupation of the compartment when it is open to at the cytoplasmic surface of the enzyme. In steady-state kinetics, the Michaelis constant for Na^+ entering the compartment for cations in human Na^+/K^+-exchanging ATPase[318] and Na^+/K^+-exchanging ATPase from *C. maenas*[257] as a reactant from the cytoplasmic solution and the Michaelis constant for K^+ entering the compartment for cations as a reactant from the extracytoplasmic solution, respectively, are significantly smaller than the inhibition constants for Na^+ as a product when it is leaving the compartment for cations into the extracytoplasmic solution or K^+ leaving the compartment for cations as a product into the cytoplasmic solution.

Although these differences in dissociation constant are not necessary for active transport to occur by this mechanism (Figure 6–38), in this way, the rates of exchange of two K^+ for three Na^+ in the E1·$MgATP^{2-}$ conformation and three Na^+ for two K^+ in the E2–P conformation are accelerated. The time between the opening to one side of the membrane of the compartment loaded with the proper number of one type of cation (the cationic products) and the closing of the compartment around the proper number of the other type of cation (the cationic reactants) can be viewed as the time it takes for the cationic products to vacate and the cationic reactants to occupy the compartment. As these exchanges proceed by random collisions of cations with the open compartment, the probability that cationic reactants will be bound in the correct number and in the absence of bound cationic products increases as the dissociation constant for cationic products from the site increases and the dissociation constant for cationic reactants from the site decreases. Furthermore, under normal circumstances, when the enzyme is actively transporting cations against their electrochemical gradients, the concentrations of cationic products are always greater than the concentrations of cationic reactants on the respective sites of the membrane. For example, at the cytoplasmic side, K^+ is the cationic

product and Na^+ is the cationic reactant, but the concentration of K^+ is significantly greater than the concentration of Na^+.

The existence of the four discrete global conformations assumed by Na^+/K^+-exchanging ATPase—$E2{\cdot}[K^+]_2$, $E1{\cdot}MgATP^{2-}$, $[Na^+]_3{\cdot}E1{\sim}P$, and E2–P—has been established in several ways other than their ability to occlude particular cations. There are several short segments of the native folded catalytic α polypeptide of Na^+/K^+-exchanging ATPase from *O. cuniculus*[330] and porcine H^+/K^+-exchanging ATPase[331] that are susceptible to cleavage by endopeptidases, presumably because they form exposed loops on the surface of the native enzyme, and the accessibilities of these segments to endopeptidases change dramatically as the conformations change.[332] The affinity of the different conformations of Na^+/K^+-exchanging ATPase for ligands such as $MgATP^{2-}$ and cardiac glycosides are dramatically different.[311,333] Finally, in addition to the observations described above, a number of fluorescent molecules have been covalently attached to various locations in canine and porcine Na^+/K^+-exchanging ATPase, and their fluorescence emission changes as changes are made in the conformation of the enzyme.[312,334] Because these various reporters of the structure of the protein are scattered over its surface, it is assumed that each change in structure being detected is a global conformational change.

Steps in the mechanism for hydrolysis of $MgATP^{2-}$ at the hydrolytic site of Na^+/K^+-exchanging ATPase are connected by global conformational changes to each change in access to the compartment through which the cations pass.

When the enzyme is in the $E2{\cdot}[K^+]_2$ conformation, two K^+ are occluded within the compartment, and the hydrolytic site is unoccupied by substrates. There are two parallel paths that the mechanism can take from this point (Figure 6–38), each of which opens the compartment to the cytoplasmic side of the enzyme. The conformational change of mammalian Na^+/K^+-exchanging ATPase from the $E2{\cdot}[K^+]_2$ conformation to the $(K^+)_2{\cdot}E1$ conformation, in which the enzyme is open to the cytoplasmic surface is slow and has an unfavorable equilibrium constant, but when it happens to occur, $MgATP^{2-}$ at low concentration can bind rapidly and with high affinity to the hydrolytic site, locking in the open $(K^+)_2{\cdot}E1$ conformation. The hydrolytic site, however, does have a large dissociation constant for $MgATP^{2-}$ in the $E2{\cdot}[K^+]_2$ conformation. If $MgATP^{2-}$ is at a high enough concentration, then it can bind before the conformational change occurs. When it binds, the enzyme opens to the cytoplasm in a fast step leading to release of the K^+.[311,335] The product of both paths is the conformation $E1{\cdot}MgATP^{2-}$. Normal cytoplasmic concentrations of $MgATP^{2-}$ are sufficient to saturate the hydrolytic site when the enzyme is in the $E2{\cdot}[K^+]_2$ conformation, even though it displays low affinity for $MgATP^{2-}$ in this conformation; and when it is in the plasma membrane of a cell, the **binding of $MgATP^{2-}$ accelerates the opening of the compartment to the cytoplasm**.[312] In addition, steady-state kinetic measurements of porcine Na^+/K^+-exchanging ATPase, when correlated to the rate at which $^{86}Rb^+$ is deoccluded in the absence of $MgATP^{2-}$, lead to the conclusion that high concentrations of Na^+ ($K_{d,app}$ = 40 mM), presumably associating with a site other than the compartment in which the two Rb^+ are occluded, also accelerate their deocclusion,[305] but the side of the membrane on which this site is located was not determined. Because $MgATP^{2-}$ can bind to the hydrolytic site by either of these two paths, the steady-state kinetics of P-type Ca^{2+} transporter from *O. cuniculus* as the concentration of $MgATP^{2-}$ is varied display positive deviations from linear behavior that appear to be cooperative,[336] although they are not because the enzyme is a monomer with only one active site for hydrolysis of $MgATP^{2-}$ and no other sites with which $MgATP^{2-}$ associates.

From a comparison of a crystallographic molecular model of P-type Ca^{2+} transporter from *O. cuniculus* in which the site for hydrolysis of $MgATP^{2-}$ is empty with one of the enzyme in which the same site is occupied by magnesium 5′-adenylic methylenediphosphonic anhydride ($MgAMPPCP^{2-}$), it can be concluded that association of $MgATP^{2-}$ with the $E2{\cdot}[H^+]_2$ conformation of the enzyme proceeds with a **major local conformational change** (Figure 6–41).[291,294,316] Three **hinged domains**, formed by 110, 160, and 240 amino acids (upper left, upper middle, and upper right, respectively, in Figure 6–41A) comprise the majority of the large portion of P-type Ca^{2+} transporter that resides in the cytoplasm. In the absence of nucleotide, these domains are splayed apart. After $MgAMPPCP^{2-}$ has been bound by the open hydrolytic site, and presumably after $MgATP^{2-}$ has been bound during normal turnover as well, these three domains have closed around the nucleotide (Figure 6–41B) and merged into a large, compact globular structure. The same hinged domains and the same conformational change are observed in Na^+/K^+-exchanging ATPase.[292,295,304,321]

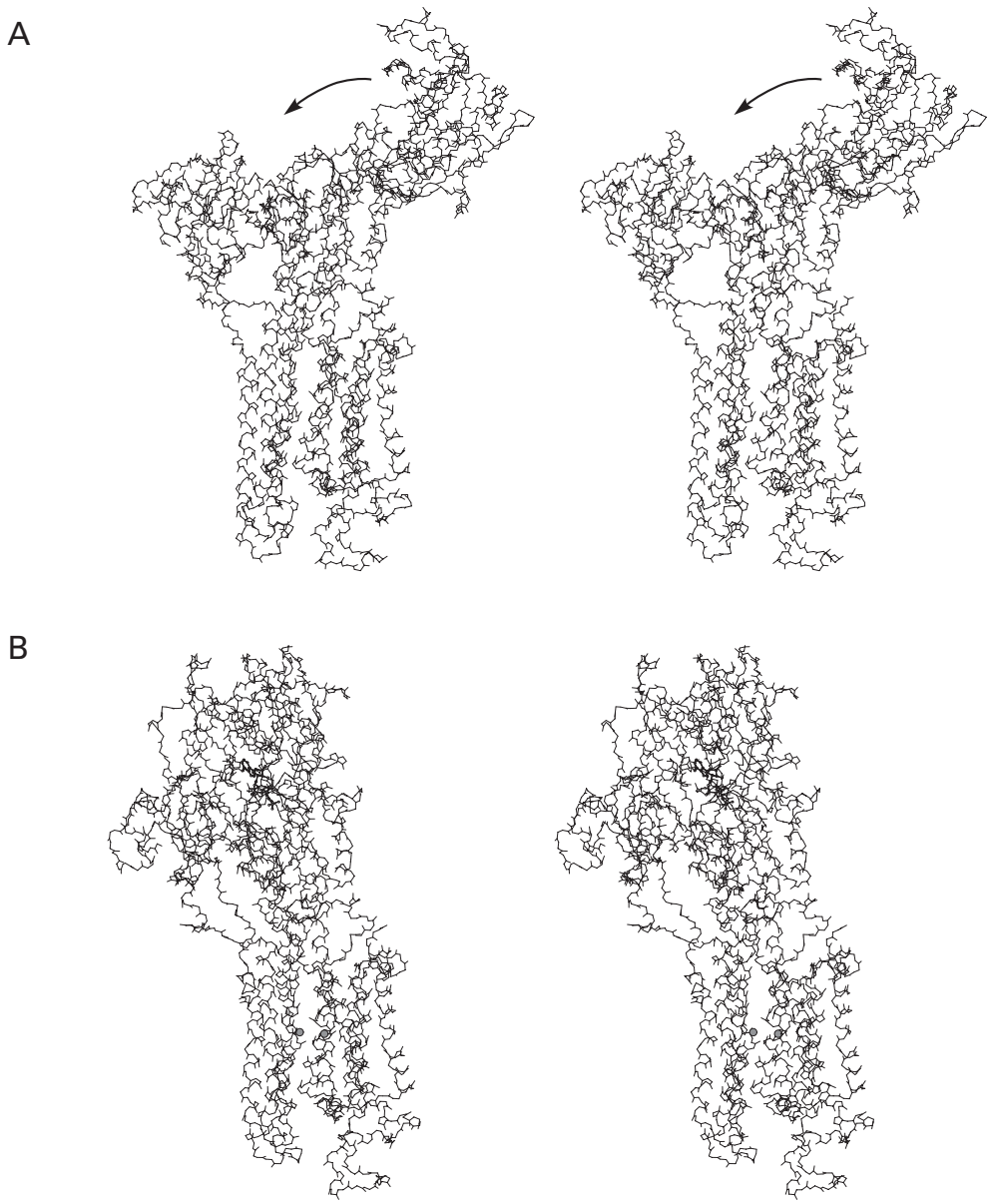

Figure 6–41: Stereodrawings[485] of crystallographic molecular models showing the local change in conformation that results when the structural domains of P-type Ca^{2+} transporter from *O. cuniculus* close around a molecule of $MgATP^{2-}$ to produce the occupied hydrolytic site. (**A**) Open hydrolytic site. To obtain this crystallographic molecular model,[294] the same preparation of P-type Ca^{2+} transporter described in the legend of Figure 6–34 was used. The enzyme, however, was crystallized from a solution of 10 mM $CaCl_2$ and 3 mM $MgCl_2$ in the absence of any nucleotide, phosphate, or compound that could produce a mimic of the phosphorylated intermediate. (**B**) Closed hydrolytic site. The same crystallographic molecular model was used to make this drawing of the enzyme with its hydrolytic site occupied by $MgAMPPCP^{2-}$ as was used for the drawing in Figure 6–34. Again, black atoms are carbons, white atoms are oxygens, small gray atoms are nitrogens, and large dark gray atoms are the three atoms of phosphorus. Only the atoms in the complete polypeptide backbones are included in the two skeletal drawings. The two Ca^{2+} occupying the compartment for cations are drawn as large gray spheres. To give the best view of the three domains that are splayed open in the drawing of the local conformation in which the hydrolytic site is open and unoccupied (Panel A), an orientation that is produced by a 40° rotation about a vertical axis in the plane of the page in Figure 6–34 was chosen. The drawing of the enzyme occupied by $MgAMPPCP^{2-}$ is in the same orientation. The major motion producing the closing of the structural domains is the pivot to the left (arrow) of the large structural domain on the right of the cytoplasmic portion of the enzyme in Panel A.

This large local change in conformation is probably what biases the conformational change from the $E2\cdot[K^+]_2$ to the $E1\cdot MgATP^{2-}$ conformation upon association of $MgATP^{2-}$.

In the resulting $E1\cdot MgATP^{2-}$ conformation, the hydrolytic site has closed around $MgATP^{2-}$ and the compartment for cations has opened to the cytoplasmic solution. Once the compartment for cations in Na^+/K^+-exchanging ATPase is open to the cytoplasm, two K^+ are eventually replaced by three Na^+ while the $MgATP^{2-}$ remains in the hydrolytic site that has closed around it. Once three Na^+ have replaced two K^+ in the compartment for cations in Na^+/K^+-exchanging ATPase, the global conformation changes, occluding the three Na^+. Alternatively, once two Ca^{2+} have replaced several H^+ in the compartment for cations of P-type Ca^{2+} transporter, the global conformation changes, occluding the two Ca^{2+}. During this conformational change in Na^+/K^+-exchanging ATPase from the $E1\cdot MgATP^{2-}$ to the $[Na^+]_3\cdot E1\sim P$ conformation, the compartment closes around three Na^+ and the γ-phosphate of $MgATP^{2-}$ is transferred simultaneously to an aspartate in the hydrolytic site to produce an aspartyl phosphate, which is a mixed anhydride[337]

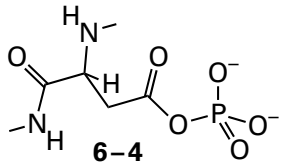

6–4

Peptides have been isolated from streptogrisin digests of Na^+/K^+-exchanging ATPase from *Cavia porcellus* and digests of P-type Ca^{2+} transporter from *O. cuniculus*, respectively, that contain this **intermediate aspartyl phosphate**.[338]

Kinetic studies of the phosphorylation that occurs during the conformational change from the $(Na^+)_3E1\cdot MgATP^{2-}$ to the $[Na^+]_3\cdot E1\sim P$ conformation demonstrate that a slower step ($500\ s^{-1}$ at 24° C), presumably the global conformational change occluding the cations, has to occur before the rapid phosphorylation ($>3000\ s^{-1}$) of the aspartate in the hydrolytic site of the enzyme and that the $MgADP^-$ that is produced at the hydrolytic site during phosphorylation of the aspartate is immediately in rapid equilibrium with $MgADP^-$ in solution.[339] In the crystallographic molecular model of the complex between P-type Ca^{2+} transporter from *O. cuniculus* and $MgAMPPCP^{2-}$, the compartment is occupied by two Ca^{2+} (Figures 6–34 and 6–41B), and it has already been occluded. This molecular model is consistent with the conclusion that the global conformational change from the $E1\cdot MgATP^{2-}$ to the E1~P conformation that occludes the compartment occurs before the aspartate is phosphorylated during the conformational change. Magnesium 5′-adenylic methylenediphosphonic anhydride cannot phosphorylate the aspartate, yet the two Ca^{2+} are occluded.

In the $[Na^+]_3\cdot E1\sim P$ conformation, the aspartyl phosphate (**6–4**) in mammalian Na^+/K^+-exchanging ATPase is in an environment causing it to have a large negative standard free energy of hydrolysis because the aspartyl phosphate and $MgADP^-$ are in rapid equilibrium with $MgATP^{2-}$ free in solution[340,341]

$$E_1COO\sim PO_3^{2-}\cdot MgADP^- \rightleftharpoons E_1COO^-\cdot MgATP^{2-} \qquad (6\text{–}129)$$

as would be expected from the large negative standard free energy of hydrolysis for acyl phosphates in solution (Table 1–3). If the next conformational change in the mechanism is blocked by binding of the inhibitor oligomycin to the enzyme or by covalent modification of the enzyme with *N*-ethylmaleimide (Figure 6–38), then this rapid equilibrium in the hydrolytic site is manifested in a rapid isotopic exchange[342] of $Mg[^{14}C]ADP^-$ with $Mg[^{12}C]ATP^{2-}$.

If, however, the next conformational change proceeds spontaneously (Figure 6–38), as it normally does, then the $[Na^+]_3\cdot E1\sim P$ conformation converts rapidly to the $E2\text{–}P\cdot(Na^+)_3$ conformation, in which the compartment for the Na^+ being transported has opened to the extracytoplasmic surface. The acyl phosphate, although still at the same aspartate in Na^+/K^+-exchanging ATPase from *Electrophorus electricus*,[343] has **changed from one with a large negative standard free energy of hydrolysis to one with a small standard free energy of hydrolysis** because in this conformation it is in rapid equilibrium with phosphate in solution[344]

$$E_2COO\text{–}PO_3^{2-} + H_2O \rightleftharpoons E_2COO^- + H^+ + HOPO_3^{2-} \qquad (6\text{–}130)$$

in Na^+/K^+-exchanging ATPase from *E. electricus* as well as the feline enzyme. In other words, in this conformation, phosphate in solution is able to easily phosphorylate the aspartate in the hydrolytic site. This phosphorylation is analogous to what occurs on the active site of myosin ATPase in the absence of actin, where $MgADP^-$ and $HOPO_3^{2-}$ are in rapid

equilibrium with $MgATP^{2-}$ (see Equation 5–259 and Figure 5–18)

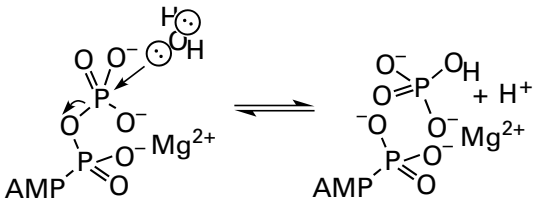

(6–131)

which at the time was an unexpected observation. In the case of Na^+/K^+-exchanging ATPase, an acyl phosphate is in equilibrium with H_2O and $HOPO_3^{2-}$, also contrary to expectation. The structure of the hydrolytic site in this conformation has dramatically shifted the value for an equilibrium constant relative to what it would be in free solution, a feat that will be duplicated by the active site of H^+-transporting two-sector ATPase.

Once three Na^+ in the compartment for cations in Na^+/K^+-exchanging ATPase have been replaced by two K^+, or in the case of P-type Ca^{2+} transporter, two Ca^{2+} by two or three H^+, the conformational change from the E2–P conformation in which two K^+ occupy the open compartment to the E2·$[K^+]_2$ conformation occurs. Coincident with the closing of the compartment to occlude the two K^+, the **acyl phosphate is hydrolyzed** to regenerate the empty hydrolytic site.[341,345] This conformational change can be followed by observing the effect of the concentration of K^+ on the rate of hydrolysis of the aspartyl phosphate (**6–4**) in the active site of bovine Na^+/K^+-exchanging ATPase[346] that has been formed from [γ-^{32}P]$MgATP^{2-}$ in the presence of Na^+. Because the aspartyl phosphate in the E2–P conformation hydrolyzes rapidly, but only upon addition of K^+, while the aspartyl phosphate in the $[Na^+]_3$·E1~P conformation rapidly transfers its phosphate to $MgADP^-$, the relative amounts of these two conformations, and hence the equilibrium constant between them, can be determined under any set of circumstances.[341] The phosphate produced by hydrolysis of the aspartyl phosphate in the E2–P conformation seems to remain associated with the hydrolytic site during the transition from the E2–P conformation to the E2·$[K^+]_2$ conformation, as there is a crystallographic molecular model of Na^+/K^+-exchanging ATPase from *S. acanthias* in which the hydrolytic site is closed around an analogue of phosphate that cannot phosphorylate the aspartate and the two K^+ are occluded.[299]

The steps in the mechanism of active transport at which standard free energy changes that represent the standard free energy of hydrolysis of $MgATP^{2-}$ are manifested are not the steps in which the covalent bonds are made and broken. The steps in which covalent bonds are made and broken are the transitions between E1·$MgATP^{2-}$ and $[Na^+]_3$·E1~PO_3^{2-}·$MgADP^-$ and E2–P and E2·$[K^+]_2$. The **steps in which the change in standard free energy are manifest** are those in which only conformational changes of the enzyme occur, which are in the spontaneous transition between $(Na^+)_3$·E1~P and E2–P and the transition between E2·$[K^+]_2$ and E1·$MgATP^{2-}$ that is strongly promoted by association of $MgATP^{2-}$. Yet again, these observations seem counterintuitive.

Active transport occurs because specific events that take place at the site where the $MgATP^{2-}$ is hydrolyzed are coupled to distinct, but also specific, events that take place in the compartment through which the cations pass into and out of the cytoplasm. This compartment is defined by its ability to occlude the cations. The distance between this compartment and the hydrolytic site is 5 nm (Figure 6–34), and the only reasonable strategy for this rigid coupling of events is through extensive global conformational changes in the enzyme.

Each global conformation through which the coupling is accomplished must be solid enough to unerringly transfer information about the status of the active site and the status of the compartment for the ions over such a long distance. The protein in each conformation cannot be soft. Because there is nothing special about the protein in these enzymes, this necessity yet again demonstrates that **proteins cannot be soft**.

Because the occluded forms, in which the cations are stationary occupants in the compartment through which they pass, exist, the actual transport of the cations involves closing of the compartment at one side, after they are bound, before it opens to the other side. Because the barrier at the closed end of an open compartment is at that instant the only barrier between the cytoplasmic and extracytoplasmic solutions, it follows that, as they are transported, **it is not the cations that move but the barrier between cytoplasm and extracytoplasmic solution that moves.**

Several drawings have been presented in which four of the crystallographic molecular models of P-type Ca^{2+} transporter have been proposed to be representatives of the four respective global conformations of the enzyme that accomplish the active transport of Ca^{2+} and H^+.[322,347] There are several problems with these presentations that make them

premature. First, there is no agreement among the crystallographers as to which molecular models represent the four conformations. Second, in many of the molecular models chosen, rather large perturbants of the structure—such as sarcolipin,[314] a peptide of 31 amino acids that forms a membrane-spanning α helix adjacent to the α helices forming the compartment for Ca^{2+} and H^+, or thapsigargin,[300,309,315,348,349] a rather large molecule, $C_{34}H_{50}O_{12}$, that binds within the compartment for cations—were bound to P-type Ca^{2+} transporter in the crystals and were present in the molecular model. In fact, the only molecular models in which the compartment is open to the cytoplasm have these perturbants associated with them.

Finally, there has been no attempt to distinguish between **local conformational changes**, which are dramatic, and global conformational changes, which are probably more subtle but are key to the process. For example, the induced fit upon association of adenine nucleotides with the active site of P-type Ca^{2+} transporter or Na^+/K^+-exchanging ATPase is a significant conformational change. It seems, however, to be associated only with occupation of the active site by an adenine nucleotide, normally the substrates $MgATP^{2-}$ or $MgADP^-$. If so, this conformational change may be a local conformational change similar to the one that occurs upon association of carbamoyl phosphate and L-aspartate with the active sites of aspartate carbamoyltransferase. Nevertheless, even if it is only a local conformational change, it probably promotes the respective global conformational changes from the $E2{\cdot}[H^+]_n$ to the $(H^+)_n{\cdot}E1{\cdot}MgATP^{2-}$ conformation and from the $E2{\cdot}[K^+]_2$ to the $(K^+)_2{\cdot}E1{\cdot}MgATP^{2-}$ conformation that follow association of $MgATP^{2-}$ at normal cellular concentrations. In another example, whenever the compartment for cations in P-type Ca^{2+} transporter is occupied by Ca^{2+}, it is in an occluded local conformation,[316] but during the catalytic cycle, Ca^{2+} must associate with and dissociate from the compartment when it is open on each side of the membrane. Nevertheless, even if closing of the compartment around the Ca^{2+} to occlude them is a local conformational change, it promotes the next global conformational change, in the sequence linking the events in the compartment with the events in the active site.

The entire process (Equation 6–128) of **active transport is reversible**, as are all enzymatic reactions. The rapid reversibility of the two halves of the mechanism, that in which Na^+ is transported and that in which K^+ is transported, can be demonstrated. The enzyme in an intact, resealed human erythrocyte in the absence of K^+ catalyzes a rapid three-for-three exchange of cytoplasmic, radioactive $^{24}Na^+$ for extracytoplasmic, nonradioactive $^{23}Na^+$ that requires the presence of both cytoplasmic $MgATP^{2-}$ and cytoplasmic $MgADP^-$ as expected if the mechanism is as described (Figure 6–38).[350,351] The enzyme in resealed human erythrocytes also catalyzes, in the absence of Na^+, a rapid two-for-two exchange of cytoplasmic, radioactive $^{42}K^+$ for extracytoplasmic, nonradioactive $^{39}K^+$ that requires[352] the presence of cytoplasmic $HOPO_3^{2-}$ as expected (Figure 6–38) but also the presence of cytoplasmic $MgATP^{2-}$. The latter requirement results from the fact that the binding of $MgATP^{2-}$ at the hydrolytic site accelerates the rate-limiting step in the K^+/K^+ exchange, that of opening the compartment to the cytoplasm to release the occluded K^+. Finally, if sufficient concentration gradients of Na^+ and K^+ are created across the plasma membranes of erythrocytes from *C. porcellus* and the concentrations of $MgADP^-$ and $HOPO_3^{2-}$ in the cytoplasm are high and the concentration of $MgATP^{2-}$ is low, then Na^+/K^+-exchanging ATPase will synthesize[353] $MgATP^{2-}$.

H^+-Transporting two-sector ATPase is an unrelated enzyme that normally, but also reversibly, catalyzes the synthesis of $MgATP^{2-}$ from $MgADP^-$ and $HOPO_3^{2-}$ by coupling that synthesis to the transport of cations.

H^+-Transporting two-sector ATPase[354]

$$MgADP^-_{neg} + HOPO_3{}^{2-}_{neg} + n\,H^+_{pos} + H^+_{neg} \rightleftharpoons n\,H^+_{neg} + MgATP^{2-}_{neg} + H_2O_{neg} \quad (6\text{–}132)$$

is responsible for most of the synthesis of $MgATP^{2-}$ in aerobic living organisms.* H^+-Transporting two-sector ATPase is embedded in and spans the inner membrane of a mitochondrion, the membrane of the thylakoid of a chloroplast, or the plasma membrane of a bacterium. The subscripts indicate that the hydrons are transported across the membrane of the organelle or cell during catalysis from the space on the side of the membrane that normally has a more positive electric potential into the space

*The hydron to the right on the first line of the equation is referred to as a "scalar" hydron. A scalar hydron is a hydron that is a reactant or product of the chemical transformation catalyzed by the enzyme, that appears on the side of the membrane where that transformation occurs, and that is not involved in the net transport of hydrons from one side of the membrane to the other.

that nomally has a more negative electric potential.* Depending on the species of the organism and the organelle in which the enzyme is located, the effective stoichiometry† of the hydrons transported, *n*, is between 8/3 and 15/3.[355] For example, the stoichiometry for mammalian mitochondria is 8/3 while that for cells of *E. coli* is 10/3. A related enzyme[356] from certain bacteria uses a gradient of Na^+ from the exterior to the interior of the bacterium to synthesize $MgATP^{2-}$. This ability is another example of Na^+ substituting for H^+, as is observed in the cation ATPases just discussed, but it does not mean that the H^+-transporting two-sector ATPases and the cation ATPases are in any way related to each other—far from it.

Under normal circumstances when there is a large **electrochemical gradient of hydrons** from the exterior intramembrane space of a mitochondrion to the matrix in its interior, from the exterior of a bacterial cell to the cytoplasm in its interior, or from the interior lumen of a thylakoid to the stroma on its exterior surface,†† H^+-transporting two-sector ATPase synthesizes $MgATP^{2-}$ from $MgADP^-$ and $HOPO_3^{2-}$, just as Na^+/K^+-exchanging ATPase will synthesize $MgATP^{2-}$ when there are large electrochemical gradients of Na^+ and K^+ across the membrane. If, however, the electrochemical gradient decreases sufficiently, H^+-transporting two-sector ATPase will then catalyze the net transport of hydrons in reverse from the interior to the exterior of a mitochondrion or bacterial cell or from the exterior to the interior of a thylakoid against the electrochemical gradient of hydrons at the expense of hydrolysis of $MgATP^{2-}$. Under these circumstances, the enzyme catalyzes the active transport of hydrons. In fact, there are related enzymes,[357] commonly referred to as V-type proton ATPases, the sole purpose of which is to transport hydrons actively across a membrane, in this instance from the cytoplasm of a eukaryotic cell into internal membrane-enclosed spaces such as lysosomes, endosomes, and the Golgi apparatus, to acidify their interior. Because the transport is from cytoplasm into the interior of these enclosed spaces, the V-type proton ATPases are presumably, as are chloroplasts, the descendants, by invagination, of an ancestral H^+-transporting two-sector ATPase in the plasma membrane of the bacterial cells that became the cells of eukaryotes rather than their mitochondria, which are the descendants of invasive bacteria. This origin places the active sites at which $MgATP^{2-}$ is hydrolyzed on the cytoplasmic surface of the respective organelles, which is where the $MgATP^{2-}$ is found.

As is the case with P-type Ca^{2+} transporter (Figure 6–34) and Na^+/K^+-exchanging ATPase, H^+-transporting two-sector ATPase is embedded in a membrane with most of its mass in the aqueous solution on one side of that membrane. In the case of H^+-transporting two-sector ATPase, however, the **majority of its mass is in the space that normally has the more negative electric potential**. As with P-type Ca^{2+} transporter and Na^+/K^+-exchanging ATPase, the **portion of the enzyme embedded in the bilayer of the membrane** is also constructed almost entirely of α helices that span or almost span that membrane. P-Type Ca^{2+} transporter, however, is composed of only one folded polypeptide while H^+-transporting two-sector ATPase is composed of many different subunits,[358] the exact number in most species still to be determined. In addition, several of these subunits are present in multiple copies. As a result, H^+-transporting two-sector ATPase is much larger than P-type Ca^{2+} transporter and Na^+/K^+-exchanging ATPase.

The major portion of the large structure located in the aqueous solution on the side of the membrane with a more negative electric potential can

*The terms cytoplasmic and extracytoplasmic or even interior or exterior are useless in this instance because the mitochondria and chloroplasts in which H^+-transporting two-sector ATPase is found are both the progeny of bacterial cells in which the enzyme is also found. The inner membrane of a mitochondrion is the plasma membrane of the ancestral bacterium so the ancient cytoplasmic space, now the matrix of the mitochondrion, is on the side of the inner membrane opposite the cytoplasm of the eukaryotic cell. A thylakoid is the progeny of an invagination in the plasma membrane of the ancestral bacterium that pinched off. Consequently, the interior of the thylakoid is the ancient extracytoplasmic space, and the ancient cytoplasmic space is on the same side of the membrane of the thylakoid as the cytoplasm of the eukaryotic cell in which it is found. The enzyme is unaware of its change of venue and is still transporting hydrons into bacterial cells, into the matrix of the mitochondion, and out of the interior of the thylakoid when $MgATP^{2-}$ is being synthesized. Consequently, positive (pos) and negative (neg) indicate the spaces that have, under normal cytoplasmic circumstances, positive and negative electric potential relative to each other.

†The stoichiometries noted are those for H^+-transporting two-sector ATPase when it is operating at its highest efficiency. Because there is not a direct chemical connection between the current of hydrons and the synthesis of $MgATP^{2-}$, the actual stochiometry is probably less than the ideal, depending on the circumstances.

††There is a "large electrochemical gradient of hydrons" from the exterior to the interior when the pH is sufficiently lower ($\Delta pH = 0.5–1.5$) in the solution on the positive, acidic side of the membrane than in the solution on the negative, basic side, and the electric potential is sufficiently more positive ($\triangle V = -50$ to -220 mV) in the solution on the positive, acidic side than in the solution on the negative, basic side.[355]

be dissociated from the rest of H⁺-transporting two-sector ATPase and purified.[359] For historical reasons,* this soluble sector of H⁺-transporting two-sector ATPase is called F_1-ATPase, and the portion that is left behind within the membrane is called the F_o sector. Together these comprise the two sectors of H⁺-transporting *two-sector* ATPase. The sector that is **F_1-ATPase contains the active sites** at which $MgATP^{2-}$ is either synthesized from or hydrolyzed to $MgADP^-$ and $HOPO_3^{2-}$. When it is detached from the F_o sector of the intact enzyme, F_1-ATPase is no longer coupled to the electrochemical gradient because it is no longer attached to the F_o sector, which is the portion of the enzyme that spans the membrane and transports hydrons across it. For H⁺-transporting two-sector ATPase to synthesize $MgATP^{2-}$, the reversible hydrolysis of $MgATP^{2-}$, which is catalyzed by the active sites on F_1-ATPase, must be coupled to the movement of hydrons down the usual electrochemical gradient, and this transport of hydrons takes place through the F_o sector. Consequently, F_1-ATPase on its own can only hydrolyze $MgATP^{2-}$, which it does quite efficiently. It follows that, under normal circumstances when they are associated with each other, the coupling between the two sectors must, necessarily, be tight.

Five different folded polypeptides comprise F_1-ATPase from bovine mitochondria.[360,361] These five folded polypeptides, of lengths 510 amino acids (α), 480 amino acids (β), 273 amino acids (γ), 146 amino acids (δ), and 50 amino acids (ε), are present in the stoichiometry $\alpha_3\beta_3\gamma\delta\varepsilon$. In the crystallographic molecular model of bovine F_1-ATPase (Figure 6–42),[362-366] the three α subunits and the three β subunits, the sequences of which are homologous to each other (23% identity; 3.2 gap percent) and the tertiary structures of which are superposable,[363] form a ring with a **sixfold rotational axis of pseudosymmetry**. Because the α and β subunits alternate around the ring (Figure 6–42), it is a heterohexamer composed of three $\alpha\beta$ dimers, and all six subunits are assembled head-to-tail.[363,364] The γ subunit, in addition to folding into a small globular domain (150 aa) below this $(\alpha\beta)_3$ ring, also forms a shaft,† composed of a long (48 aa) continuous α helix from its amino terminus and a long (73 aa) continuous α helix from its carboxy terminus. These two α helices twist around each other in half a turn of a coiled coil (Figure 6–43B).[364] The folded δ and ε polypeptides are two small globular subunits (not shown in Figures 6–42 and 6–43) attached to the protruding globular base of the γ subunit on the surface of that globular domain opposite the location of the $(\alpha\beta)_3$ heterohexameric ring. These small subunits are not involved directly in the synthesis of $MgATP^{2-}$, but they function to connect and couple, in part, the γ subunit of the F_1-ATPase to the F_o sector.

In intact F_1-ATPase from every species examined, **the three $\alpha\beta$ dimers assume different conformations**, so the central axis is a threefold rotational axis of pseudosymmetry[363] rather than, as in most trimeric proteins, a threefold rotational axis of symmetry. The $(\alpha\beta)_3$ heterohexameric ring from *Bacillus* sp. PS3 (α subunit, 59% identity; 0.4 gap percent and β subunit, 76% identity; 0.8 gap percent relative to the respective bovine subunits), in the absence of any other subunits of its F_1-ATPase, has been crystallized, and there is a crystallographic threefold rotational axis of symmetry relating the three $\alpha\beta$ heterodimers.[367] From this observation it follows that the $(\alpha\beta)_3$ heterohexameric ring from *Bacillus* sp. PS3 on its own has an exact threefold rotational axis of symmetry, as would be expected, and the conformations of its $\alpha\beta$ subunits must be identical. In the crystallographic molecular model of the intact $(\alpha\beta)_3\gamma\delta\varepsilon$ complex from *Bacillus* sp. PS3, however, the three $\alpha\beta$ heterodimers around the ring adopt the three different conformations observed in the bovine $(\alpha\beta)_3\gamma\delta\varepsilon$ complex.[368] Consequently, the asymmetry in the $(\alpha\beta)_3\gamma\delta\varepsilon$ complex of F_1-ATPase from *Bacillus* sp. PS3, and presumably in all the other F_1-ATPases, is induced by the dramatic asymmetry of the γ subunit (Figure 6–43) upon which the $(\alpha\beta)_3$ heterohexameric ring is snugly impaled. The asymmetry among the three $\alpha\beta$ heterodimers in the intact enzyme is crucial to the ability of H⁺-transporting two-sector ATPase to synthesize $MgATP^{2-}$.

As might be expected, the **active sites at which $MgATP^{2-}$ is synthesized** or hydrolyzed are located in the $(\alpha\beta)_3$ heterohexamer of F_1-ATPase. There are six sites at which either $MgATP^{2-}$ or $MgADP^-$ and $HOPO_3^{2-}$ can be bound simultaneously in the heterohexamer,[365,369] and these six sites are related by the sixfold rotational axis of pseudosymmetry, rotation around which superposes the six homologous subunits, three α subunits and three β subunits. The six sites are located within the six interfaces between α and β subunits (Figure 6–42A,B), one in each interface, and side chains from both the α and β subunits comprising a given interface form each binding site.

*and perhaps for personal reasons

†The metaphor begins.

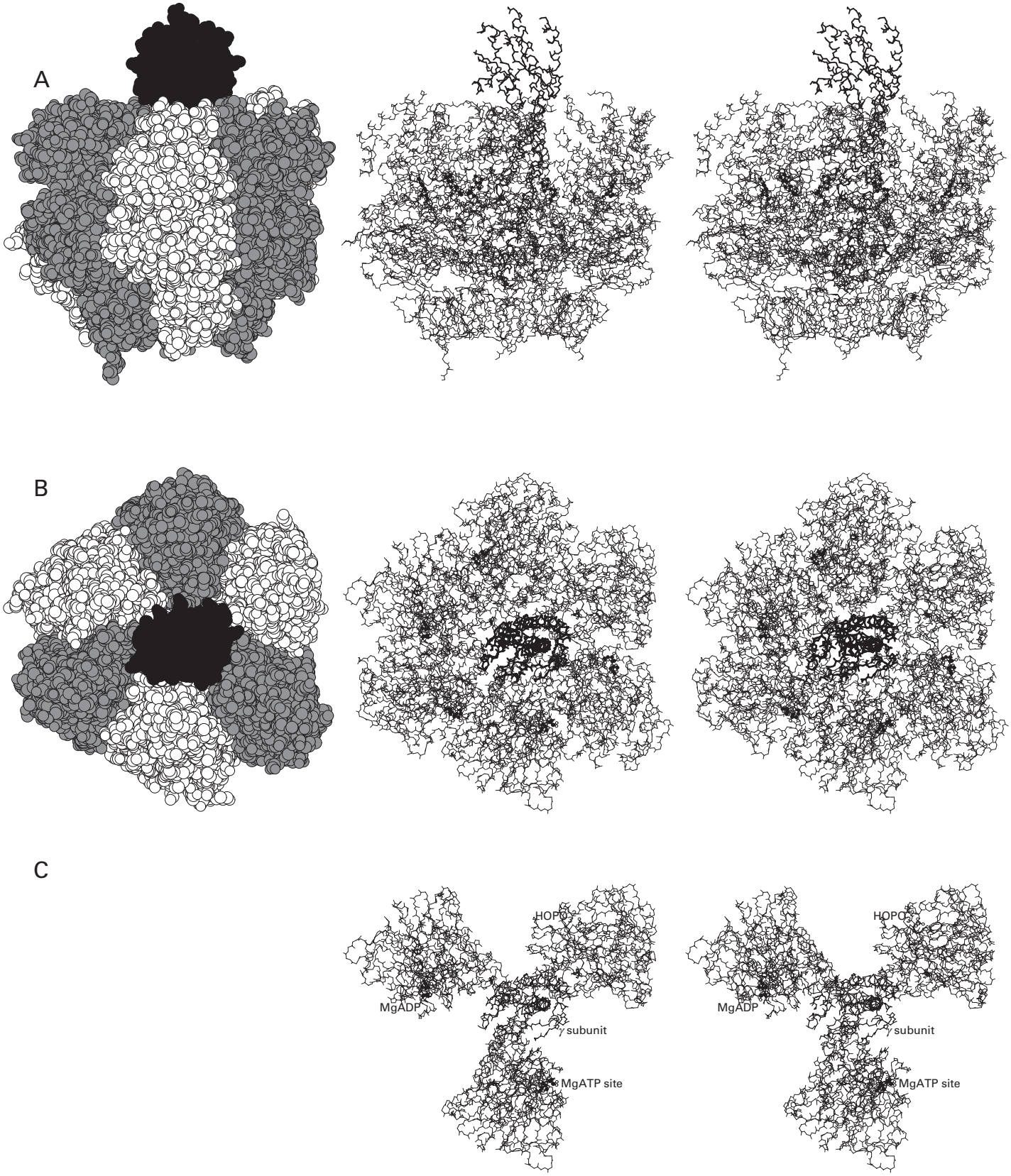
A
B
C
HOPO3
MgADP
subunit
MgATP site
HOPO3
MgADP
subunit
MgATP site

Figure 6–42: Space-filling drawings and stereodrawings[485] of a crystallographic molecular model of the $(\alpha\beta)_3\gamma$ portion of bovine F_1-ATPase.[365] Mitochondria were isolated by differential centrifugation from a homogenate of bovine heart, and these mitochondria were then sonicated to produce submitochondrial particles. During this procedure, the majority of the intramitochondrial soluble proteins were released into solution and could be removed by pelleting the submitochondrial particles. The washed submitochondrial particles in aqueous buffer were shaken with 0.5 volume of chloroform, the emulsion was broken, and the yellowish, clear aqueous phase was concentrated. The concentrate was then submitted to chromatography by molecular exclusion, and the fractions containing F_1-ATPase were concentrated and passed over a solid phase to which Cibacron Blue F3GA was covalently attached. The adsorbant removed the remaining impurities to produce a solution of purified F_1-ATPase, which was precipitated with ammonium sulfate.[362] The enzyme was redissolved and crystallized with poly(ethylene glycol) 6000 as a precipitant in 0.2 M NaCl, 3 mM sodium azide, 20 mM $MgSO_4$, 0.25 mM $MgAMPPNP^{2-}$, 5 μM $MgADP^{-}$, and 50 mM 2-amino-2-(hydroxymethyl)propane-1,3-diol at pH 8.2. Reflections from crystals were collected to Bragg spacing of 0.19 nm. The portion of the resulting refined crystallographic molecular model containing the complete polypeptides of the three α subunits, the three β subunits, and the γ subunit is presented to the left in space-filling models (γ subunit in black, α subunits in gray, and β subunits in white) and to the right as stereo line drawings of only the polypeptide backbones (γ subunit in thick lines, α subunits in lines of intermediate thickness, and β subunits in thin lines) in the same orientation as the space-filling models. The four molecules of $MgAMPPNP^{2-}$, the single molecule of $MgADP^{-}$, and the single molecule of $HOPO_3^{2-}$, which are associated one in each of the six occupied sites in the $(\alpha\beta)_3$ ring in the crystallographic molecular model, are drawn in ball-and-stick format. Again, black atoms are carbons, white atoms are oxygens, small gray atoms are nitrogens, and large dark gray atoms are atoms of phosphorus. (**A**) Side-on views with the γ subunit protruding from the top. (**B**) View from the surface of the enzyme from which the γ subunit protrudes. This orientation defines clockwise (negative rotation) and counterclockwise (positive rotation). (**C**) Stereo line drawing of the polypeptide backbones of the γ subunit and only the three catalytic β subunits with their active sites occupied. The site labeled MgATP, normally occupied by $MgATP^{2-}$, is occupied here by the analogue $MgAMPPNP^{2-}$. The site labeled MgADP, normally occupied by $MgADP^{-}$ and $HOPO_3^{2-}$ in equilibrium with $MgATP^{2-}$ and a molecule of water, is occupied here by $MgADP^{-}$ and azide ion in place of $HOPO_3^{2-}$. The site labeled $HOPO_3^{2-}$, normally occupied by various substrates associating and dissociating, is occupied here by $HOPO_3^{2-}$.

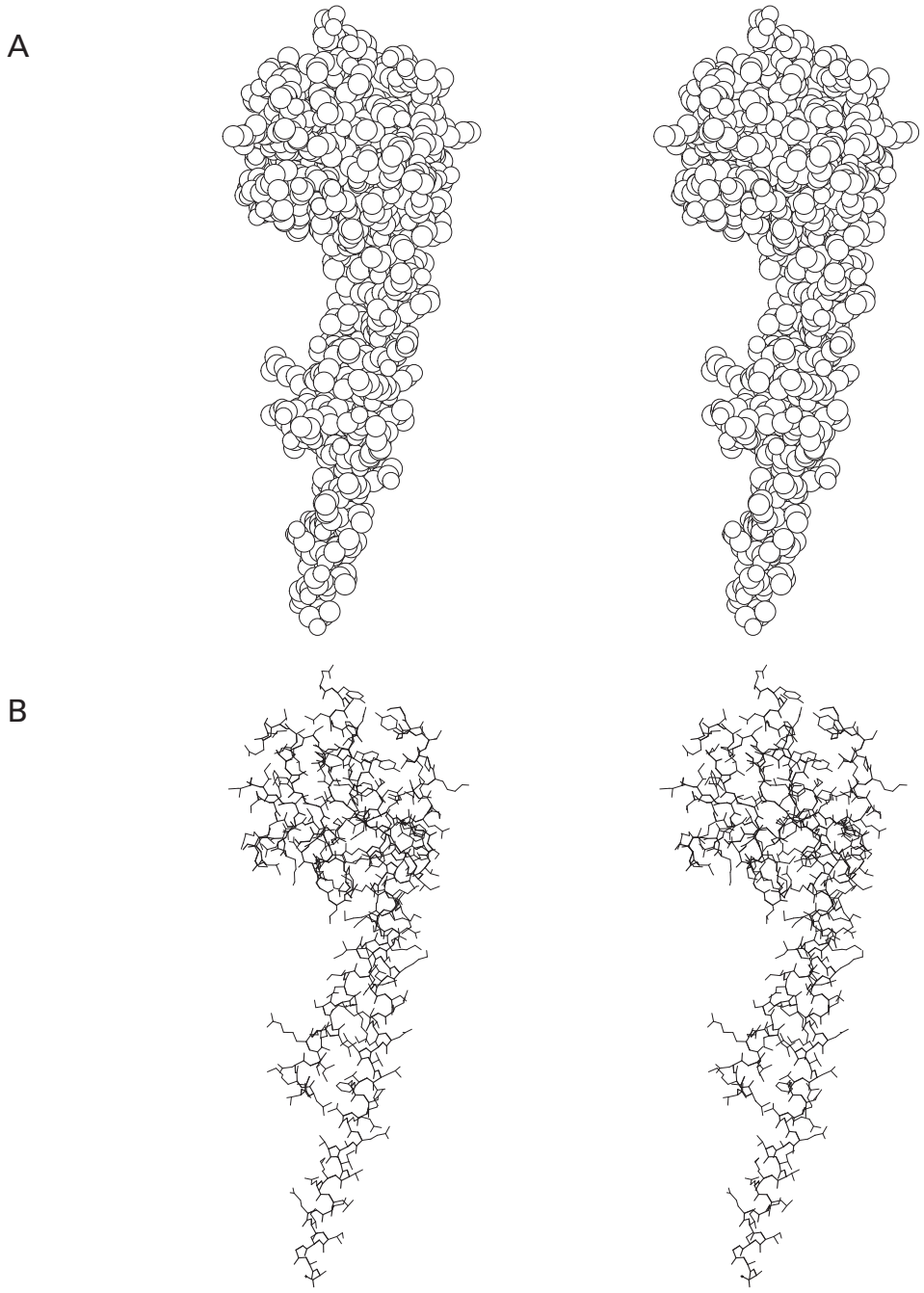

Figure 6–43: Stereodrawings[485] of a crystallographic molecular model of the γsubunit of bovine F_1-ATPase. The γsubunit is from the same crystallographic molecular model as that of Figure 6–42. (**A**) Stereo space-filling drawing of the complete γsubunit. (**B**) Stereo line drawing of all amino acids and their side chains in the complete γsubunit .

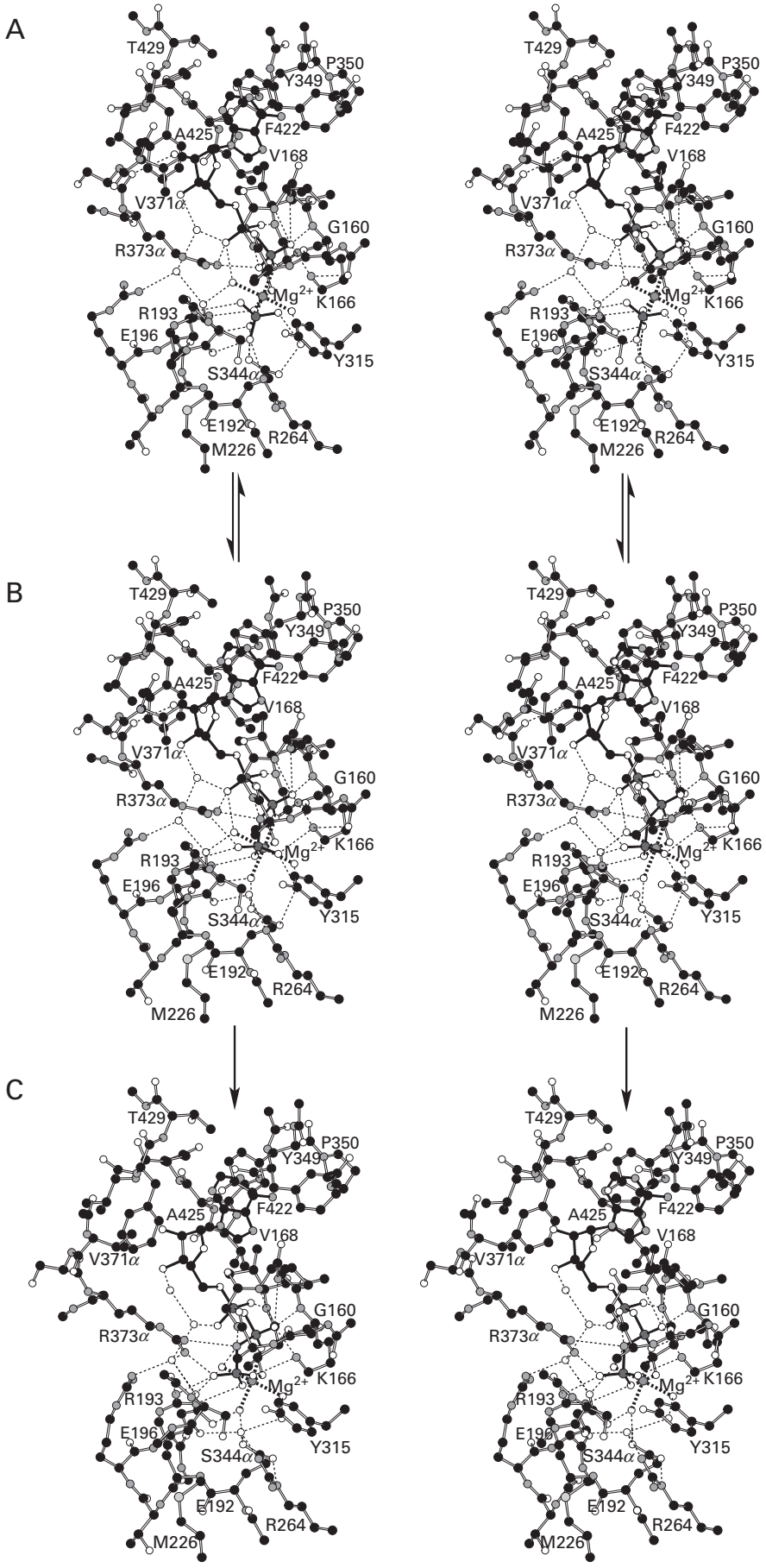
A
B
C
T429
P350
Y349
A425
F422
V168
V371α
G160
R373α
Mg2+
K166
R193
E196
Y315
S344α
E192
R264
M226

Figure 6–44: Stereodrawings[485] of crystallographic molecular models of the two active sites of bovine F_1-ATPase that are occupied by nucleotides. Black atoms are carbons, white atoms are oxygens, small gray atoms are nitrogens, large light gray atoms are sulfurs, and large dark gray atoms are atoms of phosphorus. The segments of polypeptide drawn are identified by naming and numbering the amino acids at their amino-terminal and carboxy-terminal ends. The majority of the segments are from the β subunit, and the numbers of their amino acids are unadorned. The two segments from the α subunit are designated by adding an α to the end of each number. (**A**) Active site on the β subunit in the same crystallographic molecular model as that of Figure 6–42 occupied by $MgADP^-$ (black bonds) and N_3^- ion and in the D conformation.[365] A molecule of water on Mg^{2+}, the N_3^- ion, and a second molecule of water, however, have been replaced by a drawing of $HOPO_3^{2-}$ (black bonds). This drawing is positioned in the active site so that its phosphorus is 0.31 nm from the oxygen of the $MgADP^-$ that is to become the bridging oxygen in $MgATP^{2-}$, a distance that is slightly within the sum of the van der Waals radii (0.33 nm). This position of its phosphorus places its apical oxygen in the same location as the molecule of water that is forming hydrogen bonds with Arginine β264 and Glutamate β192 and the amido oxygen of Serine α344 in the unaltered crystallographic molecular model. One of the equatorial oxygens of $HOPO_3^{2-}$ is oriented toward the Mg^{2+} in as close an approach as possible, which leaves the two other equatorial oxygens occupying positions close the two peripheral negatively charged nitrogens of N_3^-, each with a formal charge number of –0.5. This drawing represents the D conformation occupied by the two substrates $MgADP^-$ and $HOPO_3^{2-}$. (**B**) Active site of Panel A occupied instead by a molecule of $MgAMPPNP^{2-}$ (black bonds) in a different crystallographic molecular model[366] of bovine F_1-ATPase. For this molecular model, the enzyme was crystallized with poly(ethylene glycol) 6000 as a precipitant in 0.2 M NaCl, 20 mM $MgSO_4$, 0.25 mM $MgAMPPNP^{2-}$, 5 μM $MgADP^-$, and 50 mM 2-amino-2-(hydroxymethyl)propane-1,3-diol at pH 8.2. In the absence of N_3^-, this active site is occupied by $MgAMPPNP^{2-}$. Consequently, this molecular model represents the active site in the D conformation occupied by the substrates $MgATP^{2-}$ and H_2O. The molecule of H_2O that is the other substrate forms hydrogen bonds with Arginine β264 and Glutamate β192 and the amido oxygen of Serine α344; and it is in the same location as the molecule of water that was replaced by the apical oxygen of $HOPO_3^{2-}$ to draw the active site in Panel A. (**C**) Active site on the β subunit in the same crystallographic molecular model as that of Figure 6–42, occupied by $MgAMPPNP^{2-}$ (black bonds) and consequently in the T conformation. Arrows between the three panels indicate that the active site in the D conformation is the catalytic site in which the substrates $MgADP^-$ and $HOPO_3^{2-}$ and $MgATP^{2-}$ and H_2O come to equilibrium and that, at an instant in which it is occupied by $MgATP^{2-}$ and H_2O, its conformation is changed to the T conformation by rotation of the γ subunit.

Each site for binding adenine nucleotides, however, is formed mainly (85%) by side chains from only one subunit. Consequently, there are three sites formed mainly by side chains from an α subunit, and there are three sites formed mainly by side chains from a β subunit.

The three sites for the binding of adenine nucleotides formed mainly from each of the three β subunits and pseudosymmetrically arranged in the asymmetric $(\alpha\beta)_3$ heterohexamer (Figure 6–42C) are the active sites at which $MgATP^{2-}$ is synthesized and hydrolyzed.[366] This conclusion follows in part from **covalent labeling of the active sites**. A large number of reagents, both nonspecific electrophiles[370-372] and photoactive reagents[373,374] and electrophilic[375-381] and photolytically reactive[382] derivatives of adenine nucleotides, inactivate the enzymatic hydrolysis of $MgATP^{2-}$ by modifying the side chains of amino acids in a β subunit of F_1-ATPase.

Magnesium 2-azidoATP^{2-}, upon photolysis, covalently modifies Tyrosine β349 of bovine F_1-ATPase[383] and this single modification inactivates the enzyme.[384] The same tyrosine in bovine F_1-ATPase or its homologue in the F_1-ATPase from thermophilic *Bacillus* sp. PS3 is also modified by the nonspecific electrophilic reagent 7-chloro-4-nitrobenzofuran, and this exclusive modification also inactivates the enzymatic activity.[385-389] 5′-[4-Fluorosulfonylbenzoyl]inosine, an electrophilic derivative of a purine nucleoside, also inactivates the enzyme by modifying this same tyrosine in bovine F_1-ATPase.[390] Upon photolysis of 3′-*O*-(4-benzoyl)benzoyladenosine 5′-diphosphate bound in the active site of bovine F_1-ATPase, a triplet state of the carbonyl of benzophenone is formed that abstracts a hydrogen from a nearby amino acid, and the resulting radical on the benzophenone then colligates with the resulting radical on that amino acid to insert into the protein. The amino acid modified is in a tryptic nonadecapeptide containing Tyrosine β349.[382] Tyrosine β349 is in the site that was subsequently identified crystallographically (Figure 6–44)[363,365,366] as the active site of the enzyme. Its phenyl ring lies flat against the adenine of $MgATP^{2-}$ or ADP^{3-}.

Dicyclohexylcarbodiimide modifies exclusively a glutamate in F_1-ATPase from *E. coli* that is homologous to Glutamate β192 of bovine F_1-ATPase,[391,392] and this modification inactivates the ATPase activity of the enzyme.[393] Glutamate β192 is the sole catalytic acid–base in the active site (Figure 6–44).

In at least one instance, however, a reagent, in this case 2-oxo-2-phenylacetaldehyde, modifies an amino acid, the arginine in F_1-ATPase from chloroplasts of *Spinacia oleracea* that is in the homologous position of Arginine β299 in bovine F_1-ATPase. The modification inactivates the enzyme even though

this amino acid is distant (2.4 nm) from the nearest atom in $MgATP^{2-}$ when it is bound in the active site.[372]

In each instance cited above, with the informative exception of the case of Arginine β299, the **modification of only one amino acid side chain in one β subunit** in the $(\alpha\beta)_3\gamma\delta\varepsilon$ complex that is F_1-ATPase is sufficient to completely inactivate the ATPase activity.* The conclusion that has been drawn from these results is that the three active sites on the enzyme do not act independently of each other during hydrolysis of $MgATP^{2-}$ and, by microscopic reversibility, during synthesis of $MgATP^{2-}$. A number of other observations also suggest that the three active sites are required to act together in concert to hydrolyze a molecule of $MgATP^{2-}$.[394]

There are kinetic measurements and isotopic exchanges that suggest a mechanism for hydrolysis of $MgATP^{2-}$ and, in reverse, for the synthesis of $MgATP^{2-}$. When hydrolysis of $MgATP^{2-}$ by bovine F_1-ATPase is monitored under **conditions in which catalysis can occur at only one active site** on each $(\alpha\beta)_3$ heterohexamer, the reaction is dramatically different from the situation in which all three sites are hydrolyzing $MgATP^{2-}$ together.[395] When 1 μM bovine F_1-ATPase is mixed with 0.3 μM $MgATP^{2-}$ so that only one site in each $(\alpha\beta)_3$ heterohexamer can be occupied, hydrolysis of $MgATP^{2-}$ and release of $MgADP^-$, and $HOPO_3^{2-}$ into solution is extremely slow (5 h^{-1}).[396]

The reason for this slow rate is not that hydrolysis of $MgATP^{2-}$ on the active site is slow. In fact, on an active site of the enzyme in this situation, the equilibrium

$$ECOO^-\cdot MgATP^{2-}\cdot H_2O \rightleftharpoons ECOOH\cdot MgADP^-\cdot HOPO_3^{2-} \quad (6\text{–}133)$$

with an equilibrium constant of 0.5, is established rapidly. The magnitude of this **equilibrium constant for the reaction on this single active site** is another example of the ability of an active site to dramatically change the equilibrium constant observed for reactants and products in solution. Steady-state and stopped-flow kinetic measurements are consistent with this equilibrium being established even when F_1-ATPase from *E. coli* is continuously hydrolyzing $MgATP^{2-}$ in its normal steady state.[397]

Reactants and products in this equilibrium interconvert on an active site with rate constants* k_2 and k_{-2} of 12 and 24 s^{-1}, respectively.[396] Rather, as in the case of myosin ATPase, it is the **release of products that is rate-limiting** when only one site on the $(\alpha\beta)_3$ heterohexamer is catalyzing the hydrolysis. Both ADP^{3-} and $HOPO_3^{2-}$ are released into solution at the same slow rate (14 h^{-1}).[398] If, however, excess $MgATP^{2-}$ is added before the products have dissociated, the rate of dissociation of ADP^{3-} and $HOPO_3^{2-}$ increases more than 100,000-fold to a rate equal to the rate of hydrolysis of $MgATP^{2-}$ at the higher concentrations of reactant.[398-401] Consequently, association of $MgATP^{2-}$ with another of the active sites on the $(\alpha\beta)_3$ heterohexamer accelerates the dissociation of products from the active site in which they were in equilibrium with reactant.

The equilibrium between $MgATP^{2-}$ and $MgADP^-$ and $HOPO_3^{2-}$ on an active site in F_1-ATPase can also be established from the other direction. When $MgADP^-$ and $H_2PO_4^-$ are added to F_1-ATPase from chloroplasts of *S. oleracea*, the enzyme forms, on one of its active sites, 0.25 mol of $MgATP^{2-}$ for every mole of $(\alpha\beta)_3\gamma\delta\varepsilon$ F_1-ATPase.[402]

The fact that both ADP^{3-} and $HOPO_3^{2-}$ are released from the active site of bovine F_1-ATPase with the same rate constant in the absence of excess $MgATP^{2-}$ suggests that a slow rate-limiting conformational change opens the active site to the solution. Once the active site has opened, both products dissociate so rapidly that the observed rates of their dissociations are simply equal to the rate of the conformational change opening the site. If so, then association of $MgATP^{2-}$ at another site, presumably another of the three active sites, dramatically accelerates this conformational change.

The rate at which $MgATP^{2-}$ associates with this second site (6×10^6 M^{-1} s^{-1}) to enhance the rate of dissociation of products from the first active site is equal to the rate at which $MgATP^{2-}$ associates with a single active site in the unoccupied $(\alpha\beta)_3$ heterohexamer.[396,401] This equality suggests that the site to

*The truncated version of F_1-ATPase from *Bacillus* sp. PS3, which contains only α and β subunits in the stoichiometry $(\alpha\beta)_3$ and which hydrolyzes $MgATP^{2-}$, is completely inactivated by incorporation of the reagent 7-chloro-4-nitrobenzofuran into only one-third of the β subunits. This observation suggested that the $(\alpha\beta)_3$ ring in the absence of the γ subunit is asymmetric.[389] As has already been noted, however, this $(\alpha\beta)_3$ subcomplex of F_1-ATPase, in the absence of nucleotides, crystallizes in the space group $P2_13$ with an $\alpha\beta$ dimer in the asymmetric unit, a fact requiring that the $(\alpha\beta)_3$ heterohexamer in this particular crystal be threefold rotationally symmetric.[367]

*Note that, in the active site of the enzyme while it is hydrolyzing $MgATP^{2-}$, the synthesis of $MgATP^{2-}$ is nevertheless 2 times faster than its hydrolysis.

which the $MgATP^{2-}$ binds to accelerate the release of products has the same conformation as the active site to which it binds when the enzyme is completely unoccupied and that this site to which it binds is another of the three active sites. **Association of $MgATP^{2-}$ with a site in this conformation produces the conformational change** at the site at which $MgATP^{2-}$ and $MgADP^{-}$ and $HOPO_3^{2-}$ are in equilibrium, opening that active site to the solution and releasing ADP^{3-} and $HOPO_3^{2-}$ when $MgATP^{2-}$ is being hydrolyzed.

These kinetic measurements of the reaction catalyzed by F_1-ATPase clarify previous **observations of intermediate isotopic exchange**.[394] In fact, it was these earlier observations of isotopic exchange that inspired the kinetic observations just described. When $Mg[\gamma\text{-}^{18}O_3P]ATP^{2-}$ is hydrolyzed in $H_2{}^{16}O$ or $Mg[\gamma\text{-}^{16}O_3P]ATP^{2-}$ is hydrolyzed in $H_2{}^{18}O$ by bovine F_1-ATPase, as the concentration of $MgATP^{2-}$ in solution is lowered systematically, the number of oxygens from water incorporated by intermediate isotopic exchange into the $H_2PO_4^{-}$ that is the product of the enzymatic reaction increases from the stoichiometric value of 1 to greater than 3.[399,403] The explanation for these observations of intermediate isotopic exchange is that association of $MgATP^{2-}$ with one of the three catalytic sites on the $(\alpha\beta)_3\gamma\delta\varepsilon$ oligomer accelerates the release of the products of hydrolysis of $MgATP^{2-}$ at one of the other sites, as was documented in the later kinetic experiments. If this is so, then the lower the concentration of $MgATP^{2-}$, the longer the reactants and products of the reaction (Equation 6–133) between $MgATP^{2-}$ and H_2O and $MgADP^{-}$ and $HOPO_3^{2-}$ will sit at equilibrium. As the reaction sits at equilibrium, the nucleotides and $HOPO_3^{2-}$ are constantly exchanging oxygens with molecules of water. If molecules of water can enter and leave the active site but $MgATP^{2-}$, $MgADP^{-}$, and $HOPO_3^{2-}$ cannot or if there are several molecules of water locked in the active site that can participate in the isotopic exchange, then the longer reactant and product remain locked in the active site, the more exchange will be observed. From the observed rates for incorporation of oxygen from water during this intermediate isotopic exchange, it could be calculated[404] that, on the active site, the rate of the back reaction for synthesis of $MgATP^{2-}$ from $MgADP^{-}$ and $HOPO_3^{2-}$ is 60 s^{-1}, which is indistinguishable, within the margin of error, from the 24 s^{-1} measured in the experiments that were described earlier.[396]

When intact H^+-transporting two-sector ATPase embedded in its membrane is hydrolyzing $MgATP^{2-}$ in the absence of an electrochemical gradient of hydrons, it also catalyzes the intermediate isotopic exchange of $H_2{}^{18}O$ into the $H^{16}OP^{16}O_3^{2-}$ that is its product.[405-407] In reverse, when the enzyme is synthesizing $MgATP^{2-}$ from $MgADP^{-}$ and $HOPO_3^{2-}$ in the presence of a sufficient electrochemical gradient of hydrons, incorporation of oxygen-16 from $H_2{}^{16}O$ into the $Mg[\gamma\text{-}^{18}O_3P]ATP^{2-}$ formed from $H^{18}OP^{18}O_3^{2-}$ as a result of intermediate isotopic exchange is observed. This intermediate exchange during the synthesis of $MgATP^{2-}$ is accelerated when the concentration of $MgADP^{-}$ in solution is decreased by adding pyruvate kinase and phospho*enol*pyruvate[408] or by simply decreasing the initial concentration of $MgADP^{-}$.[409] Decreasing the concentration of $HOPO_3^{2-}$ also leads to an increase in this intermediate isotopic exchange.[409] The same results were observed with H^+-transporting two-sector ATPase from *S. oleracea*.[410] These observations can be explained by assuming that, in order for newly synthesized $MgATP^{2-}$ to be released into solution from the active site in which it is in equilibrium with $MgADP^{-}$ and $HOPO_3^{2-}$, both $MgADP^{-}$ and $HOPO_3^{2-}$ must occupy one of the two other active sites in the $(\alpha\beta)_3$ heterohexamer. The longer it takes for the other active site be occupied, the longer the $MgADP^{-}$ and $HOPO_3^{2-}$ and the $MgATP^{2-}$ and the molecule of water remain at equilibrium in the catalytic active site and the more intermediate isotopic exchange occurs.

All the results presented so far suggest that at least two of the three active sites on the $(\alpha\beta)_3$ heterohexamer in a molecule of F_1-ATPase must cooperate during hydrolysis of $MgATP^{2-}$. The fact, however, that a hybrid $(\alpha\beta)_2\alpha\beta'\gamma\delta\varepsilon$ oligomer of F_1-ATPase with one mutant, inactive β subunit (β') and two unmutated β subunits, one with a presumably normal active site and the other with a presumably normal site for binding of $MgATP^{2-}$, is unable to catalyze hydrolysis of $MgATP^{2-}$ at normal rates implies that **all three of the active sites on the β subunits must cooperate** under normal circumstances.[411]

An explanation for all these observations of kinetics and intermediate isotopic exchange has been provided.[408,412] It has been updated (Figure 6–45) by consideration of the crystallographic molecular models of the three active sites (Figure 6–44) and of the conformations of the three $\alpha\beta$ heterodimers (Figure 6–46).[363,365]

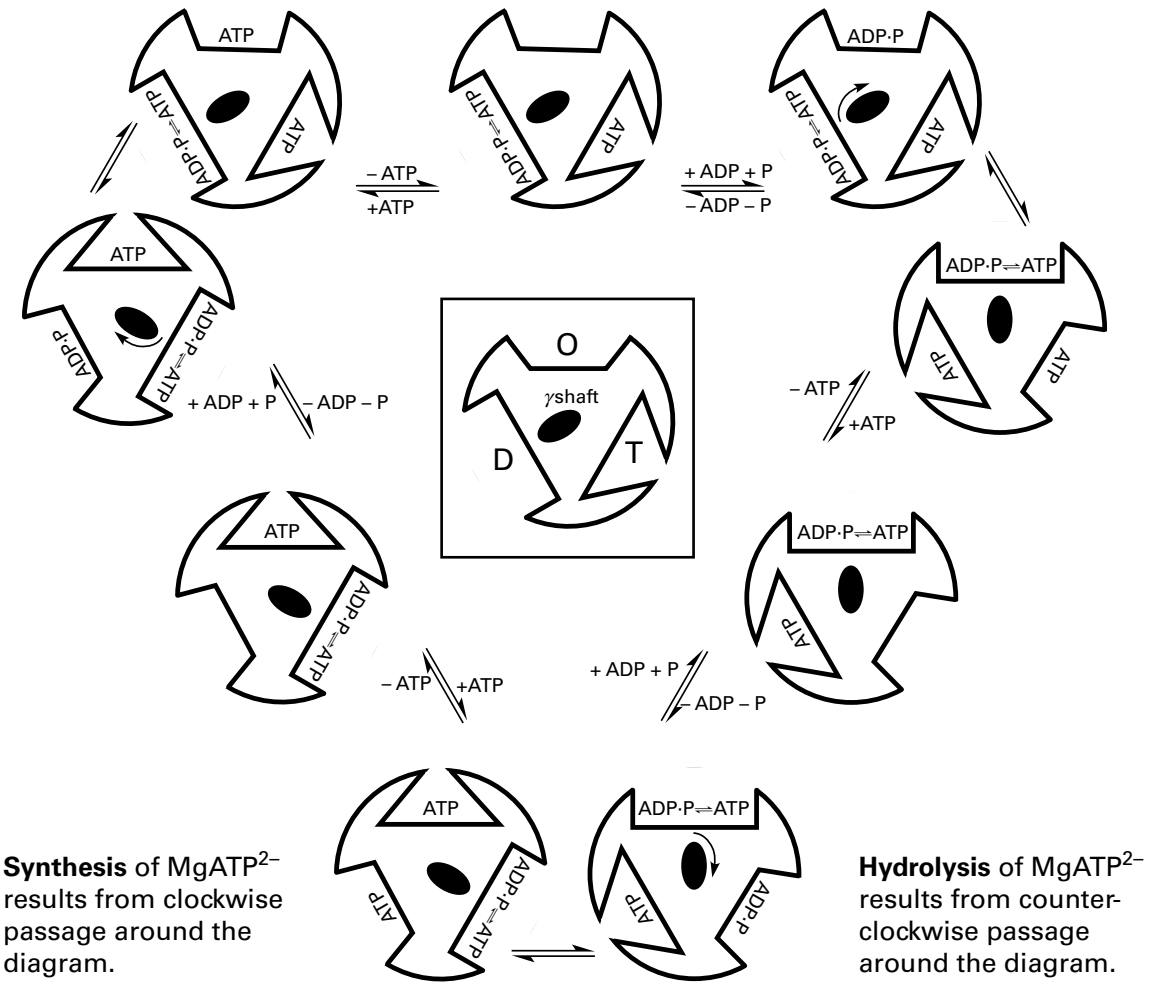

Figure 6–45: Diagrams[408,412] of a proposal for the quaternary conformational changes through which F_1-ATPase passes during the consecutive synthesis of three molecules of MgATP^{2-} from three molecules of MgADP^{-} and $HOPO_3^{2-}$. The diagramatic representations for each of the three conformations of the $\alpha\beta$ heterodimer are defined within the box in the center. The original proposal for the conformational mechanism has been updated by considering the results of the foregoing crystallographic molecular models and the conclusion that the active site in which catalysis occurs is the active site in the D conformation,[366,414] which is represented in the diagrams by the equilibria. The three conformations that each active site adopts—O, D and T—are identified in the central drawing. The reactions along each side of the equilateral triangle are dissociation of MgATP^{2-} and association of MgADP^{-} and $HOPO_3^{2-}$. The steps at the three vertices are the quaternary conformational changes produced by clockwise rotation in steps of –120° of the γ subunit, represented by the black ellipse.

Figure 6–46: Stereodrawings[485] of changes in the conformation of the β subunit of F_1-ATPase promoted by rotation of the γ subunit. Protein is presented in space-filling stereodrawings, and the ligands in each panel are portrayed in ball-and-stick format in which black atoms are carbons, white atoms are oxygens, small gray atoms are nitrogens, and large dark gray atoms are atoms of phosphorus. Drawings of the three β subunits in the crystallographic molecular model of Figure 6–42 are each presented in the same orientation, with the γ subunit in its orientation relative to that particular β subunit. In this way, the drawings reproduce the consecutive changes in one of the β subunits expected upon two consecutive –120° rotations of the γ subunit. The rotation of the γ subunit depicted is clockwise (arrow), the direction in which MgATP^{2-} is synthesized. (**A**) The β subunit in the D conformation. Here the active site is occupied by the MgADP^{-} in the crystallographic molecular model, and a drawing of $HOPO_3^{2-}$, which is not present in the crystallographic molecular model, has been added. This drawing represents the active site in which substrates are in catalytic equilibrium. (**B**) The β subunit in the T conformation. Here the active site is occupied by the MgAMPPNP^{2-} in the crystallographic molecular model. This drawing represents the active site in which the eventual product, MgATP^{2-}, is protected from hydrolysis. (**C**) The β subunit in the O conformation. This drawing represents the active site that has been thrown open. A molecule of MgATP^{2-}, which is not present in the crystallographic molecular model, has been placed in its approximate location in the T conformation to illustrate the opening of the active site that precedes dissociation of product. Notice how the two segments of polypeptide above the substrates that clasp them in the D and T conformations have spread apart to open the active site to the solution.

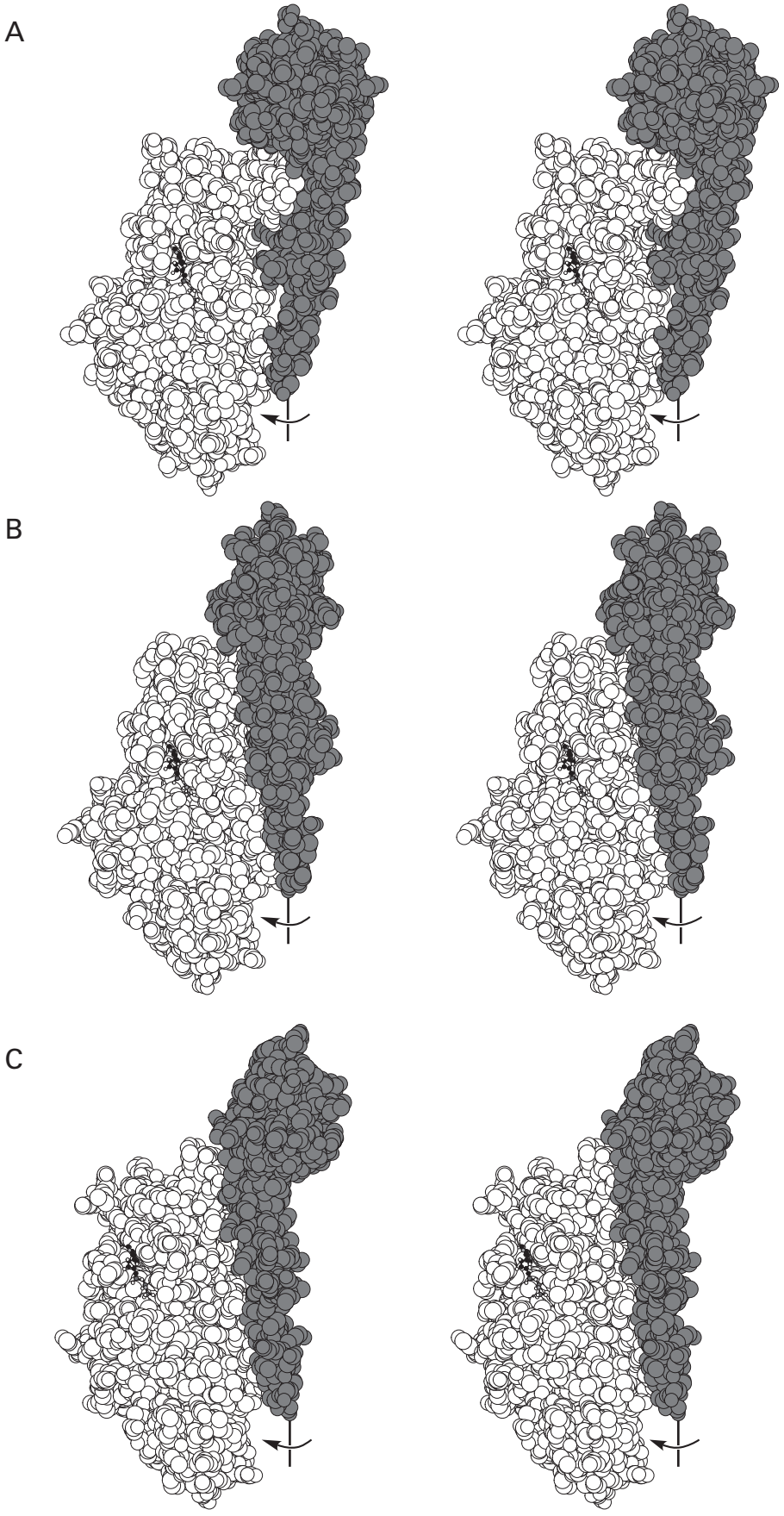
A
B
C

At any instant, the three $\alpha\beta$ heterodimers in the entire $(\alpha\beta)_3\gamma\delta\varepsilon$ complex, each of which contains one of the three active sites, are in **three different conformations.** In the O conformation, **the active site in the $\alpha\beta$ heterodimer is open to the solution**, and the substrates $MgADP^-$ and $HOPO_3^{2-}$ or the substrates $MgATP^{2-}$ and a molecule of water can associate with or dissociate from this conformation. In the D conformation, in which in a given instant the **active site in the $\alpha\beta$ heterodimer is closed around the substrates**, $MgADP^-$ and $HOPO_3^{2-}$ or $MgATP^{2-}$ and a molecule of water, these four substrates are in rapid equilibrium with each other (Equation 6–133), which by chance or design seems to favor $MgATP^{2-}$ slightly. In the T conformation, the active site is closed around $MgATP^{2-}$ but the $MgATP^{2-}$ and the molecule of water are no longer in equilibrium with $MgADP^-$ and $HOPO_3^{2-}$. The D conformation contains the only active site that is catalytically active. In the T conformation, catalysis of the equilibrium has been suspended, and instead the **active site in the $\alpha\beta$ heterodimer protects the molecule of $MgATP^{2-}$** that occupies it from adventitious hydrolysis.

This explanation is consistent with and **explains the available crystallographic molecular models.** In crystallographic molecular models of bovine F_1-ATPase (Figure 6–42), these three different conformations are easily distinguished and have been identified by the ligands that occupy their active sites.[363] The enzyme has been crystallized from a solution containing $MgADP^-$; magnesium 5′-adenylic imidodiphosphonic anhydride ($MgAMPPNP^{2-}$), a stable analogue of $MgATP^{2-}$; and azide (N_3^-), an analogue of $HOPO_3^{2-}$. In these crystals, the active site in the T conformation of the $\alpha\beta$ heterodimer is occupied by a molecule of $MgAMPPNP^{2-}$, and the active site in the D conformation of the $\alpha\beta$ heterodimer is occupied by $MgADP^-$ and azide.[365] The latter fact indicates that the D conformation of the active site has a preference for $MgADP^-$ and N_3^- over the $MgAMPPNP^{2-}$ that is also in solution because the concentration of $MgAMPPNP^{2-}$ is 50 times higher than that of $MgADP^-$. The active site in the O conformation of the $\alpha\beta$ heterodimer in this crystallographic molecular model is occupied by one $HOPO_3^{2-}$, and it is significantly distorted relative to the other two active sites into a conformation open to the solution. In two other crystallographic molecular models of F_1-ATPase, from *R. norvegicus*[369] and from *Bos taurus*,[413] both crystallized in the absence of Mg^{2+}, the O site is occupied by ADP^{3-} and has partially closed around it. When the $(\alpha\beta)_3$ ring in the molecular model of the bovine enzyme is viewed from the surface from which the γ subunit protrudes (Figure 6–42C), the conformations in counterclockwise* order are O, D, and T.

The **catalytic active site** in which $MgATP^{2-}$ and a molecule of water and $MgADP^-$ and $HOPO_3^{2-}$ are in equilibrium with each other during the normal catalysis performed by F_1-ATPase (Equation 6–133) has been identified as the active site in the D conformation (Figure 6–44A,B).[366,414] In a crystallographic molecular model[366] in which the active site in the D conformation is occupied by $MgAMPPNP^{2-}$ (Figure 6–44B), the molecule of water that is the reactant in hydrolysis of $MgATP^{2-}$ is compressed against the γ-phosphorus of $MgAMPPNP^{2-}$. The distance between the oxygen of this molecule of water and the γ-phosphorus (0.31 nm) is less than the sum of their van der Waals radii (0.335 nm), and the distance between this oxygen and one oxygen on the γ-phosphorus (0.28 nm) is also within the sum of the van der Waals radii (0.30 nm). The distance (0.48 nm) between the oxygen of this molecule of water and an oxygen on the β-phosphorus of $MgADP^-$ in the active site in the D conformation occupied by $MgADP^-$ and N_3^- (Figure 6–44A), when it is not compressed against a phosphorus atom, is the same (±0.004 nm) as that between this oxygen and the bridging nitrogen in $MgAMPPNP^{2-}$ when it is occupying the active site in the D conformation and it is compressed against the γ-phosphorus. From these indistinguishable distances, it follows that this molecule of water is rigidly held in this exact location regardless of the occupants of the active site. The α-phospho and β-phospho groups of either $MgADP^-$ or $MgATP^{2-}$ are also rigidly held. In fact, there are six donors for hydrogen bonds in addition to the Mg^{2+} anchoring firmly just the β-phospho group, the phospho group containing the oxygen that is the nucleophile in the nucleophilic substitution at the phosphorus in $HOPO_3^{2-}$ that has $MgATP^{2-}$ as its product. Consequently, when the phospho group of $HOPO_3^{2-}$, the axial oxygen of which replaces this molecule of water, is transferred to the nucleophilic oxygen on the β-phospho group of the $MgADP^-$, the phosphorus of $HOPO_3^{2-}$ must also be forced up against the nucleophilic oxygen on the β-phospho group, again within the sum of the two van der Waals radii.

When $MgAMPPNP^{2-}$ is occupying the active site in the T conformation (Figure 6–44C) rather than the D conformation, however, the molecule of

*For reasons that will become apparent later, the accepted view of F_1-ATPase for determining clockwise and counterclockwise rotation of the γ subunit is from the surface from which it protrudes, the top surface in the drawing in Figure 6–42A.

water that was a participant in the equilibrium between $MgATP^{2-}$ and $MgADP^{-}$ and $HOPO_3^{2-}$ in the active site in the D conformation, has been pulled away from the γ-phosphorus of $MgAMPPNP^{2-}$ (0.37 nm) by the conformational change (Figure 6–44). In addition, the two lone pairs of electrons on this molecule of water are occupied by donors for hydrogen bonds from Arginine β264 and one of the molecules of water on Mg^{2+}, and its two hydrogens are occupied by acceptors for hydrogen bonds from Glutamate β192 and the amido oxygen of Serine α344.[415] Consequently, this molecule of water in the active site in the T conformation is too far from the γ-phosphorus atom, and it no longer has one of its lone pairs of electrons directed at the γ-phosphorus atom. Therefore, it cannot participate in a nucleophilic substitution at the γ-phosphorus atom leading to hydrolysis of the $MgATP^{2-}$ that, under normal circumstances, would occupy this site in the T conformation. Calculations are consistent with the proposal that, in the active site in the T conformation, $MgATP^{2-}$ is thermodynamically stabilized as well as kinetically stabilized relative to $MgADP^{-}$ and $HOPO_3^{2-}$.[416] Although it seems strange, the only obvious significant difference between the active sites in the D and T conformations is the position and nucleophilicity of this molecule of water,[414] yet this **shift in the position of the molecule of water** seems to be all that is required to protect the $MgATP^{2-}$. It seems that the way this enzyme achieves one of the most important synthetic reactions in a living organism is to use a conformational change to move a molecule of water a tenth of a nanometer away from an atom of phosphorus and hold it there.

C**atalysis that is provided by the active site in the D conformation** to promote equilibration is straightforward. Three hydrogen bonds, by holding its axial oxygen firmly, compress the phosphorus of $HOPO_3^{2-}$ against the nucleophilic oxygen on the β-phospho group of $MgADP^{-}$ (Figure 6–44A) as well as compressing the molecule of water formed from the axial oxygen against the phosphorus of the γ-phospho group of $MgATP^{2-}$ (Figure 6–44B). The most important of the three groups participating in these hydrogen bonds is the amido oxygen of Serine α344 because it is in a polypeptide backbone and consequently significantly more rigidly positioned than either the guanidinio group of Arginine β264 or the carboxy group of Glutamic Acid β192. The amido oxygen of Serine α344 also has the advantage that it can only accept a hydrogen bond, thereby ensuring that the hydron on $HOPO_3^{2-}$ is on the oxygen of the hydroxy group that becomes the water that is the required leaving group in the nucleophilic substitution at phosphorus. The amido oxygen of Serine α344 also ends up as one of the four hydrogen bonds that prevent the molecule of water from being a nucleophile in the active site when it has changed to the T conformation. To convert the hydroxy group on $HOPO_3^{2-}$ into the molecule of water that is the required leaving group in the conversion of $MgADP^{-}$ and $HOPO_3^{2-}$ into $MgATP^{2-}$, the necessary hydron is provided by the catalytic carboxy group of Glutamic Acid β192, which forms a hydrogen bond with the hydroxy group on $HOPO_3^{2-}$ in the ground state.

In free solution at pH 7 and 25 °C and a concentration of Mg^{2+} of 1 mM, which are the nominal conditions of cytoplasm, the equilibrium constant is 1×10^{-4} for the reaction*

$$ADP_t + phosphate_t \rightleftharpoons ATP_t + H_2O \qquad (6\text{–}134)$$

where ADP_t is adenosine diphosphate in all its forms (about 45% $MgADP^{-}$ and 45% ADP^{3-}), ATP_t is adenosine triphosphate in all its forms (>80% $MgATP^{2-}$), and $phosphate_t$ is phosphate in all its states of hydronation (60% $HOPO_3^{2-}$).[417] In the active site of F_1-ATPase in the D conformation, the value for the equilibrium constant for the equivalent reaction is 2. This **dramatic shift in the equilibrium constant** must result from the fact that the active site has a higher affinity for $MgATP^{2-}$ and water than for $MgADP^{-}$ and $HOPO_3^{2-}$. In contrast to the fact that $MgATP^{2-}$ must associate with the active site of F_1-ATPase in the catalytic D conformation with high affinity, the Michaelis constant for $MgATP^{2-}$ as a reactant for the hydrolysis catalyzed by the enzyme from *R. norvegicus* is in the range of 0.1 mM.[418] This observation is consistent with a requirement for the binding of $MgATP^{2-}$ at an active site other than the catalytic active site on a molecule of F_1-ATPase with a dissociation constant around 0.1 mM to promote the release of products during hydrolysis of $MgATP^{2-}$.

The reason that the active site in the catalytic D conformation has a **higher affinity for $MgATP^{2-}$ than for $MgADP^{-}$ and $HOPO_3^{2-}$** can be understood

*The equilibrium constant cited[417] does not include the concentration of water in the numerator. In the present instance, it has been included so that a comparison can be made with the reaction in the active site, in which the product water is a pre-positioned, isolated molecule of water.

by placing $HOPO_3^{2-}$ in the crystallographic molecular model of the active site in the D conformation that is occupied by $MgADP^-$ and N_3^- (Figure 6–44A) after removing the N_3^- and two molecules of water that together occupy the usual positions of the four oxygens of $HOPO_3^{2-}$ in its absence.[365] The most inescapable requirement for this insertion is that the phosphorus atom of $HOPO_3^{2-}$ cannot be less than 0.31 nm away from the oxygen on the β-phospho group that acts as the nucleophile because of the van der Waals radii of the phosphorus atom (0.18 nm) and the oxygen atom (0.15 nm). Placing these two atoms at a distance of 0.31 nm also places the apical oxygen of $HOPO_3^{2-}$ in almost the exact position of the molecule of water that forms paradigmatic hydrogen bonds with Arginine β264 and Glutamate β192 and the amido oxygen of Serine α344 in the active site in the D conformation when it is occupied either by $MgADP^-$ and N_3^- or by $MgAMPPNP^{2-}$ (Figure 6–44B) and positions the bond between phosphorus and the apical oxygen of $HOPO_3^{2-}$ in the proper orientation for the nucleophilic substitution at phosphorus. The three equatorial oxygens of $HOPO_3^{2-}$ can then be positioned in the same orientation as three equatorial oxygens on the γ-phospho group in the active site in the D conformation when it is occupied by $MgAMPPNP^{2-}$.

There are several disadvantages, however, to this inescapable position for $HOPO_3^{2-}$ in the active site in the D conformation when it is also occupied by $MgADP^-$ relative to the same active site when it is occupied by $MgAMPPNP^{2-}$ and the molecule of water that is the other product of the nucleophilic substitution at phosphorus. A hydrogen bond cannot form between Lysine β166 and one of the equatorial oxygens on $HOPO_3^{2-}$, and a hydrogen bond cannot form between Arginine α373 and another of the equatorial oxygens on $HOPO_3^{2-}$ because the distances (0.33 nm) between the respective nitrogens that are donors and oxygens that are acceptors are too long (Figure 6–44A). Both hydrogen bonds (0.29 nm), however, form when $MgADP^-$ and $HOPO_3^{2-}$ become $MgATP^{2-}$ and a molecule of water (Figure 6–44B). The closest oxygen on $HOPO_3^{2-}$ is a marginal ligand to Mg^{2+} because the distance between it and Mg^{2+} is too long and its oxygen is not in an octahedral position, which is the preferred geometry of coordination for Mg^{2+}. The closest oxygen on $HOPO_3^{2-}$ to Mg^{2+} also must push aside one of the molecules of water that is a ligand to Mg^{2+} because of a steric clash, and this steric effect distorts the coordination at this position as well. When $MgADP^-$ and $HOPO_3^{2-}$ become $MgATP^{2-}$ and a molecule of water, an oxygen on the β-phospho group of $MgATP^{2-}$ and this same oxygen, which was the closest oxygen to Mg^{2+} in $HOPO_3^{2-}$ and is now on the γ-phospho group of $MgATP^{2-}$, are undistorted octahedral ligands for Mg^{2+}. This undistorted coordination is the same as that between Mg^{2+} and ATP^{4-} when $MgATP^{2-}$ is in solution. Nor can the Mg^{2+} be readily reoriented to adjust to these distortions caused by this oxygen on $HOPO_3^{2-}$ when the active site in the D conformation is occupied by $MgADP^-$ because the Mg^{2+} is coordinated by the oxygen of Threonine β167, by a molecule of water between it and one of the nonbridging oxygens of the α-phospho group of $MgADP^-$, and by an oxygen from the β-phospho group of $MgADP^-$, which is rigidly held and cannot move any closer to $HOPO_3^{2-}$ because of the steric hindrance of the van der Waals radii. For all these reasons, it seems apparent that the active site of the enzyme should have a higher affinity for $MgATP^{2-}$ and the molecule of water than for $MgADP^-$ and $HOPO_3^{2-}$.

The **structure of the opened active site** in the $\alpha\beta$ heterodimer in the O conformation is dramatically different from that of the active site of an $\alpha\beta$ heterodimer in either the D or T conformation (Figure 6–47).[363,365,366] The door that closed over the $MgADP^-$ and $HOPO_3^{2-}$ formed by the segment of polypeptide containing Phenylalanine β422 to Threonine α429 has opened to the solution, permitting dissociation of $MgATP^{2-}$ in the direction of synthesis. The cup for the β-phospho group of $MgATP^{2-}$ and $MgADP^-$, however, is still in almost the same conformation, although somewhat tilted, and is holding $HOPO_3^{2-}$ in the crystallographic molecular model, presumably ready to cup the β-phospho group of the reactant $MgADP^-$ rather than $HOPO_3^{2-}$ following dissociation of $MgATP^{2-}$ in the direction of synthesis. The methyl group of Alanine β425 and the phenyl ring of Tyrosine β349, which clamp the pyrimidinyl groups of both adenine nucleotides (0.8 nm apart) in the D and T conformations (Figure 6–44), are still opposite each other (0.95 nm apart) and ready to clamp down again. The phenyl group of Phenylalanine β422, into the π molecular orbital system of which the exocyclic amido group buries its two hydrogens (Figure 6–44) and which distinguishes adenine from guanine by electron repulsion, is ready to swing outward to perform its function. All these features prepare the site to associate with ADP^{3-}.

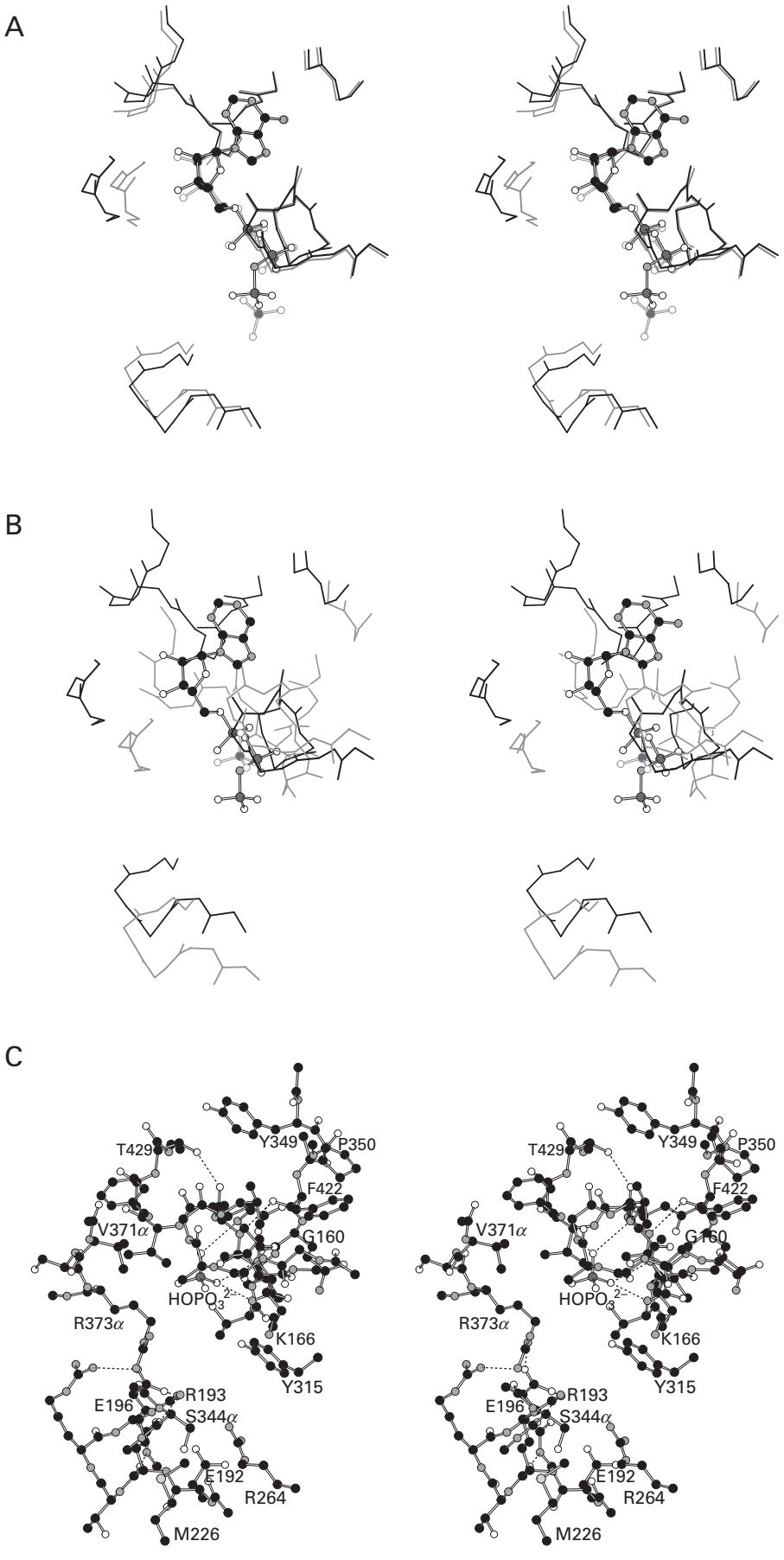
A
B
C
T429
Y349
P350
F422
V371α
G160
HOPO3 2-
R373α
K166
Y315
R193
E196
S344α
E192
R264
M226

Figure 6–47: Stereodrawings[485] of changes in the conformation of one of the active sites in F_1-ATPase upon changes in the quaternary conformation of enzyme. The polypeptide backbones of the segments of polypeptide surrounding the active sites in the crystallographic molecular model of Figure 6–42 are shown as stereo line drawings, and the adenine nucleotides and $HOPO_3^{2-}$ are shown as ball-and-stick stereodrawings in which black atoms are carbons, white atoms are oxygens, small gray atoms are nitrogens, and large dark gray atoms are atoms of phosphorus. (**A**) Superposition of the segments of polypeptide and $MgADP^-$ and $HOPO_3^{2-}$ from the active site in the D conformation (gray lines) upon the same segments of polypeptide and $MgAMPPNP^{2-}$ from the active site in the T conformation (black lines). (**B**) Superposition of the segments of polypeptide and $MgAMPPNP^{2-}$ from the active site in the T conformation (black lines) upon the same segments of polypeptide and the adventitious $HOPO_3^{2-}$ from the active site in the O conformation. (**C**) Active site in the O conformation in the crystallographic molecular model of Figure 6–42 occupied by $HOPO_3^{2-}$, labeled as in Figure 6–44. Again, the majority of the segments are from the β subunit, the numbers of their amino acids are unadorned, and the two segments from the α subunit are designated by adding an α to the end of each number. Two oxygens of $HOPO_3^{2-}$ occupy the cup that had been and will be occupied by one of the nonbridging oxygens of the β-phospho groups of $MgATP^{2-}$ and $MgADP^-$ (Figure 6–44).

In another crystallographic molecular model in which the O conformation is occupied by $HOPO_2S^{2-}$ ($pK_a = 5.4$), in which the hydron is on one of the oxygens,[419] there are hydrogen bonds between one or the other oxygen and Arginine β264, Arginine β193, and Lysine β166 and between sulfur and Arginine β264 and Arginine β193. Each side chain forms hydrogen bonds to the oxygens of $HOPO_3^{2-}$ or the γ-phospho group of $MgATP^{2-}$ in the catalytic D conformation (Figure 6–44A,B). From these facts, it has been concluded that $HOPO_2S^{2-}$ in this molecular model occupies the subsite with which the substrate $HOPO_3^{2-}$ associates in the O conformation.[420]

The **proposal for the synthesis of $MgATP^{2-}$** (Figure 6–45) includes the following sequence of events.[363,394] The reactants $MgADP^-$ and $HOPO_3^{2-}$ associate with an active site in an $\alpha\beta$ heterodimer in the O conformation, and the conformation of that active site changes from the O to the D conformation. On the basis of the crystallographic molecular model of the enzyme from *R. norvegicus* crystallized in the absence of Mg^{2+}, in which ADP^{3-} occupies the active site in the O conformation, it has been proposed that ADP^{3-} can bind to the active site of the β subunit in the O conformation, inducing a partial closing around itself before $HOPO_3^{2-}$ associates with the active site and its conformation changes completely to the D conformation,[369,413] but the arrangement of the side chains holding the $MgADP^-$ in the active site in this complex is somewhat different from that in the D conformation (Figure 6–44). However they came to be there, once Mg^{2+}, ADP^{3-}, and $HOPO_3^{2-}$ are bound to the active site in the O conformation, its conformation changes to the catalytic D conformation and the equilibrium between $MgATP^{2-}$ and a molecule of water and $MgADP^-$ and $HOPO_3^{2-}$ is established. Following establishment of this equilibrium, the active site on the same $\alpha\beta$ heterodimer undergoes its second conformational change into the T conformation at an instant when it happens to be occupied by $MgATP^{2-}$ and the molecule of water rather than by $MgADP^-$ and $HOPO_3^{2-}$. The T conformation protects $MgATP^{2-}$ from hydrolysis. This active site on the same $\alpha\beta$ heterodimer occupied by this stable molecule of $MgATP^{2-}$ then undergoes a third and final change back to the O conformation. The change from the D to the T conformation is undramatic, but the change from the T to the O conformation is dramatic (Figure 6–47). The active site swings open to the solution, and $MgATP^{2-}$, around which there are definitely no longer any catalytic groups, simply dissociates into solution. The abrupt conformational change of the active site in the T conformation, in which $MgATP^{2-}$ is enclosed and protected from catalytic hydrolysis, to the O conformation site, from which $MgATP^{2-}$ readily dissociates, is the key to the synthesis of $MgATP^{2-}$ by H^+-transporting two-sector ATPase.[405]

The reason that each of the three active sites on a molecule of F_1-ATPase passes through these three conformations during the synthesis of $MgATP^{2-}$ is the same reason that there are three conformations in the enzyme at rest: the γ subunit. When the enzyme is not at rest but synthesizing $MgATP^{2-}$, the **γ subunit rotates** clockwise in steps of -120° (Figures 6–45 and 6–46). Because the three conformations of the $\alpha\beta$ heterodimers within the $(\alpha\beta)_3$ ring are created by the asymmetry of the γ subunit, the **conformational changes must proceed in concert** with strict conservation of the global asymmetry (Figures 6–42 and 6–45) as the γ subunit rotates.[365,366] At each step, when one of the $\alpha\beta$ heterodimers changes from the O to the D conformation, its clockwise neighbor is required to change from the T to the O conformation, and its counterclockwise neighbor is required to change from the D to the T conformation. The clockwise rotation of the γ subunit cannot occur until the active site in an $\alpha\beta$ heterodimer changing from the O to the D conformation is occupied by $MgADP^-$ and $HOPO_3^{2-}$ and the active site in an $\alpha\beta$ heterodimer changing from

the D to the T conformation is occupied by $MgATP^{2-}$. The former of these two requirements explains why the incorporation of oxygen-16 from $H_2{}^{16}O$ into the $Mg[\gamma\text{-}{}^{18}O_3P]ATP^{2-}$ formed from $H^{18}OP^{18}O_3{}^{2-}$ as a result of intermediate isotopic exchange while the enzyme is synthesizing $MgATP^{2-}$ increases as the concentration of either $MgADP^-$ or $HOPO_3{}^{2-}$ is decreased.

If this is the mechanism by which F_1-ATPase synthesizes $MgATP^{2-}$, then it must be the case, by **microscopic reversibility**, that the enzyme proceeds through the same sequence of steps in reverse when it is hydrolyzing $MgATP^{2-}$. A molecule of the reactant $MgATP^{2-}$ associates with the active site in an $\alpha\beta$ heterodimer in the O conformation. During the change from the O to the T conformation caused by a counterclockwise rotation of the γsubunit, the active site closes upon the $MgATP^{2-}$ and the molecule of water. Because the key to the synthesis of $MgATP^{2-}$ is the absolute control of this molecule of water, it is engaged in four hydrogen bonds, and at this point, it is too distant to participate in hydrolysis, so the molecule of $MgATP^{2-}$ is at rest. A counterclockwise rotation of the γsubunit causes the conformation of the active site in the same $\alpha\beta$ heterodimer to change to the D conformation, in which $MgATP^{2-}$ and the molecule of water can now equilibrate rapidly with $MgADP^-$ and $HOPO_3{}^{2-}$. At an instant when $MgADP^-$ and $HOPO_3{}^{2-}$ occupy the active site in the D conformation, a counterclockwise rotation of the γsubunit causes the $\alpha\beta$ heterodimer to change from the D to the O conformation, but this can happen only if a molecule of $MgATP^{2-}$ is occupying the active site in the O conformation before the change in conformation occurs. The products of hydrolysis, $MgADP^-$ and $HOPO_3{}^{2-}$, dissociate from the open active site as products. These requirements for occupation, in addition to those for the sequence of conformational changes, follow from microscopic reversibility.

Observations that have been made of hydrolysis of $MgATP^{2-}$ by the enzyme are all consistent with this mechanism. Consequently, those observations are also evidence that it is the mechanism for the synthesis of $MgATP^{2-}$. During hydrolysis of $MgATP^{2-}$, there is an active site on the enzyme in which $MgATP^{2-}$ and a molecule of water and $MgADP^-$ and $HOPO_3{}^{2-}$ reach an equilibrium in favor of the former. The equilibrium persists until a second molecule of $MgATP^{2-}$ associates with the enzyme, after which $MgADP^-$ and $HOPO_3{}^{2-}$ dissociate from the enzyme. The second molecule of $MgATP^{2-}$ terminates the equilibration by associating at the active site in the $(\alpha\beta)_3$ trimer that is in the O conformation because the γsubunit cannot rotate until that site is occupied by a molecule of $MgATP^{2-}$. When the γsubunit is then able to rotate, the active site in the D conformation changes to the O conformation and the $MgADP^-$ and $HOPO_3{}^{2-}$ dissociate while the conformation of the active site with which $MgATP^{2-}$ has just associated changes to the T conformation. The active site previously in the T conformation, which must have been occupied by $MgATP^{2-}$, just as the three uninvolved sites in the three α subunits are always occupied by $MgATP^{2-}$, shifts in concert to the D conformation.

The **requirements for occupancy of the active sites before rotation can occur** during the synthesis of $MgATP^{2-}$ by this proposed mechanism are obvious. If the transformation from the O to the D conformation could occur when the active site in the O conformation is occupied by $MgATP^{2-}$, when the active site is occupied by only $MgADP^-$ or only $HOPO_3{}^{2-}$, or when the active site is empty, then no synthesis of $MgATP^{2-}$ at that particular active site would occur during that cycle. If the transformation from the D to the T conformation could occur at an instant when the active site is occupied with $MgADP^-$ and $HOPO_3{}^{2-}$ rather than $MgATP^{2-}$, then no synthesis of $MgATP^{2-}$ at that site would occur during that cycle. Such mistakes are made, but the more that are made, the less efficient becomes the synthesis of $MgATP^{2-}$, the normal purpose of the enzyme. Natural selection must have minimized the frequency of those mistakes. The requirements for occupancy during hydrolysis of $MgATP^{2-}$ are simply the result of microscopic reversibility. An obvious structural explanation for the requirement that the active site in the D conformation must be occupied by $MgATP^{2-}$ before the conformational change to the T conformation can occur during the synthesis of $MgATP^{2-}$ would be that it should be impossible to pull $HOPO_3{}^{2-}$ by its apical oxygen 0.06 nm away from its location in the D conformation to the location it would have to occupy in the T conformation to retain the three hydrogen bonds to this apical oxygen while a molecule of water could easily be pulled away.

There are two ways to explain the sequence of global conformational changes coincident with the rotation of the γsubunit during the synthesis of $MgATP^{2-}$.

The first explanation is an **equilibrium explanation**. The sequences of amino acids for the α and β subunits together encode all three conformations, O, D, and T, which are able to equilibrate with each other at the level of the conformation of each $\alpha\beta$ heterodimer. When the global conformation of

the $(\alpha\beta)_3$ ring in the O,D,T global conformation is occupied in turn by the proper substrates at its three active sites and then assumes the D,T,O global conformation as a result of these more local equilibrations, the γ subunit is able to rotate in the clockwise direction and sterically stabilize this D,T,O conformation. This explanation is equivalent to the explanation given for the ability of allosteric ligands to change the conformation of an allosterically controlled and cooperative enzyme such as aspartate carbamoyltransferase. The problem is that the three $\alpha\beta$ heterodimers together have to change their individual conformations coincident with the required local conformational changes in each of them, and all these conformational changes have to occur in concert before the O,D,T global conformation becomes the D,T,O global conformation that permits rotation of the γ subunit. Another way to view this explanation, however, is to consider the three conformations represented schematically in Figure 6–45 to be three global conformations that the $(\alpha\beta)_3$ heterohexameric ring can assume and that are in equilibrium with each other. When the global conformation of the moment changes to one that is adjacent in the cycle represented in the figure in either direction, synthesis of $MgATP^{2-}$ or hydrolysis of $MgATP^{2-}$, the shaft of the γ subunit rotates clockwise or counterclockwise, respectively, to fit this new global conformation, temporarily locking that conformation in place.

The second explanation is a **mechanical explanation**. The γ subunit is a camshaft on which there are two principal cams (Figure 6–43), the bulge along its length formed by the bend of the longer of the two α helices and the overhang at the top that is formed from the globular domain of the γ subunit as it emerges from its seat and perhaps a portion of the ε subunit, which rotates with the γ subunit.[421,422] As the camshaft turns, it sterically distorts the conformation of each $\alpha\beta$ heterodimer in turn into the O, the D, and then the T conformation. This explanation appeals to an observer who is familiar with machines, and the metaphor of a machine will become even more compelling as the discussion proceeds. The problem is that, as has already been noted, proteins of the size of an $\alpha\beta$ heterodimer are hard, not soft, and cannot be distorted readily.

As usual, the two explanations are not mutually exclusive. In the first case, it is reasonable that steric forces engendered by a powered rotation of the γ subunit dramatically hasten and bias the equilibration of the different permitted global conformations. In the second case, the distortion produced by the rotating γ subunit must produce only conformations that are allowed by the sequences of amino acids for the α and β subunits and hence can be achieved by them in the absence of steric forces applied by the γ subunit. The steric forces simply stabilize one of these encoded conformations at each $\alpha\beta$ heterodimer.

There are experimental observations demonstrating that the γ subunit does rotate in its seat as $MgATP^{2-}$ is hydrolyzed. That rotation of the γ subunit of some kind must occur was demonstrated by forming an $(\alpha\beta'_{rad})_2\alpha\beta'\gamma\delta\varepsilon$ hybrid of F_1-ATPase from *E. coli* with β' subunits in which Aspartate β380, which is immediately adjacent in the crystallographic molecular model to Cysteine γ87 in the γ subunit, was mutated to cysteine and in which only two of these mutated β subunits were radioactive (rad). A cystine was formed between a nonradioactive, mutant β' subunit and the γ subunit, and this crosslinked β'–γ was reconstituted with three α subunits, two radioactive, mutant β'_{rad} subunits, a δ subunit, and an ε subunit. This complex was inactive in hydrolysis of $MgATP^{2-}$ until the cystine was reduced to two cysteines. Reduction of the complex allowed it to hydrolyze $MgATP^{2-}$, after which the cystines were re-formed. Some of the γ subunits, which initially were crosslinked only to nonradioactive β' subunits, were found now to be crosslinked to radioactive β'_{rad} subunits.[423]

The γ subunit in F_1-ATPase from *S. oleracea* was modified exclusively at Cysteine 322 with eosin-5-maleimide, and this modified F_1-ATPase was immobilized on beads of crosslinked agarose. It was found that, immediately after photobleaching of the eosin with an intense flash of polarized light, the absorption of bound eosin was anisotropic. If $MgATP^{2-}$ was present, the anisotropy decayed ($k = 7\ s^{-1}$ at 37° C) as the γ subunit rotated, but no decay of anisotropy was observed when $MgAMPPNP^{2-}$ was used[424] instead of $MgATP^{2-}$.

The most convincing verification, however, of rotation of the γ subunit within its seat in the $(\alpha\beta)_3$ ring during hydrolysis of $MgATP^{2-}$ by F_1-ATPase has been **watching it rotate**.[425,426] For the explanation of the synthesis of $MgATP^{2-}$ to be correct, when F_1-ATPase is hydrolyzing $MgATP^{2-}$, the upper right subunit in Figure 6–42 converts in turn from the O to the T and then to the D conformation. These conformational changes require the γ subunit to rotate in

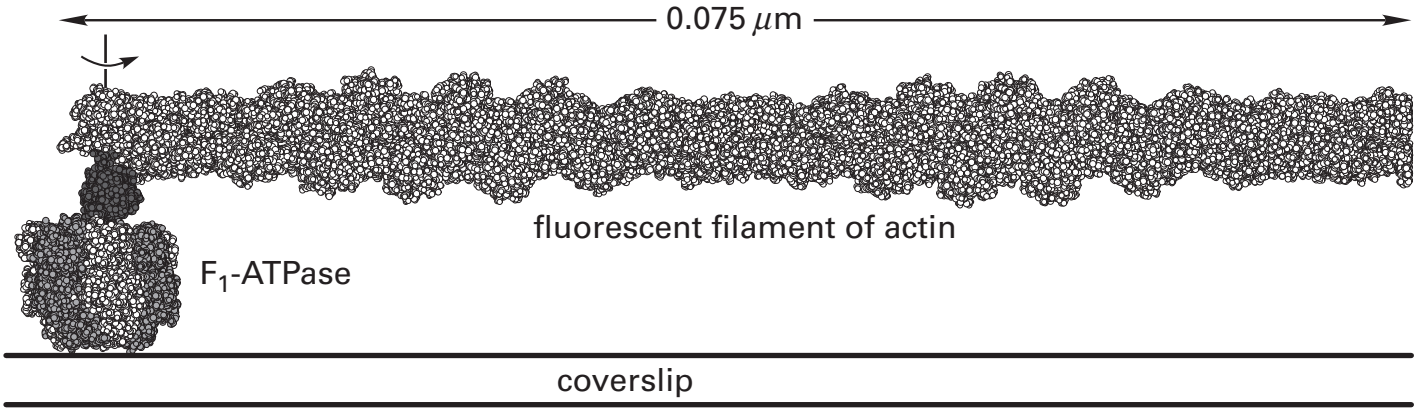

Figure 6–48: Drawing[485] of a filament of actin bound to the γsubunit of F_1-ATPase. The portion of the crystallographic molecular model of F_1-ATPase containing the complete polypeptides of the three αsubunits, the three βsubunits, and the γsubunit (Figure 6–42) is presented as a space-filling model (γsubunit in dark gray, αsubunits in light gray, and βsubunits in white). The molecular model of a filament of actin from *O. cuniculus* was constructed from a map of electron scattering density derived from 63,000 images in electron micrographs of filaments of actin frozen in amorphous ice. Crystallographic molecular models of actin monomer were then inserted into this map of electron scattering density to obtain a molecular model of the helical filament. This molecular model, in space-filling representation and at the same scale, was placed so that one end impinged upon the γsubunit of bovine F_1-ATPase (Figure 6–42). The point of attachment was arbitrarily chosen to be at one end of the filament because most of the rotating fluorescent filaments of actin had their rotation axis at one end of the filament. The filament of actin in the drawing was truncated at the other end because the actual filaments observed rotating were about 1 μm long, about 15 times longer than the segment drawn.

a counterclockwise direction when viewed on the side of the $(\alpha\beta)_3$ ring from which it protrudes (Figure 6–45). The $(\alpha\beta)_3$ ring of the $(\alpha\beta)_3\gamma F_1$-ATPase subcomplex from *Bacillus* sp. PS3 was firmly affixed to a glass coverslip through its surface opposite that from which the γsubunit protrudes. A filament of fluorescent actin was then attached to the γsubunit protruding from the affixed $(\alpha\beta)_3$ ring (Figure 6–48). Because fluorescent filaments of actin are large enough to be observed in a fluorescence microscope, individual filaments of the fluorescent actin could be observed directly. When $MgATP^{2-}$ was added, many of the filaments, which were being viewed from below the coverslip and hence from the side opposite that from which the γsubunit protrudes, rotated in a clockwise direction, as predicted. When the filament of actin was 1 μm long (13 times longer than the portion of the filament of actin depicted in Figure 6–48), rotations as rapid as 5 s^{-1} were observed.

As one might expect from the dimensions (Figure 6–48), when the actin filament turns through the solution while $MgATP^{2-}$ is being hydrolyzed, it encounters significant **frictional resistance to its rotational motion**. At a saturating concentration of 2 mM $MgATP^{2-}$, the rotational rate is a function of the length of the actin filament. The longer the filament, the slower is the rotation. From this relation, the torque exerted on the actin filament by the γsubunit within the $(\alpha\beta)_3$ ring of F_1-ATPase from *Bacillus* sp. PS3[426] or the γsubunit within the $(\alpha\beta)_3$ ring of F_1-ATPase from *E. coli*[427] can be estimated. The estimate of the **torque generated** is 50 pN nm (5×10^{-20} J rad^{-1}) when [$MgATP^{2-}$] is 2 mM, [$MgADP^{-}$] is 10 μM, and [phosphate] is 0.1 mM at pH 7.0. If a complete rotation (2π rad) requires hydrolysis of three molecules of $MgATP^{2-}$, the free energy of hydrolysis at these concentrations of $MgATP^{2-}$, $MgADP^{-}$, and phosphate should be able to generate a torque of 5.4×10^{-20} J rad^{-1}, which is the torque observed. An even more direct measurement of the torque generated on a magnetic bead attached to the γsubunit within the $(\alpha\beta)_3$ ring of F_1-ATPase from *Bacillus* sp. PS3 in an applied magnetic field as a function of the standard free energy of hydrolysis of $MgATP^{2-}$ showed the same equivalence[428] over a range of free energies of hydrolysis from −70 to −110 kJ mol^{-1}. This **equivalence between generated torque and standard free energy of hydrolysis** supports the conclusion that hydrolysis of the $MgATP^{2-}$ at three sites for every revolution is driving the rotation of the filament of actin or the magnetic bead.

That these measurements are consistent with the conclusion that the torque generated during this step is roughly equivalent to the standard free energy of hydrolysis of the molecule of $MgATP^{2-}$ suggests that rotation must be tightly coupled to hydrolysis. It necessarily follows, from microscopic

reversibility, that if a clockwise torque is applied to the γsubunit that is equal to or greater than the counterclockwise torque generated during its hydrolysis, then molecules of $MgATP^{2-}$ must be synthesized from molecules of $MgADP^{-}$ and $HOPO_3^{2-}$. This enforced synthesis has been observed. When magnetic beads are attached to γsubunits of F_1-ATPase from *Bacillus* sp. PS3 such that they are tilted off the central axis of the $(\alpha\beta)_3\gamma$subcomplex, and the subcomplex is attached to a glass slide, the bead can be forced to **drive the rotation of the γsubunit clockwise** by a rotating magnetic field. When the γsubunit is forced to rotate clockwise* within the $(\alpha\beta)_3$ ring, $MgATP^{2-}$ is synthesized[429,430] from $MgADP^{-}$ and $HOPO_3^{2-}$.

At low enough concentrations (2 μM) of $MgATP^{2-}$, so that the rate of rotation of the filament of actin is slow enough that the generation of torque does not limit the rate, its rotation is resolved into **discrete steps of +120°**.[426] If a spherical 40 nm bead of colloidal gold is used rather than a fluorescent filament of actin to visualize the rotation, then the viscous drag on the rotating γsubunit, and hence the generation of torque, is decreased dramatically. The bead is attached to the γsubunit of the $(\alpha\beta)_3\gamma$complex of F_1-ATPase from *Bacillus* sp. PS3 off-axis so that the oscillation as the bead rotates can be observed. The bead rotates when a saturating concentration of $MgATP^{2-}$ (2 mM) is present, and its rotation proceeds in discrete +120° steps (Figure 6–49),[431] as expected if the rotation is the result of discrete global conformational changes of the $(\alpha\beta)_3$ ring (Figure 6–45). Furthermore, the rate of rotation under these conditions of low torque is equal to one-third the rate of hydrolysis of $MgATP^{2-}$ in a range of concentrations of $MgATP^{2-}$ that encompasses rates over a span of 1000.

When one of the β subunits in the $(\alpha\beta)_3$ ring is replaced with a mutant β' subunit, the active site of which binds $MgATP^{2-}$ slowly, association of $MgATP^{2-}$ with just this one active site in the open conformation becomes the rate-limiting step in the overall hydrolysis of $MgATP^{2-}$,[432] and the rotation of beads

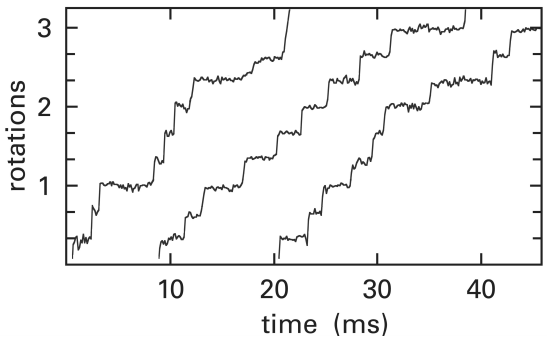

Figure 6–49: Rotation of the γsubunit of F_1-ATPase[431] in steps of +120°. A mutant of the $(\alpha\beta)_3\gamma$complex of F_1-ATPase from *Bacillus* PS3 in which Cysteine 193 in the α subunit had been mutated to serine and Serine 107 and Isoleucine 210 in the γsubunit had both been mutated to cysteines was prepared by site-directed mutation. These two cysteines introduced into the complex were then modified with 6-*N*′-[2-(*N*-maleimido)-ethyl]-*N*-piperazinylamidohexyl-D-biotinamide to attach biotinyl groups covalently to the protein. The protein was then mixed with streptavidin, a homotetrameric protein (4 × 183 aa) from *Streptomyces avidinii* with four symmetrically arranged sites for the binding of biotin (k_{diss} = 0.009 h^{-1}). The protein to which streptavidin had bound was then mixed with spheres of colloidal gold (diameter 40 nm) coated with bovine serum albumin that had been modified with with sulfosuccinimidyl-*N*-[*N*′-(D-biotinyl)-6-aminohexanoyl]-6′-aminohexanoate. The open sites on the streptavidin bound to the mutant F_1-ATPase associated with biotinyl groups on the serum albumin adsorbed to the beads, and beads became attached to γsubunits of F_1-ATPase. Molecules of F_1-ATPase to which beads were attached were adsorbed to a glass coverslip at the surface opposite that from which the γsubunit protrudes (Figures 6–42 and 6–48). When a solution containing 2 mM $MgATP^{2-}$ was introduced, some of the beads attached to the coverslip through molecules of F_1-ATPase were observed to rotate. These rotating beads ended up attached to the γsubunit with their centers displaced about 10 nm from the axis of rotation of the γsubunit so that the spheres themselves could be seen to rotate around that axis. The rotation was observed with a high-speed digital motion picture camera at 2 frames ms^{-1}. For analysis, a rotating bead in the field was chosen and placed within the transparent circle of a digital mask, and an algorithm was used to follow the rotation of that bead and convert each image into a rotational position for the centroid of the bead relative to the axis of rotation. Rotational position is plotted continuously in units of full rotation as a function of time. It can be seen that the rotation is discontinuous and occurs in steps of a third of a rotation (+120°). Reprinted with permission from reference 431. Copyright 2001 SpringerNature. https://doi.org/10.1038/35073513

of colloidal gold attached to γsubunits of the $(\alpha\beta)_2\alpha\beta'\gamma$subcomplex occurs in discrete steps of +360° rather than steps of +120°. When the active site of the unmutated $\alpha\beta$ heterodimer counterclockwise to the mutant $\alpha\beta'$ heterodimer is in the D conformation, occupied by the equilibrating mixture of $MgATP^{2-}$ and $MgADP^{-}$ and $HOPO_3^{2-}$, the rotation of +120° cannot occur until the reactant $MgATP^{2-}$ binds to the active site of the mutant $\alpha\beta'$ heterodimer. Association of $MgATP^{2-}$ with the

*As previouly noted, the accepted view of F_1-ATPase for determining clockwise and counterclockwise rotation of the γsubunit is the view of the surface from which the γsubunit protrudes (Figure 6–42). From here on, angles of rotation will be given the signs appropriate for rotation when viewed from this side of F_1-ATPase. From this side, during synthesis of $MgATP^{2-}$, the rotation of the γsubunit is clockwise; and during hydrolysis of $MgATP^{2-}$, its rotation is counterclockwise. By accepted convention (sinister, righteous), clockwise or left-handed rotation is given a negative sign, and counterclockwise or right-handed rotation is given a positive sign.

mutant is slow. As soon as it associates, the first rotation of +120° and its accompanying conformational changes occur, followed by two rapid unresolved rotations of +120° as $MgATP^{2-}$ binds rapidly, in succession, to the unmutated $\alpha\beta$ heterodimers consecutively during the rapid hydrolysis of two molecules of $MgATP^{2-}$.

The individual steps of +120° during hydrolysis of $MgATP^{2-}$ can be **resolved into two steps**. Rotation of native, unmutated $(\alpha\beta)_3\gamma$ subcomplex of F_1-ATPase from *Bacillus* sp. PS3, while hydrolyzing $MgATP^{2-}$, was followed as a function of the concentration of $MgATP^{2-}$. At 2 mM $MgATP^{2-}$, the rotation occurs in discrete steps of +120°, but at 20 μM $MgATP^{2-}$, discrete **steps of +80° and +40°** could be observed.[431] It has been concluded that the reason for these intermediate steps is that there are two global conformations through which F_1-ATPase passes while hydrolyzing or, by microscopic reversibility, while synthesizing each molecule of $MgATP^{2-}$. One conformation precedes the +80° step, and the other precedes the +40° step when the enzyme is hydrolyzing $MgATP^{2-}$. The requirements for these two conformational changes to occur have been examined.

When F_1-ATPase from *Bacillus* sp. PS3 is hydrolyzing $MgATP^{2-}$ in the intermediate range of concentrations at which the rotation takes alternating steps of +40° and +80°, the dwell time between a +40° step and an +80° step increases as the concentration of $MgATP^{2-}$ is decreased, while the dwell time between an +80° step and a +40° step does not.[431] This result suggests that the global conformation of the $(\alpha\beta)_3$ ring that precedes a +80° step and follows a +40° step cannot undergo the next conformational change that is to occur during the +80° step until $MgATP^{2-}$, the reactant for hydrolysis, associates with one of the active sites. This global conformation, during hydrolysis of $MgATP^{2-}$, is **waiting for the reactant $MgATP^{2-}$ to associate**.

When F_1-ATPase from *Bacillus* sp. PS3 is hydrolyzing magnesium adenosine 5′-[γ-thio]triphosphate, a slow reactant, or when a mutant of the enzyme in which the glutamic acid homologous to Glutamic Acid β192 in bovine F_1-ATPase has been mutated to aspartic acid is hydrolyzing $MgATP^{2-}$, the steady-state rate of hydrolysis is decreased significantly relative to the rate of hydrolysis of unmodified $MgATP^{2-}$ by the native enzyme. In each instance, the dwell time between the +80° step and the +40° step increases.[433] This result suggests that the global conformation of the $(\alpha\beta)_3$ ring that precedes a +40° step and follows a +80° step cannot undergo the next conformational change that is to occur during the +40° step **until the equilibrium between $MgATP^{2-}$ and H_2O and $MgADP^-$ and $HOPO_3^{2-}$ has been established**.

At 2 mM $MgATP^{2-}$ the rotation occurs in discrete steps of +120°; when the concentration of $MgATP^{2-}$ is decreased to 20 μM, the rotation occurs in steps of +80° and +40°; and when the concentration of $MgATP^{2-}$ is decreased further to 2 μM, the rotation again occurs in discrete steps of +120°. It follows from these observations that as the concentration of $MgATP^{2-}$ is decreased from 2 mM to 2 μM, a **change in rate-limiting step** occurs. At 2 μM $MgATP^{2-}$, the rate-limiting step is association of $MgATP^{2-}$ while at 2 mM $MgATP^{2-}$, the rate-limiting step is the establishment of the equilibrium between $MgATP^{2-}$ and H_2O and $MgADP^-$ and $HOPO_3^{2-}$. As the concentration of $MgATP^{2-}$ is decreased from 20 μM to 2 μM, the rate-limiting step becomes association of $MgATP^{2-}$ with an active site in an $\alpha\beta$ heterodimer, and the +40° step becomes rapid relative to the slow, rate-limiting +80° step. As a result, the +40° step cannot be resolved, and only +120° steps are observed. When the concentration of $MgATP^{2-}$ is increased from 20 μM to 2 mM, association of $MgATP^{2-}$ with an active site in an $\alpha\beta$ heterodimer increases, and the +80° step becomes rapid relative to the slow, rate-limiting +40° step. As a result, the +80° step cannot be resolved and only +120° steps are observed.

Measurements have been made of the orientation of a fluorophore rigidly and covalently attached to two neighboring cysteines introduced by site-directed mutation into each β subunit of F_1-ATPase from *Bacillus* sp. PS3.[434] Molecular distances have been estimated from fluorescence resonance energy transfer[435] among three fluorescent sulfoindocyanine dyes attached to three cysteines that had been inserted into the three β subunits of F_1-ATPase from *Bacillus* sp. PS3 in place of Leucines 398 by site-directed mutation.[436] These observations are consistent with the conclusion that, when $MgATP^{2-}$ is being hydrolyzed, **the conformation that precedes the +40° step is the conformation usually observed in crystallographic molecular models** (Figures 6–42, 6–44, and 6–46). In addition, fluorescence resonance energy transfer between a fluorophore attached to Cysteine γ5 and a fluorophore attached to Cysteine β3 is consistent with the orientation of the γ subunit in the conformation preceding the +80° step during hydrolysis of $MgATP^{2-}$, which proceeds with counterclockwise rotation of the γ subunit, being +40° from its rotational orientation usually observed in crystallographic molecular models.[437] This observation is

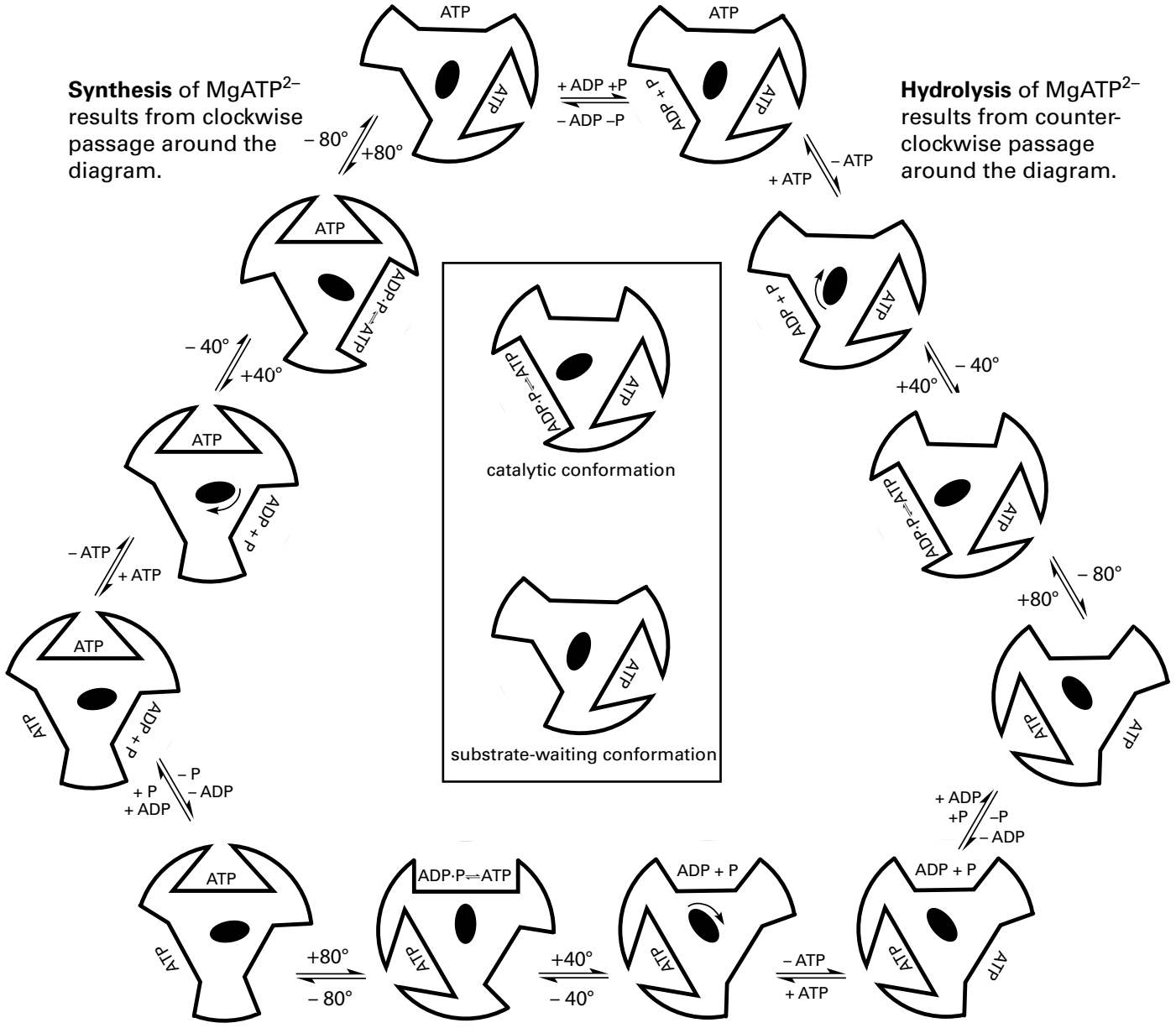

Figure 6–50: Revision of the diagram of Figure 6–45 to incorporate the properties of the intermediate conformation that, during hydrolysis of $MgATP^{2-}$, follows a discontinuous rotation of –80° and precedes a discontinuous rotation of –40° to complete a step of –120° (Figure 6–49). The diagramatic representations for each of the three conformations of the $\alpha\beta$ heterodimer in the two different global conformations are defined within the box in the center. In this diagram, the two intermediate rotations comprise the sides of the equilateral triangle with the catalytic global conformation observed in the crystallographic molecular model of Figure 6–42 in the center of each side. The quaternary conformations at the vertices are the intermediate conformations, the ATP-waiting conformations, from which the substrate $MgATP^{2-}$ dissociates in the direction of synthesis and associates in the direction of hydrolysis. The points in the sequence at which $MgADP^-$ and $HOPO_3^{2-}$ associate or dissociate, respectively, are not clear, so in the diagram, they are shown associating during the rotation of –80°, a choice for which there is some evidence.

consistent with the conclusion that **the conformation of the $(\alpha\beta)_3$ ring preceding the +80° step is different** from its crystallographic conformation.

All these observations suggest that there are two different global conformations of the $(\alpha\beta)_3$ ring in F_1-ATPase that are adopted while the enzyme is hydrolyzing $MgATP^{2-}$, or in reverse synthesizing $MgATP^{2-}$, rather than just the conformation observed crystallographically. These two conformations (Figure 6–50) are the catalytic conformation and the subtrate-waiting conformation. The crystallograph-

ically observed global conformation is the **catalytic global conformation**, the one preceding the counterclockwise step of +40° during hydrolysis of $MgATP^{2-}$**.** In this global conformation, a molecule of the reactant $MgATP^{2-}$ is protected within the active site of the $\alpha\beta$ heterodimer in the T conformation; the reactants, $MgATP^{2-}$ and the molecule of water, and the products, $MgADP^{-}$ and $HOPO_3^{2-}$, are coming to equilibrium within the active site of the $\alpha\beta$ heterodimer in the D conformation; and all the explanations of these two conformations in these two different β subunits drawn from the crystallographic molecular models are still valid. The second conformation, which results from the +40° rotation and precedes the +80° rotation during hydrolysis of $MgATP^{2-}$, is the **substrate-waiting global conformation**. The substrate-waiting global conformation is also intrinsically asymmetric, with asymmetry determined again by the γ subunit. In the substrate-waiting global conformation, in the direction of hydrolysis, one of the active sites in the $\alpha\beta$ heterodimer is open to the solution and waiting for association of $MgATP^{2-}$.

During hydrolysis, the catalytic global conformation is in a **catalytic dwell** until the reactants, $MgATP^{2-}$ and the molecule of water, and the products, $MgADP^{-}$ and $HOPO_3^{2-}$, reach equilibrium or at least until an instant in which the active site in the D conformation is occupied by the products of hydrolysis, $MgADP^{-}$ and $HOPO_3^{2-}$, at which point the counterclockwise rotation of +40° occurs. If these two conformations alternate while F_1-ATPase is hydrolyzing $MgATP^{2-}$, then they must also alternate while it is synthesizing $MgATP^{2-}$. If the rotation of +40° during hydrolysis is required to take place only when $MgADP^{-}$ and $HOPO_3^{2-}$ are occupying the $\alpha\beta$ heterodimer in the D conformation—so that they end up as products ready to dissociate from the same $\alpha\beta$ heterodimer in the open conformation produced by the rotation—then it follows, by microscopic reversibility, that the rotation of –40° during synthesis is required to take place only when $MgADP^{-}$ and $HOPO_3^{2-}$ are occupying an $\alpha\beta$ heterodimer in the same open conformation. Consequently, in the direction of synthesis, the essential purpose of this $\alpha\beta$ heterodimer in the open conformation within the substrate-waiting global conformation is to wait until the reactants $MgADP^{-}$ and $HOPO_3^{2-}$ associate and occupy their proper places before it converts to the D conformation within the catalytic global conformation.

While the magnitudes of fluorescence resonance energy transfer within the catalytic global conformation are consistent with the conclusion that it is the one observed crystallographically, the magnitudes of fluorescence resonance energy transfer within the substrate-waiting global conformation, which has not been observed crystallographically, provide some information about its structure. One of the active sites in an $\alpha\beta$ heterodimer is in a conformation that is indistinguishable by physical measurements from the T conformation in the crystallographic molecular model, and this active site is assumed to be occupied by a protected molecule of $MgATP^{2-}$. The other two active sites, although distinguishable in their resonance transfer, are about as open as the O conformation in the crystallographic molecular model, but in one of those, the interface between α and β subunits is even more open than in the O conformation.[436]

There is a problem with the original proposal for the synthesis of $MgATP^{2-}$ (Figure 6–45). There are **two essential discriminations** that H^+-transporting two-sector ATPase must make in order to synthesize $MgATP^{2-}$ by a conformational mechanism. First, the global conformation of the enzyme must change only when $MgATP^{2-}$ and the molecule of water are occupying the active site of the $\alpha\beta$ heterodimer in the D conformation in order to withdraw the molecule of water and enclose the $MgATP^{2-}$ in the T conformation. Second, the global conformation of the enzyme must change only when $MgADP^{-}$ and $HOPO_3^{2-}$ are occupying the site of the $\alpha\beta$ heterodimer in a conformation open to the solution to capture these two reactants in the D conformation. At both sites, the circumstances are changing rapidly. In the site in the D conformation, the equilibrium between $MgATP^{2-}$ and the molecule of water and $MgADP^{-}$ and $HOPO_3^{2-}$ is constantly interconverting the participants. Dissociations and associations of $MgADP^{-}$ and $HOPO_3^{2-}$ into and from solution are constantly proceeding at the open site with which they associate. It is unlikely that $MgATP^{2-}$ will be momentarily situated in the active site in the D conformation at the same time that $MgADP^{-}$ and $HOPO_3^{2-}$ will be momentarily situated in the site with which they associate.

The solution that natural selection seems to have chosen to this problem is to have two conformations that alternate with each other as the overall rotation proceeds. In the synthesis of $MgATP^{2-}$, when $MgADP^{-}$ and $HOPO_3^{2-}$ are occupying the open site in the substrate-waiting conformation, the –40° rotation occurs, trapping them in the active site of that same $\alpha\beta$ heterodimer in the D conformation. When the equilibrium between $MgADP^{-}$ and $HOPO_3^{2-}$ and $MgATP^{2-}$ and a molecule of water has

been established and at an instant when $MgATP^{2-}$ is occupying the catalytic site in the D conformation, the –80° rotation occurs, trapping the $MgATP^{2-}$ in the T conformation.

All these conclusions lead to a **revision of the earlier conformational explanation** for the synthesis of $MgATP^{2-}$. This revision (Figure 6–50)[436] attempts to assign the status of each active site and its occupants in each of the two conformations, but the overall strategy[363,394]—associating with only $MgADP^{-}$ and only $HOPO_3^{2-}$, setting them in equilibrium with each other, trapping and protecting the $MgATP^{2-}$ that has been formed before it can be unformed in this equilibrium, and opening to release the $MgATP^{2-}$ that was trapped into solution—has not been revised.

As before, during synthesis of $MgATP^{2-}$, in the catalytic global conformation a molecule of the product $MgATP^{2-}$ is at rest, withdrawn from the molecule of water, and protected within the active site of the $\alpha\beta$ heterodimer in the T conformation. The enzyme is waiting for the equilibrium within the active site of the $\alpha\beta$ heterodimer in the D conformation to be established between the reactants, $MgADP^{-}$ and $HOPO_3^{2-}$, and the products, $MgATP^{2-}$ and the molecule of water, and also waiting in the catalytic dwell for an instant in which it is occupied only by the products, $MgATP^{2-}$ and the molecule of water. In that instant, when only the products are present, the γsubunit rotates –80° to produce the also-asymmetric, substrate-waiting global conformation, in which the $MgATP^{2-}$ that was just formed and selected by the change in conformation is protected in the same $\alpha\beta$ heterodimer in a closed conformation that is indistinguishable by physical measurements from the T conformation within the catalytic global conformation. During hydrolysis of $MgATP^{2-}$, the substrate-waiting global conformation is the one with which the reactant $MgATP^{2-}$ associates. Microscopic reversibility requires that, during the synthesis of $MgATP^{2-}$, the substrate-waiting conformation is the one in which the $MgATP^{2-}$—formed and trapped in the preceding cycle and waiting in the $\alpha\beta$ heterodimer in the preceding T conformation within the catalytic global conformation—has now become untrapped. This $MgATP^{2-}$ finds itself in the same $\alpha\beta$ heterodimer that is now in an open conformation and dissociates.

The only way, however, to have the reactants $MgADP^{-}$ and $HOPO_3^{2-}$ associate with an open active site in the substrate-waiting global conformation and end up in the active site of the $\alpha\beta$ heterodimer in the D conformation within the catalytic global conformation after the rotation of –40° is for them to associate with the other open conformation within the substrate-waiting global conformation (Figure 6–50), not the one from which $MgATP^{2-}$ dissociates. It so happens that this other active site is the one that, preceding the rotation of –40°, was in the O conformation within the catalytic global conformation that is occupied by ADP^{3-} in several crystallographic molecular models. The conformation of the $\alpha\beta$ heterodimer in the O conformation within the catalytic global conformation may change very little upon the –80° rotation.*

There is no reason for association and dissociation of reactants and products in either the direction of synthesis or the direction of hydrolysis to occur in a special order because the two open active sites within the substrate-waiting conformation are on different $\alpha\beta$ heterodimers, and the physical measurements suggest that neither of them is the same as the one in the O conformation within the crytallographic molecular model of the catalytic global conformation. There are measurements of occupation of the active sites by nucleotides in the substrate-waiting conformation in the direction of hydrolysis that use a derivative of $MgATP^{2-}$ to which a fluorescent sulfoindocyanine dye has been covalently attached at the 3′-oxygen.[438] Measurements of fluorescence intensity indicate that this derivative associates with the substrate-waiting conformation when it is already occupied by two other nucleotides. These results imply that, in the direction of hydrolysis, the reactant $MgATP^{2-}$ associates before the product $MgADP^{-}$ dissociates. After association, the substrate-waiting complex has three nucleotides associated with it: the protected $MgATP^{2-}$, the just-bound $MgATP^{2-}$ in the $\alpha\beta$ heterodimer in one open conformation, and the product $MgADP^{-}$ in the $\alpha\beta$ heterodimer in the other open conformation. These observations are consistent with the conclusion that there must be an open site for $MgATP^{2-}$ and an open site for $MgADP^{-}$ in the substrate-waiting conformation. They are also consistent with the possibility of $MgADP^{-}$ associating with the active site of the $\alpha\beta$ heterodimer in the O conformation even before the rotation of –80° occurs. Other measurements, however, of the effects of the product $MgADP^{-}$ on rotation of the γsubunit during hydrolysis of $MgATP^{2-}$ are consistent with the conclusion that $MgADP^{-}$ must dissociate during or just prior to the conformational change between the substrate-waiting and catalytic global conformations.[439] Because of these observations, the order of

*In the drawing, a slight change was introduced in the region with which $HOPO_3^{2-}$ associates, although even that change may be unwarranted.

association and dissociation in Figure 6–50 was chosen even though it is not exclusive.

The maximum rate at which $MgATP^{2-}$ can be synthesized by bovine H^+-transporting two-sector ATPase[440] at 30 °C is 440 s^{-1}, which is the same as the maximum rate at which the enzyme hydrolyzes $MgATP^{2-}$ in the absence of a gradient of hydrons. The equivalence of these rates suggests that, when neither catalysis nor association nor dissociation of reactants is rate-limiting, the rotation of the γ subunit in each direction encounters equivalent barriers.

A molecular model of intact porcine H^+-transporting two-sector ATPase (Figure 6–51)[441] has been constructed from a map of electron-scattering density derived from image reconstruction of electron micrographs of molecules of the intact enzyme frozen in amorphous ice. Alignments of the sequences of amino acids for the known subunits of the porcine enzyme are 83%–99% identical to those of the bovine enzyme and contain no gaps, so the structures of the two intact enzymes must be essentially identical. In the molecular model, the shaft composed of the γ, δ, and ε subunits protruding from the $(\alpha\beta)_3$ ring of F_1-ATPase (Figure 6–42) is attached, through its flat top, to a **cylinder composed of eight c subunits** (Figure 6–52B).[441,442] There is a globular protein, formed from segments of nine of the subunits of the intact enzyme, completely within the membrane on one side of the cylinder of c subunits (Figure 6–52C). A coiled coil of α helices, beginning at the surface of the membrane, connects this globular protein within the membrane to the top of the $(\alpha\beta)_3$ ring of F_1-ATPase (Figure 6–51). The complete structure of H^+-transporting two-sector ATPase is one of the strangest structures of a protein that has been observed.

Each of the eight identical c subunits forming the cylinder is a **hairpin of two α helices**,[443] each one 20 amino acids long, arranged in such a way that one α helix in each c subunit is on the external surface of the cylinder and the other is in the interior of the cylinder. The eight c subunits are arrayed around an eightfold rotational axis of symmetry normal to the plane of the bilayer of phospholipids* forming the inner mitochondrial membrane.[442] There is a single α helix of unknown provenance with an unknown sequence of amino acids on this rotational axis of symmetry that plugs what would otherwise be a hole filled with a chain of molecules of water comprising a hydron wire. The rotational axis of symmetry of the cylinder of c subunits is coaxial with the rotational axis of pseudosymmetry in the center of the $(\alpha\beta)_3$ ring, on which axis sits the asymmetric α-helical doubly coiled coil of the γ subunit (Figures 6–42 and 6–43).

Subunit a of porcine H^+-transporting two-sector ATPase also spans the membrane (Figure 6–52A), and its entire folded polypeptide (226 aa) is within the membrane in the multisubunit globular protein, to the side of the cylinder of c subunits. Subunit a consists of seven, mostly hydrophobic, α helices of different lengths.[444] **Subunit a is flush against the cylinder of eight c subunits**, and two of its α helices come in intimate contact with four of the separate exterior α helices of four of the c subunits. The longest α helix, the fifth one in subunit a, even curves to fit flush against the cylinder (Figure 6–52B).[445-448]

The net **clockwise rotation of the cylinder of c subunits** past subunit a drives the rotation of the shaft of the γ subunit within the $(\alpha\beta)_3$ ring in F_1-ATPase during the synthesis of $MgATP^{2-}$. The $(\alpha\beta)_3$ ring of F_1-ATPase in turn is rigidly connected to subunit a by the coiled coil of α helices to prevent it from rotating relative to subunit a. This rotation of the cylinder of c subunits in concert with rotation of the γ subunit of F_1-ATPase has been directly observed[449-455] when intact H^+-transporting two-sector ATPase in a membrane is hydrolyzing $MgATP^{2-}$.

There are mutants of H^+-transporting two-sector ATPase in which a cystine has been introduced, crosslinking a c subunit to a segment of polypeptide in the globular protein within the membrane adjacent to the cylinder of c subunits (Figure 6–52C). These mutant enzymes are unable to transport hydrons into vesicles of membrane in which they had been incorporated when $MgATP^{2-}$ was added to the outside, but they are able to do so at the same rate as unmutated enzyme when the cystine is eliminated by thiol–disulfide exchange with 1,4-bis(sulfanyl)butane-2,3-diol.[456] This observation requires that the cylinder of c subunits rotate relative to the globular protein.

*Unlike a plasma membrane, which contains a significant concentration of cholesterol, the bilayer of the inner mitochondrial membrane is formed almost completely from phospholipids and also contains cardiolipin, a phospholipid unique to mitochondria.

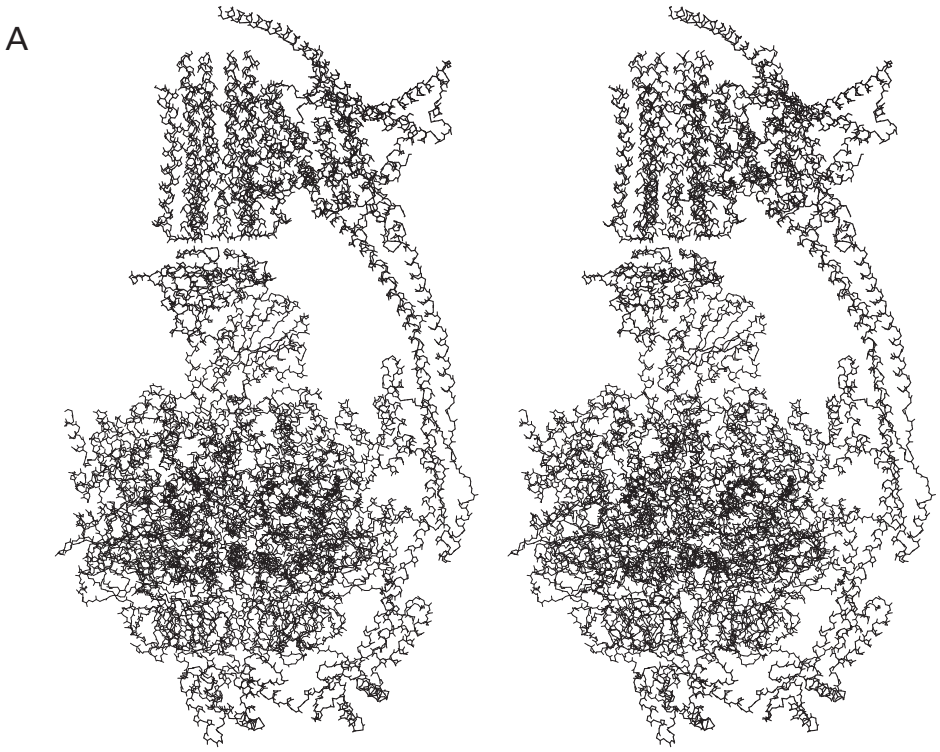
A

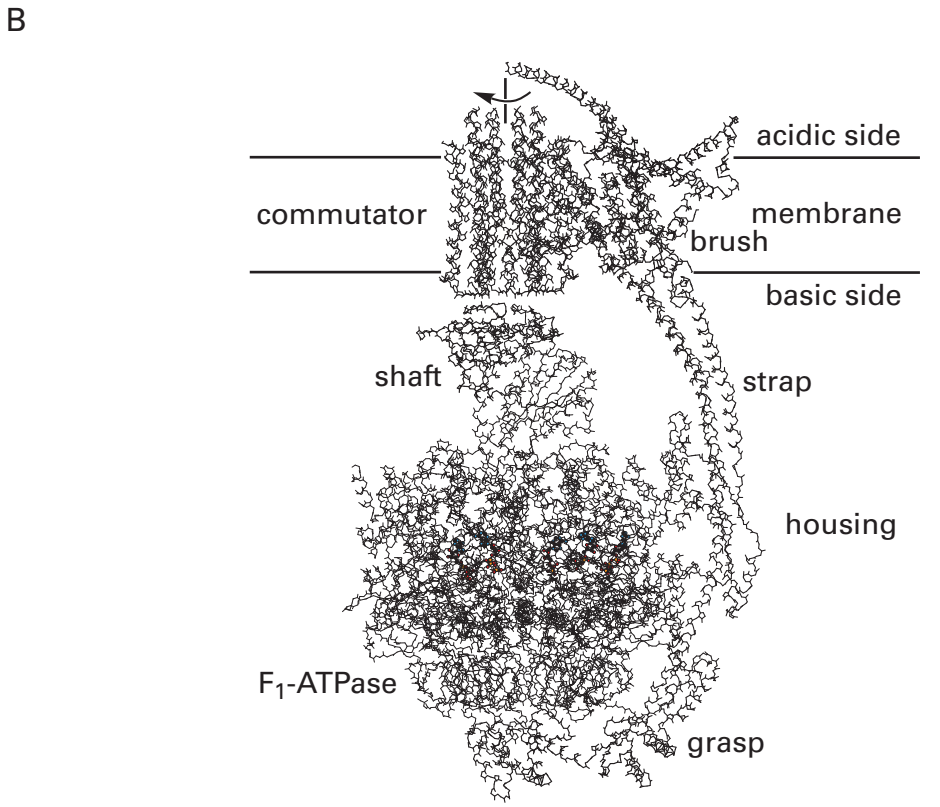
B
acidic side
commutator
membrane
brush
basic side
shaft
strap
housing
F1-ATPase
grasp

Figure 6–51: Stereodrawing[485] of a molecular model of porcine H^+-transporting two-sector ATPase from a reconstruction of images in electron micrographs.[441] Mitochondria were obtained from a homogenate of fresh porcine hearts by differential centrifugation. These mitochondria were suspended in 75 mM sorbitol, 75 mM sucrose, 20 mM KCl, 5 mM $MgCl_2$, and 10 mM 2-[4-(2-hydroxyethyl)piperazin-1-yl]ethanesulfonate at pH 7.5, and a mass of the detergent digitonin equal to 4 times the mass of the protein in the suspension was added to dissolve the mitochondria. Undissolved material was removed by centrifugation. H^+-Transporting two-sector ATPase was purified by centrifugation on a gradient of 0.4–2.0 M sucrose in a buffer containing 0.1% digitonin. Its location on the gradient was determined by electrophoresis on gels of poly(acrylamide) cast in a solution of dodecyl sulfate. The fractions collected from the gradient were concentrated and further purified by molecular-exclusion chromatography, again in a buffer containing 0.1% digitonin. Samples of an aqueous solution containing the purified enzyme were applied to grids for electron microscopy, and the grids were rapidly frozen to turn the thin film of solution into amorphous ice. High-resolution images of about 350,000 molecules of a tetrameric complex of H^+-transporting two-sector ATPase were chosen for further analysis, during which the most informative 114,103 particles were selected for the final reconstruction. The rotational orientation of each tetrameric complex was determined algorithmically, and from these assigned orientations and the individual images to which they were assigned, a three-dimensional map of electron-scattering density was computed to a nominal resolution of 0.44 nm. A crystallographic molecular model of bovine F_1-ATPase was inserted into the map of electron scattering density, and with molecular models of H^+-transporting two-sector ATPase from other species as guides, molecular models with sequences of amino acids for the polypeptides of known subunits in the porcine F_o sector were inserted into the map. Electron densities from several segments of polypeptide of unknown provenance that were left were filled with models of polypeptide backbone without side chains. The final model was then submitted to refinement. (**A**) Stereo line drawing of just the polypeptide backbones of the known subunits of the enzyme as well as the unknown segments in the final refined molecular model of porcine H^+-transporting two-sector ATPase. The $(\alpha\beta)_3\gamma$ portion of F_1-ATPase is drawn with thinner lines, and all the other polypeptide backbones, including the δ and ε subunits of F_1-ATPase, are drawn with thicker lines. The three noncatalytic sites on the $(\alpha\beta)_3$ heterohexamer are occupied by the usual molecules of $MgATP^{2-}$. The active sites in the D and T conformations are occupied by ADP^{3-}, which was included in the solution in which the enzyme was suspended when added to the grid. These five nucleotides are drawn in ball-and-stick format. Again, black atoms are carbons, white atoms are oxygens, small gray atoms are nitrogens, and large dark gray atoms are atoms of phosphorus. (**B**) Cellular orientation of H^+-transporting two-sector ATPase and its position in the bilayer. The approximate location of the bilayer of phospholipids is indicated in a line drawing of the polypeptide backbones of the final molecular model, and the various parts of H^+-transporting two-sector ATPase are labeled as if it were an appliance for making $MgATP^{2-}$, driven by the shaft of a motor.

Figure 6–52: Stereodrawings[485] of portions of the complete molecular model of porcine H^+-transporting two-sector ATPase[441] drawn in Figure 6–51. (**A**) Stereo line drawing, viewed from within the plane of the membrane. The complete polypeptide backbones in the cylinder of the eight α-helical hairpins of the eight c subunits are drawn with thin lines. The lone α helix, of unknown provenance with an unknown sequence of amino acids, in the center of the cylinder and the complete polypeptide backbone of subunit a (to the right in the drawing) are drawn with thick lines. (**B**) Stereo line drawing, viewed from the positive, acidic side of the membrane. Participants and designations are the same as in Panel A but viewed from the upper side of the drawing in Panel A. (**C**) Stereo line drawing from within the plane of the membrane and including additional segments of polypeptide. The complete polypeptide backbones in the cylinder of the eight α-helical hairpins of the eight c subunits are drawn with thin lines. The lone α helix in its center and the complete polypeptide backbones from subunit a, subunit f, and subunit DAPIT; those segments of the polypeptides of subunit B1, subunit d, and protein 8 that are in the membrane; and the complete or partial polypeptide backbones of three unknown polypeptides observed in the map of electron scattering density are drawn with thick lines (to the right in the drawing). All these latter segments of polypeptide are within the membrane and form a compact globular protein.

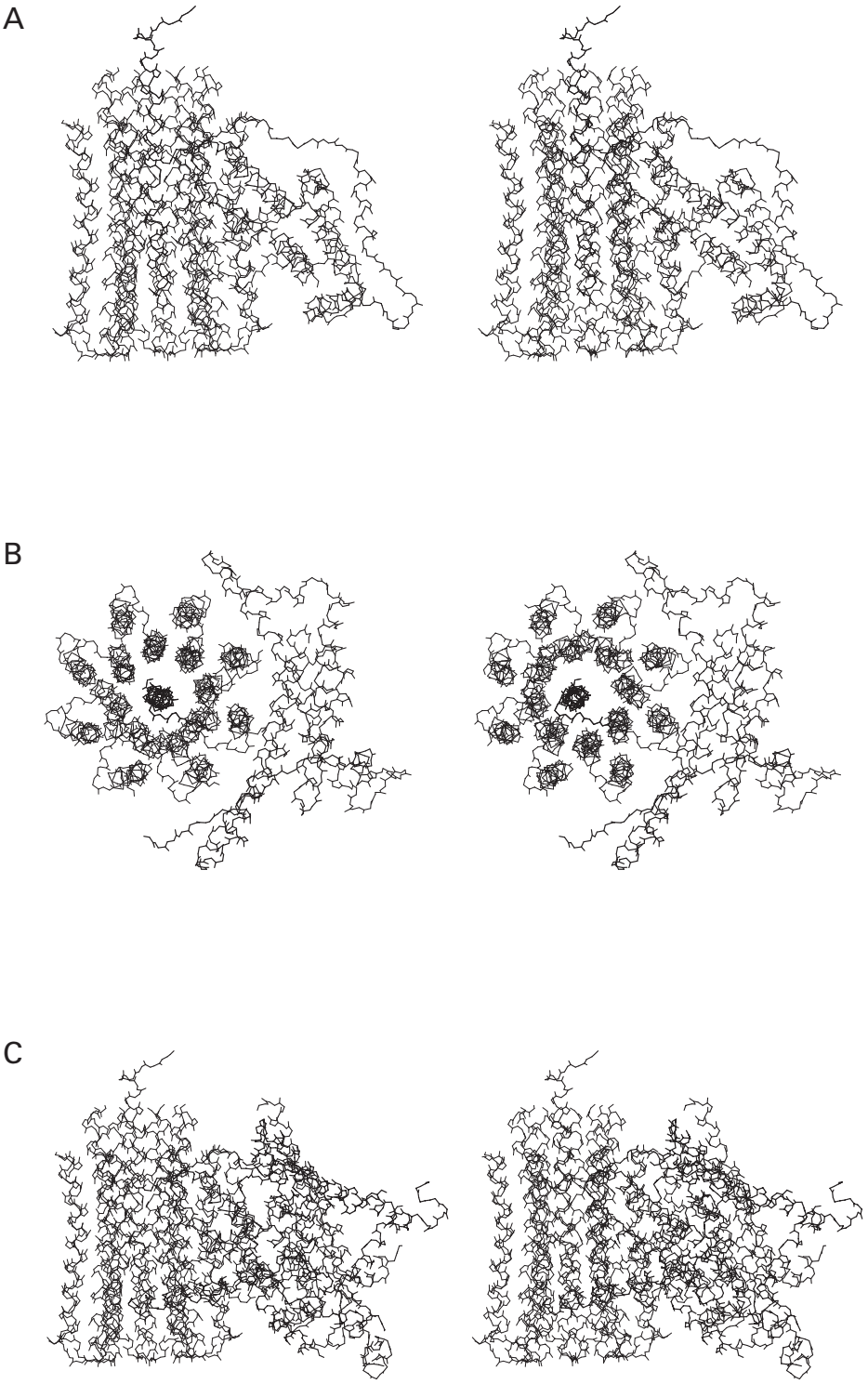
A
B
C

When the connection between the cylinder of c subunits and the shaft of the γsubunit in H^+-transporting two-sector ATPase from *S. cerevisiae* is disrupted by eliminating the δ subunit by site-directed mutation, mitochondria containing the mutated enzyme could no longer synthesize $MgATP^{2-}$ and were also unable to maintain an electrochemical gradient of hydrons because a leak for hydrons is present where one was not before.[457] Presumably, the cylinder of c subunits, no longer connected to the shaft of the γsubunit and no longer experiencing significant resistance to rotation from the synthesis of $MgATP^{2-}$, simply rotates in a net clockwise direction at will, shuttling hydrons until the electrochemical gradient is dissipated while no $MgATP^{2-}$ can be synthesized.

Within the membrane, five stretches of polypeptide from five identified and sequenced subunits of porcine H^+-transporting two-sector ATPase and three stretches of polypeptide from three unknown and hence unsequenced subunits form the structure surrounding subunit a (Figure 6–52C). Together with the entire subunit a, they form the compact globular protein to one side of the cylinder of c subunits. The other segments of polypeptide in the globular protein firmly attach subunit a to the triply coiled coil of α helices that emerges from the membrane on its negative, basic side and connects to the $(\alpha\beta)_3$ ring of the F_1-ATPase, which is within the majority of the protein on the negative, basic side of the membrane. These other eight segments of polypeptide within the membrane also act as **booms to push the bilayer of phospholipid away** from the extensive interface between subunit a and the ring of eight c subunits so that the two opposite edges of this interface are in unimpeded contact with solutions on the positive, acidic side and the negative, basic side of the membrane.

The majority of the surface of the cylinder of c subunits—those portions not in contact with subunit a and the other segments of polypeptide, in particular the majority of its midsection—is immersed within the hydrocarbon in the center of the bilayer of phospholipids, as if it were dissolved in clear machine oil bounded by the phosphoglyceroyl head groups on either side of the bilayer at its top and bottom.

The carboxy group of each Glutamic Acid 58, located on the outer α helix of each of the eight c subunits, carries one of the hydrons flowing across the membrane. Related by the eightfold rotational axis of symmetry, each Glutamate 58 around the exterior of the cylinder is located in the middle of an outer α helix and in the very middle of the membrane. During the rotation of the cylinder past subunit a, each carboxylato group of the eight Glutamates 58 in turn is loaded with a hydron from the solution on the positive, acidic side of the membrane, and then that hydron is unloaded by dissociation into the solution on the negative, basic side of the membrane. Consequently a complete rotation of the cylinder of c subunits can be divided into a number of identical steps equal to the number of c subunits in the ring. In the case of porcine H^+-transporting two-sector ATPase there are eight steps, each involving a -45° clockwise rotation of the cylinder during the synthesis of $MgATP^{2-}$.

When hydrons pass across the membrane from the solution on the positive, acidic side to the solution on the negative, basic side of the membrane during the synthesis of $MgATP^{2-}$, while the cylinder turns in a net clockwise direction relative to the position of subunit a, they pass across the interface between subunit a and the exterior α helices of the cylinder of c subunits (Figures 6–52A,B). In the middle of its journey, each hydron is carried on a Glutamate 58 as a neutral carboxy group, rotating through the hydrocarbon of the membrane. The hydron cannot dissociate in this solvent, so it remains on the carboxy group. Between the single subunit a and the cylinder of c subunits, there are **two half channels**, one between the solution on the positive, acidic side of the membrane and a location in the center of the membrane that is accessible to the carboxy group on a Glutamate 58 and the other between the solution on the negative, basic side of the membrane and a different, but nearby, location in the center of the membrane that is also accessible to a Glutamate 58.[458] Each channel is a gap in the interface between subunit a and the cylinder of c subunits.[357,441,459-467]

In porcine H^+-transporting two-sector ATPase during the synthesis of $MgATP^{2-}$, a hydron from the solution on the positive, acidic side of the membrane enters the interface between subunit a and the c subunits (Figure 6–53A).[441] There is a fairly **wide gap in the interface lined with hydrophilic side chains** from Threonines 161 and 165, Asparagine 163, and Glutamine 97 in subunit a that connects the positive, acidic solution to the space between the guanidinio group of Arginine 159 in subunit a and the carboxylato group of Glutamate 58B in the c subunit labeled B in Figure 6–53 when it is in position to accept a hydron (Figure 6–53A).

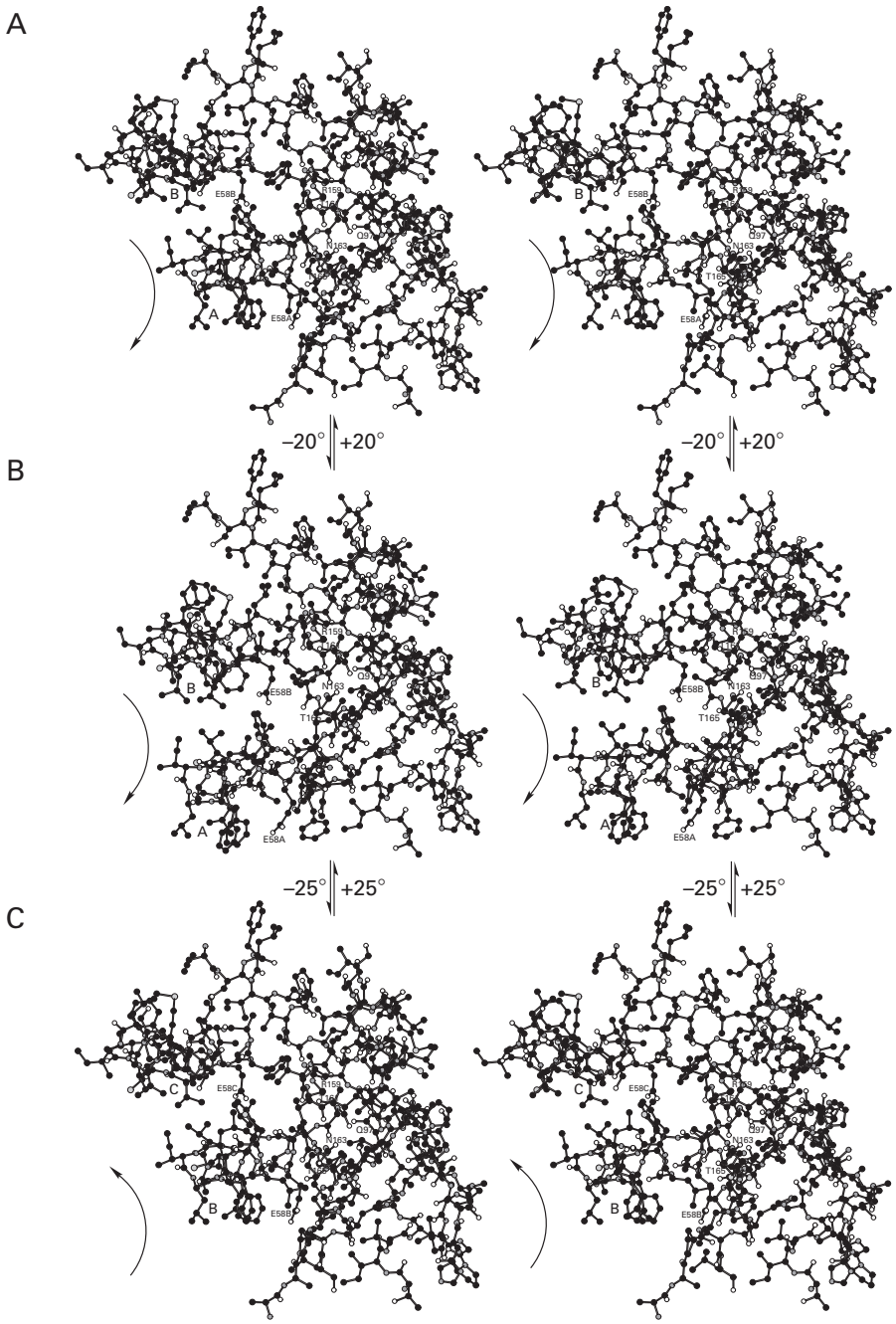
A
B
C
−20°
+20°
−20°
+20°
−25°
+25°
−25°
+25°
E58B
E58A
E58C
N163
T165
Q97
R156

Figure 6–53: Stereodrawings[485] of the half channel in the gap on the positive, acidic side of the membrane where transfer of a hydron to the carboxylato group of a Glutamate 58 in the cylinder of c subunits occurs during synthesis of $MgATP^{2-}$. Black atoms are carbons, white atoms are oxygens, small gray atoms are nitrogens, and large light gray atoms are sulfurs. The drawing shows a portion of the molecular model of porcine H^+-transporting two-sector ATPase[441] drawn in Figure 6–51 that includes the interface between subunit a and the cylinder of c subunits in which the gap that forms the channel from the positive, acidic solution is located. The segments of subunit a that line the gap forming the half channel (Isoleucine 10–Proline 18, Asparagine 83–Isoleucine 106, Isoleucine 147–Leucine 170, and Threonine 200–Serine 219) are drawn, to the right in each panel of the figure. Glutamine 97, Threonine 161, Asparagine 163, and Threonine 165, the hydrophilic side chains of which are located in the wall of the channel, are labeled. During synthesis of $MgATP^{2-}$, hydrons pass through the enzyme from the positive, acidic solution to the negative, basic solution. (**A**) Segments of two external α helices, on the positive, acidic half of the cylinder c subunits (in both cases Glycine 53–Phenylalanine 73), labeled A and B. The point at which a hydron is transferred to Glutamate 58B in the α helix of c subunit B is thought to be adjacent to Arginine 159, at the bottom of the channel and at the end of a hydron wire. It is also thought that the side chain of Glutamate 58B rotates around its β carbon–γ carbon bond to approach the guanidino group more closely before the hydron in the half channel from the positive, acidic side associates with the carboxylato group. Glutamic Acid 58A in the α helix of c subunit B is moving toward the hydrocarbon of the bilayer. (**B**) Coordinates of the molecular model for the same segments from c subunits A and B, submitted to a clockwise rotation of –20° around the axis of symmetry running through the cylinder of c subunits. Rotation of the cylinder was perfomed before the respective atoms in those segments were added to the drawing. The segments of subunit a, however, were drawn in the same orientation as in the drawing in Panel A. The clockwise rotation of –20° moves the carboxy group of Glutamic Acid 58B away from the gap to the positive, acidic side of the membrane, but only when it is the conjugate acid carrying the hydron. Glutamic Acid 58A in in the α helix of c subunit A has entered the hydrocarbon of the bilayer. (**C**) Coordinates of the molecular model for the segments of c subunit, submitted to a further clockwise rotation of –25° to complete a full step of –45°. The drawing is the same as that in Panel A, with the exception that the labels of the α helices were changed from A to B and from B to C because, upon completion of a –45° step, Glutamate 58C in the α helix of c subunit C has rotated into the loading zone for a hydron in the same position that Glutamate 58B in the α helix of c subunit B did in Panel A, and the α helix of c subunit B occupies the same position that the α helix of c subunit A did in Panel A. In this drawing, Glutamate 58C has arrived at the point at which a hydron in the half channel from the positive, acidic side is transferred to its carboxylato group. In Panel B, Glutamic Acid 58C in the α helix of c subunit C was in the unloading zone in the bottom of the channel from the negative, basic side of the membrane and its hydron had to dissociate into that channel before the rotation of –25° could occur, bringing it into the loading zone for a hydron from the positive, acidic side of the membrane. The curved arrows in Panels A and B indicate clockwise rotations. The curved arrow in Panel C, which indicates a counterclockwise rotation of the cylinder +20° in reverse, emphasizes the equilibrium between the rotational orientations, in this case returning Glutamate 58C to the channel from the negative, basic side of the membrane.

Figure 6–54: Stereodrawings[485] of the half channel in the gap on the negative, basic side of the membrane where transfer of a hydron from the carboxy group of a Glutamatic Acid 58 in the cylinder of c subunits occurs during synthesis of $MgATP^{2-}$. Black atoms are carbons, white atoms are oxygens, small gray atoms are nitrogens, and large light gray atoms are sulfurs. The drawing shows a portion of the molecular model of porcine H^+-transporting two-sector ATPase[441] that includes the interface between subunit a and the cylinder of c subunits in which the gap that forms the channel from the negative, basic solution is located. Each panel is a drawing of a portion of the same molecular model, portions of which are drawn in Figure 6–53, but it is viewed from the opposite side of the membrane. The segments of subunit a that line the gap forming the half channel (Leucine 49–Leucine 75, Methionine 100–Phenylalanine 114, Threonine 123–Leucine 160, and Leucine 208–Aspartate 224) are drawn, again to the right in each panel of the figure. Histidine 127, Glutamate 145, and Glutamine 152, the hydrophilic side chains of which are located in the wall of the channel, are labeled. (**A**) Segments of three external α helices, on the negative, basic half of the cylinder c subunits (in all three cases Leucine 46–Leucine 62) with the same labels, A, B and C, used in Figure 6–53. As in Figure 6–53A, a hydron in the gap on the positive, acidic side is associating with the carboxylato group of Glutamate 58B, and Glutamatic Acid 58A is on its way into the hydrocarbon as it was before. (**B**) Coordinates of the molecular model for the same segments from c subunits B and C, submitted to a clockwise rotation of –20° around the axis of symmetry running through the cylinder of c subunits. Recall that a clockwise rotation appears to be a counterclockwise rotation from this vantage point. The α helix from c subunit A has departed into the hydrocarbon. The segments of subunit a, however, are drawn in the same orientation as in the drawing in Panel A. The point at which hydrons dissociate from the carboxy groups of Glutamic Acids 58 is adjacent to Serine 148, at the bottom of the gap. Arginine 159 is also labeled to show the bottom of the half channel from the positive, acidic side of the membrane relative to the bottom of the half channel from the negative, basic solution. The carboxy group of Glutamic Acid 58C in c subunit C, counterclockwise to the α helix in c subunit B, has just completed its transit of the hydrocarbon. The clockwise rotation of –20° has brought this carboxy group into alignment with Serine 148, where its hydron dissociates. The clockwise rotation of –20° moves the carboxy group of Glutamic Acid 58B away from the gap to the positive, acidic side of the membrane on its way into the hydrocarbon. Glutamic Acid 58A has entered the hydrocarbon of the bilayer. (**C**) Coordinates of the molecular model for the segments of c subunit, submitted to a further clockwise rotation of –25° to complete a full step of –45°. The drawing is the same as that in Panel A, with the exception that the labels of the α helices were changed from A to B and from B to C, and the α helix of c subunit D, which has just entered from the hydrocarbon and is not yet in the unloading zone for its hydron, has been added. Glutamate 58C, from which a hydron dissociated in Panel B, has arrived at the point at which a hydron in the half channel from the positive, acidic side associates with its carboxylato group. The curved arrows in Panels A and B indicate the respective clockwise rotations. The curved arrow in Panel C, which indicates a counterclockwise rotation of the cylinder +20° in reverse, emphasizes the equilibrium between the rotational orientations, in this case returning Glutamate 58C to the channel from the negative, basic side of the membrane. Between the two orientations in this equilibrium, Glutamate 58C passes through a gap of 25°. Within this gap, it must remain unhydronated.

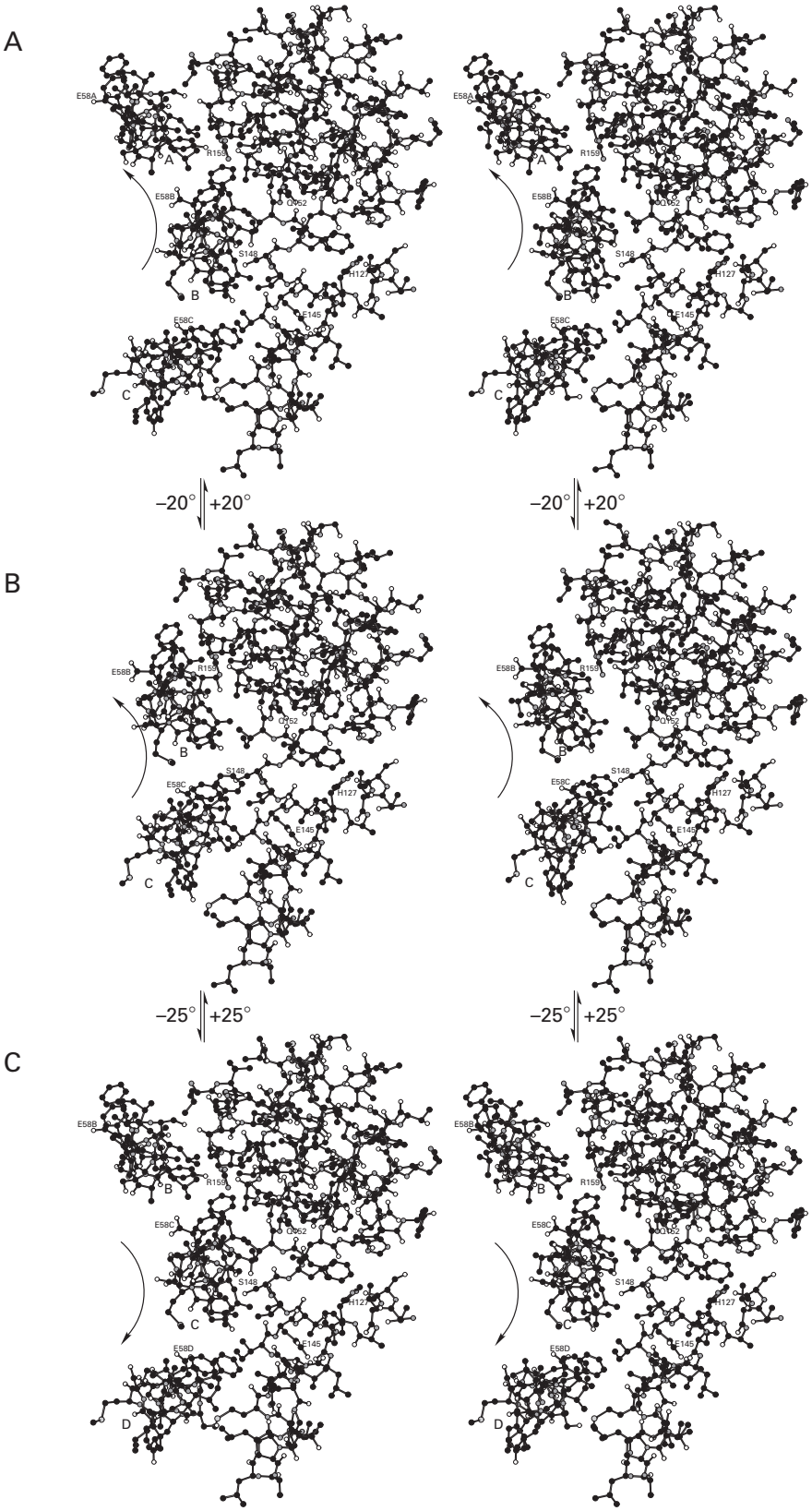
A
E58A
R159
A
E58B
D252
S148
H127
B
E145
E58C
C
−20°
+20°
−20°
+20°
B
E58B
R159
D252
B
S148
E58C
H127
E145
C
−25°
+25°
−25°
+25°
C
E58B
R159
B
E58C
D252
S148
H127
C
E145
E58D
D

The empty space in the molecular model between the van der Waals surfaces of the carboxyato group of Glutamate 58B and the guanidinio group of Arginine 159 is about 0.3 nm wide. The resolution of the model of porcine H^+-transporting two-sector ATPase derived from image reconstruction from electron micrographs is insufficient to observe **fixed molecules of water**, but the space between these two side chains must contain at least one molecule of water, forming a hydrogen bond to the carboxylato group or a hydrogen bond to the guanidinio group or bridging them. In a higher-resolution molecular model from image reconstruction of electron micrographs of H^+-transporting two-sector ATPase from *Polytomella*,[462] a molecule of water can be observed forming a hydrogen bond to the guanidinio group of the homologous arginine in subunit a (28% identity; 2.2 gap percent).

Because there is no significant empty space in a molecule of protein, the entire hydrophilic gap in the interface between subunit a and two adjacent c subunits (labeled A and B in Figure 6–53A) must also contain molecules of water, some fixed in place by donors and acceptors for hydrogen bonds on the side chains of Threonines 161 and 165, Asparagine 163, and Glutamine 97 as well as the amido groups of the polypeptide backbone. There must also be some disordered molecules of water in less confined regions within the gap. Presumably the fixed molecules of water and the hydroxy groups on Threonines 161 and 165 provide a **hydron wire** through which the **hydron moves from the intrusion of the positive, acidic solution into the gap** to the carboxylato group of Glutamate 58B in the middle of the external α helix in c subunit B (Figure 6–53A).

During the synthesis of $MgATP^{2-}$, once the carboxylato group of Glutamate 58B has been hydronated, the cylinder, and hence its α helix, rotates clockwise to remove the now-neutral carboxy group of Glutamic Acid 58B from the hydron wire (Figure 6–53B) on its way around the circle through the hydrocarbon of the phospholipids to the half channel opening to the negative, basic solution. After a further rotation of –25°, the unhydronated carboxylato group of Glutamate 58C in the α helix in c subunit C (Figure 6–53C), on the counterclockwise side of the c subunit B, arrives at the hydron wire from the positive, acidic solution and the delivery of a hydron is repeated to begin the next step.

After the hydron from the positive, acidic surface has associated with Glutamate 58B (Figure 6–53A) and the cylinder has rotated in a clockwise direction by only about –20° (the –20° rotation from Panel A to Panel B in Figure 6–53 is the same as the –20° rotation from Panel A to Panel B in Figure 6–54 but viewed from the other side of the membrane), a hydron dissociates from the carboxy group of Glutamic Acid 58C to the counterclockwise side of c subunit B. At this point, Glutamic Acid 58C has just completed its circumnavigation through the hydrocarbon carrying its hydron. That hydron then passes into the negative, basic solution on the other side of the membrane through a fairly wide gap in the interface between subunit a and the cylinder of c subunits (Figure 6–54B).[441] This gap is about +25° counterclockwise from the gap on the positive, acidic side, and it is lined with hydrophilic side chains from Histidine 127, Glutamate 145, and Glutamine 152 in subunit a. When Glutamate 58C arrives from the hydrocarbon, this gap connects the negative, basic solution to the space between the carboxy group of Glutamic Acid 58C and the hydroxy group of Serine 148 in subunit a (Figure 6–54B). The space between Serine 148 and Glutamic Acid 58C probably contains one or more fixed molecules of water. The entire gap between subunit a and two adjacent c subunits (those labeled B and C in Figure 6–54B) must also contain molecules of water, some fixed in place by donors and acceptors for hydrogen bonds on the side chains of Histidine 127, Glutamate 145, and Glutamine 152 as well as the amido groups of the polypeptide backbone and some in disordered regions.

Presumably the fixed molecules of water and the carboxy group of Glutamic Acid 145 from subunit a provide a hydron wire through which the hydron moves from the carboxy group of Glutamic Acid 58C **into the intrusion of the negative, basic solution into the gap**, and hence into the solution on the negative, basic side. In the higher-resolution molecular model of H^+-transporting two-sector ATPase from *Polytomella*, single molecules of water and pairs of molecules of water can be observed in this gap, and some of these molecules of water are probably participants in a hydron wire,[462] the complete structure of which is not resolved. In the portion of subunit a in H^+-transporting two-sector ATPase from *T. thermophilus* that is structurally homologous to subunit a in the porcine enzyme, the hydrophilic side chains projecting into this gap on the negative, basic side of the membrane, organizing the molecules of water, and participating in the hydron wire are more numerous and their alignment is more exact.[463]

During the synthesis of $MgATP^{2-}$, after the hydron dissociates from the carboxy group on Glutamic Acid 58C, the now-carboxylato group on Glutamate 58C rotates about –25° with the cylinder in the clockwise direction (Figure 6–54B,C) to arrive next to Arginine 159 at the bottom of the gap in the interface between the cylinder of c subunits and subunit a that opens to the positive, acidic side to begin the next step.

To couple the clockwise rotation of the cylinder of c subunits to the movement of hydrons down the electrochemical gradient from the positive, acidic solution to the negative, basic solution with complete stoichiometry and hence maximum efficiency, the –335° clockwise rotation between the half channel from the positive, acidic solution and the half channel to the negative, basic solution must proceed only when the carboxy group of Glutamic Acid 58 has been hydronated, and the hydron cannot dissociate between the the two half channels. In addition, the –25° clockwise rotation between the half channel to the negative, basic solution and the half channel from the positive, acidic solution must proceed only when the carboxylato group of Glutamate 58 has been unhydronated, and it must remain unhydronated. If these requirements are completely satisfied, then **the movement of each hydron from the positive, acidic solution to the negative, basic solution is coupled stoichiometrically to a clockwise rotation of 45° by the cylinder of c subunits.**[468,469]

The requirement that the carboxy group of Glutamic Acid 58 remain hydronated during the clockwise rotation between the channels is satisfied by the hydrocarbon, which provides an ingenious solution to keeping it hydronated over an arc of about –335°. More critically, however, the requirement that the clockwise rotation of only about –25° between the two channels (Figure 6–54B,C) must proceed only when the carboxylato group of Glutamate 58 has been unhydronated and the requirement that it must remain unhydronated are far more difficult to achieve because it must move through an interface between two subunits of the protein. Furthermore, because all these rotations are reversible, the movement through this small gap may actually reverse several times before proceeding forward. When the carboxylato group of Glutamate 58 returns to the gap leading to the negative, basic solution during a momentary reversal, it must also traverse the intervening space unhydrated, or an unproductive hydron leak from the positive, acidic side to the negative, basic side would occur.

Consequently, the key to accomplishing the proper stoichiometry for the clockwise and counterclockwise rotations of 25° between the negative, basic half channel on the one side of the membrane and the positive, acidic half channel on the other is the properties of the **short gap between the two half channels.** This gap sits between the channel to the negative, basic solution, at which a hydron dissociates from Glutamic Acid 58 when it is adjacent to Serine 148 on subunit a (Figure 6–54B), and the channel to the positive, acidic solution, at which a hydron associates with the same Glutamate 58 when it is adjacent to Arginine 159 on subunit a (Figure 6–54C). Every time one of the Glutamic Acids 58 moves through that gap in a clockwise or counterclockwise direction as the hydronated conjugate acid, the free energy that must be captured from the electrochemical gradient of hydrons by H^+-transporting two-sector ATPase is lost. How the protein within this short gap solves this requirement is still unclear and may require elucidation of the exact positions of the side chains and the fixed molecules of water present in that short gap. Nevertheless, the structure of this short gap must have been under significant selective presure.

For H^+-transporting two-sector ATPase to function properly, subunit a must be affixed to the $(\alpha\beta)_3$ ring so that, every time the cylinder of c subunits completes a full revolution past subunit a within the membrane, the shaft of the γ subunit completes a full revolution within the $(\alpha\beta)_3$ ring. When the cylinder of c subunits in intact H^+-transporting two-sector ATPase from *E. coli* was attached firmly to a glass coverslip and filaments of actin were attached either to a β subunit or to subunit a, the respective filaments rotated at the same rate, and the rates at which they rotated changed in concert as the viscous drag was increased.[450] This observation is consistent with the β subunit and subunit a being connected tightly together within H^+-transporting two-sector ATPase. This connection is achieved by the triply coiled coil of α helices.

All H^+-transporting two-sector ATPases have an $(\alpha\beta)_3$ ring, a $\gamma\delta\varepsilon$ shaft, a rotationally symmetric ring of c subunits, and subunit a or its equivalent, and each is homologous in its sequence of amino acids, or at the least structurally homologous, to its respective siblings in the various species of animals, plants, fungi, and bacteria.[358] The **segments of H^+-transporting two-sector ATPase that connect subunit a to the $(\alpha\beta)_3$ ring**, however, differ among animals, plants, fungi, and bacteria. In the case of

porcine H^+-transporting two-sector ATPase (Figure 6–51), the connection is made by a triply coiled coil of α helices anchored at one end in the globular protein within the membrane containing subunit a and at the other end entwined within a structure formed from subunit O and affixed tightly to the $(\alpha\beta)_3$ ring. In H^+-transporting two-sector ATPase from *Polytomella*, the connection is made by a much wider, kinked rope of five and sometimes six α helices along its length and some strands of random meander.[462] Regardless of the differences among the different species, a connection is made[445,446,448,470-474] with one or two separate α-helical coiled coils providing straps and various subunits, which differ among species, gluing these straps to the $(\alpha\beta)_3$ ring.

In addition to the differences in the number and identity of subunits forming the connection between subunit a and the $(\alpha\beta)_3$ ring among the H^+-transporting two-sector ATPases from different species is the difference in the **number of c subunits in the cylindrical ring**.[442] Bovine and porcine H^+-transporting two-sector ATPase have 8 c subunits in the ring,[442] the enzyme from *S. cerevisiae* has 10 c subunits in the ring,[475] the enzyme from *E. coli* also has 10 c subunits in the ring,[476] the enzyme from *S. oleracea* has 14 c subunits in the ring,[477] Na^+-transporting two-sector ATPase from *Ilyobacter tartaricus* has the equivalent of 11 c subunits in the ring,[478,479] and Na^+-transporting two-sector ATPase from *Enterococcus hirae* has the equivalent of 10 c subunits in the ring.[480] The number of c subunits in the cylinder from Na^+-transporting two-sector ATPase from *I. tartaricus* can be varied from 10 to 15 by site-directed mutation without affecting its function.[481] Although this relation has not been accurately validated, it usually is assumed[442] that the ratio between the number of hydrons transported down the electrochemical gradient and the number of $MgATP^{2-}$ synthesized, when the enzyme is operating at maximum efficiency and stoichiometry, is simply the ratio between the number of c subunits in the cylinder for a particular species divided by the number of active sites (3). Nothing, however, operates at maximum efficiency.

The strange aspect of this ratio is that it is usually not an integer, as it would be if the number of c subunits were usually 9 or 12.* The rotational offsets for the steps in the two distant and independent rotors are not the same as they would be if there were only 3 c subunits in the cylinder to match the 3 subunits the $(\alpha\beta)_3$ ring, or if there were 9 c subunits in the cylinder to match the alternating rotations of 80° and 40° of the γ subunit. It has been assumed that the mismatch between the number of c subunits and the number of active sites in F_1-ATPase requires that either the connection between subunit a and the $(\alpha\beta)_3$ ring or the connection between the ring of c subunits and the shaft of the γ subunit in H^+-transporting two-sector ATPase be **flexible enough to permit effective coordination** between steps in rotation of the cylinder of c subunits relative to subunit a and steps in the rotation of the γ subunit within the $(\alpha\beta)_3$ ring. Were the connection absolutely rigid, neither rotor could proceed through its steps because of the mismatch in their stoichiometry. Nevertheless, the coiled coils and their attachments ensure that every complete rotation of the cylinder of c subunits over the course of several complete rotations is always accompanied by the same number of complete rotations of the γ subunit within the $(\alpha\beta)_3$ ring.

Various global conformations of H^+-transporting two-sector ATPase from *Polytomella* have been observed in image reconstructions of electron micrographs. In the molecular models derived from these reconstructions, the connection between the $(\alpha\beta)_3$ ring and the strap of the coiled coil has flexed to accommodate different rotational orientations of the cylinder of c subunits relative to the rotational orientation of the $(\alpha\beta)_3$ ring. The only difference among these global conformations seems to be these relative rotational orientations. It has been proposed that these different global conformations permit the necessary coordination between the rotary motions.[462]

A different conclusion was reached when the stiffness of the connections between subunit a and the $(\alpha\beta)_3$ ring and the stiffness of the connection between the cylinder of c subunits and the shaft of the γ subunit were measured. Actin filaments or magnetic beads were attached to either the cylinder of c subunits or the globular structure within the membrane containing subunit a in wild-type H^+-transporting two-sector ATPase from *E. coli* or mutants of the enzyme in which cystines crosslink the γ subunit to a β subunit or a c subunit to subunit a. When these variously modified H^+-transporting two-sector ATPases were attached through the surface of their F_1-ATPase opposite the shaft of the γ subunit (Figure 6–48), measurements of the torque required to rotate the bead magnetically or the observed displacements of the bead or the filament of actin caused by random Brownian displacements for each

*This lack of an integral relationship defied expectations, much as the fact that the number of amino acids in a complete turn of a helix formed by a polypeptide defied expectations.[482]

modified form of enzyme could be used to determine the stiffness of either the connection between subunit a and the $(\alpha\beta)_3$ ring or the connection between the cylinder of c subunits and the shaft of the γsubunit. Counterintuitively, it was concluded that the stiffness between subunit a and the $(\alpha\beta)_3$ ring was about 10 times greater than the stiffness between the cylinder of c subunits and the shaft of the γsubunit and that the flexions required to coordinate the rotary motions of the γsubunit and those of the c subunit occur mostly in the connection between the cylinder of c subunits and the shaft of the γsubunit,[453,483] an interface that seems upon inspection to be rather inflexible (Figure 6–51).

In contradiction to this conclusion that the flexions occur in the connection between the cylinder of c subunits and the shaft of the γsubunit, when cystines were introduced in turn between several of the subunits that form the interfaces in the $\gamma\delta\varepsilon c_{12}$ rotor in H^+-transporting two-sector ATPase from *E. coli*, no effect was observed on the ability of each mutated and stitched enzyme to transport hydrons into vesicles into which it was incorporated or to synthesize $MgATP^{2-}$ when a large enough gradient of hydrons was established across the membranes of the vesicles.[484]

The temptation to compare H^+-transporting two-sector ATPase to an electrical appliance in which the shaft of a motor drives machinery accomplishing its purpose has been irresistible (Figure 6–51B). The $(\alpha\beta)_3$ ring of F_1-ATPase accomplishes the purpose of the appliance, that of synthesizing $MgATP^{2-}$. The $\gamma\delta\varepsilon$ shaft connects this machinery to the motor that turns the shaft. The motor is not the usual induction motor of an electric appliance, but a motor that employs a current directly without magnetic induction. The cylinder of c subunits is most analogous to a commutator ring in an induction motor and subunit a to one of its brushes. The subunits that grasp the $(\alpha\beta)_3$ ring, the α-helical coiled coils, and the segments of polypeptide surrounding subunit a in the membrane together form a rigid housing that ensures that the brush and the machinery accomplishing the purpose of the appliance are firmly fixed in a constant orientation as the shaft turns.

Given this irresistible impulse, much attention has been devoted to mechanical explanations of how the free energy in the electrochemical gradient of hydrons is converted stereochemically into the conformational changes that are responsible for the synthesis of $MgATP^{2-}$. As was the case with Na^+/K^+-exchanging ATPase, however, the only relevant chemical fact is that when eight hydrons, one after the other, move through the cylinder of c subunits in porcine H^+-transporting two-sector ATPase from the positive, acidic solution to the negative, basic solution, three molecules of $MgATP^{2-}$ are produced from three molecules of $MgADP^-$ and three molecules of $HOPO_3^{2-}$ by F_1-ATPase. If this **coupling is effectively enforced** and there is a sufficient electrochemical gradient of hydrons from the positive, acidic solution to the negative, basic solution, it necessarily follows that the equilibrium in Equation 6–132 will be in favor of the synthesis of $MgATP^{2-}$.

This consideration brings up another point that often seems to be ignored. As is the case with all enzymes, H^+-transporting two-sector ATPase catalyzes its reaction in both directions and every step is a reversible step. Although throughout this discussion preference has been given to the direction of the reaction in which $MgATP^{2-}$ is synthesized, this preference is personal and only due to the fact that this synthesis is what the enzyme usually does. The enzyme, however, also catalyzes hydrolysis of $MgATP^{2-}$, and the net direction of the reaction in a given set of circumstances depends on the change in situational free energy for Equation 6–132 under those circumstance. It follows that any molecular explanation of the role of any of the catalytic functional groups that implies that it assists the reaction in only one direction should be read with the fact that the reaction is reversible always in mind. The basis of microscopic reversibility is that any effect that lowers the standard free energy of a transition state increases the rate in each direction of the equilibrium governed by that transition state.

One is left with the impression that H^+-transporting two-sector ATPase, the source of most of the $MgATP^{2-}$ responsible for all the kinetic energy in living organisms, is one of the most bizarre enzymes in the collection, and a fit place to conclude this disquisition. The question of how it works seems to have been answered. The question of how it came to exist in the first place may never be answered.

Suggested Reading

Steinberg, M., & Karlish, S. J. D. (1988) Studies on conformational changes in Na,K-ATPase labeled with 5-iodoacetamidofluorescein, *J. Biol. Chem. 264*, 2726–2734. https://doi.org/10.1016/S0021-9258(19)81673-3

Abrahams, J. P., Leslie, A. G., Lutter, R., and Walker, J. E. (1994) Structure at 2.8 Å resolution of F_1-ATPase from bovine heart mitochondria, *Nature 370*, 621–628. https://doi.org/10.1038/370621a0

References

1. Baldwin, J., and Chothia, C. (1979) Haemoglobin: The structural changes related to ligand binding and its allosteric mechanism, *J. Mol. Biol. 129*, 175–220.
2. Fermi, G., Perutz, M. F., Shaanan, B., and Fourme, R. (1984) The crystal structure of human deoxyhaemoglobin at 1.74 Å resolution, *J. Mol. Biol. 175*, 159–174.
3. Vasquez, G. B., Ji, X., Fronticelli, C., and Gilliland, G. L. (1998) Human carboxyhemoglobin at 2.2 Å resolution: Structure and solvent comparisons of R-state, R2-state and T-state hemoglobins, *Acta Crystallogr., Sect. D: Biol. Crystallogr. 54*, 355–366.
4. Ke, H. M., Honzatko, R. B., and Lipscomb, W. N. (1984) Structure of unligated aspartate carbamoyltransferase of *Escherichia coli* at 2.6 Å resolution, *Proc. Natl. Acad. Sci. U. S. A. 81*, 4037–4040.
5. Krause, K. L., Volz, K. W., and Lipscomb, W. N. (1985) Structure at 2.9 Å resolution of aspartate carbamoyltransferase complexed with the bisubstrate analogue *N*-(phosphonacetyl)-L-aspartate, *Proc. Natl. Acad. Sci. U. S. A. 82*, 1643–1647.
6. Ke, H. M., Lipscomb, W. N., Cho, Y. J., and Honzatko, R. B. (1988) Complex of *N*-phosphonacetyl-L-aspartate with aspartate carbamoyltransferase: X-Ray refinement, analysis of conformational changes and catalytic and allosteric mechanisms, *J. Mol. Biol. 204*, 725–747.
7. Stevens, R. C., Gouaux, J. E., and Lipscomb, W. N. (1990) Structural consequences of effector binding to the T-state of aspartate carbamoyltransferase: Crystal structures of the unligated and ATP- and CTP-complexed enzymes at 2.6 Å resolution, *Biochemistry 29*, 7691–7701.
8. Gerhart, J. C., and Pardee, A. B. (1962) The enzymology of control by feedback inhibition, *J. Biol. Chem. 237*, 891–896.
9. Cockrell, G. M., Zheng, Y., Guo, W., Peterson, A. W., Truong, J. K., and Kantrowitz, E. R. (2013) New paradigm for allosteric regulation of *Escherichia coli* aspartate transcarbamoylase, *Biochemistry 52*, 8036–8047.
10. Gerhart, J. C., and Holoubek, H. (1967) The purification of aspartate transcarbamylase of *Escherichia coli* and separation of its protein subunits, *J. Biol. Chem. 242*, 2886–2892.
11. Changeux, J. P., Gerhart, J. C., and Schachman, H. K. (1968) Allosteric interactions in aspartate transcarbamylase. I. Binding of specific ligands to the native enzyme and its isolated subunits, *Biochemistry 7*, 531–538.
12. Suter, P., and Rosenbusch, J. P. (1977) Asymmetry of binding and physical assignments of CTP and ATP sites in aspartate transcarbamoylase, *J. Biol. Chem. 252*, 8136–8141.
13. Honzatko, R. B., Crawford, J. L., Monaco, H. L., Ladner, J. E., Ewards, B. F., Evans, D. R., Warren, S. G., Wiley, D. C., Ladner, R. C., and Lipscomb, W. N. (1982) Crystal and molecular structures of native and CTP-liganded aspartate carbamoyltransferase from *Escherichia coli*, *J. Mol. Biol. 160*, 219–263.
14. Honzatko, R. B., Monaco, H. L., and Lipscomb, W. N. (1979) A 3.0 Å resolution study of nucleotide complexes with aspartate carbamoyltransferase, *Proc. Natl. Acad. Sci. U. S. A. 76*, 5105–5109.
15. Monod, J., Wyman, J., and Changeux, J. P. (1965) On the nature of allosteric transitions: A plausible model, *J. Mol. Biol. 12*, 88–118.
16. Suter, P., and Rosenbusch, J. P. (1976) Determination of ligand binding: Partial and full saturation of aspartate transcarbamylase. Applicability of a filter assay to weakly binding ligands, *J. Biol. Chem. 251*, 5986–5991.
17. Courtice, F. C., and Douglas, C. G. (1947) The ferricyanide method of blood-gas analysis, *J. Physiol. (Oxford, U. K.) 105*, 345–356.
18. Hill, A. V. (1910) The possible effects of the aggregation of the molecules of haemoglobin

on its dissociation curves., *J. Physiol. (Oxford, U. K.) 40*, iv–vii.
19. Blangy, D., Buc, H., and Monod, J. (1968) Kinetics of the allosteric interactions of phosphofructokinase from *Escherichia coli*, *J. Mol. Biol. 31*, 13–35.
20. Vickrey, J. F., Herve, G., and Evans, D. R. (2002) *Pseudomonas aeruginosa* aspartate transcarbamoylase. Characterization of its catalytic and regulatory properties, *J. Biol. Chem. 277*, 24490–24498.
21. Imai, K. (1979) Thermodynamic aspects of the co-operativity in four-step oxygenation equilibria of haemoglobin, *J. Mol. Biol. 133*, 233–247.
22. Adair, G. S. (1925) The hemoglobin system. VI. The oxygen dissociation curve of hemoglobin, *J. Biol. Chem. 63*, 529–545.
23. Edsall, J. T., Felsenfeld, G., Goodman, D. S., and Gurd, F. R. N. (1954) The association of imidazole with the ions of zinc and cupric copper, *J. Am. Chem. Soc. 76*, 3054–3061.
24. West, J. M., Tsuruta, H., and Kantrowitz, E. R. (2002) Stabilization of the R-allosteric structure of *Escherichia coli* aspartate transcarbamoylase by disulfide bond formation, *J. Biol. Chem. 277*, 47300–47304.
25. Kyte, J. (2007) In *Structure in Protein Chemistry: Second Edition*, pp 452–456, Garland Science, New York.
26. Valdez, B. C., French, B. A., Younathan, E. S., and Chang, S. H. (1989) Site-directed mutagenesis in *Bacillus stearothermophilus* fructose-6-phosphate 1-kinase: Mutation at the substrate-binding site affects allosteric behavior, *J. Biol. Chem. 264*, 131–135.
27. Tian, T., Wang, C., Wu, M., Zhang, X., and Zang, J. (2018) Structural insights into the regulation of *Staphylococcus aureus* phosphofructokinase by tetramer–dimer conversion, *Biochemistry 57*, 4252–4262.
28. Schirmer, T., and Evans, P. R. (1990) Structural basis of the allosteric behaviour of phosphofructokinase, *Nature (London, U. K.) 343*, 140–145.
29. Evans, P. R., and Hudson, P. J. (1979) Structure and control of phosphofructokinase from *Bacillus stearothermophilus*, *Nature (London, U. K.) 279*, 500–504.
30. Oberfelder, R. W., Barisas, B. G., and Lee, J. C. (1984) Thermodynamic linkages in rabbit muscle pyruvate kinase: Analysis of experimental data by a two-state model, *Biochemistry 23*, 3822–3826.
31. Morgan, H. P., O'Reilly, F. J., Wear, M. A., O'Neill, J. R., Fothergill-Gilmore, L. A., Hupp, T., and Walkinshaw, M. D. (2013) M2 Pyruvate kinase provides a mechanism for nutrient sensing and regulation of cell proliferation, *Proc. Natl. Acad. Sci. U. S. A. 110*, 5881–5886.
32. Morgan, H. P., McNae, I. W., Nowicki, M. W., Hannaert, V., Michels, P. A., Fothergill-Gilmore, L. A., and Walkinshaw, M. D. (2010) Allosteric mechanism of pyruvate kinase from *Leishmania mexicana* uses a rock and lock model, *J. Biol. Chem. 285*, 12892–12898.
33. Rigden, D. J., Phillips, S. E., Michels, P. A., and Fothergill-Gilmore, L. A. (1999) The structure of pyruvate kinase from *Leishmania mexicana* reveals details of the allosteric transition and unusual effector specificity, *J. Mol. Biol. 291*, 615–635.
34. Choe, J. Y., Poland, B. W., Fromm, H. J., and Honzatko, R. B. (1998) Role of a dynamic loop in cation activation and allosteric regulation of recombinant porcine fructose-1,6-bisphosphatase, *Biochemistry 37*, 11441–11450.
35. Ke, H. M., Zhang, Y. P., Liang, J. Y., and Lipscomb, W. N. (1991) Crystal structure of the neutral form of fructose-1,6-bisphosphatase complexed with the product fructose 6-phosphate at 2.1 Å resolution, *Proc. Natl. Acad. Sci. U. S. A. 88*, 2989–2993.
36. Ke, H. M., Zhang, Y. P., and Lipscomb, W. N. (1990) Crystal structure of fructose-1,6-bisphosphatase complexed with fructose 6-phosphate, AMP, and magnesium, *Proc. Natl. Acad. Sci. U. S. A. 87*, 5243–5247.
37. Zhang, Y., Liang, J. Y., Huang, S., and Lipscomb, W. N. (1994) Toward a mechanism for the allosteric transition of pig kidney fructose-1,6-bisphosphatase, *J. Mol. Biol. 244*, 609–624.
38. Choe, J. Y., Fromm, H. J., and Honzatko, R. B. (2000) Crystal structures of fructose 1,6-bisphosphatase: Mechanism of catalysis and allosteric inhibition revealed in product complexes, *Biochemistry 39*, 8565–8574.
39. Choe, J. Y., Nelson, S. W., Arienti, K. L., Axe, F. U., Collins, T. L., Jones, T. K., Kimmich, R. D., Newman, M. J., Norvell, K., Ripka, W. C., Romano, S. J., Short, K. M., Slee, D. H., Fromm, H. J., and Honzatko, R. B. (2003) Inhibition of fructose-1,6-bisphosphatase by a

new class of allosteric effectors, *J. Biol. Chem. 278*, 51176–51183.
40. Iancu, C. V., Mukund, S., Fromm, H. J., and Honzatko, R. B. (2005) R-State AMP complex reveals initial steps of the quaternary transition of fructose-1,6-bisphosphatase, *J. Biol. Chem. 280*, 19737–19745.
41. Iwata, S., Kamata, K., Yoshida, S., Minowa, T., and Ohta, T. (1994) T and R states in the crystals of bacterial L-lactate dehydrogenase reveal the mechanism for allosteric control, *Nat. Struct. Biol. 1*, 176–185.
42. Iwata, S., and Ohta, T. (1993) Molecular basis of allosteric activation of bacterial L-lactate dehydrogenase, *J. Mol. Biol. 230*, 21–27.
43. Rypniewski, W. R., and Evans, P. R. (1989) Crystal structure of unliganded phosphofructokinase from *Escherichia coli*, *J. Mol. Biol. 207*, 805–821.
44. Johnson, L. N., and Barford, D. (1990) Glycogen phosphorylase: The structural basis of the allosteric response and comparison with other allosteric proteins, *J. Biol. Chem. 265*, 2409–2412.
45. Crow, J. P., and Beckman, J. S. (1995) Quantitation of protein tyrosine, 3-nitrotyrosine, and 3-aminotyrosine utilizing HPLC and intrinsic ultrviolet absorbance, *Methods 7*, 116–120.
46. Kirschner, M. W., and Schachman, H. K. (1973) Conformational studies on the nitrated catalytic subunit of aspartate transcarbamylase, *Biochemistry 12*, 2987–2997.
47. Kirschner, M. W., and Schachman, H. K. (1973) Local and gross conformational changes in aspartate transcarbamylase, *Biochemistry 12*, 2997–3004.
48. Beernink, P. T., Endrizzi, J. A., Alber, T., and Schachman, H. K. (1999) Assessment of the allosteric mechanism of aspartate transcarbamoylase based on the crystalline structure of the unregulated catalytic subunit, *Proc. Natl. Acad. Sci. U. S. A. 96*, 5388–5393.
49. Endrizzi, J. A., Beernink, P. T., Alber, T., and Schachman, H. K. (2000) Binding of bisubstrate analog promotes large structural changes in the unregulated catalytic trimer of aspartate transcarbamoylase: Implications for allosteric regulation, *Proc. Natl. Acad. Sci. U. S. A. 97*, 5077–5082.
50. Jin, L., Stec, B., Lipscomb, W. N., and Kantrowitz, E. R. (1999) Insights into the mechanisms of catalysis and heterotropic regulation of *Escherichia coli* aspartate transcarbamoylase based upon a structure of the enzyme complexed with the bisubstrate analogue *N*-phosphonacetyl-L-aspartate at 2.1 Å, *Proteins: Struct., Funct., Genet. 37*, 729–742.
51. Krause, K. L., Volz, K. W., and Lipscomb, W. N. (1987) 2.5 Å Structure of aspartate carbamoyltransferase complexed with the bisubstrate analog *N*-(phosphonacetyl)-L-aspartate, *J. Mol. Biol. 193*, 527–553.
52. Wang, J., Stieglitz, K. A., Cardia, J. P., and Kantrowitz, E. R. (2005) Structural basis for ordered substrate binding and cooperativity in aspartate transcarbamoylase, *Proc. Natl. Acad. Sci. U. S. A. 102*, 8881–8886.
53. Stevens, R. C., and Lipscomb, W. N. (1992) A molecular mechanism for pyrimidine and purine nucleotide control of aspartate transcarbamoylase, *Proc. Natl. Acad. Sci. U. S. A. 89*, 5281–5285.
54. Velyvis, A., Yang, Y. R., Schachman, H. K., and Kay, L. E. (2007) A solution NMR study showing that active site ligands and nucleotides directly perturb the allosteric equilibrium in aspartate transcarbamoylase, *Proc. Natl. Acad. Sci. U. S. A. 104*, 8815–8820.
55. Whitaker, A. M., Naik, M. T., Mosser, R. E., and Reinhart, G. D. (2019) Propagation of the allosteric signal in phosphofructokinase from *Bacillus stearothermophilus* examined by methyl-transverse relaxation-optimized spectroscopy nuclear magnetic resonance, *Biochemistry 58*, 5294–5304.
56. Foote, J., and Lipscomb, W. N. (1981) Kinetics of aspartate transcarbamylase from *Escherichia coli* for the reverse direction of reaction, *J. Biol. Chem. 256*, 11428–11433.
57. Foote, J., and Schachman, H. K. (1985) Homotropic effects in aspartate transcarbamoylase. What happens when the enzyme binds a single molecule of the bisubstrate analog *N*-phosphonacetyl-L-aspartate?, *J. Mol. Biol. 186*, 175–184.
58. Ladjimi, M. M., and Kantrowitz, E. R. (1988) A possible model for the concerted allosteric transition in *Escherichia coli* aspartate transcarbamylase as deduced from site-directed mutagenesis studies, *Biochemistry 27*, 276–283.
59. Ladjimi, M. M., Middleton, S. A., Kelleher, K. S., and Kantrowitz, E. R. (1988) Relationship between domain closure and binding, catal-

ysis, and regulation in *Escherichia coli* aspartate transcarbamylase, *Biochemistry 27*, 268–276.
60. Viappiani, C., Abbruzzetti, S., Ronda, L., Bettati, S., Henry, E. R., Mozzarelli, A., and Eaton, W. A. (2014) Experimental basis for a new allosteric model for multisubunit proteins, *Proc. Natl. Acad. Sci. U. S. A. 111*, 12758–12763.
61. Koshland, D. E., Jr., Nemethy, G., and Filmer, D. (1966) Comparison of experimental binding data and theoretical models in proteins containing subunits, *Biochemistry 5*, 365–385.
62. Kim, K. H., Pan, Z. X., Honzatko, R. B., Ke, H. M., and Lipscomb, W. N. (1987) Structural asymmetry in the CTP-liganded form of aspartate carbamoyltransferase from *Escherichia coli*, *J. Mol. Biol. 196*, 853–875.
63. Huang, J., and Lipscomb, W. N. (2004) Aspartate transcarbamylase (ATCase) of *Escherichia coli*: A new crystalline R-state bound to PALA, or to product analogues citrate and phosphate, *Biochemistry 43*, 6415–6421.
64. Gerhart, J. C., and Schachman, H. K. (1968) Allosteric interactions in aspartate transcarbamylase: II. Evidence for different conformational states of the protein in the presence and absence of specific ligands, *Biochemistry 7*, 538–552.
65. Kirschner, M. W., and Schachman, H. K. (1971) Conformational changes in proteins as measured by difference sedimentation studies. I. A technique for measuring small changes in sedimentation coefficient, *Biochemistry 10*, 1900–1919.
66. Howlett, G. J., and Schachman, H. K. (1977) Allosteric regulation of aspartate transcarbamoylase. Changes in the sedimentation coefficient promoted by the bisubstrate analogue *N*-(phosphonacetyl)-L-aspartate, *Biochemistry 16*, 5077–5083.
67. Yang, Y. R., and Schachman, H. K. (1980) Communication between catalytic subunits in hybrid aspartate transcarbamoylase molecules: Effect of ligand binding to active chains on the conformation of unliganded, inactive chains, *Proc. Natl. Acad. Sci. U. S. A. 77*, 5187–5191.
68. Griffiths, J. R., Price, N. C., and Radda, G. K. (1974) Conformational changes in phosphorylase *a*, studied by a spin label probe, *Biochim. Biophys. Acta, Enzymol. 358*, 275–280.
69. Gibbons, I., and Schachman, H. K. (1976) A method for the separation of hybrids of chromatographically identical oligomeric proteins. Use of 3,4,5,6-tetrahydrophthaloyl groups as a reversible "chromatographic handle", *Biochemistry 15*, 52–60.
70. Wang, C., Yang, Y. R., Hu, C. Y., and Schachman, H. K. (1981) Communication between subunits in aspartate transcarbamoylase. Effect of active site ligands on the tertiary structure of regulatory chains, *J. Biol. Chem. 256*, 7028–7034.
71. Johnson, R. S., and Schachman, H. K. (1983) Communication between catalytic and regulatory subunits in Ni(II)- and Co(II)-aspartate transcarbamoylase: Ligand-promoted structural alterations at the intersubunit bonding domains, *J. Biol. Chem. 258*, 3528–3538.
72. Johnson, R. S., and Schachman, H. K. (1980) Propagation of conformational changes in Ni(II)-substituted aspartate transcarbamoylase: Effect of active-site ligands on the regulatory chains, *Proc. Natl. Acad. Sci. U. S. A. 77*, 1995–1999.
73. Macol, C. P., Tsuruta, H., Stec, B., and Kantrowitz, E. R. (2001) Direct structural evidence for a concerted allosteric transition in *Escherichia coli* aspartate transcarbamoylase, *Nature Struct. Biol. 8*, 423–426.
74. Gouaux, J. E., and Lipscomb, W. N. (1990) Crystal structures of phosphonoacetamide ligated T and phosphonoacetamide and malonate ligated R states of aspartate carbamoyltransferase at 2.8 Å resolution and neutral pH, *Biochemistry 29*, 389–402.
75. Howlett, G. J., Blackburn, M. N., Compton, J. G., and Schachman, H. K. (1977) Allosteric regulation of aspartate transcarbamoylase: Analysis of the structural and functional behavior in terms of a two-state model, *Biochemistry 16*, 5091–5100.
76. Changeux, J. P., and Rubin, M. M. (1968) Allosteric interactions in aspartate transcarbamylase: 3. Interpretation of experimental data in terms of the model of Monod, Wyman, and Changeux, *Biochemistry 7*, 553–561.
77. Tsuruta, H., Kihara, H., Sano, T., Amemiya, Y., and Vachette, P. (2005) Influence of nucleotide effectors on the kinetics of the quaternary structure transition of allosteric aspar-

tate transcarbamylase, *J. Mol. Biol. 348*, 195–204.
78. Fetler, L., Tauc, P., Herve, G., Moody, M. F., and Vachette, P. (1995) X-Ray scattering titration of the quaternary structure transition of aspartate transcarbamylase with a bisubstrate analogue: Influence of nucleotide effectors, *J. Mol. Biol. 251*, 243–255.
79. Briggs, G. E., and Haldane, J. B. S. (1925) A note on the kinetics of enzyme action., *Biochem. J. 19*, 338–339.
80. Konishi, K., and Fujioka, M. (1988) Rat liver glycine methyltransferase. Cooperative binding of *S*-adenosylmethionine and loss of cooperativity by removal of a short NH_2-terminal segment, *J. Biol. Chem. 263*, 13381–13385.
81. Nissler, K., Kessler, R., Schellenberger, W., and Hofmann, E. (1977) Binding of fructose-6-phosphate to phosphofructokinase from yeast, *Biochem. Biophys. Res. Commun. 79*, 973–978.
82. Freyer, R., Eschrich, K., and Schellenberger, W. (1976) Kinetic modeling of yeast phosphofructokinase, *Stud. Biophys. 57*, 123–128.
83. Sanchez, J. E., Gross, P. G., Goetze, R. W., Walsh, R. M., Jr., Peeples, W. B., and Wood, Z. A. (2015) Evidence of kinetic cooperativity in dimeric ketopantoate reductase from *Staphylococcus aureus*, *Biochemistry 54*, 3360–3369.
84. Le Bras, G., and Garel, J. R. (1982) A proteolyzed derivative of *Escherichia coli* phosphofructokinase is no longer sensitive to allosteric effectors and still shows cooperativity in substrate binding, *Biochemistry 21*, 6656–6660.
85. Johnson, J. L., and Reinhart, G. D. (1992) MgATP and fructose 6-phosphate interactions with phosphofructokinase from *Escherichia coli*, *Biochemistry 31*, 11510–11518.
86. Mosser, R., Reddy, M. C. M., Bruning, J. B., Sacchettini, J. C., and Reinhart, G. D. (2013) Redefining the role of the quaternary shift in *Bacillus stearothermophilus* phosphofructokinase, *Biochemistry 52*, 5421–5429.
87. Auzat, I., Le Bras, G., and Garel, J. R. (1995) Hypercooperativity induced by interface mutations in the phosphofructokinase from *Escherichia coli*, *J. Mol. Biol. 246*, 248–253.
88. Koike, K., and Feigelson, P. (1971) Studies on the catalytic and allosteric sites in modulating the reactivity of tryptophan oxygenase with heme ligands. II. Carbon monoxide derivatives, *Biochemistry 10*, 3385–3390.
89. Koike, K., Poillon, W. N., and Feigelson, P. (1969) Influence of allosteric effector substances on the structure and catalytic activity of tryptophan oxygenase, *J. Biol. Chem. 244*, 3457–3462.
90. Neet, K. E., Keenan, R. P., and Tippett, P. S. (1990) Observation of a kinetic slow transition in monomeric glucokinase, *Biochemistry 29*, 770–777.
91. Whittington, A. C., Larion, M., Bowler, J. M., Ramsey, K. M., Bruschweiler, R., and Miller, B. G. (2015) Dual allosteric activation mechanisms in monomeric human glucokinase, *Proc. Natl. Acad. Sci. U. S. A. 112*, 11553–11558.
92. Schirch, L., and Quashnock, J. (1981) Evidence that tetrahydrofolate does not bind to serine hydroxymethyltransferase with positive homotropic cooperativity, *J. Biol. Chem. 256*, 6245–6249.
93. Gerhart, J. C., and Pardee, A. B. (1963) Effect of the feedback inhibitor, CTP, on subunit interactions of aspartic transcarbamylase, *Cold Spring Harbor Symp. Quant. Biol. 28*, 491–496.
94. Wild, J. R., Loughrey-Chen, S. J., and Corder, T. S. (1989) In the presence of CTP, UTP becomes an allosteric inhibitor of aspartate transcarbamoylase, *Proc. Natl. Acad. Sci. U. S. A. 86*, 46–50.
95. Peterson, A. W., Cockrell, G. M., and Kantrowitz, E. R. (2012) A second allosteric site in *Escherichia coli* aspartate transcarbamoylase, *Biochemistry 51*, 4776–4778.
96. Cockrell, G. M., and Kantrowitz, E. R. (2012) Metal ion involvement in the allosteric mechanism of *Escherichia coli* aspartate transcarbamoylase, *Biochemistry 51*, 7128–7137.
97. Potter, D., and Miziorko, H. M. (1997) Identification of catalytic residues in human mevalonate kinase, *J. Biol. Chem. 272*, 25449–25454.
98. Fu, Z., Voynova, N. E., Herdendorf, T. J., Miziorko, H. M., and Kim, J. J. (2008) Biochemical and structural basis for feedback inhibition of mevalonate kinase and isoprenoid metabolism, *Biochemistry 47*, 3715–3724.
99. Andi, B., West, A. H., and Cook, P. F. (2005) Regulatory mechanism of histidine-tagged

homocitrate synthase from *Saccharomyces cerevisiae*. I. Kinetic studies, *J. Biol. Chem. 280*, 31624–31632.
100. Bulfer, S. L., Scott, E. M., Pillus, L., and Trievel, R. C. (2010) Structural basis for L-lysine feedback inhibition of homocitrate synthase, *J. Biol. Chem. 285*, 10446–10453.
101. Sun, W., Shahinas, D., Bonvin, J., Hou, W., Kimber, M. S., Turnbull, J., and Christendat, D. (2009) The crystal structure of *Aquifex aeolicus* prephenate dehydrogenase reveals the mode of tyrosine inhibition, *J. Biol. Chem. 284*, 13223–13232.
102. Morollo, A. A., and Eck, M. J. (2001) Structure of the cooperative allosteric anthranilate synthase from *Salmonella typhimurium*, *Nature Struct. Biol. 8*, 243–247.
103. Spraggon, G., Kim, C., Nguyen-Huu, X., Yee, M. C., Yanofsky, C., and Mills, S. E. (2001) The structures of anthranilate synthase of *Serratia marcescens* crystallized in the presence of (I) its substrates, chorismate and glutamine, and a product, glutamate, and (II) its end-product inhibitor, L-tryptophan, *Proc. Natl. Acad. Sci. U. S. A. 98*, 6021–6026.
104. Caligiuri, M. G., and Bauerle, R. (1991) Subunit communication in the anthranilate synthase complex from *Salmonella typhimurium*, *Science 252*, 1845–1848.
105. Caligiuri, M. G., and Bauerle, R. (1991) Identification of amino acid residues involved in feedback regulation of the anthranilate synthase complex from *Salmonella typhimurium*: Evidence for an amino-terminal regulatory site, *J. Biol. Chem. 266*, 8328–8335.
106. Pilkis, S. J., El-Maghrabi, M. R., Pilkis, J., and Claus, T. (1981) Inhibition of fructose-1,6-bisphosphatase by fructose 2,6-bisphosphate, *J. Biol. Chem. 256*, 3619–3622.
107. Ke, H., Zhang, Y., and Lipscomb, W. N. (1990) Crystal structure of fructose-1,6-bisphosphatase complexed with fructose 6-phosphate, AMP, and magnesium, *Proc. Natl. Acad. Sci. U. S. A. 87*, 5243–5247.
108. Taketa, K., and Pogell, B. M. (1965) Allosteric inhibition of rat liver fructose 1,6-diphosphatase by adenosine 5′-monophosphate, *J. Biol. Chem. 240*, 651–662.
109. Underwood, A. H., and Newsholme, E. A. (1965) Some properties of fructose 1,6-diphosphatase of rat liver and their relation to the control of gluconeogenesis, *Biochem. J. 95*, 767–774.
110. Lorek, A., Wilson, K. S., Sansom, M. S., Stuart, D. I., Stura, E. A., Jenkins, J. A., Zanotti, G., Hajdu, J., and Johnson, L. N. (1984) Allosteric interactions of glycogen phosphorylase *b*: A crystallographic study of glucose 6-phosphate and inorganic phosphate binding to diimidate-cross-linked phosphorylase *b*, *Biochem. J. 218*, 45–60.
111. Barford, D., and Johnson, L. N. (1989) The allosteric transition of glycogen phosphorylase, *Nature (London, U. K.) 340*, 609–616.
112. Baskaran, S., Roach, P. J., DePaoli-Roach, A. A., and Hurley, T. D. (2010) Structural basis for glucose-6-phosphate activation of glycogen synthase, *Proc. Natl. Acad. Sci. U. S. A. 107*, 17563–17568.
113. Ramon-Maiques, S., Fernandez-Murga, M. L., Gil-Ortiz, F., Vagin, A., Fita, I., and Rubio, V. (2006) Structural bases of feed-back control of arginine biosynthesis, revealed by the structures of two hexameric *N*-acetylglutamate kinases, from *Thermotoga maritima* and *Pseudomonas aeruginosa*, *J. Mol. Biol. 356*, 695–713.
114. Ormo, M., Bystrom, C. E., and Remington, S. J. (1998) Crystal structure of a complex of *Escherichia coli* glycerol kinase and an allosteric effector fructose 1,6-bisphosphate, *Biochemistry 37*, 16565–16572.
115. MacRae, I. J., Segel, I. H., and Fisher, A. J. (2002) Allosteric inhibition via R-state destabilization in ATP sulfurylase from *Penicillium chrysogenum*, *Nature Struct. Biol. 9*, 945–949.
116. Grant, G. A., Xu, X. L., and Hu, Z. (2000) Role of an interdomain Gly-Gly sequence at the regulatory-substrate domain interface in the regulation of *Escherichia coli* D-3-phosphoglycerate dehydrogenase, *Biochemistry 39*, 7316–7319.
117. Thompson, J. R., Bell, J. K., Bratt, J., Grant, G. A., and Banaszak, L. J. (2005) V_{max} Regulation through domain and subunit changes. The active form of phosphoglycerate dehydrogenase, *Biochemistry 44*, 5763–5773.
118. Thomson, C. M., Alphey, M. S., Fisher, G., and da Silva, R. G. (2019) Mapping the structural path for allosteric inhibition of a short-form ATP phosphoribosyltransferase by histidine, *Biochemistry 58*, 3078–3086.
119. Vyazmensky, M., Sella, C., Barak, Z., and Chipman, D. M. (1996) Isolation and characterization of subunits of acetohydroxy acid

synthase isozyme III and reconstitution of the holoenzyme, *Biochemistry 35*, 10339–10346.
120. Pang, S. S., and Duggleby, R. G. (1999) Expression, purification, characterization, and reconstitution of the large and small subunits of yeast acetohydroxyacid synthase, *Biochemistry 38*, 5222–5231.
121. Lee, Y. T., and Duggleby, R. G. (2001) Identification of the regulatory subunit of *Arabidopsis thaliana* acetohydroxyacid synthase and reconstitution with its catalytic subunit, *Biochemistry 40*, 6836–6844.
122. Gill, G. N., and Garren, L. D. (1971) Role of the receptor in the mechanism of action of adenosine 3′,5′-cyclic monophosphate, *Proc. Natl. Acad. Sci. U. S. A. 68*, 786–790.
123. Kim, C., Xuong, N. H., and Taylor, S. S. (2005) Crystal structure of a complex between the catalytic and regulatory (RIα) subunits of PKA, *Science 307*, 690–696.
124. Lonhienne, T., Low, Y. S., Garcia, M. D., Croll, T., Gao, Y., Wang, Q., Brillault, L., Williams, C. M., Fraser, J. A., McGeary, R. P., West, N. P., Landsberg, M. J., Rao, Z., Schenk, G., and Guddat, L. W. (2020) Structures of fungal and plant acetohydroxyacid synthases, *Nature (London, U. K.) 586*, 317–321.
125. Anderson, K. S., Miles, E. W., and Johnson, K. A. (1991) Serine modulates substrate channeling in tryptophan synthase: A novel intersubunit triggering mechanism, *J. Biol. Chem. 266*, 8020–8033.
126. Schneider, T. R., Gerhardt, E., Lee, M., Liang, P. H., Anderson, K. S., and Schlichting, I. (1998) Loop closure and intersubunit communication in tryptophan synthase, *Biochemistry 37*, 5394–5406.
127. Niks, D., Hilario, E., Dierkers, A., Ngo, H., Borchardt, D., Neubauer, T. J., Fan, L., Mueller, L. J., and Dunn, M. F. (2013) Allostery and substrate channeling in the tryptophan synthase bienzyme complex: Evidence for two subunit conformations and four quaternary states, *Biochemistry 52*, 6396–6411.
128. Ngo, H., Harris, R., Kimmich, N., Casino, P., Niks, D., Blumenstein, L., Barends, T. R., Kulik, V., Weyand, M., Schlichting, I., and Dunn, M. F. (2007) Synthesis and characterization of allosteric probes of substrate channeling in the tryptophan synthase bienzyme complex, *Biochemistry 46*, 7713–7727.
129. Ngo, H., Kimmich, N., Harris, R., Niks, D., Blumenstein, L., Kulik, V., Barends, T. R., Schlichting, I., and Dunn, M. F. (2007) Allosteric regulation of substrate channeling in tryptophan synthase: Modulation of the L-serine reaction in stage I of the β-reaction by α-site ligands, *Biochemistry 46*, 7740–7753.
130. Casino, P., Niks, D., Ngo, H., Pan, P., Brzovic, P., Blumenstein, L., Barends, T. R., Schlichting, I., and Dunn, M. F. (2007) Allosteric regulation of tryptophan synthase channeling: The internal aldimine probed by *trans*-3-indole-3′-acrylate binding, *Biochemistry 46*, 7728–7739.
131. Weyand, M., and Schlichting, I. (1999) Crystal structure of wild-type tryptophan synthase complexed with the natural substrate indole-3-glycerol phosphate, *Biochemistry 38*, 16469–16480.
132. Xue, Y., Lipscomb, W. N., Graf, R., Schnappauf, G., and Braus, G. (1994) The crystal structure of allosteric chorismate mutase at 2.2 Å resolution, *Proc. Natl. Acad. Sci. U. S. A. 91*, 10814–10818.
133. Strater, N., Hakansson, K., Schnappauf, G., Braus, G., and Lipscomb, W. N. (1996) Crystal structure of the T state of allosteric yeast chorismate mutase and comparison with the R state, *Proc. Natl. Acad. Sci. U. S. A. 93*, 3330–3334.
134. Eriksson, M., Uhlin, U., Ramaswamy, S., Ekberg, M., Regnstrom, K., Sjoberg, B. M., and Eklund, H. (1997) Binding of allosteric effectors to ribonucleotide reductase protein R1: Reduction of active-site cysteines promotes substrate binding, *Structure 5*, 1077–1092.
135. Brown, N. C., and Reichard, P. (1969) Role of effector binding in allosteric control of ribonucleoside diphosphate reductase, *J. Mol. Biol. 46*, 39–55.
136. Changeux, J. P., and Edelstein, S. J. (2005) Allosteric mechanisms of signal transduction, *Science 308*, 1424–1428.
137. Webby, C. J., Jiao, W., Hutton, R. D., Blackmore, N. J., Baker, H. M., Baker, E. N., Jameson, G. B., and Parker, E. J. (2010) Synergistic allostery, a sophisticated regulatory network for the control of aromatic amino acid biosynthesis in *Mycobacterium tuberculosis*, *J. Biol. Chem. 285*, 30567–30576.
138. Shapiro, B. M., and Stadtman, E. R. (1968) 5′-Adenylyl-*O*-tyrosine. The novel phos-

phodiester residue of adenylylated glutamine synthetase from *Escherichia coli*, *J. Biol. Chem. 243*, 3769–3771.
139. Jiang, P., Mayo, A. E., and Ninfa, A. J. (2007) *Escherichia coli* glutamine synthetase adenylyltransferase (ATase, EC 2.7.7.49): Kinetic characterization of regulation by PII, PII-UMP, glutamine, and α-ketoglutarate, *Biochemistry 46*, 4133–4146.
140. Dobson, R. C., Griffin, M. D., Jameson, G. B., and Gerrard, J. A. (2005) The crystal structures of native and (*S*)-lysine-bound dihydrodipicolinate synthase from *Escherichia coli* with improved resolution show new features of biological significance, *Acta Crystallogr., Sect. D: Biol. Crystallogr. 61*, 1116–1124.
141. Skovpen, Y. V., and Palmer, D. R. (2013) Dihydrodipicolinate synthase from *Campylobacter jejuni*: Kinetic mechanism of cooperative allosteric inhibition and inhibitor-induced substrate cooperativity, *Biochemistry 52*, 5454–5462.
142. Min, L., Jin, Z., Caldovic, L., Morizono, H., Allewell, N. M., Tuchman, M., and Shi, D. (2009) Mechanism of allosteric inhibition of *N*-acetyl-L-glutamate synthase by L-arginine, *J. Biol. Chem. 284*, 4873–4880.
143. Scarano, E., Geraci, G., and Rossi, M. (1967) Deoxycytidylate aminohydrolase. II. Kinetic properties. The activatory effect of deoxycytidine triphosphate and the inhibitory effect of deoxythymidine triphosphate, *Biochemistry 6*, 192–201.
144. Ikehara, Y., Arai, K., Furukawa, N., Ohno, T., Miyake, T., Fushinobu, S., Nakajima, M., Miyanaga, A., and Taguchi, H. (2014) The core of allosteric motion in *Thermus caldophilus* L-lactate dehydrogenase, *J. Biol. Chem. 289*, 31550–31564.
145. Sintchak, M. D., Arjara, G., Kellogg, B. A., Stubbe, J., and Drennan, C. L. (2002) The crystal structure of class II ribonucleotide reductase reveals how an allosterically regulated monomer mimics a dimer, *Nature Struct. Biol. 9*, 293–300.
146. Vitols, E., Brownson, C., Gardiner, W., and Blakley, R. L. (1967) Cobamides and ribonucleotide reduction. V. A kinetic study of the ribonucleoside triphosphate reductase of *Lactobacillus leichmannii*, *J. Biol. Chem. 242*, 3035–3041.
147. Beck, W. S. (1967) Regulation of cobamide-dependent ribonucleotide reductase by allosteric effectors and divalent cations, *J. Biol. Chem. 242*, 3148–3158.
148. Eliasson, R., Pontis, E., Jordan, A., and Reichard, P. (1999) Allosteric control of three B_{12}-dependent (class II) ribonucleotide reductases. Implications for the evolution of ribonucleotide reduction, *J. Biol. Chem. 274*, 7182–7189.
149. Panagou, D., Orr, M. D., Dunstone, J. R., and Blakley, R. L. (1972) A monomeric, allosteric enzyme with a single polypeptide chain. Ribonucleotide reductase of *Lactobacillus leichmannii*, *Biochemistry 11*, 2378–2388.
150. Tu, J. I., and Graves, D. J. (1973) Association-dissociation properties of sodium borohydride-reduced phosphorylase b, *J. Biol. Chem. 248*, 4617–4622.
151. Johnson, J. L., and Reinhart, G. D. (1997) Failure of a two-state model to describe the influence of phospho(*enol*)pyruvate on phosphofructokinase from *Escherichia coli*, *Biochemistry 36*, 12814–12822.
152. Blackmore, N. J., Reichau, S., Jiao, W., Hutton, R. D., Baker, E. N., Jameson, G. B., and Parker, E. J. (2013) Three sites and you are out: Ternary synergistic allostery controls aromatic amino acid biosynthesis in *Mycobacterium tuberculosis*, *J. Mol. Biol. 425*, 1582–1592.
153. Shiman, R., Jones, S. H., and Gray, D. W. (1990) Mechanism of phenylalanine regulation of phenylalanine hydroxylase, *J. Biol. Chem. 265*, 11633–11642.
154. Knappskog, P. M., Flatmark, T., Aarden, J. M., Haavik, J., and Martinez, A. (1996) Structure/function relationships in human phenylalanine hydroxylase: Effect of terminal deletions on the oligomerization, activation and cooperativity of substrate binding to the enzyme, *Eur. J. Biochem. 242*, 813–821.
155. Hubner, G., Weidhase, R., and Schellenberger, A. (1978) The mechanism of substrate activation of pyruvate decarboxylase: A first approach, *Eur. J. Biochem. 92*, 175–181.
156. Dyda, F., Furey, W., Swaminathan, S., Sax, M., Farrenkopf, B., and Jordan, F. (1993) Catalytic centers in the thiamin diphosphate dependent enzyme pyruvate decarboxylase at 2.4 Å resolution, *Biochemistry 32*, 6165–6170.
157. Koon, N., Squire, C. J., and Baker, E. N. (2004) Crystal structure of LeuA from *Mycobacterium tuberculosis*, a key enzyme in leu-

cine biosynthesis, *Proc. Natl. Acad. Sci. U. S. A. 101*, 8295–8300.
158. Casey, A. K., Schwalm, E. L., Hays, B. N., and Frantom, P. A. (2013) V-type allosteric inhibition is described by a shift in the rate-determining step for α-isopropylmalate synthase from *Mycobacterium tuberculosis*, *Biochemistry 52*, 6737–6739.
159. Lietzan, A. D., Menefee, A. L., Zeczycki, T. N., Kumar, S., Attwood, P. V., Wallace, J. C., Cleland, W. W., and St Maurice, M. (2011) Interaction between the biotin carboxyl carrier domain and the biotin carboxylase domain in pyruvate carboxylase from *Rhizobium etli*, *Biochemistry 50*, 9708–9723.
160. Legge, G. B., Branson, J. P., and Attwood, P. V. (1996) Effects of acetyl CoA on the pre-steady-state kinetics of the biotin carboxylation reaction of pyruvate carboxylase, *Biochemistry 35*, 3849–3856.
161. Oberfelder, R. W., Lee, L. L., and Lee, J. C. (1984) Thermodynamic linkages in rabbit muscle pyruvate kinase: Kinetic, equilibrium, and structural studies, *Biochemistry 23*, 3813–3821.
162. Oshima, Y., Matsuura, M., and Horiuchi, T. (1972) Conformational change of the lac repressor induced with the inducer, *Biochem. Biophys. Res. Commun. 47*, 1444–1450.
163. Perutz, M. F., Ladner, J. E., Simon, S. R., and Ho, C. (1974) Influence of globin structure on the state of the heme: I. Human deoxyhemoglobin, *Biochemistry 13*, 2163–2173.
164. Sowole, M. A., Simpson, S., Skovpen, Y. V., Palmer, D. R., and Konermann, L. (2016) Evidence of allosteric enzyme regulation via changes in conformational dynamics: A hydrogen/deuterium exchange investigation of dihydrodipicolinate synthase, *Biochemistry 55*, 5413–5422.
165. Conly, C. J., Skovpen, Y. V., Li, S., Palmer, D. R., and Sanders, D. A. (2014) Tyrosine 110 plays a critical role in regulating the allosteric inhibition of *Campylobacter jejuni* dihydrodipicolinate synthase by lysine, *Biochemistry 53*, 7396–7406.
166. Mathias, M. M., and Kemp, R. G. (1972) Allosteric properties of muscle phosphofructokinase: 3. Thiol reactivity as an indicator of conformational state, *Biochemistry 11*, 578–584.
167. Hatzakis, N. S., Wei, L., Jørgensen, S. K., Kunding, A. H., Bolinger, P. Y., Ehrlich, N., Makarov, I., Skjot, M., Svendsen, A., Hedegard, P., and Stamou, D. (2012) Single enzyme studies reveal the existence of discrete functional states for monomeric enzymes and how they are "selected" upon allosteric regulation, *J. Am. Chem. Soc. 134*, 9296–9302.
168. Bruschweiler, S., Schanda, P., Kloiber, K., Brutscher, B., Kontaxis, G., Konrat, R., and Tollinger, M. (2009) Direct observation of the dynamic process underlying allosteric signal transmission, *J. Am. Chem. Soc. 131*, 3063–3068.
169. Van Schaftingen, E., Jett, M. F., Hue, L., and Hers, H. G. (1981) Control of liver 6-phosphofructokinase by fructose 2,6-bisphosphate and other effectors, *Proc. Natl. Acad. Sci. U. S. A. 78*, 3483–3486.
170. Van Schaftingen, E., and Hers, H. G. (1981) Inhibition of fructose-1,6-bisphosphatase by fructose 2,6-biphosphate, *Proc. Natl. Acad. Sci. U. S. A. 78*, 2861–2863.
171. Consler, T. G., Uberbacher, E. C., Bunick, G. J., Liebman, M. N., and Lee, J. C. (1988) Domain interaction in rabbit muscle pyruvate kinase. II. Small angle neutron scattering and computer simulation, *J. Biol. Chem. 263*, 2794–2801.
172. Yuan, M., McNae, I. W., Chen, Y., Blackburn, E. A., Wear, M. A., Michels, P. A. M., Fothergill-Gilmore, L. A., Hupp, T., and Walkinshaw, M. D. (2018) An allostatic mechanism for M2 pyruvate kinase as an amino-acid sensor, *Biochem. J. 475*, 1821–1837.
173. Eisenstein, E., Markby, D. W., and Schachman, H. K. (1990) Heterotropic effectors promote a global conformational change in aspartate transcarbamoylase, *Biochemistry 29*, 3724–3731.
174. Fetler, L., Kantrowitz, E. R., and Vachette, P. (2007) Direct observation in solution of a preexisting structural equilibrium for a mutant of the allosteric aspartate transcarbamoylase, *Proc. Natl. Acad. Sci. U. S. A. 104*, 495–500.
175. Shumilin, I. A., Zhao, C., Bauerle, R., and Kretsinger, R. H. (2002) Allosteric inhibition of 3-deoxy-D-arabino-heptulosonate-7-phosphate synthase alters the coordination of both substrates, *J. Mol. Biol. 320*, 1147–1156.
176. Ke, H. M., Liang, J. Y., Zhang, Y. P., and Lipscomb, W. N. (1991) Conformational transition of fructose-1,6-bisphosphatase: Structure comparison between the AMP complex

(T form) and the fructose 6-phosphate complex (R form), *Biochemistry 30*, 4412–4420.
177. Liu, X., Pavlovsky, A. G., and Viola, R. E. (2008) The structural basis for allosteric inhibition of a threonine-sensitive aspartokinase, *J. Biol. Chem. 283*, 16216–16225.
178. Johansson, K., Ramaswamy, S., Saarinen, M., Lemaire-Chamley, M., Issakidis-Bourguet, E., Miginiac-Maslow, M., and Eklund, H. (1999) Structural basis for light activation of a chloroplast enzyme: The structure of sorghum NADP-malate dehydrogenase in its oxidized form, *Biochemistry 38*, 4319–4326.
179. Velyvis, A., Schachman, H. K., and Kay, L. E. (2009) Application of methyl-TROSY NMR to test allosteric models describing effects of nucleotide binding to aspartate transcarbamoylase, *J. Mol. Biol. 387*, 540–547.
180. Grant, G. A. (2017) Regulatory mechanism of *Mycobacterium tuberculosis* phosphoserine phosphatase SerB2, *Biochemistry 56*, 6481–6490.
181. Sprang, S. R., Withers, S. G., Goldsmith, E. J., Fletterick, R. J., and Madsen, N. B. (1991) Structural basis for the activation of glycogen phosphorylase *b* by adenosine monophosphate, *Science 254*, 1367–1371.
182. Barford, D., Hu, S. H., and Johnson, L. N. (1991) Structural mechanism for glycogen phosphorylase control by phosphorylation and AMP, *J. Mol. Biol. 218*, 233–260.
183. Johnson, L. N., Snape, P., Martin, J. L., Acharya, K. R., Barford, D., and Oikonomakos, N. G. (1993) Crystallographic binding studies on the allosteric inhibitor glucose-6-phosphate to T state glycogen phosphorylase *b*, *J. Mol. Biol. 232*, 253–267.
184. Blickling, S., Beisel, H. G., Bozic, D., Knablein, J., Laber, B., and Huber, R. (1997) Structure of dihydrodipicolinate synthase of *Nicotiana sylvestris* reveals novel quaternary structure, *J. Mol. Biol. 274*, 608–621.
185. Villeret, V., Huang, S., Zhang, Y., and Lipscomb, W. N. (1995) Structural aspects of the allosteric inhibition of fructose-1,6-bisphosphatase by AMP: The binding of both the substrate analogue 2,5-anhydro-D-glucitol 1,6-bisphosphate and catalytic metal ions monitored by X-ray crystallography, *Biochemistry 34*, 4307–4315.
186. Hines, J. K., Chen, X., Nix, J. C., Fromm, H. J., and Honzatko, R. B. (2007) Structures of mammalian and bacterial fructose-1,6-bisphosphatase reveal the basis for synergism in AMP/fructose 2,6-bisphosphate inhibition, *J. Biol. Chem. 282*, 36121–36131.
187. Faehnle, C. R., Liu, X., Pavlovsky, A., and Viola, R. E. (2006) The initial step in the archaeal aspartate biosynthetic pathway catalyzed by a monofunctional aspartokinase, *Acta Crystallogr., Sect. F: Struct. Biol. Commun. 62*, 962–966.
188. Tauc, P., Leconte, C., Kerbiriou, D., Thiry, L., and Herve, G. (1982) Coupling of homotropic and heterotropic interactions in *Escherichia coli* aspartate transcarbamylase, *J. Mol. Biol. 155*, 155–168.
189. Fetler, L., and Vachette, P. (2001) The allosteric activator Mg-ATP modifies the quaternary structure of the R-state of *Escherichia coli* aspartate transcarbamylase without altering the T↔R equilibrium, *J. Mol. Biol. 309*, 817–832.
190. Hensley, P., and Schachman, H. K. (1979) Communication between dissimilar subunits in aspartate transcarbamoylase: Effect of inhibitor and activator on the conformation of the catalytic polypeptide chains, *Proc. Natl. Acad. Sci. U. S. A. 76*, 3732–3736.
191. Lovell, S. C., Mullick, A. H., and Muirhead, H. (1998) Cooperativity in *Bacillus stearothermophilus* pyruvate kinase, *J. Mol. Biol. 276*, 839–851.
192. Kerbiriou, D., and Herve, G. (1972) Biosynthesis of an aspartate transcarbamylase lacking co-operative interactions. I. Disconnection of homotropic and heterotropic interactions under the influence of 2-thiouracil, *J. Mol. Biol. 64*, 379–392.
193. Middleton, S. A., and Kantrowitz, E. R. (1988) Function of arginine-234 and aspartic acid-271 in domain closure, cooperativity, and catalysis in *Escherichia coli* aspartate transcarbamylase, *Biochemistry 27*, 8653–8660.
194. Newton, C. J., and Kantrowitz, E. R. (1990) Importance of domain closure for homotropic cooperativity in *Escherichia coli* aspartate transcarbamylase, *Biochemistry 29*, 1444–1451.
195. Grant, G. A., Xu, X. L., and Hu, Z. (1999) The relationship between effector binding and inhibition of activity in D-3-phosphoglycerate dehydrogenase, *Protein Sci. 8*, 2501–2505.
196. Grant, G. A., Hu, Z., and Xu, X. L. (2001) Amino acid residue mutations uncouple cooperative effects in *Escherichia coli* D-3-phos-

phoglycerate dehydrogenase, *J. Biol. Chem. 276*, 17844–17850.
197. Schnappauf, G., Lipscomb, W. N., and Braus, G. H. (1998) Separation of inhibition and activation of the allosteric yeast chorismate mutase, *Proc. Natl. Acad. Sci. U. S. A. 95*, 2868–2873.
198. Gorman, S. D., and Boehr, D. D. (2019) Energy and enzyme activity landscapes of yeast chorismate mutase at cellular concentrations of allosteric effectors, *Biochemistry 58*, 4058–4069.
199. Campbell, I. D., Dwek, R. A., Price, N. C., and Radda, G. K. (1972) Studies on the interaction of ligands with phosphorylase *b* using a spin-label probe, *Eur. J. Biochem. 30*, 339–347.
200. Henry, E. R., Bettati, S., Hofrichter, J., and Eaton, W. A. (2002) A tertiary two-state allosteric model for hemoglobin, *Biophys. Chem. 98*, 149–164.
201. Favrot, L., Amorim Franco, T. M., and Blanchard, J. S. (2018) Biochemical characterization of the *Mycobacterium smegmatis* threonine deaminase, *Biochemistry 57*, 6003–6012.
202. McGresham, M. S., Lovingshimer, M., and Reinhart, G. D. (2014) Allosteric regulation in phosphofructokinase from the extreme thermophile *Thermus thermophilus*, *Biochemistry 53*, 270–278.
203. Calhoun, D. H., Rimerman, R. A., and Hatfield, G. W. (1973) Threonine deaminase from *Escherichia coli*. I. Purification and properties, *J. Biol. Chem. 248*, 3511–3516.
204. Tomozawa, Y., and Wolfenden, R. (1970) Binding of guanosine triphosphate and adenosine triphosphate by rabbit muscle adenosine monophosphate deaminase, *Biochemistry 9*, 3400–3404.
205. Kumpaisal, R., Hashimoto, T., and Yamada, Y. (1987) Purification and characterization of dihydrodipicolinate synthase from wheat suspension cultures, *Plant Physiol. 85*, 145–151.
206. Spinka, M., Seiferheld, S., Zimmermann, P., Bergner, E., Blume, A. K., Schierhorn, A., Reichenbach, T., Pertermann, R., Ehrt, C., and Konig, S. (2017) Significance of individual residues at the regulatory site of yeast pyruvate decarboxylase for allosteric substrate activation, *Biochemistry 56*, 1285–1298.
207. Naught, L. E., Gilbert, S., Imhoff, R., Snook, C., Beamer, L., and Tipton, P. (2002) Allosterism and cooperativity in *Pseudomonas aeruginosa* GDP-mannose dehydrogenase, *Bio-Biochemistry 41*, 9637–9645.
208. Akowski, J. P., and Bauerle, R. (1997) Steady-state kinetics and inhibitor binding of 3-deoxy-D-arabino-heptulosonate-7-phosphate synthase (tryptophan sensitive) from *Escherichia coli*, *Biochemistry 36*, 15817–15822.
209. Zhu, X., Byrnes, M., Nelson, J. W., and Chang, S. H. (1995) Role of glycine 212 in the allosteric behavior of phosphofructokinase from *Bacillus stearothermophilus*, *Biochemistry 34*, 2560–2565.
210. Maeba, P., and Sanwal, B. D. (1969) Phosphoenolpyruvate carboxylase of *Salmonella*. Some chemical and allosteric properties, *J. Biol. Chem. 244*, 2549–2557.
211. Helmreich, E., and Cori, C. F. (1964) The role of adenylic acid in the activation of phosphorylase, *Proc. Natl. Acad. Sci. U. S. A. 51*, 131–138.
212. Cori, C. F., and Cori, G. T. (1936) Mechanism of formation of hexosemonophosphate in muscle and isolation of a new phosphate ester, *Proc. Soc. Exp. Biol. Med. 34*, 702–705.
213. Fletterick, R. J., and Madsen, N. B. (1980) The structures and related functions of phosphorylase *a*, *Annu. Rev. Biochem. 49*, 31–61.
214. Sprang, S., and Fletterick, R. J. (1979) The structure of glycogen phosphorylase *a* at 2.5 Å resolution, *J. Mol. Biol. 131*, 523–551.
215. Stalmans, W., Laloux, M., and Hers, H. G. (1974) The interaction of liver phosphorylase *a* with glucose and AMP, *Eur. J. Biochem. 49*, 415–427.
216. Sprang, S., Fletterick, R., Stern, M., Yang, D., Madsen, N., and Sturtevant, J. (1982) Analysis of an allosteric binding site: The nucleoside inhibitor site of phosphorylase *a*, *Biochemistry 21*, 2036–2048.
217. Kasvinsky, P. J., Shechosky, S., and Fletterick, R. J. (1978) Synergistic regulation of phosphorylase *a* by glucose and caffeine, *J. Biol. Chem. 253*, 9102–9106.
218. Kasvinsky, P. J., Madsen, N. B., Fletterick, R. J., and Sygusch, J. (1978) X-ray crystallographic and kinetic studies of oligosaccharide binding to phosphorylase, *J. Biol. Chem. 253*, 1290–1296.

219. Cammarata, M., Levantino, M., Wulff, M., and Cupane, A. (2010) Unveiling the timescale of the R-T transition in human hemoglobin, *J. Mol. Biol. 400*, 951–962.
220. Bjorling, S. C., Goldbeck, R. A., Paquette, S. J., Milder, S. J., and Kliger, D. S. (1996) Allosteric intermediates in hemoglobin: 1. Nanosecond time-resolved circular dichroism spectroscopy, *Biochemistry 35*, 8619–8627.
221. Goldbeck, R. A., Paquette, S. J., Bjorling, S. C., and Kliger, D. S. (1996) Allosteric intermediates in hemoglobin: 2. Kinetic modeling of HbCO photolysis, *Biochemistry 35*, 8628–8639.
222. Rodgers, K. R., and Spiro, T. G. (1994) Nanosecond dynamics of the R→T transition in hemoglobin: Ultraviolet raman studies, *Science 265*, 1697–1699.
223. Eckfeldt, J., Hammes, G. G., Mohr, S. C., and Wu, C. W. (1970) Relaxation spectra of aspartate transcarbamylase. I. Interaction of 5-bromocytidine triphosphate with native enzyme and regulatory subunit, *Biochemistry 9*, 3353–3362.
224. Ramaiah, A., and Tejwani, G. A. (1973) Interconvertible forms of phosphofructokinase of rabbit liver: The role of effectors on the interconversion, *Eur. J. Biochem. 39*, 183–192.
225. Singer, S. C., and Holmes, E. W. (1977) Human glutamine phosphoribosylpyrophosphate amidotransferase: Hysteretic properties, *J. Biol. Chem. 252*, 7959–7963.
226. Smith, L. C., Ravel, J. M., Lax, S. R., and Shive, W. (1962) The control of 3-deoxy-D-arabino-heptulosonic acid 7-phosphate synthesis by phenylalanine and tyrosine, *J. Biol. Chem. 237*, 3566–3570.
227. Smiley, K. L., and Suelter, C. H. (1967) Univalent cations as allosteric activators of muscle adenosine 5′-phosphate deaminase, *J. Biol. Chem. 242*, 1980–1981.
228. Fermi, G. (1975) Three-dimensional fourier synthesis of human deoxyhaemoglobin at 2.5 Å resolution: Refinement of the atomic model, *J. Mol. Biol. 97*, 237–256.
229. Shaanan, B. (1983) Structure of human oxyhaemoglobin at 2.1 Å resolution, *J. Mol. Biol. 171*, 31–59.
230. Baldwin, J. M. (1980) The structure of human carbonmonoxy haemoglobin at 2.7 Å resolution, *J. Mol. Biol. 136*, 103–128.
231. Chothia, C., Wodak, S., and Janin, J. (1976) Role of subunit interfaces in the allosteric mechanism of hemoglobin, *Proc. Natl. Acad. Sci. U. S. A. 73*, 3793–3797.
232. Ke, H., Thorpe, C. M., Seaton, B. A., Lipscomb, W. N., and Marcus, F. (1990) Structure refinement of fructose-1,6-bisphosphatase and its fructose 2,6-bisphosphate complex at 2.8 Å resolution, *J. Mol. Biol. 212*, 513–539.
233. Kyte, J. (2007) In *Structure in Protein Chemistry: Second Edition*, p 466, Garland Science, New York.
234. Kotaka, M., Ren, J., Lockyer, M., Hawkins, A. R., and Stammers, D. K. (2006) Structures of R- and T-state *Escherichia coli* aspartokinase III. Mechanisms of the allosteric transition and inhibition by lysine, *J. Biol. Chem. 281*, 31544–31552.
235. Funkhouser, J. D., Abraham, A., Smith, V. A., and Smith, W. G. (1974) Kinetic and molecular properties of lysine-sensitive aspartokinase. Factors influencing the lysine-mediated association reaction and their relationship to the cooperativity of lysine inhibition, *J. Biol. Chem. 249*, 5478–5484.
236. Smith, J. L., Zaluzec, E. J., Wery, J. P., Niu, L., Switzer, R. L., Zalkin, H., and Satow, Y. (1994) Structure of the allosteric regulatory enzyme of purine biosynthesis, *Science 264*, 1427–1433.
237. Holmes, E. W., Wyngaarden, J. B., and Kelley, W. N. (1973) Human glutamine phosphoribosylpyrophosphate amidotransferase. Two molecular forms interconvertible by purine ribonucleotides and phosphoribosylpyrophosphate, *J. Biol. Chem. 248*, 6035–6040.
238. Quinlan, R. J., and Reinhart, G. D. (2006) Effects of protein-ligand associations on the subunit interactions of phosphofructokinase from *B. stearothermophilus*, *Biochemistry 45*, 11333–11341.
239. Eisenstein, E. (1991) Cloning, expression, purification, and characterization of biosynthetic threonine deaminase from *Escherichia coli*, *J. Biol. Chem. 266*, 5801–5807.
240. Halgand, F., Wessel, P. M., Laprevote, O., and Dumas, R. (2002) Biochemical and mass spectrometric evidence for quaternary structure modifications of plant threonine deaminase induced by isoleucine, *Biochemistry 41*, 13767–13773.
241. Guidotti, G. (1967) Studies on the chemistry of hemoglobin: II. The effect of salts on the dissociation of hemoglobin into subunits, *J. Biol. Chem. 242*, 3685–3693.

242. Dai, Y. P., Lee, C. S., and O'Sullivan, W. J. (1995) Properties of uracil phosphoribosyltransferase from *Giardia intestinalis*, *Int. J. Parasitol. 25*, 207–214.
243. Schumacher, M. A., Bashor, C. J., Song, M. H., Otsu, K., Zhu, S., Parry, R. J., Ullman, B., and Brennan, R. G. (2002) The structural mechanism of GTP stabilized oligomerization and catalytic activation of the *Toxoplasma gondii* uracil phosphoribosyltransferase, *Proc. Natl. Acad. Sci. U. S. A. 99*, 78–83.
244. Karmali, A., Drake, A. F., and Spencer, N. (1983) Purification, properties and assay of D-ribulose 5-phosphate 3-epimerase from human erythrocytes, *Biochem. J. 211*, 617–623.
245. Liang, W., Ouyang, S., Shaw, N., Joachimiak, A., Zhang, R., and Liu, Z. J. (2011) Conversion of D-ribulose 5–phosphate to D-xylulose 5-phosphate: New insights from structural and biochemical studies on human RPE, *FASEB J. 25*, 497–504.
246. Andrell, J., Hicks, M. G., Palmer, T., Carpenter, E. P., Iwata, S., and Maher, M. J. (2009) Crystal structure of the acid-induced arginine decarboxylase from *Escherichia coli*: Reversible decamer assembly controls enzyme activity, *Biochemistry 48*, 3915–3927.
247. Breinig, S., Kervinen, J., Stith, L., Wasson, A. S., Fairman, R., Wlodawer, A., Zdanov, A., and Jaffe, E. K. (2003) Control of tetrapyrrole biosynthesis by alternate quaternary forms of porphobilinogen synthase, *Nat. Struct. Biol. 10*, 757–763.
248. Tang, L., Stith, L., and Jaffe, E. K. (2005) Substrate-induced interconversion of protein quaternary structure isoforms, *J. Biol. Chem. 280*, 15786–15793.
249. Mills-Davies, N., Butler, D., Norton, E., Thompson, D., Sarwar, M., Guo, J., Gill, R., Azim, N., Coker, A., Wood, S. P., Erskine, P. T., Coates, L., Cooper, J. B., Rashid, N., Akhtar, M., and Shoolingin-Jordan, P. M. (2017) Structural studies of substrate and product complexes of 5-aminolaevulinic acid dehydratase from humans, *Escherichia coli* and the hyperthermophile *Pyrobaculum calidifontis*, *Acta Crystallogr., Sect. D: Biol. Crystallogr. 73*, 9–21.
250. Schumacher, M. A., Carter, D., Scott, D. M., Roos, D. S., Ullman, B., and Brennan, R. G. (1998) Crystal structures of *Toxoplasma gondii* uracil phosphoribosyltransferase reveal the atomic basis of pyrimidine discrimination and prodrug binding, *EMBO J. 17*, 3219–3232.
251. Gallagher, D. T., Gilliland, G. L., Xiao, G., Zondlo, J., Fisher, K. E., Chinchilla, D., and Eisenstein, E. (1998) Structure and control of pyridoxal phosphate dependent allosteric threonine deaminase, *Structure 6*, 465–475.
252. Krahn, J. M., Kim, J. H., Burns, M. R., Parry, R. J., Zalkin, H., and Smith, J. L. (1997) Coupled formation of an amidotransferase interdomain ammonia channel and a phosphoribosyltransferase active site, *Biochemistry 36*, 11061–11068.
253. Evans, P. R., Farrants, G. W., and Hudson, P. J. (1981) Phosphofructokinase: Structure and control, *Philos. Trans. R. Soc., B 293*, 53–62.
254. Yu, P., and Pettigrew, D. W. (2003) Linkage between fructose 1,6-bisphosphate binding and the dimer-tetramer equilibrium of *Escherichia coli* glycerol kinase: Critical behavior arising from change of ligand stoichiometry, *Biochemistry 42*, 4243–4252.
255. Feese, M. D., Faber, H. R., Bystrom, C. E., Pettigrew, D. W., and Remington, S. J. (1998) Glycerol kinase from *Escherichia coli* and an Ala65→Thr mutant: The crystal structures reveal conformational changes with implications for allosteric regulation, *Structure 6*, 1407–1418.
256. Jencks, W. P. (1989) How does a calcium pump pump calcium?, *J. Biol. Chem. 264*, 18855–18858.
257. Skou, J. C. (1960) Further investigations on a $Mg^{++} + Na^{+}$-activated adenosintriphosphatase, possibly related to the active, linked transport of Na^{+} and K^{+} across the nerve membrane, *Biochim. Biophys. Acta 42*, 6–23.
258. Whittam, R. (1962) The asymmetrical stimulation of a membrane adenosine triphosphatase in relation to active cation transport, *Biochem. J. 84*, 110–118.
259. Whittam, R., and Ager, M. E. (1964) Vectorial aspects of adenosine-triphosphatase activity in erythrocyte membranes, *Biochem. J. 93*, 337–348.
260. Sharkey, R. G. (1983) Lactoperoxidase-catalyzed iodination of sodium and potassium ion-activated adenosine triphosphatase in the Madin-Darby canine kidney epithelial cell line and canine renal membranes, *Biochim. Biophys. Acta 730*, 327–341.

261. O'Connell, M. A. (1982) Exclusive labeling of the extracytoplasmic surface of sodium ion and potassium ion activated adenosinetriphosphatase and a determination of the distribution of surface area across the bilayer, *Biochemistry 21*, 5984–5991.
262. Jørgensen, P. L., Karlish, S. J., and Gitler, C. (1982) Evidence for the organization of the transmembrane segments of (Na,K)-ATPase based on labeling lipid-embedded and surface domains of the α-subunit, *J. Biol. Chem. 257*, 7435–7442.
263. Lytton, J., and MacLennan, D. H. (1988) Molecular cloning of cDNAs from human kidney coding for two alternatively spliced products of the cardiac Ca^{2+}-ATPase gene, *J. Biol. Chem. 263*, 15024–15031.
264. Rabon, E. C., McFall, T. L., and Sachs, G. (1982) The gastric [H,K]ATPase: H^+/ATP Stoichiometry, *J. Biol. Chem. 257*, 6296–6299.
265. Shin, J. M., Munson, K., and Sachs, G. (2011) Gastric H^+,K^+-ATPase, *Compr. Physiol. 1*, 2141–2153.
266. Skrabanja, A. T., van der Hijden, H. T., and De Pont, J. J. (1987) Transport ratios of reconstituted ($H^+ + K^+$)-ATPase, *Biochim. Biophys. Acta 903*, 434–440.
267. Hasselbach, W., and Makinose, M. (1963) On the mechanism of calcium transport across the membrane of the sarcoplasmic reticulum, *Biochem. Z. 339*, 94–111.
268. Chiesi, M., and Inesi, G. (1980) Adenosine 5′-triphosphate dependent fluxes of manganese and and hydrogen ions in sarcoplasmic reticulum vesicles, *Biochemistry 19*, 2912–2918.
269. Levy, D., Seigneuret, M., Bluzat, A., and Rigaud, J. L. (1990) Evidence for proton countertransport by the sarcoplasmic reticulum Ca^{2+}-ATPase during calcium transport in reconstituted proteoliposomes with low ionic permeability, *J. Biol. Chem. 265*, 19524–19534.
270. Niggli, V., Adunyah, E. S., Penniston, J. T., and Carafoli, E. (1981) Purified (Ca^{2+}-Mg^{2+})-ATPase of the erythrocyte membrane. Reconstitution and effect of calmodulin and phospholipids, *J. Biol. Chem. 256*, 395–401.
271. Greeb, J., and Shull, G. E. (1989) Molecular cloning of a third isoform of the calmodulin-sensitive plasma membrane Ca^{2+}-transporting ATPase that is expressed predominantly in brain and skeletal muscle, *J. Biol. Chem. 264*, 18569–18576.
272. Schatzmann, H. J., and Vincenzi, F. F. (1969) Calcium movements across the membrane of human red cells, *J. Physiol. 201*, 369–395.
273. Niggli, V., Sigel, E., and Carafoli, E. (1982) The purified Ca^{2+} pump of human erythrocyte membranes catalyzes an electroneutral Ca^{2+}-H^+ exchange in reconstituted liposomal systems, *J. Biol. Chem. 257*, 2350–2356.
274. Slayman, C. L., Long, W. S., and Lu, C. Y. (1973) The relationship between ATP and an electrogenic pump in the plasma membrane of *Neurospora crassa*, *J. Membr. Biol. 14*, 305–338.
275. Scarborough, G. A. (1976) The *Neurospora* plasma membrane ATPase is an electrogenic pump, *Proc. Natl. Acad. Sci. U. S. A. 73*, 1485–1488.
276. Hodges, T. K., Leonard, R. T., Bracker, C. E., and Keenan, T. W. (1972) Purification of an ion-stimulated adenosine triphosphatase from plant roots: Association with plasma membranes, *Proc. Natl. Acad. Sci. U. S. A. 69*, 3307–3311.
277. Pardo, J. M., and Serrano, R. (1989) Structure of a plasma membrane H^+-ATPase gene from the plant *Arabidopsis thaliana*, *J. Biol. Chem. 264*, 8557–8562.
278. Stroobant, P., and Scarborough, G. A. (1979) Active transport of calcium in *Neurospora* plasma membrane vesicles, *Proc. Natl. Acad. Sci. U. S. A. 76*, 3102–3106.
279. Wang, K., Sitsel, O., Meloni, G., Autzen, H. E., Andersson, M., Klymchuk, T., Nielsen, A. M., Rees, D. C., Nissen, P., and Gourdon, P. (2014) Structure and mechanism of Zn^{2+}-transporting P-type ATPases, *Nature (London, U. K.) 514*, 518–522.
280. Canfield, V. A., and Levenson, R. (1998) Domain swapping between Na,K- and H,K-ATPase identifies regions that specify Na,K-ATPase activity, *Biochemistry 37*, 7509–7516.
281. Kyte, J. (1972) Properties of the two polypeptides of sodium- and potassium-dependent adenosine triphosphatase, *J. Biol. Chem. 247*, 7642–7649.
282. Shull, G. E., Schwartz, A., and Lingrel, J. B. (1985) Amino-acid sequence of the catalytic subunit of the ($Na^+ + K^+$)ATPase deduced from a complementary DNA, *Nature (London, U. K.) 316*, 691–695.

283. Kawakami, K., Noguchi, S., Noda, M., Takahashi, H., Ohta, T., Kawamura, M., Nojima, H., Nagano, K., Hirose, T., Inayama, S., Hayashida, H., Miyata, T. and Numa, S. (1985) Primary structure of the α-subunit of *Torpedo californica* ($Na^+ + K^+$)ATPase deduced from cDNA sequence, *Nature (London, U. K.) 316*, 733–736.
284. Shull, G. E., Lane, L. K., and Lingrel, J. B. (1986) Amino-acid sequence of the β-subunit of the ($Na^+ + K^+$)ATPase deduced from a cDNA, *Nature (London, U. K.) 321*, 429–431.
285. Craig, W. S. (1982) Monomer of sodium and potassium ion activated adenosinetriphosphatase displays complete enzymatic function, *Biochemistry 21*, 5707–5717.
286. Zampighi, G., Kyte, J., and Freytag, W. (1984) Structural organization of ($Na^+ + K^+$)-ATPase in purified membranes, *J. Cell Biol. 98*, 1851–1864.
287. Nicholas, R. A. (1984) Purification of the membrane-spanning tryptic peptides of the α polypeptide from sodium and potassium ion activated adenosinetriphosphatase labeled with 1-tritiospiro[adamantane-4,3′-diazirine], *Biochemistry 23*, 888–898.
288. Shull, G. E., and Lingrel, J. B. (1986) Molecular cloning of the rat stomach ($H^+ + K^+$)-ATPase, *J. Biol. Chem. 261*, 16788–16791.
289. Shull, G. E., and Greeb, J. (1988) Molecular cloning of two isoforms of the plasma membrane Ca^{2+}-transporting ATPase from rat brain. Structural and functional domains exhibit similarity to Na^+,K^+- and other cation transport ATPases, *J. Biol. Chem. 263*, 8646–8657.
290. Kyte, J. (1974) The reactions of sodium and potassium ion-activated adenosine triphosphatase with specific antibodies. Implications for the mechanism of active transport, *J. Biol. Chem. 249*, 3652–3660.
291. Toyoshima, C., and Mizutani, T. (2004) Crystal structure of the calcium pump with a bound ATP analogue, *Nature (London, U. K.) 430*, 529–535.
292. Kanai, R., Ogawa, H., Vilsen, B., Cornelius, F., and Toyoshima, C. (2013) Crystal structure of a Na^+-bound Na^+,K^+-ATPase preceding the E1P state, *Nature (London, U. K.) 502*, 201–206.
293. MacLennan, D. H., Brandl, C. J., Korczak, B., and Green, N. M. (1985) Amino-acid sequence of a $Ca^{2+} + Mg^{2+}$-dependent ATPase from rabbit muscle sarcoplasmic reticulum, deduced from its complementary DNA sequence, *Nature (London, U. K.) 316*, 696–700.
294. Toyoshima, C., Nakasako, M., Nomura, H., and Ogawa, H. (2000) Crystal structure of the calcium pump of sarcoplasmic reticulum at 2.6 Å resolution, *Nature (London, U. K.) 405*, 647–655.
295. Morth, J. P., Pedersen, B. P., Toustrup-Jensen, M. S., Sorensen, T. L., Petersen, J., Andersen, J. P., Vilsen, B., and Nissen, P. (2007) Crystal structure of the sodium-potassium pump, *Nature (London, U. K.) 450*, 1043–1049.
296. Clarke, D. M., Loo, T. W., Inesi, G., and MacLennan, D. H. (1989) Location of high affinity Ca^{2+}-binding sites within the predicted transmembrane domain of the sarcoplasmic reticulum Ca^{2+}-ATPase, *Nature (London, U. K.) 339*, 476–478.
297. Nielsen, J. M., Pedersen, P. A., Karlish, S. J., and Jørgensen, P. L. (1998) Importance of intramembrane carboxylic acids for occlusion of K^+ ions at equilibrium in renal Na,K-ATPase, *Biochemistry 37*, 1961–1968.
298. Pedersen, P. A., Nielsen, J. M., Rasmussen, J. H., and Jørgensen, P. L. (1998) Contribution to Tl^+, K^+, and Na^+ binding of Asn776, Ser775, Thr774, Thr772, and Tyr771 in cytoplasmic part of fifth transmembrane segment in α-subunit of renal Na,K-ATPase, *Biochemistry 37*, 17818–17827.
299. Shinoda, T., Ogawa, H., Cornelius, F., and Toyoshima, C. (2009) Crystal structure of the sodium-potassium pump at 2.4 Å resolution, *Nature (London, U. K.) 459*, 446–450.
300. Toyoshima, C., Nomura, H., and Tsuda, T. (2004) Lumenal gating mechanism revealed in calcium pump crystal structures with phosphate analogues, *Nature (London, U. K.) 432*, 361–368.
301. Ma, J. C., and Dougherty, D. A. (1997) The cation–π interaction, *Chem. Rev. (Washington, DC, U. S.) 97*, 1303–1324.
302. Cornelius, F. (1988) Incorporation of $C_{12}E_8$–solubilized Na^+,K^+-ATPase into liposomes: Determination of sidedness and orientation, *Methods Enzymol. 156*, 156–167.
303. Ogawa, H., Shinoda, T., Cornelius, F., and Toyoshima, C. (2009) Crystal structure of the sodium-potassium pump (Na^+,K^+-ATPase)

with bound potassium and ouabain, *Proc. Natl. Acad. Sci. U. S. A. 106*, 13742–13747.
304. Laursen, M., Yatime, L., Nissen, P., and Fedosova, N. U. (2013) Crystal structure of the high-affinity Na^+K^+-ATPase-ouabain complex with Mg^{2+} bound in the cation binding site, *Proc. Natl. Acad. Sci. U. S. A. 110*, 10958–10963.
305. Monti, J. L. E., Montes, M. R., and Rossi, R. C. (2018) Steady-state analysis of enzymes with non-Michaelis-Menten kinetics: The transport mechanism of Na^+/K^+-ATPase, *J. Biol. Chem. 293*, 1373–1385.
306. Post, R. L., Hegyvary, C., and Kume, S. (1972) Activation by adenosine triphosphate in the phosphorylation kinetics of sodium and potassium ion transport adenosine triphosphatase, *J. Biol. Chem. 247*, 6530–6540.
307. Beauge, L. A., and Glynn, I. M. (1979) Occlusion of K ions in the unphosphorylated sodium pump, *Nature (London, U. K.) 280*, 510–512.
308. Glynn, I. M., and Richards, D. E. (1982) Occlusion of rubidium ions by the sodium-potassium pump: Its implications for the mechanism of potassium transport, *J. Physiol. (Oxford, U. K.) 330*, 17–43.
309. Toyoshima, C., and Nomura, H. (2002) Structural changes in the calcium pump accompanying the dissociation of calcium, *Nature (London, U. K.) 418*, 605–611.
310. Olesen, C., Sorensen, T. L., Nielsen, R. C., Moller, J. V., and Nissen, P. (2004) Dephosphorylation of the calcium pump coupled to counterion occlusion, *Science 306*, 2251–2255.
311. Karlish, S. J., and Yates, D. W. (1978) Tryptophan fluorescence of $(Na^+ + K^+)$-ATPase as a tool for study of the enzyme mechanism, *Biochim. Biophys. Acta 527*, 115–130.
312. Steinberg, M., and Karlish, S. J. (1989) Studies on conformational changes in Na,K-ATPase labeled with 5-iodoacetamidofluorescein, *J. Biol. Chem. 264*, 2726–2734.
313. Forbush, B., 3rd. (1987) Rapid release of ^{42}K and ^{86}Rb from an occluded state of the Na,K-pump in the presence of ATP or ADP, *J. Biol. Chem. 262*, 11104–11115.
314. Winther, A. M., Bublitz, M., Karlsen, J. L., Moller, J. V., Hansen, J. B., Nissen, P., and Buch-Pedersen, M. J. (2013) The sarcolipin-bound calcium pump stabilizes calcium sites exposed to the cytoplasm, *Nature (London, U. K.) 495*, 265–269.
315. Bublitz, M., Musgaard, M., Poulsen, H., Thogersen, L., Olesen, C., Schiott, B., Morth, J. P., Moller, J. V., and Nissen, P. (2013) Ion pathways in the sarcoplasmic reticulum Ca^{2+}-ATPase, *J. Biol. Chem. 288*, 10759–10765.
316. Sorensen, T. L., Moller, J. V., and Nissen, P. (2004) Phosphoryl transfer and calcium ion occlusion in the calcium pump, *Science 304*, 1672–1675.
317. Hoffman, J. F. (1962) The active transport of sodium by ghosts of human red blood cells, *J.Gen. Physiol. 45*, 837–859.
318. Post, R. L., Merritt, C. R., Kinsolving, C. R., and Albright, C. D. (1960) Membrane adenosine triphosphatase as a participant in the active transport of sodium and potassium in the human erythrocyte, *J. Biol. Chem. 235*, 1796–1802.
319. Hanel, A. M., and Jencks, W. P. (1991) Dissociation of calcium from the phosphorylated calcium-transporting adenosine triphosphatase of sarcoplasmic reticulum: Kinetic equivalence of the calcium ions bound to the phosphorylated enzyme, *Biochemistry 30*, 11320–11330.
320. Glynn, I. M., Hara, Y., and Richards, D. E. (1984) The occlusion of sodium ions within the mammalian sodium-potassium pump: Its role in sodium transport, *J. Physiol. (Oxford, U. K.) 351*, 531–547.
321. Nyblom, M., Poulsen, H., Gourdon, P., Reinhard, L., Andersson, M., Lindahl, E., Fedosova, N., and Nissen, P. (2013) Crystal structure of Na^+, K^+-ATPase in the Na^+-bound state, *Science 342*, 123–127.
322. Olesen, C., Picard, M., Winther, A. M., Gyrup, C., Morth, J. P., Oxvig, C., Moller, J. V., and Nissen, P. (2007) The structural basis of calcium transport by the calcium pump, *Nature (London, U. K.) 450*, 1036–1042.
323. Toyoshima, C., Norimatsu, Y., Iwasawa, S., Tsuda, T., and Ogawa, H. (2007) How processing of aspartylphosphate is coupled to lumenal gating of the ion pathway in the calcium pump, *Proc. Natl. Acad. Sci. U. S. A. 104*, 19831–19836.
324. Gregersen, J. L., Mattle, D., Fedosova, N. U., Nissen, P., and Reinhard, L. (2016) Isolation, crystallization and crystal structure determination of bovine kidney Na^+,K^+-ATPase, *Acta Crystallogr., Sect. F: Struct. Biol. Commun. 72*, 282–287.

325. Laursen, M., Gregersen, J. L., Yatime, L., Nissen, P., and Fedosova, N. U. (2015) Structures and characterization of digoxin- and bufalin-bound Na^+,K^+-ATPase compared with the ouabain-bound complex, *Proc. Natl. Acad. Sci. U. S. A. 112*, 1755–1760.
326. Yatime, L., Laursen, M., Morth, J. P., Esmann, M., Nissen, P., and Fedosova, N. U. (2011) Structural insights into the high affinity binding of cardiotonic steroids to the Na^+,K^+-ATPase, *J. Struct. Biol. 174*, 296–306.
327. Holmgren, M., Wagg, J., Bezanilla, F., Rakowski, R. F., De Weer, P., and Gadsby, D. C. (2000) Three distinct and sequential steps in the release of sodium ions by the Na^+/K^+-ATPase, *Nature (London, U. K.) 403*, 898–901.
328. Orlowski, S., and Champeil, P. (1991) The two calcium ions initially bound to non-phosphorylated sarcoplasmic reticulum Ca^{2+}-ATPase can no longer be kinetically distinguished when they dissociate from phosphorylated ATPase toward the lumen, *Biochemistry 30*, 11331–11342.
329. Tsunekawa, N., Ogawa, H., Tsueda, J., Akiba, T., and Toyoshima, C. (2018) Mechanism of the E2 to E1 transition in Ca^{2+} pump revealed by crystal structures of gating residue mutants, *Proc. Natl. Acad. Sci. U. S. A. 115*, 12722–12727.
330. Jørgensen, P. L. (1977) Purification and characterization of ($Na^+ + K^+$)-ATPase. VI. Differential tryptic modification of catalytic functions of the purified enzyme in presence of NaCl and KCl, *Biochim. Biophys. Acta 466*, 97–108.
331. Helmich-de Jong, M. L., van Emst-de Vries, S. E., and de Pont, J. J. (1987) Conformational states of ($K^+ + H^+$)-ATPase studied using tryptic digestion as a tool, *Biochim. Biophys. Acta 905*, 358–370.
332. Jørgensen, P. L., and Andersen, J. P. (1988) Structural basis for E1-E2 conformational transitions in Na,K-pump and Ca-pump proteins, *J. Membr. Biol. 103*, 95–120.
333. Kyte, J. (1972) The titration of the cardiac glycoside binding site of the ($Na^+ + K^+$)-adenosine triphosphatase, *J. Biol. Chem. 247*, 7634–7641.
334. Taniguchi, K., Suzuki, K., Kai, D., Matsuoka, I., Tomita, K., and Iida, S. (1984) Conformational change of sodium- and potassium-dependent adenosine triphosphatase. Conformational evidence for the Post-Albers mechanism in Na^+- and K^+-dependent hydrolysis of ATP, *J. Biol. Chem. 259*, 15228–15233.
335. Moczydlowski, E. G., and Fortes, P. A. (1981) Inhibition of sodium and potassium adenosine triphosphatase by 2′,3′-*O*-(2,4,6-trinitrocyclohexadienylidene) adenine nucleotides. Implications for the structure and mechanism of the Na:K pump, *J. Biol. Chem. 256*, 2357–2366.
336. Neet, K. E., and Green, N. M. (1977) Kinetics of the cooperativity of the Ca^{2+}-transporting adenosine triphosphatase of sarcoplasmic reticulum and the mechanism of the ATP interaction, *Arch. Biochem. Biophys. 178*, 588–597.
337. Degani, C., and Boyer, P. D. (1973) A borohydride reduction method for characterization of the acyl phosphate linkage in proteins and its application to sarcoplasmic reticulum adenosine triphosphatase, *J. Biol. Chem. 248*, 8222–8226.
338. Bastide, F., Meissner, G., Fleischer, S., and Post, R. L. (1973) Similarity of the active site of phosphorylation of the adenosine triphosphatase from transport of sodium and potassium ions in kidney to that for transport of calcium ions in the sarcoplasmic reticulum of muscle, *J. Biol. Chem. 248*, 8385–8391.
339. Keillor, J. W., and Jencks, W. P. (1996) Phosphorylation of the sodium--potassium adenosinetriphosphatase proceeds through a rate-limiting conformational change followed by rapid phosphoryl transfer, *Biochemistry 35*, 2750–2753.
340. Post, R. L., Kume, S., Tobin, T., Orcutt, B., and Sen, A. K. (1969) Flexibility of an active center in sodium-plus-potassium adenosine triphosphatase, *J. Gen. Physiol. 54*, 306–326.
341. Hara, Y., and Nakao, M. (1981) Sodium ion discharge from pig kidney Na^+, K^+-ATPase Na^+-dependency of the E1P⇌E2P equilibrium in the absence of KCl, *J. Biochem. (Tokyo) 90*, 923–931.
342. Fahn, S., Koval, G. J., and Albers, R. W. (1968) Sodium-potassium-activated adenosine triphosphatase of *Electrophorus* electric organ: V. Phosphorylation by adenosine triphosphate-^{32}P, *J. Biol. Chem. 243*, 1993–2002.
343. Siegel, G. J., Koval, G. J., and Albers, R. W. (1969) Sodium-potassium-activated adenosine triphosphatase. IV. Characterization of

the phosphoprotein formed from orthophosphate in the presence of ouabain, *J. Biol. Chem. 244*, 3264–3269.
344. Dahms, A. S., and Boyer, P. D. (1973) Occurrence and characteristics of ^{18}O exchange reactions catalyzed by sodium- and potassium-dependent adenosine triphosphatases, *J. Biol. Chem. 248*, 3155–3162.
345. Albers, R. W., Fahn, S., and Koval, G. J. (1963) The role of sodium ions in the activation of electrophorus electric organ adenosine triphosphatase, *Proc. Natl. Acad. Sci. U. S. A. 50*, 474–481.
346. Kanazawa, T., Saito, M., and Tonomura, Y. (1970) Formation and decomposition of a phosphorylated intermediate in the reaction of Na^+-K^+ dependent ATPase, *J. Biochem. (Tokyo) 67*, 693–711.
347. Norimatsu, Y., Hasegawa, K., Shimizu, N., and Toyoshima, C. (2017) Protein-phospholipid interplay revealed with crystals of a calcium pump, *Nature (London, U. K.) 545*, 193–198.
348. Jensen, A. M., Sorensen, T. L., Olesen, C., Moller, J. V., and Nissen, P. (2006) Modulatory and catalytic modes of ATP binding by the calcium pump, *EMBO J. 25*, 2305–2314.
349. Winther, A. M., Liu, H., Sonntag, Y., Olesen, C., le Maire, M., Soehoel, H., Olsen, C. E., Christensen, S. B., Nissen, P., and Moller, J. V. (2010) Critical roles of hydrophobicity and orientation of side chains for inactivation of sarcoplasmic reticulum Ca^{2+}-ATPase with thapsigargin and thapsigargin analogs, *J. Biol. Chem. 285*, 28883–28892.
350. Cavieres, J. D., and Glynn, I. M. (1976) Na-Na exchange by the Na pump requires ATP as well as ADP [proceedings], *J. Physiol. (Oxford, U. K.) 263*, 214P–215P.
351. Glynn, I. M., and Hoffman, J. F. (1971) Nucleotide requirements for sodium-sodium exchange catalysed by the sodium pump in human red cells, *J. Physiol. (Oxford, U. K.) 218*, 239–256.
352. Simons, T. J. (1974) Potassium: potassium exchange catalysed by the sodium pump in human red cells, *J. Physiol. (Oxford, U. K.) 237*, 123–155.
353. Lew, V. L., Glynn, I. M., and Ellory, J. C. (1970) Net synthesis of ATP by reversal of the sodium pump, *Nature (London, U. K.) 225*, 865–866.
354. Kasahara, M., and Penefsky, H. S. (1978) High affinity binding of monovalent P_i by beef heart mitochondrial adenosine triphosphatase, *J. Biol. Chem. 253*, 4180–4187.
355. Silverstein, T. P. (2014) An exploration of how the thermodynamic efficiency of bioenergetic membrane systems varies with c-subunit stoichiometry of F_1F_0 ATP synthases, *J. Bioenerg. Biomembr. 46*, 229–241.
356. Laubinger, W., and Dimroth, P. (1988) Characterization of the ATP synthase of *Propionigenium modestum* as a primary sodium pump, *Biochemistry 27*, 7531–7537.
357. Zhao, J., Benlekbir, S., and Rubinstein, J. L. (2015) Electron cryomicroscopy observation of rotational states in a eukaryotic V-ATPase, *Nature (London, U. K.) 521*, 241–245.
358. Ruhle, T., and Leister, D. (2015) Assembly of F_1F_0-ATP synthases, *Biochim. Biophys. Acta 1847*, 849–860.
359. Pullman, M. E., Penefsky, H. S., Datta, A., and Racker, E. (1960) Partial resolution of the enzymes catalyzing oxidative phosphorylation. I. Purification and properties of soluble dinitrophenol-stimulated adenosine triphosphatase, *J. Biol. Chem. 235*, 3322–3329.
360. Knowles, A. F., and Penefsky, H. S. (1972) The subunit structure of beef heart mitochondrial adenosine triphosphatase: Isolation procedures, *J. Biol. Chem. 247*, 6617–6623.
361. Brooks, J. C., and Senior, A. E. (1972) Methods for purification of each subunit of the mitochondrial oligomycin-insensitive adenosine triphosphatase, *Biochemistry 11*, 4675–4678.
362. Lutter, R., Abrahams, J. P., van Raaij, M. J., Todd, R. J., Lundqvist, T., Buchanan, S. K., Leslie, A. G., and Walker, J. E. (1993) Crystallization of F_1-ATPase from bovine heart mitochondria, *J. Mol. Biol. 229*, 787–790.
363. Abrahams, J. P., Leslie, A. G., Lutter, R., and Walker, J. E. (1994) Structure at 2.8 Å resolution of F_1-ATPase from bovine heart mitochondria, *Nature (London, U. K.) 370*, 621–628.
364. Gibbons, C., Montgomery, M. G., Leslie, A. G., and Walker, J. E. (2000) The structure of the central stalk in bovine F_1-ATPase at 2.4 Å resolution, *Nature Struct. Biol. 7*, 1055–1061.
365. Bowler, M. W., Montgomery, M. G., Leslie, A. G., and Walker, J. E. (2006) How azide inhib-

its ATP hydrolysis by the F-ATPases, *Proc. Natl. Acad. Sci. U. S. A. 103*, 8646–8649.
366. Bowler, M. W., Montgomery, M. G., Leslie, A. G., and Walker, J. E. (2007) Ground state structure of F_1-ATPase from bovine heart mitochondria at 1.9 Å resolution, *J. Biol. Chem. 282*, 14238–14242.
367. Shirakihara, Y., Leslie, A. G., Abrahams, J. P., Walker, J. E., Ueda, T., Sekimoto, Y., Kambara, M., Saika, K., Kagawa, Y., and Yoshida, M. (1997) The crystal structure of the nucleotide-free $\alpha_3\beta_3$ subcomplex of F_1-ATPase from the thermophilic *Bacillus* PS3 is a symmetric trimer, *Structure 5*, 825–836.
368. Shirakihara, Y., Shiratori, A., Tanikawa, H., Nakasako, M., Yoshida, M., and Suzuki, T. (2015) Structure of a thermophilic F_1-ATPase inhibited by an ε-subunit: Deeper insight into the ε-inhibition mechanism, *FEBS J. 282*, 2895–2913.
369. Bianchet, M. A., Hullihen, J., Pedersen, P. L., and Amzel, L. M. (1998) The 2.8 Å structure of rat liver F_1-ATPase: Configuration of a critical intermediate in ATP synthesis/hydrolysis, *Proc. Natl. Acad. Sci. U. S. A. 95*, 11065–11070.
370. Pougeois, R., Lauquin, G. J., and Vignais, P. V. (1983) Interaction of 4-azido-2-nitrophenyl phosphate, an inorganic phosphate photoreactive analogue, with chloroplast coupling factor 1, *Biochemistry 22*, 1241–1245.
371. Kohlbrenner, W. E., and Cross, R. L. (1978) Efrapeptin prevents modification by phenylglyoxal of an essential arginyl residue in mitochondrial adenosine triphosphatase, *J. Biol. Chem. 253*, 7609–7611.
372. Viale, A. M., and Vallejos, R. H. (1985) Identification of an essential arginine residue in the β-subunit of the chloroplast ATPase, *J. Biol. Chem. 260*, 4958–4962.
373. Pal, P. K., and Coleman, P. S. (1990) Detecting precatalytic conformational changes in F_1-ATPase with 4-benzoyl(benzoyl)-1-amidofluorescein, a novel fluorescent nucleotide site-specific photoaffinity label, *J. Biol. Chem. 265*, 14996–15002.
374. Lauquin, G., Pougeois, R., and Vignais, P. V. (1980) 4-Azido-2-nitrophenyl phosphate, a new photoaffinity derivative of inorganic phosphate: Study of its interaction with the inorganic phosphate binding site of beef heart mitochondrial adenosine triphosphatase, *Biochemistry 19*, 4620–4626.
375. Ackerman, S. H., Grubmeyer, C., and Coleman, P. S. (1987) Evidence for catalytic cooperativity during ATP hydrolysis by beef heart F_1-ATPase: Kinetics and binding studies with the photoaffinity label bzATP, *J. Biol. Chem. 262*, 13765–13772.
376. Drutsa, V. L., Kozlov, I. A., Milgrom, Y. M., Shabarova, Z. A., and Sokolova, N. I. (1979) An active-site-directed adenosine triphosphate analogue binds to the β-subunits of factor F_1 mitochondrial adenosine triphosphatase with its triphosphate moiety, *Biochem. J. 182*, 617–619.
377. Wakagi, T., and Ohta, T. (1982) Detection of the conformational change in the catalytic site of adenosine triphosphatase from beef liver mitochondria by affinity labeling with the dialdehyde derivative of ethenoadenosine triphosphate, *J. Biochem. (Tokyo) 92*, 1403–1412.
378. Scheurich, P., Schafer, H. J., and Dose, K. (1978) 8-Azido-adenosine 5′-triphosphate as a photoaffinity label for bacterial F_1 ATPase, *Eur. J. Biochem. 88*, 253–257.
379. van Dongen, M. B., and Berden, J. A. (1986) Demonstration of two exchangeable noncatalytic and two cooperative catalytic sites in isolated bovine heart mitochondrial F_1, using the photoaffinity labels [2-^{3}H]-8-azido-ATP and [2-^{3}H]-8-azido-ADP, *Biochim. Biophys. Acta 850*, 121–130.
380. Carlier, M. F., Holowka, D. A., and Hammes, G. G. (1979) Interaction of photoreactive and fluorescent nucleotides with chloroplast coupling factor 1, *Biochemistry 18*, 3452–3457.
381. Bragg, P. D., Stan-Lotter, H., and Hou, C. (1982) Adenine nucleotide binding sites in normal and mutant adenosine triphosphatases of *Escherichia coli*, *Arch. Biochem. Biophys. 213*, 669–679.
382. Aloise, P., Kagawa, Y., and Coleman, P. S. (1991) Comparative Mg^{2+}-dependent sequential covalent binding stoichiometries of 3′-*O*-(4-benzoyl)benzoyl adenosine 5′-diphosphate of MF_1, TF_1, and the $\alpha_3\beta_3$ core complex of TF_1: The binding change motif is independent of the F_1 $\gamma\delta\varepsilon$ subunits, *J. Biol. Chem. 266*, 10368–10376.
383. Cross, R. L., Cunningham, D., Miller, C. G., Xue, Z. X., Zhou, J. M., and Boyer, P. D. (1987) Adenine nucleotide binding sites on beef heart F_1 ATPase: Photoaffinity labeling of

β-subunit Tyr-368 at a noncatalytic site and βTyr-345 at a catalytic site, *Proc. Natl. Acad. Sci. U. S. A. 84*, 5715–5719.
384. van Dongen, M. B., de Geus, J. P., Korver, T., Hartog, A. F., and Berden, J. A. (1986) Binding and hydrolysis of 2-azido-ATP and 8-azido-ATP by isolated mitochondrial F_1: Characterisation of high-affinity binding sites, *Biochim. Biophys. Acta 850*, 359–368.
385. Ferguson, S. J., Lloyd, W. J., and Radda, G. K. (1975) The mitochondrial ATPase. Selective modification of a nitrogen residue in the β subunit, *Eur. J. Biochem. 54*, 127–133.
386. Ferguson, S. J., Lloyd, W. J., Lyons, M. H., and Radda, G. K. (1975) The mitochondrial ATPase. Evidence for a single essential tyrosine residue, *Eur. J. Biochem. 54*, 117–126.
387. Ferguson, S. J., Lloyd, W. J., Radda, G. K., and Slater, E. C. (1976) On the role of the essential tyrosine residue in the mitochondrial ATPase, *Biochim. Biophys. Acta 430*, 189–193.
388. Verburg, J. G., Yoshida, M., and Allison, W. S. (1986) The use of dithionite reduction to identify the essential tyrosine residue in the F_1-ATPase from the thermophilic bacterium, PS3, that reacts with 7-chloro-4-nitrobenzofurazan, *Arch. Biochem. Biophys. 245*, 8–13.
389. Yoshida, M., and Allison, W. S. (1990) The ATPase activity of the $\alpha_3\beta_3$ complex of the F_1-ATPase of the thermophilic bacterium PS3 is inactivated on modification of Tyrosine 307 in a single β subunit by 7-chloro-4-nitrobenzofurazan, *J. Biol. Chem. 265*, 2483–2487.
390. Bullough, D. A., and Allison, W. S. (1986) Inactivation of the bovine heart mitochondrial F_1-ATPase by 5′-*p*-fluorosulfonylbenzoyl-[^{3}H]inosine is accompanied by modification of Tyrosine 345 in a single β subunit, *J. Biol. Chem. 261*, 14171–14177.
391. Yoshida, M., Poser, J. W., Allison, W. S., and Esch, F. S. (1981) Identification of an essential glutamic acid residue in the β subunit of the adenosine triphosphatase from the thermophilic bacterium PS3, *J. Biol. Chem. 256*, 148–153.
392. Yoshida, M., Allison, W. S., Esch, F. S., and Futai, M. (1982) The specificity of carboxyl group modification during the inactivation of the *Escherichia coli* F_1-ATPase with dicyclohexyl[^{14}C]carbodiimide, *J. Biol. Chem. 257*, 10033–10037.
393. Satre, M., Lunardi, J., Pougeois, R., and Vignais, P. V. (1979) Inactivation of *Escherichia coli* BF_1-ATPase by dicyclohexylcarbodiimide: Chemical modification of the β subunit, *Biochemistry 18*, 3134–3140.
394. Boyer, P. D. (1993) The binding change mechanism for ATP synthase—Some probabilities and possibilities, *Biochim. Biophys. Acta 1140*, 215–250.
395. Grubmeyer, C., and Penefsky, H. S. (1981) Cooperativity between catalytic sites in the mechanism of action of beef heart mitochondrial adenosine triphosphatase, *J. Biol. Chem. 256*, 3728–3734.
396. Grubmeyer, C., Cross, R. L., and Penefsky, H. S. (1982) Mechanism of ATP hydrolysis by beef heart mitochondrial ATPase. Rate constants for elementary steps in catalysis at a single site, *J. Biol. Chem. 257*, 12092–12100.
397. Scanlon, J. A., Al-Shawi, M. K., Le, N. P., and Nakamoto, R. K. (2007) Determination of the partial reactions of rotational catalysis in F_1-ATPase, *Biochemistry 46*, 8785–8797.
398. Cunningham, D., and Cross, R. L. (1988) Catalytic site occupancy during ATP hydrolysis by MF_1-ATPase. Evidence for alternating high affinity sites during steady-state turnover, *J. Biol. Chem. 263*, 18850–18856.
399. Hutton, R. L., and Boyer, P. D. (1979) Subunit interaction during catalysis. Alternating site cooperativity of mitochondrial adenosine triphosphatase, *J. Biol. Chem. 254*, 9990–9993.
400. Penefsky, H. S. (1988) Rate of chase-promoted hydrolysis of ATP in the high affinity catalytic site of beef heart mitochondrial ATPase, *J. Biol. Chem. 263*, 6020–6022.
401. Cross, R. L., Grubmeyer, C., and Penefsky, H. S. (1982) Mechanism of ATP hydrolysis by beef heart mitochondrial ATPase: Rate enhancements resulting from cooperative interactions between multiple catalytic sites, *J. Biol. Chem. 257*, 12101–12105.
402. Feldman, R. I., and Sigman, D. S. (1982) The synthesis of enzyme-bound ATP by soluble chloroplast coupling factor 1, *J. Biol. Chem. 257*, 1676–1683.
403. Choate, G. L., Hutton, R. L., and Boyer, P. D. (1979) Occurrence and significance of oxygen exchange reactions catalyzed by mitochondrial adenosine triphosphatase preparations, *J. Biol. Chem. 254*, 286–290.

404. O'Neal, C. C., and Boyer, P. D. (1984) Assessment of the rate of bound substrate interconversion and of ATP acceleration of product release during catalysis by mitochondrial adenosine triphosphatase, *J. Biol. Chem. 259*, 5761–5767.
405. Boyer, P. D., Cross, R. L., and Momsen, W. (1973) A new concept for energy coupling in oxidative phosphorylation based on a molecular explanation of the oxygen exchange reactions, *Proc. Natl. Acad. Sci. U. S. A. 70*, 2837–2839.
406. Cross, R. L., and Boyer, P. D. (1975) The rapid labeling of adenosine triphosphate by ^{32}P-labeled inorganic phosphate and the exchange of phosphate oxygens as related to conformational coupling in oxidative phosphorylation, *Biochemistry 14*, 392–398.
407. Rosing, J., Kayalar, C., and Boyer, P. D. (1977) Evidence for energy-dependent change in phosphate binding for mitochondrial oxidative phosphorylation based on measurements of medium and intermediate phosphate-water exchanges, *J. Biol. Chem. 252*, 2478–2485.
408. Kayalar, C., Rosing, J., and Boyer, P. D. (1977) An alternating site sequence for oxidative phosphorylation suggested by measurement of substrate binding patterns and exchange reaction inhibitions, *J. Biol. Chem. 252*, 2486–2491.
409. Hackney, D. D., and Boyer, P. D. (1978) Subunit interaction during catalysis: Implications of concentration dependency of oxygen exchanges accompanying oxidative phosphorylation for alternating site cooperativity, *J. Biol. Chem. 253*, 3164–3170.
410. Hackney, D. D., Rosen, G., and Boyer, P. D. (1979) Subunit interaction during catalysis: Alternating site cooperativity in photophosphorylation shown by substrate modulation of [^{18}O]ATP species formation, *Proc. Natl. Acad. Sci. U. S. A. 76*, 3646–3650.
411. Noumi, T., Taniai, M., Kanazawa, H., and Futai, M. (1986) Replacement of Arginine 246 by histidine in the β subunit of *Escherichia coli* H^+-ATPase resulted in loss of multi-site ATPase activity, *J. Biol. Chem. 261*, 9196–9201.
412. Cross, R. L. (1981) The mechanism and regulation of ATP synthesis by F_1-ATPases, *Annu. Rev. Biochem. 50*, 681–714.
413. Rees, D. M., Montgomery, M. G., Leslie, A. G., and Walker, J. E. (2012) Structural evidence of a new catalytic intermediate in the pathway of ATP hydrolysis by F_1-ATPase from bovine heart mitochondria, *Proc. Natl. Acad. Sci. U. S. A. 109*, 11139–11143.
414. Kagawa, R., Montgomery, M. G., Braig, K., Leslie, A. G., and Walker, J. E. (2004) The structure of bovine F_1-ATPase inhibited by ADP and beryllium fluoride, *EMBO J. 23*, 2734–2744.
415. Leslie, A. G., and Walker, J. E. (2000) Structural model of F_1-ATPase and the implications for rotary catalysis, *Philos. Trans. R. Soc., B 355*, 465–471.
416. Yang, W., Gao, Y. Q., Cui, Q., Ma, J., and Karplus, M. (2003) The missing link between thermodynamics and structure in F_1-ATPase, *Proc. Natl. Acad. Sci. U. S. A. 100*, 874–879.
417. Alberty, R. A., and Goldberg, R. N. (1992) Standard thermodynamic formation properties for the adenosine 5′-triphosphate series, *Biochemistry 31*, 10610–10615.
418. Ebel, R. E., and Lardy, H. A. (1975) Stimulation of rat liver mitochondrial adenosine triphosphatase by anions, *J. Biol. Chem. 250*, 191–196.
419. Frey, P. A., and Sammons, R. D. (1985) Bond order and charge localization in nucleoside phosphorothioates, *Science 228*, 541–545.
420. Bason, J. V., Montgomery, M. G., Leslie, A. G., and Walker, J. E. (2015) How release of phosphate from mammalian F_1-ATPase generates a rotary substep, *Proc. Natl. Acad. Sci. U. S. A. 112*, 6009–6014.
421. Rodgers, A. J., and Wilce, M. C. (2000) Structure of the γ-ε complex of ATP synthase, *Nature Struct. Biol. 7*, 1051–1054.
422. Tsunoda, S. P., Rodgers, A. J., Aggeler, R., Wilce, M. C., Yoshida, M., and Capaldi, R. A. (2001) Large conformational changes of the ε subunit in the bacterial F_1F_0 ATP synthase provide a ratchet action to regulate this rotary motor enzyme, *Proc. Natl. Acad. Sci. U. S. A. 98*, 6560–6564.
423. Duncan, T. M., Bulygin, V. V., Zhou, Y., Hutcheon, M. L., and Cross, R. L. (1995) Rotation of subunits during catalysis by *Escherichia coli* F_1-ATPase, *Proc. Natl. Acad. Sci. U. S. A. 92*, 10964–10968.
424. Sabbert, D., Engelbrecht, S., and Junge, W. (1996) Intersubunit rotation in active

F-ATPase, *Nature (London, U. K.) 381*, 623–625.
425. Noji, H., Yasuda, R., Yoshida, M., and Kinosita, K., Jr. (1997) Direct observation of the rotation of F_1-ATPase, *Nature (London, U. K.) 386*, 299–302.
426. Yasuda, R., Noji, H., Kinosita, K., Jr., and Yoshida, M. (1998) F_1-ATPase is a highly efficient molecular motor that rotates with discrete 120 degree steps, *Cell (Cambridge, MA, U. S.) 93*, 1117–1124.
427. Omote, H., Sambonmatsu, N., Saito, K., Sambongi, Y., Iwamoto-Kihara, A., Yanagida, T., Wada, Y., and Futai, M. (1999) The γ-subunit rotation and torque generation in F_1-ATPase from wild-type or uncoupled mutant *Escherichia coli*, *Proc. Natl. Acad. Sci. U. S. A. 96*, 7780–7784.
428. Saita, E., Suzuki, T., Kinosita, K., Jr., and Yoshida, M. (2015) Simple mechanism whereby the F_1-ATPase motor rotates with near-perfect chemomechanical energy conversion, *Proc. Natl. Acad. Sci. U. S. A. 112*, 9626–9631.
429. Itoh, H., Takahashi, A., Adachi, K., Noji, H., Yasuda, R., Yoshida, M., and Kinosita, K. (2004) Mechanically driven ATP synthesis by F_1-ATPase, *Nature (London, U. K.) 427*, 465–468.
430. Rondelez, Y., Tresset, G., Nakashima, T., Kato-Yamada, Y., Fujita, H., Takeuchi, S., and Noji, H. (2005) Highly coupled ATP synthesis by F_1-ATPase single molecules, *Nature (London, U. K.) 433*, 773–777.
431. Yasuda, R., Noji, H., Yoshida, M., Kinosita, K., Jr., and Itoh, H. (2001) Resolution of distinct rotational substeps by submillisecond kinetic analysis of F_1-ATPase, *Nature (London, U. K.) 410*, 898–904.
432. Ariga, T., Masaike, T., Noji, H., and Yoshida, M. (2002) Stepping rotation of F_1-ATPase with one, two, or three altered catalytic sites that bind ATP only slowly, *J. Biol. Chem. 277*, 24870–24874.
433. Shimabukuro, K., Yasuda, R., Muneyuki, E., Hara, K. Y., Kinosita, K., Jr., and Yoshida, M. (2003) Catalysis and rotation of F_1 motor: Cleavage of ATP at the catalytic site occurs in 1 ms before 40 degree substep rotation, *Proc. Natl. Acad. Sci. U. S. A. 100*, 14731–14736.
434. Masaike, T., Koyama-Horibe, F., Oiwa, K., Yoshida, M., and Nishizaka, T. (2008) Cooperative three-step motions in catalytic subunits of F_1-ATPase correlate with 80 degrees and 40° substep rotations, *Nat. Struct. Mol. Biol.15*, 1326–1333.
435. Kyte, J. (2007) In *Structure in Protein Chemistry: Second Edition*, pp 601–606, Garland Science, New York.
436. Sugawa, M., Okazaki, K., Kobayashi, M., Matsui, T., Hummer, G., Masaike, T., and Nishizaka, T. (2016) F_1-ATPase conformational cycle from simultaneous single-molecule FRET and rotation measurements, *Proc. Natl. Acad. Sci. U. S. A. 113*, E2916–2924.
437. Yasuda, R., Masaike, T., Adachi, K., Noji, H., Itoh, H., and Kinosita, K., Jr. (2003) The ATP-waiting conformation of rotating F_1-ATPase revealed by single-pair fluorescence resonance energy transfer, *Proc. Natl. Acad. Sci. U. S. A. 100*, 9314–9318.
438. Nishizaka, T., Oiwa, K., Noji, H., Kimura, S., Muneyuki, E., Yoshida, M., and Kinosita, K., Jr. (2004) Chemomechanical coupling in F_1-ATPase revealed by simultaneous observation of nucleotide kinetics and rotation, *Nat. Struct. Mol. Biol. 11*, 142–148.
439. Martin, J. L., Ishmukhametov, R., Hornung, T., Ahmad, Z., and Frasch, W. D. (2014) Anatomy of F_1-ATPase powered rotation, *Proc. Natl. Acad. Sci. U. S. A. 111*, 3715–3720.
440. Matsuno-Yagi, A., and Hatefi, Y. (1988) Estimation of the turnover number of bovine heart F_0F_1 complexes for ATP synthesis, *Biochemistry 27*, 335–340.
441. Gu, J., Zhang, L., Zong, S., Guo, R., Liu, T., Yi, J., Wang, P., Zhuo, W., and Yang, M. (2019) Cryo-EM structure of the mammalian ATP synthase tetramer bound with inhibitory protein iF_1, *Science 364*, 1068–1075.
442. Watt, I. N., Montgomery, M. G., Runswick, M. J., Leslie, A. G., and Walker, J. E. (2010) Bioenergetic cost of making an adenosine triphosphate molecule in animal mitochondria, *Proc. Natl. Acad. Sci. U. S. A. 107*, 16823–16827.
443. Hoppe, J., and Sebald, W. (1980) Amino acid sequence of the proteolipid subunit of the proton-translocating ATPase complex from the thermophilic bacterium PS-3, *Eur. J. Biochem. 107*, 57–65.
444. Nielsen, J., Hansen, F. G., Hoppe, J., Friedl, P., and von Meyenburg, K. (1981) The nucleotide sequence of the ATP genes coding for the F_0 subunits a, b, c and the F_1 subunit δ of

the membrane bound ATP synthase of *Escherichia coli*, *Mol. Gen. Genet. 184*, 33–39.
445. Carbajo, R. J., Kellas, F. A., Runswick, M. J., Montgomery, M. G., Walker, J. E., and Neuhaus, D. (2005) Structure of the F_1-binding domain of the stator of bovine F_1F_o-ATPase and how it binds an α-subunit, *J. Mol. Biol. 351*, 824–838.
446. Matthies, D., Haberstock, S., Joos, F., Dotsch, V., Vonck, J., Bernhard, F., and Meier, T. (2011) Cell-free expression and assembly of ATP synthase, *J. Mol. Biol. 413*, 593–603.
447. Dong, H., and Fillingame, R. H. (2010) Chemical reactivities of cysteine substitutions in subunit a of ATP synthase define residues gating H^+ transport from each side of the membrane, *J. Biol. Chem. 285*, 39811–39818.
448. Lau, W. C., and Rubinstein, J. L. (2012) Subnanometre-resolution structure of the intact *Thermus thermophilus* H^+-driven ATP synthase, *Nature (London, U. K.) 481*, 214–218.
449. Sambongi, Y., Iko, Y., Tanabe, M., Omote, H., Iwamoto-Kihara, A., Ueda, I., Yanagida, T., Wada, Y., and Futai, M. (1999) Mechanical rotation of the c subunit oligomer in ATP synthase (F_0F_1): Direct observation, *Science 286*, 1722–1724.
450. Nishio, K., Iwamoto-Kihara, A., Yamamoto, A., Wada, Y., and Futai, M. (2002) Subunit rotation of ATP synthase embedded in membranes: a or β Subunit rotation relative to the c subunit ring, *Proc. Natl. Acad. Sci. U. S. A. 99*, 13448–13452.
451. Diez, M., Zimmermann, B., Borsch, M., Konig, M., Schweinberger, E., Steigmiller, S., Reuter, R., Felekyan, S., Kudryavtsev, V., Seidel, C. A., and Graber, P. (2004) Proton-powered subunit rotation in single membrane-bound F_0F_1-ATP synthase, *Nat. Struct. Mol. Biol.11*, 135–141.
452. Ueno, H., Suzuki, T., Kinosita, K., Jr., and Yoshida, M. (2005) ATP-driven stepwise rotation of F_oF_1-ATP synthase, *Proc. Natl. Acad. Sci. U. S. A. 102*, 1333–1338.
453. Wachter, A., Bi, Y., Dunn, S. D., Cain, B. D., Sielaff, H., Wintermann, F., Engelbrecht, S., and Junge, W. (2011) Two rotary motors in F-ATP synthase are elastically coupled by a flexible rotor and a stiff stator stalk, *Proc. Natl. Acad. Sci. U. S. A. 108*, 3924–3929.
454. Usukura, E., Suzuki, T., Furuike, S., Soga, N., Saita, E., Hisabori, T., Kinosita, K., Jr., and Yoshida, M. (2012) Torque generation and utilization in motor enzyme F_0F_1-ATP synthase: Half-torque F_1 with short-sized push-rod helix and reduced ATP synthesis by half-torque F_0F_1, *J. Biol. Chem. 287*, 1884–1891.
455. Martin, J., Hudson, J., Hornung, T., and Frasch, W. D. (2015) F_o-Driven rotation in the ATP synthase direction against the force of F_1 ATPase in the F_oF_1 ATP synthase, *J. Biol. Chem. 290*, 10717–10728.
456. Suzuki, T., Ueno, H., Mitome, N., Suzuki, J., and Yoshida, M. (2002) F_0 of ATP synthase is a rotary proton channel. Obligatory coupling of proton translocation with rotation of c-subunit ring, *J. Biol. Chem. 277*, 13281–13285.
457. Duvezin-Caubet, S., Caron, M., Giraud, M. F., Velours, J., and di Rago, J. P. (2003) The two rotor components of yeast mitochondrial ATP synthase are mechanically coupled by subunit δ, *Proc. Natl. Acad. Sci. U. S. A. 100*, 13235–13240.
458. Vik, S. B., and Antonio, B. J. (1994) A mechanism of proton translocation by F_1F_0 ATP synthases suggested by double mutants of the a subunit, *J. Biol. Chem. 269*, 30364–30369.
459. Guo, H., Bueler, S. A., and Rubinstein, J. L. (2017) Atomic model for the dimeric F_o region of mitochondrial ATP synthase, *Science 358*, 936–940.
460. Srivastava, A. P., Luo, M., Zhou, W., Symersky, J., Bai, D., Chambers, M. G., Faraldo-Gomez, J. D., Liao, M., and Mueller, D. M. (2018) High-resolution cryo-EM analysis of the yeast ATP synthase in a lipid membrane, *Science 360*, eaas9699.
461. Hahn, A., Vonck, J., Mills, D. J., Meier, T., and Kuhlbrandt, W. (2018) Structure, mechanism, and regulation of the chloroplast ATP synthase, *Science 360,* eaat4318.
462. Murphy, B. J., Klusch, N., Langer, J., Mills, D. J., Yildiz, O., and Kuhlbrandt, W. (2019) Rotary substates of mitochondrial ATP synthase reveal the basis of flexible F_1-F_o coupling, *Science 364*, eaaw9128.
463. Zhou, L., and Sazanov, L. A. (2019) Structure and conformational plasticity of the intact *Thermus thermophilus* V/A-type ATPase, *Science 365*, eaaw9144.

464. Sobti, M., Smits, C., Wong, A. S., Ishmukhametov, R., Stock, D., Sandin, S., and Stewart, A. G. (2016) Cryo-EM structures of the autoinhibited *E. coli* ATP synthase in three rotational states, *eLife 5*, e21598
465. Guo, H., Suzuki, T., and Rubinstein, J. L. (2019) Structure of a bacterial ATP synthase, *eLife 8*, e43128.
466. Zhou, A., Rohou, A., Schep, D. G., Bason, J. V., Montgomery, M. G., Walker, J. E., Grigorieff, N., and Rubinstein, J. L. (2015) Structure and conformational states of the bovine mitochondrial ATP synthase by cryo-EM, *eLife 4*, e10180.
467. Allegretti, M., Klusch, N., Mills, D. J., Vonck, J., Kuhlbrandt, W., and Davies, K. M. (2015) Horizontal membrane-intrinsic α-helices in the stator a-subunit of an F-type ATP synthase, *Nature (London, U. K.) 521*, 237–240.
468. Angevine, C. M., Herold, K. A., Vincent, O. D., and Fillingame, R. H. (2007) Aqueous access pathways in ATP synthase subunit a. Reactivity of cysteine substituted into transmembrane helices 1, 3, and 5, *J. Biol. Chem. 282*, 9001–9007.
469. Gohlke, H., Schlieper, D., and Groth, G. (2012) Resolving the negative potential side (n-side) water-accessible proton pathway of F-type ATP synthase by molecular dynamics simulations, *J. Biol. Chem. 287*, 36536–36543.
470. McLachlin, D. T., Coveny, A. M., Clark, S. M., and Dunn, S. D. (2000) Site-directed crosslinking of b to the α, β, and a subunits of the *Escherichia coli* ATP synthase, *J. Biol. Chem. 275*, 17571–17577.
471. Lokanath, N. K., Matsuura, Y., Kuroishi, C., Takahashi, N., and Kunishima, N. (2007) Dimeric core structure of modular stator subunit E of archaeal H^+ -ATPase, *J. Mol. Biol. 366*, 933–944.
472. Lau, W. C., Baker, L. A., and Rubinstein, J. L. (2008) Cryo-EM structure of the yeast ATP synthase, *J. Mol. Biol. 382*, 1256–1264.
473. Rees, D. M., Leslie, A. G., and Walker, J. E. (2009) The structure of the membrane extrinsic region of bovine ATP synthase, *Proc. Natl. Acad. Sci. U. S. A. 106*, 21597–21601.
474. Lee, L. K., Stewart, A. G., Donohoe, M., Bernal, R. A., and Stock, D. (2010) The structure of the peripheral stalk of *Thermus thermophilus* H^+-ATPase/synthase, *Nat. Struct. Mol. Biol. 17*, 373–378.
475. Stock, D., Leslie, A. G., and Walker, J. E. (1999) Molecular architecture of the rotary motor in ATP synthase, *Science 286*, 1700–1705.
476. Jiang, W., Hermolin, J., and Fillingame, R. H. (2001) The preferred stoichiometry of c subunits in the rotary motor sector of *Escherichia coli* ATP synthase is 10, *Proc. Natl. Acad. Sci. U. S. A. 98*, 4966–4971.
477. Seelert, H., Poetsch, A., Dencher, N. A., Engel, A., Stahlberg, H., and Muller, D. J. (2000) Structural biology. Proton-powered turbine of a plant motor, *Nature (London, U. K.) 405*, 418–419.
478. Vonck, J., von Nidda, T. K., Meier, T., Matthey, U., Mills, D. J., Kuhlbrandt, W., and Dimroth, P. (2002) Molecular architecture of the undecameric rotor of a bacterial Na^+-ATP synthase, *J. Mol. Biol. 321*, 307–316.
479. Meier, T., Polzer, P., Diederichs, K., Welte, W., and Dimroth, P. (2005) Structure of the rotor ring of F-type Na^+-ATPase from *Ilyobacter tartaricus*, *Science 308*, 659–662.
480. Murata, T., Yamato, I., Kakinuma, Y., Leslie, A. G., and Walker, J. E. (2005) Structure of the rotor of the V-type Na^+-ATPase from *Enterococcus hirae*, *Science 308*, 654–659.
481. Pogoryelov, D., Klyszejko, A. L., Krasnoselska, G. O., Heller, E. M., Leone, V., Langer, J. D., Vonck, J., Muller, D. J., Faraldo-Gomez, J. D., and Meier, T. (2012) Engineering rotor ring stoichiometries in the ATP synthase, *Proc. Natl. Acad. Sci. U. S. A. 109*, E1599–1608.
482. Bragg, L., Kendrew, J. C., and Perutz, M. F. (1950) Polypeptide chain configurations in crystalline proteins, *Proc. R. Soc. London, Ser. A 203*, 321–357.
483. Sielaff, H., Rennekamp, H., Wachter, A., Xie, H., Hilbers, F., Feldbauer, K., Dunn, S. D., Engelbrecht, S., and Junge, W. (2008) Domain compliance and elastic power transmission in rotary F_oF_1-ATPase, *Proc. Natl. Acad. Sci. U. S. A. 105*, 17760–17765.
484. Tsunoda, S. P., Aggeler, R., Yoshida, M., and Capaldi, R. A. (2001) Rotation of the c subunit oligomer in fully functional F_1F_o ATP synthase, *Proc. Natl. Acad. Sci. U. S. A. 98*, 898–902.
485. Kraulis, P. J. (1991) Molscript—A program to produce both detailed and schematic plots of protein structures, *J.Appl. Crystallogr. 24*, 946–950.

486. Sprang, S. R., Acharya, K. R., Goldsmith, E. J., Stuart, D. I., Varvill, K., Fletterick, R. J., Madsen, N. B., and Johnson, L. N. (1988) Structural changes in glycogen phosphorylase induced by phosphorylation, *Nature (London, U. K.) 336*, 215–221.
487. Jørgensen, P. L. (1974) Purification and characterization of (Na^+ plus K^+)-ATPase. 3. Purification from the outer medulla of mammalian kidney after selective removal of membrane components by sodium dodecylsulphate, *Biochim. Biophys. Acta 356*, 36–52.
488. Carilli, C. T., Farley, R. A., Perlman, D. M., and Cantley, L. C. (1982) The active site structure of Na^+- and K^+-stimulated ATPase. Location of a specific fluorescein isothiocyanate reactive site, *J. Biol. Chem. 257*, 5601–5606.

Glossary

Acid Acidic hydron and the atom to which it is attached.

Acid dissociation constant Equilibrium constant that relates the concentration of hydronium ion and the concentration of the conjugate base of an acid to the concentration of the acid.

Activator Ligand that binds to an enzyme and forms a dead-end complex that has a greater rate of catalysis than normal.

Active site Unique location on the surface or in the interior of one of the subunits in an enzyme molecule where the reaction catalyzed by that enzyme takes place.

Active-site label Reagent that has been designed to associate specifically, noncovalently, and in a defined orientation within the active site of a particular enzyme at the location normally occupied by a substrate and then modify covalently a particular catalytic acid–base or particular side chain that participates in association of a substrate with the active site.

Active transport of hydrons Movement of hydrons against an electrochemical gradient through the portion of an enzyme that spans the membrane, which requires that there be a continuous path for the hydrons to follow from one side of the enzyme to the other and a physical mechanism to couple the expenditure of energy, in the form of a favorable oxidation–reduction or the hydrolysis of $MgATP^{2-}$, to the unfavorable transport of the hydrons. See also *formal transport of hydrons*.

Actual reactant Reactant in an enzymatic reaction that is formed nonenzymatically from a compound originally thought to be the reactant.

Acyl oxidation state Oxidation state for a carbon that has three bonds, either σ bonds or a mixture of σ bonds and π bonds, to heteroatoms and only one σ bond to carbon or hydrogen. See *oxidation states of carbon*.

Adair equation One of two equations that are used to fit sigmoid behavior and that involve no explanation for sigmoid behavior. See also *Hill equation*, *Monod–Wyman–Changeux equation*, and *sigmoid behavior*.

Additional substrate Substrate that is not part of the formal stoichiometric equation for an enzymatic reaction because it is regenerated during the reaction but that must be present in solution for the enzymatic reaction to occur.

Affinity label Compound that contains a reactive center and that is designed to resemble the substrate of an enzyme or ligand for a protein so closely that it will bind specifically to the active site or binding site, and while it is bound the reactive center will covalently modify an amino acid in or near the site.

Agonist Ligand that binds to a protein and, upon binding, produces a measurable change in the characteristic physiological function of that protein.

Aldol condensation Nucleophilic addition of the α carbon of an enolate or enamine to a carbonyl group or imine to form a carbon–carbon bond and give an alcohol or amine.

Alkyl migration Transfer of an alkyl group, usually intramolecularly and often between two adjacent atoms (as in a 1,2-alkyl migration), during the course of a molecular rearrangement. See also *hydride migration*.

Allosteric constant Constant for the equilibrium between two conformations of an enzyme or protein that displays allosteric behavior. See also *conditional allosteric constant* and *fundamental allosteric constant*.

Allosteric effect Indirect interaction between distinct, spatially separated sites on a protein during which the conformation of the protein is altered by association of a ligand at one or more of the sites, causing a change at one or more of the other sites. See also *heterotropic allosteric effect* and *homotropic allosteric effect*.

Amphipathic molecule Extended molecule that has a hydrophilic region, usually one end, and a hydrophobic region, usually the other end.

Antagonist Ligand that binds to a protein and blocks the ability of an agonist to accomplish its normal function.

Antenna Large structure in a photosystem the prosthetic chromophores of which are responsible for absorbing photons of incident light and in which the resulting electronic excitation, an exciton, is transferring to the special pair of the reaction center.

Anti elimination Elimination in which the leaving group and the hydron or electrophile dissociate on opposite sides of a plane containing the carbons in a carbon–carbon bond to which they are attached. See also *syn elimination*.

Antiperiplanar conformation Arrangement in which two periplanar substituents of interest are oriented at a dihedral angle of $180^\circ \pm 30^\circ$ from one another. See also *synperiplanar conformation*.

Antiperiplanar push Push exerted by a lone pair of electrons in the antiperiplanar conformation to a leaving group. See also *synperiplanar push*.

Apical position Position of the substituents or ligands in a trigonal bipyramid that are collinear or almost collinear with the central atom above and below an equatorial plane, or the position in a pyramidal arrangement that is at or near the apex of the pyramid. See also *equatorial position*.

Apparent rate constant Rate constant in a rate equation that is not a function of the concentration of a reactant but that varies as the concentration of another reactant is varied.

Aromatic transition state Transition state in which there is a continuous, conjugated ring of atoms with atomic orbitals, each of which overlaps in sequence around the ring with its two nearest neighbors, so that they together form a complete cyclic molecular orbital system containing $4n + 2$ electrons.

Associative exchange Mechanism for the exchange of ligands to a metallic cation in which the entering ligand associates with the metallic cation, expanding its coordination, and then the leaving ligand dissociates. See also *dissociative exchange*.

Associative nucleophilic substitution Nucleophilic substitution that proceeds through a tetrahedral intermediate, in which the bond between the electrophile and the nucleophile has fully formed before the bond between the leaving group and the electrophile begins to break. See also *concerted nucleophilic substitution* and *dissociative nucleophilic substitution*.

Base Basic lone pair of electrons and the atom with which it is associated.

Bifurcation of two electrons Situation in which the two electrons of a two-electron reductant are required to travel singly through two different paths of electron transfer or, in reverse, two electrons that have traveled singly through two different paths are combined and transferred together to a two-electron oxidant.

Bilin Linear tetrapyrrole, derived ultimately from heme *b*, that is extensively conjugated and is one of the prosthetic chromophores found in certain antennae of photosystems.

Biochemical standard reduction potential, $E^{\circ\prime}$ Reduction potential, relative to a standard hydrogen electrode, observed when the two members of the redox couple are present at equal activity at a pH of 7.

Bisubstrate analogue Molecule composed of portions from two reactants for an enzyme.

Bond dissociation energy Enthalpy (kilojoules mole^{-1}) required to break the bond homolytically between a hydrogen and the rest of the particular molecule to form a radical, regardless of whether or not that radical was formed by the abstraction of a hydrogen.

Bond order Theoretical index of the degree of bonding between two atoms relative to that of a single bond containing a localized electron pair, which is equal to the often nonintegral difference between the population of electrons in bonding orbitals and the population in antibonding orbitals in the region between the two atoms, divided by 2.

Brønsted coefficient, β Slope of a linear Brønsted plot.

Brønsted coefficient for leaving groups, β_{lg} Slope of a linear Brønsted plot in which rate constants and pK_a values for conjugate acids of the leaving groups are plotted.

Brønsted coefficient for nucleophiles, β_{nuc} Slope of a linear Brønsted plot in which the common logarithms of rate constants for a set of nucleophiles participating in the same nucleophilic substitution are plotted as a function of the values for pK_a of the respective nucleophiles.

Brønsted correlation Any correlation between the common logarithms of a set of rate constants or equilibrium constants for the members of a set of interchangeable participants in a particular reaction—be they reactants, products, or catalysts—and the values of pK_a for the respective participants or for their conjugate acids, corrected for the number of acidic hydrons and basic lone pairs of electrons on the participating atom.

Brønsted plot Graph of a Brønsted correlation in which the common logarithms of a set of equilibrium constants or rate constants are plotted against the respective values of corrected pK_a for the chosen participant or its conjugate acid.

Brønsted relation for general acid–base catalysis Function that relates the rate constants or common logarithms of the rate constants for general acid catalysis to the acid dissociation constants or values of pK_a for the catalysts or that relates the rate constants or common logarithms of the rate constants for general base catalysis to the acid dissociation constants or values of pK_a for the conjugate acids of the catalysts.

Burst of product Rapid appearance of an amount of product equal to the molar concentration of active sites in the solution that can be distinguished kinetically from the much slower accumulation of product that follows the burst and proceeds at the normal steady-state rate.

Cage Complex of molecules of solvent that surrounds two molecules, which entered the cage from solution or formed during a dissociation, and hinders their separation by diffusion.

Cage effect Association of two molecules in a solution within a cage of solvent that permits the molecules to undergo a series of collisions within the cage in quick succession, each known as an encounter.

Caged reactant Photolabile derivative of the reactant for an enzyme that is catalytically inactive but that decomposes upon photolysis to produce the catalytically active reactant.

Captodative effect Effect on the stability of a carbon-centered radical determined by the combined action of an electron-withdrawing substituent (a captor) and an electron-releasing substituent (a dator), both attached to the radical center.

Carbanionic intermediate Diamagnetic, noncovalent intermediate that forms in an active site when a hydron or another electrophile dissociates heterolytically from a carbon in a reactant—usually a carbon adjacent to a carbonyl, imino, or acyl group—and that dissociation produces a carbanion or that forms when a nucleophile associates heterolytically with a carbon in a reactant—usually a carbon conjugated to a carbonyl, imino, or acyl carbon—and that association produces a carbanion.

Carbenium ion Carbocation containing a carbon atom with three substituents and a vacant *p* atomic orbital, generated when the leaving group dissociates from an electrophilic carbon before the nucleophile enters the reaction and having the hybridization *p*, sp^2, sp^2, sp^2 because of electron repulsion among the three occupied molecular orbitals of the three σ bonds to the substituents.

Carbocationic intermediate Diamagnetic, noncovalent intermediate that forms in an active site when a leaving group dissociates heterolytically from a carbon in a reactant and that dissociation produces a carbocation or that forms when a hydron or another electrophile associates heterolytically with carbon in a reactant and that addition produces a carbocation.

Carbonato oxidation state Oxidation state for a carbon that is entirely bonded to heteroatoms. See *oxidation states of carbon*.

μ-Carbonmonoxy group Carbon monoxide that bridges two or more metallic ions and participates in each of the coordinations of those metallic ions.

Carbonyl oxidation state Oxidation state for a carbon that has two σ bonds to either carbon or hydrogen and either two single σ bonds to heteroatoms or a σ bond and a π bond, the two components of a double bond, to a heteroatom. See *oxidation states of carbon*.

Carotenoid Tetraterpenoid formally derived from lycopene that contains 40 carbon atoms and a linear conjugated π molecular orbital system of 22 or 30 carbon atoms that is all trans and fairly rigid throughout its length and that is one of the prosthetic groups in a photosystem responsible for absorption of a photon and transfer of the resulting electronic excitation to the special pair.

Catalytic constant, k_0 Observed rate constant, which is apparently first-order with respect to the total molar concentration of active sites and zero-order with respect to reactants, for the enzymatic reaction at high concentrations of all reactants or at extrapolated infinite concentrations.

Catalytic immunoglobulin Immunoglobulin that is raised against an analogue for either a transition state or an intermediate of high energy in a particular chemical reaction and that, because it binds the corresponding transition state or intermediate of high energy tightly, catalyzes the corresponding reaction.

Channeling efficiency Percentage of initial reactant that is converted to final product intramolecularly within a multienzymatic complex relative to the total amount of initial reactant converted to final product both intramolecularly, by passing from one active site to the next within a molecule of the complex, and intermolecularly, by passing through the solution between active sites on different molecules of the complex.

Charge-transfer complex Complex between a reductant (the electron donor) and an oxidant (the electron acceptor) formed in a reversible equilibrium and characterized by an electronic transition to an excited state in which electronic charge is transferred from the donor to the acceptor.

Chemical gradient Gradient in chemical potential established when the molar concentration of uncharged substance A is greater on one side of a biological membrane than on the other side. See also *electric gradient, electrochemical gradient,* and *gradient*.

Chlorophyll Derivative of a pheophytin in which Mg^{2+} is coordinated in the center of the aromatic ring by lone pairs of electrons from the four central nitrogens.

Chloroplast Organelle in plant cells that is responsible for absorbing light and producing a reductant of low potential, that is descended from a photosynthetic bacterium, and that has an outer membrane corresponding to the plasma membrane of the ancestral photosynthetic bacterial cell within which there are thylakoids descended from chromatophores in the ancestral bacterium.

Chromatography by size exclusion Method that can be used to determine the binding of a ligand to a protein in which the protein is passed through a column of beaded, tightly crosslinked dextran that has been equilibrated with a solution containing a fixed concentration of ligand, and the protein binds ligand as it passes through the beaded dextran until the binding reaches equilibrium.

Chromatophore Cellular structure in a photosynthetic bacterium, either an invagination of the plasma membrane or a separate vesicle in the cytoplasm the interior of which is, or is derived from, the extracytoplasmic solution.

Claisen condensation Substitution of the α carbon of an enolate or enamine for a leaving group, usually an alcohol, amine, or thiolate, at the acyl carbon of the respective derivative of a carboxylic acid to give a carbonyl or the derivative of a carbonyl.

Cobalamin Prosthetic group that contains a coordinated cobalt ion to which four of the ligands are lone pairs of electrons from the four central nitrogens in a corrinoid ring.

Coenzyme Cofactor that is a small molecule relative to the enzyme itself, that associates with and dissociates from the enzyme during each turnover, either at the active site or at another site specific to the coenzyme, and that transfers chemical groups, hydrogens, or electrons among active sites. See also *cofactor* and *prosthetic group*.

Cofactor Any ion, usually a metallic cation, or any organic molecule that is required by an enzyme for its function. See also *coenzyme* and *prosthetic group*.

Col Lowest of all barriers of potential energy along all the paths between reactant and product on a surface of potential energy through which passes the reaction coordinate and, as at a pass in the mountains, at which the curvature is positive along the coordinate perpendicular to the reaction coordinate along which the curvature is negative.

Colligation Formation of a covalent bond by the combination or recombination of two radicals.

Commitment forward, c_f Ratio between the forward elementary rate constant for a specific step in the mechanism of an enzymatically catalyzed reaction and the composite rate constant for the reversal of the reaction from the form of the enzyme immediately preceding this specific step to the point at which the reactant of interest has been released back into the solution.

Commitment in reverse, c_r Ratio between the reverse elementary rate constant for a specific step in the mechanism of an enzymatically catalyzed reaction and the composite rate constant for forward flux from the form of the enzyme immediately following this step through the first kinetically irreversible step in the mechanism.

Competitive inhibition Inhibition produced by a competitive reversible inhibitor. See also *mixed inhibition*, *noncompetitive inhibition*, and *uncompetitive inhibition*.

Competitive reversible inhibitor with respect to reactant A Reversible inhibitor the addition of which to the solution decreases the observed value of the specificity constant or apparent specificity constant for reactant A while having no effect on the value of the catalytic constant or apparent catalytic constant for that reactant.

Complete kinetic mechanism Kinetic mechanism for a chemical reaction that includes explicitly every elementary step in that reaction and no steps other than elementary steps.

Composite acid–base Network of simple acid–bases, connected by hydrogen bonds, that has several tautomers in equilibrium with each other and from which hydrons can dissociate and associate at the periphery, often accompanied by shifts in the hydrons in the hydrogen bonds of the network.

Composite rate constant Rate constant for a composite reaction, or a step in a kinetic mechanism that is a composite reaction, that can be expressed as a combination of several elementary rate constants for the several constituent elementary steps. It is sometimes called net rate constant. See also *elementary rate constant*.

Composite reaction Chemical reaction, or step in the proposed kinetic mechanism for a reaction, for which the expression for the rate involves rate constants of more than a single elementary reaction and which proceeds through more than one transition state. See also *elementary reaction*.

Concerted elimination–addition Elimination–addition reaction in which there is no carbanionic or carbocationic intermediate because the bond between the one carbon and the leaving group is breaking or forming in concert with the breaking or forming of the bond between the other carbon and the electrophile or hydron in an elementary reaction.

Concerted nucleophilic substitution Nucleophilic substitution in which there is no intermediate because the bond between the leaving group and the electrophile is breaking as the bond between the electrophile and the nucleophile is forming in an elementary reaction. See also *associative nucleophilic substitution* and *dissociative nucleophilic substitution*.

Conditional allosteric constant Allosteric constant for an enzyme in the presence of saturating concentrations of one or more of its ligands. See also *allosteric constant* and *fundamental allosteric constant*.

H conformation Inhibited conformation of an enzyme from which a heterotropic allosteric inhibitor has the smaller dissociation constant. See also *V conformation*.

R conformation Conformation of a protein or enzyme that predominates when a ligand or substrate, the behavior of which is being examined and which displays cooperativity in its association with the protein, is present at saturating concentrations and often only when an allosteric activator or cosubstrate is present. See also *T conformation*.

T conformation Conformation of a protein or enzyme that predominates when a ligand or substrate, the behavior of which is being examined and which displays cooperativity in its association with the protein, is absent and often only when an allosteric inhibitor or cosubstrate is present. See also *R conformation*.

V conformation Activated conformation of an enzyme from which a heterotropic allosteric activator has the smaller dissociation constant. See also *H conformation*.

Conformational selection Sequence of events in which a conformational change occurs in the free enzyme before substrates can associate with the active site. See also *induced fit*.

Conservation of enzyme Principle that the total molar concentration of active sites, which is usually a known quantity but that always remains constant throughout the reaction, must be equal to the sum of the concentrations of all forms of the active site.

Cooperativity Allosteric interaction between two or more identical sites, usually but not always active sites, on an oligomeric protein in which the association of a ligand or substrate at one or more of the sites induces conformational changes in the remaining unoccupied sites, leading to an increase in the affinity of those sites for their ligand or substrate—or an increase in the limiting rate of the remaining active sites—and typically producing sigmoid behavior. See also *sigmoid behavior*.

Corrinoid A macrocyclic tetrapyrrole derived from the porphyrin uroporphyrinogen III in which two of the pyrrolyl groups in the macrocycle are partly reduced and the four pyrrolyl groups are joined by three methine groups and one direct carbon–carbon bond linking their α positions.

Covalent intermediate Intermediate in an enzymatic reaction in which the enzyme itself and the other atoms participating in the intermediate are covalently attached to each other.

Covalent prosthetic intermediate Intermediate in an enzymatic reaction in which the other atoms participating in the intermediate that are derived from the reactants are covalently attached to a prosthetic group that is itself covalently or noncovalently attached to the active site.

Cyclic voltammetry Procedure that can be used to determine the biochemical standard reduction potential of a prosthetic group that participates in a redox couple.

Cycloaddition Pericyclic reaction in which a total of $(2n + 1)$ double bonds from two unsaturated molecules, or two parts of the same unsaturated molecule, participate to produce a cyclic adduct in which the number of π bonds has decreased by two and the number of σ bonds has increased by two, namely, the two σ bonds creating the cyclic adduct.

Cytochrome Visibly colored protein that contains one or more hemes as prosthetic groups and that acts as an electron-transferring coenzyme.

Dead-end inhibition Situation in which a reversible inhibitor forms a complex with an enzyme, either occupied or unoccupied by substrates, that is unable to engage in any further reaction while the inhibitor is bound.

Dead time Interval between the time of mixing and the time at which the flow has ceased completely in an apparatus for stopped flow, during which no observation of changes can be made.

Deshielding Shift of electrons away from the observed nucleus that decreases the shielding those electrons would normally provide.

Desolvation Process during which the layer of solvation surrounding a molecule is stripped away.

Deuterium kinetic isotope effect Change in a rate constant produced by substitution of a deuterium for a protium in a reactant.

Diamagnetic, noncovalent intermediate Intermediate in an enzymatic reaction that forms within the active site, that is noncovalently associated with the active site, and in which all electrons are paired in atomic and molecular orbitals.

Diastereotopic faces Two faces of a trigonal atom with three different functional groups where addition to that atom of a functional group different from the other three would form one of a pair of diastereomers. See also *enantiotopic faces* and *stereoheterotopic faces*.

Diastereotopic functional groups Two identical functional groups on a prochiral atom where replacement of one of the two with a functional group different from the other two on the same atom would form one of a pair of diastereomers. See also *enantiotopic functional groups* and *stereoheterotopic functional groups*.

Diels–Alder reaction Cycloaddition in which four atoms in two adjacent, conjugated double bonds (the diene) form a cyclohexene by combining with a double bond (the dienophile) elsewhere in the same molecule or in another molecule.

Disproportionation Reaction in which two identical molecules are converted to two different molecules and, in a special case, two identical molecules at the same intermediate oxidation state are converted to one molecule at a higher oxidation state and one molecule at a lower oxidation state.

Dissociative exchange Mechanism for the exchange of ligands to a metallic cation in which the leaving ligand dissociates from the metallic cation, contracting its coordination, and then the entering ligand occupies the open site of coordination. See also *associative exchange*.

Dissociative nucleophilic substitution Nucleophilic substitution in which the bond between the leaving group and the electrophile is completely broken before the bond between the electrophile and the nucleophile begins to form and which necessarily involves an intermediate. See also *associative nucleophilic substitution* and *concerted nucleophilic substitution*.

Distributive reaction Situation in which an active site catalyzes a reaction within a particular segment of a linear homopolymer—be it a cleavage of the polymer beyond that segment, the addition of a new segment to that segment, or simply a chemical alteration of that segment—by associating from solution before and dissociating into the solution after the catalytic event within that segment. See also *processive reaction*.

Donnan effect Effect that causes a ligand that is charged to be depleted or enriched in the diffuse layer of dissolved counterions around the protein and that, consequently, decreases or increases, respectively, the measured concentration of bound ligand in the compartment containing the protein.

Double kinetic isotope effect Change in a primary kinetic isotope effect associated with the overall enzymatic reaction that is brought about by substituting a heavier isotope at another position in the molecule at which another bond is formed or broken.

Electric gradient Gradient in electric potential established when the molar concentration of ionically charged substance A is greater on one side of a biological membrane than on the other side. See also *chemical gradient, electrochemical gradient,* and *gradient*.

Electrochemical gradient Gradient in chemical activity of a substance, caused by the combination of chemical and electric gradients. See also *chemical gradient, electric gradient,* and *gradient*.

Electrochemical gradient of hydrons Sum of the free energy stored in the electric potential and the free energy stored in the difference in the concentration of hydrons (the gradient of hydrons) across a membrane.

Electrocyclic reaction Pericyclic reaction in which a σ bond is formed between the termini of a fully conjugated linear π molecular orbital system containing three (or $2n + 3$) π bonds among six (or $4n + 6$) atoms that become a ring with two (or $2n + 2$) π bonds and the σ bond connecting the former termini and in which the number of π bonds has decreased by one and the number of σ bonds has increased by one.

Electron-donating substituent Group that donates electron density to an adjacent atom or π molecular orbital system that is more electron-deficient than the donor.

Electron repulsion Positive, unfavorable free energy that results from overlap between filled orbitals.

Electron-withdrawing substituent Group that withdraws electron density from an adjacent atom or π molecular orbital system that is less electron-deficient.

Electronic matrix element, H_{AB} Term that quantifies the coupling of the electronic state of the donor of an electron with the electronic state of the acceptor of an electron in an outer-sphere electron transfer when both are in the configuration of the transition state. See also *Marcus equation*.

Electrophilic aromatic addition Addition of an electrophile to a carbon in an electron-rich and nucleophilic aromatic system to form a cationic adduct between the electrophile and an atom in the aromatic ring.

Electrophilic aromatic substitution Electrophilic aromatic addition followed by the dissociation of another electrophile from the resulting adduct, usually (but not always) from the same carbon to which the first electrophile added, with the result that one electrophile replaces another electrophile.

Electrostatic catalysis Enhancement of the rate of a reaction that results from the electrostatic field created by the formal elementary charge of one or several nearby functional groups.

Elementary rate constant Rate constant for an elementary reaction. See also *composite rate constant*.

Elementary reaction Reaction for which no reaction intermediates have been detected or need to be postulated in order to describe the chemical reaction on a molecular scale, which occurs in a single step, and which passes through only a single transition state. See also *composite reaction*.

Elimination–addition Reaction in which an acid or electrophile and a base or nucleophile are removed from two adjacent carbons or two carbons separated by one or more double bonds to produce a double bond or an additional double bond, or a reaction in which an acid or electrophile and a base or nucleophile are added to a carbon–carbon double bond or the two ends of a conjugated set of double bonds.

Enamine Vinylic amine, which is the conjugate base resulting from removal of a hydron from the carbon atom α to an iminium.

Enantiotopic faces Two opposite faces of a trigonal atom with three different achiral functional groups where addition to that atom of an achiral functional group different from the other three would form one of a pair of enantiomers. See also *diastereotopic faces* and *stereoheterotopic faces*.

Enantiotopic functional groups Two identical functional groups on a prochiral tetrahedral atom where replacement of one of the two with an achiral functional group different from the other two on the same atom would form one of a pair of enantiomers. See also *diastereotopic functional groups* and *stereoheterotopic functional groups*.

Encounter complex Complex of all the necessary molecular participants in the transition state for the production of an intermediate or product, which have been assembled together at an encounter-controlled rate; most of the time, the participants dissociate before a transition state forms, except in the case of an encounter-controlled reaction.

Encounter-controlled bimolecular rate constant Rate constant for a reaction in which every encounter between the two reactants results in product; also referred to as the "diffusion-controlled rate constant".

Endergonic Description of a reaction for which the overall standard Gibbs energy change ΔG° is positive. See also *exergonic* and *isoergonic*.

End-product inhibition Situation where one or several end products of a metabolic pathway inhibit the first committed reaction in that pathway. See also *first committed reaction*.

Ene reaction Pericyclic reaction in which the distal atom in the double bond adjacent to an allylic hydrogen adds to an atom in a second double bond unconjugated to the first, either in another molecule or within the same molecule, to form a new σ bond while the allylic hydrogen is transferred to the other atom in the second double bond so that the number of π bonds has decreased by one and the number of σ bonds has increased by one during the transfer of the hydrogen.

Enethiolate Vinylic thiolate, which is the conjugate base resulting from removal of a hydron from the carbon atom α to a thiocarbonyl.

Enol tautomer Vinylic tautomer of a ketone, aldehyde, ketimine, aldimine, or acyl derivative in which there is a hydron on the oxygen, nitrogen, or sulfur and a double bond between the carbonyl or acyl carbon and the carbon adjacent to it, and that is the conjugate acid of an enolate. See also *keto tautomer*.

Enolate Conjugate base of a ketone or aldehyde from which the acidic hydrogen on carbon adjacent to the carbonyl group has dissociated.

Enzyme Molecule of protein that acts as a catalyst for a particular chemical reaction by forming a molecular complex with the reactant or reactants and that increases the rate of the reaction, catalyzes only one specific reaction type, operates on only a limited or exclusive set of substrates, controls the regiospecificity of the reaction, and is specific to only one of the enantiomers or diastereomers of its substrates.

Equatorial position Position of the three substituents or ligands in a trigonal bipyramid or the four ligands in a pyramidal arrangement coplanar or almost coplanar with the central atom. See also *apical position*.

Equilibrium dialysis Method that can be used to determine the binding of a ligand to a protein in which the protein is placed on one side of a semipermeable membrane that separates two compartments, ligand is added to both compartments, the system is allowed to reach equilibrium, and the concentration of protein on the one side and the concentrations of the ligand on the two sides are then measured.

Equilibrium isotope effect Change in the equilibrium constant for a reaction produced by isotopic substitution at an atom in the reactant and product.

Equilibrium-ordered mechanism Kinetic mechanism in which it is proposed that the association of reactants is ordered and each association of a reactant is at equilibrium.

Equilibrium-random mechanism Kinetic mechanism in which it is proposed that the association of reactants is random and each association of a reactant is at equilibrium.

Evolutionarily shifting domains Domains that are homologous, either in amino acid sequence or because their crystallographic molecular models are superposable, and appear at different locations in the polypeptides of apparently unrelated proteins.

Exciton Electronic excitation treated as if it were a quasi-particle capable of migrating through a network of chromophores.

Exergonic Description of a reaction for which the overall standard Gibbs energy change ΔG° is negative. See also *endergonic* and *isoergonic*.

Expanded kinetic mechanism Kinetic mechanism for a chemical reaction that expands one or more of the steps in a kinetic mechanism to include additional steps.

Extradiol dioxygenase One of a family of enzymes that can dioxygenate an ortho or para dihydroxyphenyl or aminohydroxyphenyl group to turn it into the respective 6-oxohexa-2,4-dienoate by oxidatively cleaving the carbon–carbon bond adjacent to one of the hydroxy groups but not the carbon–carbon bond between two vicinal ortho hydroxy groups. See also *intradiol dioxygenase*.

Final product Product that dissociates from the active site for the last reaction in a sequence of successive reactions catalyzed by a multienzymatic complex. See also *initial reactant* and *intermediate substrate*.

First committed reaction Earliest step in any metabolic pathway in which a metabolite is produced that can only be used in that pathway. See also *end-product inhibition*.

Fixed molecule of water Molecule of water that has a fixed location in a map of electron density because, at any given instant, that site in the crystal is occupied by a molecule of water.

Fixed reactant Reactant that is held at a constant concentration in a series of experiments to determine the initial rate of an enzymatic reaction. See also *varied reactant*.

Flavin Coenzyme that can be either free in solution or a tightly bound prosthetic group; that has, as its catalytically active portion, a 7,8-dimethylisoalloxazine substituted at nitrogen 10; and that has three stable oxidation states differing sequentially by two one-electron steps between oxidized flavin, flavin semiquinone (a radical), and reduced flavin.

Flavoenzyme Enzyme with a flavin prosthetic group that is either covalently bound or tightly bound noncovalently.

Fluorescent reporter Functional group incorporated into an enzyme that can register, by changes in its fluorescence, changes occurring in the active site as reactants associate and are converted into intermediates.

Formal transport of hydrons Appearance of hydrons in the solution on one side of a membrane, resulting from their dissociation during the oxidation of one or more prosthetic groups on that side of the membrane, and disappearance of an equal number of hydrons from the solution on the other side of the membrane, resulting from their association during the reduction of one or more prosthetic groups on that side of the membrane. See also *active transport of hydrons*.

Fractionation factor Theoretically calculated or observed primary equilibrium isotope effect for transfer of a hydrogen from a particular position in a particular molecule to a reference molecule.

Franck–Condon principle Principle that an electronic transition is most likely to occur without changes in the positions of the nuclei in the molecular entity and its environment or, in other words, that the position and momentum of all nuclei in a system be the same before and after the transfer of an electron.

Free energy change, ΔG, for an oxidation–reduction Change in free energy resulting from the difference between the reduction potential of the redox couple of oxidized reactant and its reduced product in an oxidation–reduction reaction and the reduction potential of the redox couple of reduced reactant and its oxidized product.

Fundamental allosteric constant Allosteric constant for an enzyme in the absence of any of its ligands. See also *allosteric constant* and *conditional allosteric constant*.

Gap percent Number of gaps for every 100 positions that have to be added to obtain the greatest percent identity in two sequences of amino acids being aligned. See also *percent identity*.

General acid–base catalysis Increase in the rate of a reaction due only to an increase in the concentration of an added acid–base.

General acid catalysis Increase in the rate of a reaction due only to an increase in the concentration of the conjugate acid of an added acid–base, which may include hydronium ion and which is expressed as a rate constant multiplied by the concentration of the conjugate acid.

General base catalysis Increase in the rate of a reaction due only to an increase in the concentration of the conjugate base of an added acid–base, which may include hydroxide ion and which is expressed as a rate constant multiplied by the concentration of the conjugate base.

General redox couple Widely used cytoplasmic redox couple—such as NAD^+ and NADH, ubiquinone and ubiquinol, oxidized and reduced electron-transfer flavoprotein, or oxidized and reduced ferredoxin—that participates in an enzymatically catalyzed oxidation–reduction and that connects the particular reaction catalyzed by the enzyme to the overall reduction potential at which the cytoplasm is poised. See also *nominal redox couple*.

Gradient Change in a quantity—such as temperature, electric potential, or the concentration or chemical activity of a substance—with distance, expressed as a ratio or differential ratio of the quantity. See also *chemical gradient*, *electric gradient*, and *electrochemical gradient*.

Haber–Bosch process Industrial method for converting N_2 to NH_4^+ that uses a catalyst produced from a dust of magnetite (Fe_2O_3) that has been partially reduced to form a layer of ferrous oxide surrounded by a layer of porous metallic iron.

Half-reaction Oxidation or reduction of one of the two redox couples that together make up an oxidation–reduction.

Hammond postulate Principle that the transition state between a reactant or reactants and an intermediate of high energy should resemble the intermediate more closely than the reactant or reactants.

Heme Prosthetic complex, surrounded by protein, formed between an octahedrally coordinated iron ion and a porphyrin the four central nitrogens of which act as a tetradentate ligand providing four equatorial lone pairs of electrons as ligands to the iron ion, and the two axial ligands, which are opposite each other across the iron, are provided by the protein, the solvent, or solutes in the solution.

Heme P450 Prosthetic heme that is found in a group of monooxygenases that catalyze several different types of oxidations and that, upon association with carbon monoxide, displays a characteristic absorption at 450 nm in its difference spectra, caused by the presence of a thiolate in an axial position of the heme.

Heterolysis Cleavage of a covalent bond so that both bonding electrons remain with one of the two fragments between which the bond is broken. See also *homolysis*.

Heterolytic reaction Reaction in the mechanism of which covalent bonds are broken by heterolysis or, when bonds are formed, both electrons forming each bond arrive on the same reactant. See also *homolytic reaction*.

Heterotropic allosteric effect Allosteric effect that occurs when the interacting sites bind different ligands. See also *allosteric effect* and *homotropic allosteric effect*.

Heterotropic allosteric effector Ligand that acts by associating with a protein or enzyme at a site different from a site for binding another ligand or an active site and altering association of ligands or substrates with this other site or its steady-state kinetics.

High-potential [4Fe–4S] iron–sulfur cluster Iron–sulfur cluster that participates in the oxidation–reduction between the monoanionic and dianionic states and for which the standard reduction potential lies between 0 and +500 mV.

High-spin state State of the ion of a transition metal in which its $3d$ electrons are distributed so that as many of the $3d$ orbitals as possible, even if they are not degenerate because of the effects of the ligands, contain unpaired electrons of the same spin as dictated by Hund's rule.

High-valent state Formal oxidation state of a transition metal ion that is more positive than the oxidation states of that ion that are usually encountered.

Hill coefficient Slope of a plot of log $[Y\,(1 - Y)^{-1}]$ against log [L], for ligand or substrate L, where Y can be either occupancy or fraction of limiting velocity, which serves as a semiquantitative measure of the degree of cooperativity.

Hill equation One of two equations that are used to fit sigmoid behavior and that involve no explanation for sigmoid behavior. See also *Adair equation, Monod–Wyman–Changeux equation,* and *sigmoid behavior*.

Homolysis Cleavage of a bond so that each of the molecular fragments between which the bond is broken retains one of the bonding electrons. See also *heterolysis*.

Homolytic reaction Reaction in the mechanism of which covalent bonds are broken by homolysis or formed by colligation. See also *heterolytic reaction*.

Homotropic allosteric effect Allosteric effect that occurs when two or more interacting sites are composed of the same respective amino acids within two or more constituent subunits, each formed from a folded polypeptide of the same sequence, and consequently associate with the same ligand or set of ligands. See also *allosteric effect* and *heterotropic allosteric effect*.

Hydride migration Transfer of a hydrogen (formally a hydride), usually intramolecularly and often between two adjacent atoms (as in a 1,2-hydride migration), during the course of a molecular rearrangement. See also *alkyl migration*.

Hydron General name to be used without regard to the nuclear mass of the hydrogen entity, either for hydrogen in its natural abundance or where it is not desired to distinguish between the isotopes. See also *proton*.

Hydron motive force Difference in the free energy of a hydron between the two sides of a cellular membrane across which there is an electrochemical gradient of hydrons.

Hydron wire Chain of hydrogen bonds into one end of which a hydron enters and out of the other end of which a hydron emerges or out of one end of which a hydron is removed and into the other end of which a hydron enters.

Hydronium ion Species unavoidably present in aqueous solution that is composed of one hydron and either four molecules of water ($H_9O_4^+$), six molecules of water ($H_{13}O_6^+$), or 21 molecules of water ($H_{43}O_{21}^+$) in some fluctuating combination for which the mean number of waters is unknown.

Hydrophobic effect Decrease in standard free energy that results from the removal of hydrogen–carbon bonds from contact with water.

Hydroxide ion Species unavoidably present in aqueous solution that can be considered as a hydron hole, shared among the central oxygen and three, or perhaps more, of its nearest neighbors of water, in which there is one hydron fewer than two hydrogens for every oxygen.

α-Hydroxy enamine Enamine in which the nitrogen of thiamine diphosphate participates, that is formed when an electrophile dissociates from the adduct between thiamine diphosphate and an aldehyde or ketone, and that is basic and nucleophilic at its α carbon because of the electron excess usually provided at such a carbon by an enamine.

Hyperconjugation Interaction of the two electrons in a σ bond with the lowest unoccupied molecular orbital (LUMO) or a partially occupied molecular orbital of an adjacent π molecular orbital system or an adjacent unoccupied or partially occupied p atomic orbital.

Induced fit Change in the conformation of an enzyme that is thermodynamically linked to the association of its substrates and that usually produces a more competent active site. See also *conformational selection*.

Inhibition constant, K_i Dissociation constant of an inhibitor from an enzyme.

Inhibitor Chemical substance that, when added to the solution, decreases the initial rate of an enzymatically catalyzed reaction.

Initial rate, v_0 Rate of decrease in the concentration of reactant in an enzymatically catalyzed reaction, or the rate of increase in the concentration of product, observed immediately after the reaction is initiated, either by adding the enzyme or by adding the final reactant necessary to complete the set of reactants; or, if necessary, the rate extrapolated back to zero time.

Initial reactant Reactant that associates with the active site for the first reaction in a sequence of successive reactions catalyzed by a multienzymatic complex. See also *final product* and *intermediate substrate*.

Inner-sphere catalysis Increase in the rate of a reaction due to one or more reactants becoming inner-sphere ligands to a catalytic metallic cation and, during their coordination, participating in the reaction. See also *outer-sphere catalysis*.

Inner-sphere electron transfer Electron transfer, usually between two metal centers sharing a ligand or an atom in their respective coordination shells, that takes place when there is strong electronic coupling (>20 kJ mol^{-1}) between donor (the reductant) and acceptor (the oxidant) in the transition state. See also *outer-sphere electron transfer*.

Interaction coefficient Slope of the line when a series of Brønsted coefficients is plotted as a function of the values of pK_a for the conjugate acids of a series of homologous acids or bases participating in the reaction other than the participants that produced the Brønsted coefficients.

Intermediate Arrangement of atoms in the mechanism of a chemical reaction that has a lifetime longer than the time required for the intramolecular and intermolecular vibrations among those atoms to become established and that is formed from the reactants and reacts further to give the products. See also *transition state*.

Intermediate isotopic exchange Hydrogen or oxygen isotopic exchange observed at a position in one product as the reaction is proceeding in one direction, but the exchanged isotope is not an atom that would have been incorporated into the product from a stoichiometric hydron or a stoichiometric molecule of water during the normal course of the reaction.

Intermediate substrate Product of any of the successive reactions catalyzed by a multienzymatic complex except for the last reaction in the sequence. See also *final product* and *initial reactant*.

Intermolecular, bimolecular reaction Reaction that takes place between two different reactants.

Intradiol dioxygenase One of a family of enzymes that can dioxygenate an ortho dihydroxyphenyl group to turn it into a (2*Z*,4*Z*)-hexa-2,4-dienedioate by oxidatively cleaving the carbon–carbon bond between the two vicinal hydroxy groups. See also *extradiol dioxygenase*.

Intramolecular, unimolecular reaction Reaction in which a bond will be formed between two atoms within the same reactant.

Intrinsic kinetic isotope effect Kinetic isotope effect on a microscopic rate constant for a specific elementary step in the mechanism of an enzymatically catalyzed reaction, not necessarily a step in which the bond at which isotopic substitution has been made is broken.

Inverse kinetic isotope effect Counterintuitive increase in an apparent rate constant that results from substitution of a lighter isotope with a heavier isotope. See also *normal kinetic isotope effect*.

Inversion of configuration Configurational change when a chemical species having a tetrahedral arrangement of bonds to a central atom, such as carbon or phosphorus, is converted into the chemical species having the opposite relative configuration.

Iron–sulfur cluster Array of two or more iron ions, bridging sulfide ions, and nonbridging sulfido groups of cysteines from the protein, in the most common arrangements of which four sulfurs are positioned tetrahedrally around each iron ion.

[2Fe–2S] Iron–sulfur cluster Iron–sulfur cluster that contains two iron ions with two of the tetrahedral positions around each iron ion occupied by sulfide ions and the other two positions occupied by sulfido groups of cysteines in the protein.

[3Fe–4S] Iron–sulfur cluster Iron–sulfur cluster that contains three atoms of iron and that is usually derived from a [4Fe–4S] iron–sulfur cluster in which one of the four irons has dissociated because a cysteine from the protein that would normally form a strong bond with this iron is either absent or unable to do so.

[4Fe–3S] Iron–sulfur cluster Iron–sulfur cluster that is formally a [4Fe–4S] iron–sulfur cluster from which one of the sulfides has been removed.

[4Fe–4S] Iron–sulfur cluster Iron–sulfur cluster that contains four iron ions and four sulfide ions with three of the tetrahedral positions around each iron ion occupied by sulfide ions and the fourth occupied by the sulfido group of a cysteine from the protein.

Isoergonic Description of a reaction for which the overall standard Gibbs energy change ΔG° is close to zero. See also *endergonic and exergonic*.

Isoprenoid Compound formally derived from isoprene, the skeleton of which can generally be discerned in repeated occurrence of isoprenoid units in the molecule but that may differ from strict additivity of isoprene units by loss or shift of a fragment, commonly a methyl group.

Isoprenoid unit Five-carbon building block within a molecule formally, but not necessarily actually, derived from isoprene (2-methylbuta-1,3-diene), found in carotenoids, steroids, and terpenes.

Isotopic exchange Exchange of one isotope of an atom in a reactant for a different isotope of that atom catalyzed by the active site of an enzyme during which the exchanged isotope appears in either the reactant or product.

Isotopic exchange at equilibrium Isotopic exchange within one reactant that is observed when all reactants and products of the enzymatic reaction are present in the solution and the respective concentrations of reactants and products are purposely set so that they satisfy the equation for the equilibrium constant.

Isotopic exchange at initial rate Isotopic exchange that is observed at an atom in one reactant when all the reactants and none of the products are present and the reaction is proceeding only in one direction.

Keto–enol tautomerization Interconversion between keto and enol tautomers of a carbonyl carbon, with the equilibrium constant K_E.

Keto tautomer Tautomer of a ketone, aldehyde, ketimine, aldimine, or acyl derivative in which there is a hydron on the carbon adjacent to the carbonyl or acyl carbon, and the double bond is between the carbonyl or acyl carbon and the oxygen, nitrogen, or sulfur. See also *enol tautomer*.

Kinetic isotope effect Change in a rate constant produced by substitution of the isotope of one or more atoms in a reactant for another isotope. See also *primary kinetic isotope effect* and *secondary kinetic isotope effect*.

Kinetic mechanism Proposal for the steps through which a chemical reaction proceeds between reactants and products, each step of which is associated with one rate constant (if proposed to be kinetically irreversible) or two rate constants (if proposed to be an equilibrium).

Kinetic titration Titration of the sites for an activator, substrate, or inhibitor of an enzyme that is followed by its effect on the kinetics of the enzymatic reaction in a situation in which the ligand has a small enough dissociation constant so that it is stoichiometrically bound by the enzyme. See also *spectrophotometric titration*.

Kinetically irreversible step Step in which the rate of the back reaction is so slow that it has no effect on the kinetics of the overall reaction.

Leaving group Atom or group of atoms that dissociates heterolytically from an electrophilic center, leaving behind the rest of the molecule.

Leffler coefficient Slope of a linear plot in which the changes in standard free energy of activation for a set of reactants participating in the same type of reaction are plotted against the overall changes in standard free energy of each individual reaction.

Ligand Molecule that binds to but is not chemically transformed by a protein.

Light-harvesting prosthetic group Prosthetic group in the antenna of a photosystem that absorbs light and from which the resulting electronically excited state migrates through the network of prosthetic groups in the antenna to a photosynthetic reaction center.

Limiting rate, V Rate of the enzymatic reaction at a given total molar concentration of active sites at high concentrations of all reactants or at extrapolated infinite concentrations.

Local conformational change Conformational change that occurs within the tertiary structure of a single folded polypeptide, that is confined to that folded polypeptide, and that has an insignificant effect on neighboring subunits. See also *quaternary conformational change*.

Low-potential [4Fe–4S] iron–sulfur cluster Iron–sulfur cluster that participates in the oxidation–reduction between the dianionic and trianionic states and for which the standard reduction potential lies between –800 and 0 mV.

Low-spin state State of the ion of a transition metal in which its 3d electrons are distributed so that one or more of its 3d orbitals of low energy contain pairs of electrons of opposite spin while one or more of its 3d orbitals of high energy, as a result of electron repulsion from the ligands, remain vacant.

Macroviscosity Viscosity of a solution. See also *microviscosity*.

Marcus equation Relation that defines the rate constant for the outer-sphere transfer of an electron to be a thermodynamic function of temperature, electronic matrix element (H_{AB}), reorganization energy (λ), and free energy accompanying the transfer (ΔG°). See also *electronic matrix element, H_{AB}*, and *reorganization energy, λ*.

Mechanism-based label Active-site label that must be chemically altered at the active site, in a reaction resembling the one normally catalyzed by the enzyme, before it can modify a catalytic acid–base or side chain in the active site.

Mediator Small molecule that can be rapidly oxidized or reduced by one or two electrons at an electrode and also rapidly reduced or oxidized by the prosthetic group in a protein so that the concentrations of oxidized and reduced prosthetic group in the solution can be conveniently poised at the reduction potential of the electrode.

Metabolism Ensemble of the coordinated sequences of chemical reactions and physical processes that occur within all living cells to provide energy (catabolism) and to accomplish biosynthesis (anabolism).

Michael addition Addition to a carbon–carbon double bond conjugated to a carbonyl, imino, or acyl group in which a nucleophile adds to the carbon in the double bond peripheral to and a hydron or electrophile adds to the carbon distal to the carbonyl, imino, or acyl group.

Michaelis constant for reactant A, K_{mA} Concentration of reactant A at which the rate of the enzymatic reaction at a given total molar concentration of active sites is half the limiting rate when all other reactants for the enzyme are present at high concentrations or have been extrapolated to infinite concentrations.

Microscopic reversibility Principle, which is a corollary of absolute rate theory, stating that any chemical reaction must pass through the same transition states but in opposite order in the forward and reverse directions, so the mechanism in one direction is exactly the reverse of the mechanism in the other direction even though the fluxes through the steps in the two directions differ when the reaction is not at equilibrium.

Microviscosity Viscosity experienced by a molecule in a solution. See also *macroviscosity*.

Midpoint reduction potential, E_m Potential measured under a given set of conditions when the total molar concentration of the reduced participant in a redox couple, $[\text{reduced}]_t$, in all its ionization states and tautomers is equal to the total molar concentration of the oxidized participant in the same redox couple, $[\text{oxidized}]_t$, in all its ionization states and tautomers, and the conditions are such that the activity coefficients cancel, usually because the concentrations of the reactants are small.

Mitochondrion Organelle in all eukaryotic cells that is responsible for producing $MgATP^{2-}$ by oxidative phosphorylation; that is descended from an aerobic, nonphotosynthetic bacterium; and that has an inner membrane corresponding to the plasma membrane of the ancestral bacterial cell.

Mixed inhibition Inhibition produced by a mixed reversible inhibitor. See also *competitive inhibition*, *noncompetitive inhibition*, and *uncompetitive inhibition*.

Mixed reversible inhibitor with respect to reactant A Reversible inhibitor for which the inhibition constant that affects the specificity constant or apparent specificity constant for reactant A is different from the inhibition constant that affects the catalytic constant or apparent catalytic constant for reactant A, and both inhibition constants are finite.

Molecular orbital Wavefunction that describes an electron distribution over the effective field provided by the nuclei and all other electrons of a molecule, that can be expressed as a linear combination of atomic orbitals, and that is usually represented schematically as envelope encompassing a region of space in which there is an arbitrarily fixed high probability of finding the electron occupying the orbital.

π Molecular orbital system Complete set of molecular orbitals—equal to the number of atoms in the system—each orbital of which is a linear combination of p atomic orbitals, one from each of the atoms, which are all adjacent to each other, and that delocalizes the electrons that occupy the constituent molecular orbitals over all the atoms in the system and in which the distribution of electrons can be approximated by examining resonance structures.

σ Molecular orbital system System containing two molecular orbitals that results from the combination of two atomic orbitals from two adjacent atoms, either s orbitals or hybrid orbitals formed from an s orbital and an atomic orbital of higher principal quantum number, and that forms a localized covalent bond between the two atoms.

Molecular orbital system of the transition state Set of atomic and molecular orbitals that are formed by mixing of the atomic and molecular orbitals of the reactant or reactants in a chemical reaction and that can undergo permitted unmixing to generate the atomic and molecular orbitals of the product or products of the chemical reaction.

Molybdoenzyme Enzyme that contains a molybdenum ion coordinated by both sulfanyl groups from one or two molybdopterins. See also *tungstoenzyme*.

Monod–Wyman–Changeux equation General equation that explains sigmoid behavior on the basis of the proposal that the homooligomer involved undergoes a quaternary conformational change in which symmetry is conserved. See also *Adair equation*, *Hill equation*, and *sigmoid behavior*.

Monomeric metaphosphate Planar molecule in which phosphorus is trivalent, hybridized sp^2, forms a σ bond to each of the three oxygens, and contains three pairs of electrons in a π molecular orbital system.

Mononuclear iron–sulfur cluster Iron–sulfur cluster that contains one iron ion with all four tetrahedral positions occupied by the sulfido groups of cysteines from the protein.

Multienzymatic complex Assembly of the active sites for two or more different reactions in the same macromolecular complex.

Nominal redox couple Redox couple that is unique to a particular flavoenzyme and that gives the enzyme its name. See also *general redox couple*.

Noncompetitive inhibition Inhibition produced by a noncompetitive reversible inhibitor. See also *competitive inhibition*, *mixed inhibition*, and *uncompetitive inhibition*.

Noncompetitive reversible inhibitor with respect to reactant A Reversible inhibitor the addition of which to the solution decreases the specificity constant or apparent specificity constant for reactant A and the catalytic constant or apparent catalytic constant for reactant A by the same factor.

Nonprocessive enzyme Enzyme that catalyzes a distributive reaction.

Normal kinetic isotope effect Decrease in a rate constant that results from substitution of a lighter isotope with a heavier isotope. See also *inverse kinetic isotope effect*.

Nuclear Overhauser effect Increase or decrease in the integrated intensity of the absorption of one nucleus in a nuclear magnetic resonance spectrum that occurs when a neighboring nucleus is saturated by applied radio frequency at which it absorbs and that results from the intramolecular transfer of nuclear spin polarization.

Nucleophilic substitution Heterolytic transfer of an electrophile between two lone pairs of electrons, each at a nucleophilic position, by which one nucleophile is replaced by another nucleophile.

Omit map of difference electron density Map of electron density produced when the molecular model of a substrate, ligand, or inhibitor is omitted from a crystallographic molecular model, a data set is calculated from this molecular model, and refinement against the observed reflections is initiated and continued until the positive electron density for these omitted participants in the maps no longer changes.

One-electron oxidation–reduction Oxidation–reduction in which a single electron is transferred to the oxidant from the reductant.

Ordered association Situation in which two or more reactants must add to an active site in a particular order to produce a Michaelis complex between all reactants and the active site. See also *random association*.

Outer-sphere catalysis Increase in the rate of a reaction produced by ligands coordinated to a metallic cation, rather than by the metallic cation itself. See also *inner-sphere catalysis*.

Outer-sphere electron transfer Electron transfer that takes place between a donor and an acceptor, usually separated from each other by several to many atoms, when there is weak or no electronic coupling between them in the transition state. See also *inner-sphere electron transfer*.

Oxidation number Number assigned to an atom that is the charge it would bear if all the ligands were removed, along with the electron pairs that were shared with the atom, and that is largely synonymous with its oxidation state.

Oxidation–reduction Complete balanced reaction that is the sum of two redox couples, in which the oxidant of one couple is reduced by the transfer of one or two electrons from the reductant of the other couple, causing the oxidation number of the reductant to increase and the oxidation number of the oxidant to decrease, and that is usually accompanied by association and dissociation of hydrons from the participants.

Oxidation state Degree of oxidation of an atom.

Oxidation state of an alcohol Oxidation state for a carbon that has one σ bond to a heteroatom and three other σ bonds to either carbon or hydrogen. See *oxidation states of carbon*.

Oxidation state of an alkane Oxidation state for a carbon that has four σ bonds to either carbon or hydrogen. See *oxidation states of carbon*.

Oxidation states of carbon Five configurations defined by the number of bonds—none, one, two, three, or four—between a carbon atom and one or more heteroatoms, the transitions between which are oxidations–reductions that have their own distinct chemistry. See *acyl oxidation state*, *carbonato oxidation state*, *carbonyl oxidation state*, *oxidation state of an alcohol*, and *oxidation state of an alkane*.

Oxidative decarboxylation Oxidation that causes a carboxylato group to dissociate from a molecule as carbon dioxide and that usually involves the formation of a carbonyl or the derivative of a carbonyl at a carbon β to the carboxylato group that dissociates with an enolate intermediate.

Oxocarbenium ion Distinct type of carbenium ion in which one substituent of the carbon atom is an oxygen atom so that the positive charge is delocalized between carbon and oxygen.

μ-Oxo group Oxide dianion or a hydroxide that bridges two or more metallic ions and participates in the coordination of each metallic ion.

Oxyanion hole Arrangement of donors for hydrogen bonds that associates with an oxyanion in a substrate or intermediate in an enzymatic reaction, but usually it stabilizes an oxyanion in an intermediate.

Partition function of the transition state, $^{\ddagger}Q^{0\prime}$ Function calculated from all degrees of freedom available to the transition state except motion along the reaction coordinate.

Patterson map Map of all the vectors between all the atoms in the unit cell of a crystal.

Pentadienyl carbenium ion Intermediate in an electrophilic aromatic substitution on a phenyl group that is produced when the electrophile adds to one of the carbons in the ring, that is formed by mixing the five *p* atomic orbitals remaining in the ring, and that usually delocalizes a positive charge.

Percent identity Percentage of positions in two optimally aligned sequences of amino acids that are occupied by identical amino acids. See also *gap percent*.

Perfectly processive enzyme Processive enzyme that transforms every segment in a particular molecule of a polymer without dissociating from it.

Pericyclic reaction Concerted reorganization of bonding that takes place through a transition state that is a cyclic array of overlapping atomic orbitals and proceeds through an aromatic transition state. See *cycloaddition*, *electrocyclic reaction, ene reaction*, and *sigmatropic rearrangement*.

Periplanarity Location of atoms, bonds, and lone pairs of electrons that are within dihedral angles of ±30° of a plane passing through a σ bond and that allows overlaps of molecular and atomic orbitals to occur among them.

pH–rate profile Plot of the observed rate constants for a reaction as a function of pH at constant temperature and ionic strength in the absence of added general acid–bases that is usually presented as the common logarithms of the observed rate constant for the reaction as a function of pH.

Pheophytin Macrocyclic prosthetic tetrapyrrole, derived from a porphyrin, that has an aromatic ring of 18 atoms over which a single electron can be delocalized, causing it to be capable of participating in one-electron transfer.

Phosphodiester Phosphoric acid that has been esterified with two alcohols, such as two nucleotides.

Phosphomonoester Phosphoric acid that has been esterified with only one alcohol, such as the 6-hydroxy group of glucose.

***N*-(5′-Phosphopyridoxyl)enamine** Structure formed when an electrophile dissociates from the β carbon of an *N*-(5′-phosphopyridoxyl)iminium and that is (as is the case with all enamines) electron-rich, basic, and nucleophilic.

Phosphotriester Phosphoric acid that has been esterified with three alcohols.

Photoisomerization Photochemical process accomplishing an isomerization of a prosthetic group by a bond rotation that causes an initial *E* or *Z* conformation to be changed to the opposite conformation as a result of absorbing a photon of light.

Photosynthetic reaction center Membrane-spanning enzyme that forces an electron to move from a donor of more positive standard reduction potential to an acceptor of more negative standard reduction potential by coupling that movement to the consumption of the energy in a photon of visible light.

Photosystem Complex between a photosynthetic reaction center and a number of proteins containing one or more types of chromophores such as chlorophylls, carotenoids, and bilins that together act as an antenna to absorb quanta of light.

Ping-pong mechanism Kinetic mechanism in which the active site oscillates between two forms, each separated from the other by a respective irreversible step, and each form has the same pattern of rate constants relating it to the other form.

Porphyrin Prosthetic group containing four pyrrolyl groups united through their α positions by four methine groups into a macrocyclic, aromatic ring, the four nitrogens of which can act as equatorial ligands to an octahedrally coordinated transition metallic ion.

Positional isotopic exchange Intramolecular isotopic exchange of one atom in a substrate with another atom, of the same element but a different isotope, in such a way that the product of the isotopic exchange is chemically identical to the reactant except that the two isotopes within the molecule have been interchanged.

Potentiometric titration Procedure in which the reduction potential of a solution, which is monitored by an electrode, is changed while the degree of oxidation–reduction of the molecule that is the subject of the titration is monitored.

Predominantly competitive inhibition with respect to reactant A Type of mixed inhibition where the inhibitor has a greater affinity for the enzyme unoccupied by reactant A than for the active site occupied by reactant A.

Predominantly uncompetitive inhibition with respect to reactant A Type of mixed inhibition where the inhibitor has a greater affinity for the enzyme occupied by reactant A than for the active site unoccupied by reactant A.

Primary equilibrium isotope effect Equilibrium isotope effect for isotopic substitution at a particular atom that is transferred between a reactant and a product during a reaction.

Primary kinetic isotope effect Kinetic isotope effect for a reaction in which the bond between the one atom that has been isotopically substituted and an atom to which it is covalently attached is broken or in which such a bond is formed. See also *kinetic isotope effect and secondary kinetic isotope effect*.

***pro-R* Functional group** Stereoheterotopic functional group on a prochiral atom to which arbitrary assignment of higher priority relative to the other identical functional group generates the *R* configuration at that atom.

***pro-S* Functional group** Stereoheterotopic functional group on a prochiral atom to which arbitrary assignment of higher priority relative to the other identical functional group generates the *S* configuration at that atom.

Processive enzyme Enzyme that catalyzes a processive reaction.

Processive reaction Situation in which an active site catalyzes a reaction within a particular segment of a linear homopolymer—be it a cleavage of the polymer beyond that segment, the addition of a new segment to that segment, or simply a chemical alteration of that segment—and then moves, without dissociating, to an adjacent segment of that polymer to catalyze the same reaction again. See also *distributive reaction*.

Processivity Ratio of the rate at which the active site moves to the next segment of a polymer and completes its catalysis of the reaction at that location to the rate at which the polymer dissociates from the enzyme.

Prochiral carbon Tetrahedral carbon to which are attached two chemically identical functional groups and two other functional groups, each of which is different from the two identical ones and different from each other, and that is capable of becoming chiral if one of the identical functional groups were replaced by a functional group different from the other two or a trigonal carbon to which are attached three different functional groups and that is capable of becoming chiral if an additional functional group, different from the other three, were attached.

Prochiral molecule Molecule that is achiral but that is capable of becoming chiral by a single substitution or addition.

Product Substrate that is being produced in the reaction catalyzed by an enzyme; or substrate that is not present when a solution is prepared to monitor a chemical reaction catalyzed by an enzyme but that is produced during the reaction.

Promoter sequence Sequence of nucleotides in double-stranded DNA that identifies a point at which transcription is to be initiated.

Prosthetic group Molecule, in addition to the amino acids that comprise a protein, that is either covalently attached as a posttranslational modification to the protein or remains tightly bound for an extended period of time (often equal to the lifetime of the protein) and that, when it is acting as a cofactor in an active site, provides a catalytic functional group. See also *coenzyme* and *cofactor*.

Protomers Identical, constituent complexes, between one or several folded polypeptides, each different from the others, that when combined in a fixed stoichiometry form the oligomeric protein.

Proton Nuclear particle of charge number +1 and rest mass of 1.007 276 470(12) unified atomic mass units. See also *hydron*.

Proximal ligand Axial ligand derived from the protein surrounding a heme that has only one ligand from the protein.

Push Interaction with a lone pair of electrons on an adjacent oxygen or nitrogen and the central atom in a nucleophilic dissociation or in the tetrahedral intermediate in a nucleophilic substitution, or the lone pair of electrons on an oxygen or nitrogen that is conjugated to the atom adjacent to the central atom, that results from an overlap between the filled orbital of the lone pair and the unoccupied orbital in the σ bond between the central atom and the leaving group that produces electron repulsion between the lone pair of electrons and the σ bond being broken, and that accelerates the departure of a leaving group.

Pyridoxal 5′-phosphate Prosthetic group that provides an aldehyde as a catalytic functional group and that is usually bound covalently to the resting enzyme as an internal pyridoximine, formed at the aldehyde in a simple nucleophilic substitution with the primary amino group of a lysine in the active site of the enzyme.

Pyridoximine Imine formed between the carbonyl group of pyridoxal 5′-phosphate and the amino group of a lysine within the enzyme (an internal pyridoximine) or an amino group in a substrate (an external pyridoximine).

***N*-Pyruvoyl group** Pyruvoyl group that is covalently attached through an amide between its carboxy group and the amino terminus of an enzyme and that provides a ketone with a catalytic capacity similar to that of the aldehyde in pyridoxal 5′-phosphate for the decarboxylation of α-amino acids.

Q-cycle Explicit series of electron transfers catalyzed by quinol—cytochrome-*c* reductase or plastoquinol—plastocyanin reductase that occur in an obligate order among a Rieske [2Fe–2S] iron–sulfur cluster, two hemes *b*, and a heme *c*.

Quaternary conformational change Conformational change in an oligomer that includes two or more of its subunits (but usually all of them), that usually occurs with retention of the symmetry of the oligomer, and that usually involves a change in the orientation of its constituent folded polypeptides with respect to each other. See also *local conformational change*.

Quenched flow Technique for following the progress of a reaction in an apparatus in which the reaction time can be controlled by connecting the outlet from a rapid mixing chamber to a length of tubing that is connected to a second mixing chamber or that simply ends in a quench solution and varying the time between mixing and the second mixing chamber or the quench solution by changing the flow rate or the length and cross-sectional area of the tubing connecting them and that permits products of the reaction to be assayed chemically rather than only spectroscopically. See also *stopped flow*.

Quinol Cyclic aromatic compound that has two hydroxy groups ortho or para to each other, or otherwise conjugated to each other, including ubiquinols, plastoquinols, menaquinols, and phylloquinol.

Quinone Derivative of a quinol in which the two hydroxy groups have been oxidized to carbonyl groups in a fully conjugated cyclic dione but that is not aromatic.

Quinonoid intermediate Structure formed when an electrophile dissociates from the carbon immediately adjacent to the iminium nitrogen in an external pyridoximine and that, as a result of this dissociation, is basic, nucleophilic, electron-rich, and capable of push.

Radiationless transfer of energy by resonance Formalism that describes the transfer of electronic excitation without photon emission or absorption from the initially excited chromophore (the donor) to another chromophore (the acceptor) as the consequence of a dipole–dipole interaction, the magnitude of which depends on spectral overlap, intermolecular distance, and the relative orientation of the transition dipole moments of the molecules.

Radical clock Compound, such as a methylcyclopropane or *trans*-2-methyl-1-phenylcyclopropane, that rearranges rapidly at a known rate when the respective radical is produced upon abstraction of a hydrogen from its methyl group.

Radical intermediate Paramagnetic, noncovalent intermediate that possesses an unpaired electron and that forms in an active site when a hydrogen atom is abstracted from a reactant, when an electron is added or subtracted from a reactant, or when a reactant dissociates homolytically.

Random association Situation in which the two or more reactants for an enzymatic reaction can add to the active site in any order to produce the same complex between all of them and the active site. See also *ordered association*.

Rate-affecting step Step in the complete kinetic mechanism of a reaction the elementary rate constant of which appears in the kinetic equation governing the rate of a reaction other than the rate-limiting rate constant for that reaction.

Rate equation Mathematical equation, derived from a written kinetic mechanism, that relates the observed initial rate, v_0, of the reaction to the initial concentrations of reactants and total molar concentration of active sites, the only parameters of which are the rate constants in the mechanism.

Rate-limiting step Last step in a series of reaction steps, the rate constant for which appears in the kinetic equation for the multistep reaction.

Rate of dialysis Unidirectional rate at which a ligand passes through a semipermeable membrane, which is directly proportional to the ligand's free concentration.

***Re* face** Stereoheterotopic face of a trigonal atom the functional groups of which, when viewed from that side of the carbon, appear in a clockwise sense in order of priority. See also *Si face*.

Reactant Substrate that is present when a solution is prepared by an investigator to undergo a reaction catalyzed by an enzyme.

Reactant activation Acceleration of the initial rate of an enzymatic reaction by a reactant as its concentration is increased, beyond the usual increase in rate resulting only from its association with the active site.

Reactant antagonism Effect that occurs when one reactant decreases the dissociation constant for another reactant and vice versa.

Reaction coordinate Path from reactant to product on a surface of potential energy that passes through a col on the surface at the transition state.

Redox couple Reduced molecule and oxidized molecule, such as reduced flavin and oxidized flavin, that can be interconverted by subtracting or adding only electrons and hydrons.

Reduction potential, E Driving force, usually expressed as a voltage, that a redox couple, under a given set of conditions, can provide to move electrons from a standard hydrogen electrode to the oxidized molecule of the redox couple to form the reduced molecule.

Relaxation time, τ Reciprocal of the first-order rate constant observed for a given first-order relaxation, formally defined as the time t during which the overall change in concentration falls to e^{-1} of its initial value.

Reorganization energy, λ Difference between the free energy of a Franck–Condon state in which the position and momentum of the nuclei and their respective solvation are the same before and after the transfer of an electron and the sum of the free energies of the equilibrium nuclear configuration of the donor, the equilibrium nuclear configuration of the acceptor, and their respective solvations. See also *Marcus equation*.

Resonance Raman infrared spectrum Raman spectrum observed when a chromophore in the active site is excited by a beam of light from a laser that is perpendicular to the beam of the laser that is registering the spectrum.

Reverse hydronation Situation in which a minor tautomer of either unassociated reactant or unassociated active site, rather than the respective major tautomer, or a minor tautomer of the Michaelis complex of the two, rather than the major tautomer, is the active form of the active site.

Reversible inhibitor Inhibitor that exerts its effect by associating noncovalently and reversibly with the enzyme and that, when associated, decreases or eliminates its ability to catalyze the reaction.

Rieske [2Fe–2S] iron–sulfur cluster [2Fe–2S] iron–sulfur cluster in which there are two histidines from the protein as ligands to one of the irons instead of two cysteines.

Secondary kinetic isotope effect Kinetic isotope effect in which the isotopic substitution occurs at another atom that is attached covalently to an atom participating in the breaking of a bond, other than the two atoms between which the bond is broken. See also *kinetic isotope effect, primary kinetic isotope effect, α-secondary kinetic isotope effect, and β-secondary kinetic isotope effect.*

α-Secondary kinetic isotope effect Secondary kinetic isotope effect in which the isotopic substitution occurs at an atom bonded directly to one atom in a bond being broken during the reaction. See also *kinetic isotope effect, primary kinetic isotope effect, secondary kinetic isotope effect, and β-secondary kinetic isotope effect.*

β-Secondary kinetic isotope effect Secondary kinetic isotope effect in which the isotopic substitution occurs at an atom bonded to an atom that, in turn, is bonded to an atom in the bond being broken during a reaction. See also *kinetic isotope effect, primary kinetic isotope effect, secondary kinetic isotope effect, and α-secondary kinetic isotope effect.*

Selanyl group Selenium analogue (–SeH) of a sulfanyl group.

Selenocysteine Amino acid homologous to serine and cysteine, in which a selenium replaces the oxygen or sulfur, respectively.

Semipermeable membrane Polymer film with pores large enough to permit small molecules to pass through them but too small to permit the passage of macromolecules such as proteins, polysaccharides, or nucleic acids.

Semiquinone Intermediate oxidation state with an unpaired electron that is formed by the removal of one electron from a quinol or other one-electron donor (such as reduced flavin) and from which another electron can be removed to produce the respective quinone or other donor oxidized by removal of two electrons.

Shielding Effect of electrons surrounding the observed nucleus and electrons surrounding neighboring nuclei that causes the local field of the nucleus to be less than the applied external magnetic field.

***Si* face** Stereoheterotopic face of a trigonal atom the functional groups of which, when viewed from that side of the carbon, appear in a counterclockwise sense in order of priority. See also *Re face.*

Sigmatropic rearrangement Pericyclic reaction in which a σ bond allylic to a π bond in the reactant is broken, a new σ bond allylic to a π bond is formed, and two π bonds migrate to adjacent positions in a situation in which both reactant or reactants and product or products together have two (or $2n + 2$) π bonds that are capable of participating in a cyclic, conjugated transition state in which the σ bond of the reactant and the σ bond of the product can also participate.

Sigmoid behavior Deviation from ideal behavior in which the slope of the curve describing occupancy of sites for ligands or substrates or for enzymatic activity increases as the concentration of ligand or substrate is increased before it then decreases as it approaches its rectangularly hyperbolic asymptote at saturation, producing an S-shaped (sigmoid) plot. See also *cooperativity.*

Solvation Interactions, favorable or unfavorable, between a molecule of solute or a transition state and molecules of solvent in the vicinity that modify the behavior of the solvent molecules and which in turn affect the behavior of the molecule of solute or the transition state.

Solvent deuterium kinetic isotope effect Kinetic isotope effect that results from the substitution of a hydron in the molecules of solvent for a deuterium and which, in a biochemical context, is when ^2H_2O is used as solvent instead of ^1H_2O.

Solvent kinetic isotope effect Kinetic isotope effect that results from a change in the isotopic composition of the solvent, usually when another isotopic form of the solvent is substituted for the naturally occurring isotopic form.

Special pair Two chlorophylls that together make up the prosthetic group in a photosynthetic reaction center that undergoes initial excitation either directly from sunlight or indirectly by transfer of an exciton.

Specific acid catalysis Increase in the rate of a reaction due only to an increase in the concentration of hydronium ion.

Specific base catalysis Increase in the rate of a reaction due only to an increase in the concentration of hydroxide ion.

Specificity constant for reactant A, k_A Observed apparent second-order rate constant, which is first-order with respect to the total molar concentration of active sites and first-order with respect to reactant A, for the enzymatic reaction at low concentration of reactant A, or at extrapolated zero concentration, when all other reactants for the enzymatic reaction are present at high concentrations or have been extrapolated to infinite concentrations.

Spectrophotometric titration Titration of the sites for an activator, substrate, or inhibitor of an enzyme that is followed by its effect on the absorbance of the solution due to a change in the absorbance of the ligand or the protein or both of them. See also *kinetic titration*.

Standard entropy of approximation, $\Delta^{\ddagger}S^{\circ}_{\text{approx}}$ Decrease in standard entropy that results when two reactants that are free in solution form a complex within a solvent cage with the alignments required to form the transition state for the reaction in which they participate.

Standard entropy of molecularity, $\Delta^{\ddagger}S^{\circ}_{\text{molec}}$ Change in standard entropy due solely to bringing two separate reactants together into the same solvent cage.

Standard entropy of rotational restraint, $\Delta^{\ddagger}S^{\circ}_{\text{rot}}$ Decrease in standard entropy that is required to freeze rotational motions within a solvent cage enclosing two reactants during the formation of a transition state.

Standard free energy of activation, $\Delta^{\ddagger}G^{\circ\prime}$ Difference between the standard chemical potentials of the reactants in an elementary reaction when they are free in solution and when they are in the transition state.

Standard hydrogen electrode Electrode in which diatomic hydrogen gas at a pressure of 10^5 pascals is poised electrochemically at equilibrium with two hydrons at pH = 0 in aqueous solution.

Standard reduction potential, E° Reduction potential observed when the two members of a redox couple are present at equal activity at a pH of 0.

Steady-state approximation Assumption that, because the concentration of reactant is so much greater than the concentration of enzyme, after the first few molecules of reactant have been turned into product by each molecule of enzyme, the concentration of each species involving the enzyme has reached a constant, steady state.

Stereoelectronic control Control of the identity of products or rate of a reaction by particular rotational alignments among atoms in a reactant that approximate and overlap molecular and atomic orbitals in the ground state preceding a transition state.

Stereoheterotopic faces Two faces that are either enantiotopic or diastereotopic. See also *diastereotopic faces* and *enantiotopic faces*.

Stereoheterotopic functional groups Two identical functional groups that are either enantiotopic or diastereotopic. See also *diastereotopic functional groups* and *enantiotopic functional groups*.

Sticky product Product that dissociates slowly from the active site relative to either the rate of the back reaction to bound reactant or the rate of the forward reaction from bound reactant to bound product.

Sticky reactant Reactant that is converted to products free in solution faster than it can dissociate from the active site.

Stopped flow Technique for following the progress of a reaction in an apparatus where an observation chamber is located as close to a mixing chamber as possible, and rapid flow of two solutions containing reactants through the mixing chamber under high pressure is initiated and then arrested as abruptly as possible so that the progress of the reaction can be monitored in the observation chamber by some method with a rapid response, such as absorbance or fluorescence. See also *quenched flow*.

Structure–activity correlation Effect of changing the functional groups on a particular reactant on the rate of a common reaction.

Substrates All of the molecules that are interconverted by an enzyme as it catalyzes its particular chemical reaction and that appear in the equation for the equilibrium catalyzed by the enzyme.

Swain–Schaad relation Theoretical function that relates the rate constant for a reactant substituted at a particular position with tritium to the ratio of the rate constants for that reactant hydronated and deuterated, respectively, at the same position.

Swain–Scott correlation Plot of common logarithms of observed second-order rate constants for a set of nucleophiles participating in a particular nucleophilic substitution as a function of a set of parameters, also known as nucleophilicities, that are related to the common logarithms of the respective rate constants for nucleophilic substitutions between the same set of nucleophiles and a reference electrophile.

Syn elimination Elimination in which the leaving group and the hydron or electrophile dissociate on the same side of a plane containing the carbons in a carbon–carbon bond to which they are attached. See also *anti elimination*.

Synperiplanar conformation Arrangement in which the two periplanar substituents of interest are oriented at a dihedral angle of $0° \pm 30°$ from one another. See also *antiperiplanar conformation*.

Synperiplanar push Push exerted by a lone pair of electrons in the synperiplanar conformation. See also *antiperiplanar push*.

Tautomerization Dissociation of a hydron from one atom in a molecule before, after, or concurrent with the association of a hydron with another atom in the same molecule.

Temperature jump Relaxation technique in which the temperature of a chemical system is suddenly raised, the system then relaxes to a new state of equilibrium, and analysis of the relaxation process provides rate constants for the step or steps through which the system proceeds to reach the new equilibrium.

Ternary complex Complex between an active site and two reactants.

Terpene Isoprenoid of biological origin that can be designated as a monoterpene (C_{10}), sesquiterpene (C_{15}), diterpene (C_{20}), triterpene (C_{30}), or tetraterpene (C_{40}).

Terpenoid Terpene that has been modifed so that it contains atoms of oxygen.

Tetrahedral intermediate Intermediate in a reaction in which an initially double-bonded carbon atom (typically an acyl carbon atom) has been transformed from trigonal to tetrahedral.

Thiamine diphosphate Prosthetic group tightly, but noncovalently, bound to the active sites of certain enzymes, the functionally important site of which is a carbon sandwiched between the iminium nitrogen and the sulfur in a thiazolium and the conjugate base of which is an ylide.

Thylakoid Flattened vesicle of membrane, inside the outer membrane of a chloroplast in a plant cell or inside the plasma membrane of a cyanobacterium, that corresponds to a chromatophore in the ancestral photosynthetic bacterial cell that gave rise to chloroplasts.

Total molar concentration of active sites, $[E]_t$ Sum of the concentrations of unoccupied active sites and of active sites occupied by substrates and intermediates in the enzymatic reaction.

Transamination Conversion of an amino group into an oxo group at one carbon and conversion of an oxo group into an amino group at another carbon, resulting in the transfer of ammonia or an amine between the two carbons.

Transferred nuclear Overhauser effect Nuclear Overhauser effect caused by the transfer of saturation from the atom in one molecule to the atom in another molecule that results from the two molecules being in intimate contact.

Transimination Conversion of an imine formed with one amino group into an imine formed with another amino group, usually at the same carbon.

Transition state Point of maximum potential energy along the reaction coordinate between reactant and product, which is located at a col, which lasts only as long as is necessary to pass over the col, and which is an assembly of atoms at the col that has an equal probability of forming the reactants or products of the elementary reaction in which it participates. See also *intermediate*.

Transition state theory Theory applied to the rates of elementary reactions that assumes an equilibrium, with an equilibrium constant $^{\ddagger}K'$, exists between the reactants and the sole transition state for the reaction.

Trigonal bipyramid Arrangement in which three of the five substituents on a particular atom or ligands to a particular metallic cation, which are designated equatorial, lie close to or within a plane containing the central atom or metallic cation at approximately 120° angles to each other and the other two substituents or ligands, which are designated apical, are located above and below the equatorial plane, respectively, close to or on a line perpendicular to the plane that passes through the central atom or metallic cation.

Tritium kinetic isotope effect Change in a rate constant produced by substitution of a tritium for a protium in a reactant.

Tungstoenzyme Enzyme that contains a tungsten ion coordinated by both sulfanyl groups from one or two molybdopterins. See also *molybdoenzyme*.

Tunneling Process by which a particle or a set of particles crosses a barrier on a surface of potential energy without having the energy required to surmount this barrier and which is usually revealed in the behavior of isotopes.

Two-electron oxidation–reduction Oxidation–reduction in which two electrons are transferred to the oxidant from the reductant.

Ultrafiltration Method that can be used to determine the binding of a ligand to a protein in which the protein and the ligand are allowed to equilibrate in a solution, a portion of the solution is forced under pressure through a semipermeable membrane, and the concentration of protein on the unfiltered side and the concentrations of the ligand on the filtered and unfiltered sides are then measured.

Uncompetitive inhibition Inhibition produced by an uncompetitive reversible inhibitor. See also *competitive inhibition*, *mixed inhibition*, and *noncompetitive inhibition*.

Uncompetitive reversible inhibitor with respect to reactant A Reversible inhibitor the addition of which to the solution decreases the catalytic constant or apparent catalytic constant for reactant A while having no effect on the specificity constant or apparent specificity constant for reactant A.

Varied reactant Reactant that is varied at several discrete, different concentrations in a series of experiments that determine the initial rate of an enzymatic reaction. See also *fixed reactant*.

Vibrational Stark effect Shift in the frequency of the maximum of absorbance for a vibrational mode produced by an electric field.

Ylide Compound in which an anionic carbon or other anionic atom is attached directly to a heteroatom (usually nitrogen, phosphorus, or sulfur) carrying a fixed formal positive charge, a separation of charge that cannot be neutralized internally by a shift of π electrons in a π molecular orbital system.

Enzymes and Other Proteins Discussed

acetaldehyde dehydrogenase (acetylating)
acetate CoA-transferase
acetate kinase
acetoacetate decarboxylase
acetolactate synthase
acetylcholinesterase
acetyl-CoA *C*-acetyltransferase
acetyl-CoA carboxylase
acetyl-CoA carboxytransferase
acetylene hydratase
N-acetylglucosamine-6-phosphate deacetylase
N^4-(*β*-*N*-acetylglucosaminyl)-L-asparaginase
β-*N*-acetylglucosaminylglycopeptide *β*-1,4-galactosyltransferase
acetylglutamate kinase
β-*N*-acetylhexosaminidase
N-acetylneuraminate synthase
N-acetylneuraminate lyase
acireductone dioxygenase (Ni^{2+}-requiring)
acireductone synthase
aconitate Δ-isomerase
aconitate hydratase
[acyl-carrier-protein] hydrolase
[acyl-carrier-protein] *S*-acetyltransferase
[acyl-carrier-protein] *S*-malonyltransferase
acyl-CoA:acyl-CoA alkyltransferase
acyl-homoserine-lactone synthase
acyl-CoA dehydrogenase
adenine deaminase
adenine phosphoribosyltransferase
adenosine deaminase
adenosine kinase
adenosylhomocysteinase
adenosylmethionine decarboxylase
adenylate kinase
adenylosuccinate lyase
adenylosuccinate synthase
adenylyl-sulfate reductase
ADP-*glyceromanno*-heptose 6-epimerase
ADP-glucose phosphorylase
adrenodoxin-$NADP^+$ reductase
aerobic carbon monoxide dehydrogenase
alanine racemase
alanine—tRNA ligase
alcohol dehydrogenase
aldehyde dehydrogenase (FAD-independent)
aldehyde dehydrogenase (NAD^+)
aldehyde ferredoxin oxidoreductase
aldehyde oxygenase (deformylating)
aldehyde reductase
alginate lyase
aliphatic halogenase
alkaline phosphatase
1-alkyl-2-acetylglycerophosphocholine esterase
alkylglycerone-phosphate synthase
all-trans-8′-apo-*β*-carotenal 15,15′-oxygenase
allantoin racemase
alliin lyase
alliin synthase
allophycocyanin
amicyanin
amidophosphoribosyltransferase
amidoxime reductase
D-amino-acid oxidase
L-amino-acid oxidase
D-amino-acid transaminase
L-aminoadipate-semialdehyde dehydrogenase
2-(3-amino-3-carboxypropyl)histidine synthase
2-amino-4-deoxychorismate synthase
amino-acid *N*-acetyltransferase

butane monooxygenase (soluble)
butyryl-CoA dehydrogenase
calmodulin-dependent P-type Ca^{2+} transporter
cAMP-dependent protein kinase
camphor 5-monooxygenase
carbamoyl-phosphate synthase (ammonia)
carbamoyl-phosphate synthase (glutamine-hydrolyzing)
carbazole 1,9a-dioxygenase
carbide synthase
carbonic anhydrase
carboxy-*S*-adenosyl-L-methionine synthase
5-(carboxyamino)imidazole ribonucleotide mutase
5-(carboxyamino)imidazole ribonucleotide synthase
N^2-(2-carboxyethyl)arginine synthase
(carboxyethyl)arginine β-lactam-synthase
3-carboxyethylcatechol 2,3-dioxygenase
carboxylesterase
3-carboxy-*cis,cis*-muconate cycloisomerase
4-carboxymuconolactone decarboxylase
carboxypeptidase
carboxypeptidase A
carboxypeptidase C
carboxypeptidase D
5-carboxyvanillate decarboxylase
β-carotene 15,15′-dioxygenase
carotenoid oxygenase 1
catalase
catalase-peroxidase
catechol *O*-methyltransferase
catechol oxidase
CDP-4-dehydro-6-deoxyglucose reductase
CDP-6-deoxy-L-*threo*-D-*glycero*-4-hexulose-3-dehydrase
CDP-paratose 2-epimerase
cellobiose dehydrogenase (acceptor)
cellulase
cellulose 1,4-β-cellobiosidase
cellulose 1,4-β-cellobiosidase (reducing end)
cellulose synthase
cellulose synthase (UDP-forming)
cephalosporin synthase
chalcone isomerase
chalcone synthase
chitinase
chloramphenicol *O*-acetyltransferase
chloride peroxidase
chlorite O_2-lyase
4-chlorobenzoate—CoA ligase
4-chlorobenzoyl-CoA dehalogenase
cholest-4-en-3-one 26-monooxygenase [(25*S*)-3-oxocholest-4-en-26-oate forming]
cholesterol monooxygenase (side-chain-cleaving)
cholesterol oxidase
choline oxidase
chondroitin AC lyase
chorismate mutase
chorismate mutase–prephenate dehydratase
chorismate synthase
chymotrypsin
α-chymotrypsin
citrate (*pro*-3*S*)-lyase
citrate (*Re*)-synthase
citrate (*Si*)-synthase
c-Jun amino-terminal protein kinase
coenzyme-B sulfoethylthiotransferase
CO-methylating acetyl-CoA synthase
coronamic acid synthase
creatinase
creatine kinase
creatininase
crotonyl-CoA carboxylase/reductase
cupriplastocyanin
cyanamide hydratase
cyclic-AMP-dependent non-specific serine/threonine protein kinase
cycloartenol synthase
cyclohexanone monooxygenase
cyclomaltodextrin glucanotransferase
cyclopropane-fatty-acyl-phospholipid synthase
cystathionine γ-lyase

dihydropyrimidine dehydrogenase (NADP$^+$)
dihydroxy-acid dehydratase
3,4-dihydroxy-2-butanone-4-phosphate synthase
1,4-dihydroxy-2-naphthoyl-CoA synthase
3,4-dihydroxyphenylacetate 2,3-dioxygenase
dihydroxyacetanilide epoxidase
diiron hydrogenase
dimethyl sulfide:cytochrome c_2 reductase
dimethylallyl*trans*transferase
4-dimethylallyltryptophan synthase
N^1-(1,1-dimethylallyl)tryptophan synthase
dimethylglycine oxidase
N^1-(1,1-dimethylprop-2-enyl)tryptophan synthase
dimethylpropiothetin dethiomethylase
dimethylsulfoxide reductase
dinitrogenase
dinitrogenase reductase
2,6-dioxo-6-phenylhexa-3-enoate hydrolase
diphosphate—fructose-6-phosphate 1-phosphotransferase
diphosphomevalonate decarboxylase
dipicolinate synthase
DNA (cytosine-5-)-methyltransferase
DNA β-glucosyltransferase
DNA helicase
DNA helicase I
DNA helicase PcrA
DNA helicase UvrD
DNA ligase (ATP)
DNA-(apurinic or apyrimidinic site) lyase
DNA-formamidopyrimidine glycosylase
DNA-3-methyladenine glycosylase II
DNA-directed DNA polymerase
DNA-directed DNA polymerase β
DNA-directed RNA polymerase
dopamine β-monooxygenase
double-stranded uracil-DNA glycosylase
dTDP-glucose 4,6-dehydratase
dTMP kinase
dUTP diphosphatase
*Eco*RV endonuclease
elastase
electron-transferring flavoprotein
electron-transferring-flavoprotein dehydrogenase
enamidase
endo-1,4-β-xylanase
endoglucanase CelC
endothiapepsin
2-enoate reductase
enoyl thioester reductase
enoyl-[acyl-carrier-protein] reductase (NADH)
enoyl-[acyl-carrier-protein] reductase (NADPH, *Re*-specific)
enoyl-CoA hydratase
epi-isozizaene synthase
epoxidase
epoxidase AsqJ
epoxide hydrolase
ethanolamine ammonia-lyase
ethylenediamine-*N*,*N*′-disuccinate lyase
ethylmalonyl-CoA mutase
exodeoxyribonuclease (lambda-induced)
exo-(1→4)-α-D-glucan lyase
exoribonuclease II
exo-α-sialidase
F_1-ATPase
(2*E*,6*E*)-farnesyl diphosphate synthase
farnesyl*trans*transferase
fatty acid synthase system
ferredoxin
ferredoxin hydrogenase
ferredoxin reductase
ferredoxin—NADP$^+$ reductase
ferredoxin—nitrite reductase
ferredoxin:CoB-CoM heterodisulfide reductase
ferredoxin:thioredoxin reductase
flavin monooxygenase
flavin prenyltransferase
flavodoxin
flavoenzyme NADPH—hemoprotein reductase
flavoprotein of assimilatory sulfite reductase (NADPH)

glutathione transferase
glutathione-disulfide reductase
glyceraldehyde-3-phosphate dehydrogenase
glycerol dehydrogenase
glycerol kinase
glycine *C*-acetyltransferase
glycine amidinotransferase
glycine dehydrogenase (decarboxylating)
glycine hydroxymethyltransferase
glycine *N*-methyltransferase
glycine oxidase
glycine reductase
glycogen phosphorylase
glycogen synthase
glycoprotein 3-α-L-fucosyltransferase
glyoxylate reductase
GMP synthase (glutamine-hydrolysing)
GTP 3′,8-cyclase
GTP cyclohydrolase
guanidinoacetate *N*-methyltransferase
H^+/K^+-exchanging ATPase
H^+-transporting two-sector ATPase
H_2:CoB-CoM heterodisulfide
haloacetate dehalogenase
haloacid dehalogenase
haloalkane dehalogenase
halohydrin dehalogenase
heme oxygenase (biliverdin-producing, ferredoxin)
heme oxygenase (biliverdin-producing)
hemerythrin
hemocyanin
hemoglobin
hemoperoxidase
hexokinase
3-hexulose-6-phosphate synthase
histidine ammonia-lyase
histidine decarboxylase
histidinol dehydrogenase
histidinol-phosphatase
histidinol-phosphate transaminase
histone acetyltransferase
histone deacetylase
HIV-1 retropepsin
homocitrate synthase
homogentisate 1,2-dioxygenase
homoisocitrate dehydrogenase
homoserine *O*-acetyltransferase
homoserine dehydrogenase
hydrogen peroxide-dependent heme synthase
hydrogenase (acceptor)
[FeFe] hydrogenase H-cluster radical SAM maturase HydG
D-2-hydroxyacid dehydrogenase (NAD^+)
(*S*)-2-hydroxy-acid oxidase
3-hydroxyacyl-[acyl-carrier-protein] dehydratase
3-hydroxyanthranilate 3,4-dioxygenase
3-hydroxybenzoate 4-monooxygenase
3-hydroxybenzoate 6-monooxygenase
4-hydroxybenzoate 3-monooxygenase
4-hydroxybenzoate 3-monooxygenase [NAD(P)H]
4-hydroxybenzoyl-CoA reductase
4-hydroxybutanoyl-CoA dehydratase
3-hydroxybutyryl-CoA epimerase
3-hydroxydecanoyl-[acyl-carrier-protein] dehydratase
3-hydroxyisobutyryl-CoA hydrolase
2-hydroxyethylphosphonate dioxygenase
(*R*)-2-hydroxyisocaproyl-CoA dehydratase
(*R*)-2-hydroxyisocaproyl-CoA dehydratase activator
hydroxylamine dehydrogenase
hydroxylamine reductase
4-hydroxymandelate synthase
hydroxymethylbilane synthase
4-hydroxy-3-methylbut-2-en-1-yl diphosphate reductase
(*E*)-4-hydroxy-3-methylbut-2-enyl-diphosphate synthase (flavodoxin)
hydroxymethylglutaryl-CoA reductase
hydroxymethylglutaryl-CoA reductase (NADPH)
hydroxymethylglutaryl-CoA synthase
3-hydroxy-2-methylpyridinecarboxylate monooxygenase

malate synthase
maleate hydratase
maleate isomerase
mandelate racemase
(*S*)-mandelate dehydrogenase
manganese catalase
manganese peroxidase
mannose-6-phosphate isomerase
mannuronate-specific alginate lyase
medium-chain acyl-CoA dehydrogenase
melilotate 3-monooxygenase
menaquinone reductase
3-mercaptopyruvate sulfurtransferase
mercury(II) reductase
methane monooxygenase (particulate)
methane monooxygenase (soluble)
methanol dehydrogenase (cytochrome *c*)
L-methionine adenosyltransferase
methionine decarboxylase
methionine γ-lyase
L-methionine (*R*)-*S*-oxide reductase
L-methionine (*S*)-*S*-oxide reductase
methionine synthase
methionine—tRNA ligase
methionyl aminopeptidase
2-methylacyl-CoA dehydrogenase
methylamine dehydrogenase (amicyanin)
methylamine—glutamate *N*-methyltransferase
methylamine utilization protein MauG
methylaspartate mutase
methylcrotonyl-CoA carboxylase
methylated-DNA—[protein]-cysteine *S*-methyltransferase
2-methyleneglutarate mutase
methylenetetrahydrofolate dehydrogenase
methylenetetrahydrofolate reductase (NADPH)
methylenetetrahydrofolate reductase [NAD(P)H]
methylenetetrahydrofolate—tRNA-(uracil^{54}-C^5)-methyltransferase [NAD(P)H-oxidizing]
2-*C*-methyl-D-erythritol 4-phosphate cytidylyltransferase
methylglyoxal synthase
3-methyl-2-indolic acid synthase
methylisocitrate lyase
methylmalonyl-CoA carboxytransferase
methylmalonyl-CoA decarboxylase
methylmalonyl-CoA mutase
3-methyl-2-oxobutanoate dehydrogenase (2-methylpropanoyl-transferring)
3-methyl-2-oxobutanoate hydroxymethyltransferase
4-methylphenol dehydrogenase (hydroxylating)
methylphosphonate synthase
5-methyltetrahydropteroyltriglutamate—homocysteine *S*-methyltransferase
mevalonate kinase
micrococcal nuclease
monoamine oxidase
monophenol monooxygenase
morphinone reductase
mRNA interferase toxin RelE
muconate cycloisomerase
muconolactone Δ-isomerase
mycofactocin radical SAM maturase
myeloperoxidase
myoglobin
myosin
myosin II
Na^+/K^+-exchanging ATPase
NADH peroxidase
NADH:ubiquinone reductase (H^+-translocating)
NADPH—hemoprotein reductase
naphthalene 1,2-dioxygenase
neomycin C epimerase
N-formylmethionylaminoacyl-tRNA deformylase
nickel–iron hydrogenase
nicotinamidase
nicotinate dehydrogenase
nicotinate-nucleotide diphosphorylase (carboxylating)
nicotinate-nucleotide—dimethylbenzimidazole phosphoribosyltransferase
nitrate reductase (quinone)

nitric oxide reductase (cytochrome *c*)
nitric oxide reductase (menaquinol)
nitric oxide reductase [NAD(P)$^+$, nitrous oxide-forming]
nitric-oxide synthase
nitric-oxide synthase (flavodoxin)
nitric-oxide synthase (NADPH)
nitrile hydratase
nitrite reductase
nitrite reductase (cytochrome; ammonia-forming)
nitrite reductase (NO-forming)
nitroalkane oxidase
nitrocyanin
nitrogenase
nitrous-oxide reductase
nonspecific protein-tyrosine kinase Csk
nonspecific protein-tyrosine kinase v-Fps
(*S*)-norcoclaurine synthase
nucleoside deoxyribosyltransferase
nucleoside-diphosphate kinase
5′-nucleotidase
octenoyl-CoA reductase/carboxylase
olefin-forming fatty acid decarboxylase
oleoyl-[acyl-carrier-protein] hydrolase
D-ornithine 4,5-aminomutase
ornithine aminotransferase
ornithine carbamoyltransferase
ornithine cyclodeaminase
D-ornithine/D-lysine decarboxylase
L-ornithine N^5-monooxygenase
L-ornithine N^5-monooxygenase (NADPH)
L-ornithine N^5-monooxygenase [NAD(P)H]
orotate phosphoribosyltransferase
orotate reductase (NADH)
orotidine-5′-phosphate decarboxylase
oxalate decarboxylase
oxalate oxidase
oxalate oxidoreductase
3-oxoacid CoA-transferase
3-oxoacyl-[acyl-carrier-protein] synthase
4-oxalocrotonate dehydrogenase
3-oxoacyl-[acyl-carrier-protein] synthase
2-oxo-4-carboxy-3-hexenedioate hydratase
oxoglutarate dehydrogenase (succinyl-transferring)
2-oxo-hept-4-ene-1,7-dioate hydratase
2-oxo-3-hexenedioate decarboxylase
2-oxopropyl-CoM reductase (carboxylating)
palmitoyl-[glycerolipid] 7-desaturase
pancreatic ribonuclease
pectate lyase
penicillopepsin
pentalenene synthase
pepsin
pepsin A
peptide deformylase
peptidyl-glutamate 4-carboxylase
peptidylglycine monooxygenase
peptidylprolyl isomerase
peroxidase
peroxygenase
persulfide dioxygenase
phenacrylate decarboxylase
phenol 2-monooxygenase (NADPH)
phenylalanine aminomutase (D-β-phenylalanine forming)
phenylalanine aminomutase (L-β-phenylalanine forming)
phenylalanine ammonia-lyase
phenylalanine dehydrogenase
phenylalanine 4-monooxygenase
phosphate acetyltransferase
phospho*enol*pyruvate carboxykinase
phospho*enol*pyruvate carboxykinase (ATP)
phospho*enol*pyruvate carboxykinase (GTP)
phospho*enol*pyruvate carboxylase
phospho*enol*pyruvate mutase
6-phosphofructokinase
6-phosphofructo-2-kinase
β-phosphoglucomutase
phosphoglucomutase
phosphoglucomutase (α-D-glucose-1,6-bisphosphate-dependent)

phosphogluconate dehydrogenase (NADP$^+$-dependent, decarboxylating)
6-phospho-β-glucosidase
phosphoglycerate dehydrogenase
phosphoglycerate kinase
phosphoglycerate mutase
phosphoinositide-dependent protein kinase
phosphoinositide phospholipase C
phosphoketolase
phospholipase A_2
phospholipase D
phosphonate dehydrogenase
phosphonoacetaldehyde hydrolase
phosphopantothenate—cysteine ligase (CTP)
phosphopantothenoylcysteine decarboxylase
phosphoprotein phosphatase
phosphopyruvate hydratase
phosphoribosylamine—glycine ligase
phosphoribosylaminoimidazolecarboxamide formyltransferase
phosphoribosylaminoimidazolesuccino-carboxamide synthase
phosphoribosylanthranilate isomerase
phosphoribosylformylglycinamidine synthase
phosphoribosylglycinamide formyltransferase
phosphoribulokinase
phosphoserine phosphatase
O-phosphoserine sulfhydrylase
3-phosphoshikimate 1-carboxyvinyltransferase
phosphotransferase system
phosphotriesterase
photosynthetic reaction center
photosystem II
C-phycocyanin
phycocyanin
phycoerythrin
4-phytase
(+)-α-pinene synthase
L-pipecolate oxidase
pivalyl-CoA mutase
plastocyanin
plastoquinol—plastocyanin reductase
poly(ADP-ribose) glycohydrolase
poly(β-D-mannuronate) C5 epimerase
polysaccharide monooxygenase
polyunsaturated fatty acid isomerase
porphobilinogen synthase
PqqA peptide cyclase
premalbrancheamide halogenase
prephenate dehydratase
prephenate dehydrogenase
preQ1 synthase
primary-amine oxidase
procollagen-lysine 5-dioxygenase
procollagen-proline 4-dioxygenase
proline dehydrogenase
proline racemase
propanediol dehydratase
propionyl-CoA carboxylase
prosolanapyrone-III cycloisomerase
prostaglandin-endoperoxide synthase
protein deglycase DJ-1
protein farnesyltransferase
protein geranylgeranyltransferase
protein O-GlcNAcase
protein-lysine 6-oxidase
protein-tyrosine kinase
protein-tyrosine kinase Csk
protein-tyrosine-phosphatase
protocatechuate 3,4-dioxygenase
pseudouridylate synthase
D-psicose 3-epimerase
D-psicose-6-phosphate 3-epimerase
P-type Ca^{2+} transporter
P-type H^+-exporting transporter
P-type Zn^{2+} transporter
purine nucleosidase
purine-nucleoside phosphorylase
purple acid phosphatase
putidaredoxin—NAD^+ reductase
pyranose oxidase
pyridoxamine—pyruvate transaminase

ulvan lyase
unspecific monooxygenase
uracil phosphoribosyltransferase
uracil-DNA glycosylase
urate hydroxylase
urease
uridine phosphorylase
urocanate hydratase
vanadium nitrogenase
verruculogen synthase
vetispiradiene synthase
xanthine dehydrogenase
xanthine oxidase
xanthine phosphoribosyltransferase
xylose isomerase
D-xylose reductase